EurJIC
European Journal of Inorganic Chemistry

January 2003
Issue 1
Pages 1–180

Papers available ahead of print in Early View at www.interscience.wiley.com

Earliest available Table of Contents:
Automatically, free of charge by e-mail through
www.interscience.wiley.com/alerts

COVER PICTURE

The cover picture shows the structure of an unusual dinuclear $Rh^{I}-Rh^{III}$ complex obtained in the reaction of the tetradentate ligand 3,6-bis(2-pyridyl)pyridazine with cationic (diene)Rh^{I} precursors. Initially, the expected N,N-bidentate Rh^{I} complex is formed, which upon further reaction with the Rh^{I} precursor undergoes C–H bond activation of the pyridazine ring, forming a C,N-bidentate Rh^{III} center. This is followed by a unique rearrangement of the diene, which is dependent on the metal precursor and on the ligand used. Details are discussed in the article by D. Milstein et al. on p. 70ff. We thank Relli Mahager (Graphics Department, WIS) for producing the colour picture.

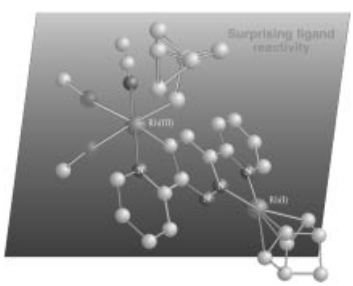

MICROREVIEW

Contents

17 **A. Antiñolo, M. Fajardo, A. Otero,* S. Prashar**

Sandwich and Half-Sandwich (Imido)niobium Complexes

Keywords: Niobium / Imido ligands / Cyclopentadienyl ligands / *ansa*-Niobocene complexes

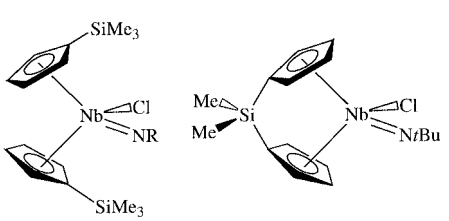

 © 2003 WILEY-VCH Verlag GmbH & Co. KGaA, 69451 Weinheim 1434–1948/03/0101–0007 $ 20.00+.50/0

SHORT COMMUNICATIONS

29 **A. V. Usatov,* E. V. Martynova, F. M. Dolgushin, A. S. Peregudov, M. Yu. Antipin, Yu. N. Novikov**

Selective Insertion of Dioxygen into an (η^2-C_{60})−Ir Bond: Synthesis and Structure of the First Metallacyclic Complex with a σ-Coordinated Fullerene Molecule

Keywords: Fullerenes / Carboranes / Iridium / Oxygen / Insertion

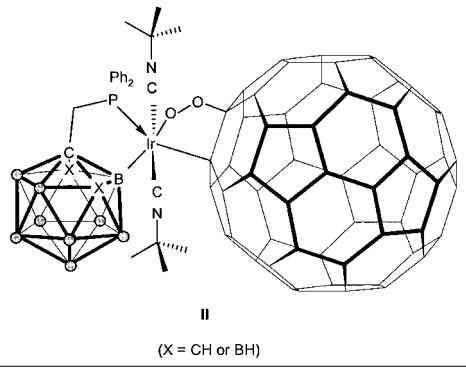

II

(X = CH or BH)

34 **P. Comba,* Y. D. Lampeka,* L. Lötzbeyer, A. I. Prikhod'ko**

Macrocyclic Melamine-Based Ligand Complexes as Building Blocks for the Metal-Directed Synthesis of Heterometallic Di- and Trinuclear Compounds

Keywords: Template reactions / Nickel / Copper / Macrocycles / N ligands

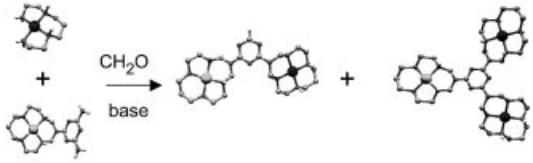

38 **D. Sun, R. Cao,* Y. Sun, W. Bi, X. Li, M. Hong, Y. Zhao**

Self-Assembly of a One-Dimensional Silver Complex Containing Two Kinds of Helical Chains

Keywords: Self-assembly / S ligands / N ligands / Silver / Helical structures

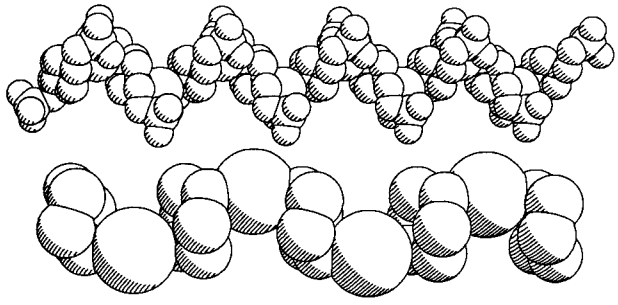

42 **O. Bortolini,* M. Carraro, V. Conte,* S. Moro**

Vanadium-Bromoperoxidase-Mimicking Systems: Direct Evidence of a Hypobromite-Like Vanadium Intermediate

Keywords: Ab initio calculations / Enzyme models / Mass spectrometry / Peroxo ligands / Vanadium

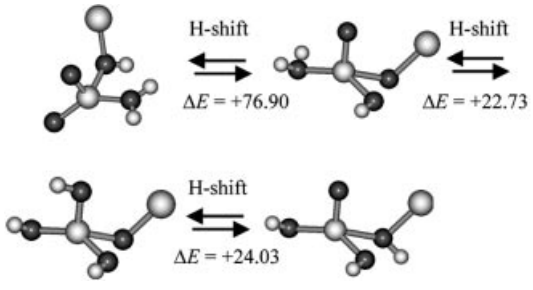

47 **B. Kozlevčar, P. Gamez, R. de Gelder, W. L. Driessen,* J. Reedijk**

Unprecedented Change of the Jahn−Teller Axis in a Centrosymmetric Cu^{II} Complex Induced by Lattice Water Molecules − Crystal and Molecular Structures of Bis[bis(3,5-dimethylpyrazol-1-yl)acetato]copper(II) and Its Dihydrate

Keywords: Copper / N ligands / Jahn−Teller distortion / EPR spectroscopy

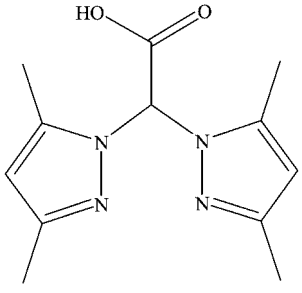

51 **K. Merz, H.-M. Hu, S. Rell, M. Driess***

Syntheses and Molecular Structures of Metallasiloxanes Containing Zn_3O_4 and $Zn_6Si_6O_{10}$ Cores

Keywords: Clusters / Oxides / Siloxides / Zinc

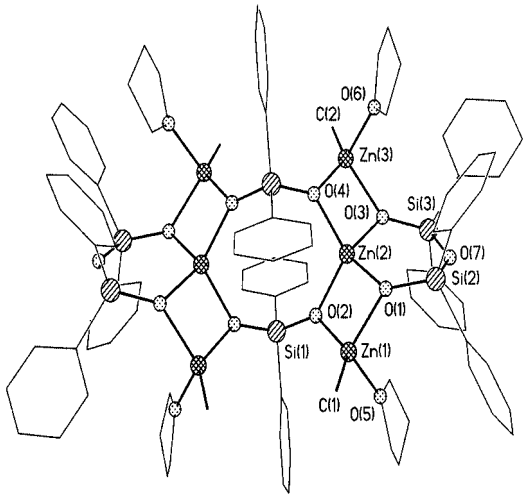

54 **I. Shevchenko,* V. Anddrushko, E. Lork, G.-V. Röschenthaler***

The Unexpected Formation of a Novel Fluorinated Triene

Keywords: Phosphanes / Bis(trifluoromethyl)acrylonitrile / Alkenes / Ylides / Carbenes

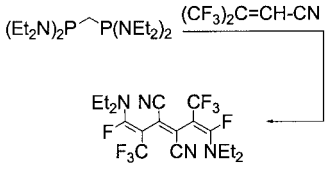

57 **A. Jouaiti, M. W. Hosseini,* N. Kyritsakas**

Molecular Tectonics: Design of 1-D Coordination Networks Based on Pyrene-Bearing Pyrazolyl Units

Keywords: N ligands / Coordination networks / Silver / Palladium

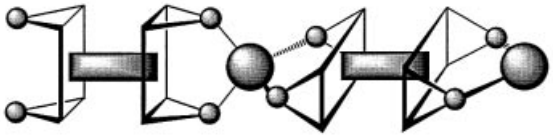

62 **L. Li,* Z. Liu, S. S. Turner, D. Liao, Z. Jiang,* S. Yan**

Unique Magnetic Behavior in a One-Dimensional Coordination Polymer $[Co(tmpyim)_2(tp)]$

Keywords: Magnetic properties / Crystal structure / Radicals / Terephthalate

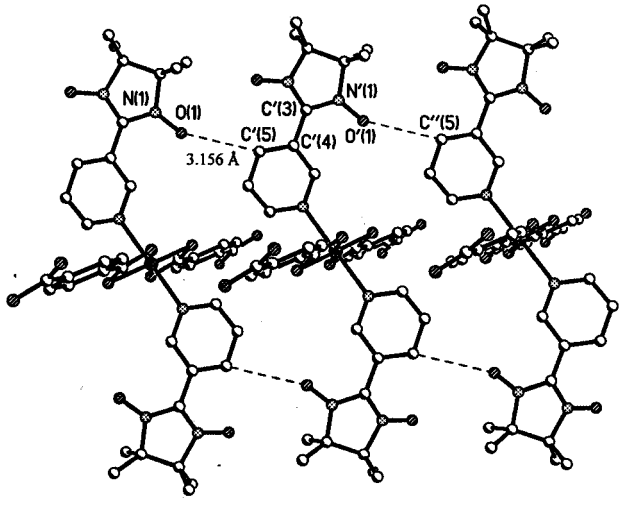

66 **C. Ackerhans, H. W. Roesky,* D. Vidovic, J. Magull**

Symmetric Tetraalkynyldisilanes

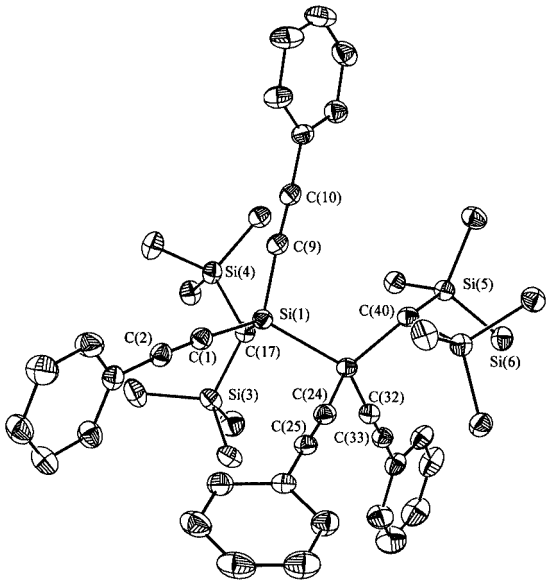

Keywords: Alkynes / Bulky ligands / Silanes / Silicon

FULL PAPERS

70 **R. Dorta, L. Konstantinovski, L. J. W. Shimon, Y. Ben-David, D. Milstein***

Chelation versus Cyclometalation in a Cationic Dppn−Rh^{I} Complex − A Unique Rearrangement of Norbornadiene via C−H Activation of the Pyridazine Ring

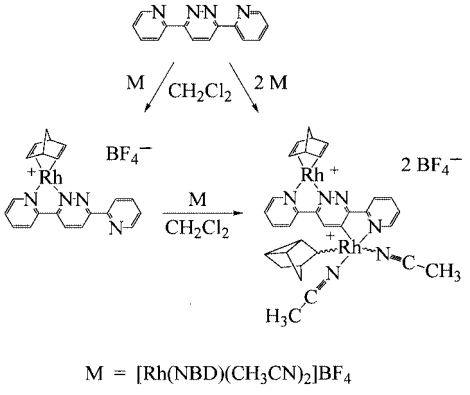

M = $[Rh(NBD)(CH_3CN)_2]BF_4$

Keywords: Rhodium complexes / Mono- and dinuclear complexes / C−H activation / Rearrangement of norbornadiene / ^{1}H-^{15}N GHMBC NMR / X-ray structure

77 **A. Y. Makarov, I. Y. Bagryanskaya, F. Blockhuys,* C. Van Alsenoy, Y. V. Gatilov, V. V. Knyazev, A. M. Maksimov, T. V. Mikhalina, V. E. Platonov, M. M. Shakirov, A. V. Zibarev***

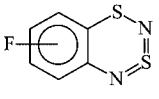

Fluorinated 1,3$\lambda^4\delta^2$,2,4-Benzodithiadiazines − A Synthetic, Structural and Theoretical Study

Keywords: Antiaromaticity / Fluorinated 1,3$\lambda^4\delta^2$,2,4-benzodithiadiazines / Electrophilic cyclisation / Molecular structure / NICS / Nucleophilic cyclisation

89 **T. Ruman, Z. Ciunik, S. Wołowiec***

The Ambivalent Bonding of the 3(5)-Isopropylpyrazolyl Moiety in Homo- and Heteroscorpionate Hydrobis(3-R_1-5-R_2-pyrazolyl)(*y*-isopropylpyrazolyl)boratocobalt(II) Complexes (*y* = 3 or 5)

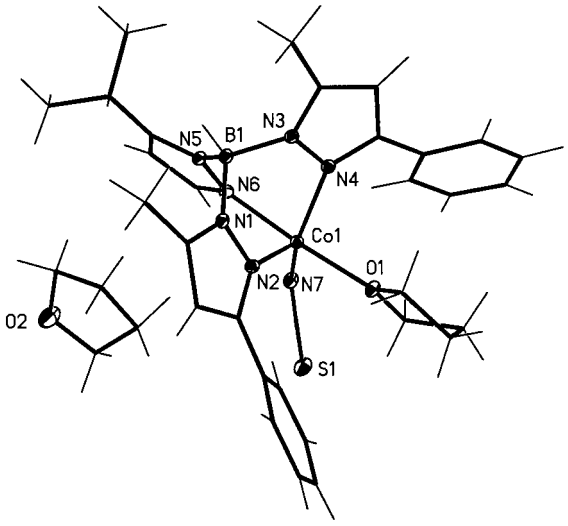

Keywords: Cobalt / Borates / N ligands / NMR spectroscopy

94 **D. Sun, R. Cao,* Y. Sun, X. Li, W. Bi, M. Hong, Y. Zhao**

Two New Zeolite-Like Supramolecular Copper Complexes

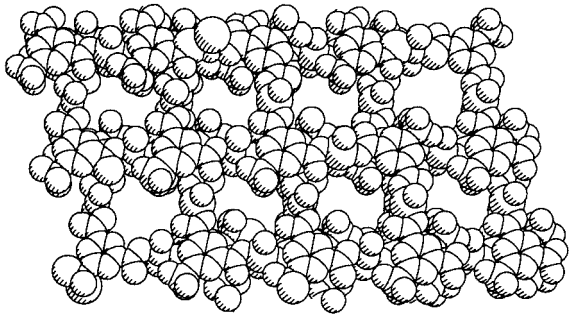

Keywords: Copper / Supramolecular chemistry / Hydrogen bonds / Zeolite analogues / Amines

99 **R. A. Findeis, L. H. Gade***

Tripodal Phosphane Ligands with Novel Linker Units and Their Rhodium Complexes as Building Blocks for Dendrimer Catalysts

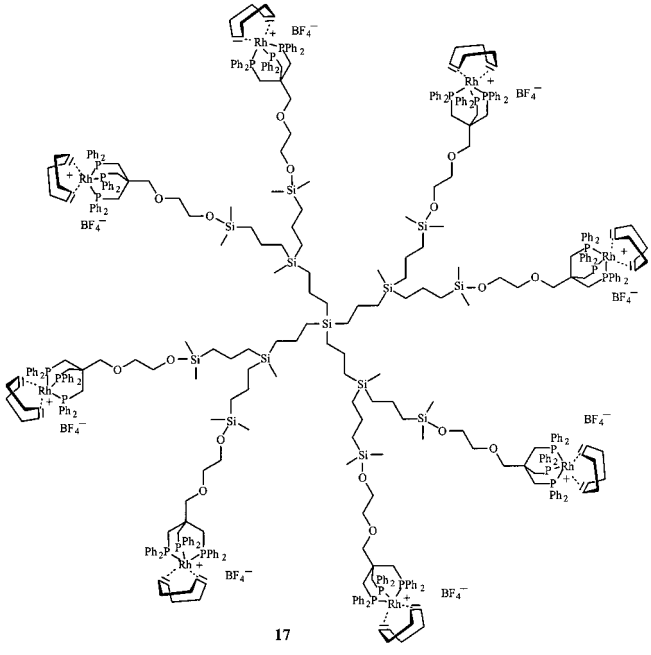

Keywords: Phosphane ligands / Hydrogenation / Catalysis / Dendrimers / Rhodium

111

M. Bremer, H. Nöth,* M. Warchhold

The Structure of Some Amine Solvates of Magnesium Bis(tetrahydroborate) and DFT Calculations on Solvates of Lithium Tetrahydroborate

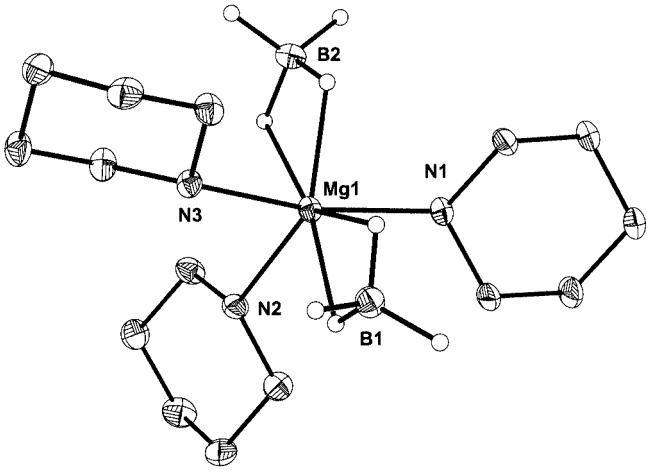

Keywords: Amine ligands / Borates / Density functional calculations / Lithium / Magnesium

120

M. R. J. Elsegood, K. E. Holmes, P. F. Kelly,* E. J. MacLean, J. Parr, J. M. Stonehouse

Preparation of the First Complexes of Bidentate Sulfimides; the X-ray Crystal Structures of $[PdBr_2\{1,4\text{-}(PhS\{NH\})_2C_6H_4\}]_2$, $[PdCl_2\{1,2\text{-}(PhS\{NH\})(PhS)C_6H_4\}]$ and *trans*-$[PdCl_2\{1,2\text{-}(PhS\{NH\})(PhS)C_6H_4\}PPh_3]$

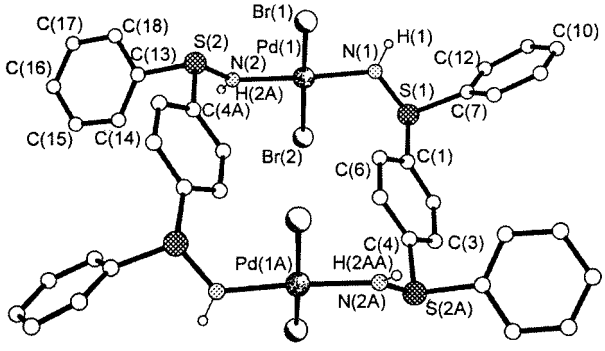

Keywords: S ligands / N ligands / Palladium / Bridging ligands

128

B. Longato, L. Pasquato, A. Mucci,* L. Schenetti*

Coordination Modes of 9-Methyladenine in *cis*-Platinum(II) Complexes with Dimethyl(phenyl)phosphanes as Ancillary Ligands − Synthesis and Characterization of *cis*-$[PtL_2(9\text{-}MeAd)_2](NO_3)_2$, *cis*-$[PtL_2\{9\text{-}MeAd(-H)\}]_3(NO_3)_3$, and *cis*-$[L_2Pt\{9\text{-}MeAd(-H)\}PtL_2](NO_3)_3$

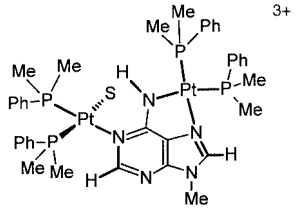

Keywords: Coordination modes / N ligands / NMR spectroscopy / P ligands / Platinum

138 **X.-M. Zhang, M.-L. Tong, M.-L. Gong, X.-M. Chen***

Supramolecular Organisation of Polymeric Coordination Chains into a Three-Dimensional Network with Nanosized Channels that Clathrate Large Organic Molecules

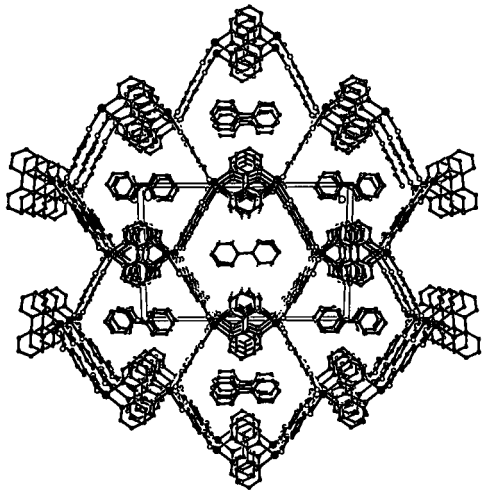

Keywords: Coordination polymers / Microporous materials / Inclusion compounds / Supramolecular chemistry

143 **T. Lébl,* A. Smička, J. Brus, C. Bruhn**

Synthesis, Structural Study, and In Vitro Trypanocidal and Antitumour Activities of Tetrakis(3-methoxypropyl)tin and (3-Methoxypropyl)tin Chlorides

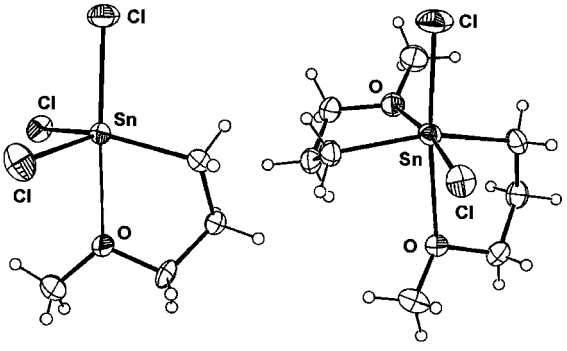

Keywords: Chelates / Drug research / O ligands / Structure elucidation / Tin

149 **A. W.-H. Lam, W.-T. Wong,* S. Gao, G. Wen, X.-X. Zhang**

Synthesis, Crystal Structure, and Photophysical and Magnetic Properties of Dimeric and Polymeric Lanthanide Complexes with Benzoic Acid and Its Derivatives

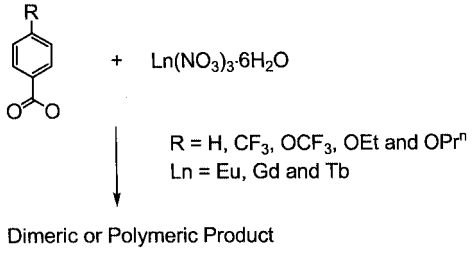

Keywords: Carboxylate ligands / Lanthanides / Luminescence / Magnetic properties

164 **J. Beckmann, D. Horn, K. Jurkschat,* F. Rosche, M. Schürmann, U. Zachwieja, D. Dakternieks,* A. Duthie, A. E. K. Lim**

Triorganotin Fluoride Structures: A Ligand Close-Packing Model with Predominantly Ionic Sn−F Bonds

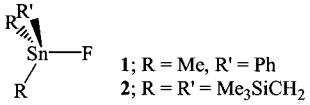

1; R = Me, R' = Ph
2; R = R' = Me_3SiCH_2

Keywords: Ab initio calculations / Chain structures / Hypervalent compounds / Tin / Fluorides / X-ray diffraction

175 **D. M. Thompson, M. Jones, M. C. Baird***

Anionic Cyclopentadienyl C_{60} Complexes of Molybdenum and Tungsten; The Strange Case of Iron

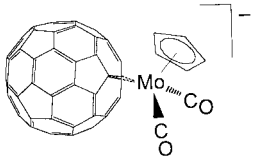

Keywords: Fullerenes / Molybdenum / Tungsten / Iron

Sandwich and Half-Sandwich (Imido)niobium Complexes

Antonio Antiñolo,[a] Mariano Fajardo,[b] Antonio Otero,*[a] and Sanjiv Prashar[b]

Keywords: Niobium / Imido ligands / Cyclopentadienyl ligands / *ansa*-Niobocene complexes

This review discusses the study we have carried out towards the synthesis, structure and reactivity of (imido)niobium complexes, which contain at least one cyclopentadienyl ligand. The following families of niobium complexes are described: (i) half-sandwich imido complexes; (ii) metallocene imido compounds; (iii) imido complexes containing *ansa*-cyclopentadienyl ligands; (iv) dinuclear imido complexes such as $[\{Nb(\eta^5\text{-}C_5H_4SiMe_3)_2Cl\}_2(\mu\text{-}1,3\text{-}N_2C_6H_4)]$. In addition we describe spectroscopic and structural features of the (imido)niobium complexes.
(© Wiley-VCH Verlag GmbH, 69451 Weinheim, Germany, 2003)

1. Introduction

The interest arising from the use of imido groups as ligands in the organometallic chemistry of the group 5 elements has experienced a rapid increase in the past decade. Half-sandwich complexes are well known in (imido)niobium chemistry.[1−25] Their metallocene counterparts have also been studied but to a lesser degree.[24−30]

The attention dedicated to imido-containing niobium complexes can be attributed firstly to the isoelectronic relationship that this ligand shares with the cyclopentadienyl moiety. Thus, the half-sandwich imido fragment Nb(=NR)Cp is isoelectronic with MCp_2 (M = Ti, Zr, Hf). Secondly, the imido group can also be bound to the metal atom in differing fashions acting either as a two- or four-electron donor.

[a] Departamento de Química Inorgánica, Orgánica y Bioquímica, Facultad de Químicas, Campus Universitario, Universidad de Castilla-La Mancha,
13071 Ciudad Real, Spain
Fax: (internat.) + 34-926/295-318
E-mail: Antonio.Otero@uclm.es
[b] Departamento de Ciencias Experimentales e Ingeniería, E.S.C.E.T., Universidad Rey Juan Carlos,
28933 Móstoles (Madrid), Spain

Antonio Antiñolo (top, left) was born in Cartagena, Spain in 1956. He obtained his graduate degree in 1978 from the University of Murcia and his Doctorate in 1982 with Prof. Pascual Royo at the University of Alcalá de Henares. After his postdoctoral appointment with Prof. Michael F. Lappert in 1984 at the University of Sussex, Antonio Antiñolo took up a lectureship position at the University of Alcalá de Henares in 1984. In 1990 he moved to the University of Castilla-La Mancha and became a Full Professor in 1999. His current research interests are centred on metallocene and ansa-metallocene derivatives of early transition metals as possible stereoselective catalysts in olefin polymerization and the activation of small molecules in polyhydride chemistry.

Mariano Fajardo (top, right) was born in Cartagena, Spain in 1956. He obtained his graduate degree in 1978 from the University of Murcia and his Doctorate in 1982 with Prof. Pascual Royo at the University of Alcalá de Henares. From 1982 to 1984 he worked as a postdoc with Prof. Jack Lewis at the University of Cambridge. On his return to Spain he took up a lectureship post at the University of Alcalá de Henares. In the year 2000 he was appointed Full Professor at the University Rey Juan Carlos in Madrid. His current research interests are centred on complexes of early transition metals as possible stereoselective catalysts in olefin polymerization and epoxidation processes and the role of metal complexes in environmental chemistry.

Antonio Otero (bottom, left) was born in Minglanilla (Cuenca), Spain in 1949. He obtained his graduate degree in 1973 from the University of Murcia and his Doctorate in 1976 with Prof. Pascual Royo. From 1978−1979, he worked as a postdoctoral fellow at the University of Oxford with Prof. Malcolm Green researching C−H bond activation processes from cyclopentadienylmolybdenum and -tungsten organometallic complexes. From 1979 to 1989 he was a lecturer at the University of Alcalá. In December 1989, he was appointed Full Professor in Inorganic Chemistry at the University of Castilla-La Mancha. He has authored more than 130 publications in reviewed journals. His current research interests include organometallic chemistry of early transition metals, particularly of group 4 and 5 elements, homogeneous catalytic processes of olefin polymerization with group 4 metallocene catalysts, and heterogeneization of homogeneous catalysts on different inorganic supports.

Sanjiv Prashar (bottom, right) was born in London, United Kingdom in 1966. He obtained his B.Sc. in 1987 and his D.Phil. in 1992 with Prof. Michael F. Lappert from the University of Sussex. His first postdoctoral appointment took him to Spain where he worked with Prof. Pascual Royo at the University of Alcalá de Henares. In 1995 he moved to Ciudad Real in the Spanish Mancha and for more than 6 years he worked at the University of Castilla-La Mancha in collaboration with Professors Antonio Antiñolo and Antonio Otero. It was here that the majority of this study of (imido)niobium compounds was carried out. In October 2001 he took up a lectureship position at the University Rey Juan Carlos in Madrid where his current research interests are centred on ansa-metallocene derivatives of early transition metals as possible stereoselective catalysts in olefin polymerization.

MICROREVIEWS: This feature introduces the readers to the author's research through a concise overview of the selected topic. Reference to important work from others in the field is included.

Imido ligands, are common ligands in high-oxidation-state transition-metal chemistry. An (imido)metal complex has the general form M=NR where there is a double bond between the metal centre and the nitrogen atom. In addition, the lone pair on the nitrogen atom usually donates electron density to the metal centre, providing a triple-bond interaction with the metal atom.

In high-valent complexes the imido unit is usually considered to be RN^{2-} whereas in low-valent complexes it tends to be considered as a neutral ligand. When specifying how many electrons an imido ligand donates it is therefore necessary to state which electron formalism one is using and to consider how the nitrogen atom is participating in the bonding (Scheme 1). It should be noted that the imido and oxo ligands are isoelectronic.

	$L_nM{=}N{-}R$	$L_nM{\leftarrow}N{\equiv}C$
Hybridization at nitrogen:	sp^2	sp
Idealized bond angle:	120°	180°
Isoelectronic to:	$L_nM{=}O$	$L_nM{\leftarrow}O$
Electron donation:		
NR^{2-}	$4e^-$	$6e^-$
neutral	$2e^-$	$4e^-$

Scheme 1. Hybridization and electron counting in imido compounds

The M−N−R bond angle can, in most cases be regarded as an indicator of the degree of π-donation from the nitrogen atom. Imido ligands are very good π-donors and thus the overwhelming majority of imido complexes are linear or near-linear (bond angles from 150 to 180°).

The imido ligand can act as a spectator ligand similar to the role played by cyclopentadienyl or can directly participate in the reactivity namely in protonation processes. Imido ligands are of interest not only for their role as ancillary ("spectator") ligands, but for the potential group transfer of the imido unit to an organic moiety.

2. Discussion

2.1 (Imido)niobium Precursors

The complexes [Nb(=NAr)Cl_3(DME)] [Ar = C_6H_4Me-4 (**1**), C_6H_4OMe-4 (**2**)][31] [Equation (1)] were prepared by a modification of the synthetic methods reported for other (imido)niobium halide complexes.[32,33] The synthesis of [Nb(=N*t*Bu)Cl_3(py)$_2$] was reported by Sundermeyer et al.[34] These complexes have been employed in the synthesis of the cyclopentadienyl-containing niobium complexes discussed hereafter.

$$NbCl_5 + ArNH_2 + DME + 2py + 2ZnCl_2 \xrightarrow{CH_2Cl_2} [Nb(=NAr)Cl_3(DME)] + 2[pyH][ZnCl_3] \quad (1)$$

Ar = C_6H_4Me-4 (**1**), C_6H_4OMe-4 (**2**)

The ^{1}H NMR spectra of **1** and **2** show clearly the inequivalence of the methyl and methylene groups of the DME adduct suggesting, for an octahedral disposition, that this ligand is bonded to the metal centre by two Nb−O links in which one oxygen atom is located *cis* to the imide group and the other oxygen atom *trans*. This has been confirmed by X-ray crystal diffraction studies (Figure 1).[35]

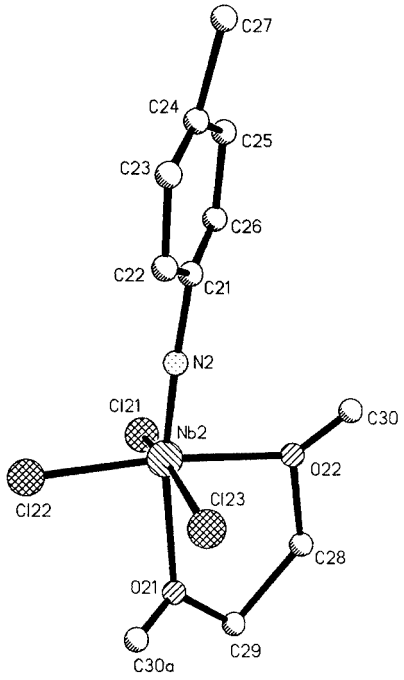

Figure 1. Molecular structure of [Nb(=NC_6H_4Me-4)Cl_3(DME)] (**1**)

2.2 Half-Sandwich (Imido)niobium Complexes

2.2.1 Synthesis

The principal synthetic routes, reported previously in the literature, for the preparation of half-sandwich (imido)niobium complexes involved the reaction of [Nb(η^5-C_5R_5)Cl_4] with the appropriate amine H_2NR' or $NR'(SiMe_3)_2$.[20,23] However, [Nb(=N*t*Bu)$CpCl_2$] (**3**) and [Nb(=NC_6H_4Me-4)$CpCl_2$] (**4**) were prepared by the straightforward reaction of 1 mol-equiv. of NaCp with [Nb(=N*t*Bu)Cl_3(py)$_2$] or **1**, respectively [Equation (2)].[31]

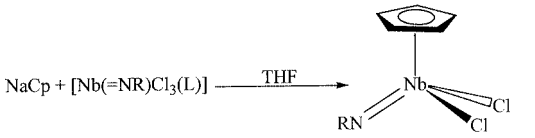

(2)

When the same reaction was carried out between [Nb(=N*t*Bu)Cl_3(py)$_2$] and LiCp′ (Cp′ = η^5-$C_5H_4SiMe_3$) both the monosubstituted [Nb(=N*t*Bu)Cp′Cl_2] (**5**) and disubstituted [Nb(=N*t*Bu)Cp′$_2$Cl] (**6**) complexes were shown to be present (Scheme 2).[31]

2.2.2 Structural Characterization

Complexes containing the unsubstituted cyclopentadienyl ligand show a unique signal in their ^{1}H NMR

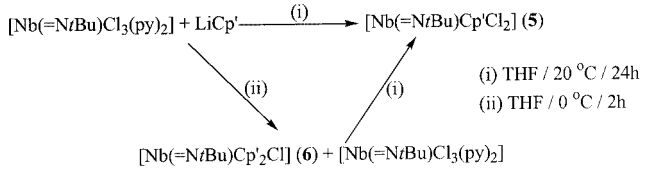

Scheme 2

spectra regardless of the surrounding symmetry for this moiety. However, when a substituent is introduced in the cyclopentadienyl ring, the resulting ring protons give signals directly related to the symmetry of the complex. Thus for **5**, an AA′BB′ system for the ring protons is observed in the ^{1}H NMR spectrum.

2.2.3 Reactivity with Allyl Grignard Reagents

The allyl(imido)niobium complexes [Nb(=N*t*Bu)Cp(η^1-$CH_2C(R)CH_2$]Cl] [R = H (**7**), Me (**8**)] were prepared by the reaction of **3** with the corresponding allylmagnesium chloride [Equation (3)].[36] In the ^{1}H NMR spectrum for **7** and **8** the signals associated with η^1-allyl systems, namely three signals corresponding to the CH_2 moiety bonded to the metal centre, the central group C(R) and the olefinic protons for the terminal CH_2, were observed. The values of the coupling constants and those of other η^1-allyl complexes discussed in this review are given in Table 1.

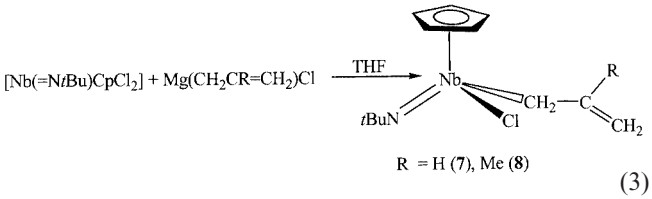

R = H (**7**), Me (**8**) (3)

2.3 (Imido)niobocene Complexes

2.3.1 Synthesis

Although the chemistry of monocyclopentadienyl(imido) complexes of niobium is well documented[1−25] far fewer examples of bent (imido)niobocene complexes can be found in the literature.[24−30] Our initial studies in this field led to the synthesis of [Nb(=NR)Cp′$_2$Cl] [R = *t*Bu (**6**), Ph (**9**), *n*Pr (**10**), *i*Pr (**11**)] along two distinctive preparative routes.[37,38] The first involved the reaction of RNH_2 with [{NbCp′$_2$Cl}$_2$] in accordance with a sequence involving initial oxidative addition of the amine, giving rise presumably to an amido intermediate which on subsequent thermolytic expulsion of H_2 affords the imido derivative [Equation (4)].[37] The second route consisted of the thermal treatment of [NbCp′$_2$(RNCO)Cl] to give the desired imido complex [see Equation (5)].[37,38]

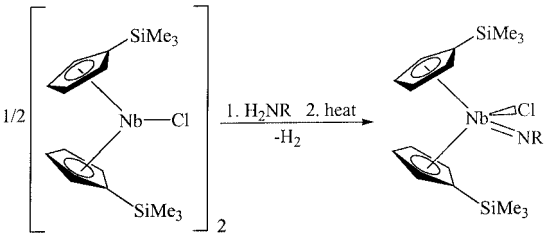

(4)

R = *t*Bu (**6**), Ph (**9**), *n*Pr (**10**), *i*Pr (**11**)

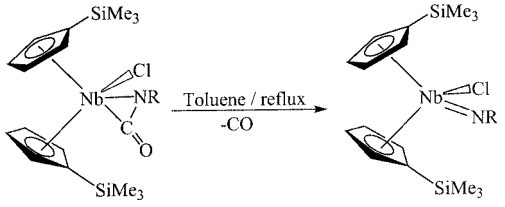

(5)

R = *t*Bu (**6**), Ph (**9**), *n*Pr (**10**), *i*Pr (**11**)

A more straightforward preparative method, by the reaction of 2 equiv. of LiCp′ with the corresponding (imido)niobium halide precursor [Equation (6)], was used in the synthesis of [Nb(=NR)Cp′$_2$Cl] [R = *t*Bu (**6**), C_6H_4Me-4 (**12**), C_6H_4OMe-4 (**13**)].[31] In a similar manner the imido complex [Nb(=NC_6H_4Me-4)Cp$_2$Cl] (**14**) was synthesized.[39] The mixed sandwich complex [Nb(=N*t*Bu)-CpCp′Cl] (**15**) was prepared by the addition of LiCp′ to a THF solution of [Nb(=N*t*Bu)CpCl$_2$] (**3**) [Equation (7)].[31]

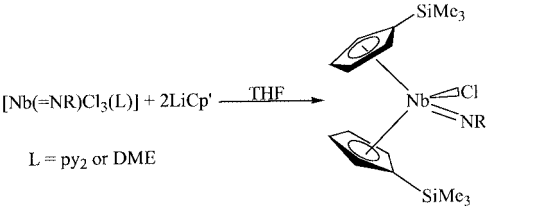

(6)

R = *t*Bu (**6**), C_6H_4Me-4 (**12**), C_6H_4OMe-4 (**13**)

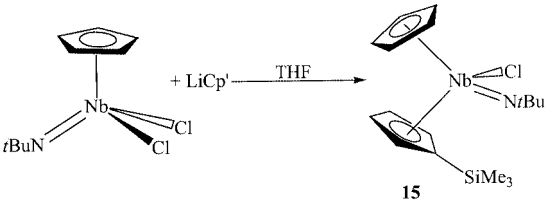

(7)

15

Table 1. Coupling constants for the η^1-allyl complexes

	^3J(^{1}H-^{1}H)	$^2J_{gem}$(^{1}H-^{1}H)	$^3J_{cis}$(^{1}H-^{1}H)	$^3J_{trans}$(^{1}H-^{1}H)
[Nb(=N*t*Bu)Cp(η^1-CH_2CHCH_2)Cl] (**7**)	8.1 Hz	2.6 Hz	9.9 Hz	16.8 Hz
[Nb(=N*t*Bu)Cp[η^1-$CH_2C(Me)CH_2$]Cl] (**8**)		3.0 Hz		
[Nb(=NC_6H_4Me-4)Cp$_2$(η^1-CH_2CHCH_2)] (**25**)	8.3 Hz	2.5 Hz	9.9 Hz	16.8 Hz
[Nb(=N*t*Bu)Cp′$_2$(η^1-CH_2CHCH_2)] (**26**)	8.5 Hz	2.5 Hz	9.9 Hz	16.9 Hz
[Nb(=NC_6H_4Me-4)Cp′$_2$(η^1-CH_2CHCH_2)] (**27**)	8.1 Hz	2.5 Hz	9.9 Hz	16.8 Hz
[Nb(=NC_6H_4OMe-4)Cp′$_2$(η^1-CH_2CHCH_2)] (**28**)	8.3 Hz	2.4 Hz	10.0 Hz	16.8 Hz
[Nb(=N*t*Bu){$Me_2Si(\eta^5$-$C_5H_4)_2$}(η^1-CH_2CHCH_2)] (**55**)	8.5 Hz	2.6 Hz	9.9 Hz	16.8 Hz

2.3.2 Structural Characterization

The ^{1}H NMR spectra of the $(Cp')_2$(imido) complexes **6**, **9**−**13** all give similar signal patterns reflecting the C_s symmetry of the molecules. Thus, there is inequivalency between the cyclopentadienyl ring protons in the same system but equivalency between the two rings. An ABCD system is therefore observed.

The molecular structures of **9** and **13**, determined by single-crystal X-ray diffraction studies are depicted in Figures 2 and 3.

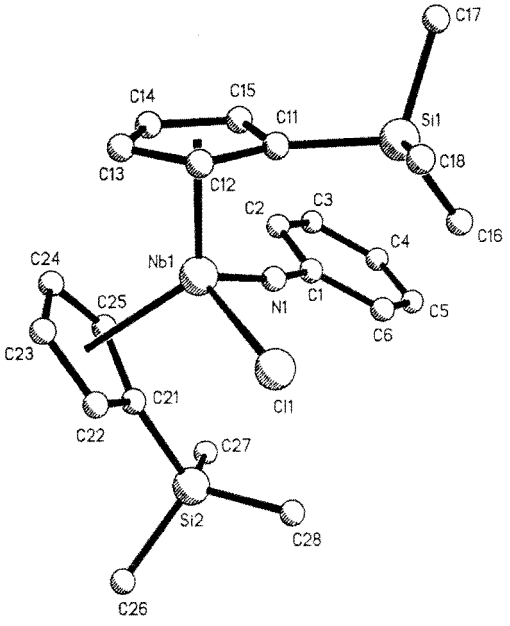

Figure 2. Molecular structure of [Nb(=NPh)Cp′$_2$Cl] (**9**)

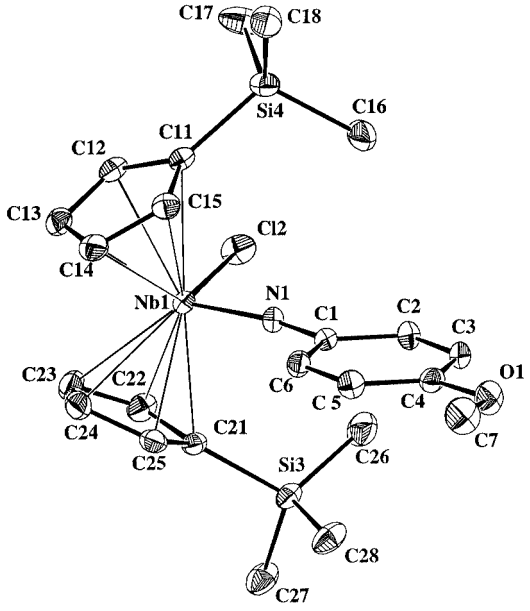

Figure 3. Molecular structure of [Nb(=NC$_6$H$_4$OMe-4)Cp′$_2$Cl] (**13**)

The structural features of **9** and **13** are nearly identical and thus for reasons of simplicity, reference is only made to the former complex.

Compound **9** is a monomer in the solid state and shows a typical bent-metallocene structure. Interestingly, the chlorine atom and the phenyl group lie practically in the equatorial plane, in a similar disposition to that found previously for [Ta(=NPh)(η^5-$C_5Me_5)_2$H] and [Ta(=NH)(η^5-$C_5Me_5)_2$Cl].[40,41] Using a frontier-orbital approach Jørgensen[42] explained why the phenyl group in this type of complexes lies in the equatorial plane and not perpendicular to it in an alternative arrangement. The Nb−N bond length is 1.792(2) Å, indicating that probably a bond order halfway between two (Nb=N) and three (Nb≡N) is present. However, the interesting structural parameter is the value of 165.1(2)° found for the Nb−N−C_{ipso} moiety. In the structures reported linear M−N−C geometries are observed for virtually all metallocene complexes (see Table 4). However, for **9** a deviation in this angle of about 15° is observed. The bent arrangement may indicate that the imido nitrogen atom is sp^2-hybridized, but in such a case the phenyl substituent should be orientated out of the equatorial plane towards one of the cyclopentadienyl ligands.[40] Therefore, in spite of the low angle for Nb−N−C_{ipso}, we propose that the nitrogen atom is sp-(not sp^2-)hybridized and that the two limiting descriptions, Nb≡N−R and Nb=N−R, proposed by Bercaw and co-workers for (η^5-$C_5Me_5)_2$Ta(=NPh)(H) may explain the true bonding situation.[40]

In order to gain more insight into the nature of the Nb−N bond, extended-Hückel molecular-orbital calculations have been performed.[43−46] Figure 4 shows an interaction diagram for the frontier orbitals of [Nb(=NPh)Cp_2Cl] from [$NbCp_2Cl]^{2+}$ to the left and NPh^{2-} to the right.[37] The results are in agreement with those found previously by Jørgensen[42] for [Ta(=NPh)(η^5-$C_5Me_5)_2$H].

A Walsh diagram for five of the frontier orbitals for bending of the phenyl group in the equatorial plane between 180 and 120° is illustrated in Figure 5, and shows that the highest occupied molecular orbital (HOMO) is unaffected by this bending in contrast to the bending out of the equatorial plane where an increase in energy similar to that described for [Ta(=NPh)(η^5-$C_5Me_5)_2$H] is observed.[37] However, the Walsh diagram shows that the second and third HOMO increase in energy upon bending the phenyl group (θ = 140°) and a change in total energy from −1717.63 eV for θ = 180° to 1714.54 eV for θ = 120° is observed. However, no significant changes in energy between θ = 180 and 140° are observed, indicating that in complex **9**, with Nb−N−C_{ipso} of 165°, electronic effects are not responsible for this deviation from linear. The Nb−N and N−C_{ipso} overlap populations decrease as a result of the bending and the charge at the niobium atom decreases as the charge at the nitrogen atom increases (see Table 2). The phenyl substituent arranges itself so as to maximize the overlap with the nitrogen p-orbital, but slight modifications of this overlap are observed in the range θ = 180−160°. We have established that the imido bond angles for "linear imide" in this class of complexes can vary to 140° with little effect on the M−N bonding.[37]

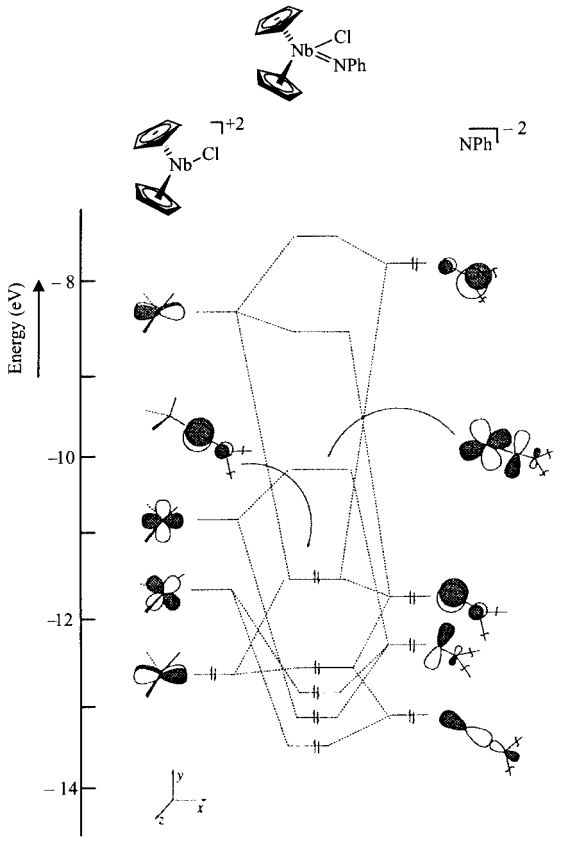

Figure 4. Interaction diagram for the formation of [Nb(=NPh)Cp_2Cl] from $[NbCp_2Cl]^{2+}$ to the left and NPh^{2-} to the right; some of the frontier orbitals are shown in the centre

The formal electron count of **9** is 20 electrons with the excess 2 electrons probably being located in a nonbonding orbital similar to that proposed by Green et al. for [Mo(=N*t*Bu)(η^5-C_5H_5)$_2$].[47] Similar "20-electron" (imido)niobocene complexes [Nb(=NR)(η^5-$C_5H_4SiMe_3$)$_2$Cl] have shown a lengthening of the Nb−centroid distances in comparison with their 18- and 17-electron analogues and this too occurs in **9** (see Table 3). Indeed, such lengthening has also been observed in (imido)metallocene complexes of titanium[48] and molybdenum.[47] The bonding in the "19-electron" vanadium complex [V(=$NC_6H_3Me_2$-2,6)(η^5-C_5Me_5)$_2$] has previously been studied by molecular orbital calculations and led to the proposal that the surplus electrons in these "high-electron" complexes are located in essentially ligand-based orbitals and thus the 18-electron rule is not violated.[49−51] Similar calculations have been carried out for "20-electron" osmium complexes [Os(NR)$_3$].[52]

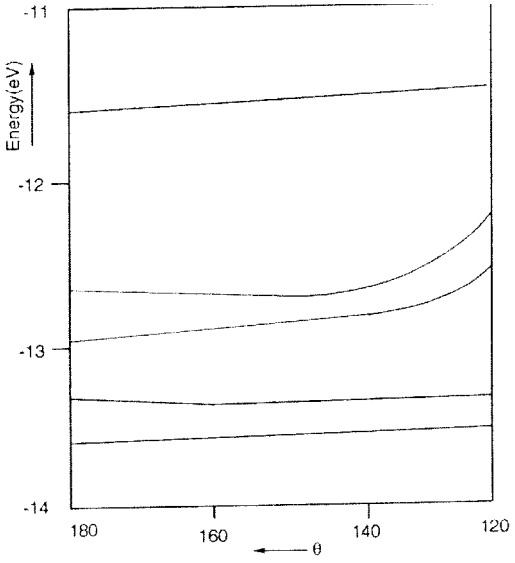

Figure 5. Walsh diagram for the bending of the phenyl group in the equatorial plane

Table 3. Comparison of Nb−Cent distances in selected Cp′-containing niobocene complexes (Cp′ = η^5-$C_5H_4SiMe_3$; Cent = the centroid of the C_5 ring)

Compound	Average Nb−Cent [Å]	Ref.
[Nb(=NC_6H_4OMe-4)Cp′$_2$Cl] (**13**)	2.189	[31]
[{NbCp′$_2$Cl}$_2$(μ-1,3-$N_2C_6H_4$)] (**61**)	2.188	[53]
[Nb(=O)Cp′$_2$Me]	2.181	[54]
[Nb(=NPh)Cp′$_2$(C≡CPh)]] (**37**)	2.180	[55]
[Nb(=NPh)Cp′$_2$Cl] (**9**)	2.180	[37]
[NbCp′$_2$Cl(η^2-*N*,*C*-OCNPh)]	2.121	[53]
[NbCp′$_2$Cl$_2$]	2.079	[54,56]
[{NbCp′$_2$Cl}$_2$]	2.07	[37]
[NbCp′$_2$(C_6F_5)(CO)]	2.04	[54]

A comparison of selected structural data of (imido)niobocene complexes is given in Table 4.

2.3.3 Alkyl Derivatives

Despite the broad scope of imido group 5 metal chemistry only a handful of alkyl-containing (imido)niobocene complexes have previously been reported.[24,25,30] We have expanded this field by the preparation of the following new

Table 2. Values for the overlap populations of the N−C and Nb−N bonds and charges (N, Nb) as a function of the bending angle Nb−N−C(Ph) in the equatorial plane

Angle θ (in the plane) [°]	120	140	160	180
Energy [eV]	−1714.54	−1716.84	−1717.50	−1717.63
Overlap population (N−C bond)	797	836	857	862
Charge on N	−1.091	−0.894	−0.806	−0.786
Charge on Nb	0.840	0.623	0.531	0.512
Overlap population (Nb−N bond)	895	978	1017	1030

Table 4. Selected structural data for (imido)niobocene complexes

	Cp−Nb−Cp [°]	Nb−N−C [°]	Nb−N [Å]	Ref.
(*S*) [Nb(=N*t*Bu){$Me_2Si(\eta^5$-$C_5Me_4)(\eta^5$-$C_5H_3Me)$}Cl] (**58**)	122.7	168.0(4)	1.790(5)	[57]
(*R*) [Nb(=N*t*Bu){$Me_2Si(\eta^5$-$C_5Me_4)(\eta^5$-$C_5H_3Me)$}Cl] (**58**)	122.3	167.5(4)	1.782(5)	[57]
[Nb(=N*t*Bu){$Me_2Si(\eta^5$-$C_5Me_4)(\eta^5$-C_5H_3*i*Pr)}Cl] (**59**)	122.1	172.3(2)	1.772(2)	[57]
[Nb(=N*t*Bu){$Me_2Si(\eta^5$-$C_5H_4)_2$}Cl]	121.21	178.8(2)	1.756(3)	[58]
[Nb(=N$SiMe_3$){$Me_2C(\eta^5$-$C_5H_4)_2$}Cl]	114.2	167.71(7)	1.777(1)	[59]
[Nb(=N*t*Bu){$Me_2C(\eta^5$-$C_5H_4)_2$}Cl]	113.3	178.4(3)	1.762(3)	[59]
[Nb(=N*t*Bu){$Me_2C(\eta^5$-$C_5H_4)_2$}Br]	113.4	178.3(2)	1.765(2)	[59]
[Nb(=N*t*Bu){$Me_2C(\eta^5$-$C_5H_4)_2$}I]	114.2	171.8(2)	1.770(2)	[59]
[Nb(=NAr){$Me_2C(\eta^5$-$C_5H_4)_2$}Cl][a]	114.4	167.5(1)	1.798(2)	[60]
[Nb(=NAr){$Me_2C(\eta^5$-$C_5H_4)_2$}(NMe_2)][$B(C_6H_5)_4$][a]	114.0	166.8(1)	1.803(2)	[60]
[Nb(=N*t*Bu)(η^5-$C_5H_5)_2$Cl][b]	122.7	173.6(4)	1.789(4)	[30]
	124.0	179.4(5)	1.737(6)	
[Nb(=NC_6H_5)(η^5-$C_5H_4SiMe_3)_2$NbCl] (**9**)	124.9	165.1(2)	1.792(2)	[37]
[Nb(=NC_6H_4OMe-4)(η^5-$C_5H_4SiMe_3)_2$Cl] (**13**)	125.23	163.0(2)	1.787(3)	[31]
[Nb(=NPh)Cp'_2(C≡CPh)]] (**37**)	128.2	167.9(6)	1.804(5)	[55]
[{$NbCp'_2Cl$}$_2$(μ-1,3-$N_2C_6H_4$)] (**61**)	124.5	167.4(14)	1.754(20)	[53]
	125.6	168.4(15)	1.763(18)	

[a] Two independent molecules exist in the unit cell.

(imido)niobocene complexes containing alkyl ligands: [Nb(=N*t*Bu)Cp_2R] [R = Et (**16**), CH_2SiMe_3 (**17**)],[39] [Nb(=NC_6H_4Me-4)Cp_2R] [R = Me (**18**), Et (**19**), CH_2Ph (**20**) CH_2SiMe_3 (**21**)][39] and [Nb(=NPh)Cp'_2R] [R = Me (**22**), Et (**23**), *i*Pr (**24**)].[53] The synthetic pathway to these complexes is determined by the reaction of the appropriate magnesium reagent MgRCl with the corresponding metallocene complex [Equation (8)].

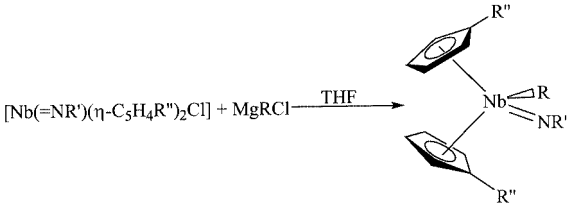

R = Et, R' = *t*Bu, R" = H (**16**);
R = CH_2SiMe_3, R' = *t*Bu, R" = H (**17**);
R = Me, R' = C_6H_4Me-4, R" = H (**18**);
R = Et, R' = C_6H_4Me-4, R" = H (**19**);
R = CH_2Ph, R' = C_6H_4Me-4, R" = H (**20**);
R = CH_2SiMe_3, R' = C_6H_4Me-4, R" = H (**21**);
R = Me, R' = Ph, R" = $SiMe_3$ (**22**);
R = Et, R' = Ph, R" = $SiMe_3$ (**23**);
R = *i*Pr, R' = Ph, R" = $SiMe_3$ (**24**). (8)

In the ^{1}H NMR spectra of the ethyl complexes **16** and **19** (Figure 6) the ethyl group displays an A_3BC pattern with typical values of J_{AB} = 7.0, J_{AC} = 7.5, J_{BC} = 14.0 Hz, similar to those reported previously in two ethyl complexes of niobium.[61,62] This observation indicates the inequivalency of the methylene protons due to either H-bonding interactions C−H···N between the alkyl and imido groups, which restrict rotation about the Nb−C bond or the presence of an unusually weak agostic interaction between an α-hydrogen atom of the ethyl group and the metal centre. The latter explication is favoured because in complexes that do not contain electronegative ligands, e.g. [$NbCp_2$-(Et)(RC≡CR)], the same phenomena of possible agostic interactions is observed in the NMR spectra.[62]

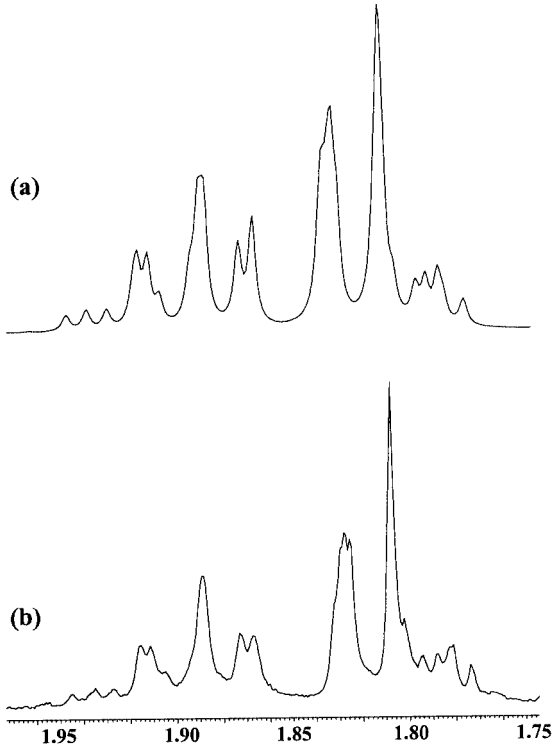

Figure 6. ^{1}H NMR spectra of [Nb(=NC_6H_4Me-4)Cp_2Et] (**19**) in the ethyl region: (a) simulated; (b) experimental

2.3.4 Allyl Derivatives

In a similar manner the η^1-allyl(imido)niobocene complexes, [Nb(=NC_6H_4Me-4)$Cp_2(\eta^1$-CH_2CHCH_2)] (**25**)[39] and [Nb(=NR)$Cp'_2(\eta^1$-CH_2CHCH_2)] [R = *t*Bu (**26**), C_6H_4Me-4 (**27**), C_6H_4OMe-4 (**28**)][31] have been synthesized [Equation (9)]. The ^{1}H NMR spectra for the η^1-allyl complexes were similar to that recorded for **7**. Couplings constants are given in Table 1.

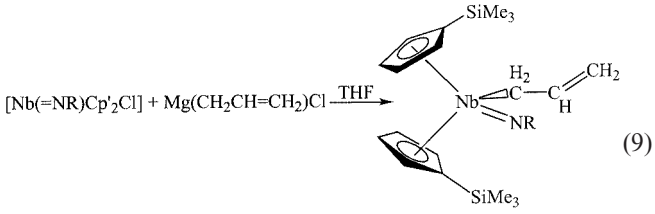

(9)

R = *t*Bu (**26**), C_6H_4Me-4 (**27**), C_6H_4OMe-4 (**28**)

Recently, we reported the preparation of first alkynyl-containing niobocene complexes[63] and by a natural extension of this work the alkynyl(imido)niobium complexes [Nb(=N*t*Bu)(η^5-C_5H_5)$_2$(C≡CR)] [R = Me (**29**), $SiMe_3$ (**30**), *t*Bu (**31**), CH_2Ph (**32**)], [Nb(=NC_6H_4Me-4)(η^5-C_5H_5)$_2$(C≡CR)] [R = $SiMe_3$ (**33**), *t*Bu (**34**)], [Nb(=N*t*Bu)(η^5-$C_5H_4SiMe_3$)$_2$(C≡CR)] [R = $SiMe_3$ (**35**), *t*Bu (**36**)], [Nb(=NPh)(η^5-$C_5H_4SiMe_3$)$_2$(C≡CR)] (R = Ph (**37**), *t*Bu (**38**)], [Nb(=NC_6H_4Me-4)(η^5-$C_5H_4SiMe_3$)$_2$(C≡CR)] [R = $SiMe_3$ (**39**), *t*Bu (**40**)], [Nb(=NC_6H_4OMe-4)(η^5-$C_5H_4SiMe_3$)$_2$(C≡CR)] [R = $SiMe_3$ (**41**), *t*Bu (**42**)], were synthesized.[55] The general synthetic method involved the reaction of dialkynylmagnesium reagents and the corresponding (imido)niobocene halide derivative. An example is given in Equation (10).

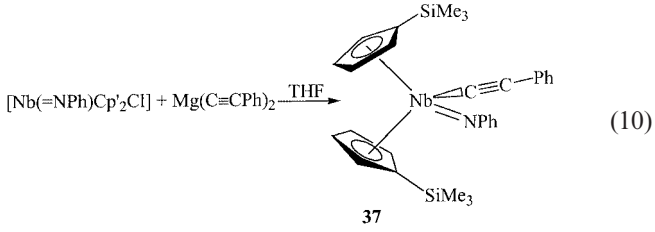

(10)

37

The molecular structure of **37**, determined by single-crystal X-ray diffraction studies is depicted in Figure 7. Complex **37** presents a typical bent-metallocene structure with two additional ligands. Both cyclopentadienyl rings are η^5-bonded to the metal atom with a Cent−Nb−Cent angle of 128.2°. The alkynyl ligand is σ-bonded to the metal atom as indicated by the C(1)−C(2) distance of 1.20(1) Å which is typical for a C−C triple bond and the Nb−C(1)−C(2) angle of 177.9(6)° whose linear nature confirms that the C(1) and C(2) atoms are sp-hybridized. The Nb−N bond length of 1.804(5) Å, is at the upper limit for those observed for (imido)niobium complexes (1.73−1.80 Å) (see Table 4) and is indicative of an Nb−N triple bond. As in complexes **9** and **13**, the formal electron count is 20.

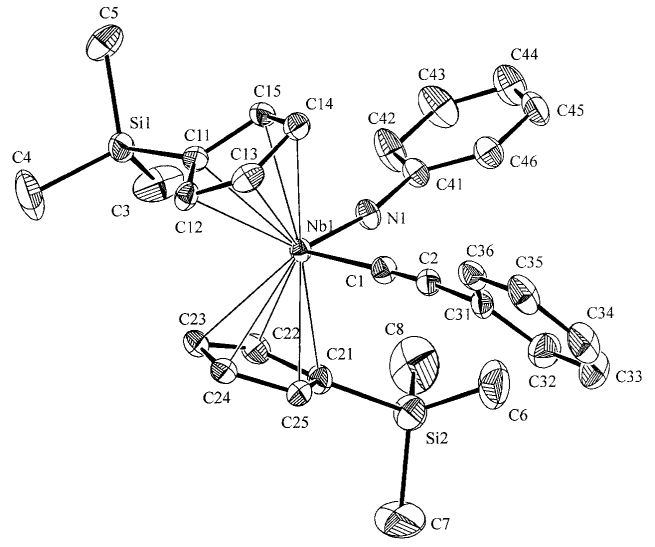

Figure 7. Molecular structure of [Nb(=NPh)(η^5-$C_5H_4SiMe_3$)$_2$-(C≡CPh)] (**37**)

2.3.5 Reactivity

The cationic niobium species, [Nb(NHPh)Cp′$_2$R]$^+$ (R = Cl (**43**), Me (**44**), Et (**45**), *i*Pr (**46**)], were obtained by the reaction of the neutral (imido)niobocene complexes **9** and **22−24** with HBF_4.[53] Protonation took place at the nitrogen atom to give the corresponding amido derivative [Equation (11)].

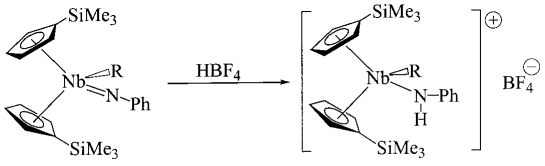

(11)

R = Cl (**43**), Me (**44**), Et (**45**), *i*Pr (**46**)

The hydride complex [Nb(=NPh)Cp′$_2$H] (**47**)[53] was prepared by initially reducing the (imido)niobocene(v) complexes **9** and **22−24** and their subsequent oxidation by hydrogen abstraction from the solvent to give the corresponding niobium(v) hydride derivative [Equation (12)].

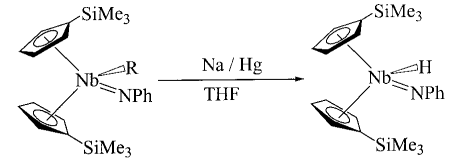

(12)

R = Cl, Me, Et, *i*Pr

47

The reactivity of the alkynyl(imido) complexes **30** and **37** with the protic reagents CF_3COOH and HBF_4 was studied.[55] Protonation of these complexes may occur at the alkynyl and/or the imido moiety as observed previously in niobocene complexes containing only one of these ligands.[53,63] In the reactions of **30** and **37** with CF_3COOH and HBF_4, respectively, the protonated compounds were isolated [Equation (13)]. It was found that in these alkynyl-(imido) complexes protonation takes place preferentially at the nitrogen atom of the imido group leading to the formation of the cationic amide species [Nb(NH*t*Bu)(η^5-C_5H_5)$_2$(C≡CSiMe$_3$)]$^+$ (**48**) and [Nb(NHPh)(η^5-$C_5H_4SiMe_3$)$_2$(C≡CPh)]$^+$ (**49**).[55]

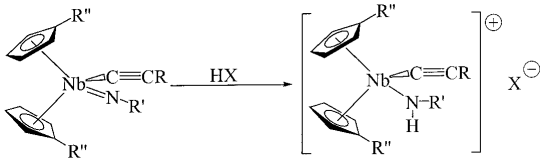

(13)

R = $SiMe_3$, R' = *t*Bu, R" = H, X = CF_3COO (**48**);
R = Ph, R' = Ph, R" = $SiMe_3$, X = BF_4 (**49**).

The normally greater Brønsted basicity of the imido ligand relative to the alkynyl ligand may explain the selective nature of the protonation reaction of these alkynyl(imido)niobocene complexes.

It was found that when [Nb(=NC$_6$H$_4$Me-4)Cp$_2$Me] (**18**) was treated with H_2O, the reaction took place at the Nb−N and not the Nb−C bond of the alkyl group. The alkyl(oxo) complex [Nb(=O)Cp$_2$Me] (**50**) was isolated by recrystallization from a hexane solution.[39] The amine $H_2NC_6H_4$Me-4 was identified by ^{1}H NMR spectroscopy to be the by-product of this reaction [Equation (14)].

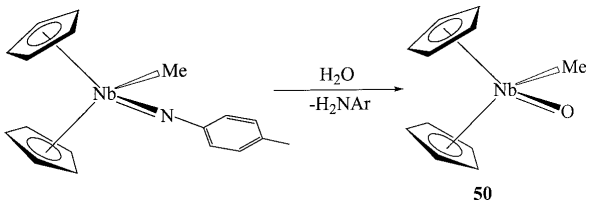

50 (14)

2.4 *ansa*-(Imido)niobocene Complexes

In 1996 we reported the first *ansa*-niobocene complexes in which both cyclopentadienyl rings are bound only in an η^5-mode to the niobium atom[64] and following from this work we prepared the *ansa*-(imido)niobocene complex [Nb(=N*t*Bu){Me$_2$Si(η^5-C$_5$H$_4$)$_2$}Cl] (**51**) [Equation (15)].[58] The ^{1}H NMR spectrum reveals the presence of a system similar to that obtained for its non-*ansa* analogues. The C_s symmetry of the molecule is such that there is only one plane of symmetry and the two methyl groups of $SiMe_2$ become inequivalent, as do the cyclopentadienyl protons, thus giving two singlets for the former and four multiplets for the latter. The molecular structure of **51**, determined by single-crystal X-ray diffraction studies, is depicted in Figure 8. The following *ansa*-(imido)-niobocene complexes have also been reported by other authors: [Nb(=NR){Me$_2$C(η^5-C$_5$H$_4$)$_2$}Cl] (R = *t*Bu, SiMe$_3$),[59] [Nb(=NC$_6$H$_3$*i*Pr$_2$-2,6){Me$_2$C(η^5-C$_5$H$_4$)$_2$}Cl].[60]

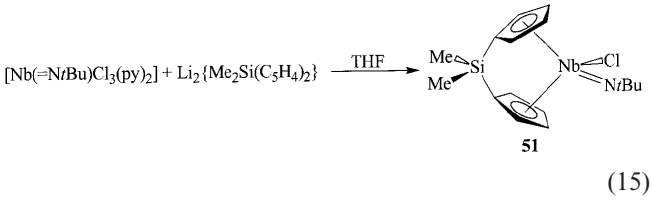

51 (15)

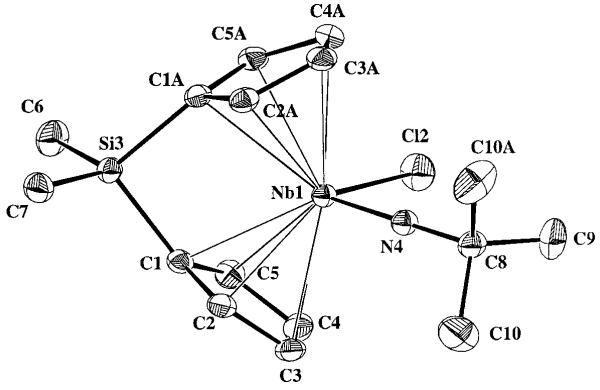

Figure 8. Molecular structure of [Nb(=N*t*Bu){Me$_2$Si(η^5-C$_5$H$_4$)$_2$}Cl] (**51**)

2.4.1 Alkyl, Allyl and Alkynyl Derivatives

The alkyl derivatives [Nb(=N*t*Bu){Me$_2$Si(η^5-C$_5$H$_4$)$_2$}R] [R = Me (**52**), Et (**53**), CH_2Ph (**54**)] were synthesized from **51** and the corresponding Grignard reagent.[58] The allyl and alkynyl products [Nb(=N*t*Bu){Me$_2$Si(η^5-C$_5$H$_4$)$_2$}(η^1-CH$_2$CHCH$_2$)] (**55**)[58] and [Nb(=N*t*Bu){Me$_2$Si(η^5-C$_5$H$_4$)$_2$}(C≡CR)] [R = SiMe$_3$ (**56**), *t*Bu (**57**)][55] were prepared in a similar manner. The ^{1}H NMR spectrum of the ethyl complex **53** showed the same characteristics as those observed for **16** and **19**. The η^1-allyl complex **55** was identical in nature to those already discussed.

2.4.2 Substituted ansa-(Imido)niobocene Complexes

We prepared the first niobocene complex containing a substituted *ansa* ligand [Nb(=N*t*Bu){Me$_2$Si(η^5-C$_5$H$_3$SiMe$_3$)$_2$}Cl] (**56**) [Equation (16)].[58] The synthesis of substituted *ansa*-ligand complexes of niobium can lead to a variety of isomers (Figure 9) depending on the configuration of the cyclopentadienyl rings. These include two *meso*-(*R*,*S*) forms **I** and **II** and the enantiomers *rac*-(*R*,*R*) (**III**) and *rac*-(*S*,*S*) (**IV**). For this complex ^{1}H NMR spectroscopy will show clearly the existence of the *meso* and *rac* isomers. Complex **56** was isolated uniquely as the *meso* isomer as was revealed by ^{1}H NMR spectroscopy. The *meso* isomer contains a plane of symmetry (C_s), which makes the cyclopentadienyl rings of the *ansa* ligand equivalent, and hence only three signals for the ring protons are observed in its ^{1}H NMR spectrum, which in addition gave the expected signals for the *t*Bu and the SiMe$_3$ groups and two for SiMe$_2$. The cyclopentadienyl rings of the *ansa* ligand, however, will be inequivalent in the *rac* complex due to the lack of symmetry (C_1). In the case of **56**, the *rac* isomer is probably disfavoured due to steric effects and for this same reason in the *meso* complex the SiMe$_3$ groups should be pointing away from the bulky imido group.

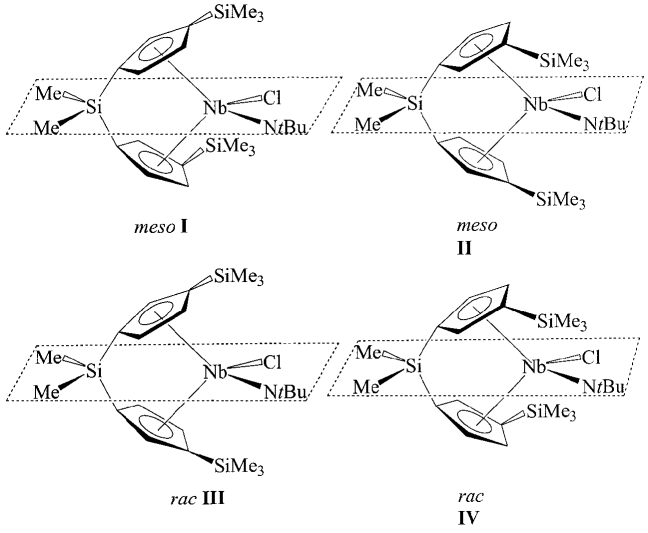

Figure 9. Possible isomers for [Nb(=N*t*Bu){Me$_2$Si(η^5-C$_5$H$_3$SiMe$_3$)$_2$}Cl] (**56**)

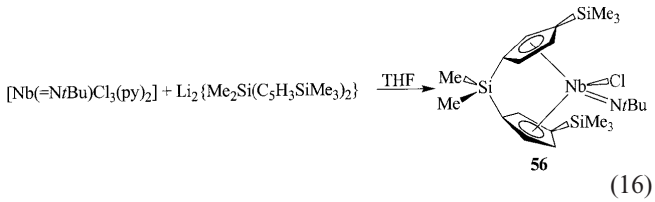

56

(16)

2.4.3 Asymmetric ansa-(Imido)niobocene Complexes

We have prepared the first (imido)niobocene complexes incorporating asymmetric *ansa* ligands. The complexes [Nb(=N*t*Bu){$Me_2Si(\eta^5$-$C_5Me_4)(\eta^5$-$C_5H_3R)$}Cl] [R = H (**57**), Me (**58**), *i*Pr (**59**), $SiMe_3$ (**60**)] were synthesized by the reaction of [Nb(=N*t*Bu)$Cl_3(py)_2$] with Li_2{$Me_2Si(\eta^5$-$C_5Me_4)(\eta^5$-$C_5H_3R)$} [Equation (17)].[57]

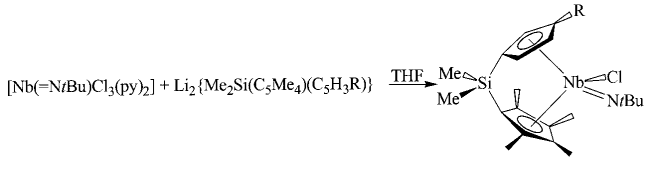

R = H (**57**); Me (**58**); *i*Pr (**59**); $SiMe_3$ (**60**)

(17)

2.4.4 Structural Characterization

The ^{1}H NMR spectrum of **57** shows the lack of symmetry in this chiral complex, with the four methyl groups attached to the cyclopentadienyl ring being inequivalent as are the methyl groups of the $SiMe_2$ bridge and the four protons of the unsubstituted cyclopentadienyl moiety.

In the case of complexes **58**−**60** the monosubstitution of one of the cyclopentadienyl rings of the *ansa* ligands gives rise to the possibility of two different isomers (**I**) and (**II**) (Figure 10) depending on the configuration of the cyclopentadienyl rings in which the substituent R can be orientated towards or away from the imido group. The niobium atom is chiral and thus in both cases **I** and **II** should exist as pairs of enantiomers.

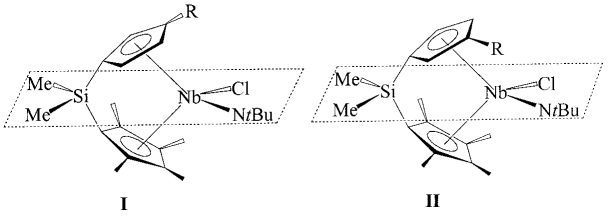

Figure 10. Possible isomers for complexes [Nb(=N*t*Bu){$Me_2Si(\eta^5$-$C_5Me_4)(\eta^5$-$C_5H_3R)$}Cl] [R = Me (**58**), *i*Pr (**59**), $SiMe_3$ (**60**)]

The ^{1}H spectra of **58**−**60** are similar to that observed in **57** and in addition show the existence exclusively of only one of the possible isomers. It is assumed that this corresponds to isomer **I**, i.e., that the substituent R is pointing away from the bulky imido group. The isomer **II** is probably heavily disfavoured due to steric effects.

The molecular structures of **58** and **59** were established by X-ray crystal structure studies; they are shown in Figures 11 and 12, respectively.[57]

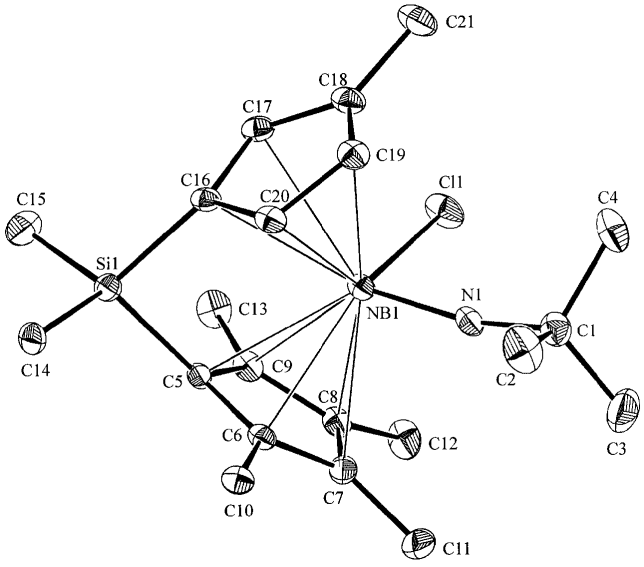

Figure 11. Molecular structure of [Nb(=N*t*Bu){$Me_2Si(\eta^5$-$C_5Me_4)(\eta^5$-$C_5H_3Me)$}Cl] (**58**)

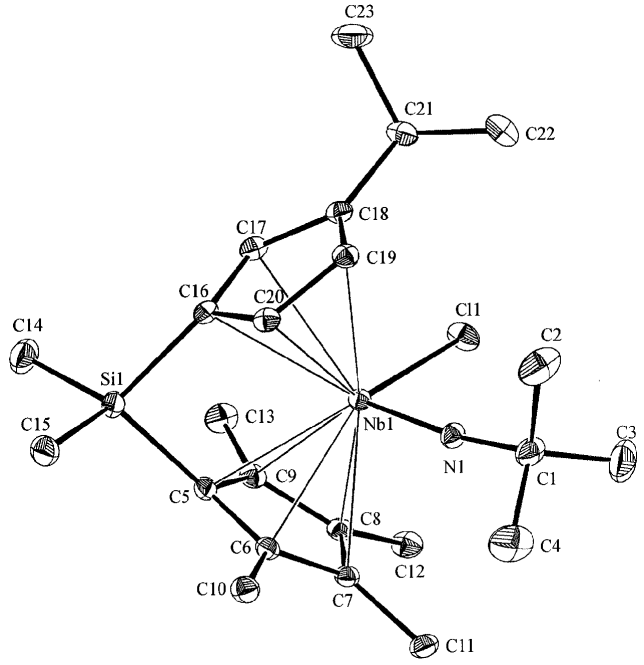

Figure 12. Molecular structure of [Nb(=N*t*Bu){$Me_2Si(\eta^5$-$C_5Me_4)(\eta^5$-C_5H_3*i*Pr)}Cl] (**59**)

The niobium atoms in both **58** and **59** show a geometry that is typical for pseudo-tetrahedral (imido)niobocene(v) derivatives. The $Me_2Si(C_5Me_4)(C_5H_3R)$ *ansa* ligand chelates the niobium centre, and both cyclopentadienyl rings are bound to the metal atom in an η^5-mode adopting the typical bent-metallocene conformation. The environment of the niobium atom is completed by a chlorine atom and the imido group bonded through the nitrogen atom to the niobium atom. The structure also reveals that the alkyl group in the monosubstituted C_5 ring is oriented away from the

imido group. The Cent−Nb−Cent angles (122.7 and 122.3° in **58**; 122.1° in **59**) are similar to those reported for other *ansa*-niobocene complexes containing the $SiMe_2$-bridged *ansa* ligand (see Table 2). The formal electron count for **58** and **59** is 20.

2.4.5 Asymmetric Complexes with Germanium-Bridged ansa Ligands

The reaction of $Li_2\{Me_2Ge(C_5Me_4)(C_5H_4)\}$ with $[Nb(=NtBu)Cl_3(py)_2]$ gave the niobium derivative $[Nb(=NtBu)\{Me_2Ge(\eta^5\text{-}C_5Me_4)(\eta^5\text{-}C_5H_4)\}Cl]$ (**61**) [Equation (18)].[65] This is the first example of a niobocene complex incorporating a germanium-bridged *ansa* ligand.

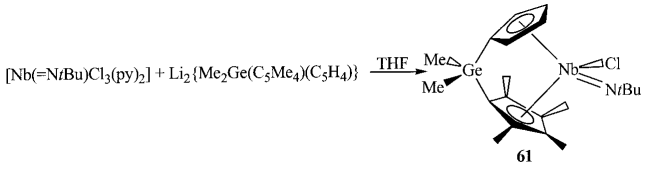

(18)

2.5 (Imido)niobocene Complexes with Phosphane-Substituted Cyclopentadienyl Ligands

The use of phosphane-substituted cyclopentadienyl ligands in the chemistry of group 5 elements has been restricted to one reference concerning the tantalum complex $[Ta(\eta\text{-}C_5Me_5)(\eta\text{-}C_5H_4PPh_2)Cl_2]$ and its reactivity.[66] To the best of our knowledge there have been no reports of this type of compounds in the chemistry of niobium.

By the reaction of the lithium derivative $Li_2\{Me_2Si(C_5Me_4)(C_5H_3PPh_2)\}$ with $[Nb(=NtBu)Cl_3(py)_2]$ we have prepared the *ansa*-phosphane(imido)niobocene complex $[Nb(=NtBu)\{Me_2Si(\eta^5\text{-}C_5Me_4)(\eta^5\text{-}C_5H_3PPh_2)\}Cl]$ (**62**) [Equation (19)].[67] The complex $[Nb(=NtBu)(\eta^5\text{-}C_5H_4PPh_2)_2Cl]$ (**63**), was prepared in a similar way by reaction of 2 equiv. of $Li(C_5H_4PPh_2)$ with $[Nb(=NtBu)Cl_3(py)_2]$.[67]

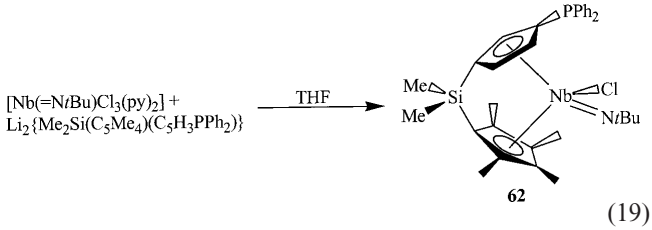

(19)

2.6 Dinuclear (Imido)niobocene Complexes

2.6.1 Synthesis

The [bis(imido)]diniobocene complexes were prepared in a similar manner to their mononuclear analogues. Thus, the complexes $[\{NbCp'_2Cl\}_2(\mu\text{-}1,3\text{-}N_2C_6H_4)]$ (**64**) and $[\{NbCp'_2Cl\}_2(\mu\text{-}1,4\text{-}N_2C_6H_4)]$ (**65**) were prepared by two distinct synthetic routes; firstly by oxidative addition of the bis(amine) and subsequent loss of H_2 [Equation (20)], alternatively by thermal treatment of $[\{NbCp'_2Cl\}_2(OCNC_6H_4NCO)]$ and elimination of CO [Equation (21)].[53]

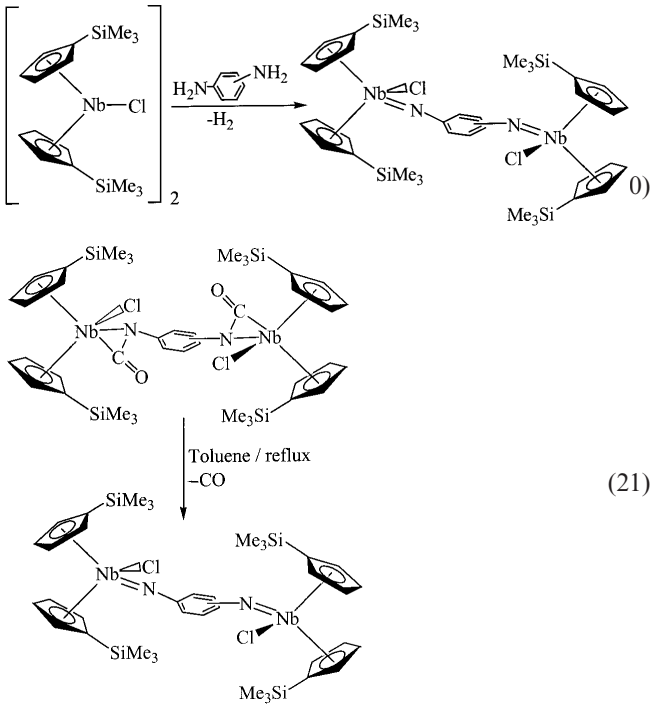

2.6.2 Characterization

Complexes **64** and **65** were characterized by ^1H NMR spectroscopy which revealed spectra similar to those obtained for other (imido)niobocene complexes. The molecular structure of **64**, determined by single-crystal X-ray diffraction studies, is illustrated in Figure 13.[53]

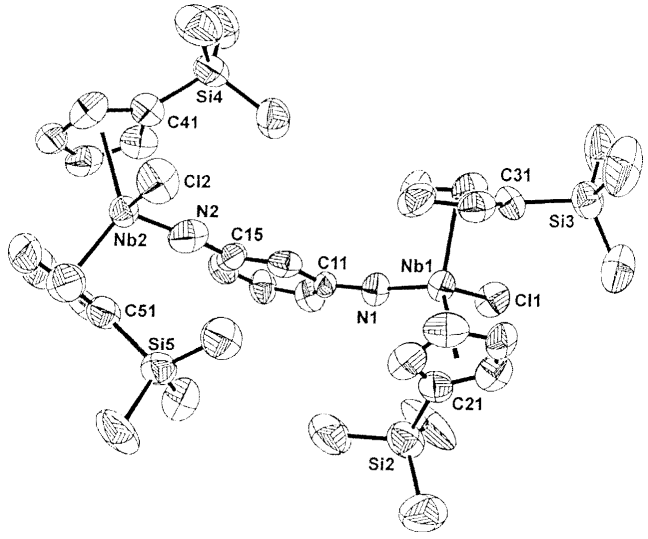

Figure 13. Molecular structure of $[\{NbCp'_2Cl\}_2(\mu\text{-}1,3\text{-}N_2C_6H_4)]$ (**64**)

The complex shows two bent niobocene units linked to a phenylenebis(imido) ligand and is to date the only known example of this type reported in the chemistry of metallocene compounds. The formal electron count is 20 at both niobium centres and the structural parameters are similar to those previously discussed for other niobium complexes (see Table 4).[53]

2.6.3 Alkyl Derivatives

The alkyl derivatives [{NbCp′$_2$R}$_2$(μ-1,3-$N_2C_6H_4$)] [R = Me (**66**), Et (**67**), *i*Pr (**68**)] and [{NbCp′$_2$R}$_2$(μ-1,4-$N_2C_6H_4$)] [R = Me (**69**), Et (**70**), *i*Pr (**71**)] were prepared by the reaction of the chloro precursor with the corresponding Grignard reagent.[53]

2.6.4 Hydride Derivatives

The hydride derivatives [{NbCp′$_2$H}$_2$(μ-1,3-$N_2C_6H_4$)] (**72**) and [{NbCp′$_2$H}$_2$(μ-1,4-$N_2C_6H_4$)] (**73**) were prepared according to Equation (22).[53]

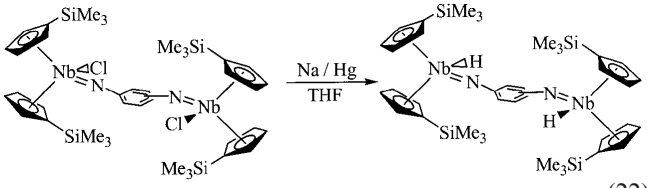

(22)

Conclusion

This review gives an insight into our work in the field of (imido)niobium complexes containing at least one cyclopentadienyl ligand. Amongst the compounds described are the first examples of: (a) symmetrically and asymmetrically substituted *ansa*-(imido)niobocene complexes, (b) germanium-bridged *ansa* ligands, (c) (imido)niobocene and *ansa*-(mido)niobocene complexes incorporating phosphane-substituted ligands. (d) [bis(imido)]diniobocene complexes.

The molecular structures for many of the niobocene complexes have been determined and show the linear or near linear nature of the imido group. This indicates that the imido group is acting as a four-electron donor. Thus, the formal electron count is 20 with surplus electrons probably being located in ligand-based orbitals. In addition we have observed in these compounds a lengthening of the niobium−cyclopentadienyl distance compared with their 18-electron analogues.

In symmetrically and asymmetrically substituted *ansa*-(imido)niobocene complexes we have observed that steric conditions are the governing factor in the final orientation of the ligands in the complexes.

Alkyl, allyl and alkynyl derivatives have been readily synthesized by reaction of the initial (imido)niobium chloride precursor with the corresponding magnesium reagent. It was found that protonation and hydrolysis take place preferentially at the imido group and not at the Nb−C σ-bond.

Acknowledgments

We gratefully acknowledge financial support from the Dirección General de Enseñanza Superior e Investigación Científica, Spain (Grants no. PB 98-0159-C02-01-02, no. BQU2000-0463 and the FEDER project 1FD97-1375).

[1] A. Galindo, M. Gómez, P. Gómez-Sal, A. Martín, D. Del Rio, F. Sánchez, *Organometallics* **2002**, *21*, 293−304.
[2] M. J. Humphries, M. L. H. Green, M. A. Leech, V. C. Gibson, M. Jolly, D. N. Williams, M. R. J. Elsegood, W. Clegg, *J. Chem. Soc., Dalton Trans.* **2000**, 4044−4051.
[3] C.-T. Chen, L. H. Doerrer, V. C. Williams, M. L. H. Green, *J. Chem. Soc., Dalton Trans.* **2000**, 967−974.
[4] A. Castro, M. V. Galakhov, M. Gómez, P. Gómez-Sal, A. Martín, F. Sánchez, *J. Organomet. Chem.* **2000**, *595*, 36−53.
[5] M. P. Coles, C. I. Dalby, V. C. Gibson, R. I. Little, E. L. Marshall, M. H. Ribeiro da Costa, S. Mastroianni, *J. Organomet. Chem.* **1999**, *591*, 78−87.
[6] A. Castro, M. V. Galakhov, M. Gómez, F. Sánchez, *J. Organomet. Chem.* **1999**, *580*, 161−168.
[7] M. I. Alcalde, P. Gómez-Sal, P. Royo, *Organometallics* **1999**, *18*, 546−554.
[8] L. Djakovitch, W. A. Herrmann, *J. Organomet. Chem.* **1998**, *562*, 71−78.
[9] M. I. Alcalde, P. Gómez-Sal, A. Martin, P. Royo, *Organometallics* **1998**, *17*, 1144−1150.
[10] M. C. W. Chan, J. M. Cole, V. C. Gibson, J. A. K. Howard, C. Lehmann, A. D. Poole, U. Siemeling, *J. Chem. Soc., Dalton Trans.* **1998**, 103−112.
[11] L. Djakovitch, W. A. Herrmann, *J. Organomet. Chem.* **1997**, *545/546*, 399−405.
[12] M. L. H. Green, J. T. James, J. F. Saunders, J. Souter, *J. Chem. Soc., Dalton Trans.* **1997**, 1281−1288.
[13] W. A. Herrmann, W. Baratta, E. Herdtweck, *Angew. Chem.* **1996**, *108*, 2098−2100; *Angew. Chem. Int. Ed. Engl.* **1996**, *35*, 1951−1953.
[14] W. A. Herrmann, W. Baratta, *J. Organomet. Chem.* **1996**, *506*, 357−361.
[15] S. Schmidt, J. Sundermeyer, F. Möeller, *J. Organomet. Chem.* **1994**, *475*, 157−166.
[16] V. C. Gibson, A. D. Poole, U. Siemeling, D. N. Williams, W. Clegg, D. C. R. Hockless, *J. Organomet. Chem.* **1993**, *462*, C12−C14.
[17] A. D. Poole, D. N. Williams, A. M. Kenwright, V. C. Gibson, W. Clegg, D. C. R. Hockless, P. A. O′Neil, *Organometallics* **1993**, *12*, 2549−2555.
[18] U. Siemeling, V. C. Gibson, *J. Chem. Soc., Chem. Commun.* **1992**, 1670−1671.
[19] J. K. Cockcroft, V. C. Gibson, J. A. K. Howard, A. D. Poole, U. Siemeling, C. Wilson, *J. Chem. Soc., Chem. Commun.* **1992**, 1668−1670.
[20] D. N. Williams, J. P. Mitchell, A. D. Poole, U. Siemeling, W. Clegg, D. C. R. Hockless, P. A. O′Neil, V. C. Gibson, *J. Chem. Soc., Dalton Trans.* **1992**, 739−751.
[21] A. D. Poole, V. C. Gibson, W. Clegg, *J. Chem. Soc., Chem. Commun.* **1992**, 237−239.
[22] U. Siemeling, V. C. Gibson, *J. Organomet. Chem.* **1992**, *426*, C25−C27.
[23] V. C. Gibson, D. N. Williams, W. Clegg, D. C. R. Hockless, *Polyhedron* **1989**, *8*, 1819−1820.
[24] M. J. Humphries, M. L. H. Green, R. E. Douthwaite, L. H. Rees, *J. Chem. Soc., Dalton Trans.* **2000**, 4555−4562.
[25] S. Schmidt, J. Sundermeyer, *J. Organomet. Chem.* **1994**, *472*, 127−138.
[26] M. J. Humphries, R. E. Douthwaite, M. L. H. Green, *J. Chem. Soc., Dalton Trans.* **2000**, 2952−2959.
[27] M. L. H. Green, J. T. James, A. N. Chernega, *J. Chem. Soc., Dalton Trans.* **1997**, 1719−1726.
[28] S. Schmidt, J. Sundermeyer, H. Werner, *Chem. Ber.* **1995**, *128*, 877−881.
[29] A. N. Chernega, M. L. H. Green, A. G. Suarez, *Can. J. Chem.* **1995**, *73*, 1157−1163.
[30] A. N. Chernega, M. L. H. Green, A. G. Suarez, *J. Chem. Soc., Dalton Trans.* **1993**, 3031−3034.
[31] A. Antiñolo, M. Fajardo, C. Huertas, A. Otero, S. Prashar, A. M. Rodriguez, *J. Organomet. Chem.* **1999**, *585*, 154−161.
[32] A. V. Korolev, A. L. Rheingold, D. S. Williams, *Inorg. Chem.* **1997**, *36*, 2647−2655.
[33] K. S. Heinselman, V. M. Miskowski, S. J. Geib, L. C. Wang, M. D. Hopkins, *Inorg. Chem.* **1997**, *36*, 5530−5538.

[34] J. Sundermeyer, J. Putterlik, M. Foth, J. S. Field, N. Ramesar, *Chem. Ber.* **1994**, *127*, 1201−1212.
[35] I. López-Solera, S. Prashar, unpublished work.
[36] A. Antiñolo, C. Huertas, I. del Hierro, M. F. Lappert, A. Otero, S. Prashar, A. M. Rodriguez, E. Villaseñor, *Organometallics* **1998**, *17*, 5874−5879.
[37] A. Antiñolo, P. Espinosa, M. Fajardo, P. Gómez-Sal, C. López-Mardomingo, A. Martín-Alonso, A. Otero, *J. Chem. Soc., Dalton Trans.* **1995**, 1007−1013.
[38] A. Antiñolo, S. Garcia-Lledó, J. Martinez de Ilarduya, A. Otero, *J. Organomet. Chem.* **1987**, *335*, 85−90.
[39] A. Antiñolo, I. López-Solera, A. Otero, S. Prashar, *J. Organomet. Chem.* **2001**, *631*, 151−156.
[40] G. Parkin, A. van Asselt, D. J. Leahy, L. R. Whinnery, N. G. Hua, R. W. Quan, L. M. Henling, W. P. Schaefer, B. D. Santarsiero, J. E. Bercaw, *Inorg. Chem.* **1992**, *31*, 82−85.
[41] D. M. Antonelli, W. P. Schaefer, G. Parkin, J. E. Bercaw, *J. Organomet. Chem.* **1993**, *462*, 213−220.
[42] K. A. Jørgensen, *Inorg. Chem.* **1993**, *32*, 1521−1522.
[43] C. Mealli, D. M. Proserpio, *J. Chem. Educ.* **1990**, *67*, 399−402.
[44] R. Hoffmann, *J. Chem. Phys.* **1963**, *39*, 1397−1412.
[45] R. Hoffmann, W. N. Lipscomb, *J. Chem. Phys.* **1962**, *36*, 2179−2189.
[46] R. Hoffmann, W. N. Lipscomb, *J. Chem. Phys.* **1962**, *37*, 2872−2888.
[47] J. C. Green, M. L. H. Green, J. T. James, P. C. Konidaris, G. H. Maunder, P. Mountford, *J. Chem. Soc., Chem. Commun.* **1992**, 1361−1364.
[48] S. C. Dunn, P. Mountford, D. A. Robson, *J. Chem. Soc., Dalton Trans.* **1997**, 293−304.
[49] J. H. Osborne, A. L. Rheingold, W. C. Trogler, *J. Am. Chem. Soc.* **1985**, *107*, 7945−7952.
[50] A. J. Bridgeman, L. Davis, S. J. Dixon, J. C. Green, I. N. Wright, *J. Chem. Soc., Dalton Trans.* **1995**, 1023−1027.
[51] J. T. Anhaus, T. P. Kee, M. H. Schofield, R. R. Schrock, *J. Am. Chem. Soc.* **1990**, *112*, 1642−1643.
[52] M. H. Schofield, T. P. Kee, J. T. Anhaus, R. R. Schrock, K. H. Johnson, W. M. Davis, *Inorg. Chem.* **1991**, *30*, 3595−3604.
[53] A. Antiñolo, F. Carrillo-Hermosilla, A. Otero, M. Fajardo, A. Garcés, P. Gómez-Sal, C. López-Mardomingo, A. Martín, C. Miranda, *J. Chem. Soc., Dalton Trans.* **1998**, 59−65.
[54] A. Antiñolo, J. M. de Ilarduya, A. Otero, P. Royo, A. M. M. Lanfredi, A. Tiripicchio, *J. Chem. Soc., Dalton Trans.* **1988**, 2685−2693.
[55] A. Antiñolo, M. Fajardo, C. López-Mardomingo, I. López-Solera, A. Otero, Y. Pérez, S. Prashar, *Organometallics* **2001**, *20*, 3132−3138.
[56] A. M. M. Lanfredi, A. Tiripicchio, M. Kapon, G. M. Reisner, *J. Chem. Soc., Dalton Trans.* **1990**, 375.
[57] A. Antiñolo, I. López-Solera, I. Orive, A. Otero, S. Prashar, A. M. Rodriguez, E. Villaseñor, *Organometallics* **2001**, *20*, 71−78.
[58] A. Antiñolo, A. Otero, S. Prashar, A. M. Rodriguez, *Organometallics* **1998**, *17*, 5454−5459.
[59] N. J. Bailey, J. A. Cooper, H. Gailus, M. L. H. Green, J. T. James, M. A. Leech, *J. Chem. Soc., Dalton Trans.* **1997**, 3579−3584.
[60] W. A. Herrmann, W. Baratta, E. Herdtweck, *J. Organomet. Chem.* **1997**, *541*, 445−460.
[61] A. Antiñolo, F. Carrillo-Hermosilla, I. del Hierro, A. Otero, M. Fajardo, Y. Mugnier, *Organometallics* **1997**, *16*, 4161−4166.
[62] H. Yasuda, H. Yamamoto, T. Arai, A. Nakamura, J. Chen, Y. Kai, N. Kasai, *Organometallics* **1991**, *10*, 4058−4066.
[63] C. García-Yebra, C. López-Mardomingo, M. Fajardo, A. Antiñolo, A. Otero, A. Rodríguez, A. Vallat, D. Lucas, Y. Mugnier, J. J. Carbó, A. Lledós, C. Bo, *Organometallics* **2000**, *19*, 1749−1765.
[64] A. Antiñolo, M. Martinez-Ripoll, Y. Mugnier, A. Otero, S. Prashar, A. M. Rodriguez, *Organometallics* **1996**, *15*, 3241−3243.
[65] C. Alonso-Moreno, A. Antiñolo, I. López-Solera, A. Otero, S. Prashar, A. M. Rodríguez, E. Villaseñor, *J. Organomet. Chem.*, in press.
[66] C. Poulard, G. Boni, P. Richard, C. Moïse, *J. Chem. Soc., Dalton Trans.* **1999**, 2725−2730.
[67] A. Antiñolo, R. Fernández-Galán, I. Orive, A. Otero, S. Prashar, *Eur. J. Inorg. Chem.*, in press.

Received June 11, 2002
[I02309]

Selective Insertion of Dioxygen into an (η^2-C_{60})−Ir Bond: Synthesis and Structure of the First Metallacyclic Complex with a σ-Coordinated Fullerene Molecule

Alexander V. Usatov,*[a] Ekaterina V. Martynova,[a] Fedor M. Dolgushin,[a] Alexander S. Peregudov,[a] Mikhail Yu. Antipin,[a] and Yurii N. Novikov[a]

Keywords: Fullerenes / Carboranes / Iridium / Oxygen / Insertion

Oxidation of the carboranyliridium fullerene complex [(η^2-C_{60})Ir(*o*-$HCB_{10}H_9CCH_2PPh_2$-*B*,*P*)(*t*BuNC)$_2$] (**I**) in $CHCl_3$ solution by O_2 occurs by a selective insertion of the dioxygen molecule into the longest Ir–C bond (in the *trans*-position relative to the B-σ-carboranyl fragment) to give a new metal complex [σ-C_{60}OO-Ir(*o*-$HCB_{10}H_9CCH_2PPh_2$-*B*,*P*)(*t*BuNC)$_2$] (**II**). Complex **II** was isolated and characterized analytically and by UV, IR, ^{1}H and ^{31}P NMR spectroscopy. An X-ray diffraction study of **II** showed that this complex contains a cyclic iridaperoxide fragment in which the fullerene cage is σ-coordinated to the iridium atom.

(© Wiley-VCH Verlag GmbH & Co. KGaA, 69451 Weinheim, Germany, 2003)

Despite considerable advances in the synthesis of metal complexes of fullerenes and their derivatives, the reactivity of these interesting compounds has been studied rather scarcely.[1] The most interesting results obtained in this field are: (i) the discovery of an interaction between polymeric compounds [$C_{60}M_n$] (M = Pd, Pt) and various phosphanes and phosphites resulting in the known monomeric complexes [(η^2-C_{60})ML_2],[2,3] and (ii) insertion of two isocyanide molecules into the Pt−C(fullerene) bonds in the complex [(η^2-C_{60})Pt(CNR)$_2$] giving rise to a new five-membered metallacyclic complex [C_{60}(C=NR)$_2$Pt(CNR)$_2$].[4]

Recently,[5] we have reported the synthesis and structure of the iridium complex [(η^2-C_{60})Ir(*o*-$HCB_{10}H_9CCH_2PPh_2$-*B*,*P*)(*t*BuNC)$_2$] (**I**) containing both an η^2-coordinated C_{60} fullerene and a chelating carboranylphosphane fragment in the coordination sphere of the metal atom. A salient feature of this complex is a distorted η^2-coordination of the fullerene ligand, which is manifested in an appreciable lengthening of one Ir−C bond relative to the other one due to the strong *trans*-effect of the B-σ-carboranyl group. Having established this fact, we started to investigate the possibility of the selective insertion of various reagents into the most reactive elongated bond.

In studies of the oxidation of complex **I** in various solutions we found that bubbling dioxygen through a solution of **I** in $CHCl_3$ at room temperature led to a gradual disappearance of the absorption band at 460 nm in the UV/Vis spectrum of the reaction mixture (this band is characteristic of (η^2-C_{60})-type metal derivatives[5−7]). The reason for this is the formation of a new complex **II** that was isolated and characterized both analytically and spectroscopically.

The IR spectrum of complex **II** exhibits a strong stretching vibration band of *trans*-arranged isocyanide ligands at 2191 cm^{-1} similar to the IR spectrum of **I**. A rather large frequency shift of this band towards the high-frequency region [cf. ν(NC) = 2168 cm^{-1} for complex **I**][5] points to a considerably higher electron-deficient character of the iridium atom in **II**. The $^{31}P\{^1H\}$ NMR spectrum of **II** exhibits a singlet at δ_P = 20.9 ppm, which is shifted appreciably to high field (δ_P = 37.8 ppm for **I**).[5] The ^{1}H NMR spectral pattern of **II** is similar to that of **I**, exhibiting two singlets for the protons of the *tert*-butyl groups of the isocyanide ligands and an ABX pattern for the protons of methylene group of the five-membered ring. This points to a retention of the molecular chirality of the carborane polyhedron. However, these spectral characteristics are insufficient to draw an unambiguous conclusion about the mutual arrangement of the components in the complex **II** and, correspondingly, to determine the addition position of the dioxygen molecule [this can be either the Ir−C bond or one (or several) of the C=C bonds of the fullerene cage]. To establish the structure of this compound, we grew a single crystal of **II** from $CHCl_3$ solution and performed an X-ray diffraction study. The molecular structure of this complex is shown in Figure 1 while selected geometric parameters are listed in Table 1. Our X-ray diffraction study showed that complex **II** is a five-membered iridaperoxide derivative [σ-C_{60}OO-Ir(*o*-$HCB_{10}H_9CCH_2PPh_2$-*B*,*P*)(*t*BuNC)$_2$] with a σ bond between the Ir atom and fullerene cage. This complex is formed as a result of selective insertion of dioxygen

[a] A.N.Nesmeyanov Institute of Organoelement Compounds, Russian Academy of Sciences,
Vavilov St. 28, Moscow 119991, Russia
Fax: (internat.) +7-095/135-5085
E-mail: usa@ineos.ac.ru

molecule into the longest Ir−C bond of the metallacyclopropane fragment of complex **I** according to Scheme 1.

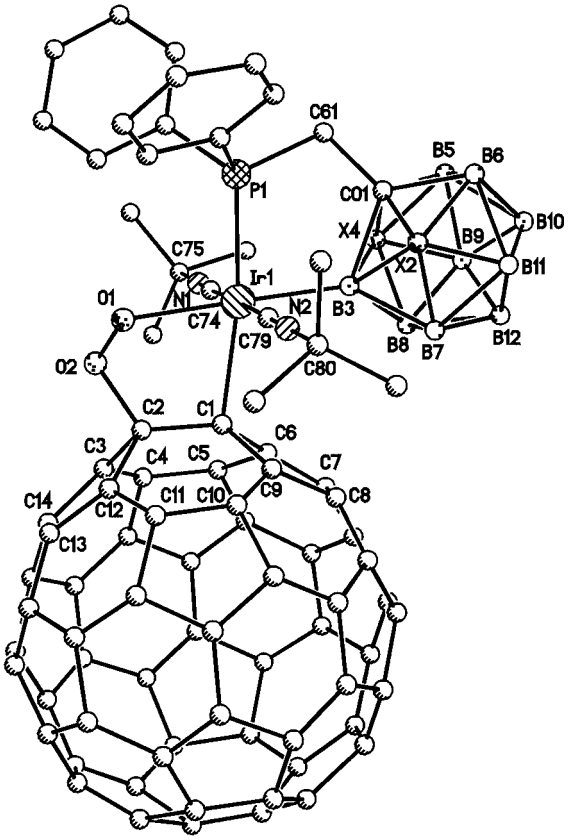

Figure 1. Molecular structure of **II**

No significant changes were found in the geometry of the carboranylphosphane ligand of **II** relative to the initial compound **I** (this was also confirmed by the spectroscopic data). This ligand is coordinated to the iridium atom by the Ir(1)−B(3) σ-bond with the boron atom in position 3(6) and the Ir(1)−P(1) coordination bond involved in the five-membered metallacycle Ir(1)P(1)C(61)C(01)B(3). The both bond lengths in **I** and **II** are essentially identical. However, the metallacycle conformations in both compounds are appreciably different. In **I**, this cycle has a flattened envelope conformation with the P(1) atom deviating by 0.43 Å from the plane of other four atoms of the cycle. In **II**, the metallacycle adopts a flattened twist-conformation characterized by slight deviations of the P(1) and C(61) atoms in opposite directions from the plane passing through the Ir(1), B(3), and C(01) atoms; the Ir(1)−P(1)−C(61)−C(01) torsion angle is 13.8°. This points to a high lability of this metallacycle in the related complexes. The carbon and boron atoms in the 2- and 4-positions of the carborane polyhedron in both **I** and **II** are disordered with equal weights (labeled X2 and X4, see Figure 1). This is due to the fact that the crystal structure is comprised of both enantiomers differing in the mutual arrangement of these boron and carbon atoms with respect to the plane passing through the C(01), B(3), B(10), and B(12) atoms as a consequence of the molecular chirality of the substituted carborane polyhedron.

Table 1. Selected geometrical parameters for **II**

Bond lengths (Å)			
Ir(1)−P(1)	2.281(2)	C(01)−B(3)	1.826(9)
Ir(1)−B(3)	2.101(8)	O(1)−O(2)	1.417(8)
Ir(1)−O(1)	2.154(5)	O(2)−C(2)	1.48(2)
Ir(1)−C(1)	2.238(6)	O(2)−C(2′)	1.41(2)
Ir(1)−C(74)	1.982(6)	C(1)−C(2)	1.46(2)
Ir(1)−C(79)	1.982(6)	C(1)−C(2′)	1.67(2)
P(1)−C(61)	1.853(7)	N(1)−C(74)	1.135(7)
C(01)−C(61)	1.508(9)	N(1)−C(75)	1.480(8)
C(01)−X(4)	1.631(10)	N(2)−C(79)	1.146(7)
C(01)−X(2)	1.657(9)	N(2)−C(80)	1.466(7)
Bond angles (°)			
B(3)−Ir(1)−O(1)	177.0(2)	C(01)−B(3)−Ir(1)	116.8(4)
C(1)−Ir(1)−P(1)	171.74(17)	C(01)−C(61)−P(1)	112.4(4)
B(3)−Ir(1)−C(1)	103.3(2)	O(2)−O(1)−Ir(1)	103.8(4)
O(1)−Ir(1)−C(1)	76.4(2)	O(1)−O(2)−C(2)	94.2(9)
B(3)−Ir(1)−P(1)	84.90(18)	O(1)−O(2)−C(2′)	109.3(7)
O(1)−Ir(1)−P(1)	95.49(17)	C(74)−N(1)−C(75)	176.7(7)
C(74)−Ir(1)−C(79)	178.1(2)	C(79)−N(2)−C(80)	176.7(7)
C(61)−P(1)−Ir(1)	110.9(2)	N(1)−C(74)−Ir(1)	177.7(6)
C(61)−C(01)−B(3)	113.5(5)	N(2)−C(79)−Ir(1)	179.3(6)

A salient feature of complex **II** is the η^1-coordination of the fullerene ligand to the iridium atom through the Ir(1)−C(1) σ-bond. To the best of our knowledge, no structurally characterized mononuclear complexes with this type of fullerene coordination to the transition metal atom have been reported so far.[1] Although Balch et al.[8a] have suggested the formation of a σ-bond between the fullerene cage and a post transition metal atom (Ag), taking compound $C_{60}[Ag(NO_3)]_5$ as an example, a strong structural disorder (including orientation disordering of the fullerene fragment and a disordering of the silver atoms over several positions) does not allow us to use their results for a reliable description of the geometrical features of this type of fullerene coordination to metal atoms. Among polynuclear complexes, a series of triosmium cluster derivatives with μ_3-η^1:η^1:η^2-C_{60} [8b] and μ_3-η^1:η^2:η^1-C_{60} [8c,8d] ligands have been recently obtained and structurally characterized by Park and coworkers. In these complexes, one of the Os atoms has a π-type coordination with a 6/6 bond of a hexagon ring in the C_{60} moiety, whereas two other Os atoms are σ-bonded to this ring with an average Os−C(C_{60}) distance of 2.24 Å.

The Ir(1)−C(1) σ-bond length in **II** is 2.238(6) Å. This value somewhat exceeds the Ir−C(fullerene) bond lengths typical for a conventional η^2-coordination {cf. 2.228(4) and 2.162(4) Å in **I**[5] and 2.19 Å in [(η^2-C_{60})Ir(CO)Cl(PPh_3)$_2$][1]}. A feature of the crystal structure of complex **II** is the unusual disordering of the fullerene cage due to the type of coordination to the metal atom. The Ir(1)−C(1) σ-bond defines a rigid axis about which the fullerene cage is rotated by about 10°. In this case, only two

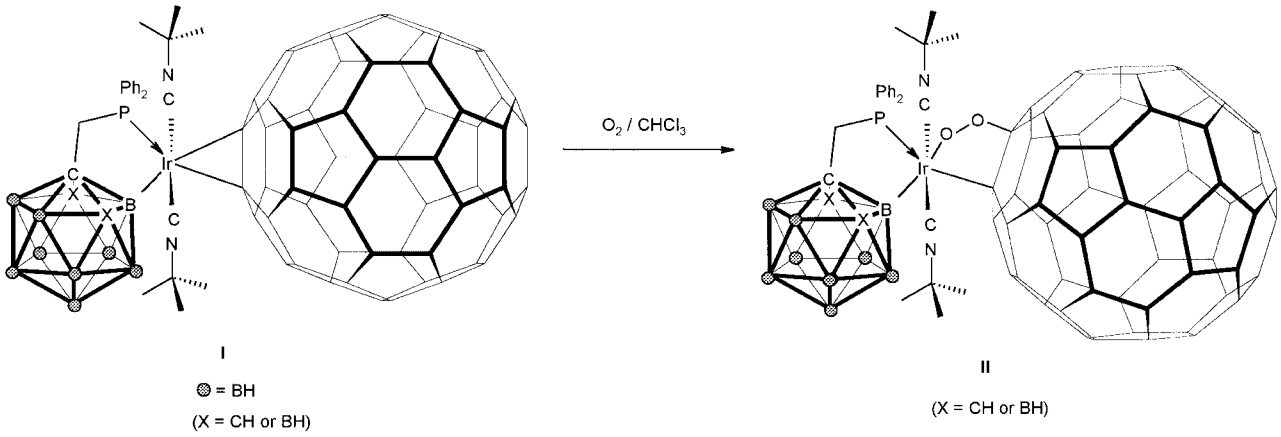

Scheme 1

out of sixty fullerene carbon atoms are ordered, namely the C(1) atom and the C(60) atom occupying the diametrically opposite position. The remaining fifty eight carbon atoms are disordered over two equally populated positions. Figure 2 shows a fragment of the complex **II** to illustrate this disordering of the fullerene ligand.

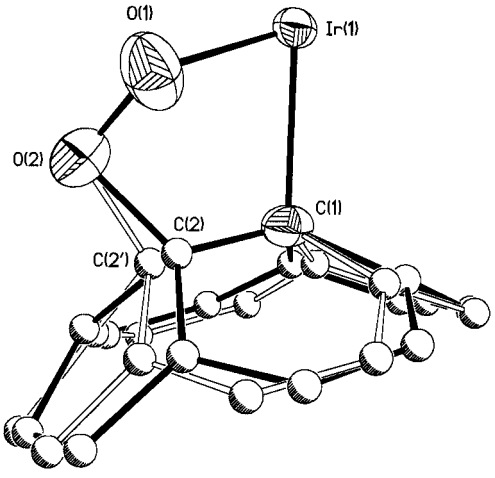

Figure 2. Disordered fragment of molecule **II**

The iridium atom in **II** is also bound to the fullerene cage through a peroxide bridge, which is part of the five-membered cycle Ir(1)−O(1)−O(2)−C(2)−C(1). The crystal structure (Figure 1) unambiguously shows that the dioxygen molecule has inserted into the longer Ir−C(fullerene) bond of the initial complex **I** [this bond is in a pseudo-*trans*-position relative to the Ir(1)−B(3) σ-bond]. As a result, the iridium atom in **II** is close to an octahedral coordination. Specifically, the O(1) atom is in a *trans*-position with respect to the B(3) atom while the C(1) atom is in a *trans*-position with respect to the phosphane ligand [the O(1)−Ir(1)−B(3) and C(1)−Ir(1)−P(1) angles are 177.0(2) and 171.7(2)°, respectively]. The M−O−O−R fragment is not uncommon in transition metal chemistry; however, five-membered metallacycles containing a peroxy group similar to that found in **II** are rarely observed, even though the formation of such compounds has been postulated for olefin oxidation catalyzed by metal complexes. The closest analog of this metallacyclic peroxide fragment is found in the platinum complex $[(PPh_3)_2Pt(O\text{-}O\text{-}C(Me)_2\text{-}C(CN)_2]$ (**III**).[9] Only three structurally characterized iridium complexes containing an Ir−O−O−R fragment are known, where R = $C(sp^3)$[10,11] or a second Ir atom.[12] All these compounds are characterized by a very wide range of their Ir−O and O−O bond lengths (1.99−2.11 and 1.43−1.59 Å, respectively). In complex **II**, the Ir(1)−O(1) and O(1)−O(2) distances are 2.154(5) and 1.417(8) Å, respectively. The dioxairidacycle has an envelope conformation and the angle of folding along the Ir(1)···O(2) line is nearly 60° [the Ir(1)−O(1)−O(2)−C(2) and Ir(1)−O(1)−O(2)−C(2′) torsion angles are 67.1 and 65.8°, respectively]. The corresponding cycle in the platinum complex **III** also has a nonplanar structure with a Pt−O−O−C torsion angle of 53.5°. Disordering of the C(2) atom in the fullerene cage causes a disorder of the oxygen atoms in the peroxy group, increasing the thermal parameters of the O(1) and O(2) atoms (see Figure 2). However, we failed to resolve this disorder due to the spatial proximity of these positions.

A disorder of the fullerene cage and, correspondingly, a low accuracy of its geometric parameters in **II** precludes a detailed consideration of changes in the structure caused by σ-coordination to the iridium atom and peroxy group. In particular, substantially different C(1)−C(2) and C(1)−C(2′) distances [1.46(2) and 1.67(2) Å, respectively; av. 1.56 Å] were obtained for two equivalent positions, C(2) and C(2′), of the C atom bound to the oxygen atom of peroxy group. Nevertheless, both disordered C_{60} cages display different distortions in the vicinity of the key atoms C(1) and C(2) [or C(2′)]. These distortions can be revealed

by comparing the distances from the center of the C_{60} moiety to the carbon atoms along different directions.[13] In particular, in both disordered fullerene cages the distance to the C(1) atom bonded to Ir atom is, on average, 3.83 Å, whereas the distances to the C(2) [or C(2′)] atom bonded to the peroxy group are longer (av. 3.90 Å). The distances to other carbon atoms of the fullerene cage lie between 3.47 and 3.60 Å. Thus, bonding to an O-atom of the peroxy group leads to a greater distortion of the fullerene ligand than that caused by the σ-bond with the Ir atom. Much smaller distortions of the fullerene ligand were found for a conventional η^2-coordination to the iridium atom in **I**, where the average Ir−C distance to the key carbon atoms is 3.73 Å.

In the crystal, there are $3^2/_3$ solvate chloroform molecules per molecule of **II**. The crystal packing (Figure 3) is characterized by shortened Cl···Cl contacts between the solvate chloroform molecules (the shortest distances are 3.31 and 3.43 Å) and by shortened Cl···C distances involving the C(19), C(20), and C(55) atoms of the fullerene ligand (3.13, 3.25 and 3.22 Å, respectively). For comparison, the shortest van der Waals intermolecular contacts are 3.65 Å for Cl···Cl and 3.45 Å for Cl···C.[14] One solvate chloroform molecule forms a weak C−H···O hydrogen bond with the O(1) atom of the peroxy group of **II** [the O(1)···C(1S) distance is 3.02(2) Å and the O(1)···H(1S)−C(1S) angle is 159°].

Thus, we have established that selective insertion reactions can occur involving only one M−C(fullerene) bond in complexes of the (η^2-C_{60})-M type to give the corresponding metallacyclic derivatives with a σ-coordinated fullerene ligand. Oxidation of [(η^2-C_{60})Ir(*o*-$HCB_{10}H_9CCH_2PPh_2$-*B*,*P*)(*t*BuNC)$_2$] by dioxygen resulting in the complex [σ-C_{60}OO-Ir(*o*-$HCB_{10}H_9CCH_2PPh_2$-*B*,*P*)(*t*BuNC)$_2$] is a good example of such a process. To the best of our knowledge, this is not only the first stable mononuclear exohedral fullerene complex in which the fullerene cage is σ-coordinated to the transition metal atom, but also the first structurally characterized complex with a peroxoiridacycle.

Experimental Section

General: IR spectra were obtained on a Specord M80 spectrometer. ^{1}H NMR spectra (400.3 MHz) and ^{31}P{^{1}H} NMR spectra (160.02 MHz) were recorded on a Bruker AMX-400 spectrometer and are quoted relative to residual signals of the solvent (internal standard) and 85% H_3PO_4 (external standard), respectively.

Synthesis of Complex [σ-C_{60}OO-Ir(*o*-$HCB_{10}H_9CCH_2PPh_2$-*B*,*P*)(*t*BuNC)$_2$] (II): Dioxygen was slowly bubbled through a stirred solution of complex **I** (0.0562 g, 0.04 mmol) in dry chloroform (15 mL) at room temperature until disappearance of the absorption band at 460 nm in the UV spectrum of the reaction mixture (ca. 60 h). Chloroform was then removed under reduced pressure and the residue was extracted with THF. The extract was filtered, concentrated to approx. 1.5 mL, and hexane was added. The resulting precipitate was filtered off, washed with hexane, and dried in vacuo

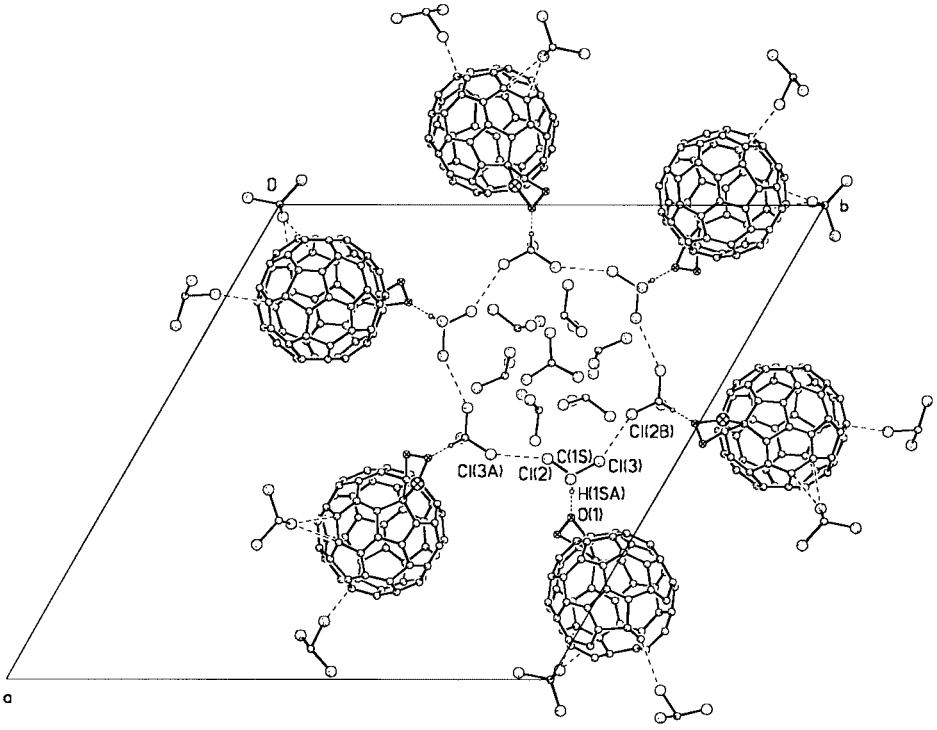

Figure 3. Fragment of crystal packing of solvate **II**·$3^2/_3CHCl_3$ viewed along the *c* direction with intermolecular contacts Cl···Cl, Cl···C and C−H···O (one of two possible orientations of fullerene moiety is shown); the ligand environment of the Ir atoms, apart from the fullerene and oxygen atoms of the peroxide bridge, has been omitted for clarity

to give the complex **II**·$6H_20$ (24.4 mg, 39%) as a dark-green powder. $C_{85}H_{40}B_{10}N_2O_2PIr·6H_20$ (1560.6): calcd. C 65.42, H 3.36; found C 65.53, H 3.73. UV/Vis ($CHCl_3$): λ = 329 nm, 404 (sh), 707. IR (Nujol): $\tilde{\nu}$ = 3568 cm^{-1} (OH), 2581 (BH), 2191 (NC). ^1H NMR ([D_8]THF): δ = 1.30 (s, 9 H, *t*Bu), 1.45 (s, 9 H, *t*Bu), 2.45 (s, 12 H, H_2O), 3.21 (dd, $^2J_{H,P}$ = 6.8, $^2J_{H,H}$ = 16.9 Hz, 1 H, CH_2), 3.50 (s, 1 H, CH^{carb}), 4.19 (dd, $^2J_{H,P}$ = 10.7, $^2J_{H,H}$ = 16.9 Hz, 1 H, CH_2), 7.48 (m, 6 H, Ph), 8.15 (m, 4 H, Ph) ppm. $^{31}P\{^1H\}$ NMR ([D_8]THF): δ = 20.9 ppm.

X-ray Structure Determination of II: Single crystals of **II**·$3^2/_3CHCl_3$ were grown from a chloroform solution of **II**·$6H_20$ at room temperature. The crystals are rhombohedral, space group $R\bar{3}$, a = 29.901(1), c = 42.955(2) Å, V = 33258(1) $Å^3$, Z = 18, $d_{calcd.}$ = 1.699 g/cm^3, and μ(Mo-K_α) = 22.83 cm^{-1}. The intensities of 19332 independent reflections (R_{int} = 0.0635) were measured on a Bruker SMART 1000 CCD diffractometer (graphite monochromated Mo-K_α radiation, λ = 0.71073 Å, ω and scan technique with a 0.3° step in ω and 10 s per frame exposure, θ ≤ 29.5°) at 100.0(2) K. Reflection intensities were integrated using the SAINT software[15] and corrected for absorption semi-empirically (SADABS program)[16] based on multiple measurements of identical reflections and equivalents. The structure was solved by direct methods and refined by full-matrix least-squares against F^2. The uncoordinated carbon atom in the carborane polyhedron is disordered over two equally populated positions labeled X(2) and X(4). The carbon atoms of the C_{60} fullerene ligand [except for the C(1) and C(60) atoms] are disordered over two equally populated positions. The methyl groups of the *tert*-butyl isocyanide ligands are rotationally disordered over two positions with a 3:1 occupancy ratio. In the crystal structure, there are three solvate chloroform molecules in general positions (one of them is disordered) and three solvate chloroform molecules in special positions (one of them occupies a position on the 3 axis and the two others occupy the $\bar{3}$ axes). All disordered atoms in the crystal structure of complex **II** were refined with isotropic thermal parameters. All H atoms of the carborane polyhedron were located from the electron density difference synthesis, while the remaining H atoms were placed geometrically and included in the refinement using a riding model. The refinement converged to wR_2 = 0.1911 and GOF = 1.013 for all independent reflections]R_1 = 0.0649 was calculated against F for a total of 12640 observed reflections with $I > 2\sigma(I)$]; the number of refined parameters was 1013. All calculations were performed using the SHELXTL-97 program[17] on an IBM PC/AT computer.

CCDC-190946 contains the supplementary crystallographic data for this paper. These data can be obtained free of charge at www.ccdc.cam.ac.uk/conts/retrieving.html [or from the Cambridge Crystallographic Data Centre, 12, Union Road, Cambridge CB2 1EZ, UK; Fax: (internat.) +44-1223/336-033; E-mail: deposit@ccdc.cam.ac.uk].

Acknowledgments

This work was supported by the Russian Foundation for Basic Research (Project No. 00-03-32807), the Russian Federation State Research Program "Fullerenes and atomic clusters" [Contr. No. 107-14 (00)-II], and by the Russian Federation Ministry of Industry, Science, and Technology Sub-Program "Fundamental Problems of Modern Chemistry" [Contr. No. 402-19.6/22.3/23.1 (00)-II]. We are grateful to referees who provided us with up-to-date information on the studies by J. T. Park and co-workers.

[1] A. L. Balch, M. M. Olmstead, *Chem. Rev.* **1998**, *98*, 2123−2165.
[2] H. Nagashima, H. Yamaguchi, Y. Kato, Y. Saito, M. Haga, K. Itoh, *Chem. Lett.* **1993**, 2153−2156.
[3] H. Nagashima, Y. Kato, H. Yamaguchi, E. Kimura, T. Kawanishi, M. Kato, Y. Saito, M. Haga, K. Itoh, *Chem. Lett.* **1994**, 1207−1210.
[4] H. Nagashima, M. Nakazawa, T. Furukawa, K. Itoh, *Chem. Lett.* **1996**, 405−406.
[5] A. V. Usatov, E. V. Martynova, F. M. Dolgushin, A. S. Peregudov, M. Yu. Antipin, Yu. N. Novikov, *Eur. J. Inorg. Chem.* **2002**, 2565−2567.
[6] F. J. Brady, D. J. Cardin, M. Domin, *J. Organomet. Chem.* **1995**, *491*, 169−172.
[7] A. V. Usatov, K. N. Kudin, E. V. Vorontsov, L. E. Vinogradova, Yu. N. Novikov, *J. Organomet. Chem.* **1996**, *522*, 147−153.
[8] [8a] M. M. Olmstead, K. Maitra, A. L. Balch, *Angew. Chem. Int. Ed.* **1998**, *38*, 231−233. [8b] H. Song, K. Lee, M.-G. Choi, J. T. Park, *Organometallics* **2002**, *21*, 1756−1758. [8c] H. Song, K. Lee, C. H. Lee, J. T. Park, H. Y. Chang, M.-G. Choi, *Angew. Chem. Int. Ed.* **2001**, *40*, 1500−1502. [8d] H. Song, C. H. Lee, K. Lee, J. T. Park, *Organometallics* **2002**, *21*, 2514−2520.
[9] G. Read, M. Urgelles, A. M. R. Galas, M. B. Hursthouse, *J. Chem. Soc., Dalton Trans.* **1983**, 911−913.
[10] J. Xiao, B. D. Santarsiero, B. A. Vaartastra, M. Cowie, *J. Am. Chem. Soc.* **1993**, *115*, 3212−3220.
[11] P. Barbaro, C. Bianchini, C. Mealli, A. Meli, *J. Am. Chem. Soc.* **1991**, *113*, 3181−3183.
[12] J. R. Bleeke, Y.-F. Xie, L. Bass, M. Y. Chiang, *J. Am. Chem. Soc.* **1991**, *113*, 4703−4704.
[13] The fullerene centroid was calculated without inclusion of the C(1) and C(2) atoms and the C(55) and C(60) atoms occupying diametrically opposed positions [or the C(1), C(2′) and C(55′), C(60) atoms for the second orientation of the C_{60} cage].
[14] Yu. V. Zefirov, P. M. Zorkii, *Russ. Chem. Rev.* **1995**, *64*, 415−428.
[15] *SMART V5.051 and SAINT V5.00, Area detector control and integration software*, **1998**, Bruker AXS.
[16] G. M. Sheldrick, *SADABS*, **1997**, Bruker AXS Inc., Madison, WI-53719,USA
[17] G. M. Sheldrick, *SHELXTL-97 V5.10*, **1997**, Bruker AXS Inc., Madison, WI-53719, USA.

Received August 12, 2002
[I02458]

Macrocyclic Melamine-Based Ligand Complexes as Building Blocks for the Metal-Directed Synthesis of Heterometallic Di- and Trinuclear Compounds

Peter Comba,*[a] Yaroslaw D. Lampeka,*[b] Lutz Lötzbeyer,[a] and Alexander I. Prikhod'ko[b]

Keywords: Template reactions / Nickel / Copper / Macrocycles / N ligands

Heterodi- and heterotrimetallic Ni^{II}/Cu^{II}, Ni^{II}_2/Cu^{II} and Ni^{II}/Cu^{II}_2 complexes of bis- and tris-macrocyclic ligands, linked by a 1,3,5-triazine spacer group, are obtained as products of copper(II)- or nickel(II)-assisted condensations of the open-chain tetraamine complexes $[M^2(2,3,2\text{-tet})]^{2+}$ [2,3,2-tet= bis-*N*,*N*′-(2-aminoethyl)propane-1,3-diamine, $M^2 = Ni^{II}$ or Cu^{II}] with formaldehyde and the monomacrocyclic ligand complexes $[M^1(L^1)]^{2+}$, where L^1 is a cyclam-type macrocycle with a pendent melamine group ($M^1 = Cu^{II}$ or Ni^{II}). The spectroscopic (UV/Vis and EPR) and electrochemical properties of the oligonuclear heterometallic compounds in comparison with those of the homometallic analogues indicate small, but significant, intramolecular metal-metal interactions.

(© Wiley-VCH Verlag GmbH & Co. KGaA, 69451 Weinheim, Germany, 2003)

Introduction

A number of metalloproteins have oligonuclear active sites,[1] cooperative effects in dinuclear enzyme mimics have been studied extensively,[2−4] and examples of very active catalysts with more than one metal center involved may indicate that there is some potential in oligonuclear metal catalysts. Generally, the two (or more) metal ions have different functions in enzymatic catalytic processes and, therefore, the two sites in model compounds and active molecular catalysts should be structurally and/or electronically different.[5] The synthesis of ligands with two different coordination sites is not easy,[5,6] and coordination of two different metal ions to symmetrical ligands leads to problems with the separation of the product mixtures, especially with labile metal ions. The sequential synthesis of oligonuclear complexes is therefore an appealing concept,[7] and for oligomacrocylic ligand complexes, consecutive metal-ion-directed processes should be an efficient preparative technique.

There are a few mixed $Ni^{II}Cu^{II}$ complexes of bis-tetraazamacrocyclic ligands[8−10] but no corresponding trinuclear complexes have been described so far. The nickel(II)- and copper(II)-directed reactions of $[M^2(2,3,2\text{-tet})]^{2+}$ [2,3,2-tet = bis *N*,*N*′-(2-aminoethyl)propane-1,3-diamine, $M^2 = Ni^{II}$ or Cu^{II}] with formaldehyde and melamine (melamine = 2,4,6-triamino-1,3,5-triazine) lead to mixtures of homometallic mono-, bis- and tris-macrocyclic ligand complexes.[11−14] The fact that products of different nuclearity are formed in the one-pot reactions suggests that the melamine amino groups of the mono- and bis-macrocyclic ligand complexes can serve as locking fragments in the formation of the second and third macrocyclic subunit. Here we report the use of the recovered mono-macrocyclic ligand complexes as starting materials for the di- and trinuclear mixed-metal complexes (see Scheme 1).

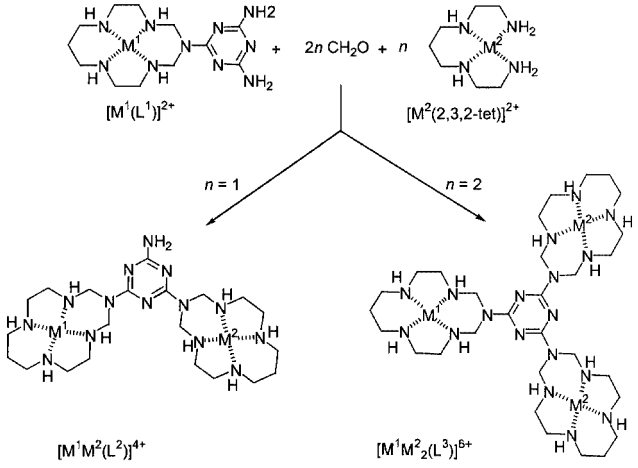

Scheme 1

[a] Universität Heidelberg, Anorganisch-Chemisches Institut, Im Neuenheimer Feld 270, 69120 Heidelberg, Germany
Fax: (internat.) +49-6221/546-617
E-mail: comba@akcomba.oci.uni-heidelberg.de
[b] L.V. Pisarzhevsky Institute of Physical Chemistry, National Academy of Science of Ukraine, Prospekt Nauki 31, 03039, Kiev-39, Ukraine
Fax: (internat.) +38-044/265-6216
E-mail: ditop@iphch.kiev.ua

Results and Discussion

The nickel(II)- or copper(II)-assisted reaction of the open-chain tetraamine 2,3,2-tet with the melamine-substituted macrocyclic ligand compounds $[M^1(L^1)]^{2+}$ results in the formation of the desired di- and trinuclear heterometallic species $[M^1M^2(L^2)]^{4+}$, $[M^1_2M^2(L^3)]^{6+}$ and $[M^1M^2_2(L^3)]^{6+}$ ($M^1 = Cu^{II}$, $M^2 = Ni^{II}$; see Scheme 1). Similar to the analogous reactions leading to the corresponding homo-oligonuclear complexes[13,14] the yields of the one-pot template reactions are low (5−10%) and higher for the copper(II)- than for the nickel(II)-directed reactions. The yields are solvent dependent and the highest were obtained in ethanol/acetonitrile mixtures. As a side-product the modified bis-macrocyclic ligand complex $[NiCu(L^{2a})]^{4+}$, in which the melamine NH_2 protons of L^2 are substituted by CH_2OH groups, is formed in appreciable yield. This complex was fully characterized by MS and elemental analysis (see Exp. Sect.).

The mass spectra of the three new hetero-oligonuclear complexes are clear evidence for the successful syntheses. Peaks for the molecular ions, with expected intensity distributions, were observed in all cases (see Figure 1 for an example). As expected, due to the inertness of the oligo-macrocyclic ligand complexes, no peaks of homo-oligonuclear species were observed; i.e., there are no transmetallation reactions. Characteristic peaks in the IR spectra of the complexes {1630 cm^{-1} (δ_{NH2}) and 1560 cm^{-1} (ν_{CN}) for $[NiCu(L^2)]^{4+}$ and 1550 cm^{-1} (ν_{CN}) for $[NiCu_2(L^3)]^{6+}$ and $[Ni_2Cu(L^3)]^{6+}$} are in good agreement with those of the corresponding homo-oligonuclear compounds.[13,14] The electronic spectra of the homo- and heteronuclear complexes are similar (Table 1). The absorption in the UV region is due to the superposition of the MLCT transition {ν_{max} = 39500 cm^{-1} (ε = 8500 $M^{-1}\cdot cm^{-1}$) and 45500 cm^{-1} (ε = 12000) for $[Cu(cyclam)]^{2+}$ and $[Ni(cyclam)]^{2+}$, respectively, cyclam = 1,4,8,11-tetraazacylotetradecane}[13,14] and a melamine-based π-π transition [ν_{max} = 49100 cm^{-1} (ε = 52000)].[13,14] The intensity of the MLCT bands are approximately proportional to the number of copper(II) and nickel(II) sites in the oligonuclear complexes.

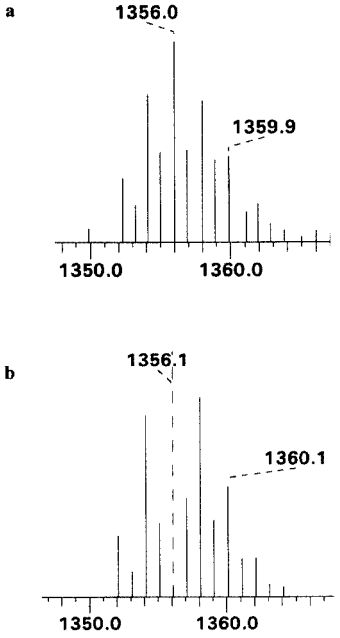

Figure 1. Experimental (a) and calculated (b) distribution of peak intensities for $\{[Ni_2Cu(L^3)](ClO_4)_5\}^+$ in the FAB mass spectrum of the trinuclear mixed-metal complex

The intensities of the d-d electronic transitions are also very similar to the sum of the spectra of the corresponding mononuclear nickel(II) and copper(II) sites (see Table 1). Nickel(II) complexes of melamine-based ligands exist in aqueous solution as equilibrium mixtures of diamagnetic four-coordinate $[NiN_4]$ and paramagnetic six-coordinate $[NiN_4(OH_2)_2]$ species.[14] Because of the larger intensity of the copper(II) d-d transitions those due to nickel(II) appear only as ill-resolved shoulders at the high energy tail of the copper(II) band. This is more pronounced at higher temperatures and in the noncoordinating solvent nitromethane,

Table 1. Spectroscopic[a] and electrochemical[b] data of the di- and trinuclear complexes

Compound	Absorption bands			Cyclic voltammograms	
	d-d	MLCT[c]	π-π[c]	0.1 M $NaNO_3$	3.33×10^{-2} M Na_2SO_4
$[Cu(L^1)]^{2+}$	19400(87)[d]	39500 (8500)	47900 (51000)		
$[Ni(L^1)]^{2+}$	22000(20)[d] 22000(64)[e]		47800 (52000)	883(65)	643(75)
$[Cu_2(L^2)]^{4+}$	19400(176)[d] 20200(157)[e]	39500 (16500)	47000 (57600)		
$[Ni_2(L^2)]^{4+}$	22000(42)[d] 22000(128)[e]		46800 (62000)	865 (70)	593(70), 703(75)
$[NiCu(L^2)]^{4+}$	19400(92)[d] 21100(120)[e]	39500 (9700)	46400 (51700)	865 (80)	600(100)
$[Cu_3(L^3)]^{6+}$	19400(260)[d]	39500 (24400)	46700 (87000)		
$[NiCu_2(L^3)]^{6+}$	19400(184)[d] 20700(201)[e]	39500 (18100)	46100 (75200)	865 (120)	620(120)
$[Ni_2Cu(L^3)]^{6+}$	19900(117)[d] 21300(193)[e]	39500 (11000)	45900 (73700)	865 (120)	605(85)

[a] ν_{max} in cm^{-1} (ε in $L\cdot mol^{-1}\cdot cm^{-1}$). [b] Aqueous solution, $E_{1/2}$ in mV vs. sat.Ag/AgCl (peak separation, ΔE, in mV). [c] Aqueous solution. [d] 0.1 M $NaNO_3$, aqueous solution. [e] Nitromethane solution.

where the amount of the diamagnetic form of nickel(II) is dominant (see Table 1).

EPR spectra of the complexes are indicative of the number of copper(II) sites in the oligomacrocyclic ligand complexes. For $[NiCu(L^2)]^{4+}$ and $[Ni_2Cu(L^3)]^{6+}$ the spectra are, as expected, almost identical (Figure 2), and similar to that of $[Cu(L^1)]^{2+}$.[11,13] The spectrum of $[NiCu_2(L^3)]^{6+}$ is similar to that of $[Cu_2(L^2)]^{4+}$ and typical for a dipole-dipole coupled bis(spin 1/2) system. The rather broad features of the two dicopper(II) compounds (spectra d and e) do not allow us to exclude small amounts of $CuNi_2$ or Cu_3 impurities in the samples. However, the spectra are compatible with pure Cu_2 and $NiCu_2$ samples and transmetallation is unexpected for this type of cyclam-based copper(II) and nickel(II) complexes under the conditions employed, and proven by the mass spectroscopic data and elemental analyses. A detailed interpretation of the EPR spectra with the aim of analyzing the solution structural properties, based on MM-EPR,[15] is in process and will be published elsewhere.[16]

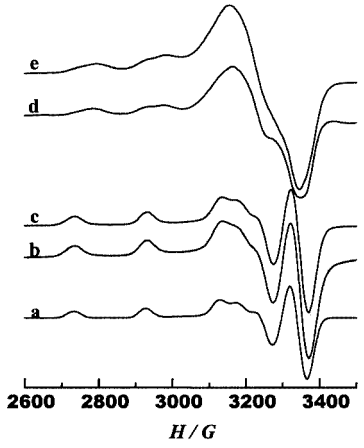

Figure 2. EPR spectra of frozen solutions [DMF/H_2O, (2:1), approx. 10^{-3} M] of: (a) $[Cu(L^1)]^{2+}$, (b) $[NiCu(L^2)]^{4+}$, (c) $[Ni_2Cu(L^3)]^{6+}$, (d) $[Cu_2(L^2)]^{4+}$ and (e) $[NiCu_2(L^3)]^{6+}$

The redox potentials of the $Ni^{III/II}$ couple in aqueous solution (0.1 M $NaNO_3$ or 3.3×10^{-2} M Na_2SO_4) were determined by cyclic voltammetry (Table 1). Due to the more positive $E_{1/2}$ values for the $Cu^{III/II}$ transformation[13] these processes were not observed in the potential range studied (0.2−1.0 V). The CV of $[Ni_2(L^2)]^{4+}$ and $[NiCu(L^2)]^{4+}$ in 0.1 M $NaNO_3$ reveal one quasi-reversible $Ni^{III/II}$ transition each, but the current of the mixed-metal species is approximately half that of the homo-dinuclear complex at the same concentration. Under the same conditions the current observed for $[NiCu_2(L^3)]^{6+}$ is smaller than for $[NiCu(L^2)]^{4+}$; this is believed to be due to a smaller diffusion coefficient of the tris(macrocyclic) ligand cationic complex. A similar effect is observed for $[Ni_2(L^2)]^{4+}$ and $[Ni_2Cu(L^3)]^{6+}$. The potentials of the $Ni^{III/II}$ couple for all hetero-oligonuclear complexes are close to that of the corresponding mononuclear compound. This indicates a negligible electrostatic influence of the copper(II) centers on the redox transformation of the nickel ions.

Due to the stabilization of nickel(III) by coordination of sulfate, the $E_{1/2}$ values in sulfate media are less anodic. As expected, $[NiCu(L^2)]^{4+}$ as well as $[NiCu_2(L^3)]^{6+}$ reveal one electrochemical process with potentials similar to the less anodic peaks observed for $[Ni_2(L^2)]^{4+}$ (Figure 3). $[Ni_2(L^2)]^{4+}$ also undergoes a second redox transformation at higher potential. This was interpreted as being due to hydrogen bonding between a water molecule coordinated to one nickel center and sulfate axially coordinated to the adjacent metal ion.[14] It was therefore unexpected that both nickel centers of $[Ni_2Cu(L^3)]^{6+}$ are electrochemically identical in sulfate media. It appears that the formation of the proposed hydrogen-bonded arrangement is less favorable when water is coordinated to copper(II); a possible reason is the differences in M−O (OH_2) bonds {approx. 2.15 and 2.5 Å for tetragonal nickel(II) and copper(II) tetramines[14]}.

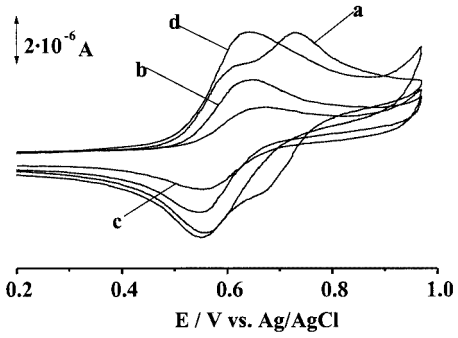

Figure 3. Cyclic voltammograms of 2.5×10^{-3} M solutions of the macrocyclic ligand complexes in 3.33×10^{-2} M Na_2SO_4: (a) $[Ni_2(L^2)]^{4+}$; (b) $[NiCu(L^2)]^{4+}$; (c) $[NiCu_2(L^3)]^{6+}$; (d) $[Ni_2Cu(L^3)]^{6+}$

Conclusion

Based on the available electrochemical and UV/Vis spectroscopic data there is only a weak interaction between the copper(II) and nickel(II) centers. This is supported by the EPR spectra of the systems with two copper centers, which are typical for dipole-dipole coupled dicopper(II) compounds. The electrochemical data indicate that the cooperativity in the binding of sulfate observed for the homometallic dinickel(II) system[14] disappears in the mixed-metal systems. This suggests that axial coordination to the mixed-metal systems is significantly different to that of the homometallic compounds, and this will lead to important differences in the rich host-guest chemistry[13] of the trinuclear systems.

Experimental Section

Physical Methods: Infrared spectra (KBr pellets) were recorded on a Specord 75 IR (Carl Zeiss) spectrometer. Electronic absorption spectra were measured on a Specord M40 (Carl Zeiss) spectrophotometer. EPR spectra were obtained with a Bruker ESP300E spectrometer (9.4635 GHz) as approx. 1×10^{-3} mol·L^{-1} frozen (liquid nitrogen temperature) solutions in DMF/water (2:1). Fast atom bombardment mass-spectra (FAB^+ mode) were obtained

with a MAT8400 mass spectrometer, using *p*-nitrobenzyl alcohol (Nibelol) as the matrix. Cyclic voltammograms were generated using a PI-50−1.1 potentiostat, equipped with a PR-8 function generator (Izmeritel, Gomel) and an N-307 X-Y recorder (ZIP, Krasnodar). A standard three-electrode scheme was used, consisting of a glassy carbon working, a Ag/AgCl reference and a Pt wire auxiliary electrode. All solutions for electrochemistry were purged with nitrogen before measurement. Analytical data were obtained from the microanalytical laboratory of the chemical institutes of the University of Heidelberg.

Materials: AR grade chemicals and solvents were used as supplied for all reactions. Open-chain amine metal complexes $[M(2,3,2\text{-tet})](ClO_4)_2$ [M = Ni or Cu; 2,3,2-tet= bis-*N*,*N*′-(2-aminoethyl)-propane-1,3-diamine] and macrocyclic ligand mononuclear $\{[Ni(L^1)](ClO_4)_2{\cdot}H_2O$ and $[Cu(L^1H)](ClO_4)_3{\cdot}H_2O\}$ and homodinuclear $\{[Ni_2(L^2)](ClO_4)_4{\cdot}2H_2O$ and $[Cu_2(L^2)](ClO_4)_4{\cdot}2.5H_2O\}$ complexes were prepared as described previously.[13,14]

Syntheses: ***Caution! Perchlorate salts of metal complexes are potentially explosive. Although we did not experience any problems, such complexes should be handled very carefully.***

In a typical procedure 4.0 mmol of $[Ni(L^1)](ClO_4)_2{\cdot}H_2O$ {or $[Cu(L^1H)](ClO_4)_3{\cdot}H_2O\}$ and 9.1 mmol of $[Cu(2,3,2\text{-tet})](ClO_4)_2$ {or $[Ni(2,3,2\text{-tet})](ClO_4)_2\}$ were dissolved in a mixture of acetonitrile (25 mL), ethanol (35 mL) and triethylamine (3 mL), and the resulting solution was brought to reflux. A solution of 37% aqueous formaldehyde (23.0 mmol) in ethanol (15 mL) was added dropwise during one hour. The reaction mixture was refluxed for an additional 48 h, then cooled to ambient temperature and filtered. The solution was diluted to 2 L and absorbed onto a Sephadex C-25 (Na^+ form) ion exchange column, which was first washed with water (0.5 L). The first band eluted with 0.25 M $NaClO_4$ contained unchanged starting materials and was discarded.

Two bands eluted from the column with 0.4 M $NaClO_4$. The first band was collected, the solvents evaporated under low pressure to a small volume and left to dry at ambient temperature. The solid red-yellow residue was treated with 30 mL of acetonitrile to extract the macrocyclic complex. This was precipitated from the purple acetonitrile solution by slow diffusion of diethyl ether, and the solid was carefully triturated in 10 mL of 1 M aqueous $NaClO_4$. The precipitate, **$[NiCu(L^{2a})](ClO_4)_4\ 3H_2O$**, was collected by filtration, washed with ethanol and dried in air. Yield 0.22 g, 5%. $C_{23}H_{55}Cl_4CuN_{14}NiO_{21}$ (1127.8): calcd. C 24.49, H 4.92, N 17.39; found C 24.28, H 4.84, N 17.62. MS: *m*/*z* = 972 ($[CuNi(L^{2a}\text{-}2H)](ClO_4)_3^+$), 944 ($[CuNi(L^{2a}\text{-}CH_2OH)](ClO_4)_3^+$), 914 ($[CuNi(L^{2a}\text{-}2CH_2OH)](ClO_4)_3^+$).

$[NiCu(L^2)](ClO_4)_4{\cdot}3H_2O$ eluted as the second band with 0.4 M $NaClO_4$. The eluate was evaporated to 40 mL under reduced pressure and cooled in a refrigerator. The red-orange precipitate was filtered, washed with ethanol and dried in air. Yield 0.47 g, 11%. The product was purified by reprecipitation from an aqueous solution by addition of $NaClO_4$. IR (KBr): $\tilde{\nu}$ = 3210m cm^{-1} [ν(NH), macrocycle], 1630m [δ(NH_2), melamine], 1560s [ν(CN), melamine], ca. 1100vs, 626m [ν(ClO_4)]. $C_{12}H_{52}Cl_4CuN_{14}NiO_{19}$ (960.7): calcd. C 23.60, H 4.90, N 18.35; found C 23.79, H 4.95, N 18.12. MS: *m*/*z* = 914 ($[CuNi(L^2)](ClO_4)_3^+$).

The tris-macrocyclic ligand complexes were eluted as the third band with 0.8 M $NaNO_3$. The eluate was reduced to a volume of 40 mL. After cooling, the precipitate of $NaNO_3$ was removed by filtration. After addition of 2 g of $NaClO_4$ the solution was left at room temperature for a few days to allow crystals to form. The product was filtered, washed with ice-cold water and ethanol and dried in air.

$[NiCu_2(L^3)](ClO_4)_3(NO_3)_3{\cdot}3H_2O$. Yield 0.36 g, 7%. IR (KBr): $\tilde{\nu}$ = 3190m cm^{-1} [ν(NH), macrocycle], 1550s [ν(CN), melamine], 1370s [ν(NO_3)], ca. 1100vs, 626m [ν(ClO_4)]. $C_{30}H_{72}Cl_3Cu_2N_{21}NiO_{24}$ (1403.2): calcd. C 25.68; H 5.17; N 20.96; found C 25.77; H 5.36; N 21.32. MS: *m*/*z* = 1248 ($[NiCu_2(L^3)](ClO_4)_2(NO_3)_3^+$).

$[NiCu_2(L^3)](ClO_4)_6{\cdot}4H_2O$: This product was obtained by addition of $NaClO_4$ to an aqueous solution of $[NiCu_2(L^3)](ClO_4)_3(NO_3)_3{\cdot}3H_2O$. Yield: nearly quantitative. IR (KBr): $\tilde{\nu}$ = 3226 cm^{-1} [ν(NH), macrocycle], 1550s [ν(CN), melamine], ca. 1100vs, 626m [ν(ClO_4)]. $C_{30}H_{74}Cl_6Cu_2N_{18}NiO_{28}$ (1533.5): calcd. C 23.50, H 4.86, N 16.44; found C 23.62, H 5.02, N 16.42.

$[Ni_2Cu(L^3)](ClO_4)_6{\cdot}5H_2O$: Yield 0.21 g, 3%. IR (KBr): $\tilde{\nu}$ = 3200m cm^{-1} [ν(NH), macrocycle], 1550s [ν(CN), melamine], ca. 1100vs, 626m [ν(ClO_4)]. $C_{30}H_{76}Cl_6CuN_{18}Ni_2O_{29}$:calcd. C 22.00, H 4.48, N 17.11; found C 22.06, H 4.65, N 16.78. MS: *m*/*z* = 1356 ($[CuNi_2(L^3)](ClO_4)_5^+$).

Acknowledgments

Financial support by the German Science Foundation (DFG) and the Department of Fundamental Research of the Ministry for Education and Science of the Ukraine are gratefully acknowledged.

[1] S. J. Lippard, J. M. Berg, *Principles of Bioinorganic Chemistry*, University Science Books, Mill Valley 1994.
[2] J. Reedijk, *Bioinorganic Catalysis*, Marcel Dekker Inc., New York Basel 1993.
[3] B. Meunier, in *Structure & Bonding, Vol. 97* (Ed.: B. Meunier), Springer, Berlin 2000.
[4] B. Meunier, *Biomimetic Oxidations Catalyzed by Transition Metal Complexes*, Imperial College Press 2000.
[5] C. Fraser, L. Johnston, A. L. Rheingold, B. S. Haggerty, G. K. Williams, J. Whelan, B. Bosnich, *Inorg. Chem.* **1992**, *31*, 1835−1844.
[6] M. Konrad, S. Wuthe, F. Meyer, E. Kaifer, *Eur. J. Inorg. Chem.* **2001**, 2233−2240.
[7] A. Mayboroda, G. Rheingold, H. Lang, *Eur. J. Inorg. Chem.* **2001**, 2263−2269.
[8] L. Fabbrizzi, L. Montagna, A. Poggi, T. A. Kaden, L. C. Siegfried, *J. Chem. Soc., Dalton* **1987**, 2631−2634.
[9] K. Mochizuki, S. Higashiya, M. Uyama, T. Kimura, *J. Chem. Soc., Chem. Commun.* **1994**, 2673−2674.
[10] A. McAuley, S. Subramanian, M. J. Zaworotko, K. Biradha, *Inorg. Chem.* **1999**, *22*, 5078−5085.
[11] P. V. Bernhardt, E. J. Hayes, *J. Chem. Soc., Dalton Trans.* **1998**, 3539−3541.
[12] P. V. Bernhardt, E. J. Hayes, *Inorg. Chem.* **1998**, *37*, 4214−4219.
[13] P. Comba, Y. D. Lampeka, A. Y. Nazarenko, A. I. Prikhod′ko, H. Pritzkow, *Eur. J. Inorg. Chem.* **2002**, 1464−1474.
[14] P. Comba, Y. D. Lampeka, A. Y. Nazarenko, A. I. Prikhod′ko, H. Pritzkow, J. Taraszewska, *Eur. J. Inorg. Chem.* **2002**, 1871−1882.
[15] P. V. Bernhardt, P. Comba, T. W. Hambley, S. S. Massoud, S. Stebler, *Inorg. Chem.* **1992**, *31*, 2644−2651.
[16] P. Comba, Y. D. Lampeka, M. Kerscher, A. I. Prikhod′ko, manuscript in preparation.

Received August 14, 2002
[I02461]

Self-Assembly of a One-Dimensional Silver Complex Containing Two Kinds of Helical Chains

Daofeng Sun,[a] Rong Cao,*[a] Yanqiong Sun,[a] Wenhua Bi,[a] Xing Li,[a] Maochun Hong,[a] and Yingjun Zhao[a]

Keywords: Self-assembly / S ligands / N ligands / Silver / Helical structures

Self-assembly of the potassium sulfonate salt K_2pesp [H_2pesp = piperazine-1,4-bis(2-ethanesulfonic acid] with piperazine (PIP) and a silver(I) salt in solution allows the preparation of a novel one-dimensional helical polymer $[Ag(PIP)]_n{\cdot}[Ag(pesd)]_n{\cdot}2nH_2O$ (**1**), which is made up of two independent silver-containing helical chains, namely $[Ag(PIP)]_n$ and $[Ag(pesd)]_n$. There is no direct bonding interaction between the two chains, and the hydrogen bonds between the chains give **1** a two-dimensional layer supramolecular architecture.
(© Wiley-VCH Verlag GmbH & Co. KGaA, 69451 Weinheim, Germany, 2003)

Inorganic supramolecular chemistry, in particular the construction of specific structural networks, is a particularly active field of chemistry.[1] In the past few decades, helical structures have received much attention from chemists due to their fundamental role in biology, and their potential applications in asymmetric catalysis and nonlinear optical materials.[2,3] Although the most effective method to construct helical polymers is to carefully design helical ligands,[4] the use of oligopyridines and other optically active ligands has resulted in a large number of helical structures, such as di- and oligonuclear, infinite single or double helical chains.[5] However, no helical structures constructed from sulfonic ligands have been reported, probably due to the weak coordinating ability of sulfonate ligands.[6,7] Recently, we began to study the reactions of the flexible sulfonate ligand[8] piperazine-1,4-bis(2-ethanesulfonic acid) (H_2pesp) with silver salts, with the aim of obtaining information on the coordination ability of sulfonic ligands, which have previously been regarded as poorly coordinating anions,[7] and for constructing novel coordination architectures. In this paper, we describe a novel silver polymer containing two independent silver helical chains $[Ag(PIP)]_n{\cdot}[Ag(pesp)]_n{\cdot}2nH_2O$ (**1**).

Complex **1** was obtained as colorless crystals by the self-assembly reaction of dipotassium salt of piperazine-1,4-bis(2-ethanesulfonic acid) (K_2pesp), piperazine hexahydrate (PIP) and $AgNO_3$ in H_2O/MeOH at room temperature. X-ray diffraction analysis shows **1** to be a one-dimensional polymer containing two independent silver-containing helical chains, namely $[Ag(pesp)]_n$ and $[Ag(PIP)]_n$. The crystal structure consists of two independent subunits, $[Ag(pesp)]^-$ and $[Ag(PIP)]^+$. In $[Ag(pesp)]^-$, the central silver is coordinated by two oxygen atoms and two nitrogen atoms from different ligands in a distorted tetrahedral geometry similar to that found in $[Ag_2(\mu_2\text{-}OH_2)(pesp)]_n$,[8] with an average Ag−O bond length of 2.433(10) Å and an average Ag−N bond length of 2.334(9) Å. Due to the presence of a flexible ethyl group, one oxygen atom of the sulfonate group and one nitrogen atom of the piperazine unit of $pesp^{2-}$ chelate the silver ion and the whole ligand acts as a μ_2-bridge. The coordination mode of the $pesp^{2-}$ ligand in **1** is quite different from that found in $[Ag_2(\mu_2\text{-}OH_2)(pesp)]_n$,[8] in which $pesp^{2-}$ is almost linear and acts as a μ_6-bridge to link six silver ions. This result illustrates that the flexible $pesp^{2-}$ ligand can adopt diverse coordination modes according to the different geometric requirements of the metal ions.[9] Thus, each $pesp^{2-}$ ligand links two silver ions and to form a one-dimensional anionic 2_1 helical chain, as shown in Figure 1. To the best of our knowledge, this is the first example of a silver(I) helical structure constructed by sulfonate ligands. The charge balance comes from another one-dimensional cationic helical chain, $[Ag(PIP)]_n$. In this $[Ag(PIP)]^+$ unit, the silver ion is coordinated by two nitrogen atoms from two PIP ligands in a linear geometry with the average Ag−N distance being 2.200(10) Å, shorter than that in the $[Ag(pesp)]^-$ unit. Each PIP links two silver ions to form a one-dimensional cationic helical chain (Figure 2). The piperazine rings in both $pesp^{2-}$ and PIP ligands adopt the most stable "chair" configuration as found in other Ag-PIP complexes.[10]

Considering that the most volatile component of the structure should be the piperazine units, thermogravimetric analyses (TGA) were performed to determine the thermal

[a] State Key Laboratory of Structural Chemistry, Fujian Institute of Research on the Structure of Matter, Chinese Academy of Sciences,
Fujian, Fuzhou, 350002, China

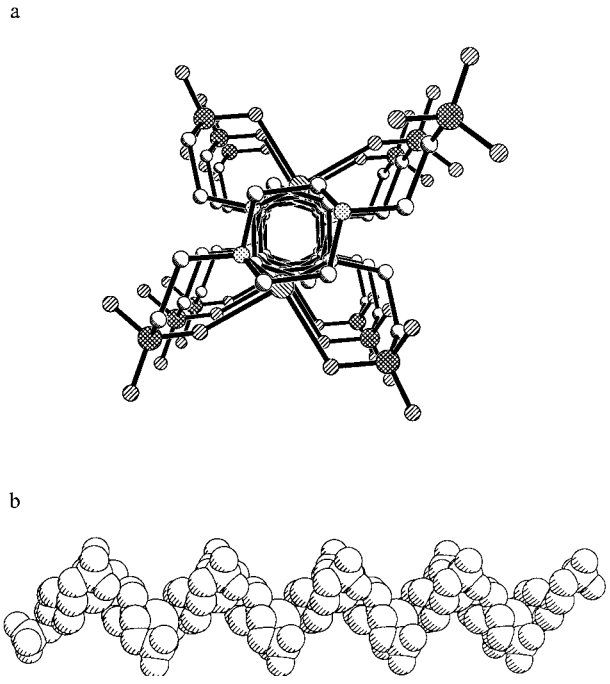

Figure 1. The $[Ag(pesp)]_n^{n-}$ anion helical chain in **1**: a) along the helical axis; b) space filling representation; selected bond lengths (Å) and angles (°): Ag(1)−N(1) 2.308(9), Ag(1)−N(2) 2.359(9), Ag(1)−O(4) 2.388(8), Ag(1)−O(1) 2.477(10); N(1)−Ag(1)−N(2) 143.1(3), N(1)−Ag(1)−O(4) 119.2(3), N(2)−Ag(1)−O(4) 88.5(3), N(1)−Ag(1)−O(1) 91.1(3), N(2)−Ag(1)−O(1), 113.2(3), O(4)−Ag(1)−O(1), 92.2(3)

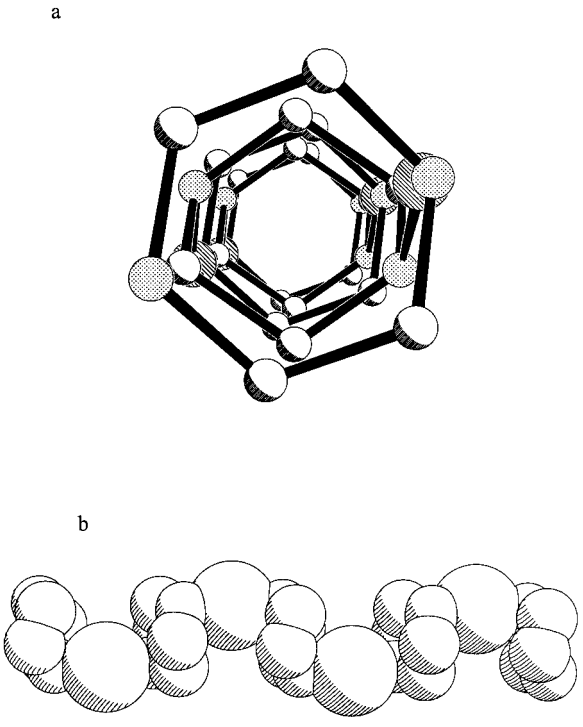

Figure 2. The $[Ag(PIP)]_n^{n+}$ cation helical chain in **1**: a) along the helical axis; b) space filling representation; selected bond lengths (Å) and angles (°): Ag(2)−N(3) 2.197(10), Ag(2)−N(4) 2.203(10); N(3)−Ag(2)−N(4) 153.9(4)

stability of complex **1**. After a total weight loss of 5.50% is achieved at 250 °C, which corresponds to the loss of two uncoordinated water molecules per formula unit, complex **1** starts to decompose gradually and the decomposition ends above 700 °C.

The most intriguing feature of **1** is the independence of the cationic and anionic helical chains. Although some polymeric complexes containing two kinds of helical chains have been reported, the chains are usually not independent and are connected by coordination bonds.[11,12] In **1**, there is no direct bonding interaction between the two chains, only hydrogen bonding interactions between some nitrogen atoms of the PIP ligands and the oxygen atoms of $pesp^{2-}$ are observed — the shortest N−O distance is 2.876(9) Å — and a two-dimensional wave-like layer structure is formed by such weak interactions (Figure 3). Aside from the hydrogen bonds between the chains, there are also weak Ag−O interactions between the layers: the sulfonate oxygen atom [O(3)] coordinates weakly to the silver ion [Ag(2)] of another layer with an Ag−O distance of 2.793 Å. This weak interaction makes the inter-layer distance much shorter (6.667 Å; Figure 4); the free water molecules are found between the layers.

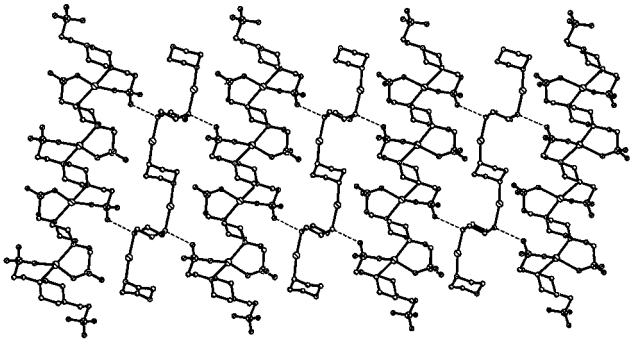

Figure 3. The 2D layer structure of **1** constructed by hydrogen bond between chains

As is well known, the self-assembly reaction is strongly influenced by many factors such as the pH value, the solvent and the metal:ligand ratio. We therefore changed the reaction conditions in order to attempt the preparation of different structures. However, when we adjusted the pH value to 7 or 8 by addition of $HClO_4$, we obtained the polymer $[Ag_2(\mu_2\text{-}OH_2)(pesp)]_n$,[8] which presumably arises from partial protonation of the piperazine moiety this pH value and subsequent loss of its coordination ability. When we attempted the reaction in different solvents and metal:ligand ratios, only an unknown precipitate was obtained, which indicates that the pH value, the solvent and the metal:ligand ratio do indeed influence the formation of **1**. Further study of this reaction is underway and will be reported shortly.

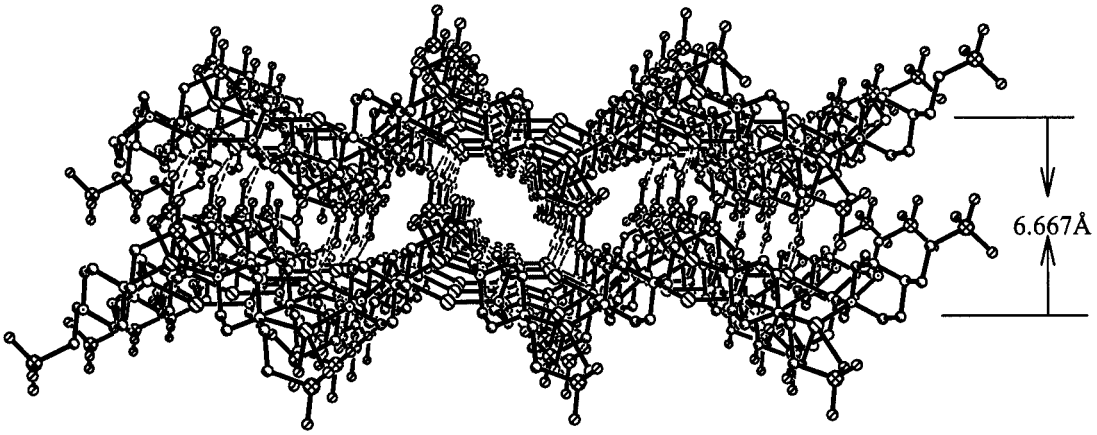

Figure 4. Structure of **1** showing the interlayer network

Experimental Section

Synthesis of 1: K_2pesp (0.045 g, 0.125 mmol) and PIP (0.021 g, 0.25 mmol) were dissolved in 10 mL of water. Then, a solution of $AgNO_3$ (0.043 g, 0.25 mmol) in MeOH (5 mL) was carefully layered on it. After standing in the dark for about two weeks, colorless prism-like crystals were obtained. Yield: 35%. $C_{12}H_{30}Ag_2N_4O_8S_2$ (638.2): calcd. C 22.58, H 4.74, N 8.78; found C 22.60, H 4.65, N 8.80. IR (KBr): $\tilde{\nu}$ = 3450(vs), 3261(m), 2827(m), 1655(m), 1552(m), 1460(m), 1358(m), 1315(s), 1250(s), 1200(vs), 1215(vs), 1167(vs), 1039(vs), 866(s), 588(vs) cm^{-1}.

X-ray Crystallography: $C_8H_{18}Ag_2N_2O_7S_2$, (**1**), M_r = 638.26, triclinic, $P\bar{1}$, a = 6.7657(8), b = 10.5093(13), c = 14.8207(18) Å, α = 101.281(2)°, β = 97.091(2)°, γ = 90.516(2)°, V = 1024.9(2) $Å^3$, Z = 2, D_c = 2.068 g/cm^3, μ(Mo-K_α) = 2.162 mm^{-1}, T = 293(2) K, R [$I < 2\sigma(I)$] = 0.0738, wR = 0.1636 for 3604 independent reflections with $F \geq 2.0\sigma(F_o)$.

Table 1. Crystallographic data for complex **1**

	1
Empirical formula	$C_8H_{18}Ag_2N_2O_7S_2$
Fw	638.26
Crystal system	Triclinic
Space group	$P\bar{1}$
a, Å	6.7657(8)
b, Å	10.5093(13)
c, Å	14.8207(18)
α, deg	101.281(2)
β, deg	97.091(2)
γ, deg	90.516(2)
V, $Å^3$	1024.9(2)
Z	2
D_c, g·cm^{-3}	2.068
μ, mm^{-1}	2.162
R_1 [$I < 2\sigma(I)$][a]	0.0738
wR_2 (all data)[b]	0.1636

[a] $R_1 = \|F_0| - |F_c\|/|F_0|$. [b] $wR_2 = [w(F_0^2 - F_c^2)^2/w(F_0^2)^2]^{1/2}$.

The intensity data were collected on a Smart CCD diffractometer with graphite-monochromated Mo-K_α (λ = 0.71073 Å) radiation at room temperature with the ω-2θ scan mode. An empirical absorption correction was applied to the data using the SADABS program. The structures were solved by direct methods. All non-hydrogen atoms were refined anisotropically. The hydrogen atoms were generated in idealized positions. All calculations were performed using the SHELXTL program. Crystallographic data for the complex **1** are given in Table 1.

CCDC-188274 contains the supplementary crystallographic data for this paper. These data can be obtained free of charge at www.ccdc.cam.ac.uk/conts/retrieving.html [or from the Cambridge Crystallographic Data Centre, 12, Union Road, Cambridge CB2 1EZ, UK; Fax: (internat.) +44-1223/336-033; E-mail: deposit@ccdc.cam.ac.uk].

Acknowledgments

The authors acknowledge financial support from the NSFC and a key project from CAS. We also thank Prof. Guoyu Yang for the thermogravimetric analysis.

[1] [1a] S. R. Batten, R. Robson, *Angew. Chem. Int. Ed.* **1998**, *37*, 1460−1494. [1b] A. J. Blake, N. R. Champness, P. Hubberstey, W.-S. Li, M. Schröder, M. A. Withersby, *Coord. Chem. Rev.* **1999**, *183*, 117−138. [1c] B. Moulton, J. J. Lu, R. Hajndl, S. Hariharan, M. J. Zaworotko, *Angew. Chem. Int. Ed.* **2002**, *41*, 2821−2824. [1d] H. Bourahma, B. Moulton, V. Kravtsov, M. J. Zaworotko, *J. Am. Chem. Soc.* **2002**, *124*, 9990−9991.

[2] C. Chen, K. S. Suslick, *Coord. Chem. Rev.* **1993**, *128*, 293−322 and references therein.

[3] [3a] J. Nishida, T. Suzuki, M. Ohkita, T. Tsuji, *Angew. Chem. Int. Ed.* **2001**, *40*, 3251−3254. [3b] R. A. van Delden, B. L. Feringa, *Angew. Chem. Int. Ed.* **2001**, *40*, 3198−3200.

[4] [4a] D. L. Reger, R. F. Semeniuc, M. D. Smith, *Eur. J. Inorg. Chem.* **2002**, 543−546. [4b] J. M. Rowland, M. M. Olmstead, P. K. Mascharak, *Inorg. Chem.* **2002**, *41*, 1545−1549. [4c] C. S. A.

Fraser, D. J. Eisler, M. C. Jennings, R. J. Puddephatt, *Chem. Commun.* **2002**, 1224−1225. [4d] A. Erxleben, *Inorg. Chem.* **2001**, *40*, 412−414. [4e] P. L. Caradoc-Davies, L. R. Hanton, *Chem. Commun.* **2001**, 1098−1099. [4f] C. Piguet, G. Bernardinelli, G. Hopfgartner, *Chem. Rev.* **1997**, *97*, 2005−2062. [4g] H. Oshio, T. Watanabe, T. Ito, *Inorg. Chem.* **1997**, *36*, 1608−1610. [4h] O. J. Gelling, F. V. Bolhuis, B. L. Feringa, *J. Chem. Soc., Chem. Commun.* **1991**, 917−919.

[5] [5a] M. J. Hannon, C. L. Painting, E. A. Plummer, L. J. Childs, N. W. Alcock, *Chem. Eur. J.* **2002**, *8*, 2226−2238. [5b] M. C. Hong, W. P. Su, R. Cao, M. Fujita, J. X. Lu, *Chem. Eur. J.* **2000**, *6*, 427−431. [5c] K. Biradha, C. Seward, M. J. Zaworotko, *Angew. Chem. Int. Ed.* **1999**, *38*, 492−495. [5d] L. Carlucci, G. Ciani, D. M. Proserpio, A. Sironi, *Inorg. Chem.* **1998**, *37*, 5941−5943. [5e] M. A. Withersby, A. J. Blake, N. R. Champness, P. Hubberstey, W. S. Li, M. Schröder, *Angew. Chem. Int. Ed. Engl.* **1997**, *36*, 2327−2329. [5f] M. L. Tong, X. M. Chen, B. H. Ye, S. W. Ng, *Inorg. Chem.* **1998**, *37*, 5278−5281. [5g] A. J. Blake, N. R. Champness, P. A. Cooke, J. E. B. Nicolson, *Chem. Commun.* **2000**, 665−666.

[6] [6a] G. K. H. Shimizu, G. D. Enright, C. I. Ratcliffe, K. F. Preston, J. L. Reid, J. A. Ripmeester, *Chem. Commun.* **1999**, 1485−1486. [6b] A. Onoda, Y. Yamada, M. Doi, T. Okamura, N. Ueyama, *Inorg. Chem.* **2001**, *40*, 516−521.

[7] G. A. Lawrance, *Chem. Rev.* **1986**, *86*, 17−33.

[8] D. F. Sun, R. Cao, Y. C. Liang, M. C. Hong, *Chem. Lett.* **2002**, 198−199 and unpublished results.

[9] [9a] P. K. Bowyer, K. A. Porter, A. D. Rae, A. C. Willis, S. B. Wild, *Chem. Commun.* **1998**, 1153−1154. [9b] B. L. Fei, W. Y. Sun, T. Okamura, W. X. Tang, N. Ueyama, *New J. Chem.* **2001**, *25*, 210−212.

[10] [10a] L. Carlucci, G. Ciani, D. M. Proserpio, A. Sironi, *Inorg. Chem.* **1995**, *34*, 5698−5700. [10b] T. Soma, T. K. Miyamoto, T. Iwamoto, *Chem. Lett.* **1997**, 319−320. [10c] S. M. Kuang, Z. Z. Zhang, Q. G. Wang, T. C. W. Mak, *Inorg. Chem.* **1998**, *37*, 6090−6092. [10d] J. Ratilainen, K. Airola, R. Frohlich, M. Nieger, K. Rissanen, *Polyhedron* **1999**, *18*, 2265−2273.

[11] [11a] A. Erxleben, *Inorg. Chem.* **2001**, *40*, 2928−2931. [11b] Z. Shi, S. H. Feng, S. Gao, L. R. Zhang, G. Y. Yang, J. Hua, *Angew. Chem. Int. Ed.* **2000**, *39*, 2325−2327. [11c] M. J. Hannon, C. L. Painting, N. W. Alcock, *Chem. Commun.* **1999**, 2023−2024. [11d] G. Baum, E. C. Constable, D. Fenske, C. E. Housecroft, T. Kulke, *Chem. Eur. J.* **1999**, *5*, 1862−1873.

[12] [12a] G. Struckmeier, U. Therwalt, J. H. Fuhrhop, *J. Am. Chem. Soc.* **1976**, *98*, 278−281. [12b] K. T. Potts, M. Keshavarz-K, F. S. Tham, K. A. Gheysen Raiford, C. Arana, H. D. Abruna, *Inorg. Chem.* **1993**, *32*, 5477−5484.

Received July 24, 2002
[I02412]

Vanadium-Bromoperoxidase-Mimicking Systems: Direct Evidence of a Hypobromite-Like Vanadium Intermediate

Olga Bortolini,*[a] Mauro Carraro,[b] Valeria Conte,*[c] and Stefano Moro[d]

Keywords: Ab initio calculations / Enzyme models / Mass spectrometry / Peroxo ligands / Vanadium

Here we report a direct observation, by electrospray ionization mass spectrometry, of the intermediate $[VO(OH_2)(OH)(OBr)]^+$, which may be involved in the catalytic cycle of the V-HalPO enzymes. Ab initio calculations also support the stability of such a species.

(© Wiley-VCH Verlag GmbH & Co. KGaA, 69451 Weinheim, Germany, 2003)

Vanadium-dependent bromoperoxidases (V-BrPOs) catalyze the oxidation of bromide ion by hydrogen peroxide.[1−3] Kinetic studies on V-BrPOs indicate a mechanism where V^V ion binds H_2O_2 to produce a peroxo complex that reacts with the Br^- ion to generate an oxidized "bromine equivalent" species, able either to halogenate organic substrates or to react again with H_2O_2 to form singlet oxygen[1−3] (Scheme 1).

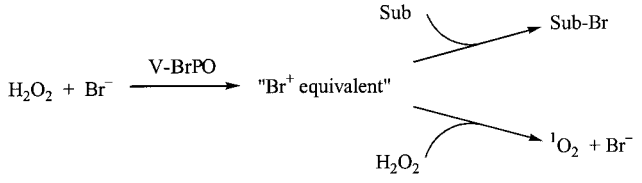

Scheme 1. General reactivity for vanadium haloperoxidases

The nature of the intermediate (e.g. HOBr, Br_2, Br_3^-, V_{enz}-OBr, enz-Br), however, is still a matter of some controversy.[1−4] With the aim of shedding light on this point several functional models of V-BrPOs have been reported.[1−4] These, however, fail to reproduce the chemistry of V-BrPOs for different reasons. A two-phase system has also been proposed as a mimicking prototype of the enzymatic activity on the basis of similar reactivity found during peroxidative bromination[5] (Scheme 2).

In this latter case, kinetic data and a product distribution analysis supported the occurrence of a V-containing hypobromite-like intermediate as the "bromine equivalent", although without direct evidence. This proposal was further justified by ab initio calculations which showed that the suggested intermediate lies at a relative minimum of potential energy in comparison with the reactants $[OV(O_2)^+]$/HBr and the couple $[O_2V(H_2O)^+]$/HOBr.[6]

An analysis of the system behaviour[5,6] as a function of the aqueous phase pH and H_2O_2 concentration was performed with styrene as the organic substrate. With this substrate, in our two-phase system, formation of two products has been observed: the corresponding bromohydrin and the dibromide. These crucial results are reported in Table 1.

Variation of the above mentioned parameters produces the selective formation of the mono- or the diperoxovanadium derivative in the aqueous phase, as indicated by ^{51}V NMR analysis of the aqueous phase of the reaction mixture.[4] In particular, at pH 1.1 ($HClO_4$) equal concentrations of NH_4VO_3 and H_2O_2 give rise to more than 95% of the monoperoxo derivative (reaction 1 in Table 1). Upon decreasing the $[NH_4VO_3]/[H_2O_2]$ ratio to 0.5, in otherwise identical conditions, mono- and diperoxovanadium complexes are formed in roughly a 1:1 ratio (reaction 2). By increasing the pH (≥3) the almost exclusive formation of the diperoxo derivative is obtained; in such conditions the efficiency of the reaction strongly decreases (reactions 3−5).[4]

Interestingly, the two reactions (1 and 2) carried out at the same pH (1.1) afforded an almost identical amounts of products. This fact indicates that the dimeric triperoxovanadium derivative, invoked as the active species in the oxybro-

[a] Dip. Chimica, Università di Ferrara,
Via Borsari 46, 44100 Ferrara, Italy
Fax: (internat.) +39-053/224-0709
E-mail: brl@unife.it
[b] Dip. Chimica Organica, Università di Padova,
Via Marzolo 1, 35131 Padova, Italy
[c] Dip. Scienze e Tecnologie Chimiche, Università di Roma "Tor Vergata",
Via della Ricerca Scientifica, 00133, Roma, Italy
Fax: (internat.) +39-053/224-0709
E-mail: valeria.conte@uniroma2.it
[d] Dip. Chimica e Tecnologie Farmaceutiche, Università di Padova,
Via Marzolo 5, 35131 Padova, Italy

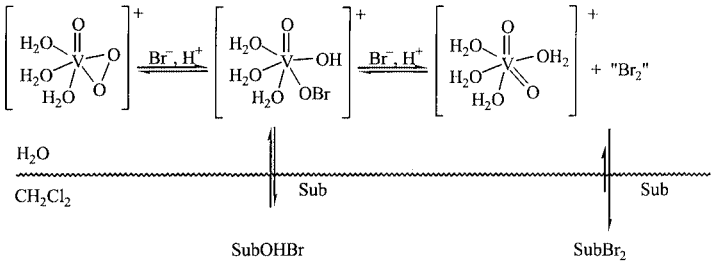

Scheme 2. Two-phase system for oxybromination of organic substrate catalyzed by V^V peroxo complexes in the presence of bromide ions

Table 1. Oxybromination reactions of styrene (1.6 mmol) with NH_4VO_3 (0.2 mmol) and H_2O_2 (0.4 mmol) in the presence of KBr (0.5 mmol) in $H_2O/CHCl_3$ 20:20 mL, T = 25 °C, stirring rate 800 rpm

	pH	H_2O_2 consumed (%)	Yield of bromohydrin (%)[b]	Yield of dibromide (%)[b]
1[c]	1.1	95	61.8	5.4
2	1.1	90	60.5	1.9
3	1.8	98	54.6	0.9
4	3.0	21	16.5	0.3
5	4.0	18	2.7	n.d.

[a] Products analysed after 4 hours. [b] Yield calculated on the basis of the consumed oxidant. [c] NH_4VO_3 0.4 mmol.

mination reaction, is not involved,[1] and probably that the only peroxo derivative implicated in the formation of the "bromine equivalent" species is the monoperoxo complex. Thus, either the reactivity of the diperoxo complex is markedly lower (reactions 4 and 5), or it acts as a reservoir of the active species.

It has been shown recently that electrospray ionization mass spectrometry (ESI-MS) in association with heteronuclear NMR spectroscopy and ab initio calculations is a powerful combination for the elucidation of solution structures of highly reactive intermediates.[7–9] Therefore, this approach has been applied to the $V/H_2O_2/H^+/Br^-$ system in order to obtain direct experimental information on the occurrence of the postulated "bromine equivalent" species.

The ESI-MS positive-ion mode full scan of solutions containing millimolar vanadate and H_2O_2 at a pH of about 1 ($HClO_4$) in 1:1 water/alcohol (MeOH or EtOH) mixtures shows the occurrence of different species identified as the monoperoxo derivatives $[OV(O_2)(H_2O)]^+$ (at m/z = 117), $[OV(O_2)(H_2O)_2]^+$ (at m/z = 135) and $[OV(O_2)(H_2O)(ROH)]^+$ (at m/z = 149 or 163), depending on the alcohol used, and the dimeric peroxo complexes $[\{OV(O_2)\}_2O(H_2O)_2(ROH)(H)_2]^{2+}$ (at m/z = 142 or 149) and $[\{OV(O_2)\}_2O(H_2O)(ROH)(H)]^+$ (at m/z = 265 or 279). Other significant peaks corresponding to the monomeric and dimeric non-peroxidic species are equally observed as well, in agreement with previously reported data.[7] The addition of a fivefold excess of Br^- to the infused H_2O/MeOH solution gives rise to the formation of a new vanadium species containing a single bromine atom, as demonstrated by the related isotopic cluster. The new complexes, although transferred in the gas-phase in low relative abundance (≤15%), were clearly detected as doublets at m/z = 179 ^{79}Br (181, ^{81}Br), 193 (195) and 197 (199) and tentatively identified as shown in Table 2.

The substitution of methanol with ethanol in the infusion solvent composition produces no significant changes in the full-scan mass spectrum, with the exception that the ionic species at m/z = 193 (195) is replaced by the homologous ethoxy-containing ion at m/z = 207 (209). Further support for the identification of the species was obtained by collision-induced decomposition (MS^2) spectra and the relevant results are collected in Table 2. For low energies (up to 0.5 V), the only peaks observed are those related to ion-molecule reactions of the selected species P with solvent molecules. At higher energies (1.5 V), decomposition takes place with loss of HBr, accompanied by addition of water molecule(s). Formation of dinuclear doubly charged species, i.e. m/z = 147 (149) $[V_2Br_2O_2H_2]^{2+}$ and $[V_2Br_2O_2C_2H_6]^{2+}$ 161 (163), formally deriving from expulsion of O_2, is also observed.[10]

Of special interest is the formal loss of water found in the MS^2 spectra of the -OCH_3 [m/z = 193 (195)] and -OCH_2CH_3 [m/z = 207 (209)] containing derivatives. This process, which corresponds to an internal oxidative decomposition, formally produces ions where a direct coordination of a carbonyl moiety to the metal may be invoked.[4] This gas-phase chemistry has also been observed with other vanadium picolinate[11] and ruthenium[12] derivatives. Synthesis of stable alkyl-V^V complexes has also been reported.[13]

The involvement of fragmentations occurring on vanadium-bound ligands other than OBr confirms that bromide ion is not bound to the complex merely as an ionic couple, but through covalent bonds probably originating from the activation of the peroxidic O–O bridge.[14]

The analysis of the $V/H_2O_2/H^+$ system, upon addition of an excess of Br^-, was completed by extending the ESI-MS inspection to solutions containing a twofold excess of H_2O_2 with respect to vanadate, at a pH of about 2. According to previous studies,[7] the diperoxo complex is the dominant species. These solutions, analyzed both in positive- and negative-ion mode, did not reveal the activation of diperoxovanadium species by bromine ions, in agreement with the reactivity reported above (Table 1).

Further support for the rational formation of the vanadium-containing "bromine equivalent" species was ob-

Table 2. MS^2 ions observed after collision-induced decomposition of the precursor ionic species (P) in mixed H_2O/CH_3OH (or CH_3CH_2OH) under ESI-MS conditions[a]

P m/z	P + CH_3OH m/z	P + H_2O m/z	P –HBr +H_2O m/z	P –H_2O m/z	P –HBr+2H_2O m/z	[b] m/z	[b] m/z
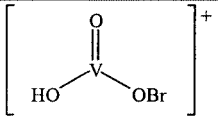 179 (181)	211 (213)	197 (199)	----	----	135 (135)	147 (149)	161 (163)
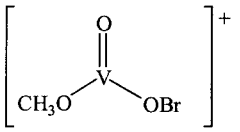 193 (195)	225 (227)	211 (213)	----	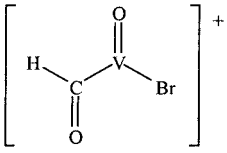 175 (177)	149 (149)	147 (149)	161 (163)
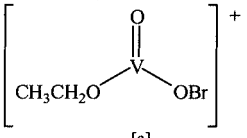 207[c] (209)	253[c] (255)	225 (229)	145 (145)	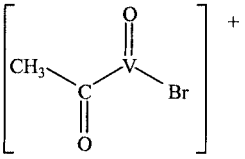 189 (191)	------	147 (149)	161 (163)
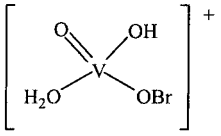 197 (199)	229 (231)	215 (217)	135 (135)	179 (181)	------	------	161[c] (163)

[a] The *m/z* values refer to the presence of ^{79}Br or ^{81}Br. [b] Doubly charged ions $[V_2Br_2O_2H_2]^{2+}$ [*m/z* = 147 (149)] and $[V_2Br_2O_2C_2H_6]^{2+}$ [*m/z* = 161 (163)], see text. [c] EtOH as the co-solvent.

tained by performing ab initio calculations on the various species that can be obtained by reaction of the monoperoxo vanadium compound and bromine, both in the presence or in the absence of a molecule of solvent in the coordination sphere of the metal. Scheme 3 collects the results obtained by effecting geometry optimization of all the structures with density functional theory (DFT) calculations carried out with Becke's hybrid three-parameter functional with Lee−Yang−Parr nonlocal correlation (B3LYP).[15,16] Calculations were conducted with the (99,302) numerical integration grid[16] and full accuracy at all stages in order to achieve SCF convergence. The 6-311G+(d,f) basis set implemented in the Gaussian 98 suite of programs was used.[16] After the geometry optimisation step, the energy values weren evaluated through single point calculations (performed using the SCF=tight option in Gaussian 98) at the B3LYP/6-311G++(3df,3dp) level of theory.[16]

The most interesting feature of the results collected in Scheme 3 is the relative stability of the conjugated acids of the species $[OV(OH)_2(OBr)]$. Such a derivative presents three distinct protonation sites: a) the oxygen atom of the V=O group, b) the -OH oxygen atom, and c) the oxygen atom of the -OBr group. The corresponding protonated species are indicated in Scheme 3. Indeed, the structure with the proton located at the -OBr residue is the one located energetically uphill with respect to the other possible species protonated at the oxygen atom of the hydroxy moiety (ca. 47 kJ mol^{-1}), at the oxo moiety (ca. 24 kJ mol^{-1}) or at both hydroxy and oxo moieties (ca. 77 kJ mol^{-1}). This intermediate, $[OV(OH)_2(OHBr)]^+$, would be the species that releases HOBr — one of the postulated brominating species — in solution. Interestingly, the most stable protonated isomer corresponds to the $[OV(OH_2)(OH)(OBr)]^+$ structure. Following this result this species may be directly involved in the Br^+ transfer process. Furthermore, it should be noted that the thermodynamically feasible coordination of bromide ion to the cationic naked monoperoxo species, a process which does not involve oxidation of the halide, if it occurs in solution during the catalytic process, is probably not located along the reaction coordinate. According to this assumption, we decided to omit from our theoretical study all the possible species with the bromine moiety directly coordinated to the vanadium atom, such as $[OVBr(O_2)(OH_2)]$ and the related protonated derivatives. All these species can

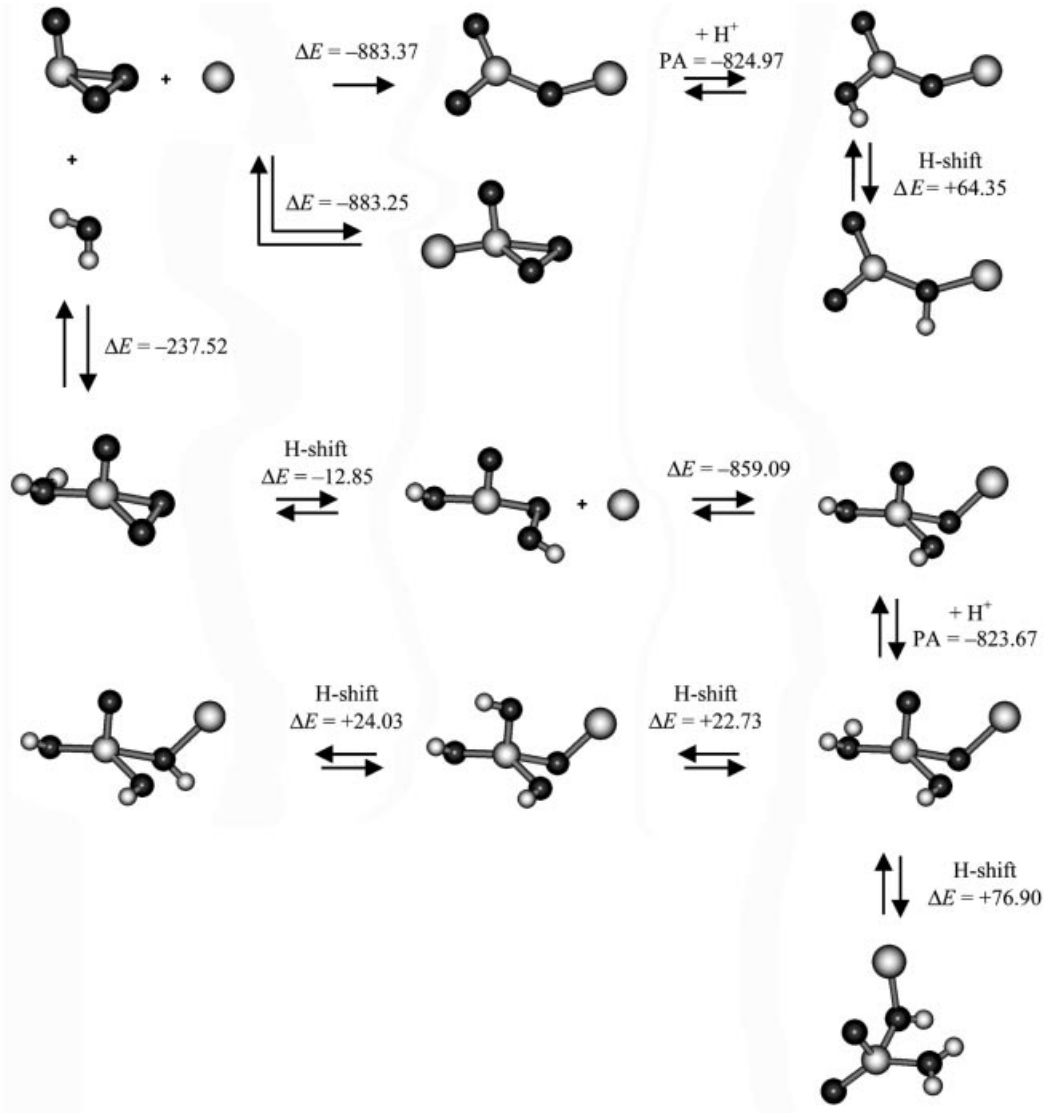

Scheme 3. Ab initio calculations on the formation of the V-OBr intermediates; energy values are reported in kJ mol^{-1}; PA = proton affinity

be considered as real ionic couples, especially in the gas phase, where the electrostatic compensation between the negatively charged bromine ion and the positively charged peroxo-vanadium complexes might be the chemical explanation for their relatively high thermodynamic stabilities.

In conclusion we have reported a direct observation of the intermediate $[OV(OH_2)(OH)(OBr)]^+$ by ESI-MS spectrometry. Ab initio calculations also support the stability of such a species confirming that the choice of an appropriate model and its analysis with suitable techniques allows the collection of significant data for a better understanding of the mechanism of action of the V-HalPO enzymes.

Experimental Section

The ESI-MS measurements (positive-ion mode) were obtained using an LCQ instrument (Thermoquest, San Jose, CA). The peroxovanadium solutions were prepared by dissolving $n Bu_4NVO_3$ (5×10^{-4} mol·L^{-1}) in MeOH/H_2O (or EtOH for the experiments conducted in this solvent) pH 1 $HClO_4$, in the presence of an equimolar amount of H_2O_2. In the experiments conducted in the presence of Br^-, a fivefold excess of KBr was used. Solution flow rate 8 μL·min^{-1}, capillary temperature 180 °C, spray voltage 2.5 kV, capillary voltage 5 V, tube lenses offset 15 V, nebulizing gas N_2 (40 units flow rate). The parameters related to octapoles and detector were achieved by the automatic set-up procedure. Collision-induced decompositions of selected ions were obtained by applying a supplementary r.f. voltage (tickle voltage) to the end-cap electrodes of the ion trap (resonance activation). For experimental details on the two-phase reactions reported in Table 1 see refs.[5,6]

Acknowledgments

We acknowledge financial support from the Italian Ministry of University and Scientific and Technological Research to the project COFIN2000: "Activation of peroxidic species in innovative selective oxidation processes" and from the Italian National Research Council.

[1] A. Butler, A. H. Baldwin, *Structure and Bonding − Metal sites in Proteins and Models, Vol. 89*, Springer Verlag, Berlin-Heidelberg, Dordrecht, **1997** pp.109−125, and references cited therein.
[2] V. Pecoraro, C. Slebodnick, B. Hamstra, *Vanadium Compounds: Chemistry Biochemistry and Therapeuthic Applications* (Eds.: D. C. Crans, A. Tracey), **1998**, ACS Symposium Series 711, chap. 12.
[3] A. Butler, *Coord. Chem. Rev.* **1999**, *187*, 17−35.
[4] V. Conte, O. Bortolini, M. Carraro, S. Moro, *J. Inorg. Biochem.* **2000**, *80*, 41−49.
[5] V. Conte, F. Di Furia, S. Moro, in *Vanadium Compounds: Chemistry Biochemistry and Therapeuthic Applications*, (Eds.: D. C. Crans, A. Tracey), **1998**, ACS Symposium Series 711, chap. 10 and refs. cited therein.
[6] V. Conte, F. Di Furia, S. Moro, S. Rabbolini, *J. Mol. Catal.* **1996**, *113*, 175−184.
[7] O. Bortolini, V. Conte, F. Di Furia, S. Moro, *Eur. J. Inorg. Chem.* **1998**, 1193−1197.
[8] O. Bortolini, M. Carraro, V. Conte, S. Moro, *Eur. J. Inorg. Chem.* **1999**, 1489−1495.
[9] M. Bonchio, O. Bortolini, V. Conte, S. Moro, *Eur. J. Inorg. Chem.* **2001**, 2913−2919.
[10] Attempts to characterize these dimeric V^{III} ions, which is out of the scope of this communication, are in progress. Stable divanadium(III) species are known, see: R. S. Czernuszewicz, Q. Yan, M. R. Bond, C.-J. Carrano, *Inorg. Chem.* **1994**, *33*, 6116−6119.
[11] O. Bortolini, D. C. Crans, V. Conte, manuscript in preparation.
[12] R. Argazzi, C. A. Bignozzi, O. Bortolini, P. Traldi, *Inorg. Chem.* **1993**, *32*, 1222−1225.
[13] J. De With, A. D. Horton, A. G. Orpen, *Organometallics* **1990**, *9*, 2207−2209.
[14] The coordination of Br^- to non-peroxidic species, such as VO_2^+ ions, followed by protonation, was not observed in the ESI-MS experiments.
[15] A. D. Becke, *J. Chem. Phys.* **1993**, *98*, 5648−5651.
[16] Gaussian 98 (Revision A.9), M. J. Frisch, G. W. Trucks, H. B. Schlegel, G. E. Scuseria, M. A. Robb, J. R. Cheeseman, V. G. Zakrzewski, J. A. Montgomery, Jr., R. E. Stratmann, J. C. Burant, S. Dapprich, J. M. Millam, A. D. Daniels, K. N. Kudin, M. C. Strain, O. Farkas, J. Tomasi, V. Barone, M. Cossi, R. Cammi, B. Mennucci, C. Pomelli, C. Adamo, S. Clifford, J. Ochterski, G. A. Petersson, P. Y. Ayala, Q. Cui, K. Morokuma, D. K. Malick, A. D. Rabuck, K. Raghavachari, J. B. Foresman, J. Cioslowski, J. V. Ortiz, A. G. Baboul, B. B. Stefanov, G. Liu, A. Liashenko, P. Piskorz, I. Komaromi, R. Gomperts, R. L. Martin, D. J. Fox, T. Keith, M. A. Al-Laham, C. Y. Peng, A. Nanayakkara, C. Gonzalez, M. Challacombe, P. M. W. Gill, B. Johnson, W. Chen, M. W. Wong, J. L. Andres, C. Gonzalez, M. Head-Gordon, E. S. Replogle, and J. A. Pople, Gaussian, Inc.: Pittsburgh, PA, 1998.

Received July 30, 2002
[I02431]

Unprecedented Change of the Jahn−Teller Axis in a Centrosymmetric Cu^{II} Complex Induced by Lattice Water Molecules − Crystal and Molecular Structures of Bis[bis(3,5-dimethylpyrazol-1-yl)acetato]copper(II) and Its Dihydrate

Bojan Kozlevčar,[a] Patrick Gamez,[a] René de Gelder,[b] Willem L. Driessen,*[a] and Jan Reedijk[a]

Keywords: Copper / N ligands / Jahn−Teller distortion / EPR spectroscopy

Two copper coordination compounds with the tridentate (NON) ligand bis(3,5-dimethylpyrazol-1-yl)acetic acid (Hbdmpza) are reported. The central coordination sphere in both compounds is fulfilled by two ligands in $[CuL_2]$. The ligands are centrosymmetrically oriented around the copper ion, thus forming a *trans*-CuN_4O_2 elongated octahedral chromophore. The atoms in both compounds are not positioned at the same places in the Jahn–Teller-distorted octahedral environment. For compound $[CuL_2]$ (**1**) two nitrogen atoms are located on the longer axis [Cu–N: 2.438(2) Å], while the other two nitrogen atoms [Cu–N: 2.006(2) Å] and the two oxygen atoms [Cu–O: 1.983(2) Å] form the basal plane of the octahedron. The coordination sphere for $[CuL_2]\cdot 2H_2O$ (**2**) is composed of four nitrogen atoms [Cu–N: 2.013(3), 2.038(2) Å] that form the basal plane, while the two oxygen atoms are at a longer distance [Cu–O: 2.293(2) Å]. The water molecules in **2** are hydrogen bonded to the non-coordinated carboxylate oxygen atoms, forming bridges between two neighbouring monomeric units and leading to an infinite chain. Significant differences are observed for both compounds by spectroscopic investigations (EPR, IR, ligand field).

(© Wiley-VCH Verlag GmbH & Co. KGaA, 69451 Weinheim, Germany, 2003)

Introduction

Many *trans*-CuN_4O_2 chromophores are reported in the literature with strong nitrogen donor ligands and weaker oxygen donor ligands. For most of them, the Jahn−Teller axis, i.e. the axis with the longest Cu−L bonds, coincides with the O−Cu−O bond in the elongated distorted octahedron.[1,2] A search of the Cambridge Structural Database revealed that in only 9 of the 277 CuN_4O_2 chromophores does the Jahn−Teller axis coincide with one of the N−Cu−N bonds, and there is only one example of a compressed octahedron (four longer and two shorter bonds).[3] No pair of compounds with the same coordinated ligands — one with the O−Cu−O unit as the Jahn−Teller axis and the other with the N−Cu−N as the Jahn−Teller axis — have been reported.[1,2] The absence of isomers is probably due to steric effects of the ligands, which favour only one of the arrangement types in the coordination sphere. With a special ligand shape, different configurations around the central copper ion may be expected. Bearing this in mind, a vicinal tridentate ligand that produces a nitrogen-oxygen-nitrogen (NON) donor set may be of special interest. In this paper, the comparison of two structures of the ligand bis(3,5-dimethylpyrazol-1-yl)acetic acid with copper(II) is presented.

[a] Leiden Institute of Chemistry, Gorlaeus Laboratories, Leiden University,
P. O. Box 9502, 2300 RA Leiden, The Netherlands
Fax: (internat.) +31-71/527-4671
E-mail: driessen@chem.leidenuniv.nl
[b] Department of Inorganic Chemistry, University of Nijmegen, P. O. Box 9010, 6500 GL Nijmegen, The Netherlands

Results and Discussion

Two copper(II) compounds were synthesised with the deprotonated tridentate ligand bis(3,5-dimethylpyrazol-1-yl)-acetic acid (Hbdmpza) in the $[CuL_2]$ coordination sphere. In both cases bdmpza coordinates through two pyrazole nitrogen atoms and one deprotonated carboxylate oxygen atom (NON donor set). Similar coordination complexes are known for other *d*-block metals and bdmpza.[4−7] The ligands are centrosymmetrically arranged around the copper ion, thus forming *trans*-CuN_4O_2 chromophores. Both new copper compounds show an elongated distorted octahedral geometry, however the coordinated atoms do not play the same role. The coordination environment of **1** (Figure 1) is particularly interesting, with the basal plane composed of two nitrogen atoms [Cu−N: 2.006(2) Å] and two oxygen atoms [Cu−O: 1.983(2) Å], and the remaining two coordinated nitrogen atoms forming the Jahn−Teller axis [Cu−N: 2.438(2) Å].

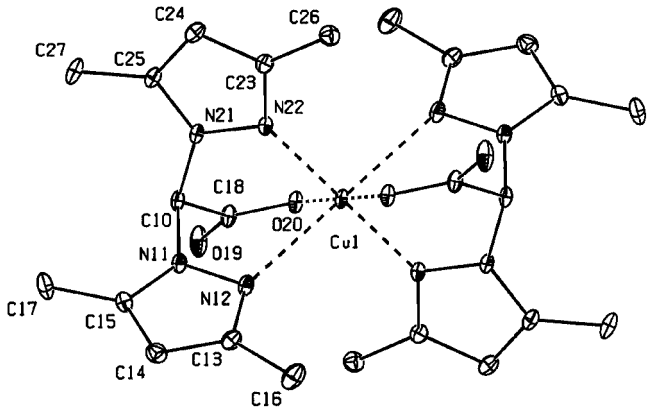

Figure 1. The centrosymmetric structure of **1** with two tridentate scorpionate ligands around the central copper; thermal ellipsoids are drawn at the 10% probability level; all hydrogen atoms have been omitted for clarity.

The more common isomer with the Jahn−Teller axis along the O−Cu−O bonds has also been obtained, but from aqueous solution. In this compound $[CuL_2]\cdot 2H_2O$ (**2**; Figure 2, the basal octahedron plane is composed of four nitrogen atoms [Cu−N: 2.013(3), 2.038(2) Å], while the oxygen atoms are located at a longer distance [Cu−O: 2.293(2) Å]. Such a conformation has also been found in Fe^{II} and Zn^{II} $[ML_2]$ analogues.[5] Each water molecule in **2** forms two hydrogen bonds to the noncoordinated carboxylate oxygen atoms [O···H−O:; 2.813(4), 2.868(4) Å], thereby connecting two neighbouring monomeric units and leading to linear chains of octahedra as shown in Figure 2.

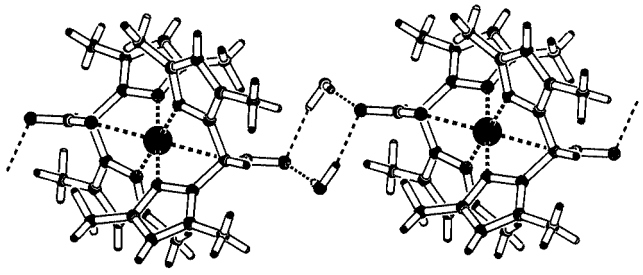

Figure 2. The intermolecular hydrogen-bonding contacts between the coordination octahedra in the structure of the hydrated compound **2**

In the anhydrous compound **1**, a significantly longer C−O distance [1.262(3) Å] is observed for the coordinated carboxylate oxygen atom than for the non-coordinated one [1.214(3) Å]. For the hydrated compound **2**, almost the same C−O distances are observed [1.245(4) and 1.241(4) Å]. These similar C−O bonds for the carboxylate group of **2** are probably due to the binding of both oxygen atoms to a Lewis acid, i.e. to the copper and to a water molecule, while only one carboxylate oxygen is coordinated in **1**.

The solid-state EPR spectrum of compound **1** measured at room temperature shows an isotropic copper(II) signal

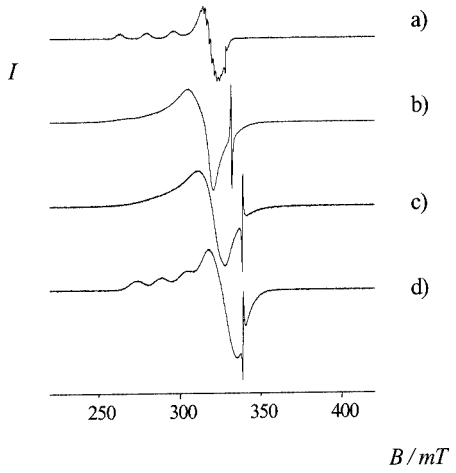

Figure 3. EPR spectra of compounds **1** and **2**, measured under different conditions: a) **1** as a frozen methanol solution at 77 K; b) **1** as a solid at 77 K; c) **1** as a solid at room temp.; d) **2** as a solid at room temp.; the sharp signal closest to 350 mT in all spectra is due to the reference

(Figure 3c). No resolution of $g_{\|}$, $g_{\perp}$ or $A_{\|}$ is observed, which is indicative of exchange narrowing due to the close distance and dipolar coupling between the Cu ions in the lattice. At 77 K, the spectrum reveals an additional low-intensity $g_{\|}$ signal at 260 mT and a small change in the shape of the $g_{\perp}$ signal (Figure 3b). A significantly different feature is observed for the room-temperature solid-state EPR spectrum of **2**. Beside the $g_{\perp}$ signal, a $g_{\|}$ signal with three distinctive $A_{\|}$ signals is present at lower field (Figure 3d). The value of $A_{\|}$ amounts to 15.0 mT, which is typical for a tetragonal Cu centre. The coupling of the *d* electron spin and the nuclear spin results in a hyperfine splitting, and agrees with the anisotropic nature of the coordination sphere that is characteristic of an elongated octahedral geometry. The EPR spectra of frozen methanolic solutions of **1** and **2** are identical (Figure 3a). This is as expected as the water molecules dissociate upon dissolution of **2** in methanol. Solvation of the monomeric complex disrupts the hydrogen-bond network of **2** as the water molecules are probably replaced by methanol molecules. Additional superhyperfine splitting was observed in the frozen solution due to interaction with ^{14}N nuclei from the ligand. Relevant parameters for the solution spectra, which were satisfactorily simulated,[8] are $g_{\|} = 2.289$, $g_{\perp} = 2.061$, $A_{Cu} = 160$ Gs, and $A_N = 15.5$ Gs.

In the region above 3000 cm^{-1} in the vibrational spectra, characteristic bands for H-bonded water O−H stretching vibrations are present only for the hydrated compound **2** (See Figure 4).

The rest of the IR spectra is almost identical for both compounds due to the presence of the same constituents. Exceptions may be found in the regions where the carboxylate group stretching vibrations are expected. Differences are observed at 1650 cm^{-1} for the asymmetric vibration ν_{as}(OOC) and at 1350 cm^{-1} for the symmetric vibration ν_s(OOC): the spectrum of the anhydrous compound **1** shows only one band in both areas, while two bands are observed in the spectrum of the solvated compound **2**. In-

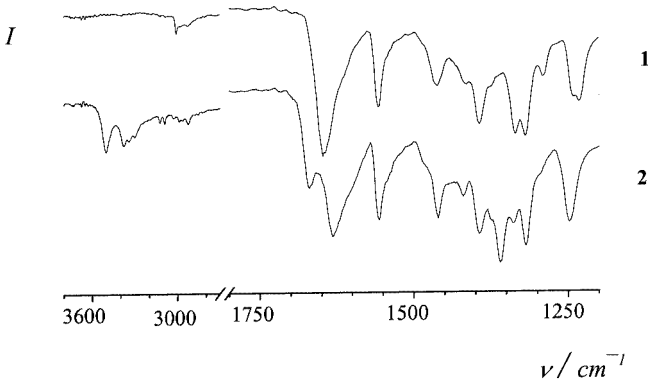

Figure 4. Comparison of two regions in the vibrational spectra of the investigated compounds

terestingly, the stronger ν_{as}(OOC) band of **2** is shifted towards lower energy and the stronger ν_s(OOC) band to higher energy relative to the corresponding bands in the spectrum of **1**. Therefore Δ [= ν_{as}(OOC) − ν_s(OOC)] [9] for **2** is smaller than for **1**. This is related to the typically monodentate carboxylate group in **1** and the pseudo-didentate group in **2**. In the carboxylate group of **1**, more single bond character for the coordinated oxygen atom is present, and more double bond character with the non-coordinated oxygen atom (O=C−O−Cu). The hydrogen bond in **2** attracts the non-coordinated oxygen atom, weakening the double bond (H−O−H···O=C−O−Cu). This is in agreement with the bigger Δ values for monodentate than for didentate carboxylate groups.[9] The IR spectrum of dry **2** is identical to the spectrum of **1**, which is stable under reduced pressure or in diethyl ether.

In the visible part of the electronic spectra, a broad d−d band is observed for compounds **1** and **2**. The peak in the spectrum of **1** is found at 13900 cm^{-1}, while in the spectrum of **2** it appears at 15300 cm^{-1}. The difference is in agreement with a weaker tetragonal chromophore CuN_2O_2 in **1** compared to CuN_4 in **2**.

The pair of compounds **1** and **2** clearly represent an unprecedented change of the Jahn−Teller axis induced by water molecules. The two copper complexes prepared show significantly different results in the vibrational, EPR and electronic spectra. The stabilization of **2** by a hydrogen-bonding network modifies the coordination of the ligand around the copper, although steric hindrance would favour the other alternative (complex **1**). The water molecules apparently direct the Cu−O bonds to be in the Jahn−Teller axis of the copper-centred octahedron.

Experimental Section

General Remarks: All reagents and solvents were purchased from commercial sources and used as received. The ligand bis(3,5-dimethylpyrazol-1-yl)acetic acid was prepared from dibromoacetic acid and 3,5-dimethylpyrazole in a basic solution as described in the literature.[5] C,H,N analyses were carried out by the Microanalysis Department of Leiden University. Infrared spectra were recorded on a Perkin−Elmer Paragon 1000 spectrophotometer, equipped with a Golden Gate Diamond ATR as a sample support. X-band EPR spectra were recorded on a JEOL ESR spectrometer, equipped with an Esprit 330 data system, at room temperature and at 77 K, with dpph as an internal reference (g = 2.0036). The ligand field spectra of the solid compounds were recorded in the 300−2000 nm range on a Perkin−Elmer Lambda 900 UV/Vis/NIR spectrometer in the diffuse reflectance mode with MgO as reference.

[CuL_2] (1): A solution of the ligand (25 mg, 0.10 mmol) in acetonitrile (10 mL) was added to copper(II) acetate hydrate (10 mg, 0.025 mmol). Pale-blue crystals started to precipitate from the transparent solution at room temperature in a few hours. They were filtered off the next day and washed with diethyl ether. $C_{24}H_{30}CuN_8O_4$ (558.1): calcd. C 51.7, H 5.42, N 20.1; found C 51.3, H 5.22, N 20.0. IR (solid): $\tilde{\nu}$ = 1645 cm^{-1} (C−O), 1558 (C−N). UV/Vis-NIR (solid): λ_{max} = 13900 cm^{-1}. EPR (solid, room temp.): g = 2.118.

[CuL_2]·$2H_2O$ (2): The ligand (50 mg, 0.20 mmol), dissolved in acidified water (10 mL), was added to copper(II) acetate hydrate (40 mg, 0.10 mmol). Blue crystals started to precipitate from the transparent solution at room temperature after a few hours. They were filtered off next day and dried for 5 minutes on a filter paper. $C_{24}H_{34}CuN_8O_6$ (594.1): calcd. C 48.5, H 5.77, N 18.9; found C 48.5, H 5.46, N 18.9. IR (solid): $\tilde{\nu}$ = 3504 cm^{-1} (O−H), 3381 (O−H), 1669 (C−O), 1634 (C−O), 1558 (C−N). UV/Vis-NIR (solid): λ_{max} = 15300 cm^{-1}. EPR (solid, room temp.): $g_{\|}$ = 2.288, $g_{\perp}$ = 2.077, $A_{\|}$ = 0.129.

X-ray Crystallography: X-ray data were collected on an Enraf−Nonius CAD4 diffractometer equipped with graphite-monochromated Mo-K_α radiation (0.71073 Å). Crystal data are collected in Table 1. The structure was solved with automated Patterson techniques using DIRDIF/PATTY [10] and refined on F us-

Table 1. Crystal data and structure determination data for the compounds **1** and **2**

Formula	$C_{24}H_{30}CuN_8O_4$ (**1**)	$C_{24}H_{34}CuN_8O_6$ (**2**)
Molecular weight	558.10	594.13
Crystal habit	block	block
Crystal colour	light blue	light blue
Crystal system	triclinic	triclinic
Space group	$P\bar{1}$	$P\bar{1}$
a (Å)	7.8946(10)	7.5745(7)
b (Å)	8.7869(13)	8.7165(9)
c (Å)	10.2039(15)	11.1364(12)
α (°)	65.456(16)	69.514(8)
β (°)	83.008(17)	85.676(12)
γ (°)	87.332(13)	89.739(9)
V (Å^3)	639.08(18)	686.61(13)
Z	1	1
$D_{calcd.}$ (g·cm^{-3})	1.45	1.44
F(000)	291	311
μ (cm^{-1})	9.0	8.5
Temperature (K)	293	293
θ Min., θ max.	2.55, 27.5	2.7, 27.5
$h/k/l$ range	−10,10/−11,10/−13,0	0,9/−11,11/−14,14
Total reflections	3102	3368
Observed reflections [$I > 2\sigma(I)$]	2815	2447
No. of refined parameters	214	229
Final R, wR [$I > 2\sigma$(I)]	0.032, 0.048	0.047, 0.083
Min. and max. residual density (e·Å^{-3})	−0.34, 0.32	−0.82, 0,71

ing full-matrix least-squares techniques with fl^{ta}L3.4.[11−12] The positions of the non-hydrogen atoms were refined with anisotropic displacement parameters. All hydrogen atoms were located in the Fourier difference maps. The positions of the hydrogen atoms were refined with fixed isotropic displacement parameters. For compound **2** an empirical absorption correction was applied.[13] Geometric calculations and molecular graphics were performed with PLATON.[14]

CCDC-190297 (**1**) and CCDC-190298 (**2**) contain the supplementary crystallographic data for this paper. These data can be obtained free of charge at www.ccdc.cam.ac.uk/conts/retrieving.html [or from the Cambridge Crystallographic Data Centre, 12, Union Road, Cambridge CB2 1EZ, UK; fax: (internat.) +44-1223/336-033; E-mail: deposit@ccdc.cam.ac.uk].

Acknowledgments

The financial support of the Ministry of Education, Science and Sport, Republic of Slovenia, through grant MŠZŠ PS-511-103 to B. K. is gratefully acknowledged. The work described here has also been supported by the Leiden University Study group WFMO (Werkgroep Fundamenteeel-Materialen Onderzoek).

[1] F. H. Allen, O. Kennard, *Chem. Des. Autom. News* **1993**, *8*, 31−37.
[2] M. Melnik, M. Kabešova, L. Macaškova, C. E. Holloway, *J. Coord. Chem.* **1998**, *45*, 31−145.
[3] J. D. Crane, O. D. Fox, E. Sinn, *J. Chem. Soc., Dalton Trans.* **1999**, 1461−1465.
[4] A. Otero, J. Fernandez-Baeza, J. Tejada, A. Antinolo, F. Carrillo-Hermosilla, E. Diez-Barra, A. Lara-Sanchez, M. Fernandez Lopez, M. Lanfranchi, M. A. Pellingelli, *J. Chem. Soc., Dalton Trans.* **1999**, 3537−3539.
[5] A. Beck, B. Weibert, N. Burzlaff, *Inorg. Chem.* **2001**, 521−527.
[6] A. Otero, J. Fernandez-Baeza, A. Antinolo, F. Carrillo-Hermosilla, J. Tejada, E. Diez-Barra, A. Lara-Sanchez, L. Sanchez-Barba, I. Lopez-Solera, M. R. Ribeiro, J. M. Campos, *Organometallics* **2001**, *20*, 2428−2430.
[7] N. Burzlaff, I. Hegelmann, B. Weibert, *J. Organomet. Chem.* **2001**, *626*, 16−23.
[8] F. Neese, The program EPR, a modelling approach, Version 1.0, University of Konstanz, **1993**.
[9] G. B. Deacon, J. Phillips, *Coord. Chem. Rev.* **1980**, *33*, 227−250.
[10] P. T. Beurskens, G. Admiraal, G. Beurskens, W. P. Bosman, S. Garcia-Granda, R. O. Gould, J. M. M. Smits, C. Smykalla, *The DIRDIF program system*, Technical Report of the Crystallography Laboratory, University of Nijmegen, The Netherlands, **1992**.
[11] S. R. Hall, G. S. D. King, J. M. Stewart, *Xtal3.4 Users Manual*, Universities of Western Australia and Maryland, **1995**.
[12] *International Tables for Crystallography* (Ed.: A. J. C. Wilson), Vol. C, Kluwer, Dordrecht, The Netherlands, **1992**.
[13] N. Walker, D. Stewart, *Acta Crystallogr.* **1983**, *39*, 158.
[14] A. L. Spek, *PLATON, A Multipurpose Crystallographic Tool*, Utrecht University, The Netherlands, **2000**.

Received July 31, 2002
[I02434]

Syntheses and Molecular Structures of Metallasiloxanes Containing Zn_3O_4 and $Zn_6Si_6O_{10}$ Cores

Klaus Merz,[a] Huai-Ming Hu,[a] Stefan Rell,[a] and Matthias Driess*[a]

Keywords: Clusters / Oxides / Siloxides / Zinc

The trinuclear zinc siloxane $[(MeZn)_2Zn(OSiPh_3)_4]$ (**1**) and the first novel siloxane-bridged hexanuclear dimer $[\{Me(THF)Zn\}_2OZn(OSiR_2)(R^1)]_2$ (R = Ph, $R^1 = OSiR_2OSiR_2O$) (**2**) are accessible by Brønsted acid/base reaction of triorganosilanols with the zinc base $ZnMe_2$. Both compounds were characterised by NMR spectroscopy and a single-crystal X-ray structure analysis. The X-ray structures of the reported complexes are discussed.
(© Wiley-VCH Verlag GmbH & Co. KGaA, 69451 Weinheim, Germany, 2003)

Introduction

In recent years, a large variety of molecular metallasiloxanes (M-O-Si) have been synthesised through metallation of organosilanols.[1] These compounds have received considerable attention as versatile precursors for metal silicates[2] and doped metal oxides[3] or as molecular models for heterogeneous silica- and zeolite-supported catalytic systems.[4,5] We discovered recently that the thermolysis of molecular M-O-Si compounds with almost identical M−O and Si−O binding energies facilitates ambident decomposition pathways, affording elemental metal and/or metal oxide particles. The composition of the products can also be easily influenced by the nature of the substituents at the M and Si atoms and the reaction conditions. Thus, solid-to-solid and solid-to-vapour decomposition (CVD) of the tetranuclear zinc siloxane $[XZnOSiR_3]_4$ (X = Me, Et, I) or its polymeric analogue $[(Me_3SiO)_2Zn]_n$ affords nanocrystalline ZnO and/or Zn particles.[6]

Results and Discussion

In order to learn more about the influence of the degree of aggregation of the zinc siloxane precursors and the nature of their organic shell on the size and morphology of the produced Zn and/or ZnO particles, we have been interested in the synthesis of differently preorganised zinc siloxane aggregates. In this contribution, we describe the synthesis and characterisation of the sterically congested trinuclear zinc siloxane $[(MeZn)_2Zn(OSiR_3)_4]$ (**1**) which can be easily expanded to its hexanuclear dimer $[\{Me(THF)Zn\}_2OZn(OSiR_2)(OSiR_2OSiR_2O)]$ (**2**). The latter represents a novel type of metallasiloxane and is the first zinc polysiloxane. In accordance with recent studies, different zinc siloxane aggregates are accessible by Brønsted acid/base reaction of triorganosilanols R_3SiOH (R = Me, Et, *i*Pr) with the zinc bases ZnR_2 (R = Me, Et). Depending on the steric demand of the substituents this reaction furnishes dimeric, trimeric and tetrameric ZnO aggregates.[7,8]

Thus, the reaction of the sterically congested triphenylsilanol Ph_3SiOH with $ZnMe_2$ leads to the Zn_3O_4 aggregate **1** in 75% yield (Scheme 1). The crystal structure of **1** (Figure 1) consists of asymmetric units with a nonlinear array of three zinc atoms [Zn···Zn···Zn = 159.27(3)°] that are bridged by four triphenylsiloxy groups The spirocyclic zinc atom Zn(2) has a distorted tetrahedral geometry, whereas the two terminal zinc atoms (Zn1 and Zn3) are only trigonal-planar coordinated. The observed Zn_3O_4 core of the aggregate is in good agreement with that of the previously reported derivatives $[(MeZn)_2Zn(OSi{\it i}Pr_3)_4]$[7] and $[Me_3SiCH_2ZnOR]_2Zn]$ [R = (2,6-iPr$_2$-C$_6$H$_4$)].[9] Remarkably, the Zn−O distances for the four-coordinate Zn(2) atom [average 1.949(3) Å] are shorter than those for the three-coordinate ones [average 1.981(3) Å] due to the greater partial positive charge at Zn(2). The inconspicuous Zn−C distances average 1.919(6) Å. While the dihedral angle between the two Zn_2O_2 planes of 86.9(1)° is close to the expected value of 90°, the endocyclic O(1)−Zn(2)−O(2) and O(3)−Zn(2)−O(4) angles are, at 84.1(1) and 86.0(1)° respectively, considerably distorted from the ideal tetrahedral value (109.5°). This large distortion is due to the strained four-membered Zn_2O_2 rings which, in turn, result in a corresponding expansion of the exocyclic O−Zn(2)−O angles [average 121.1(1)°]. To our surprise, the preference for the trinuclear structural motif of the Zn atoms in **1** is still preserved if the sterically congested Ph_3SiO groups are fully replaced by the less demanding Ph_2SiO_2 moieties.

[a] Lehrstuhl für Anorganische Chemie 1: Molekül- und Koordinationschemie, Ruhr-Universität,
Bochum,Universitätsstrasse 150, 44801 Bochum, Germany,
Fax: (internat.) +49-(0)234/321-4378
E-mail: matthias.driess@ruhr-uni-bochum.de

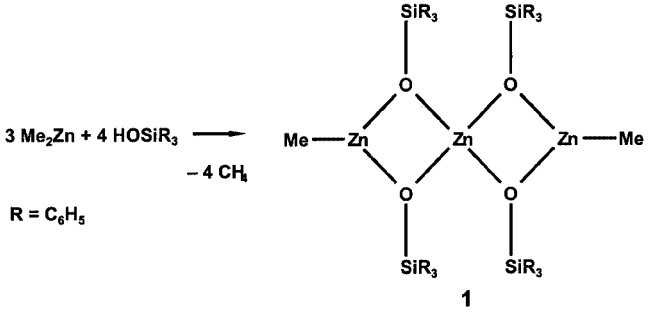

Scheme 1

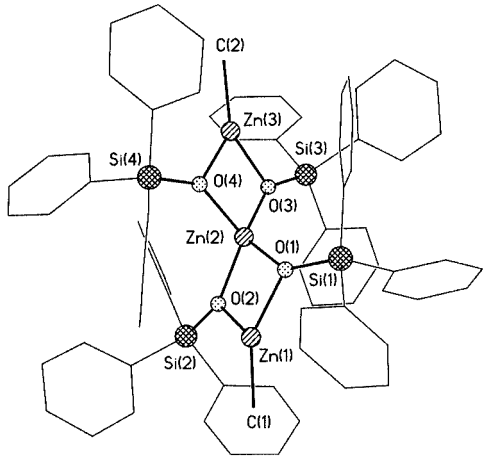

Figure 1. Molecular structure of **1**; hydrogen atoms omitted for clarity; selected distances (Å) and angles (°): Zn(2)−O(2) 1.940(3), Zn(2)−O(4) 1.949(3), Zn(2)−O(1) 1.952(3), Zn(2)−O(3) 1.957(3), Zn(1)−C(1) 1.918(5), Zn(1)−O(1) 1.954(3), Zn(1)−O(2) 2.000(3), Zn(3)−C(2) 1.919(6), Zn(3)−O(4) 1.962(3), Zn(3)−O(3) 2.011(3); O(2)−Zn(2)−O(1) 84.1(1), O(4)−Zn(2)−O(3) 86.1(1), Zn(3)−Zn(2)−Zn(1) 159.27(3), Zn(2)−O(1)−Zn(1) 96.6(1), O(4)−Zn(3)−O(3) 84.2(1), O(3)−Zn(2)−O(1) 124.4 (1), O(4)−Zn(2)−O(2) 119.6 (1), Zn(2)−O(2)−Zn(1) 95.5(1), Zn(2)−O(4)−Zn(3) 95.3(1), Zn(2)−O(3)−Zn(3) 93.5(1)

Thus, the reaction of $Ph_2Si(OH)_2$ with $ZnMe_2$ in THF leads to the hexanuclear $Zn_6Si_6O_{10}$ aggregate **2** in 52% yield (Scheme 2). Although the mechanism is still unknown, it seems likely that the initial steps involve the formation of a Zn_3O_4 core with terminal $OSi(Ph_2)OH$ functions.

Compound **2** crystallises in the monoclinic space group $P2_1/n$ with one half of the molecule in the asymmetric unit. The crystal structure of **2** (Figure 2) reveals a novel type of zinc siloxane in which two spirobicyclic Zn_3O_4 cores are linked together by two R_2Si-fragments.

Additionally, one periphery of each Zn_3O_4 core is bridged by an $Ph_2SiOSiPh_2$ moiety. The Zn atoms are tetrahedral and each of the Zn(2) and Zn(3) atoms bears one

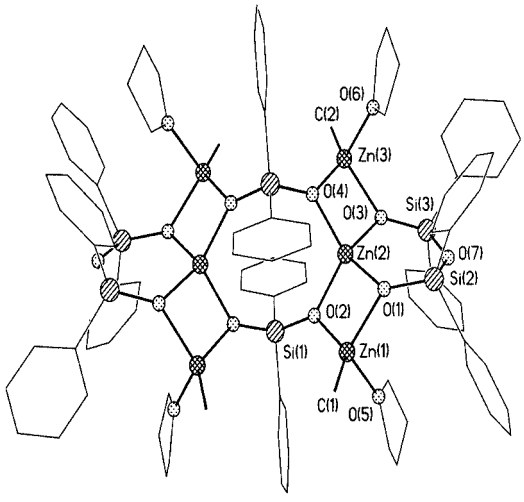

Figure 2. Molecular structure of **2**; hydrogen atoms omitted for clarity; selected distances (Å) and angles (°): Zn(2)−O(2) 1.943(2), Zn(2)−O(4) 1.947(2), Zn(2)−O(1) 1.973(2), Zn(2)−O(3) 1.983(2), Zn(1)−O(2) 2.022(2), Zn(1)−O(1) 2.026(2), Zn(3)−C(2) 1.962(3), Zn(3)−O(4) 2.003(2), Zn(3)−O(3) 2.046(2); O(2)−Zn(2)−O(1) 87.49(6), O(4)−Zn(2)−O(3) 88.08(6), Zn(3)−Zn(2)−Zn(1) 175.94(1), O(2)−Zn(1)−O(1) 83.99(6)

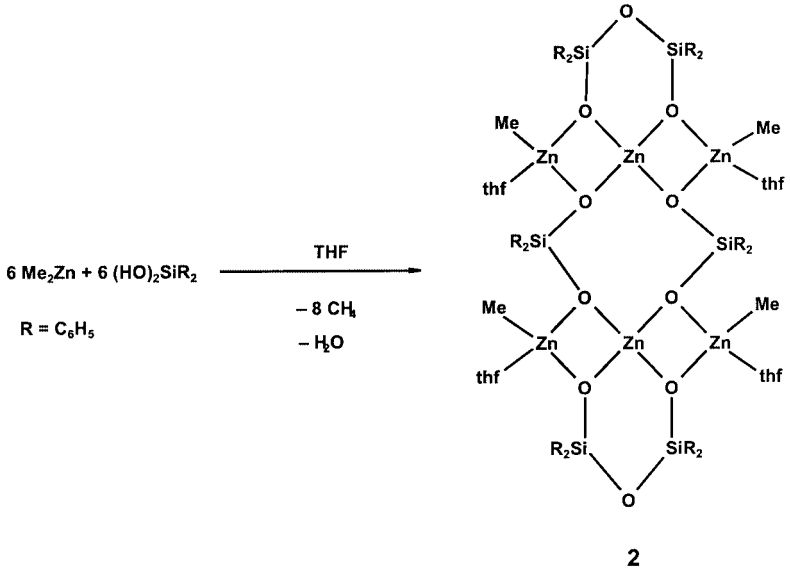

Scheme 2

methyl and one THF ligand. The observed Zn_3O_4 core is practically identical to that in **1**. However, the three Zn atoms of the cores now adopt an almost linear arrangement [Zn···Zn···Zn = 175.94 (1)°]. The Zn−C distances [average 1.954 (5) Å] are longer than those in **1** due to the higher coordination number at the Zn atoms. Another striking structural feature of **2** is that the dihedral angle between the $Zn(2)O_2Zn(3)$ and $Zn(2)O_2(Zn1)$ planes is about 20° smaller than that in **1** [86.9(1)°]. However, the O−Zn−O and Zn−O−Zn angles are almost identical with these values in **1**. Similar to the situation in **1**, the Zn−O distances for the spiro-Zn(2) atom [average 1.962(2) Å] are conspicuously smaller than the corresponding values for Zn(1)−O and Zn(3)−O [average 2.069(2) Å].

Experimental Section

General Remarks: All manipulations were carried out under anaerobic conditions under dry argon using standard Schlenk techniques. Solvents were refluxed over an appropriate drying agent, and distilled and degassed prior to use. NMR spectra were recorded on a Bruker Avance250 spectrometer at ambient temperature operating at 250.1 MHz (^{1}H) or 63 MHz (^{13}C). Chemical shifts are reported relative to TMS at δ = 0.00 ppm (^{1}H).

Preparation of $[(MeZn)_2Zn(OSiPh_3)_4]$ (1): At −78 °C, a solution of $ZnMe_2$ (1.91 g, 20 mmol, 2 M solution in toluene) in toluene (ca. 50 mL) was slowly added to a solution of Ph_3SiOH (7.37 g, 26.7 mmol) in toluene (10 mL), resulting in the immediate evolution of methane. The solution was then allowed to warm to room temperature and all volatiles were removed in vacuo (10^{-3} Torr). Recrystallisation from toluene/hexane gave pure **1** as colourless crystals. Yield: 7.17 g (5.40 mmol, 81%); m.p. 221−223 °C (decomp.). ^{1}H NMR (C_6D_6): δ = − 0.61 (s, 6 H, ZnMe), 7.12−7.83 [m, 60 H, $(C_6H_5)_3Si$] ppm. ^{13}C NMR (C_6D_6): δ = −14.9 (s, 2 C, ZnMe), 137.3−123.6 [m, 64 C, $(C_6H_5)_3Si$] ppm. $C_{74}H_{66}O_4Si_4Zn_3{\cdot}C_7H_8$ (1419.9): calcd. C 65.50, H 5.02; found C 65.30, H 5.00.

Preparation of $[\{Me(THF)Zn\}_2OZn(OSiR_2)(OSiR_2OSiR_2O)]$ (2; R = Ph): Compound **2** was prepared in a similar manner as **1**, starting from $ZnMe_2$ (1.91 g, 20 mmol, 2 M solution in toluene) in toluene (ca. 50 mL) and a solution of $Ph_2Si(OH)_2$ (4.32 g, 20 mmol) in tetrahydrofuran (10 mL). Recrystallisation of the residue from tetrahydrofuran (10 mL) afforded colourless plates. Yield: 3.45 g (1.73 mmol, 52%) of a mixture of stereoisomers. ^{1}H NMR (C_6D_6): δ = −0.53 to −1.11 (12 H, ZnMe), 7.02−8.08 [60 H, $(C_6H_5)_2Si$] ppm. ^{13}C NMR (C_6D_6): δ = −13.7 to −15.3 (m, 4 C, ZnMe), 138.1−124.2 [m, 64 C, $(C_6H_5)_3Si$] ppm. $C_{92}H_{104}O_{14}Si_6Zn_6$ (1994.51): calcd. C 55.40, H 26.00; found C 55.2, H 25.95.

X-ray Crystallographic Study

1: $C_{74}H_{66}O_4Si_4Zn_3{\cdot}C_7H_8$, M = 1419.9, triclinic, space group $P\bar{1}$, a = 13.202(7), b = 13.402(8), c = 21.69(1) Å, α = 97.175(12)°, β = 93.142(11)°, γ = 99.876(12)°, V = 3741(4) Å^3, Z = 2, $2\theta_{max}$ = 59.1°, 24158 measured reflections, 829 parameters, μ = 1.065 mm^{-1}, $R1$ = 0.0685 for 6268 observed reflections [$I > 2\sigma(I)$], $wR2$ = 0.1134 for all reflections.

2: $C_{92}H_{104}O_{14}Si_6Zn_6$, M = 1994.51, monoclinic, space group $P2_1/n$, a = 18.561(4), b = 13.162(3), c = 20.993(4) Å, V = 4690(1) Å^3, Z = 2, $2\theta_{max}$ = 50.28°, 23990 measured reflections, 532 parameters, μ = 1.646 mm^{-1}, $R1$ = 0.0305 for 6728 observed reflections [$I > 2\sigma(I)$], $wR2$ = 0.0770 for all reflections.

The intensity data were collected on a Bruker-axs-SMART 1000 diffractometer (Mo-K_α radiation, λ = 0.71707 Å, T = 203 K). Both structures were solved by direct methods and refined by full-matrix least-squares using SHELXTL-97.[10] The contribution of the disordered solvent in **1** to the structure factors was taken into account by back-Fourier transformation using PLATON/SQUEEZE.[11] All non-hydrogen atoms were refined using anisotropic thermal parameters; hydrogen atoms were included by use of a riding model and fixed isotropic thermal parameters.

CCDC-186433 (**1**) and -186434 (**2**) contain the supplementary crystallographic data for this paper. These data can be obtained free of charge at www.ccdc.cam.ac.uk/conts/retrieving.html [or from the Cambridge Crystallographic Data Centre, 12, Union Road, Cambridge CB2 1EZ, UK; fax: (internat.) +44−1223/336−033; E-mail: deposit@ccdc.cam.ac.uk].

Acknowledgments

We are grateful to the Deutsche Forschungsgemeinschaft (SFB 558), the Fonds der Chemischen Industrie and the Ministry of Science and Education of Nordrhein-Westfalen for financial support.

[1] [1a] R. Murugavel, A. Voigt, M. G. Walawalkar, H. W. Roesky, *Chem. Rev.* **1996**, *96*, 2205. [1b] L. King, A. C. Sullivan, *Coord. Chem. Rev.* **1999**, *189*, 19.
[2] [2a] S. Suh, D. M. Hoffman, L. M. Atagi, D. C. Smith, *Chem. Vap. Deposition* **2001**, *7*, 81. [2b] K. Su, T. D. Tilley, M. J. Sailor, *J. Am. Chem. Soc.* **1996**, *118*, 3459.
[3] M. Lazell, M. Motevalli, S. A. A. Shah, A. C. Sullivan, *J. Chem. Soc., Dalton Trans.* **1997**, 3363.
[4] F. J. Feher, T. A. Budzichowski, *Polyhedron* **1995**, *14*, 3239.
[5] J. A. Biscardi, G. D. Meitzner, E. Iglesia, *J. Catal.* **1998**, *179*, 192.
[6] [6a] K. Merz, R. Schoenen, M. Driess, *J. Phys. IV France* **2001**, *11*, 467. [6b] R. Schoenen, K. Merz, S. Rell, M. Driess, *J. Phys. IV France* **2001**, *11*, 547.
[7] [7a] M. Driess, K. Merz, S. Rell, *Eur. J. Inorg. Chem.* **2000**, 2517. [7b] G. Anantharaman, H. W. Roesky, J. Magull, *Angew. Chem.* **2002**, *114*, 1525; *Angew. Chem. Int. Ed.* **2002**, *41*, 1226.
[8] [8a] F. Schindler, H. Schmidbaur, U. Krüger, *Angew. Chem.* **1965**, *77*, 865. [8b] F. Schindler, H. Schmidbaur, *Angew. Chem.* **1967**, *79*, 683; *Angew. Chem. Int. Ed. Engl.* **1967**, *6*, 683.
[9] M. M. Olmstead, P. P. Power, S. C. Shoner, *J. Am. Chem. Soc.* **1991**, *113*, 3379.
[10] G. M. Sheldrick, SHELXTL-97, University of Göttingen **1997**.
[11] PLATON/SQUEEZE, P. v. d. Sluis, A. L. Spek, *Acta Crystallogr., Sect. A* **1990**, *46*, 194.

Received August 22, 2002
[I02475]

The Unexpected Formation of a Novel Fluorinated Triene

Igor Shevchenko,*[a] Vasyl Andrushko,[a] Enno Lork,[b] and Gerd-Volker Röschenthaler*[b]

Keywords: Phosphanes / Bis(trifluoromethyl)acrylonitrile / Alkenes / Ylides / Carbenes

Bis[bis(dialkylamino)phosphanyl]methane (**1**) and 4,4,4-trifluoro-3-(trifluoromethyl)-2-butenenitrile (**2**) unexpectedly gave triene **3**. According to the X-ray structure analysis compound **3** exists in the solid state exclusively as one isomer.

(© Wiley-VCH Verlag GmbH & Co. KGaA, 69451 Weinheim, Germany, 2003)

Among known compounds containing three conjugated C=C double bonds, there are only two fluorine substituted examples: perfluoro-1,3,5-hexatriene[1–5] and 1,6-dichlorohexafluoro-1,3,5-hexatriene.[6] Here we wish to report on an unusual reaction of bis[bis(dimethylamino)phosphanyl]-methane (**1**) with 4,4,4-trifluoro-3-(trifluoromethyl)-2-butenenitrile (**2**) which, unexpectedly, gave the triene **3**. The second product of this reaction was identified as the fluorine-substituted ylide **4** (Scheme 1).

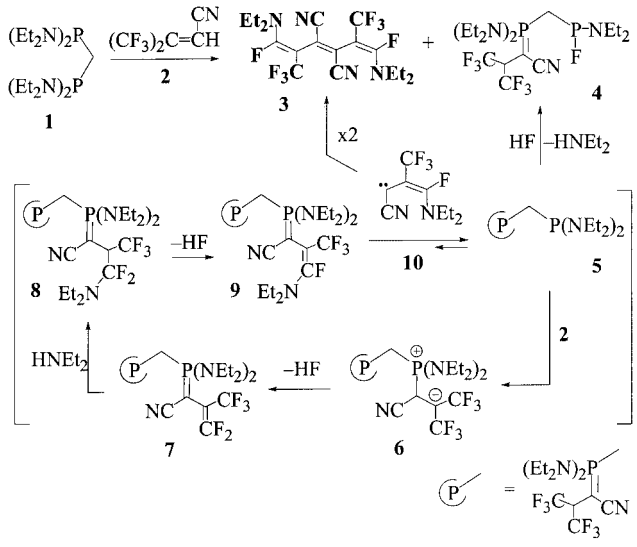

Scheme 1

[a] Institute of Bioorganic Chemistry,
Murmanskaya Street 1, 02094 Kiev, Ukraine
Fax: (internat.) +38-044/573-2552
E-mail: ishev@bpci.kiev.ua
[b] Institute of Inorganic and Physical Chemistry, Universität Bremen, NW2, C2350,
Leobener Str, 28334 Bremen, Germany
Fax: (internat.) +49-(0)421/218-4267
E-mail: gvr@chemie.uni-bremen.de

It is interesting to note that one of the trifluoromethyl groups of the starting acrylonitrile **2** loses two fluorine atoms and adds one of the diethylamino groups which was initially connected to a trivalent phosphorus atom of **1**. The mechanism of this reaction includes the intermediate formation of the ylide **5**, which was detected in the ^{31}P NMR spectrum of the reaction mixture as two characteristic doublets at δ = 73.78 and 67.18 ppm ($^2J_{P,P}$ = 102.4 Hz). These signals decrease slowly in intensity during the course of the reaction and the two doublets of the final product **4** appear. Intermediate **5** can react further with **2** to give the unstable betaine **6**, which decomposes into compound **7** and HF. The hydrogen fluoride thus formed cleaves the P–N bond of the trivalent phosphorus atom of **5** immediately to give **4** and diethylamine. This amine then adds across the C=C double bond of **7**, yielding the intermediate compound **8**, which splits off hydrogen fluoride and gives the unsymmetrical double ylide **9**. These considerations are supported by the fact that the reaction mixture contains a certain amount of diethylammonium fluoride.

The most probable route of formation of the symmetric molecule **3** is the dimerization of carbene **10**. This carbene can be formed during the disintegration of **9** into **5**; the cleavage of the ylidic bond in compound **9** is probably reversible. Of course, some aspects of the detailed mechanism shown in Scheme 1 may differ slightly; for example, some of the proposed steps may be concerted. However, the general concept of an exchange between a fluorine atom and a diethylamino group probably does not differ considerably from the proposed scheme, as a similar process has been observed recently.[7]

The triene **3** was isolated as a slightly yellow crystalline product. The structure of a single crystal was determined by X-ray analysis (Figure 1).

The three double bonds are not conjugated as they are not coplanar. The diethylamino and trifluoromethyl groups at the terminal double bonds, and the central double bond, have a *trans*-configuration. It is interesting to note that no

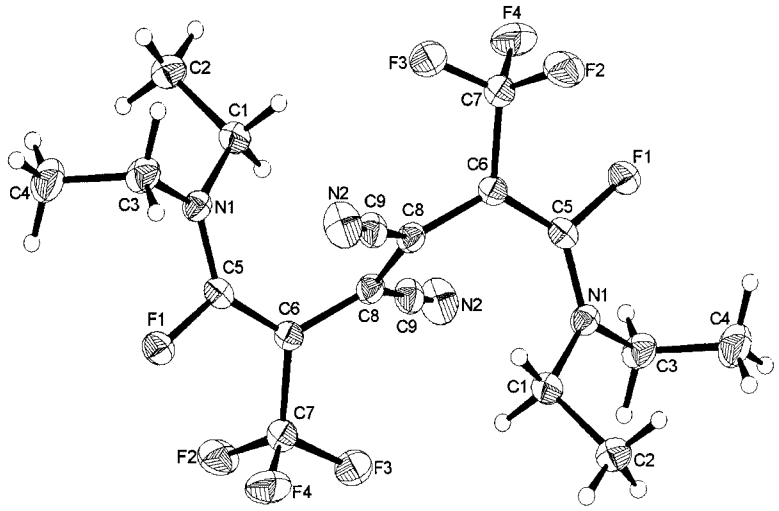

Figure 1. Selected bond lengths [Å] and angles [°]: N(1)−C(5) 1.3296(19), C(5)−F(1) 1.3523(17), C(5)−C(6) 1.361(2), C(6)−C(7) 1.496(2), C(6)−C(8) 1.470(2), C(8)−C(8) 1.365(3); N(1)−C(5)−F(1) 111.85(12), N(1)−C(5)−C(6) 132.27(14), F(1)−C(5)−C(6) 115.88(12), C(8)−C(6)−C(7) 119.23(13), C(9)−C(8)−C(6) 117.98(12), C(8)−C(8)−C(9) 117.35(17)

other possible steric isomers have been found in the crystalline form. An explanation for this phenomenon can be found in the NMR spectra, where a fast interconversion between the isomers in solution at room temperature can be seen. The ^{19}F NMR spectrum displays a doublet for the CF_3 groups ($\delta = -56.6$ ppm, $^4J_{F,F} = 18$ Hz) and a broad unresolved signal for the CF fluorine atoms ($\delta = -66.2$ ppm). At +60 °C the rate of interconversion substantially exceeds the NMR detection limit and the broad signal transforms into a quadruplet with the same coupling constant. An analysis of the low temperature spectra leads to several conclusions. Interconversion between the isomers proceeds rather easily as the other isomers begin to appear at −25 °C. At −60 °C the spectrum shows three isomers in the proportion 1:1:3 indicating that one of the isomers is more stable than the other two. The appearance of only three isomers indicates that the rotation occurs only at terminal double bonds, whereas the central C=C bond retains its *trans*-configuration (otherwise the number of isomers would be larger[4]). The relatively easy rotation around the terminal double bonds is probably accounted for by the π-electron donating ability of the diethylamino groups and the electron-accepting ability of the trifluoromethyl groups, leading to the conjugation of the free electron-pairs of the nitrogen atoms with the adjacent double bonds and formation of the betainic structure **11** (Scheme 2).

Although the lengths of all the C=C double bonds are equal, the influence of **11** should be rather large. The C(5)−N(1) bond is substantially shorter than the other two bonds to nitrogen (132.96 vs. 148.56 pm) and the diethylamino groups have an almost ideal flat conformation. Thus, rotation can occur via the resonance structure **11** to give the two other possible isomers **12** and **13**.

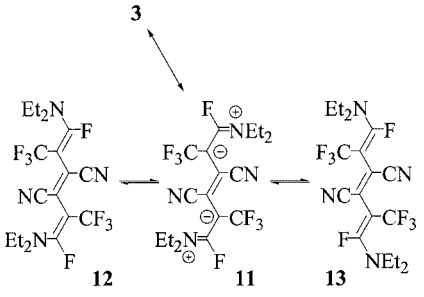

Scheme 2

Experimental Section

General Remarks: All operations were performed under nitrogen in a dry box. The solvents were dried by the usual procedures. NMR: Spectrometer Bruker AC-200 (^1H at 200.1 MHz, ^{13}C at 50.3 MHz, ^{31}P at 81.3 MHz); reference substances were $SiMe_4$ (TMS) ext. (^1H, ^{13}C), and 85% H_3PO_4 ext. (^{31}P). MS: Spectrometer Finnigan MAT 8430; E.I. at 70 eV. Materials: Compound **1** was obtained from methylenebis(dichlorophosphane) and diethyl(trimethylsilyl)amine in petroleum ether at 0 °C (yield 70%; b.p. 108−110 °C, 0.07 Torr). Compound **2** was obtained by adding gaseous hexafluoroacetone to (triphenylphosphoranylidene)acetonitrile without solvent at 20 °C (yield 90%; b.p. 88−90 °C) .

Compound 3: Compound **2** (140 mg, 0.74 mmol) was added to **1** (120 mg, 0.33 mmol) without solvent at 20 °C. After completion of the slightly exothermic reaction the mixture was heated to 50 °C for 15 min. Dichloromethane (2 mL) was then added followed by addition of diethyl ether (0.5 mL) and the mixture left at −15 °C for 2−3 days. The crystals of **3** that formed were isolated, washed

with diethyl ether (2 × 2 mL) and dried in vacuo (0.05 mm). Yield 36 mg (49%), m.p. 78−80 °C. ^{1}H NMR ($CDCl_3$): δ = 1.26 (t, $^3J_{H,H}$ = 7.0 Hz, 12 H, CH_2CH_3), 3.32 (dq, $^3J_{H,H}$ = 7.0, $^3J_{F,H}$ = 3.2 Hz, 8 H, CH_2CH_3) ppm. ^{19}F NMR ($CDCl_3$): δ = −56.6 (d, $^4J_{F,F}$ = 18 Hz, 6 F), −66.2 (broad, 2 F) ppm. MS (EI): $M_{calcd.}$ = 444.37; $M_{exp.}$ = 444. $C_{18}H_{20}F_8N_4$ (444.4): calcd. C 48.65, H 4.54, N 12.61; found C 48.64, H 4.51, N 12.56.

Compound 4: The solvent was evaporated from the mother liquor remaining after crystallisation of **3** and the resulting oil was extracted with hexane (4 × 10 mL). The extracts were combined and concentrated to a volume of 5 mL. In order to dissolve the precipitated oil the mixture was heated to boiling point, cooled to room temperature and left to stand for 30 min and then cooled to −15 °C for 3−4 days. The crystals formed were separated from the mother liquor and dried in vacuo (0.05 mm). Yield 82 mg (49%). M.p. 90−91 °C. ^{1}H NMR ($CDCl_3$): δ = 1.14 (t, $^3J_{H,H}$ = 7.03 Hz, 6 H, NCH_2CH_3), 1.16 (t, $^3J_{H,H}$ = 7.03 Hz, 12 H, NCH_2CH_3), 2.3−2.7 (m, 2 H, P-CH_2-P), 2.9−3.4 [m, 12 H, NCH_2CH_3, 1 H, $CH(CF_3)_2$] ppm. ^{13}C NMR ($CDCl_3$): δ = 12.68 (dm, $J_{P,C}$ = 238.9 Hz, 1 C, P*C*CN), 13.48 (m, 4 C, NCH_2CH_3), 15.13 (m, 2 C, NCH_2CH_3), 34.26 (ddd, $^1J_{P,C}$ = 19.5, $^1J_{P,C}$ = 87.8, $^2J_{F,C}$ = 48.8 Hz, P*C*P), 39.36 (m, 4 C, NCH_2CH_3), 42.89 (d, $^3J_{F,C}$ = 18.5 Hz, 2 C, NCH_2CH_3), 47.44 [m, 1 C, $CH(CF_3)_2$], 124.16 [q, $^1J_{F,C}$ = 281.8 Hz, 2 (CF_3)], 124.90 (d, $^2J_{P,C}$ = 12.6 Hz, CN) ppm. ^{19}F NMR ($CDCl_3$): δ = −67.04 (dd, $^3J_{H,F}$ = 7.8, $^3J_{P,F}$ = 3.6 Hz, 6 F) ppm. ^{31}P NMR ($CDCl_3$): δ = 62.23 (dd, $^2J_{P,P}$ = 68.2, $^3J_{P,F}$ = 17.1 Hz,), 155.05 (dd, $^2J_{P,P}$ = 68.2, $^1J_{F,P}$ = 958.1 Hz) ppm. $C_{18}H_{33}F_7N_4P_2$ (500.42): calcd. C 43.20, H 6.64, N 11.20; found C 44.39, H 6.98, N 12.20.

X-ray Crystallographic Study: Empirical formula $C_{18}H_{20}F_8N_4$; formula weight 444.38; monoclinic; crystal dimensions 0.70 × 0.50 × 0.50 mm; space group $P2_1/n$; a = 1002.40(10), b = 897.50(10), c = 1165.1(2) nm, β = 108.620(10)°, V = 0.9933(2) nm^3, Z = 2; $D_{calcd.}$ = 1.486 mg/mm^3; F_{000} = 456; $2\theta_{max}$ = 27.50°; reflections collected 3031; independent reflections 2269 [R(int) = 0.0209]; completeness to theta (27.50°) = 99.2%; refinement method: full-matrix least-squares on F^2; data/restraints/parameters: 2269/0/141; goodness-of-fit on F^2 = 1.041; final R indices [$I > 2\sigma(I)$] $R1$ = 0.0385, $wR2$ = 0.0930; R indices (all data) $R1$ = 0.0576, $wR2$ = 0.1031; extinction coefficient 0.019(3). CCDC-174595 contains the supplementary crystallographic data for this paper. These data can be obtained free of charge at www.ccdc.cam.ac.uk/conts/retrieving.html [or from the Cambridge Crystallographic Data Centre, 12, Union Road, Cambridge CB2 1EZ, UK; Fax: (internat.) +44-1223/336-033; E-mail: deposit@ccdc.cam.ac.uk].

Acknowledgments

We thank the Deutsche Forschungsgemeinschaft for their support of this work.

[1] V. Dedek, I. Linhart, M. Kovac, *Collect. Czech. Chem. Commun.* **1985**, *50*, 1714−1726.
[2] Patent; Dow Chem. Co; US 2705229, **1953**.
[3] R. Hrabal, Z. Chvatal, V. Dedek, *J. Fluorine Chem.* **1985**, *29*, 160.
[4] V. Dedek, Z. Chvatal, *J. Fluorine Chem.* **1986**, *31*, 363−380.
[5] N. Jing, D. M. Lemal, *J. Org. Chem.* **1994**, *59*, 1844−1848.
[6] M. M. Kremlev, P. G. Cherednichenko, L. I. Moklyachuk, L. M. Yagupol'skii, *J. Org. Chem. (USSR, Engl. Transl.)* **1989**, *25*, 2316−2320.
[7] I. Shevchenko, V. Andrushko, E. Lork, G.-V. Röschenthaler, *Chem. Commun.* **2002**, *8*, 120−121.

Received August 28, 2002
[I02483]

Molecular Tectonics: Design of 1-D Coordination Networks Based on Pyrene-Bearing Pyrazolyl Units

Abdelaziz Jouaiti,[a] Mir Wais Hosseini,*[a] and Nathalie Kyritsakas[b]

Keywords: N ligands / Coordination networks / Silver / Palladium

The synthesis of a new ligand based on a pyrene backbone bearing four pyrazolyl units is reported. Whereas this compound forms a discrete exo-binuclear complex with palladium, in the presence of silver a 1-D coordination network is obtained and structurally characterised in the solid state by X-ray diffraction method.
(© Wiley-VCH Verlag GmbH & Co. KGaA, 69451 Weinheim, Germany, 2003)

Introduction

Coordination networks i.e. periodic molecular assemblies formed by the self-assembly of organic and metallic tectons (active molecular building blocks) has attracted increasing interest over the last decade.[1] The formation of coordination networks results from the interconnection of metallic centres by organic ligands through coordination bonds. Both the metal centre and the organic ligand must permit the iteration of the coordination process in order to behave as tectons.[2] In other words, the organic tecton must posses at least two coordination sites or poles[3] divergently oriented. The dimensionality of the network depends on the number of translations of the coordination pattern in different directions of space. Thus, a 1-D coordination network is generated by a single translation of the coordination pattern. For the design of coordination networks, one must take into account the interplay between the organic (number of coordination sites, topology) and metallic (number of coordination and geometry) tectons. For 1-D coordination networks, the majority of cases reported deal with bis-monodentate tectons.[4] However, a few examples of bis-bidentate[5,6] bis-tridentate[7−9] and a combination of mono- and tridentate[3] tectons have been also published.

Here we report the formation of the 1-D coordination network **7** formed between the pyrene-based tecton **4**, bearing four pyrazolyl units, and the silver cation, and the synthesis of two discrete binuclear palladium complexes **5** and **6**.

[a] Université Louis Pasteur, Laboratoire de Chimie de Coordination Organique
4, rue Blaise Pascal, 67000 Strasbourg, France
Fax: (internat.) +33-390/241-325
E-mail: hosseini@chimie.u-strasbg.fr
[b] Service Commun des Rayons X, Institut Le Bel,
4, rue Blaise Pascal, 67000 Strasbourg, France

Results and Discussion

As stated above, examples of coordination networks containing bis-chelate tectons are rather rare. In a continuation of our efforts towards the design of new types of coordination networks,[10] we thought that the pyrene-based tecton **4** bearing four pyrazolyl units may be of interest for the formation of 1-D coordination networks in the presence of connecting transition metals. The synthesis and binding ability of pyrazole-based ligands have been reported.[11] The design of the tecton **4** was based on the use of pyrene as the backbone because the latter permits the introduction of four monodentate units in positions 4, 5, 9 and 10 in a symmetrical fashion. The pyrazolyl group was the obvious candidate as the monodentate unit. Indeed, when four such units are connected through their nitrogen atoms to the pyrene backbone at positions 4, 5, 9 and 10, due to their localisation, each set of two pyrazolyl units on each side of the backbone will behave as a chelate, thus affording a bis-chelate tecton. Pyrene has previously been used as a backbone to anchor bipyridine,[12,13] terpyridine[13] and quinoline[14] units. Due to its planarity, pyrene **1** is poorly soluble in common solvents, and so we thought that the introduction of bulky and nonplanar *tert*-butyl substituents at positions 2 and 7, remote from the binding zones of the ligand, should overcome this insolubility problem.

For the synthesis of compound **4**, pyrene **1** was the starting material. The introduction of the *tert*-butyl groups at positions 2 and 7, leading to compound **2**, was achieved following reported procedures.[15] The bromination of **2** by Br_2 in the presence of $FeCl_3$ in CCl_4, leading to the tetrabromo compound **3**, was also achieved following reported procedures.[16] Finally, the desired compound **4** (Scheme 1) was obtained in 24% yield upon treatment of the tetrabromo compound **3** with sodium pyrazolate in DMF.

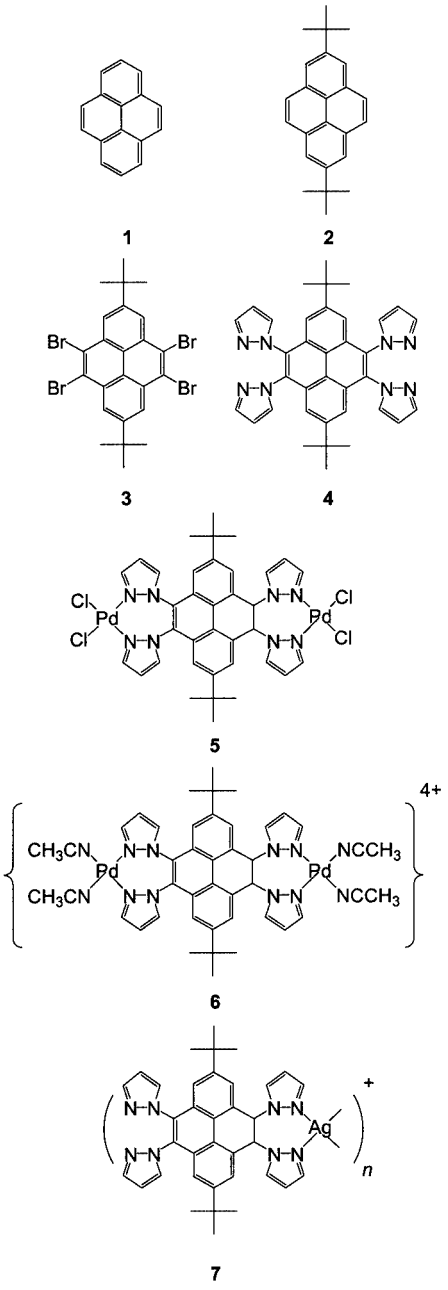

Scheme 1

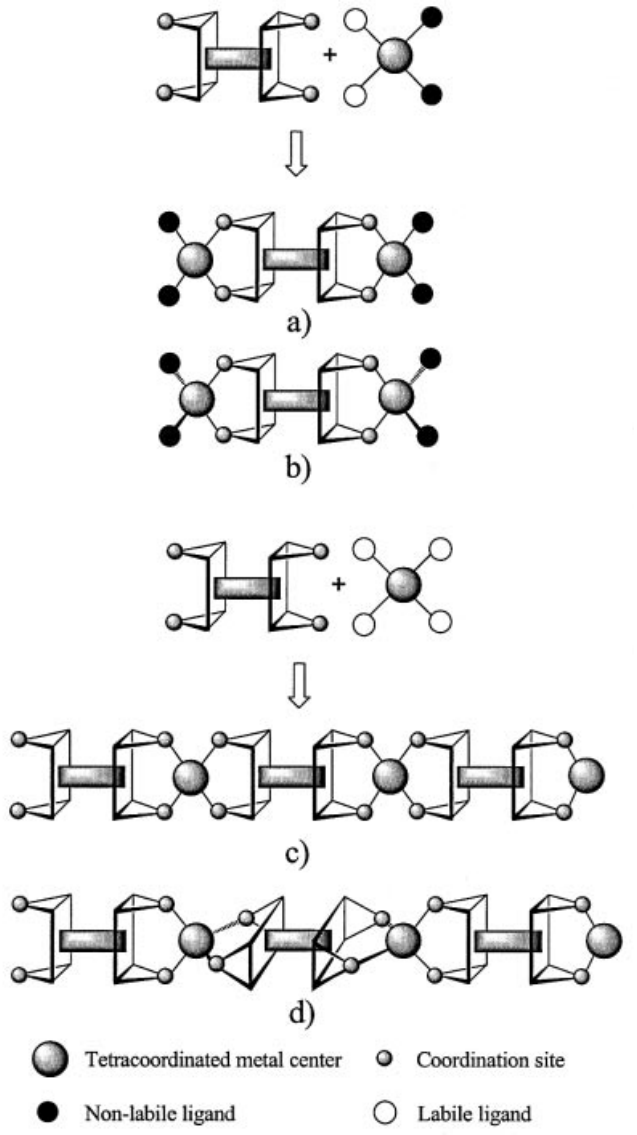

Figure 1. Schematic representation of the formation of discrete exo-binuclear complexes formed between an exo-bis-chelate ligand and deprotected metal centres adopting a square planar (a) or tetrahedral (b) coordination geometry, or infinite 1-D coordination networks in the presence of metal centres adopting a square planar (c) or tetrahedral (d) coordination geometry

Among many coordination possibilities that the bis-chelate tecton **4** may offer, one may envisage the formation of discrete exo-binuclear complexes upon binding of metal centres possessing only two available coordination sites and adopting either a square planar (Figure 1a) or a tetrahedral (Figure 1b) coordination geometry.

The quantitative formation of the exo-binuclear palladium complex **5** was demonstrated by treating the ligand **4** with $[PdCl_2(CH_3CN)_2]$ in a mixture of CH_2Cl_2 and CH_3CN at room temperature. Complex **5** is rather insoluble in common solvents. However, suitable yellow-orange single-crystals could be obtained from a DMSO/MeOH mixture. The structure of **5** was investigated in the solid state by X-ray diffraction, which revealed the following features (Figure 2). The crystal (triclinic, space group $P\bar{1}$) is composed of discrete binuclear complexes **5**, two DMSO and one water solvent molecules. Although the H_2O molecule is H-bonded to the O atom of DMSO (d_{O-O} = 2.74 Å), no specific interactions between the solvent molecules and complex **5** could be identified. For the pyrene moiety, possessing a centre of symmetry, the aromatic core, as expected, is planar. Both *tert*-butyl groups are disordered over two positions. The py-

razolyl units [average N−N distance of ca 1.35 Å and $d_{N-C(Py)}$ = 1.43 Å] are tilted with respect to the plane of pyrene (NNCC dihedral angles of −69° and 73.9°). The two sets of two pyrazolyl units forming two chelates are located above and below the main plane of the ligand. Consequently, the two square-planar Pd centres are also located above and below the main plane of the pyrene backbone. The coordination sphere around each Pd^{II} is composed of two N atoms belonging to two adjacent pyrazolyl units in *cis* configuration (average d_{Pd-N} of 2.03 Å, NPdN angle of ca 88°) and two Cl^- anions (d_{Pd-Cl} = 2.28 Å, ClPdCl angle of ca 92°).

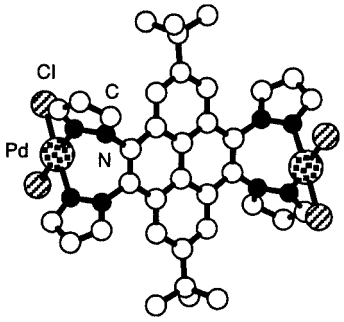

Figure 2. Crystal structures of the exo-binuclear palladium complex formed with pyrazolyl-based ligand **4**; solvent molecules (DMSO, H_2O) and H atoms are omitted for clarity; for bond lengths and angles see text

When dealing with 1-D coordination networks based on bidentate tectons, many structural frameworks may be envisaged.[17] In particular, in the presence of the tecton **4**, 1-D networks may be generated by using tetracoordinate metal centres adopting either a square planar (Figure 1c) or tetrahedral (Figure 1d) coordination geometry.

Since the Cl^- anions bound to Pd^{II} are not sufficiently labile for generating a network in the presence of free tecton **4** (neutral ligand), the binuclear complex **6**, for which the Cl^- anions are substituted by acetonitrile molecules and the positive charge on the complex is compensated by tetrafluoroborate anions, was prepared in quantitative yield upon treatment of **4** with $[Pd(CH_3CN)_4][BF_4]_2$ in a mixture of CH_2Cl_2 and CH_3CN at room temperature. The much more soluble complex **6** was characterised by NMR spectroscopy. Considering the discrete complex **6** as a metalla tecton, the formation of a 1-D network of the square-planar type shown in Figure 1c was attempted in the presence of the free ligand **4**. Unfortunately, crystallisation under different conditions (variation of the solvent and co-solvent, temperature) afforded only an amorphous and insoluble powder which could not be structurally characterised.

The formation of 1-D networks **7** of the tetrahedral type presented schematically in Figure 1d was investigated using the Ag^+ cation, which may adopt a tetrahedral coordination geometry. In a crystallisation tube, upon slow diffusion of a solution of $Ag(PF)_6$ (10 mg, excess) in EtOH (3 mL) into a solution of compound **4** (5 mg) in $CHCl_3$ (2 mL), colourless crystals of network **7** were obtained at room temp. in the dark over a period of a week and studied by X-ray diffraction of a single crystal (Figure 3). The crystal (triclinic system, space group $P\bar{1}$) is composed of **4**, the Ag^+ cation, a PF_6^- anion and $CHCl_3$ solvent molecules. Although the $CHCl_3$ molecule is rather weakly H-bonded to the PF_6^- anion (d_{H-F} = 2.35 Å), no specific interactions between the cationic part of the crystal and the solvent or anion could be observed.

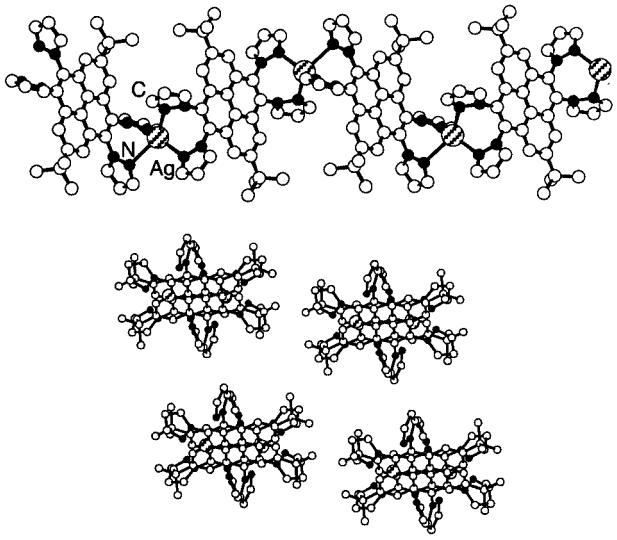

Figure 3. A portion of the crystal structures of the stair-type, 1-D coordination network formed by the self-assembly of **4** and Ag^+ cation (top) and the parallel packing of the 1-D networks (bottom); anions (PF_6^-), solvent molecules ($CHCl_3$) and H atoms are omitted for clarity; for bond lengths and angles see text.

The cationic portion of the crystal is an infinite coordination network formed upon interconnection of the organic tectons **4** by silver cations (Figure 3 top). As in the case of the square-planar discrete binuclear Pd complex mentioned above, the pyrazolyl units are tilted with respect to the plane of pyrene (NNCC dihedral angles of −82.3° and 85.0°) and located on the opposite faces of the centrosymmetric ligand **4**, thus offering two chelates, one on each face of the ligand. The coordination sphere around the silver cation is composed of four N atoms (d_{Ag-N} varying between 2.24 Å and 2.50 Å) belonging to two sets of two pyrazolyl units of consecutive ligands. The coordination geometry around the silver cation is a severely distorted tetrahedron (NAgN angle varying between 84.7° and 139.7°). The stair-type 1D network **7** may be described as the translation into a single direction of space of the coordination node composed of a tetracoordinate silver cation and two sets of two pyrazolyl units belonging to two consecutive ligands **4**. The cationic 1-D networks are packed parallel to each other (Figure 3 bottom) and the empty spaces are occupied by chloroform molecules.

In summary, the synthesis of the new ligand **4** based on a pyrene backbone bearing four pyrazolyl units was achieved. Whereas the compound **4** was shown to bind two PdX_2 moieties (X = Cl^- or CH_3CN) to form the exo-binuclear

palladium complexes **5** and **6**, respectively, in the presence of $AgPF_6$, the formation of a 1-D coordination network **7** based on the interconnection of the organic tecton **4** by silver cation adopting a tetrahedral coordination geometry was demonstrated in the solid state by X-ray diffraction on single-crystal. The preparation of either other discrete complexes or coordination networks using the ligand **4** and other transition metals is currently under investigation.

Experimental Section

Synthesis of 4: NaH (50% in oil, 0.69 g, 14.3 mmol) was added in small portions to a solution of pyrazole (1 g, 14.7 mmol) in dry DMF (45 mL) under argon and the mixture stirred at room temperature for 35 min. A solution of the tetrabromo compound **3** (1.0 g, 1.58 mmol), prepared according to published procedures,[16] was added to this mixture in one portion. The mixture turned blue instantaneously. Upon heating the mixture at 130 °C for 40 h., a dark red solution was obtained. The solvents were evaporated to dryness and the residue was taken up in water (50 mL). The brownish solid was filtered, washed with water (50 mL) and finally dried under vacuum. The pure compound **4** (0.22 g) was obtained in 24% yield after column chromatography (SiO_2, CH_2Cl_2, 0−1% MeOH). m.p. > 300 °C, ^{1}H NMR ($CDCl_3$, 200 MHz, 25 °C): δ = 1.33 (s, 18 H, CH_3), 6.37 (t, 2 Hz, 4 H, $H_{pyrazolyl}$), 7.48 (d, 2 Hz, 4 H, $H_{pyrazolyl}$), 7.86 (d, 2 Hz, 4 H, $H_{pyrazolyl}$), 7.98 (s, 4 H, H_{pyrene}) ppm. ^{13}C NMR ($CDCl_3$, 75 MHz, 25 °C): δ = 31.4, 106.7, 122.0, 127.7, 133.0, 133.1, 141.3, 151.1 ppm. $C_{36}H_{34}N_8$: (578.72): calcd. C 74.72, H 5.92, N 19.36; found C 74.33, H 5.88, N 19.12.

Synthesis of 5: A solution of $[PdCl_2(CH_3CN)_2]$ (18 mg, 0.069 mmol) in CH_3CN (4 mL) was added to a solution of **4** (20 mg, 0.035 mmol) in CH_2Cl_2 (3 mL) under argon and the mixture stirred overnight at room temperature. The solvents were evaporated to dryness and the residue was taken up in CH_2Cl_2 (5 mL) and filtered. The solid was further washed with diethyl ether (10 mL). The pure complex **5** obtained in quantitative yield (32 mg) was insoluble in all common solvents. ^{1}H NMR (DMSO, 200 MHz, 25 °C): δ = 1.29 (s, 18 H, CH_3), 6.51 (broad, 4 H, $H_{pyrazolyl}$), 6.99 (broad, 4 H, $H_{pyrazolyl}$), 8.27 (s, 4 H, H_{pyrene}), 8.86 (broad, 4 H, $H_{pyrazolyl}$) ppm. $C_{36}H_{34}Cl_4N_8Pd_2{\cdot}CH_3CN$ (974.4): calcd. C 46.84, H 3.83, N 12.94; found C 46.70, H 3.60, N 12.72.

Synthesis of 6: A solution of $[Pd(CH_3CN)_4][BF_4]_2$ (50 mg, 0.11 mmol) in a 1:1 mixture of CH_3CN and CH_2Cl_2 (10 mL) was added to a solution of **4** (30 mg, 0.05 mmol) in CH_2Cl_2 (5 mL) under argon and the mixture stirred overnight at room temperature. The solvents were evaporated to dryness affording the desired complex in quantitative yield. ^{1}H NMR (CD_3CN, 200 MHz, 25 °C): δ = 1.45 (s, 18 H, CH_3), 2.17 (s, 12 H, CH_3CN), 7.06 (t, J = 1.6 Hz, 4 H, $H_{pyrazolyl}$), 8.03 (s, 4 H, H_{pyrene}), 8.42 (d, J = 1.5 Hz, 4 H, $H_{pyrazolyl}$), 8.55 (d, J = 1.5 Hz, 4 H, $H_{pyrazolyl}$) ppm.

Crystallisation Conditions

Complex 5: In a crystallising tube, MeOH was slowly diffused into a solution of **5** in DMSO at room temperature affording, after several days, yellowish-orange crystals.

Network 7: In a crystallising tube, a solution of $AgPF_6$ (excess, 10 mg) in EtOH was slowly diffused into a solution of **5** (5 mg) in $CHCl_3$ at room temperature and in the dark. After a week, colourless crystals were obtained.

Crystal Structure Characterisation: X-ray diffraction data collection was carried out on a Kappa CCD diffractometer equipped with an Oxford Cryosystem liquid N_2 device, using graphite-monochromated Mo-K_α radiation. For all structures, diffraction data were corrected for absorption and analysed using OpenMolen package.[18] All non-H atoms were refined anisotropically.

Crystallographic Data for 5 (Yellow Crystals, 294 K): $C_{36}H_{34}Cl_4N_8Pd_2{\cdot}2DMSO{\cdot}H_2O$, M = 1107.62, triclinic, a = 13.1079(3), b = 13.6607(4), c = 15.1388(4) Å, α = 92.145(5), β = 99.638(5), γ = 115.715(5), U = 2389.3(4) Å^3, space group $P\bar{1}$, Z = 2, $D_{calcd.}$ = 1.54 g cm^{-3}; μ = 1.108 mm^{-1}, 5800 data with $I > 3\sigma(I)$, R = 0.054, Rw = 0.087.

For 7 (Colourless Crystals, 173 K): $C_{36}H_{34}AgN_8{\cdot}PF_6{\cdot}4CHCl_3$, M = 1309.07, triclinic, a = 11.4299(4), b = 15.5450(5), c = 17.8274(6) Å, α = 103.614(5), β = 101.712(5), γ = 110.022(5), U = 2749.5(6) Å^3, space group $P\bar{1}$, Z = 2, $D_{calcd.}$ = 1.58 g cm^{-3}; μ = 1.037 mm^{-1}, 6900 data with $I > 3\sigma(I)$, R = 0.085, Rw = 0.096.

CCDC-193060 (**5**) and 193061 (**7**) contain the supplementary crystallographic data for this paper. These data can be obtained free of charge at www.ccdc.cam.ac.uk/conts/retrieving.html or from the Cambridge Crystallographic data Center, 12 Union Road, Cambridge CB2 1EZ, UK; Fax: (internat.) +44-1223/336-033; E-mail: deposit@ccdc.cam.ac.uk.

[1] S. R. Batten, R. Robson, *Angew. Chem. Int. Ed.* **1998**, *37*, 1460−1494; A. J. Blake, N. R. Champness, P. Hubberstey, W.-S. Li, M. A. Withersby, M. Schöder, *Coord. Chem. Rev.* **1999**, *183*, 117−138; M. W. Hosseini, in NATO ASI Series (Eds.: D. Braga, F. Grepiono, G. Orpen), Serie c, Kluwer, Dordrecht, Netherlands, **1999**, *538*, 181−208; M. Eddaoudi, D. B. Moler, H. Li, B. Chen, T. M. Reineke, M. O'Keeffe, O. M. Yaghi, *Acc. Chem. Res.* **2001**, *34*, 319−330; B. Moulton, M. J. Zaworotko, *Chem. Rev.* **2001**, *101*, 1629−1659.

[2] M. Simard, D. Su, J. D. Wuest, *J. Am. Chem. Soc.* **1991**, *113*, 4696−4698.

[3] A. Jouaiti, M. W. Hosseini, A. De Cian, *Chem. Commun.* **2000**, 1863−1864.

[4] O. M. Yaghi, H. Li, C. Davis, D. Richardson, T. L. Groy, *Acc. Chem. Res.* **1998**, *31*, 474−484; T. L. Hennigar, D. C. MacQuarrie, P. Losier, R. D. Rogers, M. J. Zaworotko, *Angew. Chem. Int. Ed. Engl.* **1997**, *36*, 972−973; J. Blake, N. R. Champness, S. S. M. Chung, W-S. Li, M. Schröder, *Chem. Commun.* **1997**, 1675−1676; M. A. Withersby, A. J. Blake, N. R. Champness, P. Hubberstey, W-S. Li, M. Schröder, *Chem. Commun.* **1997**, 2327−2328.

[5] U. Velten, M. Rehahn, *Chem. Commun.* **1996**, 2639−2640.

[6] C. Kaes, M. W. Hosseini, C. E. F. Rickard, B. W. Skelton, A. White, *Angew. Chem. Int. Ed.* **1998**, *37*, 920−922.

[7] E. C. Constable, A. M. W. Cargill Thompson, *J. Chem. Soc., Dalton Trans.* **1992**, 3467−3475; E. C. Constable, A. J. Edwards, D. Philips, P. R. Raithby, *Supramolecular Chem.* **1995**, *5*, 93−95.

[8] S. J. Loeb, G. K. H. Shimizu, *J. Chem. Soc., Chem. Commun.* **1993**, 1395−1396; M. Ferigo, P. Bonhôte, W. Marty, H. Stoeckli-Evans, *J. Chem. Soc., Dalton Trans.* **1994**, 1549−1554; A. Neels, B. Mathez Neels, H. Stoeckli-Evans, *Inorg. Chem.* **1997**, *36*, 3402−3409.

[9] M. Loï, E. Graf, M. W. Hosseini, A. De Cian, J. Fischer, *Chem. Commun.* **1999**, 603−604; M. Loï, M. W. Hosseini, A. Jouaiti, A. De Cian, J. Fischer, *Eur. J. Inorg. Chem.* **1999**, 1981−1985.

[10] For recent publications see: B. Schmaltz, A. Jouaiti, M. W. Hosseini, A. De Cian, *Chem. Commun.* **2001**, 1242−1243; A. Jouaiti, V. Jullien, M. W. Hosseini J.-M. Planeix, A. De Cian, *Chem. Commun.* **2001**, 1114−1115; C. Klein, E. Graf, M. W. Hosseini, A. De Cian, J. Fischer, *New J. Chem.* **2001**, *25*, 207−209; S. Ferlay, S. Koenig, M. W. Hosseini, J. Pansanel, A.

De Cian, N. Kyritsakas, *Chem. Commun.* **2002**, 218−219, A. Jouaiti, M. W. Hosseini, N. Kyritsakas, *Chem. Commun.* **2002**, 1898−1899; B. Zimmer, V. Bulach, M. W. Hosseini, A. De Cian, N. Kyritsakas, *Eur. J. Inorg. Chem.* **2002**, 3079−3082; B. Zimmer, M. Hutin, V. Bulach, M. W. Hosseini, A. De Cian, N. Kyritsakas, *New J. Chem.* **2002**, *26*, 1532−1535.

[11] M. Loï, M. W. Hosseini, A. Jouaiti, A. De Cian, J. Fischer, *Eur. J. Inorg. Chem.* **1999**, 1981−1985; A. Jouaiti, M. Loï, M. W. Hosseini, A. De Cian, *Chem. Commun.* **2000**, 2085−2086.

[12] A. L. Rodriguez, G. Peron, C. Duprat, M. Vallier, E. Fouquet, F. Fages, *Tetrahedron Lett.* **1998**, *39*, 1179−1182,

[13] A. Harriman, M. Hissler, A. Khatyr, R. Ziessel, *Chem. Commun.* **1999**, 735−736.

[14] C. Bonnefous, A. Chouai, R. P. Thummel, *Inorg. Chem.* **2001**, *40*, 5851−5859.

[15] L. Rodenburg, R. Brandsma, C. Tintel, J. van Thuijl, J. Lugtenburg, J. Cornelisse, *Recl. Trav. Chim. Pays-Bas* **1986**, *105*, 156−161.

[16] Y. Miura, E. Yamano, *J. Org. Chem.* **1995**, *60*, 1070−1073.

[17] R. W. Saalfrank, H. Maid, F. Hampel, K. Peters, *Eur. J. Inorg. Chem.* **1999**, 1859−1867.

[18] OpenMolenN, Interactive Structure Solution, Nonius B. V., Delft, The Netherlands, 1997.

Received September 10, 2002
[I02507]

Unique Magnetic Behavior in a One-Dimensional Coordination Polymer [Co(tmpyim)$_2$(tp)]

Licun Li,*[a] Zhiliang Liu,[a] Scott S. Turner,[b] Daizheng Liao,[a] Zonghui Jiang,*[a] and Shiping Yan[a]

Keywords: Magnetic properties / Crystal structure / Radicals / Terephthalate

A one dimensional cobalt(II)–radical complex [Co(tmpyim)$_2$(tp)] [tmpyim = 4,4,5,5-tetramethyl-2-(3′-pyridyl)-imidazoline-1-oxyl 3-oxide and tp = terephthalate dianion] has been synthesized and characterized by X-ray crystallography. The crystal structure consists of infinite chains of Co(tmpyim)$_2$ units cross-linked by terephthalate ligands. The magnetic behavior of the complex is unique and is discussed in connection with the crystal structure.
(© Wiley-VCH Verlag GmbH & Co. KGaA, 69451 Weinheim, Germany, 2003)

In the field of molecular-based magnetic materials, it is fundamentally important to understand the interactions between organic or inorganic spin-carriers and the structure-function relationships of the magnetic systems.[1−2] The so-called "crystal engineering" approach has been used extensively to control material structure and dimensionality in which extended inorganic structures with organic bridges are synthesized to give coordination polymers or networks.[3−4]

Metal complexes based on pyridyl-substituted nitronyl nitroxides have attracted considerable attention in recent years due to the ability of these radicals to coordinate metal ions and act as magnetic couplers, giving rise to new functional materials with a variety of structural topologies.[5−12] The terephthalate ligand is a versatile ligand with good binding ability, as exemplified by the formation of polymeric structures.[13−15] In this paper we report the crystal structure and magnetic properties of a one-dimensional Co^{II}−radical complex with a terephthalate bridge, [Co(tmpyim)$_2$(tp)] (**1**) [tmpyim = 4,4,5,5-tetramethyl-2-(3′-pyridyl)imidazoline-1-oxyl 3-oxide and tp = terephthalate dianion).

The structure of **1** (Figure 1) shows that each terephthalate dianion binds to two Co^{II} ions in a bis-bidentate mode, leading to a 1-D chain structure. Two tmpyim radical ligands coordinate to the Co^{II} ion through the nitrogen atoms of their pyridyl rings. The Co^{II} ion has a distorted octahedral coordination environment, which is centrosymmetric. Four carboxylato oxygen atoms from two tp ligands form the equatorial plane. The Co−O bond lengths in the basal plane are 2.117(2) and 2.122(2) Å for Co(1)−O(3) and Co(1)−O(4), respectively. The axial positions, occupied by nitrogen atoms from the tmpyim ligands, have a Co−N bond length of 2.144(3) Å. The dihedral angle between the pyridyl ring and the nitroxide group [O(1)−N(1)−C(3)−N(2)−O(2)] is 31.6°. The shortest contact between nitroxide groups is 3.860 Å. However, it should be noted that the closest contact is observed between the oxygen atom [O(1)] of the nitroxide group and the carbon atom [C′(5)] belonging to the adjacent chain [O(1)−C′(5) = 3.156 Å; Figure 2]. The intrachain Co^{II}−Co^{II} distance is 10.633 Å and the shortest interchain Co^{II}−Co^{II} separation is 7.119 Å, which corresponds to the unit cell length (*b*).

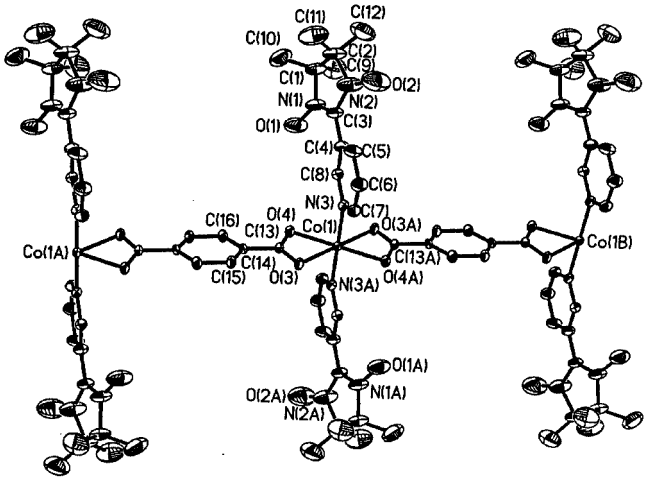

Figure 1. View of the molecular structure of [Co(tmpyim)$_2$(tp)] with atom labeling and 30% thermal ellipsoids

The magnetic susceptibility of complex **1** was measured in the temperature range 2−300 K, with an applied field of

[a] Department of Chemistry, Nankai University, Tianjin 300071, P. R. China
[b] Davy-Faraday Research Laboratory, The Royal Institution of Great Britain, 21 Albemarle, Street, London, W1S 4BS, UK

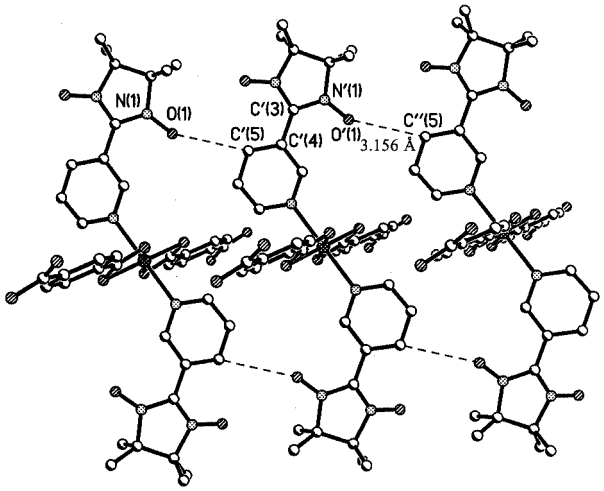

Figure 2. The closest contact in $[Co(tmpyim)_2(tp)]$ showing exchange coupling through NO···C interactions

1000 G. The plot of effective magnetic moment μ_{eff} versus T is shown in Figure 3.

At room temperature, μ_{eff} is equal to 6.13 μ_B, which is much higher than that expected for noninteracting S_{Co} = 3/2 and S_{rad} =1/2 spins, indicating that an important orbital contribution is involved. The plot of μ_{eff} versus T reveals four domains: (i) from 300 K to 55.1 K, μ_{eff} increases continuously from 6.13 μ_B to a value of 6.46 μ_B; (ii) between 55.1 K and 25 K μ_{eff} decreases gradually with decreasing temperature; (iii) from 25 K to 2 K, μ_{eff} increases rapidly to reach a maximum of 6.84 μ_B at 3 K; (iv) below 2 K, μ_{eff} decreases again on cooling. This magnetic behavior is unique. In complex **1**, there are four kinds of magnetic interactions, namely: (i) Co^{II} interacting with the coordinated tmpyim radical, (ii) a $Co^{II}-Co^{II}$ interaction *via* the terephthalate bridge, (iii) a magnetic coupling between neighboring tmpyim radicals through the NO···C pathway (3.156 Å), and (iv) a through-space interaction between neighboring NO groups of tmpyim radicals (3.860 Å). The magnetic interaction between the cobalt(II) ions should be very weakly antiferromagnetic and can be neglected since the tp bridge is long.[16] The extent of magnetic coupling of the two adjacent NO groups depends on their separation and the relative orientation of the π* orbitals.[17] In complex **1**, the shortest O−O separation between the nitroxide groups is rather large (3.860 Å) and the planes of the π systems of the nitroxide radicals form an angle of 26.8° with the plane defined by the two adjacent NO groups. These geometrical parameters are not disposed favorably for strong overlap and lead to weakly antiferromagnetic interactions.[17−19] The last kind of magnetic coupling is also weak and should be dominant only at low temperatures. Therefore the magnetic behavior of the complex between 300 K and 55.1 K must correspond to that of Co^{II} interacting with the coordinated tmpyim radical, which implies that the magnetic interaction between cobalt(II) and tmpyim radical is ferromagnetic. The decrease of μ_{eff} between 55.1 K an 25 K is attributed to the spin-orbit coupling of the cobalt(II) ion. Regarding the interaction between radicals, the crystal structure shows that the closest contact involves the oxygen atom [O(1)] of the uncoordinated NO group, which carries a large, positive spin density, and the carbon atom [C′(5)] of the adjacent tmpyim radical, which carries a small, negative spin density [O(1)···C′(5) = 3.156 Å]. These two atoms carrying opposite signs of the spin density alternate, leading to ↑N(1)−O(1)↑···↓C′(5)−↑C′(4)−↓C′(3)−↑N′(1)−↑O′(1)···↓C″(5), which matches McConnell's criteria.[20] Thus, the exchange coupling between neighboring tmpyim radicals through an NO···C pathway should be ferromagnetic and so results in the increase in μ_{eff} between 25 K and 2 K. The μ_{eff} value decreases below 2 K due to the weak antiferromagnetic interaction between neighboring NO groups of the tmpyim

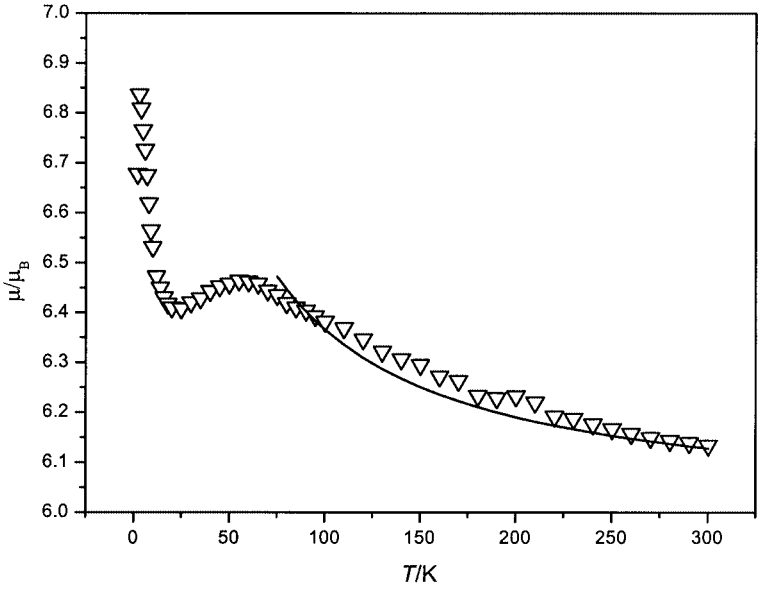

Figure 3. A plot of μ_{eff} (▽) versus T for $[Co(tmpyim)_2(tp)]$

radicals, spin-orbital coupling and zero-field splitting. It would be very difficult to incorporate all of these into a model to fit the magnetic data at the lower temperature. However, according to Sinn,[21] the higher temperature magnetic data above 70 K may be approximately interpreted by the isotropic spin Hamiltonian. For the $Co(tmpyim)_2$ unit, the spin Hamiltonian can be expressed as

$$\hat{H} = -2J\sum(\hat{S}_{Co}\hat{S}_R + \hat{S}_{Co}\hat{S}_R)$$

where J represents the magnetic interaction between the Co^{II} ion and the coordinated tmpyim radical. The expression of the magnetic susceptibility is given below:

$$\chi_M = \frac{N\beta^2}{4kT}\frac{35g_1^2 + 10g_2^2\exp(-5x) + g_3^2\exp(-8x) + 10g_4^2\exp(-3x)}{3 + 2\exp(-5x) + \exp(-8x) + 2\exp(-3x)}$$

with $x = J/kT$, $g_1 = (3g_{Co} + 2g_R)/5$, $g_2 = (11g_{Co} + 4g_R)/15$, $g_3 = (5g_{Co} - 2g_R)/3$ and $g_4 = g_{Co}$.

The best fit (line in Figure 3) for the magnetic data (70−300 K) leads to $g_{Co} = 2.86$, $g_{rad} = 2.00$, $J = 7.62$ cm^{-1}, $R = 7.67 \times 10^{-5}$ (the residual value R is defined as $[(\chi_M)_{obsd} - (\chi_M)_{calcd.}]^2/[(\chi_M)_{obsd.}]^2$). The fitting results show that the exchange coupling between the Co^{II} ion and the tmpyim radical is weakly ferromagnetic. In complex **1**, the magnetic orbital of the tmpyim radical is a π* orbital and the spin density can delocalized on the pyridyl ring by spin polarization. The cobalt ion has two magnetic orbitals with σ symmetry ($d_{x^2-y^2}$, d_{z^2}),which are orthogonal to the magnetic orbital of the nitroxide, leading to a ferromagnetic interaction, and one magnetic orbital with π symmetry (either of d_{xy}, d_{xz}, d_{yz}) that will able to overlap with the magnetic orbital of the nitroxide, leading to antiferromagnetic coupling. The magnetic coupling constant J can be expressed as $J = 1/3(J_{x^2-y^2,\pi^*} + J_{z^2,\pi^*} + J_{xy,\pi^*})$.[22] The first two terms are ferromagnetic and are capable of overcoming the third antiferromagnetic term, leading to a ferromagnetic interaction being observed between the cobalt(II) ion and the tmpyim ligand. Since the nitroxide moiety has a large dihedral angle of 31.6° to the plane of the tmpyim pyridyl ring, which reduces the possibility of delocalizing the spin density of the NO group, the exchange coupling between the cobalt(II) ion and tmpyim is weak. The obtained g_{Co} value is considered to be acceptable in view of the corresponding value of other high-spin octahedral Co^{II} complexes.[23,24]

Experimental Section

General: Elemental analysis was carried out on a Perkin−Elmer elemental analyzer model 240. Infrared spectra were recorded on a Shimadzu IR spectrophotometer model 408, as KBr pellets. Variable temperature magnetic susceptibilities on polycrystalline samples in a gelatin capsule were measured on a Quantum Design MPMS-7 SQUID magnetometer.

Preparation of 1: An aqueous solution (10 mL) of dipotassium terephthalate (0.121 g, 0.5 mmol) was added to a solution of $[Co(ClO_4)_2]\cdot 6H_2O$ (0.183 g, 0.5 mmol) and tmpyim (0.234 g, 1 mmol) in H_2O (10 mL). The reaction mixture was then stirred for 1 h. Dark blue single crystals suitable for X-ray analysis were obtained by slow evaporation at room temperature after three weeks. $C_{32}H_{36}CoN_6O_8$ (691.60): calcd. C 55.57, H 5.25, N 12.15; found C 55.46, H 5.51, N 12.50. Important IR absorptions (KBr): $\tilde{\nu}$ = 1550 (s) cm^{-1}, 1400 (s) cm^{-1}, 1370 (br) cm^{-1}.

X-ray Crystallographic Analysis of 1: A dark blue crystal (0.30 × 0.25 × 0.20 mm) was selected and mounted on a glass fiber. All measurements were made on a Bruker Smart 1000 diffractometer equipped with graphite-monochromated Mo-K_α radiation (λ = 0.71073 Å). A total of 6654 reflections including 2897 independent reflections (R_{int} = 0.0559) were collected in the 2.13 < θ < 25.03° range at room temperature. A summary of the crystallographic data is given in Table 1. The absorption correction was performed empirically.[25] The structure was solved by direct methods using the SHELXS-97 program[26] and refined with SHELXL 97[27] by full-matrix least-squares methods on F^2. All non-hydrogen atoms were refined anisotropically, while the hydrogen atoms were located geometrically and refined isotropically.

CCDC-192270 contains the supplementary crystallographic data for this paper. These data can be obtained free of charge at www.ccdc.cam.ac.uk/conts/retrieving.html [or from the Cambridge Crystallographic Data Centre, 12, Union Road, Cambridge CB2 1EZ, UK; Fax: (internat.) +44-1223/336-033; E-mail: deposit@ccdc.cam.ac.uk].

Table 1. Crystallographic data for complex **1**

Empirical formula	$C_{32}H_{36}CoN_6O_8$
Molecular weight	691.60
Crystal system	Monoclinic
Space group	C_2/c
a [Å]	20.040(5)
b [Å]	7.119(2)
c [Å]	24.717(7)
β [°]	107.652(5)
V [Å^3]	3360.1(16)
Z	4
ρ (calcd.) [g/cm^3]	1.367
μ [mm^{-1}]	0.569
F(000)	1444
θ range [°]	2.13- 25.03
Limiting indices	$-23 \le h \le 23$, $-8 \le k \le 8$, $-13 \le l \le 29$
Reflections collected	6554
Independent reflections	2897 [R_{int} = 0.0559]
Observed reflections [$I > 2\sigma(I)$]	1802
Data/restraints/parameters	2897/ 0/214
Goodness-of-fit on F^2	0.977
Final R indices [$I > 2\sigma(I)$]	R_1 = 0.0556, wR_2 = 0.1300
R indices (all data)	R_1 = 0.1005, wR_2 = 0.1481
Largest diff. peak and hole[e·Å^{-3}]	0.564 and −0.366

Acknowledgments

This work was supported by the National Science Foundation of China (Nos. 20271029,20171025) and the UK Engineering and Physical Sciences Research Council S. S. T. thanks Prof. P. Day for access to the SQUID magnetometer.

[1] *Magneto-structural Correlations in Exchange Coupled Systems*, NATO ASI Series C140 (Eds.: R. D. Willet, D. Gatteschi, O. Kahn), D. Reidel, Dordrecht, The Netherlands, **1985**.
[2] O. Kahn, *Molecular Magnetism*, VCH, New York, **1993**.
[3] E. Coronado, P. Delhaès, D. Gatteschi, J. S. Miller, *Molecular Magnetism: From Molecular Assemblies to Devices*, Klumer Academic Publishers: Dordrecht, The Netherlands, **1996**.
[4] S. Subramanian, M. J. Zaworotko, *Angew. Chem.* **1995**, *107*, 2295−2297; *Angew. Chem. Int. Ed. Engl.* **1995**, *34*, 2127−2128.
[5] A. Caneschi, D. Gatteschi, P. Rey, *Prog. Inorg. Chem.* **1991**, *39*, 331−429.
[6] F. L. De Panthou, E. Belorizky, R. Calemczuk, D. Luneau, C. Marcenat, E. Ressouche, P. Turek, P. Rey, *J. Am. Chem. Soc.* **1995**, *117*, 11247−11253.
[7] K. Fegy, D. Luneau, E. Belorizky, M. Novac, J. L. Tholence, C. Paulsen, T. Ohm, P. Rey, *Inorg. Chem.* **1998**, *37*, 4524−4532.
[8] D. Luneau, F. M. Romero, R. Ziessel, *Inorg. Chem.* **1998**, *37*, 5078−5087.
[9] I. Dasna, S. Golhen, L. Ouahab, N. Daro, J.-P. Sutter, *Polyhedron* **2001**, *20*, 1371−1374.
[10] C. J. Lee, C. H. Huang, H. H. Wei, Y. H. Liu, G. H. Lee, Y. Wang, *J. Chem. Soc., Dalton Trans.* **1998**, 171−176.
[11] Y. Yamamoto, T. Suzuki, S. Kaizaki, *J. Chem. Soc., Dalton Trans.* **2001**, 1566−1572.
[12] L. Li, D. Liao, Z. Jiang, S. Yan, *J. Chem. Soc., Dalton Trans.* **2002**, 1350−1353.
[13] C. S. Hong, Y. Do, *Inorg. Chem.* **1997**, *36*, 5684−5685.
[14] R. H. Groeneman, L. R. MacGillivray, J. L. Atwood, *Inorg. Chem.* **1999**, *38*, 208−209.
[15] L. Deakin, A. M. Arif, J. S. Miller, *Inorg. Chem.* **1999**, *38*, 5072−5077.
[16] J. Cano, G. De Munno, J. L. Sanz, R. Ruiz, J. Faus, F. Lloret, M. Julve, A. Caneschi, *J. Chem. Soc., Dalton Trans.* **1997**, 1915−1923.
[17] A. Caneschi, F. Ferraro, D. Gatteschi, P. Rey, R. Sessoli, *Inorg. Chem.* **1990**, *29*, 1756−1760.
[18] A. Caneschi, D. Gatteschi, J. Laugier, P. Rey, R. Sessoli, *Inorg. Chem.* **1988**, *27*, 1553−1557.
[19] A. Caneschi, F. Ferraro, D. Gatteschi, P. Rey, R. Sessoli, *Inorg. Chem.* **1990**, *29*, 4217−4223.
[20] H. M. McConnell, *J. Chem. Phys.* **1963**, *39*, 1910.
[21] E. Sinn, *Coord. Chem. Rev.* **1970**, *5*, 313−347.
[22] O. Kahn, *Inorg. Chim. Acta* **1982**, *62*, 3−14.
[23] A. Bencini, C. Benelli, D. Gatteschi, C. Zanchini, *Inorg. Chem.* **1980**, *19*, 1301−1304.
[24] J. Zarembowitch, O. Kahn, *Inorg. Chem.* **1984**, *23*, 589−593.
[25] G. M. Sheldrick, *SADABS*, University of Göttingen, Göttingen, Germany, 1996.
[26] G. M. Sheldrick, *SHELXS-97, Program for the Solution of Crystal Structure*, University of Göttingen, Göttingen, Germany, 1997.
[27] G. M. Sheldrick, *SHELXL-97, Program for the Refinement of Crystal Structure*, University of Göttingen, Göttingen, Germany, 1997.

Received August 27, 2002
[I02481]

Symmetric Tetraalkynyldisilanes

Carsten Ackerhans,[a] Herbert W. Roesky,*[a] Denis Vidovic,[a] and Jörg Magull[a]

Dedicated to Professor M. F. Hawthorne on the occasion of his 75th birthday

Keywords: Alkynes / Bulky ligands / Silanes / Silicon

The reaction of the tetrachlorodisilane $R_2Si_2Cl_4$ (**1**) [R = $CH(SiMe_3)_2$] with the lithium salt R*C≡CLi of the parent alkyne results in the replacement of the chlorine atoms with alkynyl groups to yield the product $R_2Si_2(C{\equiv}CR^*)_4$ [R* = Ph (**2**), *t*Bu (**3**), $SiMe_3$ (**4**), *n*-C_3H_7 (**5**)]. Compounds **2** and **3** were characterized by X-ray structural analysis.
(© Wiley-VCH Verlag GmbH & Co. KGaA, 69451 Weinheim, Germany, 2003)

Introduction

In recent years many alkynylsilicon compounds have been synthesised[1] where the number of alkynyl groups attached to the central silicon atom varies from one to four (Scheme 1: **A**). Some of these products have been isolated.[2,3] Moreover, in a few compounds the alkynyl group acts as a linker between silicon and carbon atoms or two silicon atoms, respectively, forming chains[4,5] or heterocycles.[6,11] In Scheme 1 two examples of heterocycles containing alkynyl groups are shown. In compound **B** silicon and carbon atoms and in **C** two silicon atoms are linked together. However, to the best of our knowledge, a disilane carrying four alkynyl groups has not been reported previously.

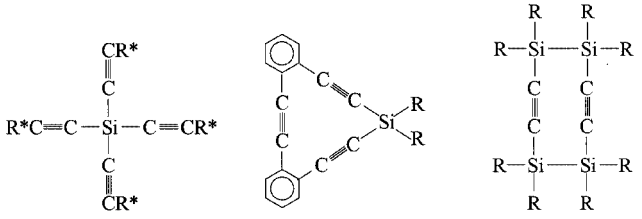

Scheme 1

Recently we have reported the reaction of the tetraaminodisilane $R_2Si_2(NH_2)_4$ [R = $CH(SiMe_3)_2$] with HBr and HI, with elimination of ammonia and formation of the halodisilanes $R_2Si_2X_4$ (X = Br, I).[12] A similar reaction using alkynes did not succeed as their acidity is lower than both HBr and HI. As an alternative approach we used the lithium salts R*C≡CLi [R* = Ph (**2**), *t*Bu (**3**), $SiMe_3$ (**4**), *n*-C_3H_7 (**5**); Scheme 2] as a starting material for the reaction with the tetrachlorodisilane $R_2Si_2Cl_4$ (**1**) [R = $CH(SiMe_3)_2$] with elimination of LiCl.

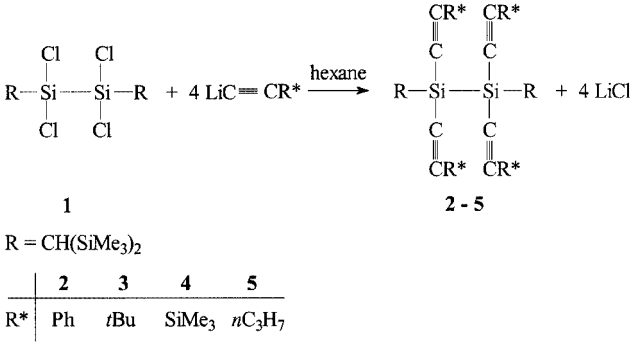

	2	3	4	5
R*	Ph	*t*Bu	$SiMe_3$	nC_3H_7

Scheme 2

Results and Discussion

Synthesis and Spectra

Lithiation of R*C≡CH was accomplished with a solution of butyllithium in hexane at −78 °C. The tetrachlorodisilane was then added at the same temperature. The reaction mixture was slowly warmed to room temperature, the LiCl separated by filtration and finally the solvent removed under vacuum to yield compounds **2**−**5**. The products **2**−**4** were obtained as colourless solids whereas **5** was isolated as a colourless oil. Single crystals of **2** and **3** suitable for X-ray crystallographic measurements were isolated from hexane solutions.

[a] Institut für Anorganische Chemie der Universität Göttingen, Tammannstraße 4, 37077 Göttingen, Germany
Fax: (internat.) + 49-(0)551/393-373
E-mail: hroesky@gwdg.de

In the mass spectra compounds **2**−**5** were identified by their molecular ion peaks [M^+] at m/z = 778 (**2**), 698 (**3**), 762 (**4**), and 642 (**5**); in the IR spectra the absorptions for the C≡C vibrations are in the range between 2100 and 2200 cm^{-1}.

The ^1H NMR spectra of **2**−**5** show resonances for the protons of the methyl groups of the bis(trimethylsilyl)methyl ligands in the range δ = 0.49 to 0.59 ppm, whereas the resonances of the corresponding CH groups are in the range between δ = 0.21 and 0.53 ppm. Additionally, the resonances of the substituents of the alkynyl groups are found in each spectrum. For compound **2** the aromatic protons are found as two multiplets, one at δ = 6.87 to 6.91 ppm (*m*-, *p*-Ph) and the other at δ = 7.47 to 7.52 ppm (*o*-Ph). The protons of the *t*Bu groups of **3** appear as a singlet at δ = 1.17 ppm and the trimethylsilyl protons resonate in the spectrum of **4** at δ = 0.13 ppm. The spectrum of **5** exhibits three multiplets for the aliphatic protons [δ = 0.83 (CH_2-CH_3), 1.38 (CH_2-CH_3), and 1.99 ppm (C≡C-CH_2)].

In the ^{13}C NMR spectra of **2**−**5** the resonances of the CH_3 groups of the ligands are in the range between δ = 3.3 and 3.5 ppm and those for the CH groups between δ = −0.3 and 0.4 ppm. The triple-bonded carbon atoms of the inner atoms with respect to the silicon atom exhibit resonances between δ = 110.6 and 120.2 ppm, while for the outer atoms they are observed between δ = 80.9 and 110.9 ppm. The resonances of the acetylenic substituents are found in the expected range.

The trimethylsilyl groups resonate in the ^{29}Si NMR spectra between δ = 0.8 and 1.2 ppm and the silicon atoms of the central disilane unit resonate between δ = −54.2 and −56.5 ppm.

X-ray Structural Analysis

The single-crystal structural analysis of compounds **2** (Figure 1) and **3** (Figure 2) shows that the central disilane unit is connected to four alkynyl groups in an anticlinic conformation. The coordination sphere of the silicon atoms is completed in each case by a bis(trimethylsilyl)methyl group.

The disilane **2** crystallises in the orthorhombic space group $Pna2_1$ and **3** in the monoclinic space group $C2/c$. The unit cell of **3** contains eight molecules of the disilane and an additional two molecules of cyclohexane and two more of *n*-hexane.

The Si−Si bond length in both compounds is essentially identical [2.378(1) Å (**2**) and 2.373(1) Å (**3**)] and is only slightly shorter than that in the chloro compound **1** [2.380(2) Å].[12]

The bond length between the central silicon atoms and the acetylenic carbon atoms averages to 1.833 Å for **2** and 1.832 Å for **3** and is similar to the corresponding bond length in $Si(C_2SiMe_3)_4$ (1.825 Å).[2] The C−Si−C angle at the silicon atom averages to 106.73° (**2**) and 107.75° (**3**). Selected bond lengths and angles for **2** and **3** are listed in Table 1.

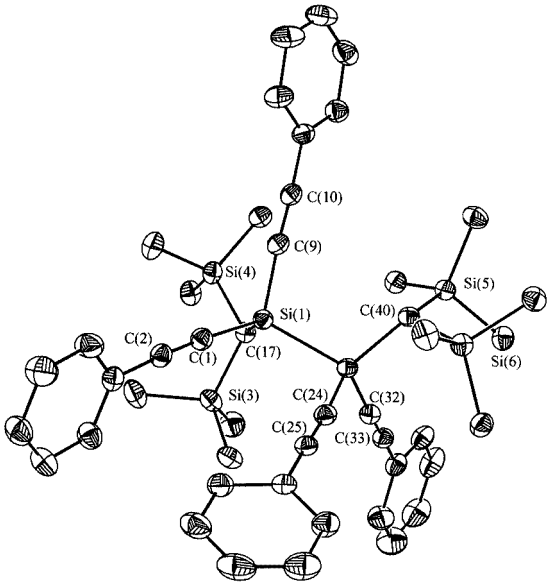

Figure 1. Molecular structure of **2** in the crystal (50% probability thermal ellipsoids)

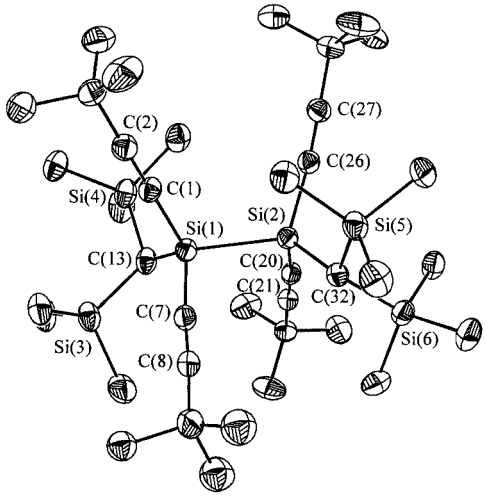

Figure 2. Molecular structure of **3** in the crystal (50% probability thermal ellipsoids)

Table 1. Selected bond lengths [Å] and angles [°] for **2** and **3**

Compound	**2**	**3**
Si(1)−Si(2)	2.378(1)	2.373(1)
Si(1)−C(1)	1.837(3)	1.827(3)
C(1)−C(2)	1.212(4)	1.200(4)
Si(1)−C(17/13)	1.863(2)	1.879(3)
C(1)−Si(1)−Si(2)	109.48(8)	114.80(9)
C(1)−Si(1)−C(9/7)	105.62(12)	106.24(13)
C(1)−Si(1)−C(17/13)	110.41(12)	109.18(13)

Conclusion

This work shows that alkynes are slim enough to allow fourfold substitution on a disilane sterically hindered by

two bis(trimethylsilyl)methyl groups. The easiest way to synthesise this class of compounds is using the lithium salt of the corresponding alkyne and the tetrachlorodisilane. The products are useful precursors for heterocyclic and polymeric silicon-containing materials after manipulation of the alkyne groups.

Experimental Section

General Remarks: All reactions were performed under dry nitrogen using standard Schlenk and syringe techniques. The solvents were dried according to literature methods[13] and freshly distilled and saturated with nitrogen prior to use. Melting points were measured on a Büchi B-540 melting point apparatus. IR spectra were recorded using a BIO-RAD Digilab FTS 7 spectrophotometer. Mass spectra (MS) were obtained on a Finnigan MAT 95 or a Finnigan MAT 8200 spectrometer using the EI technique. NMR spectra were recorded on a Bruker AC 250 or a Bruker Avance 500 spectrometer; chemical shifts are quoted relative to external $SiMe_4$. Elemental analyses were performed by the Analytical Laboratory of the Institute of Inorganic Chemistry at the University of Göttingen.

General Procedure: A solution of butyllithium (40 mmol) in *n*-hexane (25 mL, 1.6 M) was added dropwise to a solution of the alkyne (40 mmol) in hexane (100 mL) at −78 °C. Subsequently **1** (5.2 g, 10 mmol) dissolved in *n*-hexane (50 mL) was added over a period of 30 min and the mixture was allowed to warm to room temperature overnight. The precipitate was removed from the solution by filtration and the volume of solvent was reduced to 20 mL under vacuum. Products **2**−**4** were obtained as colourless solids and **5** was obtained as a colourless oil after complete removal of the solvent.

1,2-Bis[bis(trimethylsilyl)methyl]tetra(phenylethynyl)disilane (2): Yield: 6.1 g (7.8 mmol, 78%). M.p. 110 °C. ^{1}H NMR (C_6D_6): δ = 0.53 [s, 2 H, C*H*($SiMe_3$)$_2$], 0.59 [s, 36 H, Si(C*H*$_3$)$_3$], 6.87−6.91 (m, 12 H, *o*-, *p*-Ph-*H*), 7.47−7.52 (m, 8 H, *m*-Ph-*H*) ppm. ^{13}C NMR (C_6D_6): δ = 0.4 [*C*H($SiMe_3$)$_2$], 3.4 [Si(*C*H$_3$)$_3$], 92.5 (Si-C≡*C*-Ph), 110.6 (Si-*C*≡C), 123.6, 128.5, 128.9, 132.0 (arom.-*C*) ppm. ^{29}Si NMR (C_6D_6): δ = −54.2 (*Si*-C≡C-Ph), 1.4 (*Si*Me_3) ppm. IR (KBr): ṽ = 2156, 1950, 1879, 1595, 1488, 1304, 1261, 1249, 1017, 916, 844, 755, 723, 689, 538 cm^{-1}. MS (EI): *m*/*z* (%) = 778 (28) [M$^+$], 736 (13) [M$^+$ − Me], 375 (100) [1/2M$^+$ − Me]. $C_{46}H_{58}Si_6$ (779.48): calcd. C 70.9, H 7.5, Si 21.6; found C 68.1, H 7.5, Si 20.6.[14]

1,2-Bis[bis(trimethylsilyl)methyl]tetra(*tert*-butylethynyl)disilane (3): Yield: 5.0 g (7.2 mmol, 72%). M.p. 265 °C. ^{1}H NMR (C_6D_6): δ = 0.41 [s, 2 H, C*H*($SiMe_3$)$_2$], 0.52 [s, 36 H, Si(C*H*$_3$)$_3$], 1.17 [s, 36 H, C(C*H*$_3$)$_3$] ppm. ^{13}C NMR (C_6D_6): δ = 0.1 [*C*H($SiMe_3$)$_2$], 3.4 [Si(*C*H$_3$)$_3$], 28.2 [*C*(CH$_3$)$_3$], 30.3 [C(*C*H$_3$)$_3$], 80.6 (Si-C≡*C*-*t*Bu), 119.2 (Si-*C*≡C-*t*Bu) ppm. ^{29}Si NMR (C_6D_6): δ = −57.4 (*Si*-C≡C), 0.8 (*Si*Me_3) ppm. IR (KBr): ṽ = 2196, 2154, 1301, 1253, 1202, 1096, 1018, 940, 842, 796, 773, 727, 679, 535, 418 cm^{-1}. MS (EI): *m*/*z* (%) = 698 (11) [M$^+$], 641 (21) [M$^+$ − *t*Bu], 349 (100) [1/2M$^+$]. $C_{38}H_{74}Si_6$ (699.52): calcd. C 65.2, H 10.7, Si 24.1; found C 63.2, H 10.6, Si 23.7.[14]

1,2-Bis[bis(trimethylsilyl)methyl]tetrakis(trimethylsilylethynyl)-disilane (4): Yield: 5.8 g (7.6 mmol, 76%). M.p. 245 °C. ^{1}H NMR (C_6D_6): δ = 0.13 [s, 36 H, C≡CSi(C*H*$_3$)$_3$], 0.47 [s, 2 H, C*H*($SiMe_3$)$_2$], 0.52 [s, 36 H, CH(Si*Me*$_3$)$_2$] ppm. ^{13}C NMR (C_6D_6): δ = −0.5 [C≡C-Si(*C*H$_3$)$_3$] 0.2 [*C*H($SiMe_3$)$_2$], 3.5 [CH(Si*Me*$_3$)$_2$],

Table 2. X-ray structure analysis data for **2** and **3**

Compound	**2**	**3**
Formula	$C_{46}H_{58}Si_6$	$C_{38}H_{74}Si_6$·1/4C_6H_{12}·1/4C_6H_{14}
Molecular weight	779.46	720.80
Crystal system	orthorhombic	monoclinic
Space group	*Pna*2 (1)	*C* 2/*c*
Unit cell	*a* = 19.186(4) Å	*a* = 20.9598(12) Å
	b = 12.175(2) Å	*b* = 12.2564(8) Å
	c = 41.181(8) Å	*c* = 40.590(2) Å
	α = 90°	α = 90°
	β = 90°	β = 101.220(4)°
	γ = 90°	γ = 90°
Volume	9620(3) Å^3	10228.0(10) Å^3
Z	4	8
Density	0.538 g/cm^3	0.936 g/cm^3
Absorption coefficient	0.101 mm^{-1}	0.185 mm^{-1}
F(000)	1672	3186
Index range	−21 ≤ *h* ≤ 21	−22 ≤ *h* ≤ 22
	−13 ≤ *k* ≤ 13	−13 ≤ *k* ≤ 13
	−47 ≤ *l* ≤ 46	−43 ≤ *l* ≤ 43
Reflections collected	55676	80576
Independent reflections	15026 [R_{int} = 0.0556]	6680 [R_{int} = 0.0999]
Data/restr./param.	15026/1/932	6680/4/447
Data collection range	1.74 ≤ Θ ≤ 24.06°.	1.93 ≤ Θ ≤ 22.50°.
Final *R* indices [$I > 2\sigma(I)$][a]	*R*1 = 0.0370	*R*1 = 0.0490
	*wR*2 = 0.1025	*wR*2 = 0.1566
Final *R* indices (all data)	*R*1 = 0.0386	*R*1 = 0.0566
	*wR*2 = 0.1033	*wR*2 = 0.1612
Goodness-of-fit on F^2[b]	1.088	1.092
Largest diff. peak and hole	0.258 and −0.243 e·Å^{-3}	0.603 and −0.294 e·Å^{-3}

[a] $R1 = \Sigma|F_o - F_c|/\Sigma|F_o|$; $wR2 = [\Sigma w(F_o^2 - F_c^2)^2/\Sigma wF_o^4]^{1/2}$. [b] Goodness of fit $S = [\Sigma w(F_o^2 - F_c^2)^2/\Sigma$ (n-p)]$^{1/2}$).

110.9 (Si-C≡C-SiMe$_3$), 120.2 (Si-C≡C-SiMe$_3$) ppm ^{29}Si NMR (C_6D_6): δ = −58.3 (*Si*-Si-C≡C), −18.7 (C≡C-*Si*Me$_3$), 1.2 [CH(*Si*Me$_3$)$_2$] ppm. IR (KBr): ṽ = 2108, 1948, 1875, 1303, 1262, 1251, 1155, 1022, 845, 779, 760, 722, 679, 539, 429 cm^{-1}. MS (EI): *m*/*z* (%) = 762 (24) [M$^+$], 789 (19) [M$^+$ − SiMe$_3$], 381 (100) [1/2 M$^+$]. $C_{34}H_{74}Si_{10}$ (763.81): calcd. C 53.5, H 9.8, Si 36.8; found C 53.5, H 9.8, Si 35.1.

1,2-Bis[bis(trimethylsilyl)methyl]tetra(1-pentynyl)disilane (5): Yield: 4.0 g (6.2 mmol, 62%). ^{1}H NMR (C_6D_6): δ = 0.21 [s, 2 H, C*H*(SiMe$_3$)$_2$], 0.49 [s, 36 H, Si(C*H*$_3$)$_3$], 0.83 (m, C$_4$H$_4$-C*H*$_3$, 12 H), 1.38 (m, C*H*$_2$CH$_3$, 8 H), 1.99 (m, C≡C-C*H*$_2$, 8 H) ppm. ^{13}C NMR (C_6D_6): δ = −0.3 [*C*H(SiMe$_3$)$_2$], 3.3 [Si(*C*H$_3$)$_3$], 13.7, 22.0, 22.4, (*C*$_3$H$_7$), 83.2 (Si-C≡*C*-C$_3$H$_7$), 112.5 (Si-*C*≡C-C$_3$H$_7$) ppm. ^{29}Si NMR (C_6D_6): δ = −56.5 (*Si*-C≡C-C$_3$H$_7$), 1.0 (*Si*Me$_3$) ppm. IR (KBr): ṽ = 2167, 2138, 1932, 1861, 1465, 1427, 1382, 1338, 1324, 1263, 1248, 1079, 1062, 1020, 980, 840, 797, 770, 726, 680, 646, 599, 579, 539, 501, 413 cm^{-1}. MS (EI): *m*/*z* (%) = 642 (5) [M$^+$], 627 (4) [M$^+$ − Me], 321 (100) [1/2 M$^+$]. $C_{34}H_{66}Si_6$ (643.41): calcd. C 63.5, H 10.3, Si 26.2; found C 62.1, H 10.1, Si 24.8.[14]

X-ray Crystallographic Study of 2 and 3

The crystals were mounted on glass fibre in rapidly cooled mineral oil. Diffraction data (see also Table 2) were collected on a Stoe IPDS II diffractometer at 133(2) K, with graphite-monochromated Mo-K_α radiation (λ = 0.71073 Å), using the ω-scan technique. The structures were solved by direct methods using SHELXS-97[15] and refined against F^2 on all data by full-matrix least-squares with SHELXL-97.[16] All non-hydrogen atoms were refined anisotropically. All hydrogen atoms were included in the model at geometrically calculated positions and refined using a riding model. CCDC-191736 (**2**) and CCDC-191737 (**3**) contain the supplementary crystallographic data for this paper. These data can be obtained free of charge at www.ccdc.cam.ac.uk/conts/retrieving.html [or from the Cambridge Crystallographic Data Centre, 12, Union Road, Cambridge CB2 1EZ, UK; fax: (internat.) +44-1223/336-033; E-mail: deposit@ccdc.cam.ac.uk].

Acknowledgments

This work was financially supported by the Deutsche Forschungsgemeinschaft and the Göttinger Akademie der Wissenschaften.

[1] L. Brandsma, *Preparative Acetylenic Chemistry*, 2nd Ed., Elsevier, Amsterdam **1992**.
[2] H. Schmidbaur, J. Ebenhöch, G. Müller, *Z. Naturforsch., Teil B* **1988**, *43*, 49−52.
[3] T. Matsuo, K. Uchida, A. Sekiguchi, *Chem. Commun.* **1999**, 1799−1800.
[4] E. Hengge, A. Baumegger, M. Eibl, E. Hohenester, C. Kratky, *Angew. Chem.* **1990**, *102*, 722−724; *Angew. Chem. Int. Ed. Engl.* **1990**, *29*, 641−643.
[5] F. Carré, S. G. Dutremez, C. Guérin, B. J. L. Henner, A. Jolivet, V. Tomberli, F. Dahan, *Organometallics* **1999**, *18*, 770−781.
[6] H. Sakurai, Y. Nakadaira, A. Hosomi, Y. Eriyama, C. Kabuto, *J. Am. Chem. Soc.* **1983**, *105*, 3359−3360.
[7] M. Voronkov, O. Yarosh, G. Turkina, V. Vitkovskii, A. Albanov, *J. Organomet. Chem.* **1990**, *389*, 1−22.
[8] M. Ishikawa, T. Hatano, Y. Hasegawa, T. Horio, A. Kunai, A. Miyai, T. Ishida, T. Tsukihara, T. Yamanaka, T. Koike, J. Shioya, *Organometallics* **1992**, *11*, 1604−1618.
[9] L. Guo, J. D. Bradshaw, C. A. Tessier, W. J. Youngs, *Organometallics* **1995**, *14*, 586−588.
[10] G. Haberhauer, R. Gleiter, H. Irngartinger, T. Oeser, F. Rominger, *J. Chem. Soc., Perkin Trans. 2* **1999**, 2093−2097.
[11] M. Unno, T. Saito, H. Matsumoto, *Chem. Lett.* **1999**, 1235−1236.
[12] C. Ackerhans, P. Böttcher, P. Müller, H. W. Roesky, I. Usón, H.-G. Schmidt, M. Noltemeyer, *Inorg. Chem.* **2001**, *40*, 3766−3773.
[13] Autorenkollektiv, *Organikum*, 19. Aufl., Deutscher Verlag der Wissenschaften, Berlin **1993**.
[14] The formation of SiC during the elemental analysis of **2, 3** and **5** is the reason for the differences of the calcd. and found data for C and Si.
[15] G. M. Sheldrick, *Acta Crystallogr., Sect. A* **1990**, *46*, 467−473.
[16] G. M. Sheldrick, SHELX 97, Universität Göttingen, **1997**.

Received August 16, 2002
[I02465]

Chelation versus Cyclometalation in a Cationic Dppn−Rh^{I} Complex − A Unique Rearrangement of Norbornadiene via C−H Activation of the Pyridazine Ring

Reto Dorta,[a] Leonid Konstantinovski,[a] Linda J. W. Shimon,[b] Yehoshoa Ben-David,[a] and David Milstein*[a]

Keywords: Rhodium complexes / Mono- and dinuclear complexes / C−H activation / Rearrangement of norbornadiene / ^{1}H-^{15}N GHMBC NMR / X-ray structure

The tetradentate ligand 3,6-bis(2-pyridyl)pyridazine (dppn) was treated with cationic Rh^{I} precursors. The mononuclear complexes [Rh(dppn)(NBD)]BF_4 (**1**) and [Rh(dppn)(COD)]BF_4 (**5**) were obtained in quantitative yield when treating dppn with [Rh(NBD)$_2$]BF_4 or [Rh(COD)$_2$]BF_4 respectively. Treatment of **1** with a second equivalent of the metal precursor [Rh(NBD)(CH$_3$CN)$_2$]BF_4 led to the dinuclear complex [Rh$_2$(dppn-H)(NBD)(η^1-C$_7$H$_9$)(CH$_3$CN)$_2$](BF_4)$_2$ (**2**) [dppn-H = μ-C$_4$HN$_2$(C$_5$H$_4$N)$_2$-3,6], a mixed Rh^{I}–Rh^{III} complex. This complex arises from C–H activation of the pyridazine ring, followed by a unique rearrangement of the NBD ligand. Compound **2** was also obtained directly by treating dppn with 2 equiv. of [Rh(NBD)(CH$_3$CN)$_2$]BF_4. The complex [Rh$_2$(dppn-H)(NBD)(η^1-C$_7$H$_9$)(CH$_3$OH)$_2$(CH$_3$CN)](BF_4)$_2$ (**4**) was obtained by dissolving **2** in methanol. Full characterization of compounds **1**, **4** and **5** included an investigation by ^{1}H-^{15}N GHMBC NMR spectroscopy and single-crystal X-ray structures of **1** and **4**.
(© Wiley-VCH Verlag GmbH, 69451 Weinheim, Germany, 2003)

Introduction

Late transition metal systems with chelating nitrogen ligands are the subject of intense recent research due to their catalytic potential in processes such as the polymerization of olefins,[1] the selective C−H bond activation,[2] and the catalysis by monolayers.[3] The ease of C−H activation, when such ligands are employed, might depend on their inherently electron-rich nature. In particular, it has been shown that *ortho*-metalation of aromatic *N*-donor ligands by d^8-M^{I} complexes is strongly dependent on the basic properties of the metal precursor.[4] In addition, dinucleating ligands that can form homo- or heterodinuclear transition metal complexes with well-defined geometries are of considerable interest, considering the rapidly evolving area of dimetallic catalysts,[5] and supramolecular chemistry.[6] We thus decided to investigate the coordination chemistry of the tetradentate ligand 3,6-bis(2-pyridyl)pyridazine (dppn) towards cationic Rh^{I} precursors, especially in view of the fact that surprisingly little is known about its coordination behaviour and its reactivity with d^8-M^{I} metal precursors.[7]

In this paper we report the unexpected reactivity of this ligand towards cationic diene−Rh^{I} precursors (diene = norbornadiene and cyclooctadiene) giving rise to mono- and dinuclear complexes. Surprisingly, the dinuclear complex consists of an Rh^{I}−Rh^{III} complex arising from C−H activation of the pyridazine ligand, followed by a unique rearrangement of the norbornadiene ligand, rather than the expected *N*,*N*-coordinated bis(Rh^{I}) complexes. Full characterization of the resulting compounds included an investigation by ^{1}H-^{15}N GHMBC NMR spectroscopy and the single-crystal X-ray structures of two of them.

Results and Discussion

The ligand 3,6-bis(2-pyridyl)pyridazine (dppn) was synthesized in two steps in 45% overall yield. Lithiation of 2-bromopyridine with BuLi and subsequent reaction of the lithiated adduct with trimethyltin chloride yielded (2-pyridyl)trimethyltin in quantitative yield.[8] The second step consisted of a double Stille-type coupling between the organotin compound and 3,6-dichloropyridazine which was performed using Pd^0 or Pd^{II} catalyst precursors. The highest yield (45%) was obtained with 1 mol % of $PdCl(PPh_3)_2(CH_2Ph)$ as the catalyst.[9]

Upon addition of 1 equiv. of dppn to a stirred CH_2Cl_2 solution of [Rh(NBD)$_2$]BF_4 or [Rh(NBD)(CH$_3$CN)$_2$]BF_4, precipitation of a dark red solid took place within 30 min.

[a] Department of Organic Chemistry, The Weizmann Institute of Science,
76100 Rehovot, Israel
E-mail: david.milstein@weizmann.ac.il
[b] Department of Chemical Services, The Weizmann Institute of Science,
76100 Rehovot, Israel

This compound was characterized as [Rh(dppn)(NBD)]BF_4 (**1**) (Scheme 1) using various NMR techniques. As expected, the ligand dppn gave rise to ten distinct signals in the ^{1}H NMR spectrum. Except for the routine NMR methods used for such organometallic compounds, we also performed a ^{1}H-^{15}N GHMBC experiment, a technique used for the characterization of bioorganic molecules,[10] but which has very rarely been applied to transition metal complexes.[11] The resulting spectrum clearly showed the four signals of the nitrogen atoms of dppn (Figure 1). The correlation provided their ^2J and ^3J couplings to the neighboring hydrogen atoms. Very clear shifts in the nitrogen spectrum were seen for N(1), N(17) and N(18) (for atom numbering see Scheme 2) and are given in Table 1. The noncoordinated pyridine moiety [N(7)] showed essentially the same shift as seen in the free ligand.[12] Furthermore, the two nitrogen atoms coordinated to the rhodium metal gave rise to coupling constants of $J_{N\text{-}Rh}$ = 20−30 Hz.

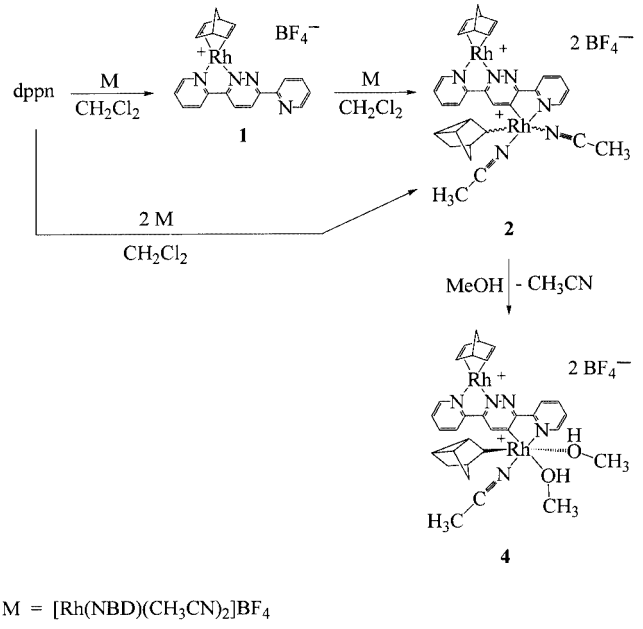

Scheme 1. Synthetic route to complexes **1**, **2** and **4**

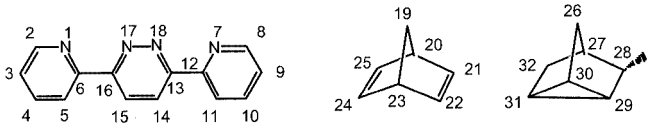

Scheme 2. Numbering scheme used for the characterization of the compounds

Crystals of **1** suitable for an X-ray crystallographic analysis were grown by diffusion of diethyl ether into a concentrated solution of **1** in methanol and confirmed the structure. The crystal consists of discrete [Rh(dppn)(NBD)]$^+$ cations, BF_4^- counterions and methanol solvent molecules. An ORTEP view of the cationic complex with the atomic numbering scheme, together with selected bond lengths and angles, is shown in Figure 2. The Rh atom is in a square-

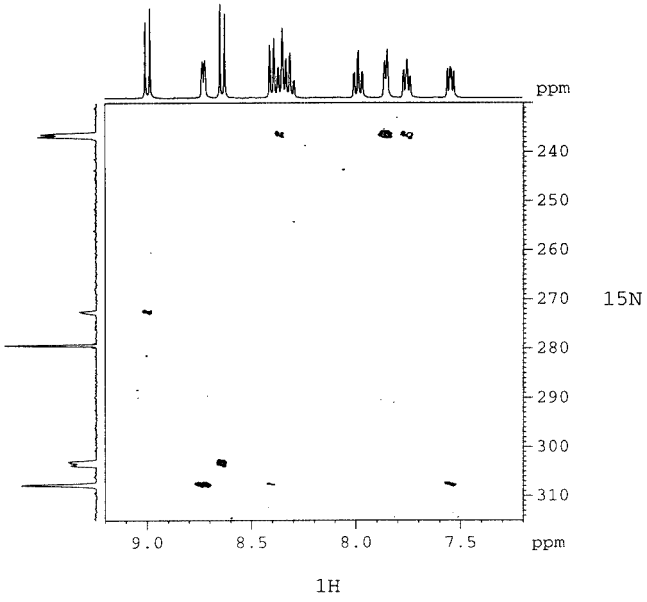

Figure 1. ^{1}H-^{15}N GHMBC NMR in CD_3NO_2 of complex **1**

planar arrangement with the two *cis*-nitrogen atoms of the dppn molecule acting as a bidentate chelating ligand through two neighboring pyridyl and pyridazinyl nitrogen atoms. As in complex **4** (see below), the N−Rh distance of the pyridazinyl is slightly shorter than the corresponding pyridyl N−Rh distance and concomitantly the Rh−olefin bond *trans* to it somewhat longer. The noncoordinating N atoms are mutually *trans* to each other with respect to the C(9)−C(10) (for atom numbering see Figure 2) axis, as previously observed in other crystallographically characterized mononuclear complexes of dppn.[7,13]

Treatment of **1** with a second equivalent of [Rh(NBD)-$(CH_3CN)_2$]BF_4 in CH_2Cl_2 led to the slow formation of a pink precipitate. The product was tentatively identified as the complex [Rh_2(dppn-H)(NBD)(η^1-C_7H_9)$(CH_3CN)_2$]-$(BF_4)_2$ (**2**) (Scheme 1) [dppn-H = μ-$C_4HN_2(C_5H_4N)_2$-3,6]. Characterization of **2** by NMR spectroscopy was hampered by its low solubility in noncoordinating, polar solvents. Despite this, the ^{1}H NMR spectrum in CD_2Cl_2 clearly showed that the dppn ligand was orthometalated on the pyridazine ring giving rise to only nine proton signals. Furthermore, two resonances at δ = 2.34 and 2.64 ppm were attributed to the two acetonitrile molecules bound to the Rh^{III} metal center.[14] The formulation of **2** was also supported by elemental analysis. When **2** was dissolved in the weakly coordinating solvent methanol, dissociation of one of the acetonitrile ligands (peak at δ = 2.34 ppm) was observed, leading most probably to a highly labile 14e-Rh^{III} complex. Slow addition of diethyl ether to a concentrated solution of **2** in methanol gave **4** as a deep red solid. Characterization of **4** by ^{1}H NMR in [D_4]methanol showed that indeed, both of the methanol molecules are highly labile and exchange rapidly with the deuterated solvent. The structure of the compound was elucidated by using various NMR techniques to assign all the protons and carbon atoms. Especially for complex **4**, the ^{1}H-^{15}N GHMBC

Table 1. Results of the ^{1}H-^{15}N GHMBC NMR experiment of dppn, **1**, **4** and **5** (for atom numbering see Scheme 2)

[a]	dppn[b]	**1**[c]	**4**[d]	**5**[c]
N(1)	306.9; ^{2}J with 2-H, ^{3}J with 3-H and 5-H	236.5; ^{2}J with 2-H, ^{3}J with 3-H and 5-H, $J^{N\text{-}Rh}$ = 19.7 Hz	238.3; ^{2}J with 2-H, ^{3}J with 3-H and 5-H, $J_{N\text{-}Rh}$ = 24.7 Hz	235.1; ^{2}J with 2-H, ^{3}J with 3-H and 5-H, $J_{N\text{-}Rh}$ = 26.0 Hz
N(7)	306.9; ^{2}J with 8-H, ^{3}J with 9-H and 11-H	307.6; ^{2}J with 8-H, ^{3}J with 9-H and 11-H	234.5; ^{2}J with 8-H, ^{3}J with 9-H and 11-H, $J_{N\text{-}Rh}$ = 42.4 Hz	307.7; ^{2}J with 8-H, ^{3}J with 9-H and 11-H
N(17)	388.0; ^{3}J with 15-H	303.2; ^{3}J with 15-H, $J_{N\text{-}Rh}$ = 24.1 Hz	283.2; ^{3}J with 15-H, $J_{N\text{-}Rh}$ = 40.2 Hz	300.2; ^{3}J with 15-H, $J_{N\text{-}Rh}$ = 20.5 Hz
N(18)	388.0; ^{3}J with 14-H	272.4; ^{3}J with 14-H		271.1; ^{3}J with 14-H
others			174.1; CH_3CN; ^{3}J with CH_3, $^{2}J_{N\text{-}Rh}$ = 45.9 Hz	

[a] Chemical shifts in ppm (referenced to liquid ammonia). [b] In $CDCl_3$. [c] In CD_3NO_2. [d] In CD_3OD.

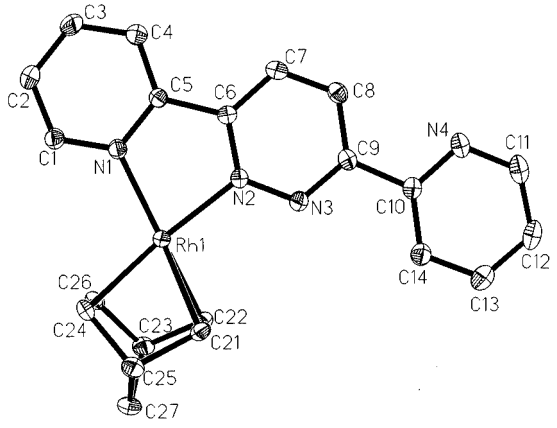

Figure 2. ORTEP drawing of a molecule of **1** (50% of probability); BF_4^-, solvent molecules and hydrogen atoms are omitted for clarity; selected bond lengths [A] and angles [°]: Rh(1)−N(1) 2.077(2), Rh(1)−N(2) 2.049(2), Rh(1)−C(21) 2.127(2), Rh(1)−C(22) 2.120(2), Rh(1)−C(24) 2.155(2), Rh(1)−C(26) 2.145(2); N(2)−Rh(1)−N(1) 78.91(8), N(2)−Rh(1)−C(22) 101.87(9), N(1)−Rh(1)−C(22) 156.99(9), N(2)−Rh(1)−C(21) 102.65(9), N(1)−Rh(1)−C(21) 164.63(9), C(22)−Rh(1)−C(21) 38.19(10), N(2)−Rh(1)−C(26) 159.45(9), N(1)−Rh(1)−C(26) 103.89(9), C(22)−Rh(1)−C(26) 67.52(10), C(21)−Rh(1)−C(26) 80.11(10), N(2)−Rh(1)−C(24) 161.69(9), N(1)−Rh(1)−C(24) 106.56(9), C(22)−Rh(1)−C(24) 80.01(10), C(21)−Rh(1)−C(24) 67.42(10), C(26)−Rh(1)−C(24) 37.53(10)

NMR experiment proved to be extremely informative (Table 1). As expected, the signal of one of the nitrogen atoms [N(18)] of the pyridazyl unit is not seen due to the lack of ^{2}J and ^{3}J coupling with any hydrogen atoms. In **4**, both pyridyl moieties are bound to the metal atom and show significant shifts of the signals of the nitrogen atoms [N(1) and N(7)] compared to those of the free ligand dppn. In addition, both nitrogen atoms [N(1) and N(7)] gave rise to coupling constants with the corresponding rhodium centers ($J_{N\text{-}Rh}$ = 24.7 and 42.4 Hz, respectively) as well as the coordinated pyridazyl nitrogen atom ($J_{N\text{-}Rh}$ = 40.2 Hz).[15] To unambiguously ascertain the exact structure of **4**, crystals suitable for X-ray crystallography were grown by slow diffusion of diethyl ether into a concentrated methanol/CH_2Cl_2 solution containing **4**. The ORTEP representation along with selected bond lengths and angles is shown in Figure 3. In complex **4**, the deprotonated ligand acts as a quadridentate ligand chelating the two metal atoms on opposite sides, one through one pyridyl and one pyridazinyl nitrogen atom, the other through one pyridyl nitrogen and one pyridazinyl carbon atom. The two metal centers differ in their geometry and their oxidation state, one being a square-planar Rh^{I} and the other an octahedral Rh^{III}. The part of the ligand with the square-planar metal atom shows nearly identical bond lengths and angles as seen in complex **1**. The octahedral metal atom is surrounded by the chelating C,N fragment of dppn, the 3-nortricyclyl unit, one acetonitrile and two methanol molecules. To the best of our knowledge, there are only two previous structural reports of methanol bonded to Rh^{III}, one involving a Cp^*Rh^{III} complex,[16] and the other one being $[RhCl_2(MeOH)(PCP)]$ [PCP = C_6H_3-2,6-$(CH_2PCy_2)_2$].[17] Interestingly, the two methanol molecules are *trans* to the two carbon fragments, whereas the acetonitrile molecule lies *trans* to the pyridine unit. The two methanol ligands show markedly different bond lengths to the metal atom: Rh(2)−O(2) is 2.202(3) Å, and Rh(2)−O(1) is 2.298(3) Å. This indicates that the latter is the additional sixth ligand with respect to the pentacoordinate complex **2**, whereas the methanol molecule *trans* to the pyridazyl moiety is the methanol ligand displacing the acetonitrile ligand of **2**. The lability of both methanol ligands is also reflected when comparing their metal−O bond lengths to the ones found in $[Cp^*Rh\{\eta^1(N7)\text{-}9\text{-}MH\}(CH_3OH)_2](OTf)_2\cdot CH_3OH$ (9-MH = 9-methylhypoxanthine).[16] In addition, the X-ray structure reveals that hydrogen bonding occurs between one of the coordinated methanol molecules and one of the fluorine atoms of tetrafluoroborate ($F_3BF\cdots HOCH_3$ 1.973 Å). Chelation on the

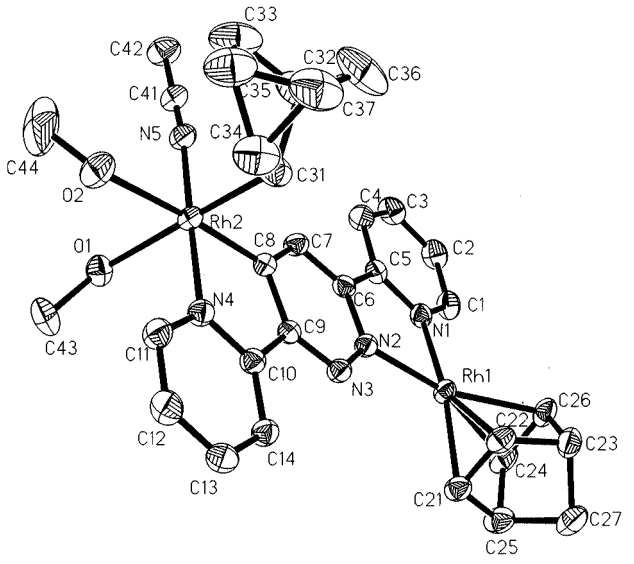

Figure 3. ORTEP drawing of a molecule of **4** (50% of probability); BF_4^-, solvent molecules and hydrogen atoms are omitted for clarity; selected bond lengths [Å] and angles [°]: Rh(1)−N(1) 2.073(3), Rh(1)−N(2) 2.047(3), Rh(1)−C(21) 2.124(4), Rh(1)−C(22) 2.114(4), Rh(1)−C(24) 2.144(4), Rh(1)−C(26) 2.132(4), Rh(2)−C(8) 1.953(4), Rh(2)−N(5) 2.010(3), Rh(2)−N(4) 2.027(3), Rh(2)−C(31) 2.054(4), Rh(2)−O(1) 2.298(3), Rh(2)−O(2) 2.202(3); N(2)−Rh(1)−N(1) 78.83(13), N(2)−Rh(1)−C(22) 101.40(15), N(1)−Rh(1)−C(22) 154.87(15), N(2)−Rh(1)−C(21) 103.82(14), N(1)−Rh(1)−C(21) 166.72(15), C(22)−Rh(1)−C(21) 38.07(17), N(2)−Rh(1)−C(26) 156.94(16), N(1)−Rh(1)−C(26) 102.71(14), C(22)−Rh(1)−C(26) 67.38(16), C(21)−Rh(1)−C(26) 80.05(16), N(2)−Rh(1)−C(24) 164.04(16), N(1)−Rh(1)−C(24) 106.79(15), C(22)−Rh(1)−C(24) 79.94(17), C(21)−Rh(1)−C(24) 67.34(16), C(26)−Rh(1)−C(24) 37.80(18), C(8)−Rh(2)−N(5) 92.58(15), C(8)−Rh(2)−N(4) 82.21(14), N(5)−Rh(2)−N(4) 173.82(13), C(8)−Rh(2)−C(31) 87.04(18), N(5)−Rh(2)−C(31) 96.10(16), N(4)−Rh(2)−C(31) 87.00(16), C(8)−Rh(2)−O(2) 175.96(14), N(5)−Rh(2)−O(2) 90.86(13), N(4)−Rh(2)−O(2) 94.22(13), C(31)−Rh(2)−O(2) 94.70(18), C(8)−Rh(2)−O(1) 94.29(13), N(5)−Rh(2)−O(1) 86.34(13), N(4)−Rh(2)−O(1) 90.70(12), C(31)−Rh(2)−O(1) 177.17(15), O(2)−Rh(2)−O(1) 83.82(12)

opposite side of the ligand gives rise to a relatively large separation between the two metal atoms (Rh···Rh 6.737 Å).

We thus clearly see that compounds **2** and **4** are the product of oxidative addition of the C−H bond on the pyridazine ring resulting in the formation of dinuclear Rh^{I}−Rh^{III} species. The C−H activation step is most probably followed by Rh−H addition to the double bond of the norbornadiene moiety and subsequent rearrangement of the norbonenyl molecule.[18] To the best of our knowledge, the rearrangement on a metal center of norbornadiene resulting in the formation of a 3-nortricyclyl ligand unit is unprecedented, although such rearrangements are thought to be involved in catalytic reactions such as the di- and trimerization of norbornadiene,[19] and catalytic amination reactions.[20] Complex **2** was also prepared directly by treating the ligand dppn with 2 equiv. of [Rh(NBD)$(CH_3CN)_2$]BF_4 in a CH_2Cl_2 solution (Scheme 1). To obtain a more detailed picture of this reaction, we monitored the transformation on a small scale in an NMR tube using deuterated dichloromethane. Although complex **1** is not very soluble in dichloromethane, the addition of 1 equiv. of [Rh(NBD)-$(CH_3CN)_2$]BF_4 to **1** gave a deep red solution. Recording the ^{1}H NMR spectrum after 10 min showed the formation of compound **A** (Scheme 3).[21] The formulation of this intermediate is supported by several characteristic peaks in the ^{1}H NMR spectrum. Firstly, the aromatic region shows 5 signals for the 10 hydrogen atoms of the ligand dppn indicating the presence of a symmetrical species. One of these signals (corresponding to 2 hydrogen atoms) is shifted downfield and is attributed to the α-hydrogen atoms on the two pyridyl moieties that are bound to the metal center. Furthermore, the signals of the NBD also indicate that both rhodium atoms are in an electronically equivalent situation. A peak at δ = 2.20 ppm for the methyl groups of the two acetonitrile ligands shows coordination of these molecules to the metal center {for [Rh(NBD)$(CH_3CN)_2$]BF_4 at δ = 2.30 ppm, the chemical shift of free CH_3CN is δ = 2.05 ppm}. After 30 min, the peaks of the product **2** can already be seen (ca. 10% by integration) and after 2 h, product **2** started to precipitate. During the transformation of **A** to **2**, the unknown dinuclear complex **3**, as shown in Scheme 3, was not observed. The X-ray structure of **1** shows that a complex such as **3** is not obtained most likely because of steric crowding of the two vicinal norbornadiene ligands. Furthermore, no hydride or norbornenyl were detected, indicating that the C−H activation step (or an earlier step) is probably rate-determining in the overall process.

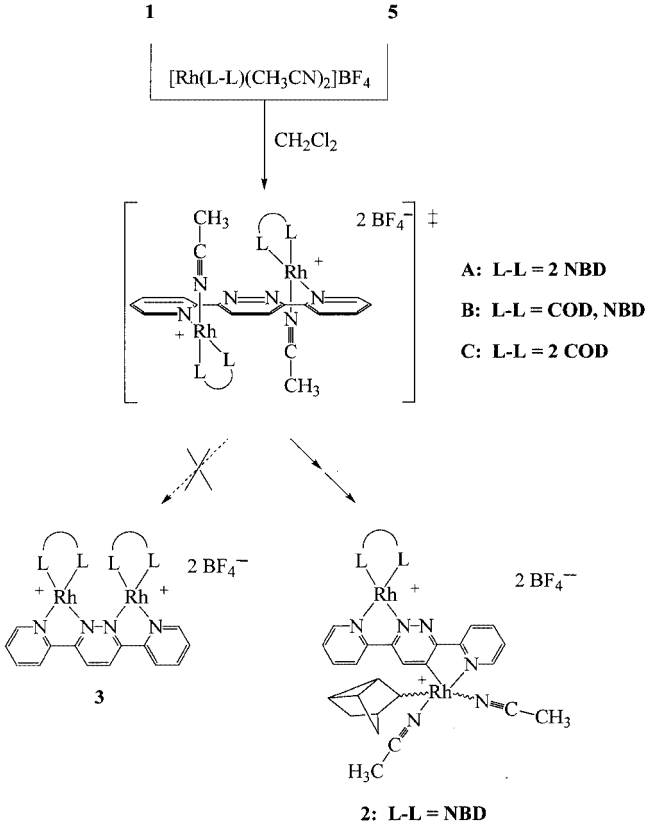

Scheme 3. Reaction pathway of the mononuclear complexes **1** and **5** with a second equivalent of [Rh(diene)$(CH_3CN)_2$]BF_4

As expected, C−H activation did not take place when complex **1** in dichloromethane was treated with the relatively electron-poor complex $[Rh(NBD)_2]BF_4$. The reaction did also not take place in coordinating solvents such as acetonitrile, pyridine, acetone or methanol. Such coordinating solvents stabilize complexes of the type $[Rh(NBD)(solvent)_2]BF_4$ and retard binding to the pyridine moiety of dppn to give **A**. The unique rearrangement of NBD to the final 3-nortricyclyl unit seems to be a prerequisite in this reaction. To test this, we synthesized the analogous mononuclear cyclooctadiene complex $[Rh(dppn)(COD)]BF_4$ (**5**), which was fully characterized including by ^1H-^{15}N GHMBC NMR (Table 1). When **5** was treated with 1 equiv. of $[Rh(COD)(CH_3CN)_2]BF_4$ in deuterated dichloromethane, products arising from C−H activation were not observed, showing that if indeed C−H activation takes place, it is reversible and the resulting labile hydride does not insert into the double bond of the diene. Instead, the dinuclear complex **C**, analogous to **A**, was formed in this case (Scheme 3). On the other hand, when complex **5** was added to 1 equiv. of $[Rh(NBD)(CH_3CN)_2]BF_4$, we observed intermediate **B** before disappearance of the NBD signals and concomitant formation of the characteristic signals for 3-nortricyclyl were seen.[22] Interestingly, reaction of 2-phenylpyridine with 1 equiv. of $[Rh(NBD)(CH_3CN)_2]PF_6$ did not give any activation of the phenyl ring of this ligand. The unique reactivity of **1** might thus arise from the hindered rotation of the pyridazine ring as shown in structure **A** and the subsequently easier approach of the metal center towards the C−H bond.[23]

Summary

We have reported the reactivity of cationic diene−Rh^I complexes with the linear tetradentate ligand dppn. Clean formation of the mononuclear complexes **1** and **5** was observed when the corresponding precursors were treated with an equimolar amount of the ligand and the X-ray study of one of them (**1**) showed the expected chelation through two neighboring nitrogen atoms of dppn. Surprisingly, further reaction of **1** or **5** with $[Rh(NBD)(CH_3CN)_2]BF_4$ gave rise to C−H activation of the pyridazine ring of the ligand and a unique rearrangement of the norbornadiene yielding a 3-nortricyclyl ligand unit. Complete characterization includes the X-ray crystallographic study of complex **4**. Complexes **1**, **4** and **5** were also characterized by ^1H-^{15}N GHMBC NMR spectroscopy, a technique which proved extremely useful for the characterization of these complexes. Several control experiments showed that this reactivity is not only crucially dependent on the basicity of the metal precursor used, but that the presence of at least one metal precursor with coordinated NBD is a prerequisite. Furthermore, it seems to be unique to the ligand used, possibly by the influence of the *N*,*N*-coordinated metal center on the C−H activation process by the second metal center. Further work is underway to extend the chemistry of these dppn−Rh systems and to explore their catalytic potential.

Experimental Section

General Procedures: All experiments were carried out under purified nitrogen in a Vacuum Atmospheres glove box equipped with an MO 40−2 inert gas purifier. All solvents were reagent-grade or better. All nondeuterated solvents were refluxed in the presence of sodium benzophenone ketyl and distilled under argon. Deuterated solvents were used as received. All the solvents were degassed with argon and kept in the glove box over molecular sieves. Commercially available reagents were used as received. The complexes $[Rh(NBD)_2]BF_4$, $[Rh(NBD)(CH_3CN)_2]BF_4$, $[Rh(COD)_2]BF_4$ and $[Rh(COD)(CH_3CN)_2]BF_4$ [24] were prepared according to literature procedures. ^1H and ^{13}C (DEPT) 1D NMR spectra were recorded with a Bruker DPX-250 spectrometer. A Bruker DRX-400 spectrometer operating at 400.13 MHz (^1H), 100.61 MHz (^{13}C) or 40.54 MHz (^{15}N) was used for 2D spectra. The spectrometer was equipped with a 5-mm Bruker inverse multinuclear resonance probe with a single-axis (*z*) gradient coil. Measurements were carried out at a probe temperature of 25 °C using concentrations of ca. 20 mg/ml. 2D ^1H-^{13}C correlation spectra were acquired with 1 K points in F_2, 128−256 complex increments in F_1 and 4−8 scans per increment for GHMQC; 1 K−2 K points in F_2, 128−256 increments in F_1 and 8−16 scans for GHMBC experiments. 2D ^1H-^{15}N correlation spectra were measured using the Bruker standard microprogram GHMBC. The GHMBC spectra were collected with 2 K × 256 (512) data points and 96−120 scans for each increment using the spectral widths in F_1 and F_2 of ca. 8−9 ppm for proton and 100−300 ppm for nitrogen-15. The long-range delay was optimized for 50−60 ms. Apodization was done with a sine bell in both dimensions. All ^{15}N spectra were referenced to liquid ammonia. Abbreviations used in the description of NMR spectroscopic data are as follows: br., broad; s, singlet; d, doublet; t, triplet; m, multiplet. The atom numbering in Scheme 2 has been used for the characterization of the compounds. Elemental analyses were performed by H. Kolbe, Mikroanalytisches Laboratorium, 45470 Mülheim, Germany.

Synthesis of dppn: (a) Preparation of 2-$(CH_3)_3Sn(C_5H_4N)$: To a solution of BuLi (50.000 mmol) in diethyl ether (50.0 mL) at −78 °C was added dropwise a solution of 2-bromopyridine (7.90 g, 50.000 mmol) in diethyl ether (25.0 mL). The resulting solution was stirred at −78 °C for 2 h. $SnCl(CH_3)_3$ (9.95 g, 50.000 mmol), dissolved in THF (10.0 mL), was added dropwise and the resulting deep-red solution was warmed to room temperature overnight during which time a heavy precipitate formed. The precipitate was filtered off and the solution was concentrated in vacuo and distilled under reduced pressure (135 °C, ca. 10 Torr). Yield: 12.10 g, 100%. **(b) Preparation of dppn:** 2,6-dichloropyridazine (2.60 g, 17.450 mmol), $Sn(C_5H_4N)(CH_3)_3$ (10.60 g, 44.000 mmol) and $PdCl(Ph_3P)_2(CH_2Ph)$ (0.50 g, 0.661 mmol) were placed in a Schlenk tube containing xylenes (300.0 mL) and refluxed under argon for 24 h. The resulting brown solution was treated at 0 °C with a saturated solution of KF (210.0 mL) and diethyl ether (300.0 mL) was added. The slurry was stirred for 40 min and poured into H_2O (750.0 mL). The product was extracted with diethyl ether, dried ($MgSO_4$), filtered and concentrated in vacuo. Chromatography on deactivated silica (eluent: hexane/diethyl ether, 1:1) gave dppn as a golden-colored, crystalline material. Yield: 1.84 g, 45%. ^1H NMR ($CDCl_3$): δ = 7.41 (ddd, ^3J = 7.6, ^3J = 4.8, ^4J = 1.2 Hz, 2 H, 3,9-H), 7.91 (ddd, ^3J = 7.7, ^4J = 1.8 Hz, 2 H, 4,10-H), 8.70 (d, 2 H, 14,15-H), 8.76 (m, 4 H, 2,5,8,10-H) ppm. ^{13}C NMR ($CDCl_3$): δ = 121.92 (2 C, C-3,9), 125.53 (2 C, C-14,15), 125.77 (2 C, C-5,11), 138.10 (2 C, C-4,10), 150.52 (2 C, C-2,8), 154.29 (2 C, C-13,16), 159.03 (2 C, C-6,12) ppm. ^{15}N ($CDCl_3$): δ = 306.89 (s,

^{2}J with 2,8-H, ^{3}J with 3,5,9,11-H, 2 N, N-1,7), 387.98 (s, ^{3}J with 14,15-H, 2 N, N-17,18) ppm. MS (EI): m/z = 235 [M^{+}].

Preparation of [Rh(dppn)(NBD)]BF$_4$ (1): A solution of dppn (100.0 mg, 0.427 mmol) in CH_2Cl_2 (3.0 mL) was added to a solution of [Rh(NBD)$_2$]BF$_4$ (159.0 mg, 0.427 mmol) in CH_2Cl_2 (3.0 mL). Stirring the resulting red solution at room temperature led to the precipitation of a deep red solid. The suspension was stirred for another 3 h, the solid filtered, washed with diethyl ether (2 times 5.0 mL) and dried in vacuo. Yield: 220.0 mg, 100%. Crystals suitable for an X-ray analysis were grown by slow concentration of a concentrated solution of **1** in methanol. ^{1}H NMR (CD_3NO_2): δ = 1.61 (br. s, 2 H, 19-H), 4.19 (br. s, 2 H, 20,23-H), 4.77 (br. s, 4 H, 21,22,24,25-H), 7.55 (ddd, ^{3}J = 7.5 Hz and 4.8, ^{4}J = 0.9 Hz, 1 H, 9-H), 7.76 (ddd, ^{3}J = 7.4 Hz and 5.3, ^{4}J = 1.3 Hz, 1 H, 3-H), 7.87 (d, ^{3}J = 5.1 Hz, 1 H, 5-H), 8.00 (ddd, ^{3}J = 7.8, ^{4}J = 1.7 Hz, 1 H, 10-H), 8.32 (ddd, ^{3}J = 7.8, ^{4}J = 1.4 Hz, 1 H, 4-H), 8.36 (d, ^{3}J = 7.7 Hz, 1 H, 2-H), 8.40 (d, ^{3}J = 8.0 Hz, 1 H, 11-H), 8.64 (d, ^{3}J = 9.0 Hz, 1 H, 15-H), 8.73 (d, ^{3}J = 4.6 Hz, 1 H, 8-H), 9.00 (d, ^{3}J = 9.0 Hz, 1 H, 14-H) ppm. ^{13}C NMR (CD_3OD): δ = 52.16 (d, $^{3}J_{Rh,C}$ = 2.5 Hz), 63.55 (d, $^{2}J_{Rh,C}$ = 6.1 Hz), 66.50 (d, $^{1}J_{Rh,C}$ = 9.8 Hz), 121.84, 123.69, 126.20, 127.84, 128.27, 128.45, 137.82, 141.25, 150.05, 150.26, 151.16, 153.59, 159.92 ppm. ^{15}N NMR (CD_3NO_2): δ = 242.45 (d, ^{2}J with 2-H, ^{3}J with 3-H and 5-H, $^{1}J_{N,Rh}$ = 19.3 Hz, 1 N, N-1), 271.03 (d, ^{3}J with 14-H, $^{2}J_{N,Rh}$ = 10.6 Hz, 1 N, N-18), 309.21 (s, ^{3}J with 9-H and 11-H, 1 N, N-7, ^{2}J with 8-H), 312.04 (d, ^{3}J with 15-H, $^{1}J_{N,Rh}$ = 20.2 Hz, 1 N, N-17) ppm. $C_{21}H_{18}BF_4N_4Rh$ (516.13): calcd. C 48.87, H 3.52, N 10.86; found C 48.81, H 3.54, N 10.80.

In situ Characterization of A: A solution of [Rh(NBD)(CH$_3$CN)$_2$]BF$_4$ (12.5 mg, 0.034 mmol) in CD_2Cl_2 (0.5 mL) was added to a suspension of [Rh(dppn)(NBD)]BF$_4$ (17.6 mg, 0.034 mmol) in CD_2Cl_2 (0.5 mL). The resulting red solution was transferred to an NMR tube and the spectrum was measured after 10 min. ^{1}H NMR (CD_2Cl_2): δ = 1.43 (s, 4 H), 2.20 (br. s, 6 H), 3.99 (br. s, 4 H), 4.45 (br. s, 8 H), 7.68 (dt, 2 H), 8.18 (dd, 2 H), 8.30 (d, 2 H), 8.36 (d, 2 H), 9.18 (s, 2 H) ppm.

In situ Characterization of C: A solution of [Rh(COD)(CH$_3$CN)$_2$]BF$_4$ (15.0 mg, 0.039 mmol) in CD_2Cl_2 (0.5 mL) was added to a suspension of [Rh(dppn)(COD)]BF$_4$ (21.0 mg, 0.039 mmol) in CD_2Cl_2 (0.5 mL). The resulting deep red solution was transferred to an NMR tube and the spectrum was measured. ^{1}H NMR (CD_2Cl_2): δ = 2.07 (d, br, 4 H), 2.28 (s, 6 H), 2.49 (br. s, 4 H), 4.58 (br. s, 8 H), 7.73 (dt, 2 H), 8.17 (dd, 2 H), 8.37 (d, 2 H), 8.48 (br, 2 H), 9.18 (s, 2 H) ppm.

Preparation of [Rh$_2$(dppn-H)(NBD)(η^1-C$_7$H$_9$)(CH$_3$CN)$_2$](BF$_4$)$_2$ (2): A solution of [Rh(NBD)(CH$_3$CN)$_2$]BF$_4$ (37.4 mg, 0.103 mmol) in CH_2Cl_2 (3.0 mL) was added to a suspension of [Rh(dppn)(NBD)]BF$_4$ (53.0 mg, 0.103 mmol) in CH_2Cl_2 (3.0 mL). The resulting red solution was stirred overnight during which time a slow precipitation of a pink solid occurred. The solid was recovered, washed with diethyl ether and dried in vacuo. Yield: 67.0 mg, 74%. ^{1}H NMR (CD_2Cl_2): δ = 0.8−1.5 (several m, 7 H), 1.54 (s, 2 H), 1.71 (br. s, 1 H), 2.34 (s, 3 H), 2.51 (br. s, 1 H), 2.64 (s, 3 H), 4.09 (br. s, 2 H), 4.56 (br. s, 4 H), 7.52−7.68 (m, 3 H), 8.04 (dt, not well defined, 1 H), 8.15 (m, 1 H), 8.28 (dt, J = 7.7 Hz, 1 H and 1.5 Hz), 8.72 (m, 2 H), 8.89 (br. s, 1 H) ppm. $C_{32}H_{32}B_2F_8N_6Rh_2$ (880.10): calcd. C 43.67, H 3.67, N 9.55; found C 44.29, H 3.76, N 9.36.

Preparation of [Rh$_2$(dppn-H)(NBD)(η^1-C$_7$H$_9$)(CH$_3$OH)$_2$(CH$_3$CN)](BF$_4$)$_2$ (4): Complex **2** (80.0 mg, 0.091 mmol) was dissolved in methanol (3.0 mL) and stirred at room temperature for 1 h. Addition of diethyl ether to the resulting red solution led to the precipitation of a red solid that was filtered, washed with additional diethyl ether and dried in vacuo. Yield: 76.0 mg, 93%. Crystals suitable for X-ray crystallography were obtained by slow diffusion of diethyl ether into a concentrated methanol/CH_2Cl_2 solution and subsequent slow concentration. ^{1}H NMR (CD_3OD): δ = 0.82 (dd, ^{3}J = 11.5 Hz, 2 H, 26-H), 0.86 (br. s, 1 H, 27-H), 1.02 (d, J = ca. 9 Hz, 1 H, 32-H), 1.10 (br. s, 1 H, 30-H), 1.04 (s, 1 H, 29-H), 1.16 (d, J ca. 9 Hz, 1 H, 32-H), 1.32 (br. s, 1 H, 31-H), 1.60 (s, 2 H, 19-H), 2.58 (br. s, 1 H, 28-H), 2.75 (s, 3 H, CH_3CN), 4.14 (br. s, 2 H, 20,23-H), 4.69 (t, ^{3}J = 2.0 Hz, 4 H, 21,22,24,25-H), 7.73 (ddd, ^{3}J = 7.7 Hz and 5.3, ^{4}J = 1.1 Hz, 1 H, 3-H), 7.76 (ddd, ^{3}J = 6.0, ^{4}J = 1.2 Hz, 1 H, 9-H), 7.92 (d, ^{3}J = 5.2 Hz, 1 H, 2-H), 8.24 (ddd, ^{3}J = 7.8, ^{4}J = 1.4 Hz, 1 H, 10-H), 8.31 (ddd, ^{3}J = 7.6 Hz,^{4}J = 1.6 Hz, 1 H, 4-H), 8.32 (d, ^{3}J = 7.4 Hz, 1 H, 8-H), 8.71 (d, 5, ^{3}J = 8.2 Hz, 1 H), 8.73 (d, ^{3}J = 8.0 Hz, 1 H, 11-H), 8.82 (s, 1 H, 15-H) ppm. ^{13}C NMR (CD_3OD): δ = 3.41 (CH_3CN), 13.45 (C-27), 13.86 (C-29), 19.18 (C-30), 33.26 (C-26), 34.27 (C-32), 37.10 (C-31), 45.29 (d, C-28), 53.31 (d, J = 2.3 Hz, 2 C, C-20,23), 64.78 (d, J = 5.8 Hz, C-19), 67.24 (t, J = 9.0 Hz, 4 C, C-21,22,24,25), 123.41 (C-8), 125.29 (C-5), 125.62 (br, CH_3CN), 128.62 (C-9), 129.22 (C-3), 135.28 (C-15), 141.53 (C-9), 142.55 (C-4), 151.37 (2 C, C-2,11), 155.08 (C-6), 156.51 (C-13), 160.56 (C-12), 169.44 (C-16) ppm. ^{15}N NMR (CD_3OD): δ = 174.10 (^{3}J with CH_3CN, $^{1}J_{N,Rh}$ = 45.9 Hz, 1 N, CH_3CN), 234.51 (d, ^{2}J with 8-H, ^{3}J with 9-H and 11-H, $^{1}J_{N,Rh}$ = 42.4 Hz, 1 N, N-7), 238.32 (d, ^{2}J with 2-H, ^{3}J with 3-H and 5-H, $^{1}J_{N,Rh}$ = 24.7 Hz, 1 N, N-1), 283.20 (d, ^{3}J with 15-H, $^{1}J_{N,Rh}$ = 40.2 Hz, 1 N, N-17) ppm. $C_{32}H_{37}B_2F_8N_5O_2Rh_2$ (903.13): calcd. C 42.56, H 4.13, N 7.75; found C 42.85, H 4.15, N 7.98.

Preparation of [Rh(dppn)(COD)]BF$_4$ (5): A solution of dppn (79.1 mg, 0.338 mmol) in CH_2Cl_2 (3.0 mL) was added to a solution of [Rh(COD)$_2$]BF$_4$ (137.1 mg, 0.338 mmol) in CH_2Cl_2 (3.0 mL). The resulting solution was stirred at room temperature for 24 h. Some of the compound readily precipitated from the solution. Addition of diethyl ether led to complete precipitation of a green compound that was washed with diethyl ether and dried in vacuo. Yield: 174.0 mg, 97%. ^{1}H NMR (CD_3NO_2): δ = 2.29 (m, 4 H, CH_2 of COD), 2.63 (m, 4 H, CH_2 of COD), 4.92 (s, 4 H, 4 olefins COD), 7.54 (ddd, ^{3}J = 7.6, 4.8, ^{4}J = 1.2 Hz, 1 H, 9-H), 7.80 (ddd, ^{3}J = 7.4, 5.4, ^{4}J = 1.4 Hz, 1 H, 3-H), 7.97 (ddd, ^{3}J = 7.8, ^{4}J = 1.7 Hz, 1 H, 10-H), 8.05 (d, 5, ^{3}J = 5.3 Hz, 1 H), 8.31 (ddd, ^{3}J = 7.8, ^{4}J = 1.5 Hz, 1 H, 4-H), 8.38 (m, 2 H, 2,11-H), 8.64 (d, ^{3}J = 9.1 Hz, 1 H, 15-H), 8.75 (dd, ^{3}J = 4.8 Hz, 1 H, 8-H), 9.09 (d, ^{3}J = 9.1 Hz, 1 H, 14-H) ppm. ^{15}N NMR (CD_3NO_2): δ = 235.13 (d, ^{2}J with 2-H, ^{3}J with 3-H and 5-H, $^{1}J_{N,Rh}$ = 26.0 Hz, 1 N, N-1), 271.05 (s, ^{3}J with 14-H, 1 N, N-18), 300.24 (d, $^{1}J_{N,Rh}$ = 20.5 Hz, ^{3}J with 15-H, 1 N, N-17), 307.71 (s, ^{3}J with 9-H and 11-H, ^{2}J with 8-H, 1 N, N-7) ppm. $C_{22}H_{22}BF_4N_4Rh$ (532.17): calcd. C 49.65, H 4.17, N 10.53; found C 49.60, H 4.14, N 10.39.

X-ray Crystal Structure Determination of 1 and 4: Single crystals of **1** and **4** were mounted on a nylon loop and flash-frozen in a nitrogen stream at 120 K. Data were collected with a Nonius Kappa CCD diffractometer mounted on an FR590 generator equipped with a sealed tube with Mo-K_α radiation (λ = 0.71073 Å) and a graphite monochromator. The structures were solved using direct method with SHELXS-97 and refined by full-matrix least-squares technique with SHELXL-97 based on F^2.[25] CCDC-183245 (**1**), and -183246 (**4**) contain the supplementary crystallographic data for this paper. These data can be obtained free of charge at www.ccdc.cam.ac.uk/conts/retrieving.html or from the Cambridge Crystallographic Data Center, 12, Union Road, Cambridge CB2 1EZ, UK [Fax: (internat.) + 44-1223/336-033; E-mail: deposit@ccdc.cam.ac.uk].

Complex 1: $C_{21}H_{18}N_4Rh{\cdot}BF_4{\cdot}CH_3OH$, dark orange, plates, 0.10 × 0.10 × 0.05 mm, triclinic, $P\bar{1}$ (no. 2), a = 7.887(2), b = 11.904(2), c = 12.564(3) Å, α = 110.10(3), β = 99.17(3), γ = 98.63(3)° from 20° of data, V = 1066.6(4) Å^3, Z = 2, M_w = 548.16, $D_{calcd.}$ = 1.707 Mg/m^3, μ = 0.859 mm^{-1}. The final cycle of refinement based on F^2 gave an agreement factor R = 0.0336 for data with $I > 2\sigma(I)$ and R = 0.0437 for all data (5490 reflections) with a goodness-of-fit of 1.017. Idealized hydrogen atoms were placed and refined in riding mode.

Complex 4: $C_{32}H_{37}N_5Rh_2{\cdot}(BF_4)_2{\cdot}CH_2Cl_2$, red, 0.2 × 0.2 × 0.2 mm, triclinic, $P\bar{1}$, a = 12.114(2), b = 12.400(2), c = 15.136(3) Å, α = 67.58(3), β = 83.86(3), γ = 69.04(3)° from 20° of data, V = 1961.6(6) Å^3, Z = 2, M_w = 988.03, $D_{calcd.}$ = 1.673 Mg/m^3, μ = 1.053 mm^{-1}. The final cycle of refinement based on F^2 gave an agreement factor R = 0.0497 for data with $I > 2\sigma(I)$ and R = 0.0537 for all data (8833 reflections) with a goodness-of-fit of 1.055. Idealized hydrogen atoms were placed and refined in riding mode.

Acknowledgments

This work was supported by the Israel Science Foundation (grant no. 83/00), by the MINERVA foundation, Munich, Germany and by the Helen and Milton Kimmel center for Molecular Design. D. M. is the Israel Matz Professor of Organic Chemistry.

[1] For two recent reviews, see: [1a] S. D. Ittel, L. K. Johnson, M. Brookhart, *Chem. Rev.* **2000**, *100*, 1169−1203, and references therein. [1b] G. J. P. Britovsek, V. C. Gibson, D. F. Wass, *Angew. Chem. Int. Ed.* **1999**, *38*, 428−447, and references therein.

[2] [2a] A. E. Shilov, G. B. Shul'pin, *Chem. Rev.* **1997**, *97*, 2879−2932. [2b] S. S. Stahl, J. A. Labinger, J. E. Bercaw, *Angew. Chem. Int. Ed.* **1998**, *37*, 2181−2192. [2c] R. A. Periana, D. J. Taube, S. Gamble, H. Taube, T. Satoh, H. Fuji, *Science* **1998**, *280*, 560−564. [2d] T. Ishiyama, J. Takagi, K. Ishida, N. Miyaura, N. R. Anastasi, J. F. Hartwig, *J. Am. Chem. Soc.* **2002**, *124*, 390−391. [2e] H. A. Zhong, J. A. Labinger, J. E. Bercaw, *J. Am. Chem. Soc.* **2002**, *124*, 1378−1399.

[3] K. Toellner, R. Popovitz-Biro, M. Lahav, D. Milstein, *Science* **1997**, *278*, 2100−2103.

[4] [4a] J. F. van Baar, K. Vrieze, D. J. Stufkens, *J. Organomet. Chem.* **1975**, *97*, 461−472. [4b] A. J. Deeming, I. P. Rothwell, M. B. Hursthouse, K. M. Abdul Malik, *J. Chem. Soc., Dalton Trans.* **1979**, 1899−1911. [4c] D. W. Evans, G. R. Baker, G. R. Newkome, *Coord. Chem. Rev.* **1989**, *93*, 155−183.

[5] For representative examples, see: [5a] M. E. Broussard, B. Juma, S. G. Train, W.-J. Peng, S. A. Laneman, G. G. Stanley, *Science* **1993**, *260*, 1784−1788. [5b] R. G. Konsler, J. Karl, E. N. Jacobsen, *J. Am. Chem. Soc.* **1998**, *120*, 10780−10781. [5c] L. Cai, H. Mahmoud, Y. Han, *Tetrahedron: Asymmetry* **1999**, *10*, 411−427. [5d] C. He, S. J. Lippard, *J. Am. Chem. Soc.* **2000**, *122*, 184−185.

[6] M.-T. Youinou, N. Rahmouni, J. Fischer, J. A. Osborn, *Angew. Chem. Int. Ed. Engl.* **1992**, *31*, 733−735. J.-M. Lehn, *Supramolecular Chemistry: Concepts and Perspectives*, VCH, Weinheim, **1995**, chapter 9.

[7] For the only example of d^8-M^{I} complexes: [7a] N. Rahmouni, A. A. Bahsoun, M.-T. Youinou, J. A. Osborn, J. Fischer, A. Ezzamarty, *Polyhedron* **1998**, *17*, 3083−3088. For d^6-M^{III} complexes: [7b] A. Tiripicchio, A. M. Manotti Lanfredi, M. Ghedini, F. Neve, *J. Chem. Soc., Chem. Commun.* **1983**, 97−98. [7c] A. M. Manotti Lanfredi, A. Tiripicchio, F. Ugozzoli, M. Ghedini, F. Neve, *J. Chem. Soc., Dalton Trans.* **1988**, 651−656. [7d] M. Ghedini, F. Neve, A. M. Manotti Lanfredi, F. Ugozzoli, *Inorg. Chim. Acta* **1988**, *147*, 243−250.

[8] U. Gilge, P. Jutzi, *J. Organomet. Chem.* **1983**, *246*, 163−168.

[9] For preparation of the catalyst, see: R. S. Y. Lau, P. K. Wong, J. K. Stille, *J. Am. Chem. Soc.* **1976**, *98*, 5832−5840.

[10] For a recent review, see: G. E. Martin, C. E. Hadden, *J. Nat. Prod.* **2000**, *63*, 543−585.

[11] [11a] A. Satake, T. Nakata, *J. Am. Chem. Soc.* **1998**, *120*, 10391−10396. [11b] A. Satake, H. Koshino, T. Nakata, *Chem. Lett.* **1999**, 49−50. [11c] A. Satake, H. Kadohama, H. Koshino, T. Nakata, *Tetrahedron Lett.* **1999**, *40*, 3557−3560. [11d] A. Jantti, M. Wagner, R. Suontamo, E. Kolehmainen, K. Rissanen, *Eur. J. Inorg. Chem.* **1998**, 1555−1562. [11e] E. Kolehmainen, J. Tamminen, R. Kauppinen, J. Linnanto, *J. Inclusion Phenom. Mol. Recognit. Chem.* **1999**, *35*, 75−84.

[12] The unexpectedly large shift for signal of the noncoordinated N(18) nitrogen atom in complexes **1** and **5** (compared to that of the free ligand) might be due to the influence of the coordinated Rh−N(17) moiety adjacent to it.

[13] [13a] A. M. Manotti Lanfredi, A. Tiripicchio, M. Ghedini, G. De Munno, *Acta Crystallogr., Sect. B* **1982**, *38*, 1165−1168. [13b] M. Ghedini, M. Longeri, F. Neve, *Inorg. Chim. Acta* **1987**, *132*, 223−228. [13c] R. Dorta, L. J. W. Shimon, D. Milstein, unpublished results.

[14] Such pentacoordinated Rh^{III} complexes are fairly common; for recent examples from this laboratory, see: R. Goikhman, D. Milstein, *Angew. Chem. Int. Ed.* **2001**, *40*, 1119−1122.

[15] In general, the Rh−N coupling constants in complexes **1, 4** and **5** seem to follow a trend with smaller coupling constants for Rh^{I} than for Rh^{III} [except for Rh−N(17) in **4**]. Studies on other rhodium complexes are needed in order to confirm this observation.

[16] D. P. Smith, M. T. Griffin, M. M. Olmstead, M. F. Maestre, R. H. Fish, *Inorg. Chem.* **1993**, *32*, 4677−4678.

[17] R. J. Cross, A. R. Kennedy, L. Manojlovic-Muir, K. W. Muir, *J. Organomet. Chem.* **1995**, *493*, 243−249.

[18] Skeletal rearrangements of dienes have been observed: [18a] R. G. Miller, P. A. Pinke, R. D. Stauffer, H. J. Golden, D. J. Baker, *J. Am. Chem. Soc.* **1974**, 4211−4220. [18b] P. A. Pinke, R. G. Miller, *J. Am. Chem. Soc.* **1974**, 4221−4229. [18c] H. J. Golden, D. J. Baker, R. G. Miller, *J. Am. Chem. Soc.* **1974**, 4235−4243. [18d] P. Eilbracht, M. Acker, B. Rosenstock, *Chem. Ber.* **1989**, 151−158. [18e] P. Eilbracht, M. Acker, G. Hüttmann, I. Winkels, *Chem. Ber.* **1989**, 159−168. For related studies involving methylenecyclopropane, see: [18f] P. Binger, M. J. Doyle, R. Benn, *Chem. Ber.* **1983**, 1−10. [18g] P. Binger, A. Brinkmann, P. Wedemann, *Chem. Ber.* **1983**, 2920−2930.

[19] M. Green, T. A. Kuc, *J. Chem. Soc., Dalton Trans.* **1972**, 832−839.

[20] [20a] J. Kiji, S. Nishimura, S. Yoshikawa, E. Sasakawa, J. Furukawa, *Bull. Chem. Soc. Jpn.* **1974**, *47*, 2523−2525. [20b] H. Trauthwein, A. Tillack, M. Beller, *Chem. Commun.* **1999**, 2029−2030.

[21] Attempts to isolate intermediates **A**, **B** and **C** gave mixtures containing some starting and/or final product.

[22] Unfortunately, the resulting complex could not be isolated as a clean compound.

[23] Alternatively, C−H activation of the electron-rich pyridazyl ring might be easier than C−H activation of a phenyl ring.

[24] M. Green, T. A. Kuc, S. H. Taylor, *J. Chem. Soc. A* **1971**, 2334−2337.

[25] G. M. Sheldrick, *SHELX-97, Program for Crystal Structure Refinement*, University of Göttingen, **1997**.

Received April 10, 2002
[I02186]

Fluorinated 1,3λ⁴δ²,2,4-Benzodithiadiazines − A Synthetic, Structural and Theoretical Study

Alexander Yu. Makarov,[a] Irina Yu. Bagryanskaya,[a] Frank Blockhuys,*[b] Christian Van Alsenoy,[b] Yuri V. Gatilov,[a] Vladimir V. Knyazev,[a] Alexander M. Maksimov,[a] Tatiana V. Mikhalina,[a] Vyacheslav E. Platonov,[a] Makhmut M. Shakirov,[a] and Andrey V. Zibarev*[a]

Dedicated to Professor Dr. Rüdiger Mews on the occasion of his 60th birthday

Keywords: Antiaromaticity / Fluorinated 1,3λ⁴δ²,2,4-benzodithiadiazines / Electrophilic cyclisation / Molecular structure / NICS / Nucleophilic cyclisation

The series of title compounds has been prepared through both electrophilic ($C_6H_nF_{5-n}$–N=S=N–$SiMe_3$ + SCl_2) and nucleophilic (C_6HF_4–S–N=S=N–$SiMe_3$ + CsF) intramolecular *ortho*-cyclisation reactions, and the former route seems to be the more effective. High regioselectivity of the ring-closing procedures is observed in both cases. The compounds were characterised by X-ray crystallography and multinuclear (^{1}H, ^{13}C, ^{15}N and ^{19}F) NMR spectroscopy. In accordance with GIAO calculations, ^{15}N{^{1}H} experiments and the effects observed on complete substitution of hydrogen by fluorine, the high-field signal in the ^{15}N NMR spectra can be assigned to N-4 and the low-field signal to N-2. In the crystal, 5,6,7-trifluoro- (**5**) and 5,6,8-trifluoro-1,3λ⁴δ²,2,4-benzodithiadiazine (**6**) are planar, whereas the 6,8-difluoro derivative **3** is bent along the S1···N4 line by 8.3°. According to NICS calculations the heterocycle moiety in this compound class is antiaromatic while the carbocycle is aromatic. The fluorine substituents increase the aromaticity – and in some cases (especially when a fluorine atom is present in the 8-position) the antiaromaticity – of the corresponding rings. The *ortho*-fluoro-containing starting material $C_6H_nF_{5-n}$–N=S=N–$SiMe_3$ (n = 2: **10**) cyclises to the fluorinated 2,1,3-benzothiadiazole **27** upon treatment with CsF instead of SCl_2. For starting compound 6-HC_6F_4–S–N=S=N–$SiMe_3$ (**14**) the planar (*Z*,*E*) configuration features a short intramolecular H···N contact, as evidenced by X-ray diffraction. Both the reaction pathways mentioned are also discussed.

(© Wiley-VCH Verlag GmbH, 69451 Weinheim, Germany, 2003)

1. Introduction

Hyperelectronic (π- and σ-excessive) 1,3λ⁴δ²,2,4-benzodithiadiazines[1−4] **1** (Scheme 1) reveal a nontrivial combination of definite features of antiaromaticity[5] with moderate thermal stability. In particular, the compounds in series **1** possess a cyclic 12π-electron system with a notably low IE_1 [6−8] in planar or nearly planar molecular conformations observed both in the gas phase[9] and in the crystal,[1−4] low-lying π*-excited states[1−4,10] localised predominantly on the heterocycle,[11] and enhanced magnetic shielding of the ^{1}H, ^{13}C and ^{19}F (for the monofluoro derivatives) nuclei attached to C-5 and C-8 − i.e., those closest to the heterocycle − with respect to those attached to C-6 and C-7,[1,3,4] this probably being due to paratropic ring currents.[5] At the same time, the compounds in series **1** are thermally stable up to ca. 100 °C. At higher temperatures and in dilute hydrocarbon solutions, compounds **1** quantitatively yield persistent 1,2,3-benzodithiazolyl radicals (Scheme 1),[10,12] which are also the products of photolysis reactions of **1**.[10,13] The key intermediates are singlet 1,2,3-benzodithiazol-2-ylnitrenes (Scheme 1), identified under matrix isolation conditions.[13] The other aspects of the heteroatom reactivity of **1** have been studied only to a limited extent. Since both the π-excess and the antiaromaticity are destabilising factors, one might believe that the heteroatom reactivity of **1** should be high; consequently, many new reactions should be found in which this reactivity takes on many different forms. Additionally, several new structures should no doubt be observed among the reaction products of **1**. Currently, however, the only fact that is known is that the compounds in series **1** are able to iminate some S^{II} [4]

[a] Institute of Organic Chemistry, Russian Academy of Sciences, 630090 Novosibirsk, Russia
Fax: (internat.) + 7-3832/344-752
E-mail: zibarev@nioch.nsc.ru
[b] Department of Chemistry, University of Antwerp (UIA), Universiteitsplein 1, 2610 Wilrijk (Antwerpen), Belgium
Fax: (internat.) + 32-3/820-2310
E-mail: Frank.Blockhuys@ua.ac.be

Supporting information for this article is available on the WWW under http://www.eurjic.org or from the author.

and P^{III} [14] derivatives oxidatively, another reaction most probably mediated by the nitrenes mentioned above. Reversible cycloaddition to norbornadiene[1] as well as reduction and hydrolysis to 2-aminobenzenethiols (isolated in the form of their corresponding disulfides)[3] have also been described.

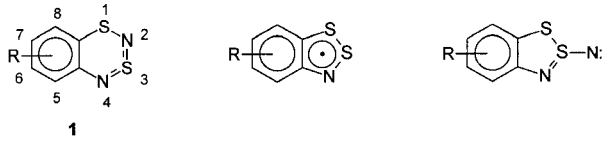

1

In this work, compounds **1**: R = H (**2**), 6,8-F_2 (**3**), 6,7-F_2 (**4**), 5,6,7-F_3 (**5**), 5,6,8-F_3 (**6**), 5,6,7,8-F_4 (**7**)

Scheme 1

The fluorinated compounds in series **1** are all unknown except for the 5-, 6- and 7-fluoro derivatives[3,4] and the 5,6,7,8-tetrafluoro derivative.[2] Nevertheless, they are interesting not only from a general point of view, but also in the context of further investigation of the peculiarities of the molecular and electronic structures of these compounds. For instance, it was found by gas electron diffraction (GED) that a free molecule of the parent 1,3$\lambda^4\delta^2$,2,4-benzodithiadiazine **2** is bent significantly, while a free molecule of its tetrafluoro derivative **7** is planar.[9] The bent geometry of the former was attributed to pseudo-Jahn−Teller distortion to minimize the antiaromaticity,[4,9] whereas the planar geometry of the latter was thought to be due to a conflict between the pseudo-Jahn−Teller effect and the perfluoro (or π-fluoro) effect, caused by the presence of a fluorine atom in the 8-position, resolved in favour of the latter.[9] To verify this conclusion it is necessary to perform GED on 6,8-difluoro- (**3**) and 5,6,7-trifluoro-1,3$\lambda^4\delta^2$,2,4-benzodithiadiazine (**5**), the free molecules of which would be expected to be planar and bent, respectively, and these experiments are currently underway.

This work deals with the preparation and X-ray structural characterisation of a number of new fluorinated derivatives of 1,3$\lambda^4\delta^2$,2,4-benzodithiadiazine **2**, as well as with the quantitative estimation of the (anti)aromaticity of the compounds in series **1** for both the fluorocarbon and the hydrocarbon series, by application of the Nucleus-Independent Chemical Shift (NICS) concept.[15] On the basis of the theoretical calculations, a more detailed structural study was also performed for all fifteen possible fluoro-substituted 1,3$\lambda^4\delta^2$,2,4-benzodithiadiazines.

2. Results and Discussion

The monofluorinated compounds of series **1** had previously been synthesised by 1:1 condensation of the corresponding Ar−N=S=N−$SiMe_3$ with SCl_2, followed by the electrophilic *ortho*-cyclisation of the [Ar−N=S=N−S−Cl] intermediates.[3,4] The tetrafluoro derivative **7** was obtained by the nucleophilic ring-closure of the intermediate $[Ph_F-S-N=S=N]^-$ anion generated from Ph_F−S−N=S=N−$SiMe_3$ and CsF.[2] Both approaches were applied in this work.

2.1. Electrophilic Cyclisation

The Ar−N=S=N−$SiMe_3$ starting materials **8**−**10** (Scheme 2) for the electrophilic ring-closure procedure were synthesised by a general method[3,4,16,17] from the corresponding Ar−N=S=O compounds and $LiN(SiMe_3)_2$. Earlier, the less common $Me_3SnN(SiMe_3)_2$ was used to transform the polyfluorinated Ar−N=S=O into Ar−N=S=N−$SiMe_3$.[18,19] Further treatment of **8**−**10** with SCl_2 afforded the desired compounds **3**−**5** (Scheme 2). From these experiments it appears that the introduction of up to three fluorine atoms into the carbocycle does not deactivate Ar−N=S=N−$SiMe_3$ toward the electrophilic cyclisation needed to obtain **1**. It should be noted that only 75% of the stoichiometric amount of SCl_2 was used in these preparations, so as to suppress any further reaction of **3**−**5** with SCl_2, it having previously been found that the compounds in series **1** readily react with SCl_2 to yield 1,2,3-benzodithiazolium chlorides (Herz salts).[4]

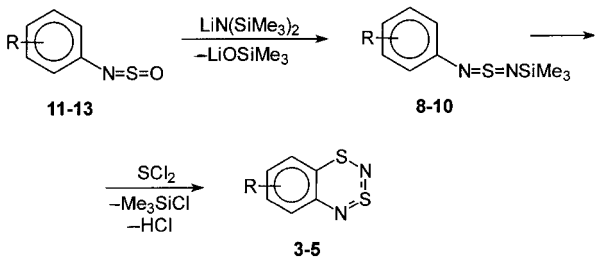

11-13 **8-10** **3-5**

3: R = 6,8-F_2; **4**: R = 6,7-F_2; **5**: R = 5,6,7-F_3;
8, **11**: R = 3,5-F_2; **9**, **12**: R = 3,4-F_2; **10**, **13**: R = 2,3,4-F_3

Scheme 2

The cyclisation proved to be effectively regioselective in the case of **9**, which possesses two non-equivalent positions at which the ring-closure may occur (cf. refs.[3,4]). Only **4** (Scheme 2) was isolated from the reaction mixture, and the second possible isomer was not detected. It had previously been shown[3] that the regioselectivity in these types of cyclisation reactions is consistent with the thermodynamics of the corresponding intermediate σ complexes as well as with factors of kinetic control for an orbital-controlled electrophile-nucleophile reaction. At the same time, the ratio of the isomers observed in the reaction mixture is obviously affected by the difference in their rates of reaction with SCl_2.[4] The structures of **3** and **5** were confirmed by X-ray crystallography (see below).

As reaction by-products, the corresponding sulfur diimides $(Ar-N=)_2S$ were identified in all cases. One can explain their formation in terms of dimerisation of [Ar−N=

S=N−S−Cl] intermediates through [2π + 2π] cycloaddition reactions, followed by decomposition of the nonsymmetric dimers to $(Ar-N=)_2S$ and the well-known $[S_3N_2Cl]Cl$.[20] Dilution of the reaction solutions reduces the yields of the $(Ar-N=)_2S$ by-products.

2.2. Nucleophilic Cyclisation

The $Ar_F-S-N=S=N-SiMe_3$ starting materials **14**−**18** (Scheme 3) for the nucleophilic cyclisation reactions were obtained through the known 1:1 condensation of the corresponding Ar_FSCl compounds with $(Me_3SiN=)_2S$.[2,3,19] The structure of **14** was confirmed by X-ray crystallography (Figure 1). The planar (*Z*,*E*) configuration features a short intramolecular H···N contact or hydrogen bond (cf. hydrocarbon analogues[21]).

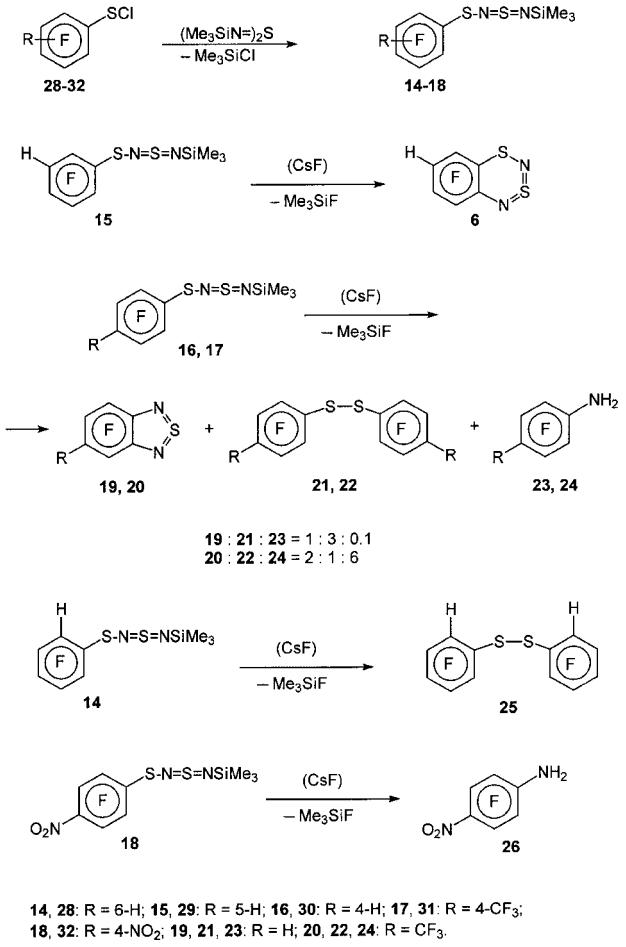

Scheme 3

The compounds **14**−**18** were treated with CsF in boiling acetonitrile (cf. ref.[2]) in an attempt to close the ring and obtain the target heterocycles; this was successful only in the case of **15** (Scheme 3). The cyclisation of **15** to **6** again proved to be highly regioselective, since the second possible isomer was not observed. It had previously been shown,[19] for the closely related nucleophilic cyclisation reactions affording polyfluorinated naphtho[1,2-*c*][1,2,5]thiadiazoles,

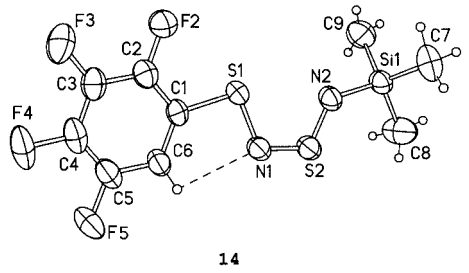

Figure 1. Molecular structure of **14**; selected bond lengths [Å] and bond angles [°]: C1−S1 1.762(3), S1−N1 1.662(3), N1−S2 1.552(3), S2−N2 1.494(3), N2−Si1 1.748(3), N1−H 2.504; C1−S1−N1 98.55(15), S1−N1−S2 116.19(15), N1−S2−N2 113.58(15), S2−N2−Si1 129.17(19)

that the preferred direction of the ring-closure is consistent with essentially the same factors as described above for the electrophilic cyclisation reactions. The structure of **6** was confirmed by X-ray crystallography (see below).

In the cases of **16** and **17**, only polyfluorinated 2,1,3-benzothiadiazoles **19** and **20** (i.e., the smaller-sized heterocycles) could be detected in the reaction mixtures, along with the corresponding Ar_FSSAr_F and Ar_FNH_2 derivatives (in different ratios). In the case of **14** (a potential precursor of **5**: see Scheme 2), however, only the disulfide **25** (Scheme 3) was identified by ^{19}F NMR in the crude reaction product, and was subsequently isolated; in the case of **18** only amine **26** (Scheme 3) was obtained in high yield.

Similar thiadiazoles, disulfides and/or amines had previously been obtained from unsuccessful attempts to prepare fluorinated naphthalene- and pyridine-fused 1,3λ⁴δ²,2,4-dithiadiazines from the corresponding $Ar_F-S-N=S=N-SiMe_3$ derivatives upon treatment with CsF[3,19] (cf. also the formation of the corresponding disulfide, rather than the target compound **2**, from $2\text{-}O_2NC_6H_4-S-N=S=N-SiMe_3$ on treatment with CsF[2]). The results were attributed then to both low nucleophilicity and thermal stability of the $[Ar_F-S-N=S=N]^-$ anions and explained in terms of: (1) *ipso*-cyclisation followed by ring-opening reactions to form $[Ar_F-N=S=N-S]^-$ anions, (2) elimination of sulfur and *ortho*-cyclisation of $[Ar_F-N=S=N]^-$ anions to form thiadiazoles, or (3) decomposition to Ar_FNH_2. The decomposition of $[Ar_F-S-N=S=N]^-$ anions before cyclisation yields Ar_FSSAr_F.[3,19]

The same explanation is obviously valid for this work. The difference between the successful $Ar_F-S-N=S=N-SiMe_3$-based syntheses of the title compounds (Ar_F = C_6F_5,[2] 5-HC_6F_4) and their failed counterparts (Ar_F = 6-HC_6F_4, 4-HC_6F_4) is in accordance with the known relative propensities of fluorine atoms in different positions of partially fluorinated aromatic compounds to nucleophilic substitution.[22] In the case of **14** one can also consider that the intramolecular H···N interaction (see Figure 1) stabilises the $[Ar_F-S-N^--S\equiv N]$ thiazylamide form of the intermediate anion (cf. refs.[17,23,24]) more than the $[Ar_F-S-N=S=N]^-$ sulfur diimide one, the former obviously being unable to cyclise in either *ortho* or *ipso* fashion. Taking into

account the high yield of cyclisation of the [4-$F_3CC_6F_4NSN]^-$ anion to the corresponding thiadiazole under the same conditions,[25] one can also explain the predominant formation of amine **24** from compound **17** (Scheme 3) by the direct decomposition of the [4-$F_3CC_6F_4NSNS]^-$ anion to the radical anion [4-$F_3CC_6F_4N]^{\cdot -}$, followed by reaction with the solvent to give the final product **24**. This explanation is also applicable to the formation of **26** from **18** (Scheme 3).

Thus, the synthetic usefulness of the nucleophilic approach to fluorinated 1,3$\lambda^4\delta^2$,2,4-benzodithiadiazines is limited. On the other hand, this type of cyclisation reaction is a convenient method for the synthesis of fluorinated 2,1,3-benzothiadiazoles.[16,19,25] For example, compound **10** (the precursor of **5** under electrophilic cyclisation conditions; Scheme 2) afforded fluorinated thiadiazole **27** in good yield upon treatment with CsF (Scheme 4).

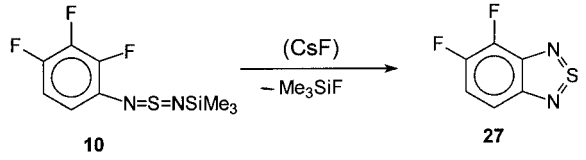

10 **27**

Scheme 4

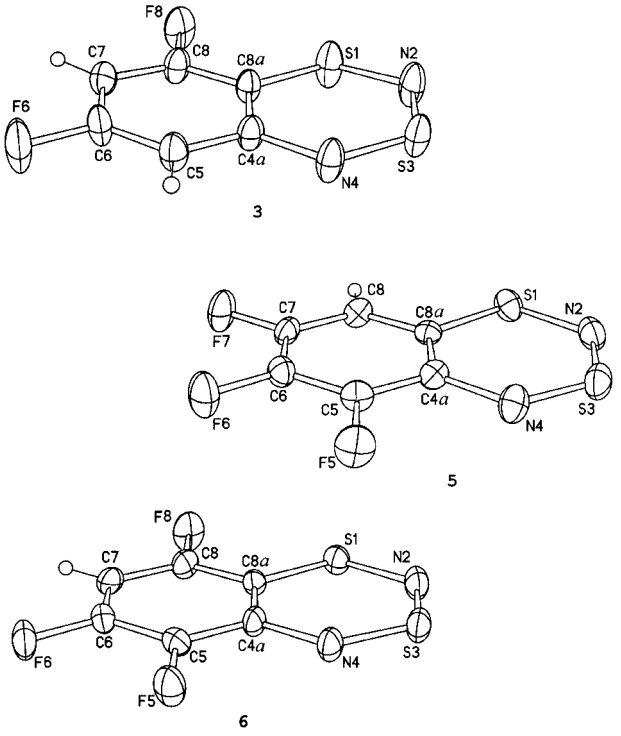

Figure 2. Molecular structures of **3**, **5** and **6**; for selected bond lengths and bond angles see Table 1

2.3. X-ray Molecular Structures and Comparison with Calculated Gas-Phase Data

According to X-ray crystallography[1–4] and gas electron diffraction[9] data, as well as post-HF and DFT calculations,[4,9,11] the compounds in series **1** are structurally nonrigid because they possess a low-energy vibrational mode that allows the molecule to be deformed easily upon going from the gas phase to the solid. For example, a molecule of **2** is significantly bent along the S1···N4 line in the gas phase[9] and perfectly planar in the crystal.[1] In contrast, a molecule of **7** is flat in the gas phase[9] and folded in the solid state.[2] (For an in-depth discussion of the structures of **2** and **7** in the two phases, including an analysis of the experimental gas-phase geometries, see ref.[9]; the results of GED measurements on **3** and **5** will be published elsewhere.) The 6-fluoro derivative of **2** is nearly planar in the crystal.[3] This structural dichotomy is also observed for compounds **3**, **5** and **6** in the crystal (Figure 2 and Table 1). According to X-ray diffraction data, molecules **5** and **6** are planar, whilst a molecule of **3** is bent along the S1···N4 line by 8.3°; this is the largest deviation from planarity so far found in the solid state for fluoro-containing compounds of series **1**.[2,3] For compound **4** the crystals obtained were not suitable for X-ray diffraction.

The bond lengths and bond angles of **3**, **5** and **6** (Table 1) are typical.[1–4,9] As in the parent compound **2** and the tetrafluoro derivative **7**, four of the π-electrons in the heterocycle are localised to some extent in two of the N–S bonds, giving rise to one long and two short bonds. We also note that the bond lengths in the N=S=N moiety of **5** are practically identical, as also found for **2**,[1] whereas for **3** and **6** they are slightly different, as found for **7**.[2]

Thus, in the crystal, compound **2** and its 5-F_3C, 6-F, 7-Br, 7-H_3CO, 5,6,7-F_3 (**5**) and 5,6,8-F_3 (**6**) derivatives are planar, whereas the 5-H_3CO, 5-Br, 6-H_3C, 8-Br, 6,8-F_2 (**3**) and 5,6,7,8-F_4 (**7**) derivatives are bent along the S1···N4 line by up to 10.8° (for the 5-H_3CO derivative) (see refs.[1–4] and this work). Of the two crystallographically independent molecules of the 6-Br derivative, one is perfectly planar whereas the other is bent by 3.1°, which directly indicates the importance of packing effects.[4]

Table 1 also compares the solid-state geometries with those obtained in the gas phase by calculation, for those derivatives for which crystal structures exist. The choice of the method/basis set combination was based on previous calculations on **2** and **7**, which showed that B3LYP/6-311+G* performs quite well for these systems, unlike MP2, which incorrectly reproduces the conformation of the heterocycle.[9] (Cartesian coordinates and energies for **2** and its fifteen fluorinated derivatives can be found in the Supporting Information; symmetries and relative energies can be found in Table 3). The calculations rigorously maintain the equal bond lengths in the N=S=N fragment for all sixteen compounds; the largest difference is 0.005 Å. However, the localisation of the π-electrons in the heterocycle is adequately reproduced. The variation in the N=S bond lengths for the various derivatives is negligible: for N2–S3 this is limited to 0.005 Å, and for S3–N4 to 0.006 Å. The values in Table 1 illustrate this. For the S–N single bond,

Table 1. Selected data comparing solid-state (XRD) and calculated gas-phase (B3LYP, r_e) geometries for **3**, **5**, **6** and 6-fluoro-1,3λ⁴δ²,2,4-benzodithiadiazine[3]

	5		**3**		**6**		6-Fluoro	
Parameter[a] [b]	XRD	B3LYP	XRD	B3LYP	XRD	B3LYP	XRD	B3LYP
S1−N2	1.683(5)	1.713	1.668(5)	1.697	1.677(6)	1.696	1.673(4)	1.713
N2−S3	1.539(5)	1.568	1.551(5)	1.565	1.537(7)	1.565	1.534(4)	1.568
S3−N4	1.532(4)	1.566	1.536(5)	1.567	1.552(5)	1.566	1.531(5)	1.568
N4−C4a	1.430(6)	1.402	1.425(6)	1.409	1.421(6)	1.401	1.425(6)	1.409
C4a−C8a	1.389(7)	1.410	1.398(7)	1.414	1.386(9)	1.415	1.405(6)	1.410
C8a−S1	1.786(5)	1.814	1.779(5)	1.826	1.784(6)	1.825	1.797(5)	1.813
S1−N2−S3	123.9(3)	121.7	123.9(3)	124.9	124.8(1)	125.0	124.3(3)	121.1
N2−S3−N4	119.7(2)	117.9	118.3(2)	118.5	119.1(3)	118.3	119.0(2)	118.0
S3−N4−C4a	121.4(4)	121.9	123.2(4)	122.9	121.2(5)	122.7	123.3(3)	121.9
N4−C4a−C8a	125.7(4)	125.6	123.6(4)	124.7	125.1(5)	125.6	123.7(5)	124.5
C4a−C8a−S1	123.9(4)	121.6	124.6(4)	125.1	125.4(4)	124.3	124.1(4)	122.0
C8a−S1−N2	105.3(2)	103.8	105.0(2)	103.9	104.1(3)	104.0	105.3(2)	103.6

[a] Bond lengths in Å and bond angles in °. [a] For atomic numbering see Scheme 1 and Figure 2.

S1−N2, the variation is larger, amounting to 0.021 Å, and seems to depend on the presence of the fluorine atom in the 8-position and thus on the conformation of the heterocycle. If the atom is present and the compound has C_s symmetry, the S1−N2 bond is shorter, as is again illustrated in Table 1. The typical C−C double/single-bond alternation, as observed in the calculations on **2** and **7**,[9] is found for all other compounds in the series and thus seems to be independent of the number and position of the fluorine atoms.

A closer look at the various C−F bond lengths displays some interesting patterns. The C−F distance for a particular position (i.e., C5, C6, C7 or C8) is shorter when that fluorine atom has another fluorine atom *ortho* to it than when it does not, which corresponds to the known shortening of the C−F bond in r_0 structures observed by microwave spectroscopy on going from fluorobenzene to 1,2-difluorobenzene.[26] The difference in the bond lengths between these two situations depends on the position of the fluorine atom: for F5 and F8 the difference is limited to 0.009 Å on average and for F6 and F7 it is 0.012 Å on average. In any of the derivatives of **2**, the C8−F8 distance is always the largest, C7−F7 and C6−F6 are intermediate and the C5−F5 bond length is the shortest. The four torsion angles that define the conformation of the heterocycle (see ref.[9] for further details) do not vary significantly with the number and the position of the fluorine atoms. The largest differences for each angle range from 1.0° for C5−C4a−C8a−S1 through 1.9° (N4−C4a−C8a−S1) and 2.4° (S3−N2−S1−C8a) to 3.8° for C4a−C8a−S1−N2.

2.4. Spectral Properties

The experimental assignment of the ^{1}H and ^{13}C NMR spectra of compound **2**, the parent compound in the **1** series, is based on double resonance, COLOC and off-resonance techniques. For the fluorinated derivatives, mono-resonance and off-resonance techniques as well as analyses of ^{1}H-^{1}H, ^{1}H-^{19}F, ^{13}C-^{19}F and ^{19}F-^{19}F spin-spin coupling constants were used to obtain full assignments. These are given in Table 2.

In the ^{15}N{^{1}H} NMR spectrum of **2**, the signal at δ = 263.1 ppm is a doublet on selective decoupling with 8-H, but a singlet on selective decoupling with 5-H. From this, it is possible to assign the signal at δ = 263.1 ppm to N-4 and the signal at δ = 269.2 ppm to N-2. This is also in agreement with an empirical analysis of the ^{15}N NMR spectroscopic data for various 5-, 6-, 7- and 8-R substituted derivatives of **2**.[3] Comparison of ^{15}N and ^{15}N{^{1}H} NMR spectra (see footnotes to Table 2; the latter feature the lack of the N^4-H^5 spin-spin coupling, cf. ref.[3]) unambiguously identifies the high-field resonance of the 6-F derivative of **2** as well as of compounds **3** and **4** as N-4 and the low-field resonance as N-2. For the previously studied compounds of series **1**, the δ^{15}N values lie in a narrow range of ca. 280−250 ppm (except for **7**[2]), with a weak dependence on the nature of the carbocyclic substituent. In the case of polyfluorinated derivatives **5**, **6** (Table 2) and **7**,[2] one nitrogen resonance is shifted to higher field (up to δ = 233 ppm for **7**[2]). It is known for related heterocycles that replacement of the four hydrogen atoms by fluorines increases the ^{15}N shielding in 2,1,3-benzothiadiazole but does not affect the δ^{15}N of 1,3λ⁴δ²,5,2,4-benzotrithiadiazepine.[27,28] Consequently, and in agreement with the discussion above, it is feasible that the high-field signal in the ^{15}N NMR spectra of **5**−**7** belongs to N-4 and the low-field signal to N-2. In agreement with the experiment, the GIAO calculations systematically predict that the N-2 nucleus of the studied compounds should be definitely deshielded relative to the N-4 nucleus for all but the 5-fluoro derivative, since the calculations for this last compound fail to predict the coincidence of both signals. For the 7-fluoro derivative the experimental assignment is difficult, but from the excellent qualitative agreement between theory and experiment for the other derivatives, one can be confident in again assigning the high-field signal to N-4 and low-field signal to N-2. Quantitative prediction of the δ^{15}N values, on the other hand, is prob-

Table 2. Calculated and experimentally determined NMR chemical shifts (ppm) for 1,3λ^{4}δ^2,2,4-benzodithiadiazine **2** and its fluoro-substituted derivatives

	2					5-Fluoro				
δ		HF		DFT		δ		HF		DFT	
7-H	6.78	7-H	7.17	7-H	6.58	7-H	6.70	7-H	7.18	7-H	6.48
6-H	6.63	6-H	7.10	6-H	6.41	6-H	6.38	6-H	6.88	6-H	6.08
5-H	5.90	5-H	6.67	5-H	5.59	8-H	5.53	8-H	6.12	8-H	5.12
8-H	5.79	8-H	6.44	8-H	5.42	5-F	36.4	5-F	31.5	5-F	40.1
C-4a	138.5	C-4a	143.3	C-4a	141.4	C-5	152.1	C-5	149.5	C-5	148.5
C-7	133.2	C-7	130.7	C-7	129.5	C-7	133.3	C-7	132.7	C-4a	130.4
C-6	130.5	C-6	129.5	C-6	125.8	C-4a	126.9	C-4a	130.9	C-7	129.3
C-8	124.0	C-8	124.8	C-8	119.5	C-8	119.4	C-8	118.5	C-6	115.9
C-5	123.0	C-5	123.0	C-5	119.1	C-6	119.0	C-6	118.1	C-8a	115.6
C-8a	115.3	C-8a	113.8	C-8a	114.2	C-8a	116.4	C-8a	117.2	C-8	114.4
N-2	269.2	N-2	396.7	N-2	354.2	N-2	268.0	N-2	390.7	N-2	350.1
N-4	263.1	N-4	353.5	N-4	313.3	N-4	268.0	N-4	338.3	N-4	297.3
	6-Fluoro					7-Fluoro				
δ		HF		DFT		δ		HF		DFT	
7-H	6.48	7-H	6.87	7-H	6.21	6-H	6.25	6-H	6.74	6-H	5.92
8-H	5.76	5-H	6.47	5-H	5.39	5-H	5.90	5-H	6.68	5-H	5.53
5-H	5.71	8-H	6.45	8-H	5.34	8-H	5.59	8-H	6.22	8-H	5.20
6-F	50.5	6-F	37.6	6-F	45.8	7-F	55.5	7-F	40.3	7-F	54.0
C-6	163.9	C-6	161.7	C-6	161.4	C-7	165.2	C-7	162.3	C-7	163.8
C-4a	140.2	C-4a	146.0	C-4a	143.0	C-4a	134.5	C-4a	137.9	C-4a	136.9
C-8	124.9	C-8	127.2	C-8	120.4	C-5	124.6	C-5	125.9	C-5	120.5
C-7	118.4	C-7	115.7	C-7	115.4	C-8a	117.5	C-8a	118.3	C-8a	116.4
C-5	111.4	C-5	110.8	C-8a	108.2	C-6	115.4	C-6	114.4	C-6	111.5
C-8a	110.1	C-8a	106.8	C-5	108.1	C-8	112.3	C-8	112.5	C-8	108.6
N-2[a]	275.7	N-2	415.8	N-2	362.6	N[b]	260.7	N-2	373.3	N-2	335.9
N-4[a]	259.6	N-4	341.8	N-4	308.9	N[b]	256.5	N-4	352.6	N-4	309.7
	3					**4**				
δ		HF		DFT		δ		HF		DFT	
7-H	6.23	7-H	6.26	7-H	5.39	5-H	5.86	5-H	6.57	5-H	5.43
5-H	5.53	5-H	5.76	5-H	4.58	8-H	5.72	8-H	6.33	8-H	5.23
6-F	53.6	6-F	41.7	6-F	49.0	7-F	29.7	7-F	18.9	7-F	29.9
8-F	47.4	8-F	36.6	8-F	41.5	6-F	25.4	6-F	17.1	6-F	22.3
C[b]	163.8	C-8	162.5	C-6	161.3	C-6,C-7[b]	152.2	C-7	148.9	C-7	151.8
C[b]	155.5	C-6	154.5	C-8	152.3	C-6,C-7[b]	150.0	C-6	147.7	C-6	148.4
C-4a	139.0	C-4a	143.2	C-4a	137.9	C-4a	135.0	C-4a	139.9	C-4a	137.6
C-5	107.8	C-8a	106.3	C-5	104.3	C-5,C-8[b]	113.6	C-8	115.4	C-8	110.3
C-7	107.1	C-7	103.3	C-7	103.7	C-5,C-8[b]	113.2	C-5	113.7	C-5	110.0
C-8a	97.6	C-5	94.8	C-8a	96.1	C-8a	111.0	C-8a	109.8	C-8a	109.0
N-2[c]	265.4	N-4	298.3	N-2	324.2	N-2[d]	265.0	N-2	394.6	N-2	347.3
N-4[c]	250.1	N-2	391.5	N-4	270.6	N-4[d]	258.8	N-4	342.8	N-4	307.4
	5					**6**				
δ		HF		DFT		δ		HF		DFT	
8-H	5.51	8-H	6.06	8-H	4.99	7-H	6.29	7-H	6.37	7-H	5.39
7-F	30.1	7-F	23.1	7-F	31.4	8-F	41.6	8-F	30.0	8-F	35.7
5-F	16.3	5-F	17.9	5-F	23.6	5-F	32.0	6-F	24.8	6-F	30.3
6-F	3.3	6-F	-0.4	6-F	3.1	6-F	10.7	5-F	6.7	5-F	12.8
C-7	152.8	C-7	150.3	C-7	152.2	C-6,C-8[b]	152.4	C-6	151.4	C-6	151.4
C-5	142.2	C-5	140.6	C-6	140.1	C-6,C-8[b]	150.4	C-8	148.7	C-8	147.3
C-6	140.6	C-6	138.4	C-5	139.9	C-5	138.7	C-5	134.5	C-5	135.4
C-4a	124.5	C-4a	128.5	C-4a	127.7	C-4a	127.2	C-4a	131.3	C-4a	128.3
C-8a	110.8	C-8a	112.3	C-8a	109.4	C-7	107.7	C-7	105.3	C-7	104.2
C-8	108.1	C-8	108.5	C-8	104.5	C-8a	97.5	C-8a	96.6	C-8a	96.1
N-2	265.1	N-2	388.3	N-2	343.4	N-2	264.2	N-2	386.7	N-2	320.8
N-4	240.9	N-4	328.0	N-4	291.4	N-4	232.8	N-4	287.4	N-4	257.0
	7										
δ		HF		DFT							
8-F,5-F[b]	18.5	8-F	11.2	8-F	15.8						
5-F,8-F[b]	12.2	5-F	11.0	5-F	14.3						
6-F,7-F[b]	9.9	6-F	3.9	7-F	8.1						
7-F,6-F[b]	6.9	7-F	2.9	6-F	5.3						
C-6,C-7[b]	143.0	C-6	139.8	C-7	141.9						
C-7,C-6[b]	141.3	C-7	139.3	C-6	141.1						
C-8,C-5[b]	140.4	C-8	139.0	C-8	138.9						
C-5,C-8[b]	139.5	C-5	136.3	C-5	136.9						
C-4a	122.0	C-4a	125.2	C-4a	122.9						
C-8a	98.9	C-8a	100.4	C-8a	98.1						
N-2	255.5	N-2	368.5	N-2	309.0						
N-4	233.1	N-4	289.7	N-4	256.7						

[a] The doublet at δ = 275.7 ppm is not changed on going to the $^{15}N\{^1H\}$ spectrum; thus, the corresponding spin-spin coupling constant (ca. 2.2 Hz) is not $^3J(N^4\text{-}H^5)$ (cf. ref.[3]) and the signal does not belong to N-4. [b] Uncertain experimental assignments. [c] The doublet of doublets of doublets at δ = 250.1 ppm becomes a doublet of doublets on going to the $^{15}N\{^1H\}$ spectrum while the triplet at δ = 265.4 ppm is not affected. [d] The quadruplet at δ = 258.8 ppm becomes a triplet on going to the $^{15}N\{^1H\}$ spectrum while the signal at δ = 265.0 ppm is not affected.

lematic: DFT performs better than HF but the rms deviation for all the compounds under consideration in Table 2 is still δ = 103.9 ppm for HF and 60.0 ppm for DFT.

A similar observation can be made for the δ^{19}F values. Here, the rms differences are 8.6 and 3.6 ppm respectively. The spread in the specific values of the different compounds is larger for this nucleus, but HF seems to do better when the number of fluorine atoms increases. Both methods do, however, qualitatively reproduce the spectrum of all compounds, except for **6**, in which 5-F and 6-F have been switched. The assignments of the ^{19}F NMR spectrum of **7**, previously uncertain,[2] can now be confidently made, on the basis of the superior DFT shifts.

For the ^{1}H NMR spectrum, the difference in performance of the two methods is a considerably smaller: the rms values are now 0.56 ppm for HF and 0.49 ppm for DFT, with HF performing better than DFT for compounds with a larger number of fluorine atoms. The only false prediction found for this nucleus, by both methods, is for the 6-fluoro derivative, in which 5-H and 8-H have been switched, but since both the calculated and the experimental differences in chemical shifts are very small, solvent effects can be used to account for this discrepancy.

For the δ^{13}C values, the rms differences for both methods are comparable: 2.6 ppm for HF and 2.7 ppm for DFT, but, in contrast to what was found for hydrogen, the performance of HF deteriorates relative to that of DFT when the number of fluorine atoms increases. The rather surprising fact that DFT falters slightly in the case of the carbon chemical shifts, when it had been clearly superior for the other nuclei, may be explained in terms of basic density functional theory. This indicates that the usual theorems do not hold in the presence of an external magnetic field and the functional has to depend both on the electron density ρ and the current density *j*, induced by the magnetic field.[29] The functionals used here, including B3LYP, do not, and this may explain why DFT would be less reliable for compounds or specific fragments of compounds in which the effect of the current density *J* is logically larger, such as the aromatic ring in these 1,3λ⁴δ²,2,4-benzodithiadiazines. Only for the parent compound **2** and its 6-fluoro and 7-fluoro derivatives are the ^{13}C chemical shifts reproduced perfectly by both methods. For both **4** and **6** the two methods agree on the chemical shifts and the previously uncertain experimental assignments can be confidently made. For the 5-fluoro derivative of **2**, DFT switches C-4a and C-7 and incorrectly reproduces the shifts of C-6, C-8 and C-8a − the small difference calculated for C-8 and C-6 might explain this, even though the HF calculation displays the same small difference yet makes a correct prediction. In the case of compound **5**, DFT switches C-5 and C-6 but the small calculated difference may again be the cause. For **7** the assignments of C-5 and C-8 can now be made unambiguously, from the results of both methods, but those of C-6 and C-7 remain doubtful. Compound **3** fares the worst where HF is concerned, since only C-4a is correctly predicted and the rest is switched; even though DFT performs better, the correct assignment of C-6 and C-8 remains a problem.

Despite the small problems that remain, the two methods used here perform generally well on a qualitative and sometimes even on a quantitative level. More sophisticated computational methods were not evaluated since computational time and efficiency become an important factor in those cases, and an evaluation of that type is beyond the scope of this study.

The most interesting feature of the NMR spectra of previously studied compounds of series **1**[1,3,4] is the enhanced shielding of the ^{1}H, ^{13}C and ^{19}F nuclei (for the *mono*fluoro derivatives) attached to C-5 and C-8 − i.e., those closest to the heterocycle − as compared to those attached to C-6 and C-7, probably due to paratropic ring currents. However, this is not the case for **3**−**6** (Table 2) and **7**.[2] The GIAO calculations at HF and B3LYP levels of theory (Table 2) reproduce these shielding patterns. However, the results of these calculations cannot be interpreted in chemical terms. One can only think that for **3**−**7** the mutual influence of the fluorine atoms dominates all other effects on δ^{19}F.

The long-wavelength absorption maxima in the UV/Vis spectra of compounds **3**−**6** (Table 5) and **7**[2] are found in the 620−635 nm range (i.e., essentially the same as for the non-fluorinated analogues),[1,3,4] with only a weak dependence upon the number and positions of the fluorine substituents. These results are in agreement with the conclusion,[11] based on resonance Raman data, that the low-energy electronic transition in the UV/Vis spectra, responsible for the blue colour of solutions of the compounds in series **1**, is localised mainly on the sulfur−nitrogen chain.

2.5. Antiaromaticity

The aromaticity or antiaromaticity of π-systems is characterised by a combination of energetic, geometric and magnetic criteria. Application of these criteria usually yields different, and very frequently contradictory, results.[5] In these situations the Nucleus-Independent Chemical Shift (NICS) concept[15] appears to be a useful criterion for the quantification of (anti)aromaticity. For all 15 possible (poly)fluorinated compounds, and also the parent, the NICS values both of the carbocycle and of the heterocycle were calculated at the HF level of theory, together with a selected number at the DFT/B3LYP level, and studied as a function of the number and the position of fluorine atoms.

The heterocyclic ring of the parent compound **2** has a positive NICS value and is antiaromatic, whilst the carbocyclic ring has a negative value and is aromatic (Table 3). In comparison, at the same level of theory, but with the B3LYP/6-31G* geometry, the NICS values for benzene, naphthalene and D_{4h}-cyclooctatetraene are δ = −9.7, −9.9 and 30.1 ppm[15] (for a minireview on the antiaromaticity of planar cyclooctatetraene, see ref.[30]). For 1,3λ⁴δ²,5,2,4-trithiadiazepine (10π-electron sulfur−nitrogen heterocycle) this value is δ = −9.3 ppm.[31] The NICS values (Table 3) also show that fluorination increases the aromaticity of the carbocyclic moieties of the compounds in series **1**. These effects have been discussed previously with respect to fluor-

Table 3. Calculated NICS values (ppm) for all possible fluoro-substituted 1,3λ^{4}δ^2,2,4-benzodithiadiazines and the parent compound **2** in their minimum energy conformations [B3LYP/6-311+G* geometries and energies, except for C_1-**7** for which the MP2/6-31G* geometry was used (see ref.[9] for details)]; values at HF/6-31+G* and B3LYP/6-31+G* levels and relative energies ΔE [kJ·mol^{-1}] are given for each isomer

Compound	ΔE	Conformation	HF/6-31+G*		B3LYP/6-31+G*	
			Carbocycle	Heterocycle	Carbocycle	Heterocycle
Parent (**2**)	0.00	C_1	−6.70	10.74	−1.64	14.99
	1.72	C_s (TS)	−5.21	16.48		
5-Fluoro	8.46	C_1	−8.14	11.02	−2.80	15.32
6-Fluoro	0.00	C_1	−8.55	10.41	−3.42	14.63
7-Fluoro	0.08	C_1	−8.24	11.12	−3.00	15.32
8-Fluoro	3.39	C_s	−6.99	16.02		
5,6-Difluoro	19.46	C_1	−9.97	10.66		
5,7-Difluoro	4.86	C_1	−9.56	11.31		
5,8-Difluoro	2.25	C_s	−8.57	15.81		
6,7-Difluoro (**4**)	9.42	C_1	−10.30	10.64	−4.96	14.77
6,8-Difluoro (**3**)	0.00	C_s	−8.62	15.67	−2.49	21.68
7,8-Difluoro	14.57	C_s	−8.75	15.37		
5,6,7-Trifluoro (**5**)	10.88	C_1	−11.58	10.85	−6.03	15.01
5,6,8-Trifluoro (**6**)	0.04	C_s	−10.13	15.36	−3.63	21.05
5,7,8-Trifluoro	0.00	C_s	−10.19	15.09		
6,7,8-Trifluoro	6.28	C_s	−10.41	15.32		
5,6,7,8-Tetrafluoro (**7**)	−	C_s	−11.77	14.94	−5.24	20.35
	−	C_1 (TS)	−14.16	5.90		

inated pyridines and pyridones and were explained in terms of the increased π-electron density in the ring system due to the positive mesomeric effect from the fluorine substituents.[32] The antiaromaticity of the heterocyclic moieties of the compounds in series **1** also depends on the number of fluorine substituents, but in a more complicated way. In some cases fluorine substituents increase the antiaromaticity (Table 3), whereas in some other cases (cf. **2**, **4** and **5**) fluorination does not affect the NICS value for the heterocycle.

The positions of the fluorine substituents seem to be of importance, especially the presence of a fluorine atom in the 8-position (cf. **2** and its 8-F, 5,8-F_2 and 6,7,8-F_3 derivatives **3**, **6** and **7** in Table 3): the very position responsible for the flattering of the heterocyclic ring on going from **2** to **7**.[9] It is clear from the results of the HF calculations in Table 3 that the presence of the fluorine atom in the 8-position and the resulting increase in symmetry to C_s reduces the aromaticity of the carbocycle and increases the antiaromaticity of the heterocycle, roughly by about 1 and 5 ppm, respectively. This effect can also be seen in the DFT calculations, but the shifts in NICS values are larger there. There is no relation between NICS values and energetic stabilisation.

The NICS values of the carbocycle at the DFT level seem unexpectedly low, at least in comparison with the data of other compounds described above, while those at the HF level "fit" better. However, from the discussion of the performance of both levels of theory in the prediction of NMR shifts it is difficult to assess which of the two methods generates the more "reasonable" values. On the other hand, if the value for **2** at the DFT level is taken at face value, one might be inclined to assume the compound's carbocycle is non-aromatic (NICS close to zero), which is clearly incorrect. Apart from the difference in scale, this is the only item that distinguishes the two methods.

Table 3 also lists data for two transition states (TS): the planar conformation of **2** and the nonplanar one of **7**. Even though the differences between TSs and ground states are not extreme, the values for the TSs − especially those for the heterocycle − are clearly located outside the set of the values for the ground states; this may be seen as an additional criterion for the assignment of the electronic states of a given conformer.

From the NICS values (Table 3 and ref.[15]), one can conclude that the antiaromaticity of the heterocycle moiety in compound **2** is about 1/3 of the antiaromaticity of D_{4h} cyclooctatetraene. According to recent estimations of resonance energy, however, the destabilization of D_{4h} cyclooctatetraene due to the cyclic interaction of the π bonds (i.e., the antiaromaticity) is negligible.[30] Taking these findings into account, along with the fact that only the heterocyclic moieties of the compounds in series **1** are antiaromatic, whereas the carbocyclic moieties are aromatic (and the C4a−C8a) bond belongs to both moieties at the same time), as well as other available data on these compounds' molecular and electronic structures[1−4,6−9,11] and thermal stabilities,[10,12] one can speculate that, in terms of the aromaticity/antiaromaticity concept,[5] 1,3λ^{4}δ^2,2,4-benzodithiadiazines could reasonably be classified on the whole as conjugated non-aromatic substances.

3. Conclusions

Novel fluorinated derivatives of 1,3λ^{4}δ^2,2,4-benzodithiadiazines (series **1**) have been prepared and characterised structurally. They are interesting not only from structural

and theoretical points of view, the latter including an extension of the aromaticity/antiaromaticity concept to non-traditional compounds, but also for applications in synthesis. As noted above, hydrolysis of the compounds in series **1** produces 2,2′-diaminodiphenyl disulfides.[3] The latter are well-known starting materials in the preparation of 1,5-benzothiadiazepines with anti-anginal and anti-hypertensive activities.[33] In this context one can believe that these fluorinated derivatives (from this work and refs.[2−4]) have some prospects in the synthesis of currently unknown fluorinated 1,5-benzothiadiazepines with potentially useful pharmacological properties.

Experimental Section

General: The ^{1}H, ^{13}C and ^{15}N NMR spectra were measured in $CDCl_3$ (unless otherwise indicated) with a Bruker DRX 500 spectrometer at frequencies of 500.13, 125.76 and 50.68 MHz, respectively, with TMS and NH_3 (liq.) as standards; the ^{19}F NMR spectra were recorded with a Bruker AC 200 machine at a frequency of 188.28 MHz with C_6F_6 as the standard. The high-resolution mass spectra (EI, 70 eV) were collected with a Finnigan MAT MS-8200 instrument, and the UV/Vis spectra were recorded with Specord M40 and HP 8453 spectrophotometers. The GC-MS measurements of solutions in CH_2Cl_2 were performed with a Hewlett−Packard G1800A GCD apparatus.

The X-ray structure determinations (Table 4) were carried out with a Bruker P4 diffractometer with the use of Mo-K_α radiation with a graphite monochromator, at −30 °C for **5** and **6**, and at 20 °C for **3** and **14**. The structures were solved by direct methods by use of the SHELXS-97 program and refined by the least-squares method in the full-matrix anisotropic (isotropic for H atoms) approximation by use of the SHELXL-93 and SHELXL-97 programs. The structure of **6** was refined as a merohedric twin (the law of twinning is 100, 0−10, 00−1). Hydrogen atoms were located on difference Fourier maps for **5** and **14**, or geometrically for **3** and **6**. Atomic coordinates, thermal parameters, bond lengths and bond angles; CCDC-178645 (**3**), -178646 (**5**), -178647 (**6**), and -178648 (**14**) contain the supplementary crystallographic data for this paper. These data can be obtained free of charge at www.ccdc.cam.ac.uk/conts/retrieving.html or from the Cambridge Crystallographic Data Centre, 12, Union Road, Cambridge CB2 1EZ, UK [Fax: (internat.) + 44-1223/336-033; E-mail: deposit@ccdc.cam.ac.uk].

Theoretical calculations were performed with Gaussian98,[34] by application of standard gradient techniques at the DFT/B3LYP level of theory using the 6-31G* and the 6-311+G* basis sets on all atoms; all basis sets were used as implemented in the program. Initially, the geometries of all compounds were optimised at the B3LYP/6-31G* level in C_s symmetry and force field calculations were used to ascertain whether the resulting structures were energy minima. When necessary, the symmetry was reduced in the subsequent B3LYP/6-311+G* calculation. Chemical shielding factors were calculated at all atomic positions and at both ring centres (non-weighted mean of the heavy-atom coordinates) for the NICS values, both at the HF/6-31+G* and B3LYP/6-31+G* levels, at the B3LYP/6-311+G* geometry, by use of the GIAO method implemented in Gaussian 98. Chemical shifts for the carbon and hydrogen atoms were obtained by subtracting the chemical shielding values of these atoms from those calculated for tetramethylsilane (TMS), which are δ = 200.7499 and 32.6074 ppm, respectively, at the HF/6-31+G* level, and δ = 191.6496 and 32.1776 ppm, respectively, at the B3LYP/6-31+G* level, based on a B3LYP/6-311+G* geometry. Chemical shifts for the fluorine atoms were obtained by subtracting the chemical shielding values of these atoms from that calculated for hexafluorobenzene (C_6F_6), which is δ = 388.5052 ppm at the HF/6-31+G* level and 347.9219 ppm at the B3LYP/6-31+G* level, based on a B3LYP/6-311+G* geometry. Chemical shifts for the nitrogen atoms were obtained by subtracting the chemical shielding values of these atoms from that calculated for ammonia (NH_3), which is 266.1027 ppm at the HF/6-

Table 4. Crystal and refinement data of compounds **3**, **5**, **6** and **14**

	3	**5**	**6**	**14**
Empirical formula	$C_6H_2F_2N_2S_2$	$C_6HF_3N_2S_2$	$C_6HF_3N_2S_2$	$C_9H_{10}F_4N_2S_2Si$
Formula mass	204.22	222.21	222.21	314.40
Crystal system	monoclinic	monoclinic	monoclinic	monoclinic
Space group	$P2_1/c$	$P2_1/c$	$P2_1/n$	$P2_1/c$
a [Å]	13.521(4)	3.8936(8)	3.8743(16)	11.6965(12)
b [Å]	7.7464(19)	5.8300(13)	7.1529(18)	17.253(2)
c [Å]	7.202(2)	32.738(6)	27.115(8)	7.1838(7)
β [°]	99.99(3)	90.60(2)	90.59(2)	99.768(8)
V [Å^3]	742.9(3)	743.1(3)	751.4(4)	1428.7(3)
Z	4	4	4	4
D_c [g cm^{-3}]	1.826	1.986	1.964	1.462
μ [mm^{-1}]	0.687	0.714	0.707	0.484
F(000)	408	440	440	640
Crystal size [mm]	3.20 × 0.09 × 0.07	1.40 × 0.20 × 0.04	5.00 × 0.24 × 0.06	0.90 × 0.14 × 0.09
Scan mode	θ-2θ	θ-2θ	ω	θ-2θ
2θ range [°]	< 50	< 50	< 52.38	< 50
Measured reflections	1315	1195	1173	2500
$F_o > 4\sigma_F$	712	843	909	1439
Transmission	0.2171−0.9535	0.8668−0.9717	0.844−0.958	0.9258−0.9631
R (obsd.)	0.0700	0.0497	0.0615	0.0463
wR_2 (all)	0.1824	0.1571	0.2183	0.1271
S	0.876	1.065	1.034	1.006

31+G* level and 263.9129 ppm at the B3LYP/6-31+G* level, based on a B3LYP/6-311+G* geometry.

The Ar_FSCl compounds **28** (Ar_F = 6-HC_6F_4)[35] and **30** (Ar_F = 4-HC_6F_4)[36] were prepared by known methods. The syntheses described below were carried out under argon (except for **29**, **31** and **32**) in absolute solvents with stirring. The reagents were added dropwise, and the solvents were distilled off at reduced pressure. CsF was calcinated and SCl_2 was distilled directly before use. Tables 5 and 6 list the physical and analytical data for the compounds synthesised.

6,8-Difluoro- (3), 6,7-Difluoro- (4) and 5,6,7-Trifluoro-1,3λ⁴δ²,2,4-benzodithiadiazine (5): Solutions of the corresponding Ar−N=S=N−$SiMe_3$ compounds (**8**−**10**, 0.010 mol) and SCl_2 (0.77 g, 7.50 mmol) in CH_2Cl_2 (30 mL) were mixed by adding them to 300 mL (600 mL in the preparation of **5**) of CH_2Cl_2 at 40 °C over a period of 1 h. After an additional hour, the reaction mixture was cooled to 20 °C and filtered, the solvent was distilled off, and the residue was sublimed under vacuum and recrystallised from hexane (to purify **5** at least three sublimation-recrystallisation cycles were necessary). Compounds **3**−**5** were obtained as black crystals.

5,6,8-Trifluoro-1,3λ⁴δ²,2,4-benzodithiadiazine (6): A solution of compound **15** (1.57 g, 0.005 mol) in MeCN (20 mL) was added over 1 h to a refluxing suspension of CsF (0.76 g, 0.005 mol) in MeCN (80 mL). After an additional 1/2 h, the reaction mixture was cooled to 20 °C and filtered, the solvent was distilled off, and the residue was sublimed under vacuum and recrystallised from hexane. Compound **6** was obtained as black crystals.

1-Fluoroaryl-3-trimethylsilyl-1,3-diaza-2-thiaallenes 8−10: A solution of the corresponding ArNSO compound **11**−**13** (0.060 mol) in hexane (25 mL) was added at −30 °C to a suspension of LiN($SiMe_3$)$_2$ (10.00 g, 0.060 mol) in hexane (50 mL). The temperature was allowed to rise to 20 °C over 2 h, and Me_3SiCl (6.60 g, 0.060 mol) in hexane (10 mL) was added. The precipitate was filtered off, the solvent was distilled off, and the residue was distilled under vacuum. Compounds **8**−**10** were obtained as orange oils.

1-Polyfluoroaryl-4-trimethylsilyl-2,4-diaza-1,3-dithia-2,3-butadienes 14−18: A solution of the corresponding Ar_FSCl compound **29**−**33** (0.025 mol) in CH_2Cl_2 (10 mL) was added at 20 °C (this temperature was −30 °C in the syntheses of **17** and **18**, followed by slow warming to 20 °C) over a period of 1 h to a solution of $Me_3SiN=)_2S$[19] (5.15 g, 0.025 mol) in CH_2Cl_2 (25 mL). After an additional 16 h, the solvent was distilled off, the residue was distilled under vacuum (for **15** and **16**) or recrystallised from hexane (for **14**, **17** and **18**), followed (for **18**) by vacuum sublimation. Compounds **15** and **16** were obtained as red oils, and compounds **14**, **17** and **18** as transparent yellow crystals.

Transformations of Compounds 14 and 16−18 by Treatment with CsF: A solution of the corresponding compound **14** or **16**−**18** (0.050 mol) in MeCN (20 mL) was added over a period of 1 h to a refluxing suspension of CsF (0.76 g, 0.005 mol) in MeCN (80 mL). After an additional 1/2 h, the reaction mixture was cooled to 20 °C and filtered, and the solvent was distilled off. The residue was worked up as follows:

Starting Compound 14: The residue was chromatographed on a silica column with hexane as the eluent. 2,2′,3,3′,4,4′,5,5′-Octafluoro-

Table 5. Spectroscopic data of the compounds

	NMR (δ[a] [ppm])				UV/Vis
Compound	^1H	^{19}F	^{13}C	^{15}N (J [Hz])	λ_{max} [nm] (log ε)[b]
3	6.23, 5.53	53.6, 47.4	163.8, 155.5, 139.0, 107.8, 107.1, 97.6	265.4 (t, 2), 250.1 (ddd, 2.5, 1.5)	632 (2.70), 365 (3.37), 277 (4.23), 264 (4.03)
4	5.86, 5.72	29.7, 25.4	152.5, 150.0, 135.0, 113.6, 113.2, 111.0	265.0 (t, 2), 258.8 (q, 2.5)	625 (2.60), 291 (4.18), 284 (4.18), 247 (3.81)
5	5.51	30.1, 16.3, 3.3	152.8, 142.2, 140.6, 124.5, 110.8, 108.1	265.1, 240.9	620 (2.58), 369 (3.12), 283 (4.11), 246 (3.79)
6	6.29	41.6, 32.0, 10.7	152.4, 150.4, 138.7, 127.2, 107.7, 97.5	264.2, 232.8	631 (2.61), 377 (3.45), 265 (4.10)
8	7.21, 6.56, 0.29	52.3			334 (3.81)
9	7.75, 7.36, 7.02, 0.24	26.4, 25.5			344 (4.13)
10	7.55, 6.89, 0.23	26.0, 25.0, 2.7			340 (3.92)
11	7.60, 7.09	58.0			309 (4.13)
12	7.46, 7.30, 6.89	33.5, 30.4			
13	8.08, 6.99	36.1, 30.3, 6.9			316 (3.95)
14	7.41, 0.33	24.3, 22.6, 7.1, 4.4			376 (4.12)
15	6.85, 0.29	54.8, 38.0, 34.5, −0.9			347 (4.06)
16	7.14, 0.32	29.1, 24.2			349 (4.11)
17	0.39	105.1, 30.7, 22.2			352 (4.18)
18	0.34	32.5, 15.4			362 (4.24)
27	7.63, 7.42	24.9, 15.9	152.4, 148.7, 145.9, 139.3, 121.2, 116.9	333.3, 323.4 (dd, 6.5, 2.7)	306 (4.04)
29	6.89	58.7, 42.5, 39.5, 0.6			
31		105.2, 35.3, 23.0			
32		37.2, 16.9			
33	6.76, 3.48	50.0, 33.2, 26.4, −1.5			
34	7.01, 6.69	53.5			411 (4.03)
35	7.46, 7.17−7.04	27.3, 25.4			418 (4.09)
36	7.20, 6.89	27.8, 24.9, 3.6			415 (3.91)

[a] Solvents: CCl_4 (**8**−**18**, **32**, **33**, **36**−**38**), neat liquid (**30**, **35**). [b] In heptane.

Table 6. Characterisation of the compounds

Compound	M.p. [°C], b.p. [°C/Torr]	Yield (%)	Empirical formula	MS: *m/z* [M^+] found (calcd.)
3	59−60	32	$C_6H_2F_2N_2S_2$	203.9625 (203.9628)
4	73−74	29	$C_6H_2F_2N_2S_2$	203.9636 (203.9628)
5	60−61	9	$C_6HF_3N_2S_2$	221.9579 (221.9533)
6	58−59	55	$C_6HF_3N_2S_2$	221.9535 (221.9533)
8	65−67/1	40	$C_9H_{12}F_2N_2SSi$	246.0458 (246.0458)
9	98−100/5	50	$C_9H_{12}F_2N_2SSi$	246.0459 (246.0458)
10	90−91/4	56	$C_9H_{11}F_3N_2SSi$	264.0363 (264.0364)
11	73−75/1, 38−39	90	$C_6H_3F_2NOS$	174.9913 (174.9915)
12	55−56/2	90	$C_6H_3F_2NOS$	174.9918 (174.9915)
13	64−65/10	92	$C_6H_2F_3NOS$	192.9809 (192.9809)
14	97−99/1, 57−58	70	$C_9H_{10}F_4N_2S_2Si$	313.9986 (313.9991)
15	107−108/1	93	$C_9H_{10}F_4N_2S_2Si$	313.9994 (313.9991)
16	115−117/1	73	$C_9H_{10}F_4N_2S_2Si$	313.9985 (313.9991)
17	111−113/2, 36−38	84	$C_{10}H_9F_7N_2S_2Si$	381.9868 (381.9865)
27	52−53	58	$C_6H_2F_2N_2S$	171.9904 (171.9907)
29	70−72/11	81	C_6HClF_4S[a]	
31	71−72/15	90	C_7ClF_7S[a]	
32	86−87	90	$C_6ClF_4NO_2S$[a]	
33	41−43/12	57	$C_6H_2F_4S$	181.9808 (181.9808)
34	99−101		$C_{12}H_6F_4N_2S$	286.0179 (286.0188)
35	84−85		$C_{12}H_6F_4N_2S$	286.0188 (286.0188)
36	88−89		$C_{12}H_4F_6N_2S$	322.0003 (321.9999)

Found (calcd.) % Cl: **29**: 16.22 (16.40); **31**: 12.25 (12.48); **32**: 13.70 (13.58).

diphenyl disulfide (**25**,[37] identified by high-resolution MS and ^1H and ^{19}F NMR) was obtained as yellow oil in a 10% yield.

Starting Compound 16: The residue was distilled under vacuum, yielding, according to GC-MS and ^{19}F NMR, 0.10 g of a 1:3:0.1 mixture of 4,5,7-trifluoro-2,1,3-benzothiadiazole (**19**)[25] 2,2′,3,3′,5,5′,6,6′-octafluorodiphenyl disulfide (**21**)[38] and 2,3,5,6-tetrafluoroaniline (**23**).[39]

Starting Compound 17: The residue was distilled under vacuum, yielding, according to GC-MS and ^{19}F NMR, 0.35 g of a 2:1:6 mixture of 4,6,7-trifluoro-5-trifluoromethyl-2,1,3-benzothiadiazole (**20**),[25] 4,4′-bis(trifluoromethyl)-2,2′,3,3′,5,5′,6,6′-octafluorodiphenyl disulfide (**22**),[40] and 2,3,5,6-tetrafluoro-4-(trifluoromethyl)-aniline (**24**).[41]

Starting Compound 18: The residue was sublimed under vacuum and recrystallised from hexane/$CHCl_3$. 2,3,5,6-Tetrafluoro-4-nitroaniline (**26**,[42] identified by comparison of its m.p. and ^1H and ^{19}F NMR spectra with those of an authentic[42] sample) was obtained as yellow crystals in 74% yield.

4,5-Difluoro-2,1,3-benzothiadiazole (27): A solution of compound **10** (1.32 g, 0.005 mol) in MeCN (20 mL) was added over 1 h to a refluxing suspension of CsF (0.76 g, 0.005 mol) in MeCN (80 mL). After an additional hour, the reaction mixture was cooled to 20 °C and filtered, the solvent was distilled off, and the residue was chromatographed on a silica column (with $CHCl_3$ as the eluent) and sublimed under vacuum followed by recrystallisation from hexane. Compound **27** was obtained as colourless crystals.

Polyfluorinated *N*-Sulfinylarylamines 11−13: The Ar−N=S=O compounds were prepared by Michaelis reaction from the corresponding $ArNH_2$ (Aldrich) and $SOCl_2$ in benzene. After the usual workup, compound **11** was obtained as yellow crystals (from hexane), and compounds **12** and **13** as yellow oils.

2,3,4,6-Tetrafluoro- (29), 2,3,5,6-Tetrafluoro-4-trifluoromethyl- (31) and 2,3,5,6-Tetrafluoro-4-nitrophenylsulfenyl Chloride (32): An excess of dry Cl_2 was slowly passed through a solution of the corresponding Ar_FSH [Ar_F = 5-HC_6F_4 (**33**), 4-$F_3CC_6F_4$,[41,43] 4-$O_2NC_6F_4$ [44]] in CCl_4 (40 mL) at ambient temperature. The solvent was distilled off and the residue was distilled (for **29** and **31**) or sublimed (for **32**) under vacuum. Compounds **29** and **31** were obtained as red oils, and compound **32** as yellow crystals.

2,3,4,6-Tetrafluorobenzenethiol (33): A solution of BuLi (4.78 g, 0.075 mol) in hexane (50 mL) was added at −80 °C to a solution of 1,2,3,5-tetrafluorobenzene (11.32 g, 0.075 mol) in Et_2O (70 mL). After 1 h, finely powdered sulfur (2.40 g, 0.075 mol) was added to the reaction solution at the same temperature. The temperature was allowed to rise to 20 °C, and the reaction mixture was quenched with 1:2 diluted HCl (25 mL). The organic layer was separated, washed with H_2O (20 mL) and dried with $CaCl_2$. The solvent was distilled off and the residue was distilled under vacuum. Compound **33** was obtained as a colourless liquid.

Fluorinated 1,3-Diaryl-1,3-diaza-2-thiaallenes (34−36): The $(Ar-N=)_2S$ compounds [Ar = 3,5-$F_2C_6H_3$ (**34**), 3,4-$F_2C_6H_3$ (**35**), 2,3,4-$F_3C_6H_2$ (**36**)] were obtained as by-products in the preparations of compounds **3**−**5**, respectively, and were isolated as orange-yellow crystals by fractional sublimation followed by recrystallisation from hexane.

Acknowledgments

The Novosibirsk authors are grateful to Mrs. Nina F. Yakusheva for her assistance in the preparations, and to the Russian Foundation for Basic Research for financial support of their work (grants 99-03-33115 and 01-03-06190) including instrumental facilities at the Collective Analytical Center of the Siberian Division of the Russian Academy of Sciences (grant 00-03-40135), and for access to the Cambridge Structural Database (grant 99-07-90133) and to the STN International databases via the STN Center at their Institute (grant 00-03-32721). A.Yu. M. is also grateful to the Siberian Division of the Russian Academy of Sciences for the N. N. Vo-

rozhtsov Award for young scientists. F. B. and C. V. A. gratefully acknowledge support by the University of Antwerp under grant GOA-BOF-UA No. 23.

[1] A. W. Cordes, M. Hojo, H. Koenig, M. C. Noble, R. T. Oakley, W. T. Pennington, *Inorg. Chem.* **1986**, *25*, 1137−1145.
[2] A. V. Zibarev, Yu. V. Gatilov, A. O. Miller, *Polyhedron* **1992**, *11*, 1137−1141.
[3] I. Yu. Bagryanskaya, Yu. V. Gatilov, A. Yu. Makarov, A. M. Maksimov, A. O. Miller, M. M. Shakirov, A. V. Zibarev, *Heteroatom Chem.* **1999**, *10*, 113−124.
[4] A. Yu. Makarov, I. Yu. Bagryanskaya, Yu. V. Gatilov, T. V. Mikhalina, M. M. Shakirov, L. N. Shchegoleva, A. V. Zibarev, *Heteroatom Chem.* **2001**, *12*, 563−576.
[5] [5a] V. I. Minkin, M. N. Glukhovtsev, B. Ya. Simkin, *Aromaticity and Antiaromaticity. Electronic and Structural Aspects*, Wiley, New York, **1994**, 336 pp. [5b] K. B. Wiberg, *Chem. Rev.* **2001**, *101*, 1317−1331 (and other articles of this special issue). [5c] M. K. Cyranski, T. M. Krygowsky, A. R. Katritzky, P. von R. Schleyer, *J. Org. Chem.* **2002**, *67*, 1333−1338.
[6] A. P. Hitchcock, R. S. DeWitte, J. M. Van Esbroek, P. Aebi, C. L. French, R. T. Oakley, N. P. C. Westwood, *J. Electron Spectrosc. Relat. Phenom.* **1991**, *57*, 165−187.
[7] N. E. Petrachenko, Yu. V. Gatilov, A. V. Zibarev, *J. Electron Spectrosc. Relat. Phenom.* **1994**, *67*, 489−492.
[8] A. V. Manaev, A. Yu. Makarov, Yu. V. Gatilov, J. N. Latosinska, V. V. Shcherbukhin, V. F. Traven, A. V. Zibarev, *J. Electron Spectrosc. Relat. Phenom.* **2000**, *107*, 33−38.
[9] F. Blockhuys, S. L. Hinchley, A. Yu. Makarov, Yu. V. Gatilov, A. V. Zibarev, J. D. Woollins, D. W. H. Rankin, *Chem. Eur. J.* **2001**, *7*, 3592−3602.
[10] I. V. Vlasyuk, V. A. Bagryansky, N. P. Gritsan, Yu. N. Molin, A. Yu. Makarov, Yu. V. Gatilov, V. V. Shcherbukhin, A. V. Zibarev, *Phys. Chem. Chem. Phys.* **2001**, *3*, 409−415.
[11] M. Schettino, R. M. Romano, C. O. Della Vedova, A. Yu. Makarov, A. V. Zibarev, *Phys. Chem. Chem. Phys.* **2001**, *3*, 1411−1418.
[12] V. A. Bagryansky, I. V. Vlasyuk, Yu. V. Gatilov, A. Yu. Makarov, Yu. N. Molin, V. V. Shcherbukhin, A. V. Zibarev, *Mendeleev Commun.* **2000**, 5−7.
[13] N. P. Gritsan, V. A. Bagryansky, I. V. Vlasyuk, Yu. N. Molin, A. Yu. Makarov, M. S. Platz, A. V. Zibarev, *Russ. Chem. Bull., Int. Ed.* **2001**, *50*, 2064−2070.
[14] A. V. Zibarev, Yu. V. Gatilov, I. Yu. Bagryanskaya, A. M. Maksimov, A. O. Miller, *J. Chem. Soc., Chem. Commun.* **1993**, 298−299.
[15] P. von R. Schleyer, C. Maerker, A. Dransfeld, H. Jiao, N. J. R. van Eikema Hommes, *J. Am. Chem. Soc.* **1996**, *118*, 6317−6318.
[16] E. Lork, R. Mews, M. M. Shakirov, P. G. Watson, A. V. Zibarev, *Eur. J. Inorg. Chem.* **2001**, 2123−2134.
[17] T. Borrmann, E. Lork, R. Mews, W. D. Stohrer, P. G. Watson, A. V. Zibarev, *Chem. Eur. J.* **2001**, *7*, 3504−3510.
[18] A. V. Zibarev, A. O. Miller, Yu. V. Gatilov, G. G. Furin, *Heteroatom Chem.* **1990**, *1*, 443−453.
[19] I. Yu. Bagryanskaya, Yu. V. Gatilov, A. O. Miller, M. M. Shakirov, A. V. Zibarev, *Heteroatom Chem.* **1994**, *5*, 561−565.
[20] T. Chivers, *Chem. Rev.* **1985**, *85*, 314−365.
[21] A. V. Zibarev, Yu. V. Gatilov, I. Yu. Bagryanskaya, S. N. Konchenko, *Polyhedron* **1992**, *11*, 2787−2793.
[22] G. M. Brooke, *J. Fluorine Chem.* **1997**, *86*, 1−76.
[23] A. V. Zibarev, E. Lork, R. Mews, *Chem. Commun.* **1998**, 991−992.
[24] T. Borrmann, A. V. Zibarev, E. Lork, G. Knitter, S. J. Chen, P. G. Watson, E. Cutin, M. M. Shakirov, W. D. Stohrer, R. Mews, *Inorg. Chem.* **2000**, *39*, 3999−4005.
[25] A. V. Zibarev, A. O. Miller, *J. Fluorine Chem.* **1990**, *50*, 359−363.
[26] [26a] S. Doraiswamy, S. D. Sharma, *J. Mol. Struct.* **1983**, *102*, 81−92. [26b] L. Nygaard, E. R. Hansen, R. L. Hansen, J. Rastrup-Andersen, G. O. Soerensen, *Spectrochim. Acta A* **1967**, *23*, 2813−2819.
[27] M. M. Shakirov, I. V. Beregovaya, A. V. Zibarev, *Khim. Geterotsikl. Soedin.* **1995**, 262−265 [*Chem. Abstr.* **1995**, *123*, 55291j].
[28] I. Yu. Bagryanskaya, H. Bock, Yu. V. Gatilov, A. Haas, M. M. Shakirov, B. Solouki, A. V. Zibarev, *Chem. Ber./Recueil* **1997**, *130*, 247−253.
[29] W. Koch, M. C. Holthausen, *A Chemist's Guide to Density Functional Theory*, Wiley-VCH, New York, **2001**, chapter 11.
[30] F. G. Klaerner, *Angew. Chem. Int. Ed.* **2001**, *40*, 3977−3981.
[31] S. Martin-Santamaria, B. Lavan, H. S. Rzepa, *Chem. Commun.* **2000**, 1089−1090.
[32] P. A. Hunt, T. Fisher, P. Schwerdtfeger, *J. Org. Chem.* **1997**, *62*, 8063−8070.
[33] A. R. Katritzky, B. V. Rogovoy, C. Chassaing, V. Vvedensky, B. Forood, B. Flatt, H. Nakai, *J. Heterocycl. Chem.* **2000**, *37*, 1655−1658.
[34] M. J. Frisch, G. W. Trucks, H. B. Schlegel, G. E. Scuseria, M. A. Robb, J. R. Cheeseman, V. G. Zakrzewski, J. A. Montgomery, Jr., R. E. Stratmann, J. C. Burrant, S. Dapprich, J. M. Millam, A. D. Daniels, K. N. Kudin, M. C. Strain, O. Farkas, J. Tomasi, V. Barone, M. Cossi, R. Cammi, B. Mennucci, C. Pomelli, C. Adamo, S. Clifford, J. Ochterski, G. A. Petersson, P. Y. Ayala, Q. Cui, K. Morokuma, D. K. Malick, A. D. Rabuck, K. Raghavachari, J. B. Foresman, J. Cioslowski, J. V. Ortiz, A. G. Baboul, B. B. Stefanov, G. Liu, A. Liashenko, P. Piskorz, I. Komaromi, R. Gomperts, R. L. Martin, D. J. Fox, T. Keith, M. A. Al-Laham. C. Y. Peng, A. Nanayakkara, C. Gonzales, M. Challacombe, P. M. W. Gill, B. Johnson, W. Chen, M. W. Wong, J. L. Andres, C. Gonzalez, M. Head-Gordon, E. S. Replogle, J. A. Pople, *Gaussian 98, Revision A.7*, Gaussian Inc., Pittsburgh PA, **1998**.
[35] T. P. Culberton, *J. Heterocycl. Chem.* **1991**, *28*, 1701−1703.
[36] P. F. Butler, M. E. Peach, *J. Fluorine Chem.* **1987**, *35*, 489−496.
[37] G. M. Brooke, M. A. Quasem, *J. Chem. Soc. C* **1967**, 865−869.
[38] P. Robson, M. Stacey, R. Stephens, J. C. Tatlow, *J. Chem. Soc.* **1960**, 4754−4760.
[39] G. M. Brooke, J. Burdon, M. Stacey, J. C. Tatlow, *J. Chem. Soc.* **1960**, 1768−1771.
[40] G. G. Furin, T. V. Terentieva, G. G. Yakobson, *Izv. Sib. Otd. Akad. Nauk SSSR Ser. Khim. Nauk* **1972**, *6*, 78−88 (in Russian).
[41] D. J. Alsop, J. Burdon, J. C. Tatlow, *J. Chem. Soc.* **1962**, 1801−1805.
[42] G. M. Brooke, J. Burdon, J. C. Tatlow, *J. Chem. Soc.* **1961**, 802−807.
[43] A. M. Maksimov, V. E. Platonov, *Fluorine Notes* **1999**, 4. www.fluorine.ru\Notes\archive.html
[44] D. J. Hupe, E. R. Pohl, *Isr. J. Chem.* **1985**, *26*, 395−399.

Received May 3, 2002
[I02284]

The Ambivalent Bonding of the 3(5)-Isopropylpyrazolyl Moiety in Homo- and Heteroscorpionate Hydrobis(3-R_1-5-R_2-pyrazolyl)(*y*-isopropylpyrazolyl)-boratocobalt(II) Complexes (y = 3 or 5)[‡]

Tomasz Ruman,[a] Zbigniew Ciunik,[b] and Stanisław Wołowiec*[a,b]

Keywords: Cobalt / Borates / N ligands / NMR spectroscopy

The synthesis of hydrotris(pyrazol-1-yl)borate ligands (Tp^x) by condensation of sodium borohydride with 3(5)-isopropylpyrazole and either 5(3)-methyl-3(5)-phenylpyrazole or 3,5-diphenylpyrazole gave the novel heteroscorpionate ligands hydrobis(5-methyl-3-phenylpyrazolyl)(5-isopropylpyrazolyl)-borate and hydrobis(3,5-diphenylpyrazolyl)(5-isopropylpyrazolyl)borate, respectively. These were converted into $CoTp^x(NCS)$ complexes as well as $CoTp^x_2$ in the case of the former ligand. In an attempted synthesis of heteroscorpionates bearing two y-isopropylpyrazolyl moieties (y = 3 or 5) formation of the homoscorpionate hydrotris(3-isopropylpyrazolyl)borate along with the above-mentioned heteroscorpionates was noticed; no formation of the desired heteroscorpionates could be detected. The bis[hydrobis(5-methyl-3-phenylpyrazolyl)(5-isopropylpyrazolyl)borato]cobalt(II) and tetrahydrofuranothiocyanatobis[hydrobis(5-methyl-3-phenylpyrazolyl)(5-isopropylpyrazolyl)borato]cobalt(II) tetrahydrofuran solvate complexes were studied by X-ray crystallography. Two Tp^x ligands provide six nitrogen donors from pyrazol-1-yl residues to form a Tp^x_2Co complex in which two 5-isopropylpyrazolyl rings are placed in a plane of symmetry, whereas the same Tp^x ligand is bound in an η^3 fashion in the pentacoordinate $[CoTp^x(NCS)(THF)]\cdot THF$ complex, in which a nitrogen atom from thiocyanate and an oxygen atom from THF complete the coordination sphere of the central metal ion. These compounds as well as the complexes thiocyanatohydrobis(3,5-diphenylpyrazolyl)(5-isopropylpyrazolyl)boratocobalt(II) and thiocyanatohydrotris(3-isopropylpyrazolyl)boratocobalt(II) were characterized by ^1H NMR and IR spectroscopy.
(© Wiley-VCH Verlag GmbH, 69451 Weinheim, Germany, 2003)

Introduction

Tris(pyrazolyl)borate anions (Tp^x) provide three *cis*-arranged nitrogen donors that are able to coordinate to transition metal ions, leaving the remaining coordination sites of the central metal ion to perform extraneous chemistry with more weakly bound ligands.[1] The stereochemistry of these reactions can be influenced by the symmetry of the Tp^x moiety, including the induction of asymmetry in catalytic reactions. One of the approaches used successfully for the latter is based on the preparation of Tp^x ligands containing chiral substituents attached to the periphery of Tp^x.[2−4] Another approach for the formation of chiral Tp^x ligands is the synthesis of heteroscorpionates composed of three different pyrazolyl residues.[5] Here we describe the synthesis of heteroscorpionates composed of two different pyrazoles, which were separated from the post-synthetic mixture as their cobalt(II) complexes.

Results and Discussion

Spontaneously formed heteroscorpionate tris(pyrazolyl)borate ligands can be obtained during the condensation of the borohydride anion with 3(5)-R-pyrazoles or 3(5)-R_1-5(3)-R_2-pyrazoles. The first spontaneous heteroscorpionate ligand was synthesized by Trofimenko, who isolated the bis-ligand complex $[Co\{HB(3\text{-}i\text{Prpz})_2(5\text{-}i\text{Prpz})\}_2]$.[6] At that time it was not clear if the heteroscorpionate was formed during the synthesis of $NaTp^x$ or exclusively during the conversion of the homoscorpionate $[HB(3\text{-}i\text{Prpz})_3]^-$ (Tp^{iPr}) into the heteroscorpionate upon heating of the $[Co(Tp^{iPr})_2]$ complex. In the latter case the driving force of the borotropic shift of the 3-isopropyl- into the 5-isopropylpyrazolyl moiety could be the release of steric clashes between six 3-isopropyl substituents around the metal ion. Later it was demonstrated that heteroscorpionate ligands are also formed during the condensation of pyrazoles with borohydrides.[7,8] This ambivalency of 3- versus 5- substitution of 3(5)-R_1-5(3)-R_2-pyrazoles can be used to construct mixed-pyrazole or even chiral Tp^x ligands.

We have used 3(5)-isopropylpyrazole for the synthesis of heteroscorpionate Tp^x ligands in order to study the bonding ambivalency of 3(5)-isopropylpyrazole in synthetic, mixed-pyrazole heteroscorpionates. The 5(3)-methyl-3(5)-phenyl-

[‡] Complexes of Heteroscorpionate Trispyrazolylborate Anionic Ligands, VII. Part VI: Ref. [9]

[a] Faculty of Chemistry, Rzeszów University of Technology, 6 Powstańców Warszawy Ave., 35-959 Rzeszów, Poland
E-mail: sw@prz.rzeszow.pl
[b] Faculty of Chemistry, University of Wrocław, 14 Joliot-Curie Str., 50-383 Wrocław, Poland

pyrazole or 3,5-diphenylpyrazole provided the additional pyrazolyl moieties to construct heteroscorpionates.

Structures of 1 and 2 in the Solid State

The heteroscorpionate obtained from condensation of $NaBH_4$ with 3-*i*PrpzH and 5-Me-3-PhpzH was found to be $[HB(5\text{-Me-3-Phpz})_2(5\text{-}i\text{Prpz})]^-$. Two cobalt(II) complexes of this anion were synthesized and studied by X-ray crystallography: the bis-ligand homoleptic complex $[Co\{HB(3\text{-Ph,5-Mepz})_2(5\text{-}i\text{Prpz})\}_2]$ (**1**) and the mono-ligand complex $[Co\{HB(3\text{-Ph,5-Mepz})_2(5\text{-}i\text{Prpz})\}(NCS)(THF)]\cdot THF$ (**2**). The molecular structures of the complexes are shown in Figure 1 and 2, respectively. The cobalt-centered bite angles (β) of the ligand in complexes **1** and **2** are 168.9° and 163.3°, respectively, while the corresponding boron-centered bite angles (α) are 88.5° and 85.2°, respectively (the bite angles were calculated as previously, i.e. disregarding hydrogen atoms).[5] The molecule of **1** is centrosymmetric. The boron-cobalt distance is 3.17 Å in **1**, while that in **2** is 3.12 Å. Thus the Tp^x ligand in **1** is bound less tightly to the cobalt center than in **2**. Accordingly, the average Co−N distance in **1** is 2.17 Å, while that in **2** is 2.09 Å (see captions to Figure 1 and 2). Such a structural difference could be anticipated due to substantial crowding around the metal ion in hexacoordinate $CoTp^x_2$ complexes. Nevertheless, this is only the second case of structurally characterized mono- and bis-ligand pentacoordinate $[CoTp^x(NCS)(THF)]$ and hexacoordinate $CoTp^x_2$ complexes constructed with the same Tp^x ligand. The first example was demonstrated for the heteroscorpionate ligand $[HB(5\text{-Me-3-Phpz})_2(3\text{-Me-5-Phpz})]^-$, for which a similar relationship was found: β = 154.6° and 149.2°, α = 85.7° and 81.9°; average Co−N bond length = 2.26 Å and 2.23 Å; Co−B distance = 3.15 Å and 3.09 Å, for $CoTp^x_2$ and $[CoTp^x(NCS)(THF)]$ complexes, respectively.[8,9]

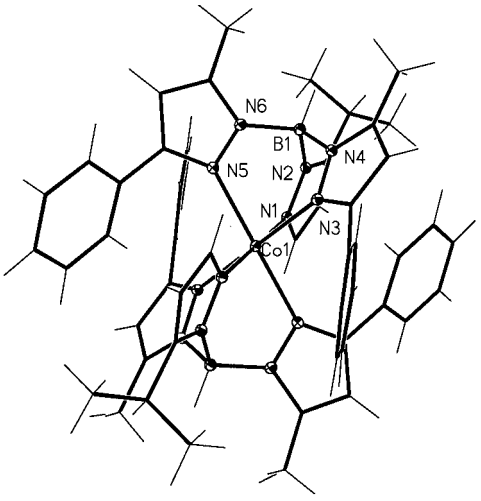

Figure 1. View of **1**; selected bond lengths [Å] and angles [°]: Co(1)−N(1) 2.0469(12), Co(1)−N(3) 2.2341(12), Co(1)−N(5) 2.2194(13); N(1)−Co(1)−N(5) 89.43(5), N(1)−Co(1)−N(3) 90.66(5), N(5)−Co(1)−N(3) 79.55(5)

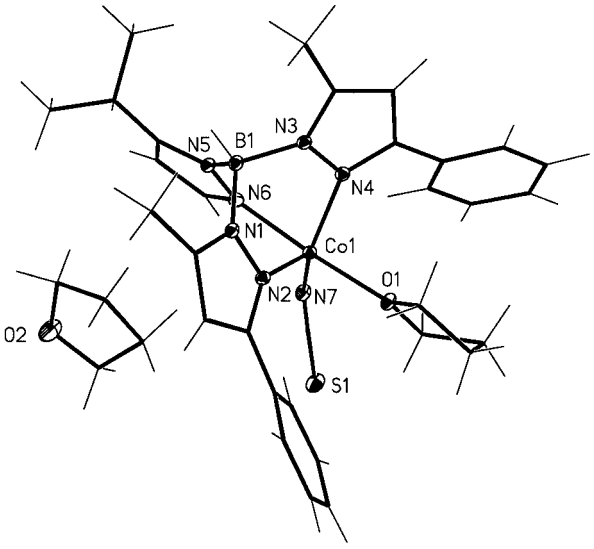

Figure 2. View of **2**; selected bond lengths [Å] and angles [°]: Co(1)−N(2) 2.0830(19), Co(1)−N(4) 2.0540(19), Co(1)−N(6) 2.1351(19), Co(1)−N(7) 1.999(2), Co(1)−O(1) 2.1193(16); N(2)−Co(1)−N(4) 93.03(7), N(2)−Co(1)−N(6) 88.05(7), N(4)−Co(1)−N(6) 84.25(7), N(7)−Co(1)−N(2) 124.92(8), N(7)−Co(1)−N(4) 141.39(8), N(7)−Co(1)−N(6) 89.73(7), N(7)−Co(1)−O(1) 88.46(7), N(2)−Co(1)−O(1) 96.76(7), N(4)−Co(1)−O(1) 94.32(7), N(6)−Co(1)−O(1) 175.06(7)

The β and α bite angles of Tp^x in **1** are much lower than those found in $[HB(3\text{-}i\text{Prpz})_2(5\text{-}i\text{Prpz})]_2Co$, which are 191.5° and 103.0°, respectively.[6] However, the Tp^x ligand in the latter is bound more tightly than that in **1**; the cobalt-boron distance is 3.15 Å. The ^1H NMR spectra of **1** and **2** are consistent with the crystal structures (see below).

A detailed analysis of the molecular structure of **2** shows some unexpected features. The 5-isopropylpyrazolyl moiety is bound more weakly than two 5-methyl-3-phenylpyrazolyl residues (see caption of Figure 2) whereas one might have expected the opposite effect due to the lack of a bulky 3-substituent and the presence of a large 5-isopropyl substituent which should result in a shortening of the Co−N(5-*i*Prpz) bond. This may be due to the specific arrangement of the remaining monodentate ligands: the coordinated THF molecule is placed within the pocket formed by the two 5-phenyl substituents, while the N-coordinated thiocyanate is very close to, and placed almost co-planar with, the 5-isopropylpyrazolyl ring. This close proximity induces a considerable weakening of the Co−N(5-*i*Prpz) bond. There are two additional intermolecular contacts (2.95 Å and 2.94 Å) between the thiocyanato sulfur atom and the *m*-H(3-Ph) and 4-H(5-Me-3-Phpz) atoms of two different molecules.

^1H NMR Spectra

The ^1H NMR spectroscopy of high-spin cobalt(II) complexes is a convenient method for the structural elucidation of $CoXTp^x$ and $CoTp^x_2$ complexes in solution[5−12] as the chemical shifts are dominated by the dipolar contribu-

tion.[12] The resonances of the 3-*i*Pr hydrogens are shifted considerably upfield, whereas those of the 5-*i*Pr hydrogens are shifted in opposite directions. The ^{1}H NMR spectrum of a side-product obtained in the synthesis of Tp^x from 3(5)-*i*PrpzH and 3,5-diPhprH, i.e. [Co(Tp^{iPr})(NCS)(CD_3OD)] (**4**, Figure 3A) indicated that heteroscorpionate [HB(3-*i*Prpz)$_2$(5-*i*Prpz)]$^-$. From this one can conclude that the driving force for the borotropic shift converting homo- to heteroscorpionates is the steric hindrance in [CoTp*i*Pr$_2$].[6] On the other hand, the ^{1}H NMR spectrum of the heteroscorpionate [Co{HB(5-*i*Prpz)(3,5-diPhpz)$_2$}(NCS)(CD_3OD)] (**3**, Figure 3B) clearly indicates the presence of a 5-*i*Pr substituent in the [CoTp^x(NCS)] complex on the basis of the methyl(*i*Pr) resonance at δ = 16.3 ppm. The presence of a 5-*i*Pr-pyrazolyl moiety in the mono-ligand complex **3** suggests that steric repulsion between the two 3-*i*Pr-pyrazolyl residues in the $CoTp^x_2$ complex is not necessary for the borotropic shift. This is strongly supported by the fact that 5-*i*Pr-pyrazolyl is present also in the synthetic heteroscorpionate Tp^x ligand both in the mono-ligand complex **2** (Figure 3C) and the bis-ligand complex **1** (Figure 3D). The symmetry of the ^{1}H NMR spectrum of **1** suggests that the Tp^x ligands are arranged in an antiperiplanar (*trans*) conformation similarly to those in [Co{HB(3-*i*Prpz)$_2$(5-*i*Prpz)}$_2$].[6] The Tp^x ligands in **1** are more sterically demanding and the boron-attached hydrogen atoms are about 0.02 Å more distant than those in [Co{HB(3-*i*Prpz)$_2$(5-*i*Prpz)}$_2$] (see above). Therefore, the 5-*i*Pr-pyrazolyl moiety is bound more weakly in **1** than in [Co{HB(3-*i*Prpz)$_2$(5-*i*Prpz)}$_2$]; the B-*H* and 3-H resonances are observed at δ = 75.2 and −29.4 ppm, respectively, while they are found at about δ = 93 and −63 ppm in the latter complex. However, the steric hindrance of [HB(3-Ph,5-Mepz)$_2$(5-*i*Prpz)]$^-$ ligand is still small enough to form the $CoTp^x_2$ complex **1**. The synthesized heteroscorpionate is a typical case of a Tp^x ligand with intermediate steric hindrance, which, depending on the synthetic procedure, forms both the stable mono-ligand complex **2** and its bis-ligand counterpart **1**. A slight structural modification by introducing a 5-phenyl- instead of a 5-methyl-substituent, resulting in formation of the heteroscorpionate [HB(5-*i*Prpz)(3,5-diPhpz)$_2$]$^-$ produces a more demanding ligand, which in the same synthetic procedure gives only the mono-ligand complex **3**.

We also varied the stoichiometry of 3(5)-*i*PrpzH and 3,5-diPhpzH in favor of the former to obtain another heteroscorpionate, [HB(*y*-*i*Prpz)$_2$(3,5-diPhpz)]$^-$ (where y = 3 or 5). However, we found that a higher percentage of homoscorpionate was obtained, without detectable amounts of the desired heteroscorpionate.

Because we were aiming for the latter, another modified pyrazole, namely 5(3)-isopropyl-3(5)-phenylpyrazole was subsequently successfully used to construct the heteroscorpionate [HB(3-Ph,5-*i*Prpz)$_2$(3,5-diMepz)]$^-$ anion which was thermally converted when isolated as its cobalt complex [CoTp^x(NCS)] into [Co{HB(5-*i*Pr-3-Phpz)(3-*i*Pr-5-Phpz)-(3,5-diMepz)}(NCS)] (**5**) in about 50% yield.[13]

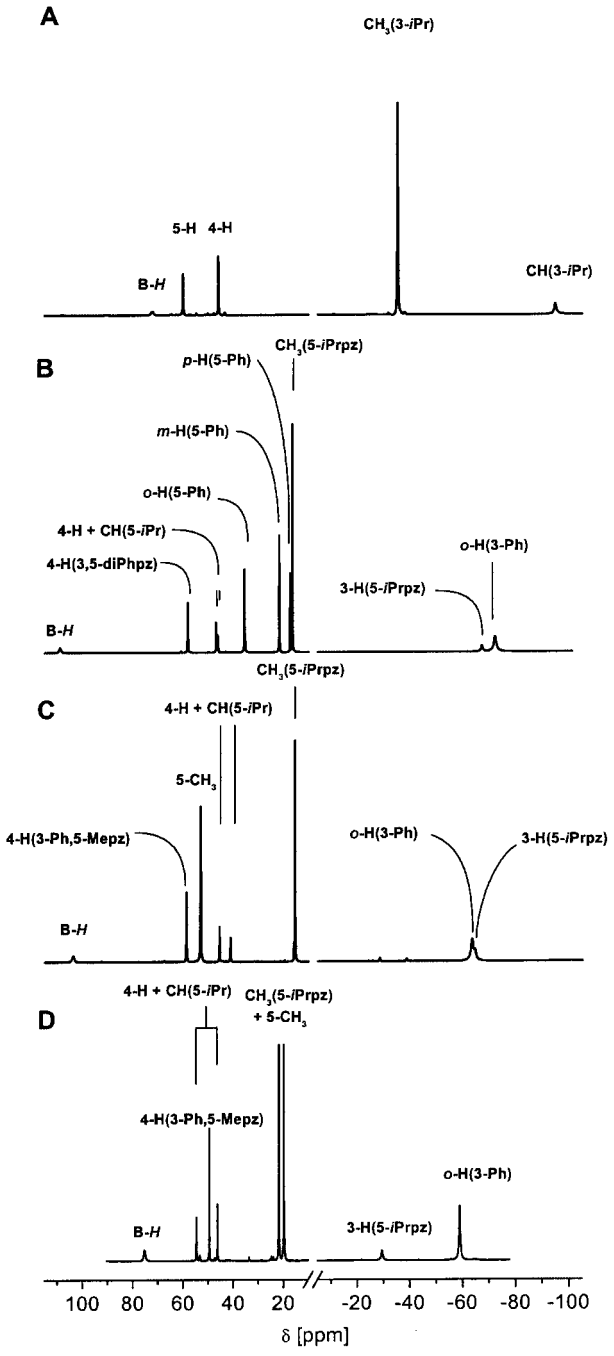

Figure 3. ^{1}H NMR spectra of: [Co(Tp^{iPr})(NCS)(CD_3OD)] (**A**); [Co{HB(5-*i*Prpz)(3,5-diPhpz)$_2$}(NCS)(CD_3OD)] (**B**); [Co{HB(5-Me-3-Phpz)$_2$(5-*i*Prpz)}(NCS)(CD_3OD)] (**C**) in [D_4]methanol; and [Co{HB(3-Ph,5-Mepz)$_2$(5-*i*Prpz)}$_2$] in [D]chloroform (**D**)

Experimental Section

Methods and Instruments: Elemental analyses were performed with Perkin−Elmer 2400 CHN analyzer. The ^{1}H NMR spectra were obtained with a Bruker AMX300 spectrometer operating in the quadrature mode at 300 MHz. The residual peaks of deuterated solvents were used as internal standards. The FT IR spectra were recorded in KBr pellets on a Perkin−Elmer 1725X instrument.

Syntheses: 5(3)-Methyl-3(5)-phenylpyrazole (5-Me-3-PhpzH), 3(5)-isopropylpyrazole (3-*i*PrpzH) and 3,5-diphenylpyrazole (3,5-diPhpzH) were synthesized by known methods.[5,6] [CoTp^x(NCS)] complexes were synthesized in the presence of an excess of metal ion and thiocyanate anion, followed by extraction of the product into dichloromethane, as previously reported.[5]

Bis[hydrobis(5-methyl-3-phenylpyrazolyl)(5-isopropylpyrazolyl)-borato]cobalt(II) ([Co{HB(3-Ph,5-Mepz)$_2$(5-*i*Prpz)}$_2$], 1), and Tetrahydrofuranothiocyanatohydrobis(5-methyl-3-phenylpyrazolyl)(5-isopropylpyrazolyl)boratocobalt(II) Tetrahydrofuran Solvate ([Co{HB-(3-Ph,5-Mepz)$_2$(5-*i*Prpz)}(NCS)(THF)]·THF, 2): $NaBH_4$ (0.57 g, 15.04 mmol) was heated with 5-Me-3-PhpzH (4.15 g, 26.2 mmol) and 3-*i*PrpzH (2.06 g, 18.75 mmol) in heptadecane (30 cm^3) with vigorous stirring in a 250-cm^3 three-necked round-bottomed flask attached to a wet-test meter and condenser. The device was flushed with nitrogen before heating was started. The temperature was gradually increased up to the boiling point of heptadecane (302 °C). Heating was continued until 1010 cm^3 of hydrogen had been collected. Heptane (60 cm^3) was added to the solution after cooling to about 100 °C and the mixture was left overnight at room temperature. The deposited precipitate was filtered off, washed with petroleum ether and vacuum dried (0.89 g, 1.94 mmol, ca. 13% yield). The crude product was converted into [CoTp^x(NCS)] complexes by standard methods. These complexes were then dissolved in THF. Dissolution was accompanied by the formation of a yellowish-white precipitate, which was filtered off, washed with small amount of THF and crystallized from dichloromethane. Yellowish-orange crystals of **1** were collected after re-concentration of the solution (256 mg, 0.275 mmol, 14.2% yield). One of the crystals was examined crystallographically (Table 1). The THF filtrate was layered with heptane. From this fraction reddish-violet crystals of **2** were collected (104 mg, 0.15 mmol, ca. 7.7% yield). One of the crystals was used for an X-ray crystallographic measurement (Table 1).

Thiocyanatohydrobis(3,5-diphenylpyrazolyl)(5-isopropylpyrazolyl)-boratocobalt(II) ([Co{HB(3,5-diPhpz)$_2$(5-*i*Prpz)}(NCS)(CH$_3$OH)], 3) and Thiocyanatohydrotris(3-isopropylpyrazolyl)boratocobalt(II) ([Co(Tp^{iPr})(NCS)], 4): $NaBH_4$ (0.46 g, 12.1 mmol) was heated with 3-*i*PrpzH (2.54 g, 23.05 mmol) and 3,5-diPhpzH (2.93 g, 13.3 mmol) in octadecane (40 cm^3) with vigorous stirring in a 250-cm^3 three-necked round-bottomed flask attached to a wet-test meter and condenser. The temperature was gradually increased up to the boiling point of octadecane (315 °C). Heating was continued until 930 cm^3 of hydrogen had been collected and then for a further hour. A white precipitate formed after cooling the mixture to about 100 °C. Heptane (80 cm^3) was then added to the suspension, which was then stirred for 2 hours at room temperature. The crude product was filtered off, washed with petroleum ether and dried to give 1.66 g of a mixture of NaTp^x salts.

NaTp^x (210 mg) was converted into a mixture of [CoTp^x(NCS)] complexes and this mixture was dissolved in methanol (5 cm^3). The insoluble blue material, identified as [Co(Tp$^{Ph}{}_2$)(NCS)],[7] was separated by passing the solution through a short bed of celite. The filtrate contained 44% [Co(Tp^{iPr})(NCS)] and 56% [Co{HB(3,5-diPhpz)$_2$(5-*i*Prpz)}(NCS)] which were identified by their ^{1}H NMR spectra. The filtrate was left to crystallize by slow evaporation of methanol. In the first instance pink, plate-shaped crystals of [Co{HB(3,5-diPhpz)$_2$(5-*i*Prpz}(NCS)(CH$_3$OH)]·CH$_3$OH were separated and collected (yield 65 mg, 0.092 mmol), and finally pink, cube-shaped crystals of [Co(Tp^{iPr})(NCS)] were collected, which turned blue upon drying at high vacuum (48 mg, 0.105 mmol).

1: $C_{52}H_{56}B_2CoN_{12}$ (929.64): calcd. C 67.18, H 6.07, N 18.81; found C 66.98, H 6.16, N 18.64. ^{1}H NMR ($CDCl_3$, 298 K): δ: = −59.0 [4 H, *o*-H(3-Ph)], −29.4 [1 H, 3-H(5-*i*Prpz)], 0.2 [4 H, *m*-H(3-Ph)], 2.5[2 H, *p*-H(3-Ph)], 19.7 and 21.7 [6 H and 6 H, 5-CH$_3$(3-Ph,5-Mepz) and CH$_3$(5-*i*Prpz)], 46.2 [1 H, HC(5-*i*Pr) or 4-H(5-*i*Prpz)], 49.4 [2 H, 4-H(3-Ph,5-Mepz)], 54.5 [1 H, 4-H(5-*i*Prpz) or HC(5-*i*Pr)], 75.2 (1 H, BH) ppm. IR (KBr): $\tilde{\nu}$ = 2536 cm^{-1} ν(BH).

2: $C_{35}H_{44}BCoN_7O_2S$ (696.57): calcd. C 60.35, H 6.37, N 14.76; found C 60.20, H 6.28, N 14.66. ^{1}H NMR (CD_3OD, 298 K): δ = −64.7 [1 H, 3-H(5-*i*Prpz)], −63.2 [4 H, *o*-H(3-Ph)], 1.7 [4 H, *m*-H(3-Ph)], 3.6 [2 H, *p*-H(3-Ph)], 15.4 (6 H, CH$_3$, 5-*i*Prpz), 41.1 and 45.5 [1 H, CH(5-*i*Prpz) and 1 H, 4-H(5-*i*Prpz)], 53.1 (6 H, 5-CH$_3$), 58.7 [2 H, 4-H(3-Ph,5-Mepz)], 103.8 (B-H) ppm. IR (KBr): $\tilde{\nu}$ = 2545 cm^{-1} ν(BH), 2056 ν(NCS).

3: $C_{38}H_{36}BCoN_7OS$ (708.56): calcd. C 64.41, H 5.12, N 13.84; found C 64.86, H 5.37, N 13.89. ^{1}H NMR (CD_3OD, 298 K): δ = −72.4 [4 H, *o*-H(3-Ph)], −67.4 [1 H, 3-H(5-*i*Prpz)], 1.5 [4 H, *m*-H(3-Ph)], 3.4 [2 H, *p*-H(3-Ph)], 16.3 (6 H, CH$_3$, 5-*i*Prpz), 17.2 [2 H, *p*-H(5-Ph)], 21.6 [4 H, *m*-H(5-Ph)], 35.3 [4 H, *p*-H(5-Ph)], 46.2 and 46.8 [1 H, CH(5-*i*Prpz) and 1 H, 4-H(5-*i*Prpz)], 58.1 [2 H, 4-H(3,5-diPhpz)], 109.0 (1 H, BH) ppm. IR (KBr): $\tilde{\nu}$ = 2579 cm^{-1} ν(BH), 2063 ν(NCS).

4: $C_{19}H_{28}BCoN_7S$ (456.29): calcd. C 50 01, H 6.18, N 21.49; found C 50.21, H 5.71, N 21.32. ^{1}H NMR (CD_3OD, 298 K): δ = −86.0 [3 H, CH(3-*i*Prpz)], −28.6 [18 H, CH$_3$(3-*i*Prpz)], 49.7 [3 H, 5-H(3-*i*Prpz)], 63.2 [3 H, 4-H(3-*i*Prpz)], 75.0 (1 H, B-H) ppm. IR (KBr): $\tilde{\nu}$ = 2484 cm^{-1} ν(BH), 2059 ν(NCS).

Crystal data are given in Table 2, together with refinement details. All measurements of crystals were performed on a Kuma KM4CCD κ-axis diffractometer with graphite-monochromated Mo-K_α radiation. Both crystals were positioned at 65 mm from the KM4CCD camera. 612 Frames were measured at 0.75° intervals with a counting time of 45 sec. The data were corrected for Lorentz and polarization effects. Data reduction and analysis were carried out with the Oxford Diffraction (Poland) (formerly Kuma Diffrac-

Table 1. The structure-chemical shift relationship

Compound	Geometric factors[a]			Chemical shifts[b]			
	β [°]	α [°]	B···Co [Å]	δ(B-*H*) [ppm]	δ(C*H*,3-*i*Pr) [ppm]	δ(C*H*$_3$,3-*i*Pr) [ppm]	δ(*o*-H,3-Ph) [ppm]
1-CD$_3$OD	140.6	75.5	3.07	93.7	−	−	−57.4
2-CD$_3$OD[c]	−	−	−	92.7	−34.8	−24.8	−57.9
3-CD$_3$OD	159.0	86.4	3.11	86.7	−71.1	−29.8[d]	−81.2
4-CD$_3$OD[e]	141.3	77.6	2.97	95.6	−	−	−69.6
5-CD$_3$OD[e]	152.5	83.0	3.11	85.0	−70.2	−29.1[d]	−78.2

[a] Data from X-ray crystallographic measurements for [CoTp^x(NCS)(THF)] complexes, unless stated otherwise. [b] Measured in [D$_4$]methanol. [c] No X-ray data available. [d] Average value for two separate resonances. [e] Geometric factors measured for tetracoordinate [CoTp^x(NCS)] and pentacoordinate [CoTp^x(NCS)]$_2$, respectively

Table 2. Crystal data and structure refinement

Compound	**1**	**2**
Empirical formula	$C_{52}H_{56}B_2N_{12}Co$	$C_{35}H_{44}BN_7O_2SCo$
Molecular weight	929.64	696.57
T /K	100(2)	100(2)
λ (Å)	0.71073	0.71073
Crystal system	Triclinic	Orthorhombic
Space group	$P\bar{1}$	Pbca
a (Å)	10.782(2)	15.6114(15)
b (Å)	10.905(3)	19.8342(15)
c (Å)	12.2209(19)	22.0406(17)
α (°)	87.45(2)	–
β (°)	74.763(16)	–
γ (°)	60.72(2)	–
V (Å^3)	1203.3(5)	6824.6(10)
Z	1	8
D_c (Mg·m^{-3})	1.283	1.356
μ (mm^{-1})	0.407	0.607
F(000)	489	2936
Crystal size (mm)	0.20 × 0.18 × 0.16	0.20 × 0.17 × 0.14
θ range for data collection (°)	3.47–28.41	3.23–28.53
Ranges of *h*,*k*,*l*	−14→14, −12→14, −16→14	−20→12, −26→26, −28→29
Reflections collected	8288	45044
Independent reflections(R_{int})	5285 (0.0187)	8203 (0.0527)
Data/parameters	5285/416	8203/601
GOF(F^2)	1.078	1.161
Final R_1/wR_2 indices [$I > 2\sigma(I)$]	0.0323/0.0810	0.0565/0.0970
Extinction	–	0.00012(12)
Largest diff. peak/hole (e·Å^{-3})	0.337/-0.429	0.620/-0.303

tion Wrocław, Poland) programs. The structures were solved by the heavy-atom method (program SHELXS-97) and refined by full-matrix least-squares on all F^2 data using the SHELXL-97 programs.[14,15] Non-hydrogen atoms were refined with anisotropic vibrational parameters; hydrogen atoms were included from geometry of molecules and/or Δρ maps and were refined with isotropic vibrational parameters.

CCDC-185198 (**1**) and -185199 (**2**) contain the supplementary crystallographic data for this paper. These data can be obtained free of charge at www.ccdc.cam.ac.uk/conts/retrieving.html [or from the Cambridge Crystallographic Data Centre, 12, Union Road, Cambridge CB2 1EZ, UK; Fax: (internat.) +44-1223/336-033; E-mail: deposit@ccdc.cam.ac.uk].

Acknowledgments

The authors thank KBN (Poland) for a grant (3 T09A 05219).

[1] S. Trofimenko, *Scorpionates: The Coordination Chemistry of Polypyrazolylborate Ligands*, Imperial College Press; London, U. K., 1999.
[2] D. LeCloux, M. C. Keyes, M. Osawa, V. Reynolds, W. B. Tolman, *Inorg. Chem.* **1994**, *33*, 6361–6368.
[3] M. C. Keyes, M. B. Chamberlein, S. A. Caltagirone, J. A. Halfen, W. B. Tolman, *Organometallics* **1998**, *17*, 1984–1992.
[4] G. R. Motson, O. Mamula, J. C. Jeffery, J. A. McCleverty, M. D. Ward, A. von Zelevsky, *J. Chem. Soc., Dalton Trans.* **2001**, 1389–1391.
[5] T. Ruman, M. Łukasiewicz, Z. Ciunik, S. Wołowiec, *Polyhedron* **2001**, *20*, 2551–2558.
[6] S. Trofimenko, J. C. Calabrese, P. J. Domaille, G. S. Thompson, *Inorg. Chem.* **1989**, *28*, 1091–1101.
[7] S. Trofimenko, A. L. Rheingold, L. Liable-Sands, *Inorg. Chem.* **2002**, *41*, 1889–1896.
[8] M. Łukasiewicz, Z. Ciunik, T. Ruman, M. Skóra, S. Wołowiec, *Polyhedron* **2001**, *20*, 237–244.
[9] T. Ruman, Z. Ciunik, E. Szklanny, S. Wołowiec, *Polyhedron*, in press.
[10] T. Ruman, Z. Ciunik, J. Mazurek, S. Wołowiec, *Eur. J. Inorg. Chem.* **2002**, 754–760.
[11] J. C. Calabrese, P. J. Domaille, G. Thompson, S. Trofimenko, *Inorg. Chem.* **1990**, *29*, 4429–4437.
[12] G. N. LaMar, J. P. Jesson, P. J. Meakin, *J. Am. Chem. Soc.* **1971**, *93*, 1286–1288.
[13] T. Ruman, Z. Ciunik, S. Wołowiec, manuscript in preparation.
[14] G. M. Sheldrick, SHELXS-97, *program for solution of crystal structures*, University of Göttingen, 1997.
[15] G. M. Sheldrick, SHELXL-97, *program for crystal structure refinement*, University of Göttingen, 1997.

Received June 21, 2002
[I02341]

Two New Zeolite-Like Supramolecular Copper Complexes

Daofeng Sun,[a] Rong Cao,*[a] Yanqiong Sun,[a] Xing Li,[a] Wenhua Bi,[a] Maochun Hong,[a] and Yingjun Zhao[a]

Keywords: Copper / Supramolecular chemistry / Hydrogen bonds / Zeolite analogues / Amines

Assembly of sodium 5-sulfoisophthalate (NaH_2SIPA) with copper(II) nitrate in the presence of an amine results in the formation of two new types of supramolecular copper complexes $[\{Cu(H_2O)_2(HSIPA)\}\cdot 2H_2O\cdot(PIP)_{1/2}]_n$ (**1**) and $[\{Cu(H_2O)_3(HSIPA)\}\cdot 6H_2O\cdot(hmt)_{1/2}]_n$ (**2**). Both complexes have 1D zigzag chain structures formed by the interconnection of four- or five-coordinate copper ions by carboxylate ligands. The 3D supramolecular architectures are dependent on the guest amine.

(© Wiley-VCH Verlag GmbH & Co. KGaA, 69451 Weinheim, Germany, 2003)

Introduction

Crystal engineering of supramolecular architectures or metal-organic coordination polymers is a maturing field and has attracted much attention in the past decades.[1−4] With the recent development of self-assembly supramolecular chemistry, it is possible to rationally design and synthesize supramolecular architectures or metal-organic coordination polymers based on covalent or supramolecular contacts (such as hydrogen bond, π-π interactions etc.).[5−7] However, the assembly of porous materials from organic ligands and metal-ion building blocks to generate new supramolecular architectures is still a challenge.[8−10] Based on the different interactions between building blocks, two principle methods can be achieved to construct open supramolecular architectures: one is based upon covalent bonds and the other on supramolecular contacts.[11] The use of covalent bonds to engage metal ions and organic ligands, such as polycarboxylic acids or 4,4′-bipy, has resulted in a large number of porous frameworks with various dimensionalities and topologies.[12−15] In contrast, the use of supramolecular contacts to construct porous supramolecular frameworks is much less common, although a few examples have been reported.[16−20]

Currently, one of the problems when constructing porous networks is the presence of an interpenetrated network if the void is more than 50% of the crystal by volume.[21] The use of guest molecules as templates — as in zeolite-like metal phosphates — can reduce the interpenetration, and this has been well documented.[4,21,22] Furthermore, the porous architectures can be tailored by changing the structure of the guest molecules.[23] In this paper, we report two new zeolite-like supramolecular copper(II) complexes, $[\{Cu(H_2O)_2(HSIPA)\}\cdot 2H_2O\cdot(PIP)_{1/2}]_n$ (**1**) and $[\{Cu(H_2O)_3(HSIPA)\}\cdot 6H_2O\cdot(hmt)_{1/2}]_n$ (**2**) (H_3SIPA = 5-sulfoisophthalic acid, PIP = piperazine, hmt = hexamethylenetetramine), constructed by a combination of coordination and hydrogen bonds. These two complexes possess quite different architectures based on the guest amine molecules.

[a] State Key Laboratory of Structural Chemistry, Fujian Institute of Research on the Structure of Matter, Chinese Academy of Sciences,
Fujian, Fuzhou, 350002, China

Results and Discussion

Complexes **1** and **2** were prepared in the presence of an amine in solution at room temperature. X-ray diffraction shows that both **1** and **2** possess one-dimensional zigzag chain structures and the hydrogen-bond interactions between chains make them three-dimensional channel-like frameworks in which the guest amine molecules reside.

Complex **1** possesses a one-dimensional zigzag chain structure. As shown in Figure 1, the central copper ion is coordinated by two oxygen atoms from two different $HSIPA^{2-}$ ligands and two coordinated water molecules — with the average $Cu-O_{SIPA}$ distance being 1.951(5) and $Cu-O_w$ being 1.965(7) Å — in a square -planar geometry, whereas the protonated sulfonate group does not participate in the coordination. Thus, every copper ion is linked by two $HSIPA^{2-}$ ligands to form a one-dimensional zigzag chain. The organic amine molecules (PIP) are found on the same side of the chain. Three kinds of strong hydrogen bonds are found between the chains: a) hydrogen bonds between uncoordinated carboxylate oxygen atoms and coordinated water molecules (O···O distances: 2.626 and 2.756 Å); b) hydrogen bonds between sulfonate oxygen atoms and the coordinated water molecules (O···O distances: 2.660 Å); and c) hydrogen bonds between uncoordinated carboxylate or sulfonate oxygen atoms and the guest amine or water molecules. The hydrogen-bond interactions between chains

make the complex a three-dimensional open supramolecular architecture with channels along the *a* axis (Figure 2). These channels possess approximate dimensions of 11.016 × 9.894 Å and are occupied by amine and free water molecules that form hydrogen bonds with the oxygen atoms of the sulfonate group and with coordinated water molecules (O···O distance: 2.636−2.819 Å; O···N distance: 2.819 Å).

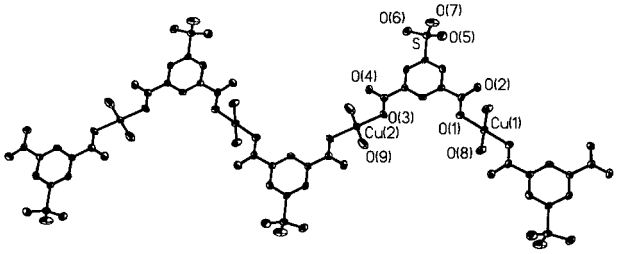

Figure 1. The one-dimensional zigzag chain structure of **1**, showing the coordination environment of the central metal ion

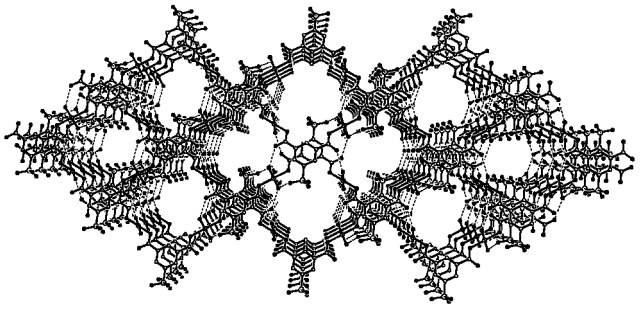

Figure 2. The 3D channel-like supramolecular architecture of **1** along the *a* axis; guest amine and water molecules are omitted for clarity

Complex **2** also has a one-dimensional zigzag chain, different from **1**, where the central copper ion is coordinated by two oxygen atoms from two different $HSIPA^{2-}$ ligands and three coordinated water molecules — with the average $Cu-O_{SIPA}$ distance being 1.960 Å, $Cu-O_w$ being 2.068 Å — in a pyramidal geometry (Figure 3). Two carboxylate oxygen atoms and two coordinated water molecules form the equatorial plane, and another coordinated water molecule occupies the axial position. As in $[Zn(ta)(phen)(H_2O)]_n$ and other similar complexes,[24,25] an axial elongation of the M−O bonds is observed [$Cu-O_w$ distance: 2.241(7) Å which is much longer than others]. Similar to **1**, every copper ion is linked by two $HSIPA^{2-}$ ligands to form a one-dimensional zigzag chain and the amine molecules (hmt) are found on the same side of the chain. Three kinds of hydrogen bonds are observed in **2**: a) hydrogen bonds between uncoordinated carboxylate oxygen atoms and coordinated water molecules (O···O distances: 2.634−2.729 Å); b) hydrogen bonds between sulfonate oxygen atoms and the free water molecules (O···O distances: 2.746−2.954 Å); and c) hydrogen bonds between sulfonate oxygen atoms or coordinated water molecules and the guest amine molecules. The chain is linked by hydrogen bonds of type *a* to generate a two-dimensional porous layer structure (Figure 4), which is further linked by hydrogen bonds of type *b* in an $O_{SIPA}\cdots O_w\cdots O_{SIPA}$ fashion to form a 3D open supramolecular framework with channels along the *c* axis (Figure 5). These channels, with approximate dimensions of 16.445 × 6.474 Å, are occupied by amine (hmt) and free water molecules that form hydrogen bonds with the oxygen atoms of the sulfonate group and with coordinated water molecules (O···O distance: 2.644−2.788 Å; O···N distance: 2.711−2.879 Å).

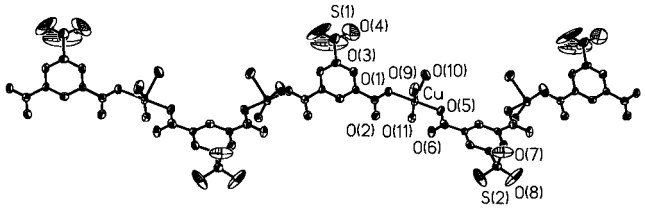

Figure 3. The one-dimensional zigzag chain structure of **2**, showing the coordination environment of the central metal ion

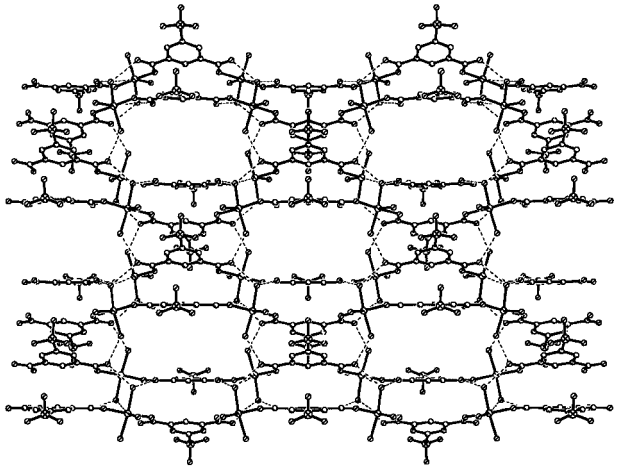

Figure 4. The 2D porous supramolecular architecture of **2** along the *c* axis

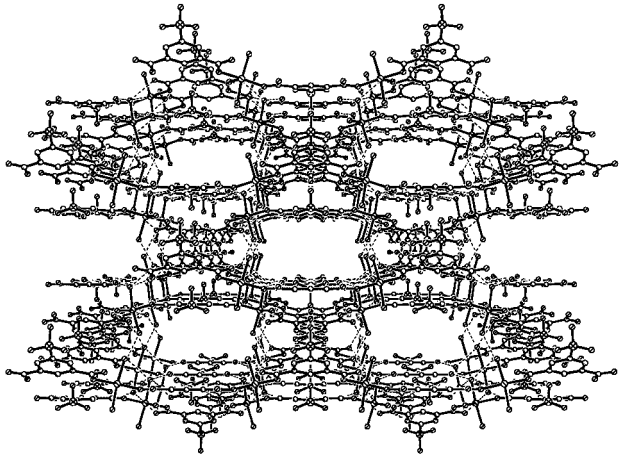

Figure 5. The 3D channel-like supramolecular architecture of **2** along the *c* axis; guest amine and water molecules are omitted for clarity

Thermogravimetric analysis (TGA) determined the thermal stability of complexes **1** and **2**. For **1**, the weight loss of 4.41% from 25 to 93 °C is equivalent to the loss of one uncoordinated water molecule (calcd. 3.71%). A total weight loss of 12.02% is achieved at 280 °C, which corresponds to the loss of another uncoordinated water molecule and 0.5 guest amine molecules per formula unit (calcd. 12.55%). However, the loss of the coordinated water molecules in **1** is not observed before 300 °C where the decomposition starts; decomposition ends above 800°C. For **2**, there is three-step weight loss in the range from 25 to 800 °C. The first weight loss of 21.20% from 25 to 145 °C corresponds to the loss of the six free water molecules per formula unit (calcd. 20.38%); the second weight loss of 12.80% from 145 to 300 °C corresponds to the loss of 0.5 guest amine molecules per formula unit (calcd. 13.21%) and the third weight loss of 10.25% from 300 to 325 °C corresponds to the loss of the coordinated water molecules (calcd. 10.19%); after 325 °C, complex **2** starts to decompose and the decomposition ends above 800 °C. This result may indicate that the guest molecules are difficult to remove from the host molecules due to the existence of strong hydrogen bonds between the host and guest molecules.

Although both **1** and **2** have three-dimensional supramolecular architectures, they are quite different due to the influence of the amine molecules. In **1**, the central copper ion is four-coordinate in a square planar geometry, and the uncoordinated carboxylate oxygen atoms, which act as hydrogen-bond acceptors, point toward different sides of the chain (Figure 6a), which makes the angle of the zigzag chain almost 90°. The chains are superimposed above each other in a staggered arrangement through hydrogen bonds between the uncoordinated carboxylate oxygen atoms and coordinated water molecules (Figure 7a). In **2**, the copper ion is five-coordinate in a pyramidal geometry, and the uncoordinated carboxylate oxygen atoms, which act as hydrogen-bond acceptors, point toward the same side of the chain (Figure 6b), which makes the angle of the zigzag chain about 120°. The superposition of the chains in **2** is quite different from that in **1**: first, two chains are linked by hydrogen bonds in staggered arrangement to form a double chain, which is further linked to generate a 2D porous layer. Secondly, the hydrogen bonds between the oxygen atoms of the sulfonate group and free water molecules in an $O_{SIPA}\cdots O_w\cdots O_{SIPA}$ fashion give rise to the final 3D open framework (Figure 7b). We propose that the structural differences between **1** and **2** arise from the influence of the guest amine molecules: the difference in the backbone of the guest molecules results in a difference of the coordination modes of the central metal ions, which further influences the arrangement of the hydrogen-bond acceptor, and leads to the difference in the final 3D supramolecular architectures. This result indicates that the host structures assembled are greatly affected by the guests,[23] and therefore changing the guest molecule, even only slightly, should lead to different structural supramolecular complexes constructed from covalent or supramolecular contacts, or a combination of the two.

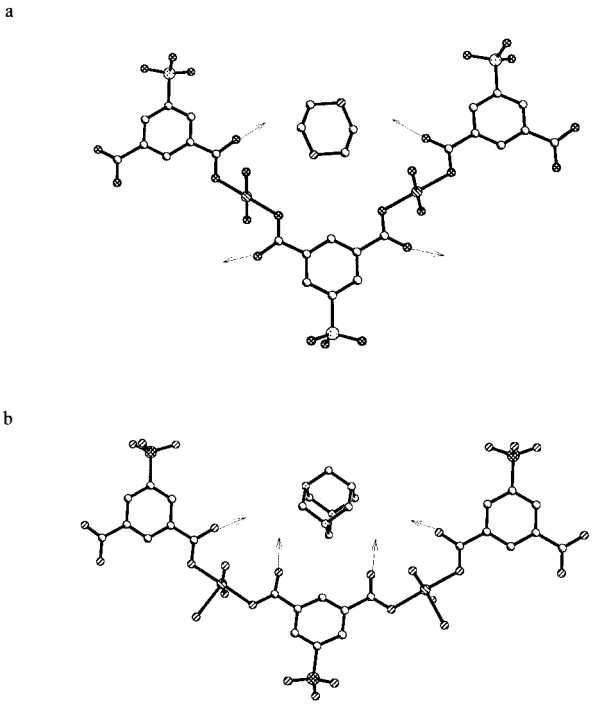

Figure 6. The different arrangement of the uncoordinated carboxylate oxygen atoms for **1** (a) and **2** (b)

Conclusion

In conclusion, two new zeolite-like supramolecular copper complexes have been prepared in the presence of amines at room temperature. Although both complexes possess one-dimension zigzag chain structures, the different guest amines result in different three-dimensional supramolecular architectures. Although guest-dependent supramolecular structures are known, their construction is still a challenge to chemists and will be an active field in the future.

Experimental Section

General Remarks: All chemicals were used as purchased without purification. Thermogravimetric experiments were performed using a TGA/SDTA851 instrument (heating rate of 10 °C/min, argon stream). IR spectra were recorded on a Magna 750 FT-IR spectrophotometer as KBr pallets. Elementary analyses were carried out in the elementary analysis group of this institute.

Synthesis of $[\{Cu(H_2O)_2(HSIPA)\}\cdot 2H_2O\cdot(PIP)_{1/2}]_n$ (1): NaH_2SIPA (0.034 g, 0.125 mmol) was dissolved in 15 mL water and $Cu(NO_3)_2\cdot 5H_2O$ (0.06 g, 0.25 mmol) was added with stirring at 60 °C. After stirring for 15 min, a solution of PIP (0.02 g, 0.25 mmol) in ethanol (5 mL) was added, and 15 min later a blue precipitate had formed. After filtration, the light-blue solution was allowed to stand in air at room temperature until blue prism-like crystals were obtained. Yield: 40%. $C_{10}H_{16}CuNO_{11}S$ (485.38): calcd. C 28.51, H 3.83, N 3.33; found C 28.60, H 3.75, N 3.40. IR (KBr): $\tilde{\nu}$ = 3211

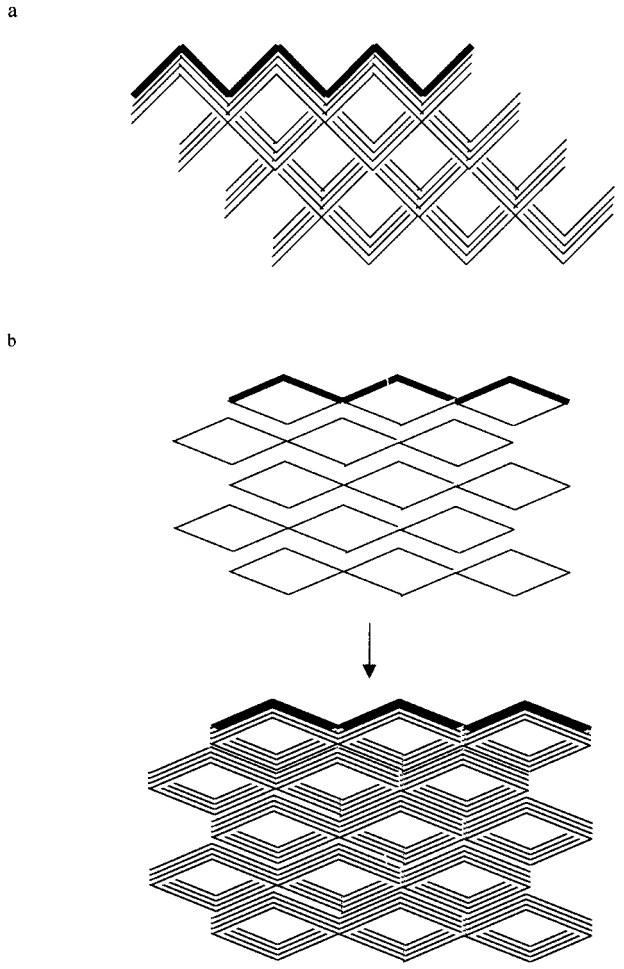

Figure 7. Schematic representation of the arrangement of the chains constructed by hydrogen bonding in **1** (a) and **2** (b)

cm^{-1} (vs), 3035 (vs), 2829 (s), 1605 (vs), 1556 (vs), 1444 (s), 1362 (vs), 1174 (s), 1043 (vs), 771 (s), 733 (m), 623 (s).

Synthesis of $[\{Cu(H_2O)_3(HSIPA)\}\cdot 6H_2O\cdot(hmt)_{1/2}]_n$ (2): The procedure was the same as that for **1** except that PIP was replaced by hmt. Yield: 50%. $C_{11}H_{26}CuN_2O_{15.5}S$ (529.94): calcd. C 24.95, H 4.95, N 5.29; found C 24.70, H 5.10, N 5.50. IR (KBr): $\tilde{\nu}$ = 3440 cm^{-1} (vs), 3120 (vs), 1637 (vs), 1574 (s), 1441 (vs), 1358 (vs), 1259 (s), 1178 (vs), 1109 (s), 1047 (vs), 1024 (s), 976 (m), 775 (s), 725 (vs), 633 (s).

X-ray Crystallographic Study: $C_{10}H_{16}CuNO_{11}S$ (**1**), M_r = 485.38, triclinic, $P\bar{1}$, a = 7.5666(4), b = 10.4595(3), c = 10.5323(5) Å, α = 75.387(2), β = 76.875(2), γ = 87.483(2)°, V = 785.44(6) $Å^3$, Z = 2, D_c = 2.052 $g\cdot cm^{-3}$, μ(Mo-K_α) = 2.901 mm^{-1}, T = 293(2) K, R [$I < 2\sigma(I)$] = 0.0753, wR = 0.1807 for 2749 independent reflections with $F \geq 2.0\ \sigma(F_o)$.
$C_{11}H_{26}CuN_2O_{15.50}S$ (**2**), M_r = 529.94, monoclinic, $C2/m$, a = 15.3759(3), b = 18.8359(6), c = 14.1292(2) Å, β = 90.324(2)°, V = 4092.02(16) $Å^3$, Z = 8, D_c = 1.720 $g\cdot cm^{-3}$, μ(Mo-K_α) = 1.251 mm^{-1}, T = 293(2) K, R [$I < 2\sigma(I)$] = 0.0864, wR = 0.1939 for 3711 independent reflections with $F \geq 2.0\ \sigma(F_o)$.

The intensity data were collected on a Smart CCD diffractometer with graphite-monochromated Mo-K_α (λ = 0.71073 Å) radiation at room temperature in the ω-2θ scan mode. An empirical absorption correction was applied to the data using the SADABS program. The structures were solved by direct methods. All non-hydrogen atoms were refined anisotropically. The hydrogen atoms were generated in idealized positions. All calculations were performed using the SHELXTL program. Selected bond lengths and angles for the two complexes are given in Table 1.
CCDC-189986 (**1**) and -189987 (**2**) contain the supplementary crystallographic data for this paper. These data can be obtained free of charge at www.ccdc.cam.ac.uk/conts/retrieving.html [or from the Cambridge Crystallographic Data Centre, 12, Union Road, Cambridge CB2 1EZ, UK; Fax: (internat.) +44−1223/336-033; E-mail: deposit@ccdc.cam.ac.uk].

Table 1. Selected bond lengths [Å] and angles [°] for **1** and **2**

1[a]			
Cu(1)−O(1)#1[a]	1.969(5)	Cu(2)−O(3)	1.933(5)
Cu(1)−O(1)	1.969(5)	Cu(2)−O(3)#2	1.933(5)
Cu(1)−O(8)#1	1.983(5)	Cu(2)−O(9)	1.946(7)
Cu(1)−O(8)	1.983(5)	Cu(2)−O(9)#2	1.946(7)
O(1)#1−Cu(1)−O(1)	180.0	O(3)−Cu(2)−O(3)#2	180.0(3)
O(1)#1−Cu(1)−O(8)#1	87.0(2)	O(3)−Cu(2)−O(9)	88.8(2)
O(1)−Cu(1)−O(8)#1	92.9(2)	O(3)#2−Cu(2)−O(9)	91.2(2)
O(1)#1−Cu(1)−O(8)	93.0(2)	O(3)−Cu(2)−O(9)#2	91.2(2)
O(1)−Cu(1)−O(8)	87.0(2)	O(3)#2−Cu(2)−O(9)#2	88.8(2)
O(8)#1−Cu(1)−O(8)	180.0(3)		
2			
Cu−O(5)	1.955(5)	Cu−O(11)	1.988(6)
Cu−O(1)	1.964(5)	Cu−O(10)	2.241(7)
Cu−O(9)	1.975(6)		
O(5)−Cu−O(1)	177.9(2)	O(9)−Cu−O(11)	165.3(3)
O(5)−Cu−O(9)	93.2(3)	O(5)−Cu−O(10)	90.0(2)
O(1)−Cu−O(9)	88.8(3)	O(1)−Cu−O(10)	89.1(2)
O(5)−Cu−O(11)	87.4(2)	O(9)−Cu−O(10)	96.0(3)
O(1)−Cu−O(11)	90.8(2)	O(11)−Cu−O(10)	98.7(2)

[a] Symmetry transformations used to generate equivalent atoms: #1 $-x, -y+1, -z$; #2 $-x, -y-z-1$; #3 $-x, -y+2, -z$.

Acknowledgments

The authors thank financial support from NNSFC, and a key project from CAS. We also thank Prof. Guoyu Yang for the thermogravimetric analysis.

[1] P. Lightfoot, A. Snedden, *J. Chem. Soc., Dalton Trans.* **1999**, 3549−3551.
[2] Y. B. Dong, M. D. Smith, R. C. Layland, H. C. Zur Loye, *J. Chem. Soc., Dalton Trans.* **2000**, 775−780.
[3] K. Biradha, K. V. Domasevitch, B. Moulton, C. Seward, M. J. Zaworotko, *Chem. Commun.* **1999**, 1327−1328.
[4] H. Gudbjartson, K. Biradha, K. M. Poirier, M. J. Zaworotko, *J. Am. Chem. Soc.* **1999**, *121*, 2599−2600.
[5] M. L. Tong, H. K. Lee, X. M. Chen, R. B. Huang, T. C. M. Mak, *J. Chem. Soc., Dalton Trans.* **1999**, 3657−3659.
[6] L. R. Macgillivray, R. H. Groeneman, J. L. Atwood, *J. Am. Chem. Soc.* **1998**, *120*, 2676−2677.
[7] C. H. Chang, K. C. Hwang, C. S. Liu, Y. Chi, A. J. Carty, L. Scoles, S. M. Peng, G. H. Lee, J. Reedijk, *Angew. Chem. Int. Ed.* **2001**, *40*, 4651−4653.
[8] O. M. Yaghi, C. E. Davis, G. Li, H. L. Li, *J. Am. Chem. Soc.* **1997**, *119*, 2861−2868.

[9] Y. Cui, H. L. Ngo, W. B. Lin, *Inorg. Chem.* **2002**, *41*, 1033−1035.
[10] J. W. Ko, K. S. Min, M. P. Suh, *Inorg. Chem.* **2002**, *41*, 2151−2157.
[11] V. G. Albano, M. C. Aragoni, M. Arca, C. Castellari, F. Demartin, F. A. Devillanova, F. Isaia, V. Lippolis, L. Loddo, G. Verani, *Chem. Commun.* **2002**, 1170−1171.
[12] S. S. Y. Chui, S. M. F. Lo, J. P. H. Charmant, A. G. Orpen, I. D. Williams, *Science* **1999**, *283*, 1148−1150.
[13] R. Cao, D. F. Sun, Y. C. Liang, M. C. Hong, K. Tatsumi, Q. Shi, *Inorg. Chem.* **2002**, *41*, 2087−2094.
[14] P. M. Forster, A. K. Cheetham, *Angew. Chem. Int. Ed.* **2002**, *41*, 457−459.
[15] M. Eddaoudi, D. B. Moler, H. L. Li, B. L. Chen, T. M. Reineke, M. O'Keeffe, O. M. Yaghi, *Acc. Chem. Res.* **2001**, *34*, 319−330.
[16] T. P. Vaid, O. L. Sydora, R. E. Douthwaite, P. T. Wolczanski, E. B. Lobkovsky, *Chem. Commun.* **2001**, 1300−1301.
[17] P. J. Nichols, C. L. Raston, J. W. Steed, *Chem. Commun.* **2001**, 1062−1063.
[18] S. F. Lai, C. Y. Cheng, K. J. Lin, *Chem. Commun.* **2001**, 1082−1083.
[19] O. M. Yaghi, H. L. Li, T. L. Groy, *J. Am. Chem. Soc.* **1996**, *118*, 9096−9101.
[20] V. R. Pedireddi, S. Chatterjee, A. Ranganathan, C. N. R. Rao, *J. Am. Chem. Soc.* **1997**, *119*, 10867−10868.
[21] P. Losier, M. J. Zaworotko, *Angew. Chem. Int. Ed. Engl.* **1996**, *35*, 2779−2782.
[22] J. C. Dai, X. T. Wu, Z. Y. Fu, S. M. Hu, W. X. Du, C. P. Cui, L. M. Wu, H. H. Zhang, R. Q. Sun, *Chem. Commun.* **2002**, 12−13.
[23] H. J. Choi, M. P. Suh, *J. Am. Chem. Soc.* **1998**, *120*, 10622−10628.
[24] D. F. Sun, R. Cao, Y. C. Liang, Q. Shi, W. P. Su, M. C. Hong, *J. Chem. Soc., Dalton Trans.* **2001**, 2335−2340.
[25] J. Cano, G. D. Munno, J. L. Sanz, R. Ruiz, J. Faus, F. Lloret, M. Julve, A. Caneschi, *J. Chem. Soc., Dalton Trans.* **1997**, 1915−1920.

Received July 18, 2002
[I02401]

Tripodal Phosphane Ligands with Novel Linker Units and Their Rhodium Complexes as Building Blocks for Dendrimer Catalysts

Ralf A. Findeis[a] and Lutz H. Gade*[a]

Dedicated to Professor Gottfried Huttner on the occasion of his 65th birthday

Keywords: Phosphane ligands / Hydrogenation / Catalysis / Dendrimers / Rhodium

An efficient strategy for the backbone functionalization of a tripodal phosphane ligand which allows its attachment to solid supports and polymers has been developed. Using pentaerythrol (**1**) as the starting material, the functionalized phosphane tripod $HOCH_2CH_2OCH_2C(CH_2PPh_2)_3$ (**9**) was obtained in good yield in a four-step synthesis. Reaction of **9** with $[Mo(CO)_3(MeCN)_3]$ and $[Rh(COD)_2][A]$ gave the complexes $[\{HOCH_2CH_2OCH_2C(CH_2PPh_2)_3\}Mo(CO)_3]$ (**10**) and $[\{HOCH_2CH_2OCH_2C(CH_2PPh_2)_3\}Rh(COD)][A]$ (A = BF_4: **11a**, PF_6: **11b**), respectively, two of which were characterised by X-ray diffraction. The carbosilane dendrimer $Si\{(CH_2)_3SiMe_2Cl\}_4$ "G[0]-[Cl]$_4$" (**12**) and its first generation analogue $Si[(CH_2)_3SiMe\{(CH_2)_3SiMe_2Cl\}_2]_4$ "G[1]-[Cl]$_8$" (**15**) were reacted with, respectively, four and eight molar equivalents of the lithium alkoxy derivative of **9** giving the two functionalized dendrimers G[0]-$[OCH_2CH_2Otriphos]_4$ (**13**) and G[1]-$[OCH_2CH_2Otriphos]_8$ (**16**). These were metallated with four and eight molar equivalents of $[Rh(COD)_2][BF_4]$ in CH_2Cl_2, selectively yielding the metallated dendrimers G[0]-$[OCH_2CH_2OtriphosRh(COD)BF_4]_4$ (**14**) and G[1]-$[OCH_2CH_2OtriphosRh(COD)BF_4]_8$ (**17**). Comparative catalytic hydrogenation of styrene and 1-hexene using $[Rh(triphos)(COD)][BF_4]$ (**11a)** and the metallodendrimers **14** and **17** showed that the fixation to the low generation dendrimers did not alter the catalytic hydrogenation properties of the catalysts.

(© Wiley-VCH Verlag GmbH & Co. KGaA, 69451 Weinheim, Germany, 2003)

Introduction

The immobilization of molecular catalysts may lead to catalytic phases which combine the virtues of homogeneous catalysis (high activity and selectivity, directed catalyst design) with those of heterogeneous catalysts (e.g. facile catalyst separation and recycling).[1] However, leaching of the metal is a major practical problem, regardless of the method of catalyst fixation and the nature of the support material.[2] This may be suppressed to various degrees by using polydentate ligands which form thermally and kinetically stable complexes with the catalyst metal. Polydentate phosphanes have been widely employed in this context and tripodal systems, such as the "triphos" ligand $MeC(CH_2PPh_2)_3$, are good examples of this capacity.[3] Their use as ligands in heterogenized metal catalysts requires the functionalization of their backbone structure, preferentially in the apical position. Modified triphos ligands have been employed for the physisorption of Ru and Rh complexes on oxidic supports[4] and the covalent fixation of such catalyst precursors to polystyrene.[5] Immobilized triphos-based catalysts have been studied in catalytic hydrogenation and hydroformylation as well as the isomerization of allylic alcohols.[6] Additionally, backbone-functionalized triphos complexes have been employed in two-phase catalysis.[7]

Since the first reports of the dendrimer fixation of molecular catalysts,[8] a variety of ligands and catalytically active complexes has been immobilized on the inside and outside of dendritic polymers.[9] Due to the importance of phosphanes in homogeneous catalysis, the immobilization of both chiral and achiral phosphane ligands has been studied in a range of such systems.[10] However, there is as yet no report of the fixation of triphos derivatives to dendrimers. To this end, efficient preparative methods for the synthesis of functionalized triphos ligands were required. Important contributions to this field have been reported by Bianchini and Huttner and their co-workers in recent years.[3–7,11–16]

Previously published syntheses of such derivatives partially suffer from the nontolerance of certain functional groups (e.g. C-C multiple bonds)[11] or the fact that the phosphanyl groups are introduced at a very early stage of the reaction sequence, making subsequent work up more difficult.[12–16] Moreover, if expensive (chiral) phosphanyl functions are to be introduced in an early reaction step of the synthetic pathway[17] the loss of phosphane during the overall sequence may be considerable. A strategy in which the phosphane is introduced in the final step of the ligand-linker synthesis, was therefore an important objective of our work. In this paper

[a] Laboratoire de Chimie Organométallique et de Catalyse, CNRS UMR 7513, Institut Le Bel, Université Louis Pasteur, 4, rue Blaise Pascal, 67070 Strasbourg, France

we report the efficient synthesis of triphos derivatives containing an ether-alcohol function in the apical position of the ligand backbone, their fixation to zeroth- and first-generation carbosilane dendrimers and their metallation to give cationic rhodium complexes. These were then employed in a comparative study as hydrogenation catalysts.

Results and Discussion

Synthesis of the Tripodal Phosphane $HOCH_2CH_2OCH_2C(CH_2PPh_2)_3$ (9)

We chose pentaerythol (**1**) as the starting material for the synthesis of an apically functionalized *triphos* ligand. This tetraalcohol is a cheap basic chemical which possesses a functionalized neopentane structure and thus appears to be well suited for the synthetic objective. There are several reports in the literature, namely from Huttner and coworkers, of the use of this starting material in *triphos* chemistry; however, these workers decided to functionalize the apical position after introduction of the phosphane groups.[13−16] As stated above, this sequence will reduce the overall yields based upon the phosphane starting material. Since the diphenylphosphanyl groups referred to in this work are model systems for more complex tridentate P-donor ligands, this point was of particular importance to us.

The four hydroxyl functions in **1** are chemically equivalent, and in order to attach a linker group to only one of these it had to be differentiated with respect to the others. This is readily achieved by reaction of **1** with triethyl orthoacetate in toluene to give the known methyl trioxabicyclooctane derivative **2** (Scheme 1).[18] The unchanged "apical" OH-function was then coupled with benzyl-protected 2-chloroethanol[19] as a linker unit to give $BzOCH_2CH_2OCH_2C(CH_2O)_3CCH_3$ (**3**), which, in turn, was hydrolysed yielding the triol $BzOCH_2CH_2OCH_2C(CH_2OH)_3$ (**4**). After functional group interconversion with $SOCl_2$ in dry pyridine, giving the trichloride **5**, and hydrogenolytic deprotection, compound **6** was reacted with Ph_2PH under strongly basic reaction conditions to yield the target phosphane $HOCH_2CH_2OCH_2C(CH_2PPh_2)_3$ (**9**) in good yield.

The differentiation of the OH groups by orthoester protection requires the multistep sequence in the synthesis of **9** as discussed above. This leads to moderate overall yields of the triphos derivative in spite of the relatively high yields in each individual reaction step. It was therefore desirable to devise a shorter route to compound **9**. This was possible via the 3-chloro-2,2-bis(chloromethyl)propan-1-ol (**7**), which is directly accessible from pentaerythrol (Scheme 1).[20] Reaction of **7** with THP-protected 2-bromoethanol gave $THPOCH_2CH_2OCH_2C(CH_2Cl)_3$ (**8**), which was converted into compound **6** by hydrolytic deprotection. This strategy provided a facile access to large quantities of the key intermediate **6**.

Synthesis and Structural Characterization of the Tripod-Metal Complexes $[\{HOCH_2CH_2OCH_2C(CH_2PPh_2)_3\}Mo(CO)_3]$ (10) and $[\{HOCH_2CH_2OCH_2C(CH_2PPh_2)_3\}Rh(COD)][A]$ ($A^- = BF_4^-$: 11a; $A^- = PF_6^-$: 11b).

In order to assess the structural details and the ligand properties of the triphosphane $HOCH_2CH_2OCH_2C(CH_2PPh_2)_3$ (**9**), it was reacted with one molar equivalent of $[Mo(CO)_3(MeCN)_3]$ to yield the yellow, air stable triphosphane-molybdenum complex $[\{HOCH_2CH_2OCH_2C(CH_2PPh_2)_3\}Mo(CO)_3]$ (**10**; Scheme 2). The ^{31}P NMR resonance of the coordinated phosphane ligand is observed at $\delta = 15.6$ ppm (**9**: $\delta = -25.8$ ppm) and the ν(CO) bands appear in the IR spectrum at 1929 and 1834 cm^{-1}. The molecular ion peak at $m/z = 866$ in the mass spectrum confirms the formulation of the complex.

Single crystals of complex **10**, which were suitable for an X-ray diffraction study, were obtained by slow diffusion of diethyl ether into a CH_2Cl_2 solution of the compound. The molecular structure of **10** is displayed in Figure 1a along with its principal bond lengths and angles. The phosphane ligand adopts the expected facial coordination mode in a molybdenum complex having a slightly distorted octahedral coordination geometry. The Mo−P distances of 2.5242(9) to 2.5302(8) Å and the M−CO bond lengths of 1.965(3) to 1.968(3) Å are within the expected range. Both the P−Mo−P and the C−Mo−C angles, which lie in the ranges of 81.11(3) to 84.67(3)° and 84.4(1) to 86.8(1)°, respectively, are below 90° defining a slightly elongated trigonal antiprismatic first coordination sphere (Figure 1b).

In view of the principal objective of this work, the synthesis of cationic triphos-rhodium hydrogenation catalysts attached to dendritic supports, the ligand-linker unit **9** was reacted with $[Rh(COD)_2]BF_4$ to give the Rh^I complex $[\{HOCH_2CH_2OCH_2C(CH_2PPh_2)_3\}Rh(COD)][BF_4]$ (**11a**; Scheme 2) which was characterised by elemental analysis and ^1H, ^{13}C and ^{31}P NMR spectroscopy. The most characteristic spectroscopic feature is the doublet at $\delta = 4.3$ ppm in the ^{31}P NMR spectrum ($^1J_{Rh,P} = 106.8$ Hz) indicating the equivalence of all three phosphorus nuclei on the NMR time scale at 293 K. The observation of an essentially unchanged single phosphorus resonance even at −80 °C is consistent with a rapid dynamic exchange, probably according to a turnstile mechanism, as was previously observed for $[Rh(triphos)(COD)]PF_6$ and $[Ir(triphos)(COD)]PF_6$.[21] We were unable to obtain single crystals of compound **11a** which were suitable for X-ray diffraction. This was achieved, however, after anion exchange with $NH_4[PF_6]$ giving the yellow crystalline complex $[\{HOCH_2CH_2OCH_2C(CH_2PPh_2)_3\}Rh(COD)][PF_6]$ (**11b**; Scheme 2). A single crystal X-ray structure analysis of complex **11b** established its molecular structure, which is displayed in Figure 2a, while the inner coordination environment of the rhodium atom is highlighted in Figure 2b.

The coordination geometry of the complex displayed in Figure 2b is a distorted trigonal bipyramid, the apical position being occupied by the phosphorus atom P(1) and the centroid of the olefinic double bond C(5)−C(6). Whereas

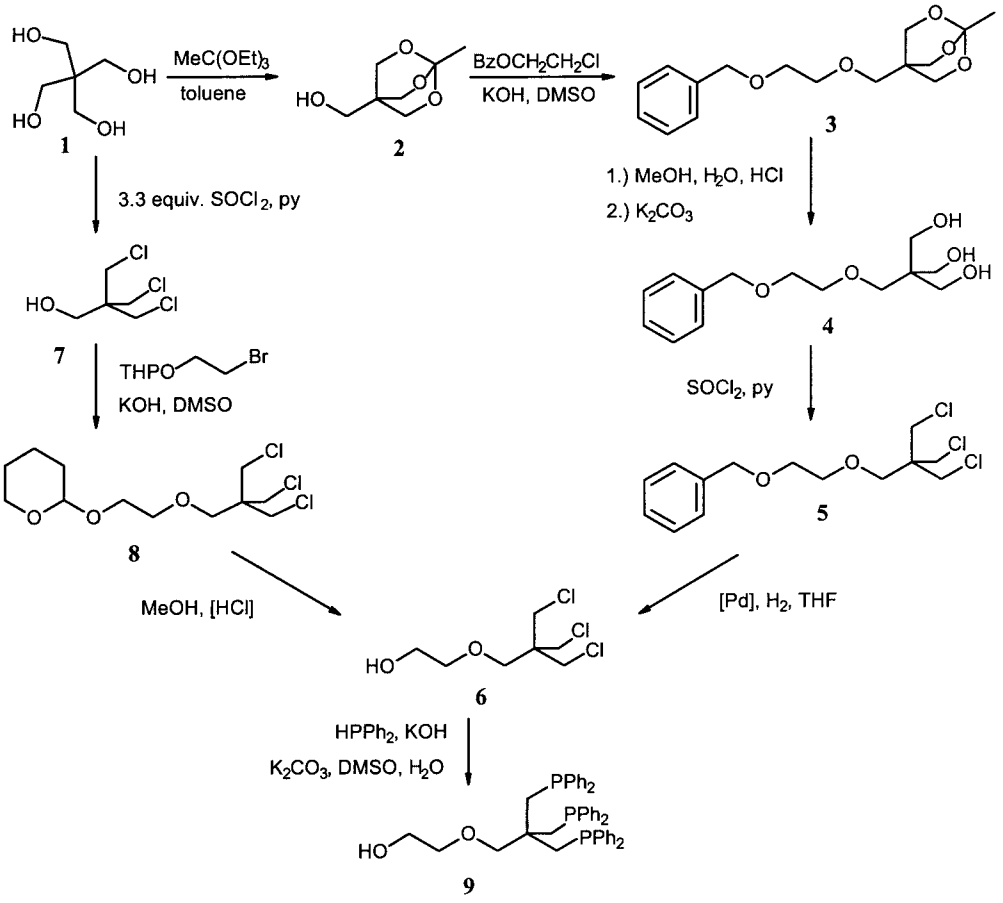

Scheme 1. The two synthetic strategies for the preparation of the ligand-linker **9**

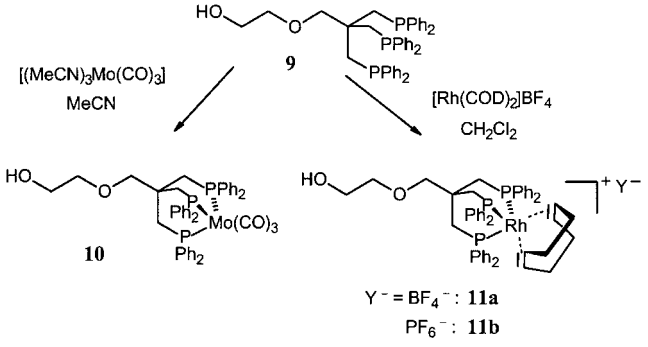

Scheme 2. Synthesis of the tripod-metal complexes **10** and **11a/b**

the Rh−P bond length to the apical phosphane unit [Rh−P(1) 2.303(2) Å] is significantly shorter than for those of the two equatorial phosphanes [Rh−P(2) 2.405(2), Rh−P(3) 2.406(2) Å], the Rh−C distances to the apical olefin carbon atoms [Rh−C(5) 2.264(6), Rh−C(6) 2.327(6) Å] are significantly greater than for the equatorial π-olefin ligands [Rh−C(1) 2.180(6), Rh−C(2) 2.155(6) Å]. The P(1)−Rh−centroid{C(5)/C(6)} angle of 170.13(4) deviates slightly from the ideal of 180°, while the P(1)−Rh−P(2/3) and P(1)−Rh−centroid{C(1)/C(2)} angles are close to 90°. As observed in the crystal structure of the molybdenum complex **10**, the oxygen atoms in the $HOCH_2CH_2O$- spacer in **11b** adopt a gauche conformation.

The packing of the molecules of **11b** in the unit cell is displayed in Figure 2c. For the sake of clarity, the phenyl groups of the diphenylphosphane units, and the lattice solvent molecules (CH_2Cl_2), have been omitted. The molecules are arranged in such a way that the apical alcohol units of the tripod ligands face each other forming intermolecular hydrogen bonds while the PF_6 anions are arranged along channels in the crystal near to the positively charged rhodium complex units.

Fixation of [{$HOCH_2CH_2OCH_2C(CH_2PPh_2)_3$}-Rh(COD)][$BF_4$] (11a) to Zeroth and First Generation Carbosilane Dendrimers

In order to asses the suitability of the apically derivatized *triphos* ligand **9** for the fixation of rhodium hydrogenation catalysts to carbosilane dendrimers, the known zeroth generation dendrimer $Si\{(CH_2)_3SiMe_2Cl\}_4$, "G[0]-$[Cl]_4$" (**12**) and its first generation analogue $Si[(CH_2)_3SiMe\{(CH_2)_3SiMe_2Cl\}_2]_4$, "G[1]-$[Cl]_8$" (**15**) [22] were reacted with, respectively, four and eight molar equivalents of the lithium alkoxy derivative of **9**. After work up the two func-

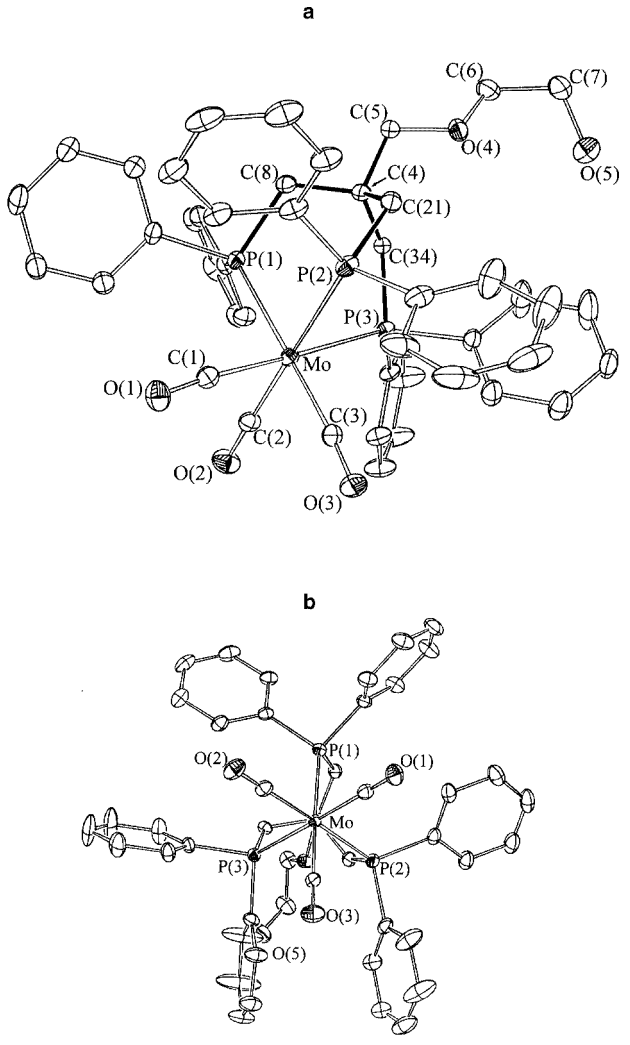

Figure 1. a) Molecular structure of complex **10**; principal bond lengths (Å) and angles (°): Mo−P(1) 2.5292(7), Mo−C(3) 1.966(3), O(4)−C(6) 1.427(4), Mo−P(2) 2.5242(9), C(1)−O(1) 1.165(3), C(6)−C(7) 1.497(5), Mo−P(3) 2.5302(8), C(2)−O(2), 1.164(4), C(7)−O(5) 1.423(4), Mo−C(1) 1.968(3), C(3)−O(3) 1.155(3), O(4)−O(5) 2.751(3), Mo−C(2) 1.965(3), C(5)−O(4) 1.403(4); P(1)−Mo−P(2) 84.67(3), C(1)−Mo−C(2) 84.4(1), C(4)−C(8)−P(1) 116.4(4), P(1)−Mo−P(3) 84.49(2), C(1)−Mo−C(3) 84.9(1), C(4)−C(21)−P(2) 117.3(2), P(2)−Mo−P(3) 81.11(3), C(2)−Mo−C(3) 86.8(1), C(4)−C(34)−P(3) 116.7(2); b) view along the virtual threefold molecular axis of the tripohos-$Mo(CO)_3$ unit

tionalized dendrimers G[0]-[OCH_2CH_2Otriphos]$_4$ (**13**) and G[1]-[OCH_2CH_2Otriphos]$_8$ (**16**) were isolated in high yield (Scheme 3 and 4).

The dendrimer phosphanes **13** and **16** were characterised by elemental analysis, ^{1}H, ^{13}C, ^{29}Si and ^{31}P NMR spectroscopy as well as FAB (**13**) and MALDI-TOF (**16**) mass spectrometry. Stirring of **13** and **16** with, respectively, four and eight molar equivalents of [$Rh(COD)_2$][BF_4] in CH_2Cl_2 selectively gave the metallated dendrimers G[0]-[OCH_2CH_2OtriphosRh(COD)BF_4]$_4$ (**14**) (Scheme 3) and G[1]-[OCH_2CH_2OtriphosRh(COD)BF_4]$_8$ (**17**) (Figure 3). These were characterised by the analytical and NMR spectroscopic techniques applied to the phosphane precursors as well as

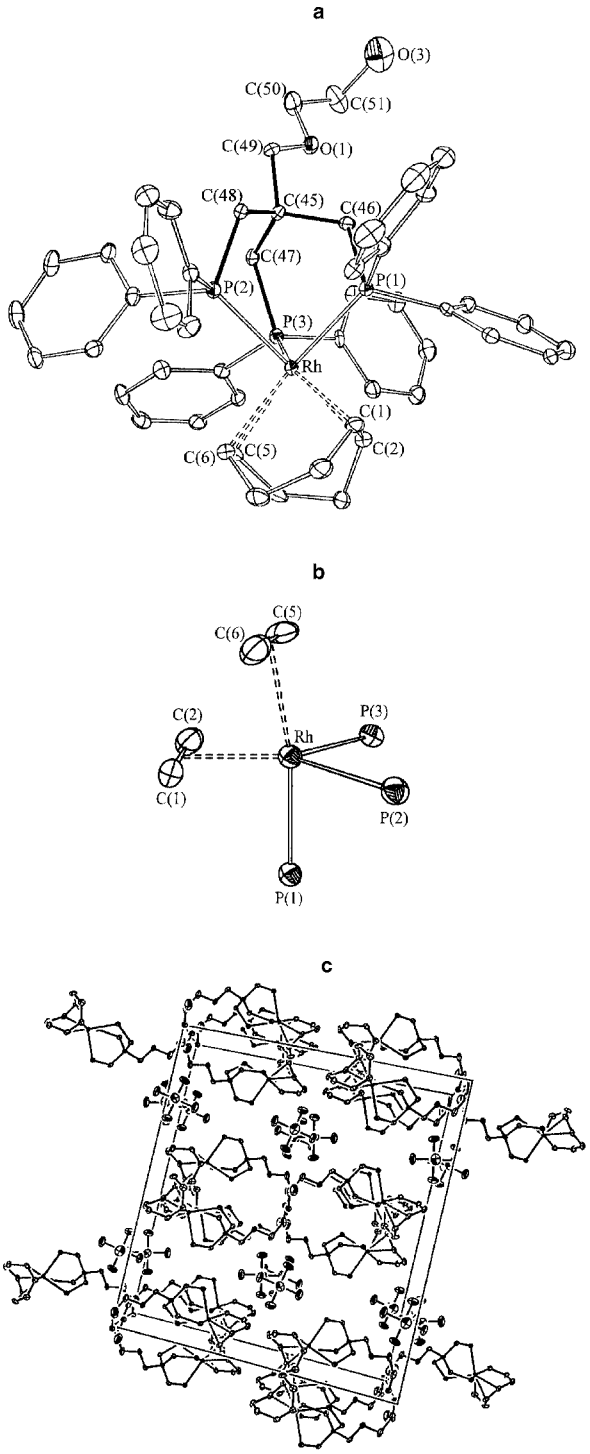

Figure 2. a) Molecular structure of complex **11b**; principal bond lengths (Å) and angles (°):Rh−P(1) 2.303(2), Rh−C(5) 2.264(6), O(1)−C(49) 1.411(7), Rh−P(2) 2.405(2), Rh−C(6) 2.327(6), O(1)−C(50) 1.412(7), Rh−P(3) 2.406(2), P(1)−C(46) 1.851(5), C(50)−C(51) 1.53(1), Rh−C(1) 2.180(6), P(2)−C(48) 1.843(6), O(2)−C(51) 1.55(2), Rh−C(2) 2.155(6), P(3)−C(47) 1.849(6); P(1)−Rh−P(2) 87.56(6), P(1)−C(46)−C(45) 115.0(4), C(49)−O(1)−C(50) 112.9(5), P(1)−Rh−P(3) 87.11(5), P(2)−C(48)−C(45) 116.8(4), O(1)−C(50)−C(51) 109.5(6), P(2)−Rh−P(3) 89.52(5), P(3)−C(47)−C(45) 117.4(4), C(50)−C(51)−O(2) 100.8(9); b) ligand arrangement in the first coordination sphere of complex **11b**; c) the packing of the molecules of **11b** in the unit cell; for the sake of clarity, the phenyl groups of the diphenylphosphane units, and the lattice solvent molecules (CH_2Cl_2) have been omitted

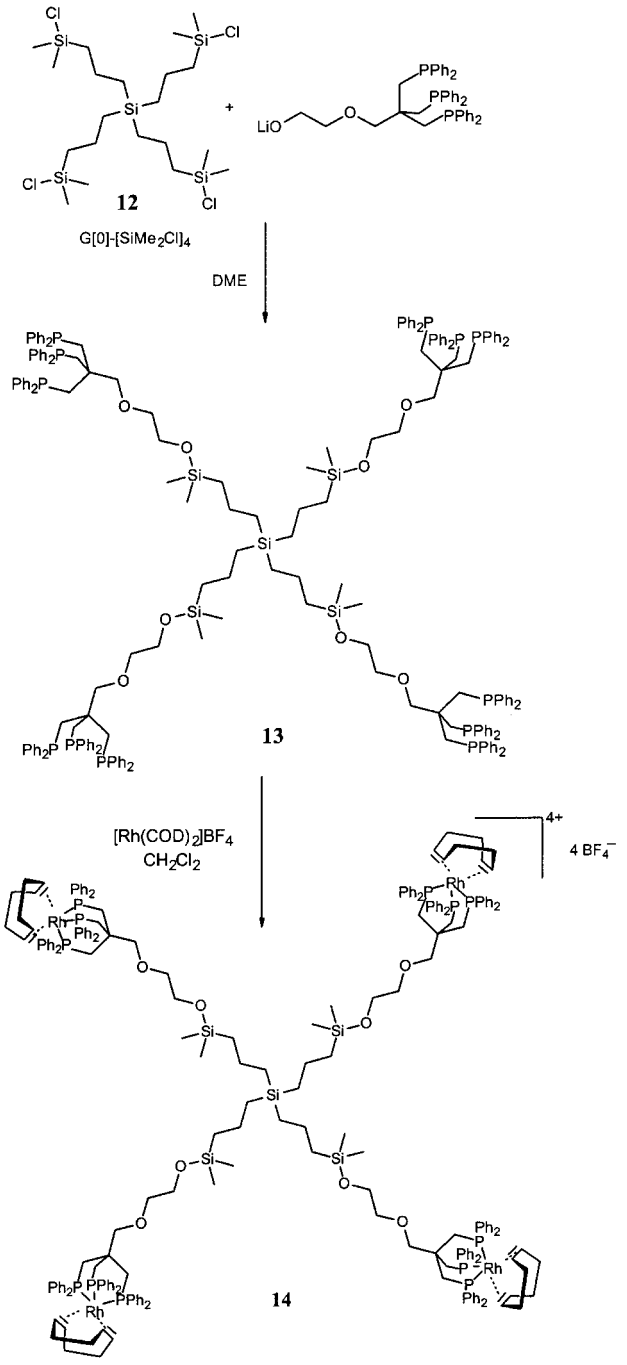

Scheme 3. Fixation of **9** to the end groups of the zeroth generation dendrimer G[0]-[$SiMe_2Cl$]$_4$ (**12**) to give G[0]-[OCH_2CH_2Otriphos]$_4$ (**13**) and subsequent metallation yielding G[0]-[OCH_2CH_2OtriphosRh(COD)BF_4]$_4$ (**14**)

by electrospray mass spectrometry, which confirmed the uniformity of the products. The molecular ion peaks were observed at m/z = 1002.2 for compound **14**, corresponding to the $[(M - 4BF_4)/4]^+$ ion, and at m/z = 1041.3 for the octametallated dendrimer **17**, corresponding to the $[(M - 8BF_4)/8]^+$ ion.

Comparison of the Catalytic Behavior of the Rhodium Complexes [Rh(triphos)(COD)][BF_4], 11a, 14 and 16 (cat1−4) in the Hydrogenation of Styrene and 1-Hexene

As outlined in the introduction, the hydrogenation of olefins was to be investigated in a comparative study of the catalytic properties of the mononuclear *triphos*-rhodium complexes [Rh(triphos)(COD)][BF_4] (**cat1**) and **11a** (**cat2**) as well as their dendrimer-linked derivatives **14** (**cat3**) and **16** (**cat4**). Mononuclear triphos-rhodium catalysts have been studied previously and were found to be active hydrogenation catalysts for simple nonfunctionalized alkenes.[17,21a,23,24] All catalytic tests were carried out at 1 bar of H_2 pressure and 20 ± 1 °C with an equivalent amount of catalyst (1 mol %), i.e. a constant number of catalytic sites in the system.

As simple substrates for catalytic hydrogenations styrene and 1-hexene are frequently chosen, the latter in order to assess the competition between hydrogenation and alkene isomerization within the coordination sphere of the catalyst.[25] After an initial induction period, during which the COD ligand is reduced, the hydrogenation of the styrene occurs at a constant rate until an almost quantitative conversion of the substrate. The catalytic activities of the catalysts **cat1** − **cat4** did not vary significantly and were found to be at TOF = 10 h^{-1} under the standard conditions cited above.

As has been shown by van Leeuwen and co-workers, carbosilane metallodendrimer catalysts of the first and second generation may possess the required molecular dimensions to allow recycling by membrane filtration.[11] If performed in batch reactors, this requires catalysts which retain their original activity after separation and reintroduction to a catalytic conversion. The dendrimer catalysts **cat3** and **cat4** were found to be isolable (removal of the solvent and reaction product under vacuum) after a complete conversion and re-usable for a subsequent cycle without significant decrease in activity during the first three cycles of catalyst isolation and reintroduction to a new batch of substrates.

In order to test the activity of the new dendritic catalysts towards a second standard substrate employed in hydrogenation tests, the hydrogenation at 1 bar H_2 pressure was carried out using 1-hexene. A competing reaction in this transformation is the isomerization of the alkene to a mixture of (*E*)- and (*Z*)-2-hexene. The typical course of this reaction, as followed by GC-MS, is again represented for **cat4** in Figure 4.

After an induction period, during which the catalytically active species is generated, the conversion of 1-hexene sets in, giving hexane, (*Z*)-2-hexene and (*E*)-2-hexene with a turnover frequency of 30 h^{-1} based on the 1-hexene consumed. After the complete consumption of 1-hexene, the hydrogenation of (*Z*)-2-hexene leads to the further production of hexane, albeit at a lower rate. The curve representing the generation of hexane levels off when the concentration of the *Z*-isomer has dropped to about 30% of its maximum value. As observed for practically all cationic rhodium hydrogenation catalysts, the conversion of the *E*-isomer is

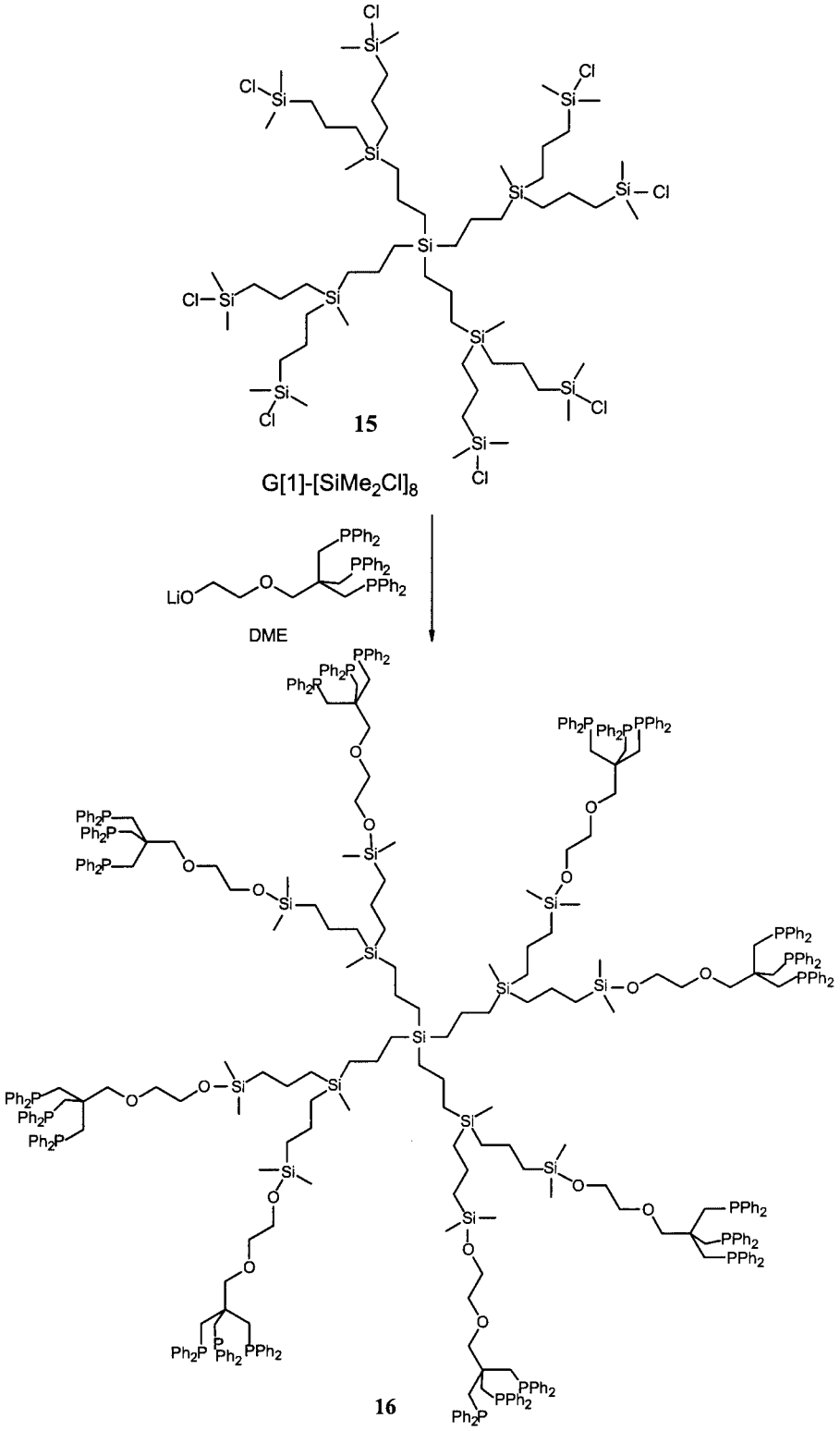

Scheme 4. Fixation of **9** to the end groups of the first generation dendrimer G[1]-[$SiMe_2Cl$]$_8$ (**15**) to give G[1]-[OCH_2CH_2Otriphos]$_8$ (**16**)

much slower and essentially insignificant on the chosen time scale.[25] Comparison of **cat1** − **cat4** showed an overall identical catalytic behaviour.

Conclusions

In this paper we have presented an efficient strategy for the backbone functionalization of the *triphos* ligand which

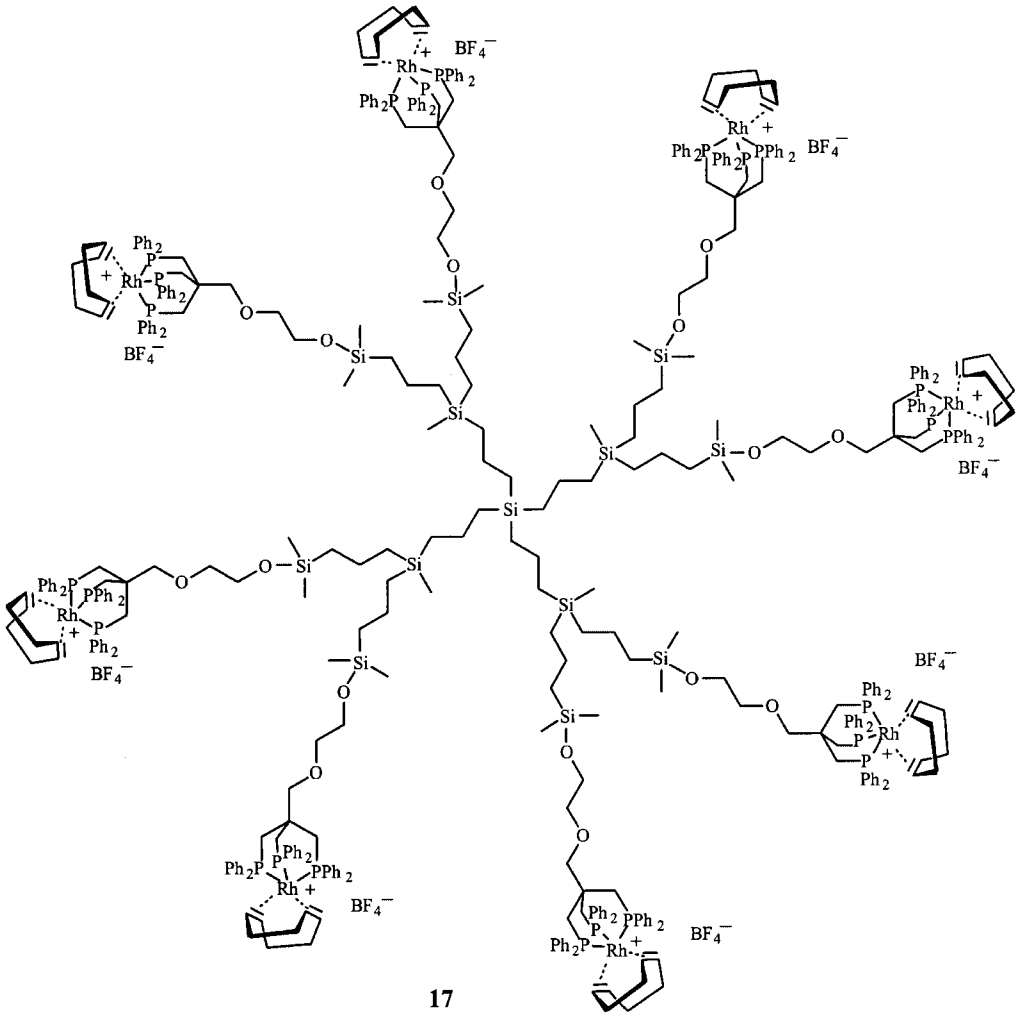

17

Figure 3. First generation rhododendrimer G[1]-[OCH_2CH_2OtriphosRh(COD)BF_4]$_8$ (**17**)

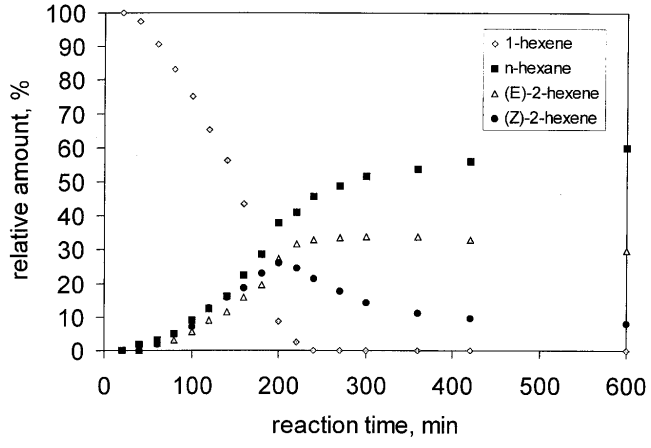

Figure 4. A typical conversion diagram for the hydrogenation of 1-hexene, represented here for the rhododendrimer **16** (**cat4**)

allows its attachment to solid supports and polymers. We have also been able to completely characterise two carbosilane dendrimer derivatives and found them to be sufficiently robust to allow for several recycling steps. Fixation to the low-generation dendrimers did not alter the catalytic hydrogenation properties of the triphos-rhodium catalyst. This constitutes the basis for the extension of this work to higher dendrimer generations which is currently under way.

Experimental Section

All manipulations were performed under nitrogen (desiccant P_4O_{10}, Granusic®, J. T. Baker) on a high vacuum line using standard Schlenk techniques, or in a glovebox. All reaction flasks were heated prior to use by means of three evacuation-refill cycles. Solvents and solutions were transferred by needle-septa techniques. Solvents were dried according to standard methods and saturated with nitrogen. The deuterated solvents used for the NMR spectroscopic measurements were degassed by three successive "freeze-pump-thaw" cycles and stored over 4 Å molecular sieves. Solids were separated from suspensions by filtration through dried Celite or by centrifugation. The ^1H, ^{13}C, ^{19}F, ^{29}Si and ^{31}P NMR spectra were recorded on Bruker AC 200, Bruker Avance 250 and Bruker AMX 400 FT NMR spectrometers. ^1H and ^{13}C data are listed in parts per million [ppm] relative to tetramethylsilane and were refer-

enced using the residual protonated solvent peak (^{1}H) or the carbon resonance (^{13}C). ^{29}Si, ^{19}F and ^{31}P NMR spectroscopic data are listed in ppm relative to, respectively, tetramethylsilane, $FCCl_3$ and 85% H_3PO_4 as external standards. Infrared spectra were recorded on a Nicolet Magna IRTM 750 spectrometer. Elemental analyses were carried out by the microanalytical service at the chemistry department at Strasbourg. 4-(Hydroxymethyl)-1-methyl-2,6,7-trioxabicyclo[2.2.2]octane (**2**),[18] benzyl 2-chloroethyl ether,[19] diphenylphosphane,[26] 3-chloro-(2,2-chloromethyl)-propan-1-ol (**7**),[20] 2-(2-Bromoethoxy)tetrahydropyran,[27] $[(MeCN)_3Mo(CO)_3]$,[28] $[Rh(COD)_2]BF_4$,[29] G[0]-$[Cl]_4$ (**12**),[30] G[1]-$[Cl]_8$ (**15**) [31] and $[CH_3C(CH_2PPh_2)_3Rh(COD)]BF_4$ [21] were prepared according to published procedures. All other chemicals used as starting materials were obtained commercially and used without further purification.

Preparation of $BzOCH_2CH_2OCH_2C(CH_2O)_3CCH_3$ (3): 4-(Hydroxymethyl)-1-methyl-2,6,7-trioxabicyclo[2.2.2]octane (**2**; 14.3 g, 89.0 mmol) was added to a stirred suspension of finely powdered KOH (11.2 g, 200 mmol) and benzyl 2-chloroethyl ether (30.9 g, 181 mmol) in 150 mL of DMSO. The reaction mixture was stirred at 60 °C for 2 h and then cooled to room temperature. Water (500 mL) was then added and the solution thus obtained was extracted with three portions of Et_2O (200 mL). The combined organic extracts were washed with 100 mL of a saturated aqueous solution of NaCl, then with 100 mL of water and subsequently dried over Na_2SO_4. After removal of the solvent by distillation, the yellow oily residue was purified by column chromatography to yield $BzOCH_2CH_2OCH_2C(CH_2O)_3CCH_3$ (**3**) as a colourless, viscous liquid. Yield: 20.5 g (70.2 mmol, 79%). R_f (Al_2O_3 60 neutral, EtOAc/*n*-hexane = 2:8): 0.49. ^{1}H NMR (300.17 MHz, $CDCl_3$, 295 K): δ = 1.42 (s, 3 H, H-1), 3.23 (s, 2 H, H-5), 3.54−3.60 (m, 4 H, H-6,7), 4.00 (s, 6 H, H-3), 4.54 (s, 2 H, H-8), 7.25−7.35 (m, 5 H, H-10,11,12) ppm. $^{13}C\{^1H\}$ NMR (75.48 MHz, $CDCl_3$, 295 K): δ = 23.2 (CH_3, C-1), 34.6 (C, C-4), 69.0 (CH_2, C-3), 69.1(CH_2, C-6/7), 69.3 (CH_2, C-6/7), 70.9 (CH_2, C-8), 72.8 (CH_2, C-5), 108.1 (C, C-2), 127.2 (CH, C-12), 127.3 (CH, C-11), 128.1 (CH, C-10), 137.9 (C, C-9) ppm. IR (film): $\tilde{\nu}$ = 3007 (w), 2876 (m), 1485 (m), 1453 (m), 1401 (s) 1354 (m), 1296 (m), 1209 (m), 1165 (m), 1127 (s), 1055 (s), 989 (m), 930 (m), 864 (s), 739 (m), 698 (m), 617 (m) cm^{-1}. $C_{16}H_{22}O_5$ (294.35) calcd. C 65.29. H 7.53: found C 65.41. H 7.62.

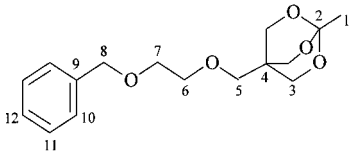

Preparation of $BzOCH_2CH_2OCH_2C(CH_2OH)_3$ (4): A solution of (18.2 g, 61.8 mmol) of $BzOCH_2CH_2OCH_2C(CH_2O)_3CCH_3$ (**3**) in 40 mL of methanol and 50 mL of 2 N HCl was stirred at room temperature for 6 h. Solid Na_2CO_3 (7.51 g, 71.3 mmol) was carefully added to the reaction mixture in small portions and the solution was subsequently stirred for another 18 h at ambient temperature. The solvents were removed by distillation, the residue was extracted with methanol and the solution was evaporated to dryness to yield pure $BzOCH_2CH_2OCH_2C(CH_2OH)_3$ (**4**) as a soft amorphous solid. Yield: 14.4 g (53.1 mmol, 86%). ^{1}H NMR (300.17 MHz, $CDCl_3$, 295 K): δ = 3.53 (s, 2 H, H-3), 3.60 (br. s, 4 H, H-4,5), 3.65 (s, 6 H, H-1), 4.54 (s, 2 H, H-6), 7.25−7.35 (m, 5 H, H-8,9,10) ppm. $^{13}C\{^1H\}$ NMR (75.48 MHz, $CDCl_3$, 295 K): δ = 45.0 (C, C-2), 64.5 (CH_2, C-4/5), 69.0 (CH_2, C-4/5), 70.8 (CH_2, C-6), 72.8 (CH_2, C-3), 73.2 (CH_2, C-1) 127.7 (CH, C-10), 127.8 (CH, C-9), 128.4 (CH, C-8), 137.6 (C, C-7) ppm. IR (film): $\tilde{\nu}$ = 3413 (vs), 2931 (s), 2878 (s), 1448 (s), 1410 (s), 1094 (s), 1040 (s), 837 (m), 746 (m), 699 (s) cm^{-1}. $C_{14}H_{22}O_5$ (270.33) calcd. C 62.20, H 8.20: found C 61.88. H 8.03.

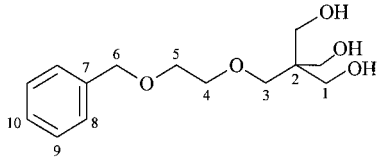

Preparation of $BzOCH_2CH_2OCH_2C(CH_2Cl)_3$ (5): $SOCl_2$ (20.5 g, 172 mmol) was added dropwise to a stirred mixture of $BzOCH_2CH_2OCH_2C(CH_2OH)_3$ (**4**; 14.1 g, 52.2 mmol) and dry pyridine (13.6 g, 172 mmol) at 0 °C. After complete addition, the reaction mixture was stirred for 30 min at 0 °C, then for 30 min at room temperature, and finally at 110−120 °C for 2.5 h. After cooling to 0 °C 150 mL of iced water was added and the aqueous phase thus obtained was twice extracted with 50 mL of CH_2Cl_2. The combined organic layers were treated with 100 mL of dilute HCl and with 2 × 100 mL of water and were then dried over Na_2SO_4. The solvent was removed by distillation at normal pressure, and the residue was purified by column chromatography to give $BzOCH_2CH_2OCH_2C(CH_2Cl)_3$ (**5**) as a colourless liquid. Yield: 9.52 g (29.2 mmol, 56%). R_f (Kieselgel, EtOAc/*n*-hexane = 1:9) = 0.34. ^{1}H NMR (300.17 MHz, $CDCl_3$, 295 K): δ = 3.53 (s, 2 H, H-3), 3.59−3.67 (m, 4 H, H-4,5), 3.64 (s, 6 H, H-1), 4.54 (s, 2 H, H-6), 7.25−7.34 (m, 5 H, H-8,9,10) ppm. $^{13}C\{^1H\}$ NMR (75.48 MHz, $CDCl_3$, 295 K): δ = 44.3 (CH_2, C-1), 46.3 (C, C-2), 68.6 (CH_2, C-4/5), 69.3 (CH_2, C-4/5), 71.0 (CH_2, C-6), 73.2 (CH_2, C-3), 127.6 (CH, C-10), 127.7 (CH, C-9), 128.4 (CH, C-8), 138.2 (C, C-7) ppm. IR (film): $\tilde{\nu}$ = 3029 (w), 2920 (m), 1495 (w), 1453 (m), 1434 (m), 1354 (m), 1307 (m), 1267 (m), 1104 (s), 871 (m), 798 (m), 741 (m), 698 (s), 616 (w) cm^{-1}. $C_{14}H_{19}Cl_3O_2$ (325.66): calcd. C 51.63. H 5.88: found C 51.89. H 5.74.

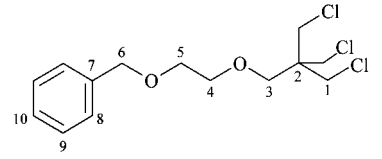

Preparation of $HOCH_2CH_2OCH_2C(CH_2Cl)_3$ (6) by Deprotection of $BzOCH_2CH_2OCH_2C(CH_2Cl)_3$ (5): A mixture of $BzOCH_2CH_2OCH_2C(CH_2Cl)_3$ (**5**; (8.32 mg 25.5 mmol) and 310 mg of Pd/C was stirred in THF at room temp under 1 bar of H_2 for 12 h. The reaction mixture was then filtered through celite, the solvent removed by distillation at normal pressure and the oily residue purified by fractional distillation at reduced pressure giving compound $HOCH_2CH_2OCH_2C(CH_2Cl)_3$ (**6**) as a colourless liquid. Yield: 4.88 g (20.7 mmol, 81%). B.p.: 97−99 °C/0.64 Torr. ^{1}H NMR (400.1 MHz, $CDCl_3$, 295 K): δ = 3.48 (s, 2 H, H-3), 3.54 (t, $^3J_{H,H}$ = 4.3 Hz, 2 H, H-4/5), 3.59 (s, 6 H, H-1), 3.68 (t, $^3J_{H,H}$ = 4.3 Hz, 2 H, H-4/5) ppm. $^{13}C\{^1H\}$ NMR (100.6 MHz, $CDCl_3$, 295 K): δ = 44.5 (CH_2, C-1), 46.5 (C, C-2), 62.0 (CH_2, C-5), 68.8 (CH_2, C-4), 73.0 (CH_2, C-3) ppm. IR (film): $\tilde{\nu}$ = 3373 (br), 2962 (s), 2877 (s), 1476 (m), 1434 (s), 1360 (m), 1308 (m), 1126 (s), 1062 (s), 871 (s), 806 (m), 759 (m), 742 (m), 701 (m) cm^{-1}. $C_7H_{13}Cl_3O_2$ (235.54): calcd. C 35.69, H 5.56; found C 35.23, H 5.50.

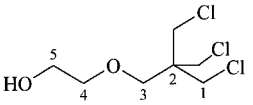

Preparation of $THPOCH_2CH_2OCH_2C(CH_2Cl)_3$ (8): Finely powdered KOH (9.45 g, 168 mmol) was added at room temperature to a vigorously stirred solution of 3-chloro-2,2-bis(chloromethyl)propan-1-ol (**7**; 8.02 g, 41.9 mmol) and (2-bromoethoxy)tetrahydropyran (26.2 g, 125 mmol) in 40 mL of DMSO. There was a strong evolution of heat during the addition and the temperature was controlled by occasional cooling with an ice bath. After complete addition of the solid KOH the reaction mixture was stirred at 60 °C for another 2 h and then cooled to room temperature. Water (180 mL) was added, and the aqueous phase was extracted with 3 × 50 mL of CH_2Cl_2. The combined organic extracts were washed with 3 × 50 mL H_2O and then dried over Na_2SO_4. After removal of the solvent by distillation the residue was subjected to fractional distillation under reduced pressure to give $THPOCH_2CH_2OCH_2C(CH_2Cl)_3$ (**10**) as a colourless liquid. Yield: 9.78 g (30.6 mmol, 73%). B.p.: 115 °C/0.19 Torr. ^1H NMR (400.1 MHz, $CDCl_3$, 295 K): δ = 1.43−1.57 (m, 6 H, H-7,8,9), 3.44 (s, 2 H, H-3), 3.46−3.62 (m, 4 H, H-4,5), 3.59 (s, 6 H, H-1), 3.77−3.85 (m, 2 H, H-10), 4.69 (t, $^3J_{H,H}$ = 3.3 Hz, 1 H, H-6) ppm. $^{13}C\{^1H\}$ NMR (100.6 MHz, $CDCl_3$, 295 K): δ = 19.5 (CH_2, C-7/8/9), 25.6 (CH_2, C-7/8/9), 30.8 (CH_2, C-7/8/9), 44.5 (CH_2, C-1), 46.5 (C, C-2), 62.3 (CH_2, C-5), 66.7 (CH_2, C-10), 68.8 (CH_2, C-4), 70.8 (CH_2, C-3), 99.1 (CH, C-6) ppm. IR (film): $\tilde{\nu}$ =2942 (s), 2871 (m), 1440 (m), 1352 (m), 1260 (m), 1201 (m), 1128 (s), 1076 (s), 1036 (s), 1020 (m), 986 (m), 871 (m), 814 (w), 742 (w), 702 (w) cm^{-1}. $C_{15}H_{27}Cl_3O_3$ (319.66): calcd. C 45.09, H 6.62; found C 45.39, H 6.38.

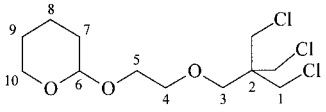

Preparation of $HOCH_2CH_2OCH_2C(CH_2Cl)_3$ (6) by Deprotection of $THPOCH_2CH_2OCH_2C(CH_2Cl)_3$ (8): Solid *p*-toluenesulfonic acid (220 mg) was added to a solution of $THPOCH_2CH_2OCH_2C(CH_2Cl)_3$ (**10**; 11.2 g, 35.1 mmol) in 50 mL of methanol. The reaction mixture was stirred at room temperature for 15 h, neutralised with solid K_2CO_3 and the solvent removed by distillation. The remaining residue was subjected to a fractional distillation as described above to give **6**. Yield: 7.78 g (32.9 mmol, 93%).

Preparation of $HOCH_2CH_2OCH_2C(CH_2PPh_2)_3$ (9): A solution of $HPPh_2$ (7.80 g, 41.9 mmol) in 10 mL of DMSO was added to a vigorously stirred suspension of K_2CO_3 (32.1 g, 233 mmol) in 45 mL of DMSO and this was followed by the addition of KOH (3.95 g, 70.4 mmol) in 3.0 mL of degassed water. The deep-red suspension thus obtained was stirred for 30 min at room temperature and then a solution of of $HOCH_2CH_2OCH_2C(CH_2Cl)_3$ (**6**; 3.14 g, 13.3 mmol) in 15 mL of DMSO was added with a syringe. The reaction mixture was stirred at 90 °C for 2 h and then at 110 °C for another hour. After cooling, 250 mL of water was added, the aqueous phase separated and the volatile organic components removed in vacuo. The residue was extracted with 2 × 20 mL of toluene, the solution treated with 2 × 10 mL of degassed water and then dried over Na_2SO_4. After removal of the solvent the residue was extracted with methanol and the target compound $HOCH_2CH_2OCH_2C(CH_2PPh_2)_3$ (**9**) was obtained as a colourless solid directly from the extract. Yield: 6.64 g (9.71 mmol, 73%). M.p.: 138 °C. ^1H NMR (400.14 MHz, $CDCl_3$, 295 K): δ = 2.38 (d, $^1J_{P,H}$ = 2.9 Hz, 6 H, H-1), 2.81 (t, $^3J_{H,H}$ = 4.4 Hz, 2 H, H-4/5), 3.24 (s, 2 H, H-3), 3.27 (t, $^3J_{H,H}$ = 4.4 Hz, 2 H, H-4/5), 7.16−7.25 (m, 30 H, aromat. H) ppm. $^{13}C\{^1H\}$ NMR (100.63 MHz, $CDCl_3$, 295 K): δ = 37.5−37.9 (m, CH_2, C-1), 41.7 (q, C, $^2J_{PC}$ = 11.4 Hz, C-2), 60.0 (s, CH_2, C-5), 70.5 (s, CH_2, C-4), 76.5 (q, CH_2, $^3J_{PC}$ = 7.6 Hz, C-3), 127.2−127.5 (m, CH, aromat. C), 131.8−132.1 (m, CH, aromat. C), 138.3 (m, C, aromat. C) ppm. $^{31}P\{^1H\}$ NMR (161.9 MHz, $CDCl_3$, 295 K): δ = −25.8 (s) ppm. IR (CH_2Cl_2): $\tilde{\nu}$ = 3395 (br), 3072 (m), 2864 (m), 1585 (w), 1481 (m), 1434 (s), 1405 (m), 1307 (w), 1259 (m), 1120 (s), 1061 (s), 1026 (m), 999 (m), 869 (m), 831 (m), 693 (m) cm^{-1}. $C_{43}H_{43}O_2P_3$ (684.73): calcd. C 75.43, H 6.33; found C 75.26, H 6.42.

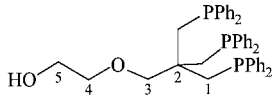

Preparation of $[\{HOCH_2CH_2OCH_2C(CH_2PPh_2)_3\}Mo(CO)_3]$ (10): A solution of $[(MeCN)_3Mo(CO)_3]$ (368 mg, 1.21 mmol) in 5 mL of acetonitrile was slowly added to a stirred suspension of $HOCH_2CH_2OCH_2C(CH_2PPh_2)_3$ (**9**; 831 mg, 1.21 mmol) in 10 mL of acetonitrile. The reaction mixture was stirred at ambient temperature for 16 h and the product was then precipitated by addition of Et_2O. The light brown solid was isolated by filtration, washed with Et_2O and dried under vacuum. Complex $[\{HOCH_2CH_2OCH_2C(CH_2PPh_2)_3\}Mo(CO)_3]$ (**10**) was obtained as an ochre microcrystalline solid after recrystallisation from acetonitrile/Et_2O. Yield: 963 mg (1.11 mmol, 92%). M.p.: 293 °C (dec.). ^1H NMR (300.17 MHz, CD_2Cl_2, 295 K): δ = 2.36 (m, 6 H, H-1), 3.43 (s, 2 H, H-3), 3.69 (t, $^3J_{H,H}$ = 5.6 Hz, 2 H, H-4/5), 3.81 (t, $^3J_{H,H}$ = 5.6 Hz, 2 H, H-4/5), 7.08−7.39 (m, 30 H, aromat. H) ppm. $^{13}C\{^1H\}$ NMR (75.48 MHz, CD_2Cl_2, 295 K): δ = 31.2 (m, CH_2, C-1), 41.7 (q, C, $^2J_{PC}$ = 7.1 Hz, C-2), 62.4 (s, CH_2, C-5), 73.3 (s, CH_2, C-4), 84.4 (q, CH_2, $^3J_{PC}$ = 9.8 Hz, C-3), 128.4−129.3 (m, aromat. C), 132.0−132.2 (m, aromat. C), 138.8−139.2 (m, aromat. C), 221.3 (m, CO, C-6) ppm. $^{31}P\{^1H\}$ NMR (161.9 MHz, CD_2Cl_2, 295 K): δ = 15.6 (s) ppm. IR (KBr): $\tilde{\nu}$ = 3444 (br), 3057 (w), 2901 (w), 1929 (vs), 1834 (vs), 1481 (m), 1433 (s), 1118 (m), 1082 (m), 999 (w), 831 (m), 737 (m), 697 (s), 623 (m) cm^{-1}. MS (FAB): *m/z* = 866.0 $[M + H]^+$. $C_{46}H_{43}MoO_5P_3$ (864.71): calcd. C 63.90, H 5.01; found C 63.72, H 4.88.

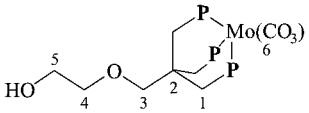

Preparation of $[\{HOCH_2CH_2OCH_2C(CH_2PPh_2)_3\}Rh(COD)]BF_4$ (11a) and of $[\{HOCH_2CH_2OCH_2C(CH_2PPh_2)_3\}Rh(COD)]PF_6$ (11b): A solution of $HOCH_2CH_2OCH_2C(CH_2PPh_2)_3$ (**9**; 766.9 mg, 1.12 mmol) in 15 mL of CH_2Cl_2 was slowly added to a stirred solution of $[Rh(COD)_2]BF_4$ (454.8 mg, 1.12 mmol) in 15 mL of CH_2Cl_2. The reaction mixture was stirred at room temperature for 14 h, accompanied by a change of colour from red-brown to orange and the product was then precipitated by addition of pentane. The yellow, microcrystalline solid obtained after washing with *n*-pentane and drying in vacuo was the pure complex $[\{HOCH_2CH_2OCH_2C(CH_2PPh_2)_3Rh(COD)\}]BF_4$ (**11a**).

11a: Yield: 1.03 g (1.05 mmol, 94%). M.p.: 165 °C (dec.). ^{1}H NMR (300.17 MHz, CD_2Cl_2, 295 K): δ = 2.41−2.46 (m, 4 H, H-7$_{exo}$), 2.60 (s, 6 H, H-1), 2.76−2.82 (m, 4 H, H-7$_{endo}$), 3.65 (s, 2 H, H-3), 3.75 (t, $^3J_{H,H}$ = 5.2 Hz, 2 H, H-4/5), 3.84 (t, $^3J_{H,H}$ = 5.2 Hz, 2 H, H-4/5), 4.08 (s, 4 H, H-6), 7.10−7.39 (m, 30 H, aromat. H) ppm. ^{13}C{^{1}H} NMR (75.48 MHz, CD_2Cl_2, 295 K): δ = 30.8 (m, CH_2, C-1), 33.6 (s, CH_2, C-6), 41.0 (m, C, C-2), 62.3 (s, CH_2, C-5), 73.6 (s, CH_2, C-4), 83.3 (q, CH_2, $^3J_{PC}$ = 11.0 Hz C-3), 84.8 (m, CH, C-7), 128−135 (m, aromat. C) ppm. ^{31}P{^{1}H} NMR (121.5 MHz, CD_2Cl_2, 295 K): δ = 4.3 (d, $^1J_{RhP}$ = 106.8 Hz) ppm. IR (film): $\tilde{\nu}$ = 3418 (br), 3051 (w), 2933 (w), 2870 (w), 1483 (m), 1433 (s), 1083 (vs), 1054 (s), 830 (m), 744 (m), 696 (s) cm^{-1}. $C_{51}H_{55}BF_4O_2P_3Rh$ (982.63): calcd. C 62.34, H 5.64; found C 62.11, H 5.75.

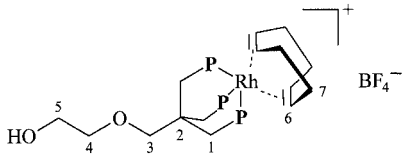

Complex **11b** was obtained by addition of NH_4PF_6 (163 mg, 3.46 mmol) in 5 mL of methanol to a solution of [{$HOCH_2CH_2OCH_2C(CH_2PPh_2)_3$}Rh(COD)]$BF_4$ (**11a**; 170 mg, 0.173 mmol) in 5 mL of methanol. The reaction mixture was stirred at room temperature for 15 h, the precipitate separated by filtration, washed with 2 × 3 mL of methanol and 2 × 5 mL of *n*-pentane and then dried in vacuo. The complex [{$HOCH_2CH_2OCH_2C(CH_2PPh_2)_3$}Rh(COD)]$PF_6$ (**11b**) was isolated as a yellow microcrystalline solid. Yield: 160.3 mg (0.153 mmol, 89%). M.p.: 185 °C (dec.). ^{1}H NMR (300.17 MHz, CD_2Cl_2, 295 K): δ = 2.43−2.49 (m, 4 H, H-7$_{exo}$), 2.63 (s, 6 H, H-1), 2.78−2.85 (m, 4 H, H-7$_{endo}$), 3.67 (s, 2 H, H-3), 3.78 (t, $^3J_{H,H}$ = 5.2 Hz, 2 H, H-4/5), 3.85 (t, $^3J_{H,H}$ = 5.2 Hz, 2 H, H-4/5), 4.11 (s, 4 H, H-6), 7.11−7.42 (m, 30 H, aromat. H) ppm. ^{13}C{^{1}H} NMR (75.48 MHz, CD_2Cl_2, 295 K): δ = 31.2 (m, CH_2, C-1), 33.2 (CH_2, C-6), 41.1 (m, C, C-2), 62.5 (CH_2, C-5), 73.7 (CH_2, C-4), 83.5 (q, CH_2, $^3J_{PC}$ = 10.9 Hz C-3), 85.0 (m, CH, C-7), 128−135 (m, aromat. C) ppm. ^{19}F{^{1}H} NMR (376.47 MHz, CD_2Cl_2, 295 K): δ = −73.8 (d, $^1J_{P,F}$ = 715 Hz) ppm. ^{31}P{^{1}H} NMR (121.51 MHz, CD_2Cl_2, 295 K): δ = −143.2 (sept), 5.5 (d, $^1J_{Rh,P}$ = 104.4 Hz) ppm. IR (film): $\tilde{\nu}$ = 3419 (br), 2929 (w), 2862 (w), 2815 (w), 1482 (m), 1434 (s), 1122 (m), 1085 (m), 844 (s), 745 (m), 697 (m) cm^{-1}. $C_{51}H_{55}F_6O_2P_4Rh$ (1040.79): calcd. C 58.86, H 5.33; found C 59.10, H 5.21.

Preparation of G[0]-[OCH_2CH_2Otriphos]$_4$ (13): A 1.6 M solution of *n*BuLi in hexanes (1.40 mL, 2.23 mmol) was added to a stirred solution of $HOCH_2CH_2OCH_2C(CH_2PPh_2)_3$ (**9**; 1.53 mg, 2.23 mmol) in 15 mL of DME at −78 °C. The reaction mixture was warmed to ambient temperature and then stirred for another 30 min. After re-cooling to −78 °C a solution of G[0]-[Cl]$_4$ (**12**; 318.9 mg, 559 μmol) in 10 mL of DME was added dropwise and the reaction mixture was then stirred at ambient temperature for 36 h. After removal of the volatiles, the residue was extracted with toluene and the extract filtered through Celite. Compound G[0]-[OCH_2CH_2Otriphos]$_4$ (**13**) was obtained as a soft amorphous solid after removal of the solvent and drying under vacuum. Yield: 1.66 g (525 μmol, 94%). ^{1}H NMR (300.17 MHz, $CDCl_3$, 295 K): δ = 0.04 (s, 24 H, H-6), 0.50−0.61 (m, 16 H, H-7, 9), 1.22−1.35 (m, 8 H, H-8), 2.55 (s, 24 H, H-1), 2.76 (t, $^3J_{H,H}$ = 4.3 Hz, 8 H, H-4/5), 3.15 (s, 8 H, H-3), 3.21 (t, $^3J_{H,H}$ = 4.3 Hz, 8 H, H-4/5), 7.21−7.36 (m, 120 H, aromat. H) ppm. ^{13}C{^{1}H} NMR (75.48 MHz, $CDCl_3$, 295 K): δ = −0.1 (s, CH_3, C-6), 19.3 (s, CH_2, C-7/8/9), 20.0 (s, CH_2, C-7/8/9), 27.3 (s, CH_2, C-7/8/9), 40.4 (m, CH_2, C-1), 44.9 (q, CH_2, $^2J_{PC}$ = 12.4 Hz, C-2), 63.2 (s, CH_2, C-4/5), 73.5 (s, CH_2, C-4/5), 79.5 (q, CH_2, $^3J_{PC}$ = 17.0 Hz, C-3), 129.8−135.2 (m, aromat. C) ppm. ^{29}Si{^{1}H} NMR (79.49 MHz, CD_2Cl_2, 295 K): δ = 0.4 (s, *Si*), 18.7 (s, *Si*−O) ppm. ^{31}P{^{1}H} NMR (121.51 MHz, CD_2Cl_2, 295 K): δ = −26.9 (s) ppm. MS (FAB): *m*/*z* = 3164.3 [M + H]$^+$. $C_{192}H_{216}O_8P_{12}Si_5$ (3163.93): calcd. C 72.89, H 6.88; found C 72.41, H 6.76.

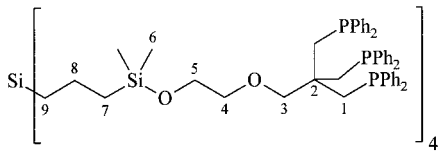

Preparation of G[0]-[OCH_2CH_2OtriphosRh(COD)BF_4]$_4$ (14): A solution of G[0]-[OCH_2CH_2Otriphos]$_4$ (**13**; 305 mg, 96.3 μmol) in 15 mL of CH_2Cl_2 was slowly added with a cannula to a stirred solution of [Rh(COD)$_2$]BF_4 (385 mg, 949 μmol) in 10 mL of CH_2Cl_2. The reaction mixture was stirred at room temperature for 24 h and the product was then precipitated by addition of *n*-pentane. The precipitate was separated by filtration, washed with 3 × 10 mL of *n*-pentane and then dried in vacuo. The reaction product G[0]-[OCH_2CH_2OtriphosRh(COD)BF_4]$_4$ (**14**) was obtained as a yellow solid. Yield: 369 mg (84.7 μmol, 88%). M.p.: 161 °C (dec.). ^{1}H NMR (300.17 MHz, CD_2Cl_2, 295 K): δ = 0.01 (s, 24 H, H-6), 0.49−0.55 (m, 8 H, H-9), 0.60−0.66 (m, 8 H, H-8), 0.86−0.91 (m, 8 H, H-7), 2.43 (br. s, 16 H, H-11$_{exo}$), 2.58 (s, 24 H, H-1), 2.77 (br. s, 16 H, H-11$_{endo}$), 3.61 (s, 8 H, H-3), 3.69 (t, $^3J_{H,H}$ = 4.9 Hz, 8 H, H-4/5), 3.82 (t, $^3J_{H,H}$ = 4.9 Hz, 8 H, H-4/5), 4.09 (br. s, 16 H, H-10), 7.09−7.37 (m, 120 H, aromat. H) ppm. ^{13}C{^{1}H} NMR (75.48 MHz, CD_2Cl_2, 295 K): δ = −2.0 (s, CH_3, C-6), 17.3 (s, CH_2, C-7/8/9), 17.9 (s, CH_2, C-7/8/9), 21.1 (s, CH_2, C-7/8/9), 30.8 (m, CH_2, C-1), 33.2 (s, CH_2, C-10), 40.6 (m, C, C-2), 61.9 (s, CH_2, C-5), 73.1 (s, CH_2, C-4), 83.0 (q, $^3J_{P,C}$ = 10.2 Hz, CH_2, C-3), 84.5 (m, CH, C-10), 128.2−135.5 (m, aromat. C) ppm. ^{29}Si{^{1}H} NMR (79.49 MHz, CD_2Cl_2, 295 K): δ = 0.2 (s, *Si*), 17.8 (s, *Si*−O) ppm. ^{31}P{^{1}H} NMR (121.51 MHz, CD_2Cl_2, 295 K): δ = 4.5 (d, $^1J_{Rh,P}$ = 104.3 Hz) ppm. IR (KBr): $\tilde{\nu}$ = 2913 (m), 2870 (m), 1432 (m), 1250 (w), 1084 (s), 1047 (m), 833 (m), 737 (m), 696 (s) cm^{-1}. MS (ESI): *m*/*z* = 1002.2 [(M − 4BF_4)/4]$^+$. $C_{224}H_{264}B_4F_{16}O_8P_{12}Rh_4Si_5$ (4355.50): calcd. C 61.77, H 6.11; found C 61.32, H 6.02.

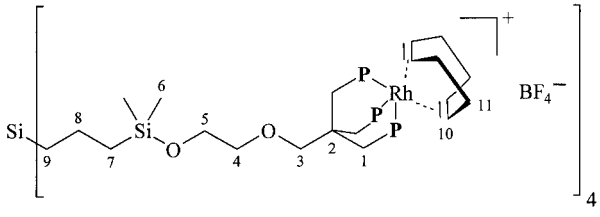

Preparation of G[1]-[OCH_2CH_2Otriphos]$_8$ (16): A 1.6 M solution of *n*BuLi in *n*-hexane (1.77 mL, 2.83 mmol) was added to a solution of $HOCH_2CH_2OCH_2C(CH_2PPh_2)_3$ (**9**; 1.94 g, 2.83 mmol) in 10 mL of DME at −78 °C. The reaction mixture was warmed to room temperature and then subsequently stirred for 30 min. After re-cooling to −78 °C, a solution of G[1]-[Cl]$_8$ (**15**; 514.0 mg, 353 μmol) in 15 mL of DME was added with the aid of a syringe and the reaction mixture was then stirred for 36 h at ambient temperature. After removal of the volatiles, the residue was extracted with toluene and the extract filtered through Celite. After removing the solvent in vacuo, the reaction product G[1]-[OCH_2CH_2Otriphos]$_8$ (**16**) was obtained as an analytically pure soft solid. Yield: 2.13 g (321 μmol, 91%). ^{1}H NMR (300.17 MHz, $CDCl_3$, 295 K): δ = 0.16 (s, 48 H, H-6), 0.20 (s, 12 H, H-10), 0.67−0.77 (m, 48 H, H-7, 9,

11, 13), 1.41−1.51 (m, 24 H, H-8, 12), 2.71 (s, 48 H, H-1), 2.92 (t, $^3J_{H,H}$ = 5.4 Hz, 16 H, H-4/5), 3.29 (s, 16 H, H-3), 3.37 92 (t, $^3J_{H,H}$ = 5.4 Hz, 16 H, H-4/5), 7.33−7.51 (m, 240 H, aromat. H) ppm. $^{13}C\{^1H\}$ NMR (75.48 MHz, $CDCl_3$, 295 K): δ = −1.9 (s, CH_3, C-10), −1.5 (s, CH_3, C-6), 17.7 (s, CH_2, C-7/8/9), 17.8 (s, CH_2, C-11/12/13), 20.8 (s, CH_2, C-7/8/9), 21.8 (s, CH_2, C-7/8/9), 22.3 (s, CH_2, C-11/12/13), 22.9 (s, CH_2, C-11/12/13), 38.1 (m, CH_2, C-1), 42.8 (q, $^2J_{P,C}$ = 12.5 Hz, C, C-2), 61.3 (s, CH_2, C-4/5), 71.5 (s, CH_2, C-4/5), 77.4 (q, $^3J_{P,C}$ = 12.5 Hz, CH_2, C-2), 128.1−140.0 (m, aromat. C) ppm. $^{29}Si\{^1H\}$ NMR (79.49 MHz, CD_2Cl_2, 295 K): δ =0.5 (s, *Si*), 0.9 (s, *Si*Me), 17.6 (s, *Si*Me_2O) ppm. $^{31}P\{^1H\}$ NMR (121.51 MHz, $CDCl_3$, 295 K): δ = −27.3 (s) ppm. MS (MALDI-TOF): *m*/*z* = 6642.9 $[M]^+$. $C_{400}H_{468}O_{16}P_{24}Si_{13}$ (6640.59): calcd. C 72.35, H 7.10; found C 71.83, H 6.93.

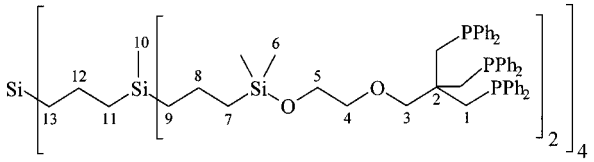

Preparation of G[1]-[OCH_2CH_2OtriphosRh(COD)BF_4]$_8$ (17): A solution of G[1]-[OCH_2CH_2Otriphos]$_8$ (**16**; 717.2 mg, 108 μmol) in 15 mL of CH_2Cl_2 was added to a stirred solution of $[Rh(COD)_2]BF_4$ (351 mg, 864 μmol) in 10 mL of CH_2Cl_2. The reaction mixture was stirred at ambient temperature for 24 h and the product subsequently precipitated by addition of pentane. After centrifugation, the precipitate was washed with 3 × 10 mL of *n*-pentane and then dried in vacuo. The metallodendrimer G[1]-[OCH_2CH_2OtriphosRh(COD)BF_4]$_8$ (**17**) was obtained as a yellow powder. Yield: 945 mg (97.2 μmol, 90%). M.p.: 156C (dec.). ^1H NMR (400.2 MHz, CD_2Cl_2, 295 K): δ = 0.09 (s, 12 H, H-10), 0.20 (s, 48 H, H-6), 0.51−0.67 (m, 48 H, H-7,9,11,13), 1.28−1.38 (m, 24 H, H-8,12), 2.45 (m, 32 H, H-15), 2.60 (s, 48 H, H-1), 2.78 (m, 32 H, H-15), 3.62 (s, 16 H, H-3), 3.70 (m, $^3J_{H,H}$ = 6.1 Hz, 32 H, H-14), 7.08−7.50 (m, 120 H, aromat. H) ppm. $^{13}C\{^1H\}$ NMR (75.48 MHz, CD_2Cl_2, 295 K): δ = δ = −1.6 (s, CH_3, C-6), 17.9 (s, CH_2, C-7/8/9), 18.2 (s, CH_2, C-11/12/13), 18.6 (s, CH_2, C-7/8/9), 18.6 (s, CH_2, C-11/12/13), 20.9 (s, CH_2, C-7/8/9), 23.2 (s, CH_2, C-11/12/13), 31.2 (m, CH_2, C-1), 33.5 (s, CH_2, C-15), 41.1 (m, C, C-2), 62.3 (s, CH_2, C-5), 73.7 (s, CH_2, C-4), 83.4 (q, $^3J_{P,C}$ = 10.2 Hz, CH_2, C-3), 84.9 (m, CH, C-14), 128.2−135.3 (m, aromat. C) ppm. $^{29}Si\{^1H\}$ NMR (79.49 MHz, CD_2Cl_2, 295 K): δ = 0.5 (s, *Si*Me), 17.6 (s, *Si*Me_2O) ppm. $^{31}P\{^1H\}$ NMR (121.51 MHz, CD_2Cl_2, 295 K): δ = 4.4 (d, $^1J_{Rh,P}$ = 106.8 Hz) ppm. IR (KBr): $\tilde{\nu}$ = 2912 (m), 2870 (m), 1482 (m), 1433 (s), 1250 (m), 1084 (s), 1051 (s), 833 (m), 743 (m), 695 (s), cm^{-1}. MS (ESI): *m*/*z* = 1041.3 $[(M - 8\ BF_4)/8]^+$. $C_{464}H_{564}B_8F_{32}O_{16}P_{24}Rh_8Si_{13}$ (9023.73) calcd. C 61.76, H 6.30; found C 61.21, H 6.09.

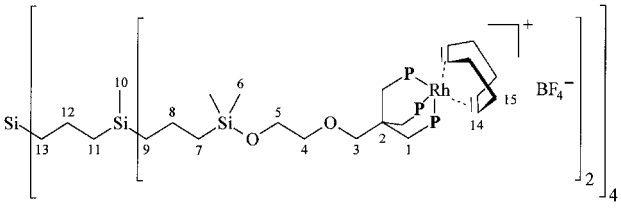

Catalyst Testing: The catalyst tests were carried out in THF at 1 bar H_2 pressure using 1 mol % of rhodium. The course of the catalytic hydrogenation was monitored by GC/MS spectrometry performed with a Shimadzu GC-17A/GCMS-QP5050A. Column: SGE BPX5, 5% phenyl, polysilyphenylene-siloxane, nonpolar, 30 m, 0.22 mm, carrier gas He. The products were analysed by comparison of the recorded mass spectra and retention times with those of authentic samples. The measured relative ratio of the products was calibrated by comparative measurements with known substance ratios using pure substances.

X-ray Diffraction Study of Compounds 10 and 11b: Suitable crystals of the complexes **10** and **11b** were obtained by layering concentrated solutions of the compounds in dichloromethane with hexanes and allowing slow diffusion at room temperature. The crystal data were collected on a Nonius Kappa CCD diffractometer at −100 °C and transferred to a DEC Alpha workstation; for all subsequent calculations the Nonius OpenMoleN package was used.[32] The structures were solved by direct methods with absorption corrections being part of the scaling procedure of the data reductions. After refinement of the heavy atoms, difference Fourier maps revealed the maxima of residual electron density close to the positions expected for the hydrogen atoms; they were introduced as fixed contributors in the structure factor calculations with fixed coordinates (C−H: 0.95 Å) and isotropic temperature factors [B(H) = 1.3 B_{eqv}(C) Å^2] but not refined. Full least-square refinements on F^2. A final difference map revealed no significant maxima of electron density. The scattering factor coefficients and the anomalous dispersion coefficients were taken from ref.[33] Crystal data and experimental details for the crystals of **10** and **11b** are given in Table 1.

Table 1. X-ray experimental data of compounds **10** and **11b**

	10	**11b**
Formula	$C_{46}H_{43}MoO_5P_3$	$C_{52}H_{57}Cl_2F_6O_2P_4Rh$
Molecular weight	864.7	11125.73
Crystal system	monoclinic	monoclinic
Space group	$P2_1/n$	$C2/c$
a (Å)	11.1938(2)	24.0051(5)
b (Å)	21.3216(4)	23.5811(5)
c (Å)	17.5362(3)	18.9749(5)
β (deg)	97.901(5)	114.302(5)
V (Å^3)	4145.6(1)	9789.3(4)
Z	4	8
$D_{calcd.}$ (g·cm^{-3})	1.39	1.53
*F*000	1784	4624
μ (mm^{-1})	0.477	0.653
Temperature (K)	173	173
Wavelength (Å)	0.71073	0.71073
Radiation	Mo-K_α	Mo-K_α
Theta limits (deg)	2.5/27.50	2.5/27.46
Number of data measd.	17070	18508
Number of data with $I > 3\sigma(I)$	5986	5327
Number of variables	496	614
R	0.036	0.042
Rw	0.046	0.067
GOF	1.058	1.118
Largest peak in final difference (e Å^{-3})	0.743	0.338

CCDC-190059 (**10**) and -190060 (**11b**) contain the supplementary crystallographic data for this paper. These data can be obtained free of charge at www.ccdc.cam.ac.uk/conts/retrieving.html [or from the Cambridge Crystallographic Data Center, 12, Union Road, Cambridge CB2 1EZ, UK; Fax: (internat.) +44−1223/336−033; E-mail: deposit@ccdc.cam.ac.uk].

Acknowledgments

We thank the Deutsche Forschungsgemeinschaft, the CNRS, and the Institut Universitaire de France for funding and Wacker

Chemie AG for a generous gifts of basic chemicals. We thank Dr. André Decian and Natalie Gruber for carrying out the X-ray diffraction studies.

[1] [1a] B. C. Gates, *Catalytic Chemistry*, Wiley, New York, **1982**. [1b]C. Lecuyer, F. Quignard, A. Choplin, D. Olivier, J.-M. Basset, *Angew. Chem. Int. Ed. Engl.* **1991**, *30*, 1660−1161. [1c] T. A. Budzichowski, S. T. Chacon, M. H. Chisholm, F. J. Feher, W. Streib, *J. Am. Chem. Soc.* **1991**, *113*, 689−691.

[2] [2a] F. R. Hartley, *Supported Metal Complexes − A New Generation of Catalysts*, D. Reidel Publishing Company, Dortrecht, **1989**. [2b] Yu. I Yermakov, B. N. Kuznetsov, V. A. Zakharov, *Catalysis by Supported Complexes*, Elsevier, Amsterdam, **1981**. [2c]W. A. Herrmann, C. W. Kohlpaintner, *Angew. Chem. Int. Ed. Engl.* **1993**, *32*, 1524−1544.

[3] [3a] C. Bianchini, A. Meli, M. Peruzzini, F. Vizza, F. Zanobini, *Coord. Chem. Rev.* **1992**, *120*, 193−208. [3b] H. A. Mayer, W. C. Kaska, *Chem. Rev.* **1994**, *94*, 1239−1272.

[4] [4a] C. Bianchini, D. G. Burnaby, J. Evans, P. Frediani, A. Meli, W. Oberhauser, R. Psaro, L. Sordelli, F. Vizza, *J. Am. Chem. Soc.* **1999**, *121*, 5961−5971. [4b] C. Bianchini, V. Dal Santo, A. Meli, W. Oberhauser, R. Psaro, F. Vizza, *Organometallics* **2000**, *19*, 2433−2444.

[5] [5a] P. Schober, G. Huttner, L. Zsolnai, A. Jacobi, *J. Organomet. Chem.* **1998**, *571*, 279−288. [5b] C. Bianchini, M. Frediani, F. Vizza, *Chem. Commun.* **2001**, 479−480. [5c] C. Bianchini, M. Frediani, G. Mantovani, F. Vizza, *Organometallics* **2001**, *20*, 2660−2662.

[6] C. Bianchini, A. Meli, W. Oberhauser, *New J. Chem.* **2001**, *25*, 11−12.

[7] [7a] C. Bianchini, A. Meli, V. Patinec, V. Sernau, F. Vizza, *J. Am. Chem. Soc.* **1997**, *119*, 4945−4954. [7b] I. Rojas, F. L. Linares, N. Valencia, C. Bianchini, *J. Mol. Catal. A* **1999**, *144*, 1−6.

[8] [8a] J. W. J. Knapen, A. W. van der Made, J. C. de Wilde, P. W. N. M. van Leeuwen, P. Wijkens, D. M. Grove, G. van Koten, *Nature* **1994**, *372*, 659−663. [8b] R. A. Gossage, L. A. van de Kuil, G. van Koten, *Acc. Chem. Res.* **1998**, *31*, 423−431. [8c] A. W. Kleij, H. Kleijn, J. T. B. H. Jastrzebski, W. J. J. Smeets, A. L. Spek, G. van Koten, *Organometallics* **1999**, *18*, 268−276. [8d] A. W. Kleij, H. Kleijn, J. T. B. H. Jastrzebski, A. L. Spek, G. van Koten, *Organometallics* **1999**, *18*, 277−285. [8e] R. A. Gossage, J. T. B. H. Jastrzebski, J. van Ameijde, S. J. E. Mulders, A. J. Brouwser, R. M. J. Liskamp, G. van Koten, *Tetrahedron Lett.* **1999**, *40*, 1413−1416.

[9] For reviews of dendrimer catalysis, see: [9a] G. E. Oosterom, J. N. H. Reek, P. C. J. Kramer, P. W. N. M. van Leeuwen, *Angew. Chem. Int. Ed.* **2001**, *40*, 1828−1849. [9b] D. Astruc, F. Chardac, *Chem. Rev.* **2001**, *101*, 2991−3023.

[10] [10a] A. Miedaner, C. J. Curtis, R. M. Barkley, D. L. DuBois, *Inorg. Chem.* **1994**, *33*, 5482−5490. [10b] D. de Groot, E. B. Eggeling, J. C. de Wilde, H. Kooijman, R. J. van Haaren, A. W. van der Made, A. L. Spek, D. Vogt, J. N. H. Reek, P. C. J. Kamer, P. W. N. M. van Leeuwen, *Chem. Commun.* **1999**, 1623−1624. [10c] P. Wijkens, J. T. B. H. Jastrzebski, P. A. van der Schaaf, R. Kolly, A. Hafner, G. van Koten, *Org. Lett.* **2000**, *2*, 1621−1624. [10d] M. Benito, O. Rossell, M. Seco, G. Segales, *Organometallics* **1999**, *18*, 5191−5193. [10e] S. C. Bourque, F. Maltais, W.-J. Xiao, O. Tardif, H. Alper, P. Arya, L. E. Manzer, *J. Am. Chem. Soc.* **1999**, *121*, 3035−3038. [10f] S. C. Bourque, H. Alper, L. E. Manzer, P. Arya, *J. Am. Chem. Soc.* **2000**, *122*, 956−957. [10g] P. Arya, N. V. Ran, J. Singkhonrat, H. Alper, S. C. Bourque, L. E. Manzer, *J. Org. Chem.* **2000**, *65*, 1881−1885. [10h] M. Bardaji, M. Kustos, A.-M. Caminade, J.-P. Majoral, B. Chaudret, *Organometallics* **1997**, *16*, 403−410. [10i] V. Maraval, R. Laurent, A.-M. Caminade, J.-P. Majoral, *Organometallics* **2000**, *19*, 4025−4029. [10j] N. Hovestad, E. B. Eggeling, H. J. Heidbuechel, J. T. B. H. Jastrzebski, U. Kragl, W. Keim, D. Vogt, G. van Koten, *Angew. Chem. Int. Ed.* **1999**, *38*, 1655−1658.

[11] B. C. Janssen, V. Sernau, G. Huttner, A. Asam, O. Walter, M. Büchner, L. Zsolnai, *Chem. Ber.* **1995**, *128*, 63−70.

[12] A. Muth, A. Asam, G. Huttner, A. Barth, L. Zsolnai, *Chem. Ber.* **1994**, *127*, 305−311.

[13] T. Seitz, A. Muth, G. Huttner, T. Klein, O. Walter, M. Fritz, L. Zsolnai, *J. Organomet. Chem.* **1994**, *469*, 155−162.

[14] T. Seitz, G. Huttner, M. Büchner, *Z. Naturforsch., Teil B* **1994**, *49*, 1813−1817.

[15] T. Seitz, A. Asam, G. Huttner, O. Walter, L. Zsolnai, *Z. Naturforsch., Teil B* **1995**, *50*, 1287−1306.

[16] P. Schober, R. Soltek, G. Huttner, L. Zsolnai, K. Heinze, *Eur. J. Inorg. Chem.* **1998**, 1407−1415.

[17] [17a] M. J. Burk, R. L. Harlow, *Angew. Chem. Int. Ed. Engl.* **1990**, *29*, 1462−1464. [17b] M. J. Burk, J. E. Feaster, R. L. Harlow, *Tetrahedron: Asymmetry* **1991**, *2*, 569−592.

[18] T. J. Dunn, W. L. Neumann, M. M. Rogic, S. R. Woulfe, *J. Org. Chem.* **1990**, *55*, 6368−6373.

[19] S. M. Ludeman, D. L. Bartlett, G. Zon, *J. Org. Chem.* **1979**, *44*, 1163−1166.

[20] [20a] M. Y. Etienne, R. Soulas, *Bull. Soc. Chim. Fr.* **1957**, 978. [20b] K. M. Lynch, W. P. Dailey, *J. Org. Chem.* **1995**, *60*, 4666−4668.

[21] [21a] J. Scherer, G. Huttner, O. Walter, B. C. Janssen, L. Zsolnai, *Chem. Ber.* **1996**, *129*, 1603−1615. [21b] J. F. Frazier, J. S. Merola, *Polyhedron* **1992**, *11*, 2917−2927.

[22] [22a] A. van der Made, P. W. N. M. van Leeuwen, J. C. de Wilde, R. A. C. Brandes, *Adv. Mater.* **1993**, *5*, 466−468. [22b] L.-L. Zhou, J. Roovers, *Macromolecules* **1993**, *26*, 963−968. [22c] J. Roovers, L.-L. Zhou, P. M. Toporowski, M. van Zwan, H. Iatrou, N. Hadjichristidis, *Macromolecules* **1993**, *26*, 4324−4331. [22d] D. Seyferth, D. Y. Son, A. C. Rheingold, R. L. Ostrander, *Organometallics* **1994**, *13*, 2682−2690. [22e] D. Seyferth, T. Kugita, A. L. Rheingold, G. P. A. Yap, *Organometallics* **1995**, *14*, 5362−5366.

[23] [23a] C. Bianchini, A. Meli, M. Peruzzini, F. Vizza, Y. Fujiwara, T. Jintoku, H. Taniguchi, *J. Chem. Soc., Chem. Commun.* **1988**, 299−301. [23b] C. Bianchini, A. Meli, F. Laschi, J. A. Ramirez, P. Zanello, A. Vacca, *Inorg. Chem.* **1988**, *27*, 4429−4435.

[24] [24a] C. Bianchini, A. Meli, M. Peruzzini, F. Vizza, P. Frediani, J. A. Ramirez, *Organometallics* **1990**, *9*, 226−240. [24b] C. Bianchini, A. Meli, M. Peruzzini, F. Vizza, A. Albinati, *Organometallics* **1990**, *9*, 2283−2291.

[25] [25a] R. R. Schrock, J. A. Osborn, *J. Am. Chem. Soc.* **1976**, *98*, 4450−4455. [25b] R. R. Schrock, J. A. Osborn, *J. Am. Chem. Soc.* **1976**, *98*, 2134−2143. [25c] R. R. Schrock, J. A. Osborn, *J. Am. Chem. Soc.* **1976**, *98*, 2143−2147.

[26] W. Gee, R. A. Shaw, B. C. Smith, *Inorg. Synth.* **1967**, *9*, 19−24.

[27] [27a] W. E. Parham, E. L. Anderson, *J. Am. Chem. Soc.* **1948**, *70*, 4187−4189. [27b] Y. Xu, A. L. Roughton, P. Soucy, S. Goldstein, P. Deslongchamps, *Can. J. Chem.* **1993**, *71*, 1169−1183. −

[28] D. P. Tate, W. R. Knipple, J. M. Augl, *Inorg. Chem.* **1962**, *1*, 433 434.

[29] [29a] T. G. Schenk, J. M. Downes, C. R. C. Milae, P. B. Mackenzie, H. Boucher, J. Whelan, B. Bosnich, *Inorg. Chem.* **1985**, *24*, 2334−2337. [29b] J. A. Osborn, R. R. Schrock, *J. Am. Chem. Soc.* **1971**, *93*, 3089−3091.

[30] A. W. van der Made, P. W. N. M. van Leeuwen, *J. Chem. Soc., Chem. Commun.* **1992**, 1400−1401.

[31] [31a] I. Cuadrado, M. Móran, J. Losada, C. M. Casado, C. Pascual, B. Alonso, F. Lobete, in *Advances of Dendritic Macromolecules* (Ed.: G. R. Newkome), JAI Press: Greenwich, CT, **1996**, *3*, 151. [31b] I. Cuadrado, C. M. Casado, B. Alonso, M. Móran, J. Losada, V. Belsky, *J. Am. Chem. Soc.* **1997**, *119*, 7613−7614.

[32] Nonius *OpenMoleN, Interactive Structure Solution*, Delft, **1997**.

[33] D. T. Cromer, J. T. Waber, *International Tables for X-ray Crystallography*, The Kynoch Press, Birmingham, **1974**.

Received July 22, 2002
[I02407]

The Structure of Some Amine Solvates of Magnesium Bis(tetrahydroborate) and DFT Calculations on Solvates of Lithium Tetrahydroborate[‡]

Mathias Bremer,[a] Heinrich Nöth,*[a] and Marcus Warchhold[a]

Dedicated to Professor Gottfried Huttner on the occasion of his 65th birthday

Keywords: Amine ligands / Borates / Density functional calculations / Lithium / Magnesium

Eight solvates of magnesium bis(tetrahydroborate) have been prepared and characterised by NMR and IR spectroscopy, and five of them also by X-ray crystallography. Compounds $Mg(BH_4)_2 \cdot 3NH_2tBu$ and $Mg(BH_4)_2 \cdot 3pip$ each have a distorted trigonal-bipyramidal structure (with the BH_4 group viewed as a simple ligand) while the putative $Mg(BH_4)_2 \cdot 6py$ proved to be $[Mg(BH_4)_2 \cdot 4py]$ with a pseudooctahedral structure, two py molecules being present as solvent of crystallization. Similarly, $Mg(BH_4)_2 \cdot 8DMSO$ contains the cation $[Mg(DMSO)_6]^{2+}$ in the crystal, and $Mg(BH_4)_2 \cdot 6NH_2Bzl$ has an ionic lattice made up of $Mg(NH_2Bzl)_6^{2+}$ and BH_4^- ions. The BH_4 groups in the molecular compounds are bonded to the Mg centre through double hydrogen bonds. In order to study the bonding in alkali and alkali earth metal tetrahydroborates, DFT calculations were performed for $LiBH_4$ and its ammonia and dimethyl ether solvates. The minimum-energy structure for a $LiBH_4$ molecule has C_{3v} symmetry; this is not changed when one ammonia molecule is added and is also the result for $LiBH_4 \cdot 3NH_3$. Addition of the first NH_3 or Me_2O molecule contributes more to the stabilisation than a second or a third molecule.

(© Wiley-VCH Verlag GmbH & Co. KGaA, 69451 Weinheim, Germany, 2003)

Introduction

The BH_4 anion is a versatile ligand. In mononuclear complexes, one, two or three of its hydrogen atoms may bond to the metal centre. In di-, tri-, and tetranuclear complexes, and also in polymeric compounds, two, three, or even all four hydrogen atoms of the BH_4 ion may be involved in coordination to the metal centres.[1,2] While the structures of the diethyl ether and amine solvates of the alkali metal tetrahydroborates, particularly those of lithium, are fairly well known, there is little structural information on solvates of magnesium bis(tetrahydroborate). So far, only two compounds − $Mg(BH_4)_2 \cdot 3thf$[3,4] and $Mg(BH_4)_2 \cdot$diglyme − have been structurally investigated.[5] Both are mononuclear, with $Mg(\mu\text{-}H_2BH_2)_2$ units to which the diethyl ether ligands are coordinated. Although many other solvates of magnesium bis(tetrahydroborate) have been reported,[6−10] no structural information as to the bonding of the BH_4 group is known. In pursuit of our interest in studying the structures of tetrahydroborates of main group metals systematically we have prepared a number of new solvates of $Mg(BH_4)_2$ and determined their crystal structures. Moreover, we also performed DFT calculations on mononuclear $LiBH_4 \cdot n OMe_2$ and $LiBH_4 \cdot n NH_3$ in the expectation that they might offer insights into the hydrogen bonding of the BH_4 group and the stability of the solvates.

Preparation and Spectra

Magnesium bis(tetrahydroborate) is regarded as a salt-like compound, due to its comparatively high melting point (180 °C)[11] and very low solubility in non-polar solvents. It was first prepared by Wiberg and Bauer,[12] from Et_2Mg and diborane in diethyl ether solution, while it was later shown by Ashby and Becker that dimeric $EtMgBH_4 \cdot OEt_2$ is a better starting material.[13] It reacts with diborane in diethyl ether solution to give a solid 2:3 diethyl ether adduct of magnesium tetrahydroborate. Under similar conditions we obtained $Mg(BH_4)_2 \cdot 2OEt_2$ as a viscous oil, which reacts rapidly with moisture [see Equation (1)].

$$EtMg(BH_4) + B_2H_6 \rightarrow Mg(BH_4)_2 + \text{“}EtBH_2\text{''} \quad (1)$$

It is clear that the formation of $Mg(BH_4)_2$ as in Equation (1) requires several steps. ^{11}B NMR spectroscopy gives an insight into the course of the reaction. Figure 1 shows spectra taken at different ratios of $EtMgBH_4/B_2H_6$ in diethyl ether solution. Trace 1 shows the (undecoupled) ^{11}B quintuplet signal of the starting material at $\delta = -43.1$ ppm.

[‡] Metal Tetrahydroborates and Tetrahydroborato Metallates, 28. Part 27: Ref.[1]

[a] Department of Chemistry, University of Munich, Butenandstr. 5−13, 81377 Munich, Germany

Trace 2 shows in addition a quadruplet and a triplet at δ = −27 and −18 ppm; these are typical for $EtBH_3^-$ and $Et_2BH_2^-$. More diborane (trace 3) gives rise to the formation of more $Et_2BH_2^-$ besides BEt_3 (signal at δ = 86 ppm). Trace 5 reveals that the addition of even more diborane transforms the ethylhydridoborates completely into BH_4^- and ethyldiboranes. Moreover, BEt_3 reacts with diborane to give the ethyldiboranes and the former compound vanishes completely, as shown in trace 6. The 1:1 signal ratio of the broad signal at δ = 42.9 ppm and the triplet of triplets at δ = 4.8 ppm are indicative of the preferred formation of asymmetrically substituted diethyldiborane $Et_2BH_2BH_2$. After removal of all volatiles, only the quintuplet signal of magnesium tetrahydroborate could be noted. The most striking feature of this process is that the anion Et_3BH^- is not observed. We assume that this species reacts very rapidly with "BH_3" to give BEt_3 and BH_4^-. In a similar reaction, Et_2BH is formed by hydride abstraction from $Et_2BH_2^-$ by diborane. Et_2BH then picks up BH_3 to give asymmetrical diethyldiborane. The characterising NMR spectroscopic data are listed in the legend of Figure 1.

It is known from previous work[6−10] that $Mg(BH_4)_2$ readily forms solvates with diethyl ethers and amines. Adducts with ammonia[8,9] and with methylamines[10] are readily available, as is the complex with isopropylamine,[10] but all these adducts deteriorate quickly at ambient temperature. We were, however, able to obtain the last of these compounds as single crystals, but these became rapidly turbid during their isolation at low temperature (ca. −30 °C). In contrast, $Mg(BH_4)_2{\cdot}3H_2NCMe_3$ (**1**) was isolable and stable at −30 °C. All the new compounds, as well as a previously described pyridine adduct,[10] were obtained either by dissolving $Mg(BH_4)_2$ in the amine as solvent or by replacement of THF from $Mg(BH_4)_2{\cdot}3$thf with a new ligand L′, and crystallisation of the complexes by addition of cyclohexane to the resulting solutions. Reactions proceeded as shown in Equation (2). The compounds listed in Table 1 were obtained. The yields were not optimised, only the material that crystallised or precipitated being isolated.

$$Mg(BH_4)_2{\cdot}n\mathrm{L} + n\,\mathrm{L}' \rightarrow Mg(BH_4)_2{\cdot}n\mathrm{L}' + n\,\mathrm{L} \quad (2)$$

^{11}B NMR spectra were recorded either in the corresponding amine as solvent or in DMSO. The shielding of the boron nuclei and the coupling constants observed are practically independent of the coordinated ligand (diethyl ethers, amines). The small but significant low-field shift of the ^{11}B NMR signal relative to $NaBH_4$ [$\delta^{11}B$ = −41; $^1J(BH)$ = 82 Hz] suggests that there is a weak interaction between the tetrahydroborate anion and the Mg cation, but on the other hand, the fairly similar shielding also suggests that $Mg(BH_4)_2$ is present in amine solution as a salt [Mg(amine)$_n$]$(BH_4)_2$, and hence that the solution state is different to the structure in the solid state except in the case of compound **4**. As with most tetrahydroborates, neither the ^{11}B chemical shift nor the coupling constant give a reliable in-

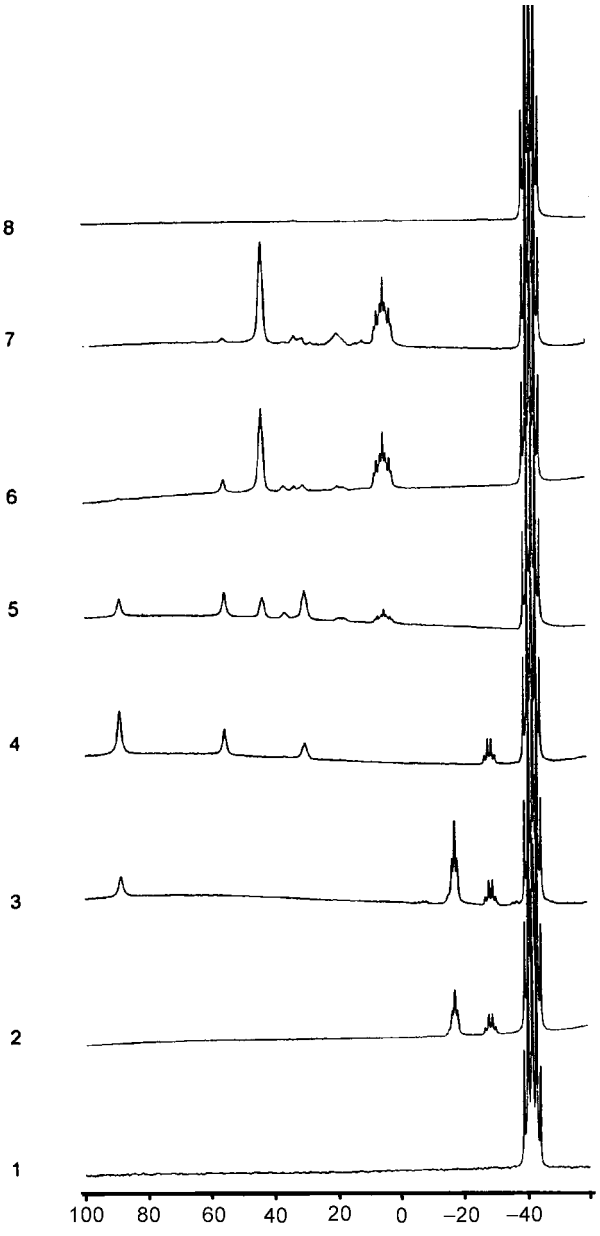

Figure 1. ^{11}B NMR spectra of a solution of $EtMgBH_4$ to which diborane dissolved in diethyl ether was added incrementally; assignment of chemical shifts (in $\delta^{11}B$) are as follows: BH_4^- −43.1, H_3BEt^- −30.3, $H_2BEt_2^-$ −18.1, $H_2BH_2BEt_2$ 4.8, H_2BEt 29.8, $H_2BH_2BEt_2$ 42.9, $HBEt_2$ 54.9, BEt_3 87.3

Table 1. $\delta^{11}B$ [ppm] and $^1J(BH)$ [Hz] values of compounds **1**−**8**

		$\delta^{11}B$	$^1J(BH)$
$Mg(BH_4)_2{\cdot}3H_2NtBu$	**1**	−38.5	82
$Mg(BH_4)_2{\cdot}3HNC_5H_{10}$	**2**	−40.3	82
$Mg(BH_4)_2{\cdot}6py$	**3**	−37.6	82
$Mg(BH_4)_2{\cdot}6H_2NCH_2Ph$	**4**	−37.8	81
$Mg(BH_4)_2{\cdot}2$(18-crown-5)	**5**	−34.9	81
$Mg(BH_4)_2{\cdot}8$DMSO	**6**	−33.8	79
$Mg(BH_4)_2{\cdot}2$deta	**7**	35.8	82
$Mg(BH_4)_2{\cdot}$pmdta	**8**	−34.5	82

Table 2. Typical IR bands [cm^{-1}]in the B−H stretching region (for ^{11}B isotope) of the tetrahydroborates **1**−**8** and $Mg(BH_4)_2 \cdot 2OEt_2$ (**9**)

1	2369 st	2325 st			2228 st	
4		2327 st	2216 st	2252 st		2182 m
5			2283.4 st		2219.3 st	2149.3 m
6			2282.8 st		2214.1 st	2146.9 st
7			2299.8 st		2234.2 st	2159.0 st
8	2368.8 st	2322.2 st	2275.8 st	2240.9 st	2197.1 st	
9	2391.7 st	2350.8sh	2234.5sh	2185.2st		
$NaBH_4$ [11]	2393 st		2291 st		2229 st	

dication as to the bonding of the BH_4 group to Mg^{2+}. The quintuplet structure of the signal shows four chemically equivalent hydrogen atoms: this may be due to a free anion or to rapid exchange between bridging and terminal hydrogen atoms.[14]

Thanks to its higher time resolution, IR spectroscopy may be more informative as far as the interaction of the cation with the BH_4 anion is concerned. Depending on the type of hydrogen bond the local symmetry of the BH_4 anion changes from C_{3v} to C_{2v} and then to C_{3v} for the single bridge $Mg(H-BH_3)$ to the double bridge $Mg(H_2BH_2)$ and then to the triple bridge $Mg(H_3BH)$. The expected spectra are different for the three types of bonding. For double hydride bridges, four active IR bands, due to two $\nu_{as}BH_2$ vibrations and two $\nu_{sym}BH_2$ vibrations, would be expected, while for C_{3v} symmetry three bands, due to ν_{as} and ν_{sym} for the H_3B group and one stretching frequency for the single B−H bond, should be observable.

The presence of four bands in the IR spectrum of $Mg(BH_4)_2 \cdot 2OEt_2$ thus points to double hydride bridges, and this suggests hexacoordination at the Mg centre (two oxygen and four hydrogen atoms, see Table 2).

In contrast, the crown diethyl ether complex exhibits only three bands, which are found in the same region as for $NaBH_4$,[15] and this is indicative of an ionic structure. The same feature is found for the DMSO compound **6**, but this is not compatible with its $\delta^{11}B$ value (−33.8). The structure in DMSO solution may therefore be different from that in the solid state. One can imagine an equilibrium in solution of a type as shown in Equation (3).

$$Mg(DMSO)_6^{2+} + 2\,BH_4^- \rightleftarrows Mg(DMSO)_5BH_4^+ + BH_4^- + DMSO \quad (3)$$

The diethylenetriamine complex **7** shows an IR spectrum typical of free BH_4 anions in the BH stretching range. This compound should therefore have the constitution $[Mg(dta)_2](BH_4)_2$, with hexacoordinated Mg ions. In contrast, complex **8** − which contains only one molecule of the amine − has five BH bands in the stretching region. This indicates that it most probably has the structure $[Mg(pmdta)H_2BH_2]BH_4$.

Crystal Structures

In order to investigate the type of hydride bridging between the BH_4 anion and the Mg ion in the solid state, single crystals of **1**−**4** and also of **6** were studied by X-ray crystallography. The tBuNH$_2$ solvate **1** crystallises in the monoclinic space group $P2_1/n$ with $Z = 8$ (i.e., there are two independent molecules in the asymmetric unit). The molecular parameters of the two molecules are fairly similar, and so only one of them is depicted in Figure 2. Both BH_4 groups in the molecule are bonded to the magnesium ion through two hydrogen atoms. A distorted trigonal-bipyramidal arrangement of two boron and three nitrogen atoms around the magnesium centre is observed, with two nitrogen atoms in the apical positions. The apical Mg−N distances are longer [2.243(2), 2.277(2) Å] than the equatorial Mg−N bond [2.212(2) Å]. The atoms Mg1, B1, B2, and N2 lie almost in a perfect plane. Interestingly, the B−Mg−B angle is quite open, at 137.87(8)°. The Mg···B distances in **1** are on average 0.097 Å longer than in $Mg(BH_4)_2 \cdot 3thf$.[3,4] Although all hydrogen positions around the boron atoms were found in the difference Fourier map and refined well, the B−H distances nevertheless have to be regarded as approximate distances.

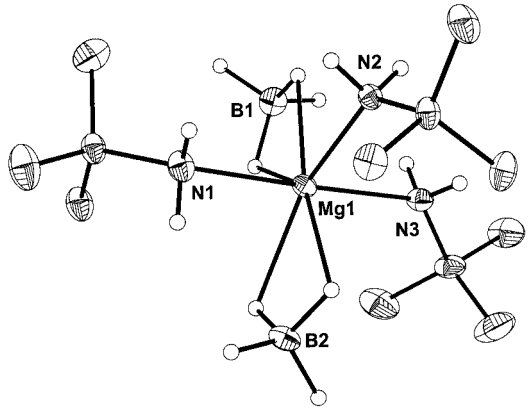

Figure 2. The molecular structure of compound **1**; thermal ellipsoids are represented on a 25% probability scale; selected atom distances (in Å) and bond angles (in °): Mg1−N1 2.243(2), Mg1−N2 2.212(2), Mg1−N3 2.227(2), Mg···B1 2.549(2), Mg1···B2 2.521(2), Mg−H_{br} 2.08 (aver.), B−H_{br} 1.15(1) (aver.), B−H_{term} 1.12(1) (aver.); B1−Mg1−B2 137.8(8), N1−Mg1−N2 89.48(6), N1−Mg1−N3 177.55(7), N2−Mg−N3 90.44(7)

In principle, the same molecular structure as for **1** was found for **2** (see Figure 3). However, this molecule crystallises in the triclinic system with the centrosymmetric space group $P\bar{1}$, $Z = 2$. In contrast to **1**, one of the two apical N atoms has a short Mg−N bond [2.233(4) Å] while the second [2.249(4) Å] is longer, practically as long the

equatorial Mg−N distance [2.244(4) Å]. Moreover, the two Mg···B distances are quite different, although their average value corresponds to the Mg···B distance found for **1**.

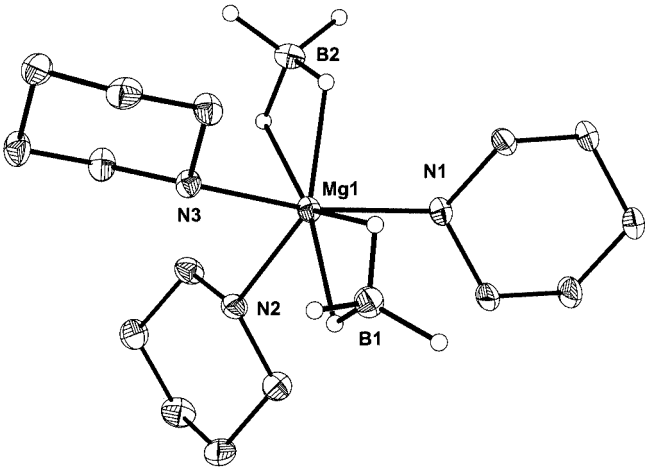

Figure 3. The molecular structure of compound **2**; thermal ellipsoids are represented on a 25% probability scale; selected atom distances (in Å) and bond angles (in °): Mg1−N1 2.233(4), Mg1−N2 2.244(4), Mg1−N3 2.249(4), Mg1···B1 2.536(6), Mg1···B2 2.520(6), Mg−H 1.99(5) (aver.), B−H_{br} 1.12(5) (aver.), B−H_{term} 1.15(5) (aver.); B1−Mg1−B2 143.6(2), N1−Mg1−N2 102.2(2), N1−Mg1−M3 165.0(2), N2−Mg1−N3 92.7(2)

The composition of the pyridine complex of $Mg(BH_4)_2$ suggested an ionic structure $[Mg(py)_6](BH_4)_2$. This is not the case, however, as shown by the X-ray structure analysis of the orthorhombic crystals, space group *Ccca* (see Figure 4). The asymmetric unit contains molecular $Mg(BH_4)_2$·4py, and in addition there are two pyridine molecules. The $Mg(BH_4)_2$·4py molecule possesses D_2 point group symmetry. All its pyridine molecules are arranged in a plane around the Mg centre, while the boron atoms stand perpendicularly on the MgN_4 plane. Thus, the geometry for the MgB_2N_4 unit is a distorted octahedron with the Mg atom in its centre. In agreement with the higher coordination number, the Mg···B distances are longer than those in **1** and **2**, but these lengths are considerably greater than would be expected. As a consequence, the Mg−H bond lengths are also long, and one should note, although with caution, that the bridging hydrogen B−H bond lengths are shorter than those of the terminal B−H bonds. On the other hand, the Mg−N bond lengths [varying from 2.197(2) to 2.224(3) Å] are longer than in **1** or **2**. One might argue that the difference in Mg−N bond length could be smaller because of the sp^2-type N atoms of the pyridine molecules.

In contrast to the molecular compounds, the benzylamine adduct **4** proved to be ionic. The crystals are monoclinic, space group $P2_1/c$, $Z = 4$. Figure 5 shows the cation, together with a BH_4 anion and two further boron atoms. The sites of these two boron atoms are occupied with SOFs of 0.5 on inversion centres. Although the highest residual electron densities are found around these boron atoms, assignment to boron-bonded hydrogen atoms was not possible. It should be noted that a set of tetrahedrally oriented H atoms would, by symmetry, be transformed into eight H positions about these boron atoms, and SOFs of 0.5 would be expected for these hydrogen atoms. It follows that it would be unlikely that these could be well located, because of the expected very low electron density for these hydrogen atoms.

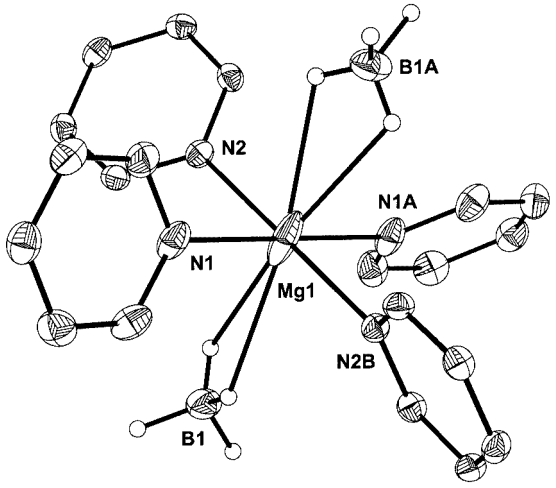

Figure 4. The molecular structure of compound **3**; thermal ellipsoids are represented on a 25% probability scale; selected atom distances (in Å) and bond angles (in °): Mg1−N1 2.224(3), Mg1−N2 2.197(2), Mg1···B1 2.988(4), Mg1−H_{br} 2.40(4) (aver.), B−H_{br} 0.98(5), B−H_{term} 1.13(3); B1−Mg1−B1A 180, B1−Mg1−N1 90, N1−Mg1−N1A 180

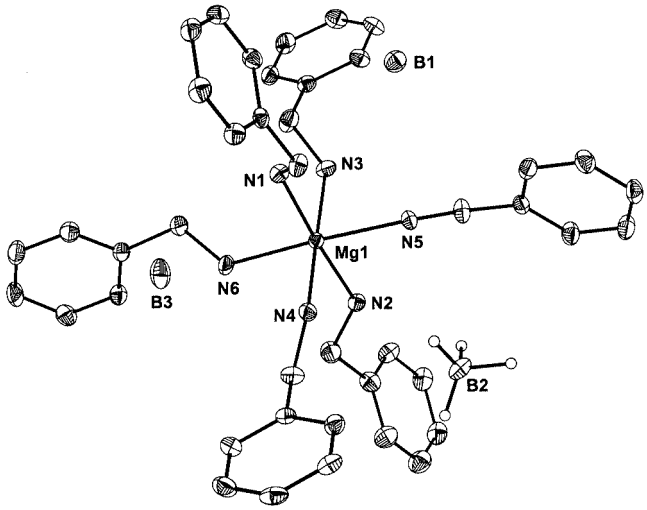

Figure 5. The molecular structure of compound **4**; thermal ellipsoids are represented on a 25% probability scale; selected atom distances (in Å) and bond angles (in °): Mg1−N1 2.252(2), Mg1−N2 2.247(2), Mg1−N3 2.263(2), Mg1−N4 2.258(2), Mg1−N5 2.258(2), Mg1−N6 2.233(2); N1−Mg1−N2 176.50(9), N1−Mg1−N3 89.92(8), N1−Mg1−N4 87.88(8), N1−Mg1−N5 89.62(8), N1−Mg1−N6 91.23(9), N3−Mg1−N4 176.89(6), N5−Mg1−N6 176.95(5)

The Mg ion occupies a slightly distorted octahedral environment. One of the six Mg−N bonds is significantly shorter [2.233(2) Å] than the other five [2.247−2.263(2) Å]. The N−Mg−N bond angles of adjacent N atoms range from 87.88(8) to 91.23(9)°, while those of opposite N atoms are practically identical [176.89(9) to 176.95(9)°].

Figure 6 shows the structure of compound **6**. The asymmetric unit of the cell is $[Mg(DMSO)_6]_{1/2}\cdot(BH_4)\cdot DMSO$. A symmetry operation through an inversion centre generates the cation $Mg(DMSO)_6^{2+}$ and an additional BH_4, besides a DMSO molecule. The Mg−O distances range from 2.056 through 2.072 to 2.093(2) Å, and the O−Mg1−O bond angles are consequently 180° for opposite oxygen atoms and very close to 90° for adjacent oxygen atoms. The S−O bond lengths of the coordinated DMSO molecules are slightly longer [1.516 to 1.521(2) Å] than those in the free DMSO molecule [1.501(3) Å], while the S−C bonds are slightly shorter for coordinated DMSO [aver. 1.769(5) Å] than for non-coordinated DMSO (1.779 Å). On the other hand the O−S−C bond angles in the coordinated DMSO molecules are slightly smaller than those in free DMSO.

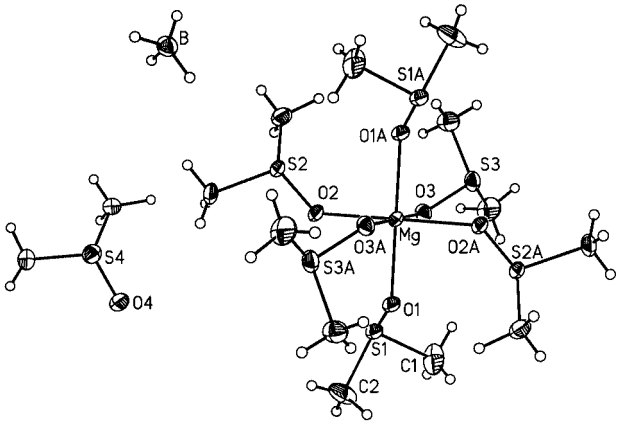

Figure 6. The molecular structure of compound **6**; thermal ellipsoids are represented on a 25% probability scale; selected atom distances (in Å) and bond angles (in °): Mg1−O1 2.056(2), Mg1−O2 2.093(2), Mg1−O3 2.072(2), B1−H1 1.10(4), B1−H2 0.75(4), B1−H3 1.02(4), B1−H4 1.15(4), S1−O1 1.520(2), S1−C1 1.769(5), S1−C2 1.769(5), S2−O2 1.521(2), S3−O3 1.516(2), S4−O4 1.501(3), S4−C7 1.781(5), S4−C8 1.777(5); O1−Mg1−O1A 180; O1−Mg1−O2 89.86(9), O1−Mg1−O2A 90.14(9), O1−Mg1−O3 90−20(9), O1−Mg1−O3A 89.80(9), H−B−H 92−122(3), S1−O1−Mg1 124.8(1), O1−S1−C1 104.9(2), O1−S1−C2 103.7(2), C1−S1−C2 97.4(2), S2−O2−Mg1 118.6(1), O2−S2−C3 105.2(2), O2−S2−C4 105.1(2), C3−S2−C4 98.4(3), S3−O3−Mg1 122.7(1), O3−S3−C5 105.9(2), O3−S3−C6 104.1(2), O4−S4−C7 107.1(2), O4−S4−C8 106.2(2), C7−S4−C8 96.7(2)

DFT Calculations

As far as magnesium tetrahydroborates are concerned, the structures determined so far show that only $\mu_2{}^1$ bonding (double hydride bridge to a single central atom) of the tetrahydroborate ion is present irrespective of the solvate ligand. In contrast, $LiBH_4$ forms a large variety of solvates with different types of bonded BH_4 groups ranging from molecular units with $\mu_2{}^1$-$\mu_3{}^1$-bonded BH_4 anions to dimers with two $2\mu_1{}^1$-$\mu_1{}^2$ BH_4 groups (two single and one H atom bridging two Li ions) to polymeric structures in which all H atoms of the BH_4 anion are involved.[1,16] Such a situation is also observed in the linear polymeric structure of $Ba(BH_4)\cdot 2thf$.[17] It was therefore of interest to obtain some insight into what should be expected when the $LiBH_4$ molecule is solvated, as these results may also be important for other alkali metal and alkaline earth metal tetrahydroborate compounds. For this reason we conducted DFT calculations on free $LiBH_4$ molecules and some of their ammonia and dimethyl ether solvates. These calculations were performed by use of the Gaussian 98 program package.[18] All calculations were conducted at the B3LYP level of theory[18,19] with the triple ξ basis set 6-311++G(d,p).[20] A frequency analysis after geometry optimisation showed no imaginary frequencies, and so the geometry represents a minimum on the energy hypersurface.

As the BH_4 anion approaches the Li cation, one would expect that the bond of the bridging hydrogen atoms should become longer than the terminal B−H bonds. This difference should increase as the BH_4 group becomes more polarized by the Li cation. Since it is difficult to determine the B−H distances reliably by X-ray diffractometry it is advisable to inspect the stretching frequencies of the B−H bonds (Scheme 1). Tables 3, 4, and 5 summarise the point group symmetries, the calculated wavenumbers of the B−H stretching vibrations and the calculated B−H bond lengths. Calculations with H_2O as a ligand could not be performed successfully as there is always a hydride−proton interaction giving rise to a very strong distortion. We therefore used dimethyl ether as the model for Li−O interactions. It should be noted that a distorted μ_2 coordination was found for $LiBH_4\cdot 2NH_3$; it is not included in the data of Table 5.

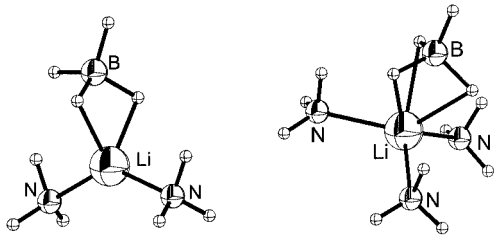

Scheme 1. Calculated geometries for $LiBH_4$ |1582NH_3 and $LiBH_4$ |1583NH_3 (see Table 3)

First, it follows that, on using a larger basis set for the $LiBH_4$ molecules of point group symmetry C_{3v}, significant differences result for $\nu_{sym}BH_{br}$ but particularly for νBH_{term}. Addition of NH_3 to $LiBH_4$ strengthens the bridging B−H bonds and weakens the terminal B−H bond, while addition of three ammonia molecules produces a remarkable weakening of the BH_{term} bond and a strengthening of the bridging B−H bonds. The same trend holds for the dimethyl ether adducts.

On the other hand, the calculated B−H distances, and in particular the Li···B atom distances, increase with increasing coordination number at the cation. Table 3 shows a comparison of calculated and observed Li···B, Li···N, and Li−H distances. The calculated and observed data (but not the trend) are compatible.

Moreover, the trend in bonding should be reflected by the calculated electronic energies (Table 4). The data given are corrected by unscaled zero point energies and are relative to $LiBH_4$ with C_{3v} point group symmetry and triple hydride bridging. Data for the solvated $LiBH_4$ molecule are

Table 3. Relative changes in energy with variation of coordination of the tetrahydridoborate anion and the solvation of the Li cation

Compound	Point group	Relative energy[a] [kJ/mol]	Ref.[b] [kJ/mol]	Ref.[c] [kJ/mol]	Ref.[d] [kJ/mol]
$Li(\mu_1\text{-}HBH_3)$	C_{3v}	109[e]	125	113	
$Li(\mu_2\text{-}H_2BH_2)$[b]	C_{2v}	19[f]	24	23	15
$Li(\mu_3\text{-}H_3BH)$	C_{3v}	0	0	0	0
$(LiBH_4)_2$	C_1	−68			−79
$LiBH_4{\cdot}NH_3$	C_3	−84			
$LiBH_4{\cdot}2NH_3$	C_1	−132			
$LiBH_4{\cdot}3NH_3$	C_1	−165			
$(LiBH_4{\cdot}NH_3)_2$	C_1	−172			
$LiBH_4{\cdot}OMe_2$	C_1	−87			
$LiBH_4{\cdot}2OMe_2$	C_1	−141			
$LiBH_4{\cdot}3OMe_2$	C_1	−175			

[a] Method B3LYP/6-311++G(d,p). [b] Method HF/6-31G(d,p); A. A. Gorbik, O. P. Carkin, *Russ. J. Inorg. Chem.* **1985**, *30*, 1711−1714. [c] Method HF/6-31G(d)//HF/STO-3G; J. D. Dill, P. v. R. Schleyer, J. S. Binkley, J. A. Pople, *J. Am. Chem. Soc.* **1977**, *99*, 6159−6173. [d] Method HF/6-31G; geometries partially fixed; D. R. Armstrong, W. Clegg, D. S. Jones, W. N. Lipscomb, *Chem. Phys. Lett.* **1987**, 630−632. [e] Forced by fixed geometry; two imaginary frequencies. [f] Forced by fixed geometry; one imaginary frequency.

Table 4. Comparison between calculated [B3LYP/6-311++G(d,p)] and experimentally determined (X-ray) bond lengths (values in Å are in part averaged)

	Calculation	X-ray structure	Calculation	X-ray structure
	$LiBH_4{\cdot}2NH_3$	$LiBH_4{\cdot}2$(collidine) (**2**)	$LiBH_4{\cdot}3NH_3$	$LiBH_4{\cdot}3$(aniline) (**7**)
Li−B	2.172	2.252(6)	2.232	2.135(2)
Li−N	2.056	2.051(3)	2.129	2.279(6)
$B-H_{br}$	1.246	1.17(2)	1.235	1.10(4)
$B-H_{term}$	1.215	1.14(2)	1.205	0.86(5)
$Li-H_{br}$	1.819	1.81(2)	2.129	1.96(4)

Table 5. Effect on coordination and solvation of the tetrahydroborate ion [B3LYP/6-311++G(d,p), if not otherwise stated]

Compound	Point group	Vibration frequencies (in cm^{-1})			Bond lengths (in Å)		
		$\nu_{asym}(BH_{br})$	$\nu_{sym}(BH_{br})$	$\nu(BH_{term})$	$B-H_{br}$	$B-H_{term}$	M−B
BH_4^-	T_d	2226 (T)				1.238	−
$LiBH_4$	C_{3v}	2210 (E)	2249	2594	1.244	1.193	1.914
$LiBH_4$ [a]	C_{3v}	2216 (E)	2256	2606	1.243	1.191	1.914
$NaBH_4$	C_{3v}	2206 (E)	2240	2521	1.242	1.201	2.288
KBH_4	C_{3v}	2215 (E)	2248	2493	1.241	1.205	2.648
$HMgBH_4$	C_{3v}	2217 (E)	2241	2640	1.246	1.187	2.117
$NH_3{\cdot}LiBH_4$	C_3	2220 (E)	2253	2566	1.243	1.196	1.954
$3NH_3{\cdot}LiBH_4$	C_1	2271/2273	2284	2488	1.235	1.205	2.232
$OMe_2{\cdot}LiBH_4$	C_1	2216/2226	2255	2565	1.243	1.196	1.955
$2OMe_2{\cdot}LiBH_4$	C_1	2231/2247	2311	2526	1.238	1.201	2.044
$3OMe_2{\cdot}LiBH_4$	C_1	2268/2284	2296	2499	1.235	1.204	2.116

[a] Calculated with a larger basis set B3LYP/6-311++G(3df,3pd).

also scaled for $Li(H_3BH)$ and free solvent molecules with $E = 0$ kJ/mol.

There is an energy difference of 90 kJ/mol between singly and doubly bridged $LiBH_4$, while the energy difference between the latter and the triply bridged molecule is only 19 kJ/mol. Dimerization of $LiBH_4$ affords a stabilization by 68 kJ/mol, and successive addition of ammonia produces a large stabilization for the addition of the first molecule, and less for each other step as one adds two or three molecules. $LiBH_4{\cdot}3NH_3$ is the most stable monomeric arrangement. Calculations also show that $(LiBH_4{\cdot}NH_3)_2$ is 7 kJ/mol more stable than $LiBH_4{\cdot}3NH_3$. A similar trend holds for the dimethyl ether adducts of $LiBH_4$. These adducts are more stable than the solvates with ammonia molecules.

Discussion

At present, only two types of magnesium bis(tetrahydroborates) are known: molecular mononuclear solvates and ionic mononuclear complexes. The structure of solvent-free $Mg(BH_4)_2$ is still unknown, but in view of the effective radii of Br^- and BH_4^-, which are very similar, one might expect that $Mg(BH_4)_2$ should have the same structure as $MgBr_2$. Thus, $MgBr_2$ forms THF solvates such as $MgBr_2{\cdot}3THF$.[21,22] While a multitude of different bonding situations has been found for $LiBH_4$, ranging from solvated mononuclear to polymeric species,[1,16] only one type of bonding has so far been detected for $Mg(BH_4)_2$: $Mg(\mu_2^1\text{-}H_2BH_2)$, irrespective of the number of additional ligands associated with Mg^{2+}. For instance, $Mg(BH_4)_2{\cdot}3THF$, **1** and **2** can be regarded as deriving from a trigonal-bipyramidal geometry[3,4] if we involve the boron atoms in bonding and neglect the bridging hydrogen atoms. If we consider only the nearest neighbours to magnesium, then the coordination number is 7 (four H and three N or O atoms). Compound **3** can be viewed as distorted octahedral, the Mg ion coordinated to four N and two B atoms, or as octacoordinated (four H and four N atoms).

The second type is ionic, with the general composition $[MgL_6](BH_4)_2$ (compounds **4**, **6** and most probably also **7**). These compounds are formed if the donor numbers of the solvent molecules are high.[23] The order of increasing donor strength found for $Mg(BH_4)_2$ is: ether < THF < $NH_2tBu \approx$ pip < py < NH_2Bzl < DMSO. In comparison with complexes of the other alkali earth metals, the order $Ba^{2+} < Sr^{2+} < Ca^{2+} < Mg^{2+}$ demonstrated by Irvin and Williams[24,25] is compatible with the solvates of these alkali earth metal tetrahydroborates.

It is astonishing that no di- or trinuclear solvates of magnesium bis(tetrahydroborate) are yet known; one might expect that solvates of the type $L_2(BH_4)Mg(BH_4)_2Mg(BH_4)L_2$ should be stable by analogy to $MgBr_2{\cdot}2THF$, which forms a polymer in the solid state with hexacoordinated Mg^{2+}.[22] Thus, there is no reason why solvates of magnesium bis(tetrahydroborate) should not have as rich a structural chemistry as the solvates of $LiBH_4$.

Experimental Section

General: All experiments were performed under anhydrous conditions by use of Schlenk techniques and dinitrogen as a protecting gas. The amines used were distilled before use. $Mg(BH_4)_2$ was prepared from $EtMgBH_4$ [13,26] and diborane in diethyl ether. NMR: Jeol XL400, $BF_3{\cdot}OEt_2$ as external standard. IR: Nicolet 520 FT-IR or Perkin−Elmer 325 (samples in Nujol): X-ray: Siemens P4 diffractometer equipped with an LT2 low-temperature device and a CCD area detector for compounds **1**−**4**. Data for compound **6** were collected with a scintillation counter in the ω/2θ mode. Mo-K_α radiation, graphite monochromator.

Magnesium Bis(tetrahydridoborate) Bis(diethyl ether) (9): A solution of iodine (25.4 g, 100 mmol) in diglyme (50 mL) was slowly added to a stirred solution of $NaBH_4$ (7.5 g, 200 mmol) in diglyme (30 ml). The diborane generated was carried by a stream of N_2 into a solution of $EtMgBH_4$ (25 mmol) in diethyl ether (100 mL). After this solution had been stirred for 2 h, all volatile components were removed in vacuo (1 Torr). The diethyl ether adduct of $Mg(BH_4)_2$ was a solid that liquefied on standing at ambient temperature. The coordinated diethyl ether could be removed (monitoring by weight loss) by keeping the compound in high vacuum (0.001 Torr) for 12 h. Yield of **9**: 4.75 g (93.8%). $\delta^{11}B$ (ether) = −43.0 [^1J(BH) = 82.4 Hz] ppm. δ^1H (C_6D_6) = 0.21 [q, ^1J(HB) = 82 Hz], 0.90 (t, CH_3), 3.61 (q, CH_2) ppm. $\delta^{13}C$ (C_6D_6) = 65.7 (CH_2), 13.7 (CH_3) ppm. $C_8H_{28}B_2MgO_2$ (202.25): calcd. H^- 3.98, B 10.69, Mg 12.02; found H^- 3.71, B 10.55, Mg 12.03.

Magnesium Bis(tetrahydroborate) Tris(*tert*-butylamine) (1): $Mg(BH_4)_2$ (134 mg, 2.78 mmol) was dissolved in *tert*-butylamine (15 mL). Methylcyclohexane (5 mL) was added with stirring. This addition caused the precipitation of a small amount of a solid, which was discarded. The filtrate was kept at 8 °C for a week. Colourless prisms separated and were isolated by filtration. The crystals deteriorated rapidly when a stream of dinitrogen was passed over them. Therefore, some of these crystals were removed from the supernatant liquid and placed in perfluoroether oil for X-ray diffraction. The composition is the result of the structure determined by X-ray crystallography. Yield: 280 mg (37%). M.p. 134−136 °C (dec., sealed capillary). $\delta^{11}B$ = −38.5 [^1J(BH) = 82 Hz] ppm. IR: $\tilde{\nu}$ = 2422 (sh), 2369 (st), 2325 (st), 228 (st) cm^{-1}.

Magnesium Bis(tetrahydroborate) Tris(piperidine) (2): $Mg(BH_4)_2$ (178 mg, 3.29 mmol) was dissolved in piperidine (10 mL), and cyclohexane (5 mL) was added to the stirred solution. Insoluble material was removed from the turbid solution. The filtrate was stored at 8 °C. Colourless prisms of composition $Mg(BH_4)_2{\cdot}3pip$ (as determined by X-ray crystallography) were isolated. Yield: 298 mg (29%). M.p. 50−53 °C (dec.). $\delta^{11}B$ (piperidine) = −40.3 [^1J(BH) = 82 Hz] ppm.

Magnesium Bis(tetrahydroborate) Hexakis(pyridine) (3): $Mg(BH_4)_2$ (94 mg, 1.7 mmol) and 1,3,5-trimethyl-1,3,5-triazine (0.25 mL, 1.78 mmol) were dissolved in pyridine (10 mL). Cyclohexane (2 mL) was added with stirring. A colourless solid precipitated and was removed by filtration. Storage at 8 °C gave crystals of composition $Mg(BH_4){\cdot}6py$. Yield: 130 mg (14%). M.p. 57 − 59 °C (dec.). Attempts to obtain compound **3** from $Mg(BH_2)_4$ and pyridine in the absence of the triazine gave no crystals but only oily products. $\delta^{11}B$ = −37.6 [^1J(BH) = 82 Hz] ppm.

Magnesium Bis(tetrahydroborate) Hexakis(benzylamine) (4): Cyclohexane (5 mL) was added to a solution of $Mg(BH_4)_2$ (196 mg, 3.62 mmol) in benzylamine (25 mL). The solid that formed was removed by filtration and the filtrate was cooled to −35 °C. After 3 weeks, colourless prisms had formed and were isolated. Yield: 1.33 g (53%). M.p. 59−60 °C (dec.). $\delta^{11}B$ (benzylamine) = −37.8 [^1J(BH) = 83 Hz)] ppm. IR: $\tilde{\nu}$ = 2327 (sh), 2316 (st), 2252 (st), 2182 (st) cm^{-1}. $C_{42}H_{62}B_2MgN_6$ (696.5): calcd. C 72.38, H 8.97, N 12.06; found C 71.10, H 8.55, N 12.00.

Magnesium Bis(tetrahydroborate) Bis(15-crown-5) (5): $Mg(BH_4)_2{\cdot}3THF$[3] (3.78 g, 14.0 mmol) was dissolved in THF (40 mL), and 15-crown-5 (5.6 mL, 28 mmol) was added dropwise to the stirred solution. This resulted in the formation of a precipitate, which was isolated by centrifugation and then dried in vacuo. No single crystal could be obtained. Yield: 6.64 g (96.1%). M.p. 311−313 °C. $C_{20}H_{48}B_2MgO_{10}$ (494.52): calcd. C 48.58, H 9.78, H^- 1.63, B 4.37; found C 48.92, H 9.91, H^- 1.59, B 4.31.

Magnesium Bis(tetrahydroborate) Octakis(dimethyl sulfoxide) (6): $tBuSMg(BH_4){\cdot}OEt_2$[26] (1.24 g, 5.7 mmol) was dissolved in a min-

Table 6. Data relating to crystallography, data collection and structure solution of compounds **1**−**4** and **6**

	1	**2**	**3**	**4**	**6**
Empirical formula	$C_{12}H_{41}B_2MgN_3$	$C_{15}H_{41}B_2MgN_3$	$C_{30}H_{38}B_2MgN_6$	$C_{42}H_{58}B_2MgN_6$	$C_{16}H_{56}B_2MgO_8S_8$
Formula mass	273.41	309.44	528.59	692.87	679.02
Crystal size [mm]	0.30×0.30×0.30	0.10×0.30×0.30	0.20×0.20×0.30	0.20×0.30×0.30	0.35×0.2×0.15
Crystal system	monoclinic	triclinic	orthorhombic	monoclinic	triclinic
Space group	*P*2(1)/*n*	$P\bar{1}$	*Ccca*	*P*2(1)/*c*	$P\bar{1}$
a [Å]	18.9389(9)	10.758(2)	11.604(2)	14.421(1)	9.853(3)
b [Å]	12.4814(6)	10.983(2)	15.114(2)	20.223(2)	10.073(3)
c [Å]	18.9867(9)	11.184(2)	17.190(2)	14.528(1)	11.430(3)
α [°]	90	86.201(3)	90	9	64.66(1)
β [°]	111.4190(1)	61.602(4)	90	90.1720(1)	68.05(2)
γ [°]	90	61.788(3)	90	90	84.72(2)
V [Å^3]	4178.2(3)	1002.7(3)	3014.7(7)	4237.0(6)	948.7(5)
Z	4	2	4	4	1
ρ(calcd.) [Mg/m^3]	0.869	1.025	1.165	1.086	1.189
μ [mm^{-1}]	0.077	0.087	0.088	0.077	0.518
F(000)	1248	348	1128	1496	366
Index range	$-24 \le h \le 24$	$-14 \le h \le 13$	$-13 \le h \le 13$	$-18 \le h \le 18$	$-1 \le h \le 10$
	$-16 \le k \le 16$	$-14 \le k \le 14$	$-16 \le k \le 16$	$-26 \le k \le 26$	$-10 \le k \le 10$
	$-24 \le l \le 24$	$-14 \le l \le 14$	$-20 \le l \le 20$	$-14 \le l \le 19$	$-12 \le l \le 12$
2θ [°]	58.00	58.02	49.38	58.96	59.98
T [K]	183(2)	193(2)	183(2)	193(2)	173(2)
Refl. collected	23965	5915	7201	24949	3992
Refl. unique	8161	3109	1233	8120	3443
Refl. observed (4σ)	4143	2578	948	4870	3100
R (int.)	0.0442	0.0241	0.0285	0.0489	0.0255
No. variables	422	230	95	479	244
Weighting scheme[a] *x*/*y*	0.0538/0.000	0.0991/3.071	0.0611/3.4174	0.0945/1.6511	0.0652/0.4550
GOOF	0.888	1.152	1.077	1.037	1.043
Final *R* (4σ)	0.0434	0.0938	0.0464	0.0634	0.0482
Final *wR*2	0.0929	0.2626	0.1305	0.1694	0.0772
Largest residual peak [e/Å^3]	0.216	0.520	0.368	0.625	0.419

[a] $w^{-1} = \sigma^2 F_o^2 + (xP)^2 + yP$; $P = (F_o^2 + 2F_c^2)/3$.

imum amount of DMSO. Ether was allowed to diffuse into this solution over 3 d. Colourless, clear crystals formed during this period and proved to be **6**. The compound hydrolyses only very slowly in air. Yield: 0.88 g (22%). M.p. 118−121 °C. δ^1H ([D$_6$]DMSO) = −0.33 [q, ^1J(HB) = 79.1 Hz] ppm. $C_{16}H_{56}B_2MgO_8S_8$ (679.07): calcd. C 28.30, H 8.31, H$^-$ 1.18, B 3.18, Mg 3.58; found C 27.80, H 8.35, H$^-$ 1.22, B 3.24, Mg 3.48.

Magnesium Bis(tetrahydroborate) Bis(diethylenetriamine) (7): Diethylenetriamine (5 mL, 49 mmol) was added dropwise to a stirred THF solution (50 mL) of $Mg(BH_4)_2$·3THF (3.38 g, 12.5 mmol). This resulted in the immediate precipitation of a colourless solid. After the mixture had been stirred for an additional hour, the solid was isolated by centrifugation. The product did not dissolve in diethyl ether but did so readily in DMSO. Ether was allowed to diffuse into this solution over several days. Clear crystals of **7** separated. These can be kept in air for several minutes without noticeable hydrolysis. Yield: 3.12 g (96.3% before crystallisation). M.p. 298−301 °C. δ^1H ([D$_6$]DMSO) = −0.33 [q, ^1J(HB) = 81.5 Hz], [sept, ^1J(H^{10}B) = 27.3], 3.40 (m, 4 H), 3.31 (m, 4 H) ppm. δ^{13}C (DMSO) = 52.3, 41.4 ppm. $C_8H_{34}B_2MgN_6$ (260.32): calcd. C 36.91, H 13.16, H$^-$ 3.09, B 8.38, Mg 9.34, N 32.27; found C 37.97, H 12.73, H$^-$ 2.98, B 8.31, Mg 9.29, N 31.99.

Magnesium Bis(tetrahydroborate) *N*,*N*,*N*′,*N*′,*N*′′-Pentamethyldiethylenetriamine (8): Pentamethyldiethylenetriamine (5 ml, 38 mmol) was added with stirring to a solution of $Mg(BH_4)_2$·3THF (2.87 g, 10.6 mmol) in THF (50 mL). The solution was kept at −18 °C for 24 h. Over this time clear needles separated; these hydrolysed rapidly on contact with air or water. Yield: 1.52 g (63.1%). δ^1H ([D$_6$]DMSO) = −0.32 [q, ^1J(H^{11}B) = 81.9 Hz, sept, ^1J(H^{10}B) = 28.0 Hz], 2.51 (s, 3 H, MeN), 2.62 (t, 4 H, Me_2NCH_2), 2.71 (t, 4 H, $MeNCH_2$), 3.73 (s, 12 H, NMe_2) ppm. δ^{13}C = 42.9 (MeN), 45.8 (NMe_2), 56.0 (Me_2NC), 57.9 ($MeNC$) ppm. $C_9H_{31}B_2MgN_3$ (227.29): calcd. C 47.56, H 13.75, H$^-$ 3.54, B 9.51, N 18.49, Mg 10.69; found C 46.39, H 12.96, H$^-$ 3.47, B 9.43, N 16.57, Mg 10.58.

X-ray Structure Determinations: Crystals were covered with perfluoropolyether oil and selected under dinitrogen gas. They were placed on a glass fibre, mounted on a goniometer head and cooled to −80 °C by means of a Siemens LT2 low-temperature device. After cell determination, the data were collected in the hemisphere mode (implemented in the program SMART[27]) on 1284 frames. Data reduction was performed with the program SAINT,[28] and the structure was solved and refined with the SHELX programmes.[29] Parameters for non-hydrogen atoms were anisotropically refined, and the hydrogen atoms bonded to the boron atoms were placed in the found positions while the CH hydrogen atoms were placed in calculated positions. Isotropic thermal parameters for the boron-bonded hydrogen atoms were freely refined but fixed in the final cycles of the refinement. A summary of relevant data is given in Table 6. Additional crystallographic data for the structures were deposited with the Cambridge Crystallographic Data Centre as supplementary publications numbers CCDC-186646 (**1**), -186647 (**2**), -186648 (**3**), -186649 (**4**) and -186650 (**6**). These can be obtained free of charge on application to CCDC, 12 Union Road, Cambridge CB2 1EZ, UK [Fax: (internat.) + 44-1223/336033; E-mail: deposit@ccdc.cam.as.uk].

Acknowledgments

We thank the Fonds der Chemischen Industrie and particularly Chemetall GmbH for support of this work. We also acknowledge the help by Mr. Peter Mayer for many measurements, and Mrs. E. Kiesewetter for recording IR spectra.

[1] J. Knizek, H. Nöth, *J. Organomet. Chem.* **2000**, *614/615*, 168−187.
[2] H. H. Giese, J. Knizek, H. Nöth, M. Warchhold, *Eur. J. Inorg. Chem.* **2001**, 1195−1206.
[3] H. Nöth, *Z. Naturforsch., Teil B* **1982**, *37*, 1499−1503.
[4] E. B. Lobkovski, L. V. Titov, S. B. Psirka, M. Yu, *Antipin Zh. Struct. Khim.* **1982**, *23*, 172−174.
[5] V. N. Konoplev, T. A. Silina, *Koord. Khim.* **1988**, *33*, 2363−2366; E. B. Lobkovski, L. V. Titov, M. D. Lecicheva, A. N. Chelkhov, *Zh. Strukt. Khim.* **1990**, *31*, 147−153.
[6] V. N. Konoplev, T. A. Silina, A. S. Sizarea, *Koord. Khim.* **1988**, *18*, 451−455.
[7] V. N. Konoplev, V. I. Mikheeva, *Zh. Neorg. Khim.* **1965**, *10*, 2363−2364.
[8] V. N. Konoplev, T. A. Silina, *Zh. Neorg. Khim.* **1985**, *5*, 1125−1127.
[9] R. W. Parry, D. R. Shultz, *J. Am. Chem. Soc.* **1958**, *80*, 4−8.
[10] S. Heřmanek, J. Plešek, *Collect. Czech. Chem. Commun.* **1966**, *31*, 3845−3849.
[11] E. Wiberg, R. Bauer, *Z. Naturforsch., Teil B* **1952**, *5*, 58−59.
[12] E. Wiberg, R. Bauer, *Z. Naturforsch., Teil B* **1950**, *3*, 397.
[13] E. C. Ashby, W. Becker, *Inorg. Chem.* **1975**, *4*, 1816−1818.
[14] For a survey see: H. Nöth, B. Wrackmeyer, "Nuclear Magnetic Resonance Spectroscopy of Boron Compounds", in: *NMR Basic Principle and Progress* (Eds.: P. Diehl, E. Fluck, R. Kosfeld), Springer Publishers, Berlin, Heidelberg, New York, **1978**, p. 76 ff.
[15] For a detailed discussion of IR spectra of alkali metal tetrahydroborates see: *Gmelin, Handbuch der Anorganischen Chemie, Ergängungswerk zur 8. Auflage*, vol. 33, pp. 8−11. It should be noted that usually four bands are observed although only one IR-active vibration is to be expected for tetrahedral symmetry. The four bands result from the ν_3, $2\nu_4$, $\nu_2 + \nu_4$, and $2\nu_2$ vibrations.
[16] H. H. Giese, H. Nöth, W. Ponikwar, *Eur. J. Inorg. Chem.* **1999**, 1931−1937.
[17] M. Bremer, H. Nöth, W. Ponikwar, *Chem. Ber.* **1995**, *128*, 455−460.
[18] M. J. Frisch, G. W. Trucks, H. B. Schlegel, G. E. Scuseria, M. A. Robb, J. R. Cheeseman, V. G. Zakrzewski, J. A. Montgomery, R. E. Stratmann, J. C. Burant, S. Dapprich, J. M. Millam, A. D. Daniels, K. N. Kudin, M. C. Strain, O. Farkas, J. Tomasi, V. Barone, M. Cossi, R. Cammi, B. Mennucci, C. Pomelli, C. Adamo, S. Clifford, J. Ochterski, G. A. Petersson, P. Y. Ayala, Q. Cui, K. Morokuma, D. K. Malick, A. D. Rabuck, K. Raghavachari, J. B. Foresman, J. Cioslowski, J. V. Ortiz, B. B. Stefanov, G. Liu, A. Liashenko, P. Piskorz, I. Komaromi, R. Gomperts, R. L. Martin, D. J. Fox, T. Keith, M. A. Al-Laham, C. Y. Peng, A. Nanayakkara, C. Gonzalez, M. Challacombe, P. M. W. Gill, B. G. Johnson, W. Chen, M. W. Wong, J. L. Andres, M. Head-Gordon, E. S. Replogle, J. A. Pople, *Gaussian 98* (Revision A.7), Gaussian, Inc., Pittsburgh, PA, **1998**.
[19] A. Becke, *J. Chem. Phys.* **1993**, *98*, 5648−5652; C. Lee, W. Yang, R. Parr, *Phys. Rev. B* **1988**, *37*, 785−789.
[20] R. Krishnan, J. S. Binley, R. Seeger, J. A. Pople, *J. Chem. Phys.* **1980**, *72*, 650−654.
[21] F. Ramirez, R. Sarma, Y. F. Chaw, T. M. McCaffrey, J. F. Maracek, B. McKeever, D. Nierman, *J. Am. Chem. Soc.* **1977**, *99*, 5285−5289.
[22] R. Sarma, F. Ramirez, B. McKeever, Y.F. Chaw, J. F. Maracek, D. Nierman, T. M. McCaffrey, *J. Am. Chem. Soc.* **1977**, *99*, 5289−5295.
[23] V. Gutmann, *The Donor-Acceptor Approach to Molecular Interactions*, Plenum Press, New York, **1978**; V. Gutmann, U. Mayer, *Adv. Inorg. Radiochem.* **1975**, *17*, 189−223.
[24] H. Irving, R. J. P. Williams, *Nature* **1948**, *162*, 746−754
[25] H. Irving, R. J. P. Williams, *J. Chem. Soc.* **1953**, 3192−3210.
[26] M. Bremer, PhD Thesis, University of Munich, **1995**.
[27] *SMART*: Siemens Analytical Instruments, Version 5.1, Madison, **1995**.
[28] *SAINT*: Siemens Analytical Instruments, Version 5.1, Madison, **1996**.
[29] *SHELX97*: G. M. Sheldrick, University of Göttingen, **1997**.
[30] A. A. Gorbik, O. P. Carkin, *Russ. J. Inorg. Chem.* **1985**, *30*, 1711−1714.
[31] J. D. Dill, P. v. R. Schleyer, J. S. Binkley, J. A. Pople, *J. Am. Chem. Soc.* **1977**, *99*, 6159−617.

Received May 28, 2002
[I02273]

Preparation of the First Complexes of Bidentate Sulfimides; the X-ray Crystal Structures of $[PdBr_2\{1,4\text{-}(PhS\{NH\})_2C_6H_4\}]_2$, $[PdCl_2\{1,2\text{-}(PhS\{NH\})(PhS)C_6H_4\}]$ and *trans*-$[PdCl_2\{1,2\text{-}(PhS\{NH\})(PhS)C_6H_4\}PPh_3]$

Mark R. J. Elsegood,[a] Kathryn E. Holmes,[a] Paul F. Kelly,*[a] Elizabeth J. MacLean,[b] Jonathon Parr,[c] and Julia M. Stonehouse[a]

Keywords: S ligands / N ligands / Palladium / Bridging ligands

Reaction of $[PPh_4]_2[Pd_2X_6]$ (where X = Cl, Br or I) with 1,4-$(PhS\{NH\})_2C_6H_4$ (**1**) in dichloromethane results in the formation of $[Pd\{1,4\text{-}(PhS\{NH\})_2C_6H_4\}X_2]_2$ (**2**). X-ray crystallography (performed using a synchrotron source) confirms that in the case where X = Br (**2a**) both the bis-sulfimides act as bridging ligands through N–Pd bonds producing an 18-membered ring system linking the four sulfur atoms into an almost perfect square. Changing the reaction solvent to methanol/dichloromethane results in the formation of a polymeric material. Reaction of $[PdCl_2(PhCN)_2]$ with 1,2-$(PhS\{NH\})(PhS)C_6H_4$ (**3**) results in the formation of $[PdCl_2\{1,2\text{-}(PhS\{NH\})(PhS)C_6H_4\}]$ (**4**) in which **3** acts as a bidentate ligand, bound by N–Pd and S–Pd bonds to form a unique MSCCSN metallacycle. The Pd–S bond is broken upon reaction with one equivalent of PPh_3, generating *trans*-$[PdCl_2\{1,2\text{-}(PhS\{NH\})(PhS)C_6H_4\}PPh_3]$ (**5**); further reaction with PPh_3 results in complete removal of **3** from the system and formation of *trans*-$[PdCl_2(PPh_3)_2]$.
(© Wiley-VCH Verlag GmbH & Co. KGaA, 69451 Weinheim, Germany, 2003)

Introduction

Recent work within our group has demonstrated that the mononuclear sulfimide Ph_2SNH is an excellent ligand insofar as it readily forms N-bound complexes with a range of transition metal centres.[1] In addition, its importance as a ligand is enhanced by the fact that it is capable of stabilising unusual coordination geometries[2] and that significant hydrogen-bonding effects can be observed between the ligand and counterions.[3] In order to build upon these results, we have recently reported the preparation of a range of new sulfimide systems based upon polysulfide starting materials.[4] These include the bis-sulfimide 1,4-$(PhS\{NH\})_2C_6H_4$ (**1**) and the mixed sulfide/sulfimide 1,2-$(PhS\{NH\})(PhS)C_6H_4$ (**3**), both of which prove to have an interesting structure in their own right thanks to the appearance of hydrogen-bonding arrays generated by interactions between the sulfimide units and waters of crystallisation. They both also have clear potential as new ligands. Ligand **1** has the obvious potential to act as a bidentate bridge between two metal centres. Examples of such ligands are, of course, well-known and they can often act as the lynchpin for much important chemistry. By way of example, Godfrey et al. recently demonstrated the ability of 1,3-bis(diphenylphosphinoyl)propane to bridge manganese centres in binuclear complexes.[5] In this particular case the ligand is crucial to the product's ability to reversibly take up SO_2. Such properties highlight the need to investigate new ligand systems of this type, and here we demonstrate for the first time that **1** can act in this way and in doing so highlight the potential of an entirely new class of bidentate ligand. In the case of **3** the presence of both nitrogen and sulfur atoms capable of binding to metal centres provides the potential for the system to act as a bidentate chelating ligand. The use of ligands containing coordination sites of different binding strengths continues to be of importance (for example with the use of hemilabile ligands within catalytically important systems)[6] and here we show that **3** can indeed act as a bidentate ligand.

[a] Department of Chemistry, Loughborough University
Loughborough LE11 3TU, UK
Fax: (internat.) +44-(0)1509/223-925
E-mail: p.f.kelly@lboro.ac.uk
[b] CLRC Daresbury Laboratory,
Daresbury, Warrington, WA4 4AD, UK
Fax: (internat.) +44-(0)1025/603-193
E-mail: e.j.maclean@dl.ac.uk
[c] Department of Chemistry, Yale University,
225 Prospect Street, New Haven
CT 06520-8107, USA.
Fax: (internat.) +1-203/423-9990
E-mail: parr@jaxindy.chem.yale.edu

Results and Discussion

We have recently demonstrated that reaction of 1,4-$(PhS)_2C_6H_4$ with MSH (*O*-mesitylsulfonylhydroxylamine) results in the formation of a salt of the protonated bis-sulf-

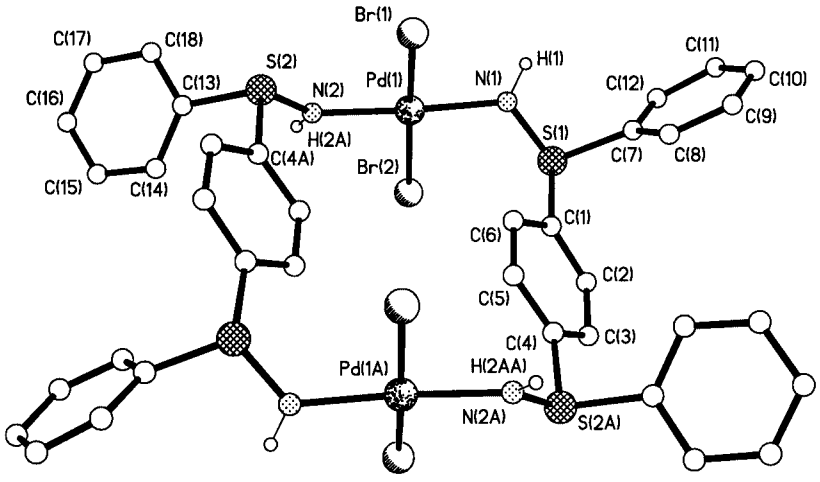

Figure 1. The X-ray crystal structure of one of the two unique molecules in the unit cell of **2a**; selected bond lengths (Å) and angles (°): Pd(1)−N(1) 2.020(5), Pd(1)−N(2) 2.025(5), Pd(1)−Br(1) 2.4411(9), Pd(1)−Br(2) 2.4227(9), N(1)−S(1) 1.622(5), N(2)−S(2) 1.618(5); Pd(1)−N(2)−S(2) 122.4(3), Pd(1)−N(1)−S(1) 122.2(3), Br(2)−Pd(1)−Br(1) 170.91(3), N(1)−Pd(1)−N(2) 174.7(2)

imide $[1,4\text{-}(PhS\{NH_2\})_2C_6H_4]^{2+}$ from which the free bis-sulfimide **1** may be generated by treatment with the base DBU. Compound **1** is an air-stable, colourless material which may be crystallised in hydrated or water-free forms, both of which have structures containing extended hydrogen-bonding arrays. In the light of the high affinity of the related monosulfimide Ph_2SNH for metal centres one might expect **1** to readily react with transition metal complexes and we have now found this to indeed be the case.

Reaction of a stirred suspension of **1** with $[PPh_4]_2[Pd_2Br_6]$ in CH_2Cl_2 results in the formation of an insoluble orange/red product **2a**. The IR spectrum of **2a** clearly indicates the presence of **1** as a ligand. We have previously shown that in complexes of Ph_2SNH the two key features which vary in the IR spectra are the SN and NH stretches, and in this case they are shifted from 928 and 3111 cm^{-1} respectively in the free ligand to 880 and 3260 cm^{-1} upon coordination. In addition, microanalysis confirms the formulation "$[PdBr_2\{1,4\text{-}(PhS\{NH\})_2C_6H_4\}]_n$", although, of course, it provides no information as to the value of *n*. Standard crystallisation techniques cannot be used upon **2a** as, once formed, it appears to be totally insoluble in a range of solvents. Small microcrystals of the product can, however, be obtained by changing the reaction conditions. If CH_2Cl_2 is added to a solid mixture of the two reagents without stirring, then a slow reaction occurs and **2a** forms as crystals large enough to be investigated by X-ray crystallography using a synchrotron source.

X-ray crystallography performed in this manner reveals that the structure of **2a** consists of two $PdBr_2$ units linked by two bis-sulfimide ligands, resulting in an overall binuclear 18-membered ring arrangement (Figure 1).

The resulting relative dispositions of the Pd−Br, P−N, S−N and bridging phenyl units are best illustrated by the side on view shown in Figure 2 (this illustrates the structure of one of the two independent molecules in the unit cell − see X-ray text below). The Pd−Br bonds are almost perpendicular to the Pd_2N_4 plane [N(2)−Pd(1)−Br(2) = 85.7°] while the S−N bonds of each of the ligands also project on either side of this plane (in what has been referred to as a "sofa-bed" arrangement).[7] The linking phenyl units of each ligand are parallel to each other and inclined at an angle of 52.8° to the Pd_2N_4 plane. Perhaps the most intriguing thing about the structure is that the positions of the sulfur atoms are such that they define an almost perfect square, with S(2)−S(1) = 6.325 Å, S(2)−S(1A) = 6.326 Å and S(1)−S(2)−S(1A) = 91.5°. As Figure 2 shows, the fact that the bridging phenyls are offset relative to each other precludes any π-π interactions. Unlike many of the complexes of Ph_2SNH we have previously investigated there appear to be no significant interactions between the N−H groups of the ligands and halide ligands of adjacent molecules.

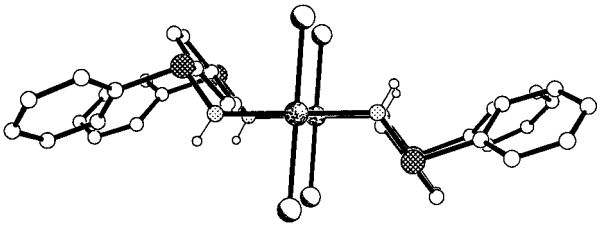

Figure 2. The X-ray crystal structure of **2a** viewed side-on, illustrating the relative disposition of the sulfimide groups and the bridging phenyls

Complex **2a** appears to be the only isolable material from this reaction. The initial yield equates to 67% based upon palladium and more of the same material is obtained when the reaction filtrate is treated with Et_2O. The latter proced-

ure generates **2a** as an orange solid which does not then redissolve back into the CH_2Cl_2. From this observation we can conclude that a small amount of another, soluble, complex of **1** is present in the initial filtrate; however, all attempts to isolate this result in formation of **2a** and so it is difficult to speculate as to its nature. The reaction of $[PPh_4]_2[Pd_2I_6]$ with **1** appears to proceed in an identical manner to that of its bromo counterpart (Scheme 1). Again, the product is an insoluble orange/red material whose IR spectrum is extremely similar to that of **2a**. Taken together with microanalysis this allows us to formulate it as $[PdI_2\{1,4\text{-}(PhS\{NH\})_2C_6H_4\}]_2$ (**2b**) with confidence. Although we have yet to produce crystals suitable for X-ray crystallographic confirmation, we have every reason to believe that **2b** has the same kind of binuclear structure as **2a**. Likewise $[PdCl_2\{1,4\text{-}(PhS\{NH\})_2C_6H_4\}]_2$ (**2c**) forms in the analogous reaction with $[PPh_4]_2[Pd_2Cl_6]$; in this case microanalysis results indicate that the dichloromethane solvate forms. The IR spectrum of this material is, however, very similar to that of **2a** and **2b** and in this case Pd−Cl stretches at 346 and 304 cm^{-1} consistent with the *trans*-halides are observed.

The reaction time needed for the formation of compounds **2** is long (typically three days), a fact dictated by the insolubility of **1** in CH_2Cl_2. Although this would appear inefficient, in fact it is key to the formation of the binuclear product; changing the solvent system has a dramatic effect upon the course of the reaction (Scheme 1). Compound **1** is actually soluble in methanol and so addition of a solution of the ligand in this solvent to a solution of $[PPh_4]_2[Pd_2Br_6]$ in CH_2Cl_2 results in an immediate reaction. Again, an insoluble product is generated (with just $[PPh_4]Br$ left in solution, as shown by IR spectroscopy) but in this case rather than the bright orange red colour of **2a** the product is a pale brown colour. IR spectroscopy reveals the presence of bands due to **1** but the key stretches, ν[N−H] and ν[N−S], are both stronger and broader than those in **2a** and are shifted to 3220 and 897 cm^{-1}, respectively. Microanalysis supports the formulation $[PdBr_2\{1,4\text{-}(PhS\{NH\})_2C_6H_4\}]$ but unlike **2a** (which shows the peaks which may be predicted from the aforementioned single crystal data) the X-ray powder pattern of this product shows no discernible peaks. This leads us to believe that this product is an amorphous polymeric material rather than the binuclear structure of **2a**. Interestingly, it forms even when only one equivalent of **1** is used in the reaction. In this case the expected $[PPh_4]_2[(PdBr_3)_2\{1,4\text{-}(PhS\{NH\})_2C_6H_4\}]$ (in which the bis-sulfimide would link two $[PdBr_3]^-$ units) does not form. Rather, the polymeric material is generated, while the reaction filtrate contains just $[PPh_4]Br$ and unchanged $[PPh_4]_2[Pd_2Br_6]$ (as shown by IR spectroscopy). Given that it is reasonable to assume this reaction proceeds via a transient intermediate of the form $[PdBr_3\mathbf{1}]^-$ in which one of the nitrogen atoms of the ligand is bound to palladium, it would appear that the halide *trans* to N in this case is activated towards displacement by another nitrogen. Similar results are observed for reactions involving $[Pd_2Cl_2]^{2-}$ and $[Pd_2I_2]^{2-}$, generating insoluble polymeric products which are very pale brown and dark brown, respectively. The IR spectra of both products are analogous to that of the bromide product with broad ν[N−H] (3211 and 3217 cm^{-1} for chloride and iodide, respectively) and very broad ν[N−S] peaks (centred on 897 cm^{-1} in both cases).

It would appear, therefore, that only when the reaction of **1** with $[Pd_2X_6]^{2-}$ is slowed down by the use of CH_2Cl_2 as solvent is a molecular product seen; the use of methanol

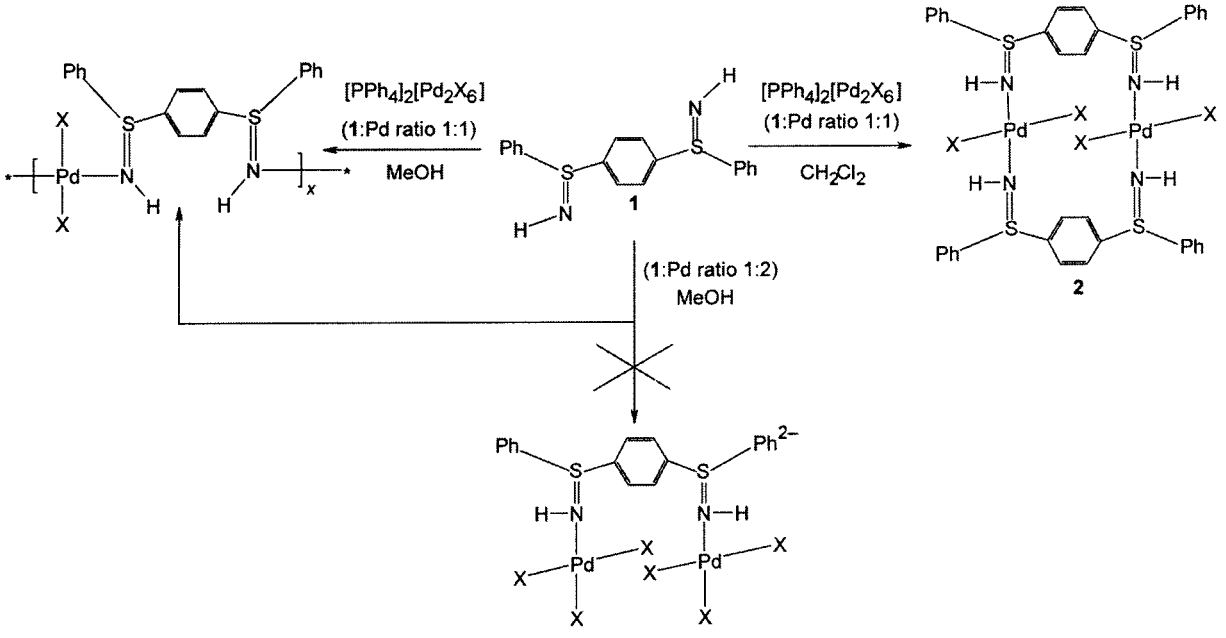

Scheme 1

encourages the fast formation of a polymeric material. It should be noted, though, that in some solvents the reaction does not proceed at all. For example, if the reactions are attempted in MeCN then after three days of stirring the mixture simply consists of a suspension of unchanged **1** in the solution of the palladium starting material. As for the structure of the polymeric complexes we can only speculate that they possess a linear polymeric arrangement made up of alternating PdX_2**1** units. Of course other structural motifs could be envisaged and it may even be that the material contains a mixture of different oligomers (although we can be sure that none of the binuclear complex is present thanks to the IR and powder X-ray results); only single crystal X-ray crystallography would provide an unequivocal answer and we have yet to obtain crystalline samples. Once formed the material is totally insoluble in all solvents and techniques used to obtain single crystals of **2a** are not amenable in this case due to the fast reaction time.

Reaction of $[PdCl_2(PhCN)_2]$ with 1,2-(PhS{NH})-(PhS)C_6H_4 (**3**; molar ratio 1:1) in CH_2Cl_2 results in the formation of an orange solution from which a mass of dark orange/red crystals appears upon standing overnight. X-ray crystallography reveals that this product is $[PdCl_2\{1,2-(PhS\{NH\})(PhS)C_6H_4\}]$ (**4**) in which **3** acts as a bidentate ligand bound to the palladium through the sulfimide nitrogen and the thioether sulfur (Figure 3) (Scheme 2).

The resulting metallacycle, which shows significant deviation from planarity (thus, for example, the two sulfurs ap-

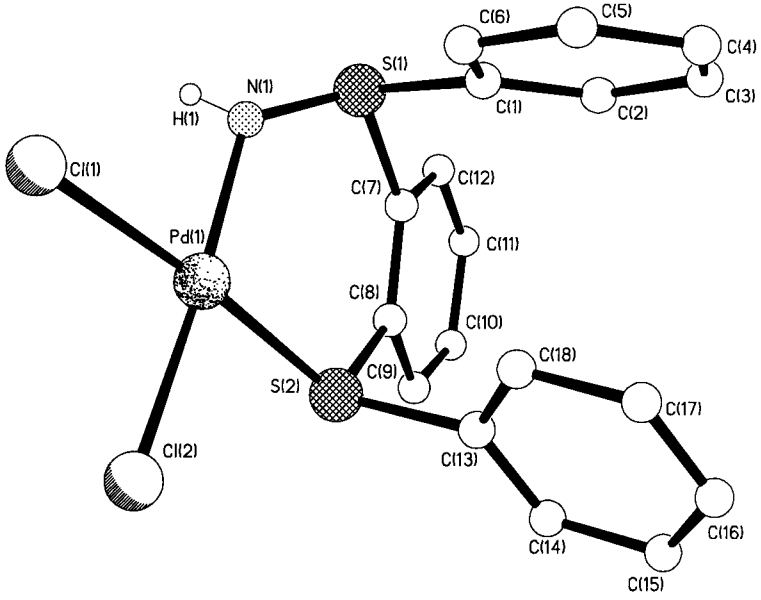

Figure 3. The X-ray crystal structure of **4**; selected bond lengths (Å) and angles (°): Pd(1)−N(1) 2.0203(19), N(1)−S(1) 1.5971(19), S(1)−C(7) 1.7969(2), C(7)−C(8) 1.396(3), C(8)−S(2) 1.791(2), S(2)−Pd(1) 2.2771(6), Pd(1)−Cl(1) 2.3056(6), Pd(1)−Cl(2) 2.3271(6); Pd(1)−N(1)−S(1) 128.28(11), N(1)−S(1)−C(7) 113.75(10), S(1)−C(7)−C(8)125.82(17), C(7)−C(8)−S(2) 126.45(17), C(8)−S(2)−Pd(1) 114.14(8), Cl(1)−Pd(1)−N(1) 85.58(6), Cl(2)−Pd(1)−S(2) 84.25(2)

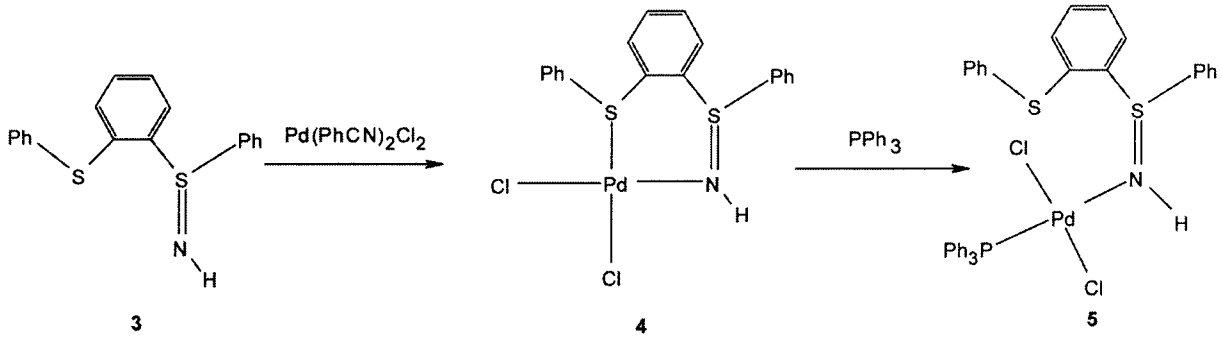

Scheme 2

pear 0.2821 Å (S1) and 0.2162 Å (S2) above the mean plane of the six atoms in the metallacycle), constitutes a rare example of an XNSCCS ring. A search of the Cambridge Structural Database[8] reveals only eight examples within which such an arrangement is observed. As Figure 4 shows, the only examples (**a** and **b**) in which atom X is a metal contain a tridentate ligand.[9] The rest consist of the two examples shown wherein X is a nitrogen atom (**c** and **d**) together with four examples in which this atom is carbon (including the one shown, **e**).[10a−10f]

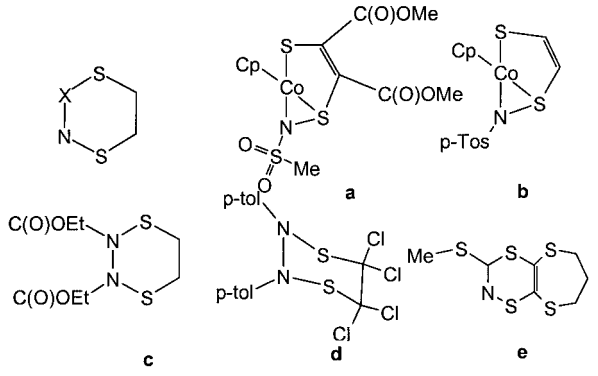

Figure 4. Previous examples of species exhibiting the XSCCSN cyclic unit observed in **4**

Perhaps the most intriguing feature of the structure of **4** is the fact that the molecules arrange themselves into dimers (Figure 5). These units are held together by hydrogen bonding between the N−H groups and chlorides of opposite molecules. The contact between molecules is close, with a Pd−Pd distance of 3.512 Å. Interestingly, this value is almost exactly the same as the closest Pd−Pd interactions in $[Pd(S_2N_2H)(PMe_2Ph)_2][BF_4]$ which also has Pd attached to a sulfur and to an N−H unit on an S−N bond.[11] In that case a 1-D structure was formed by an infinite array of the cations; in the case of **4** this cannot take place as the orientation of the non-bridging phenyl groups — both to one side of the plane of each metallacycle — precludes the close approach of further molecules.

That the thioether group of **3** should coordinate to a metal centre is of no great surprise given that the coordination chemistry of such units is extensive. In general, however, such ligands are relatively weakly bound and, indeed, can often act as easily substituted leaving groups. Of the two coordination sites in **4** one would thus expect the Pd−S bond to be broken by an incoming ligand and this can be demonstrated by the reaction of **4** with triphenylphosphane. Slow addition of the solid phosphane to a stirred solution of **4** in CH_2Cl_2 results in lightening of the colour of the solution; removal of the solvent in vacuo followed by trituration with petroleum ether results in a yellow solid **5** (Scheme 2) The ^{31}P NMR spectrum of this solid ($CDCl_3$) consists of a singlet at $\delta = 27.7$ ppm while the IR spectrum confirms the presence of bands typically associated with both sulfimide units (911 cm^{-1}) and with phosphanes (1096 cm^{-1}). Slow diffusion of diethyl ether into a CH_2Cl_2 solution of the product results in the formation of orange crystals for which X-ray crystallography reveals the structure shown in Figure 6. As Figure 6 shows, **5** consists of a palladium centre coordinated to a PPh_3 ligand and to **3** (acting in this case as a monodentate N-bound ligand) bound in a *trans* fashion. Two *trans*-chloride ligands make up the rest of the coordination sphere.

The course of the reaction of **4** with PPh_3 thus involves two steps: substitution of the Pd−S bond by the phosphane, followed by isomerisation to the observed *trans* arrangement. Presumably the latter effect is brought about by the significant steric interactions that would be present between the six phenyl groups in the initially formed *cis*

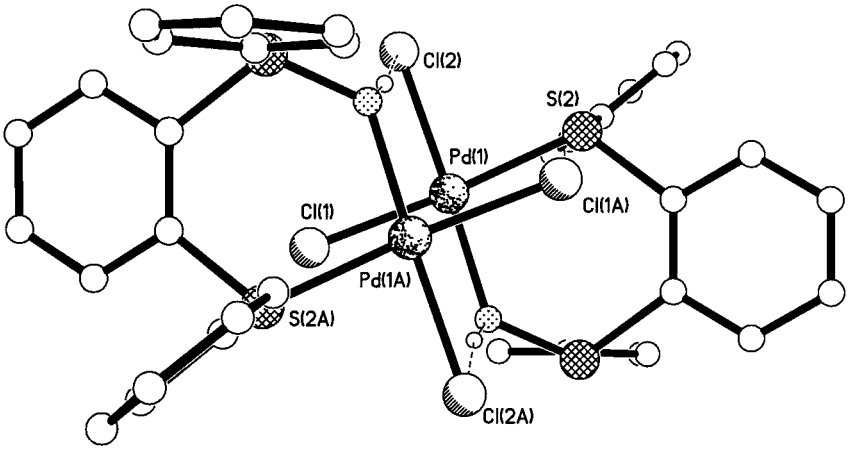

Figure 5. The formation of dimers within the overall structure of **4**; intra-dimer distances (Å) and angles (°): Pd(1)−Pd(1A) 3.512, S(2)−Cl(1A) 3.428, N(1)−Cl(2A) 3.469(2), N(1)−H(1)−Cl(2A) 165(3)

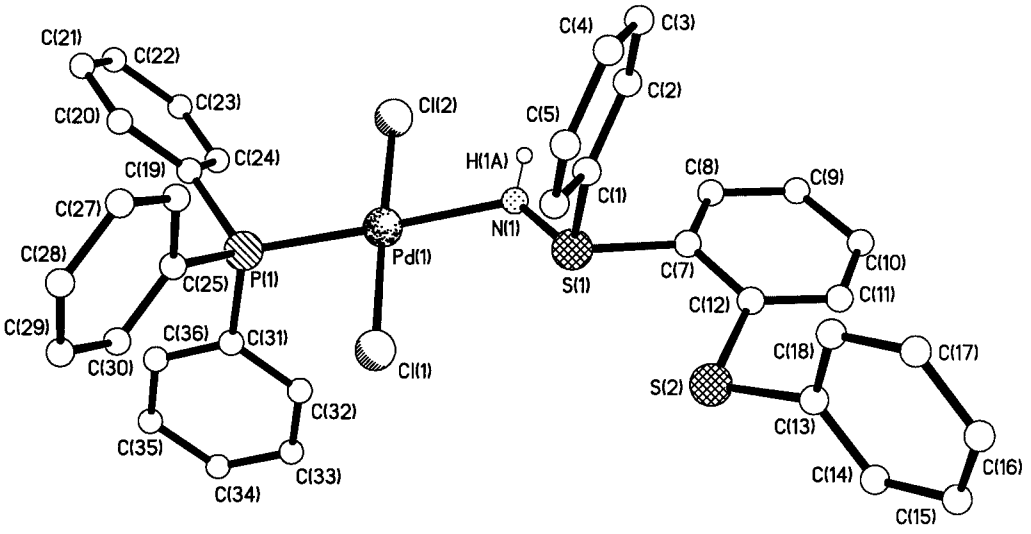

Figure 6. The X-ray crystal structure of **5**; selected bond lengths (Å) and angles (°): Pd(1)−N(1) 2.094(6), N(1)−S(1) 1.603(6), S(1)−C(7) 1.823(7), C(7)−C(12) 1.382(9), C(12)−S(2) 1.798(8), S(2)−C(13) 1.773(7), Pd(1)−Cl(1) 2.2873(18), Pd(1)−Cl(2) 2.3010(17), Pd(1)−P(1) 2.2331(14); Pd(1)−N(1)−S(1) 121.6(3), N(1)−S(1)−C(7) 106.0(3), S(1)−C(7)−C(12)115.9(6), C(12)−S(2)−C(13) 102.8(3), Cl(1)−Pd(1)−N(1) 94.79(18), Cl(2)−Pd(1)−N(1) 84.47(18)

intermediate. The ^{31}P chemical shift of the phosphane group is consistent with it being *trans* to an N−H unit.

Addition of the phosphane to **4** has to be very slow in order to obtain pure **5**. If this is not carefully observed then variable amounts of a yellow, far less soluble product are obtained. Microanalysis indicates that this product is $[PdCl_2(PPh_3)_2]$ and in such cases it appears in the ^{31}P NMR spectrum of the product as a peak at $\delta = 23.4$ ppm. The ability of PPh_3 to break the Pd−N bond as well as the Pd−S bond of the starting material can be confirmed by addition of one molar equivalent of the phosphane to **5**. This results in the immediate precipitation of the sparingly soluble $[PdCl_2(PPh_3)_2]$.

Conclusion

The isolation and full characterisation of **2a** (together with **2b** and **2c**) constitutes the first successful use of a bis-sulfimide system as a ligand. It is, therefore, the first example of the use of an entirely new class of bidentate ligand and this observation strongly suggests that many more examples of complexes of **1** should be isolable (although the observed polymer formation upon using methanol as solvent does highlight a problem which may need to be resolved in other systems). Such results also indicate that the coordination chemistry of other examples of bis-sulfimides should be extensive. Although (as shown in previous work) the *ortho*-isomer 1,2-$(PhS\{NH\})_2C_6H_4$ cannot be formed in the same manner as **1**, the mixed sulfimide/sulfide 1,2-$(PhS\{NH\})(PhS)C_6H_4$ (**3**) is known and the isolation of complex **4** confirms its potential as a chelating ligand. The isolation of **5** also confirms that the Pd−S bond within this molecule is significantly weaker than the Pd−N bond.

Experimental Section

Compounds **1** and **3** were prepared by the reaction of MSH with appropriate thioether starting materials.[4] Salts of the type $[PPh_4]_2[Pd_2X_6]$ were prepared from $PdCl_2$ (X = Cl or Br) as reported previously[12] or, in the case of X = I, by addition of a hot solution of NaI (20 mmol) and PdI_2 (2.2 mmol) in EtOH (100 mL) to a hot solution of $[PPh_4]I$ (2.2 mmol) in the same solvent (100 mL) followed by filtration. $[PdCl_2(PhCN)_2]$ was prepared by the dissolution of $PdCl_2$ into hot benzonitrile followed by precipitation with 60:80 petroleum ether. Microanalysis was performed by the Loughborough Departmental service. ^{31}P NMR spectra were recorded on a Jeol FX90Q spectrometer operating at 36.21 MHz. IR spectra were run on a Perkin Elmer PE2000 spectrometer.

$[PdBr_2\{1,4\text{-}(PhS\{NH\})_2C_6H_4\}]_2$ (2a): A solution of $[PPh_4]_2[Pd_2Br_6]$ (0.102 g, 0.074 mmol) in CH_2Cl_2 (20 mL) was treated with **1** (0.05 g, 0.15 mmol) added in one portion with stirring. The resulting mixture was then stirred for three days during which time a red/orange precipitate formed. The latter was filtered from the solution, washed with CH_2Cl_2 (50 mL), Et_2O (20 mL) and then dried in vacuo yielding 60 mg of red/orange solid. A further 10 mg was obtained when the filtrate was treated with Et_2O. Total yield 70 mg, 79%. $C_{36}H_{32}Br_4N_4S_4Pd_2$ (1181.3): calcd. C 36.8, H 2.7, N 4.8; found C 36.3, H 2.6, N 4.4. IR (KBr): $\tilde{\nu} = 3260$ cm^{-1} (ν N−H), 880 (ν N−S).

Microcrystalline material of sufficient size for use in synchrotron X-ray crystallography was generated by a variation on the above procedure wherein the starting materials were mixed (in the same amounts as above) as solids and then the CH_2Cl_2 added without

stirring. After one week the solution was decanted from the resulting crystalline mass which was then washed with CH_2Cl_2. The IR spectrum of the material prepared this way was identical to that prepared above.

[PdI$_2${1,4-(PhS{NH})$_2$C$_6$H$_4$}]$_2$ (2b): This was prepared as a red/orange solid by reaction of $[PPh_4]_2[Pd_2I_6]$ (0.202 g, 0.122 mmol) with **1** (0.079 g, 0.244 mmol) in exactly the same way as for **3**. Yield 105 mg, 63%. $C_{36}H_{32}I_4N_4Pd_2S_4$ (1369.3): calcd. C 31.6, H 2.4, N 4.1; found C 31.9, H 2.4, N 4.1. IR (KBr): $\tilde{\nu}$ = 3260 cm^{-1} (ν N−H), 880 (ν N−S).

[PdCl$_2${1,4-(PhS{NH})$_2$C$_6$H$_4$}]$_2$·CH$_2$Cl$_2$ (2c): This was prepared as a red/orange solid by reaction of $[PPh_4]_2[Pd_2Cl_6]$ (0.082 g, 0.077 mmol) with **1** (0.050 g, 0.154 mmol) in exactly the same way as for **3**. Yield 45 mg, 61%. $C_{37}H_{34}Cl_6N_4Pd_2S_4$ (1088.5): calcd. C 40.8, H 3.1, N 5.1; found C 40.3, H 3.1, N 4.8. IR (KBr): $\tilde{\nu}$ = 3260 cm^{-1} (ν N−H), 898 (ν N−S).

[PdCl$_2${1,2-(PhS{NH})(PhS)C$_6$H$_4$}] (4): A solution of $[PdCl_2(PhCN)_2]$ (0.176 g, 0.460 mmol) in dichloromethane (10 mL) was treated with a solution of 1,2-(PhS{NH})(PhS)C_6H_4 (0.142 g, 0.460 mmol) in an equal volume of the same solvent added dropwise with stirring. After addition of the ligand a precipitate was present which then redissolved after a minute of stirring. The solution was then left to stand for 48 hours and the resulting orange/red or brown crystals were collected. Yield: 0.165 g (86%). $C_{18}H_{15}Cl_2NPdS_2$ (486.7): calcd. C 44.4, H 3.1, N 2.9; found C 44.4, H 3.0, N 2.8. IR (KBr): $\tilde{\nu}$ = 3215, 3053, 944 cm^{-1}.

***trans*-[PdCl$_2${1,2-(PhS{NH})(PhS)C$_6$H$_4$}PPh$_3$] (5):** A solution of **4** (0.039 g, 0.08 mmol) in dichloromethane (10 mL) was treated with solid PPh_3 (21 mg, 0.08 mmol) added slowly in small portions with vigorous stirring. After complete addition of the PPh_3 the clear solution was reduced in volume and petroleum ether 40:60 (50 mL) was added. The resulting solid was then recrystallised from dichloromethane/Et_2O giving orange crystals. Yield: 0.036 g (61%). $C_{36}H_{30}Cl_2NPPdS_2$ (749.0): calcd. C 57.2, H 3.9, N 1.7; found C 57.7, H 4.0, N 1.9. ^{31}P NMR ($CDCl_3$): δ = 27.7 ppm. IR (KBr): $\tilde{\nu}$ = 3294, 3048, 1096, 911 cm^{-1}.

X-ray Crystallographic Study: Data (Table 1) for **2a** were collected at 150 K on a Bruker AXS SMART 1 K CCD area-detector diffractometer using synchrotron radiation (λ = 0.6879 Å) at Daresbury SRS Station 9.8.[13,14] Absorption correction was applied semi-empirically from equivalent and repeated data. The structure was solved by direct methods and refined by full-matrix least-squares on F^2. The asymmetric unit comprises two half molecules on centres of symmetry. Some disorder is present within one of the molecules with alternative positions for the sulfimide SNH unit with 90.4:9.6 (4)% refined occupancies. Hydrogen atoms were placed in geometrical positions and allowed to ride on their attached atom with U_{iso}(H) set to be 1.2 times U_{eq} of the carrier atom.

Data for **4** and **5** were collected at 150 K with a Bruker AXS SMART 1000 CCD diffractometer using Mo-K_α radiation (λ = 0.71073 Å). Both structures were solved by Patterson synthesis and refined by full-matrix least-squares methods on F^2. NH hydrogens were located from the difference map and their coordinates were freely refined. All other hydrogens were placed in geometrical positions using a riding model as described above. Some disorder is present in **5** with alternative positions for the sulfur and nitrogen atoms with refined occupancies of 84.0:16.0 (5)%.

The programs used were Bruker SMART,[15a] SAINT,[15a] SHELXTL[15b] and local programs.

CCDC-176115 (**2a**), -186575 (**4**) and -186576 (**5**) contain the supplementary crystallographic data for this paper. These data can be obtained free of charge at www.ccdc.cam.ac.uk/conts/retrieving.html

Table 1. Crystallographic data of **2a**, **4**, **5**

Compound	**2a**	**4**	**5**
Formula	$C_{36}H_{32}Br_4N_4Pd_2S_4$	$C_{18}H_{15}Cl_2NPdS_2$	$C_{36}H_{30}Cl_2NPPdS_2$
Mol. wt.	1181.34	486.73	749.00
Crystal dimensions	0.070 × 0.020 × 0.005	0.19 × 0.11 × 0.08	0.33 × 0.15 × 0.05
Crystal system	Triclinic	Triclinic	Triclinic
Space group	$P\bar{1}$	$P\bar{1}$	$P\bar{1}$
a (Å)	8.4402(15)	9.5236(8)	9.5178(7)
b (Å)	11.044(2)	10.7767(9)	9.9441(7)
c (Å)	22.519(4)	11.1578(9)	17.7459(13)
α (°)	94.962(3)	61.497(2)	90.768(2)
β (°)	98.383(3)	66.767(2)	99.786(2)
γ (°)	101.418(2)	67.985(2)	96.508(2)
V (Å^3)	2021.2(6)	899.72(13)	1643.6(2)
Z	2	2	2
Absorption coefficient, μ (mm^{-1})	5.082	1.560	0.930
Min. and max. transmission	0.717 and 0.975	0.756 and 0.885	0.749 and 0.955
θ range (°)	1.83 to 25.46	2.15 to 28.89	2.06 to 25.00
Wavelength (Å)	0.6877	0.71073	0.71073
Decay	20%	0%	0%
Measured reflections	16679	7941	12081
Independent reflections	8215	4144	5772
Observed reflections [$F^2 > 2\sigma(F^2)$]	5244	3678	4576
R_{int}	0.0430	0.0142	0.0276
R [$F^2 > 2\sigma(F^2)$][a]	0.0453	0.0236	0.0553
$wR2$ [all data][b]	0.0991	0.0622	0.1313
Largest difference map features (e·Å^{-3})	0.942 and −1.144	0.953 and −0.698	2.943 and −1.503

[a] $R = ||F_o| - |F_c||/|F_o|$. [b] $wR2 = \{[w(F_o^2 - F_c^2)^2]/[w(F_o^2)^2]\}^{1/2}$.

[or from the Cambridge Crystallographic Data Centre, 12, Union Road, Cambridge CB2 1EZ, UK; Fax: (internat.) +44-1223/336-033; E-mail: deposit@ccdc.cam.ac.uk].

Acknowledgments

We acknowledge the provision of time on *DARTS*, the UK national synchrotron radiation service at the CLRC Daresbury Laboratory, through funding by the EPSRC. We are also grateful to Johnson Matthey for loans of precious metals, and to Pauline King for the running of X-ray powder diffraction patterns.

[1] P. F. Kelly, A. C. Macklin, A. M. Z. Slawin, K. W. Waring, *Polyhedron* **2000**, *19*, 2077−2081 and references therein.
[2] P. F. Kelly, A. M. Z. Slawin, K. W. Waring, *J. Chem. Soc., Dalton Trans.* **1997**, 2583−2584.
[3] P. F. Kelly, A. M. Z. Slawin, K. W. Waring, *Inorg. Chem. Commun.* **1998**, *1*, 249−250.
[4] M. R. J. Elsegood, K. E. Holmes, P. F. Kelly, J. Parr, J. M. Stonehouse, *New. J. Chem.* **2002**, *26*, 202−206.
[5] W. I. Cross, S. M. Godfrey, C. A. McAuliffe, R. G. Pritchard, *Chem. Commun.* **2001**, 1764−1765.
[6] See, for example: A. Bader, E. Lindner, *Coord. Chem. Rev.* **1991**, *108*, 27−110.
[7] A. G. Constable, W. S. McDonald, B. L. Shaw, *J. Chem. Soc., Dalton Trans.* **1979**, 1109−1111.
[8] F. H. Allen, O. Kennard, *Chem. Des. Autom. News* **1993**, *8*, 1; F. H. Allen, O. Kennard, *Chem. Des. Autom. News* **1993**, *8*, 31−37.
[9] M. Nomura, T. Yagisawa, C. Takayama, T. Sugiyama, Y. Yokaguma, K. Shimizu, A. Sugimori, M. Kajitani, *J. Organomet. Chem.* **2000**, *611*, 376−385.
[10] [10a] V. A. Starodub, *J. Struct. Chem.* **1998**, *39*, 88−92. [10b] M. R. Bryce, G. R. Davison, A. S. Batsanov, J. A. K. Howard, *J. Chem. Soc., Perkin Trans. 1* **1992**, 2295−2302. [10c] M. R. Bryce, S. Yoshida, A. S. Batsanov, J. A. K. Howard, *J. Chem. Soc., Perkin Trans. 1*. **1997**, 1157−1161. [10d] M. R. Bryce, G. R. Davison, A. S. Batsanov, J. A. K. Howard, *J. Chem. Soc., Chem. Commun.* **1992**, 478−480. [10e] K. T. Potts, J. S. Baum, *J. Heterocycl. Chem.* **1991**, *28*, 1637−1639. [10f] K.-H. Linke, H. G. Kalker, *Z. Anorg. Allg. Chem.* **1977**, *434*, 157−164.
[11] R. Jones, P. F. Kelly, D. J. Williams, J. D. Woollins, *J. Chem. Soc., Dalton Trans.* **1988**, 803−807.
[12] P. F. Kelly, A. M. Z. Slawin, A. Soriano-Rama, *J. Chem. Soc., Dalton Trans.* **1996**, 53−59.
[13] R. J. Cernik, W. Clegg, C. R. A. Catlow, G. Bushnell-Wye, J. V. Flaherty, G. N. Greaves, I. Burrows, D. J. Taylor, S. J. Teat, M. Hamichi, *J. Synchrotron Rad.* **1997**, *4*, 279−286.
[14] W. Clegg, M. R. J. Elsegood, S. J. Teat, C. Redshaw, V. C. Gibson, *J. Chem. Soc., Dalton Trans.* **1998**, 3037−3039.
[15] [15a] SMART and SAINT software for CCD diffractometers, Bruker AXS Inc, Madison, WI, **1994**. [15b] G. M. Sheldrick. *SHELXTL user manual*, version 5, Bruker AXS Inc., Madison, WI, **1994**.

Received June 3, 2002
[I02289]

Coordination Modes of 9-Methyladenine in *cis*-Platinum(II) Complexes with Dimethyl(phenyl)phosphanes as Ancillary Ligands − Synthesis and Characterization of *cis*-$[PtL_2(9\text{-MeAd})_2](NO_3)_2$, *cis*-$[PtL_2\{9\text{-MeAd}(-H)\}]_3(NO_3)_3$, and *cis*-$[L_2Pt\{9\text{-MeAd}(-H)\}PtL_2](NO_3)_3$

Bruno Longato,*[a] Lucia Pasquato,[b] Adele Mucci,*[c] and Luisa Schenetti*[c]

Keywords: Coordination modes / N ligands / NMR spectroscopy / P ligands / Platinum

Treatment of 9-methyladenine (9-MeAd) with *cis*-$[PtL_2(NO_3)_2]$ (**1**) (L = PMe_2Ph) in a 2:1 molar ratio generated the bis(adduct) *cis*-$[PtL_2(9\text{-MeAd})_2](NO_3)_2$ (**2**), which was isolated and fully characterized by multinuclear (^1H, ^{31}P, ^{13}C, ^{195}Pt and ^{15}N) NMR analysis, which showed that the two nucleobases are selectively coordinated through the N1 atom. Small amounts of a mono(adduct) *cis*-$[PtL_2(S)(9\text{-MeAd})]^{2+}$ (**3**) (S = solvent) and of a diplatinated species *cis*-$[L_2Pt(S)\{9\text{-MeAd}(-H)\}PtL_2]^{3+}$ (**4**) are formed in DMSO solution when 9-MeAd is present in smaller quantities than **1**. Complex **3** is platinated at N1, with a solvent molecule representing the fourth ligand around the metal center. Complex **4** contains an adenine molecule deprotonated and platinated at N1,N6,N7, with two *cis*-L_2Pt units bonded to nitrogen atom N1 and to nitrogen atoms N6 and N7, respectively. With increasing relative concentration of the nucleobase, both complexes **3** and **4** progressively convert into the bis(adduct) **2**, the only species detectable in solution when the Ad/Pt molar ratio is 2:1. The trinuclear compound *cis*-$[L_2Pt\{9\text{-MeAd}(-H)\}]_3(NO_3)_3$ (**5**) (L = PMe_2Ph), containing an NH_2-deprotonated nucleobase bridging the metal centers through the N1 and N6 atoms, is quantitatively formed when the dinuclear hydroxo complex *cis*-$[Pt(\mu\text{-OH})L_2]_2(NO_3)_2$ (**6**) reacts with 9-MeAd in CH_3CN solution. The isolated complex was fully characterized by multinuclear NMR spectroscopy and mass spectrometry. It appears to be stable in solution in CH_3CN and chlorinated solvents, whereas in DMSO it partially converts into a new species, probably the dinuclear analog *cis*-$[PtL_2\{9\text{-MeAd}(-H)\}]_2(NO_3)_2$, in which the adenine maintains its coordination mode. At equilibrium the trinuclear/dinuclear species molar ratio is 20:1. Through the addition of a stoichiometric amount of nitrate **1** to a DMSO solution of **5** we were able to generate the diplatinated compound **4** in high yield. Complex **4** displays a new coordination mode for the adeninate ion, with N1 bonded to one platinum atom whereas N6 and N7 are chelated to a second one.
(© Wiley-VCH Verlag GmbH & Co. KGaA, 69451 Weinheim, Germany, 2003)

Introduction

Among the model nucleobases, 9-substituted adenine exhibits the most versatile coordination properties.[1] As a neutral molecule it generally binds a metal atom at the N7 position, less frequently at the N1 atom, and only rarely through both these donor atoms (Scheme 1).[2,3]

Deprotonation of the exocyclic NH_2 group affords an additional site for metal coordination, and adducts of the adeninate ligand in which N1 and N6 bridge two metal atoms have been characterized.[4] More recently, chelation of a metal atom with the involvement of the adeninate N1 and N6 atoms, followed by conversion into the more stable N6/N7 isomer, has also been described.[5]

As part of a study dealing with the role of the ancillary ligands in the reactivity of platinum complexes toward model nucleobases, we have found that coordination of the neutral 9-methyladenine (9-MeAd) at the metal center of the water-soluble *cis*-$[Pt(NO_3)_2(PMe_3)_2]$ complex occurs selectively at the N1 atom, as indicated by a comprehensive multinuclear NMR analysis of the isolated bis(adduct) *cis*-$[Pt(PMe_3)_2(9\text{-MeAd})_2]^{2+}$.[6] We have also shown that the dinuclear hydroxo complex *cis*-$[Pt(\mu\text{-OH})(PMe_3)_2]_2^{2+}$ is able to deprotonate the NH_2 group of the adenine, as shown in Equation (1).

$$cis\text{-}[Pt(\mu\text{-OH})L_2]_2^{2+} + 2\,(9\text{-MeAd}) \rightarrow cis\text{-}[PtL_2\{9\text{-MeAd}(-H)\}]_2^{2+} + 2\,H_2O \quad (1)$$

The resulting cation, *cis*-$[Pt(PMe_3)_2\{9\text{-MeAd}(-H)\}]_2^{2+}$, contains adeninate ions bridging two *cis*-L_2Pt^{2+} units through the N1 and N6 atoms, a coordination mode previously established for the 9-ethyladenine (9-EtAd) analog

[a] Istituto di Scienze e Tecnologie Molecolari − C.N.R., c/o Dipartimento di Chimica Inorganica, Metallorganica ed Analitica, Universita' di Padova,
Via Marzolo 1, 35131 Padova, Italy
Fax: (internat.) + 39-049/827-5161
E-mail: longato@chin.unipd.it
[b] Dipartimento di Chimica Inorganica, Metallorganica ed Analitica, Universita' di Padova,
via Marzolo 1, 35131 Padova, Italy
[c] Dipartimento di Chimica, Universita' di Modena e Reggio Emilia,
Via Campi 183, 41100 Modena, Italy
Fax: (internat.) + 39-059/373543
E-mail: mucci.adele@unimo.it
schene@unimo.it
Supporting information for this article is available on the WWW under http://www.eurjic.org or from the author.

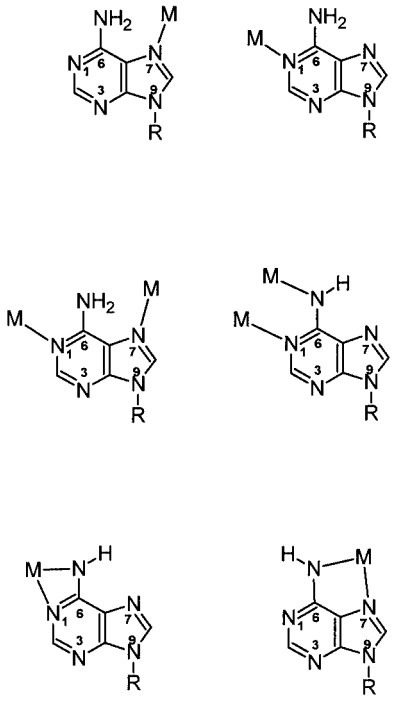

Scheme 1. Coordination modes of neutral and deprotonated 9-substituted adenines

cis-$[Pt(PMe_3)_2\{9\text{-EtAd}(-H)\}]_2(NO_3)_2$ by X-ray diffraction.[7]

In this paper we present the synthesis and characterization of three new (adenine)platinum(II) complexes with dimethyl(phenyl)phosphanes (L= PMe_2Ph) as ancillary ligands. The addition of a stoichiometric amount of nucleobase to *cis*-$[PtL_2(NO_3)_2]$ (**1**) in DMSO solution quantitatively forms the complex *cis*-$[PtL_2(9\text{-MeAd})_2](NO_3)_2$ (**2**). Similarly to the trimethylphosphane analog,[6] the bis(adduct) **2** contains the neutral 9-MeAd ligands coordinated at the N1 site. In order to investigate the possible involvement of the N7 site, we also examined mixtures of 9-MeAd and nitrate **1**, by ^{31}P NMR spectroscopy, at Ad/Pt molar ratios lower than 2. Under these conditions we noticed, concomitantly with the formation of the mono(adduct) *cis*-$[PtL_2(S)(9\text{-MeAd})]^{2+}$ (**3**, S = solvent), the presence of significant amounts of the diplatinated complex *cis*-$[L_2Pt(S)\{9\text{-MeAd}(-H)\}PtL_2]^{3+}$ (**4**), containing a deprotonated adenine molecule binding two *cis*-L_2Pt^{2+} units through the N1 and the N6/N7 atoms, as shown in Scheme 2.

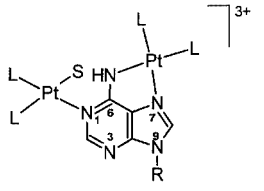

Scheme 2. Proposed structure for complex **4**; S represents a solvent molecule

The deprotonation of the nucleobase induced by simultaneous platination at the N1 and the N7 sites is a reversible process, since the bis(adduct) **2** is the only product obtained when the Ad/Pt ratio is adjusted to 2. Together with the details of the spectroscopic characterization of this diplatinated species **4**, we report here on the synthesis of *cis*-$[PtL_2\{9\text{-MeAd}(-H)\}]_3(NO_3)_3$ (**5**), a cyclic trinuclear complex formed by condensation of the dinuclear hydroxo complex *cis*-$[Pt(\mu\text{-OH})L_2]_2(NO_3)_2$ (**6**) with adenine. The trinuclear complex **5**, in which the NH_2-deprotonated adenines bridge the metal centers through the N1 and N6 atoms, converts easily, although not quantitatively, into the diplatinated species **4** upon treatment with the nitrate **1** in DMSO solution. A detailed multinuclear (^1H, ^{13}C, ^{31}P, ^{195}Pt and ^{15}N at natural abundance) NMR study of the reaction mixture allowed the complete characterization of the complex **4**, in which the adenine exhibits an unprecedented coordination mode.

Results and Discussion

Treatment of 9-Methyladenine with *cis*-$[PtL_2(NO_3)_2$ (1) − Characterization of *cis*-$[PtL_2(9\text{-MeAd})_2](NO_3)_2$ (2) and *cis*-$[PtL_2(S)(9\text{-MeAd})](NO_3)_2$ (3)

In spite of the low solubility of *cis*-PtL_2Cl_2 (L = PMe_2Ph) in water, substitution of the chloride ligands occurs easily when a suspension of the compound is treated with $AgNO_3$. The resulting dinitrato complex **1** dissolves in coordinating solvents such as DMSO, CH_3CN, H_2O and DMF to form the ionic complexes *cis*-$[PtL_2S_2]^{2+}$ (S represents a solvent molecule). As would be expected,[8] solutions of **1** in water are acidic as a result of an acid/base equilibrium [Equation (2)] and the dinuclear hydroxo complex **6** is obtained in good yield when the solutions are neutralized with a strong base.[8,9]

$$2\ cis\text{-}[PtL_2(H_2O)_2]^{2+} \rightleftarrows cis\text{-}[Pt(\mu\text{-OH})L_2]_2^{2+} + 2\ H_3O^+ \quad (2)$$

Both the nitrato complex **1** and the hydroxo complex **6** appear to be very reactive towards the model nucleobase 9-MeAd. Thus, addition of 2 equiv. of 9-MeAd to a DMSO solution of **1** causes the dissolution of the nucleobase within a few minutes, with the quantitative formation of the bis(adduct) **2**. This complex was isolated and fully characterized by multinuclear NMR spectroscopy and the pertinent data are reported in Tables 1−4.

All the NMR spectra display two sets of resonances, attributed to two species (in a 48:52 ratio) containing two N1-coordinated adenine units. The correct assignment of the coordination sites requires the use of suitable two-dimensional inverse detection NMR techniques, as underlined in a previous report.[6] The first step is the contextual assignment of all protons and carbon atoms of the adenine moiety through ^1H,^{13}C correlation experiments. In particular, 2-H and 8-H are distinguishable by their $^1J_{H,C}$ coupling constants [^1J(2-H,C2) = 200 Hz; ^1J(8-H,C8) = 212 Hz] and their cross-peaks with C6 (detected through 2-H and NH_2) and C5 (detected through 8-H and NH_2) which are the

Table 1. ^{1}H NMR spectroscopic data (δ in ppm) for 9-MeAd and complexes **2**−**5** (L = PMe_2Ph)

Compound	2-H	8-H	NH_2/NH	NMe	PMe_2
9-MeAd	8.13	8.06	7.13	3.69	–
$[PtL_2(9\text{-MeAd})_2]^{2+}$ [a]	8.84	8.22	8.6	3.66	1.86; 1.64
2	8.73	8.20	8.6	3.64	1.81; 1.73
$[PtL_2(S)(9\text{-MeAd})]^{2+}$	8.74	8.34	8.75	3.76	1.74, 1.74
3					1.63, 1.54
$[L_2Pt(S)\{9\text{-MeAd}(-H)\}PtL_2]^{3+}$	8.46	8.44	6.5[b]	3.79	1.55; 1.61
4					1.77; 1.78
					1.92; 1.99
					2.01; 2.11
$[PtL_2\{9\text{-MeAd}(-H)\}]_3^{3+}$	8.12	8.38	7.17	3.58	1.08; 1.14
5					1.78; 1.84

[a] The first row refers to the 48% abundant conformer. [b] The NH proton of complex **4** displays $^2J_{H,Pt}$ = 89 Hz and $^3J_{H,P}$ = 6.5 Hz.

Table 2. ^{13}C NMR spectroscopic data (δ in ppm) for 9-MeAd and complexes **2**−**5** (L = PMe_2Ph)

Compound	C2	C4	C5	C6	C8	NMe	PMe_2
9-MeAd	152.4	149.8	118.3	155.8	141.3	29.3	–
$[PtL_2(9\text{-MeAd})_2]^{2+}$ [a]	150.8	147.6	118.9	153.8	143.7	29.7	12.3/11.9
2	151.5	147.3	119.3	153.2	143.5	29.7	12.2/11.9
$[PtL_2(S)(9\text{-MeAd})]^{2+}$	152.3	147.9	119.1	153.2	143.7	29.8	11.9/11.9
3							12.7/13.2
$[L_2Pt(S)\{9\text{-MeAd}(-H)\}PtL_2]^{3+}$	156.1	145.5	126.2	161.6	144.0	31.1	12.8/12.5
4							11.5/11.3
							14.9/15.3
							13.9/13.7
$[PtL_2\{9\text{-MeAd}(-H)\}]_3^{3+}$	154.3	146.4	120.2	157.8	141.0	29.5	12.7/13.0
5							14.0/11.4

[a] The first row refers to the 48% abundance conformer.

Table 3. ^{31}P and ^{195}Pt NMR spectroscopic data (δ in ppm; *J* in Hz) for complexes **2**−**5** (L = PMe_2Ph); the chemical shift values of the protons correlating with ^{31}P and ^{195}Pt are given in parentheses

Complex	^{31}P	$^1J_{P,Pt}$	^{195}Pt
$[PtL_2(9\text{-MeAd})_2]^{2+}$ [a]	−19.61	3225	−4350
	(8.84, 1.64, 1.86)	3230	(8.84, 1.64, 1.86)
2	−19.73		−4325
	(8.73, 1.73, 1.81)		(8.73, 1.73, 1.81)
$[PtL_2(S)(9\text{-MeAd})]^{2+}$	−12.07	3360	−4280
3	(8.74, 1.74)	3750	(8.74, 1.54, 1.63, 1.74)
	−20.14		
	(1.54, 1.63)		
$[L_2Pt(S)\{9\text{-MeAd}(-H)\}PtL_2]^{3+}$	−11.98	3320	−4272
4	(8.46, 1.77, 1.78)	3660	(8.46, 1.55, 1.61, 1.77, 1.78)
	−20.96	3650	−4378
	(1.55, 1.61)	3170	(6.5, 1.92, 1.99, 2.01, 2.11)
	−15.12		
	(8.44, 2.01, 2.11)		
	−16.19		
	(6.5, 1.92, 1.99)		
$[PtL_2\{9\text{-MeAd}(-H)\}]_3^{3+}$	−16.15	3170	−4277
5	(7.17, 1.08, 1.14)	3325	(7.17, 8.12, 1.08, 1.14, 1.78, 1.84)
	−18.94		
	(8.12, 1.78, 1.84)		

[a] The first row refers to the 48% abundance conformer.

Table 4. ^{15}N NMR spectroscopic data (δ in ppm; *J* in Hz) for 9-MeAd and complexes **2**−**5** (L = PMe_2Ph)

Compound	N1	N3	N6	N7	N9
9-MeAd	−141.1	−151.0	−296.9	−137.1	−225.9
$[PtL_2(9\text{-MeAd})_2]^{2+}$ [a]	−200.3	−142.2	−284.5	−132.8	−218.2
2	$^2J_{N,P}$ = 60	−144.3	−284.5	−132.8	−218.2
	−202.5				
	$^2J_{N,P}$ = 60				
$[PtL_2(S)(9\text{-MeAd})]^{2+}$	−195.5	−144.0	−284.0	−131.5	−218.5
3	$^2J_{N,P}$ = 60				
$[L_2Pt(S)\{9\text{-MeAd}(-H)\}PtL_2]^{3+}$	−190.0	−149.1	−243.6	−187.5	−214.0
4	$^2J_{N,P}$ = 50		$^2J_{N,P}$ = 45	$^2J_{N,P}$ = 50	
$[PtL_2\{9\text{-MeAd}(-H)\}]_3^{3+}$	−199.2	−157.2	−270.8	−127.4	−219.7
5	$^2J_{N,P}$ = 50		$^2J_{N,P}$ = 50		

[a] The first row refers to the 48% conformer.

most deshielded and shielded adenine carbon atoms, respectively (Table 2). The second step is represented by $^1H,^{15}N$ inverse detection experiments, which show that only the 2-H protons correlate with platinated nitrogen atoms (recognisable by the presence of a $^2J_{N,P}$ coupling constant of about 50 Hz), enabling the presence of an isomeric mixture of N1- and N7-coordinated bases to be definitely ruled out. The presence of two species must be due to the hindered rotation of the nucleobases around the platinum−nitrogen bond, resulting in a *head-to-head* and *head-to-tail* arrangement of the adenines. This finding is in agreement with results previously reported for the complex with L = PMe_3,[6] showing that it is the phenyl group in the ancillary ligand − and not the adenine coordination site − that influences the conformer ratio. It should be noted that each conformer displays a couple of diastereotopic methyl signals readily attributable to the corresponding phosphorus atom through $^1H,^{31}P$ correlation experiments. The methyl proton signals allow the ^{195}Pt resonances to be detected in inverse detection mode. The same ^{31}P and ^{195}Pt signals are detectable, even though more weakly, through the 2-H protons, confirming the platination of atom N1.

The coordination of the adenine is a reversible process. In fact, addition of nitrate **1** to a solution of bis(adduct) **2** causes the immediate appearance of an AB multiplet at δ = −12.07 and −20.14 ppm in the ^{31}P NMR spectrum (Table 3), in addition to the resonances of **2**. It is reasonable to attribute the AB multiplet to the mono(adduct) **3**, in which the fourth ligand should be a solvent molecule, as suggested by the large difference between the $^1J_{P,Pt}$ values for the two ^{31}P resonances. The multinuclear NMR characterization of this species (Table 1−4) supports the hypothesis of the formation of a mono(adduct). In fact, almost all the adenine signals are very similar to those of the bis(adduct) **2**, and only 8-H, NMe and N1, which in this case is also the only platinated nitrogen atom, are slightly deshielded with respect to **2**. The highest chemical shift difference is that observed above for one phosphorus resonance, found at δ = −12.07 ppm, relative to δ ≈ −19.7 ppm in the bis(adduct) **2** and attributable with confidence to the substitution of an adenine moiety by a solvent molecule to form the mono(adduct) **3**. The presence of a cross-peak between the adenine 2-H and the deshielded P at δ = −12.07 ppm in the inverse detection correlation experiment indicates that this signal is due to the phosphane group *trans* to N1, and hence *cis* to the entering solvent molecule.

In addition to the mono- and bis(adducts), solutions of 9-MeAd and nitrate **1** contain a third species (complex **4**), readily detectable when the Ad/Pt molar ratio is about 1:3. This minor component (ca. 8%) features two AB multiplets, with the same relative intensities, in the ^{31}P NMR spectrum (Figure 1).

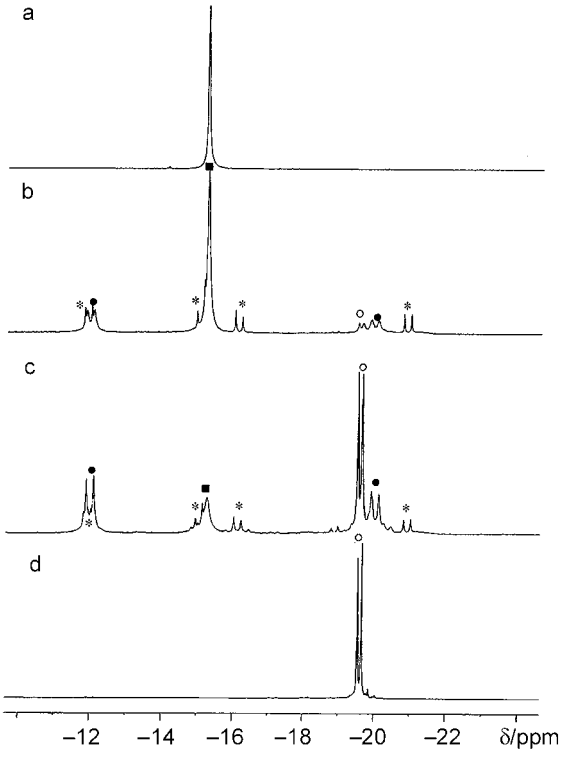

Figure 1. ^{31}P NMR spectra (central part, at 121.5 MHz in $[D_6]$DMSO) of: a) approximately 0.1 M solution of nitrate **1**; b) after addition of nucleobase (molar ratio Ad/Pt = 1:2.85); c) molar ratio Ad/Pt = 1:1; d) molar ratio Ad/Pt = 2:1; ■ denotes nitrate **1**, ○ denotes bis(adduct) **2**, • denotes mono(adduct) **3**, * denotes complex **4**

The resonances labelled by stars in Figure 1 (part b and c) disappear when the Ad/Pt molar ratio is increased to 2, leaving the singlets of the bis adduct **2** at δ = −19.61 and −19.73 ppm as the only detectable signals (Figure 1, part d). The characterization of the adenine complex **4** is discussed later.

Treatment of 9-Methyladenine with *cis*-[Pt(μ-OH)L_2]$_2$(NO_3)$_2$ (6) − Characterization of the Trinuclear Complex *cis*-[PtL_2{9-MeAd(−H)}]$_3$(NO_3)$_3$ (5)

We have shown that the dinuclear hydroxo complex *cis*-[Pt(μ-OH)L_2]$_2^{2+}$ (L = PMe_3) reacts with 9-MeAd (or 9-EtAd) in water as shown in Equation (1), to give the dinuclear complex *cis*-[PtL_2{9-MeAd(−H)}]$_2^{2+}$ containing the NH_2-deprotonated nucleobase, bridging two metal centers through atoms N1 and N6.[6,7] Under the same conditions, the dinuclear hydroxo complex **6** gives a very complex mixture of products, as indicated by the plethora of resonances in the ^{31}P NMR spectrum of the resulting solution, whereas in aprotic solvents a much simpler pattern is obtained. Thus, a suspension of **6** and 9-MeAd (molar ratio 1:2) in [D_6]DMSO becomes clear in ca. 30 min and the ^{31}P NMR spectrum of the resulting solution shows the presence of two AB systems at δ = −18.94/−16.15 and −21.69/−20.95 ppm, the relative intensities of which (20:1) have not changed significantly after several days, indicating that an equilibrium has already been reached. Moreover, in CD_3CN only one AB system is obtained, at δ = −20.03/−17.58 ppm, with well-resolved ^{195}Pt satellites. This spectrum also remains unchanged after several days. The elemental analysis of the product formed in acetonitrile is consistent with the formulation [PtL_2{9-MeAd(−H)}]$_n$(NO_3)$_n$, whereas the ESI-MS spectrum shows the highest *m*/*z* value at 1982, with the expected isotopic distribution, due to the cation {[PtL_2{9-MeAd(−H)}]$_3$(NO_3)$_2$}$^+$, strongly supporting the trinuclear nature of **5**. The stability of isolated **5** is confirmed by the presence of a single set of resonances in the ^{1}H and ^{31}P NMR spectra in $CDCl_3$ or CD_3CN solutions. In contrast, partial conversion into a new species occurs after a few hours at room temperature in [D_6]DMSO, since the ^{31}P NMR spectrum exhibits the same pattern as found when the condensation reaction [Equation (1)] was performed in this solvent. The NMR spectroscopic data obtained through multinuclear experiments are collected in Tables 1−4. ^{1}H,^{15}N NMR correlation spectra (Figure 2) clearly show that platination involves atoms N1 and N6.

The nitrogen signals at δ = −199.2 ppm (detected through the 2-H proton at δ = 8.12 ppm) and δ = −270.8 ppm (detected through the NH proton at δ = 7.17 ppm) are clearly attributable to atoms N1 and N6, respectively. These two resonances in fact display the typical *f*1 modulation due to $^2J_{N,P}$ couplings, in addition to the *f*2 modulation due to $J_{H,N}$ coupling constants. The ^{15}N chemical shift changes of the platinated nitrogen atoms, a shielding of δ = 58 ppm for N1 and a deshielding of δ = 26 ppm for N6, are similar to those found for the dinuclear analog *cis*-[$Pt(PMe_3)_2${9-MeAd(−H)}]$_2$(NO_3)$_2$.[7] In the current case, however, the ^{31}P NMR spectrum obtained for **5** at a low field (36.23 MHz) does not exhibit the long-range platinum-phosphorus couplings found in structurally authentic-

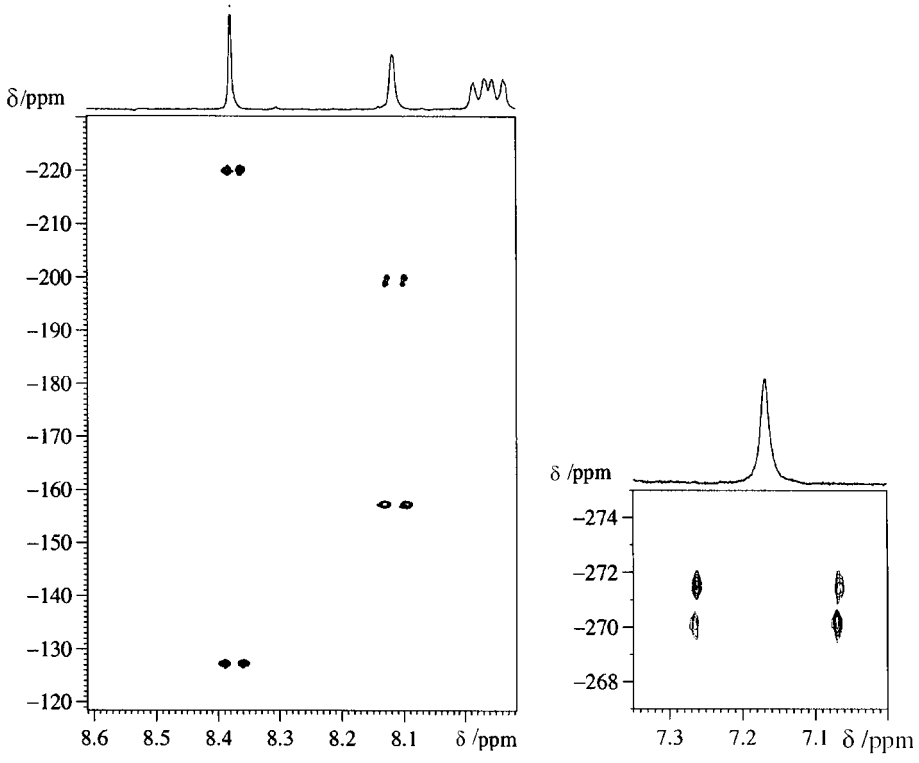

Figure 2. ^{1}H,^{15}N inverse detected spectra of complex **5**; left: HMBC experiment (aromatic region, evolution time 50 ms); right: HMQC experiment (NH region, evolution time 5.6 ms)

ated dinuclear species,[7] in agreement with the higher nuclearity of the complex **5** evidenced by mass spectrometry. The minor component found in the [D_6]DMSO solution of **5** is tentatively attributable to the dinuclear cation *cis*-[PtL_2{9-MeAd(−H)}]$_2^{2+}$ in equilibrium with the predominant trinuclear one. The ^{31}P NMR parameters of the dinuclear species (δ = −21.69/−20.95 ppm) indicate more shielded and less differentiated ^{31}P nuclei than in the trinuclear analog. These spectroscopic features have also been observed with other di- and trinuclear cyclic oligomers containing bridging nucleobases.[10]

Spectroscopic Characterization of the Diplatinated Complex *cis*-[L_2Pt(S){9-MeAd(−H)}PtL_2](NO_3)$_3$ (4)

Solutions of nitrate **1** and 9-MeAd at low Ad/Pt molar ratios contain, in addition to the mono- and bis(adducts), a third species, labelled above as complex **4**, characterized by two AB systems in the ^{31}P NMR spectrum (Figure 1, part b). Its characterization was accomplished by the same multinuclear approach as used for the bis and mono(adducts) on a sample containing Ad/Pt in a 1:3.4 ratio and the results are reported in Tables 1−4. The inverse detection ^{1}H,^{13}C, ^{1}H,^{31}P and ^{1}H,^{195}Pt correlation experiments clearly show that this species contains a single adeninate unit coordinated to two different metal centers, as shown in Scheme 2. The three signals at δ = 8.46, 8.44 and 6.5 ppm (with the same relative intensities) are readily attributable to the 2-H, 8-H and NH protons and belong to the same deprotonated adenine molecule, as inferred from the ^{1}H,^{13}C heteronuclear multiple bond correlation spectrum (Figure 3).

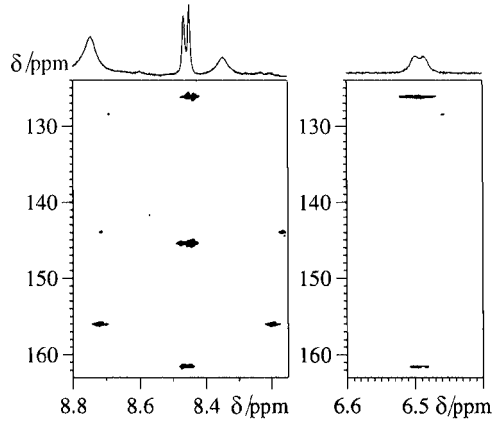

Figure 3. ^{1}H,^{13}C inverse detected spectrum of complex **4** acquired, with a 42 ms evolution delay, on the sample containing Ad/Pt in a 1:3.4 ratio; the spectrum displays, besides the long-range correlations, residual one-bond correlations at δ = 156.1 and 144.0 ppm

In fact, we observe that the 2-H and 8-H protons both detect C4 at δ = 145.5 ppm, the 8-H and NH protons C5 at δ = 126.2 ppm, and the 2-H and NH protons C6 at δ = 161.6 ppm. Furthermore, in the ^{1}H,^{31}P spectrum (Figure 4), 2-H correlates with ^{31}P at δ = −11.98 ppm, 8-H with ^{31}P at δ = −15.12 ppm, and NH with ^{31}P at δ = −16.19 ppm. This is a behavior typical of protons close to or bonded to platinated nitrogen atoms, suggesting three-site (N1, N6 and N7) platination of the deprotonated nucleobase.

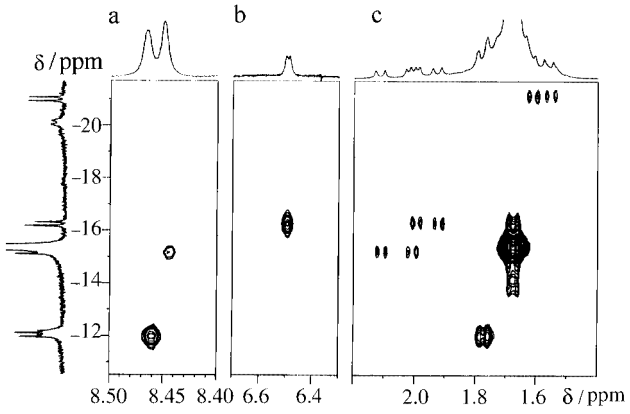

Figure 4. ^{1}H,^{31}P inverse detected spectrum of complex **4** acquired, with a 42 ms evolution delay, on a sample containing Ad/Pt in a 1:3.4 ratio: a) aromatic region, b) NH region, c) aliphatic region; the highest correlation in the aliphatic region is due to unchanged nitrate **1** (methylphosphane signals are found at δ = 1.67 ppm in the ^{1}H NMR spectrum, whereas the ^{31}P NMR signal is at δ = −15.3 ppm)

In addition, the ^{1}H,^{195}Pt spectrum confirms that NH metalation occurs with a ^{195}Pt signal that resonates at δ = −4378 ppm, even though the cross peaks are of low intensity under these conditions. The same experiment performed at low field (200 MHz) allows a second correlation to be detected between 2-H and a ^{195}Pt at δ = −4272 ppm. The low concentration of the diplatinated species did not allow us to detect these two signals in the directly acquired ^{195}Pt spectrum and all ^{15}N signals in the ^{1}H,^{15}N inverse detection mode.

The presence of a deprotonated adenine moiety in this intriguing species prompted us to investigate the involvement of the N7 sites of the trinuclear complex **5** in the platination process when the nitrate **1** is added. The ^{31}P NMR spectrum of a [D_6]DMSO solution of **5** and **1** in 1:3 molar ratio, measured immediately after the mixing of the reactants, is reported in Figure 5.

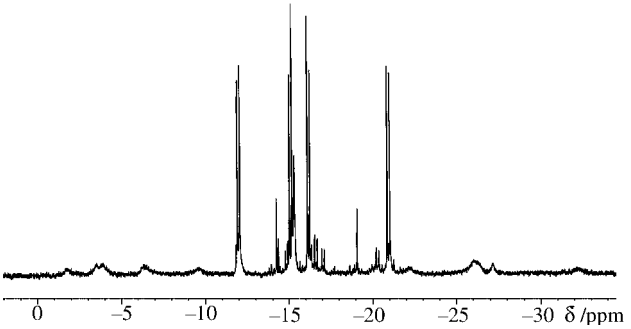

Figure 5. ^{31}P NMR spectrum of a [D_6]DMSO solution of **5** and **1** in 1:3 molar ratio

Figure 5 shows that we were able to obtain a solution containing a major product (80%) displaying the spectroscopic characteristics already found for the diplatinated spe-

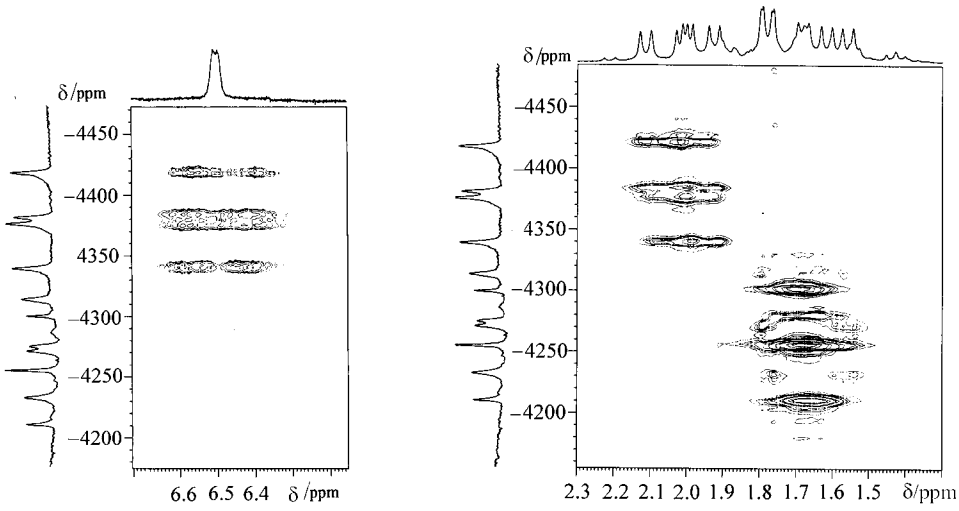

Figure 6. $^{1}H,^{195}Pt$ inverse detected spectra of complex **4** obtained from **5** and **1** in 1:3 molar ratio; left: HMBC experiment (NH region, evolution time 6.2 ms); right: HMBC experiment (aliphatic region, evolution time 12.5 ms); a high correlation in the aliphatic region due to unchanged nitrate **1** ($\delta^{195}Pt = -4254$ ppm) is also present

cies **4**, the unchanged nitrate **1** and other minor species. The directly acquired ^{195}Pt spectrum (displayed as *f*1 trace in Figure 6) reveals the presence of two well-resolved double doublets at the expected chemical shifts, together with the triplet due to the unchanged nitrate **1**. The $^{1}H,^{195}Pt$ spectrum (Figure 6) shows the correlations already found for the diplatinated complex **4** in the sample with Ad/Pt in a 1:3.4 ratio. Furthermore, the signals of the methyl groups bonded to the phosphorus nuclei at $\delta = -15.12$ and -16.19 ppm (see Figure 4) detect ^{195}Pt at $\delta = -4378$ ppm, whereas the signals of the methyl groups bonded to the phosphorus nuclei at $\delta = -11.98$ and -20.96 ppm detect ^{195}Pt at $\delta = -4272$ ppm. Overall, the H,Pt and H,P correlations strongly suggest that nitrogen atoms N6 and N7 chelate or bridge a platinum atom at $\delta = -4378$ ppm, whereas N1 of the same adeninate unit is bonded to a platinum atom at $\delta = -4272$ ppm.

The high concentration of the diplatinated complex **4** allowed us to determine all $^{1}H,^{15}N$ correlations and $^{2}J_{N,P}$ couplings (Figure 7 and Table 4) and to confirm the three-site platination of adenine.

It is evident from Figure 7 that NH and the two aromatic adenine protons detect platinated nitrogen atoms: NH detects N6 at $\delta = -243.6$ ppm, whereas 2-H and 8-H detect N1 at $\delta = -190.0$ ppm and N7 at $\delta = -187.5$ ppm, respectively. These three signals, in addition to a *f*2 modulation due to $J_{H,N}$ couplings, display the *f*1 modulation due to $^{2}J_{N,P}$ typical of metalation, definitely establishing that the adenine unit has three platinated sites. The N1 and N7 coordination shifts ($\delta \approx -50$ ppm) are very similar to those previously observed for platinated N1 sites, while a more marked shift ($\delta = -53$ ppm) is observed for N6 in the diplatinated complex **4** with respect to N6 in the trinuclear complex **5** ($\delta = -26$ ppm). It is also worth mentioning that the NH proton of **4** shows (in ^{1}H NMR spectra recorded at low field or in coupled $^{1}H,^{195}Pt$ correlation spectra) a

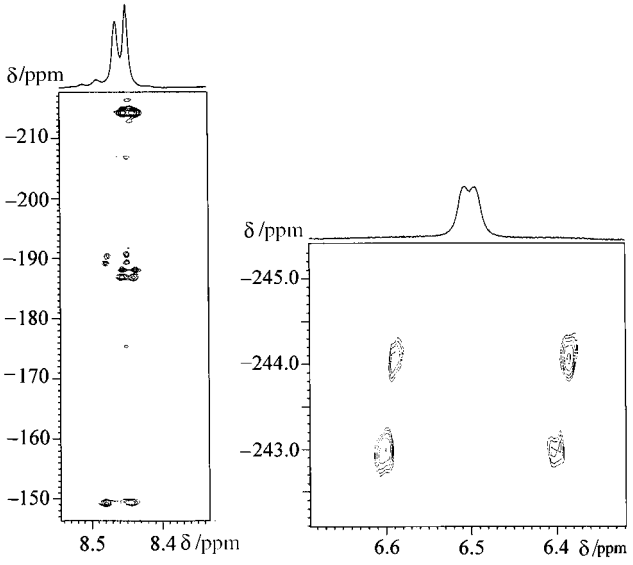

Figure 7. $^{1}H,^{15}N$ inverse detected spectra of complex **4** obtained from **5** and **1** in 1:3 molar ratio; left: HMBC experiment (aromatic region, evolution time 50 ms); right: HMQC experiment (NH region, evolution time 5.6 ms)

$^{2}J_{H,Pt}$ value of 89 Hz, while the corresponding coupling is unresolved in the trinuclear complex **5**. Both these observations suggest probable chelation in the case of **4**.

To gain further insight into the structure of this interesting complex, a nuclear Overhauser effect[11] study was undertaken, in order to find protons spatially close together. The results validate all the attributions previously derived on the bases of heteronuclear correlations and are graphically summarized in Scheme 3.

Both NOESY (nuclear Overhauser enhancement spectroscopy) and ROESY (rotating-frame Overhauser enhancement spectroscopy) experiments[10] were performed, but the

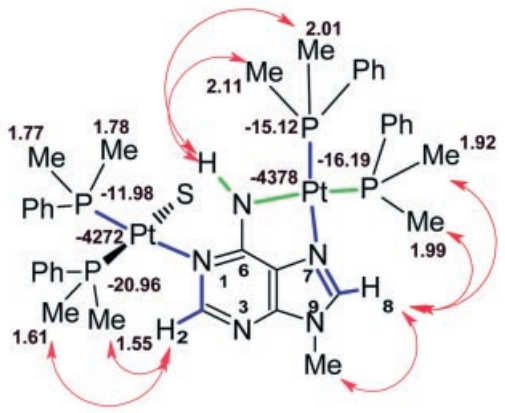

Scheme 3. The most significant NOE correlations (red arrows) and heteronuclear H,P correlations (blue and green paths) for complex **4**

best results were achieved through the second type of experiment. In the NOESY spectra, indeed, not all the cross peaks were detected and those present were of both signs. This means that the correlation time of complex **4** is $\omega_0\tau_c \approx 1.1$ (at 400 MHz), as is the case for molecules of molecular weight around 1200 Da at this field value,[10] confirming that the diplatinated species **4** has the nuclearity depicted in Scheme 2. The same experiment carried out on the trinuclear complex **5** shows, in fact, only negative cross-peaks, as to be expected for species of higher molecular weight. The nuclear Overhauser study confirms that, in this class of platinum complexes, the higher long-range coupling constants are those between a phosphorus atom and the nuclei of the ligand in a *trans* relationship to it (see Scheme 3). In the case of **4**, for instance, 2-H − which correlates with ^{31}P at δ = −11.98 ppm − is spatially closer to the methyl groups (δ = 1.55 and 1.61 ppm) bonded to ^{31}P at δ = −20.96 ppm, the NH proton that correlates with ^{31}P at δ = −16.19 ppm is spatially closer to the methyl groups (δ = 2.01 and 2.11 ppm) bonded to ^{31}P at δ = −15.12 ppm, and 8-H − which correlates with ^{31}P at δ = −15.12 ppm − is spatially closer to the methyl groups (δ = 1.92 and 1.99 ppm) bonded to ^{31}P at δ = −16.19 ppm. In addition, a weak Overhauser effect is detected between the NH proton and the methyl groups at δ = 1.55 and 1.61 ppm, but is higher than that with the methyl groups at δ = 1.77 and 1.78 ppm. This strongly suggests a distortion of the coordination plane of the platinum atom bonded to N1 (δ = −4272 ppm) with respect to the adenine plane, in agreement with previous findings.[3] Additional evidence is provided by the significant deshielding experienced by the methyl groups of the two phosphane ligands bonded to the chelated ^{195}Pt atom at δ = −4378 ppm, consistent with their proximity to the aromatic plane. The chemical shifts of the phosphane ligands bonded to ^{195}Pt at δ = −4272 ppm are very similar to those found for the mono(adduct) **3** and indicate the presence of a solvent molecule in the fourth coordination platinum site. Finally, we observe that the N6/N7 complexation could hardly be deduced from trends in ^{13}C or ^{1}H chemical shifts. More significant are the changes observed in the ^{15}N chemical shifts upon coordination and the value of the coupling constant (89 Hz) between the NH proton and the chelated ^{195}Pt at δ = −4378 ppm.

The formation of the diplatinated complex **4** under the two different sets of conditions described deserves further comment. Concomitant platination at the N1 and N7 sites of neutral adenines is known when the donor atoms in ancillary ligands are nitrogen or chlorine atoms.[3,12] As observed above, N1 is the preferred metalation site of neutral adenine when phosphanes are used as ancillary ligands, but N6/N7 platination also occurs in the presence of a large excess of platinum. The formation of complex **4** could be explained in terms of the initial formation of an N1- and N7-diplatinated intermediate in which the pK_a of NH_2 is lowered by the phosphane ligands, with the consequent formation of an adeninate ion that eventually chelates one platinum atom through N6 and N7. This hypothesis requires the presence of a base in the reaction medium, a role that can be played by the solvent and/or by residual water molecules. The participation of water molecules in the deprotonation is indicated by the observed changes to the signal of a trace of water in [D_6]DMSO solution. This signal is shifted significantly downfield when platinum is in large excess, and progressively moves upfield to its normal δ value (δ = 3.3 ppm) when the Ad/Pt ratio is enhanced. Nevertheless, a direct contribute of the solvent as a base cannot be ruled out.

The disruption of the original N1/N6-bridged trinuclear complex **5** is required when it is treated with the nitrate **1** to form **4**; metalation at N7 probably occurs, forming highly charged, sterically crowded and unstable species that rearrange to less charged and crowded complexes. This process could, in the simplest case, produce two isomeric diplatinated and chelated N1/N6 or N6/N7 complexes. The latter of these is the more stable form found in DMSO solution, in agreement with the higher stability of five-membered rings with respect to four-membered rings, as already reported for mononuclear molybdenum adeninate complexes.[5]

Conclusion

We have reported here on the different coordination modes of 9-MeAd in platinum complexes with phosphanes as ancillary ligands. The results can be summarized as follows:

i) 9-MeAd in its neutral form binds selectively at the N1 site to the metal center of the *cis*-L_2Pt^{2+} units. The role of the different substituents on the phosphane ligands (L = PMe_3, PMe_2Ph) is merely to change slightly the relative stability of the conformers in the bis (adduct) **2**.

ii) The deprotonation of the nucleobase at the NH_2 amino group, promoted by the hydroxo ligand present in the reacting platinum complex **6**, results in the formation of cyclic adducts *cis*-$[PtL_2\{9\text{-MeAd}(-H)\}]_n^{n+}$, in which the

adeninate ions selectively bind the metal atom at the N1 and N6 positions. The relative stability of the oligomers is dependent on the ancillary ligands and on the solvent. The dinuclear complex ($_n$ = 2) is the more stable species when L is PMe_3, whereas the trinuclear **5** appears to be the more stable form with the more sterically demanding PMe_2Ph ligand.

iii) The involvement of the N7 adenine atom in the platination process occurs concomitantly with the N6 chelation, which in turn requires NH_2 deprotonation. The three-site platination of the same adenine unit observed in complex **4** represents an unprecedented coordination mode of 9-MeAd in platinum(II) complexes.

Experimental Section

Materials and Methods: The nucleobase 9-MeAd[13] and the platinum complexes *cis*-[$PtCl_2(PMe_2Ph)_2$][14] were synthesized as previously reported. ^{1}H, ^{13}C, ^{31}P, ^{195}Pt and ^{15}N NMR spectra were obtained in [D_6]DMSO solutions at 300 K in 5-mm sample tubes with Bruker 400AMX WB (operating at 400.13, 100.61, 161.98, 85.88 and 40.56 MHz, respectively) or Bruker AVANCE 300 MHz (operating at 121.5 MHz for ^{31}P) spectrometers, unless otherwise stated. The ^{1}H and ^{13}C chemical shifts were referenced by assigning ^{1}H impurity in the solvent at δ = 2.49 ppm and the ^{13}C multiplet at δ = 39.5 ppm, respectively. The external references were H_3PO_4 (85% w/w in D_2O) for ^{31}P, Na_2PtCl_4 in D_2O (adjusted to δ = −1628 ppm from Na_2PtCl_6) for ^{195}Pt and CH_3NO_2 (in $CDCl_3$ at 50% w/w) for ^{15}N. Inverse detected spectra were obtained through heteronuclear multiple-quantum or multiple-bond correlation (HMQC or HMBC) experiments,[15,16] using parameters similar to those previously reported.[6] The conditions for NOESY and ROESY phase-sensitive spectra[11] by time-proportional phase incrementation (TPPI) were: mixing time 200 ms, spectral width 8.7 ppm with 4096 complex points in *f*2; 512 *t*1 values and 128 scans for *t*1 value. A squared sine function (SSB 2) in *f*2 and in *f*1 was applied prior to Fourier transformation. For the ROESY experiment the spin-lock field was 4000 Hz.

Synthesis of *cis*-[$Pt(NO_3)_2(PMe_2Ph)_2$] (1): A solution of $AgNO_3$ (1.26 g, 7.44 mmol) in H_2O (15 mL) was added to a water (100 mL) suspension of *cis*-[$PtCl_2(PMe_2Ph)_2$] (2.02 g, 3.72 mmol). The AgCl precipitate was eliminated by filtration and the filtrate was concentrated under vacuum to provide **1** as a white solid (1.43 g, 65%). ^{1}H NMR (400.13 MHz, [D_6]DMSO): δ = 1.67 (d, $^2J_{H,P}$ = 11.9 Hz, 6 H, PMe_2), 7.48 (m, 2 H, *m*-H), 7.56 (m, 1 H, *p*-H), 7.70 (m, 2 H, *o*-H) ppm. ^{13}C NMR (100.61 MHz, [D_6]DMSO): δ = 11.8 (m, $^1J_{C,P}$ = 45 Hz, PMe), 128.9 (d, $^1J_{C,P}$ = 67.2 Hz, C1), 128.9 (t, $^2J_{C,P}$ = 5.7 Hz, C_{ortho}), 131.4 (t, $^3J_{C,P}$ = 5.5 Hz, C_{meta}), 138.0 (s, C_{para}). ^{195}Pt NMR (85.88 MHz, [D_6]DMSO): δ = −4254 (t, $^1J_{Pt,P}$ = 3840 Hz) ppm. ^{31}P NMR (161.98 MHz, [D_6]DMSO): δ = −15.32 (s, $^1J_{P,Pt}$ = 3842 Hz) ppm. ^{31}P NMR (121 MHz, CD_3CN): δ = −18.3 (br. s, $^1J_{P,Pt}$ approximately 3800 Hz), in D_2O: δ = −17.2 (s, $^1J_{P,Pt}$ 3824 Hz). $C_{16}H_{22}N_2O_6P_2Pt$ (595.4): calcd. C 32.28, H 3.72, N 4.70; found C 32.22, H 3.65, N 4.72.

Synthesis of *cis*-[$Pt(PMe_2Ph)_2$(9-MeAd)$_2$]$(NO_3)_2$ (2): A suspension of *cis*-[$Pt(NO_3)_2(PMe_2Ph)_2$] (250 mg, 0.41 mmol) and 9-MeAd (125 mg, 0.84 mmol) in water (50 mL) was stirred at room temperature for approximately 1 h. The resulting solution was concentrated under vacuum and the residue was dissolved in MeOH (20 mL). The solution was filtered to eliminate traces of platinum, and addition of Et_2O afforded a white, microcrystalline precipitate, which was further purified from MeOH/Et_2O, filtered and dried under vacuum. The yield of pure product was 222 mg (61%). $C_{28}H_{36}N_{12}O_6P_2Pt$ (893.7): calcd. C 37.63, H 4.06, N 18.80; found C 37.53, H 4.15, N 18.68. ^{1}H NMR (400.13 MHz, [D_6]DMSO): major conformer: δ = 1.73 (d, $^2J_{H,P}$ = 11.2 Hz, 3 H, PMe), 1.80 (d, $^2J_{H,P}$ = 11.2 Hz, 3 H, PMe), 3.64 (s, 3 H, NMe), 7.3−7.7 (m, 5 H, Ph), 8.20 (s, 1 H, 8-H), 8.73 (s, 1 H, 2-H); minor conformer: δ = 1.64 (d, $^2J_{H,P}$ = 11.2 Hz, 3 H, PMe), 1.86 (d, $^2J_{H,P}$ = 11.2 Hz, 3 H, PMe), 3.66 (s, 3 H, NMe), 7.3−7.7 (m, 5 H, Ph), 8.22 (s, 1 H, 8-H), 8.84 (s, 1 H, 2-H) ppm. ^{31}P NMR (161.98 MHz, [D_6]DMSO): major conformer: δ = −19.73 (s, $^1J_{P,Pt}$ = 3231 Hz); minor conformer: δ = −19.61 (s, $^1J_{P,Pt}$ = 3225 Hz) ppm. ^{31}P NMR (36.23 MHz, D_2O): δ = −22.14 (s, $^1J_{P,Pt}$ = 3140 Hz) and −22.45 (s, $^1J_{P,Pt}$ = 3142 Hz) ppm.

Preparation of *cis*-[{$Pt(\mu$-OH)$(PMe_2Ph)_2$}$_2$]$(NO_3)_2$ (6): A solution of $AgNO_3$ (0.98 g, 5.78 mmol) in H_2O (12 mL) was added to a suspension of *cis*-[$PtCl_2(PMe_2Ph)_2$] (1.57 g, 2.89 mmol) in water (67 mL). The immediately formed precipitate of AgCl was filtered and the resulting solution was neutralized with a solution (31.0 mL) of NaOH (0.092 M). After the mixture had been stirred at room temperature for 0.5 h, the white precipitate that separated was recovered by filtration, washed twice with H_2O (10 mL), recrystallized from EtOH/Et_2O and dried under vacuum to give **6** (0.72 g, 45%). ^{1}H NMR (300 MHz, [D_6]DMSO): δ = 1.54 (d, $^2J_{P,H}$ = 11.7 Hz, 6 H, PMe), 4.09 (s broad, 1 H, OH), 7.74−7.49 (m, 5 H, Ph) ppm. ^{31}P NMR (161.98 MHz, [D_6]DMSO): δ = −14.50 (s, $^1J_{P,Pt}$ = 3456 Hz) ppm. $C_{32}H_{46}N_2O_8P_4Pt_2$ (1100.8): calcd. C 34.98, H 4.03, N 2.54; found C 35.02, H 3.98, N 2.61.

Synthesis of *cis*-[$Pt(PMe_2Ph)_2${9-MeAd(−H)}$]_3(NO_3)_3$ (5): A suspension of *cis*-[$Pt(\mu$-OH$)_2(PMe_2Ph)_2$]$(NO_3)_2$ (210 mg, 0.19 mmol) and 9-MeAd (57 mg, 0.38 mmol) in CH_3CN (3 mL) was stirred at room temperature for approximately 1 h. Addition of Et_2O to the resulting solution afforded a white, microcrystalline precipitate, which was filtered off, washed with Et_2O and dried under vacuum to give **5** (184 mg, 71%). ^{1}H NMR (300 MHz, $CDCl_3$): δ = 8.31 (s, 1 H, 8-H), 8.15 (s, 1 H, 2-H), 7.85−7.37 (m, 10 H, Ph), 7.22 (s, 1 H, NH), 3.71 (s, 3 H, NMe), 1.89 (d, $^2J_{H,P}$ = 11.5 Hz, 3 H, PMe), 1.71 (d, $^2J_{H,P}$ = 11.6 Hz, 3 H, PMe), 1.13 (d, $^2J_{H,P}$ = 10.0 Hz, 3 H, PMe), 1.11 (d, $^2J_{H,P}$ = 10.3 Hz, 3 H, PMe) ppm. ^{31}P NMR (161.98 MHz, $CDCl_3$): δ = −21.88 (d, $^2J_{P,P}$ = 23.9, $^1J_{P,Pt}$ = 3842 Hz), −18.06 (d, $^2J_{P,P}$ = 23.9, $^1J_{P,Pt}$ = 3163 Hz) ppm. ^{1}H NMR (300 MHz, CD_3CN): δ = 8.175 (s, 1 H, 8-H), 8.06 (s, 1 H, 2-H), 7.85−7.37 (m, 10 H, Ph), 7.24 (s, 1 H, NH), 3.71 (s, 3 H, NMe), 1.82 (d, $^2J_{H,P}$ = 11.5 Hz, 3 H, PMe), 1.73 (d, $^2J_{H,P}$ = 11.6 Hz, 3 H, PMe), 1.09 (d, $^2J_{H,P}$ = 10.0 Hz, 3 H, PMe), 1.078 (d, $^2J_{H,P}$ = 10.3 Hz, 3 H, PMe) ppm. ^{31}P NMR (161.98 MHz, CD_3CN): δ = −20.69 (d, $^2J_{P,P}$ = 24.3, $^1J_{P,Pt}$ = 3340 Hz), −18.06 (d, $^2J_{P,P}$ = 24.3, $^1J_{P,Pt}$ = 3190 Hz) ppm. ^{1}H NMR (300 MHz, [D_6]DMSO): δ = 1.08/1.14 (d, $^2J_{H,P}$ = 10.7 Hz, 18 H, PMe), 1.78/1.84 (d, $^2J_{H,P}$ = 11.7 Hz, 18 H, PMe), 3.58 (s, 9 H, NMe), 7.17 (d, $J_{H,P}$ = 6.5 Hz, NH), 7.3−7.6 (m, 18 H, $H_{meta,para}$), 7.84 (m, 6 H, H_{ortho}), 7.96 (m, 6 H, H_{ortho}), 8.12 (s, 3 H, 2-H), 8.38 (s, 3 H, 8-H) ppm. ^{31}P NMR (161.98 MHz, [D_6]DMSO): δ = −16.15 (d, $^2J_{P,P}$ = 24.4, $^1J_{P,Pt}$ = 3170 Hz), −18.94 (d, $^2J_{P,P}$ = 24.4, $^1J_{P,Pt}$ = 3320 Hz). $C_{66}H_{84}N_{18}O_9P_6Pt_3$ (2044.6): calcd. C 38.77, H 4.14, N 12.33; found C 38.85, H 4.24, N 11.88.

Acknowledgments

We would like to thank Dr. Roberta Seraglia of the Istituto di Scienze e Tecnologie Molecolari − C.N.R. (Padova) for the mass spec-

trum. Thanks are due to the Centro Interdipartimentale Grandi Strumenti of Modena University for the use of the Bruker AMX 400 WB spectrometer. This work was financially supported by the Ministero dell'Universita' e della Ricerca Scientifica e Tecnologica (PRIN 2001).

[1] B. Lippert, *Prog. Inorg. Chem.* **1989**, *37*, 1−97.
[2] F. Schwarz, B. Lippert, H. Schollhorn, U. Thewalt, *Inorg. Chim. Acta* **1990**, *176*, 113−121.
[3] S. Jaworski, S. Menzer, B. Lippert, M. Sabat, *Inorg. Chim. Acta* **1993**, *205*, 31−34.
[4] L. Prizant, M. J. Olivier, R. Rivest, A. L. Beauchamp, *J. Am. Chem. Soc.* **1979**, *101*, 2765−2767.
[5] L. Y. Kuo, M. G. Kanatzidis, T. J. Marks, *J. Am. Chem. Soc.* **1987**, *109*, 7207−7209.
[6] L. Schenetti, A. Mucci, B. Longato, *J. Chem. Soc., Dalton Trans.* **1996**, 299−303.
[7] G. Trovo′, G. Bandoli, M. Nicolini, B. Longato, *Inorg. Chim. Acta* **1993**, *211*, 95−99.
[8] G. Trovo′, G. Bandoli, U. Casellato, B. Corain, M. Nicolini, B. Longato, *Inorg. Chem.* **1990**, *29*, 4616−4621.
[9] J. J. Li, W. Li, P. R. Sharp, *Inorg. Chem.* **1996**, *35*, 604−613.
[10] L. Schenetti, G. Bandoli, A. Dolmella, G. Trovò, B. Longato, *Inorg. Chem.* **1994**, *33*, 3169−3176.
[11] D. Neuhaus, M. P. Williamson, *The Nuclear Overhauser Effect in Structural and Conformational Analysis*, VCH, New York, **1989**.
[12] C. J. L. Lock, R. A. Speranzini, G. Turner, J. Powell, *J. Am. Chem. Soc.* **1976**, *98*, 7865−7866.
[13] G. Kruger, *Z. Physiol. Chem.* **1893**, *18*, 434.
[14] J. M. Jenkins, L. Shaw, *J. Chem. Soc. A* **1966**, 773−775.
[15] A. Bax, R. H. Griffey, B. L. Hawkins, *J. Magn. Reson.* **1983**, *55*, 301−315.
[16] A. Bax, M. F. Summers, *J. Am. Chem. Soc.* **1986**, *108*, 2093−2094.

Received June 15, 2002
[I02318]

Supramolecular Organisation of Polymeric Coordination Chains into a Three-Dimensional Network with Nanosized Channels that Clathrate Large Organic Molecules

Xian-Ming Zhang,[a,b] Ming-Liang Tong,[a] Meng-Lian Gong,[a] and Xiao-Ming Chen*[a]

Keywords: Coordination polymers / Microporous materials / Inclusion compounds / Supramolecular chemistry

Hydrothermal treatment of a mixture of $[Zn(MeCO_2)_2]\cdot H_2O$, terephthalic acid, and 2,2′-bipyridine resulted in a coordination polymer [Zn(bpy)(tp)](bpy) (**1**; bpy = 2,2′-bipyridine, H_2tp = terephthalic acid) which crystallizes in the monoclinic space group $C2/c$, $M_r = 541.85$, $a = 15.388(11)$, $b = 21.963(11)$, $c = 7.670(8)$ Å, $\beta = 112.82(2)°$, $V = 2387(3)$ Å^3, $Z = 4$, $D_c = 1.506$ g·cm^{-3}. An X-ray single-crystal structural analysis reveals that **1** is a three-dimensional network with nanosized channels constructed from one-dimensional coordination chains via C–H···O hydrogen bonds and aromatic intercalations. TGA and XRPD showed that the porous network of **1** is very stable while the guest 2,2′-bipyridine molecules in the channels are removable. Compound **1** shows a strong ligand-centred emission at room temperature in the solid state.
(© Wiley-VCH Verlag GmbH & Co. KGaA, 69451 Weinheim, Germany, 2003)

Introduction

Microporous inorganic materials including zeolites, aluminium phosphates, and transition metal phosphates are particularly important for their applications as molecular sieves, desiccants, ion exchangers, and catalysts,[1−7] and thus they have been studied in detail in the past decades. Several years ago, microporous compounds were extended to pure organic and metal-organic frameworks, or coordination polymers.[8−20] Compared with inorganic compounds, organic and coordination polymers built from molecular building blocks hold great promise for their ease of processability, flexibility, structural diversity, and geometrical control, such as the size, shape, and symmetry.[12] However, most pure organic and coordination polymers do not possess a porous structure because of the interpenetration of two or more independent networks and the collapse of the network in the absence of guest molecules.[21] Thus, the designed construction of extended porous organic or metal-organic frameworks from molecular building blocks is one of the most challenging issues in current synthetic chemistry.

Recent progress in the design and synthesis of porous metal-organic frameworks has been recently made by Yaghi, Williams, Kitagawa, and their co-workers, in particular, using the concept of secondary building units (SBUs) for understanding and predicting the topologies of structures.[12] The terephthalate (tp) anion is one of the best ligands for the design and construction of inorganic-organic hybrid porous frameworks owing to its thermal stability and symmetry. Hong and co-workers[22] recently attempted to construct a porous coordination polymer with mixed tp and 1,10-phenanthroline (phen) ligands via aromatic π-π stacking interactions, but, due to the ill-suited orientation of the phen and tp groups, and the existence of coordinated water molecules, the networks obtained were not porous. From entropic and kinetic points of view, it is advantageous to arrange the building blocks in a more orderly fashion and remove the coordinated water molecules by reaction at higher temperatures and for longer times.[8] We report here a new porous compound [Zn(bpy)(tp)](bpy) (**1**) generated by a high temperature hydrothermal reaction, which is constructed from infinite zigzag coordination polymeric chains via C−H···O hydrogen bonds and aromatic π-π stacking interactions.

Results and Discussion

Synthesis and Characterization

While well established for the syntheses of zeolites, the hydrothermal method has more recently been adapted to the preparation of complexes. There are a variety of hydrothermal parameters such as reaction time, temperature, pH value, and molar ratio of reactants, and small changes in one or more of the parameters may have a profound influence on the final reaction outcome. Compared with typical hydrothermal conditions for the synthesis of coordination

[a] School of Chemistry and Chemical Engineering Sun Yat-Sen University
Guangzhou 510275, China
Fax: (internat.) +86-20/8411-2245
E-mail: cescxm@zsu.edu.cn
[b] Department of Chemistry Shanxi Teachers University
Linfen Shanxi 041004, China

polymers (120−180 °C and 2−7 days), compound **1** was synthesized at a higher reaction temperature (200 °C) during an exceptionally long reaction time (25 days).

Description of Crystal Structure

X-ray crystallography reveals that **1** consists of one-dimensional zigzag $[Zn(bpy)(tp)]_n$ chains and free bpy groups. There are 0.5 zinc atoms, and 0.5 tp, 0.5 coordinated bpy and 0.5 free bpy ligands in each asymmetric unit. The zinc atom in **1** has a highly distorted octahedral coordination environment with four oxygen atoms [Zn(1)−O(1) 2.380(4), Zn(1)−O(2) 2.057(4) Å, O(1)−Zn(1)−O(2) 59.3(2)°] from two tp groups and two nitrogen atoms [Zn(1)−N(1) 2.132(4) Å and N(1)−Zn(1)−N(1a) 77.2(2)°] from a chelating bpy ligand, as shown in Figure 1. Each tp group acts in a bis-bidentate mode and bridges two zinc atoms, resulting in $[Zn(bpy)(tp)]_n$ chains with additional bpy ligands found alternately on both sides. The Zn···Zn···Zn angle formed by three adjacent zinc atoms is 128°. Both carboxylate ends function in an asymmetric chelate mode, as evidenced by the Zn(1)−O(1) and Zn(1)−O(2) bond lengths.

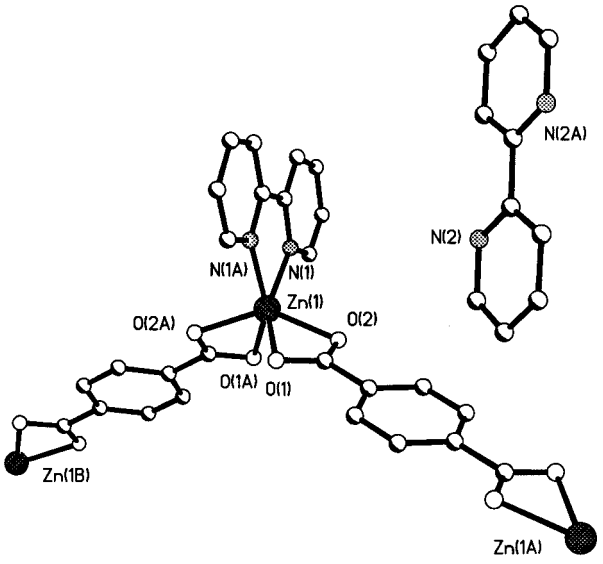

Figure 1. Perspective view of the coordination environment of the zinc atom and the guest bpy molecule in **1**

Two strong bands at 1563 (s) and 1395 (s) cm^{-1} in the IR spectrum are due to the antisymmetric and symmetric stretching vibrations of the carboxylate group, respectively. The difference (Δ = 168 cm^{-1}) between $\nu_{asym}(CO_2)$ and $\nu_{sym}(CO_2)$ is similar to that of an ionic carboxylate, which may be attributed to existence of the C−H···O hydrogen bond associated with the carboxylate oxygen atoms (see below), hence the carboxylate end behaves like a bridging carboxylate-*O*,*O*′ group in the IR spectrum of **1**.

It should be noted that there are persistent one-dimensional C−H···O hydrogen bond interactions between adjacent $[Zn(bpy)(tp)]_n$ chains. Recent studies[23] have revealed that the C···O distance (*D*) in C−H···O hydrogen bond is in the range of 3.0−4.0 Å. The C−H···O angle θ in the range of 110−180° is acceptable, although a linear C−H···O bond (150° < θ < 180°) is structurally more important. In **1** the C(3)···O(1) distance of 3.489 Å and C(3)−H(3a)···O(1) angle of 157.3° indicate a strong C−H···O hydrogen bond. Two complementary C−H···O hydrogen bonds form a double-linked C−H···O hydrogen bond interaction which further extends the $[Zn(bpy)(tp)]_n$ chains into undulating $[Zn(bpy)(tp)]_n$ layers, as shown in Figure 2a. Within the layer, the separation between two adjacent bpy ligands is ca. 7.0 Å. Hydrogen bond interactions are usually important in the synthesis of supramolecular architectures,[24] and in **1** they undoubtedly play an important role in the stabilization of the layer structure and the control of the orientation of the tp ligands. Besides the C−H···O hydrogen bond, the pyridyl C(8) [with H(8a)] atom also forms a hydrogen bond with the carboxy O(2) atom from an adjacent layer, in which the C(8)···O(2) distance and C(8)−H(8a)···O(2) angle are 3.254 Å and 129.3°, respectively (Figure 2b).

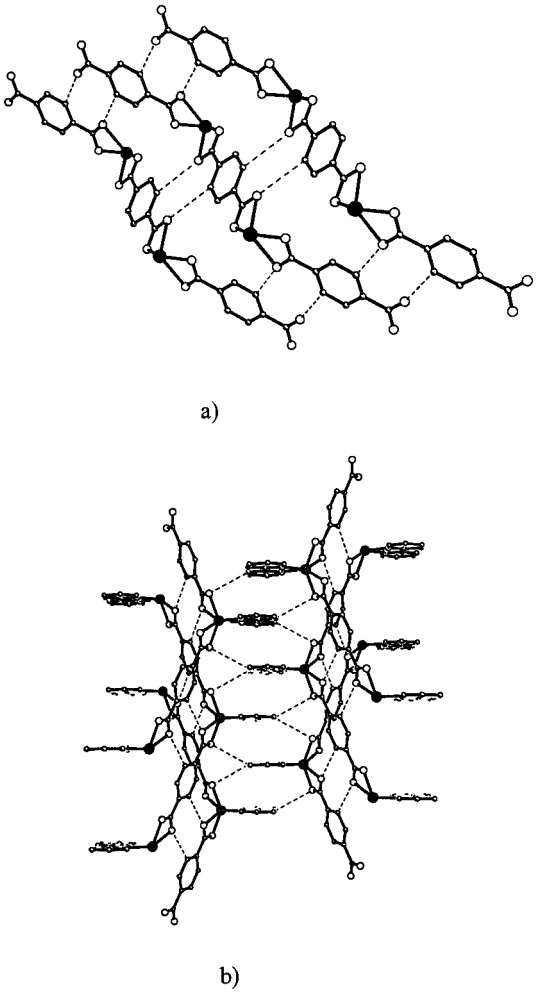

Figure 2. Perspective views of the two-dimensional layers constructed by the zigzag chains and C−H···O hydrogen bonds: (a) top-view of a single layer; (b) side-view of two layers exhibiting the intercalation of the lateral bpy ligands

Aromatic π-π stacking interactions are also apparent in **1**, as shown in Figure 2b. Aromatic π-π stacking interactions can be depicted by centroid-centroid distance, plane-to-plane distance, and displacement angle.[25] The displacement angle means the angle formed between the ring-centroid vector and the ring normal to one of the pyridine planes. In **1**, the centroid-centroid distance (3.85 Å) between two coordinated pyridine fragments, plane-to-plane distance (3.46 Å) and displacement angle (26°) indicate strong π-π stacking interactions between adjacent bpy ligands. All lateral bpy ligands from adjacent undulating $[Zn(bpy)(tp)]_n$ layers are parallel-displaced and intercalated in a zipper-like mode similar to some previously documented examples,[26] which, in combination with the C(8)−H(8a)···O(2) hydrogen bond, further extends the undulating layers into a three-dimensional supramolecular network featuring one-dimensional nanosized saddle-like channels running along the *c* axis (Figure 3). The guest bpy molecules reside in the channels and exhibit an intermolecular parallel-displaced stacking geometry (plane-to-plane distance 3.5 Å) between themselves. Although the three-dimensional structure of **1** is somewhat similar to that of $[Cu(4,7\text{-phen})(H_2O)_3](ClO_4)_2\cdot(4,7\text{-phen})_2$,[27] it is, in fact, constructed in a significantly different fashion. The three-dimensional architecture of this copper compound is formed by the parallel stacking of adjacent S-shaped "triple chains"; in contrast, that of **1** is formed by the zipper-like intercalation of the lateral bpy ligands.

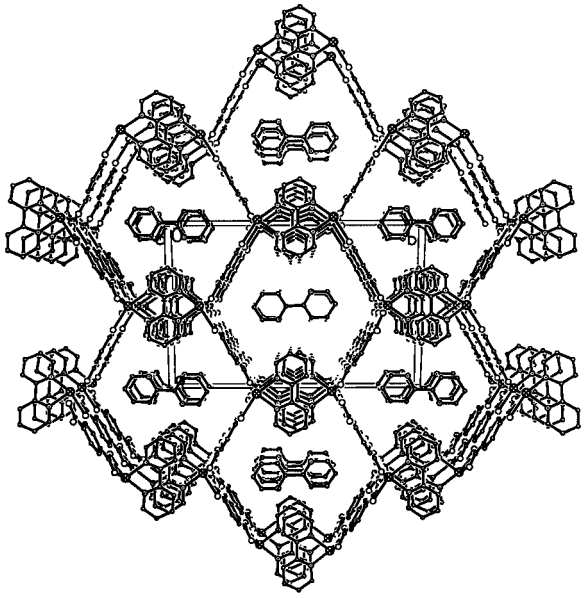

Figure 3. Perspective view of the three-dimensional network along the *c* axis

It is worthwhile to note that the free dimensions (13 × 7 Å) of these channels produced after calcination of **1** occupy as much as 40.7% of the crystal volume,[28,29] a figure similar to those of $[Cu_3(TMA)_2(H_2O)_3]$[8] and $[Zn_2(BTC)(NO_3)](H_2O)(EtOH)_5$ [30] (41% and 43.6%, respectively) and those (47% to 50%) of the most open zeolites, such as the faujasite, paulingite, and zeolite A families.[2] In the formation of the channels in **1**, the C−H···O hydrogen bonds play a critical role because they make the tp ligands arranged in an orderly fashion, which minimizes the volume occupied by the network skeleton by controlling the orientation of the tp building blocks, leaving the large one-dimensional channels that are occupied by the guest bpy molecules.

In order to study the microporosity chemistry of **1**, thermogravimetric analysis (TGA) was performed in air and at 1 atm. pressure at a heating rate of 10 °C·min^{-1} on a polycrystalline sample of this material, which showed the following clear and well-separated weight loss steps. As shown in Figure 4, a total weight loss of 29.0% occurred over the temperature range 190−310 °C, corresponding to the removal of one free bpy molecule per formula unit (calcd. 28.8%), followed by a two-step total weight loss of 56.3% between 340 and 640 °C consistent with the removal of coordinated bpy and tp ligands. The remaining weight of 14.7% corresponds to the percentage (15.0%) of the Zn and O components, indicating that the final product is ZnO. It should be noted that no weight loss was observed in the temperature range 310−340 °C. Therefore the TGA curve of **1** indicates that: 1) the free bpy molecules are removed from the channels in the temperature range 190−310 °C, whereas the coordinated bpy and tp ligands do not decompose over this temperature range; 2) in air and under 1 atm. pressure, a phase formulated as [Zn(bpy)(tp)] is stable in the temperature range 310−340 °C, which is unusually high for a one-dimensional coordination polymer.

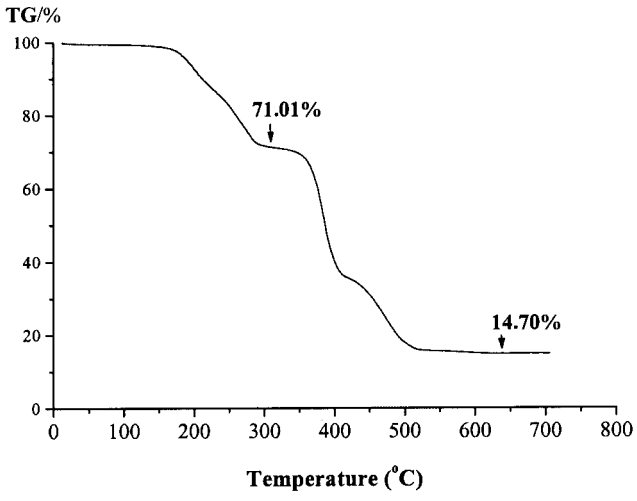

Figure 4. Thermogravimetric analysis curve of **1**

The above conclusions have also been supported by calcination of **1**. Elemental microanalysis (C 56.05, H 3.14, N 7.26) of **1** after calcination (designated as **1′**) in air at 220 °C and 10^{-2} Torr for 10 hours shows that the free bpy molecules are removed in the course of calcination. The X-ray powder diffraction patterns (Figure 5) of **1** and **1′** are similar while the positions, intensities and widths of some

peaks show minor differences, thus indicating that the porous network of **1** is retained after the calcination and removal of guests.

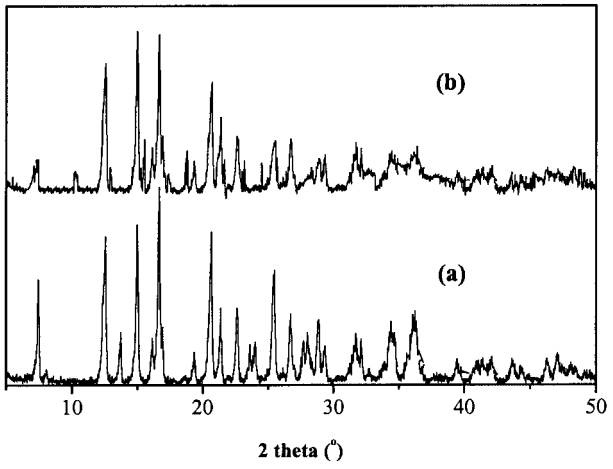

Figure 5. The XRPD patterns for: (a) as-synthesized **1** with bpy in the channels, and (b) the calcinated material

Photoluminescence

In the solid state, **1** shows an intense and broad emission band ranging from 400 to 600 nm upon photoexcitation (λ_{ex} = 260 nm; Figure 6). The maxima of the emission bands are located at 468 and 540 nm. According to the literature,[31,32] the emission at 468 nm can be assigned to the $^1\pi,\pi^*$ state of the bpy ligands and the small shoulder at 540 nm to the $^1\pi,\pi^*$ state of free bpy molecules. The blue shift of the emission at 468 nm compared to that of free bpy ligand is possibly due to the fact that the bpy ligands are not allowed to relax along the inter-ring torsional mode upon photoexcitation.

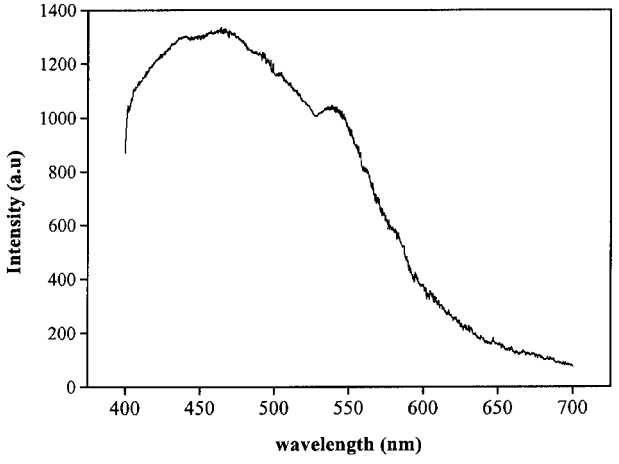

Figure 6. Photoluminescent spectrum of **1** excited at 260 nm

Experimental Section

General Remarks: Elemental analyses were performed on a Perkin−Elmer 240 elemental analyzer. The FT-IR spectra were recorded from KBr pellets between 400 and 4000 cm^{-1} on a Nicolet 5DX spectrometer. Thermal gravimetric analyses (TGA) were performed under a static air atmosphere using a Perkin−Elmer 7 thermogravimetric analyzer with a heating rate of 10 °C·min^{-1}. The XRPD patterns were recorded a Rigaku D/Max 3III diffractometer with a scanning rate of 4 deg·min^{-1}. Photoluminescence of **1** was performed at room temperature on a Hitachi F-4500 spectrometer.

Preparation of 1: A mixture of $Zn(MeCO_2)_2{\cdot}H_2O$ (0.112 g), H_2tp (0.083 g), NaOH (0.040 g), bpy (0.079 g), and water (10 mL) in a 1:1:2:1:1100 molar ratio was stirred for 20 min in air, then sealed in a 23 mL Teflon-lined stainless steel container, which was heated to 200 °C for 25 days. After cooling to room temperature at a rate of 5 °C per hour, pale-yellow large block crystals (ca. 3.2 × 2.3 × 1.5 mm) of **1** were recovered in 60% yield based on bpy. $C_{28}H_{20}N_4O_4Zn$ (541.85): calcd. C 60.06, H 3.72, N 10.34; found C 59.87, H 3.81, N 10.26. IR (KBr): $\tilde{\nu}$ = 3436 cm^{-1} m, 3069 w, 1563 s, 1443 m, 1395 s, 1294 m, 1174 w, 1018 w, 903 m, 842 s, 760 s, 546 m.

Preparation of the Porous Framework 1′: Compound **1** was calcinated in a vacuum oven at 220 °C under a pressure of ca. 10^{-2} Torr for 10 h. $C_{18}H_{12}N_2O_4Zn$ (385.69): calcd. C 56.05, H 3.14, N 7.26; found C 55.94, H 3.07, N 7.21.

X-ray Crystallographic Study: Diffraction intensities were collected at 293 K on a Siemens R3 diffractometer (Mo-K_α, λ = 0.71073 Å). Lorentz-polarization and absorption corrections were applied. The structures were solved by direct methods (SHELXS-97)[33] and refined by full-matrix least-squares techniques (SHELXL-97). Analytical expressions of neutral-atom scattering factors were employed, and anomalous dispersion corrections were incorporated. In all cases, all non-hydrogen atoms were refined anisotropically and hydrogen atoms of organic ligands were geometrically placed. The crystallographic data are listed in Table 1 and selected interatomic distances and angles are given in Table 2.

Table 1 Crystal and structure refinement for complex **1**

Empirical formula	$C_{28}H_{20}N_4O_4Zn$
Formual weight	541.85
Temperature [K]	293(2)
Wavelength [Å]	0.71073
Crystal system	monoclinic
Space group	*C*2/*c*
a [Å]	15.388(11)
b [Å]	21.963(11)
c [Å]	7.670(8)
β [°]	112.82(2)
V [$Å^3$]	2389(3)
Z	4
Density [Mg/m^3]	1.506
Absorption coefficient [mm^{-1}]	1.072
F(000)	1112
No. indep. refl.	2100
No. obs. refl.	1662
Data/restrains/parameters	2100/0/169
Goodness-of-fit on F^2	1.084
R_1 [$I > 2\sigma(I)$]	0.0603
wR_2	0.1741
Extinction coefficient	0.0039(9)
Largest diff. peak and hole [e·$Å^{-3}$]	0.532 and −0.645

CCDC-173807 contains the supplementary crystallographic data for this paper. These data can be obtained free of charge at www.ccdc.cam.ac.uk/conts/retrieving.html [or from the Cambridge

Table 2. Selected bond lengths [Å] and angles [°] for **1**

Zn(1)−O(2)	2.057(4)	N(1a)1−Zn(1)−N(1)	77.2(2)
Zn(1)−N(1)	2.132(4)	O(2)−Zn(1)−O(1a)[a]	98.5(2)
Zn(1)−O(1)	2.380(4)	N(1)−Zn(1)−O(1a)	88.3(2)
		O(2)−Zn(1)−O(1)	59.3(2)
O(2a)−Zn(1)−O(2)	140.5(2)	N(1a)−Zn(1)−O(1)	88.3(2)
O(2)−Zn(1)−N(1a)	109.8(2)	N(1)−Zn(1)−O(1)	150.1(2)
O(2)−Zn(1)−N(1)	101.0(2)	O(1a)−Zn(1)−O(1)	115.2(2)

[a] Symmetry code: a) $-x, y, -z + 1/2$.

Crystallographic Data Centre, 12, Union Road, Cambridge CB2 1EZ, UK; Fax: (internat.) +44−1223/336-033; E-mail: deposit@ccdc.cam.ac.uk].

Acknowledgments

This work was supported by the National Natural Science Foundation of China (No. 20131020 & 29971033) and the Ministry of Education of China (No. 01134).

[1] A. K. Cheetham, G. Férey, T. Loiseau, *Angew. Chem. Int. Ed.* **1999**, *38*, 3268−3292.
[2] D. W. Breck, *Zeolite Molecular Sieves*, Kreiger, Malabar, **1974**.
[3] S. T. Wilson, B. M. Lok, C. A. Messina, T. R. Cannan, E. M. Flanigen, *J. Am. Chem. Soc.* **1982**, *104*, 1146−1147.
[4] T. E. Gier, G. D. Stucky, *Nature* **1991**, *349*, 508−510.
[5] M. E. Davis, *Acc. Chem. Res.* **1993**, *26*, 111−115.
[6] T. E. Gier, X. Bu, P. Feng, G. D. Stucky, *Nature* **1998**, *395*, 154−157.
[7] P. Feng, X. Bu, G. D. Stucky, *Nature* **1997**, *388*, 735−741.
[8] S. S.-Y. Chui, S. M.-F. Lo, J. P. H. Charmant, A. G. Orpen, I. D. Williams, *Science* **1999**, *283*, 1148−1150.
[9] L. Chen, M. Eddaoudi, S. T. Hyde, M. O'Keeffe, O. M. Yaghi, *Science* **2001**, *291*, 1021−1023.
[10] S.-I. Noro, S. Kitagawa, M. Kondo, K. Seki, *Angew. Chem. Int. Ed.* **2000**, *39*, 2082−2084.
[11] M. Eddaoudi, J. Kim, M. O'Keeffe, O. M. Yaghi, *J. Am. Chem. Soc.* **2002**, *124*, 376−377.
[12] O. M. Yaghi, H.-L. Li, C. Davis, D. Richardson, T. L. Groy, *Acc. Chem. Res.* **1998**, *31*, 474−484.
[13] H. K. Chae, M. Eddaoudi, J. Kim, S. I. Hauck, J. F. Hartwig, M. O'Keeffe, O. M. Yaghi, *J. Am. Chem. Soc.* **2001**, *123*, 11482−11483.
[14] J. Kim, B. Chen, T. M. Reineke, H. Li, M. Eddaoudi, D. B. Moler, M. O′Keeffe, O. M. Yaghi, *J. Am. Chem. Soc.* **2001**, *123*, 8239−8247.
[15] M. Eddaoudi, J. Kim, J. B. Wachter, H. K. Chae, M. O′Keeffe, O. M. Yaghi, *J. Am. Chem. Soc.* **2001**, *123*, 4368−4369.
[16] H. Li, M. Eddaoudi, M. O'Keeffe, O. M. Yaghi, *Nature* **1999**, *402*, 276−279.
[17] M. J. Zaworotko, *Angew. Chem. Int. Ed.* **2000**, *39*, 3052−3054.
[18] K. Biradha, C. Seward, M. J. Zaworotko, *Angew. Chem. Int. Ed.* **1999**, *38*, 492−495.
[19] K. Biradha, Y. H. Hongo, M. Fujita, *Angew. Chem. Int. Ed.* **2000**, *39*, 3843−3845.
[20] M. Eddaoudi, D. B. Moler, H. Li, B. Chen, T. M. Reineke, M. O′Keeffe, O. M. Yaghi, *Acc. Chem. Res.* **2001**, *34*, 319−330.
[21] S. R. Batten, R. Robson, *Angew. Chem. Int. Ed.* **1998**, *37*, 1460−1496
[22] D.-F. Sun, R. Cao, Y.-C. Liang, Q. Shi, W.-P. Su, M.-C. Hong, *J. Chem. Soc., Dalton Trans.* **2001**, 2335−2340.
[23] G. R. Desiraju, *Acc. Chem. Res.* **1996**, *29*, 441−449.
[24] M. J. Krische, J.-M. Lehn, *Struct. Bonding* **2000**, *96*, 3−29.
[25] C. Janiak, *J. Chem. Soc., Dalton Trans.* **2000**, 3885−3896.
[26] S.-L. Zheng, M.-L. Tong, R.-W. Fu, X.-M. Chen, S.W. Ng, *Inorg. Chem.* **2001**, *40*, 3562−3569.
[27] M.-L. Tong, S.-L. Zheng, X.-M. Chen, T. Yuen, C. L. Lin, X.-Y. Huang, J. Li, *New J. Chem.* **2001**, 1482−1485.
[28] The channel dimensions are estimated from the van der Waals radii for carbon (1.70 Å), nitrogen (1.55 Å), and oxygen (1.40 Å).
[29] A. L. Spek, *PLATON, A Multipurpose Crystallographic Tool*, Untrecht University: Utrecht, The Netherlands, **1999**.
[30] M. Yaghi, C. E. Davis, G. Li, H. Li, *J. Am. Chem. Soc.* **1997**, *119*, 2861−2868.
[31] K. D. Ley, K. S. Schanze, *Coord. Chem. Rev.* **1998**, *171*, 287−307.
[32] V. W. W. Yam, K. K. W. Lo, *Chem. Soc. Rev.* **1999**, *28*, 323−334.
[33] G. M. Sheldrick, *SHELX-97, Program for X-ray Crystal Structure Solution and Refinement*, Göttingen University, Germany (**1997**).

Received June 20, 2002
[I02339]

Synthesis, Structural Study, and In Vitro Trypanocidal and Antitumour Activities of Tetrakis(3-methoxypropyl)tin and (3-Methoxypropyl)tin Chlorides

Tomáš Lébl,*[a] Aleš Smička,[a][†] Jiří Brus,[b] and Clemens Bruhn[c]

Dedicated to Professor Jaroslav Holeček on the occasion of his 70th birthday

Keywords: Chelates / Drug research / O ligands / Structure elucidation / Tin

A set of four water-soluble (3-methoxypropyl)stannanes of general formula $(CH_3OCH_2CH_2CH_2)_xSnCl_{4-x}$, where x = 4 (**1**), x = 3 (**2**), x = 2 (**3**), and x = 1 (**4**), was prepared. For **3** and **4**, which were isolated in the crystalline state, it was shown by X-ray diffraction that the tin atom is coordinated in distorted octahedral and trigonal-bipyramidal geometries, respectively (i.e., the oxygen atoms of the 3-methoxypropyl groups were coordinated to the central tin atom in both cases, forming chelates). For all compounds, structures in $CDCl_3$ and [D_6]DMSO solutions were proposed on the basis of their ^{13}C and ^{119}Sn NMR spectra. In $CDCl_3$ solution, the degree of donor-acceptor bonding between the central tin atom and oxygen atom of the 3-methoxypropyl substituent was evaluated on the basis of ^{17}O NMR chemical shifts and $^{3,6}J(^1H,^{119}Sn)$ long-range coupling constants. Compounds **2** and **3** exhibited promising in vitro antitumour and trypanocidal activities.

(© Wiley-VCH Verlag GmbH, 69451 Weinheim, Germany, 2003)

Introduction

Organotin compounds have shown a wide spectrum of biological merits. Their antitumour properties in vitro against a wide panel of tumour cell lines of human origin are fairly well known,[1] and it has also been proposed that anticancer reagents could also be used against trypanosomal diseases (human sleeping sickness and domesticated live stock diseases).[2] Recently, it was found that several organotin thiolates exhibit high in vitro levels of activity in comparison with the arsenic derivatives used for chemotherapy.[3] However, the antitumour and trypanocidal efficiencies of organotin derivatives seem to be limited by their low water solubility.[4] Particular attention has therefore recently been paid to the synthesis of organotin compounds with higher water solubilities.[5]

In 1997, Susperregui et al. reported the synthesis and structures of water-soluble [3-(2-methoxy)ethoxy]propyltin chlorides.[6] Interesting in vitro and vivo trypanocidal activity was later described for bis[3-(2-methoxy)ethoxy]-propyltin dichloride and the corresponding oxide.[7] Those papers suggest that the replacement of alkyl by alkoxyalkyl substituents could constitute a route to water-soluble organotin derivatives. In order to check whether the replacement of a 1-butyltin moiety, as conventionally used in organotin drug research, by a 3-methoxypropyltin one would deliver water-soluble and biologically active derivatives, (3-methoxypropyl)stannanes of general formula $(CH_3OCH_2CH_2CH_2)_xSnCl_{4-x}$ (x = 1−4) have been synthesized and structurally characterized, both in the solid state and in solution, and their in vitro antitumour and trypanocidal activities were tested.

[a] Department of General and Inorganic Chemistry, University of Pardubice,
Cs. Legií, 565, 532 10 Pardubice, Czech Republic
Fax: (internat.) + 420-40/603-7068
E-mail: tomas.lebl@upce.cz
[b] Institute of Macromolecular Chemistry of the Academy of Sciences of the Czech Republic,
Heyrovský sq. 2, 16206 Praha 6, Czech Republic
E-mail: brus@imc.cas.cz
[c] Department of Inorganic Chemistry, Martin-Luther-Universität Halle-Wittenberg,
Kurt-Mothes-Straße 2, 06120 Halle (Saale), Germany
E-mail: bruhn@chemie.uni-halle.de
[†] Suddenly and tragically died on June 19, 2001 in Pardubice

Results and Discussion

Synthesis

Tetrakis(3-methoxypropyl)tin (**1**) was synthesised as shown in Scheme 1, by treatment of tin tetrachloride with excess (3-methoxypropyl)magnesium chloride (previously prepared from 3-methoxypropyl chloride and magnesium chips in THF). Tetraorganostannane **1** was isolated by vacuum distillation as a colourless liquid in a yield of 92% with respect to $SnCl_4$.

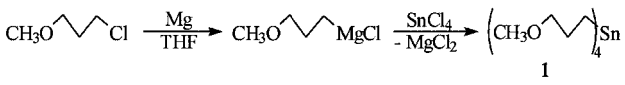

Scheme 1

(3-Methoxypropyl)tin chlorides **2**−**4** were synthesised by means of a Kocheshkov redistribution reaction (Scheme 2),[8] by treatment of tetraorganostannane **1** with the appropriate amount of tin tetrachloride (3:1, 1:1, and 1:3 for **2**, **3**, and **4**, respectively). Although Kocheshkov reactions usually display low selectivity, the (3-methoxypropyl)tin chlorides **2**−**4** could be isolated by vacuum distillation in yields of about 95%. Such a high selectivity might be explained by suppression of 3-methoxypropyl group cleavage by intramolecular O→Sn coordination (see below) and consequently lower reactivities in the products **2**, **3**, and **4**.

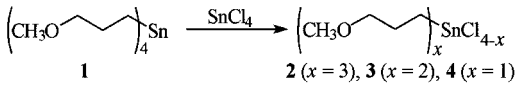

Scheme 2

Solid-State Structures

Only the (3-methoxypropyl)tin chlorides **3** and **4** were isolated in a crystalline state, and their structures were determined by X-ray diffraction (Figure 1 and Figure 2). Selected bond lengths and angles are listed in Table 1 and Table 2, respectively.

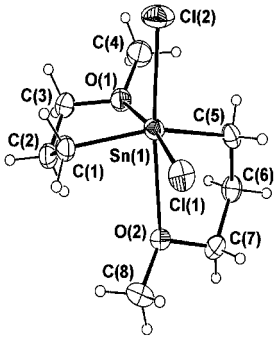

Figure 1. Solid-state structure of bis(3-methoxypropyl)tin dichloride (**3**)

Both complexes consist of discrete molecules. For compound **3**, the environment around the central tin atom has a deformed octahedral geometry (skew) with both oxygen atoms coordinated to the tin atom in a *cis* configuration [O−Sn−O 89.4(1)°]. Two chlorine atoms are also mutually *cis* [Cl−Sn−Cl 97.26(7)°], while two C−Sn bonds are at an angle of 148.5(2)°. The shape of the coordination polyhedron is thus similar to that of the analogous bis[3-(2-methoxy)-ethoxy]propyltin dichloride.[6] The tin atom in **4**, on the other hand, is coordinated as a distorted trigonal-bipyramid with the carbon atom and the two chlorine atoms in the equatorial plane [C−Sn−Cl(1) = 129.3(9), C−Sn−Cl(3) = 120.5(9), Cl(1)−Sn−Cl(3) = 102.31(5)°] and the oxygen atom and the third chlorine atom in axial positions [O−Sn−Cl(2) = 175.7(1)°]. The whole equatorial plane is tilted towards the oxygen atom [C−Sn−Cl(2) = 102.9(6), Cl(1)−Sn−Cl(2) = 95.80(5), Cl(3)−Sn−Cl(2) = 98.17(6)°]. The crystal-state structure of **4** differs from that of the analogous [3-(2-methoxy)ethoxy]propyltin trichloride in that the oxygen atom of one water molecule is used in order to reach an octahedral coordination.[6]

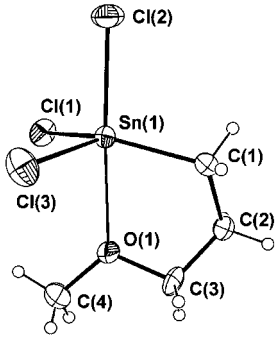

Figure 2. Solid-state structure of (3-methoxypropyl)tin trichloride (**4**)

Table 1. Selected bond lengths [Å] and angles [°] for **3**

Sn(1)−O(1)	2.559(4)	Sn(1)−Cl(2)	2.419(2)
Sn(1)−O(2)	2.556(4)	Sn(1)−C(1)	2.136(6)
Sn(1)−Cl(1)	2.432(2)	Sn(1)−C(5)	2.138(6)
C(1)−Sn(1)−C(5)	148.5(2)	C(1)−Sn(1)−Cl(1)	100.3(2)
O(1)−Sn(1)−O(2)	89.4 (1)	C(1)−Sn(1)−Cl(2)	102.5(2)
Cl(1)−Sn(1)−Cl(2)	97.26(7)	C(5)−Sn(1)−Cl(1)	99.7(2)
Cl(1)−Sn(1)−O(1)	84.9(1)	C(5)−Sn(1)−Cl(2)	98.9(2)
Cl(2)−Sn(1)−O(2)	173.4(1)	C(1)−Sn(1)−O(2)	83.2(2)

Table 2. Selected bond lengths [Å] and angles [°] for **4** (values are given for one split layer)

Sn(1)−Cl(1)	2.332(1)	Sn(1)−O(1)	2.394(3)
Sn(1)−Cl(2)	2.390(1)	Sn(1)−C(1)	2.09(3)
Sn(1)−Cl(3)	2.327(1)		
O(1)−Sn(1)−Cl(2)	175.7(1)	Cl(1)−Sn(1)−Cl(2)	95.80(5)
C(1)−Sn(1)−Cl(1)	129.3(9)	Cl(1)−Sn(1)−Cl(3)	102.31(5)
C(1)−Sn(1)−Cl(2)	102.9(6)	Cl(3)−Sn(1)−Cl(2)	98.17(6)
C(1)−Sn(1)−Cl(3)	120.6(9)		

The Sn−O bond length in the distorted trigonal-bipyramidal geometry of **4** [2.394(40) Å] is slightly shorter than the Sn−O bond lengths found in the distorted octahedral geometry of **3** [2.559(4) and 2.556(4) Å]. This is in agreement with increasing Lewis acidity of the central tin atom. The Sn−O bonds are in both cases shorter than those in the analogous [3-(2-methoxy)ethoxy]propyltin chlorides [2.442(2), 2.65(1), and 2.67(1) Å, respectively].[6] However, the oxygen atom of the water molecule in [3-(2-methoxy)-ethoxy]propyltin trichloride has a significantly stronger bond [Sn−O 2.292(5) Å] than oxygen atoms of chelating alkoxypropyl groups.[6]

The Sn−C [2.09(3)−2.145(4) Å] and Sn−Cl [2.3274(12)−2.4328(12) Å] bond lengths in compounds **3** and **4** are similar to those found in the analogous [3-(2-methoxy)ethoxy]propyltin chlorides [2.127−2.15(2) and 2.351−2.426(6) Å, respectively].[6] In the trigonal-bipyramidal geometry of **4**, the apical chlorine atom has a slightly weaker bond to the central tin atom [Sn−Cl(2) = 2.3904(12) Å] than the equatorial ones [Sn−Cl(1) = 2.3317(14), Sn−Cl(3) = 2.3274(12) Å], due to the *trans* effect of the coordinated oxygen atom of the 3-methoxypropyl group.

The sixfold- and fivefold-coordinated tin atoms observed for (3-methoxypropyl)tin chlorides **3** and **4** in the crystalline state are in accordance with ^{119}Sn solid-state NMR chemical shifts of δ = −133 and −157 ppm, respectively. Moreover, the ^{119}Sn CP/MAS spectrum of **3** showed a 1:2:4:1:4:4 splitting pattern due to the interaction of ^{119}Sn nuclei with two equivalent $^{35/37}$Cl spins (Figure 3).[9]

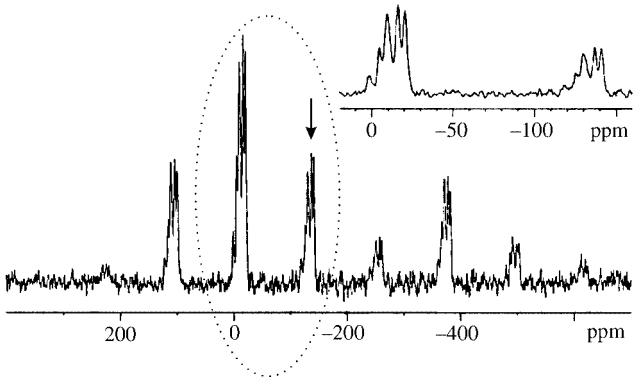

Figure 3. ^{119}Sn CP/MAS NMR spectrum of bis(3-methoxypropyl)-tin dichloride (**3**); the vertical arrow indicates the centre band

Structures in Solution

Methoxypropylstannanes **1**−**4** were characterised in $CDCl_3$ solution by ^{1}H NMR spectroscopy (see Exp. Sect.). In order to evaluate these solution structures both in non-coordinating and in coordinating solvents, their ^{13}C, ^{17}O, and ^{119}Sn NMR spectra were measured in $CDCl_3$ and [D_6]DMSO. All relevant NMR parameters are summarised in Table 3. The values of the $J(^1H,^{119}Sn)$ coupling constants obtained from gradient-assisted 1D ^{1}H,^{119}Sn HMQC and 2D ^{1}H,^{119}Sn J-HMBC spectra are given in Table 4.[10] The numbering scheme used for the hydrogen and carbon atoms is given in Scheme 3.

The ^{119}Sn chemical shift values of the (3-methoxypropyl)-stannanes **1**−**4** in $CDCl_3$ solution are shifted upfield [$\Delta\delta(^{119}Sn)$ = 1.3, 103.8, 234.9, and 132.4 ppm, respectively] with respect to analogous 1-butyltin compounds.[11] The ^{119}Sn chemical shifts were found not to be concentration-dependent, and so only intramolecular side-arm donation can be assumed. In the case of tetra-organotin compound **1**, the value of $\Delta\delta(^{119}Sn)$ is negligible. Accordingly, O→Sn interaction, if present, must be very weak. The tin atom is coordinated as a slightly distorted tetrahedron, as is evident from $^1J(^{13}C,^{119}Sn)$ = 324.5 Hz (average angle C−Sn−C 107°).[12] For triorganotin compound **2**, the significant upfield shift [$\Delta\delta(^{119}Sn)$ = 103.8 ppm] indicates a pentacoordinated tin atom. The value of $^1J(^{13}C,^{119}Sn)$ = 434.6 Hz (average angle C−Sn−C 118°) shows that coordination polyhedron of **2** has a *trans*-trigonal-bipyramidal shape.[12] Consequently, one oxygen atom has to be coordinated to the central tin atom while the other two are not. However, only one set of signals for the 3-methoxypropyl groups was observed in the ^{1}H and ^{13}C NMR spectra at room temperature and in [D_8]toluene at 180 K. This indicates the existence of an exchange that is fast on the NMR timescale even at 180 K. In the case of (3-methoxypropyl)tin chlorides **3** and **4**, the moderate differences between the ^{119}Sn chemical shifts in $CDCl_3$ solution and in the solid state (δ = 24 and 18 ppm, respectively) show that the distorted octahedral (Figure 2) and trigonal-bipyramidal (Figure 3) structures determined by X-ray diffraction are retained upon dissolution in $CDCl_3$.[9] The agreement of the C−Sn−C angles as calculated from the coupling constant $^1J(^{13}C,^{119}Sn)$ = 731.6 Hz (148°) and as determined by X-ray diffraction [148.5(2)°] confirms the suitability of the equation used for calculation.[12]

The values of $\delta(^{17}O)$ are shifted downfield as the Lewis acidity of the central tin atom increases (Table 3). Since the oxygen atom in the 3-methoxypropyl substituent is regarded as a pure σ-donor, this denotes an increasing degree of donor-acceptor bonding between the central tin atom and the oxygen atom in the organic substituent.[13] The values of the $^{3,6}J(^1H,^{119}Sn)$ long-range coupling constants between the ^{119}Sn nucleus and the CH_3O protons also increase with the same trend (Table 4). On the assumption that the contributions of the scalar coupling pathways through the CH_3O→Sn coordinative bond [$^3J(^1H,^{119}Sn)$] and through the covalent bonds of 3-methoxypropyl chain [$^6J(^1H,^{119}Sn)$] have the same signs, their sum and the increasing strength of CH_3O→Sn coordinative bonding could be responsible for this increasing trend.

For (3-methoxypropyl)tin chlorides **2**−**4** in deuteriochloroform solutions, the values of $^2J(^{119}Sn,^{13}C)$ are higher and the values of $^3J(^{13}C,^{119}Sn)$ lower than the corresponding values for analogous 1-butyltin chlorides. In the case of **3**, $^2J(^{13}C,^{119}Sn)$ was even higher than $^3J(^{13}C,^{119}Sn)$ (i.e., opposite to the trend usually observed for 1-butylstannes (Table 3).[11] It is likely that this represents the sum of two scalar coupling pathways contributions − through the co-

Table 3. ^{13}C, ^{17}O, and ^{119}Sn NMR spectral parameters for (3-methoxypropyl)stannanes **1**−**4** in non-coordinating solvent ($CDCl_3$) and in coordinating solvent ([D_6]DMSO) at 300 K

Compound	Solvent	δ(^{13}C) [ppm] (J(^{13}C,^{119}Sn) [Hz])				δ(^{119}Sn)	δ(^{17}O)
		C1	C2	C3	C4	[ppm]	[ppm]
1	$CDCl_3$	4.9 (324.5)	26.7 (18.6)	76.0 (59.3)	58.4 (−)	−4.3	−17.0
	[D_6]DMSO	5.2 (325.3)	26.2 (19.3)	75.2 (52.3)	57.7 (−)	−1.2	−
2	$CDCl_3$	14.7 (434.6)	25.6 (26.5)	74.7 (55.7)	58.5 (−)	49.0	−15.8
	[D_6]DMSO	15.6 (456.5)	25.3 (27.2)	74.3 (65.2)	57.9 (−)	27.4	−
3	$CDCl_3$	26.6 (731.6)	24.5 (42.7)	72.4 (34.0)	58.6 (−)	−108.6	−13.0
	[D_6]DMSO	30.8 (840.4)	24.7 (44.7)	73.0 (95.1)	58.2 (−)	−170.5	−
4	$CDCl_3$	26.0 (845.2)	23.8 (67.0)	70.2 (79.3)	58.5 (−)	−138.5	−3.0
	[D_6]DMSO	[a]	25.6 (62.5)	73.8 (229.6)	57.8 (−)	−445.6	−

[a] Not obtained, probably due to the existence of a dynamic equilibrium (Scheme 4).

Table 4. J(^1H,^{119}Sn) coupling constants for (3-methoxypropyl)stannanes **1**−**4** in $CDCl_3$

Compound	J(^1H,^{119}Sn) [Hz]			
	H1[a]	H2[a]	H3[b]	H4[b]
1	51.2	47.8	[c]	0.52
2'	60.8	86.2	1.31	[d]
3	95.9	195.8	7.73	1.86
4	104.9	254.2	5.07	2.24

[a] Obtained from the ^1H,^{119}Sn HMQC spectra. [b] Obtained by 2D ^1H,^{119}Sn J-HMBC. [c] Not obtained due to an overlap. [d] Not obtained, probably due to the existence of a fast dynamic equilibrium as discussed in the text.

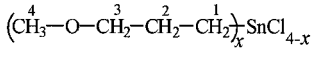

Scheme 3

valent bonds of the 3-methoxypropyl chain and through the coordinative O→Sn bond − of opposite signs in this case. In [D_6]DMSO solution, the values of δ(^{119}Sn) and the coupling constants J(^{13}C,^{119}Sn) of compounds **1**−**4** and their 1-butyltin analogues are not very different.[11] It therefore seems highly probable that the oxastannacycles are cleaved because of an equilibrium in which the donor oxygen atoms of the 3-methoxypropyl substituents are replaced by the stronger Lewis base [D_6]DMSO (Scheme 4). Unfortunately, this dynamic equilibrium disables the measurement of ^1H,^{119}Sn J-HMBC and the determination of long-range J(^1H,^{119}Sn) coupling constants.

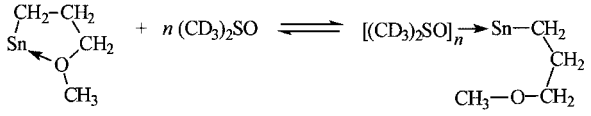

Scheme 4

Trypanocidal and Antitumour Activities

All four (3-methoxypropyl)stannanes **1**−**4** have moderate water solubility (0.6, 3.0, 4.0, and 6.6 g/L H_2O at 25 °C, respectively). For compounds **1**, **2**, and **3**, trypanocidal activity tests afforded MEC values of 24000, 3300, and 3700 nM, respectively. Compound **4** showed no trypanocidal activity. The trypanocidal activity of compounds **2** and **3** is slightly higher than that of bis[3-(2-methoxy)ethoxy]propyltin dichloride and oxide (5900 and 6800 nM, respectively) but is significantly lower than those of the arsenic derivatives Arsobal and Cymelarsan (5 and 0.6 nM, respectively).[7] Compounds **1** and **4** exhibited no antitumour activity (ID_{50} > 62500). For compounds **2** and **3** the ID_{50} values were in the ranges of 1259−2443 and 9200−31512 ng/mL, respectively, and hence markedly below the standard of the clinically used drugs cisplatin (ID_{50} = 169−3269 ng/ml), doxorubicine (ID_{50} = 8−199 ng/mL) and taxol (ID_{50} < 3 ng/mL).

The very low activity and the complete absence of activity observed for compounds **1** and **4** are in accord with the usually low biological activities of tetra- and monoorganotin compounds.[14] The antitumour and trypanocidal activity of (3-methoxypropyl)tin chlorides **2** and **3** are rather poor, but still promising. It can be concluded that the replacement of a 1-butyl substituent by a 3-methoxypropyl moiety can considerably increase the water solubility of organotin derivatives, whereas antitumour and trypanocidal activity is preserved. The substitution of chlorine atoms by moieties that might improve targeting of the parasite and/or tumours could also improve the activity.

Experimental Section

Preparative Techniques and Starting Materials: All reactions were carried out under argon by standard Schlenk techniques.[15] THF was distilled from sodium benzophenone ketyl. Methanol was dried by distillation from CH_3ONa. Tin tetrachloride was distilled prior to use. All other starting compounds were used without further purification.

Preparation of 3-Methoxypropyl Chloride: A solution of CH_3ONa in methanol (5 M, 64 mL, 0.32 mol) was added dropwise over 3 h, with vigorous stirring, to 1-bromo-3-chloropropane (50.0 g, 0.32

mol). The reaction mixture was stirred overnight at room temperature and then heated under reflux as long as the solution remained basic. Afterwards, water (150 mL) was added and the obtained solution was extracted with diethyl ether (3 × 100 mL). The organic layers were combined and dried with Na_2SO_4. The diethyl ether was removed by distillation. Rectification of the residue afforded 3-methoxypropyl chloride (16.2 g, yield 47%) as a colourless liquid, boiling at 110−112 °C. ^{1}H NMR ($CDCl_3$): δ = 2.09 (m, 2 H), 3.42 (s, 3 H), 3.58 (t, $^3J_{H,H}$ = 5.9 Hz, 2 H), 3.70 (t, $^3J_{H,H}$ = 6.5 Hz, 2 H) ppm. ^{13}C NMR ($CDCl_3$): δ = 32.61, 41.82, 58.68, 69.01 ppm.

Preparation of Tetrakis(3-methoxypropyl)tin (1): A solution of 3-methoxypropyl chloride (10.0 g, 0.92 mol) in THF (15 mL) was added to Mg chips (2.2 g, 0.92 mol, activated by I_2). About 10% of the solution was added at once and the reaction was initiated by addition of 2 drops of 1,2-dibromethane. The remaining solution was then added dropwise in such a manner as to maintain the reaction mixture at reflux. The reaction mixture was then heated under reflux for 30 min. After the mixture had then been cooled to −50 °C, neat $SnCl_4$ (5.2 g, 20 mmol) was added dropwise with vigorous stirring. The reaction mixture was left to warm to room temperature and then heated under reflux for 5 h. Water (10 mL) was added and the resulting precipitate was filtered off and washed with benzene. The THF and benzene solutions were combined and dried with Na_2SO_4, and the solvents were removed by rotary evaporation. The residue was distilled at 3−4 Pa, and **1** (7.6 g, yield 92%) was obtained as a colourless liquid, boiling at 120−126 °C. ^{1}H NMR ($CDCl_3$): δ = 0.73 (m, 8 H), 1.69 (m, 8 H), 3.29 (t, $^3J_{H,H}$ = 6.6 Hz, 8 H), 3.31 (s, 12 H) ppm. $C_{16}H_{36}O_4Sn$ (411.14): calcd. C 46.74, H 8.83, Sn 28.87; found C 46.66, H 8.79, Sn 28.43.

Preparation of (3-Methoxypropyl)tin Chlorides 2−4: A mixture of **1** (1.50 g, 1.23 mmol) and $SnCl_4$ [0.32 g, 1.23 mmol for $(CH_3OCH_2CH_2CH_2)_3SnCl$ (**2**); 0.95 g, 3.65 mmol for $(CH_3OCH_2CH_2CH_2)_2SnCl_2$ (**3**); 2.90 g, 11.13 mmol for $CH_3OCH_2CH_2CH_2SnCl_3$ (**4**)] was heated at 200 °C for 3 h. The resulting (3-methoxypropyl)tin chlorides **2**−**4** were purified by vacuum distillation.

Compound 2: 1.73 g, yield 95%, colourless liquid, b.p. 114−116 °C/1−2 Pa. ^{1}H NMR ($CDCl_3$): δ = 1.20 (t, $^3J_{H,H}$ = 7.7 Hz, 8 H), 1.91 (m, 8 H), 3.34 (s, 12 H), 3.39 (t, $^3J_{H,H}$ = 6.1 Hz, 8 H) ppm. $C_{12}H_{27}ClO_3Sn$ (373.48): calcd. C 38.59, H 7.29, Cl 9.49, Sn 31.78; found C 38.65, H 7.31, Cl 9.73, Sn 31.26.

Compound 3: 2.36 g, yield 96%, colourless crystals, b.p. 128−132 °C/7 Pa, m.p. 80−83 °C. ^{1}H NMR ($CDCl_3$): δ = 1.67 (m, 8 H), 2.05 (m, 8 H), 3.44 (s, 12 H), 3.54 (t, $^3J_{H,H}$ = 5.5 Hz, 8 H) ppm. $C_8H_{18}Cl_2O_2Sn$ (335.82): calcd. C 28.61, H 5.40, Cl 21.11, Sn 35.34; found C 28.65, H 5.34, Cl 20.95, Sn 35.67.

Compound 4: 4.22 g, yield 96%, colourless crystals, b.p. 95−100 °C/1 Pa, m.p. 69−71 °C. ^{1}H NMR ($CDCl_3$): δ = 2.11 (m, 8 H), 2.21 (m, 8 H), 3.53 (s, 12 H), 3.61 (t, $^3J_{H,H}$ = 5.5 Hz, 8 H) ppm.

Table 5. Experimental details for the X-ray crystal structure determination of **3** and **4**

	3	**4**
Crystal data		
Empirical formula	$C_8H_{18}Cl_2O_2Sn$	$C_4H_9Cl_3OSn$
Formula mass	335.81	298.15
Crystal system	monoclinic	monoclinic
Space group	$P2_1/c$	$P2_1/n$
Z	4	4
a, b, c [Å]	7.626(1), 15.364(4), 11.499(2)	6.3055(16), 22.325(5), 7.670(2)
β [°]	100.71(2)	113.66(3)
V [Å^3]	1323.7(5)	988.9(4)
D_x [g·cm^{-3}]	1.685	2.003
λ [Å]	0.71073	0.71073
μ (Mo-K_α) [mm^{-1}]	2.307	3.328
Temperature [K]	203(2)	220(1)
F (000)	664	568
Crystal size [mm]	0.24 × 0.24 × 0.21	0.30 × 0.21 × 0.19
Data collection		
Scan range θ [°]	2.24−25.0	3.43−26.00
Index ranges	$-8 \le h \le 8$, $-18 \le k \le 18$, $-13 \le l \le 13$	$-7 \le h \le 7$, $-27 \le k \le 27$, $-9 \le l \le 9$
Reflections collected	9170	13196
Independent reflections	2183 (R_{int} = 0.1329)	1879 (R_{int} = 0.0515)
Reflections observed	1998	1754
Refinement		
Refinement method	Full-matrix, least squares on F^2	Full-matrix, least squares on F^2
Parameters refined	118	110
Goodness-of-fit on F^2	1.105	1.318
Final R indices [$I > 2\sigma(I)$]	$R1$ = 0.0706, $wR2$ = 0.1130	$R1$ = 0.0259, $wR2$ = 0.0607
R indices (all data)	$R1$ = 0.0784, $wR2$ = 0.1198	$R1$ = 0.0291, $wR2$ = 0.0682
$\Delta\rho_{max;}\ \Delta\rho_{min}$ [e·Å^{-3}]	0.711; −0.786	0.569; −0.541

$C_4H_9Cl_3OSn$ (298.16): calcd. C 16.11, H 3.04, Cl 35.67, Sn 39.81; found C 16.16, H 3.10, Cl 36.20, Sn 39.56.

X-ray Diffraction Measurements: Diffraction experiments were carried out with Mo-K_α radiation using a Stoe IPDS diffractometer at 203(2) K (**3**) and 220(1) K (**4**). The structures were successfully solved by direct methods (SHELXS-86).[16] Further refinements were carried out against F^2 (SHELXL-97).[17] All non-H atoms were refined with anisotropic displacement parameters, hydrogen atoms were placed in calculated positions and refined according to the riding model. Crystal data and details of data collection and refinement are given in Table 1, Table 2, and Table 5. CCDC-178265 (**3**) and -178264 (**4**) contain the supplementary crystallographic data for this paper. These data can be obtained free of charge at www.ccdc.cam.ac.uk/conts/retrieving.html or from the Cambridge Crystallographic Data Centre, 12, Union Road, Cambridge CB2 1EZ, UK [Fax: (internat.) + 44-1223/336-033; E-mail: deposit@ccdc.cam.ac.uk].

Microanalyses: Microanalyses (C, H, Sn, Cl) were carried out with a Fison EA 1108 instrument in the Microanalytical Laboratory at the University of Pardubice.

NMR Measurements: ^{1}H, ^{13}C, ^{17}O, and ^{119}Sn NMR spectra were recorded in a 5-mm tuneable probe with a Bruker AMX 360 (^{1}H: 360.14 MHz; ^{13}C: 90.57 MHz; ^{17}O: 48.82 MHz; ^{119}Sn: 134.28 MHz) and a Bruker AVANCE 500 spectrometer (^{1}H: 500.13 MHz; ^{13}C: 125.77 MHz; ^{119}Sn: 186.48 MHz). ^{1}H and ^{13}C chemical shifts are given in ppm with respect to Me_4Si, and ^{119}Sn chemical shifts with respect to Me_4Sn. The gradient-assisted 1D ^{1}H,^{119}Sn HMQC and 2D ^{1}H,^{119}Sn J-HMBC spectra were recorded as explained elsewhere,[10] with the Bruker AVANCE 500 spectrometer. ^{119}Sn CP/MAS NMR spectra were recorded with a Bruker DSX 200 spectrometer equipped with a double-bearing CP/MAS probe at room temperature. The ^{119}Sn chemical shifts were calibrated indirectly with reference to tetracyclohexyltin (δ = −97.35 ppm) and were allocated approximately to the centre of gravity of the signals.

Trypanocidal and Antitumour Screening: The trypanocidal activity tests were carried out in vitro on cultures of *Trypanosoma equiperdum*.[18] The MEC values indicated for these activities correspond to the minimal efficient concentration that would allow complete depletion of trypanosome population within 24 h. In vitro antitumour screening against seven tumoural cell lines of human origin (A, 498 − a renal cancer, EVSA-T − a breast cancer, H 226 − a non-small cell lung cancer, IGROV − an ovarian cancer, M19 − a melanoma, MCF-7 − a breast cancer, WiDr − a colon carcinoma) were performed in accordance with procedures already described elsewhere.[19]

Acknowledgments

The financial support from the Ministry of Education, Youth and Sports of the Czech Republic (Project LN 00 A028) and the Grant Agency of the Czech Republic (grant 203/00920) is gratefully acknowledged. We are grateful to Prof. T. Baltz and Prof. C. Giroud for performing the trypanocidal screening and to Prof. M. Gielen for arranging antitumour screening. T. L. and A. S. thank Prof. Jaroslav Holeček for fruitful discussions about chemistry and life, and all that helped us to finish this paper.

[1] [1a] M. Gielen, *Coord. Chem. Rev.* **1996**, *151*, 41−51. [1b] D. de Vos, R. Willem, M. Gielen, K. E. van Wingerden, K. Nooter, *Met.-Based Drugs* **1998**, *5*, 179 and literature cited therein.
[2] S. V. Barrett, M. P. Barret, *Parasitol. Today* **2000**, *16*, 7−9.
[3] J. Susperregui, A. Petsom, M. Bayle, G. Lain, C. Giroud, T. Baltz, G. Déléris, *Eur. J. Med. Chem.* **1997**, *32*, 123−128.
[4] G. Atassi, *Rev. Silicon, Germanium, Tin Lead Compd.* **1985**, *8*, 219−235.
[5] For example: [5a] M. Gielen, *Main Group Met. Chem.* **1994**, *17*, 6. [5b] M. G. Mirisola, A. Pellerito, T. Fiore, G. C. Stocco, A. Cestelli, I. Di Liegro, *Appl. Organomet. Chem.* **1997**, *11*, 499−511. [5c] M. Kemmer, M. Gielen, M. Biesemans, D. de Vos, R. Willem, *Met.-Based Drugs* **1998**, *5*, 189−196.
[6] J. Susperregui, M. Bayle, J. M. Léger, G. Déléris, M. Biesemans, R. Willem, M. Kemmer, M. Gielen, *J. Organomet. Chem.* **1997**, *545/546*, 559−565.
[7] J. Susperregui, M. Bayle, G. Lain, Ch. Giroud, T. Baltz, G. Déléris, *Eur. J. Med. Chem.* **1999**, *34*, 617−623.
[8] [8a] K. A. Kozeshkow, *Ber. Dtsch. Chem. Ges.* **1933**, *66*, 1661−1665. [8b] W. P Neumann, G. Burkhardt, *Justus Liebigs Ann. Chem.* **1963**, *663*, 11−21.
[9] R. K. Harris, A. Sebald, D. Furiani, G. Tagliavini, *Organometallics* **1988**, *7*, 388−394.
[10] [10a] J. C. Martins, M. Biesemans, R. Willem, *Prog. Nucl. Magn. Reson. Spectrosc.* **2000**, *36*, 271−322. [10b] M. Biesemans, J. C. Martins, R. Willem, A. Lyčka, A. Ružička, J. Holeček, *Magn. Reson. Chem.* **2002**, *40*, 65−69.
[11] [11a] M. Nádvorník, J. Holeček, K. Handlíř, A. Lyčka, *J. Organomet. Chem.* **1984**, *275*, 43−51. [11b] J. Holeček, M. Nádvorník, K. Handlíř, A. Lyčka, *J. Organomet. Chem.* **1986**, *315*, 299−308. [11c] V. Pejchal, J. Holeček, M. Nádvorník, A. Lyčka, *Collect. Czech. Chem. Commun.* **1995**, *60*, 1492−1501.
[12] The C−Sn−C angles in the 3-methoxypopylstannenes **1**−**3** were calculated by use of the equation derived for analogous 1-butyltin compounds (A. Lyčka, J. Holeček, *Inorg. Chim. Acta* **1986**, *118*, L15−L16). This approach can be considered appropriate because the values of slope and intercept for linear dependence of C−Sn−C angle and ^1J(^{119}Sn,^{13}C) are dominantly dependent on the type of hybridisation at the carbon atom. For comparison see also: T. P. Lockhart, W. F. Manders, *Inorg. Chem.* **1986**, *25*, 892−895; J. Holeček, K. Handlíř, M. Nádvorník, A. Lyčka, *Z. Chem.* **1990**, *30*, 265−266.
[13] O. Exner, H. Dahn, P. Pechie, *Magn. Reson. Chem.* **1992**, *30*, 381−386.
[14] J. M. Barnes, L. Magos, *Organomet. Chem. Rev.* **1968**, *3*, 137−150.
[15] S. Herzog, J. Dehnert, *Z. Chem.* **1964**, *4*, 1.
[16] G. M. Sheldrick, *SHELXS-86, A Program for Crystal Structure Solution*, University of Göttingen, Germany, **1986**.
[17] G. M. Sheldrick, *SHELXL-97, A Program for Crystal Structure Refinement*, University of Göttingen, Germany, **1997**.
[18] Z. Q. Zhang, C. Giroud, T. Baltz, *Acta Trop.* **1992**, *50*, 101−110.
[19] [19a] V. T. DeVita Jr., S. Hellman, S. A. Rosenberg, *Cancer: principles and practice of oncology*, 5th ed., Lippincott-Raven Publ., Philadelphia, **1997**. [19b] Y. P. Kepers, G. J. Peters, J. Van Ark-Otte, B. Winograd, H. M. Pinedo, *Eur. J. Cancer* **1991**, *27*, 897−900.

Received June 25, 2002
[I02364]

Synthesis, Crystal Structure, and Photophysical and Magnetic Properties of Dimeric and Polymeric Lanthanide Complexes with Benzoic Acid and Its Derivatives

Alex Wai-Hing Lam,[a] Wing-Tak Wong,*[a,b] Song Gao,[b] Gehui Wen,[c] and Xi-Xiang Zhang[c]

Keywords: Carboxylate ligands / Lanthanides / Luminescence / Magnetic properties

A new family of lanthanide carboxylate complexes with benzoic acid and its derivatives was synthesised and characterised. The structures of the complexes were established by X-ray crystallography, which revealed that various chelating modes of the carboxylate ligands are present on the metal ion, resulting in the formation of dimeric and polymeric skeletons. The photophysical properties of the Eu and Tb complexes were studied: the complexes exhibited sensitised luminescence in the visible spectral region, but the luminescence intensities and lifetimes were very sensitive to quenching by the OH groups of methanol molecules. The solid-state magnetic properties of the Gd and Tb complexes demonstrated the presence of weak antiferromagnetic exchange interactions at very low temperatures, caused by interaction between the neighbouring ions along the chain.

(© Wiley-VCH Verlag GmbH, 69451 Weinheim, Germany, 2003)

Introduction

The design of molecular systems that combine binding abilities and photosensitising properties for the construction of efficient photoluminescent lanthanide complexes continues to be an active area of research. Several classes of ligand have been utilised for the preparation of such complexes; they include cryptands,[1] podands,[2] calixarenes,[3] macrocyclic ligands,[4] β-diketones,[5] carboxylic acid derivatives,[6] terphenyl ligands,[7] and proteins.[8] Most of the complexes investigated emit red or green light (Eu^{3+} and Tb^{3+} luminescence, respectively), but there are also complexes of different Ln^{3+} ions that luminesce in other spectral regions. Efficient luminescent materials may have several applications: as luminescent probes in biomedical assays,[9] as luminescent sensors for chemical species (H^+, O_2, halide ions, OH^-),[4c] and as electroluminescent devices,[10] for example. Besides the quantum yield of the luminescent lanthanide materials, other aspects such as light output, solubility, volatility, and photo-, thermo- and thermodynamic stabilities may be critical to many applications, and must also be controlled.

Variation of the coordination geometries of the central metal atom, and also of the carboxylate ions in the lanthanide carboxylate complexes, are interesting themes of structural chemistry.[11] Over the past twenty years, many structural studies of lanthanide carboxylates have been reported, and diverse coordination types recognised. A large number of lanthanide carboxylate complexes have been found to be dimeric or polymeric.[11a] A one-dimensional system is believed to impose the greatest restriction on metal−metal interaction, and energy migration that depends on such interaction between nearest neighbours in the lattice will thus be dominant in the chain direction. Research studies on polynuclear lanthanide complexes may therefore provide information concerning exchange and magnetic interaction mechanisms. Numerous aromatic carboxylic acids of europium and terbium are chelated in binary or ternary fashion and exhibit high stability and strong luminescence. Tb^{3+} luminescence is enhanced by more than 10^4-fold by dipicolinic acid, and Eu^{3+} luminescence is similarly enhanced by diketonates. The common feature for strong sensitisation is the direct coordination of a conjugated π-electron system to the metal ions. Photoluminescence properties notwithstanding, several studies have demonstrated that luminescent lanthanide complexes have potential for application as emitters in electroluminescent (EL) devices.[12] Kido et al.[13] reported organic electroluminescent devices based on trivalent terbium or europium complexes with β-diketones.

[a] Department of Chemistry, The University of Hong Kong, Pokfulam Road, Hong Kong, P. R. China,
Fax: (internat.) + 852/25472933 or 28571586
[b] PKU-HKU Joint Laboratory on Rare Earth Materials and Bioinorganic Chemistry, Peking University, Beijing 100871, P. R. China
[c] Department of Physics, Hong Kong University of Science and Technology, Clear Water Bay, Kowloon, Hong Kong, P. R. China

Supporting information for this article is available on the WWW under http://www.eurjic.org or from the author.

However, these complexes were limited by their poor photostabilities. As complexes with unlimited polymeric chain structures, lanthanide carboxylates have not only good luminescent properties, but also good ultraviolet absorption properties. Some representative examples of lanthanide carboxylate complexes that can be fabricated as EL devices are $[Tb(AHB)_3]$ (AHBA = 2-amino-4-hexadecylbenzoic acid),[14] $[Tb(MeOBB)_3]$ and $[Eu(MeOBB)_3]$ [MeOBB = 2-(4-methoxybenzoyl)benzoic acid].[15]

In view of the potential applications of lanthanide carboxylates and the fascinating properties of carboxylate ligands, a new series of lanthanide carboxylate complexes (Eu, Gd, and Tb) with benzoic acid and its derivatives were synthesised: $[Ln_2(Bz)_6(MeOH)_4]_n$ (**1a**−**c**), $[Ln(Bz)_3(DMF)]_n$ (**2a**−**c**) (HBz = benzoic acid), $[Ln(cf_3)_3(MeOH)_2]_n$ (**3a**−**c**) (Hcf_3 = 4-trifluoromethylbenzoic acid), $[Ln(ocf_3)_3(MeOH)_2]_n$ (**4a**−**c**) ($Hocf_3$ = 4-trifluoromethoxybenzoic acid), $[Ln(oet)_3(DMF)(H_2O)]_2$ (**5a**−**c**) (Hoet = 4-ethoxybenzoic acid), and $[Ln(opr)_2(NO_3)(MeOH)_2]_n$ (**6a**−**c**) (Hopr = 4-*n*-propoxybenzoic acid). Their structures demonstrate the rich coordination chemistry of lanthanide carboxylate complexes, and the structures of Eu, Gd and Tb complexes with the same ligand are isomorphous. The luminescent and magnetic properties of these lanthanide complexes have also been studied and are discussed.

Results and Discussion

Syntheses and Crystal Structures of Lanthanide Complexes

Treatment of hydrated lanthanide (Eu, Gd, and Tb) nitrates with NaOH and the corresponding benzoic acid ligands in MeOH (1:3:3 ratio) afforded precipitates of the complexes (Scheme 1). The complexation of the lanthanide complexes was confirmed by IR spectroscopy, the absence of ν(COOH) absorption bands of the ligands at about 1700 cm^{-1} in all spectra indicating the coordination of ligands to the metal. All the IR spectra show the presence of absorption bands characteristic of the carboxylate groups. The bands at about 1600−1500 cm^{-1} correspond to the asymmetric vibrations of COO^- groups, while those at about 1450−1350 cm^{-1} are attributable to their symmetric vibrations. Several $\nu(COO^-)_{as}$ bands suggest that different coordination modes of carboxylate groups are present in the complexes, as is confirmed by structural analyses. Complexes with coordinated MeOH molecules exhibited a broad

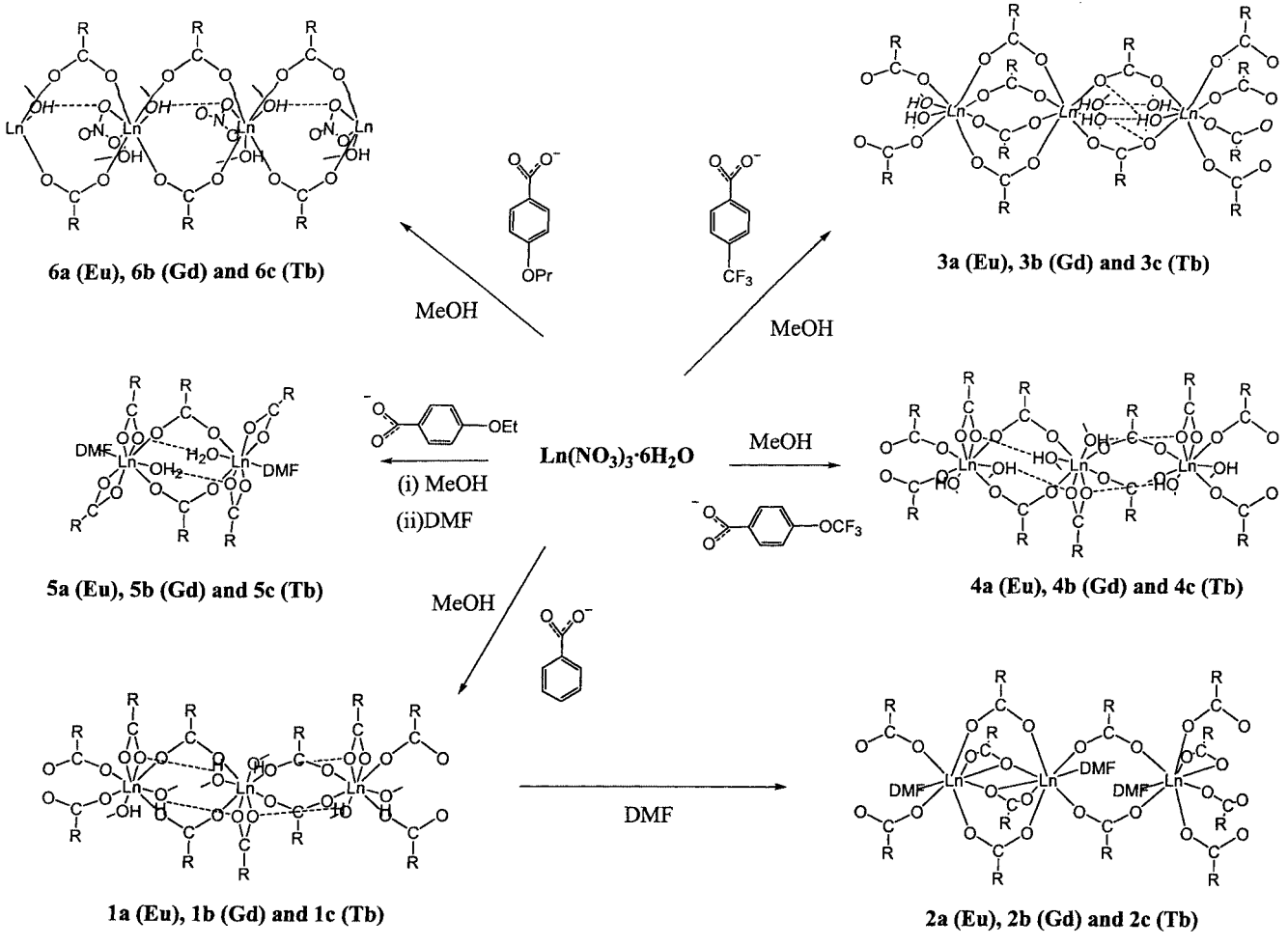

Scheme 1

ν(O−H) band at about 3500 cm^{-1}, and those complexes containing the fluorinated benzoate ligands showed the corresponding ν(C−F) stretching range from 1300 to 1100 cm^{-1}. The presence of absorption bands at about 1660 cm^{-1} is attributable to the ν(C=O) of the DMF molecule, which confirms the successful replacement of MeOH by DMF molecules in complexes **2a**−**c** and **5a**−**c**. According to the ESI-MS studies of the complexes, a series of characteristic peaks were observed, the most intense peaks corresponding to the formulation of anionic fragments being $[LnL_4]^-$ and $[Ln_2L_7]^-$, where L is the respective benzoate ligand. This observation revealed that dimeric or oligomeric complexes would retain their dimeric/oligomeric natures in solution. The thermal decomposition behaviour of the complexes was investigated by a TGA study, although no attempt was made to identify the intermediate products formed during this thermolysis. The first step in the thermogram corresponds to the distinct loss of coordinated solvent molecules [MeOH (ca. 30−120 °C) or DMF (ca. 100−160 °C)], in line with their X-ray crystallographic results. The total weight losses are compatible with the formulas, and the masses of the final products correspond to the complete combustion of the complexes to their corresponding oxides (Eu_2O_3, Gd_2O_3, Tb_2O_3, or Tb_4O_7) at 900 °C.

Single crystals of complexes **1a**−**c**, **2a**−**c**, **3a**, **3c**, **4a**−**c**, **5b**, **5c**, and **6c** were obtained by slow evaporation of their corresponding solvents for a period of time, and their structures were established by X-ray crystallography. Structures of complexes (Eu, Gd, and Tb) with a particular ligand are isostructural, so a detailed structural description of the complexes is exemplified by one of them.

The polymeric structure of complex **1a** is displayed in Figure 1, and selected bond lengths and bond angles are given in Table 1. This analysis revealed that there are two independent and distinct Eu^{3+} ions, bridged through four ligand carboxylate groups to form an infinite chain along the *a* axis. Each Eu^{3+} ion is coordinated by two O atoms from a bidentate chelating carboxylate group, four from four different ligands in a bridging mode, and two O atoms from two methanol molecules. Along the chain, the metal−metal distances and angle are: Eu(1)···Eu(2) = 4.90 Å, Eu(1)···Eu(2*) = 4.93 Å and Eu(2*)−Eu(1)−Eu(2) = 165.7°. The coordination geometry around the Eu(1) atom can be described as a distorted square antiprism, in which the top square face is defined by O(2), O(4), O(5), and O(14), and the bottom one is formed by O(6), O(7), O(9), and O(13). The dihedral angle between the square faces is 9.16°. Meanwhile, the geometry of the Eu(1) atom can also be described as a distorted bicapped trigonal prism, in which the top plane is defined by O(2), O(5), and O(7), and the bottom plane is completed by O(4), O(9), and O(14). The O(6) and O(13) atoms cap two quadrilateral faces of the trigonal prism. The dihedral angle between the planes is 10.35°. This observation of coordination polyhedra also applies for the Eu(2) atom, which can be described as a distorted square antiprism or a bicapped trigonal prism. The dihedral angles between the square and the trigonal planes are 8.55 and 12.17°, respectively. The Eu−O bond lengths range from 2.309(6) to 2.535(6) Å for both Eu^{3+} ions. The Eu−O(CO) carboxylate bond lengths of the bidentate chelating species [2.468(6)−2.527(6) Å] are longer than those of the bridging one [2.309(6)−2.367(6) Å], due to the formation of an unstable four-membered ring.[16] The Eu−O(MeOH) distances range from 2.496(6) to 2.537(6) Å. Intra-chain hydrogen bonding is observed between the methanol H atoms and the carboxylate O atoms [O(13)···O(11) = 2.72 Å, O(14)···O(12*) = 2.83 Å, O(15)···O(5*) = 2.76 Å, O(16)···O(6) = 2.82 Å]. Although the methanol H atoms could not be located, an analysis of the spatial relationships of the proximal potential donors and acceptors indicated an unambiguous pattern for the hydrogen bonding interactions. This type of coordination mode of ligands has been observed in the complex $\{[Eu(\alpha\text{-}C_5H_3O_3)_3(H_2O)_2]\cdot NO_3(4,4'\text{-Hbpy})\}_n$.[17]

A perspective view of the polymeric structure of complex **2a** is shown in Figure 2 and selected bond lengths and bond angles are summarised in Table 2. The structure demonstrates that each Eu^{3+} ion is connected to two neighbouring ones by six ligands through the carboxylate groups, to form an endless polymer. The carboxylate groups of the six molecules of benzoate are bidentate bridging and tridentate chelating-bridging. Four of the six carboxylate groups simultaneously bridge two Eu^{3+} ions, while the other two carboxylate groups chelate one Eu^{3+} ion and at the same time bridge two Eu^{3+} ions. Each Eu^{3+} ion is further coordinated to one DMF molecule to form eight-coordinate metal ions. The intra-chain Eu···Eu distances within the structure are Eu(1)···Eu(1*) = 3.93 Å and Eu(1)···Eu(1′) = 5.34 Å. The angle Eu(1′)−Eu(1)−Eu(1*) is 169.5°, and we can regard this as a linear chain along the *c* axis. The alternating metal−metal distances along the chain can be explained by the chelating-bridging carboxylate groups linking the Eu^{3+} ions, which result in shorter Eu···Eu distances than seen in other polymeric lanthanide carboxylates.[18] In addition, the larger steric effect of DMF relative to MeOH may cause the lengthening of the Eu···Eu distances; a similar observation has been noted in the Eu^{3+} complex with *N*-methylglycine.[19] The Eu−O(CO) bond lengths of bidentate bridging carboxylate groups [2.306(3)−2.403(3) Å] are smaller than those of the tridentate chelating-bridging moieties [2.333(3)−2.580(3) Å].

A crystal of complex **3a** suitable for X-ray analysis was sealed in a capillary and the molecular structure was established by X-ray crystallography. As illustrated in Figure 3, the Eu^{3+} ion in complex **3a** is coordinated by eight oxygen atoms, six of which [O(1), O(2), O(3), O(4*), O(5), and O(6)] are from six different carboxylate groups, while the other two [O(7) and O(8)] are from two coordinated methanol molecules. The Eu(1) atom is connected to two neighbouring Eu atoms [Eu(1′), Eu(1*)] alternatively by two bridging carboxylate groups and by four bridging carboxylate groups, to form an infinite one-dimensional chain along the *a* axis. Thus, along the chain, the Eu···Eu distances in the complex are alternatively long [Eu(1)···Eu(1′) = 5.42 Å] and short [Eu(1)···Eu(1*) = 4.19 Å]. With the alternating Eu···Eu distances and the chain

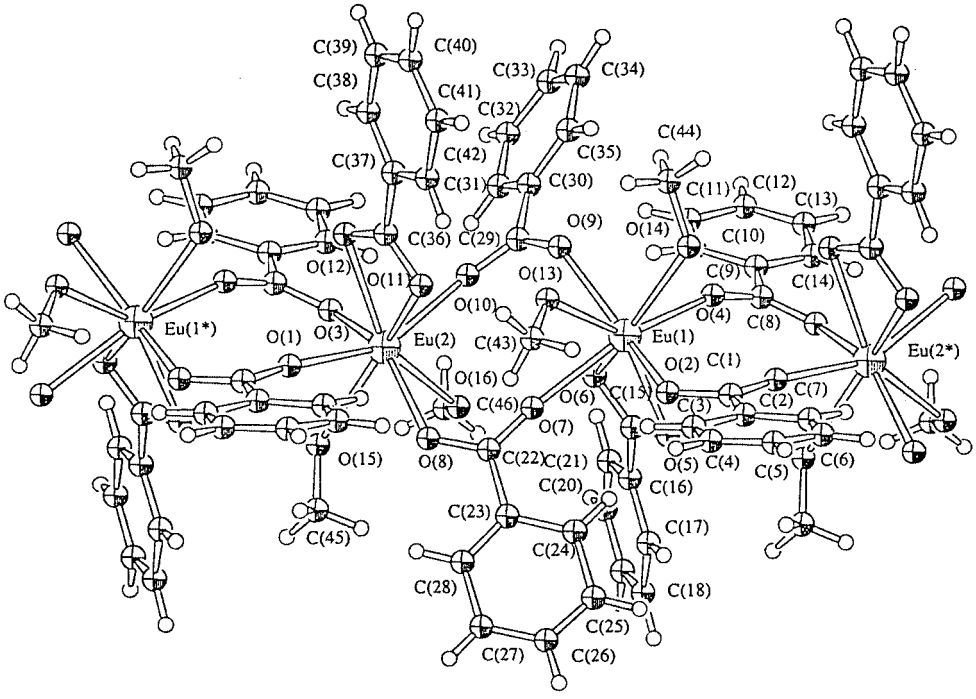

Figure 1. Polymeric structure of $[Eu_2(Bz)_6(MeOH)_4]_n$ (**1a**) with the atomic numbering scheme for non-hydrogen atoms

Table 1. Selected bond lengths [Å] and bond angles [°] for complexes **1a**−**c**

1a		**1b**		**1c**	
Eu(1)···Eu(2)	4.90	Gd(1)···Gd(2)	4.89	Tb(1)···Tb(2)	4.88
Eu(1)···Eu(2*)	4.93	Gd(1)···Gd(2*)	4.92	Tb(1)···Tb(2*)	4.91
Eu(1)−O(2)	2.344(6)	Gd(1)−O(2)	2.326(6)	Tb(1)−O(2)	2.30(1)
Eu(1)−O(4)	2.320(6)	Gd(1)−O(4)	2.297(7)	Tb(1)−O(4)	2.30(1)
Eu(1)−O(5)	2.476(6)	Gd(1)−O(5)	2.506(7)	Tb(1)−O(5)	2.43(1)
Eu(1)−O(6)	2.510(6)	Gd(1)−O(6)	2.476(7)	Tb(1)−O(6)	2.48(1)
Eu(1)−O(7)	2.333(6)	Gd(1)−O(7)	2.355(7)	Tb(1)−O(7)	2.28(1)
Eu(1)−O(9)	2.309(6)	Gd(1)−O(9)	2.305(7)	Tb(1)−O(9)	2.29(1)
Eu(1)−O(13)	2.523(6)	Gd(1)−O(13)	2.516(7)	Tb(1)−O(13)	2.49(1)
Eu(1)−O(14)	2.496(6)	Gd(1)−O(14)	2.481(7)	Tb(1)−O(14)	2.46(1)
Eu(2)−O(1)	2.314(6)	Gd(2)−O(1)	2.377(7)	Tb(2)−O(1*)	2.28(1)
Eu(2)−O(3)	2.315(6)	Gd(2)−O(3)	2.336(7)	Tb(2)−O(3*)	2.29(1)
Eu(2)−O(8)	2.367(6)	Gd(2)−O(8)	2.316(6)	Tb(2)−O(8)	2.32(1)
Eu(2)−O(10)	2.348(6)	Gd(2)−O(10)	2.323(7)	Tb(2)−O(10)	2.32(1)
Eu(2)−O(11)	2.468(6)	Gd(2)−O(11)	2.491(8)	Tb(2)−O(11)	2.42(1)
Eu(2)−O(12)	2.527(6)	Gd(2)−O(12)	2.455(7)	Tb(2)−O(12)	2.48(1)
Eu(2)−O(15)	2.535(6)	Gd(2)−O(15)	2.494(7)	Tb(2)−O(15)	2.50(1)
Eu(2)−O(16)	2.507(6)	Gd(2)−O(16)	2.517(7)	Tb(2)−O(16)	2.49(1)
O(13)···O(11)	2.72	O(13)···O(12*)	2.74	O(13)···O(11)	2.73
O(14)···O(12*)	2.83	O(14)···O(11)	2.87	O(14)···O(12*)	2.88
O(15)···O(5*)	2.76	O(15)···O(5*)	2.83	O(15)···O(5*)	2.76
O(16)···O(6)	2.82	O(16)···O(6)	2.76	O(16)···O(6)	2.82
Eu(2*)−Eu(1)−Eu(2)	165.7	Gd(2*)−Gd(1)−Gd(2)	165.8	Tb(2*)−Tb(1)−Tb(2)	166.2

angle [Eu(1′)−Eu(1)−Eu(1*) = 158.4°], the carboxylate linked one-dimensional array can be best described as a linear chain. Intra-chain hydrogen bonding is observed between the doubly bridged Eu(1)···Eu(1′) unit, arising from a coordinated methanol H atom and carboxylate O atoms [O(8)−H(20)···O(1*) = 2.22 Å and O(8)−H(20)···O(7*) = 2.20 Å, respectively]. The single coordination mode may be accounted for by the presence of a bulky CF_3 group. This matches well with the results reported by Tahir et al.[20] for a cerium 3,5-dinitrobenzoate dihydrate complex $[Ce_2(C_7H_3N_2O_6)_6(H_2O)_4]_n$. The outer sphere in each repeating unit of $[Eu(cf_3)_3(MeOH)_2]$ contains one solvated methanol molecule. Two CF_3 groups of the ligands are disordered in the monomeric unit. Like those in complexes **1a**−**c**, the coor-

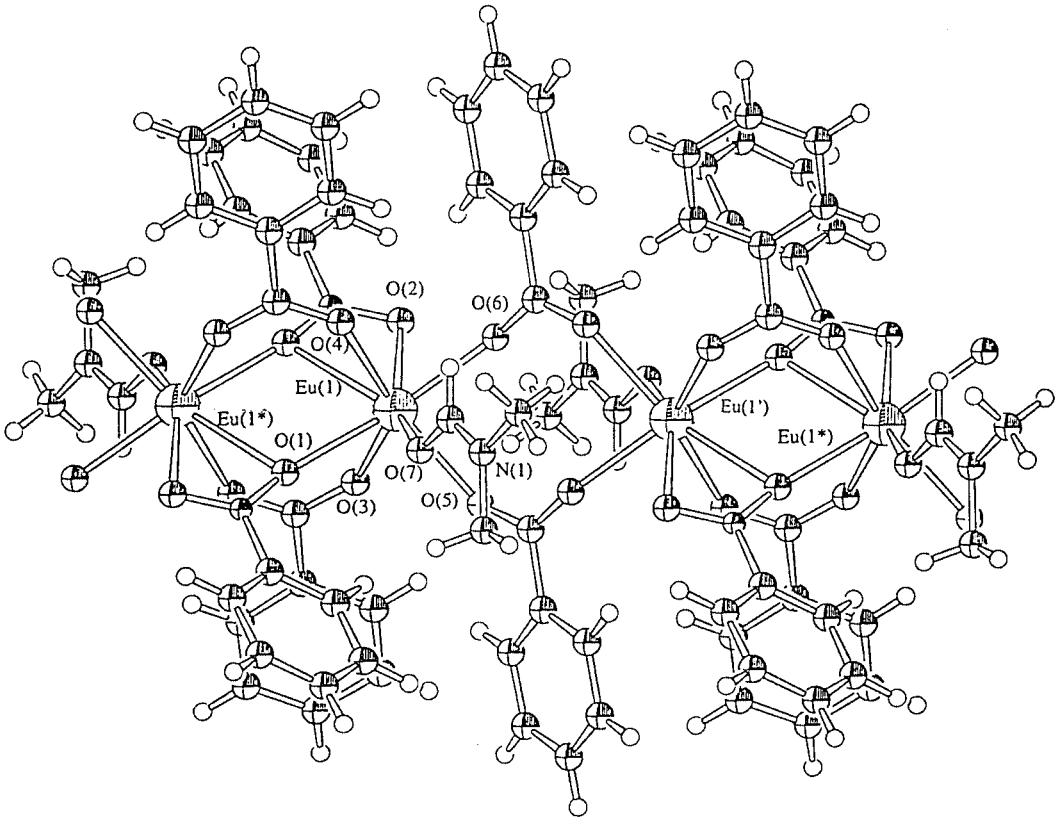

Figure 2. Polymeric structure of $[Eu(Bz)_3(DMF)]_n$ (**2a**) with the atomic numbering scheme for Eu and O atoms

Table 2. Selected bond lengths [Å] and bond angles [°] for complexes **2a−c**

2a		**2b**		**2c**	
Eu(1)···Eu(1*)	3.93	Gd(1)···Gd(1*)	3.91	Tb(1)···Tb(1*)	3.90
Eu(1)···Eu(1′)	5.34	Gd(1)···Gd(1′)	5.33	Tb(1)···Tb(1′)	5.33
Eu(1)−O(1)	2.333(3)	Gd(1)−O(1)	2.325(2)	Tb(1)−O(1)	2.30(2)
Eu(1)−O(1*)	2.580(3)	Gd(1)−O(1*)	2.579(2)	Tb(1)−O(1*)	2.52(2)
Eu(1)−O(2)	2.513(3)	Gd(1)−O(2*)	2.492(2)	Tb(1)−O(2*)	2.48(2)
Eu(1)−O(3)	2.403(3)	Gd(1)−O(3)	2.395(2)	Tb(1)−O(3)	2.38(2)
Eu(1)−O(4)	2.382(3)	Gd(1)−O(4)	2.371(2)	Tb(1)−O(4)	2.41(2)
Eu(1)−O(5)	2.354(3)	Gd(1)−O(5)	2.349(2)	Tb(1)−O(5)	2.28(2)
Eu(1)−O(6)	2.306(3)	Gd(1)−O(6)	2.299(2)	Tb(1)−O(6)	2.28(2)
Eu(1)−O(7)	2.422(3)	Gd(1)−O(7)	2.415(2)	Tb(1)−O(7)	2.31(2)
Eu(1′)−Eu(1)−Eu(1*)	169.5	Gd(1′)−Gd(1)−Gd(1*)	169.6	Tb(1′)−Tb(1)−Tb(1*)	169.6

dination polyhedron of complex **3a** can best be described as either a distorted square antiprism or a bicapped trigonal prism, with the dihedral angles between the corresponding planes being 3.78 and 7.10°, respectively. For the square antiprism geometry, the top square plane is defined by O(1), O(2), O(7), and O(8), and the bottom plane is completed by O(3), O(4*), O(5), and O(6). For the distorted bicapped trigonal geometry the top plane is formed by O(1), O(3), and O(5), and the bottom plane is composed of O(2), O(4*), and O(6), while the O(7) and O(8) atoms cap two quadrilateral faces of the trigonal prism. The Eu−O(CO) distances [2.360(5)−2.446(4) Å] and the Eu−O(MeOH) distances [2.521(5)−2.600(5) Å] are similar to those in complex **1a**. Table 3 summarises selected bond lengths and bond angles in complexes **3a** and **3c**.

The coordination geometry of the carboxylate ligands in complexes **4a−c** is similar to that in the lanthanide benzoate complexes **1a−c**. A perspective drawing of complex **4a** is illustrated in Figure 4, and selected bond lengths and bond angles are shown in Table 4. Each Eu^{3+} ion is connected to two neighbouring ones through four bridging carboxylate groups to form an infinite one-dimensional chain along the *a* axis. The coordination sphere is completed by a bidentate chelating carboxylate group and two

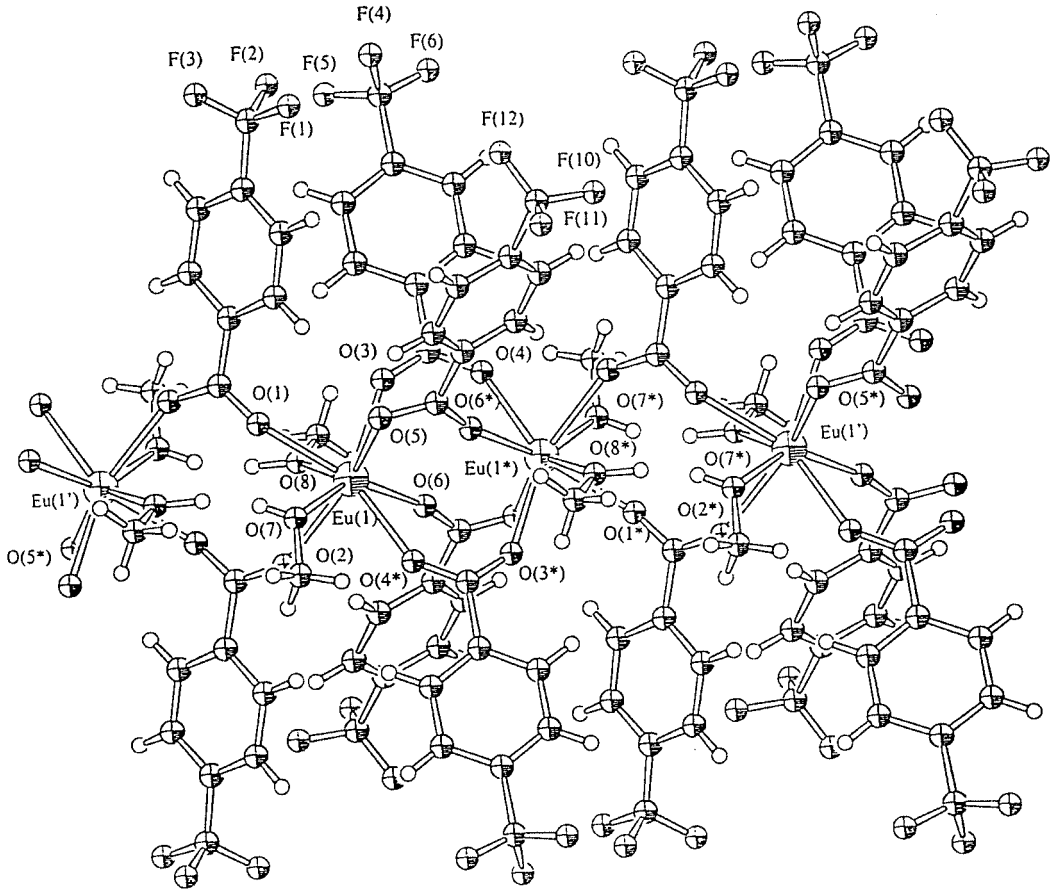

Figure 3. Polymeric structure of $[Eu(cf_3)_3(MeOH)_2]_n$ (**3a**) with the atomic numbering scheme for Eu, F and O atoms

Table 3. Selected bond lengths [Å] and bond angles [°] for complexes **3a** and **3c**

3a		**3c**	
Eu(1)−Eu(1*)	4.19	Tb(1)−Tb(1*)	4.21
Eu(1)−Eu(1′)	5.42	Tb(1)−Tb(1′)	5.37
Eu(1)−O(1)	2.362(4)	Tb(1)−O(1)	2.335(2)
Eu(1)−O(2)	2.378(4)	Tb(1)−O(2)	2.345(2)
Eu(1)−O(3)	2.363(4)	Tb(1)−O(3)	2.339(3)
Eu(1)−O(4*)	2.369(4)	Tb(1)−O(4*)	2.346(3)
Eu(1)−O(5)	2.446(4)	Tb(1)−O(5)	2.418(3)
Eu(1)−O(6)	2.360(5)	Tb(1)−O(6)	2.325(3)
Eu(1)−O(7)	2.600(5)	Tb(1)−O(7)	2.591(3)
Eu(1)−O(8)	2.521(5)	Tb(1)−O(8)	2.515(3)
O(8)−H(20)···O(1*)	2.22	O(8)−H(20)···O(1*)	2.27
O(8)−H(20)···O(7*)	2.20	O(8)−H(20)···O(7*)	2.30
Eu(1′)−Eu(1)−Eu(1*)	158.4	Tb(1′)−Tb(1)−Tb(1*)	159.1

methanol molecules. An intra-chain hydrogen bond between the coordinated methanol H atoms and chelating carboxylate O atoms is observed [O(10)−H(14)···O(5*) = 1.82 Å] and [O(11)−H(13)···O(4*) = 2.47 Å]. Along the infinite chain, the Eu···Eu distances in complex **4a** are alternatively long [Eu(1)···Eu(1′) = 5.03 Å] and short [Eu(1)···Eu(1*) = 4.86 Å]. With the alternating Eu···Eu distances and the chain angle [Eu(1′)−Eu(1)−Eu(1*) = 159.3°], the carboxylate-linked one-dimensional array can best be described as a linear chain. The difference between the alternating metal−metal distances is smaller than in complex **2a**, because the bridging unit in **4a** is made up of the same number of ligands and coordinating modes. However, this coordination geometry should not cause such a difference in the metal−metal distances along the chain. This can be explained by studying the molecular structure, in which the orientations of the carboxylate ligands align in the same direction in the alternating monomeric unit. Increased steric hindrance in that unit would result in a slightly longer metal−metal distance. Similarly to that in complex **3a**, the coordination geometry about the Eu(1) atom may be described either as a distorted square antiprism or as a bicapped trigonal prism. The square planes formed around the Eu(1) atom by O(1*)−O(2)−O(4)−O(11) and O(5)−O(7)−O(8)−O(10) adopt a distorted square antiprism geometry, with the dihedral angle between these planes being 11.74°. Meanwhile, the geometry of the distorted bicapped trigonal prism is made up of the top plane [O(1*)−O(4)−O(8)] and the bottom plane [O(2)−O(7)−O(11)], while the quadrilateral faces of the trigonal prism are capped by atoms O(5) and O(10). The dihedral angle between the planes is 16.46°. The

Eu−O(CO) bond lengths of the chelating and bridging carboxylate groups are 2.513(5)−2.532(7) Å and 2.296(6)−2.369(6) Å, respectively, while the Eu−O(MeOH) distances are 2.486(6) and 2.541(6) Å. These Eu−O bond lengths fall in the usual range of other known lanthanide carboxylates.[18a,18b]

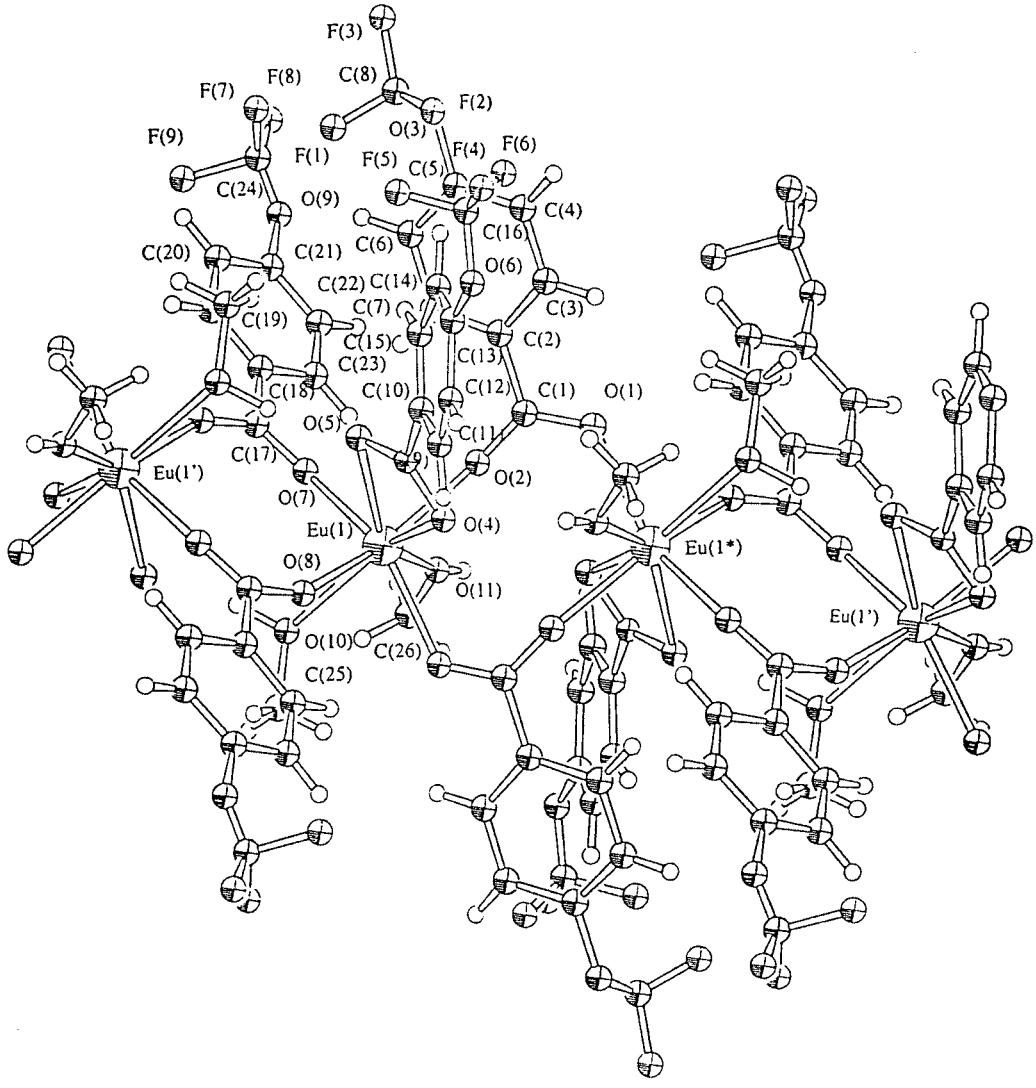

Figure 4. Polymeric structure of $[Eu(ocf_3)_3(MeOH)_2]_n$ (**4a**) with the atomic numbering scheme for non-hydrogen atoms

Table 4. Selected bond lengths [Å] and bond angles [°] for complexes **4a−c**

4a		**4b**		**4c**	
Eu(1)···Eu(1*)	4.86	Gd(1)···Gd(1*)	4.86	Tb(1)···Tb(1*)	4.79
Eu(1)···Eu(1′)	5.03	Gd(1)···Gd(1′)	5.00	Tb(1)···Tb(1′)	5.05
Eu(1)−O(1*)	2.369(6)	Gd(1)−O(1)	2.326(4)	Tb(1)−O(1)	2.394(3)
Eu(1)−O(2)	2.337(6)	Gd(1)−O(2*)	2.341(4)	Tb(1)−O(2*)	2.229(3)
Eu(1)−O(4)	2.532(7)	Gd(1)−O(4)	2.526(4)	Tb(1)−O(4)	2.363(3)
Eu(1)−O(5)	2.513(5)	Gd(1)−O(5)	2.488(4)	Tb(1)−O(5)	2.925(3)
Eu(1)−O(7)	2.296(6)	Gd(1)−O(7)	2.311(4)	Tb(1)−O(7)	2.025(3)
Eu(1)−O(8)	2.319(6)	Gd(1)−O(8*)	2.289(5)	Tb(1)−O(8)	2.621(3)
Eu(1)−O(10)	2.541(6)	Gd(1)−O(10)	2.503(4)	Tb(1)−O(10)	2.236(4)
Eu(1)−O(11)	2.486(6)	Gd(1)−O(11)	2.475(5)	Tb(1)−O(11)	2.757(4)
O(10)−H(14)···O(5*)	1.82	O(10)−H(19)···O(5*)	1.87	O(10)−H(20)···O(5*)	2.23
O(11)−H(13)···O(4*)	2.47	O(11)−H(20)···O(4*)	1.85	O(11)−H(13)···O(4*)	1.86
Eu(1′)−Eu(1)−Eu(1*)	159.3	Gd(1′)−Gd(1)−Gd(1*)	159.3	Tb(1′)−Tb(1)−Tb(1*)	159.0

The molecular structure of complex **5b** was established by X-ray crystallography, and the polymeric structure of the complex is depicted in Figure 5. Selected bond lengths are given in Table 5. The structure consists of an asymmetric dimer in which Gd^{3+} ions, in non-equivalent positions, are connected by two ligands through the carboxylate groups. These two carboxylate groups are bidentate bridging, and bind to two Gd^{3+} ions simultaneously. Each Gd^{3+} ion is further coordinated to two bidentate chelating carboxylate groups, one water molecule and one dimethylformamide (DMF) to form eight-coordinate metal ions. Furthermore, intramolecular hydrogen bonding interaction links the two Gd^{3+} ions through the coordinated water H atom and carboxylate O atom of the ligands [O(21)−H(72)···O(13) = 2.35 Å and O(22)−H(70)···O(2) = 1.75 Å]. The Gd···Gd distance is 4.46 Å, longer than that in the Gd^{3+} complex $[Gd(C_3H_5O_2)_3(H_2O)_2]_2{\cdot}4H_2O{\cdot}2(CH_4N_2S)$[21] because of the larger steric effect from the ethoxybenzoate ligand. The coordination polyhedron of the Gd(1) atom can be described either as a distorted bicapped trigonal prism or as a square antiprism. In the bicapped trigonal prism description, the top plane is formed by O(2), O(4), and O(7), and the bottom plane is completed by O(10), O(19), and O(21), while the quadrilateral faces of the trigonal prism [O(2)−O(4)−O(10)−O(19) and O(4)−O(7)−O(19)−O(21)] are capped by O(1) and O(5), respectively. The dihedral angle between the trigonal faces is 5.50°. Besides this description, it can also be treated as a distorted square antiprism. One square face is defined by O(1), O(4), O(5), and O(19), whereas the other face is completed by O(2), O(7), O(10), and O(21). The dihedral angle between the square faces is 7.60° and the Gd(1)−O bond lengths range from 2.333(5) to 2.541(5) Å. The Gd(1)−O distances for the chelating carboxylate groups [2.414(5)−2.541(5) Å] are significantly longer than those of the bridging carboxylate groups [2.333(5)−2.359(6) Å], since lengthening of the chelating carboxylate group is caused by the formation of an unstable four-membered chelate ring with the Gd^{3+} ion. In addition,

Table 5. Selected bond lengths [Å] for complexes **5a** and **5b**

5a		**5b**	
Gd(1)···Gd(2)	4.46	Tb(1)···Tb(2)	4.50
Gd(1)−O(1)	2.463(5)	Tb(1)−O(1)	2.444(5)
Gd(1)−O(2)	2.414(5)	Tb(1)−O(2)	2.427(4)
Gd(1)−O(4)	2.422(5)	Tb(1)−O(4)	2.391(6)
Gd(1)−O(5)	2.541(5)	Tb(1)−O(5)	2.511(5)
Gd(1)−O(7)	2.359(6)	Tb(1)−O(7)	2.341(6)
Gd(1)−O(10)	2.333(5)	Tb(1)−O(10)	2.320(5)
Gd(1)−O(19)	2.368(6)	Tb(1)−O(19)	2.310(6)
Gd(1)−O(21)	2.408(5)	Tb(1)−O(21)	2.395(5)
Gd(2)−O(8)	2.326(5)	Tb(2)−O(8)	2.283(6)
Gd(2)−O(11)	2.365(6)	Tb(2)−O(11)	2.340(6)
Gd(2)−O(13)	2.453(5)	Tb(2)−O(13)	2.447(6)
Gd(2)−O(14)	2.473(6)	Tb(2)−O(14)	2.406(4)
Gd(2)−O(16)	2.532(5)	Tb(2)−O(16)	2.530(5)
Gd(2)−O(17)	2.418(5)	Tb(2)−O(17)	2.394(6)
Gd(2)−O(20)	2.342(5)	Tb(2)−O(20)	2.378(5)
Gd(2)−O(22)	2.410(5)	Tb(2)−O(22)	2.395(5)
O(21)−H(72)···O(13)	2.35	O(21)−H(57)···O(14)	1.79
O(22)−H(70)···O(2)	1.75	O(22)−H(58)···O(2)	2.01

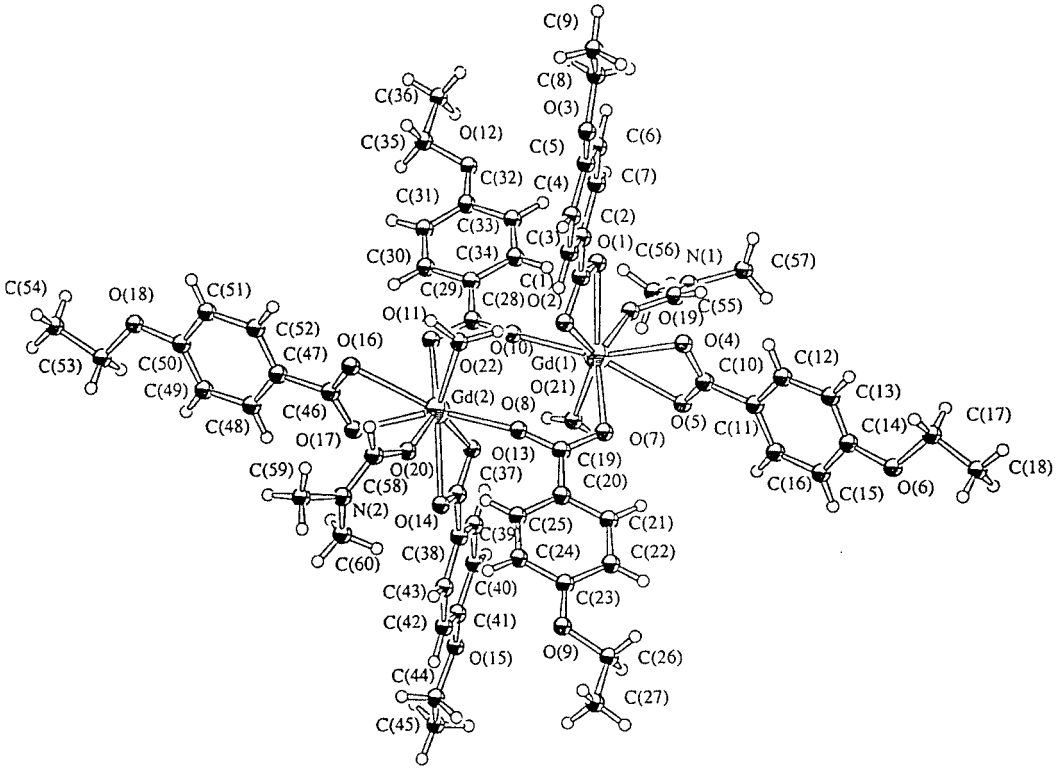

Figure 5. Molecular structure of $[Gd(oet)_3(DMF)(H_2O)]_2$ (**5b**) with the atomic numbering scheme for non-hydrogen atoms

the description of the coordination sphere around the Gd(2) atom is similar to that of Gd(1). The distorted bicapped trigonal prism consists of the top plane [O(11)−O(13)−O(17)] and the bottom plane [O(8)−O(20)−O(22)], with a dihedral angle of 5.74° between them. For the distorted square antiprism, the defining planes are made up by O(8)−O(11)−O(13)−O(22) and O(14)−O(16)−O(17)−O(20), with a dihedral angle of 6.25°. The Gd(2)−O distances [2.326(5)−2.532(5) Å] are close to the value of the Gd(1)−O distances, and the Gd(2)−O distances of chelating carboxylate [2.418(5)−2.532(5) Å] are longer than those of the bridging carboxylate [2.326(5)−2.365(6) Å], which are consistent with the Gd(1) values.

The molecular structure of complex **6c** is shown in Figure 6, and selected bond lengths and bond angles are tabulated in Table 6. The Tb^{3+} ion is connected to two neighbouring metal ions through four bidentate bridging carboxylate ligands to form an infinite chain along the *c* axis, and it is coordinated by eight oxygen atoms: four from carboxylate ligands, two from a nitrate ion and two from the methanol molecules. Along the chain, the Tb···Tb distance is 5.35 Å and the Tb(1*)−Tb(1)−Tb(1*) angle is 173.6°, and the structure of the complex can thus be de-

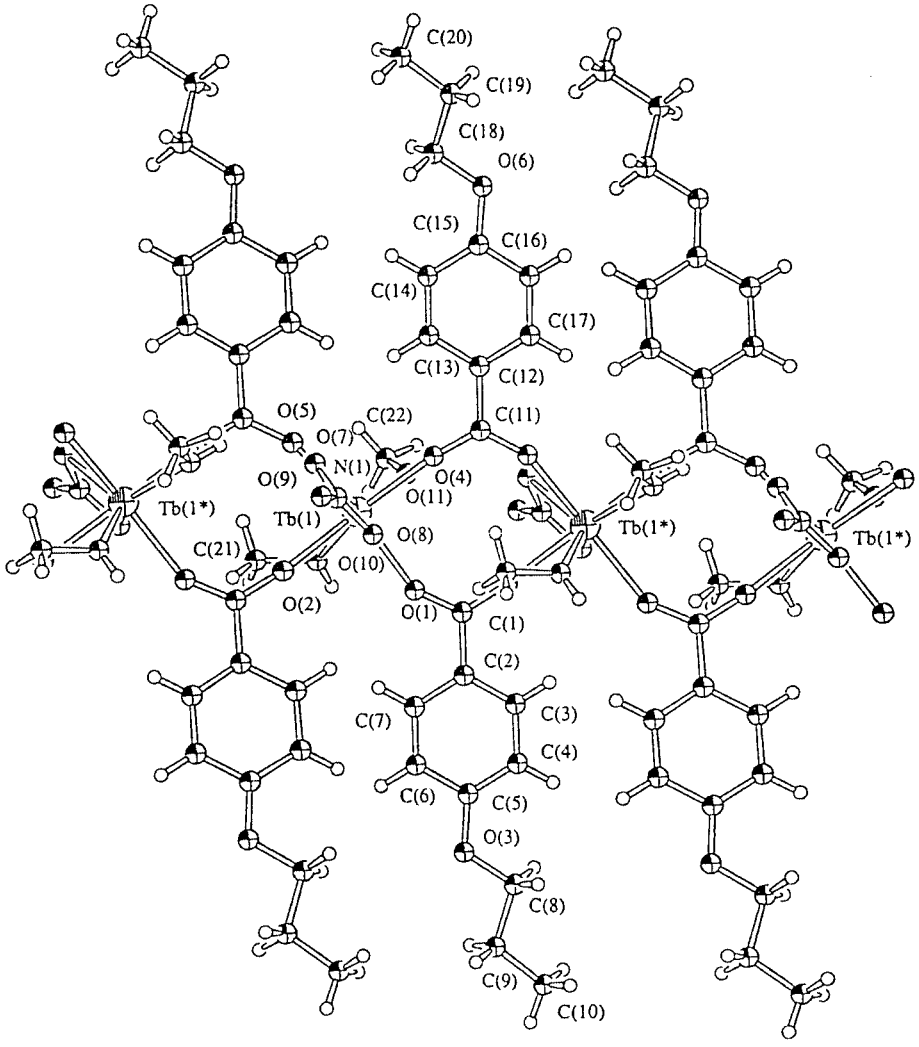

Figure 6. Molecular structure of $[Tb(opr)_2(NO_3)(MeOH)_2]_n$ (**6c**) with the atomic numbering scheme for non-hydrogen atoms

Table 6. Selected bond lengths [Å] and bond angles [°] for complex **6c**

			6c		
Tb(1)···Tb(1*)	5.35	Tb(1)−O(7)	2.521(4)	N(1)−O(8)	1.256(7)
Tb(1)−O(1)	2.273(4)	Tb(1)−O(8)	2.564(4)	N(1)−O(9)	1.234(7)
Tb(1)−O(2)	2.282(4)	Tb(1)−O(10)	2.413(4)	O(11)−H(30)···O(7*)	2.19
Tb(1)−O(4)	2.288(4)	Tb(1)−O(11)	2.474(4)		
Tb(1)−O(5)	2.277(4)	N(1)−O(7)	1.255(6)	Tb(1*)−Tb(1)−Tb(1*)	173.6

scribed as a linear chain skeleton. Intra-chain hydrogen bonding was observed between the coordinated methanol H atom and the O atom of the coordinated nitrate [O(11)−H(30)···O(7*) = 2.19 Å]. The coordination polyhedron around the Tb^{3+} ion can be described both as a distorted square antiprism and as a bicapped trigonal prism. It is hard to distinguish the polyhedron from these two typical coordination geometries, so both are illustrated here. For the distorted square antiprism geometry, the top square plane can be defined by O(1), O(2), O(8), and O(10), whereas the bottom plane is completed by O(4), O(5), O(7), and O(11). The dihedral angle between these two planes is 12.33°. For the distorted bicapped trigonal prism, on the other hand, the top plane is defined by O(1), O(4), and O(11), and the bottom plane is formed by O(2), O(5), and O(7), while O(8) and O(10) cap the quadrilateral faces of the trigonal prisms O(1)−O(2)−O(4)−O(7) and O(1)−O(2)−O(5)−O(11), respectively. The dihedral angle between the trigonal planes is 5.93°. The Tb−O(CO), Tb−O(NO_2), and Tb−O(MeOH) distances are 2.273(4)−2.288(4) Å, 2.521(4)−2.564(4) Å, and 2.413(4)−2.474(4) Å, respectively. The significant differences between the N−O bond lengths [1.234(7), 1.255(6), and 1.258(7) Å] indicate that the nitrate ion is bonded to the metal ion in a bidentate mode, as is evident from the IR spectra. Only two ligands are coordinated to the metal ion instead of the three in the previously described lanthanide carboxylates, and this is believed to be caused by steric hindrance by the propoxy groups, which prevents another ligand from coordinating to the metal to result in a longer metal−metal distance. An interesting feature of this complex is the propoxy groups on the benzoate ligands "bobbing up and down" along the chain.

Photophysical Properties

All complexes are soluble in hot MeOH or DMF solution, the improved solubility of the complexes being due to the *para*-substituted alkoxy and fluorinated groups. Consequently, the photophysical investigations were mainly carried out in MeOH solution, and solid-state luminescence was also studied.

Both the solid-state and the solution-state excitation spectra of the europium and terbium complexes match the corresponding electronic absorption profiles of the respective ligands throughout the UV spectral region, showing that ligand-to-metal energy transfer occurs. In addition, the absence of observable *f-f* absorption transitions in the excitation spectra reveals that the sensitisation process is favoured by indirect excitation. Excitation of the ligand-centred (LC) absorption bands results in the well-known narrow emission bands of the Eu^{3+} and Tb^{3+} ions, and their emission spectra are essentially identical in the solid state and in the solution state. Europium complex **1a** emits red light upon LC excitation, originating from the $^5D_0 \rightarrow {}^7F_n$ (n = 0, 1, 2, 3, 4) transitions, with the strongest emission due to the $^5D_0 \rightarrow {}^7F_2$ transition at 618 nm (Figure 7). The terbium complex **1c**, on the other hand, exhibits bright green luminescence in which the peaks in the emission spectrum correspond to the $^5D_4 \rightarrow {}^7F_n$ (n = 6, 5, 4, 3) transitions, with the strongest emission corresponding to the $^5D_4 \rightarrow {}^7F_5$ transition at 545 nm (Figure 8). Both of their time-resolved luminescence spectra show monoexponential decay, with luminescence lifetimes of 0.43 and 1.30 ms, respectively. A summary of the luminescent properties of the complexes is given in Table 7. The solid-state luminescent properties of both Eu and Tb benzoate complexes are similar to those reported by Wang[22] and Ronda,[23] in which the benzoate complexes have different structures. Degassed samples exhibit nearly identical luminescence observations and lifetime values, suggesting that oxygen quenching of the excited state can be neglected in this case. Although we have not been able to evaluate the efficiency of the energy transfer involved in these complexes quantitatively, there is an almost negligible emission intensity from the benzoate ligand, suggesting that the energy transfer process from ligand to metal is fairly efficient. This phenomenon is similar to those seen in other lanthanide benzoate complexes.[22−24]

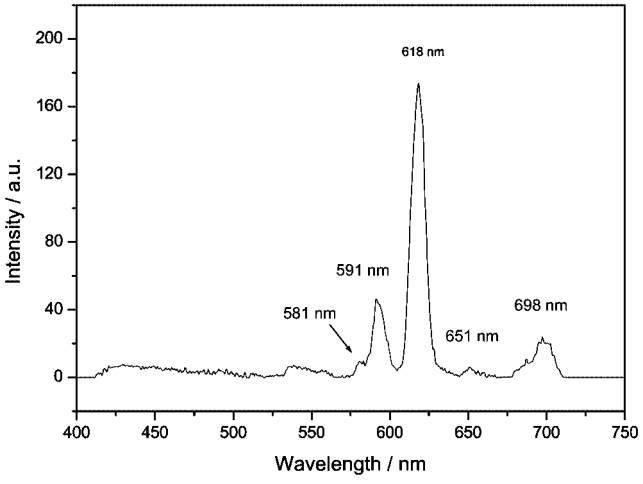

Figure 7. Emission spectrum of $[Eu_2(Bz)_6(MeOH)_4]_n$ (**1a**) in methanol at 298 K

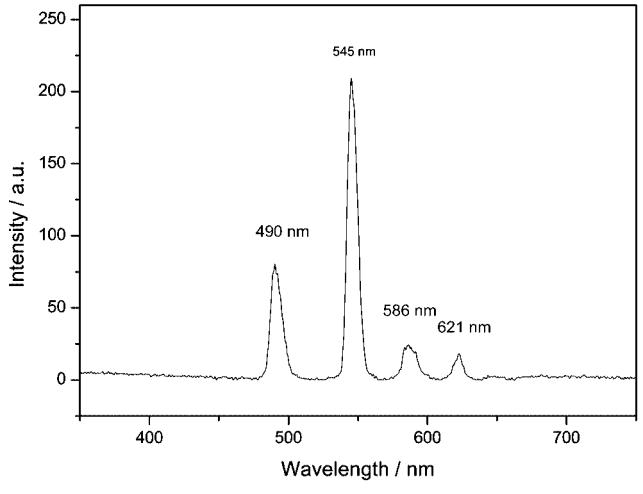

Figure 8. Emission spectrum of $[Tb_2(Bz)_6(MeOH)_4]_n$ (**1c**) in methanol at 298 K

Table 7. Luminescence lifetime of the europium and terbium carboxylate complexes measured in MeOH (τ_{MeOH}) and MeOD (τ_{MeOD}), as well as the number of coordinated solvent molecules (q) as determined by Horrocks' equation

Complex	τ_{MeOH} [ms]	τ_{MeOD} [ms]	q
1a	0.48	2.17	3.4±0.5
1c	1.30	1.59	1.2±0.5
3a	0.39	1.98	4.3±0.5
3c	0.98	1.21	1.6±0.5
4a	0.40	2.12	4.2±0.5
4c	0.90	1.12	1.8±0.5
6a	0.45	1.90	3.6±0.5
6c	1.03	1.36	2.0±0.5

The known sensitivity of Eu^{3+} and Tb^{3+} luminescence towards quenching by hydroxy groups in the solvent provides an experimental tool with which to estimate the degree of shielding by the ligands. An empirical relationship has been established by Horrocks and Sudnich,[25] estimating the number of coordinated methanol molecules (q) as $q = A(\tau_{MeOH}^{-1} - \tau_{MeOD}^{-1})$, where A is 2.1 for the Eu^{3+} and 8.4 for the Tb^{3+} complexes, and τ^{-1} is the reciprocal luminescence lifetime, measured separately in MeOH and in [D_4]methanol.

The luminescence lifetime of the complexes increases significantly in deuterated MeOH, indicating the quenching effect of the excited state of Ln^{3+} ions by the O−H oscillators of the coordinated methanol. The solvation parameter q determined is 3.4±0.5 and 1.2±0.5 for **1a** and **1c**, respectively (the error of ±0.5 is generally assumed to be reasonable for this calculation).[25b] This is consistent with three and one coordinated methanol molecule(s) in the first coordination sphere for the Eu^{3+} and Tb^{3+} ions. Additional contribution of solvent-based quenching from the second-sphere interaction may be considered. Parker et al.[26] have shown that significant lifetime differences can also be observed even when no solvent molecules are directly coordinated to the lanthanide ion. This is attributable to the contribution of second-sphere interaction and/or hydrogen bonding of solvent molecules to the ligand, giving rise to apparent q values of anywhere between 0 and 1.

Georges et al.[6a] reported the luminescent properties of terbium chelated with benzoic acid derivatives in aqueous solution, and suggested that, if the benzoic acid derivatives have similar triplet-state energy levels, sensitisation of the terbium luminescence is mainly determined by the ability of the acid to bind to the lanthanide ion. An electron-donating substituent group will increase the negative charge shift of the carboxylic carbon atom and hence also the stability constant of the complex. They also showed that the triplet-state energy levels of benzoic acid derivatives with *para*- and *ortho*-substituted OH and NH_2 groups are in the range of 23500−25500 cm^{-1}, which is above the emission level of $^5D_0$ for Eu^{3+} and $^5D_4$ for Tb^{3+} ions. This therefore supports the observation of stronger sensitisation of the terbium complexes than of the europium complexes, because of the smaller overlap between the ligand triplet and europium ion excited states. The above ligands' triplet state values can be used as a reference for our benzoate ligands and support the luminescent behaviour of the lanthanide complexes in our systems, in which stronger terbium emissions were observed.

The luminescence properties of lanthanide benzoate DMF complexes **2a** and **2c** display characteristic narrow-line emission bands, similar to those observed in complexes **1a** and **1c**, upon excitation of the LC absorption band at 277 nm in DMF and in the solid state. The reason for preparing these complexes with coordinated DMF molecules was to enhance the luminescence intensity and lifetime by eliminating the O−H oscillators that quenched the excited state of lanthanide ions from the coordinated methanol. Unfortunately, complexes **2a** and **2c** exhibit relatively weak luminescence upon LC excitation. This can be accounted for by the instability of the complexes in solution, arising from the possible association/dissociation process, since DMF is a strong O-donor solvent that may compete with the benzoate ligand to coordinate to the Ln^{3+} ions. The smaller antenna effect therefore results in lower sensitisation from the ligand to the metal ions, and thus lowers the luminescence intensity. Similar observation are made for complexes **5a** and **5c**.

Complexes **3a**, **3c**, **4a**, **4c**, **6a**, and **6c** show luminescent behaviour similar to that of complexes **1a** and **1b** in the solid state and in the solution state. Comparison of the lanthanide complexes with different benzoate ligands suggests that, according to their luminescent properties, electron-donating substituted groups such as ethoxy and propoxy increased the stability of the complexes, resulting in longer lifetimes and stronger intensities than seen for the benzoate lanthanides, while relatively shorter lifetimes were observed for electron-withdrawing groups such as trifluoromethyl and trifluoromethoxy. Concentrations of the complexes below 10^{-5} M result in changes of the excitation spectra as time passes, indicating that partial decomplexation occurs, which is understandable in view of the relatively weak coordination of bidentate carboxylate ligands. No attempts at quantum yield measurements were therefore made.

Magnetic Properties

The short metal−metal distance within the molecules demonstrated significant potential interest in terms of the study of the magnetic exchange interactions between those ions. We have previously reported the magnetic properties of the tetranuclear μ_4-oxo complexes, which exhibit antiferromagnetic coupling at low temperature.[27] From the evidence of the X-ray analyses of the complexes, they all have metal−metal distances (3.90−5.35 Å) believed to correspond to some magnetic interaction between the ions along the chain. Solid-state magnetic measurements were therefore carried out for the gadolinium and terbium complexes. Table 8 summarises the magnetic properties of these complexes.

The temperature dependence of the magnetic properties of the dimeric complexes **5b** and **5c** were investigated at 100

Table 8. Magnetic data of the gadolinium and terbium carboxylate complexes

Complex	$\chi_M T$ at 298 K [$cm^3 \cdot K \cdot mol^{-1}$]	$\chi_M T$ at 2 K [$cm^3 \cdot K \cdot mol^{-1}$]	Curie constant C [$cm^3 \cdot K \cdot mol^{-1}$]	Weiss constant θ [K]	J value [cm^{-1}]	g value
1b	17.04	15.55	16.97	−0.26	−0.021[a]	2.02[a]
1c	24.60	20.71	24.77	−4.62	−	−
2b	8.01	5.45	8.07	−1.09	−0.097[b]	1.97[b]
2c	12.10	4.07	12.24	−4.15	−	−
3b	7.89	7.88	7.91	0.14	−	−
3c	10.78	7.59	10.61	−1.65	−	−
4b	7.62	4.67	7.58	−1.91	−0.028[a]	1.95[a]
4c	11.56	8.54	11.77	−4.15	−	−
5b	15.86	10.74	15.48	−1.34	−0.068[b]	1.98[b]
5c	20.77	11.57	21.28	−10.50	−	−
6b	7.23	6.58	7.21	−0.58	−0.019[a]	1.92[a]
6c	10.5	8.94	10.70	−2.30	−	−

[a] Fitted by Equation (2). [b] Fitted by Equation (1).

Oe and 10 kOe field, respectively, over a temperature range of 2−300 K. Plots of χ_M^{-1} vs. T for these complexes obey the Curie−Weiss law, giving C = 15.48 and 21.28 $cm^3 \cdot K \cdot mol^{-1}$ and θ = −1.34 and −10.50 K for **5b** and **5c**, respectively. The $\chi_M T$ value (15.86 $cm^3 \cdot K \cdot mol^{-1}$) of complex **5b** remain almost constant − and close to the expected value of two non-interacting free Gd^{3+} ions − from 300 to 25 K.[28] A dramatic drop in value below 25 K to 10.74 $cm^3 \cdot K \cdot mol^{-1}$ at 2 K was observed (Figure 9). This feature is indicative of weak antiferromagnetic coupling between the Gd^{3+} ions in the molecule. We can analyse the data quantitatively by using the equation deduced from the isotropic spin Hamiltonian, $H = -JS_{Gd1}S_{Gd2}$, with the quantum numbers $S_{Gd1} = S_{Gd2} = 7/2$. Equation (1) is for the magnetic susceptibility of dimeric system[29] with $x = J/kT$ and N = Avogadro's number, β = Bohr magneton, k = Boltzmann constant.

$$\chi_M = \left(\frac{2N\beta^2 g^2}{kT}\right)\left(\frac{e^x + 5e^{3x} + 14e^{6x} + 30e^{10x} + 55e^{15x} + 91e^{21x} + 140e^{28x}}{1 + 3e^x + 5e^{3x} + 7e^{6x} + 9e^{10x} + 11e^{15x} + 13e^{21x} + 15e^{28x}}\right) \quad (1)$$

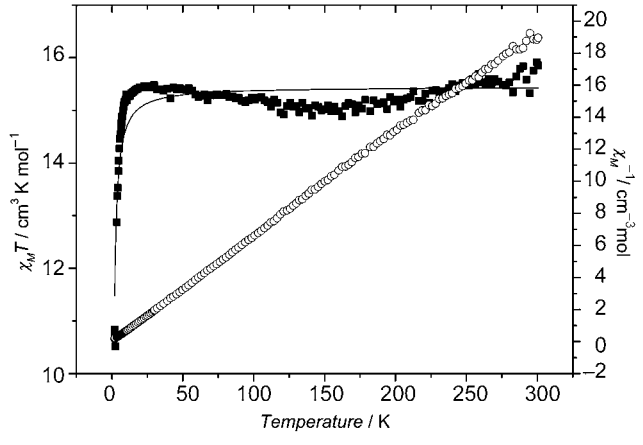

Figure 9. Temperature dependence of $\chi_M T$ (filled squares) and χ_M^{-1} (open circles) of $[Gd(oet)_3(DMF)(H_2O)]_2$ (**5b**) with diamagnetic correction; the solid line represents the best calculated curve

The magnetic interaction parameter J can be evaluated by fitting the data for the dimer system with Equation (1). The J value is −0.068 cm^{-1} whereas g is 1.98. A good agreement between the experimental and calculated values is reflected by the small R value [$R = \Sigma(\chi_M T_{calcd.} - \chi_M T_{obsd.})^2/\Sigma(\chi_M T_{obsd.})^2$] of $4.8 \cdot 10^{-4}$. Meanwhile, the $\chi_M T$ value of complex **5c** decreases gradually from room temperature (20.77 $cm^3 \cdot K \cdot mol^{-1}$) to 2 K (11.57 $cm^3 \cdot K \cdot mol^{-1}$). This room-temperature value is smaller than the expected values for two free non-interacting Tb^{3+} ions, which is primarily a consequence of the ligand field effect that the lowest J multiplet of the Russell−Saunders ground term was perturbed. The dramatic drop in $\chi_M T$ is mainly due to the splitting of the ligand field of the Tb^{3+} ions because of strong spin-orbit coupling, and partly contributed to the possible antiferromagnetic coupling between the Tb^{3+} ions in the dimer unit at a lower temperature.

A relatively longer metal−metal distance than seen in complexes **5b** and **5c** is associated with complex **6c** (5.35 Å). We believed such a large separation might give rise to some magnetic exchange behaviour, and so the solid-state magnetic properties of complexes **6b** and **6c** were studied over the 2−300 K temperature range, at 100 Oe applied field; χ_M is the molar magnetic susceptibility per monomer unit of the polymeric chain. For complex **6b**, the $\chi_M T$ value at room temperature is 7.23 $cm^3 \cdot K \cdot mol^{-1}$, close to the expected value for one isolated Gd^{3+} ion ($^8S_{7/2}$). However, the whole profile of the $\chi_M T$ vs. T plot is indicative of weak antiferromagnetic coupling, resulting in a nonmagnetic ground state for the Gd^{3+} ions. The abrupt drop of $\chi_M T$ at below 60 K, to the minimum value of 6.58 $cm^3 \cdot K \cdot mol^{-1}$, together with the negative θ value of −0.58 K, suggests the presence of weak antiferromagnetic coupling between the metal ions. As complex **6b** consists of an infinite chain with equal spacing, it can be quantitatively analysed by use of the equation deduced from the isotropic spin Hamiltonian, $H = -JS_{Gd1}S_{Gd2}$, with the quantum numbers $S_{Gd1} = S_{Gd2} = 7/2$. The analytical expression of Equation (2) for

the magnetic susceptibility of an infinite chain of classical spins was derived by Fisher[30] with

$$u = \coth\left[\frac{2JS(S+1)}{kT}\right] - \left[\frac{kT}{2JS(S+1)}\right]$$

and the other symbols as defined in Equation (1).

$$\chi_M = \frac{Ng^2\beta^2 S(S+1)}{3kT}\frac{1+u}{1-u} \quad (2)$$

A quantitative analysis of the data, based on Equation (2), shows a good fit of $\chi_M T$ with $J = -0.019$ cm^{-1}, $g = 1.92$ and $R = 1.17 \cdot 10^{-5}$. The magnetic behaviour of complex **6c** is similar to that of the Gd complex, indicating the possible presence of antiferromagnetic interaction between the Tb^{3+} ions. The data fit well with the Curie−Weiss law, with $C = 10.70$ cm^3 K·mol^{-1} and $\theta = -2.30$ K. The $\chi_M T$ value exhibits a continuous decrease upon cooling, from 10.5 cm^3·K·mol^{-1} at room temperature to 10.58 cm^3·K·mol^{-1} at ca. 130 K, and then drop very rapidly to 8.94 cm^3·K·mol^{-1} at 2 K. The continuous decrease in $\chi_M T$ as the temperature is lowered is probably primarily a result of the ligand field effect stemming from the strong spin-orbit coupling of the Tb^{3+} ions together with possible contribution from weak intra- and intermolecular antiferromagnetic coupling between the Tb^{3+} ions. The other complexes **1b**, **1c**, **2b**, **2c**, **3c**, **4b** and **4c**, but not **3b**, exhibit weak antiferromagnetic coupling between the lanthanide ions at low temperature, with behaviour similar to that of other homoleptic lanthanide complexes.[29,31]

Conclusion

A new series of lanthanide carboxylate complexes with benzoate-type ligands were successfully synthesised and demonstrated a rich coordination chemistry in the solid state. All benzoate ligands can sensitise lanthanide luminescence, especially for the terbium ion, but coordinated methanol molecules cause the quenching of lanthanide excited states. Although the use of *para*-substituted benzoate ligands improved the solubilities of the complexes, it gives rise to steric hindrance between the ligands, so that they have relatively shorter luminescence lifetimes than the complexes with benzoate ligands. Weak antiferromagnetic interactions between the neighbouring ions along the chain were observed at low temperature in studies of magnetic properties.

Experimental Section

General: All chemicals were purchased from commercial sources and were used as received without any further purification. The solid-state infrared spectra were recorded with a Bio-Rad FTS-7 FT-IR spectrometer on KBr pellets. Elemental analyses were performed by Butterworth Laboratories, UK. Thermal gravimetric analysis (TGA) was conducted with a Perkin−Elmer TGA 7 thermogravimetric analyser under nitrogen, over the 30−900 °C temperature range and with a heating rate of 20 °C/min. Electronic absorption spectra were recorded with a Hewlett Packard 8453 UV/Vis spectrophotometer at room temperature. Luminescence spectra were recorded with a Perkin−Elmer LS-50B luminescence spectrometer equipped with a Hamamatse R928 photomultiplier tube, with excitation and emission slit widths of 2.5−15 nm depending on the intensity of the emission. Solid samples were ground into fine powders prior to the luminescence measurements. Both aerated and deoxygenated solution luminescence spectra were measured at room temperature in the $1 \cdot 10^{-4}$ to $2 \cdot 10^{-5}$ M concentration range. For deoxygenated samples, the solutions were subjected to at least three freeze-pump-thaw cycles. Corrections were made for all excitation and emission spectra. Luminescence lifetimes, τ, were measured with the instrument in time-resolved mode, and are averages of at least three independent measurements made by monitoring the decay at a wavelength corresponding to the maximum intensity in the emission spectrum (618 nm for Eu and 545 nm for Tb), after pulsed excitation. The resulting first-order decay curve gave linear plots of ln(*Int*) vs. *t* from which the lifetime was calculated by $\tau = -1/\text{slope}$. Temperature-dependent magnetic susceptibilities of solid samples were recorded on a Quantum Design SQUID magnetometer (MPMS-5S) and a Oxford MagLab2000 magnetometer in the 2−300 K temperature range with applied fields of 100 Oe and 10000 Oe, respectively. The diamagnetic correction was estimated by use of Pascal's constants. Quantitative analyses of the magnetic susceptibility data for the complexes were performed by use of the Nonlin fitting program (Version 3.0).

Syntheses of the Lanthanide Complexes: Since the syntheses of the lanthanide complexes used similar procedures, the synthesis of complex **1a** is described as a general method. The respective ligands 4-(trifluoromethyl)benzoic acid, 4-(trifluoromethoxy)benzoic acid, 4-ethoxybenzoic acid, and 4-*n*-propoxybenzoic acid were used instead of benzoic acid for the preparation of complexes **2a**−**c**, **3a**−**c**, **4a**−**c**, **5a**−**c**, and **6a**−**c**.

General Method: Benzoic acid (82 mg, 0.672 mmol) and NaOH (26.9 mg, 0.672 mmol) in methanol (5 mL) were stirred at room temperature for 30 min. $Eu(NO_3)_3 \cdot 6H_2O$ (100 mg, 0.224 mmol) in methanol (2 mL) was added to the reaction mixture, and a white precipitate appeared after 1 d. The reaction mixture was further stirred for 12 h, and the precipitate was filtered and washed with methanol. **1a:** Yield: 202 mg, 78 %. IR (KBr disc): $\tilde{\nu}$ = 3527 br, 3450 br, 3072 m, 3060 m, 3029 w, 1593 s, 1539 vs, 1520 vs, 1428 vs, 714 s, 551 w cm^{-1}. ESI-MS (negative mode): *m*/*z* = 1152, 637. $C_{46}H_{46}Eu_2O_{16}$ (1158.78): calcd. C 47.68, H 4.00; found C 47.6, H 4.0. **1b:** Yield: 195 mg, 75 %. IR (KBr disc): $\tilde{\nu}$ = 3530 br, 3445 br, 3071 m, 3055 m, 3027 w, 1593 s, 1543 vs, 1522 vs, 1429 vs, 715 s, 553 w cm^{-1}. ESI-MS (negative mode): *m*/*z* = 1162, 642. $C_{46}H_{46}Gd_2O_{16}$ (1169.36): calcd. C 47.25, H 3.97; found C 47.3, H 4.0. **1c:** Yield: 210 mg, 81 %. IR (KBr disc): $\tilde{\nu}$ = 3528 br, 3449 br, 3072 m, 3058 m, 3030 w, 1594 s, 1541 vs, 1521 vs, 1430 vs, 714 s, 554 w cm^{-1}. ESI-MS (negative mode): *m*/*z* = 1166, 644. $C_{46}H_{46}O_{16}Tb_2$ (1172.71): calcd. C 47.11, H 3.95; found C 47.3, H 3.9. The product was dissolved in hot methanol for crystallisation and colourless single crystals of **1a**−**c** were obtained on slow evaporation of the solvent over a few days.

Complexes **2a**−**c** were prepared by dissolving complexes **1a**−**c**, respectively, in a minimum amount of hot dimethylformamide, colourless single crystals of **2a**−**c** being obtained after 2 d. **2a:** Yield: 80 mg, 61 %. IR (KBr disc): $\tilde{\nu}$ = 3065 m, 1661 s, 1603 s, 1558 s, 1527 s, 1446 m, 1422 s, 1399 s, 1374 m, 1107 w, 857 m, 723 s cm^{-1}. $C_{24}H_{22}EuNO_7$ (588.40): calcd. C 48.99, H 3.77, N 2.38; found C

49.0, H 3.7, N 2.4. **2b:** Yield: 76 mg, 58 %. IR (KBr disc): $\tilde{\nu}$ = 3060 m, 1658 s, 1603 s, 1559 s, 1530 s 1450 m, 1422 s, 1402 s, 1376 m, 1107 w, 855 m, 724 s cm^{-1}. $C_{24}H_{22}GdNO_7$ (593.69): calcd. C 48.55, H 3.74, N 2.36; found C 48.6, H 3.8, N 2.4. **2c:** Yield: 85 mg, 65 %. IR (KBr disc): $\tilde{\nu}$ = 3061 m, 1657 s, 1605 s, 1558 s, 1527 s 1448 m, 1423 s, 1400 s, 1375 m, 1107 w, 856 m, 723 s cm^{-1}. $C_{24}H_{22}NO_7Tb$ (595.37): calcd. C 48.42, H 3.72, N 2.35; found C 48.4, H 3.7, N 2.3.

The synthesis of complexes **3a**−**c** was similar to that described in the General Method. **3a:** Yield: 97 mg, 55 %. IR (KBr disc): $\tilde{\nu}$ = 3503 br, 3389 br, 3183 w, 3067 w, 1595 s, 1543 s, 1527 s, 1431 s, 1329 s, 1163 m, 1118 s, 1066 s, 1020 m, 868 m, 789 s, 709 m, 490 m cm^{-1}. ESI-MS (negative mode): *m*/*z* = 1628, 908. $C_{26}H_{20}EuF_9O_8$ (783.38): calcd. C 39.86, H 2.57; found C 39.8, H 2.6. **3b:** Yield: 86 mg, 49 %. IR (KBr disc): $\tilde{\nu}$ = 3505 br, 3389 br, 3175 w, 3072 w, 1599 s, 1547 s, 1531 s, 1437 s, 1335 s, 1165 m, 1118 s, 1068 s, 1018 m, 868 m, 789 s, 711 m, 490 m cm^{-1}. ESI-MS (negative mode): *m*/*z* = 1638, 914. $C_{26}H_{20}F_9Gd_8O$ (788.67): calcd. C 39.60, H 2.56; found C 39.6, H 2.5. **3c:** Yield: 105 mg, 60 %. IR (KBr disc): $\tilde{\nu}$ = 3503 br, 3393 br, 3185 w, 3073 w, 1597 s, 1551 s, 1531 s, 1435 s, 1333 s, 1165 m, 1118 s, 1068 s, 1018 m, 870 m, 791 s, 711 m, 490 m cm^{-1}. ESI-MS (negative mode): *m*/*z* = 1642, 915. $C_{26}H_{20}F_9O_8Tb$ (790.34): calcd. C 39.51, H 2.55; found C 39.6, H 2.6. Colourless block-shaped single crystals of **3a** and **3c** were obtained from the filtrate on slow evaporation of the solvent for 3 d.

The synthesis of complexes **4a**−**c** was similar to that described in the General Method. **4a:** Yield: 110 mg, 59 %. IR (KBr disc): $\tilde{\nu}$ = 3447 br, 1601 s, 1559 s, 1541 s, 1437 s, 1319 s, 1288 s, 1206 s, 1167 s, 783 m cm^{-1}. ESI-MS (negative mode): *m*/*z* = 1740, 972. $C_{26}H_{20}EuF_9O_{11}$ (831.38): calcd. C 37.56, H 2.42; found C 37.5, H 2.5. **4b:** Yield: 117 mg, 63 %. IR (KBr disc): $\tilde{\nu}$ = 3437 br, 1605 s, 1560 s, 1545 s, 1437 s, 1313 s, 1286 s, 1209 s, 1169 s, 783 m cm^{-1}. ESI-MS (negative mode): *m*/*z* = 1750, 978. $C_{26}H_{20}F_9GdO_{11}$ (836.67): calcd. C 37.32, H 2.41; found C 37.3, H 2.4. **4c:** Yield: 119 mg, 65 %. IR (KBr disc): $\tilde{\nu}$ = 3420 br, 1605 s, 1557 s, 1541 s, 1433 s, 1311 s, 1279 s, 1211 s, 1167 s, 783 m cm^{-1}. ESI-MS (negative mode): *m*/*z* = 1754, 979. $C_{26}H_{20}F_9O_{11}Tb$ (838.35): calcd. C 37.25, H 2.40; found C 37.3, H 2.4. Colourless rod-shaped single crystals of **4a**−**c** were obtained from the filtrate on slow evaporation of solvent for a week.

The synthesis of complexes **5a**−**c** was similar to that described in the General Method. **5a:** Yield: 182 mg, 55%. IR (KBr disc): $\tilde{\nu}$ = 3003 w, 2978 m, 2935 m, 2887 m, 1660 s, 1609 s, 1589 s, 1558 s, 1522 s, 1437 m, 1421 s, 1389 m, 1255 s, 784 w cm^{-1}. ESI-MS (−ve): *m*/*z* = 1460, 813. $C_{60}H_{72}Eu_2N_2O_{22}$ (1477.14): calcd. C 48.79, H 4.91, N 1.90; found C 48.8, H 5.0, N 1.9. **5b:** Yield: 172 mg, 52%. IR (KBr disc): $\tilde{\nu}$ = 3005 w, 2979 m, 2934 m, 2890 m, 1659 s, 1610 s, 1588 s, 1557 s, 1524 s, 1440 m, 1420 s, 1388 m, 1253 s, 783 w cm^{-1}. ESI-MS (negative mode): *m*/*z* = 1471, 818. $C_{60}H_{72}Gd_2N_2O_{22}$ (1487.73): calcd. C 48.44, H 4.88, N 1.88; found C 48.5, H 5.0, N 1.9. **5c:** Yield: 187 mg, 57%. IR (KBr disc): $\tilde{\nu}$ = 3003 w, 2978 m, 2934 m, 2888 m, 1659 s, 1607 s, 1589 s, 1558 s, 1524 s, 1439 m, 1419 s, 1389 m, 1255 s, 783 w cm^{-1}. ESI-MS (negative mode): *m*/*z* = 1474, 820. $C_{60}H_{72}N_2O_{22}Tb_2$ (1491.08): calcd. C 48.33, H 4.87, N 1.88; found C 48.4, H 4.9, N 1.9. Recrystallisation of the products from hot DMF afforded colourless rod-shaped single crystals of **5b** and **5c** after a few weeks.

The synthesis of complexes **6a**−**c** was similar to that described in the General Method. **6a:** Yield: 103 mg, 72 %. IR (KBr disc): $\tilde{\nu}$ = 3405 br, 3079 w, 2966 m, 2938 m, 2878 m, 1607 s, 1522 m, 1507 s, 1421 s, 1388 s, 1312 m, 1257 s, 1171 m, 786 w cm^{-1}. ESI-MS (negative mode): *m*/*z* = 1558, 869. $C_{22}H_{30}EuNO_{11}$ (636.44): calcd. C 41.52, H 4.75, N 2.20; found C 41.6, H 4.8, N 2.3. **6b:** Yield: 115 mg, 81%. IR (KBr disc): $\tilde{\nu}$ = 3406 br, 3079 w, 2965 m, 2938 m, 2878 m, 1607 s, 1522 m, 1508 s, 1421 s, 1389 s, 1311 m, 1257 s, 1173 m, 787 w cm^{-1}. ESI-MS (negative mode): *m*/*z* = 1569, 874. $C_{22}H_{30}GdNO_{11}$ (641.72): calcd. C 41.18, H 4.71, N 2.18; found C 41.2, H 4.8, N 2.2. **6c:** Yield: 128 mg, 90%. IR (KBr disc): $\tilde{\nu}$ = 3416 br, 3082 w, 2967 m, 2938 m, 2876 m, 1609 s, 1524 m, 1506 s, 1419 s, 1385 s, 1314 m, 1257 s, 1171 m, 787 w cm^{-1}. ESI-MS (negative mode): *m*/*z* = 1572, 875. $C_{22}H_{30}NO_{11}Tb$ (642.40): calcd. C 41.07, H 4.70, N 2.18; found C 41.1, H 4.7, N 2.2. A mixture of 4-*n*-propoxybenzoic acid, NaOH and $Tb(NO_3)_3{\cdot}6H_2O$ was left standing at room temperature, and colourless rod-shaped single crystals of **6c** were obtained on slow evaporation of the solvent for a few days.

Crystallography: Single crystals suitable for X-ray crystallographic analyses were mounted on sealed glass capillaries by use of epoxy resin. Diffraction data were collected at ambient temperature with a Rigaku AFC7R diffractometer, a Marresearch Image Plate Scanner or a Bruker AXS SMART-CCD 1000 diffractometer by use of graphite-monochromated Mo-K_α radiation (λ = 0.71073 Å) with ω-2θ and ω scan techniques. A summary of crystallographic data and structure refinements is listed in the Supporting Infornmation. All data sets were collected for Lorentz and polarisation effects and the absorption corrections based on ψ-scan methods[32] or inter-image scaling were also applied. All structures were solved by a combination of Patterson methods (DIRDIF92, PATTY)[33] or direct methods (SIR92[34] or SHELXS-86[35]) and difference Fourier techniques. The solutions were refined on *F* by full-matrix, least-squares analysis, with all metal and non-hydrogen atoms refined anisotropically for structures **2a**−**b**, **3c**, **4a**−**c**, and **6c**, while structures **1a**−**c**, **2c**, **3a**, **5b**, and **5c** were refined anisotropically for all metal and heavy atoms. All hydrogen atoms were included in the structure factor calculations but were not refined. All calculations were performed with a Silicon-Graphics workstation with the aid of the program package TeXsan.[36] CCDC-195568 to -195581 contain the supplementary crystallographic data for this paper. These data can be obtained free of charge at www.ccdc.cam.ac.uk/conts/retrieving.html or from the Cambridge Crystallographic Data Centre, 12, Union Road, Cambridge CB2 1EZ, UK [Fax: (internat.) + 44-1223/336-033; E-mail: deposit@ccdc.cam.ac.uk].

Supporting Information: A summary of crystallographic data, including the data collection and structure solution parameters for complexes **1a**−**c**, **2a**−**c**, **3a**, **3c**, **4a**−**c**, **5b**−**c** and **6c** is shown in Table S1. Magnetic data of complexes **5c**, **6b** and **6c** are illustrated in Figures S1−3, respectively (see also footnote on the first page of this article).

Acknowledgments

We gratefully acknowledge financial support from the Hong Kong Research Grants Council and the University of Hong Kong. A. W.-H. L. acknowledges the receipt of a postgraduate studentship and Hung Hing Ying scholarship administered by the University of Hong Kong. This work is partially supported by Hong Kong RGC (HKUST6157/00E) (X.-X. Z.).

[1] [1a] C. Galaup, C. Picard, B. Cathala, L. Cazaux, P. Tisnès, *Helv. Chim. Acta* **1999**, *82*, 543−560. [1b] N. Sabbatini, M. Guardigli, J.-M. Lehn, *Coord. Chem. Rev.* **1993**, *123*, 201−228. [1c] G. Blasse, G. J. Dirksen, N. Sabbatini, S. Perathoner, *Inorg. Chim. Acta* **1987**, *133*, 167−173.

[2] [2a] D. A. Bardwell, J. C. Jeffery, P. L. Jones, J. A. McCleverty, E. Psillakis, Z. Reeves, M. D. Ward, *J. Chem. Soc., Dalton Trans.* **1997**, 2079−2086. [2b] P. L. Jones, A. J. Amoroso, J. C. Jeffery, J. A. McCleverty, E. Psillakis, L. H. Ree, M. D. Ward, *Inorg. Chem.* **1997**, *36*, 10−18.

[3] [3a] L. Prodi, S. Pivari, F. Bolletta, M. Hissler, R. Ziessel, *Eur. J. Inorg. Chem.* **1998**, 1959−1965. [3b] J.-C. G. Bünzli, P. Froidevaux, J. M. Harrowfield, *Inorg. Chem.* **1993**, *32*, 3306−3311.

[4] [4a] A. Beeby, R. S. Dickins, S. Faulkner, D. Parker, J. A. G. Williams, *Chem. Commun.* **1997**, 1401−1402. [4b] A. Beeby, S. Faulkner, *Chem. Phys. Lett.* **1997**, *266*, 116−122. [4c] D. Parker, P. Kanthi-Senanayake, J. A. G. Williams, *J. Chem. Soc., Perkin Trans. 2* **1998**, 2129−2139.

[5] [5a] E. J. Nassar, P. S. Calefi, I. L. V. Rosa, O. A. Serra, *J. Alloys Comp.* **1998**, *275−255*, 838−840. [5b] J.-C. G. Bünzli, F. Ihringer, *Inorg. Chim. Acta* **1996**, *246*, 195−205. [5c] P. K. Sharma, A. R. van Doorn, A. G. J. Staring, *J. Lumin.* **1994**, *62*, 219−225.

[6] [6a] N. Arnaud, J. Georges, *Analyst* **2000**, *125*, 1487−1490. [6b] S. T. Mullins, P. G. Sammes, R. M. West, G. Yahioglu, *J. Chem. Soc., Perkin Trans. 1* **1996**, 75−81. [6c] J. B. Lamture, Z. H. Zhou, A. S. Kumar, T. G. Wensel, *Inorg. Chem.* **1995**, *34*, 864−869. [6d] G.F. de Sá, L. H. A. Nunes, Z.-M. Wang, G. R. Choppin, *J. Alloys Comp.* **1993**, *196*, 17−23.

[7] [7a] M. P. Oude Wolbers, F. C. J. M. Van Veggel, B. H. M. Snellink-Ruel, J. W. Hofstraat, F. A. J. Geurts, D. N. Reinhoudt, *J. Chem. Soc., Perkin Trans. 2* **1998**, 2141−2150. [7b] S. Petoud, J.-C. G. Bunzli, K. J. Schenk, C. Piguet, *Inorg. Chem.* **1997**, *36*, 1345−1353.

[8] W. W. Horrocks De Jr., P. Bolender, W. D. Smith, R. M. Supkowski, *J. Am. Chem. Soc.* **1997**, *119*, 5972−5973.

[9] [9a] I. Hemmilä, *J. Alloys Comp.* **1995**, *225*, 480−485. [9b] J. Coates, P. G. Sammes, G. Yahioglu, R. M. West, A. J. Garman, *J. Chem. Soc., Chem. Commun.* **1994**, 2311−2312. [9c] I. Hemmilä, *Applications of Fluorescence in Immunoassays*, Wiley, New York, **1991**.

[10] J. Kido, W. Ikeda, M. Kimura, K. Nagai, *Jpn. J. Appl. Phys.* **1996**, *35*, 394−396.

[11] [11a] J. P. Costes, J. M. Clemente-Juan, F. Dahan, F. Nicodme, M. Verelst, *Angew. Chem. Int. Ed.* **2002**, *41*, 323−325. [11b] A. Ouchi, Y. Suzuki, Y. Ohku, Y. Koizumi, *Coord. Chem. Rev.* **1988**, *92*, 29−43. [11c] R. C. Mehrotra, R. Bohra, *Metal Carboxylates*, Acad. Press, London, U.K., **1983**.

[12] [12a] G. Yu, Y. Q. Liu, X. Wu, D. B. Zhu, H. Y. Li, L. P. Jin, M. Z. Wang, *Chem. Mater.* **2000**, *12*, 2537−2541. [12b] S. Capecchi, O. Renault, D.-G. Moon, M. Halim, M. Etchells, P. J. Dobson, O. V. Salata, V. Christou, *Adv. Mater.* **2000**, *12*, 1591−1594. [12c] W. L. Li, Z. Q. Gao, Z. Y. Hong, C. S. Lee, S. T. Lee, *Synth. Met.* **2000**, *111−112*, 53−56. [12d] J. Kido, K. Nagai, Y. Okamoto, *J. Alloys Comp.* **1993**, *192*, 30−33.

[13] [13a] J. Kido, K. Nagai, Y. Okamoto, T. Skotheim, *Chem. Lett.* **1991**, *235*, 1267−1270. [13b] J. Kido, K. Nagai, Y. Ohashi, *Chem. Lett.* **1990**, *220*, 657−660.

[14] Y. X. Zheng, C. Y. Shi, Y. J. Liang, Q. Lin, C. Guo, H. J. Zhang, *Synth. Met.* **2000**, *114*, 321−323.

[15] A. Edward, C. Claude, I. Sokolik, T. Y. Chu, Y. Okamoto, R. Dorsinville, *J. Appl. Phys.* **1997**, *82*, 1841−1846.

[16] J. F. Ma, Z. S. Jin, J. Z. Ni, *J. Struct. Chem.* **1991**, *10*, 56−59.

[17] X. Li, X. Zheng, L. Jin, S. Lu, J. Zhang, *J. Mol. Struct.* **2001**, *559*, 341−346.

[18] [18a] G. Yang, H. A. Chen, Z. Y. Zhou, X. M. Chen, *J. Chem. Crystallogr.* **1999**, *29*, 309−317. [18b] E. Huskowska, I. Turowska-Tyrk, J. Legandziewicz, T. Glowiak, *J. Alloys Comp.* **1998**, *275*, 852−858. [18c] T. Imai, M. Shimoi, A. Ouchi, *Bull. Chem. Soc. Jpn.* **1987**, *60*, 159−167. [18d] Y. Sugita, A. Ouchi, *Bull. Chem. Soc. Jpn.* **1987**, *60*, 171−178.

[19] P. P. Gawryszewska, L. Jerrykiewicz, P. Sobota, J. Legendziewicz, *J. Alloys Comp.* **2000**, *300/301*, 275−282, references therein.

[20] M. N. Tahir, D. Ulku, C. Unaleroglu, E. M. Movsumov, *Acta Crystallogr., Sect. C* **1996**, *52*, 1449−1451.

[21] G. V. Romanenko, N. V. Podberezskaya, V. V. Bakakin, *Zh. Strukt. Khim.* **1981**, *22*, 185−188.

[22] C. Seward, N. X. Hu, S. N. Wang, *J. Chem. Soc., Dalton Trans.* **2001**, 134−137.

[23] M. Bredol, U. Kynast, C. Ronda, *Adv. Mater.* **1991**, *3*, 361−367.

[24] R. F. Wang, L. P. Jin, L. S. Li, S. Z. Lu, J. H. Zhang, *J. Coord. Chem.* **1999**, *47*, 279−287.

[25] [25a] R. C. Holz, C. A. Chang, W. D. Horrocks, *Inorg. Chem.* **1991**, *30*, 3270−3275. [25b] W. D. Horrocks, D. R. Sudnick, *Acc. Chem. Res.* **1981**, *14*, 384−392.

[26] S. Aime, M. Botta, D. Parker, J. A. G. Williams, *J. Chem. Soc., Dalton Trans.* **1996**, 17−20.

[27] A. W. H. Lam, W. T. Wong, G. H. Wen, X. X. Zhang, S. Gao, *New J. Chem.* **2001**, *25*, 531−533.

[28] [28a] E. A. Boundreaux, L. N. Mulay, *Theory and Applications of Molecular Paramagnetism*, J. Wiley & Sons: New York, **1976**. [28b] O. Kahn, *Molecular Magnetism*, VCH Publishers, New York, **1993**.

[29] A. Panagiotopoulos, T. F. Zafiropoulos, S. P. Perlepes, E. Bakalbassis, I. Masson-Ramade, O. Kahn, A. Terzis, C. P. Raptopoulou, *Inorg. Chem.* **1995**, *34*, 4918−4920.

[30] M. E. Fisher, *Am. J. Phys.* **1964**, *32*, 343−351.

[31] J. Legendziewicz, M. Borzechowska, G. Oezko, G. Meyer, *New J. Chem.* **2000**, *24*, 53−59.

[32] A. C. T. North, D. C. Phillips, F. S. Mathews, *Acta Crystallogr., Sect. A* **1968**, *24*, 351−359.

[33] P. T. Beursken, G. Admiraal, G. Beurskens, W. P. Bosman, S. Garcia-Granda, R. O. Gould, J. M. M. Smits, C. Smykalla, *The DIRDIF program system*, Technical Report of the Crystallography Laboratory, University of Nijmegen, The Netherlands, **1992**.

[34] *SIR92:* A. Altomare, M. C. Burla, M. Camalli, M. Cascarano, C. Giacovazzo, A. Guagliardi, G. Polidori, *J. Appl. Crystallogr.* **1994**, *27*, 435−436.

[35] *SHELXS 86*, Program for Crystal Structure Solution: G. M. Sheldrick, *Acta Crystallgr., Sect. A* **1990**, *46*, 467−473.

[36] *TeXsan:* Crystal Structure Analysis Package, Molecular Structure Corp., **1985** and **1992**.

Received July 4, 2002
[I02365]

Triorganotin Fluoride Structures: A Ligand Close-Packing Model with Predominantly Ionic Sn−F Bonds

Jens Beckmann,[a] Dagmar Horn,[a] Klaus Jurkschat,*[a] Fred Rosche,[a] Markus Schürmann,[a] Uwe Zachwieja,[a] Dainis Dakternieks,*[b] Andrew Duthie,[b] and Allan E. K. Lim[b]

Keywords: Ab initio calculations / Chain structures / Hypervalent compounds / Tin / Fluorides / X-ray diffraction

The synthesis and complete characterization by multinuclear NMR, infrared, and Mössbauer spectroscopy, by single crystal X-ray analysis, as well as by electrospray mass spectrometry of the new soluble triorganotin fluoride Me_2PhSnF (**1**) is reported. The crystal structure of **1** reveals a *rod-like* polymeric structure in the solid state. Solutions of **1** in apolar solvents, such as toluene, contain mixtures of interconvertible oligomers. Ab initio MO calculations on model compounds H_3SnF, $[H_3SnFSnH_3]^+$, and $[FH_3SnFSnH_3F]^-$ indicate that the Sn–F bonds are substantially ionic in character, and suggest open-chain species, rather than cyclic species. In donor solvents, such as pyridine, **1** forms complexes with the solvent, such as Me_2PhSnF·pyridine. The solid-state structure of $(Me_3SiCH_2)_3SnF$ (**2**) is reformulated as monomeric with a weak intermolecular Sn···F interaction that gives rise to a [4+1] coordination. The relative short Sn–Sn separation enables the fluorine atoms to oscillate (flip-flop) between two neighboring $(Me_3SiCH_2)_3Sn$– groups, which is expressed in the X-ray experiment by a dynamic disorder. Ab initio MO calculations on a model compound, $[H_3SnFSnH_3]^+$, suggest only a small energy barrier for the flip-flop motion.

(© Wiley-VCH Verlag GmbH, 69451 Weinheim, Germany, 2003)

Introduction

Organometallic fluorides have received considerable attention owing to their structural diversity, which is associated with the ambivalent nature of fluorine. Fluorine is both monovalent and an excellent donor.[1] As it is also the most electronegative element, fluorine typically forms very polar or ionic bonds with most main-group elements[2] and transition metals.[3]

Triorganotin fluorides, R_3SnF, have been known for many decades,[4,5] and the nature of the Sn−F bonds remains controversial. Owing to its high melting point and virtual insolubility in organic solvents, Okawara et al. originally proposed an ionic structure for Me_3SnF.[6] However, on the basis of an early X-ray structure and IR and Raman spectroscopy, the structure of Me_3SnF was reformulated as a polymeric arrangement consisting of planar trimethyltin groups bridged by fluorine atoms.[7] Despite the fact that disorder precluded a satisfactory refinement of the X-ray structure of Me_3SnF, the comparatively short Sn−F bond lengths (2.15, 2.45 Å) and the slightly bent Sn−F−Sn bond angle (141°) were interpreted in terms of a predominantly covalent Sn−F bond character.[8−10] A similar arrangement was observed in the X-ray structure of nBu_3SnF; however, disorder again prevented the complete refinement of this structure.[11] Due to their bent Sn−F−Sn linkages, Me_3SnF and nBu_3SnF were both classified as *zigzag* polymers (**I**).[12] In contrast, the structures of the polymeric triorganotin fluorides Ph_3SnF[13] and $(PhCH_2)_3SnF$[14] consist of symmetric Sn−F−Sn bridges with equal Sn−F bond lengths (2.15 Å and 2.16 Å), whereas $cHex_3SnF$[15] contains unsymmetric bridges (2.05/2.30 Å). The latter compounds reveal (almost) linear Sn−F−Sn linkages and hence, are classified as *rod-like* polymers (**II**).[12]

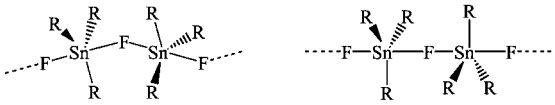

I **II**

The X-ray structure of $(Me_3SiCH_2)_3SnF$ deserves a special comment.[16] The authors suggested a *rod-like* polymer with symmetric Sn−F−Sn bridges. The two equally long Sn−F bonds (2.57 Å) were interpreted in terms of a highly ionic bond character.[15]

Monomeric structures have been reported for triorganotin fluorides containing more sterically demanding substitu-

[a] Fachbereich Chemie der Universität Dortmund, Lehrstuhl für Anorganische Chemie II,
44221 Dortmund, Germany
Fax: (internat.) + 49-(0)231/755-5048
E-mail: kjur@platon.chemie.uni-dortmund.de
[b] Centre for Chiral and Molecular Technologies, Deakin University,
Geelong, Vic. 3217, Australia
Fax: (internat.) + 61-0352/272218
E-mail: dainis@deakin.edu.au

ents, such as $[(Me_2PhSi)_3C]Me_2SnF$, $[(Me_3Si)_3C]Ph_2SnF$,[17] and $(2,4,6\text{-}Me_3C_6H_2)_3SnF$.[18] The latter compound was used to establish a standard "covalent" Sn−F bond length (1.96 Å).[18] Monomeric triorganotin fluorides were also obtained using the intramolecular coordination of the so-called *built-in* ligands.[19−23] Similarly, triorganotin fluorides react with additional fluoride ions to form monomeric triorganodifluorostannates, $R_3SnF_2^-$.[24−27]

Besides X-ray diffraction studies, ^{119}Sn Mössbauer spectroscopy,[12,28−41] ^{119}Sn MAS NMR spectroscopy,[42−47] IR spectroscopy,[6,10,36,48−52] and Raman spectroscopy[36,39,52] have been applied to distinguish between polymeric and monomeric triorganotin fluorides. Consequently, iBu$_3$SnF,[44] $(PhCH_2CH_2CH_2)_3SnF$,[53] and $(F_3C)_3SnF$[54] were assigned as polymeric structures, whereas $(PhMe_2CCH_2)_3SnF$,[53,55] $[(Me_3Si)_3C]Me_2SnF$,[17] $[(Me_3Si)(Me_2FSi)_2C]Me_2SnF$,[56] and $[(Me_3Si)_2(Me_2FSi)C]Me_2SnF$[57] have been identified as monomers. Furthermore, in the presumed polymeric triorganotin fluorides, R_3SnF (R = Me, Et, *n*Pr, *n*Bu, *n*Pen, *n*Hex, *n*Oct, *n*Dec), the effect of the lengths of the alkyl chain on the melting point, solubility, and the degree of crystallinity were studied, however, without the support of spectroscopy.[58]

Recently, Gillespie et al. used results from ab initio calculations to reinterpret the nature of bonds containing fluorine.[59] They concluded that a large majority of element−fluorine bonds, including Si−F bonds, possess substantial ionic character, and molecules such as SiF_4 are therefore more appropriately described using a ligand close-packing model with predominately ionic Si−F bonds.[60,61] A search of the literature revealed only two publications that included ab initio studies of molecules containing tin−fluorine bonds,[62,63] although neither of these studies focused directly on the nature of the Sn−F bonds.

The unusually high solubility of the new triorganotin fluoride $PhMe_2SnF$ enabled a comprehensive study of a polymeric triorganotin fluoride in solution. We now report on the results of this study, as well as on the reinvestigation of the structure of $(Me_3SiCH_2)_3SnF$.[16] The ab initio electronic structure calculations of the model compounds H_3SnF, $[H_3SnFSnH_3]^+$, and $[FH_3SnFSnH_3F]^-$ are also reported.

Results and Discussion

Dimethylphenyltin fluoride Me_2PhSnF (**1**) and tris(trimethylsilylmethyl)tin fluoride $(Me_3SiCH_2)_3SnF$ (**2**) were prepared in good yields from Me_2PhSnI and $(Me_3SiCH_2)_3SnCl$ (**2a**) by halide exchange reactions with KF and NH_4F, respectively, in a two-layer solvent system (water/diethyl ether) [Equation (1)].

$$R_2R'SnX \xrightarrow[-\ NH_4Cl\ or\ -\ KCl]{KF\ (ex)\ or\ NH_4F\ (ex)/H_2O/ether} R_2R'SnF \quad (1)$$

X = Cl, I

1, R = Me, R' = Ph

2, R = R' = CH_2SiMe_3

For putative polymeric triorganotin fluorides, **1** and **2** reveal very low melting points, 124−126 °C and 123−127 °C, respectively. In comparison, Me_3SnF and Ph_3SnF melt at temperatures exceeding 250 °C or decompose without melting.[4,5] This observation prompted us to investigate the structures of **1** and **2** in greater detail.

Characterization of 1 and 2 in the Solid State

The ^{119}Sn MAS NMR spectrum of Me_2PhSnF (**1**) exhibits a triplet centered at $\delta = -49.3$ ppm with a $^1J(^{119}Sn\text{-}^{19}F)$ coupling of 1235 Hz, thus unambiguously revealing a polymeric arrangement with symmetric Sn−F−Sn bridges on the NMR time scale. The ^{119}Sn MAS NMR parameters of **1** agree well with those reported for the polymeric parent compounds Me_3SnF [triplet at $\delta = 24.3$ ppm, $^1J(^{119}Sn\text{-}^{19}F) = 1300$ Hz] and Ph_3SnF [triplet at $\delta = -211.9$ ppm, $^1J(^{119}Sn\text{-}^{19}F) = 1530$ Hz].[44] The integration over all spinning sidebands of the three independent manifolds confirms the 1:2:1 ratio required for a triplet. The large sideband manifolds were also utilized to perform a tensor analysis according to the method of Herzfeld and Berger.[64,65] The isotropic chemical shielding (δ_{iso}), anisotropy (ζ), asymmetry (η) and chemical shift tensor components (σ_{11}, σ_{22}, σ_{33}) are presented in Table 1, alongside the same parameters for the related compounds Me_3SnF, Ph_3SnF, and $[Ph_3SnF_2]^-$.[27,44,45] Comparison of the data reveals that the average anisotropy for **1** is substantially larger ($|\zeta_{avg}| = 312$ ppm) than for Me_3SnF ($|\zeta_{avg}| = 221$ ppm), Ph_3SnF ($|\zeta_{avg}| = 250$ ppm) and $[Ph_3SnF_2]^-$ ($|\zeta_{avg}| = 219$ ppm), which clearly indicates that this parameter not only depends on the coordination number, but also on the local symmetry around the tin atoms. The lower symmetry in **1** as compared with Me_3SnF and Ph_3SnF is also reflected in the asymmetry, which is in the range between 0.80 and 1.00 for the three manifolds. For the parent compounds, which possess threefold symmetry axes, group theory requires the asymmetry to be 0.00,[66] which is indeed what was observed.[44,45]

In sharp contrast, the ^{119}Sn MAS NMR spectrum of $(Me_3SiCH_2)_3SnF$ (**2**) shows a doublet centered at 165.8 with a $^1J(^{119}Sn\text{-}^{19}F)$ coupling of 2167 Hz, indicating a monomer with tetracoordinated tin atoms. The ^{119}Sn MAS NMR parameters of **2** are similar to those of monomeric $(2,4,6\text{-}Me_3C_6H_2)_3SnF$ [two doublets due to crystallographically independent tin atoms at $\delta = -70.6$ ppm, $^1J(^{119}Sn\text{-}^{19}F) = 2300$ Hz; and $\delta = -82.2$ ppm, $^1J(^{119}Sn\text{-}^{19}F) = 2256$ Hz].[45] The integration over the two spinning sideband manifolds confirms that both sites of the doublet are of equal intensity. The reasonably small sideband manifolds of **2** were used to perform a tensor analysis as described above; the parameters obtained along with those for $(2,4,6\text{-}Me_3C_6H_2)_3SnF$ are presented in Table 1.[44] It is interesting to note that, for compound **2**, the asymmetry η is 0.00, which strongly indicates the presence of a threefold symmetry axis for the geometry around the tin atom;[66] this result is indeed confirmed by the single-crystal X-ray structure analysis (see below). The average anisotropy of **2** ($|\zeta_{avg}| = 95$ ppm) lies between those of the (symmetrically substituted) pentacoordi-

Table 1. Selected ^{119}Sn MAS NMR parameters for **1**, **2** and related compounds

Compound	δ_{iso}	ζ [ppm]	η	σ_{11} [ppm]	σ_{22} [ppm]	σ_{33} [ppm]
1	−39.3	−350.1	0.85	363	66	−311
	−48.2	−306.3	1.00	354	48	−258
	−57.0	+281.3	0.80	−196	29	338
Me_3SnF	41.5	−329	0.0	123	123	−370
	24.1	−221	0.0	87	87	−245
	6.7	−113	0.0	50	50	−120
Ph_3SnF	−198.1	−306	0.0	351	351	−108
	−211.9	−255	0.0	340	340	−43
	−225.2	−188	0.0	321	321	37
$[Ph_2SnF_2]^-$	−348.8	−276.5	0.20	515	459	72
	−362.7	−222.7	0.00	474	474	140
	−376.5	−158.0	0.20	471	440	218
2	154.7	154.7	0.00	−119	−119	−226
	169.4	169.4	0.00	−110	−110	−289
Mes_3SnF[a]						
(site 1)	−54.0	−51	0.2	85	74	3
	−84.8	75	0.1	42	53	160
(site 2)	−65.9	−62	0.3	107	87	3
	−96.0	63	0.3	55	74	159

[a] Mes = 2,4,6-$Me_3C_6H_2$.

nated compounds (Me_3SnF, Ph_3SnF, $[Ph_3SnF_2]^-$) and monomeric $(2,4,6\text{-}Me_3C_6H_2)_3SnF$ ($|\zeta_{avg}|$ = 63 ppm). Given that the symmetry of **2** is higher than that in $(2,4,6\text{-}Me_3C_6H_2)_3SnF$,[18] this observation may indicate a weak intermolecular Sn···F interaction ([4+1] coordination). Since this additional interaction is indeed confirmed by the single-crystal X-ray structure analysis (see below), it seems that the anisotropy ζ is more sensitive than the $^1J(^{119}Sn\text{-}^{19}F)$ coupling towards weak interactions. However, more systematic work is needed to prove this hypothesis.

The ^{119}Sn Mössbauer spectrum of **1** is also in good agreement with a polymeric structure.[37] The quadrupole splitting and the isomeric shift, 3.87 and 1.30 mm·s^{-1}, respectively, are indicative of pentacoordinated tin atoms. Notably, the quadrupole splitting and the isomeric shift for Me_3SnF and Ph_3SnF were reported to be 3.80 and 1.36 mm·s^{-1}, and 3.62 and 1.32 mm·s^{-1}, respectively.[36] In contrast, the Mössbauer spectrum of **2** is consistent with a monomeric structure containing tetracoordinated tin atoms; the quadrupole splitting and the isomeric shift are 2.97 and 1.29 mm·s^{-1}, respectively.[37]

In the pioneering work of Kriegsmann et al., the IR spectra of the triorganotin fluorides, R_3SnF (R = Me, Et, *n*Pr, *n*Bu), were compared, both in the solid state (polymeric) and in the gas phase (monomeric). They concluded that the asymmetric Sn−F stretching vibration for polymeric triorganotin fluoride compounds lies between 340 and 360 cm^{-1}, whereas for monomeric compounds the Sn−F stretching vibrations are between 530 and 590 cm^{-1}.[36,48,50] The IR spectrum (KBr pellet) of **1** shows a broad absorption at 340 cm^{-1}, consistent with a polymeric structure. In contrast, the IR spectrum (KBr pellet) of **2** shows no band between 300 and 400 cm^{-1}, but a band, which appears at 471 cm^{-1}, is tentatively assigned to an Sn−F stretching vibration. The position of this band lies between those of monomeric and polymeric triorganotin fluoride compounds. This supports the interpretation of the single-crystal X-ray diffraction analysis which shows that compound **2** exhibits a structure between the polymeric and monomeric forms, with a [4+1]-coordinated tin atom (see below).[36,48,50]

Single-Crystal X-ray Analyses of 1, 2, and 2a

The X-ray structure of Me_2PhSnF (**1**) is illustrated in Figure 1; selected bond parameters are collected in the caption of the figure, and details of the structure solution are listed in Table 3. Compound **1** features a slightly distorted *rod-like* polymeric arrangement with almost symmetric Sn−F bond lengths. All tin atoms in **1** are crystallographically related and adopt slightly distorted trigonal-bipyramidal geometries [geometrical goodness $\Delta\Sigma(\theta)$ = 88.4°], with the axial and equatorial positions occupied by two fluorine and three carbon atoms, respectively.[67,68] The slight distortion is best reflected in the C(1)−Sn(1)−C(11) and F(1)−Sn(1)−F(1a) bond angles, which are 116.5(1) and 179.44(7)°, respectively. The Sn−F bond lengths of **1** are 2.162(1) and 2.179(1) Å, and are only 0.016 and 0.033 Å longer than those of Ph_3SnF.[13] The tin atom is displaced by 0.030(2) Å from the plane defined by C(1), C(2), C(11), in the direction of F(1). In the crystal lattice, Me_2PhSnF (**1**) forms stapled layers of parallel but isolated polymer chains (Figure 2). The shortest distance between these polymer chains is 3.656(4) Å, between C(14) and C(16c) (c = 0.5 + x, y, −0.5 − z) of neighboring phenyl groups.

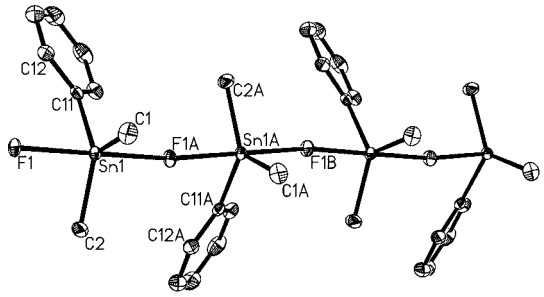

Figure 1. General view (SHELXTL) of a part of the polymeric chain of **1** showing 30% probability displacement ellipsoids and the atom numbering (SHELXTL-PLUS); selected bond lengths [Å] and angles [°]: Sn(1)−C(1) 2.112(3), Sn(1)−C(2) 2.115(3), Sn(1)−C(11) 2.123(3), Sn(1)−F(1) 2.162(1), Sn(1)−F(1a) 2.179(1), C(1)−Sn(1)−C(2) 121.7(1), C(1)−Sn(1)−C(11) 116.5(1), C(2)−Sn(1)−C(11) 121.7(1), C(1)−Sn(1)−F(1) 91.78(9), C(2)−Sn(1)−F(1) 89.99(8), C(11)−Sn(1)−F(1) 90.72(7), C(1)−Sn(1)−F(1a) 88.63(8), C(2)−Sn(1)−F(1a) 90.12(8), C(11)−Sn(1)−F(1a) 88.76(7), F(1)−Sn(1)−F(1a) 179.44(7), Sn(1)−F(1)−Sn(1b) 172.57(7) (symmetry transformation used to generate equivalent atoms: a = $-x$ + 1/2, y + 1/2, z; b = x, y − 1, z)

Despite having a very low melting point, Me_2PhSnF (**1**) is a polymer in the solid state. Apparently, this observation may simply be explained by the well-known correlation between the symmetry and the melting point of a molecule. It

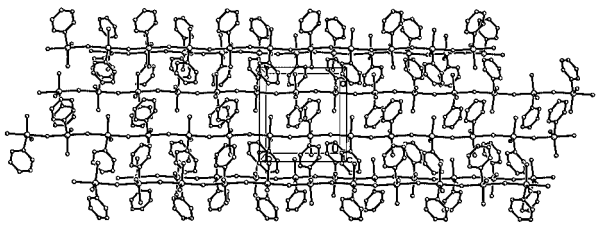

Figure 2. Perspective view (SHELXTL) of stapled layers of parallel polymer chains running through the crystal lattice of **1**

has been suggested that highly symmetrical molecules can absorb appreciable amounts of energy, before vibrations induce disruption from the crystal lattice.[69] In fact, all other structurally investigated polymeric triorganotin fluoride complexes bear three identical organic substituents and hence, possess a higher degree of symmetry than **1**.

The X-ray structure of $(Me_3SiCH_2)_3SnF$ (**2**) is illustrated in Figure 3; selected bond parameters are collected in the caption of the figure, and details of the structure solution are listed in Table 3. As previously reported by Zakharov et al.,[16] the structure of **2** is characterized by an infinite chain of tin atoms, with an Sn−Sn separation of 5.151(1) Å. However, the Sn−F distances are not equal [2.565(8) Å],[16] but show two pairs of different values [2.027(6)/3.125(6) Å and 2.377(6)/2.774(6) Å] as result of the dynamic disorder of the tin and fluorine atoms, respectively. The tin atoms exhibit strongly distorted trigonal-bipyramidal configurations [geometrical goodness $\Delta\Sigma(\theta)$ = 47.1° (Sn1), 54.0° (Sn1′)],[67,68] and represent positions halfway along the tetrahedron−trigonal bipyramid pathway. The distortion from the ideal trigonal bipyramid is reflected in the C−Sn(1)−C and C−Sn(1′)−C angles of 116.5(2) and 117.4(2)°, respectively. The origin for the deviation of these angles from tetrahedral is not mostly due to the steric hindrance of the organic substituents, as observed for Mes_3SnF (mean C−Sn−C 116.8°),[18] nor due to substituent electronegativity (Bent's rule),[70] but is rather the result of the intermolecular Sn(1)···F(1A) and Sn(1′)···F(1A) distances of 2.774(6) and 3.125(6) Å, respectively, being shorter than the sum of the van der Waals radii of tin and fluorine (3.63 Å).[70] This view is supported by the solid-state structure of $(Me_3SiCH_2)_3SnI$,[71] which shows C−Sn−C angles (111.7−115.2°) that are closer to those in a tetrahedral geometry.[72] Most interestingly, it appears that the intermolecular Sn···F interactions are not unambiguously reflected by the ^{119}Sn MAS NMR spectrum of **2**, which reveals a doublet and not a doublet of doublets (see above). The latter observation further strongly supports a dynamic rather than a statistical disorder in the structure of **2**. Given the sensitivity of ^{119}Sn MAS NMR spectroscopy, statistically disordered tin sites would give rise to the observation of two independent doublets. It is also worth mentioning that the molecular structure of $(Me_3SiCH_2)_3SnCl$ (**2a**) exhibits an analogous disorder, as shown in Figure 4; selected bond parameters are collected in the caption of the figure and details of the structure solution are listed in Table 2. The Sn−Sn separation in the infinite chain of tin atoms is 5.564(2) Å, and the pairs of Sn−Cl distances are 2.508(9)/3.056(9) and 2.498(10)/3.066(10) Å.[72] The geometrical goodness $\Delta\Sigma(\theta)$ of the respective tin atoms is 54.45° (Sn1) and 70.02° (Sn1′).[67,68]

Characterization of 1 and 2 in Solution

$PhMe_2SnF$ (**1**) and $(Me_3SiCH_2)_3SnF$ (**2**) are highly soluble in common organic solvents, such as chloroform, tolu-

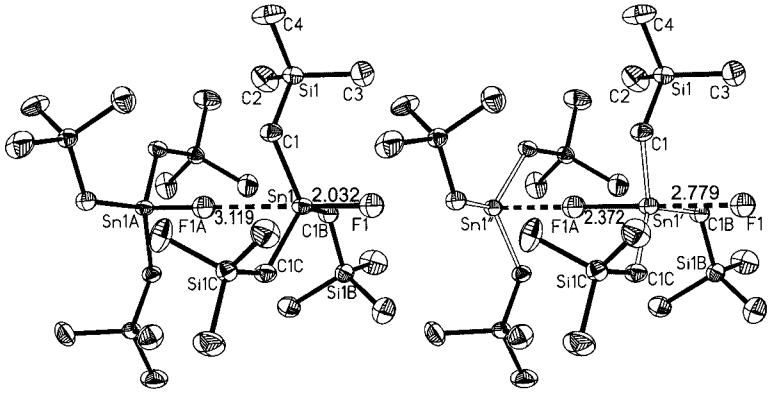

Figure 3. General view (SHELXTL) of **2** showing 30% probability displacement ellipsoids and the atom numbering scheme; selected bond lengths [Å] and angles [°]: disordered site 1: Sn(1)−C(1) 2.131(3), Sn(1)−F(1) 2.027(7), Sn(1)−F(1a) 3.125(7), C(1)−Sn(1)−C(1b) 116.5(2), C(1)−Sn(1)−F(1) 100.8(4), C(1)−Sn(1)−F(1a) 79.2(4), F(1)−Sn(1)−F(1a) 180.0; disordered site 2: Sn(1′)−C(1) 2.122(3), Sn(1′)−F(1) 2.774(6), Sn(1′)−F(1a) 2.377(6), C(1)−Sn(1′)−C(1b) 117.4(2), C(1)−Sn(1′)−F(1) 80.6(4), C(1)−Sn(1′)−F(1a) 99.4(4), F(1)−Sn(1′)−F(1a) 180.0 (symmetry transformations used to generate equivalent atoms: $a = -x, -y, z - 1/2$; $b = -y, x - y, z$; $c = -x + y, -x, z$)

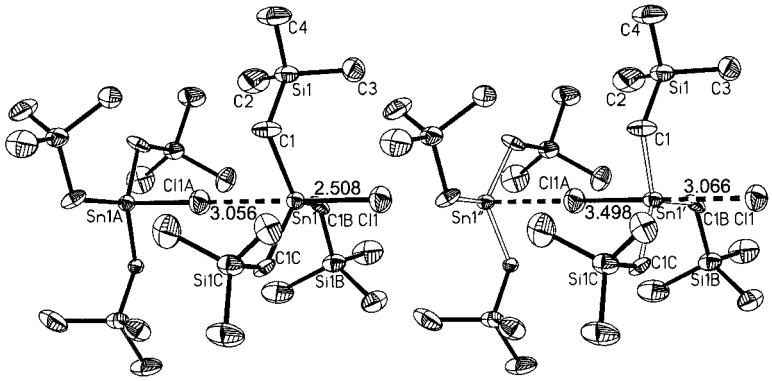

Figure 4. General view (SHELXTL) of **2a** showing 30% probability displacement ellipsoids and the atom numbering scheme; selected bond lengths [Å] and angles [°]: disordered site 1: Sn(1)−C(1) 2.154(4), Sn(1)−Cl(1) 2.508(9), Sn(1)−F(1a) 3.056(9), C(1)−Sn(1)−C(1b) 117.5(2), C(1)−Sn(1)−Cl(1) 99.3(3), C(1)−Sn(1)−Cl(1a) 80.7(3), Cl(1)−Sn(1)−Cl(1a) 180.0; disordered site 2: Sn(1′)−C(1) 2.136(3), Sn(1′)−Cl(1) 3.066(10), Sn(1′)−Cl(1a) 2.498(10), C(1)−Sn(1′)−C(1b) 119.0(1), C(1)−Sn(1′)−Cl(1) 94.3(3), C(1)−Sn(1′)−Cl(1a) 95.7(3), Cl(1)−Sn(1′)−Cl(1a) 180.0 (symmetry transformations used to generate equivalent atoms: $a = -x, -y, z - 1/2$; $b = -y, x - y, z$; $c = -x + y, -x, z$)

Table 2. Calculated NPA atomic charges for **3** and the staggered conformers of **4** and **5**

Molecule	$-q$(F) [au]	q(Sn) [au]	$-q$(H) [au]
3	0.723	1.545	0.274
4	0.743	1.522	0.217
5		1.607	0.302
bridging F	0.809		
terminal F	0.796		

ene, or methanol, which is in contrast to most polymeric triorganotin fluorides.[4,5]

The osmometric molecular weight determination of **1** (in toluene) reveals a strong, but steady concentration and temperature dependence, as illustrated in Figure 5. The highest molecular mass observed was 12000 g·mol^{-1}, corresponding to a degree of association exceeding 50 molecular units. In contrast, the molecular weight determination of **2** (in CH_2Cl_2) showed only the presence of monomers.5

Being consistent with the afore-mentioned ^{119}Sn MAS NMR spectrum, the ^{119}Sn NMR spectrum of **1** in [D$_8$]toluene displays a broad triplet at $\delta = -53.0$ ppm [$\nu_{1/2} = 250$, $^1J(^{119}\text{Sn-}^{19}\text{F}) = 1334$ Hz], the shape of which is somewhat distorted and similar to that reported for nBu$_3$SnF.[46] The ^{19}F NMR spectrum of **1** in [D$_8$]toluene shows a signal at $\delta = -139.0$ ppm ($\nu_{1/2} = 150$ Hz) with an unresolved $^1J(^{19}\text{F-}^{119/117}\text{Sn})$ coupling of 1260 Hz. Bearing in mind the natural abundance of the isotopes ^{119}Sn and ^{117}Sn, the magnitude of the integral ratio between the main signal and the tin satellites confirms the Sn−F−Sn connectivity. The presence of only one signal in both the ^{119}Sn and ^{19}F NMR spectrum suggests the fast exchange, on the ^{119}Sn and ^{19}F NMR time scales, of rapidly interconverting oligomers with varying degrees of association. We speculate that the $^1J(^{119}\text{Sn-}^{19}\text{F})$ coupling is maintained because the majority of F−Sn−F

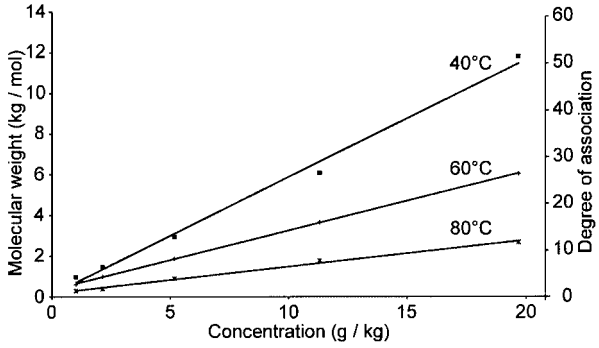

Figure 5. Osmometric molecular mass determination of **1** in toluene at 40, 60, and 80 °C (concentrations: 1.0, 2.1, 5.1, 11.3, 19.7 g·kg^{-1})

fragments present in these oligomers possess lifetimes that are comparatively long on the ^{119}Sn and ^{19}F NMR time scales.[46] Attempts to slow down the exchange process at −80 °C indeed show that the ^{119}Sn and ^{19}F spectra in [D$_8$]toluene become more complex. However, the broadness of the signals precluded the recognition of distinctive NMR multiplets or signals. All attempts to identify monomers at 80 °C or very low concentration (10 mg·mL^{-1} for ^{119}Sn; 0.25 mg·mL^{-1} for ^{19}F) failed. The IR spectrum of a saturated solution of **1** in CH_2Cl_2 shows a very strong asymmetric stretching Sn−F vibration at 339 cm^{-1}, which is almost identical to the corresponding band in the solid state and indicates bridging fluorine atoms.

At high molecular weights, a remarkable viscosity was noticed for solutions of **1** in toluene, which increases with higher concentrations and lower temperatures. Similar ob-

servations have already been reported for solutions of nBu$_3$SnF in different solvents, for which the effect was studied in greater detail.[73−75] Additives, such as pyridine or aniline, reduce the viscosity to that of the pure solvent.[73] No attempts were made to determine the viscosity of **1** in different solvents. Instead, a solution of **1** in [D$_5$]pyridine was investigated by ^{119}Sn NMR spectroscopy, which shows a broad signal centered at $\delta = -84.0$ ppm ($\nu_{1/2}$ = 800 Hz) at room temperature, and a doublet centered at $\delta = -91.5$ ppm ($\nu_{1/2}$ = 350 Hz) with a $^1J(^{119}\text{Sn-}^{19}\text{F})$ coupling of 1905 Hz at −25 °C. The ^{19}F NMR spectrum of the same solution at room temperature and at −25 °C shows a signal centered at $\delta = -168.6$ ppm [$^1J(^{19}\text{F-}^{119}\text{Sn}) = 1840$ Hz], and at $\delta = -164.4$ ppm [$^1J(^{19}\text{F-}^{119}\text{Sn}) = 2100$ Hz], respectively. The observation of a doublet in the ^{119}Sn NMR spectrum, and the intensity ratio of the satellites to the main signal in the ^{19}F NMR spectrum suggest the formation a monomeric complex, PhMe$_2$SnF·pyridine. An analogous complex, namely Ph$_3$SnF·pyridine, has already been mentioned in the literature.[24]

The ^{119}Sn NMR spectrum ($CDCl_3$) of **2** shows a doublet centered at $\delta = 193.0$ ppm with a $^1J(^{119}\text{Sn-}^{19}\text{F})$ coupling of 2340 Hz, which agrees reasonably well with the ^{119}Sn MAS NMR parameters (see above), although the difference in the chemical shift in solution and in the solid state (δ = 31.0 ppm) is much bigger than that in compound **1** (δ = 4.8 ppm). One possible explanation is that in solution the tetrahedral configuration of the tin atom in **2** is much less distorted than in the solid state, i.e. compound **2** is entirely monomeric. The ^{19}F NMR spectrum of **2** reveals a signal at $\delta = -207.2$ ppm, with a well-resolved $^1J(^{19}\text{F-}^{119}\text{Sn})$ coupling of 2370 Hz. The integration of the main signal with respect to the tin satellites confirms the monomeric structure.

Electrospray Mass Spectrometry

In order to identify the association of organotin ions with the parent compounds by autoionization, ESI MS spectra of PhMe$_2$SnF (**1**) and (Me$_3$SiCH$_2$)$_3$SnF (**2**) were recorded in acetonitrile. The following mass clusters showing the expected isotopic patterns were observed: **1**, negative mode: $Me_2PhSnF_2^-$ (265.0), $(Me_2PhSn)_2F_3^-$ (509.0), $(Me_2PhSn)_3F_4^-$ (753.0), positive mode: Me_2PhSn^+ (227.0), $(Me_2PhSn)_2F^+$ (471.0), $(Me_2PhSn)_3F_2^+$ (715.0), $(Me_2PhSn)_4F_3^+$ (961.0); **2**, negative mode: $(Me_3SiCH_2)_3SnF_2^-$ (419.1), positive mode: $(Me_3SiCH_2)_3Sn^+$ (381.1), $[(Me_3SiCH_2)_3Sn]_2F^+$ (779.2).

The ready formation of charged species suggests a highly ionic character of the Sn−F bonds in **1** and **2**. The degree of association is generally higher for species related to **1** than for those related to **2**, which correlates well with the observed Lewis acidities of the parent compounds. For some of the organotin anions detected under electrospray conditions, analogs were already identified in previous studies by ^{119}Sn NMR and ^{19}F NMR spectroscopy, e.g. $R_3SnF_2^-$ and $(R_3SnF)_2F^-$ (R = Me, nBu, Ph).[25,76,77] The observation of the uncoordinated (solvent-free) triorganotin cations, Me_2PhSn^+ (227.0) and $(Me_3SiCH_2)_3Sn^+$ (381.1), is also worth mentioning as the stabilities of such species were questioned for a long time.[78,79] Recently, the crystal structure of an isolated nBu$_3$Sn$^+$ cation (counter anion $CB_{11}Me_{12}^-$) undeniably proved the stabilities of these species.[80]

Conductivity measurements of **2** in acetonitrile, at $c = 10^{-3}$ mol·L^{-1}, reveal no change in conductivity compared with that of the pure solvent (1.7 μS). The result is consistent with extensive ion-pairing.

Ab Initio Computational Study of Model Compounds Containing Sn−F Bonds

The three model compounds H$_3$SnF (**3**), [H$_3$SnFSnH$_3$]$^+$ (**4**), and [FH$_3$SnFSnH$_3$F]$^-$ (**5**) were selected as subjects for the computational investigation. H$_3$SnF (**3**) is the simplest example of a monomeric tetravalent tin compound containing a tin−fluorine bond, whereas [H$_3$SnFSnH$_3$]$^+$ (**4**) and [FH$_3$SnFSnH$_3$F]$^-$ (**5**) represent two possible ways of defining a subsection of a polymeric tin fluoride chain. It is expected that the actual properties of the Sn−F−Sn linkages in a polymeric chain would be intermediate between those of the two extremes modeled herein. Furthermore, **4** and **5** resemble the corresponding ditin ions that have been detected in the ESI MS analyses of **1** and **2**.

The B3LYP/TZ-optimized structures of the model compounds, alongside selected geometric parameters are depicted in Figure 6. The calculated Sn−F bond length of H$_3$SnF (**3**) of 1.946 Å appears to agree with the Sn−F bond length of 1.961(4) Å observed in the monomeric triorganotin fluoride (2,4,6-Me$_3$C$_6$H$_2$)$_3$SnF.[18] For [H$_3$SnFSnH$_3$]$^+$ (**4**) and [FH$_3$SnFSnH$_3$F]$^-$ (**5**), staggered and eclipsed conformations were located on the potential energy surfaces; however, the differences in calculated bond lengths and angles between rotamers are negligible in both cases. Therefore, only the staggered conformations will be discussed here. As expected, the Sn−F distances increase when the coordination numbers of both tin and fluorine are increased: the Sn−F distance in **4** is 2.124 Å, and the distance from Sn to the bridging F atom in **5** increases further to 2.255 Å when the coordination number of tin is raised from four to five. This result is consistent with the experimentally obtained Sn−F bond lengths in polymeric organotin fluorides. For instance, the mean Sn−F bond lengths in **1**, Ph$_3$SnF, and cHex$_3$SnF are 2.171(2), 2.145(1), and 2.177(1) Å, respectively. The distance between the tin and the nonbridging fluorine atoms in **5** (2.041 Å) is also somewhat larger than the Sn−F distance in H$_3$SnF (**3**). The equilibrium Sn−F−Sn angles for all four fluorine-bridged ditin systems are calculated to be 180°. The SnH$_3$ moieties in **4** and **5** are effectively able to undergo free internal rotation, the calculated energy difference between the staggered and eclipsed conformations is only 0.02 kcal·mol^{-1} and 0.05 kcal·mol^{-1} for **4** and **5**, respectively. Both conformers of **4** and the staggered conformer of **5** are calculated to be minima on the B3LYP/TZ potential energy surface, whereas the eclipsed conformer of **5** is a first-order saddle point possessing one imaginary frequency (30i cm^{-1}) associated with rotation of the SnH$_3$ moieties towards the staggered con-

formation. The fact that the eclipsed conformer of **4** is calculated to be a minimum instead of a transition state analogous to the eclipsed conformer of **5**, could be an artifact due to the extreme flatness of the potential energy surface around the calculated stationary points, as illustrated by the very small difference in energy between the staggered and eclipsed conformations in **4**.

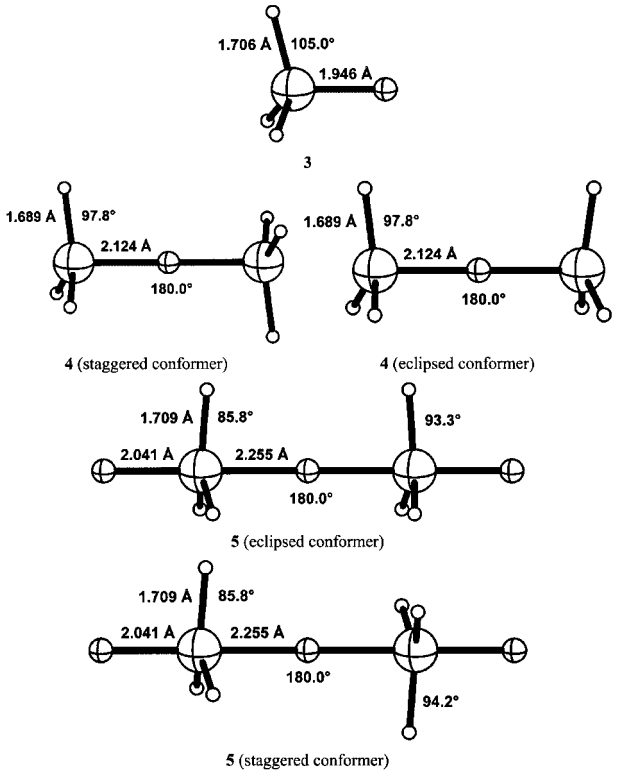

Figure 6. B3LYP/TZ-optimized structures and selected geometrical parameters of the model compounds **3**, and both eclipsed and staggered conformers of **4** and **5**

The Sn−F−Sn bending potential curves for both conformers of **4** and **5** are plotted in Figure 7. For both cases, it was found that the staggered conformation is slightly lower in energy than the eclipsed conformation at all Sn−F−Sn angles studied. The energy difference between the two conformers is smallest at the equilibrium Sn−F−Sn angle of 180°, and increases slightly as the Sn−F−Sn angle is reduced. This is consistent with the observation of staggered conformations in crystal structures of polymeric triorganotin fluorides, e.g. **1**, Ph_3SnF[13] and *c*Hex_3SnF.[15] However, the small energy differences calculated herein imply that the experimentally observed preference for polymeric triorganotin fluorides to adopt staggered conformations could be due to crystal-packing or steric effects, rather than electronic factors. All four curves are indicative of a very flat bending potential surface around the equilibrium Sn−F−Sn angle of 180°. Both curves corresponding to **4** lie below room temp. (= 0.6 kcal·mol^{-1}) between 160 and 180°, whereas the curves corresponding to **5** lie below room temp. between 140 and 180°. According to the criteria set forth by Gillespie et al., the linear Sn−F−Sn equilibrium angle and the high flexibility of the Sn−F−Sn linkages are indicative of highly ionic Sn−F bonds.[59] Thus, the observation of *zigzag* polymeric structures (bent Sn−F−Sn linkages) for Me_3SnF[8−10] and nBu_3SnF,[11] may be attributed to a combination of this flexibility and crystal packing effects, rather than being an indication of covalent bond character.[8−10] Despite the high flexibility of the Sn−F−Sn linkages, the preference of the F−Sn−F angles to be close to 180° (Bent's rule) precludes the formation of small or medium-sized rings in solution, e.g. similar to *cyclo*-$(R_2AlF)_3$.[81] The average internal angle of a *n*-membered ring is required by three-dimensional geometry to be less than (for puckered rings) or equal to (for flat rings) $[(n-2)/n] \times 180°$.[82] Constraining the F−Sn−F angles to be linear, would therefore necessitate large values of *n* before the Sn−F−Sn linkages are able to adopt favorable angles (> 150°).

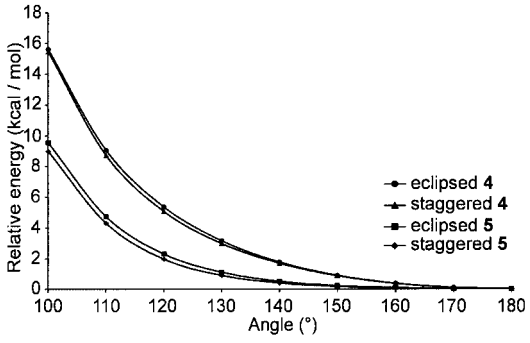

Figure 7. Energy profiles for the Sn−F−Sn bending deformations of both eclipsed and staggered conformers of **4** and **5**

Natural Population Analysis (NPA)[83] atomic charges calculated for **3** and the staggered conformers of **4** and **5** clearly show a significant localization of negative charge on the fluorine atoms in the model compounds, hence providing further evidence of the high ionic character of the Sn−F bond (Table 2). The bonds between tin and the bridging fluorine atoms are apparently slightly more ionic than the bonds between tin and non-bridging fluorine atoms.

In order to investigate the possibility that an oscillating (flip-flop) motion of the fluorine atoms between two neighboring tin atoms could be the reason for the disorder observed in the X-ray structure solution of **2**, a potential energy surface scan of the staggered conformer of **4** was performed, where the Sn−Sn separation is fixed at various values and the fluorine atom is moved from one tin atom to another. The calculated energy profiles are plotted in Figure 8. At a small Sn−Sn separation of 4.25 Å, which is extremely close to the equilibrium distance of 4.248 Å calculated for **4**, and a reasonable approximation to the measured Sn−Sn separations in the X-ray structures of all polymeric triorganotin fluorides, e.g. Ph_3SnF (4.29 Å),[13] $(PhCH_2)_3SnF$ (4.33 Å),[14] and **1** (4.33 Å), the curve re-

sembles a parabola with a minimum at the halfway point, where both Sn−F distances are 2.125 Å. However, when the Sn−Sn separation is increased, the curves become double-minimum potentials, which possess two minima approximately 2 Å away from the two tin atoms and a local maximum at the halfway point between the two tin atoms. This situation resembles that found in monomeric triorganotin fluorides, e.g. (2,4,6-$Me_3C_6H_2)_3SnF$ (Sn−Sn separation 6.42 Å, mean Sn−F distance 1.96 Å).[18] Most interestingly, the energy barrier between the two minima is found to increase substantially with increasing Sn−Sn separation. Thus, for very large Sn−Sn separations, as observed in (2,4,6-$Me_3C_6H_2)_3SnF$, the fluorine atoms are trapped in their respective potential wells. However, for reasonably small Sn−Sn separations, as observed in **2** (5.15 Å), the energy barrier is low enough to be exceeded and the fluorine atoms may oscillate (flip-flop) between the two potential wells. In the X-ray experiment of **2**, this motion is evidenced by a dynamic disorder (see above). It was further noticed that disorder prevented the complete refinement of the X-ray structure of Me_3SnF.[8−10] From the indisputable Sn−Sn separation (4.6 Å) it can be surmised that the disorder in Me_3SnF might also be due to dynamic factors rather than on statistical grounds.[84] In contrast, the Sn−Sn separation in the unsymmetric polymer *c*Hex_3SnF (4.35 Å)[15] is only marginally greater than in symmetric polymers, such as Ph_3SnF,[13] $(PhCH_2)_3SnF$,[14] and **1**. In view of the calculated energy profiles and the two unsymmetric Sn−F bonds (2.05/2.30 Å), the structure of *c*Hex_3SnF should also reveal a dynamic disorder reflected on the low energy barrier found for small Sn−Sn separations. In fact, the disorder of almost all carbon atoms in the structure of *c*Hex_3SnF strongly supports this assumption.[15]

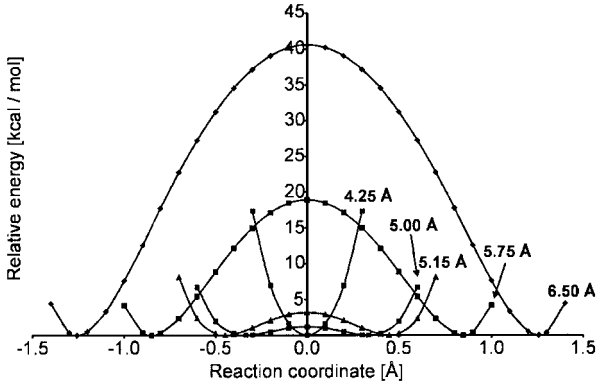

Figure 8. Energy profiles for the motion of the fluorine atoms from one tin atom to another in the staggered conformer of **4**, at Sn−Sn separations of 4.25, 5.0, 5.15, 5.75, and 6.5 Å; the zero of the reaction coordinate is set to the halfway point between the two tin atoms, where both Sn−F bond lengths are equal; calculated equilibrium Sn−F distances are 2.125, 2.165, 2.112, 2.026, and 1.992 Å, respectively

Experimental Section

General: ($Me_3SiCH_2)_3SnCl$ [$\delta(^{119}Sn)$ = 172.6 ppm] was prepared according to literature procedures.[85] Solution ^1H, ^{13}C, ^{19}F, ^{29}Si, and ^{119}Sn NMR spectra were obtained using a Bruker DRX 400 spectrometer. Chemical shifts (δ) are given in ppm and are referenced against $SiMe_4$, $SnMe_4$, and $CFCl_3$. ^{119}Sn MAS NMR spectra were recorded with a Bruker MSL 400 spectrometer using cross-polarization and high-power proton decoupling. An 8-μs 90° pulse, 5 ms of contact time and a recycle delay of 10 s were used. Chemical shifts (δ_{iso}) are quoted relative to $SnMe_4$, using solid *c*Hex_4Sn (δ_{iso} = −97.35 ppm) as a secondary reference. Typically, 12−15 K transitions were recorded for a signal-to-noise ratio suitable for tensor analyses. At least two experiments at independent spinning frequencies ranging from 4−12 kHz were recorded to determine the isotropic chemical shifts. The tensor analyses were performed according to the method developed by Herzfeld and Berger;[64][65] WINFIT software (Bruker) was used to analyze the spectra.[86] The principle components of the shielding tensors are reported using Haeberlen's notation as the isotropic chemical shift ($\delta_{iso} = -\sigma_{iso}$), the anisotropy ($\zeta = \sigma_{33} - \sigma_{iso}$) and the asymmetry ($\eta = |\sigma_{22} - \sigma_{11}|/|\sigma_{33} - \sigma_{iso}|$), σ_{11}, σ_{22}, σ_{33} are the three components of the shielding tensor expressed in its principal axis system with the following convention: $|\sigma_{33} - \sigma_{iso}| \geq |\sigma_{11} - \sigma_{iso}| \geq |\sigma_{22} - \sigma_{iso}|$.[87] With this convention, ζ is a signed value expressed in ppm and η is a dimensionless parameter, the value of which varies between 0 and 1. The Mössbauer spectra were recorded in constant-acceleration mode with a homemade instrument, designed and built by the Institut voor Kernen Stralingsfysica (IKS), Leuven, Belgium. The isomer shifts refer to a source of $Ca^{119m}SnO_3$ from Amersham, U.K., with the samples being maintained at 90(2) K. The data were treated with a least-squares iterative program that deconvoluted the spectrum into a sum of Lorentzians. FT infrared spectra were recorded using a Bruker IFS28 spectrometer. Electrospray mass spectra were obtained with a Platform II single quadrupole mass spectrometer (Micromass, Altrincham, U.K.) using an acetonitrile mobile phase. Acetonitrile solutions (0.1 mM) of the compounds were injected directly into the spectrometer via a Rheodyne injector equipped with a 50-μL loop. A Harvard 22 syringe pump delivered the solutions to the vaporization nozzle of the electrospray ion source at a flow rate of 10 $\mu L \cdot min^{-1}$. Nitrogen was used as both a drying gas and for nebulization with flow rates of approx. 200 $mL \cdot min^{-1}$ and 20 $mL \cdot min^{-1}$, respectively. Pressure in the mass analyzer region was usually about $4 \cdot 10^{-5}$ mbar. Typically 10 signal-averaged spectra were collected. Microanalyses were performed using an instrument from Carlo Erba Strumentazione (Model 1106). Molecular weight determinations were performed with a Gonotec Osmomat 070 osmometer.

Dimethylphenyltin Fluoride, Me_2PhSnF (1): A solution of PhMgBr (80 mL, 50.0 mmol) in THF, which was prepared from C_6H_5Br (7.85 g) and magnesium turnings (1.22 g), was added dropwise at 0 °C to a solution of Me_2SnCl_2 (5.00 g, 22.8 mmol) in THF (80 mL). The reaction mixture was heated at reflux for 1.5 h and the THF was distilled off. Diethyl ether (150 mL) was added to the residue and the resulting suspension was stirred for 15 min. This suspension was hydrolyzed with an aqueous HCl solution (50 mL, 4%), while cooling with ice. The organic layer was separated and the aqueous layer extracted three times with diethyl ether (30 mL). The combined organic phases were dried with Na_2SO_4. Filtration of the sodium sulfate and evaporation of the diethyl ether in vacuo gave Me_2Ph_2Sn (10.15 g, 33.5 mmol) as a yellow oil [$\delta^{119}Sn(CH_2Cl_2/D_2O$ capillary) = −60.1 ppm] of sufficient purity. Iodine (5.71 g, 45 mmol) was added in small portions to an ice-cooled magnetic-

ally stirred solution of Me_2Ph_2Sn (10.15 g, 22.5 mmol) in CH_2Cl_2 (100 mL). The reaction mixture was stirred at 0 °C for 2.5 h followed by the removal of dichloromethane and benzene in vacuo, giving a yellow oil, Me_2PhSnI (17.69 g) consisting of Me_2PhSnI [$\delta^{119}Sn(CH_2Cl_2/D_2O$ capillary) = −15.3 ppm]. A solution of KF (1.88 g, 32.4 mmol) in water (30 mL) was added to a solution of Me_2PhSnI (2.86 g, 8.1 mmol) in diethyl ether (30 mL). The reaction mixture was stirred for 24 h and was then left for a few hours without stirring giving rise to the formation of colorless crystals of Me_2PhSnF at the phase boundary (1.36 g, 6.7 mmol, 83% yield), m.p. 124−126 °C. ^1H NMR ($CDCl_3$): δ = 7.38 [complex pattern, $^2J(^1H\text{-}^{117/119}Sn)$ = 30 Hz, 2 H, *o*-H], 7.27 (complex pattern, 3 H, *m*-, *p*-H), 0.34 [s, $^2J(^1H\text{-}C\text{-}^{119/117}Sn)$ = 71 Hz, 6 H, *Me*] ppm. $^{13}C\{^1H\}$ NMR ($CDCl_3$, c = 0.228 mol·L^{-1}): δ = 144.6 [$^1J(^{13}C\text{-}^{117/119}Sn)$ = 707/741 Hz, C_i], 135.3 [$^2J(^{13}C\text{-}^{117/119}Sn)$ = 49 Hz, C_o], 128.6 (C_p), 127.9 [$^3J(^{13}C\text{-}^{117/119}Sn)$ = 65 Hz, C_m], −0.05 [$^1J(^{13}C\text{-}^{117/119}Sn)$ = 544/568 Hz, CH_3] ppm. ^{19}F NMR ($CDCl_3$): δ = −137.4 [$^1J(^{19}F\text{-}^{119/117}Sn)$ = 1255 Hz] ppm; ([D$_8$]toluene): δ = −139.0 [$^1J(^{19}F\text{-}^{119/117}Sn)$ = 1260 Hz] ppm. $^{119}Sn\{^1H\}$ NMR ($CDCl_3$): δ = −52.3 [$^1J(^{119}Sn\text{-}^{19}F)$ = 1340 Hz]; ([D$_8$]toluene): δ = −53.0 ppm [$^1J(^{119}Sn\text{-}^{19}F)$ = 1334 Hz] ppm. $^{13}C\{^1H\}$ MAS NMR: δ = −0.3, 1.6 (CH_3), 144.8, 136.6, 134.4, 128.5 (phenyl carbon atoms) ppm. $^{119}Sn\{^1H\}$ MAS NMR: δ = −49.5 [$^1J(^{119}Sn\text{-}^{19}F)$ = 1235 Hz] ppm. IR (KBr): $\tilde{\nu}$ = 3066 w, 2995 w, 2912 wbr, 1431 s, 1197 s, 1082 s, 998 w, 778 vs, 727 vs, 699 vs, 561 s, 531 s, 340 vs cm^{-1}. $C_8H_{11}FSn$ (244.91): calcd. C 39.2, H 4.5; found C 39.3, H 4.5.

Tris(trimethylsilylmethyl)tin Fluoride, $(Me_3SiCH_2)_3SnF$ (2): A saturated aqueous solution of NH_4F (30 mL) was added to a solution of $(Me_3SiCH_2)_3SnCl$ (0.80 g, 1.9 mmol) in diethyl ether (50 mL). The reaction mixture was stirred for 24 h and the organic layer was separated. The aqueous layer was extracted twice with diethyl ether (20 mL) and the combined organic phases were dried with Na_2SO_4. After filtration from the latter, the diethyl ether was distilled leaving a colorless residue which was recrystallized from dichloromethane giving $(Me_3SiCH_2)_3SnF$ (0.71 g, 1.8 mmol, 92% yield) of m.p. 123−127 °C. ^1H NMR ($CDCl_3$): δ = 0.11 (s, 27 H, CH_3), 0.23 [d, $^3J(^1H\text{-}^{19}F)$ = 4.2, $^2J(^1H\text{-}^{117/119}Sn)$ = 72.5/75.3 Hz, CH_2] ppm. $^{13}C\{^1H\}$ NMR ($CDCl_3$): δ = 6.1 [$^1J(^{13}C\text{-}^{119}Sn)$ = 286, $^2J(^{13}C\text{-}^{19}F)$ = 10 Hz; Sn*C*H$_2$Si], 1.5 (Si*Me*$_3$) ppm. ^{19}F NMR ($CDCl_3$): δ = −207.2 [$^1J(^{19}F\text{-}^{119}Sn)$ = 2369 Hz] ppm. $^{29}Si\{^1H\}$ NMR ($CDCl_3$): δ = 2.0 [$^2J(^{29}Si\text{-}^{119/117}Sn)$ = 29 Hz] ppm. $^{119}Sn\{^1H\}$ NMR ($CDCl_3$): δ = 196.4 [$^1J(^{119}Sn\text{-}^{19}F)$ = 2340, $^1J(^{119}Sn\text{-}^{13}C)$ = 282, $^2J(^{119}Sn\text{-}^{29}Si)$ = 30 Hz] ppm. $^{13}C\{^1H\}$ MAS NMR: δ = 3.7 (CH_3), 8.0 (broad, CH_2) ppm. $^{119}Sn\{^1H\}$ MAS NMR: δ = 165.8 [$^1J(^{119}Sn\text{-}^{19}F)$ = 2167 Hz] ppm. IR (KBr): $\tilde{\nu}$ = 2954 s, 2897 s, 1450 w, 1407 w, 1353 w, 1307 w, 1248 vs, 1023 vs, 833 vsbr, 752 s, 719 s, 689 s, 616 w, 596 s, 577 w, 529 s, 471 sbr, 283 w cm^{-1}. $C_{12}H_{33}FSi_3Sn$ (399.38): calcd. C 36.1, H 8.3; found C 36.2, H 8.1. Molecular weight (5.04 mg·g^{-1} CH_2Cl_2, T = 30 °C): 464 g·mol^{-1}.

X-ray Crystallographic Study: Intensity data for the colorless crystals were collected with a Nonius KappaCCD diffractometer with graphite-monochromated Mo-K_α radiation. The data collections covered almost the whole sphere of reciprocal space with 2 sets at different κ angles and 185 frames (**1**) and 360 frames via ω rotation (Δ/ω = 1°) (**2**, **2a**) at two times 5 s (**2a**), 10 s (**1**), and 30 s (**2**) per frame (Table 3). The crystal-to-detector distance was 3.0 cm (**2**, **2a**) and 3.4 cm (**1**). Crystal decay was monitored by repeating the initial frames at the end of the data collection. There was no indication for any decay when analyzing the duplicate reflections. The structure was solved by direct methods using SHELXS-97[88] and successive difference Fourier syntheses. Refinement was performed with full-matrix least-squares methods using SHELXL-97.[89] The

Table 3. Crystal data and structure refinement for **1**, **2**, and **2a**

	1	**2**	**2a**
Empirical formula	$C_8H_{11}FSn$	$C_{12}H_{33}FSi_3Sn$	$C_{12}H_{33}ClSi_3Sn$
Formula mass [g/mol]	244.86	399.34	415.79
Crystal system	orthorhombic	hexagonal	hexagonal
Crystal size [mm]	0.30 × 0.06 × 0.06	0.15 × 0.13 × 0.12	0.25 × 0.23 × 0.23
Space group	*Pbca*	*P*6(3)	*P*6(3)
a [Å]	9.3997(3)	10.6877(3)	10.6330(4)
b [Å]	8.6639(2)	10.6877(3)	10.6330(4)
c [Å]	22.3783(7)	10.3022(2)	11.1281(3)
V [Å^3]	1822.45(9)	1019.13(5)	1089.59(6)
Z	8	2	2
$\rho_{calcd.}$ [Mg/m^3]	1.785	1.301	1.267
T [K]	173(1)	291(1)	291(1)
μ [mm^{-1}]	2.748	1.423	1.446
F(000)	944	412	428
θ range [°]	3.68 to 27.48	2.96 to 24.98	3.83 to 25.02
Index ranges	$-12 \le h \le 12$ $-10 \le k \le 10$ $-29 \le l \le 29$	$-12 \le h \le 12$ $-10 \le k \le 10$ $-10 \le l \le 10$	$-12 \le h \le 12$ $-10 \le k \le 10$ $-11 \le l \le 11$
No. of reflections collected	10202	11175	12312
Completeness to θ_{max}	95.4%	93.8%	94.3%
No. of independent reflections/R_{int}	1998	1128	1226
No. of reflections observed with [$I > 2\sigma(I)$]	1246	820	833
No. of refined parameters	93	58	59
GooF (F^2)	1.014	0.912	0.940
$R1(F)$ [$I > 2\sigma(I)$]	0.0223	0.0228	0.0276
$wR2(F2)$ (all data)	0.0504	0.0538	0.0746
$(\Delta/\sigma)_{max}$	< 0.001	< 0.001	< 0.001
Largest difference peak/hole [e/Å^3]	0.793/−0.693	0.394/−0.182	0.376/−0.226

H atoms were placed in geometrically calculated positions using a riding model with U_{iso} constrained at 1.2 (for aryl groups) and 1.5 (for methyl groups) times U_{eq} of the carrier C atom. TWIN refinements were applied for **2** and **2a**, because a racemic twinning was present with a Flack parameter of 0.47(12) (**2**) and 0.52(13) (**2a**).[90] The TWIN refinement improved the *R* values of *R*1 [(0.0002) (**2**), (0.0003) (**2a**)] and of *wR*2 [(0.0004) (**2**), (0.0005) (**2a**)]. Atomic scattering factors for neutral atoms and real and imaginary dispersion terms were taken from International Tables for X-ray Crystallography.[91] The figures were created by SHELXTL.[92] CCDC-179688 (**1**), -179689 (**2**), and -179690 (**2a**) contain the supplementary crystallographic data for this paper. These data can be obtained free of charge at www.ccdc.cam.ac.uk/conts/retrieving.html or from the Cambridge Crystallographic Data Centre, 12 Union Road, Cambridge CB2 1EZ, UK [Fax: (internat.) + 44-1223/336-033; E-mail: deposit@ccdc.cam.ac.uk].

Acknowledgments

We thank the Deutsche Forschungsgemeinschaft, the Fonds der Chemischen Industrie and the Australian Research Council for financial support. The Australian National University Supercomputer Facility is acknowledged for a grant of supercomputer time. A. E. K. L. acknowledges an Overseas Postgraduate Research Scholarship from Deakin University. We acknowledge B. Mahieu (Louvain-la-Neuve, Belgium) for recording the Mössbauer spectra.

[1] H. W. Roesky, I. Haiduc, *J. Chem. Soc., Dalton Trans.* **1999**, 2249−2264.
[2] B. R. Jagirdar, E. F. Murphy, H. W. Roesky, *Prog. Inorg. Chem.* **1999**, *48*, 351−455.
[3] E. F. Murphy, H. W. Roesky, *Chem. Rev.* **1997**, *97*, 3425−3468.
[4] R. K. Ingham, S. D. Rosenberg, H. Gilman, *Chem. Rev.* **1960**, *60*, 459−539.
[5] *Gmelin Handbook of Inorganic Chemistry: Tin, Pt. 5: Organotin Fluorides, Triorganotin Chlorides*, Springer, Berlin, **1978**.
[6] R. Okawara, D. E. Webster, E. G. Rochow, *J. Am. Chem. Soc.* **1960**, *82*, 3287−3290.
[7] R. Okawara, M. Wada, *Adv. Organomet. Chem.* **1967**, *5*, 137−167.
[8] H. C. Clark, R. J. O′Brien, J. Trotter, *Proc. Chem. Soc.* **1964**, 85.
[9] H. C. Clark, R. J. O′Brien, J. Trotter, *J. Chem. Soc.* **1964**, 2332−2336.
[10] K. Yasuda, Y. Kawasaki, N. Kasai, T. Tanaka, *Bull. Chem. Soc. Jpn.* **1965**, *38*, 1216−1218.
[11] D. Williams, *Austr. Def. Stand. Lab., Annu. Rep.* **1967/8**, p. 37.
[12] K. C. Molloy, K. Quill, *J. Chem. Soc., Dalton Trans.* **1985**, 1417−1423.
[13] D. Tudela, E. Gutierrez-Puebla, A. Monge, *J. Chem. Soc., Dalton Trans.* **1992**, 1069−1071.
[14] H. Reuter, Ph.D. thesis, University of Bonn, **1986**.
[15] D. Tudela, R. Fernandez, V. K. Belsky, V. E. Zavodnik, *J. Chem. Soc., Dalton Trans.* **1996**, 2123−2126.
[16] L. N. Zakharov, Y. T. Struchkov, E. A. Kuz′min, B. I. Petrov, *Kristallografiya* **1983**, *28*, 271−275.
[17] S. S. Al-Juaid, S. M. Dhaher, C. Eaborn, P. B. Hitchcock, J. D. Smith, *J. Organomet. Chem.* **1987**, *325*, 117−127.
[18] H. Reuter, H. Puff, *J. Organomet. Chem.* **1989**, *379*, 223−234.
[19] M. Ochiai, S. Iwaki, T. Ukita, Y. Matsuura, M. Shiro, Y. Nagao, *J. Am. Chem. Soc.* **1988**, *110*, 4606−4610.
[20] U. Kolb, M. Dräger, B. Jousseaume, *Organometallics* **1991**, *10*, 2737−2742.
[21] U. Kolb, M. Dräger, M. Dargatz, K. Jurkschat, *Organometallics* **1995**, *14*, 2827−2834.
[22] I. Wharf, A. M. Lebuis, G. A. Roper, *Inorg. Chim. Acta* **1999**, *294*, 224−231.
[23] D. Dakternieks, K. Dunn, B. R. Vincent, E. R. T. Tiekink, *Main Group Met. Chem.* **2000**, *23*, 327−328.
[24] A. C. Sau, L. A. Carpino, R. R. Holmes, *J. Organomet. Chem.* **1980**, *197*, 181−197.
[25] S. J. Blunden, R. Hill, *J. Organomet. Chem.* **1989**, *371*, 145−154.
[26] M. Gingras, *Tetrahedron Lett.* **1991**, *32*, 7381−7384.
[27] J. Beckmann, D. Dakternieks, A. Duthie, E. R. T. Tiekink, *J. Organomet. Chem.*, **2002**, *648*, 204−208.
[28] R. V. Parish, R. H. Platt, *J. Chem. Soc., Chem. Commun.* **1968**, 1118−1120.
[29] R. V. Parish, R. H. Platt, *J. Chem. Soc. A* **1969**, *14*, 2145−2150.
[30] H. A. Stoeckler, H. Sano, *J. Chem. Soc. D* **1969**, 954−955.
[31] J. Devooght, M. Gielen, S. Lejeune, *J. Organomet. Chem.* **1970**, *21*, 333−343.
[32] R. V. Parish, R. H. Platt, *Inorg. Chim. Acta* **1970**, *4*, 65−72.
[33] N. N. Greenwood, B. A. Goodman, *J. Chem. Soc. A* **1971**, 1862−1865.
[34] R. H. Herber, S. Chandra, *J. Chem. Phys.* **1971**, *54*, 1847−1851.
[35] R. H. Herber, *J. Chem. Phys.* **1971**, *54*, 3755−3760.
[36] K. Licht, H. Geissler, P. Köhler, K. Hottmann, H. Schnorr, H. Kriegsmann, *Z. Anorg. Allg. Chem.* **1971**, *385*, 271−288.
[37] R. H. Platt, A. G. Maddock, *J. Chem. Soc. A* **1971**, 1191−1195.
[38] R. C. Poller, J. N. R. Ruddick, *J. Organomet. Chem.* **1972**, *39*, 121−128.
[39] R. H. Herber, J. Fischer, Y. Hazony, *J. Chem. Phys.* **1973**, *58*, 5185−5187.
[40] H. Negita, R. Boku, M. Sugiya, S. Ichiba, *Bull. Chem. Soc. Jpn.* **1980**, *53*, 3021−3022.
[41] R. Barbieri, A. Silvestri, G. Ruisi, G. Alonzo, *Inorg. Chim. Acta* **1985**, *97*, 113−117.
[42] R. K. Harris, K. J. Packer, P. Reams, *Chem. Phys. Lett.* **1985**, *115*, 16−18.
[43] R. K. Harris, P. Reams, K. J. Packer, *J. Mol. Struct.* **1986**, *141*, 13−25.
[44] H. Bai, R. K. Harris, H. Reuter, *J. Organomet. Chem.* **1991**, *408*, 167−172.
[45] H. Bai, R. K. Harris, *J. Magn. Reson.* **1992**, *96*, 24−30.
[46] Y. W. Kim, A. Labouriau, C. M. Taylor, W. L. Earl, L. G. Werbelow, *J. Phys. Chem.* **1994**, *98*, 4919−4922.
[47] J. C. Cherryman, R. K. Harris, *J. Magn. Reson.* **1997**, *128*, 21−29.
[48] K. Licht, H. Geissler, P. Köhler, K. Müller, *Z. Chem.* **1971**, *11*, 272−273.
[49] J. R. May, W. R. McWhinnie, R. C. Poller, *Spectrochim. Acta Part A* **1971**, *27*, 969−974.
[50] K. Licht, P. Köhler, H. Kriegsmann, *Z. Anorg. Allg. Chem.* **1975**, *415*, 31−42.
[51] R. H. Herber, *Polyhedron* **1985**, *4*, 1969−1974.
[52] A. S. Sall, O. Sarr, L. Diop, *Spectrochim. Acta* **1992**, *48A*, 613−614.
[53] H. Zimmer, O. A. Homberg, M. D. Jayawant, *J. Org. Chem.* **1966**, *31*, 3857−3860.
[54] R. Eujen, U. Thurmann, *J. Organomet. Chem.* **1992**, *433*, 63−77.
[55] W. T. Reichle, *Inorg. Chem.* **1966**, *5*, 87−91.
[56] D. A. Antonov, C. Eaborn, J. D. Smith, P. B. Hitchcock, E. Molla, V. I. Rozenberg, W. A. Stancyk, A. Kowaleska, *J. Organomet. Chem.* **1996**, *521*, 109−112.
[57] S. S. Al-Juaid, M. Al-Rawi, C. Eaborn, P. B. Hitchcock, J. D. Smith, *J. Organomet. Chem.* **1998**, *564*, 215−226.
[58] D. K. Dandge, C. Taylor, J. P. Heller, *J. Polym. Sci., Part A: Polym. Chem.* **1989**, *27*, 1053−1063.
[59] E. A. Robinson, S. A. Johnson, T.-H. Tang, R. J. Gillespie, *Inorg. Chem.* **1997**, *36*, 3022−3030.
[60] E. A. Robinson, G. L. Heard, R. J. Gillespie, *J. Mol. Struct.* **1999**, *485/486*, 305−319.
[61] R. J. Gillespie, *Coord. Chem. Rev.* **2000**, *197*, 51−69.

[62] K. O. Christe, D. A. Dixon, D. McLemore, W. W. Wilson, J. A. Sheehy, J. A. Boatz, *J. Fluorine Chem.* **2000**, *101*, 151−153.
[63] M. Kaupp, B. Metz, H. Stoll, *Angew. Chem. Int. Ed.* **2000**, *39*, 4607−4609.
[64] J. Herzfeld, A. E. Berger, *J. Chem. Phys.* **1980**, *73*, 6021−6030.
[65] J. Herzfeld, X. Chen, in: *Encyclopedia of Nuclear Magnetic Resonance*, John Wiley & Sons, New York, **1996**, vol. 7, pp. 4362−4369.
[66] A. D. Buckingham, S. M. Malm, *Mol. Phys.* **1971**, *22*, 1127−1130.
[67] M. Dräger, *Z. Anorg. Allg. Chem.* **1976**, *423*, 53−66.
[68] U. Kolb, M. Beuter, M. Dräger, *Inorg. Chem.* **1994**, *33*, 4522−4530.
[69] J. Timmerman, *J. Chim. Phys.* **1938**, *35*, 331.
[70] J. E. Huheey, E. A. Keiter, R. L. Keiter, *Inorganic Chemistry − Principles of Structure and Reactivity*, 4th ed., Harper Collins College Publishers, New York, **1993**.
[71] L. N. Zakharov, B. I. Petrov, V. A. Lebedev, E. A. Kuz′min, N. V. Belov, *Kristallografiya* **1978**, *23*, 1049−1051.
[72] M. Beuter, U. Kolb, A. Zickgraf, E. Brau, M. Bletz, M. Dräger, *Polyhedron* **1997**, *16*, 4005−4015.
[73] P. Dunn, D. Oldfield, *J. Macromol. Sci., Chem.* **1970**, *4*, 1157−1168.
[74] A. P. Evans, *J. Appl. Polym. Sci.* **1974**, *18*, 1919−1925.
[75] D. K. Dandge, C. Taylor, J. P. Heller, K. V. Wilson, N. Brumley, *J. Macromol. Sci., Chem.* **1989**, *A26*, 1451−1464.
[76] D. Dakternieks, H. Zhu, *Inorg. Chim. Acta* **1992**, *196*, 19−25.
[77] M. Jang, A. F. Janzen, *J. Fluorine Chem.* **1994**, *66*, 129−135.
[78] J. B. Lambert, B. Kuhlmann, *J. Chem. Soc., Chem. Commun.* **1992**, 931−932.
[79] J. B. Lambert, S. M. Ciro, C. L. Stern, *J. Organomet. Chem.* **1995**, *499*, 49−55.
[80] I. Zharov, B. T. King, Z. Havlas, A. Pardi, J. Michl, *J. Am. Chem. Soc.* **2000**, *122*, 10253−10254.
[81] C. Schnitter, K. Klimek, H. W. Roesky, T. Albers, H.-G. Schmidt, C. Roepken, E. Parisini, *Organometallics* **1998**, *17*, 2249−2257.
[82] J. Beckmann, D. Dakternieks, A. E. K. Lim, K. F. Lim, K. Jurkschat, *Organometallics*, manuscript submitted.
[83] A. E. Reed, R. B. Weinstock, F. Weinhold, *J. Chem. Phys.* **1985**, *83*, 735−746.
[84] S. P. Ionov, G. V. Ionova, *Zh. Fiz. Khim.* **1972**, *46*, 845−850.
[85] O. A. Kruglaya, G. S. Kalinina, B. I. Petrov, N. S. Vyazankin, *J. Organomet. Chem.* **1972**, *46*, 51−58.
[86] A. Massiot, H. Thiele, A. Germanus, *Bruker Report* **1994**, *140*, 43.
[87] U. Haeberlen, *Advances in Magnetic Resonance, Suppl. 1: High Resolution NMR in Solids: Selective Averaging*, Academic Press, New York, **1976**.
[88] G. M. Sheldrick, *Acta Crystallogr., Sect. A* **1990**, *46*, 467−473.
[89] G. M. Sheldrick, University of Göttingen, **1997**.
[90] H. D. Flack, *Acta Crystallogr., Sect. A* **1983**, *39*, 876−881.
[91] *International Tables for Crystallography*, vol. C, Kluwer Academic Publishers, Dordrecht, **1992**.
[92] G. M. Sheldrick, *SHELXTL, Release 5.1, Software Reference Manual*, Bruker AXS, Inc., Madison, **1997**.
[93] M. J. Frisch, G. W. Trucks, H. B. Schlegel, G. E. Scuseria, M. A. Robb, J. R. Cheeseman, V. G. Zakrzewski, J. A. Montgomery, R. E. Stratmann, J. C. Burant, S. Dapprich, J. M. Millam, A. D. Daniels, K. N. Kudin, M. C. Strain, O. Farkas, J. Tomasi, V. Barone, M. Cossi, R. Cammi, B. Mennucci, C. Pomelli, C. Adamo, S. Clifford, J. Ochterski, G. A. Petersson, P. Y. Ayala, Q. Cui, K. Morokuma, D. K. Malick, A. D. Rabuck, K. Raghavachari, J. B. Foresman, J. Cioslowski, J. V. Ortiz, B. B. Stefanov, G. Liu, A. Liashenko, P. Piskorz, I. Komaromi, R. Gomperts, R. L. Martin, D. J. Fox, T. Keith, M. A. Al-Laham, C. Y. Peng, A. Nanayakkara, C. Gonzalez, M. Challacombe, P. M. W. Gill, B. G. Johnson, W. Chen, M. W. Wong, J. L. Andres, M. Head-Gordon, E. S. Replogle, J. A. Pople, *Gaussian 98 (Revision A.7)*, Gaussian, Inc., Pittsburgh, PA, **1998**..
[94] A. Bergner, M. Dolg, W. Kuechle, H. Stoll, H. Preuss, *Mol. Phys.* **1993**, *80*, 1431−1441.
[95] S. Huzinaga, *Gaussian Basis Sets for Molecular Calculations*, Elsevier, New York, **1984**.
[96] A. Höllwarth, M. Böhme, S. Dapprich, A. W. Ehlers, A. Gobbi, V. Jonas, K. F. Köhler, R. Stegmann, A. Veldkamp, G. Frenking, *Chem. Phys. Lett.* **1993**, *208*, 237−240.
[97] A. D. Becke, *J. Chem. Phys.* **1993**, *98*, 5648−5652.
[98] C. Lee, W. Yang, R. G. Parr, *Phys. Rev. B: Condens. Matter* **1988**, *37*, 785−789.

Received July 9, 2002
[I02373]

Anionic Cyclopentadienyl C_{60} Complexes of Molybdenum and Tungsten; The Strange Case of Iron

David M. Thompson,[a] Marni Jones,[a] and Michael C. Baird*[a]

Keywords: Fullerenes / Molybdenum / Tungsten / Iron

Thermal and photochemical reactions of the carbonylate salts A[(η^5-C_5H_5)Fe$(CO)_2$], A[(η^5-C_5H_5)Mo$(CO)_3$] and A[(η^5-C_5H_5)W$(CO)_3$] (A = Na, PPN) in THF with C_{60} result in all cases in electron transfer to give $[C_{60}]^-$ and the transient 17-electron, metal-centered radicals CpFe$(CO)_2$, CpMo$(CO)_3$ and CpW$(CO)_3$, respectively. Subsequent self-coupling of the three metal-centred radicals then results in the formation of the metal-metal bonded dimers [CpFe$(CO)_2]_2$, [CpMo$(CO)_3]_2$ and [CpW$(CO)_3]_2$. In contrast, while the mixture of Na[C_{60}] and [CpFe$(CO)_2]_2$ does not react further under photochemical conditions, photolysis of mixtures of Na[C_{60}] and both [CpMo$(CO)_3]_2$ and [CpW$(CO)_3]_2$ ultimately results in complete homolysis of the dimers and regeneration of the corresponding metal-centered radicals, which then combine with the $[C_{60}]^-$ remaining in solution to form the η^2-C_{60} complexes A[CpMo$(CO)_2$(η^2-C_{60}] and A[CpW$(CO)_2$(η^2-C_{60}].
(© Wiley-VCH Verlag GmbH & Co. KGaA, 69451 Weinheim, Germany, 2003)

Introduction

Molecular transition metal-fullerene compounds generally fall into two main classes, endohedral compounds in which the metal atom is confined within a fullerene molecule,[1] and η^2-transition metal complexes in which the fullerene behaves essentially as a weakly conjugated, electron-deficient alkene ligand η^2-bonded to the metal via a [6-6] ring junction.[2] Most known examples of η^2-complexes are neutral compounds in which the fullerene has either added to a neutral precursor, thus increasing the coordination number about the metal, or has displaced a ligand such as CO or a phosphane.[2] We have recently described a third synthetic methodology, an approach which results in the formation of unusually stable anionic η^2-fullerene complexes.[3]

It is well-known that C_{60} contains a low lying, triply degenerate LUMO and is therefore readily reduced,[4] and we have found that the carbonylate anions $[M(CO)_n]^-$ (M = Co, n = 4; M = Mn, Re, n = 5) are sufficiently reducing in THF solution that they convert C_{60} to the radical anion $[C_{60}]^-$ as in step (a) of Scheme 1.[3] When reduction is carried out in refluxing THF with A[$M(CO)_5$] (A = Na, PPN; M = Mn, Re), the rates at which the 17-electron intermediates $M(CO)_5$ couple [step (b) of Scheme 1] and undergo CO substitution [step (c) of Scheme 1] are similar and comparable amounts of $M_2(CO)_{10}$ and the stable complexes A[$Mn(CO)_4$(η^2-C_{60})] are formed.[3b−3d] However, under photolytic conditions, the 18-electron dimers $M_2(CO)_{10}$ undergo dissociation back to the radicals [reverse of step (b)] which then react with the $[C_{60}]^-$ remaining in solution to give higher yields of the η^2-C_{60} products.[3b−3d] In contrast, with A[$Co(CO)_4$] (A = Na, PPN), no $Co_2(CO)_8$ is formed in either the thermal or the photochemical reactions, possibly because the rate of dimerization of the $Co(CO)_4$ radical is slow relative to the rate of CO substitution by $[C_{60}]^-$.[3d] Interestingly, the η^2-fullerene complex $[Co(CO)_3(\eta^2\text{-}C_{60})]^-$ is thermally rather labile, and the sodium salt Na[$Co(CO)_3$(η^2-C_{60})] decomposes in refluxing THF to give the unusual mixed-metal fulleride compound $NaCoC_{60}$·3THF.[3a,3d]

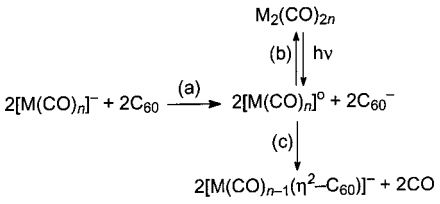

Scheme 1

In view of the rich variety of chemistry observed with these three carbonylate anions, we have extended our studies to anionic cyclopentadienyl analogues of iron, molybdenum and tungsten, A[(η^5-C_5H_5)$M(CO)_n$] (A = Na, PPN; M = Fe, n = 2; M = Mo, W, n = 3); these are found to exhibit analogous but different patterns of reactivity.

Results and Discussion

As an extension of our earlier research on reactions of the carbonylate anions $[Co(CO)_4]^-$ $[Mn(CO)_5]^-$ and $[Re(CO)_5]^-$ with C_{60},[3] we have now investigated the analogous reactions of C_{60} with the anionic complexes

[a] Department of Chemistry, Queen's University, Kingston, Ontario, K7L 3N6, Canada

$[CpFe(CO)_2]^-$, $[CpMo(CO)_3]^-$ and $[CpMo(CO)_3]^-$. These anions are all highly reducing,[7] and we anticipated chemistry rather similar to that outlined in Scheme 1, that is single-electron transfer processes followed by dimerization of the resulting metal-centered radicals and/or combination of the metal-centered radicals with the $[C_{60}]^-$ radical anion. Sodium salts were utilized in all cases because of their ease of preparation, while PPN salts were also utilized in the case of molybdenum and tungsten in unsuccessful attempts to obtain suitable crystals of the new η^2-C_{60} complexes for crystallographic purposes, as we had done previously with the manganese system.[3b]

Reactions of A[CpFe(CO)$_2$] (A = Na$^+$, PPN$^+$) with C$_{60}$

The thermal reactions of $A[CpFe(CO)_2]$ ($A = Na^+$, PPN^+) proceeded extremely rapidly. The first IR spectrum run following the addition of C_{60} to a THF solution of either salt (recorded within 1−2 min) revealed only the ν_{CO} bands of $[CpFe(CO)_2]_2$ with intensities similar to those of the starting $CpFe(CO)_2^-$, while ES-MS revealed a strong peak at 720 Da/e and with an isotope distribution consistent with $[C_{60}]^-$. Consistent with the presence of $[C_{60}]^-$ in solution, a near IR spectrum of a THF solution exhibited a peak at 1078 nm.[4] Refluxing these solutions over several hours resulted in no further changes to any of the spectra, and we were able to selectively precipitate $A[C_{60}]$ from the THF solutions by adding a small amount of pentane.

The reactions appear to involve extremely facile initial electron transfer from $[CpFe(CO)_2]^-$ to C_{60} and subsequent dimerization of the $CpFe(CO)_2$ radicals [Equation (1) and (2)].

$$[CpFe(CO)_2]^- + C_{60} \rightarrow CpFe(CO)_2 + [C_{60}]^- \quad (1)$$

$$CpFe(CO)_2 \rightarrow 0.5[CpFe(CO)_2]_2 \quad (2)$$

It was initially thought that $[CpFe(CO)(C_{60})]^-$ was perhaps not being formed because the rate of $CpFe(CO)_2$ radical dimerization is very nearly diffusion controlled[8] and, possibly, much higher than the rate of CO substitution by $[C_{60}]^-$. However, since photolysis of $[CpFe(CO)_2]_2$ is known to result in metal-metal bond homolysis, it was anticipated that continued photolysis would provide a source of $CpFe(CO)_2$ radicals which would be able to react with $[C_{60}]^-$ at least to some extent.[8]

To our surprise, however, the photochemical reactions of $A[CpFe(CO)_2]$ ($A = Na^+$, PPN^+) with C_{60} proceeded in an analogous fashion to the thermal reactions, the only product detected in IR spectra being, again, the dimer $[CpFe(CO)_2]_2$ in high yield. Subsequent photolyses run for up to 96 h revealed no changes to the IR spectra. Tandem ES-MS measurements revealed the strong peak of C_{60}^- at 720 Da/e.

It seems possible that the Cp ring provides steric hindrance and prevents coordination of fulleride to the relatively small iron. While other complexes have been reported containing both metal-fullerene and metal-Cp bonds,[2] there are no examples of the smaller first row transition metals showing both ligands coordinated. Thus the steric argument seems reasonable.

Reactions of A[CpM(CO)$_3$] (M = Mo, W; A = Na$^+$, PPN$^+$) with C$_{60}$

Thermal reactions of $A[CpMo(CO)_3]$ ($A = Na^+$, PPN^+) with C_{60} in refluxing THF resulted in a gradual loss (over 3 h) of the ν_{CO} bands of $[CpMo(CO)_3]^-$ and the appearance of the ν_{CO} bands of $[CpMo(CO)_3]_2$.

The intensities of the product peaks were in both cases similar to those of the starting carbonylate anion before reaction. The presence of $[C_{60}]^-$ in the solutions was confirmed by observation of a peak at 720 Da/e in the ES mass spectrum and a peak at 1074 nm in the near NIR spectrum.[4] As with the iron system, continued refluxing of the solutions resulted in no further changes to any of the spectra, and thus the reactions were as in Equation (3) and (4).

$$[CpMo(CO)_3]^- + C_{60} \rightarrow CpMo(CO)_3 + [C_{60}]^- \quad (3)$$

$$CpMo(CO)_3 \rightarrow 0.5[CpMo(CO)_3]_2 \quad (4)$$

In contrast, photolysis of THF solutions of $A[CpM(CO)_3]$ (A = Na, PPN) in the presence of C_{60} yielded much more interesting results. In the case of $A[CpMo(CO)_3]$, the ν_{CO} bands of $[CpMo(CO)_3]^-$ were replaced over the course of about 3 h by two sets of ν_{CO} bands, those at 1911, 1956 and 2012 cm^{-1} attributable to $[CpMo(CO)_3]_2$, and two new ν_{CO} bands at 1818 and 1900 cm^{-1}. After 48 h, the latter pair of peaks dominated the IR spectrum.

ESMS monitoring of these reactions at times when the ν_{CO} bands of $[CpMo(CO)_3]_2$ and the new pair at 1900 and 1818 cm^{-1} were present in the IR spectrum revealed peaks at 720 and 939 Da/e with isotope distributions consistent with attributions to $[C_{60}]^-$ and $[CpMo(CO)_2(C_{60})]^-$, respectively. As the reaction continued and the intensities of the ν_{CO} band of $[CpMo(CO)_3]_2$ decreased, the intensity of the peak at 720 Da/e in the ESMS also decreased. When only the ν_{CO} bands at 1818 and 1900 cm^{-1} were present, photolysis was discontinued and the reaction mixtures were worked up as above to give $A[CpMo(CO)_2(C_{60})]$. The latter complexes are soluble in THF, and IR spectra of their THF solutions revealed the two ν_{CO} bands at 1800 and 1900 cm^{-1}. Furthermore, ESMS revealed a single peak at 939 Da/e, consistent with the isotope distribution anticipated for $[CpMo(CO)_2(C_{60})]^-$ (Figure 1).

On this basis, the course of the photochemical process clearly involves electron transfer and molybdenum-centered radical coupling, as in Equation (3) and (4), but the latter is reversed photochemically[9] and gives rise to coupling of molybdenum-centered and fulleride radicals, as in Equation (5) [M = Mo].

$$CpM(CO)_3 + [C_{60}]^- \rightarrow [CpM(CO)_2(C_{60})]^- + CO \quad (5)$$

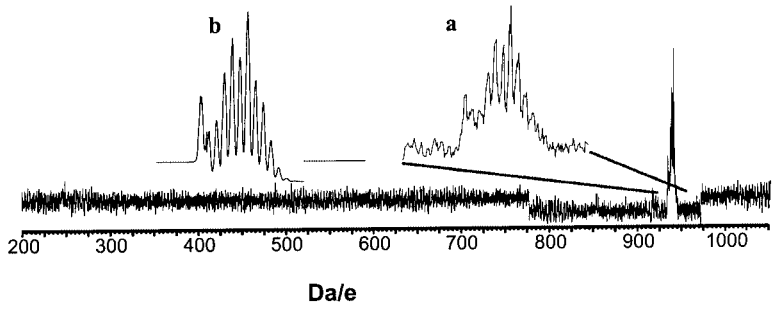

Figure 1. Negative-ion mode ES mass spectrum of PPN[CpMo(CO)$_2$(C_{60})]: (a) observed; (b) calculated

Interestingly, it was also observed that increasing the cone voltage from 10 mV to 30−50 mV resulted in loss of intensity from the peak at 939 Da/e and gain in intensity of a peak at 909 Da/e, a new peak with a position and isotope distribution consistent with [CpMo(CO)(C_{60})]$^-$. As has been established previously,[5c] successive decarbonylation of transition metal carbonylates with increasing cone voltage is a general phenomenon and this result was anticipated. Further increasing the cone voltage above 50 mV resulted in the observation of a peak at 720 Da/e with an isotope distribution consistent with [C_{60}]$^-$. No anionic daughter ions of the type [CpMo(CO)$_x$]$^-$ (x = 1−2) were observed.

A ^{1}H NMR spectrum of the complex was recorded in [D_8]THF, and exhibited a singlet at δ = 5.65 ppm attributable to the Cp ring protons. A ^{13}C NMR spectrum of PPN[CpMo(CO)$_2$(C_{60})] was also recorded in [D_8]THF, and the chemical shifts of the resonances are listed in Table 1, where the approximate relative intensities of the sp^2-hybridized carbon resonances are also given. As with the ^{13}C NMR spectra of other transition metal fullerene complexes,[2b] rigorous assignments of the sp^2-carbon resonances are not possible, although the numbers and intensities of the peaks between δ = 135 and 180 ppm can be used to determine the symmetry of the anion. Resonances in this region at δ = 134.7, 133.6, 130.5 and 128.4 ppm are attributed to the phenyl ring carbons on the PPN$^+$ cation on the basis of comparison with the spectrum of the chloride salt. Of the remaining 18 resonances, one (δ = 125.99 ppm) is readily attributed to the Cp ring carbons, and 17 to fullerene cage carbons. A fullerene bound to a metal by a [6-6] ring junction in an olefinic coordination mode (C_{2v} symmetry) should exhibit 17 ^{13}C resonances, one for the two coordinated (sp^3-hybridized) carbons and 16 attributable to the sp^2-carbons,[2b] and thus the ^{13}C NMR spectroscopic data are consistent with a structure of C_{2v} symmetry.

The near-IR spectra of solutions of A[CpMo(CO)$_2$(η^2-C_{60})] revealed no absorptions in the range 800−1400 nm, results consistent with observations made previously for A[Mn(CO)$_4$(η^2-C_{60})].[3d] Despite many attempts to obtain X-ray quality crystals, none of the crystals obtained proved to be amenable to solution by X-ray crystallography. Confirmation of the correct elemental composition was provided, however, by high resolution ESMS experiments on PPN[CpMo(CO)$_2$(C_{60})]; a peak at 938.9491 Da/e was observed, differing by 14.7 mDa (15.7 ppm) from the theoretical mass of 938.9344 Da/e.

Table 1. ^{13}C NMR spectroscopic data for PPN[CpMo(CO)$_2$(η^2-C_{60})]

Chemical shift of peak (δ)	Relative intensity[a]	Assignment
93.36		sp^3-C_{60}
125.99		Cp
128.40		PPN$^+$
130.53		PPN$^+$
133.39		PPN$^+$
134.74		PPN$^+$
136.60	1.60	sp^2-C_{60}
142.01	2.00	sp^2-C_{60}
142.64	1.96	sp^2-C_{60}
143.37	3.44	sp^2-C_{60}
144.20	2.29	sp^2-C_{60}
145.77	1.26	sp^2-C_{60}
145.90	2.29	sp^2-C_{60}
146.19	1.86	sp^2-C_{60}
146.39	2.16	sp^2-C_{60}
146.43	2.18	sp^2-C_{60}
146.50	1.00	sp^2-C_{60}
147.41	2.36	sp^2-C_{60}
148.08	0.97	sp^2-C_{60}
151.48	1.98	sp^2-C_{60}
156.89	0.77	sp^2-C_{60}
179.32	1.61	sp^2-C_{60}

[a] The relative intensities were calculated arbitrarily as ratios of the intensity of the peak at δ = 146.50 ppm. The intensities calculated in this way are approximate at best and are probably only valid for carbons in the general environment (sp^2 carbons)

The thermal and photochemical reactions of A[CpW(CO)$_3$] (A = Na$^+$, PPN$^+$) with C_{60} in THF parallel those of molybdenum. Reactions in refluxing THF were monitored by IR spectroscopy and ESMS, and the sole products were [CpW(CO)$_3$]$_2$ (in high yield) and A[C_{60}]. These products presumably arise as postulated in Equation (3) and (4) for molybdenum, and involve initial electron transfer from [CpW(CO)$_3$]$^-$ to C_{60} to give the CpW(CO)$_3$ radical and the [C_{60}]$^-$ radical anion followed by dimerization of CpW(CO)$_3$

In contrast, the photochemical reactions of A[CpW(CO)$_3$] (A = Na$^+$, PPN$^+$) with C_{60} in THF resulted in the slow but clean formation of A[CpW(CO)$_2$(C_{60})] (A = Na$^+$, PPN$^+$), via the same intermediates — the CpW(CO)$_3$

radical and the $[C_{60}]^-$ radical anion — observed in the thermal reactions. The photochemical reactions were monitored by IR spectroscopy and ESMS, and the ν_{CO} bands of $A[CpW(CO)_3]$ were found to be replaced initially by the ν_{CO} bands of $[CpW(CO)_3]_2$, and then by the ν_{CO} bands of $[CpW(CO)_2(C_{60})]^-$ (1809, 1894 cm^{-1}) over several hours. Tandem ESMS measurements revealed peaks at 720 Da/e and 1025 Da/e with intensities linked to the intensities of the carbonyl absorptions of $[CpW(CO)_3]_2$ and those at 1809 and 1894 cm^{-1}, respectively.

When only the ν_{CO} bands at 1809 and 1894 cm^{-1} were evident in the IR spectrum (96 h for the Na^+ salt, 48 h for the PPN^+ salt), photolysis was discontinued and the black product was precipitated from the solution by the addition of pentane and identified by IR spectroscopy and ESMS. The latter exhibits a peak at 1025 Da/e with an isotope pattern consistent with $[CpW(CO)_2(C_{60})]^-$ (Figure 2). Increasing the cone voltage from 10 to 30−50 V resulted in the appearance of a peak at 997 Da/e^- with an isotope distribution consistent with $[CpW(CO)(C_{60})]^-$. Further increasing the cone voltage beyond 50 V resulted in the observation of the peak of $[C_{60}]^-$ at 720 Da/e.

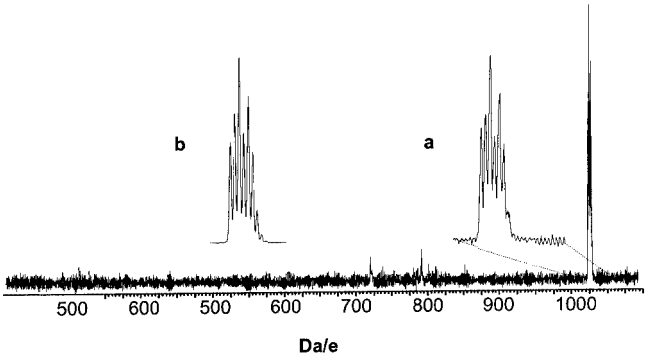

Figure 2. Negative-ion mode ES mass spectrum of $PPN[CpW(CO)_2(C_{60})]$: (a) observed; (b) calculated

Although we could again obtain crystals by layering THF solutions with pentane, the X-ray diffraction pattern generated by the crystals gave insufficient data for a structure solution. However, a ^1H NMR spectrum was obtained (δ_{Cp} = 5.56 in $[D_8]$THF), and confirmation of the elemental composition for $PPN[CpW(CO)_2(C_{60})]$ was provided by high resolution ESMS experiments in which a peak at 1024.9689 Da/e was observed, differing by 11.0 mDa (10.8 ppm) from the theoretical mass of 1024.9799 Da/e.

Thus the photochemical reactions of $PPN[CpW(CO)_3]$ and $PPN[CpW(CO)_3]$ with C_{60} both proceed as in Equations 3−5 and result in the formation of the complexes $PPN[CpM(CO)(C_{60})]$ (M = Mo, W) via a mechanism similar to those found for the manganese and cobalt complexes reported previously.[3b−3d] Given that no $[CpM(CO)_2(C_{60})]^-$ is observed in the thermal reactions, it seems that the rate of metal-centered radical dimerization is considerably higher than the rate of $[C_{60}]^-$ substitution. However, photolysis provides a constant supply of $CpM(CO)_3$ radicals through dimer homolysis, and the apparently irreversible nature of $[C_{60}]^-$ substitution for CO leads to an accumulation of $[CpM(CO)_2(C_{60})]^-$. By further analogy with $PPN[Mn(CO)(C_{60})]$, for which η^2-coordination of the fullerene has been established crystallographically,[3b] we presume that the molybdenum and tungsten complexes should also be formulated as η^2-complexes with the C_{60} coordinated via a [6-6] ring junction, as in Figure 3.

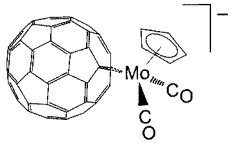

Figure 3. Proposed Structure of the $[CpMo(CO)_2(C_{60})]^-$ anion

Conclusions

Thermal and photochemical reactions of the carbonylate salts $A[(\eta^5\text{-}C_5H_5)M(CO)_n]$ (A = Na, PPN; M = Fe, n = 2; M = Mo, W, n = 3) with C_{60} result in all cases in electron transfer to give $[C_{60}]^-$ and the transient 17-electron, metal-centered radicals $CpFe(CO)_2$ or $CpM(CO)_3$. Subsequent self-coupling of $CpFe(CO)_2$ and $CpM(CO)_3$ then gives the metal-metal bonded dimers $[CpFe(CO)_2]_2$ and $[CpM(CO)_3]_2$. Interestingly, while the mixture of $Na[C_{60}]$ and $[CpFe(CO)_2]_2$ does not react further under photochemical conditions, photolysis of the mixtures of $Na[C_{60}]$ and $[CpM(CO)_3]_2$ ultimately results also in complete homolysis of the dimers and regeneration of the metal-centered radicals, which then combine with the $[C_{60}]^-$ remaining in solution to form the η^2-C_{60} complexes $A[CpM(CO)_2(\eta^2\text{-}C_{60})]$.

Experimental Section

All reactions were carried out using standard Schlenk line techniques or under Vacuum Atmospheres or MBraun glove boxes. Argon and nitrogen were purified by passing over a column of BASF catalyst heated to 140 °C and subsequently over a second column containing 5 Å molecular sieves. Solvents were purified by distillation over a drying agent under a blanket of nitrogen or argon. In most cases Na wire was used as the drying agent, the exceptions being dichloromethane and acetonitrile for which CaH_2 and P_2O_5 were used, respectively.

Infrared (IR) spectra were recorded on a Bruker IFS 25 FTIR spectrometer, and negative ion mode electrospray mass spectrometry (henceforth ESMS)[5] experiments on a VG Quattro spectrometer with nitrogen as the nebulizing gas. Typical concentrations of the species being studied were 1−5 mM, and the capillary voltage, cone voltage, lens parameters, ionization energy and ramp, position of the source, flow rate of the sample and time of acquisition were all varied in order to optimize the intensity of the peak being studied. Low cone voltages <30 V were normally used to observe parent ions in solution, and higher cone voltages (up to 150 V) to observe fragmentation products. High resolution ESMS experiments were carried out on a Micromass Q-TOF-2 quadrupole time-of-flight mass spectrometer. Mass-to-charge ratios reported below refer in all cases to the strongest peak in what are always complex distributions of isotopomers.

^{1}H NMR spectra were recorded on a Bruker AC-200 spectrometer and were referenced internally to the known residual ^{1}H signal in the deuterated solvent relative to TMS. ^{13}C NMR spectra were recorded on a Bruker AM-500 spectrometer, and were internally referenced relative to the solvent resonances. Near-IR spectra in the region 800−1300 nm were run on a Cary 17 UV/Vis spectrophotometer, and UV/Vis spectra in the region 190 nm−820 nm on a HP 8452A Diode Array Spectrophotometer.

Unless explicitly stated otherwise, all chemicals were obtained from Aldrich, Fisher or Strem and were used as received. C_{60} was obtained from MER Corporation. The compounds Na[(η^5-C_5H_5)Fe(CO)$_2$],[6a] Na[(η^5-C_5H_5)Mo(CO)$_3$][6a] and Na[(η^5-C_5H_5)W(CO)$_3$][6a] were prepared as in the literature.

PPN[(η^5-C_5H_5)Fe(CO)$_2$]: This compound was prepared utilizing a modification of a reported procedure.[6b] A solution of [(η^5-C_5H_5)Fe(CO)$_2$]$_2$ (2.0 g) in 30 mL of THF was stirred over 80 g of 1% sodium amalgam for 30 min. The resulting red supernatant was then cannulated into a 250 mL flask and a solution containing an excess of [PPN]Cl in dry CH_3CN was added. The solution was stirred vigorously for 30 min, by which time a white precipitate of NaCl was evident. The solution was separated from the solid by filtration through Celite and the solvent was removed under reduced pressure to give PPN[(η^5-C_5H_5)Fe(CO)$_2$] as a deep red solid.[6b]

PPN[(η^5-C_5H_5)M(CO)$_3$] (M = Mo, W): These compounds were prepared from the corresponding sodium salts as described for the iron analogue except that dichloromethane was used as a solvent for the [PPN]Cl; yellow products were obtained. The products were characterized by ^{1}H NMR and IR spectroscopy. For PPN[(η^5-C_5H_5)Mo(CO)$_3$], ν_{CO} = 1782, 1895 cm^{-1} (CH_2Cl_2).[6a] For PPN[(η^5-C_5H_5)W(CO)$_3$], ν_{CO} = 1775, 1892 cm^{-1} (CH_2Cl_2).[6a]

Thermal Reactions of A[CpFe(CO)$_2$] (A = Na, PPN) with C_{60}: C_{60} (100 mg, 0.14 mmol) was added to a solution of Na[CpFe(CO)$_2$] (0.40 g, 0.14 mmol) in 10 mL of THF. The solution immediately turned a deep red color, and an IR spectrum recorded within 2 min revealed only the ν_{CO} bands of [CpFe(CO)$_2$]$_2$ at 1782 and 1992 cm^{-1}. The reaction was refluxed for 3 h, but no further changes occurred in the carbonyl region. The solution was filtered through Celite, 25 mL of hexanes was added to the filtrate and a black solid precipitated from the red solution. The black solid was filtered and characterized as NaC_{60} on the basis of an absorption at 1078 nm in the NIR[4] and a peak at 720 Da/e in the ES mass spectrum (both THF solutions). Removal of the solvent from the red solution under reduced pressure yielded [CpFe(CO)$_2$]$_2$, identified by IR spectroscopy (1782 and 1992 cm^{-1} in THF). Very similar observations were made with PPN[CpFe(CO)$_2$].

Thermal Reactions of A[CpMo(CO)$_3$] (A = Na, PPN) with C_{60}: A solution of Na[CpMo(CO)$_3$] (37 mg, 0.14 mmol) in 10 mL of THF was treated with C_{60} (100 mg, 0.14 mmol) and the mixture was refluxed. The color of the solution quickly turned deep red and the ν_{CO} bands of [CpMo(CO)$_3$]$^-$ were gradually replaced by those of [CpMo(CO)$_3$]$_2$ (1911, 1956, and 2012 cm^{-1}) over 3 h. ESMS monitoring revealed the presence of a peak at 720 Da/e. After 4 h of refluxing, no further changes to the carbonyl region of the IR spectrum were evident and the solution was filtered. The filtrate was treated with 25 mL of pentane to give a black precipitate of NaC_{60}, identified as above by ESMS and near IR spectroscopy (characteristic peak at 1078 nm[4]). [CpMo(CO)$_3$]$_2$ was recovered by removing solvent from the filtrate under reduced pressure (ν_{CO} 1911, 1956, 2012 cm^{-1}). The compounds PPN[CpMo(CO)$_3$] and A[CpW(CO)$_3$] (A = Na, PPN) reacted similarly.

Photochemical Reactions of A[CpFe(CO)$_2$] (A = Na, PPN) with C_{60}: C_{60} (100 mg, 0.14 mmol) was added to a solution of Na[CpFe(CO)$_2$] (0.40 g, 0.14 mmol) in 10 mL of THF. The solution immediately turned deep red, and an IR spectrum recorded immediately revealed only the ν_{CO} bands of [CpFe(CO)$_2$]$_2$ at 1782 and 1992 cm^{-1}. A Hanovia lamp, placed inside a water-cooled quartz tube, was situated 10−12 cm away from the reaction vessel and the stirred reaction mixture was photolyzed for 96 h. During this time no further changes in the IR occurred while ESMS revealed only a peak at 720 Da/e. Workup procedures were as described above for the thermal reactions, and again yielded only NaC_{60} and [CpFe(CO)$_2$]$_2$. Similar results were obtained with PPN[CpFe(CO)$_2$].

Photochemical Reactions of A[CpMo(CO)$_3$] (A = Na, PPN) with C_{60}. Syntheses of A[CpMo(CO)$_3$(η^2-C_{60})]: A solution of Na[CpMo(CO)$_3$] (37 mg, 0.14 mmol) in 10 mL THF was treated with C_{60} (100 mg, 0.14 mmol) and the mixture was photolyzed as above. The solution quickly turned deep red, and the ν_{CO} bands of Na[CpMo(CO)$_3$] decreased over 3 h as ν_{CO} bands at 1818, 1900, 1911, 1956, and 2012 cm^{-1} appeared and gained in intensity. On further photolysis, the solution turned brown as the ν_{CO} bands at 1818 and 1900 cm^{-1} continued to gain intensity while those at 1911, 1956, and 2012 cm^{-1}, attributable to [CpMo(CO)$_3$]$_2$, decreased. ESMS monitoring of the solution revealed peaks at 720 and 937 Da/e which increased in intensity over the first 3 hours, but the latter thereafter gained intensity at the expense of the former. Increasing the cone voltage in any ESMS experiment resulted in a loss of intensity from the peak at 937 Da/e$^-$, an increase in the intensity of the peak at 720 Da/e and the appearance of a new peak 909 Da/e. The reaction was halted after 96 h, the solution was then filtered through Celite and pentane was added to the now green filtrate to precipitate Na[CpMo(CO)$_2$(η^2-C_{60})]. This was washed with pentane and dried under reduced pressure; yield 77 mg (58%). The compound was characterized by IR spectroscopy (ν_{CO} 1818, 1900 cm^{-1} in THF) and ESMS (937 Da/e, THF).

The synthesis of PPN[CpMo(CO)$_3$(η^2-C_{60})] proceeded similarly and was carried out several times; it was typically finished within 36 h to give amber-green solutions of the product in 70−90% isolated yield (140−180 mg). PPN[CpMo(CO)$_2$(η^2-C_{60})] was characterized by ESMS (939 Da/e) as well as IR (ν_{CO} 1818, 1900 cm^{-1}), ^{1}H NMR (δ_{Cp} = 5.65 in [D$_8$]THF) and ^{13}C NMR spectroscopy (Table 1; in [D$_8$]THF). The near IR spectrum (THF) exhibited no absorptions between 800 and 1400 nm, but the UV/Vis spectrum (THF) exhibited absorptions at 336, 400−600 (broad band) and 583 nm. While crystals of this compound were obtained by layering THF solutions with hexanes, they did not give useful elemental analyses and were not of sufficient quality for X-ray crystallographic analysis. However the anion was characterized unambiguously by high resolution ESMS; 938.9491 Da/e; calc. 938.9344; difference 15.7 ppm.

Photochemical Reactions of A[CpW(CO)$_3$] (A = Na, PPN) with C_{60}. Syntheses of A[CpW(CO)$_3$(η^2-C_{60})]: These reactions were carried out as described for the molybdenum analogues and proceeded similarly. Combining Na[CpW(CO)$_3$] with C_{60} resulted in the formation of a red solution, loss of intensities of the ν_{CO} bands of Na[CpW(CO)$_3$] (1744, 1793 and 1895 cm^{-1}) over 3 h and appearance of ν_{CO} bands at 1809, 1894, 1904, 1953, and 2010 cm^{-1}. On further photolysis, the ν_{CO} bands at 1809 and 1894 cm^{-1}, attributed to [CpW(CO)$_2$(η^2-C_{60})]$^-$, continued to gain intensity while the ν_{CO} bands (of [CpW(CO)$_3$]$_2$) at 1904, 1953, and 2010 cm^{-1} grew weaker. ESMS monitoring of the reaction revealed peaks at 720 Da/e and 1025 Da/e which increased in intensity over the first

3 h, at which point that at 720 Da/e began to lose intensity in favor of the peak at 1025 Da/e, attributed to $[CpW(CO)_2(\eta^2\text{-}C_{60})]^-$. The reaction was stopped after 96 h, and the solution was then filtered through Celite and worked up as above to give 67 mg of $Na[CpW(CO)_2(\eta^2\text{-}C_{60})]$ (46% yield).

A similar procedure was used to synthesize $PPN[CpW(CO)_2(\eta^2\text{-}C_{60})]$ from $PPN[CpW(CO)_3]$ in yields ranging from 141−198 mg (65−91%). The product was characterized using IR (ν_{CO} 1809, 1894 cm^{-1}), ^1H NMR (δ = 5.56 ppm in $[D_8]$THF) and near IR (no absorptions in the region 800−1400 nm) spectroscopy and ESMS (1025 Da/e). Although crystals were obtained by layering THF solutions with hexanes, they did not give useful elemental analyses and were not of sufficient quality for X-ray crystallographic analysis. Therefore the anion was characterized unambiguously as such by high resolution ESMS: 1024.9689 Da/e; calcd. 1024.9799; difference 10.8 ppm.

Acknowledgments

We thank the Natural Sciences and Engineering Research Council for a Research Grant to MCB and a Graduate Fellowship to DMT, and ALCAN for a Graduate Fellowship to DMT. We also thank Prof. J. A. Stone, Mr. T. Hunter and Dr. I. Galetich for assistance with the mass spectrometry measurements.

[1] [1a] D. S. Bethune, R. D. Johnson, J. R. Salem, M. S. de Vries, C. C. Yannoni, *Nature (London)* **1993**, *366*, 123. [1b] I. Holleman, M. G. H. Boogaarts, G. Meijer, *Recl. Trav. Chim. Pays-Bas* **1994**, *113*, 543. [1c] F. T. Edelmann, *Angew. Chem. Int. Ed. Engl.* **1995**, *34*, 981. [1d] S. Nagase, K. Kobayashi, T. Akasaka, *Bull. Chem. Soc. Jpn.* **1996**, *69*, 2131.

[2] [2a] W. Śliwa, *Transition Met. Chem.* **1996**, *21*, 583. [2b] A. H. H. Stephens, M. L. H. Green, *Adv. Inorg. Chem.* **1997**, *44*, 1. [2c] A. L. Balch, M. M. Olmstead, *Chem. Rev.* **1998**, *98*, 2123.

[3] [3a] D. K. Patel, D. M. Thompson, M. C. Baird, L. K. Thompson, K. F. Preston, *J. Organomet. Chem.* **1997**, *546*, 607. [3b] M. Bengough, D. M. Thompson, M. C. Baird, *Organometallics* **1999**, *18*, 2950. [3c] D. M. Thompson, J. McLeod, M. C. Baird, *Pure Appl. Chem.* **2001**, *273*, 287. [3d] D. M. Thompson, M. Bengough, M. C. Baird, *Organometallics*, in press.

[4] [4a] M. S. Dresselhaus, G. Dresselhaus, P. C. Eklund, *Science of Fullerenes and Carbon Nanotubes*, Academic Press, 1996. [4b] M. J. Rosseinsky, *Chem. Mat.* **1998**, *10*, 2665.

[5] For information on electrospray mass spectrometry and applications to organometallic and fullerene chemistry, see: [5a] S. J. Gaskell, *J. Mass Spectrom.* **1997**, *32*, 677. [5b] R. Colton, A. D'Agostino, J. C. Traeger, *Mass Spectrom. Rev.* **1995**, *14*, 79. [5c] W. Henderson, B. K. Nicholson, L. J. McCaffrey, *Polyhedron* **1998**, *17*, 4291. [5d] W. Henderson, J. S. McIndoe, B. K. Nicholson, P. J. Dyson, *J. Chem. Soc., Dalton Trans.* **1998**, 519. [5e] M. Ferrer, R. Reina, O. Rossell, M. Seco, G. Segales, *J. Organomet. Chem.* **1996**, *515*, 205. [5f] G. Khairallah, J. B. Peel, *Chem. Commun.* **1997**, 253. [5g] M. P. Barrow, X. Feng, J. I. Wallace, O. V. Boltalina, R. Taylor, P. J. Derrick, T. Drewello, *Chem. Phys. Lett.* **2000**, *330*, 267.

[6] [6a] R. Faltynek, M. S. Wrighton, *J. Am. Chem. Soc.* **1978**, *100*, 2701. [6b] J. K. Ruff, W. J. Schlientz, *Inorg. Synth.* **1976**, *15*, 85.

[7] [7a] N. G. Connelly, W. E. Geiger, *Chem. Rev.* **1996**, *96*, 877. [7b] C.-K. Lai, W. G. Feighery, Y. Zhen, J. D. Atwood, *Inorg. Chem.* **1989**, *28*, 3929. [7c] M. S. Corraine, J. D. Atwood, *Organometallics* **1991**, *10*, 2315. [7d] C. K. Lai, M. S. Corraine, J. D. Atwood, *Organometallics* **1992**, *11*, 582.

[8] [8a] J. V. Caspar, T. J. Meyer, *J. Am. Chem. Soc.* **1980**, *102*, 7794. [8b] B. D. Moore, M. B. Simpson, M. Poliakoff, J. J. Turner, *J. Chem. Soc., Chem. Commun.* **1984**, 972.

[9] [9a] M. S. Wrighton, D. S. Ginley, *J. Am. Chem. Soc.* **1975**, *97*, 4246. [9b] J. L. Hughey, C. B. Bock, T. J. Meyer, *J. Am. Chem. Soc.* **1975**, *97*, 4440. [9c] R. M. Laine, P. C. Ford, *Inorg. Chem.* **1977**, *16*, 388.

Received August 6, 2002
[I02453]

EurJIC
European Journal of Inorganic Chemistry

January 2003
Issue 2
Pages 181–378

Papers available ahead of print in Early View at www.interscience.wiley.com

Earliest available Table of Contents:
Automatically, free of charge by e-mail through
www.interscience.wiley.com/alerts

COVER PICTURE

The cover picture shows a self-assembled [2]catenane, with two interpenetrating 24-membered digold rings and with intermolecular aurophilic attractions as a key feature. Details are discussed in the article by R. J. Puddephatt et al. on p. 217ff.

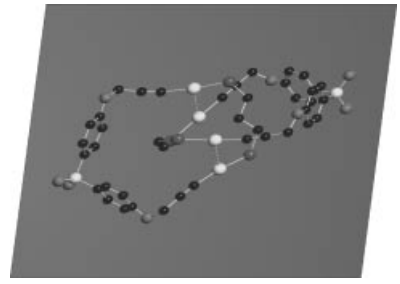

MICROREVIEW

Contents

195 **A. Macchioni**

Elucidation of the Solution Structures of Transition Metal Complex Ion Pairs by NOE NMR Experiments

Keywords: Ion pairs / NMR spectroscopy / Transition metals

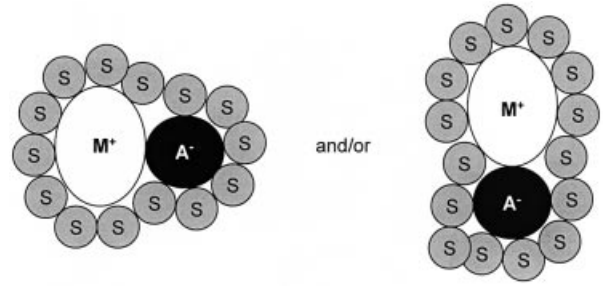

 © WILEY-VCH Verlag GmbH, 69451 Weinheim, Germany, 2003 1434–1948/03/0102–0185 $ 20.00+.50/0

SHORT COMMUNICATIONS

207 **M. Soleilhavoup, L. Viau, G. Commenges, C. Lepetit, R. Chauvin***

The η^5-(σ-P,ν-Arene) Chelating H-MOP Ligand in an Optically and Catalytically Active Rhodium(I) Complex

Keywords: Phosphane ligands / Arene ligands / Atropisomerism / Rhodium / NMR spectroscopy / Asymmetric catalysis

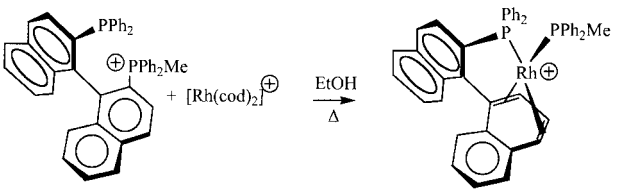

213 **R. Della Pergola,* E. Comensoli, L. Garlaschelli, M. Manassero,* M. Sansoni, D. Strumolo**

Rhodium Clusters Substituted by Cycloheptatrienyl Ligands: Synthesis and Solid-State Structure of $[Rh_{11}(CO)_{14}(\mu_3\text{-}\eta^2\text{:}\eta^3\text{:}\eta^2\text{-}C_7H_7)_3]$

Keywords: Rhodium / Carbocycles / Cluster compounds / Carbonyl ligands

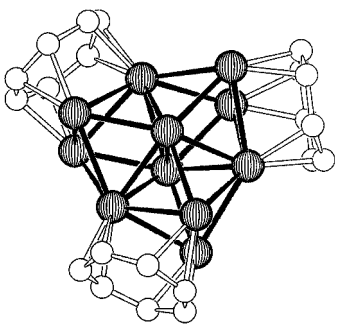

FULL PAPERS

217 **F. Mohr, M. C. Jennings, R. J. Puddephatt***

Gold(I) Macrocycles and [2]Catenanes Containing Sulfone-Functionalised Diacetylide Ligands

Keywords: Self assembly / Catenanes / Macrocycles / Gold / Aurophilicity

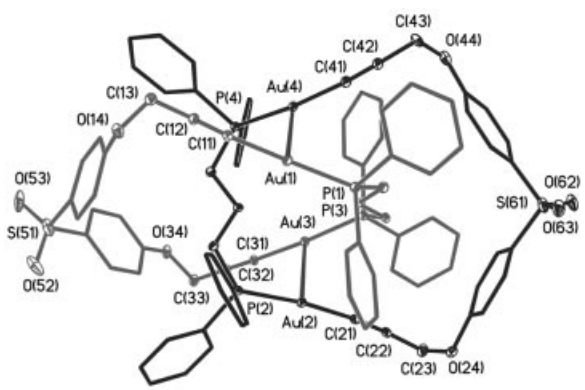

224 **M. K. Denk,* K. Hatano, A. J. Lough**

Synthesis and Characterization of a Carbene•SO_2 Adduct

Keywords: Carbenes / Sulfenes / Density functional calculations / Thermochemistry / Sulfur ylides

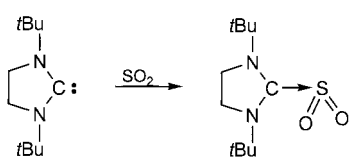

1 **2**

232 **H.-F. Klein,* R. Beck, O. Hetche**

Dynamic Properties of Methyl(trimethylphosphane)nickel Complexes Containing (2-Diphenylphosphanyl)phenylamido Ligands

Keywords: Solution dynamics / Nickel / Coordination numbers 4 and 5 / Structure elucidation

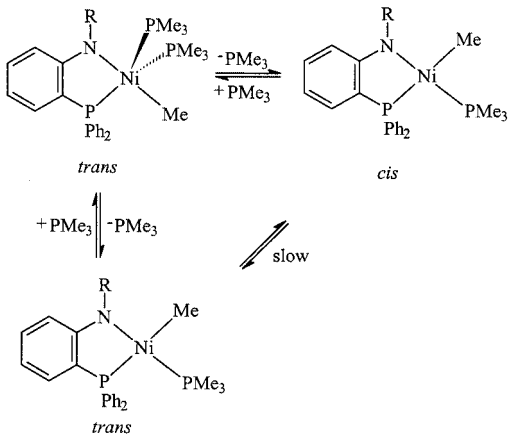

240 **H.-F. Klein,* R. Beck, U. Flörke, H.-J. Haupt**

Fluxional and Rigid (Trimethylphosphane)-cobalt Complexes Containing Chelating (2-Diphenylphosphanyl)anilido Ligands

Keywords: Chelates / Cobalt / P ligands / Structure elucidation

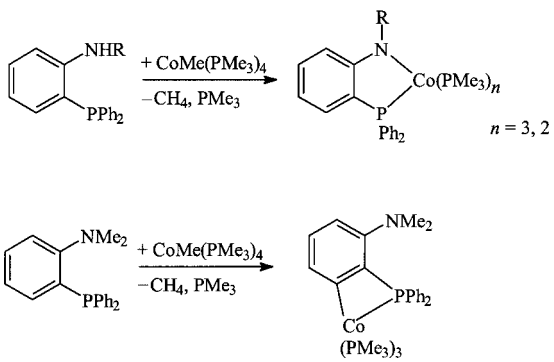

249 **P. Kilian, D. Philp, A. M. Z. Slawin, J. D. Woollins***

Use of Molecular Scaffolding for the Stabilization of an Intramolecular Dative P^{III}-P^{V} System

Keywords: Phosphorus heterocycles / Strained molecules / Neighbouring-group effects / Phosphorus−phosphorus bond

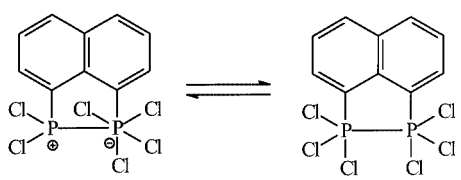

255 **J.-L. Zuo, W.-F. Fu, C.-M. Che,* K.-K. Cheung**

Synthesis, Crystal Structure, and Photoluminescent Properties of a Tetracarbonyl(naphthyridylcarbamoyl)rhenium(I) Complex and a Highly Emissive Tetracarbonyl(naphthyridylamido)-rhenium(I) Complex

Keywords: Carbonyl ligands / N ligands / Photoluminescence / Rhenium / Structure elucidation

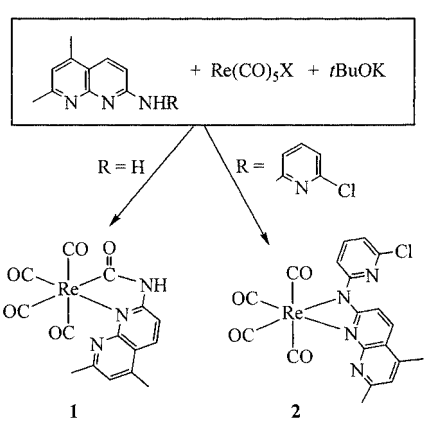

263 **S. Lhuachan, S. Siripaisarnpipat,* N. Chaichit**

Synthesis, Spectra and Crystal Structure of Two Copper(I) Complexes of Acetonethiosemicarbazone

Keywords: Copper / Electrochemistry / Schiff bases / IR spectroscopy

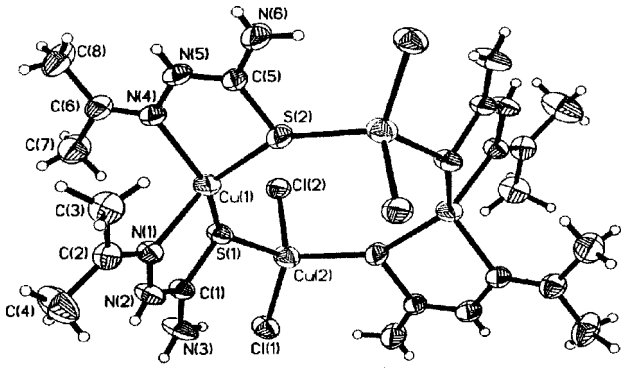

$[Cu_2(tscac)_2Cl_2]_2$

268 **M. S. A. Hamza, Y. Zou, K. L. Brown, R. van Eldik***

Thermodynamic and Kinetic Data for the Base-On/Base-Off Equilibration of Alkylcobalamins

Keywords: Alkylcobalamins / Metal−carbon bond / Kinetics / High-pressure chemistry / Catalysis

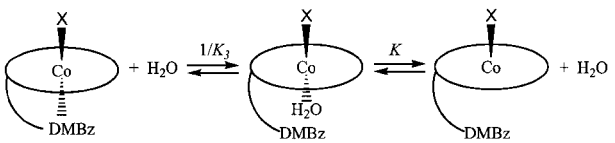

277 **J. S. L. Yeo, J. J. Vittal, T. S. A. Hor***

Facile Metal-Mediated Synthesis of Macrocyclic Diselenoethers

Keywords: Platinum / Selenium / Alkylation / Metallacycles / Synthesis design

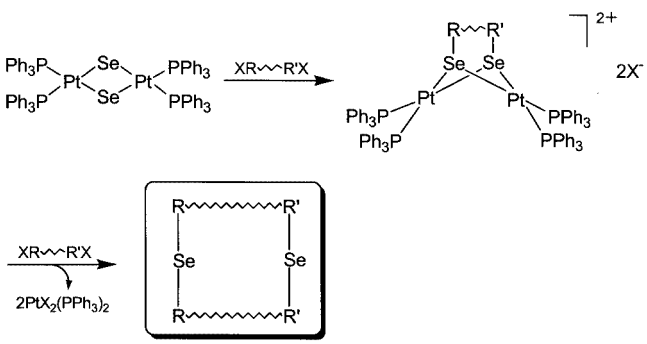

281 **G. Bodes, F. W. Heinemann, G. Jobi, J. Klodwig, S. Neumann, U. Zenneck***

Halogen Atoms as Reactive Centers for the Introduction of Functional Side Chains into (Arene)ruthenium(0) Complexes

Keywords: Arene complexes / Electrophilic substitution / Lithiation / Ruthenium

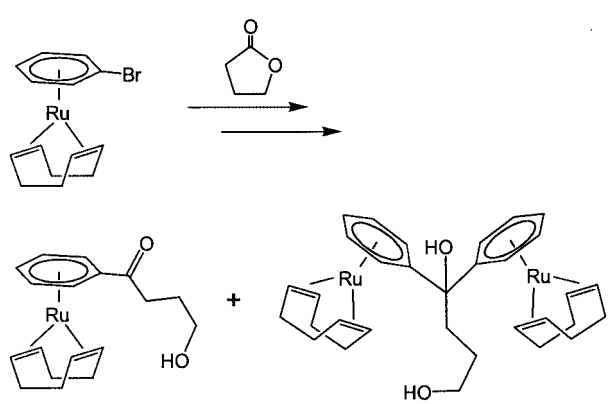

293 **B. A. Messerle,* V.-A. Tolhurst, P. Turner**

Synthesis, Structure and Reactivity of Ruthenium(II) Carbonyl Complexes Containing Bis(pyrazol-1-yl)methane and Bis(*N*-methylimidazol-2-yl)methane

Keywords: N ligands / Ruthenium / Structure elucidation / Reactivity

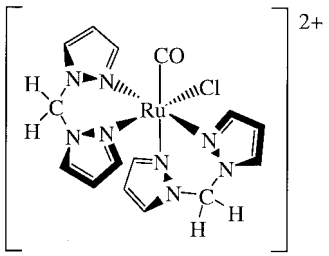

301 **T. Ressler,* J. Wienold, R. E. Jentoft, F. Girgsdies**

Evolution of Defects in the Bulk Structure of MoO_3 During the Catalytic Oxidation of Propene

Keywords: Molybdenum / EXAFS spectroscopy / X-ray diffraction / Heterogeneous catalysis / Oxidation

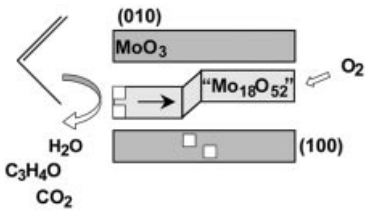

313 **X. Zhang, M. H. Prosenc, T. Meyer-Friedrichsen, J. Heck***

[(η^6-Cyclooctatetraene){η^5-(+)-neomenthylcyclopentadienyl}ruthenium(II)] Hexafluorophosphate: Synthesis and Characterization of a Chiral Mixed Sandwich Complex

Keywords: Chirality / Cyclopentadienyl ligands / Sandwich complexes / Ruthenium

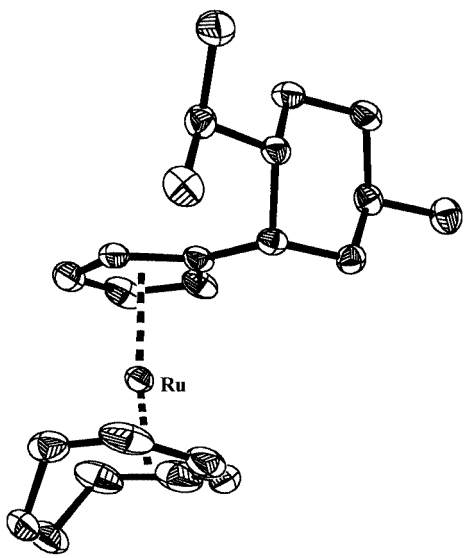

318 **Y. Luo, Y. Yao, Q. Shen,* K. Yu, L. Weng**

Synthesis and Characterization of Lanthanide(III) Bis(guanidinate) Derivatives and the Catalytic Activity of Methyllanthanide Bis(guanidinate) Complexes for the Polymerization of ε-Caprolactone and Methyl Methacrylate

Keywords: Lanthanides / N ligands / Structure elucidation / Polymerization / ε-Caprolactone / Methyl methacrylate

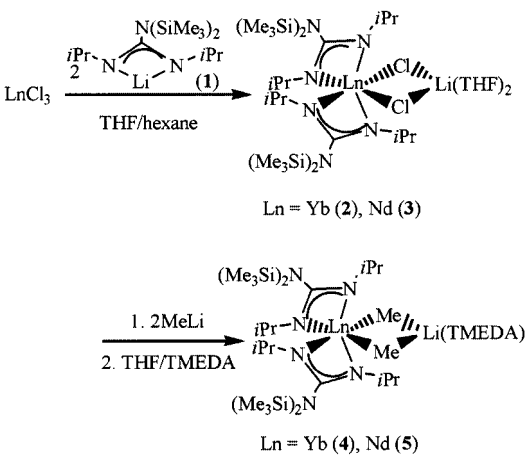

324 E. Polo,* A. Barbieri, O. Traverso

The Effect of Phenyl Substituents on the Activity of Some Zirconocene Photoinitiators

Keywords: Homogeneous catalysis / Metallocenes / Photolysis / Polymerisation / Zirconium

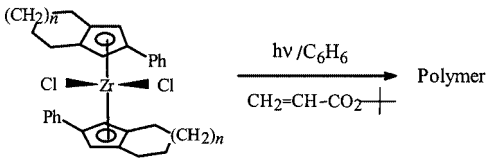

331 A. Lafuma, S. Chodorowski-Kimmes, F. X. Quinn, C. Sanchez*

Photochromic Properties of a Spirooxazine and a Spiropyran in Alcoholic Solutions of Zirconium and Aluminium Alkoxides: Influence of the Ethyl Acetoacetate Chelating Agent on the Optical Properties

Keywords: Alkoxides / Sol-gel processes / Spiro compounds / Photochromism / Aluminium / Zirconium

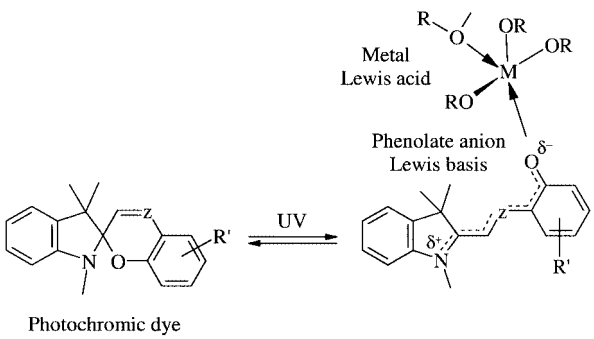

339 I. Hegelmann, A. Beck, C. Eichhorn, B. Weibert, N. Burzlaff*

Alkylzinc Complexes with Achiral and Chiral Monoanionic *N,N,O* Heteroscorpionate Ligands

Keywords: Scorpionate ligands / Zinc / Bioinorganic chemistry / Tripodal ligands / N ligands

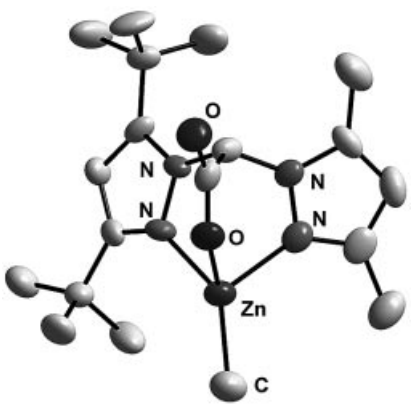

348 A. Romerosa,* C. López-Magaña, M. Saoud, S. Mañas

New Dinuclear Palladium Phosphane Complexes Stabilised by 8-Thiotheophylline

Keywords: Palladium / Nucleobases / Bioinorganic chemistry / P ligands

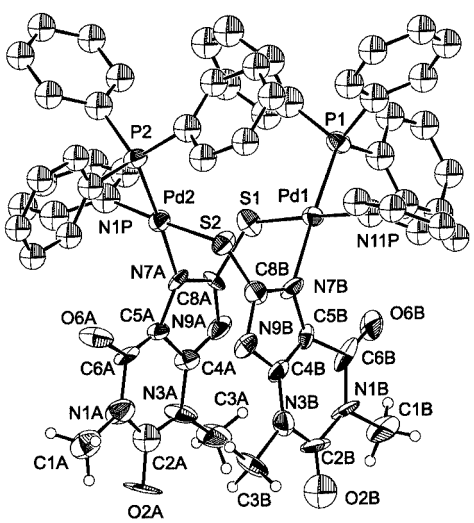

356 **Y. Garcia,* P. J. van Koningsbruggen, G. Bravic, D. Chasseau, O. Kahn**

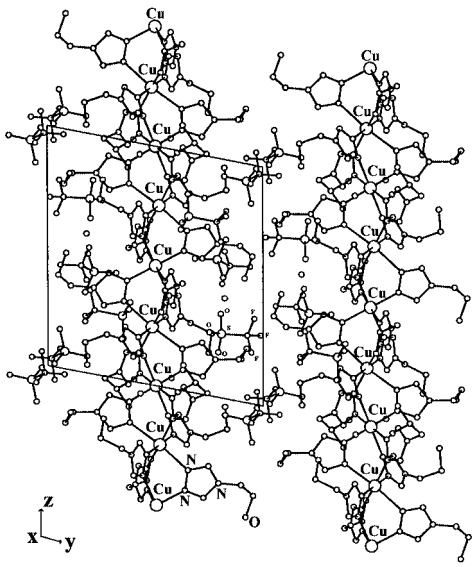

A Cu^{II} Chain Compound Showing a Ferromagnetic Coupling through Triple N^1,N^2-1,2,4-Triazole Bridges

Keywords: Chain structures / Copper / N ligands / Bridging ligands / Magnetic properties

363 **R. Dinda, P. Sengupta, S. Ghosh,* W. S. Sheldrick**

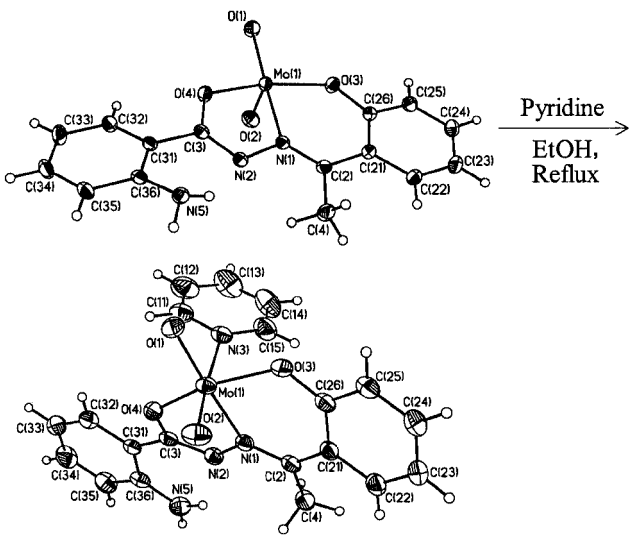

Synthesis, Structure, and Reactivity of a New Mononuclear Molybdenum(VI) Complex Resembling the Active Center of Molybdenum Oxotransferases

Keywords: Molybdenum / Bioinorganic chemistry / Substrate binding / Enzyme models

370 **Z. Kang, E. Wang,* M. Jiang, S. Lian, Y. Li, C. Hu**

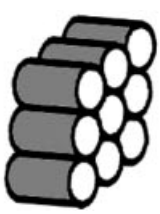

Convenient Controllable Synthesis of Inorganic 1D Nanocrystals and 3D High-Ordered Microtubes

Keywords: Nanotubes / Polyoxometalates / Synthetic methods

CORRECTION

377 **S. Sjövall, M. H. Johansson, C. Andersson***

A New Highly Active Diphosphane-Palladium(II) Complex as a Catalyst Precursor for the Heck Reaction

Elucidation of the Solution Structures of Transition Metal Complex Ion Pairs by NOE NMR Experiments

Alceo Macchioni[a]

Keywords: Ion pairs / NMR spectroscopy / Transition metals

Our results from structural investigations of transition metal complex ion pairs in solution by homonuclear and heteronuclear 1D- and 2D-NOE NMR spectroscopy are reviewed. Both model (**A**) and catalytically active (**B**) complexes have been taken into account; their general formulas are: *trans*-$[ML_2(N,X)(Y)(Z)]^+A^-$ (**A**) {M = Fe^{II}, Ru^{II} and Os^{II}, L = PMe_3, Y = CO, Z = COMe, A^- = BPh_3R^-, $CF_3SO_3^-$, BF_4^-, PF_6^- and $B[3,5\text{-}(CF_3)_2C_6H_3]_4^-$; M = Ir^{III}, L = PR_3, Y = Z = H and A^- = BPh_4^-, $CF_3SO_3^-$, BF_4^-, PF_6^-} and $[M'(N,X)(R,olefin)]^+A^-$ (**B**) {M′ = Pt, R = Me, olefin = ethene, propene and CH_2=CHCOOMe, A^- = BF_4^-; M′ = Pd, (R,olefin) = η^1,η^2-5-methoxycyclooctenyl, A^- = BPh_4^-, $CF_3SO_3^-$, BF_4^-, PF_6^-, SbF_6^- and $B[3,5\text{-}(CF_3)_2C_6H_3]_4^-$}, where N,X = bis(pyrazolyl)methane, bipyridine, α-diimines, α-diamines or α-oxo imines. The detection of dipolar interionic interactions in ^{1}H-NOESY and ^{19}F,^{1}H-HOESY NMR spectra allowed relative anion-cation orientations to be determined, these being well defined in most cases, with one orientation predominating in solution. We often found that the anion approaches the complexes from the side of the N,X-ligands, due to an accumulation of positive charge at the junction of the moieties containing the N- and X-donor atoms. In square-planar complexes **B**, the apparently favoured apical positions were often protected either by electronic factors [N,X = bis(2-pyridyl)amine or bis(pyrazolyl)methane] or by a combination of electronic and steric factors (N,X = α-diimines). For M′ complexes, bearing Ar–N=C(Me)–C(Me)=N–Ar ligands, the position of the counter-anion is finely modulated by the steric hindrance of the *ortho*-aryl substituents. The accessibility of the metal centre, which is directly associated with the catalytic performances of the complexes, was determined by using the counter-anion as a probe. Finally, average interionic distances were estimated for model complexes **A**, bearing unsymmetrical BPh_3R^- counter-anions, based on the quantification of interionic NOEs.

(© Wiley-VCH Verlag GmbH, 69451 Weinheim, Germany, 2003)

1 Introduction

Several stoichiometric and catalytic reactions mediated by cationic transition metal complexes are strongly affected by the phenomenon of ion-pairing. In most cases the counter-anion effect is carried out through competition with the substrate for coordination to the metal ion; consequently, in terms of reaction rate and yield, better results are obtained when less strongly coordinating anions are used.[1] As an example, Evans et al.[2] showed in 1995 that the degree and rate of conversion of the Diels−Alder reaction between methacrolein and cyclopentadiene, catalysed by dicationic Cu^{II} compounds bearing bis(oxazoline) ligands, was significantly affected by the nature of the counter-anion, and that higher performances were obtained with use

[a] Department of Chemistry, University of Perugia,
Via Elce di Sotto 8, 06123 Perugia, Italy
Fax: (internat.) + 39-075/585-5598
E-mail: alceo@unipg.it

Alceo Macchioni was born in Città della Pieve, Italy, in 1963. He obtained his "Laurea" in Chemistry from the University of Perugia in 1988. He received his Ph.D. degree in Chemistry in 1992 from the same university under the supervision of Giuseppe Cardaci. After a postdoctoral stay (November 1992 until February 1995) with Paul S. Pregosin and Luigi M. Venanzi, Zürich, Switzerland, he returned to Italy as a Researcher at the University of Perugia. In April 2001 he obtained the "Idoneità" to be Associate Professor in General and Inorganic Chemistry. He has recently received the "Raffaello Nasini" prize from the Inorganic Division of the Italian Chemical Society. His main research interests are the synthesis and characterization of ruthenium and palladium complexes and their application in homogeneous catalysis, with particular attention to the role of noncovalent interactions in their structure and reactivity in solution.

MICROREVIEWS: This feature introduces the readers to the authors' research through a concise overview of the selected topic. Reference to important work from others in the field is included.

of the least strongly coordinating anion (SbF_6^-) of those tested. Kündig et al. found a similar counter-anion influence[3] in the same reaction with catalysis by monocationic Ru^{II} compounds.

Consequently, new types of anions have been engineered in order to diminish their coordinating power. The strategy of introducing large and highly fluorinated moieties, or electron-withdrawing substituents in general, into the counter-anions has often been used to achieve this goal.[4,5]

In some cases the anion plays a direct role in the stoichiometric and catalytic processes.[6−8] RajanBabu et al.,[9] for instance, showed the synergistic effect of hemilabile coordination and the counter-anion effect in hydrovinylation catalysed by cationic Ni^{II} compounds. Faita et al.[10] found that the enantioselectivity of a reaction could be inverted by use of a suitable counter-anion, while Marks and Chen[11] suggested that ion-pairing affects the stereochemistry of propylene chain formation during single-site olefin polymerization. Finally, Arndtsen et al.[12] showed that the use of chiral counter-anions[13] may provide a novel method for inducing enantioselectivity.

It seems clear from the examples reported above that the ion-pairing phenomenon has an established relevance in transition metal chemistry. Until seven years ago, however, there had been no detailed investigations into the structures of transition metal complex ion pairs in solution; that is, the environment in which they "work". Very little was known about the relative anion-cation orientation and, consequently, of the possibility of having one or more favoured points of anchorage for the two ionic moieties. A few structural studies in solution, concerning organolithium[14,15] and organoammonium[16] ion pairs, appeared in the literature after the mid 1980s. They were based on Nuclear Overhauser Effect (NOE) NMR spectroscopy; that is, on the detection of inter-ionic dipolar interactions[17] between the atoms of the cations (lithium or hydrogen) and those of the anions (hydrogen or fluorine).

Our laboratory decided to investigate transition metal complex ion pairs by application of 1D- and 2D-NOE NMR spectroscopy (both homonuclear and heteronuclear). We began by developing appropriate methodologies on "model" systems. We then considered transition metal complexes with structures or reactivities that were affected by the nature of the counter-anion, in the hope of obtaining a better understanding of the role of anion-cation interactions and, possibly, of correlating them with the reactivity of the complexes. During the course of our studies we realized that the detection of anion-cation interactions can afford precious information about the electron density distribution around the metal ion. In particular, the accessibility of the metal centre in square-planar complexes for a generic nucleophile can be accurately determined by assuming that the anion is a good probe.

The main results of our studies to date are reviewed here. After an examination of some basic aspects of NOE theory essential for facilitating the reading of this paper, the results of qualitative NOE NMR investigations and the consequent interionic structures are reported for compounds grouped according to the geometry of the metal centre. When the analysed complexes are active catalysts, the connections between the interionic interactions and the catalytic performances are outlined. The last paragraph illustrates the results of quantitative NOE measurements, which have allowed average interionic distances to be estimated.

2 NOE and Suitable Systems for Investigation

In an ideal two-spin (I = 1/2) system, the NOE, defined as the fractional change in the intensity of one nucleus (I) on perturbation of the nucleus (S), dipolar coupled to it, is related to the cross-relaxation rate constant (σ_{IS}) and the dipolar longitudinal relaxation rate constant (ρ_{IS}) according to Equation (1),[18] where I^0 is the equilibrium intensity of I, and γ_S and γ_I are the giromagnetic ratios;[19] σ_{IS} can be related to the molecular tumbling rate by Equation (2), where μ_0 is the permeability constant in a vacuum, $\hbar$ is Planck's constant divided by 2π, τ_c is the rotational correlation time, and ω_I and ω_S are the resonance frequencies of the I and S nuclei, respectively.

$$NOE = f_I\{S\} = \frac{(I - I^0)}{I^0} = \frac{\gamma_S}{\gamma_I}\frac{\sigma_{IS}}{\rho_{IS}} \quad (1)$$

$$\sigma_{IS} = \frac{1}{10}\left[\left(\frac{\mu_0}{4\pi}\right)\hbar\gamma_I\gamma_S r_{IS}^{-3}\right]^2 \tau_c\left[\frac{6}{1+(\omega_I+\omega_S)^2\tau_c^2} - \frac{1}{1+(\omega_I-\omega_S)^2\tau_c^2}\right] \quad (2)$$

When small molecules in nonviscous solvents are considered (as in all our cases) the *extreme narrowing limit* approximation is reached. In such a situation $\omega_{I(or\ S)}\tau_c << 1$ and, consequently, σ_{IS} simply depends on τ_c and r_{IS} according to Equation (3).

$$\sigma_{IS} \propto \tau_c r_{IS}^{-6} \quad (3)$$

Because σ_{IS} is related to the internuclear distance (r_{IS}), the NOE is often *qualitatively* used to obtain information about the proximity of the I and S nuclei.

By considering Equation (4) (where I_z is the macroscopic longitudinal magnetization due to I, and τ_m is the mixing time[20]), σ_{IS} can be *quantitatively* derived (a) by limiting attention to the linear build-up of the I enhancement for short mixing times ($\tau_m \rightarrow 0$), or (b) by measuring the complete kinetics of NOE build-up and fitting the experimental data with the theoretical Equations derived from integration of Equation (4), in which the proportionality constant between $dI_z/d\tau_m$ and σ_{IS} depends on the type of NOE NMR experiment.[21]

$$\left.\frac{dI_z}{d\tau_m}\right|_{\tau_m=0} \propto \sigma_{IS} \quad (4)$$

By comparison of σ_{IS} with that relative to two nuclei (A and B) of known internuclear distance (r_{AB} = calibration or reference distance), an estimation of r_{IS} can be obtained by Equation (5), if it is assumed that the proportionality constant between σ and r^{-6} is the same for the two couples of nuclei (IS and AB); this condition is satisfied when the rotational correlation times (τ_c), the other variable on which σ depends, of the I-S and A-B vectors are the same.

$$\frac{\sigma_{IS}}{\sigma_{AB}} = \left(\frac{r_{IS}}{r_{AB}}\right)^{-6} \quad (5)$$

The essential features of NOE illustrated above should be sufficient for understanding of which systems can be successfully investigated and what precautions must be taken. Some obvious requirements for the systems are: (1) the presence of NMR-active nuclei with high receptivity (H or F) in both ionic moieties, and (2) the presence of magnetically nonequivalent nuclei, spatially dispersed around the ionic moieties, that will make it possible to discriminate different anion-cation orientations. Protons or fluorine atoms are frequently present in cationic moieties bearing the transition metal ion and in its usual counter-anions, and condition (1) is respected. Requirement (2) is often satisfied by the transition metal cation but rarely by its counter-anion.

NOEs strongly decrease with increasing r_{IS}. As a consequence, NOEs can be observed only if the internuclear distances are shorter than ca. 5 Å, thereby introducing the apparent limitation that only intimate ion pairs can be structurally investigated. However, this is only an apparent limitation, because, if we are interested in studying systems in which ion-pairing affects the reactivity, an acceptable percentage of intimate ion pairs have to be present. A real limitation, however, is that when a quantitative analysis is carried out, the correlation times of the reference and distances of interest must be the same. In fact, the reference distance must refer to a pair of nuclei belonging to the cation or the anion (intramolecular distance), while the distances that we want to estimate are between the nuclei of the cation and those of the anion (interionic distances). Their correlation times are not necessarily the same and have to be determined in order to verify that the interionic distances are reasonably accurate. These last are inevitably average distances, because of the presence of several motions in ionic compounds: (1) overall rotation of ion pairs and/or ions constituting them, (2) ion pair dissociation and formation, and (3) internal motions (Me group rotations around single bonds and chair-boat inversion of the six-member cycles etc.). Although these motions could affect both τ_c and r_{IS}, it has been found[22] that the distances calculated from the observed σ by assuming rigid isotropic motion are not often in error by more than about 10%.

3 Qualitative NMR Investigations

The results illustrated in this section derive from NOESY and HOESY NMR studies carried out in deuterated solvents with low dielectric constants ([D_2]dichloromethane: ε = 8.93 at 298 K; [D]chloroform: ε = 4.81 at 293 K) for 10^{-2}–10^{-1} M solutions. Under such conditions, compounds are mainly present in solution as intimate ion pairs.[23] The interionic NOEs observed in the spectra were classified as strong, medium and weak. Consequently, the relative anion-cation orientation is qualitatively, or perhaps better semiquantitatively, deduced by means of simple triangulations. Most of the complexes considered in this paper were synthesized in our laboratory. Nevertheless, the synthetic procedures are not illustrated here, but can be found in the quoted references.

3.1 Octahedral Iron(II), Ruthenium(II), Osmium(II) and Iridium(III) Complex Ion Pairs

The interionic structure of *trans*-[Ru(COMe)-{(pz_2)CHR}(CO)(PMe_3)$_2$]BPh_4 (R = H or pz; pz = pyrazol-1-yl ring) in [D_2]dichloromethane was investigated first.[24,25] The interionic contacts, between the *ortho*-protons of the anion and the 5- and CHR protons (medium) of the cation and the phosphane protons (weak) observed in the ^{1}H-NOESY NMR spectra, and the absence of interactions with the COMe protons, allowed us to conclude that the anion is specifically located close to the bis(pyrazolyl) ligand (Scheme 1).

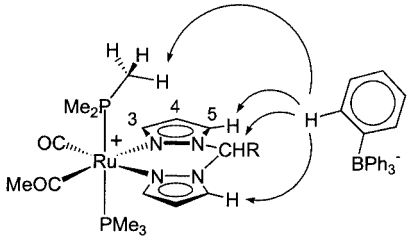

Scheme 1

The same relative anion-cation orientation was found (a) by ^{19}F,^{1}H-HOESY NMR studies with fluorinated counterions (BF_4^-, PF_6^- and $CF_3SO_3^-$) (Figure 1), (b) for isoelectronic and isostructural iron(II) and osmium(II)[26] complexes, and (c) for similar ruthenium(II) complexes containing neutral N,O-ligands.[27] An explanation of the observed specific localization of the anion with respect to the cation was found with the help of quantum mechanical and mechanical docking calculations.[28] There is, in fact, an accumulation of positive charge at the −CHR carbon atom, while the negative charge is concentrated on the oxygen atom of the COMe group. The ion pair with the counteranion on the side of the pyrazolyl rings is consequently dictated by a gain in the electrostatic interaction energy. When BPh_4^- is taken into account, the observed relative anion-cation position is further stabilized by the favourable lipophilic interactions between the phenyl groups of the anion and the pyrazolyl rings. Very interesting studies carried out by Schneider and co-workers on organic ion pairs in water[29,30] show that π-stacking interactions give the ion pairs additional stabilization of about 2 kJ/mol for every

phenyl moiety. In our complexes, we found that two phenyl groups of BPh_4^- are oriented in such a way that they are almost parallel to the two pyrazolyl rings, as illustrated in Scheme 2 for *cis*-[Ru(COMe){$(pz_2)CH_2$}$(CO)_2(PMe_3)$]-BPh_4.[28]

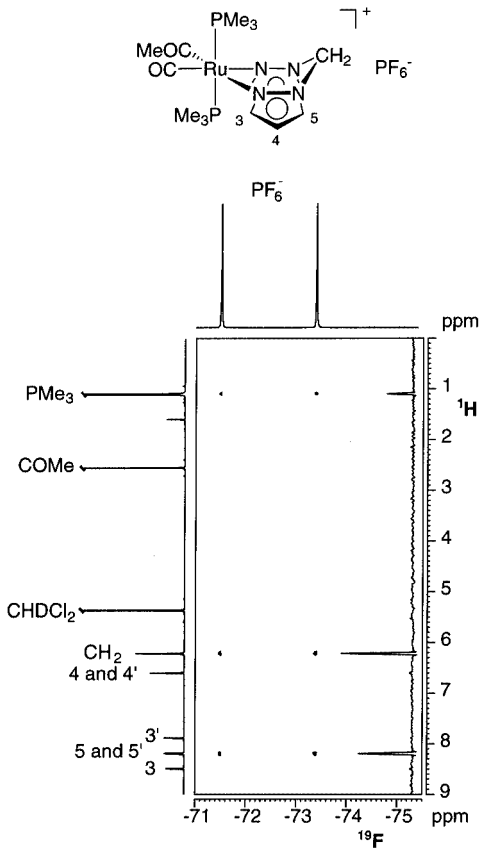

Figure 1. ^{19}F, ^1H-HOESY NMR spectrum of the *trans*-[Ru(COMe){$(pz_2)CH_2$}$(CO)(PMe_3)_2$]PF_6 complex, showing the heteronuclear interionic contacts of PF_6^- with CH_2, H5/H5′ and PMe_3 protons; the F1 trace (indirect dimension) relative to one component of the fluorine doublet is reported on the right (376.65 MHz, 298 K, [D_2]dichloromethane, τ_m = 0.8 s); reproduced from ref.[37] with the permission of the American Chemical Society

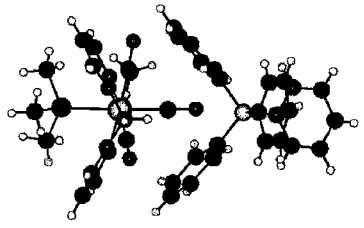

Scheme 2. Reproduced from ref.[28] with the permission of the American Chemical Society

According to Schneider this should give rise to a consequent energy gain of about 4 kJ/mol, which could compensate for the reduction of favourable Coulomb interaction due to an increase in the average anion-cation distance on going from BF_4^- or PF_6^- to BPh_4^-. Studies in more polar solvents (acetone, methanol and nitromethane) indicated that the same interionic structure is maintained but the anion-cation dipolar interactions are more difficult to detect because the increased solvent polarity decreases the percentage of intimate ion pairs. The effect of increasing the polarity of the solvent is also mimed by the reduction of the coordinating property of the counter-anion when, for instance, the poorly coordinating B[3,5-$(CF_3)_2(C_6H_3)$]$_4^-$ counter-ion is used. Very weak interionic contacts were observed for *trans*-[Ru(COMe){$(pz_2)CH_2$}$(CO)(PMe_3)_2$]B[3,5-$(CF_3)_2C_6H_3]_4$ complex in [D_2]dichloromethane, while interionic interactions of acceptable intensity between the fluorine atoms of the counter-anion and the "usual" protons of the cation in [D]chloroform were visible in the ^{19}F,^1H-HOESY NMR spectra.

Interestingly, results from NOE and Pulsed-Field Gradient Spin-Echo (PGSE)[31−34] NMR experiments in [D]chloroform for analogous complexes bearing the more coordinating BPh_4^- anion indicated that the same anion-cation orientation is present, but that aggregates higher than ion pairs form at elevated concentrations in solution.[35]

With the aim of obtaining even more detailed information about anion-cation orientation in solution, *trans*-[Ru(COMe){$(pz_2)CH_2$}$(CO)(PMe_3)_2$]BPh_3R (R = Me, *n*Bu and *n*Hex) compounds, with unsymmetrical counter-anions, were synthesized and investigated.[36,37] The results obtained corresponded to our expectations: the counter-anion is located in the same position, but it orients the aliphatic chain far from the cationic organometallic moiety. By assuming this orientation, the anion maximizes the favourable lipophilic interactions allowing two π-stackings with the energetic gain mentioned above.

The possibility that the high specificity in the anion-cation interactions could be confined to the presence of N-aromatic ligands was excluded by synthesis and investigation of analogous ruthenium(II) compounds bearing α-diimines or substituted ethylenediamines.[38] A section of the ^1H-NOESY NMR spectra, relating to the simplest compound taken into account, is reported in Figure 2, and shows interionic interactions between the anion and the protons of the ethylenediamine, the intensity decreasing on moving from NH_2^d to NH_2^a. In the absence of conjugation, the anion is not only still located close to the N,N-ligand, but it even prefers the N-arm *trans* to the COMe group, where the electron density is less, due to the high *trans* influence of COMe. The introduction of steric hindrance in the N,N-ligand (by use of $NRHCH_2CH_2NR'H$ ligands) affords a fine modulation of the anion position that shifts toward less crowded "places". For example, when R = R′ = $CH_2C_6H_5$ (bz), two stereoisomers are present, depending on the orientation of the bz groups with respect to the phosphanes. In the stereoisomer with the two bz groups oriented toward the same phosphane, the anion stays close to the N,N-ligand but preferentially interacts with the protons of the other phosphane group.

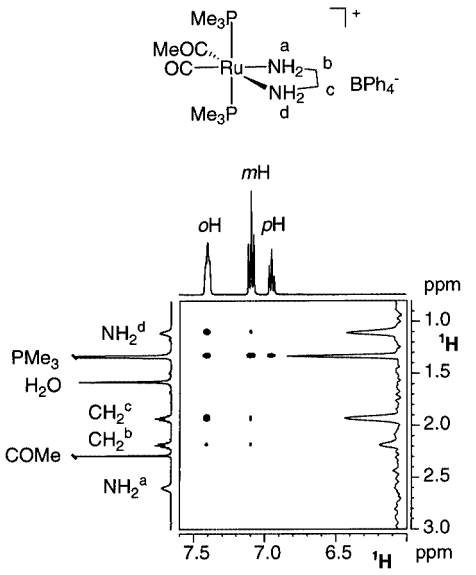

Figure 2. A section of the ^{1}H-NOESY NMR spectrum of the illustrated complex, showing the gradual decrease of the interionic contact intensity on passing from positions d to a; the 1D trace relative to the *ortho*-proton column is reported on the right (400.13 MHz, 298 K, [D_2]dichloromethane, τ_m = 0.8 s)

Inspection of *cis,trans*-[Ir(bipy)H_2($PRPh_2$)$_2$]A complex ion pairs (A^- = PF_6^-, BF_4^-, $CF_3SO_3^-$ and BPh_4^-; R = Me and Ph) afforded other hints about the tendency of the anion to stay close to N,N-ligands.[39] In such complexes, the anion would have the apparently favourable possibility to bind near the MH_2 group, which would give the closest M−anion distance and allow hydrogen bonding.[40] Instead, the anion is specifically located near to the bipy ligand interacting with the 3- (strong), 4- (medium), 5- (weak) and phosphane protons (Scheme 3); the interaction specificity falls off with increasing anion size. Calculations identify the predominant location of the positive charge at the bipyridyl ring carbon atoms that take part in the interring C−C bond. The electrostatic potential calculated for the cation confirms the location of the preferred binding site. Pregosin et al.[41] recently reported specific anion-cation interactions in similar dihydridoiridium(II) complexes.

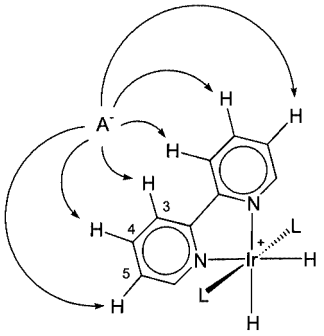

Scheme 3

3.2 Square-Planar Platinum(II) and Palladium(II) Complex Ion Pairs

In the case of ionic square-planar complexes, the determination of the relative anion-cation position might appear to be trivial because of the apparently favoured option for the anion to approach the organometallic moiety from the apical positions. In our studies we soon realized that the apical positions are usually protected both by electronic and by steric properties of the coordinated ligands. The first square-planar complex that we investigated[42] was [PtMe(dpa)(Me_2SO)]PF_6 [where dpa = bis(2-pyridyl)amine], and we found that the anion is located in the periphery of the N,N-ligand, close to the amine NH-proton. The ^{19}F,^{1}H-HOESY NMR spectra showed only selective interionic interactions between the fluorine nuclei and the bridging NH (strong), 3- and 3′- (strong) and DMSO (very weak) protons (Scheme 4).

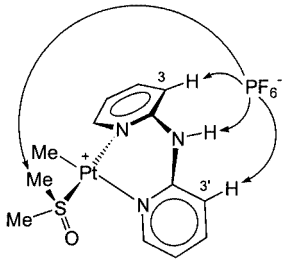

Scheme 4

The most reasonable explanation of this observation is the formation of NH···FPF_5^- hydrogen bonds, providing electronic protection of the metal centre.

Access to the metal centre can also be denied by a synergistic effect between electrostatic attraction and the introduction of suitable steric hindrance in the apical positions. This was made evident in an investigation of the interionic structures of [PtMe(η^2-olefin)(α-diimines)]BF_4 complexes[43] {where α-diimines = [2,6-$(R)_2$-C_6H_3]N=C(R′)-C(R′)=N[2,6-$(R)_2$-C_6H_3], R = H, Me, Et and *i*Pr, R′ = H and Me, olefin = CH_2=CHR′′ with R′′ = H, Me and COOMe}. In these complex ion pairs, the anion is located on the side of the diimine ligands, but accessibility of the metal centre for it is finely modulated by the steric hindrance of the R and R′′ groups (Scheme 5) which protect the apical positions.[44]

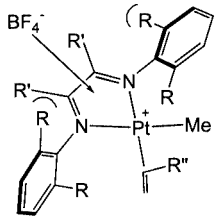

Scheme 5

When R′′ = Me and R ≥ Et, the anion is completely trapped between the R and R′ substituents and does not interact with any olefin or Me protons. For R′′ = Me and R = H and Me, weak interionic NOEs between fluorine nuclei of the anion and olefin and Me protons are visible in the $^{19}F,^{1}H$-HOESY NMR spectra (Figure 3). Interestingly, in agreement with our findings for these platinum(II) complexes and our calculations on octahedral complexes, Tilset et al. showed[45] by DFT calculations that the association of solvent molecules such as H_2O or TFE (trifluoroethanol) to the cationic square-planar σ-complex [(α-diimine)PtMe(CH_4)]$^+$ occurs at the C−C diimine bond where the positive charge accumulates.

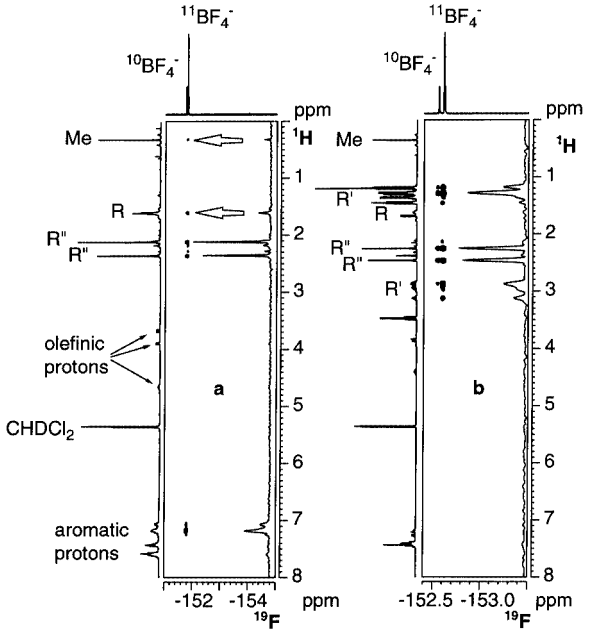

Figure 3. The two ^{19}F, ^{1}H-HOESY NMR spectra (376.65 MHz, 298 K, [D_2]dichloromethane, τ_m = 0.8 s) show the disappearance of interionic interactions between BF_4^- and Me−Pt and R′′ (indicated with arrows) on going from R = H (a) to R = *i*Pr (b); the F1 trace (indirect dimension) relative to one component of the fluorine doublet is reported on the right of every spectrum

The complexes illustrated in Scheme 5 were studied because they are analogous to nickel(II) and palladium(II) compounds that have been established to be the catalytic resting state of olefin polymerization[46,47] and for which R substituents have been found to affect their catalytic activity.[48,49] Bulky substituents block the axial coordination sites and consequently slow the chain-transfer rate relative to propagation, resulting in the formation of polymers with higher molecular weights. Our results confirm the protection of the axial coordination sites exerted by R groups but they also allow the steric hindrance necessary to afford complete protection to be directly evaluated, if it is assumed that BF_4^- is a good nucleophilic probe.

In the absence of specific F···H interactions and/or steric protection, the two axial positions are preferred and equally populated by the counter-anion. As an example, in [Pd(η^1,η^2-C_8H_{12}OMe)(bipy)]A complexes {where bipy = 2,2′-bipyridine and A$^-$ = BPh_4^-, $CF_3SO_3^-$, BF_4^-, PF_6^-, SbF_6^- and B[3,5-$(CF_3)_2C_6H_3]_4^-$} the anion occupies the axial positions even if it slightly prefers to locate close to the bipy ligand and, in particular, close to the N-arm *trans* to the Pd−C σ-bond (Figure 4).[50] This anion-cation relative orientation is always observed independently of the nature of the counter-anions; instead the intensity of the interionic NOEs decreases with decreasing coordinating tendency of the anion: $CF_3SO_3^-$ > BF_4^- > PF_6^- > B[3,5-$(CF_3)_2C_6H_3]_4^-$.

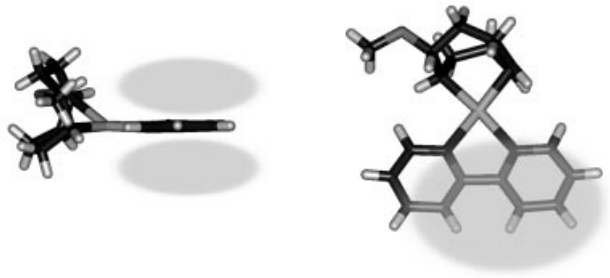

Figure 4. Two views of the solution interionic structure of [Pd(η^1,η^2-C_8H_{12}OMe)(bipy)]A complexes, in which the gray clouds represent the action space of the A$^-$ counter-anion; the two positions above and below the coordination plane are equally populated, and the anion is shifted on the side of bipy ligand with a slight preference for the ring *trans* to the Pd−C σ-bond

It is known that complexes [Pd(η^1,η^2-C_8H_{12}OMe)(bipy)]A are good catalysts for alternating CO/styrene co-polymerization carried out under mild conditions[51] and that the A$^-$ counter-anion strongly affects the catalytic performances.[50] Higher catalytic efficiency is obtained by use of less strongly coordinating anions: that is, those showing weaker interionic interactions. The persistence of the same anion-cation orientation on changing the anion features (size and electron density distribution) and the correlation between the catalytic performances of the complexes with the noncoordinating power of the anion, clearly indicate that the anion competes with the substrates for coordination to the metal ion. Interestingly, the interionic solid-state structure is different from that observed in solution. In fact, due to the stack between two cation moieties, in the solid state the counter-anions are located sideways surrounding the coordination plane (Figure 5).

The substitution of bipy with the nonplanar $(pz_2)CH_2$ ligand results in a very specific localization of the counter-anion (PF_6^-), far from the apical positions and close to the CH_2 moiety of the N,N-ligand.[52] Because of the small axial steric hindrance introduced by the $(pz_2)CH_2$ ligand, the reason for such an unexpected specificity has to be sought in the formation of $^-F_5P-F\cdots H_2C(pz_2)$ weak interactions. As a confirmation, analogous five-coordinated palladium complexes [Pd(η^1,η^2-C_8H_{12}OMe)(pz_3)CH)]PF_6 showed a remarkable specificity of interaction between the counter-ion and the (pz_3)CH and 5′/5′′′-protons (Figure 6) in solution; in the solid state, H-bonding between the highly polarized (pz_3)CH proton and fluorine lone pairs (3.16−3.20 Å) gives rise to a sort of anion-cation recognition.[52]

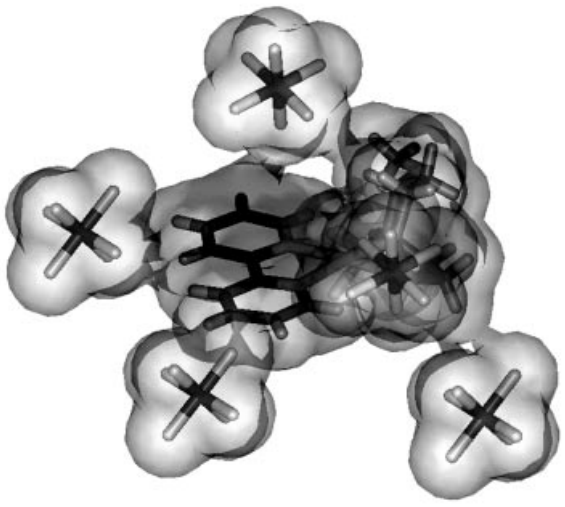

Figure 5. Solid-state structure of [Pd(η^1,η^2-C_8H_{12}OMe)(bipy)]PF_6, showing one cationic moiety surrounded by five counter-anions lying in the periphery of the coordination plane leaving the apical positions free; the van der Waals surface is also shown

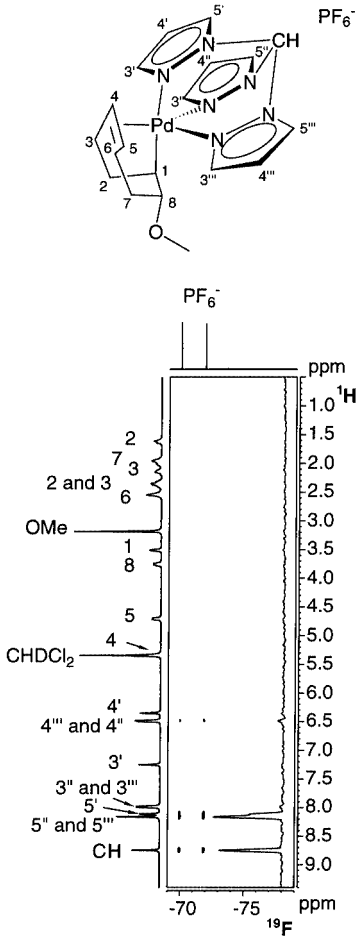

Figure 6. ^{19}F, ^1H-HOESY NMR spectrum (376.65 MHz, 188 K, [D_2]dichloromethane, τ_m = 0.8 s) of [Pd(η^1,η^2-C_8H_{12}OMe)-{(pz_3)CH}]PF_6 recorded showing the remarkable specificity of interaction between PF_6^- and the 5′-5′′′ and 4′-4′′′ (very weak) protons of the cation; the 1D-trace relative to the PF_6^- column is reported on the right; reproduced from ref.[52] with the permission of the American Chemical Society

The introduction of more hindered substituents, such as α-diimines {[2,6-$(R)_2$-C_6H_3]N=C(R′)-C(R′)=N[2,6-$(R)_2$-C_6H_3] where R = H, Me, Et and *i*Pr, R′$_2$ = Me_2 and An}, the steric contribution of which in the axial positions is easily tuned, afforded results similar to those found for the platinum complexes discussed above.[53] Two new pieces of information were produced: a) for R′$_2$ = Me_2, complete steric protection of the metal centre already occurs with R = Me, and b) for R′$_2$ = An (9-Anthryl) and R′ = *i*Pr, nonspecific interionic structure was observed. The first point indicates that the steric hindrance in the axial positions was additive over all the ligands coordinated to the metal ion. Consequently, when there is a methoxycyclooctenyl moiety as well as the α-diimine ligand, it is sufficient that R = Me to protect the metal centre completely. As a confirmation, in the case of platinum complexes shown in Scheme 5, complete protection occurs for R′′ = Me and R = Et but not for R′′ = H and R = Et. Point b) allows even more interesting deductions. In fact, the substitution of the two R′ methyl groups with the An moiety[54] has the effect of dispersing the positive charge on the side of the N,N-ligand or of making it difficult to approach. Consequently, the anion no longer has its "anchorage" point and it interacts with several protons, including those belonging to the methoxycyclooctenyl moiety. One implication is that steric protection alone does not guarantee a specific interionic structure, but that, if for electronic reasons, the latter is present, modulation of the introduced steric hindrance finely determines the relative anion-cation position. This point may have interesting connections with the catalytic performances of [PdMe(η^2-olefin)(α-diimines)]A complexes toward olefin polymerization. From the literature, it is known that the molecular weights of the obtained polymers increase in the following order: R′ = Me > An > H.[47] It seems reasonable that, when R′ = H, the reduced steric protection deriving from the less restricted rotation around the N−C(*ipso*) bond favours the chain-transfer process, with polymers of lower molecular weight consequently being obtained. The reason why higher polymers are obtained with R′ = Me relative to R′ = An, however, is not obvious. Our results indicate that, in complexes in which R groups are the same, there is a greater dispersion of the positive charge for R′ = An than for R′ = Me. It could be that, in the latter case, the association of olefin is slowed by its favourable interaction with the C−C diimine carbon atoms, affording a sort of added electronic protection of the axial coordination sites and reducing the chain-transfer process rate.

All [Pd(η^1,η^2-C_8H_{12}OMe)(N,N)]A complexes are active catalysts for the CO/*p*-methylstyrene alternating copolymerization, and the counter-anion effect has been discussed above. As far as the N,N-ligand effect is concerned, in contrast to olefin polymerization, increased steric hindrance on the apical positions decreases the catalytic performance. For example, when N,N = [2,6-$(R)_2$-C_6H_3]N=C(Me)−C(Me)=N[2,6-$(R)_2$-C_6H_3] for R = H, the compound is a reasonably

good catalyst for the CO/styrene copolymerization reaction. In contrast, the complex with R = *i*Pr is completely inactive in the copolymerization, but catalyses the formation of the homopolymer (polystyrene). This is probably due to the need for initial CO coordination at the fifth coordination site[55] in the copolymerization reaction; this is difficult to approach when sterically protected by the substituents in the N,N-ligands. The information derived from investigation of the interionic structure could also be useful for probing accessibility of the metal centre in this case.

Another example of reduced anion-cation interaction specificity was observed during the investigation of $[Pt(Me)(PPh_3)(dmphen)]PF_6$ complexes (where dmphen = 2,9-dimethyl-1,10-phenanthroline).[56] In such tetrahedral distorted square-planar complexes, the anion is located on the side of the phenanthroline but has sufficient mobility to interact with all the protons, with the exception of those of the Me group bonded directly to the platinum centre. The explanation can be found in (a) the difficulty that the anion has in approaching the carbon atoms of the pyridyl ring junctions, where it is reasonable to assume that the positive charge accumulates, and (b) the inclination (42.6°) of the coordination plane with respect to that containing the phenanthroline ligand.

Finally, we have recently synthesized $[Pd(\eta^1,\eta^2\text{-}C_8H_{12}O\text{-}Me)(N,O)]BF_4$ compounds {where N,O = $[2,6\text{-}(i\text{Pr})_2\text{-}C_6H_3]N{=}C(Ph){-}C(Ph){=}O$, $[2,6\text{-}(i\text{Pr})_2\text{-}C_6H_3]N{=}C(Me){-}C(Ph){=}O$} in which only the N-arm affords steric protection of the axial positions.[57] The counter-anion can choose between the least crowded side, close to the O-arm, or the electronically favoured position close to the $-N{=}C(R)$ bond. The interionic contacts observed in $^{19}F,^1H$-HOESY NMR spectra suggest that the two anion-cation orientations are simultaneously present in solution with almost equal probability.

4 Quantitative NMR Investigations

After we had found preferred anion-cation orientations in most of the investigated transition metal complex ion pairs in solution, we then attempted to quantify the NOEs for estimation of average interionic distances. The first systems to be investigated were chosen on the basis of (a) their stabilities, because quantitative NOE measurements are rather time-consuming, especially if the complete kinetics of NOE build-up has to be recorded, and (b) the existence of a well-defined anion-cation "anchorage" point, in that the deduced interionic distances, already averaged by fast internal motions and ion dissociation and re-association, would be difficult to interpret if more than one anion-cation orientation were present in solution. Considering these two points, we decided to start our investigations with *trans*-$[Ru(COMe)\{(pz_2)CH_2\}(CO)(PMe_3)_2]BPh_3R$ (R = Me and Ph) complexes,[37] the semiquantitative interionic structures of which were already known. As anticipated in Section 2, the interionic NOEs can be related to σ_{IS} and consequently to the interionic distances by fitting the experimental NOE data of the complete kinetics of the NOE build-up or the initial linear trends for short mixing times. A reference distance is needed in both cases, and it inevitably refers to two nuclei belonging to the same ionic moiety. The possibility of applying Equation (5) to estimate the average interionic distances is subordinated to inspection of the correlation time of the reference distance (intramolecular) and those of interest (interionic). The *o*-H/*m*-H distance in BPh_3R^- was chosen as the reference distance, because its value in the solid state (2.47 Å) was known from neutron diffraction investigations relating to a cationic platinum(II) dinuclear single hydrido-bridged complex.[58] The complete kinetics of NOE build-up was measured by selective inversion of several target resonances by use of the *selno* (*se*lective *no*esy)[59,60] and *selnogp* (*se*lective *no*esy with field *g*radient *p*ulses)[61,62] NMR pulse sequences. An example is reported in Figure 7, in which the kinetics of NOE build-up for H4, CH_2 and *o*-H upon irradiation of H5 are reported (R = Ph). The determined structure and selected internuclear distances for the complex with the BPh_3Me^- counter-anion are illustrated in Scheme 6.

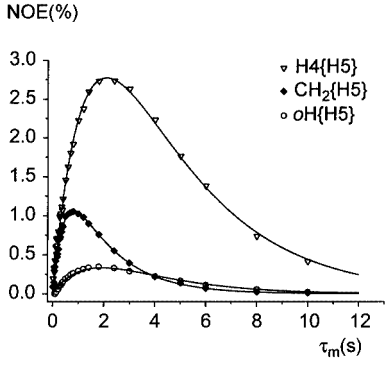

Figure 7. Experimental data relating to % NOE as a function of τ for the irradiation of H5 protons for the complex *trans*-$[Ru(COMe)\{(pz_2)CH_2\}(CO)(PMe_3)_2]BPh_4$ (400.13 MHz, 302 K, $[D_2]$dichloromethane, Gaussian-shaped pulse); reproduced from ref.[37] with the permission of the American Chemical Society

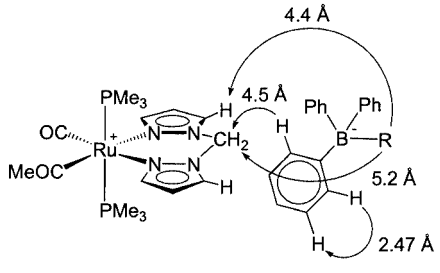

Scheme 6

An interesting point is the difference between <r>(CH_2-*o*H) (= 4.5 Å) and <r>(CH_2−BMe) (= 5.2 Å). In fact,

$\Delta<r> = 0.7$ Å and this agrees perfectly with a situation in which the anion orients the Me group far away from the metal centre.

The distances involving the protons of the counter-anion, which can undergo dynamic motion (demonstrated by the equivalence of the four phenyl groups) and those of CH_2 and H5 protons (involved in the chair-boat inversion of the six-membered Ru−N−N−CH_2−N−N ring) were increased by 10% in order to correct, at least partially, for overestimation of the short distances.

In order to check the accuracy of the determined average interionic distances, rotational correlation times were estimated by two independent NMR methodologies: ^{13}C relaxation measurements[63−65] and the dependence of ^1H-^1H cross-relaxation on the temperature. The latter methodology is based on nonlinear fitting of the experimental σ_{IS} values against T (see Figure 8), in which the dependence of the rotational correlation time on temperature is introduced by means of Equation (6), where E_R is the activation energy for rotational reorientation, τ_0 is a constant, and k is the Boltzmann constant.[66,67]

$$\tau_c = \tau_0 \cdot e^{\frac{E_R}{kT}} \quad (6)$$

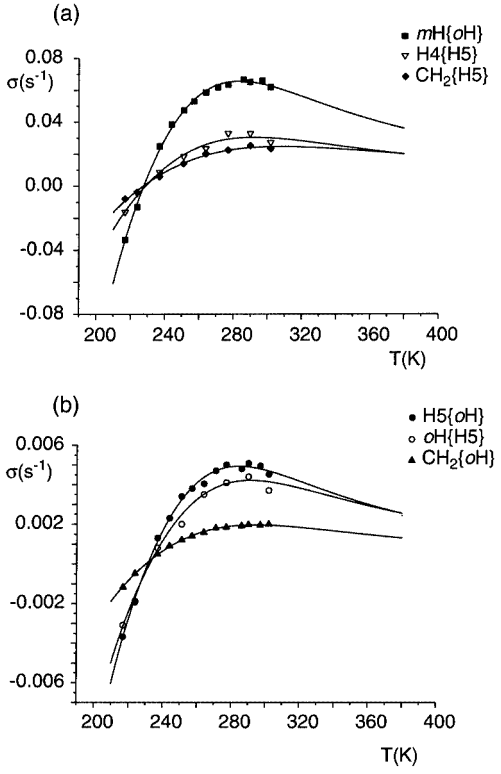

Figure 8. Intramolecular (a) and interionic (b) experimental values of σ_{IS} as a function of temperature and best nonlinear least-squares fits for the complex *trans*-[Ru(COMe){$(pz_2)CH_2$}-$(CO)(PMe_3)_2$]BPh_4; it can be seen that the temperature values of the σ zero cross and maximum points are the same for both intermolecular and interionic couples of nuclei, indicating the same correlation times (400.13 MHz, 298 K, [D_2]dichloromethane); reproduced from ref.[37] with the permission of the American Chemical Society

With both methodologies, it was found that intramolecular and interionic couples of nuclei have rotational correlation times that are the same within experimental error (ca. 100 ps)[37] and are about 3.8 times higher than those relating to pairs of nuclei belonging to *trans*-[Ru(COMe){$(pz_2)BH_2$}(CO)$(PMe_3)_2$]. The latter compound[68] is isosteric with, and has almost the same mass as, the cationic fragment of the investigated ruthenium(II) ion pairs. Consequently, it was concluded that the overall ion pair rotation contributes mainly to the dipolar relaxation processes and that the determined interionic average distances were accurate. The error on r_{IS} was estimated to be ± 0.2 Å in view both of the goodness of the fittings and of the presence of the exchange processes mentioned above.

The usefulness of the average interionic distances can be seen by considering the complexes containing unsymmetrical BPh_3R^- counter-anions. While the tendency of the anion to orient the R aliphatic chain far away from the metal centre is clearly illustrated when R = *n*Bu and *n*-Hex, by the absence of interionic NOEs in the ^1H-NOESY NMR spectra of the terminal Me, when R = Me, this is not true because, while also orienting the methyl group far away from the metal centre, it remains close enough to interact with CH_2 and H5 cationic protons. Only the $\Delta<r>$ value mentioned above allows us to conclude that B−Me is oriented like the other B−R moieties.

5 Conclusion

The structures of transition metal complex ion pairs in solution can be determined by the use of NOE NMR spectroscopy, which provides valuable information about the interplay between interionic weak interactions and the reactivity of complexes. ^1H-NOESY and ^{19}F,^1H-HOESY investigations of several Fe^{II}, Ru^{II}, Os^{II}, Pd^{II}, Pt^{II} and Ir^{III} complex ion pairs have shown that in most cases there is a predominant relative anion-cation orientation, determined mainly by a gain in electrostatic interaction energy. This in turn is derived from positioning the anion close to the cationic moiety where the positive charge accumulates; we have very often found this to be far away from the metal centre. In complexes bearing N,N-ligands, the positive charge is concentrated in the bridging units of the two moieties containing the N-donor. Steric effects are important in the modulation of the fine anion-cation orientation, and two different cases have been observed, depending on whether or not the "steric protection" acted on the point at which the positive charge was located. In the first case, a general loss of specificity was observed; in the second case a remarkably well-defined interionic structure was observed. Quantitative NOE measurements were carried out on systems belonging to this second case and the average interionic distances were estimated. Despite the precautions that must be taken and the careful checks that must be made, the possibility of determining average interionic distances offers a unique tool for detailed structural investigation of ion pairs in solution.

Acknowledgments

I would like to thank all the co-workers who participated in obtaining the results reviewed here. This work was supported by grants from the Ministero dell'Istruzione, dell'Università e della Ricerca (MIUR, Rome, Italy), Programma di Rilevante Interesse Nazionale, Cofinanziamento 2000−2001.

[1] S. H. Strauss, *Chem. Rev.* **1993**, *93*, 929−942. C. A. Reed, *Acc. Chem. Res.* **1998**, *31*, 133−139.
[2] D. A. Evans, J. A. Murry, P. von Matt, R. D. Norcross, S. J. Miller, *Angew. Chem. Int. Ed. Engl.* **1995**, *34*, 798−800.
[3] E. P. Kündig, C. M. Saudan, G. Bernardinelli, *Angew. Chem. Int. Ed.* **1999**, *38*, 1220−1223.
[4] E. Y. −X Chen, T. J. Marks, *Chem. Rev.* **2000**, *100*, 1391−1434.
[5] S. D. Ittel, L. Johnson, M. Brookhart, *Chem. Rev.* **2000**, *100*, 1169−1203.
[6] R. Romeo, G. Arena, L. M. Scolaro, M. R. Plutino, *Inorg. Chim. Acta* **1995**, *240*, 81−92.
[7] A. Lightfoot, P. Schnider, A. Pfaltz, *Angew. Chem. Int. Ed.* **1998**, *37*, 2897−2899.
[8] G. Bellachioma, G. Cardaci, A. Macchioni, C. Zuccaccia, *J. Organomet. Chem.* **2000**, *594*, 119−126.
[9] M. Nandi, J. Jin, T. V. RajanBabu, *J. Am. Chem. Soc.* **1999**, *121*, 9899−9900.
[10] G. Desimoni, G. Faita, A. Martoni, P. Righetti, *Tetrahedron Lett.* **1999**, *40*, 2001−2004.
[11] M.-C. Chen, T. J. Marks, *J. Am. Chem. Soc.* **2001**, *123*, 11803−11804.
[12] D. B. Llewellyn, D. Adamson, B. A. Arndtsen, *Org. Lett.* **2000**, *2*, 4165−4168.
[13] J. Lacour, J. J. Jodry, C. Ginglinger, S. Torche-Haldimann, *Angew. Chem. Int. Ed.* **1998**, *37*, 2379−2380.
[14] W. Bauer, G. Müller, P. v. R. Schleyer, *Angew. Chem. Int. Ed. Engl.* **1986**, *25*, 1103−1104.
[15] A. G. Avent, C. Eaborn, M. N. A. El-Kheli, M. E. Molla, J. D. Smith, A. C. Sullivan, *J. Am. Chem. Soc.* **1986**, *108*, 3854−3855.
[16] T. C. Pochapsky, P. M. Stone, *J. Am. Chem. Soc.* **1990**, *112*, 6714−6715.
[17] For a review on intermolecular NOE investigations see: H. Mo, T. C. Pochapsky, *Prog. NMR Spectrosc.* **1997**, *30*, 1−38.
[18] D. Neuhaus, Michael Williamson, *The Nuclear Overhauser Effect in Structural and Conformational Analysis*, VCH, Weinheim, **1989**, chapters 2 and 3.
[19] A term ρ_I* has to be added to ρ_{IS} when relaxation of other dipole-dipole systems occurs. ρ_I* accounts for intermolecular dipole-dipole interaction with paramagnetic species, quadrupolar relaxation, chemical shift anisotropy (CSA) relaxation, scalar relaxation and spin rotation relaxation. The effect of the term ρ_I* is to reduce the NOE enhancement.
[20] In this paper both the evolution periods of 1D transient experiments and the mixing times of the NOESY or HOESY experiments are indicated with τ_m. τ_m represents the time during which the NOE develops after (a) the selective inversion of a single resonance in 1D experiments or (b) frequency labelling of all resonances in 2D experiments.
[21] D. Neuhaus, Michael Williamson, *The Nuclear Overhauser Effect in Structural and Conformational Analysis*, VCH, Weinheim, **1989**, chapter 4.
[22] D. Neuhaus, Michael Williamson, *The Nuclear Overhauser Effect in Structural and Conformational Analysis*, VCH, Weinheim, **1989**, chapter 5.
[23] G. Bellachioma, G. Cardaci, A. Macchioni, G. Reichenbach, *Gazz. Chim. It.* **1991**, *121*, 101−106.
[24] G. Bellachioma, G. Cardaci, A. Macchioni, G. Reichenbach, S. Terenzi, *Organometallics* **1996**, *15*, 4349−4351.
[25] A. Macchioni, G. Bellachioma, G. Cardaci, V. Gramlich, H. Rüegger, S. Terenzi, L. M. Venanzi, *Organometallics* **1997**, *16*, 2139−2145.
[26] G. Bellachioma, G. Cardaci, A. Macchioni, F. Valentini, C. Zuccaccia, E. Foresti, P. Sabatino, *Organometallics* **2000**, *19*, 4320−4326.
[27] G. Bellachioma, G. Cardaci, V. Gramlich, A. Macchioni, M. Valentini, C. Zuccaccia, *Organometallics* **1998**, *17*, 5025−5030.
[28] A. Macchioni, G. Bellachioma, G. Cardaci, G. Cruciani, E. Foresti, P. Sabatino, C. Zuccaccia, *Organometallics* **1998**, *17*, 5549−5556.
[29] H.-J. Schneider, T. Schiestel, P. Zimmermann, *J. Am. Chem. Soc.* **1992**, *114*, 7698−7703.
[30] H.-J. Schneider, *Chem. Soc. Rev.* **1994**, 227−234.
[31] P. Stilbs, *Prog. Nucl. Magn. Reson. Spectrosc.* **1987**, *19*, 1−45.
[32] C. S. Johnson Jr., *Prog. Nucl. Magn. Reson. Spectrosc.* **1999**, *34*, 203−256.
[33] W. S. Price, *Concepts Magn. Reson.* **1997**, *9*, 299−336.
[34] W. S. Price, *Concepts Magn. Reson.* **1998**, *10*, 197−237.
[35] C. Zuccaccia, G. Bellachioma, G. Cardaci, A. Macchioni, *Organometallics* **2000**, *19*, 4663−4665.
[36] C. Zuccaccia, G. Bellachioma, G. Cardaci, A. Macchioni, *Organometallics* **1999**, *18*, 1−3.
[37] C. Zuccaccia, G. Bellachioma, G. Cardaci, A. Macchioni, *J. Am. Chem. Soc.* **2001**, *123*, 11020−11028.
[38] G. Bellachioma, G. Cardaci, F. D'Onofrio, A. Macchioni, S. Sabatini, C. Zuccaccia, *Eur. J. Inorg. Chem.* **2001**, 1605−1611.
[39] A. Macchioni, C. Zuccaccia, E. Clot, K. Gruet, R. H. Crabtree, *Organometallics* **2001**, *20*, 2367−2373.
[40] P. Desmurs, K. Kavallieratos, W. Yao, R. H. Crabtree, *New. J. Chem.* **1999**, *23*, 1111−1115.
[41] D. Drago, P. S. Pregosin, A. Pfaltz, *Chem. Commun.* **2002**, 286−287.
[42] R. Romeo, N. Nastasi, L. Monsù Scolaro, M. R. Plutino, A. Albinati, A. Macchioni, *Inorg. Chem.* **1998**, *37*, 5460−5466.
[43] C. Zuccaccia, A. Macchioni, I. Orabona, F. Ruffo, *Organometallics* **1999**, *18*, 4367−4372.
[44] R. van Asselt, C. J. Elsevier, W. J. J. Smeets, A. L. Spek, R. Benedix, *Recl. Trav. Chim. Pays-Bas* **1994**, *113*, 88−98.
[45] H. Heiberg, L. Johansson, O. Gropen, O. B. Ryan, O. Swang, M. Tilset, *J. Am. Chem. Soc.* **2000**, *122*, 10831−10845.
[46] L. K. Johnson, C. M. Killian, M. Brookhart, *J. Am. Chem. Soc.* **1995**, *117*, 6414−6415.
[47] D. J. Tempel, L. K. Johnson, R. L. Huff, P. S. White, M. Brookhart, *J. Am. Chem. Soc.* **2000**, *122*, 6686−6700.
[48] L. Deng, T. K. Woo, L. Cavallo, P. M. Margl, T. Ziegler, *J. Am. Chem. Soc.* **1997**, *119*, 6177−6186.
[49] R. D. J. Froese, D. G. Musaev, K. Morokuma, *J. Am. Chem. Soc.* **1998**, *120*, 1581−1587.
[50] A. Macchioni, G. Bellachioma, G. Cardaci, M. Travaglia, C. Zuccaccia, B. Milani, G. Corso, E. Zangrando, G. Mestroni, C. Carfagna, M. Formica, *Organometallics* **1999**, *18*, 3061−3069.
[51] B. Milani, G. Mestroni, A. Sommazzi, F. Garbassi, Italian Patent no. MI 95/A 000337, **1995**; European Patent no. 96101967.6-2102, **1996**.
[52] B. Binotti, G. Bellachioma, G. Cardaci, A. Macchioni, C. Zuccaccia, E. Foresti, P. Sabatino, *Organometallics* **2002**, *21*, 346−354.
[53] G. Bellachioma, B. Binotti, G. Cardaci, C. Carfagna, A. Macchioni, S. Sabatini, C. Zuccaccia, *Inorg. Chim. Acta* **2002**, *330*, 44−51.
[54] R. van Asselt, E. C. G. Gielens, R. E. Rulke, K. Vrieze, C. J. Elsevier, *J. Am. Chem. Soc.* **1994**, *116*, 977−985.
[55] C. Bianchini, A. Meli, *Coord. Chem. Rev.* **2002**, *225*, 35−66.
[56] R. Romeo, L. Fenech, L. Monsù Scolaro, A. Albinati, A. Macchioni, C. Zuccaccia, *Inorg. Chem.* **2001**, *40*, 3293−3302.
[57] A. Macchioni, C. Zuccaccia, B. Binotti, C. Carfagna, E. Foresti, P. Sabatino, *Inorg. Chem. Commun.* **2002**, *5*, 319−322.
[58] A. Albinati, G. Bracher, D. Carmona, J. H. P. Jans, W. T. Klooster, T. F. Koetzle, A. Macchioni, J. S. Ricci, R. Thouvenot, L. M. Venanzi, *Inorg. Chim. Acta* **1997**, *265*, 255−265.
[59] H. Kessler, H. Oschinat, G. Griesinger, W. Bermel, *J. Magn. Reson.* **1986**, *70*, 106−133.

[60] C. J. Bauer, R. Freeman, T. Frenkiel, J. Keeler, J. Shaka, *J. Magn. Reson.* **1984**, *58*, 442−457.
[61] J. Stonehouse, P. Adel, J. Keeler, J. Shaka, *J. Am. Chem. Soc.* **1994**, *116*, 6037−6038.
[62] K. Stott, J. Stonehouse, J. Keeler, T.-L. Hwang, J. Shaka, *J. Am. Chem. Soc.* **1995**, *117*, 4199−4200.
[63] A. Abragam, *The Principle of Nuclear Magnetism*, Claredon Press, Oxford, **1961**.
[64] M. Bühl, G. Hopp, W. von Philipsborn, S. Beck, M.-H. Prosenc, U. Rief, H.-H. Brintzinger, *Organometallics* **1996**, *15*, 778−785.
[65] S. Gaemers, J. van Slageren, C. M. O'Connor, J. G. Vos, R. Hage, C. J. Elsevier, *Organometallics* **1999**, *18*, 5238−5244.
[66] D. M. Doddrell, M. R. Bendall, A. J. O'Connor, D. T. Pegg, *Aust. J. Chem.* **1977**, *30*, 943−956.
[67] T. C. Farrar, E. D. Becker, *Pulse and Fourier Transform N. M. R.*, Academic Press, New York, **1971**.
[68] G. Bellachioma, G. Cardaci, V. Gramlich, A. Macchioni, F. Pieroni, L. M. Venanzi, *J. Chem. Soc., Dalton Trans.* **1998**, 947−951.

Received May 15, 2002
[I02258]

The η^5-(σ-P,π-Arene) Chelating H-MOP Ligand in an Optically and Catalytically Active Rhodium(I) Complex

Michèle Soleilhavoup,[a] Lydie Viau,[a] Gérard Commenges,[a] Christine Lepetit,[a] and Remi Chauvin*[a]

Keywords: Phosphane ligands / Arene ligands / Atropisomerism / Rhodium / NMR spectroscopy / Asymmetric catalysis

(*R*)-methylbinapium, a Hayashi-type phosphonium-MOP ligand, reacts with $[Rh(cod)_2][BF_4]$ in ethanol to afford the chiral mixed bis(monophosphane)rhodium(I) complex $[Rh(\eta^5$-H-MOP)$(MePh_2P)][BF_4]$. The constitutional and geometrical features of this complex have been determined by exhaustive ^1H, ^{11}B, ^{13}C, ^{31}P and ^{103}Rh 1-D, 2-D and NOE NMR spectroscopy and optical rotation measurements. The chelating η^5-(γ-phosphanyldiene) ligand character of H-MOP in this complex is an extension to Rh^I of similar coordination modes studied by Pregosin in the coordination sphere of Ru^{II}. The process of its formation relies on an enantiospecific reductive cleavage of a P^+–C bond, which is also reminiscent of Pregosin's P–C bond cleavages in the ruthenium series. The complex is a catalytic precursor for the hydrogenation of (Z)-α-acetamidocinnamic acid.

(© Wiley-VCH Verlag GmbH & Co. KGaA, 69451 Weinheim, Germany, 2003)

Introduction

According to the recent literature, the dogma stating that only chelating chiral *di*phosphane ligands can lead to high *ee*'s in reductive asymmetric catalysis has exceptions provided that the alternative *mono*phosphane ligands contain a resolved atropisomeric biaryl axis.[1] Monophosphite, monophosphonites and phosphoramidites of binaphthol are thus efficient ligands for the rhodium-catalyzed asymmetric hydrogenation of acrylic acid derivatives,[1,2] while Hayashi's X-MOP ligands (Scheme 1) are efficient ligands for the palladium-catalyzed reduction of allylic alcohols,[3] palladium-catalyzed hydrosilylation of olefins,[4] or rhodium-catalyzed arylation of imines.[5] The intriguing stereochemical efficiency of the X-MOP ligands is similar to that of the homoleptic binap ligand **1** (formally PPh_2-MOP).[6] This is assumed to mainly result from steric/electronic effects, but it might also be enhanced by the transient coordination of one or more C=C bonds of the naphthyl groups. Indeed, Pregosin's work definitely shows that binap and biphep can act as two-, four-, six-, or eight-electron donors in ruthenium(II) complexes.[7,8] On the other hand, binap- and MeO-biphep-ruthenium complexes have been reported to undergo selective hydrolytic P−C bond cleavage leading to complexes containing both a monophosphane H-MOP ligand and a diphenylphosphinoyl ligand.[9,10] In a few cases, the H-MOP ligand displays an η^4-coordination of one naphthyl substituent.[7,9]

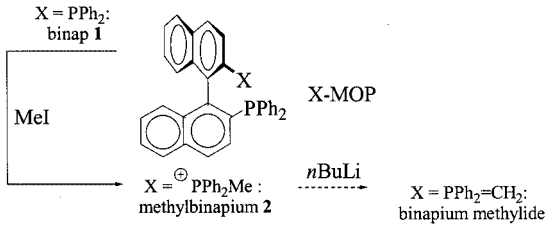

Scheme 1. X-MOP ligands

Our initial goal was to look for chiral phosphoniophosphane ligands capable of providing hybrid chelation by primary P→$[Rh]^{\delta-}$ dative and secondary electrostatic $P^+\cdots[Rh]^{\delta-}$ interactions.[11] The results with "methyldiopium" as a ligand prototype suggested that the electrostatic interaction might be too loose due to the flexibility of the diopium skeleton.[12] The 1,1-binaphthyl core of **2**, a P^+-MOP ligand previously termed as "methylbinapium" (Scheme 1),[13] was therefore devised as a more rigid skeleton. The coordination chemistry of binapium **2** is, however, quite versatile.[12,13] While the methylbinapium skeleton is known to enter the coordination sphere of rhodium(I) as its ylide form (Scheme 1, X = PPh_2=CH_2),[14] the outcome of our attempts to introduce methylbinapium **2** (X = $^+PPh_2CH_3$) directly into the coordination sphere of rhodium(I) is here disclosed.

[a] Laboratoire de Chimie de Coordination du CNRS, UPR 8241, 205 Route de Narbonne, 31077 Toulouse cedex 4, France
Fax: (internat.) +33-5/6155-3003
E-mail: chauvin@lcc-toulouse.fr

Results and Discussion

Reactivity of Methylbinapium 2 with [Rh(cod)$_2$][BF$_4$]

"(*R*)-methylbinapium" **2** was prepared by a one-step symmetry breaking of the parent C_2-symmetric diphosphane **1** with MeI.[13] The steric hindrance exerted by the phosphonium terminus towards the P^{III} terminus was illustrated by both the X-ray-crystal structure of binapium iodide **2·I**, and by its lack of reactivity toward electrophiles [e.g. MeI or Fe(CO)$_4$(NMe$_3$)].[13] It is therefore not surprising that **2·I** did not react with either [RhCl(cod)]$_2$ or [Rh(cod)$_2$][BF$_4$] under conventional conditions. Under harsher conditions, however, namely in boiling ethanol for two days, [Rh(cod)$_2$][BF$_4$] did react with a single equivalent of binapium iodide **2·I**. The expected product [RhI(cod)-(**2**)][BF$_4$] was not observed, but column chromatography allowed the separation of two complexes. An apolar complex was eluted first and assigned to structure **4** on the basis of its ^{1}H, ^{13}C and ^{31}P NMR spectroscopic data. The major polar complex was then eluted. Its ^{1}H and ^{31}P NMR spectra indicate the absence of both a cyclooctadiene ligand and any phosphonium group, and display two coupled nonequivalent P atoms at a rhodium center. The structure of this complex was later assigned as the H-MOP complex **3·BF$_4$** (Scheme 2, see below). Surprisingly, in the presence of two equivalents of **2·I**, the conversion of [Rh(cod)$_2$][BF$_4$] was much slower. This was ascribed to a harmful effect of the excess iodide ions competing with the hindered P^{III} center of **2**. Indeed, reaction of [Rh(cod)$_2$][BF$_4$] with the tetrafluoroborate salt **2·BF$_4$** proceeded more rapidly and more selectively: after refluxing for 20 h in ethanol, complex **3·BF$_4$** was the sole rhodium complex observed by ^{31}P NMR analysis of the crude material.

Structure Determination of Complex 3.

The major signal in the ES-MS spectrum at m/z = 741.2 is consistent with the parent cationic fragment [(MePh$_2$P)(H-MOP)Rh]$^+$. The complete multinuclear NMR assignment and the corresponding structure were determined in $CDCl_3$ solution. The ionic nature of the complex could be first refined as a [RhPP′]$^+$[BF$_4$]$^-$ form from the ^{11}B and ^{103}Rh NMR signals at δ = −0.59 ppm and −391 ppm (dd, $^1J_{PRh}$ = 199.6, $^1J_{P'Rh}$ = 206.0 Hz), respectively. The shielded ^{103}Rh signal is typical for a rhodium(I) complex in this environment.[15] The HMQC ^{1}H-^{31}P spectrum (Figure 1) displays a strong coupling of the ^{31}P/^{103}Rh ABX pattern [δ = 18.31 ppm (dd) and 57.39 ppm (dd), $^1J_{PRh}$ = 200, $^1J_{PRh}$ = 206, $^2J_{PP}$ = 39 Hz] with five inequivalent aromatic protons, and three equivalent shielded protons of a methylphosphane unit at δ = 1.50 ppm (d, $^2J_{PH}$ = 9 Hz). This observation supports a [Rh(PAr$_3$)(PAr$_2$Me)]$^+$ complexation pattern.

A weaker coupling of the ^{31}P nuclei also occurs with an intriguing ^{1}H nucleus at δ = 5.44 ppm. According to the ^{1}H-^{1}H COSY spectrum, this proton shows a $^3J_{H,H}$ coupling of 6.2 Hz with a proton whose signal appears at δ = 7.57 ppm, itself similarly coupled with a third proton (δ = 7.07 ppm). These latter three protons, referred to as H4, H3, and H2 (see Scheme 3), are also weakly coupled with ^{31}P nuclei ($J_{PH} \leq 1$ Hz). They were assigned to the protons of the η^4-diene-Rh moiety of a chelating H-MOP ligand. The η^4-coordination was confirmed by the high field resonance (δ = 97.3−105.5 ppm) of the corresponding carbon atoms C2, C3, C4 and C1, as well as by their $^1J_{RhC}$ values (c.a. 5 Hz). By contrast, the resonance at lower field of the adjacent C5 and C10 carbons (δ = 119.7 and 122.4 ppm) and the absence of coupling to the ^{103}Rh nucleus rule out the possibility of an η^6-coordination mode previously encountered in other cationic phosphane-rhodium complexes.[16] In the ruthenium series, due to the absence of $^1J_{RuC}$ information, it is more difficult to draw the line between η^4- and η^6-coordination. Nevertheless, in the related complex [Ru(η^5-H-MOP)(PPhEt$_2$)(PPh$_2$OH)]$^{2+}$[OTf]$_2$, which was assigned an η^4-diolefin structure, the effect of the proximate Ru atom on the uncoordinated C5 and C10 atoms was reported to result in chemical shifts of δ = 116.2 and 116.4 ppm, respectively. These are of the same order of magnitude as those of C5 and C10 in the rhodium complex **3**.[7] It is also worth noting that the η^4-coordination mode in **3** is consistent with a classical 16-electron count in the coordination sphere of phosphanylrhodium(I) complexes.

Although we were unable to isolate a crystal suitable for an X-ray diffraction analysis, the structure of the complex is probably very static, as indicated by VTP NMR analysis at 313 and 223 K: apart from a slight broadening, no significant shift nor decoalescence of the ^{1}H and ^{31}P signals was observed. ^{1}H-^{1}H NOE experiments allowed us to confirm the above topological assignment and to gain insights into the geometrical relationships between protons (Scheme 3). In particular, they show that in the preferred conformation, the methyl group is oriented towards the PPh$_2$ terminus of the naphthylphosphane ligand, while both phenyl rings of the methyldiphenylphosphane ligand are oriented towards the diene moiety. Although direct information on the conformation of the η^4-naphthyl group is not available, the absence of an NOE between the latter phenyl ring protons

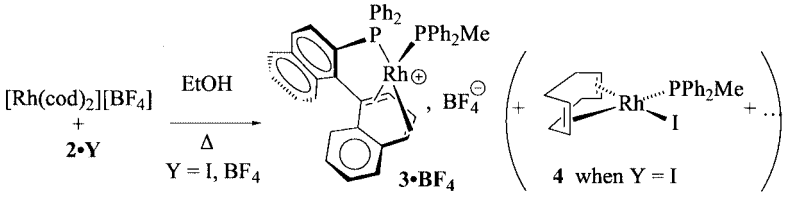

Scheme 2. Reaction of methylbinapium **2** with [Rh(cod)$_2$][BF$_4$]

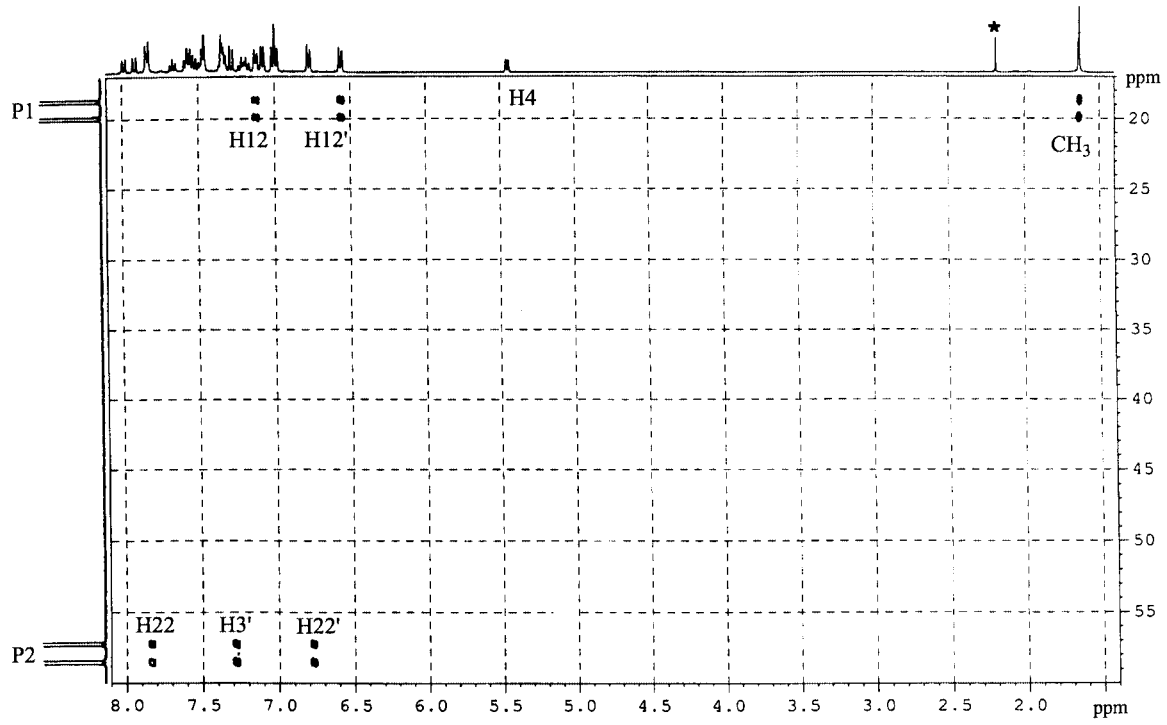

Figure 1. 400−162 MHz HMQC ^{1}H-^{31}P NMR spectrum of **3·BF$_4$** in $CDCl_3$ solution at 298 K; a weaker correlation of H4 with P1 and P2 is also seen at a lower threshold of the 2D plot (atom numbering in Scheme 3); *: residual acetone peak

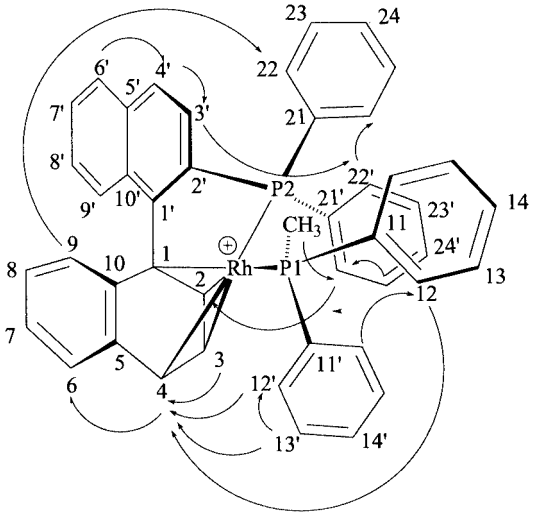

Scheme 3. 3D structural assignment based on ^{1}H-^{1}H NOE experiments

and the H6−H9 protons would be consistent with a folding along the C1···C4 axis. Such a folding (ca. 35°) was indeed reported to occur in the related complex [(η^4-naphthalene)RhCp].[17] Finally, NOE data also support a classical face-to-edge conformation of the phenyl substituents in both the $RhPPh_2$ units.

The optical rotation of complex **3·BF$_4$** is high: $[\alpha]_D^{25} = +175$ ($c = 0.1$, CH_2Cl_2). For comparison, the optical rotation of the enantiomerically pure complex [{(*R*)-binap}(cod)Rh][ClO_4] is $[\alpha]_D^{20} = +180$ ($c = 0.05$, CH_2Cl_2),[6] and that of free (*S*)-H-MOP prepared by Hayashi is $[\alpha]_D^{25} = +102$ ($c = 2.03$, $CHCl_3$).[18] The chiral information brought by the (*R*)-binapium reactant is therefore qualitatively preserved: the complex is enantiospecifically obtained as an enriched scalemic mixture.

In summary, the complex thus contains both an η^5-(σ-P, π-arene) (*S*)-H-MOP ligand and an independent η^1,σ-P methyldiphenylphosphane ligand. It provides a generalization to rhodium(I) of similar well-documented complexation patterns in ruthenium(II) complexes.[7−9] It is, however, worth noting that other chelating ω-phosphanylalkene ligands associated with an independent monophosphorus(III) ligand at a rhodium(I) center are known.[19]

Reaction Mechanism via Reductive P$^+$−C Bond Cleavage

The formation of complex **3** formally results from a complexation-reduction process. The reducing agent here is the ethanol solvent, which is also commonly used to convert rhodium(III) salts to rhodium(I) complexes.[24] A plausible mechanism involving elementary processes at Rh^I and Rh^{III} centers is depicted in Scheme 4. Starting from (*R*)-binapium, the final stereoselective reductive elimination would finally lead to an (*S*)-H-MOP ligand.[18] The overall P$^+$−C bond cleavage process is reducing in nature, and is therefore basically complementary to the related "acid-induced" and "solvent-induced" P−C bond cleavage processes identified by Pregosin in the coordination sphere of ruthenium complexes.[7] A related reductive P−C bond cleavage was also invoked in the coordination sphere of a rhodium complex converting PPh_3 to PPh_2(*n*-Pr) under hydrogen in the pres-

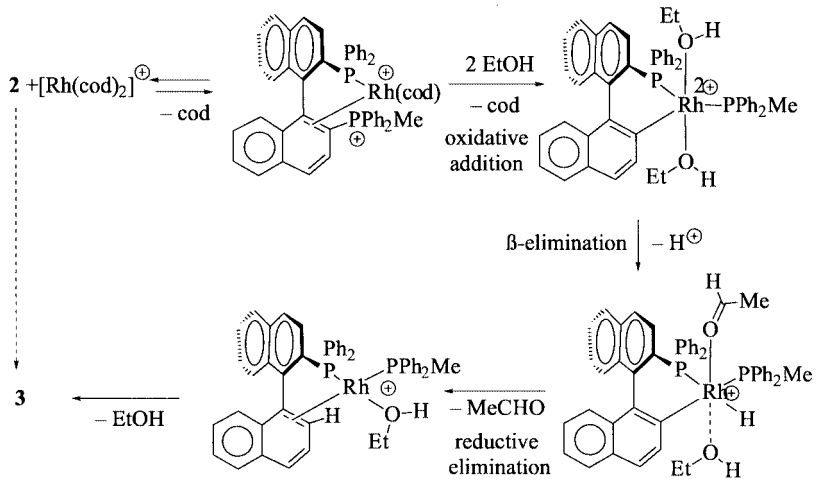

Scheme 4. Plausible mechanism for the formation of complex **3**

ence of propylene at 130 °C.[20] It is also worth noting that Hayashi recently reported a selective P^V-C bond cleavage by *n*BuLi in neutral $P(O)Ph_2$-MOP derivatives.[21]

Catalytic Hydrogenation with Complex 3

The chiral structure of complex **3** combines the essential features of classical $[P_2Rh(diene)]^+$ catalytic precursors for asymmetric hydrogenation of prochiral acrylic acid derivatives,[22] albeit in another connectivity pattern, $[P(Pdiene)Rh]^+$. These features prompted us to test complex **3** in a 1% catalytic ratio for the hydrogenation of (*Z*)-α-acetamidocinnamic acid, a reference substrate. Under 1 bar of hydrogen in methanol, the conversion into *N*-acetylphenylalanine reached only 6% after 40 h. Under 20 bar of hydrogen, however, the conversion reached 95%, although no significant enantioselectivity was obtained. According to the generally accepted mechanism for rhodium-catalyzed hydrogenation,[22] the η^4-diene moiety should be hydrogenated in situ to a putative (but likely) tetralinyl-substituted naphthylphosphane complex **5**. In this complex, the (*S*) configuration of the chiral carbon center should result from the initial (*S*)-configuration of the chirality axis of H-MOP (Scheme 5). The fate of the 1,1′-tetralinylnaphthtylphosphane ligand has been investigated by MM2 calculations. The latter suggest that, in contrast to H-MOP, this ligand no longer contains a frozen atropisomeric axis.[23] Both "atropisomers" are essentially isoenergetic,[23b] and the rotation barrier could be estimated at approx. 45 kcal·mol^{-1}.[23c] In qualitative accordance with the experimental observations, the same method applied to the parent H-MOP ligand affords a much higher barrier of about 130 kcal·mol^{-1}.[3,4] The 1,1′-tetralinylnaphthtylphosphane ligand can therefore be qualified as "weakly" chiral. The negligible *ee* is therefore consistent with all reports on the enantioselectivity control by monophosphane ligands bearing a remote chiral center on their backbone.[22]

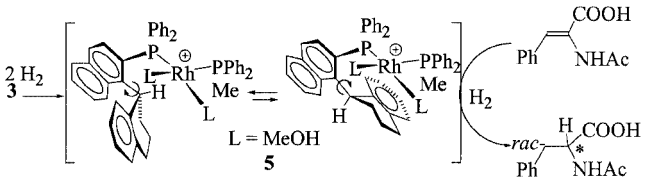

Scheme 5. Catalytic hydrogenation of (*Z*)-α-acetamidocinnamic acid with complex **3** as precursor

Conclusion

The novelty of the above results comes from two points: (i) the η^5-(σ-P,π-arene) hetero-chelating behaviour of an atropisomeric biarylphosphane at a rhodium(I) center; (ii) a selective reductive P^+-C bond cleavage leading to a mixed bis(monophosphane)rhodium(I) complex. This peculiar organometallic chemistry and the preliminary catalytic results pave the way to more general studies of this type of complexes in other Rh-catalyzed processes, such as C–C bond forming reactions.[3,4,5]

Experimental Section

Reactions were carried out under a nitrogen atmosphere using Schlenk tube and vacuum line techniques. Ethanol was distilled over drierite. Dichloromethane was distilled over P_2O_5. (−)-(*R*)-Binap and methyl iodide were purchased from Fluka. Ammonium tetrafluoroborate was purchased from Aldrich. $[Rh(cod)_2][BF_4]$ was prepared from $[RhCl(cod)]_2$, itself prepared from cyclooctadiene and $RhCl_3{\cdot}3H_2O$ (Johnson–Mattey) according a modified described procedure (no carbonate was added).[24] NMR spectra were recorded in $CDCl_3$ solution, on Bruker AC 200 and AMX 400 spectrometers. Positive chemical shifts at low field are expressed in ppm relative to internal TMS for ^1H and ^{13}C, and external 85% H_3PO_4 in D_2O for ^{31}P. ^{103}Rh chemical shifts are given to high fre-

quency of Ξ(^{103}Rh) = 3.16 MHz. Optical rotations were measured in a 1-dm cell with a Perkin−Elmer 241 polarimeter.

Methylbinapium 2: (*R*)-Methylbinapium iodide **2·I** (m.p. 307−310 °C) was prepared in 97% yield from (*R*)-binap **1** according to described procedures.[13,14] The tetrafluoroborate salt **2·BF$_4$** was obtained quantitatively by metathesis of **2·I** and [NH$_4$][BF$_4$].

Complex 3·BF4: (*R*)-Binapium tetrafluoroborate **2·BF$_4$** (0.115 g, 0.16 mmol) and [Rh(cod)$_2$][BF$_4$] (0.065 g, 0.16 mmol) were mixed in ethanol (15 mL). The suspension was heated, and the resulting deep orange solution was refluxed for 20 h. The solvent was then evaporated under reduced pressure. ^{31}P NMR analysis of the crude material indicated the presence of complex **3·BF$_4$** along with traces of binapium oxide [^{31}P NMR (81 MHz, CDCl$_3$): δ = 26.52 (s, 1 P, MePh$_2$*P*$^+$), 31.67 (s, 1 P, Ph$_2$*P*=O)]. Further purification was achieved by chromatography over silica gel eluting with CH$_2$Cl$_2$/acetone mixtures of increasing polarity (from 100:0 to 80:20). The most colored fractions were collected and the solvents evaporated, leading to an orange solid (0.060 g, 45%) which was used for full spectroscopic analysis and optical rotation measurement. TLC (SiO$_2$, CH$_2$Cl$_2$/acetone 80:20) R_f = 0.60. (+)ES-MS: *m*/*z* = 741.2 with consistent isotopic pattern. $[\alpha]_D^{25}$ = +175, $[\alpha]_{578}^{25}$ = +202. $[\alpha]_{546}^{25}$ = +278 (c = 0.1, CH$_2$Cl$_2$). ^{11}B (128.4 MHz, CDCl$_3$): δ = −0.59 (q, $^1J_{FB}$ = 1.0 Hz, *B*F$_4$). Other NMR assignments were achieved with the help of ^{1}H{^{31}P}, ^{31}P{^{1}H}, ^{13}C{^{1}H}, ^{13}C{^{1}H, ^{31}P}, ^{1}H-^{31}P{^{1}H} HMQC, ^{31}P-^{103}Rh ^{1}J-HMQC, ^{1}H-^{13}C{^{31}P}, ^{1}H-^{1}H{^{31}P} GS-HMQC, ^{1}H-^{1}H GS-COSY45, ^{1}H{^{31}P} dpfgse TOCSY, and ^{1}H-^{1}H{^{31}P} dpfgse (t_m = 600 ms) NOE experiments.

^{31}P NMR (162 MHz, CDCl$_3$): δ = 57.89 (dd, $^1J_{PRh}$ = 206.0, $^2J_{PP}$ = 38.6 Hz, NaphtPh$_2$*P*), 19.28 (dd, $^1J_{PRh}$ = 199.6, $^2J_{PP}$ = 38.6 Hz, MePh$_2$*P*) ppm. ^{103}Rh NMR (12.6 MHz, CDCl$_3$): δ = −391 (dd, $^1J_{PRh}$ = 206.0, $^1J_{PRh}$ = 199.6 Hz, PP′*Rh*$^+$) ppm. ^{1}H NMR (400 MHz, CDCl$_3$): δ = 1.63 (ddd, $^2J_{P1H}$ = 9.3 Hz, $^3J_{RhH}$ = 1.3 Hz, $^4J_{P2H}$ = 0.6 Hz, 3 H, P1C*H*$_3$), 5.44 (dt, $^3J_{H4H3}$ = 6.2 Hz, $^3J_{P1H4} \approx {}^2J_{P2H4} \approx$ 1 Hz, 1 H, *H*4), 6.56 (dd, $^3J_{H12'H13'}$ = 7.6, $^3J_{P1H12'}$ = 11.8 Hz, 2 H, *H*12′), 6.77 (dd, $^3J_{H22'H23'}$ = 7.7, $^3J_{P2H22'}$ = 12.0 Hz, 2 H, *H*22′), 7.00 (dt, $^3J_{H23'H22'} \approx {}^3J_{H23'H24'}$ = 7.6, $^4J_{P2H23'}$ = 1.3 Hz, 2 H, *H*23′), 7.00 (dt, $^3J_{H13'H12'} \approx {}^3J_{H13'H14'}$ = 7.6, $^4J_{P1H13'}$ = 1.3 Hz, 2 H, *H*13′), 7.07 (dd, $^3J_{H2H3}$ = 6.2 Hz, $^2J_{P1H2}$ = 0.7 Hz, 1 H, *H*2), 7.07 (dm, $^3J_{H9H8} \approx$ 7 Hz, 1 H, *H*9), 7.11 (dm, $^3J_{P1H12}$ = 11.8 Hz, 2 H, *H*12), 7.18 (ttd, $^3J_{H24'H23'}$ = 7.8, $^4J_{H24'H22'}$ = 1.3, $^3J_{P2H24'}$ = 1.8 Hz, 1 H, *H*24′), 7.21 (ttd, $^3J_{H14'H13'}$ = 7.5, $^4J_{H14'H12'}$ = 1.3, $^5J_{P1H14'}$ = 1.8 Hz, 1 H, *H*14′), 7.25 (dm, $^5J_{P2H24}$ = 2.0 Hz, 1 H, *H*24), 7.27 (dm, $^4J_{P2H23}$ = 2.0 Hz, 2 H, *H*23), 7.27 (dd, $^3J_{H3'H4'}$ = 8.4, $^3J_{P2H3'}$ = 8.5 Hz, 1 H, *H*3′), 7.33 (d, $^3J_{H6H7}$ = 7.2 Hz, 1 H, *H*6), 7.33 (m, 1 H, *H*14), 7.35 (dm, $^4J_{P1H13}$ = 2.0 Hz, 2 H, *H*13), 7.51 (t, $^3J_{H8H7} = {}^3J_{H8H9}$ = 7.2 Hz, 1 H, *H*8), 7.55 (m, 1 H, *H*8′), 7.57 (t, $^3J_{H3H2} \approx {}^3J_{H3H4}$ = 6.2 Hz, 1 H, *H*3), 7.57 (m, 1 H, *H*7), 7.66 (dt, $^3J_{H7'H6'} \approx {}^3J_{H7'H8'}$ = 8.3, $^4J_{H7'H9'}$ = 1.2 Hz, 1 H, *H*7′), 7.82 (dm, $^3J_{P2H22}$ = 7.8 Hz, 2 H, *H*22), 7.82 (d, $^3J_{H9'H8'}$ = 8.6 Hz, 1 H, *H*9′), 7.91 (dd, $^3J_{H4'H3'}$ = 8.4, $^4J_{P2H4'}$ = 1.6 Hz, 1 H, *H*4′), 7.98 (d, $^3J_{H6'H7'}$ = 8.3 Hz, 1 H, *H*6′) ppm. ^{13}C{^{1}H} NMR (100 MHz, CDCl$_3$): δ = 17.29 (ddd, $^1J_{PC}$ = 32, $^2J_{RhC}$ = 2, $^3J_{P2C}$ = 2 Hz, P1*C*H$_3$), 97.32 (ddd, $^1J_{RhC4}$ = 5, $^3J_{P1C4}$ = 4.8, $^3J_{P2C4}$ = 8.0 Hz, *C*4), 97.56 (ddd, $^1J_{RhC2}$ = 5, $^2J_{P1C2}$ = 4.0, $^2J_{P2C2}$ < 1 Hz, *C*2), 101.74 (ddd, $^1J_{RhC3}$ = 4, $^2J_{P1C3}$ < 1, $^2J_{P2C3}$ = 2.0 Hz, *C*3), 105.54 (ddd, $^1J_{RhC1}$ = 5, $^2J_{P1C1}$ = 10.4, $^2J_{P2C1}$ = 4.3 Hz, *C*1), 119.67 (s, *C*5),122.36 (s, *C*10), 122.90 (s, *C*9), 125.46 (s, *C*6), 126.44 (s, *C*9′), 127.71 (s, *C*3′), 128.78 (d, $^3J_{P1C13'}$ = 10.5 Hz, *C*13′), 128.78 (s, *C*6′), 128.97 (d, $^3J_{P2C23'}$ = 10.5 Hz, *C*23′), 128.94 (s, *C*8′),129.19 (d, $^3J_{P1C13}$ = 10.5 Hz, *C*13), 129.43 (s, *C*7′), 129.66 (s, *C*7), 129.69 (d, $^3J_{P2C23}$ = 11.5 Hz, *C*23), 129.84 (dd, $^1J_{P2C21}$ = 52, $^2J_{RhC21}$ = 3 Hz, *C*21), 130.08 (s, *C*8), 130.68 (d, $^4J_{P1C14}$ = 2.5 Hz, *C*14), 130.79 (d, $^4J_{P1C14'}$ = 2.5 Hz, *C*14′), 131.11 (d, $^4J_{P2C24'}$ = 2.0 Hz, *C*24′), 131.20 (d, $^2J_{P1C12}$ = 12.0 Hz, *C*12), 131.30 (d, $^1J_{P2C21'}$ = 48 Hz, *C*21′), 131.30 (s, *C*4′), 131.47 (d, $^3J_{P2C10'}$ = 15 Hz, *C*10′), 132.00 (d, $^2J_{P2C22'}$ = 11.5 Hz, *C*22′), 132.35 (d, $^4J_{P2C24}$ = 3 Hz, *C*22), 132.40 (d, $^2J_{P1C12'}$ = 12.0 Hz,; *C*12′), 132.50 (d, $^1J_{P1C11'}$ = 47.5 Hz, *C*11′), 134.44 (d, $^4J_{P2C5'}$ = 2.0 Hz, *C*5′), 134.72 (d, $^2J_{P2C22}$ = 13.5 Hz, *C*22), 137.62 (d, $^1J_{P1C11}$ = 46.2 Hz, *C*11), 142.27 (d, $^2J_{P2C1'}$ = 21.0 Hz, *C*1′), 146.21 (dd, $^1J_{P2C2'}$ = 49.0, $^2J_{P1C2'}$ = 3.0 Hz, *C*2′) ppm.

Hydrogenation Procedure: Complex **3·BF$_4$** (0.005 g, 0.006 mmol) and (*Z*)-α-acetamidocinnamic acid (0.123 g, 0.6 mmol) were placed in a glass vessel in a steel autoclave under 1 bar of nitrogen atmosphere. Methanol was then syringed in, and the autoclave was pressurized to 21 bar with hydrogen gas. After stirring at 25 °C for 40 h, the autoclave was opened and the solvent evaporated to dryness to give an orange solid. ^{1}H NMR analysis of the crude material in [D$_6$]DMSO indicated an exclusive 95% conversion of the staring material to *N*-acetylphenylalanine. The catalyst residue was removed by treatment with a 5 N aqueous NaOH solution and washing with Et$_2$O. After acidification with HCl, the aqueous layer was extracted with Et$_2$O. The organic layer was dried over MgSO$_4$ and the solvents evaporated giving a white powder (0.87 g) consisting in 95% *N*-acetylphenylalanine and 5% unchanged olefin according to ^{1}H NMR spectroscopy. $[\alpha]_D^{25}$ = +0.007 (*c* = 1, EtOH).

[1] M. T. Reetz, G. Mehler, *Angew. Chem.* **2000**, *112*, 4047−4049; M. T. Reetz, G. Mehler, *Angew. Chem. Int. Ed.* **2000**, *39*, 3889−3890.

[2] [2a] C. Claver, E. Fernandez, A. Gillon, K. Heslop, D. J. Hyett, A. Martorell, A. G. Orpen, P. G. Pringle, *Chem. Commun.* **2000**, 961−962. [2b] M. van den Berg, A. J. Minnaard, E. P. Schudde, J. van Esch, A. H. M. de Vries, J. G. de Vries, B. L. Feringa, *J. Am. Chem. Soc.* **2000**, *122*, 11539−11450. [2c] A. Bayer, P. Murszat, U. Thewalt, B. Rieger, *Eur. J. Inorg. Chem.* **2002**, 2614−2624. [2d] M. van den Berg, R. M. Haak, A. J. Minnaard, A. H. M. de Vries, J. G. de Vries, B. L. Feringa, *Adv. Synth. Catal.* **2002**, *344*, 1003−1007.

[3] T. Hayashi, *Acc. Chem. Res.* **2000**, *33*, 354−362.

[4] [4a] K. Kitayama, Y. Uozumi, T. Hayashi, *Chem. Commun.* **1995**, 1533−1534. [4b] K. Kitayama, H. Tsuji, Y. Uozumi, T. Hayashi, *Tetrahedron Lett.* **1996**, 4169−4172.

[5] T. Hayashi, M. Ishigedani, *J. Am. Chem. Soc.* **2000**, *122*, 976−977.

[6] R. Noyori, R. H. Takaya, *Acc. Chem. Res.* **1990**, *23*, 345−350, and references therein.

[7] T. J. Geldbach, P. S. Pregosin, *Eur. J. Inorg. Chem.* **2002**, 1907−1918.

[8] [8a] N. Feiken, P. S. Pregosin, G. Trabesinger, *Organometallics* **1997**, *16*, 537−543. [8b] N. Feiken, P. S. Pregosin, G. Trabesinger, *Organometallics* **1997**, *16*, 3735−3736. [8c] N. Feiken, P. S. Pregosin, G. Trabesinger, *Organometallics* **1997**, *16*, 5756−5762. [8d] C. J. den Reijer, P. Dotta, P. S. Pregosin, A. Albinati, *Can. J. Chem.* **2001**, *79*, 693−704. [8e] T. J. Geldbach, D. Drago, P. S. Pregosin, *J. Orgamomet. Chem.* **2002**, *643−644*, 214−222.

[9] A. S. C. Chan, S. Laneman, *Inorg. Chim. Acta* **1994**, *223*, 165−167.

[10] C. J. den Reijer, M. Wörle, P. S. Pregosin, *Organometallics* **2000**, *19*, 309−316.

[11] [11a] J. J. Brunet, R. Chauvin, G. Commenges, B. Donnadieu, P. Leglaye, *Organometallics* **1996**, *5*, 1752−1754. [11b] R. Chauvin, *Eur. J. Inorg. Chem.* **2000**, 577−591.

[12] L. Viau, R. Chauvin, *J. Organomet. Chem.* **2002**, *654*, 180−186.

[13] P. Leglaye, B. Donnadieu, J.-J. Brunet, R. Chauvin, *Tetrahedron Lett.* **1998**, *39*, 9179−9182.

[14] L. Viau, C. Lepetit, G. Commenges, R. Chauvin, *Organometallics* **2001**, *20*, 808−810.
[15] B. E. Mann, in *Transition Metal Nuclear Magnetic Resonance* (Ed.: P. S. Pregosin), Elsevier, Amsterdam, 1991, *Studies in Inorganic Chemistry* vol. 13, p. 177.
[16] E. T. Singewald, X. Shi, C. A. Mirkin, S. J. Schofer, C. L. Stern, *Organometallics* **1996**, *15*, 3062−3069.
[17] J. Müller, P. E. Gaede, C. Hirsch, K. Qiao, *J. Organomet. Chem.* **1994**, *472*, 329−335.
[18] Y. Uozumi, N. Suzuki, T. Hayashi, *Tetrahedron* **1994**, *50*, 4293−4302.
[19] See for example: S. Deblon, H. Rüegger, H. Schönberg, S. Loss, V. Gramlich, H. Grutzmacher, *New. J. Chem.* **2001**, *25*, 83−92.
[20] A. G. Abatjoglou, E. Billig, D. R. Bryant, *Organometallics* **1984**, *3*, 923−926.
[21] T. Shimada, H. Kurushima, Y.-H. Cho, T. Hayashi, *J. Org. Chem.* **2001**, *66*, 8854−8858.
[22] [22a] H. B. Kagan, in *Comprehensive Asymmetric Catalysis* (Eds.: E. N. Jacobsen, A. Pfaltz, H. Yamamoto), Vol. 1, Springer, Heidelberg, 1999, Chap. 2, p. 9.J. [22b] M. Brown, in *Comprehensive Asymmetric Catalysis* (Eds.: E. N. Jacobsen, A. Pfaltz, H. Yamamoto), Vol. 1, Springer, Heidelberg, 1999, Chap. 5, p. 121.
[23] [23a] MM calculations were carried out using the MM2 force field implemented in the software, CAChe Scientific, release 3.8, Oxford Molecular, **1995**. [23b] The absolute minimum steric energy of the (S_C,R_{Ar-CH}) rotamer is −32.8 kcal·mol^{-1}. It lies merely 0.7 kcal·mol^{-1} lower than the steric energy of the (S_C,S_{Ar-CH}) rotamer. [23c] The whole steric energy hypersurface was not mapped, but several 360° rotations (by 10° and then 1° increments) afforded maximum energy structures in the range 10−20 kcal·mol^{-1}.

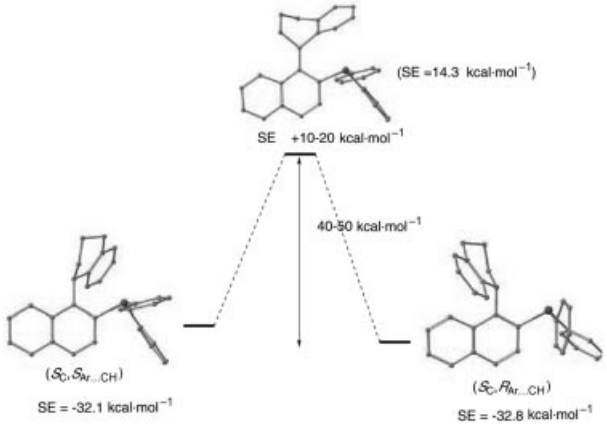

[24] Addition of carbonate is not necessary and affords impure greenish samples. G. Giordano, R. H. Crabtree, R. M. Heintz, D. Forster, D. E. Morris, in *Inorganic Synthesis*, vol. 28, John Wiley & Sons, New York, **1991**, p. 88.

Received September 19, 2002
[I02534]

Rhodium Clusters Substituted by Cycloheptatrienyl Ligands: Synthesis and Solid-State Structure of $[Rh_{11}(CO)_{14}(\mu_3\text{-}\eta^2\text{:}\eta^3\text{:}\eta^2\text{-}C_7H_7)_3]$

Roberto Della Pergola,*[a] Emanuela Comensoli,[b] Luigi Garlaschelli,[b] Mario Manassero,*[c] Mirella Sansoni,[c] and Donatella Strumolo[b]

Keywords: Rhodium / Carbocycles / Cluster compounds / Carbonyl ligands

The cluster $[Rh_{11}(CO)_{14}(C_7H_7)_3]$ (**1**) was obtained from the reaction of $[Rh_6(CO)_{16}]$ and an excess of cycloheptatriene in refluxing toluene. Initially, the substituted cluster $[Rh_6(CO)_{13}(C_7H_8)]$ (**2**) could be identified spectroscopically, which is transformed into **1** after prolonged refluxing. In the solid state, the eleven rhodium atoms define a trioctahedral metal cage, condensed through a common edge. The three planar, equivalent C_7 rings sit on the top of triangular faces. The spectroscopic characterisation of the product is hampered by its low solubility.
(© Wiley-VCH Verlag GmbH & Co. KGaA, 69451 Weinheim, Germany, 2003)

Ligands derived from cycloheptatriene are widely employed in organometallic chemistry; mononuclear[1] and cluster compounds[2] containing such a ring are well documented in the literature. When supported by a cluster, the C_7 rings can bind one, two or three metal atoms. Relevant examples of these different bonding modes are: (i) $[Ru_6C(CO)_{11}(C_7H_9)(C_7H_7)]$[3] and $[Co_4(CO)_6(C_7H_9)(C_7H_7)]$,[4] where η^5-C_7H_9 and μ_3-η^7-C_7H_7 binding modes are displayed in the same molecule, (ii) $[Ru_4(CO)_7(C_7H_7)_2]$, which contains edge-bridging μ_2-η^3:η^4 units,[5] and (iii) $[Ru_6C(CO)_{14}(C_7H_8)]$, where a facial μ_3-η^2:η^2:η^2 binding mode is present.[3] Upon coordination to several metal atoms, the reactivity of the ring is modified, and the hapticity of the ligand can be changed either by a ring contraction,[3] by reductive coupling,[6] or by a ligand-to-ligand hydrogen transfer.[3,4]

We have recently isolated $[Ir_6(CO)_{13}(C_7H_8)]$, and described its peculiar reactivity toward reducing agents, which is assisted by a reversible modification of the bonding mode of the cyclic ligand.[7]

The substitution of rhodium clusters with carbocyclic ligands is relatively unexplored: reactions of $Rh_4(CO)_{12}$ and $Rh_6(CO)_{16}$ with polyenes have been described,[8] but only $[Rh_6(CO)_{14}(\eta^4\text{-}C_6H_8)]$,[9] $[Rh_4(CO)_8(\mu_3\text{-}C_8H_8)]$ and $[Rh_4(CO)_6(\mu_3\text{-}C_8H_6R_2)(\eta^4\text{-}C_8H_6R_2)]$[10] have been structurally characterised. For these reasons we have re-examined the substitution of $[Rh_6(CO)_{16}]$ with cycloheptatriene. We found a behaviour different from that already reported,[8] and from that of $Ir_6(CO)_{16}$,[7] which allowed us to isolate a new rhodium cluster that is highly substituted by the C_7 ring.

Results

The carbonyl substitution of $Rh_6(CO)_{16}$ with cycloheptatriene proceeds in boiling toluene. After about six hours most of the starting material has been converted into a new, soluble cluster. The infrared spectrum of the toluene solution allows the unequivocal identification of this primary product as $[Rh_6(CO)_{13}(C_7H_8)]$ (**2**), since its carbonyl stretching bands (2093s, 2064vs, 2035s, 2006m, 1794m cm^{-1}) are almost superimposable with those of the corresponding iridium analogue $[Ir_6(CO)_{13}(C_7H_8)]$.[7] All attempts to grow crystals, isolate in the solid state, purify, or convert **2** into an anionic derivative failed, owing to its high solubility and moderate stability. Currently, we are trying to identify the decomposition products, to reconstruct the steps of the subsequent cluster build-up. At this early stage of the reaction, a brown microcrystalline precipitate is also present, which can be easily confused with unreacted $Rh_6(CO)_{16}$.[8] However, $[Ir_6(CO)_{13}(C_7H_8)]$ is poorly soluble in toluene and it crystallizes directly on cooling the reaction mixture.[7] Therefore we measured the crystallographic parameters of the dark solid residue, and found a com-

[a] Dipartimento di Scienze dell' Ambiente e del Territorio – Università di Milano Bicocca
Piazza della Scienza 1, 20126 Milano, Italy
Fax: (internat.) +39-026448-2890
E-mail: roberto.dellapergola@unimib.it
[b] Dipartimento di Chimica Inorganica, Metallorganica ed Analitica, Università di Milano
Via G. Venezian 21, 20133 Milano, Italy
[c] Dipartimento di Chimica Strutturale e Stereochimica Inorganica, Università di Milano
Via G. Venezian 21, 20133 Milano, Italy
E-mail: m.manassero@istm.cnr.it
Supporting information for this article is available on the WWW under http://www.eurjic.org or from the author.

pletely unexpected unit cell. Thus, the course of the reaction was investigated more deeply. The solution was subjected to a few additional cycles of heating and cooling: after 10 additional hours the solution was colourless, and **2** had been completely converted into a material that is very insoluble in THF, CH_2Cl_2, MeCN and hydrocarbon solvents. Several of the well-shaped crystals were big enough for a X-ray analysis, and a structural characterisation of the new cluster $[Rh_{11}(CO)_{14}(C_7H_7)_3]$ (**1**) was performed. The powder residue could only be partially characterised. The elemental analysis established a Rh/C_7 ring ratio of 2, and its infrared spectrum, as a nujol mull, showed bands at 1977m, 1954s, 1804m cm^{-1}. It was found, by XRPD, to be poorly crystalline. These data suggest that this material, which is the main product of the reaction, is composed of highly substituted clusters whose formulation can be related neither to **1** nor to **2**.

The solid state structure of **1**, together with the numbering scheme, is shown in Figure 1. Figure 2 shows, with two different orientations, the connectivity of the CO's and the C_7H_7 rings to the metallic framework, which can be described as three octahedra, mutually fused through a face and all sharing a common edge [Rh(1)−Rh(1′)]. Owing to the crystallographic symmetry, only three metal atoms, three independent carbonyl groups and four carbon atoms of the C_7H_7 ring occupy the asymmetric unit. The molecule contains terminal [CO(1)], edge-bridging [CO(2)] and face-bridging [CO(3)] CO ligands, 15 sites in total, which are all indicated in the figures. However, we strongly believe that **1** contains only 14 CO molecules, and that the six equivalent

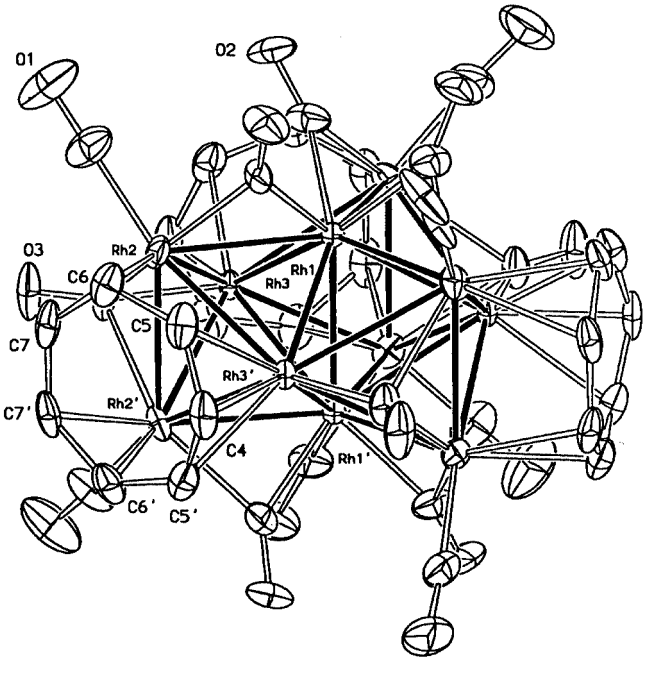

Figure 1. The solid state structure of $[Rh_{11}(CO)_{14}(C_7H_7)_3]$; relevant bond lengths (Å): Rh(1)−Rh(1′) 2.821(1), Rh(1)−Rh(2) 2.684(1), Rh(1)−Rh(3) 2.720(1), Rh(2)−Rh(2′) 2.733(1), Rh(2)−Rh(3) 2.885(1), Rh(2)−Rh(3′) 2.855(1), Rh(3)−C(4) 2.142(4), Rh(3)−C(5) 2.323(4), Rh(2)−C(6) 2.159(4), Rh(2)−C(7) 2.209(5); average C−C(ring) 1.416

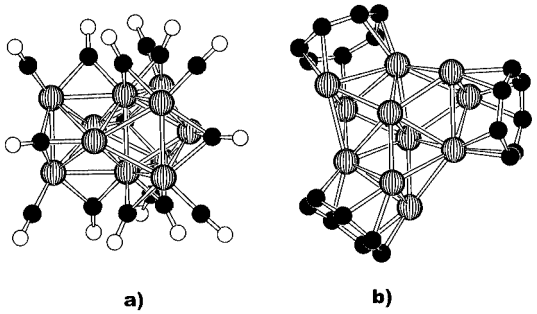

Figure 2. The disposition of the carbonyls (a) and the C_7H_7 (b) around the metallic framework of $[Rh_{11}(CO)_{14}(C_7H_7)_3]$

CO(2) sites are randomly occupied by five ligands. As a matter of fact the occupancy factor of CO(2) is lower than unity, and close to the expected value of 5/6 (0.83). Under this assumption, **1** possesses 148 valence electrons, a number which has been observed in Rh,[11] Pt−Rh[12] or Ir[13] clusters with the same framework. The three independent metal atoms are very different for the number of Rh−Rh, Rh−CO and $Rh-C_{ring}$ connectivities; however, local electron counts[13] at the three sites differ by less than one electron, and the small discrepancies cannot be rationalized in terms of bond-length variations, even if the asymmetry of the face bridging CO(3) [2.335(3) Å for Rh(2)−CO(3) and 1.977(7) for Rh(3)−CO(3)] is consistent with the unbalanced distribution of electrons. For example, Rh(1) has a (formal) excess of one electron, but the longest bonds within the cluster are the Rh(2)−Rh(3) interactions. It is likely that the lengths of the Rh−Rh bonds reflect the steric and electronic requirements of the carbocycle. In keeping with this, the bond lengths of the organic unit are spread over a wide range: 2.142(4)−2.323(4) for $Rh-C_{ring}$ and 1.378(6)−1.447(7) Å for C−C bonds.

The almost planar cycloheptatrienyl rings are bound to triangular faces in the μ_3-η^2:η^3:η^2 fashion and are coordinated through one allylic system to Rh(3) and through two C=C double bonds to Rh(2). A slightly different arrangement for the same ligand has frequently been observed: in the μ_3-η^2:η^3:η^3 bonding mode one carbon atom, shared by two allylic moieties, is connected to two metal atoms with comparable distances.[4,7] In **1** the two external atoms of the allylic systems are very far from the nonbonded rhodium atom [Rh(2)−C(5) is about 2.9 Å] and the cluster can be classified as a genuine example of μ_3-η^2:η^3:η^2 hapticity. In any case, the neutral ligand must be considered as a seven-electron donor. Alternatively, the molecule can be described as being derived from the homoleptic $[Rh_{11}(CO)_{23}]^{3-}$,[11] by formal substitution of nine CO's with three tropylium cations ($[C_7H_7]^+$ is a six-electron donor).

Unfortunately, the analytical and spectroscopic characterisation of **1** is hampered by its low solubility, which is not unexpected for a neutral, high-nuclearity cluster. Even if the compound were available in larger amounts, it is unlikely that the number of CO ligands could be confirmed by microanalysis, since the differences would be below the experimental errors. To confirm the presence of **1** among

the products of the reaction, the determination of the cell parameters is more straightforward than infrared spectroscopy as five crystals, selected from among the bigger ones with difficulty, were not sufficient to record an infrared spectrum of reasonable quality.

Despite the lack of spectroscopic data on $[Rh_{11}(CO)_{14}(C_7H_7)_3]$, this compound is important since it sheds a new light on the reactivity of rhodium clusters[8,10] with cyclic unsaturated hydrocarbons: the carbonyl substitution can be accompanied by unpredictable cluster reconstruction, leading to highly substituted, high-nuclearity clusters. The reproducible preparation and the symmetrical structure of **1** are strong evidences of its high stability. Among the group 9 metal clusters it may be compared to $[Ir_7(CO)_{12}(C_8H_{12})(C_8H_{11})(C_8H_{10})]$, which shows stages of cyclooctadiene dehydrogenation.[14]

Experimental Section

In a typical preparation, $[Rh_6(CO_{16}]$ (0.30 g, 0.28 mmol) and cycloheptatriene (0.3 mL, 3 mmol) were suspended in 10 mL of toluene. The mixture was refluxed for five days, without stirring, switching the heating on and off at the beginning and at the end of the day's work. The residue, insoluble in most common solvents, was collected by filtration, and washed with toluene. $[Rh_2(CO)_4(C_7H_7)]_n$: calcd. for C 32.3, H 1.7; found C 31.7, H 1.9.

Well-shaped, prismatic crystals of **1** were selected under the lens of a microscope and used for characterisation.

Crystal data and other experimental details are summarized in Table 1. The diffraction experiment was carried out on a Bruker SMART CCD area-detector diffractometer at 223 K using Mo-K_α radiation (λ = 0.71073 Å) with a graphite monochromator in the incident beam. Intensity data were processed with the software SAINT,[15a] and an empirical absorption correction was applied (SADABS).[15b] The calculations were performed using the Personal Structure Determination Package[16] and the physical constants tabulated therein. Scattering factors and anomalous dispersion corrections were taken from ref.[17] The structure was solved by direct methods (SHELXS 86)[18] and refined by full-matrix least-squares using all reflections and minimizing the function $\Sigma w(F_o^2 - kF_c^2)^2$ (refinement on F^2). Anisotropic thermal factors were refined for all the non-hydrogen atoms. Hydrogen atoms were placed in their ideal positions and not refined. In the final difference Fourier map the maximum residual electron density was 1.40(49) e·Å^{-3} at 0.66 Å from Rh(2).

Table 1. Selected crystallographic data (more detailed information can be found in the Supporting Information)

Formula	$C_{35}H_{21}O_{14}Rh_{11}$
M	1797.50
Crystal system	hexagonal
Space group	$P6_3/m$
a (Å)	11.821(1)
c (Å)	16.492(2)
U (Å^3)	1995.8(4)
Z	2
T (K)	223
θ-range/°	3−26
Reciprocal space explored	hemisphere
No. of reflections (total; independent)	16288, 2095
R_{int}	0.059
Final R_2 and R_{2w} indices (F^2, all reflections)	0.047, 0.054
Conventional R_1 index [$I > 2\sigma(I)$]	0.028
Reflections with $I > 2\sigma(I)$	1440

CCDC-194777 contains the supplementary crystallographic data for this paper. These data can be obtained free of charge at www.ccdc.cam.ac.uk/conts/retrieving.html [or at Cambridge crystallographic Data Centre, 12 Union Road, Cambridge CB2 1EZ, UK; Fax: (internat.) +44-122/336-033; E-mail: deposit@ccdc.cam.ac.uk].

Acknowledgments

This work was funded by MIUR (COFIN and FAR). We are indebted to N. Masciocchi for the XRPD spectra

[1] M. L. H. Green, D. K. P. Ng, *Chem. Rev.* **1995**, *95*, 439−473.
[2] H. Wadepohl, *Coord. Chem. Rev.* **1999**, *185−186*, 551−568.
[3] D. Braga, F. Grepioni, L. Scaccianoce, B. F. G. Johnson, *J. Chem. Soc., Dalton Trans.* **1998**, 1321−1325.
[4] H. Wadepohl, S. Gebert, H. Pritzkow, F. Grepioni, D. Braga, *Chem. Eur. J.* **1998**, *4*, 279−288.
[5] D. Braga, P. J. Dyson, F. Grepioni, B. F. G. Johnson, C. M. Martin, L. Scaccianoce, A. Steiner, *Chem. Commun.* **1997**, 1259−1260.
[6] H. Wadepohl, S. Gebert, H. Pritzkow, D. Osella, C. Nervi, J. Fiedler, *Eur. J. Inorg. Chem.* **2000**, 1833−1843.
[7] R. Della Pergola, A. Bianchi, F. Fabrizi de Biani, L. Garlaschelli, M. Manassero, M. Sansoni, D. Strumolo, P. Zanello, *Organometallics* **2002**, in press
[8] T. Kitamura, T. Joh, *J. Organomet. Chem.* **1974**, *65*, 235−243.
[9] P. J. Dyson, S. L. Ingham, B. F. G. Johnson, A. J. Blake, *J. Organomet. Chem.* **1995**, *498*, 237−240.
[10] H. Wadepohl, R. Merkel, H. Pritzkow, S. Rihm, *J. Chem. Soc., Dalton Trans.* **2001**, 3617−3625.
[11] A. Fumagalli, S. Martinengo, G. Ciani, A. Sironi, B. T. Heaton, *J. Chem. Soc., Dalton Trans.* **1988**, 163−171.
[12] A. Fumagalli, S. Martinengo, G. Ciani, *J. Organomet. Chem.* **1984**, *273*, C46−C49.
[13] R. Della Pergola, L. Garlaschelli, M. Manassero, M. Sansoni, *J. Cluster Sci.* **1999**, *10*, 109−119 and references therein
[14] C. G. Pierpont, *Inorg. Chem.* **1979**, *18*, 2972−2977.
[15] [15a] SAINT Reference manual, Siemens Energy and Automation, Madison, WI, **1994−1996**. [15b] G. M. Sheldrick, SADABS, Empirical Absorption Correction Program, University of Gottingen, **1997**.
[16] [16a] B. A. Frenz, *Comput. Phys.* **1988**, *2*, 42. [16b] Crystallographic Computing 5, Oxford University Press: Oxford, U. K., **1991**; Chapter 11, p. 126.
[17] International Tables for X-ray Crystallography, Vol.4, Kynoch Press, Birmingham, **1974**.
[18] G. M. Sheldrick, SHELXS-86, Program for the solution of crystal structures, University of Gottingen, Germany, **1985**.

Received October 14, 2002
[I02549]

Gold(I) Macrocycles and [2]Catenanes Containing Sulfone-Functionalised Diacetylide Ligands

Fabian Mohr,[a] Michael C. Jennings,[a] and Richard J. Puddephatt*[a]

Keywords: Self assembly / Catenanes / Macrocycles / Gold / Aurophilicity

The reaction of the polymeric digold(I) diacetylide $[(AuCCCH_2OC_6H_4)_2SO_2]_n$ with diphosphane ligands PP leads to the formation of either macrocyclic ring complexes $[(AuCCCH_2OC_6H_4)_2SO_2(\mu\text{-PP})]$ or [2]catenanes $[(AuCCCH_2OC_6H_4)_2SO_2(\mu\text{-PP})]_2$ by a self-assembly process. With the diphosphane ligands $Ph_2PCCPPh_2$, $[Fe(C_5H_4PPh_2)_2]$ and $Ph_2P(CH_2)_nPPh_2$ (n = 4, 5 and 6), macrocyclic ring complexes result, but with the diphosphane ligand $Ph_2P(CH_2)_3PPh_2$, the [2]catenane selectively crystallises from an isomeric mixture of products.
(© Wiley-VCH Verlag GmbH & Co. KGaA, 69451 Weinheim, Germany, 2003)

Introduction

The promise of useful applications of nanoscale devices has stimulated intense research into the synthesis and properties of mechanically interlocked molecules such as catenanes and rotaxanes.[1−5] Synthetic strategies based on ideas such as π-π interactions, metal ion templation, hydrophobic forces and hydrogen bonding have been developed to assemble such supramolecular structures.[6,7] The vast majority of catenanes and rotaxanes prepared to date are based either on organic or inorganic molecules, and the first organometallic [2]catenane was reported only in 1993.[8]

Gold(I) has proven to be a versatile building-block for constructing organometallic network polymers, rings and catenanes because of the low steric effects associated with its tendency for linear coordination and the potential to form Au···Au aurophilic attractions that can enhance association between gold(I) centers.[9,10] These aurophilic attractions (bond energies of ca. 7−11 kcal mol^{-1}) result in gold−gold distances ranging from 2.75 to 3.40 Å.[11] Gold(I) is a labile metal center and so easy rearrangements can occur to give thermodynamic control of the self-assembly processes. Recently, the first detailed studies of organometallic [2]catenanes containing gold(I) centres and diacetylide bridging ligands have been reported.[12−15] This work has shown that both the "hinge group" (X) in the diacetylide ligand and the "spacer group" between the phosphorus atoms (Y) (Figure 1) determine whether [2]catenanes or macrocyclic complexes are formed. Short and sterically demanding spacer groups Y such as $(CH_2)_2$, HC=CH, C≡C and $[Fe(C_5H_4)_2]$ form macrocycles, whilst longer spacer groups such as $(CH_2)_4$ and $(CH_2)_5$ may form [2]catenanes, depending on the nature of the hinge group. The case where the spacer group is $(CH_2)_3$ represents the borderline between macrocycle and [2]catenane formation: mixtures of both structural forms are usually observed. The hinge group effect depends at least in part on the orientation of the aryl groups (the twist angles of the two aryl groups with respect to the plane of the hinge atom, Figure 2), with the combinations of angles approximating to 90, 45 or 45, 45 (found with X = CH_2, CMe_2 or CHAr) favouring [2]catenane formation, while the combination 90, 0 (found with X = O or S) is particularly unfavourable to [2]catenane formation and so leads to formation of the simple macrocycles only. The unfavourable combination of angles 90, 0 found with X = S arises from π-bonding between the sulfur atom and adjacent aryl groups. This p_π-p_π bonding should not be present on oxidation of S to SO_2, and so catenation might then be possible. In order to study this potential method of triggering catenation, the selectivity of formation of [2]catenanes or macrocyclic rings with gold(I) bound to the sulfone-functionalized diacetylide and diphosphane ligands has been studied, and the results are presented below.

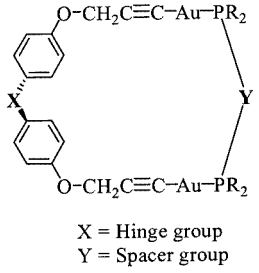

Figure 1. Schematic diagram of a macrocyclic gold(I) complex

[a] Department of Chemistry, University of Western Ontario, London, ON, N6A 5B7, Canada
Fax: (internat.) + 1-519/661-3022
E-mail: pudd@uwo.ca

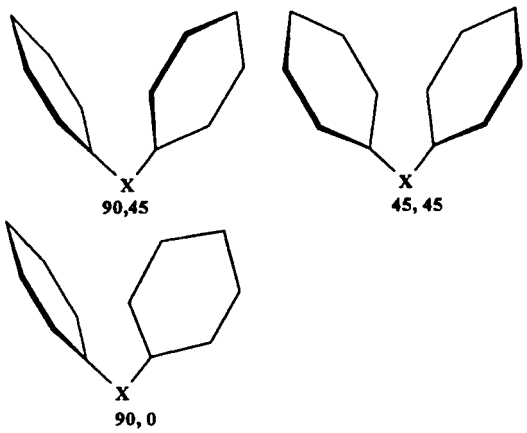

Figure 2. Orientation of aryl groups at the hinge atom X

Results and Discussion

Ligand and Gold(I) Oligomer Synthesis

Reaction of bis(4-hydroxyphenyl) sulfone with propargyl bromide under basic conditions gives the bis(alkyne) compound **1** (Scheme 1) in high yield. This was easily converted into the oligomeric digold(I) diacetylide complex **2** by reaction with [AuCl(SMe$_2$)] in the presence of triethylamine (Scheme 1). Complex **2** was isolated in high yield as a yellow powder, which was insoluble in common organic solvents. Like other gold(I) acetylides, it is presumed to have a polymeric structure in which each acetylide group is σ-bonded (η^1) to one gold atom and π-bonded (η^2) to another.[16] This is supported by the IR spectrum of **2**, which exhibits a weak band at 1996 cm^{-1}, considerably lower (133 cm^{-1}) than the corresponding band in the precursor **1** as would be expected if the alkynyl groups act as π donors.

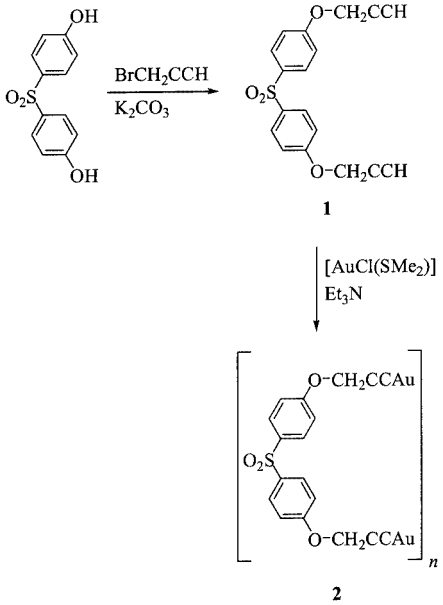

Scheme 1

Reactions with Diphosphane Ligands

Macrocyclic Ring Complexes

Reactions of complex **2** with a variety of diphosphane ligands gave colourless or pale-yellow, air-stable solids in good yields (Scheme 2). The new complexes were characterized by ^{1}H and ^{31}P NMR spectroscopy, MALDI-TOF mass spectrometry, elemental analyses and, in a number of cases, by X-ray crystallography. The ^{31}P NMR spectra of the complexes show one singlet, with chemical shifts ranging from δ = 18.59 (**3a**) to 37.57 ppm (**3e**). The ^{1}H NMR spectra show, in addition to the spacer group and OCH_2 resonances, two pairs of doublets at δ ≈ 7.8 and 7.1 ppm, corresponding to the protons on the *p*-disubstituted SC_6H_4O rings. The simple ^{1}H NMR spectra as well as the presence of only one singlet in the ^{31}P NMR spectra show that these molecules have a high degree of symmetry and exist as single isomers in solution. The spectroscopic data are consistent with macrocyclic ring structures for the complexes containing the diphosphane ligands $Ph_2PCCPPh_2$ (**3a**), [Fe($C_5H_4PPh_2$)$_2$] (**3b**) and $Ph_2P(CH_2)_nPPh_2$ [*n* = 4 (**3c**), 5 (**3d**) and 6 (**3e**)]. The MALDI-TOF mass spectra show molecular ion peaks in each case, with no peak corresponding to the potential [2]catenane but this is not definitive evidence since the mechanical bond of a [2]catenane may be easily broken. The proposed macrocyclic structures of complexes **3a**, **3b** and **3d** have been confirmed crystallographically. Figures 3, 4, and 5 show the molecular structures, while selected bond lengths and angles are listed in Tables 1, 2, and 3.

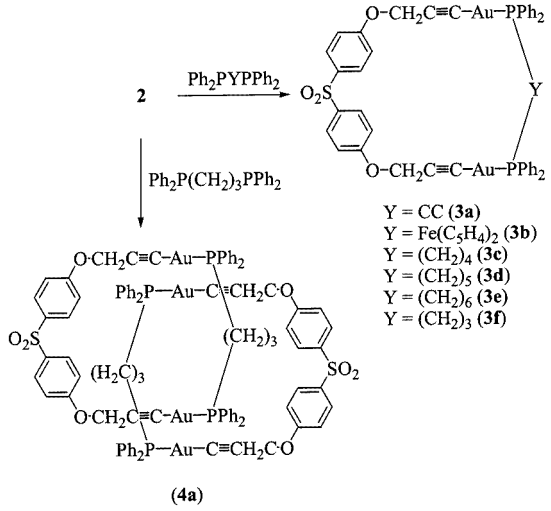

Scheme 2

The complexes consist of 23- (**3a**), 24- (**3b**) and 26-membered (**3d**) rings in which one diphosphane and one diacetylide ligand bridge two gold(I) centers. The angles C−Au−P are close to linearity in each case, as expected for gold(I). The molecular structures of the macrocyclic complexes are similar, but the three complexes pack very differently in the crystal space. Complex **3a** forms a polymeric

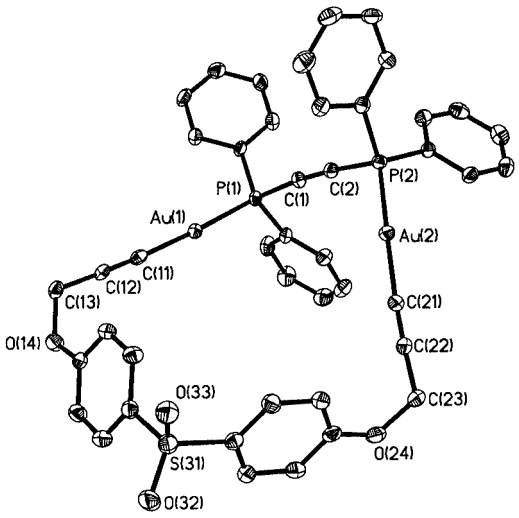

Figure 3. Molecular structure of complex **3a**; ellipsoids show 50% probability levels, hydrogen atoms have been omitted for clarity

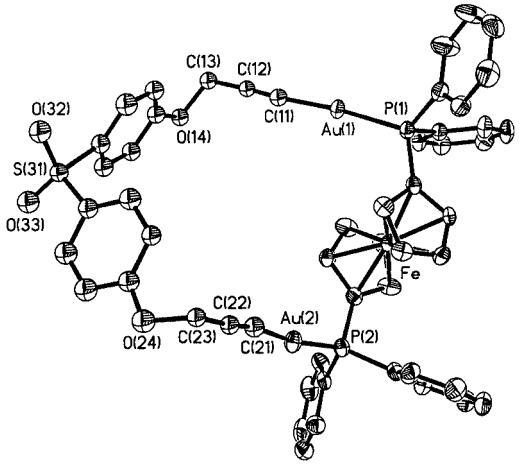

Figure 4. Molecular structure of complex **3b**; ellipsoids show 50% probability levels, hydrogen atoms have been omitted for clarity

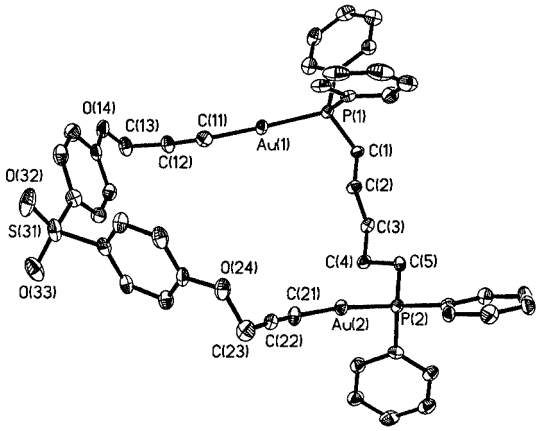

Figure 5. Molecular structure of complex **3d**; ellipsoids show 50% probability levels, hydrogen atoms have been omitted for clarity.

Table 1. Selected bond lengths [Å] and angles [°] in complex **3a**

Au(1)−P(1)	2.2709(18)	Au(2)−P(2)	2.2749(15)
Au(1)−C(11)	2.010(7)	Au(2)−C(21)	2.008(6)
C(11)−C(12)	1.192(9)	C(21)−C(22)	1.201(8)
C(1)−C(2)	1.212(8)	Au(1)···Au(2A)	3.1819(3)
C(11)−Au(1)−P(1)	176.27(17)	C(21)−Au(2)−P(2)	171.85(19)
C(12)−C(11)−Au(1)	176.1(6)	C(22)−C(21)−Au(2)	176.0(6)

Table 2. Selected bond lengths [Å] and angles [°] in complex **3b**

Au(1)−P(1)	2.2644(19)	Au(2)−P(2)	2.2729(19)
Au(1)−C(11)	1.968(18)	Au(2)−C(21)	2.032(19)
C(11)−C(12)	1.18(2)	C(21)−C(22)	1.19(3)
		Au(2)···Au(2A)	3.1488(7)
C(11)−Au(1)−P(1)	171.3(5)	C(21)−Au(2)−P(2)	175.5(6)
C(12)−C(11)−Au(1)	171.7(15)	C(22)−C(21)−Au(2)	170.6(18)

Table 3. Selected bond lengths [Å] and angles [°] in complex **3d**

Au(1)−P(1)	2.288(2)	Au(2)−P(2)	2.276(2)
Au(1)−C(11)	1.994(11)	Au(2)−C(21)	1.984(8)
C(11)−C(12)	1.233(13)	C(21)−C(22)	1.208(11)
C(11)−Au(1)−P(1)	178.0(3)	C(21)−Au(2)−P(2)	171.0(3)
C(12)−C(11)−Au(1)	176.5(9)	C(22)−C(21)−Au(2)	168.3(8)

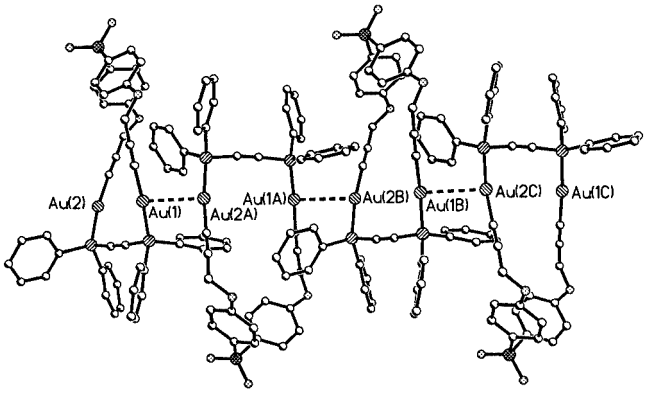

Figure 6. Packing of complex **3a** to form a polymeric chain

structure (Figure 6), resulting from aurophilic attractions [Au(1)···Au(2A) 3.1819(3) Å] between adjacent rings. Related polymers, formed by aurophilic attractions, are known with phosphane−gold(I) units in combination with halides, thiolates or acetylides.[9,11,17] In addition, the macrocycles in **3a** adopt an *anti* arrangement to minimise steric interactions. Macrocycle **3b** forms discrete dimeric units consisting of two rings connected by close gold−gold contacts [Au(2)···Au(2A) 3.1488(7) Å] (Figure 7), again the rings adopt an *anti* arrangement. In contrast, complex **3d** forms neither dimeric units nor a polymer: discrete macrocycles fill the crystal space.

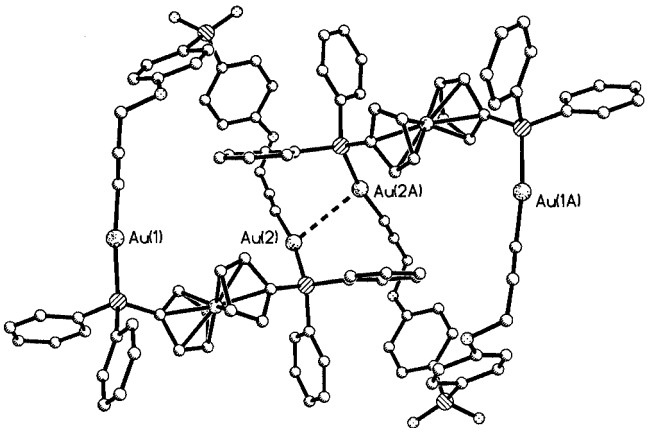

Figure 7. Packing of complex **3d** to form dimeric units

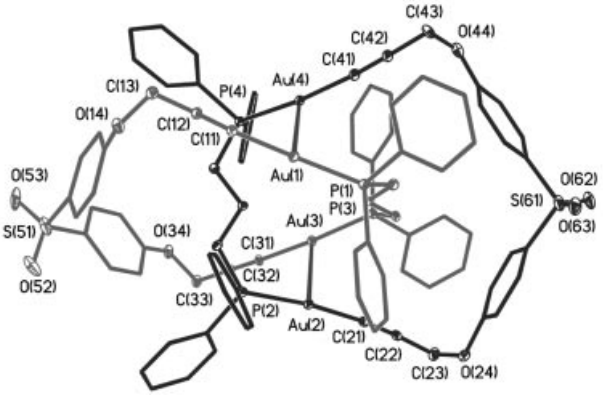

Figure 8. Molecular structure of complex **4a**; ellipsoids show 25% probability levels, C_6H_4 and phenyl rings are shown as lines and hydrogen atoms have been omitted for clarity

A [2]Catenane and Its Equilibrium with a Macrocycle

Reaction of complex **2** with $Ph_2P(CH_2)_3PPh_2$ gives a colourless, air-stable solid (Scheme 2). The ^{31}P NMR spectrum of this product contained two major singlet resonances, and the ^1H NMR spectrum contained two major pairs of doublets for the C_6H_4 protons. There was also a third minor set of resonances. This indicates that the compound exists as a mixture of three isomers, as discussed previously for the complex $[Me_2C(C_6H_4OCH_2CC)_2Au_2(Ph_2PCH_2CH_2CH_2PPh_2)]$.[15] The two major isomers are assigned as the macrocyclic ring **3f** and the [2]catenane **4a** (Scheme 2). The [2]catenane is characterized by lower chemical shifts for the C_6H_4 protons (**4a**: δ = 6.16 and 7.30 ppm; **3f**: δ = 7.07 and 7.78 ppm) and for the phosphorus atoms (**4a**: δ = 31.47 ppm; **3f**: δ = 35.32 ppm). The proton shielding arises as a result of the rigid structure of the [2]catenane with close edge-to-face contact between the C_6H_4 groups and phenyl groups of the interlocked molecule, and is characteristic of the [2]catenane structure with $Ph_2P(CH_2)_3PPh_2$ ligands.[15] Curiously, single crystals of the pure [2]catenane **4a** were insoluble in common organic solvents. The MALDI-TOF mass spectrum of the crystals of **4a** does not show a molecular ion peak for the [2]catenane, but only a molecular ion peak for the simple macrocycle **3f**. Presumably the mechanical link is broken under the conditions used.

The structure of the [2]catenane **4a** is shown in Figure 8 and selected bond lengths and angles are listed in Table 4. The two macrocyclic rings are interlocked across the diphosphane ligand backbones. There are two close gold−gold contacts [Au(1)···Au(4) 3.2392(7) Å and Au(2)···Au(3) 3.3164(6) Å] and these aurophilic attractions no doubt favour the [2]catenane formation. In addition, there are several close phenyl−C_6H_4 and phenyl−phenyl interactions (Figure 8), and the sum of these secondary bonding energies is clearly enough to overcome the negative entropy associated with [2]catenane formation.

Table 4. Selected bond lengths [Å] and angles [°] in complex **4a**

Au(1)−P(1)	2.279(2)	Au(2)−P(2)	2.275(3)
Au(3)−P(3)	2.279(2)	Au(4)−P(4)	2.273(2)
Au(1)···Au(4)	3.2392(7)	Au(2)···Au(3)	3.3164(6)
Au(1)−C(11)	2.011(10)	Au(2)−C(21)	1.998(10)
Au(3)−C(31)	2.007(9)	Au(4)−C(41)	1.996(10)
C(11)−C(12)	1.181(12)	C(21)−C(22)	1.220(13)
C(31)−C(32)	1.192(12)	C(41)−C(42)	1.193(14)
C(11)−Au(1)−P(1)	172.1(3)	C(21)−Au(2)−P(2)	172.9(3)
C(31)−Au(3)−P(3)	171.7(3)	C(41)−Au(4)−P(4)	170.4(4)

Conclusion

It is shown that the reaction of the sulfone-functionalised polymeric dialkynyldigold(I) complex **2** (Scheme 1) with diphosphane ligands can lead to the self-assembly of macrocyclic rings or of a [2]catenane, depending on the nature of the spacer group in the diphosphane ligand. Short or bulky spacer groups form macrocyclic rings, because the ring cavity is too small to allow interlocking to form the [2]catenane. A [2]catenane is formed, in equilibrium with the macrocyclic complex, with the intermediate-length $(CH_2)_3$ spacer group. A macrocycle is formed with the longer $(CH_2)_5$ spacer group and, probably, also with the $(CH_2)_4$ spacer group. The aim of this work was to study the influence of the sulfone unit as a "hinge group" X (Figure 1), in supporting [2]catenane formation. Compared to the hinge groups studied previously, it is clear that the SO_2 group is better than X = S or O, but not so good as X = CH_2, CMe_2, C_6H_{10} (cyclohexylidene) or $CH(C_6H_4Br)$ for promoting formation of [2]catenanes. Thus, when X = S or O, no [2]catenane is detected in any case, whereas the carbon-based hinge groups give catenanes when the diphosphane is $Ph_2P(CH_2)_nPPh_2$, with n = 3−5.[12−15] Some key structural parameters are listed in Table 5. The hinge angles are not greatly distorted from the ideal tetrahedral angles and are slightly more open than for the sulfide hinge group (Table 5). The aryl groups in all complexes studied are twisted out of the plane defined by the C−S−C group with angles between the 90, 90° and 90, 45° combinations that are favourable for [2]catenane formation and very different from the case with X = S (Table 5). It is therefore not obvious why [2]catenane formation is less favoured when X = SO_2 than when X = CH_2 or CMe_2 (Table 5). The differ-

Table 5. The hinge angles and aryl twist angles [°] for selected complexes

Hinge group X	Spacer group Y	Hinge angle	Aryl twists	Structure
SO_2	CC	104.7(3)	100, 100	ring
SO_2	$Fe(C_5H_4)_2$	109.4(7)	97(95), 87(43)[a]	ring
SO_2	$(CH_2)_5$	105.9(4)	95, 65	ring
SO_2	$(CH_2)_3$	105.4(5)/ 107.9(5)	89, 69/87, 71[b]	catenane
S	$(CH_2)_4$	104.3(3)	97, 1	ring
CH_2	$(CH_2)_4$	115.0(6)/115.3(5)	92, 33/93, 29 [b]	catenane
CMe_2	$(CH_2)_4$	111.2(7)/111.9(9)	52, 47/49, 39 [b]	catenane

[a] Two values because of structural disorder. [b] Two values for two independent rings.

ences could be caused by subtle differences in hinge angles, or by electronic effects of the hinge groups on the strengths of phenyl−aryl attractions. Nevertheless, the comparison of the hinge groups S and SO_2 does show how the orientation of the aryl groups can be controlled and the effect could in principle be used to trigger catenation on oxidation of S to SO_2. Our attempts to demonstrate the effect directly have been unsuccessful since the Au−C bonds are not stable to strongly oxidising conditions.

Experimental Section

General Remarks: NMR spectra were recorded using Varian Mercury 400 and Inova 600 MHz spectrometers. ^1H and ^{13}C NMR chemical shifts are reported relative to tetramethylsilane, while ^{31}P NMR chemical shifts are reported relative to 85% H_3PO_4 as an external standard. IR spectra were recorded using a Perkin−Elmer 2000 FT-IR as Nujol mulls on NaCl plates. MALDI-TOF spectra were recorded using a Micromass MALDI-LR instrument in positive ion mode. The samples were dissolved in CH_2Cl_2 and spotted onto a dried layer of matrix [1 μL of α-cyano-4-hydroxycinnamic acid (10 mg/mL in CAN/EtOH, 50:50)]. The samples were analysed in reflection mode and mass spectra were externally calibrated using a tryptic digest of alcohol dehydrogenase. The complex [AuCl(SMe$_2$)] was prepared by a literature procedure.[18] All other chemicals and solvents were from commercial sources and used as received. All reactions involving gold complexes were carried out in reactions vessels shielded from light. Elemental analyses were carried out by Guelph Chemical Laboratories, Guelph, Canada.

Diacetylide Ligand 1: $BrCH_2C{\equiv}CH$ (2.4 g, 17.58 mmol) and K_2CO_3 (1.6 g, 11.58 mmol) were added to a solution of $O_2S(4\text{-}C_6H_4OH)_2$ (2.0 g, 7.99 mmol) in acetone (50 mL). The mixture was heated under reflux for about 24 h. The cooled solution was filtered to give a pale yellow filtrate. The solvent was removed under reduced pressure and the resultant off-white solid dried under vacuum. Yield: 2.3 g, 88%. IR (nujol): $\tilde{\nu}$ = 2080 (br, w) 2129 cm^{-1} (s) (C≡C). ^1H NMR (400 MHz, [D$_6$]acetone, 25 °C): δ = 7.91 (d, J = 9.4 Hz, 4 H, C_6H_4), 7.16 (d, J = 8.6 Hz, 4 H, C_6H_4), 4.89 (d, J = 2.4 Hz, 2 H, OCH_2), 3.14 (t, J = 2.4 Hz, 2 H, C≡H) ppm. ^{13}C NMR (100 MHz, [D$_6$]acetone, 25 °C): δ = 161.2, 135.2, 129.6, 115.6 (all C_6H_4), 78.2 (C≡CH), 77.2 (C≡*C*H), 56.2 (OCH_2) ppm. MS: *m*/*z* (%) = 326 (72) $[M]^+$. $C_{18}H_{14}O_4S$ (326.4): calcd. C 66.24, H .32; found C 65.79, H 4.57.

Digold(I) Diacetylide 2: [AuCl(SMe$_2$)] (0.452 g, 1.53 mmol) was dissolved in THF (50 mL)/MeOH (30 mL). A solution of **1** (0.250 g, 0.77 mmol) and Et_3N (0.4 mL, 2.87 mmol) in THF (20 mL)/MeOH (10 mL) was added to this. The resulting mixture was stirred for 3 h to produce a yellow precipitate. The solid was then collected by filtration, washed with THF, MeOH, Et_2O and pentane, and dried. Yield: 0.499 g, 91%. The product was insoluble in common organic solvents. IR (nujol): $\tilde{\nu}$ = 1996 cm^{-1} (w) (C≡C). $C_{18}H_{12}Au_2O_4S$ (718.3): calcd. C 30.10, H 1.68; found C 30.56, H 1.92.

Macrocycle 3a: A mixture of **2** (0.100 g, 0.139 mmol) and $Ph_2PCCPPh_2$ (0.044 g, 0.112 mmol) in CH_2Cl_2 (10 mL) was stirred for 3 h at room temperature. The mixture was filtered through Celite and the filtrate concentrated under vacuum (ca. 2−3 mL). Addition of Et_2O precipitated an off-white solid. The powder was collected by filtration, washed with Et_2O and pentane, and dried. Yield 0.078 g, 51%. ^{31}P NMR (162 MHz, $CDCl_3$, 25 °C): δ = 18.59 ppm. ^1H NMR (400 MHz, $CDCl_3$, 25 °C): δ = 7.86 (d, J = 7.9 Hz, 4 H, C_6H_4), 7.62−7.69 (m, 8 H, Ph), 7.52−7.58 (m, 4 H, Ph), 7.43−7.49 (m, 8 H, Ph), 7.13 (d, J = 9.3 Hz, 4 H, C_6H_4), 4.91 (s, 4 H, OCH_2) ppm. MALDI-TOF MS: *m*/*z* (%) = 1113 (19) $[MH]^+$. $C_{44}H_{32}Au_2O_4PS{\cdot}1/2Et_2O$ (1149.7): calcd. C 48.05, H 3.24; found C 48.86, H 2.92. Crystals suitable for X-ray diffraction were grown by slow diffusion of hexane into a concentrated CH_2Cl_2 solution.

Macrocycle 3b: This was prepared by the procedure described for **3a** from **2** (0.075 g, 0.104 mmol) and [Fe($C_5H_4PPh_2$)$_2$] (0.046 g, 0.083 mmol). The product was isolated as a pale-yellow solid. Yield 0.097 g, 74%. ^{31}P NMR (162 MHz, $CDCl_3$, 25 °C): δ = 36.79 ppm. ^1H NMR (400 MHz, $CDCl_3$, 25 °C): δ = 7.87 (d, J = 8.6 Hz, 4 H, C_6H_4), 7.36−7.51 (m, 20 H, Ph), 7.16 (d, J = 9.3 Hz, 4 H, C_6H_4), 4.94 (s, 4 H, OCH_2), 4.33 (s, 4 H, C_5H_4), 4.27 (s, 4 H, C_5H_4) ppm. MALDI-TOF MS: *m*/*z* (%) = 1273 (100) $[MH]^+$. $C_{52}H_{40}Au_2FeO_4P_2S{\cdot}0.2CH_2Cl_2$ (1289.7): calcd. C 48.50, H 3.15; found C 48.54, H 3.18. Crystals suitable for X-ray diffraction were grown by slow diffusion of Et_2O into a concentrated nitrobenzene solution.

Macrocycle 3c: This was prepared by the procedure described for **3a** from **2** (0.100 g, 0.139 mmol) and $Ph_2P(CH_2)_4PPh_2$ (0.113 g, 0.083 mmol). The product was isolated as a colourless solid. Yield 0.110 g, 71%. ^{31}P NMR (162 MHz, $CDCl_3$, 25 °C): δ = 38.27 ppm. ^1H NMR (400 MHz, $CDCl_3$, 25 °C): δ = 7.85 (d, J = 8.6 Hz, 4 H, C_6H_4), 7.60−7.38 (m, 20 H, Ph), 7.15 (d, J = 8.6 Hz, 4 H, C_6H_4), 4.90 (s, 4 H, OCH_2), 2.27 (m, 4 H, CH_2), 1.65 (m, 4 H, CH_2) ppm. MALDI-TOF MS: *m*/*z* (%) = 1144 (100) $[MH]^+$. $C_{46}H_{40}Au_2O_4P_2S$ (1144.8): calcd. C 48.26, H 3.52; found C 48.16, H 3.75.

Macrocycle 3d This was prepared by the procedure described for **3a** from **2** (0.100 g, 0.139 mmol) and $Ph_2P(CH_2)_5PPh_2$ (0.052 g, 0.118 mmol). The product was isolated as a cream-coloured solid. Yield 0.126 g, 80%. ^{31}P NMR (162 MHz, $CDCl_3$, 25 °C): δ = 37.06 ppm. ^1H NMR (400 MHz, $CDCl_3$, 25 °C): δ = 7.87 (d, J = 8.6 Hz, 4 H, C_6H_4), 7.54−7.62 (m, 8 H, Ph), 7.39−7.51 (m, 12 H, Ph), 7.16 (d, J = 8.6 Hz, 4 H, C_6H_4), 4.95 (s, 4 H, OCH_2), 2.29 (m, 4 H,

CH_2), 1.50 (m, 6 H, CH_2) ppm. MALDI-TOF MS: *m/z* (%) = 1159 (100) $[MH]^+$. $C_{47}H_{42}Au_2O_4P_2S{\cdot}1/2CH_2Cl_2$ (1201.2): calcd. C 47.49, H 3.61; found C 47.62, H 3.70. Crystals suitable for X-ray diffraction were grown by slow diffusion of hexane into a concentrated CH_2Cl_2 solution.

Macrocycle 3e: This was prepared by the procedure described for **3a** from **2** (0.075 g, 0.104 mmol) and $Ph_2P(CH_2)_6PPh_2$ (0.038 g, 0.084 mmol). The product was isolated as a colourless solid. Yield 0.073 g, 61%. ^{31}P NMR (162 MHz, $CDCl_3$, 25 °C): δ = 37.57 ppm. ^1H NMR (400 MHz, $CDCl_3$, 25 °C): δ = 7.83 (d, *J* = 8.6 Hz, 4 H, C_6H_4), 7.37−7.65 (m, 20 H, Ph), 7.09 (d, *J* = 9.3 Hz, 4 H, C_6H_4), 4.84 (s, 4 H, OCH_2), 2.31, 1.51, 1.36 (m, 4 H, CH_2) ppm. MALDI-TOF MS: *m/z* (%) = 1173 (100) $[MH]^+$. $C_{48}H_{44}Au_2O_4P_2S{\cdot}CH_2Cl_2{\cdot}Et_2O$ (2502.7): calcd. C 48.47, H 3.95; found C 48.58, H 3.79.

Macrocycle 3f and [2]Catenane 4a: This was prepared as an equilibrium mixture by the procedure described for **3a** from **2** (0.075 g, 0.104 mmol) and $Ph_2P(CH_2)_3PPh_2$ (0.035 g, 0.085 mmol). The product was isolated as a colourless solid. Yield 0.093 g, 80%. **3f**: ^{31}P NMR (162 MHz, $CDCl_3$, 25 °C): δ = 35.32 ppm. ^1H NMR (600 MHz, $CDCl_3$, 25 °C): δ = 7.78 (d, *J* = 9 Hz, 4 H, C_6H_4), 7.36−7.51 (m, 20 H, Ph), 7.07 (d, *J* = 9 Hz, 4 H, C_6H_4), 4.95 (s, 4 H, OCH_2), 2.42 (m, 8 H, CH_2), 1.78 (m, 4 H, CH_2). **4a**: ^{31}P NMR (162 MHz, $CDCl_3$, 25 °C): δ = 31.47 ppm. ^1H NMR (600 MHz, $CDCl_3$, 25 °C): δ = 7.30 (d, *J* = 9 Hz, 4 H, C_6H_4), 7.36−7.51 (m, 20 H, Ph), 6.16 (d, *J* = 9 Hz, 4 H, C_6H_4), 4.94 (s, 4 H, OCH_2), 2.73 (m, 8 H, CH_2), 1.82 (m, 4 H, CH_2) ppm. MALDI-TOF MS: *m/z* (%) = 1131 (100) $[M/2 + H]^+$. $C_{90}H_{76}Au_4O_8P_4S_2$ (2261.5): calcd. C 47.80, H 3.39; found C 47.47, H 3.62. Crystals of **4a** suitable for X-ray diffraction were grown by slow diffusion of hexane into a concentrated CH_2Cl_2 solution.

X-ray Crystallographic Study: Data for **3a**, **3b**, **3d** and **4a** were collected at −73 °C by using a Nonius Kappa CCD diffractometer operating with Mo-K_α radiation (graphite monochromator, λ = 0.7107 Å) using COLLECT software.[19] The unit cell parameters were calculated and refined from the full data set. Crystal cell refinement and data reduction was carried out using DENZO and absorption correction was carried out using SCALEPACK.[20] The structures were solved by direct methods[21] (**3a**, **3b** and **4a**) or Patterson methods[22] (**3d**) and were refined using Fourier techniques.[23] Hydrogen atoms were included at geometrically determined positions riding on their respective carbon atoms. The atomic scattering factors were taken from standard sources.[24,25] All calculations were performed using the SHELXTL 5.1 program package.[26] Table 6 summarises the crystallographic and refinement details for all complexes. CCDC-185297 (**3a**), -185298 (**3b**), -185299 (**3d**) and -185300 (**4a**) contain the supplementary crystallographic data for this paper. These data can be obtained free of charge at www.ccdc.cam.ac.uk/conts/retrieving.html or from the Cambridge Crystallographic Data Centre, 12, Union Road, Cambridge CB2 1EZ, UK [Fax: (internat.) + 44-1223/336-033; E-mail: deposit@ccdc.cam.ac.uk].

3a: A colourless needle of $[(\mu\text{-}Ph_2PCCPPh_2)Au_2(\mu\text{-}CCCH_2\text{-}OC_6H_4S(O)_2C_6H_4OCH_2CC)]{\cdot}3CH_2Cl_2$ was mounted on a glass fibre. All of the non-hydrogen atoms were refined with anisotropic thermal parameters. One of the three occluded solvent molecules showed some occupational disorder. All three solvent molecules were refined with the bond lengths fixed (C−Cl = 1.65 Å and Cl···Cl = 2.74 Å). Solvent molecule one (C41) and two (C51) were refined anisotropically. The third solvent molecule (C61) was refined isotropically as a 70:30 disorder. The hydrogen atoms were included for all solvent molecules.

Table 6. Crystal and refinement data for complexes **3a**, **3b**, **3d** and **4a**

	3a	**3b**	**3d**	**4a**
Empirical formula	$C_{47}H_{38}Au_2Cl_6O_4P_2S$	$C_{59}H_{52.5}Au_2N_{0.5}O_6P_2S$	$C_{49.75}H_{47.50}Au_2Cl_{5.50}O_4P_2S$	$C_{92}H_{81}Au_4Cl_4O_8P_4S_2$
Formula mass	1367.41	1408.30	1392.29	2432.23
Crystal size [mm]	0.40 × 0.10 × 0.08	0.10 × 0.10 × 0.04	0.46 × 0.10 × 0.03	0.30 × 0.18 × 0.10
T [K]	200(2)	200(2)	200(2)	200(2)
Crystal system	monoclinic	monoclinic	triclinic	monoclinic
Space group	$P2_1/c$	$C2/c$	$P\bar{1}$	$P2_1/n$
a [Å]	16.5607(2)	33.0021(4)	14.1532(3)	12.56950(10)
b [Å]	13.8361(2)	15.6311(2)	14.4715(4)	22.4692(3)
c [Å]	22.9485(4)	22.1400(3)	14.6846(4)	31.4742(4)
α [°]	90	90	72.9000(10)	90
β [°]	111.0280(10)	97.756(7)	67.81130(10)	97.9920(10)
γ [°]	90	90	73.7070(10)	90
V [Å^3]	4908.14(13)	11316.6(3)	2612.58(12)	8802.81(18)
Z	4	8	2	4
$\rho_{calcd.}$ [g cm^{-1}]	1.851	1.653	1.770	1.835
μ [mm^{-1}]	6.448	5.568	6.033	6.943
F(000)	2632	5504	1351	4692
Absorption correction	integration	integration	integration	integration
Transmission range	0.6434−0.1824	0.8080−0.6059	0.8397−0.1678	0.5436−0.2299
θ limits [°]	2.64/27.60	2.55/27.50	2.73/27.50	2.59/27.49
Measured reflections	49456	83894	23715	59691
Unique reflections	11314 (R_{int} = 0.055)	12954 (R_{int} = 0.091)	11886 (R_{int} = 0.090)	19849 (R_{int} = 0.068)
Parameters	503	475	535	931
GOF on F^2	1.055	1.025	1.019	1.202
*R*1 [$I > 2\sigma(I)$]	0.0420	0.0518	0.0605	0.0595
*wR*2 (on F^2, all data)	0.1136	0.1460	0.1686	0.1288
$\Delta\rho_{min/max}$ [e Å^{-3}]	2.579/−2.242	1.867/−0.751	2.744/−1.677	1.678/−1.224

3b: A yellow-orange diamond plate of [μ-[Fe($C_5H_4PPh_2$)$_2$]Au$_2$(μ-$CCH_2OC_6H_4S(O)_2C_6H_4OCH_2CC$)]·1/2$PhNO_2$·$Et_2O$ was mounted on a glass fibre. The SO_2 bridging ligand was disordered. It was modeled as a mixture of two isotropic moieties (60:40). All of the remaining non-hydrogen atoms were refined with anisotropic thermal parameters. The nitrobenzene was modeled at a half occupancy and the ether at full occupancy. Both solvent molecules were kept isotropic.

3d: A colourless plate of [(μ-$Ph_2P(CH_2)_5PPh_2$)Au$_2$(μ-$CCCH_2OC_6H_4S(O)_2C_6H_4OCH_2CC$)]·2.75$CH_2Cl_2$ was mounted on a glass fibre. All of the non-hydrogen atoms were refined with anisotropic thermal parameters. The solvent molecules showed some disorder. One solvent molecule (C41) was refined anisotropically. The second solvent molecule (C51) was refined at 75% occupancy with the bond lengths fixed as above. The third solvent molecule (C61) was refined isotropically as a 70:30 disorder, with fixed bond lengths. The hydrogen atoms were included for all solvent molecules.

4a: A colourless crystal of [(μ-$Ph_2P(CH_2)_3PPh_2$)Au$_2$(μ-$CCCH_2OC_6H_4S(O)_2C_6H_4OCH_2CC$)]$_2$·2$CH_2Cl_2$ was mounted on a glass fibre. All of the non-hydrogen atoms were refined with anisotropic thermal parameters. The two solvent molecules were refined anisotropically, with hydrogen atoms included and with bond lengths fixed as above.

Acknowledgments

We thank the National Science and Engineering Research Council (Canada) for financial support. R. J. P. thanks the Government of Canada for a Canada Research Chair.

[1] *Molecular Catenanes, Rotaxanes and Knots* (Eds.: J.-P. Sauvage, C. Dietrich-Buchecker), Wiley-VCH, Weinheim, **1999**.
[2] M. Fujita, *Acc. Chem. Res.* **1999**, *32*, 53−61.
[3] A. R. Pease, J. O. Jeppesen, J. F. Stoddart, Y. Lio, C. P. Collier, J. R. Heath, *Acc. Chem. Res.* **2001**, *34*, 433−444.
[4] G. F. Swiegers, T. J. Malefetse, *Chem. Rev.* **2000**, *100*, 3483−3573.
[5] V. Balzani, A. Credi, F. M. Raymo, J. F. Stoddart, *Angew. Chem.* **2000**, *112*, 3484−3530; *Angew. Chem. Int. Ed.* **2000**, *39*, 3348−3391.
[6] S. Leininger, B. Olenyuk, P. J. Stang, *Chem. Rev.* **2000**, *100*, 853−908.
[7] G. Schill, *Catenanes, Rotaxanes and Knots*, Academic Press, New York, **1971**.
[8] G.-J. M. Gruter, F. J. J. de Kanter, P. R. Markies, T. Nomoto, O. S. Akkerman, F. Bickelhaupt, *J. Am. Chem. Soc.* **1993**, *115*, 12179−12180.
[9] R. J. Puddephatt, *Coord. Chem. Rev.* **2001**, *216−217*, 313−332.
[10] R. J. Puddephatt, *Chem. Commun.* **1998**, 1055−1062.
[11] H. Schmidbaur, *Chem. Soc. Rev.* **1995**, *24*, 391−400.
[12] C. P. McArdle, M. C. Irwin, M. C. Jennings, R. J. Puddephatt, *Angew. Chem. Int. Edn. Engl.* **1999**, *38*, 3376−3378.
[13] C. P. McArdle, J. J. Vittal, R. J. Puddephatt, *Angew. Chem. Int. Ed.* **2000**, *39*, 3819−3822.
[14] C. P. McArdle, M. C. Jennings, J. J. Vittal, R. J. Puddephatt, *Chem. Eur. J.* **2001**, *7*, 3572−3583.
[15] C. P. McArdle, M. C. Irwin, M. C. Jennings, J. J. Vittal, R. J. Puddephatt, *Chem. Eur. J.* **2002**, *8*, 723−734.
[16] D. M. P. Mingos, J. Yau, S. Menzer, D. J. Williams, *Angew. Chem. Int. Edn.* **1995**, *34*, 1894−1895.
[17] P.M. van Calcar, M.M. Olmstead, A.L. Balch, *Inorg. Chem.* **1997**, *36*, 5231−5238.
[18] A. Tamaki, J. K. Kochi, *J. Organomet. Chem.* **1974**, *64*, 411−425.
[19] *COLLECT, data collection software*, Nonius BV, **1999**.
[20] Z. Otwinowski, W. Minor in *Methods in Enzymology* (Ed.: R. M. Sweet), Academic Press, New York, **1997**.
[21] A. Altomare, M. Cascarano, C. Giacovazzo, A. Guagliardi, M. C. Burla, G. Polidori, M. Camalli, *J. Appl. Crystallogr.* **1994**, *27*, 1045−1050.
[22] P. T. Beurskens, G. Admiraal, G. Beurskens, W. P. Bosman, S. Garcia-Granda, R. O. Gould, J. M. M. Smits, C. Smykalla, *PATTY: The DIRDIF Program System*, Technical Report of the Crystallography Laboratory; University of Nijmegen, **1992**.
[23] P. T. Beurskens, G. Admiraal, G. Beurskens, W. P. Bosman, R. de Gelder, R. Israel, J. M. M. Smits, *The DIRDIF-94 Program System, Technical Report of the Crystallography Laboratory; University of Nijmegen*, **1994**.
[24] D. T. Cromer, J. T. Waber, *International Tables for X-ray Crystallography*, Kynoch Press, Birmingham, England, **1974**.
[25] *International Tables for Crystallography*, Kluwer Academic, Dordrecht, The Netherlands, **1992**.
[26] G. M. Sheldrick, *SHELXTL 5.1*, Universität Göttingen, **1998**.
Received August 30, 2002
[I02491]

Synthesis and Characterization of a Carbene·SO_2 Adduct − New Insights into the Structure and Bonding of Thiourea *S,S*-Dioxides[‡][‡‡]

Michael K. Denk,*[a] Ken Hatano,[b] and Alan J. Lough[c]

Keywords: Carbenes / Sulfenes / Density functional calculations / Thermochemistry / Sulfur ylides

The title compound 1,3-di-*tert*-butylimidazol-2-ylidene·SO_2 (**2**) was obtained from the respective stable carbene **1** and SO_2 in quantitative yield and investigated by single crystal X-ray crystallography and NMR spectroscopy. Quantum chemical calculations show that thiourea-*S,S*-dioxides like **2** are Lewis acid-base adducts of the respective diamino carbenes with SO_2 (CS bond energies < 20 kcal·mol^{-1}). They possess long CS bonds and a pyramidal sulfur atom and are thus structurally distinct from sulfur ylides or sulfenes.

(© Wiley-VCH Verlag GmbH & Co. KGaA, 69451 Weinheim, Germany, 2003)

Introduction

Despite the frequent assumption of their involvement as reactive intermediates, sulfenes ($R_2C{=}SO_2$)[1] have remained elusive and are thus clearly distinct from the growing list of isolable compounds featuring carbon-sulfur double[1,2] and even triple bonds.[2]

Sulfenes can be generated in situ by the 1,2-elimination of HCl from sulfonyl chlorides (R_2CH-SO_2Cl) or by fluorodesilylation of 2-silylsulfochlorides.[1h] The reaction of carbenes with SO_2 can result in the formation of sulfenes but has found little synthetic use. While the formation of sulfene, $CH_2{=}SO_2$, from methylene and SO_2 was deduced from the formation of secondary products only,[3] diphenylsulfene has been isolated in a frozen matrix and characterized by its IR and Raman spectra at 100 K.[4]

Thiourea *S,S*-dioxide (**2**),[5−7] a stable, commercially available compound has been known since 1910[5] and is readily obtained by oxidation of thiourea (**1**) with peracids. It could be described as a donor-stabilized sulfene but the X-ray structure of **2** shows a long C-S bond (185 pm) and a pyramidal sulfur atom.[8] The C-S double bond of a sulfene would imply a short C-S bond and a planar or close to planar C-SO_2 fragment.

Using X-ray data[8c] and EHMO calculations,[8d] Chen and Wang[8d] have concluded that the C-S bond in **2** is essentially a single bond. Despite this attempt to clarify the bonding situation, **2** is still usually written with a C-S double bond.

In 1994, Skrypnik and Lyashchuk reported the isolation of the diamino ketene **4′**[9a,9c] and the stable sulfene **5′** (Scheme 1).[9b,9c] The existence of **4′** has since been refuted through high level ab initio calculations[10] which demonstrated that **4′** would only have the marginal stability of a van-der-Waals complex.[10] Two notes questioning the existence of **5′**[10b,10c] have appeared in the literature, but, in the absence of additional experimental or computational data, the issue remains unresolved. X-ray data reported for **5′**[9b] are limited to selected bond lengths and bond angles and have not been deposited in the Cambridge database.

Our interest in the subject was triggered by our previous investigations of stable diamino carbenes,[11] diamino silylenes[12] and related species and, in particular, by the question whether thiourea *S,S*-dioxides like **2** or **5′** could act as synthons for diamino carbenes. We now present experimental evidence (NMR spectroscopy, X-ray crystallographic data) and quantum chemical calculations which indicate that thiourea *S,S*-dioxides (including **5′**) are not sulfenes or sulfur ylides but Lewis acid-base adducts of diamino carbenes.

Results and Discussion

Reaction of the stable carbene **3** or **3′** with SO_2 did not give any indication of the formation of **5** (previously unknown) or **5′** (ref.[9b]).

[‡] Synthesis and Reactivity of Subvalent Compounds, 12. Part 11: Michael K. Denk, José M. Rodezno, Shilpi Gupta and Alan J. Lough, Oxidation, Hydrogenation and Hydrolysis of Stable Diamino Carbenes, *J. Organomet. Chem.* **2001**, *617/618*, 242−253.

[‡‡] Results presented at the Canadian Society for Chemistry Meeting. June 1. - June 6. 2002, Vancouver.

[a] Department of Chemistry and Biochemistry, University of Guelph,
Guelph, Ontario N1G 2 W1, Canada

[b] Organometallic Photodynamics Group, Photodynamics Research Center,
RIKEN 19−1399, Koeji, Nagamachi, Aoba-ku, Sendai 980−0868, Japan

[c] X-ray Laboratory, Department of Chemistry, University of Toronto,
80 St. George Street, Toronto, Ontario M5S 3H6, Canada

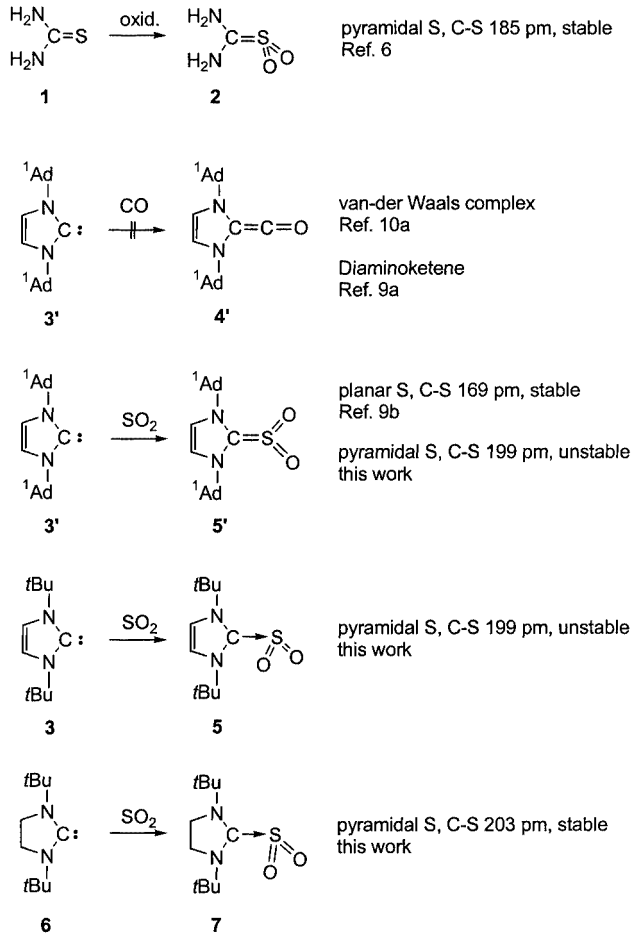

Scheme 1. Reactions of stable carbenes with CO and SO_2

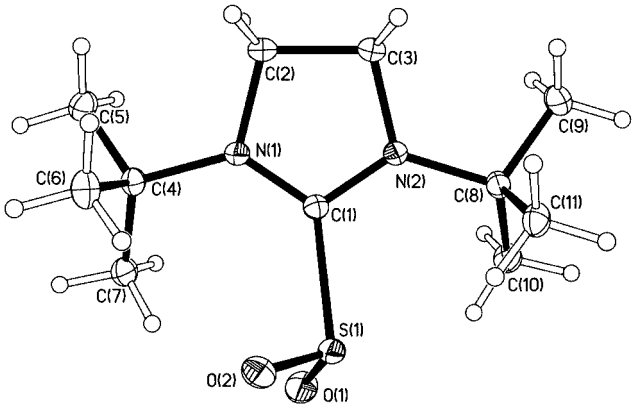

Figure 1. Molecular structure of **7**; selected bond lengths [pm] and angles [°]: C(1)−S(1) 203.0(2), S(1)−O(2) 146.85(13), S(1)−O(1) 146.93(13), C(1)−N(1) 132.9(2); C(1)−N(2) 133.9(2), O(1)−S(1)−O(2) 113.09(8), O(1)−S(1)−C(1) 104.04(7), O(2)−S(1)−C(1) 100.25(7), N(1)−C(1)−N(2) 111.61(3), N(1)−C(1)−S(1) 129.94(11), N(2)−C(1)−S(1) 117.33(11); selected torsional angles: O(1)−S(1)−C(1)−N(1) 77.93(15), O(2)−S(1)−C(1)−N(1), −39.20(15), C(2)−N(1)−C(1)−S(1) 162.89(11), C(4)−N(1)−C(1)−S(1) −12.20(23)

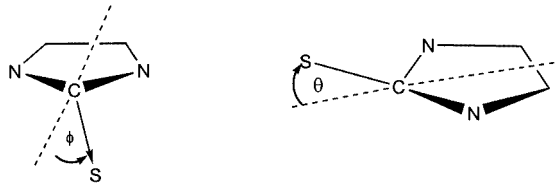

Figure 2. horizontal (φ) and vertical (θ) tilt angles used in the description of **7**

Much to our surprise, reaction of the closely related but electronically less stabilized[12] carbene **6**[11a] with SO_2 led to the clean formation of **7**, which was characterized by single crystal X-ray crystallography (Figure 1),[14−17] multinuclear NMR spectroscopy, and computational methods.[18−22]

Compound **7** is poorly soluble in hydrocarbons such as hexane and toluene but dissolves well in THF and dichloromethane. These solutions are unreactive towards oxygen, pyridine and CsF but are sensitive to moisture.[13] Attempts to sublime **7** ($T \leq 110$ °C, 0.05 Torr) resulted in decomposition. The compound is undissociated in benzene solution (^{1}H NMR spectroscopy) and is unaffected by prolonged storage under vacuum. Samples heated to 100 °C for 24 h show no signs of decomposition (^{1}H NMR, IR spectroscopy) but decomposition occurs upon melting (123 °C).

The C-S bond length of 203.0(2) pm in **7** exceeds the sum of the covalent single-bond-radii of sulfur and carbon (187 pm).[23] The pyramidal SO_2 fragment is off-center from its idealized position (C-S bond axis bisecting the N−C−N angle) by $\varphi = 6.3°$ and is also tilted away from the N−C−N plane by $\theta = 10.8°$ (Figure 2).

The C-S bond length in **7** is also significantly longer than that reported for **2**, which may be related to the fact that **2**, unlike **7**, shows hydrogen bonding in the solid state (NH···OS 186 pm).[8] Hydrogen bonding can enhance the Lewis acidity of the SO_2 fragment by reducing its electron density. Despite the difference of the C-S bond lengths in **2** and **7**, the C-S bond energies (see below) are very similar so that fundamental differences in the bonding situation for **2** and **7** must be ruled out.

Preservation of the solid-state structure of **7** in solution would give rise to an AA′BB′ spin system for the ring protons. However, between −100 °C and 25 °C the VT ^{1}H NMR spectrum of **7** shows only two singlets, one for the ethylene protons (4 H) and the one for the two *tert*-butyl groups (18 H).

A rapid equilibrium between the conformers **7a**/**7b** (Figure 3) can occur through rotation of the SO_2 group or inversion of the sulfur atom and can explain the observed be-

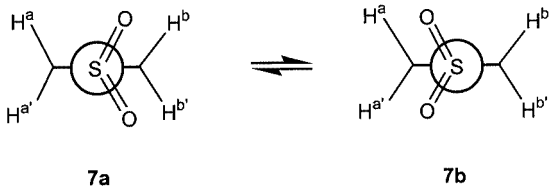

Figure 3. Dynamic behavior of **7**

havior of **7**. The high configurational stability of the pseudo-tetrahedral sulfur geometry (e.g. in sulfoxides) seems incompatible with the observed dynamic behavior and the rotational mechanism is more likely.[27]

The ^1H and ^{13}C NMR shifts of **7** resemble that of the stable carbene **6**. Coordination of **6** to SO_2 leads to a moderate shielding of the carbene carbon atom [$\delta^{13}C$ = +238 (**6**), +231 ppm (**7**)], a trend that is analogous to the shielding effect caused by protonation of **6** ($\delta^{13}C$, [**6H**]$^+$**SCN**$^-$, $CDCl_3$, N_2CH +152.4 ppm).[11e]

The structural and spectroscopic data characterize **7** as a Lewis acid-base adduct of the carbene **6** and are inconsistent with those presented for **5′** which has been described as a stable sulfene (short C-S bond, planar N_2CSO_2 framework).[9b] This discrepancy and the doubts raised about the existence of **5′** elsewhere,[10b,10c] have prompted us to study the bonding situation through high level quantum chemical methods.[18–22]

Computational Structures of Sulfene *S,S*-Dioxides

A method for the calculation of accurate structures of **7** was established by comparison of computational structures with the experimental structures. Computational structures[19] were obtained with Gaussian 98[18] at the HF and DFT[20,21] levels. The respective methyl-substituted compounds **5Me** and **7Me** were chosen as model compounds for **5** and **7**.

Table 1. Molecular structure of SO_2 at different levels of theory

Method	Basis set	Gaussians	S–O [pm]	O–S–O [deg]	E_o [a]
Exp.[b]	–	–	143.08	119.33	–
HF	6-31G(d)	108	141.40	118.82	−547.169006
B3LYP	6-31G(d)	108	146.40	119.13	−548.587479
MPW1PW91	6-31G(d)	108	145.40	119.07	−548.540504
MPW1PW91	6-311G(d)	110	144.72	118.81	−548.604023
MPW1PW91	6-31+G(d)	120	145.52	118.70	−548.550124
MPW1PW91	6-311+G(d)	122	144.83	118.73	−548.611774
HF	6-31G(2d)	126	140.18	118.74	−548.563322
MPW1PW91	6-31G(2d)	126	143.92	119.10	−547.184484
B3LYP	6-31G(2d)	126	144.69	119.20	−548.609993
MPW1PW91	6-311G(2d)	128	143.65	119.08	−548.635021
MPW1PW91	6-31G(df)	138	145.01	118.94	−548.552992
MPW1PW91	cc-pVDZ	139	147.01	117.77	−548.556824
MPW1PW91	6-31G(3d)	144	143.37	119.34	−548.580389
MPW1PW91	6-311G(3d)	146	143.18	119.37	−548.646360
B3LYP	6-311G(3d)	146	143.99	119.43	−548.690367

[a] Zero-point energies were added without scaling. [b] Microwave structure, *CRC Handbook of Chemistry and Physics*, 81st edition, 9–22.

Table 2. Computational (**5Me**) and experimental (**5′**[9b]) structures of imidazol-2-ylidene·SO_2 adducts

	HF 6-31G(d)	MPW1PW91 6-31G(d)	MPW1PW91 6-31G(2d)	B3LYP 6-31G(2d)	X-ray [9b]
S–C	192.54	199.56	198.96	237.89	169
S–O	146.30	148.86	147.56	146.78	161
	146.43	149.21	147.83	146.78	?
C–N	132.34	133.88	133.75	135.35	?
	132.56	134.09	133.92	135.35	?
C–C_{ring}	133.61	135.63	135.48	135.56	?
O–S–O	114.46	114.83	114.14	115.54	127
O–S–C	97.86	96.73	96.74	98.25	?
	98.10	98.28	97.88	98.36	?
S–C–N	127.86	128.80	130.10	127.84	?
	124.48	124.24	123.21	127.52	?
N–C–N	107.92	106.57	106.57	104.62	112
O–S–C–N[a]	59.18	56.56	57.33	31.99	?
	−57.18	−60.81	−58.27	149.47	?
φ [b]	1.69	2.36	3.45	0.85	?
θ[b]	2.56	6.99	3.92	0.16	?
ν_1 [c]	56	54	50	22	
Symmetry	C_1	C_1	C_1	C_1	?

[a] Torsional angles with *syn*-nitrogen. [b] See Figure 2. [c] Lowest vibrational mode in cm^{-1}.

Structures obtained with density functional methods are usually more accurate than Hartree−Fock structures but the effect can be obscured by internal error compensation and can become apparent only for larger than usual basis sets. The MPW1PW91/6-31G(d)[20] structure of SO_2 (Table 1) is very similar to the HF/6-31G(d) structure, but the higher accuracy of the MPW1PW91 approach becomes obvious for more extended basis sets.

The superior accuracy of MPW1PW91 structures[20] has been established through calculations on large test sets of organic and inorganic compounds[20a] and is also obvious for the structures calculated in this study. While the C-S bond length of **7Me** calculated at the MPW1PW91/6-31G(2d) level (202.02 pm) is in excellent agreement with the experimental value[24] [**7**: 203.0(2) pm], the B3LYP/6-31G(2d) value of 234.27 pm deviates significantly.

At the MPW1PW91/6-31G(2d) level, the structures of **5Me** (Table 2) and **7Me** (Table 3) are very similar. In particular, they display a *pyramidal* geometry at the sulfur atom and *long* C-S bonds (**5Me**: 199 pm, **7Me**: 202 pm). The computational structure of **5Me** is thus in qualitative disagreement with the structure published for **5′**. The possibility of a second minimum with a planar CSO_2 geometry and a short C-S bond was considered as a possible source for the discrepancy and studied by starting the optimization pro-

Table 4. Natural charges of selected carbenes (**3Me**, **6Me**) and their SO_2 adducts (**5Me**, **7Me**); MPw1PW91/ 6-31G(2d)//MPw1PW91/ 6-31G(2d) level

Atom	7Me		5Me	SO_2	6Me	3Me
S	1.60	1.60	+1.64	−	−	
O	−0.99	−0.99	−0.82	−	−	
N_2C	+0.31	+0.22	−	+0.22	+0.13	
N	−0.45	−0.40	−	−0.51	−0.46	
C*C*	−0.29	−0.07	−	−0.30	−0.10	
H_3C	−0.45	−0.50	−	−0.48	−0.48	

Table 3. Computational (**7Me**) and experimental (**7**) structures of imidazolidine-2-ylidene•SO_2 adducts

	HF 6-31G(d)	MPW1PW91 6-31G(d)	MPW1PW91 6-31G(2d)	B3LYP 6-31G(2d)	X-ray this work
S−C	194.50	201.55	202.02	234.27	203.0(2)
S−O	146.17	148.91	147.55	146.69	146.85(13)
	146.13	148.91	147.54	146.85	146.93(13)
C−N	131.78	132.07	132.69	133.40	132.9(2)
	131.05	132.01	132.18	132.97	133.9(2)
ring C−C	153.60	153.54	153.59	154.13	151.8(2)
O−S−O	114.75	115.08	114.81	115.32	113.09(8)
O−S−C	99.27	94.79	95.24	94.89	100.25(7)
	96.91	99.74	99.38	99.38	104.04(7)
S−C−N	123.84	123.30	125.23	127.03	129.94(11)
	124.88	124.86	123.41	121.48	117.33(11)
N−C−N	111.23	110.72	110.60	109.13	111.61(3)
O−S−C−N[a]	59.19	54.09	54.26	52.93	77.93(15)
	−57.17	−62.38	−61.98	−63.75	−39.20(15)
φ [b]	0.52	0.78	0.91	2.78	6.3
θ[b]	2.50	10.64	9.69	17.4	10.8
ν_1 [c]	56	54	52	26	−
Symmetry	C_1	C_1	C_1	C_1	C_1

[a] Torsional angles with *syn*-nitrogen. [b] See Figure 2. [c] Lowest vibrational mode in cm^{-1}.

Table 5. Experimental (**3**,[11] **6**[12]) and computational (**3Me**, **6Me**) structures of selected carbenes

		X-ray	HF 6-31G(d)	MPW1PW91 6-31G(d)	MPW1PW91 6-31G(2d)	B3LYP 6-31G(2d)
6	$C-N_{ring}$	134.83(13)	134.15	134.66	134.40	134.94
		134.73(13)	134.15	134.66	134.40	134.94
	$C-C_{ring}$	151.2(2)	153.22	153.16	153.09	153.80
	N−C−N	106.44(9)	105.55	105.05	105.23	105.36
	Point group	C_1	C_1	C_1	C_1	C_1
3	$C-N_{ring}$	136.6(2)	135.20	134.60	136.42	137.07
		138.0(2)	135.20	134.61	136.42	137.07
	$C-C_{ring}$	134.1(2)	133.27	153.29	135.12	135.44
	N−C−N	102.19(2)	102.52	105.065	101.50	101.51
	Point group	C_1	C_1	C_1	C_1	C_1

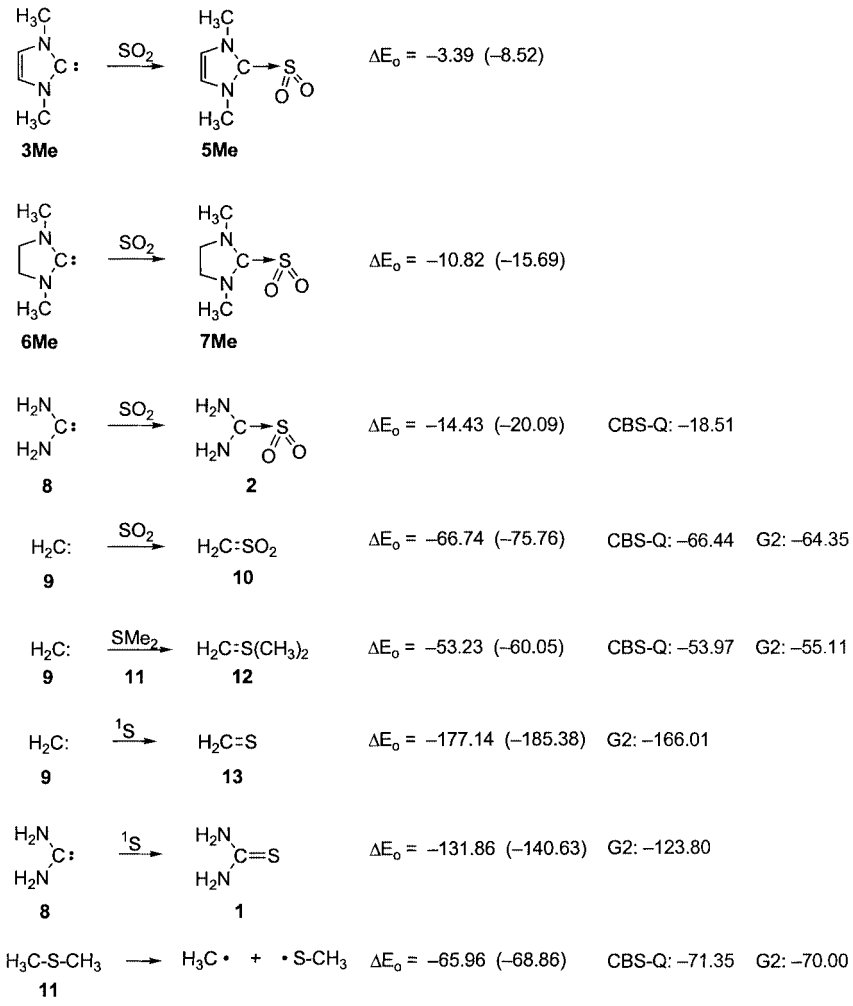

Scheme 2. CS bond energies of selected sulfur compounds; B3LYP/6-311G(3df,p)//MPW1PW91/6-31G(2d) and, in parentheses), MPW1PW91/6-311G(3df,p)//MPW1PW91/6-31G(2d); zero-point energies of the DFT calculations are at the MPW1PW91/6-31G(2d) level and were added without scaling

cess of **5Me** with a sulfene structure analogous to **5′**. The sulfene geometry reported for **5′** (Table 2) is unstable at all levels investigated (HF, MPW1PW91, or B3LYP methods with 6-31G(d) or 6-31G(2d) basis sets) and reverts to structures with long C-S bonds and pyramidally coordinated sulfur atoms.

The computational instability of the sulfene structure and the fact that we were unable to obtain **5′** or to observe the spectroscopic data (^{1}H NMR, ^{13}C NMR) published for it suggest that the compound may indeed be nonexistent.[10b]

Computational charge densities (Table 4) of **5Me** and **7Me** show a net transfer of charge density from the carbenes **3Me** and **6Me** to SO_2 and are consistent with the description of SO_2 acting as a Lewis acid. The net transfer of charge density occurring in the formation of **5Me** and **7Me** is very similar. The electron-deficient sulfur atom in SO_2 (+1.64) accepts only a small additional charge (0.04) from the carbene in both cases: most of the transferred electron density ultimately resides on the more electronegative oxygen atoms. The carbene carbon atoms show a loss of 0.09 charge units, with some of the electron depletion relayed to the nitrogen atoms (0.06 in **7Me** and 0.09 in **5Me**)

To further study the possible existence of **5′**, C-S bond-dissociation energies were obtained from DFT, CBS-Q, and G2 calculations.

Thermochemistry of the C-S bond

The C-S bond energies of **2**, **5Me**, **7Me**, sulfene ($H_2C=SO_2$, **10**), *S*,*S*-dimethylsulfoniumylide [$H_2C=S(CH_3)_2$, **12**], thioformaldehyde ($H_2C=S$, **13**), and dimethyl sulfide [$(CH_3)_2S$, **11**] were calculated from the reaction energies ΔE_o of the respective bond formation reactions (Scheme 2 and Table 6). The established accuracy of the G2 and CBS-Q method assures an absolute error of less than 2 kcal·mol^{-1} which is significantly better than the maximum absolute error of about 10 kcal·mol^{-1} obtained with current DFT methods.[22,26]

The computationally derived C-S bond energies fall into four distinct groups which are readily identified with dative bonds (**2**, **5**, **7**), single bonds (**11**), double bonds (**1**, **13**) and

Table 6. Selected electronic (E_o) and zero-point vibrational energies used for the determination of carbon sulfur bond energies (Scheme 2)

	ZPE MPW1PW9/6-31G(2d)	E_o MPW1PW91/6-311G(3df,p)[a]	E_o B3LYP/6-311G(3df,p)[a]	E_o CBS-Q (G2)	E_o G2
SO_2	0.007004	−548.659528	−548.703037	−548.035075	−548.015737
1	0.062112	−548.209841	−548.249307	547.533352	−547.525021
2	0.068589	−698.615621	−698.694602	−697.784525	–
3Me	0.127553	−304.686454	−304.767787	–	–
5Me	0.148869	−853.359555	−853.476229	–	–
6Me	0.150455	−305.867894	−305.948725	–	–
7Me	0.161255	−854.552419	−854.668997	–	–
8	0.057466	−149.921832	−149.966888	−149.719961	−149.716975
9	0.016713	−39.109961	−39.130423	−39.056539	−39.058392
10	0.034253	−587.890200	−587.939822	−587.197478	−587.176680
11	0.076207	−477.976372	−477.999719	−477.375022	−477.369000
12	0.101272	−517.182016	−517.214969	−516.517553	−516.515213
$CH_3^{\cdot}$	0.029693	−39.810590	−39.825444	−39.745168	−39.745086
$CH_3S^{\cdot}$	0.036749	−438.056051	438.069180	−437.516154	−437.512381
13	0.024867	−437.469279	−437.484993	−436.937353	−436.933692
S	0	−398.063932	−398.072317	–	−397.610779

[a] Single point energies of MPW1PW91/6-31G(2d) structures with zero-point energies (first column) added without scaling.

bond orders which are intermediate between single and double bonds (sulfur ylides **10**, **12**).

The C-S bond dissociation energy of sulfene (**10**; CBS-Q: 66.44 kcal·mol^{-1}) is significantly lower than that of thioformaldehyde (**13**; G2: 166.01 kcal·mol^{-1}) and only slightly higher than that of the sulfur ylide **12** (G2: 55.11 kcal·mol^{-1}). This allows the conclusion that the C-S bond in **10**, despite its short distance and the planar coordination of the sulfur atom, is also ylidic in nature. The C-S bond dissociation energies of **2**, **5** and **7** (3.39−20.09 kcal·mol^{-1}) are of a magnitude commonly observed for Lewis acid-base adducts and rule out a description of these compounds as sulfur ylides.

While the accuracy of the CBS-Q and G2 approach leaves little room for interpretation, the modifying influence of steric hindrance remains to be discussed.

The free rotation of the SO_2 group in **7**[27] is evidence against the presence of a strong steric interaction between the *tert*-butyl groups and the SO_2 fragment. The presence of steric effects would also manifest itself in a specific elongation of the C-S bond lengths. However, the computational C-S bond length obtained for the methyl-substituted **7Me** is virtually identical to that observed for the *tert*-butyl-substituted compound **7**.

A sterically induced transformation of a dative C-S bond (**5Me**) into a double bond (as the one claimed for **5′**) can be ruled out because steric hindrance can only lead to a decrease of the C-S bond energy. The marginal C-S bond energy of **5Me** correlates well with the fact that the formation of **5** and **5′** could not be observed in this study.

Conclusion

Based on thermochemical data, thiourea *S*,*S*-dioxides must be described as Lewis acid-base complexes of diaminocarbenes with SO_2. This description of the bonding situation is consistent with their reactivity as reducing agent[4] and formamidine synthons.[4] The synthesis of the carbene complex, thiourea *S*,*S*-dioxide (**2**), by de Berry Barnett in 1910,[5] thus precedes the synthesis of the first transition metal carbene complex reported by Fischer and Maasböl[25] by more than 50 years.

Experimental Section

All operations were performed under argon (99.995%) with usual Schlenk techniques. The stable carbenes **3**[11b−11d] and **6**[11a] were obtained by published procedures.

Synthesis and Characterization of 1,3-Di-*tert*-butylimidazolidin-2-ylidene·SO_2 (7): A slow stream of SO_2 was passed over a magnetically stirred solution of **6**[11a] (5.20 g, 28.2 mmol) in 150 mL of dry THF at 25 °C. The colorless solution became slightly turbid and a crystalline, colorless precipitate formed after a few minutes. Filtration through a medium porosity Schlenk frit gave 6.94 g of **7** (quantitative yield). m.p. 123 °C (dec.). ^{1}H NMR (C_6D_6): δ = 1.25 (s, 18 H, *t*Bu), 2.78 (s, 4 H, CH_2). ^{13}C(C_6D_6): 29.7 [C(CH_3)$_3$], 44.6 (CH_2), 55.2 [C(CH_3)$_3$], 231.0 ppm (N_2C) ppm. MS (CI^+, Methane): *m*/*z* (%) = 245 (14) $[M]^+$, 229 (10), 183 (62) $[LC-H]^+$, 167 (10), 126 (61), 111 (56), 99 (31), 84 (10), 71 (100) $[C_3H_7N_2]^+$, 57 (51). IR (Nujol): $\tilde{\nu}$ = 1629 cm^{-1} m, 1490 s, 1404 m, 1284 s, 1230 s, 1198 s, 1158 s, 1091 w, 1052 s, 1018 m, 905 m, 646 w, 613 s.

Acknowledgments

We thank the *Natural Sciences and Engineering Research Council of Canada* (*NSERC*) for continued support of this work through an operating grant. The comments of Prof. Ian Still and Prof. Adrian Schwan on parts of the manuscript are gratefully acknowledged. We thank José Rodezno and Dr. Tim Burrow for VT NMR measurements.

[1] [1a] G. Opitz, E. Tempel, *Liebigs. Ann. Chem.* **1966**, *699*, 74−87. [1b] G. Opitz, *Angew. Chem. Int. Ed. Engl.* **1967**, *6*, 107−123. [1c] J. F. King, P. de Mayo, D. L. Verdun, *Can. J. Chem.* **1969**, *47*, 4509−4511. [1d] J. F. King, R. A. Marty, P. de Mayo, P. L. Verdun, *J. Am. Chem. Soc.* **1971**, *93*, 6304−6305. [1e] S. Hünig, H. Hoch, *Chem. Ber.* **1972**, *105*, 2197−2215. [1f] R. Langendries, F. C. De Schryver, P. de Mayo, R. A. Marty, J. Schutyser, *J. Am. Chem. Soc.* **1974**, *96*, 2964−2968. [1g] J. F. King, J. Y. L. Lam, S. Skonieczny, *J. Am. Chem. Soc.* **1992**, *114*, 1743−1749. [1h] E. Block, A. Schwan, D. A. Dixon, *J. Am. Chem. Soc.* **1992**, *114*, 3492−3499. [1i] M. F. Reich, V. J. Lee, J. Ashcroft, G. O. Morton, *J. Org. Chem.* **1993**, *58*, 5288−5290. [1j] J. F. King, in *The Chemistry of Functional Groups*, "The Chemistry of Sulfonic Acids" (Ed.: S. Patai), Wiley, **1991**, p697.

[2] For recent discussions of carbon-sulfur multiple bonds see: K. Seppelt, *Angew. Chem.* **1991**, *103*, 399−413; *Angew. Chem. Int. Ed. Engl.* **1991**, *30*, 361−374. J. A. Dobado, H. Martínez-Garcia, J. M. Molina, *Inorg. Chem.* **1999**, *38*, 6257−6260.

[3] H. Hiraoka, *J. Chem. Soc., Chem. Commun.* **1974**, 1014−1015.

[4] W. Sander, M. Kirschfeld, M. Halupka, *J. Am. Chem. Soc.* **1997**, *119*, 981−986.

[5] E. de Berry Barnett, *J. Chem. Soc.* **1910**, *97*, 63−65.

[6] [6a] I. V. Prokof'eva, A. E. Bukanova, *Zh. Neorg. Khim.* **1968**, *13*, 522−525. [6b] W. Walter, G. Randau, *Justus Liebigs Ann. Chem.* **1969**, *722*, 52−79. [6c] W. Walter, G. Randau, *Justus Liebigs Ann. Chem.* **1969**, *722*, 80−97. [6d] D. Gupta, R. Soman, S. Dev, *Tetrahedron* **1982**, 3013−3018.

[7] [7a] B. Quiclet-Sire, I. Thevenot, S. Z. Zard, *Tetrahedron Lett.* **1995**, *36*, 9469−9470. [7b] B. S. Jursic, D. Neumann, A. McPherson, *Synthesis* **2000**, 1656−1658. [7c] R. Balicki, U. Chmielowiec, *Monatsh. Chem.* **2000**, *131*, 1105−1107.

[8] [8a] R. A. L. Sullivan, A. Hargreaves, *Acta Crystallogr.* **1962**, *15*, 675−676. [8b] A. Hargreaves, *Acta Crystallogr.* **1963**, *16*, 1133−1137. [8c] I-C. Chen, Y. Wang, *Acta Crystallogr., Sect. C* **1984**, *40*, 1937−1983. [8d] Y. Wang, N.-L. Chang, C.-T. Pai, *Inorg. Chem.* **1990**, *29*, 3256−3259.

[9] [9a] S. N. Lyashchuk, Y. G. Skrypnik, *Tetrahedron Lett.* **1994**, *35*, 5271−5274. [9b] Y. G. Skrypnik, S. N. Lyashchuk, *Sulfur Lett.* **1994**, *17*, 287−294. [9c] primed compounds refer to the 1-adamantyl-substituted systems while the non-primed ones refer to the *tert*-butyl-substituted ones.

[10] [10a] D. A. Dixon, A. J. Arduengo, K. D. Dobbs, D. V. Khasnis, *Tetrahedron Lett.* **1995**, *36*, 646−648. [10b] A. Senning, *Sulfur Lett.* **1996**, *20*, 105. [10c] J. F. King, K. M. Baines, M. R. Netherton, V. Dave, *Can. J. Chem.* **2001**, *79*, 461.

[11] [11a] M. K. Denk, A. Thadani, K. Hatano, A. J. Lough, *Angew. Chem. Int. Ed. Engl.* **1997**, *36*, 2607−2609; *Angew. Chem.* **1997**, *109*, 2719−2721. [11b] M. K. Denk, K. Hatano, M. J. Ma, *Tetrahedron Lett.* **1999**, *40*, 2057−2060. [11c] M. K. Denk, J. Rodezno, S. Gupta, A. J. Lough, *J. Organomet. Chem.* **2001**, *617−618*, 242−253. [11d] M. K. Denk, J. Rodezno, *J. Organomet. Chem.* **2000**, *608*, 122−125. [11e] M. K. Denk, S. Gupta, J. Brownie, S. Tajammul, A. J. Lough, *Chem. Eur. J.* **2001**, *7*, 4477−4486.

[12] [12a] A. P. Hitchcock, L. E. Ennis, J. F. Lehmann, M. K. Denk, *J. El. Spec.* **2001**, *114*, 1037−1041. [12b] L. A. Leites, S. S. Bukalov, M. K. Denk, R. West, M. Haaf, *J. Molecular Structure − THEOCHEM* **2000**, *550*, 329−335. [12c] M. K. Denk, S. Gupta, R. Ramachandran, *Eur. J. Inorg. Chem.* **1999**, 41−49. [12d] J. F. Lehmann, S. G. Urquhart, L. E. Ennis, A. P. Hitchcock, K. Hatano, S. Gupta, M. K. Denk, *Organometallics* **1999**, *18*, 1862−1872. [12e] M. Haaf, A. Schmiedl, T. A. Schmedake, R. A. Powell, A. J. Millevolte, M. K. Denk, R. West, *J. Am. Chem. Soc.* **1998**, *120*, 12714−12719. [12f] M. K. Denk, K. Hatano, A. J. Lough, *Eur. J. Inorg. Chem.* **1998**, 1067−1070. [12g] S. Urquhart, A. P. Hitchcock, M. K. Denk, *Organometallics* **1998**, *17*, 2352−2360. [12h] M. K. Denk, S. Gupta, R. Ramachandran, *Tetrahedron Lett.* **1996**, 9025−9028. [12i] N. Metzler, M. K. Denk, *Chem. Commun.* **1996**, 2657−2658. [12j] M. K. Denk, R. Lennon, R. Hayashi, R. West, A. Haaland, A. V. Belyakov, H. P. Verne, M. Wagner, N. Metzler, *J. Am. Chem. Soc.* **1994**, *116*, 2691−2692. [12k] M. Denk, R. K. Hayashi, R. West, *J. Am. Chem. Soc.* **1994**, *116*, 10813−10814. [12l] M. Denk, J. C. Green, N. Metzler, M. Wagner, *J. Chem. Soc., Dalton Trans.* **1994**, 2405−2410. [12m] M. Denk, R. K. Hayashi, R. West, *J. Chem. Soc., Chem. Commun.* **1994**, 33−34.

[13] ^{1}H NMR and tentative assignment of the hydrolysis product **[6 H]$^+$[HSO$_3^-$]**: ^{1}H NMR ($CDCl_3$): δ = 1.50 [C(CH_3)$_3$], 4.03 (CH_2), 8.31 (N_2CH^+).

[14] **Crystal data for 7:** $C_{11}H_{22}N_2O_2S_2$, M_r = 246.37, monoclinic, space group $P2_1/n$, a = 7.649(1), b = 19.239(1), c = 8.736(1) Å, β = 95.51(1)°, V = 1279.6(4) Å^3, Z = 4, $\rho_{calcd.}$ = 1.284 g cm^{-3}, λ(Mo-K_α) = 0.71073 Å, μ(Mo-K_α) = 0.243 mm^{-1}, T = 150.0(1) K, total number of collected reflections 10008, independent reflections 3162. (4.15 < θ < 28.29°) and scalepack absorption correction. Structure refined on F^2 (full-matrix-least-squares) and hydrogen atoms were refined with isotropic thermal parameters. Final $R1$ [$I > 2\sigma(I)$] = 0.0365 for 3162 observed reflections and $wR2$ (all data) = 0.0523. Maximum and minimum peaks in final ΔF map were 0.329 and −0.428 e·Å^{-3}.

[15] Structures solved and refined using SHELXTL/PC.[16] Crystallographic data (excluding structure factors) for **7** have been deposited. CCDC-165466 contains the supplementary crystallographic data for this paper. These data can be obtained free of charge at www.ccdc.cam.ac.uk/conts/retrieving.html [or from the Cambridge Crystallographic Data Centre, 12, Union Road, Cambridge CB2 1EZ, UK; Fax: (internat.) +44-1223/336-033; E-mail: deposit@ccdc.cam.ac.uk].

[16] [16a] G. M. Sheldrick, *Acta Crystallogr., Sect. A* **1990**, *46*, 467−473. [b] *Bruker Analytical X-ray Systems*, Madison, Wisconsin, USA, **1998**.

[17] C. K. Johnson, *ORTEP, FORTRAN Thermal Ellipsoid Plot Program for Crystal Structure Illustrations*, National Laboratories, Oak Ridge/Tennessee, USA, 1965.

[18] Gaussian 98, Revision A.7: M. J. Frisch, G. W. Trucks, H. B. Schlegel, G. E. Scuseria, M. A. Robb, J. R. Cheeseman, V. G. Zakrzewski, J. A. Montgomery, Jr., R. E. Stratmann, J. C. Burant, S. Dapprich, J. M. Millam, A. D. Daniels, K. N. Kudin, M. C. Strain, O. Farkas, J. Tomasi, V. Barone, M. Cossi, R. Cammi, B. Mennucci, C. Pomelli, C. Adamo, S. Clifford, J. Ochterski, G. A. Petersson, P. Y. Ayala, Q. Cui, K. Morokuma, D. K. Malick, A. D. Rabuck, K. Raghavachari, J. B. Foresman, J. Cioslowski, J. V. Ortiz, A. G. Baboul, B. B. Stefanov, G. Liu, A. Liashenko, P. Piskorz, I. Komaromi, R. Gomperts, R. L. Martin, D. J. Fox, T. Keith, M. A. Al-Laham, C. Y. Peng, A. Nanayakkara, C. Gonzalez, M. Challacombe, P. M. W. Gill, B. Johnson, W. Chen, M. W. Wong, J. L. Andres, C. Gonzalez, M. Head-Gordon, E. S. Replogle, and J. A. Pople, Gaussian, Inc., Pittsburgh PA, 1998.

[19] The structures are optimized with tight optimization and verified as local minima through frequency calculations. The calculations were performed without symmetry restrictions. Without this precaution, structures with virtual frequencies corresponding to methyl rotations or SO_2 rocking vibrations can be obtained. Zero point energies were obtained at the MPw1PW91/6-31G(2d)//MPw1PW91/6-31G(2d) level and were included without scaling. The energies were converted using the factor 1 Hartree = 627.5905 kcal·mol^{-1}.

[20] [20a] C. Adamo, V. Barone, *J. Chem. Phys.* **1998**, *108*, 664−675. [20b] K. B. Wiberg, J. D. Hammer, K. W. Zilm, J. R. Cheeseman, *J. Org. Chem.* **1999**, *64*, 6394−6400. [20c] G. de Oliveira, J. M. L. Martin, F. de Proft, P. Geerlings, *Phys. Rev. A* **1999**, *60*, 1034−1045. [20d] G. Scalmani, J. L. Bredas, V. Barone, *J. Chem. Phys.* **2000**, *112*, 1178−1191.

[21] [21a] A. D. Becke, *Phys. Rev.* **1988**, *A38*, 3098. [21b] C. Lee, W. Yang, R. G. Parr, *Phys. Rev.* **1988**, *B37*, 785. [21c] A. D. Becke, *J. Chem. Phys.* **1993**, *98*, 5648−5652.

[22] [22a] M. R. Nyden, G. A. Petersson, *J. Chem. Phys.* **1981**, *75*, 1843−1862. [22b] G. A. Petersson, M. A. Al-Laham, *J. Chem. Phys.* **1991**, *94*, 6081−6090. [22c] G. A. Petersson, T. Tensfeldt,

J. A. Montgomery, *J. Chem. Phys.* **1991**, *94*, 6091−6101. [22d] J. A. Montgomery, J. W. Ochterski, G. A. Petersson, *J. Chem. Phys.* **1994**, *101*, 5900−5909.

[23] J. Emsley, *The Elements*, 2nd ed., Clarendon Press, Oxford, **1991**.

[24] Irrespective of the employed basis set [6-31G(d), 6-31G(2d)], the B3LYP structures of **7Me** give unrealistic CS bond lengths (>230 pm vs. exp. 203 pm). Equally unsatisfactory CS distances are obtained for other commonly used density functionals (SVWN5, B3PW91, G96LYP, BH&HLYP, B1LYP). For the test case of SO_2, The quality of the MPW1PW91 structures increases smoothly with the total number of primitive gaussians (6-31G(d) < 6-311G(d) < 6-31G(2d) < 6-311G(2d) < 6-31G(3d) < 6-311G(3d) while the quality of the HF structures is inconsistent. For example, the HF/6-31(2d) structure of SO_2 is *less accurate* than the HF/6-31(d) structure. The inclusion of diffuse functions, which are typically added to improve the structures of electron-rich systems, in particular anions, did not lead to improved structures of SO_2.

[25] E. O. Fischer, A. Maasböl, *Angew. Chem. Int. Ed. Engl.* **1964**, *3*, 580.

[26] L. A. Curtiss, K. Raghavachari, G. W. Trucks, J. A. Pople, *J. Chem. Phys.* **1991**, *94*, 7221−7230.

[27] PM3 calculations show low rotational barriers for **7Me** (3.65 kcal·mol^{-1}) and **7** (5.75 kcal·mol^{-1}).

[28] Estimated errors for the computational structures of **7Me/5Me** can be inferred from a comparison of the MPW1PW91/6-31G(d) structure of SO_2 with the experimental structure. This leads to estimated errors of 0.84 pm (0.59%) for the SO bond lengths and 0.23 deg (0.19%) for the O−S−O angles. For the remainder of the geometrical parameters, the errors obtained for the G2 test set of molecules (ref.[20]) may be assumed.

Received April 8, 2002
[I02181]

Dynamic Properties of Methyl(trimethylphosphane)nickel Complexes Containing (2-Diphenylphosphanyl)phenylamido Ligands

Hans-Friedrich Klein,*[a] Robert Beck,[a] and Olaf Hetche[a]

Keywords: Solution dynamics / Nickel / Coordination numbers 4 and 5 / Structure elucidation

P,N-chelates of nickel NiCl[2-(Ph_2P)C_6H_4NR](PMe_3) (**1**: R = H; **2**: R = $SiMe_3$) have been obtained from $NiCl_2(PMe_3)_2$ and 2-(Ph_2P)C_6H_4NRLi. Reaction with MeLi affords methylnickel compounds NiMe[2-(Ph_2P)C_6H_4NR](PMe_3) (**3**: R = H; **4**: R = Me; **5**: R = $SiMe_3$). By the same route NiMe[2-(R^1R^2P)C_6H_4NR](PMe_3) (**6**: R^1 = R^2 = $CHMe_2$) was synthesized. Solutions in THF contain *cis* and *trans* isomers of square-planar complexes, and dynamic NMR spectroscopy shows dissociation of trimethylphosphane to be more rapid in the *trans* isomers. In a crystal of **5** the molecular structure is *cis*-**5**. Out of these complexes only **3** and **4** add trimethylphosphane to form pentacoordinate compounds NiMe[2-(Ph_2P)C_6H_4NR](PMe_3)$_2$ (**7**, **8**) in the crystal as shown by the molecular structure of **7** while in THF equilibria **7** ⇄ *cis*-**1** and **8** ⇄ *cis*-**2** are observed by NMR spectroscopy. The same solution properties are found with NiMe[2-(R^1R^2P)C_6H_4NR](PMe_3)$_2$ (**9**: R^1 = CMe_3, R^2 = Ph).

(© Wiley-VCH Verlag GmbH & Co. KGaA, 69451 Weinheim, Germany, 2003)

Introduction

A well-known strategy to avoid a bridging coordination mode in transition metal amides is the use of chelating ligands. As a convenient anchoring group the 2-(diphenylphosphanyl) group induces P,N-chelating systems to form five-membered metallacyles. Usually these are derived from 2-(diphenylphosphanyl)aniline which is isoelectronic with P,O-chelating 2-(diphenylphosphanyl)phenol and because of its potential in homogeneous catalysis of olefin reactions merits further investigation. 2-(Diphenylphosphanyl)aniline has been shown by Cooper et al.[1] to form mononuclear bis(chelate) compounds of platinum and nickel acting either as a neutral or as an anionic 4-electron donor (Scheme 1).

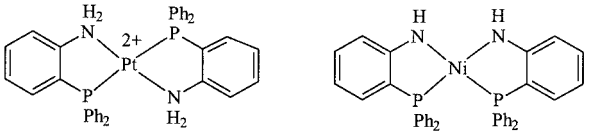

trans-bis(amino)platinum(II) *cis*-bis(amido)nickel(II)

Scheme 1. Square-planar bis(P,N-chelates)

2-(Diphenylphosphanyl)-*N*-methylanilido compounds of rhodium(I) and iridium(I) have been investigated by Dahlenburg et al.,[2] while 2-(diphenylphosphanyl)-*N*,*N*-dimethylaniline in penta- and tetracoordinate complexes of nickel(II) with added Et_2AlCl turns out to be a catalyst in the oligomerization of propene as described by Corain et al.[3]. As a model of a growing alkylmetal chain we have synthesized some methylnickel complexes containing P,N-chelating and trimethylphosphane ligands and report here on molecular structures and dynamic properties in solution.

Results and Discussion

N-Lithiated 2-(diphenylphosphanyl)anilines react with *trans*-$NiCl_2(PMe_3)_2$ [Equation (1)] to afford the chloronickel complexes **1** and **2** as green solids which are sparingly soluble in pentane or ether.

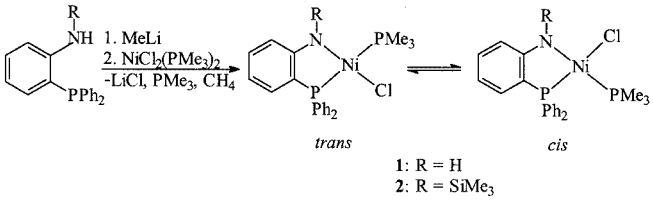

(1)

The ^{31}P NMR spectrum obtained from a THF solution of **1** or **2** at 233 K shows four doublet resonances. The pair containing the large P,P coupling is assigned to *trans*-**1** (62%) and *trans*-**2** (66%), while the pair showing the small P,P coupling is due to *cis*-**1** (38%) and *cis*-**2** (34%), respectively. Similar mixtures of isomers have been observed with related cationic palladium complexes.[4]

Added trimethylphosphane accelerates the exchange of ligands but does not alter the green color of these solutions

[a] Eduard-Zintl-Institut für Anorganische and Physikalische Chemie der Technischen Universität Darmstadt, Petersenstrasse 18, 64285 Darmstadt, Germany

and thereby indicates the absence of a pentacoordinate compound. Addition of a second mol-equiv. of LiMe or use of *trans*-NiMeCl(PMe_3)$_2$ as a reactant [Equation (2)] furnishes the corresponding methylnickel compounds.

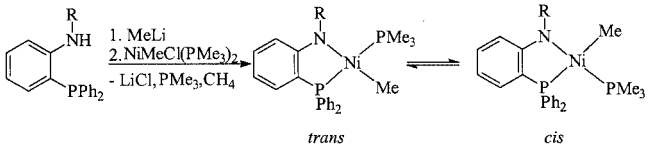

3: R = H
4: R = Me
5: R = $SiMe_3$

(2)

The reaction mixture displays a deep red color, while removal of THF solvent together with 1 mol-equiv. of trimethylphosphane during workup causes a change to orange-yellow, finally yielding orange solids **3**−**5**. The microcrystalline compounds are highly hygroscopic and under argon decompose above 122 °C, 105 °C, and 83 °C, respectively.

Using 2-(diisopropylphosphanyl)-*N*-methylaniline in a similar synthesis [Equation (3)] affords red crystals of **6** that decompose above 104 °C. NMR spectra of THF solutions of **3**−**6** again each display a double set of the expected resonances which are assigned to *cis* and *trans* isomers. In particular, $NiCH_3$ protons opposite to the chelating ^{31}P donor resonate between δ = −0.82 and −0.77 ppm with unresolved *trans* coupling ($_{cis}{}^3J_{P,H}$ = 4.5−6.1 Hz) while for those opposite to the amide donor at δ = −0.04(3) ppm a doublet of doublets pattern is observed ($^3J_{P,H}$ = 3.8−4.1 Hz). In toluene solution the *trans* isomers are observed as the dominant species (> 95%).

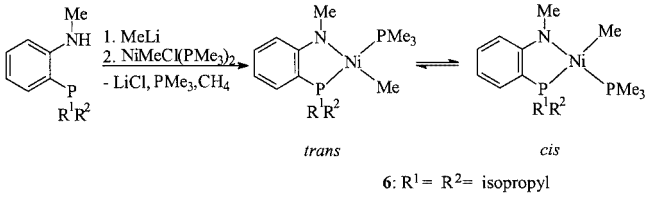

6: R^1 = R^2 = isopropyl

(3)

The ^{31}P NMR spectra in THF show a large coordination chemical shift of the chelate-P nucleus by 52 ppm to low field and a resonance for the coordinated trimethylphosphane ligand at δ ≈ −2 ppm. Surprisingly, the *cis* and *trans* isomers show different behavior at variable temperatures. Only the *cis* isomers continue to display a doublet of doublets ($^2J_{P,P}$ ≈ 30 Hz) between 298 and 213 K (Figure 1) while the large *trans* coupling ($^2J_{P,P}$ ≈ 300 Hz) is attained in the low-temperature limit. Upon warming, both doublet resonances of *trans*-**3**−**6** collapse to singlets caused by incipient dissociation of trimethylphosphane. Therefore, the slightly shifted broad singlet at δ = −5 ppm (298 K) must be regarded as an average of rapidly exchanging free and coordinated trimethylphosphane which also involves the pentacoordinate species (see below).

Single crystals of **5** obtained from pentane when subject to an X-ray diffraction experiment were shown to consist of *cis*-**5** (Figure 2). The unit cell contains two molecules that differ mainly in the rotational position of a phenyl substituent. The nickel atom is located in a square-planar arrangement of ligand functions. Bond lengths C−Ni and N−Ni are as usual[5] but opposite N,P and C,P donor atoms deviate from linearity by 10 and 20°, respectively. The chelate bond Ni−P1 is by 8 pm longer than Ni−P2 due to the

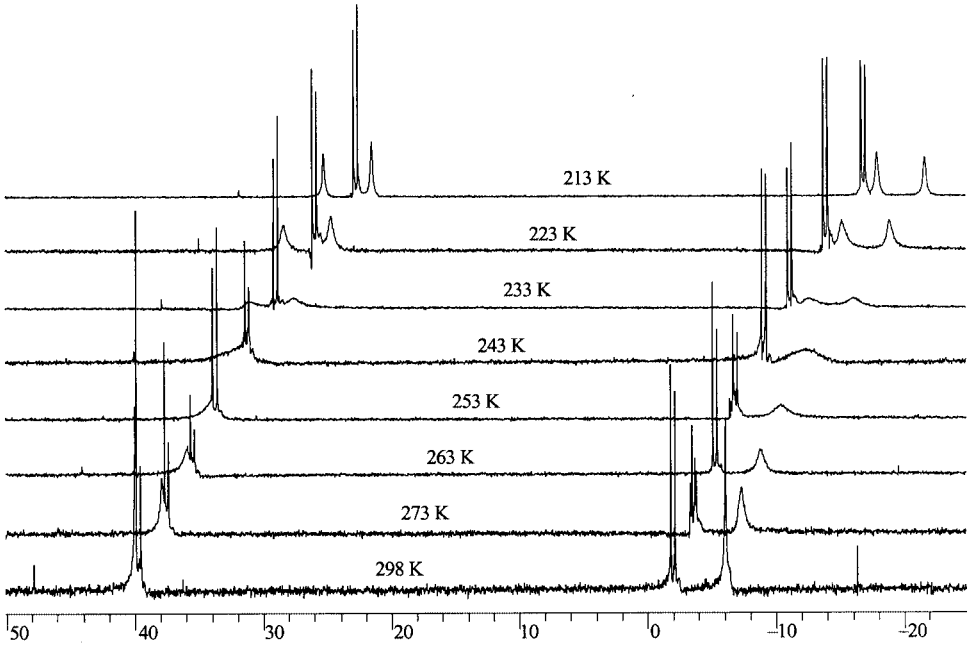

Figure 1. ^{31}P NMR spectra of **3** (THF, 213−298K)

larger *trans* influence of the NiMe group relative to the amide donor. The Me_3Si group is clearly oriented above the plane of the metallacycle.

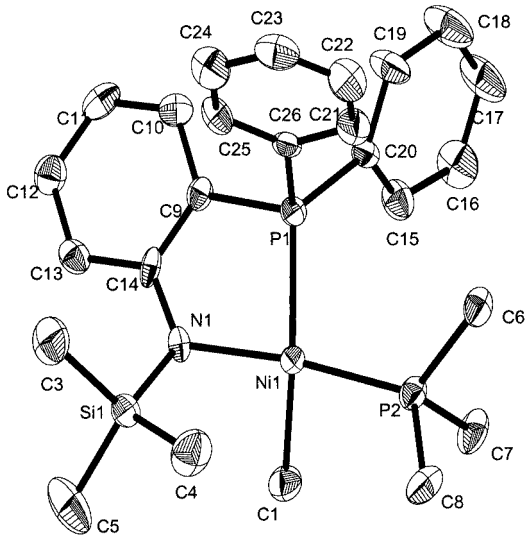

Figure 2. Molecular structure of *cis*-**5** (ORTEP plot with hydrogen atoms omitted); selected bond lengths [Å] and angles [°]: Ni−C1 1.971(11), Ni−N 1.956(8), Ni−P1 2.219(3), Ni−P2 2.124(3), P1−C9 1.814(10), C9−C14 1.387(15), C14−N 1.367(14), N−Si 1.731(8); N−Ni−P2 170.0(3), N−Ni−P1 84.0(3), C1−Ni−P1 160.8(4), N−Ni−C1 91.6(4), P1−Ni−P2 102.26(11), C1−Ni−P2 84.9(4), C9−P1−Ni 96.3(3), C14−N−Ni 117.6(6), Si−N−Ni 115.8(5), C14−N−Si 123.6(6)

Added trimethylphosphane makes **3** and **4** better soluble in pentane and causes a deep red color. Upon cooling, dark red crystals of **7** and **8** are isolated that show an even better thermal stability than their parent complexes reminding one of the pair $NiMe_2(PMe_3)_2$ and $NiMe_2(PMe_3)_3$.[6] Only **6** does not change color under these conditions and is recovered unchanged. Analytical and spectroscopic data are consistent with pentacoordinate compounds **7** and **8**. In solution dissociation of the ligands is excessive, and in ^{31}P NMR experiments a low-temperature limit of ligand motions was only attained with **7** revealing the coordination geometry. A doublet at $\delta = -16$ ppm (2 P) for trimethylphosphane and a triplet at $\delta = 23$ ppm for the PPh_2 group with $^2J_{P,P} = 192$ Hz are consistent with all three phosphorus donor atoms in equatorial sites leaving methyl and amide groups in axial positions of a trigonal bipyramid.

The molecular structure (Figure 3) confirms the configuration of **7** as derived from spectroscopic data. The nickel atom is centered in a trigonal bipyramid with axial C and N and three equatorial P donor atoms. Bond lengths are not notably different from those in *cis*-**5**, and the chelate bite angle [P1−Ni−N 85.60(13)°] is only slightly larger than in *cis*-**5** [P1−Ni−N 84.0(3)°]. A difference is recognized in a trigonal-planar arrangement of bonds to N in **7** (sum of angles 359.7°) as compared with a more pyramidal geometry in *cis*-**5** (sum of angles 357.0°). Interestingly, the sum of internal angles in the metallacycle of **7** (539.7°) is closer to the value of a regular pentagon (540°) than in *cis*-**5** (530.0°) suggesting a better fit of the former and a slight thermodynamic advantage for the pentacoordinate complex molecule.

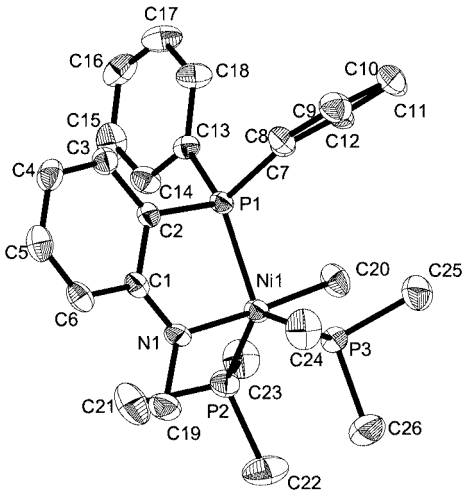

Figure 3. Molecular structure of **7** (ORTEP plot with hydrogen atoms omitted); selected bond lengths [Å] and angles [°]: Ni−C20 1.996(6), Ni−N 1.974(4), Ni−P1 2.202(2), Ni−P2 2.224(2), Ni−P3 2.253(2), N−C1 1.452(6), N−C19 1.452(6), C1−C2 1.423(7); N−Ni−C20 176.7(3), P1−Ni−P2 125.90(6), P1−Ni−P3 110.71(6), P2−Ni−P3 123.36(7), P1−Ni−N 85.60(13), P1−Ni−C20 91.1(2), Ni−N−C1 120.9(3), C1−N−C19 116.5(4), Ni−N−C19 122.3(3)

A prochiral P-donor function was introduced using 2-[*tert*-butyl(phenyl)phosphanyl]-*N*-methylaniline as a prechelate reactant [Equation (4)]. The red crystals of pentacoordinate **9** are highly soluble in pentane and under argon decompose above 115 °C.

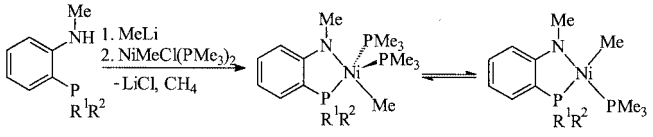

7: $R^1 = R^2 = H$
8: $R^1 = R^2 = Me$
9: $R^1 = Ph$, $R^2 = CMe_3$ (4)

One bulky alkyl substituent in the 2-(phosphanyl) group does not interfere with the reversible uptake of trimethylphosphane. With **9** we have not been able to isolate a 16-VE species in an analytically pure state.

A close structural relationship between **8** and [2-(diphenylphosphanyl)phenolato-*O*,*P*]methylbis(trimethylphosphane)nickel[7] is found in agreement with expectation for isoelectronic molecules (Table 1).

Ligand mobility in P,N-chelates of nickel appears to be generally higher than in P,O-chelates, but only the first dissociation step (Scheme 2) could be demonstrated by experiment.

While removal of the second trimethylphosphane ligand was achieved with P,O-chelating ligands by formation of μ_2-

Table 1. Structural relations between isoelectronic P,O and P,N compounds of nickel(II)

	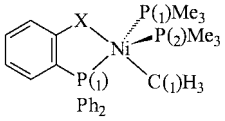	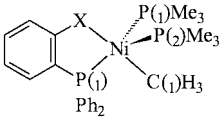
	X = O[7]	X = NMe (**8**)
Selected bond lenghts [pm]:		
Ni−C(1)	198.1(5)	199.6(6)
Ni−P(1)	219.1(2)	220.2(2)
Ni−P(2)	224.5(2)	225.3(2)
Ni−P(3)	222.4(2)	222.4(2)
Ni−X	198.4(3)	197.4(4)
Selected bond angles [°]:		
X−Ni−C(1)	177.7(2)	176.7(3)
X−Ni−P(1)	86.35(10)	85.60(13)
P(1)−Ni−P(3)	125.16(6)	125.90(6)
P(1)−Ni−P(2)	114.02(6)	110.71(6)
P(3)−Ni−P(2)	120.71(7)	123.36(7)
Σ five-membered metallacycle [°]:	538.8	539.7

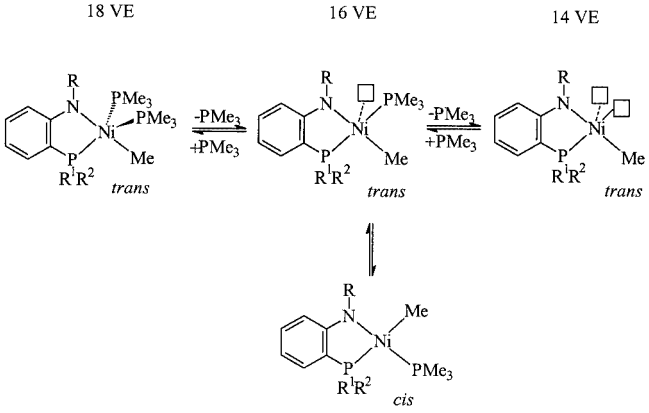

Scheme 2. Dynamic coordination in methylnickel P,N-chelates

O-bridged dinuclear complexes,[8] our attempts to remove the last trimethylphosphane ligand from the metal atom by favoring a bridging coordination mode of the amide function met with thermal decomposition (in boiling toluene). However, this result does not exclude a 14-electron species as an intermediate providing still another vacant coordination site for substrate binding.

Therefore, the tetracoordinate complexes **3**−**5** as prime candidates were examined with respect to catalytic activity in ethene oligomerization under otherwise same conditions as with the isoelectronic and highly active P,O-chelates.[7] A toluene solution (80 mL) containing 0.1 mmol of complex was kept in a steel autoclave under 50 bar of ethene at 80 °C. No drop of pressure was observed within 12 h which corresponds with no activity.

Conclusion

Methyl(trimethylphosphane)nickel complexes of P,N-chelating 2-(phosphanyl)anilines can be smoothly synthesized from convenient starting compounds as thermally stable materials. Solution dynamics of ligand motions and solvent-dependent equilibria of square-planar *cis* and *trans* isomers are novel and characteristic properties when compared with isoelectronic P,O-chelates. Rapid addition and dissociation of trimethylphosphane exclusively involve equatorial positions of a trigonal bipyramid with axial methyl and N-donor groups. Replacing an oxygen by a nitrogen donor atom in five-membered metallacycles of nickel brings about gross electronic changes whereby catalytic activity in oligomerization of ethene is completely lost. A coarse tuning by electronic effects of substituents attached to the metallacycle would be necessary to recover such activity.

Experimental Section

General Procedures and Materials: All air-sensitive and volatile materials were handled using standard vacuum techniques and were kept under argon. Microanalyses: Kolbe Microanalytical Laboratory, Mülheim/Ruhr, FRG. Melting points/decomposition temperatures: Sealed capillaries, uncorrected values. Chemicals (Merck/Schuchardt) were used as purchased. Literature methods were applied in the preparation of $NiCl_2(PMe_3)_2$, $NiMeCl(PMe_3)_2$,[6] 2-(diphenylphosphanyl)aniline,[9] 2-(diphenylphosphanyl)-*N*-methylaniline, 2-(diisopopylphosphanyl)aniline[10] and 2-[*tert*-butyl(phenyl)phosphanyl]-*N*-methylaniline.[11] IR: Nujol mulls between KBr discs, Bruker spectrophotometer type FRA

106. ^{1}H and ^{13}C NMR spectra (300 MHz and 75 MHz, respectively) were recorded with a Bruker ARX-300 spectrometer, ^{31}P NMR spectra (81 MHz) with a Bruker AM-200 instrument. ^{13}C and ^{31}P resonances were obtained with broad-band proton decoupling.

2-(Diphenylphosphanyl)-*N*-(trimethylsilyl)aniline: 2-(Diphenylphosphanyl)aniline (1.20 g, 4.32 mmol) in diethyl ether (80 mL) was combined with 1.6 M BuLi solution in hexane (2.7 mL, 4.32 mmol) and kept at 20 °C for 30 min. Chlorotrimethylsilane (470 mg, 4.32 mmol) was added, and after 16 h, LiCl was filtered off and the solution concentrated to a volume of 40 mL. Cooling to 4 °C afforded white crystals. Yield 1.10 g (73%); m.p. 76−77 °C. ^{1}H NMR (300 MHz, [D$_8$]THF): δ = 0.01 (s, 9 H, SiCH$_3$), 4.30 (d, $^4J_{P,H}$ = 9.3 Hz, 1 H, NH), 6.45 (dt, ^3J = 7.6, ^4J = 0.7 Hz, 1 H, CH), 6.65 (m, 2 H, CH), 7.01 (dt, ^3J = 6.5, ^4J = 1.5 Hz, 2 H, CH), 7.13−7.20 (m, 10 H, CH) ppm. ^{13}C NMR (75 MHz, [D$_8$]THF): δ = −1.89 (s, CH$_3$), 114.7 (s, CH), 116.9 (d, $^4J_{P,C}$ = 2.2 Hz, CH), 120.9 (d, $^3J_{P,C}$ = 5.6 Hz, C), 127.4 (s, CH), 127.6 (d, $^2J_{P,C}$ = 7.8 Hz, CH), 129.1 (s, CH), 132.5 (d, $^1J_{P,C}$ =18.7 Hz, CH), 133.7 (d, $^3J_{P,C}$ = 5.5 Hz, C), 135.1 (d, $^2J_{P,C}$ = 7.7 Hz, C), 150.1 (d, $^1J_{P,C}$ = 19.5 Hz, CH) ppm. ^{31}P NMR (81 MHz, [D$_8$]THF): δ = −10 (s) ppm. $C_{21}H_{24}NPSi$ (349.5): calcd. C 72.17, H 6.92, N 4.01; found C 72.45, H 6.63, N 3.95.

2-[*tert*-Butyl(phenyl)phosphanyl]-*N*-methylaniline: This prechelate ligand was obtained in a procedure given for 2-(diphenylphosphanyl)-*N*-methylaniline[10] starting from *N*-methylaniline and chloro(*tert*-butyl)phenylphosphane. Yield 52%, yellow oil; b.p. 189−190 °C/7 mbar. IR (Nujol, 4000−400 cm^{-1}): ṽ = 3349 vs (νN−H), 3052 m, 2926 m (νH−C=), 2810 (νNC−H), 1587 s, 1569 s (νC=C), 1518 s, 1454 s, 1435 s, 1419 m, 1312 m (δ_{as}PCH), 1289 m (δ_sPCH), 1165 m, 1089 w, 1046 w, 1029 vw, 999 vw, 912 vw, 746 vs, 729 w, 698 vs (γC−H), 515 m, 496 m, 482 m. ^{31}P NMR (81 MHz, CD_2Cl_2, 296 K): δ = −16 (s) ppm.

Chloro[2-(diphenylphosphanyl)anilido-*N*,*P*](trimethylphosphane)-nickel (1): 2-(Diphenylphosphanyl)aniline (750 mg, 2.70 mmol) in 50 mL of THF was combined at −70 °C with 1.6 M MeLi in diethyl ether (1.7 mL, 2.70 mmol), and this solution was added dropwise at −70 °C to $NiCl_2(PMe_3)_2$ (762 mg, 2.70 mmol) in 50 mL of THF causing the red color to turn green. The mixture was warmed to 20 °C and concentrated to dryness in vacuo. The solid residue was extracted with three 80-mL portions of diethyl ether through a glass-sinter disc (G3) and the green solution cooled to 4 °C to afford green crystals. Yield 710 mg (59%); m.p. 95−96 °C (dec.). IR (Nujol): ṽ = 3377 cm^{-1} (N−H). ^{1}H NMR (200 MHz, [D$_8$]THF, 233 K): *cis*-**1** (63%): δ = 1.07 (d, $^2J_{P,H}$ = 10.1, 9 H, PCH$_3$), 3.65 (s, 1 H, NH), 5.91 (m, 1 H, CH), 6.22 (m, 1 H, CH), 6.67 (m, 1 H, CH), 7.15 (m, 1 H, CH), 7.45−7.55 (m, 6 H, CH), 7.82−7.86 (m, 4 H, CH); *trans*-**1** (37%): δ = 1.33 (d, $^2J_{P,H}$ = 10.0 Hz, 9 H, PCH$_3$), 4.59 (s, 1 H, NH), 6.10 (m, 1 H, CH), 6.37 (m, 1 H, CH), 6.67 (m, 1 H, CH), 7.01 (m, 1 H, CH), 7.15 (m, 1 H, CH), 7.31 (m, 1 H, CH), 7.55−7.59 (m, 6 H, CH), 7.98−8.07 (m, 4 H, CH) ppm. ^{31}P NMR (81 MHz, [D$_8$]THF, 233 K): *cis*-**1** (63%): δ = −9 (d, $^2J_{P,P}$ = 89 Hz, 1 P, PCH$_3$), 52 (d, $^2J_{P,P}$ = 89 Hz, 1 P, PC_6H_5); *trans*-**1** (37%): δ = −9 (d, $^2J_{P,P}$ = 347 Hz, 1 P, PCH$_3$), 31 (d, $^2J_{P,P}$ = 347 Hz, 1 P, PC_6H_5) ppm. $C_{21}H_{24}ClNNiP_2$ (445.0): calcd. C 56.49, H 5.42, N 3.14; found C 56.68, H 5.50, N 3.05.

Chloro[2-(diphenylphosphanyl)-*N*-(trimethylsilyl)anilido-*N*,*P*](trimethylphosphane)nickel (2): 2-(Diphenylphosphanyl)-*N*-(trimethylsilyl)aniline (840 mg, 2.40 mmol) in 50 mL of THF was combined at −70 °C with 1.6 M MeLi in diethyl ether (1.5 mL, 2.40 mmol), and this solution was added as above to $NiCl_2(PMe_3)_2$ (677 mg, 2.40 mmol) in 50 mL of THF causing the red color to turn green. The mixture was warmed to 20 °C, stirred for 3 h, and concentrated to dryness in vacuo. The residue was extracted with three 80-mL portions of diethyl ether and the green solution cooled to 4 °C to afford green rectangular crystals. Yield 745 mg (60%); m.p. 108−109 °C (dec.). ^{1}H NMR (200 MHz, [D$_8$]THF, 233 K): *cis*-**2** (66%): δ = 0.02 (s, 9 H, SiCH$_3$), 1.06 (d, $^2J_{P,H}$ = 9.2 Hz, 9 H, PCH$_3$), 5.93 (m, 1 H, CH), 6.23 (m, 1 H, CH), 6.71 (m, 2 H, CH), 6.83 (m, 2 H, CH), 7.41−7.49 (m, 6 H, CH), 7.76−7.85 (m, 4 H, CH); *trans*-**2** (34%): δ = 0.06 (s, 9 H, SiCH$_3$), 1.39 (d, $^2J_{P,H}$ = 11.1 Hz, 9 H, PCH$_3$), 6.15 (m, 1 H, CH), 6.40 (m 1 H, CH), 7.05 (m, 2 H, CH), 7.49−7.58 (m, 6 H, CH), 8.00−8.02 (m, 4 H, CH) ppm. ^{31}P NMR (81 MHz, [D$_8$]THF, 233 K): *cis*-**2** (66%): δ = −8 (d, $^2J_{P,P}$ = 88 Hz, 1 P, PCH$_3$), 52 (d, $^2J_{P,P}$ = 88 Hz, 1 P, PC_6H_5); *trans*-**2** (34%): δ = −9 (d, $^2J_{P,P}$ = 348 Hz, 1 P, PCH$_3$), 32 (d, $^2J_{P,P}$ = 348 Hz, 1 P, PC_6H_5) ppm. $C_{24}H_{32}ClNNiP_2Si$ (517.1): calcd. C 55.57, H 6.22, N 2.70, P 11.94; found C 55.18, H 5.78, N 2.66, P 11.95.

[2-(Diphenylphosphanyl)anilido-*N*,*P*](methyl)(trimethylphosphane)-nickel (3): 2-(Diphenylphosphanyl)aniline (910 mg, 3.28 mmol) in 70 mL of diethyl ether was combined at −70 °C with 1.6 M MeLi in diethyl ether (2.1 mL, 3.28 mmol), and this solution was added dropwise at −70 °C to $NiMeCl(PMe_3)_2$ (860 mg, 3.28 mmol) in 50 mL of diethyl ether. The mixture was warmed to 20 °C and concentrated to dryness in vacuo. The resulting orange solid was extracted with three 70-mL portions of fresh diethyl ether and the solution concentrated at 20 °C to afford orange crystals of **3** (358 mg). From the mother liquor at −27 °C a light yellow solid (632 mg) was obtained which consisted of **3** only (NMR). Combined yields 990 mg (71%); m.p. 105−106 °C (dec.). IR (Nujol): ṽ = 3348 cm^{-1} (N−H). ^{1}H NMR (300 MHz, [D$_8$]THF): *cis*-**3** (60%): δ = −0.07 (dd, $_{trans}{}^3J_{P,H}$ = 4.1, $_{cis}{}^3J_{P,H}$ = 8.8 Hz, 3 H, NiCH$_3$), 1.29 (d, $^2J_{P,H}$ = 3.6 Hz, 9 H, PCH$_3$), 3.44 (s, 1 H, NH), 5.85 (m, 1 H, CH), 6.64−6.67 (m, 1 H, CH), 6.85 (t, ^3J = 6.9 Hz, 1 H, CH), 7.31 (m, 1 H, CH), 7.33−7.36 (m, 6 H, CH), 7.62−7.67 (m, 4 H, CH); *trans*-**3** (40%): δ = −0.82 (d, $^3J_{P,H}$ = 6.1 Hz, 3 H, NiCH$_3$), 1.09 (d, $^2J_{P,H}$ = 8.6 Hz, 9 H, PCH$_3$), 3.06 (s, 1 H, NH), 5.88 (dd, ^3J= 7.0, ^4J= 1.4 Hz, 1 H, CH), 5.91 (dd, ^3J = 8.2, $^4J_{P,H}$ = 5.0 Hz, 1 H, CH), 6.64−6.67 (m, 2 H, CH), 7.36−7.41 (m, 6 H, CH), 7.70−7.77 (m, 4 H, CH) ppm. ^{13}C NMR (75.4 MHz, [D$_8$]THF, 296 K): *cis*-**3** (60%): δ = 4.2 (dd, $^2J_{P,C}$ = 33.8, $^2J_{P,C}$ = 62.6 Hz, NiCH$_3$), 12.6 (d, $^1J_{P,C}$ = 21.9 Hz, PCH$_3$), 108.8 (d, $^3J_{P,C}$ = 6.2 Hz, C-2), 115.9 (d, $^2J_{P,C}$ = 9.5 Hz, *m*-C), 128.9 (d, $^2J_{P,C}$ = 9.3 Hz, *p*-C), 130.2 (s, C-5), 134.1 (d, $^2J_{P,C}$ = 11.4 Hz, *o*-C), 134.3 (s, C-3), 134.7 (s, *i*-C), 134.9 s, C-6), 171.4 (d, $^2J_{P,C}$ = 31.0 Hz, NC-1); *trans*-**3** (40%): δ = −16.8 (d, $^2J_{P,C}$ = 24.1 Hz, NiCH$_3$), 16.3 (d, $^1J_{P,C}$ = 28.9 Hz, PCH$_3$), 110.4 (d, $^3J_{P,C}$ = 5.6 Hz, C-2), 114.8 (d, $^3J_{P,C}$ = 3.0 Hz, C-5), 128.9 (d, $^2J_{P,C}$ = 8.6 Hz, *m*-C), 130.4 (s, *p*-C), 132.6 (d, $^2J_{P,C}$ = 10.2 Hz, *o*-C), 133.2 (s, C-3), 134.7 (s, C-4), 134.9 (s, *i*-C), 135.2 (s, C-6), 169.9 (d, $^2J_{P,C}$ = 32.7 Hz, NC-1) ppm. ^{31}P NMR (81 MHz, [D$_8$]THF): *cis*-**1** (60%, 193 K): δ = −2 (d, $^2J_{P,P}$ = 27 Hz, 1 P, PCH$_3$), 40 (d, $^2J_{P,P}$ = 27 Hz, 1 P, PC_6H_5); *trans*-**3** (40%, 193 K): δ = −2 (d, $^2J_{P,P}$ = 303 Hz, 1 P, PCH$_3$), 40 (d, $^2J_{P,P}$ = 303 Hz, 1 P, PC_6H_5); *cis*-**1** (60%, 296 K): δ = −2 (d, $^2J_{P,P}$ = 25 Hz, 1 P, PCH$_3$), 40 (d, $^2J_{P,P}$ = 25 Hz, 1 P, PC_6H_5); *trans*-**3** (40%, 296 K): δ = −5 (s, 1 P, PCH$_3$), 37 (s, 1 P, PC_6H_5) ppm. $C_{22}H_{27}NNiP_2$ (425.1): calcd. C 62.01, H 6.38, N 3.28, P 14.53; found C 61.52, H 6.51, N 3.16, P 14.48.

[2-(Diphenylphosphanyl)-*N*-methylanilido-*N*,*P*](methyl)(trimethylphosphane)nickel (4): 2-(Diphenylphosphanyl)-*N*-methylaniline (970 mg, 3.32 mmol) in 50 mL of diethyl ether was combined at −70 °C with 1.6 M MeLi in diethyl ether (2.2 mL, 3.32 mmol), and

this solution was added dropwise at −70 °C to $NiMeCl(PMe_3)_2$ (870 mg, 3.32 mmol) in 80 mL of diethyl ether. The orange-red mixture was warmed to 20 °C, filtered, and concentrated to dryness in vacuo. The resulting solid was washed with 5 mL of pentane and dried at 20 °C in vacuo to afford a yellow solid of **4** (1.18 g). Single orange crystals obtained from toluene were found suitable for X-ray diffraction. Yield 71%; m.p. 122−124 °C (dec.). ^{1}H NMR (300 MHz, [D$_8$]THF): *cis*-**4** (88%): δ = 0.13 (m, 3 H, $NiCH_3$), 1.15 (d, $^2J_{P,H}$ = 6.9 Hz, 9 H, PCH_3), 2.60 (s, 3 H, NCH_3), 5.89 (m, 1 H, CH), 6.15 (m, 1 H, CH), 6.62 (m, 1 H, CH), 6.84 (m, 1 H, CH), 7.39 (m, 6 H, CH), 7.59−7.73 (m, 4 H, CH); *trans*-**4** (12%): δ = −0.77 (m, 3 H, $NiCH_3$), 1.05 (d, $^2J_{P,H}$ = 8.9 Hz, 9 H, PCH_3), 2.80 (s, NCH_3) ppm. ^{13}C NMR (75.4 MHz, [D$_8$]THF, 296 K): *cis*-**4**: δ = 4.9 (m, $NiCH_3$), 14.5 (d, $^1J_{P,C}$ = 30.6 Hz, PCH_3), 35.2 (s, NCH_3), 108.4 (s, C-2), 108.7 (s, C-5), 127.1 (d, $^1J_{P,C}$ = 16.9 Hz, *m*-C), 127.4−131.1 (m, C-3/C-4), 131.7 (d, $^1J_{P,C}$ = 26.7 Hz, *o*-C), 132.2 (d, $^2J_{P,C}$ = 12.1 Hz, *p*-C), 153.6 (s, C-6) ppm. ^{31}P NMR (81 MHz, [D$_8$]THF, 233 K): *cis*-**4** (88%): δ = −1 (d, $^2J_{P,P}$ = 32 Hz, 1 P, PCH_3), 38 (d, $^2J_{P,P}$ = 32 Hz, 1 P, PC_6H_5); *trans*-**4** (12%): δ = −9 (d, $^2J_{P,P}$ = 329 Hz, 1 P, PCH_3), 34 (d, $^2J_{P,P}$ = 329 Hz, 1 P, PC_6H_5) ppm. $C_{22}H_{27}NNiP_2$ (425.1): calcd. C 62.76, H 6.64, N 3.18, P 14.07; found C 63.15, H 7.19, N 3.04, P 13.70.

[2-(Diphenylphosphanyl)-*N*-(trimethylsilyl)anilido-*N*,*P*](methyl)-(trimethylphosphane)nickel (5): 2-(Diphenylphosphanyl)-*N*-(trimethylsilyl)aniline (830 mg, 2.37 mmol) in 80 mL of diethyl ether was combined at −70 °C with 1.6 M MeLi in diethyl ether (1.5 mL, 2.40 mmol), and to the fluorescent solution was added at −70 °C solid $NiMeCl(PMe_3)_2$ (620 mg, 2.37 mmol) to form a deep red mixture. The mixture was warmed to 20 °C, stirred for 1 h, and concentrated to dryness in vacuo. The residue was extracted with two 70-mL portions of diethyl ether and the red solution cooled to −27 °C to afford deep orange crystals of **5** (732 mg). Yield 62%; m.p. 83−84 °C (dec.). ^{1}H NMR (300 MHz, [D$_8$]THF): *cis*-**5** (58%): δ = −0.01 (dd, $_{trans}{}^3J_{P,H}$ = 3.8 Hz, $_{cis}{}^3J_{P,H}$ = 8.8 Hz, 3 H, $NiCH_3$), 0.09 (s, 9 H, $SiCH_3$), 1.09 (d, $^2J_{P,H}$ = 4.1 Hz, 9 H, PCH_3), 5.86 (m, 1 H, CH), 6.55 (m, 1 H, CH), 6.75 (m, 1 H, CH), 7.25 (m, 1 H, CH), 7.31−7.35 (m, 6 H, CH), 7.64−7.70 (m, 4 H, CH); *trans*-**5** (42%): δ = 0.82 (d, $^3J_{P,H}$ = 4.5 Hz, 3 H, $NiCH_3$), 0.07 (s, 9 H, $SiCH_3$), 1.08 (d, $^2J_{P,H}$ = 8.6 Hz, 9 H, PCH_3), 5.88 (m, 1 H, CH), 6.19 (dd, ^3J = 8.0, ^4J = 4.7 Hz, 1 H, CH), 6.55−6.63 (m, 1 H, CH), 6.85 (m, 1 H, CH), 7.36−7.41 (m, 6 H, CH), 7.71−7.77 (m, 4 H, CH) ppm. ^{13}C NMR (75.4 MHz, [D$_8$]THF): *cis*-**5** (58%): δ = 1.6 (s, $SiCH_3$), 4.2 (m, $NiCH_3$), 12.7 (d, $^1J_{P,C}$ = 21.9 Hz, PCH_3), 110.8 (s, C-2), 115.9 (s, C-5), 129.3 (d, $^2J_{P,C}$ = 9.2 Hz, *m*-C), 133.2−134.6 (s, C-1, *o*-C, *p*-C), 135.0 (s, C-6), 172.3 (d, $^2J_{P,C}$ = 31.5 Hz, NC-1); *trans*-**5** (42%): δ = −16.9 (d, $^2J_{P,C}$ = 24.9 Hz, $NiCH_3$), 1.9 (s, $SiCH_3$), 16.1 (d, $^1J_{P,C}$ = 25.9 Hz, PCH_3), 111.2 (d, $^3J_{P,C}$ = 6.1 Hz, C-2), 114.8 (s, C-5), 129.0 (s, C-3), 130.5 (d, $^2J_{P,C}$ = 18.7 Hz, *o*-C), 132.7 (d, $^2J_{P,C}$ = 9.8 Hz, *m*-C), 133.2 (s, *p*-C), 134.1 (d, $^2J_{P,C}$ = 11.9 Hz, *i*-C), 134.7 (s, C-4), 135.2 (s, C-6), 171.2 (d, $^2J_{P,C}$ = 30.8 Hz, NC-1) ppm. ^{31}P NMR (81 MHz, [D$_8$]THF, 233 K) *cis*-**5** (58%): δ = 1 (d, $^2J_{P,P}$ = 27 Hz, 1 P, PCH_3), 40 (d, $^2J_{P,P}$ = 27 Hz, 1 P, PC_6H_5); *trans*-**5** (42%): δ = −3 (d, $^2J_{P,P}$ = 297 Hz, 1 P, PCH_3), 40 (d, $^2J_{P,P}$ = 297 Hz, 1 P, PC_6H_5) ppm. $C_{25}H_{35}NNiP_2Si$ (497.1): calcd. C 6.26, H 7.08, N 2.81, P 12.40; found C 60.36, H 6.75, N 2.78, P 12.15.

[2-(Diisopropylphosphanyl)-*N*-methylanilido-*N*,*P*](methyl)(trimethylphosphane)nickel (6): 2-(Diphenylphosphanyl)-*N*-methylaniline (780 mg, 3.49 mmol) in 50 mL of diethyl ether was combined at −70 °C with 1.6 M MeLi in diethyl ether (2.3 mL, 3.50 mmol), and to the yellow fluorescent solution was added solid $NiMeCl(PMe_3)_2$ (912 mg, 3.49 mmol). The mixture was warmed to 20 °C and concentrated to dryness in vacuo. The resulting orange solid was extracted with two 50-mL portions of pentane, and the combined solutions after repeatedly concentrating and cooling to −27 °C afforded red crystals of **6** (751 mg). Yield 58%; m.p. 104−105 °C (dec.). ^{1}H NMR (300 MHz, [D$_8$]THF, 296 K): *trans*-**6** (78%): δ = −0.65 (d, $^3J_{P,H}$ = 9.1 Hz, 3 H, $NiCH_3$), 1.00 (d, $^2J_{P,H}$ = 3.6 Hz, 18 H, PCH_3), 2.67 (s, 3 H, NCH_3), 5.82 (m, 1 H, CH), 5.89 (d, ^3J = 7.2 Hz, 1 H, CH), 6.57−6.63 (m, 2 H, CH), 7.22−7.27 (m, 6 H, CH), 7.46− 7.48 (m, 4 H, CH); *cis*-**6** (22%): δ = −0.07 (dd, $_{trans}{}^3J_{P,H}$ = 3.7, $_{cis}{}^3J_{P,H}$ = 6.5 Hz, 3 H, $NiCH_3$), 1.00 (br. s, 9 H, PCH_3), 2.48 (s, 3 H, NCH_3). ^{1}H NMR (300 MHz, [D$_8$]toluene): *trans*-**6** (> 98%): δ = 0.33 (dd, $^3J_{P,H}$ = 4.1 and 8.2 Hz, 3 H, $NiCH_3$), 1.00 (d, $^2J_{P,H}$ = 6.2 Hz, 9 H, PCH_3), 1.24 (br. d, $^3J_{P,H}$ = 7.1 Hz, 6 H, $PCHCH_3$), 1.28 (br. d, $^3J_{P,H}$ = 7.1 Hz, 6 H, $PCHCH_3$), 2.34 (m, 2 H, PCH), 2.98 (s, 3 H, NCH_3), 6.40 (t, ^3J = 7.1 Hz, 1 H, CH), 6.49 (dd, ^3J = 8.4, ^4J = 2.2 Hz, 1 H, CH), 7.12 (t, ^3J = 7.4 Hz, 1 H, CH), 7.31 (dt, ^3J = 7.1, $^4J_{P,H}$ = 1.4 Hz, 1 H, CH) ppm. ^{13}C NMR (75.4 MHz, [D$_8$]THF, 296 K): *trans*-**6**: δ = −14.3 (d, $^2J_{P,C}$ = 16.8 Hz, $NiCH_3$), 16.7 (d, $^1J_{P,C}$ = 7.6 Hz, PCH_3), 44.4 (s, N*C*H$_3$), 108.5 (s, C-2), 110.4 (d, $^2J_{P,C}$ = 12.5 Hz, 5-C), 128.9 (d, $^2J_{P,C}$ = 8.6 Hz, *m*-C), 129.4−131.9 (m, *p*-C/C-3), 133.3 (d, $^2J_{P,C}$ = 11.5 Hz, *o*-C), 134.4 (d, $^2J_{P,C}$ = 12.4 Hz, C-4), 135.3 (s, *i*-C), 139.8 (s, C-6) ppm. ^{31}P NMR (81 MHz, [D$_8$]THF, 193 K): *trans*-**6** (78%): δ = −11 (d, $^2J_{P,P}$ = 326 Hz, 1 P, PCH_3), 45 (d, $^2J_{P,P}$ = 297 Hz, 1 P, $PCHCH_3$); *cis*-**1** (22%): δ = −1 (d, $^2J_{P,P}$ = 25 Hz, 1 P, PCH_3), 45 (d, $^2J_{P,P}$ = 25 Hz, 1 P, $PCHCH_3$) ppm. ^{31}P NMR (81 MHz, [D$_8$]toluene): *trans*-**6** (> 98%): δ = −18 (d, $^2J_{P,P}$ = 327 Hz, 1 P, PCH_3), 40 (d, $^2J_{P,P}$ = 327 Hz, 1 P, $PCHCH_3$) ppm. $C_{17}H_{33}NNiP_2$ (371.1): calcd. C 54.87, H 8.94, N 3.76, P 16.65; found C 54.88, H 8.83, N 3.71, P 16.70.

[2-(Diphenylphosphanyl)anilido-*N*,*P*](methyl)bis(trimethylphosphane)nickel (7): 2-(Diphenylphosphanyl)aniline (810 mg, 2.92 mmol) in 50 mL of diethyl ether was combined at −70 °C with 1.6 M MeLi in diethyl ether (1.8 mL, 2.92 mmol), and this solution was added dropwise at −70 °C to $NiMeCl(PMe_3)_2$ (763 mg, 2.92 mmol) in 50 mL of diethyl ether. Workup proceeded as with **3**, and crystallization from 70 mL of pentane, containing excess PMe_3 (1.23 g, 16.1 mmol), afforded dark red crystals that were dried in vacuo at −5 °C for 10 min. Yield 790 mg of **7** (54%); m.p. 110−111 °C (dec.). IR (Nujol): $\tilde{\nu}$ = 3361 cm^{-1} (N−H). ^{1}H NMR (300 MHz, [D$_8$]THF, 296 K): *trans*-**7** (66%): δ = −0.75 (d, $^3J_{P,H}$ = 8.6 Hz, 3 H, $NiCH_3$), 1.00 (d, $^2J_{P,H}$ = 3.6 Hz, 18 H, PCH_3), 2.78 (NH 3,44s, 1 H, NH), 5.86 (m, 1 H, CH), 6.19 (dd, ^3J = 6.2, ^4J = 1.6 Hz, 1 H, CH), 6.66 (m, 1 H, CH), 6.85 (m, 1 H, CH), 7.30−7.38 (m, 6 H, CH), 7.64−7.74 (m, 4 H, CH); *cis*-**7** (34%): δ = −0.06 (m, 3 H, $NiCH_3$), 1.00 (d, $^2J_{P,H}$ = 3.6 Hz, 9 H, PCH_3), 3.44 (s, 1 H, NH), 5.88 (m, 1 H, CH), 6.20 (m, 1 H, CH) ppm. ^{13}C NMR (75.4 MHz, [D$_8$]THF, 296 K): *trans*-**7**: δ = −14.1 (m, $NiCH_3$), 16.7 (d, $^1J_{P,C}$ = 7.2 Hz, PCH_3), 45.1 (s, NCH_3), 108.5−135.4 (s, 10 C) ppm. ^{31}P NMR (81 MHz, [D$_8$]THF, 233 K): *trans*-**7** (66%): δ = −26 (br. s, 2 P, PCH_3), 27 (br. s, 1 P, PC_6H_5); *cis*-**7** (34%): δ = −1 (d, $^2J_{P,P}$ = 26 Hz, 1 P, PCH_3), 39 (d, $^2J_{P,P}$ = 26 Hz, 1 P, PC_6H_5) ppm. $C_{25}H_{35}NNiP_3$ (501.1): calcd. C 59.79, H 7.23, N 2.79, P 18.50; found C 58.80, H 7.39, N 2.74, P 18.33.

[2-(Diphenylphosphanyl)-*N*-methylanilido-*N*,*P*](methyl)bis(trimethylphosphane)nickel (8). Method a: 2-(Diphenylphosphanyl)-*N*-methylaniline (845 mg, 2.90 mmol) in 70 mL of THF was combined at −70 °C with $NiMe_2(PMe_3)_3$ (920 mg, 2.90 mmol) in 80 mL of diethyl ether. Warming to 20 °C caused evolution of gas and a dark red color. After 3 h, the volatiles were removed in vacuo and the residue was extracted with 70 mL of pentane, containing excess PMe_3 (610 mg, 8.0 mmol). Cooling to −27 °C afforded dark

red crystals of **8**: Yield 478 mg (32%). **Method b:** 2-(Diphenylphosphanyl)-*N*-methylaniline (770 mg, 2.64 mmol) in 70 mL of diethyl ether was combined at −70 °C with 1.6 M MeLi in diethyl ether (1.7 mL, 2.64 mmol), and to the yellow fluorescent solution was added $NiMeCl(PMe_3)_2$ (690 mg, 2.64 mmol) in 50 mL of diethyl ether. The deep red mixture was warmed to 20 °C and after 3 h concentrated to dryness in vacuo. The resulting solid was worked up as above affording crystals of **8**. Yield 912 mg (67%); m.p. 117−119 °C (dec.). ^{1}H NMR (300 MHz, [D$_8$]THF, 296 K): *trans*-**8** (79%): δ = −0.74 (d, $^3J_{P,H}$ = 10.1 Hz, 3 H, $NiCH_3$), 1.02 (d, $^2J_{P,H}$ = 4.8 Hz, 18 H, PCH_3), 1.24 (d, $^2J_{P,H}$ = 12.6 Hz, 9 H, PCH_3), 2.66 (s, 3 H, NCH_3), 5.95 (t, ^3J = 7.2 Hz, 1 H, CH), 6.12 (dd, $^4J_{P,H}$ = 5.0, ^3J = 8.5 Hz, 1 H, CH), 6.86 (dt, ^3J = 8.1, ^4J = 1.5 Hz, 1 H, CH), 7.22 (dt, ^3J = 7.4, ^4J = 1.5 Hz, 1 H, CH), 7.21−7.29 (m, 3 H, CH), 7.59−7.67 (m, 2 H, CH); *cis*-**8** (21%): δ = −0.07 (dd, $^3J_{P,H}$ = 4.2, $^3J_{P,H}$ = 8.2 Hz, 3 H, $NiCH_3$), 1.12 (d, $^2J_{P,H}$ = 4.8 Hz, 9 H, PCH_3), 1.47 (d, $^2J_{P,H}$ = 13.2 Hz, 9 H, PCH_3), 2.59 (s, 3 H, NCH_3), 5.83 (t, ^3J = 7.1 Hz, 1 H, CH), 6.17 (dd, $^4J_{P,H}$ = 5.2, ^3J = 8.2 Hz, 1 H, CH), 6.41 (dt, ^3J = 8.8, ^4J = 1.5 Hz, 1 H, CH), 6.86 (dt, ^3J = 8.1, ^4J = 1.5 Hz, 1 H, CH), 7.31−7.33 (m, 3 H, CH), 7.70−7.80 (m, 2 H, CH) ppm. ^{13}C NMR (75.4 MHz, [D$_8$]THF, 296 K): *trans*-**8**: δ = −14.4 (d, $^2J_{P,C}$ = 14.5 Hz, $NiCH_3$), 16.3 (d, $^2J_{P,C}$ = 6.9 Hz, PCH_3), 29.1 (d, $^1J_{P,C}$ = 5.8 Hz, CCH_3), 36.3 d $^2J_{P,C}$ = 11.9 Hz, CCH_3), 44.6 (s, NCH_3), 107.5 (s, C-2), 110.1 (s, C-5), 110.7 (d, $^2J_{P,C}$ = 10.8 Hz, *o*-C), 127.9 (s, C-3), 128.5 (d, $^3J_{P,C}$ = 6.8 Hz, *p*-C), 131.8 (s, C-4), 132.8 (d, $^3J_{P,C}$ = 8.4 Hz, *m*-C), 133.9 (s, *i*-C), 134.8 (s, C-6), 170.5 (m, NC-1) ppm. ^{31}P NMR (81 MHz, [D$_8$]THF, 233 K): *trans*-**8** (79%): δ = −16 (d, $^2J_{P,P}$ = 181 Hz, 2 P, PCH_3), 31 (t, $^2J_{P,P}$ = 181 Hz, 1 P, PC_6H_5); *cis*-**8** (21%): δ = −1 (d, $^2J_{P,P}$ = 29 Hz, 1 P, PCH_3), 57 (d, $^2J_{P,P}$ = 29 Hz, 1 P, PC_6H_5) ppm. $C_{26}H_{38}NNiP_3$ (515.2): calcd. C 60.49, H 7.42, N 2.71, P 18.00; found C 60.71, H 7.30, N 2.75, P 18.10.

{2-[*tert*-Butyl(phenyl)phosphanyl]-*N*-methylanilido-*N*,*P*}(methyl)bis-(trimethylphosphane)nickel (9): 2-[*tert*-Butyl(phenyl)phosphanyl]-*N*-methylaniline (680 mg, 2.50 mmol) in 80 mL of diethyl ether was treated at − 50 °C whilst stirring with 1.6 M MeLi in diethyl ether (1.6 mL, 2.50 mmol). After warming to 20 °C, the mixture was stirred until evolution of gas had ceased. At − 50 °C this reagent was combined with $NiClMe(PMe_3)_2$ (655 mg, 2.50 mmol) in 50 mL of diethyl ether. The mixture was stirred at 20 °C for 3 h and concentrated to dryness in vacuo. The resulting orange solid was extracted with two 50-mL portions of pentane and the solution concentrated at 20 °C to afford short red rods of **9**. Yield 583 mg (47%), m.p. 115−117 °C (dec.). ^{1}H NMR (300 MHz, [D$_8$]THF, 296 K): *trans*-**9** (79%): δ = −0.74 (d, $^3J_{P,H}$ = 10.1 Hz, 3 H, $NiCH_3$), 1.02 (d, $^2J_{P,H}$ = 4.8 Hz, 18 H, PCH_3), 1.24 (d, $^2J_{P,H}$ = 12.6 Hz, 9 H, PCH_3), 2.66 (s, 3 H, NCH_3), 5.95 (t, ^3J = 7.2 Hz, 1 H, CH), 6.12 (dd, $^4J_{P,H}$ = 5.0, ^3J = 8.5 Hz, 1 H, CH), 6.86 (dt, ^3J = 8.1, ^4J = 1.5 Hz, 1 H, CH), 7.22 (dt, ^3J = 7.4, ^4J = 1.5 Hz, 1 H, CH), 7.21−7.29 (m, 3 H, CH), 7.59−7.67 (m, 2 H, CH); *cis*-**9** (21%): δ = −0.07 (dd, $_{trans}{}^3J_{P,H}$ = 4.2 Hz, $_{cis}{}^3J_{P,H}$ = 8.2 Hz, 3 H, $NiCH_3$), 1.12 (d, $^2J_{P,H}$ = 4.8 Hz, 9 H, PCH_3), 1.47 (d, $^2J_{P,H}$ = 13.2 Hz, 9 H, PCH_3), 2.59 (s, 3 H, NCH_3), 5.83 (t, ^3J = 7.1 Hz, 1 H, CH), 6.17 (dd, $^4J_{P,H}$ = 5.2, ^3J = 8.2 Hz, 1 H, CH), 6.41 (dt, ^3J = 8.8, ^4J = 1.5 Hz, 1 H, CH), 6.86 (dt, ^3J = 8.1, ^4J = 1.5 Hz, 1 H, CH), 7.31−7.33 (m, 3 H, CH), 7.70−7.80 (m, 2 H, CH) ppm. ^{13}C NMR (75.4 MHz, [D$_8$]THF, 296 K): *trans*-**9**: δ = −14.4 (d, $^2J_{P,C}$ = 14.5 Hz, $NiCH_3$), 16.3 (d, $^2J_{P,C}$ = 6.9 Hz, PCH_3), 29.1 (d, $^1J_{P,C}$ = 5.8 Hz, CCH_3), 36.3 (d, $^2J_{P,C}$ = 11.9 Hz, CCH_3), 44.6 (s, NCH_3), 107.5 (s, C-2), 110.1 (s, C-5), 110.7 (d, $^2J_{P,C}$ = 10.8 Hz, *o*-C), 127.9 (s, C-3), 128.5 (d, $^3J_{P,C}$ = 6.8 Hz, *p*-C), 131.8 (s, C-4), 132.8 (d, $^3J_{P,C}$ = 8.4 Hz, *m*-C), 133.9 (s, *i*-C), 134.8 (s, C-6), 170.5 (m, NC-1) ppm. ^{31}P NMR (81 MHz, [D$_8$]THF, 233 K): *trans*-**9** (79%): δ = −16 (d, $^2J_{P,P}$ = 181 Hz, 2 P, PCH_3), 31 (t, $^2J_{P,P}$ = 181 Hz, 1 P, PC_6H_5); *cis*-**9** (21%): δ = −1 (d, $^2J_{P,P}$ = 29 Hz, 1 P, PCH_3), 57 (d, $^2J_{P,P}$ = 29 Hz, 1 P, PC_6H_5) ppm. $C_{24}H_{42}NNiP_3$ (495.2): calcd. C 58.09, H 8.53, N 2.82, P 18.73; found C 58.06, H 8.40, N 2.73, P 18.70.

Crystal Structure Analyses: Crystal data are presented in Table 2. Data collection: Complex *cis*-**5**: A crystal was sealed under argon in a glass capillary and mounted on a Stoe Stadi-4 diffractometer. Reflections were collected (ω-scans) using graphite-monochromated Mo-K_α radiation; absorption corrections based on ψ-scans were applied. The structure was solved by direct and conventional Fourier methods. All non-hydrogen atoms were treated anisotropically, hydrogen atoms were treated with a riding model in idealized positions. The final *wR*2 value is high due to poor crystal quality, but there is no doubt about the space group. Complex **7**: Crystal mounting, data collection, structure solution, and refinement as for *cis*-**5**. Crystallographic data (excluding structure factors) for the structures reported in this paper have been deposited with the Cambridge Crystallographic Data Centre. Copies of the data [CCDC-186327 (*cis*-**5**) and -186328 (**7**)] can be obtained free of charge on application to CCDC, 12 Union Road, Cambridge CB2 1EZ, UK [Fax: (internat.) + 44-1223/336-033, E-mail: deposit@ccdc.cam.ac.uk].

Table 2. Crystal data for compounds *cis*-**5** and **7**

	cis-**5**	**7**
Empirical formula	$C_{25}H_{35}NNiP_2Si$	$C_{26}H_{38}NNiP_3$
Formula mass	498.4	516.3
Crystal size [mm]	0.38 × 0.20 × 0.19	0.41 × 0.30 ×0.18
Crystal system	monoclinic	monoclinic
Space group	$P2_1/c$	$P2_1/c$
a [Å]	10.6570(9)	8.558(3)
b [Å]	18.9000(11)	19.911(10)
c [Å]	26.19900(17)	15.817(7)
β [°]	90.870(5)	93.13(3)
V [Å^3]	5276.32(40)	2726.2(2)
Z	4	4
$D_{calcd.}$ [g/cm^3]	1.255	1.255
μ(Mo-K_α) [mm^{-1}]	0.856	0.843
T [K]	293(2)	293(2)
Data coll. range [°]	5.8 ≤ 2Θ ≤ 50	4.9 ≤ 2Θ ≤ 50
h	−10 ≤ *h* ≤ 10	−8 ≤ *h* ≤ 8
k	0 ≤ *k* ≤ 18	0 ≤ *k* ≤ 19
l	0 ≤ *l* ≤ 25	0 ≤ *l* ≤ 15
No. reflect. measured	13711	8166
No. unique data	4834 (R_{int} = 0.0367)	2535 (R_{int} = 0.0222)
Parameters	541	292
GoF on F^2	1.172	1.163
R_1 [$I \geq 2\sigma(I)$]	0.0727	0.0389
*wR*2 (all data)	0.3110	0.1295

Acknowledgments

Financial support of this work by the Fonds der Chemischen Industrie is gratefully acknowledged.

[1] [1a] C. W. G. Ansell, M. McPartlin, P. A. Tasker, M. K. Cooper, *Inorg. Chim. Acta* **1983**, *76*, 135. [1b] M. K. Cooper, J. M. Downes, H. J. Goodwin, M. McPartlin, *Inorg. Chim. Acta*

1983, *76*, 155−156. [1c] M. K. Cooper, J. M. Downes, H. J. Goodwin, M. McPartlin, *Inorg. Chim. Acta* **1983**, *76*, 157−158.
[2] L. Dahlenburg, K. Herbst, *Chem. Ber./Recueil* **1997**, *130*, 1693−1698.
[3] [3a] L. Crociani, F. Refosco, F. Tisato, S. Gatto, B. Corain, *Inorg. Chim. Acta* **1996**, *249*, 131−133. [3b] L. Crociani, F. Refosco, F. Tisato, S. Gatto, G. Bandoli, *Z. Crystallogr.* **1997**, *212*, 745−751. [3c] L. Crociani, F. Refosco, F. Tisato, G. Bandoli, B. Corain, *Eur. J. Inorg. Chem.* **1998**, 1687−1689.
[4] L. Crociani, G. Bandoli, A. Dolmella, M. Basato, B. Corain, *Eur. J. Inorg. Chem.* **1998**, 1811−1920.
[5] A. G. Orpen, L. Brammer, F. H. Allen, O. Kennard, D. G. Watson, R. Taylor, *J. Chem. Soc., Dalton Trans.* **1989**, S1−S83.
[6] H.-F. Klein, H. H. Karsch, *Chem. Ber.* **1973**, *106*, 1433−1452.
[7] J. Heinicke, M. He, A. Dal, H.-F. Klein, O. Hetche, W. Keim, U. Flörke, H.-J. Haupt, *Eur. J. Inorg. Chem.* **2000**, 431−440.
[8] O. Hetche, doctoral thesis, TU Darmstadt, **2000**.
[9] M. K. Cooper, J. M. Downes, P. A. Duckworth, R. T. Tiekink, *Aust. J. Chem.* **1992**, *45*, 595−609.
[10] A. B. van Oort, P. H. M. Budzelaar, J. H. G. Frijns, A. G. Orpen, *J. Organomet. Chem.* **1990**, *396*, 33−47.
[11] R. Beck, Doctoral thesis, TU Darmstadt, **2001**.

Received May 24, 2002
[I02269]

Fluxional and Rigid (Trimethylphosphane)cobalt Complexes Containing Chelating (2-Diphenylphosphanyl)anilido Ligands

Hans-Friedrich Klein,*[a] Robert Beck,[a] Ulrich Flörke,[b] and Hans-Jürgen Haupt[b]

Keywords: Chelates / Cobalt / P ligands / Structure elucidation

2-(Diphenylphosphanyl)anilines (P^NHR) eliminate methane upon reaction with $[CoMe(PMe_3)_4]$ forming the complexes $[Co(\eta^2\text{-}P\text{^}NR)(PMe_3)_3]$ (**1**: R = H; **2**: R = Me) and $[Co(\eta^2\text{-}P\text{^}NR)(PMe_3)_2]$ (**3**: R = Me). Reaction with HCl gives $[CoCl(\eta^1\text{-}P\text{^}NHR)(PMe_3)_2]$ (**4**: R = H; **5**: R = Me) and reaction with CO or olefin gives $[Co(\eta^2\text{-}P\text{^}NR)(CO)(PMe_3)_2]$ (**6**: R = H; **7**: R = Me) and $[Co(\eta^2\text{-}P\text{^}NR)(olefin)(PMe_3)_2]$ (**8**: R = H, olefin = C_2H_4; **9**: R = Me, olefin = C_2H_4; **10**: R = Me, olefin = C_3H_6), respectively. No catalytic transformation of the olefins was observed. Oxidation by iodomethane yields a cobalt(II) compound $[CoI(\eta^2\text{-}P\text{^}NR)(PMe_3)_2]$ (**11**: R = Me). By treating 2-(diphenylphosphanyl)aniline with $[CoMe_2(PMe_3)_3]$ a methylcobalt(II) complex $[CoMe(\eta^2\text{-}P\text{^}NR)(PMe_3)_2]$ (**12**: R = H) is obtained, while an excess of the aniline produces $[Co(\eta^2\text{-}P\text{^}NR)_2]$ (**13**: R = H; **14**: R = Me) or $[Co(\eta^2\text{-}P\text{^}NR)_2(PMe_3)]$ (**15**: R = H; **16**: R = Me). The methylcobalt(III) complexes *mer-trans*-$[CoIMe_2(\eta^2\text{-}P\text{^}NR)(PMe_3)_2]$ were obtained from LiP^NR and $[CoClMe_2(PMe_3)_3]$. Dynamic ^{31}P NMR spectra and the structures of complexes **3**, **6**, **12**, and **13** are discussed.
(© Wiley-VCH Verlag GmbH & Co. KGaA, 69451 Weinheim, Germany, 2003)

Introduction

Molecular derivatives of 2-(diphenylphosphanyl)aniline are well known as P,N-chelating ligands for the late transition metals,[1] and palladium(II), in particular, has been extensively investigated regarding certain aspects of homogeneous catalysis. Examples of first-row transition metals in early studies by Venanzi et al.[2] are molecular dihalides of cobalt and nickel (high-spin) which have a tetrahedral coordination geometry.

Formulae A

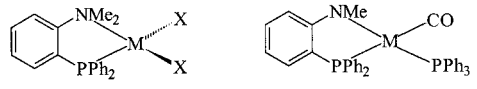

M = Co, Ni; X = Cl, Br, I M = Rh, Ir

Vaska-type square-planar complexes of rhodium(I) and iridium(I) containing 2-(diphenylphosphanyl)-*N*-methylanilido ligands have been investigated by Dahlenburg et al.,[3] and examples of a μ^2-bridging coordination mode of the 2-(diphenylphosphanyl)anilido ligand have been found in triangular clusters of ruthenium[4] and osmium.[5]

Here we describe the synthesis and structural properties of some novel mononuclear complexes of cobalt(I) and their transformation by oxidative addition reactions including an unexpected cyclometallation reaction.

Results and Discussion

2-(Diphenylphosphanyl)anilines react with $[CoMe(PMe_3)_4]$ [Equation (1)] with the elimination of methane to afford the pentacoordinate cobalt(I) complexes **1** and **2** as brown solids that are freely soluble in pentane or diethyl ether.

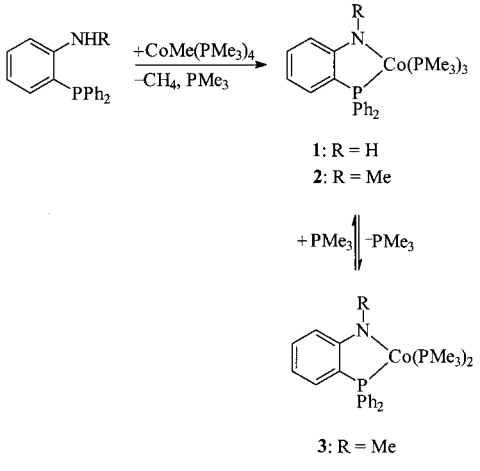

1: R = H
2: R = Me

(1)

3: R = Me

[a] Eduard-Zintl-Institut für Anorganische und Physikalische Chemie der Technischen Universität Darmstadt, Petersenstrasse 18, 64285 Darmstadt, Germany
[b] Anorganische und Analytische Chemie der Universität Paderborn, Warburger Straße, 33098 Paderborn, Germany

Complex **1** forms dark brown crystals, while **2** is obtained as a solid wax, in moderate yield, from pentane containing excess trimethylphosphane. When dissociation of ligands is favoured, by applying fresh solvent or warming solid **2** in vacuo, a gradual transformation to the tetracoordinate complex **3** is achieved which eventually forms small red brown rods that are highly air-sensitive but thermally stable up to 135 °C. The observed magnetic susceptibility ($\mu_{eff}/\mu_B = 2.97$) is typical for tetrahedral complexes of cobalt(I).

Complexes **1** and **2** show a characteristic pattern of ^{31}P NMR signals: a doublet of triplets at $\delta = 52$ ppm for the chelating P nucleus, which experiences a coordination chemical shift of $\delta = 70$ ppm, a doublet of doublets at $\delta = -7$ ppm for two isochronic P nuclei and a doublet of triplets at $\delta = 28$ ppm for a third trimethylphosphane P nucleus (Figure 1).

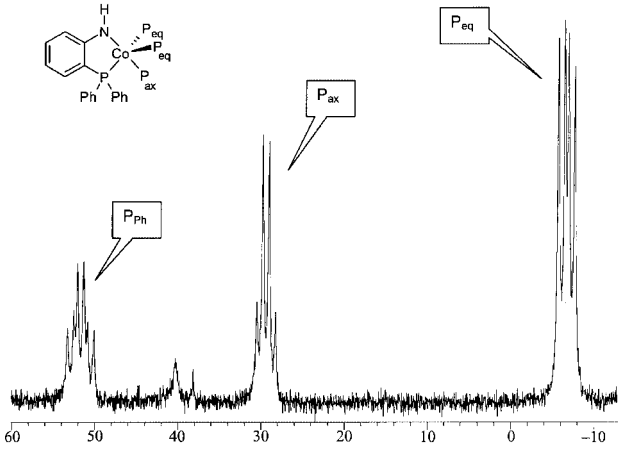

Figure 1. ^{31}P NMR spectrum of **1** (81 MHz, [D$_8$]THF, 233 K)

The values of the coupling constants ($J = 99$ and 61 Hz) fall in the range expected for the angles P−Co−P (90−110°) and suggest a trigonal-bipyramidal coordination geometry with two trimethylphosphane groups in equatorial positions.

In the molecular structure of **3** (Figure 2) a tetrahedral coordination geometry is confirmed by the angles P−Co−P (108−109°). The chelate bite angle P1−Co−N [86.34(8)°] is slightly larger than that found in a related pentacoordinate nickel(II) complex,[6] and the sum of the internal angles in the metallacycle (539.9°) equals that of a regular pentagon; N coordination to the cobalt(I) ion (16 valence electrons) [Co−N 1.926(2) Å] is found to be a normal distance,[7] and remarkably, the sum of the angles at the nitrogen atom (359.9°) indicates planarity as is the case in the nickel complex (18 valence electrons).

Reactions

Ethereal HCl protonates the N donor and one of the trimethylphosphane groups, thereby opening the chelate ring in **1** or **2** while retaining the Ph_2P donor group and generating the tetracoordinate complexes **4** and **5** [Equation (2)]. The process can be reversed by treating the compound with methyllithium. In a most convenient synthesis $CoCl(PMe_3)_3$ is treated with the appropriate 2-(diphenylphosphanyl)aniline [Equation (3)].

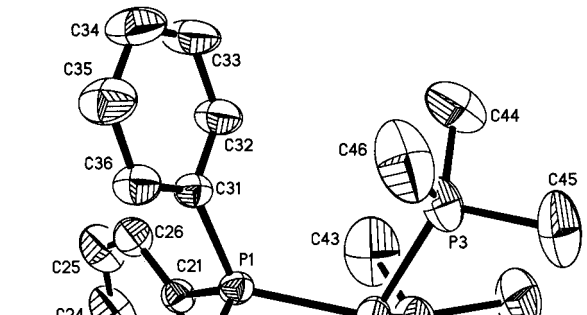

Figure 2. Molecular structure of **3** (ORTEP plot with hydrogen atoms omitted); selected bond lengths [Å] and angles [°]: Co−N1 1.926(2), Co−P1 2.2374(9), Co−P2 2.2243(10), Co−P3 2.2473(12), P1−C11 1.815(3), C11−C16 1.426(4), C16−N1 1.363(4); N1−Co−P1 86.34(8), N1−Co−P2 128.00(9), N1−Co−P3 118.97(9), C1−N1−Co 121.3(2), C16−N1−Co 122.24(18), C1−N1−C16 116.4(3), P1−Co−P2 108.58(4), P1−Co−P3 107.87(4), P2−Co−P3 103.64(4), Co−P1−C11 98.72(9), P1−C11−C16 114.4(2)

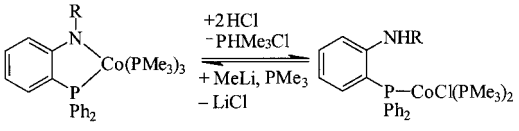

1, 2 **4**: R = H, **5**: R = Me (2)

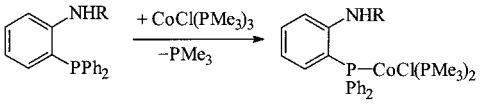

4: R = H, **5**: R = Me (3)

Complexes **4** and **5** form green solids that are insoluble in pentane, highly soluble in THF, and are best recrystallised from diethyl ether. IR spectra in the ν(NH) region show the expected number of bands at 3404 and 3318 cm^{-1} (**4**) that are close to those of 2-(diphenylphosphanyl)aniline.

A band occurring at 3332 cm^{-1} (**5**) is shifted by 30 cm^{-1} with respect to 2-(diphenylphosphanyl)-*N*-methylaniline indicating an intramolecular hydrogen bond N−H···Cl in **5**.

The values of the magnetic susceptibilities (**4**: μ_{eff}/μ_B = 3.29; **5**: μ_{eff}/μ_B = 3.25) are consistent for tetrahedral high-spin complexes.[8] Under 1 bar of CO **1** and **2** smoothly form monocarbonyl complexes [Equation (4)].

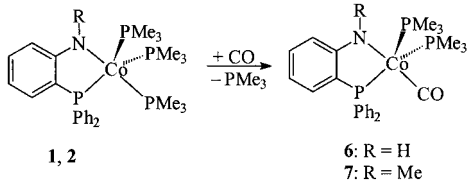

1, 2 **6**: R = H, **7**: R = Me (4)

From pentane, red crystals of **6** and **7** are obtained that are thermally stable up to 150 °C. IR spectra contain single ν(CO) bands of terminal carbonyl ligands (**6**: 1887 cm^{-1}; **7**: 1906 cm^{-1}) indicating that only one of the possible two isomers is present. The ^{31}P NMR doublet and triplet resonances at characteristic shifts, along with the larger coupling (J = 97 Hz) indicate that the carbonyl ligand resides in an axial position. This configuration is also adopted in the

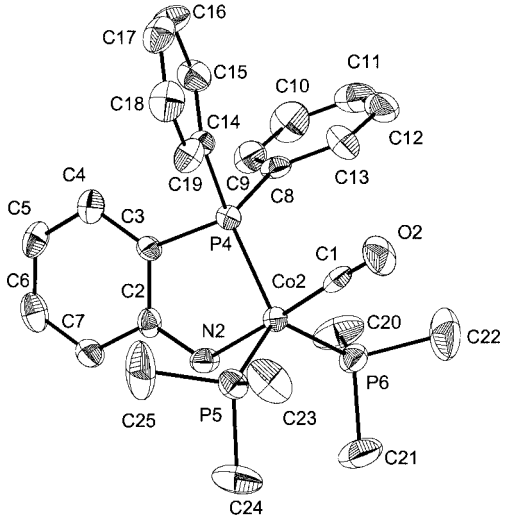

Figure 3. Molecular structure of **6** (ORTEP plot with hydrogen atoms omitted); selected bond lengths [Å] and angles [°]: Co−C1 1.754(14), C1−O2 1.157(15), Co−P4 2.210(3), Co−P5 2.184(3), Co−P6 2.194(3), Co−N2 1.907(9), N2−C2 1.360(14), C2−C3 1.411(15), P4−C3 1.80(1); N2−Co−C1 176.9(5), N2−Co−P4 84.3(3), N2−Co−P5 86.1(3), N2−Co−P6 88.2(3), Co−N2−C2 122.6(8), N2−C2−C3 118.8(9), C2−C3−P4 111.6(8), C3−P4−Co 100.6(4)

crystal, as shown by the molecular structure of **6** (Figure 3).

The carbonyl and amide ligands occupy axial positions with tighter bonding [Co−N = 1.907(9) Å] than that in **3** which arises from a push-pull stabilisation of ligands in *trans* positions [C−Co−N 176.9(5)°]. The chelate bite angle P4−Co−N [84.3(3)°] is only 2° larger than it is in **3**, and the sum of the internal angles in the metallacycle is 537.9°. There is a close structural correspondence between **6** and a related carbonylbis(trimethylphosphane)cobalt(I)(*P*,*O*-chelate) complex[9] as can be expected of isoelectronic O and NH donors.

Brown solutions of **1** or **2** in pentane under 1 bar of ethene or propene turn red and upon cooling afford red crystals of monoolefin complexes **8**−**10** [Equation (5)], in the case of **6** and **7** together with crystals of **3**. No reaction is observed in neat cyclopentene.

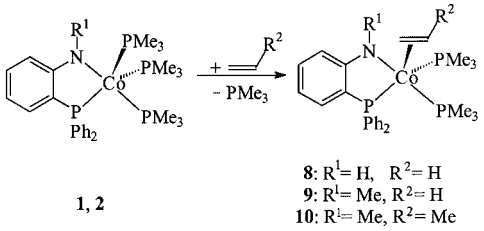

1, 2 **8**: R^1 = H, R^2 = H; **9**: R^1 = Me, R^2 = H; **10**: R^1 = Me, R^2 = Me (5)

Careful drying under a gas blanket of olefin and manual selection of crystals gives analytically pure samples of **8**−**10**. All three compounds are solids with low melting points that are sensitive towards heat and oxygen, already releasing olefin at 20 °C in vacuo. As no structural proof has been obtained by X-ray diffraction on single crystals, ^{31}P NMR spectroscopy was used to support pentacoordination in compounds **8**−**10**. At 193 K ligand mobility is slow enough to reveal the ground-state geometry through a doublet of doublets pattern of three ^{31}P NMR signals (Table 1).

Table 1. ^{31}P NMR spectroscopic data (81 MHz, [D_8]THF, 193 K) for (olefin)cobalt compounds **8**−**10** [δ in ppm, J in Hz]

	δ(P_{Ph})		δ(P_{ax})		δ(P_{eq})	
	$^2J(P_{Ph}P_{eq})$	$^2J(P_{Ph}P_{ax})$	$^2J(P_{ax}P_{Ph})$	$^2J(P_{ax}P_{eq})$	$^2J(P_{eq}P_{Ph})$	$^2J(P_{eq}P_{ax})$
8	61 (dd)		23 (dd)		3 (dd)	
	34	30	30	52	34	52
9	61 (dd)		23 (dd)		3 (dd)	
	36	32	32	56	36	56
10	61 (dd)		22 (dd)		3 (dd)	
	38	30	30	52	38	52

^{31}P nuclei of axial and equatorial trimethylphosphane groups are coupled with an equatorial chelating ^{31}P nucleus leaving an equatorial position for the olefin ligand. Reaction of **2** with iodomethane [Equation (6)] − oxidative substitution of a trimethylphosphane group and quaternisation − takes an unexpected course.

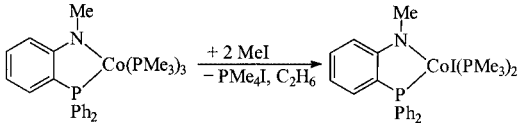

2 **11** (6)

Black crystals of an iodocobalt(II) complex **11** are obtained from diethyl ether. Elemental analysis shows that the cobalt atom has lost the initial methylmetal function and is coordinated to five ligands. Accordingly, the magnetic susceptibility (μ_{eff}/μ_B = 2.09) is as expected for a pentacoordin-

ate cobalt (d^7) compound.[10] A corresponding methylcobalt(II) complex **12** is obtained by reaction of 2-(diphenylphosphanyl)aniline with $CoMe_2(PMe_3)_3$ [Equation (7)].

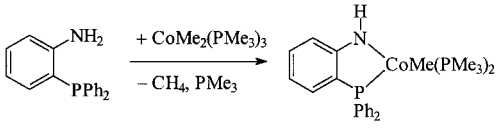

12 (7)

The black crystals of **12** are freely soluble in pentane and are thermally even more stable than **11**. The magnetic susceptibility (μ_{eff}/μ_B = 1.65) is at the lower end of that expected for a trigonal-bipyramidal configuration of the Co atom (d^7, 17 valence electrons).[10] While no solution structure of **12** could be derived from spectroscopic data, the molecular structure was revealed by X-ray diffraction (Figure 4).

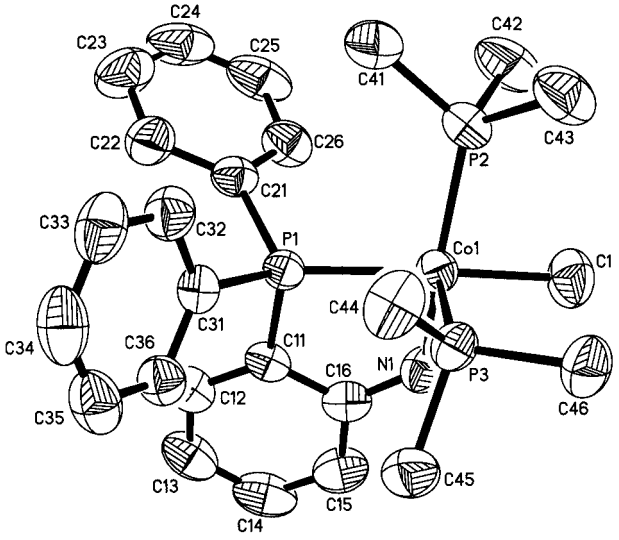

Figure 4. Molecular structure of **12** (ORTEP plot with hydrogen atoms omitted); selected bond lengths [Å] and angles [°]: Co–C1 2.019(3), Co–N1 1.929(2), Co–P1 2.2472(8), Co–P2 2.1858(9), Co–P3 2.2833(8), N1–C16 1.351(3), C16–C11 1.407(4), C11–P1 1.808(3); P1–Co–C1 162.43(10), N1–Co–P2 154.60(7), N1–Co–P3 102.47(7), N1–Co–P1 82.64(7), Co–N1–C16 125.32(18), N1–C16–C11 118.5(2), C16–C11–P1 111.83(19), C11–P1–Co 101.65(9)

The cobalt centre of **12** is located above an almost square plane (P1,P2,C1,N1) with an apical trimethylphosphane group (P3) attached to it at the longest Co–P distance. The void *trans* to P3 is large enough for, although not occupied by, a hydride ligand. This is seen from the IR spectrum where the ν(CoH) region is empty along with the d^7 valence state of the Co atom. The methyl ligand (C1) is arranged in the opposite position to the chelating P donor (P1) which is different from an otherwise related pentacoordinate methylnickel(II) complex (18 electrons), where it is *trans* to the amide donor.[6] The chelate bite angle is close to that in **3**, and the sum of the internal angles (539.9°) indicates a relaxed metallacycle. Reactivity of the methylmetal function is sufficient to afford bis(P,N)chelate compounds of cobalt(II) [Equation (8)].

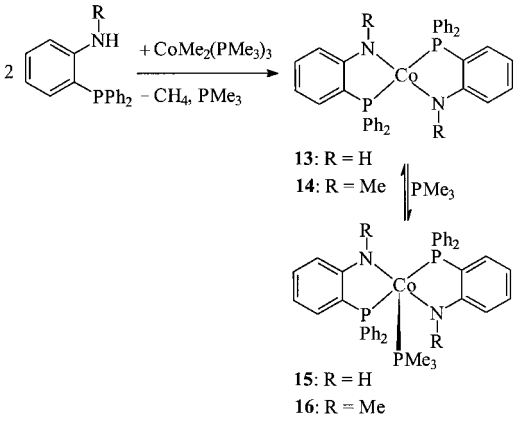

(8)

The molecular complexes **13** and **14** (15 metal valence electrons) are stable up to 250 and 200 °C, respectively. Only when additional trimethylphosphane is supplied in excess, does it coordinate to afford the pentacoordinate species **15** and **16**. Magnetic susceptibilities (**13**: μ_{eff}/μ_B = 2.05; **14**: μ_{eff}/μ_B = 2.33; **15**: μ_{eff}/μ_B = 2.10; **16**: μ_{eff}/μ_B = 2.04) fall in the range expected for tetracoordinate (low-spin)[9,11] and pentacoordinate[9,10] cobalt(II) compounds but give no further clue to the configuration of the complexes.

In the molecular structure of **13** (Figure 5) a *trans* square-planar arrangement of ligands is revealed around a cobalt atom sitting in a centre of inversion. The chelate bite angle is normal [P–Co–N 83.6(2)°] and so are the bond lengths [Co–N 1.858(6), Co–P 2.212(6) Å]. The structure of **13** is the first for this type of bis(*P*,*N*)chelate cobalt complex, with the *trans* configuration differing from that of isoelectronic *cis*-bis(*P*,*O*)chelate cobalt compounds.[9]

In an attempted synthesis of methylcobalt(III) complexes containing chelating 2-(diphenylphosphanyl)anilido ligands no reaction of $CoMe_3(PMe_3)_3$ with 2-(diphenylphosphanyl)aniline or 2-(diphenylphosphanyl)-*N*-methylaniline was observed. An alternative route [Equation (9)] afforded the dimethylcobalt(III) compounds **17** and **18**.

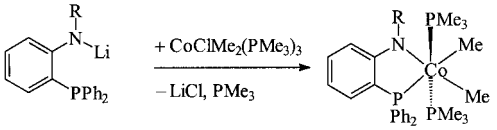

17: R = H
18: R = Me (9)

Highly soluble short orange rods of **17** and **18** are crystallised from pentane and melt at 85 and 89 °C, respectively. Under conditions of low ligand mobility (193 K) the ^{31}P NMR signals recorded as a triplet (1 P) and doublet (2 P) indicate a meridional arrangement of P donor functions in

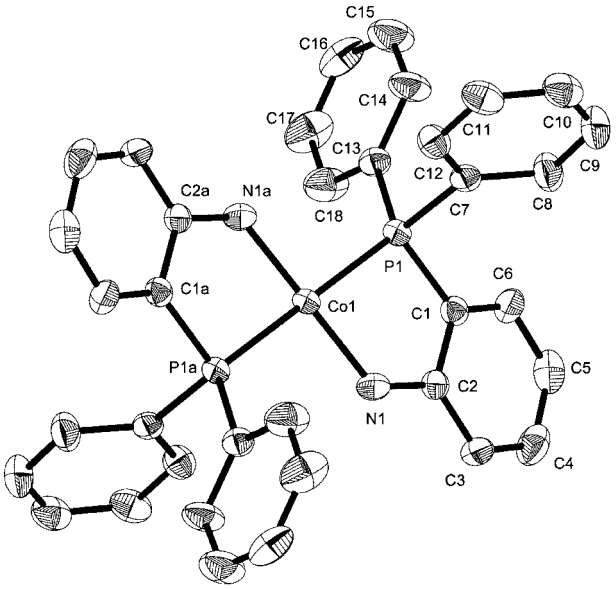

Figure 5. Molecular structure of **13** (ORTEP plot with hydrogen atoms omitted); selected bond lengths [Å] and angles [°]: Co−N1 1.858(6), Co−P1 2.212(2), P1−C1 1.798(8), C1−C2 1.398(10), C2−N1 1.389(9); C2−N1−Co 124.6(5), N1−C2−C1 117.0(7), C2−C1−P1 111.5(6), C1−P1−Co 100.8(3)

octahedral complexes of a low-spin Co (d^6) ion. Complex **15** tends to lose one of the methyl groups since after repeated recrystallisations black crystals of **12** were obtained.

Reactions involving methylcobalt compounds thus far have been directed towards a prechelate NH function and proceed with the elimination of methane. Surprisingly, [CoMe(PMe_3)$_4$] was found to react smoothly at −70 °C with 2-(diphenylphosphanyl)-*N*,*N*-dimethylaniline. Evolution of gas was observed while heating to 20 °C, and eventually dark red crystals of **19** were obtained and found to arise from a cyclometallation reaction [Equation (10)].

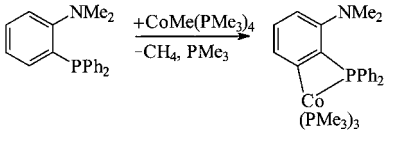

(10)

19

The ^{31}P NMR spectrum at 233 K clearly shows the characteristic shifts and coupling pattern of an *ortho*-metallated tris(trimethylphosphane)cobalt complex.[12] As no further signals are detected, the absence of possible isomers of **19** is confirmed. This unusual result is supported by the ^{13}C NMR spectroscopic data. Only ten resonances of aromatic carbon nuclei were detected whereas eighteen are expected to arise from altogether five available *ortho*-CH groups.

Consequently, a thorough search for isomers of **19** was undertaken. In view of an 80% yield the synthesis was repeated on a larger scale (see Exp. Sect.) to afford 85% of the product, and 270 mg of solid residue could be scrutinised by IR and ^{13}C NMR spectroscopy. Again only the signals of **19** were detected besides some trimethylphosphane oxide and the well-known marks of silicon grease, which amounts to an estimated regioselectivity of better than 99%.

Complexes of rhodium and iridium, containing 2-(diphenylphosphanyl)-*N*,*N*-dimethylaniline as a bidentate ligand, have been described,[13] and no *ortho*-metallation was reported. Clearly, this spontaneous transformation with cobalt and its unexpected absolute selectivity merit further investigation.

Experimental Section

General Procedures and Materials: All air-sensitive and volatile materials were handled using standard vacuum techniques and were kept under argon. Microanalyses: Kolbe Microanalytical Laboratory, Mülheim/Ruhr, FRG. Melting points/decomposition temperatures: Sealed capillaries, uncorrected values. Chemicals (Merck/Schuchardt) were used as purchased. Literature methods were applied in the preparation of [CoCl(PMe_3)$_3$],[14] [CoMe(PMe_3)$_4$],[15] [CoMe$_2$(PMe_3)$_3$],[10] [CoClMe$_2$(PMe_3)$_3$],[16] 2-(diphenylphosphanyl)aniline,[17] 2-(diphenylphosphanyl)-*N*-methylaniline,[18] and 2-(diphenylphosphanyl)-*N*,*N*-dimethylaniline.[19] IR: Nujol mulls between KBr discs, Bruker spectrophotometer type FRA 106. ^{1}H and ^{13}C NMR spectra (300 MHz and 75 MHz, respectively) were recorded with a Bruker ARX-300 spectrometer, ^{31}P NMR spectra (81 MHz) with a Bruker AM-200 instrument. ^{13}C and ^{31}P NMR resonances were obtained with broad-band proton decoupling. MS: Varian Mat-311 (FD). Magnetic susceptibility data were obtained by the Faraday method, Cahn D 200 torsion balance and Bruker BMN-200/60 magnet system at 1.5 Tesla.

[2-(Diphenylphosphanyl)anilido-*N*,*P*]tris(trimethylphosphane)cobalt (1). Method a: 2-(Diphenylphosphanyl)aniline (1202 mg, 3.70 mmol) in diethyl ether (40 mL) was combined with [CoMe(PMe_3)$_4$] (1400 mg, 3.70 mmol) in diethyl ether (40 mL) at −70 °C causing the evolution of gas and giving a brown heterogeneous mixture. This was heated to 20 °C and stirred for 1 h. The dark solid of **1** was isolated by decanting and washing with cold pentane and dried in vacuo. From the liquor, at 4 °C, another 260 mg of black crystals of **1** were obtained. Combined yield 1710 mg (82%). **Method b:** Chloro[2-(diphenylphosphanyl)anilido-*N*,*P*]bis(trimethylphosphane)cobalt (**4**) (980 mg, 1.87 mmol) and trimethylphosphane (1500 mg, 19.7 mmol) in THF (40 mL) were combined at −70 °C with MeLi (1.6 M) in diethyl ether (1.2 mL, 1.80 mmol) causing the dark green colour to turn red brown. The mixture was heated to 20 °C and stirred for 30 min. The volatiles were removed in vacuo and the residue was extracted with three portions of diethyl ether (80 mL). Fractional crystallisation at 4 °C afforded black crystals of **1**. Yield 664 mg (63%); m.p. 118−119 °C (dec.). IR (Nujol): $\tilde{\nu}$ = 3331 cm^{-1} (N−H). ^{1}H NMR (300 MHz, [D$_8$]THF, 233 K): δ = 0.88 (br. s, 9 H, PCH_3), 1.28 (br. s, 18 H, PCH_3), 2.95 (s, 1 H, NH), 5.69 (t, ^3J = 6.8 Hz, 1 H, CH), 6.23 (t, ^3J = 4.9 Hz, 1 H, CH), 6.38 (t, ^3J = 7.1 Hz, 1 H, CH), 7.06 (t, ^3J = 7.4 Hz, 1 H, CH), 7.19−7.25 (m, 6 H, CH), 7.62−7.66 (m, 4 H, CH) ppm. ^{31}P NMR (81 MHz, [D$_8$]THF, 233 K): δ = −7 (dd, $^2J_{P,P}$ = 99 and 61 Hz, 2 P, PCH_3), 28 (dt, $^2J_{P,P}$ = 61 and 60 Hz, 1 P, PC_6H_5), 52 (dt, $^2J_{P,P}$ = 99 and 61 Hz, 1 P, PCH_3) ppm. $C_{27}H_{42}CoNP_4$ (563.5): calcd. C 57.55, H 7.51, N 2.49, P 21.99; found C 58.29, H 7.53, N 2.48, P 21.60.

[2-(Diphenylphosphanyl)-*N*-methylanilido-*N*,*P*]tris(trimethylphosphane)cobalt (2). Method a: 2-(Diphenylphosphanyl)-*N*-

methylaniline (750 mg, 1.95 mmol) in THF (50 mL) was combined with $CoMe(PMe_3)_4$ (740 mg, 1.95 mmol) in THF (50 mL) at 20 °C. The mixture was stirred for 16 h and the solvents were evaporated to dryness in vacuo. The residue was extracted with two portions of pentane (50 mL) and the red brown solution cooled to −27 °C to afford a black solid which was isolated by decanting and drying in vacuo to give a waxy solid of **2**. Yield 395 mg (35%). **Method b:** Chloro[2-(diphenylphosphanyl)-*N*-methylaniline]bis(trimethylphosphane)cobalt (**5**) (580 mg, 1.08 mmol) and trimethylphosphane (1100 mg, 14.4 mmol) in THF (70 mL) were combined at −70 °C with MeLi (1.6 M) in diethyl ether (0.67 mL, 1.08 mmol) causing the dark green colour to turn red brown. The mixture was warmed to 20 °C and stirred for 30 min. The volatiles were removed in vacuo and the residue was extracted with three 50 mL portions of pentane. Crystallisation at 4 °C afforded black crystals of **2**. Yield 395 mg (29%); m.p. 130−135 °C (dec.). ^{1}H NMR (300 MHz, [D$_8$]THF, 233 K): δ = 0.90 (br. s, 9 H, PCH_3), 1.25 (br. s, 18 H, PCH_3), 2.66 (s, 3 H, NCH_3), 5.80−7.78 (m, 14 H, CH) ppm. ^{31}P NMR (81 MHz, [D$_8$]THF, 233 K): δ = −8 (dd, $^2J_{P,P}$ = 103 and 59 Hz, 2 P, PCH_3), 29 (dt, $^2J_{P,P}$ = 60 and 59 Hz, 1 P, PC_6H_5), 52 (dt, $^2J_{P,P}$ = 103 and 59 Hz, 1 P, PCH_3) ppm. MS (70 eV): *m/z* (%) = 577 (20) [M$^+$], 501 (30) [M$^+$ − PMe_3].

[2-(Diphenylphosphanyl)-*N*-methylanilido-*N*,*P*]bis(trimethylphosphane)cobalt (3): 2-(Diphenylphosphanyl)aniline (685 mg, 2.35 mmol) in THF (50 mL) was combined with [$CoMe(PMe_3)_4$] (890 mg, 2.35 mmol) in THF (50 mL), at −70 °C, and after heating to 20 °C, the mixture was stirred for 16 h. The volatiles were removed in vacuo and the residue was extracted with two portions of pentane (50 mL). Crystallisation at 4 °C afforded red brown rods of **3**. Yield 763 mg (69%); m.p. 135−136 °C (dec.). Magnetic moment (299 K): μ_{eff} = 2.97 μ_B. $C_{25}H_{35}CoNP_3$ (501.4): calcd. C 59.89, H 7.04, N 2.79, P 18.53; found C 59.78, H 7.00, N 2.83, P 18.75.

Chloro[2-(diphenylphosphanyl)aniline]bis(trimethylphosphane)cobalt (4): 2-(Diphenylphosphanyl)aniline (584 mg, 2.10 mmol) in THF (50 mL) was combined with $CoCl(PMe_3)_3$ (680 mg, 2.10 mmol) in THF (50 mL) and within 10 min a dark green solution formed. After 1 h, the volatiles were removed in vacuo and the residue was extracted with three portions of diethyl ether (80 mL). Crystallisation at 4 °C afforded dark green prisms of **4**. Yield 716 mg (65%); m.p. 126−127 °C (dec.). Magnetic moment (299 K): μ_{eff} = 3.25 μ_B. IR (Nujol): $\tilde{\nu}$ = 3404, 3211 cm^{-1} (N−H). $C_{24}H_{34}ClCoNP_3$ (523.8): calcd. C 55.03, H 6.54, N 2.67, P 17.74; found C 55.09, H 6.40, N 2.66, P 17.89.

Chloro[2-(diphenylphosphanyl)-*N*-methylaniline]bis(trimethylphosphane)cobalt (5): 2-(Diphenylphosphanyl)-*N*-methylaniline (803 mg, 2.75 mmol) in THF (50 mL) and [$CoCl(PMe_3)_3$] (890 mg, 2.75 mmol) in THF (50 mL) formed a dark green solution. After 1 h, the volatiles were removed in vacuo and the residue was extracted as above. Crystallisation at 4 °C afforded dark green platelets of **5**. Yield 1130 mg (77%); m.p. 130−131 °C (dec.). Magnetic moment (299 K): μ_{eff} = 3.29 μ_B. IR (Nujol): $\tilde{\nu}$ = 3332 cm^{-1} (N−H). $C_{25}H_{36}ClCoNP_3$ (537.9): calcd. C 55.83, H 6.75, N 2.60, P 17.28; found C 55.78, H 6.52, N 2.58, P 17.33.

Carbonyl[2-(diphenylphosphanyl)anilido-*N*,*P*]bis(trimethylphosphane)cobalt (6): A sample of **1** (710 mg, 1.26 mmol) in THF (70 mL) was stirred under 1 bar of CO for 30 min and afforded a red solution. The volatiles were removed in vacuo and the residue was extracted with two portions of pentane (70 mL). At 4 °C short orange red rods of **6** were obtained. Yield 487 mg (75%); m.p. 153−157 °C (dec.). IR (Nujol): $\tilde{\nu}$ = 3375 cm^{-1} (N−H), 1887 cm^{-1} (CO). ^{1}H NMR (300 MHz, [D$_8$]THF, 296 K): δ = 1.15 (s, 18 H, PCH_3), 1.35 (br. s, 1 H, NH), 5.93 (dd, ^3J = 7.2, ^4J = 1.1 Hz, 1 H, CH), 6.34 (dd, ^3J = 5.1, $^4J_{P,H}$ = 3.1 Hz, 1 H, CH), 6.60 (dd, ^3J = 6.7, ^4J = 1.4 Hz, 1 H, CH), 7.06 (dt, ^3J = 7.8, ^4J = 1.4 Hz, 1 H, CH), 7.25−7.31 (m, 6 H, CH), 7.52−7.61 (m, 4 H, CH) ppm. ^{13}C NMR (75.4 MHz, [D$_8$]THF, 296 K): δ = 18.6 (s, PCH_3), 109.7 (d, $^3J_{P,C}$ = 4.5 Hz, CH), 116.7 (d, $^1J_{P,C}$ = 13.2 Hz, CH), 128.5 (d, $^2J_{P,C}$ = 9.4 Hz, CH), 130.3 (s, CH), 132.7 (d, $^2J_{P,C}$ = 12.5 Hz, CH), 133.8 (s, CH), 135.0, 142.0 (s, C) ppm. ^{31}P NMR (81 MHz, [D$_8$]THF, 233 K): δ = 5 (d, $^2J_{P,P}$ = 97 Hz, 2 P, PCH_3), 63 (t, $^2J_{P,P}$ = 97 Hz, 1 P, PC_6H_5) ppm. $C_{25}H_{33}CoNOP_3$ (515.4): calcd. C 58.26, H 6.45, N 2.72, P 18.03; found C 58.03, H 6.64, N 2.66, P 18.11.

Carbonyl[2-(diphenylphosphanyl)-*N*-methylanilido-*N*,*P*]bis(trimethylphosphane)cobalt (7): A sample of **2** (590 mg, 1.02 mmol) in THF (70 mL) was stirred under 1 bar of CO for 30 min to afford a light red solution. The volatiles were removed in vacuo and the residue was extracted with two portions of pentane (70 mL). At 4 °C short dark red rods of **7** were obtained. Yield 492 mg (91%); m.p. 165−170 °C (dec.). IR (Nujol): $\tilde{\nu}$ = 1906 cm^{-1} (CO). ^{1}H NMR (300 MHz, [D$_8$]THF, 296 K): δ = 1.17 (s, 18 H, PCH_3), 2.74 (s, 3 H, NCH_3), 5.72 (dd, ^3J = 7.4, ^4J = 1.3 Hz, 1 H, CH), 6.22 (dd, ^3J = 6.2, $^4J_{P,H}$ = 2.8 Hz, 1 H, CH), 6.60 (dd, ^3J = 6.2, ^4J = 1.4 Hz, 1 H, CH), 7.15 (dd, ^3J = 7.4, ^4J = 1.4 Hz, 1 H, CH), 7.31−7.36 (m, 6 H, CH), 7.45−7.52 (m, 4 H, CH) ppm. ^{13}C NMR (75.4 MHz, [D$_8$]THF, 296 K): δ = 18.1 (s, PCH_3), 39.4 (s, NCH_3), 109.2 (s, CH), 112.5 (d, $^4J_{P,C}$ = 4.9 Hz, CH), 117.2 (d, $^1J_{P,C}$ = 14.9 Hz, CH), 127.4 (d, $^2J_{P,C}$ = 12.3 Hz, CH), 130.3 (s, CH), 133.4 (d, $^2J_{P,C}$ = 12.5 Hz, CH), 133.7, 135.0 (s, C), 169.1 (d, $^2J_{P,C}$ = 30.5 Hz, NC) ppm. ^{31}P NMR (81 MHz, [D$_8$]THF, 233 K): δ = 6 (d, $^2J_{P,P}$ = 97 Hz, 2 P, PCH_3), 65 (t, $^2J_{P,P}$ = 97 Hz, 1 P, PC_6H_5) ppm. $C_{26}H_{35}CoNOP_3$ (529.4): calcd. C 58.99, H 6.66, N 2.65, P 17.55; found C 58.98, H 6.73, N 2.55, P 17.48.

[2-(Diphenylphosphanyl)anilido-*N*,*P*](ethene)bis(trimethylphosphane)cobalt (8): A sample of **1** (580 mg, 1.02 mmol), suspended in pentane (70 mL), was stirred under 1 bar of C_2H_4 for 30 min to afford a red solution which was filtered and cooled to −27 °C. Short red rods of **8** were dried in a stream of ethene at 20 °C. Yield 281 mg (53%); m.p. 45−50 °C (dec.). IR (Nujol): $\tilde{\nu}$ = 3342 cm^{-1} (N−H). ^{1}H NMR (300 MHz, [D$_8$]THF, 296 K): δ = 1.17 (d, $^2J_{P,H}$ = 7.3 Hz, 9 H, PCH_3), 1.32 (d, $^2J_{P,H}$ = 4.5 Hz, 9 H, PCH_3), 1.74 (m, 2 H, C=CH_2), 2.85 (m, 2 H, C=CH_2), 4.21 (br. s, 1 H, NH), 5.85 (m, 1 H, CH), 5.94 (m, 1 H, CH), 6.71 (m, 2 H, CH), 7.35−7.39 (m, 6 H, CH), 7.75−7.78 (m, 4 H, CH) ppm. ^{13}C NMR (75.4 MHz, [D$_8$]THF, 296 K): δ = 17.8 (d, $^1J_{P,C}$ = 19.4 Hz, PCH_3), 20.4 (d, $^1J_{P,C}$ = 16.3 Hz, PCH_3), 44.1 (m, CH_2), 108.1, 111.5, 123.2 (s, CH), 127.3 (m, C), 128.8, 130.7, 133.2 (s, CH), 134.4 (d, $^2J_{P,C}$ = 25.3 Hz, C), 141.7 (s, CH) ppm. ^{31}P NMR (81 MHz, [D$_8$]THF, 193 K): δ = 3 (dd, $^2J_{P,P}$ = 34 and 52 Hz, 1 P, PCH_3), 24 (dd, $^2J_{P,P}$ = 30 and 52 Hz, 1 P, PCH_3), 61 (dd, $^2J_{P,P}$ = 34 and 30 Hz, 1 P, PC_6H_5) ppm. $C_{26}H_{37}CoNP_3$ (515.4): calcd. C 60.59, H 7.24, N 2.72, P 18.03; found C 60.54, H 7.43, N 2.74, P 17.92.

[2-(Diphenylphosphanyl)-*N*-methylanilido-*N*,*P*](ethene)bis(trimethylphosphane)cobalt (9): A sample of **2** (720 mg, 1.24 mmol) in pentane (70 mL) was stirred under 1 bar of C_2H_4 for 30 min to afford a red solution which was filtered and cooled to 4 °C. Short red rods of **9** were dried in a stream of ethene at 20 °C. Yield 410 mg (62%); m.p. 45−50 °C (dec.). ^{1}H NMR (300 MHz, [D$_8$]THF, 296 K): δ = 0.72 (d, $^2J_{P,H}$ = 7.2 Hz, 9 H, PCH_3), 1.30 (d, $^2J_{P,H}$ = 3.9 Hz, 9 H, PCH_3), 1.73 (m, 2 H, C=CH_2), 2.16 (s, 3 H, NCH_3), 2.81 (m, 2 H, C=CH_2), 5.80 (m, 2 H, CH), 6.66−6.68 (m, 2 H, CH), 7.31−7.33 (m, 6 H, CH), 7.67−7.75 (m, 4 H, CH) ppm. ^{13}C NMR (75.4 MHz, [D$_8$]THF, 296 K): δ = 17.8 (d, $^1J_{P,C}$ = 22.6 Hz, PCH_3), 20.4 (d, $^1J_{P,C}$ = 14.6 Hz, PCH_3), 38.2 (s, NCH_3), 45.3 (d,

$^2J_{P,C}$ = 18.3 Hz, CH_2), 45.9 (m, CH_2), 108.4, 111.0, 123.3 (s, CH), 128.4 (d, $^1J_{P,C}$ = 19.1 Hz, C), 128.8, 130.7, 133.2 (s, CH), 133.8 (d, $^2J_{P,C}$ = 24.3 Hz, C), 141.7 (s, CH), 166.0 (s, NC) ppm. ^{31}P NMR (81 MHz, [D$_8$]THF, 193 K): δ = 3 (dd, $^2J_{P,P}$ = 36 and 56 Hz, 1 P, PCH_3), 23 (dd, $^2J_{P,P}$ = 32 and 56 Hz, 1 P, PCH_3), 61 (dd, $^2J_{P,P}$ = 36 and 32 Hz, 1 P, PC_6H_5) ppm. $C_{27}H_{39}CoNP_3$ (529.2): calcd. C 61.25, H 7.42, N 2.65, P 17.55; found C 61.18, H 7.52, N 2.51, P 17.62.

[2-(Diphenylphosphanyl)-*N*-methylanilido-*N*,*P*](propene)bis(trimethylphosphane)cobalt (10): A sample of **2** (830 mg, 1.43 mmol) in pentane (70 mL) was stirred under 1 bar of C_3H_6 for 30 min to afford a red solution which was filtered and cooled to −27 °C. Red triangular platelets of **10** together with those of **2** were dried in a stream of propene at 20 °C and separated mechanically. Yield 179 mg (23%); m.p. 85−87 °C (dec.). ^{1}H NMR (300 MHz, [D$_8$]THF, 296 K): δ = 0.74 (d, $^2J_{P,H}$ = 8.0 Hz, 9 H, PCH_3), 1.30 (d, $^2J_{P,H}$ = 6.1 Hz, 9 H, PCH_3), 1.36 (m, 3 H, CCH_3), 2.42 (s, 3 H, NCH_3), 2.79 (m, 1 H, C=CH), 2.81 (m, 2 H, C=CH_2), 6.55 (m, 1 H, CH), 6.61 (m, 1 H, CH), 6.55 (m, 2 H, CH), 7.21−7.35 (m, 6 H, CH), 7.65−7.80 (m, 4 H, CH) ppm. ^{31}P NMR (81 MHz, [D$_8$]THF, 193 K): δ = 3 (dd, $^2J_{P,P}$ = 38 and 52 Hz, 1 P, PCH_3), 22 (dd, $^2J_{P,P}$ = 30 and 52 Hz, 1 P, PCH_3), 61 (dd, $^2J_{P,P}$ = 38 and 30 Hz, 1 P, PC_6H_5) ppm. $C_{28}H_{41}CoNP_3$ (543.2): calcd. C 61.88, H 7.60, N 2.58, P 17.10; found C 61.08, H 7.65, N 2.56, P 17.41.

[2-(Diphenylphosphanyl)-*N*-methylanilido-*N*,*P*](iodo)bis(trimethylphosphane)cobalt(diethyl ether) (11): A sample of **2** (780 mg, 1.35 mmol) in THF (50 mL) was combined with iodomethane (441 mg, 3.10 mmol), at −70 °C, and the solution heated to 20 °C to form a heterogeneous mixture. After 3 h, an off-white solid of tetramethylphosphonium iodide (IR) was removed by filtration and the dark brown solution concentrated to dryness in vacuo. Extraction with three portions of diethyl ether (80 mL) and crystallisation at 4 °C afforded black cubic crystals of **11**. Yield 426 mg (45%); m.p. 85−86 °C (dec.). Magnetic moment (299 K): μ_{eff} = 2.09 μ_B. $C_{29}H_{45}CoINOP_3$ (702.4): calcd. C 49.59, H 6.46, N 1.99, P 13.23; found C 50.20, H 6.12, N 2.10, P 14.03.

[2-(Diphenylphosphanyl)anilido-*N*,*P*](methyl)bis(trimethylphosphane)cobalt (12): 2-(Diphenylphosphanyl)aniline (615 mg, 2.11 mmol) in diethyl ether (50 mL) and $CoMe_2(PMe_3)_3$ (670 mg, 2.11 mmol) in diethyl ether (50 mL) were combined at −70 °C and heated to 20 °C. After 16 h, the volatiles were removed in vacuo, and the solid residue was extracted with two portions of pentane (50 mL). Crystallisation at 4 °C afforded black crystals of **12**. Yield 752 mg (71%); m.p. 117−119 °C (dec.). IR (Nujol): $\tilde{\nu}$ = 3341 cm^{-1} (N−H). Magnetic moment (299 K): μ_{eff} = 1.65 μ_B. MS (70 eV): *m*/*z* (%) = 502 (14) [M$^+$], 350 (30) [M$^+$ − 2 PMe_3]. $C_{25}H_{36}CoNP_3$ (502.4): calcd. C 59.77, H 7.22, N 2.79, P 18.49; found C 59.78, H 7.12, N 2.78, P 18.31.

Bis[2-(diphenylphosphanyl)anilido-*N*,*P*]cobalt (13). Method a: 2-(Diphenylphosphanyl)aniline (1060 mg, 3.84 mmol) in diethyl ether (50 mL) and $CoMe_2(PMe_3)_3$ (610 mg, 1.92 mmol) in diethyl ether (50 mL) were combined at −70 °C and heated to 20 °C. After 16 h, the volatiles were removed in vacuo, the solid residue was washed with cold pentane (5 mL) and extracted with two portions of diethyl ether (50 mL). Crystallisation at 4 °C afforded dark red crystals of **13**. Yield 458 mg (39%). **Method b:** 2-(Diphenylphosphanyl)-aniline (2050 mg, 7.39 mmol) in THF (30 mL) and $CoCl_2$ (480 mg, 3.69 mmol) in THF (50 mL) were combined at −70 °C and MeLi (1.6 M) in diethyl ether (4.6 mL, 7.39 mmol) was added causing the colour to turn dark red. The mixture was warmed to 20 °C and the volatiles were removed in vacuo. The residue was extracted with two portions of diethyl ether (50 mL) and kept at 4 °C to afford crystals of **13**. Yield 1150 mg (51%); decomp. > 250 °C. IR (Nujol): $\tilde{\nu}$ = 3337 cm^{-1} (N−H). Magnetic moment (299 K): μ_{eff} = 2.05 μ_B. $C_{36}H_{30}CoN_2P_2$ (611.5): calcd. C 70.71, H 4.95, N 4.58, P 10.13; found C 71.09, H 5.33, N 4.39, P 10.46.

Bis[2-(diphenylphosphanyl)-*N*-methylanilido-*N*,*P*]cobalt (14). Method a: 2-(Diphenylphosphanyl)-*N*-methylaniline (1040 mg, 3.59 mmol) in diethyl ether (40 mL) and $CoMe_2(PMe_3)_3$ (570 mg, 1.79 mmol) in diethyl ether (70 mL) were combined at −70 °C and heated to 20 °C. After 5 h, the volatiles were removed in vacuo, the solid residue was extracted with two portions of diethyl ether (70 mL). Crystallisation at 4 °C afforded dark red crystals of **14**.Yield 551 mg (48%). **Method b:** 2-(Diphenylphosphanyl)aniline (1130 mg, 3.86 mmol) in THF (30 mL) and $CoCl_2$ (250 mg, 1.93 mmol) in THF (70 mL) were combined at −70 °C and MeLi (1.6 M) in diethyl ether (2.42 mL, 3.86 mmol) was added causing the colour to turn dark red. The mixture was heated to 20 °C and the volatiles were removed in vacuo. The residue was extracted with two portions of diethyl ether (50 mL) and kept at 4 °C to afford crystals of **14**. Yield 390 mg (32%); decomp. > 202 °C. Magnetic moment (299 K): μ_{eff} = 2.33 μ_B. $C_{38}H_{34}CoN_2P_2$ (639.6): calcd. C 71.36, H 5.36, N 4.38, P 9.69; found C 70.78, H 5.46, N 4.39, P 9.88.

Bis[2-(diphenylphosphanyl)anilido-*N*,*P*](trimethylphosphane)cobalt (15): A sample of **13** (660 mg, 1.07 mmol) was recrystallised from diethyl ether (40 mL) containing excess trimethylphosphane (280 mg, 3.67 mmol) at 4 °C to afford bunches of red brown crystals. Yield 248 mg **15** (47%); m.p. 148−150 °C (dec.). IR (Nujol): $\tilde{\nu}$ = 3337 cm^{-1} (N−H). Magnetic moment (299 K): μ_{eff} = 2.10 μ_B. $C_{39}H_{39}CoN_2P_3$ (687.6): calcd. C 68.12, H 5.72, N 4.07, P 13.51; found C 68.10, H 5.85, N 4.02, P 13.61.

Bis[2-(diphenylphosphanyl)-*N*-methylanilido-*N*,*P*](trimethylphosphane)cobalt (16): A sample of **14** (450 mg, 0.70 mmol) was recrystallised from diethyl ether (50 mL) containing excess trimethylphosphane (730 mg, 9.59 mmol) at −27 °C to afford bunches of short red brown rods of **16**. Yield 206 mg (41%); m.p. 165−167 °C (dec.). Magnetic moment (299 K): μ_{eff} = 2.04 μ_B. $C_{41}H_{43}CoN_2P_3$ (715.7): calcd. C 68.81, H 6.06, N 3.91, P 12.98; found C 68.79, H 5.45, N 4.06, P 13.25.

***mer-trans*-Dimethyl[2-(diphenylphosphanyl)anilido-*N*,*P*]bis(trimethylphosphane)cobalt (17):** 2-(Diphenylphosphanyl)aniline (850 mg, 3.06 mmol) in diethyl ether (70 mL) were treated with MeLi (1.6 M) in diethyl ether (1.9 mL, 3.06 mmol). At −70 °C, $CoClMe_2(PMe_3)_3$ (1080 mg, 3.06 mmol) in diethyl ether (50 mL) was added to the mixture which was heated to 20 °C and stirred for 16 h. The volatiles were removed in vacuo, and the solid residue was extracted with two portions of pentane (70 mL). Crystallisation at −27 °C afforded short orange rods of **17**. Yield 1030 mg (65%); m.p. 85−87 °C (dec.). IR (Nujol): $\tilde{\nu}$ = 3338 cm^{-1} (N−H). ^{1}H NMR (200 MHz, [D$_8$]THF, 233 K): δ = −0.65 (q, $^3J_{P,H}$ = 6.6 Hz, 3 H, $CoCH_3$), 0.50 (t, $^3J_{P,H}$ = 9.9 Hz, 3 H, $CoCH_3$), 0.67 (br. s, 18 H, PCH_3), 1.47 (br. s, 1 H, NH), 6.02 (t, ^3J = 6.9 Hz, 1 H, CH), 6.37 (t, ^3J = 5.9 Hz, 1 H, CH), 6.67 (t, ^3J = 7.5 Hz, 1 H, CH), 7.19−7.26 (m, 6 H, CH), 7.49 (m, 1 H, CH). 7.78−7.82 (m, 4 H, CH) ppm. ^{31}P NMR (81 MHz, [D$_8$]THF, 193 K): δ = 12 (br. s, 2 P, PCH_3), 41 (br. s, 1 P, PC_6H_5) ppm. $C_{26}H_{39}CoNP_3$ (517.5): calcd. C 60.35, H 7.60, N 2.71, P 17.96; found C 60.09, H 7.60, N 2.65, P 17.99.

***mer-trans*-[2-(Diphenylphosphanyl)-*N*-methylanilido-*N*,*P*]dimethylbis(trimethylphosphane)cobalt (18):** 2-(Diphenylphosphanyl)-*N*-methylaniline (345 mg, 1.18 mmol) in diethyl ether (70 mL) was

treated with MeLi (1.6 M) in diethyl ether (0.74 mL, 1.18 mmol). At −70 °C, $CoClMe_2(PMe_3)_3$ (417 mg, 1.18 mmol) in diethyl ether (50 mL) was added to the mixture which was heated to 20 °C and stirred for 16 h. The volatiles were removed in vacuo, and the solid residue was extracted with two portions of pentane (70 mL). Crystallisation at −27 °C afforded short orange rods of **18**. Yield 630 mg (59%); m.p. 89−91 °C (dec.). ^{1}H NMR (300 MHz, [D$_8$]THF, 233 K): δ = −0.60 (q, $^3J_{P,H}$ = 6.7 Hz, 3 H, $CoCH_3$), 0.53 (t, $^3J_{P,H}$ = 9.2 Hz, 3 H, $CoCH_3$), 0.64 (br. s, 18 H, PCH_3), 2.48 (s, 3 H, NCH_3), 6.20 (t, ^3J = 6.8 Hz, 1 H, CH), 6.35 (t, ^3J = 7.0 Hz, 1 H, CH), 6.67 (t, ^3J = 7.9 Hz, 1 H, CH), 6.96−7.01 (m, 6 H, CH), 7.55 (t, ^3J = 6.8 Hz, 1 H, CH), 7.69−7.75 (m, 4 H, CH) ppm. ^{31}P NMR (81 MHz, [D$_8$]THF, 193 K): δ = 15 [d(br), $^2J_{P,P}$ = 35 Hz, 2 P, PCH_3), 40 (t, $^2J_{P,P}$ = 35 Hz, 1 P, PC_6H_5) ppm. $C_{27}H_{41}CoNP_3$ (531.5): calcd. C 61.02, H 7.78, N 2.64, P 17.48; found C 61.08, H 7.43, N 2.64, P 17.43.

[3-(Dimethylamino)-2-(diphenylphosphanyl)phenyl-*C*^{1},*P*]tris(trimethylphosphane)cobalt (19): 2-(Diphenylphosphanyl)-*N*,*N*-dimethylaniline (1100 mg, 3.60 mmol) in diethyl ether (50 mL) was combined at −70 °C with $CoMe(PMe_3)_4$ (1360 mg, 3.60 mmol) in diethyl ether (80 mL), with the evolution of a gas. The mixture was heated to 20 °C and turned red brown. The volatiles were removed in vacuo, the residue was extracted with two portions of pentane (80 mL), and from the red solution dark red crystals of **19** were obtained. Yield 1550 mg (85%); m.p. 112−113 °C (dec.). ^{1}H NMR (300 MHz, [D$_8$]THF, 296 K): δ = 1.02 (d, $^2J_{P,H}$ = 5.6 Hz, 9 H, PCH_3), 1.23 (br. s, 18 H, PCH_3), 2.13 (s, 6 H, NCH_3), 5.90 (m, 1 H, CH), 6.19−6.28 (m, 2 H, CH), 7.22−7.24 (m, 6 H, CH), 7.75−7.79 (m, 4 H, CH) ppm. ^{13}C NMR (75.4 MHz, [D$_8$]THF, 296 K): δ = 22.2−22.7 (m, PCH_3), 23.3 (m, PCH_3), 43.3 (s, NCH_3), 109.3 (s, CH), 125.9 (d, $^3J_{P,C}$ = 3.1 Hz, CH), 126.0 (s, CH), 126.3 (d, $^3J_{P,C}$ = 5.6 Hz, CH), 126.9 (s, CH), 133.2 (d, $^3J_{P,C}$ = 7.6 Hz, CH), 133.3 (d, $^3J_{P,C}$ = 7.6 Hz, CH), 139.1 (d, $^1J_{P,C}$ = 9.6 Hz, C), 171.3 (m, CoC) ppm. ^{31}P NMR (81 MHz, [D$_8$]THF, 233 K): δ = −24 (dt, $^2J_{P,P}$ = 89 and 68 Hz, 1 P, PC_6H_5), −4 (dt, $^2J_{P,P}$ = 89 and 47 Hz, 2 P, PCH_3), 22 (dt, $^2J_{P,P}$ = 68 and 47 Hz, 1 P, PCH_3) ppm. $C_{29}H_{46}CoNP_4$ (591.5): calcd. C 58.89, H 7.84, N 2.37, P 20.95; found C 58.92, H 7.82, N 2.27, P 20.83.

Crystal Structure Analyses: Crystal data are presented in Tables 2 and 3. Data collection: Complex **3**: A crystal was sealed under argon in a glass capillary and mounted on a Bruker AXS P4 diffractometer. Reflections were measured (ω-scans) using graphite-monochromated Mo-K_α radiation; Lp correction and absorption correction based on ψ-scans were applied. The structure was solved by direct and conventional Fourier methods. All non-hydrogen atoms were treated anisotropically, hydrogen atoms were treated with a riding model in idealised positions. Complex **6**: A crystal was sealed under argon in a glass capillary and mounted on a Stoe Stadi-4 diffractometer. Intensities were collected (ω-scans) using graphite-monochromated Mo-K_α radiation. No absorption correction was applied. The structure was solved as for **3**. Complex **12**: Crystal mounting, data collection, structure solution and refinement as for **3**. Complex **13**: A crystal was sealed under argon in a glass capillary and mounted on a Stoe Stadi-4 diffractometer. Reflections were collected (ω-scans) using graphite-monochromated Mo-K_α radiation. Absorption corrections based on ψ-scans were applied. The structure was solved as for **3**. Crystallographic data (excluding structure factors) for the structures reported in this paper have been deposited with the Cambridge Crystallographic Data Centre. Copies of the data (CCDC-184429 for **3**, -186376 for **6**, -184430 for **12**, -186377 for **13**) can be obtained free of charge on application to CCDC, 12 Union Road, Cambridge CB2 1EZ, UK [Fax: (internat.) + 44-1223/336-033; E-mail: deposit@ccdc.cam.ac.uk].

Table 2. Crystal data for compounds **3** and **6**

	3	**6**
Empirical formula	$C_{25}H_{35}CoNP_3$	$C_{25}H_{33}CoNOP_3$
Formula mass	501.4	515.4
Crystal size [mm]	0.44 × 0.40 × 0.36	0.44 × 0.30 × 0.26
Crystal system	monoclinic	monoclinic
Space group	$P2_1/c$	$P2_1$
a [Å]	9.385(3)	9.8330(5)
b [Å]	12.502(2)	15.1030(7)
c [Å]	23.190(4)	18.1480(8)
β [°]	92.66(2)	89.940(4)
V [Å^3]	2718.0(11)	2695.1(2)
Z	4	2
$D_{calcd.}$ [g/cm^3]	1.225	1.270
μ(Mo-K_α) [mm^{-1}]	0.820	0.386
Temperature [K]	293(2)	293(2)
Data coll. range [°]	$4.8 \le 2\Theta \le 55$	$4.8 \le 2\Theta \le 48$
h	$-1 \le h \le 12$	$-11 \le h \le 11$
k	$-1 \le k \le 16$	$0 \le k \le 17$
l	$-30 \le l \le 30$	$0 \le l \le 20$
No. reflect. measured	8023	8138
No. unique data	6232 (R_{int} = 0.020)	4209 (R_{int} = 0.0494)
Parameters	278	544
GoF on F^2	1.008	1.117
$R1$ [$I \ge 2\sigma(I)$]	0.0515	0.0607
$wR2$ (all data)	0.1171	0.1639

Table 3. Crystal data for compounds **12** and **13**

	12	**13**
Empirical formula	$C_{36}H_{30}CoN_2P_2$	$C_{28}H_{42}CoIO_{0.5}P_3$
Formula mass	502.4	611.6
Crystal size [mm]	0.46 × 0.40 × 0.37	0.49 × 0.38 × 0.31
Crystal system	monoclinic	monoclinic
Space group	$P2_1/n$	$P2_1/a$
a [Å]	9.908(2)	11.5617(10)
b [Å]	20.075(4)	14.9016(17)
c [Å]	13.311(2)	17.8507(18)
β [°]	94.36(1)	101.384(9)
V [Å^3]	2639.9(8)	3015.0(5)
Z	4	4
$D_{calcd.}$ [g/cm^3]	1.264	1.347
μ(Mo-K_α) [mm^{-1}]	0.844	0.649
Temperature [K]	293(2)	293(2)
Data coll. range [°]	$4.0 \le 2\Theta \le 55$	$5.4 \le 2\Theta \le 50$
h	$-12 \le h \le 1$	$-13 \le h \le 13$
k	$-26 \le k \le 1$	$0 \le k \le 17$
l	$-17 \le l \le 17$	$0 \le l \le 21$
No. reflect. measured	7476	5689
No. unique data	6052 (R_{int} = 0.0200)	5267 (R_{int} = 0.0593)
Parameters	278	373
GoF on F^2	1.046	1.131
$R1$ [$I \ge 2\sigma(I)$]	0.0403	0.0657
$wR2$ (all data)	0.0985	0.2085

Acknowledgments

Financial support of this work by Fonds der Chemischen Industrie is gratefully acknowledged.

[1] [1a] H. P. Fritz, I. R. Gordon, K. E. Schwarzhans, L. M. Venanzi, *J. Chem. Soc., Dalton Trans.* **1960**, 5210−5216. [1b] M. Graciani, *J. Am. Chem. Soc.* **1998**, *120*, 2973−2974. [1c] E. Farnetti, G. Nardin, M. Graciani, *J. Chem. Soc., Chem. Commun.* **1988**, 1264−1265.
[2] T. B. Rauchfuss, F. T. Patino, D. M. Roundhill, *Inorg. Chem.* **1975**, *14*, 652−655.
[3] L. Dahlenburg, K. Herbst, *Chem. Ber./Recueil* **1997**, *130*, 1693−1698.
[4] C. J. Adams, M. I. Bruce, P. A. Duckworth, P. A. Huphrey, O. Kühl, W. R. Cullen, P. Braunstein, S. C. Cea, W. B. Skelton, A. H. White, *J. Organomet. Chem.* **1994**, *467*, 251−281.
[5] W. Ainscough, A. M. Brodie, S. L. Ingham, J. M. Waters, *J. Organomet. Chem.* **1994**, *468*, 229−234.
[6] H.-F. Klein, R. Beck, O. Hetche, *Eur. J. Inorg. Chem.* **2003**, 232−239, preceding paper.
[7] M. M. Olmstead, P. P. Power, G. Siegel, *Inorg. Chem.* **1986**, *25*, 1027−1028.
[8] [8a] D. G. Holah, A. N. Hughes, B. C. Hui, *Inorg. Nucl. Chem. Lett.* **1974**, *10*, 427. [8b] D. G. Holah, A. N. Hughes, B. C. Hui, K. Wright, *Can. J. Chem.* **1974**, *52*, 2990−2995.
[9] H.-F. Klein, A. Brand, G. Cordier, *Z. Naturforsch., Teil B* **1998**, *53*, 307−314.
[10] [10a] K. K. Chou, C. A. McAuliffe, *Inorg. Chim. Acta* **1975**, *14*, 121. [10b] H.-F. Klein, H. H. Karsch, *Chem. Ber.* **1976**, *109*, 1453−1464.
[11] [11a] P. Rigo, M. Bressan, *J. Inorg. Nucl. Chem.* **1975**, *37*, 1812−1814. [11b] B. N. Figgis, J. Lewis, *Prog. Inorg. Chem.* **1964**, *6*, 37−222.
[12] H.-F. Klein, S. Schneider, M. He, U. Flörke, H.-J. Haupt, *Eur. J. Inorg. Chem.* **2000**, 2295−2301.
[13] T. B. Rauchfuss, J. L. Clements, S. F. Agnew, D. M. Roundhill, *Inorg. Chem.* **1977**, *16*, 775−778.
[14] H.-F. Klein, H. H. Karsch, *Inorg. Chem.* **1975**, *14*, 473−477.
[15] H.-F. Klein, H. H. Karsch, *Chem. Ber.* **1975**, *108*, 944−954.
[16] H.-F. Klein, H. H. Karsch, *Chem. Ber.* **1975**, *108*, 956−966.
[17] M. K. Cooper, J. M. Downes, P. A. Duckworth, R. T. Tiekink, *Aust. J. Chem.* **1992**, *45*, 595−609.
[18] A. B. van Oort, P. H. M. Budzelaar, J. H. G. Frijns, A. G. Orpen, *J. Organomet. Chem.* **1990**, *396*, 33−47.
[19] L. Horner, G. Simons, *Phosphorus Sulfur* **1983**, *15*, 165−176.

Received May 31, 2002
[I02281]

Use of Molecular Scaffolding for the Stabilization of an Intramolecular Dative P^{III}-P^{V} System

Petr Kilian,[a] Douglas Philp,[a] Alexandra M. Z. Slawin,[a] and J. Derek Woollins*[a]

Keywords: Phosphorus heterocycles / Strained molecules / Neighbouring-group effects / Phosphorus−phosphorus bond

The reaction of $NapP_2S_4$ (**1**; Nap = naphthalene-1,8-diyl) with chlorine gas gave [$Nap(PCl_2)(PCl_4)$] (**2**), displaying a rare σ^4P-σ^6P bonding interaction. An X-ray structure analysis confirmed the PCl_5-like, P–P bond containing phosphonium-phosphoride structure of **2** in the crystal, which was also found in solution at low temperature. At ambient and higher temperatures, dynamic behaviour on the NMR time-scale was observed, which was assigned to interchange of the ionic phosphonium-phosphoride form **2** and the molecular bis(phosphorane) $Nap(PCl_3)_2$ form **3**, rather than to the ionic phosphonium salt-phosphorane form [$Nap(PCl_3)(PCl_2)$][Cl] **4**. Electronic structure calculations were performed at the B3LYP/6–31G(d,p) level of theory on structures **2** and **3**; structure **3** was located as a local minimum on the potential energy surface, 15 kcal·mol^{-1} higher in energy than structure **2**. The crystal structure and calculated P–P distances are 2.34 and 2.31 Å for **2** and **3**, respectively. An activation energy of 19.7 kcal·mol^{-1} was found for the transition state structure by coordinate driving calculations; the line-shape analysis of variable temperature $^{31}P\{^1H\}$ NMR spectra gave an activation energy of 14.4 kcal·mol^{-1}.

(© Wiley-VCH Verlag GmbH & Co. KGaA, 69451 Weinheim, Germany, 2003)

Introduction

Sterically overcrowded and therefore structurally distorted molecules or molecular ions have attracted the attention of chemists for many years. Bay region substituted polycyclic aromatic hydrocarbons, such as 1,8-disubstituted naphthalenes, are one of the most intensively studied systems in this field. The rigidity of the naphthalene backbone combined with the close proximity of functional groups in these species offer an ideal scaffolding for unusual chemistry as well as interesting bonding and geometry.

In the case of 1,8-diphospha-substituted naphthalenes, $NapP_2S_4$ (**1**, Nap = naphthalene-1,8-diyl) has been widely used as a synthon,[1−3] however there is an obvious lack of further suitably versatile, easily accessible starting materials, such as $Nap(PCl_2)_2$ or $Nap(PH_2)_2$. Halophosphoranes and halophosphanes are especially valuable synthons in organophosphorus chemistry. The preparation of the most desirable derivative $Nap(PCl_2)_2$ has been published recently.[4] As the direct method of preparation from lithiated naphthalene ($NapLi_2$) and PCl_3 was not successful (Scheme 1), protection was employed. Thus the reaction of $NapLi_2$ and protected chlorophosphane, followed by deprotection (Scheme 1) gave the desired $Nap(PCl_2)_2$. Formation of stable intermediates in the deprotection step, though, resulted in a low overall yield, which seems to restrain broader synthetic use of this method. In the search for further methods for the preparation of halogenated 1,8-diphosphanaphthalene synthons, we have obtained a new derivative $Nap(PCl_4)(PCl_2)$ **2**, which is not only a promising synthon, but also contains a very rare $\sigma^4P-\sigma^6P$ bond as well as showing interesting fluxionality on the NMR timescale.

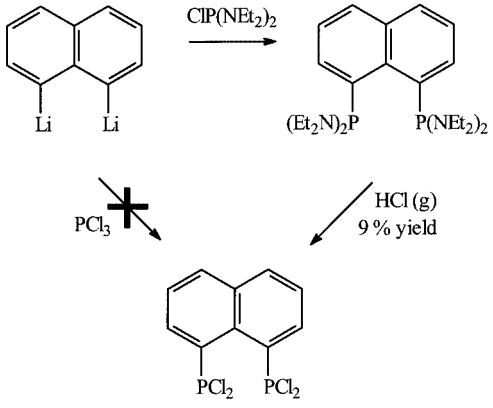

Scheme 1. Route to $Nap(PCl_2)_2$ via $NapLi_2$

Results and Discussion

Synthesis

The reaction of $NapP_2S_4$ **1** with a slight excess of chlorine gas proceeded with complete desulfuration, yielding the yellow solid $Nap(PCl_4)(PCl_2)$ **2** (Scheme 2). A plausible mechanism for the chlorination involves consequential meta-

[a] School of Chemistry, University of St. Andrews, St. Andrews, Fife, KY16 9ST, United Kingdom
E-mail: jdw3@st-andrews.ac.uk

thesis of a) bridging and b) terminal sulfur atoms, leading to the bis(phosphorane) $Nap(PCl_4)_2$. The next step — a spontaneous elimination of Cl_2 from $Nap(PCl_4)_2$ with formation of **2** — is obviously a consequence of the excessive steric strain connected with such an overcrowded molecular geometry: $Nap(PCl_4)_2$ would contain two five-coordinate P atoms kept in close proximity by the rigid organic backbone causing extensive shielding of the coordination sphere of each P atom. Instead of back formation of $Nap(PCl_4)_2$, a simultaneous P−P and P−C bond cleavage leading to PCl_5 and chlorinated naphthalenes on prolonged chlorination was observed by ^{31}P and ^{1}H NMR spectroscopy.

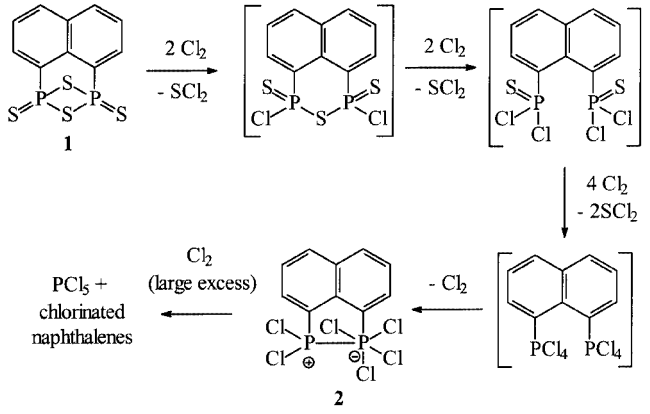

Scheme 2. Reaction of $NapP_2S_4$ (**1**) with chlorine gas.; undetected intermediates are in square brackets

The purification of the crude product **2** was performed by subliming off the major by-product (PCl_5) and further volatiles, followed by twofold recrystallisation from hot THF, resulting in a moderate yield 20% of pure **2.** The oxidation state of the phosphorus atoms in **2** is +4, thus the formation of **2** represents a formal reduction of P^V to P^{IV}.

X-ray Investigations

A single crystal X-ray structure determination (Figure 1, Table 1) proved the phosphonium-phosphoride structure of **2** in the crystal. Compound **2** possesses approximate C_S symmetry, with the carbon atoms of the naphthalene backbone, the two P atoms as well as Cl(4) and Cl(6) forming a nearly ideal plane (mean deviation of 0.02 Å) with atoms Cl(6) and P(1) lying only 0.05 Å above and below this plane; the dihedral angle P(1)−C(1)···C(9)−P(2) is 2°. The P−P interaction in **2** is clearly attractive, the P−P bond length (2.34 Å) is slightly shorter than the peri-separation [C(1)···C(9) distance] of 2.51 Å in the organic backbone. It is only very recently that the first examples of P−P bonding interaction (σ^3P-σ^4P^+ type) in 1,8-P,P-naphthalenes were described.[5] The vast majority of nonbridged 1,8-P,P-naphthalenes show significantly longer P···P distances, twisting of the naphthalene ring and distortions of the *ipso*-C geometries as a result of repulsive P···P interactions. For example, no evidence of a P···P attractive interaction (e.g. dative bond) was found in the phosphonium salts **A** (Figure 2, P···P distances: 3.19 and 3.26 Å), where the P environments are similar to those in **2**.[6] Compound **2** thus represents only the second type of attractive P−P interaction in 1,8-P,P-naphthalenes proved by means of a single crystal X-ray structure determination.

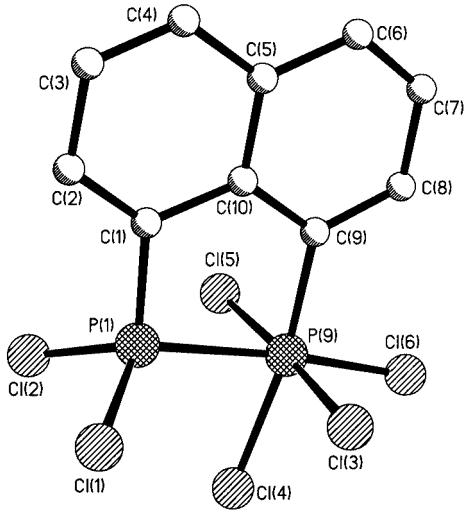

Figure 1. Crystal structure of **2** (H atoms omitted for clarity); for selected bond lengths and angles see Table 1

Table 1. Comparison of selected bond lengths [Å] and angles [°] for the crystal structure of **2** and calculated [B3LYP/6−31G(d,p)] structures **2** and **3**

	2 (X-ray)	**2** (calcd.)	**3** (calcd.)
P(1)−P(9)	2.338(2)	2.390	2.313
P(1)−C(1)	1.755(4)	1.755	1.904
P(9)−C(9)	1.883(4)	1.883	1.800
P(1)−Cl(1)	1.988(2)	1.995	2.075
P(1)−Cl(2)	1.978(2)	1.995	2.075
P(9)−Cl(3)	2.164(2)	2.162	2.216
P(9)−Cl(4)	2.178(2)	2.160	−
P(1)−Cl(4)	−	−	2.277
P(9)−Cl(5)	2.149(2)	2.158	2.216
P(9)−Cl(6)	2.088(2)	2.082	2.077
C(1)−C(10)	1.422(6)	1.430	1.429
C(9)−C(10)	1.425(6)	1.431	1.430
C(1)−P(1)−P(9)	99.7(2)	99.0	85.9
C(9)−P(9)−P(1)	86.1(1)	84.8	98.9
C(10)−C(1)−P(1)	111.6(3)	112.8	119.9
C(10)−C(9)−P(9)	118.4(3)	120.4	112.5
C(1)−C(10)−C(9)	124.0(4)	123.1	122.8

The P−P distance of 2.34 Å in **2** lies near to the upper limit of the range for P−P single bonds (2.20−2.35 Å) and is the longest observed for σ^4P-σ^6P bonds reported to date [range 2.165−2.2962(6) Å].[7,8] The rather long P−P bond length may be accounted for by: i) a released, but still significant, strain in the structure of **2** (indicated by angular distortions of both P environments), ii) a mismatch between the optimal P−P bond length and the peri separation on

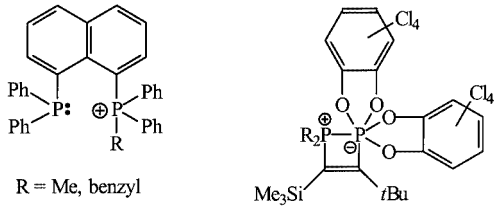

Figure 2. Structural formula of phosphonium salts **A** and $\sigma^4P\rightarrow\sigma^6P$ ylide **B**.; non-coordinating counteranions were present in salts **A**

the naphthalene skeleton, and iii) the lower basicity of the organo-PCl_2 group compared, for example, to the trialkylphosphanyl group. The P(1) environment is distorted tetrahedral [C(1)−P(1)−P(9) angle 99.7(2)°], whilst the P(9) environment is distorted octahedral [C(9)−P(9)−Cl(6) angle 99.1(2)°]. As expected, the P−Cl bond lengths of the four-coordinate P(1) atom are shorter than these of the six-coordinate P(9) atom [1.978(2)−1.988(2) vs. 2.088(2)−2.178(2) Å]. It should be noted that **2** represents a rare examples of an organochlorophosphorane having a solid-state structure similar to that of solid $[PCl_4][PCl_6]$.[9]

From the few examples of the donor type $\sigma^4P\rightarrow\sigma^6P$ linkage known,[7,8,10−13] it can be concluded that a strong donor-acceptor interaction is required for its stabilisation. This interaction is facilitated by both the high Lewis acidity and the basicity of the σ^6P and σ^4P atoms, respectively, which are dictated by the electron-withdrawing or -donating nature of the substituents. As the organo-PCl_2 group in **2** cannot be regarded as a strong donor, the release of the steric strain by formation of a P−P bond and the coherent transformation of the naphthalene ring into a planar geometry is probably the important factor contributing to the stabilization of the unusual $\sigma^4P\rightarrow\sigma^6P$ bond in **2**. Indeed, a similar "scaffolding" mechanism was found to play an important role in the stabilisation of unusual P−P interactions (including $\sigma^4P\rightarrow\sigma^6P$) in the unsaturated four-membered ring skeleton **B** (Figure 2).[11]

NMR Investigations and Study of the Equilibrium Processes

The $^{31}P\{^1H\}$ NMR spectrum of **2** at 303 K ([D8]THF, 109.4 MHz) indicated a dynamic behaviour on the NMR timescale. The spectrum consists of two broad doublets (AX system, δ_P = 82.9 and −225.9 ppm; $^1J_{P,P}$ = 118.5 Hz). At low temperature (213 K) the two doublets sharpen (δ_P = 82.9 and −227.9 ppm; $^1J_{P,P}$ = 88.3 Hz). Such a spectrum results from an ionic phosphonium-phosphoride structure; the chemical shifts are similar to those of PCl_4^+ (δ_P = 86 ppm) and PCl_6^-(δ_P = −290 ppm) as well as to those observed in the solid state ^{31}P MAS spectrum of ionic $[P(CH_2Cl)Cl_3][P(CH_2Cl)Cl_5]$ (δ_P = 111 and −206 ppm).[9] The relatively small magnitude of the $^1J_{P,P}$ coupling observed in **2** is not without precedent, a similar magnitude of 122 Hz was observed in a diphosphete[8] containing a σ^4P-σ^6P bond with a slightly shorter P−P bond length of 2.30 Å. Both the linewidth and $^1J_{P,P}$ increase substantially with temperature, only subtle δ_P changes were observed (Figure 3). At temperatures higher than 303 K the linewidth is so high that a determination of $^1J_{P,P}$ is impossible; at 333 K ([D8]THF) approximate coalescence temperature was reached, as virtually no ^{31}P resonances were observed.

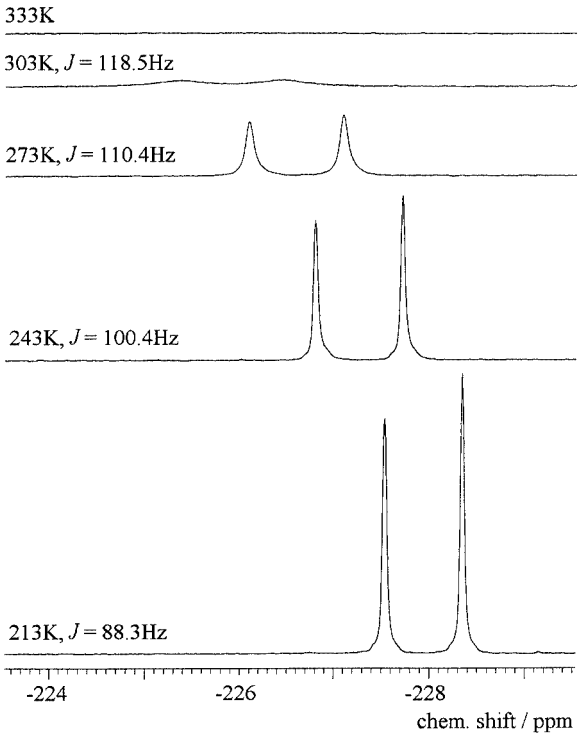

Figure 3. Variable temperature $^{31}P\{^1H\}$ NMR spectra (109.4 MHz) of a saturated solution of **2** in [D8]THF; high-field half spectrum region is shown, 1024 scans for each temperature; the same line shapes were observed in the low-field half spectrum region

Considerable theoretical and stereochemical interest is attached to phosphorus pentahalides and their organo-substituted relatives because of the variety of structures they adopt. There are three possible structures available for the R_2PCl_3 organochlorophosphoranes, these being ionic $[R_2PCl_2][R_2PCl_4]$ (like PCl_5), molecular pseudo-trigonal bipyramidal R_2PCl_3 (like PF_5) and ionic phosphonium salt $[R_2PCl_2][Cl]$ (like PBr_5). The relevant bisfunctional equivalents to these structures are depicted in Figure 4, compound **2** representing an intramolecular equivalent of the PCl_5-like structure. This structure (**2**) has been found both in the solid state and in solution at low temperatures. In order to explain the NMR fluxionality observed at ambient and higher temperatures described above, the interchange between **2** and **3** or **4** may thus be considered (Figure 4).

The interchange between **2** and **4** would involve the presence of Cl^- in the solution. Measurement of the ^{35}Cl NMR spectra of a solution of **2** ([D8]toluene, 49.0 MHz, 298 K, 45000 scans) showed no evidence for the presence of Cl^- ions, and thus mitigated against the presence of **4** under these conditions.

Further uncertainty about the presence of **4** in the system arises from the unexpected features found in the ^{31}P NMR spectra of an equilibrium mixture with respect to those of

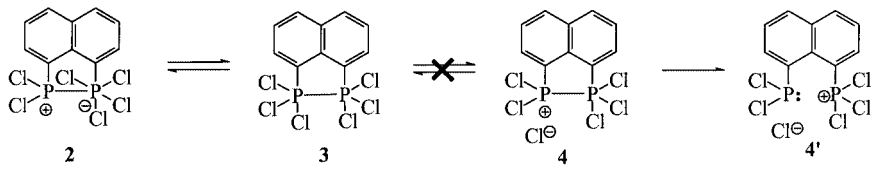

Figure 4. Possible equilibrium structures in solution at ambient and higher temperatures; **2**: ionic phosphonium phosphoride; **3**: molecular bis(pseudo-trigonal bipyramidal); **4**: ionic phosphonium salt-phosphorane; **4′**: ionic phosphanyl-phosphonium salt

the isostructural phosphonium salts **A** (Figure 2). The NMR and X-ray data of **A** (Figure 2) were discussed recently[6] and we assume that some parallels between phosphonium salts **A** and **4** can be drawn. The X-ray data show that there is no P→P$^+$ bonding interaction in **A**. The NMR spectroscopic data of **A** are consistent with this (although dynamic behaviour was observed due to hindered rotation), the magnitudes of $J_{P,P}$ (27−32 Hz) observed were too small for a conventional P−P bond. Although there are differences in the electronegativities of the substituents in **4** and **A**, we expect repulsive P−P interaction in **4**, the more precise description of bonding thus being **4′** (Figure 4). The measurement of a VT $^{31}P\{^1H\}$ NMR spectrum of a solution of **2** showed an increase of the magnitude of $J_{P,P}$ with increasing temperature (Figure 3). The preservation of $^1J_{P,P}$ at higher temperatures indicates that the P−P bond is retained throughout. This behaviour is obviously inconsistent with the P···P nonbonding interaction in **4′**, providing further support that **3** is involved.

In order to gain further insight into the equilibrium processes depicted in Figure 4, we performed electronic structure calculations on structures **2** and **3** at the B3LYP/6−31G(d,p) level of theory. The calculated structures are shown in Figure 5. The geometry around the two P centres in **2** is reproduced well by the calculations (Table 1). Structure **3** was located as a local minimum on the potential energy surface 15 kcal·mol^{-1} higher in energy than structure **2**. A shorter P−P bond length (2.31 Å) was found in **3**. Although both σ^5P environments in **3** are approximately trigonal bipyramidal, and the phosphorus atoms lie in the plane of the naphthalene ring, they are not related by any symmetry element in the molecule. In the trigonal bipyramidal geometry of P(1) the C(1) and Cl(4) atoms are axial, whereas in the trigonal bipyramidal geometry of P(9), Cl(3) and Cl(5) occupy the axial positions.

This result again demonstrates the stabilisation of an unusual bonding geometry in peri-substituted naphthalenes. Up to now, only two X-ray structures of compounds containing a σ^5P-σ^5P bond have been reported, in which the P−P bond was axial[14] and equatorial.[15,16]

In order to further assess the fluxional behaviour of **2**, we performed coordinate driving calculations in which one chlorine atom from the octahedral P centre was transferred in a concerted manner to the tetrahedral P centre, thus converting **2** into **3**. The calculations indicated that these interconversions are plausible and a transition state structure (Figure 6) is obtained for the axial chlorine [Cl(4)] transfer

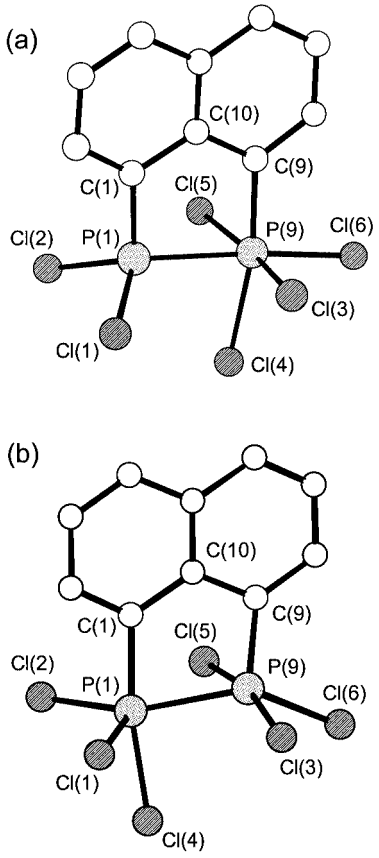

Figure 5. Calculated [B3LYP/6−31G(d,p)] structures of: (a) compound **2**, and (b): compound **3** (H atoms omitted for clarity); for selected bond lengths and angles see Table 1

pathway. The calculated activation energy is 19.7 kcal·mol^{-1} for the conversion of **2** to **3**.

The approximate activation energy of 14.4 kcal·mol^{-1} was found by line shape analysis of the variable temperature $^{31}P\{^1H\}$ NMR spectra, using the expression $k = \pi(\Delta\nu)$, where $\Delta\nu$ is the difference (Hz) between the line width at a temperature T, where exchange of sites is taking place (273 K), and the line width in the absence of exchange (183 K). The Eyring equation was subsequently employed to calculate the $\Delta G^{\ddagger}$ value at T. The values obtained independently from NMR spectroscopic data and coordinate driving calculations show good agreement; the relatively high barrier probably reflects the significant shortening of the P−P distance in the transition state.

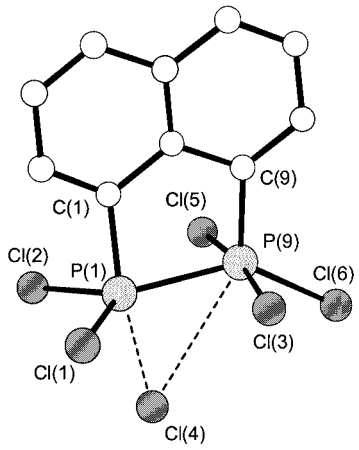

Figure 6. Calculated [B3LYP/6−31G(d,p)] transition state structure for the conversion of **2** to **3** (H atoms omitted for clarity); selected bond lengths [Å] and angles [°] P(1)−P(9) 2.256, Cl(4)−P(1) 2.460, Cl(4)−P(9) 2.970, P(1)−Cl(4)−P(9) 67.0

By analogy with $P(CH_2Cl)Cl_4$, which has δ_P = −39.0 ppm for the pseudo-trigonal bipyramidal structure (in solution),[9] we anticipate a similar chemical shift in **3**. Not surprisingly, given the inequality in the populations of **2** and **3** suggested by our calculations, separated signals were not observed in the 121.4 MHz ^{31}P NMR spectrum at any temperature studied (193−373 K). However, changes were observed in linewidth, $^1J_{P,P}$ and δ_P, which is consistent with a dominant population (namely **2**) being in exchange on the NMR timescale with a second minor population (namely **3**) at higher temperatures. The observed increase of $^1J_{P,P}$ with increasing temperature probably reflects an increasing population of **3** (where a shorter P−P bond is found) with increasing temperature. Note that in **3**, the two phosphorus centres are not necessarily magnetically equivalent. The degree of inequivalence depends on the rate of ligand exchange (a process similar to pseudorotation), which is necessarily a concerted process in the sterically overcrowded environment. The presence of an ionic-molecular equilibrium would suggest substantial solvent-dependence of $^1J_{P,P}$. The magnitude of $^1J_{P,P}$ at 273 K, determined from the 121.4 MHz ^{31}P NMR spectra, is 131 Hz in [D_8]toluene solution and 100 Hz in [D_2]dichloromethane solution. Thus, the less-polar solvent (toluene) shifts the equilibrium to the molecular form **3**.

Conclusion

$NapP_2S_4$ (**1**) was used previously as a source of the $NapP_2$ moiety in many reactions with nucleophiles, though generally P−S−P bridge or P=S moieties were retained in their products. In this paper we have shown that **1** can be completely desulfurated in the reaction with chlorine gas, giving $NapP_2Cl_6$ (**2**). In analogy to PCl_5 or $PhPCl_4$, **2** is expected to allow access to new main-group derivatives of 1,8-P,P-naphthalene with interesting bonding and chemistry. NMR spectroscopic data and calculations suggest that the dynamic process observed in solutions of **2** might be explained by interchange between the ionic phosphonium-phosphoride form **2** and the molecular bis(phosphorane) form **3**; an intramolecular equivalent to the dynamic equilibrium of ionic $[PCl_4][PCl_6]$ and molecular PCl_5 forms.

Experimental Section

General Remarks: All manipulations were performed using standard Schlenk techniques with carefully dried and deoxygenated solvents under an oxygen-free argon atmosphere. Compound **1** was prepared as described previously.[17] NMR: Varian Unity Plus 500, Bruker AM 300 and Jeol GSX 270; Ra: Perkin−Elmer System 2000. MS: VG Autospec.

$NapP_2Cl_6$ (2): Chlorine gas was bubbled through an externally cooled (0 °C), vigorously stirred suspension of **1** (14.3 g, 45.2 mmol) in dichloromethane (90 cm^3). The reaction was completed after ca. 10 min, during which time the solid dissolved completely, and a new yellow solid (**2**) precipitated. The product was collected by filtration, washed with dichloromethane (30 cm^3) and dried in vacuo. PCl_5 and further volatile by-products were sublimed off at 120−130 °C in vacuo (≈ 13 Pa). The remaining solid was of sufficient purity for further synthetic use, although its ^{31}P NMR spectrum (in THF, −30 °C, external lock) showed the presence of small amounts of partially oxidized/hydrolysed by-products. These impurities can be removed by twofold recrystallisation from hot THF. Yield after twofold recrystallisation 3.60 g (20%) of **2** in the form of yellow, extremely moisture sensitive crystals. Compound **2** is barely soluble in cold dichloromethane and toluene, but more soluble in THF. The crystals used for X-ray work were obtained from hot toluene. M.p. 208−211 °C with gas evolution. ^1H NMR (500 MHz, CD_2Cl_2, 258 K, TMS): δ = 7.75 [m, 1 H, H(3)], 7.95 [t, $^3J_{H,H}$ = $^3J_{H,P}$ = 7.7 Hz, 1 H, H(8)], 8.02 [t, $^3J_{H,H} \approx {}^4J_{H,H} \approx$ 6.0 Hz, 1 H, H(4)], 8.42−8.50 [m (overlapped), 2 H, H(6) and H(7)], 8.76 [dd, $^3J_{H,P}$ = 33.1, $^3J_{H,H}$ = 7.6 Hz, 1 H, H(2)] ppm. $^{13}C\{^1H\}$(125.7 MHz, [D_8]THF, 258 K, TMS), only signals of tertiary carbons could be assigned as the solubility of **2** at low temperatures was very low: δ = 124.9 [t (virtual), $^2J_{C,P} \approx$ 14.1 Hz, C(2)], 129.9−129.5 [m (overlapped), C(8) and C(3)], 131.8 [s, C(4)], 135.6 [s, C(7)], 140.7 [s; C(6)] ppm. $^{31}P\{^1H\}$ (121.4 MHz, CD_2Cl_2, external reference 85% H_3PO_4, for numbering of atoms see Figure 1): at 298 K 2× broad d (AX system), δ_P −225.4 [P(9)] and 83.2 [P(1)], $^1J_{P,P}$ = 105.7 Hz; at 223 K 2×d (AX system), δ_P −227.9 [P(9)] and 82.2 [P(1)], $^1J_{P,P}$ = 83.8 Hz. Raman (sealed capillary): $\tilde{\nu}$ = 3068 (s, Ar-H), 1556 (s), 1365 (s), 435 and 420 (m, P-Cl), 322 cm^{-1} (vs). MS (EI+, 70 eV, sampled neat): *m/z* = 365 [M − Cl], 330 [M − 2Cl], 293 [M − 3Cl, base peak].

Computational Methodology: All calculations were performed on a dual processor Silicon Graphics Octane^2 Workstation. Initial guess structures were constructed using Maestro (Version 3.0.r38) and computations were carried out using Jaguar (Version 4.1.r53).[18] The identity of ground and transition states was verified by vibrational frequency analysis and the calculated transition state possessed one imaginary vibration which corresponded to the reaction coordinate.

X-ray Crystallographic Study: Crystal data for **2**: $C_{10}H_6Cl_6P_2$, mol. wt. 400.8, yellow plates, 0.1 × 0.1 × 0.1 mm, monoclinic, space group $P2_1/n$, Z = 4, a = 8.1613(9), b = 18.053(2), c = 10.0490(9) Å, β = 97.197(3)°, V = 1468.9(3) $Å^3$, $\rho_{calcd.}$ 1.363 $Mg{\cdot}m^{-3}$, $2\theta_{max}$ = 46.46°, graphite monochromated Mo-K_α radiation (λ = 0.71073

Å), μ(Mo-K_α) = 1.363 mm^{-1}, T = 293 K. Data were measured on a Bruker SMART CCD, and Lorentzian polarisation and absorption (SADABS, max./min. transmission 1.0000/0.7767) corrections were performed. Of 6227 measured data, 2085 were unique and 1706 observed [$I > 2\sigma(I)$]. The structure was solved by direct methods. The non-hydrogen atoms were refined anisotropically, the hydrogen atoms were idealised and refined isotropically using a riding model. Structural refinements were performed with the full-matrix least-squares method on F^2 using the program SHELXTL (Version 5.10, Bruker AXS, 1997) to give R_1 = 0.0438 and wR_2 = 0.1114, with a residual electron density of 0.82 eÅ^{-3}.

CCDC-182100 contains the supplementary crystallographic data for **2**. These data can be obtained free of charge at www.ccdc.cam.ac.uk/conts/retrieving.html [or from the Cambridge Crystallographic Data Centre, 12, Union Road, Cambridge CB2 1EZ, UK; Fax: (internat.) +44−1223/336−033; E-mail: deposit@ccdc.cam.ac.uk].

Acknowledgments

We thank the EPSRC for funding.

[1] M. R. St. J. Foreman, J. D. Woollins, *J. Chem. Soc., Dalton Trans.* **2000**, 1533−1543.
[2] P. Kilian, A. M. Z. Slawin, J. D. Woollins, *Eur. J. Inorg. Chem.* **1999**, 2327−3333.
[3] P. Kilian, J. Marek, R. Marek, J. Tousek, O. Humpa, A. M. Z. Slawin, J. Touzín, J. Novosad, J. D. Woollins, *J. Chem. Soc., Dalton Trans.* **1999**, 2231−2236.
[4] A. Karacar, H. Thonnessen, P. G. Jones, R. Bartsch, R. Schmutzler, *Chem. Ber./Recueil* **1997**, *130*, 1485−1489.
[5] A. Karacar, M. Freytag, H. Thonnessen, P. G. Jones, R. Bartsch, R. Schmutzler, *J. Organomet. Chem.* **2002**, *643−644*, 68−80.
[6] A. Karacar, V. Klaukien, M. Freytag, H. Thonnessen, J. Omelanczuk, P. G. Jones, R. Bartsch, R. Schmutzler, *Z. Anorg. Allg. Chem.* **2001**, *627*, 2589−2603.
[7] D. Schomburg, *Acta Crystallogr., Sect. A* **1984**, *40*, C265.
[8] M. Sanchez, R. Reau, F. Dahan, M. Regitz, G. Bertrand, *Angew. Chem.* **1996**, *108*, 2386−2388; *Angew. Chem. Int. Ed. Engl.* **1996**, *35*, 2228−2230.
[9] K. B. Dillon, T. A. Straw, *J. Chem. Soc., Chem. Commun.* **1991**, 234−235.
[10] H. Luo, R. McDonald, R. G. Cavell, *Angew. Chem.* **1998**, *110*, 1172−1174; *Angew. Chem. Int. Ed.* **1998**, *37*, 1098−1099.
[11] M. Sanchez, R. Reau, H. Gornitzka, F. Dahan, M. Regitz, G. Bertrand, *J. Am. Chem. Soc.* **1997**, *119*, 9720−9728.
[12] W. S. Sheldrick, J. A. Gibson, G.-V. Roschenthaler, *Z. Naturforsch., Teil B* **1978**, *33*, 1102−1105.
[13] C. W. Schultz, R. W. Rudolph, *J. Am. Chem. Soc.* **1971**, *93*, 1898−1903.
[14] H. W. Roesky, D. Amirzadeh-Asl, W. S. Sheldrick, *J. Am. Chem. Soc.* **1982**, *104*, 2919−2920.
[15] J. E. Richman, R. O. Day, R. R. Holmes, *Inorg. Chem.* **1981**, *20*, 3378−3381.
[16] J. E. Richman, R. O. Day, R. R. Holmes, *J. Am. Chem. Soc.* **1980**, *102*, 3955.
[17] M. R. St. J. Foreman, J. Novosad, A. M. Z. Slawin, J. D. Woollins, *J. Chem. Soc., Dalton Trans.* **1997**, 1347−1350.
[18] Schrodinger Inc., Portland, Or, USA, 2001.

Received June 11, 2002
[I02308]

Synthesis, Crystal Structure, and Photoluminescent Properties of a Tetracarbonyl(naphthyridylcarbamoyl)rhenium(I) Complex and a Highly Emissive Tetracarbonyl(naphthyridylamido)rhenium(I) Complex

Jing-Lin Zuo,[a] Wen-Fu Fu,[b] Chi-Ming Che,*[a,b] and Kung-Kai Cheung[b]

Keywords: Carbonyl ligands / N ligands / Photoluminescence / Rhenium / Structure elucidation

The reactions of $Re(CO)_5X$ (X = Cl, Br) with 7-amino-2,4-dimethyl-1,8-naphthyridine (H_2L^1) and 7-[2-(6-chloropyridyl)-amino]-2,4-dimethyl-1,8-naphthyridine (HL^2) in the presence of *t*BuOK afforded the η^1-naphthyridylcarbamoyl complex $[Re(CO)_4(HL^1CO)]$ (**1**) and the naphthyridylamido complex $[Re(CO)_4(L^2)]$ (**2**), respectively. The structures of HL^2, **1**·$CHCl_3$, **1**·HL^3·$2CH_2Cl_2$ [HL^3 = (7-chloronaphthyridyl)(5,7-dimethylnaphthyridyl)amine], and **2** have been determined by X-ray crystallography. Complex **1** displays a weak emission at 453 nm in an EtOH/MeOH (1:4, v/v) glassy solution at 77 K; complex **2** exhibits an intense (quantum yield: 0.22 in CH_2Cl_2) and long-lived emission (46 μs in CH_2Cl_2), with a solvent-sensitive λ_{max}, in degassed solutions at room temperature.
(© Wiley-VCH Verlag GmbH, 69451 Weinheim, Germany, 2003)

Introduction

Carbonylrhenium(I) complexes have been the subject of extensive photochemical and photophysical studies over the past several decades. These complexes display interesting photochemical,[1] and rich photoluminescent and electroluminescent properties.[2−4] Recent studies have also demonstrated their applications as luminescent probes for chemosensing.[5] In the course of our studies on the photoluminescent properties of carbonylrhenium(I) complexes, we have paid attention to the species containing tetracarbonylrhenium(I) units. This class of carbonylrhenium(I) complexes, such as the $[Re(CO)_4(bpm)]^+$ cation (bpm = 2,2′-bipyrimidine) and some neutral *ortho*-metalated species, exhibits substantially long emission life-times and high emission quantum yields compared with the extensively studied tricarbonylrhenium(I) species $Re(CO)_3(L-L)X$ (L−L = a bidentate *N*,*N*′-chelating ligand such as 1,10-phenanthroline and 2,2′-bipyridine; X = a monodentate anionic ligand such as Cl^- or Br^-).[6]

In the present paper, we report on the synthesis and the photophysical properties of the tetracarbonyl(η^1-naphthyridylcarbamoyl)rhenium(I) complex $[Re(CO)_4(HL^1CO)]$ (**1**, H_2L^1 = 7-amino-2,4-dimethyl-1,8-naphthyridine), and the naphthyridylamido complex $[Re(CO)_4L^2]$ {**2**, HL^2 = 7-[2-(6-chloropyridyl)amino]-2,4-dimethyl-1,8-naphthyridine}, both of which have been characterized by X-ray crystallography. The η^1-carbamoyl complex **1** was prepared from the reaction between $Re(CO)_5Cl$ and H_2L^1, probably by an interesting intramolecular migratory insertion of CO into the Re^I−amide bond. The amido complex **2** exhibits an intense, long-lived emission in degassed solutions at room temperature.

Results and Discussion

Synthesis and Spectral Features

Treatment of $Re(CO)_5Cl$ with naphthyridylamine H_2L^1 in dichloromethane in the presence of *t*BuOK afforded complex **1** in a 40% yield (Scheme 1). The η^1-carbamoyl group in this complex probably results from the migratory insertion of CO into the rhenium(I)−amide bond. We propose that the reaction might first generate the amine intermediate **I** (Scheme 2), followed by the deprotonation of the coordinated amine ligand in **I** by *t*BuOK to give the arylamide intermediate **II**.[7] This then readily undergoes an intramolecular migratory insertion of CO into the Re−amide bond, giving complex **1**. The synergistic action of the naph-

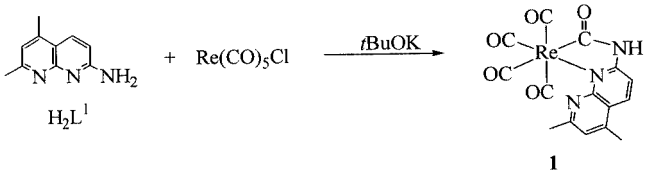

H_2L^1 **1**

Scheme 1. Synthesis of the η^1-naphthyridylcarbamoyl complex **1**

[a] Coordination Chemistry Institute and the State Key Laboratory of Coordination Chemistry, Nanjing University, Nanjing 210093, P. R. China
[b] Department of Chemistry, The University of Hong Kong, Pokfulam Road, Hong Kong

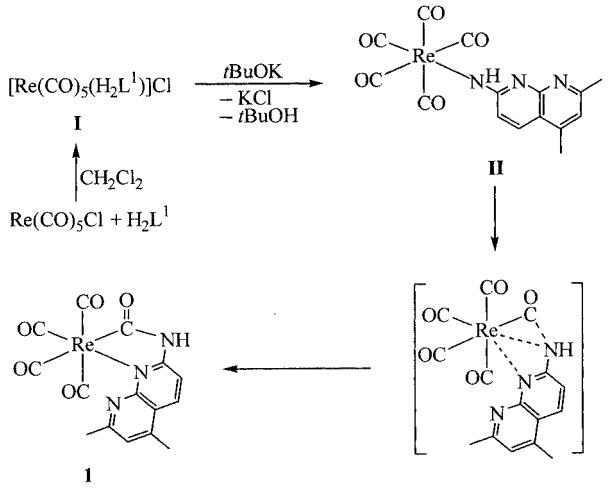

Scheme 2. Proposed mechanism for the formation of complex **1** by migratory insertion of CO into a Re−amido bond

thyridyl group should facilitate such CO insertion processes.

Migratory insertion of CO into a low-valent metal−nitrogen bond is not unprecedented,[8a,9] but is less common than the migratory insertion of CO into an M−R or M−H bond (which has been widely encountered in organometallic chemistry).[10] The mechanism we propose here (Scheme 2) is similar to that of the *ortho*-metalation of the (arylamido)iridium(I) complex *trans*-$Ir(PPh_3)_2(CO)(NHAr)$,[8] and to the formation of the (η^1-carbamoyl)dicarbonylrhenium complex $[(CO)_2RReC(=O)N(CH_3)CH_2CH_2(\eta^5\text{-}C_5H_4)]$ by insertion of CO into an Re−N bond.[9a]

We speculate that replacement of the H atom of the NH group in **II** by a bulky group may prevent or retard the foregoing CO insertion reaction. To test this possibility, we converted H_2L^1 into two new naphthyridylamine ligands HL^2 and (7-chloronaphthyridyl)(5,7-dimethylnaphthyridyl)-amine (HL^3), according to the reactions shown in Scheme 3. Indeed, reaction of $Re(CO)_5Br$ with HL^2 under conditions similar to those for the reaction between $Re(CO)_5Cl$ and H_2L^1 did not give an η^1-carbamoyl complex. Instead, the reaction afforded the amido complex **2** in an 80% isolated yield (Scheme 4).

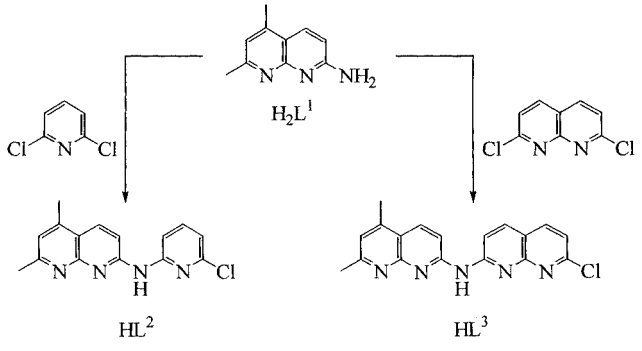

Scheme 3. Synthesis of HL^2 and HL^3

The reaction of HL^3 with $Re(CO)_5Br$ was also examined, but no identifiable rhenium complexes were obtained in this case. Ligand HL^3 was found to be less reactive than H_2L^1 and HL^2. For example, treatment of $Re(CO)_5Br$ with a 1:1 mixture of HL^3 and H_2L^1 in dichloromethane produced a mixture of **1** and free HL^3, and gave crystals of $\mathbf{1}\cdot HL^3\cdot 2CH_2Cl_2$ on recrystallization from dichloromethane/hexane.

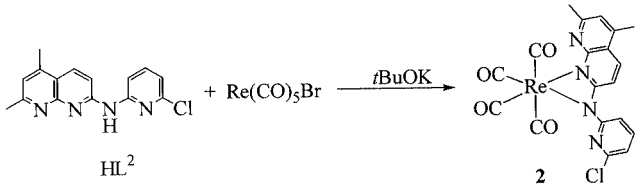

Scheme 4. Synthesis of the naphthyridylamido complex **2**

All the new compounds in this work display parent ion peaks in their mass spectra. The IR spectra of complexes **1** and **2** show CO stretches at frequencies ranging from 1928 to 2103 cm^{-1}; this ν(CO) frequency range is similar to that of the cyclometalated tetracarbonylrhenium(I) complex $[Re(CO)_4\{\mu_2\text{-}C(NHR)(NHC_6H_4)\}]$ (1916−2081 cm^{-1}),[11] but different from the typical ν(CO) frequency range of tricarbonylrhenium(I) complexes (ca. 1700−2000 cm^{-1}).[12] The ν(CO) band at 2087 cm^{-1} for **1**, and at 2103 cm^{-1} for **2**, could be assigned to the *trans*-$Re(CO)_2$ subunits of the $Re(CO)_4$ moieties in the two complexes, since the strong *trans* influence of CO would weaken the Re−CO π-back bonding and thus increase the ν(CO) frequency. However, we cannot exclude the possibility of mixing between the stretching vibrations of the *trans*- and *cis*-$Re(CO)_2$ subunits.

Crystal Structures

Table 6 shows the crystal and refinement data for HL^2, $\mathbf{1}\cdot CHCl_3$, $\mathbf{1}\cdot HL^3\cdot 2CH_2Cl_2$, and **2**. The ORTEP drawings or unit cell diagrams for these crystals are depicted in Figures 1−5. Selected bond lengths and angles are compiled in Tables 1−4.

The free ligand HL^2 is basically planar (Figure 1) and adopts a configuration that is similar to the *anti-syn* configuration of the dimer of 2,2′-dipyridylamine.[13] The N(2)−C(6) and N(2)−C(8) distances are 1.378(6) and 1.400(6) Å, respectively (see Table 1). These are longer than the corresponding C−N distances in pyridine or naphthyridine.

Complex **1** exhibits a distorted octahedral rhenium(I) center and has a strained five-membered metallacycle involving the Re(1), N(1), C(6), N(2), and C(1) atoms (Figure 2) and the Re1, N2, C6, N1, and C5 atoms (Figure 3). The C−Re−N angle in the metallacycle is 76.2(3)° for $\mathbf{1}\cdot CHCl_3$ (Table 2), and 75.8(2)° for $\mathbf{1}\cdot HL^3\cdot 2CH_2Cl_2$ (Table 3). The average Re−CO bond length for the terminal CO groups *trans* to the HL^1CO ligand (1.952 Å) is shorter than the average Re−CO bond length of the *trans*-$Re(CO)_2$ subunit (1.994 Å). The Re−C(carbamoyl) bond lengths of 2.146(7) Å in $\mathbf{1}\cdot CHCl_3$, and of 2.158(7) Å in $\mathbf{1}\cdot HL^3\cdot 2CH_2Cl_2$, are similar to that in $[(CO)_2BrReC(=O)N(CH_3)CH_2CH_2(\eta^5\text{-}C_5H_4)]$ (2.19 Å).[9a] There are hydrogen bonds between complex **1** and the free ligand HL^3 in $\mathbf{1}\cdot HL^3\cdot 2CH_2Cl_2$

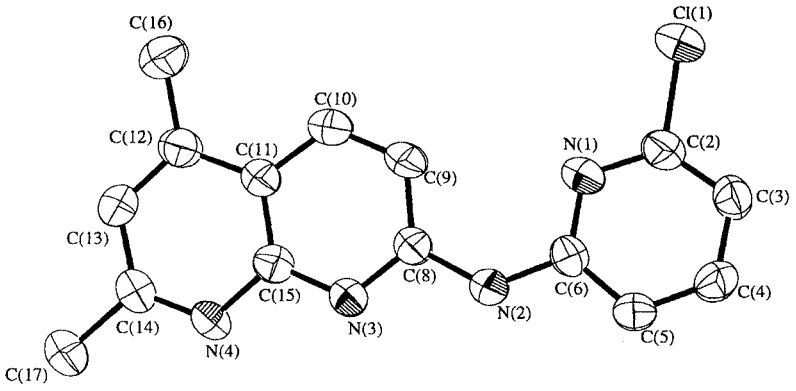

Figure 1. Molecular structure and atomic numbering scheme of HL^2 (probability level of thermal ellipsoids: 50%); hydrogen atoms are not shown

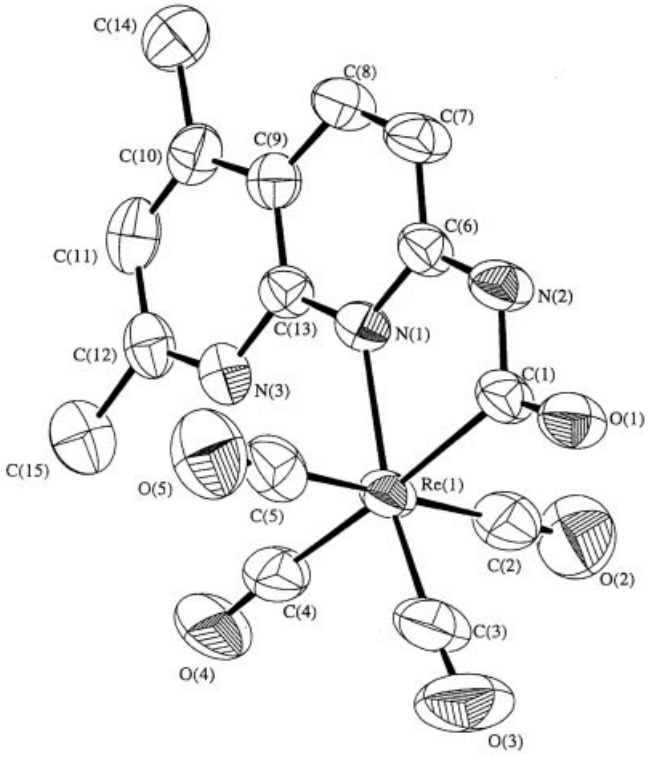

Figure 2. Molecular structure and atomic numbering scheme of **1**·$CHCl_3$ (probability level of thermal ellipsoids: 50%); the hydrogen atoms and the solvent molecules are not shown

[N(1)−H(1)···N(7)* 3.17 Å, O(5)*···H(2)−N(6) 2.86 Å], as shown in Figure 4. Accordingly, the HL^3 ligand in this crystal can be considered as an organic guest incorporated into the host complex **1** (incorporation of an organic guest into organometallic complexes may be potentially useful for nonlinear optical, conducting and ferromagnetic materials[14]).

Complex **2**, which also exhibits a distorted octahedral rhenium(I) center, features a highly strained four-membered metallacycle consisting of the Re(1), N(1), C(10), and N(2) atoms with an N(1)−Re−N(2) angle of 59.5° (Figure 5). The average Re−CO distance for the CO groups *trans* to the naphthyridylamide ligand (1.932 Å) is shorter, while the average Re−CO bond length of the *trans*-$Re(CO)_2$ subunit (2.04 Å) is longer than the corresponding average Re−CO distances in **1**·$CHCl_3$ and **1**·HL^3·$2CH_2Cl_2$. The Re−N(amide) and Re−N(naphthyridine) distances are 2.206(5) and 2.152(5) Å, respectively, which are similar to the average Re−N(bpm) distance of 2.16 Å in [$Re(CO)_4$(bpm)][BF_4].[6] The conformation of the naphthyridylamido ligand L^2 in **2** is similar to that in the free amine HL^2. However, the N(1)−C(5) [1.358(8) Å] and N(1)−C(10) [1.351(8) Å] bonds of the ligand L^2 in **2** are shorter than the corresponding N−C bonds [1.378(6) and 1.400(6) Å, respectively] in the free ligand HL^2.

Electronic Absorption Spectra

Table 5 shows the UV/Vis spectroscopic data of complexes **1** and **2**, together with those of the free ligand HL^2. The absorptions of **1** and **2** at $\lambda < 330$ nm are similar to those of the (carbonyl)(diimine)Re^I complexes;[6,15] we assign these bands mainly to $\pi\rightarrow\pi^*$ transitions. In dichloromethane solution, complex **2** exhibits a broad lower energy absorption band at λ_{max} = 415 nm ($\varepsilon = 1.7\cdot10^4$ $mol^{-1}\cdot dm^3\cdot cm^{-1}$) and a shoulder at 432 nm ($\varepsilon = 1.5\cdot10^4$ $mol^{-1}\cdot dm^3\cdot cm^{-1}$), both of which are absent in the spectra of HL^2 in the same solvent. The 415-nm absorption is solvent-sensitive and is blue-shifted to 410 nm in acetonitrile (see Table 5). We assign this absorption to the $d\pi(Re)\rightarrow\pi^*$ (heterocyclic ligand) transition.[16] Note that on going from **2** to **1** the lowest-energy absorption band shifts to considerably higher energies (from 432 to 358 nm). This may be attributed to the different electronic properties of the coordinated naphthyridylamido and -carbamoyl groups. For example, the partial delocalization of electron density from the metal center to the carbamoyl moiety in complex **1** would raise the energy of the MLCT transition, whereas in complex **2**, the Re($d\pi$) orbitals would be destabilized due to coordination of the electron-rich naphthyridylamido group to Re^I, leading to a reduction in MLCT transition energy.

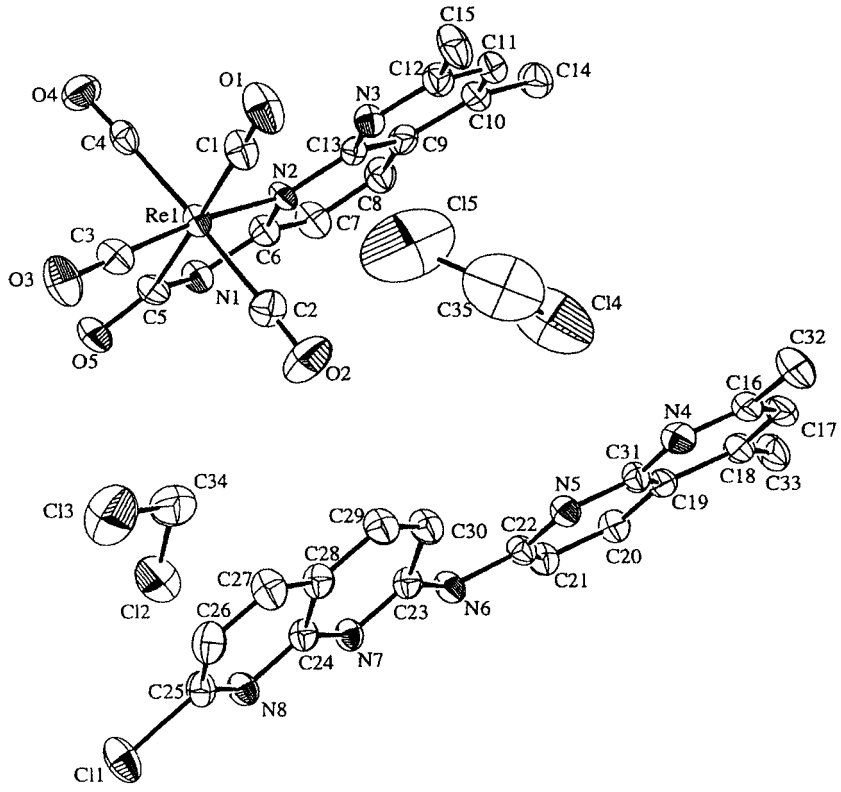

Figure 3. Molecular structure and atomic numbering scheme of **1**·HL^3·$2CH_2Cl_2$ (probability level of thermal ellipsoids: 50%); hydrogen atoms are not shown

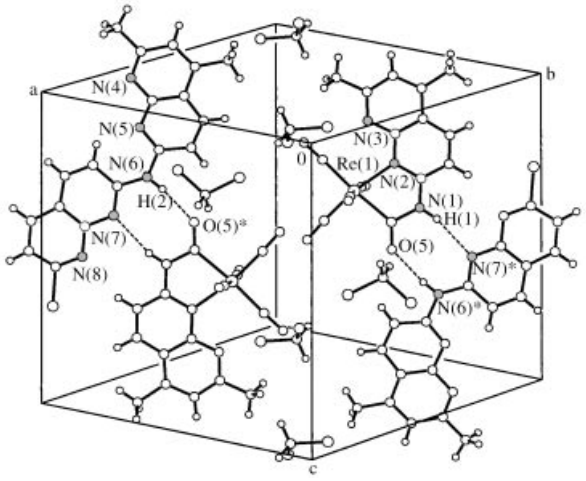

Figure 4. Unit cell diagram for **1**·HL^3·$2CH_2Cl_2$

Photoluminescent Properties

Complex **1** displays a weak emission at λ_{max} = 453 nm in an EtOH/MeOH (1:4, v/v) glassy solution at 77 K. However, no emission was detected when this complex was dissolved in dichloromethane or acetonitrile at room temperature.

On excitation at 400−430 nm, complex **2** exhibits an intense structured emission in an EtOH/MeOH (1:4, v/v) glassy solution at 77 K (λ_{max} = 499 and 533 nm), with a vibrational shift of 1280 cm^{-1} (Figure 6). The emission of **2** in dichloromethane at 77 K is intense and structured (λ_{max} = 512 and 550 nm). On the basis of previous work,[15,17] we tentatively assign the structured 77 K emission to be $^3(\pi\pi^*)$ in nature.

Complex **2** emits strongly in fluid solutions as well. A broad emission analogous to the ^{3}MLCT emission of $[Re(CO)_4(bpm)]^+$ or $[Re^I(CO)_3(L-L)X]$ (L−L = aromatic diimines)[17] was observed at λ_{max} = 520 nm in dichloromethane, 535 nm in acetonitrile, 522 nm in toluene, 505 nm in benzene, and 515 nm in tetrahydrofuran at room temperature (Table 5). We suggest that this solvent-dependent broad emission has an admixture of ^{3}IL and ^{3}MLCT characters (the ^{3}MLCT emissions from (carbonyl)Re^I complexes of aromatic diimines are also solvent-dependent).

Note that the free ligand HL^2 gives a broad emission at λ_{max} = 400 nm in acetonitrile at room temperature. This emission has a substantially higher energy than that of complex **2**, and is assigned to be a $^1(\pi\pi^*)$ emission in nature. As expected, the intraligand fluorescence of HL^2 has a short life-time ($\leq 10^{-3}$ μs, Table 5).

It is interesting to note the very long emission life-times (25−46 μs in degassed solutions, 142 and 150 μs in EtOH/MeOH and CH_2Cl_2 glassy solutions at 77 K) and high emission quantum yields (up to 0.22) for complex **2** (Table 5), which are in contrast to those reported for $[Re(CO)_4(L-L)]^+$ (life-time < 10 μs and quantum yield < 0.05).[15] The long emission life-time is characteristic of an organic triplet emission and reflects substantial ^{3}IL character in the excited state.

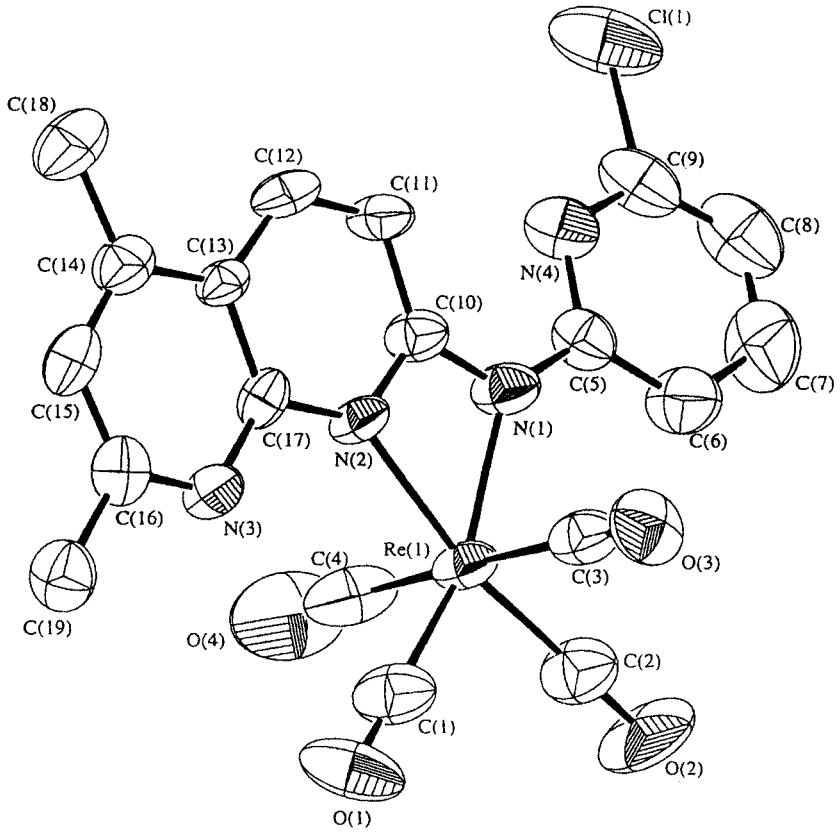

Figure 5. Molecular structure and atomic numbering scheme of **2** (probability level of thermal ellipsoids: 50%); hydrogen atoms are not shown

Table 1. Selected bond lengths and angles in ligand HL^2

Bond lengths [Å]			
Cl(1)−C(2)	1.761(5)	N(1)−C(2)	1.330(7)
N(1)−C(6)	1.336(6)	N(2)−C(6)	1.378(6)
N(2)−C(8)	1.400(6)	N(3)−C(8)	1.335(6)
N(3)−C(15)	1.347(7)	N(4)−C(14)	1.321(7)
N(4)−C(15)	1.375(6)		
Bond angles [°]			
C(2)−N(1)−C(6)	117.0(5)	C(6)−N(2)−C(8)	130.2(4)
C(8)−N(3)−C(15)	117.6(4)	C(14)−N(4)−C(15)	117.6(4)
Cl(1)−C(2)−N(1)	115.8(4)	Cl(1)−C(2)−C(3)	117.7(4)
N(1)−C(2)−C(3)	126.5(5)	C(2)−C(3)−C(4)	115.3(5)
N(1)−C(6)−N(2)	119.8(5)	N(1)−C(6)−C(5)	121.9(5)

Table 2. Selected bond lengths and angles in complex **1**·$CHCl_3$

Bond lengths [Å]			
Re(1)−N(1)	2.205(6)	Re(1)−C(1)	2.146(7)
Re(1)−C(2)	1.99(1)	Re(1)−C(3)	1.91(1)
Re(1)−C(4)	2.000(9)	Re(1)−C(5)	2.00(1)
O(1)−C(1)	1.228(9)	O(2)−C(2)	1.13(1)
O(3)−C(3)	1.14(1)	O(4)−C(4)	1.13(1)
O(5)−C(5)	1.13(1)	N(2)−C(1)	1.41(1)
Bond angles [°]			
N(1)−Re(1)−C(1)	76.2(3)	N(1)−Re(1)−C(2)	91.3(3)
N(1)−Re(1)−C(3)	168.6(3)	N(1)−Re(1)−C(4)	99.6(3)
N(1)−Re(1)−C(5)	90.1(3)	C(1)−Re(1)−C(2)	88.7(3)
C(1)−Re(1)−C(3)	92.4(3)	C(2)−Re(1)−C(3)	88.3(5)
C(2)−Re(1)−C(4)	91.7(4)	C(2)−Re(1)−C(5)	177.5(4)
C(4)−Re(1)−C(5)	90.2(4)	C(1)−N(2)−C(6)	120.4(6)
Re(1)−C(1)−O(1)	132.1(6)		

Experimental Section

General: 7-Amino-2,4-dimethyl-1,8-naphthyridine (H_2L^1) and 2,7-dichloro-1,8-naphthyridine were prepared by literature methods.[18] All reactions were performed under nitrogen using standard Schlenk techniques. ^1H and $^{13}C\{^1H\}$ NMR spectra were recorded with a Bruker DPX 300 or DRX 500 FT NMR spectrometer. Chemical shifts were referenced to tetramethylsilane. Fast atom bombardment (FAB) mass spectra were obtained with a Finnigan Mat 95 mass spectrometer using a 3-nitrobenzyl alcohol matrix. UV/Vis absorption spectra were measured with a Perkin−Elmer Lambda 19 UV/Vis spectrophotometer. Elemental analyses were performed by Butterworth Laboratory. Steady-state emission measurements were performed with a SPEX Fluorolog-2 spectrophotometer. The emission spectra were corrected for monochromator and photomultiplier efficiency and for xenon lamp stability. Quantum yields of the complexes were determined relative to quinine sulfate in 1.0 N sulfuric acid at 298 K ($\Phi = 0.54$). Emission lifetime measurements were performed with a Quanta Ray DCR-3 Nd-YAG laser (pulse output 355 nm, 8 ns). The fluorescent lifetimes were obtained by a picosecond laser spectrophotometer equipped with a C4334 streakscope connected to the C4792-01

Tble 3. Selected bond lengths and angles in complex $1{\cdot}HL^3{\cdot}2CH_2Cl_2$

Bond lengths [Å]			
Re(1)−N(2)	2.204(5)	Re(1)−C(1)	1.983(8)
Re(1)−C(2)	1.992(9)	Re(1)−C(3)	1.916(9)
Re(1)−C(4)	1.993(9)	Re(1)−C(5)	2.158(7)
Cl(1)−C(25)	1.771(8)	O(1)−C(1)	1.15(1)
O(2)−C(2)	1.14(1)	O(3)−C(3)	1.16(1)
O(4)−C(4)	1.116(9)	O(5)−C(5)	1.236(9)
N(1)−C(5)	1.396(9)	N(1)−C(6)	1.362(9)
N(2)−C(6)	1.345(9)	N(2)−C(13)	1.393(8)
N(6)−C(22)	1.389(8)	N(6)−C(23)	1.388(9)
Bond angles [°]			
N(2)−Re(1)−C(1)	99.4(3)	N(2)−Re(1)−C(2)	88.0(3)
N(2)−Re(1)−C(3)	170.1(3)	N(2)−Re(1)−C(4)	90.7(2)
N(2)−Re(1)−C(5)	75.8(2)	C(1)−Re(1)−C(2)	91.2(4)
C(1)−Re(1)−C(3)	90.4(3)	C(1)−Re(1)−C(4)	92.9(3)
C(1)−Re(1)−C(5)	174.8(3)	C(2)−Re(1)−C(3)	90.2(4)
C(2)−Re(1)−C(4)	175.8(3)	C(2)−Re(1)−C(5)	90.8(3)
C(3)−Re(1)−C(4)	90.3(3)	C(3)−Re(1)−C(5)	94.4(3)
C(4)−Re(1)−C(5)	85.0(3)	C(5)−N(1)−C(6)	119.7(6)
Re(1)−N(2)−C(6)	114.0(4)	Re(1)−N(2)−C(13)	127.4(4)
C(6)−N(2)−C(13)	118.6(6)	C(22)−N(6)−C(23)	130.3(6)

Table 4. Selected bond lengths and angles in complex **2**

Bond lengths [Å]			
Re(1)−N(1)	2.206(5)	Re(1)−N(2)	2.152(5)
Re(1)−C(1)	1.925(9)	Re(1)−C(2)	1.94(1)
Re(1)−C(3)	2.06(1)	Re(1)-C(4)	2.02(1)
Cl(1)−C(9)	1.751(8)	O(1)−C(1)	1.15(1)
O(2)−C(2)	1.15(1)	O(3)−C(3)	1.07(1)
O(4)−C(4)	1.11(1)	N(1)−C(5)	1.358(8)
N(1)−C(10)	1.351(8)	N(2)−C(10)	1.349(9)
N(2)−C(17)	1.363(8)		
Bond angles [°]			
N(1)−Re(1)−N(2)	59.5(2)	N(1)−Re(1)−C(1)	162.4(2)
N(1)−Re(1)−C(2)	107.5(3)	N(1)−Re(1)−C(3)	89.3(3)
N(1)−Re(1)−C(4)	91.6(3)	N(2)−Re(1)−C(1)	102.9(3)
N(2)−Re(1)−C(2)	166.9(3)	N(2)−Re(1)−C(3)	90.9(2)
N(2)−Re(1)−C(4)	90.1(2)	C(1)−Re(1)−C(2)	90.1(3)
C(1)−Re(1)−C(3)	91.0(4)	C(1)−Re(1)−C(4)	88.3(4)
C(2)−Re(1)−C(3)	90.4(3)	C(2)−Re(1)−C(4)	88.7(3)
C(3)−Re(1)−C(4)	178.9(3)	Re(1)−N(1)−C(5)	136.9(5)
Re(1)−N(1)−C(10)	95.7(4)	C(5)−N(1)−C(10)	127.3(6)
Re(1)−N(2)−C(10)	98.3(4)	Re(1)−N(2)−C(17)	138.6(5)

streak trigger. The decay signal was recorded with a R928 PMT (Hamamatsu), which was connected to a Tektronix 2430 digital oscilloscope. Solutions for the photophysical experiments were degassed by at least four freeze-pump-thaw cycles.

Syntheses

7-[2-(6-Chloropyridyl)amino]-2,4-dimethyl-1,8-naphthyridine (HL^2): A suspension of H_2L^1 (1.73 g, 0.01 mol), 2,6-dichloropyridine (1.48 g, 0.01 mol), and powdered KOH (0.7 g, 0.012 mol) in toluene (300 mL) was refluxed for 24 h. On removal of the solvent, the residue was washed with water and diluted aqueous HCl, followed by chromatography on a silica gel (70−230 mesh) column using petroleum ether (boiling range 40−60 °C) and ethyl acetate (4:1, v/v) as the eluent. The pale yellow fraction was collected and the solvents were evaporated to give a pale yellow product. Yield: 1.19 g (42%). ^{1}H NMR ($CDCl_3$, 300 MHz): δ = 2.6−2.7 (s, 6 H, CH_3), 7.0−8.5 (m, 6 H, aryl H), 7.6 (s, 1 H, NH) ppm. FAB-MS: *m/z* = 285 $[M]^+$. IR (KBr): $\tilde{\nu}$ = 3233, 1587, 1505, 1458, 1344, 983, 784, 713, 554 cm^{-1}.

Table 5. Spectroscopic and photophysical properties of HL^2, **1**, and **2**

Compound	Medium (T [K])	λ_{max}^{abs} [nm] ($\varepsilon \times 10^{-4}$ [$dm^3{\cdot}mol^{-1}{\cdot}cm^{-1}$])	λ_{max}^{em} [nm]/τ [μs]	φ_{em}
HL^2	CH_2Cl_2 (298)	259 (4.0), 345 (3.1), 357 (3.5)		
	CH_3CN (298)		400/≤ 10^{-3}	0.30
1	CH_2Cl_2 (298)	241 (3.6), 327 (0.99), 342 (1.1), 358 (0.98)	non-emissive	
	CH_3CN (298)	236 (4.6), 307 (0.81), 342 (0.99), 356 (0.83)	non-emissive	
	EtOH/MeOH[a] (77)		weak emission (453 nm)	
2	CH_2Cl_2 (298)	289 (2.6), 317 (1.0, sh), 415 (1.7), 432 (1.5, sh)	520/46	0.22
	CH_3CN (298)	286 (3.0), 316 (1.4, sh), 410 (1.7), 426 (1.6, sh)	535/26	0.19
	$C_6H_5CH_3$ (298)		522/25	0.11
	C_6H_6 (298)	290 (3.0), 317 (1.3, sh), 416 (1.6), 436 (1.4, sh)	505/26	0.16
	THF (298)	291 (2.4), 318 (1.0, sh), 415 (1.3), 437 (1.1, sh)	515/31	0.06
	EtOH/MeOH[a] (77)		499/150 533/150	
	CH_2Cl_2 (77)		512/142 550/142	

[a] 1:4 (v/v).

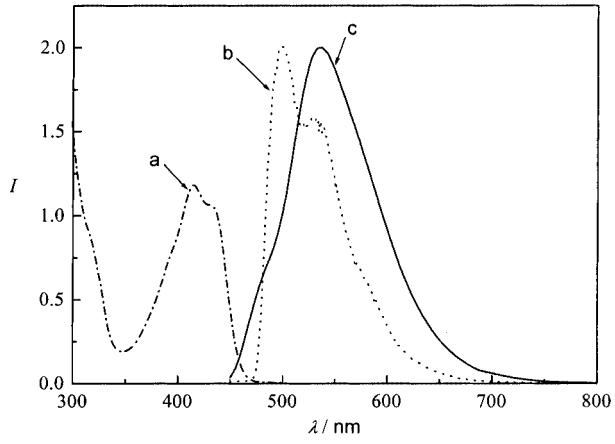

Figure 6. Electronic absorption spectrum (a) and emission spectra (b, c) of **2**; the absorption spectrum was measured in CH_3CN at 298 K, whereas the emission spectra were measured in EtOH/MeOH (1:4, v/v) glassy solutions at 77 K (b) and in degassed acetonitrile at 298 K (c); I = intensity (arbitrary units)

(7-Chloronaphthyridyl)(5,7-dimethylnaphthyridyl)amine (HL^3): This ligand was prepared according to the same procedure as that for HL^2, except that 2,7-dichloro-1,8-naphthyridine was used instead of 2,6-dichloropyridine and the eluent for the chromatography was methanol/dichloromethane (5:95, v/v). Yield: 1.18 g (35%). ^1H NMR ($CDCl_3$, 300 MHz): δ = 2.6−2.7(s, 6 H, CH_3), 6.7−8.1(m, 7 H, aryl H), 8.3 (s, 1 H, NH) ppm. FAB-MS: m/z = 336 $[M]^+$. IR (KBr): $\tilde{\nu}$ = 3223, 3046, 1674, 1593, 1486, 1313, 1147, 850, 789, 595, 462 cm^{-1}. UV/Vis (CH_2Cl_2): λ_{max} (ε): 253 ($2.1\cdot10^4$), 329 ($1.1\cdot10^4$), 359 ($1.8\cdot10^4$), 375 ($2.6\cdot10^4$), 419 ($5.9\cdot10^3$), 443 nm ($6.8\cdot10^3$).

$[Re(CO)_4(HL^1CO)]$ (1): A mixture of H_2L^1 (173 mg, 1 mmol), $Re(CO)_5Cl$ (362 mg, 1 mmol), and *t*BuOK (112 mg, 1 mmol) in CH_2Cl_2 (20 mL) was refluxed overnight. After filtration and concentration, a yellow solid was obtained. The solid was washed with toluene and recrystallized from chloroform/pentane. Yield: 203 g (40%). $C_{15}H_{10}N_3O_5Re\cdot0.5H_2O$ (507.47): calcd. C 35.5, H 2.2, N 8.3; found C 35.4, H 2.3, N 8.7. ^1H NMR ($CDCl_3$, 300 MHz): δ = 2.67 (s, 3 H, CH_3), 2.75 (s, 3 H, CH_3), 7.15 (s, 1 H, aryl H), 7.30 (d, $^3J_{H,H}$ = 9.3 Hz, 1 H, aryl H), 8.23 (d, $^3J_{H,H}$ = 8.4 Hz, 1 H, aryl H), 10.37 (s, 1 H, NH) ppm. $^{13}C\{^1H\}$ NMR ($CDCl_3$, 500 MHz): δ = 18.1 (CH_3), 23.7 (CH_3), [109.7, 116.1, 122.7, 136.2, 146.2, 153.7, 161.2] (aryl C), 163.5 (carbamoyl C), [187.1, 190.1, 191.8] (terminal CO) ppm. FAB-MS: m/z = 498 $[M]^+$. IR (KBr): $\tilde{\nu}$ = 3310 (w), 2087 (s), 2008 (s), 1928 (s), 1653 (m), 1614 (s), 1593 (s), 1538 (s), 1044 (s), 862 (s), 701 (s), 615 (s), 580 (s) cm^{-1}.

$[Re(CO)_4L^2]$ (2): A mixture of HL^2 (284 mg, 1 mmol) and *t*BuOK (112 mg, 1 mmol) in CH_2Cl_2 (20 mL) was heated under reflux for 30 min, followed by the addition of $Re(CO)_5Br$ (406 mg, 1 mmol). The mixture was then stirred for 6 h. After filtration and concentration, a yellow solid was obtained, which was chromatographed on a silica gel column using dichloromethane as the eluent. Recrystallization from dichloromethane/hexane afforded complex **2** as yellow prismatic crystals. Yield: 466 mg (80%). $C_{19}H_{12}ClN_4O_4Re$ (581.98): calcd. C 39.2, H 2.1, N 9.6; found C 39.5, H 2.2, N 9.4. ^1H NMR ($CDCl_3$, 300 MHz): δ = 2.58 (s, 3 H, CH_3), 2.65 (s, 3 H, CH_3), 6.62−8.29 (m, 6 H, aryl H) ppm. $^{13}C\{^1H\}$ NMR ($CDCl_3$, 500 MHz): δ = 17.8 (CH_3), 25.2 (CH_3), [113.4, 114.8, 115.0, 120.6, 135.7, 140.1, 145.4, 148.4, 152.5, 159.6, 162.1, 177.7] (aryl C), [185.6, 189.2, 189.3, 191.0] (terminal CO) ppm. FAB-MS: m/z = 581 $[M]^+$. IR (KBr): $\tilde{\nu}$ = 2925 (w), 2103 (m), 2009 (s), 1981 (s), 1946 (s), 1931 (s), 1682 (m), 1579 (m), 1455 (s), 1336 (m), 1152 (m), 776 (m), 626 (w), 585 (m) cm^{-1}.

Table 6. Crystal and refinement data

	HL^2	**1**·$CHCl_3$	**1**·HL^3·$2CH_2Cl_2$	**2**
Empirical formula	$C_{15}H_{13}ClN_4$	$C_{16}H_{11}Cl_3N_3O_5Re$	$C_{35}H_{28}Cl_5N_8O_5Re$	$C_{19}H_{12}ClN_4O_4Re$
Formula mass	284.75	617.85	1004.13	581.99
Crystal size [mm]	0.15×0.07×0.25	0.30×0.10×0.07	0.15×0.07×0.20	0.05×0.30×0.35
Crystal system	monoclinic	triclinic	triclinic	monoclinic
Space group	$P2_1/c$	$P\bar{1}$	$P\bar{1}$	$P2_1/a$
a [Å]	13.292(2)	7.419(1)	12.761(2)	9.176(2)
b [Å]	7.497(2)	10.684(2)	13.560(3)	13.378(2)
c [Å]	14.322(3)	14.668(2)	13.829(3)	16.754(3)
α [°]	90	106.06(1)	105.88(2)	90
β [°]	102.74(2)	98.18(1)	101.80(2)	98.73(2)
γ [°]	90	105.56(1)	114.82(2)	90
V [$Å^3$]	1392.1(5)	1046.4(7)	1944(1)	2032.8(6)
Z	4	2	2	4
D_c [g cm^{-3}]	1.359	1.961	1.715	1.901
F(000)	592	588	988	1112
μ [cm^{-1}]	2.69	62.23	35.22	61.44
T [K]	301	301	301	301
$2\theta_{max}$ [°]	51.0	50.0	51.2	51.2
hkl range	$0 \le h \le 16$	$-8 \le h \le 8$	$0 \le h \le 15$	$0 \le h \le 11$
	$0 \le k \le 7$	$0 \le k \le 12$	$-16 \le k \le 14$	$0 \le k \le 16$
	$-16 \le l \le 15$	$-17 \le l \le 16$	$-15 \le l \le 14$	$-20 \le l \le 19$
Measured reflns	13412	3916	17861	18515
Unique reflns	1826	3700	6645	3934
Reflns with $I > 3\sigma(I)$	1006	2966	5526	3081
Parameters	184	248	493	262
R, $_wR$	0.055, 0.064	0.035, 0.045	0.049, 0.063	0.044, 0.059
Goodness of fit	2.09	1.709	1.43	1.81
(D map) max./min. [e·$Å^{-3}$]	0.23/−0.25	1.18/−1.22	1.35/−2.36	1.67/−1.47

X-ray Crystallography: The data of HL^2, **1**·HL^3·$2CH_2Cl_2$, and **2** were collected with a Mar diffractometer equipped with a 300-mm image plate detector, whereas those of **1**·$CHCl_3$ were collected with a Rigaku AFC7R diffractometer, using graphite-monochromatized Mo-K_α radiation (λ = 0.71073 Å for **1**·$CHCl_3$ and **2**, and 0.71069 Å for the others; data see Table 6). The structures were solved by direct methods (SIR92:[19] HL^2 and **1**·HL^3·$2CH_2Cl_2$) or by Patterson methods (PATTY:[20] **1**·$CHCl_3$ and **2**), expanded by Fourier methods, and refined by full-matrix least squares using the software package TeXsan[21] with a Silicon Graphics Indy computer. Note that the chlorine atoms of the $CHCl_3$ solvent molecule in **1**·$CHCl_3$ were disordered, with Cl(1), Cl(1′), Cl(2), Cl(2′), Cl(3), and Cl(3′) each having an occupation number of 0.5. In the least-squares refinements, all the non-H atoms, except C(16) and the disordered Cl atoms in **1**·$CHCl_3$, were refined anisotropically. The H atoms bonded to the N(2) atom in HL^2 and to the N(1) and N(6) atoms in **1**·HL^3·$2CH_2Cl_2$ found in the difference Fourier synthesis were refined. All the other H atoms placed at calculated positions with thermal parameters equal to 1.3 times that of the attached C atoms were not refined. CCDC-176086 (HL^2), -176087 (**1**·$CHCl_3$), -176088 (**1**·HL^3·$2CH_2Cl_2$), and -176089 (**2**) contain the supplementary crystallographic data for this paper. These data can be obtained free of charge at www.ccdc.cam.ac.uk/conts/retrieving.html or from the Cambridge Crystallographic Data Centre, 12 Union Road, Cambridge CB2 1EZ, UK [Fax: (internat.) + 44-1223/336-033; E-mail: deposit@ccdc.cam.ac.uk].

Acknowledgments

We acknowledge support from The University of Hong Kong, the Hong Kong Research Grants Council (HKU 7298/99P), the Innovation and Technology Commission of the Hong Kong SAR Government (ITS/053/01), and the Distinguished Young Scholar Fund to CMC from the National Natural Science Foundation of China (NSF, 29929001).

[1] [1a] O. Ishitani, M. W. George, T. Ibusuki, F. P. A. Johnson, K. Koike, K. Nozaki, C. Pac, J. J. Turner, J. R. Westwell, *Inorg. Chem.* **1994**, *33*, 4712. [1b] J. Hawecker, J.-M. Lehn, R. Ziessel, *J. Chem. Soc., Chem. Commun.* **1983**, 536. [1c] C. Kutal, A. J. Corbin, G. Ferraudi, *Organometallics* **1987**, *6*, 553.

[2] A. Vogler, H. Kunkely, *Angew. Chem. Int. Ed. Engl.* **1981**, *20*, 469.

[3] [3a] J. C. Luong, L. Nadjo, M. S. Wrighton, *J. Am. Chem. Soc.* **1978**, *100*, 5790. [3b] H. Kunkely, A. Merz, A. Vogler, *J. Am. Chem. Soc.* **1983**, *105*, 7241.

[4] A. Vogler, H. Kunkely, *Inorg. Chim. Acta* **1980**, *45*, L265.

[5] [5a] T. G. Kotch, A. J. Lees, S. J. Fuerniss, K. I. Papathomas, *Chem. Mater.* **1991**, *3*, 25. [5b] T. A. Oriskovich, P. S. White, H. H. Thorp, *Inorg. Chem.* **1995**, *34*, 1629.

[6] [6a] R. J. Shaver, D. P. Rillema, C. Woods, *J. Chem. Soc., Chem. Commun.* **1990**, 179. [6b] P. Spellane, R. J. Watts, A. Vogler, *Inorg. Chem.* **1993**, *32*, 5633.

[7] D. S. Glueck, J. Wu, F. J. Hollander, R. G. Bergman, *J. Am. Chem. Soc.* **1991**, *113*, 2041.

[8] [8a] M. Rahim, K. J. Ahmed, *Organometallics* **1994**, *13*, 1751. [8b] M. Rahim, C. White, A. L. Rheingold, K. J. Ahmed, *Organometallics* **1993**, *12*, 2401.

[9] [9a] T.-F. Wang, C.-C. Hwu, C.-W. Tsai, Y.-S. Wen, *Organometallics* **1998**, *17*, 131. [9b] M. H. Chisholm, C. E. Hammond, J. C. Huffman, *Organometallics* **1987**, *6*, 210.

[10] G. W. Parshall, S. D. Ittel, *Homogeneous Catalysis*, John-Wiley, New York, **1992**, chapter 5.4.

[11] K.-L. Lu, C.-M. Wang, H.-H. Lee, L.-C. Chen, Y.-S. Wen, *J. Chem. Soc., Chem. Commun.* **1993**, 706.

[12] M. Wrighton, D. L. Morse, *J. Am. Chem. Soc.* **1974**, *96*, 998.

[13] J. E. Johnson, R. A. Jacobson, *Acta Crystallogr., Sect. B* **1973**, *29*, 1669.

[14] M. M. Chowdhry, D. M. P. Mingos, A. J. P. White, D. J. Williams, *Chem. Commun.* **1996**, 899.

[15] R. J. Shaver, D. P. Rillema, *Inorg. Chem.* **1992**, *31*, 4101.

[16] [16a] W. E. Ford, M. Calvin, *Chem. Phys. Lett.* **1980**, *76*, 105. [16b] W.-M. Xue, M. C.-W. Chan, Z.-M. Su, K.-K. Cheung, S.-T. Liu, C.-M. Che, *Organometallics* **1998**, *17*, 1622. [16c] A. Nakamura, T. Imai, Y. Oda, S. Okutsu, A. Ueno, F. Toda, *J. Electroanal. Chem.* **1997**, *438*, 159.

[17] L. Sacksteder, A. P. Zipp, E. A. Brown, J. Streich, J. N. Demas, B. A. DeGraff, *Inorg. Chem.* **1990**, *29*, 4335.

[18] [18a] R. A. Henry, P. R. Hammond, *J. Heterocycl. Chem.* **1977**, *14*, 1109. [18b] G. R. Newkome, S. J. Garbis, V. K. Majestic, F. R. Fronczek, G. Chiari, *J. Org. Chem.* **1981**, *46*, 833.

[19] *SIR92:* A. Altomare, M. Cascarano, C. Giacovazzo, A. Guagliardi, M. C. Burla, G. Polidori, M. Camalli, *J. Appl. Crystallogr.* **1994**, *27*, 435.

[20] *PATTY:* P. T. Beurskens, G. Admiraal, G. Beurskens, W. P. Bosman, S. Garcia-Granda, R. O. Gould, J. M. M. Smits, C. Smykalla, The DIRDIF Program System, Technical Report of the Crystallography Laboratory, University of Nijmegen, The Netherlands, **1992**.

[21] *TeXsan:* Crystal Structure Analysis Package, Molecular Structure Corporation, The Woodlands, Texas, USA, **1985** and **1992**.

Received December 18, 2001
[I01513]

Synthesis, Spectra and Crystal Structure of Two Copper(I) Complexes of Acetonethiosemicarbazone

Sanchai Lhuachan,[a] Sutatip Siripaisarnpipat,*[b] and Narongsak Chaichit[c]

Keywords: Copper / Electrochemistry / Schiff bases / IR spectroscopy

The reaction of copper(I) chloride with acetonethiosemicarbazone (tscac) in a copper to tscac molar ratio of 1:2 forms the cationic complex $[Cu(tscac)_2]Cl$ (**1**). When the ratio of the copper to tscac was reduced to 1:1, a dimeric complex $[Cu_2Cl_2(tscac)_2]_2$ (**2**) was obtained. In complex **2**, two $CuCl_2$ species act as bridging groups between two $Cu(tscac)_2$ moieties forming an eight-membered ring, whereas in complex **1**, there is no $CuCl_2$ moiety in the structure. In both complexes the copper(I) center is coordinated in a distorted tetrahedral geometry to two tscac groups through the sulfur and the imine nitrogen atom. In dimeric complex **2**, the sulfur atom in each tscac ligand coordinates weakly to copper(I) in the $CuCl_2$ moiety giving the distorted tetrahedral geometry. For the free ligand, the $\nu_{c=s}$ vibration at 789 cm^{-1} appears at lower energy than in complexes **1** and **2** (754 and 744 cm^{-1} respectively) indicating coordination at the sulfur atom. The complexes synthesized by either electrochemical or chemical methods are identical.
(© Wiley-VCH Verlag GmbH & Co. KGaA, 69451 Weinheim, Germany, 2003)

Introduction

Thiosemicarbazone and its derivatives are chelating ligands with sulfur and nitrogen donor atoms forming a five-membered chelate ring. In a few cases they behave as monodentate ligands and bond through the sulfur atom only.[1] These ligands show antitubercular activity and activity against influenza and have been suggested as possible pesticides and fungicides. These activities are due to their ability to chelate trace metals. It has been reported that copper ions enhance the antitubercular activity of thiosemicarbazone,[2] leading to an increased interest in the chemistry of transition metal chelates of thiosemicarbazone and its derivatives. The preparation and crystal structures of copper(II) complexes of thiosemicarbazide, thiosemicarbazone and their derivatives have been reported.[3–8] The copper(I) complexes of some *N*- and *S*-substituted thiosemicarbazones are polymeric, the metal ion being bonded through the nitrogen and sulfur of the thiosemicarbazone moiety.[1] We report here a comparison of the crystal structures of two copper(I) complexes of acetonethiosemicarbazone, i.e. $[Cu(tscac)_2]Cl$ (**1**) and $[Cu_2Cl_2(tscac)_2]_2$ (**2**) which were prepared by both chemical and electrochemical methods. Their spectroscopic data are also reported.

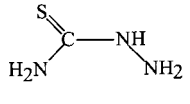

(Tsc)

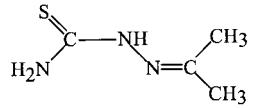

(tscac)

Results and Discussion

Electrolysis of elemental copper in an ammonium chloride solution containing the ligand for half an hour at 4.5 V and 40 mA was found to be optimum for the formation of complex **1** with the highest yield (98%). A total of 72 coulombs of electricity was passed leading to the dissolution of 0.054 g of copper. The electrochemical efficiency (E_f), which is defined as mol of metal dissolved per Faraday of electricity, was found to be 1.14. This means the anodic reaction involves a one-electron transfer. For the preparation of complex **2**, the optimum conditions for the electrolysis were one hour at 3.5 V and 40 mA. The 144 coulombs of electricity applied led to the dissolution of 0.108 g of copper. The electrochemical efficiency (E_f) was found to be 0.96. This means the anodic reaction also involves a one-electron transfer.[9] X-ray analyses for these complexes showed that the complexes prepared by both chemical and electrochemical methods have the same molecular and crystal structures. Consequently, only the crystal structures of com-

[a] Chemistry Program, Faculty of Science and Technology, Rajabhat Institute Saun Dusit
295 Ratchasima Rd., Dusit, Bangkok 10300, Thailand
[b] Laboratory of Crystallography and Gemology, Department of Chemistry, Faculty of Science, Kasetsart University
P. O. Box 1011 Kasetsart, Jatuchak, Bangkok 10903, Thailand
Fax: (internat.) +66-2/942-8900 ext. 302
E-mail: fscists@ku.ac.th
[c] Department of Physics, Faculty of Science and Technology, Thammasart University,
Rangsit, Pathum Thani, 12121, Thailand

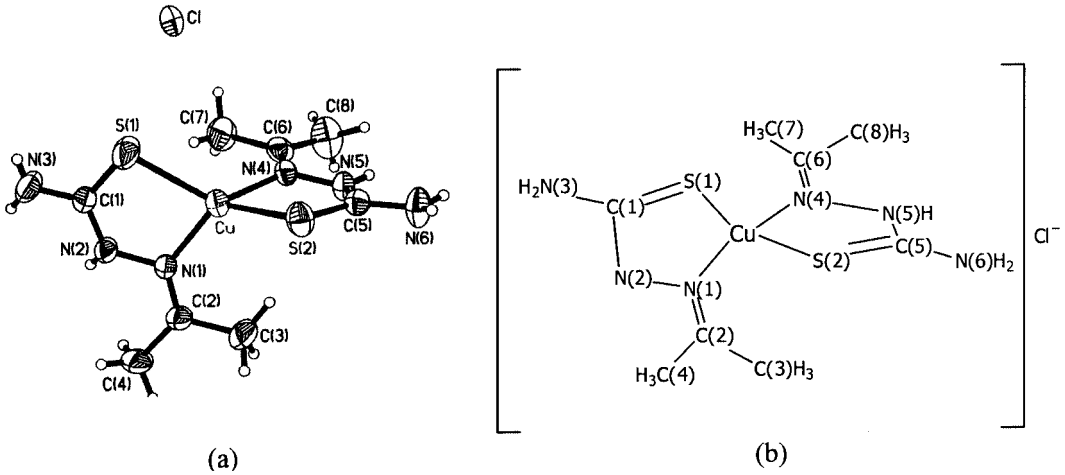

Figure 1. (a) Perspective view of complex **1** with thermal ellipsoids at the 50% probability level; (b) structural formula

plexes **1** and **2** prepared by chemical methods are discussed below.

Complex **1** consists of a distorted tetrahedral $[Cu(tscac)_2]^+$ cation and a chloride counteranion (Figure 1). The copper tetrahedron consists of two sulfurs and two nitrogens of two acetonethiosemicarbazone ligands forming two five-membered chelate rings. All the atoms of the five-membered rings are essentially coplanar and the planes of those rings are almost perpendicular. The average Cu−S distance is similar to the Cu−S distance in $[Cu(tsc)Cl_2]$.[3]

Complex **2** crystallizes as a neutral tetranuclear copper(I) complex with general formula $[Cu_2Cl_2(tscac)_2]_2$. Two $Cu(tscac)_2$ moieties are bridged by two $CuCl_2$ groups forming an eight-membered ring. In each $Cu(tscac)_2$ moiety, a copper center [Cu(1)] is coordinated in a distorted tetrahedral geometry by two sulfur atoms [S(1) and S(2)] and two nitrogen atoms [N(1) and N(4)] of two tscac ligands, forming two five-membered rings as in complex **1**. The coordination around the other copper center [Cu(2)] in the bridging $CuCl_2$ is also tetrahedral. Each $CuCl_2$ acts as a bridging group between two $Cu(tscac)_2$ moieties through the S(1) and S(2) atoms and gives rise to the tetranuclear copper(II) complex shown in Figure 2. The imino protons of the two tscac ligands are non-equivalent and give rise to NMR signals at $\delta = 10.31$ and 11.41 ppm. The center of each molecule is a crystallographic center of symmetry which is surrounded by four copper and four sulfur atoms forming an eight-membered ring. The two Cu−Cl distances are significantly different by 0.08 Å and longer than those for $[Cu^{II}(tsc)Cl_2]$.[3] The elongation of the Cu−Cl bond in this complex may be a result of the spatial arrangement of a hydrogen bonding interaction between the amino group and the chloride ion. The closest hydrogen bond length is 3.159 Å between N(3) and Cl(1). This interaction causes the non-equivalence of the amino protons. The torsion angles Cl(1)−Cu(2)−S(1)−C(1), Cl(2)−Cu(2)−S(1)−C(1) and Cu(2)−S(1)−C(1)−N(3) are 22.19(15)°, 140.89(14)° and −22.3(4)°, respectively, showing that the Cl(1) and N(3) atoms are in a suitable position for the formation of an intramolecular hydrogen bond. The Cu(1)−S bond length is 0.01 Å shorter than the Cu(2)−S bond length, indicating the weaker nature of the Cu(2)−S bond. As Cu(1) is part of two five-membered rings the length of the Cu(1)−S bond must be squeezed. The molecule forms weak intermolecular hydrogen bonds as indicated in Figure 3. The formation of two five-membered rings around Cu(1) causes the deviation of the angles around Cu(1) from tetrahedral angles, and this deviation is greater than that around Cu(2). The angle between the planes of the two five-membered rings is almost perpendicular (approx. 80°). All the atoms of the five-

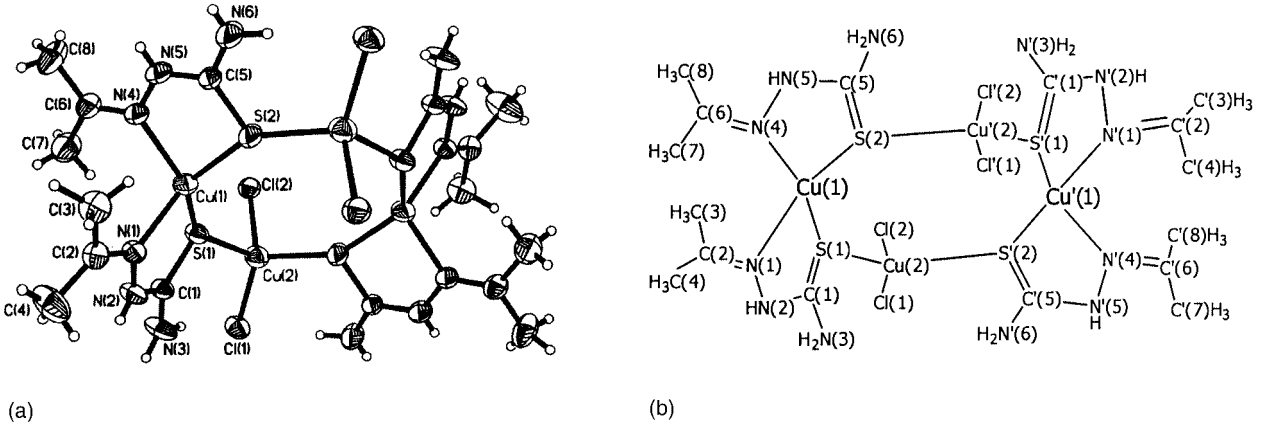

Figure 2. (a) Perspective view of complex **2** with thermal ellipsoids at the 50% probability level; (b) structural formula

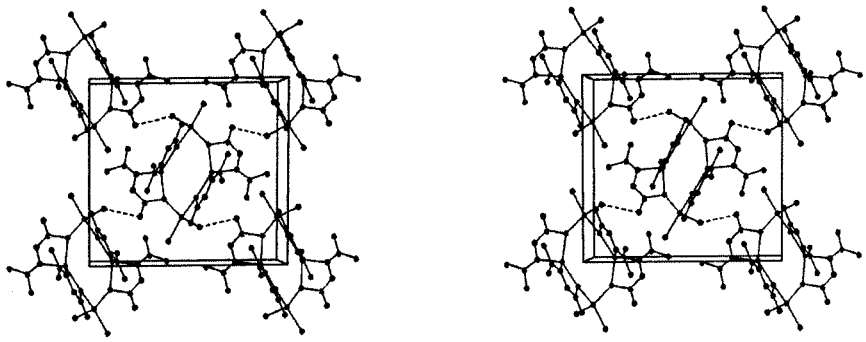

Figure 3. A stereoscopic view of the packing in the unit cell of $[Cu_2Cl_2(tscac)_2]_2$ (**2**) showing the intermolecular hydrogen bonding

Table 1. Selected bond lengths (Å) and angles (°) for compounds **1** and **2**

Compound **1**			
Cu−N(1)	2.1031(14)	Cu−N (4)	2.1657(14)
Cu−S(1)	2.2598(5)	Cu−S(2)	2.2737(6)
S(1)−C(1)	1.6900(19)	S(2)−C(5)	1.6988(17)
N(1)−C(2)	1.289(2)	N(1)−N(2)	1.3921(19)
N(2)−C(1)	1.350(2)	N(3)−C(1)	1.327(2)
N(4)−C(6)	1.285(2)	N(4)−N(5)	1.3930(19)
N(5)−C(5)	1.349(2)	N(6)−C(5)	1.328(2)
C(2)−C(3)	1.493(3)	C(2)−C(4)	1.494(3)
C(6)−C(8)	1.493(3)	C(6)−C(7)	1.494(3)
N(1)−Cu−N(4)	107.80(5)	N(1)−Cu−S(2)	127.69(4)
N(4)−Cu−S(2)	85.10(4)	N(1)−Cu−S(1)	86.30(4)
N(4)−Cu−S(1)	124.05(4)	S(2)−Cu−S(1)	128.51(2)
Compound **2**			
Cu(1)−N(4)	2.084(3)	Cu(1)−N(1)	2.117(3)
Cu(1)−S(1)	2.2647(11)	Cu(1)−S(2)	2.2762(11)
Cu(2)−Cl(1)	2.3157(11)	Cu(2)−S(2)*	2.3405(12)
Cu(2)−S(1)	2.3678(11)	Cu(2)−Cl(2)	2.3936(12)
S(1)−C(1)	1.708(4)	S(2)−C(5)	1.713(4)
S(2)−Cu(2)*	2.3405(12)	N(1)−C(2)	1.290(5)
N(1)−N(2)	1.396(4)	N(2)−C(1)	1.340(5)
N(3)−C(1)	1.325(5)	N(4)−C(6)	1.280(5)
N(4)−N(5)	1.402(5)	N(5)−C(5)	1.336(5)
N(6)−C(5)	1.317(5)	C(2)−C(3)	1.482(6)
C(2)−C(4)	1.503(7)	C(6)−C(8)	1.495(7)
C(6)−C(7)	1.505(7)		
N(4)−Cu(1)−N(1)	105.49(12)	N(4)−Cu(1)−S(1)	126.81(10)
N(1)−Cu(1)−S(1)	86.10(8)	N(4)−Cu(1)−S(2)	85.99(9)
N(1)−Cu(1)−S(2)	125.08(9)	S(1)−Cu(1)−S(2)	129.33(5)
Cl(1)−Cu(2)−S(2)*	114.85(4)	Cl(1)−Cu(2)−S(1)	114.37(4)
S(2)*−Cu(2)−S(1)	106.76(4)	Cl(1)−Cu(2)−Cl(2)	111.21(4)
S(2)*−Cu(2)−Cl(2)	108.78(5)	S(1)−Cu(2)−Cl(2)	99.68(4)

membered rings are essentially coplanar. The principle distances and angles are presented in Table 1.

A comparison between the vibrational bands of tscac in $[Cu(tscac)_2]Cl$ and $[Cu_2Cl_2(tscac)_2]_2$ leads to the following observations:

(1) The absorption bands at 2800−3300 cm^{-1} are assigned to NH_2 and N−H stretching modes.[8] A broad peak at 3554 cm^{-1} in the spectrum of $[Cu_2Cl_2(tscac)_2]_2$ indicates the existence of weak hydrogen bonding (N−H···Cl) as seen in the crystal structure.

(2) The $\nu_{C=N}$ band at 1594 cm^{-1} in the free ligand is shifted to lower frequency in the complexes {1546 cm^{-1} in $[Cu(tscac)_2]Cl$ and 1555 cm^{-1} in $[Cu_2Cl_2(tscac)_2]_2$}. This shift supports the coordination of copper to the imine nitrogen.[8] The bands between 1400−1500 cm^{-1} in the spectra of the free ligands and the complexes can be assigned to the ν_{C-N} band.

(3) The absorptions at 789, 754 and 744 cm^{-1} can be assigned to the C=S stretching in the free ligand, $[Cu(tscac)_2]Cl$ and $[Cu_2Cl_2(tscac)_2]_2$ respectively. These shifts to lower energy in the complexes indicate a weaker C=S bond upon coordination with copper. A comparison of the vibrational frequencies in the tscac ligand and the complexes is shown in Table 2.

Table 2. Comparison of some vibration frequencies and bond lengths in tscac and the complexes

Compound	C=S		C=N	
	$\tilde{\nu}$ (cm^{-1})	Distance (Å)	$\tilde{\nu}$ (cm^{-1})	Distance (Å)
tscac	789 s	1.690[2]	1594 s	1.292[2]
$[Cu(tscac)_2]Cl$	752 s	1.6900(19)	1546 s	1.289(2)
		1.6988(17)		1.285(2)
$[Cu_2Cl_2(tscac)_2]_2$	744 s	1.708(4)	1555 s	1.290(5)
		1.713(4)		1.280(5)

Both complexes are ESR silent and display no d-d electronic spectra, consistent with the presence of Cu^I species.

The reactions at the anode were established by the weight loss of the copper sheet, which was weighed before and after the reaction. The electrochemical efficiency of 0.96 and 1.14 found for both complexes indicates that the anode material loses one electron per atom. The colorless gas observed at the cathode is formed as a result of the reduction of hydrogen ion either from the ligand or the acid. Mabrouk and co-workers[9] have suggested that in the electrochemical synthesis of metal complexes with thiosemicarbazide the ligand loses a proton and becomes negatively charged. If the reactions in this study occurred as described above, the number of tscac protons in the complexes should not be equal to the number of protons in the free ligand. The ^1H NMR spectra, however, show an equal number of protons in the free ligand and the complexes. In addition, the preparative results show that hydrochloric acid must be

added to the reaction mixture otherwise the electrolysis will not occur. Therefore the hydrogen gas must be formed from the protons in the hydrochloric acid not in the ligand.

Conclusion

It can be concluded from the electrolysis data (see Exp. Sect.) that the electrolysis of copper in the presence of acetonethiosemicarbazone occurs as follows [Equation (1) and (2)]:

$$\text{Cu} + 2\,\text{Tscac} + \text{Cl}^-_{(aq)} \xrightarrow{\text{for 1 : 2 adduct } ([\text{Cu(tscac)}_2]\text{Cl})} \text{complex } \mathbf{1} + e^- \quad (1)$$

$$\text{and for 1 : 1 adduct } ([\text{Cu}_2(\text{tscac})_2\text{Cl}_2]_2)\quad 4\,\text{Cu} + 4\,\text{Tscac} + 4\,\text{Cl}^- \longrightarrow \text{complex } \mathbf{2} + 4\,e^- \quad (2)$$

Alternatively the complexes may be prepared by chemical synthesis as outlined below

Experimental Section

Materials and Instruments: All chemicals are commercially available (BDH Co., Carlo Erba, Merck Co., Fluka, May & Baker Co. Ltd., Mallinckvodt Co.) and used without further purification. The infrared spectra were measured as KBr discs on a Perkin−Elmer Model SYSTEM 2000 spectrophotometer. ^{1}H NMR spectra were recorded on a JEOL Model JNM-A500 FT NMR 500 MHz spectrometer with deuterated dimethyl sulfoxide (DMSO) as solvent and internal standard. X-ray analyses were carried out using a Siemens Smart CCD diffractometer.

The electrochemical cell consists of a platinum cathode and the sacrificial copper anode immersed in an ammonium chloride solution containing acetonethiosemicarbazone. The complexes were prepared using the method described by Mabrouk and coworkers[9] with slight modification. After each electrolysis the electrochemical efficiency(E_f) was determined. The electrochemical efficiency is defined as mol of metal dissolved per Faraday of electricity. The amount of electricity used for each experiment in this study is equal to 72 coulomb or 7.5×10^{-4} Faradays. Theoretically, this amount of electricity dissolves Cu^+ 7.5×10^{-4} mol or Cu^{2+} 3.75×10^{-4} mol. Therefore, the E_f for Cu^+ and Cu^{2+} must be close to 1 and 0.5 mol·F^{-1}. This means that after electrolysis the E_f for one-electron transfer must be close to 1 and for two-electron transfer to 0.5. The variation of voltage, current and time was performed in order to determine the optimum electrolysis conditions. The electrochemical conditions described below are the optimum conditions for each complex.

Acetonethiosemicarbazone (tscac): The ligand was prepared using the method described by Sunner[10] with a slight modification. Thiosemicarbazide (2 mmol) was added to acetone (50 mL) and the mixture was heated and stirred until a white precipitate had formed. The compound was collected (yield 98%) and recrystallized from a mixture of water and acetone. ^{1}H NMR (500 MHz, [D$_6$]DMSO, 25 °C): δ = 1.89 (s, 3 H, CH$_3$), 1.90 δ (s, 3 H, CH$_3$), 7.49 (br, 1 H, NH$_2$), 7.95 (br, 1 H, NH$_2$) and 9.87 (br, 1 H, NH) ppm.

Complex 1 by Chemical Synthesis: In this synthesis the mol ratio of Cu:tscac is 1:2. A 6 M solution of NH_3 was added to a solution of CuCl (1.5 mmol in 6 M HCl) until the pH of the solution was 4−5. After adding thiosemicarbazone (3.0 mmol in 50 mL acetone) dropwise with stirring at room temperature, the reaction mixture formed two layers. Concentrated ammonium chloride solution was then added to the two layers until a single layer formed. The reaction mixture became pale yellow and was then filtered. Upon slow evaporation for 12−24 hours at room temperature, yellow octahedral crystals were formed. The product was collected, washed with water and acetone and dried in an oven at 60−70 °C. Yield: 40% (0.109 g). The infrared spectrum shows the presence of the tscac ligand in the yellow product. ^{1}H NMR (500 MHz, [D$_6$]DMSO, 25 °C): δ = 2.00 (m, 12 H, CH$_3$), 7.63 and 8.86 (br, 4 H, NH$_2$), 10.92 (s, 2 H, NH).

Complex 2 by Chemical Synthesis: This complex was prepared in a similar procedure to that described above, but using a mol ratio of Cu:tscac of 1:1. After slow evaporation of the solvent from the pale yellow solution for 1−2 days at room temperature, colorless needles were formed. The product was filtered, washed with water and acetone, and dried in an oven at 60−70 °C. Yield: 38% (0.132 g). The infrared spectrum shows the presence of tscac in the product. This complex turns green when exposed to air for several weeks. ^{1}H NMR (500 MHz, [D$_6$]DMSO, 25 °C): δ = 2.00 (m, 12 H, CH$_3$), 7.98 and 8.47 (s, 4 H, NH$_2$), 10.31 and 11.41 (s, 2 H, NH).

Complex 1 by Electrochemical Synthesis: The electrochemical oxidation of a copper anode in an acidic solution containing acetone (50 mL), 6 M HCl (0.5 mL), acetonethiosemicarbazone (1.5 mmol) and ammonium chloride (0.5 g) for half hour at 4.5 V and 40 mA led to the dissolution of 47.4 mg of copper as the Cu^I ion. The reaction mixture became pale yellow and was then filtered to remove insoluble impurities. The solvent was then slowly evaporated from the filtrate at room temperature. After 6 hours, yellow crystals formed. These were then filtered off, washed with water and acetone successively and dried in an oven at 60−70 °C. Yield: 98% (0.266 g). The infrared spectrum shows the presence of tscac in the yellow crystals. The electrochemical efficiency of this reaction was evaluated (see above).

Complex 2 by Electrochemical Synthesis: The electrochemical oxidation of a copper anode in an acidic solution containing acetone (50 mL), 6 M HCl (0.5 mL), acetonethiosemicarbazone (1.5 mmol) and ammonium chloride (0.5 g) for one hour at 3.5 V and 40 mA led to the dissolution of 94.8 mg of copper as the Cu^I ion. The reaction mixture was pale yellow solution and then was filtered to remove the impure particles. The reaction mixture became pale yellow and was then filtered to remove insoluble impurities. The solvent was then slowly evaporated from the filtrate at room temperature. After 8 hours, pale yellow crystals had formed. These were then filtered off, washed with water and acetone successively and dried in an oven at 60−70 °C). Yield: 69% (0.273 g). The infrared spectrum shows the presence of coordination between Cu and tscac. The electrochemical efficiency of this reaction was evaluated (see above). This complex did not give a suitable crystal for the collection of X-ray diffraction data.

X-ray Crystallographic Study: The diffraction data for all complexes with appropriate size crystals were collected at 298(2) K on a 1 K Bruker Smart CCD area detector diffractometer using ω rotation scans with a scan width of 0.3° and graphite-monochromated Mo-K_α radiation (λ = 0.71073 Å). For data collection and data integration, the SMART and SAINT programs were used[11] and empirical absorption correction was performed with the pro-

gram SADABS.[12] The structures were solved by direct methods using the SHELXTL program system[13] for all complexes and were refined by full-matrix least-squares first with isotropic and then with anisotropic thermal parameters for all non-hydrogen atoms. For all complexes the hydrogen atoms were located from a Fourier difference map and refined. Crystal parameters and refinement results for all complexes showed that the complexes prepared by both methods resulted in the same crystal structure. Crystal data and refinement results of complexes **1** and **2** prepared by chemical method are listed in Table 3.

Table 3. Crystallographic data

	1	**2**
Complex	$[Cu(tscac)_2]Cl$	$[Cu_2Cl_2(tscac)_2]_2$
Formula	$C_8H_{18}ClCuN_6S_2$	$C_{16}H_{36}Cl_4Cu_4N_{12}S_4$
Crystal system	Orthorhombic	Monoclinic
Space group	$P2_12_12_1$	$P2_1/c$
a [Å]	11.3795(1)	8.0512(2)
b [Å]	11.5664(1)	15.8665(3)
c [Å]	12.1246(2)	13.6949(3)
α, β, γ [°]	90, 90, 90	90, 94.212(1), 90
V [Å^3]	1595.84(3)	1744.72(7)
Z	4	2
D_m [g cm^{-3}], flotation	1.506	1.748
D_c [g cm^{-3}]	1.504	1.753
μ [mm^{-1}]	1.790	2.981
$2\theta_{max}$ [°]	56.65	61.15
No. reflections measured	10818	12546
Independent	3918	5006
R	0.0225	0.0553
R_w	0.0518	0.0809

CCDC-182401 (**1**) and -182402 (**2**) contain the supplementary crystallographic data for this paper. These data can be obtained free of charge at www.ccdc.cam.ac.uk/conts/retrieving.html [or from the Cambridge Crystallographic Data Center, 12, Union Road, Cambridge CB2 1EZ, UK; Fax: (internat.) +44-1223/336-033; E-mail: deposit@ccdc.cam.ac.uk].

Acknowledgments

This work is financially supported by the Kasetsart University Research and Development Institute. We also thank Dr. John Jeffery from University of Bristol for his kind assistance.

[1] M. A. Ali, S. E. Livingstone, *Coord. Chem. Rev.* **1974**, *13*, 101−132.
[2] M. J. M. Campbell, *Coord. Chem. Rev.* **1975**, *15*, 279−319.
[3] D. Chattopadyay, S. K. Majumdar, P. Lowe, C. H. Schwalbe, S. K. Chattopadhyay, S. Ghosh, *J. Chem. Soc., Dalton Trans.* **1991**, *8*, 2121−2124.
[4] M. B. Ferrari, G. G. Fava, P. Tarasconi, R. Albertini, S. Pinelli, R. Starcich, *J. Inorg. Biochem.* **1994**, *53*, 13−25.
[5] J. V. Martinez, R. A. Toscano, J. R. Ortiz, *Polyhedron* **1995**, *14*, 579−583.
[6] M. A. Ali, K. K. Dey, M. Nazimuddin, F. E. Smith, R. J. Butcher, J. P. Jasinski, J. M. Jasinski, *Polyhedron* **1996**, *15*, 3331−3339.
[7] J. G. Tojai, J. G. Jaca, R. Cortes, T. Rojo, M. K. Urtiaga, M. I. Arriortua, *Inorg. Chim. Acta* **1996**, *249*, 25−32.
[8] M. B. Ferrari, G. G. Fava, E. Leporati, G. Pelosi, R. Rossi, P. Tarasconi, R. Albertini, A. Bonati, P. Lunghi, S. Pinelli, *J. Inorg. Biochem.* **1998**, *70*, 145−154.
[9] H. E. Mabrouk, A. A. Fl-Asmy, T. Y. Al-Ansi, M. Mounir, *Bull. Soc. Chim. Fr.* **1991**, *128*, 309−313.
[10] S. Sunner, *Kgi. Fysiograf. Sällskap. Lund. Förh.* **1948**, *18*, 139−148.
[11] SMART, Data Collection Software, Version 4.0 and SAINT, Data Integration Software, Version 4.0; Bruker AXS, Inc., Madison, WI, **1997**.
[12] G. M. Sheldrick, *SADABS, Program for Empirical Absorption of Göttingen.* **1996**.
[13] G. M. Sheldrick, *SHELXTL version 5.1*, University of Göttingen, Göttingen, Germany, **1993**.

Received April 16, 2002
[I02199]

Thermodynamic and Kinetic Data for the Base-On/Base-Off Equilibration of Alkylcobalamins

Mohamed S. A. Hamza,[a,b] Xiang Zou,[c] Kenneth L. Brown,[c] and Rudi van Eldik*[a]

Keywords: Alkylcobalamins / Metal−carbon bond / Kinetics / High-pressure chemistry / Catalysis

The base-on/base-off equilibration of a series of alkylcobalamins (XCbl) was studied as a function of the electronic properties of X. A square scheme was developed to incorporate all species that participate in this equilibration. The equilibrium between five- and six-coordinate species was studied for several alkylcobalamins (protonated base-off) and alkylcobinamides as a function of pressure by using UV/Vis spectroscopy. In addition, the kinetics of the acid-induced base-on/base-off equilibration of β-$NCCH_2$Cbl, β-CF_3Cbl and CNCbl were studied; the data obtained reveal evidence for an acid-catalysed reaction path. The results of this study and the observed correlations are discussed in reference to those reported in the past, and enable the formulation of an overall equilibration scheme.
(© Wiley-VCH Verlag GmbH & Co. KGaA, 69451 Weinheim, Germany, 2003)

Introduction

In general there is a need to investigate ligand substitution reactions *trans* to the axial alkyl ligand in coenzyme B_{12} and other β-alkylcobalamins, for comparison with the work performed on substitution reactions *trans* to a non-alkyl ligand. Methylcobalamin (CH_3Cbl) and coenzyme B_{12} (AdoCbl) undergo substitution of their axial benzimidazole ligand by a protein histidine residue during complexation to the CH_3Cbl-dependent methionine synthase,[1] the class I[2] AdoCbl-dependent mutases, methylmalonyl coenzyme A mutase, and glutamate mutase,[3] and the class III AdoCbl-dependent D-lysine-5,6-aminomutase.[4]

One of the most characteristic chemical properties of cobalamins is the base-on/base-off equilibrium in which the axially coordinated dimethylbenzimidazole (DMBz) nucleotide is displaced by H_2O and protonated. This reaction is accompanied by a large change in the electronic spectrum upon conversion of the (red) base-on to the (yellow) base-off form. The base-on/base-off equilibrium can best be described by the reactions outlined in Scheme 1.

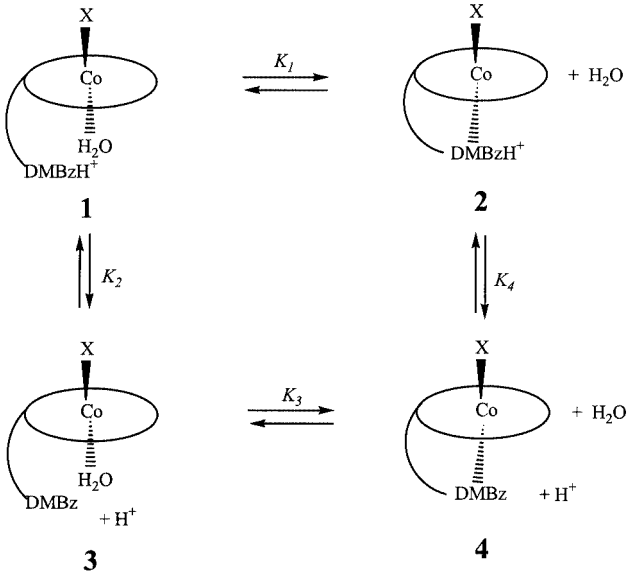

Scheme 1

In this square scheme, **1** represents the protonated base-off cobalamin species, by far the major contributor at low pH, **2** the protonated base-on species, which must be a minor contributor at all pH values, **3** the deprotonated base-off species, which can be a significant contributor at neutral pH for some X, and **4** the deprotonated base-on species, the major species at neutral pH. The introduction of **2** is new and is based on the kinetic data for the base-on/base-off equilibration presented in this report. Coordination (ring closure) of the protonated base-off cobalamin species

[a] Institute for Inorganic Chemistry, University of Erlangen-Nürnberg,
Egerlandstr. 1, 91058 Erlangen, Germany
Fax. (internat.) + 49-(0)9131/8527387
E-mail: vaneldik@chemie.uni-erlangen.de
[b] Department of Chemistry, Faculty of Science, Ain Shams University,
Cairo, Egypt
[c] Department of Chemistry and Biochemistry, Ohio University, Athens, Ohio 45701, USA
Supporting information for this article is available on the WWW under http://www.eurjic.org or from the author.

1 is expected to be unfavorable with respect to chelation of the deprotonated base-off species **3**, such that $K_1 << K_3$.

Although it is known that the base-on form (**4**) is a six-coordinate species, one of the remaining questions is whether the base-off forms (**1** and **3**) are six-coordinate aqua complexes or five-coordinate species without a water molecule occupying the sixth coordination site, or whether they exist in equilibrium between the five- and six-coordinate forms. Physicochemical measurements including electronic absorption, IR and NMR spectra of corrinoid Co^{III} complexes have suggested that the presence of an alkyl group as a strong donor ligand increases the fraction of the five-coordinate species.[5−8] The temperature dependence of the UV/Vis spectra of alkyl cobinamides (RCbi's, derivatives in which the axial nucleotide is chemically removed) suggests that the ratio of six-coordinate to five-coordinate species increases on decreasing the temperature.[5] Increasing temperature also favours the five-coordinate form when diethyl phosphite is the upper axial ligand, and in this case it was also shown qualitatively that increasing pressure favours the six-coordinate form.[9] No structural data on the five-coordinate forms have yet been reported and more direct evidence for the reversible coordination of water is clearly desirable.

Wirt and Chance[10] provided evidence for a five-coordinate/six-coordinate equilibrium in base-off CH_3Cbl and AdoCbl from the temperature dependence of the 1s-3d pre-edge transition in the X-ray absorption edge spectra of these complexes. In addition to the spectroscopic evidence, thermodynamic parameters for this equilibrium provide evidence that the base-off RCbl's exist as an equilibrium mixture of six-coordinate aqua and five-coordinate species, and that this equilibrium is sensitive to the nature of the organic ligand.[11]

Recently, the equilibrium between the five- and six-coordinate base-off forms of both methylcobalamin and vinylcobinamide was studied as a function of pressure, and it was found that this equilibrium is shifted towards the formation of the six-coordinate species upon increasing pressure.[12] This has led us to investigate the equilibrium between the five- and six-coordinate species [shown by way of example for the protonated base-off species **1** in Equation (1)] for many of the available alkylcobalamins (protonated base-off) and cobinamides, in order to investigate the influence of the group X on this equilibrium and to understand the mechanistic implications of its occurrence.

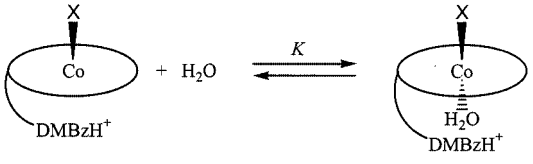

5 **1** (1)

In addition, a systematic study of the kinetics of the base-on/base-off equilibration for β-$NCCH_2$Cbl, β-CF_3Cbl and CNCbl was undertaken, and the data obtained reveal evidence for the acid-catalysed reaction path shown in Scheme 1. The reported results enable us to draw a consistent mechanistic picture for such ligand displacement reactions.

Results

According to Scheme 1, the base-on/base-off reaction must be viewed as the sum of two consecutive equilibria, either deprotonation of **1** followed by coordination (ring closure) of **3**, involving dissociation of a coordinated water molecule, or coordination (ring closure) of **1** followed by deprotonation of the base-on species **2**. It follows from the square scheme that $K_2K_3 = K_1K_4$. Values of $pK_{base\text{-}off}$ [Equation (2), where $K_{base\text{-}off}$ represents the apparent acid dissociation constant of a mixture of species **1** and **2**] have been reported for a large number of cobalamins, and range from about 4.0 (*n*-heptylCbl) to −2.4 in the case of H_2OCbl.[13,14] The pK_a of the detached axial nucleoside α-ribazole ($pK_a = 5.56$),[15] or the virtually identical value for the appropriate microscopic pK_a of the detached axial nucleotide, α-ribazole-3′-phosphate ($pK_a = 5.54$),[16] can be used for the value of pK_2.

$$K_{base\text{-}off} = \frac{K_2(1+K_3)}{(1+K_1)} \quad (2)$$

Based on the definition of $K_{base\text{-}off}$ [Equation (2)], it can be shown (see Supporting Information; see also footnote on the first page of this article) that f_{off}, the fraction of base-off species, is given by Equation (3).

$$f_{off} = \frac{([H^+]+K_2)}{([H^+]+K_{base\text{-}off})(1+K_1)} \quad (3)$$

Equations (2) and (3) simplify to Equations (4) and (5) on the basis that it is reasonable to expect K_1 to be very small, so that $1 + K_1 \approx 1$.

$$K_{base\text{-}off} = K_2(1+K_3) \quad (4)$$

$$f_{off} = \frac{([H^+]+K_2)}{([H^+]+K_{base\text{-}off})} \quad (5)$$

Equation (5) indicates that the fraction of base-off cobalamin depends on the pH, such that an increase in $[H^+]$ will increase the concentration of **1**, and therefore the fraction of base-off species in solution. However, under neutral experimental conditions (pH ≥ 7) or under conditions in which typical cyanation reactions were studied (pH = 11), Equation (5) simplifies to Equation (6). Equations (5) and (6) allow the calculation of the fraction of base-off form from $K_{base\text{-}off}$, K_2 and $[H^+]$ under all experimental

conditions, where Equation (6) is identical to that used before for pH ≥ 7.[13]

$$f_{off} = \frac{K_2}{K_{base\text{-}off}} \quad (6)$$

Effect of Pressure on the UV/Vis Spectra of XCbl and XCbi

There is good evidence that Cbi's (and protonated, base-off Cbl's) with strong donor ligands (e.g. vinyl, methyl, sulfite, dialkyl phosphites) exist as temperature-dependent mixtures of five- and six-coordinate aqua forms based on UV/Vis and EXAFS data.[5,10,17] Increasing temperature favours the five-coordinate form, and with diethyl phosphite as the β-axial ligand, it has also been shown qualitatively that increasing pressure favours the six-coordinate form.[9]

Organocobalamins (XCbl) with different X (Ado, Et, Me, $BrCH_2$, CF_3CH_2, $NCCH_2$, CF_3, CN) are believed to exist in aqueous solution in a base-on form (**4**) and two base-off forms (**1** and **3**), which can both be either five- or six-coordinate, as shown for **1** in Equation (1). UV/Vis spectra of cobalamins such as AdoCbl and ethylcobalamin in their protonated, base-off forms, exhibit reversible changes on heating the solution, changing the solvent or drying the solid (when a thin film was used to record the reflectance spectrum).[5,18] The spectrum of protonated base-off cobalamin at high temperature is similar to the spectra of cobinamides, suggesting that temperature affects the spectra of base-off cobalamin and the analogous cobinamides in the same way. The UV/Vis spectra of methylcobinamide, isopropylcobinamide and sulfitocobinamide at low temperature (−180 °C in ethanol or a mixture of ethanol, methanol and propan-2-ol) were assigned to the six-coordinate complexes. However, the spectra of these complexes at 20 °C were assigned to the five-coordinate complexes.[5] In the case of ethylcobalamin, the calculated[13] fraction of base-off cobalamin [ca. 4.7% from Table 1 for the two base-off forms **1** and **5** in Equation (1)] at equilibrium is in reasonable agreement with the values of 13 and ca. 15%, from NMR measurements and optical spectra, respectively.[5,18] The ratio of the species in Equation (1) is probably similar for ethylcobinamide, so that ethylcobalamin exists as a mixture of 85% **4**, 0% **3** and 15% **5**.[19] For AdoCbl, calculations suggest ca. 1.3% **3** and **5** in aqueous solution at room temperature, whereas the spectrum indicates the presence of ca. 90% **4** and ca. 10% **3** and **5**; by analogy with ethylcobalamin, one may assume 0% **3** and 10% **5**. We conclude that the base-off forms of AdoCbl and ethylcobalamin are mainly five-coordinate species at room temperature.

In addition to the spectroscopic evidence for the existence of a five-coordinate/six-coordinate equilibrium for corrinoid alkyl(aqua)cobalt complexes, and the sensitivity of this equilibrium to the inductive effect of the alkyl ligand, there are thermodynamic results that suggest the same equilibrium occurs in the base-off alkylcobalamins.[11] It was found that this equilibrium is displaced toward the six-coordinate aqua species as the organic ligand becomes more electron-withdrawing, where there is an increasing compensation for the entropy loss from the entropy gain of H_2O dissociation, and the entropy change no longer varies with the alkyl ligand. However, for some compounds with the highest value of $-\Delta S$ (and the lowest $-\Delta G$), the loss of entropy upon coordination of the pendent axial nucleotide is largely uncompensated for by the entropic effect of the loss of an axial water ligand, i.e. these compounds are largely five-coordinate.[11] The UV/Vis spectrum of protonated base-off AdoCbl (3×10^{-5} M in 1 M $HClO_4$), exhibits a band at ca. 450 nm as shown in Figure 1. Increasing the pressure to 150 MPa resulted in a small increase in absorbance at the maximum with no isosbestic points being observed. Similar UV/Vis spectra were observed in the case of *n*PrCbl. On the basis that such five-coordinate species exhibit a band at ca. 440−460 nm, compared to a band at ca. 500−522 nm for six-coordinate cobalamins or cobinamides,[8,18] the observed spectral changes suggest that the protonated base-off forms of these complexes mainly exist as five-coordinate species in solution irrespective of pressure. The fractions of the six-coordinate species are apparently very small, i.e., no shift in the equilibrium towards six-coordinate species can be induced by pressure.

Table 1. Electrochemical, thermodynamic and activation parameters for base-on/base-off reactions for a series of cobalamins (XCbl's)

X	p*K* base-off [a]	K_3 [b]	Fraction base-off[c]	Δδ(^{31}P) [Hz][d]	ΔG_3 [kJ·mol^{-1}][e]	ΔH_3 [kJ·mol^{-1}][f]	ΔS_3 [J K^{-1} mol^{-1}][f]	$E_{1/2}$[g]
Et	4.16	20	4.7×10^{-2}			−37 ± 3	−100 ± 12	−1.54
*n*Pr	4.1	23.7	4.05×10^{-2}	−11.98	−8.23	−35 ± 3	−92 ± 12	−1.55
Ado	3.67	76.6	1.3×10^{-2}	−10.45	−10.74			−1.35
CH_3	2.89	467	2.1×10^{-3}	2.81	−15.21	−32 ± 2	−54 ± 4	−1.6
CH_2CF_3	2.6	923	1.1×10^{-3}	0.6	−16.89	−33 ± 3	−58 ± 8	
CF_2H	2.15	2600	3.84×10^{-4}	7.89	−19.48	−28 ± 2	−30 ± 6	
$NCCH_2$	1.81	5620	1.78×10^{-4}	8.42	−21.69			
CF_3	1.44	1.3×10^4	7.7×10^{-5}	24.71	−23.49	−29 ± 1	−20 ± 5	−1.27
CN	0.1	2.9×10^5	3.4×10^{-6}	35.68	−31.10	−38 ± 1	−21 ± 5	−1.00
H_2O	−2.13	4.9×10^7	2.0×10^{-8}	51.01	−43.81			−0.07

[a] See Equation (2) in the text. [b] See Equation (4) and Scheme 1 in the text. [c] Fraction base-off = $K_2/K_{base\text{-}off}$. [d] Ref.[21] [e] At 25 °C, ref.[21] [f] Refs.[11,13] [g] Refs.[34,35]

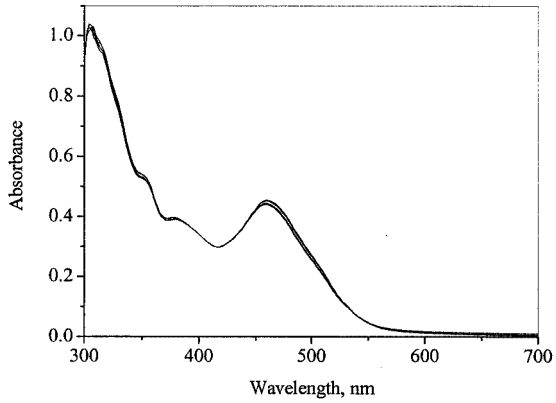

Figure 1. UV/Vis spectra of β-AdoCbl (base-off) (0.5 M $HClO_4$) recorded as a function of pressure (5, 50, 100 and 150 MPa)

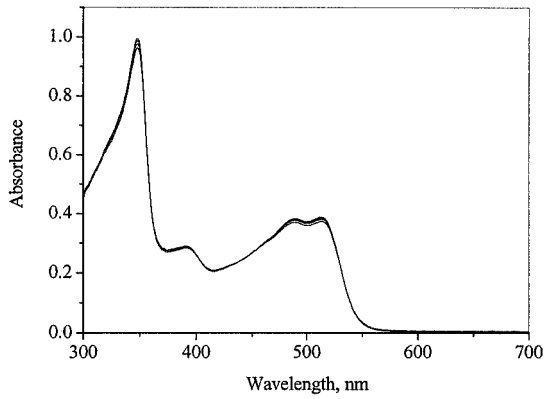

Figure 2. UV/Vis spectra of β-CF_3Cbl (base-off) (0.5 M $HClO_4$) recorded as a function of pressure (5, 50, 100 and 150 MPa).

The UV/Vis spectra of β-CF_3Cbi, β-CF_3Cbl (protonated base-off), H_2O(CN)Cbi (exists as a mixture of α- and β-isomers), and $(H_2O)_2$Cbi exhibit bands at 500−520 and 520−540 nm. Increasing the pressure to 150 MPa again resulted in a very small increase in absorbance with no isosbestic points observed [as shown in Figure 2 for β-CF_3Cbl (base-off)], suggesting that these complexes mainly exist as six-coordinate species irrespective of pressure. Thus, the fraction of the five-coordinate species in these compounds is very small. Interestingly, β-CF_3CH_2Cbl (protonated base-off), β-$NCCH_2$Cbl (protonated base-off) and the cobinamides of these complexes exhibit the main band at 454 and 478 nm, respectively.[20] The absorbance at these maxima increases slightly and is accompanied by a slight shift in the band position on increasing pressure. More importantly, however, a significant increase in absorbance at ca. 480−540 nm was observed upon increasing the pressure step-wise from 5 to 150 MPa. These changes in the UV/Vis spectra are accompanied by isosbestic points at 304, 365, 450 and 595 nm as shown in Figure 3 for β-$NCCH_2$Cbl (protonated base-off), suggesting that an equilibrium between the five- and six-coordinate species occurs [see also Supporting Information, Figure S-1 for the UV/Vis spectra of β-CF_3CH_2Cbl (protonated base-off) as a function of pressure]. Similar changes to those obtained upon increasing the pressure were obtained upon decreasing the temperature. This equilibration involves the coordination of a water molecule to the five-coordinate species to form the six-coordinate aqua complex, and indicates that these complexes exist as a mixture of five- and six-coordinate species in solution.

We recently studied this equilibrium for both MeCbl (protonated base-off) and vinylcobinamide,[12] and found that increasing pressure displaces the observed equilibrium [Equation (1)] from the five-coordinate towards the six-coordinate form for both complexes. A significant increase in the absorbance at ca. 490 nm was observed, accompanied by good isosbestic points. Values of the equilibrium constant {K = [six-coordinate]/[five-coordinate] as defined in Equation (1)} as a function of pressure were calculated

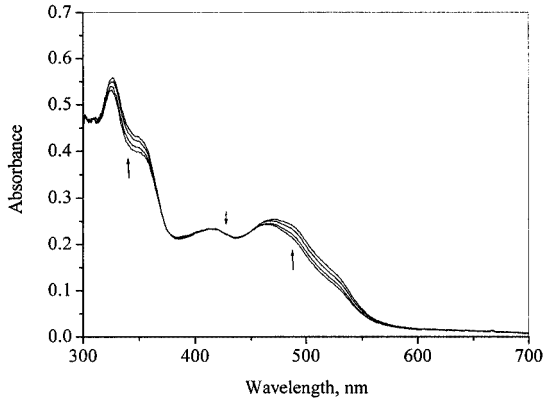

Figure 3. UV/Vis spectra of β-$NCCH_2$Cbl (base-off) (0.5 M $HClO_4$) recorded as a function of pressure (5, 50, 100, and 150 MPa, accompanied by an increase in absorbance around 480−540 nm)

from the increase in absorbance at 490 nm using the relative optical density for the fully formed six-coordinate and five-coordinate species derived from the temperature-dependence studies.[5] The reaction volume, ΔV, was found to be -12.4 ± 1.0 and -12.5 ± 1.2 cm^3 mol^{-1} for the conversion of the five- to the six-coordinate species in vinylcobinamide and MeCbl (base-off), respectively.[12] Their identical values underline the close parallel between Cbi's and protonated Cbl's, and their agreement with the theoretical value of -13.1 cm^3 mol^{-1} expected for the coordination of a water molecule to a five-coordinate species confirm that conversion of the five- to the six-coordinate form involves the coordination of one water molecule to the five-coordinate form.[12]

Based on the UV/Vis spectra recorded under pressure, we conclude that the protonated base-off species of the first two compounds (AdoCbl and *n*PrCbl) of the series of alkylcobalamins (see Table 1 for a list of these XCbl's) investigated during the course of this work are mainly five-coordinate species irrespective of pressure. For some of the XCbl's (X = Me, CF_3CH_2, $NCCH_2$ and vinyl) we suggest that the protonated base-off forms exist in solution as an equilibrium between five- and six-coordinate species. However, for

the last three complexes in the XCbl series (X = CF_3, CN and H_2O), the base-off forms of these compounds are mainly six-coordinate aqua species irrespective of pressure. It seems clear that the X group in the upper, β-axial position has a significant influence on this equilibrium, and by increasing the electron-withdrawing ability of the alkyl group the equilibrium is shifted towards the six-coordinate complexes.

Kinetics of the Base-On/Base-Off Equilibration

β-CF_3Cbl, β-$NCCH_2$Cbl and CNCbl were selected for this study, since the p$K_{base\text{-}off}$ values of these complexes are 1.81, 1.44 and 0.1, respectively.[15,21,22] These p$K_{base\text{-}off}$ values are in the range which allow a titration with acid to be carried out in order to dechelate the DMBz in the α-position. At the same time, the DMBz dissociation rate of these compounds can be monitored with stopped-flow techniques, since, from the electron-inductive effect of these X, the rate of DMBz dissociation is expected to be much slower for these complexes than for those with strongly donating X. The DMBz dissociation rates of other XCbl's such as MeCbl and CF_3CH_2Cbl are much too fast to be monitored by the stopped-flow technique.[23,24]

The kinetic results for the stopped-flow "pH-jump" reaction of 3×10^{-5} M β-$NCCH_2$Cbl (pH = 5, unbuffered solution) with different concentrations of $HClO_4$ (0.01−0.3 M) at I = 1 M ($NaClO_4$) and 5 °C are shown in Figure 4. The values of $k_{obsd.}$ first decrease with increasing acid concentration in the lower concentration range (0.005−0.05 M), and then increase linearly with increasing acid concentration at higher concentrations (0.05−0.3 M). A combination of these concentration dependencies results in the curved dependence observed in Figure 4. The first part of the plot at low acid concentration is incomplete since the reaction becomes too fast to be monitored by stopped-flow and the change in absorbance at 530 or 478 nm becomes too small. The second part of the plot is expected to level off (base-off, k_{-3}), but shows a significant increase in $k_{obsd.}$ with increasing acid concentration. This linear increase in $k_{obsd.}$ is ascribed to an acid-catalysed dechelation reaction, the slope of which represents the rate constant for the acid-catalysed reaction (k^H) and the intercept of which represents the rate constant for the spontaneous dechelation of DMBz (k_{-3}). We conclude that dechelation of DMBz to give β-$NCCH_2$Cbl (base-off) is catalysed by acid. Reenstra and Jencks previously reported that the reaction between CNCbl and HCN is also catalysed by acid, but no kinetic data were given.[25] In terms of the overall base-on/base-off equilibration presented in Scheme 1, the rate law for the acidification reaction of β-$NCCH_2$Cbl is given in Equation (7), in which k_{-3} and k_3 represent the rate constants for the spontaneous dechelation of **4** and chelation of **3**, respectively, $K_2/(K_2 + [H^+])$ represents the fraction of the base-off species in the form of **3** that can undergo chelation, and k^H represents the acid-catalysed reaction path, i.e. the product of the protonation constant for **4** and the dechelation rate constant k_{-1} of **2**, such that $k^H = k_{-1}/K_4$.

$$k_{obs} = k_{-3} + \frac{k_3 K_2}{K_2 + [H^+]} + k^H [H^+] \quad (7)$$

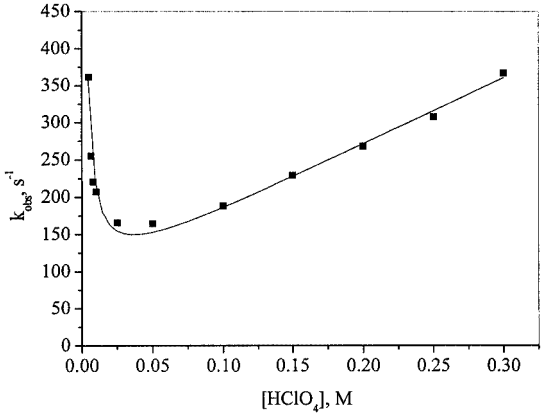

Figure 4. $k_{obsd.}$ versus [$HClO_4$] for the reaction between β-$NCCH_2$Cbl and $HClO_4$ at 5 °C and I = 1 M ($NaClO_4$); the solid line is a fit to Equation (7) in the text.

A non-linear least-squares fit of the data shown in Figure 4 to the rate law in Equation (7), with pK_2 = pK_{Bz} = 5.56,[15] results in $k_3 = (4.4 \pm 0.3) \times 10^5$ s^{-1}, $k_{-3} = 83 \pm 13$ s^{-1} and $k^H = 913 \pm 71$ M^{-1} s^{-1}. It follows that K_3 (= k_3/k_{-3}) equals 5300, which is in very good agreement with the value of 5620 previously reported from thermodynamic considerations.[13] Also, the value of k_{-3} is in good agreement with the acid-independent limiting rate constant obtained when the nucleophile concentration dependence was studied for the reaction of β-$NCCH_2$Cbl and CN^-.[26]

Similar results to those obtained for β-$NCCH_2$Cbl, were obtained for the reaction of β-CF_3Cbl with $HClO_4$. The data for the reaction of 3×10^{-5} M β-CF_3Cbl with $HClO_4$ (0.01−1 M) are shown in Figure 5. The data again show a decrease in $k_{obsd.}$, followed by an increase in $k_{obsd.}$ at higher acid concentrations. The non-linear least-squares fit of the data to the rate-law in Equation (7) resulted in $k_3 = (7.80 \pm 0.07) \times 10^4$ s^{-1}, $k_{-3} = 7.7 \pm 0.2$ s^{-1} and $k^H = 31.8 \pm 0.4$ M^{-1} s^{-1}. It follows that $K_3 = 1.01 \times 10^4$, which is in good agreement with the reported value of 1.3×10^4.[13] Also k_{-3} is in good agreement with the acid-independent limiting rate constant (8.2 s^{-1}) previously determined from the concentration dependence of the reaction of CN^- with β-CF_3Cbl.[27]

Similar results to those obtained for the acidification of β-$NCCH_2$Cbl and β-CF_3Cbl, were obtained for the reaction of CNCbl with $HClO_4$. The data for the reaction of 3×10^{-5} M CNCbl with $HClO_4$ (0.01−1.0 M) at 25 °C again show a decrease in $k_{obsd.}$ followed by a slight increase in $k_{obsd.}$ at higher acid concentrations (see Figure S-2 in the Supporting Information). The increase in $k_{obsd.}$ in this case was not as prominent as in the previous two cases because the value of p$K_{base\text{-}off}$ in this case is only 0.1,[22] which means that more acidic conditions are required to give signific-

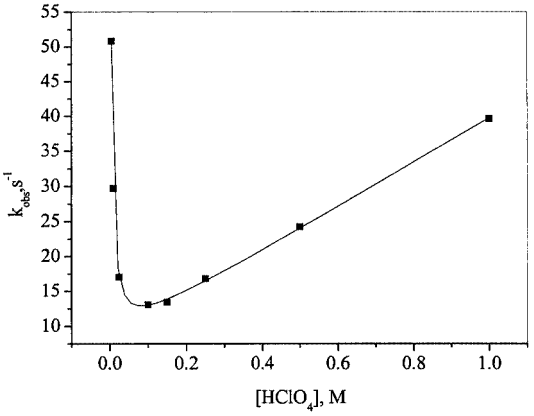

Figure 5. $k_{obsd.}$ versus [$HClO_4$] for the reaction between β-CF_3Cbl and $HClO_4$ at 10 °C and I = 1 M ($NaClO_4$); the solid line is a fit to Equation (7) in the text

ant proportions of the protonated base-off cobalamin. The non-linear least-squares fit of the data resulted in k_3 = (9.2 ± 0.6) × 10^3 s^{-1}, k_{-3} = 0.19 ± 0.04 s^{-1} and k^H = 0.28 ± 0.06 M^{-1} s^{-1}, from which it follows that K_3 = 4.85 × 10^4, which is significantly smaller than the value determined previously (2.9 × 10^5).[13] The value of k_{-3} is also higher than the limiting rate constant (0.042 s^{-1}) determined from the concentration dependence of the reaction of CN^- with CNCbl.[25,26] These differences are in part caused by the lower value of $pK_{base-off}$ and the consequently much higher concentration of $HClO_4$ required to obtain the base-off form.

By way of comparison, the values of k_{-3} for the spontaneous ring opening of β-$NCCH_2$Cbl, β-CF_3Cbl, and CNCbl to give the corresponding unprotonated base-off cobalamins were found to be 83, 7.7 and 0.19 s^{-1}, respectively. The rate constant k_3 for ring closure of the unprotonated base-off forms of these cobalamins was found to be 4.4 × 10^5, 7.8 × 10^4 and 9.2 × 10^3 s^{-1}, respectively, and the acid catalysed rate constant k^H for the ring opening of the unprotonated base-on forms was found to be 913, 31.8 and 0.28 M^{-1} s^{-1}, respectively. These rate constants all follow the same trend for the three complexes, which can be ascribed to the influence of the axial group (X) in the upper, β-position (see further discussion related to Table 1). Thus, our systematic study of the acid dependence of the base-on/base-off reactions has revealed rate constants for the individual reaction steps that present a consistent picture of the overall mechanism and are in agreement with the earlier reported overall equilibrium data for this process, which plays a crucial role in the ligand substitution reactions at the DMBz site of the complexes.

Discussion

It seems clear that the alkyl group (X) in the *trans* position, which controls the equilibrium between the base-on and base-off cobalamin species shown in Scheme 1, as well as the ratio between the five- and six-coordinate species shown in Equation (1), must play a crucial role in controlling the ligand displacement mechanism of these complexes.

The complex-formation constants for the substitution of the α-axial water molecule in a series of alkyl cobinamides by nitrogenous ligands decrease and approach zero as the *trans* ligand is varied in the order H_2O > cyanide > CF_3 > $NCCH_2$ > CH_2CF_3 > methyl > Ado > ethyl.[5,18,28] This weakening of the bond between cobalt and all other ligands (X) only makes sense if the bond to H_2O is also being weakened in the same way in the above *trans* effect order. One would therefore expect that the Co−OH_2 bond could be weakened to such an extent that a five-coordinate complex could be formed. In the case of Co^{II} complexes, [$CoL_5(H_2O)$] where L = CN^-, MeNC and PhNC, water can readily be removed to produce a five-coordinate complex when L = PhNC, or a dimer with a metal−metal bond when L = CN^- or MeNC, and the formation constant is indeed very low.[29]

The stretching frequency ν_{CN} (for cyanide *trans* to X), when X = H_2O, was found to be 2133 cm^{-1}. However, this value was found to be 2082 cm^{-1}, when X = Et, which is close to the stretching frequency for free CN^- (2079 cm^{-1}),[18,29c] i.e., the coordinated cyanide ion becomes more ionic in character. It is clear from this argument that the positive charge on Co decreases from X = H_2O to X = Et. It was also found that the Co−N and Co−C bond lengths in RCbl's increase in the order H_2O < CN < CF_3 < $NCCH_2$ < CF_2H < CF_3CH_2 < CH_3 < Ado.[30−32] This suggests that AdoCbl is a labile complex for ligand substitution reactions. Furthermore, in the case of AdoCbl steric effects may also play an important role in controlling its substitution behaviour.[33]

Table 1 shows that there is a significant increase in $E_{1/2}$ from −1.54 V (X = Et) to −0.07 V (X = H_2O), which reflects the effect of the X group on $E_{1/2}$.[34,35] These data suggest that there is a relationship between the electrochemical behavior and electron density on the Co centre in XCbl's. However, electrochemical studies on XCbl [X = CH_3, CH_3CH_2, $CH_2CH_2CH_3$, $CH_2CH(CH_3)_2$ and $CH_2C(CH_3)_3$], suggest that the bulkiness of X may have a significant influence on the $E_{1/2}$ values.[35] The decrease in $E_{1/2}$ may reflect changes in the Co−X distance which modulates the energy of the lowest σ-type MO (LUMO) of these complexes. The energy of the σ-LUMO (the orbital in which the electron added to RCo must enter) increases when the Co−X distance decreases.[35]

Kräutler et al.[36,37] have compared the crystal structure of AdoCbl with that of cob(II)alamin, which is the intermediate that arises from homolytic cleavage of the β-axial bond. It was found that the two structures are indeed very similar, indicating that it is not just a distortion of the corrin moiety that leads to the homolysis products, but rather strong stabilisation of the radicals by the environment. The structure of cob(II)alamin showed that the cobalt ion is shifted 0.12 Å out of the plane of the corrin nitrogen atoms towards the DMBz ligand. More recently, Jensen et al.[38] ascribed the difference between MeCbl and AdoCbl to the

different electronic nature of the two Co−C bonds. According to B3LYP DFT calculations, the HOMO energy is higher in AdoCbl than in MeCbl, favoring homolytic cleavage. This is due to the 5′-deoxyadenosyl group, which interacts with the corrin ring and induces more electron density on the cobalt centre.

As mentioned previously, most of the known cobalt corrinoid complexes are six-coordinate species, except when one of the axial ligands is a polarizable group such as SO_3^{2-} or an organic ligand, where there is a possibility of a five-coordinate complex.[5] The ratio of the base-on form (six-coordinate species) to the base-off forms (five- and six-coordinate aqua species) is related to the value of K_3 for the formation of the base-on species from the base-off species. Thus, when the $pK_{base\text{-}off}$ value of the protonated base-off complex is high and close to the value for free DMBz (viz. 5.54),[15,16] the fraction of five-coordinate species in this equilibrium will be significant. It was found that the change in the spectrum on drying or heating cobalamin (a qualitative measure of the ease with which DMBz is displaced) does depend on the nature of the axial ligand in the order expected from the $pK_{base\text{-}off}$ values: CN ($pK_{base\text{-}off}$ = 0.1) ≈ ethynyl (0.7) < CF_3 (1.44) < vinyl (2.4) < methyl (2.89) < Ado (3.67) < ethyl (4.14).[14,39]

The values of K_3, the fraction of base-off species, the values of $pK_{base\text{-}off}$ and the thermodynamic parameters associated with the base-off/base-on equilibrium of XCbl are summarized in Table 1. This table shows the effect of the alkyl group (X) located in the *trans* position and the *trans* effect order for the different XCbl complexes. The value of K_3 varies from 20 in the case of CH_3CH_2Cbl to 4.9×10^7 in the case of H_2OCbl. Consequently, the fraction of the base-off form of XCbl decreases significantly from 0.047 in the case of CH_3CH_2Cbl to 2×10^{-8} for H_2OCbl.

The differences between the ^{31}P NMR chemical shifts for the base-on and base-off forms of XCbl, $\Delta\delta(^{31}P)$, are also included in Table 1. These values show a regular variation with the apparent free energy of coordination of the pendant axial DMBz ligand.[21] These effects are interpreted in terms of variations in the axial Co−N bond length leading to progressive changes in the base-on phosphodiester conformation throughout the series of cobalamins. Interestingly, $\delta(^{31}P)$ for base-on Cbl's is linearly related to the axial Co−N bond length (slope = −2.26 ± 0.08 ppm/Å),[32] but $\delta(^{31}P)$ for the base-off Cbl's is the same for all XCbl. When the axial ligand is bound moderately weakly in a base-on cobalamin such as MeCbl (K_3 = 467) or CF_3CH_2Cbl (K_3 = 923), the RO−P−OR bond angle is nearly identical for the base-on and base-off species and hence a negligible value of $\Delta\delta(^{31}P)$ results. However, for those cobalamins such as AdoCbl (K_3 = 76.6) or EtCbl (K_3 = 20) in which the axial base is bound more weakly, the axial Co−N bond becomes longer (2.24 Å in AdoCbl), the RO−P−OR bond angle decreases and the ^{31}P resonance is shifted upfield, producing a negative $\Delta\delta(^{31}P)$. However, in the case of CNCbl, where the axial ligand is bound significantly more tightly (K_3 = 2.9×10^5), the Co−N bond length is short (1.97 Å), the RO−P−OR bond angle increases, and the ^{31}P resonance is shifted downfield and produces a positive $\Delta\delta(^{31}P)$.[21]

Table 1 also shows that the enthalpy of formation of the base-on species, ΔH_3, (the average value is −33 ± 6 kJ·mol^{-1})[11,13] is independent of the nature of the upper axial group (X), despite the variation in K_3. Thus, all the variation in K_3 and $pK_{base\text{-}off}$ must be due to variation in the entropy change, ΔS_3, upon coordination of the axial nucleotide; ΔS_3 varies from −100 ± 12 (X = Et) to −20 ± 5 (X = CF_3) and −21 ± 5 J K^{-1} mol^{-1} (X = CN). This suggests that for the compounds with the strongest electron-donating group (X = Et and Pr) and the most negative ΔS_3 values, the entropy loss associated with the restriction of the pendant axial nucleotide during formation of the base-on species is largely uncompensated by any gain in entropy due to loss of an axial water ligand. This in turn suggests that the base-off species of these complexes are largely pentacoordinated under these conditions. The equilibrium in Equation (1) is displaced towards the formation of the six-coordinate species by increasing electron-withdrawing X groups; thus, for X = CF_3 and CN, the loss of entropy associated with the axial DMBz coordination is compensated for by an increase in entropy due to axial water loss.[11] These results are in agreement with our findings for the equilibrium between five- and six-coordinate species obtained from the UV/Vis spectra recorded under pressure.

We conclude from the above discussion, and based on the trends observed in Table 1, that the base-off forms of some XCbl's such as AdoCbl and ethylcobalamin are mainly five-coordinate. However, in the case of CF_3Cbl, CNCbl and H_2OCbl, the percentage of the base-off forms is very small and they mainly exist as six-coordinate species. The structure of the base-off forms of the other cobalamins (X = Me, CH_2Br, CH_2CF_3, vinyl, etc.) are intermediate and exist as an equilibrium mixture of the five- and six-coordinate species. A decrease in the labilisation effect of X on going from adenosyl to CH_2CF_3 and CF_3 causes a drastic decrease in the fraction of the base-off species and also in the fraction of the five-coordinate species. These effects can play a significant role in the ligand substitution behaviour of the investigated complexes.

Our systematic study of the acid dependence of the base-on/base-off reactions has revealed rate constants for the individual reaction steps that present a consistent picture for the overall mechanism and are in agreement with the earlier reported overall equilibrium data for this process. In addition, the reported kinetic data reveal evidence for an acid-catalysed pathway for the dechelation of DMBz.

Experimental Section

Materials: All the chemicals used were p.A. grade and used as received without further purification. $HClO_4$ and $NaClO_4$ were purchased from Merck. Ultrapure water was used in the kinetic and thermodynamic measurements. The preparations and measurements were carried out in diffuse light since all the alkylcobalamins are known to be very light-sensitive.[18,40] Cyanocobalamin and Ad-

oCbl were supplied by Sigma and H_2Ocbl acetate by Roussel. The other alkylCbl's were prepared as described in the literature[20,41] by treating Co^{II} cobalamin with suitable alkylating agents. In a typical reductive alkylation, H_2OCbl (10 mg, ca. 0.01 mmol) in 5.0 mL of 10% acetic acid or 5% NH_4Cl was purged with argon for 1 h, zinc wool (0.01 mol), freshly activated with 1.0 M HCl, was added, and the reduction was allowed to proceed for 30 min. Alkyl halide (ca. 1 mmol; R = *n*Pr, CF_3CH_2, CF_3 and $NCCH_2$ for the preparation of *n*PrCbl, CF_3CH_2Cbl, CF_3Cbl and $NCCH_2$Cbl, respectively) was introduced, and the reaction was allowed to proceed for 30 min. Alkylcobinamides were prepared by treating (cobinamide)Co^{II}, generated by zinc reduction of Factor B[42,43] [a mixture of the two diastereomers of (aqua)(cyano)cobinamide], with the appropriate alkyl halides. The reaction mixtures were desalted by chromatography on Amberlite XAD-2[15] and the β-isomers were separated by HPLC.[20,44,45]

Instrumentation and Measurements: The pH of the solutions was measured using a Mettler Delta 350 pH meter with a combined glass electrode, calibrated with standard buffer solutions at pH = 4.0, 7.0 and 10.0. UV/Vis spectra were recorded with Shimadzu UV-2101 and Cary 1 spectrophotometers. UV/Vis spectra under high pressure were recorded with the Shimadzu spectrophotometer utilizing a home-made high-pressure unit.[46] Analytical HPLC was performed on a 4.6 × 250 mm Beckman C_8 ultrasphere column while semipreparative HPLC was performed on a 10 × 250 mm Beckman C_8 ultrasphere column, using 50 mM aqueous ammonium phosphate buffer (pH = 3.0) and acetonitrile as described previously.[20,44,45] Kinetic measurements were carried out with an Applied Photophysics SX 18MV stopped-flow instrument coupled to an online data acquisition system. At least eight kinetic runs were recorded under all conditions, and the reported rate constants represent the mean values. All kinetic measurements (pH jump experiments) were carried out under pseudo-first-order conditions, i.e. the acid concentration was in at least tenfold excess over the cobalamin concentration. The UV/Vis spectrophotometers and stopped-flow instruments were thermostatted to the desired temperature ±0.1 °C.

Acknowledgments

The authors gratefully acknowledge financial support from the Deutsche Forschungsgemeinschaft and the Fonds der Chemischen Industrie (to R. v. E.), the Alexander von Humboldt Foundation (fellowship to M. S. A. H.), and the National Institute of General Medical Sciences, USA (Grant GM 48858 to K. L. B.). M. S. A. H. thanks the Ain Shams University, Cairo, Egypt for a sabbatical leave.

[1] [1a] C. L. Drennan, S. Huang, J. T. Drummond, R. G. Matthews, M. L. Ludwig, *Science* **1994**, *266*, 1669−1674. [1b] C. L. Drennan, R. G. Matthews, M. L. Ludwig, *Curr. Opin. Struc. Biol.* **1994**, *4*, 919−929.
[2] B. T. Golding, W. Buckel, in *Comprehensive Biological Catalysis* (Ed.: M. L. Sinnott), Academic Press, London, **1997**, vol. III, pp. 239−259.
[3] [3a] F. Mancia, N. H. Keep, A. Nakagawa, P. F. Leadlay, S. McSweeney, B. Ramussen, P. Boscke, O. Diat, P. R. Evans, *Structure* **1996**, *4*, 339−350. [3b] R. Reitzer, K. Gruber, G. Jogl, U. G. Wagner, H. Bothe, W. Buckel, C. Kratky, *Structure* **1999**, *7*, 891−902.
[4] C. H. Chang, P. A. Frey, *J. Biol. Chem.* **2000**, *275*, 106−114.
[5] R. A. Firth, H. A. O. Hill, B. E. Mann, J. M. Pratt, R. G. Thorp, R. J. P. Williams, *J. Chem. Soc. A* **1968**, 2419−2428.
[6] R. A. Firth, H. A. O. Hill, B. E. Mann, J. M. Pratt, R. G. Thorp, *J. Chem. Soc., Chem. Commun.* **1967**, 1013−1014.
[7] H. A. O. Hill, J. M. Pratt, R. J. P. Williams, *Discuss. Faraday Soc.* **1969**, *47*, 165−171.
[8] S. M. Chemaly, J. M. Pratt, *J. Chem. Soc., Dalton Trans.* **1980**, 2259−2266.
[9] S. M. Chemaly, *J. Inorg. Biochem.* **1991**, *44*, 1−15.
[10] M. D. Wirt, M. R. Chance, *J. Inorg. Biochem.* **1993**, *49*, 265−273.
[11] K. L. Brown, G-.Z. Wu, *Inorg. Chem.* **1994**, *33*, 4122−4127.
[12] M. S. A. Hamza, R. van Eldik, L. S. Harper, J. M. Pratt, E. A. Betterton, *Eur. J. Inorg. Chem.* **2002**, 580−583.
[13] K. L. Brown, S. Peck-Siler, *Inorg. Chem.* **1988**, *27*, 3548−3555.
[14] G. C. Hayward, H. A. O. Hill, J. M. Pratt, N. J. Vanston, R. J. P. Williams, *J. Chem. Soc.* **1965**, 6485−6493.
[15] K. L. Brown, J. M. Hakimi, D. M. Nuss, Y. D. Montejano, D. W. Jacobsen, *Inorg. Chem.* **1984**, *23*, 1463−1471.
[16] K. L. Brown, *J. Am. Chem. Soc.* **1987**, *109*, 2277−2284.
[17] *Chemistry and Biochemistry of B12* (Ed.: R. Banerjee), Wiley & Sons, Inc., New York, **1999**, pp.73−112, 113−164.
[18] J. M. Pratt, *Inorg. Chem. of Vitamin B12*, Academic Press, London, **1972**.
[19] For some of the RCbl, there is the possibility of an intramolecular complex in which the DMBz nucleotide is associated with the *g* acetamide side chain via a hydrogen bond. This additional species for unprotonated base-off cobalamin (tuck-in) was characterized by ^{13}C and ^{15}N NMR spectroscopy.[13]
[20] K. L. Brown, X. Zou, L. Salmon, *Inorg. Chem.* **1991**, *30*, 1949−1953.
[21] K. L. Brown, J. M. Hakimi, D. W. Jacobsen, *J. Am. Chem. Soc.* **1984**, *106*, 7894−7899.
[22] K. L. Brown, J. M. Hakimi, *Inorg. Chem.* **1984**, *23*, 1756−1764.
[23] P. A. Milton, T. L. Brown, *J. Am. Chem. Soc.* **1977**, *99*, 1390−1396.
[24] K. L. Brown, A. W. Awtrey, P. B. Chock, S. G. Rhee, in *Vitamin B_{12}: Proceedings of the 3rd European Symposium on Vitamin B_{12} and Intrinsic Factor* (Eds.: B. Zagalak, W. Friedrich), de Gruyter, Berlin, **1979**.
[25] W. W. Reenstra, W. P. Jencks, *J. Am. Chem. Soc.* **1979**, *101*, 5780−5791.
[26] M. S. A. Hamza, X. Zou, K. L. Brown, R. van Eldik, *J. Chem. Soc., Dalton Trans.*, in press.
[27] M. S. A. Hamza, X. Zou, K. L. Brown, R. van Eldik, *Inorg. Chem.* **2001**, *40*, 5440−5447.
[28] M. S. A. Hamza, K. L. Brown, *Inorg. Chim. Acta* **1997**, *279*, 178−185.
[29] [29a] J. M. Pratt, P. R. Silverman, *J. Chem. Soc. A* **1967**, 1286−1291. [29b] J. M. Pratt, R. J. P. Williams, *J. Chem. Soc. A* **1967**, 1291−1298. [29c] D. A. Baldwin, E. A. Betterton, J. M. Pratt, *S. Afr. J. Chem.* **1982**, *35*, 173−175.
[30] L. Randaccio, M. Furlan, S. Geremia, M. Slouf, I. Srnova, D. Toffoli, *Inorg. Chem.* **2000**, *39*, 3403−3413.
[31] T. Wagner, C. E. Afshar, H. L. Carrell, J. P. Glusker, U. Englert, H. P. C. Hogenkamp, *Inorg. Chem.* **1999**, *38*, 1785−1794.
[32] X. Zou, K. L. Brown, *Inorg. Chim. Acta* **1998**, *267*, 305−308.
[33] [33a] F. Mancia, P. R. Evans, *Structure* **1998**, *6*, 711−720. [33b] F. Champloy, G. Jogl, R. Reitzer, W. Buckel, H. Bothe, B. Beatrix, G. Broeker, A. Michalowicz, W. Meyer-Klaucke, C. Kratky, *J. Am. Chem. Soc.* **1999**, *121*, 11780−11789. [33c] B. Kräutler, W. Keller, C. Kratky, *J. Am. Chem. Soc.* **1989**, *111*, 8936−8938.
[34] A. M. Calafat, L. G. Marzilli, *J. Am. Chem. Soc.* **1993**, *115*, 9182−9190.
[35] R. E. Shepherd, S. Zhang, P. Dowd, G. Choi, B. Wilk, S. C. Chol, *Inorg. Chim. Acta* **1990**, *174*, 249−256.
[36] B. Kräutler, W. Keller, C. Kratky, *J. Am. Chem. Soc.* **1989**, *111*, 8936−8938.
[37] C. Kratky, G. Färber, K. Gruber, K. Wilson, Z. Dauter, H.-

F. Nolting, R. Konrat, B. Kräutler, *J. Am. Chem. Soc.* **1995**, *117*, 4654−4670.
[38] K. P. Jensen, S. P. A. Sauer, T. Liljefors, P.-O. Norrby, *Organometallics* **2001**, *20*, 550−556.
[39] H. P. C. Hogenkamp, J. E. Rush, C. A. Swenson, *J. Biol. Chem.* **1965**, *240*, 3641−3644.
[40] *Chemistry and Biochemistry of B_{12} (Ed.: R. Banerjee), Wiley & Sons, Inc., New York,* **1999**.
[41] K. L. Brown, X. Zou, M. Richardson, W. P. Henry, *Inorg. Chem.* **1991**, *30*, 4834−4838.
[42] P. Renz, *Methods Enzymol.* **1971**, *18*, 82−92.
[43] X. Zou, D. R. Evans, K. L. Brown, *Inorg. Chem.* **1995**, *34*, 1634−1635.
[44] K. L. Brown, D. R. Evans, *Inorg. Chem.* **1990**, *29*, 2559−2561.
[45] D. W. Jacobsen, R. Green, K. L. Brown, *Methods Enzymol.* **1986**, *123*, 14−22.
[46] R. van Eldik, W. Gaede, S. Wieland, J. Kraft, M. Spitzer, D. A. Palmer, *Rev. Sci. Instrum.* **1993**, *64*, 1355−1357.

Received April 19, 2002
[I02205]

Facile Metal-Mediated Synthesis of Macrocyclic Diselenoethers

Jeremy S. L. Yeo,[a] Jagadese J. Vittal,[a] and T. S. Andy Hor*[a]

Keywords: Platinum / Selenium / Alkylation / Metallacycles / Synthesis design

Nucleophilic attack of $[Pt_2(\mu\text{-}Se)_2(PPh_3)_4]$ on dihaloalkanes gives stable diselenolato complexes, which release macrocyclic diselenoethers upon treatment with dihaloalkanes. The overhead-bridged diplatinum intermediates have been isolated and structurally characterized by single-crystal X-ray crystallography.
(© Wiley-VCH Verlag GmbH, 69451 Weinheim, Germany, 2003)

Introduction

Organoselenium compounds are particularly valuable in electronic,[1] magnetic,[2] catalytic[3] as well as numerous chemotherapeutic[4] and biomedical[5] applications. However, the synthesis of many of these reagents is often tedious and cumbersome.[6] For example, the multi-step preparation of 1,2-bis[(3-chloro-1-propyl)selenio]benzene requires purification by column chromatography and gives a low yield of 31%.[6a] We are therefore interested in the use of organometallic selenido complexes as a source of new organoselenium compounds or an alternative convenient means to prepare known substrates. The complex $[Pt_2(\mu\text{-}Se)_2(PPh_3)_4]$[7] (**1**) is particularly attractive because it can be prepared easily in good yields, is stable with a good shelf-life, and, most importantly, has two nucleophilic selenide centres where functionalization and transformation can take place. We hereby demonstrate a number of possibilities to activate selenide using common organic halides. In doing so, we prepared a range of new organoselenide ligands[8] that could have a significant bearing towards our ultimate goal in metal-assisted syntheses of new organoselenium materials.

Results and Discussion

Treatment of **1** in MeOH with an almost twofold excess of 1,4-dibromobutane at room temperature resulted in a solution which gave a yellow precipitate upon reaction with NH_4PF_6. Positive-mode ESMS analysis (CH_2Cl_2/MeOH) suggested alkylation at both selenide centres to give a dicationic selenolato complex $[Pt_2(\mu,\eta\text{-}Se_2C_4H_8)(PPh_3)_4]^{2+}$ (**2**; m/z = 825). A single-crystal X-ray structural determination of its acetone solvate revealed a hinged $\{Pt_2Se_2\}$ core [θ Pt(1)-Se(1)···Se(1A)−Pt(1A) 140.2°] with a C_4 overhead bridge across the two selenide atoms, thus giving a C_2 symmetry at the molecular centre (Figure 1). The inner C_2 moiety is disordered with an occupancy of 0.7 for C(2) and 0.3 for C(2A). Its ^{31}P NMR spectrum at room temp. suggests that all phosphanes are equivalent (δ = 19.1 ppm).

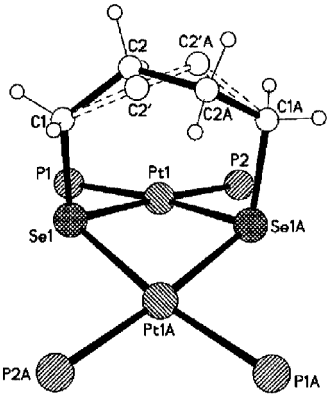

Figure 1. The cation of the molecular structure of $[Pt_2(\mu,\eta\text{-}Se_2C_4H_8)(PPh_3)_4][PF_6]_{1.5}[Cl]_{0.5}$ **2·2(CH$_3$)$_2$CO** with the phenyl rings omitted for clarity; selected bond lengths [A] and angles [°]: Pt(1)−P(1) 2.31(5), Pt(1)−P(2) 2.29(5), Pt(1)-Se(1) 2.48(2), Pt(1)−Se(1A) 2.46(2), Se(1)−C(1) 2.0(3), C(1)−C(2) 1.5(4), C(2)−C(2A) 1.540(19), C(1A)−C(2A) 1.4(3), Pt(1)−Se(1)−Pt(1A) 93.8(7), Se(1)−Pt(1)−Se(1A) 81.8(8), P(1)−Pt(1)−P(2) 99(2), P(1)−Pt(1)−Se(1) 87.1(15), P(2)−Pt(1)−Se(1) 174.0(15), P(1)−Pt(1)−Se(1A) 168.8(15), C(2)−C(1)−Se(1) 116(10), C(1)−C(2)−C(2A) 116(10)

Repeating the preparation with a 100-fold excess of 1,4-dibromobutane (DBB) gave an orange oil which was characterized by ESMS to contain 1,6-diselenacyclodecane **P1** {[**P1** + MeCN + H]$^+$: m/z = 312; [**P1** + MeCN + Na]$^+$: m/z = 335} (Figure 2). Extraction with C_6H_6 followed by careful evaporation of the solvents in vacuo afforded pure **P1** as a white powder (71%); its composition was verified by ^1H and ^{13}C NMR spectroscopy.[9] Fujihara et al. reported the synthesis[9] of **P1** in low yields (3%) by the

[a] Department of Chemistry, National University of Singapore, 3 Science Drive 3, Singapore 117543, Singapore
Fax: (internat.) +65/6779-1691
E-mail: andyhor@nus.edu.sg

method given in Equation (1). **P1** can also be obtained by reacting **2** with a large excess of 1,4-dibromobutane.

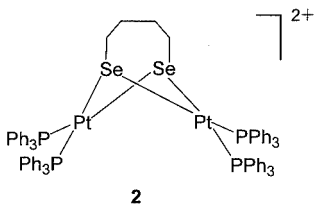

2

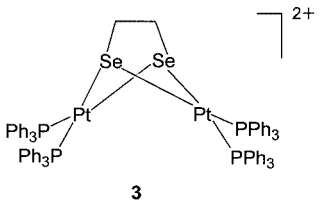

3

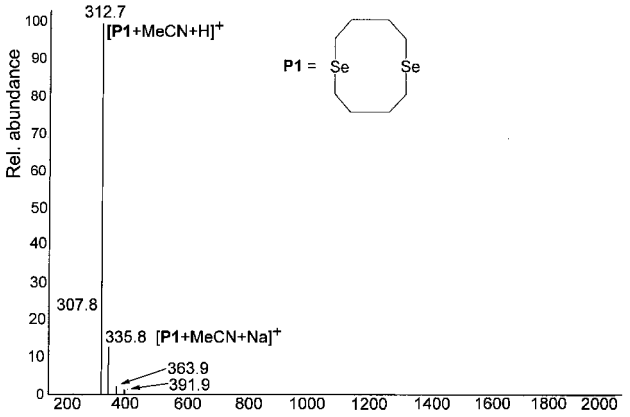

Figure 2. Positive-ion ESMS spectrum of 1,6-diselenacyclodecane (**P1**) in MeCN/H_2O (50:50) solution

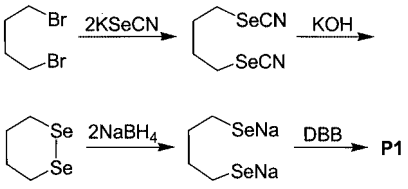

(1)

Reaction of **1** with 1,2-dichloroethane gave another stable selenolato-bridged compound $[Pt_2(\mu,\eta\text{-}Se_2C_2H_4)(PPh_3)_4]^{2+}$ (**3**; Figure 3). The shorter alkyl chain does not appear to affect the stability of the $\{Pt_2Se_2\}$ core or the bridging or chelating ability of the diselenolate ligand. We are currently studying the synthesis of other $[Pt_2(\mu,\eta\text{-}Se_2R)_2(PPh_3)_4]^{2+}$ (R = $CH_2C{=}CCH_2$ and $CH_2C_6H_4CH_2$) and their synthetic utility.

The formation and/or isolation of these organoselenium products illustrates the potential use of a selenide complex such as **1** as a stoichiometric reagent for the synthesis of selenium-containing macrocycles. A likely formation pathway is illustrated in Scheme 1.

A key to this function is the nucleophilic nature of the μ_2-selenide. The stability of similar chalcogenolato complexes has been reported elsewhere.[10] The second alkylation would considerably weaken the metal-ligand bonds which facilitate the liberation of the organoselenium moiety. Re-entry of the chloride to the coordination sphere regenerates $[PtCl_2(PPh_3)_2]$, which is the precursor of **1**, and turns this from a stoichiometric to a potentially catalytic synthesis. The value of this cycle lies in its simplicity in terms of principle and experimental procedures, the use of simple reagents and ambient conditions, and the ease of isolation through extraction. The major advantages are the ability to choose a wide range of alkyl and aryl halides and the flexibility of the $\{Pt_2Se_2\}$ core in accommodating different organic residues as its overhead bridge. These collectively determine the molecular skeleton of the desirable products and make this a potentially powerful entry to selenium macrocycles.

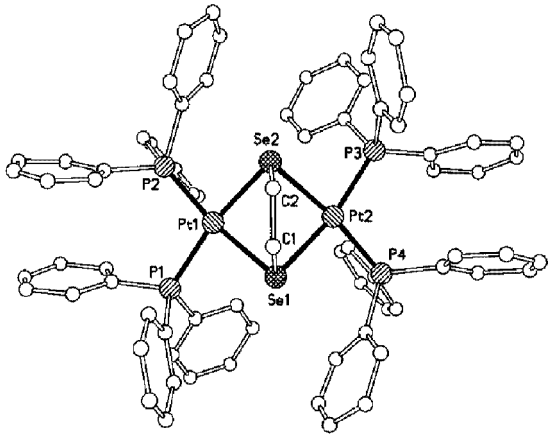

Figure 3. The cation of the molecular structure of $[Pt_2(\mu,\eta\text{-}Se_2C_2H_4)(PPh_3)_4][PF_6]_2$, **3·0.33$CH_2Cl_2$·0.17MeCN·2.83$H_2O$**; selected bond lengths [Å] and angles [°]: Pt(1)−P(1) 2.300(15), Pt(1)−P(2) 2.293(14), Pt(1)−Se(1) 2.478(6), Pt(1)−Se(2) 2.476(6), Se(1)−C(1) 2.00(6), Se(2)−C(2) 1.98(5), C(1)−C(2) 1.50(7), Pt(1)−Se(1)−Pt(2) 86.34(18), Se(1)−Pt(1)−Se(2) 77.78(19), P(1)−Pt(1)−P(2) 97.6(5), P(2)−Pt(1)−Se(1) 172.2(4), P(1)−Pt(1)−Se(2) 167.4(4), C(1)−C(2)−Se(2) 112(4)

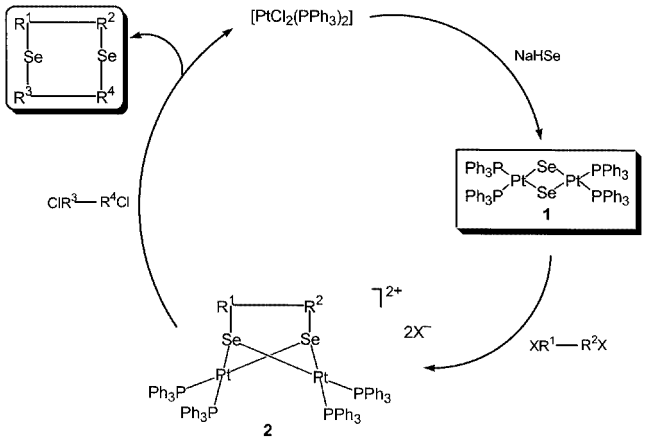

Scheme 1. A stoichiometric pathway with a catalytic-like cycle showing the roles played by **1** and a general representation of **2** and **3** in the preparation of organoselenium compounds

Conclusion

The high nucleophilicity of bridging selenide towards various organic halides makes **1** a potentially rich source of organoselenium substrates. This could lead to many new materials since **1** is reactive to many forms of organic halides. The question is the delicate control of the disintegration of the dinuclear core, stabilization of the mononuclear complex, and its subsequent breakdown to liberate the organoselenium residue. Our next target is to understand the subtle balance of these sequential, yet competing, processes. Such understanding is a prerequisite for us to harness a complex disintegration process whereby we can develop synthetically viable methods for laboratory-scale preparation of materials that are otherwise difficult to obtain.

Experimental Section

General Procedures and Chemicals: All substrates used for analysis were commercially available from Aldrich. We followed a modified preparation of $[Pt_2(\mu\text{-}Se)_2(PPh_3)_4]$ (**1**).[11] All reactions were performed under a positive pressure of purified Ar unless otherwise stated. Solvents were distilled and degassed before use.

Instrumental: Samples for ESMS analysis were prepared in 1 mL MeCN solutions of the analytes. Electrospray mass spectra were obtained with a Finnigan/MAT TSQ 7000 mass spectrometer with the MeCN/H_2O (50:50) mobile phase driven at 0.03 mL min^{-1} using a Thermo Separation products SpectraSystem TSP4000 LC pump. Samples were injected through a Rheodyne valve fitted with a 5 μL sample loop. The source temperature was 200 °C. The capillary potential tip was 4500 V, with nitrogen used both as a drying and a nebulizing gas. Peaks were assigned from the *m*/*z* values and from the isotope distribution patterns that were simulated using the ISOTOPE program.[12] The *m*/*z* values given are for the most intense peak in the envelope in each case. ^1H NMR and ^{13}C NMR spectra were recorded at 25 °C on a Bruker ACF 300 spectrometer (at, 300 and 75.47 MHz respectively) with Me_4Si as internal standard. The ^{31}P NMR spectra were recorded at 121.39 MHz with 85% H_3PO_4 as external reference. Elemental analyses were performed by the microanalytical laboratory of the Department of Chemistry at the National University of Singapore.

$[Pt_2(\mu\text{-}Se_2C_4H_8)(PPh_3)_4][PF_6]_{1.5}[Cl]_{0.5}$ (2): Excess 1,4-dibromobutane (11.1 mg, 20.0 μL, 0.0512 mmol) was added to a brown suspension of **1** (44.1 mg, 0.0276 mmol) in methanol (20 mL). The resultant yellow solution was stirred for 3 h, after which excess NH_4PF_6 (10.0 mg, 0.0614 mol) was added to give a yellow suspension. After stirring for 1 h, deionized water (50 mL) was added to induce precipitation. The suspension was filtered, the solid washed successively with 100 mL portions of deionized water and diethyl ether, and dried under vacuum yielding a yellow powder of **2**. The solid was dissolved in dichloromethane/acetone and this solution layered with hexane. Pale yellow crystals suitable for X-ray analysis were obtained. Yield: 24.2 mg (46%). $C_{76}H_{68}Cl_{0.5}F_9P_{5.5}Pt_2Se_2$ (1888.6): calcd. C 48.3, H 3.6, P 9.0; found C 47.6, H 3.6, P 8.2. ^1H NMR ($CDCl_3$): δ = 1.18−1.26 (m, 8 H, $4CH_2$), 6.92−7.74 (m, 60 H, 12 C_6H_5) ppm. $^{31}P\{^1H\}$ NMR ($CDCl_3$): δ = 19.1 (t, $^1J_{P,Pt}$ = 2964 Hz) ppm.

$[Pt_2(\mu\text{-}SeC_2H_4)_2(PPh_3)_4][PF_6]_2$ (3): By using a similar procedure as for **2**, excess 1,2-dichloroethane (8.1 mg, 10.2 μL, 0.0821 mmol) and **1** (50.7 mg, 0.0317 mmol) gave an orange powder of **3**. The solid was dissolved in dichloromethane/acetonitrile and this solution layered with hexane. Orange crystals suitable for X-ray analysis were obtained. Yield: 26.4 mg (43%). $C_{74}H_{64}F_{12}P_6Pt_2Se_2$ (1915.3): calcd. C 46.4, H 3.4, P 9.7; found C 46.0, H 3.3, P 9.0. ^1H NMR ($CDCl_3$): δ = 1.18 (s, 4 H, $2CH_2$), 6.98−7.77 (m, 60 H, 12 C_6H_5) ppm. $^{31}P\{^1H\}$ NMR ($CDCl_3$): δ = 12.9 (t, $^1J_{P,Pt}$ = 3117 Hz) ppm.

X-ray Crystal Structure Determinations

$2\cdot 2(CH_3)_2CO$: $C_{82}H_{80}Cl_{0.5}F_9O_2P_{5.5}Pt_2Se_2$: M = 2004.62, crystal dimensions: 0.32 × 0.30 × 0.08 mm^3. Monoclinic, space group *I*2/*m*, a = 17.6277(16), b = 24.464(2), c = 20.905(3) Å, β = 91.887(2)°, V = 9010.2(18) $Å^3$, Z = 4, $d_{calcd.}$ = 1.478 $g\cdot cm^{-3}$, μ(Mo-K_α) = 4.081 mm^{-1}. 25888 Reflections measured, 8126 unique (R_{int} = 0.0812), final $R1$ and $wR2$ values 0.0639 and 0.1775 for 4807 independent reflections [$I \geq 2\sigma(I)$] and 424 parameters.

$3\cdot 0.33CH_2Cl_2\cdot 0.17MeCN\cdot 2.83H_2O$:
$C_{74.67}H_{70.83}Cl_{0.67}F_{12}N_{0.17}O_{2.83}P_6Pt_2Se_2$: M = 2001.37, crystal dimensions: 0.20 × 0.10 × 0.08 mm^3. Monoclinic, space group $P2_1/c$, a = 32.6363(19), b = 18.0886(10), c = 43.093(3) Å, β = 100.262(2)°, V = 25033(3) $Å^3$, Z = 12, $d_{calcd.}$ = 1.593 $g\cdot cm^{-3}$, μ(Mo-K_α) = 4.427 mm^{-1}. 145023 Reflections measured, 44105 unique (R_{int} = 0.1330), final $R1$ and $wR2$ values 0.0678 and 0.1710 for 16422 independent reflections [$I \geq 2\sigma(I)$] and 942 parameters.

The data collection was performed on a Bruker AXS APEX diffractometer, equipped with a CCD area-detector using Mo-K_α radiation (λ = 0.71073 Å) at −50 °C. The SMART[13] software package was used for collecting frames of data, indexing reflections, and the determination of lattice parameters, SAINT[13] for integration of intensity of reflections and scaling, SADABS[14] for empirical absorption correction, and SHELXTL[15] for space group and structure determination, refinements, graphics, and structure reporting. Hydrogen atoms were not located. The structures were refined by full-matrix least-squares on F^2 with anisotropic thermal parameters for non-hydrogen atoms, unless otherwise indicated [$R_1 = \Sigma||F_0| - |F_c||/\Sigma|F_0|$, and $wR_2 = \{\Sigma[w(F_0^2 - F_c^2)^2]/\Sigma[w(F_0^2)^2]\}^{1/2}$ (where $w^{-1} = \sigma^2(F_0^2) + (aP)^2 + (bP)$].

For **$2\cdot 2(CH_3)_2CO$**, the original cell data in *C*2/*m* were transformed to the equivalent nonstandard space group *I*2/*m*. The cation has a crystallographic twofold symmetry and the C(2) carbon was found to be disordered. Two positions for this methylene carbon atom were resolved with occupancies of 0.7 and 0.3. Only isotropic thermal parameters were refined for these carbon atoms. The carbon atoms C(1F) to C(6F) of a phenyl ring were treated as a regular hexagon and only isotropic thermal parameters were refined. During the metathesis reaction with NH_4PF_6 half a molecule of chloride ions were retained in the compound which was found to be severely disordered. They were found in seven places in the asymmetric unit and each chloride was found on the mirror plane. In total two acetone molecules were disordered over three locations on the twofold crystallographic axis. All the hydrogen atoms were added in the calculated positions for the purpose of structure factor calculations only. In the final least-squares refinement based on F^2, the model converged at $R1$ = 0.0639 and $wR2$ = 0.1775 for 4807 reflections with $I \geq 2\sigma(I)$ and 424 variables. Despite the disorder of the methylene group and the chloride anions, the structural connectivity is proved beyond any doubt in the cation. We were unable to solve the structure in *C*2. In any case, between centrosymmetric and noncentrosymmetric space groups, the centrosymmetric description is recommended by Marsh.[16]

For **3·0.33CH_2Cl_2·0.17MeCN·2.83H_2O** all the carbon atoms of the phenyl rings were treated as regular hexagons and only isotropic thermal parameters were refined. Common isotropic thermal parameters were refined for the F atoms of each PF_6^- anion and soft constraints were imposed to maintain the octahedral geometry around the phosphorus atom. All the hydrogen atoms were added in their calculated positions for the purpose of structure factor calculations only. From the Fourier-difference routines a molecule of CH_2Cl_2 and half a molecule of MeCN were located. Hard geometrical constraints were imposed for these molecules in the least-squares refinement. Of the twelve sites of the asymmetric unit containing 8.5 H_2O molecules, seven were assigned to disordered O atoms with occupancies of 0.5. In the final least-squares refinement based on F^2, the model converged at $R1 = 0.0678$ and $wR2 = 0.1710$ for 16422 reflections with $I \geq 2\sigma(I)$ and 942 variables. Despite the weak data, the structural connectivity is proved beyond any doubt in the cation.

CCDC-175722 and CCDC-175723 contain the supplementary crystallographic data for this paper. These data can be obtained free of charge at www.ccdc.cam.ac.uk/conts/retrieving.html [or from the Cambridge Crystallographic Data Centre, 12, Union Road, Cambridge CB2 1EZ, UK; Fax: (internat.) +44-1223/336-033; E-mail: deposit@ccdc.cam.ac.uk].

Acknowledgments

The authors acknowledge the National University of Singapore (NUS) for support (R143-000-053-112) and J. S. L. Y. thanks NUS for a research scholarship. We thank G. K. Tan for assistance in X-ray analysis.

[1] [1a] M. S. Hannu, R. Oilunkaniemi, R. S. Laitinen, M. Ahlgén, *Inorg. Chem. Commun.* **2000**, *3*, 397−399. [1b] R. Oilunkaniemi, R. S. Laitinen, M. Ahlgén, *J. Organomet. Chem.* **1999**, *587*, 200−206. [1c] A. Singhal, V. K. Jain, B. Varghese, E. R. T. Tiekink, *Inorg. Chim. Acta* **1999**, *285*, 190−196. [1d] L.-B. Han, N. Choi, M. Tanaka, *J. Am. Chem. Soc.* **1997**, *119*, 1795−1796.

[2] [2a] N. Kobayashi, T. Naito, T. Inabe, *Synth. Met.* **2001**, *120*, 1055−1056. [2b] R. Kato, M. Fujiwara, Y. Kashimura, J. Yamaura, *Synth. Met.* **2001**, *120*, 675−678. [2c] A. S. Batsanov, M. R. Bryce, A. S. Dhindsa, J. A. K. Howard, A. E. Underhill, *Polyhedron* **2001**, *20*, 537−540.

[3] [3a] K. Wang, E. I. Stiefel, *Science* **2001**, *291*, 106−109. [3b] H. Kunkely, A. Vogler, *Inorg. Chim. Acta* **2001**, *319*, 183−186.

[4] M. L. Scott, J. L. Martin, J. R. Shapiro, D. L. Klayman, A. Shrift, *Organic Selenium Compounds: Their Chemistry and Biology* (Eds.: D. L. Klayman, W. H. H. Günther), Wiley-Interscience, New York, **1973**, Chapter 13.

[5] [5a] B. S. Lim, M. W. Willer, M. Miao, R. H. Holm, *J. Am. Chem. Soc.* **2001**, *123*, 8343−8349. [5b] K.-M. Sung, R. H. Holm, *Inorg. Chem.* **2001**, *40*, 4518−4525. [5c] R. C. Bray, B. Adams, A. T. Smith, B. Bennett, S. Bailey, *Biochemistry* **2000**, *39*, 11258−11269.

[6] [6a] R. J. Batchelor, F. W. B. Einstein, I. D. Gay, J.-H. Gu, S. Mehta, B. M. Pinto, X.-M. Zhou, *Inorg. Chem.* **2000**, *39*, 2558−2571. [6b] R. D. Adams, K. T. McBride, *Chem. Commun.* **1997**, *6*, 525−526. [6c] R. D. Adams, K. T. McBride, R. D. Rogers, *Organometallics* **1997**, *16*, 3895−3901. [6d] R. J. Batchelor, F. W. B. Einstein, I. D. Gay, J. Gu, B. M. Pinto, X. Zhou, *Inorg. Chem.* **1996**, *35*, 3667−3674.

[7] A. Bencini, M. D. Vaira, R. Morassi, P. Stoppioni, *Polyhedron* **1996**, *15*, 2079−2086.

[8] J. S. L. Yeo, J. J. Vittal, W. Henderson, T. S. A. Hor, *Organometallics* **2002**, *21*, 2944−2949.

[9] H. Fujihara, R. Akaishi, N. Furukawa, *Tetrahedron* **1993**, *49*, 1605−1618.

[10] [10a] S.-W. A. Fong, T. S. A. Hor, *J. Chem. Soc., Dalton Trans.* **1999**, 639−651. [10b] C. E. Briant, C. J. Gardner, T. S. A. Hor, N. D. Howells, D. M. P. Mingos, *J. Chem. Soc., Dalton Trans.* **1984**, 2645−2651.

[11] J. S. L. Yeo, J. J. Vittal, W. Henderson, T. S. A. Hor, *J. Chem. Soc., Dalton Trans.* **2001**, 315−321.

[12] L. J. Arnold, *J. Chem. Educ.* **1992**, *69*, 811−811.

[13] *SMART & SAINT Software Reference Manuals*, version 4.0, Siemens Energy & Automation, Inc., Analytical Instrumentation, Madison, WI, **1996**.

[14] G. M. Sheldrick, *SADABS, a software for empirical absorption correction*, University of Göttingen, **1993**.

[15] G. M. Sheldrick, *SHELXTL*, version 5.03, Siemens Energy & Automation, Inc., Analytical Instrumentation, Madison, WI, **1996**.

[16] R. E. Marsh, *Acta Crystallogr., Sect. B* **1986**, *42*, 193−193.

Received May 2, 2002
[I02240]

Halogen Atoms as Reactive Centers for the Introduction of Functional Side Chains into (Arene)ruthenium(0) Complexes[‡]

Gregor Bodes,[a] Frank W. Heinemann,[a] Günter Jobi,[a] Jens Klodwig,[a] Stefan Neumann,[a] and Ulrich Zenneck*[a]

Dedicated to Professor Horst Kisch on the occasion of his 60th birthday

Keywords: Arene complexes / Electrophilic substitution / Lithiation / Ruthenium

Substitution of the naphthalene ligand of [(COD)(η⁶-naphthalene)Ru] (**2**) (COD = 1,5-cyclooctadiene) by suitable haloarenes (halogen = F, Cl, Br, I) affords several new mono- and dihaloarene(cyclooctadiene)ruthenium complexes. Depending on the number and position of the halogen and organyl substituents, the haloarenes form achiral or planar-chiral π-ligands; [(η⁶-bromoarene)(COD)Ru] complexes are prone to rapid bromine/lithium exchange with *n*BuLi at low temperatures, while the chloro and fluoro derivatives undergo *ortho*-metalation under the same conditions. The lithiated species react readily with chiral or achiral electrophiles such as chlorodiorganophosphanes, carbonyl chlorides, aldehydes, lactones, ketones, and epoxides to yield substituted [(η⁶-arene)(COD)Ru] complexes with donor functions in their side chains, inaccessible by other routes. Enantiopure complexes are obtained when achiral lithioarene complexes are combined with chiral electrophiles, but pairs of diastereomers are formed if the lithioarene ligand is a planar-chiral species. Dinuclear ruthenium complexes [1,1-bis{(COD)(η⁶-phenyl)Ru}-1,4-butanediol] (**28**) and [1,1-bis{(COD)(η⁶-4-fluorophenyl)Ru}-1,4-butanediol] (**30**) with two (η⁶-aryl)-(COD)Ru units linked by a common 1,4-butanediol side chain are formed through the reactions between the appropriate lithioarene complexes and γ-butyrolactone.
(© Wiley-VCH Verlag GmbH, 69451 Weinheim, Germany, 2003)

Introduction

(Arene)ruthenium(0) complexes are useful catalysts for hydrogenation,[2,3] isomerization,[4] and dimerization[5,6] reactions of alkenes. Their (arene)ruthenium(II) counterparts catalyze enantioselective hydrogen transfer to ketones[7,8] and imines[9] in the presence of enantiomerically pure chiral β-amino alcohols[7] or 1,2-diamines,[8,9] affording high yields and high *ee*s at the same time. Thanks to the particular stability of the arene−metal bond,[10] (arene)ruthenium complexes may be converted from Ru^0 into Ru^{II} without the loss of the arene ligand, simply by addition of hydrochloric acid.[2] Only the co-ligands that complete the coordination sphere are exchanged in parallel with the redox process. Of course, it would be very promising to perform the catalytic reactions of (arene)ruthenium complexes in both redox states with enantiopure species whose chirality was connected with the arene ligand. The preparation of [(η⁶-arene)-(COD)Ru] complexes is well known since the work of Bennett, Vitulli, and Pertici,[3,11,12] who introduced [(COD)(η⁶-1,3,5-cyclooctatriene)Ru] (**1**) and [(COD)(η⁶-naphthalene)Ru] (**2**) as suitable starting materials (Scheme 1).

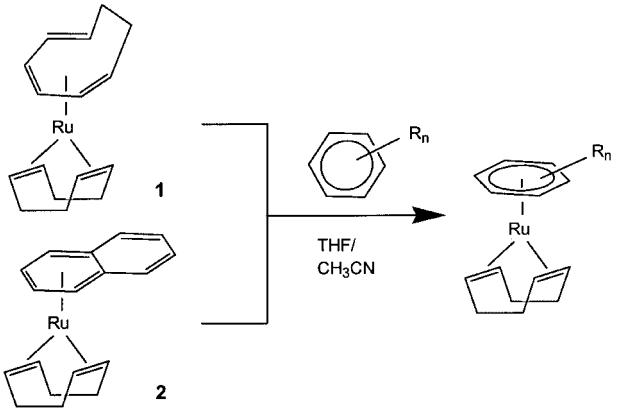

Scheme 1. Synthesis of [(η⁶-arene)(COD)Ru] complexes by ligand exchange

However, bulky, polar, or highly substituted arenes cannot be introduced in this way. An alternative route to such complexes utilizes bromine/lithium exchange between [(η⁶-bromoarene)(COD)Ru] complexes and *n*-butyllithium at

[‡] Chiral Arene Ruthenium Complexes, 4. Part 3: Ref.[1]

[a] Institut für Anorganische Chemie der Universität Erlangen-Nürnberg,
Egerlandstr. 1, 91058 Erlangen, Germany
Fax: (internat.) + 49-(0)9131/852-7367
E-mail: Zenneck@chemie.uni-erlangen.de

low temperatures.[13] The lithiated species can be treated with alkyl chloroformates to form ester-substituted [(η^6-arene)(COD)Ru] compounds. Through the introduction of chiral alkyl chloroformates [alkyl = (−)-menthyl], this directly affords enantiopure asymmetric complexes. To develop the high potential of this approach, we investigated the preparation and reactivity of (mono- and dihaloarene)ruthenium(0) complexes systematically. These allow the introduction of many electrophiles of choice. Examples are provided for chlorodiorganophosphanes, carbonyl chlorides, aldehydes, lactones, ketones, and epoxides. Novel (arene)ruthenium(0) complexes with donor functions such as PR_2 and OH in the side chain are of interest, as these functions should offer the potential to control the reactivity of the different types of (arene)ruthenium catalysts.

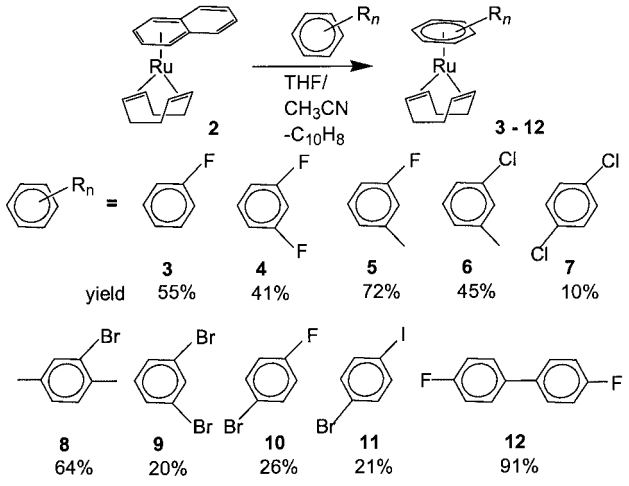

Scheme 2. Preparation of [(COD)(η^6-haloarene)Ru] complexes

Results and Discussion

Preparation of [(COD)(η^6-haloarene)Ru] Complexes

Mono- or dihaloarenes (fluorobenzene, 1,3-difluorobenzene, 3-fluorotoluene, 3-chlorotoluene, 1,4-dichlorobenzene, 2-bromo-1,4-xylene, 1,3-dibromobenzene, 1-bromo-4-fluorobenzene, 1-bromo-4-iodobenzene, and 4,4′-difluoro-1,1′-biphenyl) replace the naphthalene ligand of [(COD)(η^6-naphthalene)Ru] (**2**) in the presence of acetonitrile at room temperature in moderate to excellent yield (Scheme 2). The reaction fails with the triply substituted arenes 3,5-dibromotoluene, 1,2,3- and 1,3,5-tribromobenzene, and 1,2,3-trichlorobenzene.

Two different tendencies are exemplified by the experimental results. If one halogen atom of an incoming arene ligand is accompanied by one or two organyl substituents, the yield increases, but it is reduced with a second halogen atom. So far, no trihalobenzenes have been coordinated successfully. The only dihalobenzene that gives yields of more than 50% is 1,4-dibromobenzene;[13] in all other cases it is between 10 and 21%. As the minimum yield is obtained with 1,4-dichlorobenzene, there must be more than one reason for the diminishing effect, but electronegativity is most probably one of them. The electron-donating effects of the alkyl substituents favor π-complexation directly. As a consequence, even multiply alkyl-substituted arenes can be introduced. Not only 1,2,4-trimethylbenzene, but also 1,2,3,4-tetramethylbenzene, are prone to this type of reaction.[3] Two of the (dihalobenzene)ruthenium complexes have been characterized by X-ray diffraction: [(η^6-1-bromo-4-fluorobenzene)(COD)Ru] (**10**) and [(η^6-1-bromo-4-iodobenzene)(COD)Ru] (**11**) (Figure 1). Thanks to the pronounced chemical differences between their halogen atoms, **10** and **11** are both suitable for stepwise substitution reactions.

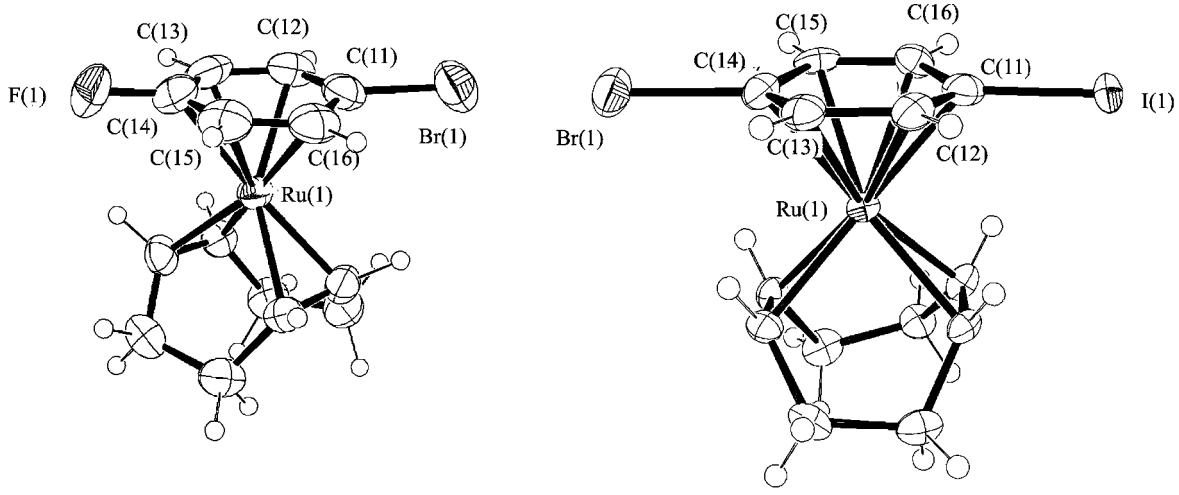

Figure 1. Molecular structures of **10** (left) and **11** (right) in the solid state; selected bond lengths [pm] for **10**: Ru(1)−C(11) 225.4(6), Ru(1)−C(12) 219.6(7), Ru(1)−C(13) 226.4(7), Ru(1)−C(14) 224.2(7), Ru(1)−C(15) 220.4(7), Ru(1)−C(16) 224.6(7); selected bond lengths [pm] for **11**: Ru(1)−C(11) 217.1(9), Ru(1)−C(12) 226.8(9), Ru(1)−C(13) 226.5(9), Ru(1)−C(14) 219.4(9), Ru(1)−C(15) 227.8(9), Ru(1)−C(16) 226.4(9)

The coordinated arene ring is boat-like and distorted in both cases, as two *para*-positioned ring carbon atoms are situated significantly closer to the central metal atom than the other four. In the case of **10** the average value is 220 pm for Ru(1)−C(12) and Ru(1)−C(15), but 225 pm for the other Ru−C_{ring} distances. The corresponding values for **11** are 218 pm for Ru(1)−C(11)/(14) versus 226 pm. This deviation from planarity is a known effect in [(η⁶-arene)(COD)Ru] complexes.[13,14] Its observation, undisturbed in the case of [(COD)(η⁶-1,4-dihalobenzene)Ru] complexes, provides evidence for the interligand influence of COD and arene ligands even in the case of electronegative 1,4-disubstitution of the arene.

Electrophilic Substitution of [(η⁶-bromoarene)(COD)Ru] Complexes

Metalation and subsequent reactions of organometallic compounds are standard derivatization methods.[15] The electrophilic substitution of [(η⁶-bromoarene)(COD)Ru] complexes is initiated by a rapid bromine/lithium exchange at low temperatures. Examples are given for [(η⁶-2-bromo-1,4-xylene)(COD)Ru] (**8**), [(η⁶-1-bromo-4-fluorobenzene)(COD)Ru] (**10**), [(η⁶-bromobenzene)(COD)Ru] (**13**), [(η⁶-2-bromotoluene)(COD)Ru] (**14**),[13] and *n*-butyllithium as the metalation agent. In all cases, the bromine/lithium exchange is accomplished within a few minutes in THF as the solvent at −80 °C, and the electrophiles are added at the same temperature immediately after its completion. In the case of OH-group formation, the reaction sequence finishes with a hydrolysis. We tested this type of reaction with chlorodiorganophosphanes, carbonyl chlorides, ketones, epoxides, aldehydes, and lactones as electrophiles. (Scheme 3, Table 1)

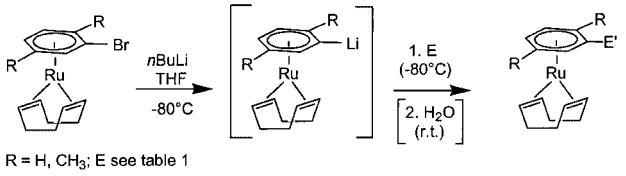

Scheme 3. Electrophilic substitution reaction of [(η⁶-bromoarene)(COD)Ru] complexes

The reaction sequence proceeds very well, and so the introduction of side chains with phosphanyl, ester, oxo, and hydroxy groups, including phenolic hydroxy functions, is a favorable preparative route. The mononuclear and dinuclear complexes **15**−**34** are accessible in this way. We had previously attempted the direct preparation of some related complexes by ligand exchange as an alternative and straightforward approach and had failed in several interesting cases. Acidic hydrogen atoms, phosphanyl groups, and bulky substituents on incoming arene ligands block the arene ligand exchange reaction of ruthenium(0).[1] Neither the NMR spectra, nor other experimental observations point to direct interactions between the donor centers of the side chains and the ruthenium atoms in **15**−**34**. As [(η⁶-arene)(COD)Ru] complexes are closed-shell 18-valence electron species, there is no driving force for such an effect. The potential interaction will come into play when an electron-deficient situation is created for the ruthenium atom by oxidation or COD ligand displacement, through a catalytic application of the complexes.[16]

Table 1. Products of electrophilic substitution of [(η⁶-bromoarene)(COD)Ru] complexes

Starting material	Electrophile E	Product	Yield (%)
13	$ClP(iPr)_2$	[(COD)(diisopropyl-η⁶-phenylphosphane)Ru] (**15**)	83
14	$ClP(iPr)_2$	[(COD)(diisopropyl-η⁶-2-tolylphosphane)Ru] (**16**)	86
13	$ClP(tBu)_2$	[(COD)(di-*tert*-butyl-η⁶-phenylphosphane)Ru] (**17**)	78
14	$ClPPh_2$	[(COD)(diphenyl-η⁶-2-tolylphosphane)Ru] (**18**)	73
14	acetyl chloride	[(COD)(η⁶-2-methylacetophenone)Ru] (**19**)	90
13	pivalyl chloride	[(COD)(*tert*-butyl η⁶-phenyl ketone)Ru] (**20**)	94
14	pivalyl chloride	[(COD)(*tert*-butyl η⁶-2-tolyl ketone)Ru] (**21**)	91
13	ClCOPh*t*Bu	[(COD)(4-*tert*-butylphenyl η⁶-phenyl ketone)Ru] (**22**)	67
13	(1*S*)-(−)-camphanic chloride	(−)-[(COD)(camphanoyl η⁶-phenyl ketone)Ru] (**23**)	43
14	(*R*)-(+)-styrene epoxide	[(COD){1-phenyl-2-(η⁶-2-tolyl)ethanol}Ru] (**24a**, **24b**)	31
13	acetone	[(COD){dimethyl(η⁶-phenyl)methanol}Ru] (**25**)	65
13	cyclohexanone	[(COD)(η⁶-phenylcyclohexanol)Ru] (**26**)	69
13	γ-butyrolactone	[(COD)(3-hydroxypropyl η⁶-phenyl ketone)Ru] (**27**) [1,1-bis-{(COD)(η⁶-phenyl)Ru}-1,4-butanediol] (**28**)	21 45
10	γ-butyrolactone	[(COD)(η⁶-4-fluorophenyl 3-hydroxypropyl ketone)Ru] (**29**) [1,1-bis-{(COD)(η⁶-4-fluorophenyl)Ru}-1,4-butanediol] (**30**)	40 16
14	γ-butyrolactone	[(COD)(3-hydroxypropyl η⁶-2-tolyl ketone)Ru] (**31**)	44
13	1,2-*O* isopropylidene-3-*O*-methyl-α-D-xylopento-dialdofuranose-(1,4)	[(COD){(6-methoxy-2,2-dimethyltetrahydrofuro[2,3-*d*]-[1,3]dioxol-5-yl)(η⁶-phenyl)methanol}Ru] (**32a**, **32b**)	48
8	(−)-menthyl chloroformate	[(COD)(menthyl η⁶-1,4-xylene-2-carboxylate)Ru] (**33a**, **33b**)	42
14	*o*-acetylsalicoyl chloride	[(COD)(*o*-hydroxyphenyl η⁶-2-tolyl ketone)Ru] (**34**)	60

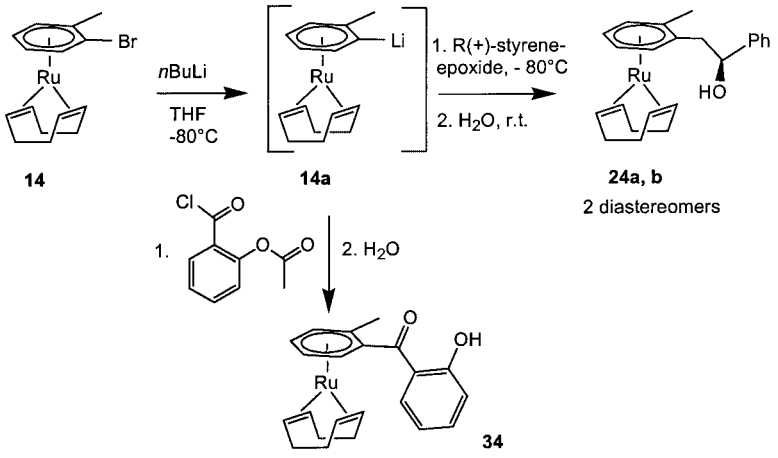

Scheme 4. Electrophilic substitution reactions of [(η^6-2-bromotoluene)(COD)Ru] (**14**)

[(η^6-bromobenzene)(COD)Ru] (**13**) is an achiral starting material and the same is true for its lithium exchange product [(η^6-lithiobenzene)(COD)Ru] (**13a**). Treatment with optically pure (1*S*)-(−)-camphanoyl chloride therefore directly affords enantiopure (−)-[(COD)(camphanoyl η^6-phenyl ketone)Ru] (**23**). The electrophilic substitution reaction does not affect the stereogenic centers of the incoming electrophile. Because of the planar chirality of their arene ligands, **8** and **14** consist of racemic mixtures of asymmetric compounds, and so a subsequent reaction with enantiopure electrophiles produces pairs of diastereomers. An example is the combination of **14** with (*R*)-(+)-styrene epoxide. The two C_1-symmetric diastereomers **24a** and **24b** are formed in this way (Scheme 4).

Diastereomers **32a** and **32b** are also obtained by treatment of achiral **13** with 2-*O* isopropylidene-3-*O*-methyl-α-D-xylopentodialdofuranose-(1,4), as the transformation of its aldehyde function into a secondary benzyl alcohol by addition to the (arene)ruthenium fragment is not diastereoselective (Scheme 5).

To our surprise, electrophilic substitution of **14** with *o*-acetylsalicoyl chloride causes a spontaneous cleavage of the ester group, which was replaced by a phenolic OH group in the end product. Lithiated **14a** thus yields [(3-hydroxyphenyl η^6-2-tolyl ketone)(COD)Ru] (**34**) as the only isolable product. (Scheme 4) Complex **34** was our target product from the beginning, as it contains an OH group at a suitable distance from the metal atom, but the experimental finding represents a nice shortcut in the right direction. As in the case of the (bromoarene)ruthenium complexes, the handling of the novel compounds **15** to **34** causes no problems. All are stable in the solid state, show no sign of hydrolysis, and are only slightly air-sensitive in solution.

Another surprising result occurred when the bromine/lithium exchange product **13a** of bromobenzene complex **13** was treated with γ-butyrolactone. Not only was the designed ring-opening/addition product [(COD)(3-hydroxypropyl η^6-phenyl ketone)Ru] (**27**) formed (in moderate yield), but dinuclear [1,1-bis{(COD)(η^6-phenyl)Ru}-1,4-butanediol] (**28**) was isolated as the main product. The results obtained from the combination of the 1-bromo-4-fluorobenzene complex **10** and γ-butyrolactone are very similar, except that the yield of mononuclear product [(COD)(η^6-4-fluorophenyl 3-hydroxypropyl ketone)Ru] (**29**) exceeds that of dinuclear [1,1-bis{(COD)(η^6-4-fluorophenyl)Ru}-1,4-butanediol] (**30**).

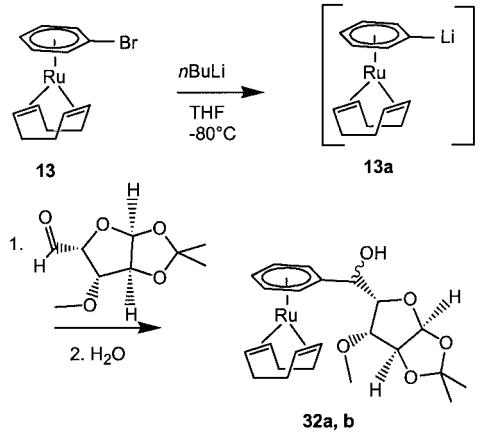

Scheme 5. Preparation of diastereomeric furanose-substituted complexes **32a** and **32b**

The first addition intermediate **27a**, most probably due to a high ketone reactivity,[1] couples with its lithiobenzene precursor complex **13a** to form a 1,4-butanediolate interme-

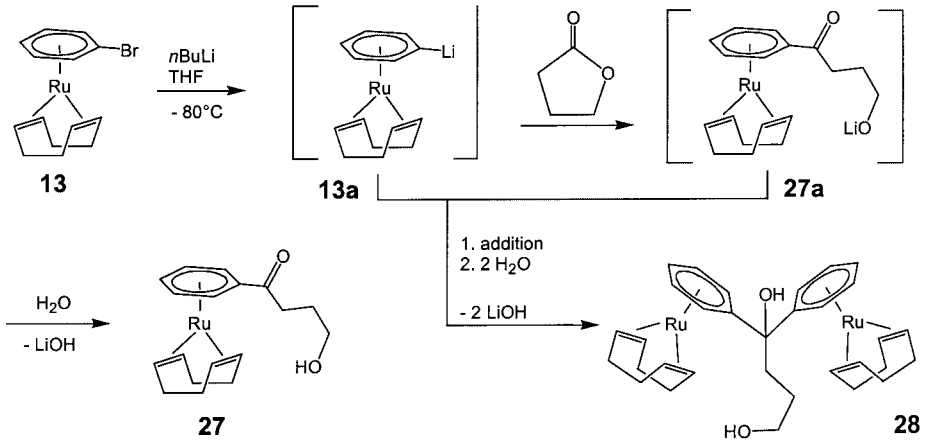

Scheme 6. Formation of dinuclear (arene)ruthenium complex **28**

diate. Both branches of the reaction sequence are terminated by hydrolysis, the lithium ions being replaced by hydrogen atoms. (Scheme 6)

This route represents a new and effective pathway to benzyl carbon atom linked (bisarene)diruthenium complexes. A special property is the bifunctionalization of the common 1,4-butanediol side chain. Both dinuclear complexes **28** and **30** have been characterized by X-ray diffraction: their molecular structures are depicted in Figure 2.

The X-ray results are in full accordance with the analytical and spectroscopic findings on the complexes, which confirm their dinuclear nature, the introduction of only one side chain per $\{(\eta^6\text{-aryl})(\text{COD})\text{Ru}\}_2$ unit, and the absence of ketone functions. The molecular structures of **28** and **30** in the solid state represent different rotamers. This applies to the relative orientation of the $(\eta^6\text{-aryl})(\text{COD})\text{Ru}$ complex units as well as for the 1,4-butanediol chains. In the case of **28** the two (COD)Ru fragments are located opposite to the C116−C117−C214 bond angle of the bridging benzyl carbon atom C117. Its reduction to 106.3° is a consequence of that arrangement. In contrast to that, the (COD)Ru(2) fragment of **30** interacts directly with the arene ligand of Ru(1) and the corresponding C116−C117−C216 benzyl carbon bond angle of **30** is increased significantly. The

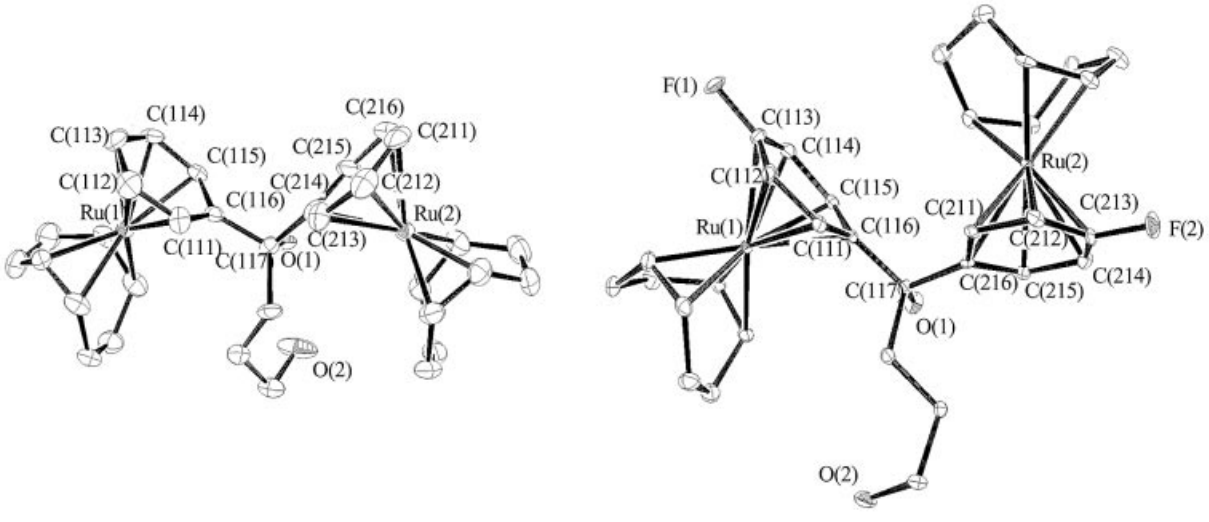

Figure 2. Molecular structures of [1,1-bis{(COD)(η^6-phenyl)Ru}-1,4-butanediol] (**28**, left) and [1,1-bis{(COD)(η^6-4-fluorophenyl)Ru}-1,4-butanediol] (**30**, right) in the solid state; hydrogen atoms have been omitted for clarity; selected bond lengths [ppm] of **28**: Ru(1)−C(111) 227.6(7), Ru(1)−C(112) 220.0(8), Ru(1)−C(113) 225.9(7), Ru(1)−C(114) 225.3(7), Ru(1)−C(115) 222.0(6), Ru(1)−C(116) 231.1(6); bond angle [°]: C(116)−C(117)−C(214) = 106.3(5); selected bond lengths [ppm] of **30**: Ru(1)−C(111) 223.7(3), Ru(1)−C(112) 219.3(3), Ru(1)−C(113) 225.9(2), Ru(1)−C(114) 228.0(3), Ru(1)−C(115) 220.7(3), Ru(1)−C(116) 229.4(2); bond angle [°]: C(116)−C(117)−C(216) = 112.19(19)

$Ru-C_{aryl}$ bond lengths of both species cover a range from 220 to 231 pm. As in the case of the dihaloarene complexes, the arene ligands are slightly boat-like distorted.

The molecular packing of the dinuclear complexes in the solid state is dominated by the formation of infinite zigzag chains of the 1,4-butanediol substituents by intermolecular O−H−O bridges. (Figure 3).

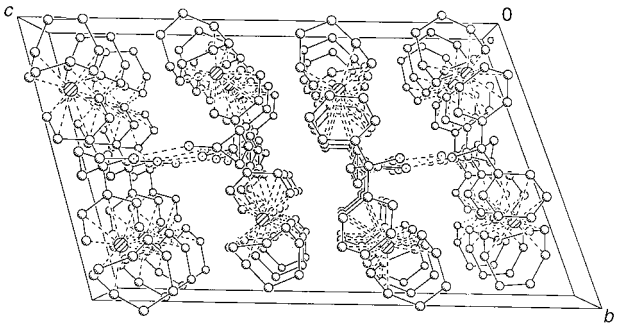

Figure 3. Molecular packing of **28** in the solid state; O−H−O bridges are indicated by the dotted lines between the stacks

Interestingly, a single *o*-methyl group is a steric protector sufficiently powerful to disfavor the formation of dinuclear 1,4-butanediol complexes in the γ-butyrolactone reactions almost completely. 2-Bromotoluene complex **14** therefore forms [(COD)(3-hydroxypropyl η^6-2-tolyl ketone)Ru] (**31**) as the isolable main product. A dinuclear analogue to **28** and **30** can only be detected by mass spectrometry, as a small side product.

Electrophilic Substitution through *ortho*-Metalation of (Chloro- and fluoroarene)ruthenium Complexes

(Chloro- and fluoroarene)metal complexes follow a different reaction pathway when they are attacked by organolithium agents. The main route is no longer halogen/lithium exchange, but *ortho*-metalation is observed instead.[17] This type of reactivity was tested by treatment of *n*BuLi with [(COD)(η^6-3-fluorotoluene)Ru] (**5**) and [(η^6-3-chlorotoluene)(COD)Ru] (**6**). *o*-Acetylsalicoyl chloride was treated with metalated fluoro derivative **5a**, and α-phenylcinnamoyl chloride with the corresponding chloro complex **6a**. (Scheme 7)

As in the case of the bromine/lithium exchange products, the *ortho*-metalation intermediates **5a** and **6a** allow effective introduction of electrophiles. The metalation takes place selectively at the less sterically hindered *o*-position with respect to the halogen substituent. As the chlorine and fluorine atoms remain in the complexes they might be usable a second time for subsequent modification of complexes **35** and **36**. In analogy to phenol complex **34**, the ester function of *o*-acetylsalicoyl chloride is again split spontaneously in the reaction and the target phenolic side chain OH group is formed directly.

Conclusions

[(COD)(η^6-haloarene)Ru] complexes are easily accessible by arene ligand substitution of [(COD)(η^6-naphthalene)Ru] (**2**) by suitable mono- and dihaloarenes. The reaction works with F, Cl, Br, and I as arene ring substituents, and the incoming haloarene may have one or two halogen atoms and a maximum number of three substituents. Depending on the number and position of the halogen atom(s) and organyl substituent(s), the haloarenes form achiral or planar-chiral π-ligands. [(COD)(η^6-haloarene)Ru] complexes are valuable starting materials for the introduction of arene ligand side chains with functional groups that would otherwise block the π-complexation of arene ligands to Ru^0 or Ru^{II}. The bromine atom of [(η^6-bromoarene)(COD)Ru] complexes is rapidly exchanged for a lithium atom when they are treated with *n*BuLi at low temperatures, but the chloro and fluoro derivatives undergo *ortho*-metalation under the same conditions. The re-

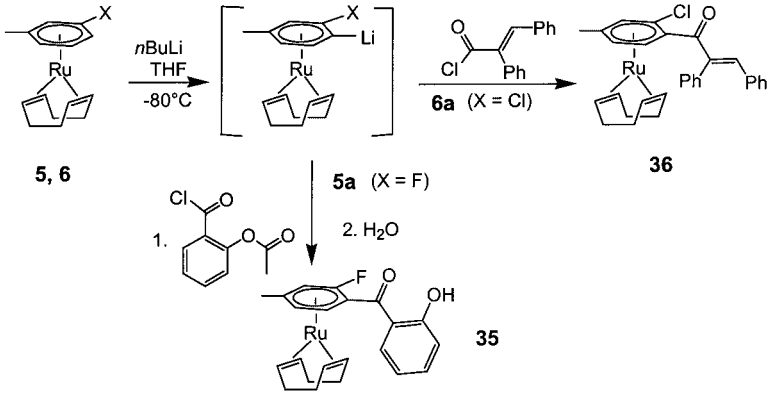

Scheme 7. Electrophilic substitution reaction by *ortho*-metalation

sulting lithiobenzene species react effectively with a great variety of chiral or achiral electrophiles to yield substituted [(η^6-arene)(COD)Ru] complexes with donor functions such as OH or PR_2 groups in the side chains. Enantiopure complexes are obtained when achiral lithioarene complexes are combined with chiral electrophiles, but pairs of diastereomers are formed if the lithioarene ligand is a planar chiral species. Because of the high reactivity of the primary products, the combination of sterically unhindered lithiobenzene complexes and γ-butyrolactone results in the formation of dinuclear [1,1-bis{(η^6-aryl)(COD)Ru}-1,4-butanediol] complexes, each with two [(η^6-aryl)(COD)Ru] units linked by a common 1,4-butanediol side chain.

The new reaction sequences allow a completely new means of ligand design for (arene)ruthenium catalysts of interest, the selectivity and reactivity of which may now be controlled by highly variable side chains with σ-ligand properties of choice. This point is currently under investigation. In a subsequent paper we will report on the oxidation of some of the (η^6-arene)Ru^0 complexes with the donor side chains reported here to form corresponding (η^6-arene)Ru^{II} species, the tethering of the donor function to the metal atom, and first insights into their potential as hydrogen-transfer catalysts.[16]

Experimental Section

General: All reactions were carried out under dry, oxygen-free nitrogen. Solvents were purified by conventional methods, distilled, and stored under nitrogen. NMR spectra were recorded at close to room temperature with Jeol JNM-PMX 60, FT-JNM-EX 270, and FT-JNM-GX 270 spectrometers, with dimethylpolysiloxane and the solvent signals as internal standards. Mass spectra were recorded with a Varian MAT 212 spectrometer. Microanalyses were performed at the analytical department of the institute, on Carlo Erba Elemental Analyzers Mod. 1106 and Mod. 1108, for crystalline products only. Column chromatography (15 × 1 cm) was accomplished on neutral degassed alumina (Merck), deactivated with 5% degassed water. The starting materials [(COD)(η^6-naphthalene)Ru] (**2**),[12] [(η^6-bromobenzene)(COD)Ru] (**13**),[13] and [(η^6-2-bromotoluene)(COD)Ru] (**14**)[13] were prepared as reported in the literature.

Preparation of [(COD)(η^6-haloarene)Ru] Complexes (General Procedure): [(COD)(η^6-naphthalene)Ru] (**2**) and an excess of the haloarene were dissolved in THF and acetonitrile. After the mixture had been stirred at room temperature (room temp.) for 3 d, all volatile components were removed in vacuo at 45 °C. Filtering of the obtained oils through alumina/5%H_2O and recrystallization (if possible) yielded the products.

Bromine/Lithium Exchange and Electrophilic Substitution Reactions of [(η^6-Bromoarene) (COD)Ru] Complexes (General Procedure): The bromoarene complex was dissolved in THF and cooled to −80 °C, and a solution of *n*-butyllithium in hexane was added by syringe. The reaction mixture was stirred for 10 min and a solution of the electrophile in THF was added at the same temperature. The mixture was then allowed to warm slowly to room temp. over 2 h. In the case of Li alkoxide intermediates, a small portion of degassed water was added by syringe to produce the OH groups. The mixture was stirred for a few minutes and the solvents were removed in vacuo. The residue was extracted with *n*-hexane and toluene and the combined liquids were filtered through Al_2O_3/5%H_2O. If necessary, the product was purified by column chromatography on Al_2O_3/5%H_2O with *n*-hexane as the mobile phase.

***o*-Lithiation and Electrophilic Substitution Reactions of (η^6-Chloro- and η^6-fluoroarene)ruthenium Complexes (General Procedure):** The chloro- or fluoroarene complex was dissolved in THF and cooled to −80 °C, and a solution of *n*-butyllithium in hexane was added by syringe. After 5 min, a solution of the electrophile in THF was added at the same temperature, and the mixture was allowed to come to room temp. over 2 h. All volatile components were removed in vacuo. The residue was extracted with *n*-hexane and toluene and the product was purified by column chromatography on Al_2O_3/5%H_2O with *n*-hexane as the mobile phase.

[(COD)(η^6-fluorobenzene)Ru] (3): Reaction mixture: [(COD)(η^6-naphthalene)Ru] (**2**) (1300 mg, 3.84 mmol), fluorobenzene (10 mL, 106.6 mmol) in 20 mL of THF and 1 mL of acetonitrile. Yield 650 mg (2.12 mmol, 55%) of **3**. MS (FD+): *m*/*z* = 306 [M^+]. ^{1}H NMR (269.7 MHz, C_6D_6): δ = 5.14 (dd,$^3J\{H_oH_m\}$ = 5.5, $^3J\{H_oF\}$ = 2.7 Hz, 2 H, H_o); 4.74 (td, $^3J\{HH\}$ = 5, $^4J\{H_mF\}$ = 2.7 Hz, 2 H, H_m); 4.20 (td, $^3J\{H_pH_m\}$ = 5, $^3J\{H_pF\}$ = 3.8 Hz, 1 H, H_p); 3.60 (m, 4 H, olefin. COD); 2.39 (m, 8 H, aliphat. COD) ppm. $^{13}C\{^1H\}$ NMR (100.4 MHz, C_6D_6): δ = 138.0 (d, $^1J\{CF\}$ = −271 Hz, *ipso*-C); 86.1 (s, C_p); 81.1 (d, $^4J\{CF\}$ = 6 Hz, C_m); 80.6 (d, $^3J\{CF\}$ = 22.4 Hz, C_o); 61.6 (C olefin. COD); 33.0 (C aliphat. COD) ppm. $C_{14}H_{17}FRu$ (305.2): calcd. C 55.1, H 5.6; found C 54.6, H 6.3.

[(COD)(η^6-1,3-difluorobenzene)Ru] (4): Reaction mixture: **2** (1300 mg, 3.84 mmol), 1,3-difluorobenzene (10 mL, 101.4 mmol) in 20 mL of THF and 1 mL of acetonitrile. Yield 510 mg (1.57 mmol, 41%) of **4**. ^{1}H NMR (399.65 MHz, C_6D_6): δ = 5.61 (s, 1 H, aromat. H); 4.76 (m, 1 H, aromat. H); 4.48 (m, 2 H, aromat. H); 3.57 (m, 4 H, olefin. COD); 2.24 (m, 8 H, aliphat. COD) ppm. $C_{14}H_{16}F_2Ru$ (233.2): calcd. C 52.01, H 4.99; found C 52.19, H 5.35.

[(COD (η^6-3-fluorotoluene))Ru] (5): Reaction mixture: **2** (1300 mg, 3.84 mmol), 3-fluorotoluene (10 mL, 90.5 mmol) in 30 mL of THF and 1 mL of acetonitrile. Yield 930 mg (2.76 mmol, 72%) of **5**. MS (FD+): *m*/*z* = 320 [M^+]. ^{1}H NMR (399.65 MHz, C_6D_6): δ = 5.12 (s, 1 H, H^1); 5.00 (d, $^3J\{H^2H^3\}$ = 5 Hz, 1 H, H^2); 4.96 (td, $^3J\{H^{2/4}H^3\}$ = 5, $^4J\{H^3F\}$ = 3 Hz, 1 H, H^3); 4.00 (dd, $^3J\{H^4H^3\}$ = 5, $^3J\{H^4F\}$ = 4.5 Hz, 1 H, H^4); 3.38 (m, 4 H, olefin. COD); 2.28 (m, 8 H, aliphat. COD); 1.57 (s, 3 H, CH_3) ppm. $^{13}C\{^1H\}$ NMR (100.4 MHz, C_6D_6): δ = 138.0 (d, $^1J\{CF\}$ = −271 Hz, C^6); 98.0 (d, $^3J\{CF\}$ = 6 Hz, C^4); 87.3 (C^3); 80.6 (d, $^3J\{CF\}$ = 6 Hz, C^2); 77.3 (d, $^2J\{CF\}$ = 22 Hz, $C^{1/5}$); 76.5 (d, $^2J\{CF\}$ = 22 Hz), $C^{1/5}$; 63.9, 63.4 (C olefin. COD); 34.5, 33.8 (C aliphat. COD); 17.9 (C-methyl) ppm. $C_{15}H_{19}FRu$ (319.2): calcd. C 56.4, H 6.0; found C 56.3, H 6.2.

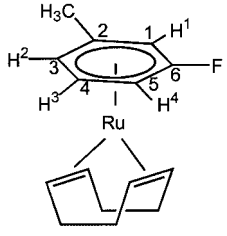

[(η^6-3-Chlorotoluene)(COD)Ru] (6): Reaction mixture: **2** (1200 mg, 3.55 mmol), 3-chlorotoluene (10 mL, 84.6 mmol) in 10 mL of THF and 1 mL of acetonitrile. Yield 540 mg (1.61 mmol, 45%) of **6**. MS (FD+): *m*/*z* = 336 [M^+]. ^{1}H NMR (399.65 MHz, C_6D_6): δ = 5.36 (s, 1 H, H^1); 5.31 (d, $^3J\{H^4H^3\}$ = 5 Hz), 1 H, H^4; 4.96 (t, $^3J\{H^{2/}$

$^4H^3\}$ = 5 Hz, 1 H, H^3); 4.03 (d, $^3J\{H^2H^3\}$ = 5 Hz, 1 H, H^2); 3.44 (m, 4 H, olefin. COD); 2.37 (m, 8 H, aliphat. COD); 1.67 (s, 3 H, CH_3) ppm. $^{13}C\{^1H\}$ NMR (100.4 MHz, C_6D_6): δ = 125.7, 101.4, 100.4 (aromat. C), 88.7 (d, C-Cl), 84.7, 83.3 (aromat. C); 65.6, 64.8 (C olefin. COD); 34.2, 33.5 (C aliphat. COD); 17.9 (C-methyl) ppm.

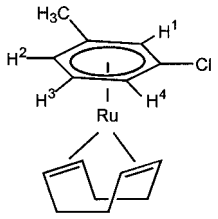

[(COD)(η⁶-1,4-dichlorobenzene)Ru] (7): Reaction mixture: **2** (180 mg, 0.53 mmol), 1,4-dichlorobenzene (735 mg, 5 mmol) in 10 mL of THF and 1 mL of acetonitrile. Yield 20 mg (0.06 mmol, 10%) of **7**. MS (EI, 70 eV): *m*/*z* = 356 [M⁺]. ^1H NMR (269.6 MHz, C_6D_6): δ = 5.05 (s, 4 H, aromat. H); 3.50 (m, 4 H, olefin. COD); 2.30 (m, 8 H, aliphat. COD) ppm. $C_{14}H_{16}Cl_2Ru$ (356.2): calcd. C 47.2, H 4.52; found C 46.06, H 4.38.

[(η⁶-2-Bromo-1,4-xylene)(COD)Ru] (8): Reaction mixture: **2** (500 mg, 1.5 mmol), 2-bromo-1,4-xylene (5 g, 27 mmol) in 25 mL of THF and 1 mL of acetonitrile. Yield 380 mg (0.96 mmol, 64%) of **8**. MS (FD+): *m*/*z* = 394 [M⁺]. ^1H NMR (269.6 MHz, C_6D_6): δ = 5.36 (s, 1 H, aromat. H); 4.34 (d, ^3J = 8 Hz, 1 H, arom-H); 4.04 (d, ^3J = 8 Hz, 1 H, aromat. H); 3.35 (m, 2 H, olefin. COD); 3.03 (m, 2 H, olefin. COD); 2.2−2.4 (m, 8 H, aliphat. COD); 1.95, 1.60 (s, 3 H, CH_3) ppm. $^{13}C\{^1H\}$ NMR (67.7 MHz, C_6D_6): δ = 104.0, 102.9, 92.4, 90.2, 86.0, 83.6 (aromat. C); 68.5, 66.6 (C olefin. COD); 35.0, 33.6 (C aliphat. COD); 19.1,17.8 (CH_3) ppm.

[(COD)(η⁶-1,3-Dibromobenzene)Ru] (9): Reaction mixture: **2** (950 mg, 2.81 mmol), 1,3-dibromobenzene (10 mL, 82.8 mmol) in 50 mL of THF and 1 mL of acetonitrile. Yield 310 mg (0.7 mmol, 20%) of **9**. MS (FD+): *m*/*z* = 444 [M⁺]. ^1H NMR (399.65 MHz, C_6D_6): δ = 5.91 (s, 1 H, H^1); 4.77 (t, $^3J\{H^{2/4}H^3\}$ = 6 Hz, 1 H, H^3); 4.68 (d, $^3J\{H^{2/4}H^3\}$ = 6 Hz, 2 H, $H^{2/4}$); 3.49 (m, 4 H, olefin. COD); 2.26 (m, 8H, aliphat. COD) ppm. $^{13}C\{^1H\}$ NMR (100.4 MHz, C_6D_6): δ = 93.0, 89.2, 87.5, 86.3 (aromat. C); 69.8 (C olefin. COD); 34.6, 33.8 (C aliphat. COD) ppm. $C_{14}H_{16}Br_2Ru$ (445.1): calcd. C 37.77, H 3.62; found C 38.37, H 3.71.

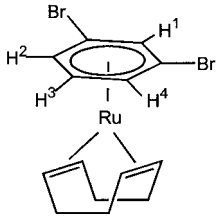

[(η⁶-1-Bromo-4-fluorobenzene)(COD)Ru] (10): Reaction mixture: **2** (1729 mg, 5.12 mmol), 1-bromo-4-fluorobenzene (10 g, 57 mmol) in 60 mL of THF and 1.5 mL of acetonitrile. Yield 512 mg (1.33 mmol, 26%) of **10**. MS (EI, 70 eV): *m*/*z* = 384 [M⁺]. ^1H NMR (269.6 MHz, C_6D_6): δ = 5.02 (m, 2 H, aromat. H); 4.87 (m, 2 H, aromat. H); 3.55 (m, 4 H, olefin. COD); 2.30 (m, 8 H, aliphat. COD) ppm. $^{13}C\{^1H\}$ NMR (67.7 MHz, C_6D_6): δ = 126.0, 88.7 (aromat. C), 86.0 (d, CF), 75.9, 75.7 (aromat. C); 67.8 (C olefin. COD); 34.0 (C aliphat. COD) ppm. $^{13}C\{^1H\}$ NMR (67.8 MHz, C_6D_6): δ = 88.7 (aromat. C), 86.0 (d, CF), 75.9, 75.6 (aromat. C); 67.9 (C olefin. COD); 34.0 (C aliphat. COD) ppm. $C_{14}H_{16}BrFRu$ (384.2): calcd. C 43.76, H 4.19; found C 43.29, H 4.01.

[(η⁶-1-Bromo-4-iodobenzene)(COD)Ru] (11): Reaction mixture: **2** (1400 mg, 4.1 mmol), 1-bromo-4-iodobenzene (10 g, 35.3 mmol) in 20 mL of THF and 1 mL of acetonitrile. Yield 420 mg (0.85 mmol, 21%) of **11**. MS (FD+): *m*/*z* = 494 [M]⁺. ^1H NMR (399.65 MHz, C_6D_6): δ = 5.22 (d, ^3J = 5 Hz, 2 H, aromat. H); 5,12 (d, ^3J = 5 Hz, 2 H, aromat. H); 3.39 (s, 4 H, olefin. COD); 2.29 (m, 8 H, aliphat. COD) ppm. $^{13}C\{^1H\}$ NMR (100.4 MHz, C_6D_6): δ = 97.0, 96.2, 92.8, 91.9, 88.7 (aromat. C); 70.3 (C olefin. COD); 34.7 (C aliphat. COD) ppm. $C_{14}H_{16}BrIRu$ (492.2): calcd. C 34.2, H 3.3; found C 34.4, H 3.1.

[(COD)(η⁶-4,4′-difluoro-1,1′-biphenyl)Ru] (12): Reaction mixture: **2** (960 mg, 2.84 mmol), 4,4′-difluoro-1,1′-biphenyl (2,03 g, 10,7 mmol) in 50 mL of THF and 1.5 mL of acetonitrile. Yield 1035 mg (2.59 mmol, 91%) of **12**. MS (FD+): *m*/*z* = 399 [M⁺]. ^1H NMR (269.7 MHz, C_6D_6): δ = 6.99 (m, 4 H, free aromat. H); 4.95 (dd, 2 H, coord. aromat. H, C*H*CF); 4.72 (dd, 2 H, coord. aromat. H); 3.35 (s, 4 H, olefin. COD); 2.28 (m, 8 H, aliphat. COD) ppm.

[(COD)(diisopropyl-η⁶-phenylphosphane)Ru] (15): Reaction mixture: [(η⁶-bromobenzene)(COD)Ru] (**13**) (150 mg, 0.41 mmol) in 25 mL of Et_2O, *n*-butyllithium (0.24 mL, 0.6 mmol), and chlorodiisopropylphosphane (0.095 mL, 0.6 mmol). Yield 137 mg (0.34 mmol, 83%) of **15**. MS (EI, 70 eV): *m*/*z* = 404 [M⁺]. ^1H NMR (269.6 MHz, C_6D_6): δ = 5.45 (t, 1 H, H_p); 4.63 (dd$_o$, $^3J\{H_oH_m\}$ = 6, $^3J\{H_oP\}$ = 5 Hz, 2 H, H); 4.45 (t, 2 H, H_m); 3.67 (s, 4 H, olefin. COD); 2.15−2.40 (m, 8 H, aliphat. COD), 1.81 (dh, $^2J\{HP\}$ = 1.5, $^3J\{HH\}$ = 10.7 Hz, 2 H, CH isoprop.); 1.17 (dd, $^3J\{HP\}$ = 9.2, $^3J\{HH\}$ = 6.7 Hz, 6 H, CH_3 isoprop.); 0.95 (dd, $^3J\{HP\}$ = 15.6, $^3J\{HH\}$ = 6.7 H, 6 H, CH_3 isoprop.) ppm. $^{13}C\{^1H\}$ NMR (100.4 MHz, C_6D_6): δ = 98.1 (d, $^1J\{CP\}$ = 29.72 Hz, C-*ipso*); 89.4 (C^4), 88.3 (d, $^2J\{CP\}$ = 17.4 Hz, $C^{2/6}$); 84.4 (d, $^3J\{CP\}$ = 4.9 Hz, $C^{3/5}$); 62.5 (C olefin. COD); 33.9 (C aliphat. COD); 22.6 (d, $J\{CP\}$ = 14.8 Hz, C isoprop.); 19.9 (d, $J\{CP\}$ = 16.6 Hz, C isoprop.); 19.4 (d, $J\{CP\}$ = 9 Hz, C isoprop.) ppm. ^{31}P NMR (109.6 MHz, C_6D_6): δ = 4.75 (s) ppm.

[(COD)(diisopropyl-η⁶-2-tolylphosphane)Ru] (16): Reaction mixture: [(η⁶-2-bromotoluene)(COD)Ru] (**14**) (185 mg, 0.48 mmol) in 25 mL of Et_2O, *n*-butyllithium (0.26 mL, 0.65 mmol), and chlorodiisopropylphosphane (0.10 mL, 0.65 mmol). Yield 174 mg (0.42 mmol, 86%) of **16**. MS (EI, 70 eV): *m*/*z* = 417 [M⁺]. ^1H NMR (269.6 MHz, C_6D_6): δ = 5.51 (t, $^3J\{H_pH_m\}$ = $\{H_pH_{m'}\}$ = 6 Hz, 1 H, $H_{p/m}$); 5.11 (d, $^3J\{H_{m'}H_p\}$ = 6 Hz, 1 H, $H_{m'}$); 5.10 (dd, $^3J\{H_oH_m\}$ = 6, $^3J\{H_oP\}$ = 5 Hz, 1 H, H_o); 3.82 (t, $^3J\{H_mH_p\}$ = $^3J\{H_mH_o\}$ = 6 Hz, 1 H, $H_{m/p}$); 3.43 (s, 4 H, H olefin. COD); 2.00−2.40 (m, 10 H, H aliphat. COD, H isoprop.); 1.75 (s, 3 H, CH_3); 1.57 (dd, $^3J\{HH\}$ = 10.7, $^3J\{HP\}$ = 18.8 Hz, 3 H, H isoprop. CH_3); 1.13 (dd, $^3J\{HH\}$ = 10.7, $^3J\{HP\}$ = 14.8 Hz, 3 H, H isoprop. CH_3); 0.94 (dd, $^3J\{HH\}$ = 10.7, $^3J\{HP\}$ = 14.8 Hz, 3 H, H isoprop. CH_3); 0.86 (dd, $^3J\{HH\}$ = 10.7, $^3J\{HP\}$ = 10.3 Hz, 3 H, H isoprop. CH_3) ppm. $^{13}C\{^1H\}$ NMR (67.7 MHz, C_6D_6): δ = 98.9 (d, $^1J\{CP\}$ = 32.11 Hz, C-*ipso*); 96.5 (d, $J\{CP\}$ = 26.2 Hz, aromat. C); 92.8 (d, $J\{CP\}$ = 2.78 Hz, aromat. C); 91.6 (d, $J\{CP\}$ = 2.71 Hz, aromat. C); 87.3, 79.7 (aromat. C); 62.9, 61.7 (C olefin. COD); 34.3; 33.5 (C aliphat. COD); 25.2 (d, $J\{CP\}$ = 17.9 Hz, C isoprop.); 22.3 (d, $J\{CP\}$ = 13.7 Hz, C isoprop.); 22.1 (d, $J\{CP\}$ = 20.6 Hz), C isoprop.; 20.2 (d, $J\{CP\}$ = 15.2 Hz, C isoprop.); 19.8 (d, $J\{CP\}$ = 16.6 Hz, C isoprop.); 18.7 (d, $^3J\{CP\}$ = 5.6 Hz, CH_3 tolyl.); 18.3 (d, $J\{CP\}$ = 22.1 Hz, C isoprop.) ppm. ^{31}P NMR (109.6 MHz, C_6D_6): δ = −6.8 (s).

[(COD)(di-*tert*-butyl-η⁶-phenylphosphane)Ru] (17): Reaction mixture: **13** (170 mg, 0.46 mmol) in 25 mL of Et_2O, *n*-butyllithium (0.24 mL, 0.6 mmol), and di-*tert*-butylchlorophosphane (0.11 mL,

0.6 mmol). Yield 156 mg (0.36 mmol, 78%) of **16**. MS (EI, 70 eV): *m*/*z* = 432 [M$^+$]. ^{1}H NMR (269.6 MHz, C_6D_6): δ = 5.55 (t, $^3J\{H_pH_m\}$ = 6 Hz, 1 H, H_p); 4.85 (dd, $^3J\{H_oH_m\}$ = 6, $^3J\{H_oP\}$ = 5 Hz, 2 H, H_o); 4.40 (t, 2 H, H_m); 3.55 (s, 4 H, H olefin. COD); 2.10−2.40 (m, 8 H, H aliphat. COD); 1.25 (d, $^3J\{HP\}$ = 13.4 Hz, 18 H, H-*t*Bu) ppm. $^{13}C\{^1H\}$ NMR (67.7 MHz, C_6D_6): δ = 100.2 (d, $^1J\{CP\}$ = 13.8 Hz, C-*ipso*); 91.8 (d, $^2J\{CP\}$ = 21.3 Hz, $C^{2/6}$); 87.7 (s, C^4); 85.1 (d, $^3J\{CP\}$ = 3.9 Hz), $C^{3/5}$; 62.8 (C olefin. COD); 34.0 (C aliphat. COD); 32.8 (d, *J*{CP} = 22.8 Hz, C-*t*Bu); 31.2 (d, *J*{CP} = 13.6 Hz, C-*t*Bu) ppm. ^{31}P NMR (109.6 MHz, C_6D_6): δ = 33.7 (s) ppm. $C_{22}H_{35}PRu$ (431.6): calcd. C 61.26, H 8.17; found C 61.01, H 8.37.

[(COD)(diphenyl-η^6-2-tolylphosphane)Ru] (18): Reaction mixture: **14** (250 mg, 0.65 mmol) in 20 mL of THF, *n*-butyllithium (0.32 mL, 0.8 mmol), and chlorodiphenylphosphane (0.15 mL, 0.8 mmol). Yield 230 mg (0.474 mmol, 73%) of **18**. MS (EI, 70 eV): *m*/*z* = 486 [M$^+$]. ^{1}H NMR (269.6 MHz, C_6D_6): δ = 7.7 (dt, $^3J\{HH\}$ = 12, $^3J\{HP\}$ = 5 Hz, 2 H, aromat. H); 7.45 (dt, $^3J\{HH\}$ = 12, $^3J\{HP\}$ = 13.7 Hz, 2 H, aromat. H); 7.17−7.0 (m, 6 H, aromat. H). 5.47 (t, $^3J\{H_pH_m\}$ = $^3J\{H_pH_{m'}\}$ = 6 Hz, 1 H, $H_{p/m}$); 4.73 (dd, $^3J\{H_oH_m\}$ = 6, $^3J\{H_oP\}$ = 5 Hz, 1 H, H_o); 4.65 (d, $^3J\{H_{m'}Hp\}$ = 6 Hz, 1 H, $H_{m'}$); 4.05 (t, $^3J\{H_mH_p\}$ = $^3J\{H_mH_o\}$ = 6 Hz, 1 H, $H_{m/p}$); 3.43 (s, 4 H, H olefin. COD); 2.25−2.40 (m, 8 H, H aliphat. COD); 1.63 (s, 3 H, CH_3) ppm. $^{13}C\{^1H\}$ NMR (100.4 MHz, C_6D_6): δ = 137.5, 136.3 (d, $^1J\{CP\}$ = 13.2 Hz, aromat. C); 135.3 (d, $^2J\{CP\}$ = 20.7 Hz, aromat. $C^{2/6}$); 133.6 (d, $^2J\{CP\}$ = 19.8 Hz, aromat. $C^{2'/6'}$); 128.83 (d, $^3J\{CP\}$ = 6.6 Hz, aromat. $C^{3/5}$); 128.6 (d, $^3J\{CP\}$ = 6.6 Hz, aromat. $C^{3'/5'}$); 128.81, 128.5 (aromat. C^4), 99.7 (d, $^1J\{CP\}$ = 24.8 Hz, C^1-*ipso*); 96.1 (d, $^2J\{CP\}$ = 18.2 Hz, aromat.C); 90.9 (d, $^2J\{CP\}$ = 3.3 Hz, aromat. C); 90.1, 85.9, 84.1 (aromat. C); 64.1, 62.2 (C olefin. COD); 34.2 (C aliphat. COD); 17.4 (d, $^3J\{CP\}$ = 19.7 Hz, CH_3) ppm. ^{31}P NMR (109.6 MHz, C_6D_6): δ = −17.6 (s) ppm.

[(COD)(η^6-2-methylacetophenone)Ru] (19): MS (EI, 70 eV): *m*/*z* = 343 [M$^+$]. ^{1}H NMR (269.9 MHz, C_6D_6): δ = 4.95 (t, 1 H, aromat. H); 4.77 (d, 1 H, aromat. H); 4.51 (t, 1 H, aromat. H); 4.40 (d, all $^3J_{arom}$ = 6 Hz, 1 H, aromat. H); 3.45−3.35 (m, 2 H, H olefin. COD); 3.30−3.20 (m, 2 H, H olefin. COD); 2.40−2.10 (m, 8 H, H aliphat. COD); 2.25 (s, 3 H, CH_3); 2.12 (s, 3 H, CH_3) ppm. $^{13}C\{^1H\}$ NMR (100.4 MHz, C_6D_6): δ = 189.9 (CO); 101.6; 93.0, 91.4; 88.7, 87.8, 82.4 (aromat. C); 65.6; 63.9 (C olefin. COD); 34.5, 33.4 (C aliphat. COD); 28.5, 19.6 (C-*C*H$_3$) ppm. $C_{17}H_{22}ORu$, M = 343.4.

[(COD)(*tert*-butyl η^6-phenyl ketone)Ru] (20): Reaction mixture: **13** (240 mg, 0.65 mmol) in 20 mL of THF, *n*-butyllithium (0.31 mL, 0.78 mmol), and pivalyl chloride (0.1 mL, 0.78 mmol). Yield 252 mg (0.68 mmol, 94%) of **20**. MS (EI, 70 eV): *m*/*z* = 372 [M$^+$]. ^{1}H NMR (399.65 MHz, C_6D_6): δ = 5.17 (t, $J\{H_pH_m\}$ = 5.4 Hz, 1 H, H_p); 5.16 (d, $J\{H_oH_m\}$ = 6.3 Hz, 2 H, H_o); 4.16 (t, 2 H, H_m); 3.21 (m, 4 H, H olefin. COD); 1.92 (s, 8 H, H aliphat. COD), 1.06 (s, 9 H, H *t*Bu) ppm. $^{13}C\{^1H\}$ NMR (100.40 MHz, C_6D_6): 203.6 (CO); 91.7, 87.8, 87.3, 84.4 (aromat.C); 65.2 (C olefin. COD); 44.1 (C_{quart} *t*Bu); 34.1 (C aliphat. COD); 29.1 (C *t*Bu) ppm. $C_{19}H_{26}ORu$ (371.5): calcd. C 61.43, H 7.05; found C 61.96, H 7.42.

[(COD)(*tert*-butyl η^6-2-tolyl ketone)Ru] (21): Reaction mixture: **14** (207 mg, 0.54 mmol) in 20 mL of THF, *n*-butyllithium (0.25 mL, 0.6 mmol), and pivalyl chloride (0.075 mL, 0.6 mmol). Yield 191 mg (0.49 mmol, 91%) of **21**. MS (EI, 70 eV): *m*/*z* = 386 [M$^+$]. ^{1}H NMR (269.6 MHz, C_6D_6): δ = 5.15 (t, 1 H, aromat. H); 4.65 (d, 1 H, aromat. H); 4.55 (t, 1 H, aromat. H); 4.40 (d, all *J* = 6 Hz, 1 H, aromat. H); 3.65−3.50 (m, 2 H, H olefin. COD); 3.48−3.38 (m, 2 H, H olefin. COD); 2.40−2.10 (m, 8 H, H aliphat. COD); 1.70 (s, 3 H, CH_3); 1.07 (s, 9 H, CH_3 *t*Bu) ppm. $^{13}C\{^1H\}$ NMR (67.7 MHz, C_6D_6): δ = 208 (CO); 104.5, 97.7, 86.0, 85.4, 84.4, 81.9 (aromat. C); 64.6, 63.9 (C olefin. COD); 45.2 (C_{quart} *t*Bu); 34.6, 33.6 (C aliphat. COD); 27.5 (CH_3 *t*Bu); 17.4 (CH_3 tolyl) ppm. $C_{20}H_{28}ORu$ (385.5): calcd. C 62.31, H 7.32; found C 62.93, H 7.48.

[(COD)(4-*tert*-butylphenyl η^6-phenyl ketone)Ru] (22): Reaction mixture: **13** (264 mg, 0.72 mmol) in 20 mL of THF, *n*-butyllithium (0.34 mL, 0.86 mmol), and 4-*tert*-butylbenzoyl chloride (0.17 mL, 0.86 mmol). Yield 202 mg (0.45 mmol, 67%) of **22**. MS (EI, 70 eV): *m*/*z* = 448 [M$^+$]. ^{1}H NMR (269.6 MHz, C_6D_6): δ = 8.22 (d, $J\{H^{6/9}H^{7/8}\}$ = 8.0 Hz, 2 H, $H^{6/9}$); 7.33 (d, $J\{H^{6/9}H^{7/8}\}$ = 8.0 Hz, 2 H, $H^{7/8}$); 5.48 (d, $J\{H_oH_m\}$ = 6.2 Hz, 2 H, H_o); 5.38 (t, $J\{H_pH_m\}$ = 5.7 Hz, 1 H, H_p); 4.53 (t, 2 H, H_m); 3.55 (m, 4 H, H olefin. COD); 2.25 (m, 8 H, H aliphat. COD), 1.28 (s, 9 H, H *t*Bu) ppm. $^{13}C\{^1H\}$ NMR (67.70 MHz, C_6D_6): δ = 194.8 (CO); 155.0, 136.7, 129.7; 125.4, 93.3, 88.3, 87.5, 84.6 (aromat. C); 64.9 (C olefin. COD); 34.9 (C_{quart} *t*Bu); 33.8 (C aliphat. COD); 31.1 (C-*t*Bu) ppm.

(−)-[(COD)(camphanoyl η^6-phenyl ketone)Ru] (23): Reaction mixture: **13** (300 mg, 0.8 mmol) in 15 mL of THF, *n*-butyllithium (0.3 mL, 0.75 mmol), and (1*S*)-(−)-camphanoyl chloride (177 mg, 0.8 mmol). Yield 160 mg (0.34 mmol, 43%) of **23**. MS (FD+): *m*/*z* = 468 [M$^+$]. ^{1}H NMR (269.6 MHz, C_6D_6): δ = 6.0 (d, $^3J\{HH\}$ = 6 Hz, 1 H, H_o); 5.5 (m, 2 H, $H_{o/p}$); 4.55 (t, $^3J\{H\ H\}$ = 6 Hz, 1 H, H_m); 3.58 (m, 4 H, H olefin. COD); 2.24 (m, 8 H, H aliphat. COD); 0.97, 0.88 (s, 3 H, CH_3) ppm. $^{13}C\{^1H\}$ NMR (100.4 MHz, C_6D_6): δ = 194.3 (CO); 177.7, 129.3, 128.5, 125.6, 96.6 (aromat. *ipso*-C); 91.0, 90.9, 90.4, 87.5, 86.1 (aromat. C); 66.3, 65.5 (C olefin. COD); 34.2, 33.8 (C aliphat. COD); 16.9, 9.7 (CH_3) ppm. $C_{24}H_{30}O_3Ru$ (467.6): calcd. C 61.65, H 6.46; found C 59.44, H 6.66. $[\alpha]^D$ = −312, $[\alpha]^{578}$ = −152, $[\alpha]^{633}$ = −92 (25 °C, toluene).

[(COD){1-phenyl-2-(η^6-2-tolyl)ethanol}Ru] (24a, b): Reaction mixture: **14** (500 mg, 1.3 mmol) in 100 mL of THF, *n*-butyllithium (0.6 mL, 1.5 mmol), and (*R*)-(+)-styrene epoxide (0.18 mL, 1.5 mmol). Yield 169 mg (0.4 mmol, 31%) of **24a** and **24b** as a 1:1 mixture of diastereomers. MS (EI, 70 eV): *m*/*z* = 422 [M$^+$]. ^{1}H NMR (269.6 MHz, C_6D_6): δ = 7.16 (d, *J* = 14.8 Hz, 2 H, aromat. H); 7.14 (d, *J* = 14.8 Hz, 2 H, aromat. H); 7.03−6.87 (m, 6 H, aromat. H); 5.12 (t, $^3J\{H_pH_m\}$ = $^3J\{H_pH_{m'}\}$ = 8 Hz, 1 H, H_p); 5.00 (t, $^3J\{H_{p2}H_{m2}\}$ = $^3J\{H_{p2}H_{m'2}\}$ = 8 Hz, 1 H, H_{p2}); 4.55 (d, *J* = 8 Hz, 1 H, aromat. H); 4.5−4.38 (m, 2 H, aromat. H); 4.27 (d, 1 H, aromat. H); 4.10 (d, $^3J\{HH\}$ = 3 Hz, 1 H, OH); 4.02 (m, 2 H, arom H); 3.62 (d, $^3J\{HH\}$ = 3 Hz, 1 H, OH); 3.25−3.05, 3.00−2.90 [m, 4 H, H olefin. COD, COD(2)]; 2.45−1.85 [m, 20 H, H aliphat. COD, COD(2), H aliphat. CH_2 and CH_2(2)]; 1.35 (s, 3 H, CH_3); 1.34 [s, 3 H, CH_3(2)] ppm. $^{13}C\{^1H\}$ NMR (67.7 MHz, C_6D_6): δ = 144.8, 129.2, 128.6, 127.8, 127.4, 126.2, 126, 101.3, 101.1, 100.5, 97.4, 91.2, 90.4, 88.0, 87.5, 86.3, 86.1, 86.0, 84.5 (aromat.C); 73.2, 72.5 (C-alcohol); 62.9, 62.3, 61.3, 61.1 (C olefin. COD); 41.8, 41.0 (C aliphat. CH_2); 34.6; 34.5, 33.7, 33.6 (C aliphat. COD); 17.0,16.5 (CH_3) ppm.

[(COD)(dimethyl-η^6-phenylmethanol)Ru] (25): Reaction mixture: **13** (220 mg, 0.59 mmol) in 20 mL of THF, *n*-butyllithium (0.35 mL, 0.88 mmol), and acetone (0.06 mL, 0.88 mmol). Yield 132 mg (0.38 mmol, 65%) of **25**. MS (EI, 70 eV): *m*/*z* = 346 [M$^+$]. ^{1}H NMR (399.65 MHz, C_6D_6): δ = 5.29 (t, $J\{H_pH_m\}$ = 5.4 Hz, 1 H, H_p); 4.60 (d, $J\{H_oH_m\}$ = 5.7 Hz, 2 H, H_o); 4.14 (t, 2 H, H_m); 3.17 (m, 4 H, H olefin. COD); 1.94 (m, 8 H, H aliphat. COD), 1.23 (s, 6 H, CH_3) ppm. $^{13}C\{^1H\}$ NMR (100.40 MHz, C_6D_6): δ = 115.2, 86.1, 85.7, 84.8 (aromat. C); 70.8 (C alcohol.); 60.2 (C olefin. COD); 34.1 (C aliphat. COD); 31.3 (CH_3) ppm.

[(COD)(η^6-phenylcyclohexanol)Ru] (26): Reaction mixture: **13** (350 mg, 0.91 mmol) in 20 mL of THF, *n*-butyllithium (0.44 mL,

1.1 mmol), and cyclohexanone (0.11 mL, 1.1 mmol). Yield 242 mg (0.63 mmol, 69%) of **26**. MS (EI, 70 eV): *m*/*z* = 386 [M$^+$]. ^{1}H NMR (399.65 MHz, C_6D_6): δ = 5.32 (t, $J\{H_pH_m\}$ = 5.5 Hz, 1 H, H_p); 4.63 (d,, $J\{H_oH_m\}$ = 6.0 Hz 2 H, H_o); 4.14 (t, 2 H, H_m); 3.18 (m, 4 H, H olefin. COD); 1.95 (m, 8 H, H aliphat. COD), 1.68 (m, 4 H, H aliphat. cyclohexane), 1.28 (m, 6H, H aliphat. cyclohexane) ppm. ^{13}C{^{1}H} NMR (100.40 MHz, C_6D_6): δ = 116.2, 86.2, 85.8, 85.1 (aromat.C); 70.1 (C alcohol.); 60.1 (C olefin. COD); 39.2 (C aliphat. cyclohexane); 34.3 (C aliphat. COD); 26.1 (C aliphat. cyclohexane); 22.8 (C aliphat. cyclohexane) ppm.

[(COD)(3-hydroxypropyl η^6-phenyl ketone)Ru] (27): Reaction mixture: **13** (380 mg, 1.03 mmol) in 30 mL of THF, *n*-butyllithium (0.44 mL, 1.1 mmol), and γ-butyrolactone (88.7 mg, 1.03 mmol). Yield 80 mg (0.21 mmol, 21%) of **27** and 150 mg (0.23 mmol, 45%) of **28**. MS (FD+): *m*/*z* = 374 [M$^+$]. ^{1}H NMR (399.65 MHz, C_6D_6): δ = 5.31 (d, $^3J\{HH\}$ = 6 Hz, 2 H, H_o); 5.24 (t, $^3J\{HH\}$ = 6 Hz; 1 H, H_p); 4.52 (t, $^3J\{HH\}$ = 6 Hz, 1 H, H_m); 3.45 (m, 2 H, CH_2OH); 3.40 (m, 4 H, H olefin. COD); 2.59 (t, 2 H, CH_2CO); 2.10 (m, 8 H, H aliphat. COD); 1.88 (quint, 2 H, $CH_2CH_2CH_2$) ppm. ^{13}C{^{1}H} NMR (100.40 MHz, C_6D_6): δ = 199.0 (CO); 91.3, 88.8, 86.8, 82.9 (aromat. C); 64.4 (C olefin. COD); 62.1 (COH); 34.5 (*C*CO); 33.9 (C aliphat. COD); 27.7 (CH_2) ppm.

Data for 1,1-Bis[(COD)(η^6-phenyl)Ru]-1,4-butanediol (28): MS (FD+): *m*/*z* = 662 [M$^+$]. ^{1}H NMR (399.65 MHz, C_6D_6): δ = 5.52 (t, ^3J = 6 Hz, 2 H, aromat. H); 5.21 (d, 2 H, aromat. H); 5.03 (d, 2 H, aromat. H); 4.39 (tt, all ^3J = 6 Hz, 4 H, aromat. H); 3.4 (m, 4 H, H$^{2/4}$; 8 H, H olefin. COD); 2.20 (m, 16 H, H aliphat. COD); 1.79 (m, 2 H, H^3) ppm. ^{13}C{^{1}H} NMR (100.40 MHz, C_6D_6): δ = 114.5, 86.5, 85.8, 85.7, 84.8 (aromat. C); 75.2 (C^1); 63.2 (C^4); 61.3, 61.1 (C olefin. COD); 40.5 (C^2); 34.3, 34.2 (C aliphat. COD); 27.6 (C^3) ppm.

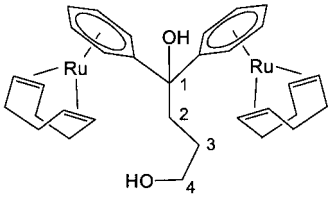

[(COD)(η^6-4-fluorophenyl 3-hydroxypropyl ketone)Ru] (29): Reaction mixture: **10** (353 mg, 0.92 mmol) in 45 mL of THF, *n*-butyllithium (0.58 mL, 0.92 mmol), and γ-butyrolactone (79 mg, 0.92 mmol). Yield 140 mg (0.36 mmol, 40%) of **29** and 50 mg (0.07 mmol, 16%) of **30**. MS (FD+): *m*/*z* = 392 [M$^+$]. ^{1}H NMR (269.71 MHz, C_6D_6): δ = 5.39 (dd, 2 H, aromat. H); 5.02 (dd, 2 H, aromat. H); 3.54 (m, 4 H, H olefin. COD); 3.54 (t, 2 H, CH_2OH); 2.58 (t, 2 H, CH_2CO); 2.25 (m, 8 H, H aliphat. COD); 1.86 (m, 2 H, $CH_2CH_2CH_2$) ppm. ^{13}C{^{1}H} NMR (67.8 MHz, C_6D_6): δ = 197.9 (CO); 139.8, 135.8, 92.1 (aromat. C); 82.8 (d, CF); 77.3, 77.0 (aromat. C) 66.8 (C olefin. COD); 61.8 (COH); 34.8 (*C*CO); 33.8 (C aliphat. COD); 27.3 (*C*H$_2$) ppm.

Data for [1,1-bis{[COD(η^6-4-fluoropheny)Ru}-1,4-butanediol] (30): MS (FD+): *m*/*z* = 697 [M$^+$], 488 [M − Ru(COD)]$^+$. ^{1}H NMR (269.71 MHz, C_6D_6): δ = 5.02 (m, 2 H, aromat.H); 4.95 (m; 2 H, aromat. H); 4.90 (m; 2 H, aromat. H); 4.74 (m, 2 H, aromat. H); 3.66 (m, 8 H, H olefin. COD); 3.23 (q, 2 H, H_3); 2.32 (m, 16 H, H aliphat. COD); 2.11 (t, 2 H, H_3); 1.68 (m, 2 H, H_2) ppm. ^{13}C{^{1}H} NMR (67.8 MHz, C_6D_6): δ = 143.6, 139.6, 116.0 (aromat. C), 80.8, 79.8 (d, C-F), 74.7, 74.4, 73.1 (aromat. C); 72.7 (C^1); 63.9, 63.7 (C olefin. COD); 62.8 (C^4); 40.1 (C^2); 34.2, 33.6 (C aliphat. COD); 26.6 (C^3) ppm.

[(COD)(3-hydroxypropyl η^6-2-tolyl ketone)Ru] (31): Reaction mixture: **14** (180 mg, 0.47 mmol) in 20 mL of THF, *n*-butyllithium (0.3 mL, 0.48 mmol), and γ-butyrolactone (0.036 mL, 0.47 mmol). Yield 80 mg (0.21 mmol, 44%) of **31**. MS (FD+): *m*/*z* = 388 [M$^+$]. ^{1}H NMR (399.65 MHz, C_6D_6): δ = 5.36 (t, $^3J\{HH\}$ = 8 Hz, 1 H, aromat. H); 4.82 (d,$^3J\{HH\}$ = 8 Hz, 1 H, aromat. H); 4.43 (t, $^3J\{HH\}$ = 8 Hz, 1 H, aromat. H); 4.31 (t, $^3J\{HH\}$ = 8 Hz, 1 H, aromat. H); 3.42 (m, 2 H, CH_2OH); 3.37 (m, 2 H, H olefin. COD); 3.20 (m, 2 H, H olefin.COD); 2.72 (m, 1 H, CH_2CO); 2.63 (m, 1 H, CH_2CO); 2.19 (m, 8 H, H aliphat. COD); 2.02 (s, 3 H, CH_3); 1.86 (quint, 2 H, CH_2) ppm. ^{13}C{^{1}H} NMR (100.40 MHz, C_6D_6): δ = 202.3 (CO); 101.3, 93.2, 91.6, 88.6, 87.6, 82.3 (aromat. C); 65.7, 64.0 (C olefin. COD); 62.17 (CH_2OH); 37.1 (*C*H$_2$ CO); 34.4, 33.6 (C aliphat. COD); 27.8 (CH_2); 19.6 (CH_3) ppm.

[(COD){(6-methoxy-2,2-dimethyltetrahydrofuro[2,3-*d*][1,3]dioxol-5-yl)(η^6-phenyl)methanol}Ru] (32a, 32b): Reaction mixture: **13** (455 mg, 1.24 mmol) in 15 mL of THF, *n*-butyllithium (0.75 mL, 1.2 mmol), and 1,2-*O*-isopropylidene-3-*O*-methyl-α-D-xylopentodialdofuranose-(1,4) (250 mg, 1.24 mmol). Yield 290 mg (0.59 mmol, 48%) of **32a**, **32b**. MS (FD+): *m*/*z* = 490 [M$^+$]. ^{1}H NMR (399.65 MHz, C_6D_6): δ = 5.91 (d, $^3J\{HH\}$ = 4 Hz, 1 H, aromat. H); 5.84 (d, $^3J\{HH\}$ = 4 Hz, 1 H, aromat. H); 5.51 (d, $^3J\{HH\}$ = 5 Hz, 2 H, aromat. H); 5.36 (t, $^3J\{HH\}$ = 5 Hz, 1 H, aromat. H); 5.19 (t, $^3J\{HH\}$ = 5 Hz, 1 H, aromat. H); 4.87 (t, $^3J\{HH\}$ = 5 Hz, 1 H, aromat. H); 4.84 (t, $^3J\{HH\}$ = 5 Hz, 1 H, aromat. H); 4.79 (t, $^3J\{HH\}$ = 5 Hz, 1 H, aromat. H); 4.70 (d, $^3J\{HH\}$ = 5 Hz, 2 H, aromat. H); 4.54 (d, $^3J\{HH\}$ = 5 Hz, 1 H, aromat. H); 4.47 (td, $^3J\{HH\}$ = 4 Hz, 2 H, aromat. H); 4.43 (t, $^3J\{HH\}$ = 5 Hz, 1 H, aromat. H); 4.34 (d, $^3J\{HH\}$ = 4 Hz, 1 H, aromat. H); 4.26 (d, $^3J\{HH\}$ = 4 Hz, 1 H, aromat. H); 4.10 (t, $^3J\{HH\}$ = 5 Hz, 1 H, aromat. H); 4.05 (d, $^3J\{HH\}$ = 3 Hz, 2 H, aromat. H); 3.46 (d, $^3J\{HH\}$ = 3 Hz, 2 H, aromat. H); 3.58−3.33 (m, 4 H, H olefin. COD); 3.20 (s, 3 H, H OMe); 3.01 (s, 1 H, O*H*); 2.83 (s, 3 H, H OMe); 2.81 (d, $J\{HH\}$ = 7 Hz, 1 H, HO*H*); 2.38−2.05 (m, 8 H, H aliphat. COD); 1.40 (d, 3 H , H isoprop. *endo*); 1.11 (d, 3 H, H isoprop. *exo*) ppm. ^{13}C{^{1}H} NMR (100.40 MHz, C_6D_6): δ = 112.0, 111.8 (aromat. C); 110.0, 106.0 (isoprop. C); 106.0 (d, C-OH); 88.7, 87.7, 87.6, 87.4, 87.0, 86.6, 86.5 (aromat. C); 85.4,84.9, 84.8 ($C_{furanose}$); 84.5 (aromat. C); 84.2 ($C_{furanose}$); 83.9, 83.7 (aromat. C); 82.4, 82.0, 71.2, 69.5 ($C_{furanose}$); 61.4, 60.6 (C olefin. COD); 58.2, 57.0 (*C*OMe); 34.8, 34.3 (C aliphat. COD); 27.4, 27.3, 26.7. 26.6 (CH_3 isoprop.) ppm.

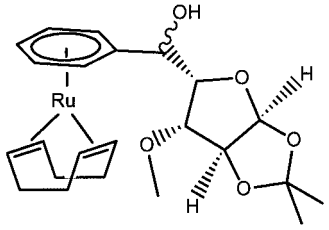

[(COD)(menthyl η^6-1,4-xylene-2-carboxylate)Ru] (33a and 33b): Reaction mixture: **8** (380 mg, 0.96 mmol) in 10 mL of THF, *n*-butyllithium (0.5 mL, 1.25 mmol), and (−)-menthyl chloroformate (0.3 mL, 1.3 mmol). Yield 200 mg (0.4 mmol, 42%) of **33a** and **33b**. MS (FD+): *m*/*z*: 497 [M$^+$]. ^{1}H NMR (269.6 MHz, C_6D_6): δ = 5.52 (s, 1 H, aromat. H); 5.13 (m, 1 H, ester H); 4.88 (dt, 1 H, aromat. H); 4.75 (dt, 1 H, aromat. H); 4.32 (t, 1 H, aromat. H); 4.04 (t, 1 H, aromat. H); 3.48 (m, 2 H, H olefin. COD); 3.14 (m, 2 H, H olefin. COD); 2.2−2.4 (m, 8 H, H aliphat. COD); 0.7−1.7 (19 H, menthyl) ppm.

[(COD)(*o*-hydroxyphenyl η⁶-2-tolyl ketone)Ru] (34): Reaction mixture: **14** (300 mg, 0.79 mmol) in 30 mL of THF, *n*-butyllithium (0.32 mL, 0.79 mmol), and *o*-acetylsalicoyl chloride (156 mg, 0.79 mmol). Yield 200 mg (0.47 mmol, 60%) of **34**. MS (FD+): *m*/*z* = 422 [M⁺]. ^{1}H NMR (399.65 MHz, [D$_8$]THF): δ = 12.62 (s, 1 H, phenol. H); 8.50 (d, $^3J\{H^5H^6\}$ = 8 Hz, 1 H, H$_5$); 7.08 (t, $^3J\{H^{5/8}H^{6/7}\}$ = 8 Hz, 1 H, H$^{6/7}$); 7.01 (d, $^3J\{H^7H^8\}$ = 8 Hz, 1 H, H^8); 6.56 (t, $^3J\{H^{5/8}H^{6/7}\}$ = 8 Hz, 1 H, H$^{6/7}$); 5.24 (t, $^3J\{H^2H^{1/3}\}$ = 5.5 Hz), 1 H, H^2; 4.78 (d, $^3J\{H^4H^3\}$ = 5.5 Hz, 1 H, H^4); 4.60 (d, $^3J\{H^1H^2\}$ = 5.5 Hz, 1 H, H^1); 4.31 (t, $^3J\{H^3H^{2/4}\}$ = 5.5 Hz, 1 H, H^3); 3.48 (m, 4 H, H olefin. COD); 2.38 (m, 8 H, H aliphat. COD); 1.63 (s, 3 H, CH$_3$) ppm. ^{13}C{^{1}H} NMR (100.40 MHz, [D$_8$]THF): δ = 201.8 (CO); 163.7 (C-OH); 136.8, 134.0, 120.6, 118.8, 118.4 (aromat. C); 99.4 (*ipso*-C); 96.0 (π-tolyl-C); 89.4, 88.6, 85.0, 83.6 (arom-C), 65.3 (C olefin. COD); 64.3;34.1 (C aliphat. COD); 33.5; 17.2 (CH$_3$) ppm.

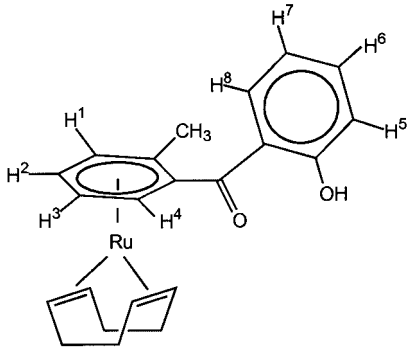

[(COD)(η⁶-1-{2-fluoro-4-tolyl} *o*-hydroxyphenyl ketone)Ru] (35): Reaction mixture: **5** (550 mg, 1.7 mmol) in 30 mL of THF, *n*-butyllithium (0.68 mL, 1.7 mmol), and *o*-acetylsalicoyl chloride (300 mg, 1.5 mmol). Yield 300 mg (0.68 mmol, 40%) of **35**. MS (FD+): *m*/*z* = 440 [M⁺]. ^{1}H NMR (300.13 MHz, C$_6$D$_6$):δ = 12.46 (s, 1 H, phenol. H); 8.81 (m, 1 H, aromat. H); 7.06 (m, 2 H, aromat. H); 6.66 (m, 1 H, aromat. H); 4.50 (dd, $^3J\{HH\}$ = 6, $J\{HF\}$ = 3 Hz, 1 H, aromat. H); 4.41 (dd, $^3J\{HH\}$ = 6, $J\{HF\}$ = 3 Hz, 1 H, aromat. H); 4.27 (d, $^3J\{HF\}$ = 4 Hz, 1 H, aromat. H); 3.54 (m, 4 H, H, olefin. COD); 2.18 (m, 8 H, H aliphat. COD); 1.72 (s, 3 H, CH$_3$) ppm. ^{13}C{^{1}H} NMR (75.47 MHz, C$_6$D$_6$): δ = 197.2 (CO); 163.4 (C-OH); 137.4, 134.2 (aromat. C); 127.3 ($^1J\{CF\}$ = −271 Hz, π-aromat. C); 120.8, 118.8,118.6 (aromat. C); 99.4 ($^3J\{CF\}$ = 6 Hz, π-aromat. C); 89.2 (d, $^2J\{CF\}$ = 17 Hz, π-aromat. C), 79.7 ($^3J\{CF\}$ = 2 Hz, π-aromat. C); 85.0 (π-aromat. C); 75.2 (d, π-aromat. C, $^2J\{CF\}$ = 22 Hz); 67.6 (C olefin. COD); 33.5 (C aliphat. COD); 18.3 (CH$_3$) ppm.

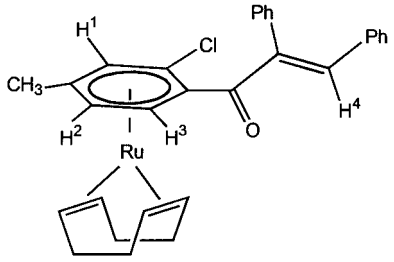

[(η⁶-1-{2-chloro-4-tolyl}-2,3-diphenylprop-2-en-1-one)(COD)Ru] (36): Reaction mixture: **6** (275 mg, 0.82 mmol) in 20 mL of THF, *n*-butyllithium (0.36 mL, 0.9 mmol), and α-phenylcinnamoyl chloride (218 mg, 0.9 mmol). Yield 180 mg (0.33 mmol, 41%) of **36**. MS (FD+): *m*/*z* = 542 [M⁺]. ^{1}H NMR (399.65 MHz, C$_6$D$_6$): δ = 7.93 (s, 1 H, olefin. H); 7.1 (m, 10 H, phenyl. H); 5.25 (d, $^3J\{H^2H^3\}$ = 5.5 Hz, 1 H, H^2); 5.03 (s, 1 H, H^1); 4.10 (d, $^3J\{H^2H^3\}$ = 5.5 Hz, 1 H, H^3); 3.59 (m, 4 H, H olefin. COD); 2.25 (m, 8 H, H aliphat. COD); 1.68 (s, 3 H, CH$_3$) ppm. ^{13}C{^{1}H} NMR (100.40 MHz, C$_6$D$_6$): δ = 193.8 (CO); 142. 3, 141.4, 138.1, 136.7, 136.6, 135.7, 130.9, 130.7, 129.5, 129.4, 129.1, 128.7, 128.7, 125.9 (phenyl. C, olefin. C); 102.2, 101.9, 99.4, 88.8, 86.2, 83.4 (aromat. C); 70.2, 68.4 (C olefin. COD); 34.5, 33.8 (C aliphat. COD); 18.4 (CH$_3$) ppm.

Crystal Structure Determinations: Suitable crystals of **10**, **11**, **28**, and **30** were taken directly from the mother liquor. Data were collected with a Siemens P4 diffractometer for **10**, **11**, and **28** and with a Nonius KappaCCD for **30**, with use of Mo-K_α radiation (λ = 0.71073 Å) and a graphite monochromator. The crystal structures were solved by direct methods and refined by use of the SHELXTL 5.03[18] programs for **10** and **28**, and SHELXTL NT 5.10[19] for **11** and **30**. Non-hydrogen atoms were refined anisotropically. Hydrogen atoms are either geometrically positioned (**10** and **28**) or their positions were derived from a difference Fourier map and refined with a fixed common isotropic displacement parameter (**11** and **30**). Other experimental details are given in Tables 2 and 3. Crystallographic data for the structures reported in this paper have been deposited with the Cambridge Crystallographic Data Center as supplementary publication nos. CCDC-186921 (**10**), -186922 (**11**), -186923 (**28**), and -186924 (**30**). Copies of the data can be obtained free of charge on application to CCDC, 12 Union Road, Cambridge CB21EZ, UK [Fax: (internat.) + 44-1223/336-033; E-mail: deposit@ccdc.cam.ac.uk or www: http://www.ccdc.ca.ac.uk].

Table 2. Crystallographic data for **10** and **11**

	10	**11**
Empirical formula	$C_{14}H_{16}BrFRu$	$C_{14}H_{16}BrIRu$
Formula mass	384.25	492.15
Color, shape	yellow, plate	yellow, needle
Size [mm]	0.90×0.52×0.10	0.70×0.35×0.20
Crystal system	monoclinic	monoclinic
Space group	$P2_1/c$	$P2_1/n$
a [Å]	13.003(1)	14.702(2)
b [Å]	8.316(1)	6.369(2)
c [Å]	12.586(1)	16.062(3)
β [°]	110.04(1)	113.14(1)
Volume [Å^3]	1278.6(2)	1383.0(5)
Z	4	4
$\rho_{calcd.}$ [g·cm^{-1}]	1.996	2.364
μ [mm^{-1}]	4.337	6.230
T [K]	294(2)	200(2)
Absorption correction	ψ-scan	ψ-scan
T_{min}/T_{max}	0.017/0.059	0.049/0.120
F(000)	752	928
Reflections measured	3606	4362
Independent reflections	2795	3335
Observed reflections [$F_o \geq 4\sigma(F)$]	2063	2630
No. refined parameters	202	154
Goodness-of-fit on F^2	1.029	1.077
R_1 [$F_o \geq 4\sigma(F)$]	0.0550	0.0585
wR_2 (all data)	0.1470	0.1766
Max/min resid. density [e·Å^{-3}]	1.034/−1.487	3.007/−3.076

Acknowledgments

We thank the Deutsche Forschungsgemeinschaft (SFB, 583) and the Fonds der Chemischen Industrie for financial support.

Table 3. Crystallographic data for **28** and **30**

	28	**30**
Empirical formula	$C_{32}H_{42}O_2Ru_2$	$C_{39}H_{48}F_2O_2Ru_2$ [a]
Formula mass	660.80	788.91[a]
Color, shape	Yellow, block	Yellow, block
Size [mm]	0.75×0.38×0.30	0.28×0.24×0.15
Crystal system	triclinic	monoclinic
Space group	$P\bar{1}$	$C2/c$
a [Å]	8.725(4)	36.1071(6)
b [Å]	14.455(5)	8.9293(2)
c [Å]	23.190(9)	21.7669(4)
α [°]	107.14(2)	90.0
β [°]	90.76(4)	112.294(1)
γ [°]	106.38(4)	90.0
Volume [Å^3]	2667(2)	6493.3(2)
Z	4	8
$\rho_{calcd.}$ [g·cm^{-1}]	1.646	1.614
μ [mm^{-1}]	1.161	0.977
T [K]	200(2)	100(2)
Absorption correction	ψ-scan	multi-scan
T_{min}/T_{max}	0.501/0.712	0.701/0.769
F(000)	1352	3232
Reflections measured	13619	33917
Independent reflections	11365	9246
Observed reflections [$F_o \geq 4\sigma(F)$]	8342	6534
No. refined parameters	663	544
Goodness-of-fit at F^2	1.093	1.011
R_1 [$F_o \geq 4\sigma(F)$]	0.0636	0.0346
wR_2 (all data)	0.1723	0.0728
Max/min resid. density [e·Å^{-3}]	2.608/−1.175	0.604/−0.590

[a] Includes one molecule of solvent (toluene).

[1] G. Bodes, F. W. Heinemann, G. Marconi, S. Neumann, U. Zenneck, *J. Organomet. Chem.* **2002**, *641*, 90.
[2] P. Pertici, G. Vitulli, C. Bigelli, R. Lazzaroni, *J. Organomet. Chem.* **1984**, *275*, 113.
[3] M.A. Bennett, H. Neumann, M. Thomas, X. Wang, G. Vitulli, P. Pertici, P. Salvadori, *Organometallics* **1991**, *10*, 3237.
[4] P. Pertici, G. Uccello Barretta, F. Burzagli, P. Salvadori, M. A. Bennett, *J. Organomet. Chem.* **1991**, *413*, 303.
[5] Y. Ohgomori, S. Ichikawa, T. Yoneyama, N. Sumitani (Mitsubishi Petrochemical Co., Ltd.), Eur. Pat. Appl. EP 537,625 (*Chem. Abstr.* **1993**, *119*, 94953p); J. Ookago, S. Ichikawa, T. Yoneyama, N. Sumya (Mitsubishi Petrochemical Co.), Jpn. Kokai Tokyo Koho JP 05,186,377 (93,186,377) (*Chem. Abstr.* **1993**, *119*, 250721u); J. Ookago, N. Sumya, S. Ichikawa (Mitsubishi Petrochemical Co.), Jpn. Kokai Tokyo Koho JP 05,310,631 (93,310,631) (*Chem. Abstr.* **1994**, *120*, 269654s).
[6] P. Pertici, V. Ballantini, P. Salvadori, M. A. Bennett, *Organometallics* **1995**, *14*, 2565.
[7] J. Takehara, S. Hashiguchi, A. Fujii, S. Inoue, T. Ikariya, R. Noyori, *Chem. Commun.* **1996**, 233.
[8] A. Fujii, S. Hasahiguchi, N. Uematsu, T. Ikariya, R. Noyori, *J. Am. Chem. Soc.* **1996**, *118*, 2521.
[9] N. Uematsu, A. Fujii, S. Hashiguchi, T. Ikariya, R. Noyori, *J. Am. Chem. Soc.* **1996**, *118*, 4916.
[10] E. L. Muetterties, J. R. Bleeke, A. C. Sievert, *J. Organomet. Chem.* **1979**, *178*, 197; P.M. Maitlis, *Chem. Soc. Rev.* **1981**, *10*, 1.
[11] P. Pertici, G. Vitulli, S. Bertozzi, R. Lazzaroni, *Inorg. Chim. Acta* **1988**, *149*, 235.
[12] P. Pertici, G. Vitulli, R. Lazzaroni, P. Salvadori, P. L. Barili, *J. Chem. Soc., Dalton Trans.* **1982**, 1019; G. Vitulli, P. Pertici, P. Salvadori, *J. Chem. Soc., Dalton Trans.* **1984**, 2255; P. Pertici, E. Pitzalis, F. Marchetti, C. Rosini, P. Salvadori, M. A. Bennett, *J.Organomet. Chem.* **1994**, *466*, 221.
[13] F. Heinemann, J. Klodwig, F. Knoch, M. Wündisch, U. Zenneck, *Chem. Ber./Recueil* **1997**, *130*, 123.
[14] H. Schmidt, M. L. Ziegler, *Chem. Ber.* **1976**, *109*, 132.
[15] Some examples: M. D. Rausch, D. J. Ciappenelli, *J. Organomet. Chem.* **1967**, *10*, 127; C. Elschenbroich, *J. Organomet. Chem.* **1968**, *14*, 157; M. F. Semmelhack, J. Bisaha, M. Czarny, *J. Am. Chem. Soc.* **1979**, *101*, 168; M. Uemura, K. Isobe, Y. Hayashi, *Chem. Lett.* **1985**, 91; F. Rose-Munch, E. Rose, *Curr. Org. Chem.* **1999**, *3*, 445.
[16] G. Marconi, H. Baier, F. W. Heinemann, P. Pinto, H. Pritzkow, U. Zenneck, in preparation.
[17] Some examples: R. J. Card, W. S. Trahanovsky, *J. Org. Chem.* **1980**, *45*, 2560; M. F. Semmelhack, G. R. Clark, J. L. Garcia, J. J. Harrison, Y.Thebtaranonth, W. Wulff, A. Yamashita, *Tetrahedron* **1981**, *37*, 3957; C. Bohm, K. Muniz, C. Ganter, *New J. Chem.* **1998**, 1371; S. Pache, C. Botuha, R. Franz, J. Einhorn, E. P. Kündig, *Helv. Chim. Acta* **2000**, *83*, 2436.
[18] *SHELXTL 5.03*, Siemens Analytical X-ray Instrument, Madison, WI, U.S.A., **1995**.
[19] *SHELXTL NT 5.10*, Bruker AXS, Madison, WI, U.S.A., **1998**.

Received June 6, 2002
[I02300]

Synthesis, Structure and Reactivity of Ruthenium(II) Carbonyl Complexes Containing Bis(pyrazol-1-yl)methane and Bis(*N*-methylimidazol-2-yl)methane

Barbara A. Messerle,*[a] Vicki-Anne Tolhurst,[a] and Peter Turner[b]

Keywords: N ligands / Ruthenium / Structure elucidation / Reactivity

A series of ruthenium(II) complexes with the pyrazolylalkane ligands bis(pyrazol-1-yl)methane (BPM) (**I**) and bis(3,5-dimethylpyrazol-1-yl)methane (dmBPM) (**II**), and the imidazolylalkane ligand bis(*N*-methylimidazol-2-yl)methane (BIM) (**III**) have been synthesised and characterised. The complexes $[Ru(N\text{-}N)(CO)_2X_2]$ [N-N = BPM, X = Cl (**1a**), Br (**1b**); N-N = dmBPM, X = Cl (**2**); N-N = BIM, X = Cl (**3**)] were prepared from the stoichiometric reaction of $[Ru(CO)_2X_2]_n$ and the bidentate N-donor ligand in refluxing methanol. The crystal structure of **2** showed the complex to have octahedral geometry about the ruthenium centre, with the carbonyl and chloride ligands being coordinated *cis* and *trans*, respectively. The complex $[Ru(BPM)_2(CO)(Cl)][BPh_4]$ (**4**) was prepared from the reaction of $RuCl_3$ and BPM in refluxing DMF, or from the decarbonylation of $[Ru(BPM)(CO)_2Cl_2]$ (**1a**) in the presence of BPM and $NaBPh_4$. The NMR spectra of **4** were fully assigned from 2D NMR experiments. The NOESY showed a *cis* coordination of the chloride and carbonyl ligands, and this was confirmed by single crystal X-ray diffraction studies.
(© Wiley-VCH Verlag GmbH & Co. KGaA, 69451 Weinheim, Germany, 2003)

Introduction

Organometallic ruthenium complexes are efficient catalysts for a variety of processes,[1] such as the coupling of pyridine, carbon monoxide and hexenes,[2] the coupling of aromatic carbon-hydrogen bonds with olefins,[3] and the intramolecular cyclisation of hydroxyenynes to form furan derivatives.[4,5] Catalytically active ruthenium complexes containing N-donor ligands are becoming more significant, leading to the development of new ruthenium complexes with N-donor ligands and suitable co-ligands for optimum catalytic activity. The preparation of a number of ruthenium carbonyl systems containing 2,2′-dipyridyl and its derivatives has been reported,[6−8] and in some cases these complexes are efficient catalysts for processes such as the reduction[9] and hydrogenation[10] of CO_2 and, in particular, the water-gas shift reaction, in both homogeneous[11−14] and heterogeneous environments.[15−17]

The sp^2-N donor poly(pyrazol-1-yl)methane and poly(imidazol-2-yl)methane ligands, such as bis(pyrazol-1-yl)methane (**I**) (BPM),[18] bis(3,5-dimethylpyrazol-1-yl)methane (**II**),[18] tris(pyrazol-1-yl)methane (**III**) (TPM),[18] bis(*N*-methylimidazol-2-yl)methane (**IV**) (BIM),[19] and tris(*N*-methylimidazol-2-yl)methanol (**V**; TIM) are neutral ligands closely related to the poly(pyrazolyl)borate ligands.[20] The basicity of the sp^2-N donor atoms of the five-membered heterocycles of BPM and BIM are considerably different to that of N-atoms of other ligands containing heterocycles, such as 2,2′-bipyridyl (BIPY), which has a significant effect on the relative degree of electron donation to the metal by the ligand.[21] A number of complexes containing poly(pyrazol-1-yl)methane ligands have been synthesised for metals in groups 5, 6, 9 and 10.[22] Only a limited number of poly(pyrazol-1-yl)methane complexes of metals of group 8 have been reported;[23,24] these include $[Ru(TPM)(OH_2)_3](p\text{-}CH_3C_6H_4SO_3)_2\cdot 1.5H_2O$[25] and [Ru(TPM)(COD)Cl]Cl (COD = 1,5-cyclooctadiene).[26] Group 8 metal complexes containing poly(imidazol-2-yl)methane ligands have also been reported and include $[Ru(BIM)(CO)(PPh_3)H]Cl$,[27] $[M(TIM)(CO)(PPh_3)H]Cl$ (M = Ru, Os)[28] and $[Fe(TIM)_2][FeCl_4]$.[29] We have recently reported a series of ruthenium(II) complexes with the pyrazolylalkane ligands TPM and BPM, $[RuCl(PPh_3)_2(TPM)]X$ (X = Cl, BF_4), $[Ru(CO)H(PPh_3)(BPM)_2]Cl$ and $[Ru(PPh_3)(BPM)(\mu\text{-}Cl)_3Ru(PPh_3)(BPM)]Cl$.[30]

[a] School of Chemical Sciences, The University of New South Wales,
Sydney, NSW 2052, Australia
Fax: (internat.) +61-2/9385-6141
E-mail: b.messerle@unsw.edu.au
[b] School of Chemistry, The University of Sydney,
Sydney, NSW 2006, Australia

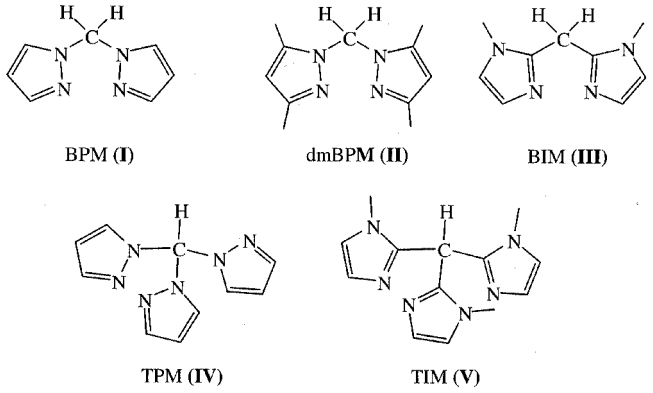

Herein we report the preparation of a series of neutral and charged ruthenium carbonyl complexes containing the N-donor ligands BPM, dmBPM, and BIM. These complexes are of interest for their possible application in hydrogenation catalysis. The complexes $[Ru(N\text{-}N)(CO)_2X_2]$ [N-N = BPM, X = Cl (**1a**), Br (**1b**); N-N = dmBPM, X = Cl (**2**); N-N = BIM, X = Cl (**3**)] were prepared from the stoichiometric reaction of $[Ru(CO)_2X_2]_n$ and the bidentate ligand in refluxing methanol. The ionic complex $[Ru(BPM)_2(CO)Cl][BPh_4]$ (**4**) was prepared from the reaction of $RuCl_3$ and BPM in refluxing DMF, and from the decarbonylation of $[Ru(BPM)(CO)_2Cl_2]$, followed by the addition of BPM and $NaBPh_4$.

Results And Discussion

Synthesis of $[Ru(N\text{-}N)(CO)_2X_2]$ Complexes

Preparations of the complexes $[Ru(N\text{-}N)(CO)_2X_2]$ are outlined in Scheme 1. Treatment of $[Ru(CO)_2Cl_2]_n$ with the bidentate nitrogen ligands in refluxing methanol results in the isolation of $[Ru(N\text{-}N)(CO)_2Cl_2]$ [N-N = bis(pyrazol-1-yl)methane (BPM) (**1a**), bis(3,5-dimethylpyrazol-1-yl)methane (dmBPM) (**2**), bis(N-methylimidazol-2-yl)methane

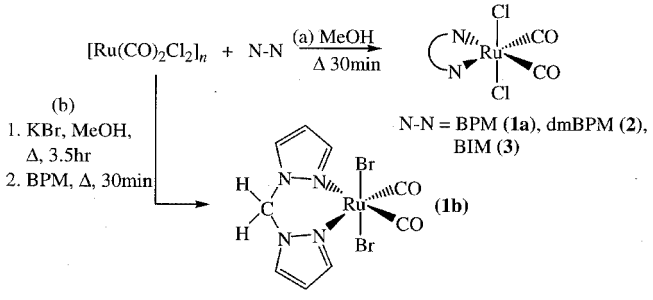

Scheme 1. Preparation of neutral organoruthenium complexes **1(a,b)**, **2** and **3**

(BIM) (**3**)] in good yields as yellow solids (Scheme 1a). The preparation of $[Ru(BPM)(CO)_2Br_2]$ (**1b**) involved an initial halide exchange reaction between $[Ru(CO)_2Cl_2]_n$ and KBr, followed by the addition of BPM (Scheme 1b). This complex was isolated in fair yield as an orange solid. Attempts to prepare the complex $[Ru(BPM)(CO)_2I_2]$ from the reaction of $[Ru(CO)_2Cl_2]_n$ with NaI resulted in an orange solid. Unfortunately, residual NaI remained and a pure complex could not be obtained. CI mass spectra of the chloride complexes exhibit peaks corresponding to M^+ ions for all complexes, confirming the complexes to be monomeric. Subsequent loss of CO ligands are observed followed by peaks corresponding to the [M − 2CO − Cl] and [M − 2CO − 2Cl] ions. FAB mass spectra of the bromide complex show similar results, exhibiting peaks corresponding to the M^+ ions with subsequent loss of CO ligands.

The ^1H NMR spectra of **1(a, b)**, **2** and **3** exhibit resonances typical of symmetrical complexes containing such ligands. The protons of the two nitrogen-containing rings of each ligand are equivalent, with only one set of resonances observed for the aromatic protons of the pyrazolyl or imidazolyl rings. Broad singlets are observed for the methylene protons of the BPM and dmBPM ligands of **1(a, b)**, due to the fluxionality of the puckered six-membered ring containing the central Ru atom. At room temperature, the resonance due to the methylene protons of the dmBPM ligand of **2** is not observed, however, on reducing the temperature to −28 °C two resonances due to the two inequivalent protons of the methylene group of dmBPM are observed, where the six-membered ring is in a nonexchanging boat conformation. A similar ligand geometry was observed in the complex $[Ru(BPM)_2(PPh_3)Cl]Cl$.[30] The assignments are consistent with the *cis*-(CO), *trans*-(halide) structure of the complexes. The $^{13}C\{^1H\}$ NMR spectra for each of the complexes **1(a, b)** and **2** are also consistent with the ^{13}C nuclei of the two aromatic rings of the ligands being equivalent.

The IR spectra of these complexes in the ν(C≡O) region show two C≡O stretches at typical wavenumbers for terminal carbonyl ligands, indicating that the complexes have octahedral ruthenium centres with C_{2v} symmetry, and that the coordination sphere about the ruthenium centre is *cis*(CO)-*trans*(halide). The ν(C≡O) frequencies and $^{13}C\{^1H\}$ NMR carbonyl resonances are listed in Table 1. A shift in ν(C≡O) frequencies towards lower wavenumbers is observed in the order BPM > dmBPM > BIM, which is associated with a downfield shift for the ^{13}C CO resonance. The additional four electron-donating methyl groups on the dmBPM ligand give the ligand a better electron-donating ability than BPM. The trend also shows that the imidazolyl ligand is a better electron donor than pyrazolyl ligands. A marginal shift in ν(C≡O) frequencies to lower wavenumber

Table 1. Infrared ν(CO) absorptions and ^{13}C CO shifts of *cis*(CO)-*trans*(X)-$[Ru(N\text{-}N)(CO)_2X_2]$ complexes

Complex	ν(CO) (cm^{-1})	^{13}C (ppm)
$[Ru(BPM)(CO)_2Cl_2]$ (**1a**)	2064, 2011	196.4
$[Ru(BPM)(CO)_2Br_2]$ (**1b**)	2064, 2007	196.3
$[Ru(dmBPM)(CO)_2Cl_2]$ (**2**)	2061, 1998	197.1
$[Ru(BIM)(CO)_2Cl_2]$ (**3**)	2051, 1986	198.4
$[Ru(bipy)(CO)_2Cl_2]$	2066, 2003	196.3
$[Ru(bipy)(CO)_2Br_2]$	2062, 2004	197.2
$[Ru(bipy)(CO)_2I_2]$	2056, 2000	198.5

is also observed for the complexes $[Ru(BPM)(CO)_2X_2]$ (Cl > Br). This trend has been observed on a number of occasions for dipyridylruthenium complexes.[6,31,32]

Synthesis of $[Ru(BPM)_2(CO)Cl][BPh_4]$

The complex $[Ru(BPM)_2(CO)Cl][BPh_4]$ (**4**) was prepared by two methods (Scheme 2). Firstly, $RuCl_3{\cdot}xH_2O$ was allowed to react with two equivalents of BPM in refluxing DMF for 8 hours (Scheme 2a). After cooling, the solvent volume was reduced by distillation and $NaBPh_4$ was added. Et_2O was then added to the reaction to afford an off-white precipitate. This was recrystallised from acetone and diethyl ether to afford $[Ru(BPM)_2(CO)Cl][BPh_4]$ (**4**). This method is analogous to the preparation of $[Ru(BIPY)_2(CO)Cl][ClO_4]$.[33] Complex **4** was also prepared by the monodecarbonylation of $[Ru(BPM)(CO)_2Cl_2]$ **(1a)**. Complex **1a** was reacted with excess Me_3NO in refluxing MeCN after which one equivalent of BPM was added and the reaction refluxed for a further 16 hours. The addition of $NaBPh_4$ after this time resulted in the formation of compound **4** (Scheme 2b). This method proved to be the more efficient, with 37% yield obtained. The positive electrospray mass spectrum of the cation of **4** gave a M^+ ion mass of 460.9, consistent with the cation formula. Loss of CO is observed (432.9 $[M - CO]^+$) followed by loss of chlorine (396.9 $[M - CO - Cl]^+$). The infrared spectrum of $[Ru(BPM)_2(CO)Cl][BPh_4]$ exhibits a ν(CO) frequency of 1970 cm^{-1}. This is similar to the CO(str) frequency of $[Ru(BIPY)_2(CO)Cl][ClO_4]$,[33] again showing that the two ligands have similar electron-donating properties to the ruthenium centre.

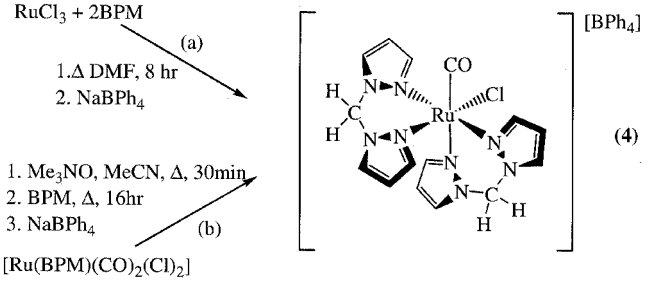

Scheme 2. Preparation of $[Ru(BPM)_2(CO)Cl][BPh_4]$ (**4**)

Attempts to prepare the halogen-free compounds $[Ru(BPM)_2(CO)_2][BPh_4]_2$ and $[Ru(BIM)_2(CO)_2][BPh_4]_2$ by dechlorination with trifluoromethanesulfonic acid or silver triflate, followed by the addition of BPM and $NaBPh_4$, were unsuccessful. These methods have been reported for the preparation of $[Ru(BIPY)_2(CO)_2]^{2+}$. No product could be isolated from the reaction of $[Ru(BPM)(CO)_2Cl_2]$ or $[Ru(BIM)(CO)_2Cl_2]$ and silver triflate, while the reaction of $[Ru(BIM)(CO)_2Cl_2]$ with trifluoromethanesulfonic acid followed by the addition of $NaBPh_4$ resulted in the quantitative protonation of the BIM ligand affording an ionic compound (Figure 1). Important crystal data are given in Table 2 with important bond lengths and bond angles listed in Table 3. Figure 2 shows the dimeric nature of the cation through H-bonding.

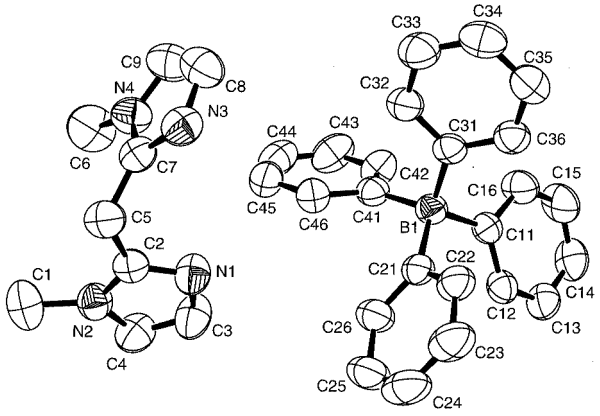

Figure 1. Molecular projection of the asymmetric unit of [HBIM][BPh_4], showing atom labelling scheme; thermal ellipsoids are drawn at the 50% probability level; H-atoms removed for clarity

NMR Spectroscopic Studies of $[Ru(BPM)_2(CO)(Cl)][BPh_4]$

The ^1H and $^{13}C\{^1H\}$ NMR spectra were completely assigned for $[Ru(BPM)_2(CO)Cl][BPh_4]$ (**4**) (at 250 K). At room temperature, rapid conformational exchange is observed, so that the resonances of the protons of the two BPM ligands are completely equivalent. At 250 K, the resonances of the protons of the four pyrazole rings of the ligands are found to be inequivalent, indicating that the two BPM ligands are mutually *cis*, and that the chloride and carbonyl ligands are mutually *cis*. It was not possible to distinguish the positions of the carbonyl and the chloride ligands. The NOESY spectrum shows the chelating ligands to be puckered and the six-membered chelate ring to have a boat conformation with only one methylene proton interacting with the closest protons of the pyrazole rings. A similar geometry is observed in the complex $[Ru(BPM)_2(PPh_3)Cl]Cl$, where the complete coordination sphere of the ruthenium centre could be determined because of strong NOESY interactions between the protons of the pyrazole rings and the triphenylphosphane ligand.[30] The atom labelling used for the assignment of NMR spectra of **4** is shown in Figure 3.

Structures of $[Ru(dmBPM)(CO)_2Cl_2]$ (2) and $[Ru(BPM)_2(CO)Cl][BPh_4]$ (4)

Important crystal data are listed in Table 2 with important bond lengths and bond angles of $[Ru(dmBPM)(CO)_2Cl_2]$ (**2**) and $[Ru(BPM)_2(CO)Cl][BPh_4]$ (**4**) listed in Table 4 and 5, respectively. Both compounds are noncentrosymmetric and crystallise in the $P\bar{1}$ (#2) space group. The ruthenium centres in both complexes have a distorted octahedral geometry, with the bis(pyrazol-1-yl)methane ligands chelating the ruthenium centres to form six-membered chelate rings with boat conformations. The structure of $[Ru(dmBPM)(CO)_2Cl_2]$ (Figure 4) shows the carbonyl and chloride ligands to have *cis* and *trans* arrangements, respectively. The structures of both *cis*(CO), *cis*(Cl)-

Table 1. Crystallographic data for [Ru(dmBPM)$(CO)_2Cl_2$] (**2**), [Ru$(BPM)_2$(CO)Cl][BPh_4] (**4**) and [HBIM][BPh_4]

	[Ru(dmBPM)$(CO)_2Cl_2$]	[Ru$(BPM)_2$(CO)Cl][BPh_4]	[HBIM][BPh_4]
Formula	$C_{13}H_{16}N_4O_2RuCl_2$	$C_{39}H_{36}N_8OBRuCl$	$C_{33}H_{33}BN_4$
M	432.27	780.09	496.45
Crystal system	triclinic	triclinic	monoclinic
Space group	$P\bar{1}$ (#2)	$P\bar{1}$ (#2)	$P2_1/c$ (#14)
a/ Å	7.9834(6)	13.167(3)	10.5867(4)
b/ Å	8.8530(6)	15.354(3)	14.9348(6)
c/ Å	12.4069(9)	9.952(2)	18.2777(7)
α/°	98.9100(10)	106.188(4)	90.00
β/°	90.4100(10)	98.774(4)	105.9330(10)
γ/°	94.1650(10)	89.101(4)	90.00
V/ Å^3	863.86(11)	1908.8(7)	2778.87(19)
D_c/mg cm^{-3}	1.662	1.357	1.187
Z	2	2	4
F(000)	432	444	1056
μ/mm^{-1}	1.227	0.5223	0.070
$T^*_{(min, max)}$	0.830, 1.000	0.85370, 0.96303	0.980, 0.993
$2\theta_{max}$/°	56.54	56.40	56.56
No. unique reflections	4020	8483	6695
No. observed data [$I_o < 2(I)$]	3497	5241	2914
R[a]	3.15	5.16	3.97
R′[a]	7.42	14.67	8.41
GooF	1.027	1.262	1.064
Absorption Correction	Empirical	Gaussian	Gaussian

[a] *R* and *R′* defined as residual factor and weighted residual factor, respectively, for observed reflections satisfying $F_0^2 \geq 2\sigma F^2$. (w = 1/[$\sigma^2(F_0^2)$ + (0.0332P)^2 + 0.6217*P*] (**2**), w = 1/[$\sigma^2(F_0^2)$ + (0.0550*P*)^2] (**4**), (w = 1/[$\sigma^2(F_0^2)$ + (0.0300*P*)^2] ([HBIM][BPh_4], where *P* = (F_0^2 + 2F_c^2)/3).

Table 2. Selected bond lengths and angles for [HBIM][BPh_4]

Bond lengths (Å)			
N(1)−C(2)	1.3167(18)	N(3)−C(7)	1.3259(19)
N(1)−C(3)	1.3683(19)	N(3)−C(8)	1.369(2)
N(2)−C(2)	1.3493(18)	N(4)−C(7)	1.3294(18)
N(2)−C(4)	1.3619(19)	N(4)−C(9)	1.371(2)
N(2)−C(1)	1.4618(19)	N(4)−C(6)	1.4627(19)
C(2)−C(5)	1.494(2)	C(5)−C(7)	1.483(2)
C(3)−C(4)	1.337(2)	C(8)−C(9)	1.331(2)
Bond angles (°)			
C(2)−N(1)−C(3)	105.33(14)	C(7)−N(3)−C(8)	109.10(16)
C(2)−N(2)−C(4)	107.05(13)	C(7)−N(4)−C(9)	108.84(15)
C(2)−N(2)−C(1)	127.58(15)	C(7)−N(4)−C(6)	125.60(15)
C(4)−N(2)−C(1)	125.36(15)	C(9)−N(4)−C(6)	125.56(16)
N(1)−C(2)−N(2)	110.93(14)	N(3)−C(7)−N(4)	107.60(15)
N(1)−C(2)−C(5)	123.61(15)	N(3)−C(7)−C(5)	126.13(15)
N(2)−C(2)−C(5)	125.46(15)	N(4)−C(7)−C(5)	126.23(16)
C(4)−C(3)−N(1)	110.29(16)	C(9)−C(8)−N(3)	107.18(17)
C(3)−C(4)−N(2)	106.40(16)	C(8)−C(9)−N(4)	107.28(16)

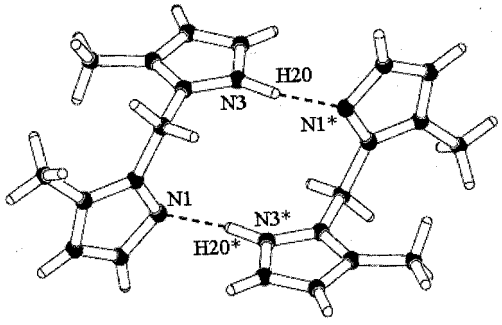

Figure 2. Molecular projection of [$(HBIM)_2$]$^{2+}$, showing dimeric nature through H-bonding

[Ru(BIPY)$(CO)_2Cl_2$] and *cis*(CO), *trans*(Cl)-[Ru(BIPY)-$(CO)_2Cl_2$] have been reported previously.[34] The structure of the [Ru$(BPM)_2$(CO)Cl]$^+$ cation (Figure 5) shows the carbonyl and chloride ligands to have *cis* coordination with respect to each other, as was observed for the complex in solution at low temperatures using NMR spectroscopy.

The Ru−N distances for **2** [2.165(2) and 2.167(2) Å] are significantly longer than those seen in the analogous bipyridine complexes *cis*(CO), *cis*(Cl)-[Ru(BIPY)$(CO)_2Cl_2$] and *cis*(CO), *trans*(Cl)-[Ru(BIPY)$(CO)_2Cl_2$] [2.117(8) and 2.090(8), 2.112(12) and 2.102(9) Å, respectively],[34] where the longer Ru−N bond length corresponds to the bond *trans* to the carbonyl ligand in the *cis*(CO), *cis*(Cl)-[Ru(BIPY)$(CO)_2Cl_2$] structure. The Ru−N bond lengths of **2** are also considerably longer than those in the cation of **4** [2.076(4)−2.140(4) Å] and can be attributed to the increased steric interaction caused by the methyl substituents present on the pyrazolyl rings. The Ru−Cl bond lengths [2.3941(7), 2.4155(7) Å] are similar, as would be expected for a *cis*(CO), *trans*(Cl) geometry. Both distances are similar to those of *cis*(CO), *trans*(Cl)-[Ru(BIPY)$(CO)_2Cl_2$] [2.391(5), 2.390(5) Å (Ru−Cl); 1.85(17), 1.817(8) Å (Ru−C)].[34] The distortion in the octahedral geometry about the ruthenium centre is evident by the slight deviation from ideal bond angles about the ruthenium centre. The

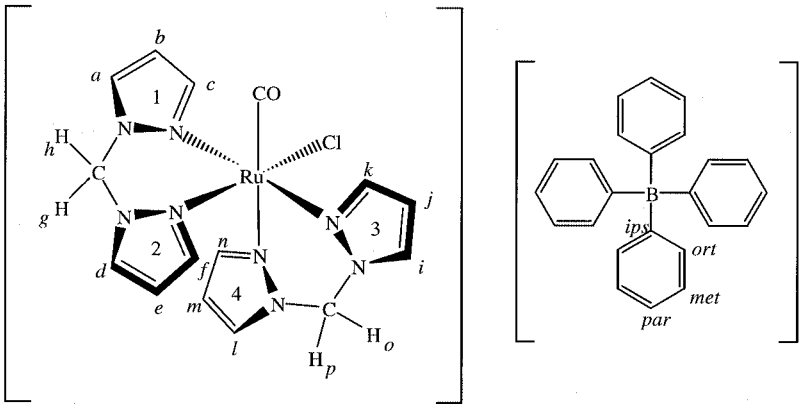

Figure 3. Atom labelling scheme of $[Ru(BPM)_2(CO)Cl][BPh_4]$ (**4**) for NMR spectra

Table 4. Selected bond lengths and angles for $[Ru(dmBPM)(CO)_2Cl_2]$ (**2**)

Bond lengths (Å)			
Ru−N(2	2.165(2)	Ru−C(2)	1.868(3)
Ru−N(4)	2.167(2)	Ru−Cl(3)	2.3941(7)
Ru−C(1)	1.869(3)	Ru−Cl(2)	2.4155(7)
Bond Angles (°)			
N(2)−Ru−N(4)	86.38(8)	Cl(3)−Ru−C(2)	91.95(10)
N(2)−Ru−C(2)	94.94(11)	Cl(3)−Ru−C(1)	91.23(10)
N(2)−Ru−C(1)	178.27(11)	Cl(2)−Ru−C(2	88.55(10)
N(4)−Ru−C(1)	94.44(11)	Cl(2)−Ru−C(1)	89.33(10)
N(4)−Ru−C(2)	178.68(10)	Cl(3)−Ru−N(2)	87.27(6)
C(1)−Ru−C(2)	84.24(13)	Cl(3)−Ru−N(4)	88.12(6)
Cl(3)−Ru−Cl(2)	179.28(3)	Cl(2)−Ru−N(2)	92.17(6)
Cl(2)−Ru−N(4)	91.38(6)		

Table 5. Selected bond lengths and angles of $[Ru(BPM)_2(CO)Cl][BPh_4]$ (**4**)

Bond lengths (Å)			
Ru−N(4)	2.071(4)	Ru−N(6)	2.095(4)
Ru−N(2)	2.090(4)	Ru−N(8)	2.142(4)
Ru−C(15)	1.930(5)	Ru−Cl(1)	2.3986(16)
Bond angles (°)			
N(4)−Ru−N(6)	173.88(15)	N(4)−Ru−N(2)	88.66(15)
N(6)−Ru−N(2)	88.44(15)	N(4)−Ru−N(8)	87.35(15)
N(6)−Ru−N(8)	87.01(14)	N(2)−Ru−N(8)	84.54(15)
N(4)−Ru−C(15)	91.50(17)	N(6)−Ru−C(15)	94.19(17)
Cl−Ru−N(4)	90.81(12)	Cl−Ru−N(6)	91.63(12)
N(2)−Ru−C(15)	96.72(18)	N(8)−Ru−C(15)	178.27(19)
Cl−Ru−N(2)	175.26(11)	Cl−Ru−N(8)	90.73(11)
Cl−Ru−C(15)	88.00(15)		

bite angle of the dmBPM ligand [86.38(8)°] is similar to that in *trans*-$[Ru(BPM)(CO)(PMe_3)_2(COMe)]^+$ [84.3(5)°][35] and $[Ru_2(PPh_3)_2(BPM)_2(\mu\text{-}Cl)_3]Cl$ [88.4(3)°].[30]

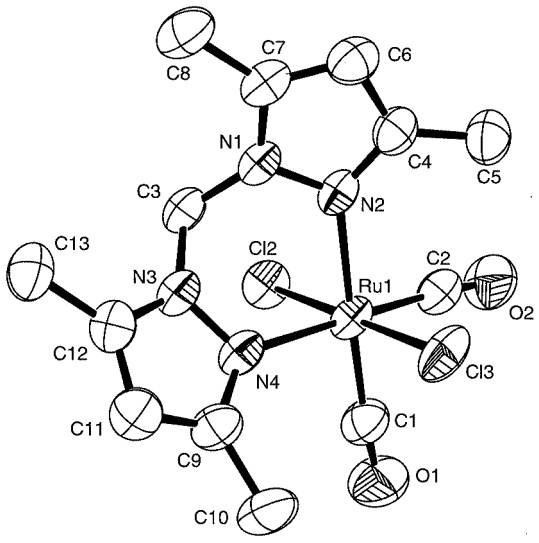

Figure 4. Molecular projection of $[Ru(dmBPM)(CO)_2Cl_2]$ (**2**) showing atom labelling scheme; thermal ellipsoids are drawn at the 50% probability level; H-atoms removed for clarity

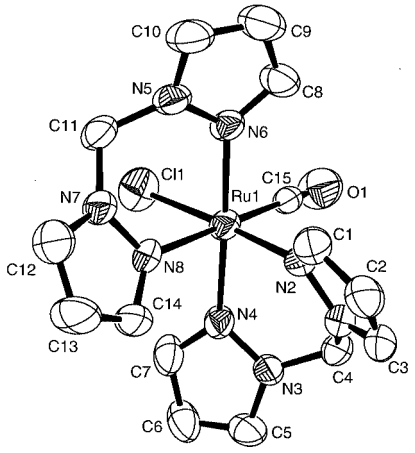

Figure 5. Molecular projection of $[Ru(BPM)_2(CO)Cl][BPh_4]$ (**4**) showing atom labelling scheme; thermal ellipsoids are drawn at the 50% probability level; H-atoms removed for clarity

The structure of the cation of **4** shows the CO and Cl ligands to have *cis* coordination with respect to each other. The Ru−N bond lengths are shorter than those of the neutral complex **2** because of the absence of the methyl moieties on the pyrazolyl rings of the ligands, but are similar to those of $[Ru(BIPY)_2(CO)Cl]^+$ [mean value 2.10(2) Å].[33] Similar to $[Ru(BIPY)_2(CO)Cl]^+$, three Ru−N bond lengths of **4** are similar, ranging from 2.071(4) to 2.095(4) Å, with one longer bond [2.140(4) Å], corresponding to the Ru−N bond *trans* to the carbonyl ligand; this is in accordance with the increased *trans* influence, CO > N_{ligand} > Cl. The Ru−Cl and Ru−C bond lengths in **4** of 2.3986(16) and 1.930(5) Å, respectively, are also similar to those reported for $[Ru(BIPY)_2(CO)Cl]^+$.[33] The slightly distorted octahedral geometry about the ruthenium centre in **4** is not unlike related structures, with the bite angle of the ligands being 88.66(15) and 87.01(14)°, similar to those in the compounds described above.

Reactivity of $[Ru(N\text{-}N)(CO)_2Cl_2]$ Compounds

The catalytic activity of the $[Ru(N\text{-}N)(CO)_2Cl_2]$ compounds was investigated. The analogous dipyridylruthenium compounds are active in the water-gas shift reaction as well as a number of other catalytic processes. The processes we investigated included hydrogenation, hydrosilylation, intramolecular cyclisation of unsaturated carboxylic acids to form lactones, and intermolecular coupling reactions. All reactions were conducted at 60 °C over several days. All coupling reactions were unsuccessful, as were the hydrogenation reactions. The activity of the complexes toward H_2 was monitored using *para*-hydrogen NMR experiments (4 atm H_2). No activation of H_2 by the ruthenium compounds was observed, at various temperatures or under photolytic conditions.

Conclusions

A series of organoruthenium compounds containing the bidentate ligands bis(*N*-methylimidazol-1-yl)methane and bis(pyrazol-1-yl)methane ligands have been prepared that are free of phosphane coligands. Structural elucidation of $[Ru(dmBPM)(CO)_2Cl_2]$ (**2**) shows it to be a mononuclear compound with *cis*(CO), *trans*(Cl) coordination in a distorted octahedral geometry. All other prepared analogous compounds are assigned with the same coordination environment based on spectral similarities. The ionic compound $[Ru(BPM)_2(CO)Cl][BPh_4]$ (**4**) was prepared by two routes. Structural elucidation of $[Ru(BPM)_2(CO)Cl][BPh_4]$ (**4**) shows it to have a *cis* arrangement of the two bis(pyrazol-1-yl)methane ligands. This was also confirmed by NOESY and COSY NMR spectroscopy and is similar to the previously reported $[Ru(BPM)_2(PPh_3)Cl]Cl$.[14] We were unable to prepare the halide-free compound $[Ru(BPM)_2(CO)_2][BPh_4]$. The activation of small molecules by the ruthenium compounds was investigated, with the ruthenium compounds described herein having quite different reactivity to that of $[Ru(BIPY)(CO)_2Cl_2]$.

Experimental Section

All reactions were performed under nitrogen gas using standard Schlenk techniques. Ruthenium(III) trichloride hydrate was obtained from Johnson−Matthey, and used without purification. The ruthenium complex $[Ru(CO)_2Cl_2]_n$ [36] and the ligands bis(pyrazol-1-yl)methane (BPM),[18] bis(3,5-dimethylpyrazol-1-yl)methane (dmBPM)[18] and bis(*N*-methylimidazol-1-yl)methane (BIM)[19] were prepared according to literature procedures. All solvents were degassed prior to use. DMF was freshly distilled under reduced pressure from $MgSO_4$ prior to use.

The positive electrospray mass spectra of the complexes were recorded on a Finnigan/MAT TSQ7000 LCMS mass spectrometer. CI mass spectra were recorded on a Finnigan PolarisQ GCMS/MS ion trap mass spectrometer and LSIMS mass spectra were recorded on a Kratos Analytical Concept ISQ mass spectrometer using an mnba matrix. Infrared spectra (cm^{-1}) were recorded using an ATI Mattson *Genesis Series* FTIR Spectrometer. ^1H and $^{13}C\{^1H\}$ NMR spectra were recorded on Bruker DPX300, DPX400, DPX500 or Varian Gemini 200 spectrometers at 300 K unless otherwise stated. Chemical shifts are internally referenced to residual solvent.

$[Ru(BPM)(CO)_2Cl_2]$ (1a): $[Ru(CO)_2Cl_2]_n$ (99 mg, 0.43 mmol) and BPM (70 mg, 0.44 mmol) were refluxed in MeOH (40 mL) for 30 mins. The yellow solution was cooled to room temperature and the volume reduced in vacuo (to about 5 mL) to afford a pale yellow precipitate. The solid was collected and washed with Et_2O (yield 90 mg, 55%). Recrystallisation by vapour diffusion of $MeNO_2$ and Et_2O at −30 °C afforded pale yellow block crystals. ^1H NMR (200 MHz, [D$_6$]acetone): δ = 6.63 (t, $^3J_{H\text{-}H}$ = 2.50 Hz, 2 H, pz-H), 7.26 (br. s, 2 H, CH_2), 8.16 (d, $^3J_{H\text{-}H}$ = 2.30 Hz, 4 H, pz-H), 8.24 (d, $^3J_{H\text{-}H}$ = 2.20 Hz, 4 H, pz-H) ppm. $^{13}C\{^1H\}$ NMR (100 MHz, [D$_6$]acetone): δ = 63.4 (CH_2), 108.5 (C4), 135.3 (C5), 147.2 (C3), 196.4 (CO) ppm. CI-MS: *m*/*z* = 376 [M^+; $^{101}Ru(^{12}C_7N_4H_9)(^{12}CO)_2{}^{35}Cl_2$], 348 [M − CO; $^{101}Ru(^{12}C_7N_4H_9)(^{12}CO)^{35}Cl_2$], 320 [$M^+$ − 2CO; $^{101}Ru(^{12}C_7N_4H_9)^{35}Cl_2$], 285 [$M^+$ − 2CO-Cl; $^{101}Ru(^{12}C_7N_4H_9)^{35}Cl$], 250 [$M^+$ − 2CO − 2Cl; $^{101}Ru(^{12}C_7N_4H_9)$] 148 (L). $C_9H_8Cl_2N_4O_2Ru$ (376.18) calcd. C 28.74, H 2.14, N 14.90; found C 28.95, H 2.04, N 14.89.

$[Ru(dmBPM)(CO)_2Cl_2]$ (2): Procedure as above using dmBPM (yield 54 mg, 30%). Recrystallisation by vapour diffusion of $MeNO_2$ and Et_2O at −30 °C afforded pale yellow block crystals. ^1H NMR (500 MHz, [D$_8$]THF, −28 °C): δ = 2.48 (s, 6 H, pz-CH_3), 2.63 (s, 6 H, pz-CH_3), 6.15 (s, 2 H, pz-H), 6.20 (d, $^2J_{H\text{-}H}$ = 15.09 Hz, 1 H, CH_2), 7.53 (d, $^2J_{H\text{-}H}$ = 15.09 Hz, 1 H, CH_2) ppm. ^1H NMR (500 MHz, [D$_8$]THF, 27 °C): δ = 2.46 (s, 6 H, pz-CH_3), 2.63 (s, 6 H, pz-CH_3), 6.09 (s, 2 H, pz-H) ppm. $^{13}C\{^1H\}$ NMR (75 MHz, [D$_8$]THF, 27 °C): δ = 10.8, 15.5, 56.3, 108.8, 142.7, 155.3, 197.1 (C≡O) ppm. CI MS: *m*/*z* = 431 [M^+; $^{101}Ru(^{12}C_{11}N_4H_{16})(^{12}CO)_2{}^{35}Cl_2$], 403 [$M^+$ − CO; $^{101}Ru(^{12}C_{11}N_4H_{16})(^{12}CO)^{35}Cl_2$], 375 [$M^+$ − 2CO; $^{101}Ru(^{12}C_{11}N_4H_{16})^{35}Cl_2$], 340 [$M^+$ − 2CO − Cl; $^{101}Ru(^{12}C_{11}N_4H_{16})^{35}Cl$], 305 [$M^+$ − 2CO − 2Cl; $^{101}Ru(^{12}C_{11}N_4H_{16})$], 204 [L; $^{12}C_{11}N_4H_{16}$]. $C_{13}H_{16}Cl_2N_4O_2Ru$ (432.27): calcd. C 36.11, H 3.73, N 12.97; found C 36.04, H 3.76, N 12.86.

$[Ru(BIM)(CO)_2Cl_2]$ (3): Procedure as above using BIM (yield 197 mg, 55%). Recrystallisation from $MeNO_2$ at −30 °C afforded pale yellow block crystals. ^1H NMR (300 MHz, CD_3NO_2, 27 °C): δ = 6.16 (s, 6 H, CH_3), 6.77 (s, 2 H, CH_2), 8.65 (d, $^3J_{H\text{-}H}$ = 1.11 Hz, 2 H, mim-H), 8.81 (d, $^3J_{H\text{-}H}$ = 1.50 Hz, 2 H, mim-H) ppm. $^{13}C\{^1H\}$ NMR (75 MHz, CD_3NO_2, 27 °C): δ = 23.9, 34.6, 123.8, 130.7, 144.1, 198.4 ppm. CI-MS: *m*/*z* = 375 [M^+ − CO;

$^{101}Ru(^{12}C_9N_4H_{12})(CO)^{35}Cl_2]$, 347 [$M^+$ − 2CO; $^{101}Ru(^{12}C_9N_4H_{12})^{35}Cl_2]$, 312 [$M^+$ − 2CO − Cl; $^{101}Ru(^{12}C_9N_4H_{12})^{35}Cl]$, 176 [$M^+$ − 2CO − 2Cl − Ru; $^{12}C_9N_4H_{12}$]. $C_{11}H_{12}Cl_2N_4O_2Ru$ (404.22): calcd. C 32.69, H 2.99, N 13.86; found C 32.76, H 2.90, N 13.80.

[Ru(BPM)(CO)$_2$Br$_2$] (1b): $[Ru(CO)_2Cl_2]_n$ (202 mg, 0.87 mmol) and KBr (1.0 g, 8.40 mmol) were refluxed in degassed MeOH (40 mL) for 3.5 hours. BPM (147 mg, 0.99 mmol) was then added to the orange solution and the reaction was refluxed for a further 30 mins. The orange solution was cooled to room temperature affording a colourless precipitate which was collected by filtration. The solvent of the filtrate was removed in vacuo and the resulting orange solid was isolated and washed with MeOH (184 mg, 50%). ^{1}H NMR (200 MHz, [D$_6$]acetone, 27 °C): δ = 6.64 (t, $^3J_{H\text{-}H}$ = 2.58 Hz, 2 H, pz-H), 7.29 (br. s, 2 H, CH_2), 8.20 (d, $^3J_{H\text{-}H}$ = 2.34 Hz, 4 H, pz-H), 8.25 (d, $^3J_{H\text{-}H}$ = 2.06 Hz, 4 H, pz-H) ppm. $^{13}C\{^1H\}$ NMR (50 MHz, [D$_6$]acetone, 27 °C): δ = 64.19 (CH_2), 108.83 (C4), 135.76 (C5),148.45 (C3), 197.72 (CO) ppm. LSIMS: *m*/*z* = 466 [M^+; $^{101}Ru(^{12}C_7N_4H_9)(^{12}CO)_2{}^{80}Br_2]$, 438 [$M^+$ − CO; $^{101}Ru(^{12}C_7N_4H_9)(^{12}CO)^{80}Br_2]$, 410 [$M^+$ − 2CO) [$^{101}Ru(^{12}C_7N_4H_9)^{80}Br_2$ 410], 386 [M^+ − Br; $^{101}Ru(^{12}C_7N_4H_9)(^{12}CO)_2{}^{80}Br_2]$, 358 [$M^+$ − CO − Br; $^{101}Ru(^{12}C_7N_4H_9)(^{12}CO)^{80}Br]$. $C_9H_8Br_2N_4O_2Ru$ (465.06): calcd. C 23.24, H 1.73, N 12.05; found C 23.44, H 1.78, N 12.01.

[Ru(BPM)$_2$(CO)Cl][BPh$_4$] (4): Method 1. $RuCl_3{\cdot}3H_2O$ (100 mg, 0.48 mmol) and BPM (123 mg, 0.83 mmol) were refluxed in DMF for 8 hours. The reaction mixture was cooled, $NaBH_4$ (2.62 mg, 0.77 mmol) was added and the reaction stirred for 1 hour. The solution was then cooled and the volume of solvent reduced to about 5 mL. Et_2O was then added to the solution resulting in an off-white precipitate which was collected and washed with Et_2O. The off-white compound was recrystallised from acetone and Et_2O (89 mg, 15%). NMR assignments refer to the numbering given in Figure 3. ^{1}H NMR (500 MHz, [D$_6$]acetone, −23 °C): δ = 5.92 (d, $^3J_{H\text{-}H}$ = 2.36 Hz, H*r*), 6.25 (d, $^3J_{H\text{-}H}$ = 2.13 Hz, H*h*), 6.29 (d, $^3J_{H\text{-}H}$ = 2.52, $^3J_{H\text{-}H}$ = 2.60 Hz, H*q*), 6.40 (t, $^3J_{H\text{-}H}$ = 2.36 Hz, H*g*), 6.63 (d, $^3J_{H\text{-}H}$ = 14.66 Hz, H*n*), 6.70 (t, $^3J_{H\text{-}H}$ = 2.60 Hz, H*l*), 6.71 (t, $^3J_{H\text{-}H}$ = 2.44 Hz, H*b*), 6.77 (t, BPh_4), 6.92 (t, BPh_4), 7.11 (d, $^3J_{H\text{-}H}$ = 13.79 Hz, H*d*), 7.24 (d, $^3J_{H\text{-}H}$ = 14.98 Hz, H*o*), 7.32 (t, BPh_4), 7.63 (d, $^3J_{H\text{-}H}$ = 13.87 Hz, H*e*), 8.09 (d, $^3J_{H\text{-}H}$ = 2.21 Hz, H*a*), 8.14 (d, $^3J_{H\text{-}H}$ = 2.13 Hz, H*k*), 8.23 (d, $^3J_{H\text{-}H}$ = 3.00 Hz, H*p*), 8.29 (t, $^3J_{H\text{-}H}$ = 2.68, $^3J_{H\text{-}H}$ = 3.00 Hz, H*f*), 8.38 (d, $^3J_{H\text{-}H}$ = 2.68 Hz, H*m*), 8.41 (d, $^3J_{H\text{-}H}$ = 2.84 Hz, H*c*) ppm. ^{13}C NMR (125 MHz, [D$_6$]acetone, −23 °C): δ = 64.1 (C*d,e*), 64.7 (C*o,n*), 109.1 (C*g*), 109.3 (C*l*), 109.6 (C*q*), 110.0 (C*b*), 122.9 (BPh_4), 126.6 (BPh_4), 135.8 (C*f*), 136.8 (C*p*), 137.4 (BPh_4), 137.4 (C*m*), 137.7 (C*c*), 144.0 (C*h*), 145.7 (C*r*), 147.2 (C*k*), 149.5 (C*a*) ppm. IR (nujol): $\tilde{\nu}$ = 1970 cm^{-1} (C≡O str). $^+$ES MS: *m*/*z* = 460.9 [M^+; $^{101}Ru(^{12}C_7N_4H_9)_2(^{12}CO)^{35}Cl]$. $C_{39}H_{36}BClN_8ORu$ (780.13): calcd. C 60.04, H 4.65, N 14.37; found C 60.16, H 4.99, N 14.07.

Method 2. A mixture of $[Ru(BPM)(CO)_2Cl_2]$ (103 mg, 0.452 mmol) and Me_3NO (90 mg, 2.00 mmol) in MeCN was refluxed for 30 mins. BPM (150 mg, 1.01 mmol) was then added to the reaction mixture which was then refluxed for a further 16 hours. The yellow solution was allowed to cool slightly, after which $NaBPh_4$ (459 mg, 1.34 mmol) was added. A pale yellow precipitate was formed on cooling, which was collected and washed with Et_2O (132 mg, 37%). Suitable crystals for X-ray diffraction were grown from $MeNO_2/Et_2O$.

Catalysis Reactions

Coupling of HC≡CPh and HSiEt$_3$: *Typical reaction*. Phenylacetylene (25 mg, 0.25 mmol), triethylsilane (29 mg, 0.25 mmol), [Ru(BIM)(CO)$_2$Cl$_2$] (5.3 mg, 14.1 μmol) and [D$_3$]$MeNO_2$ were sealed in an NMR tube. The mixture was heated to 60 °C and the reaction was monitored using NMR spectroscopy. After one week, no coupling product was observed.

Coupling of Acetophenone and 1-Pentene: *Typical reaction*. Acetophenone (35 mg, 0.29 mmol), 1-pentene (17 mg, 0.25 mmol), [Ru(dmBPM)(CO)$_2$Cl$_2$] (5.7 mg, 12.9 μmol) and [D$_8$]THF were sealed in an NMR tube. The mixture was heated to 60 °C and the reaction was monitored using NMR spectroscopy. After one week, no coupling product was observed.

Cyclisation of *cis*-3-Methyl-2-pentene-4-yn-1-ol to 2,3-Dimethylfuran: *Typical reaction*. *cis*-3-Methyl-2-pentene-4-yn-1-ol (63 mg, 0.66 mmol), [Ru(BIM)(CO)$_2$Cl$_2$] (2.8 mg, 6.9 μmol) and [D$_8$]THF were sealed in an NMR tube. The mixture was heated to 60 °C and the reaction was monitored using NMR spectroscopy. After one week, no cyclisation product was observed.

Cyclisation of 4-Pentynoic acid to γ-Methylene-γ-butyrolactone: *Typical reaction*. 4-Pentynoic acid (58 mg, 0.59 mmol), [Ru(BIM)(CO)$_2$Cl$_2$] (2.4 mg, 5.9 μmol) and [D$_8$]THF were sealed in an NMR tube. The mixture was heated to 60 °C and the reaction was monitored using NMR spectroscopy. After one week, no cyclisation product was observed.

Parahydrogen Experiments: Hydrogen enriched in the *para* spin state was prepared by cooling H_2 to 77 K over a paramagnetic catalyst. An atmosphere of H_2 equivalent to ca. 3 atm. pressure at 298 K was introduced into the resealable NMR tube on a high vacuum line already containing the sample and deuterated solvent. The samples were thawed immediately prior to use and introduced into the NMR spectrometer at the pre-set temperature.

X-ray diffraction studies

Data collection used a Bruker SMART 1000 CCD diffractometer equipped with an Oxford System Cryostream low-temperature attachment, with graphite monochromated Mo-K_α radiation (λ_{max} = 0.71073 Å), *T* = 173 K ([Ru(dmBPM)(CO)$_2$Cl$_2$]) or 293 K ([HBIM][BPh$_4$] and [Ru(BPM)$_2$(CO)Cl][BPh$_4$]). Data integration and reduction were performed with SAINT and XPREP.[37] A Gaussian absorption correction was applied to the data of [Ru(BPM)$_2$(CO)Cl][BPh$_4$] and [HBIM][BPh$_4$].[37,38] A semi-empirical correction was determined with SADABS[39] for [Ru(dmBPM)(CO)$_2$Cl$_2$]. Molecular projections of all structures were generated with Ortep-3.[40] All structures were solved by direct methods using SHELXS-97[41] and structure refinement was done using SHELXL-97.[42] All non-hydrogen sites for the three structures were treated anisotropically. All hydrogen atoms were calculated and refined isotropically. H(20) in [HBIM][BPh$_4$] was modelled with isotropic displacement parameters.

CCDC-184163 (**2**), -184164 (**4**) and -184165 ([HBIM][BPh$_4$]) contains the supplementary crystallographic data for this paper. These data can be obtained free of charge at www.ccdc.cam.ac.uk/conts/retrieving.html [or from the Cambridge Crystallographic Data Centre, 12, Union Road, Cambridge CB2 1EZ, UK; fax: (internat.) +44−1223/336−033; E-mail: deposit@ccdc.cam.ac.uk].

Acknowledgments

We thank the ARC for funding and an RSC Journal Travel Grant for funding a visit to the University of York (VAT). We thank Johnson−Matthey for the loan of $RuCl_3{\cdot}xH_2O$. We also thank Simon Duckett (University of York) for the loan of his NMR probe for in situ photolysis, and Sarah Wren for her assistance.

[1] M. A. Bennett, in *Comprehensive Organometallic Chemistry* (Eds.: G. Wilkinson, F. G. A. Stone, E. W. Abel), Pergamon Press, **1982**, Vol 4, Ch 32.9, p. 931−967.
[2] E. J. Moore, W. R. Pretzler, T. J. O'Connell, J. Harris, L. LaBounty, L. Chou, S. S. Grimmer, *J. Am. Chem. Soc.* **1992**, *114*, 5888−5890.
[3] S. Murai, F. Kakiuchi, S. Sekine, Y. Tanaka, A. Kamatani, M. Sonoda, N. Chatani, *Nature* **1993**, *366*, 529−531.
[4] T. Kondo, K. Kodoi, T. Mitsudo, Y. Watanabe, *J. Chem. Soc., Chem. Commun.* **1994**, 755−756.
[5] B. Seiller, B. Bruneau, P. H. Dixneuf, *J. Chem. Soc., Chem. Commun.* **1994**, 493−494.
[6] D. St. C. Black, G. B. Deacon, N. C. Thomas, *Aust. J. Chem.* **1982**, *35*, 2445−2453.
[7] S. Chardon-Noblat, A. Deronzier, R. Ziessel, D. Zsoldos, *Inorg. Chem.* **1997**, *36*, 5384−5389.
[8] D. St. C. Black, G. B. Deacon, N. C. Thomas, *Transition Met. Chem.* **1980**, *5*, 317−318.
[9] J.-M. Lehn, R. Ziessel, *J. Organomet. Chem.* **1990**, *382*, 157−173.
[10] C. Yin, Z. Xu, S.-Y. Yang, S. M. Ng, K. Y. Wong, Z. Lin, C. P. Lau, *Organometallics* **2001**, *20*, 1216−1222.
[11] M. G. Richmond, *J. Organomet. Chem.* **1993**, *457*, 121−165.
[12] J. M. Kelly, J. G. Vos, *Angew. Chem. Int. Ed. Engl.* **1982**, *21*, 628−629; *Angew. Chem.* **1982**, *94*, 644−645.
[13] J. G. Haasnoot, W. Hinrichs, O. Weir, J. Vos, *Inorg. Chem.* **1986**, *25*, 4140−4143.
[14] H. Ishida, K. Tanaka, M. Morimoto, T. Tanaka, *Organometallics* **1986**, *5*, 724−730.
[15] C. Ungermann, V. Landis, S. A. Moya, H. Cohen, H. Walker, R. G. Pearson, R. G. Rinker, P. C. Ford, *J. Am. Chem. Soc.* **1979**, *101*, 5922−5929.
[16] P. C. Ford, R. G. Rinker, C. Ungermann, R. M. Laine, V. Landis, S. A. Moya, *J. Am. Chem. Soc.* **1978**, *100*, 4595−4597.
[17] S. Luukkanen, P. Homanen, M. Haukka, T. A. Pakkanen, A. Deronzier, S. Chardon-Noblat, D. Zsoldos, R. Ziessel, *Appl. Catal., A* **1999**, *185*, 157−164.
[18] S. Julia, J. M. del Mazo, L. Avila, J. Elguero, *Org. Prep. Proced. Int.* **1984**, *16*, 299−307.
[19] P. K. Byers, A. J. Canty, *Organometallics* **1990**, *9*, 210−220.
[20] S. Trofimenko, *Acc. Chem. Res.* **1971**, *4*, 17−22.
[21] A. J. Canty, C. V. Lee, *Organometallics* **1982**, *1*, 1063−1066.
[22] S. Trofimenko, *The Coordination Chemistry of Pyrazole-Derived Ligands* (Ed.: S. J. Lippard), J. Wiley and Sons, NY, **1986**, Vol 34, p. 115−210.
[23] F. Mani, *Inorg. Nucl. Chem. Lett.* **1979**, *15*, 297−302.
[24] [24a] A. Llobet, M. E. Curry, H. T. Evans, T. J. Meyer, *Inorg. Chem.* **1989**, *28*, 3131−3137. [24b] A. Llobet, P. Doppelt, T. J. Meyer, *Inorg. Chem.* **1988**, *27*, 514−520.
[25] A. Llobet, D. J. Hodgson, T. J. Meyer, *Inorg. Chem.* **1990**, *29*, 3760−3766.
[26] M. Fajardo, A. de la Hoz, E. Diez-Barra, F. A. Jalon, A. Otero, A. Rodriguez, J. Tejeda, D. Belletti, M. Lanfranchi, M. A. Pellinghelli, *J. Chem. Soc., Dalton Trans.* **1993**, 1935−1939.
[27] S. Elgafi, L. D. Field, B. A. Messerle, T. W. Hambley, P. Turner, *J. Chem. Soc., Dalton Trans.* **1997**, 2341−2345.
[28] S. Elgafi, L. D. Field, B. A. Messerle, I. E. Buys, T. W. Hambley, *J. Organomet. Chem.* **1997**, *538*, 119−128.
[29] L. P. Wu, Y. Yamagiwa, I. Ino, K. Sugimoto, T. Kuroda-Sowa, T. Kamikawa, M. Munakata, *Polyhedron* **1999**, *18*, 2047−2053.
[30] L. D. Field, B. A. Messerle, L. P. Soler, I. E. Buys, T. W. Hambley, *J. Chem. Soc., Dalton Trans.* **2001**, 1959−1965.
[31] M. Haukka, M. Ahlgrén, T. A. Pakkanen, *J. Chem. Soc., Dalton Trans.* **1996**, 1927−1933.
[32] G. B. Deacon, J. M. Patrick, B. W. Skelton, N. C. Thomas, A. H. White, *Aust. J. Chem.* **1984**, *37*, 929−945.
[33] J. M. Clear, J. M. Kelly, C. M. O'Connell, J. G. Vos, C. J. Cardin, S. R. Costa, *J. Chem. Soc., Chem. Commun.* **1980**, 750−751.
[34] M. Haukka, J. Kiviaho, M. Ahlgrén, T. A. Pakkanen, *Organometallics* **1995**, *14*, 825−833.
[35] A. Macchioni, G. Bellachioma, G. Cardaci, V. Gramlich, H. Rügger, S. Terenzi, L. M. Venanzi, *Organometallics* **1997**, *16*, 2139−2145.
[36] M. J. Cleare, W. P. Griffith, *J. Chem. Soc., A* **1969**, 372−380.
[37] Bruker SMART, SAINT and XPREP: Area detector control and data integration and reduction software; Bruker Analytical X-ray Instruments, Inc., Madison, WI, 1995.
[38] P. Coppens, L. Leiserowitz, D. Rabinovich, *Acta Crystallogr.* **1965**, *18*, 1035−1038.
[39] [39a] R. H. Blessing, *Acta Crystallogr., Sect. A* **1995**, *51*, 33−38. [39b] G. M. Sheldrick, SADABS: Empirical absorption correction program for area detector data, University of Göttingen, Germany, 1996.
[40] Ortep-3 for Windows: L. J. Farrugia, *J. Appl. Cryst.* **1997**, *30*, 565−566.
[41] G. M. Sheldrick, SHELXS-97: *Program for crystal structure solution*, University of Göttingen, 1996.
[42] G. M. Sheldrick, SHELX97: *Program for crystal structure refinement*, University of Göttingen, 1996.

Received June 11, 2002
[I02307]

Evolution of Defects in the Bulk Structure of MoO_3 During the Catalytic Oxidation of Propene

Thorsten Ressler,*[a] Julia Wienold,[a] Rolf E. Jentoft,[a] and Frank Girgsdies[a]

Keywords: Molybdenum / EXAFS spectroscopy / X-ray diffraction / Heterogeneous catalysis / Oxidation

The evolution of characteristic defects in the bulk structure of MoO_3 under propene oxidation conditions was investigated by in situ X-ray absorption spectroscopy and X-ray diffraction. Under the reaction conditions employed (273 K to 773 K, and propene to oxygen ratios from 1:1 to 1:5), orthorhombic MoO_3 remains the only crystalline phase detected by XRD. The starting temperature for the reaction of propene and oxygen in the presence of MoO_3 coincides with the temperature at which reduction of MoO_3 begins in He, H_2 and propene ($\approx$ 620 K). At temperatures below 720 K, and independent of the atmosphere used, partial reduction of MoO_3 is observed resulting in the formation of "$Mo_{18}O_{52}$" type defects in the layer structure of α-MoO_3. At temperatures above 720 K, and under oxygen or in an oxidizing atmosphere, the "$Mo_{18}O_{52}$" type defects are reoxidized to MoO_3. Evidently, the catalytically active molybdenum oxide phase develops under partial oxidation conditions at temperatures below 720 K, and does not possess the undisturbed ideal layer structure of orthorhombic α-MoO_3. The results presented clearly show the necessity and the potential for bulk structural investigations of heterogeneous catalysts under the reaction conditions used. The bulk structure, and particularly the type and number of defects in the material ("real" structure) considerably affect the catalytic properties. Hence, in order to rationally design a most active heterogeneous catalyst, both the structure and reactions of the surface, and the structure, defects, and reactions of the bulk need to be known in detail, and carefully considered.
(© Wiley-VCH Verlag GmbH & Co. KGaA, 69451 Weinheim, Germany, 2003)

Introduction

Molybdenum trioxide, MoO_3, is an active catalyst for the oxidation of propene in the presence of gaseous dioxygen at temperatures above about 600 K. Moreover, MoO_3 constitutes a suitable three-dimensional model system for the more complex molybdenum based mixed oxide catalysts that are employed industrially for various partial oxidation reactions. Hence, the structural features and the catalytic properties of MoO_3 have been investigated in detail over the last five decades in order to reveal structure-activity relationships and to aid the rational design of improved catalyst materials.[1−4] Accordingly, the various steps of the molecular mechanism of the oxidation of propene in the presence of MoO_3 have been suggested to include adsorption of propene on the surface of the catalyst, abstraction of hydrogen, and the formation of an allylic species.[5,6] Subsequently, oxygen from the lattice of MoO_3 is incorporated in the allylic species, forming the partial oxidation product acrolein, or the total oxidation product carbon dioxide. The bulk of the metal oxide is then reoxidized by oxygen from the gas phase ("redox mechanism" or "Mars−van Krevelen mechanism").[7−9]

Although it is assumed that the lattice oxygen of MoO_3 participates in the oxidation of propene, little is known about defects in the regular layer structure of MoO_3 that may form under the reaction conditions, or about the structural properties and the role of these defects in the partial oxidation reactions proceeding on the surface of the MoO_3 catalyst. The question remains, how close is the "real" bulk structure of MoO_3 under the reaction conditions to the "ideal" structure of orthorhombic α-MoO_3?

Under propene oxidation reaction conditions, MoO_3 exhibits a slightly reduced average valence, which, according to the conventional redox mechanism, has to be attributed to different rates for the reduction and the re-oxidation of the molybdenum trioxide.[1] Since molybdenum is known to form a number of well-defined suboxides with average valences between 6.0 (MoO_3) and 4.0 (MoO_2) (i.e. $Mo_{18}O_{52}$, $Mo_{17}O_{47}$, Mo_9O_{26}, Mo_8O_{23}, Mo_5O_{14}, Mo_4O_{11}), it has been speculated that one of these suboxides constitutes the active phase in a molybdenum oxide partial oxidation catalyst. Thus, stoichiometric reduction and oxidation of various molybdenum oxides have been studied extensively in the past, with various attempts to correlate the observations made with the catalytic behavior of the materials investigated.[1] Those studies have proven extremely valu-

[a] Department of Inorganic Chemistry, Fritz-Haber-Institut der MPG,
Faradayweg 4−6, 14195 Berlin, Germany
Fax: (internat.) + 49-(0)30/8413−4405
E-mail: Ressler@fhi-berlin.mpg.de

able to elucidate the evolution of the phase composition and the bulk structure during reduction and oxidation of the molybdenum oxides, and to determine the solid-state kinetics of these reactions. Recently, we were able to show that only $Mo_{18}O_{52}$ is a possible intermediate of the reduction of MoO_3 in propene and the oxidation of MoO_2 in oxygen,[10] while none of the well-defined suboxides were detected during reduction of MoO_3 in hydrogen at temperatures below about 700 K.[11] However, the evolution of the bulk structure of MoO_3 under catalytic reaction conditions and the formation of defects have largely been neglected in the past.

Investigations of the relationships between the structure and the reactivity of a heterogeneous catalyst need to be performed in situ (i.e. under "real" reaction conditions), with simultaneous monitoring of the catalyst structure and the gas phase composition.[12] Naturally, "post mortem" investigations of catalysts at room temperature, in air or in an inert atmosphere, cannot provide unambiguous correlations between the structure and the reactivity of the solid. Only few bulk structural techniques can readily be employed to study an active heterogeneous catalyst under "real" reaction conditions at elevated temperatures ($\geq$ 473 K) and pressures ($\geq$ 1 bar). Due to the low absorbance of hard X-rays (photon energy $\geq$ 5 keV) by gases or window materials, conventional experimental set-ups for X-ray diffraction (XRD) and X-ray absorption spectroscopy (XAS) can easily be combined with suitable environmental cells for catalytic studies. In addition to steady-state investigations, both techniques permit experiments with a suitable time-resolution (approx. 1 min) to monitor the structural evolution of the bulk phases, which can be used to elucidate the solid-state kinetics of the reactions involved.[10,13,14]

XAS and XRD are complementary techniques because together they provide information on the quantitative phase composition of amorphous and crystalline phases, the short-range and long-range order structure of the phases present, the electronic structure, and the crystallite size, microstrain, and morphology. As this data is of paramount importance to reveal structure-reactivity relationships in heterogeneous catalysis, XAS and XRD have been extensively employed under these reaction conditions.[15] However, the evolution of defects in the regular bulk structure of heterogeneous catalysts, and the relationships between the "real" structure of a solid catalyst and its reactivity has received little attention. In the future, new insight into the importance of defects in the "real" structure of solid heterogeneous catalysts, for the catalytic properties of the material can be expected from time-resolved in situ bulk structural investigations.

In this work in situ XAS and XRD combined with mass spectrometry are employed to elucidate the phase compositions, and the long-range and short-range structural evolution of MoO_3 during the temperature-programmed reaction of propene and oxygen. The formation of characteristic defects in the bulk structure of MoO_3 under reaction conditions is described as a function of the reaction temperature and the reducing potential of the gas phase.

Results

In Situ XRD − Evolution of the Long-Range Structure

Figure 1 shows the evolution of XRD patterns measured during the temperature-programmed treatment of MoO_3 in helium in the temperature range 573−773 K, with a heating rate of 0.1 K/min. The onset temperature for the reduction of MoO_3 to form MoO_2 is at about 620 K. At temperatures between 620 K and 720 K only MoO_2 and MoO_3 are detected, whereas at temperatures above 720 K Mo_4O_{11} is formed from a parallel reaction of MoO_3 and MoO_2.[11]

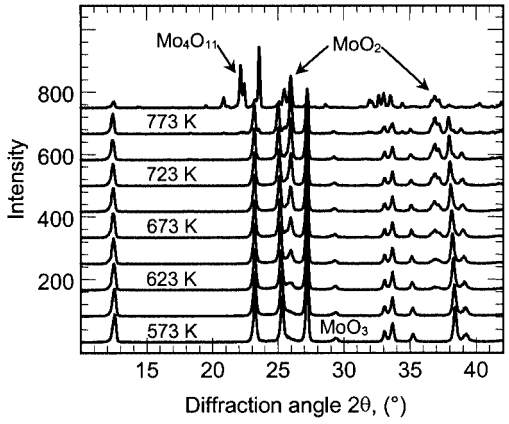

Figure 1. Evolution of XRD patterns during thermal treatment of MoO_3 in helium (573−773 K, about 0.1 K/min). The crystalline phases detected (MoO_3, MoO_2, Mo_4O_{11}) are indicated

During the temperature-programmed treatment of MoO_3 in oxygen (20% in He) in the temperature range 473−773 K with a heating rate of 0.1 K/min, MoO_3 remains the only crystalline phase detected by XRD. The evolution of ratios of integrated intensities of selected *hkl* reflections and the crystallite sizes calculated for these reflections during thermal treatment of MoO_3 in oxygen are shown in Figure 2, part (a) and (b), respectively. While the ratios shown remain nearly constant up to about 620 K, the ratios 110/101 and 020/101 increase substantially between about 620 K and about 700 K, and almost return to their original room temperature value at about 720 K. The ratio 020/110 does not change significantly in the temperature range studied. The apparent crystallite sizes calculated for the 101 and 110 reflections exhibit an increase above 673 K, while the crystallite size calculated for the 002 reflection shows a decrease between 573 K and 673 K. On cooling to room temperature, the crystallite sizes calculated for the *hkl* reflections shown are similar to those determined prior to the temperature treatment. A Williamson−Hall analysis,[16] using selected *hkl* reflections in a 2θ range from 6.0 to 55.0, only shows minor strain in the original MoO_3 materials. A certain anisotropy in the direction of the strain in the MoO_3 lattice can be deduced from the considerable scatter of the individual points in the Williamson−Hall plot obtained. However, the lack of suitable higher-order reflections did not permit a direction-dependent strain analysis. During treatment in oxygen, a slight increase in the strain occurred

at about 620 K, followed by a decrease at about 720 K (inset in Figure 2). This behavior coincides with the deviations observed in the ratios of integrated intensities [Figure 2 (a)].

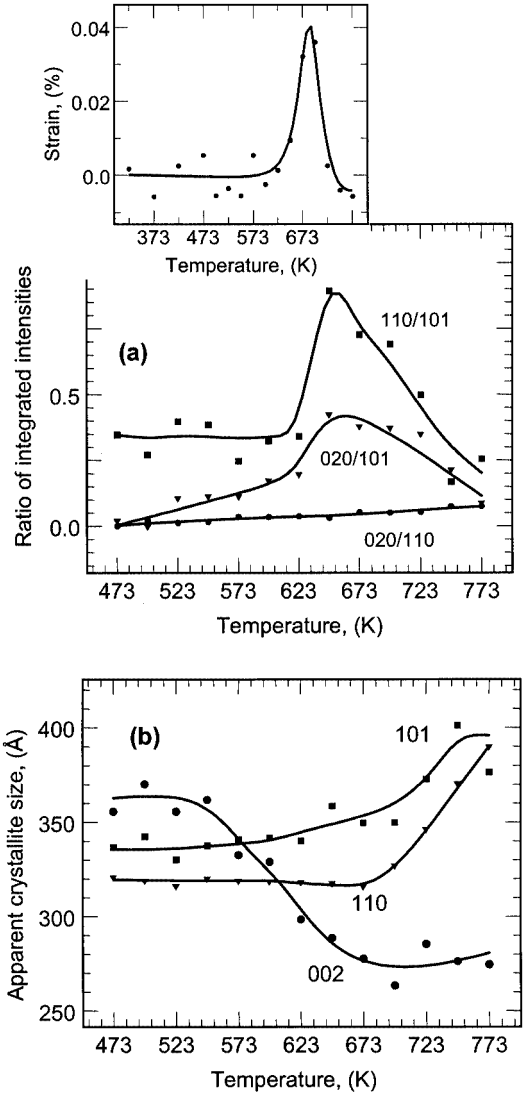

Figure 2. Evolution of ratio of integrated intensities (a) [for MoO_3 at 300 K, initial values are $A(110/101) = 4.6$, $A(020/101) = 1.9$, and $A(020/110) = 0.4$; ratios are arbitrarily displaced on y axis] and particle size (b) of selected *hkl* reflections of MoO_3 during thermal treatment of MoO_3 in oxygen (20% O_2 in He, 473−773 K, about 0.1 K/min). The inset in (a) shows the evolution of strain in the MoO_3 structure obtained from a Williamson−Hall analysis

During the temperature-programmed reaction (TPR) of propene (10 vol-%) and oxygen (10 vol-%) in the presence of MoO_3 from 473 K to 773 K, with a heating rate of 0.1 K/min, MoO_3 remains the only crystalline phase detected by XRD. The evolution of ratios of integrated intensities of selected *hkl* reflections and apparent crystallite sizes calculated for these reflections are shown in Figure 3, part (a) and part (b), respectively. Similar to the treatment in oxygen, the ratio 020/101 increases at temperatures above about 620 K, while the ratio 020/110 remains unaffected. On the other hand, the ratio 020/101 does not decrease above 720 K, but remains at a higher value. The ratio 110/101 continuously decreases between 473 K and 773 K. The apparent crystallite sizes calculated for the 110 and 002 reflections are similar to those observed during the treatment in oxygen [Figure 2, part (b)]. A Williamson−Hall analysis, using selected *hkl* reflections in the 2θ range from 6.0 to 55.0 of the diffraction patterns measured during the TPR of propene and oxygen, shows a considerable increase in the strain at temperatures above 620 K [inset in Figure 3, (a)]. This behavior coincides with the deviations observed in the ratios of integrated intensities [Figure 3, (a)].

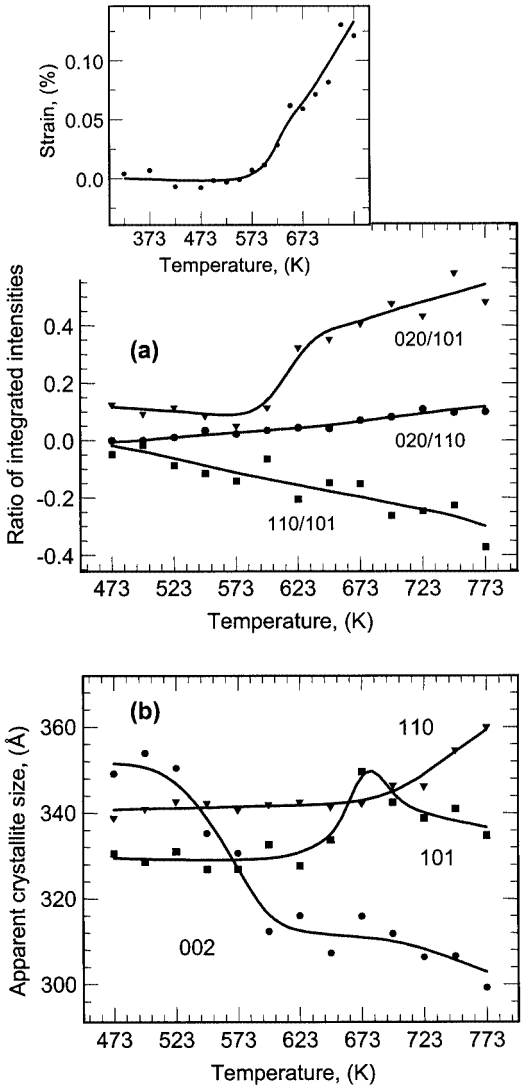

Figure 3. Evolution of ratio of integrated intensities (a) (for clarity, ratios are arbitrarily displaced on *y* axis) and particle size (b) of selected *hkl* reflections of MoO_3 during the temperature-programmed reaction of propene and oxygen (10% O_2 and 10% propene in He, 473−773 K, about 0.1 K/min). The inset in (a) shows the evolution of strain in the MoO_3 structure obtained from a Williamson−Hall analysis

In Situ XAFS − Evolution of Average Valence and Short-Range Structure

The development of the Mo-*K* edge position seen in the time-resolved XAFS spectra measured during the treatment

of MoO_3 in oxygen, and during the TPR of propene (10 vol-%) and oxygen (ratios 1:1, 1:3, and 1:5) in the presence of MoO_3 (473−773 K, 10 K/min), is depicted in Figure 4. The large number of spectra measured in the energy-dispersive mode permits reliable interpretation of small changes (< 0.1 eV) in the Mo-*K* edge position. The shift of the Mo-*K* edge position towards smaller photon energy at a temperature of about 620 K indicates the reduction of molybdenum. According to the calibration curve shown in ref.10,[10] a Mo-*K* edge shift of 0.2 eV corresponds to a difference in average valence of about 0.033. The degree of reduction under the reaction conditions for temperatures between 620 K and 720 K is related to the reducing potential of the gas phase (1:1 > 1:3 > 1:5). For the treatment of MoO_3 at temperatures above 720 K in oxygen, and in propene and oxygen with a ratio of 1:5, a shift of the Mo-*K* edge position towards higher photon energies indicates a re-oxidation of the partially reduced MoO_3. Conversely, for the reaction of propene and oxygen (ratios 1:1 and 1:3) in the presence of MoO_3, no shift of the Mo-*K* edge to higher photon energies is observed and the molybdenum oxide phase remains partially reduced at temperatures up to 773 K.

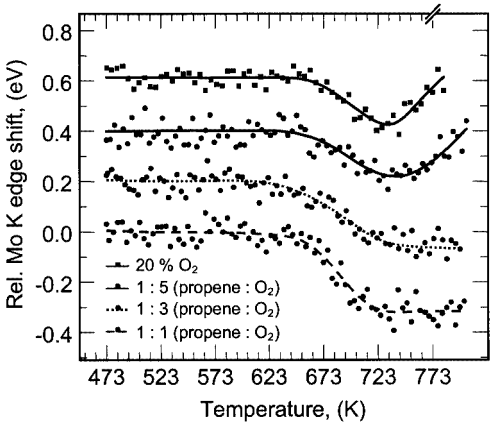

Figure 4. Evolution of Mo-*K* edge position (relative to the edge position of MoO_3, and displaced for clarity) during thermal treatment of MoO_3 in oxygen (20% in He) and during the temperature-programmed reaction of propene and oxygen in the presence of MoO_3 (10% O_2 and 10% propene in He) (473−773 K, 10 K/min, held at 773). The three different ratios of oxygen and propene employed are indicated

A principal component analysis of the XAFS spectra measured during the TPR did not afford conclusive results on the identity of the molybdenum oxide phases present. However, in addition to the temperature effect on the near-edge spectra, at least two primary components appear to be necessary to reconstruct the experimental spectra. Furthermore, the evolution of the mixing coefficients of the least important primary component shows a behavior similar to the Mo-*K* edge-shift data depicted in Figure 4.

The evolution of Mo-*K* near-edge spectra measured in the conventional XAFS mode during the TPR of propene (10%) and oxygen (10%) (300−773 K, 5 K/min) in the presence of MoO_3, together with the corresponding evolution of the average molybdenum valence, is depicted in Figure 5, part (a). Besides temperature broadening, no significant changes to the shape of the XAFS spectrum of MoO_3 occur under the reaction conditions. However, a detailed analysis of the Mo-*K* edge position again reveals a slight reduction of the molybdenum oxide at temperatures above about 620 K. Using a previously reported calibration to transform the edge-shift into average valence,[10] results in an average valence of about 5.94 for the molybdenum oxide under the reaction conditions, at temperatures above 673 K. If the type of defects formed under the TPR conditions were consistent with an "$Mo_{18}O_{52}$" type shear structure, an average valence of 5.94 would correspond to a phase composition of 75% MoO_3 and 25% $Mo_{18}O_{52}$. The evolution of the gas phase composition during the TPR of oxygen and propene in the presence of MoO_3 in a ratio of 1:1 is depicted in Figure 5, part (b). The onset temperature for the reaction is about about 620 K, producing both the partial oxidation product, acrolein and the total oxidation product, carbon dioxide. The onset temperature for the oxidation of propene was the same for all ratios of propene to oxygen measured (ratios 1:1 > 1:3 > 1:5).

Since the mass spectrometer used for the XRD and XAS experiments was not calibrated, only qualitative catalysis data can be provided. However, at 713 K, the conversion of propene in the presence of MoO_3 has been reported to be 7%, with an acrolein yield of 2%,[5] and it is assumed that the catalytic behavior of the material used here is similar. A comparison of the ratio of the ion currents of CO_2 and acrolein measured during the TPR indicates a minimum selectivity towards acrolein at about 673 K (Figure 6). This minimum selectivity is most pronounced for a ratio of propene and oxygen of 1:1.

The evolution of the Fourier-transformed Mo-*K* edge $\chi(k)$ of MoO_3 during the TPR of propene and oxygen (ratio 1:1) is depicted in Figure 7. A continuous decrease in amplitude of the higher Mo−Mo backscattering shells can be seen. As reported previously, $Mo_{18}O_{52}$ constitutes a suitable reference phase for the type of structural defects observed during reduction of MoO_3 in propene.[10] A schematic representation of the structures of orthorhombic α-MoO_3 (*Pbnm*, a = 3.936 Å, b = 13.855 Å, c = 3.696 Å)[17] and $Mo_{18}O_{52}$ ($P\bar{1}$, a = 8.145 Å, b = 11.890 Å, c = 21.230 Å, α = 102.7 °, β = 67.8 °, γ = 110.0 °)[18] is depicted in Figure 8.

The $Mo_{18}O_{52}$ structure is derived from the MoO_3 structure by crystallographic-shear operations. Hence, both contain a van der Waals gap between the individual layers, in contrast to other molybdenum oxides possessing crystallographic-shear structures such as Mo_8O_{23} and Mo_9O_{26}.[19] A comparison of the radial distribution functions of MoO_3 and $Mo_{18}O_{52}$ for a 1 nm cluster is shown in Figure 9.

The magnitude of the Fourier-transformed (FT) XAFS $\chi(k)$ of $Mo_{18}O_{52}$ will be considerably smaller than that of MoO_3 as a result of the large number of slightly different distances in the structure of $Mo_{18}O_{52}$.

In order to simulate the influence of adding certain amounts of $Mo_{18}O_{52}$ to MoO_3 on the FT[$\chi(k)$] of the re-

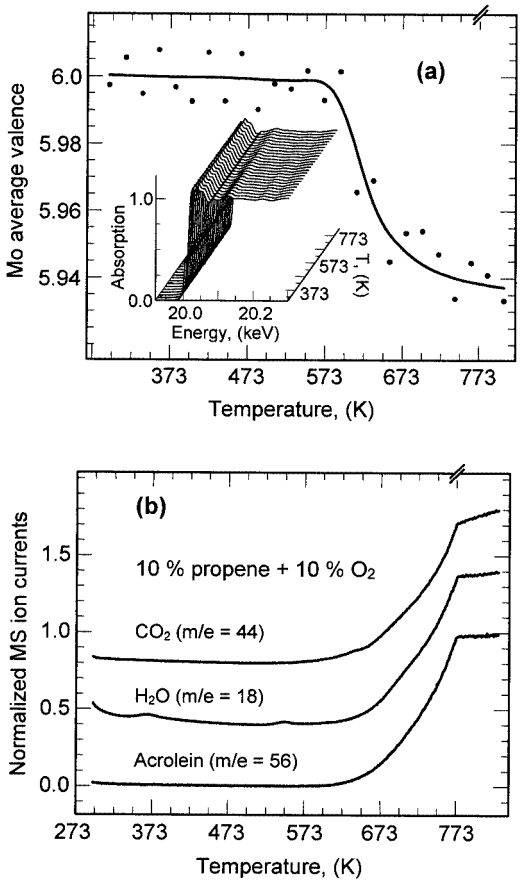

Figure 5. (a) Evolution of Mo-*K* edge position (relative to the edge position of MoO_3, and displaced for clarity) during the temperature-programmed reaction of propene and oxygen in the presence of MoO_3 (10% O_2 and 10% propene in He) (300−773 K, 5 K/min, held at 773) (inset shows evolution of XANES spectra during the TPR). (b) Evolution of the corresponding gas phase composition [CO_2 (*m/e* = 44), H_2O (*m/e* = 18), acrolein (*m/e* = 56)] during the temperature-programmed reaction of propene and oxygen

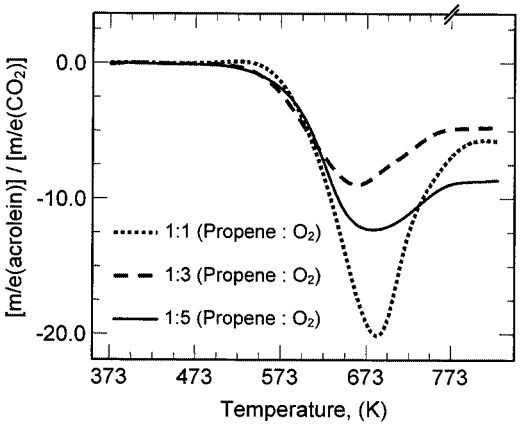

Figure 6. Ratio of the ion currents of CO_2 (*m/e* = 44) and acrolein (*m/e* = 56) measured the during temperature-programmed reaction of propene (10%) and oxygen (10% [dotted], 30% [solid], 50% [dashed]) in the presence of MoO_3 (values are displaced on the *y* axis)

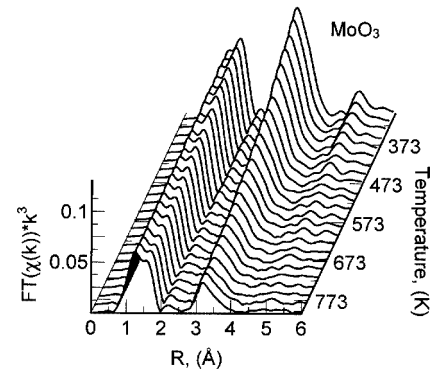

Figure 7. Evolution of Fourier-transformed $\chi(k)$ of MoO_3 during the temperature programmed reaction of propene and oxygen (10% O_2 and 10% propene in He) (300−773 K, 5 K/min, held at 773) (note inverse temperature scale) (Figure 5)

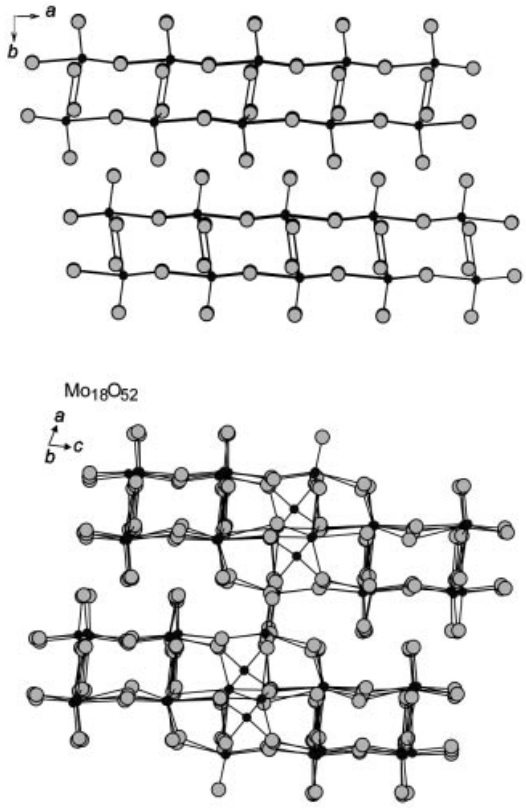

Figure 8. Schematic representations of the layer structures of MoO_3 (projection parallel to 001) and $Mo_{18}O_{52}$ (arbitrary projection for comparison with MoO_3)

sulting mixture, numerical mixtures of the experimental $\chi(k)$ of MoO_3 and $Mo_{18}O_{52}$ were calculated. The evolution of the Fourier-transformed $\chi(k)$ of these mixtures of MoO_3 and $Mo_{18}O_{52}$ is shown in Figure 10. Evidently, adding $Mo_{18}O_{52}$ to MoO_3 results in a decrease in the amplitude of all backscattering shells, in particular of the higher Mo−Mo shells. However, even for concentrations of $Mo_{18}O_{52}$ as large as 40%, the resulting FT[$\chi(k)$] strongly resembles that of MoO_3.

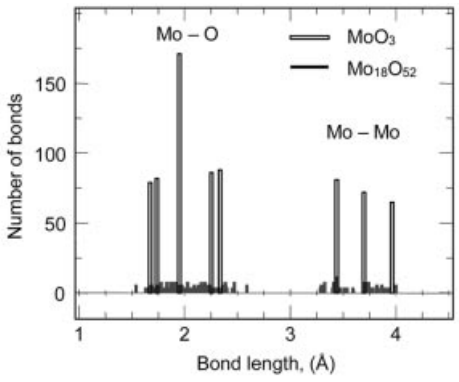

Figure 9. Comparison of radial distribution functions of MoO_3 and $Mo_{18}O_{52}$ calculated for cluster sizes of about 10 Å in both structures (≈ 330 atoms, about 670 Mo−O and Mo−Mo bonds)

Table 1. Structural parameters [coordination number (CN) and distance R of Mo−O and Mo−Mo coordination shells] of a MoO_3 model structure (*Pbnm*, a = 3.936 Å, b = 13.855 Å, c = 3.696 Å) obtained from a refinement of the model structure to the experimental XAFS functions $\chi(k)$ of MoO_3 (N_{ind} = 25, N_{free} = 13, 8 single scattering paths and 11 multiple scattering paths). Additional parameters refined are Θ(O) = 1383 K, Θ(Mo) = 442 K, E_0 = −1.5 eV (Θ: Debye temperature). The fit residual is 4.6

Shell	CN	R_{model}, (Å)	R_{MoO3}, (Å)	ΔR, (Å)	Weight (%)
Mo−O	1	1.671	1.683	0.012	71
Mo−O	1	1.735	1.710	−0.025	69
Mo−O	2	1.948	1.938	−0.01	100
Mo−O	1	2.251	2.227	−0.024	36
Mo−O	1	2.332	2.349	0.017	32
Mo−Mo	2	3.438	3.421	−0.017	91
Mo−Mo	2	3.696	3.693	−0.003	75
Mo−Mo	2	3.963	3.946	0.017	62

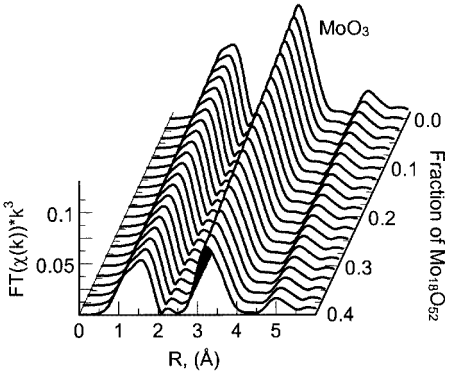

Figure 10. Evolution of Fourier-transformed $\chi(k)$ of calculated mixtures of experimental $\chi(k)$ of MoO_3 and $Mo_{18}O_{52}$, with increasing concentration of $Mo_{18}O_{52}$ (100% to 60% MoO_3)

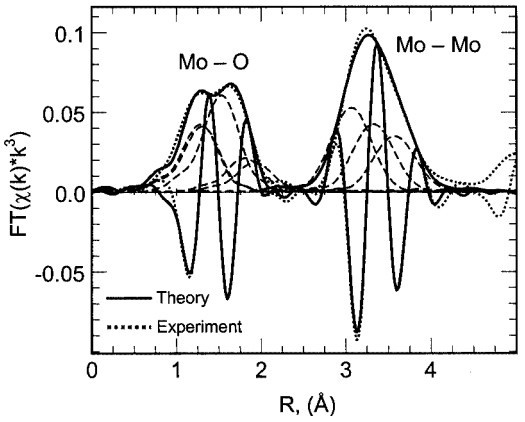

Figure 11. XAFS refinement of a theoretical Mo-K edge $\chi(k)$ (solid) to an experimental Fourier-transformed $\chi(k)$ of MoO_3 (dotted) (Table 1). The main Mo−O and Mo−Mo single-scattering paths are indicated (dashed)

The large number of different distances in the structures of MoO_3 and $Mo_{18}O_{52}$ prevents a conventional XAFS refinement of each individual distance and coordination number. Therefore, using theoretical XAFS phases and amplitudes calculated for the structure of orthorhombic α-MoO_3, structural parameters of the most prominent single-scattering and multiple-scattering paths (Table 1) in MoO_3 were refined to the calculated and measured $\chi(k)$, according to the XAFS analysis procedure described above. Thus, a detailed XAFS analysis of the set of $\chi(k)$ values of the numerical mixtures of MoO_3 and $Mo_{18}O_{52}$ (Figure 10), and the experimental spectra measured during the TPR of propene and oxygen (1:1) in the presence of MoO_3 (Figure 7) was performed to quantify the effect of the contribution of $Mo_{18}O_{52}$ on the structural parameters obtained for the MoO_3 phase. The very good agreement between refinement and experimental data that can be achieved using this fitting procedure is evident from the results of the refinement shown in Figure 11 and Table 1. For the numerical mixtures of MoO_3 and $Mo_{18}O_{52}$, the XAFS refinement procedure described above failed for concentrations of $Mo_{18}O_{52}$ larger than 27%.

The evolution of the Debye temperatures of molybdenum and oxygen backscatterers in the MoO_3 structure as a function of the concentration of $Mo_{18}O_{52}$ in the numerical mixtures and as a function of temperature during the TPR of propene and oxygen are depicted in Figure 12 (a) and Figure 12 (b), respectively. For the numerical mixtures, the Debye temperature of oxygen continuously increases for concentrations of $Mo_{18}O_{52}$ larger than 5%. The Debye temperature of molybdenum decreases linearly over the concentration range studied. For the TPR experiment, both Debye temperatures decrease almost linearly in the temperature range from 300 K to about 620 K. Above about 620 K, the Debye temperature of oxygen greatly increases, whereas the Debye temperature of molybdenum continues to decrease. For the series of XAFS spectra measured during the treatment of MoO_3 in oxygen, the increase of the Debye temperature of oxygen starting at about 620 K is followed by a decrease at temperatures above about 720 K.

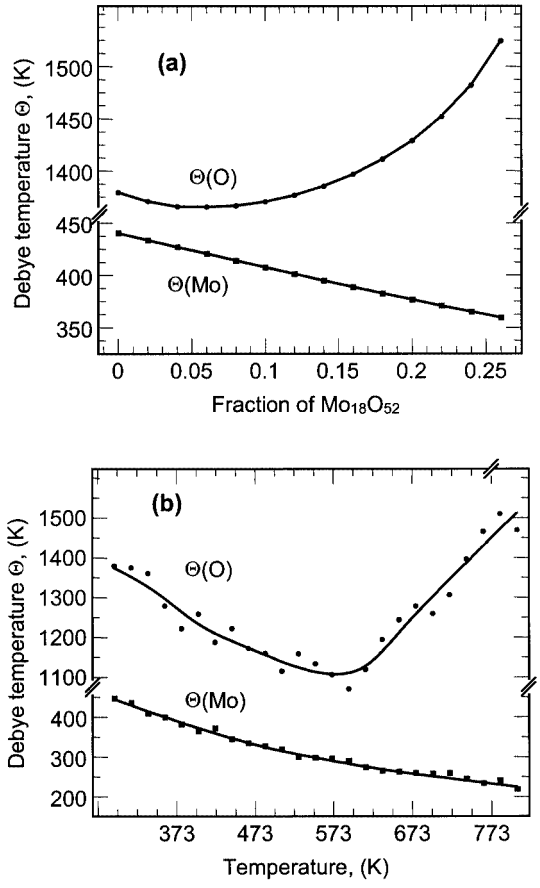

Figure 12. Evolution of Debye temperatures of molybdenum and oxygen backscatterers in the structure of MoO_3 obtained from XAFS refinement, (a) as a function of the concentration of $Mo_{18}O_{52}$ in the mixtures of MoO_3 and $Mo_{18}O_{52}$ in Figure 10 and (b) during the temperature-programmed reaction of propene and oxygen in the presence of MoO_3 (Figure 7) (10% O_2 and 10% propene in He) (300−773 K, 5 K/min, held at 773)

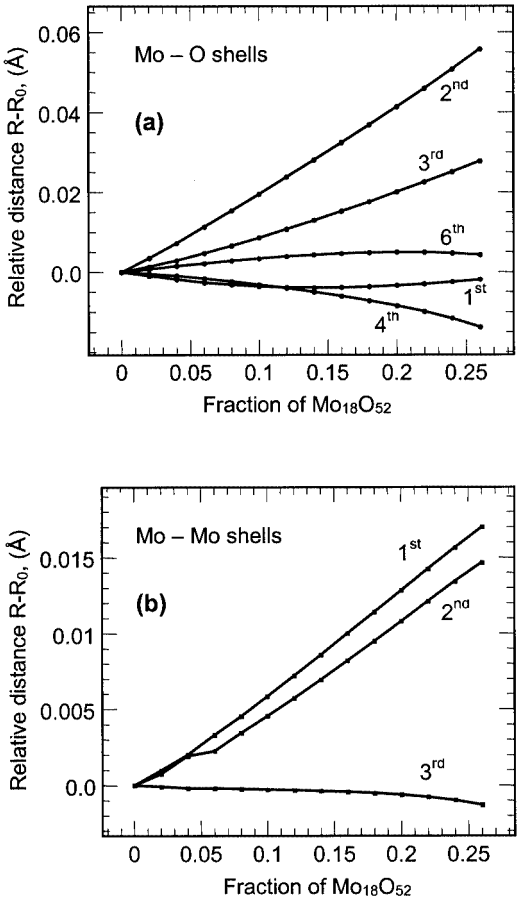

Figure 13. Evolution of relative Mo−O (a) (R_0 1st = 1.683 Å, 2nd = 1.710 Å, 3rd = 1.938 Å, 4th = 2.227 Å, 6th = 2.349 Å) and Mo−Mo (b) (R_0 1st = 3.421 Å, 2nd = 3.693 Å, 3rd = 3.946 Å) distances in the structure of MoO_3 obtained from XAFS refinement to the mixtures of MoO_3 and $Mo_{18}O_{52}$ in Figure 10

The evolution of the Mo−O and Mo−Mo distances in the first neighboring shells of the structure of MoO_3 as a function of the concentration of $Mo_{18}O_{52}$ in the numerical mixtures is displayed in Figure 13 (a and b), respectively. Figure 14 (a and b) show the evolution of Mo−O and Mo−Mo distances during the TPR of propene and oxygen. For the numerical mixtures, a pattern of increasing and decreasing distances are seen in the Mo−O and Mo−Mo distances. For the TPR experiment, there is a minor increase in the Mo−O distances in the temperature range from 300 K to about 620 K, corresponding to the anisotropic thermal expansion of MoO_3. At temperatures above about 620 K, several Mo−O distances show a strong deviation from their behavior at lower temperatures, resulting in a pattern of increasing and decreasing Mo−O distances very similar to that observed for the numerical mixtures. At temperatures above about 620 K, the Mo−Mo distances show a distinct deviation from their behavior at temperatures between 300 K and 620 K.

In order to validate the analysis procedure chosen, the suitability of other suboxides (i.e. Mo_4O_{11}, Mo_5O_{14}, and Mo_8O_{23}) to explain the deviations observed in the XAFS fit parameters was tested accordingly. Addition of more than 10% of Mo_4O_{11} and Mo_8O_{23} resulted in a considerable distortion of the FT[$\chi(k)$] and, hence, the failure of the XAFS fitting procedure used. For tetragonal Mo_5O_{14}, the radial distribution function also consists of a number of slightly different Mo−O and Mo−Mo distances. However, the XAFS parameters obtained from an analysis of numerical mixtures of the experimental $\chi(k)$ of MoO_3 and Mo_5O_{14} did not exhibit the characteristic increase in the Debye temperature of oxygen, or the characteristic pattern of increasing and decreasing Mo−O distances at temperatures above about 620 K. Hence, of the suboxides tested, only the shear-structure $Mo_{18}O_{52}$ constitutes a suitable reference for the type of defects observed in MoO_3 under reaction conditions.

Discussion

Changes in the bulk structure of an alkene oxidation catalyst under reaction conditions can occur when the lat-

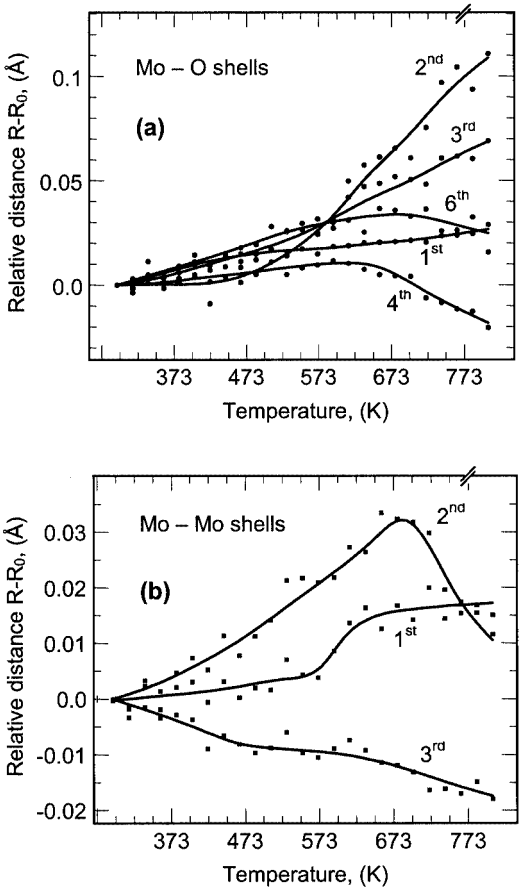

Figure 14. Evolution of relative Mo−O (a) and Mo−Mo (b) distances in the structure of MoO_3 during the temperature-programmed reaction of propene and oxygen in the presence of MoO_3 (Figure 7) (10% O_2 and 10% propene in He) (300−773 K, 5 K/min, held at 773)

tice oxygen of the catalyst participates in the oxidation of the alkene (''redox'' mechanism), and if the corresponding reduction and re-oxidation of the catalyst bulk proceed at different rates. In this work we investigated the evolution of the bulk structure of MoO_3, in combination with the catalytic activity under the reaction conditions of propene oxidation by oxygen. In order to reveal structure-reactivity relationships for MoO_3, this study focused on two characteristic features. First, the onset temperature of the oxidation of propene was correlated to changes in the molybdenum average valence and the bulk structure of MoO_3. Second, the nature of the structural defects induced in the layer structure of MoO_3 under reaction conditions was elucidated.

Onset of Reduction of MoO_3 in He, H_2, Propene, and Propene and Oxygen

From the data presented here and in previous reports it becomes evident, that the onset temperature for the reduction of MoO_3 in He (Figure 1), H_2,[13] propene,[10] and propene and oxygen (Figure 4) is approximately the same (≈ 620 K), and independent of the composition of the gas phase. Only in hydrogen, where the incorporation of hydrogen into the MoO_3 lattice facilitates the formation of MoO_2 product nuclei, is the onset temperature slightly shifted towards lower temperatures (≈ 600 K).[20] Apparently, the onset temperature for the reduction of MoO_3 coincides with the attainment of oxygen vacancies in the MoO_3 lattice with sufficient mobility. Only when the molybdenum-oxygen bonds in the MoO_3 lattice are weakened, and the oxygen in the lattice is sufficiently mobile and can participate in oxidation reactions proceeding at the surface of the catalyst, can stoichiometric reduction of MoO_3 with hydrogen or propene take place. Moreover, the onset of the reduction of MoO_3 coincides with the onset of propene oxidation on this material. This holds for both reduction of MoO_3 in propene and for the reaction of propene and oxygen in the presence of MoO_3. Again, it seems that both partial and total oxidation of propene on MoO_3 require a certain mobility of the lattice oxygen of MoO_3 and the formation of partially reduced defects, in order to proceed. Abstraction of a proton from propene to form an allylic species is a necessary prerequisite for the oxidation of propene to proceed on MoO_3 and determines the rate of conversion of propene. However, catalytic activity of MoO_3 is observed only after the Mo−O bonds in the lattice have become sufficiently weak to permit defect formation and activation of oxygen from the gas phase.

Evolution of the Average Valence of MoO_3 under the Reaction Conditions

The degree of reduction and, hence, the degree of defects in MoO_3 under partial oxidation conditions, can be estimated from the average valence of the molybdenum oxide (Figure 5), obtained from comparing the Mo-*K* edge position to that of suitable references. At a temperature of about 620 K, slight reduction of the molybdenum oxide occurs (Figure 4), independent of the composition of the gas phase. This is in agreement with the proposition that in this temperature range the oxygen ions in the lattice are mobile enough to be exchanged with oxygen in the gas phase (in oxygen), or to participate in the oxidation of propene (propene and oxygen), resulting in partially reduced MoO_3. In the temperature range from about 620 K to about 720 K, this partially reduced MoO_3 is not completely reoxidized by the oxygen in the gas phase. This may be because of the different rates of reduction (release of oxygen from the bulk) and re-oxidation of the bulk, or because, within this temperature range, the shear-structure defects formed do not readily back-transform into oxygen vacancies that could diffuse through the bulk to the surface and be filled with oxygen from the gas phase.

At reaction temperatures above about 720 K, re-oxidation of the partially reduced MoO_3 occurs during the treatment of MoO_3 in oxygen, and in propene and oxygen (ratio of 1:5) (Figure 4). Conversely, during the reaction of propene and oxygen (ratio of 1:1 and 1:3), re-oxidation of molybdenum is not detected at reaction temperatures above about 720 K. Apparently, at these ratios, the reducing potential of the gas phase with respect to the MoO_3 bulk is still too high to allow reoxidation of the molybdenum oxide.

Evidently, the ability of the atmosphere to reduce or oxidize the bulk material depends not only on the presence of oxygen in the gas phase, but also on the ratio of the reductant (propene) and the oxidant (oxygen). With an increasing concentration of oxygen, the reducing potential of the gas phase decreases until the partially reduced molybdenum oxide is reoxidized at temperatures above about 720 K.

Bulk Structural Evolution of MoO_3 under the Reaction Conditions

During the treatment of MoO_3 in oxygen or during the TPR in propene and oxygen, MoO_3 remains the only crystalline phase detected. In the temperature-programmed experiments, the evolution of the lattice parameters of MoO_3 is dominated by the anisotropic thermal expansion of MoO_3.[10] Therefore, the analysis described focused on integrated intensities and apparent crystallite sizes calculated for selected *hkl* reflections. The non-uniform behavior of the ratios of integrated intensities and apparent crystallite sizes (i.e. integral breadth) at temperatures above about 620 K (Figure 2 and Figure 3) indicates the formation of characteristic defects in the parent layer structure of MoO_3 without resulting in a long-range ordered separate phase under these reaction conditions. On the basis of our previous results on the reduction of MoO_3 in propene,[10] we suggest that the structure of molybdenum trioxide under propene oxidation reaction conditions corresponds to a defect-rich MoO_3 containing "$Mo_{18}O_{52}$" type defects. The close relationship between the structures of MoO_3 and $Mo_{18}O_{52}$ (Figure 8) facilitates the formation of "$Mo_{18}O_{52}$" type defects under these reaction conditions. Conversely, formation of other partially reduced molybdenum oxides that also contain shear-structures or tetrahedrally coordinated Mo, would require massive restructuring. Hence, they are less probable intermediates or structures formed at temperatures below 700 K. Therefore, the deviations observed in the ratios of integrated intensities (*h0l* > *hk0*, *hkl*) and apparent crystallite sizes, and the increase of strain in the MoO_3 lattice at temperatures above about 620 K, are caused by the formation of shear-structural defects (e.g. Wadsley defects) in the layer structure of MoO_3 under the reaction conditions (Figure 2 and Figure 3). In future work, these characteristic deviations may serve as starting points for a detailed investigation of the structural relationships between MoO_3 and $Mo_{18}O_{52}$, and of the effects of a transition between the two structures on the XRD patterns measured under reaction conditions.

The number of "$Mo_{18}O_{52}$" type defects formed cannot readily be estimated from the effect on the Fourier transform of the Mo-*K* edge XAFS measured under reaction conditions. A comparison of the radial distribution functions of MoO_3 and $Mo_{18}O_{52}$ for a 1 nm cluster (Figure 9) indicates that because of the large number of slightly different distances in the structure of $Mo_{18}O_{52}$, the magnitude of the Fourier transform of $Mo_{18}O_{52}$ is considerably smaller than that of MoO_3. Hence, even major fractions of $Mo_{18}O_{52}$ in MoO_3 may hardly be noticed from changes in the MoO_3 Fourier transform (Figure 10). Thus, the Mo-*K* XAFS spectra of MoO_3 under the reaction conditions correspond largely to that of pure defect-free MoO_3 (Figure 7) at elevated temperatures. The considerable number of defects in the MoO_3 structure (≈ 25% as estimated from the average Mo valence) is only accessible from their second order influence on the structural parameters, as obtained from an XAFS refinement of a MoO_3 model structure to the spectra of MoO_3 under reaction conditions (Figure 11).

Simulating the effect of the presence of "$Mo_{18}O_{52}$" in MoO_3 by calculating XAFS functions that correspond to mixtures of these two oxides, resulted in characteristic deviations in the XAFS fit parameters obtained for MoO_3 [i.e. increase in the Debye temperatures, and increase and decrease in the Mo−O distances in the 1st coordination shell, Figure 12, part (a) and Figure 13]. For the experimental spectra measured under the reaction conditions, at temperatures below about 620 K, the evolution of the XAFS fit parameters is dominated by the regular effect of the increasing reaction temperature [i.e. decreasing Debye temperatures and slightly increasing Mo−O distances, Figure 12, part (b) and Figure 14]. However, at temperatures above about 620 K, the oxygen Debye temperatures increase drastically, while the Mo−O distances in the 1st coordination shell exhibit a characteristic pattern of increasing and decreasing distances. The deviations observed in the XAFS fit parameters obtained for MoO_3 under reaction conditions at temperatures above about 620 K are similar to those obtained for the analysis of the mixtures of MoO_3 and $Mo_{18}O_{52}$. Therefore, the XAFS analysis of the Mo-*K* edge spectra measured under the reaction conditions corroborates the formation of "$Mo_{18}O_{52}$" type defects in the layer structure of MoO_3 during oxidation of propene at temperatures below 720 K.

Regarding the evolution of the bulk structure of MoO_3 in a reducing atmosphere of propene and oxygen (ratio of 1:1) at temperatures above 720 K, two possibilities with respect to the formation of oxygen vacancies can be envisioned. First, the "$Mo_{18}O_{52}$" type defects in the structure vanish at the expense of an increasing number of free oxygen vacancies in the MoO_3 structure. This would result in an average valence below 6.0 and an overall structure of the material close to that of MoO_3. Second, the "$Mo_{18}O_{52}$" type defects persist even at higher temperatures, resulting in an average valence below 6.0 and a disturbed bulk structure of MoO_3. The experimental data shown corroborate the second possibility (Figure 5, Figure 12, and Figure 13). Apparently, this very dynamic system under these reaction conditions is not governed by the energy necessary to break up the "$Mo_{18}O_{52}$" type defects and to form vacancies that can be filled with gas phase oxygen. Instead, the density of vacancies in the MoO_3 layer structure, resulting from the ratio of the rate of reduction of the MoO_3 lattice by propene and the rate of re-oxidation by gas phase oxygen, energetically favors the shear-structure defects, rather than the free oxygen vacancies.[21,22] Only at an increased oxygen partial pressure and temperatures above about 720 K, is the rate of re-oxidation of the MoO_3 lattice sufficient to allow the release of oxygen vacancies from the shear-structure de-

fects and, subsequently, filling of the oxygen vacancies by gas phase oxygen.

A schematic model for the behavior of MoO_3 under propene oxidation conditions is depicted in Figure 15.

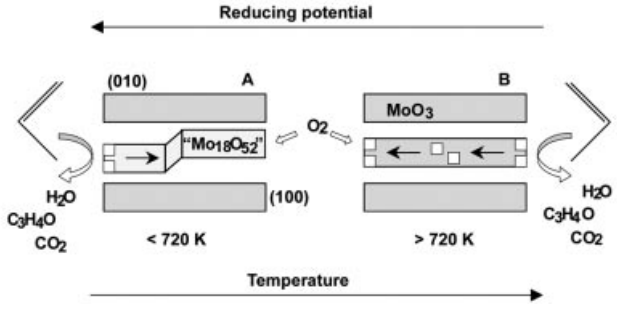

Figure 15. Schematic representation of the structure of MoO_3 under the reaction conditions (propene and oxygen), as a function of temperature and reducing potential of the gas phase. A) Below 720 K, **or** in a reducing gas phase. B) Above 720 K, **and** in an oxidizing gas phase. "$Mo_{18}O_{52}$" refers to crystallographic-shear type defects in the MoO_3 structure (squares indicate oxygen vacancies)

Oxygen vacancies are generated mostly at the side facets of the MoO_3 layer structure and can diffuse easily along the [100] or the [001] direction into the bulk.[23–26] Evidently, both reaction temperature and the reducing potential of the gas phase influence the bulk structure of the molybdenum oxide material under reaction conditions. By varying the reducing potential in the gas phase, the degree of reduction of the MoO_3 bulk can be adjusted. If the gas phase becomes oxidizing with respect to the bulk, at temperatures above about 720 K re-oxidation of the "$Mo_{18}O_{52}$" type defects in the MoO_3 layer structure takes place (B in Figure 15). Conversely, under a reducing atmosphere with respect to the MoO_3 bulk, "$Mo_{18}O_{52}$" type defects persist in the MoO_3 structure and the material is not completely reoxidized at elevated temperatures (A in Figure 15).

Evidently, under propene oxidation reaction conditions, the structure of the molybdenum oxide catalyst is not identical to that of the initial MoO_3. Rather, given the oxidation and reduction kinetics of molybdenum oxides at temperatures below about 720 K, the material corresponds to partially reduced metastable MoO_3 with a considerable number of "$Mo_{18}O_{52}$" type defects in the parent layer structure. From Figure 6 it can be seen that the catalytically most active and selective molybdenum oxide phase for propene oxidation to form acrolein develops under the reaction conditions. Possibly, a certain number of "$Mo_{18}O_{52}$" type defects have to be present in the bulk structure of MoO_3 to result in an improved selectivity in the partial oxidation of propene in the presence of MoO_3. The minor total oxidation activity at temperatures below about 600 K (Figure 6), which is not accompanied by a change in the average valence of the molybdenum oxide, may be assigned to adsorbed oxygen species.[27] However, a detailed analysis of the effect of oxygen partial pressure and temperature on the reactivity and selectivity of MoO_3 is not the subject of this report and shall be pursued in future studies. Furthermore, molybdenum trioxide obtained by various preparation routes will be investigated to elucidate the dependence of the defect type and the catalytic properties on the preparation conditions. In order to obtain more active and selective molybdenum oxide phases (e.g. Mo_5O_{14}), ternary oxides such as mixed molybdenum vanadium oxides are needed. It has to be clarified if these oxides need to be prepared, or if they can be obtained as binary molybdenum oxides by careful tailoring of the preparation conditions.

Many of the attempts to reveal the catalytic properties of MoO_3 described in the literature are restricted to "post-mortem" investigations, or studies on stoichiometric reactions involving molybdenum oxides and, for instance, oxidation by oxygen, or reduction by hydrogen or propene. Those investigations are valuable to elucidate the structural evolution of the material under noncatalytic conditions. Our previous investigations on the reduction and re-oxidation of MoO_3 allowed us to interpret the structural changes described here. However, only investigating the catalyst under reaction conditions (in situ) employing the modern in situ techniques available will eventually result in a complete description of the evolution of the bulk structure of the catalytically relevant material.

Naturally, an investigation of the evolution of the bulk structure of MoO_3 under reaction conditions cannot provide information on the individual steps of the partial oxidation of propene proceeding on the surface of the molybdenum oxide material used. However, while studying these surface reaction steps on defined model systems such as thin films or molecular molybdenum oxides, one needs to be aware of the importance of the bulk structure for the catalytic properties of a "real" heterogeneous catalyst. Attempting to access the reactivity of individual molybdenum oxide polyhedra, in order to model partial oxidation reactions proceeding on the surface of a bulk molybdenum oxide catalyst, requires taking into account the paramount role of the underlying bulk structure of the catalyst. By neglecting either the bulk or the surface, all the properties essential for the material to function as a heterogeneous catalyst cannot be comprehended and, hence, any attempts to design an improved catalyst based on this incomplete picture will fail. Eventually, a rational design of a most active heterogeneous catalyst will only be possible if both the structure and reactions of the surface, and the structure and reactions of the bulk are adequately understood and considered.

Conclusion

In this work we presented investigations on the evolution of characteristic defects in the bulk structure of MoO_3 under propene oxidation conditions using in situ X-ray absorption spectroscopy and X-ray diffraction. Under the reaction conditions employed (273 K to 773 K, and propene to oxygen ratios from 1:1 to 1:5), MoO_3 remains the only crystalline phase detected by XRD. The onset temperature for the temperature-programmed reaction of propene and oxygen in the presence of MoO_3 coincides with the onset

of the reduction of MoO_3 in He, H_2, or propene ($\approx$ 620 K). Thus, the weakening of Mo−O bonds in MoO_3, the sufficient mobility of oxygen ions, and the formation of defects are essential for the reduction of MoO_3 and for its function as a heterogeneous catalyst.

Various in situ experiments indicate that the structural evolution of MoO_3 during the TPR, reduction, and treatment in He is surprisingly similar. At temperatures below about 720 K, and independent of the atmosphere used, partial reduction of MoO_3 is observed, resulting in the formation of "$Mo_{18}O_{52}$" type defects in the bulk structure. At temperatures above about 720 K, and in oxygen or in an oxidizing atmosphere (sufficiently low propene to oxygen ratio), the "$Mo_{18}O_{52}$" type defects are reoxidized to MoO_3. Evidently, the catalytically active molybdenum oxide phase under partial oxidation conditions at temperatures below 720 K does not correspond to the original MoO_3 possessing the undisturbed ideal layer structure of orthorhombic α-MoO_3. Instead, at these temperatures, the catalytically active phase, which is partially reduced and possesses a large number of "$Mo_{18}O_{52}$" type defects (crystallographic-shear structures) in the layer structure of MoO_3, develops under reaction conditions.

The results presented clearly show the necessity and the great potential for bulk structural investigations of heterogeneous catalysts under reaction conditions. Evidently, the bulk structure and particularly the type and number of defects in the material ("real" structure) considerably affect the catalytic properties. Hence, in order to rationally design a most active heterogeneous catalyst, both the structure and reactions of the surface, and the structure, defects, and reactions of the bulk need to be known in detail, and carefully considered.

Experimental Section

MoO_3 Preparation and Characterization

Molybdenum trioxide (MoO_3) was prepared by thermal decomposition of ammonium heptamolybdate (AHM), $(NH_4)_6Mo_7O_{24}{\cdot}4H_2O$[28] (Aldrich Co.), under a stream of synthetic air (room temp. − 773 K with 2 K/min, held for 2 h at 773 K). The phase purity of the compound obtained was verified by XRD. The molybdenum trioxide used in this study is identical to that used in ref. 10 and 11.[10,11]

X-ray Diffraction

In situ XRD experiments were performed on a STOE STADI P powder diffractometer equipped with a secondary monochromator (Cu-K_α radiation) and a scintillation counter operated in the stepping mode. The in situ cell consisted of a Bühler HDK S1 high temperature diffraction chamber. The gas phase composition at the cell outlet was analyzed on line with a Pfeiffer Prisma 200 quadropole mass spectrometer in the multiple ion detection mode. In situ XRD measurements were conducted under atmospheric pressure with flowing reactants ($\approx$ 100 mL/min). Details on the XRD setup used can be found elsewhere.[11] Crystallite sizes were calculated from the integral breadth of selected *hkl* reflections using the Scherrer formula.[29]

In situ X-ray Absorption Spectroscopy

For in situ XAS experiments, MoO_3 was mixed with boron nitride (ratio 1:4) and 37 mg of the mixture was pressed with a force of 1 ton into a 5 mm diameter self-supporting pellet. The absorption jump, $\Delta\mu x$, at the Mo-*K* edge was about 1.5. In situ XAS experiments were performed in transmission in a flow-reactor[30] at atmospheric pressure with flowing reactants ($\approx$ 30 mL/min). The gas phase composition at the cell outlet was continuously monitored using a mass spectrometer in the multiple ion detection mode (QMS200 from Pfeiffer). Further details about the experimental XAS set-up used can be found in ref.[11].

In situ transmission XAS experiments were performed at the Mo-*K* edge (19.999 keV) at beamline X1 at the Hamburg Synchrotron Radiation Laboratory, HASYLAB, using a Si(311) double crystal monochromator (measuring time about 4.5 min/scan). The storage ring operated at 4.4 GeV with injection currents of 150 mA. Time-resolved in situ XAS experiments were carried out at the Mo-*K* edge utilizing an energy-dispersive spectrometer (European Synchrotron Radiation Facility, ESRF, ID24[31]) equipped with a curved Si(111) polychromator in the transmission mode[32] (measuring time about 3 s/scan). The storage ring operated at 6.0 GeV with injection currents of 90 mA in the 16-bunch mode.

XAFS Data Analysis

X-ray absorption fine structure (XAFS) analysis was performed using the software package WinXAS v2.2,[33] following recommended procedures from the literature.[34] Background subtraction and normalization were carried out by fitting linear polynomials to the pre-edge and the post-edge region of an absorption spectrum. The Mo-*K* edge absorption threshold was determined from the first root in the first derivative of the near-edge region (XANES). Principal component analysis (PCA)[35] was used to identify the number and type of Mo oxide phases[10] present during the thermal treatment of MoO_3 under various atmospheres.

The X-ray absorption fine structure (EXAFS) $\chi(k)$ was extracted by using cubic splines to obtain a smooth atomic background, $\mu_0(k)$. The radial distribution function $FT[\chi(k)]$ was calculated by Fourier transformation of the k^3-weighted experimental $\chi(k)$ function, multiplied by a Bessel window, into the R space. EXAFS data analysis was performed using theoretical backscattering phases and amplitudes calculated with the ab initio multiple-scattering code FEFF7.[36] Single scattering and multiple scattering paths in the MoO_3 model structure were calculated up to 5.0 Å, with a lower limit of 2.0% in amplitude with respect to the strongest backscattering path. EXAFS refinements were performed in the *R* space to the magnitude and the imaginary part of a Fourier-transformed k^3-weighted experimental $\chi(k)$, by using the standard EXAFS formula (k range from 3.1 to 15.4 $Å^{-1}$, *R* range 0.9 to 4.1 Å).[37] Structural parameters that were determined by a least-squares EXAFS fit to the experimental spectra are (i) one E_0 shift for oxygen and molybdenum backscatterers, (ii) two Debye temperatures for oxygen and molybdenum backscatterers, (iii) distances of the single-scattering paths with an amplitude larger than 10% were allowed to vary, distances of multiple-scattering paths were correlated to the corresponding single-scattering paths, (iv) one third cumulant for all scattering paths. Coordination numbers (CN) were kept constant in the refinement.

Acknowledgments

The synchrotron radiation facilities HASYLAB, Hamburg, Germany, and ESRF, Grenoble, France, are acknowledged for provid-

ing beamtime for this work. TR thanks the Deutsche Forschungsgemeinschaft, DFG, for financial support (Habilitations-Stipendium). T. Neisius and O. Timpe are acknowledged for participating in the XAS experiments. The authors are grateful to Prof. R. Schlögl for many fruitful discussions and continuous support.

[1] B. Grzybowska-Swierkosz, *Topics in Catalysis* **2000**, *11/12*, 23−42.
[2] R. K. Grasselli, *Catalysis Today* **1999,** *49*, 141−153.
[3] J. Haber, E. Lalik, *Catalysis Today* **1997,** *33*, 119−137.
[4] M. M. Bettahar, G. Costentin, L. Savary, J. C. Lavalley, *Appl. Cat. A* **1996**, *145*, 1−48.
[5] B. Grzybowska, J. Haber, J. Janas, *J. Catal.* **1977**, *49*, 150−163.
[6] K. Brückmann, R. Grabowski, J. Haber, A. Mazurkiewicz, J. Sloczynski, T. Wiltowski, *J. Catal.* **1987**, *104*, 71−79.
[7] P. Mars, D. W. van Krevelen, *Chem. Ing. Sci.* **1954**, *3*, 41.
[8] L. D. Krenzke, G. W. Keulks, *J. Catal.* **1980**, *61*, 316−325.
[9] W. Ueda, Y. Moro-Oka, T. Ikawa, *J. Catal.* **1981**, *70*, 409−417.
[10] T. Ressler, J. Wienold, R. E. Jentoft, O. Timpe, T. Neisius, *J. Catal.* **2002**, *210*, 67−83.
[11] T. Ressler, R. E. Jentoft, J. Wienold, M. M. Günter, O. Timpe, *J. Phys. Chem. B* **2000**, *104*, 6360−6370.
[12] R. Schlögl, *Angew. Chem. Int. Ed. Engl.* **1993**, *32*, 381−383.
[13] T. Ressler, J. Wienold, R. E. Jentoft, T. Neisius, M. M. Günter, *Topics in Catalysis* **2002**, *18*, 45−42.
[14] T. Ressler, J. Wienold, R. E. Jentoft, O. Timpe, T. Neisius, *Solid State Communications* **2001**, *119*, 169.
[15] D. C. Koningsberger, B. L. Mojet, *Topics in Catalysis* **2000**, *10*, 3.
[16] G. K. Williamson, W. H. Hall, *Acta Metall* **1953**, *1*, 22.
[17] L. Kihlborg, *Ark. Kemi* **1963**, *21*, 357.
[18] L. Kihlborg, *Ark. Kemi* **1963**, *21*, 443.
[19] R. L. Smith, G. S. Rohrer, *J. Solid State Chem.* **1996**, *124*, 104−115.
[20] T. Ressler, J. Wienold, R. E. Jentoft, *Solid State Ionics* **2001**, *141−142*, 243−251.
[21] E. Broclawik, J. Haber, *J. Catal.* **1981**, *72*, 379−382.
[22] R. Tokarz−Sobieraj, K. Hermann, M. Witko, A. Blume, G. Mestl, R. Schlögl, *Surface Science* **2001**, *489*, 107−125.
[23] A. Guerrero-Ruiz, J. M. Blanco, M. Aguilar, I. Rodriguez-Ramos, J. L. G. Fierro, *J. Catal.* **1992**, *137*, 429−436.
[24] A. Guerrero-Ruiz, I. Rodriguez-Ramos, P. Ferreira-Aparicio, M. Abon, J. C. Volta, *Catalysis Today* **1996**, *32*, 223−227.
[25] N. Floquet, O. Bertrand, J. J. Heizmann, *Oxidation of Metals* **1992**, *37*, 253−280.
[26] P. A. Batist, C. J. Kapteijns, B. C. Lippens, G. C. A. Schuit, *J. Catal.* **1967**, *7*, 33−49.
[27] J. Haber, W. Turek, *J. Catal.* **2000**, *190*, 320−326.
[28] J. Wienold, R. E. Jentoft, T. Ressler, *Eur. J. Inorg. Chem.* **2002**, submitted.
[29] R. J. Matyi, L. H. Schwartz, J. B. Butt, *Catal. Rev. Sci. Eng.* **1987**, *29*, 41.
[30] Designed by M. Hagelstein, T. Neisius, et al.,((***Author: please list all authors)***) ESRF, France, in a collaborative effort with the Fritz−Haber-Institut, Berlin, Germany
[31] M. Hagelstein, A. San Miguel, A. Fontaine, J. Goulon, *J. de Physique IV* **1997**, *7*, C2−303.
[32] M. Hagelstein, C. Ferrero, U. Hatje, T. Ressler, W. Metz, *J. Synch. Rad.* **1995**, *2*, 174−179.
[33] T. Ressler, *J. Synch. Rad.* **1998**, *5*, 118−122.
[34] D. C. Koningsberger, R. Prins, *X-ray Absorption Spectroscopy, Chemical Analysis*, 92, Wiley, New York, **1988**.
[35] T. Ressler, J. Wong, J. Roos, I. L. Smith, *Environ. Sci. & Technol.* **2000**, *34*, 950−958.
[36] J. J. Rehr, C. H. Booth, F. Bridges, S. I. Zabinsky, *Phys. Rev. B* **1994**, *49*, 12347−12350.
[37] T. Ressler, S. L. Brock, J. Wong, S. L. Suib, *J. Phys. Chem. B* **1999**, *103*, 6407−6420.

Received June 21, 2002
[I02332]

[(η⁶-Cyclooctatetraene){η⁵-(+)-neomenthylcyclopentadienyl}ruthenium(II)] Hexafluorophosphate: Synthesis and Characterization of a Chiral Mixed Sandwich Complex

Xiaofeng Zhang,[a][‡] Marc H. Prosenc,[a] Timo Meyer-Friedrichsen,[a][‡‡] and Jürgen Heck*[a]

Dedicated to Prof. Dr. Rüdiger Mews on the occasion of his 60th birthday

Keywords: Chirality / Cyclopentadienyl ligands / Sandwich complexes / Ruthenium

Three different {η⁵-(+)-neomenthylcyclopentadienyl}ruthenium complexes have been synthesized from (–)-menthol: [(η⁶-benzene){η⁵-(+)-neomenthylcyclopentadienyl}ruthenium(II)] hexafluorophosphate (**1**), [tris(acetonitrile){η⁵-(+)-neomenthylcyclopentadienyl}ruthenium(II)] hexafluorophosphate (**2**) and [(η⁶-cyclooctatetraene){η⁵-(+)-neomenthylcyclopentadienyl}ruthenium(II)] hexafluorophosphate (**3**). X-ray structural determination (space group $P2_12_12_1$) and NMR spectroscopic studies of **3** show it exists as a single stereoisomer in both the solid and solution phase, with $[\alpha]_D^{20} = +92.5$. The chiral modification of the Cp ligand induces anisochrony for all of the magnetically active nuclei of the unsubstituted COT ligand.

(© Wiley-VCH Verlag GmbH & Co KGaA, 69451 Weinheim, Germany, 2003)

Introduction

Iterative nucleophilic and electrophilic addition to a coordinated cyclooctatetraene (COT) in $[(\eta^6\text{-COT})(\eta^5\text{-Cp})M]^+$ (Cp = cyclopentadienyl; M = Fe, Ru) has been shown to be a powerful tool for the formation of stereo- and regioselectively substituted cycloocta-1,3-dienes.[1,2] Since the first nucleophilic addition creates a stereogenic carbon atom in the *cyclo*-C_8 ligand (Figure 1), we attempted to synthesize a starting COT complex containing a chiral modified Cp ligand, which would be expected to influence the stereochemical selectivity of the initial nucleophilic addition. We chose the (+)-neomenthyl substituent as a chiral auxiliary on the cyclopentadienyl ring [(+)-NMCp];[3] this has widely been used in the synthesis of Cp complexes active in enantioselective transformations.[4]

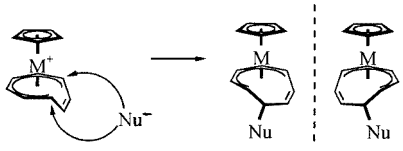

Figure 1. Nucleophilic attack on the two enantiotopic sites in $[(\eta^6\text{-COT})(\eta^5\text{-Cp})M]^+$ (M = Fe, Ru)

Results and Discussion

Synthesis

(+)-Neomenthylcyclopentadiene [(+)-NMCpH] was prepared according to a known procedure[3] and subsequently transformed into the thallium salt by addition of TlOEt (Scheme 1).

The thallium salt [(+)-NMCp]Tl reacts with $[(\eta^6\text{-}C_6H_6)RuCl_2]_2$ [5] in acetonitrile, yielding $[(\eta^6\text{-}C_6H_6)\{\eta^5\text{-}(+)\text{-NMCp}\}Ru]X$ [X = Cl, Scheme 1, b; X = PF_6 (**1**), Scheme 1, c]. Irradiation of complex **1** in acetonitrile with a high-pressure mercury lamp gives the {η⁵-(+)-NMCp}Ru half-sandwich complex **2**. Addition of COT to a solution of **2** in acetonitrile affords product **3** as a light yellow powder in very good yields. Crystals of **3** are air-stable and soluble in dichloromethane but almost insoluble in diethyl ether.

X-ray Structure Analysis

Crystals of **3** suitable for X-ray structural analysis were grown by slow diffusion of diethyl ether into a CH_2Cl_2 solution of **3** at room temperature. Data collection parameters and selected bond lengths and angles are listed in Table 1 and Table 2, respectively. Complex **3** crystallizes in the chiral orthorhombic space group $P2_12_12_1$. The cation (Fig-

[a] Institut für Anorganische und Angewandte Chemie, Universität Hamburg,
Martin-Luther-King-Platz 6, 20146 Hamburg, Germany
Fax: (internat.) + 49-(0)40/428386945
E-mail: juergen.heck@chemie.uni-hamburg.de
[‡] Present address: Changchun Institute of Applied Chemistry, Chinese Academy of Sciences,
Changchun 130022, P. R. China
[‡‡] Present address: Bayer AG Leverkusen, Werk Uerdingen, Rheinuferstraße 7–9, 47829 Krefeld, Germany

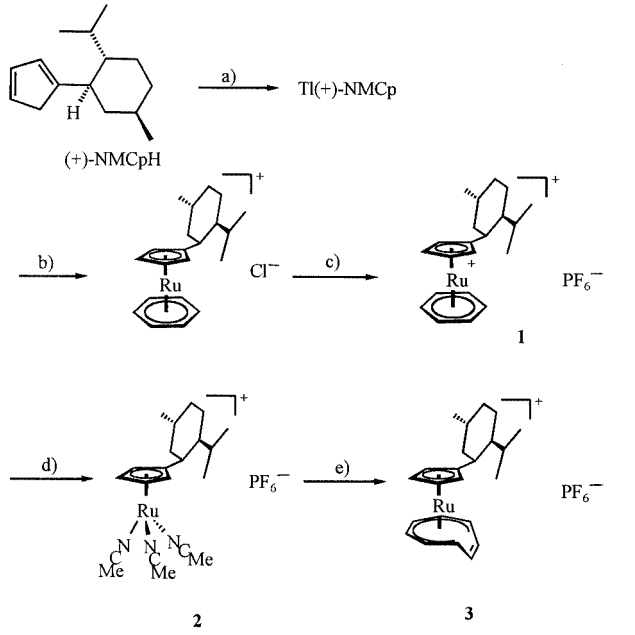

Scheme 1. Synthesis of [(η⁶-cyclooctatetraene){η⁵-(+)-neomenthylcyclopentadienyl}ruthenium(II)] hexafluorophosphate (**3**): a) TlOEt, THF, room temperature; b) MeCN, $[(\eta^6\text{-}C_6H_6)RuCl_2]_2$, room temperature; c) MeOH, NH_4PF_6; d) MeCN, hν; e) COT, MeCN

ure 2) adopts a typical sandwich-like structure with the Cp ligand and the η⁶-coordinated part of the COT ligand almost parallel. The uncoordinated double bond of the COT ligand, C7−C8, protrudes from the plane of the metal-bound carbon atoms *exo* with respect to the metal center. The dihedral angle between the "best" planes of the coordinated carbon atoms C1−C2−C5−C6 and of the carbon atoms C1−C6−C7−C8 is 120°, very similar to the corresponding structural feature in $[(\eta^6\text{-COT})(\eta^5\text{-Cp})Fe]^+$.[6] The COT ring exhibits slight rotational disorder by a torsion around the axis connecting the Ru atom and the six coordinated carbon atoms. This results in large anisotropic temperature factors for the atoms in the COT ring and a very short C7−C8 bond length of 128.9(3) pm (typical C=C double bond length of 134 pm).

Attempts to resolve this disorder did not improve the model; the *R*1 value rises about 0.5% and standard deviations increase as well. Most notably, the C7−C8 bond lengths in the disordered model were not chemically sensible; a nondisordered model was thus used and refined anisotropically. The Ru−C(COT) bond lengths of 214.1−222.6 pm are in the typical range of cationic $(\eta^6\text{-}cyclo\text{-}C_8)Ru$ complexes.[1b] The distances between the Ru center and the carbon atoms of the Cp ligand of 218.1(2)−222.98(19) pm correspond to Ru−C(Cp) bond lengths of other cationic CpRu complexes[7] except for the bond to C9 [226.14(16) pm], the atom which bears the (+)-neomenthyl substituent. This slight elongation of the Ru−C9 bond may be due to packing effects within the crystal.

Table 1. Crystal data and structure refinement for [(η⁶-cyclooctatetraene){η⁵-(+)-neomenthylcyclopentadienyl}ruthenium(II)] hexafluorophosphate (**3**)

	3
Empirical formula	$C_{23}H_{31}F_6PRu$
Formula mass	553.52
T [K]	153(2)
λ [pm]	71.073
Crystal system	orthorhombic *P*
Space group	$P2_12_12_1$
a [pm]	1062.36(6)
b [pm]	1211.68(7)
c [pm]	1769.78(11)
V [10^6 pm^3]	2278.1(2)
Z	4
$\rho_{calcd.}$ [Mg/m^3]	1.614
μ [mm^{-1}]	0.815
F(000)	1128
Crystal size [mm]	0.3 × 0.3 × 0.1
Scan range [°]	2.30−27.99
Index range	$-14 \le h \le 14$ $-16 \le k \le 15$ $-22 \le l \le 23$
Reflections measured	27406
Reflections unique	5218
R_{int}	0.0397
Parameters	308
Reflections [$I > 4\,\sigma(I)$]	5218
GoF[a]	1.052
$R1/wR^2$ [$I > 2\sigma(I)$][b]	0.0227/0.0581
$R1/wR^2$ (all data)[b]	0.0233/0.0584
Residual min./max. [e/Å^3]	0.452/−0.342

[a] GoF (goodness of fit) = $[\Sigma w(F_o^2 - F_c^2)^2/(n-p)]^{1/2}$ (n = numbers of reflections, p = numbers of parameters). [b] Weight = $1/[\sigma^2(F_o^2) + 0.0351 \times P)^2 + 0.440P]$, $P = [\max(F_o^2,0) + 2\,F_c^2]/3$.

Table 2. Selected bond lengths [pm] and angles [°] for [(η⁶-cyclooctatetraene){η⁵-(+)-neomenthylcyclopentadienyl}ruthenium(II)] hexafluorophosphate (**3**)

Ru1−C1	222.62	C2−C3	141.9(5)
Ru1−C2	214.1(2)	C3−C4	142.8(5)
Ru1−C3	220.2(2)	C4−C5	140.3(6)
Ru1−C4	220.9(3)	C5−C6	139.5(4)
Ru1−C5	215.7(2)	C6−C7	148.5(3)
Ru1−C6	222.0(2)	C7−C8	128.9(3)
Ru1−C9	226.14(16)	C9−C13	142.2(3)
Ru1−C10	218.57(19)	C9−C10	144.2(3)
Ru1−C11	218.1(2)	C9−C14	152.7(2)
Ru1−C12	220.0(2)	C10−C11	143.0(3)
Ru1−C13	222.98(19)	C11−C12	142.0(3)
C1−C2	139.0(4)	C12−C13	143.0(3)
C1−C8	148.6(3)		
Xa−Ru1−Xb[a]	166.7		
P1[b]−P2[c]	120.0		
P2−P3[d]	156.7		

[a] Xa, Xb = pivots of the Cp ligand and coordinated part of the COT ligand, respectively. [b] P1: Best plane of C1, C2, C5, C6. [c] P2: Best plane of C1, C6, C7, C8. [d] P3: Best plane of C2, C3, C4, C5.

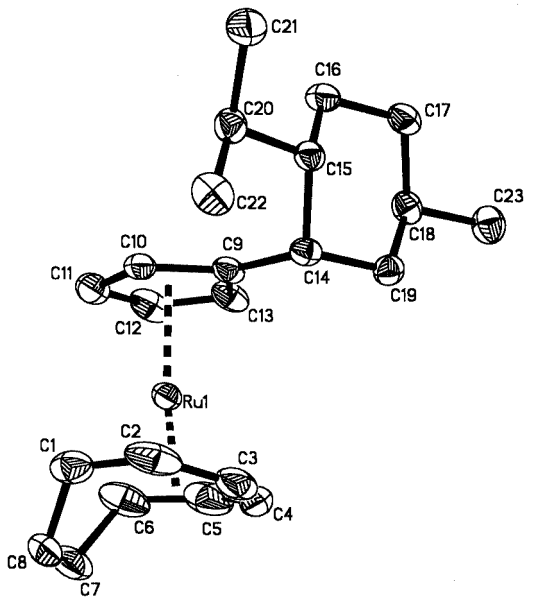

Figure 2. Molecular structure of [(η^6-cyclooctatetraene){η^5-(+)-neomenthylcyclopentadienyl}ruthenium(II)] hexafluorophosphate (**3**); thermal ellipsoids are drawn at the 50% probability level and the hydrogen atoms and the PF_6^- counterion are omitted for clarity

The most important result of this structural analysis is the unambiguous identification of the presence of only one stereoisomer, the (+)-neomenthyl derivative; this is also confirmed by ^1H and ^{13}C NMR spectra of **3** (vide infra). The (+)-neomenthyl substituent adopts a conformation which places it at the most remote position with respect to the sandwich moiety.

NMR Spectroscopy

Complex **3** displays ^1H and ^{13}C NMR signals due to the (+)-neomenthyl substituent (^1H: δ = 0.7−2.9 ppm; ^{13}C: δ = 20−50 ppm), and the Cp and COT ligands (^1H: δ = 5.0−6.3 ppm; ^{13}C: δ = 82−138 ppm). The ^1H and ^{13}C chemical shifts of the metal-bound hydrocarbon units clearly testify to the cationic nature of **3**,[1b] and the number of signals confirms the formation of a single stereoisomer. Due to the chiral (+)-neomenthyl substituent all of the Cp protons are inequivalent and give rise to four multiplets in the range δ = 5.3−5.6 ppm, consistent with the chemical shifts observed in other monocationic CpRu sandwich complexes.[1,8]

Remarkably, the chiral (+)-neomenthyl substituent also induces anisochrony in all of the nuclei of the COT ligand. In Figure 3, both experimental (bottom) and calculated (top) ^1H NMR spectra of the COT region display signals due to eight chemically inequivalent hydrogen atoms. Even the uncoordinated C=C double bond, which is most distant from the chiral neomenthyl group, displays two different resonance signals in the ^1H and ^{13}C NMR spectra (δ = 5.0840 and 5.0934 ppm for 7-H and 8-H, δ =134.99 and 135.07 ppm for C-7 and C-8). The largest shift difference of the resonance signals of nuclei which are equivalent in the COT ligand of a corresponding complex without a chiral induction, for example [(η^5-Cp)Ru(η^6-COT)]$^+$, is found for 1-H and 6-H (δ = 5.6937 and 5.7903 ppm), and C-3 and C-4 (δ = 104.1 and 103.2 ppm).

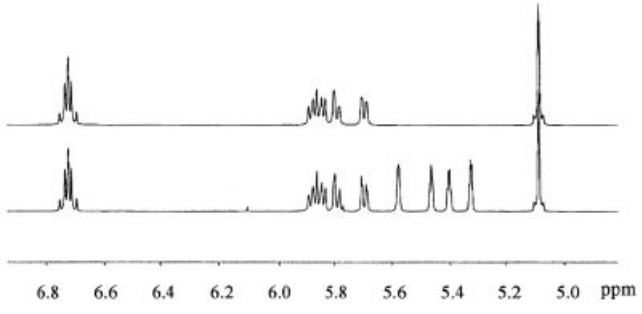

Figure 3. Experimental (bottom) and calculated (top) ^1H NMR spectra of [(η^6-cyclooctatetraene){η^5-(+)-neomenthylcyclopentadienyl}ruthenium(II)] hexafluorophosphate (**3**); signals due to theCp ligand are omitted from the calculated spectrum for simplicity [parameters used for the calculation: δ = 5.0840, 5.0934 (7-H, 8-H), 5.6937, 5.7903 (1-H, 6-H), 5.8419, 5.8717 (2-H, 5-H), 6.7085, 6.7294 ppm (3-H, 4-H); $^3J_{1\text{-}2}$ = 8.474, $^3J_{1\text{-}8}$ = 2.644, $^3J_{2\text{-}3}$ = 6.940, $^3J_{3\text{-}4}$ = 8.963, $^3J_{4\text{-}5}$ = 6.968, $^3J_{5\text{-}6}$ = 8.764, $^3J_{6\text{-}7}$ = 2.514, $^3J_{7\text{-}8}$ = 6.558 Hz; significant changes in the calculated spectra are observed on changing the shifts by 0.001 ppm and the coupling constants by 0.001 Hz]

Optical Activity

A specific optical rotation of $[\alpha]_D^{20}$= +92.5 was determined for **3**. The optical activity of complex **3** is consistent with a Cotton effect observed in CD spectra of **3**, which is negative for the electronic absorption at higher energy (λ = 267 nm: [θ] = −6760 °·L·mol^{-1}·cm^{-1}) and positive at lower energy (λ = 325 nm: [θ] = +3500 °·L·mol^{-1}·cm^{-1}). Since the molar extinction coefficient of these absorption bands is very low [ε (267 nm) = 1726 L·mol^{-1}·cm^{-1}; ε (325 nm) = 673 L·mol^{-1}·cm^{-1}], we assign these Cotton effects to d-d transitions.

Conclusions

The introduction of the chiral (+)-neomenthyl substituent on the cyclopentadienyl ligand allows the synthesis of the [(η^6-cyclooctatetraene){η^5-(+)-neomenthylcyclopentadienyl}ruthenium(II)] cation, which is the first structurally characterized chiral cyclooctatetraene complex. The chiral Cp ligand even induces inequivalence at all positions of the COT ligand as demonstrated by NMR experiments. This inequivalence suggests that chiral induction in nucleophilic additions to the COT ligand may be possible, and this is currently under investigation.

Experimental Section

General: All reactions were carried out under nitrogen. Solvents were saturated with nitrogen and freshly distilled from an appropriate drying agent. NMR: Bruker WM 500, AM 360 and Varian

Gemini 200. IR (KBr disks): FT-IR 1720 X (Perkin−Elmer). UV/Vis (MeCN solution): Perkin−Elmer, Model 554. CD (MeCN solution): Jasco, Model J 500-C. Elemental analysis: Heraeus-CHN-O-Rapid (Zentrale Elementanalytik, Fachbereich Chemie, Universität Hamburg). (+)-Neomenthylcyclopentadiene[3] and $[(\eta^6\text{-}C_6H_6)RuCl_2]_2$ [5] were synthesized according to literature procedures. $RuCl_3{\cdot}xH_2O$ was a gift from Degussa AG. Cyclohexadiene and TlOEt were purchased from Aldrich and Merck, respectively.

[(+)-Neomenthylcyclopentadienyl]thallium: A solution of TlOEt (4.0 mL, 56.1 mmol) in THF (10 mL) was added to a solution of (+)-NMCpH (11.27 g, 55.1 mmol) in THF (120 mL) at room temperature. After stirring for 17 h, about 100 mL of the solvent was evaporated in vacuo. The resulting off-white precipitate was collected on a filter and washed with small amounts of toluene. The solid material was dried in vacuo. Yield: 6.98 g (31.1%) of [(+)-NMCp]Tl. The product is air-sensitive and was used without further purification.

[(η^6-Benzene){η^5-(+)-neomenthylcyclopentadienyl}ruthenium(II)] Hexafluorophosphate (1): Solid [(+)-NMCp]Tl (5.9 g, 14.47 mmol) was added to a suspension of $[(\eta^6\text{-}C_6H_6)RuCl_2]_2$ (3.14 g, 6.28 mmol) in acetonitrile (300 mL). After stirring at room temperature for 20 h, the reaction mixture was filtered through Celite and the filter was washed four times with 10 mL of acetonitrile. The acetonitrile solution was concentrated to dryness, and the residue was dissolved in absolute methanol (40 mL). Solid NH_4PF_6 (2.21 g, 13.56 mmol) was added to the methanol solution, whereupon the product precipitated. After 3.5 h of stirring, the reaction mixture was filtered, and the solid material was washed three times with methanol and once with diethyl ether. The light yellow solid material was dried in vacuo yielding 4.30 g (64.9%) of **1**. IR: $\tilde{\nu}$ = 3094 (m), 2943 (s), 2871 (m), 2845 (m), 1443 (s), 1410 (m), 1391 (m), 1382 (w), 1367 (w), 840 (broad vs), 558 (vs), 443 (m), 423 (m) cm^{-1}. ^1H NMR (360 MHz, CD_3CN): δ = 0.727 (d, ^3J = 6.5 Hz, 3 H, Me), 0.882 (d, ^3J = 6.4 Hz, 3 H, Me), 0.930 (d, ^3J = 6.3 Hz, 3 H, Me), 0.84−1.17 [m, 3 H, (+)-neomenthyl], 1.22 [m, 1 H, (+)-neomenthyl], 1.60−1.82 [m, 4 H, (+)-neomenthyl], 2.80 [m, 1 H, (+)-neomenthyl], 5.21 (m, 1 H, Cp), 5.25 (m, 1 H, Cp), 5.32 (m, 1 H, Cp), 5.44 (m, 1 H, Cp), 6.10 (s, 6 H, C_6H_6) ppm. ^{13}C NMR (50 MHz, CD_3CN): δ = 20.76, 22.05, 23.02, 24.87, 28.42, 30.26, 35.78, 36.26, 44.25, 48.46 [(+)-neomenthyl], 79.05 (Cp), 80.46 (Cp), 82.37 (Cp), 83.48 (Cp), 87.13 (C_6H_6), 118.25 (C_qCp) ppm. $C_{21}H_{29}F_6PRu$ (527.50): calcd. C 47.82, H 5.54; found C 48.18, H 5.74.

[Tris(acetonitrile){η^5-(+)-neomenthylcyclopentadienyl}-ruthenium(II)] Hexafluorophosphate by Photolysis of 1: A solution of **1** (3.62 g, 6.86 mmol) in acetonitrile (300 mL) was irradiated with a high-pressure Hg lamp for 26 h. The solution was then concentrated to dryness and the residue identified as $[(MeCN)_3(\eta^5\text{-}NMCp)Ru]PF_6$ (**2**) by means of ^1H NMR spectroscopy. This was used for the reaction with COT (vide infra) without further purification. ^1H NMR (200 MHz, CD_2Cl_2): δ = 0.84 (d, ^3J = 6.2 Hz, Me), 0.95 (d, ^3J = 6.2 Hz, Me), 0.97 (d, ^3J = 6.2 Hz, Me), 0.9−1.7 [m, 9 H, (+)-neomenthyl], 2.44 (s, 9 H, MeCN), 2.7 [m, 1 H, (+)-neomenthyl], 4.13 (m, 1 H, Cp), 4.21 (m, 1 H, Cp), 4.30 (m, 1 H, Cp), 4.51 (m, 1 H, Cp) ppm.

[(η^6-Cyclooctatetraene){η^5-(+)-neomenthylcyclopentadienyl}-ruthenium(II)] Hexafluorophosphate (3): COT (3.1 mL, 27.6 mmol) was added to a solution of **2** (3.9 g, 6.8 mmol) in acetonitrile (180 mL). The solution was stirred overnight at room temperature and then concentrated to dryness. The residue was suspended in a mixture of diethyl ether (10 mL) and CH_2Cl_2 (4 mL). The light yellow solid material was filtered and dried in vacuo. Yield: 3.5 g (93%) of **3** as a light yellow powder. IR (KBr): $\tilde{\nu}$ = 3130 (m), 2974 (s), 2952 (s), 2924 (s), 2868 (s), 2853 (s), 2844 (m), 1690 (m), 1460 (s), 1447 (m), 1401 (m), 1386 (s), 1370 (m), 1332 (m), 1148 (m), 831 (vs), 798 (s), 742 (m), 640 (w), 558 (vs), 519 (w), 427 (m), 421 (m) cm^{-1}. ^1H NMR (500 MHz, CD_3CN): δ = 0.709 (d, ^3J = 6.4 Hz, 3 H, Me), 0.874 (d, ^3J = 6.1 Hz, 3 H, Me), 0.929 (d, ^3J = 6.1, 3 H, Me), 0.9−1.5 [m, 3 H, (+)-neomenthyl], 1.28 [m, 1 H, (+)-neomenthyl], 1.44 [m, 1 H, (+)-neomenthyl], 1.65 [m, 2 H, (+)-neomenthyl], 1.82 [m, 1 H, (+)-neomenthyl], 1.97 [m, 1 H, (+)-neomenthyl], 2.87 [m, 1 H, (+)-neomenthyl], 5.084 (m, 1 H, 7-H or 8-H), 5.093 (m, 1 H, 8-H or 7-H), 5.33 (m, 1 H, Cp), 5.40 (m, 1 H, Cp), 5.46 (m, 1 H, Cp), 5.57 (m, 1 H, Cp), 5.694 (dm, 1 H, 1H or 6-H), 5.790 (dm, 1 H, 6-H or 1-H), 5.842 (m, 1 H, 2-H or 5-H), 5.872 (m, 1 H, 5H or 2H), 6.709 (m, 1 H, 3-H or 4-H), 6.729 (m, 1 H, 4-H or 5-H) ppm (the chemical shifts for the COT protons were taken from the calculated spectra, see Figure 3). ^{13}C NMR (50 MHz, CD_3CN): δ = 20.6, 22.0, 22.9, 24.8, 28.7, 30.2, 35.7, 36.3, 43.8, 48.5, [(+)-neomenthyl], 83.0, 84.3, 84.9, 86.9 (Cp), 88.7, 88.9, 94.1, 94.5, 103.2, 104.1 (COT), 114.3 (C_qCp), 134.99, 135.07 (COT) ppm. $[\alpha]_D^{20}$ = +92.5 (*c* = 0.6, CH_2Cl_2). CD (MeCN): λ_{max} (ε, [θ]) = 267 (1726, −6760), 325 (673, +3500) nm ($L{\cdot}mol^{-1}{\cdot}cm^{-1}$, $°{\cdot}L{\cdot}mol^{-1}{\cdot}cm^{-1}$). $C_{23}H_{31}F_6PRu$ (553.52): calcd. C 49.91, H 5.64; found C 49.14, H 5.71.

X-ray Structural Analysis of 3: Suitable crystals were obtained by slow diffusion of diethyl ether into a CH_2Cl_2 solution of **3**. Determination of cell parameters and collection of reflection intensities were carried out using a Bruker−Apex three-circle diffractometer with a CCD detector at −120 °C. An absorption correction was applied using the SADABS Program (see Table 1). The structure was solved by direct methods using SHELXS-97[9] and refined using SHELXL-97.[10] All non-hydrogen atoms were refined anisotropically and the hydrogen atoms were included in calculated positions using a riding model approach. For more details see Table 1. CCDC-188541 contains the supplementary crystallographic data for this paper. These data can be obtained free of charge at www.ccdc.cam.ac.uk/conts/retrieving.html or from the Cambridge Crystallographic Data Centre, 12 Union Road, Cambridge CB2 1EZ, UK [Fax: (internat.) + 44-1223/336-033; E-mail: deposit@ccdc.cam.ac.uk].

Acknowledgments

This work was supported by the Deutsche Forschungsgemeinschaft (DFG) HE 1309/2 and by the Fonds der Chemischen Industrie. We thank the BASF for the donation of cyclooctatetraene and the Degussa AG for the donation of $RuCl_3$. M. H. P. thanks the DFG for a fellowship PR 654-1/1.

[1] [1a] J. Heck, G. Lange, O. Reimelt, *Angew. Chem.* **1998**, *110*, 533−535; *Angew. Chem. Int. Ed.* **1998**, *37*, 520−522. [1b] G. Lange, O. Reimelt, L. Jessen, J. Heck, *Eur. J. Inorg. Chem.* **2000**, 1941−1952.
[2] O. Reimelt, J. Heck, *Organometallics*, submitted.
[3] [3a] E. Cesarotti, H. B. Kagan, R. Goddard, C. Krüger, *J. Organomet. Chem.* **1978**, *162*, 297−309. [3b] M. A. Giardello, V. P. Conticello, L. Brard, M. Sabat, A. L. Rheingold, C. L. Stern, T. J. Marks, *J. Am. Chem. Soc.* **1994**, *116*, 10212−10240.
[4] [4a] P. A. Schofield, H. Adams, N. A. Bailey, E. Cesarotti, C. White, *J. Organomet. Chem.* **1991**, *412*, 273−289. [4b] Y. Ma, R. G. Bergman, *Organometallics* **1994**, *13*, 2548−2550. [4c] C.

M. Haar, C. L. Stern, T. J. Marks, *Organometallics* **1996**, *15*, 1765−1784. [4d] P. W. Roesky, U. Denninger, C. L. Stern, T. J. Marks, *Organometallics* **1997**, *16*, 4486−4492. [4e] M. R. Douglass, M. Ogasawara, S. Hong, M. V. Metz, T. J. Marks, *Organometallics* **2002**, *21*, 283−292.

[5] [5a] M. C. Baird, R. A. Zelonka, *Can. J. Chem.* **1972**, *50*, 3063−3072. [5b] M. C. Baird, R. A. Zelonka, *J. Organomet. Chem.* **1972**, *44*, 383−389. [5c] B. M. Trost, C. M. Older, *Organometallics* **2002**, *21*, 2544−2546.

[6] J. Heck, W. Massa, *J. Organomet. Chem.* **1989**, *376*, C15−C19.

[7] F. Grepioni, G. Cojazzi, D. Braga, E. Marseglia, L. Scaccianoce, B. F. G. Johnson, *J. Chem. Soc., Dalton Trans.* **1999**, 553−558.

[8] T. P. Gill, R. Mann, *Organometallics* **1982**, *1*, 485−488.

[9] G. M. Sheldrick, *SHELXS-97*, University of Göttingen, Germany, **1997**.

[10] G. M. Sheldrick, *SHELXL-97*, University of Göttingen, Germany, **1997**.

Received June 24, 2002
[I02344]

Synthesis and Characterization of Lanthanide(III) Bis(guanidinate) Derivatives and the Catalytic Activity of Methyllanthanide Bis(guanidinate) Complexes for the Polymerization of ε-Caprolactone and Methyl Methacrylate

Yunjie Luo,[a] Yingming Yao,[a] Qi Shen,*[a] Kaibei Yu,[b] and Linhong Weng[c]

Keywords: Lanthanides / N ligands / Structure elucidation / Polymerization / ε-Caprolactone / Methyl methacrylate

The synthesis and structure of new lanthanide complexes with the guanidinate ligand $[(Me_3Si)_2NC(NiPr)_2^-]$ are described. Reaction of a THF slurry of $LnCl_3$ with a hexane solution of $[(SiMe_3)_2NC(NiPr)_2]Li$ (**1**) in a 1:2 molar ratio afforded the new soluble organolanthanide complexes $[(SiMe_3)_2NC(NiPr)_2]Ln(\mu\text{-}Cl)_2Li(THF)_2$ [Ln = Yb (**2**), Nd (**3**)]. Alkylation of **2** and **3** with 2 equiv. of MeLi in hexane gave $[(SiMe_3)_2NC(NiPr)_2]Ln(\mu\text{-}Me)_2Li(TMEDA)$ [Ln = Yb (**4**), Nd (**5**)] in good yield as crystalline solids. The molecular structures of **2** and **5** were determined by single-crystal X-ray analysis. The lanthanide ions in these complexes display a distorted pseudo-octahedral coordination geometry. Complexes **4** and **5** exhibited extremely high activity for the ring-opening polymerization of ε-caprolactone to give high molecular weight polymers. Complex **5** also showed good catalytic activity for the syndiotactic polymerization of methyl methacrylate.
(© Wiley-VCH Verlag GmbH & Co KGaA, 69451 Weinheim, Germany, 2002)

Introduction

Guanidinate anions, $[(RN)_2C(NR_2')]^-$, are isoelectronic alternatives to cyclopentadienyl ligands and their electronic properties and steric bulk can be modified by variation of the substituents on the nitrogen atoms. As a result, guanidinates have attracted increasing attention as ancillary ligands in the coordination and organometallic chemistry of main group and transition metals,[1] and some of these complexes have been reported to exhibit interesting reactivity. For example, neutral and cationic Zr^{IV} bis(guanidinate) complexes are catalysts for the polymerization of α-olefins,[2] and mono- and dianionic guanidinate complexes of Ta^{IV} and (hydrocarbyl)Zr^{IV} bis(guanidinate) complexes react with Me_3SiCl, ArNC,[3] and 2,6-dimethylphenyl isocyanide,[4] respectively. However, the application of guanidinate ligands in organolanthanide chemistry has been quite limited; to date, only three papers concerning the synthesis and characterization of lanthanide guanidinate complexes have been published,[5–7] with one of these discussing the catalytic activity of $La[CyNC\{N(SiMe_3)_2\}NCy](OC_6H_3tBu_2\text{-}2,6)_2$ complexes for the ring-opening polymerization of D,L-lactide.[7]

We have recently become interested in understanding the chemistry of organolanthanide complexes with nitrogen-based polydentate ligands.[8] As an extension of our studies in this area, we have prepared the lanthanide guanidinate complexes $[(SiMe_3)_2NC(NiPr)_2]Ln(\mu\text{-}Cl)_2Li(THF)_2$ [Ln = Yb (**2**), Nd (**3**)] and $[(SiMe_3)_2NC(NiPr)_2]Ln(\mu\text{-}Me)_2Li(TMEDA)$ [Ln = Yb (**4**), Nd (**5**)]. Complexes **4** and **5** are highly active for the ring-opening polymerization of ε-caprolactone, and **5** is also able to catalyze the polymerization of methyl methacrylate.

Results and Discussion

Synthesis and Characterization of the Chloro and Methyl Complexes 2, 3 and 4, 5

The reaction of *N*,*N*′-diisopropylcarbodiimide with 1 equiv. of $LiN(SiMe_3)_2$ in hexane gives a quantitative yield of $[(SiMe_3)_2NC(NiPr)_2]Li$ (**1**); thus, in most cases a freshly prepared solution of the lithium guanidinate was used directly in the following metathesis reactions. Treatment of a hexane solution of **1** with a THF slurry of $LnCl_3$ in a 2:1 molar ratio at room temperature afforded after workup the chlorolanthanide guanidinate complexes $[(SiMe_3)_2NC(NiPr)_2]_2Ln(\mu\text{-}Cl)_2Li(THF)_2$ [Ln = Yb (**2**), Nd (**3**)] in 76 and 82% yield, respectively.

[a] Department of Chemistry and Chemical Engineering, Suzhou University,
Suzhou 215006, People's Republic of China
Fax: (internat.) + 86-0512/65112371
E-mail: qshen@suda.edu.cn
[b] Chengdu Institute of Organic Chemistry, Chinese Academy of Sciences,
Chengdu 610041, People's Republic of China
[c] Department of Chemistry, Fudan University,
Shanghai 200433, People's Republic of China

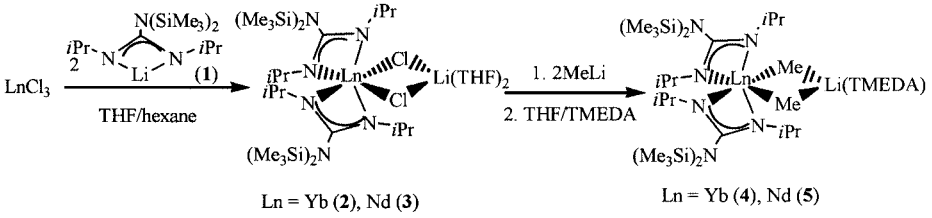

Scheme 1

Elemental analyses show both **2** and **3** to be lanthanide monochloride bis(guanidinates), complexed with LiCl·2THF. An X-ray determination of the structure of **2** reveals it to be an "ate" complex possessing two chloro bridges to an Li cation as shown in Scheme 1 and Figure 1.

Complexes **2** and **3** are useful precursors for further transformation. They react with 2 equiv. of MeLi in hexane to produce the μ-methyl "ate" derivatives **4** and **5** in 72 and 76% yield, respectively (Scheme 1). Use of 1 equiv. of MeLi gave the same methyl complexes, albeit in quite low yield.

All the complexes synthesized are air- and moisture-sensitive and have good solubility in toluene, diethyl ether and tetrahydrofuran (THF).

The N=C=N stretch of the parent carbodiimide (2117 cm^{-1}) is absent in the IR spectra of these complexes while a C=N stretch at approximately 1640 cm^{-1} is observed. These data suggest that the π-electrons within the double bonds of the N−C−N linkage are delocalized in all the complexes.[9]

Crystals of **2** suitable for X-ray diffraction were grown from THF, while **5** crystallized from a solution of a mixture of THF and TMEDA.

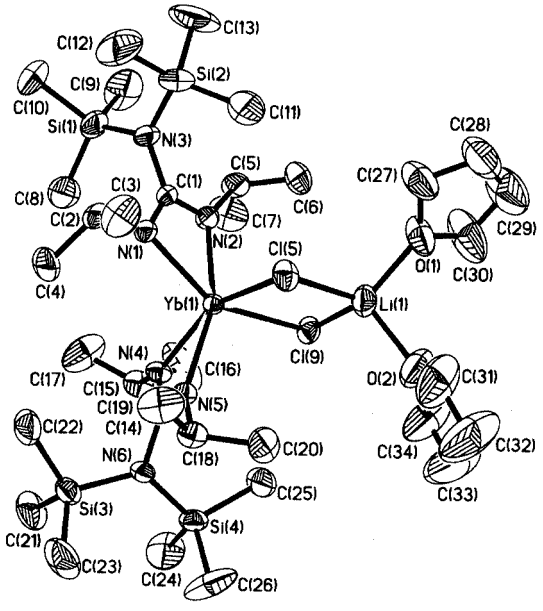

Figure 1. ORTEP diagram of $[(SiMe_3)_2NC(NiPr)_2]_2Yb(\mu\text{-}Cl)_2Li(THF)_2$ (**2**) showing non-hydrogen atom numbering scheme

An ORTEP diagram of **2** is shown in Figure 1. Crystal and structural refinement data are listed in Table 1, and selected bond lengths and angles are given in Table 2. As shown in Figure 1, **2** is a dinuclear lanthanide−lithium complex with two chloro bridges. The $[(SiMe_3)_2NC(NiPr)_2]_2Yb$ moiety is bonded through two chloro bridges to a lithium cation, which in turn is bonded to two oxygen atoms of two THF molecules. The Yb ion displays a distorted octahedral geometry defined by the four nitrogen atoms of the two chelating bidentate guanidinate ligands and the two chloride ligands, while the Li ion adopts a distorted tetrahedral geometry. The nearly identical C−N distances within the chelating guanidinate ligands (see Table 2) suggest that the π-electrons within the NCN fragments are delocalized. The guanidinate ligands bind to Yb through two nitrogen atoms to yield a planar four-membered ring with bite angles of 57.09(13)° and 57.18(12)°. The Yb−N bond lengths vary from 2.295(3) to 2.332(3) Å, similar to the values reported for $[(SiMe_3)_2NC(NCy)_2]_2[N(SiMe_2)]Yb$[5] and $\{[(SiMe_3)_2NC(NiPr)_2]_2Y(\mu\text{-}Cl)\}_2$.[6] The Yb−Cl bond lengths are 2.6076(14) and 2.6306(13) Å, respectively, which are similar to those in $Li[YbCl_2(C_5H_4SiCH_3Ph_2)_2](Et_2O)_2$.[10] The C(1)−Yb−C(14) angle is 131.09(12)°, similar to that found in $[(SiMe_3)_2NC(NCy)_2]_2YbN(SiMe)_2$ (130.5°),[5] but greater than the corresponding angle in $\{[(SiMe_3)_2NC(NiPr)_2]_2Y(\mu\text{-}Cl)\}_2$ [123.09(15)°].[6] The Cl(1)−Yb−Cl(2) angle [84.42(4)°] is also greater than that in $\{[(SiMe_3)_2NC(NiPr)_2]_2Y(\mu\text{-}Cl)\}_2$ [76.30(4)°],[6] and smaller than that in $Li[YbCl_2(C_5H_4SiCH_3Ph_2)_2](Et_2O)_2$ [87.14(3)°].[10]

The orientation of the $N(SiMe_3)_2$ groups relative to the NCNYb plane is approximately perpendicular and is similar to the analogous Sm,[5] Yb,[5] and Y[6] complexes. This disposition prevents π-overlapping between these two moieties; however, it increases the steric bulk above and below the planar guanidinate ligand.

An ORTEP diagram of **5** is presented in Figure 2. Details concerning the data collection are listed in Table 1 and selected bond lengths and angles are given in Table 3.

The crystal structure of **5** is similar to that of **2**, even though **5** is only monomeric in the solid state. The geometry of the Nd ion is best described as a distorted pseudo-octahedron defined by the four nitrogen atoms of the two chelating bidentate guanidinate ligands and the two μ-methyl groups. The Li ion adopts a distorted tetrahedral geometry with two μ-Me groups and two N atoms of a TMEDA molecule coordinated to it.

Table 1. Details of the crystallographic data and refinements for **2** and **5**

	2	**5**
Empirical formula	$C_{34}H_{80}Cl_2LiN_6O_2Si_4Yb$	$C_{34}H_{86}LiNdN_8Si_4 \cdot 0.375C_6H_{12}$
Formula mass	968.28	902.21
T [K]	293(2)	291(2)
λ [Å]	0.71073	0.71073
Crystal system	Triclinic	triclinic
Space group	$P\bar{1}$	$P\bar{1}$
Unit cell dimensions		
a [Å]	9.972(3)	12.981(6)
b [Å]	14.912(5)	14.008(5)
c [Å]	18.456(6)	17.476(7)
α [°]	75.717(4)	101.16(2)
β [°]	87.347(4)	93.52(4)
γ [°]	79.438(4)	108.87(3)
V [Å^3]	2614.8(15)	2924(2)
Z	2	2
Density [Mg/m^3]	1.230	1.025
μ [mm^{-1}]	2.013	0.997
F(000)	1010	966
θ range [°]	1.60−25.01	1.58−25.00
No. of reflns. collected	10703	11029
No. of ind. reflections	9112 [R(int) = 0.0298]	10189[R(int) = 0.0327]
No.of data/restraints/param.	9112/0/452	10189/7/464
Final R [$I > 2\sigma(I)$]	0.0352	0.0597
Rw	0.0816	0.1716
GOF on F^2	1.056	1.005

Table 2. Selected Bond lengths [Å] and angles [°] for **2**

Yb(1)−N(4)	2.295(3)	Yb(1)−N(1)	2.299(3)
Yb(1)−N(2)	2.330(4)	Yb(1)−N(5)	2.332(3)
Yb(1)−Cl(1)	2.6076(14)	Yb(1)−Cl(2)	2.6306(13)
Yb(1)−C(1)	2.742(4)	Yb(1)−C(14)	2.745(4)
Yb(1)−Li(1)	3.470(9)	Li(1)−O(1)	1.916(12)
Li(1)−O(2)	1.946(12)	Li(1)−Cl(1)	2.318(11)
Li(1)−Cl(2)	2.348(11)	N(1)−C(1)	1.310(6)
N(4)−C(14)	1.316(5)	N(2)−C(1)	1.322(6)
N(5)−C(14)	1.328(5)	N(3)−C(1)	1.448(6)
N(6)−C(14)	1.437(5)		
N(1)−Yb(1)−N(2)	57.09(13)	N(4)−Yb(1)−N(5)	57.18(12)
Cl(1)−Yb(1)−Cl(2)	84.42(4)	C(1)−Yb(1)−C(14)	131.09(12)
C(1)−Yb(1)−Li(1)	112.4(2)	C(14)−Yb(1)−Li(1)	116.5(2)
O(1)−Li(1)−O(2)	103.3(5)	Cl(1)−Li(1)−Cl(2)	97.9(3)
Li(1)−Cl(1)−Yb(1)	89.4(3)	Li(1)−Cl(2)−Yb(1)	88.2(3)
C(1)−N(3)−Si(1)	117.0(4)	C(1)−N(3)−Si(2)	118.6(4)
C(14)−N(6)−Si(4)	118.3(3)	C(14)−N(6)−Si(3)	118.4(3)
N(1)−C(1)−N(2)	114.4(4)	N(3)−C(1)−Yb(1)	173.6(3)
N(4)−C(14)−N(5)	113.7(4)	N(6)−C(14)−Yb(1)	171.4(3)

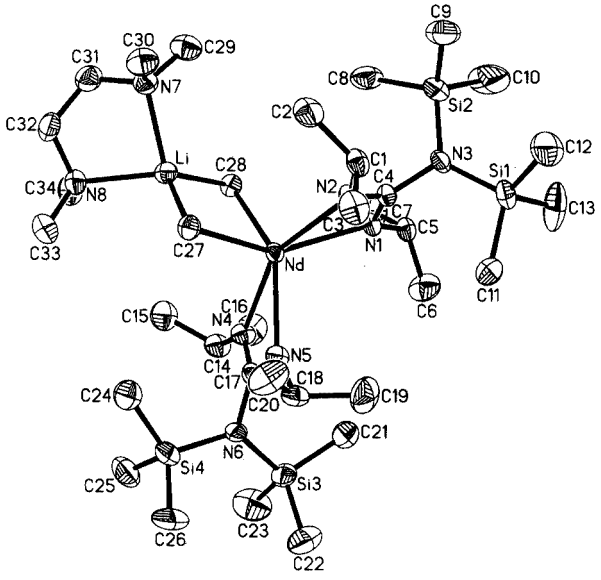

Figure 2. ORTEP diagram of $[(SiMe_3)_2NC(NiPr)_2]_2Nd(\mu\text{-}Me)_2Li(TMEDA)$ (**5**) showing the atom-numbering scheme; hydrogen atoms have been omitted for clarity

The Nd−N bond lengths within each NdN_2C moiety differ by approximately 0.05 Å. The Nd−C_{methyl} bond lengths are 2.590(8) and 2.595(8) Å, which are identical to those in $[(tBuCp)_2Nd(\mu\text{-}Me)]_2$ [2.594(15) Å][11] and similar to those in $[(SiMe_3)_2NC(NiPr)_2]_2Y(\mu\text{-}Me)_2Li(TMEDA)$ [2.505(4) and 2.508(4) Å].[6] The bite angles of the two ligands are 53.5(2) and 54.0(2)°, which are close to that found in $[(SiMe_3)_2NC(NiPr)_2]_2Y(\mu\text{-}Me)_2Li(TMEDA)$ [55.36(10)°].[6] The Me−Nd−Me angle of 89.3(2)° is similar to the angle in $[(tBuCp)_2Nd(\mu\text{-}Me)]_2$ [88.4(7)°].[11]

Polymerization of ε-Caprolactone and Methyl Methacrylate by Complexes 4 and 5

Both **4** and **5** were found to catalyze the polymerization of ε-caprolactone and methyl methacrylate in toluene solution. The preliminary results are listed in Tables 4 and 5, respectively.

Table 3. Selected bond lengths [Å] and angles [°] for **5**

Nd−N(5)	2.476(7)	Li−N(8)	2.191(15)
Nd−N(1)	2.477(6)	Li−C(27)	2.215(16)
Nd−N(2)	2.513(6)	Li−C(28)	2.244(15)
Nd−N(4)	2.523(6)	N1−C(4)	1.338(9)
Nd−C(27)	2.590(8)	N2−C(4)	1.315(9)
Nd−C(28)	2.595(8)	N3−C(4)	1.457(9)
Nd−C(4)	2.931(7)	N4−C(17)	1.352(10)
Nd−C(17)	2.936(8)	N5−C(17)	1.328(9)
Nd−Li	3.129(13)	N6−C(17)	1.455(10)
Li−N(7)	2.147(15)		
N(1)−Nd−N(2)	53.5(2)	C(4)−N(3)−Si(1)	118.8(5)
N(5)−Nd−N(4)	54.0(2)	C(4)−N(3)−Si(2)	117.2(5)
C(27)−Nd−C(28)	89.3(2)	C(17)−N(4)−Nd	93.6(4)
C(4)−Nd−C(17)	128.5(2)	C(17)−N(5)−Nd	96.3(5)
C(4)−Nd−Li	116.0(3)	C(17)−N(6)−Si(4)	116.6(5)
C(17)−Nd−Li	115.5(3)	C(17)−N(6)−Si(3)	118.5(5)
N(7)−Li−N(8)	85.3(5)	N(2)−C(4)−N(1)	115.6(6)
C(27)−Li−C(28)	109.6(6)	N(3)−C(4)−Nd	174.0(5)
C(4)−N(1)−Nd	95.7(4)	N(5)−C(17)−N(4)	115.7(7)
C(4)−N(2)−Nd	94.8(4)	N(6)−C(17)−Nd	174.7(5)

Table 4. Ring-opening polymerization of ε-caprolactone initiated by $[(SiMe_3)_2NC(NiPr)_2]_2Ln(\mu\text{-}Me)_2Li(TMEDA)$ [Ln = Yb (**4**), Nd (**5**)]

Entry[a]	Initiator	T_p [°C]	$[M]/[I]$	Yield[b] (%)	M_n ($\times 10^{-4}$)	M_w/M_n [c]
1	**5**	20	300	100	7.44	1.92
2	**5**	20	500	100	9.18	1.99
3	**5**	20	700	100	8.08	2.35
4	**5**	20	1000	100	6.35	2.21
5	**5**	40	1000	100	6.45	2.20
6	**5**[d]	20	1000	100	11.03	2.54
7	**5**[e]	20	1000	100	9.87	2.96
8	**4**	20	500	61.2	8.68	2.33
9	**4**	20	700	46.6	9.59	2.35
10	**4**	20	1000	27.2	9.22	2.18

[a] General polymerization conditions: in toluene, 15 min, solvent/monomer = 10 (v/v). [b] Yield: weight of polymer obtained/weight of monomer used. [c] Measured by GPC calibrated with standard polystyrene samples. [d] Polymerization time: 60 min. [e] Polymerization time: 14 h.

Table 5. Polymerization of methyl methacrylate by $[(SiMe_3)_2NC(NiPr)_2]_2Nd(\mu\text{-}Me)_2Li(TMEDA)$ (**5**)

Entry[a]	T_p [°C]	Yield[b] (%)	M_n ($\times 10^{-4}$)	M_w/M_n[c]	Stereochemistry (%)		
					rr	mr	mm
1	−78	10	15.7	2.15	58.90	19.16	21.94
2	−35	12	7.8	2.59	56.96	29.86	13.18
3	4	21	5.6	1.98	53.22	25.67	21.11
4	25	36	6.0	3.21	49.56	28.67	21.77
5	40	82	10.8	2.16	44.59	26.15	29.26

[a] General polymerization conditions: catalyst concentration 0.5 mol % monomer, solvent toluene, solvent/monomer 2 (v/v), polymerization time 3 h. [b] Yield: weight of polymer obtained/weight of monomer used. [c] Measured by GPC calibrated with standard polystyrene samples.

Both complexes showed high activity for the ring-opening polymerization of ε-caprolactone (Scheme 2). The identity of the central metal atom has a large effect on the catalytic activity. For example, using **5** as a catalyst gives yields as high as 100% in 15 min over $[M]/[I]$ mol ratios of 500:1 to 1000:1 at 20 °C, while under the same conditions **4** gave yields of only 61.2−27.2%. The order of reactivity Nd > Yb is in agreement with that found for metallocene-based organolanthanide catalysts.[12] The polymerization systems give high molecular weight polymers ($M_n > 10^4$). The molecular mass distributions are broader than those obtained with the homoleptic (phosphoraniminato)lanthanide complexes,[13] especially when long reaction times are used (Entries 4, 6 and 7); this may be due to a transesterification reaction.

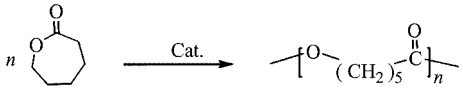

Scheme 2

Complex **5** also exhibits good catalytic activity for the polymerization of methyl methacrylate (Scheme 3). Triad microstructural analysis of the polymers was carried out using ^1H NMR spectra in $CDCl_3$. The catalytic activity increased with increasing polymerization temperature. For example, only a 10% yield was obtained at −78 °C, while at 40 °C, a yield of 82% could be realized. Moreover, the present polymerization system gives the syndio-rich polymers, and the syndiotacticity decreases with increasing polymerization temperature.

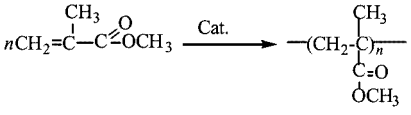

Scheme 3

Conclusions

In summary, we have successfully synthesized a series of new soluble lanthanide bis(guanidinate) complexes free of cyclopentadienyl ligands, and characterized some of their structural features by X-ray crystallography. Moreover, we have found that the "ate" methyllanthanide bis(guanidinate) complexes show highly catalytic activity for the ring-opening polymerization of ε-caprolactone, and good catalytic activity for the polymerization of methyl methacrylate to give syndiotactic polymers. A systematic study of the catalytic activity of methyllanthanide guanidinate complexes in the polymerization of other monomers is ongoing in our laboratory.

Experimental Section

General Procedures: All manipulations were performed under pure argon with rigorous exclusion of air and moisture using standard Schlenk techniques. Solvents were distilled from Na/benzophenone ketyl prior to use. Deuterated benzene was dried with sodium and vacuum-transferred. Anhydrous $LnCl_3$ [14] and $LiN(SiMe_3)_2$ [15] were prepared according to literature procedures. *N*,*N*′-Diisopropylcarbodiimide was purchased from Aldrich and purified by distillation. ε-Caprolactone was purchased from Acros, dried by stirring with CaH_2 for 48 h, then distilled under reduced pressure. Methyl methacrylate was dried by stirring with CaH_2 for 48 h, then distilled under reduced pressure. Melting points were determined in argon-filled capillary tubes and are uncorrected. Lanthanide metal analyses were carried out by complexometric titration. The content of lithium was determined with a Hitachi 180−80 polarized Zeeman atomic absorption spectrophotometer. Carbon, hydrogen, and nitrogen analyses were performed by direct combustion with a Carlo−Erba EA-1110 instrument. The IR spectra were recorded with a Nicolet Magna-IR 550 spectrometer. ^1H and ^{13}C NMR spectra were obtained using a Unity Inova-400 spectrometer. Molecular weight and molecular weight distributions were determined against polystyrene standards by gel permeation chromatography (GPC) at 30 °C with a Waters 1515 apparatus with three HR columns (HR-1, HR-2 and HR-4) using THF as the eluent.

Synthesis of [(SiMe$_3$)$_2$NC(N*i*Pr)$_2$]Li (1): $LiN(SiMe_3)_2$ (1.67 g, 10.00 mmol) in hexane (30 mL) was added dropwise to a hexane solution (50 mL) of *N*,*N*′-diisopropylcarbodiimide (1.6 mL, 10.00 mmol) at room temperature. The resulting reaction mixture was stirred for 30 min and gave a clear pale-yellow solution. After removal of the reaction solvent, crude **1** was isolated as a white powder (2.88 g, 9.81 mmol, 98.3%). $C_{13}H_{32}LiN_3Si_2$ (293.60): calcd. C 53.19, H 11.01, N 14.32; found C 52.79, H 11.24, N 13.82. ^1H NMR ([D$_6$]benzene): δ = 3.78 (m, 2 H, C*H*Me$_2$), 1.17 [d, 12 H, CH(C*H*$_3$)$_2$], 0.35 [s, 18 H, Si(C*H*$_3$)$_3$] ppm. ^{13}C NMR ([D$_6$]benzene): δ = 164.36 (*C*N$_3$), 46.17 (*C*HMe$_2$), 28.19 [(*C*H$_3$)$_2$CH], 3.03 [CN[Si(*C*H$_3$)$_3$]$_2$) ppm. IR (KBr pellets): $\tilde{\nu}$ = 3449 (s), 2963 (m), 1636 (s), 1450 (m), 1389 (m), 1327 (m), 1258 (m), 1173 (m), 1049 (m), 957 (m), 841 (s), 686 (m) cm^{-1}.

Synthesis of [(SiMe$_3$)$_2$NC(N*i*Pr)$_2$]$_2$Yb(μ-Cl)$_2$Li(THF)$_2$ (2): A hexane solution (50 mL) of in situ generated [(SiMe$_3$)$_2$NC(N*i*Pr)$_2$]Li (**1**) (3.90 g, 13.30 mmol) was added to a slurry of $YbCl_3$ (1.85 g, 6.62 mmol) in THF (30 mL). The reaction mixture was stirred for 24 h at room temperature and the solvents were stripped off in vacuo. The residual yellow powder was extracted with diethyl ether and LiCl was centrifuged off. The yellow supernatant was then concentrated and cooled to −15 °C overnight to give bright-yellow crystals. Yield: 4.87 g (5.03 mmol, 76%). M.p.165−168 °C. $C_{34}H_{80}Cl_2LiN_6O_2Si_4Yb$ (968.28): calcd. C 42.17, H 8.34, Li 0.72, N 8.68, Yb 17.87; found C 41.63, H 8.26, Li 0.81, N 8.41, Yb 18.52. ^1H NMR ([D$_6$]benzene): δ = 4.15, 3.84 (m, 4 H, C*H*Me$_2$), 3.64 (m, 8 H, THF-α-C*H*$_2$), 1.47 (m, 8 H, THF-β-C*H*$_2$), 1.33, 1.09 [d, 24 H, CH(C*H*$_3$)$_2$], 0.23 [s, 36 H, Si(C*H*)$_3$] ppm. IR (KBr pellets): $\tilde{\nu}$ = 3283 (m), 3182 (m), 2966 (m), 1635 (s), 1466 (m), 1388 (m), 1321 (m), 1253 (s), 1172 (m), 1057 (s), 952 (m), 841 (s), 756 (m), 686 (m) cm^{-1}.

Synthesis of [(SiMe$_3$)$_2$NC(N*i*Pr)$_2$]$_2$Nd(μ-Cl)$_2$Li(THF)$_2$ (3): As for the synthesis of **2**, using **1** (11.38 mmol), $NdCl_3$ (1.40 g, 5.59 mmol), and THF (60 mL). Recrystallization from toluene yielded blue purple needles of **3** (4.31 g, 4.58 mmol, 82%). M.p. 176−178 °C. $C_{34}H_{80}Cl_2LiN_6NdO_2Si_4$ (939.48): calcd. C 43.46, H 8.60, Li 0.74, N 8.95, Nd 15.35; found C 42.76, H 8.78, Li 0.71, N 8.34, Nd 15.72. ^1H NMR ([D$_6$]benzene): δ = 4.15, 3.85 (m, 4 H, C*H*Me$_2$), 3.61 (m, 8 H, THF-α-C*H*$_2$), 1.45 (m, 8 H, THF-β-C*H*$_2$), 1.33, 1.09 [d, 24 H, CH(C*H*$_3$)$_2$], 0.23 [s, 36 H, Si(C*H*)$_3$] ppm. IR (KBr pellets): $\tilde{\nu}$ = 3296 (m), 2971 (m), 1636 (s), 1466 (m), 1373 (m), 1327 (m), 1258 (s), 1172 (m), 1057 (s), 941 (s), 833 (s), 756 (m), 686 (m) cm^{-1}.

Synthesis of [(SiMe$_3$)$_2$NC(N*i*Pr)$_2$]$_2$Yb(μ-Me)$_2$Li(TMEDA) (4): A Schlenk bottle was charged with **2** (8.23 g, 8.5 mmol) and hexane (100 mL). The solution was cooled to −78 °C, and MeLi (11.4 mL, 16.99 mmol) was added by syringe. The reaction mixture was kept at −78 °C for 1 h, then slowly warmed to room temperature and stirred overnight. After removal of volatiles under vacuum, the yellow residue was extracted with toluene, and LiCl was removed by centrifugation. The supernatant was removed in vacuo, and THF (20 mL) containing TMEDA (1 mL) was added. Cooling to −15 °C overnight gave **3** as bright yellow cubic crystals. Yield 6.1 g (6.12 mmol, 72%). M.p. 100−102 °C. $C_{34.25}H_{90.50}LiN_8Si_4Yb$ (931.01): calcd. C 44.18, H 9.82, Li 0.75, N 12.04, Yb 18.59; found C 43.81, H 9.54, Li 0.71, N 11.98, Yb 18.32. ^1H NMR ([D$_6$]benzene): δ = 2.15 (m, 4 H, C*H*Me$_2$), 1.25 [m, 24 H, CH(C*H*$_3$)$_2$], 0.33 [s, 36 H, Si(C*H*)$_3$], −6.11 (s, 12 H, TMEDA-C*H*$_3$), −7.74 (br, 4 H, TMEDA-C*H*$_2$), −9.81 (s, 4.5 H, C$_6$*H*$_{12}$), −15.45 (br, 6 H, μ-C*H*$_3$) ppm. IR (KBr pellets): $\tilde{\nu}$ = 3449 (m), 2963 (s), 1636 (s), 1466 (m), 1381 (m), 1327 (m), 1258 (s), 1180 (m), 1049 (m), 957 (s), 918 (m), 841 (s), 756 (m), 686 (m) cm^{-1}.

Synthesis of [(SiMe$_3$)$_2$NC(N*i*Pr)$_2$]$_2$Nd(μ-Me)$_2$Li(TMEDA) (5): As for the synthesis of **4**, using **3** (5.60 mmol), MeLi (7.6 mL, 11.32 mmol), and hexane (60 mL). Recrystallization from THF containing TMEDA gave blue-purple cubic crystals. Yield 3.84 g (4.26 mmol, 76%). M.p. 118−120 °C. $C_{34.25}H_{90.50}LiN_8NdSi_4$ (902.21): calcd. C 48.26, H 10.13, N 12.42, Nd 15.99. Li 0.77; found C 47.86, H 9.90, N 11.83, Nd 15.86, Li 0.75. ^1H NMR ([D$_6$]benzene, ppm): δ = 3.51 (m, 4 H, C*H*Me$_2$), 2.83 [m, 24 H, CH(C*H*$_3$)$_2$], 2.16 [s, 36 H, Si(C*H*)$_3$], 1.24 (s, 12 H, TMEDA-C*H*$_3$), 0.51 (br, 4 H, TMEDA-C*H*$_2$), 0.19 (s, 4.5 H, C$_6$*H*$_{12}$), −2.21 (br, 6 H, μ-C*H*$_3$) ppm. IR (KBr pellets): $\tilde{\nu}$ = 3442 (m), 2963 (s), 1636 (s), 1466 (m), 1373 (m), 1327 (m), 1258 (s), 1180 (m), 1049 (s), 957 (s), 918 (m), 841 (s), 756 (m), 686 (m) cm^{-1}.

A Typical Procedure for Polymerization Reactions: The procedures for the polymerization of ε-caprolactone and methyl methacrylate are similar (Table 5), and a typical polymerization procedure is given below (Entry 1, Table 5). A 50-mL Schlenk flask, equipped with a magnetic stirring bar, was charged with a 2.7 mM solution of initiator in toluene. To this solution was added 1 mL of ε-caprolactone using a syringe. The contents of the flask were then stirred vigorously at 20 °C for 15 min , during which time the mixture became very viscous, thus disrupting the stirring. The reaction mixture was quenched by the addition of 1 M HCl solution and was then poured into ethanol to precipitate the polymer, which was dried under vacuum and weighed.

X-ray Structural Determination of 2 and 5: Single crystals were sealed in a thin-walled glass capillary filled with argon for X-ray structural analysis. Diffraction data for **2** were collected with a Bruker SMART CCD area detector using and ω scans. Data for **5** were collected with a Siemens P4 four-circle diffractometer. The structures were solved by direct methods and refined by full-matrix least-squares procedures based on $|F|^2$. All non-hydrogen atoms were refined with anisotropic displacement coefficients. Hydrogen atoms were treated as idealized contributions. The structures of both **2** and **5** were solved and refined using SHELXS-97 and SHELXL-97 programs, respectively. CCDC-192647 (**2**) and

-192648 (**5**) contain the supplementary crystallographic data for this paper. These data can be obtained free of charge at www.ccdc.cam.ac.uk/conts/retrieving.html or from the Cambridge Crystallographic Data Centre, 12 Union Road, Cambridge CB2 1EZ, UK [Fax: (internat.) + 44-1223/336-033; E-mail: deposit@ccdc.cam.ac.uk].

Acknowledgments

The authors are grateful for the Chinese National Natural Science Foundation and the Department of Education of Jingsu Province for financial support.

[1] P. J. Bailey, S. Pace, *Coord. Chem. Rev.* **2001**, *214*, 91.
[2] A. P. Duncan, S. M. Mullins, J. Arnold, R. G. Bergman, *Organometallics* **2001**, *20*, 1808.
[3] N. Thirupathi, G. P. A. Yap, D. S. Richeson, *Organometallics* **2000**, *19*, 2573.
[4] T. G. Ong, D. Wood, G. P. A. Yap, D. S. Richeson, *Organometallics* **2002**, *21*, 1.
[5] Y. L. Zhou, G. P. A. Yap, D. S. Richeson, *Organometallics* **1998**, *17*, 4387.
[6] Z. P. Lu, G. P. A. Yap, D. S. Richeson, *Organometallics* **2001**, *20*, 706.
[7] G. R. Giesbrecht, G. D. Whitener, J. Arnold, *J. Chem. Soc., Dalton Trans.* **2001**, 923.
[8] Y. M. Yao, Y. Zhang, Q. Shen, K. B. Yu, *Organometallics* **2002**, *21*, 819.
[9] G. R. Giesbrecht, A. Shafir, J. Arnold, *J. Chem. Soc., Dalton Trans.* **1999**, 3601.
[10] P. L. Watson, J. F. Whitney, R. L. Harlow, *Inorg. Chem.* **1981**, *20*, 3271.
[11] Q. Shen, Y. X. Chen, Y. H. Lin, *J. Organomet. Chem.* **1991**, *419*, 293.
[12] M. Yamashita, Y. Takemoto, E. Ihara, H. Yasuda, *Macromolecules* **1996**, *29*, 1798.
[13] T. Gröb, G. Seybert, W. Massa, F. Weller, R. Palaniswami, A. Greiner, K. Dehnicke, *Angew. Chem. Int. Ed.* **2000**, *39*, 4373.
[14] M. D. Taylor, C. P. Carter, *J. Inorg. Nucl. Chem.* **1962**, *24*, 387.
[15] L. E. Manzer, *Inorg. Chem.* **1978**, *17*, 1552.

Received June 22, 2002
[I02346]

The Effect of Phenyl Substituents on the Activity of Some Zirconocene Photoinitiators[‡]

Eleonora Polo,*[a] Andrea Barbieri,[a] and Orazio Traverso[b]

Keywords: Homogeneous catalysis / Metallocenes / Photolysis / Polymerisation / Zirconium

In this paper we report the synthesis of several unbridged zirconocenes, **1a**–**c**, **2** and **5**, each bearing a phenyl substituent in the 2-position of the cyclopentadienyl ring. We also report their photochemical behaviour and we compare the results with those obtained with the corresponding unsubstituted metallocenes **3a**–**c** and **4**. Study of their electronic spectra and EPR/spin trapping experiments showed photogeneration of ligand- and zirconium-centred radicals, thus making these complexes suitable as photoinitiators for radical polymerisation processes. The substitution of the hydrogen atom in the 2-position with a phenyl group had positive effects both on the absorption coefficients, improving the light absorption efficiency, and on the reaction yields of *tert*-butyl acrylate polymerisation. These results can be explained in terms of the combined effects of greater persistence of the radical in solution and/or increased efficiency of the radical in initiating the polymerisation process.

(© Wiley-VCH Verlag GmbH & Co. KGaA, 69451 Weinheim, Germany, 2003)

Introduction

A growing area of interest in photochemistry is the design of new photoinitiators for use in pigmented coatings, photoresists, adhesives, and holography;[2−4] of these, initiators with absorption peaks at wavelengths longer than 300 nm are of particular interest since they can be used with the visible light produced by continuous wave lasers.[5]

Since the absorption of a photon generates an electronically excited state that does not occur thermally or occurs only at very high temperatures, photoinitiated reactions and thermally activated processes can induce different reaction pathways. Light can be used as a clean, tuneable and versatile "reagent", thus allowing selective activation of a photoinitiator, also in the presence of organic solvents and chemical contaminants. Another advantage offered by photoinitiation is that the light can be spatially directed and turned on or off simply.

The desirability of expanding the application of photoinitiated chemistry has recently resulted in the discovery of several classes of inorganic and organometallic photoinitiators.[6−9] Among these, metallocenes have attracted increasing interest due to the "tuneability" of their structures and because they leave few toxic residues and photobleach with high efficiency, thus leaving clear or colourless coatings after exposure to argon lasers.

In the context of our research into metallocenes suitable as photoinitiators in radical polymerisation processes, we have recently[1] explored the possible use of several known and new zirconocenes. In the light of the encouraging results obtained, we then investigated possible improvements to their activity as photoinitiators through the introduction of particular substituents in the cyclopentadienyl moiety to modify the electronic distribution.

In this paper we report the photochemical behaviour of several unbridged zirconocenes, each bearing a phenyl substituent in the 2-position of the cyclopentadienyl ring. This substitution should help in stabilising the radical of the polymerisation initiator and enhance the polymerisation efficiency, due to the potential delocalisation of the spare electron offered by the phenyl ring, thus prolonging its life in solution. The introduction of this substituent should increase the absorption coefficients, thus improving the light absorption efficiency.

Several zirconium complexes were synthesised and studied: bis[η^5-(2-phenyl-4,5,6,7-tetrahydro-1*h*-indenyl)]zirconium dichloride [**1a**, $(C6Ph)_2ZrCl_2$], bis[η^5-(2-phenyl-4,5,6,7,8-hexahydroazulenyl)]zirconium dichloride [**1b**, $(C7Ph)_2ZrCl_2$], bis[η^5-(2-phenyl-4,5,6,7,8,9-hexahydro-1*H*-cyclopenta[8]annulenyl)]zirconium dichloride [**1c**, $(C8Ph)_2ZrCl_2$] and bis[η^5-(2-phenylindenyl)]zirconium dichloride [**2**, $(IndPh)_2ZrCl_2$]. The results were compared with those obtained with the corresponding unsubstituted

[‡] Zirconocenes as Photoinitiators for Free Radical Polymerisation of Acrylates, 2. Part 1: Ref.[1]

[a] C.N.R., I.S.O.F. sez. Ferrara,
Via L. Borsari 46, 44100 Ferrara, Italy
Fax: (internat.) + 39-0532/240709
E-mail: tr3@unife.it
tr1@unife.it
[b] Dip. di Chimica dell'Università di Ferrara,
Via L. Borsari 46, 44100 Ferrara, Italy
Fax: (internat.) + 39-0532/240709
E-mail: tr2@unife.it

metallocenes: bis[η^5-(4,5,6,7-tetrahydro-1*H*-indenyl)]zirconium dichloride [**3a**, $(C6)_2ZrCl_2$], bis[η^5-(4,5,6,7,8-hexahydroazulenyl)]zirconium dichloride [**3b**, $(C7)_2ZrCl_2$], bis[η^5-(4,5,6,7,8,9-hexahydro-1*H*-cyclopenta[8]annulenyl)]-zirconium dichloride [**3c**, $(C8)_2ZrCl_2$], and bis(η^5-indenyl)-zirconium dichloride (**4**, Ind_2ZrCl_2).

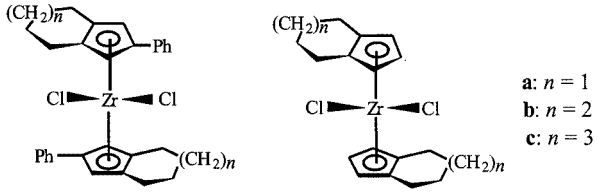

1a–c **3a–c**

Another similar complex, bis(4-methyl-1,2-diphenylcyclopentadienyl)zirconium dichloride [**5**, $(CpMePh_2)_2ZrCl_2$], was also synthesised and tested. It should combine the above advantages with a shorter and cheaper synthetic procedure.

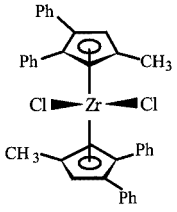

5

Results and Discussion

Ligand and Complex Synthesis

The synthetic approach is outlined in Scheme 1. The starting enones **6a–c** were obtained by a synthetic procedure previously designed in our laboratories.[10]

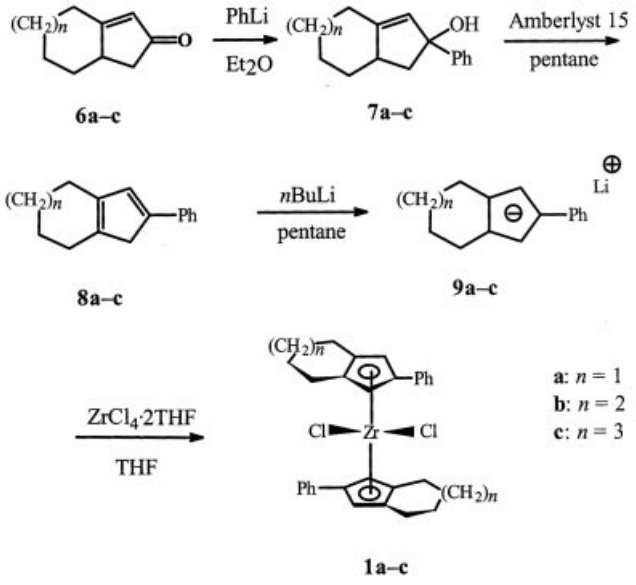

Scheme 1

2-Phenyl-substituted ligands can easily be obtained in three steps from the enones **6a–c**. Treatment of **6a–c** with phenyllithium gave the allyl alcohols **7a–c**, which were dehydrated under very mild conditions by treatment at room temp. with Amberlyst 15, a strongly acidic ion-exchange resin. Since the resulting dienes **8a–c** polymerise quite easily, it is crucial to use low temperatures and short workup times for the dehydration step in order to improve the reaction yields. The use of an ion-exchange resin gave better yields than the usual acid workup, since the reagent can be easily and rapidly removed from the reaction medium by simple filtration. Furthermore, in the case of these phenyl-substituted ligands, filtration through Florisil afforded only one of the three possible isomeric dienes, thus making the hydrogen abstraction easier, since only the isomer bearing an allylic $-CH_2-$ group can easily be dehydrogenated.[11]

Treatment of the dienes with a slight excess of *n*-butyllithium gave the corresponding lithium salts **9a–c**, with overall yields over the three preceding steps ranging from 60 to 70%. Treatment of the lithium salts **9a–c** with $ZrCl_4$·2THF in THF in a 2.3:1 molar ratio resulted in the formation of the corresponding metallocenes **1a–c**, in yields ranging from 68 to 72%.

The synthesis of the complex **5** was performed according to Scheme 2, starting from 4-hydroxy-3,4-diphenylcyclopent-2-en-1-one.

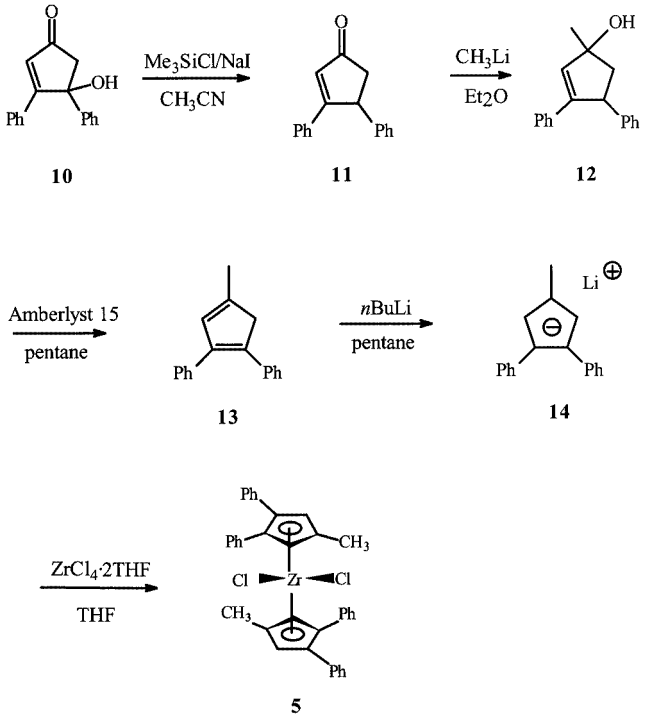

Scheme 2

The synthesis of the ligand **14**[12,13] and of the corresponding metallocenes have already been described by others,[14,15] but we have found that the reaction yields were hardly reproducible. Our modified procedure proved more reliable and gave higher yields both of the intermediates and of the metallocene **5**.

The starting compound was converted into the enone **11** by treatment with the reagent Me_3SiCl/NaI in acetonitrile (a synthetic equivalent of Me_3SiI)[16,17] under very mild conditions. Treatment with methyllithium, followed by dehydration with Amberlyst 15, gave the diene **13** as the sole isomer, if Florisil treatment was used. Treatment with *n*-butyllithium and metallation with $ZrCl_4 \cdot 2THF$ gave the metallocene **5**.

Photochemistry

UV/Vis spectra of the complexes **1a**−**c**, **2** and **5** were recorded in benzene and compared with those obtained previously[1] for the complexes **3a**−**c** and **4**. While we did not observe significant variations in the position of the λ maxima (just a slight shift towards shorter wavelengths), we did see that the substituents in the cyclopentadienyl ring increased the extinction coefficients by more than one order of magnitude (Table 1), a feature particularly interesting for the efficiency of the process.

Table 1. Spectroscopic properties of the complexes in benzene

Complex		λ_{max} [nm]	ε_{max} [$mol^{-1} \cdot L \cdot cm^{-1}$]
1a	$(C6Ph)_2ZrCl_2$	320	23500
1b	$(C7Ph)_2ZrCl_2$	300	18000
1c	$(C8Ph)_2ZrCl_2$	300	14000
2	$(IndPh)_2ZrCl_2$	300	60500
		310	60500
		330	41000
3a	$(C6)_2ZrCl_2$	310	1600
		350	1100
3b	$(C7)_2ZrCl_2$	310	2380
		345	1540
3c	$(C8)_2ZrCl_2$	305	2920
		345	1720
4	$(Ind)_2ZrCl_2$	310	1475
		380	720
5	$(CpMePh_2)_2ZrCl_2$	290	12000

These zirconium(IV) complexes possess d^0 configuration, so any dominant effect of Ligand-Field (LF) and/or Metal-to-Ligand Charge Transfer (MLCT) transitions can reasonably be excluded. Since the free ligand shows absorption bands at lower energies ($\lambda \geq 330$ nm), the observed shift supports the hypothesis of a prevalent Ligand-to-Metal Charge Transfer (LMCT) character for the electronic transition, consistent with the formation of ligand- and metal-centred radicals (Scheme 3). The photochemistry of the complexes strongly supports the LMCT assignment.[18,19]

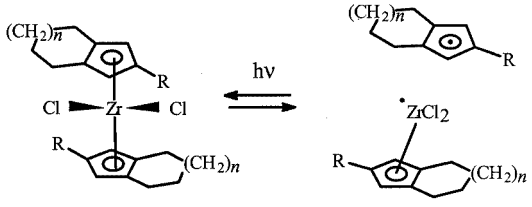

Scheme 3

Selective photolysis was carried out on the complexes in benzene at the wavelengths corresponding to their LMCT transitions, in order to test their photoreactivity in solution and whether they might be possible candidates for free radical photopolymerisation. The nature of the complexes has a significant influence on their photoreactivity in solution; in particular, the introduction of the phenyl substituent seems to accelerate the initial decomposition of the complexes, but only to a certain extent. In the cases of complexes **1a**−**c**, **4** and **5**, we observed percentages of degradation (estimated by UV/Vis spectroscopy) varying from 10 to 40% with respect to the initial values after only 10 min (Figure 1). After that time, though, a sort of plateau was reached, and this persisted for the rest of the irradiation time, as if a photostationary equilibrium had been established. The photodecomposition was reversible; after 24 h of storage in the dark, the initial spectral pattern and absorbance values were almost completely recovered. In contrast, only 15% of the unsubstituted complexes **3a**−**c** was degraded even after 1 h of irradiation.

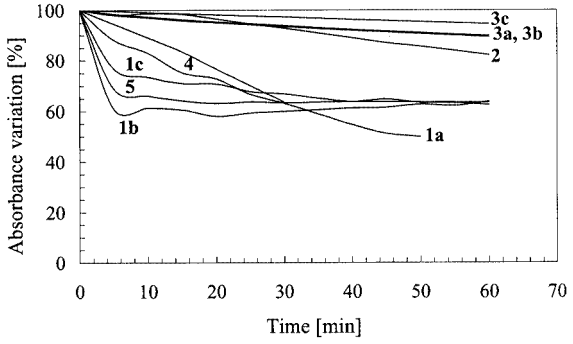

Figure 1. Percentage variation of the absorption band maxima of complexes in benzene as a function of the irradiation time

A particular case is represented by complex **2**, which shows a similar photostability to the complexes **3a**−**c**, despite its phenyl substituent. This effect can be attributed to the extra stabilisation given by the indenyl aromatic system.

EPR Spin Trapping Investigation

To establish the nature of the species produced upon irradiation, EPR/spin trapping experiments were carried out by direct irradiation of benzene solutions of the zirconocenes inside the spectrometer cavity. The spin trap *N-tert*-butyl-α-phenylnitrone (PBN) was used to identify the nature of the radical species (Scheme 4).[20,21]

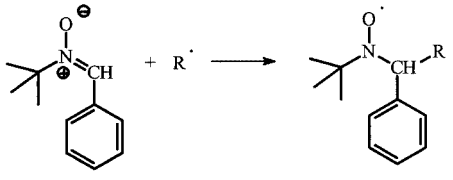

Scheme 4

Besides the signals already recorded with the reference complexes **3a**−**c** and **4**, the spectra of the phenyl-substituted complexes **1a**−**c**, **2** and **5** showed the presence of a

second radical species, consistent with the presence of a cyclopentadienyl radical.[22] Since the hyperfine coupling constant (*hfcc*) values are common to all the phenyl-substituted complexes, including the metallocene **5**, which does not possess a second ring, they can reasonably be assigned to a radical delocalised on the phenyl ring.

Table 2. *hfcc* values of the radical spin adducts with PBN in benzene

Complex		Species I			Species II		
		a_N [G]	a_H [G]	[%]	a_N [G]	a_H [G]	[%]
1a	$(C6Ph)_2ZrCl_2$	14.6	2.4	61	15.3	2.6	39
1b	$(C7Ph)_2ZrCl_2$	14.2	2.1	60	15.0	4.7	40
1c	$(C8Ph)_2ZrCl_2$	14.6	2.7	70	15.0	3.8	30
2	$(IndPh)_2ZrCl_2$	14.5	2.6	66	15.4	3.3	34
3a	$(C6)_2ZrCl_2$	14.6	3.2	100	–	–	–
3b	$(C7)_2ZrCl_2$	14.5	2.9	100	–	–	–
3c	$(C8)_2ZrCl_2$	14.7	3.0	100	–	–	–
4	$(Ind)_2ZrCl_2$	14.6	2.5	100	–	–	–
5	$(CpMePh_2)_2ZrCl_2$	14.6	2.3	71	14.9	3.5	29

Polymerisation Activity

The polymerisation of acrylates has great industrial significance and has been the subject of intensive experimental investigations and practical applications. On the basis of the photochemical findings, polymerisation tests were performed on *tert*-butyl acrylate (*t*BA), the least reactive monomer in the acrylates series. For this reason, the commercial product does not contain stabilisers as the other acrylates do, and its chemical sluggishness makes it a good terminating agent for the polymerisation of the other acrylate monomers. A positive result obtained in *t*BA polymerisation can be considered evidence of a high efficiency of a metallorganic complex as a radical initiator and can rule out the possibility that the polymer obtained may have come from direct photochemical activation of the monomer.

The polymerisation tests were carried out in benzene and the tacticity of the polymer formed was estimated by deconvolution of the methine peaks of poly(*t*BA) at $\delta \approx 42$ ppm in the $^{13}C\{^1H\}$ NMR spectra.

The final result of the polymerisation might be due to the combined effects of two factors: i) the photoreactivity of the complex in solution, and ii) the efficiency of the radical in promoting the polymerisation process.

The polymer yields obtained with the complexes **1a**,**b**, **2** and **5** were at least twice as high as those obtained with the corresponding unsubstituted metallocenes **3a**–**c** and **4**. This improvement in the polymerisation outcome can be explained by better persistence of the radical initiating species in solution. The extra stabilisation provided by the phenyl ring can slow down recombination and fragmentation processes, thus guaranteeing higher concentrations of radical initiators in solution. Particularly interesting is the bis(2-phenylindenyl)zirconium dichloride (**2**), which offers the highest percentage in conversion combined with the best photostability in solution. Complex **5** also deserves more studies, since it combines good monomer conversion with a shorter synthetic preparation.

Another interesting feature is that the polymerisation yields are linear with the irradiation time. This result could be a possible sign of a living radical process.[23] Further studies in order to ascertain the nature of this process unambiguously are currently in progress.

As was to be expected, the stereochemical outcome of the reaction was quite independent of the complex used and the data were quite similar to those reported with the unsubstituted complexes, with a content of syndiotactic triads [rr] ranging from 30 to 35% and of isotactic triads [mm] around 6%. This result is consistent with the radical nature of the process.

Table 3. *tert*-Butyl acrylate polymerisation data

Complex		20% (v/v) *t*BA in C_6H_6 [a]			
		Yield [%][b]	Stereochemistry [%][c]		
			[rr]	[mr]	[mm]
1a	$(C6Ph)_2ZrCl_2$	46	30	65	05
1b	$(C7Ph)_2ZrCl_2$	46	34	60	06
1c	$(C8Ph)_2ZrCl_2$	39	36	58	06
2	$(IndPh)_2ZrCl_2$	56	35	59	06
3a	$(C6)_2ZrCl_2$	24	37	52	11
3b	$(C7)_2ZrCl_2$	22	40	45	15
3c	$(C8)_2ZrCl_2$	24	35	50	15
4	$(Ind)_2ZrCl_2$	25	36	51	13
5	$(CpMePh_2)_2ZrCl_2$	40	35	60	05

[a] Polymerisation conditions: a 20% (v/v) monomer solution in benzene in a 4-mL cuvette was irradiated ($\lambda > 320$ nm) for 1 h in the presence of 7 mg of the metallocene. [b] Degree of polymerisation: (weight of polymer obtained/weight of starting monomer) × 100. [c] Percentage composition of syndiotactic [rr], atactic [mr], and isotactic [mm] triads in the polymer, calculated from deconvolution of the ^{13}C NMR peaks at $\delta = 41-43$ ppm.

Conclusion

On the basis of their photochemical behaviour in solution, known and new phenyl-substituted metallocene complexes **1a**–**c**, **2** and **5** have been used here for the first time as photoinitiators for radical polymerisation processes.

An interesting feature is the high extinction coefficients of these new complexes, which improve the light absorption efficiency of the irradiation process, and the possibility to shift their λ maxima towards lower energies by a judicious choice of phenyl substituents without the necessity to modify the entire synthetic procedure.

The radical species involved in the photoinduced cleavage of the metal–ligand bond have been identified and *t*BA polymerisation has been studied in detail and the results compared with those obtained with the complexes **3a**–**c** and **4**, already described in the first paper of this series.[1]

The substitution of the hydrogen atom in position 2 of the cyclopentadienyl ring with a phenyl group increased the polymerisation yields significantly, due to the combined effects of a longer persistence of the radical in solution and/

or increased efficiency of the radical in initiating the polymerisation process.

Experimental Section

General Remarks: All manipulations of air- and/or moisture-sensitive materials were carried out under an inert gas by use of a dual vacuum/argon line and standard Schlenk techniques. All solvents were thoroughly dehydrated and deoxygenated under argon before use. They were dried and purified by heating at reflux under argon in the presence of a suitable drying agent (pentane, petroleum ether, diethyl ether, benzene, toluene and THF: Na/benzophenone ketyl or potassium; CH_2Cl_2: CaH_2) followed by distillation and storage under argon in Young's ampoules. CH_3CN was dried with 4 Å molecular sieves. Solvents and solutions were transferred under positive argon pressure through stainless steel cannulas (diameter 0.5−2.0 mm) and mixtures were filtered in a similar way with modified cannulas that could be fitted with glass fibre filter disks (Whatman GFC). Unless otherwise specified, all reagents were purchased from commercial suppliers (Aldrich and Fluka) and used without further purification. Reaction courses and product mixtures were routinely monitored by thin layer chromatography (TLC) on pre-coated silica gel F_{254} plates. Preparative flash chromatography was carried out with 60 Å silica gel (230−400 mesh ASTM). Anhydrous magnesium sulfate was used for drying. Elemental analyses were performed with a Carlo Erba 1106 Elemental Analysis apparatus.

NMR Spectra: ^1H (200.13 MHz) and ^{13}C (50.32 MHz) NMR spectra were recorded at room temperature with a Bruker AC 200 spectrometer. Spectra were referenced internally to the residual protio solvent resonance relative to tetramethylsilane (δ = 0 ppm). Deuterated solvents were dried and distilled under argon in the presence of a suitable drying agent ($CDCl_3$: CaH_2; C_6D_6: K) and stored under argon in Young's ampoules.

EPR Studies: The spin trap PBN was purchased from Sigma−Aldrich Chem. Co. and used without further purification. The EPR/spin trapping experiments were performed with a Bruker EMX spectrometer, operating in the X-band (microwave frequency = 9.74 GHz, microwave power = 20 mW, magnetic field modulation frequency = 100 kHz, magnetic field modulation amplitude = 1 G). Sample solutions were freeze-pump-thaw-degassed and then irradiated with a 350-W medium-pressure Hg lamp directly in the EPR spectrometer cavity (Bruker ER-4104OR, TE102). Hyperfine coupling constants (*hfcc*s) were calculated by best-fit simulation of experimental spectra with NIEHS WinSim software.[24]

Photochemical Experiments: Irradiation was performed with an Oriel 500-W high-pressure Hg lamp equipped with cut-off filters for wavelength selection and a water filter to prevent thermal processes. UV/Vis spectra were recorded with a Perkin−Elmer Lambda 40 double-beam spectrophotometer.

Polymerisation Tests: *tert*-Butyl acrylate was dehydrated with CaH_2 and vacuum-distilled immediately before sample preparation. In a typical experiment, a 20% (v/v) monomer solution in benzene in a 4-mL cuvette was irradiated at λ > 320 nm for 1 h in the presence of 7 mg of the metallocene. All polymerisations were carried out at 20 °C. The reaction was quenched by addition of a small amount of aqueous hydrochloric acid, and the polymer was precipitated by pouring CH_3OH/HCl (10:1) into the reaction mixture. The polymer was collected by filtration and dried overnight under high vacuum.

Preparation of the Complexes: The enones **6a**−**c**,[11] 4-hydroxy-3,4-diphenylcyclopent-2-en-1-one (**10**),[13] the metallocenes Ind_2ZrCl_2 (**3**)[25] and (2-phenylindenyl)$_2ZrCl_2$ (**4**)[26] were prepared as described in the literature.

Allylic Alcohols 7. General Procedure: Enone **6** (8.80 mmol) in anhydrous diethyl ether (20 mL) was cooled to 0 °C under nitrogen. Phenyllithium (6.5 mL, 10.4 mmol, 1.6 M in cyclohexane/ether) was slowly added, and the yellow solution became brown. The cooling bath was removed and the mixture was stirred at room temp. until TLC (eluent: diethyl ether/petroleum ether, 1:1) showed only traces of the starting material (about 2 h). The reaction mixture was then cooled to 0 °C, the excess of alkylating agent was decomposed by careful addition of iced water, and the separated organic phase was washed several times with diethyl ether. The collected organic fractions were dried and the solvent was evaporated under reduced pressure. The crude alcohol **7** was obtained in quantitative yield as a mixture of two diastereoisomers.

2-phenyl-2,4,5,6,7,7a-hexahydro-1*H*-inden-2-ol (7a). Major Isomer: ^1H NMR ($CDCl_3$): δ = 1.20−1.50 (m, 3 H), 1.60 (s, 1 H, exchanged on D_2O addition, O*H*), 1.70−2.20 (m, 6 H), 2.40−2.65 (m, 2 H, CH_2Cp), 5.40 (m, 1 H, =C*H*Cp), 7.10−7.60 (m, 5 H, Ar*H*) ppm. **Minor Isomer:** ^1H NMR ($CDCl_3$): δ = 1.20−1.50 (m, 3 H), 1.60 (s, 1 H, exchanged on D_2O addition, O*H*), 1.70−2.20 (m, 6 H), 2.40−2.65 (m, 2 H, CH_2Cp), 5.50 (m, 1 H, =C*H*Cp), 7.10−7.60 (m, 5 H, Ar*H*) ppm.

2-phenyl-1,2,4,5,6,7,8,8a-octahydroazulen-2-ol (7b). Major Isomer: ^1H NMR ($CDCl_3$): δ = 1.35−1.95 (m, 11 H), 2.35−2.60 (m, 2 H), 2.65−2.81 (m, 1 H), 5.48 (m, 1 H, =C*H*Cp), 7.15−7.60 (m, 5 H, Ar*H*) ppm. **Minor Isomer:** ^1H NMR ($CDCl_3$): δ = 1.35−1.95 (m, 11 H), 2.35−2.60 (m, 2 H), 2.65−2.81 (m, 1 H), 5.58 (m, 1 H, =C*H*Cp), 7.15−7.60 (m, 5 H, Ar*H*) ppm.

2-phenyl-2,4,5,6,7,8,9,9a-octahydro-1*H*-cyclopenta[8]annulen-2-ol (7c). Major Isomer: ^1H NMR ($CDCl_3$): δ = 1.38−2.40 (m, 13 H), 2.40−2.60 (m, 2 H), 2.62−2.70 (m, 1 H), 5.52 (m, 1 H, =C*H*Cp), 7.10−7.65 (m, 5 H, Ar*H*) ppm. **Minor Isomer:** ^1H NMR ($CDCl_3$): δ = 1.38−2.40 (m, 13 H), 2.40−2.60 (m, 2 H), 2.62−2.70 (m, 1 H), 5.60 (m, 1 H, =C*H*Cp), 7.10−7.65 (m, 5 H, Ar*H*) ppm.

Dienes 8. General Procedure: Crude alcohol **7** (max, 8.80 mmol), partially dissolved in pentane (30 mL), was stirred at room temp. with Amberlyst 15 (1.27 g). After 1 h, the reaction was complete (TLC: diethyl ether/petroleum ether, 2:1). Magnesium sulfate was added and, after a further 5 min of stirring, the suspension was filtered through a short column (*h* = 6 cm; i.d. = 3 cm) of Florisil (100−200 mesh) and the solvents were evaporated under reduced pressure, keeping the temperature below 30 °C. A yellow solid was obtained.

2-phenyl-4,5,6,7-tetrahydro-1*H*-indene (8a): ^1H NMR ($CDCl_3$): δ = 1.60−1.80 (m, 4 H, CCH$_2$CH_2), 2.20−2.45 (m, 4 H, CCH_2CH$_2$), 3.25 (d, *J* = 1.17 Hz, 2 H, CH_2Cp), 6.70 (d, *J* = 1.17 Hz, 1 H, =C*H*Cp), 7.10−7.70 (m, 5 H, Ar*H*) ppm.

2-phenyl-4,5,6,7,8-hexahydroazulene (8b): ^1H NMR ($CDCl_3$): δ = 1.55−1.82 (m, 6 H, CCH$_2$CH_2), 2.40−2.52 (m, 4 H, CCH_2CH$_2$), 3.25 (d, *J* = 1.08 Hz, 2 H, CH_2Cp), 6.70 (d, *J* = 1.08 Hz, 1 H, =C*H*Cp), 7.15−7.20 (m, 1 H, Ar*H*), 7.20−7.35 (m, 2 H, Ar*H*), 7.35−7.50 (m, 2 H, Ar*H*) ppm.

2-phenyl-4,5,6,7,8,9-hexahydro-1*H*-cyclopenta[8]annulene (8c): ^1H NMR ($CDCl_3$): δ = 1.40−1.60 (m, 4 H, CCH$_2$CH_2), 1.60−1.80 (m, 4 H, CCH$_2$CH_2), 2.45−2.60 (m, 4 H, CCH_2CH$_2$), 3.25 (s, 2 H, CH_2Cp), 6.72 (s, 1 H, =C*H*Cp), 7.10−7.65 (m, 5 H, Ar*H*) ppm.

Lithium Salts 9. General Procedure: Diene **8** (max, 8.80 mmol) was placed in a Schlenk flask, degassed, dissolved in anhydrous petroleum ether (30 mL) and cooled to 0 °C. *n*-Butyllithium (5 mL, 2.5 M solution in hexanes, 12.5 mmol) was added dropwise, and the solution was stirred at 0 °C for 30 min, then allowed to reach room temp. and stirred overnight. Lithium salt **8** separated from the solution as powdery solid, which was filtered through a cannula and washed twice with petroleum ether. The residual solvent was pumped off, leaving the lithium salt **9** as yellow pyrophoric powder.

2-Phenyl-4,5,6,7-tetrahydro-1*H*-indenyllithium (9a): 1.07 g. Yield over three steps: 60%; average yield per step 84%.

2-Phenyl-4,5,6,7,8-hexahydroazulenyllithium (9b): 1.24 g. Yield over three steps: 65%; average yield per step 87%.

2-Phenyl-4,5,6,7,8,9-hexahydro-1*H*-cyclopenta[8]annulenyllithium (9c): 1.44 g. Yield over three steps: 71%; average yield per step 89%.

Metallocene Dichlorides 1. General Procedure: $ZrCl_4 \cdot 2THF$ (4.5 mmol) in THF (20 mL) was added dropwise to solutions of the lithium salts **9** (9.6 mmol) in anhydrous THF (20 mL). The reaction mixtures were stirred overnight. The solvent was then removed under vacuum, and the residues were extracted with toluene, filtered, concentrated and layered with pentane. Fine, deep yellow solids precipitated and were isolated by filtration, washing with pentane and concentration under high vacuum.

Bis[η^5-(2-phenyl-4,5,6,7-tetrahydro-1*H*-indenyl)]zirconium Dichloride (1a): 1.80 g. Yield 68%. $C_{30}H_{30}Cl_2Zr$ (552.69): calcd. C 65.2, H 5.5, Cl 12.8; found C 65.8, H 5.7, Cl 12.4. ^{1}H NMR ($CDCl_3$): δ = 1.2−1.5 (m, 4 H, CCH_2CH_2), 1.6−1.9 (m, 4 H, CCH_2CH_2), 2.1−2.4 (m, 8 H, CCH_2CH_2), 6.1 (s, 4 H, CHCp), 7.0−7.4 (m, 10 H, ArH) ppm. ^{13}C NMR ($CDCl_3$): δ = 22.0 (CCH_2CH_2), 23.8 (CCH_2CH_2), 113.7 (CH Cp), 123.9 (C=CH Cp), 125.2 (*m*CH Ar), 127.3 (*p*CH Ar), 129.0 (*o*CH Ar), 130.8 (CH_2C=CCp), 133.3 (CC= Ar) ppm.

Bis[η^5-(2-phenyl-4,5,6,7,8-hexahydroazulenyl)]zirconium Dichloride (1b): 2.17 g. Yield 78%. $C_{32}H_{34}Cl_2Zr$ (580.74): calcd. C 66.2, H 5.9, Cl 12.2; found C 65.8, H 6.2, Cl 12.0. ^{1}H NMR ($CDCl_3$): δ = 1.6−2.1 (m, 12 H, CCH_2CH_2), 2.2−2.7 (m, 8 H, CCH_2CH_2), 6.3 (s, 4 H, CH Cp), 7.1−7.6 (m, 10 H, ArH) ppm. ^{13}C NMR ($CDCl_3$): δ = 28.6 (CH_2), 30.0 (CH_2), 32.0 (CH_2), 116.4 (CH Cp), 124.4 (C= CH Cp), 125.3 (*m*CH Ar), 127.2 (*p*CH Ar), 129.0 (*o*CH Ar), 133.3 (CC=Ar), 134.6 (CH_2C=C Cp) ppm.

Bis[η^5-(2-phenyl-4,5,6,7,8,9-hexahydro-1*H*-cyclopenta[8]annulenyl)]-zirconium Dichloride (1c): 2.10 g. Yield 72%. $C_{34}H_{38}Cl_2Zr$ (608.80): calcd. C 67.1, H 6.3, Cl 11.7; found C 66.8, H 6.8, Cl 11.3. ^{1}H NMR ($CDCl_3$): δ = 1.0−1.5 (m, 12 H, CCH_2CH_2), 1.6−1.9 (m, 4 H, CCH_2CH_2), 2.0−2.3 (m, 4 H, CCH_2CH_2), 2.3−2.6 (m, 4 H, CCH_2CH_2), 5.6 (s, 4 H, CH Cp), 7.0−7.5 (m, 10 H, ArH) ppm. ^{13}C NMR ($CDCl_3$): δ = 25.9 (CH_2), 26.4 (CH_2), 31.1 (CH_2), 32.3 (CH_2), 107.6 (CH Cp), 124.3 (*m*CH Ar), 124.7 (C=CH Cp), 126.0 (*p*CH Ar), 127.5 (CH_2C=C Cp), 128.6 (*o*CH Ar), 134.9 (CC= Ar) ppm.

3,4-Diphenylcyclopent-2-en-1-one (11): The alcohol **10** (0.5 g, 2 mmol), dissolved in dry benzene (10 mL), and Me_3SiCl (12 mmol, a slightly exothermic reaction occurs) were added to a suspension of NaI (12 mmol) in anhydrous CH_3CN (0.6 mL, 12 mmol). The mixture was stirred at room temp. in the dark until TLC (eluent: diethyl ether/petroleum ether, 1:5:1), showed only traces of the starting alcohol (about 1 h). The reaction mixture was then cooled to 0 °C, quenched with water and extracted several times with diethyl ether. The collected organic fractions were washed with aqueous sodium thiosulfate, water and brine and dried. The solvent was evaporated under reduced pressure to give a deep yellow solid, which was purified by flash chromatography (eluent: diethyl ether/petroleum ether, 1:1.5) to give the enone **11** (0.44 g, 1.86 mmol). (Yield 93%). M.p. 108−110 °C. ^{1}H NMR ($CDCl_3$): δ = 2.46 (dd, *J* = 2.0, 18.8 Hz, 1 H, *cis*-PhCHCH_2), 3.14 (dd, *J* = 7.3, 18.8 Hz, 1 H, *trans*-PhCHCH_2), 4.65 (dt, *J* = 7.3, 1.7 Hz, 1 H, PhC*H*CH$_2$), 6.77 (d, *J* = 1.5 Hz, 1 H, COC*H*), 7.11−7.42 (m, 8 H, Ar*H*), 7.47−7.61 (m, 2 H, Ar*H*) ppm. ^{13}C NMR ($CDCl_3$): δ = 46.68, 46.75, 126.96, 127.06, 127.90, 128.70, 129.06, 129.11, 130.79, 133.18, 141.22, 142.41, 175.12, 208.12 ppm.

1-Methyl-3,4-diphenylcyclopent-2-en-1-ol (12): Methyllithium (2.15 mmol, 1.5 M in diethyl ether) was added dropwise to a solution of enone **11** (0.44 g, 1.86 mmol) in anhydrous THF (20 mL), cooled to 0 °C. The yellow solution turned orange. The mixture was stirred for 30 min at 0 °C and for 30 min at room temperature (TLC: diethyl ether/petroleum ether, 1.5:1). The reaction mixture was then again cooled to 0 °C, the excess of alkylating agent was decomposed by careful addition of iced water, and the separated organic phase was washed several times with diethyl ether. The collected organic fractions were dried and the solvent was evaporated under reduced pressure. The crude alcohol **12** was obtained in quantitative yield as a mixture of two diastereoisomers. **Major Isomer:** ^{1}H NMR ($CDCl_3$): δ = 1.59 (s, 3 H, CH_3), 1.68 (s, 1 H, O*H*), 1.96−2.12 (m, 1 H, *cis*-PhCHCH_2), 2.63−2.82 (m, 1 H, *trans*-PhCHCH_2), 4.27−4.42 (m, 1 H, PhC*H*CH$_2$), 6.34 (d, *J* = 1.5 Hz, 1 H, COC*H*), 7.18−7.41 (m, 10 H, Ar*H*) ppm. **Minor Isomer:** ^{1}H NMR ($CDCl_3$): δ = 1.50 (s, 3 H, CH_3), 1.72 (s, 1 H, O*H*), 1.96−2.12 (m, 1 H, *cis*-PhCHCH_2), 2.63−2.82 (m, 1 H, *trans*-PhCHCH_2), 4.27−4.42 (m, 1 H, PhC*H*CH$_2$), 6.78 (d, *J* = 1.5 Hz, 1 H, COC*H*), 7.08−7.41 (m, 10 H, Ar*H*) ppm.

4-Methyl-1,2-diphenylcyclopentadiene (13): The crude alcohol **12** (max. 1.56 mmol) in diethyl ether (30 mL) was stirred at room temp. with Amberlyst 15 (1.27 g). After 1 h, the reaction was complete (TLC: diethyl ether/petroleum ether, 2:1). Magnesium sulfate was added and, after a further 5 min of stirring, the suspension was filtered and the solvents were evaporated under reduced pressure. The residue was dissolved in petroleum ether and filtered through a short column (*h* = 6 cm; i.d. = 3 cm) of Florisil (100−200 mesh) and the solvents were evaporated under reduced pressure, keeping the temperature below 30 °C. A yellow solid (0.30 g, 1.31 mmol) was obtained (yield over two steps: 80%; average yield per step: 89%). ^{1}H NMR ($CDCl_3$): δ = 2.19 (d, *J* = 1.5 Hz, 3 H, CH_3), 3.49 (d, *J* = 1.1 Hz, 2 H, CH_2Ph), 6.37 (d, *J* = 1.3 Hz, 1 H, C=C*H*), 7.11−7.46 (m, 10 H, Ar*H*) ppm. ^{13}C NMR ($CDCl_3$): δ = 16.2, 48.8, 126.0, 126.9, 127.7, 128.2, 128.35, 132.1, 137.6, 137.5, 136.6, 141.4, 144.0 ppm.

4-Methyl-1,2-diphenylcyclopentadienyllithium (14): The diene **13** (0.30 g, 1.31 mmol) was placed in a Schlenk flask, degassed, dissolved in anhydrous petroleum ether (30 mL) and cooled to −20 °C. *n*-Butyllithium (2.20 mmol, 2.5 M solution in hexanes) was added dropwise, and the solution was stirred at −20 °C for 2 h and then allowed slowly to reach room temp. and stirred overnight. The lithium salt **14** separated from the solution as a powdery solid, which was filtered through a cannula and washed twice with petroleum ether. The residual solvent was pumped off, leaving the lithium salt **14** (0.30 g, 1.24 mmol) as a pale yellow pyrophoric powder (yield 95%).

Bis(1,2-diphenyl-4-methylcyclopentadienyl)zirconium Dichloride (5): The lithium salt **14** (0.30 g, 1.24 mmol) was dissolved in anhydrous THF (20 mL), and a solution of $ZrCl_4 \cdot 2THF$ (4.5 mmol) in THF

(20 mL) was added dropwise. The reaction mixture was stirred overnight. The solvent was then removed under vacuum, and the residue was extracted with toluene, filtered, concentrated and layered with pentane. A powdery, deep yellow solid (0.62 g, 0.99 mmol) precipitated and was isolated by filtration and washing with pentane (yield 80%). $C_{36}H_{30}Cl_2Zr$ (624.35): calcd. C, 69.2, H 4.8; Cl, 11.4; found C 69.1, H 4.9; Cl, 11.3. ^{1}H NMR ($CDCl_3$): δ = 1.73 (s, 6 H, C*H*$_3$), 6.38 (s, 4 H, Cp*H*), 7.11−7.49 (m, 20 H, Ar*H*) ppm. ^{13}C NMR ($CDCl_3$): δ = 15.2, 118.9, 127.4, 128.0, 128.8, 129.4, 133.2 ppm.

[1] E. Polo, A. Barbieri, S. Sostero, M. L. H. Green, *Eur. J. Inorg. Chem.* **2002**, *8*, 405−409.
[2] N. S. Allen (Ed.), *Photopolymerization and Photoimaging Science and Technology*, Elsevier, Amsterdam, **1989**.
[3] S. P. Pappas (Ed.), *Radiation Curing: Science and Technology*, Plenum Press, New York, **1992**.
[4] A. B. Scranton, C. N. Bowman, R. W. Peiffer (Eds.), *Photopolymerization: Fundamentals and Applications*, ACS Symposium Series, no. 673, American Chemical Society, Washington, DC, **1997**.
[5] *Photoinitiators for UV curing. Key Products Selection Guide. Additives*, Ciba, Basel, **1998**, available at http://www.cibasc.com
[6] B. M. Monroe, G. C. Weed, *Chem. Rev.* **1993**, *93*, 435−448.
[7] R. S. Davidson, *J. Photochem. Photobiol., A* **1993**, *69*, 263−275.
[8] R. S. Davidson, *J. Photochem. Photobiol., A* **1993**, *73*, 81−96.
[9] C. Kutal, *Coord. Chem. Rev.* **2001**, *211*, 353−368.
[10] E. Polo, R. M. Bellabarba, G. Prini, O. Traverso, M. L. H. Green, *J. Organomet. Chem.* **1999**, *577*, 211−218. For other synthetic strategies, see references cited herein.
[11] W. A. Herrmann, R. Anwander, H. Riepl, W. Scherer, C. R. Whitaker, *Organometallics* **1993**, *12*, 4342−4349.
[12] R. Guy, C. Mahmoud, *Bull. Soc. Chim. Fr.* **1970**, *10*, 3585−3598.
[13] H. Plenio, D. Burth, *Organometallics* **1996**, *15*, 4054−4062.
[14] F. Zhang, Y. Mu, L. Zhao, Y. Zhang, W. Bu, C. Chen, H. Zhai, H. Hong, *J. Organomet. Chem.* **2000**, *613*, 68−76.
[15] F. Zhang, Y. Mu, J. Wang, Z. Shi, W. Bu, S. Hu, Y. Zhang, S. Feng, *Polyhedron* **2000**, *19*, 1941−1947.
[16] G. A. Olah, A. Husain, B. P. Singh, A. K. Mehrotra, *J. Org. Chem.* **1983**, *48*, 3667−3672.
[17] T. Sakai, K. Miyata, M. Utaka, A. Takeda, *Tetrahedron* **1987**, *28*, 3817−3818.
[18] G. L. Geoffroy, M. S. Wrighton, *Organometallic Photochemistry*, Academic Press, **1979**.
[19] A. Barbieri, A. Droghetti, S. Sostero, O. Traverso, *J. Photochem. Photobiol., A* **1999**, *129*, 137−142.
[20] S. Sostero, D. Rehorek, O. Traverso, E. Polo, *Inorg. Chim. Acta* **1993**, *209*, 171−176.
[21] S. Di Martino, S. Sostero, O. Traverso, D. Rehorek, T. J. Kemp, *Inorg. Chim. Acta* **1990**, *176*, 107−112.
[22] D. R. Duling, *J. Magn. Reson. Ser. B* **1994**, *104*, 105−110.
[23] B. A. Howell, *J. Polym. Sci., Part A: Polym. Chem.* **2000**, *38*, 1727−1729.
[24] A. S. W. Li, K. B. Cummings, H. P. RoethLing, G. R. Buetner, C. F. Chignell, *J. Magn. Reson.* **1988**, *79*, 140−142.
[25] E. Samuel, *Bull. Soc. Chim. Fr.* **1966**, *11*, 3548−3564.
[26] G. W. Coates, R. M. Waymouth, *Science* **1995**, *267*, 217−219.

Received July 2, 2002
[I02359]

Photochromic Properties of a Spirooxazine and a Spiropyran in Alcoholic Solutions of Zirconium and Aluminium Alkoxides: Influence of the Ethyl Acetoacetate Chelating Agent on the Optical Properties

Aurélie Lafuma,[a] Sandrine Chodorowski-Kimmes,[b] Francis X. Quinn,[b] and Clément Sanchez*[a]

Keywords: Alkoxides / Sol-gel processes / Spiro compounds / Photochromism / Aluminium / Zirconium

The photochromism of two spiro compounds, a spiropyran and a spirooxazine, dissolved in alcoholic solutions of metal alkoxides $M(OR)_n$ (M = Zr, Al) has been studied. In the case of the aluminium alkoxide $Al(OsBu)_3$, special photochromic behaviour is observed characteristic of complexation between the coloured form of the dyes and the aluminium. This chemical interaction induces a considerable shift in the absorption spectra and a significant retardation rate in the dark. Addition of ethyl acetoacetate, a bidentate chelate of aluminium, leads to the disappearance of this particular photochromic behaviour.

(© Wiley-VCH Verlag GmbH & Co KGaA, 69451 Weinheim, Germany, 2003)

Introduction

Photochromism involving changes in the visible absorption spectrum has drawn much attention over the last decades because of the variety of practical applications of photochromic systems.[1] In particular, the synthesis of solid photochromic materials using the sol-gel process has been studied extensively.[2−18] Little is known, however, about the dye−matrix interaction. The photochromic properties of spiro compounds are well known. Spiropyrans have been widely studied in the past[1,19−21] and, more recently, spirooxazines have been investigated.[1,22,23] Interest in these compounds is in part explained by their high durability with respect to photoexcitation.

The photochromism of these molecules is due to photocleavage of the spiro bond under UV irradiation, creating an open merocyanine structure (photomerocyanine) which absorbs in the visible region. The reverse reaction proceeds thermally or under irradiation with visible light. Two spiro compounds (Figure 1) have been used in this study: a spiropyran denoted **SP** (1′,3′,3′-trimethyl-6-nitrospiro[2*H*-1-benzopyran-2,2′-indoline]) and a spirooxazine denoted **SO** (1,3,3-trimethylspiro[indoline-2,3′-3′*H*-naphtho[2,1-*b*][1,4]-oxazine]). The photochromism of these two dyes in different solvents is well documented,[24,25] and is very sensitive to the chemical environment of the molecule. In particular, the photochromic band of merocyanine in the visible region is known to be solvatochromic. This absorption band shifts as a function of the polarity of the solvent and the colour changes. **SP** presents a negative solvatochromism characteristic of a prevalent zwitterionic coloured form, whereas **SO** presents a positive solvatochromism characteristic of a prevalent quinonic coloured form. In this paper, we report the photochromic properties (absorption properties and kinetics of thermal bleaching of the coloured form) of **SO** and **SP** in several alcoholic solutions of metal alkoxides $M(OR)_n$ (M = Zr, Al).

Usually such alkoxides are used for the synthesis of sol-gel materials in which **SO** and **SP** can be doped. The physicochemical properties of these materials depend on the chemical nature of the alkoxide(s) and especially on their possible complexation by a chelating agent. Since in solid media photochromism is directly linked to the local envir-

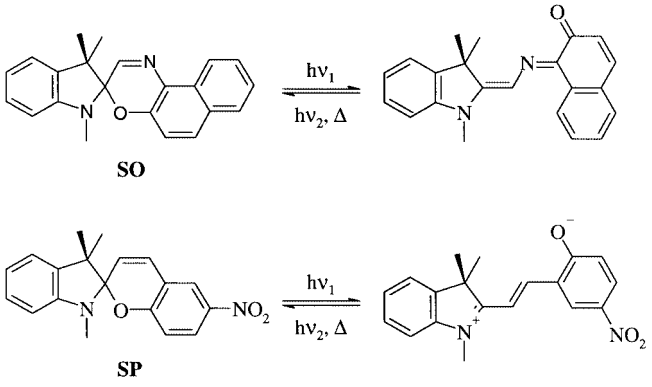

Figure 1. Molecular structures of **SO** and **SP** photochromic dyes

[a] Chimie de la Matière Condensée, Université Pierre et Marie Curie, T54-55,
4 place Jussieu, 75252 Paris Cedex 05, France
E-mail: clems@ccr.jussieu.fr
[b] L'Oréal, Recherche Avancée,
1, avn. Eugène Schueller, B. P. 22, 93601 Aulnay-sous-Bois Cedex, France

onment of the organic doped dye, it is important to determine the possible chemical interaction likely to occur with corresponding molecular precursor(s). Thus, we have studied the photochromic behaviour of **SO** and **SP** in these alkoxides modified or not by a chelating agent. This study will help us in future work on solid media using **SO** and **SP** as local probes of their environment and for understanding their photochromic behaviour in terms of physicochemical dye−matrix interactions.

In the case of the aluminium alkoxide Al(O*s*Bu)$_3$ we observed a significant modification of the photochromic behaviour of **SO** and **SP**, which can be attributed to a complexation of the photomerocyanine by aluminium. Addition of the aluminium chelating agent ethyl acetoacetate (EtacH) to the alkoxide Al(O*s*Bu)$_3$ leads to the superposition of both the complexed and the normal photochromisms for **SP** as well as the sudden disappearance of the complexed photochromism for **SO**.

Results

Characterisation of Metal Alkoxides

Metal alkoxides M(OR)$_n$ in alcoholic solutions can exist as a variety of oligomeric species,[26,27] especially if the charge on the metal ion is less than its usual coordination number. The principal oligomeric structures proposed in the literature[28−34] for the three commercial alkoxides used in this study Zr(O*n*Pr)$_4$, Al(O*s*Bu)$_3$ and [Al(O*s*Bu)$_2$(Etac)] are shown in Figure 2. For Zr(O*n*Pr)$_4$ the oligomeric structures contain solvent molecules.

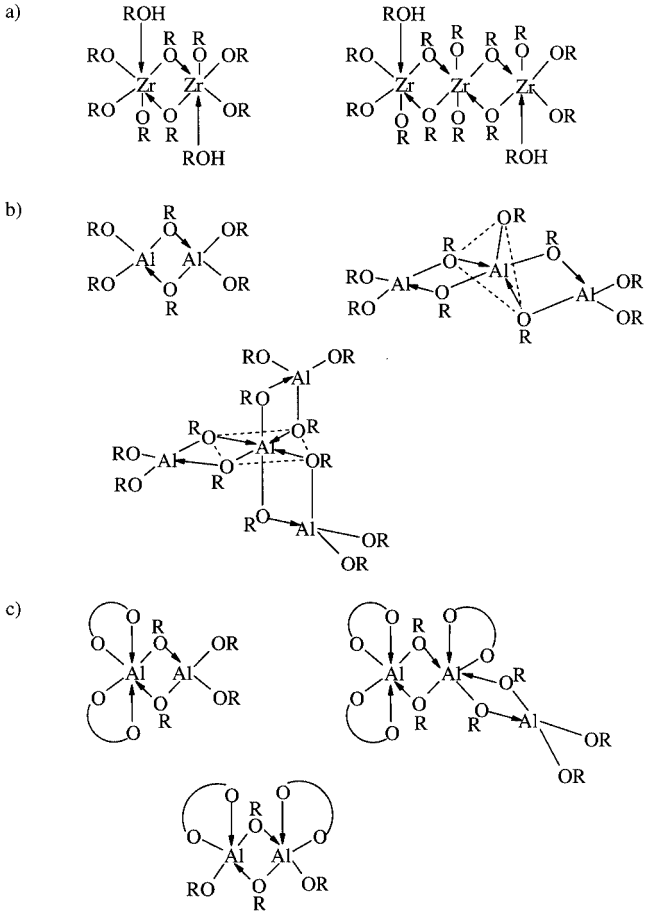

Figure 2. Prevalent oligomeric structures proposed for the metal alkoxides: (a) Zr(O*n*Pr)$_4$; (b) Al(O*s*Bu)$_3$; (c) [Al(O*s*Bu)$_2$(Etac)]

To follow the influence of EtacH on [Al(O*s*Bu)$_2$(Etac)] we synthesised intermediate alkoxides denoted [Al(O*s*Bu)$_{3-x}$(Etac)$_x$], by mixing Al(O*s*Bu)$_3$ with ethyl acetoacetate in molar ratios x = EtacH/Al with x = 0.2, 0.3, 0.4, 0.5, 0.6, 0.8 and 1. The reaction was exothermic.

The complexation between the bidentate chelate EtacH and aluminium was monitored by FTIR spectroscopy (Figure 3). The characteristic bands for EtacH are between 1745−1720 cm^{-1} and 1650−1630 cm^{-1} due to the stretching vibrations ν_{C-O} of the ketonic and enolic forms, respectively. In pure EtacH the ketonic isomer predominates[35] (Figure 4). There is no band due to the ketonic form of the Etac groups in the spectrum of Al(O*s*Bu)$_{3-x}$(Etac)$_x$ or Al(O*s*Bu)$_2$(Etac). Only the bands characteristic of the enolic form appear between 1630−1610 cm^{-1} and 1525 cm^{-1} (ν_{C-O} and ν_{C-C}, respectively). This suggests that Equation (1) occurs.

$$Al(OsBu)_3 + x\ EtacH \rightarrow Al(OsBu)_{3-x}(Etac)_x + x\ sBuOH \quad (1)$$

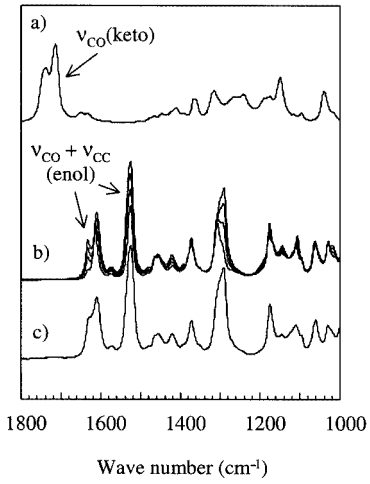

Figure 3. Infrared spectra of a) EtacH, b) Al(O*s*Bu)$_{3-x}$(Etac)$_x$, c) [Al(O*s*Bu)$_2$(Etac)]

We used ^{13}C NMR spectroscopy to look for free EtacH in the alkoxides Al(O*s*Bu)$_{3-x}$(Etac)$_x$. The spectra of Al(O*s*-Bu)$_{2.7}$(Etac)$_{0.3}$ and Al(O*s*Bu)$_2$(Etac)$_1$ (Figure 5) display two broad bands at $\delta \approx$ 175.6 and 188.7 ppm. These two bands are characteristic of carbon atoms C-4 and C-2 of the Etac ligand chelated to the aluminium atom, and they confirm that the Etac groups are bonded to the aluminium centres in an enolic form (Figure 4). In comparison, the peaks indicating free EtacH are at δ = 173.5 and 176.7 ppm for the enolic form and at δ = 167.9 and 200.9 ppm for the diketonic form. Thus, the prevalent ketonic isomer of free Et-

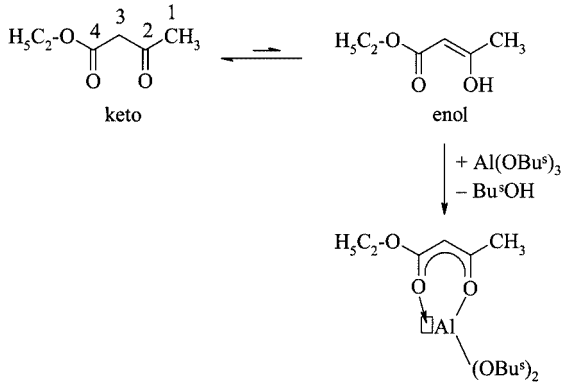

Figure 4. Keto-enol equilibrium of ethyl acetoacetate (EtacH), and schematic representation of the complexation of Al(O*s*Bu)$_3$ with the enol form of EtacH

acH is not present in the alkoxide Al(O*s*Bu)$_{3-x}$(Etac)$_x$: ^{13}C NMR spectroscopy suggests that the reaction in Equation (1) is quantitative in agreement with the reported behaviour of the reactions between metal alkoxides and chelating agents.[26]

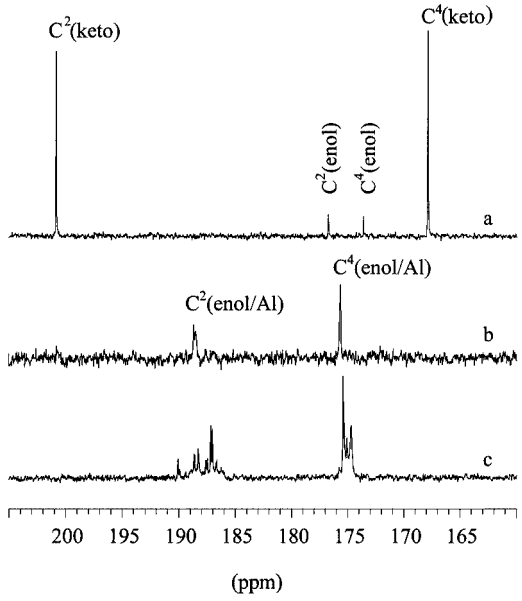

Figure 5. ^{13}C NMR spectra of (a) EtacH, (b) Al(O*s*Bu)$_{2.7}$(Etac)$_{0.3}$, (c) Al(O*s*Bu)$_2$(Etac)$_1$

^{27}Al NMR spectroscopy is very sensitive to the coordination number of aluminium.[33,34,36] The experimental and simulated ^{27}Al NMR spectra of the alkoxides Al(O*s*Bu)$_3$, Al(O*s*Bu)$_2$(Etac) (commercial) and Al(O*s*Bu)$_2$(Etac)$_1$ (prepared by mixing Al(O*s*Bu)$_3$ and EtacH at a molar ratio Etac/Al = 1) are presented in Figure 6. In Al(O*s*Bu)$_3$, the aluminium centres are mainly in tetracoordinate and pentacoordinate sites. The spectrum of Al(O*s*Bu)$_2$(Etac) is clearly different, however, with an observed increase in the coordination number of the aluminium atoms, with evidence for pentacoordinate and hexacoordinate sites. The spectra of Al(O*s*Bu)$_2$(Etac) and Al(O*s*Bu)$_2$(Etac)$_1$ are quite similar and indicate mainly hexacoordinate sites. The ^{27}Al NMR spectra of the alkoxides Al(O*s*Bu)$_{3-x}$(Etac)$_x$ (Figure 7) and their simulations (Table 1) reveal the direct influence of the bidentate ligand on the increase in aluminium's coordination number leading to a decrease of the Lewis acidity of the aluminium atom as *x* increases.

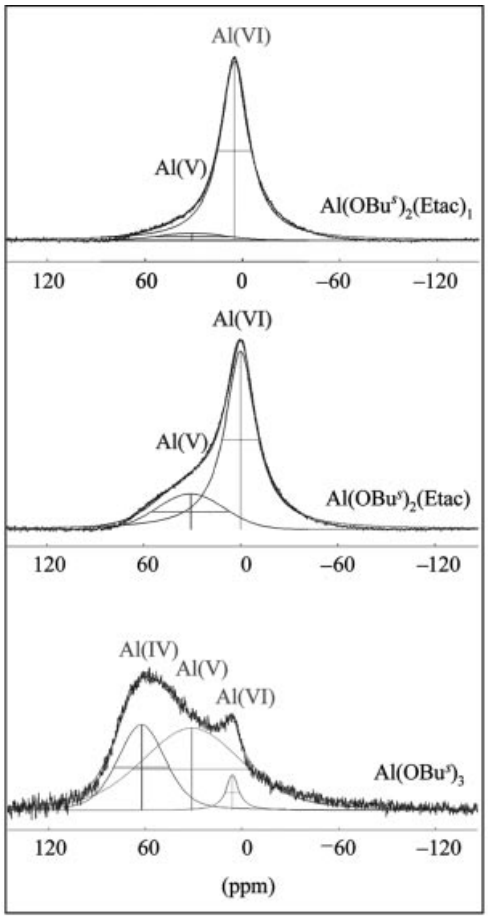

Figure 6. ^{27}Al NMR spectra of Al(O*s*Bu)$_3$, Al(O*s*Bu)$_2$(Etac)$_1$ and Al(O*s*Bu)$_2$(Etac) and their simulations

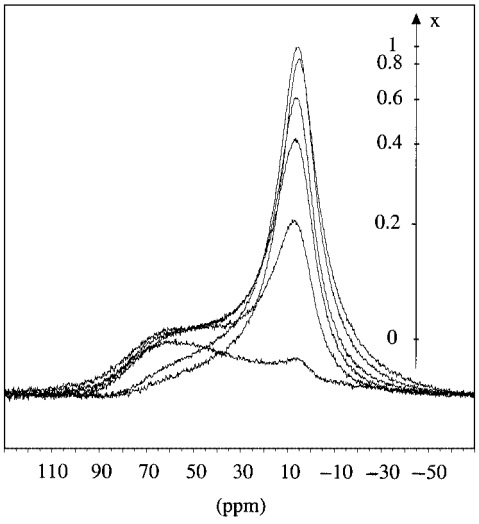

Figure 7. ^{27}Al NMR spectra of Al(O*s*Bu)$_3$ and Al(O*s*Bu)$_{3-x}$(Etac)$_x$ ($0.2 \leq x \leq 1$)

Table 1. Percentage of tetracoordinate, pentacoordinate and hexacoordinate aluminium in the alkoxides $Al(OsBu)_3$ 75%, $Al(OsBu)_{3-x}(Etac)_x$ and $Al(OsBu)_2(Etac)$

Alkoxide	Al^{IV} (%)	Al^{V} (%)	Al^{VI} (%)
$Al(OsBu)_3$ 75%	32	63	5
$Al(OsBu)_{2.8}(Etac)_{0.2}$	28	29	43
$Al(OsBu)_{2.6}(Etac)_{0.4}$	10	39	51
$Al(OsBu)_{2.4}(Etac)_{0.6}$	4	42	54
$Al(OsBu)_{2.2}(Etac)_{0.8}$	1	16	83
$Al(OsBu)_2(Etac)_1$	0	6	94
$Al(OsBu)_2(Etac)$	0	23	77

The oligomeric structures of the alkoxides $Al(OsBu)_{3-x}(Etac)_x$ can therefore be considered as intermediates between the oligomers of $Al(OsBu)_3$ and $Al(OsBu)_2(Etac)$ (see b and c in Figure 2).

Absorption Spectra

The absorption properties of the coloured forms of **SO** and **SP** in alcoholic solutions of zirconium and aluminium alkoxides were compared with those obtained in the corresponding solvent of the alkoxide (PrOH or *s*BuOH) or in the chelating agent EtacH (Table 2). Several metal alkoxides noted as $M(OR)_n$ x% (M = Zr, Al) were used at different percentage x by weight in the corresponding alcohol ROH.

Table 2. Absorption maxima [nm] of **SO** and **SP** in metal alkoxides $M(OR)_n$ [$M(OR)_n$ at a concentration c in ROH]

		SO $\lambda_{B,max}$ [nm]	SP $\lambda_{B,max}$ [nm]	
Solvent:				
PrOH		611	541	
*s*BuOH		611	551	
EtacH		600	567	
	c[M(OR)n] [mol·L^{-1}]	$\lambda_{B,max}$ [nm]	$\lambda_{B1,max}$ [nm]	$\lambda_{B2,max}$ [nm]
Alkoxide:				
$Zr(OnPr)_4$ 70%	2.1	610	496	–
$Zr(OnPr)_4$ 7%	0.17	611	530	–
$Al(OsBu)_3$ 75%	2.8	595	464	–
$Al(OsBu)_3$ 10%	0.33	593	457	–
$Al(OsBu)_{2.8}(Etac)_{0.2}$	2.5	594	463	–
$Al(OsBu)_{2.7}(Etac)_{0.3}$	2.5	605	462	550
$Al(OsBu)_{2.6}(Etac)_{0.4}$	2.5	–	461	555
$Al(OsBu)_{2.4}(Etac)_{0.6}$	2.3	–	466	555
$Al(OsBu)_{2.2}(Etac)_{0.8}$	2.2	–	469	555
$Al(OsBu)_2(Etac)_1$	2.1	609	469	555
$Al(OsBu)_2(Etac)$	2.2	610	460	557

The absorption spectrum of **SO** in the alkoxide $Zr(OnPr)_4$ in PrOH at 70% by weight is similar to that obtained in PrOH. For **SP**, the maximum absorption wavelength measured in $Zr(OnPr)_4$ shows a hypsochromic shift of 45 nm relative to **SP** in PrOH, which suggests a weak stabilizing interaction between the coloured form of **SP** and zirconium (see a in Figure 8). This shift is reduced to 11 nm with a dilution of $Zr(OnPr)_4$ in PrOH at 7% by weight.

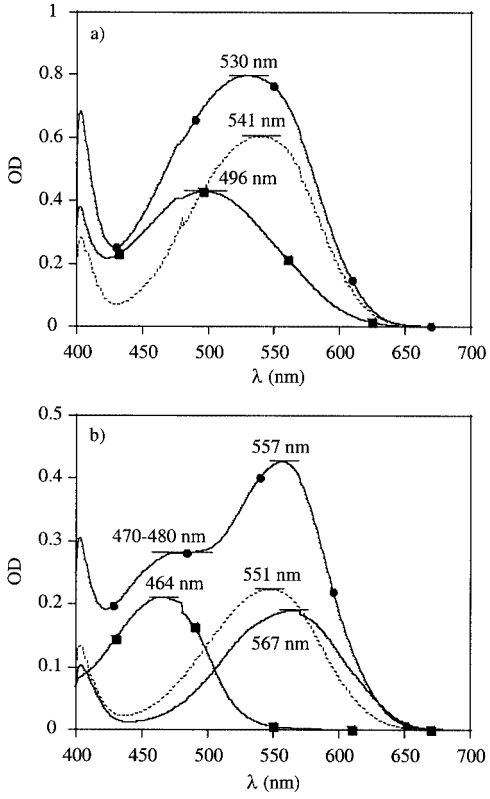

Figure 8. Visible absorption spectra of **SP** under UV irradiation in: (a) $Zr(OnPr)_4$ 70% (squares), $Zr(OnPr)_4$ 7% (dots) and PrOH (···); (b) $Al(OsBu)_3$ 75% (squares), $Al(OsBu)_2(Etac)$ (dots), *s*BuOH (···) and EtacH (—)

A drastic change in the absorption spectra of the coloured form of these dyes is observed in $Al(OsBu)_3$. The absorptions of the photomerocyanine isomers that exist before irradiation are shifted hypsochromically by 20 and 90 nm for **SO** and **SP**, respectively, relative to the values observed in *s*BuOH. This reveals a strong interaction between the photomerocyanine of the dyes and the aluminium alkoxide. This specific photochromic behaviour does not disappear with dilution of $Al(OsBu)_3$ in *s*BuOH by up to 10% by weight.

In the alkoxide $Al(OsBu)_2(Etac)$, **SO** exhibits classic photochromism whereas **SP** presents an absorption spectrum with two bands: one at 460 nm characteristic of a complexed photomerocyanine and the other at 555 nm close to the value obtained in EtacH (Figure 8, part b) revealing the direct influence of Etac on the photochromic behaviour. The absorption spectra of **SP** in the alkoxides $Al(OsBu)_{3-x}(Etac)_x$ before and during UV irradiation (Figure 9) confirm the direct link between the molar ratio x and the behaviour of the complexed dyes. Two distinct situ-

ations are observed: (a) only when x is less than 0.3 do **SO** and **SP** show photochromism whose characteristic features correspond to a complexed dye, and (b) when x is greater than or equal to 0.3 **SO** displays its usual photochromic response whereas **SP** shows a superposition of free and complexed photochromic dyes. This suggests competition between the chelation of aluminium by the ligand EtacH and its chemical interaction with the photomerocyanine of the dye.

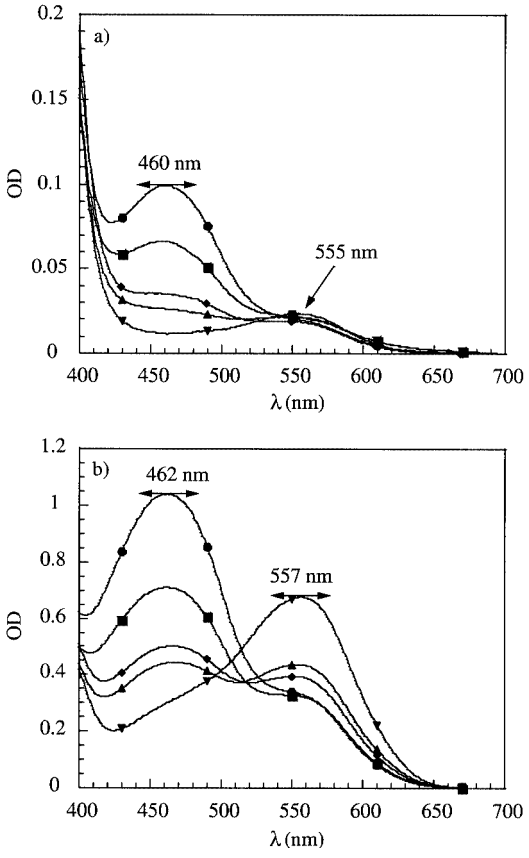

Figure 9. Visible absorption spectra of **SP** in $Al(OsBu)_{2.7}(Etac)_{0.3}$ (dots), $Al(OsBu)_{2.6}(Etac)_{0.4}$ (squares), $Al(OsBu)_{2.4}(Etac)_{0.6}$ (diamonds), $Al(OsBu)_{2.2}(Etac)_{0.8}$ (tringles, up), $Al(OsBu)_2(Etac)_1$ (triangles, down): (a) of initial coloured state and (b) under UV irradiation

Kinetics of Thermal Bleaching

The kinetics of thermal bleaching of photomerocyanines were investigated in solutions of aluminium alkoxides (Table 3) The kinetic fading rate constants k_Δ at the absorption maximum of **SO** and **SP** were obtained using a mono-exponential simulation of the thermal fading versus time. When the dye exhibited superposition between a free and a complexed photochromism two kinetics of thermal bleaching $k_\Delta(\lambda_1)$ and $k_\Delta(\lambda_2)$ at each maximum of absorption λ_1 and λ_2 were observed. This suggests that no exchange between the two coloured photomerocyanines occurs during fading. To control the effect of viscosity on the fading rate we also report the relative viscosity of several aluminium alkoxides (Table 3).

Table 3. Relative viscosity η of aluminium alkoxides and thermal fading k_Δ of **SO** and **SP** in these media

	SO k_Δ [s^{-1}]	**SP** k_Δ [s^{-1}]		
Solvent:				
*s*BuOH	0.5	$2.6\ 10^{-3}$		
EtacH	1.1	$1.5\ 10^{-2}$		
	η [cP]	k_Δ [s^{-1}]	$k_\Delta(460)$ [s^{-1}]	$k_\Delta(555)$ [s^{-1}]
Alkoxide:				
$Al(OsBu)_3$ 75%	28	$2.6\ 10^{-2}$		–
$Al(OsBu)_3$ 10%	–	$5.6\ 10^{-2}$	$2.8\ 10^{-4}$	–
$Al(OsBu)_{2.8}(Etac)_{0.2}$	25	$5.4\ 10^{-2}$	$1.2\ 10^{-4}$	–
$Al(OsBu)_{2.7}(Etac)_{0.3}$	–	0.4	$3.6\ 10^{-4}$	$6\ 10^{-4}$
$Al(OsBu)_{2.6}(Etac)_{0.4}$	23	–	$7.3\ 10^{-4}$	$5.2\ 10^{-4}$
$Al(OsBu)_{2.4}(Etac)_{0.6}$	21	–	$1.1\ 10^{-3}$	10^{-3}
$Al(OsBu)_{2.2}(Etac)_{0.8}$	17	–	$1.4\ 10^{-3}$	$1.5\ 10^{-3}$
$Al(OsBu)_2(Etac)_1$	16	0.8	$2.7\ 10^{-3}$	$2.2\ 10^{-3}$
$Al(OsBu)_2(Etac)$	33	0.81	$8.8\ 10^{-4}$	$1.2\ 10^{-3}$

For **SO** when x is less than 0.3 the kinetics of thermal bleaching of the complexed coloured isomer are especially slow, indicating chemical stabilisation of the photomerocyanine by aluminium. For x greater than or equal to 0.3 the chemical interaction between **SO** and aluminium disappears but we still observe an increase in the fading rate with x. This might be due to the increase of the hydrophobic nature of the medium combined with the addition of Etac, for which the thermal fading k_Δ is especially fast: $k_\Delta(\text{EtacH}) \leq k_\Delta[Al(OsBu)_{3-x}(Etac)_x] \leq k_\Delta(s\text{BuOH})$ for $x \geq 0.3$.

For **SP** when x is less than 0.3 the kinetics of thermal bleaching of the complexed isomer are slower than for the free isomer. This reveals a strong chemical stabilisation of the coloured photomerocyanine by aluminium. For x greater than 0.3 the thermal fading $k_\Delta(465)$ and $k_\Delta(555)$ are quite similar and become faster as x increases (Figure 10). These two values probably correspond to an average value $<k_\Delta>$ resulting from a fast chemical exchange of the metal/ligand type[37–39] between aluminium and the photomerocyanine of **SP**. The increase of this average value $<k_\Delta>$ with x could result from the decrease of the medium's viscosity and from the percentage of the complexed population of **SP**.

Discussion

The observed changes in the photochromic properties of **SO** and **SP** obtained in $Al(OsBu)_3$ are characteristic of strong chemical interactions between the coloured forms of these dyes and the aluminium. For **SO** in $Al(OsBu)_3$ we observed a hypsochromic shift of 15 nm for the complexed photomerocyanine. This is surprising given that **SO** is known to show a positive solvatochromism associated with its prevalent quinonic structure. This shift could be ex-

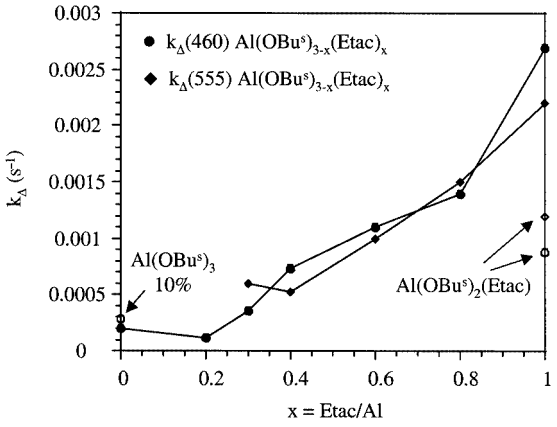

Figure 10. Evolution of the thermal fading of the free, k_Δ(555), and the complexed, k_Δ(460), photomerocyanines of **SP** with the molar ratio x = Etac/Al of the aluminium alkoxides

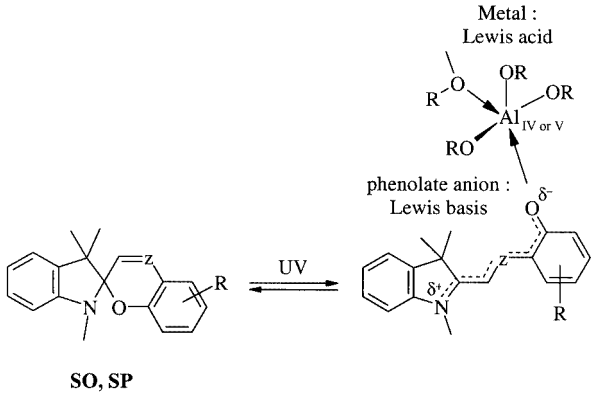

Figure 11. Schematic representation of the chemical interaction between the aluminium alkoxide and the photomerocyanine of **SO** and **SP** (Z = C or N); the depicted Al site is a representation of a trivalent aluminium cation with unsaturated coordination (tetra- or pentacoordinated)

plained by the stabilisation of the zwitterionic photomerocyanine of **SO** complexed with aluminium. The thermal fading of **SO** in 10% Al(O*s*Bu)$_3$ of low viscosity is, surprisingly, ten times slower than the fading rate usually observed in butanol. This confirms the chemical stabilisation of the coloured form of **SO**. A similar, but more noticeable, result was observed for **SP**, with a hypsochromic shift of 90 nm and a fading rate ten times slower in 10% Al(O*s*Bu)$_3$ than in butanol.

Addition of the chelating agent EtacH decreases the Lewis acidity of the aluminium atoms (its coordination increases), and this leads to the appearance of the free photochromic behaviour of the two dyes for x greater than or equal to 0.3. This result proves that the coloured form of the dye is sensitive to the low coordinate aluminium sites. Thus, we suggest that a monodentate Lewis acid/base interaction between the phenolate anion of the zwitterionic form of the photomerocyanine and the electronic lacuna of the tetracoordinate or pentacoordinate aluminium might be responsible for the changes in the photochromic properties (Figure 11). This interaction is monodentate since the photochromism of the **SP** complex still exists in the alkoxides Al(O*s*Bu)$_2$(Etac)$_1$ and Al(O*s*Bu)$_2$(Etac) without tetracoordinate aluminium according to the ^{27}Al NMR simulations. This would explain the sudden and progressive disappearance of the photochromism of the complexed forms of **SO** and **SP** for x greater than or equal to 0.3 in Al(O*s*Bu)$_{3-x}$(Etac)$_x$, since the complexation of the tetracoordinate or pentacoordinate aluminium by the chelating agent EtacH is in competition with the complexation of the coloured form of **SO** and **SP**.

In Zr(O*n*Pr)$_4$, **SP** displays a weak stabilizing interaction with zirconium (small hypsochromic shift of 45 nm) whereas the photochromism of **SO** is similar to that in PrOH. The affinity of zirconium for alcohols has been discussed in the literature.[40,41] In particular it is well known that zirconium alkoxide solvates are quite stable. Indeed, the XRD structure of [Zr(O*i*Pr)$_4$,HO*i*Pr]$_2$ has been reported [42] but such affinity for alcohol ligands should be less effective for aluminium alkoxides. Besides, Al(O*s*Bu)$_3$ is known to be a much stronger Lewis acid than Zr(O*n*Pr)$_4$. This could explain both why the chemical complexation of the coloured forms of the dyes occurs more easily in Al(O*s*Bu)$_3$ in *s*BuOH than in Zr(O*n*Pr)$_4$ in PrOH, and the greater sensitivity of Zr(O*n*Pr)$_4$ upon dilution in PrOH compared with Al(O*s*Bu)$_3$ in *s*BuOH.

Conclusion

We have studied the photochromic properties of **SO** and **SP** in alcoholic solutions of zirconium and aluminium alkoxides. The photochromism of **SP** in Zr(O*n*Pr)$_4$ reveals a weak stabilizing interaction with zirconium, whereas the photochromism of **SO** is not affected by this medium. In Al(O*s*Bu)$_3$ both **SO** and **SP** show specific photochromism characteristic of a strong chemical interaction between the coloured form of the dyes and the aluminium (hypsochromic shift of the absorption maxima and decrease of the thermal fading). This complexed photochromism can be attributed to an acid/base Lewis interaction between the phenolate anion of the zwitterionic photomerocyanine and the electronic lacuna of the tetracoordinate or pentacoordinate aluminium centre. Addition of the chelating agent EtacH to Al(O*s*Bu)$_3$ leads to the disappearance of the complexed photochromism from the molar ratio Etac/Al = 0.3. Thus, the Etac/Al ratio controls the photochromic behaviour of **SO** and **SP** in the alkoxides Al(O*s*Bu)$_{3-x}$(Etac)$_x$ and the colour obtained under UV irradiation.

Finally this study provides useful data for a good understanding of the photochromism observed in solid materials obtained by the sol-gel process of these alkoxides.

Experimental Section

Synthesis: Zr(O*n*Pr)$_4$ (70% in PrOH by weight), PrOH and *s*BuOH were purchased from Fluka. Al(O*s*Bu)$_3$ (75% in *s*BuOH by weight)

and Al(O*s*Bu)$_2$(Etac) (Etac = $C_6H_9O_3$) (95% in *s*BuOH by weight) were purchased from Gelest. Ethyl acetoacetate (EtacH), and the **SO** and **SP** dyes were purchased from Aldrich. Zr(O*n*Pr)$_4$ was used at 70% and 7% by weight in PrOH, Al(O*s*Bu)$_3$ was used at 75% and 10% by weight in *s*BuOH, Al(O*s*Bu)$_2$(Etac) was used at 70% by weight in *s*BuOH. Al(O*s*Bu)$_{3-x}$(Etac)$_x$ alkoxides were synthesised by mixing Al(O*s*Bu)$_3$ with ethyl acetoacetate at a molar ratio x = EtacH/Al with x = 0.2, 0.3, 0.4, 0.5, 0.6, 0.8 and 1. Solutions of **SO** and **SP** with these different metal alkoxides were prepared at a constant concentration of 5 10^{-3} mol·L^{-1}.

FTIR Spectroscopy: FTIR spectra were recorded with a 550 Magna Nicolet spectrometer using the ATR technique and a ZnSe crystal.

NMR Spectroscopy: ^{13}C NMR spectra were recorded in C_6D_6 with a Bruker AC 300 spectrometer in 5-mm tubes. Chemical shifts are given with respect to tetramethylsilane (TMS). ^{27}Al NMR spectra were recorded with a Bruker MSL 400 (104.26 MHz) spectrometer at room temperature. The reference (δ = 0 ppm) was an acidic aqueous solution of aluminium nitrate. The sample was held in an 8-mm tube which was in turn placed in a 10-mm tube with C_6D_6 in the annulus as the lock solvent; 144 transients were accumulated for each sample with pulse widths of 10 μs and recycle delays of 10 s. A blank spectrum (including the probe signal) was recorded under the same experimental conditions and subtracted from each spectrum.

Viscosity Measurements: Relative viscosities were measured with a Carri-med CHR apparatus using a cylindrical geometry. Measurements were obtained under a constant pressure of 10 Pa, the equipment could not detect viscosity under 10^{-2} kg·m^{-1}·s^{-1}.

Optical Experiments: A schematic representation of the basic set-up is given in Figure 12. UV light was filtered from a 400-W Xe lamp and used to activate the photocolouration of the photochromic samples. The light beam was then turned off to follow the dark fading for 10 min. The absorption spectra before and during UV irradiation, and kinetics of dark fading were recorded with a Uvikon 940 spectrophotometer in 1-mm thick quartz cells at room temperature. The kinetics of bleaching were studied by monitoring the fading of the absorbance at each wavelength of absorption maxima of the visible spectrum. The thermal bleachings were fitted ($R^2 > 0.95$) by using a mono-exponential equation: $A = B \exp(-k_\Delta t) + C$ (with C being the initial optical density before UV irradiation).

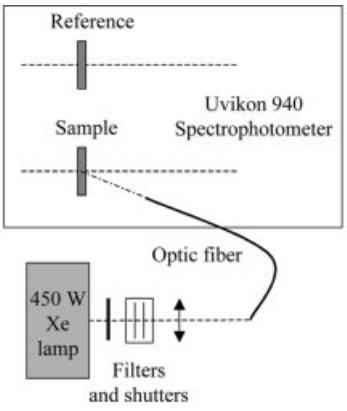

Figure 12. Schematic diagram of the apparatus used for the measurements of the photochromic samples during and after UV irradiation

Acknowledgments

We would like to gratefully acknowledge Jocelyne Maquet for technical assistance with the NMR measurements. We also wish to thank L'Oréal Research for supporting this work.

[1] H. Dürr, H. Bouas-Laurent, *Photochromism: Molecules and Systems*, Elsevier, Amsterdam, **1990**.
[2] B. Dunn, J. I. Zink, *J. Mater. Chem.* **1991**, *1*, 903−913.
[3] E. J. A. Pope, *J. Sol-Gel Sci. Techn.* **1994**, *2*, 717−722.
[4] D. Levy, D. Avnir, *J. Phys. Chem.* **1988**, *92*, 4734−4738.
[5] D. Levy, S. Einhorn, D. Avnir, *J. Non-Cryst. Sol.* **1989**, *113*, 137−145.
[6] D. Preston, J. C. Pouxviel, T. Novinson, W. C. Kaska, B. Dunn, J. I. Zink, *J. Phys. Chem.* **1990**, *94*, 4167.
[7] H. Nakazumi, R. Nagashiro, S. Matsumoto, K. Isagawa, *Sol-Gel Optics III (SPIE)* **1994**, *2288*, 402−409.
[8] J. Biteau, F. Chaput, J. P. Boilot, *J. Phys. Chem.* **1996**, *100*, 9024.
[9] L. Hou, M. Mennig, H. Schmidt, *Proc. Eurogel '92* **1992**, 173.
[10] L. Hou, B. Hoffmann, M. Mennig, H. Schmidt, *J. Sol-Gel Sci. Techn.* **1994**, *2*, 635−639.
[11] L. Hou, H. Schmidt, *J. Mater. Sci.* **1996**, *31*, 3427−3434.
[12] D. Levy, *Chem. Mat.* **1997**, *9*, 2666−2670.
[13] M. Mennig, K. Fries, H. Schmidt, *Mat. Res. Soc. Symp. Proc.* **1999**, *576*, 409−414.
[14] B. Schaudel, C. Guermeur, C. Sanchez, K. Nakatani, J. A. Delaire, *J. Mater. Chem.* **1997**, *7*, 61−65.
[15] Y. Imai, K. Adachi, K. Naka, Y. Chujo, *Polym. Bull.* **2000**, *44*, 9−15.
[16] T. R. Evans, A. F. Toth, P. A. Leermakers, *J. Am. Chem. Soc.* **1967**, *89*, 5060−5061.
[17] M. Nogami, T. Sugiura, *J. Mat. Sci. Lett.* **1993**, *12*, 1544−1546.
[18] G. Wirnsberger, B. J. Scott, B. F. Chmelka, G. D. Stucky, *Adv. Mater.* **2000**, *12*, 1450−1454.
[19] R. Heiligman-Rim, Y. Hirshberg, E. Fischer, *J. Phys. Chem.* **1962**, 2465−2470.
[20] I. Shimizu, H. Kokado, E. Inoue, *Bull. Chem. Soc. Jpn.* **1969**, *42*, 1726−1729.
[21] J. J. B. Flannery, *J. Am. Chem. Soc.* **1968**, *90*, 5660−5671.
[22] N. Y. C. Chu, *Can. J. Chem.* **1983**, *61*, 300−304.
[23] A. Kellmann, F. Tfibel, R. Dubest, P. Levoir, J. Aubard, E. Pottier, R. Guglielmetti, *J. Photochem. Photobiol., A: Chem.* **1989**, *49*, 63−73.
[24] S. R. Keum, M. S. Hur, P. M. Kazmaier, E. Buncel, *Can. J. Chem.* **1991**, *69*, 1940−1947.
[25] J. L. Pozzo, A. Samat, R. Guglielmetti, D. D. Keurkeleire, *J. Chem. Soc., Perkin Trans. 2* **1993**, 1327−1332.
[26] D. C. Bradley, *Coordin. Chem. Rev.* **1967**, *2*, 299−318.
[27] R. C. Mehrotra, A. Singh, *Chem. Soc. Rev.* **1996**, *25*, 1−13.
[28] B. A. Vaartstra, J. C. Huffman, P. S. Gradeff, L. G. Hubert-Pfalzgraf, J. C. Daran, S. Parraud, K. Yunlun, K. G. Caulton, *Inorg. Chem.* **1990**, *29*, 3126−3131.
[29] D. Peter, T. S. Ertel, H. Bertagnolli, *J. Sol-Gel Sci. Technol.* **1994**, *3*, 91−99.
[30] O. Kriz, B. Casensky, A. Lycka, J. Fusek, S. Hermanek, *J. Magn. Reson.* **1984**, *60*, 375−381.
[31] J. H. Wengrovius, M. F. Garbauskas, E. A. Williams, R. C. Going, P. E. Donahue, J. F. Smith, *J. Am. Chem. Soc.* **1986**, *108*, 982−989.
[32] L. Coury, Thèse, Université Paris VI, **1990**.
[33] L. Bonhomme-Coury, F. Babonneau, J. Livage, *J. Sol-Gel Sci. Techn.* **1994**, *3*, 157−168.
[34] F. Babonneau, L. Coury, J. Livage, *J. Non-Cryst. Sol.* **1990**, *121*, 153−157.
[35] J. L. Burdett, M. T. Rogers, *J. Am. Chem. Soc.* **1964**, *86*, 2105−2109.

[36] L. Bonhomme-Coury, F. Babonneau, J. Livage, *Chem. Mater.* **1993**, *5*, 323−330.
[37] A. C. Adams, E. M. Larsen, *Inorg. Chem.* **1966**, *5*, 814−819.
[38] T. J. Pinnavaia, R. C. Fay, *Inorg. Chem.* **1966**, *5*, 233−238.
[39] R. L. Lintvedt, H. F. Holtzclaw, *Inorg. Chem.* **1966**, *5*, 239−241.
[40] D. C. Bradley, *Nature* **1958**, *182*, 1211.
[41] D. C. Bradley, *Coord. Chem. Rev.* **1967**, *2*, 299−318.
[42] B. A. Vaartstra, J. C. Huffman, P. S. Gradeff, L. G. Hubert-Pfalzgraf, J. C. Daran, S. Parraud, K. Yunlun, K. G. Caulton, *Inorg. Chem.* **1990**, *29*, 3126−3131.

Received July 8, 2002
[i02371]

Alkylzinc Complexes with Achiral and Chiral Monoanionic *N,N,O* Heteroscorpionate Ligands

Ina Hegelmann,[a] Alexander Beck,[a] Christian Eichhorn,[b] Bernhard Weibert,[a] and Nicolai Burzlaff*[a]

Keywords: Scorpionate ligands / Zinc / Bioinorganic chemistry / Tripodal ligands / N ligands

The synthesis of the new chiral ligand (3,5-di-*tert*-butylpyrazol-1-yl)(3′,5′-dimethylpyrazol-1-yl)acetic acid (bpaH^{tBu2,Me2}) (**4**) has been achieved. Two different synthetic routes to its precursor 3,5-di-*tert*-butyl-1-[(3,5-dimethyl-1*H*-pyrazol-1-yl)methyl]-1*H*-pyrazole (bpm^{tBu2,Me2}) (**3**) are reported. Deprotonation at the methylene group, followed by reaction with carbon dioxide, yielded a racemic mixture of **4**. The chemical behaviour of bis(3,5-di-*tert*-butylpyrazol-1-yl)acetic acid (bd*t*bpzaH) (**2**) and the new chiral *N,N,O* scorpionate ligand **4** involving their coordination to zinc ions was studied. [Zn(bpa^{tBu2,Me2})Cl] (**5**) was formed from a mixture of $ZnCl_2$, **4** and base. Reaction of bis(3,5-di-*tert*-butylpyrazol-1-yl)acetic acid (bd*t*bpzaH) (**2**) with $Zn(CH_3)_2$ or $Zn(CH_2CH_3)_2$ gave the alkylzinc complexes [Zn(bd*t*bpza)(CH_3)] (**6**) and [Zn(bd*t*bpza)(CH_2CH_3)] (**7**). [Zn(bpa^{tBu2,Me2})(CH_3)] (**8**) was obtained from a synthesis analogous to that of **6** with **4**. The further reactions of **6** and **8** with acetic acid resulted in the acetato complexes [Zn(OAc)(bd*t*bpza)] (**9**) and [Zn(OAc)(bpa^{tBu2,Me2})] (**10**). The chiral methyl complex **8** may serve as a precursor for structural model complexes of the active sites of zinc enzymes, such as thermolysin or carboxypeptidase A. [Zn(bpa^{tBu2,Me2})$_2$] (**11**) was formed from a side reaction. Crystal structures of **4**, **5**, **8** and **11** were obtained; **5** crystallised as the dimer [Zn(bpa^{tBu2,Me2})Cl]$_2$; **11** presents an unusual zinc binding geometry.

(© Wiley-VCH Verlag GmbH & Co KGaA, 69451 Weinheim, Germany, 2003)

Introduction

Zinc complexes with *N,N,O* ligands can serve as models for the active site of zinc-containing enzymes that bind the metal ion with two histidine groups and one aspartate or glutamate group. Examples are carboxypeptidase A, thermolysin (Figure 1) and other proteases.[1–5]

There are only a few examples of *N,N,O* tripod ligands that mimic this motif. Carrano et al. used the scorpionate ligand (3-*tert*-butyl-2-hydroxy-5-methylphenyl)bis(3,5-dimethylpyrazol-1-yl)methane to generate model complexes of zinc-containing enzymes.[6] However, instead of a carboxylate *O*-donor, this ligand contained a phenolate *O*-donor. By insertion of formaldehyde or carbon dioxide into a B–H bond of zinc bis(pyrazol-1-yl)hydroborate complexes, Parkin et al. also formed *N,N,O* model complexes.[7] Recently, we reported on the synthesis of structural models for this class of enzymes by using bis(3,5-di-*tert*-butylpyrazol-1-yl)acetic acid.[8]

Since enzymes are chiral compounds there has been a major effort in bioinorganic chemistry to supply chiral models for the active sites of metalloenzymes. Alsfasser et al.[9] and Vahrenkamp et al.[10] achieved this by including amino acids in the ligand systems. Modification of hydrotris(pyrazol-1-yl)borate (Tp) ligands by chiral pyrazoles de-

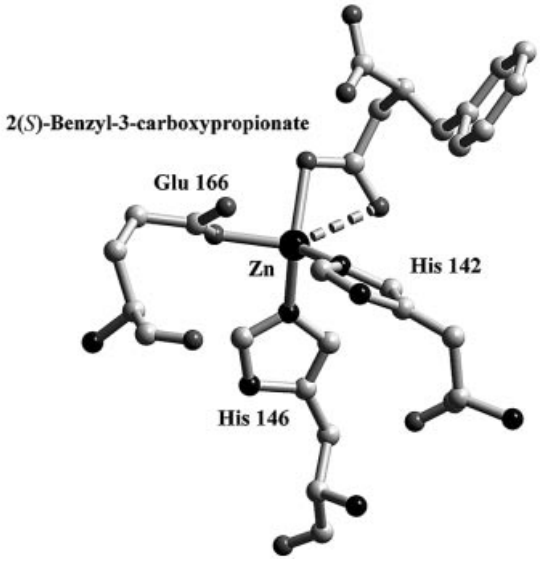

Figure 1. Active site of thermolysin with inhibitor (2*S*)-2-benzyl-3-carboxypropionic acid bound to a zinc ion (PDB-Code: 1HYT)[5]

[a] Fachbereich Chemie der Universität Konstanz,
Universitätsstraße 10, Fach M728, 78457 Konstanz, Germany
Fax: (internat.) + 49-(0)7531/88-3136
E-mail: nicolai@chemie.uni-konstanz.de
[b] Institut für Anorganische Chemie der Universität Würzburg,
Am Hubland, 97074 Würzburg, Germany

rived from the chiral pool is another way to form chiral *N*,*N*,*N* tripod ligands. This was the method used by Tolman et al.[11]

In recent years some of these zinc model complexes have been tested as catalysts for CO_2 activation.[12] Major progress has been made by using Zn^{II}-based catalysts for the copolymerisation of carbon dioxide and epoxides with the focus being on the tacticity of the polycarbonates.[13,14]

Results and Discussion

Based on the ligand synthesis of bdmpza published by Otero et al.,[15] we recently developed a simple synthesis for the sterically hindered bd*t*bpzaH (**2**) suitable for use in forming the model complexes [Zn(bd*t*bpza)Cl].[8] This route was also applied in the synthesis of a racemic mixture of a new chiral *N*,*N*,*O* scorpionate ligand. The unsymmetrical 3,5-di-*tert*-butyl-1-[(3,5-dimethyl-1*H*-pyrazol-1-yl)methyl]-1*H*-pyrazole (bpm^{tBu2,Me2}) (**3**) served as the starting material.[16] It was obtained by a phase-transfer-catalysed reaction of 1-chloromethyl-3,5-dimethylpyrazole hydrochloride with 3,5-di-*tert*-butylpyrazole under basic conditions (Scheme 1). However, the one-step phase-transfer-catalysed reaction of 3,5-dimethylpyrazole with 3,5-di-*tert*-butylpyrazole, dichloromethane and base was more convenient (Scheme 1).

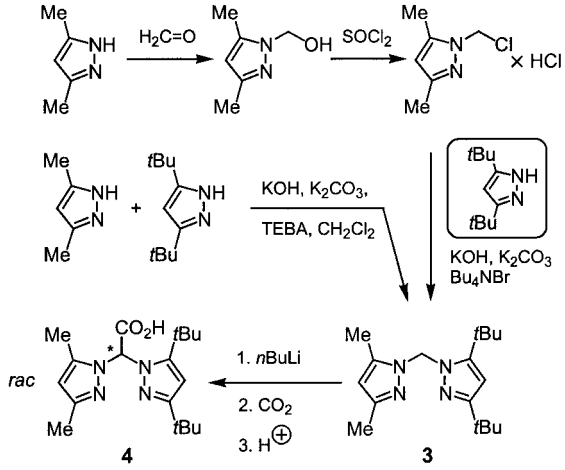

Scheme 1

After separation by column chromatography on silica, **3** was isolated in a yield of up to 17% from the reaction mixture of the three possible products. Since the other two products bis(3,5-dimethylpyrazol-1-yl)methane and especially bis(3,5-di-*tert*-butylpyrazol-1-yl)methane (**1**) can also be isolated in pure form and used for further syntheses, the second synthetic route is currently preferred. Two sets of signals are detected for the two different pyrazolyl rings in the ^1H and ^{13}C NMR spectra. Two medium-intensive IR bands at 1559 and 1541 cm^{-1} are also found for these two pyrazolyl rings.

Deprotonation of a methylene group in **3** followed by reaction with carbon dioxide and acidic workup yielded a racemic mixture of (3,5-di-*tert*-butylpyrazol-1-yl)(3′,5′-dimethylpyrazol-1-yl)acetic acid (bpaH^{tBu2,Me2}) (**4**) (Scheme 1). As in **3** two sets of signals are found in the IR, ^1H and ^{13}C NMR spectra. A strong IR band at 1758 cm^{-1} and a ^1H NMR signal at $\delta = 11.09$ ppm are an indication of the carboxylate group. Crystals of **4** suitable for X-ray structure determination were obtained by crystallisation from acetone (Figure 2). Bond lengths and bond angles in **4** (Table 1) are in good agreement with those reported earlier for bd*t*bpzaH (**2**).[8]

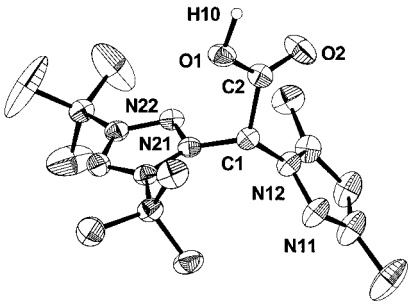

Figure 2. Molecular structure of bpaH^{tBu2,Me2} (**4**); thermal ellipsoids are drawn at the 50% probability level

Table 1. Selected bond lengths and angles of **4**

Distance [Å]	**4**	Angle [°]	**4**
C(1)−C(2)	1.540(3)	O(1)−C(2)−O(2)	125.2(2)
C(2)−O(1)	1.318(3)	C(2)−C(1)−N(12)	113.17(17)
C(2)−O(2)	1.205(3)	C(2)−C(1)−N(22)	111.26(17)
C(1)−N(12)	1.463(3)	N(12)−C(1)−N(22)	113.88(17)
C(1)−N(22)	1.454(3)		

The proton of the carboxylate group was located. It forms an intermolecular hydrogen bond to a pyrazole nitrogen atom of another molecule [*d*(H10−N11) = 1.576(3) Å].

Reaction of **4** with base and water-free $ZnCl_2$ yielded [Zn(bpa^{tBu2,Me2})Cl] (**5**) [Equation (1)]. Suitable crystals of **5** were obtained from dichloromethane. Complex **5** crystallised as a cross-linked dimer [Zn(bpa^{tBu2,Me2})Cl]$_2$ (Figure 3). Selected bond lengths and bond angles of **5** are summarised in Table 2.

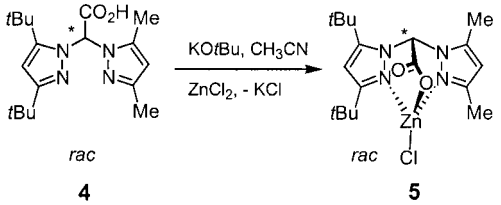

(1)

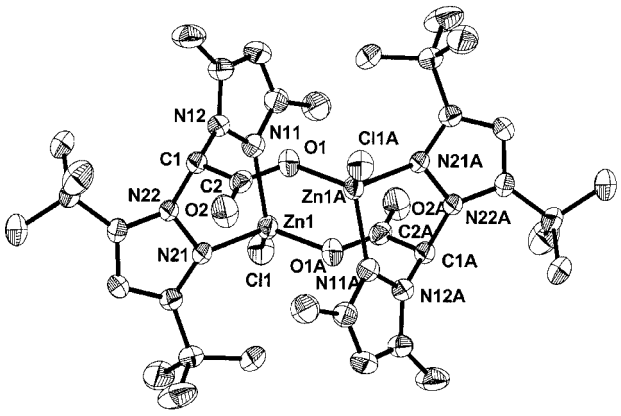

Figure 3. Molecular structure of $[Zn(bpa^{tBu2,Me2})Cl]_2$ (**5**); thermal ellipsoids are drawn at the 50% probability level

Table 2. Selected bond lengths and angles of complex **5**

Distance [Å]	**5**	Angle [°]	**5**
Zn(1)−N(11)	2.031(3)	N(11)−Zn(1)−N(21)	95.17(10)
Zn(1)−N(21)	2.095(2)	O(1A)−Zn(1)−N(11)	112.43(9)
Zn(1)−O(1A)	1.942(2)	O(1A)−Zn(1)−N(21)	103.95(9)
Zn(1)−Cl(1)	2.233(2)	N(11)−Zn(1)−Cl(1)	109.77(8)
		N(21)−Zn(1)−Cl(1)	115.91(6)
		O(1A)−Zn(1)−Cl(1)	117.42(9)

The coordination sphere around the zinc atom is almost tetrahedral, although the angle N(11)−Zn−N(21) [95.17(10)°] is smaller than the ideal tetrahedral one would be. Nevertheless, this tetrahedron is less flattened compared to that previously observed in the structure of the monomer [Zn(bd*t*bpza)Cl].[8] The coordination of the carboxylate group to the zinc atom is less of an *anti*- and more of a *syn*-type compared with the structure of [Zn(bd*t*bpza)Cl].[8] The better donor properties of this *syn*-type coordination may explain the high $\nu_{as}(CO_2^-)$ absorption around 1696 cm^{-1} (KBr pellet). This $\nu_{as}(CO_2^-)$ absorption is rather broad in solution and is found at 1687 cm^{-1}. An IR signal at 1468 cm^{-1} is assigned to $\nu_s(CO_2^-)$. The proposal of a *syn*-type coordination is also supported by a significantly shorter Zn−O(1) distance [1.942(2) Å] and a longer Zn−Cl distance [2.233(2) Å] compared to those in [Zn(bd*t*bpza)Cl] [1.990(2) and 2.170(2) Å].[8] Again, two sets of signals are observed in the NMR spectra due to the two different pyrazolyl groups. Not all of the quaternary signals are detected in the ^{13}C NMR spectrum that might be caused by a monomer/dimer equilibrium.

In the presence of Lewis base type ligands such as pyridine (py) an equimolar amount of acetic acid selectively cleaves one of the Zn−C bonds of dimethylzinc to form methane and the dimer $[Zn(OAc)(CH_3)(py)]_2$.[17] We have observed, that with sterically demanding bis(pyrazol-1-yl)-acetic acids, monomeric four-coordinated alkyl[bis(pyrazol-1-yl)acetato]zinc complexes are obtained in a similar way. Thus, reaction of bis(3,5-di-*tert*-butylpyrazol-1-yl)acetic acid (**2**) with dialkylzinc ZnR_2 (R = CH_3, CH_2CH_3) generates alkylzinc complexes [Zn(bd*t*bpza)(CH_3)] (**6**) and [Zn(bd*t*bpza)(CH_2CH_3)] (**7**) [Equation (2)] with the elimination of alkane.

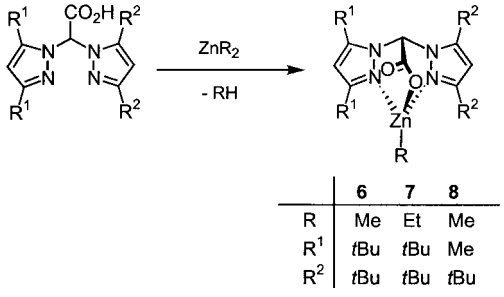

(2)

	6	**7**	**8**
R	Me	Et	Me
R^1	*t*Bu	*t*Bu	Me
R^2	*t*Bu	*t*Bu	*t*Bu

Earlier studies by H. Vahrenkamp et al.[18] and G. Parkin et al.[19] have already shown that four-coordinated alkyl[hydrotris(pyrazol-1-yl)borato]zinc complexes can be obtained by metathesis of ZnR_2 with potassium or thallium salts of sterically demanding hydrotris(pyrazol-1-yl)borate ligands. Since bis(pyrazol-1-yl)acetic acid, and not an alkali carboxylate ligand salt, was used for this synthesis, the workup procedure was simple and **6** and **7** were obtained in high yield and purity; [Zn(bd*t*bpza)(CH_3)] (**6**) is characterised by resonances attributed to the Zn−Me group at δ = −0.35 ppm (^1H NMR) and δ = −10.1 ppm (^{13}C NMR). For the Zn−Et group of [Zn(bd*t*bpza)(CH_2CH_3)] (**7**) signals are found in the ^1H NMR spectrum at δ = 0.52 ppm (q, $^3J_{H,H}$ = 8.0 Hz, CH_2) and δ = 1.29 ppm (t, $^3J_{H,H}$ = 8.0 Hz, CH_3) and in the ^{13}C NMR spectrum at δ = 3.3 ppm (CH_2) and δ = 11.9 ppm (CH_3). The remaining resonances of **6** and **7** can be assigned to the bis(3,5-di-*tert*-butylpyrazol-1-yl)acetato ligand. The analogous reaction of (3,5-di-*tert*-butylpyrazol-1-yl)(3′,5′-dimethylpyrazol-1-yl)acetic acid ($bpaH^{tBu2,Me2}$) (**4**) with dimethylzinc gave the chiral methylzinc complex $[Zn(bpa^{tBu2,Me2})(CH_3)]$ (**8**) [Equation (2)]. The resonances attributed to the Zn−Me group are observed at δ = −0.42 ppm (^1H NMR) and δ = −14.1 ppm (^{13}C NMR). In the infrared spectrum the $\nu_{as}(CO_2^-)$ absorption is assigned to a band at 1669 cm^{-1} and $\nu_s(CO_2^-)$ is assigned to a band at 1466 cm^{-1}. Two sets of NMR and IR signals are found for the two different pyrazolyl groups of the (3,5-di-*tert*-butylpyrazol-1-yl)(3′,5′-dimethylpyrazol-1-yl)acetato ligand. Complex **8** was obtained as a racemic mixture of a chiral complex. Crystals of **8** suitable for X-ray structure determination were obtained from a racemic solution of **8** in CH_2Cl_2. The structure of complex **8** represents one of the rare examples of monomeric four-coordinated alkylzinc complexes and is the first with a carboxylate *O*-donor ligand. Monomers of both enantiomers crystallised in the cell as a result of the centrosymmetric space group (Figure 4). Selected bond lengths and bond angles of **8** are summarised in Table 3.

The Zn−CH_3 bond length in complex **8** [1.962(8) Å] is similar to that in $[Zn(CH_3)Tp^{Me2}]$ [1.981(8) Å].[19] The most striking features of the molecular structure of **8** are

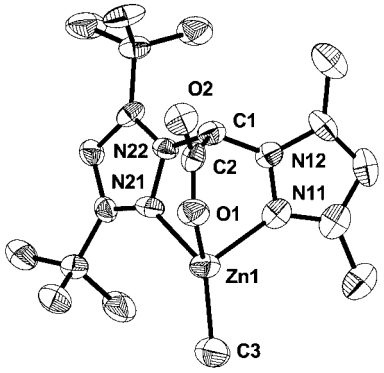

Figure 4. Molecular structure of [Zn(bpa^{tBu2,Me2})(CH$_3$)] (**8**); thermal ellipsoids are drawn at the 50% probability level

Table 3. Selected bond lengths and angles of complex **8**

Distance [Å]	**8**	Angle [°]	**8**
Zn(1)−N(11)	2.085(7)	N(11)−Zn(1)−N(21)	88.3(3)
Zn(1)−N(21)	2.104(6)	O(1)−Zn(1)−N(11)	88.5(2)
Zn(1)−O(1)	2.054(6)	O(1)−Zn(1)−N(21)	87.0(2)
Zn(1)−C(3)	1.962(8)	C(3)−Zn(1)−N(11)	119.8(3)
		C(3)−Zn(1)−N(21)	133.1(3)
		C(3)−Zn(1)−O(1)	126.8(3)

the two different angles C(3)−Zn−N(11) [119.8(3)°] and C(3)−Zn−N(21) [133.1(3)°]. Obviously, the methyl group C(3) is avoiding the bulky *tert*-butyl group. This implies a possible stereoselective induction for future alkyl-transfer reactions.

The reactivity of **6** and **8** towards acetic acid has been examined to provide acetato complexes as useful precursors to enzyme models. A slight excess of acetic acid cleaves the Zn−CH$_3$ bond with the elimination of methane and yields [Zn(OAc)(bd*t*bpza)] (**9**) and [Zn(OAc)(bpa^{tBu2,Me2})] (**10**) [Equation (3)].

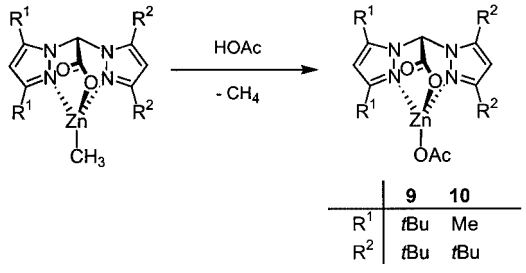

(3)

Therefore, **6** and **8** exhibit a reactivity similar to that of [Zn(CH$_3$)(Tp^{Ph})] and [Zn(CH$_3$)(Tp^{tBu})].[18,19] Signals at δ = 2.12 ppm in the ^{1}H NMR and δ = 21.1 ppm in the ^{13}C NMR spectra of **9** are assigned to the methyl group of the acetato ligand. The carboxylate signal of the acetato ligand was found at δ = 178.2 ppm in the ^{13}C NMR spectrum. Most of the NMR signals of **9** are broad compared to those of the recently published [Zn(bd*t*bpza)Cl] complex. These broad resonances may indicate an η^1/η^2 equilibrium of the acetato ligand. Two additional IR signals at 1633 cm^{-1} and 1602 cm^{-1} are therefore assigned to $\nu_{as}(CO_2^-)$ of η^1- and η^2-bound acetato ligands. The IR signals at 1681 cm^{-1} and 1467 cm^{-1} are assigned to $\nu_{as}(CO_2^-)$ and $\nu_s(CO_2^-)$ of the bd*t*bpza ligand. This is proof of the monomeric structure of **9**, since the monomer [Zn(bd*t*bpza)Cl] shows a similar $\nu_{as}(CO_2^-)$ signal at 1681 cm^{-1}.[8] The value of $\Delta\nu_{as\text{-}s}$ indicates the binding mode of the carboxylate ligand. Values of $\Delta\nu_{as\text{-}s} \geq 200$ cm^{-1} are typical for a unidentate binding mode of acetates which is in good agreement with the $\Delta\nu_{as\text{-}s}$ values of the bis(pyrazol-1-yl)acetato ligands in the complexes **5**−**9**.[20]

The NMR spectra of the complex [Zn(OAc)(bpa^{tBu2,Me2})] (**10**) formed in benzene are similar to those of **9** although two sets of signals for the two different pyrazolyl groups are visible. Three ^{1}H NMR signals at δ = 2.10 ppm, δ = 2.36 ppm and δ = 2.49 ppm are ascribed to two methyl groups of the bpa^{tBu2,Me2} ligand and one of the acetato ligand. A resonance at δ = 22.1 ppm in the ^{13}C NMR spectrum is assigned to the methyl group of the acetato ligand. The carboxylate signal of the acetato ligand was found at δ = 181.2 ppm in the ^{13}C NMR spectrum of **10**. Most of the NMR signals of **10** are broader than those of **9**. Quaternary carbon atoms are difficult to detect in the ^{13}C NMR spectrum due to the signals being broad. A ^{1}H NMR spectrum at −70 °C shows two sets of signals, again indicating an η^1/η^2 equilibrium of the acetato ligand. These slight differences compared with **9** might be explained by the fact that complex **10** is sterically less hindered. In addition to two acetato $\nu_{as}(CO_2^-)$ absorptions at 1624 cm^{-1} and 1601 cm^{-1}, weak IR signals are visible at 1442 cm^{-1} and 1427 cm^{-1} which might be assigned to $\nu_s(CO_2^-)$. The resulting $\Delta\nu_{as\text{-}s}$ values of 159 cm^{-1} and 197 cm^{-1} also verify an η^1/η^2 equilibrium.

[Zn(OAc)(bd*t*bpza)] (**9**) and [Zn(OAc)(bpa^{tBu2,Me2})] (**10**) may also be prepared by reaction of bd*t*bpzaH (**2**) or (bpaH^{tBu2,Me2}) (**4**) with Zn(OAc)$_2$ or from the reaction of

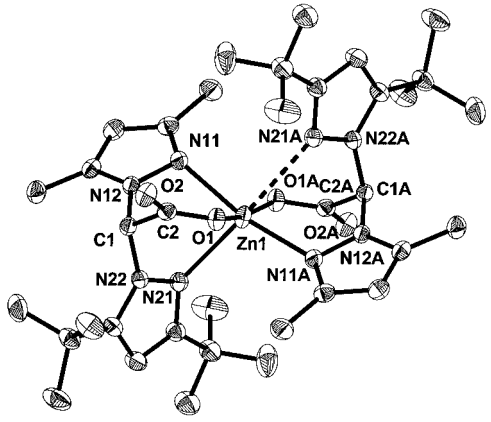

Figure 5. Molecular structure of [Zn(bpa^{tBu2,Me2})$_2$] (**11**); thermal ellipsoids are drawn at the 50% probability level; only one of the zinc positions is shown

the chloro complexes [Zn(bd*t*bpza)Cl] or [Zn(bpa^{tBu2,Me2})Cl] (**5**) with silver acetate. Due to a more complicated workup in these routes along with the formation of by-products we prefer the alkylzinc route.

During the synthesis of **10** in an acetonitrile solution a sandwich complex [Zn(bpa^{tBu2,Me2})$_2$] (**11**) was formed as a by-product. The facile formation of the related six-coordinated complexes [Zn(Tp^R)$_2$] in the reactions of [Zn(Tp^R)X] (X = OH, CH_3, Cl) has already been reported by H. Vahrenkamp et al.,[18] G. Parkin et al.[19] and Kläui et al.[21] with either octahedral[19] or tetrahedral[21] structures of the complexes [Zn(Tp^R)$_2$]. This redistribution seems to be favoured by polar solvents and sterically less demanding ligands, since the synthesis of [Zn(OAc)(bd*t*bpza)] (**9**) is less problematic. Crystals of compound **11** suitable for X-ray analysis were obtained from a solution in $CHCl_3$ (Figure 5). Bond lengths and bond angles of **11** are summarised in Table 4.

Table 4. Selected bond lengths and angles of complex **11**

Distance [Å]	**11**	Angle [°]	**11**
Zn(1)−N(11)	2.156(3)	N(11)−Zn(1)−N(21)	83.99(9)
Zn(1)−N(21)	2.3456(17)	O(1)−Zn(1)−N(11)	86.66(10)
Zn(1)−N(21A)	2.7319(18)	O(1)−Zn(1)−N(21)	89.62(8)
Zn(1)−O(1)	2.006(3)		
Zn(1)−Zn(1A)	0.405(2)		

A structural model with the zinc atom in the centre of the symmetry resembled that of [Zn(bdmpza)$_2$], which we reported recently.[8] The main differences were the extraordinary long bonds of the Zn atom to each of the nitrogen atoms of the two 3,5-di-*tert*-butylpyrazol-1-yl rings. This distance Zn−N(21) [2.5369(14) Å] was in between that of [Zn(bdmpza)$_2$] [2.180(3) Å] and the sum of the van der Waals radii [N 1.55 Å; Zn 1.40 Å]. Until now examples of octahedral zinc complexes with a longer Zn−N distance were rare, and in most cases were caused by a disorder.[22] In addition to the long bond the thermal ellipsoid of the zinc atom is rather elongated towards the two 3,5-di-*tert*-butylpyrazol-1-yl rings. Therefore, the zinc atom in **11** is disordered with two equally occupied positions slightly off the centre of symmetry; **11** exhibits a distorted square-pyramidal coordination with the 3,5-di-*tert*-butylpyrazol-1-yl group slightly bent away from the Zn−N(21) axis and the other 3,5-di-*tert*-butylpyrazol-1-yl group has a weak interaction with the zinc ion from the base direction of the pyramid.

Conclusions

A synthetic route to a racemic mixture of the new chiral scorpionate ligand (3,5-di-*tert*-butylpyrazol-1-yl)(3′,5′-dimethylpyrazol-1-yl)acetic acid (**4**) was found via 3,5-di-*tert*-butyl-1-[(3,5-dimethyl-1*H*-pyrazol-1-yl)methyl]-1*H*-pyrazole (**3**). It is sterically less hindered than the recently published bis(3,5-di-*tert*-butylpyrazol-1-yl)acetic acid (**2**), but its coordination properties are similar to those of **2**. The reaction of **2** or **4** with dialkylzinc yields the new alkylzinc complexes [Zn(bd*t*bpza)(CH_3)] (**6**), [Zn(bd*t*bpza)(CH_2-CH_3)] (**7**) and [Zn(bpa^{tBu2,Me2})(CH_3)] (**8**). Complex **8** is an example of rare monomeric alkylzinc complexes and is the first one with a carboxylate *O*-donor ligand. Acetato complexes [Zn(OAc)(bd*t*bpza)] (**9**) and [Zn(OAc)(bpa^{tBu2,Me2})] (**10**), that serve as models for the active sites of the zinc-containing enzymes carboxypeptidase A or thermolysin, were obtained by reaction of **6** and **8** with acetic acid. Future work has to define a synthetic way to obtain enantiomerically pure bis(pyrazol-1-yl)acetic acids and has to prove whether the configuration of these is stable. This might be useful for structural model complexes of metalloenzymes as well as for organometallic complexes with bis(pyrazol-1-yl)acetate ligands. The first examples of manganese, rhenium and ruthenium complexes with non-chiral bis(pyrazol-1-yl)acetate ligands have already been published.[23]

Experimental Section

General: All experiments were carried out in Schlenk tubes using suitable purified solvents. Microcrystalline precipitates were separated by centrifugation with a Hettich Rotina 46 R Schlenk tube centrifuge. IR: Biorad FTS 60, CaF_2 cuvets (0.5 mm). ^1H and ^{13}C NMR: Bruker WM 250, Bruker AC 250, JEOL GX 400, δ values relative to TMS; in some cases the ^{13}C NMR signals of quaternary carbon atoms were too weak to be detected. EI-MS and FAB MS: modified Finnigan MAT 312. Elemental analyses: Analytical Laboratory of the Fachbereich Chemie, Universität Konstanz. A modified Siemens P4 diffractometer was used for X-ray structure determinations. 3,5-Dimethylpyrazole, 2,2,6,6-tetramethyl-3,5-heptanedione, Zn(CH_3)$_2$ solution, Zn(CH_2CH_3)$_2$ solution and $ZnCl_2$ were used as purchased. 1-Chloromethyl-3,5-dimethylpyrazole hydrochloride was synthesised according to the literature.[24] 3,5-Di-*tert*-butylpyrazole was obtained by a standard literature method from 2,2,6,6-tetramethyl-3,5-heptanedione and hydrazine hydrate.[25] The synthesis of bis(3,5-di-*tert*-butylpyrazol-1-yl)acetic acid (bd*t*bpzaH) (**2**) via bis(3,5-di-*tert*-butylpyrazol-1-yl)methane (**1**) was reported recently.[8]

Ligand Syntheses

Synthesis of 3,5-Di-*tert*-butyl-1-[(3,5-dimethyl-1*H*-pyrazol-1-yl)methyl]-1*H*-pyrazole (bpm^{tBu2,Me2}) (3): 3,5-Dimethylpyrazole (6.93 g, 72.1 mmol), 3,5-di-*tert*-butylpyrazole (13.0 g, 72.1 mmol), KOH (8.42 g, 150 mmol), K_2CO_3 (20.7 g, 150 mmol) and benzyltriethylammonium chloride (2.00 g) were dissolved in dichloromethane (300 mL) and heated under reflux for 12 h. Salts were removed by filtration and the filtrate was concentrated in vacuo to dryness. The white residue was dissolved in water and extracted with pentane (4 × 200 mL). The organic layer was dried (Na_2SO_4) and the solvent removed in vacuo yielding a crude mixture of bis(3,5-dimethylpyrazol-1-yl)methane (bdmpzm), bis(3,5-di-*tert*-butylpyrazol-1-yl)methane (bd*t*bpzm) (**1**) and 3,5-di-*tert*-butyl-1-[(3,5-dimethyl-1*H*-pyrazol-1-yl)methyl]-1*H*-pyrazole (bpm^{tBu2,Me2}) (**3**). Column chromatography with pentane on silica (20 cm) yielded a fraction of bd*t*bpzm (**1**) and with pentane/ethyl acetate (14:1) a pure fraction of bpm^{tBu2,Me2} (**3**). The solutions were dried (Na_2SO_4) and solvents were evaporated; bd*t*bpzm (yield 8.52 g, 63%) was used as described earlier to synthesise bd*t*bpza (**3**).[8] The white residue of

bpm^{tBu2,Me2} (**3**) was recrystallised from acetone to give **3** as colourless crystals, which were dried in vacuo. R_f (pentane/ethyl acetate, 14:1, v/v, silica 60 plate, ammonium vanadate stain) = 0.78 [bd*t*bpzm (**1**)], 0.30 [bpm^{tBu2,Me2} (**3**)]; yield (**3**) 3.52 g (17%); m.p. 75 °C. ^{1}H NMR ($CDCl_3$, 250 MHz): δ = 1.25 (s, 9 H, CH_3), 1.37 (s, 9 H, CH_3), 2.18 (s, 3 H, CH_3), 2.32 (s, 3 H, CH_3), 5.78 (s, 1 H, H_{pz}), 5.86 (s, 1 H, H_{pz}), 6.27 (s, 2 H, CH_2) ppm. ^{13}C NMR ($CDCl_3$, 62.5 MHz): δ = 11.4 (CH_3), 13.4 (CH_3), 30.3 (CH_3), 30.4 (CH_3), 31.6 (C-*t*Bu), 31.9 (C-*t*Bu), 63.1 (CH_2), 101.0 (C_{pz}), 106.5 (C_{pz}), 141.2 (C_{pz}), 147.6 (C_{pz}), 152.6 (C_{pz}), 160.1 (C_{pz}) ppm. EI MS (70 eV): *m*/*z* (%) = 288 (26) [M^+], 193 (30) [$M^+ - C_5H_7N_2$], 108 (100) [$M^+ - C_{11}H_{19}N_2$]. IR (THF): $\tilde{\nu}$ = 1559 (C=N), 1541 (C=N) cm^{-1}. $C_{17}H_{28}N_4$ (288.44): calcd. C 70.79, H 9.78, N 19.42; found C 70.99, H 9.88, N 19.17. Reaction of 1-chloromethyl-3,5-dimethylpyrazole hydrochloride with 1 equiv. of 3,5-di-*tert*-butylpyrazole, traces of benzyltriethylammonium chloride and excess of KOH and K_2CO_3 in THF yielded an identical sample of **3**.

Synthesis of (3,5-Di-*tert*-butylpyrazol-1-yl)(3′,5′-dimethylpyrazol-1-yl)acetic Acid (bpaH^{rBu2,Me2}) (4): A solution of 3,5-di-*tert*-butyl-1-[(3,5-dimethyl-1*H*-pyrazol-1-yl)methyl]-1*H*-pyrazole (bpm^{tBu2,Me2}) (**3**) (6.50 g, 22.5 mmol) in THF (100 mL) was treated with *n*BuLi (ca. 1.6 M solution in hexane, 15.0 mL, 24.0 mmol) at −70 °C. The solution was heated to −45 °C over a period of 2 h and finally flushed with a flow of carbon dioxide. At ambient temperature, the solvent was removed in vacuo and the white residue dissolved in water (100 mL). The aqueous solution was acidified with concentrated HCl to a pH value of 1 and extracted with diethyl ether (4 × 200 mL). The combined organic layers were dried (Na_2SO_4) and concentrated in vacuo to give a white residue. The residue was washed with pentane (2 × 200 mL) to remove unchanged bpm^{tBu2,Me2} (**3**) and dried in vacuo to yield (3,5-di-*tert*-butylpyrazol-1-yl)(3′,5′-dimethylpyrazol-1-yl)acetic acid (bpaH^{tBu2,Me2}) (**4**) as a colourless powder. Yield 4.00 g (53%); m.p. 172 °C (dec.). ^{1}H NMR ($CDCl_3$, 250 MHz): δ = 1.25 (s, 9 H, CH_3), 1.28 (s, 9 H, CH_3), 2.11 (s, 3 H, CH_3), 2.19 (s, 3 H, CH_3), 5.82 (s, 1 H, H_{pz}), 5.98 (s, 1 H, H_{pz}), 7.14 (s, 1 H, CH), 11.09 (br. s, 1 H, CO_2H) ppm. ^{13}C NMR ($CDCl_3$, 62.5 MHz): δ = 11.5 (CH_3), 13.1 (CH_3), 30.1 (CH_3), 30.3 (CH_3), 31.6 (C-*t*Bu), 32.1 (C-*t*Bu), 72.6 (CH), 102.0 (C_{pz}), 108.1 (C_{pz}), 141.3 (C_{pz}), 148.6 (C_{pz}), 154.7 (C_{pz}), 160.3 (C_{pz}), 166.1 (CO_2H) ppm. EI MS (70 eV, 160 °C): *m*/*z* (%) = 332 (7) [M^+], 288 (20) [$M^+ - CO_2$], 193 (100) [$M^+ - C_5H_7N_2 - CO_2$], 109 (58) [$M^+ - C_{11}H_{19}N_2 - CO_2$], 57 (20) [$C_4H_9$]. IR (THF): $\tilde{\nu}$ = 1758 (CO_2H), 1560 (C=N), 1546 (C=N) cm^{-1}. $C_{18}H_{28}N_4O_2$ (332.45): calcd. C 65.03, H 8.49, N 16.85; found C 64.79, H 8.76, N 16.31.

Synthesis of Model Compounds

Synthesis of [Zn(bpa^{rBu2,Me2})Cl]$_2$ (5): $ZnCl_2$ (200 mg, 1.47 mmol) was added to a solution of (3,5-di-*tert*-butylpyrazol-1-yl)(3,5-dimethylpyrazol-1-yl)acetic acid (bpaH^{tBu2,Me2}) (**4**) (400 mg, 1.20 mmol) in acetonitrile (30 mL), and the solution was stirred vigorously at ambient temperature. After 5 min, potassium *tert*-butoxide (135 mg, 1.20 mmol) was added. Within 1 min, a white precipitate formed. After 2 h, the solvent was removed in vacuo. The residue was dissolved in dichloromethane (15 mL) and salts were separated by centrifugation or filtration through Celite. Dichloromethane was removed in vacuo, the residue washed with diethyl ether (2 × 10 mL) and dried in vacuo to afford [Zn(bpa^{tBu2,Me2})Cl]$_2$ (**5**) as a white crystal powder. An air-exposed solution in dichloromethane at room temperature yielded, within 1 d, prism-like colourless crystals suitable for X-ray structure determination. Yield 390 mg (75%); m.p. 259 °C. ^{1}H NMR ($CDCl_3$, 250 MHz): δ = 1.37 (s, 9 H, CH_3), 1.48 (s, 9 H, CH_3), 2.47 (s, 3 H, CH_3), 2.50 (s, 3 H, CH_3), 6.00 (s, 1 H, H_{pz}), 6.09 (s, 1 H, H_{pz}), 6.82 (s, 1 H, CH) ppm. ^{13}C NMR ($CDCl_3$, 62.5 MHz): δ = 11.5 (CH_3), 13.6 (CH_3), 30.1 (CH_3), 30.4 (CH_3), 31.6 (C-*t*Bu), 32.5 (C-*t*Bu), 70.0 (CH), 103.1 (C_{pz}), 107.8 (C_{pz}), four C_{pz} signals not detected, 164.6 (CO_2^-) ppm. EI MS (70 eV, 270 °C): *m*/*z* (%) = 430 (2) [M^+], 386 (48) [$M^+ - CO_2$], 329 (100) [$M^+ - CO_2 - C_4H_9$], 290 (22) [$M^+ - C_5H_8N_2 - CO_2$], 108 (39) [$C_6H_8N_2$]. IR (CH_2Cl_2): $\tilde{\nu}$ = 1687 br (*as*-CO_2^-), 1561 (C=N), 1548 (C=N), 1468 (*s*-CO_2^-) cm^{-1}. IR (KBr): $\tilde{\nu}$ = 1696 (*as*-CO_2^-), 1558 (C=N), 1547 (C=N), 1467 (*s*-CO_2^-) cm^{-1}. $C_{18}H_{27}ClN_4O_2Zn$ (432.27): calcd. C 50.01, H 6.30, N 12.96; found C 49.86, H 6.51, N 12.68.

Method A. General Procedure for Bis(pyrazol-1-yl)acetato(alkyl)-zinc Complexes: A solution of a sterically demanding bis(pyrazol-1-yl)acetic acid in diethyl ether was added to a slight excess of dialkylzinc in diethyl ether. Gas evolution was observed. The solution was stirred at ambient temperature for 1 h. After this time, gas evolution had ceased and the solvent was evaporated. The white residue was dissolved in CH_2Cl_2 or benzene and filtered through Celite. The solvent was again removed in vacuo to yield the product as a white residue.

Synthesis of [Zn(bd*t*bpza)(CH$_3$)] (6): Reaction of bis(3,5-di-*tert*-butylpyrazol-1-yl)acetic acid (bd*t*bpzaH) (**2**) (500 mg, 1.20 mmol) in diethyl ether (10 mL) with $Zn(CH_3)_2$ (0.620 mL of a 2 M solution in toluene, 1.24 mmol) in diethyl ether (10 mL) according to Method A and subsequent workup with CH_2Cl_2 (20 mL) yielded product **6** as a white residue. Yield 550 mg (92%); m.p. 229 °C (dec.). ^{1}H NMR ($CDCl_3$, 250 MHz): δ = −0.35 (s, 3 H, CH_3), 1.36 (s, 18 H, CH_3), 1.53 (s, 18 H, CH_3), 6.08 (s, 2 H, H_{pz}), 7.32 (s, 1 H, CH) ppm. ^{13}C NMR ($CDCl_3$, 62.5 MHz): δ = −10.1 (CH_3-Zn), 30.2 (CH_3), 31.2 (CH_3), 32.0 (C-*t*Bu), 32.3 (C-*t*Bu), 72.1 (CH), 103.1 (C_{pz}), 155.1 (C_{pz}), 163.1 (C_{pz}), 166.3 (CO_2^-) ppm. EI MS (70 eV, 180 °C): *m*/*z* (%) = 481 (18) [$M^+ - CH_3$], 452 (8) [$M^+ - CO_2$], 435 (100) [$M^+ - C_4H_9$], 393 (83) [$M^+ - CO_2 - C_4H_9$], 371 (71) [$M^+ - Zn - CH_3 - CO_2$], 321 (12) [$M^+ - Zn - CH_3 - CO_2 - 2\ C_4H_9$], 57 (62) [$C_4H_9$]. IR ($CH_2Cl_2$): $\tilde{\nu}$ = 1673 (*as*-CO_2^-), 1543 (C=N), 1465 (*s*-CO_2^-) cm^{-1}. $C_{25}H_{42}N_4O_2Zn$ (496.01): calcd. C 60.54, H 8.53, N 11.30; found C 60.50, H 8.72, N 11.30.

Synthesis of [Zn(bd*t*bpza)(CH$_2$CH$_3$)] (7): Reaction of bis(3,5-di-*tert*-butylpyrazol-1-yl)acetic acid (bd*t*bpzaH) (**2**) (500 mg, 1.20 mmol) in diethyl ether (20 mL) with $Zn(CH_2CH_3)_2$ (1.30 mL of a 1 M solution in hexane, 1.30 mmol) in diethyl ether (10 mL) according to Method A and subsequent workup with CH_2Cl_2 (20 mL) yielded product **7** as a white residue. Yield 502 mg (82%); m.p. 168−170 °C. ^{1}H NMR ($CDCl_3$, 250 MHz): δ = 0.52 (q, $^3J_{H,H}$ = 8.0 Hz, 2 H, CH_2), 1.29 (t, $^3J_{H,H}$ = 8.0 Hz, 3 H, CH_3), 1.35 (s, 18 H, CH_3), 1.52 (s, 18 H, CH_3), 6.06 (s, 2 H, H_{pz}), 7.30 (s, 1 H, CH) ppm. ^{13}C NMR ($CDCl_3$, 62.5 MHz): δ = 3.3 (CH_2), 11.9 (CH_3), 30.2 (CH_3), 31.2 (CH_3), 32.0 (C-*t*Bu), 32.3 (C-*t*Bu), 72.1 (CH), 103.1 (C_{pz}), 155.1 (C_{pz}), 163.0 (C_{pz}), 166.6 (CO_2^-) ppm. EI MS (70 eV, 240 °C): *m*/*z* (%) = 479 (40) [$M^+ - CH_2CH_3$], 435 (96) [$M^+ - CH_2CH_3 - CO_2$], 407 (56) [$M^+ - CO_2 - C_4H_9$], 371 (100) [$M^+ - CH_2CH_3 - CO_2 - Zn$], 321 (14) [$M^+ - CH_2CH_3 - CO_2 - Zn - 2\ C_4H_9$], 193 (53) [$C_{12}H_{21}N_2$], 57 (43) [$C_4H_9$]. IR ($CH_2Cl_2$): $\tilde{\nu}$ = 1671 (*as*-CO_2^-), 1544 (C=N), 1465 (*s*-CO_2^-) cm^{-1}. $C_{26}H_{44}N_4O_2Zn$ (510.04): calcd. C 61.23, H 8.70, N 10.98; found C 60.75, H 8.82, N 10.43.

Synthesis of [Zn(bpa^{rBu2,Me2})(CH$_3$)] (8): Reaction of (3,5-di-*tert*-butylpyrazol-1-yl)(3,5-dimethylpyrazol-1-yl)acetic acid (bpaH^{tBu2,Me2}) (**4**) (0.970 g, 2.92 mmol) in diethyl ether (20 mL) with $Zn(CH_3)_2$ (1.65 mL of a 2 M solution in toluene, 3.30 mmol) in diethyl ether (20 mL) according to Method A and subsequent workup with

CH_2Cl_2 (20 mL) yielded product **8** as a white residue. Yield 1.12 g (93%); m.p. 187 °C. ^{1}H NMR ($CDCl_3$, 250 MHz): δ = −0.42 (s, 3 H, CH_3), 1.38 (s, 9 H, CH_3), 1.52 (s, 9 H, CH_3), 2.30 (s, 3 H, CH_3), 2.50 (s, 3 H, CH_3), 5.99 (s, 1 H, H_{pz}), 6.01 (s, 1 H, H_{pz}), 6.89 (s, 1 H, CH) ppm. ^{13}C NMR ($CDCl_3$, 62.5 MHz): δ = −14.1 (CH_3-Zn), 11.5 (CH_3), 12.9 (CH_3), 30.3 (CH_3), 30.5 (CH_3), 31.5 (C-*t*Bu), 32.1 (C-*t*Bu), 70.2 (CH), 102.1 (C_{pz}), 107.3 (C_{pz}), 141.6 (C_{pz}), 150.7 (C_{pz}), 154.1 (C_{pz}), 162.7 (C_{pz}), 165.4 (CO_2^-) ppm. FAB MS (NBOH matrix): *m*/*z* (%) = 809 (21) [$M_2H^+ - CH_3$], 763 (10) [$M_2H^+ - CH_3 - CO_2$], 411 (100) [MH^+], 395 (9) [$M^+ - CH_3$], 365 (31) [$M^+ - CO_2H$], 351 (78) [$M^+ - CH_3 - CO_2$], 287 (86) [$M^+ - CH_3 - CO_2 - Zn$]. IR (CH_2Cl_2): $\tilde{\nu}$ = 1669 (*as*-CO_2^-), 1559 (C=N), 1539 (C=N), 1466 (*s*-CO_2^-) cm^{-1}. $C_{19}H_{30}N_4O_2Zn$ (411.85): calcd. C 55.41, H 7.34, N 13.60; found C 55.02, H 7.21, N 13.62.

Method B. General Procedure for Acetato[bis(pyrazol-1-yl)acetato]-zinc Complexes: An excess of acetic acid was added to a solution of a methyl[bis(pyrazol-1-yl)acetato]zinc complex in benzene. Gas evolution was observed. The solution was stirred at ambient temperature for 30 min. After this time, gas evolution had ceased, the solution was filtered through Celite and the volume of the solution was reduced in vacuo to 1 mL. The product was precipitated with hexane and dried in vacuo to yield the product as a white solid.

Synthesis of [Zn(OAc)(bd*t*bpza)] (9): Reaction of [Zn(bd*t*bpza)-(CH_3)] (**6**) (480 mg, 0.968 mmol) in benzene (10 mL) with acetic acid (100%, 70.0 μL, 1.22 mmol) according to Method B afforded [ZnOAc(bd*t*bpza)] (**9**) as a white crystalline powder. A similar result in yield and purity was obtained from an acetonitrile solution. Yield 400 mg (77%); m.p. 109−111 °C. ^{1}H NMR ($CDCl_3$, 250 MHz): δ = 1.37 (s, 18 H, CH_3), 1.53 (s, 18 H, CH_3), 2.12 (s, 3 H, CH_3−Ac), 6.12 (s, 2 H, H_{pz}), 7.36 (s, 1 H, CH) ppm. ^{1}H NMR (C_6D_6, 250 MHz): δ = 1.21 (s, 18 H, CH_3), 1.43 (s, 18 H, CH_3), 1.93 (s, 3 H, CH_3−Ac), 6.01 (s, 2 H, H_{pz}), 7.55 (s, 1 H, CH) ppm. ^{13}C NMR ($CDCl_3$, 62.5 MHz): δ = 21.1 (CH_3-Ac), 29.9 (CH_3), 31.0 (CH_3), 32.0 (C-*t*Bu), 32.3 (C-*t*Bu), 72.6 (CH), 103.4 (C_{pz}), 155.7 (C_{pz}), 163.2 (C_{pz}), 166.0 (CO_2^-), 178.2 (CO_2^-) ppm. ^{13}C NMR (C_6D_6, 62.5 MHz): δ = 21.9 (CH_3-Ac), 30.5 (CH_3), 30.8 (CH_3), 32.2 (C-*t*Bu), 32.4 (C-*t*Bu), 75.0 (CH), 103.0 (C_{pz}), 154.7 (C_{pz}), 161.8 (C_{pz}), 168.5 (CO_2^-), 179.8 (CO_2^-) ppm. EI MS (70 eV, 200 °C): *m*/*z* (%) = 494 (55) [$M^+ - CO_2$], 479 (43) [$M^+ - CO_2CH_3$], 437 (85) [$M^+ - CO_2 - C_4H_9$], 371 (61) [$M^+ - CO_2CH_3 - CO_2 - Zn$], 193 (100) [$C_{12}H_{21}N_2$], 179 (66) [$C_{11}H_{19}N_2$]. IR ($CH_2Cl_2$): $\tilde{\nu}$ = 1681 (*as*-CO_2^-), 1633 (*as*-CO_2^-), 1602 (*as*-CO_2^-), 1546 (C=N), 1467 (*s*-CO_2^-) cm^{-1}. $C_{26}H_{42}N_4O_4Zn$ (540.02): calcd. C 57.83, H 7.84, N 10.37; found C 58.00, H 8.20, N 10.98.

Synthesis of [Zn(OAc)(bpa^{rBu2,Me2})] (10): Reaction of [Zn-(bpa^{tBu2,Me2})(CH_3)] (**8**) (400 mg, 0.971 mmol) in benzene (5 mL) with acetic acid (100%, 57.0 μL, 1.00 mmol) according to Method B but without filtration through Celite afforded [Zn(OAc)(bpa^{tBu2,Me2})] (**10**) as a white crystalline powder. Yield 401 mg (91%); m.p.

Table 5. Structure determination details of compounds **4**, **5**, **8** and **11**

	4	**5**	**8**	**11**
Empirical formula	$C_{18}H_{28}N_4O_2$ × 1/3 C_3H_6O	$C_{18}H_{27}ClN_4O_2Zn$ × 1.5 CH_2Cl_2	$C_{19}H_{30}N_4O_2Zn$ × CH_2Cl_2	$C_{18}H_{27}N_4O_2Zn_{0.5}$ × $CHCl_3$
Formula mass	351.80	559.65	496.77	483.49
Crystal colour/habit	colourless plate	colourless column	colourless plate	colourless block
Crystal system	rhombohedral	monoclinic C	monoclinic P	monoclinic P
Space group	*R*-3	*C*2/*c*	$P2_1/c$	$P2_1/n$
a [Å]	17.691(3)	14.008(14)	11.599(14)	9.8566(4)
b [Å]	17.691(3)	20.489(15)	21.658(17)	22.2125(9)
c [Å]	17.691(3)	19.101(19)	11.130(8)	11.3820(5)
α [°]	115.061(12)	90.00	90.00	90.000(1)
β [°]	115.061(12)	104.15(4)	116.35(8)	112.300(1)
γ [°]	115.061(12)	90.00	90.00	90.000(1)
V [Å^3]	3081.4(22)	5316(8)	2505(4)	2305.60(17)
θ [°]	2.32−27.00	2.20−27.01	2.17−24.01	1.83−28.20
h	−19 to 22	−17 to 17	−13 to 12	−12 to 12
k	−22 to 22	−26 to 26	−1 to 24	−29 to 28
l	−22 to 22	−24 to 24	−1 to 12	−15 to 15
F(000)	1144	2312	1040	1008
Z	6	8	4	4
μ(Mo-K_α) [mm^{-1}]	0.076	1.348	1.215	0.927
Crystal size [mm]	0.5 × 0.3 × 0.15	0.5 × 0.3 × 0.3	0.2 × 0.15 × 0.1	0.3 × 0.2 × 0.2
$D_{calcd.}$ [gcm^{-1}]	1.138	1.399	1.317	1.393
T [K]	188(2)	231(2)	258(2)	143(2)
Reflections collected	9037	11494	4869	36682
Independent reflections	4371	5797	3926	5423
Obsd. refl. ($> 2\sigma I$)	3396	4321	1787	4866
Parameter	242	307	262	262
Weight parameter *a*	0.1050	0.0465	0.0411	0.0527
Weight parameter *b*	2.1776	3.8902	0.2667	1.1558
R_1 (obsd.)	0.0700	0.0412	0.0748	0.0377
R_1 (overall)	0.0868	0.0635	0.1887	0.0421
wR_2 (obsd.)	0.1875	0.0954	0.1155	0.1011
wR_2 (overall)	0.2035	0.1055	0.1512	0.1035
Diff. peak/hole [e/Å^3]	0.812/−0.617	0.497/−0.609	0.316/−0.387	0.681/−0.631

196 °C (dec.). ^{1}H NMR ($CDCl_3$, 250 MHz): δ = 1.33 (s, 9 H, CH_3), 1.51 (s, 9 H, CH_3), 2.10 (s, 3 H, CH_3), 2.36 (s, 3 H, CH_3), 2.49 (s, 3 H, CH_3−OAc), 6.00 (s, 1 H, H_{pz}), 6.07 (s, 1 H, H_{pz}), 6.88 (s, 1 H, CH) ppm. ^{1}H NMR (C_6D_6, 250 MHz): δ = 1.24 (s, 9 H, CH_3), 1.36 (s, 9 H, CH_3), 1.92 (s, 3 H, CH_3), 1.97 (s, 3 H, CH_3), 2.31 (s, 3 H, CH_3-OAc), 5.39 (s, 1 H, H_{pz}), 5.96 (s, 1 H, H_{pz}), 6.97 (s, 1 H, CH) ppm. ^{13}C NMR ($CDCl_3$, 62.5 MHz): δ = 11.8 (CH_3), 13.1 (CH_3), 22.1 (CH_3-OAc), 30.1 (CH_3), 30.7 (CH_3), 31.8 (C-*t*Bu), 32.3 (C-*t*Bu), 70.5 (CH), 102.9 (C_{pz}), 108.0 (C_{pz}), 142.6 (C_{pz}), 152.3 (C_{pz}), 156.0 (C_{pz}), 164.3 (C_{pz}), 165.1 (CO_2^-), 181.2 (CO_2^-) ppm. EI MS (70 eV, 230 °C): *m*/*z* (%) = 410 (18) [$M^+ - CO_2$], 353 (58) [$M^+ - CO_2 - C_4H_9$], 288 (100) [$M^+ - CO_2 - O_2CCH_3 - Zn$], 193 (30) [$C_{12}H_{21}N_2$], 109 (44) [$C_6H_9N_2$]. IR ($CH_2Cl_2$): $\tilde{\nu}$ = 1677 (*as*-CO_2^-), 1624 (*as*-CO_2^-), 1601 (*as*-CO_2^-), 1562 (C=N), 1544 (C=N), 1467 (*s*-CO_2^-), 1442 (*s*-CO_2^-), 1427 (*s*-CO_2^-) cm^{-1}. $C_{20}H_{30}N_4O_4Zn$ (455.86): calcd. C 52.70, H 6.63, N 12.29; found C 52.55, H 6.51, N 11.74.

Synthesis of [Zn(OAc)(bpa^{rBu2,Me2})] (10) in Acetonitrile: Reaction of [Zn(bpa^{tBu2,Me2})(CH_3)] (**8**) (310 mg, 0.753 mmol) in acetonitrile (5 mL) with acetic acid (100%, 80.0 μL, 1.40 mmol) according to Method B afforded [Zn(OAc)(bpa^{tBu2,Me2})] (**10**) as a white crystalline powder. The spectroscopic data are identical to those of **10** that was obtained in benzene solution. Yield (**10**) 162 mg (47%).

[Zn(bpa^{rBu2,Me2})$_2$] (11): During the synthesis of **10** in acetonitrile a white precipitate formed in the solution that was filtered off. This white residue was dissolved in CH_2Cl_2, filtered through Celite and dried in vacuo to yield [Zn(bpa^{tBu2,Me2})$_2$] (**11**) as a white crystalline powder. Additional purification can be achieved by extraction with CH_2Cl_2 from a water suspension. Crystals suitable for X-ray structure determination were obtained from a solution in $CHCl_3$. Yield 80.0 mg (29%); m.p. 207 °C (dec.). ^{1}H NMR ($CDCl_3$, 400 MHz): δ = 1.08 (s, 9 H, CH_3), 1.53 (s, 9 H, CH_3), 1.92 (s, 3 H, CH_3) 2.42 (s, 3 H, CH_3), 5.86 (s, 1 H, H_{pz}), 5.96 (s, 1 H, H_{pz}), 6.90 (s, 1 H, CH) ppm. ^{13}C NMR ($CDCl_3$, 62.5 MHz): δ = 11.8 (CH_3), 13.1 (CH_3), 30.1 (CH_3), 30.8 (CH_3), 31.6 (C-*t*Bu), 32.3 (C-*t*Bu), 70.5 (CH), 102.6 (C_{pz}), 107.6 (C_{pz}), 140.8 (C_{pz}), 150.8 (C_{pz}), 153.0 (C_{pz}), 163.0 (C_{pz}), 166.4 (CO_2^-) ppm. EI MS (70 eV, 250 °C): *m*/*z* (%) = 684 (0.5) [$M^+ - CO_2$], 353 (2) [$C_{17}H_{28}N_4$ + Zn], 288 (5.5) [$C_{17}H_{28}N_4$], 192 (26) [$C_{12}H_{20}N_2$], 177 (100) [$C_{11}H_{17}N_2$]. IR (CH_2Cl_2): $\tilde{\nu}$ = 1664 (*as*-CO_2^-), 1562 (C=N), 1540 (C=N), 1466 (*s*-CO_2^-) cm^{-1}. $C_{36}H_{54}N_8O_4Zn \cdot 2\,CHCl_3$ (967.01): calcd. C 47.39, H 5.87, N 11.64; found C 47.08, H 6.02, N 11.41.

X-ray Structure Determinations: Single crystals of **4**, **5** and **8** were sealed in glass capillaries at room temperature. A modified Siemens P4 diffractometer was used for data collection (Wyckhoff technique, graphite monochromator, Mo-K_α radiation, λ = 0.71073 Å, scan rate 4−30°min^{-1} in ω). The data set of **11** was collected with a Bruker Smart Apex. The structures were solved using direct methods {Siemens SHELXS-93[26]} and refined with full-matrix least squares against F^2 {Siemens SHELXL-97[26]}. A weighting scheme was applied in the last steps of the refinement with $w = 1/[\sigma^2(F_o^2) + (aP)^2 + bP]$ and $P = [2F_c^2 + \max(F_o^2,0)]/3$. Hydrogen atoms were included in their calculated positions and refined in a riding model. Compound **4** crystallised with one third of an acetone molecule in a special position. The carboxylic proton of **4** was found. In the case of **5** the asymmetric unit is filled by half of a dimer of the molecule. In the asymmetric unit of structure **5** one and a half molecules of dichloromethane were found and refined. The half molecule was found in a special position. One molecule of dichloromethane co-crystallised with **8**. In the case of complex **11** one molecule of $CHCl_3$ crystallised with half of the molecule. All details and parameters of the measurements are summarised in Table 5. The structure pictures were prepared with the program Diamond 2.1c.[27] CCDC-184127 [Zn(bpa^{tBu2,Me2})Cl]$_2$ (**5**), -184128 [Zn(bpa^{tBu2,Me2})(CH_3)] (**8**) and -184129 [Zn(bpa^{tBu2,Me2})$_2$] (**11**) contain the supplementary crystallographic data for this paper. These data can be obtained free of charge at www.ccdc.cam.ac.uk/conts/retrieving.html or from the Cambridge Crystallographic Data Centre, 12, Union Road, Cambridge CB2 1EZ, UK [Fax: (internat.) + 44-1223/336-033; E-mail: deposit@ccdc.cam.ac.uk].

Acknowledgments

Generous financial support by the Fonds der Chemischen Industrie (Liebig-Stipendium to N. B.) and the European Commission (Copernicus 2 Program, Contract no. ICA2-CT-2000−10002) is gratefully acknowledged. Special thanks to Prof. Dr. H. Fischer for support and discussion and also to Prof. Dr. W. A. Schenk for giving us access to a Bruker Smart Apex in Würzburg. We are indebted to Mr. Hägele and Mr. Galetskiy for recording mass spectra.

[1] Reviews: [1a] W. N. Lipscomb, N. Sträter, *Chem. Rev.* **1996**, *96*, 2375−2433. [1b] H. Vahrenkamp, *Acc. Chem. Res.* **1999**, *32*, 589−596. [1c] G. Parkin, *Chem. Commun.* **2000**, 1971−1985. [1d] H. Strasdeit, *Angew. Chem.* **2001**, *113*, 730−732; *Angew. Chem. Int. Ed.* **2001**, *40*, 707−709.
[2] M. A. Holmes, B. W. Matthews, *J. Mol. Biol.* **1982**, *160*, 623−639.
[3] W. R. Kester, B. W. Matthews, *J. Biol. Chem.* **1977**, *252*, 7704−7710.
[4] A. C. Hausrath, B. W. Matthews, *J. Biol. Chem.* **1994**, *269*, 18839−18842.
[5] G. Kurisu, Y. Kai, S. Harada, *J. Inorg. Biochem.* **2000**, *82*, 225−228.
[6] [6a] B. S. Hammes, C. J. Carrano, *Inorg. Chem.* **1999**, *38*, 3562−3568. [6b] B. S. Hammes, C. J. Carrano, *Inorg. Chem.* **1999**, *38*, 4593−4600.
[7] [7a] C. Dowling, G. Parkin, *Polyhedron* **1996**, *15*, 2463−2465. [7b] P. Ghosh, G. Parkin, *J. Chem. Soc., Dalton Trans.* **1998**, 2281−2283.
[8] A. Beck, B. Weibert, N. Burzlaff, *Eur. J. Inorg. Chem.* **2001**, 521−527.
[9] N. Niklas, O. Walter, R. Alsfasser, *Eur. J. Inorg. Chem.* **2000**, 1723−1731.
[10] P. Gockel, M. Gelinsky, R. Vogler, H. Vahrenkamp, *Inorg. Chim. Acta* **1998**, *272*, 115−124.
[11] D. D. LeCloux, C. J. Tokar, M. Osawa, R. P. Houser, M. C. Keyes, W. B. Tolman, *Organometallics* **1994**, *13*, 2855−2866.
[12] M. Kunert, M. Bräuer, O. Klobes, H. Görls, E. Dinjus, E. Anders, *Eur. J. Inorg. Chem.* **2000**, 1803−1809 and cited references.
[13] [13a] D. J. Darensbourg, J. R. Wildeson, J. C. Yarbrough, J. H. Reibenspies, *J. Am. Chem. Soc.* **2000**, *122*, 12487−12496. [13b] D. J. Darensbourg, M. W. Holtcamp, G. E. Struck, M. S. Zimmer, S. A. Niezgoda, P. Rainey, J. B. Robertson, J. D. Draper, J. H. Reibenspies, *J. Am. Chem. Soc.* **1999**, *121*, 107−116.
[14] M. Cheng, E. B. Lobkovsky, G. W. Coates, *J. Am. Chem. Soc.* **1998**, *120*, 11018−11019.
[15] [15a] A. Otero, J. Fernández-Baeza, J. Tejeda, A. Antiñolo, F. Carrillo-Hermosilla, E. Diez-Barra, A. Lara-Sánchez, M. Fernández-López, M. Lanfranchi, M. A. Pellinghelli, *J. Chem. Soc., Dalton Trans.* **1999**, 3537−3539. [15b] A. Otero, J. Fernández-Baeza, J. Tejeda, A. Antiñolo, F. Carrillo-Hermosilla, E. Diez-Barra, A. Lara-Sánchez, M. Fernández-López, *J. Chem. Soc., Dalton Trans.* **2000**, 2367−2374.
[16] Due to otherwise extraordinary long abbreviations for compound **4** and its precursor **3**, the abbreviation system for Tp ligands introduced by S. Trofimenko was transferred to this

problem. This resulted in the abbreviations bpm^{tBu2,Me2} (**3**), bpaH^{tBu2,Me2} (**4**) and bpa^{tBu2,Me2} for the anion of **4**. For further details see: S. Trofimenko, *Scorpionates − The Coordination Chemistry of Polypyrazolylborate Ligands*, Imperial College Press, London, **1999**, pp. 5−9.

[17] G. E. Coates, D. Ridley, *J. Chem. Soc.* **1965**, 1870−1877.

[18] [18a] R. Alsfasser, A. K. Powell, H. Vahrenkamp, *Angew. Chem.* **1990**, *102*, 939−941; *Angew. Chem. Int. Ed. Engl.* **1990**, *29*, 898−899. [18b] R. Alsfasser, A. K. Powell, S. Trofimenko, H. Vahrenkamp, *Chem. Ber.* **1993**, *126*, 685−694.

[19] [19a] I. B. Gorrell, A. Looney, G. Parkin, *J. Chem. Soc., Chem. Commun.* **1990**, 220−222. [19b] A. Looney, R. Han, I. B. Gorrell, M. Cornebise, K. Yoon, G. Parkin, A. L. Rheingold, *Organometallics* **1995**, *14*, 274−288.

[20] [20a] G. B. Deacon, R. J. Phillips, *Coord. Chem. Rev.* **1980**, *33*, 227−250. [20b] K. Nakamoto, *Infrared and Raman Spectra of Inorganic and Coordination Compounds*, Wiley-VCH, New York, **1997**, pp. 59−62.

[21] F. Hartmann, W. Kläui, A. Kremer-Aach, D. Mootz, A. Strerath, H. Wunderlich, *Z. Anorg. Allg. Chem.* **1993**, *619*, 2071−2076.

[22] P. Bhyrappa, V. Krishnan, M. Nethaji, *J. Chem. Soc., Dalton Trans.* **1993**, 1901−1906.

[23] [23a] N. Burzlaff, I. Hegelmann, B. Weibert, *J. Organomet. Chem.* **2001**, *626*, 16−23. [23b] A. López-Hernández, R. Müller, H. Kopf, N. Burzlaff, *Eur. J. Inorg. Chem.* **2002**, 671−677.

[24] S. Juliá, C. Martínez-Martorell, J. Elguero, *Heterocycles* **1986**, *24*, 2233−2237.

[25] C. Fernández-Castaño, C. Foces-Foces, N. Jagerovic, J. Elguero, *J. Mol. Struct.* **1995**, *355*, 265−271.

[26] G. M. Sheldrick, *SHELX-97, Programs for Crystal Structure Analysis*, University of Göttingen, Göttingen, Germany, **1997**.

[27] K. Brandenburg, M. Berndt, Diamond − *Visual Crystal Structure Information System*, Crystal Impact GbR, Bonn,Germany, **1999**; for software review see: W. T. Pennington, *J. Appl. Crystallogr.* **1999**, *32*, 1028−1029.

Received May 24, 2002
[I02399]

New Dinuclear Palladium Phosphane Complexes Stabilised by 8-Thiotheophylline

Antonio Romerosa,*[a] Carlos López-Magaña,[a] Mustapha Saoud,[a] and Sonia Mañas[a]

Keywords: Palladium / Nucleobases / Bioinorganic chemistry / P ligands

The new purine derivatives SS-bis-8-(thio)-theophylline (8-$BTTH_2$) and 8-phenylthiotheophylline (8-PhTTH), have been synthesised and characterised by elemental analysis, mass spectrometry and standard spectroscopic measurements. Reaction of 8-$BTTH_2$ with *cis*-$[PdCl_2(PPh_3)_2]$ leads to the formation of the binuclear palladium complex $[Pd(PPh_3)(\mu\text{-}Cl)(8\text{-}TT)]_2$ (8-TTH_2 = 8-thiotheophylline) in which PPh_3-induced cleavage of the S–S bridge takes place. This complex reacts with pyridine to give a different dimeric palladium complex, $[Pd(\mu\text{-}S,N\text{-}8\text{-}TT)(PPh_3)Py]_2$, in which each of the two 8-thio-(theophylline) anions binds two metals through the N7 and S atoms. The process leading to the palladium complex has also been elucidated.

(© Wiley-VCH Verlag GmbH & Co. KGaA, 69451 Weinheim, Germany, 2003)

Introduction

The interaction between metal ions and purine bases has been an important area of research in recent years. This is mainly a consequence of the biological relevance of purines, which are one of the principal constituents of nucleic acid derivatives.[1,2] Purines possess a variety of potential donor groups in their molecular skeleton and consequently behave as effective ligands towards a wide range of metal ions. Coordination to a metal ion often alters the main chemical properties of the purine molecules.[3,4] As a consequence, some metal complexes are active drugs for medical purposes.[5] The most well-known and best studied metal-based drugs are the anticancer compounds of platinum.[6]

A deep knowledge of the action mechanism of the drugs is indispensable in designing improved drugs with increased potency and reduced side effects. Ligand exchange plays an important role in determining the biological activity, as very few metal-based drugs reach the biological target without being modified. Most of them interact with different macromolecules, such as S-donor compounds, and/or water. Therefore, understanding how a drug is transformed upon interacting with biological ligands has become of paramount importance. Usually, the biomolecules that interact with and alter the metal-based drug, provoking a specialised therapeutic effect, are structurally complicated. As a consequence, it is useful to mimic their reactivity towards the metal centre through simplified model molecules. Aiming at obtaining a new simple model for addressing the interaction of purines with transition metal ions, we have synthesised the new ligand *S*,*S*-bis(8-thiotheophylline) (**1**,8-$BTTH_2$) (Scheme 1) in which two purines are linked by a disulfide group bonded through the C8 atom. This ligand can indeed interact with a metal ion through either the imidazolic N7 atom or the exocyclic O atoms, but the possibility of the sulfur atoms of the disulfide group coordinating to the metal also exists. Accomplishing the latter S-coordination is also important to mimic the coordination abilities of disulfide groups in biomolecules.

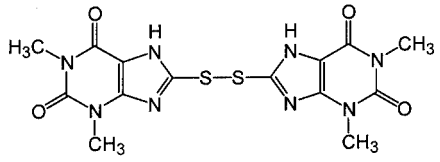

8-$BTTH_2$ (**1**)

Scheme 1

The evaluation of the chemical properties of the interaction of **1** with *cis*-$[PdCl_2(PPh_3)_2]$ shows that it is of interest as a biological model. Palladium is a biologically active metal, somewhat similar to platinum, although more reactive, and widely used to promote homogeneous catalytic processes and highly efficient organic syntheses.[7] In the case at hand, the presence of two PPh_3 ancillary ligands, not only makes the palladium complexes soluble in common organic solvents but also provides an NMR-active label, the P-nucleus of the phosphane, which allows us to study its reaction with **1** by $^{31}P\{^1H\}$ NMR spectroscopy.

[a] Departamento de Química Física, Bioquímica y Química Inorgánica, Facultad de Ciencias Experimentales, Universidad de Almería, 04071, Almería, Spain
E-mail: romerosa@ual.es

Results and Discussion

Synthesis and Characterisation of *S*,*S*-bis(8-thitheophylline) (1)

The oxidation of the 8-thiotheophillinate potassium salt by the smooth oxidant I_2, which was prepared in situ by reaction of 8-thiotheophylline (8-TTH_2) with KOH, affords the new purine derivative *S*,*S*-bis(8-thiotheophylline) in which two theophylline molecules are held together, through their C8 atoms, by a disulfide bridge.

The IR spectrum of **1** shows a simplification and an intensity reduction of the absorption bands between 2500 and 3700 cm^{-1} compared to that of the parent 8-TTH_2 molecule, which is in agreement with the formation of the disulfide bridge. Key points of the ^1H NMR spectroscopic analysis are the absence of the 8-TTH_2 N−H resonances[8] (δ = 12.95 and 13.36 ppm) and the observation of a unique broad signal at δ = 4.67 ppm that can only be assigned to the imidazolic N−H resonance. The chemical shift of the N7−H proton in **1** appears in the range expected for aliphatic amines, in agreement with their basic character. This fact is better understood by assuming the existence of a partial negative charge on the purine imidazolic ring (Scheme 2). The charge separation may simply be accomplished by moving a lone pair from each of the two S atoms to each of the C8 purine imidazolic carbon atoms. In the resonance structure (b), the S atoms bear a positive charge and, therefore, are well suited to be attacked by nucleophiles. The low acidity of the N7 proton indeed suggests a large contribution of the structure (b) and points to the tendency of this new purine derivative to react with electron rich species through the disulfide group.

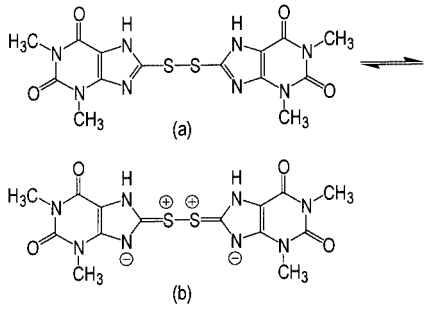

Scheme 2

The $^{13}C\{^1H\}$ NMR spectrum provides the conclusive evidence that confirms the proposed structure for **1**. Particularly, and in keeping with the presence of a substituted S atom, the C-8 resonance appears much closer (δ = 148 ppm) to that in 8-methylthiotheophylline (δ = 153.0 ppm)[12] than in 8-TTH_2 (δ = 163.8 ppm).[13]

Characterisation and Mechanistic Studies of the Formation of the Palladium Complexes 6 and 7

Different synthetic strategies may be used to prepare **6**: (i) the reaction of **1** with *cis*-$[PdCl_2(PPh_3)_2]$ and KOH in refluxing EtOH, (ii) the reaction of **1** with KOH and $Na_2[PdCl_4]$ and PPh_3 in EtOH/H_2O, and (iii) the reaction of **2**, (**3** or **4**) with *cis*-$[PdCl_2(PPh_3)_2]$ (or $Na_2[PdCl_4]$ and PPh_3) in EtOH under reflux. It is also important to point out that **6** was obtained from the above reactions with high yields irrespective of the molar ratio used. However, a higher yield was obtained from method (ii) using a 1:2:2:4 molar ratio between **1**, KOH, Pd^{2+}, and PPh_3.

Unfortunately, **6** was not soluble enough in the non-coordinating solvent to obtain its ^1H, $^{31}P\{^1H\}$ and $^{13}C\{^1H\}$ NMR spectra.[9] We could conclude that the palladium complex **6** contains a PPh_3 group, a chloride ligand and an 8-TTH^- ligand, the latter coordinated through the S donor atom [ν(N7-H) = 3059−2790 cm^{-1}] on the basis of the synthetic procedures, the elemental analysis and IR spectrum. In order to complete the square-planar geometry around the palladium atom, one can hypothesise that a dimeric structure exists in which the bridging tethering ligand is either the chloride (I) or the sulfur atom of the purine group (II) (Scheme 3). Both structures are realistic and have several precedents in the relevant literature.[10−13]

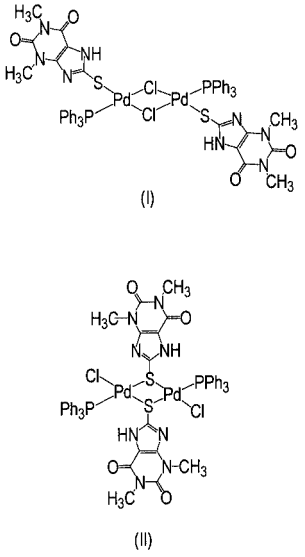

Scheme 3

Although a definitive comparison between the two proposed structures was not possible on the basis of the data collected, an important element in distinguishing between them comes from the observation that dimeric palladium(II) complexes with halide bridges are readily cleaved by unidentate ligands such as pyridine or PPh_3, while the corresponding palladium(II) thiolato bridges are not.[14−16] Since **6** readily reacts with pyridine to give **7**, we may reasonably assume that structure (I) is much more probable than (II).

In order to understand better the metal-purine interaction in the present palladium complexes, we have decided to study the mechanism responsible for the surprising formation of complex **7**, carrying out a variety of experiments that are discussed below. The first aim of our study was to elucidate the process responsible for the S−S bond

breakage, a result which is quite surprising. The rupture of the S−S bond during the reaction leading to **6** and **7** needs a reducing agent that provides the necessary electrons to accomplish the reduction. Therefore, it is conceivable that the disulfide bond of **1** breaks during the synthetic process leading to **6** and, therefore, it is plausible that one or more compounds implicated in the reaction should take the role of the reducing agent.

Of the several experiments carried out in order to understand the nature of the compounds responsible for the in situ reduction of the disulfide it is worth mentioning the stability tests of **1** in different solvents and pH, and the reactivity tests of 8-TTH_2, **1**, **2**, **3**, and **4** with *cis*-$[PdCl_2(PPh_3)_2]$ (or $[PdCl_4]^{2-}$ and PPh_3) carried out using different stoichiometries and pH conditions. From a perusal of these experiments we may conclude that: a) EtOH and MeOH, in both basic (KOH, pyridine) or acidic (HCl) conditions, do not reduce **1** even after prolonged reflux (up to two days); b) compound **6** was obtained irrespective of the molar proportion of the reagents; c) there are many pathways to access **6** in refluxing EtOH; d) to obtain **6** from 8-TTH_2 a basic medium (KOH or NaOH) is mandatory.

Monitoring the reaction between **1** and *cis*-$[PdCl_2(PPh_3)_2]$ by $^{31}P\{^1H\}$ and ^1H NMR spectroscopy provided additional pieces of information to clarify the reduction step of the S−S bond. This study was carried out as follows: ligand **1** and *cis*-$[PdCl_2(PPh_3)_2]$ (1:2 molar ratio) were placed into an NMR tube and CD_3OD was added from a syringe at 20 °C. At this temperature a $^{31}P\{^1H\}$ NMR spectrum was immediately acquired, showing only the *cis*-$[PdCl_2(PPh_3)_2]$ resonance. A reaction only took place after heating the solution to 50 °C. After 6 hours of heating at this temperature, the *cis*-$[PdCl_2(PPh_3)_2]$ resonance was no longer observed while the $^{31}P\{^1H\}$ resonance of $O{=}PPh_3$ appeared (δ = 29.58 ppm, confirmed also by GC-MS analysis) and a red orange precipitate was formed. This precipitate was filtered out from the solution, washed with ethanol and dried. On the basis of IR data the red solid was assigned as **6**.

An interpretation of the above results suggests that the reducing agent responsible for the S−S bond cleavage should be the PPh_3. In effect, the phosphane may be readily produced from *cis*-$[PdCl_2(PPh_3)_2]$ (Scheme 4) through a dissociation equilibrium[17,18] and its capacity to efficiently reduce disulfide groups in proteins and other disulfide derivatives has been documented.[19] In order to confirm whether PPh_3 is the only reducing agent or whether the palladium metal also plays a role in this process, the reactivity of **1** with PPh_3 in MeOH and DMSO as well as of **3** with PPh_3 in MeOH were studied in situ, carrying out bulk experiments.

From these experiments, we may conclude that PPh_3 alone is responsible for the cleavage of the S−S bond in **1** while the metal plays no role in the process. In this regard, it is important to stress that during the in situ reaction between **1** and PPh_3 in CD_3OD, $O{=}PPh_3$ is produced in quantitative yield. On carrying out the same reaction in DMSO (Scheme 5) the phenylthiotheophylline (**5**, 8-PhTTH), a new thiopurine containing an S-PPh_3 group, was formed. Compound **5** was fully characterised (see Exp. Sect.), but for the present discussion it is important to stress that in the $^{13}C\{^1H\}$ NMR spectrum, C8 resonates at δ = 170.3 ppm ([D_6]DMSO), very deshielded with respect to the corresponding signal for the *S*-alkyl-substituted 8-TTH_2 derivatives[11] ($\delta \approx 150$ ppm).

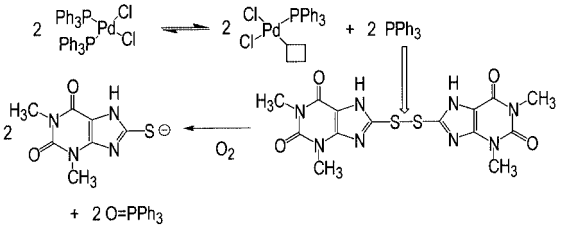

Scheme 4

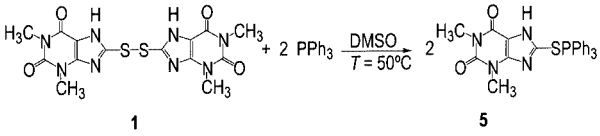

Scheme 5

Finally, the orange compound **6** reacts simply with pyridine to give **7** which likely forms via cleavage of the bridging structure followed by nucleophilic substitution of the bridging chloride ligand by pyridine (Scheme 6).[21,22] In this basic medium, deprotonation of the N7 imidazolic nitrogen easily takes place to yield the corresponding anion which may coordinate to the palladium metal. Moreover, and in keeping with this overall mechanism, formation of PPh_3 is not observed by NMR spectroscopic methods when **6** is dissolved in [D_5]pyridine.

Crystal Structure of $[Pd(\mu\text{-S},N\text{-8-TT})(PPh_3)Py]_2{\cdot}9H_2O$ (7)

Orange prismatic crystals of the dimeric palladium complex $[Pd(\mu\text{-S},N\text{-8-TT})(PPh_3)Py]_2{\cdot}9H_2O$ (**7**) suitable for an X-ray study were obtained from a pyridine/acetonitrile solution of complex **6**. Although both IR and $^{31}P\{^1H\}$ NMR ($CDCl_3$) spectra are in good agreement with the solid-state structure of **7**, the ^1H NMR spectrum recorded in $CDCl_3$ does not match up with it. The most significant discrepancy is the appearance of four different singlets in the range typical of the $N{-}CH_3$ groups of the purines (δ = 3.14, 3.22, 3.40 and 3.52 ppm). Such behaviour points to the magnetic inequivalence of the purine $N{-}CH_3$ groups and also indicates that the two purines have different chemical environments. Other important ^1H NMR spectroscopic features are a broad signal at δ = 13.21 ppm, suggesting that the N7 purine atom is protonated, and a resonance at δ = 11.38 ppm that cannot easily be assigned, even though an N7 purine imidazolic proton seems a realistic assignment for this low-field shifted resonance.[1,20] Recording the ^1H NMR spectrum at different temperatures in $CDCl_3$ points

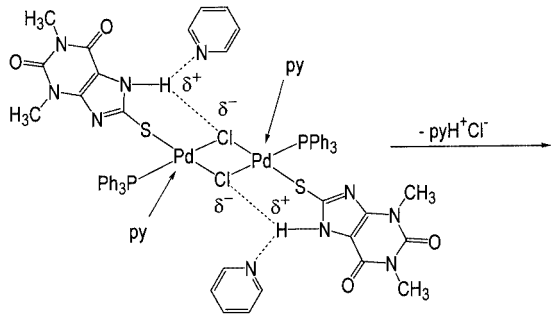

6

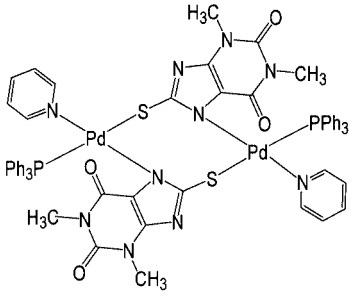

7

Scheme 6

towards the existence of a temperature dependent equilibrium for **7**. Notably, while the N−CH_3, pyridine and PPh_3 signals do not vary significantly with the temperature in the -60 to +60 °C range, the two low-field signals at δ = 11.38 and 13.21 ppm are lost at higher temperatures. This fact suggests that complex **7** encompasses an equilibrium between two different species. Recording the ^{1}H NMR spectrum of **7** in [D_5]pyridine further corroborates this finding as the proton spectrum contains only two signals in the purine N−CH_3 region (δ = 3.14 ppm for N1−CH_3; δ = 3.29 ppm for N3−CH_3) while the N7−H signals are no longer evident. By slow evaporation of the [D_5]pyridine solution orange crystals are obtained, which display IR and ^{1}H NMR ($CDCl_3$) spectra identical to those of the original compound **7**.[21]

In order to determine the structure of the palladium compound **7** and to collect important geometrical information on this class of compounds, an X-ray analysis has been carried out on a single crystal. The diffraction study showed that a dinuclear palladium complex and nine water molecules form the asymmetric unit cell. Four water molecules are located in a precise position of the lattice while the remaining five are disordered. An ORTEP drawing of the complex is shown in Figure 1 with the atomic numbering scheme. Details of crystal data and relevant information are summarized in Table 1.

Each metal atom in **7** displays a distorted square-planar coordination with the triphenylphosphane molecule located *cis* to a pyridine N atom and *cis* to the S atom of an 8-

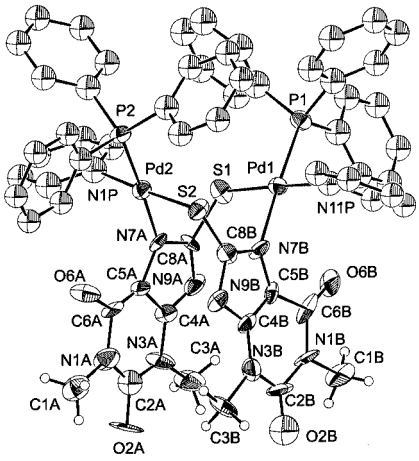

Figure 1. ORTEP drawing of **7**

Table 1. Summary of crystal data for [Pd(μ-*S*,*N*-8-BTT)-(PPh_3)Py]$_2$·9H_2O (**7**)

Formula	$C_{60}H_{52}N_{10}O_4S_2P_2Pd_2$·9$H_2O$
Mol. wt.	1478.18
T, K	296
λ, Å (Mo-K_α radiation)	0.71073
Crystal dimen., mm	0.25 × 0.15 × 0.11
Cryst. syst.	Monoclinic
space group	Cc
a, Å	22.178 (5)
b, Å	17.612 (5)
c, Å	19.575 (5)
β, °	117.656 (5)
V, Å^3	6772 (3)
Z	2
ρ_{calcd}, g/cm^{-3}	1.402
Abs coeff/mm^{-1}	0.705
F(000)	2820
θ range	1.55−25.00
Total no. of reflns	5943
No. of unique reflns	4267
R,[a] %	0.0701
R_w,[b] %	0.1661
Goodness of fit	1.117

[a] $R = \sum||F_0| - |F_c||/\sum|F_0|$. [b] $R_w = [\sum w(|F_0| - |F_c|)^2/\sum wF_0^2)]^{1/2}$.

TT^{2-} ligand. A *trans*-located N7 imidazolic atom from a second 8-TT^{2-} ligand completes the coordination polyhedron about each palladium atom. A remarkable feature of the present structure is that each palladium atom is linked by two different molecules of purine, i.e. each purine ligand in the dimeric structure binds two different palladium atoms, the first one using the S-atom and the second one through the imidazolic N7 atom. Thus, an eight-membered ring containing Pd1-S1-C8A-N7A-Pd2-S2-C8B-N7B and featuring a boat geometry is formed (Figure 2). For both metals, the square-planar coordination deviates slightly from planarity (Pd1, rms deviation 0.024; Pd2, rms deviation 0.070), the largest deviation being 4.15(69)° Å (for

Pd1) and 3.87(81)° Å (for Pd2). The dihedral (OR torsion) angle between the palladium planes is 71.00(31)°.

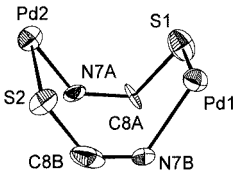

Figure 2

The two purine molecules are practically planar (the torsional angles between the imidazolic and pyrimidinic mean planes are: 3.10(1.34)°, (molecule A); and 4.12(1.24)°, (molecule B) and also non parallel to one another [angle between imidazolic mean plane of A and B purine molecules: 16.12(45)°], while the exocyclic groups do not show any significant deviation from the plane containing the purine ligand.

The bond lengths between palladium and the NNSP donor set are similar for both metal atoms, the largest difference being only 0.0423(399) Å between the N7A−Pd2 and N7B−Pd1 bond length. The analysis of the coordination distances showed the well-known *trans*-effect exerted by the P atoms. In fact, the longer P−Pd separation [P1−Pd1: 2.2655(75) Å] is opposite to the shorter N7 metal distance [N7B−Pd1: 2.0601(190) Å] and vice versa [P2−Pd2: 2.2863(77) Å; N7A−Pd2 2.1024(209) Å]. The distances N(pyridine)−Pd, and S−Pd are similar for both metal centres [N11P−Pd1: 2.0791(92) Å; N1P−Pd2: 2.0791(100) Å]. The two Pd−N(pyridine) distances are longer than the covalent Pd−N bond length (1.98 Å) and are even longer than the Pd−N bond lengths of other Pd−N(pyridine) complexes (1.98−2.04 Å) according to a search in the Cambridge Structural Database,[22] although they are similar to those found in palladium complexes in which pyridine is *trans* to an alkyl C atom.[23] Palladium complexes featuring a coordination sphere containing N, S, P and N atoms are unknown, and therefore no comparative information is available to discuss the *trans*-effect seen in **7** in detail.

A final comment relevant to the Pd1−Pd2 separation [4.1364(70) Å], is that this distance excludes any significant bonding interactions between the two metal centres. The rest of the bond lengths and angles are similar to those found in other N(7)-bonded purine complexes,[6,24] and do not deserve any additional comments.

Conclusions

The mild oxidation of 8-thiotheophylline (8-TTH_2) with I_2 leads to the formation of **1**, a new thiopurine derivative containing two theophylline units bonded through the C8 carbon atoms by a S−S bridge. Reaction of **1** with *cis*-[$PdCl_2(PPh_3)_2$] gives **6** in which two palladium atoms are likely to be bridged by two chlorides and each metal is additionally coordinated to one PPh_3 group and to the deprotonated thiol group of the 8-thiotheophylline ligand. It is conceivable that PPh_3 released from the *cis*-[$PdCl_2(PPh_3)_2$], is responsible for the cleavage of the S−S bond in **1**. Complex **6** reacts with pyridine to give the dimetallic complex **7** which was authenticated by X-ray methods. In the latter complex two palladium atoms are held together by two molecules of 8-TT^{2-} through the N7 and S atom. Each metal completes a square-planar coordination by using one PPh_3 and one pyridine molecule. The bonding pattern of the thiotheophyllinate anion in **7** is without precedent and represents a remarkable and curious coordination mode of purine derivatives. The process leading to **7** has been rationalised and likely proceeds via nucleophilic substitution of the two chloride bridges and subsequent deprotonation of the 8-TTH^- by pyridine.

The experimental results suggest: a) The coordination of the present thiopurine occurs through the S-atom; b) phosphane metal complexes, like the palladium one used in this work as the starting material, may be biologically relevant due to their capacity of easily dissociating the phosphane ligand, which, in turn, may react with disulfide groups of sulfur-containing proteins resulting in the cleavage of the S−S bridges. Although the solubility of the present palladium complexes do not allow any possible application in medicinal chemistry, this kind of study, possibly extended to other nucleobases and/or to different transition metal complexes and phosphanes, is important because it can bring about new metal-nucleobase interactions. Current studies are in progress in our laboratories in order to verify whether the use of palladium and platinum complexes, stabilised by water soluble phosphanes, may lead to the synthesis of metal-purine derivatives of higher solubility in biological conditions.

Experimental Section

All reagents were of analytical grade and were used without further purification. The complexes *cis*-[$PdCl_2(PPh_3)_2$],[6] $Na_2[PdCl_4]$ and the ligand 8-thiotheophylline[25] (8-TTH_2) were prepared as described previously. All reactions were routinely performed under argon by using standard Schlenk-tube techniques. Deuterated solvents for NMR spectroscopic measurements were dried over molecular sieves (4 Å). ^1H, $^{13}C\{^1H\}$ and $^{31}P\{^1H\}$ NMR spectra were recorded on a Bruker AVANCE DPX 300 spectrometer. Peak positions are relative to tetramethylsilane (^1H, $^{13}C\{^1H\}$) and were calibrated with respect to the residual protonated solvent (^1H) or to the solvent resonance ($^{13}C\{^1H\}$). The $^{31}P\{^1H\}$ NMR spectra are given with respect to external 85% H_3PO_4 in D_2O with downfield values taken as positive. Infrared spectra were recorded on KBr discs on a IR-ATI Mattson Infinity Series. Elemental analyses (C, H N, S) were performed on a Fisons Instruments EA 1108 elemental analyser. GC/MS analyses were carried out using a Varian GC/MS Saturn 3 gas chromatograph-ion-trap mass spectrometer, using a stationary phase column DB-5MS (J&W Scientific,Folsom, Ca, USA), 30 m × 0.25 mm I.D. × 0.25 μm film thickness. Melting points were measured on a BÜCHI 530 instrument.

Synthesis of *S,S*-Bis(8-thiotheophylline) [1, 8-$BTTH_2$]: The ligand **1** was prepared by stirring 8-thiotheophylline (8-TTH_2) (1.00 g,

5.0 mmol) with KOH (0.28 g, 4.8 mmols) in EtOH (20 mL) for 30 min. Further addition of I_2 (1.32 g, 5.2 mmol) at room temperature, and reflux for 6 hours gave **1** as a pale yellow powder that was filtered off, washed with H_2O (2 × 2 mL), EtOH (2 × 2 mL) and finally vacuum dried. Yield: 1.37 g, 65%. m.p.: 294−295 °C. $C_{14}H_{14}N_8O_4S_2$ (422.44): calcd. C 39.8, H 3.3, N 26.5, S 14.2; found C 41.2, H 3.4, N 24.6, S 14.0. M.p.: 294−295 °C. IR: ν(N−H) 3115−2660 cm^{-1} (br. w.); ν(C6=O) 1717 (s); ν(C2=O) 1640 (s). ^1H NMR (22 °C, [D_6]DMSO): δ = 3.33 (s, N1-CH_3), 3.56 (s, N3-CH_3), 4.67 (w, N7−H) ppm. $^{13}C\{^1H\}$ NMR (22 °C, [D_6]DMSO): δ = 27.5 (N1-CH_3), 29.8 (N3-CH_3), 112.2 (C5), 146.9 (C4), 148.80 (C8), 151.0 (C6), 154.8 (C2) ppm.

Synthesis of the Potassium Salts of 8-Thiotheophyllinate [2, K_2(8-TT)] and *S,S*-Bis(8-thiotheophyllinate) [3, K_2(8-BTT)]: 8-TTH_2 (for **2**; 5 mmol, 1 g) or 8-$BTTH_2$ (for **3**; 2.5 mmol, 1 g) was introduced, via a dropping funnel, to a solution of KOH (0.27 g. 4.8 mmol) in EtOH (10 mL); a white precipitate immediately separated. The mixture was stirred and refluxed for 2 hours, slowly cooled down to room temperature, the precipitate filtered off, washed with two portions (2 mL) of cold EtOH and, finally, dried under vacuum.
2: Yield: 0.86 g, 60%. $C_7H_6K_2N_4O_2S$ (288.41): calcd. C 29.1, H 2.1, N 19.4, S 11.1; found C 29.1, H 2.3, N 19.2, S 10.9. IR: ν(C6=O) 1672 cm^{-1} (s); ν(C2=O) 1631 (s); ν(C=C) + ν(C=N) 1526, 1518, 1553, 1445. ^1H NMR (22 °C, CD_3OD): δ = 3.25 (s, N1-CH_3), 3.41 (s, N3-CH_3) ppm.
3: Yield: 0.87 g, 70%. $C_{14}H_{12}K_2N_8O_4S_2$ (498.62): calcd. C 33.7, H 2.4, N 22.5, S 12.9; found C 33.5, H 2.5, N 22.2, S 12.5. IR: ν(C6=O) 1687 cm^{-1} (s); ν(C2=O) 1631 (s); ν(C=C) + ν(C=N) 1565, 1525, 1454. ^1H NMR (22 °C, CD_3OD): δ = 3.36 (s, N1-CH_3), 3.51 (s, N3-CH_3) ppm.

Synthesis of the Pyridinium Salt of *S,S*-Bis(8-thiotheophyllinate) [4, $(PyH)_2$(8-BTT)]: Pyridine (5 mL) was added to a vigorously stirred suspension of **1** (0.5 g, 1.18 mmol) in EtOH (15 mL). The yellow solution obtained was stirred for 2 h at room temperature and concentrated to ca. 5 mL. The addition of pentane (10 mL) gave a pale yellow precipitate that was filtered off, washed twice with pentane (5 mL) and dried under vacuum. The crude yellow powder thus obtained contained some pyridine and did not give reproducible elemental analyses. Nevertheless, an analytically pure compound was obtained by recrystallisation from hot EtOH.

An in situ NMR spectroscopy experiment in which **1** (20 mg, 0.0047 mmol) was dissolved in [D_5]pyridine (0.5 mL) showed that **4** was the only product formed. Yield: 0.24 g, 35%. $C_{24}H_{22}N_{10}O_4S_2$ (578.62): calcd. C 49.8, H 3.8, N 24.2, S 11.1; found C 49.4, H 4.2, N 23.8, S 10.7. IR: ν(PyN-H) 3110 cm^{-1} (w.); ν(C6=O) 1718, 1704 (s); ν(C2=O) 1644 (s); ν(C=C)+ν(C=N) 1594, 1547, 1485 (s). ^1H NMR (22 °C, [D_5]pyridine): δ = 3.43 (s, N1-CH_3, 6 H), 3.70 (s, N3-CH_3, 6 H), 8.67−7.72 (m, Py, 20 H) ppm.

Reaction of 1 with PPh_3 in Ethanol: A suspension of **1** (0.5 g, 1.18 mmol), KOH (0.07 g, 1.25 mmol) and PPh_3 (0.62 g, 2.34 mmol) in EtOH (5 mL) was refluxed for 3 hours. The resulting colourless solution was kept at room temperature overnight to leave a pale yellow precipitate, which was filtered off, washed with cold EtOH and vacuum dried. NMR spectroscopy and elemental analysis allowed us to confirm that this compound is **2** (Yield: 0.44 g, 65%). A second crop of **2** was obtained from the mother liquor. Total yield: 0.52 g, 76%.

An in situ NMR spectroscopy experiment (0.5 mL CD_3OD, T = 50 °C) showed that O=PPh_3 and an insoluble white precipitate, which was separated and identified as **2**, were formed during the reaction of **1** (0.017 g, 0.04 mmol) with KOH (0.003 g, 0.05 mmol) and PPh_3 (0.025 g, 0.09 mmol).

Reaction of 1 with PPh_3 in DMSO or Dioxane. Synthesis of 8-Phenylthiotheophylline [(5), 8-PhTTH]: Compound **1** (0.5 g, 1.18 mmol) and PPh_3 (0.65, 2.48 mmol) were added to 5 mL of DMSO (or dioxane). The suspension was stirred at 30 °C for 1 h and then heated to 50 °C for 2 h. The addition of heptane (15 mL) to the hot solution yielded a pale yellow precipitate that was filtered off, washed with pentane (2 × 10 mL) and vacuum dried. The crude compound was recrystallised twice from hot EtOH to give analytically pure yellow microcrystals of **5**.

In situ NMR spectroscopy monitoring of this reaction ([D_6]DMSO, T = 60 °C) confirmed that the only soluble compound formed was **5**. Yield: 0.17 g, 30%. $C_{25}H_{22}N_4O_2PS$ (473.51): calcd. C 63.4, H 4.7, N 11.8, S 6.8; found C 63.2, H 4.5, N 11.6, S 6.5. IR: ν(N−H) 3200−2620 cm^{-1} (br. w.); ν(C6=O) 1690 (s); ν(C2=O) 1642 (s). ^1H NMR (22 °C, [D_6]DMSO): δ = 3.15 (s, N1-CH_3, 3 H), 3.35 (s, N3-CH_3, 3 H), 7.24−7.65 (m, Ph, 5 H), 11.33 (w, N7−H, 1 H) ppm. $^{13}C\{^1H\}$ NMR (22 °C, [D_6]DMSO): δ = 27.7 (N1-CH_3), 29.8 (N3-CH_3), 104.3 (C5), 129.1−133.8 (m, Ph), 149.9 (C4), 151.1 (C2), 151.6 (C6), 170.3 (C8) ppm. $^{31}P\{^1H\}$ NMR (22 °C, [D_6]DMSO): δ = 27.5 ppm.

Synthesis of [Pd(PPh_3)(μ-Cl)(8-TT)]$_2$ (6). Method A: Compound **1** (0.1 g, 0.24 mmol) was added to a solution of KOH (0.028 g, 0.5 mmol) in EtOH (20 mL). After 5 min, *cis*-[$PdCl_2(PPh_3)_2$] (0.350 g, 0.50 mmol) was added to the reaction mixture to yield a red orange suspension. This was left for 30 min at room temperature and then heated to reflux for 2 hours. A red orange precipitate formed, which was filtered off, washed twice with EtOH (5 mL) and air dried. Yield: 0.27 g, 91%.

Method B: A solution of $Na_2[PdCl_4]$ (0.06 g, 0.20 mmol) in 5 mL of water was added at room temperature to a suspension of PPh_3 (0.131 g, 0.5 mmol), 1 (0.05 g, 0.12 mmol) and KOH (0.012 g, 0.2 mmol) in 15 mL of EtOH. The mixture was stirred at room temperature for 1 h and then refluxed for 2 h. The red orange precipitate of 6 was isolated as described above. Yield: 0.1 g, 70%.

Method C: One equivalent of **3** (or **4**) was reacted in refluxing EtOH with two mol equivalents of *cis*-[$PdCl_2(PPh_3)_2$] (or $Na_2[PdCl_4]$ and PPh_3 in a 1:2 molar ratio). After 1 h the precipitate was separated, washed and dried as described previously. Yield: 73%.

Method D: Reaction of one equivalent of **2** with a stoichiometric amount of *cis*-[$PdCl_2(PPh_3)_2$] (or 1 $Na_2[PdCl_4]$ + 2 PPh_3) in refluxing EtOH, gave **6** as a red orange precipitate within 1 h. The compound was separated, washed and dried as described previously. Yield: 73%.

$C_{50}H_{44}Cl_2N_8O_4P_2Pd_2S_2$ (1230.76): calcd. C 48.8, H 3.6, N 9.1, S 5.2; found C 48.5, H 3.8, N 9.2, S 4.9. IR: ν(N7 H) 3059−2790 cm^{-1} (w); ν(C6=O) 1673 (s); ν(C2=O) 1625 (s); ν(C=C) + ν(C=N) 1583, 1535, 1520 (s); δ(Ph−H) 740, 703, 688, 516, 507.

In Situ Reaction of 1 with *cis*-[$PdCl_2(PPh_3)_2$] in CD_3OD: Compound **1** (30 mg, 0.071 mmol), *cis*-[$PdCl_2(PPh_3)_2$] (100 mg, 0.142 mmol) and CD_3OD (0.5 mL) were placed into a 5-mm NMR tube maintained at 20 °C. A $^{31}P\{^1H\}$ NMR spectrum was immediately acquired, showing only the resonance due to the starting metal complex *cis*-[$PdCl_2(PPh_3)_2$]. The temperature was then raised to 50 °C causing the separation of a red orange solid within 6 h. Formation of O=PPh_3 was observed by $^{31}P\{^1H\}$ NMR spectroscopy and GC-MS analysis. The red precipitate was separated,

Table 2. Selected bond lengths (Å) and angles (°) for $[(8\text{-BzTT})_2\text{-Pd}(PPh_3)_2]_2$ (**7**)

Pd1−N11P	2.079(9)
Pd1−N7B	2.10(2)
Pd1−P1	2.266(8)
Pd1−S1	2.294(8)
Pd2−N7A	2.060(19)
Pd2−N1P	2.087(10)
Pd2−P2	2.286(8)
Pd2−S2	2.301(8)
P1−C121	1.796(13)
P1−C101	1.824(13)
P1−C111	1.857(13)
P2−C201	1.847(12)
P2−C211	1.821(12)
P2− C221	1.842(13)
S1−C8A	1.76(2)
S2−C8B	1.73(3)
N7A−C8A	1.38(3)
N7A−C5A	1.40(3)
C8A−N9A	1.34(3)
N7B−C8B	1.29(3)
N7B−C5B	1.34(3)
C8B−N9B	1.44(3)
N11P−Pd1−N7B	85.3(8)
N11P−Pd1−P1	94.7(5)
N7B−Pd1−P1	176.4(6)
N11P−Pd1−S1	178.4(5)
N7B−Pd1−S1	93.3(7)
P1−Pd1− S1	86.7(3)
N7A−Pd2−N1P	85.6(7)
N7A−Pd2−P2.	176.7(6)
N1P−Pd2−P2	94.7(5)
N7A−Pd2−S2	93.4(5)
N1P−Pd2−S2	175.7(5)
C8A−S1−Pd1	106.2(8)
C8B−S2−Pd2	103.1(10)
C8A−N7A−Pd2	129.8(15)
C5A−N7A−Pd2	127.8(16)
N9A−C8A−N7A	113.5(18)
N9A−C8A−S1	127.0(17)
N7A−C8A−S1	119.5(17)
C4A−N9A−C8A	107(2)
C8B−N7B−Pd1	123.5(17)
C5B−N7B−Pd1	128.5(17)
N7B−C8B−N9B	114(2)
N7B−C8B−S2	128(2)
N9B−C8B−S2	118(2)
C4B−N9B−C8B	99(2)

washed with two portions (0.5 mL) of CH_3OH and vacuum dried. This residue was dissolved in $[D_6]$DMSO (0.5 mL) and $^{31}P\{^1H\}$ NMR spectroscopy confirmed that it was **6**.

Synthesis of $[Pd(PPh_3)Py(\mu\text{-S,N-8-TT})]_2\cdot 9H_2O$ (7): Compound **6** (0.15 g, 0.12 mmol) was introduced into a vessel containing acetonitrile (5 mL). The temperature was kept at 50 °C and pyridine (1 mL) was then added. The red orange solution obtained from this was left to stand at room temperature. Orange prismatic crystals were obtained by slow evaporation of the solvent. Yield: 0.05 g, 30%. $C_{60}H_{52}N_{10}O_4P_2Pd_2S_2\cdot 9H_2O$ (1478.05): calcd. C 48.7, H 4.8, N 9.5, S 4.3; found C 49.0, H 5.1, N 9.2, S 4.1. IR: ν(C6=O) 1673 cm^{-1} (s); ν(C2=O) 1625 (s); ν(C=C) + ν(C=N) 1603, 1521 (s); δ(Ph−H) 762, 696, 534, 514, 491. ^1H NMR (22 °C, $CDCl_3$): δ = 3.14, 3.22 (s, N1-CH_3, 3 H), 3.40, 3.52 (s, N3-CH_3, 3 H), 7.18−7.70 (m, Ph, 5 H), 7.18−8.62 (m, Py, 5 H), 11.40 (s, 1 H), 13.23 (w, 1 H) ppm. $^{31}P\{^1H\}$ NMR (22 °C, $CDCl_3$): δ = 27.35 ppm. ^1H NMR (22 °C, $[D_5]$pyridine): δ = 3.14 (s, N1-CH_3, 6 H), 3.29 (s, N3-CH_3, 6 H), 7.02−7.70 (m, Ph, 5 H), 7.02−7.78 (m, Py, 5 H) ppm. $^{31}P\{^1H\}$ NMR (22 °C, $[D_5]$pyridine): δ = 36.18 ppm.

In Situ Reaction of 6 with $[D_5]$pyridine: Compound **6** (35 mg, 0.028 mmol) was placed into an NMR tube and $[D_5]$pyridine (0.5 mL) was added. Dissolution took place after heating at 50 °C to give a red orange solution. $^{31}P\{^1H\}$ NMR spectroscopic monitoring showed the presence of several compounds with **7** being the most abundant (82%). Formation of $O{=}PPh_3$ or PPh_3 was not observed. Compound **7** was precipitated as an orange microcrystalline solid by addition of acetonitrile (2 mL).The compound was confirmed by IR and NMR spectroscopy. The identification of the secondary compounds that accompany the formation of **7** was not attempted.

X-ray Crystallography: Crystals suitable for the X-ray diffraction study were obtained from a solution of **7** in acetonitrile/pyridine (1:1) by slow evaporation. Data were collected at 293 K on a Stoe-Siemens AED diffractometer, using graphite-monochromatised Mo-K_α radiation (λ = 0.71069 Å). The unit cell parameters were obtained from least-squares refinement of 32 well-centred reflections ($12.5° < \theta < 15.9°$). The data were collected by the ω − 2θ scan mode ($1.55° < 2\theta < 25°$) and were corrected for Lorentz and polarisation effects as well as for absorption effects. Details of crystal data and relevant information are summarised in Table 1. The structure was solved using the Sir97 program.[26] In the final refinement the SHELX-96 program[27] was used and in the graphic representation the ORTEP program.[28] Refinement was done by full-matrix least-squares calculations, initially with isotropic thermal parameters. In the final refinement, all purine non-hydrogen atoms and water oxygen atoms were refined anisotropically, whereas purine hydrogen atoms were placed at their calculated positions and then refined isotropically. All of the phenyl rings were treated as rigid bodies with D_{6h} symmetry and C−C distances fixed at 1.39 Å. No significant peaks were detected in the final least-squares cycles. Selected bond lengths and angles are listed in Table 2.

CCDC-194639 contains the supplementary crystallographic data for this paper. These data can be obtained free of charge at www.ccdc.cam.ac.uk/conts/retrieving.html [or from the Cambridge Crystallographic Data Centre, 12, Union Road, Cambridge CB2 1EZ, UK; fax: (internat.) +44-1223/336-033; E-mail: deposit@ccdc.cam.ac.uk].

Acknowledgments

We acknowledge Antonio Valverde and Ana Aguilera for GS-MS analyses. Thanks are due to the bilateral project "Programa Hispano-Marroquí" (AECI, MAE) and Junta de Andalucía (A29/00 project) for supporting the stay of M. S. in Almería.

[1] B. Lippert, *Coord, Chem. Rev.* **2000**, *200*, 487−516.
[2] I. Bertini, H. B. Gray, S. J. Lippard, J. S. Valentine, *Bioinorganic Chemistry*, University Science Books, Mill Valley, **1994**.
[3] U. Bierbach, N. Farrell, *Inorg. Chem.* **1997**, *36*, 3657−3665.
[4] Z. Guo, P. J. Sadler, *Angew. Chem. Int. Ed.* **1999**, *38*, 1512−1537.
[5] M. J. Clarke, F. Zhu, D. R. Frasca, *Chem. Rev.* **1999**, *99*, 2511−2533.
[6] E. Wong, C. M. Giandomenico, *Chem. Rev.* **1999**, *99*, 2451−2466.
[7] J. Tsuji, *Palladium Reagents and Catalysts*, John Wiley & Sons, **1995**.
[8] E. Colacio, A. Romerosa, J. Ruiz, P. Román, J. M. Gutiérrez-

Zorrilla, A. Vegas, M. Martínez-Ripoll, *Inorg. Chem.* **1991**, *30*, 3743−3749.
[9] A. Romerosa, C. López-Magaña, M. Saoud, S. Mañas, E. Colacio, J. Suárez-Varela, *Inorg. Chim. Acta* **2000**, *307*, 125−130.
[10] P. M. Maitlis, P. Espinet, M. J. H. Russell, *Comprehensive Organometallic Chemistry*, first edition (Ed.: G. Wilkinson, F. G. A. Stone, E. W. Abel), Pergamon Press, **1982**, p. 279.
[11] A. T. Hutton, C. P. Morley, *Comprehensive Coordination Chemistry*, first edition (Eds.: G. Wilkinson, R. D. Gillard, J. A. McCleverty), Pergamon Press, **1987**, p. 1157.
[12] A. T. Hutton, C. P. Morley, *Comprehensive Coordination Chemistry*, first edition (Eds.: G. Wilkinson, R. D. Gillard, J. A. McCleverty), Pergamon Press, **1987**, p. 1131.
[13] J. Forniés, R. Navarro, V. Sicilia, M. Tomás, *Inorg. Chim. Acta* **1990**, *168*, 201−207.
[14] J. Chatt, F. G. J. Mann, *J. Chem. Soc.* **1938**, 1949−1956.
[15] J. Chatt, F. A. Hart, *J. Chem. Soc.* **1953**, 2363−2371.
[16] T. Boschi, B. Crociani, M. Nicolini, U. Belluco, *Inorg. Chim. Acta* **1975**, *12*, 39−44.
[17] Ch. Elschenbroich, A. Salzer, *Organometallics: A Concise Introduction*, 2nd ed., VCH, 1992.
[18] J. W. Suggs, *Encyclopedia of Inorganic Chemistry* (Ed.: R. B. King), Wiley, **1994**, p. 3023.
[19] L. E. Overman, *Synthesis* **1974**, 59.
[20] B. Lippert, *Prog. Inorg. Chem.* **1989**, *37*, 1−97.
[21] A ^{13}C NMR spectrum could not be obtained due to the low solubility of **7** in all of the common solvents.
[22] F. H. Allen, O. Kennard, R. Taylor, *Acc. Chem. Res.* **1983**, *16*, 146−153.
[23] F. Iwasaki, N. Manabe, M. Yasui, N. Matsumura, N. Kamiya, H. Iwasaki, *Bull. Chem. Soc. Jpn.* **1996**, *69*, 2749−2757 and references therein.
[24] E. Colacio, R. Cuesta, J. M. Moreno, *Inorg. Chem.* **1997**, *36*, 1084−1087.
[25] E. Colacio, R. Cuesta, M. Ghazi, M. A. Huertas, J. M. Moreno, A. Navarrete, *Inorg. Chem.* **1997**, *36*, 1652−1656.
[26] K. W. Merz, P. H. Sthal, *Arzneim. Forsch.* **1965**, *15*, 10.
[27] A. Altomare, G. Cascarano, C. Giacovazzo, A. Guagliardi, A. G. Moliterni, M. C. Burla, G. Polidori, M. Carmalli, R. Spagna, *SIR 97 Package Program*, **1997**.
[28] G. M. Sheldrick, *SHELX-96 Program for Crystal Structure Determination*, University of Göttingen, **1996**.
[29] C. K. Johnson, *ORTEP:* Report ORNL-5318, OAK Ridge national Laboratory: Oak Ridge, TN, **1976**.

Received March 13, 2002
[I02135]

A Cu^{II} Chain Compound Showing a Ferromagnetic Coupling through Triple N^1,N^2-1,2,4-Triazole Bridges

Yann Garcia,*[a][‡] Petra J. van Koningsbruggen,[b] Georges Bravic,[a] Daniel Chasseau,[a] and Olivier Kahn†[a]

Keywords: Chain structures / Copper / N ligands / Bridging ligands / Magnetic properties

$[Cu(hyetrz)_3](CF_3SO_3)_2\cdot H_2O$ [hyetrz = 4-(2′-hydroxyethyl)-1,2,4-triazole] represents the first structurally characterised ferromagnetically coupled Cu^{II} chain compound containing triple N^1,N^2-1,2,4-triazole bridges. *catena*-[μ-Tris{4-(2′-hydroxyethyl)-1,2,4-triazole-N^1,N^2}copper(II)] bis(trifluoromethanesulfonate) hydrate ($C_{14}H_{23}F_6S_2O_{10}CuN_9$) crystallises in the triclinic space group $P\bar{1}$, a = 13.54(3), b = 14.37(3), c = 15.61(4) Å, α = 95.9(1), β = 104.9(1), γ = 106.5(1)°, V = 2763(11) Å^3, Z = 4 (Cu^{II} units). The Cu^{II} ions are linked by triple N^1,N^2-1,2,4-triazole bridges yielding an alternating chain with Cu1–Cu2 = 3.8842(4) Å and Cu2–Cu3 = 3.9354(4) Å. Analysis of the magnetic data according to a high-temperature series expansion gives a J value of +1.45(3) cm^{-1}. The nature and the magnitude of the ferromagnetic exchange have been discussed on the basis of the structural features.

(© Wiley-VCH Verlag GmbH & Co. KGaA, 69451 Weinheim, Germany, 2003)

Introduction

Polynuclear coordination compounds containing derivatives of 1,2,4-triazole have been of increasing interest during the last decade. Several studies have dealt with the search for magneto-structural correlations for transition metal(II) compounds containing N^1,N^2-1,2,4-triazole bridges.[1−14] On the other hand, polynuclear (1,2,4-triazole)iron(II) compounds have been found to yield spin transition materials exhibiting cooperative behaviour.[15−17]

Although a wealth of polynuclear transition metal(II) compounds have been structurally and magnetically characterised, an incomplete picture concerning the interplay of the 1,2,4-triazole derivatives and noncoordinated anions still exists when determining the structural features and the associated magnetic behaviour. Dinuclear Cu^{II} compounds could be obtained by using polyfunctional 1,2,4-triazole derivatives with N-donating substituents, forming five-membered chelate rings. The magnetic properties of these could be fine-tuned by playing upon the coordination geometry of the double N^1,N^2-1,2,4-triazole bridges residing in the equatorial plane of the Cu^{II} ions.[1−7] A correlation between the magnitude of the antiferromagnetic (AF) interaction and the ligand bridge geometry could be established for the first time for this class of compounds.[5,10,11] The geometry of the bridging ligand network appears mainly to be determined by the geometric requirements of the Cu^{II} atom and the spatial disposition of the ligands. Therefore, no direct influence of the incorporated noncoordinated anions in determining the crystal packing and its possible effect on the 1,2,4-triazole bridge geometry could be proposed.

Generally, depending upon the experimental conditions, the reaction of 4-R-substituted 1,2,4-triazole ligands with Cu^{II} salts of potentially noncoordinating anions either yield linear chain Cu^{II} compounds[8,18,19] or linear trinuclear Cu^{II} entities.[20−23] The propagation of the AF exchange is indeed drastically decreased in these triply N^1,N^2-1,2,4-triazole-bridged trinuclear[20] and linear-chain Cu^{II} compounds[8] compared with the dinuclear bis(μ-N^1,N^2-1,2,4-triazole) compounds.[1−7,10] Actually, in these dinuclear systems, the propagation of the AF exchange may proceed very efficiently via the $d_{x^2-y^2}$ orbitals on the Cu^{II} ions which interact with the σ-orbitals of the nitrogen atoms of the bridging ligand, which are all situated in the equatorial plane. The introduction of an additional ligand in the Cu···Cu linkage, as in the case of the linear tri- and polynuclear Cu^{II} systems, brings the equatorial planes of the Jahn−Teller-distorted octahedral Cu^{II} ions in positions canted by about 60° towards one another. Consequently, the AF coupling can only proceed efficiently via a single 1,2,4-triazole ligand, and will be very weak, typically of the order of a few wavenumbers.

Indeed, the AF coupling between nearest-neighbour Cu^{II} ions within the linear trinuclear $[Cu_3\{4\text{-(2-pyridyl)-1,2,4-triazole}\}_{10}(H_2O)_2](ClO_4)_6\cdot 7H_2O$ has been found to be

[a] Laboratoire des Sciences Moléculaires, Institut de Chimie de la Matière Condensée de Bordeaux, UPR CNRS No 9048, 33608 Pessac, France
[b] Department of Chemistry, University of Utah, Salt Lake City, UT 84112, USA
[‡] Present address: Département de Chimie, Unité de Chimie des Matériaux Inorganiques et Organiques, Faculté des Sciences, Université catholique de Louvain, Place L. Pasteur 1, 1348 Louvain-la-Neuve, Belgium
Fax: (internat.) + 32-10/47-2330
E-mail: garcia@chim.ucl.ac.be

-5.41 cm^{-1},[20] whereas the isotropic exchange constant is only $-1.01(2)$ cm^{-1} for the 3-D network built up from linear trinuclear Cu^{II} cations, $[Cu_3\{1,2\text{-bis}(1,2,4\text{-triazol-4-yl})\text{ethane}\}_5(H_2O)_2]^{6+}$.[23] Furthermore, the linear-chain compound $[Cu(hyetrz)_3](ClO_4)_2\cdot 3H_2O$ [hyetrz = 4-(2′-hydroxyethyl)-1,2,4-triazole] also exhibits a very weak AF coupling of $J = -1.18(2)$ cm^{-1}.[8]

Surprisingly, the magnetic data for the linear trinuclear Cu^{II} compounds $[Cu_3(metrz)_6(H_2O)_4](CF_3SO_3)_6(H_2O)_4$ (metrz = 3-methyl-4-ethyl-1,2,4-triazole)[21] and $[Cu_3(etrz)_9(H_2O)_3](CF_3SO_3)_6$ (etrz = 4-ethyl-1,2,4-triazole),[22] indicate a weak overall ferromagnetic (F) interaction. Unfortunately, the magnetic data could not be satisfactorily interpreted, nor could it be related to the structural features, possibly due to the lack of detailed crystallographic data.

These unprecedented magnetic data might be related to the presence of the trifluoromethanesulfonate anion, which could play an important role in determining the crystal packing of these compounds, thereby indirectly influencing the orientation of the 1,2,4-triazole ligands. In order to check this hypothesis, an extended crystallographic and magnetic study on $[Cu(hyetrz)_3](CF_3SO_3)_2\cdot H_2O$ has been carried out, which would allow an excellent comparison with the perchlorate derivative on which we reported previously.[8]

Results and Discussion

Description of the X-ray Structure of $[Cu(hyetrz)_3](CF_3SO_3)_2\cdot H_2O$

A projection of the cationic linear Cu^{II} chain is depicted in Figure 1, and the relevant bond length and bond angle information is given in Table 1.

The coordination polymer consists of a crystallographically independent unit comprising two Cu^{II} ions, Cu1 and Cu3, in special positions and another Cu^{II} ion in a general position (Cu2), along with six symmetry-independent hyetrz ligands. The linear chain running along the *c* axis (see Figure 2) is generated by the inversion involving the crystallographic centres of symmetry located on Cu1 and Cu3. $[Cu(hyetrz)_3](ClO_4)_2\cdot 3H_2O$[8] crystallises in the monoclinic space group $P2_1/n$, whereas the title compound crystallises in the triclinic space group $P\bar{1}$. However, this does not change the local symmetry around the Cu^{II} ions, since in both compounds the inversion centres are located on the metal ions.

Three hyetrz ligands act as bidentate ligands linking the Cu^{II} ions via the nitrogen atoms N1 and N2. All metal ions are in a distorted (4+2) octahedral environment formed by six N-donating hyetrz ligands. The basal plane is formed by four nitrogen donor atoms with distances between 1.989(3)

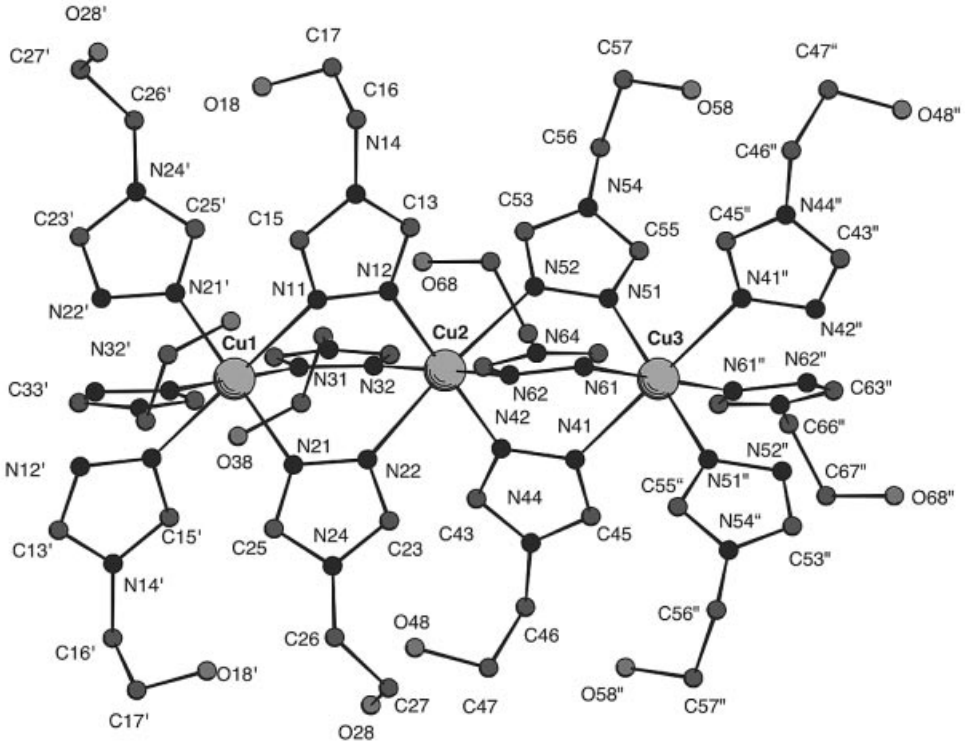

Figure 1. Drawing and atomic labeling system showing the structure of $[Cu(hyetrz)_3](CF_3SO_3)_2\cdot H_2O$; hydrogen atoms, noncoordinating counter anions, and water molecules have been omitted for clarity

Table 1. Selected bond lengths [Å] and angles [°] for $[Cu(hyetrz)_3](CF_3SO_3)_2\cdot H_2O$

Cu1−Cu2	3.8843(2)	Cu2−N32	2.066(2)
Cu2−Cu3	3.9352(2)	Cu2−N42	1.989(2)
Cu1−N11	2.370(2)	Cu2−N52	2.409(2)
Cu1−N21	2.018(2)	Cu2−N62	2.064(2)
Cu1−N31	2.067(2)	Cu3−N41	2.331(2)
Cu2−N12	1.994(2)	Cu3−N51	2.009(2)
Cu2−N22	2.360(2)	Cu3−N61	2.116(2)
N11−Cu1−N21	89.93(7)	N32−Cu2−N42	90.73(8)
N11−Cu1−N31	86.24(7)	N32−Cu2−N52	98.19(7)
N21−Cu1−N31	91.18(7)	N32−Cu2−N62	175.77(8)
N12−Cu2−N22	91.50(7)	N42−Cu2−N52	87.30(7)
N12−Cu2−N32	88.70(7)	N42−Cu2−N62	92.19(8)
N12−Cu2−N42	179.13(8)	N52−Cu2−N62	85.01(7)
N12−Cu2−N52	92.12(7)	N41−Cu3−N51	88.42(7)
N12−Cu2−N62	88.41(7)	N41−Cu3−N61	86.66(7)
N22−Cu2−N32	86.75(7)	N51−Cu3−N61	89.98(7)
N22−Cu2−N42	89.12(7)		
N22−Cu2−N52	173.93(7)		
N22−Cu2−N62	90.23(7)		
Cu1−N11−N12	123.8(1)	Cu2−N32−C33	127.1(2)
Cu1−N11−C15	125.2(2)	Cu3−N41−N42	126.7(1)
Cu2−N12−N11	122.3(1)	Cu3−N41−C45	125.9(2)
Cu2−N12−C13	129.8(2)	Cu2−N42−N41	124.7(1)
Cu1−N21−N22	120.3(1)	Cu2−N42−C43	127.4(2)
Cu1−N21−C25	131.5(2)	Cu3−N51−N52	125.0(1)
Cu2−N22−N21	128.2(1)	Cu3−N51−C55	126.7(2)
Cu2−N22−C23	124.6(2)	Cu3−N61−N62	125.5(1)
Cu1−N31−N32	129.3(1)	Cu3−N61−C65	127.8(2)
Cu1−N31−C35	124.5(2)	Cu2−N62−N61	128.4(1)
Cu2−N32−N31	125.3(1)	Cu2−N62−C63	122.3(2)

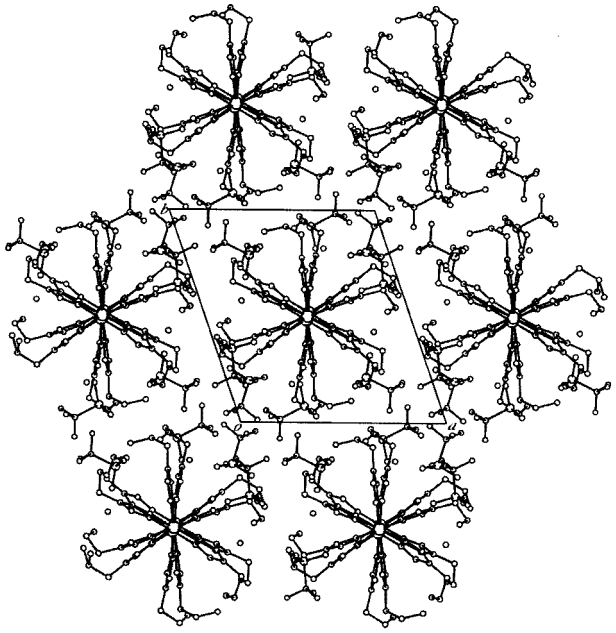

Figure 2. View of the crystal structure of $[Cu(hyetrz)_3](CF_3SO_3)_2\cdot H_2O$ along the *c* axis

and 2.116(3) Å, whereas two hyetrz ligands are coordinated in the axial positions at significantly longer distances [2.328(3)−2.409(3) Å]. This distribution of Cu−N distances is the signature for a static Jahn−Teller distortion, as has comparably been found for $[Cu(hyetrz)_3](ClO_4)_2\cdot 3H_2O$[8] and $[Cu(4\text{-amino-}1,2,4\text{-triazole})_3](ClO_4)_2\cdot 0.5H_2O$.[18] The range of Cu−N distances is, however, slightly larger for $[Cu(hyetrz)_3](CF_3SO_3)_2\cdot H_2O$. All Cu^{II} ions are not significantly displaced from their equatorial coordination plane [δ(Cu2) ≈ 0.02 Å]. The least-squares planes through the equatorial planes of the Cu^{II} octahedra make angles of 55.51(7)° for Cu1 and Cu2, 50.40(6)° for Cu2 and Cu3, which is slightly different from what has been found for $[Cu(hyetrz)_3](ClO_4)_2\cdot 3H_2O$. In that case, the least-squares planes through the equatorial planes of the octahedrally coordinated Cu^{II} ions make angles of 46(1)° for Cu1 and Cu2, 53(3)° for Cu2 and Cu3.[8] The important distortions from O_h symmetry around the Cu^{II} ions imply that the three hyetrz ligands linking neighbouring Cu^{II} ions do not conserve a perfect trigonal symmetry, as has been observed for the perchlorate derivative. The deviation from threefold symmetry is, however, significantly more pronounced for the present compound. All 1,2,4-triazole rings are fairly planar; the deviation from the least-squares plane through the ring atoms is smaller than 0.01(1) Å. The least-squares planes through the hyetrz ligands linking Cu1 and Cu2 are 52.4(1)° for hyetrz-1 and hyetrz-2, 59.3(1)° for hyetrz-2 and hyetrz-3, and 74.1(1)° for hyetrz-1 and hyetrz-3. This very much resembles the bridging mode between Cu1 and Cu2 in the perchlorate derivative with angles between the least-squares planes of 54(2)° for hyetrz-1 and hyetrz-2, 69(2)° for hyetrz-2 and hyetrz-3, and 64.6(4)° for hyetrz-1 and hyetrz-3. It is important to notice that there are significant differences in the bridging mode between Cu2 and Cu3 for both Cu^{II} hyetrz linear-chain compounds. In fact, for $[Cu(hyetrz)_3](CF_3SO_3)_2\cdot H_2O$ the threefold symmetry of the triple hyetrz linkage between Cu2 and Cu3 shows severe distortions, yielding angles of 77.1(1)° between hyetrz-4 and hyetrz-5, 61.4(1)° between hyetrz-5 and hyetrz-6, and 46.3(1)° between hyetrz-6 and hyetrz-4. On the other hand for $[Cu(hyetrz)_3](ClO_4)_2\cdot 3H_2O$,[8] the threefold symmetry of the triple hyetrz linkage between Cu2 and Cu3 shows comparable distortions as does Cu1 and Cu2 with angles of 50(3)° between hyetrz-4 and hyetrz-5, 71(1)° between hyetrz-5 and hyetrz-6, and 66(3)° between hyetrz-6 and hyetrz-4.

These differences in the hyetrz bridging geometry for $[Cu(hyetrz)_3](CF_3SO_3)_2\cdot H_2O$ is also reflected by the Cu−Cu distances, which are significantly different for the two pairs of the Cu^{II} ions, i.e., Cu1−Cu2 = 3.8843(2) Å, whereas Cu2−Cu3 = 3.9352(2) Å. This indeed is in contrast to $[Cu(hyetrz)_3](ClO_4)_2\cdot 3H_2O$, where the analogy between the two linkages leads to quasi equal Cu−Cu separations with Cu1−Cu2 = 3.8530(8) Å and Cu2−Cu3 = 3.8293(2) Å.[8]

Careful inspection of the triple N^1,N^2-1,2,4-triazole geometry between Cu1 and Cu2 reveals similar features as found in $[Cu(hyetrz)_3](ClO_4)_2\cdot 3H_2O$ for both Cu−Cu linkages; hyetrz-1 links Cu1 and Cu2 with a long distance [Cu1−N11 = 2.370(2) Å] and a rather small angle [Cu1−N11−N12 = 123.8(1)°] involving Cu1, whereas the

distance (Cu2−N12 = 1.994(2) Å] and angle [Cu2−N12−N11 = 122.3(1)°] involving Cu2 may be considered as normal. Maintaining these Cu^{II} ions under these geometric dispositions, apparently requires an extremely large Cu1−N11−N12−Cu2 torsion angle of −28.98(9)°. Also, hyetrz-2 shows considerable asymmetry in the bridging mode with respect to the Cu−N bond lengths. As for hyetrz-1, the short distance [Cu1−N21 = 2.018(2) Å] corresponds to a normal Cu1−N21−N22 angle of 120.3(1)°. However, for hyetrz-2 the long Cu2−N22 distance of 2.360(2) Å is now accompanied by a much larger Cu2−N22−N21 angle of 128.2(1)°. In this case, a torsion angle of −16.31(9)° is required. In contrast, hyetrz-3 links Cu1 and Cu2 with approximately identical Cu1−N31 = 2.067(2) Å and Cu2−N32 = 2.066(2) Å distances. However, the N^1,N^2-1,2,4-triazole bridging mode shows a rather high degree of asymmetry with respect to the Cu−N−N bond angles, which are Cu1−N31−N32 = 129.3(1)° and Cu2−N32−N31 = 125.3(1)°. The torsion angle Cu1−N31−N32−Cu2 is only −3.27(9)°.

The difference observed in the two unequal bridging modes is confirmed by the torsion angles for the ligands linking Cu2 and Cu3: −13.5(1), −11.3(1), and −20.3(1)° for hyetrz-4, hyetrz-5, and hyetrz-6, respectively. This is in sharp contrast to $[Cu(hyetrz)_3](ClO_4)_2\cdot 3H_2O$, where the torsion angles for the hyetrz ligands, having short Cu−N distances, are about −11°. The triflate derivative has corresponding ligands with torsion angles of up to −20°.

The large deviation from threefold symmetry for the present linear Cu^{II} chain is also confirmed by the fact that Cu2 is displaced by 0.238(1) Å from the Cu1−Cu3 axis, as well as by the zig-zag character of the linear chain. The latter is illustrated by the angle of 173.003(6)° between the vectors through the pairs of Cu^{II} ions (Cu1,Cu2) and (Cu2,Cu3), which is slightly smaller than the 175.18(2)° found for the perchlorate analogue. Clearly, in order to establish the linkage of Cu^{II} ions in Jahn−Teller-distorted octahedra, by triple μ-N^1,N^2-1,2,4-triazole bridges, the geometrical disposition of the ligands becomes such that important deviations from the ideal threefold axis running through the Cu^{II} ions are required. This may be illustrated by Figure 2 showing a view of the linear-chain structure along the *c* axis.

The third coordination sphere is occupied by the noncoordinated water molecules and triflate anions, which are situated between the linear chains. It is important to notice the orientation of the triflate anions, which appear to direct themselves towards the hydroxyethyl substituents of the hyetrz ligands. The relatively short O···O contacts listed in Table 2 provide evidence for a pronounced hydrogen bonding network between the triflate anions, the hydroxyethyl groups and the lattice water molecules as observed in the trinuclear Fe^{II} spin crossover compound $[Fe_3(hyetrz)_6(H_2O)_6](CF_3SO_3)_6$.[24] Unfortunately, an extended analysis of the hydrogen bonding interactions could not be carried out, since the hydrogen atoms concerned could not be located and because of the positional disorder in the triflate anions. As observed for $[Cu(hyetrz)_3](ClO_4)_2\cdot 3H_2O$, the terminal hydroxy groups of the ligands are highly agitated. The hyetrz-3 oxygen atom is shared between two split locations O38 and O39 with occupancy of 1/2 on each site. There appears to be a short O28···O48 contact of 2.690(5) Å. This would imply the occurrence of a hydrogen bond between hydroxy groups from hyetrz ligands, originating from neighbouring (i.e., intrachain) triple μ-triazole links. Also in the present compound, there is no indication for hydrogen bonding interactions taking place between hydroxyethyl groups of hyetrz ligands originating from different linear Cu^{II} chains (i.e., interchain).

Table 2. Interatomic distances (up to 3 Å) for the hydrogen bonding interactions in $[Cu(hyetrz)_3](CF_3SO_3)_2\cdot H_2O$ (labeled atoms are generated by symmetry operations: a: 1 − *x*, −*y*, −*z*; b: 1 − *x*, 1−*y*, −*z*)

O18···O87a	2.961(5)
O38···O96b	2.821(8)
O58···O106	2.791(4)
O39···O120	2.825(9)
O48···O120	2.883(5)
O58···O110	2.874(5)
O28···O48	2.690(5)
O110···O95	2.857(6)

Even if the substitution of the perchlorate anion by the triflate anion does not change the local Cu^{II} symmetry, the respective position of the cationic chains is affected by the cell difference between the two compounds. An illustration of this change is the triangle drawn normally to the axes of three adjacent chains. In the perchlorate compound it is equilateral with the length of one side being 13.6±0.2 Å, whereas in the triflate compound it is distorted at 13.0, 14.1, and 16.3 Å.

Spectroscopic Properties

The UV/Vis spectrum of $[Cu(hyetrz)_3](CF_3SO_3)_2\cdot H_2O$ shows a broad asymmetric band with a maximum situated at $15.4\cdot 10^3$ cm^{-1}, which is in agreement with the presence of CuN_6 chromophores, as well as with the tetragonal distortion of the Cu^{II} octahedra.[25]

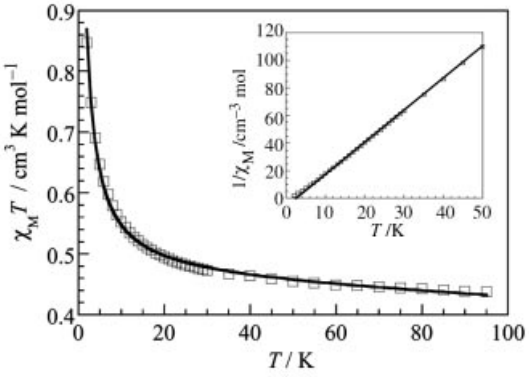

Figure 3. Observed (white squares) and calculated [line; J = +1.45(3) cm^{-1}, g = 2.20(1)] $\chi_M T$ vs. T curves for $[Cu(hyetrz)_3](CF_3SO_3)_2\cdot H_2O$; the $1/\chi_M$ vs. T curve is displayed in the insert

Magnetic Measurements

The magnetic behaviour of $[Cu(hyetrz)_3](CF_3SO_3)_2 \cdot H_2O$ is shown in Figure 3 in the form of a $\chi_M T$ vs. T plot, χ_M being the molar magnetic susceptibility and T the temperature.

At 300 K, the $\chi_M T$ value is 0.409 $cm^3 \cdot mol^{-1} \cdot K$, which is approximately the value expected for a single uncoupled Cu^{II} ion. The value of $\chi_M T$ progressively increases upon cooling, after which the $\chi_M T$ value starts to increase rather abruptly below 40 K reaching a value of 0.847 $cm^3 \cdot mol^{-1} \cdot K$ at 2 K. This behaviour is characteristic for compounds with an overall F interaction between the metal(II) ions. The occurrence of an F interaction is also illustrated by the $1/\chi_M$ vs. T plot displayed in the insert of Figure 3. A qualitative analysis of the magnitude of the F interaction has been made based on the Curie−Weiss law, $1/\chi_M = (T - \theta)/C$, yielding a Curie constant C of 0.41(1) $cm^3 \cdot K \cdot mol^{-1}$ and a Curie−Weiss temperature θ of 3.9(2) K. The magnetic data have been interpreted using the expression for the molar magnetic susceptibility of an $S = 1/2$ linear chain with a high-temperature series expansion proposed by Baker [Equation (1)],[26] in which $x = J/2kT$ and J is the isotropic exchange parameter defined by the phenomenological spin Hamiltonian [Equation (2)].

$$\chi_M = \left(\frac{Ng^2\mu_B{}^2}{4kT}\right) \cdot \left(\frac{1+5.79799x+16.902653x^2+29.376885x^3+29.832959x^4+14.036918x^5}{1+2.79799x+7.008678x^2+8.6538644x^3+4.5743114x^4}\right)^{2/3} \quad (1)$$

$$\mathbf{H} = -J[\Sigma_{i<j}\mathbf{S}_i\mathbf{S}_j] - g\mu_B H \Sigma_i \mathbf{S}_i \quad (2)$$

In Equation (1), N, g, μ_B, k, and T have their usual meanings. The g factor must be considered as an average value of the local Zeeman factors and intercluster exchange interactions were supposed to be negligible. The assumption of negligible magnetic exchange between second neighbour Cu^{II} ions is justified in view of the study of the triply N^1,N^2-1,2,4-triazole-bridged $Fe^{II}-Fe^{II}-Fe^{II}$ [24,27] and $Co^{II}-Co^{III}-Co^{II}$ [28] trinuclear clusters, where the central metal ion is diamagnetic, and no magnetic interactions could be detected between the paramagnetic terminal metal ions. A good fit in the temperature range 2−100 K has been obtained for the parameters $g = 2.20(1)$ and $J = +1.45(3)$ cm^{-1} (see Figure 3).

The magnetisation as a function of the applied magnetic field has been recorded at 2 K (see Figure 4). Upon applying a magnetic field, the magnetisation increases progressively, reaching a value of 1.007 $N\mu_B$ at 50 kOe. The value corresponds to the theoretical value of ca. 1 $N\mu_B$ expected for an $S = 1/2$ ion, as may be calculated from Equation (3).

$$M_{sat} = Ng\mu_B S \quad (3)$$

The X-band powder EPR spectrum recorded for $[Cu(hyetrz)_3](CF_3SO_3)_2 \cdot H_2O$ at 298 K only shows a rather broad (about 2000 Gauss) isotropic signal at $g = 2.09$, which may be the signature for exchange broadening. Furthermore, no indication for Cu···Cu exchange splittings is observed.[25]

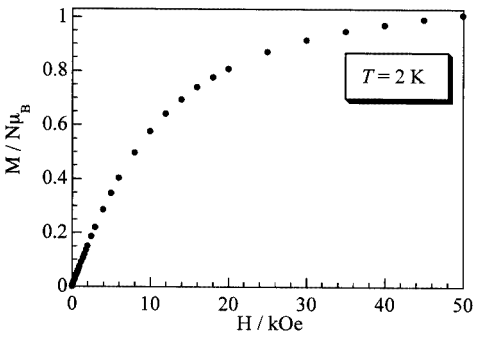

Figure 4. Magnetisation as a function of the applied magnetic field recorded at 2 K for $[Cu(hyetrz)_3](CF_3SO_3)_2 \cdot H_2O$

Concluding Remarks

X-ray structures of polymeric chain compounds containing triple N^1,N^2-1,2,4-triazole bridges have long been hard to establish and only a few examples forming Cu^{II} structures are known.[8,18,19] Structural information on these compounds are of great interest since the fascinating X-ray structure of the corresponding Fe^{II} spin transition materials has not yet been solved.[16] $[Cu(hyetrz)_3](CF_3SO_3)_2 \cdot H_2O$ represents the first example of a linear Cu^{II} chain of this family exhibiting an overall F interaction. This F coupling of $J = +1.45(3)$ cm^{-1} is rather weak, but certainly significant. The isotropic exchange J results from the competition between ferromagnetic and antiferromagnetic contributions [Equation (4)].[29]

$$J = J_{AF} + J_F \quad (4)$$

Generally, it may be expected that for Cu^{II} ions linked by polyatomic bridging ligands such as μ-N^1,N^2-1,2,4-triazoles, the F contribution is very small, and only the AF part significantly contributes to the overall magnetic interaction.[26] This for instance is the case for $[Cu(hyetrz)_3](ClO_4)_2 \cdot 3H_2O$, where a weak AF coupling [$J = -1.18(2)$ cm^{-1}] has been found.[8] The reasons for these differences in magnetic behaviour are likely to originate from significant differences in structural parameters.

Actually, the present complex has a linear-chain structure, which deviates somewhat more from threefold symmetry as compared with $[Cu(hyetrz)_3](ClO_4)_2 \cdot 3H_2O$. This mainly originates from the larger distortions observed in the Cu2−Cu3 linkage, leading to a more pronounced zigzag character of the linear chain, and importantly, to larger Cu−N−N−Cu torsion angles, which reach values of up to −20°. In both chains, the AF contribution of the exchange

only proceeds via one N^1,N^2-1,2,4-triazole bridge out of the three bridging ligands. These are the ligands linking the Cu^{II} ions with short Cu−N distances, i.e., hyetrz-3 and hyetrz-6. In both compounds, these ligands are indeed differently oriented with respect to the Cu^{II} ions, and thus with respect to the magnetic orbital situated on the Cu^{II} ions; these subtle variations in the structural parameters may change the magnetic properties. All of these factors may contribute to a reduction of the magnitude of the J_{AF} component, and for particular values of the structural parameters the J_F component may start to dominate. As a consequence the overall magnetic interaction may switch from AF to F. Apparently, the two linear-chain compounds represent two borderline cases, where either AF or F coupling is taking over. At this stage, it is rather hazardous to draw conclusions concerning the influence of a change in a structural parameter on the magnetic orbital overlap, and thus on the magnitude of the J_{AF} component. For this purpose, theoretical calculations would probably be worthwhile.

It is remarkable that in all the antiferromagnetically coupled triple N^1,N^2-1,2,4-triazole-bridged Cu^{II} compounds, the Cu−N−N−Cu torsion angles, involving the ligands responsible for the exchange coupling, are very low, i.e., 7.9(7)° and 4.9(8)° for $[Cu_3\{1,2\text{-bis}(1,2,4\text{-triazol-4-yl})\text{ethane}\}_5(H_2O)_2]^{6+}$,[23] or close to −11° for $[Cu(hyetrz)_3](ClO_4)_2\cdot 3H_2O$,[8] whereas these are rather large for the present ferromagnetically coupled triflate chain.

An overall weak F coupling has also been found for the linear trinuclear Cu^{II} compounds $[Cu_3(metrz)_6(H_2O)_4](CF_3SO_3)_6(H_2O)_4$,[21] and $[Cu_3(etrz)_9(H_2O)_3](CF_3SO_3)_6$.[22] The magnetic data could not, however, be related to the structural parameters. Only an X-ray crystallographic study of a low quality at 298 K has been reported for $[Cu_3(metrz)_6(H_2O)_4](CF_3SO_3)_6(H_2O)_4$, revealing rather short Cu···Cu separations of 3.719(7) Å, which could be related to the dynamic Jahn−Teller effect involving the central Cu^{II} ion leading to a perfectly symmetric octahedron with six relatively short Cu−N distances of 2.14(5) Å. It may be expected that upon decreasing temperature the dynamic Jahn−Teller distortion freezes into a static Jahn−Teller distortion. Since the F coupling occurs at these low temperatures, the non-detailed room-temperature structure could not provide any information on how the structural features may be related to the magnetic interaction observed for this compound.

An interesting structural feature in the ferromagnetically coupled Cu^{II} systems mentioned above, as well as in $[Cu(hyetrz)_3](CF_3SO_3)_2\cdot H_2O$ is the presence of the noncoordinated trifluoromethanesulfonate anion. It may be thought that this type of bulky anion determines, in some way, the crystal packing and in turn indirectly the geometry of the triple N^1,N^2-1,2,4-triazole bridge network. This may proceed in such a way that accidental orthogonality may occur, i.e., for certain values of the structural parameters the competition of J_{AF} and J_F results in taking over the F component, yielding an overall F interaction in triple 1,2,4-triazole-bridged Cu^{II} compounds.

Derivatives of 1,2,4-triazole are very useful for obtaining diazine-type bridged polynuclear transition metal(II) compounds having relatively short metal−metal distances. All possibilities are provided for fine-tuning the magnetic properties of the corresponding polynuclear Cu^{II} compounds by playing on the nature of the bridging units (number and geometry). Now these possibilities can also be extended towards F interactions for the chain compounds.

Experimental Section

Starting Materials: Commercially available solvents, hydrazine monohydrate, triethyl orthoformate, 2-hydroxyethylamine, and copper(II) trifluoromethanesulfonate were used without further purification.

Synthesis of 4-(2′-hydroxyethyl)-1,2,4-triazole (hyetrz): The ligand hyetrz has been prepared as already described.[8]

Synthesis of $[Cu(hyetrz)_3](CF_3SO_3)_2\cdot H_2O$: $Cu(CF_3SO_3)_2$ (0.21 g, 0.6 mmol), dissolved in water (10 mL), was added to hyetrz (0.2 g, 1.8 mmol), dissolved in water (10 mL). The reaction mixture was filtered. After a couple of weeks, blue prism-shaped single crystals were collected after slow evaporation of the solvent at room temperature. Crystals were washed with water and air-dried. Yield: 175 mg, 40%. IR (KBr): $\nu_{as}(SO_3^-) = 1269\ cm^{-1}$.

Physical Measurements: IR spectra were carried out with a Perkin−Elmer Paragon 1000 FT-IR spectrophotometer. UV/Vis spectra were recorded with a CARY 5E spectrophotometer using the diffuse reflectance technique, with polytetrafluoroethylene as a reference. X-band powder EPR spectra were obtained with a Bruker ER083CS electron spin resonance spectrometer. Magnetic susceptibilities were carried out in the temperature range 300−2 K with a quantum design MPMS-5S SQUID magnetometer. Magnetic data were corrected for diamagnetic contributions, which were estimated from the Pascal constants and were fitted to theoretical expressions by means of a Simplex routine. All parameters (J, g) were varied independently during the fitting procedure. This routine minimises the function $R = (\chi_{obs} - \chi_{calc})^2/[(\chi_{obs})^2]^{1/2}$.

Crystallographic Data Collection and Structure Determination: A blue, hexagonal crystal of approximate dimensions 0.60 × 0.50 × 0.35 mm was analysed at room temperature with an ENRAF-NONIUS CAD4 diffractometer using the monochromated Mo-K_α X-ray radiation ($\lambda = 0.7073$ Å). Accurate unit-cell parameters were obtained by least-squares refinement from 20 centred reflections in the range $15° \le \theta \le 16°$. Crystal data and details of data collection and refinement are given in Table 3. The intensities of three standard reflections, each monitored over 2 h, revealed no significant decay over the course of data collection. A semiempiric correction of absorption, based on ψ scans of three axial reflections, was applied.[31] The structure was solved by direct methods with the program SIR92.[32] Structure refinement based on F^2 was carried out by extended block-diagonal matrix methods, each block constituted by a chemical entity as Cu, hyetrz, CF_3SO_3, H_2O. Locations of hydrogen atoms which can be predicted were generated geometrically (C−H = 1.0 Å) and included in the refinement with an isotropic fixed thermal parameter. All non-hydrogen atoms were refined with anisotropic thermal parameters. The high values of thermal parameters of the oxygen atoms of the triflate and the hydroxy groups suggest disordered positions of these entities. One oxygen atom belonging to a hydroxy group was located on two

different disordered sites with an occupancy factor of 1/2. Final reliability factors converged to $R(F) = 0.038$ and $wR(F^2) = 0.120$. Neutral atom scattering factors and anomalous dispersion corrections were taken from International Tables for Crystallography.[33] A final difference Fourier map showed residual density less than ± 0.24 e·Å^{-3}. Final positional parameters are listed in the supplementary material deposited at the CCDC. Illustrations and calculations were carried out using programs written or modified locally. Crystallographic data have been deposited at the Cambridge Crystallographic Data Centre as supplementary publication no CCDC-185233. Copies of the data can be obtained free of charge on application to CCDC, 12 Union Road, Cambridge CB21EZ, UK [Fax: (internat.) + 44-1223/336-033; E-mail: deposit@ccdc.cam.ac.uk].

Table 3. Crystal data for $[Cu(hyetrz)_3](CF_3SO_3)_2 \cdot H_2O$

Empirical formula	$C_{14}H_{23}CuF_6N_9O_{10}S_2$
Formula mass	719.1
T [K]	298
Colour	blue
Dimensions [mm]	0.60 × 0.50 × 0.35
Crystal system	triclinic
Space group	$P\bar{1}$
a [Å]	13.54(3)
b [Å]	14.37(3)
c [Å]	15.61(4)
α [°]	95.9(1)
β [°]	104.9(1)
γ [°]	106.5(1)
V [Å^3]	2763(11)
Z	4
$\rho_{calcd.}$ [g·cm^{-3}]	1.729
λ [Å] (Mo-K_α)	0.71073
μ [mm^{-3}]	1.031
Measured reflections	18256
Observed reflections	10448
R(int.)	0.010
S	1.09
R[a]	0.038
wR[a]	0.120

[a] $R = |F_o| - |F_c|/|F_o|$ for observed reflections, $wR = [w(F_o^2 - F_c^2)^2/wF_o^2]^{1/2}$, $w = 1/(\sigma^2(F_o^2) + 0.025F^2)$, $F = (2F_o + F_c)/3$.

Acknowledgments

We thank the referees for useful comments.

[1] R. Prins, P. J. M. Birker, J. G. Haasnoot, G. C. Verschoor, J. Reedijk, *Inorg. Chem.* **1985**, *24*, 4128.
[2] A. Bencini, D. Gatteschi, C. Zanchini, J. G. Haasnoot, R. Prins, J. Reedijk, *Inorg. Chem.* **1985**, *24*, 2812.
[3] W. M. E Koomen-van Oudenniel, R. A. G. de Graaff, J. G. Haasnoot, R. Prins, J. Reedijk, *Inorg. Chem.* **1989**, *28*, 1128.
[4] P. J. van Koningsbruggen, J. G. Haasnoot, R. A. G. de Graaff, J. Reedijk, S. Slingerland, *Acta Crystallogr., Sect. C* **1992**, *48*, 1923.
[5] P. M. Slangen, P. J. van Koningsbruggen, K. Goubitz, J. G. Haasnoot, J. Reedijk, *Inorg. Chem.* **1994**, *33*, 1121.
[6] P. M. Slangen, P. J. van Koningsbruggen, J. G. Haasnoot, J. Jansen, S. Gorter, J. Reedijk, H. Kooijman, W. J. J. Smeets, A. L. Spek, *Inorg. Chim. Acta* **1993**, *212*, 289.
[7] P. J. van Koningsbruggen, J. G. Haasnoot, H. Kooijman, J. Reedijk, A. L. Spek, *Inorg. Chem.* **1997**, *36*, 2487.
[8] Y. Garcia, P. J. van Koningsbruggen, G. Bravic, P. Guionneau, D. Chasseau, G. L. Cascarano, J. Moscovici, K. Lambert, A. Michalowicz, *Inorg. Chem.* **1997**, *36*, 6357.
[9] P. J. van Koningsbruggen, M. W. Gluth, V. Ksenofontov, D. Walcher, D. Schollmeyer, G. Levchenko, P. Gütlich, *Inorg. Chim. Acta* **1998**, *273*, 54.
[10] S. Ferrer, P. J. van Koningsbruggen, J. G. Haasnoot, J. Reedijk, H. Kooijman, A. L. Spek, L. Lezama, A. M. Arif, J. S. Miller, *J. Chem. Soc., Dalton Trans.* **1999**, 4269.
[11] S. Ferrer, J. G. Haasnoot, J. Reedijk, E. Müller, M. Biagini Cingi, M. Lanfranchi, A. M. Manotti Lanfredi, J. Ribas, *Inorg. Chem.* **2000**, *39*, 1859.
[12] J.-C. Liu, D.-G. Fu, J. Z. Zhuang, C.-Y. Duan, X.-Z. You, *J. Chem. Soc., Dalton Trans.* **1999**, 2337.
[13] J.-C. Liu, J.-Z. Zhuang, X. Z. You, X. Y. Huang, *Chem. Lett.* **1999**, 651.
[14] J. K. Tang, H. M. Wang, P. Cheng, X. Liu, D.-Z. Liao, Z.-H. Jiang, S.-P. Yan, *Polyhedron* **2001**, *20*, 675.
[15] O. Kahn, E. Codjovi, Y. Garcia, P. J. van Koningsbruggen, R. Lapouyade, L. Sommier, *ACS Symp. Ser.* **1996**, *644*, 298.
[16] O. Kahn, C. Jay-Martinez, *Science* **1998**, *79*, 44.
[17] J. G. Haasnoot, *Coord. Chem. Rev.* **2000**, *200−202*, 131.
[18] V. P. Sinditskii, V. I. Sokol, A. E. Fogel'zang, M. D. Dutov, V. V. Serushkin, V. M. A. Porai-Koshits, B. S. Svetlov, *Russ. J. Inorg. Chem.* **1987**, *32*, 1149.
[19] K. Drabent, Z. Ciunik, *Chem. Commun.* **2001**, 1254.
[20] J. Liu, Y. Song, Z. Yu, J. Zhuang, X. Huang, X. You, *Polyhedron* **1999**, *18*, 1491.
[21] W. Vreugdenhil, J. G. Haasnoot, J. Reedijk, J. S. Wood, *Inorg. Chim. Acta* **1990**, *167*, 109.
[22] G. Vos, J. G. Haasnoot, G. C. Verschoor, J. Reedijk, P. E. L. Schaminee, *Inorg. Chim. Acta* **1985**, *105*, 31.
[23] Y. Garcia, P. J. van Koningsbruggen, H. Kooijman, A. L. Spek, J. G. Haasnoot, O. Kahn, *Eur. J. Inorg. Chem.* **2000**, 307 and 514.
[24] Y. Garcia, P. Guionneau, G. Bravic, D. Chasseau, J. A. K. Howard, O. Kahn, V. Ksenofontov, S. Reiman, P. Gütlich, *Eur. J. Inorg. Chem.* **2000**, 1531.
[25] B. J. Hathaway, D. E. Billing, *Coord. Chem. Rev.* **1972**, *5*, 143.
[26] G. A. Baker, G. S. Rushbrooke, H. E. Gilbert, *Phys. Rev. A* **1964**, *135*, 1272.
[27] [27a] G. Vos, R. A. Le Fêbre, R. A. G. de Graaff, J. G. Haasnoot, J. Reedijk, *J. Am. Chem. Soc.* **1983**, *105*, 1682. [27b] G. Vos, R. A. G. de Graaff, J. G. Haasnoot, A. M. van der Kraan, P. de Vaal, J. Reedijk, *Inorg. Chem.* **1984**, *23*, 2905.
[28] L. Antolini, A. C. Fabretti, D. Gatteschi, A. Giusti, R. Sessoli, *Inorg. Chem.* **1991**, *30*, 4858.
[29] O. Kahn, *Molecular Magnetism*, **1993**, VCH, New York.
[30] O. Kahn, *Angew. Chem. Int. Ed. Engl.* **1985**, *24*, 834.
[31] A. C. T. North, D. C. Phillips, F. S. Mathew, *Acta Crystallogr., Sect. A* **1968**, *24*, 351.
[32] A. Altomare, G. Cascarano, C. Giacovazzo, A. Guagliardi, M. C. Burla, G. Polidori, M. Camalli, *J. Appl. Crystallogr.* **1994**, *27*, 435−435.
[33] *International Tables for Crystallography* (Eds.: A. J. C. Wilson, E. Prince), Kluwer Academic Publishers, **1999**, vol. C, Tables 4.2.6.8 and 6.1.1.4.

Received May 8, 2002
[I02245]

Synthesis, Structure, and Reactivity of a New Mononuclear Molybdenum(VI) Complex Resembling the Active Center of Molybdenum Oxotransferases

Rupam Dinda,[a] Parbati Sengupta,[a] Saktiprosad Ghosh,*[a] and William S. Sheldrick[b]

Keywords: Molybdenum / Bioinorganic chemistry / Substrate binding / Enzyme models

The design, synthesis, and structure determination of a pentacoordinate square-pyramidal molybdenum(VI) complex MoO_2L (where LH_2 is a diacidic tridentate ONO donor ligand) is reported. The substrate binding capacity of MoO_2L has been demonstrated by the formation and isolation of six-coordinate octahedral complexes $[MoO_2L(B)]$ (where B = imidazole, 1-methylimidazole, pyridine, or γ-picoline) and the structures of $[MoO_2L(Imz)]$ and $[MoO_2L(Py)]$ have been solved by X-ray crystallography. Oxo transfer of MoO_2L to the substrate PPh_3 has been demonstrated by the formation of MoOL and [MoOL(bipy)]. Thus, the complex MoO_2L behaves as a model for the active center of oxotransfer molybdoenzymes and is of interest in bioinorganic chemistry.

(© Wiley-VCH Verlag GmbH & Co. KGaA, 69451 Weinheim, Germany, 2003)

Introduction

It is now established that suitable models for the active centers of oxotransfer molybdoenzymes should be capable of: (1) oxygen atom transfer to or from the substrate,[1] (2) approaching the coordination environment of the oxomolybdenum center of the relevant enzyme(s), and (3) being unresponsive to the formation of (μ-oxo)Mo^V dimers.[2] To meet criterion (3) sterically hindered ligands, like 2,6-bis(2,2-diphenyl-2-mercaptoethenyl)pyridine $[LN(SH)_2]$, have been synthesized. The Mo^{VI} complex (MoO_2LNS_2) was subsequently isolated and structurally characterized by single-crystal X-ray analysis.[3,4] This complex was shown to be a viable structural model of the active sites of several oxotransfer molybdoenzymes and it was proposed that the presence of at least one coordinated sulfur atom as well as a proper steric environment provided by the ligand to prevent Mo^V-O-Mo^V dimer formation are essential features of a model complex.[3] One of our studies on the Mo^{VI} complexes of thiosemicarbazone-type ONS donor ligands showed for the first time that the steric factor is not absolutely essential[5] to prevent the (μ-oxo)Mo^V dimer formation. In this paper we report our recent findings that indicate that even Mo^{VI} complexes of some selected ONO donor ligands may mimic the active sites of some oxotransfer molybdoenzymes.

We report the synthesis, characterization, substrate binding, and oxo transfer reactions of the complex MoO_2L, where H_2L is the ONO donor ligand 2-hydroxyacetophenone hydrazone of 2-aminobenzoylhydrazine. The five-coordinate complex (MoO_2L) is quite interesting with respect to coordination chemistry because pentacoordinated Mo^{VI} complexes, in general, are rare[2,6,7] and those with an ONO donor environment are rarer still. Most pentacoordinate Mo^{VI} complexes with oxygen−sulfur donor ligands are mono(μ-oxo)-bridged dimers, each Mo^{VI} center featuring an S_2O_3 coordination, and are trigonal-bipyramidal.[6] The structures of the pentacoordinate complex MoO_2L (**1**) and its adducts $MoO_2L(Imz)$ (**2**) and $MoO_2L(Py)$ (**4**) are determined by a single-crystal X-ray diffraction technique.

The (oxo)Mo^{IV} complexes MoOL (**6**) and [MoOL(bipy)] (**7**), obtained by oxo transfer of MoO_2L to the substrate PPh_3, are isolated and characterized. MoO_2L (**1**) is found to mimic the active center of oxotransfer molybdoenzymes and hence is of interest in bioinorganic chemistry.

Results and Discussion

In this work, a tridentate diacidic Schiff base (H_2L) is used as ligand. It is prepared by condensing 2-hydroxyacetophenone with anthranilhydrazide in ethanol.[8] The stoichiometric reaction (Scheme 1) of bis(acetylacetonato)-dioxomolybdenum(VI) with H_2L in refluxing ethanol afforded the orange five-coordinate complex MoO_2L (**1**) in excellent yield. The $[MoO_2L(B)]$ complexes **2**−**5** were prepared by reaction of MoO_2L with different heterocyclic bases (B) in ethanol [B = imidazole (**2**), 1-methylimidazole (**3**), pyridine (**4**), or γ-picoline (**5**)].

[a] Department of Inorganic Chemistry, Indian Association for the Cultivation of Science, Jadavpur, Kolkata 700032, India
Fax: (internat.) + 91-33/473-2805
E-mail: icspg@mahendra.iacs.res.in
[b] Lehrstuhl für Analytische Chemie, Ruhr-Universität Bochum, 44780 Bochum, Germany

Supporting information for this article is available on the WWW under http://www.eurjoc.org or from the author.

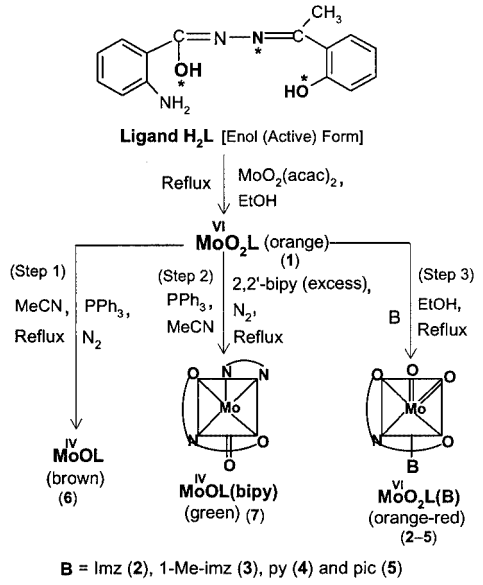

Scheme 1. Reaction diagram for the isolation of dioxomolybdenum(VI) and oxomolybdenum(IV) complexes

All these complexes are diamagnetic, indicating the presence of molybdenum in the +6 oxidation state, and are nonconducting in solution.

Selected spectroscopic data of the complexes are summarized in Table 1. In all of them, the ligand is found to act in its enol form coordinating through the deprotonated phenolate oxygen, enolate oxygen, and the azomethine nitrogen atoms. The IR spectra of the complexes do not exhibit the ligand bands at 3477 cm^{-1} [ν(OH)], 3209 cm^{-1} [ν(NH)], and 1640 cm^{-1} [ν(C=O)].[9,10] Characteristic strong bands at 1600 and 1540 cm^{-1} due to ν(C=N) and ν(C=C/aromatic) stretching modes of the ligand[10,11] are located in the spectra of both the ligand and the complexes. The Mo=O stretching modes occur as a pair of sharp strong peaks in the 930−894 cm^{-1} range.[5,12−14]

Table 1. Characteristics IR bands [cm^{-1}] and electronic spectral data [nm ($dm^3 \cdot mol^{-1} \cdot cm^{-1}$)] for the complexes

	ν(Mo=O)[a]	λ_{max} (ε)[b]
MoO_2L (**1**)	912, 894	420 (10034), 312 (15419)
MoO_2L(Imz) (**2**)	920, 895	428 (8352), 316 (17032)
MoO_2L(1-Me-Imz) (**3**)	923, 889	429 (8492), 318 (16912)
MoO_2L(Py) (**4**)	929, 902	432 (9400), 327 (14272)
MoO_2L(γ-Pic) (**5**)	929, 912	427 (8372), 319 (16703)
MoOL (**6**)	964	691 (265), 426 (1091), 312 (1997)
MoOL(bipy) (**7**)	937	679 (121), 427 (2067), 318 (5345)

[a] In KBr pellet. [b] In DMF.

Electronic spectra of the complexes in DMF display an intense band in the 440−420-nm region associated with a relatively weak band in the 330−310-nm region; these are believed to be of O (phenolate and enolate) → Mo LMCT origin.[5,14−16]

The ^1H NMR ([D_6]DMSO) spectrum of the free ligand exhibits an OH (phenolic) resonance at δ = 13.4 ppm. Signals for CH_3 protons at δ = 2.46 ppm and aromatic protons at 7.64−6.57 ppm are also found.[8] In the complex, the signal for the OH proton disappears, indicating deprotonation of the phenolic OH group in the complex MoO_2L. The NMR spectroscopic data of all the complexes are given in the Exp. Sect.

The relevant electrochemical data for the Mo^{VI} complexes **1**−**5** in DMF vs. SCE are summarized in Table 2. All reductions are irreversible. The cyclic voltammograms of the parent complex **1** show (Figure 1) only one reductive response at −1.22 V. The process may be represented as a metal-centered one-electron transfer involving the Mo^{VI} and the Mo^{V} oxidation states.[17−19] The CV traces of complexes **2**−**5** (Figure 2) exhibit two irreversible reductive responses[5,14−16] within the potential window −0.6 to −1.4 V, which are assigned to Mo^{VI}/Mo^{V} and Mo^{V}/Mo^{IV} processes, respectively. The lack of anodic response, even at a high scan rate, is clearly due to rapid decomposition of the reduced species.[19]

Table 2. Cyclic voltammetric results for dioxomolybdenum(VI) complexes at 298 K

Complex	E_{pc} [V][a]
1	−1.22
2	−0.72, −1.02
3	−0.64, −0.93
4	−0.82, −1.28
5	−0.78, −1.23

[a] Solvent: DMF; working electrode: platinum; reference electrode: SCE; supporting electrolyte: 0.1 M TEAP; scan rate: 100 mVs^{-1}. E_{pc} is the cathodic peak potential.

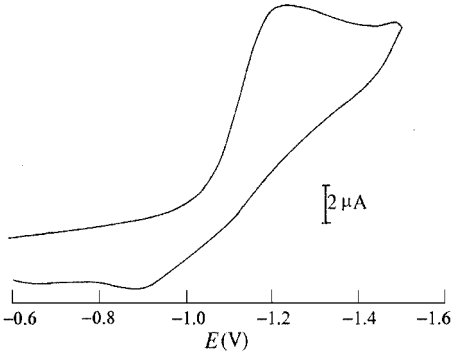

Figure 1. Cyclic voltammograms of MoO_2L (**1**) in DMF (0.1 M TEAP) at a platinum electrode; scan rate 100 mV/s and potentials recorded vs SCE

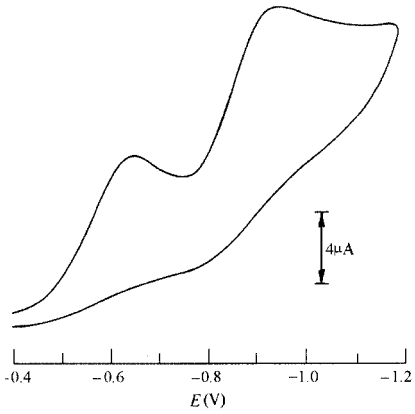

Figure 2. Cyclic voltammograms of [MoO_2L(1-Me-Imz)] (**3**) in DMF (0.1 M TEAP) at a platinum electrode; scan rate 100 mV/s and potentials recorded vs SCE

Description of the Crystal Structures

MoO_2L

Crystals of this orange compound consist of discrete molecules of MoO_2L. The structure is presented in Figure 3 and the geometric data are given in Tables 3 and 4. The coordination environment of the Mo^{VI} acceptor center consists of two oxo oxygen atoms, one enolate oxygen, one phenolate oxygen, and an azomethine nitrogen atom. This is a rare example of a five-coordinate Mo^{VI} complex.[2] No structural evidence for the achievement of hexacoordination through Mo=O···Mo bridging is observed. This MoO_2L complex could be isolated from an alcohol (MeOH, EtOH) or acetonitrile medium, from which it is found to crystallize without any solvent molecule. The molecular geometry of MoO_2L is best represented as a distorted square-pyramid with one axial oxo oxygen atom [O(2)], and three O atoms [O(1,3,4)] and the N(1) atom describing the equatorial plane. Distortion of the square plane is evident from the difference in the Mo−O(1), Mo−O(3), Mo−N(1), and Mo−O(4) bond lengths as well as the difference in the bond angles at the Mo atom [72.51(6) to 155.20(8)°]. The length of the Mo=O(1) bond lying *trans* to N(1) is practically equal to Mo=O(2); the position *trans* to O(2) remains unoccupied. The length of the two Mo−O bonds corresponding to the enolate [O(3)] and phenolate [O(4)] oxygen atoms are found to differ by only 0.077 Å. The bite angles of the ligand at Mo, O(4)−Mo−N(1) and O(3)−Mo−N(1), are 72.51(6) and 81.11(7)°, respectively, generating five-membered and six-membered chelate rings at the Mo^{VI} center. The tendency of the *cis* MoO_2 group to compress bond angles is reflected in the mean value of 76.81° for these bite angles. The lengths of the Mo=O, Mo−O and Mo−N bonds are unexceptional.[12,14,20,21] The Mo acceptor center is displaced from the average equatorial plane described by O(1)−O(3)−N(1)−O(4) towards the axial oxo oxygen atom O(2), the distance of O(2) from this plane being 2.0511 Å. Such a displacement of the Mo atom from the equatorial plane towards the apical oxo oxygen atom is also found in the aldehyde oxidoreductase of *Desulfovibrio gigas*.[22,23] This displacement, naturally, makes the Mo^{VI} acceptor center somewhat inaccessible to the donor approaching from the opposite direction. Hence, it is evident that the discrete MoO_2L molecule has a square-pyramidal structure with the sixth position, *trans* to the oxo oxygen atom O(2), vacant. This vacant sixth position is expected to act like the substrate-binding site of a molybdoenzyme. This expectation was fulfilled when MoO_2L yielded a host of six-coordinate adducts of the type MoO_2L(B), where B is a monodentate Lewis base like imidazole, substituted imidazole, pyridine or picoline. The structures of two such adduct molecules [MoO_2L(Imz)] (**2**) and [MoO_2L(Py)] (**4**) were determined by single-crystal X-ray diffraction techniques and one (**4**) is discussed below. As the structures of **2** and **4** are similar, all crystallographic data, as well as the corresponding ORTEP diagram of **2**, are included in the Supporting Information.

[MoO_2L(Py)]

Crystals of [MoO_2L(Py)] (**4**) consist of discrete molecular species and the structure is presented as Figure 4. The molybdenum(VI) center is present in a distorted octahedral donor environment consisting of *cis*-oxo atoms O(1,2), *trans*-phenolate and enolate oxygen atoms O(3,4), which are

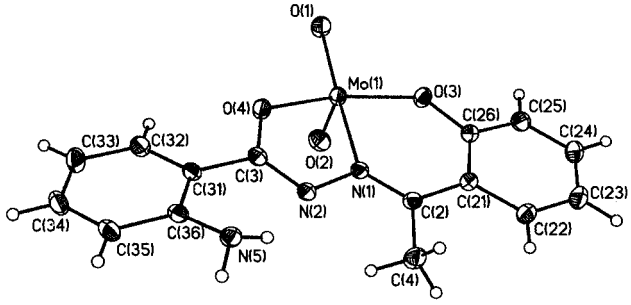

Figure 3. ORTEP plot of MoO_2L (**1**) with atom labeling scheme

Table 3. Crystal and refinement data for complexes **1** and **4**

	1	**4**
Empirical formula	$C_{15}H_{13}MoN_3O_4$	$C_{20}H_{18}MoN_4O_4$
Formula mass	395.22	474.32
Crystal symmetry	monoclinic	monoclinic
Space group	*P*2(1)/*n*	*C*2/*c*
a [Å]	7.0559(14)	20.800(5)
b [Å]	11.131(2)	10.970(2)
c [Å]	18.321(4)	17.532(4)
β [°]	95.68(3)	97.724(16)
V [Å^3]	1431.8(5)	3964.1(16)
Z	4	8
$D_{calcd.}$ [g.cm^{-3}]	1.833	1.590
F(000)	792	1920
μ(Mo-K_α) [mm^{-1}]	0.941	0.696
Collected refl.	6907	7134
Independent refl.	3288	3464
R_1 [$I > 2\sigma(I)$]	0.0271	0.0427
wR_2 (all data)	0.0614	0.1034
S (goodness of fit)	1.085	1.076
Min./max. res. [e·Å^{-3}]	0.59/−0.46	0.440/−0.685

Table 4. Selected bond lengths [Å] and bond angles [°] for complexes **1** and **4**

	Complex **1**	Complex **4**
Mo(1)−O(2)	1.696(19)	1.695(3)
Mo(1)−O(1)	1.704(16)	1.701(3)
Mo(1)−O(3)	1.906(16)	1.919(3)
Mo(1)−O(4)	2.003(16)	1.996(3)
Mo(1)−N(1)	2.249(18)	2.262(3)
Mo(1)−N(3)	−	2.433(4)
O(2)−Mo(1)−O(1)	105.95(9)	106.41(17)
O(2)−Mo(1)−O(3)	100.32(9)	100.28(16)
O(1)−Mo(1)−O(3)	102.08(8)	102.71(14)
O(2)−Mo(1)−O(4)	96.89(8)	98.09(15)
O(1)−Mo(1)−O(4)	96.39(8)	98.58(14)
O(3)−Mo(1)−O(4)	150.11(7)	146.52(13)
O(2)−Mo(1)−N(1)	97.51(8)	92.76(14)
O(1)−Mo(1)−N(1)	155.20(8)	159.70(14)
O(3)−Mo(1)−N(1)	81.11(7)	79.80(12)
O(4)−Mo(1)−N(1)	72.51(6)	71.55(12)
O(2)−Mo(1)−N(3)	−	170.04(14)
O(1)−Mo(1)−N(3)	−	82.87(14)
O(3)−Mo(1)−N(3)	−	80.76(14)
O(4)−Mo(1)−N(3)	−	76.56(12)

cis to O(1,2), an azomethine nitrogen atom N(1) and the tertiary nitrogen atom N(3). The structure of complex **4** can be derived from the structure of the coordinately unsaturated pentacoordinate square-pyramidal complex MoO_2L (**1**) by the addition of pyridine to the vacant axial position *trans* to the oxo atom O(2). The angle between the equatorial plane defined by O(1)−O(3)−N(1)−O(4) and that of the coordinated pyridine ring is 95.7°. The angle O(2)−Mo−N(3) is 170.04°, pointing to considerable distortion of the coordination octahedron around the Mo^{VI} center in compound **4**. A remarkable feature is that the values of the bond lengths and bond angles around the Mo^{VI} center in **1** are essentially the same in **4** (Table 4). Even the length of the metal−oxygen double bond (Mo=O) axial to the coordinated pyridine ligand, which is known to be highly influenced by axial coordination in many (oxo)metal complexes and is thought to be a measure of σ-donor capacity of the coordinated ligand, remains practically unchanged.[12,14,20,21] The length of the relevant bond [N(3)−Mo] is found to be longer than the other type of molybdenum−nitrogen (azomethine) bond N(1)−Mo, and indicates rather weak attachment of the pyridine ligand to the MoO_2^{2+} moiety. This is substantiated by TG and DTA studies of **4**, which reveal rather easy loss of the pyridine ligand on controlled heating.

Reactivity of the Complex 1 (MoO_2L)

Substrate Binding

The reaction (Scheme 1, step 3) can be considered as a substrate-binding reaction of the MoO_2L core when a heterocyclic base (substrate) binds to the distorted square-pyramidal MoO_2L moiety forming a distorted octahedral species. This reaction reminds us of the substrate binding of molybdoenzymes.

Oxo Transfer to Substrate

The tendency of the Mo^{VI} complex MoO_2L to transfer an oxygen atom to substrates has been examined in CH_3CN using PPh_3 as the substrate. The parent complex **1** has a band at 420 nm due to an L(O)→ M(Mo) LMCT transition. When the complex is treated with PPh_3, this band is found to be shifted towards a lower energy region and a new band appears at 691 nm. The oxo-transfer reaction may be represented as $Mo^{VI}O_2L + PPh_3 \rightarrow Mo^{IV}OL + OPPh_3$.

PPh_3O has been isolated and identified by IR and ^{31}P NMR spectroscopic data. This oxo-transfer reaction may be visualized[24] as a simple bimolecular reaction.[5]

Oxomolybdenum(IV) Complexes

The oxomolybdenum(IV) complexes were synthesized by two different methods (Scheme 1, steps 1 and 2) described later. Complexes **6** and **7** have poor solubility in many common organic solvents but are highly soluble in DMF and DMSO, and when the solutions are exposed to air they slowly oxidize to the parent MoO_2L in solution. As four-coordinate (oxo)Mo^{IV} complexes are unlikely, they are probably polymeric species in the solid state.[5] All the complexes are nonelectrolytes in DMF, and measurement of magnetic susceptibility indicated that they are diamagnetic at room temperature.[5,25,26]

Some spectral characteristics of compounds **6** and **7** are listed in Table 1. As already found in the case of its MoO_2^{2+} complexes, the ligand H_2L binds in a dianionic tridentate manner in its Mo^{IV} complexes. The IR spectra of these MoO^{IV} complexes clearly reveal that coordination takes place from the deprotonated phenolic and enolic oxygen atoms and the azomethine nitrogen atom. These complexes exhibit a single strong sharp band in the 964−937-cm^{-1} region,[5] representing the $\nu(Mo{=}O)_t$ mode.

The electronic spectra of the (oxo)Mo^{IV} compounds were recorded in dry DMF solution, and the compounds are found to display (Table 1) several absorption maxima in the 691−320-nm range, including a new band of moderate intensity in the low-energy 691−679-nm region. Absorption in this region is a characteristic feature of the $[MoO]^{2+}$ core.[5,27,28]

The proposed structure of **7**, which can be derived from the structure of its precursor complex **1**, is shown in Scheme 1.

The electron-transfer behavior of the complexes **6** and **7** (Table 5) was examined in CH_3CN using the conditions described in the Exp. Sect. The representative cyclic voltammograms of the complexes are shown in Figure 5. Controlled-potential coulometry indicates that these are one-electron processes. The (oxo)Mo^{IV} complexes undergo one-electron reduction to the corresponding Mo^{III} complexes and are oxidized by a one-electron process to Mo^{V} complexes. Similar observations were noted by Boyd and Spence,[27] as well as our own group.[5]

Table 5. Cyclic Voltammetric Results for Oxomolybdenum (IV) Complexes at 298 K

Complex[a]	Mo^{V}/Mo^{IV}	Mo^{IV}/Mo^{III}			
	E_{pa} [V]	E_{pc} [V]	E_{pa} [V]	ΔE_p [mV]	$E_{1/2}$ [V]
6	+1.02	−1.03	–	–	–
7	+1.10	−0.24	−0.15	90	−0.195

[a] Solvent: CH_3CN; working electrode: platinum; reference electrode: SCE; $E_{1/2} = 0.5\ (E_{pa} + E_{pc})$; $\Delta E_p = E_{pc} - E_{pa}$; E_{pc} and E_{pa} are the cathodic and anodic peak potentials, respectively; scan rate: 100 mVs^{-1}.

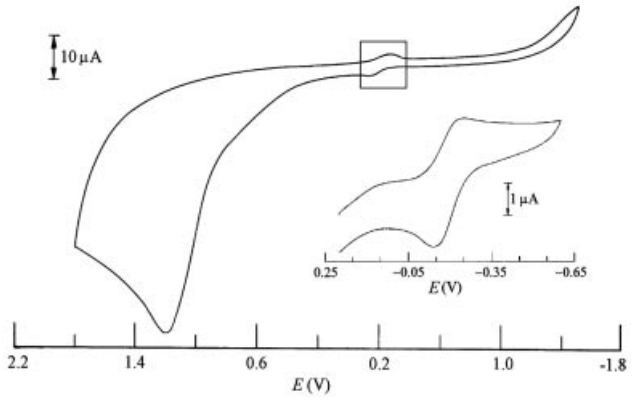

Figure 5. Cyclic voltammograms (scan rate 100 mV/s, solvent CH_3CN, 0.1 M TEAP) of MoOL(bipy) (**7**), cathodic scan (inset)

MoOL (6)

The redox behavior of this complex is found to be irreversible. At a scan rate of 100 mV s^{-1}, there is a reduction peak near −1.03 V corresponding to Mo^{IV} to Mo^{III} reduction and an anodic peak at +1.02 V for the Mo^{IV} to Mo^{V} oxidation.

MoOL(bipy) (7)

The cyclic voltammogram of this complex exhibits an irreversible anodic response (Figure 5) and a quasi-reversible cathodic response (inset, Figure 5). An initial anodic scan at a rate of 100 mV s^{-1} reveals an irreversible oxidation wave near +1.10 V, which is assigned to the one-electron oxidation of the Mo^{IV} complex to the corresponding Mo^{V} species. On the cathodic side, there is a minor reversible peak at $E_{1/2} = -0.195$ V whose current height is less than 1/10 that of the anodic peak. This small peak probably arises due to the generation of a very small amount of an Mo^{V} or Mo^{VI} species from the parent Mo^{IV} complex **7** during the preparation of the solution and performing the CV experiment. As Mo^{V} or Mo^{VI} species are expected to be more easily reduced than the corresponding Mo^{IV} species, this couple is observed at a much less negative potential than the Mo^{IV}/Mo^{III} couple observed in complex **6**. Due to the introduction of a strong donor bipy ligand the Mo^{IV}/Mo^{III} couple for **7** is expected to shift to a more negative potential and was therefore not observed within the potential window scanned in our experiment.

Conclusion

Preparation and characterization of dioxomolybdenum(VI) and oxomolybdenum(IV) complexes involving a diacidic tridentate ONO donor in the form of the 2-hydroxyacetophenone hydrazone of *o*-aminobenzoylhydrazine (LH_2) is reported. The main complex MoO_2L is a structurally characterized pentacoordinate distorted square-pyramidal species with one vacant position (*trans* to one of the M=O oxygen atoms). This vacant position is found to act as a substrate-binding site, and six-coordinate adducts, like $[MoO_2L(Py)]$ and $[MoO_2L(Imz)]$, are easily formed by the attachment of pyridine or imidazole to this position. The molybdenum center of MoO_2L is found to mimic the active site of some oxotransfer molybdoenzymes, as evidenced by the transfer of an oxo oxygen atom to the substrate PPh_3. Careful analysis of the structural data of MoO_2L indicates that the metric values of the structural features of the complex resemble those of the aldehyde oxidoreductase from *Desulfovibrio gigas* in which the Mo^{VI} center is also pentacoordinate and distorted square-pyramidal.[22,23] The magnitude of the deviation of the Mo^{VI} center towards the apical oxygen atom O(2) is also similar to that found in the molybdoenzymes referred to above.[22,23] It is known that the active sites of some oxotransfer molybdoenzymes contain at least one S donor atom around MoO_2^{2+} or MoO^{2+} cores along with N and O donor points. However, in the present case, the donor environment around the MoO_2^{2+}/MoO^{2+} core consists only of N and O donor points. This work suggests that the presence of at least one sulfur donor in the coordination sphere of the oxomolybdenum core may not be absolutely essential for all oxotransfer molybdoenzymes.

Experimental Section

General Remarks: $[MoO_2(acac)_2]$ was prepared as described in the literature.[29] Reagent grade solvents were dried and distilled prior to use. All other chemicals were reagent grade, available commercially, and used as received. Tetraethylammonium perchlorate (TEAP) used for electrochemical work was prepared as reported in the literature.[30] Elemental analyses were performed with a Perkin−Elmer 240 C, H, N analyzer. IR spectra were recorded with a Perkin−Elmer 783 spectrometer. ^1H NMR spectra were recorded with a Bruker AVANCE DPX 300 MHz spectrometer using $SiMe_4$ as an internal standard. Electronic spectra were recorded with a Shimadzu UV/Vis recording spectrophotometer. Magnetic susceptibility was measured with a PAR model 155 vibrating sample magnetometer with $Hg[Co(SCN)_4]$ as calibrant. Electrochemical data were collected using an EG&G PARC electrochemical analysis system (model 250/5/0) and a PC-controlled EG&G/PARC−VERSASTAT2 potentiostat at 298 K under dry nitrogen. Cyclic voltammetry experiments were carried out with a platinum working electrode, a platinum auxiliary electrode, SCE as the reference electrode, and TEAP as the supporting electrolyte. The value

for the ferrocenium/ferrocene couple under the experimental conditions was 0.40 V.

Synthesis of Ligand H_2L: The Schiff base ligand 2-aminobenzoylhydrazone of 2-hydroxyacetophenone was prepared by the same procedure reported in our previous work.[8]

Synthesis of $[MoO_2L]$ (1): A sample of H_2L (0.28 g, 1.04 mmol) was dissolved in 30 mL of ethanol by warming in a water bath, solid $MoO_2(acac)_2$ (0.33 g, 1.01 mmol) was added to the ligand solution and the mixture was refluxed for 3 h and then filtered. Slow concentration of the orange filtrate over 3 d produced dark orange crystals. Yield 0.32 g (81%). $C_{15}H_{13}MoN_3O_4$ (395.04): calcd. C 45.54, H 3.32, N 10.63; found C 45.94, H 3.30, N 10.01. ^{1}H NMR ([D$_6$]DMSO): δ = 7.93−6.57 (m, 8 H, C_6H_4), 2.78 (s, 3 H, CH_3) ppm.

Synthesis of $[MoO_2L(Imz)]$ (2; Imz = Imidazole): Imidazole (0.05 g, 0.75 mmol) was added to a clear orange solution (obtained by refluxing) of **1** (0.22 g, 0.55 mmol) in ethanol (50 mL) and the mixture was allowed to reflux for 3 h. The volume of this dark orange solution was reduced to 20 mL in a rotary evaporator. On standing at room temperature, the solution deposited shiny brown crystals. Yield 0.21 g (80%). $C_{18}H_{17}MoN_5O_4$ (463.08): calcd. C 46.62, H 3.69, N 15.10; found C 46.31, H 3.49, N 15.07. ^{1}H NMR ([D$_6$]DMSO): δ = 7.94−6.57 (m, 8 H, 3 H, C_6H_4, $C_3N_2H_4$), 2.77 (s, 3 H, CH_3), 12.01 (s, NH, $C_3N_2H_4$) ppm.

Synthesis of $[MoO_2L(1\text{-}Me\text{-}Imz)]$ (3; 1-Me-Imz = 1-Methylimidazol): This compound was prepared using the same procedure as for compound **2**. Yield 0.21 g (78%). $C_{19}H_{19}MoN_5O_4$ (477.09): calcd. C 47.76, H 4.01, N 14.66; found C 47.61, H 3.95, N 14.49. ^{1}H NMR ([D$_6$]DMSO): δ = 7.93−6.57 (m, 8 H, 3 H C_6H_4, $C_4N_2H_6$), 2.78 (s, 3 H, CH_3), 3.71 (s, 3 H, $C_4N_2H_6$) ppm.

Synthesis of $[MoO_2L(py)]$ (4; py = Pyridine): Complex **1** (0.22 g, 0.55 mmol) was treated with 2 mL of pyridine and the mixture was heated until a clear deep yellow solution was produced. Dry ethanol (20 mL) was added to this solution, which was then refluxed for 3 h. Slow concentration of the reaction mixture over 5 d produced yellow crystals. Yield 0.19 g (74%). $C_{20}H_{18}MoN_4O_4$ (474.08): calcd. C 50.59, H 3.82, N 11.80; found C 49.94, H 3.85, N 12.09. ^{1}H NMR ([D$_6$]DMSO): δ = 8.58−6.57 (m, 8 H, 5 H, C_6H_4, C_5H_5N), 2.77 (s, 3 H, CH_3) ppm.

Synthesis of $[MoO_2L(\gamma\text{-}pic)]$ (5; γ-pic = Picoline): This compound was prepared using the same procedure as above (compound **4**). Yield 0.19 g (70%). $C_{21}H_{20}MoN_4O_4$ (488.10): calcd. C 51.60, H 4.12, N 11.46; found C 51.84, H 3.90, N 11.51. ^{1}H NMR ([D$_6$]DMSO): δ = 8.42−6.57 (m, 8 H, 4 H, C_6H_4, C_6H_7N), 2.77 (s, 3 H, CH_3), 2.31 (s, 3 H, CH_3, C_6H_7N) ppm.

Synthesis of [MoOL] (6): A solution of PPh_3 (0.393 g, 1.5 mmol) in 5 mL of acetonitrile was added to a refluxing solution of MoO_2L (0.22 g, 0.55 mmol) in 25 mL of degassed acetonitrile. The reddish orange solution turned dark brown and a brown compound separated within 1 h. The brown compound was collected by rapid filtration of the hot mixture, washed well with hot acetonitrile and dried in vacuo; yield 0.15 g (70%). $C_{15}H_{13}MoN_3O_3$ (379.04): calcd. C 47.46, H 3.45, N 11.07; found C 47.34, H 3.12, N 11.23. ^{1}H NMR ([D$_6$]DMSO): δ = 7.94−6.57 (m, 8 H, C_6H_4), 2.78 (s, 3 H, CH_3) ppm.

Synthesis of [MoOL(bipy)] (7; bipy = 2,2′-Bipyridine): A solution of 2,2′-bipyridine (bipy; 0.78 g, 5.0 mmol) and PPh_3 (0.393 g, 1.5 mmol) in 5 mL of degassed acetonitrile was added to a refluxing solution of 0.22 g (0.55 mmol) of MoO_2L in 25 mL of degassed acetonitrile. The orange-red solution turned green after 1 h of refluxing and refluxing was continued for another 4 h. The green product was precipitated by adding excess dichloromethane (50 mL) followed by excess *n*-hexane (50 mL). The precipitate was rapidly filtered and washed well with *n*-hexane and dried in vacuo; yield 0.18 g (60%). $C_{25}H_{21}MoN_5O_3$ (535.10): calcd. C 55.02, H 3.88, N 12.83; found C 54.91, H 3.90, N 12.41. ^{1}H NMR ([D$_6$]DMSO): δ = 8.70−6.59 (m, 8 H, 8 H, C_6H_4, $C_{10}H_8N_2$), 2.77 (s, 3 H, CH_3) ppm.

Crystallography: Crystal data for compounds **1** and **4**, along with other experimental details, are summarized in Tables 3 and 4. Single-crystal data collection was performed at 293(2) K with a Siemens P4 four-circle diffractometer using graphite-monochromatized Mo-K_α radiation (λ = 0.71073 Å). The complex MoO_2L (**1**) crystallizes in the monoclinic space group $P2_1/n$ whereas the complex $MoO_2L(Py)$ (**4**) crystallizes in the monoclinic space group $C2/c$. The intensities were corrected for Lorentz and polarization effects and semi-empirical absorption corrections were performed on the basis of Ψ scans for nine chosen reflections with high χ values. Following structural solution, positional parameters and temperature factors were refined by full-matrix least squares against F_o^2 with SHELX 97.[31] All non-hydrogen atoms were refined anisotropically and a riding model with isotropic temperature factors was employed for hydrogen atoms. The X-ray crystallographic structure and the corresponding data for the complex **2** [MoO_2L-(Imz)] are reported as Supporting Information. CCDC-186348 (**1**), -186349 (**2**) and -186350 (**4**) contain the supplementary crystallographic data for this paper. These data can be obtained free of charge at www.ccdc.cam.ac.uk/conts/retrieving.html or from the Cambridge Crystallographic Data Center, 12 Union Road, Cambridge CB2 1EZ, UK [Fax: (internat.) + 44-1223/336-033; E-mail: deposit@ccdc.cam.ac.uk].

Acknowledgments

We thank Dr. S. K. Chattopadhyay, Bengal Engineering College (Deemed University) for fruitful discussions.

[1] R. H. Holm, *Coord. Chem. Rev.* **1990**, *100*, 183−221.
[2] R. H. Holm, J. M. Berg, *Acc. Chem. Res.* **1986**, *19*, 363−370.
[3] J. M. Berg, R. H. Holm, *J. Am. Chem. Soc.* **1985**, *107*, 917−925.
[4] B. E. Schultz, S. F. Gheller, M. C. Muetterties, M. J. Scott, R. H. Holm, *J. Am. Chem. Soc.* **1993**, *115*, 2714−2722.
[5] S. Purohit, A. P. Koley, L. S. Prasad, P. T. Manoharan, S. Ghosh, *Inorg. Chem.* **1989**, *28*, 3735−3742.
[6] H. Oku, N. Ueyama, A. Nakamura, *Bull. Chem. Soc. Jpn.* **1999**, *72*, 2261−2270.
[7] J. M. Berg, R. H. Holm, *J. Am. Chem. Soc.* **1985**, *107*, 925−932.
[8] R. Dinda, P. Sengupta, T. C. W. Mak, S. Ghosh, *Inorg. Chem.* **2002**, *41*, 1684−1688.
[9] [9a] W. Kemp, *Organic Spectroscopy*, Macmillan, Hampshire, **1987**, p. 62. [9b] K. Nakamoto, *Infrared and Raman Spectra of Inorganic and Coordination Compounds*, Wiley, New York, **1986**, p. 241.
[10] S. Ghosh, T. K. Bandyopadhyay, P. K. Ray, M. S. Mitra, *J. Inorg. Biochem.* **1984**, *20*, 79−86.
[11] N. S Biradar, B. R. Havinale, *Inorg. Chim. Acta* **1976**, *17*, 157−160.
[12] J. Liimatainen, A. Lehtonen, R. Sillanpaa, *Polyhedron* **2000**, *19*, 1133−1138.
[13] F. J. Arnaiz, R. Aguado, M. R. Podrosa, A. D. Cian, J. Fischer, *Polyheron.* **2000**, *19*, 2141−2147.
[14] A. Rana, R. Dinda, P. Sengupta, L. R. Falvello, S. Ghosh, *Polyhedron* **2002**, *21*, 1023−1030.

[15] [15a] S. Purohit, A. P. Koley, S. Ghosh, *Polyhedron.* **1990**, *9*, 881−890. [15b] S. Purohit, S. Ghosh, *J. Chem. Res. (S)* **1988**, 158−159.
[16] C. Bustos, O. Burckhardt, R. Schrebler, D. Carrillo, A. M. Arif, A. H. Cowley, C. M. Nunn, *Inorg. Chem.* **1990**, *29*, 3996−4001.
[17] J. Topich, *Inorg. Chem.* **1981**, *20*, 3704−3707.
[18] N. S. Rao, D. D. Mishra, R. C. Maurya, N. N. Rao, *Bull. Chem. Soc. Jpn.* **1995**, *68*, 1589−1592.
[19] M. Chaudhury, *J. Chem. Soc., Dalton Trans.* **1984**, 115−120.
[20] J. M. Berg, R. H. Holm, *J. Am. Chem. Soc.* **1984**, *106*, 3035−3036.
[21] S. K. Dutta, D. B. McConville, W. J. Youngs, M. Chaudhury, *Inorg. Chem.* **1997**, *36*, 2517−2522.
[22] R. Hille, *Chem. Rev.* **1996**, *96*, 2757−2816.
[23] M. J. Romao, M. Archer, J. Moura, J. J. G. Moura, J. Legall, R. Engh, M. Scheneidar, M. Hof, P. Hof, R. Huber, *Science* **1995**, *270*, 1170−1176.
[24] J. Topich, J. T. Lyon, *Inorg. Chem.* **1984**, *23*, 3202−3206.
[25] E. I. Stiefel, *Prog. Inorg. Chem.* **1977**, *22*, 102.
[26] R. N. Jowitt, P. C. H. Mitchell, *J. Chem. Soc. A* **1969**, 2632−2636.
[27] I. W. Boyd, J. T. Spence, *Inorg. Chem.* **1982**, *21*, 1602−1606.
[28] B. B. Kaul, J. H. Enemark, S. L. Merbs, J. T. Spence, *J. Am. Chem. Soc.* **1985**, *107*, 2885−289.
[29] G. J. J. Chen, J. W. McDonald, W. E. Newton, *Inorg. Chem.* **1976**, *15*, 2612−2615.
[30] D. T. Sawyer, J. L. Roberts, *Experimental Electrochemistry for Chemists*, John Wiley & Sons, New York, **1974**, p. 212.
[31] G. M. Sheldrick, *SHELX-97, Programs for structure solution and refinement*, Göttingen, Germany, **1997**.

Received May 23, 2002
[I02270]

Convenient Controllable Synthesis of Inorganic 1D Nanocrystals and 3D High-Ordered Microtubes

Zhenhui Kang,[a] Enbo Wang,*[a,b] Min Jiang,[a] Suoyuan Lian,[a] Yangguang Li,[a] and Changwen Hu[a]

Keywords: Nanotubes / Polyoxometalates / Synthetic methods

Polyoxometalates (POMs) nanorods, hollow particles, microtubes, and 3D-ordered tube systems were prepared using a novel and simple PEG/H_2O liquid system. POM nanorods with various diameters (30–400 nm) and lengths (500 nm to 2 μm) were produced in a well-controlled manner.

(© Wiley-VCH Verlag GmbH & Co. KGaA, 69451 Weinheim, Germany, 2003)

Introduction

Many interesting and technologically important phenomena occur in systems that have a spatial dimension similar to that of fundamental physical, chemical, or biological processes.[1] As a bridge between the molecular and the macroscopic world, mesosystems have become one of the most attractive subjects in physics, materials science, chemistry, and biology.[1] Nanosystems with characteristic lengths between 1 and 100 nm exhibit fascinating properties, such as quantized excitation, coulomb blocking, single-electron tunneling (SET), and metal−insulator transitions.[1] One-dimensional (1D) nanomaterials are of great fundamental and practical interest owing to their novel properties, which depend on their particular sizes and shapes.[1] Recently, much attention has been paid to the construction of advanced materials with such nanoscale building blocks.[2] Therefore, the exploration of preparation methods to control the sizes and shapes of nanomaterials is one of the focuses for the development of nanotechniques.[2−4]

A number of methods have been employed for the preparation of 1D nanomaterials, including template-assisted,[5] vapor-liquid-solid-(VLS-)assisted,[6] and electrochemical processes.[7] For most of these strategies, however, complicated process control, high reaction temperature, and long synthesis time are required. Recently, the introduction of microemulsions (or reverse micelles) has provided a relatively simple and powerful method for controlling the size, shape, and surface texture of nanoparticles and nanorods. In such microenvironments, the nanomaterials are encapsulated in the closed shells of surfactant molecules. The size and shape of nanoclusters can be well controlled by the size of the capsules, which can be controlled by changing the ratios of water and oil.[8] From this model of reaction fields, we speculate that if the closed capsules composed of surfactant molecules could be opened in one direction, a linear reaction field could be formed and a 1D nanomaterial could grow in such a microenvironment. Based on this speculation, we chose the nonionized surfactant polyethylene glycol (PEG) mixed with water so as to form a linear reaction field and explore the controllable synthesis of polyoxometalate (POM) nanocrystals and their nano/microstructure material forms.

As one of the typical inorganic metal oxide clusters, POMs have recently received much attention owing to their novel compositions, structures, and applications in the fields of catalysis, pharmacology, electronic, and magnetic materials.[9,12] They can be regarded as extremely versatile inorganic entities for the construction of functionally active solids and are one of the favorite candidates to be transformed into nanometer-sized materials.

It is noteworthy that POMs are nanosized polyoxometalate clusters that form by a self-assembly process in solution and can be isolated as solids. They have unique physicochemical properties such as strong Brønsted acidity, reversible multielectron redox transformations, activation of molecular oxygen and hydrogen peroxide, high proton mobility across their discrete ionic structure, etc.[9] These properties make POMs promising acid, redox, and bifunctional catalysts in homogeneous and heterogeneous systems. POMs are widely used as model systems for fundamental research, providing unique opportunities for mechanistic studies on

[a] Institute of Polyoxometalate Chemistry, Department of Chemistry, Northeast Normal University,
Changchun, Jilin 130024, P. R. China
Fax: (internat.) + 86-431/568-4009
E-mail: wangenbo@public.cc.jl.cn
[b] Institute of Coordination Chemistry, State Key Laboratory Nanjing University,
Nanjing, Jiangsu 210093, P. R. China

the molecular level. They have also become increasingly important for applied catalysis. Several new industrial processes based on POM catalysis have been commercialized.[12k] Current studies of catalysis by POMs and related systems concentrate on the catalyst preparation, characterization and monitoring, mechanistic aspects, application for organic synthesis and fine and specialty chemicals, and alkane activation. Other topics of interest include the design of advanced solid acid catalysts based on POMs incorporated into mesoporous zeolites.[9,12] POM crystalline nanomaterials, especially nano/microtubes and their 3D-ordered systems, will provide an opportunity to explore their unique properties on catalysis in many fields.

Müller et al.[10] have ingeniously synthesized many giant clusters of POMs on the nanometer scale, including novel kinds of large rings and wheel-shaped systems with 176 or even more Mo atoms. Recently, Misono et al. have studied the growth process of polyoxotungstate $(NH_4)_3PW_{12}O_{40}$ crystalline nanoparticles.[11] However, the rational design and controllable preparation of POM-based crystalline nanomaterials are still huge challenges. Because numerous well-characterized POMs are available,[12] it is extremely important to develop new strategies for the preparation of POM nanocrystals and nano/micro systems to explore their novel properties.

In this paper, we report on the 1D POM crystalline nanorods, hollow particles, nano/microtubes and 3D high-ordered tube systems prepared by a convenient and novel controllable synthesis method. Both the size and shape of these POM crystalline nanorods can be controlled by the use of different kinds of PEG and various volumes of water.

Results and Discussion

POMs Crystalline Nanorods

In our experiments, $AgNO_3$ (0.25 g) and $H_4SiW_{12}O_{40}{\cdot}nH_2O$ (1 g) were dissolved in a mixture of two different PEG/H_2O systems, one with w = 2.5:1 and the other with w = 2.5:2.5 (w = [PEG]/[H_2O]). Both of the systems were stirred before to give transparent sticky fluids. After the two systems were mixed, the reaction mixture remained clear. However, a large amount of white flocculent precipitate formed when a fourfold excess of ethanol was added. Element analysis of the white products give a molar ratio of Ag/Si/W = 4:1:12. The FT-IR spectrum exhibits characteristic peaks at 1100, 1011, 970, 919, 882, and 795 cm^{-1}, which are attributed to the ν(Si=Oa), ν(W=Ot), ν(W−Ob−W), and ν(W−Oc−W) absorptions of a Keggin-type structure, respectively. Transmission electron microscopy (TEM) images of samples taken from the PEG-400/H_2O (w = 2.5:1.5) system showed $Ag_4SiW_{12}O_{40}$ nanorods with a regular shape and size (Figure 1, a and c). The electron diffraction (Figure 1, b) and XRD patterns (Figure 1, d) confirm that these $Ag_4SiW_{12}O_{40}$ nanorods are crystalline.

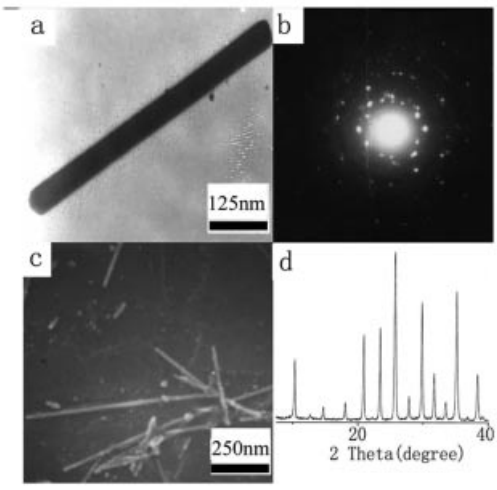

Figure 1. (a) TEM image of $Ag_4SiW_{12}O_{40}$ nanorods taken from the PEG-400/H_2O (w = 2.5:1.5) system; (b) electron diffraction pattern of the nanocrystals of $Ag_4SiW_{12}O_{40}$; (c) SEM image of $Ag_4SiW_{12}O_{40}$ nanorods; (d) XRD patterns of $Ag_4SiW_{12}O_{40}$ nanorods

In these experiments, the surfactant PEG molecules act as the most important component introduced into the reaction system. It is known that the nonionized surfactant PEG molecules form chain-like structures due to the assembly in water.[13] Therefore, we can imagine that many 1D liquid reaction fields could be formed when the PEG and a small amount of water are mixed together. The metathetical reactions of $AgNO_3$ and $H_4SiW_{12}O_{40}{\cdot}nH_2O$ and the growth of $Ag_4SiW_{12}O_{40}$ nanoclusters are strictly limited in such divided linear reactions along the directional space. Owing to the inhibition of surfactant PEG, further agglomeration will be stopped and the nanorods are therefore formed and fixed in the linear environments. Scheme 1 illustrates the possible mechanism. The TEM images of POM nanorods shown in Figure 2 proved these assumptions to be correct. Nanorods with various regular sizes and shapes can be prepared in different PEG/H_2O systems.

It is noteworthy that different molecular masses of PEG molecules lead to a variety of lengths of nanorods. Lower molecular weight surfactant of PEG-400 could be selected to prepare shorter POM nanorods with average lengths of 500−800 nm. PEG-600, which has a higher molecular weight, could be used to synthesize longer POM nanorods with average lengths of 1−2 μm. Figure 2, a and b, show the nanorods produced by the PEG-400/H_2O systems. Figure 2, c and d, illustrate the nanorods prepared by the PEG-600/H_2O systems. With increasing molecular mass of PEG, the length of the linear reaction fields is probably greater, and thus the size of nanorods is increased. Therefore, the length of POM nanorods can be controlled by adjustment of the molecular weight of PEG.

We further showed that the content of water in the preparation of 1D POM nanomaterials has a direct influence on the diameter of the nanorods. The relationship between

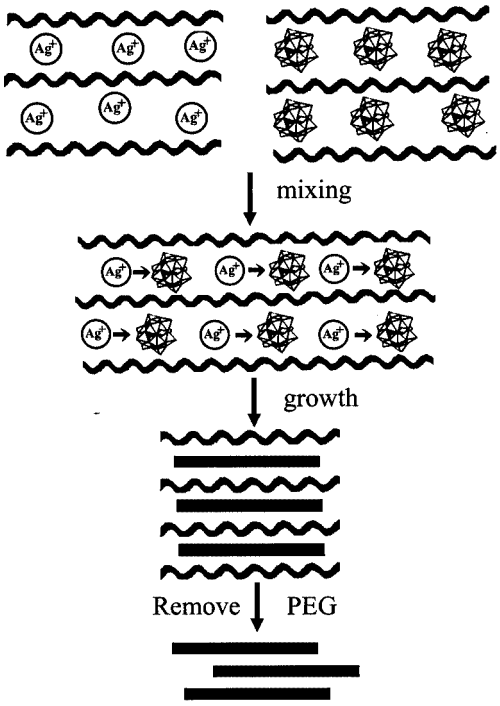

Scheme 1. Schematic diagram of the proposed formation process of POM nanorods

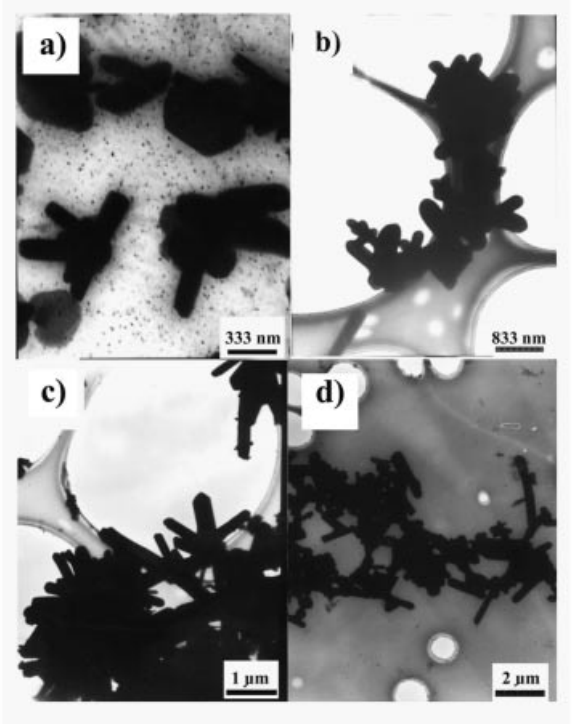

Figure 2. TEM images of $Ag_4SiW_{12}O_{40}$ nanorods with a length of: (a) and (b) 500−800 nm in the PEG-400/H_2O system; (c) and (d) 1−2 μm in the PEG-600/H_2O system

the size of 1D POM nanomaterials and the content of water is shown in Table 1. It is noteworthy that the diameter of the nanorods increases with increasing water content. As noted above, in this liquid system, many linear reaction fields exist, and the nanorods can be formed and fixed there. With the addition of water, the linear reaction field, i.e. the reaction space, will become larger, and thus the nanorods will also have larger diameters. Figure 3 shows nanorods with different diameters prepared in PEG-400/H_2O systems containing different amounts of water. Their diameters vary with the content of water in PEG-400/H_2O systems, namely 30, 70, and 90 nm for (a) PEG-400/H_2O = 2.5:1.0, (b) PEG-400/H_2O = 2.5:1.5, and (c) PEG-400/H_2O = 2.5:2.0, respectively. Similar results are also found in the PEG-600/H_2O (w = 2.5:1.5, 2.5:2.0, 2.5:2.5) systems (as shown in Figure 4), in which nanorods with diameters of (a) 200 nm, (b) 300 nm, and (c) 400 nm are obtained, respectively. Figure 5 shows the SEM images of POM nanorods with different diameters and lengths.

Table 1. Influence of the amount of water in PEG/H_2O systems on the diameters of the POM 1D nanomaterials

Surfactants	$Ag_4SiW_{12}O_{40}$ nanorods/nanowires [nm]	Content of water PEG/H_2O [mL/mL]
PEG-400	30	2.5:1.0
	70	2.5:1.5
	90	2.5:2.0
PEG-600	200	2.5:1.5
	300	2.5:2.0
	400	2.5:2.5

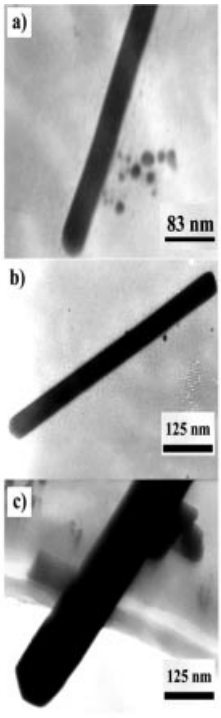

Figure 3. TEM images of nanorods taken from the PEG-400/H_2O systems; the diameters of these nanorods vary with the amount of water, namely 30, 70, and 90 nm for (a) PEG-400/H_2O = 2.5:1.0; (b) PEG-400/H_2O = 2.5:1.5; (c) PEG-400/H_2O = 2.5:2.0 (mL/mL)

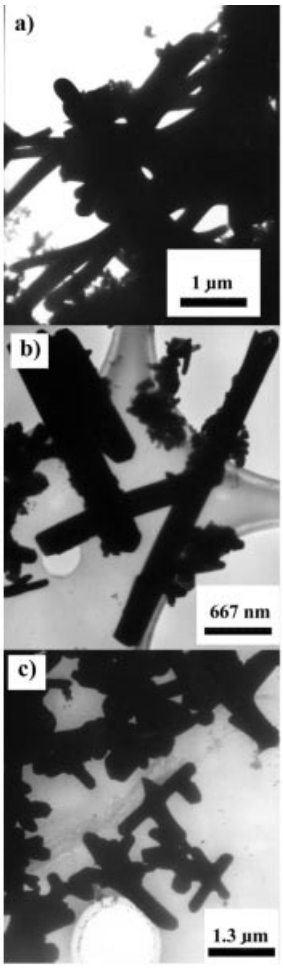

Figure 4. TEM images of nanorods taken from the PEG-600/H_2O systems; the diameters of these nanorods vary with the amount of water, namely 200, 300, and 400 nm for (a) PEG-600/H_2O = 2.5:1.5; (b) PEG-600/H_2O = 2.5:2.0; (c) PEG-600/H_2O = 2.5:2.5 (mL/mL)

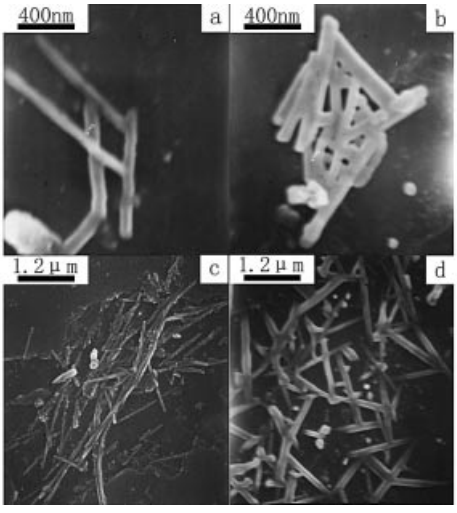

Figure 5. SEM images of POM nanorods with different diameters and lengths

In order to investigate the action of PEG in this liquid system, control experiments without PEG addition were carried out. Figure 6, a−c, show the SEM images of $Ag_4SiW_{12}O_{40}$ particles with a diameter of about 5 μm. Figure 6, d, is the XRD pattern of $Ag_4SiW_{12}O_{40}$ particles. From this figure we can see that the products are huge particles in the ordinary liquid system, hence PEG is a very important factor in controlling the shape and size of products.

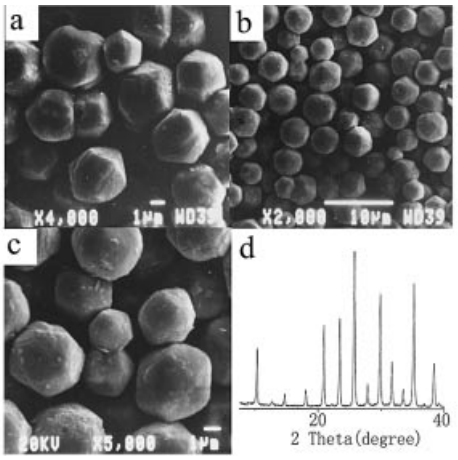

Figure 6. SEM images and XRD pattern of $Ag_4SiW_{12}O_{40}$ particles

In this liquid system, the reaction process was analyzed by conductometry. Figure 7 shows the relationship between the time and the conductivity in the PEG-400/H_2O (w = 2.5:1.5) system. Curve (a) shows the conductivity during the reaction when the solution containing PEG, water, and $AgNO_3$ was added to the other solution containing PEG, water, and $H_4SiW_{12}O_{40}$. Curve (b) shows the conductivity during the reaction when the solution containing PEG, water, and $H_4SiW_{12}O_{40}$ was added to the other solution containing PEG, water, and $AgNO_3$. Because of the coordination action between the Ag^+ and O atom in the PEG, the conductivity of the solution containing PEG, water, and $AgNO_3$ is lower than the solution that contains PEG, water, and $H_4SiW_{12}O_{40}$. When the reaction happens in the linear reaction fields, the formation of $Ag_4SiW_{12}O_{40}$ nanocrystals leads to a decrease of the electrolyte concentration. Thus, the conductivity of the reaction system decreases with the growth of nanocrystals. Curve (b) exhibits a sharp rise at the beginning of the reaction. This is due to the fact that the solution containing PEG, water, and $H_4SiW_{12}O_{40}$ has a higher conductivity than that of the solution that contains PEG, water, and $AgNO_3$.

According to these experimental results, these liquid-phase reactions can be regarded as a method that can be used to control the length and diameter of 1D POM nanomaterials rationally and effectively. During the preparation of 1D POM nanomaterials, the sticky solution, in which the uniform POM nanorods and/or nanowires could be obtained and exist stably without further agglomeration, is one of the important factors.

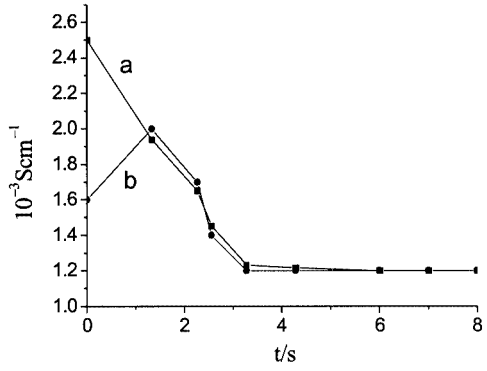

Figure 7. Relationship between the time and the conductivity

POM Hollow Particles

We wanted to produce short POM nanorods by means of the PEG-200/H_2O system, but, hollow particles were obtained instead of the expected short nanorods. This result can be attributed to the following. PEG assembly structures in water are flexible and chain-like. Surfactant PEG with lower molecular weight becomes more flexible and looser aggregates form. For PEG-200, the aggregates in water are different from those that form with higher molecular weight PEGs. The aggregates of PEG 200 in water are so soft that they cannot template the synthesis of POM nanorods. Thus, the soft and crimped aggregates lead to the formation of hollow particles. The diameters of these hollow particles are about 800 nm with homogeneous wall thickness (70 nm). Typical SEM images of hollow POM particles are shown in Figure 8. As noted above, many unique properties make POMs promising acid, redox, and bifunctional catalysts in homogeneous and heterogeneous systems. These hollow POM particles could be useful in a rich variety of applications. For instance, they may be suggested or demonstrated as extremely small containers for microencapsulation − a process that plays an important role in many areas such as catalysis, delivery of drugs, development of artificial cells, and protection of biologically active materials (e.g., enzymes, proteins, or deoxyribonucleic acids, DNAs).[14]

POM Microtubes and a 3D Ordered Microtube System

We can imagine that many 1D liquid reaction fields can be formed when PEG and a small quantity of water are mixed together. The larger the amount of water, the broader the reaction fields become. If the reaction fields are so broad that they can embrace the PEG aggregate then cannular structures may be obtained from PEG/H_2O systems. Figure 9, a, shows the half-tube obtained when PEG-400/H_2O = 2.5:3.5 (mL/mL) was used. Whole microtubes (shown in Figure 9, b−f) with diameters of about 700 nm were obtained using PEG-400/H_2O = 2.5:5 (mL/mL). Here, another important factor is the speed of stirring. High-speed stirring leads to the degradation of POM microtubes. On the contrary, well-grown microtubes were prepared at low stirring speeds (shown in Figure 9, d−f).

During the course of preparing the microtubes, an interesting phenomenon (shown in Figure 10, a) was observed:

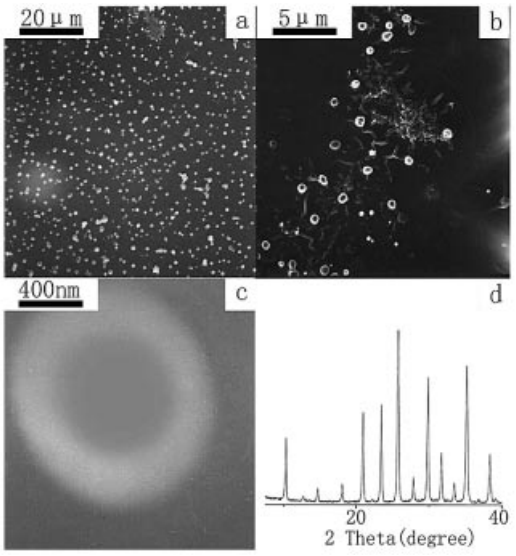

Figure 8. SEM images and XRD pattern of hollow $Ag_4SiW_{12}O_{40}$ particles

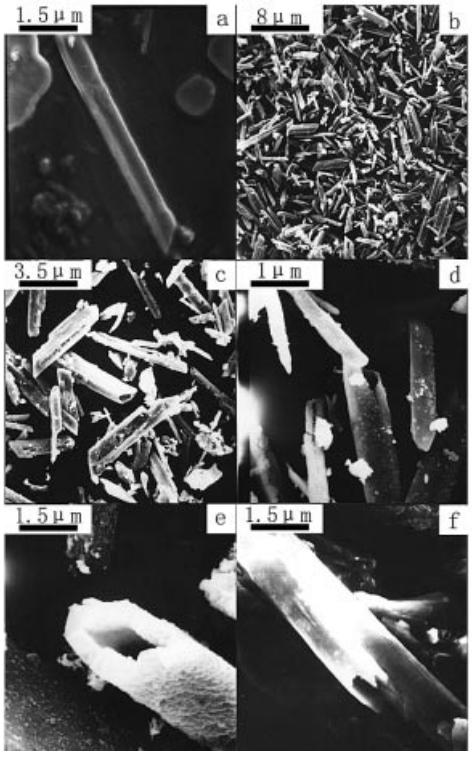

Figure 9. SEM images of $Ag_4SiW_{12}O_{40}$ microtubes

several microtubes fused together. So, we have developed a low-temperature controlled hydrothermal method using PEG/H_2O systems to synthesize 3D highly ordered microtunnel arrays. We mixed an $AgNO_3$/PEG/H_2O system and an $H_4SiW_{12}O_{40}$/PEG/H_2O system and then stirred slowly in order to make the mixture homogeneous. Then, the mixture was sealed in a 25-mL Teflon-lined reactor, with 70% filling, and heated at about 70 °C for 72 h. Figure 10, b and c,

show the SEM images of 3D-ordered microtunnel POM materials with diameters of about 1 μm. These ordered tunnels may be used as a microreactor. They should be useful in various applications, such as catalysis, selective delivery, and template for the synthesis of nanostructure materials.

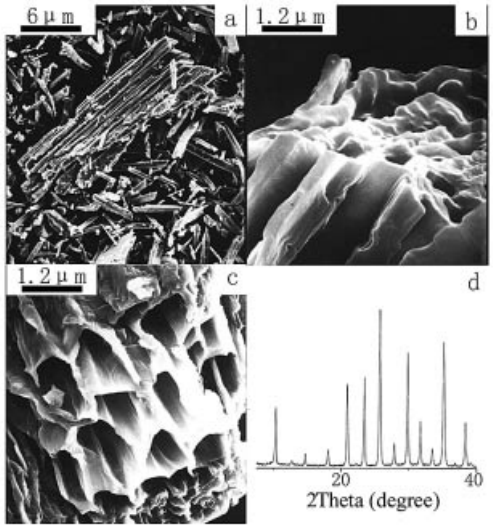

Figure 10. SEM images and XRD pattern of $Ag_4SiW_{12}O_{40}$ 3D-ordered microtubes

Figure 11 shows N_2 adsorption isotherms of the hollow particles, microtubes, and 3D-ordered tubes. In these systems there are many very large cavities. These isotherms have the typical shape of large porous materials.

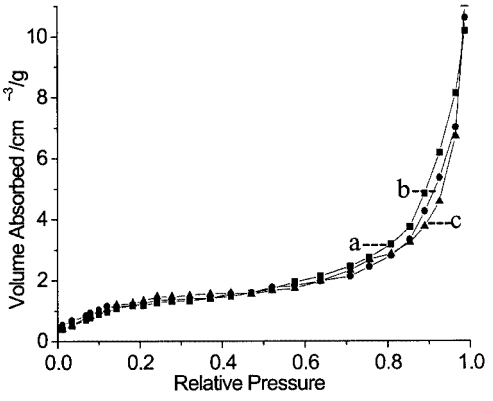

Figure 11. Isotherms of N_2 adsorption at 77 K: (a) hollow particles; (b) microtubes; (c) 3D-ordered tubes

Conclusion

In conclusion, the novel, and simple liquid PEG/H_2O system was applied in the preparation of POM nanorods, hollow particles, microtubes, and 3D-ordered tube systems. A possible mechanism is that chain-like PEG molecules segment the liquid reaction fields to form many linear microenvironments, in which the interaction of reactants and the growth of nanomaterials are limited in the directional space. From this reaction model, we presume that many other 1D nanomaterials such as metal salts ($BaSO_4$, CdS) and metal oxides (ZnO, CuO, Fe_3O_4) could also be prepared.

Furthermore, 1D POM nanorods, hollow particles, microtubes, and 3D-ordered tube system have been prepared. The regular sizes and shapes are well controlled by the PEG/H_2O systems. Owing to the extensive applications of POMs in catalysis, medicine, and functional materials, the preparation of POM nanostructured materials could provide a new route to explore their excellent properties.

Experimental Section

General: All reagents were purchased from commercial suppliers and used without further purification. The SEM images were obtained with a JEOL JSM-840 operating at 20 kV. The XRD patterns were obtained with a Rigaku D/max 2500V PC diffractometer with Cu-K_α radiation. A JEM-2010 transmission electron microscope was used to examine the morphology of the POMs nanocrystals.

General Preparation of $Ag_4SiW_{12}O_{40}$ Nanorods: $H_4SiW_{12}O_{40}{\cdot}nH_2O$ (1 g) was dissolved in a mixture of PEG-400 (or PEG-600)/H_2O (2.5 mL/1 mL, about 2.5 mL of the mixture) whilst stirring to give a clear and homodisperse system. Another 2.5 mL of PEG-400 (or PEG-600), mixed with 1−2 mL of H_2O and 0.23 g of $AgNO_3$, was stirred until it became clear. The above two solutions were then mixed and stirred for 1 min. Then, a fourfold excess of ethanol was added to form a white precipitate. The white precipitate was centrifuged, washed with ethanol, and dried in air at 50 °C for 1 h. The yield was 90% ($Ag_4SiW_{12}O_{40}$, 1.14 g, based on W). A similar approach was used for the synthesis of POM hollow particles using the PEG-200/H_2O (2.5 mL/1.5 mL) system. A clear and homodisperse system of $AgNO_3$/PEG-200/H_2O (0.5 g/2.5 mL/1.5 mL) and a similar system of $H_4SiW_{12}O_{40}$/PEG-200/H_2O (0.5 g/2.5 mL/1.5 mL) were prepared according to the above procedure. Then, the two systems were mixed and stirred. A fourfold excess of ethanol was added to form a white precipitate. The white precipitate was also centrifuged, washed with ethanol, and dried in air at 50 °C for 1 h. A very similar approach was employed to prepare the $Ag_4SiW_{12}O_{40}$ microtubes. A large amount of water (PEG/H_2O = 1:2) was added to the reaction system, with slow stirring. This mixture was sealed in a 25-mL Teflon-lined reactor, with 70% filling, and heated to about 70 °C for 72 h, to give the 3D-ordered microtube arrays.

Acknowledgments

This work was financially supported by the National Natural Science Foundation of China (20171010).

[1] [1a] Y. N. Xia, J. A. Rogers, K. E. Paul, G. M. Whitesides, *Chem. Rev.* **1999**, *99*, 1823−1848. [1b] X. F. Duan, Y. Huang, Y. Cui, J. F. Wang, C. M. Lieber, *Nature* **2001**, *409*, 66−69. [1c] M. H. Huang, S. Mao, H. Feick, H. Q. Yan, Y. Y. Wu, H. Kind, E. Weber, R. Russo, P. D. Yang, *Science* **2001**, *292*, 1897−1899.
[2] V. F. Puntes, K. M. Krishnan, A. P. Alivisatos, *Science* **2001**, *291*, 2115−2117, and references therein.
[3] M. Li, H. Schnablegger, S. Mann, *Nature* **1999**, *402*, 393−395.
[4] R. Y. Wang, J. Yang, Z. P. Zheng, M. D. Carducci, J. Jiao, S. Seraphin, *Angew. Chem. Int. Ed.* **2001**, *40*, 549−552.
[5] B. R. Martin, D. J. Dermody, B. D. Resis, M. M. Fang, L. A.

Lyon, M. J. Natan, T. E. Mallouk, *Adv. Mater.* **1999**, *11*, 1021−1025.
[6] J. T. Hu, T. W. Odom, C. M. Lieber, *Acc. Chem. Res.* **1999**, *32*, 435−445.
[7] M. B. Mohamed, K. Z. Ismail, S. Link, M. A. El-Sayed, *J. Phys. Chem. B* **1998**, *102*, 9370−9374.
[8] [8a] S. Vaucher, M. Li, S. Mann, *Angew. Chem. Int. Ed.* **2000**, *39*, 1793−1796. [8b] J. D. Hopwood, S. Mann, *Chem. Mater.* **1997**, *9*, 1819−1828. [8c] M. A. López-Quintela, J. Rivas, *J. Colloid Interface Sci.* **1993**, *158*, 446−451.
[9] [9a] M. T. Pope, A. Müller, *Angew. Chem. Int. Ed. Engl.* **1991**, *30*, 34−48. [9b] A. Müller, F. Petters, M. T. Pope, D. Gatteschi, *Chem. Rev.* **1998**, *98*, 239−272. [9c] J. T. Rhule, C. L. Hill, D. A. Judd, R. F. Schinazi, *Chem. Rev.* **1998**, *98*, 327−357. [9d] E. Coronado, C. J. Gomez-Garcia, *Chem. Rev.* **1998**, *98*, 273−296. [9e] N. Mizuno, M. Misono, *Chem. Rev.* **1998**, *98*, 199−217.
[10] [10a] A. Müller, S. Q. N. Shah, H. Bogge, M. Schmidtmann, *Nature* **1999**, *397*, 48−50. [10b] A. Müller, S. K. Das, P. Kögerler, H. Bögge, M. Schmidtmann, A. X. Trautwein, V. Schünemann, E. Krickemeyer, W. Preetz, *Angew. Chem. Int. Ed.* **2000**, *39*, 3413−3417.
[11] T. Ito, K. Inumaru, M. Misono, *Chem. Mater.* **2001**, *13*, 824−831.
[12] [12a] L. H. Bi, E. B. Wang, J. Peng, R. D. Huang, L. Xu, C. W. Hu, *Inorg. Chem.* **2000**, *39*, 671−679. [12b] W. S. You, E. B. Wang, Y. Xu, Y. G. Li, L. Xu, C. W. Hu, *Inorg. Chem.* **2001**, *40*, 5468−5471. [12c] L. H. Bi, R. D. Huang, J. Peng, E. B. Wang, Y. H. Wang, C. W. Hu, *J. Chem. Soc., Dalton Trans.* **2001**, 121−129. [12d] Y. H. Guo, E. B. Wang, Y. N. Zhou, S. H. Feng, *Chem. Mater.* **2000**, *12*, 3501−3508. [12e] Y. H. Guo, C. W. Hu, X. L Wang, E. B. Wang, Y. N. Zhou, S. H. Feng, *Chem. Mater.* **2001**, *13*, 4058−4064. [12f] L. Xu, Y. Q. Sun, E. B. Wang, E. H. Shen, Z. R. Liu, C. W. Hu, *New J. Chem.* **1999**, *23*, 1041−1044. [12g] Y. H. Guo, D. F. Li, C. W. Hu, Y. H. Wang, E. B. Wang, *Appl. Catal. B (Environment)* **2001**, *30*, 337−349. [12h] J. Peng, W. Z. Li, E. B. Wang, Q. L. Bai, *J. Chem. Soc., Dalton Trans.* **2001**, 3668−3671. [12i] C. W. Hu, Q. L. He, Y. H. Zhang, Y. Y. Liu, Y. F. Zhang, Y. D. Tang, J. Y. Zhang, E. B. Wang, *Chem. Commun.* **1996**, 121−122. [12j] W. S. You, Y. B. Wang, E. B. Wang, L. Xu, C. W. Hu, X. Q. Xin, F. Li, *Chem. J. Chin. Univ.* **2000**, *21*, 1636−1638. [12k] E. B. Wang, C. W. Hu, L. Xu, *Concise course of polyoxometalates chemistry [M]*, Chemical Industry Press, Beijing, **1997**, pp. 170−211.
[13] [13a] J. H. Sun, Y. J. Gong, W. H. Fan, Y. H. Sun, *Chem. J. Chin. Univ.* **2000**, *21*, 95−99, and references therein. [13b] W. Z. Wang, Y. J. Zhan, G. H. Wang, *Chem. Commun.* **2001**, 727−728.
[14] Y. Lu, Y. D. Yin, Y. N. Xia, *Adv. Mater.* **2001**, *13*, 271−274.

Received June 9, 2002
[I02302]

A New Highly Active Diphosphane-Palladium(II) Complex as a Catalyst Precursor for the Heck Reaction

Sven Sjövall, Maria H. Johansson, Carlaxel Andersson*

Eur. J. Inorg. Chem. **2001**, 2907–2912

In Table 1 on page 2910 the given amounts of added olefin and aryl halide were inadvertently misplaced. The correct version of this table is printed below.

Table 1. Selected results of the Heck reaction with complex **6**; experiments conducted with 1.2 equivalents of Bu_3N in NMP except where noted

No.	Olefin (mmol)[a]	ArX (mmol)[b]	**6** (mmol) × 10^{-5}	time/temp (h)/(°C)	TON[c]	Yield (%)[d]	TOF (h^{-1})[e]
1	mac (9)	PhI (6)	6	9/120	100 000	100	11 111
2	mac (36)	PhI (24)	2	100/120	1176 000	98	11 760
3	bac (15)	PhI (10)	2	56/120	495 000	99	8 840
4	sty (15)	PhI (10)	2	54/120	490 000	98[f]	9 075
5[g]	mac (15)	PhI (10)	3	36/120	333 000	99	9 250
6[h]	mac (15)	PhI (10)	3	95/120	320 000	95	3 370
7	mac (15)	4-bba (10)	3	32/120	333 000	99	10 410
8	bac (15)	4-bba (10)	3	41/120	333 000	99	8 125
9	mac (15)	PhBr (10)	4	79/140	235 000	94	2 975
10	bac (15)	PhBr (10)	4	90/140	207 500	83	2 310

[a] mac = methyl acrylate, bac = *n*-butyl acrylate, sty = styrene. – [b] 4-bba = 4-bromobenzaldehyde. – [c] TON = Turnover number (mol product/mol catalyst). – [d] GC yield using 2-methylnaphthalene as internal standard. – [e] TOF = Turnover frequency (mol product/mol catalyst × time). – [f] *trans*-stilbene/*cis*-stilbene = 9. – [g] Dioxane as solvent. – [h] Mesitylene as solvent.

In the first paragraph of the Exp. Sect. on page 2910 it was inadvertently stated that $LiPPh_2$ was prepared from nBuLi and PPh_2Cl. It should correctly say that $LiPPh_2$ was prepared from nBuLi and $HPPh_2$.

C. Andersson
[I01138 C]

 © 2003 WILEY-VCH Verlag GmbH & Co. KGaA, 69451 Weinheim 1434–1948/03/0102–0377 $ 20.00+.50/0

EurJIC
European Journal of Inorganic Chemistry

February 2003
Issue 3
Pages 379–568

Papers available ahead of print in Early View at www.interscience.wiley.com

Earliest available Table of Contents:
Automatically, free of charge by e-mail through
www.interscience.wiley.com/alerts

COVER PICTURE

The cover picture shows a mixed-valence copper(I,II) coordination polymer $[Cu^{I}_{2}Cu^{II}(4,4'\text{-bpy})_2(pydc)_2]\cdot 4H_2O$ (4,4′-bpy = 4,4′-bipyridine; pydc = pyridine-2,4-dicarboxylate) featuring the "metal-complex ligands" $[Cu^{II}(pydc)_2]^{2-}$ synthesized hydrothermally using $Cu(MeCO_2)_2$, pyridine-2,4-dicarboxylate, 4,4′-bipyridine and NaOH. Single-crystal structure analysis exhibits this compound to be the first porous 3-D framework constructed from five-fold parallel interpenetration of 2-D (6,3) nets (right-hand side). The one-dimensional channels in the 3-D framework (left-hand side) occupying 17.4% of the crystal volume are occupied by guest water molecules. The porous network is stable after removal of the lattice water molecules, which may be attributed to the multiple entanglement of the 2-D nets. Details are discussed in the article by X.-M. Zhang and X.-M. Chen on p. 413ff.

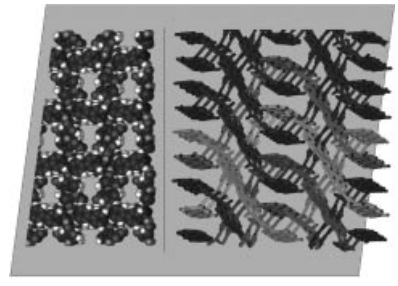

MICROREVIEW

Contents

393 **H. Braunschweig,* M. Colling**

The Chemistry of Borylene Complexes

Keywords: Boron / Borylene complexes / Transition metals

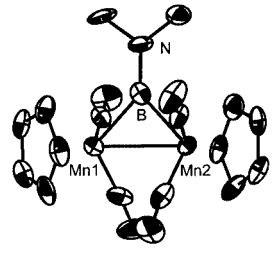

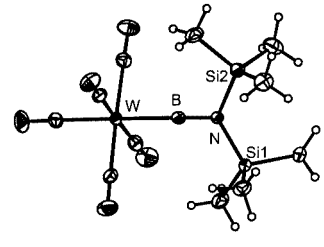

 © 2003 WILEY-VCH Verlag GmbH & Co. KGaA, 69451 Weinheim 1434–1948/03/0203–0383 $ 20.00+.50/0

SHORT COMMUNICATIONS

405 **C. Richardson, P. J. Steel***

3,6-Di(2-pyridyl)-1,4,2,5-dioxadiazine and a Silver Coordination Polymer with an Unprecedented Metallosupramolecular Topology

Keywords: Silver / Coordination polymers / Bridging ligands / N ligands

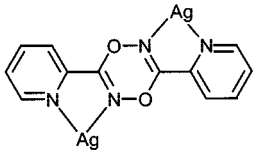

409 **I. Hegelmann, N. Burzlaff***

Direct Synthesis of Enantiopure Tripod Ligands from C_2-Symmetric Precursors

Keywords: N ligands / Tripod ligands / Chirality / Prochirality / Ruthenium

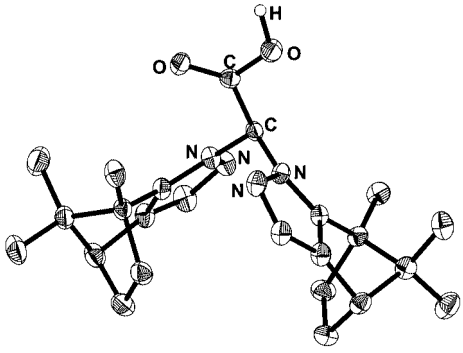

FULL PAPERS

413 **X.-M. Zhang, X.-M. Chen***

A New Porous 3-D Framework Constructed From Fivefold Parallel Interpenetration of 2-D (6,3) Nets: A Mixed-Valence Copper(I,II) Coordination Polymer $[Cu^{I}_{2}Cu^{II}(4,4'\text{-bpy})_2(pydc)_2]\cdot 4H_2O$

Keywords: Coordination polymers / Microporous materials / Mixed-valent compounds / Copper / N ligands

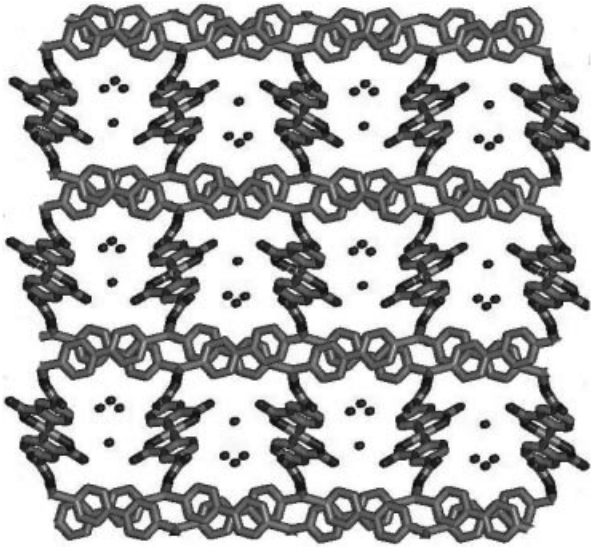

418 **D. Sellmann,* D. C. F. Blum, F. W. Heinemann, J. Sutter**

Synthesis, Structure and Reactivity of Sulfur-Rich $[Fe(L^1)(L^2)(\text{'}tpS_4\text{'})]$ Complexes with Rigid $[Fe(\text{'}tpS_4\text{'}]$ Cores and $\sigma-\pi$ Co-Ligands ($\text{'}tpS_4\text{'}^{2-}$ = 1,2-Bis(2-mercaptophenylthio)phenylene(2−); L^1, L^2 = CO, PR_3, NO)

Keywords: Helical structures / Iron / S ligands

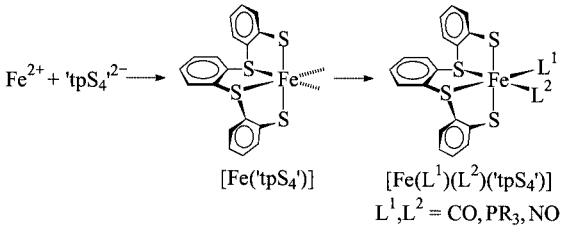

427 **W. J. van Meerendonk, K. Schröder, E. A. C. Brussee, A. Meetsma, B. Hessen,* J. H. Teuben**

Chloro- and Alkyltitanium Complexes of a New Dianionic Ancillary Ligand: A Linked Amidinate−Amide

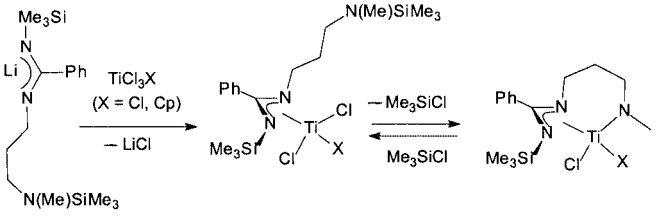

Keywords: N ligands / Tridentate ligands / Titanium / Alkyl complexes

433 **G. B. Nikiforov, H. W. Roesky,* T. Labahn, D. Vidovic, D. Neculai**

Synthesis and Structure of the First Holmium and Erbium Diiodide Complexes of Composition $LLnI_2$ (Ln = Ho, Er)

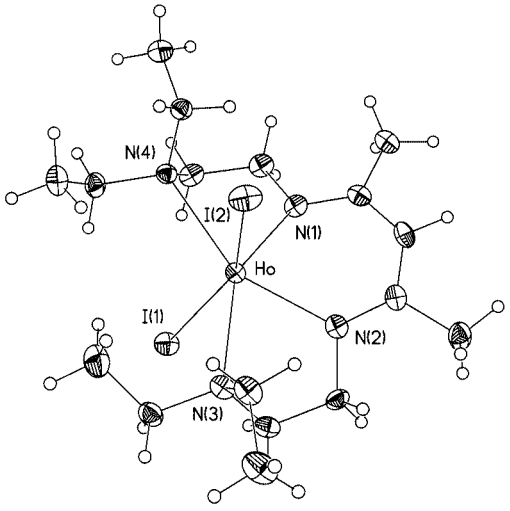

Keywords: Lanthanides / Iodides / Coordination chemistry / N ligands

437 **G. B. Nikiforov, H. W. Roesky,* J. Magull, M. Noltemeyer, H.-G. Schmidt, E. G. Ilyin, Y. B. Kokunov, A. Demsar**

Synthesis and Structure of the First Non-Metallocene Ti^{III} Fluoride Complex $LTiF_2 \cdot 2Me_3SnCl$ Supported by a β-Diketiminato Ligand

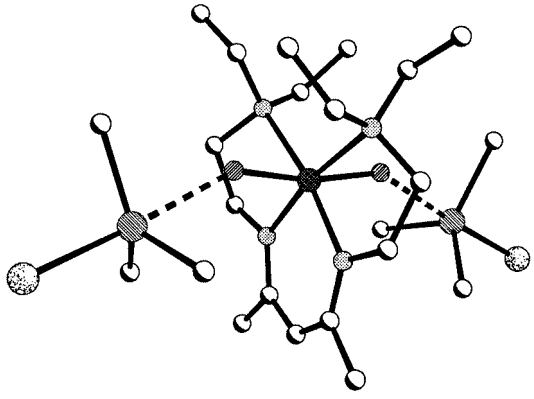

Keywords: Titanium / Fluorides / Coordination chemistry / N ligands

442 **N. D. Reddy, S. S. Kumar, H. W. Roesky,* D. Vidovic, J. Magull, M. Noltemeyer, H.-G. Schmidt**

Synthesis of a Hexadentate Hexameric Aluminum Imide and Its Metathesis Reactions

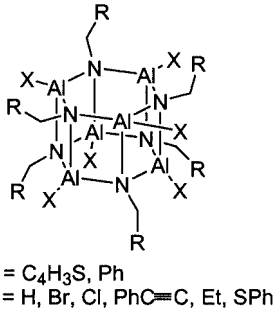

Keywords: Aluminum / Hydride ligands / N ligands / S ligands / Cluster compounds

449 **J.-L. Zuo, F. F. de Biani, A. M. Santos, K. Köhler, F. E. Kühn***

4-Ethynylpyridine as a Bridging Moiety in Mixed Rh/Re Complexes

Keywords: N ligands / Metal-metal interactions / Oligomers / Rhenium / Rhodium

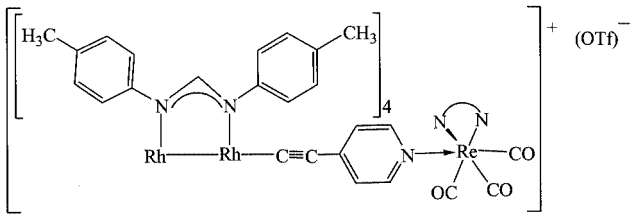

453 **M.-C. Chalbot, A. M. Mills, A. L. Spek, G. J. Long, E. Bouwman***

Structure and Electronic Properties of $[Ni(dsdm)\{Fe(CO)_3\}_2]$, an Unusual, Triangular Nickel Diiron Compound

Keywords: Carbonyl ligands / Cluster compounds / Iron / Nickel

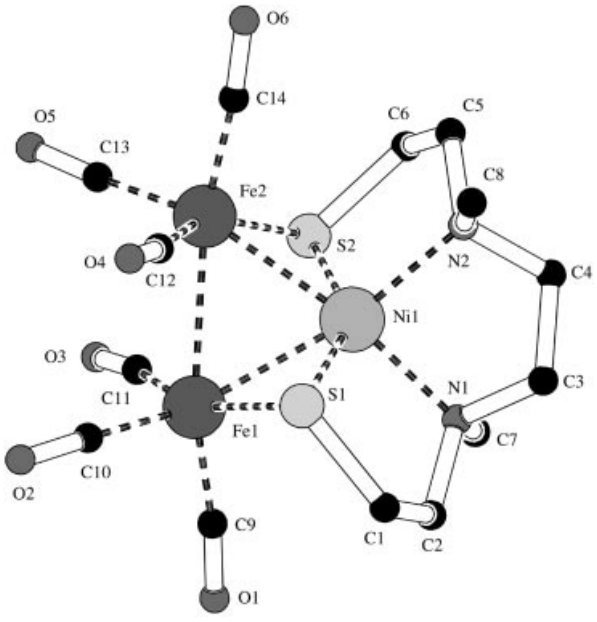

458 **J. P. Dunne, M. Bockmeyer, M. Tacke***

Co-Condensation Reactions of Substituted Aromatic Compounds with Lithium Atoms at 77 K

Keywords: Lithium / C−H bond activation / Co-condensation / Density functional calculations

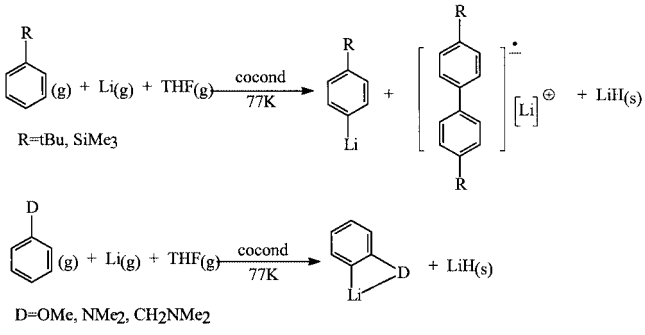

467 **A.-C. Laemmel, J.-P. Collin,* J.-P. Sauvage,* G. Accorsi, N. Armaroli***

Macrocyclic Complexes of $[Ru(N\text{-}N)_2]^{2+}$ Units [N-N = 1,10 Phenanthroline or 4-(*p*-Anisyl)-1,10-Phenanthroline]: Synthesis and Photochemical Expulsion Studies

Keywords: Ruthenium / Macrocycles / Receptors / Photochemistry / Molecular machines

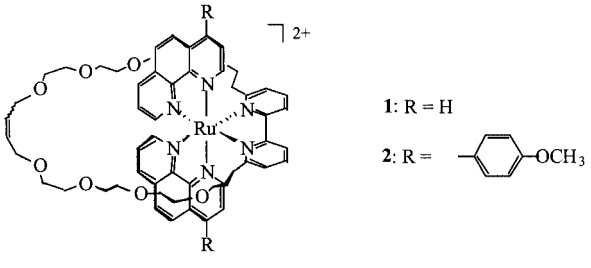

475 **T. C. Harrop, L. A. Tyler, M. M. Olmstead, P. K. Mascharak***

Change in the Spin State of an Fe^{III} Center upon One N-to-O Switch in the Coordination of a 2,6-Pyridinedicarboxamido Unit: The Effect of Methyl Thioether and Methyl Ether Appendages at the Ligand Periphery

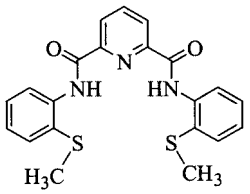

$PyPSMeH_2$

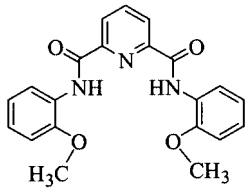

$PyPOMeH_2$

Keywords: Iron / N ligands / S ligands / Spin states / EPR spectroscopy

482 **J. Gun,* A. Modestov, O. Lev, D. Saurenz, M. A. Vorotyntsev, R. Poli***

Studies on the Reduction of $[(C_5Me_5)_2Mo_2O_5]$ in Methanol/Water/Acetate Solutions by On-Line Electrochemical Flowcell and Electrospray Mass Spectrometry

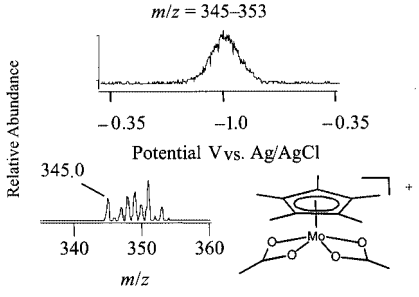

Keywords: Cyclopentadienyl ligands / Electrochemistry / Mass spectrometry / Molybdenum / Oxo ligands

493 **R. Fandos,* C. Hernández, A. Otero,* A. Rodríguez, M. J. Ruiz, P. Terreros**

New Monocyclopentadienyl Complexes of Tantalum(V) and Titanium(IV) with Chelating Pyrimidinethiolate and Oxypyridine Ligands − Molecular Structure of $[Cp^*TaCl_3(SC_6H_7N_2)]$

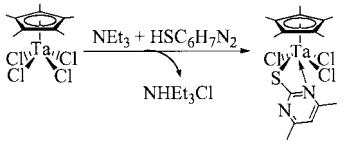

Keywords: N ligands / S ligands / Tantalum / Titanium / Cyclopentadienyl ligands

499 **R. Caspar, H. Amouri,* M. Gruselle, C. Cordier, B. Malézieux, R. Duval, H. Leveque**

Efficient Asymmetric Synthesis of Δ- and Λ-Enantiomers of (Bipyridyl)ruthenium Complexes and Crystallographic Analysis of Δ-Bis(2,2′-bipyridine)(2,2′-bipyridine-4,4′-dicarboxylato)-ruthenium: Diastereoselective Homo- and Heterochiral Ion Pairing Revisited

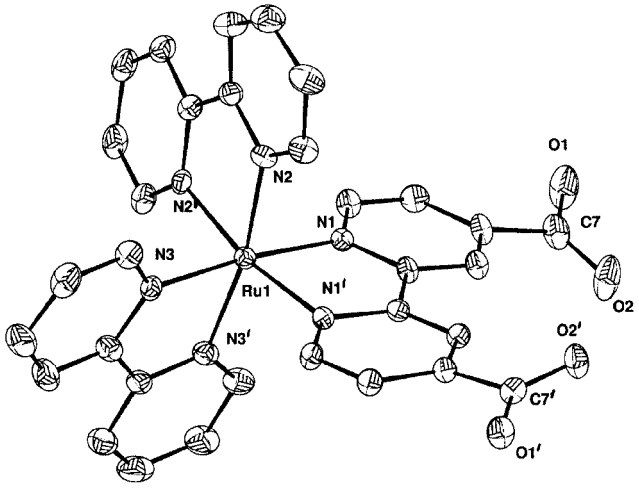

Keywords: Ruthenium / Chiral resolution / Circular dichroism

506 **L. Engelke,* M. Schaefer, F. Porsch, W. Bensch**

In-situ Energy-Dispersive X-ray Diffraction Studies of Crystal Growth and Compound Conversion Under Solvothermal Conditions

Keywords: X-ray diffraction / Cell design / Kinetics / Solvothermal synthesis / Thioantimonates

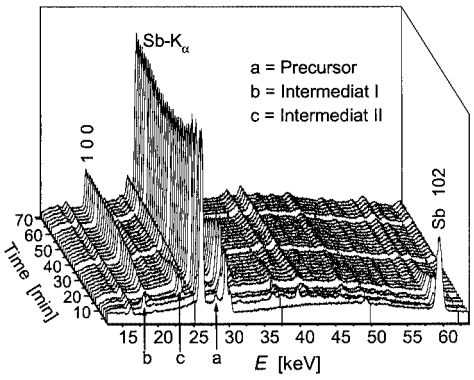

514 **M. Knorr,* G. Schmitt*, M. M. Kubicki, E. Vigier**

Formation of (σ-Alkenyl)- and (μ-Vinylidene)palladium and -platinum Complexes by Oxidative Addition of 4,4-Dichloro-1,1-diphenyl-2-azabuta-1,3-diene − The Molecular Structure of an Unusual Asymmetric (μ-Vinylidene)Pd−Pd Complex

Keywords: Palladium / Vinylidene ligands / Platinum / Metal-metal interactions

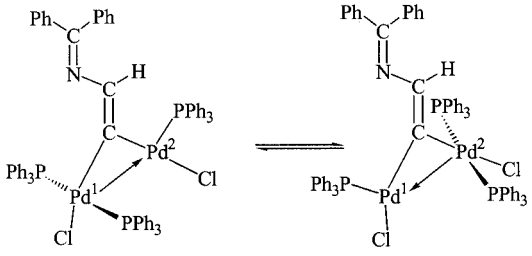

518 **P. Gómez-Saiz, J. García-Tojal,* A. Mendia, B. Donnadieu, L. Lezama, J. L. Pizarro, M. I. Arriortua, T. Rojo**

Coordination Modes in a Tridentate NNS (Thiosemicarbazonato)copper(II) System Containing Oxygen-Donor Coligands − Structures of [{Cu(L)(X)}$_2$] (X = Formato, Propionato, Nitrito)

Keywords: Copper / Magnetic properties / Stacking interactions / Thiosemicarbazone complexes

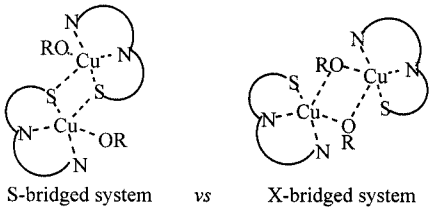

528 **M. Pitié, C. Boldron, H. Gornitzka, C. Hemmert, B. Donnadieu, B. Meunier***

DNA Cleavage by Copper Complexes of 2- and 3-Clip-Phen Derivatives

Keywords: Copper / DNA cleavage / Helical structures / Ligand design / N ligands

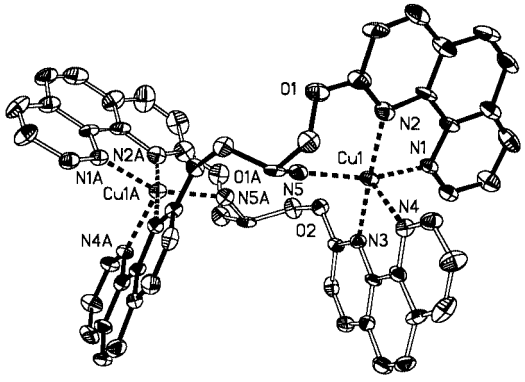

541 **P. Chaudhuri,* E. Rentschler, F. Birkelbach, C. Krebs, E. Bill, T. Weyhermüller, U. Flörke**

Ground Spin State Variation in Carboxylate-Bridged Tetranuclear $[Fe_2Mn_2O_2]^{8+}$ Cores and a Comparison with Their $[Fe_4O_2]^{8+}$ and $[Mn_4O_2]^{8+}$ Congeners

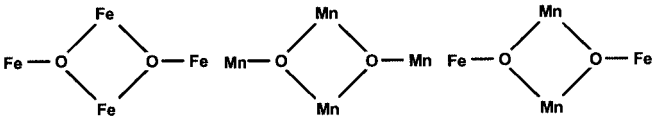

Keywords: Oxo ligands / Carboxylate ligands / Iron / Manganese / Magnetic properties / Tetranuclear complexes

556 **S. Gladiali,* F. Grepioni, S. Medici, A. Zucca, Z. Berente, L. Kollár**

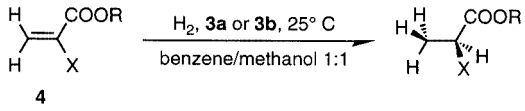

Up to 94% conversion and up to 60% ee

Chiral Complexes of Rh^I Containing Binaphthalene-Core P,S-Heterobidentate Ligands − Synthesis, Characterization, and Catalytic Activity in Asymmetric Hydrogenation of α,β-Unsaturated Acids and Esters

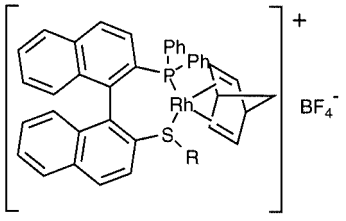

3a R = Me
3b R = *i*Pr

Keywords: S ligands / P ligands / Rhodium / Asymmetric catalysis / Hydrogenations

562 **C. Alvarez-Toledano, E. Delgado,* B. Donnadieu, M. A. Gómez, E. Hernández, G. Martín, F. Ortega-Jiménez, F. Zamora**

Activation of C−S Bonds in Organosulfur Compounds Containing α,β-Unsaturated Ketone Systems by Carbonylruthenium and -iron Complexes

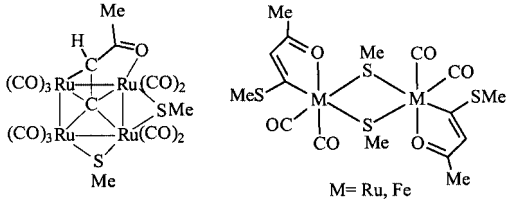

Keywords: Vinylidene ligands / Clusters / Iron / Carbonyl ligands / Ruthenium

The Chemistry of Borylene Complexes

Holger Braunschweig*[a][‡] and Miriam Colling[b]

Keywords: Boron / Borylene complexes / Transition metals

Over the past seven years, complexes of various transition metals with bridged or terminal borylene ligands BR have for the first time been reported and fully characterised. Being closely related to important organometallic compounds, such as carbene, vinylidene, and carbonyl complexes, they have already attracted considerable interest both from experimental and computational points of view. Those studies have provided some detailed information about the nature of the metal–boron bond and about the nature of metal and borylene moieties required for the formation of stable complexes. Various methods for their preparation have been developed and the first studies on their reactivity have demonstrated an interesting chemistry.

(© Wiley-VCH Verlag GmbH, 69451 Weinheim, Germany, 2003)

1. Introduction

Transition metal complexes with electron-precise, two-centre, two-electron (2c-2e) bonds linking the metal centre to a main group element have now been well established for decades, and for almost any main group element from group 13 to 17. Corresponding complexes with metal−boron bonds, however, became known only much later, indicating the difficulties associated with the synthesis and characterisation of these compounds. Despite very early investigations in this area (vide infra),[1] the first structurally authenticated transition metal complexes of boron date back only to 1990.[2,3] Until then, confirmed knowledge of compounds with direct transition metal−boron bonds was restricted to borides,[4−6] metallaboranes[7−9] and complexes with π-bonded boron-containing ligands such as borole,[10−12] diborolene,[13] borabenzene,[14,15] borazine,[16,17] and diazadiboretidine.[17] The natures of the metal−boron interactions in these classes of compounds are diverse, but none of them is characterised by classical 2c-2e bonds.

Thanks to the vigorous research into transition metal complexes of boron since 1990,[18−21] a variety of different coordination modes for boron-centred ligands have been obtained, allowing for a systematic classification of those compounds (Figure 1). According to the coordination number of boron and the number of metal−boron bonds, one can distinguish between borane (**I**), boryl (**II**), bridged (**III**) and terminal borylene (**IV**) complexes. Borane complexes can be understood as Lewis acid−base adducts of basic metal centres and acidic boranes BR_3, giving rise to fourfold coordination of the boron atom. Boryl complexes, however, show boron in coordination number three, achieved by the linking of a BR_2 group to a metal centre. The borylene ligand BR can adopt two different coordination modes: either bridging between two metal centres − also showing boron in coordination number three − or terminal to one metal centre with formation of a formal

[a] Department of Chemistry, Imperial College
London SW7 2AY, UK
Fax: (internat.) + 44-20/7594-5900
E-mail: h.braunschweig@ic.ac.uk
[b] Institut für Anorganische Chemie der Technischen Hochschule
Templergraben 55, 52056 Aachen, Germany
[‡] New address: Institut für Anorganische Chemie der Universität
Würzburg,
Am Hubland, 97074 Würzburg, Germany

Holger Braunschweig was born in 1961 in Aachen and took up his studies in chemistry at the RWTH Aachen in 1983. He obtained his doctoral degree in 1990 (with Prof. P. Paetzold), spent a year at the University of Sussex, UK (with Prof. M. F. Lappert, FRS), and obtained his venia legendi in 1998 from the RWTH Aachen, after his habilitation with Prof. P. Paetzold. From 2000 he spent two years as a Senior Lecturer and Reader at the Imperial College, London, until being appointed to a chair of Inorganic Chemistry at the University of Würzburg. His research interests are concerned with boron and transition metal chemistry, catalysis, and organometallic polymers.

Miriam Colling was born in 1972 in Geilenkirchen (Germany). After studying chemistry at the RWTH Aachen from 1991 to 1999, she completed her PhD in 2002 (with Dr. H. Braunschweig) on the synthesis, reactivity, and structure of boryl and borylene transition metal complexes.

MICROREVIEWS: This feature introduces the readers to the authors' research through a concise overview of the selected topic. Reference to important work from others in the field is included.

double bond and a decrease in the coordination number to two. Provided that the boron atom in **II**−**IV** is still Lewis acidic, there is the possibility to add a suitable base L, which results in the formation of the corresponding adducts of boryl (**IIa**) and both bridged (**IIIa**) and terminal (**IVa**) borylene complexes. Examples of all types of compounds **I**−**IV** had already been described in earlier literature between 1963 and 1970, but without structural confirmation.[1] The spectroscopic data reported for these compounds are in disagreement with more recent findings and the proposed constitutions of those complexes have to some extent been disproved.

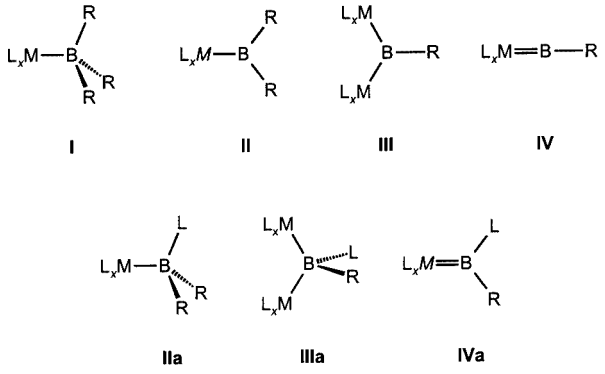

Figure 1. Different types of transition metal complexes of boron

The production of borylene complexes with either bridging or terminal BR ligands is one of the most recent achievements in the field of transition metal complexes of boron, and these compounds are still exceptionally rare in comparison with boryl and other group 13 "elementdiyl" complexes.[22] Thanks to their close relationship to pivotal organometallic compounds such as carbene, vinylidene and especially carbonyl complexes, borylene complexes have already attracted considerable interest.[23−25] This is also reflected by the numerous theoretical studies[26−32] (vide infra), which greatly outnumber the experimental reports. Furthermore, borylene complexes allow for the stabilisation of the hypovalent borylene **:**BR in the coordination sphere of a transition metal centre. In contrast to related subvalent main group element species such as carbenes, silylenes, or alanediyls, no free borylenes are known at ambient temperature and in condensed phase.

2. Terminal Borylene Complexes

2.1. Synthesis

The salt elimination reaction between mononuclear anionic transition metal carbonyl complexes $M'[L_xM(CO)_y]$ and main group element halides $HalER_z$ is a fundamental reaction in transition metal chemistry, and has had a pivotal role in establishing complexes of the type $[L_x(OC)_yM-ER_z]$ with transition metal−element bonds.[33,34] Over the past decade, salt elimination reactions have also become a very facile method for the synthesis of boryl complexes $[L_x(OC)_yM-BR_2]$ [Equation (1a)]. We have reported, however, that the formation of (boryloxy)-carbyne complexes $[L_x(OC)_{y-1}M{\equiv}C-O-BR_2]$ [Equation (1b)] with nucleophilic attack of the CO oxygen atom represents an alternative reaction pathway to the expected synthesis of boryl complexes in certain cases.[35−37]

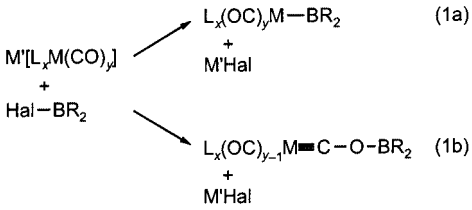

(1)

Extension of this synthetic approach to dianionic carbonylates and suitable dihaloboranes [Equation (2)] gave access to the first structurally authenticated terminal borylene complexes $[(OC)_4Fe-B(\eta^5\text{-}C_5Me_5)]$ (**1**)[38] and $[(OC)_5W=B=N(SiMe_3)_2]$ (**2**),[39] reported by Cowley and by us in 1998 (Figure 2). By applying the corresponding precursors $K_2[Fe(CO)_4]$ and $Na_2[Cr(CO)_5]$ we also obtained the related aminoborylene complexes $[(OC)_4Fe=B=N(SiMe_3)_2]$ (**3**)[39] and $[(OC)_5Cr=B=N(SiMe_3)_2]$ (**4**)[39] (Figure 2), the latter of which was subsequently characterised by X-ray structure analysis.[40] The formation of **1**−**4** implies that the boron centre in such terminal borylene complexes requires stabilisation by a sterically demanding and electron-releasing ligand. Evidently, both the $\eta^5\text{-}C_5Me_5$ and the $N(SiMe_3)_2$ ligands provide sufficient steric shielding and π-electron stabilisation. In the case of the former, an alternative point of view may be applied, namely that the electron deficiency of the boron centre is relieved by its incorporation into a non-classical pentacarba-*nido*-hexaborane cage. From our experience with the formation of transition metal−boron bonds by salt elimination reactions, the aminoborane $Br_2B=N(SiMe_3)_2$ appeared to be the most promising borane precursor for the synthesis of terminal aminoborylene complexes because of the increased electrophilicity of the boron centre in relation to (dialkylamino)boranes, and consequent facilitation of the nucleophilic substitution of the halides by transition metals.[41,42]

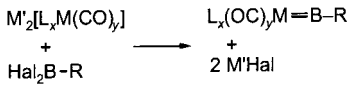

(2)

Despite significant efforts[43−45] and the vast amount of various borane precursors at hand, all attempts to obtain corresponding $[(OC)_xM=B=NR_2]$ complexes from any other aminoborane $Hal_2B=NR_2$ have so far failed, thus emphasising the particular significance of $Br_2B=N(SiMe_3)_2$ for the production of terminal borylene complexes. The failure to undergo salt elimination reactions with dianionic metal carbonylates according to Equation (2) appears to extend to common alkyl- and aryl(dihalo)boranes Hal_2B-R,[43−45] thus hampering the synthesis of terminal borylene complexes of the type $[(OC)_xM=B-R]$. These compounds are of particular interest, however, since the boron centre is both coordinatively and electronically unsaturated and thus represents a very unusual bonding situation in boron chemistry, known only in a very few methyl-

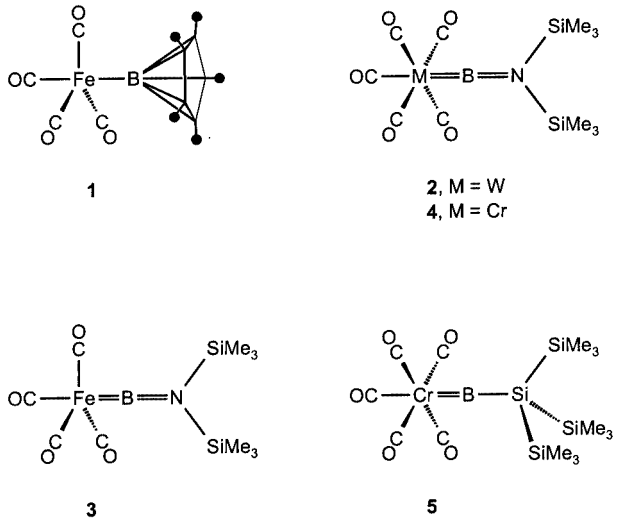

Figure 2. Selected terminal borylene complexes

eneboranes of the $(Me_3Si)_2C{=}B{-}R$ type (R = Me, *t*Bu, 2,3,5,6-tetramethylphenyl, 2,4,6-trimethylphenyl).[46−50] Because of their obvious significance[23] for the understanding of metal−boron bonding, alkyl- and arylborylene complexes $[(OC)_xM{=}B{-}R]$ had already been the subjects of several theoretical studies[28−31] before we succeeded in providing the first experimental evidence for such a compound. The use of the sterically demanding silylborane $Cl_2B{-}Si(SiMe_3)_3$ finally allowed for the synthesis and full characterisation of $[(OC)_5Cr{=}B{-}Si(SiMe_3)_3]$ (**5**) as the first terminal borylene complex with a both coordinatively and electronically unsaturated boron atom[51] (Figure 2). This silylborylene complex proved to be extremely sensitive, in contrast to its rather stable amino analogue $[(OC)_5Cr{=}B{=}N(SiMe_3)_2]$ (**4**), and shows significant decomposition in solution and even in the solid state after several hours at ambient temperature. The enhanced sensitivity of **5** is obviously due to the lack of ligand-to-boron π-interaction, as its steric shielding must be considered equal to or even larger than that in **4**.

As mentioned above, a low-coordinated boron centre displays some potential Lewis acidic character, which in the case of terminal borylene complexes might provide access to corresponding base-stabilised species of the type $[L_xM{=}B(L){-}R]$ (**IVa**, Figure 1). The only example so far was reported in 2000 by Roper, who obtained $[Os(=BNHC_9H_6N)Cl_2(CO)(PPh_3)_2]$[52] (**6**) by treatment of the borylosmium complex $[Cl_2BOsCl(CO)(PPh_3)_2]$ with 8-aminoquinoline as shown in Figure 3.

Subsequent treatment of **6** with $[Bu_4N]I$ yielded the corresponding borylene complex $[Os(=BNHC_9H_6N)Cl(I)(CO)(PPh_3)_2]$ (**7**), in which the chloro ligand *trans* to the boron atom was replaced by iodine, thus providing evidence for the *trans* influence of the borylene ligand.[52]

Obviously, this synthesis of **6** is very specific, but even the salt elimination reaction as in Equation (2) suffers from a certain lack of wider applicability in borylene chemistry. The restriction to a rather narrow range of dihaloboranes has already been discussed, but the same also appears to be

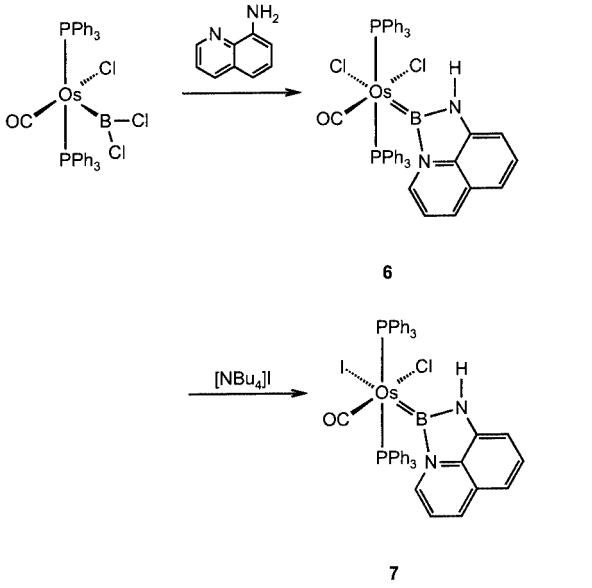

Figure 3. Synthesis of **7**

true for the dianionic transition metal precursor. Over the past few years we have employed a wide variety of such dianionic complexes or corresponding synthetic equivalents[53,54] in combination with various dihaloboranes, but without much success.[43−45]

The need for alternative synthetic methods in this chemistry initiated our studies on the potential use of complexes of the type $[(OC)_5M{=}B{=}N(SiMe_3)_2]$ (**2**: M = W; **4**: M = Cr) as a source of the aminoborylene $B{=}N(SiMe_3)_2$. The generation of such hypovalent borylenes B−R − the boron analogues of carbenes CR_2 − usually requires drastic conditions: Timms' classical method involves the reduction of boron trihalides at temperatures above 2000 °C,[55,56] while alternatively, West obtained the silylborylene $B{-}SiPh_3$ photochemically from $RB(SiPh_3)_2$ (R = Me, Mes) in hydrocarbon matrices at −196 °C.[57] The reductive[58,59] or photochemical[60] generation of species B−R in condensed phase might be assumed from the nature of the corresponding trapping products. There is, however, no direct proof for the intermediacy of borylenes − the system $MeBBr_2/2{\cdot}C_8K$ as a source for B−Me in particular has been reported to be questionable.[61] As early as 1973 Timms recognised borylene complexes as a potentially useful source of borylenes in cases in which gaseous species cannot be used.[56] We have recently reported on the first photochemically induced intermetal borylene transfer, as shown in Equation (3), thus proving that terminal borylene complexes may indeed act as a unique source of hypovalent borylenes in condensed phase and close to ambient temperature.[62]

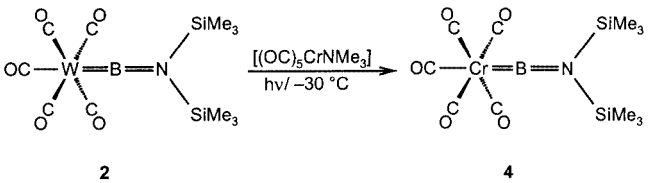

(3)

The formation of **4** as in Equation (3) merely represents an alternative synthesis of an already known compound. However, the generation of $[(\eta^5\text{-}C_5H_5)(OC)_3V{=}B{=}N(SiMe_3)_2]$ (**8**), similarly obtained from **4** and $[(\eta^5\text{-}C_5H_5)V(CO)_4]$ as shown in Equation (4),[63] emphasises the significance of photochemically induced intermetal borylene transfer, since all attempts to obtain the vanadium complex **8** by salt elimination reactions from $Na_2[(\eta^5\text{-}C_5H_5)V(CO)_3]$ and $Hal_2B{=}N(SiMe_3)_2$ failed.[43−45]

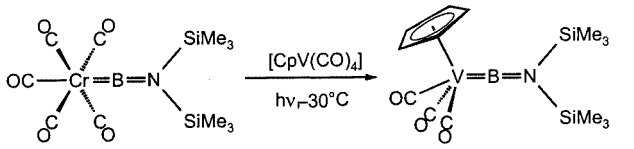

4 **8** (4)

2.2. Structure

In solution, the common and most characteristic spectroscopic feature of all terminal borylene complexes with coordinatively unsaturated (i.e., two-coordinate) boron atoms are the ^{11}B NMR resonances, which are significantly deshielded with respect to those of corresponding amino- and silylboryl complexes of the types $[L_xM{-}B(X)NR_2]$[18−21] and $[L_xM{-}B(X)SiR_3]$.[64] The aminoborylene complexes **2**−**4**, and **8** exhibit ^{11}B NMR shifts in the range from δ = 87 to 93 ppm (Table 1), thus resembling those of corresponding bridged borylene complexes with π-donating ligands at the boron atom (vide infra). The silylborylene complex $[(OC)_5Cr{=}B{-}Si(SiMe_3)_3]$ (**5**) is characterised by a strikingly deshielded ^{11}B NMR resonance at δ = 204.3 ppm, and so greatly extends the known dispersion of the ^{11}B nucleus for classical boranes. Similarly low-field-shifted resonances have been reported only for metal clusters containing interstitial boron atoms, such as *cis*- and *trans*-$[Fe_4Rh_2(CO)_{16}B]^-$ (δ = 211 and 205 ppm).[65,66] The observed significant difference between **2** and **5** could be expected for terminal borylene complexes in which the boron centre was not part of a boron−ligand π-system,[23] if one compares the bridged amino- and alkylborylene complexes of the type $[(\mu\text{-}BR)\{(\eta^5\text{-}C_5H_5)Mn(CO)_2\}_2]$ (R = NMe_2: $\delta^{11}B$ = 103 ppm; R = *t*Bu: $\delta^{11}B$ = 170 ppm).[67−69] Because of the higher coordination numbers of the boron centres, $[(OC)_4Fe{-}B(\eta^5\text{-}C_5Me_5)]$ (**1**)[70] and $[Os(=BNHC_9H_6N)Cl(I)(CO)(PPh_3)_2]$ (**7**)[52] display much more shielded ^{11}B NMR resonances − at δ = −35.3 and 51.7 ppm, respectively − with the former being characteristic for apical boron atoms in such *nido*-carboranes.

Crystal structure data are available for the following terminal borylene complexes: $[(OC)_4Fe{-}B(\eta^5\text{-}C_5Me_5)]$ (**1**),[38] $[(OC)_5W{=}B{=}N(SiMe_3)_2]$ (**2**),[39] $[(OC)_5Cr{=}B{=}N(SiMe_3)_2]$

Table 1. Metal−boron distances and ^{11}B NMR shifts

Compound	Synthesis	*d*(M−B) [pm]	$\delta^{11}B$ [ppm]	Ref.
$[(OC)_4Fe{-}B(\eta^5\text{-}C_5Me_5)]$ (**1**)	a[a]	201.0(3)	−35.3	[38]
$[(OC)_5W{=}B{=}N(SiMe_3)_2]$ (**2**)	a	215.1(7)	86.6	[39]
$[(OC)_4Fe{=}B{=}N(SiMe_3)_2]$ (**3**)	a	X	88.2	[39]
$[(OC)_5Cr{=}B{=}N(SiMe_3)_2]$ (**4**)	a, c	199.6(6)	92.3	[39][40]
$[(OC)_5Cr{=}B{-}Si(SiMe_3)_3]$ (**5**)	a	187.8(10)	204.3	[51]
$[Os(=BNHC_9H_6N)Cl_2(CO)(PPh_3)_2]$ (**6**)	c	X	y	[52]
$[Os(=BNHC_9H_6N)Cl(I)(CO)(PPh_3)_2]$ (**7**)	c	205.5(8)	51.7	[52]
$[(\eta^5\text{-}C_5H_5)(OC)_3V{=}B{=}N(SiMe_3)_2]$ (**8**)	c	197.1(8)	98.3	[63]
$[(OC)_5W{=}B{=}N(SiH_3)_2\}]$ (**9**)	−	215.2*	y	[29][30]
$[(OC)_4Fe{-}B(\eta^5\text{-}C_5H_5)]$ (**10**)	−	196.2*	y	[29][30]
$[\mu\text{-}B(NMe_2)\{(\eta^5\text{-}(C_5H_5)Mn(CO)_2\}_2]$ (**12**)	b	203(1)	103.0	[90][91]
$[\mu\text{-}B(NMe_2)\{(\eta^5\text{-}(C_5H_5)Mn(CO)_2\}_2]$ (**12**)	−	204.9*	y	[26]
$[\mu\text{-}B(NMe_2)\{(\eta^5\text{-}(C_5H_4Me)Mn(CO)_2\}_2]$ (**13**)	b	X	102.8	[90][91]
$[\mu\text{-}BtBu\{(\eta^5\text{-}(C_5H_4Me)Mn(CO)_2\}_2]$ (**14**)	b	X	170.0	[90][91]
$[\mu\text{-}B\{N(C_4H_8)\}\{(\eta^5\text{-}(C_5H_4Me)Mn(CO)_2\}_2]$ (**15**)	b	X	100.3	[88]
$[\mu\text{-}B\{N(C_5H_{10})\}\{(\eta^5\text{-}(C_5H_4Me)Mn(CO)_2\}_2]$ (**16**)	b	X	101.1	[88]
$[\mu\text{-}BH(PMe_3)(\mu\text{-}CO)\{Co(CO)_3\}_2]$ (**17**)	b	211.2(9), 210.8(11)	17.5	[92]
$[\mu\text{-}B\{N(SiMe_3)_2\}(\mu\text{-}CO)\{(\eta^5\text{-}C_5H_5)Fe(CO)\}_2]$ (**18**)	a	X	118.4	[93]
$[\mu\text{-}B\{N(SiMe_3)_2\}(\mu\text{-}CO)\{(\eta^5\text{-}C_5H_4Me)Fe(CO)\}_2]$ (**19**)	a	200.7(3), 200.2(3)	119.1	[93]
$[\mu\text{-}B\{N(SiMe_3)_2\}(\mu\text{-}CO)\{(\eta^5\text{-}C_5H_5)Ru(CO)\}_2]$ (**20**)	a	X	105.9	[94]
$[\mu\text{-}B\{N(SiMe_3)_2\}\{(\eta^5\text{-}C_5H_5)Re(CO)_2\}$ (**21**)	c	X	100.4	[40]
$[\mu\text{-}BCl\{(C_5H_4Me)Mn(CO)_2\}_2]$ (**22**)	c	203.9(11), 197.6(9)	133.5	[103]
$[\mu\text{-}B(NHtBu)\{(\eta^5\text{-}C_5H_4Me)Mn(CO)_2\}_2]$ (**23**)	c	X	102.4	[102]
$[\mu\text{-}B(NHPh)\{(\eta^5\text{-}C_5H_4Me)Mn(CO)_2\}_2]$ (**24**)	c	X	107.6	[102]
$[\mu\text{-}B(OMe)\{(\eta^5\text{-}C_5H_4Me)Mn(CO)_2\}_2]$ (**25**)	c	X	98.8	[102]
$[\mu\text{-}B(OEt)\{(\eta^5\text{-}C_5H_4Me)Mn(CO)_2\}_2]$ (**26**)	c	198.8(2), 202.1(2)	97.6	[102]
$[\mu\text{-}B(OiPr)\{(\eta^5\text{-}C_5H_4Me)Mn(CO)_2\}_2]$ (**27**)	c	X	96.5	[44]
$[\mu\text{-}B(OH)\{(\eta^5\text{-}C_5H_4Me)Mn(CO)_2\}_2]$ (**28**)	c	X	101.6	[102]

[a] a: From monoboranes; b: from diboranes(4); c: other method; X: no X-ray data available; y: no ^{11}B NMR spectroscopic data available; * geometry from ab initio calculation.

(**4**),[40] $[(OC)_5Cr{=}B{-}Si(SiMe_3)_3]$ (**5**),[51] $[Os(=BNHC_9H_6N)Cl(I)(CO)(PPh_3)_2]$ (**7**),[52] and $[(\eta^5\text{-}C_5H_5)(OC)_3V{=}B{=}N(SiMe_3)_2]$ (**8**)[63] (Table 1). The metal−boron distances in the aminoborylene complexes **2**, **4**, and **8** range from 197.1 to 215.1 pm, which, together with further spectroscopic and structural data, suggests strong boron-to-metal σ-donation and weaker metal-to-boron π-backbonding. For aminoborylene complexes of first row transition metal complexes this situation was predicted on the basis of ab initio calculations.[26] For **1**, which features a six-coordinate borylene ligand in an axial position, an iron−boron distance of 201.0 pm was reported, indicating a corresponding single bond. The base-stabilised borylene complex **7** is characterised by an osmium−boron distance of 205.5 pm, and so is longer than expected for a double bond. Corresponding findings have been made for related base-stabilised silylene complexes.[71−73]

The decisive influence of the boron-bound ligand R on the metal−boron linkage in terminal borylene complexes $[L_xM{=}B{-}R]$ has already to some extent been demonstrated by the mentioned differences in the ^{11}B NMR shifts. In the solid state, this influence becomes even more evident if one compares the results of the X-ray structure analyses of $[(OC)_5Cr{=}B{=}N(SiMe_3)_2]$ (**4**)[40] and $[(OC)_5Cr{=}B{-}Si(SiMe_3)_3]$ (**5**)[51] (Figure 4).

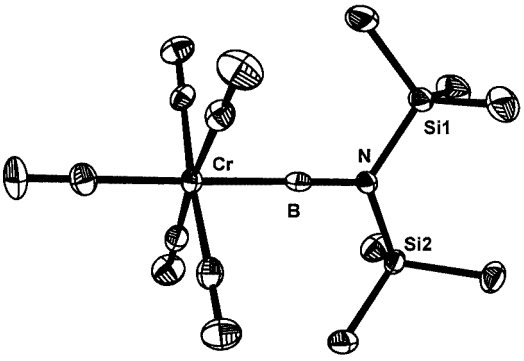

4

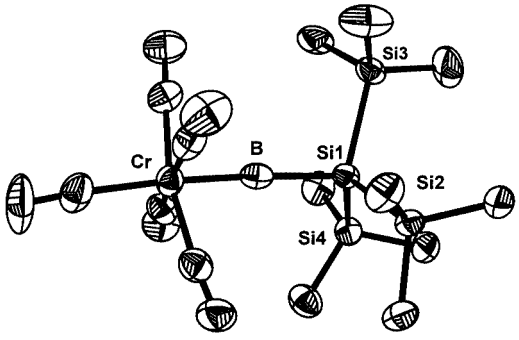

5

Figure 4. Structures of **4** and **5** in the crystal

The $Cr(CO)_4$ moieties in both molecules exhibit approximate C_{4v} symmetry, and the central Cr−B−E fragment (E = N, Si) adopts a linear arrangement. The Cr−B distance in **5** was found to be 187.8 pm, and thus 12 pm shorter than in the amino counterpart **4**. Obviously, the electron deficiency of the boron centre in the silylborylene complex demands enhanced Cr−B π-backbonding. Further evidence for increased backbonding in **5** stems from the umbrella effect detected for the equatorial CO ligands and the pronounced *trans* effect the $B{-}Si(SiMe_3)_3$ ligand has on the axial CO ligand.[51] Unlike in the previously mentioned methyleneboranes $(Me_3Si)_2C{=}B{-}R$, there is no spectroscopic, structural, or computational evidence for the presence of nonclassical B−Si−Si three-centre, two-electron bonds (hyperconjugation) − well known to relieve electron deficiency at such coordinatively and electronically unsaturated boron centres − in the case of **5**.[46−50]

The question of the nature of the metal−boron bond in terminal borlyene complexes has been addressed in many theoretical studies in the recent past,[26−32] and the selected examples $[(OC)_5W{=}B{=}N(SiH_3)_2\}]$ (**9**) and $[(OC)_4Fe{-}B(\eta^5\text{-}C_5H_5)]$ (**10**) in particular have been investigated as model compounds for complexes **1** and **2**. It was concluded that borylene ligands BR in general have both good σ-donor and π-acceptor properties, but because of the electrophilicity of the boron centre, terminal borylene complexes should only be stable with sterically protecting and electron-releasing substituents such as $N(SiMe_3)_2$ or $\eta^5\text{-}C_5Me_5$ on the boron atom.[26] The nature of the transition metal−boron bond in $[L_xM{=}B{-}R]$ is obviously strongly influenced by the boron-bonded ligand R. Descriptions based on calculations range from an almost purely RB→TM σ-bonded model (TM = transition metal), for R being a good π-donor, up to a strong TM→BR π-back-donation model when R is a weaker π-donor.[28−30] Recent studies, however, have made the point that the sum of the covalent interactions does not even give a bond order of 1, but the nature of the TM−BR bond is mainly ionic.[29−31]

2.3. Reactivity

In addition to the photochemically induced borylene transfer discussed in Sect. 2.2, knowledge about the reactivity of terminal borylene complexes is restricted to only one recent report by Roper.[52] The base-stabilised borylene complex $[Os(=BNHC_9H_6N)Cl_2(CO)(PPh_3)_2]$ (**6**) undergoes a reaction with ethanol to yield the amino(ethoxy)boryl complex $[Os\{B(OEt)NHC_9H_6N\}Cl(CO)(PPh_3)_2]$ (**11**) as shown in Equation (5), with a 1,2-shift of the quinoline nitrogen atom from the boron to the osmium centre. This alcoholysis of **6** indicated that even the boron atom in base-stabilised borylene complexes displays some electrophilic

character − a fact already predicted by a theoretical study.[26]

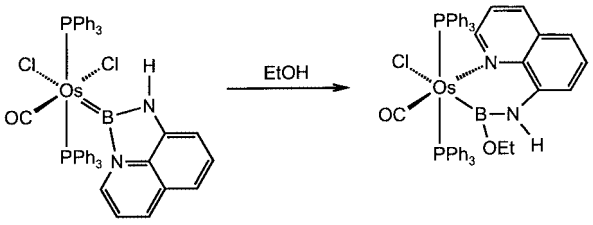

6 11 (5)

3. Bridged Borylene Complexes

Although bridged borylene complexes [μ-BR(ML_x)$_2$] (**III**) and corresponding base adducts [{μ-BR(L)}(ML_x)$_2$] (**IIIa**) are still rare, they have been known for slightly longer than their terminal counterparts, and their chemistry, briefly summarised in 2000,[24] has developed to a somewhat greater extent. There is now some knowledge about their reactivity, and three different methods for their synthesis have been developed.

3.1. Synthesis

3.1.1. From Diboranes(4)

From 1994 onwards, Hartwig, Marder, Norman, and others have been reporting that certain diboranes(4) of the general formula X_2B-BX_2 (X = OR, F) may undergo oxidative additions to suitable transition metal centres, with cleavage of the boron−boron bond and formation of mono-, bis-, or trisboryl complexes [$L_xM(BX_2)_n$] (n = 1−3).[74−85] Subsequently, we have been able to show that salt elimination reactions between 1,2-dihalodiboranes(4) and anionic transition metal complexes proceed without cleavage of the diborane and hence can provide access to novel complexes of the type [L_xM{B(R)−B(R)X}] (X = Cl, Br, I), featuring η^1-coordinated diborane(4)yl ligands.[35,37][86−89] Our attempts to achieve an η^2- or side-on coordination mode for the diborane(4) moiety as in Equation (6a), by treatment of $ClB(NMe_2)-B(NMe_2)Cl$ with K[η^5-(C_5H_4R)Mn($CO)_2$(Si$MePh_2$)] as a synthetic equivalent for a dianionic transition metal complex,[53] resulted in the unexpected formation [Equation (6b)] of the first borylene complexes [μ-B(NMe_2){η^5-(C_5H_4R)Mn($CO)_2$}$_2$] (**12**: R = H; **13**: R = Me).[90] The dinuclear borylene complexes **12** and **13** are the products of a nonstoichiometric and obviously complex reaction, accompanied by cleavage of the boron−boron bond and the formation of a corresponding diborane(6) derivative ($Me_2N-BH_2)_2$ − the origin of the hydrogen atoms and the fate of the metal-bound silyl group, however, remained unclear.[90] A significant improvement in this synthesis was achieved by employing the related hydride complex K[(η^5-(C_5H_4R)Mn$H(CO)_2$] as a precursor, giving the complexes **12** and **13** in higher yields as products of a stoichiometric reaction, as shown in Equation (7). In this case, a hydrogen transfer from the manganese to the boron centre occurred and resulted in the formation of ($Me_2N-BH_2)_2$. Our further studies have shown that the cleavage of the boron−boron bond in the starting diboranes(4) decisively contributes to the formation of the bridged borylene complexes, since no products with B−Mn bonds were formed from related monoboranes $RBCl_2$.[91] In addition to complexes **12** and **13** we were able to obtain further bridged borylene complexes of the type [μ-BR{η^5-(C_5H_4Me)Mn($CO)_2$}$_2$] {**14**: R = *t*Bu; **15**: R = N(C_4H_8); **16**: N(C_5H_{10})}[88,90,91] by treatment of K[η^5-(C_5H_4Me)MnR-($CO)_2$] (R = H, Si$MePh_2$) with corresponding diboranes(4).

In 1998 Shimoi succeeded in another approach to bridged borylene complexes.[92] By starting from [$Co_2(CO)_8$] and B_2H_4·2PMe_3 it was possible to produce the cobalt borylene complex [μ-BH(PMe_3)(μ-CO){$Co(CO)_3$}$_2$] (**17**) in a cleavage reaction similar to that of a diborane(4). Fragmentation of the 1,2-bis(trimethylphosphane)diborane(4) into BH_3·PMe_3 and BH·PMe_3 and the liberation of one CO group afforded **17** [Equation (8)], which represents the only example of a donor-stabilised bridged borylene complex.

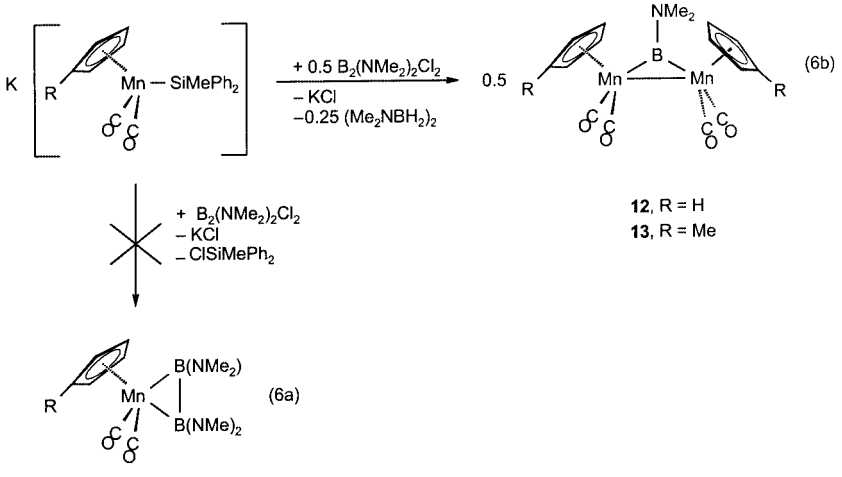

(6)

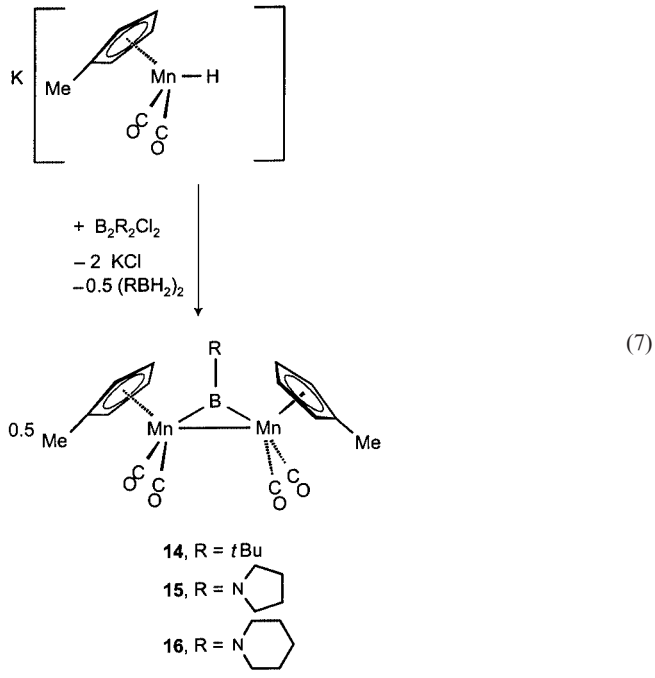

(7)

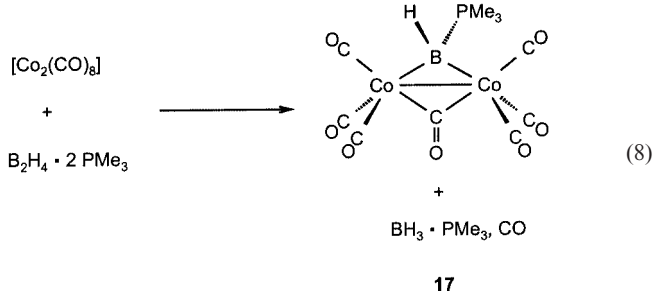

(8)

3.1.2. From Monoboranes

The previously mentioned syntheses of dinuclear borylene complexes are very specific, and are restricted to the two systems discussed. In order to provide a more general route to bridged borylene complexes, we investigated reactions between aminodihaloboranes and anionic transitionmetal compounds in a 1:2 ratio. The bridged borylene complexes $[\mu\text{-}B\{N(SiMe_3)_2\}(\mu\text{-}CO)\{(\eta^5\text{-}C_5H_4R)Fe(CO)\}_2]$ (**18**: R = H; **19**: R = Me)[93] and $[\mu\text{-}B\{N(SiMe_3)_2\}(\mu\text{-}CO)\{(\eta^5\text{-}C_5H_5)Ru(CO)\}_2]$ (**20**)[94] were obtained from $(Me_3Si)_2NBCl_2$ and $Na[(\eta^5\text{-}C_5H_4R)M(CO)_2]$ (M = Fe, R = H, Me; M = Ru, R = H) as shown in Equation (9), with salt elimination and cleavage of one carbonyl ligand.

The formation of the boryleneiron complexes **18** and **19** was observed under all conditions, while the formation of the corresponding ruthenium complex **20** depended on the reaction conditions and stoichiometry employed. Only an excess of $Na[(\eta^5\text{-}C_5H_5)Ru(CO)_2]$ and slow addition of the borane, for example, provided **20** as the sole product. Interestingly, sterically less demanding aminodichloroboranes such as Me_2NBCl_2 reacted in both cases with substitution of only one boron-bonded chloride ion and formation of

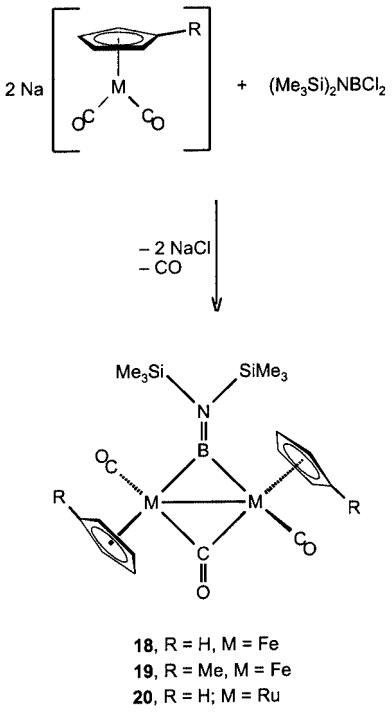

(9)

the corresponding boryl complexes. This result was attributed to the electron-withdrawing effect of the silyl groups, which in the case of $(Me_3Si)_2NBCl_2$ make the boron centre more electrophilic and hence more reactive.[93,94]

3.1.3. By Borylene Transfer

Photochemically induced borylene transfer has already been discussed as a valuable synthetic method for the generation of terminal borylene complexes not accessible through conventional salt elimination reactions. At least in one case, we have recently been able to demonstrate that this method also has similar potential for the synthesis of bridged borylene complexes. While $K[(\eta^5\text{-}C_5H_5)MnR(CO)_2]$ (R = H, $SiMePh_2$) proved to be a versatile precursor for the generation of bridged borylene complexes (vide supra), all of our attempts to extend this to the rhenium analogues by treatment of $K[(\eta^5\text{-}C_5H_5)ReR(CO)_2]$ (R = H, $SiMePh_2$) with mono- or diboranes(4) disappointingly failed.[43–45] Photolysis of $[(OC)_5W{=}B{=}N(SiMe_3)_2]$ (**2**) in the presence of $[(\eta^5\text{-}C_5H_5)Re(CO)_3]$, however, yielded the bridged borylene complex $[\mu\text{-}B\{N(SiMe_3)_2\}\{(\eta^5\text{-}C_5H_5)Re(CO)_2\}$ (**21**) as the only boron-containing species, as in Equation (10).[40]

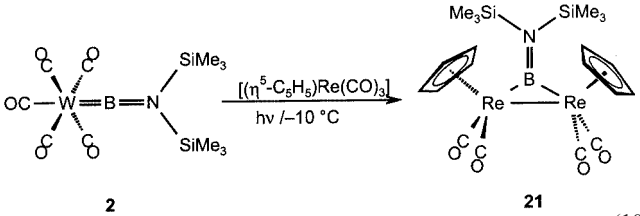

(10)

3.2. Structure

Because of the formation of two metal−boron bonds, all bridged borylene complexes show characteristically deshielded ^{11}B NMR resonances, ranging from δ = 100 to 120 ppm in the cases of the (amino)borylene complexes **12**, **13**, **15**, **16**, and **18**−**21**, in which B−N π-bonding components are present, (Table 1). For the (*tert*-butyl)borylene complex **14**, which is free of boron−ligand π-interaction, an even more deshielded signal is observed at δ = 170.0 ppm. As in the case of terminal borylene complexes, the base-stabilised complex [μ-BH(PMe$_3$)(μ-CO){Co(CO)$_3$}$_2$] (**17**) is characterised by a significantly shielded ^{11}B NMR resonance at δ = 17.5 ppm, due to the increased coordination number of the boron centre.

X-ray structural data are available for [μ-B(NMe$_2$){(η^5-C$_5$H$_5$)Mn(CO)$_2$}$_2$] (**12**), [μ-BH(PMe$_3$)(μ-CO){Co(CO)$_3$}$_2$] (**17**), [μ-B{N(SiMe$_3$)$_2$}(μ-CO){(η^5-C$_5$H$_4$Me)Fe(CO)}$_2$] (**19**), and two further derivatives of the type [μ-BX{(η^5-C$_5$H$_4$Me)Mn(CO)$_2$}$_2$] (vide infra). The metal and boron atoms in both aminoborylene complexes form isosceles triangles, with metal−metal and metal−boron distances in the range expected for corresponding single bonds (Table 1). The overall molecular structure data resemble those of the isoelectronic vinylidene[95,96] or the corresponding bridged methylene complexes,[97−99] which can be viewed as dimetallacyclopropane derivatives. The tetrahedrally coordinated boron centre in the base-stabilised complex **17** shows the expected increase in the metal−boron distances, which thus range between those in borylcobalt complexes[76,100] and those in cobaltaboranes.[101]

Recently, complex **12** was subject to theoretical investigations, and the theoretically predicted and the experimentally derived structural parameters were found to be in very good agreement (Table 1).[26] From density functional theoretical studies it was found that borylenes BX can be viable ligands in the design of transition metal complexes, which are thermodynamically stable with respect to a homolytic metal−boron bond dissociation. On the one hand, the high thermodynamic stability is traceable to the good σ-donor and π-acceptor properties of BX ligands, owing to the σ- and π-orbital energies. On the other hand, the high polarity and the small HOMO−LUMO gap of the uncoordinated BX ligand suggest low kinetic stability. Increasing the HOMO−LUMO gap by complexation also increases the kinetic stability to a certain extent, but the imbalance between σ-donation and π-acceptance produces a positive charge on BX and promotes nucleophilic attack. In complex **12**, the kinetic stability is enhanced by steric protection of the reactive frontier orbitals of the BNMe$_2$ ligand by complexation at a bridging site and additionally by the bulky methyl substituents. The dinuclear Mn$_2$(η^5-C$_5$H$_5$)$_2$(CO)$_4$ fragment also reduces the build-up of positive charge at BNMe$_2$, since it is an excellent π-donor with just the right frontier orbitals to restore the M−BNMe$_2$ σ-donation and π-back-donation balance.

3.3. Reactivity

In agreement with the previously mentioned computational studies, we found that the (amino)borylene complexes **12** and **13** displayed extremely low reactivity towards nucleophilic substitution at the bridging boron centre. Stability to both air and moisture is the consequence, and these compounds can even be obtained in high yields by aqueous workup.[69] Treatment of **13** with an excess of gaseous HCl, however, provided the (chloro)borylene complex [μ-BCl{(C$_5$H$_4$Me)Mn(CO)$_2$}$_2$] (**22**), which, because of its

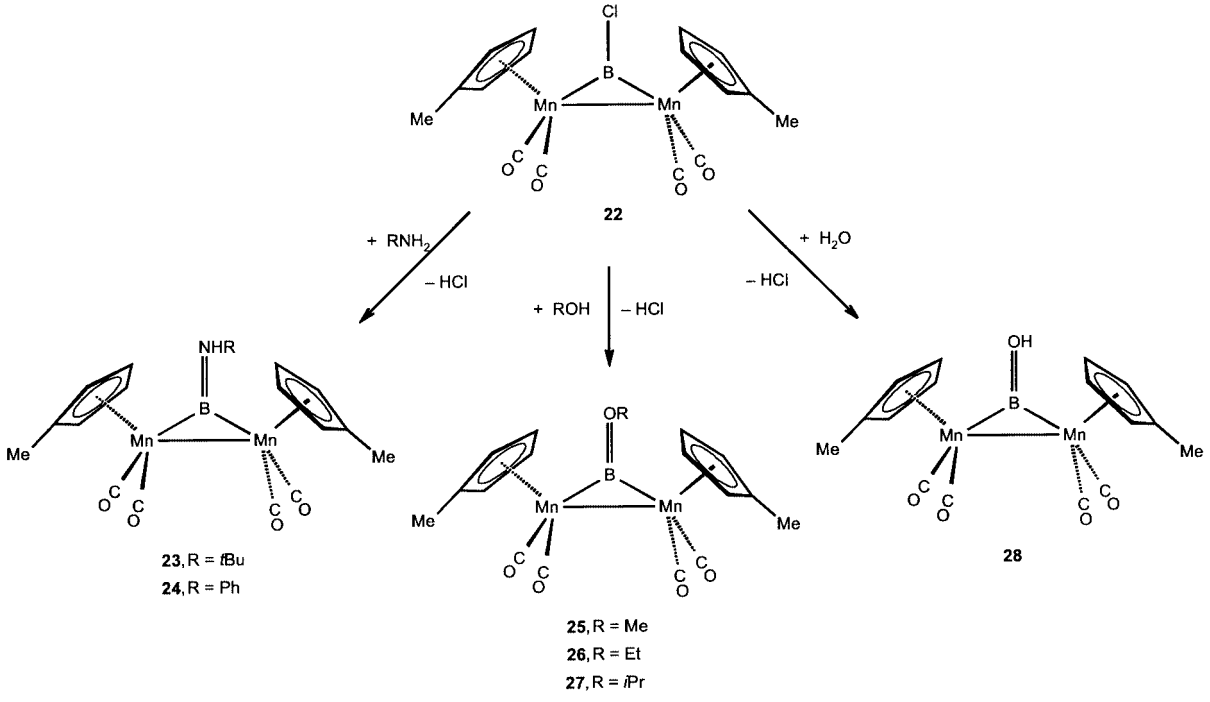

Figure 5. Substitution reactions at the metal-coordinated boryelene ligand

increased reactivity, served as starting material for further substitution reactions at the borylene centre. Treatment with protic reagents such as primary amines, alcohols and water afforded the corresponding substituted borylene complexes [μ-BX{$(C_5H_4Me)Mn(CO)_2$}$_2$] (**23**: X = NH*t*Bu; **24**: X = NHPh; **25**: X = OMe; **26**: X = OEt; **27**: X = O*i*Pr; **28**: X = OH) in high yields (Figure 5).[44,102] Structural data are available for complexes **22**[103] and **26**[44] (Table 1), and match those of the corresponding amino derivative **12**. It should be noted that such reactions at the boron centre with retention of the M−B linkage are very rare for both boryl and borylene complexes, due to the kinetic lability of the metal−boron bond, and have subsequently been observed (by Roper) only in the case of one boryl complex.[104]

Our very recent studies have shown that the photochemistry of bridged borylene complexes differs significantly from that of their terminal counterparts. Irradiation of the bridged (chloro)borylene complex **22** in the presence of $[M(CO)_6]$ (M = Cr, Mo, W) resulted not in the formation of an M=B−Cl species with borylene transfer, but in the novel dimetalla-*nido*-tetraborane [B_2Cl_2{$(\eta^5$-$C_5H_4CH_3)Mn(CO)_2$}$_2$] (**29**) as shown in Equation (11), thus establishing the first synthetic link between electron-precise borylene complexes and electron-deficient metallaboranes.[103]

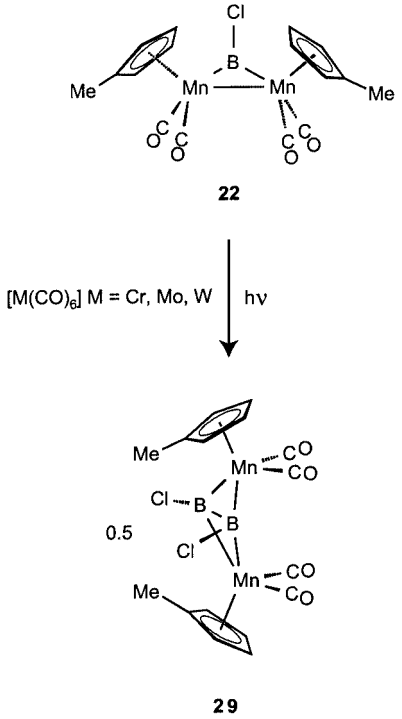

(11)

Conclusion

Since the first report on a structurally authenticated borylene complex in 1995, the chemistry of these compounds has developed considerably, due to the ambitious experimental and computational effort of several research groups worldwide. As a consequence, there is now a more detailed understanding of the bonding situation in borylene complexes, and some of the reasons why these compounds eluded researchers for such a long time have probably become clearer. Several methods for the preparation of both bridged and terminal species are now at hand, and so future studies can focus now more on the reactivity of theses complexes − the chemistry of terminal borylene complexes especially is as yet virtually unexplored. In view of their close relationship to important organometallics such as carbene or carbonyl complexes, one might even envisage similar applications in stoichiometric or catalytic reactions.

[1] G. Schmid, *Angew. Chem.* **1970**, *82*, 920−930; *Angew. Chem. Int. Ed. Engl.* **1970**, *9*, 819−828.
[2] J. R. Knorr, J. S. Merola, *Organometallics* **1990**, *9*, 3008−3010.
[3] R. T. Baker, D. W. Ovenall, J. C. Calabrese, S. A. Westcott, N. J. Taylor, I. D. Williams, T. B. Marder, *J. Am. Chem. Soc.* **1990**, *112*, 9399−9400.
[4] B. Post, in: *Rare Earth Research II* (Ed.: K. S. Korres), Gordon and Breach, New York, **1964**, pp. 107−116.
[5] R. Thompson, in: *Progress in Boron Chemistry* (Eds.: R. J. Brotherton, H. Steinberg), Pergamon, Oxford, **1970**, pp. 173−230.
[6] T. Lundström, in: *Encyclopedia of Inorganic Chemistry*, vol. 1 (Ed.: R. B. King), Wiley, New York, **1994**, pp. 328−338.
[7] C. E. Housecroft, T. P. Fehlner, in: *Advances in Organometallic Chemistry*, vol. 21 (Eds.: F. G. A. Stone, R. West), Academic Press, New York, **1981**, pp. 57−112.
[8] C. E. Housecroft, *Boranes and Metalloboranes*, Wiley, New York, **1990**.
[9] T. P. Fehlner, in: *Electron Deficient Boron and Carbon Clusters* (Eds.: G. A. Olah, K. Wade, R. E. Williams), Wiley, New York, **1991**, pp. 287−307.
[10] G. E. Herberich, in: *Comprehensive Organometallic Chemistry*, vol. 1 (Eds.: G. Wilkinson, F. G. A. Stone, E. W. Abel), Pergamon, Oxford, **1982**, pp. 381−410.
[11] G. E. Herberich, B. Buller, B. Hessner, W. Oschmann, *J. Organomet. Chem.* **1980**, *195*, 253−259.
[12] G. E. Herberich, B. Hessner, R. Saive, *J. Organomet. Chem.* **1987**, *319*, 9−27.
[13] W. Siebert, *Angew. Chem.* **1985**, *97*, 924−939; *Angew. Chem. Int. Ed. Engl.* **1985**, *24*, 943−958.
[14] A. J. Ashe, III, E. Meyers, P. Shu, T. von Lehmann, J. Bastide, *J. Am. Chem. Soc.* **1975**, *97*, 6865−6866.
[15] G. E. Herberich, C. Engelke, W. Pahlmann, *Chem. Ber.* **1979**, *112*, 607−624.
[16] H. Werner, R. Prinz, E. Deckelmann, *Chem. Ber.* **1969**, *102*, 95−103.
[17] K. Delpy, D. Schmitz, P. Paetzold, *Chem. Ber.* **1983**, *116*, 2994−2999.
[18] H. Braunschweig, *Angew. Chem.* **1998**, *110*, 1882−1898, *Angew. Chem. Int. Ed.* **1998**, *37*, 1786−1801.
[19] G. I. Irvine, M. J. G. Lesley, T. B. Marder, N. C. Norman, C. R. Rice, E. G. Robins, W. R. Roper, G. R. Whittell, L. J. Wright, *Chem. Rev.* **1998**, *98*, 2685−2722.
[20] M. R. Smith, III, in: *Progress in Inorganic Chemistry*, vol. 48 (Ed.: K. D. Karlin), Wiley, New York, **1999**, pp. 505−567.
[21] H. Braunschweig, M. Colling, *Coord. Chem. Rev.* **2001**, *223*, 1−51.
[22] R. A. Fischer, J. Weiß, *Angew. Chem.* **1999**, *111*, 3002−3022; *Angew. Chem. Int. Ed.* **1999**, *38*, 2830−2850.
[23] B. Wrackmeyer, *Angew. Chem.* **1999**, *111*, 817−819; *Angew. Chem. Int. Ed.* **1999**, *38*, 771−773.
[24] H. Braunschweig, M. Colling, *J. Organomet. Chem.* **2000**, *614*, 18−26.

[25] H. Braunschweig, in: *Inorganic Chemical Highlights* (Eds.: G. Meyer, D. Naumann, L. Wesemann), Wiley-VCH, Weinheim, New York, **2001**, pp. 213−218.
[26] W. Ehlers, E. J. Baerends, F. M. Bickelhaupt, U. Radius, *Chem. Eur. J.* **1998**, *4*, 210−221.
[27] U. Radius, F. M. Bickelhaupt, A. W. Ehlers, N. Goldberg, R. Hoffmann, *Inorg. Chem.* **1998**, *37*, 1080−1090.
[28] C. L. B. Macdonald, A. H. Cowley, *J. Am. Chem. Soc.* **1999**, *121*, 12113−12126.
[29] J. Uddin, C. Boehme, G. Frenking, *Organometallics* **2000**, *19*, 571−582.
[30] C. Boehme, J. Uddin, G. Frenking, *Coord. Chem. Rev.* **2000**, *197*, 249−276.
[31] J. Uddin, G. Frenking, *J. Am. Chem. Soc.* **2001**, *123*, 1683−1693.
[32] Y. Chen, G. Frenking, *J. Chem. Soc., Dalton Trans.* **2001**, 434−441.
[33] D. A. Robertus, G. L. Geoffrey, in: *Comprehensive Organometallic Chemistry*, vol. 2 (Eds.: G. Wilkinson, F. G. A. Stone, E. W. Abel) Pergamon, Oxford, **1982**, pp. 763−879.
[34] R. B. King, *Acc. Chem. Res.* **1970**, *3*, 417−427.
[35] H. Braunschweig, M. Koster, K. W. Klinkhammer, *Angew. Chem.* **1999**, *111*, 2368−2370, *Angew. Chem. Int. Ed.* **1999**, *38*, 2229−2231.
[36] H. Braunschweig, C. Kollann, M. Koster, U. Englert, M. Müller, *Eur. J. Inorg. Chem.* **1999**, 2277−2281.
[37] H. Braunschweig, K. W. Klinkhammer, M. Koster, K. Radacki, *Eur. J. Inorg. Chem.*, in preparation.
[38] A. H. Cowley, V. Lomelí, A. Voigt, *J. Am. Chem. Soc.* **1998**, *120*, 6401−6402.
[39] H. Braunschweig, C. Kollann, U. Englert, *Angew. Chem.* **1998**, *110*, 3355−3357; *Angew. Chem. Int. Ed.* **1998**, *37*, 3179−3180.
[40] H. Braunschweig, M. Colling, C. Kollann, H.-G. Stammler, *Angew. Chem.* **2001**, *113*, 2298−2300; *Angew. Chem. Int. Ed.* **2001**, *38*, 2229−2231.
[41] H. Braunschweig, C. Kollann, U. Englert, *Eur. J. Inorg. Chem.* **1998**, 465−468.
[42] H. Braunschweig, C. Kollann, K. W. Klinkhammer, *Eur. J. Inorg. Chem.* **1999**, 1523−1529.
[43] C. Kollann, Dissertation, RWTH Aachen, Germany, **1999**.
[44] M. Colling, Dissertation, RWTH Aachen, Germany, **2002**.
[45] H. Braunschweig, unpublished results.
[46] R. Boese, P. Paetzold, A. Tapper, *Chem. Ber.* **1987**, *120*, 1069−1073.
[47] R. Boese, P. Paetzold, A. Tapper, R. Ziembinski, *Chem. Ber.* **1989**, *122*, 1057−1060.
[48] M. Pilz, M. Stadler, R. Hunold, J. Allwohn, W. Massa, A. Berndt, *Angew. Chem.* **1989**, *101*, 761−763; *Angew. Chem. Int. Ed. Engl.* **1989**, *28*, 784−786.
[49] M. Pilz, H. Michel, A. Berndt, *Angew. Chem.* **1990**, *102*, 438; *Angew. Chem. Int. Ed. Engl.* **1990**, *29*, 401.
[50] For a review on methyleneboranes see: A. Berndt, *Angew. Chem.* **1993**, *105*, 921−933; *Angew. Chem. Int. Ed. Engl.* **1993**, *32*, 985−997.
[51] H. Braunschweig, M. Colling, C. Kollann, K. Merz, K. Radacki, *Angew. Chem.* **2001**, *113*, 4327−4329; *Angew. Chem. Int. Ed.* **2001**, *38*, 4198−4200.
[52] G. J. Irvine, C. E. F. Rickard, W. R. Roper, A. Williamson, L. J. Wright, *Angew. Chem.* **2000**, *112*, 978−980; *Angew. Chem. Int. Ed.* **2000**, *39*, 948−950.
[53] U. Schubert, U. Kirchgässner, J. Grönen, H. Piana, *Polyhedron* **1989**, *8*, 1589−1593 and references therein.
[54] E. Colomer, R. P. Corriu, C. Marzin, A. Vioux, *Inorg. Chem.* **1982**, *21*, 368−373.
[55] P. L. Timms, *J. Am. Chem. Soc.* **1967**, *89*, 1629−1631.
[56] P. L. Timms, *Acc. Chem. Res.* **1973**, *6*, 118−123 and references therein.
[57] B. Pachaly, R. West, *Angew. Chem.* **1984**, *96*, 444−445; *Angew. Chem. Int. Ed. Engl.* **1984**, *23*, 454−455.
[58] S. M. van der Kerk, P. H. M. Budzelaar, A. L. M. van Beijnen, G. J. M. van der Kerk, *Polyhedron* **1984**, *3*, 271−280.
[59] A. Meller, *Pure. Appl. Chem.* **1991**, *63*, 395−398 and references therein.
[60] B. G. Ramsey, D. M. Anjo, *J. Am. Chem. Soc.* **1977**, *99*, 3182−3183.
[61] R. Schlögl, B. Wrackmeyer, *Polyhedron* **1985**, *4*, 885−892.
[62] H. Braunschweig, M. Colling, C. Kollann, H.-G. Stammler, *Angew. Chem.* **2001**, *113*, 2298−2300; *Angew. Chem. Int. Ed.* **2001**, *38*, 2229−2231.
[63] H. Braunschweig, M. Colling, *Angew. Chem.*, in press.
[64] H. Braunschweig, M. Colling, C. Kollann, U. Englert, *J. Chem. Soc., Dalton Trans.*, in press.
[65] A. K. Bandyopadhyay, R. Khattar, J. Puga, T. P. Fehlner, A. L. Rheingold, *Inorg. Chem.* **1992**, *31*, 465−472.
[66] C. E. Housecroft, *Coord. Chem. Rev.* **1995**, *143*, 297−330.
[67] H. Braunschweig, T. Wagner, *Angew. Chem.* **1995**, *107*, 904−906; *Angew. Chem. Int. Ed. Engl.* **1995**, *34*, 825−826.
[68] H. Braunschweig, B. Ganter, *J. Organomet. Chem.* **1997**, *545*, 163−167.
[69] H. Braunschweig, M. Koster, *J. Organomet. Chem.* **1999**, *588*, 231−234.
[70] A. H. Cowley, V. Lomelí, A. Voigt, *J. Am. Chem. Soc.* **1998**, *120*, 6401−6402.
[71] K. Ueno, H. Tobita, M. Shimoi, H. Ogino, *J. Am. Chem. Soc.* **1988**, *110*, 4092−4093.
[72] C. Zybill, H. Handwerker, H. Friedrich, in: *Advances in Organometallic Chemistry*, vol. 36 (Eds.: F. G. A. Stone, R. West), Acadamic Press, New York, **1994**, pp. 229−282.
[73] P. D. Lickiss, *Chem. Soc. Rev.* **1992**, *21*, 271−279.
[74] J. F. Hartwig, X. He, *Angew. Chem.* **1996**, *108*, 352−354; *Angew. Chem. Int. Ed. Engl.* **1996**, *35*, 315−317.
[75] X. He, J. F. Hartwig, *Organometallics* **1996**, *15*, 400−407.
[76] C. Dai, G. Stringer, J. F. Corrigan, N. J. Taylor, T. B. Marder, N. C. Norman, *J. Organomet. Chem.* **1996**, *513*, 273−275.
[77] P. Nguyen, G. Lesley, N. J. Taylor, T. B. Marder, N. L. Pickett, W. Clegg, M. R. J. Elsegood, N. C. Norman, *Inorg. Chem.* **1994**, *33*, 4623−4624.
[78] T. B. Marder, N. C. Norman, C. R. Rice, E. G. Robins, *Chem. Commun.* **1997**, 53−54.
[79] W. Clegg, F. J. Lawlor, T. B. Marder, P. Nguyen, N. C. Norman, A. G. Orpen, M. J. Quayle, C. R. Rice, E. G. Robins, A. J. Scott, F. E. S. Souza, G. Stringer, G. R. Whittell, *J. Chem. Soc., Dalton Trans.* **1998**, 301−309.
[80] C. Dai, G. Stringer, T. B. Marder, A. J. Scott, W. Clegg, N. C. Norman, *Inorg. Chem.* **1997**, *36*, 272−273.
[81] C. Dai, G. Stringer, T. B. Marder, A. J. Scott, W. Clegg, N. C. Norman, *Can. J. Chem.* **1996**, *74*, 2026−2031.
[82] C. N. Iverson, M. R. Smith III, *J. Am. Chem. Soc.* **1995**, *117*, 4403−4404.
[83] G. Lesley, P. Nguyen, N. J. Taylor, T. B. Marder, A. J. Scott, W. Clegg, N. C. Norman, *Organometallics* **1996**, *15*, 5137−5154.
[84] W. Clegg, F. J. Lawlor, G. Lesley, T. B. Marder, N. C. Norman, A. G. Orpen, M. J. Quayle, C. R. Rice, A. J. Scott, F. E. S. Souza, *J. Organomet. Chem.* **1998**, *550*, 183−192.
[85] T. Ishiyama, N. Matsuda, M. Murata, F. Ozawa, A. Suzuki, N. Miyaura, *Organometallics* **1996**, *15*, 713−720.
[86] H. Braunschweig, B. Ganter, M. Koster, T. Wagner, *Chem. Ber.* **1996**, *129*, 1099−1101.
[87] H. Braunschweig, M. Koster, R. Wang, *Inorg. Chem.* **1999**, *38*, 415−416.
[88] H. Braunschweig, M. Koster, *J. Organomet. Chem.* **1999**, *588*, 231−234.
[89] H. Braunschweig, M. Koster, *Z. Naturforsch.*, in press.
[90] H. Braunschweig, T. Wagner, *Angew. Chem.* **1995**, *107*, 904−905, *Angew. Chem. Int. Ed. Engl.* **1995**, *34*, 825−826.
[91] H. Braunschweig, B. Ganter, *J. Organomet. Chem.* **1997**, *545*, 163−167.
[92] M. Shimoi, S. Ikubo, Y. Kawano, *J. Am. Chem. Soc.* **1998**, *120*, 4222−4223.
[93] H. Braunschweig, C. Kollann, U. Englert, *Eur. J. Inorg. Chem.* **1998**, 465−468.

[94] H. Braunschweig, C. Kollann, K. W. Klinkhammer, *Eur. J. Inorg. Chem.* **1999**, 1523−1529.
[95] K. Folting, J. C. Huffman, L. N. Lewis, K. G. Caulton, *Inorg. Chem.* **1979**, *18*, 3483−3486.
[96] M. Akita, S. Kato, M. Terada, Y. Masaki, M. Tanaka, Y. Moro-oka, *Organometallics* **1997**, *16*, 2392−2412.
[97] W. A. Herrmann, B. Reiter, H. Biersack, *J. Organomet. Chem.* **1975**, *97*, 245−251.
[98] M. Creswick, I. Bernal, W. A. Herrmann, *J. Organomet. Chem.* **1979**, *172*, C39−C42.
[99] W. A. Hermann, *Adv. Organomet. Chem.* **1982**, *20*, 159.
[100] D. J. Elliot, C. J. Levy, R. J. Puddephatt, D. G. Holah, A. N. Hughes, V. R. Magnuson, I. M. Moser, *Inorg. Chem.* **1990**, *29*, 5014−5015.
[101] K. J. Deck, T. P. Fehlner, A. L. Rheingold, *Inorg. Chem.* **1993**, *32*, 2794−2795.
[102] H. Braunschweig, M. Müller, *Chem. Ber./Recueil* **1997**, *130*, 1295−1298.
[103] H. Braunschweig, M. Colling, C. Hu, K. Radacki, *Angew. Chem.*, **2002**, *114*, 1359−1361; *Angew. Chem. Int. Ed.* **2002**, *39*, 1415−1417.
[104] G. R. Clark, G. J. Irvine, C. E. F. Rickard, W. R. Roper, A. Willimson, L. J. Wright, in: *Contemporary Boron Chemistry* (Eds.: M. Davidson, A. K. Hughes, T. B. Marder, K. Wade), MPG Books, Bodmin, **2000**, pp. 379−387.
[105] Note added during revision (August 15, 2002): Very recently Aldridge reported the synthesis and structure of the bridged borylene complex [μ-BMes{(η^5-C_5H_5)Fe$(CO)_2$}$_2$], obtained from $MesBBr_2$ by salt elimination (Mes = 2,4,6-Me_3-C_6H_2): S. Aldridge, D. L. Coombs, C. Jones, *Chem. Commun.* **2002**, 856−857.

Received May 1, 2002
[I02231]

3,6-Di(2-pyridyl)-1,4,2,5-dioxadiazine and a Silver Coordination Polymer with an Unprecedented Metallosupramolecular Topology

Chris Richardson[a] and Peter J. Steel*[a]

Keywords: Silver / Coordination polymers / Bridging ligands / N ligands

The new ligand 3,6-di(2-pyridyl)-1,4,2,5-dioxadiazine (**6**) has been prepared and reacted with silver tetrafluoroborate to form a novel coordination polymer in which adjacent chains are interdigitated and π-stacked.

(© Wiley-VCH Verlag GmbH & Co. KGaA, 69451 Weinheim, Germany, 2003)

Introduction

The use of bridging ligands for the controlled self-assembly of one-, two- or three-dimensional metallosupramolecular species has been the subject of enormous study in recent years.[1] Particularly stable entities can be obtained by employing ligands with chelating binding domains at the metal centres, with 2,2′-bipyridine subunits being the most commonly employed.[2] Similarly well studied are the binuclear ruthenium(II) complexes[3] of *N*,*N*′-chelating bridging ligands, such as 2,3-di(2-pyridyl)pyrazine (**1**),[4,5] 4,6-di(2-pyridyl)pyrimidine (**2**),[6] 2,5-di(2-pyridyl)pyrazine (**3**),[5] and 3,6-di(2-pyridyl)-1,2,4,5-tetrazine (**4**),[5,7] which have been the subject of detailed physicochemical studies of the fundamental nature of metal-metal interactions.

For some time now we have been involved in the synthesis of new heterocyclic ligands that incorporate less-commonly encountered heterocyclic ring systems as donors to metal acceptors. For example, we have reported a number of chelating ligands that contain tetrazole,[8] furoxan,[9] benzotriazole,[10] benzisoxazole,[11] 1,2,5-thiadiazole[12] and 1,2,3-chalcogenadiazole groups.[13] Most recently, we described a study of the binuclear ruthenium(II) complexes of 3,4-di(2-pyridyl)-1,2,5-oxadiazole (**5**),[14] which revealed remarkably strong metal-metal interactions, the magnitude of which was dependent on the specific diastereoisomer. In an attempt to probe the origin of this intriguing result, we have embarked on the synthesis of new ligands that might be used to prepare metal complexes that provide a means to test the mechanism of the observed metal-metal interactions systematically. One such issue is the role of the oxygen atom in ligand **5**.

In this context, we now describe the preparation of the new ligand 3,6-di(2-pyridyl)-1,4,2,5-dioxadiazine (**6**), which is structurally similar to ligands **3** and **4** but differs by being nonaromatic and having two oxygen atoms in the central ring. We then describe a novel coordination polymer obtained from its reaction with silver tetrafluoroborate. Surprisingly, despite the fact that 3,6-diaryl-1,4,2,5-dioxadiazines are readily synthesised,[15] no coordination complexes of any ligands containing this heterocyclic ring system have previously been reported.

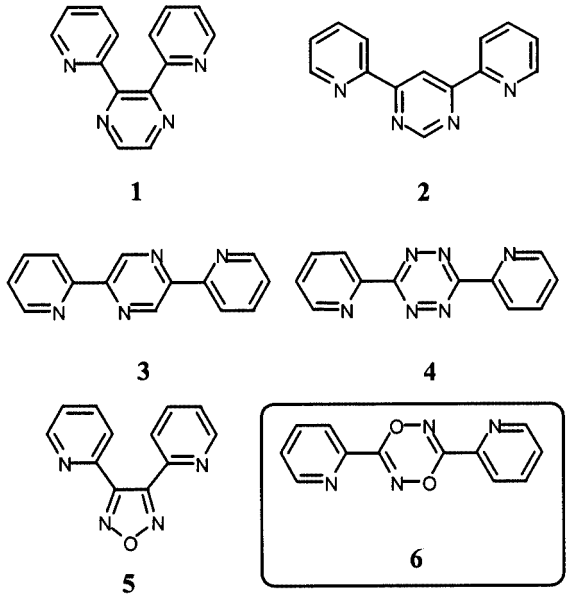

Results and Discussion

The new ligand **6** was prepared in three steps from 2-pyridinecarboxaldehyde by conversion into the oxime, chlorination to the known[16] hydroximinoyl chloride and subsequent dehydrochlorination-dimerisation to give **6** in yields that ranged between 55−60%. This reaction proceeds

[a] Department of Chemistry, University of Canterbury, Christchurch, New Zealand
Fax: (internat.) + 64-3/364-2110
E-mail: p.steel@chem.canterbury.ac.nz

via a nitrile oxide intermediate.[15] The ligand was initially characterised by melting point, elemental analysis, mass spectrometry and ^{1}H and ^{13}C NMR spectroscopy.[17] However, attempts to prepare bis(2,2′-bipyridine)ruthenium(II) complexes of **6** consistently resulted in the isolation of products containing coordinated picolinate or picolinamide ligands, as determined by FAB mass spectrometric analysis. At this point we became concerned about the integrity of the ligand itself and therefore undertook a single crystal X-ray crystal structure determination of **6**. Interestingly, a search of the Cambridge Crystallographic database located only one structure containing this heterocyclic ring system.[18]

Suitable crystals were readily obtained by slow evaporation of an ethyl acetate solution of the ligand. However, we were disappointed to discover that, although the structure solved and refined well,[19] the central ring was disordered with respect to the positions of the nitrogen and oxygen atoms of the ring, despite the fact that the outer pyridine rings did not show any such disorder (Figure 1). The molecule crystallizes about a crystallographic centre of inversion in the monoclinic space group $P2_1/n$ (see Table 1 for data collection and refinement parameters). The plane of the pyridine ring is inclined to the plane of the central ring at an angle of 21.3(1)° and the molecules pack with the typical herringbone pattern common for aromatic molecules in this space group.[20] Thus, in the crystallization process the molecules pack with the pyridine rings faithfully aligned, but with the central ring equally arranged in the two possible conformations. Notwithstanding this result, the structure of the ligand seemed assured and complexes with other transition metal precursors were sought.

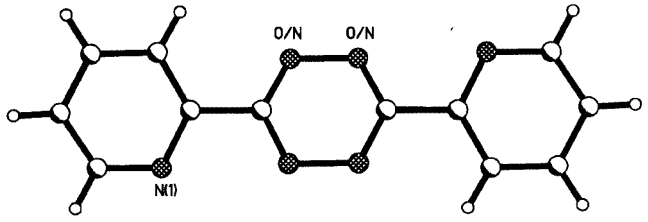

Figure 1. X-ray structure of **6** with a disordered central ring

Since we,[21] and others,[22] have found silver salts to be useful precursors to a variety of interesting metallosupramolecular compounds, including novel coordination polymers,[23] we reacted **6** with silver nitrate in methanol solution to obtain a 1:1 complex $AgL(NO_3)$ (**7**),[24] in excellent yield (96%). All attempts to produce crystals of this product suitable for X-ray structure determination were in vain. Pleasingly, however, reaction of **6** with silver tetrafluoroborate produced the 1:1 M:L complex $AgL(BF_4)$ (**8**),[25] that upon recystallization from acetonitrile underwent reorganisation to a 1:2 complex $AgL_2(BF_4)$, (**9**), which did furnish X-ray quality crystals.

This complex proved to be an intriguing coordination polymer with an unprecedented architecture. Figure 2 shows a perspective view of the contents of the asymmetric unit, along with selected atom labelling and bonding geometry. The asymmetric unit contains one silver atom, two molecules of **6** and a tetrafluoroborate counterion. One of the molecules of **6** acts as a tetradentate ligand, chelating two silver atoms separated by one unit cell translation along the *a* axis [8.011(1) Å]. The other acts as a bidentate ligand coordinating through only two of its four nitrogens, and has its mean plane approximately orthogonal to the first. The silver atom is chelated by three ligands, with bonds to the

Table 1. X-ray crystal data and details of data collections and structure refinements

Compound	**6**	**9**
Formula	$C_{12}H_8N_4O_2$	$C_{24}H_{16}AgBF_4N_8O_4$
Molecular weight	240.22	675.13
Crystal System	monoclinic	triclinic
a (Å)	6.330(2)	8.011(3)
b (Å)	5.781(2)	12.672(5)
c (Å)	14.431(5)	12.792(5)
α (°)	90	97.402(10)
β (°)	97.449(4)	99.304(18)
γ (°)	90	104.756(14)
V (Å^3)	523.6(3)	1219.4(8)
Space group	$P2_1/n$	$P\bar{1}$
Z	2	2
D_c (Mg·m^{-3})	1.524	1.839
F(000)	672	908
Temperature (K)	163(2)	163(2)
Crystal form	colourless block	colourless plate
Crystal size (mm)	0.56 × 0.44 × 0.30	0.52 × 0.20 × 0.04
μ (mm^{-1})	0.109	0.910
$2\theta_{max}$ (°)	53	53
Unique reflections	1065	4833
Parameters	83	379
R[a] [$I > 2\sigma(I)$]	0.0383	0.0285
wR[b] (all data)	0.1058	0.0753

[a] $R = \Sigma(|F_0| - |F_c|)/\Sigma|F_0|$. [b] $wR = (\Sigma[w(F_0^2 - F_c^2)^2]/\Sigma[w(F_0^2)^2])^{1/2}$.

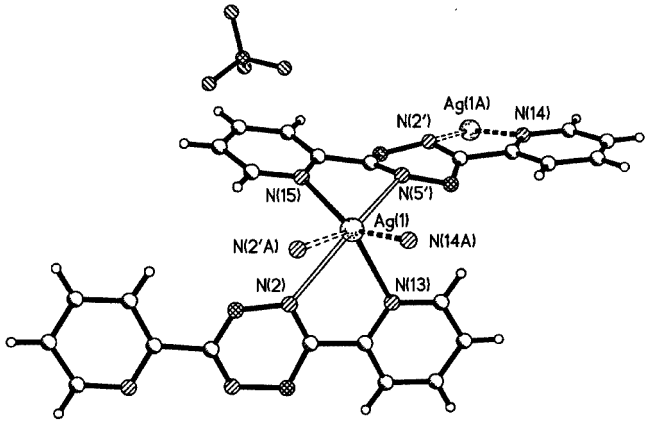

Figure 2. Perspective view and selected atom labelling of the contents of the asymmetric unit in the X-ray structure of $AgL_2(BF_4)$, (**9**); selected interatomic distances (Å) and angles(°): Ag(1)−N(15) 2.294(2), Ag(1)−N(14A) 2.296(2), Ag(1)−N(13) 2.460(2), Ag(1)−N(2) 2.619(2), Ag(1)−N(5) 2.697(2), Ag(1)−N(2′A) 2.702(2); N(15)−Ag(1)−N(14A) 147.96(7), N(15)−Ag(1)−N(13) 117.10(7), N(14A)−Ag(1)−N(13) 92.08(7), N(15)−Ag(1)−N(2) 86.31(7), N(14A)−Ag(1)−N(2) 120.16(7), N(13)−Ag(1)−N(2) 64.47(7), N(5′)−Ag(1)−N(15) 65.8(1), N(2′A)−Ag(1)−N(14A) 65.9(1)

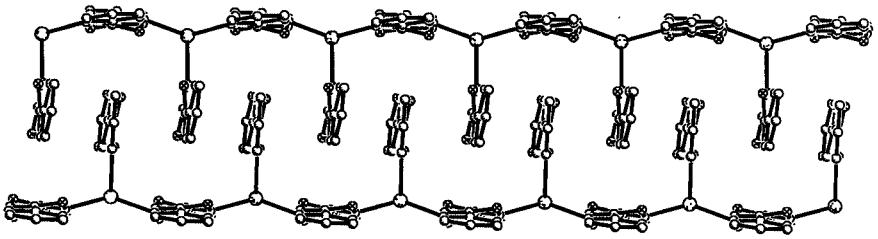

Figure 3. Projection showing the interdigitation of polymer chains

pyridine nitrogens being significantly shorter than those to the dioxadiazine nitrogens, which provide only weak interactions with the metal. These long bonds lead to small bite angles (ca. 65°) at the metal. The resulting hexacoordinate geometry at the metal is trigonal prismatic. Relatively few X-ray crystal structures have been reported that include an AgN_6 coordination environment[26] and these show various coordination geometries consistent with the filled-shell nature of the metal ion.

In both independent molecules of **6** within the complex, the central dioxadiazine ring is far from planar; these exist in boat conformations with the oxygen atoms being displaced from the planes of the carbon and nitrogen atoms by ca. 0.20 Å for the bridging ligand and ca. 0.28 Å for the terminal ligand. In the only other reported crystal structure containing this heterocyclic ring system[18] there are two independent molecules, one of which has the dioxadiazine ring in a chair form and the other in a boat form similar to that found here.

As a consequence of the bridging nature of one of the ligands, the complex extends into a fascinating coordination polymer. As shown in Figure 3, the extended structure consists of two coordination polymer chains which assemble in such a way that the terminal ligands of each chain are interdigitated as a result of π-π stacking interactions. The planes of the individual rings are separated by distances ranging between 3.0 and 3.5 Å and interacting rings have their centroids displaced at distances ranging between 3.38 and 3.81 Å. We believe that this is an unprecedented metallosupramolecular topology, in which the two sides of a ladder-like structure are separated and the rungs are held together by aromatic interactions.

In conclusion, we have shown for the first time that the dioxadiazine ring can be incorporated into chelating and bridging ligands. Studies are in progress to prepare binuclear complexes of this and related ligands with various transition metals.

Acknowledgments

We thank the Royal Society of New Zealand Marsden Fund for financial support.

[1] For recent reviews, see: [1a] S. Leininger, B. Olenyuk, P. J. Stang, *Chem. Rev.* **2000**, *100*, 853−908. [1b] G. F. Swiegers, T. J. Malefetse, *Chem. Rev.* **2000**, *100*, 3483−3538. [1c] B. Moulton, M. J. Zaworotko, *Chem. Rev.* **2001**, *101*, 1629−1658. [1d] M. Fujita, K. Umemoto, M. Yoshizawa, N. Fujita, T. Kusukawa, K. Biradha, *Chem. Commun.* **2001**, 509−518. [1e] D. W. Johnson, K. N. Raymond, *Supramol. Chem.* **2001**, *13*, 639−659. [1f] B. J. Holliday, C. A. Mirkin, *Angew. Chem. Int. Ed.* **2001**, *40*, 2022−2043. [1g] G. F. Swiegers, T. J. Malefetse, *Coord. Chem. Rev.* **2002**, *225*, 91−121.

[2] C. Kaes, A. Katz, M. W. Hosseini, *Chem. Rev.* **2000**, *100*, 3553−3590.

[3] [3a] A. Juris, V. Balzani, F. Barigelletti, S. Campagna, P. Belser, A. von Zelewsky, *Coord. Chem. Rev.* **1988**, *84*, 85−277. [3b] V. Balzani, A. Juris, M. Venturi, S. Campagna, S. Serroni, *Chem. Rev.* **1996**, *96*, 759−834.

[4] [4a] C. H. Braunstein, A. D. Baker, T. C. Strekas, H. D. Gafney, *Inorg. Chem.* **1984**, *23*, 857−864. [4b] Y. Fuchs, S. Lofters, T. Dieter, W. Shi, R. Morgan, T. C. Strekas, H. D. Gafney, A. D. Baker, *J. Am. Chem. Soc.* **1987**, *109*, 2691−2699. [4c] A. W. Wallace, W. R. Murphy, J. D. Petersen, *Inorg. Chim. Acta* **1989**, *166*, 47−54. [4d] K. Kalyanasundaram, M. K. Nazeeruddin, *Inorg. Chem.* **1990**, *29*, 1888−1897. [4e] R. M. Berger, *Inorg. Chem.* **1990**, *29*, 1920−1924. [4f] M. Haga, M. M. Ali, S. Koseki, A. Yoshimura, K. Nozaki, T. Ohno, *Inorg. Chim. Acta* **1994**, *226*, 17−24.

[5] [5a] S. Campagna, G. Denti, G. De Rosa, L. Sabatino, M. Ciano, V. Balzani, *Inorg. Chem.* **1989**, *28*, 2565−2570. [5b] G. Denti, S. Campagna, L. Sabatino, S. Serroni, M. Ciano, V. Balzani, *Inorg. Chem.* **1990**, *30*, 4750−4758. [5c] A. Juris, V. Balzani, S. Campagna, G. Denti, S. Serroni, G. Frei, G. Güdel, *Inorg. Chem.* **1994**, *33*, 1491−1496. [5d] H. B. Baudin, J. Davidsson, S. Serroni, A. Juris, V. Balzani, S. Campagna, L. Hammarstroem, *J. Phys. Chem. A* **2002**, *106*, 4312−4319.

[6] [6a] X. Hua, A. von Zelewsky, *Inorg. Chem.* **1995**, *34*, 5791−5797. [6b] I. G. Phillips, P. J. Steel, *Aust. J. Chem.* **1998**, *51*, 371−382.

[7] [7a] Q. Jaradat, K. Barqawi, T. S. Akashek, *Inorg. Chim. Acta* **1986**, *116*, 63−73. [7b] S. D. Ernst, V. Kasack, W. Kaim, *Inorg. Chem.* **1988**, *27*, 1146−1148. [7c] S. D. Ernst, W. Kaim, *Inorg. Chem.* **1989**, *28*, 1520−1528. [7d] J. Poppe, M. Moscherosch, W. Kaim, *Inorg. Chem.* **1993**, *32*, 2640−2643. [7e] K. C. Gordon, A. K. Burrell, T. J. Simpson, S. E. Page, G. Kelso, M. I. J. Polson, A. Flood, *Eur. J. Inorg. Chem.* **2002**, 554−563. [7f] C. S. Araujo, M. G. B. Drew, V. Felix, L. Jack, J. Madureira, M. Newell, S. Roche, T. M. Santos, J. A. Thomas, L. Yellowlees, *Inorg. Chem.* **2002**, *41*, 2250−2259.

[8] A. J. Downard, P. J. Steel, J. Steenwijk, *Aust. J. Chem.* **1995**, *48*, 1625−1642.

[9] C. Richardson, P. J. Steel, *Aust. J. Chem.* **2000**, *53*, 93−97.

[10] C. Richardson, P. J. Steel, *J. Chem. Soc., Dalton Trans.* **2002**, in press.

[11] C. Richardson, P. J. Steel, *Inorg. Chem. Commun.* **2000**, *3*, 155−158.

[12] C. Richardson, P. J. Steel, *Acta Crystallogr., Sect. C* **2001**, *57*, 197−198.

[13] C. Richardson, P. J. Steel, *Aust. J. Chem.* **2002**, in press.

[14] C. Richardson, P. J. Steel, D. M. D'Alessandro, P. C. Junk, F. R. Keene, *J. Chem. Soc., Dalton Trans.* **2002**, 2775−2785.

[15] F. De Sarlo, *J. Chem. Soc., Perkin Trans. 1* **1974**, 1951−1953.

[16] R. H. Wiley, B. J. Wakefield, *J. Org. Chem.* **1960**, *25*, 546−551.

[17] **Preparation of 3,6-Di(2-pyridyl)-1,4,2,5-dioxadiazine (6)**: 2-Pyr-

idine hydroximinoyl chloride hydrochloride[16] (0.51 g, 2.6 mmol) was dissolved in ethanol (25 mL). Triethylamine (0.73 mL, 5.3 mmol) and pyridine (0.64 mL, 7.9 mmol) were added and the solution stirred. The resulting yellow solution was left overnight, the precipitate was filtered off, and the filtrate taken to dryness in vacuo. The resulting solid was recrystallized from water. M. p. 154−158 °C; yield 0.18 g (59%). $C_{12}H_8N_4O_2$ (240.2): calcd. C 60.00, H 3.36, N 23.32; found C 60.05, H 3.19, N 23.47. Positive-ion EI-MS: calcd. for $C_{12}H_8N_4O_2$ 240.0647; found 240.0648. *m/z* = 240.1 (1.8) [M^+], 120.0 (20) [$PyCNO^+$], 104.0 (100) [$PyCN^+$], 78.0 (62) [Py^+]. ^{1}H NMR ($CDCl_3$): δ = 7.94 (H3′), 7.80 (H4′), 7.44 (H5′), 8.73 (H6′) ppm. ^{13}C NMR ($CDCl_3$): δ = 144.66 (C2′), 123.26 (C3′), 136.99 (C4′), 126.69 (C5′), 150.30 (C6′), 160.63 (C3/C6).

[18] R. Fruttero, B. Ferrarotti, A. Gasco, G. Calestani, C. Rizzoli, *Liebigs Ann. Chem.* **1988**, 1017−1023.

[19] The crystal data, data collection and refinement parameters for the X-ray structures are listed in Table 1. Data were collected with a Siemens SMART CCD area detector, using graphite-monochromatized Mo-K_α radiation (λ = 0.71073 Å). The structures were solved by direct methods, and refined on F^2 using all data by full-matrix least-squares procedures.
CCDC-191057 (**6**) and -191058 (**9**) contains the supplementary crystallographic data for this paper. These data can be obtained free of charge at www.ccdc.cam.ac.uk/conts/retrieving.html [or from the Cambridge Crystallographic Data Centre, 12 Union Road, Cambridge CB2 1EZ, UK; fax: (internat.) + 44-1223/336-033; Email: deposit@ccdc.cam.ac.uk].

[20] G. R. Desiraju, A. Gavezzotti, *Acta Crystallogr., Sect. B* **1989**, *45*, 473−482.

[21] [21a] C. M. Hartshorn, P. J. Steel, *Inorg. Chem.* **1996**, *35*, 6902−6903. [21b] C. M. Hartshorn, P. J. Steel, *J. Chem. Soc., Dalton Trans.* **1998**, 3927−3934. [21c] C. M. Hartshorn, P. J. Steel, *J. Chem. Soc., Dalton Trans.* **1998**, 3935−3940. [21d] R. J. Anderson, P. J. Steel, *Acta Crystallogr., Sect. C* **1998**, *54*, 223−225. [21e] B. J. O'Keefe, P. J. Steel, *Inorg. Chem. Commun.* **1998**, *1*, 147−149. [21f] C. Richardson, P. J. Steel, *Inorg. Chem. Commun.* **1998**, *1*, 260−262. [21g] C. M. Fitchett, P. J. Steel, *New J. Chem.* **2000**, *24*, 945−947. [21h] B. J. O'Keefe, P. J. Steel, *Inorg. Chem. Commun.* **2000**, *3*, 473−475. [21i] C. M. Hartshorn, P. J. Steel, *Inorg. Chem. Commun.* **2000**, *3*, 476−481. [21j] C. M. Fitchett, P. J. Steel, *Inorg. Chim. Acta* **2000**, *310*, 127−132. [21k] P. J. Steel, C. J. Sumby, *Chem. Commun.* **2002**, 322−323. [21l] P. J. Steel, C. J. Sumby, *Inorg. Chem. Commun.* **2002**, *5*, 323−327. [21m] P. J. Steel, N. C. Webb, *Eur. J. Inorg. Chem.* **2002**, 2257−2260. [21n] D. A. McMorran, P. J. Steel, *J. Chem. Soc., Dalton Trans.* **2002**, 3321−3326.

[22] M. Munakata, L. P. Wu, T. Kuroda-Sowa, *Adv. Inorg. Chem.* **1999**, *46*, 173−303.

[23] A. N. Khlobystov, A. J. Blake, N. R. Champness, D. A. Lemenovskii, A. G. Majouga, N. V. Zyk, M. Schröder, *Coord. Chem. Rev.* **2001**, *222*, 155−192.

[24] **Preparation of Silver Nitrate Complex AgL(NO_3) (7):** $AgNO_3$ (22.4 mg, 0.13 mmol) dissolved in hot MeOH (3 mL) was added to ligand **6** (31.3 mg, 0.13 mmol) in warm MeOH (2 mL). A colourless precipitate formed immediately and was collected by filtration. Yield 51.4 mg (96%). $C_{12}H_8AgN_5O_5$ (410.1): calcd. C 35.15, H 1.97, N 17.07; found C 34.94, H 1.79, N 16.80.

[25] **Preparation of Silver Tetrafluoroborate Complex 9:** Ligand **6** (35.7 mg, 0.15 mmol) was dissolved in warm MeOH (3 mL) and added to $AgBF_4$ (30.1 mg, 0.16 mmol) dissolved in MeOH (1 mL). The colourless precipitate of AgL(BF_4) (**8**), that formed was collected by filtration and washed with MeOH. M.p. 189−192 °C; yield 51.5 mg (79%). $C_{12}H_8AgBF_4N_4O_2$ (434.9): calcd. C 33.14, H 1.85, N 12.88; found C 33.38, H 2.07, N 12.62. Recrystallization of the colourless solid from acetonitrile gave plate-like crystals of $AgL_2(BF_4)$ (**9**).

[26] [26a] H. Adams, N. A. Bailey, W. D. Carlisle, D. E. Fenton, G. Rossi, *J. Chem. Soc., Dalton Trans.* **1990**, 1271−1283. [26b] E. C. Constable, M. S. Khan, M. C. Liptrot, J. Lewis, P. R. Raithby, *Inorg. Chim. Acta* **1991**, *179*, 239−244. [26c] J. de Mendoza, E. Mesa, J.-C. Rodriguez-Ubis, P. Vazquez, F. Vögtle, P.-M. Windscheif, K. Rissanen, J.-M. Lehn, D. Lilienbaum, R. Ziessel, *Angew. Chem. Int. Ed. Engl.* **1991**, *30*, 1331−1333. [26d] C. Stockheim, K. Wieghardt, B. Nuber, J. Weiss, U. Flörke, H.-J. Haupt, *J. Chem. Soc., Dalton Trans.* **1991**, 1487−1490. [26e] H. Adams, N. A. Bailey, M. J. S. Dwyer, D. E. Fenton, P. C. Hellier, P. D. Jempstead, J. M. Latour, *J. Chem. Soc., Dalton Trans.* **1993**, 1207−1216. [26f] L. Carlucci, G. Ciani, D. M. Proserpio, A. Sironi, *Angew. Chem. Int. Ed. Engl.* **1995**, *34*, 1895−1897. [26g] D. L. Reger, J. E. Collins, A. L. Rheingold, L. M. Liable-Sands, G. P. A. Yap, *Organometallics* **1997**, *16*, 349−353. [26h] M. Munakata, J. C. Zhong, T. Kuroda-Sowa, M. Maekawa, Y. Suenaga, N. Oiji, *Inorg. Chim. Acta* **2001**, *317*, 268−275. [26i] M. Jorgensen, F. C. Krebs, *Tetrahedron Lett.* **2001**, *42*, 4717−4720. [26j] A. Cingolani, Effendy, D. Martini, M. Pellei, C. Pettinari, B. W. Skelton, A. H. White, *Inorg. Chim. Acta* **2002**, *328*, 87−95.

Received August 5, 2002
[I02442]

Direct Synthesis of Enantiopure Tripod Ligands from C_2-Symmetric Precursors

Ina Hegelmann[a] and Nicolai Burzlaff*[a]

Keywords: N ligands / Tripod ligands / Chirality / Prochirality / Ruthenium

A new enantiopure chiral tripod ligand is obtained from C_2-symmetric bis(camphorpyrazol-1-yl)methane by introducing a carboxylate group at the bridging carbon atom. A prochiral centre is formed rather than an additional stereocentre. Therefore, a homochiral tripod ligand is achieved without separation of the stereoisomers.
(© Wiley-VCH Verlag GmbH & Co. KGaA, 69451 Weinheim, Germany, 2003)

Chiral facially coordinating tripod ligands play an important role in stereoselective synthesis.[1] Recently we reported a racemic example of a bis(pyrazol-1-yl)acetato tripod ligand, namely (3,5-di-*tert*-butylpyrazol-1-yl)(3′,5′-dimethylpyrazol-1-yl)acetate (bpa$^{t\mathrm{Bu2,Me2}}$; Figure 1a).[2] Usually, the chirality of these ligands originates from three different donor groups that are bound to a bridging atom with a noncoordinating group, atom or lone pair.

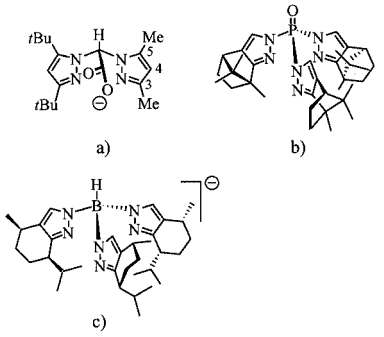

Figure 1. Chiral tripod ligands

For asymmetric induction two problems have to be solved: (a) enantiomeric purity, and (b) a stable configuration of the stereogenic centres. Separation of the enantiomers is often an elaborate, low-yield process and demands a measurement of the enantiomeric purity. If one of the donor groups is chiral and enantiopure, or derived from the chiral pool, the problem is converted into one of separation of the diastereomers. This can be avoided if C_3-symmetric ligands with three identical, chiral donor groups are applied.[3] Chiral pool derived ligands such as [OP(pz$^{\mathrm{cam}}$)$_3$] or [BH(pz$^{\mathrm{menth}}$)$_3$]$^-$ (Figure 1b, c) are often cited as examples.[4] Due to the steric hindrance of the three chiral donor groups, however, the application of these ligands is limited, especially in octahedral complexes. We now report on a general concept to obtain new enantiopure facially binding tripod ligands from C_2-symmetric precursors.

C_2 symmetry is a common feature in chiral bidentate ligands.[5] If two identical enantiopure donor groups Y* are connected by a tetrahedral bridging atom, any additional group Z at this atom will form a prochiral centre rather than an additional stereocentre (Figure 2a).[6] Trihydroxyglutaric acid, either *S*,*S* or *R*,*R*, is a textbook example of this.[6] Inversion of configuration at C3 in (*S*,*S*)-trihydroxyglutaric acid (Figure 2b) yields the identical compound.

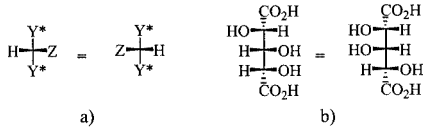

Figure 2. Prochiral centre of (*S*,*S*)-trihydroxyglutaric acid[6]

Therefore, a homochiral tripod ligand can be obtained from a C_2-symmetric precursor without additional separation of enantiomers or diastereomers. As an example of this concept we chose bis(camphorpyrazol-1-yl)methane, an enantiopure but C_2-symmetric bidentate ligand which is obtained in three steps from (+)-camphor (Scheme 1).

As reported by Steel et al., three structural isomers of bis(camphorpyrazol-1-yl)methane (**2a**, **2b** and **2c**) are formed by coupling of camphorpyrazole **1** with CH_2Cl_2 in a two-phase system.[7] Reaction with CH_2Cl_2 as both reactant and solvent reduces the reaction time to 8 hours compared to the 10 days reported previously. Compound **2c** can be separated from the other two structural isomers in two crystallisation steps from pentane and acetone, respectively, to give colourless crystals. A single-crystal X-ray diffraction experiment proved the desired constitution of **2c**.[8] According to Steel et al. isomer **2b** can also be isolated.[7]

By analogy with the synthesis of bis(3,5-dialkylpyrazol-1-yl)acetic acids,[2,9] deprotonation at the bridging carbon

[a] Fachbereich Chemie der Universität Konstanz,
Universitätsstraße 10, Fach M728, 78457 Konstanz, Germany
Fax: (internat.) + 49-(0)7531/88-3136
E-mail: nicolai@chemie.uni-konstanz.de

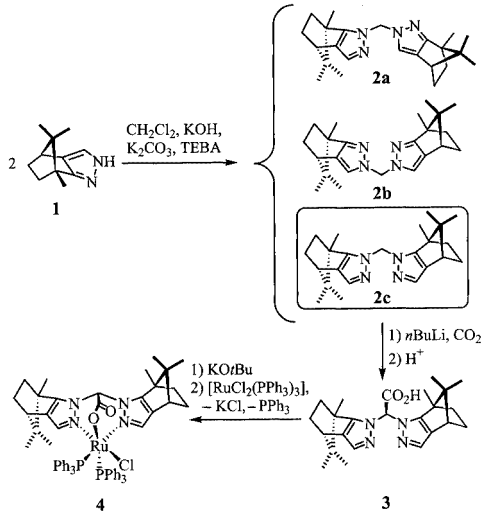

Scheme 1. Synthesis and coordination of bis(camphorpyrazol-1-yl) acetic acid

atom and subsequent reaction with carbon dioxide introduces a carboxylate group at this position. Due to missing substituents at the pyrazolyl carbon C5, **2b** is also deprotonated at C5. A similar deprotonation at C5 has been published recently by Otero et al. for an achiral bis(pyrazol-1-yl)methane.[10] Therefore, only the minor isomer **2c** out of the two C_2-symmetric isomers **2b** and **2c** is suitable for this reaction sequence. Acidic workup yields the enantiopure bis(camphorpyrazol-1-yl)acetic acid bpa^{cam2}H (**3**; Scheme 1).[11] Two sets of signals are found for the camphorpyrazolyl groups in the ^{1}H and ^{13}C NMR spectra. A strong IR band at $\tilde{\nu}$ = 1712 cm^{-1} and a ^{1}H NMR signal at δ = 11.59 ppm confirm the presence of the carboxylate group. Crystals of **3** suitable for X-ray structure determination were obtained from CH_2Cl_2 (Figure 3).[8] The bond lengths and bond angles in **3** are in good agreement with those reported earlier for other achiral bis(3,5-dialkylpyrazol-1-yl)acetic acids.[9,12]

Reaction of the potassium salt of bpa^{cam2}H (**3**) with [$RuCl_2(PPh_3)_3$] yields [Ru(bpa^{cam2})Cl(PPh_3)$_2$] (**4**; Scheme 1). Recently we reported the formation of the ruthenium complexes [Ru(bpza)Cl(PPh_3)$_2$] and [Ru(bdmpza)Cl(PPh_3)$_2$] [bpza = bis(pyrazol-1-yl)acetate; bdmpza = bis(3,5-dimethylpyrazol-1-yl)acetate] in a similar reaction.[13] An asymmetric carboxylate signal ($\tilde{\nu}_{as}$ = 1656 cm^{-1}) in the IR spectrum and the molecular ion peak (MH$^+$ = 1069) in the FAB mass spectrum indicate the coordination of the ligand. As in **3** two sets of signals are observed in the ^{1}H and ^{13}C NMR spectra for the camphorpyrazolyl groups. Two sets of signals in these spectra and two doublets in the ^{31}P NMR spectrum at δ = 39.2 and 42.7 ppm ($^2J_{P,P}$ = 35.6 Hz and 32.4 Hz) are expected for two PPh_3 ligands in a chiral environment. According to the cross coupling observed in the COSY spectrum, two singlets in the ^{1}H NMR spectrum are assigned to the bridging CH group (^{1}H NMR: δ = 6.30 ppm; ^{13}C NMR: δ = 72.9 ppm) and one of the two pyrazole C3 protons (^{1}H NMR: δ = 5.99 ppm; ^{13}C NMR: δ = 138.5 ppm). The second pyrazole C3 proton signal is probably hidden underneath the PPh_3 signals. A rather similar downfield shift of such a C3 proton signal was observed for the asymmetrical isomer of the related ruthenium complex [Ru(bpza)Cl(PPh_3)$_2$], in which one PPh_3 ligand is *trans* to the carboxylate group.[13] Therefore, a geometry with one of the PPh_3 ligands *trans* to the carboxylate group and the other *trans* to the camphorpyrazolyl group is assumed for complex **4**.

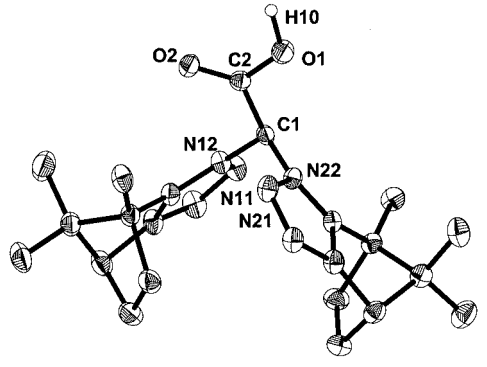

Figure 3. Molecular structure of bpa^{cam2}H (**3**); thermal ellipsoids at 50% probability level; selected bond lengths (Å) and angles (°): C1–C2 1.534(5), C2–O1 1.320(4), C2–O2 1.198(4), C1–N12 1.457(4), C1–N22 1.446(4); O1–C2–O2 126.0(3), C2–C1–N12 111.4(3), C2–C1–N22 112.9(3), N12–C1–N22 111.2(3)[8]

Our results show that new enantiopure facially binding tripod ligands can be obtained from C_2-symmetric precursors. In this concept an additional donor group is introduced at the bridging atom, forming a prochiral centre rather than an additional stereocentre. Therefore, a homochiral ligand is obtained by a simple separation of structural isomers without any separation of enantiomers or diastereomers. Future work to extend this concept will focus on the conversion of other C_2-symmetric ligands into enantiopure tripod ligands.

Experimental Section

bpa^{cam2}H (3): A solution of bpm^{cam2} (**2c**) (288 mg, 0.790 mmol) in THF (20 mL) was treated with *n*BuLi (1.6 M in *n*-hexane, 0.500 mL, 0.800 mmol) at −70 °C. The solution was allowed to warm to −45 °C over a period of 2 h and finally flushed with a flow of CO_2 for 10 min. The solvent was removed in vacuo at ambient temperature and the residue dissolved in water (50 mL). The aqueous solution was acidified with HCl (6 M) to pH 1 and extracted with Et_2O (4 × 50 mL). The combined organic layers were dried (Na_2SO_4) and concentrated in vacuo. Recrystallisation from acetone yielded the acid bpa^{cam2}H (**3**) as a colourless crystalline powder. Yield 247 mg (77%); m.p. 175 °C (dec.). $[\alpha]_D^{23}$ = +55.3 (*c* = 0.01, CH_2Cl_2). ^{1}H NMR (250 MHz, $CDCl_3$): δ = 0.68 (m, 1 H, CH_2), 0.77 (s, 3 H, CH_3), 0.78 (s, 3 H, CH_3), 0.88 (s, 3 H, CH_3), 0.92 (s, 3 H, CH_3), 0.97 (m, 2 H, CH_2), 1.30 (m, 1 H, CH_2), 1.33 (s, 3 H, CH_3), 1.48 (s, 3 H, CH_3), 1.59 (m, 1 H, CH_2), 1.75 (m, 1 H, CH_2), 1.98 (m, 2 H, CH_2), 2.76 (d, $^3J_{H,H}$ = 3.7 Hz, 1 H, CH), 2.82 (d, $^3J_{H,H}$ = 3.7 Hz, 1 H, CH), 6.78 (s, 1 H, H_{pz}), 7.17 (s, 1 H, H_{pz}), 7.37 (s, 1 H, CH), 11.59 (br. s, 1 H, CO_2H) ppm. ^{13}C NMR (62.9 MHz, $CDCl_3$): δ = 11.2, 11.4, 19.3, 19.5, 20.3, 20.4 (6 × CH_3), 27.2, 27.3, 32.1, 33.0 (4 × CH_2), 47.4, 47.5 (2 × CH), 53.2, 53.8, 62.8, 63.1 (4 × C_q), 69.7 (CH), 130.5, 130.6 (2 × C_{pz}), 131.2, 133.0 (2 × CH_{pz}),

154.1, 155.9 (2 × C_{pz}), 165.6 (CO_2H) ppm. FAB MS (NBOH): *m/z* (%) = 409 (10) [MH^+], 189 (100) [$(C_{11}H_{15}N_2)CH_2$]. IR (CH_2Cl_2): $\tilde{\nu}$ = 1712 (CO_2H) cm^{-1}. $C_{24}H_{32}N_4O_2$ (408.54): calcd. C 70.56, H 7.89, N 13.71; found C 70.43, H 7.80, N 13.65.

[Ru(bpa^{cam2})Cl(PPh$_3$)$_2$] (4): A solution of bpa^{cam2}H (585 mg, 1.43 mmol) and KO*t*Bu (137 mg, 1.22 mmol) in THF (40 mL) was stirred at ambient temperature for 1 h. [$RuCl_2(PPh_3)_3$] (1.06 g, 1.11 mmol) was then added and the solvent was removed in vacuo after 1 h. The residue was dissolved in Et_2O (5 mL), precipitated by addition of pentane (50 mL) and filtered off. It was washed with H_2O (2 × 10 mL) and pentane (40 mL) and dried in vacuo to afford [Ru(bpa^{cam2})Cl(PPh_3)$_2$] (**4**) as an amber crystalline powder. Yield 604 mg (51%); m.p. 162 °C (dec.). ^{1}H NMR (600 MHz, $CDCl_3$): δ = 0.46 (m, 3 H, CH_3), 0.54 (m, 1 H, CH_2), 0.67 (s, 3 H, CH_3), 0.80 (s, 3 H, CH_3), 0.85 (s, 3 H, CH_3), 0.88 (m, 1 H, CH_2), 1.03 (m, 2 H, CH_2), 1.44 (s, 3 H, CH_3), 1.47 (s, 3 H, CH_3), 1.71 (m, 1 H, CH_2), 1.78 (m, 2 H, CH_2), 1.86 (m, 1 H, CH_2), 2.43 (d, $^3J_{H,H}$ = 3.4 Hz, 1 H, CH), 2.49 (d, $^3J_{H,H}$ = 3.4 Hz, 1 H, CH), 5.99 (s, 1 H, H_{pz}), 6.30 (s, 1 H, CH), 7.00−7.42 (m, 31 H, H_{pz} and 2 PPh_3) ppm. ^{13}C NMR (150.9 MHz, $CDCl_3$): δ = 11.1, 12.1, 19.1, 19.4, 20.4, 20.5 (6 × CH_3), 26.7, 26.9, 32.7, 34.4 (4 × CH_2), 47.1, 47.2 (2 × CH), 53.2, 54.0, 61.9, 65.0 (4 × C_q), 72.6 (CH), 126.9 (d, $^2J_{C,P}$ = 8.8 Hz, *o*-PPh_3), 127.1 (d, $^2J_{C,P}$ = 8.8 Hz, *o*-PPh_3), 128.5 (s, *p*-PPh_3), 128.6 (s, *p*-PPh_3), 129.3, 129.6 (2 × C_{pz}), 131.9 (CH_{pz}), 134.7 (d, $^3J_{C,P}$ = 9.1 Hz, *m*-PPh_3), 135.0 (d, $^1J_{C,P}$ = 39.2 Hz, *i*-PPh_3), 135.4 (d, $^3J_{C,P}$ = 9.2 Hz, *m*-PPh_3), 136.1 (d, $^1J_{C,P}$ = 38.3 Hz, *i*-PPh_3), 138.6 (CH_{pz}), 155.3, 156.0 (2 × C_{pz}), 166.3 (CO_2^-) ppm. ^{31}P NMR (161.8 MHz, $CDCl_3$): δ = 39.2 (d, $^2J_{P,P}$ = 35.6 Hz), 42.7 (d, $^2J_{P,P}$ = 32.4 Hz). FAB MS (NBOH): *m/z* (%) = 1069 (39) [MH^+], 1034 (53) [M^+ − Cl], 807 (100) [MH^+ − PPh_3], 772 (43) [MH^+ − PPh_3 − Cl]. IR (CH_2Cl_2): $\tilde{\nu}$ = 1656 s (*as*-CO_2^-), 1482 (C=C) cm^{-1}. $C_{60}H_{61}ClN_4O_2P_2Ru$ (1068.64): calcd. C 67.44, H 5.75, N 5.24; found C 67.41, H 6.10, N 4.85.

Acknowledgments

This work was supported by the Fonds der Chemischen Industrie (Liebig-Stipendium to N.B.) and the Deutsche Forschungsgemeinschaft (DFG). We are indebted to Dr. F. Schaper for help on collecting an X-ray dataset. Special thanks also go to Prof. Dr. H. Fischer for his support and helpful discussions.

[1] Reviews: [1a] A. Togni, L. M. Venanzi, *Angew. Chem.* **1994**, *106*, 517−547; *Angew. Chem. Int. Ed. Engl.* **1994**, *33*, 497−527. [1b] F. Fache, E. Schulz, M. Lorraine Tommasino, M. Lemaire, *Chem. Rev.* **2000**, *100*, 2159−2231.

[2] I. Hegelmann, A. Beck, C. Eichhorn, B. Weibert, N. Burzlaff, *Eur. J. Inorg. Chem.* **2002**, in press.

[3] C. Moberg, *Angew. Chem.* **1998**, *110*, 260−281; *Angew. Chem. Int. Ed.* **1998**, *37*, 249−268.

[4] [4a] C. J. Tokar, P. B. Kettler, W. B. Tolman, *Organometallics* **1992**, *11*, 2737−2739. [4b] D. D. LeCloux, C. J. Tokar, M. Osawa, R. P. Houser, M. C. Keyes, W. B. Tolman, *Organometallics* **1994**, *13*, 2855−2866.

[5] For a review on C_2 symmetry see: J. K. Whitesell, *Chem. Rev.* **1989**, *89*, 1581−1590.

[6] H. Hirschmann, K. R. Hanson, *Tetrahedron* **1974**, *30*, 3649−3656.

[7] D. A. House, P. J. Steel, A. A. Watson, *Aust. J. Chem.* **1986**, *39*, 1525−1536.

[8] [8a] **Crystal data for 2c**: $C_{23}H_{32}N_4$, M_r = 364.53, orthorhombic space group $P2_12_12_1$, *a* = 11.0364(18), *b* = 11.975(3), *c* = 15.597(2) Å, *V* = 2061.3(6) Å^3, *Z* = 4, $\rho_{calcd.}$ = 1.175 g cm^{-3}. Final *R* indices: R_1 = 0.0382, wR_2 = 0.0960 {for 2363 reflections considered observed [$I > 2\sigma(I)$]}; R_1 = 0.0412, wR_2 = 0.0983 (all data) for the 245 parameters. **Crystal data for 3**: $C_{24}H_{32}N_4O_2{\cdot}CH_2Cl_2$, M_r = 493.46, orthorhombic space group $P2_12_12_1$, *a* = 8.4259(17), *b* = 14.990(3), *c* = 20.490(4) Å, *V* = 2588.1(9) Å^3, *Z* = 4, $\rho_{calcd.}$ = 1.266 g cm^{-3}. Final *R* indices: R_1 = 0.0656, wR_2 = 0.1572 {for 4139 reflections considered observed [$I > 2\sigma(I)$]}; R_1 = 0.0950, wR_2 = 0.1754 (all data) for the 302 parameters. CCDC-195681 (bpm^{cam2}; **2c**) and CCDC-195682 (bpa^{cam2}H; **3**) contain the supplementary crystallographic data for this paper. These data can be obtained free of charge at www.ccdc.cam.ac.uk/conts/retrieving.html [or from the Cambridge Crystallographic Data Centre, 12, Union Road, Cambridge CB2 1EZ, UK; Fax: (internat.) +44-1223/336-033; E-mail: deposit@ccdc.cam.ac.uk]. [8b] G. M. Sheldrick, SHELX-97, Programs for Crystal Structure Analysis, University of Göttingen, Göttingen (Germany), **1997**.

[9] [9a] A. Otero, J. Fernández-Baeza, J. Tejeda, A. Antiñolo, F. Carrillo-Hermosilla, E. Díez-Barra, A. Lara-Sánchez, M. Fernández-López, M. Lanfranchi, M. A. Pellinghelli, *J. Chem. Soc., Dalton Trans.* **1999**, 3537−3539. [9b] A. Otero, J. Fernández-Baeza, J. Tejeda, A. Antiñolo, F. Carrillo-Hermosilla, E. Díez-Barra, A. Lara-Sánchez, M. Fernández-López, *J. Chem. Soc., Dalton Trans.* **2000**, 2367−2374. [9c] A. Beck, B. Weibert, N. Burzlaff, *Eur. J. Inorg. Chem.* **2001**, 521−527.

[10] A. Antiñolo, F. Carrillo-Hermosilla, E. Díez-Barra, J. Fernández-Baeza, M. Fernández-López, A. Lara-Sánchez, A. Moreno, A. Otero, *J. Chem. Soc., Dalton Trans.* **1998**, 3737−3743.

[11] To avoid extraordinarily long abbreviations for **3** and **2c**, the abbreviation system for Tp ligands introduced by S. Trofimenko was used. This resulted in the abbreviations bpm^{cam2} (**2c**), bpa^{cam2}H (**3**) and bpa^{cam2} for the anion of **3**. For further details see: S. Trofimenko, *Scorpionates − The Coordination Chemistry of Polypyrazolylborate Ligands*, Imperial College Press, London, **1999**, pp. 5−9.

[12] N. Burzlaff, I. Hegelmann, B. Weibert, *J. Organomet. Chem.* **2001**, *626*, 16−23.

[13] A. López-Hernández, R. Müller, H. Kopf, N. Burzlaff, *Eur. J. Inorg. Chem.* **2002**, 671−677.

Received November 7, 2002
[I02611]

A New Porous 3-D Framework Constructed From Fivefold Parallel Interpenetration of 2-D (6,3) Nets: A Mixed-Valence Copper(I,II) Coordination Polymer $[Cu^{I}_{2}Cu^{II}(4,4'\text{-bpy})_2(pydc)_2]\cdot 4H_2O$

Xian-Ming Zhang[a,b] and Xiao-Ming Chen*[a]

Keywords: Coordination polymers / Microporous materials / Mixed-valent compounds / Copper / N ligands

A mixed-valence copper(I,II) coordination polymer $[Cu^{I}_{2}Cu^{II}(4,4'\text{-bpy})_2(pydc)_2]\cdot 4H_2O$ (4,4′-bpy = 4,4′-bipyridine and pydc = pyridine-2,4-dicarboxylate) featuring the "metal-complex ligands" $[Cu^{II}(pydc)_2]^{2-}$ was designed and synthesized hydrothermally from $Cu(MeCO_2)_2$, pyridine-2,4-dicarboxylate, 4,4′-bipyridine and NaOH. This compound was shown by single-crystal structure analysis to be the first porous 3-D framework constructed from fivefold parallel interpenetration of 2-D (6,3) nets. The one-dimensional channels occupying 17.4% of the crystal volume are occupied by guest water molecules and the porous network is stable after removal of the lattice water molecules, as indicated by TGA and PXRD measurements. The high stability of the 3-D framework may be attributed to the multiple entanglement of the 2-D nets.

(© Wiley-VCH Verlag GmbH & Co. KGaA, 69451 Weinheim, Germany, 2003)

Introduction

Within the currently very active research field of coordination polymers, microporous coordination frameworks are functionally related to zeolites, while intertwining networks show intriguing topologies in inorganic chemistry and may enhance the stability of the porous materials.[1−5] Both porous and intertwining frameworks are of fundamental importance in structural design and in the understanding of structure-property correlation. A two-dimensional (2-D) (6,3) net — similar to a brick-wall — is one of the most common topologies in coordination polymers; intertwining of these 2-D (6,3) nets can also ccur in parallel way.[6−8] Surprisingly, most networks consisting of parallel intertwining of (6,3) nets are overall 2-D arrays and only a single 3-D framework constructed from doubly parallel interpenetration of (6,3) nets has been reported to date.[9] Furthermore, the numbers of parallel intertwining (6,3) nets are limited to two, three and six in the known complexes.[6−8,10−13] Recently, we and others have developed routes to mixed-valence copper(I,II)[14−17] and "metal-complex ligand" (or metallo-ligand) complexes[18−20] under hydrothermal or solvothermal conditions. As a sequel, we report here a new porous mixed-valence copper(I,II) coordination polymer $[Cu^{I}_{2}Cu^{II}(4,4'\text{-bpy})_2(pydc)_2]\cdot 4H_2O$ (4,4′-bpy = 4,4′-bipyridine and pydc = pyridine-2,4-dicarboxylate), which contains "metal-complex ligands" and is the first 3-D framework constructed from fivefold parallel intertwining of two-dimensional (6,3) nets.

[a] School of Chemistry and Chemical Engineering, Sun Yat-Sen University,
Guangzhou 510275, China
Fax: (internat.) + 86-20/8411-2245
E-mail: cescxm@zsu.edu.cn
[b] Department of Chemistry, Shanxi Normal University,
Linfen, Shanxi 041004, China

Results and Discussion

Compound **1** was synthesized under mild hydrothermal conditions (160 °C and 72 hours) and its formation is strongly influenced by the reaction conditions, especially the temperature, reaction time and pH value. The dark brown colour of **1** indicates that it is possibly a mixed-valence copper(I,II) complex. The IR spectrum of complex **1** shows characteristic bands of the dicarboxylate groups at 1634 and 1607 cm^{-1} for the antisymmetric stretching and at 1373 and 1339 for symmetric stretching.[21] The separations (Δ) between $\nu_{asym}(CO_2)$ and $\nu_{sym}(CO_2)$ are 261 and 268 cm^{-1}, respectively. The splitting of $\nu_{asym}(CO_2)$ indicates that the carboxylate groups in **1** function in two different coordination fashions.

An X-ray single-crystal analysis reveals that **1** has a porous three-dimensional framework constructed from fivefold parallel interpenetration of two-dimensional (6,3) nets. Selected bond distances and angles for **1** are listed in Table 1. There are two crystallographically independent copper atoms in **1**, as shown in Figure 1. The Cu(1) atom is trigonally coordinated by two nitrogen atoms from two 4,4′-bpy ligands and one oxygen atom from a pydc ligand. Cu(2), which is located at an inversion center and is coordinated

to two nitrogen and two oxygen atoms from two pydc ligands, shows a slightly distorted square-planar geometry. The Cu(2)−O(3) and Cu(2)−N(1) distances are 1.967(5) and 1.973(6) Å, respectively, and the O(3a)−Cu(2)−N(1) and O(3)−Cu(2)−N(1) bond angles are 95.6(2) and 84.4(2)°, respectively. In fact, there are also two carboxylate oxygen atoms of pydc ligands from adjacent layers weakly bonded to Cu(2), with a Cu−O distance of 2.689(6) Å in the axial direction [Figure 1 (bottom)], and thus the Cu(2) site can be described as having a "4+2" coordination geometry. The Cu^{II} ion with d^9 configuration tends to have a "4+1" or "4+2" coordination geometry because of a strong Jahn−Teller effect, but the Cu^{I} ion with d^{10} configuration tends to have a trigonal or tetrahedral coordination geometry. The coordination symmetry of copper(II) ions in combination with charge balance indicates that Cu(1) is monovalent and Cu(2) is divalent.

Table 1. Selected bond distances [Å] and angles [°] for **1**[a]

Cu(1)−N(2)	1.935(6)	Cu(2)−O(3)	1.967(5)
Cu(1)−N(3a)	1.965(6)	Cu(2)−N(1)	1.973(6)
Cu(1)−O(2)	2.074(6)	Cu(1)···Cu(1a)	11.070
Cu(2)−O(3b)	1.967(5)	Cu(1)···Cu(2)	8.935
Cu(2)−O(1)	2.689(6)		
N(2)−Cu(1)−N(3a)	149.9(3)	O(3)−Cu(2)−N(1)	84.4(2)
N(2)−Cu(1)−O(2)	116.0(2)	O(3b)−Cu(2)−N(1b)	84.4(2)
N(3a)−Cu(1)−O(2)	93.1(2)	O(3)−Cu(2)−N(1b)	95.6(2)
O(3b)−Cu(2)−O(3)	180.0(1)	N(1)−Cu(2)−N(1b)	180.0(1)
O(3b)−Cu(2)−N(1)	95.6(2)		

[a] Symmetry codes: a = $x + 1/2, -y + 1/2, z - 1/2$; b = $-x + 2, -y, -z + 1$.

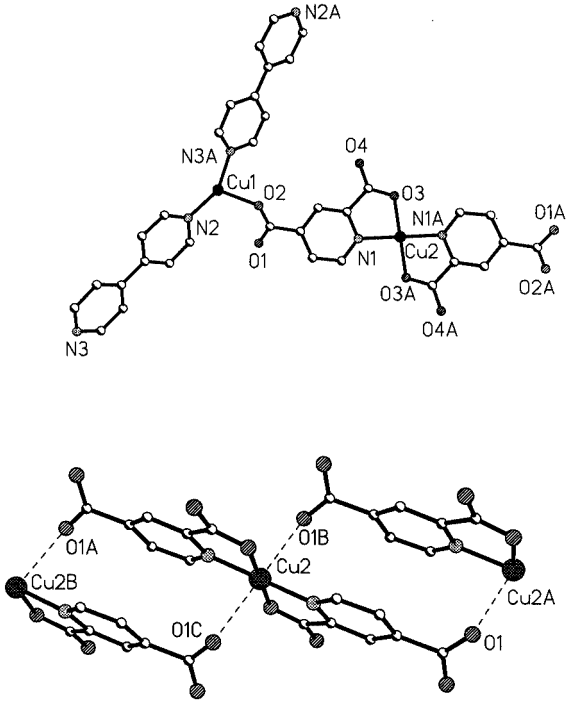

Figure 1. The coordination environments of the copper atoms in **1**

The coordination modes of pydc in its coordination polymers observed up to now are shown in Scheme 1.[18−20] As can be seen, the nitrogen and one of the 2-carboxylate oxygen atoms prefer to chelate one metal atom, and the 4-carboxylate tends to ligate one metal in a bidentate or monodentate mode, to bridge two metal atoms in a carboxylate-*O*,*O*′ mode, or be pendent. The coordination mode of pydc in **1** is shown Scheme 1 (b). In addition, we recently found two other coordination modes in cobalt complexes of pydc, as shown in Scheme 1 (e and f).[22]

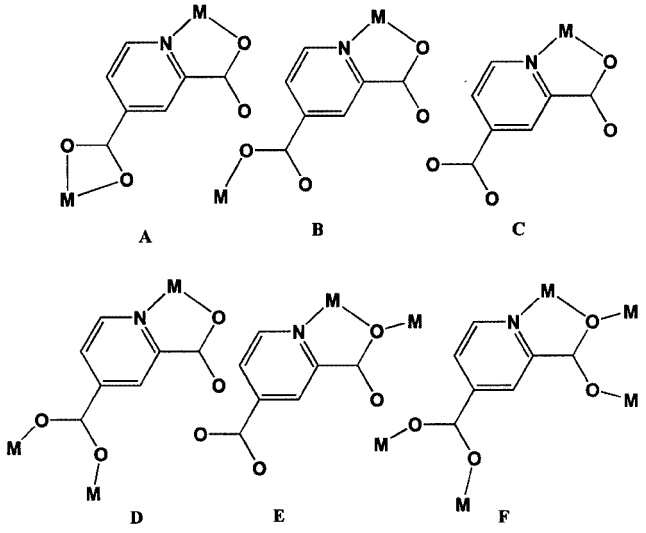

Scheme 1. Schematic representation of the observed coordination modes of pydc

In **1**, Cu(2) and two pydc ligands form a $[Cu^{II}(pydc)_2]^{2-}$ "metal-complex ligand', which bridges $[Cu^{I}(4,4'\text{-bpy})]_n^{n+}$ zigzag chains to generate a 2-D wave-like (6,3) brick-wall array [Figure 2 (top)]. The tricoordinate nodes are provided by Cu(1) and the dicoordinate nodes are provided by 4,4′-bpy and the $[Cu^{II}(pydc)_2]^{2-}$ "metal-complex ligand". The shortest Cu(1)···Cu(1) and Cu(1)···Cu(2) distances are ca. 11.07 and 8.94 Å, respectively. Within the layer, there are large brick-like units (size ca. 18 × 16 Å), each of which is formed by four 4,4′-bpy and two $[Cu^{II}(pydc)_2]^{2-}$ "metal-complex ligands". Compared with other known (6,3) networks, the overall structure of **1** is unprecedented, as shown in Figure 2 (bottom). Each single (6,3) network is intertwined with four other networks and the fivefold interpenetration of (6,3) networks results in a 3-D framework. Any two interpenetrating 2-D (6,3) nets in **1** show an interpenetrating mode topologically identical to that of the $[Cu_2^{I}(CN)\{N(CN)_2\}_2]^-$ polyanion.[23,24] Interpenetration in nature is a space-filling effect to produce dense framework but, surprisingly, the fivefold interpenetration of 2-D (6,3) networks in **1** does not occupy all the voids formed by one independent 2-D network [Figure 3 (top)]. A space-filling plot [Figure 3 (bottom)] clearly shows there are one-dimensional channels running along the *a*-axis direction in **1** which are filled by the guest water molecules. Calculations

using PLATON[25] reveal that the free dimensions of these channels in **1** occupy 17.4% of the crystal volume.

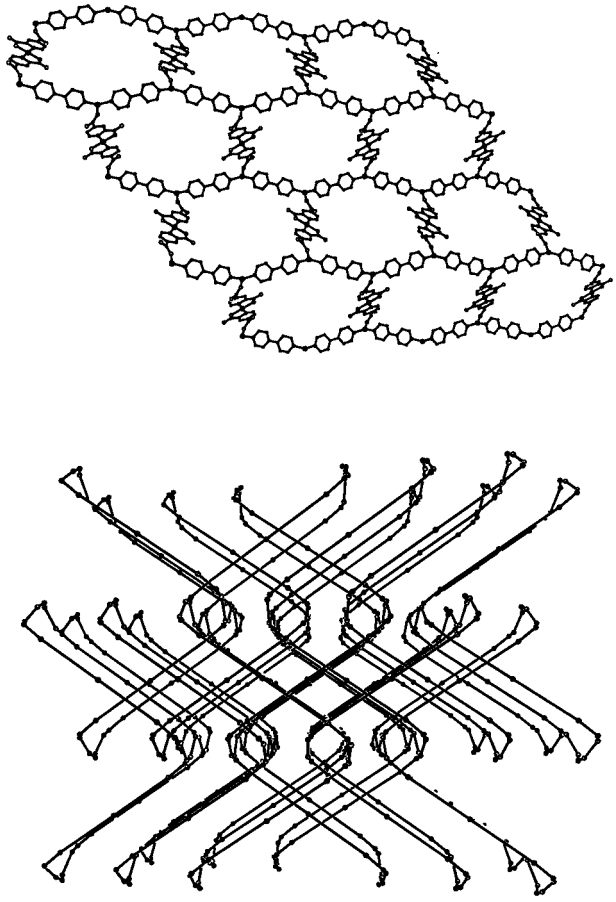

Figure 2. Perspective view of the 2-D (6,3) net in **1** (top) and the fivefold interpenetration of 2-D (6,3) nets (bottom)

Thermogravimetric analysis (Figure 4) in air showed one well-separated weight loss of 9.2% occurring in the temperature range 50−180 °C, corresponding to the removal of water molecules. It should be noted that no weight loss was observed in the temperature range 180−235 °C, indicating the formation of a stable phase formulated as $[Cu^{I}_{2}Cu^{II}(pydc)_2(4,4'\text{-bpy})_2]$ (**1′**). The X-ray powder diffraction patterns (Figure 5) of the as-synthesized **1** and calcinated **1′** are similar, although the intensities and widths of some peaks show some differences, indicating that the porous network of **1** is retained after the calcination and removal of the lattice water molecules.

In summary, a new mixed-valence copper(I,II) coordination polymer $[Cu^{I}_{2}Cu^{II}(4,4'\text{- bpy})_2(pydc)_2]$ has been hydrothermally synthesized, and is the first porous 3-D framework constructed from fivefold parallel interpenetration of 2-D (6,3) nets. The one-dimensional channels are occupied by guest water molecules. The porous network of **1** is stable after removal of the water molecules, which may be due to the multiple entanglement of the 2-D nets.

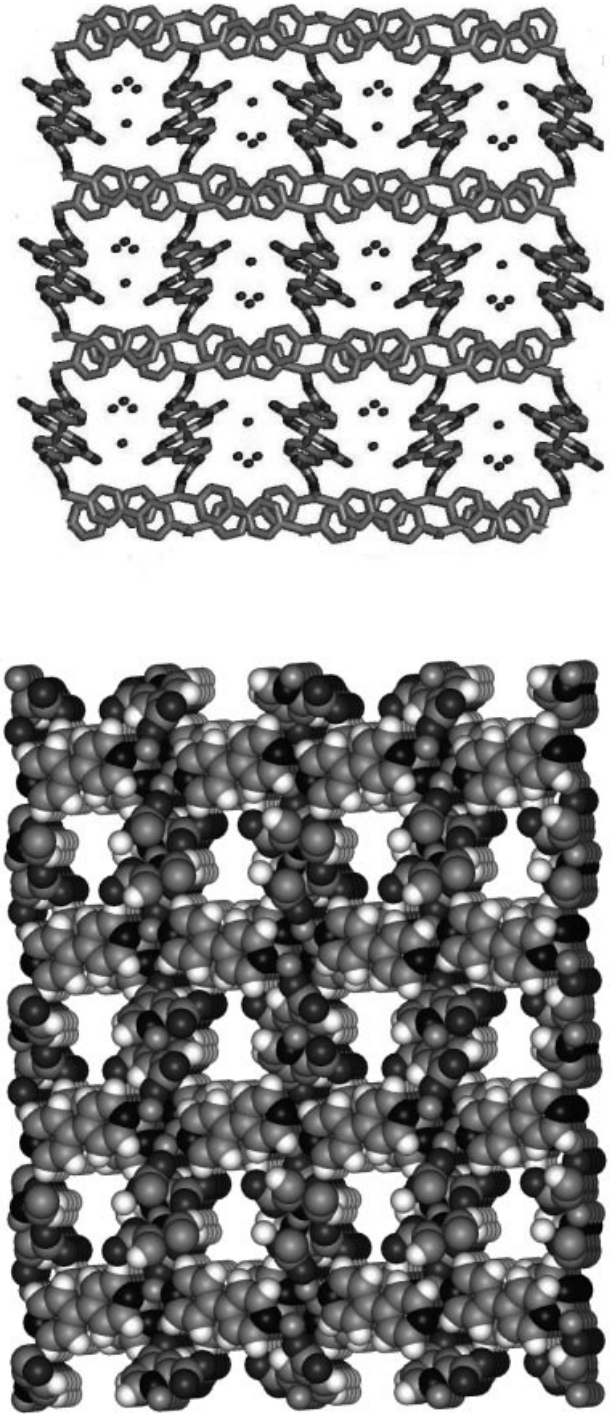

Figure 3. Plots of the 3-D array of **1** viewed along the *a*-axis: (top) ball-and-stick model showing the guest water molecules; (bottom) space-filling model omitting the guest water molecules

Experimental Section

General Remarks: Elemental analyses were performed on a Perkin−Elmer 240 elemental analyzer. The FT-IR spectra were recorded from KBr pellets in the range 400−4000 cm^{-1} on a Nicolet 5DX spectrometer. Thermal gravimetric analyses (TGA) were performed under a static air atmosphere with a Perkin−Elmer 7 thermogravimetric analyzer at a heating rate of 10 °C min^{-1}. The

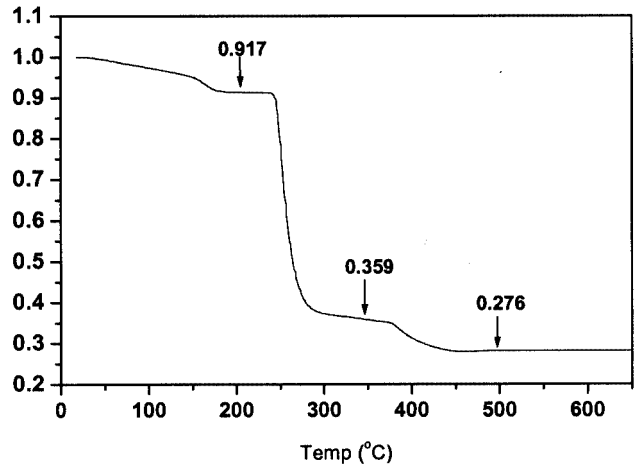

Figure 4. TGA curve of **1** in air

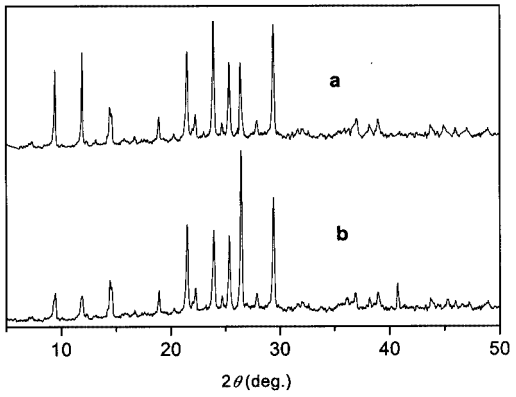

Figure 5. The X-ray powder-diffraction patterns of the as-synthesized **1** (top) and calcinated **1′** (bottom)

XRPD patterns were recorded on a Rigaku D/Max 3III diffractometer with a scanning rate of 4 °min^{-1}.

Preparation: A mixture of $Cu(MeCO_2)_2{\cdot}H_2O$ (0.075 g, 0.5 mmol), H_2pydc (0.042 g, 0.25 mmol), 4,4′-bpy (0.039 g, 0.25 mmol), NaOH (0.02 g, 0.5 mmol) and water (10 mL) in a molar ratio 1.5:1:1:2:2200 was stirred for 20 min in air, then transferred and sealed into a 23 mL Teflon-lined stainless steel container, which was heated to 160 °C for 72 hours. After cooling to room temperature at a rate of 5 °C per hour, dark-brown block crystals of **1** were recovered in 45% yield based on 4,4′-bpy. $C_{34}H_{30}Cu_3N_6O_{12}$ (905.3): calcd. C 45.11, H 3.34, N 9.28; found C 45.06, H 3.37, N 9.22. IR (KBr): $\tilde{\nu}$ = 3444bs, 3096w, 1634s, 1607s, 1552s, 1486m, 1415m, 1373s, 1339s, 1262m, 1091w, 818m, 782w, 732w, 694w cm^{-1}.

X-ray Crystallographic Study: Diffraction data were collected at 293 K on a Siemens R3 diffractometer (Mo-K_α, λ = 0.71073 Å). Lorentz-polarization and absorption corrections were applied. The structure was solved by direct methods (SHELXS-97) and refined by the full-matrix least-squares technique (SHELXL-97).[26] Analytical expressions of neutral-atom scattering factors were employed, and anomalous dispersion corrections were incorporated. In all cases, all non-hydrogen atoms were refined anisotropically and the hydrogen atoms of the organic ligands were placed geometrically. The crystallographic data for **1** are listed in Table 2.

Table 2 Crystal and structure refinement for complex **1**

Empirical formula	$C_{34}H_{30}Cu_3N_6O_{12}$
Molecular weight	905.27
Temperature (K)	293(2)
Wavelength (Å)	0.71073
Crystal system	Monoclinic
Space group	*C*2/*c*
a (Å)	8.058(5)
b (Å)	24.64(2)
c (Å)	19.203(16)
β (°)	95.75(1)
V (Å^3)	3794(5)
Z	4
Density (Mg/m^3)	1.548
μ (mm^{-1})	1.731
F(000)	1784
Absorption correction	Empirical
Max. and min. Trans.	0.4663 and 0.4133
Refl. Ind.	2978
Refinement method	Full-matrix least-squares on F^2
Data/restraints/parameters	2978/0/246
Ggoodness-of-fit on F^2	1.076
R_1	0.0679
wR_2	0.2178
$\Delta\rho_{max}/\Delta\rho_{min}$ (e·A^{-3})	1.131and −0.442

CCDC-192197 contains the supplementary crystallographic data for this paper. These data can be obtained free of charge at www.ccdc.cam.ac.uk/conts/retrieving.html [or from the Cambridge Crystallographic Data Centre, 12, Union Road, Cambridge CB2 1EZ, UK; fax: (internat.) +44-1223/336-033; E-mail: deposit@ccdc.cam.ac.uk].

Acknowledgments

This work was supported by the National Natural Science Foundation of China (No. 20131020) and the Ministry of Education of China (No. 01134).

[1] M. Eddaoudi, D. B. Moler, H. Li, B. Chen, T. M. Reineke, M. O′Keeffe, O. M. Yaghi, *Acc. Chem. Res.* **2001**, *34*, 319−330.
[2] S. R. Batten, R. Robson, *Angew. Chem. Int. Ed.* **1998**, *37*, 1460−1494.
[3] M. J. Zaworotko, *Angew. Chem. Int. Ed.* **2000**, *39*, 3052−3054.
[4] P. J. Hagrman, D. Hagrman, J. Zubieta, *Angew. Chem. Int. Ed.* **1999**, *38*, 2638−2684.
[5] C. Janiak, *Angew. Chem. Int. Ed. Engl.* **1997**, *36*, 1431−1434.
[6] M. Fujita, Y. J. Kwon, O. Sasaki, K. Yamaguchi, K. Ogura, *J. Am. Chem. Soc.* **1995**, *117*, 7287−7288.
[7] L. Carlucci, G. Ciani, D. M. Proserpio, A. Sironi, *Angew. Chem. Int. Ed. Engl.* **1996**, *35*, 1088−1090.
[8] S. R. Batten, B. F. Hoskins, R. Robson, *New. J. Chem.* **1998**, *22*, 173−176.
[9] M.-L. Tong, X.-M. Chen, B.-H. Ye, L.-N. Ji, *Angew. Chem. Int. Ed.* **1999**, *38*, 2237−2240.
[10] L. Carlucci, G. Ciani, D. M. Proserpio, *J. Chem. Soc., Dalton Trans.* **1999**, 1799−1804.
[11] M. A. Withersby, A. J. Blake, N. R. Champness, P. A. Cooke, P. Hubberstey, M. Schröder, *New J. Chem.* **1999**, *23*, 573−576.
[12] M. Kondo, M. Shimamura, S. Noro, S. Minakoshi, A. Asami, K. Seki, S. Kitagawa, *Chem. Mater.* **2000**, *12*, 1288−1299.
[13] D. Venkataraman, S. Lee, J. S. Moore, P. Zhang, K. A. Hirsch,

G. B. Gardner, A. C. Covey, C. L. Prentice, *Chem. Mater.* **1996**, *8*, 2030−2040.
[14] X.-M. Zhang, M.-L. Tong, X.-M. Chen, *Angew. Chem. Int. Ed.* **2002**, *41*, 1029−1031.
[15] X.-M. Zhang, M.-L. Tong, M.-L. Gong, H.-K. Lee, L. Luo, K.-F. Li, Y.-X. Tong, X.-M. Chen, *Chem. Eur. J.* **2002**, *8*, 3187−3194.
[16] J. Tao, Y. Zhang, M.-L. Tong, X.-M. Chen, T. Yuen, C. L. Lin, X.-Y. Huang, J. Li, *Chem. Commun.* **2002**, 1342−1343.
[17] S. M.-F. Lo, S. S.-Y. Chui, L.-Y. Shek, Z. Lin, X.-X. Zhang, G.-H. Wen, I. D. Williams, *J. Am. Chem. Soc.* **2000**, *122*, 6293−6294.
[18] L. A. Gerrard, P. T. Wood, *Chem. Commun.* **2000**, 2107−2108.
[19] D. Min, S. S. Yoon, D.-Y. Jung, C. Y. Lee, Y. Kim, W. S. Han, S. W. Lee, *Inorg. Chim. Acta* **2001**, *324*, 293−229.
[20] S.-I. Noro, S. Kitagawa, M. Yamashita, T. Wada, *Chem. Commun.* **2002**, 222−223.
[21] J. Tao, M.-L. Tong, X.-M. Chen, *J. Chem. Soc., Dalton Trans.* **2000**, 3669−3674.
[22] X.-M. Zhang et al, unpublished data.
[23] G. Saito, H. Yamochi, T. Nakamura, T. Komatsu, N. Matsukawa, T. Inoue, H. Ito, T. Ishiguro, M. Kusunoki, K. Sakaguchi, T. Mori, *Synth. Met.* **1993**, *55−57*, 2883−2890.
[24] T. Komatsu, H. Sato, T. Nakamura, N. Matsukawa, H. Yamochi, G. Saito, M. Kusunoki, K. Sakaguchi, S. Kagoshima, *Bull. Chem. Soc. Jpn.* **1995**, *68*, 2233−2244.
[25] A. L. Spek, *PLATON, A Multipurpose Crystallographic Tool*, Utrecht University: Utrecht, The Netherlands, 1999.
[26] G. M. Sheldrick, *SHELXS-97, Program for Crystal Structure Determination*, University of Göttingen, Germany, 1997.

Received October 3, 2002
[I02546]

Synthesis, Structure and Reactivity of Sulfur-Rich [Fe(L^1)(L^2)('tpS$_4$')] Complexes with Rigid [Fe('tpS$_4$'] Cores and σ−π Co-Ligands ('tpS$_4$'$^{2-}$ = 1,2-Bis(2-mercaptophenylthio)phenylene(2−); L^1, L^2 = CO, PR_3, NO)[‡]

Dieter Sellmann,*[a] David C. F. Blum,[a] Frank W. Heinemann,[a] and Jörg Sutter[a]

Dedicated to Professor Gottfried Huttner on the occasion of his 65th birthday

Keywords: Helical structures / Iron / S ligands

Optimisation of synthesis and purification steps has made the new ligand 'tpS$_4$'$^{2-}$ available in preparative amounts. Treatment of $FeCl_2 \cdot 4H_2O$ with 'tpS$_4$'-Li_2 or 'tpS$_4$'-Na_2 yielded [Fe('tpS$_4$')] (**1**), which in the solid state and in the absence of co-ligands probably trimerises to give paramagnetic [Fe('tpS$_4$')]$_3$. The [Fe('tpS$_4$')] fragment displays helical coordination of the 'tpS$_4$'$^{2-}$ ligand and binds σ–π ligands such as CO, NO and phosphanes to give diamagnetic 18-valence-electron complexes of general formula [Fe(L^1)(L^2)('tpS$_4$')]. The *cis*-dicarbonyl complex [Fe(CO)$_2$('tpS$_4$')] (**2**) is labile and readily dissociates CO to give dinuclear [Fe(CO)('tpS$_4$')]$_2$ (**3**). Simultaneous coordination of CO and phosphanes yielded [Fe(CO)(PR_3)('tpS$_4$')] with R = Me (**4**), Et (**5**), Pr (**6**) and Bu (**7**), but it proved impossible to obtain analogous complexes with bulky PPh_3 or PCy_3 ligands. Bis(phosphane) complexes could be obtained only with PMe_3 and the bidentate dppe, which yielded [Fe(PMe_3)$_2$('tpS$_4$')] (**8**) and [Fe(dppe)('tpS$_4$')] (**11**). Alkylphosphanes with longer alkyl substituents, such as P*n*Pr$_3$ and P*n*Bu$_3$, gave the labile derivatives [Fe(PR_3)$_2$('tpS$_4$')] with R = *n*Pr (**9**) and *n*Bu (**10**). Complexes **9** and **10** reversibly dissociate one PR_3 ligand, yielding diamagnetic [Fe(PR_3)('tpS$_4$')] fragments. These findings explain the decisive and hitherto inexplicable influence of PPr_3 and PBu_3 ligands upon the stabilisation of N_2H_2 in the diazene complexes [μ-N_2H_2{Fe(PR_3)('tpS$_4$')}$_2$] with R = Pr, Bu. Treatment of [Fe('tpS$_4$')] (**1**) or [Fe(CO)('tpS$_4$')]$_2$ (**3**) with NO or NO^+ yielded [Fe(NO)$_2$('tpS$_4$')] (**12**). The molecular structures of **3**, **4**, **7** and **8** were determined by X-ray structure analysis. Spectroscopic and structural results indicate that the differences in reactivity between [Fe(L^1)(L^2)('tpS$_4$')] and homologous [Fe(L^1)(L^2)('S$_4$')] complexes can be traced back to subtle electronic and structural effects.
(© Wiley-VCH Verlag GmbH & Co. KGaA, 69451 Weinheim, Germany, 2003)

Introduction

The goal of modelling and understanding the activation and turnover of small molecules at the metal/sulfur sites of nitrogenases and hydrogenases accounts for much of the interest in low-molecular-weight iron complexes with sulfur-dominated coordination spheres that are able to bind molecules relevant to enzyme activity.[1,2] In the search for such complexes we have found that iron complexes with the [Fe('S$_4$')] fragment (Scheme 1) are capable in particular of binding CO, NO, N_2H_2, N_2H_4 and NH_3, though not yet N_2.[3] It was also found that the 'S$_4$'$^{2-}$ ligand in the resulting [Fe('S$_4$')] complexes exhibits a pronounced tendency to release the C_2H_4 bridge, yielding 1,2-benzenedithiolate ligands, under photolytic and/or strongly reducing reaction conditions.[4] These findings and the well-known fact that steric constraints exerted by ligands can have a marked influence upon the reactivity of otherwise identical complexes prompted us to synthesise 'tpS$_4$'-H_2 = 1,2-bis(2-mercaptophenylthio)phenylene (Scheme 1).[5]

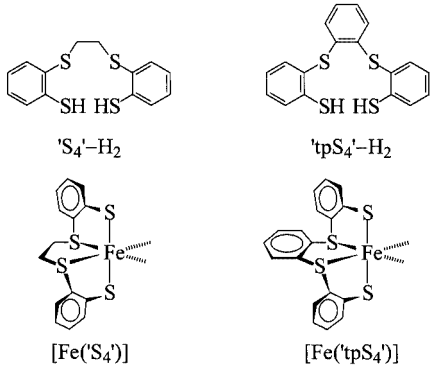

Scheme 1. Ligands and iron complex fragments with S_4 donor atom sets

[‡] Transition Metal Complexes with Sulfur Ligands, 156. Part 155: Ref.[6]

[a] Institut für Anorganische Chemie der Universität Erlangen-Nürnberg,
Egerlandstraße 1, 91058 Erlangen, Germany
Fax: (internat.) + 49-9131/852-7367
E-mail: sellmann@anorganik.chemie.uni-erlangen.de

The 'tpS_4'$^{2-}$ anion is analogous to the 'S_4'$^{2-}$ anion, but has a rigid *o*-phenylene group in place of the flexible C_2H_4 bridge and exclusively aromatic C−S bonds, which are significantly more stable towards C−S cleavage.

In our recent first paper on [Fe('tpS_4')] complexes we reported the diazene complexes [μ-N_2H_2{Fe(PR_3)('tpS_4')}$_2$] with R = Pr, Bu.[6] A strange and previously inexplicable result was that these complexes were accessible only with PPr_3 and PBu_3, but not with smaller or larger phosphanes such as PMe_3 or PPh_3. Another characteristic feature of these diazene complexes is their tendency to form hydrogen-bridge diastereomers, and [μ-N_2H_2{Fe(PPr_3)('tpS_4')}$_2$] is the first example for which these diastereomers have been characterised by X-ray structure analysis.

In this paper we report an optimised synthesis of 'tpS_4'-H_2 and give an account of the general reactivity of [Fe('tpS_4')] complex fragments with CO and phosphanes, emphasizing the similarities as well as the differences between [Fe('S_4')] and [Fe('tpS_4')] complexes.

Results and Discussion

Optimisation of the Synthesis of 'tpS_4'-H_2

The synthesis of 'tpS_4'-H_2 is a multistep procedure comprising aromatic substitution, reduction, diazotisation and diazonium salt substitution reactions, as shown in Scheme 2.[5]

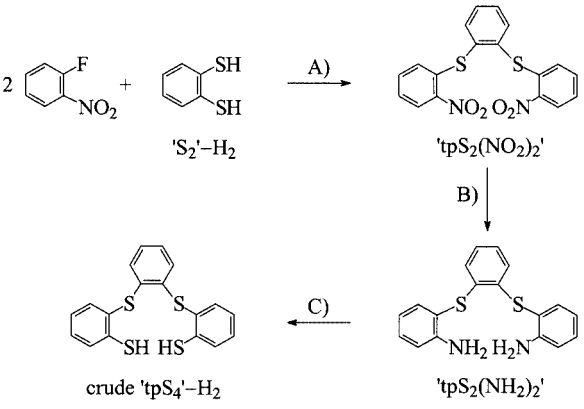

Scheme 2. Synthesis of crude 'tpS_4'-H_2: (A) + 2 NaOMe, MeOH, 12 h reflux; (B) Zn, NH_4Cl, THF, 3 h reflux; (C) (a) H_2SO_4, $NaNO_2$, H_2O, 0 °C; (b) + KSC(S)OEt, H_2O, 85 °C; (c) + KOH, EtOH, 19 h reflux; (d) + HCl, H_2O

Polyfunctional species are involved in all these steps, and the final crude product was usually heavily contaminated by side-products. Removal of these side-products had previously been achievable only in a very laborious way that included treatment of the crude 'tpS_4'-H_2 with LiOMe to give crude 'tpS_4'-Li_2, and the synthesis of the nickel complex [Ni('tpS_4')]$_2$. Recrystallisation of this nickel complex was the essential purification step. Acidolysis of [Ni('tpS_4')]$_2$ finally yielded pure 'tpS_4'-H_2, which could be converted into pure 'tpS_4'-Li_2 as a storable form. In the end, pure 'tpS_4'-H_2 or 'tpS_4'-Li_2 were obtained only in 100 mg amounts and yields that rarely exceeded 20%.[6]

In optimisation of the reaction conditions we have now found that the steps A and B of Scheme 1 can be scaled up and improved such that the intermediates '$tpS_2(NO_2)_2$' and '$tpS_2(NH_2)_2$' are obtained in nearly quantitative yields. The steps leading to 'tpS_4'-H_2 can also be scaled up, and the resulting crude product is obtained in a form that directly gives white 'tpS_4'-Na_2 in yields of ca. 70% and in gram amounts upon treatment with NaOH. The procedure described here (cf. Exp. Sect.) now makes 'tpS_4'-H_2 readily available in preparative amounts for the synthesis of metal complexes.

Syntheses of [Fe('tpS_4')] Complexes

Scheme 3 summarises the syntheses of [Fe('tpS_4'] complexes.

Coordination of anionic 'tpS_4'$^{2-}$ to Fe^{II} centres was readily achieved by treating methanolic solutions of 'tpS_4'-Li_2 (or 'tpS_4'-Na_2) with $FeCl_2{\cdot}4H_2O$. Light brown [Fe('tpS_4')] (**1**) was obtained. This is soluble in coordinating solvents such as THF or MeOH, but also in noncoordinating CH_2Cl_2. In this regard, [Fe('tpS_4')] (**1**) differs remarkably from tetranuclear [Fe('S_4')]$_4$, which is practically insoluble in all common organic solvents.[7] This solubility in THF, MeOH and CH_2Cl_2 made [Fe('tpS_4')] (**1**) the best-suited precursor for [Fe(L^1)(L^2)('tpS_4')] complexes.

The nuclearity of [Fe('tpS_4')] (**1**) remained undetermined. FD mass spectra of **1** showed peaks at *m*/*z* = 412, 824 and 1236, assignable to mono-, di- and trinuclear [Fe('tpS_4')] species. The mass peak at *m*/*z* = 1236 is compatible with the assumption that in the solid state and in the absence of co-ligands, [Fe('tpS_4')] (**1**) trimerises through thiolate bridges in such a way that coordinatively saturated hexacoordinate iron centres result. All X-ray structure determinations of [Fe(L^1)(L^2)('tpS_4')] complexes established a helical coordination of 'tpS_4'$^{2-}$ to the Fe centre (vide infra). Such a coordination can also be assumed for [Fe('tpS_4')] (**1**), the fifth and sixth coordination sites of which may be occupied by solvent molecules in solution. In the solid state, complex **1** is paramagnetic and exhibits μ_{eff} = 3.13 μ_B at room temperature.

Treatment of **1** in THF solution with an excess of CO yielded the *cis*-dicarbonyl complex [Fe$(CO)_2$('tpS_4')] (**2**), as indicated by two ν(CO) bands at 2047 and 2004 cm^{-1} in the IR spectrum. In stark contrast to the analogous [Fe$(CO)_2$('S_4')],[8] which is stable in solution and in the solid state, [Fe$(CO)_2$('tpS_4')] (**2**) is highly labile and could not be isolated in the solid state. Attempts to separate **2** from solution always yielded red-brown powders with IR spectra exhibiting strong ν(CO) bands at 1979 cm^{-1}, indicating that complex **2** had dissociated one CO ligand and that the resulting complex fragments had dimerised to give [Fe(CO)('tpS_4')]$_2$ (**3**).

This indication could be corroborated by independent experiments. Treatment of an MeOH solution of **1** with exactly 1 equiv. of CO directly gave [Fe(CO)('tpS_4')]$_2$ (**3**). Complex **3** is sparingly soluble in all common solvents and

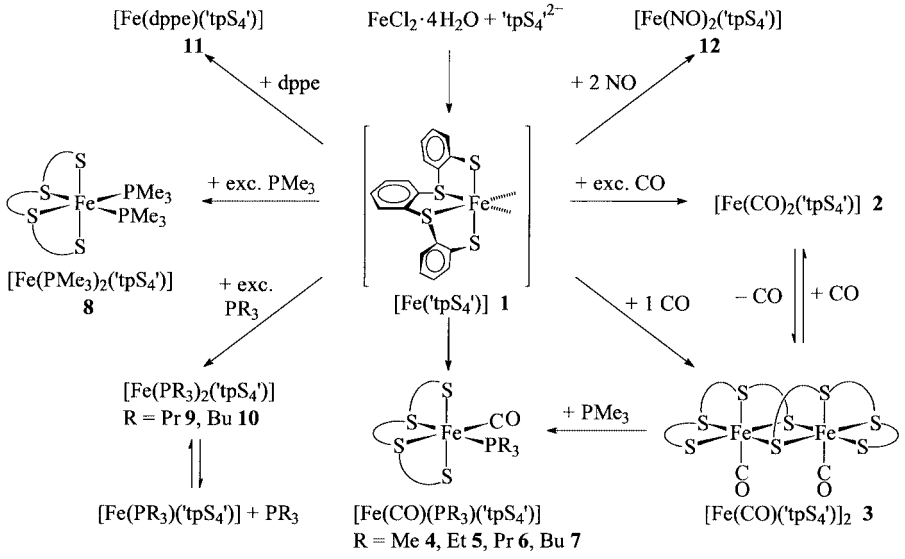

Scheme 3. Synthesis of [Fe('tpS$_4$')] complexes

precipitated from solution. Its dinuclear structure was established by X-ray crystallography.

The dissociation of CO from [Fe(CO)$_2$('tpS$_4$')] (**2**) is reversible. Treatment of an MeOH or THF suspension of **3** with an excess of CO gave a clear solution of [Fe(CO)$_2$('tpS$_4$')] (**2**), from which **3** precipitated again when the atmosphere of CO was replaced by N_2. These observations enabled us to conclude that an equilibrium exists between **2**, **3** and CO. This is driven in the direction of **3** by that compound's low solubility when the partial pressure of CO is decreased.

One more possible reason for the labile bonding of CO in [Fe(CO)$_2$('tpS$_4$')] (**2**) could be the electron density at the iron centre. Comparison of the ν(CO) bands (in KBr) of [Fe(CO)$_2$('tpS$_4$')] and [Fe(CO)$_2$('S$_4$')] (2048/2002 cm^{-1} vs. 2036/1992 cm^{-1}) and [Fe(CO)('tpS$_4$')]$_2$ and [Fe(CO)('S$_4$')]$_2$ (1979 vs. 1965 cm^{-1})[9] shows that the iron centres have a lower electron density in the [Fe('tpS$_4$')] species than in [Fe('S$_4$')], disfavouring the bonding of the π-acceptor CO.

Dinuclear [Fe(CO)('tpS$_4$')]$_2$ (**3**) could also be cleaved by PMe_3 to give mononuclear [Fe(CO)(PMe_3)('tpS$_4$')] (**4**). Complex **4** and the homologous compounds [Fe(CO)(PR$_3$)('tpS$_4$')] with R = Et (**5**), Pr (**6**) and Bu (**7**) were similarly accessible directly from [Fe('tpS$_4$')] (**1**) and equivalent amounts of CO and the corresponding PR_3. The series of complexes **4**–**7** revealed another difference between [Fe('tpS$_4$')] and [Fe('S$_4$')] complexes. While [Fe(CO)(PR$_3$)('S$_4$')] species could be obtained with practically every phosphane, ranging from PMe_3 over PBu_3 up to bulky PPh_3 and PCy_3,[10] [Fe(CO)(PR$_3$)('tpS$_4$')] complexes were accessible only with alkylphosphanes with relatively small cone angles.[11] No evidence could be found for the coordination of PPh_3 or PCy_3 to [Fe(CO)('tpS$_4$')] fragments.

As judged by their NMR spectra, all complexes **4**–**7** are diamagnetic. They each show a characteristic ν(CO) band in the 1959–1955 cm^{-1} range. The influence of the size of the PR_3 moiety for coordination of phosphanes to [Fe('tpS$_4$')] fragments became even more apparent with bis(phosphane) complexes [Fe(PR$_3$)$_2$('tpS$_4$')]. Isolable complexes could be obtained only with PMe_3 and the chelating dppe. Treatment of **1** with an excess of PMe_3 or equivalent amounts of dppe gave [Fe(PMe_3)$_2$('tpS$_4$')] (**8**) and [Fe(dppe)('tpS$_4$')] (**11**), respectively, which could be completely characterised. Treatment of [Fe('tpS$_4$')] (**1**) with PPr_3 or PBu_3, however, yielded very labile [Fe(PR$_3$)$_2$('tpS$_4$')] with R = Pr (**9**) or Bu (**10**), which could be identified only by their molecular ions in their FD mass spectra and by ^{31}P NMR spectroscopy in solution in the presence of excess phosphane. Attempts to isolate **9** or **10** in the solid state resulted in phosphane dissociation and products that gave unsatisfactory elemental analyses. The lability of the bis(phosphane) complexes [Fe(PR$_3$)$_2$('tpS$_4$')] **9** (Pr) and **10** (Bu), which prevents their isolation in the solid state, however, has considerable synthetic value and explains the hitherto unexplained decisive influence of the R substituents for trapping diazene, N_2H_2, from solution and the stabilisation of the diazene complexes [μ-N_2H_2{Fe(PR$_3$)('tpS$_4$')}$_2$] with R = Pr, Bu.

As evidenced by the diamagnetism of complexes **4**–**8** or **11**, binding of σ–π ligands to [Fe('tpS$_4$')] fragments produces a low-spin state in the Fe^{II} centres. The NMR spectra and chemical behaviour of **9** and **10**, on the other hand, indicate that their lability is due to an equilibrium according to Equation (1).

$$[Fe(PR_3)_2('tpS_4')] \rightleftharpoons [Fe(PR_3)('tpS_4')] + PR_3 \quad (1)$$

The resulting five-coordinate [Fe(PR$_3$)('tpS$_4$')] fragment has a vacant coordination site and a low-spin (diamagnetic) Fe^{II} centre, both of which are necessary to enable the coordination and stabilisation of N_2H_2. (In molecular orbital

theory terms, the diamagnetism of [Fe(PR_3)('tpS_4')] means that no electrons occupy antibonding orbitals.)

In concluding experiments, the coordination of NO and NO^+ to [Fe('tpS_4')] fragments was examined. The same complex was formed in all cases, its elemental analysis and spectroscopic data being compatible with the formula [Fe($NO)_2$('tpS_4')] (**12**). In CH_2Cl_2 solution, complex **12** shows two strong ν(NO) bands at 1779 and 1750 cm^{-1}, indicative of a *cis*-Fe($NO)_2$ entity. The strong tendency towards the formation of **12** became evident from the various reactions in which it was formed. For example, complex **12** was produced when [Fe('tpS_4')] (**1**) in CH_2Cl_2 was treated with 2 equiv. of NO gas. The two ν(NO) bands of **12** became visible in the IR spectrum of the solution even after injection of only the first equivalent. Injection of the second equivalent increased the ν(NO) band intensity. Likewise, successive treatment of [Fe(CO)('tpS_4')]$_2$ (**3**) in CH_2Cl_2 with 2 equiv. of NO gas instantaneously gave rise to the formation of [Fe($NO)_2$('tpS_4')] (**12**). No intermediates such as the 19-VE species [Fe(CO)(NO)('tpS_4')] or [Fe(NO)('tpS_4')]$_2$ could be observed by IR spectroscopy. That 19-VE complexes such as [Fe(CO)(NO)('tpS_4')], which may be expected to be labile, may occur can be concluded from the fact that [Fe($CO)_2$('tpS_4')] was formed as the second product in the reaction between [Fe(CO)('tpS_4')]$_2$ (**3**) and NO gas (Figure 1).

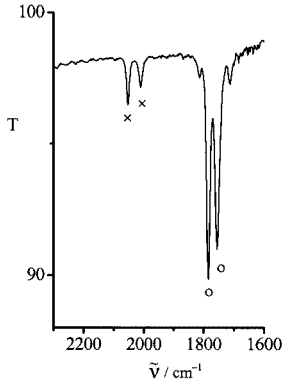

Figure 1. ν(CO)/ν(NO) region of the reaction solution (CH_2Cl_2) when [Fe(CO)('tpS_4')]$_2$ (**3**) is treated with 2 equiv. of NO gas {× = [Fe($CO)_2$('tpS_4')] (**2**), o = [Fe($NO)_2$('tpS_4')] (**12**)}

The formation of [Fe($CO)_2$('tpS_4')] can be explained by CO dissociation and transfer reactions between the labile [Fe(CO)(NO)('tpS_4')] and dinuclear **3**. Treatment of **1** or **3** with $NOBF_4$ also yielded [Fe($NO)_2$('tpS_4')]. No other nitrosyl complexes were observed, and the reducing agent necessary for the $NO^+ \rightarrow NO$ conversion was not identified.

The ^1H NMR spectrum of **12** shows only a multiplet for the aromatic protons of the [Fe('tpS_4')] fragment and indicates diamagnetism of **12**, but is inconclusive in any other respect. The insufficient solubility of **12** prevented the recording of ^{13}C NMR spectra. The FD mass spectra showed a minor peak for the molecular ion at m/z = 472 and strong peaks at m/z = 442 as well as at 412, 824 and 1236, assignable to [Fe(NO)('tpS_4')] and [Fe('tpS_4')]$_x$ species with x = 1, 2 and 3. The diamagnetism of **12**, the fact that all [Fe('tpS_4')] complexes with σ−π co-ligands obey the 18-valence-electron rule and the other data are compatible with the alternative structures **I** and **II**.

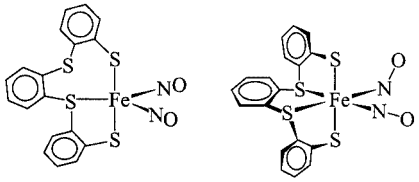

I **II**

In formula **I**, the two [FeNO] groups are linear and one sulfur donor atom of 'tpS_4'$^{2-}$ is decoordinated. In formula **II**, the 'tpS_4'$^{2-}$ ligand stays tetradentate, but one NO ligand acts as a $1e^-$ donor, the other one as a $3e^-$ donor, and both types of NO possibly isomerise quickly as in, for example, $[Ru(NO)_2Cl(PPh_3)_2]^+$.[12]

In order to examine the stability of [Fe('tpS_4')] fragments towards photolysis, solutions of [Fe(CO)('tpS_4')]$_2$ (**3**), [Fe($PMe_3)_2$('tpS_4')] (**8**) and [Fe(CO)(PMe_3)('tpS_4')] (**4**) were UV-irradiated for prolonged periods of time. The CO ligands of **3** and **4** dissociated, but in no case could decomposition of

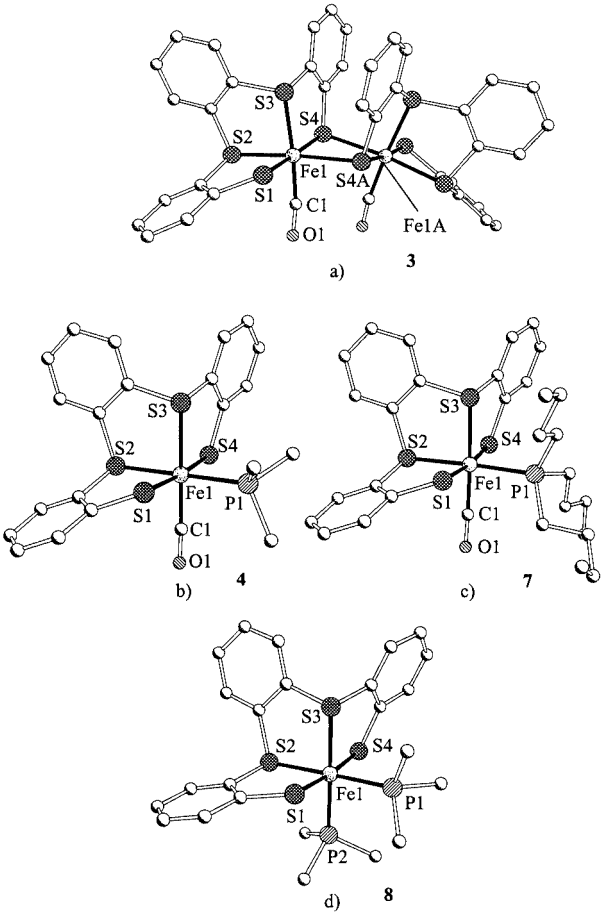

Figure 2. Molecular structures of a) [Fe(CO)('tpS_4')]$_2$·MeOH (**3**·MeOH), b) [Fe(CO)(PMe_3)('tpS_4')] (**4**), c) [Fe(CO)(PBu_3)('tpS_4')] (**7**) and d) [Fe($PMe_3)_2$('tpS_4')] (**8**) (H atoms and solvent molecules omitted)

Table 1. Selected distances [pm] and angles [°] of [Fe(CO)('tpS_4')]$_2$·MeOH (**3**·MeOH), [Fe(CO)(PMe_3)('tpS_4')] (**4**), [Fe(CO)(PBu_3)('tpS_4')] (**7**) and [Fe(PMe_3)$_2$('tpS_4')] (**8**)

	3·MeOH		**4**	**7**		**8**
Fe1−S1	228.9(3)	Fe1−S1	230.9(2)	230.5(2)	Fe1−S1	231.7(2)
Fe1−S2	224.1(3)	Fe1−S2	227.6(3)	225.7(2)	Fe1−S2	224.9(2)
Fe1−S3	228.5(3)	Fe1−S3	226.2(3)	227.1(2)	Fe1−S3	224.8(2)
Fe1−S4	228.5(3)	Fe1−S4	229.8(3)	231.0(2)	Fe1−S4	230.3(2)
Fe1−S4A	234.5(3)	Fe1−P1	225.0(3)	225.2(2)	Fe1−P1	225.1(2)
Fe1−C1	176.4(9)	Fe1−C1	177(1)	175.2(6)	Fe1−P2	224.7(2)
C1−O1	113.2(9)	C1−O1	113(2)	114.8(7)		
Fe1−Fe1A	341.0(2)					
S1−Fe1−S4	174.6(2)	S1−Fe1−S4	175.5(2)	173.71(7)	S1−Fe1−S4	174.94(9)
S2−Fe1−S4A	174.0(2)	S2−Fe1−P1	176.0(1)	177.38(6)	S2−Fe1−P1	173.81(8)
S3−Fe1−C1	174.7(4)	S3−Fe1−C1	178.5(4)	177.8(2)	S3−Fe1−P2	174.71(8)
S1−Fe1−S4A	93.6(2)	S1−Fe1−P1	89.6(1)	91.54(6)	S1−Fe1−P1	87.60(7)
S1−Fe1−C1	87.9(4)	S1−Fe1−C1	90.4(3)	90.1(2)	S1−Fe1−P2	95.56(8)
C1−Fe1−S4A	87.1(3)	P1−Fe1−C1	89.6(4)	89.2(2)	P1−Fe1−P2	93.15(8)
Fe1−C1−O1	172(2)	Fe1−C1−O1	177(1)	178.1(5)		

the [Fe('tpS_4')] fragments by C−S cleavage reactions be observed.

X-ray Structure Analyses

The molecular structures of [Fe(CO)('tpS_4')]$_2$·MeOH (**3**·MeOH), [Fe(CO)(PMe_3)('tpS_4')] (**4**), [Fe(CO)(PBu_3)('tpS_4')] (**7**) and [Fe(PMe_3)$_2$('tpS_4')] (**8**) were determined by X-ray crystallography and are shown in Figure 2. Table 1 lists selected distances and angles.

All complexes exhibit six-coordinate Fe centres and helical coordination of the 'tpS_4'$^{2-}$ ligands, resulting in chiral [Fe('tpS_4')] fragments with *trans*-thiolate and *cis*-thioether donors. Figure 1 shows the respective (*R*) enantiomers of **4**, **7** and **8**. In [Fe(CO)('tpS_4')]$_2$ (**3**), two such homochiral (*R*)-[Fe('tpS_4')] fragments are bridged through thiolate donors to give C_2-symmetrical **3**. The structure of **3** is noteworthy because it appears to be favoured in spite of the strikingly different spatial filling of the coordination sphere and the evident resulting steric strain. While the top "half" of **3** is heavily overloaded, the bottom "half" is occupied only by the two CO ligands. The electronic inequivalence of the thiolate donors in C_1-symmetrical [Fe(CO)('tpS_4')] fragments is a potential factor in favour of this type of structure. A precedent has been observed with [Fe(CO)('S_4')][9] and, according to the classification introduced then, the structure shown in Figure 1 (part a) is the αα-*Z*(*RR*) isomer of **3**.

The bond lengths of all four compounds lie in the ranges characteristic for this type of diamagnetic Fe^{II} complexes.[10] For example, terminal Fe−S distances are found in the 224−230 pm range, and Fe−S−Fe bridging distances can be elongated up to 234 pm, indicating the tendency of dinuclear complexes to dissociate into mononuclear species. As also observed for [Fe('S_4')] complexes, no marked *trans* influence of such different donors as S(thiolate), CO or PR_3 upon the respective *trans* bonds can be recognised in any of the [Fe('tpS_4')] complexes. The following structural differences between [Fe(L^1)(L^2)('tpS_4')] and the corresponding [Fe(L^1)(L^2)('S_4')] complexes are to be noted.

In [Fe(L^1)(L^2)('S_4')] complexes, the Fe−S(thioether) and Fe−S(thiolate) distances tend to be equivalent, frequently identical.[3] In [Fe(L^1)(L^2)('tpS_4')] complexes, however, the Fe−S(thioether) distances are usually distinctly shorter than the Fe−S(thiolate) distances. This is certainly not due to a better donor capability of the thioether donors but rather results from the bite angle of the *o*-phenylenebis(thioether) entity, which is smaller than that of the [SC_2H_4S] bridge in the 'S_4'$^{2-}$ ligand. Another major difference is the conformation of the central five-membered chelate ring in [Fe('S_4')] and [Fe('tpS_4')] fragments. Figure 3 shows that this [FeS(2)S(3)] ring adopts a puckered (envelope) conformation in [Fe('S_4')], whereas the chelate ring is virtually planar (coplanar to within 20 pm with the benzene ring) in [Fe('tpS_4')].

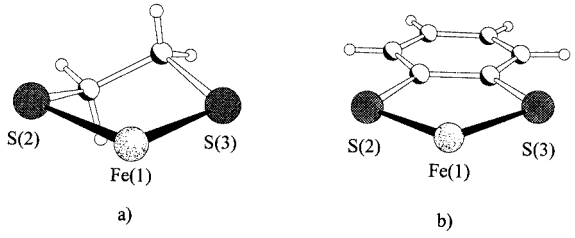

Figure 3. Comparison of the central five-membered [FeS_2C_2] rings in a) [Fe('S_4')] and b) [Fe('tpS_4')] complexes

Thus, the small but significantly different reactivities of [Fe('S_4')] and [Fe('tpS_4')] fragments with regard to the coordination of co-ligands such as CO and phosphanes can be traced back to slightly different electron densities at the Fe centres [cf. the ν(CO) frequencies] as well as to the structural flexibility or rigidity of the central [FeS_2C_2] chelate rings in these complexes.

Conclusion

Optimised synthesis and purification steps have now made 'tpS_4'-H_2 available in the preparative amounts needed

for thorough investigation of its coordination properties. Comparison of the [Fe(L^1)(L^2)('tpS_4')] complexes described in this work with the [Fe(L^1)(L^2)('S_4')] complexes obtained in previous studies shows that [Fe('tpS_4')] and [Fe('S_4')] complex fragments exhibit both close similarities and distinctive differences. While the similarities can be traced back to the identical coordination of Fe^{II} centres by two *trans*-thiolate and two *cis*-thioether donors, the differences result from a slightly lower electron density at the Fe centres and the more rigid core structure of [Fe('tpS_4')] vs. [Fe('S_4')] fragments. These differences are illustrated by, for example, the [Fe(CO)(PR_3)('tpS_4')] and [Fe(CO)(PR_3)('S_4')] complexes. While the [Fe(CO)('tpS_4')] fragment binds only small alkylphosphanes, the [Fe(CO)('S_4')] fragment can also coordinate bulky phosphanes such as PPh_3 and PCy_3. The lability of [Fe(PR_3)$_2$('tpS_4')] with R = Pr (**9**), Bu (**10**), resulting in the reversible dissociation of one PR_3 ligand, explains the decisive influence of PPr_3 and PBu_3 ligands for the stabilisation of N_2H_2 in the diazene complexes [μ-N_2H_2{Fe(PR_3)('tpS_4')}$_2$] with R = Pr, Bu. While PMe_3 gives stable [Fe(PMe_3)$_2$('tpS_4')] (**8**) and PPh_3 or PCy_3 do not coordinate at all to [Fe('tpS_4')] fragments, the medium-sized phosphanes PPr_3 and PBu_3 in solution give rise to five-coordinate [Fe(PR_3)('tpS_4')] species that are diamagnetic and have a vacant site. Diamagnetism and a vacant site are both necessary requirements for the binding and stabilisation of unstable N_2H_2 to [Fe(PR_3)('tpS_4')] fragments. The previously inexplicable stabilisation effect of PPr_3 and PBu_3 in the iron diazene complexes is thus in the end due neither to pronounced electronic nor steric effects, but to a simple dissociation equilibrium between [Fe(PR_3)$_2$('tpS_4')], [Fe(PR_3)('tpS_4')] and PR_3.

Experimental Section

General Methods: Unless noted otherwise, all reactions and operations were carried out at room temperature under nitrogen by use of standard Schlenk techniques. Solvents were dried and distilled before use. As far as possible, reactions were monitored by IR or NMR spectroscopy. Spectra were recorded with the following instruments: IR (KBr disks or CaF_2 cuvettes, solvent bands were compensated): Perkin−Elmer 16 PC FT-IR; NMR: Jeol FT-JNM-GX 270, EX 270 and Lambda LA 400, with the protio solvent signals used as a reference, chemical shifts are quoted on the δ scale (downfield shifts are positive) relative to tetramethylsilane (^{1}H, ^{13}C{^{1}H} NMR) or 85% H_3PO_4 (^{31}P{^{1}H} NMR). Spectra were recorded at 25 °C; MS: JEOL MSTATION 700 spectrometer; elemental analyses: Carlo Erba EA 1106 and 1108 analyser. Magnetic moments were determined with a Johnson−Matthey susceptibility balance. 'tpS_4'-Li_2,[5] PMe_3, PEt_3, P*n*Pr_3 and P*n*Bu_3 [13] were prepared as described in the literature, dppe was purchased from Aldrich.

'$tpS_2(NO_2)_2$': *o*-$C_6H_4(SH)_2$ (15.1 mL, 118.8 mmol) and 2-fluoronitrobenzene (35.1 mL, 332.6 mmol) were added to a solution of NaOMe (13.16 g, 243.6 mmol) in MeOH (400 mL). The solution was heated to reflux for 12 h, in the course of which a bright yellow precipitate formed. After the suspension had cooled to room temperature, the precipitate was separated, washed with MeOH (80 mL), H_2O (120 mL), and again MeOH (30 mL) and dried in vacuo. Yield: 39.64 g (95%). The product was identified by ^{1}H NMR spectroscopy and mass spectrometry.

'$tpS_2(NH_2)_2$': Zinc powder (67.4 g, 1.031 mol) and NH_4Cl (55.2 g, 1.031 mol) were added to a yellow suspension of '$tpS_2(NO_2)_2$' (39.64 g, 103.1 mmol) in THF (600 mL). The resulting grey suspension was heated to reflux for 3 h and filtered while hot. The solid residue was thoroughly extracted with hot THF (400 mL). The filtrate and combined THF washing solutions were concentrated under reduced pressure, yielding a colourless oily residue. This residue was treated with hot EtOH (50 mL) to give a white powder, which was separated, washed with EtOH (50 mL) and dried in vacuo. Additional product precipitated from the combined EtOH filtrates overnight. Yield: 32.79 g (98%). The product was identified by IR and ^{1}H NMR spectroscopy and mass spectrometry.

'tpS_4'-H_2 (Crude Product): Whilst stirring, a white suspension of powdered '$tpS_2(NH_2)_2$' (21.64 g, 66.7 mmol) in H_2O (200 mL) was cooled to 0 °C. In order to keep the suspension at 0 °C, ice (90 g) was added. After addition of a solution of H_2SO_4 (15.9 g, 161.9 mmol) in H_2O (100 mL), an aqueous solution of $NaNO_2$ (9.67 g, 140.1 mmol, 100 mL) was added dropwise. The resulting yellow orange suspension was stirred at 0 °C for another hour and subsequently added dropwise to a hot solution (85 °C) of potassium *O*-ethylxanthogenate (86.5 g, 539.9 mmol) in H_2O (200 mL), yielding a red-brown oil. The reaction mixture was stirred for another 30 min at 85 °C, cooled to room temperature and extracted with CH_2Cl_2 (600 mL). The combined CH_2Cl_2 extracts were dried with Na_2SO_4 and filtered, and the solvents were evaporated to give a dark red oil as residue. EtOH (250 mL) and powdered KOH (42.9 g, 764.6 mmol) were added, and the resulting suspension was heated to reflux for 19 h to give a dark red solution. EtOH was removed in vacuo, the remaining orange-brown residue was dissolved in H_2O (250 mL), and the resulting aqueous solution was extracted with CH_2Cl_2 (300 mL) in a separating funnel. The aqueous solution was separated and acidified with concentrated hydrochloric acid to pH = 0.5, whereupon a red oil separated. The oil/water mixture was extracted several times with CH_2Cl_2 (400 mL), the combined CH_2Cl_2 extracts were dried with Na_2SO_4 and filtered, and the solvents were evaporated to yield an orange-red oily residue, which was dried in vacuo for 12 h. Yield: 18.5 g (77%) of crude product, which contained approximately 62% of 'tpS_4'-H_2 according to the ^{1}H NMR spectrum in CD_2Cl_2.

'tpS_4'-Na_2: A dark red solution of the crude product [12.33 g, containing ca. 62% (21 mmol) of 'tpS_4'-H_2] in THF (50 mL) was combined with an MeOH solution (80 mL) of NaOMe (2.30 g, 42.6 mmol). Volatile components were removed, and the brown-red residue was dried in vacuo for 12 h and subsequently suspended in THF (200 mL). Stirring of the suspension for 1 h resulted in a white solid, which was separated, washed with THF (120 mL) and dried in vacuo for 12 h. Yield: 6.39 g (74%, referred to 'tpS_4'-H_2 contained in the crude product). The product contained traces of THF, which could not be removed by drying in vacuo for 48 h. ^{1}H NMR ([D$_4$]MeOH, 269.72 MHz): δ = 7.52−7.40 (m, 2 H), 7.30−7.18 (m, 2 H), 7.14−7.03 (m, 2 H), 6.82−6.57 (m, 6 H, C_6H_4), 3.70 (m, 4 H), 1.84 (m, 4 H, THF) ppm. ^{13}C{^{1}H} NMR ([D$_4$]MeOH, 100.40 MHz): δ = 149.25, 139.63, 137.98, 134.05, 132.91, 128.42, 126.82, 124.69, 120.90 [C (aryl)], 67.52, 25.16 (THF) ppm. IR (KBr): $\tilde{\nu}$ = 1565 m, 1437 s, 1422 s [ν(C=C)], 739 cm^{-1} vs [δ(C−H)].

[Fe('tpS_4')] (1): $FeCl_2 \cdot 4H_2O$ (68 mg, 0.34 mmol) was added to a light yellow solution of 'tpS_4'-Li_2 (126 mg, 0.34 mmol) in MeOH (30 mL). After stirring for 1 h, the reaction mixture was filtered

and concentrated to dryness. The resulting yellow-brown residue was dried in vacuo overnight and redissolved in CH_2Cl_2 (25 mL) to remove LiCl. The resulting suspension was filtered and the brown-red filtrate was evaporated to dryness. Stirring of the residue with Et_2O (20 mL) yielded brown microcrystals, which were separated, washed with Et_2O (30 mL) and dried in vacuo. Yield: 102 mg (**1**·0.25 CH_2Cl_2) (69%). IR (KBr): $\tilde{\nu}$ = 1566 m [ν(C=C)], 746 cm^{-1} vs [δ(C−H)]. MS (FD, THF, ^{56}Fe): *m*/*z*: 412 [Fe('tpS_4')]$^+$, 824 [Fe('tpS_4')]$_2^+$, 1236 [Fe('tpS_4')]$_3^+$; μ_{eff} (295 K) = 3.13 μ_B. $C_{18.25}H_{12.5}Cl_{0.5}FeS_4$ (**1**·0.25CH_2Cl_2) (433.63): calcd. C 50.55, H 2.91, S 29.58; found C 50.52, H 3.06, S 29.68.

[Fe(CO)('tpS_4')]$_2$ (3): $FeCl_2·4H_2O$ (126 mg, 0.64 mmol) was added to a light yellow solution of 'tpS_4'-Li_2 (236 mg, 0.64 mmol) in MeOH (50 mL). The orange-red reaction mixture was stirred for 1 h and filtered, and CO gas (14.3 mL, 0.64 mmol) was injected into the filtrate by syringe. A brick-red precipitate formed; after 6 h this was separated, washed with MeOH (45 mL) and Et_2O (30 mL), and dried in vacuo. Yield: 234 mg (**3**·MeOH) (81%). IR (KBr): $\tilde{\nu}$ = 1979 cm^{-1} vs [ν(CO)]. MS (FD, THF, ^{56}Fe): *m*/*z*: 412 [Fe('tpS_4')]$^+$, 824 [Fe('tpS_4')]$_2^+$, 1236 [Fe('tpS_4')]$_3^+$. $C_{39}H_{28}Fe_2O_3S_8$ (**3**·MeOH) (912.87): calcd. C 51.32, H 3.09, S 28.10; found C 51.13, H 3.08, S 28.13. Because of the low solubility of **3**, no NMR spectra could be recorded.

[Fe(CO)(PMe_3)('tpS_4')] (4): $FeCl_2·4H_2O$ (59 mg, 0.30 mmol) and PMe_3 (59 μL, 0.30 mmol) were added to a light yellow solution of 'tpS_4'-Li_2 (110 mg, 0.30 mmol) in THF (20 mL) and MeOH (10 mL) to give an olive-green reaction mixture, into which CO gas (16.8 mL, 0.30 mmol) was injected by syringe. A red solution resulted, and this was filtered, reduced in volume to 2 mL and combined with MeOH (20 mL). A light green precipitate formed and was separated, washed with MeOH (20 mL) and Et_2O (20 mL) and dried in vacuo. Yield: 80 mg (**4**·0.5MeOH) (51%). ^{1}H NMR (CD_2Cl_2, 269.72 MHz): δ = 8.25−6.70 (m, 12 H, C_6H_4), 1.44 (br. s, 9 H, CH_3) ppm. ^{13}C{^{1}H} NMR (CD_2Cl_2, 100.40 MHz): δ = 217.25 (d, J_{PC} = 31.1 Hz, *C*O), 157.59, 156.44 (d, J_{PC} = 2.7 Hz), 139.13, 138.97, 137.57, 136.01, 132.23, 132.11, 131.18, 131.04, 130.74, 130.69, 130.33, 129.78, 129.67, 129.40, 122.60, 122.53 [*C* (aryl)], 16.44 (d, J_{PC} = 29.2 Hz, CH_3) ppm. ^{31}P{^{1}H} NMR (CD_2Cl_2, 161.70 MHz): δ = 21.50 (s, PMe_3) ppm. IR (KBr): $\tilde{\nu}$ = 1966, 1957 vs [ν(CO)], 952 cm^{-1} m [δ(PCH)]. IR (THF): $\tilde{\nu}$ = 1959 cm^{-1} vs [ν(CO)]. MS (FD, THF, ^{56}Fe): *m*/*z*: 516 [Fe(CO)(PMe_3)('tpS_4')]$^+$, 412 [Fe('tpS_4')]$^+$, 824 [Fe('tpS_4')]$_2^+$, 1236 [Fe('tpS_4')]$_3^+$. $C_{22.5}H_{23}FeO_{1.5}PS_4$ (**4**·0.5MeOH) (532.51): calcd. C 50.75, H 4.35, S 24.09; found C 50.76, H 4.43, S 23.92.

[Fe(CO)(PEt_3)('tpS_4')] (5): $FeCl_2·4H_2O$ (99 mg, 0.50 mmol) and PEt_3 (158 μL, 0.50 mmol) were added to a light yellow solution of 'tpS_4'-Na_2 (200 mg, 0.50 mmol) in MeOH (10 mL) and THF (20 mL). An olive-green solution resulted, into which CO gas (11.2 mL, 0.50 mmol) was injected by syringe. The reaction mixture was stirred for 2.5 h and filtered, and the dark red filtrate was reduced in volume to 2 mL. Upon addition of MeOH (20 mL), light brown microcrystals formed, and were separated, washed with MeOH (20 mL) and dried in vacuo. Yield: 53 mg (19%). ^{1}H NMR (CD_2Cl_2, 269.72 MHz): δ = 8.07−7.73 (m, 4 H), 7.44−7.25 (m, 4 H), 7.00−6.81 (m, 4 H, C_6H_4), 1.96−1.63 (m, 6 H), 1.28−1.10 [m, 9 H, P(C_2H_5)$_3$] ppm. ^{13}C{^{1}H} NMR (CD_2Cl_2, 67.83 MHz): δ = 217.79 (d, J_{PC} = 30.1 Hz, *C*O), 157.73, 156.83 (d, J_{PC} = 7.3 Hz), 139.11 (d, J_{PC} = 11.9 Hz), 137.11, 136.29, 132.27, 131.97, 131.07, 130.90, 130.66, 130.63, 130.19, 129.74, 129.64, 129.42, 122.48 [*C* (aryl), partly superimposed], 17.83 (d, J_{PC} = 24.9 Hz), 7.99 [d, J_{PC} = 4.7 Hz, P(C_2H_5)$_3$] ppm. ^{31}P{^{1}H} NMR (CD_2Cl_2, 161.70 MHz): δ = 42.56 (s, PEt_3) ppm. IR (KBr): $\tilde{\nu}$ = 1951 cm^{-1} vs [ν(CO)]. IR (THF): $\tilde{\nu}$ = 1955 cm^{-1} vs [ν(CO)]. MS (FD, THF, ^{56}Fe): *m*/*z*: 558 [Fe(CO)(PEt_3)('tpS_4')]$^+$, 412 [Fe('tpS_4')]$^+$, 824 [Fe('tpS_4')]$_2^+$, 1236 [Fe('tpS_4')]$_3^+$. $C_{25}H_{27}FeOPS_4$ (558.57): calcd. C 53.76, H 4.87, S 22.96; found C 53.62, H 5.14, S 22.93.

[Fe(CO)(P*n*Pr_3)('tpS_4')] (6): $FeCl_2·4H_2O$ (157 mg, 0.79 mmol) and P*n*Pr_3 (158 μL, 0.79 mmol) were added to a light yellow solution of 'tpS_4'-Li_2 (292 mg, 0.79 mmol) in THF (25 mL) and MeOH (10 mL). CO gas (17.7 mL, 0.79 mmol) was injected by syringe into the olive-green mixture, which turned into a dark-red solution within 3 h. The solution was filtered, reduced in volume to 5 mL and combined with MeOH (20 mL). Grey microcrystals formed, and were separated, washed with MeOH (30 mL) and Et_2O (20 mL) and dried in vacuo. Yield: 314 mg (**6**·MeOH) (63%). ^{1}H NMR (CD_2Cl_2, 269.72 MHz): δ = 8.08−7.69 (m, 4 H), 7.46−7.23 (m, 4 H), 7.02−6.79 (m, 4 H, C_6H_4), 1.88−1.42 (m, 12 H), 1.01 [t, 9 H, P(C_3H_7)$_3$] ppm. ^{13}C{^{1}H} NMR (CD_2Cl_2, 100.40 MHz): δ = 217.78 (d, J_{PC} = 30.2 Hz, *C*O), 158.01, 156.81 (d, J_{PC} = 7.3 Hz), 139.15, 138.98, 138.84 (d, J_{PC} = 0.9 Hz), 137.02, 136.43, 132.24, 131.98, 131.13, 130.91, 130.64, 130.59, 130.22, 129.70, 129.62, 129.48, 122.49 [*C* (aryl)], 27.98 (d, J_{PC} = 23.8 Hz), 17.52 (d, J_{PC} = 2.0 Hz), 15.99 [d, J_{PC} = 12.9 Hz, P(C_3H_7)$_3$] ppm. ^{31}P{^{1}H} NMR (CD_2Cl_2, 161.70 MHz): δ = 35.88 (s, *Pn*Pr_3) ppm. IR (KBr): $\tilde{\nu}$ = 1957, 1953 cm^{-1} vs [ν(CO)]. IR (THF): $\tilde{\nu}$ = 1955 cm^{-1} vs [ν(CO)]. MS (FD, THF, ^{56}Fe): *m*/*z*: 600 [Fe(CO)(P*n*Pr_3)('tpS_4')]$^+$, 412 [Fe('tpS_4')]$^+$, 824 [Fe('tpS_4')]$_2^+$, 1236 [Fe('tpS_4')]$_3^+$. $C_{29}H_{37}FeO_2PS_4$ (**6**·MeOH) (632.69): calcd. C 55.05, H 5.89, S 20.27; found C 54.56, H 5.78, S 20.57.

[Fe(CO)(P*n*Bu_3)('tpS_4')] (7): $FeCl_2·4H_2O$ (257 mg, 1.29 mmol) and P*n*Bu_3 (257 μL, 1.29 mmol) were added to a light yellow solution of 'tpS_4'-Li_2 (479 mg, 1.29 mmol) in THF (45 mL) and MeOH (20 mL). CO gas (28.9 mL, 1.29 mmol) was injected into the resulting olive-green solution by syringe. The reaction mixture was stirred for 3 h and filtered, and the dark red filtrate was reduced in volume to 5 mL. After addition of MeOH (20 mL), grey-brown microcrystals precipitated and were separated, washed with MeOH (45 mL) and Et_2O (20 mL) and dried in vacuo. Yield: 482 mg (58%). ^{1}H NMR (CD_2Cl_2, 269.72 MHz): δ = 8.08−7.68 (m, 4 H), 7.47−7.20 (m, 4 H), 7.03−6.79 (m, 4 H, C_6H_4), 1.89−1.31 (m, 18 H), 0.94 [t, 9 H, P(C_4H_9)$_3$] ppm. ^{13}C{^{1}H} NMR (CD_2Cl_2, 67.83 MHz): δ = 217.49 (d, J_{PC} = 30.5 Hz, *C*O), 157.78, 156.59 (d, J_{PC} = 7.5 Hz), 138.87, 138.75, 138.56, 136.74, 136.17, 131.93, 131.67, 130.78, 130.58, 130.29, 130.26, 129.89, 129.40, 129.29, 129.13, 122.14 [*C* (aryl)], 25.45 (d, J_{PC} = 3.7 Hz), 25.14 (d, J_{PC} = 23.6 Hz), 24.38 (d, J_{PC} = 12.4 Hz), 13.51 [s, P(C_4H_9)$_3$] ppm. ^{31}P{^{1}H} NMR (CD_2Cl_2, 161.70 MHz): δ = 34.80 (s, *Pn*Bu_3) ppm. IR (KBr): $\tilde{\nu}$ = 1956, 1953 cm^{-1} vs [ν(CO)]. IR (THF): $\tilde{\nu}$ = 1955 cm^{-1} vs [ν(CO)]. MS (FD, THF, ^{56}Fe): *m*/*z* = 642 [Fe(CO)(P*n*Bu_3)('tpS_4')]$^+$, 412 [Fe('tpS_4')]$^+$, 824 [Fe('tpS_4')]$_2^+$, 1236 [Fe('tpS_4')]$_3^+$. $C_{31}H_{39}FeOPS_4$ (642.73): calcd. C 57.93, H 6.12, S 19.96; found C 57.90, H 6.34, S 19.84.

[Fe(PMe_3)$_2$('tpS_4')] (8): $FeCl_2·4H_2O$ (62 mg, 0.31 mmol) and PMe_3 (0.65 mL, 6.21 mmol) were added to a light yellow solution of 'tpS_4'-Li_2 (115 mg, 0.31 mmol) in THF (30 mL) and MeOH (5 mL). The resulting dark green solution was stirred for 17 h, filtered and reduced in volume nearly to dryness. Upon addition of MeOH (20 mL), olive-green microcrystals precipitated, and were separated, washed with MeOH (30 mL) and Et_2O (12 mL) and dried in vacuo. Yield: 108 mg (62%). ^{1}H NMR (CD_2Cl_2, 269.72 MHz): δ = 7.99−7.93 (m, 2 H), 7.86−7.81 (vdd, 2 H), 7.31−7.24 (m, 4 H), 6.88−6.77 (m, 4 H, C_6H_4), 1.38 (vt, 18 H, P(CH_3)$_3$] ppm. ^{13}C{^{1}H} NMR (CD_2Cl_2, 100.40 MHz): δ = 160.17, 140.85, 138.74, 131.22, 130.82, 129.87, 129.65, 128.58, 121.49 [*C*

(aryl)], 18.14 (t, J_{PC} = 12.0 Hz, P(CH_3)$_3$] ppm. $^{31}P\{^1H\}$ NMR (CD_2Cl_2, 161.70 MHz): δ = 22.09 (s, PMe_3) ppm. IR (KBr): $\tilde{\nu}$ = 956, 944 cm^{-1} vs [δ(PCH)]. MS (FD, CH_2Cl_2, ^{56}Fe): *m*/*z*: 564 [Fe(PMe_3)$_2$('tpS$_4$')]$^+$, 412 [Fe('tpS$_4$')]$^+$, 824 [Fe('tpS$_4$')]$_2^+$, 1236 [Fe('tpS$_4$')]$_3^+$. $C_{24}H_{30}FeP_2S_4$ (564.56): calcd. C 51.06, H 5.36, S 22.72; found C 50.51, H 5.64, S 22.96.

[Fe(P*n*Pr$_3$)$_2$('tpS$_4$')] (9): $FeCl_2{\cdot}4H_2O$ (17 mg, 0.08 mmol) and P*n*Pr$_3$ (0.17 mL, 0.8 mmol) were added to a light yellow solution of 'tpS$_4$'-Li$_2$ (31 mg, 0.08 mmol) in THF (6 mL) and MeOH (1 mL). The resulting solution was stirred for 14 h and concentrated to dryness. A dark green residue resulted, and was dried in vacuo for 20 min and dissolved in CD_2Cl_2 (0.7 mL) to which a few drops of P*n*Pr$_3$ had been added, in order to record NMR spectra. $^{31}P\{^1H\}$ NMR (CD_2Cl_2, 161.70 MHz): δ = 29.1 (s, *Pn*Pr$_3$), −33.4 (s, exc. *Pn*Pr$_3$) ppm. MS (FD, CH_2Cl_2, ^{56}Fe): *m*/*z*: 732 [Fe(P*n*Pr$_3$)$_2$('tpS$_4$')]$^+$, 412 [Fe('tpS$_4$')]$^+$, 824 [Fe('tpS$_4$')]$_2^+$, 1236 [Fe('tpS$_4$')]$_3^+$.

[Fe(P*n*Bu$_3$)$_2$('tpS$_4$')] (10): $FeCl_2{\cdot}4H_2O$ (23 mg, 0.12 mmol) and P*n*Bu$_3$ (0.23 mL, 1.2 mmol) were added to a light yellow solution of 'tpS$_4$'-Li$_2$ (43 mg, 0.12 mmol) in THF (10 mL) and MeOH (2 mL). The resulting solution was stirred for 15 h and concentrated to dryness. The resulting dark green residue was dried in vacuo for 15 min and dissolved in CD_2Cl_2 (0.7 mL) to which a few drops of P*n*Bu$_3$ had been added in order to record NMR spectra. $^{31}P\{^1H\}$ NMR (CD_2Cl_2, 161.70 MHz): δ = 30.3 (s, *Pn*Bu$_3$), −30.2 (s, exc. *Pn*Bu$_3$) ppm. MS (FD, CH_2Cl_2, ^{56}Fe): *m*/*z*: 816 [Fe(P*n*Bu$_3$)$_2$('tpS$_4$')]$^+$, 412 [Fe('tpS$_4$')]$^+$, 824 [Fe('tpS$_4$')]$_2^+$, 1236 [Fe('tpS$_4$')]$_3^+$.

[Fe(dppe)('tpS$_4$')] (11): $FeCl_2{\cdot}4H_2O$ (98 mg, 0.49 mmol) and dppe (196 mg, 0.49 mmol) were added to a light yellow solution of 'tpS$_4$'-Li$_2$ (183 mg, 0.49 mmol) in THF (20 mL) and MeOH (8 mL). The resulting dark green solution was stirred for 90 min, filtered, reduced in volume to 5 mL and combined with MeOH (30 mL). A light green precipitate formed, and this was separated, washed with MeOH (30 mL) and Et_2O (10 mL) and dried in vacuo. Yield: 274 mg (**11**·2MeOH) (63%). ^1H NMR (CD_2Cl_2, 269.72 MHz): δ = 8.15−7.97 (m, 6 H), 7.61−7.43 (m, 8 H), 7.34−7.23 (m, 2 H), 7.05 (vt, 4 H), 6.89−6.66 (m, 6 H), 6.59−6.43 (m, 4 H), 6.30 (vdt, 2 H, C_6H_4, C_6H_5), 3.27−2.76 (m, 4 H, $Ph_2PC_2H_4PPh_2$) ppm. $^{13}C\{^1H\}$ NMR (CD_2Cl_2, 100.40 MHz): δ = 157.90 (t, J_{PC} = 4.1 Hz), 140.79 (t, J_{PC} = 6.0 Hz), 138.41, 134.33, 134.15, 134.13, 134.00, 133.97, 133.83, 133.36 (t, J_{PC} = 4.2 Hz), 131.70 (t, J_{PC} = 4.1 Hz), 131.24, 130.42, 130.17, 130.02, 129.70, 128.43 (t, J_{PC} = 3.6 Hz), 127.95, 126.50 (t, J_{PC} = 4.6 Hz), 121.10 (C_6H_4, C_6H_5, partly covered), 26.23 (t, J_{PC} = 21.0 Hz, $Ph_2PC_2H_4PPh_2$) ppm. $^{31}P\{^1H\}$ NMR (CD_2Cl_2, 161.70 MHz): δ = 74.01 (s, $Ph_2PC_2H_4PPh_2$) ppm. IR (KBr): $\tilde{\nu}$ = 735, 695 cm^{-1} vs [δ(PCH)]. MS (FD, CH_2Cl_2, ^{56}Fe): *m*/*z*: 810 [Fe(dppe)('tpS$_4$')]$_3^+$. $C_{46}H_{44}FeO_2P_2S_4$ (**11**·2MeOH) (874.91): calcd. C 63.15, H 5.07, S 14.66; found C 63.39, H 4.87, S 14.65.

[Fe(NO)$_2$('tpS$_4$')] (12): $FeCl_2{\cdot}4H_2O$ (52 mg, 0.25 mmol) was added to a light yellow solution of 'tpS$_4$'-Li$_2$ (93 mg, 0.25 mmol) in CH_2Cl_2 (30 mL) and MeOH (10 mL). The reaction mixture was filtered, and NO gas (11.4 mL, 0.50 mmol) was injected into the dark orange filtrate by syringe. After stirring for 1 h, the solution was reduced in volume to 4 mL. A red-brown solid precipitated, and this was separated, washed with MeOH (20 mL) and Et_2O (20 mL) and dried in vacuo. Yield: 50 mg (**12**·1.5MeOH) (38%). ^1H NMR (CD_2Cl_2, 269.72 MHz): δ = 7.85−6.45 (m, C_6H_4) ppm. MS (FD, CH_2Cl_2, ^{56}Fe): *m*/*z*: 472 [Fe(NO)$_2$('tpS$_4$')]$^+$, 442 [Fe(NO)('tpS$_4$')]$^+$, 412 [Fe('tpS$_4$')]$^+$, 824 [Fe('tpS$_4$')]$_2^+$, 1236

Table 2. Selected crystallographic data of [Fe(CO)('tpS$_4$')]$_2$·MeOH (**3**·MeOH), [Fe(CO)(PMe_3)('tpS$_4$')] (**4**), [Fe(CO)(PBu_3)('tpS$_4$')] (**7**) and [Fe(PMe_3)$_2$('tpS$_4$')] (**8**)

	3·MeOH	**4**	**7**	**8**
Empirical formula	$C_{39}H_{28}Fe_2O_3S_8$	$C_{22}H_{21}FeOPS_4$	$C_{31}H_{39}FeOPS_4$	$C_{24}H_{30}FeP_2S_4$
M_r [g mol^{-1}]	912.79	516.45	642.68	564.51
T [K]	298	294	200	298
Crystal size [mm]	0.30 × 0.18 × 0.12	0.62 × 0.40 × 0.04	0.50 × 0.42 × 0.30	0.55 × 0.45 × 0.18
Crystal system	tetragonal	monoclinic	monoclinic	monoclinic
Space group	$I4_1/a$	$C2/c$	$P2_1/c$	Cc
F(000)	3728	2128	1352	2352
a [pm]	1484.7(2)	2979.0(7)	2081.8(5)	1993.1(7)
b [pm]	1484.7(2)	1128.1(6)	1109.5(3)	1895.6(6)
c [pm]	3551.0(10)	1419.0(4)	1435.2(3)	1505.0(6)
β [°]	90	106.88(1)	108.86(1)	110.17(3)
V [nm^3]	7.83(1)	4.563(3)	3.137(2)	5.34(1)
Z	8	8	4	8
$\rho_{calcd.}$ [g cm^{-3}]	1.549	1.503	1.361	1.405
μ [mm^{-1}]	1.206	1.109	0.821	1.009
Diffractometer	Nicolet R3m/V	Siemens P4	Siemens P4	Nicolet R3m/V
Radiation [pm]	Mo-K_α (λ = 71.073)	Mo-K_α (λ = 71.073)	Mo-K_α (λ = 71.073)	Mo-K_α (λ = 71.073)
Scan technique	ω-scan	ω-scan	ω-scan	ω-scan
2Θ range [°]	4.4−54.0	3.8−50.0	4.0−54.0	3.6−54.0
Scan speed [° min^{-1}]	5	2	8	5
Measured refl.	5503	4959	8456	7285
Unique refl.	4284	3805	6839	6498
R_{int} [%]	8.39	8.35	5.28	2.75
Observed refl.	764	1973	4403	3795
σ criterion	$F_o \geq 4.0\sigma(F)$	$F_o \geq 4.0\sigma(F)$	$F_o \geq 4.0\sigma(F)$	$F_o \geq 4.0\sigma(F)$
Parameters	240	265	431	559
*R*1; *wR*2 [%]	4.80; 9.62	6.90; 15.71	7.18; 17.86	3.78; 7.13
Abs. structure parameter	−	−	−	−0.02(2)

[Fe('tpS_4')]$_3^+$. IR (KBr): $\tilde{\nu}$ = 1812 w, 1779 vs, 1750 cm^{-1} vs [ν(NO)]. IR (CH_2Cl_2): $\tilde{\nu}$ = 1814 w, 1784 vs, 1756 cm^{-1} vs [ν(NO)]. $C_{19.5}H_{18}FeN_2O_{3.5}S_4$ (**12**·1.5MeOH) (520.48): calcd. C 45.00, H 3.49, N 5.38, S 24.64; found C 44.09, H 2.95, N 5.23, S 24.71.

X-ray Structure Analyses of [Fe(CO)('tpS_4')]$_2$·MeOH (3·MeOH), [Fe(CO)(PMe_3)('tpS_4')] (4), [Fe(CO)(PBu_3)('tpS_4')] (7) and [Fe(PMe_3)$_2$('tpS_4')] (8): Dark red single crystals of **3**·MeOH were formed by layering a saturated THF solution of **3** with MeOH. Green platelets of **4** and brown crystals of **7** were grown by layering saturated CH_2Cl_2 solutions of **4** and **7** with MeOH. Black single crystals of **8** were obtained by layering a saturated THF solution of **8** with Et_2O. Suitable single crystals were either embedded in protective perfluoro polyalkyl ether oil or sealed in a glass capillary under N_2. The structures were solved by direct methods, and full-matrix, least-squares refinement was carried out on F^2 values.[14] All non-hydrogen atoms were refined anisotropically. All hydrogen atoms are geometrically positioned. The MeOH solvate molecule in **3**·MeOH is disordered on a crystallographic 4_1 axis, no hydrogen atoms have been taken into account for this molecule. The PBu_3 ligand in **7** is strongly disordered. Selected crystallographic data are summarised in Table 2.[15]

Acknowledgments

Financial support of this work by the Deutsche Forschungsgemeinschaft, SFB 583 "Redoxaktive Metallkomplexe − Reaktivitätssteuerung durch molekulare Architekturen", and the Fonds der Chemischen Industrie is gratefully acknowledged.

[1] [1a] B. K. Burgess, D. J. Lowe, *Chem. Rev.* **1996**, *96*, 2983−3011. [1b] R. R. Eady, *Chem. Rev.* **1996**, *96*, 2965−2982.
[2] M. Y. Darensbourg, E. J. Lyon, J. J. Smee, *Coord. Chem. Rev.* **2000**, *206/207*, 533−561.
[3] D. Sellmann, J. Sutter, *Acc. Chem. Res.* **1997**, *30*, 460−469 and literature cited there.
[4] D. Sellmann, J. Reißer, *J. Organomet. Chem.* **1985**, *294*, 333−346.
[5] D. Sellmann, K. Engl, T. Gottschalk-Gaudig, F. W. Heinemann, *Eur. J. Inorg. Chem.* **1999**, 333−339.
[6] D. Sellmann, D. C. F. Blum, F. W. Heinemann, *Inorg. Chim. Acta*, **2002**, *337*, 1−10.
[7] D. Sellmann, H. F. Friedrich, F. Knoch, *Z. Naturforsch., Teil B* **1993**, *48*, 1675−1680.
[8] D. Sellmann, H. E. Jonk, H. R. Pfeil, G. Huttner, J. von Seyerl, *J. Organomet. Chem.* **1980**, *191*, 171−179.
[9] [9a] D. Sellmann, R. Weiß, F. Knoch, *Angew. Chem.* **1989**, *101*, 1719−1721; *Angew. Chem. Int., Ed. Engl.* **1989**, *28*, 1703−1705. [9b] D. Sellmann, R. Weiß, F. Knoch, G. Ritter, J. Dengler, *Inorg. Chem.* **1990**, *29*, 4107−4114.
[10] D. Sellmann, A. Hennige, F. W. Heinemann, *Inorg. Chim. Acta* **1998**, *280*, 39−49.
[11] C. A. McAuliffe, in *Comprehensive Coordination Chemistry* (Eds.: G. Wilkinson, R. D. Gillard, J. A. McCleverty), Pergamon Press, Oxford, **1987**, *2*, p. 1015.
[12] L. K. Bell, J. Mason, D. M. P. Mingos, D. G. Tew, *Inorg. Chem.* **1983**, *22*, 3497−3502.
[13] W. Wolfsberger, H. Schmidbaur, *Syn. Reactiv. Inorg. Metal-Org. Chem.* **1974**, *4*, 149−156.
[14] SHELXTL NT 5.10, Bruker AXS, Inc., Madison, WI, **1998**.
[15] CCDC-187351 (**3**·MeOH), -187352 (**4**), -187353 (**7**), and -187354 (**8**) contain the supplementary crystallographic data for this paper. These data can be obtained free of charge at www.ccdc.cam.ac.uk/conts/retrieving.html or from the Cambridge Crystallographic Data Centre, 12 Union Road, Cambridge CB2 1EZ, UK [Fax: (internat.) + 44-1223/336-033; E-mail: deposit@ccdc.cam.ac.uk].

Received June 19, 2002
[I02323]

Chloro- and Alkyltitanium Complexes of a New Dianionic Ancillary Ligand: A Linked Amidinate−Amide[‡]

Wouter J. van Meerendonk,[a] Kai Schröder,[a] Edward A. C. Brussee,[a] Auke Meetsma,[a] Bart Hessen,*[a] and Jan H. Teuben[a]

Keywords: N ligands / Tridentate ligands / Titanium / Alkyl complexes

The lithium amidinate $[Me_3SiNC(Ph)N(CH_2)_3N(Me)SiMe_3]$-Li(THF) (**2**), with a pendant methyl(trimethylsilyl)amine functionality, was prepared and found to react with $[TiCl_4(THF)_2]$ to give the titanium amidinate–amide dichloride complex $[\eta^2,\eta^1$-$Me_3SiNC(Ph)N(CH_2)_3NMe]TiCl_2$ (**3**) by elimination of LiCl and Me_3SiCl. The elimination of Me_3SiCl from the cyclopentadienyl derivative $Cp[\eta^2$-$Me_3SiNC(Ph)N(CH_2)_3N(SiMe_3)Me]TiCl_2$ (**5**) to give $Cp[\eta^2,\eta^1$-$Me_3SiNC(Ph)N(CH_2)_3NMe]TiCl$ (**4**) is much less favorable, and was found to be readily reversible. Dialkyltitanium complexes $[\eta^2,\eta^1$-$Me_3SiNC(Ph)N(CH_2)_3NMe]Ti(CH_2R)_2$ [R = Ph (**6**), $SiMe_3$ (**7**)] were prepared, but could not be activated for catalytic ethene polymerization.

(© Wiley-VCH Verlag GmbH & Co. KGaA, 69451 Weinheim, Germany, 2003)

Introduction

Amidinate monoanions $[RC(NR')_2]^-$ (R = aryl, alkyl; R′ = aryl, alkyl, $SiMe_3$) form a group of versatile ancillary ligands (binding predominantly in an *N*,*N*′-bidentate fashion) that have been employed extensively in main-group and transition-metal coordination chemistry, organometallic chemistry and catalysis.[1−5] They can also be incorporated as a functionality in polydentate ligand systems. Examples have been reported recently of the synthesis and complexation chemistry of monoanionic tridentate amidinate Lewis base[6−9] and dianionic tetradentate bis(amidinate) ligands.[10−12] One way to prepare amidinate-based polydentate ligands is the reaction of functionalized trimethylsilylamides with nitriles.[6,8,9,12] Here we report the use of this method to prepare the amidinate $[Me_3SiNC(Ph)N(CH_2)_3N(SiMe_3)Me]^-$ with a pendant alkyl(trimethylsilyl)amine functionality. Reaction of the Li salt of this amidinate with titanium chlorides leads to the formation of titanium complexes of the new dianionic amidinate−amide tridentate ligand $[Me_3SiNC(Ph)N(CH_2)_3NMe]^{2-}$ by sequential salt metathesis and Me_3SiCl elimination reactions. The synthesis, structure and reactivity of two of these titanium complexes, $[Me_3SiNC(Ph)N(CH_2)_3NMe]TiCl_2$ and Cp-$[Me_3SiNC(Ph)N(CH_2)_3NMe]TiCl$, are described.

[‡] Netherlands Institute for Catalysis Research (NIOK) publication RUG 02-04-05
[a] Center for Catalytic Olefin Polymerization, Stratingh Institute for Chemistry and Chemical Engineering, University of Groningen,
Nijenborgh 4, 9747 AG Groningen, The Netherlands
Fax: (internat.) + 31-50/363-4315
E-mail: hessen@chem.rug.nl

Results and Discussion

The Li salt of an amidinate with a pendant alkyl(trimethylsilyl)amine group, $[Me_3SiNC(Ph)N(CH_2)_3N(SiMe_3)Me]^-$, was prepared by the deprotonation of the diamine Me_3Si-$N(H)(CH_2)_3N(Me)SiMe_3$ (**1**) with *n*BuLi/hexane in THF, followed by reaction with benzonitrile (Scheme 1). After recrystallization from pentane, the resulting Li amidinate was obtained analytically pure as its THF solvate $[Me_3Si$-$NC(Ph)N(CH_2)_3N(Me)SiMe_3]Li(THF)$ (**2**) in 55% isolated yield. The presence of THF in **2** probably indicates that the pendant methyl(trimethylsilyl)amine functionality is not coordinated to the Li ion, in contrast to the THF-free Li amidinate−amine $[Me_3SiNC(Ph)N(CH_2)_3NMe_2]Li$, which was found to adopt a dimeric structure with a coordinated amine functionality.[9]

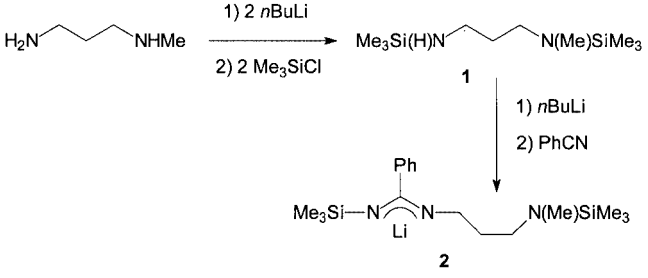

Scheme 1

The Li amidinate **2** reacts with $[TiCl_4(THF)_2]$ in THF to give the titanium amidinate−amide complex $[\eta^2,\eta^1$-Me_3Si-$NC(Ph)N(CH_2)_3NMe]TiCl_2$ (**3**) by elimination of LiCl and

Me_3SiCl (Scheme 2). After recrystallization from diethyl ether, complex **3** was obtained as orange-red crystals, analytically pure, in 56% yield.

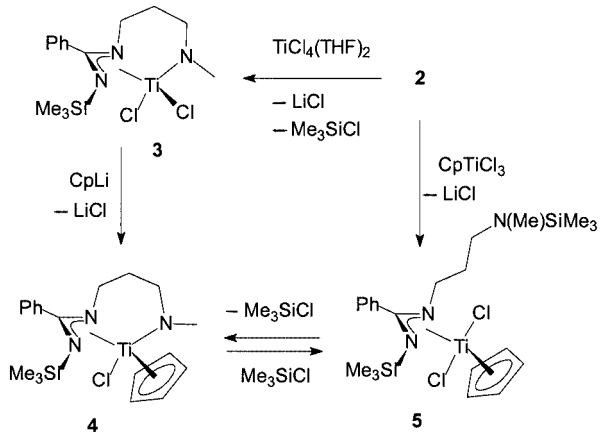

Scheme 2

A single-crystal X-ray structure determination of **3** (Figure 1) showed that the amidinate moiety of the ligand is *N*,*N*′-dihapto bound to the metal center [Ti−N(1) = 2.077(2) Å and Ti−N(2) = 2.059(2) Å]. The Ti−N distance to the amido nitrogen atom is significantly shorter [Ti−N(3) = 1.863(2) Å] than those to the amidinate nitrogen atoms, probably in response to an amide N(p) π-donation to Ti(d). The amidinate nitrogen atom linked to the alkylamide moiety deviates somewhat from planarity [the sum of the angles around N(2) is 353.8°], but this deviation is not as pronounced as in the vanadium amidinate−amine complex [η^2,η^1-$Me_3SiNC(Ph)N(CH_2)_2NMe_2$]$VCl_2$(THF) in which the sum of the angles around N is 336.4°[6] and where the amidinate−amine tridentate ligand clearly adopts a *fac* coordination geometry. The amide nitrogen atom in **3** is planar [the sum of the angles around N(3) is 360.0°], again indicative of efficient amide-to-metal π-donation. The angles around this atom show significant asymmetry, with the Ti−N−C angle within the six-membered ring [Ti−N(3)−C(13) = 137.0(2)°] being significantly larger than the Ti−N−C(Me) angle [Ti−N(3)−C(14) = 110.2(2)°]. The solution NMR spectra of **3** are consistent with C_s symmetry, indicating that the amidinate−amide acts as a meridional-type ligand, and that the six-membered TiN_2C_3 ring, which adopts a boat-like conformation in the crystal structure, readily inverts.

The rapid formation in high yield of the amidinate−amide complex **3** in the reaction of $TiCl_4(THF)_2$ with the Li amidinate **2** indicates that the Me_3SiCl elimination reaction from [η^2-Me_3Si-$NC(Ph)N(CH_2)_3N(SiMe_3)Me]TiCl_3$, the likely primary product of the salt metathesis reaction, is facile. The reverse reaction − formation of group-4 metal chlorides by reaction of group-4 metal amides with an excess of Me_3SiCl − was reported as a clean, salt-free route to generate group-4 metallocene dichlorides from their corresponding bis(amides).[13−15] Apparently, in our case the chelate effect

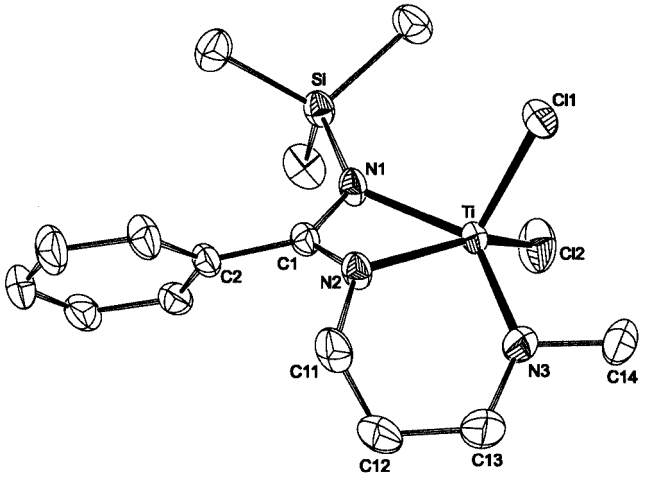

Figure 1. Molecular structure of compound **3**; thermal ellipsoids are drawn at the 50% probability level; Ti−Cl(1) 2.2464(6), Ti−Cl(2) 2.2954(7), Ti−N(1) 2.077(2), Ti−N(2) 2.059(2), Ti−N(3) 1.863(2) Å; Cl(1)−Ti−Cl(2) 107.26(2), N(1)−Ti−N(2) 64.03(6), N(1)−Ti−N(3) 139.40(7), N(2)−Ti−N(3) 84.08(7), N(3)−Ti−Cl(1) 107.72(6), N(3)−Ti−Cl(2) 100.83(6), Ti−N(3)−C(13) 137.0(2), Ti−N(3)−C(14) 110.2(2)°

leads to a thermodynamically favored elimination of Me_3SiCl and formation of the metal−amide bond in **3**.

The reaction of [$CpTiCl_3$] with the Li amidinate **2** in THF, followed by extraction with, and crystallization from, diethyl ether, resulted only in a low isolated yield (13%) of the corresponding amidinate−amide complex Cp[η^2,η^1-$Me_3SiNC(Ph)N(CH_2)_3NMe]TiCl$ (**4**), which was characterized by single-crystal X-ray diffraction (vide infra). Workup of the reaction mixture was made more difficult by the presence of a substantial amount of an orange oil, which appeared to be the major product of the reaction, but which defied crystallization. Investigation of the reaction between [$CpTiCl_3$] and **2** in [D_8]THF at ambient temperature initially showed rapid formation of a primary product, identified as Cp[η^2-$Me_3SiNC(Ph)N(CH_2)_3N(SiMe_3)Me]TiCl_2$ (**5**) from its NMR characteristics (which are identical to those of the orange oil observed in the reaction on preparative scale). This initial reaction is followed by slow release of Me_3SiCl and concomitant formation of the amidinate−amide complex **4** (Scheme 2). Characteristic for the latter are the significant downfield shift of the NMR resonances associated with the NMe group (^{1}H: δ = 3.21 ppm; ^{13}C: δ = 51.0 ppm) relative to those in **5** (^{1}H: δ = 2.29 ppm; ^{13}C: δ = 35.3 ppm). The secondary reaction can be accelerated by increasing the reaction temperature (50−80 °C), but this is then accompanied by the formation of unidentified degradation products. The Me_3SiCl elimination reaction appears to be noticeably faster when the reaction is performed in C_6D_6 rather than in the Lewis basic solvent [D_8]THF, proceeding readily at ambient temperature. The reaction was observed to reach an equilibrium (in C_6D_6 and 25 °C within 30 min), suggesting that the reaction is readily reversible in the mono(cyclopentadienyl)titanium system. Indeed, upon addition of Me_3SiCl to C_6D_6 solutions of the amidinate−amide complex **4** the formation

of **5** could be observed. Examination of C_6D_6 solutions of **4** of known concentration to which 1, 2 or 3 equiv. of Me_3SiCl were added allowed a determination of the equilibrium constant at 25 °C of the equilibrium of **4** + Me_3SiCl with **5** as K = [**5**]/([**4**] + [Me_3SiCl]) = 32(3) L mol^{-1}. Compound **4** was also prepared independently, in 38% isolated yield, by the reaction of the dichloride **3** with CpLi, in which this equilibrium is avoided. This reaction appears to suffer from some reduction of the metal center, as seen from the dark residue left after extraction of the reaction mixture with hexane and the relatively modest isolated yield.

The molecular structure of **4** (Figure 2) shows a fully symmetrically bound η^5-cyclopentadienyl ligand and an η^2,η^1-amidinate−amide ligand in which the TiN_2C_3 ring now adopts a twisted conformation. The amidinate nitrogen atom attached to the alkylamide moiety is significantly less planar [sum of the angles around N(2) is 340.6°] than in **3**. The angles around the (planar) amide nitrogen atom are again highly asymmetric, but in the opposite direction than in **3**: the Ti−N−C angle within the six-membered ring [Ti−N(1)−C(7) = 105.6(2)°] is now significantly smaller than the Ti−N−C(Me) angle [Ti−N(1)−C(6) = 141.6(2)°]. This is probably in response to the twisted conformation of the six-membered ring. It also reduces the steric interaction of the amide methyl group with the cyclopentadienyl ligand, towards which it is pointing. Overall, the metal−ligand distances in **4** are larger than those in **3** [especially the Ti−Cl distance of 2.4038(7) Å, compared to 2.2464(6) and 2.2954(7) Å in **3**] but the metal−amide distances are similar [1.887(2) Å in **4**, 1.863(2) Å in **3**], indicating the importance of the amide-to-metal π-donation.

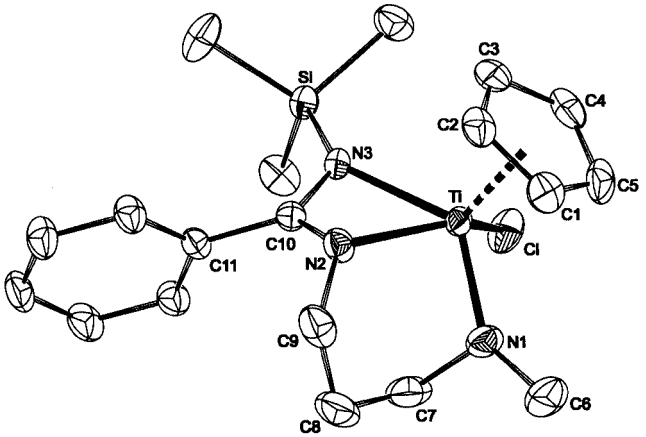

Figure 2. Molecular structure of compound **4**; thermal ellipsoids are drawn at the 50% probability level; Ti−Cl 2,4038(7), Ti−N(1) 1.887(2), Ti−N(2) 2.095(2), Ti−N(3) 2.170(2) Å; N(1)−Ti−N(2) 85.12(7), N(1)−Ti−N(3) 128.61(7), N(2)−Ti−N(3) 61.96(6), N(1)−Ti−Cl 93.96(6), Ti−N(1)−C(6) 141.6(2), Ti−N(1)−C(7) 105.6(2)°

The amidinate−amide dichloride **3** may be converted into the corresponding dialkyltitanium amidinate−amide complexes, which are precursors to cationic monoalkyl species that are interesting as potential olefin polymerization catalysts. Reaction of **3** with 2 equiv. of either $PhCH_2MgBr$ or Me_3SiCH_2Li results in the formation of the dialkyl complexes [η^2,η^1-$Me_3SiNC(Ph)N(CH_2)_3NMe$]-$Ti(CH_2R)_2$ [R = Ph (**6**), $SiMe_3$ (**7**); Scheme 3]. Compound **6** was obtained in 74% yield as yellow crystals by crystallization from pentane, whereas **7** is an extremely soluble oil that only gradually solidifies on standing. The compounds are thermally rather labile, and are best handled and stored below 0 °C. Their solution NMR spectra are consistent with an average C_s symmetry, and each show two doublets for the diastereotopic alkyl methylene protons in the ^{1}H NMR spectrum (**6**: δ = 2.75 and 3.09 ppm, $^2J_{H,H}$ = 9.0 Hz; **7**: δ = 1.56 and 1.86 ppm, $^2J_{H,H}$ = 11.0 Hz).

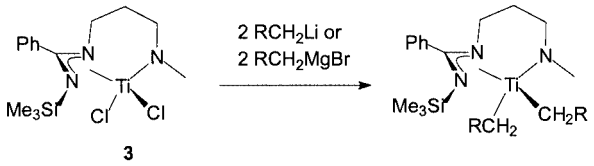

Scheme 3

The dibenzyl complex **6** was treated with the Lewis acid $B(C_6F_5)_3$ in C_6D_6 and in [D_5]bromobenzene solvents in order to effect the abstraction of a benzyl anion. As the ligand system is sterically not very demanding, the formation of a contact ion pair with an η^6-$PhCH_2B(C_6F_5)_3$ interaction might be anticipated, as was observed recently for titanium in the reaction of [(2,6-diphenylphenoxide)$_2$Ti(CH_2Ph)$_2$] with $B(C_6F_5)_3$.[16,17] However, in both solvents rapid decomposition to a mixture of unidentified products was observed, even when the reaction in [D_5]bromobenzene was performed at −20 °C. Attempts at catalytic ethene polymerization (5 bar of ethene, 150 mL of toluene solvent, 50 °C, 15 μmol of Ti) by treating **6** with $B(C_6F_5)_3$ or **7** with [$PhNMe_2H$][$B(C_6F_5)_4$] in the presence of monomer did not result in ethene uptake, suggesting that the decomposition of the cationic species generated is rapid. It is likely that the present amidinate−amide ligand is either reactive itself and/or provides insufficient steric protection to the highly electron-deficient metal center.

Conclusion

Titanium complexes of the new dianionic η^2,η^1-amidinate−amide ligand can be prepared by sequential salt metathesis and Me_3SiCl elimination reactions that occur upon combining titanium chlorides with a lithium amidinate containing a pendant (trimethylsilyl)amide functionality. The Me_3SiCl elimination reaction forming the titanium−amide bond is thermodynamically favored by its intramolecular nature, but it is reversible, and the equilibrium is dependent on what is probably a combination of electronic and steric factors. The formation of the TiN_2C_3 six-membered ring is clearly less favorable in the more electron-rich and sterically more encumbered [Cp(amidinate)-$TiCl_2$] species **5** than in the (amidinate)$TiCl_3$ intermediate

proposed in the formation of **3**. The dialkyltitanium derivatives [η^2,η^1-$Me_3SiNC(Ph)N(CH_2)_3NMe$]$Ti(CH_2R)_2$ (R = Ph, $SiMe_3$) are readily prepared but are thermally rather labile, and could not be converted into well-defined cationic alkyl compounds that are active in catalytic olefin polymerization. Possibly the present substitution pattern of the ligand ($SiMe_3$ on the amidinate nitrogen atom, Me on the amido nitrogen atom) renders it incapable of stabilizing such highly reactive species, and sterically more demanding substituents may be required for catalytic activity.

Experimental Section

General Remarks: All experiments were carried out under purified dinitrogen using standard Schlenk and glove-box techniques. Solvents were distilled from Na/K alloy (THF, diethyl ether, pentane, hexane) or sodium (toluene) under nitrogen before use. Deuterated solvents were either dried with Na/K alloy and vacuum-transferred before use (C_6D_6, [D_8]THF) or degassed and stored over 4-Å molecular sieves ([D_5]bromobenzene). $[TiCl_4(THF)_2]$[18] and $[CpTiCl_3]$,[19] were prepared according to published procedures. Benzonitrile, *n*BuLi/hexane, Me_3SiCl and $MeNH(CH_3)_3NH_2$ were purchased and used as received. NMR spectra were recorded with Varian Gemini 200, VXR 300 and Unity 500 spectrometers. The ^{1}H NMR spectra were referenced to the resonances of residual protons in the deuterated solvent. Chemical shifts (δ) are given relative to tetramethylsilane (downfield shifts are positive). Elemental analyses were performed at the Microanalytical Department of the University of Groningen. All values are the average of at least two independent determinations.

Synthesis of $Me_3SiN(H)(CH_2)_3N(Me)SiMe_3$ (1): This compound was prepared according to a modification of a published procedure.[20] A 2.5 M solution of *n*BuLi in hexane (160 mL, 0.40 mol) was slowly added to a solution of $MeNH(CH_3)_3NH_2$ (20.9 mL, 0.20 mol) in 50 mL of hexane. After refluxing for 2.5 h, Me_3SiCl (50.5 mL, 0.40 mol) was added dropwise, and the mixture was subsequently refluxed for one more hour. From the resulting deep orange suspension, the volatiles were flash-distilled at 90 °C and 0.05 Torr. Subsequent vacuum distillation of this liquid (14 Torr) yielded the product as a spectroscopically pure colorless liquid at 98−101 °C (29.3 g, 0.126 mol, 63%). ^{1}H NMR (300 MHz, C_6D_6): δ = 0.09 (s, 18 H, $SiMe_3$), 1.46 (m, 2 H, $CH_2CH_2CH_2$), 2.39 (s, 3 H, NCH_3), 2.70 (t, $^3J_{H,H}$ = 7.7 Hz, 2 H, $HNCH_2$), 2.64 (t, $^3J_{H,H}$ = 7.0 Hz, 2 H, $MeNCH_2$) ppm. ^{13}C{^{1}H} NMR (75 MHz, C_6D_6): δ = 0.2 [$Si(CH_3)_3$], 34.0 ($CH_2CH_2CH_2$), 34.1 (NCH_3), 39.8 ($HNCH_2$), 49.0 ($MeNCH_2$) ppm. IR (neat, KBr): $\tilde{\nu}$ = 3420 (br. w), 2969 (s), 2854 (m), 2795 (w), 1453 (w), 1400 (m), 1375 (w), 1330 (w), 1253 (s), 1189 (w), 1144 (m), 1110 (m), 1020 (w), 980 (w), 943 (w), 835 (s), 746 (m), 677 (m) cm^{-1}.

Synthesis of $[Me_3SiNC(Ph)N(CH_2)_3N(Me)SiMe_3]Li(THF)$ (2): A solution of **1** (4.2 mL, 18 mmol) in 50 mL of THF was cooled to −80 °C after which a 2.5 M solution of *n*BuLi in hexane (8 mL, 20 mmol) was added dropwise. The solution was allowed to warm to room temperature and was subsequently stirred for 2 h. The light yellow mixture was cooled to −80 °C and benzonitrile (1.8 mL, 17 mmol) was added, after which the mixture was allowed to warm to room temperature. The volatiles from the orange-yellow mixture were removed in vacuo, and the solid residue was recrystallized twice from pentane. Yield: 4.13 g (9.93 mmol, 55%) of a light yellow solid. ^{1}H NMR (300 MHz, C_6D_6): δ = −0.08 [s, 9 H, $Si(CH_3)_3$], −0.03 [s, 9 H, $Si(CH_3)_3$], 1.28 (m, 4 H, THF β-H), 1.58 (m, 2 H, $CH_2CH_2CH_2$), 2.44 (s, 3 H, NCH_3), 2.47 (t, $^3J_{H,H}$ = 7.0 Hz, 2 H, NCH_2), 2.98 [t, $^3J_{H,H}$ = 7.3 Hz, 2 H, $N(Me)CH_2$], 3.58 (m, 4 H, THF α-H), 7.0−7.2 (m, 5 H, Ph) ppm. ^{13}C{^{1}H} NMR (50 MHz, C_6D_6): δ = −0.9 and 3.6 [$Si(CH_3)_3$], 25.7 (THF β-C), 32.6 ($CH_2CH_2CH_2$), 34.3 (NCH_3), 48.4 and 49.3 (NCH_2), 68.3 (THF α-C), 126.9, 127.8, 128.1 (Ph *C*H), 143.3 (Ph *C*), 177.5 (*N*CN) ppm. $C_{21}H_{40}N_3LiOSi_2$ (413.68): calcd. C 60.97, H 9.75, N 10.16; found C 61.17, H 9.60, N 10.45.

Synthesis of $[Me_3SiNC(Ph)N(CH_2)_3NMe]TiCl_2$ (3): A solution of **2** (2.45 g, 5.93 mmol) and $TiCl_4(THF)_2$ (1.98 g, 5.93 mmol) in 70 mL of THF was stirred overnight at room temperature. The dark red solution was stirred for another 8 h, during which the flask was periodically briefly evacuated. The volatiles were removed in vacuo, and the residue was freed of residual THF by stirring twice with diethyl ether (15 mL), which was subsequently removed in vacuo. The residue was extracted three times with diethyl ether (30 mL) after which the extract was concentrated and cooled to −80 °C, yielding microcrystalline orange-red **3** (1.26 g, 3.31 mmol, 56%). Crystals suitable for X-ray diffraction were obtained by cooling a solution of **3** in diethyl ether to −20 °C. ^{1}H NMR (300 MHz, C_6D_6): δ = 0.24 [s, 9 H, $Si(CH_3)_3$], 1.35 (m, 2 H, $CH_2CH_2CH_2$), 2.60 (m, 2 H, NCH_2), 2.99 (m, 2 H, $MeNCH_2$), 3.74 (s, 3 H, NCH_3), 6.93−6.99 (m, 5 H, Ph) ppm. ^{13}C{^{1}H} NMR (75 MHz, C_6D_6): δ = 0.2 [$Si(CH_3)_3$], 31.8 ($CH_2CH_2CH_2$), 43.0 (NCH_2), 46.6 (NCH_3), 61.8 (NCH_2), 126.8, 127.7, 130.4 (Ph *C*H), 132.7 (Ph *C*) ppm; *N*CN signal not observed. $C_{14}H_{23}Cl_2N_3SiTi$ (380.23): calcd. C 44.22, H 6.10, N 11.05, Ti 12.60; found C 44.36, H 6.03, N 11.12, Ti 12.50.

Synthesis of $Cp[Me_3SiNC(Ph)N(CH_2)_3NMe]TiCl$ (4). Method 1: A solution of **2** (1.07 g, 2.56 mmol) in 40 mL of THF was cooled to −80 °C, after which $CpTiCl_3$ (0.57 g, 2.59 mmol) was added. The solution was allowed to warm to room temperature, during which time the color changed from yellow to orange-red. After stirring for 2 h, the volatiles were removed in vacuo and the residual THF was removed by stirring the mixture in pentane, which was subsequently pumped off. The residue was extracted twice with diethyl ether (20 mL). Concentrating and cooling the extract to −20 °C yielded red crystalline **4** (0.14 g, 0.34 mmol, 13%). Crystals suitable for X-ray diffraction were obtained by cooling a concentrated solution of **4** in diethyl ether from room temperature to 7 °C. **Method 2:** Hexane (15 mL) was condensed onto a mixture of solid **3** (0.11 g, 0.28 mmol) and CpLi (20 mg, 0.28 mmol), frozen in liquid nitrogen. The mixture was allowed to thaw and warm to room temperature. After stirring for one more hour, the suspension was filtered and the volatiles were removed from the filtrate in vacuo. Extraction of the residue with hexane, and concentrating and cooling the extract to −20 °C, yielded microcrystalline **4** (54 mg, 0.13 mmol, 38%). ^{1}H NMR (500 MHz, C_6D_6): δ = 0.17 [s, 9 H, $Si(CH_3)_3$], 1.13, 1.33 (m, 1 H each, $CH_2CH_2CH_2$), 2.43 (ddd, $^2J_{H,H}$ = 12.4, $^3J_{H,H}$ = 8.8, 5.7 Hz, 1 H, $NCHH$), 2.65 (ddd, $^2J_{H,H}$ = 14.8, $^3J_{H,H}$ = 6.2, 4.4 Hz, 1 H, $MeNCHH$), 3.03 (ddd, overlapped, 1 H, $NCHH$), 3.04 (s, 3 H, NCH_3), 3.38 (ddd, $^2J_{H,H}$ = 14.8, $^3J_{H,H}$ = 7.6, 4.3 Hz, 1 H, $NCHH$), 6.24 (s, 5 H, C_5H_5), 6.98−7.03 (m, 5 H, Ph) ppm. ^{13}C{^{1}H} NMR (126 MHz, C_6D_6): δ = 2.6 [$Si(CH_3)_3$], 29.8 ($CH_2CH_2CH_2$), 44.8 ($MeNCH_2$), 49.8 (NCH_3), 58.6 (NCH_2), 114.5 (C_5H_5), 127.0, 128.6, 129.3 (Ph *C*H), 135.0 (Ph *C*), 174.3 (*N*CN) ppm. $C_{19}H_{28}ClN_3SiTi$ (409.89): calcd. C 55.68, H 6.89, N 10.25; found C 55.10, H 6.89, N 9.75.

Reaction of $[CpTiCl_3]$ with 2 in [D_8]THF: Separately prepared solutions of $[CpTiCl_3]$ (17 mg, 0.08 mmol) and **2** (33 mg, 0.08 mmol), each in 0.4 mL of [D_8]THF, were mixed at ambient temperature,

resulting in a rapid color change from light yellow to orange, and the mixture was added into an NMR tube, equipped with a Teflon valve. The ^{1}H and ^{13}C NMR spectra indicated formation of Cp[$Me_3SiNC(Ph)N(CH_2)_3N(Me)SiMe_3$]TiCl (**5**). ^{1}H NMR (300 MHz, [D_8]THF): δ = −0.11, −0.05 [s, 9 H each, Si(CH_3)$_3$], 1.66 (m, 2 H, CH_2), 2.29 (s, 3 H, NCH_3), 2.52 (t, $^3J_{H,H}$ = 6.8 Hz, 2 H, MeNCH_2), 3.03 (m, 2 H, NCH_2), 6.83 (s, 5 H, C_5H_5), 7.33 (m, 2 H, Ph *m*-H), 7.45 (m, 3 H, Ph *o*-H and *p*-H) ppm. ^{13}C(APT) NMR (75 MHz, [D_8] THF): δ = 0.4, 3.3 [Si(CH_3)$_3$], 31.6 (CH_2), 35.3 (NCH_3), 49.8, 52.2 (NCH_2), 122.0 (C_5H_5), 128.7, 130.4, 131.5 (Ph *C*H), 135.2 (Ph *C*), 172.2 (N*C*N) ppm. Upon standing at ambient temperature or 50 °C, gradual formation of **4** and Me_3SiCl was observed. At 50 °C a maximum conversion of 34% was reached (after 24 h, with concomitant formation of some degradation products). ^{1}H NMR (300 MHz, [D_8]THF, characteristic resonances): δ = −0.11 [s, Si(CH_3)$_3$], 3.21 (s, 3 H, NCH_3), 6.30 (s, 5 H, C_5H_5) ppm. ^{13}C(APT) NMR (75 MHz, [D_8]THF): δ = 51.0 (NCH_3), 116.1 (C_5H_5) ppm.

Reaction of 4 with Me_3SiCl: Three NMR tubes were charged each with a solution of **4** in C_6D_6 to which measured amounts of a stock solution of Me_3SiCl in C_6D_6 was added. Initial concentrations of [**4**]/[Me_3SiCl] in the three tubes were: 0.030:0.035, 0.029:0.069 and 0.029:0.100 mol L^{-1}. After 30 min at 25 °C, the relative amounts of **4**, **5** and Me_3SiCl were determined by ^{1}H NMR spectroscopy. Observed ratios after 1 h were the same, indicating that equilibrium had been reached. Values determined for K = [**5**]/([**4**] + [Me_3SiCl]) were 32, 33 and 33(2) L mol^{-1}, respectively, for the three samples. Cp[$Me_3SiNC(Ph)N(CH_2)_3N(Me)SiMe_3$]$TiCl_2$ (**5**): ^{1}H NMR (500 MHz, C_6D_6): δ = −0.04 [s, 9 H, Si(CH_3)$_3$], 0.04 [s, 9 H, Si(CH_3)$_3$], 1.63 (m, 2 H, $CH_2CH_2CH_2$), 2.27 (s, 3 H, NCH_3), 2.49 (t, $^3J_{H,H}$ = 7.3 Hz, 2 H, NCH_2), 3.22 (m, 2 H, NCH_2), 6.55 (s, 5 H, C_5H_5), 6.70−6.95 (m, 5 H, Ph) ppm.

Synthesis of [$Me_3SiNC(Ph)N(CH_2)_3NMe$]$Ti(CH_2Ph)_2$ (6): A solution of **3** (0.316 g, 0.83 mmol) in 30 mL of diethyl ether was cooled to −100 °C and a 1.56 M solution of $PhCH_2MgBr$ in diethyl ether (1.07 mL, 1.66 mmol) was slowly added. The solution was allowed to warm to −15 °C, at which temperature the mixture was stirred for 2 h. During workup the temperature of the mixture was kept at or below −15 °C. The volatiles were removed in vacuo and the mixture was stirred twice with 10 mL of precooled pentane, which was subsequently pumped off. The residue was extracted with pentane, after which the extract was concentrated and cooled to −60 °C. This yielded crystalline **6** (0.302 g, 0.62 mmol, 74%). ^{1}H NMR (300 MHz, C_6D_6): δ = 0.26 [s, 9 H, Si(CH_3)$_3$], 1.07 (m, 2 H, $CH_2CH_2CH_2$), 2.63 (m, 2 H, NCH_2), 2.75, 3.09 (d, $^2J_{H,H}$ = 9.0 Hz, 2 H each, TiCH_2), 3.80 (s, 3 H, NCH_3), 6.9−7.2 (m, 15 H, Ph) ppm. ^{13}C{^{1}H} NMR (75 MHz, C_6D_6): δ = 3.0 [Si(CH_3)$_3$], 31.2 ($CH_2CH_2CH_2$), 40.8 (MeNCH_2), 45.4 (NCH_3), 59.9 (NCH_2), 84.5 (TiCH_2), 122.2, 126.5, 127.2, 128.6, 128.8, 129.3 (Ph *C*H), 134.6 (Ph *C*), 144.4 (CH_2Ph *C*), 177.4 (N*C*N) ppm. $C_{28}H_{37}N_3SiTi$ (491.59): calcd. C 68.41, H 7.59, N 8.55; found C 68.32, H 7.53, N 8.44.

Synthesis of [$Me_3SiNC(Ph)N(CH_2)_3NMe$]$Ti(CH_2SiMe_3)_2$ (7): Pentane (30 mL) was condensed into a vessel containing a solid mixture of **3** (0.31 g, 0.81 mmol) and Me_3SiCH_2Li (0.15 g, 1.63 mmol) that was frozen in liquid nitrogen. The solution was allowed to thaw and warm to −15 °C, at which temperature it was stirred for 2 h. The solution was filtered and the residue was extracted with 30 mL of pentane. From the combined filtrates the volatiles were removed in vacuo to leave **7** as a yellow oil that slowly solidified on standing. Attempts to recrystallize this material from pentane were unsuccessful due to the extreme solubility of the product. The yield of the material (> 95% pure by NMR spectroscopy) was essentially quantitative. ^{1}H NMR (300 MHz, C_6D_6): δ = 0.18 [s, 18 H,

Table 1. Crystallographic data for compounds **3** and **4**

	3	**4**
Empirical formula	$C_{14}H_{23}Cl_2N_3SiTi$	$C_{19}H_{28}ClN_3SiTi$
Molecular mass	380.21	409.86
Temperature [K]	130	130
Wavelength [Å]	0.71073	0.71073
Crystal system	monoclinic	monoclinic
Space group	$P2_1/n$	$P2_1/c$
Unit cell dimensions	a = 11.570(1) Å	a = 12.130(1) Å
	b = 8.992(1) Å	b = 15.168(1) Å
	c = 18.177(1) Å	c = 12.278(1) Å
	β = 94.129(5)°	β = 112.607(6)°
Volume	1886.2(3) Å^3	2805.4(3) Å^3
Z	4	4
Density (calculated)	1.339 Mg/m^3	1.305 Mg/m^3
Absorption coefficient	0.8 mm^{-1}	0.6 mm^{-1}
F(000)	792	864
Crystal size	0.25 × 0.30 × 0.61 mm	0.08 × 0.38 × 0.50 mm
θ range for data collection	1.12−28.0°	1.34−27.0°
Index ranges	$-15 \le h \le 1$	$-14 \le h \le 10$
	$0 \le k \le 11$	$0 \le k \le 19$
	$-23 \le l \le 23$	$-15 \le l \le 0$
Reflections collected	5514	4934
Independent reflections	4529	4531
Data/restraints/parameters	4529/0/282	4531/0/338
Goodness-of-fit on F^2	1.012	1.067
Final R indices	R_1 = 0.0352, wR_2 = 0.1012	R_1 = 0.0326, wR_2 = 0.0827
Largest difference peak and hole [e Å^{-3}]	0.59 and −0.51(7)	0.42 and −0.27(5)

$CH_2Si(CH_3)_3$], 0.22 [s, 9 H, $Si(CH_3)_3$], 1.54 (m, 2 H, $CH_2CH_2CH_2$), 1.56, 1.86 (d, $^2J_{H,H}$ = 11.0 Hz, 2 H each, $TiCH_2$), 2.87 (m, 2 H, $MeNCH_2$), 3.05 (m, 2 H, NCH_2), 3.69 (s, 3 H, NCH_3), 7.1−7.3 (m, 5 H, Ph) ppm. $^{13}C\{^1H\}$ NMR (75 MHz, C_6D_6): δ = 2.6 [$CH_2Si(CH_3)_3$], 2.7 [$NSi(CH_3)_3$], 32.4 ($CH_2CH_2CH_2$), 42.4 ($MeNCH_2$), 45.5 (NCH_3), 60.0 (NCH_2), 78.3 ($TiCH_2$), 126.5, 128.8, 129.6 (Ph *C*H), 134.9 (Ph *C*), 180.5 (N*C*N) ppm.

X-ray Crystallographic Study: Single crystals of **3** and **4** were mounted on a glass fibre in a nitrogen-filled glove-box and transferred to the cold nitrogen stream of an Enraf−Nonius CAD-4F diffractometer (graphite-monochromated Mo-K_α radiation, λ = 0.71073 Å) using inert-gas handling techniques. The structures were solved by Patterson methods and extension of the model was accomplished by direct methods applied to difference structure factors using the program DIRDIF.[21] All hydrogen atoms were located from the difference Fourier map and refined with isotropic displacement parameters. Final refinements on F^2 were carried out by full-matrix least-squares techniques (SHELXL-97[22]). CCDC-183877 (**3**) and -183876 (**4**) contain the supplementary crystallographic data for this paper. These data can be obtained free of charge at www.ccdc.cam.ac.uk/conts/retrieving.html [or from the Cambridge Crystallographic Data Centre, 12 Union Road, Cambridge CB2 1EZ, UK; Fax: (internat.) + 44-1223/336−033; E-mail: deposit@ccdc.cam.ac.uk].

[1] J. Barker, M. Kilner, *Coord. Chem. Rev.* **1994**, *133*, 219−300.
[2] F. T. Edelmann, *Coord. Chem. Rev.* **1994**, *137*, 403−481.
[3] C. Averbuj, M. S. Eisen, *J. Am. Chem. Soc.* **1999**, *121*, 8755−8759 and references cited therein.
[4] S. Dagorne, I. A. Guzei, M. P. Coles, R. F. Jordan, *J. Am. Chem. Soc.* **2000**, *122*, 274−289 and references cited therein.
[5] R. J. Keaton, K. C. Jayaratne, D. A. Henningson, L. A. Koterwas, L. R. Sita, *J. Am. Chem. Soc.* **2001**, *123*, 6197−6198 and references cited therein.
[6] M. J. R. Brandsma, E. A. C. Brussee, A. Meetsma, B. Hessen, J. H. Teuben, *Eur. J. Inorg. Chem.* **1998**, 1867−1870.
[7] K. Kincaid, C. P. Gerlach, G. R. Giesbrecht, J. R. Hagadorn, G. D. Whitener, A. Shafir, J. Arnold, *Organometallics* **1999**, *18*, 5360−5366.
[8] S. Bambirra, M. J. R. Brandsma, E. A. C. Brussee, A. Meetsma, B. Hessen, J. H. Teuben, *Organometallics* **2000**, *19*, 3197−3204.
[9] D. Doyle, Y. K. Gun'ko, P. B. Hitchcock, M. F. Lappert, *J. Chem. Soc., Dalton Trans.* **2000**, 4093−4097.
[10] J. R. Hagadorn, J. Arnold, *Angew. Chem.* **1998**, *110*, 1813−1815; *Angew. Chem. Int. Ed.* **1998**, *37*, 1729−1731.
[11] G. D. Whitener, J. R. Hagadorn, J. Arnold, *J. Chem. Soc., Dalton Trans.* **1999**, 1249−1255.
[12] S. Bambirra, A. Meetsma, B. Hessen, J. H. Teuben, *Organometallics* **2001**, *20*, 782−785.
[13] G. M. Diamond, R. F. Jordan, J. L. Petersen, *J. Am. Chem. Soc.* **1996**, *118*, 8024−8033.
[14] J. N. Christopher, G. M. Diamond, R. F. Jordan, J. L. Petersen, *Organometallics* **1996**, *15*, 4038−4044.
[15] G. M. Diamond, R. F. Jordan, J. L. Petersen, *Organometallics* **1996**, *15*, 4045−4053.
[16] M. G. Thorn, Z. C. Etheridge, P. E. Fanwick, I. P. Rothwell, *Organometallics* **1998**, *17*, 3636−3638.
[17] M. G. Thorn, Z. C. Etheridge, P. E. Fanwick, I. P. Rothwell, *J. Organomet. Chem.* **1999**, *591*, 148−162.
[18] L. E. Manzer, *Inorg. Synth.* **1982**, *21*, 135−140.
[19] R. D. Gorsich, *J. Am. Chem. Soc.* **1960**, *82*, 4212−4214.
[20] É. Ya. Lukevits, L. I. Libert, M. G. Voronkov, *J. Gen. Chem. USSR* **1969**, *39*, 768−771.
[21] P. T. Beurskens, G. Beurskens, R. de Gelder, S. García-Granda, R. O. Gould, R. Israël, J. M. M. Smits, *DIRDIF-99 program system*, Crystallography Laboratory, University of Nijmegen, The Netherlands **1999**.
[22] G. M. Sheldrick, *SHELXL-97, program for refinement of crystal structures*, University of Göttingen, Germany, **1997**.

Received July 16, 2002
[I02390]

Synthesis and Structure of the First Holmium and Erbium Diiodide Complexes of Composition $LLnI_2$ (Ln = Ho, Er)

Grigori B. Nikiforov,[a] Herbert W. Roesky,*[a] Thomas Labahn,[a] Denis Vidovic,[a] and Dante Neculai[a]

Dedicated to Professor M. Mikolajczyk on the occasion of his 65th birthday

Keywords: Lanthanides / Iodides / Coordination chemistry / N ligands

Two new diiodide complexes of stoichiometry $LLnI_2$ [Ln = Ho (**1**), Er (**2**)] with the β-diketiminato ligand 2-{[2-(diethylamino)ethyl]amino}-4-{[2-(diethylamino)ethyl]imino}pent-2-ene have been synthesized by the reaction of the lithium salt of the ligand with the corresponding triiodides. The complexes are thermally stable and soluble in common organic solvents. The X-ray structural and elemental analysis show that $LLnI_2$ is neutral, and as well free of solvent and lithium salt. The complexes adopt a pseudo-octahedral geometry with the two iodine atoms arranged in *trans* position to each other.

(© Wiley-VCH Verlag GmbH & Co. KGaA, 69451 Weinheim, Germany, 2003)

Introduction

Nitrogen-based ligands for preparing lanthanide complexes have been explored increasingly during the last decade.[1−6] Several samarium and gadolinium complexes of stoichiometry $(L1)GdBr_2$, $(L1)_3Ln$,[7] $(L2)_2LnBr$[8] (Ln = Sm, Gd) with different diimine ligands (Scheme 1) have been prepared by Magull et al. Recently, we reported the synthesis of β-diketiminato complexes of praseodymium $(L3)PrX_2$ (X = Cl, Br, BH_4.[9] All these compounds are thermally stable, monomeric in the solid state and soluble in common organic solvents.

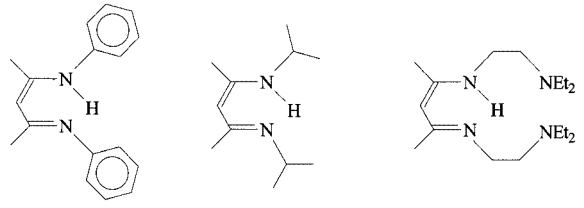

L 1 L 2 L 3

Scheme 1. The proton-containing ligands L1, L2, and L3

Iodide complexes of lanthanides are less well known than the corresponding chloride derivatives, presumably due to the lower availability, higher instability, and higher price of the starting material LnI_3.[10,11] Several lanthanide iodide complexes of La^{III},[12] Ce^{III},[13,14] Sm^{III},[15,16,17] Yb^{III},[15,18,19] Lu^{III} [20] have been reported in the literature. The first erbium iodide complex Cp_2ErI was obtained by Maginn et al.[21] in 1963 and characterized by elemental analysis. So far only one iodide complex of erbium $[\{(Me_3Si)_2C_5H_3\}_2ErI](THF)$[20] has been structurally characterized. However, complexes of the lanthanides Tb to Ho are less well known and no reports on holmium iodide complexes can be found in the literature.

Organolanthanide iodide complexes have unique chemical properties due to the more labile Ln−I bond compared to the Ln−Cl ones. This allows metathesis reactions with iodine-containing derivatives. For instance, treatment of the iodide complex with $AgSbF_6$ produces the corresponding fluoride complex;[22] the reaction of $Cp''_2CeI{\cdot}2MeCN$ [Cp'' = 1,3-$C_5H_3(SiMe_3)_2$] with the silver(I) salt $AgBF_4$ in toluene gave the cationic complex in high yield.[12] Similar reactions with the closely related chlorides, however, result in complicated mixtures.[23]

Herein we report the synthesis and characterization of the first monomeric and solvent-free iodide complexes of stoichiometry $LLnI_2$ (Ln = Ho, Er) with the β-diketiminato ligand 2-{[2-(diethylamino)ethyl]amino}-4-{[2-(diethylamino)ethyl]imino}pent-2-ene (L3). The structural characterization of these complexes provides useful data in the rapidly growing field of organolanthanide chemistry. The synthetic methods used to obtain these complexes are also informative with respect to lanthanide halide chemistry. The latter species are important precursor for further reactions.

Results and Discussion

The lanthanide complexes **1** and **2** were prepared in a one-step synthesis from the corresponding THF adducts

[a] Institut für Anorganische Chemie, Universität Göttingen, Tammannstrasse 4, 37077, Göttingen, Germany
Fax: (internat.) + 49-551/393373
E-mail: hroesky@gwdg.de

and stoichiometric amounts of the lithium salt of the ligand in THF followed by recrystallization from toluene (Scheme 2).

$$LnI_3(THF)_x + (L3)Li \xrightarrow[2.\ toluene,\ -LiI]{1.\ THF,\ r.t.} (L3)LnI_2 \quad \begin{matrix} Ln = Ho & \mathbf{1} \\ = Er & \mathbf{2} \end{matrix}$$

$$L3{=}Et_2NCH_2CH_2NC(Me)CHC(Me)NCH_2CH_2NEt_2$$

Scheme 2. Preparation of the compounds **1** and **2**

The yield of the reaction of $LnI_3(THF)_x$ with (L3)Li in THF depends highly on the quality of the triiodide. The LnI_3 compounds can be obtained by a modified procedure[24] from Ln powder and iodine vapour followed by sublimation under vacuum. The high purity LnI_3 received from Aldrich in sealed ampoules under argon is also suitable for the experiment. The precursor LnI_3 can be dissolved by heating the reaction mixture for several hours. Compounds **1** and **2** are soluble in toluene, THF, acetonitrile, and dichloromethane. The ^1H NMR spectra of **1** and **2** in C_6D_6 and CD_2Cl_2, respectively, at room temperature show a set of broad resonances ($\Delta\nu_{1/2}$ ranges from 100 to 1000 Hz) with chemical shifts ranging from $\delta = 60$ to -80 ppm. Lowering of the temperature leads to more distinct resonances; however, the fine structure of the resonances could not be observed due to the paramagnetic nature of holmium and erbium.

The complexes $(L3)LnI_2$ are thermally stable, and their melting points are in the range 192−196 °C. Mass spectrometry and elemental analysis show that compounds **1** and **2** are monomeric, solvent-free and contain no lithium halides. The molecular ions of **1** and **2** in the EI mass spectra are weak. Both compounds exhibit two sets of strong signals in the EI-MS, which correspond to $[(L3)LnI]^+$ and $[M^+ - C_5H_{12}N]$ ions. The theoretical results of an isotope pattern calculation for $[(L3)LnI]^+$ and $[M^+ - C_5H_{12}N]$ are in good agreement with the experimental data. The relative intensities of these signals are nearly the same in both the spectra of **1** and **2** (3.2:1 and 2.9:1 respectively). Thus, in conclusion it is possible to use EI-MS analysis effectively for the characterization of these complexes.

X-ray Structural Analysis of $LLnI_2$

A summary of the crystallographic data and refinement parameters for the structures of **1** and **2** are given in Table 2. Selected bond lengths and angles are listed in Table 1.

Single crystals of **1** and **2** suitable for X-ray diffraction analysis were obtained from a concentrated toluene solution. $(L3)HoI_2$ crystallizes in the triclinic $P\bar{1}$ space group; while $(L3)ErI_2$ crystallizes in the monoclinic $C2/c$ space group and has two symmetrically nonequivalent molecules in the unit cell. The X-ray structural analysis revealed that compounds **1** and **2** are monomeric in the solid state. The X-ray crystal structure of **1** resembles that of **2**, therefore only **1** is shown (Figure 1).

In both compounds the ligand coordinates to the metal center through the four nitrogen atoms. All four nitrogen atoms and the holmium or erbium atom are in the same plane. The iodine atoms in **1** and **2** are almost perpendicularly arranged within the equatorial plane, which is evident from the angles I(2)−Ho−I(1) [153.715(9)°] and

Table 1. Selected bond lengths [Å] and angles [°] for compounds **1** and **2**

Compound **1**			
Ho−N(1)	2.313(3)	N(1)−Ho−N(2)	79.51(10)
Ho−N(2)	2.314(3)	N(1)−Ho−N(3)	149.98(9)
Ho−N(3)	2.596(3)	N(2)−Ho−N(3)	70.70(9)
Ho−N(4)	2.617(3)	N(1)−Ho−N(4)	69.79(9)
Ho−I(2)	2.980(1)	N(2)−Ho−N(4)	149.22(9)
Ho−I(1)	3.058(1)	N(3)−Ho−N(4)	140.08(8)
		N(1)−Ho−I(2)	100.33(7)
		N(2)−Ho−I(2)	97.83(7)
		N(3)−Ho−I(2)	87.58(6)
		N(4)−Ho−I(2)	85.86(6)
		N(1)−Ho−I(1)	99.59(7)
		N(2)−Ho−I(1)	102.53(7)
		N(3)−Ho−I(1)	83.68(6)
		N(4)−Ho−I(1)	85.10(6)
		I(2)−Ho−I(1)	153.715(9)
Compound **2**			
Er−N(3)	2.300(5)	N(3)−Er−N(2)	80.87(19)
Er−N(2)	2.318(5)	N(3)−Er−N(4)	71.12(18)
Er−N(4)	2.595(6)	N(2)−Er−N(4)	151.73(19)
Er−N(1)	2.608(6)	N(3)−Er−N(1)	153.05(18)
Er−I(1)	2.962(1)	N(2)−Er−N(1)	72.41(19)
Er−I(2)	3.045(1)	N(4)−Er−N(1)	135.76(17)
		N(3)−Er−I(1)	97.72(14)
		N(2)−Er−I(1)	95.58(14)
		N(4)−Er−I(1)	84.70(13)
		N(1)−Er−I(1)	88.51(14)
		N(3)−Er−I(2)	97.96(14)
		N(2)−Er−I(2)	99.02(14)
		N(4)−Er−I(2)	88.78(13)
		N(1)−Er−I(2)	83.07(14)
		I(1)−Er−I(2)	160.050(16)

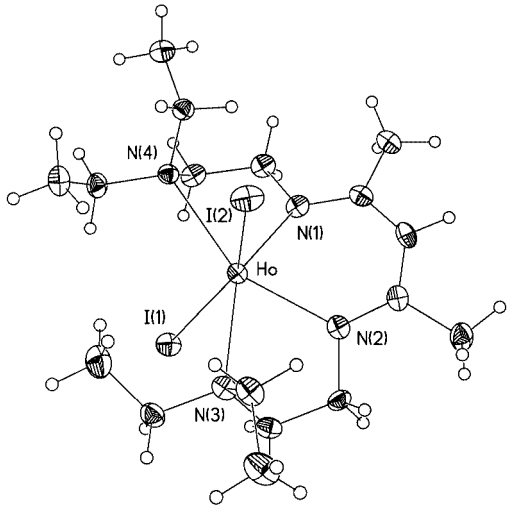

Figure 1. ORTEP drawing (50% thermal probability ellipsoids) of the crystal structure of **1** with atomic numbering scheme

I(1)−Er(1)−I(2) [160.050(16)°] (Table 1). Moreover, each iodine atom is tilted slightly toward the pendant arm. It should be pointed out that the angles between the iodine atoms in **1** and **2** are naturally larger than those between the halogen atoms in $(L3)PrX_2$ (X = Cl, Br) [Cl(2)−Pr−Cl(1) = 136.42(3)°; Br(1)−Pr−Br(2) = 137.080(12)°][9] due to the larger diameter of the praseodymium atom and the smaller ones of chlorine and bromine. For both complexes the metal atoms lie slightly out of the plane of the diimine ligand framework. The coordination number at the holmium and erbium atoms in **1** and **2** is six and the geometry around the metal atom is pseudo-octahedral.

The Ln−N bond lengths of the pendant arm are longer than those of the backbone, as for the distances in the praseodymium complex $(L3)PrX_2$ (X = Cl, Br),[9] due to the coordinative and covalent character involved in different bonding modes. The Er−I bond length is similar to those found in the literature (Er−I: 2.931 Å).[20]

Conclusions

We have reported the synthesis and characterization of two new diiodide complexes of stoichiometry $(L3)LnI_2$. These compounds are easily available when a β-diketiminato-based ligand and holmium or erbium triiodides are used. The X-ray structural and elemental analysis show that $(L3)LnI_2$ is neutral, and free of solvent and lithium salt. The complexes are thermally stable, soluble in common organic solvents and could be used as versatile starting material for studying the chemistry of water- and oxygen-free lanthanide compounds.

Experimental Section

General Remarks: All operations were performed using standard Schlenk line and dry box techniques under purified nitrogen or argon. High-purity water-free holmium and erbium triiodides were

Table 2. Crystallographic data of the X-ray diffraction studies of **1** and **2**

	1	**2**
Empirical formula	$C_{17}H_{35}HoI_2N_4$	$C_{34}H_{70}Er_2I_4N_8$
M_r	714.22	1433.10
Temperature [K]	133(2)	133(2)
Radiation used (λ [Å])	Mo-K_α (0.71073)	Mo-K_α (0.71073)
Crystal description	yellow block	yellow block
Crystal size [mm]	0.5 × 0.6 × 1.1	0.6 × 0.8 × 1.1
Crystal system	triclinic	monoclinic
Space group	$P\bar{1}$	$C2/c$
a [Å]	8.6723(10)	18.757(4)
b [Å]	11.6655(14)	14.450(3)
c [Å]	12.1951(14)	34.233(7)
α [°]	82.839(9)	90
β [°]	73.226(9)	95.37(3)
γ [°]	79.433(9)	90
V [Å^3]	1157.8(2)	9238(3)
Z,	2	8
F (000)	676	5424
$\rho_{calcd.}$ [g·cm^{-3}]	2.049	2.061
μ [mm^{-1}]	6.090	6.314
Total reflections	17725	25044
Unique reflections	3634	7600
R(int)	0.0879	0.1355
Scan range Θ [°]	1.78 to 24.00	1.78 to 24.98
Completeness to Θ_{max} [%]	100.0	93.8
Index ranges	$-9 \le h \le 9$	$-22 \le h \le 22$
	$-13 \le k \le 13$	$-17 \le k \le 17$
	$-13 \le l \le 13$	$-40 \le l \le 40$
Data/restrains/parameters	3634/0/223	7600/0/433
$R1$,[a] [b] $wR2$ [$I > 2\sigma(I)$][c]	0.0192, 0.0468	0.0390, 0.1003
$R1$,[a] [d] $wR2$ (all data)[c] [d]	0.0216, 0.0476	0.0449, 0.1041
Refinement method	Full-matrix least-squares on F^2	Full-matrix least-squares on F^2
Goodness-of-fit on F^2 [e]	1.018	1.077
Max./min. electr. dens. [e·Å^{-3}]	1.088, −0.804	2.112, −1.514

[a] $R1 = \Sigma||F_o| - |F_c||/\Sigma|F_o|$. [b] Denotes the value of the residual considering only the reflections with $I > 2\sigma(I)$. [c] $wR2 = \{\Sigma[w(F_o^2 - F_c^2)^2]/\Sigma[w(F_o^2)^2]\}^{1/2}$; $w = 1/[\sigma^2(F_o^2) + (aP)^2 + bP]$, $P = [\max(F_o^2 \text{ or } 0) + 2(F_c^2)/3$. [d] Denotes the value of the residual considering all reflections. [e] $S = [\Sigma[w(F_o^2 - F_c^2)^2]/[(n - p)^{1/2}]]$, n: number of data, p: parameters used.

purchased from Aldrich in ampoules sealed under argon. Compound (L3)H [L3 = $Et_2NCH_2CH_2NC(Me)CHC(Me)NCH_2CH_2NEt_2$] was prepared by known literature methods.[9,25,26] The purity of (L3)H was checked by elemental analysis, and ^1H and ^{13}C NMR spectroscopy. Toluene and THF were dried with Na/benzophenone and distilled under nitrogen prior to use; C_6D_6 was dried with Na and degassed; CD_2Cl_2 was dried with CaH_2 and degassed. ^1H NMR spectra were recorded using a Bruker AM 200 spectrometer. Chemical shifts are reported in δ units downfield from Me_4Si with the solvent as the reference signal. Mass spectra were recorded using a Finnigan MAT 8230 instrument, and elemental analysis were carried out at the Analytical Laboratories of the Institute of Inorganic Chemistry at the University of Göttingen. Melting points were determined in sealed capillary tubes under nitrogen and are not corrected.

Synthesis of Complexes 1 and 2. (L3)HoI_2: The methods for the preparation of **1** and **2** are the same, therefore only the method for (L3)HoI_2 is described. Compound (L3)H (0.6 g, 0.64 mL, 2.0 mmol) was added to dry THF (30 mL) in a 50-mL Schlenk flask. The mixture was cooled to −78 °C and a solution of MeLi in Et_2O (1.26 mL, 1.6 M, 2.0 mmol) was added dropwise. The solution was stirred for 1 h at −78 °C, allowed to warm to room temperature, and then stirred at room temp. until methane evolution had ceased. This solution was added dropwise to a suspension of HoI_3 (1.09 g, 2.0 mmol) in THF (30 mL) at room temp. in a 100-mL Schlenk flask. Then the reaction mixture was heated until all the precipitate dissolved. THF was removed under vacuum, and the residue was extracted with 60 mL of toluene. The yellow toluene solution was allowed to stand overnight at room temperature, when a white powder (LiI) separated from a clear yellow solution. The solution was filtered and concentrated to 20 mL. The resulting solution was left undisturbed overnight. Finally, yellow crystals formed, which were separated by filtration, washed with pentane (10 mL), and dried in vacuo. The next portions of crystals was obtained from the toluene solution. Yield of **1** 1.10 g (75%). M.p. 194−196 °C. $C_{17}H_{35}HoI_2N_4$ (714.22): calcd. C 28.58, H 4.90, I 35.59, N 7.85; found C 28.50, H 4.93, I 35.71, N 7.75. EI-MS: *m*/*z* (%) = 714 (1) [M^+], 628 (27) [$M^+ - C_5H_{12}N$], 587 (86) [(L3)HoI^+], 557 (2) [$M^+ - C_{10}H_{24}N$], 536 (3) [$M^+ - C_{12}H_{18}N_2$], 495 (2) [(L3)$HoI^+ - C_5H_{12}N$], 419 (3) [HoI_2^+], 296 (2) [$(L3)^+$], 210 (7) [$(L3)^+ - C_5H_{12}N$], 100 (11) [$C_6H_{14}N$], 86 (100) [$C_5H_{12}N$]. **LErI_2:** Yield of **2** 1.10 g (75%). M.p. 192−194 °C. $C_{17}H_{35}ErI_2N_4$ (716.55): calcd. C 28.49, H 4.89, I 35.48, N 7.82; found C 28.50, H 4.92, I 35.44, N 7.85. EI-MS: *m*/*z* (%) = 715 (1) [M^+], 629 (4.6) [$M^+ - C_5H_{12}N$], 588 (15) [(L3)ErI^+], 558 (2) [$M^+ - C_{10}H_{24}N$], 537 (2) [$M^+ - C_{12}H_{18}N_2$], 499 (2) [(L3)$ErI^+ - C_5H_{12}N$], 296 (5) [$(L3)^+$], 210 (5) [$(L3)^+ - C_5H_{12}N$], 100 (12) [$C_6H_{14}N$], 86 (100) [$C_5H_{12}N$].

X-ray Crystallographic Study: Crystal data and experimental conditions are listed in Table 2. Selected bond lengths and bond angles with standard deviations in parentheses are presented in Table 1. Intensity data for the crystal structures of **1** and **2** were collected with a Stoe image plate IPDS II-system. All structures were solved by direct methods (SHELXS-97) and refined against F^2 using SHELXL-97.[27] The heavy atoms were refined anisotropically. Hydrogen atoms were included using the riding model with U_{iso} tied to U_{iso} of the parent atoms. CCDC-187724 (**1**) and -187725 (**2**) contain the supplementary crystallographic data for this paper. These data can be obtained free of charge at www.ccdc.cam.ac.uk/conts/retrieving.html or from the Cambridge Crystallographic Data Centre, 12 Union Road, Cambridge CB2 1EZ, UK [Fax: (internat.) + 44-1223/336-033; E-mail: deposit@ccdc.cam.ac.uk].

Acknowledgments

We are thankful to the Deutsche Forschungsgemeinschaft, the Göttinger Akademie der Wissenschaften and the Fonds der Chemischen Industrie for financial support.

[1] F. T. Edelmann, *Angew. Chem.* **1995**, *107*, 2647−2669; *Angew. Chem. Int. Ed. Engl.* **1995**, *34*, 2466−2488.
[2] J. A. R. Schmidt, J. Arnold, *Chem. Commun.* **1999**, 2149−2150.
[3] P. W. Roesky, *Inorg. Chem.* **1996**, *37*, 4507−4511.
[4] T. Dubbe, S. Gambarotta, G. Yap, *Organometallics* **1998**, *17*, 3967−3973.
[5] C. Apostolidis, A. Carvalho, A. Domingos, B. Kanellakopulos, R. Maier, N. Marques, A. P. de Matos, J. Rebizant, *Polyhedron* **1999**, *18*, 263−272.
[6] S. Bambirra, M. J. R. Brandsma, E. A. C. Brussee, A. Meetsma, B. Hessen, J. H. Teuben, *Organometallics* **2000**, *19*, 3197−3204.
[7] D. Dress, J. Magull, *Z. Anorg. Allg. Chem.* **1994**, *620*, 814−818.
[8] D. Dress, J. Magull, *Z. Anorg. Allg. Chem.* **1995**, *621*, 948−952.
[9] D. Neculai, H. W. Roesky, A. M. Neculai, J. Magull, H.-G. Schmidt, M. Noltemeyer, *J. Organomet. Chem.* **2002**, *643/644*, 47−52.
[10] H. Schumann, J. A. Meese-Marktscheffel, L. Esser, *Chem. Rev.* **1995**, *95*, 865−986.
[11] F. T. Edelmann, M. F. Lappert, *Comprehensive Organometallic Chemistry II*, Pergamon Press, Oxford, **1995**, vol. 4, p. 11−87.
[12] P. N. Hazin, J. W. Bruno, G. K. Schulte, *Organometallics.* **1990**, *9*, 416−423.
[13] P. N. Hazin, C. Lakshminarayan, L. S. Brinen, J. L. Knee, J. W. Bruno, W. E. Streib, K. Folting, *Inorg. Chem.* **1988**, *27*, 1393−1400.
[14] H. J. Heeres, J. Renkema, M. Booji, A. Meetsma, J. H. Teuben, *Organometallics* **1988**, *7*, 2495−2502.
[15] D. Deng, C. Qian, F. Song, Z. Wang, G. Wu, P. Zheng, S. Jin, Y. Lin, *J. Organomet. Chem.* **1993**, *458*, 83−88.
[16] S. P. Nolan, D. Stern, T. J. Marks, *J. Am. Chem. Soc.* **1989**, *111*, 7844−7853.
[17] W. J. Evans, J. W. Grate, K. R. Levan, I. Bloom, T. T. Peterson, R. J. Doedens, H. Zhang, J. L. Atwood, *Inorg. Chem.* **1986**, *25*, 3614−3619.
[18] P. L. Watson, J. F. Whitney, R. L. Harlow, *Inorg. Chem.* **1981**, *20*, 3271−3278.
[19] G. B. Deacon, G. D. Fallon, P. I. MacKinnon, R. H. Newnham, G. N. Pain, T. D. Tuong, D. L. Wilkinson, *J. Organomet. Chem.* **1984**, *277*, 21−32.
[20] Z. Xie, Z. Liu, F. Xue, Z. Zhang, T. C. W. Mak, *J. Organomet. Chem.* **1997**, *542*, 285−289.
[21] R. E. Maginn, S. Manastyrskyj, M. Dubeck, *J. Am. Chem. Soc.* **1963**, *85*, 672−676.
[22] Z. Xie, Z. Liu, F. Xue, T. C. W. Mac, *J. Organomet. Chem.* **1997**, *539*, 127−130.
[23] W. J. Evans, T. A. Ulibarri, L. R. Chamberlain, J. W. Ziller, D. Alvarez Jr., *Organometallics* **1990**, *9*, 2124−2130.
[24] G. Brauer, *Handbook of Preparative Inorganic Chemistry*, Academic Press, New York, **1965**.
[25] S. G. McGeachin, *Can. J. Chem.* **1968**, *46*, 1903−1912.
[26] N. Kuhn, H. Lanfermann, P. Schmitz, *Liebigs Ann. Chem.* **1987**, 727−728.
[27] G. M. Sheldrick, *SHELXL: Program for Crystal Structure Refinement*, University of Göttingen, Göttingen, Germany, **1997**.

Received June 26, 2002
[I02347]

Synthesis and Structure of the First Non-Metallocene Ti^{III} Fluoride Complex $LTiF_2 \cdot 2Me_3SnCl$ Supported by a β-Diketiminato Ligand

Grigori B. Nikiforov,[a] Herbert W. Roesky,*[a] Jörg Magull,[a] Mathias Noltemeyer,[a] Hans-Georg Schmidt,[a] Evgeny G. Ilyin,[b] Yuri B. Kokunov,[b] and Alojz Demsar[a]

Dedicated to Professor F. A. Kuznetsov on the occasion of his 70th birthday

Keywords: Titanium / Fluorides / Coordination chemistry / N ligands

The Ti^{III} dichloride complex $LTiCl_2$ (**1**) and the first non-metallocene Ti^{III} fluoride complex $LTiF_2 \cdot 2Me_3SnCl$ (**2**) supported by the β-diketiminato ligand 2-{[2-(diethylamino)-ethyl]amino}-4-{[2-(diethylamino)ethyl]imino}pent-2-ene have been synthesized. Elemental analysis, mass spectrometry and X-ray structural analysis show that **1** is monomeric, neutral, and free of solvent and lithium salt. The complex adopts a pseudo-octahedral geometry with the two chlorine atoms arranged in *trans* position to each other. Compound **1** is soluble in common organic solvents and thermally surprisingly robust. Complex **2** was prepared using Me_3SnF as a fluorinating agent. X-ray structural analysis revealed that complex **2** consists of the $LTiF_2$ unit and two molecules of Me_3SnCl coordinated through a fluorine bridge to the titanium center. The fluorine atoms in **2** are located in *trans* positions to each other and the geometry around the titanium atom is distorted octahedral. Elemental analysis and mass spectrometry proved that **2** releases the coordinated Me_3SnCl under vacuum or during sublimation.

(© Wiley-VCH Verlag GmbH & Co. KGaA, 69451 Weinheim, Germany, 2003)

Introduction

The chemistry of trivalent titanium fluorides has proven to be a promising area of research with far-reaching results. At the moment this area is restricted mainly to cyclopentadienyl-substituted complexes. During the last decade our group has been successful in obtaining and structurally characterizing several Ti^{III} fluoride complexes, namely large clusters[1,2] based on fluorine-bridged organometallic units and the tetranuclear complexes $[\{[C_5H_4(SiMe_3)]_2TiF_2\}_3M]$ (M = Ti,[3] Ga,[3] Al[4]) with the four-membered MF_2Ti rings surrounded by the central metal atom in a propeller like fashion. Furthermore, the dimeric titanium complex $[(C_5H_4Me)_2TiF]_2$[5] has been prepared from the corresponding chlorine derivative.

There is widespread interest in the chemistry of low-valent titanium fluorine species from several perspectives, including synthetic methodology, and structural and theoretical implications. More pertinent to this study, however, is the high catalytic activity displayed by pentamethylcyclopentadienyl-substituted titanium fluorides in combination with methylaluminoxane (MAO) in the polymerization of styrene:[6] β-diketiminato complexes of Ti^{III} with the general formula $LTiCl_2$,[7,8] in the presence of excess methylaluminoxane[7] or $B(C_6F_5)_3$,[8] catalyse the homopolymerization of ethylene and the copolymerization of ethylene with α-olefins. Thus, our interest in the chemistry of titanium fluoride complexes stems from the potential use of Ti^{III} fluoride complexes supported by a new β-diketiminato ligand as a novel olefin polymerisation catalyst.

Mono β-diketiminato Ti^{III} dichlorides are accessible from $TiCl_3$ and the corresponding LiL salt in THF.[8] Access to a fluoride complex of Ti^{III} is possible by the reaction of trimethyltin fluoride with the corresponding chloride complex in non-aqueous solvents.[5]

Herein we report the synthesis and characterization of the new β-diketiminato Ti^{III} dichloride complex $LTiCl_2$ (**1**) [L = $Et_2NCH_2CH_2NC(Me)CHC(Me)NCH_2CH_2NEt_2$] and the first non-metallocene, neutral, solvent-free Ti^{III} fluoride complex $LTiF_2 \cdot 2Me_3SnCl$ (**2**).

[a] Institut für Anorganische Chemie, Universität Göttingen, Tammannstrasse 4, 37077, Göttingen, Germany
Fax: (internat.) + 49-551/393373
E-mail: hroesky@gwdg.de
[b] N. S. Kurnakov Institute of General and Inorganic Chemistry of Russian Academy of Sciences
Leninsky Prospect 31, 117907 Moscow GSP-1, Russia

Results and Discussion

The titanium complex **1** was prepared in a one-step synthesis from titanium trichloride and stoichiometric amounts of the lithium salt of the ligand in THF (Scheme 1). The

reaction proceeds at room temperature within 2 h and crystals are easily obtained from the original solution in high yield. Compound **1** is soluble in toluene, THF and dichloromethane, and can be recrystallized from toluene and THF. Complex **1** is thermally stable and can be refluxed in THF without observing any appreciable decomposition. Solid compound **1**, and especially its solution, are air-sensitive, but crystals of **1** are stable in a glove box for one month.

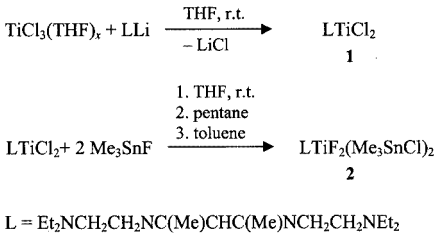

Scheme 1. Synthesis of the complexes **1** and **2**

The melting point of **1** is in the range 144−145 °C. Mass spectrometry and elemental analysis show that compound **1** is monomeric, solvent-free and contains no lithium chloride. Complex **1** exhibits a signal of the molecular ion $[M]^+$ in the EI-MS as well as strong fragments of $[C_5H_{12}N]^+$ and $[C_6H_{14}N]^+$ due to the decomposition of the titanium complex during the EI-MS experiment.

These properties indicate that **1** is a versatile starting material for studying the chemistry of low-valent titanium compounds.

Reaction of **1** with 2 equiv. of Me_3SnF in THF affords a clear solution. After evaporation of the solvent and washing with pentane, the residue was extracted with toluene. Initial addition of toluene caused the precipitate to dissolve, but after several minutes some solid deposited again. This solid is insoluble in toluene and THF and contains titanium, fluorine and non-stoichiometric amounts of the ligand. Complex **2** was purified by crystallization from toluene (Scheme 1). It should be pointed out that crystals of **2** are poorly soluble in toluene and can be obtained from the toluene solution. Complex **2** has good solubility in dichloromethane. Solutions of **2** and the solid are air-sensitive, but crystals of **2** can be kept in the glove box for several months.

The melting point of **2** is in the range 149−151 °C. Elemental analysis shows that complex **2** contains two molecules of Me_3SnCl. The composition was confirmed by EI-MS spectrometry. In the temperature range from room temp. to 120 °C $[Me_3SnCl]^+$ and several other fragments are observed. The elimination of Me_3SnCl ceases at 120 °C and in the temperature range from 155 to 200 °C compound **2** exhibits the molecular ion of $[LTiF_2]^+$.

Complex **2** decomposes and eliminates Me_3SnCl on standing under vacuum over a long period of time at 100−120 °C. The elemental analysis, however, shows that the remaining product does not correspond to the pure fluoride complex $LTiF_2$. Thus, by standing under vacuum it is possible to remove almost all coordinated Me_3SnCl, although the residue is not a pure fluoride complex. Further purification by sublimation at 150−160 °C resulted in a brown powder. The elemental analysis of the sublimate revealed that it is essentially $LTiF_2$. The EI-MS spectrum of this sublimate exhibits the molecular ion $[LTiF_2]^+$ and its corresponding fragments. Unfortunately, all the attempts to recrystallize this product were unsuccessful. Initially, this compound dissolved in toluene, but after several hours an amorphous precipitate deposited from solution.

Complexes **1** and **2** are paramagnetic and exhibit strong broadened proton NMR resonances ($\Delta\nu_{1/2}$ ranged from 50 to 1000 Hz); a fluorine resonance of **2** was not observed. A resonance at $\delta = 0.6$ ppm in the ^1H NMR spectrum of **2** in CD_2Cl_2 can be assigned to Me_3SnCl.

X-ray Structural Analysis of $LTiCl_2$

A summary of the crystallographic data and refinement parameters for the structure of **1** is given in Table 2. Selected bond lengths and angles are listed in Table 1.

Table 1. Selected bond lengths [Å] and angles [°] for compounds **1** and **2**

Complex **1**			
Ti−N(1)	2.065(2)	N(1)−Ti−N(2)	90.26(7)
Ti−N(2)	2.074(2)	N(1)−Ti−Cl(2)	92.75(7)
Ti−Cl(2)	2.372(1)	Cl(2)−Ti−Cl(1)	173.34(2)
Ti−Cl(1)	2.372(1)	N(1)−Ti−N(3)	170.24(7)
Ti−N(3)	2.434(2)	Cl(2)−Ti−N(3)	88.55(6)
Ti−N(4)	2.454(2)	N(1)−Ti−N(4)	79.84(8)
		Cl(2)−Ti−N(4)	87.57(6)
		N(3)−Ti−N(4)	109.89(6)

Complex **2**			
Ti(1)−F(1)	1.912(2)	F(1)−Ti(1)−F(1A)	169.03(1)
Ti(1)−F(1A)	1.912(2)	F(1)−Ti(1)−N(1)	94.31(1)
Ti(1)−N(1)	2.077(3)	N(1)−Ti(1)−N(1A)	89.37(2)
Ti(1)−N(2)	2.373(3)	F(1)−Ti(1)−N(2)	88.70(9)
Sn(1)−C(13)	2.112(4)	N(1)−Ti(1)−N(2)	79.99(1)
Sn(1)−Cl(1)	2.462(1)	N(1)−Ti(1)−N(2A)	169.28(1)
Sn(1)−F(1)	2.559(4)	N(2)−Ti(1)−N(2A)	110.67(1)
		Sn(1)−F(1)−Ti(1)	148.20(1)
		C(13)−Sn(1)−C(12)	114.88(2)
		C(13)−Sn(1)−Cl(1)	96.28(1)
		Cl(1)−Sn(1)−F(1A)	176.60(2)
		C(12)−Sn(1)−F(1A)	84.20(9)

Single crystals of **1** suitable for X-ray diffraction analysis were obtained by recrystallization from THF. $LTiCl_2$ crystallizes in the orthorhombic space group $Pna2_1$. The X-ray structural analysis proves that compound **1** is free of solvent and lithium salt and monomeric in the solid state (Figure 1).

In this complex the ligand coordinates to the metal center through the four nitrogen atoms. All four nitrogen atoms and the titanium atom are in the same plane. The geometry of this complex is similar to those of the praseodymium complexes $LPrX_2$ (X= Cl, Br)[9] containing the same ligand. The chlorine atoms in **1** are almost perpendicular to the equatorial plane, with the Cl(2)−Ti−Cl(1) angle [173.34(2)°] (Table 1) indicating that each chlorine atom is

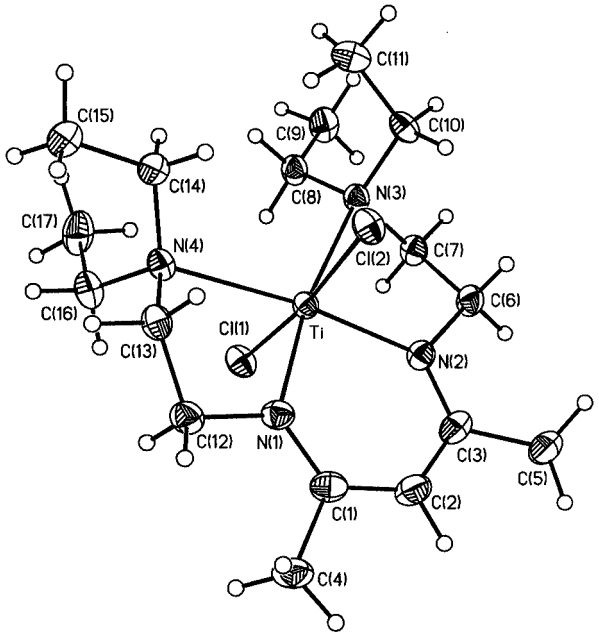

Figure 1. ORTEP drawing (50% thermal probability ellipsoids) of the crystal structure of **1** with atomic numbering scheme

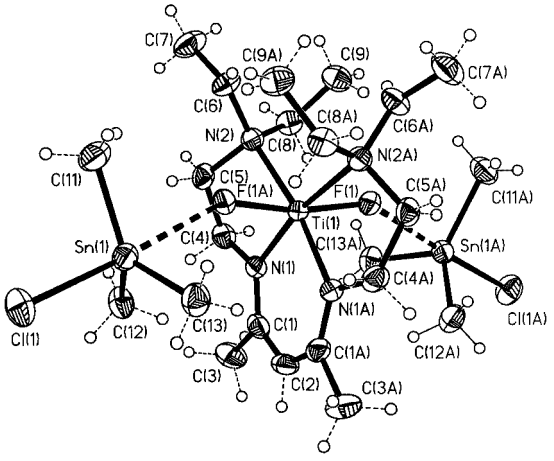

Figure 2. ORTEP drawing (50% thermal probability ellipsoids) of the crystal structure of **2** with atomic numbering scheme

slightly tilted towards the pendant arm. For this complex the titanium atom lies slightly out of the plane of the diimine ligand framework. The coordination number at the titanium atom in **1** is six and the geometry around the metal atom is pseudo-octahedral.

The Ti−N bonds of the pendant arm are longer than those of the backbone, as for the distances in the praseodymium complex $LPrX_2$ (X = Cl, Br),[9] due to the coordinative and covalent character involved in different bonding modes. The Ti−Cl bond length is similar to those found in the literature for β-diketiminato complexes of Ti^{III} (Ti−Cl 2.395 Å[7]).

X-ray Structural Analysis of $LTiF_2 \cdot 2Me_3SnCl$

A summary of the crystallographic data and refinement parameters for the structure of **2** is given in Table 2. Selected bond lengths and angles are listed in Table 1.

Single crystals of **2** suitable for X-ray diffraction analysis were obtained by crystallization from toluene. Complex **2** crystallizes in the monoclinic space group *C*2/*c*. The X-ray structural analysis reveals that compound **2** consists of an $LTiF_2$ unit and two coordinated molecules of Me_3SnCl. Trimethyltin chloride is coordinated through a fluoride bridge to the titanium center (Figure 2). The Sn−F distances [Sn(1)−F(1) 2.559(5) Å] in **2** are considerably longer than those in tin fluoride complexes [Sn−F 2.041(5)[10] Å, 2.126(3)[11] Å for five-coordinate tin] and are similar to those found for $[(acac)_2(\eta^5\text{-}C_5Me_5)Zr(\mu\text{-}F)SnMe_3Cl]$ [Sn−F 2.462(2) Å],[12] where Me_3SnCl is coordinated by a fluorine bridge to the zirconium center. Each Me_3SnCl molecule is tilted slightly towards the pendant arm of the $LTiF_2$ unit [Sn(1)−F−Ti(1) 148.20(1)°] due to repulsion between Me_3SnCl and the ethyl groups of the backbone of the β-diketiminato ligand. The coordination number at the tin atom in **2** is five and the geometry around the tin is pseudo-trigonal-bipyramidal. The fluorine and chlorine atoms in the Me_3SnFCl unit are almost in *trans* positions to each other [F(1)−Ti−Cl(1) 176.60(2)°] (Table 1).

In complex **2** the β-diketiminato ligand coordinates to the titanium center through the four nitrogen atoms. All four nitrogen atoms and the titanium atom lie in the same plane. The fluorine atoms in **2** are almost perpendicular to the equatorial plane [F(1)−Ti−F(1)#1 169.03(1)°] (Table 1) and each fluorine atom is tilted slightly towards the pendant arm. The coordination number at the titanium atom in **2** is six and the geometry around the metal atom is distorted octahedral.

The Ti−N bonds of the pendant arm are longer than those of the backbone, like those in complex **1** and $LPrX_2$ (X = Cl, Br).[9] The Ti−F bond is shorter than that found in the literature for titanium(III) fluoride complexes [Ti−F 1.975(1),[4] 2.094(1),[4] 2.092(2)[5] Å].

Conclusion

We have reported the synthesis and characterization of the Ti^{III} dichloride $LTiCl_2$ and the Ti^{III} fluoride complex $LTiF_2 \cdot 2Me_3SnCl$ supported by the β-diketiminato ligand 2-{[2-(diethylamino)ethyl]amino}-4-{[2-(diethylamino)-ethyl]imino}pent-2-ene. Compound **2** is easily prepared. It has been shown for the first time that Me_3SnF is a good fluorinating reagent for non-metallocene Ti^{III} compounds. Elemental analysis, mass spectrometry and X-ray structural analysis show that **2** is monomeric. Moreover, **2** is thermally unstable and gives off Me_3SnCl under vacuum. The uncoordinated $LTiF_2$ aggregates in toluene solution and therefore we were not able to obtain reliable results in polymerization reactions.

Experimental Section

General Remarks: All operations were performed using standard Schlenk line and dry box techniques under purified nitrogen or argon. Anhydrous titanium trichloride was of commercial reagent quality. The compound LH [L = $Et_2NCH_2CH_2NC(Me)$-$CHC(Me)NCH_2CH_2NEt_2$] was prepared by a known method.[9,13,14] The purity of LH was checked by elemental analysis, and ^1H and ^{13}C NMR spectroscopy. Me_3SnF was prepared by a literature method.[15] The purity of Me_3SnF was checked by elemental analysis and was found to contain less than 1% chlorine. Toluene, pentane and THF were dried with Na/benzophenone and distilled under nitrogen prior to use. C_6D_6 and [D_8]THF were dried with Na and degassed. CD_2Cl_2 was dried with CaH_2 and degassed. ^1H NMR spectra were recorded using a Bruker AM 200 spectrometer. Chemical shifts are reported in δ units downfield from Me_4Si with the solvent as the reference signal. Mass spectra were recorded using a Finnigan MAT 8230 instrument, and elemental analyses were carried out at the Analytical Laboratories of the Institute of Inorganic Chemistry at the University of Göttingen. Melting points were determined in sealed capillary tubes under nitrogen and are not corrected.

Synthesis of Complexes

$LTiCl_2$: LH (1.2 g, 1.28 mL, 4.0 mmol) was added to dry THF (30 mL) in a 50-mL Schlenk flask. The mixture was cooled to −78 °C and a solution of LiMe (2.52 mL; 1.6 M, 4.0 mmol) in Et_2O was added dropwise. The reaction mixture was stirred for 1 h at −78 °C, allowed to warm to room temperature and stirred at room temp. until methane evolution had ceased. This solution was added dropwise to a suspension of $TiCl_3$ (0.62 g, 4.0 mmol) in THF (30 mL) at room temp. in a 100-mL Schlenk flask. Then, the reaction mixture was stirred overnight. The suspension was filtered and concentrated. Finally, the resulting solution was left at −26 °C for 2 d. The red crystals that formed were separated by filtration, washed with pentane (20 mL) and dried in vacuo. Yield of $LTiCl_2$ (1.10 g, 66%). M.p. 144−145 °C. $C_{17}H_{35}Cl_2N_4Ti$ (414.3): calcd. C 49.28, H 8.45, N 13.53; found C 49.20, H 8.39, N 13.45. EI-MS: *m/z* (%) = 414 (6.4) [M^+], 378 (1.2) [LTiCl], 349 (0.6) [LTiCl − C_2H_6], 327 (1.0) [$M^+ - C_5H_{12}N$], 100 (4.0) [$C_6H_{14}N$], 86 (100.0) [$C_5H_{12}N$].

$LTiF_2 \cdot 2Me_3SnCl$: A mixture of $LTiCl_2$ (1.0 g, 2.4 mmol) and Me_3SnF (0.88 g, 4.8 mmol) in a 100-mL Schlenk flask was stirred in THF (40 mL) until all the precipitate dissolved (2 h). Then, the

Table 2. Crystallographic data of the X-ray diffraction studies of **1** and **2**

	1	**2**
Empirical formula	$C_{17}H_{35}Cl_2N_4Ti$	$C_{23}H_{53}Cl_2F_2N_4Sn_2Ti$
M_r	414.29	779.86
Temperature [K]	133(2)	200(2)
Radiation Used (λ [Å])	Mo-K_α (0.71073)	Mo-K_α (0.71073)
Crystal description	red plates	green block
Crystal size [mm]	0.8 × 0.8 × 0.2	1.00 × 0.80 × 0.6
Crystal system	orthorhombic	monoclinic
Space group	$Pna2_1$	$C2/c$
a [Å]	20.582(4)	10.736(2)
b [Å]	9.488(2)	17.181(3)
c [Å]	10.700(2)	18.294(4)
α [°]	90	90
β [°]	90	104.18(3)
γ [°]	90	90
V [Å^3]	2089.6(7)	3271.5(1)
Z	4	4
F (000)	884	1564
$\rho_{calcd.}$ [g·cm^{-3}]	1.317	1.579
μ [mm^{-1}]	0.672	1.946
Total reflections	16494	4650
Unique reflections	3566	2838
R(int)	0.0541	0.0506
Scan range Θ [°]	1.98 to 24.76	3.57 to 24.97
Completeness to Θ_{max} [%]	99.7	98.8
Index ranges	$-24 \le h \le 24$	$-12 \le h \le 12$
	$-11 \le k \le 9$	$-20 \le k \le 20$
	$-12 \le l \le 12$	$-21 \le l \le 21$
Data/restrains/parameters	3566/1/224	2838/0/161
*R*1,[a]	0.0308, 0.0736	0.0294, 0.0762
*R*1,[a] *wR*2 (all data)[c] [d]	0.0334, 0.0743	0.0323, 0.0781
Refinement method	Full-matrix least-squares on F^2	Full-matrix least-squares on F^2
Goodness-of-fit on F^2 [e]	1.010	1.111
Max./min. electr. dens. [e·Å^{-3}]	0.591/−0.270	1.134/−0.640

[a] $R1 = \Sigma||F_o| - |F_c||/\Sigma|F_o|$. [b] Denotes the value of the residual considering only the reflections with $I > 2\sigma(I)$. [c] $wR2$ [$I > 2\sigma(I)$] $wR2 = \{\Sigma[w(F_o^2 - F_c^2)^2]/\Sigma[w(F_o^2)^2]\}^{1/2}$; $w = 1/[\sigma^2(F_o^2) + (aP)^2 + bP]$, $P = [\max(F_o^2 \text{ or } 0) + 2(F_c^2)/3$. [d] Denotes the value of the residual considering all the reflections. [e] $S = [\Sigma[w(F_o^2 - F_c^2)^2]/[(n - p)^{1/2}]]$, *n*: number of data, *p*: parameters used.

THF was evaporated under vacuum, and the residue was washed portionwise (20 mL) with pentane. The residue was extracted with toluene (30 mL), the suspension was filtered and concentrated to approximately 7 mL. Finally, the resulting solution was left undisturbed for 3 d at room temp. The green crystals that formed were separated by filtration and washed with pentane (10 mL). Yield of $LTiF_2 \cdot 2Me_3SnCl$ (0.54 g, 29%). M.p. 149−151 °C. $C_{23}H_{53}Cl_2F_2N_4Sn_2Ti$ (779.0): calcd. C 35.38, H 6.80, N 7.18; found C 35.40, H 6.78, N 7.16. EI-MS ($T < 120$ °C): *m/z* (%) = 200 (5) [Me_3SnCl], 185 (100) [Me_2SnCl], 165 (54) [Me_3Sn], 155 (35) [SnCl], 134 (24) [MeSn], 119 (18) [Sn]; ($T > 155$ °C): *m/z* (%) = 381 (12) [M^+], 362 (1) [$LTiF]^+$, 333 (0.5) [$LTiF^+ - C_2H_6$], 309 (0.5) [$M^+ - NC_4H_{10}$], 295 (7) [$M^+ - C_5H_{12}N$], 100 (4.0) [$C_6H_{14}N$], 86 (100.0) [$C_5H_{12}N$].

Sublimation Experiment: Complex **2** (0.265 g, 0.34 mmol) was kept under vacuum at 90−110 °C for 6 h, until evolution of Me_3SnCl ceased. The amount of residue was 0.15 g (calcd. yield of the pure $LTiF_2$ 0.13 g). M.p. 152−156 °C. $C_{17}H_{35}F_2N_4Ti$ (381.5): calcd. C 53.54, H 9.19, N 14.70; found C 49.09, H 8.43, N 13.00. EI-MS: *m/z* (%) = 381 (12) [M^+], 362 (1) [LTiF], 333 (0.5) [$LTiF^+ - C_2H_6$], 309 (0.5) [$M^+ - NC_4H_{10}$], 295 (8) [$M^+ - C_5H_{12}N$], 100 (14) [$C_6H_{14}N$], 86 (100.0) [$C_5H_{12}N$]. This residue was sublimed at 150−160 °C to give 0.09 g of a dark brown powder. M.p. 122−123 °C. $C_{17}H_{35}F_2N_4Ti$ (381.5): calcd. C 53.54, H 9.19, N 14.70; found C 52.88, H 9.18, N 13.96. EI-MS: *m/z* (%) = 397 (1.5), 381 (6) [M^+], 362 (1) [LTiF], 333 (0.5) [$LTiF^+ - C_2H_6$], 309 (0.5) [$M^+ - NC_4H_{10}$], 295 (8) [$M^+ - C_5H_{12}N$], 210 (30) [$L^+ - C_5H_{12}N$], 100 (52) [$C_6H_{14}N$], 86 (100.0) [$C_5H_{12}N$].

X-ray Crystallographic Study: Crystal data and experimental conditions are listed in Table 2. Selected bond lengths and bond angles with standard deviations in parentheses are presented in Table 1. Intensity data for the crystal structure of $LTiCl_2$ were collected with a Stoe image-plate IPDS II-system. Data for the crystal structure of $LTiF_2 \cdot 2Me_3SnCl$ was collected with a Stoe−Siemens four-circle diffractometer. All structures were solved by direct methods (SHELXS-97) and refined against F^2 using SHELXS-97.[16] The heavy atoms were refined anisotropically. Hydrogen atoms were included using the riding model with U_{iso} tied to U_{iso} of the parent atoms. CCDC-189244 (**1**) and -189245 (**2**) contain the supplementary crystallographic data for this paper. These data can be obtained free of charge at www.ccdc.cam.ac.uk/conts/retrieving.html or from the Cambridge Crystallographic Data Centre, 12 Union Road, Cambridge CB2 1EZ, UK [Fax: (internat.) + 44-1223/336-033; E-mail: deposit@ccdc.cam.ac.uk].

Acknowledgments

Financial support by the Deutsche Forschungsgemeinschaft is highly acknowledged.

[1] F.-Q. Liu, A. Kuhn, R. Herbst-Irmer, D. Stalke, H. W. Roesky, *Angew. Chem.* **1994**, *106*, 577−578; *Angew. Chem. Int. Ed. Engl.* **1994**, *33*, 555−556.
[2] F.-Q. Liu, D. Stalke, H. W. Roesky, *Angew. Chem.* **1995**, *107*, 2004−2006; *Angew. Chem. Int. Ed. Engl.* **1995**, *34*, 1872−1874.
[3] F.-Q. Liu, A. Künzel, A. Herzog, H. W. Roesky, M. Noltemeyer, R. Fleischer, D. Stalke, *Polyhedron* **1997**, *16*, 61−65.
[4] F.-Q. Liu, H. Gornitzka, D. Stalke, H. W. Roesky, *Angew. Chem.* **1993**, *105*, 447−448; *Angew. Chem. Int. Ed. Engl.* **1993**, *32*, 442−443.
[5] A. Herzog, F.-Q. Liu, H. W. Roesky, A. Demsar, K. Keller, M. Noltemeyer, F. Pauer, *Organometallics* **1994**, *13*, 1521−1526.
[6] W. Kaminsky, S. Lenk, V. Scholz, H. W. Roesky, A. Herzog, *Macromolecules* **1997**, *30*, 7647−7650.
[7] W.-K. Kim, M. J. Fevola, L. M. Liable-Sands, A. L. Rheingold, K. H. Theopold, *Organometallics* **1998**, *17*, 4541−4543.
[8] P. H. M. Budzelaar, A. B. van Oort, A. G. Orpen, *Eur. J. Inorg. Chem.* **1998**, 1485−1494.
[9] D. Neculai, H. W. Roesky, A. M. Neculai, J. Magull, H.-G. Schmidt, M. Noltemeyer, *J. Organomet. Chem.* **2002**, *643/644*, 47−52.
[10] J. F. Follano, R. O. Day, R. R. Holmes, *Organometallics.* **1984**, *3*, 750−755.
[11] H. Puff, H. Hevendehl, K. Höfer, H. Reuter, W. Schuh, *J. Organomet. Chem.* **1985**, *287*, 163−178.
[12] E. F. Murphy, P. Yu, S. Dietrich, H. W. Roesky, E. Parisini, M. Noltemeyer, *J. Chem. Soc., Dalton Trans.* **1996**, 1983−1987.
[13] S. G. McGeachin, *Can. J. Chem.* **1968**, *46*, 1903−1912.
[14] N. Kuhn, H. Lanfermann, P. Schmitz, *Liebigs Ann. Chem.* **1987**, 727−728.
[15] E. Krause, *Ber. Dtsch. Chem. Ges.* **1918**, *51*, 1447−1456.
[16] G. M. Sheldrick, *SHELXL: Program for Crystal Structure Refinement*, University of Göttingen, Göttingen, Germany, **1997**.

Received July 18, 2002
[I02397]

Synthesis of a Hexadentate Hexameric Aluminum Imide and Its Metathesis Reactions

N. Dastagiri Reddy,[a] S. Shravan Kumar,[a] Herbert W. Roesky,*[a] Denis Vidovic,[a] Jörg Magull,[a] Mathias Noltemeyer,[a] and Hans-Georg Schmidt[a]

Dedicated to Professor Bernt Krebs on the occasion of his 65th birthday

Keywords: Aluminum / Hydride ligands / N ligands / S ligands / Cluster compounds

The reaction of $AlH_3{\cdot}NMe_3$ with one equivalent of 2-cyanothiophene in toluene afforded $[HAlNCH_2(C_4H_3S)]_6$ (**2**) in good yield. Treatment of **2** with $SiMe_3Br$ and $SiMe_3Cl$ in toluene under refluxing conditions resulted in the formation of compounds $[BrAlNCH_2(C_4H_3S)]_6$ (**3**) and $[ClAlNCH_2(C_4H_3S)]_6$ (**4**), respectively. In a similar way $[PhC{\equiv}CAlNCH_2(C_4H_3S)]_6$ (**5**) was readily obtained from the reaction between **2** and PhC≡CH. When **2** was treated with PhSH the Al-N cluster core dissociated and a four-membered ring compound $[(PhS)_2AlNHCH_2(C_4H_3S)]_2$ (**6**) was formed. In contrast, a similar hexameric aluminum imide $(HAlNCH_2Ph)_6$ (**1**) retains its Al-N network when treated with PhSH to yield $(PhSAlNCH_2Ph)_6$ (**7**). An exchange of ethyl groups and hydrides occurred when **2** was treated with excess of $ZnEt_2$, forming $[EtAlNCH_2(C_4H_3S)]_6$ **8**. Compounds **2**–**4** and **6**–**8** were characterized by X-ray single-crystal analysis.
(© Wiley-VCH Verlag GmbH & Co. KGaA, 69451 Weinheim, Germany, 2003)

Introduction

Recently, we have been actively involved in exploring the reactions of $AlH_3{\cdot}NMe_3$ with compounds containing C-N and C-C multiple bonds.[1] Such reactions lead to the formation of structurally interesting Al-N and Al-C clusters. In particular, a hexameric aluminum imide $(HAlNCH_2Ph)_6$ **1** can be synthesized by the treatment of PhCN with $AlH_3{\cdot}NMe_3$.[1a] We have also demonstrated that the imide **1** is stable toward certain reagents and can be functionalized easily. In our continuing efforts to synthesize functionalized aluminum imides, which can act as potential complexation agents, we have treated 2-cyanothiophene with $AlH_3{\cdot}NMe_3$. Herein we report the synthesis and metathesis reactions of an aluminum imide containing six thiophene groups, $[HAlNCH_2(C_4H_3S)]_6$ (**2**).

Results and Discussion

An interesting feature of the structure of **1** is the orientation of the benzyl groups. Three of them are aligned in one direction while the remaining three are aligned in another direction. This observation has prompted us to synthesize a hexadentate (tridentate on each side of the cluster core), hexameric aluminum imide and we have chosen 2-cyanothiophene for this purpose. Addition of a slight excess of $AlH_3{\cdot}NMe_3$ to one equivalent of 2-cyanothiophene in toluene at −78 °C and refluxing the resultant solution until the evolution of NMe_3 had ceased gave $[HAlNCH_2(C_4H_3S)]_6$ (**2**) in good yield (Scheme 1).

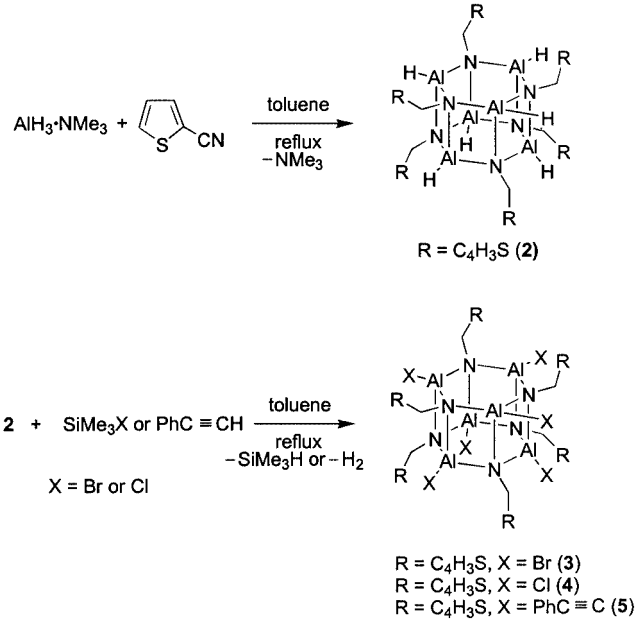

Scheme 1

[a] Institut für Anorganische Chemie der Universität Göttingen, Tammannstrasse 4, 37077, Göttingen, Germany
Fax: (internat.) +49-(0)551/393-373
E-mail: hroesky@gwdg.de

Altering the stoichiometry of the reactants decreased the yield drastically. Six thiophene groups dangling over the Al-N network make **2** hexadentate. A thorough literature search for this type of compounds was done and we found that a hexameric aluminum imide with six NMe_2 groups has been reported.[2] Treatment of **2** with $SiMe_3Br$ or $SiMe_3Cl$ in toluene under refluxing conditions resulted in the formation of compounds $[BrAlNCH_2(C_4H_3S)]_6$ (**3**) and $[ClAlNCH_2(C_4H_3S)]_6$ (**4**), respectively. In a similar way, PhC≡CH reacts with **2** to give $[PhC{\equiv}CAlNCH_2(C_4H_3S)]_6$ (**5**) and evolution of H_2 (Scheme 1). Compounds **3**−**5** were the only isolable products of the respective reactions. In all these cases, all six hydridic hydrogens in **2** are replaced by the corresponding nucleophilic moieties and the Al-N cluster core remains intact. However, when **2** was treated with PhSH the Al-N cluster core dissociated to a four-membered ring $[(PhS)_2AlNHCH_2(C_4H_3S)]_2$ (**6**). In this reaction, migration of a proton from sulfur to nitrogen was observed (Scheme 2).

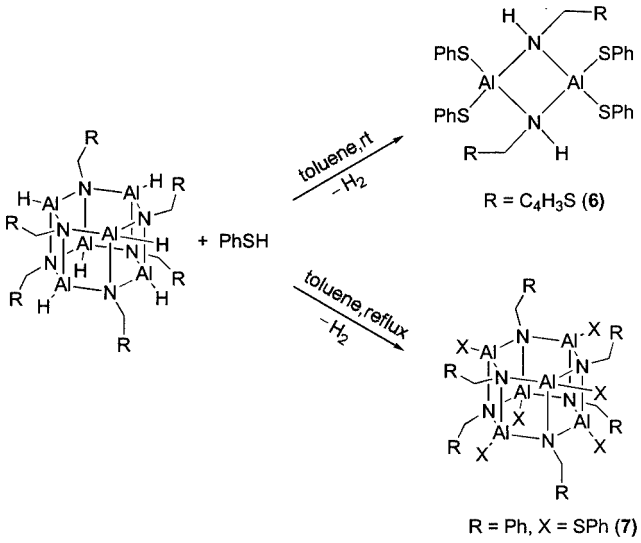

Scheme 2

There are several four-membered Al-N rings known in the literature.[3] However, none of them carries as many as six sulfur atoms. Hence, compound **6** is the first four-membered aluminum imide carrying six sulfur atoms, of which four are connected directly to the ring aluminum atoms. To compare the stability of **2** with **1** the latter was also treated with PhSH. To our surprise, in contrast to the results of the reaction between **2** and PhSH, the Al-N network of **1** remained intact even under reflux conditions and a hexa-substituted product $(PhSAlNCH_2Ph)_6$ (**7**) was formed. The reaction between $ZnEt_2$ and **2** was also carried out in order to examine the reactivity of the Al−H bonds in **2** toward exchange reactions. Only one such example, in which $AlMe_3$ exchanges methyl groups with the hydrides of $(HAlNiPr)_6$,

Table 1. Crystallographic data for the structural analyses of compounds **2**−**4** and **6**−**8**

	2	**3**	**4**	**6**	**7**·$C_6H_5CH_3$	**8**
Formula	$C_{30}H_{36}Al_6N_6S_6$	$C_{30}H_{30}Al_6Br_6N_6S_6$	$C_{30}H_{30}Al_6Cl_6N_6S_6$	$C_{34}H_{32}Al_2N_2S_6$	$C_{85}H_{80}Al_6N_6S_6$	$C_{42}H_{60}Al_6N_6S_6$
Mol. wt.	834.89	1308.30	1041.54	714.94	1539.79	1003.20
T/K	133(2)	203(2)	293(2)	293(2)	133(2)	133(2)
λ/ Å	0.71073	0.71073	0.71073	0.71073	0.71073	0.71073
Cryst system	trigonal	cubic	triclinic	monoclinic	monoclinic	cubic
Space group	$R\bar{3}$	$Pa\bar{3}$	$P\bar{1}$	$P2_1/c$	C_2/c	$Pa\bar{3}$
a (Å)	15.192(2)	16.4721(19)	10.108(2)	13.105(3)	23.525(5)	16.969(2)
b (Å)	15.192(2)	16.4721(19)	10.116(2)	9.1795(18)	14.529(3)	16.969(2)
c (Å)	14.349(3)	16.4721(19)	10.968(2)	14.822(3)	23.911(5)	16.969(2)
α (°)	90	90	98.74(3)	90	90	90
β (°)	90	90	100.97(3)	107.84(3)	111.16(3)	90
γ (°)	120	90	98.71(3)	90	90	90
V (Å^3)	2868.0(8)	4469.4(9)	1069.3(4)	1697.2(6)	7622(3)	4886.2(10)
Z	3	4	1	2	4	4
D(calcd) (g·cm^{-3})	1.450	1.944	1.617	1.399	1.342	1.364
μ(Mo-$K_α$) (cm^{-1})	0.528	0.5822	0.852	0.483	0.300	0.426
F(000)	1296	2544	528	744	3224	2112
$θ$ range (°)	2.10−24.69	3.71−24.94	1.92−24.77	1.63−24.82	1.68−24.79	2.08−24.79
Index range	$-17 \le h \le 17$	$-19 \le h \le 19$	$-11 \le h \le 11$	$-15 \le h \le 15$	$-25 \le h \le 27$	$-6 \le h \le 18$
	$-17 \le k \le 17$	$-19 \le k \le 19$	$-11 \le k \le 11$	$-10 \le k \le 10$	$-17 \le k \le 17$	$-15 \le k \le 19$
	$-16 \le l \le 16$	$-1 \le l \le 11$	$-12 \le l \le 12$	$-17 \le l \le 17$	$-28 \le l \le 24$	$-19 \le l \le 19$
Reflns collected	6025	1968	6310	13640	21707	9292
Independent reflns	1093	1311	3342	2910	6377	1398
Refinement method	Full-matrix least-squares on F^2					
Data/restraints/parameters	1093/0/77	1311/166/101	3342/0/251	2910/0/203	6377/0/462	1398/0/91
$R1$, $R2$ [$I > 2σ(I)$][a]	0.0567, 0.1698	0.0754, 0.1689	0.0443, 0.1169	0.0342, 0.0923	0.0288, 0.0742	0.0404, 0.0791
$R1$, $R2$ (all data)[a]	0.0622, 0.1773	0.1209, 0.1965	0.0535, 0.1197	0.0397, 0.0942	0.0370, 0.0763	0.0791, 0.0867
S	1.145	1.028	0.961	1.015	0.955	0.833
$Δρ$(min), $Δρ$(max)/e·Å^3	1.027, −0.536	0.643, −0.591	0.513, −0.545	0.552, −0.396	0.399, −0.272	0.274, −0.256

[a] $R1 = Σ||F_o| - |F_c||/Σ|F_o|$. $R2 = [Σw(|F_o^2| - |F_c^2|)^2/Σw|F_o^2|^2]^{1/2}$.

is known in the literature.[4] Compound **2** reacts with an excess of $ZnEt_2$ rapidly at room temperature with replacement of all its hydrides by ethyl groups, giving $[EtAlNCH_2(C_4H_3S)]_6$ (**8**; Scheme 3).[5]

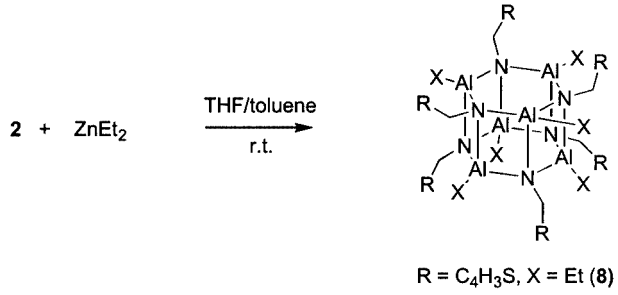

Sdheme 3

Compounds **2**−**4** and **6**−**8** were characterized by single-crystal X-ray structural analysis and the results were compared with IR, mass and elemental analysis data. A strong absorption band at 1860 cm^{-1} in the IR spectrum of **2** can be attributed to ν(Al−H).[6] The absence of this band in the IR spectra of compounds **3**−**6** indicates the lack of an Al−H bond in those compounds. In addition, a sharp band of strong intensity at 2129 cm^{-1} in the IR spectrum of **5** shows the presence of a C≡C moiety in the molecule.[7] Strong evidence for the presence of N−H in compound **6** comes from its IR spectrum, which contains a sharp band at 3248 cm^{-1}. The EI mass spectra of **2**, **3**, **4** and **6** exhibit the molecular ion peaks, whereas a peak related to $[M^+ - C_2H_5]$ is observed in the case of **8**. No molecular ion peak is found in the EI mass spectra of **5** and **7**.

Crystallographic data for the structural analyses of compounds **2**−**4** and **6**−**8** are given in Table 1, and important bond parameters are listed in Table 2. Compound **2** crystallizes in a trigonal space group ($R\bar{3}$) with one sixth of the molecule in the asymmetric unit. An ORTEP plot of **2** is given in Figure 1. The basic central core of the structure is comprised of an Al-N network containing six aluminum atoms and six nitrogen atoms in alternate positions, forming a hexagonal prism. Three of the six thiophenyl methyl groups dangling over one of the hexagonal faces of the polyhedron are oriented in one direction while those on the other hexagonal face are oriented in the opposite direction. The thiophene rings are oriented in such a way that the sulfur atoms are positioned slightly toward the vertical axis of the polyhedron. The bond parameters are similar to the previously studied structures and the Al−N bonds forming the hexagonal faces are significantly shorter than the transverse bonds.[1a,2,8]

Compound **3** crystallizes in the cubic space group $Pa\bar{3}$ with one sixth of the molecule in the asymmetric unit. An ORTEP plot depicting the spatial arrangement of the atoms in compound **3** is shown in Figure 2.

The sulfur atom of the thiophene group is disordered with an occupancy of 0.628(12). ORTEP plots of compounds **4** and **6**−**8** are given in Figures 3−6, respectively.

Table 2. Selected bond lengths and bond angles for compounds **2**−**4**, **6** and **7**

Bond lengths (Å)		Bond angles (deg)	
		Compound **2**	
N(1)−Al(1)	1.892(3)	N(3)−Al(3)−N(2)	115.38(15)
N(3)−Al(3)	1.894(3)	Al(1)−N(1)−Al(2)	124.33(15)
N(3)−Al(1)	1.974(3)	N(3)−Al(1)−N(1)	90.83(13)
		N(3)−Al(3)−N(1)	90.89(13)
		Al(3)−N(1)−Al(1)	89.00(12)
		Al(1)−N(3)−Al(3)	88.94(12)
		Compound **3**	
N(1)−Al(2)	1.873(8)	Al(2)−N(1)−Al(3)	124.7(4)
N(1)−Al(3)	1.876(8)	N(3)−Al(1)−N(2)	114.8(4)
N(1)−Al(1)	1.963(8)	N(3)−Al(3)−N(1)	91.3(3)
Al(1)−Br(1)	2.253(3)	N(3)−Al(1)−N(1)	91.2(3)
		Al(1)−N(3)−Al(3)	88.6(3)
		Al(3)−N(1)−Al(1)	88.5(3)
		Br(1)−Al(1)−N(1)	111.0(2)
		Br(1)−Al(1)−N(3)	119.3(3)
		Compound **4**	
N(1)−Al(2)	1.880(3)	Al(2)−N(1)−Al(3)	124.64(15)
N(1)−Al(3)	1.884(3)	N(3)−Al(1)−N(2)	115.67(12)
N(1)−Al(1)	1.972(3)	N(3)−Al(3)−N(1)	91.80(13)
Al(1)−Cl(1)	2.099(1)	N(3)−Al(1)−N(1)	91.47(12)
		Al(1)−N(3)−Al(3)	88.41(12)
		Al(3)−N(1)−Al(1)	88.42(11)
		Cl(1)−Al(1)−N(1)	112.38(9)
		Cl(1)−Al(1)−N(3)	118.75(9)
		Compound **6**	
N(1)−Al(1)	1.933(2)	Al(1)−N(1)−Al(2)	90.62(7)
N(1)−Al(2)	1.946(2)	N(1)−Al(2)−N(2)	89.38(7)
S(1)−Al(1)	2.209(1)	S(1)−Al(1)−S(2)	123.81(3)
S(2)−Al(1)	2.220(1)	S(2)−Al(1)−N(1)	104.40(6)
		S(2)−Al(1)−N(2)	110.29(6)
		Compound **7**	
N(1)−Al(1)	1.890(2)	Al(2)−N(3)−Al(3)	125.10(7)
N(3)−Al(2)	1.902(2)	N(1)−Al(1)−N(2)	115.86(6)
N(1)−Al(2)	1.975(2)	N(1)−Al(1)−N(3)	91.65(6)
N(3)−Al(1)	1.973(2)	Al(1)−N(3)−Al(3)	88.34(6)
Al(1)−S(1)	2.220(1)	S(1)−Al(1)−N(1)	117.24(5)
		S(2)−Al(2)−N(1)	120.86(4)
		S(3)−Al(3)−N(2)	111.75(5)
		Compound **8**	
N(1)−Al(2)	1.897(3)	Al(2)−N(1)−Al(3)	125.32(13)
N(1)−Al(3)	1.898(3)	N(3)−Al(1)−N(2)	114.12(14)
N(1)−Al(1)	1.987(3)	N(3)−Al(3)−N(1)	91.36(11)
Al(1)−C(1)	1.940(4)	Al(1)−N(3)−Al(3)	88.40(10)
		C(1)−Al(1)−N(1)	114.38(15)
		C(1)−Al(1)−N(2)	122.20(15)
		C(1)−Al(1)−N(3)	115.80(14)

The bond parameters and the basic structure of the Al-N network in compounds **4** and **8** are similar to those of **2**. However, the orientation of the thiophene groups in compound **8** is quite different from that in the other com-

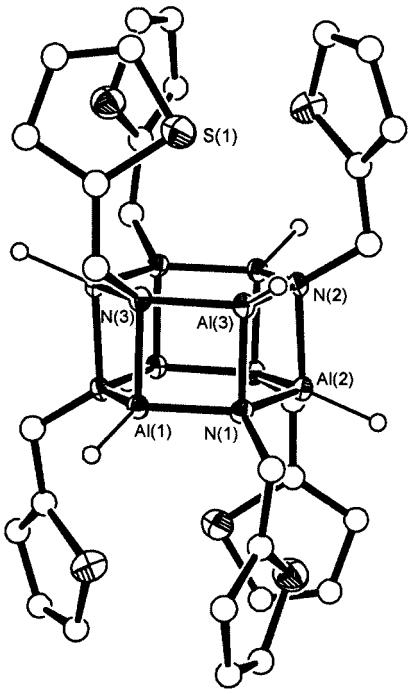

Figure 1. Crystal structure of compound $[HAlNCH_2(C_4H_3S)]_6$ (**2**); all hydrogen atoms, except those on Al, have been omitted for clarity

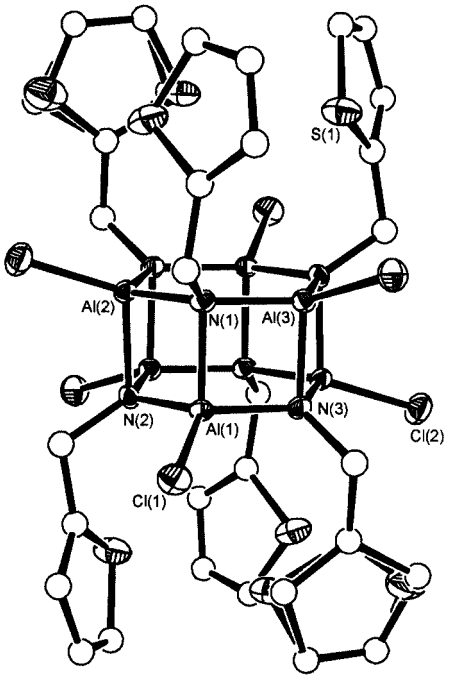

Figure 3. Crystal structure of compound $[ClAlNCH_2(C_4H_3S)]_6$ (**4**); all hydrogen atoms have been omitted for clarity

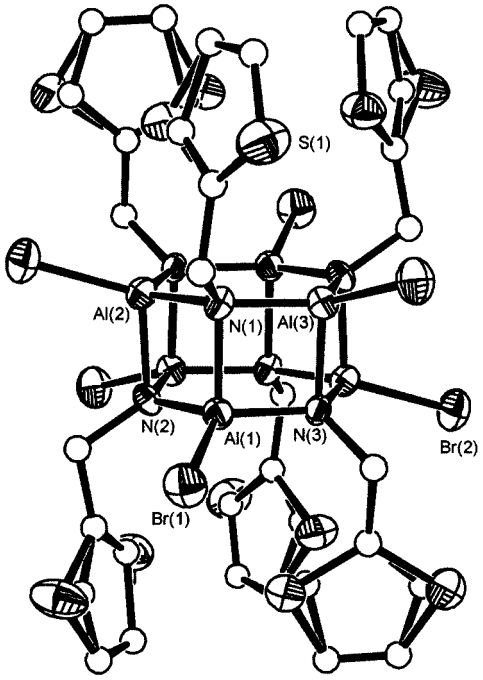

Figure 2. Crystal structure of compound $[BrAlNCH_2(C_4H_3S)]_6$ (**3**); all hydrogen atoms have been omitted for clarity

pounds. The sulfur atoms in **8** are projected away from the vertical axis, whereas they are projected toward the vertical axis in compounds **2**−**4**.

Compound **6** crystallizes in the cubic space group $Pa\bar{3}$ with half of the molecule in the asymmetric unit. Figure 4 shows the molecular structure of **6**. Two thiophenyl methyl groups are mutually *trans* and the phenyl groups on the same side of the plane of the Al-N ring are oriented in the same direction. The average Al−N bond length [1.940(2) Å] is in accordance with those reported in the literature.[3]

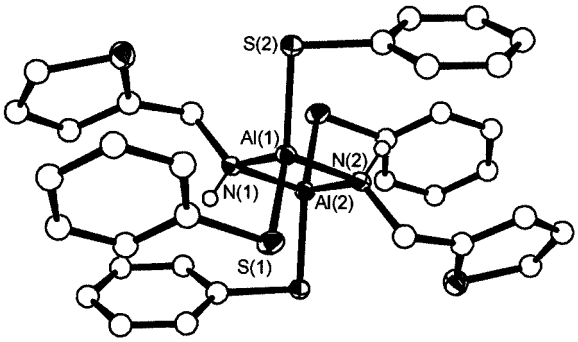

Figure 4. Crystal structure of compound $[(PhS)_2AlNHCH_2(C_4H_3S)]_2$ (**6**); all hydrogen atoms, except those on N, have been omitted for clarity

Compound **7** crystallizes in the monoclinic space group *C*2/*c* with half of the molecule in the asymmetric unit (Figure 5). The Al-N polyhedron is completely surrounded by organic moieties on all sides. While the bond parameters are similar to those of **1**, the bond angles between the transverse Al−N bonds and the Al−S bonds in **7** vary significantly from each other, which is not the case with compounds **3**, **4** and **8** (Figure 6; Table 2).

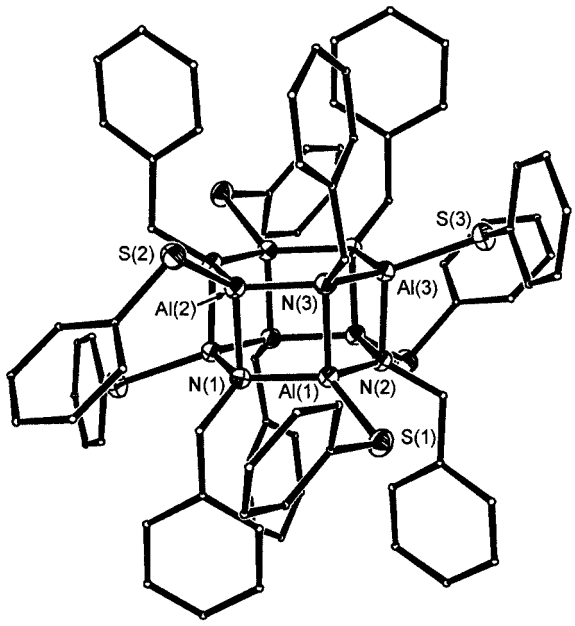

fiture 5. Crystal structure of compound $(PhSAlNCH_2Ph)_6$ (**7**); all hydrogen atoms have been excluded for clarity

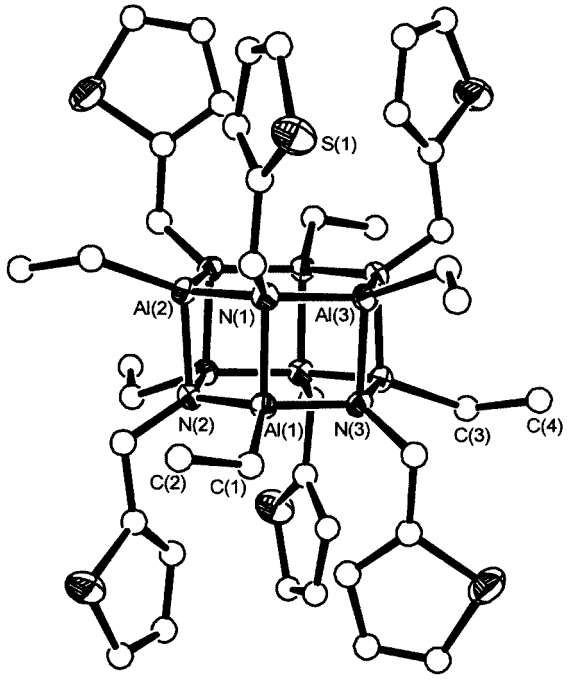

Figure 6. Crystal structure of compound $[EtAlNCH_2(C_4H_3S)]_6$ (**8**); all hydrogen atoms have been excluded for clarity

Conclusion

A hexadentate hexameric aluminum imide $[HAlNCH_2(C_4H_3S)]_6$ **2** has been synthesized and structurally characterized. Its reactivity toward reagents like $SiMe_3Br$, $SiMe_3Cl$, PhC≡CH and PhSH has been examined. We found that the Al−N network in **2** is stable toward $SiMe_3Br$, $SiMe_3Cl$ and PhC≡CH while it dissociates to form a four-membered ring with PhSH. We are currently investigating the ability of **2** and **5** to form complexes with transition metals.

Experimental Section

General Remarks: All experimental manipulations were carried out under an atmosphere of dry nitrogen using standard Schlenk techniques. The samples for spectral measurements were prepared in a dry box. Solvents were purified according to conventional procedures and were freshly distilled prior to use. $AlH_3{\cdot}NMe_3$ [9] and **1**[1a] were prepared as described in the literature. 2-Cyanothiophene, $SiMe_3Br$, $SiMe_3Cl$, PhSH, $ZnEt_2$ and PhC≡CH were procured from Aldrich and used as such. NMR spectra were recorded on a Bruker AM 200 instrument; chemical shifts are reported with reference to TMS. IR spectra were recorded on a Bio-Rad Digilab FTS7 spectrometer. Melting points were obtained on a HWS-SG 3000 apparatus and are uncorrected. CHN analyses were performed at the Analytical Laboratory of the Institute of Inorganic Chemistry at Göttingen, Germany.

Reaction of $AlH_3{\cdot}NMe_3$ with 2-Cyanothiophene. Synthesis of 2: $AlH_3{\cdot}NMe_3$ (30 mL, 0.5 M solution in toluene) was added to a solution of 2-cyanothiophene (1.50 g, 13.74 mmol) in toluene (30 mL) at −78 °C whilst stirring. The reaction mixture was allowed to warm to room temperature and then refluxed until the evolution of NMe_3 ceased. Storing the resultant solution overnight at room temperature afforded colorless crystals of **2**. Yield: 1.23 g (64%). M.p. 238−240 °C. ^1H NMR (200 MHz, $CDCl_3$): δ = 4.31 (s, 12 H, CH_2), 6.74, 6.83, 7.06 (m, 18 H, C_4H_3S) ppm. ^{13}C NMR (125 MHz, $CDCl_3$): δ = 44.07 (CH_2), 124.35, 125.28, 127.23, 146.95 (C_4H_3S) ppm. IR (KBr, nujol mull): $\tilde{\nu}$ = 1860 (s), 1718 (w), 1648 (w), 1596 (w), 1528 (w), 1339 (m), 1269 (m), 1216 (m), 1156 (m), 1075 (w), 1040 (w), 1013 (w), 969 (w), 854 (s), 819 (s), 753 (w), 723 (w), 693 (w), 658 (w), 637 (w), 621 (w), 529 (m), 481 (m), 438 (m), 413 (w) cm^{-1}. EI-MS: *m*/*z* (%) = 834 (20) $[M^+]$, 737 (28) $[M^+ - CH_2C_4H_3S]$, 653 (36) $[M^+ - (CH_2C_4H_3S + C_4H_4S)]$, 113 (100) $[H_2NCH_2C_4H_3S^+]$. $C_{30}H_{36}Al_6N_6S_6$ (834.89): calcd. C 43.16, H 4.35, N 10.07; found C 43.23, H 4.46, N 9.35.

Reaction of 2 with $SiMe_3Br$. Synthesis of 3: $SiMe_3Br$ (1.07 g, 6.99 mmol) was added at room temperature to a suspension of **2** (0.73 g, 0.87 mmol) in toluene (30 mL). The reaction mixture was stirred overnight at room temperature and refluxed for an hour. The solution was filtered and cooled to room temperature to obtain colorless crystals of **3**. Yield: 0.77 g (68%). M.p. 284−287 °C. IR (KBr, nujol mull): $\tilde{\nu}$ = 1887 (m), 1780 (w), 1714 (w), 1647 (w), 1602 (w), 1532 (w), 1433 (m), 1335 (s), 1272 (s), 1226 (m), 1216 (m), 1162 (s), 1135 (w), 1074 (w), 1043 (w), 977 (w), 891 (w), 850 (s), 826 (s), 757 (w), 723 (w), 655 (m), 617 (m), 562 (s), 520 (m), 504 (s), 465 (m), 435 (s) cm^{-1}. EI-MS: *m*/*z* (%) = 1308 (5) $[M^+]$, 179 (100), 113 (16) $[H_2NCH_2C_4H_3S^+]$. $C_{30}H_{30}Al_6Br_6N_6S_6$ (1308.30): calcd. C 27.54, H 2.31, N 6.42; found C 27.15, H 2.85, N 6.19.

Reaction of 2 with $SiMe_3Cl$. Synthesis of 4: The reaction between **2** (0.50 g, 0.60 mmol) and $SiMe_3Cl$ (0.45 g, 4.14 mmol) was carried out in a similar manner to that between **2** and $SiMe_3Br$. Yield: 0.44 g (71%). M.p. 218−223 °C. IR (NaCl, nujol mull): $\tilde{\nu}$ = 1889 (w), 1797 (w), 1724 (w), 1650 (w), 1594 (w), 1531 (w) 1495 (w), 1435 (m), 1341 (s), 1272 (s), 1219 (s), 1158 (s), 1135 (w), 1074 (w), 1042 (w), 972 (w), 896 (w), 855 (s), 824 (s), 753 (w), 728 (w), 685 (w), 653 (w), 622 (m), 593 (m), 564 (w), 540 (w) cm^{-1}. EI-MS:

m/z (%) = 1040 (10) [M^+], 943 (10) [$M^+ - CH_2C_4H_3S$], 97 (100) [$CH_2C_4H_3S^+$]. $C_{30}H_{30}Al_6Cl_6N_6S_6$ (1041.54): calcd. C 34.59, H 2.90, N 8.07; found C 33.57, H 3.47, N 7.64.

Reaction of 2 with PhC≡CH. Synthesis of 5: PhC≡CH (0.42 g, 4.11 mmol) was added at room temperature to a suspension of **2** (0.50 g, 0.60 mmol) in toluene (30 mL). The reaction mixture was stirred for half an hour at room temperature before refluxing it until the evolution of H_2 ceased. The resultant dark brown solution was filtered and kept for crystallisation at room temperature. Yield: 0.55 g (64%). M.p. 270 °C (decomp). ^{1}H NMR (200 MHz, $CDCl_3$): δ = 4.68 (s, 12 H, CH_2), 6.79, 6.95, 7.04 (m, 18 H, C_4H_3S), 7.27 (m, 18 H, *m*- and *p*-C_6H_5), 7.46 (m, 12 H, *o*-C_6H_5) ppm. ^{13}C NMR (125 MHz, $CDCl_3$): δ = 41.28 (CH_2), 67.98 (Al − C), 83.15 (Al − C≡C), 122.14, 128.30, 128.77, 132.14 (C_6H_5), 125.30, 128.23, 129.04, 137.88 (C_4H_3S) ppm. IR (NaCl, nujol mull): $\tilde{\nu}$ = 2129 (s), 2030 (w), 1951 (w), 1880 (w), 1801 (w), 1675 (w), 1653 (w), 1594 (w), 1572 (w), 1540 (w), 1486 (m), 1341 (w), 1276 (w), 1214 (s), 1175 (w), 1156 (m), 1098 (w), 1068 (w), 1044 (w), 1025 (w), 996 (w), 971 (w), 915 (w), 894 (w), 851 (m), 817 (m), 799 (w), 755 (m), 726 (w), 690 (w), 647 (w), 610 (w), 565 (w), 535 (w) cm^{-1}. In the EI-MS spectrum only low molecular weight fragments were found. $C_{78}H_{60}Al_6N_6S_6$ (1434.21): calcd. C 65.26, H 4.21, N 5.85; found C 64.93, H 4.76, N 5.77.

Reaction of 2 with PhSH. Synthesis of 6: PhSH (0.46 g, 4.17 mmol) was added slowly at room temperature to a suspension of **2** (0.50 g, 0.60 mmol) in toluene (30 mL). Evolution of H_2 was observed during the addition. The reaction mixture was stirred overnight and filtered. Colorless crystals of **6** were obtained when the filtrate was stored at room temperature. Yield: 0.63 g (84% based on PhSH). M.p. 143−153 °C. ^{1}H NMR (200 MHz, $CDCl_3$): δ = 2.80 (s, 2 H, NH), 3.90 (s, 4 H, CH_2), 6.42, 6.82 (m, 4 H, C_4H_3S), 7.21 (m, 14 H, C_6H_5S, C_4H_3S), 7.55 (m, 8 H, C_6H_5S) ppm. ^{13}C NMR (125 MHz, $CDCl_3$): δ = 41.38 (CH_2), 123.95, 125.63, 127.17, 137.07 (C_4H_3S), 125.63, 129.07, 129.46, 130.74 (C_6H_5S) ppm. IR (KBr, nujol mull): $\tilde{\nu}$ = 3248 (m), 3231 (w), 3160 (w), 1954 (w), 1882 (w), 1655 (w), 1579 (m), 1473 (m), 1436 (m), 1380 (m), 1326 (w), 1303 (w), 1257 (m), 1205 (m), 1147 (w), 1082 (m), 1066 (w), 1043 (w), 1023 (m), 971 (s), 907 (w), 864 (s), 828 (m), 740 (s), 709 (m), 691 (s), 647 (m), 574 (m), 554 (m), 530 (s), 492 (w), 483 (w), 472 (s) cm^{-1}. EI-MS: *m/z* (%) = 714 (5) [M^+], 605 (68) [M^+ − PhSH], 110 (100) [$PhSH^+$]. $C_{34}H_{32}Al_2N_2S_6$ (714.94): calcd. C 57.12, H 4.51, N 3.92; found C 56.76, H 4.63, N 3.74.

Reaction of 1 with PhSH. Synthesis of 7: PhSH (0.50 g, 4.54 mmol) was added at room temperature to a suspension of **1** (0.52 g, 0.65 mmol) in toluene (30 mL). The reaction mixture was stirred for an hour at room temperature before refluxing it until the evolution of H_2 ceased. The solution was filtered and kept for crystallisation at room temperature. Yield: 0.66 g (70%). ^{1}H NMR (200 MHz, $CDCl_3$): δ = 4.22 (s, 12 H, CH_2), 6.95 (m, 24 H, *o*-$CH_2C_6H_5$ and *o*-SC_6H_5), 7.22 (m, 36 H, *m*-, *p*-$CH_2C_6H_5$ and *m*-, *p*-SC_6H_5) ppm. ^{13}C NMR (125 MHz, $CDCl_3$): δ = 29.70 (CH_2), 126.97 (*p*-$CH_2C_6H_5$), 127.16 (*m*-$CH_2C_6H_5$), 127.56 (*o*-$CH_2C_6H_5$), 137.06 (CH_2-*C*), 128.49 (*p*-SC_6H_5), 128.59 (*m*-SC_6H_5), 129.06 (*o*-SC_6H_5), 130.74 (S-C) ppm. IR (KBr, nujol mull): $\tilde{\nu}$ = 1579 (m), 1496 (m), 1437 (w), 1367 (w), 1300 (w), 1282 (w), 1260 (w), 1198 (w), 1156 (w), 1079 (w), 1066 (w), 1031 (w), 1023 (w), 1003 (w), 974 (w), 810 (w), 735 (s), 693 (w), 667 (w), 547 (s), 524 (m), 480 (s), 459 (w), 439 (w) cm^{-1}. $C_{85}H_{80}Al_6N_6S_6$ (**7**·$C_6H_5CH_3$) (1539.79): calcd. C 66.30, H 5.24, N 5.46; found C 66.67, H 5.35, N 5.16. In the EI-MS spectrum only low molecular weight fragments were found.

Reaction of 2 with $ZnEt_2$. Synthesis of 8: A solution of $ZnEt_2$ (15 mL, 1.1 M solution) in toluene was added dropwise to a solution of **2** (0.85 g, 1.02 mmol) in THF (20 mL). The resultant mixture was stirred overnight at room temperature and then filtered. The filtrate was reduced in volume to 15 mL and stored at 0 °C to obtain colorless crystals of **8**. Yield: 0.81 g (79%). M.p. 262 °C. ^{1}H NMR (200 MHz, $CDCl_3$): δ = 0.20 (m, 12 H, $AlCH_2$), 1.11 (t, 18 H, CH_3), 4.38 (s, 12 H, NCH_2), 6.65, 6.79, 7.09 (m, 18 H, C_4H_3S) ppm. ^{13}C NMR (125 MHz, $CDCl_3$): δ = −1.09 (Al-CH_2), 9.81 (CH_3), 43.45 (NCH_2), 123.63, 124.88, 126.72, 147.37 (C_4H_3S) ppm. IR (NaCl, nujol mull): $\tilde{\nu}$ = 1337 (m), 1269 (m), 1225 (s), 1199 (w), 1157 (w), 1125 (w), 1072 (w), 1006 (s), 990 (s), 973 (s), 927 (s), 848 (s), 823 (s), 767 (s), 717 (s), 696 (s), 636 (s) cm^{-1}. EI-MS: *m/z* (%) = 974 (45) [$M^+ - C_2H_5$], 973 (100) [$M^+ - C_2H_6$]. $C_{42}H_{60}Al_6N_6S_6$ (1003.20): calcd. C 50.28, H 6.03, N 8.38; found C 50.56, H 6.03, N 8.02.

X-ray Structure Determination of 2−4, 6 and 7: A suitable crystal of each compound was mounted on a glass fiber and coated with paraffin oil. Diffraction data for **3** were collected on a Siemens−Stoe AED2 four-circle instrument, and for **2**, **4**, **6**, **7** and **8** the data were collected on a STOE IPDS II diffractometer. All measurements were made with graphite-monochromated Mo-K_α radiation (λ = 0.71073 Å). The structures were solved by direct methods using SHELXS-97[10] and refined against F^2 on all data by full-matrix least-squares with SHELXL-97.[11] All non-hydrogen atoms were refined anisotropically. Neutral-atom scattering factors (including anomalous scattering) were taken from International Tables for X-ray Crystallography.[12] Hydrogen atoms were included at geometrically calculated positions and refined using a riding model.

CCDC-192059 to -192063 and CCDC-192424 contain the supplementary crystallographic data for this paper. These data can be obtained free of charge at www.ccdc.cam.ac.uk/conts/retrieving.html [or from the Cambridge Crystallographic Data Centre, 12, Union Road, Cambridge CB2 1EZ, UK; Fax: (internat.) +44-1223/336-033; E-mail: deposit@ccdc.cam.ac.uk].

Acknowledgments

This work was supported by the Deutsche Forschungsgemeinschaft and the Göttinger Akademie der Wissenschaften. NDR thanks the Alexander von Humboldt-Stiftung for a research fellowship.

[1] [1a] N. D. Reddy, H. W. Roesky, M. Noltemeyer, H.-G. Schmidt, *Inorg. Chem.* **2002**, *41*, 2374−2378. [1b] W. Zheng, A. Stasch, J. Prust, H. W. Roesky, F. Cimpoesu, M. Noltemeyer, H.-G. Schmidt, *Angew. Chem.* **2001**, *113*, 3569−3572; *Angew. Chem. Int. Ed.* **2001**, *40*, 3461−3464. [1c] A. Stasch, M. Ferbinteanu, J. Prust, W. Zheng, F. Cimpoesu, H. W. Roesky, J. Magull, H.-G. Schmidt, M. Noltemeyer, *J. Am. Chem. Soc.* **2002**, *124*, 5441−5448.

[2] J. E. Park, B. -J. Bae, Y. Kim, J. T. Park, I. -H. Suh, *Organometallics* **1999**, *18*, 1059−1067.

[3] [3a] H. Rahbarnoohi, R. Kumar, M. J. Heeg, J. P. Oliver, *Organometallics* **1994**, *13*, 3300−3308. [3b] R. J. Wehmschulte, P. P. Power, *Inorg. Chem.* **1998**, *37*, 6906−6911. [3c] M. Cesari, S. Cucinella, *The Chemistry of Inorganic Homo- and Heterocycles* (Eds.: I. Haiduc, D. B. Sowerby), Academic Press: London. **1987**; Vol I, p 167−190. [3d] K. M. Waggoner, M. M. Olmstead, P. P. Power, *Polyhedron* **1990**, *9*, 257−263.

[4] S. Cucinella, T. Salvatori, C. Busetto, M. Cesari, *J. Organomet. Chem.* **1976**, *121*, 137−147.

[5] The yield of the products in Scheme 3 are not quantitative. We found metallic zinc as a by-product which we assume is formed from the disproportionation of EtZnH into Et_2Zn, Zn and H_2.
[6] [6a] M. G. Gardiner, G. A. Koutsantonis, S. M. Lawrence, F. -C. Lee, C. L. Raston, *Chem. Ber.* **1996**, *129*, 545−549. [6b] C. Jones, F. -C. Lee, G. A. Koutsantonis, M. G. Gardiner, C. L. Raston, *J. Chem. Soc., Dalton Trans.* **1996**, 829−833.
[7] H. A. Szymanski, *Interpreted Infrared Spectra*; Plenum Press Data Division: New York. **1966**; Vol 2, p 5.
[8] [8a] A.-A. I. Al-Wassil, P. B. Hitchcock, S. Sarisaban, J. D. Smith, C. L. Wilson, *J. Chem. Soc., Dalton Trans.* **1985**, 1929−1934 and references therein. [8b] G. D. Piero, S. Cucinella, M. Cesari, *J. Organomet. Chem.* **1979**, *173*, 263−268 and references therein.
[9] J. K. Ruff, M. F. Hawthorne, *J. Am. Chem. Soc.* **1960**, *82*, 2141−2144.
[10] G. M. Sheldrick, *Acta Crystallgr., Sect. A* **1990**, *46*, 467−473.
[11] G. M. Sheldrick, SHELXL-97, *Program for Crystal Structure Refinement*, University of Göttingen, Göttingen, Germany, **1997**.
[12] *International Tables for X-ray Crystallography*; Kynoch Press: Birmingham, England, **1969**; Vol. IV, p 55, 99, 149.

Received August 29, 2002
[I02488]

4-Ethynylpyridine as a Bridging Moiety in Mixed Rh/Re Complexes

Jing-Lin Zuo,[a] Fabrizia Fabrizi de Biani,[b] Ana M. Santos,[a,c] Klaus Köhler,[a] and Fritz E. Kühn*[a]

Keywords: N ligands / Metal-metal interactions / Oligomers / Rhenium / Rhodium

A paramagnetic, dimeric $Rh^{III}Rh^{II}$ complex of the formula $[Rh_2(form)_4(C{\equiv}CC_5H_4N)]$ (**1**) [form = *N*,*N*′-di-*p*-tolylformamidinate; C_5H_4N = pyridyl (py)] has been synthesized and used as starting material to prepare heterotrimetallic complexes of composition $[Rh_2(form)_4(C{\equiv}Cpy)\{Re(CO)_3(bipy)\}][OS(=O)_2CF_3]$ (**2**) and $[Rh_2(form)_4(C{\equiv}Cpy)\{Re(CO)_3(t\text{bu}_2\text{bipy})\}][OS(=O)_2CF_3]$ (**3**). These complexes have been examined by vibrational spectroscopy, EPR spectroscopy, thermogravimetry and cyclic voltammetry. They are heat-stable and can be handled in air without problems. The observed interactions between the Rh_2 and the Re subunits, however, are weak, and a significant charge transfer does not seem to take place. (© Wiley-VCH Verlag GmbH & Co. KGaA, 69451 Weinheim, Germany, 2003)

Introduction

Dimeric rhodium complexes were first reported in the 1960s.[1] Since then a large number of compounds containing RhRh units have been described.[2] However, the number of Rh_2 compounds containing axial Rh−C bonds is rather limited.[3] Metal-metal units, containing axial M−C bonds in general, however, have been shown to be useful building blocks for linear organometallic oligomers and polymers.[3a,4] These oligomers and polymers may display interesting and novel optical and magnetic properties.[5] RN−RhRh as well as RN−RhRh−NR units [R = $C_5H_4NRe(bipy)(CO)_3$, $C_5H_4{-}C_5H_4NRe(Br)(CO)_3$-$NC_5H_4{-}C_5H_4N$, $C_5H_4C{\equiv}CC_5H_4FeC_5H_4C{\equiv}CC_5H_4N$, $C_5H_4C{\equiv}CC_5H_4FeC_5H_5$, etc.], which we used previously as building blocks for organometallic oligomers and polymers, suffer from their weaker nitrogen-rhodium interactions and are more sensitive to temperature, air, moisture and donor solvents.[6] In this work we report on an RhRh moiety with one axial 4-ethynylpyridyl ligand. This axial ligand can act as a useful linker to other transition metal complexes, as exemplified by the formation of [carbonyl(bipyridyl)-rhenium] complexes.

[a] Anorganisch-Chemisches Institut der Technischen Universität München,
Lichtenbergstraße 4, 85747 Garching bei München, Germany
E-mail: fritz.kuehn@ch.tum.de
[b] Dipartimento di Chimica dell'Universita di Siena,
Via Aldo Moro, 53100 Siena, Italy
[c] Instituto de Tecnologia Química e Biológica da Universidade Nova de Lisboa,
Quinta do Marquês, EAN, Apt 127, 2781-901 Oeiras, Portugal

Results and Discussion

Synthesis and Characterization

Our aim was to synthesize compounds with the $[Rh_2(form)_4]$ (form = *N*,*N*′-di-*p*-tolylformamidinate) building block containing the two metal atoms in different oxidation states and only one axial σ-alkynyl moiety as connecting unit. To achieve this, an equimolar amount of *n*BuLi was added dropwise to a solution of 4-ethynylpyridine in dry THF at dry ice temperature. $[Rh_2(form)_4Cl]$ was added, the mixture was allowed to react for 5 h and then slowly brought to room temperature. Stirring was continued for 24 h and then the reaction mixture was exposed to air for another 24 h. The green residue formed was dissolved in CH_2Cl_2 and chromatographed to afford the paramagnetic, neutral $[Rh_2(form)_4(C{\equiv}Cpy)]$ (**1**) as a dark green solid (Scheme 1). Complex **1** displays its asymmetric C≡C vibration at 2120 cm^{-1}. The NC pyridine vibration is observed at 1590 cm^{-1}.

Under FAB-MS conditions the molecular peak $[M]^+$ is observed, as well as $[M - C{\equiv}Cpy]^+$. As in the case of the related Ru derivatives of formula $[Ru_2(form)_4(C{\equiv}Cpy)_2]$,[4d] the axial metal−carbon bond is easy to break under FAB conditions. Under TG conditions the complex starts decomposing at 373 °C by losing its C≡Cpy ligand. A second, distinct decomposition onset is observed at 435 °C when the "form" ligands start to break down. The remaining mass at 650 °C is ca. 45% of the original mass.

A solution of compound **1** and $[Re(CO)_3(L_2)(MeCN)(CF_3SO_3)]$ (L_2 = bipy, $t\text{bu}_2$bipy) in THF was refluxed in the dark for 3 h. The reaction mixture was then cooled to room temperature and the residue was dissolved in CH_2Cl_2 and chromatographed to yield the pale green,

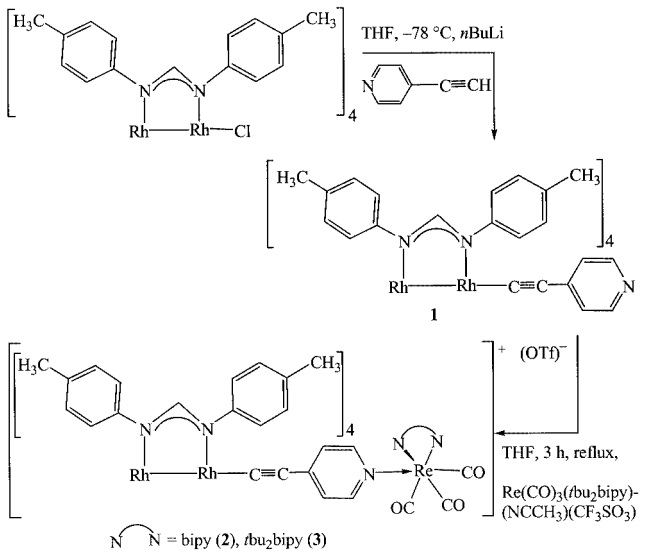

Scheme 1

paramagnetic solids $[Re(CO)_3(bipy)Rh_2(form)_4(C{\equiv}Cpy-4)][OTf]$ (**2**) and $[Re(CO)_3(tbu_2bipy)Rh_2(form)_4(C{\equiv}Cpy-4)][OTf]$ (**3**), respectively (Scheme 1). They display their C≡C vibration at 2108 and 2107 cm^{-1}, respectively, indicating a slightly weakened triple bond in comparison to the precursor complex **1**. The pyridine CN vibrations are observed at 1603 and 1606 cm^{-1}, shifted 13 and 16 cm^{-1}, respectively, in comparison to complex **1**, thus indicating a slight strengthening of the CN bond, possibly due to the increased electron density in the pyridine ring because of its bridging function between the RhRh and the Re units.

In the FAB mass spectrum the $[M]^+$ signals of the cations are observed with low intensities (< 5%) as well as the $[M - Re(CO)_3(L_2)]^+$ and the $[M - C{\equiv}Cpy - Re(CO)_3(L_2)]^+$ signal. The most intense peak in both mass spectra is the $[Re(CO)_3(L_2)]^+$ peak. Under TG conditions the decomposition onset of the complexes **2** and **3** is observed at 365 and 341 °C, respectively, in both cases below the onset of compound **1**, but above the decomposition onset of the Re ligands. This shows that the decomposition of the complexes **2** and **3** starts with the degradation of the Re moiety. Further clearly pronounced decomposition onsets are not observed until the end of the measurement, probably due to a simultaneous decomposition of the different organic ligands above 400 °C. Due to the coordination to the $Rh_2(form)_4(C{\equiv}Cpy)$ building block the Re^I moiety is significantly stabilized {the first decomposition onset of the Re^I precursor, $[Re(CO)_3(tbu_2bipy)(NCCH_3)]$ is observed at 163 °C}. Above a certain temperature level (in the temperature range of 340–370 °C), however, it starts decomposing regardless of the attached molecule. Similar observations have been made for the $[Re(CO)_3(L_2)]$ moiety connected to other dimetallic transition metal complexes by 4-ethynylpyridine units and will be reported elsewhere.

Electrochemical Properties

Cyclic voltammetric measurements of compounds **1**–**3** were performed in a dichloromethane solution containing $[tBu_4N]PF_6$ (0.2 M) as supporting electrolyte. Potentials are quoted vs. an Ag/AgCl reference electrode.

As a main feature, the cyclic voltammetric profile of the parent dinuclear complex **1**, presented in Figure 1, shows a one-electron oxidation ($E^{\circ\prime}$ = +0.55 V) and a one-electron reduction ($E^{\circ\prime}$ = −0.50 V). Both these processes are chemically and electrochemically reversible (peak current ratio at different scan rates is constantly close to 1; ΔE_p departs slightly from the theoretical value of 59 mV). Asymmetric complexes like **1** are commonly described both as an $(Rh_2)^{5+}$ or $Rh^{II}-Rh^{III}$ system.[7a] Nevertheless, it has also been suggested that, while the addition of two axial ligands does not substantially modify the Rh–Rh bonding system, asymmetric complexes such as **1** should present a large polarization toward the formally pentacoordinate rhodium atom.[7b] In spite of this, for reasons which will be discussed shortly, we adopted here the "delocalized" description. The above-mentioned processes are therefore ascribed to formal $(Rh_2)^{5+}/(Rh_2)^{6+}$ electron removal and to $(Rh_2)^{5+}/(Rh_2)^{4+}$ electron addition, respectively. The redox change $(Rh_2)^{6+}/(Rh_2)^{7+}$ is also visible at +1.3 V. This irreversible process results in the decomposition of complex **1** and generates an unknown species which gives rise to a new series of three signals at +1.38, +0.68, −0.36 V (shown in Figure 1).

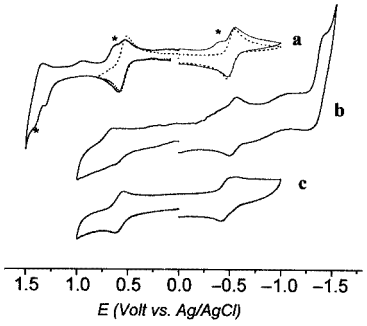

Figure 1. Cyclic voltammograms of a CH_2Cl_2 solution of $[tBu_4N]PF_6$ (0.2 mol dm^{-3}) and the complexes (a) **1**, (b) **2**, (c) **3**; scan rate 0.2 Vs^{-1}

The main features of the cyclic voltammetric profile of the compounds **2** and **3**, also shown in Figure 1, are visible and allow some conclusions to be drawn. The main features of the redox profile of **1** appear in both complexes **2** and **3**. The more anodic irreversible processes are probably masked by the solvent discharge. In the cyclic voltammetric profile of **2** a further reduction process, possessing features of chemical quasi-reversibility, is also visible at $E^{\circ\prime}$ = −1.36 V. We ascribe this redox process to an electron addition to the bipy ligand coordinated to the rhenium atom.[7a] The equivalent redox process, expected for **3**, is not found, as it is probably cathodically shifted because of the presence of the *tert*-butyl substituents and is therefore masked by the solvent discharge. The redox potential values for the visible processes of **2** and **3** remain unaffected with respect to **1**.

The most important change is the anodic shift of 80 mV for the $(Rh_2)^{5+}/(Rh_2)^{6+}$ oxidation process of complex **2** (a minor anodic shift of 30 mV is also visible for complex **3**). This effect is probably due to the electron-withdrawing effect of the Re moiety on the central Rh_2 core. Remarkably, the $(Rh_2)^{5+}/(Rh_2)^{4+}$ reduction process, in which one electron is formally added to the axially ligated formal Rh^{III} ion, is practically unchanged in **1**−**3**. Therefore, it seems that such a substituent effect is mainly transmitted to the axially nonligated formal Rh^{II} ion. In this respect, it is also interesting to compare the redox behavior of complexes **1**−**3** with that of the parent complex $Rh_2(form)_4$, whose electrochemistry has been extensively studied by Piraino et al.[7c] In this complex the redox potential for the $(Rh_2)^{4+}/(Rh_2)^{5+}$ and $(Rh_2)^{5+}/(Rh_2)^{6+}$ changes are +0.25[7d] and +1.06 V,[7d] respectively, compared with −0.50 and +0.55 V for **1**. It is evident that the introduction of the (C≡Cpy) unit as a ligand in the axial position of the Rh−Rh core has a strong effect, inducing a significant cathodic shift on both redox changes. We interpret this behavior as evidence for the strong interaction between the two Rh ions. The formal electrode potentials of the above discussed redox changes are summarized in Table 1.

Table 1. Formal electrode potentials [V] vs. Ag/AgCl for the redox changes exhibited by complexes **1**−**3** in CH_2Cl_2 with $[tBu_4N]PF_6$ (0.2 M) as supporting electrolyte

Complex	$E^{\circ\prime}$ [V], (ΔE [mV])[a], i_p *ratio*[a]						
	$(Rh_2)^{6+}/(Rh_2)^{7+}$	$(Rh_2)^{5+}/(Rh_2)^{6+}$			$(Rh_2)^{5+}/(Rh_2)^{4+}$		
1	+1.30[b]	+0.55	(62)	0.98	−0.50	(72)	0.95
2	–	+0.63	–	*0.90*[c]	−0.53	(50)	*0.90*[c]
3	–	+0.58	(66)	*1.00*[c]	−0.51	(66)	*0.90*[c]

[a] Measured at 0.2 Vs^{-1}. [b] Irreversible redox process. [c] Estimated values.

EPR Spectra

The EPR spectra of the dirhodium complexes are best described by a spin-Hamiltonian of axial symmetry for one rhodium(II) ion ($4d^7$ "low-spin"). The corresponding EPR parameters are: $g_\perp = 2.110$, $g_\parallel = 1.938$ and $A_\parallel$ (^{103}Rh) = $28{\cdot}10^{-4}$ cm^{-1}, for complex **1**; $g_\perp = 2.105$, $g_\parallel = 1.939$ and $A_\parallel(^{103}Rh) = 29{\cdot}10^{-4}$ cm^{-1} for complex **2** (N−N = bipy, Figure 2); and $g_\perp = 2.103$, $g_\parallel = 1.937$ and $A_\parallel(^{103}Rh) = 27{\cdot}10^{-4}$ cm^{-1} for complex **3** (N−N = $t$bu$_2$bipy). Although not absolutely symmetric, the ^{103}Rh hyperfine structure ($I = 1/2$, natural abundance 100%) was resolved or indicated for $B_o \| z$ in all spectra.

Similar EPR spectra and parameters have been reported for Rh_2 complexes in the literature,[3,7c,8] as, for example, for $[(ap)_4Rh_2(C{\equiv}CH)]$,[3b] $[(ap)_4Rh_2(C{\equiv}C)_2Si(CH_3)_3]$[3a] and $[(ap)_4Rh_2(C{\equiv}C)_2Rh_2(ap)_4]$[3a] (ap = 2-anilinopyridinate). The EPR spectra confirm for all complexes the presence of an $Rh_2^{II,III}$ unit with an electronic configuration of $(\sigma)^2(\pi)^4(\delta)^2(\pi^*)^4(\delta^*)^1$ for the Rh^{II} ion.[3b] The Rh^{III} ion of the $Rh_2^{II,III}$ unit is probably the one bound to the C≡Cpy unit since this ligand is known to be a σ-donor.

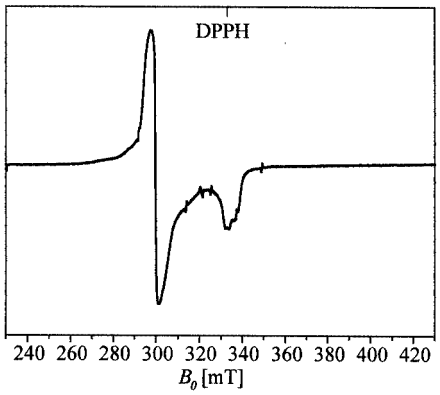

Figure 2. X-band EPR spectrum of complex **2** in a frozen solution of CH_2Cl_2; T_{rec} = 140 K (the spectrum is superimposed by small narrow lines of the standard Mn^{2+} in MgO)

Further conclusions, for example concerning partial spin density distribution to the Rh^{III} ion,[3a] are difficult to draw due to the limited resolution of the parallel features in the EPR spectra. The unequal distribution of the spin density (unpaired electron) over the two rhodium ions is underlined, however, by the observation of an additional hyperfine structure for complex **2** (Figure 2), which could be interpreted as a doublet of doublets [$A_\parallel(^{103}Rh) = 12{\cdot}10^{-4}$ cm^{-1}] observed in the parallel features for this particular EPR experiment.[3a] Regarding the EPR line-widths, the dirhodium unit is (magnetically) independent of the rhenium core connected via a bridging ligand.

Conclusions

Rh-based σ-alkynylpyridine complexes have been synthesized. They are stable to air, moisture and elevated temperatures (TG evidence) and can therefore be handled in air without any problems. However, the interactions along the RhRhC≡CpyRe axis do not allow significant electronic communication between the Rh_2 and the Re unit, as has been shown by CV and EPR experiments. However, the complexes are nevertheless of interest in the context of supramolecular chemistry. Work to replace the N−M bond by a C−M bond in closely related complexes is currently also under way in our laboratory. Furthermore, based on the findings presented here it should be possible to synthesize stable molecular rods based on Rh units ligated with two, instead of one, σ-alkynylpyridine ligands. This approach is also under examination in our laboratory.

Experimental Section

General: Unless stated otherwise, all reactions and manipulations were carried out in dry glassware under nitrogen or argon. Solvents were dried by standard procedures. 4-Ethynylpyridine,[9] $[Rh_2(O_2C{-}CH_3)_4]$,[10a] $[Rh_2(O_2CCF_3)_4]$,[10b] $[Re(N{-}N)(CO)_3(MeCN)]OTf$ (N−N = bipy, $t$bu$_2$bipy; OTf = CF_3SO_3)[11] were prepared according to literature methods. $Rh_2(form)_4Cl$ was prepared according to

the method described for $[Rh_2(ap)_4Cl]$ (ap = 2-anilinopyrinate), using "form" instead of "ap".[12] Elemental analyses were performed in the Mikroanalytisches Laboratorium of the TU München in Garching (Mr. M. Barth). IR (KBr pellets) and Raman spectra (powder samples) were obtained with a Bio-Rad FTS-575C spectrometer at room temperature. Mass spectra were obtained with Finnigan MAT 311 A and MAT 90 spectrometers. Cyclic voltammograms were recorded with a computer-controlled Model 173 Potentiostat/Galvanostat (EG&G Princeton Applied Research). The working electrode was platinum and the reference electrode was silver. Measurements were performed in a dichloromethane solution containing $[tBu_4N]PF_6$ as supporting electrolyte (0.2 M). Potentials are quoted vs. an Ag/AgCl reference electrode. The EPR spectra were recorded with a Jeol JES RE2X at X-band frequency ($\nu \approx 9.05$ GHz, microwave power 2 mW, modulation frequency 100 kHz).

$[Rh_2(form)_4(C{\equiv}Cpy\text{-}4)]$ (1): An equimolar amount of *n*BuLi was added dropwise to a solution of 4-ethynylpyridine (126.0 mg, 1.22 mmol) in 40 mL of dry THF at −78 °C under argon. $[Rh_2(form)_4Cl]$ (190 mg, 0.17 mmol) was added and the mixture was allowed to react at −78 °C for 5 h and then slowly brought to room temperature. Stirring was continued for 24 h and then the reaction mixture was exposed to air for another 24 h. The green residue was dissolved in CH_2Cl_2 and chromatographed on neutral Al_2O_3, eluting with CH_2Cl_2 to afford **1** as a dark green solid. Yield: 100 mg (50%). Dark green crystals were obtained by slow diffusion of Et_2O into a CH_2Cl_2 solution of the complex. $C_{67}H_{64}N_9Rh_2$ (1201.12): calcd. C 67.00, H 5.37, N 10.50; found C 66.55, H 5.70, N 10.36. IR (KBr): $\tilde{\nu}$ = 3019 (w), 2920 (w), 2120 (m, $\nu_{C\equiv C}$), 1590 (m), 1542 (s), 1504 (s), 1332 (m), 1219 (s), 938 (m), 821 (m), 756 (m), 710 (w), 441 (m) cm^{-1}. UV (CH_2Cl_2) = λ_{max} (ε) = 421 (10600), 591 (4200) and 905 (430 $M^{-1}\,cm^{-1}$) nm. FAB-MS (nitrobenzyl alcohol as FAB matrix, ^{103}Rh): *m/z* (%) = 1201 (4) $[M]^+$, 1098 (100) $[Rh_2(form)_4]^+$, 875 (5) $[Rh_2(form)_3]^+$, 652 (9) $[Rh_2(form)_2]^+$, 429 (21) $[Rh_2(form)]^+$.

$[Re(CO)_3(bipy)Rh_2(form)_4(C{\equiv}Cpy\text{-}4)][OTf]$ (2): A solution of compound **1** (60.0 mg, 0.05 mmol) and $[Re(CO)_3(bipy)(MeCN)][CF_3SO_3]$ (31.0 mg, 0.05 mmol) in THF (20 mL) was refluxed in the dark for 3 h. The reaction mixture was then cooled to room temperature and the residue was dissolved in CH_2Cl_2 and chromatographed on neutral Al_2O_3, eluting with CH_2Cl_2/MeOH (100:1) to yield the pale green solid **2** (51.9 mg, 55%). $C_{81}H_{72}N_{11}F_3O_6ReRh_2S$ (1776.62): calcd. C 54.76, H 4.09, N 8.67; found C 55.01, H 3.99, N 8.72. IR (KBr): $\tilde{\nu}$ = 2960 (w), 2923 (w), 2860 (w), 2108 (m), 2023 (s), 1891 (s), 1590 (m), 1543 (s), 1503 (s), 1332 (m), 1260 (m), 1219 (s), 1105 (br), 1020 (m), 812 (s), 765 (m) cm^{-1}. UV (CH_2Cl_2): λ_{max} (ε) = 336 (9120), 590 (2070), 875 (460 $M^{-1}\,cm^{-1}$) nm.

$[Re(CO)_3(tbu_2bipy)Rh_2(form)_4(C{\equiv}Cpy\text{-}4)][OTf]$ (3): A solution of compound **1** (60.0 mg, 0.05 mmol) and $[Re(CO)_3(tBu_2bipy)(MeCN)][CF_3SO_3]$ (36.5 mg, 0.05 mmol) in THF (20 mL) was refluxed in the dark for 3 h. The reaction mixture was then cooled to room temperature and the residue was dissolved in CH_2Cl_2 and chromatographed on neutral Al_2O_3, eluting with CH_2Cl_2/MeOH (200:1) to yield the pale green solid **3** (51.9 mg, 55%). $C_{89}H_{88}N_{11}F_3O_6ReRh_2S$ (1888.83): calcd. C 56.59, H 4.70, N 8.16; found C 56.72, H 4.55, N 8.22. IR (KBr): $\tilde{\nu}$ = 2961 (m), 2922 (m), 2867 (w), 2107 (m), 2027 (s), 1914 (s), 1605 (m), 1546 (s), 1503 (s), 1332 (m), 1261 (s), 1220 (s), 1096 (br), 1030 (m), 814 (s), 637 (w), 442 (w) cm^{-1}. UV (CH_2Cl_2): λ_{max} (ε) = 418 (8930, sh), 574 (1990), 885 (390 $M^{-1}\,cm^{-1}$) nm. FAB-MS (nitrobenzyl alcohol as FAB matrix, ^{103}Rh, ^{187}Re): *m/z* (%) = 1738 (16) $[M]^+$, 1198 (5) $[M - Re(CO)_3(tbu_2bipy)]^+$, 1096 (8) $[M - C{\equiv}Cpy - Re(CO)_3(tbu_2bipy)]^+$, 539 (53) $[Re(CO)_3(tbu_2bipy)]^+$, 429.

Acknowledgments

The authors are greatly indebted to the FCI for financial support. J.-L. Z. thanks the Alexander von Humboldt Foundation for a postdoctoral research associate fellowship. A. M. S. is grateful to the PRAXIS XXI for a postdoctoral research fellowship.

[1] I. I. Chernyaev, E. V. Shenderetskaya, A. A. Karyagina, *Russ. J. Inorg. Chem.* **1960**, *5*, 1163−1163.
[2] [2a] F. A. Cotton, R. A. Walton, *Multiple Bonds between Metal Atoms*, 2nd ed., Oxford University Press, London, **1993** and references cited therein. [2b]C. E. Housecroft, *Coord. Chem. Rev.* **1992**, *115*, 191−230. [2c] F. A. Cotton, E. V. Dikarev, M. A. Petrukhina, S. E. Stiriba, *Organometallics* **2000**, *19*, 1402−1405. [2d] J. M. Asara, J. S. Hess, E. Lozada, K. R. Dunbar, J. Allison, *J. Am. Chem. Soc.* **2000**, *122*, 8−13. [2e] D. L. Lichtenberger, J. R. Pollard, M. A. Lynn, F. A. Cotton, X. Feng, *J. Am. Chem. Soc.* **2000**, *122*, 3182−3190.
[3] [3a] J. L. Bear, B. Han, Z. Wu, E. v. Caemelbecke, K. M. Kadish, *Inorg. Chem.* **2001**, *40*, 2275−2281 and references cited therein. [3b] C. L. Yao, K. H. Park, A. R. Khokhar, M. J. Jun, J. L. Bear, *Inorg. Chem.* **1990**, *29*, 4033−4039.
[4] [4a] G. L. Xu, T. Ren, *J. Organomet. Chem.* **2002**, *655*, 239−243. [4b] J. Stahl, J. C. Bohling, E. B. Bauer, T. B. Peters, W. Mohr, J. M. Martin-Alvarez, F. Hampel, J. A. Gladysz, *Angew. Chem. Int. Ed.* **2002**, *41*, 1872−1876. [4c] J. L. Zuo, E. Herdtweck, F. Fabrizi de Biani, A. M. Santos, F. E. Kühn, *New. J. Chem.* **2002**, *26*, 889−894. [4d] J. L. Zuo, E. Herdtweck, F. E. Kühn, *J. Chem. Soc., Dalton Trans.* **2002**, 1244−1246. [4e] F. Coat, P. Thominot, C. Lapinte, *J. Organomet. Chem.* **2001**, *629*, 39−43. [4f] F. J. Fernández, O. Placque, M. Alfonso, H. Berke, *Chem. Commun.* **2001**, 1266−1267. [4g] G. Xu, T. Ren, *Organometallics* **2001**, *20*, 2400−2404. [4h] H. Miyasaka, R. Clérac, C. S. Campos-Fernández, K. R. Dunbar, *Inorg. Chem.* **2001**, *40*, 1663−1671. [4i] T. Ren, G. Zou, J. C. Alvarez, *Chem. Commun.* **2000**, 1197−1198. [4j] J. L. Wesemann, M. H. Chisholm, *Inorg. Chem.* **1997**, *36*, 3258−3267.
[5] M. H. Chisholm, *Acc. Chem. Res.* **2000**, *33*, 53−61 and references cited therein.
[6] [6a] W. M. Xue, F. E. Kühn, *Eur. J. Inorg. Chem.* **2001**, 2041−2047. [6b] W. M. Xue, F. E. Kühn, E. Herdtweck, *Polyhedron* **2001**, *20*, 791−798. [6c] W. M. Xue, F. E. Kühn, E. Herdtweck, Q. Li, *Eur. J. Inorg. Chem.* **2001**, 213−221.
[7] [7a] T. Ren, *Coord. Chem. Rev.* **1998**, *175*, 43−58. [7b] J. Guerrero, O. E. Piro, E. Wolcan, M. R. Feliz, G. Ferraudi, S. A. Moya, *Organometallics* **2001**, *20*, 2842−2853[7c] P. Piraino, G. Bruno, S. Lo Schiavo, F. Laschi, P. Zanello, *Inorg. Chem.* **1987**, *26*, 2205−2211. [7d] Values vs. SCE; ΔE° (SCE − AgCl) = 0.019 V.
[8] [8a] J. C. Le, M. Y. Chavan, L. K. Chau, J. L. Bear, K. M. Kadish, *J. Am. Chem. Soc.* **1985**, *107*, 7195−7197. [8b] S. Lo Schiavo, G. Bruno, P. Zanello, F. Laschi, P. Piraino, *Inorg. Chem.* **1997**, *36*, 1004−1012. [8c] G. Tresoldi, S. Lo Schiavo, P. Piraino, P. Zanello, *J. Chem. Soc., Dalton Trans.* **1996**, 885−892.
[9] L. Dellaciana, A. Haim, *J. Heterocycl. Chem.* **1984**, *12*, 607−608.
[10] [10a] T. A. Stephenson, G. Wilkinson, *J. Inorg. Nucl. Chem.* **1966**, *28*, 2285−2291. [10b] J. Kitchens, J. L. Bear, *J. Inorg. Nucl. Chem.* **1970**, *32*, 49−58.
[11] J. V. Caspar, T. J. Meyer, *J. Phys. Chem.* **1983**, *87*, 952−957.
[12] J. L. Bear, C. L. Yao, L. M. Liu, F. J. Capdevielle, J. D. Korp, T. A. Albright, S. K. Kang, *Inorg. Chem.* **1989**, *28*, 1254−1262.

Received July 31, 2002
[I02432]

Structure and Electronic Properties of [Ni(dsdm){Fe(CO)$_3$}$_2$], an Unusual, Triangular Nickel Diiron Compound

Marie-Cécile Chalbot,[a] Allison M. Mills,[b] Anthony L. Spek,[b] Gary J. Long,[c] and Elisabeth Bouwman*[a]

Keywords: Carbonyl ligands / Cluster compounds / Iron / Nickel

Reaction of the low-spin complex [Ni(dsdm)] with Fe_2CO_9 results in the unique trinuclear cluster [Ni(dsdm){Fe(CO)$_3$}$_2$]. NMR spectroscopy shows that the structure is diamagnetic, and, moreover, that the complex is stable in solution and C_2-symmetric. The X-ray structure reveals short distances between the distorted octahedral nickel(II) ion and the two octahedral iron(0) centers. The observed diamagnetism is explained by the formation of a triangular metal core with three two-electron two-center bonds. The Mössbauer spectra, which are typical of iron(0), are composed of asymmetric quadrupole doublets as a result of the presence of two chemically similar, but crystallographically distinct, iron sites.
(© Wiley-VCH Verlag GmbH & Co. KGaA, 69451 Weinheim, Germany, 2003)

In recent years the discovery of organometallic-like fragments in the active sites of hydrogenase enzymes has given a new impetus to research pertaining to iron carbonyl chemistry. The active site of the enzyme extracted from *D. gigas* has been described as a heterodimetallic nickel-iron cluster in a sulfur-rich environment containing small diatomic CO or CN molecules coordinated to iron,[1] and the structure of the active site in the Fe-only hydrogenase isolated from *D. desulfuricans* comprises a diiron subcluster also containing CO and CN ligands.[2] Although few model compounds that properly match the active-site structure of [NiFe] hydrogenases have been reported, some do show various features of the metal coordination environment.[3−6] In spite of the research both in organometallic chemistry and in bioinorganic chemistry, the number of compounds containing both Ni and Fe bridged by a sulfur donor is rather limited.[7] Of bioinorganic interest among these are the Fe_3Ni cubane clusters and Fe_4S_4 clusters bridged to mononuclear nickel complexes, both cluster types being relevant to the active site in acetyl coenzyme-A synthase,[8,9] as well as a few heterodinuclear complexes relevant to the hydrogenase active site.[10]

In the field of organometallic cluster chemistry a huge number of structures containing the (μ-S)-Fe_2CO_6 fragment have been reported.[11] This Fe_2CO_6 fragment has recently gained renewed attention because of its importance in modeling the active site of Fe-only hydrogenases.[12] Research efforts by organometallic chemists have resulted in several complexes with a cyclopentadienylnickel unit bound to Fe(CO)$_3$ moieties.[13,14]

The mononuclear compound [Ni(dsdm)] {H_2dsdm = [*N*,*N*′-dimethyl-*N*,*N*′-bis(2-sulfanylethyl)ethylenediamine]} is a nickel thiolate complex used in biomimetic studies of [NiFe] hydrogenases.[15] [Ni(dsdm)] contains two *cis* sulfur atoms which are particularly reactive towards dioxygen. Indeed, the oxidation of [Ni(dsdm)] with H_2O_2 or O_2 leads to the fully oxidized [Ni(dsodm)(H_2O)$_2$] complex in which nickel is coordinated to the sulfonato groups.[16,17] Moreover, [Ni(dsdm)] has also been used in attempts to synthesize thiolato-bridged nickel-iron complexes. The reaction of [Ni(dsdm)] with K[HFe(CO)$_4$] leads to [Fe(dsdm)Ni(CO)$_3$]$_2$ and involves the reduction of nickel(II) to nickel(0) followed by the coordination of the dsdm ligand to the iron(II).[18]

We present herein the reaction of [Ni(dsdm)] with Fe_2CO_9, which results in the formation of the novel trinuclear sulfur-bridged nickel-iron complex [Ni(dsdm){Fe(CO)$_3$}$_2$], a diamagnetic compound that contains three metal centers in a compact triangular metal core.

Results and Discussion

A projection of the structure of [Ni(dsdm){Fe(CO)$_3$}$_2$] is shown in Figure 1, and the corresponding bond lengths and angles are listed in Table 1. In this trinuclear compound the Ni(dsdm) moiety coordinates to a diiron hexacarbonyl fragment and the three metals are in a nearly equilateral trian-

[a] Leiden Institute of Chemistry, Gorlaeus Laboratories, Leiden University,
P. O. Box 9502, 2300 RA Leiden, The Netherlands
Fax: (internat.) +31-71/527-4451
E-mail: bouwman@chem.leidenuniv.nl
[b] Bijvoet Center for Biomolecular Research, Crystal and Structural Chemistry, Utrecht University,
Padualaan 8, 3584 CH Utrecht, The Netherlands
[c] Department of Chemistry,University of Missouri-Rolla,
Rolla, MO 65409-0010, USA

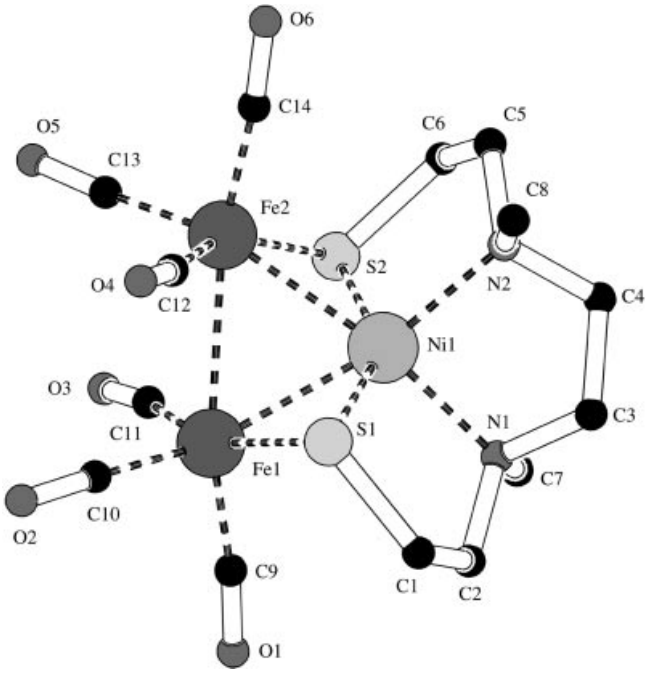

Figure 1. A PLUTON[27] projection of [Ni(dsdm){Fe(CO)$_3$}$_2$]; for clarity the hydrogen atoms have been omitted

gular arrangement with short metal-metal distances. The nickel ion is tetracoordinate to two sulfur and two nitrogen donor atoms of the dsdm ligand, in a distorted tetrahedral geometry. The two sulfur atoms each bridge the nickel ion to one of the iron tricarbonyl moieties. The dihedral angle between the planes of the two five-membered rings formed by Ni with the N,C,C,S atoms of each sulfanylethyl portion of dsdm is 87.91(16)°, indicating a nonplanar [Ni-N_2S_2] environment. The Ni−S distances of 2.1602(11) and 2.1724(11) Å are in the range reported for the trinuclear complex [Ni_3(dsdm)$_2$]Cl_2, a complex that has pseudo-square planar nickel ions, whereas the Ni−N bond lengths of 2.061(3) and 2.077(4) Å are significantly longer.[15] If one includes the two iron centers in the coordination environment of the nickel ion, the geometry of the nickel(II) ion can be regarded as that of a distorted octahedron.

The structure contains two crystallographically distinct iron sites with small variations in the Fe−C distances and Fe−C−O angles. Each iron atom is pentacoordinate in a square-pyramidal geometry with the carbonyl C10 and C13 carbon atoms at the apex. The Fe−S bonds of 2.2553(14)−2.2567(12) Å and the Fe−C and C−O bond lengths of 1.769(4)−1.793(5) Å and 1.145(6)−1.173(5) Å, respectively, are similar to those reported for [EtS-$Fe^I(CO)_3]_2$.[19] The Fe−Fe bond length of 2.6618(9) Å is significantly longer than the 2.523 and 2.537 Å values found in the starting Fe_2CO_9 complex[20] and in the sulfur-bridged diiron complex [EtSFe(CO)$_3$]$_2$,[19] respectively. From structural and spectroscopic information it appears that the two Ni−Fe interactions, at distances of 2.5061(8) and 2.5131(10) Å, must be considered as metal-metal bonds. Including those in the coordination environment of the iron(0) centers, the geometry of the latter can also be regarded as that of a distorted octahedron.

At first sight it appears that a similar arrangement of nickel bridged through sulfur to $Fe_2(CO)_6$ fragments has been reported by Holliday et. al.[21] In the reported struc-

Table 1. Bond distances and angles in [Ni(dsdm){Fe(CO)$_3$}$_2$]

Bond distances (Å)					
Ni1···Fe1	2.5130(8)	Ni1···Fe2	2.5061(8)	Fe1···Fe2	2.6617(8)
Ni1−S1	2.1724(11)	Fe1−S1	2.2553(11)	Fe2−S2	2.2566(12)
Ni1−S2	2.1602(11)	Fe1−C9	1.781(5)	Fe2−C12	1.769(5)
Ni1−N1	2.061(3)	Fe1−C10	1.789(5)	Fe2−C13	1.794(5)
Ni1−N2	2.077(4)	Fe1−C11	1.770(4)	Fe2−C14	1.777(5)
Angles (°)					
Fe1−Ni1−Fe2	64.05(2)	Ni1−Fe1−Fe2	57.85(2)	Ni1−Fe2−Fe1	58.10(2)
Fe1−Ni1−S1	56.99(3)	Ni1−Fe1−S1	53.88(3)	Ni1−Fe2−S2	53.63(3)
Fe1−Ni1−S2	90.84(4)	Ni1−Fe1−C9	108.69(14)	Ni1−Fe2−C12	98.47(13)
Fe1−Ni1−N1	106.85(10)	Ni1−Fe1−C10	146.75(14)	Ni1−Fe2−C13	149.04(14)
Fe1−Ni1−N2	163.71(10)	Ni1−Fe1−C11	104.83(14)	Ni1−Fe2−C14	110.06(14)
Fe2−Ni1−S1	93.29(4)	Fe2−Fe1−S1	87.39(3)	Fe1−Fe2−S2	85.05(3)
Fe2−Ni1−S2	57.27(3)	Fe2−Fe1−C9	154.66(15)	Fe1−Fe2−C12	74.28(15)
Fe2−Ni1−N1	165.14(10)	Fe2−Fe1−C10	106.44(14)	Fe1−Fe2−C13	104.91(14)
Fe2−Ni1−N2	104.33(10)	Fe2−Fe1−C11	74.44(14)	Fe1−Fe2−C14	159.76(14)
S1−Ni1−S2	145.10(5)	S1−Fe1−C9	101.52(14)	S2−Fe2−C12	151.71(14)
S1−Ni1−N1	90.71(10)	S1−Fe1−C10	99.89(14)	S2−Fe2−C13	102.76(14)
S1−Ni1−N2	115.35(9)	S1−Fe1−C11	157.92(14)	S2−Fe2−C14	100.91(15)
S2−Ni1−N1	113.43(10)	C9−Fe1−C10	95.4(2)	C12−Fe2−C13	101.12(19)
S2−Ni1−N2	91.81(9)	C9−Fe1−C11	90.5(2)	C12−Fe2−C14	92.9(2)
N1−Ni1−N2	86.77(13)	C10−Fe1−C11	97.3(2)	C13−Fe2−C14	92.7(2)
Ni1−S1−Fe1	69.13(4)	Ni1−S2−Fe2	69.10(4)		

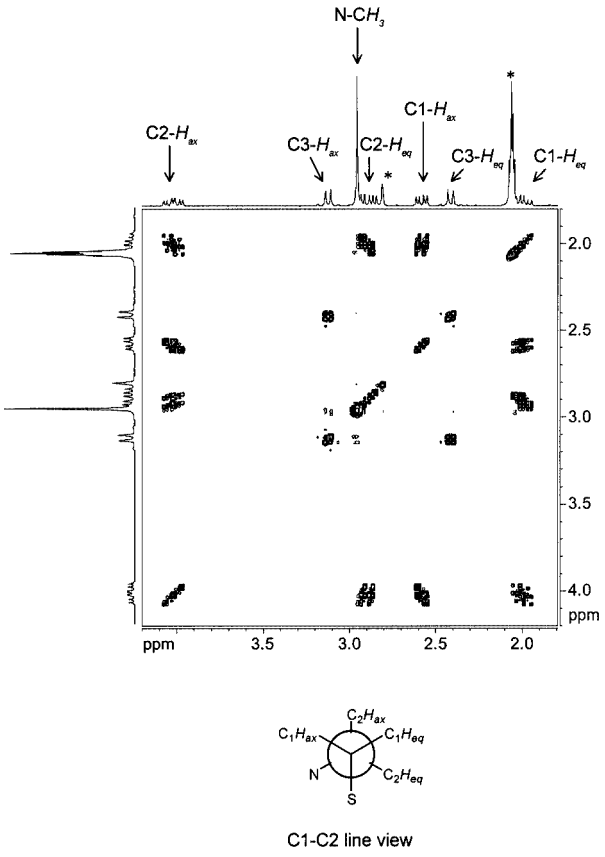

Figure 2. ^{1}H-^{1}H COSY 2D NMR spectrum of [Ni(dsdm){Fe(CO)$_3$}$_2$] at 300 MHz in [D$_6$]acetone; the asterisks denote signals from solvent and impurities

ture the two iron centers are bridged symmetrically by two sulfides, with a sulfur-sulfur distance of 2.83 Å, leading to a structure which, in all aspects, is more similar to the parent [(RS)Fe(CO)$_3$]$_2$ complex[19] if one includes the central NiS_4 unit as a chelating dithiolene group. In [Ni(dsdm){Fe(CO)$_3$}$_2$] the sulfur-sulfur distance in the dithiolate group formed by the tetrahedral Ni(dsdm) unit is too large (4.13 Å) for each sulfur to bind both Fe atoms; thus a $FeSC_3$ chromophore rather than the typical FeS_2C_3 chromophore is observed. The resulting electron deficiency of the iron center in [Ni(dsdm){Fe(CO)$_3$}$_2$] is compensated for by the additional Ni−Fe interactions. The total electron count of the trinuclear cluster is 48, similar to $Fe_3(CO)_{12}$.

[Ni(dsdm){Fe(CO)$_3$}$_2$] is diamagnetic and has been characterized by ^{1}H and ^{13}C NMR spectroscopy in solution. The NMR spectrum exhibits six sharp multiplets and a singlet, which have been assigned to the aliphatic hydrogens by ^{1}H-^{1}H COSY 2-D NMR spectroscopy (Figure 2). The presence of only seven signals indicates that, in solution, the two iron atoms are equivalent. The diamagnetism of the compound arises through the formation of a triangular metal core with three two-electron two-center bonds.

The Mössbauer spectra of [Ni(dsdm){Fe(CO)$_3$}$_2$] obtained at 80 and 297 K are shown in Figure 3. The spectra are composed of asymmetric doublets as a result of the presence of two chemically similar, but crystallographically distinct, iron sites. The spectra have been fitted at a given temperature with two quadrupole doublets both with the same line-width and area.

In Table 2 a comparison of the hyperfine parameters observed for [Ni(dsdm){Fe(CO)$_3$}$_2$] with those of other {Fe(CO)$_3$}$_2$ adducts such as ([Fe(CO)$_3$NH$_2$]$_2$, [Fe(CO)$_3$SMe]$_2$, and [Fe(CO)$_3$SPh]$_2$) is given, revealing the similarity of the chemical bonding found in these adducts.[22−24] In contrast, the hyperfine parameters of [Ni(dsdm){Fe(CO)$_3$}$_2$] are significantly different from those reported for $Fe_2(CO)_9$.[25] In all cases the adduct coordin-

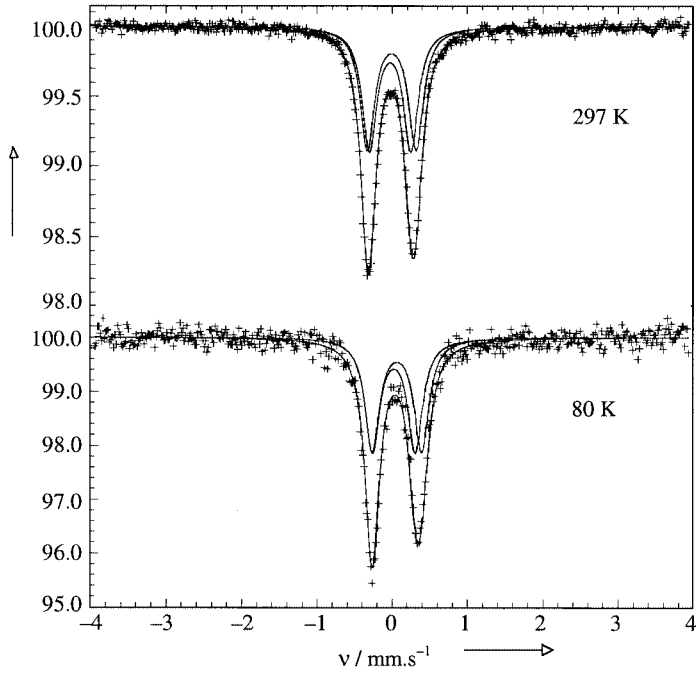

Figure 3. The Mössbauer spectra of [Ni(dsdm){Fe(CO)$_3$}$_2$] obtained at 80 and 297 K

Table 2. Mössbauer spectroscopic hyperfine parameters for [Ni(dsdm){$Fe(CO)_3$}$_2$] and related {$Fe(CO)_3$} adducts

Compound	T (K)	δ (mm/s)[a]	ΔE_Q (mm/s)	Γ (mm/s)	Area (%)	Ref
[Ni(dsdm){$FeCO_3$}$_2$]	297	−0.005	0.65	0.23[b]	50[b]	[c]
		−0.025	0.55	0.23[b]	50[b]	[c]
	80	0.066	0.66	0.23[b]	50[b]	[c]
		0.027	0.57	0.23[b]	50[b]	[c]
[$Fe(CO)_3NH_2$]$_2$,	80	0.02	0.85	–	–	[22]
syn-[$Fe(CO)_3SMe$]$_2$	80	0.03	1.00	–	–	[23]
anti-[$Fe(CO)_3SMe$]$_2$	80	0.03	0.88	–	–	[23]
[$Fe(CO)_3SPh$]$_2$	80	0.06	1.07	–	–	[24]
Fe_2CO_9	80	0.17	0.42	–	–	[25]

[a] The isomer shifts are given relative to room temperature α-iron foil. [b] These parameters were constrained to be equivalent at a given temperature. [c] This work.

ated to the iron center has reduced the isomer shift relative to that found in $Fe_2(CO)_9$. This reduction corresponds to the expected increase in the *s*-electron density at the iron-57 nucleus. Furthermore, the quadrupole splittings observed for [Ni(dsdm){$Fe(CO)_3$}$_2$] are intermediate between those of the other adducts and $Fe_2(CO)_9$, indicating that the presence of S1 and S2 coordinated to $Fe_2(CO)_6$ in [Ni(dsdm){$Fe(CO)_3$}$_2$] has reduced the electronic asymmetry at the iron site, but to a lesser extent than is found in $Fe_2(CO)_9$.

Conclusion

To supplement the large number of organometallic clusters containing the $Fe_2(CO)_6$ fragment that have been reported, we have described herein the first cluster in which additional Ni−Fe metal-metal bonds are present. The unique nature of [Ni(dsdm){$Fe(CO)_3$}$_2$] is related to the atypical binding of the two thiolate sulfurs to the $Fe_2(CO)_6$ fragment, resulting in short distances between the octahedral, high-spin nickel(II) ion and the two octahedral iron(0) centers. This remarkable structure provides an additional, interesting example of the structural versatility possible for the reaction products formed from the nickel *cis* thiolate complex [Ni(dsdm)]. For comparison, the reaction of the related, but more rigid, [Ni(bme-daco)] complex with Fe_2CO_9 produces a dinuclear nickel-iron tetracarbonyl compound, in which the nickel(II) ion remains low-spin in a square-planar environment.[10]

Experimental Section

General Remarks: [Ni(dsdm)] was synthesized according to standard procedures.[15] The Mössbauer spectra were measured at 80 and 297 K on a constant-acceleration spectrometer, which utilized a room temperature rhodium matrix cobalt-57 source and was calibrated at room temperature with α-iron foil. The spectra were fitted as two symmetric quadrupole doublets and the estimated absolute errors are ± 0.005 mm·s^{-1} for the isomer shifts, ± 0.01 mm·s^{-1} for the quadrupole splittings and line widths, and ± 0.02 (%ε) (mm·s^{-1}) for the absolute spectral areas. UV/Vis-NIR measurements were performed on a Perkin−Elmer Lambda 900 UV/Vis/NIR spectrometer. IR spectra were recorded on a Perkin−Elmer FT-IR Paragon 1000 spectrometer. ^{1}H, ^{13}C, and ^{1}H−^{1}H 2D COSY NMR spectra were recorded on a Bruker 300 DPX MHz spectrometer. Elemental analyses were performed with a Perkin−Elmer series II CHNS/O analyzer 2400.

[Ni(dsdm){$Fe(CO)_3$}$_2$]: The preparation was carried out in dry degassed solvent under an argon atmosphere by using standard Schlenk techniques. Fe_2CO_9 (0.357 g, 1 mmol) was added to a suspension of [Ni(dsdm)] (0.265 g, 1 mmol) in 10 mL of toluene. The reaction mixture was stirred for 48 hours, during which time the toluene solution developed a dark-brown color. The toluene solution was filtered to remove the insoluble material. Crystals suitable for X-ray crystallography were obtained from toluene/hexane two-layer crystallization within one day (yield 0.60 g, 11%). Attempts to optimize the yield were not undertaken. UV/Vis (CH_3CN): λ_{max} (ε) = 1007 (50), 495 (shoulder), 394 (5150) nm. IR (diamond): ν(CO) = 2009, 1956, 1917, 1900, and 1885 cm^{-1}. $C_{14}H_{18}Fe_2N_2NiO_6S_2$: calcd. 30.86, H 3.33, N 5.14, S 11.77, Ni 10.77, Fe 20.50; found C 30.99, H 3.49, N 5.30, S 11.00, Ni 10.70, Fe 19.94. ^{1}H NMR (300 MHz, [D$_6$]acetone): δ = 4.02 (m, 2 H, C2-H_{ax}), 3.13 (d, 2 H, C3-H_{ax}), 2.96 (s, 6 H, N-CH_3), 2.91 (m, 2 H, C2-H_{eq}), 2.58 (dd, 2 H, C1-H_{ax}), 2.42 (d, 2 H, C3-H_{eq}), 1.99 (m, 2 H, C1-H_{eq}) ppm. ^{13}C NMR (300 MHz, $CDCl_3$): δ = 214 (C=O), 60 (*C3*), 54 (*C2*), 51 (CH_3), 38 (*C1*).

X-ray Crystallographic Study: $C_{14}H_{18}Fe_2N_2NiO_6S_2$, M_r = 544.83, dark purple rectangular plates (0.05 × 0.12 × 0.24 mm), monoclinic, $P2_1/c$, a = 9.7562(2), b = 13.9094(4), c = 17.2651(4) Å, β = 121.0760(13)°, V = 2006.68(9) Å^3, Z = 4, ρ_c = 1.803 g·cm^{-3}, μ = 2.595 mm^{-1}; intensity data were collected on a Nonius Kappa CCD diffractometer with rotating anode (Mo-K_α, λ = 0.71073 Å) at 150 K to a maximum resolution of θ_{max} = 27.5°, 20667 measured reflections, 4588 unique reflections, 3081 observed data [$I > 2.0\sigma(I)$], R_{int} = 0.060; convergence was reached at $R1$ [$I > 2.0\sigma(I)$] = 0.0421, $wR2$ = 0.0934, and S = 1.08 for 4588 reflections and 246 parameters, $\Delta\rho_{max/min}$ = 0.49/−0.54 e·Å^{-3}. The structure was solved by direct methods using SHELXS-97[26] and refined on F^2 using SHELXL-97; an empirical absorption correction was applied using DELABS in PLATON[27] (0.589−0.876 transmission); geometrical calculations and molecular graphics preparation were performed with PLATON; all non hydrogen atoms were refined with anisotropic displacement parameters; hydrogen atom were constrained to idealized geometries and allowed to ride on their carrier atoms with an isotropic displacement parameter related to the equivalent displacement parameter of their carrier atoms.
CCDC-184378 contains the supplementary crystallographic data for this paper. These data can be obtained free of charge at

www.ccdc.cam.ac.uk/conts/retrieving.html [or from the Cambridge Crystallographic Data Centre, 12, Union Road, Cambridge CB2 1EZ, UK; Fax: (internat.) +44-1223/336-033; E-mail: deposit@ccdc.cam.ac.uk].

Acknowledgments

This work has been carried out within the framework of the Council for Chemical Sciences of the Netherlands Foundation for Scientific Research (CW-NWO), through a grant from the special program for "Young Chemists". The authors thank Mr. David Akers for his assistance in obtaining the Mössbauer spectroscopic data, and Prof. Dr. Jan Reedijk for stimulating discussions.

[1] A. Volbeda, M. H. Charon, C. Piras, E. C. Hatchikian, M. Frey, J. C. Fontecilla-Camps, *Nature* **1995**, *373*, 580−587.
[2] Y. Nicolet, C. Piras, P. Legrand, E. C. Hatchikian, J. C. Fontecilla-Camps, *Struct. Fold. Des.* **1999**, *7*, 13−23.
[3] J. C. Fontecilla-Camps, *J. Biol. Inorg. Chem.* **1996**, *1*, 91−98.
[4] M. Y. Darensbourg, E. J. Lyon, J. J. Smee, *Coord. Chem. Rev.* **2000**, *206−207*, 533−561.
[5] R. B. King, T. E. Bitterwolf, *Coord. Chem. Rev.* **2000**, *206−207*, 563−579.
[6] A. C. Marr, D. J. E. Spencer, M. Schroder, *Coord. Chem. Rev.* **2001**, *219−221*, 1055−1074.
[7] A search in the Cambridge Structural Database for Ni−S−Fe resulted in only 30 independent hits.
[8] J. Zhou, M. J. Scott, Z. Hu, G. Peng, E. Münck, R. H. Holm, *J. Am. Chem. Soc.* **1992**, *114*, 10843−10854.
[9] F. Osterloh, W. Saak, S. Pohl, *J. Am. Chem. Soc.* **1997**, *119*, 5648−5656.
[10] C.-H. Lai, J. H. Reibenspies, M. Y. Darensbourg, *Angew. Chem. Int. Ed. Engl.* **1996**, *35*, 2390−2393.
[11] A search in the Cambridge Structural Database for $(CO)_3Fe-S-Fe(CO)_3$ resulted in over 350 hits.
[12] E. J. Lyon, I. P. Georgakaki, J. H. Reibenspies, M. Y. Darensbourg, *Angew. Chem. Int. Ed.* **1999**, *38*, 3178−3180.
[13] P. Braunstein, E. Sappa, A. Tiripicchio, M. Tiripicchio Camellini, *Inorg. Chim. Acta* **1980**, *45*, L191−L193.
[14] L.-C. Song, Y.-B. Dong, Q.-M. Hu, X.-Y. Huang, J. Sun, *Organometallics* **1997**, *16*, 4540−4545.
[15] M. A. Turner, W. L. Driessen, J. Reedijk, *Inorg. Chem.* **1990**, *29*, 3331−3335.
[16] R. K. Henderson, E. Bouwman, A. L. Spek, J. Reedijk, *Inorg. Chem.* **1997**, *36*, 4616−4617.
[17] V. E. Kaasjager, E. Bouwman, M. Y. Darensbourg, A. Derecskei-Kovacs, S. Gorter, C. A. Grapperhaus, J. Reedijk, J. H. Reibenspies, J. J. Smee, L. M. Thomson, *Inorg. Chem.* **2002**, *41*, 1837−1844.
[18] E. Bouwman, R. K. Henderson, A. L. Spek, J. Reedijk, *Eur. J. Inorg. Chem.* **1999**, 217−219.
[19] L. F. Dahl, C.-H. Wei, *Inorg. Chem.* **1963**, *2*, 328−333.
[20] F. A. Cotton, J. M. Troup, *J. Chem. Soc., Dalton Trans.* **1974**, 800−802.
[21] R. L. Holliday, L. C. Roof, B. Hargus, D. M. Smith, P. T. Wood, W. T. Pennington, J. W. Kolis, *Inorg. Chem.* **1995**, *34*, 4392−4401.
[22] R. B. King, L. M. Epstein, E. W. Gowling, *J. Inorg. Nucl. Chem.* **1970**, *32*, 441−445.
[23] J. P. Crow, W. R. Cullen, F. G. Herring, J. R. Sams, R. L. Tapping, *Inorg. Chem.* **1971**, *10*, 1616−1623.
[24] E. Kostiner, A. G. Massey, *J. Organomet. Chem.* **1969**, *19*, 233−236.
[25] K. Farmery, M. Kilner, R. Greatrex, N. N. Greenwood, *J. Chem. Soc. A* **1969**, 2339−2345.
[26] G. M. Sheldrick, SHELXS-97 and SHELXL-97, University of Göttingen (Germany) **1997**.
[27] A. L. Spek, PLATON, A multipurpose crystallographic tool, Utrecht University (The Netherlands) **2002**.

Received September 19, 2002
[I02530]

Co-Condensation Reactions of Substituted Aromatic Compounds with Lithium Atoms at 77 K

John P. Dunne,[a] Matthias Bockmeyer,[a] and Matthias Tacke*[a]

Keywords: Lithium / C−H bond activation / Co-condensation / Density functional calculations

Lithium atoms were co-condensed with +I-substituted benzene derivatives like trimethyl(phenyl)silane and *tert*-butylbenzene in the presence of THF at 77 K, which resulted in C–H bond activation, to produce the aryllithium compound as well as the coupling of the substituted phenyl radicals. Other +I-substituted benzene derivatives like xylene and mesitylene failed to react with lithium atoms in the presence of THF. Oxygen and nitrogen donor substituted benzene derivatives (anisole, *N*,*N*-dimethylaniline, and *N*,*N*-dimethylbenzylamine) showed activation of the *ortho* C–H bond when co-condensed with lithium atoms in the presence of THF. However, when thioanisole was co-condensed with lithium atoms and THF, a C–S bond cleavage occurred instead. These results were interpreted with the aid of DFT calculations, which show π- and σ-complexes between the lithium clusters and benzene derivatives as reactive intermediates.
(© Wiley-VCH Verlag GmbH & Co. KGaA, 69451 Weinheim, Germany, 2003)

Introduction

The activation of carbon−hydrogen bonds has been a major topic of research for the last 30 years.[1−3] Numerous methods have been developed to perform these reactions. Most of these have centred on the oxidative addition of the hydrocarbon moiety to a highly sub-coordinated metal complex as shown in Figure 1,[4,5] however, C−H bond activation is not limited to transition metal chemistry. Another commonly used method is σ-bond metathesis using extremely electrophilic lanthanide centres as outlined below.[6]

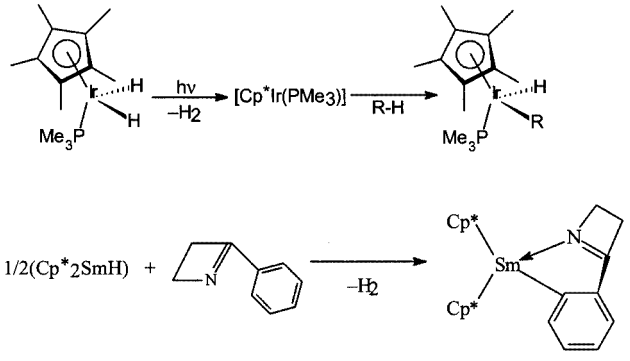

Figure 1. Selected examples of C−H bond activation using metal complexes

To date there has been very little preparative-scale work using metal atoms to perform oxidative addition reactions. Many metals are known to activate methane in a matrix under photochemical conditions,[3,7] but these types of reactions are of no use for preparative scale chemistry. For example, iron atoms when photolysed react with methane to form CH_3FeH at 10 K in an argon matrix.[8]

$$Fe + CH_4 \xrightarrow[Ar,\ 10K]{hv} HFeCH_3$$

Work performed by this group in the 1990s showed that lithium atoms could selectively activate the C−H bond of benzene and toluene in the presence of THF without the need for further photochemical excitation.[9−11] This resulted in the direct synthesis of aryllithium compounds on a synthetic scale.

$$8\ Li(g) + 4\ PhH(g) + 4\ THF(g) \xrightarrow[77K]{cocond.} \left[\text{C}_6\text{H}_5\text{Li(THF)}\right]_4 + 4\ LiH(s)$$

One of the key intermediates in this reaction is an Li_2−benzene π-complex. This complex is capable of undergoing two single electron transfers from the Li_2 cluster to the LUMO of the aromatic ring, resulting in the activation of the aromatic C−H bond.

$$2\ Li(g) + 4\ PhH(g) \xrightarrow[77K]{cocond.} \left[Li{-}Li{\leftarrow}PhH\right] \longrightarrow \left[H\begin{smallmatrix}Li\\ \diagup\ \diagdown\\ Li\end{smallmatrix}Ph\right] \longrightarrow LiH(s) + PhLi(s)$$

The aim of this paper was to (a) expand the number of aromatic substrates for this C−H bond activation, (b) to study how different substituents alter the selectivity of the reaction, and (c) to gain an insight into the electronic limits

[a] Department of Chemistry, University College Dublin, Belfield, Dublin 4, Ireland
E-mail: matthias.tacke@ucd.ie

of this reaction. For this purpose the following +I-substituted [$C(CH_3)_3$, $SiMe_3$, *p*- and *m*-xylene] benzene derivatives were chosen, as well as a series of donor-substituted (OMe, NMe_2, CH_2NMe_2, SMe) benzene derivatives.

Results

Experimental Study

The +I-substituted benzene derivatives mesitylene and (*meta*- or *para*-)xylene failed to react with lithium atoms at 77 K in the presence of THF as shown in Scheme 1. However, when an $SiMe_3$ substituent was placed on the aromatic ring [as for trimethyl(phenyl)silane] a reaction with lithium atoms was observed at 77 K. The yield for this reaction was 32%, based on the amount of lithium vapourised. A broadened set of signals corresponding to the species 4,4′-bis(trimethylsilyl)biphenyl was observed in the ^{13}C NMR spectrum. However, the ^{7}Li NMR spectrum showed a broad peak at $\delta = -2.99$ ppm, which indicates the presence of an $Li^+(THF)_4$ solvent-separated ion-pair species. These NMR spectroscopic data in conjunction with the dark red/black colour of the solution indicates that the broadened ^{13}C NMR signals are actually of the 4,4′-bis(trimethylsilyl)-biphenyl radical anion. It is formed by the reduction of 4,4′-bis(trimethylsilyl)biphenyl by excess lithium metal, as shown in Scheme 2. When the co-condensation product was redissolved in THF and treated with dimethyl disulfide a full characterisation was achieved (Scheme 2). This showed that the major product is 4,4′-bis(trimethylsilyl)biphenyl (80%) and the minor product trimethyl[4-(methylsulfanyl)-phenyl]silane (20%), identified by NMR spectroscopy and GC MS.[12,13]

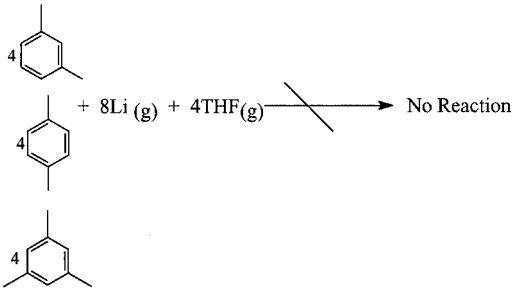

Scheme 1. Failed reaction of lithium atoms with +I-substituted benzene derivatives

A similar reaction series is seen when *tert*-butylbenzene was co-condensed with lithium atoms and THF at 77 K as outlined in Scheme 2. The yield for this reaction was lower (1% based on the amount of lithium metal vapourised) than the trimethyl(phenyl)silane co-condensation. When the co-condensation product was treated in situ with Me_2S_2, NMR spectroscopic and GC-MS data identified the major product (70%) as 4,4′-di-*tert*-butylbiphenyl[14] and a minor product (30%) as 1-*tert*-butyl-4-(methylsulfanyl)benzene.[15]

When a donor-substituted aromatic compound was used the observed direction of lithiation changed from *para* to *ortho*. Co-condensation of anisole with lithium atoms and THF at 77 K, led to the observed lithiated compound 2-methoxyphenyllithium, shown by NMR spectroscopy (as shown in Scheme 3). The *ipso*-carbon signal at $\delta = 169.6$ ppm and a singlet at $\delta = 1.56$ ppm in the ^{7}Li NMR spectrum, as well as the integration in the ^{1}H NMR spectrum clearly indicate a tetrameric structure in C_6D_6.[16] The yield of this reaction increased to 30% compared to 12% when toluene was used.[9,10] As in previous co-condensations, a further confirmation of the regiochemistry was gained by the reaction of 2-methoxyphenyllithium with dimethyl disulfide. The observed product of this reaction was 1-methoxy-2-(methylsulfanyl)benzene in a quantitative yield, which was identified from NMR spectroscopic data and GC MS data[17,18] as shown in Scheme 3.

When the sulfur donor thioanisole was used, a different reaction occurred, resulting in a cleavage of the C−S bond instead of C−H bond activation. This time the major product was diphenyl disulfide as shown in Scheme 4. When the co-condensation product was washed with pentane, it yielded a white air-sensitive product. This was shown to be MeLi by treating it with benzaldehyde to produce 1-phenylethanol upon an aqueous work up (as outlined in Scheme 4). When the pentane solution was treated with chlorotrimethylsilane (Scheme 4), the lithiated product identified by NMR spectroscopy and GC MS measurements was shown to be trimethyl(phenylsulfanyl)silane.[19]

Changing the donor substituent to a nitrogen donor like *N*,*N*-dimethylaniline resulted in the formation of 2-(dimethylamino)phenyllithium as identified by NMR spectroscopy in a low yield of 1% as shown in Scheme 3. In the ^{13}C NMR spectrum in C_6D_6 an *ipso* carbon signal $\delta = 171.6$ ppm, in conjunction with the integration of the ^{1}H NMR peaks indicates a tetrameric structure with four coordinated THF molecules resulting in a species of the composition $Ar_4Li_4{\cdot}THF_4$. It was not possible to determine if the dimethylaniline group was intramolecularly coordinated to Li from the NMR spectroscopic data. The reaction of 2-(dimethylamino)phenyllithium with S_2Me_2 resulted in the formation of dimethyl[(2-methylsulfanyl)phenyl]amine, thus confirming that the regiochemistry is *ortho* to the NMe_2.[20,21]

When *N*,*N*-benzylamine was co-condensed with lithium atoms and THF, it yielded a pyrophoric beige solid in 36% yield that was only sparingly soluble in aromatic solvents. NMR spectroscopy in C_6D_6 confirmed the *ortho* activation and the formation of 2-[(dimethylamino)methyl]phenyllithium.[21,22] Examination of the NMR spectroscopic data indicates a tetrameric structure of the composition Ar_4Li_4 in benzene, with no coordinated THF being present as outlined in Scheme 3. The reaction of 2-[(dimethylamino)methyl]phenyllithium with Me_2S_2 confirmed the regiochemistry as being *ortho* to the benzyl group. The isolated product was identified as dimethyl[2-(methylsulfanyl)benzyl]amine by GC-MS and NMR spectroscopic techniques as shown in Scheme 3.[23]

Theoretical Study

The previously reported mechanism for the reaction of lithium atoms with benzene was performed at the

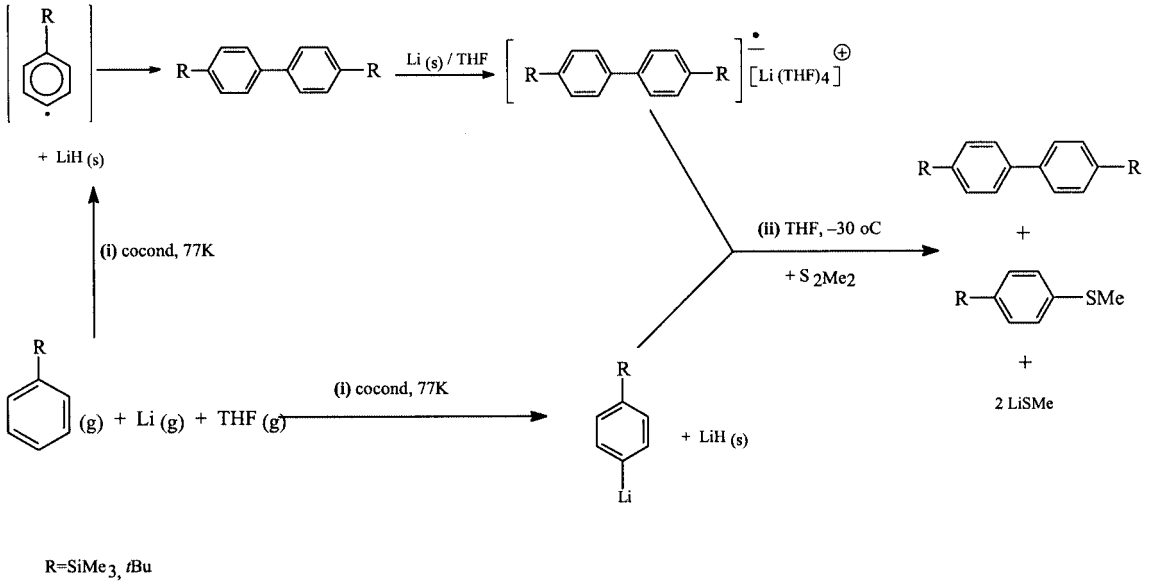

Scheme 2. The reductive coupling of +I-substituted benzene derivatives by lithium atoms

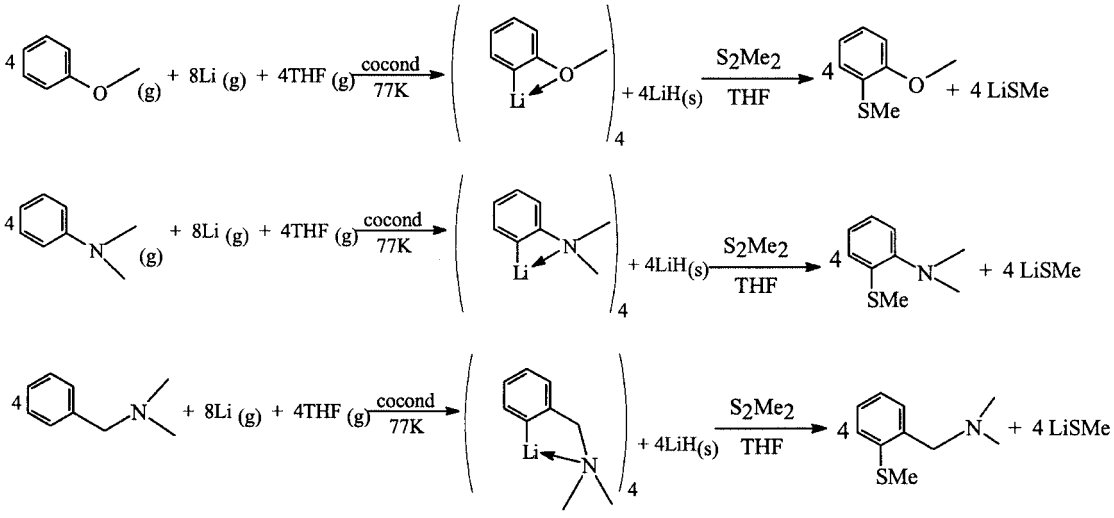

Scheme 3. Reaction of donor-substituted aromatic compounds with lithium atoms in THF

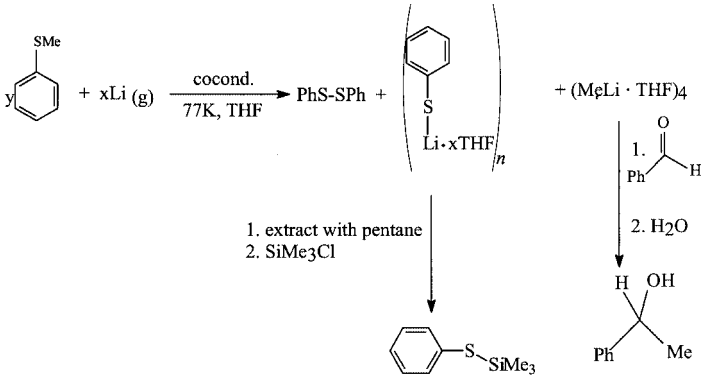

Scheme 4. Co-condensation of lithium atoms with thioanisole in the presence of THF

Hartree−Fock level of theory.[9,10] We report here the recalculation of the key intermediates for this benzene co-condensation, using a DFT method, B3LYP, and the expansion of this mechanism to include other +I- and donor-substituted benzene derivatives. In the benzene system a similar trend is seen using the B3LYP/6-31G** method as was reported earlier.[9,10] The first step of the reaction, the formation of a π-complex (**1a**), resulted in a calculated reaction enthalpy of −8.2 kcal/mol. This is larger than the previously reported value (HF/6-31G**) of −5.9 kcal/mol.[10] The next step is a double electron transfer via the aromatic system, resulting in the insertion of the Li_2 cluster into the C−H bond (the formation of **1b**). This was calculated to be −15.8 kcal/mol. This is also larger than the previously calculated value of −8.0 kcal/mol.[10] These reaction enthalpies are outlined in Figure 2.

The calculated reaction enthalpies shown in Figure 2 for the intermediate species, from the reaction involving toluene with lithium atoms, agreed with the proposed mechanism reported earlier.[9,10] From these calculations it can be seen that the Li_2 cluster forms a π-complex (**1c**) with toluene resulting in a reaction enthalpy of −9.1 kcal/mol. This is larger than in the benzene experiment (−8.2 kcal/mol). The intermediate **1c** then undergoes a double electron transfer via the aromatic system in an exothermic step of −15.0 kcal/mol. However, this enthalpy is slightly lower in energy than that of the benzene system (−15.8 kcal/mol). In the resultant species **1d** the Li_2 cluster has inserted into the *para* C−H bond. When the CH_3 group of toluene was replaced by a *tert*-butyl group as in *tert*-butylbenzene, an identical series of reaction enthalpies was found.

When the aromatic compound is trimethyl(phenyl)silane, the energies for each step in the mechanism change slightly as described in Figure 2. For the first step, the coordination of the lithium cluster to the aromatic system to form the π-complex **1e**, the reaction enthalpy is −8.6 kcal/mol. This value is larger than it is in the benzene system but lower than it is for toluene or *tert*-butylbenzene. The second step, which is the formation of the insertion product **1f**, has a reaction enthalpy of −15.4 kcal/mol. This is larger than the reaction enthalpies for the benzene and toluene/*tert*-butylbenzene systems.

When *p*-xylene is used, the energies for each step in the mechanism also differ slightly compared to the previous cases. For the first step, the formation of **1i**, the reaction enthalpy (−9.8 kcal/mol) is the most exothermic of the +I-substituted benzene derivatives. The second step, the formation of **1j** is the lowest of the reaction enthalpies (−14.6 kcal/mol) of all the +I-substituted benzene derivatives.

When the substituent on the aromatic ring is a Lewis base (e.g. O, N, P, S donors) the reaction pathway is more complicated. Now there are two possibilities for coordination of the lithium cluster as shown in Figure 3. The first possibility is the formation of a π-complex (**2a**), as in the previous compounds (**1a**−**1j**). The second possibility is coordination of the Li_2 cluster to the donor moiety in an η^1-fashion (**2b**). When an oxygen donor is involved, e.g. anisole, the preferred pathway is via the η^1 complex. The energy difference between complex **2a** and **2b** is −2.6 kcal/mol, showing that the η^1 complex **2b** is more stable than the π-complex. As in the previous mechanism the next step is a double single-electron transfer step from the Li_2 cluster to the LUMO of the aromatic ring. However, for the anisole co-condensation this step has a larger reaction enthalpy of −24.7 kcal/mol, compared with the +I-substituted derivatives shown in Figure 2. In the η^1 species **2b** there is an agostic interaction between the *ortho* C−H bond and the coordinated Li_2 cluster, with an Li−H distance of 2.586 Å as detailed in Table 1. This explains the experimentally observed *ortho* activation of the C−H bond.

If the donor atom is changed from an oxygen to a nitrogen donor, for example *N*,*N*-dimethylbenzylamine as outlined in Figure 4, the formation energy for **3b**, the η^1-coordinated Li_2 species, is −15.5 kcal/mol, while for the π-com-

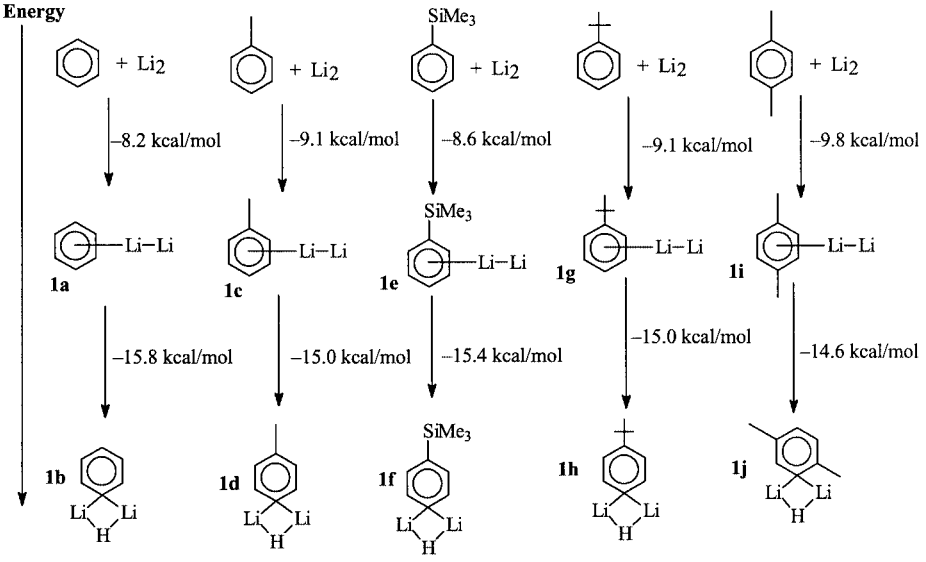

Figure 2. Calculated reaction enthalpies for +I-substituted benzene derivatives and Li_2

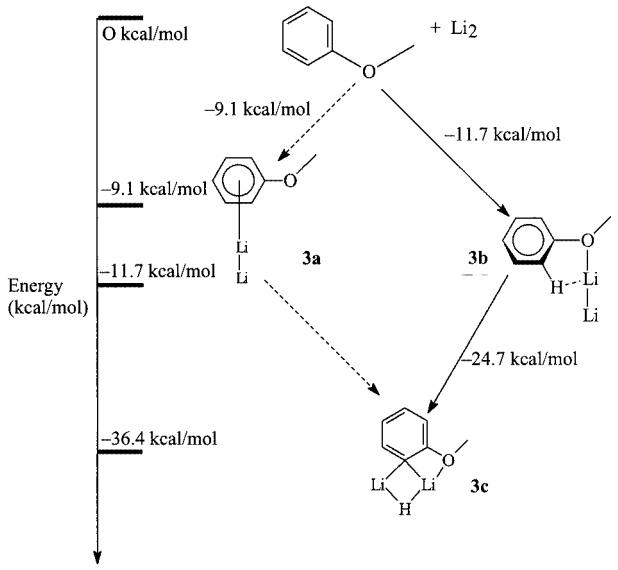

Figure 3. Calculated reaction mechanism for the co-condensation of lithium atoms with anisole

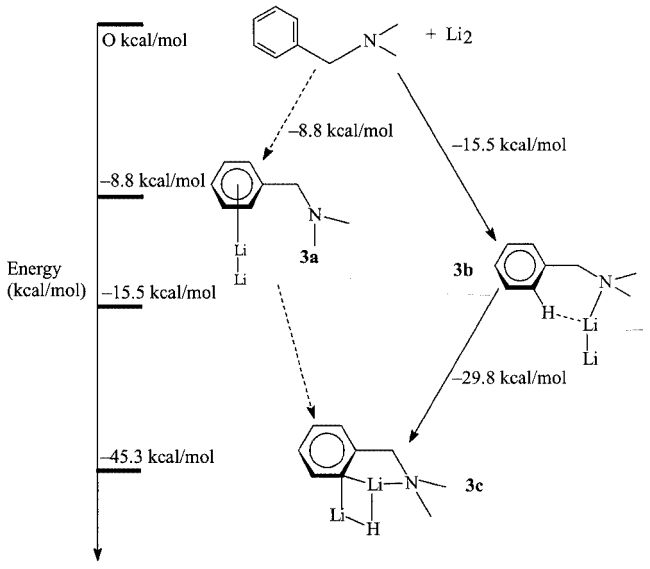

Figure 4. Calculated reaction mechanism for the co-condensation of lithium atoms with benzylamine

Table 1. Agostic H_{ortho}–Li interaction in η^1 complexes

	Li_a–H_{ortho} [Å]
Anisole	2.586
N,*N*-Dimethylaniline	2.777
N,*N*-Dimethylbenzylamine	2.669
Thioanisole	3.001
Dimethylphenylphosphane	3.109

plex **3a** the reaction enthalpy (−8.8 kcal/mol) is less exothermic. It is clear from this difference of −6.7 kcal/mol that the preferred pathway is by coordination to the donor moiety. As in the anisole case the energy for the insertion of the Li_2 cluster into the C−H bond (**3c**) is higher (at −23.1 kcal/mol) than via the π-complex types listed in Figure 2. In the calculated structure **3b** there is also an agostic-type interaction between the *ortho* C−H bond and the coordinated Li_2 cluster as detailed in Table 1. However, in this case the Li−H distance is longer (2.669 Å) than it is in the anisole species **2b** (2.586 Å).

A different preference is seen when the N-donor is *N*,*N*-dimethylaniline. In this reaction there is no clear preference between the η^1-coordination mode (**4b**) and the formation of a π-complex (**4a**) as shown in Figure 5. The difference in energy between these two species is small (−0.8 kcal/mol) and is in favour of an η^1 complex (**4b**). As in the previous two systems, there is an interaction between the *ortho* C−H bond and the coordinated Li_2 cluster **4b** with a long Li−H interaction of 2.777 Å compared to 2.586 Å in the anisole example **2b** (outlined in Table 1). The energy for the insertion into the *ortho* C−H bond of the aromatic ring is −21.9 kcal/mol, which is lower than it is in the other donor species (anisole and *N*,*N*-dimethylbenzylamine).

For soft donor atoms like phosphorus and sulfur, as defined by the Pearson concept, we see a different trend, outlined in Figure 6. When a similar theoretical study is performed on a phosphorus donor like dimethylphenylphosphane, the η^1-coordination mode (**5b**) is preferred over a π-complex (**5a**) with a calculated energy difference of −1.6 kcal/mol (shown in Figure 6). Unlike previous examples outlined above, there is no interaction between the *ortho* C−H bond and the coordinated Li_2 cluster as shown in Table 1. This can be seen from an extremely long Li−H distance of 3.109 Å. The reaction enthalpy for the insertion of the Li_2 into the C−H bond is −20.6 kcal/mol. This is smaller (compared to −21.9 kcal/mol and −24.7 kcal/mol

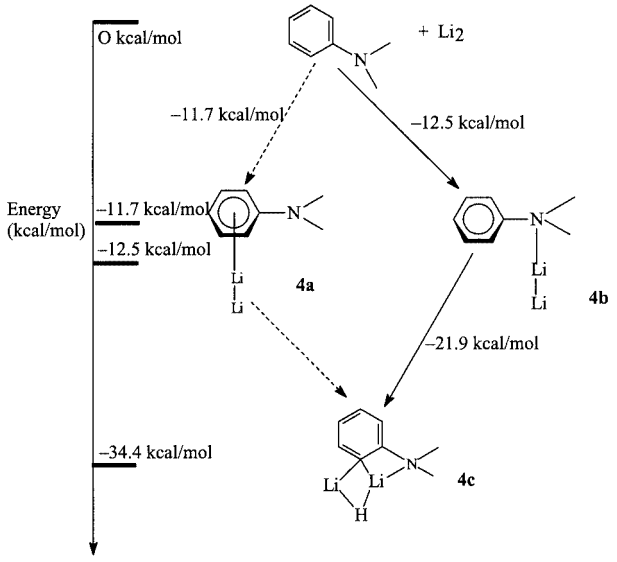

Figure 5. Calculated reaction mechanism for the co-condensation of lithium atoms with *N*,*N*-dimethylaniline

for the anisole system) than the other reaction enthalpies for this step.

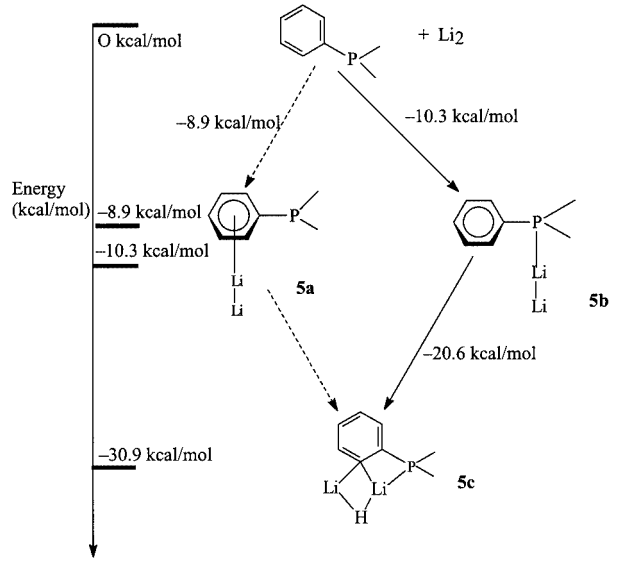

Figure 6. Calculated reaction mechanism for the co-condensation of lithium atoms with dimethylphenylphosphane

However, when the same calculation is performed on a sulfur donor like thioanisole, the situation changes. This time there is no favoured pathway, with the π-complex **6a** being just 0.1 kcal/mol lower in energy than the η^1-species **6b** as shown in Figure 7. Again there is no interaction between the *ortho* C−H bond and the η^1-coordinated Li_2 cluster. In this species the $Li-H_{agostic}$ distance is longer (3.001 Å) than it is in the corresponding η^1 complexes with oxygen and nitrogen donor substituents as outlined in Table 1. However the Li−S distance of 2.452 Å is significantly larger than in the anisole species (Li−O distance of 1.948 Å). This is a clear indication of weaker bonding due to the unfavourable hard/soft donor interaction. When a single electron is placed onto the free thioanisole there is a substantial elongation of the S−Me bond from 1.821 to 1.993 Å and the S−Ph bond length decreases from 1.785 to 1.739 Å. It was possible to predict the experimental observed C−S bond activation from this calculation.

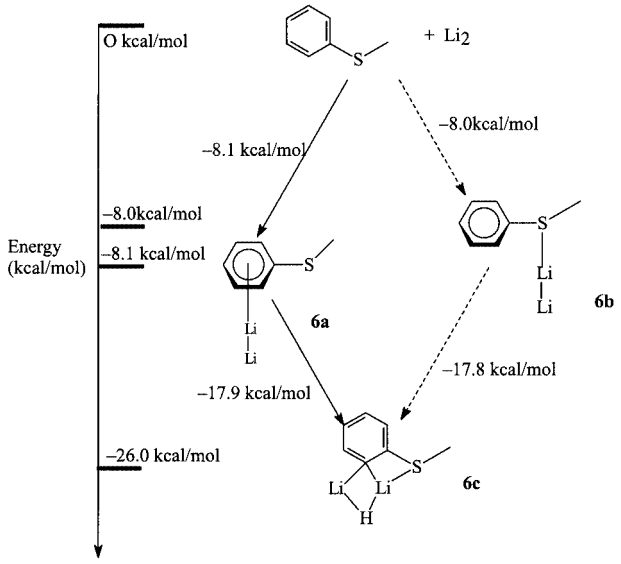

Figure 7. Calculated reaction mechanism for the co-condensation of lithium atoms with thioanisole

Discussion

Previous research in this area showed that toluene reacted with lithium atoms in the presence of THF under co-condensation conditions. The thermodynamic product benzyllithium was not formed; however, the isolated compound was identified as *p*-tolyllithium.[9,10] This interested us in the examination of the effect that other +I substituents have on the reaction. A delicate balance between +I enhancing complex formation ability and LUMO energy, allowing reductive cleavage of the aromatic C−H bond, is needed for successful C−H activation.

The electron-deficient Li_2 cluster **1** as shown in Scheme 5, will accept electron density from the aromatic system to form an unusual main group element π-complex (**2**). When the substituent on the aromatic ring donates electron density to the π-system (the +I effect), the interaction with the lithium cluster will strengthen. This can be observed by the decrease in the calculated Li−C and Li−Li bond lengths shown in Tables 2 and 3. For example in the case of toluene the Li−C distance decreases to 2.610 Å, while for mesitylene the Li−C distance is 2.591 Å compared with the longer Li−C of 2.626 Å for the benzene system. This means that there will be a stronger interaction between the aromatic rings of the +I-substituted benzene derivatives [for example xylene, *tert*-butylbenzene, mesitylene, and trimethyl(phenyl)silane] than benzene. However, the next mechanistic step is crucial. This involves the double single-elec-

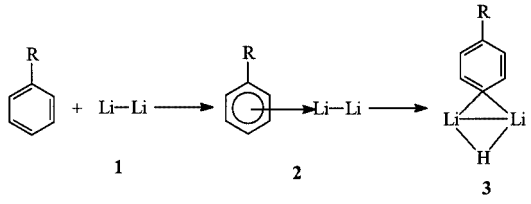

Scheme 5. Key mechanistic steps in aromatic C−H bond activation using lithium atoms

Table 2. Selected Li−C bond lengths for the +I-substituted benzene derivatives

	Li−C distance [Å]
Benzene	2.625
Toluene	2.591
p-Xylene	2.570
Mesitylene	2.547
tert-Butylbenzene	2.595
Trimethyl(phenyl)silane	2.601

Table 3. Selected Li−Li bond lengths for all calculated intermediates

Li−Li distance [Å] in:	π complex	D*-η^1 complex	C−H activated species	Free Li_2
Benzene	2.769	N/A	N/A	2.723 Å
Toluene	2.776	N/A	2.281	
Trimethyl(phenyl)silane	2.781	N/A	2.283	
Anisole	2.772	2.746	2.299	
Thioanisole	2.774	2.762	2.299	
N,*N*-Dimethylaniline	2.795	2.767	2.295	
N,*N*-Dimethylbenzylamine	2.781	2.785	2.296	
Dimethylphenylphosphane	2.782	2.769	2.293	

tron transfer from the π-bonded Li_2 cluster **3** to the LUMO of the aromatic ring. The outcome of the reaction depends on how the substituents affect the LUMO, and not its +I ability. If the LUMO energy is increased in relation to toluene and benzene, as it is for mesitylene and xylene (as outlined in Table 4), it is impossible to place electron density into it, thereby preventing the reaction from occurring. This can be seen from the lack of reaction between lithium atoms and xylene or mesitylene (as described in Scheme 1). If the substituent lowers the LUMO energy, as for trimethyl(phenyl)silane and *tert*-butylbenzene (as shown in Table 4) the reaction will proceed quite readily. If the LUMO energy of the aromatic ring is lowered too much, a single electron reduction of the aromatic compound to its stable radical anion will occur instead of C−H bond activation.

Table 4. Calculated LUMO energies of selected reactants using B3LYP/6-31G**

	LUMO [eV]
N,*N*-Dimethylaniline	0.387
Mesitylene	0.261
m-Xylene	0.197
o-Xylene	0.194
p-Xylene	0.164
Toluene	0.123
tert-Butylbenzene	0.102
Anisole	0.085
Benzene	0.072
N,*N*-Dimethylbenzylamine	0.057
Thioanisole	−0.041
Trimethyl(phenyl)silane	−0.180
4,4′-Di-*tert*-butylbiphenyl	−0.579
4,4′-Bis(trimethylsilanyl)biphenyl	−0.898

For the reaction of trimethyl(phenyl)silane with lithium atoms in the presence of THF, a reaction sequence different from the toluene co-condensation was observed. This is governed by the ability of the $SiMe_3$ group to stabilise an aromatic radical. The major product identified was 4,4′-bis-(trimethylsilanyl)biphenyl. This is the coupled product of the free phenyltrimethylsilyl radical. This indicates that a reduction of trimethyl(phenyl)silane occurs at 77 K, which then couples to form the substituted biphenyl derivative as outlined in Scheme 2. In this case the $SiMe_3$ substituent stabilises the radical long enough to allow it to form the coupled product 4,4′-bis(trimethylsilanyl)biphenyl. On warming in the MVS reactor, excess solid lithium reduces 4,4′-bis(trimethylsilanyl)biphenyl to its radical anion, in an analogous reaction to the reduction in solution of 4,4′-di-*tert*-butylbiphenyl by lithium metal.[14] From the calculated LUMO energies of these two biphenyl species (Table 4) a comparison can be made in relation to the ease of reduction of 4,4′-bis(trimethylsilanyl)biphenyl. The calculated LUMO energies for 4,4′-di-*tert*-butylbiphenyl is −0.579 eV, while 4,4′-bis(trimethylsilanyl)biphenyl has a lower LUMO energy of −0.898 eV. This shows that the reduction of 4,4′-bis(trimethylsilanyl)biphenyl by lithium metal can readily occur in THF solution.

However, a secondary C−H activated product was also identified. This was the *para*-lithiated aromatic 4-(trimethylsilyl)phenyllithium. It could not be identified in solution but treating this species with S_2Me_2 to form trimethyl[4-(methylsulfanyl)phenyl]silane, allowed a further full characterisation of the substitution pattern on the ring as outlined in Scheme 2.

The co-condensation of *tert*-butylbenzene and lithium atoms in the presence of THF was similar to the reaction involving trimethyl(phenyl)silane (as detailed in Scheme 2). The major product was found to be 4,4′-di-*tert*-butylbiphenyl. This is formed from the coupling of the *tert*-butylphenyl radical. On warming in the MVS machine it is believed that 4,4′-di-*tert*-butylbiphenyl is reduced by solid lithium metal to its radical anion. Because of this no direct NMR spectroscopy was attempted, instead the co-condensation product was treated with S_2Me_2. A minor product was observed to be *tert*-butyl-4-(methylsulfanyl)benzene, this corresponds to a secondary reaction occurring at 77 K, the activation of the *para* C−H bond of *tert*-butylbenzene.

When a Lewis base function is used, the +I inductive effect versus LUMO effect is no longer important, because the favoured donation mode to the Li_2 cluster is now via the η^1-coordination mode through the donor moiety as shown by a series of DFT calculations described in Figures 3−7. This mode of bonding is energetically favoured over the formation of a π-complex with the Li_2 cluster. Due to this change in the coordination mode, a change

in regiochemistry occurs, resulting in *ortho* C−H bond activation.

When an oxygen donor was used as in the case of anisole, the NMR spectroscopic data, which is in good agreement with the literature data,[16] showed an *ortho*-lithiated product. NMR spectroscopic data indicate a tetrameric structure of the composition Ar_4Li_4. In contrast to the benzene and toluene experiments reported previously,[9,10] the yield was increased to 30% from 12%, which is extremely high for an MVS experiment. As in the trimethyl(phenyl)silane co-condensation, treating it with dimethyl disulfide as outlined in Scheme 3, allowed a further characterisation of the lithiated product. This reaction confirms the *ortho* lithiation by the formation of 1-methoxy-2-(methylsulfanyl)benzene, which was identified from NMR spectroscopic data and GC MS data.[17,18]

When the oxygen donor substituent of anisole is changed to the softer sulfur atom as in thioanisole, a similar result was expected. However, no C−H bond activation was observed, instead NMR spectroscopic data indicated a cleavage of the S−Me bond. This resulted in the formation of the Ph−S˙ radical, which dimerises to form diphenyl disulfide. Secondary products were shown to be $(MeLi{\cdot}THF)_4$ and PhSLi·THF by derivatisation reactions and this is described in Scheme 4. This result is not unexpected since the S−Me bond strength of 69.4 kcal/mol is weaker than that of the C−H bond of 100 kcal/mol. The selectivity for the S−C sp^3 bond is due to its lower bond strength compared with the S−Ph sp^2 bond of 86.5 kcal/mol.[24]

When the donor substituent was a nitrogen donor as in *N*,*N*-dimethylaniline, the observed product was 2-(dimethylamino)phenyllithium (as outlined in Scheme 3). This reaction type is similar to the anisole case, but with a much lower yield of 1%. This is possibly due to the high LUMO energy (0.387 eV) of the *N*,*N*-dimethylaniline, as described in Table 4. This reaction is surprising since some +I-substituted aromatic compounds like mesitylene and xylenes, which have lower LUMO energies, do not react with lithium atoms. Presumably, the change in coordination mode to η^1 facilitates this reaction.

In an ether solution *N*,*N*-dimethylbenzylamine is known to react with BuLi to form 2-[(dimethylamino)methyl]phenyllithium. The factors controlling the selectivity are not well investigated.[20,21] It is reported as being tetrameric (Ar_4Li_4) in the solid state with the NMe_2 group intramoleculary coordinated to Li, while in THF solution it is dimeric with the composition $Ar_2Li_2{\cdot}4THF$. When benzylamine is co-condensed with lithium atoms and THF as outlined in Scheme 3, a pyrophoric beige solid is obtained in a larger yield (36%) than in the *N*,*N*-dimethylaniline experiment (1%). ^1H and ^{13}C NMR spectroscopic data show the presence of 2-[(dimethylamino)methyl]phenyllithium with no coordinated THF. This composition is in agreement with the published solid-state structure.[21] No activation was detected in the benzyl position. Confirmation of the regiochemistry was obtained as in previous co-condensations by the reaction with S_2Me_2.

Conclusion

Lithium atoms are able to activate +I- and donor-substituted benzene derivatives. In the case of +I-aromatic compounds like trimethyl(phenyl)silane and *tert*-butylbenzene, two products were observed, the major product was the coupled biphenyl and the minor product the C−H-activated *para*-lithiated aromatic compound. However, other +I benzene derivatives with higher LUMO energies than toluene, like xylenes and mesitylene, failed to react. It appears that this reaction type has a narrow range based on the LUMO energy of the aromatic compound. When donor substituted benzene derivatives like anisole, *N*,*N*-dimethylaniline, and *N*,*N*-benzylamine were co-condensed with lithium atoms in the presence of THF, *ortho* C−H bond activation was exclusively observed. This results from a mechanistic change from a π-bonded Li_2 cluster via the phenyl ring to a η^1-bonded Li_2 via the donor atom. For this reaction type, the LUMO energy is not as important as in the series of reactions using +I-substituted benzene derivatives. For the co-condensation of thioanisole with lithium atoms in THF, an activation of the C−S bond as well as a reductive coupling of thioanisole was observed.

Experimental Section

General: All experimental procedures were performed using standard Schlenk techniques under dry argon. THF, toluene, *m*-, *p*-xylene, anisole, and *tert*-butylbenzene were dried and distilled from sodium benzophenone ketyl under argon. Trimethyl(phenyl)silane, thioanisole, *N*,*N*-dimethylaniline, *N*,*N*-dimethylbenzylamine were dried and distilled from calcium dihydride under argon. All solvents were then degassed by three freeze-pump-thaw cycles. Celite was stored overnight in an oven at 120 °C and was dried under vacuum for 3 h before use. For each filtration layers of approximately 6 cm of Celite were used. ^1H and ^{13}C NMR spectra were obtained using either a Varian 300 MHz or a Varian 500 MHz NMR machine. All chemical shifts are reported in ppm and are referenced to TMS. The ^7Li NMR spectra in this study were obtained with a Jeol 300 MHz machine. The chemical shifts for the ^7Li NMR spectra are reported in ppm and are referenced to an internal standard of LiBr in D_2O. All GC MS samples were run as dichloromethane solutions using a Finnigan Trace GC MS, with an RTX-5MS 15-m column.

Typical Co-condensation Experiment: Lithium metal (0.53 g, 0.076 mol) was vapourised from an aluminium crucible protected by a stainless-steel inlet at around 800 °C over 90 min and co-condensed with a mixture of the aromatic compound (20 mL) and THF (80 mL, 1.12 mol). After removal of the solvent mixture, the residue was dissolved in dry toluene and the solution was filtered through Celite from the solid lithium hydride by-product and unreacted lithium metal. After removal of the toluene in vacuo a dark red solid was isolated and washed with dry pentane (20 mL). The lithiated aromatic compound was identified by ^1H and ^{13}C NMR spectroscopy.

Typical Derivatisation of the Lithiated Aromatic Compound with Me_2S_2: Dimethyl disulfide (0.3 mol/L) was added dropwise with vigorous stirring to a solution of of the lithiated aromatic compound (0.25 g) in THF (20 mL) at room temperature. The reaction

was thought to be complete when a colour change from red to yellow occurred. Water (10 mL) was added to this solution and the organic phase separated. The aqueous phase was washed three times with dichloromethane (10 mL). The combined organic extracts were dried with $MgSO_4$ and the solvent was then removed under reduced pressure, affording the derivatised compound as a brown oil. GC MS and ^1H and ^{13}C NMR spectroscopy were used to identify the product.

Theoretical Methods Used in this Study: With a view to determining the structures and reaction enthalpies of intermediates in the reaction mechanism, the application of theoretical methods has proven advantageous. For this purpose the program package used was GAUSSIAN 98[25] implemented on a DEC Alpha work station (500 MHz CPU/256 MB RAM) or an Origin 200 eight-processor cluster (SGI 180 MHz CPU/2 GB RAM). Ab-initio calculations were performed at the DFT level of theory (B3LYP) using the 6-31G** basis set for C, H, O, N, S, P, and Li. Harmonic vibrational frequencies, calculated at the same level, characterised stationary points and gave the zero-point energy. The difference in the sum of the electronic and the zero-point energies were interpreted as reaction enthalpies at 0 K. LUMO energies for each aromatic compound were obtained from geometry-optimised structures using B3LYP/6-31G**.

Acknowledgments

The authors want to thank Prof. Dr. Dietmar Stalke for the access to his NMR spectroscopy facilities in Würzburg. This work was supported by the Centre for High-Performance Computing Applications at University College Dublin, Ireland.

[1] A. E. Shilov, G. B. Shul'pin, *Chem. Rev.* **1997**, *97*, 8; A. E. Shilov, G. B. Shul'pin, *Chem. Rev.* **1997**, *97*, 2905.
[2] B. A. Arndtsen, R. G. Bergmann, T. A. Mobley, T. H. Petersen, *Acc. Chem. Res.* **1995**, *28*, 154.
[3] R. H. Crabtree, *Chem. Rev.* **1995**, *95*, 987.
[4] A. H. Janowicz, R. G. Bergman, *J. Am. Chem. Soc.* **1982**, *104*, 352.
[5] A. H. Janowicz, R. G. Bergman, *J. Am. Chem. Soc.* **1983**, *154*, 3929.
[6] N. S. Radu, S. L. Buchwald, B. Scott, C. J. Burns, *Organometallics* **1996**, *15*, 19; N. S. Radu, S. L. Buchwald, B. Scott, C. J. Burns, *Organometallics* **1996**, *15*, 3913.
[7] R. H. Hauge, J. L. Margrave, *Reactions of First-Row Transition Metal Atoms and Small Clusters in Matrices*, in: *Chemistry and Physics of Matrix-Isolated Species* (Eds.: L. Andrews, M. Moskowits), North Holland, Amsterdam, **1989**, pp. 277−302.
[8] W. E. Billups, M. M. Konars, R. H. Hauge, J. L. Margrave, *J. Am. Chem. Soc.* **1980**, *102*, 7393.
[9] M. Tacke, *Chem. Ber.* **1995**, *128*, 91.
[10] M. Tacke, *Chem. Ber.* **1996**, *129*, 1369.
[11] M. Tacke, *Eur. J. Inorg. Chem.* **1998**, 537.
[12] M. D. Curtis, A. L. Allred, *J. Am. Chem. Soc.* **1965**, *12*, 2554.
[13] C. A. Walree, X. Y. van Lauteslager, A. M. Wageningen, J. W. van Zwikker, L. A. Jenneskens, *J. Organomet. Chem.* **1995**, *496*, 117.
[14] T. Cohen, I. H. Jeong, B. Murdryk, M. Bhupathy, M. M. A. Awad, *J. Org. Chem.* **1990**, *55*, 1528.
[15] R. S. Cooke, G. S. Hammond, *J. Am. Chem. Soc.* **1970**, *92*, 2739.
[16] S. Harder, J. Boersma, L. Brandsma, G. P. M. v. Mier, J. A. Kanters, *J. Organomet. Chem.* **1989**, *364*, 1.
[17] A. Perez-Encabo, S. Perrio, A. M. Z. Slawin, S. E. Thomas, A. T. Wierzchleyski, D. J. Williams, *J. Chem. Soc., Perkin Trans. 1* **1994**, 629.
[18] J. H. Bowie, S. O. Lawesson, J. Ø. Madson, G. Schroll, D. H. Williams, *J. Chem. Soc. B* **1966**, 951.
[19] M. R. Detty, G. P. Wood, *J. Org. Chem.* **1980**, *45*, 80.
[20] C. H. Yoder, K. F. Sheffey, R. Howell, R. E. Hess, C. Pascala, C. D. Schaeffer, J. J. Zuckerman, *J. Org. Chem.* **1976**, 1511.
[21] F. T. Oakes, J. F. Sebastian, *J. Organomet. Chem.* **1978**, *159*, 363.
[22] J. T. B. H. Jastrzebski, G. van Koten, M. Konijn, C. H. Stam, *J. Am. Chem. Soc.* **1982**, *104*, 5490.
[23] K. Ohkata, K. Takee, K. Akiba, *Bull. Chem. Soc. Jpn.* **1985**, *7*, 1946.
[24] D. F. McMillen, D. M. Golden, *J. Phys. Chem.* **1984**, *88*, 3175.
[25] M. J. Frisch, G. W. Trucks, H. B. Schlegel, G. E. Scuseria, M. A. Robb, J. R. Cheeseman, V. G. Zakrzewski, J. A. Montgomery, Jr., R. E. Stratmann, J. C. Burant, S. Dapprich, J. M. Millam, A. D. Daniels, K. N. Kudin, M. C. Strain, O. Farkas, J. Tomasi, V. Barone, M. Cossi, R. Cammi, B. Mennucci, C. Pomelli, C. Adamo, S. Clifford, J. Ochterski, G. A. Petersson, P. Y. Ayala, Q. Cui, K. Morokuma, D. K. Malick, A. D. Rabuck, K. Raghavachari, J. B. Foresman, J. Cioslowski, J. V. Ortiz, A. G. Baboul, B. B. Stefanov, G. Liu, A. Liashenko, P. Piskorz, I. Komaromi, R. Gomperts, R. L. Martin, D. J. Fox, T. Keith, M. A. Al-Laham, C. Y. Peng, A. Nanayakkara, C. Gonzalez, M. Challacombe, P. M. W. Gill, B. Johnson, W. Chen, M. W. Wong, J. L. Andres, C. Gonzalez, M. Head-Gordon, E. S. Replogle, J. A. Pople, *Gaussian 98*, Revision A.7, Gaussian, Inc., Pittsburgh PA, **1998**.

Received May 6, 2002
[I02230]

Macrocyclic Complexes of $[Ru(N\text{-}N)_2]^{2+}$ Units [N-N = 1,10 Phenanthroline or 4-(*p*-Anisyl)-1,10-Phenanthroline]: Synthesis and Photochemical Expulsion Studies

Anne-Chantal Laemmel,[a] Jean-Paul Collin,*[a] Jean-Pierre Sauvage,*[a] Gianluca Accorsi,[b] and Nicola Armaroli*[b]

Keywords: Ruthenium / Macrocycles / Receptors / Photochemistry / Molecular machines

Two ruthenium complexes $[Ru(phen)_2(m\text{-}36)]^{2+}$ and $[Ru(aphen)_2(m\text{-}36)]^{2+}$, indicated as **1** and **2** respectively, which contain a 36-membered macrocycle incorporating a sterically hindered bipyridine (m-36), and two 1,10-phenanthroline (phen) or 4-(*p*-anisyl)-1,10-phenanthroline (aphen) ligands, have been synthesised. Under light irradiation, as seen from the metal-to-ligand-charge-transfer (MLCT) bands of the visible spectral region, the $[Ru(phen)]_2^{2+}$ core of **1** and **2** is selectively expelled from the macrocycle to give the corresponding bis-acetonitrile derivative. This photochemical process was found to be notably less efficient than that observed in a simpler related complex $[Ru(phen)_2dmbp]^{2+}$ (dmbp = 6,6′dimethyl-2,2′-bipyridine), that lacks the macrocyclic motif. In the case of **1** thermal back reaction takes place quantitatively affording a completely reversible system. The isolation, by chromatographic techniques, of the axial-axial *cis*-$[(a,a)Ru(aphen)_2Cl_2]$ isomer, where the two aphen ligands bear two *p*-anisyl groups disposed trans to one another enabled the preparation of **2**. This type of complex undergoes a more complicated photochemical process, in fact, following the expected photolabilisation of the $[Ru(aphen)_2]^{2+}$ unit, photoisomerisation of the primary photo-product occurs and gives a statistical mixture of the three geometrical isomers: *cis*-$[(a,a)Ru(aphen)_2(CH_3CN)_2](PF_6)_2$, *cis*-$[(a,e)Ru(aphen)_2(CH_3CN)_2](PF_6)_2$ and *cis*-$[(e,e)Ru(aphen)_2(CH_3CN)_2](PF_6)_2$. This side-reaction precludes its use as rotaxane precursor suggesting that, for this purpose, a bis-phenanthroline ligand stabilising the ruthenium core is needed.
(© Wiley-VCH Verlag GmbH & Co. KGaA, 69451 Weinheim, Germany, 2003)

Introduction

The accessibility to rotaxanes and catenanes by strategies based on various template effects allowed their involvement in different research fields such as photo-induced energy and electron transfer or molecular machines.[1] The presence of mechanical bonds, an intrinsic property of such species, should confer good reversibility to systems designed for specific tasks related to large amplitude movements. The control of molecular motion for example is an essential function in artificial[2] as well as in biological systems[3] (ATPsynthase, myosin-actin, etc.).Very often, motions in the molecules or molecular assemblies have been triggered by chemical[4] or electrochemical signals.[5] Relatively few systems rely on *purely photonic* input.[6] We now report on a transition metal light-driven system based on dissociative photoexcited states. Ru^{II} complexes of the $[Ru(diimine)_3]^{2+}$ family (diimine = bidentate ligand) seem to be promising in building light-driven machines, since the use of a sterically hindered chelate (e.g. a 6,6′ substituted bipy) associated with a $[Ru(phen)_2]^{2+}$ core (phen = 1,10-phenanthroline) leads to the specific and quantitative photolabilisation of the chelate.[7] Indeed, excitation into the absorption bands of Ru^{II}-polyimine complexes corresponding to the singlet metal-to-ligand-charge-transfer transitions (^{1}MLCT) is followed by intersystem crossing to the lowest-lying triplet level (^{3}MLCT) which, by thermal redistribution, may populate upper-lying dissociative d-d metal centred (MC) states.[8] The MC/MLCT energy gap is small and the thermal deactivation of the ^{3}MLCT state is particularly effective when the ligand field is weakened by distortions due to the sterically hindering ligands. A recent communication described a system constituted by a $[Ru(phen)_2]^{2+}$-type fragment hosted in a macrocyclic receptor.[9] The present article extends this previous example to a possible rotaxane precursor and evidences the limitations brought by a competitive photoisomerisation reaction. Figure 1 displays the basis of the photochemical expulsion of the ruthenium unit from a macrocycle and its thermal back re-coordination.

Results and Discussion

The ruthenium complexes $[Ru(phen)_2(m\text{-}36)]^{2+}$ (**1**) and $[Ru(aphen)_2(m\text{-}36)]^{2+}$ (**2**) [see a) in Figure 2] in which a bipyridine unit is incorporated in a macrocycle have been synthesised as possible rotaxane precursors. Indeed, the re-

[a] Laboratoire de Chimie Organo-minérale, Institut Le Bel, Université Louis Pasteur,
4 rue Blaise Pascal, 67 070 Strasbourg, France
E-mail: sauvage@chimie.u-strasbg.fr
[b] Istituto per la Sintesi Organica e la Fotoreattività del CNR,
via Gobetti 101, 40129 Bologna, Italy
E-mail: armaroli@frae.bo.cnr.it

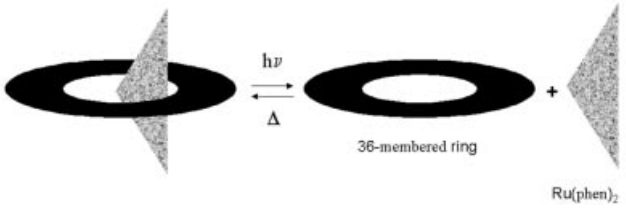

Figure 1. Principle of the photochemically driven motion and the thermal backward reaction

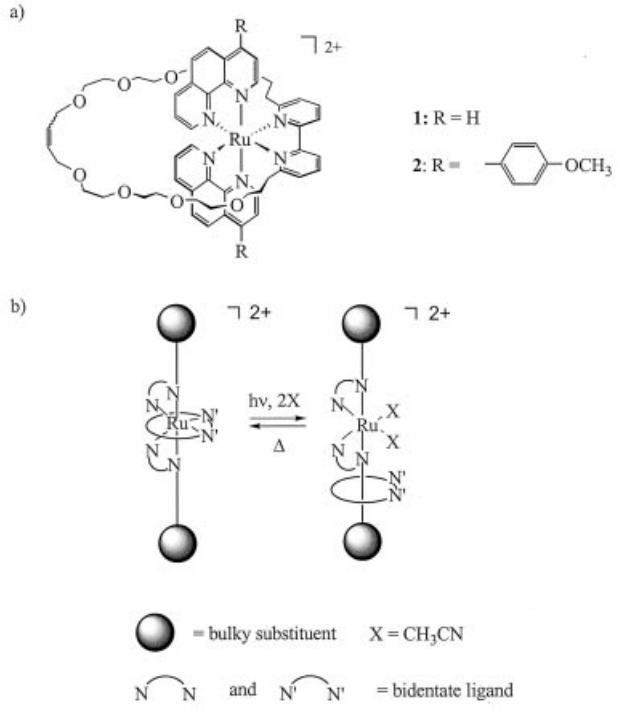

Figure 2. (a) Chemical structures of complexes **1** and **2**. (b) Possible photochemical reaction leading to a rotaxane if bulky stoppers are attached in the 4 positions

placement of the R group by bulky substituents and the photosubstitution of the bipyridine-based macrocycle by two molecules of solvent (CH_3CN) could lead to a real rotaxane as depicted in Figure 2, b). The synthesis of **1** and **2** is accomplished by applying the strategy of threading or clipping.

In this latter strategy the complexation of an appropriate bipyridine derivative bearing terminal olefins (**3**) precedes the closure of the macrocycle (Scheme 1 and 2).

The 2,2′-bipyridine ligand **3** substituted at its 6 and 6′ positions by two long chains terminated by olefinic groups was prepared in five steps from the 6,6′-dimethyl-2,2′-bipyridine (dmbp).[10] By deprotonation of dmbp with LDA in THF and reaction with two equivalents of THP-protected bromoethanol (THP = tetrahydropyran-2-yl) **4** was obtained in 63% yield. Deprotection of **4** afforded **5** in 70% yield. This alcohol was converted into **6** following the Williamson methodology (NaH/DME) by reaction with 2-{2-[2-(2-chloroethoxy)ethoxy)]ethoxy}tetrahydro-2*H*-pyran (53% yield). Deprotection with catalytic amounts of *para*-

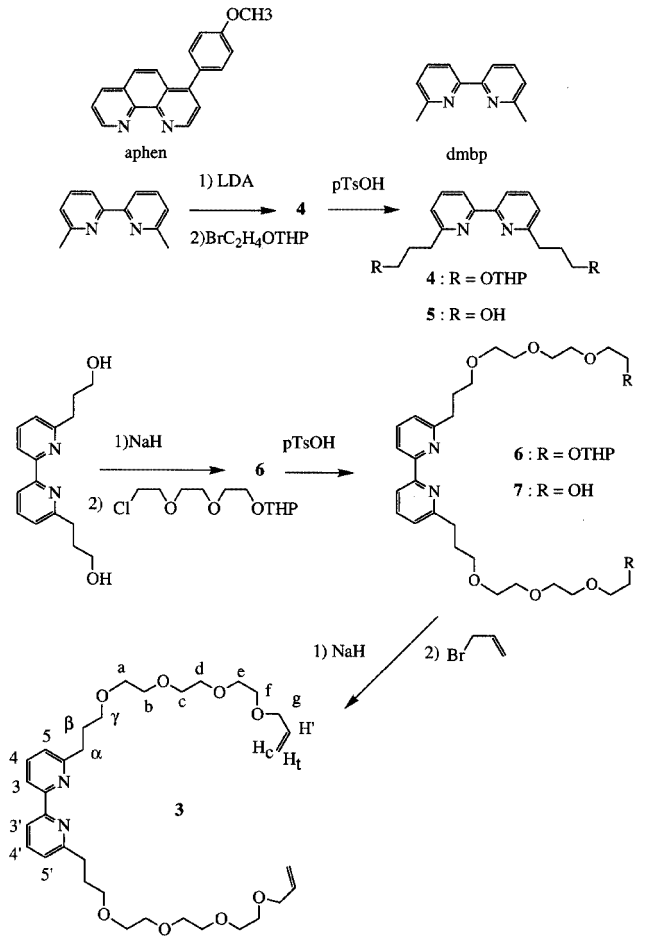

Scheme 1

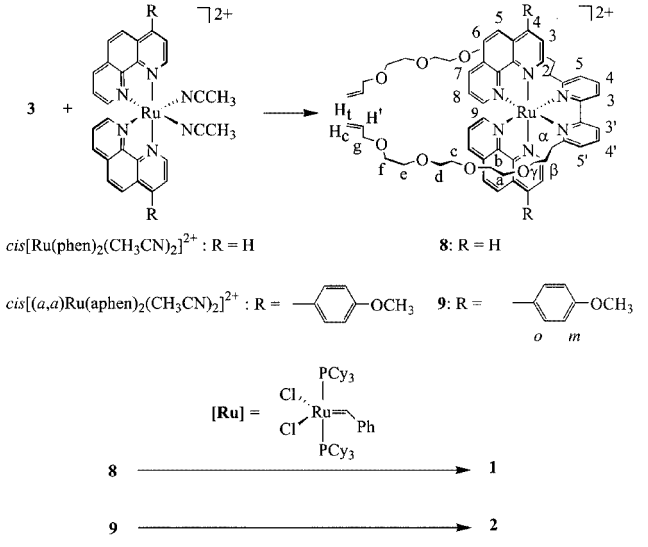

Scheme 2

toluenesulfonic acid (*p*TsOH) in ethanol led to the corresponding diol **7** in good yield (84%). The conversion of **7** to ligand **3** bearing terminal olefins was achieved with a large excess of allyl bromide in the presence of NaH in DME (75% yield).

It was recently shown that *cis*-$[Ru(phen)_2(CH_3CN)_2]^{2+}$ is a more efficient starting material than the classical bis-chloro derivative *cis*-$[Ru(phen)_2Cl_2]$ for introducing a third chelate onto the ruthenium centre.[11] Good yields of **8** were obtained by heating a stoichiometric mixture of *cis*-$[Ru(phen)_2(CH_3CN)_2]^{2+}$ [12] and **3** in ethylene glycol at 140 °C for 2 h. After column chromatography and anion exchange with PF_6^-, **8** was recovered as a red powder. The preparation of the analogous precursor **9** requires the isomeric form *cis*-$[(a,a)Ru(aphen)_2(CH_3CN)_2](PF_6)_2$ as the axle of the rotaxane (see b in Figure 2). It is itself obtained by solvolysis of the dichloride derivative *cis*-$[(a,a)Ru(aphen)_2Cl_2]$ (Figure 3).

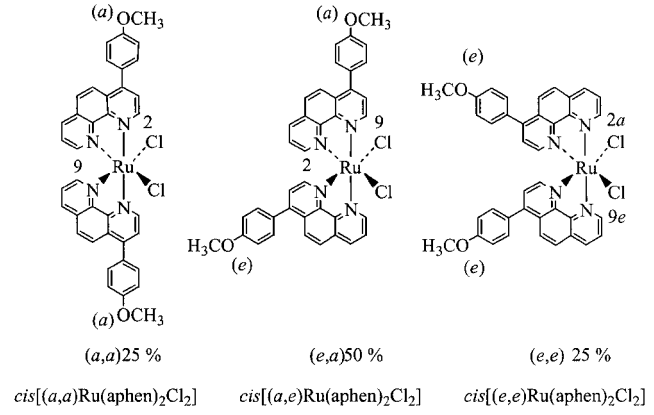

Figure 3. Schematic view of the isomeric complexes for the general species *cis*-$[Ru(aphen)_2Cl_2]^{2+}$ (*a* for axial, *e* for equatorial)

The use of an unsymmetrical ligand such as 4-(*p*-anisyl)-1,10-phenanthroline (aphen) is a challenging task since stereo- and geometric isomers are expected. The sequential addition of different bidentate polypyridyl ligands onto the ruthenium centre is actually described in the literature but several attempts following these methodologies failed.[13,14] Recently, $[Ru(CH_3CN)_4Cl_2]$ was used by von Zelewsky et al.[15] to prepare ruthenium bis-chloro complexes with a bis-bidentate ligand (chiragen). With this starting material and two equivalents of aphen a statistical mixture of three isomers as represented in Figure 3 was recovered in 46% yield. The separation of the geometric isomer *cis*-$[(a,a)Ru(aphen)_2Cl_2]$ from the mixture turned out to be possible on silica columns and on numerous acidic alumina columns with a yield of 87% being obtained. The identification of each isomer was made possible by analysing their ^1H NMR spectra (COSY and ROESY experiments). On heating the *cis*-$[(a,a)Ru(aphen)_2Cl_2]$ isomer in a CH_3CN/H_2O (50:50) mixture the bis-acetonitrile derivative *cis*-$[(a,a)Ru(aphen)_2(CH_3CN)_2]$ was isolated as a single isomer proving that no isomerisation occurs under these conditions. The reaction of ligand **7** with the complex *cis*-$[(a,a)Ru(aphen)_2(CH_3CN)_2](PF_6)_2$ gave the precursor complex **9** in 90% yield.

The cyclisation of the two terminal olefinic functions following the method developed by Grubbs et al.[16] (ring closing metathesis or RCM) turned out to be efficient. This method is compatible with a large variety of functions and has also been proved to be well suited to the synthesis of catenanes and molecular knots.[17] By using a relatively high concentration of the precursor complexes **8** and **9** (0.01 M, CH_2Cl_2 solution) and 7% of the ruthenium complex [Ru] (Scheme 2) as a catalyst the targeted complexes **1** and **2** were obtained in 67 and 45% yield, respectively. The progress of the cyclisation reactions can be monitored by the disappearance of the characteristic ^1H NMR signals of the terminal olefins and the concomitant appearance of signals corresponding to the cyclic olefin in its *cis* and *trans* isomeric forms. The electronic and mass spectra (FAB-MS) as well as the assignment of their ^1H NMR spectra (ROESY experiments) confirm the expected structures of **1** and **2**.

Upon irradiation at 404 nm (isosbestic point, see below) of an acetonitrile solution of **1**, a photochemical reaction is triggered that can be monitored by absorption and ^1H NMR spectroscopy. The starting 2.5×10^{-5} M red solution of **1** gradually changes its colour into yellow, as a consequence of the changes in position and intensity of the MLCT absorption bands. In particular, the band that peaked at 450 nm decreases with irradiation time and a new absorption band with a maximum at 380 nm grows (Figure 4).

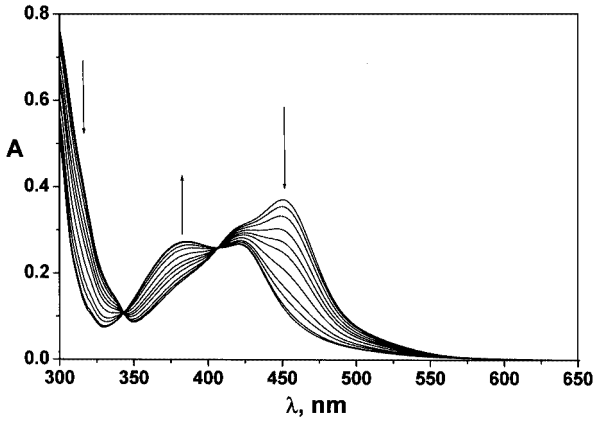

Figure 4. Changes in the electronic absorption spectra of a 2.5×10^{-5} M acetonitrile solution of **1** under irradiation with a 150 W xenon lamp at 404 nm. Spectra are recorded at t = 0, 2, 5, 10, 15, 20, 30, 45, 60, 90, 120 min of irradiation

Neat isosbestic points appear at 342 and 404 nm, emphasising the selectivity of the photochemical process and the final spectrum (Figure 4) is identical to that of the *cis*-$[Ru(phen)_2(CH_3CN)_2]^{2+}$ species. Importantly, **1** is stable when kept in the dark for indefinite periods. The experimental data led us to conclude that an efficient photolabilisation of the $[Ru(phen)_2]^{2+}$ unit takes place, analogous with the results obtained for the simpler $[Ru(phen)_2(dmbp)]^{2+}$ complex.[7] Notably, in the case of **1**, under the same experimental conditions (150 W xenon lamp, λ_{exc} = 404 nm) the time required to complete the reaction (120 min) is longer than that for $[Ru(phen)_2(dmbp)]^{2+}$ (50 min), suggesting that the expulsion of the dmbp-containing macrocycle is kinetically less favoured than the loss of a plain dmbp ligand in $[Ru(phen)_2(dmbp)]^{2+}$, due to steric hindrance.

Experiments performed by ^{1}H NMR spectroscopy confirmed the above results. The spectrum obtained after irradiating an NMR tube containing **1** in CD_3CN corresponds to a mixture of *cis*-$[Ru(phen)_2(CD_3CN)_2]^{2+}$ and the free macrocycle m-36. Once again, the efficiency of this photochemical reaction is found to decrease in comparison with the previously studied system in which a $[Ru(phen)_2]^{2+}$ core is associated with dmbp.[7]

Complexes **1** and $[Ru(phen)_2dmbp]^{2+}$ are not luminescent at room temperature due to thermally induced deactivation of the potentially luminescent MLCT state via the upper lying MC level (possibly leading to photodissociation, see above). Lowering the temperature prevents this thermal deactivation process. Very intense, long-lived luminescence is observed at 77 K for both compounds (Table 1, Figure 5). *cis*-$[Ru(phen)_2(CH_3CN)_2]^{2+}$ also exhibits intense MLCT luminescence at 77 K, and its maximum peak is substantially blue-shifted relative to **1** and $[Ru(phen)_2dmbp]^{2+}$.[18] Notably, after irradiation the emission spectra of **1** and $[Ru(phen)_2dmbp]^{2+}$ strongly resemble that of *cis*-$[Ru(phen)_2(CH_3CN)_2]^{2+}$, revealing the presence of only a small residual amount (< 10%) of starting material (see spectral shoulder at 625 nm, Table 1). The excited state lifetime (3.0 μs) also strongly supports the view that photochemical induced expulsion of the bipy-type fragment has occurred, leading to the formation of a *cis*-$[Ru(phen)_2(CH_3CN)_2]^{2+}$ coordination centre for both complexes.

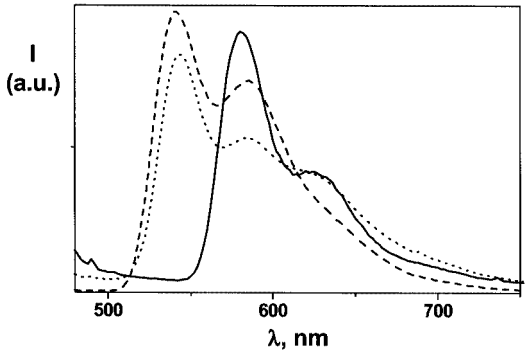

Figure 5. Emission spectra at 77 K of a CH_3CN rigid matrix of **1** before (full line, λ_{exc} = 449 nm) and after (dotted line, λ_{exc} = 420 nm) irradiation and of *cis*-$[Ru(phen)_2(CH_3CN)_2]^{2+}$ (dashed line, λ_{exc} = 420 nm). O. D. = 0.5 for all samples at the excitation wavelength

At 25 °C, quantum yields for photolabilisation are 0.020 ± 0.002 and 0.008 ± 0.001 in the case of $[Ru(phen)_2dmbp]^{2+}$ and **1,** respectively. Since the steric hindrance is more pronounced in **1** than in $[Ru(phen)_2dmbp]^{2+}$, it seems that some decoordination steps of the chelate unit are slower due to the presence of the macrocyclic chain. The cyclic nature of the complex is also expected to favour a *cis* conformation of the alkene group of the bipy-based macrocycle, making the stepwise decomplexation slightly more difficult than it is with its unconstrained analogue, dmbp.

After irradiation, it was possible to quantitatively recover complex **1** by refluxing the equimolar mixture of *cis*-$[Ru(phen)_2(CH_3CN)_2]^{2+}$ and macrocycle m-36 in ethylene glycol for two hours. The principle of the photochemically driven motion and the thermal backward reaction is indicated in Scheme 3.

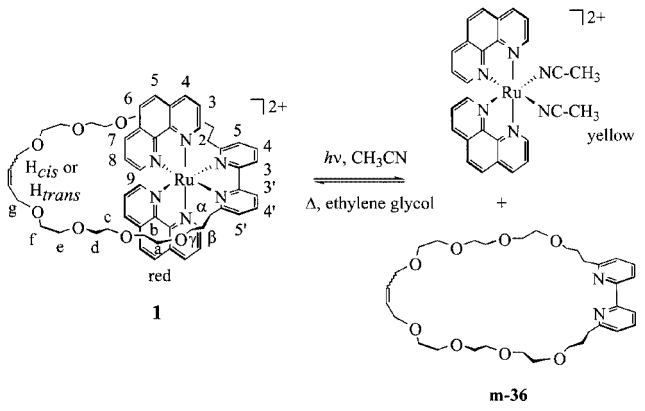

Scheme 3

The photochemical behaviour of complex **2** has also been studied under similar conditions as for complex **1**, i.e. with an efficiency similar to that observed for the same process in **1**. However, a careful examination of the area around the isosbestic point (417 nm) shows that some by-products were formed during the photoirradiation. By monitoring the photochemical reaction using ^{1}H NMR spectroscopy (CD_3CN, 500 MHz) the appearance of the free macrocycle is concomitant with the formation of the three isomeric forms of the complex *cis*-$[Ru(aphen)_2(CD_3CN)_2]^{2+}$ in the ratio 1(*a*,*a*)/2(*a*,*e*)/1(*e*,*e*). This experiment suggests that a photochemical isomerisation of the primary photo-product *cis*-[(*a*,*a*)$Ru(aphen)_2(CD_3CN)_2]^{2+}$ takes place at a similar or higher rate than that of the photosubstitution of the macrocycle m-36. A bis-phenanthroline ligand[19], that is able to stabilise the ruthenium core in a single isomeric form, is

Table 1. Luminescence Properties of the CH_3CN rigid matrix at 77 K

	$[Ru(phen)_2dmbp]^{2+}$ before irradiation	$[Ru(phen)_2dmbp]^{2+}$ after irradiation	**1** before irradiation	**1** after irradiation	$[Ru(phen)_2(CH_3CN)_2]^{2+}$
λ_{max}[a] (nm)	592, 644	545, 584, 625(sh)	584, 634	545, 584, 625(sh)	545, 584
τ[b] (μs)	2.7	3.0	5.7	3.0	3.0

[a] Band maxima from uncorrected emission spectra, excitation wavelengths are the maxima of the room temperature MLCT absorption spectra, namely 450 nm for $[Ru(phen)_2dmbp]^{2+}$ and **1** before irradiation and 420 nm for these compounds after irradiation and $[Ru(phen)_2(CH_3CN)_2]^{2+}$. [b] Excited state lifetimes, λ_{exc} = 337 nm.

needed to circumvent this undesirable process. Preliminary experiments show that no photoisomerisation occurs when the phenanthroline ligands are linked by a *p*-xylyl bridge. We are currently working on a ruthenium complex that incorporates both this bis-phenanthroline ligand and a bipy-based macrocycle.

Experimental Section

Physical Measurements: ^{1}H NMR spectra were obtained with Bruker WP200 SY (200 MHz), Bruker AM 400 and ARX 500(400 and 500 MHz, respectively) spectrometers. Chemical shifts reported are referenced to Me_4Si as an internal standard. All the photochemical and photophysical experiments were carried out in acetonitrile (Carlo−Erba for spectroscopy). The absorption spectra were recorded with a Perkin−Elmer λ5 spectrophotometer. Emission spectra were obtained with a Spex Fluorolog II spectrofluorimeter (continuous 150-W Xe lamp), equipped with a Hamamatsu R-928 photomultiplier tube. Excited state lifetimes were determined with an IBH single photon counting spectrometer equipped with a thyratron gated nitrogen lamp working in the 4−30 kHz range (λ_{exc} = 337 nm, 0.5 ns time resolution); the detector was a red-sensitive (185−850 nm) Hamamatsu R-3237−01 photomultiplier tube.

Photochemical reactions were performed as follows: dilute solutions of the complexes (about 2.5×10^{-5} M), were put into 1 cm path spectrophotometric cuvettes and irradiated under continuous stirring with a 150 W xenon lamp (Osram XBOW/1) at 404 nm using slits of 2.5 mm (9.4 nm) at the entrance and exit of a Spex 1681 0.22M monochromator. At the end of the photoreaction, after removing CH_3CN under vacuum, the orange residue was dried under vacuum to give, quantitatively, the complex $[Ru(phen)_2(CH_3CN)_2]^{2+}$ and the macrocycle.

Quantum yields of the photoreaction at 436 nm were obtained by measuring the intensity of the light source with the "micro-version" of the ferric oxalate actinometer.[20]

Synthesis of Ligands and Complexes

Some ligands and complexes were prepared following literature procedures: 3-chloro-1-(*p*-methoxyphenyl)propanone,[21] 6,6′-dimethyl-2,2′-bipyridine (6,6′-dmbp),[10] *cis*-$[Ru(phen)_2(CH_3CN)_2](PF_6)_2$,[12] $[Ru(phen)_2(6,6'\text{-dmbp})](PF_6)_2$.[7] All charged species were isolated as PF_6^- salts. The solvents were distilled over the appropriate drying agents.

4-(*p*-Anisyl)-1,10-phenanthroline (aphen): In a three-neck round-bottomed flask equipped with a reflux condenser and a thermometer, a mixture of 8-aminoquinoline (20.0 g, 0.139 mol), arsenic pentoxide As_2O_5 (18.7 g, 0.081 mol), concentrated H_2SO_4 (30 mL) and H_2O (10 mL) was heated to 100 °C under strong magnetic stirring. 3-chloro-1-(*p*-methoxyphenyl)propanone (39.0 g, 0.197 mol) was then added rapidly. The reaction mixture was heated at reflux for 2.5 h, and then poured onto ice and made alkaline with concentrated aqueous 7 M KOH. After addition of CH_2Cl_2, the organic phase was separated, the aqueous layer was extracted 5 times with CH_2Cl_2 (500 mL) and the combined organic layers were washed with water (3 times), then dried over $MgSO_4$. The black oil was collected by filtration, washed with CH_2Cl_2 and was purified by repeated chromatography (silica, CH_2Cl_2, eluent: CH_2Cl_2/MeOH, 97:3; alumina, hexane/ether, 50:50, eluent: CH_2Cl_2/MeOH, 95:5; alumina, ether/EtOAc, 50:50, eluent: CH_2Cl_2/MeOH, 99:1) and recrystallised from ethyl acetate. A sand-brown powder was isolated (10.0 g, 0.035 mol) in 25% yield. Sand-brown powder (m.p. 138 °C). ^{1}H NMR (CD_2Cl_2, 200 MHz): δ = 9.14 (dd, *J* = 4.18 and 1.48 Hz, 1 H, 9-H), 9.12 (d, *J* = 4.42 Hz, 1 H, 2-H), 8.26 (dd, *J* = 7.99 and 1.85 Hz, 1 H, 7-H), 7.75 (d, *J* = 9.10 Hz, 1 H, 5-H), 7.68 (d, *J* = 9.10 Hz, 1 H, 6-H), 7.64 (dd*J* = 7.99 and 4.31 Hz, 1 H, 8-H,), 7.55 (d, *J* = 4.66 Hz, 1 H, 3-H), 7.49 (d, *J* = 8.84 Hz, 2 H, H_o), 7.09, *J* = 8.86 Hz(d, 2 H, H_m), 3.90 (s, 3 H, Me) ppm. $C_{19}H_{14}N_{20}$: calcd. C 79.70, H 4.93, N 9.78; found C 78.74, H 5.05, N 8.23.

6,6′-Bis(γ-tetrahydropyranylpropyl)-2,2′-bipyridine (4): A 1.64 M *n*BuLi (14.0 mL, 23.0 mmol) solution was added dropwise to a solution of diisopropylamine (3.4 mL, 24.3 mmol) in THF (21 mL), under argon. A degassed solution of 6,6′-dmbp (2.0 g, 10.8 mmol) in anhydrous THF (20 mL) was cooled to − 78 °C and the freshly prepared LDA solution was added via a cannula. The solution turned from yellow to blue-purple and was stirred for a further 2 h at − 78 °C, after which the temperature was allowed to rise to 5 °C. The deep red solution was once again cooled to − 78 °C. Meanwhile, a solution of tetrahydropyrannyl-2-bromoethyl-ethyl (4.7 g, 24.0 mmol) in anhydrous THF (5 mL) was cooled to − 78 °C and degassed. This solution was then transferred, under argon, to the solution of 6,6′-dmbp at − 78 °C and the mixture turned deep green. The solution was then stirred for 16 h at room temperature. The clear orange-brown solution was hydrolysed with water (80 mL) and turned yellow. After the solvent was removed and the residue treated with CH_2Cl_2, the organic layers were washed with water, dried over $MgSO_4$, and the solvent was evaporated. The resulting orange oil was purified by column chromatography on alumina (eluent: hexane/diethyl ether, 50:50). The product was obtained in 63% yield (3.0 g, 6.8 mmol). Yellow oil. ^{1}H NMR (CD_2Cl_2, 200 MHz): δ = 8.26 (dd, *J* = 7.87 Hz, 0.99 Hz, 2 H, 3,3′-H), 7.71 (t, *J* = 7.74 Hz, 2 H, 4,4′-H), 7.18 (dd, *J* = 7.60 and 0.99 Hz, 2 H, 5,5′-H), 4.57 (t, *J* = 3.44 Hz, 2 H, H_a), 3.80 (m, 4 H, H_e), 3.41 (m, 4 H, Hγ), 2.93 (t, *J* = 7.75 Hz, 4 H, H_α), 2.12 (m, 4 H, H_β), 1.59 (m, 12 H, $H_{b,c,d}$) ppm.

6,6′-Bis(γ-hydroxypropyl)-2,2′-bipyridine (5): The bipyridine derivative **4** (2.90 g, 6.61 mmol) was dissolved in 95% EtOH (45 mL) and heated to reflux. A spatula of *p*-toluenesulfonic acid (1.27 g, 6.54 mmol) was then added. The reaction was followed by TLC (SiO_2, eluent: CH_2Cl_2/5% MeOH) and the reflux was maintained for 4 h. Additional aliquots of acid (0.80 g, 4.12 mmol) were added and the solution was refluxed for a further 4 h. The ethanol was then removed and the residue was dissolved in a CH_2Cl_2/H_2O mixture. After neutralisation by an aqueous solution of K_2CO_3, the aqueous phase was extracted 3 times with CH_2Cl_2 and the organic layers were washed with water, dried over $MgSO_4$, filtered and the solvent evaporated. The crude mixture was purified by column chromatography on silica (eluent: CH_2Cl_2/MeOH, 94.5:5.5) to give the product (1.24 g, 4.55 mmol) in 69% yield. Yellow oil. ^{1}H NMR (CD_2Cl_2, 200 MHz): δ = 8.09 (dd, *J* = 7.75 Hz, 0.61 Hz, 2 H, 3,3′-H), 7.75 (t, *J* = 7.74 Hz, 2 H, 4,4′-H), 7.21 (dd, *J* = 7.75 Hz, 0.87 Hz, 2 H, 5,5′-H), 3.90 (br. s, 2 H, OH), 3.68 (t, *J* = 5.91 Hz, 4 H, H_γ), 3.01 (t, *J* = 6.89 Hz, 4 H, H_α), 2.01 (m, 4 H, H_β) ppm.

Bis-THP Derivative of 2,2′-Bipyridine (6): A degassed solution of **5** (1.19 g, 4.36 mmol) in DME (25 mL) was added dropwise at 0 °C under argon to a suspension of NaH (0.60 g, 13.7 mmol) in DME (50 mL) for 40 min, upon which the mixture turned white. The ice bath was removed and at room temperature a degassed solution of 2-[2-(chloroethoxy)ethoxy)]ethoxy}tetrahydro-2*H*-pyran (3.64 g, 14.40 mmol) in DME (35 mL) was added dropwise to the mixture which was then heated at 50 °C for 3 h after which the temperature

was increased and the reaction heated at reflux for 14 h. The reaction was monitored by TLC (Alumina, eluent: CH_2Cl_2/5% MeOH). More NaH (0.21 g, 4.80 mmol) and a solution of tetrahydropyrannyl derivative (2.00 g, 7.91 mmol) in DME (20 mL) was added. The reaction mixture was maintained under reflux under argon for a further 34 h, then it was cooled to 0 °C. Excess NaH was neutralised by the gradual addition of EtOH until no further evolution of gas was observed (12 mL overall). The solvent was then evaporated and the residue was dissolved in a 1:1 H_2O/CH_2Cl_2 mixture. The organic layer was separated, and the aqueous layer was extracted 4 times with CH_2Cl_2. The organic layers were combined, washed with water, dried over $MgSO_4$ and filtered. Following evaporation of the solvent, the orange oil was purified twice by column chromatography on alumina eluting with a CH_2Cl_2/MeOH mixture (98.7:1.3; 99.9:0.1). Pure **6** was isolated (0.65 g, 0.92 mmol) along with a mixture of the starting material and of the monosubstituted product (1.30 g) which was treated as follows. This mixture was added to a suspension of DMSO (10 mL) containing KOH powder (3.16 g, 47.60 mmol). To this orange-brown solution, tetrahydropyrannyl derivative (4.81 g, 19.04 mmol) was added and the stirring was maintained for 3.5 h.. The mixture was then heated at 50 °C for 35 min. After cooling and addition of H_2O/CH_2Cl_2, the organic phase was separated and the aqueous phase was extracted with $CHCl_3$ (twice, 150 mL) and also CH_2Cl_2 (twice, 150 mL). The combined organic layers were washed, dried over $MgSO_4$, filtered and the solvents evaporated. The crude oil was purified four times by column chromatography on alumina (CH_2Cl_2/MeOH, 98:0.2; 99.6:0.4) to give pure **7** (0.99 g, 1.41 mmol). The overall yield of **7** (1.64 g, 2.33 mmol) from the two reactions was 53%. Colourless oil. ^{1}H NMR ($CDCl_3$, 200 MHz): δ = 8.23 (d, *J* = 7.51 Hz, 2 H, 3,3′-H), 7.68 (t, *J* = 7.75 Hz, 2 H, 4,4′-H), 7.14 (d, *J* = 7.62 Hz, 2 H, 5,5′-H), 4.62 (t, *J* = 3.32 Hz, 2 H, H_a), 3.84 (m, 4 H, H_e), 3.64 (m, 24 H, 6 × $-CH_2-CH_2-$), 3.55 (t, 4 H, H_γ), 2.92 (t, *J* = 7.63 Hz, 4 H, H_α), 2.11 (tt, 4 H, H_β), 1.90−1.30 (m, 12 H, 4 H_b, 4 H_c, 4 H_d) ppm.

2,2'-Bipyridine 7: 6 (1.62 g, 2.30 mmol) was heated to reflux in 95% EtOH (16 mL) and then *p*-toluenesulfonic acid (0.45 g, 2.30 mmol) was added. The reaction was followed by TLC (SiO_2; eluent: CH_2Cl_2/5% MeOH) and reflux was maintained for 27 h. After evaporation of the solvent, the residue was dissolved in a CH_2Cl_2/H_2O mixture and neutralised with an aqueous solution of $NaHCO_3$. The aqueous phase was extracted 3 times with CH_2Cl_2 and the organic layers were combined, washed with water, dried over $MgSO_4$ and the solvent was evaporated. **6** was isolated (1.03 g, 1.92 mmol) in 84% yield and was used without further purification (purity > 95% by NMR). Colourless oil. ^{1}H NMR ($CDCl_3$, 200 MHz): δ = 8.23 (d, *J* = 7.25 Hz, 2 H, 3,3′-H), 7.69 (t, *J* = 7.75 Hz, 2 H, 4,4′-H), 7.15 (dd, *J* = 7.64 and 0.77 Hz, 2 H, 3,3′-H), 3.80−3.52 (m, 26 H, 2 × −OH, 6 × $-CH_2-CH_2-$), 3.56 (m, 4 H, H_γ), 2.92 (t, *J* = 7.63 Hz, 4 H, H_α), 2.12 (tt, 4 H, H_β) ppm.

3: In a degassed solution of **7** (1.03 g, 1.92 mmol) in DME (45 mL), NaH (0.93 g, 21.3 mmol) was added with a spatula and the mixture was heated to 50 °C. Allyl bromide (16 mL, 181.00 mmol) was then added via the cannula transfer technique. The reaction mixture was heated at reflux for 20 h and then monitored by TLC (Alumina; CH_2Cl_2/5% MeOH). The white solution was cooled to 0 °C and excess NaH was neutralised by adding small portions (3 mL) of absolute ethanol until there was no further evolution of gas. The solvent was then evaporated and the residue dissolved in a CH_2Cl_2/H_2O (1:1) mixture. The organic phase was separated and the aqueous phase was extracted 4 times with CH_2Cl_2. The organic phases were combined, washed with H_2O and dried over $MgSO_4$. After filtration of the solution and removal of the solvent, the oily residue was purified twice by column chromatography on alumina (eluent: CH_2Cl_2/MeOH, 99.5:0.5) to afford **3** (0.89 g, 1.44 mmol) in 75% yield. Pale yellow oil. ^{1}H NMR ($CDCl_3$, 200 MHz): δ = 8.24 (d, *J* = 7.86 Hz, 2 H, 3,3′-H), 7.68 (t, *J* = 7.75 Hz, 2 H, 4,4′-H), 7.14 (dd, *J* = 7.62 and 0.98 Hz, 2 H, 5,5′-H), 5.91 (ddt, *J* = 17.22, 10.32 and 5.66 Hz, 2 H, H′), 5.26 (dtd, *J* = 17.10, 3.44 and 1.60 Hz, 2 H, H_t), 5.16 (m, *J* = 10.32, 1.72 and 1 Hz, 2 H_c), 4.01 (dt, *J* = 5.66 and 1.36 Hz, 4 H, H_g), 3.67−3.50 (m, 28 H, $H_{a,b,c,d,e,f}$, 4 H_γ), 2.92 (t, *J* = 7.50 Hz, 4 H, H_α), 2.11 (tt, *J* = 6.52 and 6.88 Hz, 4 H_β) ppm. FAB-MS for $C_{34}H_{52}N_2O_8$: *m*/*z* = 617.5 $[M + H]^+$, calcd. 617.4, 100%.

***cis*-[Ru(aphen)$_2$Cl$_2$]:** Following the complete dissolution of complex $[Ru(CH_3CN)_4Cl_2]$ (410.0 mg, 1.22 mmol) in a degassed solution of 1,2-dichloroethane (130 mL), the ligand aphen (684.0 mg, 2.39 mmol) was added and the orange-brown mixture was heated at reflux for 2 h. After evaporation of the solvent, the purple-brown residue was purified twice by flash chromatography on silica gel (Silica gel 60, 0.063−0.200 mm, Merck 7734) eluting with EtOH. The mixture of isomeric complexes *cis*-$[Ru(aphen)_2Cl_2]$ was obtained in 46% yield (412.5 mg, 0.55 mmol). The complexes obtained were purple in colour.

Separation of the Three Isomers of *cis*-[Ru(aphen)$_2$Cl$_2$]

The three isomers (460 mg, 0.620 mmol) were separated 13 times by flash chromatography on alumina (aluminium oxide 90, acidic, activity I, 0.063−0.200 mm, Merck 1078). The eluent was a mixture of CH_2Cl_2/MeOH (3%). The purple isomer **(*a*,*a*)**, which migrates as the first band, (100 mg, 0.134 mmol) was isolated as 87% of the theoretical yield (25%).

Isomer (*a*,*a*): ^{1}H NMR (CD_2Cl_2, 400 MHz): δ = 10.50 (d, *J* = 5.56 Hz, 2 H, 2-H), 8.23 (, *J* = 9.04 Hz d, 2 H, 5-H), 7.98 (d, *J* = 5.52 Hz, 2 H, 3-H), 7.97 (dd, *J* = 7.96 and 1.12 Hz, 2 H, 7-H), 7.93 (dd, *J* = 5.44 and 1.00 Hz, 2 H, 9-H), 7.88 (d, *J* = 9.28 Hz, 2 H, 6-H), 7.71 (d, *J* = 8.64 Hz, 4 H, H_o), 7.21 (d, *J* = 8.60 Hz, 4 H, H_m), 7.19 (m, 2 H, 8-H), 3.96 (s, 6 H, 2 Me) ppm. UV/Vis (CH_2Cl_2): λ = 553 (7400) nm. **Isomer (*a*,*e*):** ^{1}H NMR (CD_2Cl_2, 200 MHz): δ = 10.43 (m, 2 H, 2-H_a, 9-H_e), 8.43 (dd, *J* = 8.12 Hz, 1 H, 7-H_e), 8.23 (d, *J* = 9.10 Hz, 1 H, 5-H_a), 8.04 (dd, 2 H, 5-H_e, 6-H_e), 8.00−7.85 (m, 4 H, 3-H_a, 7-H_a, 9-H_a, 8-H_e), 7.86 (d, *J* = 9.10 Hz, 1 H, 6-H_a), 7.70 (d, *J* = 8.86 Hz, 2 H, $H_{o,a}$), 7.70 (m, 1 H, 2-H_e), 7.38 (d, *J* = 8.86 Hz, 2 H, $H_{o,e}$), 7.20 (d, *J* = 8.86 Hz, 2 H, $H_{m,a}$), 7.19 (m, 2 H, 8-H_a, 3-H_e), 7.04 (d, *J* = 8.86 Hz, 2 H, $H_{m,e}$), 3.95 (s, 3 H, Me a), 3.86 (s, 3 H, Me_e) ppm. UV/Vis (CH_2Cl_2): λ = 550 (9200) nm. **Isomer (*e*,*e*):** ^{1}H NMR (CD_2Cl_2, 400 MHz): δ = 10.48 (m, 2 × 9-H), 8.43 (d, *J* = 7.72 Hz, 2 H, 7-H), 8.06 (d,*J* = 8.80 Hz, 2 H, 6-H), 8.03 (, *J* = 9.16 Hz d, 2 H, 5-H), 8.01 (m, 2 H, 8-H), 7.71 (d, *J* = 8.80 Hz, 2 H, 2-H), 7.38 (dd, *J* = 8.44 Hz, 4 H, H_o), 7.20 (d, *J* = 8.80 Hz, 2 H, 3-H), 7.04 (d, *J* = 8.44 Hz, 4 H, H_m), 3.86 (s, 6 H, 2 Me) ppm. UV/Vis (CH_2Cl_2): λ = 547 (5800) nm.

***cis*-[(*a*,*a*)Ru(aphen)$_2$(CH$_3$CN)$_2$](PF$_6$)$_2$:** In a round bottomed flask, *cis*-[(*a*,*a*)Ru(aphen)$_2$Cl$_2$] (80 mg, 0.107 mmol) was heated at reflux under argon in a mixture of CH_3CN/H_2O 50:50 (12 mL) for 2.5 h. After cooling to room temperature, a saturated solution of aqueous KPF_6 (10 mL) and CH_3CN (5 mL) were added. The evaporation of the solvent caused a brown-orange solid to precipitate that was separated by filtration, washed with water and diethyl ether and then air-dried. *cis*-[(*a*,*a*)Ru(aphen)$_2$(CH$_3$CN)$_2$](PF$_6$)$_2$ was obtained in a yield of 45% (50 mg, 0.048 mmol). Brown-orange powder. ^{1}H NMR (CD_2Cl_2, 200 MHz): δ = 9.76 (d, *J* = 5.40 Hz, 2 H, 2-H), 8.38 (d, *J* = 9.10 Hz, 2 H, 5-H), 8.35 (dd, *J* = 8.36 Hz, 1.24 Hz, 2

H, 7-H), 8.20 (d, J = 5.42 Hz, 2 H, 3-H), 8.04 (d, J = 9.10 Hz, 2 H, 6-H), 7.87 (dd, J = 5.41 and 1.23 Hz, 2 H, 9-H), 7.76 (d, J = 8.84 Hz, 4 H, H_o), 7.50 (dd, J = 5.29 and 8.25 Hz, 2 H, 8-H), 7.25 (d, J = 8.60 Hz, 4 H, H_m), 3.97 (s, 6 H, 2 Me) ppm.

Compound 8: A stoichiometric mixture of *cis*-$[Ru(phen)_2(CH_3CN)_2](PF_6)_2$ (69.7 mg, 0.084 mmol) and **3** (51.8 mg, 0.084 mmol) was heated at 140 °C in degassed ethylene glycol (6 mL) for 2 h. After cooling to room temperature, water (8 mL) and then a saturated solution of aqueous KPF_6 (6 mL) were added. The precipitate obtained was collected by filtration and washed with water and diethyl ether. The crude product was purified by chromatography on silica gel eluting with an acetone/water/aqueous saturated KNO_3 (100:4:2) mixture. The cation was precipitated from the eluent by addition of an aqueous solution of KPF_6 and the resultant solid was filtered off to give **8** (86.2 mg, 0.063 mmol) in 75% yield. Red compound. ^{1}H NMR ([D$_6$]acetone, 200 MHz): δ = 8.94 (dd, J = 8.15 and 1.10 Hz, 2 H, 4-H), 8.74 (dd, J = 5.17 and 1.22 Hz, 2 H, 2-H), 8.67 (dd, J = 8.35 and 1.22 Hz, 2 H, 7-H), 8.63 (d, J = 8.86 Hz, 2 H, 3,3′-H), 8.47 (d, J = 8.86 Hz, 2 H, 5-H), 8.38 (d, J = 8.86 Hz, 2 H, 6-H), 8.10 (dd, J = 7.86 and 7.88 Hz, 2 H, 4,4′-H), 8.10 (dd, J = 5.23 and 8.24 Hz, 2 H, 3-H), 7.97 (dd, J = 5.40 and 1.23 Hz, 2 H, 9-H), 7.62 (dd, J = 5.28 and 8.24 Hz, 2 H, 8-H), 7.44 (dd, J = 7.87 and 0.99 Hz, 2 H, 5,5′-H), 5.82 (, J = 17.34, 10.44 and 5.23 Hz ddt, 2 H, H′), 5.18 (m, 2 H, H_t), 5.04 (m, 2 H, H_c), 3.88 (dt, J = 5.42 and 1.54 Hz, 4 H, H_g), 3.60−3.20 (m, 24 H, $H_{a,b,c,d,e,f}$), 3.20−1.00 (12 H, $H_{\alpha,\beta,\gamma}$) ppm.

$[Ru(phen)_2(m\text{-}36)](PF_6)_2$ (1): To a degassed Schlenk containing **8** (117.0 mg, 0.086 mmol) and the catalyst (Grubbs ruthenium(II) carbene: [Ru], (Scheme 2), 4.9 mg, 7% mol), freshly distilled and degassed CH_2Cl_2 (8.5 mL) was added via a cannula to obtain a 0.01 M solution. This mixture was stirred at room temperature for 18 h during which a syringe needle was periodically inserted into the reaction vessel to allow the ethylene gas to escape. The reaction was monitored by ^{1}H NMR spectroscopy. A further 7 mol percent of the catalyst was added and further solvent was added in order to maintain the desired concentration of the reaction mixture. The stirring was continued for 5 days. The solvent was then evaporated and the crude product was purified by chromatography on silica gel (eluent: acetone/H_2O/KNO_3, 100:5:2). Pure **1** was isolated (77.2 mg, 0.058 mmol) in 67% yield. Red compound. ^{1}H NMR ([D$_6$]acetone, 200 MHz): δ = 8.94 (dd, J = 8.36 and 1.24 Hz, 2 H, 4-H), 8.76 (dd, J = 5.41 and 1.23 Hz, 2 H, 2-H), 8.68 (dd, J = 8.37 and 1.23 Hz, 2 H, 7-H), 8.62 (d, J = 7.38 Hz, 2 H, 3,3′-H), 8.47 (d, J = 8.86 Hz, 2 H, 5-H), 8.38 (d, J = 8.86 Hz, 2 H, 6-H), 8.09 (dd, J = 8.12 and 7.14 Hz, 2 H, 4,4′-H), 8.09 (dd, 2 H, 3-H), 7.92 (dd, J = 5.29 and 1.11 Hz, 2 H, 9-H), 7.67 (dd, J = 5.42 and 8.12 Hz, 2 H, 8-H), 7.43 (d, J = 7.88 Hz, 2 H, 5,5′-H), 5.39 (m, 2 H, $H_{cis,}$ 75%), 5.31 (m, 2 H, $H_{trans,}$ 25%), 3.90−1.50 (m, 40 H, H_g, $H_{a,b,c,d,e,f}$, $H_{\alpha,\beta,\gamma}$) ppm. FAB-MS for $RuC_{56}H_{64}N_6O_8P_2F_{12}$: m/z = 1195.3 $[M - PF_6]^+$, calcd. 1195.3, 8%; 1049.3 $[M - 2\ PF_6 + e^-]^+$, calcd. 1050.3, 11%; 462.0 $[M - 2\ PF_6 - m_{36} + e^-]^+$, calcd. 462.0, 32%. UV/Vis (CH_3CN): 450 nm (9200).

9: A stoichiometric mixture of *cis*-[(*a*,*a*)Ru(aphen)$_2$(CH$_3$CN)$_2$](PF$_6$)$_2$ (50.0 mg, 0.048 mmol) and **3** (29.5 mg, 0.084 mmol) was heated at 140 °C in degassed ethylene glycol (7 mL) for 2.5 h. After cooling to room temperature, water (5 mL) and then a saturated solution of aqueous KPF_6 (10 mL) were added. The precipitate obtained was collected by filtration and washed with water and diethyl ether. The crude product **9** was isolated (68.8 mg, 0.044 mmol) and was used without further purification. Red compound. FAB-MS for $RuC_{72}H_{80}N_6O_{10}P_2F_{12}$: m/z = 1435.3 $[M - PF_6]^+$, calcd. 1435.4, 5%, 1289.4 $[M - 2\ PF_6 + e^-]^+$, calcd. 1290.5, 6%; 674.1 $[M - 2\ PF_{6-}$**3** $+ e^-]^+$, calcd. 674.1, 46%.

$[Ru(aphen)_2(m\text{-}36)](PF_6)_2$ (2): To a degassed Schlenk containing **9** (68.8 mg, 0.044 mmol) and the catalyst [Ru], 3 mg, 8% mol), freshly distilled and degassed CH_2Cl_2 (5 mL) was added via a cannula to obtain a 0.01 M solution. This mixture was stirred at room temperature for one day during which a syringe needle was periodically inserted into the reaction vessel to allow the escape of ethylene gas. A further 9 mol percent of the catalyst (3.5 mg) was added and after 4 days further solvent added in order to maintain the desired concentration of the reaction mixture. Further catalyst (5 mg, 14% mol) was added. The stirring was continued for 1 day (overall duration of reaction: 6 days). The solvent was then evaporated and addition of water (3 mL) and a saturated solution of aqueous KPF_6 (5 mL) allowed the precipitation of a crude product which was collected by filtration, washed with water and diethyl ether and was purified by chromatography (silica, eluent: acetone/H_2O/KNO_3, 100:7:0.7; alumina, eluent: toluene/CH_3CN 35:65; alumina, eluent: toluene/CH_3CN, 40:60). **2,** not completely pure, was isolated (30.4 mg, 0.020 mmol) in 45% yield. Preparative chromatography on silica (eluent: $CH_3CN/H_2O/KPF_6$, 100:10:2), performed twice, afforded pure **2**. Red compound. ^{1}H NMR (CD_3CN, 500 MHz): δ = 8.45 (dd, J = 8.25 and 1.15 Hz, 2 H, 7-H), 8.42 (dd, J = 5.55 Hz, 2 H, 2-H), 8.36 (d, J = 9.55 Hz, 2 H, 3,3′-H), 8.34 (d, J = 9.10 Hz, 2 H, 5-H), 8.16 (d, J = 9.25 Hz, 2 H, 6-H), 7.97 (dd, J = 7.85 and 8.15 Hz, 2 H, 4,4′-H), 7.80 (d, J = 5.55 Hz, 2 H, 3-H), 7.74 (dd, J = 5.32 and 1.17 Hz, 2 H, 9-H), 7.67 (d, J = 8.75 Hz, 4 H, H_o), 7.46 (dd, J = 5.37 and 8.17 Hz, 2 H, 8-H), 7.29 (d, J = 7.85 Hz, 2 H, 5,5′-H), 7.23 (d, J = 8.95 Hz, 4 H, H_m), 5.34 (m, 2 H, H_c), 5.21 (m, 2 H, H_t), 3.92 (s, 6 H, 2 OMe), 4.30−0.08 (m, 40 H, $H_{a,b,c,d,e,f,g,\alpha,\beta,\gamma}$) ppm. FAB-MS for $RuC_{70}H_{76}N_6O_{10}P_2F_{12}$: m/z = 1407.2 $[M - PF_6]^+$, calcd. 1407.4, 8%; 1262.3 $[M - 2\ PF_6 + e^-]^+$, calcd. 1262.4, 9%; 674.0 $[M - 2\ PF_6$ − m-36 $+ e^-]^+$, calcd. 674.1, 78%. UV/Vis (CH_3CN): λ = 457 (9700) nm.

Acknowledgments

This work was supported by the French CNRS and the Italian CNR. We thank the European Commission COST programme D11/0004/98, the French Ministry of Education, Research and Technology for a fellowship to A.C.L., and the Italian MIUR for a fellowship to G.A. (Progetto 5%). We are also grateful to Johnson Matthey for a loan of $RuCl_3$.

[1] [1a] J.-P. Collin, C. O. Dietrich Buchecker, P. Gaviña, M. C. Jimenez-Molero, J.-P. Sauvage, *Acc. Chem. Res.* **2001**, *34*, 477−487. [1b] V Balzani, A. Credi, F. M. Raymo, J. F. Stoddart, *Angew. Chem. Int. Ed.* **2000**, *39*, 3348−3391. [1c] N. Armaroli, *Chem. Soc. Rev.* **2001**, *30*, 113−124.

[2] J.-P. Sauvage, *Acc. Chem. Res.* **1998**, *31*, 611−619.

[3] [3a] J. Howard, *Nature* **1997**, *389*, 561−567. [3b] T. El ston, H. Wang, G. Oster, *Nature* **1998**, *391*, 510−513.

[4] T. R. Kelly, H. De Silva, R. A. Silva, *Nature* **1999**, *401*, 150−152.

[5] [5a] R. Ballardini, V. Balzani, M. T. Gandolfi, L. Prodi, M. Venturi, D. Philp, H. G. Ricketts, J. F. Stoddart, *Angew. Chem. Int. Ed. Engl.* **1993**, *32*, 1301−1303. [5b] A. Livoreil, J.-P. Sauvage, N. Armaroli, V. Balzani, L. Flamigni, B. Ventura, *J. Am. Chem. Soc.* **1997**, *119*, 12114−12124. [5c] N. Armaroli, V. Balzani, J.-P. Collin, P. Gaviña, J.-P. Sauvage, B. Ventura, *J. Am. Chem. Soc.* **1999**, *121*, 4397−4408.

[6] N. Koumura, R. W. J. Zijlstra, R. A. Van Delden, N. Harada, B. L. Feringa, Nature **1999**, *401*, 152−155.

[7] A.-C. Laemmel, J.-P. Collin, J.-P. Sauvage, *Eur. J. Inorg. Chem.* **1999**, 383−386.

[8] [8a] J. Van Houten, R. J. Watts, *Inorg. Chem.* **1978**, *17*, 3381−3385. [8b] B. Durham, J. V. Caspar, J. K. Nagle, T. J. Meyer, *J. Am. Chem. Soc.* **1982**, *104*, 4804−4810.
[9] J.-P. Collin, A.-C. Laemmel, J.-P. Sauvage, *New J. Chem.* **2001**, *25*, 22−24.
[10] G. R. Newkome, D. C. Pantaleo, W. E. Puckett, P. L. Ziefle, W. A. Deutsh, *J. Inorg. Nucl. Chem.* **1981**, *43*, 1529−1531.
[11] E. Baranoff, J.-P. Collin, J. Furusho, Y. Furusho, A.-C. Laemmel, J.-P. Sauvage, *Inorg. Chem.* **2002**, *41*, 1215−1222.
[12] P. Bonneson, J. L. Walsh, W. T. Pennington, A. W. Cordes, B. Durham, *Inorg. Chem.* **1983**, *22*, 1761−1765.
[13] G. F. Strouse, P. A. Anderson, J. R. Schoonover, T. J. Meyer, F. R. Keene, *Inorg. Chem.* **1992**, *31*, 3004−3006.
[14] J. A. Treadway, T. J. Meyer, *Inorg. Chem.* **1999**, *38*, 2267−2278.
[15] H. Mürner, P. Belser, A. von Zelewsky, *J. Am. Chem. Soc.* **1996**, *118*, 7989−7994.
[16] [16a] P. Schwab, M. B. France, J. W. Ziller, R. H. Grubbs, *Angew. Chem. Int. Ed. Engl.* **1995**, *34*, 2039−2041. [16b] P. Schwab, R. H. Grubbs, J. W. Ziller, *J. Am. Chem. Soc.* **1996**, *118*, 100−110.
[17] [17a] M. Weck, B. Mohr, J.-P. Sauvage, R. H. Grubbs, *J. Org. Chem.* **1999**, *64*, 5463−5471. [17b] C. O. Dietrich-Buchecker, G. Rapenne, J.-P. Sauvage, *Chem. Commun.* **1997**, 2053−2054. [17c] G. Rapenne, C. O. Dietrich-Buchecker, J.-P. Sauvage, *J. Am. Chem. Soc.* **1999**, *121*, 994−1001.
[18] A. Juris, V. Balzani, F. Barigelletti, S. Campagna, P. Belser, A. von Zelewsky, *Coord. Chem. Rev.* **1988**, *84*, 85−277.
[19] D. Pommeranc, V. Heitz, J.-C. Chambron, J.-P. Sauvage, *J. Am. Chem. Soc.* **2001**, *123*, 12215−12221.
[20] E. Fisher, *EPA NewsL* July **1983**, 33.
[21] P. C. Alford, M. J. Cook, A. P. Lewis, G. S. G. McAuliffe, V. Skarda, A. J. Thomson, J. L. Glasper, D. J. Robbins, *J. Chem. Soc., Perkin Trans. 2* **1985**, 705−709.

Received May 31, 2002
[I02286]

Change in the Spin State of an Fe^{III} Center upon One N-to-O Switch in the Coordination of a 2,6-Pyridinedicarboxamido Unit: The Effect of Methyl Thioether and Methyl Ether Appendages at the Ligand Periphery

Todd C. Harrop,[a] Laurie A. Tyler,[a] Marilyn M. Olmstead,[b] and Pradip K. Mascharak*[a]

Keywords: Iron / N ligands / S ligands / Spin states / EPR spectroscopy

Two ligands bearing the 2,6-pyridinedicarboxamide unit, namely $PyPSMeH_2$ and $PyPOMeH_2$, have been used to prepare complexes of Fe^{III} which have been structurally characterised. The potentially pentadentate thioether ligand $PyPSMeH_2$ affords only the bis complex $(Et_4N)[Fe(PyPSMe)_2]$ (**1**), irrespective of the metal to ligand ratio, due to the weak affinity of the thioether groups for the Fe^{III} center. In $[Fe(PyPSMe)_2]^-$, the two $PyPSMe^{2-}$ ligands bind to the iron center in a *mer* fashion and steric crowding among the pendant thioether groups forces one of the four deprotonated carboxamido moieties to bind to the Fe^{III} center through the carbonyl oxygen, giving rise to an FeN_5O chromophore. The tridentate ligand $PyPOMeH_2$, in its deprotonated form, also gives rise to a bis complex, $(Et_4N)[Fe(PyPOMe)_2]$ (**2**), in which the two $PyPOMe^{2-}$ ligands bind to the iron center in a *mer* fashion. In this case, however, less steric crowding among the smaller pendant ether groups allows binding of all four carboxamido nitrogens to the Fe^{III} center in $[Fe(PyPOMe)_2]^-$ giving rise to an FeN_6 chromophore. This one N-to-O switch in donor atom makes the two complexes **1** and **2** very different. While complex **2** is low spin (g = 2.18, 1.94) much like the other reported Fe^{III} bis complexes with two ligated 2,6-pyridinedicarboxamido units, complex **1** is high spin (g = 4.3). The spin flip due to a switch in only one N or O donor atom in these two complexes is unprecedented. The two complexes also exhibit different stability towards water.

(© Wiley-VCH Verlag GmbH & Co. KGaA, 69451 Weinheim, Germany, 2003)

Introduction

In recent years, coordination of carboxamido nitrogen(s) to iron centers and the spectroscopic, redox and reactivity properties of the resulting complexes have received much interest following the discovery of iron$-N_{amido}$ (N_{amido} = carboxamido N) bonds in nitrogenase[1] and nitrile hydratase.[2,3] Initially, this type of coordination was thought to be highly unlikely since Fe^{III} rapidly precipitates out as its hydroxide at much lower pH values than that required for the deprotonation of carboxamido nitrogens.[4] During the past ten years, however, research by us,[5−10] and others[11−15] has demonstrated that coordination of carboxamido nitrogens to Fe^{III} centers can afford sufficiently stable and isolable complexes. Indeed, coordination of this group results in highly negative $E_{1/2}$ values (up to −1.10 V) indicating that carboxamido nitrogens provide significant stability to iron in the +3 oxidation state.[7] Furthermore, the majority of Fe^{III} complexes coordinated to one, two, or four carboxamido nitrogens contain low spin Fe^{III} centers.[7,8,9] In addition, it appears that Fe^{III} complexes with $Fe^{III}-N_{amido}$ bonds are resistant toward hydrolysis despite the common belief that the highly basic carboxamido nitrogens could be readily attacked by water. Collectively, these results indicate that carboxamido nitrogens have a high affinity for Fe^{III} centers and impart stability towards hydrolysis of the resultant complexes.

Coordination of designed ligands with built-in 2,6-pyridinedicarboxamido unit (Figure 1) to Fe^{III} centers has resulted in complexes with novel structures and properties.[5,6,9,11,15] Recent work in this laboratory has afforded a variety of Fe^{III} complexes based on this tridentate moiety in the first coordination sphere.[5,6,10] For example, coordination of the pentadentate ligand $POPyH_4$ to Fe^{III} (H represents dissociable amide protons) results in high-spin, seven-coordinate, pentagonal bipyramidal complexes with the entire ligand in the basal plane and with two exogenous axial ligands (structure i, Figure 2).[6] In contrast, the Fe^{III} complex of the similar pentadentate ligand $PyPSH_4$ is high spin, five-coordinate with a distorted trigonal bipyramidal geometry due to the steric bulk of the thiolato sulfur (structure ii, Figure 2).[10] It is interesting to note that the potentially pentadentate ligands Py_3PH_2 and $MePy_3PH_2$ invariably afford six-coordinate bis complexes in which the two ligands are coordinated to the Fe^{III} center through the 2,6-pyridinedicarboxamido moiety with *unbound* pendant

[a] Department of Chemistry and Biochemistry, University of California,
Santa Cruz, CA 95064, USA
Fax: (internat.) +1-831/459-2935
E-mail: pradip@chemistry.ucsc.edu
[b] Department of Chemistry, University of California,
Davis, CA 95616, USA

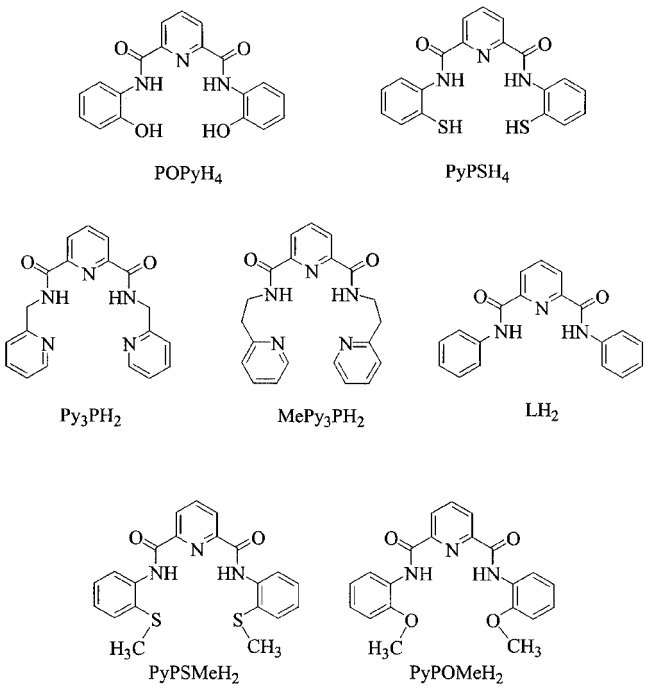

Figure 1. Ligands with the 2,6-pyridinedicarboxamide moiety (P stands for the peptide functionality in all abbreviations)

pyridine groups (structure iii, Figure 2).[5] The Fe^{III} centers in both of these complexes are low spin, much like the Fe^{III} complex of LH_2, namely $[FeL_2]^-$, reported by Mukherjee and co-workers.[11] The failure of the pendant pyridine units to bind to the Fe^{III} centers in these complexes is not related to any steric effect, since Py_3PH_2 gives rise to many $[Co(Py_3P)(L)]^{+/0}$ complexes.[16] We believe that formation of the bis complex $[Fe(Py_3P)_2]^-$ instead of $[Fe(Py_3P)(L)]^{+/0}$ with weak Fe^{III}-py interactions is a result of the high stability derived from coordination of four carboxamido nitrogens.

In order to elucidate the effect(s) of steric hindrance on the mode of coordination of carboxamido nitrogens to Fe^{III} centers and the spin-states of the resulting complexes, we have synthesized additional ligands with the 2,6-pyridinedicarboxamide moiety. The two designed ligands employed in this study are the potentially pentadentate ligand $PyPSMeH_2$ and the tridentate ligand $PyPOMeH_2$. Although $PyPSMeH_2$ is expected to bind to iron much like $PyPSH_4$, we report here that the deprotonated form, $PyPSMe^{2-}$, coordinates to Fe^{III} in a bis fashion irrespective of the ligand to Fe ratio and in the resulting complex, $(Et_4N)[Fe(PyPSMe)_2]$ (**1**), all the thioether groups remain unbound. Clearly, thioether sulfur (like pyridine nitrogen) is not a good donor for Fe^{III} and hence $PyPSMeH_2$ behaves like Py_3PH_2. It is also interesting to note that due to the steric repulsion among the pendant thioether groups in **1**, one of the carboxamido groups employs the carbonyl oxygen instead of the carboxamido nitrogen, as a donor atom, resulting in an FeN_5O chromophore. As a result of this N-to-O donor switch around the Fe^{III} center in **1**, the complex is high spin, which is in contrast to other similar bis complexes with two bound 2,6-pyridinedicarboxamido units (FeN_6 chromophore and all low spin).[5,11] In order to further substantiate our hypothesis that the steric repulsion among the pendant thioether groups in **1** is responsible for this N-to-O donor switch, we have also synthesized the bis Fe^{III} complex of the tridentate ligand $PyPOMeH_2$. The pendant ether groups in $(Et_4N)[Fe(PyPOMe)_2]$ (**2**) give rise to steric hindrance around the Fe^{III} center much like the crowding in **1**. As shown later, the structure of **2** is very similar to that of **1** except for the crucial fact that the extent of the steric repulsion among the pendant ether groups in **2** is slightly less than that among the pendant thioether groups in **1**. This allows the four carboxamido nitrogens of the two $PyPOMe^{2-}$ ligands to bind to the Fe^{III} center in **2**. Since there is no N-to-O switch, complex **2** is once again low spin much like $[FeL_2]^-$ and $[Fe(Py_3P)_2]^-$.

In this paper, we report (a) the syntheses of complexes **1** and **2**, (b) comparisons of the structures of **1** and **2** with other related Fe^{III} complexes with bound 2,6-pyridinedicarboxamide moieties, and (c) studies on spin-flip due to the N-to-O switch in **1** and **2**.

Results and Discussion

The potentially pentadentate ligand $PyPSMeH_2$ was synthesized by following a procedure previously reported by this group.[17] $PyPOMeH_2$ was prepared by reacting *o*-anisidine with 2,6-pyridinedicarbonyl dichloride (prepared from 2,6-pyridinedicarboxylic acid and thionyl chloride) in chloroform. Reaction of $(Et_4N)[FeCl_4]$ with $PyPSMe^{2-}$ in DMF

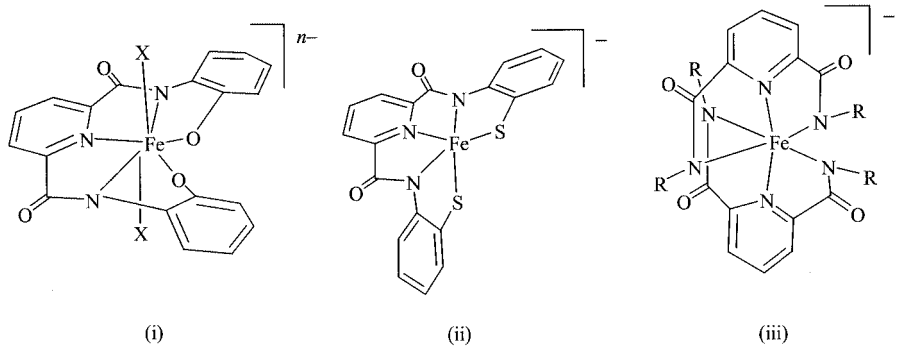

Figure 2. Different structures of Fe^{III} complexes of ligands with the 2,6-pyridinedicarboxamide moiety

afforded the red-brown Fe^{III} complex $(Et_4N)[Fe(PyPSMe)_2]$ (**1**) in good yield. It is important to note that the bis complex **1** is the only product isolated from this reaction irrespective of the ligand to Fe ratio. Thus when a 1:1 ligand to Fe ratio is used, only half of the iron is complexed by the ligand while the rest remains in solution in the form of $[FeCl_4]^-$. Clearly, the strong preference of the carboxamido nitrogens for Fe^{III}, and the weak affinity of the thioether sulfur for Fe^{III} lead to the formation of **1** as the sole product. The bright red complex $(Et_4N)[Fe(PyPOMe)_2]$ (**2**) was synthesized in high yield by reacting $(Et_4N)[FeCl_4]$ with two equivalents of $PyPOMeH_2$ and four equivalents of NaH (both relative to iron) in DMF.

Molecular Structure of $(Et_4N)[Fe(PyPSMe)_2]$ (1)

An X-ray crystallographic study of **1** (Table 1) revealed that the coordination geometry around the Fe^{III} center is distorted octahedral, with two $PyPSMe^{2-}$ units ligated in a *mer* fashion (Figure 3). Interestingly the $Fe^{III}N_5O$ chromophore consists of two pyridine nitrogens, three deprotonated carboxamido nitrogens, and the carbonyl oxygen of the fourth deprotonated carboxamido moiety. This observed mode of binding of the two $PyPSMe^{2-}$ ligands in **1** is not accidental and has also been noted in the corresponding Co^{III} complex $(Et_4N)[Co(PyPSMe)_2]$ (**3**).[17] The last carboxamido nitrogen moiety fails to bind through nitrogen due to the steric repulsion that builds up between the pendant thioether groups as an increasing number of carboxamido nitrogens become ligated to the M^{III} center. To the best of our knowledge, there is no other example of such an N-to-O donor switch in Fe^{III} complexes containing carboxamido group(s). A few examples of N-to-O linkage isomerization have been reported with ruthenium complexes[18] but these complexes contain neutral and not deprotonated carboxamide unit(s).

Table 1. Summary of crystal data and intensity collection and structure refinement parameters for $(Et_4N)[Fe(PyPSMe)_2]\cdot 1.7CH_3CN\cdot Et_2O$ (**1**·$1.7CH_3CN\cdot Et_2O$) and $(Et_4N)[Fe(PyPOMe)_2]\cdot 2H_2O$ (**2**·$2H_2O$)

Parameters	**1**·$1.7CH_3CN\cdot Et_2O$	**2**·$2H_2O$
Empirical formula	$C_{57.40}H_{69.10}FeN_{8.70}O_5S_4$	$C_{50}H_{58}FeN_7O_{10}$
Molecular weight	1145.00	972.88
a [Å]	18.772(4)	11.0430(13)
b [Å]	14.548(3)	12.3769(17)
c [Å]	21.297(4)	17.997(2)
α [°]	90	89.039(3)
β [°]	90.787(8)	76.953(3)
γ [°]	90	75.930(2)
V [Å^3]	5816(2)	2322.5(5)
Z	4	2
Crystal system	monoclinic	triclinic
Space group	$P2_1/n$	$P\bar{1}$
ρ [g·cm^{-3}]	1.308	1.391
T (K)	91(2)	91(2)
μ, [mm^{-1}]	0.458	0.393
GOF[a] on F^2	1.019	1.024
R_1 [b]	6.76	3.77
R_{w2} [c]	14.97	9.04

[a] GOF = $[\Sigma[w(F_0^2 - F_c^2)^2]/(M - N)]^{1/2}$ (M = number of reflections, N = number of parameters refined). [b] $R_1 = \Sigma||F_0| - |F_c||/\Sigma|F_0|$. [c] $Rw_2 = \{\Sigma[w(F_0^2 - F_c^2)^2]/\Sigma[w(F_0^2)^2]\}^{1/2}$.

The $Fe^{III}-N_{amido}$ [av. 2.093(3) Å] and $Fe^{III}-N_{py}$ [av. 2.081(3) Å] bond lengths in **1** are significantly longer than those reported for similar Fe^{III} complexes containing *two* coordinated 2,6-pyridinedicarboxamido moieties in their primary coordination sphere.[5,11] A close examination of the literature reveals three bis complexes of Fe^{III} that contain the 2,6-pyridinedicarboxamido unit, namely $(Et_4N)[FeL_2]$,[11] $Na[Fe(Py_3P)_2]$,[5] and $Na[Fe(MePy_3P)_2]$.[5] All three complexes consist of an $Fe^{III}N_6$ chromophore with four deprotonated carboxamido nitrogens in the basal

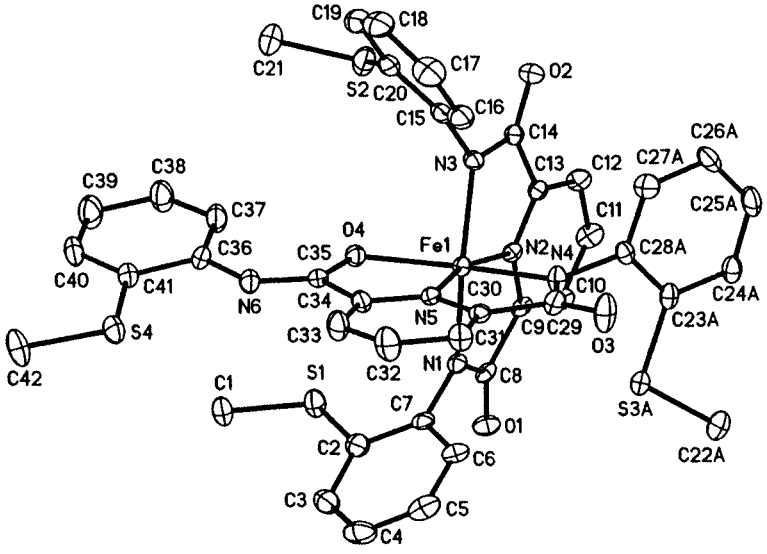

Figure 3. Thermal ellipsoid plot of $[Fe(PyPSMe)_2]^-$, the anion of **1** (at the 50% probability level); H atoms are omitted for the sake of clarity

plane and two axial pyridine donors. As a result of the strong ligand field of the carboxamido nitrogens, these Fe^{III} complexes are all low spin (vide infra) and exhibit shorter $Fe^{III}-N_{amido}$ [av. 1.961 Å] and $Fe^{III}-N_{py}$ [av. 1.877 Å] bond lengths.[5,11] Interestingly, the bond lengths of **1** compare well with those noted for high spin (vide infra) Fe^{III} complexes that contain *one* 2,6-pyridinedicarboxamido unit in the primary coordination sphere.[6,10,15] The C−O bond length of the O-bound carbonyl group [1.286(4) Å] is significantly longer than the C−O bond of the N-bound carbonyl groups [av. 1.236 Å] as a result of coordination of the carbonyl oxygen to the Fe^{III} center. Similarly, the C−N bond of the O-bound carboxamido unit [1.299(4) Å] is, as expected, shorter than the C−N bond of the N-bound carboxamido group [av. 1.336 Å] (Table 2).

Table 2. Selected bond lengths [Å] and angles [°] for $(Et_4N)[Fe(PyPSMe)_2]\cdot 1.7CH_3CN\cdot Et_2O$ (**1**·$1.7CH_3CN\cdot Et_2O$) and $(Et_4N)[Fe(PyPOMe)_2]\cdot 2H_2O$ (**2**·$2H_2O$)

Complex **1**			
Fe−O(4)	2.014(2)	Fe−N(4)	2.111(3)
Fe−N(5)	2.072(3)	O(1)−C(8)	1.236(4)
Fe−N(3)	2.077(3)	N(1)−C(8)	1.336(4)
Fe−N(2)	2.090(3)	O(4)−C(35)	1.286(4)
Fe−N(1)	2.091(3)	N(6)−C(35)	1.299(4)
O(4)−Fe−N(5)	75.73(10)	N(5)−Fe−N(4)	74.50(11)
O(4)−Fe−N(3)	90.39(10)	N(3)−Fe−N(4)	94.25(12)
N(5)−Fe−N(3)	112.90(11)	N(2)−Fe−N(4)	94.81(11)
O(4)−Fe−N(2)	115.67(10)	N(1)−Fe−N(4)	99.59(12)
N(5)−Fe−N(2)	166.85(10)	O(4)−C(35)−N(6)	129.7(3)
N(3)−Fe−N(2)	74.92(11)	O(4)−C(35)−C(34)	114.3(3)
O(4)−Fe−N(1)	92.37(10)	N(6)−C(35)−C(34)	115.9(3)
N(5)−Fe−N(1)	99.07(11)	O(1)−C(8)−N(1)	129.0(3)
N(3)−Fe−N(1)	147.56(12)	O(1)−C(8)−C(9)	119.8(3)
N(2)−Fe−N(1)	74.80(11)	N(1)−C(8)−C(9)	111.3(3)
O(4)−Fe−N(4)	149.29(11)		
Complex 2			
Fe−N(2)	1.8743(12)	Fe−N(2)	1.9842(12)
Fe−N(5)	1.8757(12)	Fe−N(4)	1.9924(12)
Fe−N(3)	1.9591(11)	N(1)−C(1)	1.3430(18)
Fe−N(1)	1.9802(12)	O(1)−C(1)	1.2438(17)
N(2)−Fe−N(5)	178.14(5)	N(1)−Fe−N(6)	91.06(5)
N(2)−Fe−N(3)	81.52(5)	N(2)−Fe−N(4)	97.86(5)
N(5)−Fe−N(3)	96.98(5)	N(5)−Fe−N(4)	81.04(5)
N(2)−Fe−N(1)	81.01(5)	N(3)−Fe−N(4)	91.12(5)
N(5)−Fe−N(1)	100.49(5)	N(1)−Fe−N(4)	91.20(5)
N(3)−Fe−N(1)	162.52(5)	N(6)−Fe−N(4)	162.23(5)
N(2)−Fe−N(6)	99.89(5)	O(1)−C(1)−N(1)	128.20(13)
N(5)−Fe−N(6)	81.22(5)	O(1)−C(1)−C(2)	120.41(13)
N(3)−Fe−N(6)	92.00(5)	N(1)−C(1)−C(2)	111.39(12)

Molecular Structure of $(Et_4N)[Fe(PyPOMe)_2]$ (2)

The coordination geometry around the Fe^{III} center in $[Fe(PyPOMe)_2]^-$ is distorted octahedral with two $PyPOMe^{2-}$ ligands coordinated in a *mer* fashion (Figure 4). Unlike **1**, complex **2** consists of an $Fe^{III}N_6$ chromophore with two axial pyridine nitrogens and *four* equatorial carboxamido nitrogens in its coordination sphere and hence resembles typical bis complexes with bound 2,6-pyridinedicarboxamido units such as $[Fe(Py_3P)_2]^-$. It is interesting to note that by simply decreasing the size of the pendant groups from SMe to OMe at the ligand periphery, a more sterically favorable situation can be created such that all six nitrogens are able to bind to the Fe^{III} center.

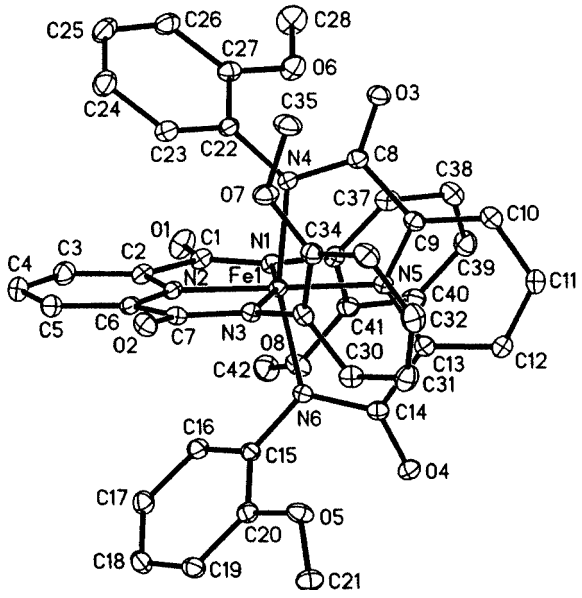

Figure 4. Thermal ellipsoid plot of $[Fe(PyPOMe)_2]^-$, the anion of **2** (at the 50% probability level); H atoms are omitted for the sake of clarity.

The $Fe^{III}-N_{amido}$ [av. 1.979(3) Å] and $Fe^{III}-N_{py}$ [av. 1.875(3) Å] bond lengths of **2** are similar to those noted in Fe^{III} complexes with FeN_6 chromophores arising from coordination of *two* 2,6-pyridinedicarboxamido units.[5,11] However, these bonds are consistently shorter than those in **1** due to the low spin nature of the Fe^{III} center in **2** (vide infra). Furthermore, the octahedral geometry of the N_6 framework in **2** is less distorted than that formed by the N_5O framework in **2**. For example, the $N_{py}-Fe-N_{py}$ and $N_{amido}-Fe-N_{amido}$ angles in **1** (166.85° and 147.56° respectively) are substantially smaller than the corresponding angles in **2** (178.14 ° and 162.23° respectively, Table 2).

Spectroscopic Properties

Coordination of $PyPSMe^{2-}$ and $PyPOMe^{2-}$ to the Fe^{III} centers is readily indicated by the IR spectra of the complexes. Ligation of the deprotonated carboxamido nitrogens to the metal centers results in a red-shift of the carbonyl stretching frequency (ν_{co}) from 1684 cm^{-1} (in both $PyPSMeH_2$ and $PyPOMeH_2$) to 1593 cm^{-1} in **1** and 1603 cm^{-1} in **2**. Also, the N−H stretching frequency of the free ligand (≈ 3200 cm^{-1} for both ligands) is absent in the IR spectra of the iron complexes confirming coordination of the ligands in their deprotonated forms.

The EPR spectrum of **1** in DMF glass at 80K confirms the high spin nature of the Fe^{III} center, displaying a strong signal at $g = 4.3$ (Figure 5). This is contrary to other bis Fe^{III} complexes with coordinated 2,6-pyridinedicarboxamido units.[5,11] The Fe^{III} centers in such complexes are exclusively low spin and exhibit axial EPR resonances with g values in the range of 2.19−1.94. This is also true for complex **2**. In the same DMF glass, complex **2** exhibits an axial EPR spectrum ($g = 2.18$, 1.94) typical of a low spin Fe^{III} center (Figure 5). The only difference between the two bis complexes **1** and **2** is the fact that in **1**, one of the four carboxamido moieties employs the carbonyl oxygen to bind the Fe^{III} center giving rise to an FeN_5O chromophore. This rather simple N-to-O switch in the donor set causes a spin flip and gives rise to the high spin complex **1**. In **2**, all six nitrogens from the two 2,6-pyridinedicarboxamido units are bonded to Fe^{III}, and the FeN_6 chromophore is low spin much like the other complexes of a similar kind.[5,11] To the best of our knowledge, change in the spin state due to only one N-to-O donor switch in otherwise similar complexes of Fe^{III} with carboxamide ligands has not been observed before. It appears that the $Fe-O_{carbonyl}$ interaction exerts a crucial effect on the strong ligand field of the carboxamido nitrogens in these species and just one such interaction can change the overall spin state of the complex. A similar trend in spin state has also been observed in other Fe^{III} complexes that contain $Fe-N_{amido}$ bonds in the presence of $Fe-O_{phen}$ bonds (where phen = phenolato oxygen).[8]

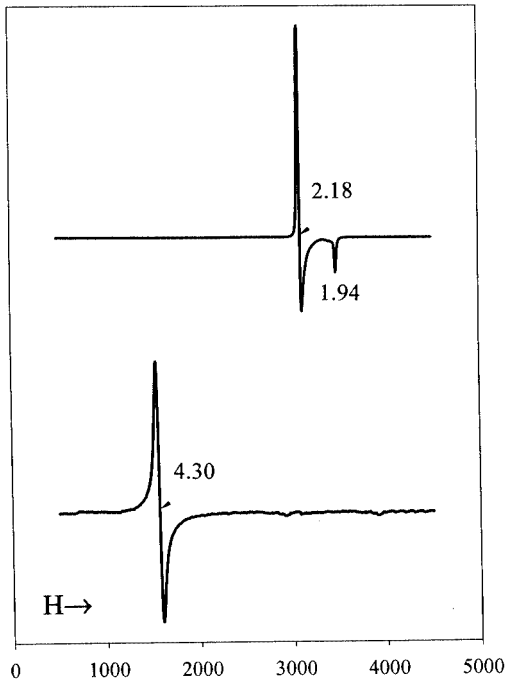

Figure 5. X-band EPR spectra of **1** (bottom panel) and **2** (top panel) in DMF glass at 80 K; instrument settings: microwave power 13 mW, microwave frequency 9.43 GHz, modulation frequency 100 KHz, modulation amplitude 2 G; selected g values are shown

Complexes **1** and **2** are soluble in a variety of solvents such as DMF and CH_3CN giving deep red-orange solutions. This color arises from strong ligand-to-metal charge transfer (LMCT) absorptions at 450 nm for **1** and 440 nm for **2** (both in DMF). Similar LMCT bands have been observed with analogous iron(III) complexes.[5,11] Although **1** is stable in aprotic solvents, it decomposes readily in water. The initial red solution loses its color within minutes and free $PyPSMeH_2$ precipitates from the solution as a white solid. This behavior contrasts sharply with that of other Fe^{III} complexes with FeN_6 chromophores, such as $Na[Fe(Py_3P)_2]$,[5] $Na[Fe(MePy_3P)_2]$,[5] and especially complex **2**. It is therefore evident that the O-bonded Fe^{III} complex **1** is inherently unstable, presumably due to its high spin nature.

Conclusion

In conclusion, we have synthesized and structurally characterized two new, six-coordinate Fe^{III} complexes that contain the 2,6-pyridinedicarboxamido unit. With the potentially pentadentate thioether ligand $PyPSMeH_2$, only the bis complex $(Et_4N)[Fe(PyPSMe)_2]$ (**1**) is obtained irrespective of the ligand to Fe ratio. This strongly suggests that *thioether sulfurs are not good donor groups for Fe^{III} in the presence of carboxamido groups.* On inspection of the few Fe^{III} complexes with bound thioether groups, it becomes evident that coordination of a thioether sulfur to Fe^{III} occurs only when the thioether group(s) exist between other strong donor groups on the ligand frame.[19−21] The steric repulsion among the pendant thioether groups in **1** gives rise to an FeN_5O coordination sphere in which one carbonyl oxygen binds to the Fe^{III} center. It appears that this subtle N-to-O switch in donor atom results in a high spin Fe^{III} center in **1**. In the case of the other Fe^{III} complex $(Et_4N)[Fe(PyPOMe)_2]$ (**2**), the smaller pendant ether groups allow coordination of all four carboxamido nitrogens resulting in a low spin complex with an FeN_6 chromophore. Collectively, these results indicate that the spin state of an Fe^{III} center coordinated by 2,6-pyridinedicarboxamido moieties can be influenced by simple addition of bulky groups to the ligand periphery. Further modifications to the 2,6-pyridinedicarboxamide ligand frame should enable the preparation of other Fe^{III} complexes with novel structural and spectroscopic properties. Such investigations are currently being performed in this laboratory.

Experimental Section

Physical Measurements: Infrared spectra were recorded with a Perkin−Elmer 1600 FTIR spectrophotometer. Absorption spectra were recorded on a Perkin−Elmer Lambda 9 spectrophotometer. ^1H and ^{13}C NMR spectra were recorded at 25 °C on a 500 MHz Varian Unity Plus spectrometer. EPR spectra at X-band frequencies were obtained at 80K with a Bruker ESP-300 spectrometer.

Materials and Methods: All manipulations were carried out using standard Schlenk techniques. 2,6-Pyridinedicarboxylic acid, 2-

(methylthio)aniline, *o*-anisidine, and sodium hydride were purchased from Aldrich and used without further purification. $(Et_4N)[FeCl_4]$[22] and $PyPSMeH_2$ [17] were synthesized by following published procedures. 2,6-Pyridinedicarbonyl dichloride was prepared by refluxing 2,6-pyridinedicarboxylic acid in neat thionyl chloride. All solvents were distilled from the appropriate drying agents prior to use: DMF from BaO, CH_3CN from CaH_2, THF from Na/benzophenone, Et_2O from Na, and $CHCl_3$ from $CaCl_2$.

Preparation of $PyPOMeH_2$: A solution of *o*-anisidine (3.79 g, 30 mmol) and Et_3N (5.00 g, 50 mmol) in $CHCl_3$ (40 mL) was slowly added to a solution of 2,6-pyridinedicarbonyl dichloride (3.11 g, 15 mmol) and Et_3N (5.00 g, 50 mmol) in $CHCl_3$ (50 mL) at 0 °C. The mixture was stirred at room temperature for 24 h. The resultant red solution was washed with aqueous $NaHCO_3$ and NaCl. The $CHCl_3$ layer was then dried over $MgSO_4$, filtered, and the solvent was removed by rotary evaporation to yield a red oil. The oil was triturated with Et_2O (25 mL) to yield a light brown solid (3.75 g, 65% yield). ^1H NMR (500 MHz, $CDCl_3$): δ = 3.95 (s, 6 H, OCH_3), 7.00 (d, 2 H, ArH), 7.10 (t, 2 H, ArH), 7.15 (t, 2 H, ArH), 8.14 (t, 1 H, ArH), 8.55 (d, 2 H, ArH), 8.61 (d, 2 H, ArH), 10.36 (s, 2 H, NH) ppm. ^{13}C NMR (500 MHz, $CDCl_3$): δ = 56.14 (OCH_3), 110.54 (ArC), 120.24 (ArC), 121.50 (ArC), 124.55 (ArC), 125.34 (ArC), 127.44 (ArC), 139.56 (ArC), 148.97 (ArC), 149.41 (ArC), 161.15 (C=O) ppm. Selected IR absorption bands (KBr pellet): $\tilde{\nu}$ = 3371 cm^{-1} (s, N−H), 3014 (w), 2979 (w), 1684 (vs, C=O), 1602 (s), 1536 (s), 1488 (s), 1461 (s), 1334 (m), 1291 (m), 1248 (s), 1220 (m), 1175 (w), 1138 (w), 1110 (m), 1070 (m), 1047 (m), 1029 (s), 1000 (w), 947 (w), 925 (w), 890 (w), 845 (w), 790 (w), 758 (w), 702 (w), 671 (s), 594 (w).

$(Et_4N)[Fe(PyPSMe)_2]$ (1): NaH (0.037 g, 1.54 mmol) was added to a solution of $PyPSMeH_2$ (0.310 g, 0.76 mmol) in DMF (15 mL) and the mixture was stirred until all the NaH had reacted. To the resultant yellow solution was added a solution of $(Et_4N)[FeCl_4]$ (0.120 g, 0.38 mmol) in DMF (2 mL). The resultant dark red solution was stirred for 2 h at 25 °C. The solvent was then removed under vacuum and the residue dissolved in CH_3CN (15 mL) and filtered to remove NaCl. Diethyl ether (7 mL) was added to the CH_3CN filtrate and the resulting solution was stored at −20 °C for 48 h. The dark red crystalline solid thus obtained was collected by filtration and dried under vacuum (0.190 g, 51% yield). Selected IR absorption bands: (KBr pellet): $\tilde{\nu}$ = 3049 cm^{-1} (w), 2983 (w), 2918 (w), 1593 (vs, ν_{CO}), 1461 (m), 1438 (w), 1377 (m), 1342 (w), 1144 (w), 1068 (w), 968 (w), 749 (w). Absorption spectrum in DMF: λ_{max} (ε, $M^{-1}\cdot cm^{-1}$) = 550 nm sh, 450 (7000), 365 (12 000).

$(Et_4N)[Fe(PyPOMe)_2]$ (2): $PyPOMeH_2$ (0.310 g, 0.82 mmol) was dissolved in DMF (10 mL) and to this was added solid NaH (0.046 g, 1.90 mmol). The mixture was stirred for 20 min and $(Et_4N)[FeCl_4]$ (0.140 g, 0.43 mmol) in DMF (2 mL) was then added. The resultant bright red solution was stirred at 25 °C for 2 h. The solvent was then removed in vacuo and the residue dissolved in CH_3CN (15 mL) and filtered to remove NaCl. To the CH_3CN filtrate was added Et_2O (5 mL) and THF (5 mL) and the solution was stored at −20 °C for three days. The bright red crystalline solid thus obtained was collected by filtration (0.290 g, 73% yield). Selected IR absorption bands: (KBr pellet): $\tilde{\nu}$ = 3072 cm^{-1} (w), 2989 (w), 2943 (w), 1603 (vs, C = O), 1578 (s), 1491 (s), 1458 (m), 1374 (m), 1249 (m), 1156 (w), 1112 (m), 1026 (m), 760 (m), 684 (w). Absorption spectrum in DMF: λ_{max} (ε, $M^{-1}\cdot cm^{-1}$) = 440 nm (6600), 305 (18 000).

X-ray Crystal Structure Analysis: Dark red/brown crystals of $(Et_4N)[Fe(PyPSMe)_2]\cdot 1.7CH_3CN\cdot Et_2O$ (**1**·$1.7CH_3CN\cdot Et_2O$) were grown from CH_3CN/Et_2O (3:1) at −20 °C. Bright red X-ray quality blocks of $(Et_4N)[Fe(PyPOMe)_2]\cdot 2H_2O$ (**2**·$2H_2O$) were grown from CH_3CN/Et_2O/THF (3:1:1) at −20 °C. Diffraction data for both complexes were collected at 90 K on a Bruker SMART 1000 diffractometer using Mo-K_α (0.71073 Å) radiation, and an absorption correction was applied in each case. The structures were solved by direct methods (SHELXS-97). In the structure of **1**·$1.7CH_3CN\cdot Et_2O$, there is disorder of one of the terminal groups of the ligand containing C22−S3−C28. This disorder has been omitted in Figure 3 for sake of clarity. Instrument parameters, crystal data, and data collection parameters for **1**·$1.7CH_3CN\cdot Et_2O$ and **2**·$2H_2O$ are summarized in Table 1. Selected bond lengths and angles are listed in Table 2.

CCDC-187840 (**1**·$1.7CH_3CN\cdot Et_2O$) and CCDC-187841 (**2**·$2H_2O$) contain the supplementary crystallographic data for this paper. These data may be obtained free of charge at www.ccdc.cam.ac.uk/conts/retrieving.html [or from the Cambridge Crystallographic Data Centre, 12 Union Road, Cambridge, CB2 1EZ, UK (Fax: (internat.) +44-1223-336-033; E-mail: deposit@ccdc.cam.ac.uk].

Acknowledgments

This research was supported by a grant from the NIH (GM61636). T.C.H. received support from the NIH IMSD grant GM 58903. L. A. T. was a recipient of a GAAN fellowship from the U. S. Department of Education.

[1] J. W. Peters, M.H. Stowell, M. Soltis, M. G. Finnegan, M. K. Johnson, D. C. Rees, *Biochemistry* **1997**, *36*, 1181−1187.
[2] S. Nagashima, M. Nakasako, N. Dohmae, M. Tsujimura, K. Takio, M. Odaka, M. Yohda, N. Kamiya, I. Endo, *Nature Struct. Biol.* **1998**, *5*, 347−351.
[3] W. Huang, J. Jia, J. Cummings, M. Nelson, G. Schneider, Y. Lindqvist, *Structure* **1997**, *5*, 691−699.
[4] H. Sigel, R. B. Martin, *Chem. Rev.* **1982**, *82*, 385−426.
[5] D. S. Marlin, M. M. Olmstead, P. K. Mascharak, *Inorg. Chem.* **1999**, *38*, 3258−3260.
[6] D. S. Marlin, M. M. Olmstead, P. K. Mascharak, *Inorg. Chim. Acta* **2000**, *297*, 106−114.
[7] D. S. Marlin, P. K. Mascharak, *Chem. Soc. Rev.* **2000**, *29*, 69−74.
[8] D. S. Marlin, M. M. Olmstead, P. K. Mascharak, *Eur. J. Inorg. Chem.* **2002**, *38*, 859−865.
[9] J. M. Rowland, M. M. Olmstead, P. K. Mascharak, *Inorg. Chem.* **2001**, *40*, 2810−2817.
[10] J. C. Noveron, M. M. Olmstead, P. K. Mascharak, *J. Am. Chem. Soc.* **2001**, *123*, 3247−3259.
[11] M. Ray, D. Ghosh, Z. Shirin, R. N. Mukherjee, *Inorg. Chem.* **1997**, *36*, 3568−3572.
[12] C.-M. Che, W.-H. Leung, C.-K. Li, H.-Y. Cheng, S.-M. Peng, *Inorg. Chim. Acta* **1992**, *196*, 43−48.
[13] M. Ray, R. N. Mukherjee, J. F. Richardson, R. M. Buchannan, *J. Chem. Soc., Dalton Trans.* **1993**, *36*, 2451−2457.
[14] M. J. Bartos, C. Kidwell, K. E. Kauffmann, S. W. Gordon-Wylie, T. J. Collins, G. C. Clark, E. Munck, S. T. Weintraub, *Angew. Chem. Intl. Ed. Engl.* **1995**, *34*, 1216−1219.
[15] R. W. Saalfrank, S. Trummer, H. Krautscheid, V. Schunemann, A. X. Trautwein, S. Hien, C. Stadler, J. Daub, *Angew. Chem. Intl. Ed. Engl.* **1996**, *35*, 2206−2208.
[16] F. A. Chavez, J. M. Rowland, M. M. Olmstead, P. K. Mascharak, *J. Am. Chem. Soc.* **1998**, *120*, 9015−9027.

[17] L. A. Tyler, M. M. Olmstead, P. K. Mascharak, *Inorg. Chim. Acta* **2001**, *321*, 135−141.
[18] D. P. Farlie, Y. Illan, H. Taube, *Inorg. Chem.* **1997**, *36*, 1029−1037.
[19] S. Karmakar, S. B. Choudhury, A. Chakravorty, *Inorg. Chem.* **1994**, *33*, 6148−6153.
[20] P. Chakraborty, S. K. Chandra, A. Chakravorty, *Inorg. Chem.* **1994**, *33*, 6429−6431.
[21] C. A. Grapperhaus, A. K. Patra, M. S. Mashuta, *Inorg. Chem.* **2002**, *41*, 1039−1041.
[22] N. S. Gill, F. B. Taylor, *Inorg. Synth.* **1967**, *9*, 136−142.
Received June 19, 2002
[I02324]

Studies on the Reduction of $[(C_5Me_5)_2Mo_2O_5]$ in Methanol/Water/Acetate Solutions by On-Line Electrochemical Flowcell and Electrospray Mass Spectrometry

Jenny Gun,*[a] Alexandre Modestov,[a] Ovadia Lev,[a] Dirk Saurenz,[b] Mikhail A. Vorotyntsev,[b] and Rinaldo Poli*[b]

Keywords: Cyclopentadienyl ligands / Electrochemistry / Mass spectrometry / Molybdenum / Oxo ligands

The complex $[Cp^*_2Mo_2O_5]$ ($Cp^* = \eta^5$-C_5Me_5) and its electrochemical reduction products in acetic acid/acetate-buffered (pH = 4.0) water/methanol solutions were investigated by combined electrochemical (EC) flowcell and on-line electrospray ionization mass spectrometry (ESI-MS). Mono-, di-, tri-, and tetranuclear organometallic molybdenum oxides were identified in the starting solution. The effect of the relevant ESI-MS parameters (ionic mode, heated capillary voltage, and heated capillary temperature) and of the concentration on the observed distribution of ions in the mass spectrometer was studied in order to minimize side reactions in the ESI chamber. It was verified that reduction in the ESI-MS is undetectable under open-circuit conditions. The on-line electrochemical study revealed the potential-dependent formation of previously unknown mono-, di-, tri-, and tetranuclear Mo^V, Mo^{IV}, and mixed-valence complexes. The compounds were identified by their characteristic isotope patterns and their ion trap MS^n fragmentations. The observed formation potentials reflect the higher stability of the multinuclear species relative to the mononuclear ones with the same oxidation state.

(© Wiley-VCH Verlag GmbH & Co. KGaA, 69451 Weinheim, Germany, 2003)

Introduction

The rapid development and eventual commercialization of Electrospray Ionization Mass Spectrometers (ESI-MS) in the 1980s and 1990s has opened the door to the determination of nonvolatile inorganic, organic, and organometallic compounds by mass spectrometry.[1,2] ESI-MS is an atmospheric-pressure technique that uses an electrostatic sprayer to transfer ionic solutes from the sample solution to the gas phase.[3,4] The ESI-MS technique is gradually becoming a valuable tool for the investigation of organometallic compounds in both protic and aprotic solvents[4] and has proven especially useful in combination with investigations of redox processes, particularly reduction processes.

Electrochemical methods are the method of choice for obtaining reduced organometallic compounds, since potential-dependent information can readily be obtained, reversibility is easily checked, and complexation by the chemical reducing agents or their by-products is minimized. Bond et al. have made extensive use of ESI-MS for the investigation of complex electrochemical transformations of organometallic compounds such as the reductions of *cis*-$[(Et_2\text{-dcbpy})_2RuX_2]$ (X = Cl^-, I^-, NCS^-, CN^-)[5] and 17-electron carbonyl(phosphane)rhenium(II) complexes.[6] These works are based on the combination of preparative electrochemistry and subsequent ESI-MS analysis. However, preparative electrochemistry suffers from several disadvantages. Firstly, considerable time is needed in order to achieve full conversion, thereby limiting the resolution of potential-dependent investigations. Secondly, the long reduction times often involve fouling of the electrode surface by polymeric by-products. Thirdly, the reduced compounds have ample time to participate in unwanted subsequent chemical reactions among themselves or with the oxidized forms. Fourthly, preparative electrochemistry monitored by ESI-MS studies involves considerable sample handling, which may result in oxygen penetration and impurity introduction.

The importance of flow-through electrochemical cells connected to a mass spectrometer and the instrumentation involved have recently been reviewed.[7] Cole et al.,[8,9] Bond et al.,[10] and Van Berkel et al.,[11,12] used different configurations of electrochemical cells coupled to on-line ESI mass spectrometers for the investigation of redox reactions. We have devised an on-line concentric electrochemical cell

[a] Laboratory of Environmental Chemistry, Division of Environmental Sciences and The Casali Institute, The Hebrew University of Jerusalem
Jerusalem, Israel
Fax: (internat.) + 972-2/658-6155
E-mail: gunjen@pob.huji.ac.il
[b] Laboratoire de Synthèse et d'Electrosynthèse Organométalliques, Faculté des Sciences "Gabriel", Université de Bourgogne,
6 Boulevard Gabriel, 21000 Dijon, France
Fax: (internat.) + 33-3/80393720
E-mail: poli@u-bouregogne.fr

connected to ESI-MS in which the counter-electrode and its products are separated from the reacting stream reaching the ESI-MS in order to isolate and protect the reduced compounds from the oxidized substances generated at the counter-electrode.

Oxygen-containing organomolybdenum complexes are especially intriguing since, in spite of their ability to attain a large number of oxidation states, relatively little is known about their speciation in protic solutions or about their electrochemistry. More information, on the other hand, is available on inorganic oxomolybdenum compounds, including ESI-MS speciation studies. Singly, doubly, and triply charged heteropoly- and isopolymolybdate anions were studied in organic and aqueous organic solutions,[13,14] though the reduction products of these compounds were not investigated by mass spectrometry. The subject of this study is the identification of the electrochemical reduction products of the complex $[Cp^*_2Mo_2O_5]$ in aqueous methanol solution. $[Cp^*_2Mo_2O_5]$ is a member of a relatively broad family of high-oxidation organometallic compounds, some of which have displayed some remarkable stoichiometric and/or catalytic chemical transformations. Although some of these molecules are stable in aqueous environments and have even been synthesized in water, their aqueous chemistry has rarely been investigated. In the particular case of $[Cp^*_2Mo_2O_5]$, while most studies have been carried out in organic solvents,[15−19] other contributions have restricted the use of aqueous media to some aspects of the synthetic procedure.[20−23] Some of us have recently reported an improved aqueous synthesis[24] of $[Cp^*_2Mo_2O_5]$ and a detailed investigation of its speciation in a $MeOH/H_2O$ mixture by conductivity studies.[25] An additional point of interest of this molybdenum system is the redox-richness of the metal. Exploration of the redox behavior of $[Cp^*_2Mo_2O_5]$ as a prototype compound may thus open up avenues for the development of new stoichiometric or catalytic redox chemistry.

Results and Discussion

(a) Studies of $[Cp^*_2Mo_2O_5]$ Solutions and Optimization of ESI-MS Conditions

The speciation of $[Cp^*_2Mo_2O_5]$ in water/methanol mixtures at various pH values is known from recent kinetic and conductivity studies in one of our laboratories.[25] The use of a mixed water/methanol medium was dictated by the insolubility of $[Cp^*_2Mo_2O_5]$ in pure water, while the hydrosoluble (but lipophobic) $[Cp^*MoO_3^-]$ ion is obtained under basic conditions. As a brief summary of the speciation studies, compound $[Cp^*_2Mo_2O_5]$ was found to exist as a dinuclear molecular species in organic solvents, but self-ionization to $[Cp^*MoO_2^+]$ and $[Cp^*MoO_3^-]$ occurs to a larger and larger extent as the water content in the solvent mixture increases. In 20% $MeOH/H_2O$, the compound behaves as a strong electrolyte, affording as the preponderant species $[Cp^*MoO_2^+]$ at pH < 2 and $[Cp^*MoO_3^-]$ at pH $>$ 5. Both species, plus a minor quantity of $[Cp^*MoO_2(OH)]$, are present at intermediate pH values.[25]

The first part of our investigation was devoted to ESI-MS studies of the reactant $[Cp^*_2Mo_2O_5]$ in order to find the analytical conditions that would most closely reflect its speciation in solution. It is worth noting in this respect that ESI-MS provides a sensitivity advantage over the previous analyses, which may have missed some less dominant species. On the other hand, even though ESI-MS is amongst the least intrusive mass spectrometric techniques,[26] the ionization process may nevertheless introduce fragmentation and rearrangement processes resulting in the observation of peaks of species that are not present in the solution. The experimental conditions must therefore be carefully optimized in order to minimize these phenomena. It is also important to verify that no redox process takes place in the ESI chamber in the absence of an applied electrochemical potential. For practical reasons, the ESI-MS studies were conducted in an $MeOH/H_2O$ (1:1) mixture containing a 0.1 M CH_3COONH_4/CH_3COOH buffer at pH = 4. Under these conditions, a substantial amount of dimolybdenum species (either the neutral $[Cp^*_2Mo_2O_5]$ or the tight ion pair $[Cp^*MoO_2^+]$,$[Cp^*MoO_3^-]$) is also present in solution.

Figure 1 compares ESI-MS analyses of a 0.1 mM solution of $[Cp^*_2Mo_2O_5]$ in positive (a) and negative (b) detection modes. The positive-mode ESI-MS spectrum exhibits four major isotopic patterns, corresponding to mono-, di-, tri-, and tetranuclear species, respectively. The mononuclear region shows two major species [see left insert in Figure 1 (a)], both exhibiting the characteristic, seven-peak isotopic pattern of a single Mo atom. The first species is characterized by an isotopic pattern at m/z = 259−267 and corresponds to the $[Cp^*MoO_2^+]$ cation, while the second one, starting 18 m/z units higher (m/z = 277−285), is attributable to the protonated hydroxo species $[Cp^*MoO_3H_2^+]$. While the former is a solution-borne species, the latter results from the protonation of $[Cp^*MoO_2(OH)]$ and $[Cp^*MoO_3^-]$ in the ESI chamber (its pK_a was estimated as ca. −2). Because of this protonation process, the ESI-MS fails to duplicate the known acid-base speciation.[25]

Two major species appear in the dimolybdenum region, both characterized by the expected isotopic distributions for species containing two Mo centers (see second insert of Figure 1 (a)]. The most abundant isotopic pattern is at m/z = 535−551, which corresponds to the protonated form of $[Cp^*_2Mo_2O_5]$. As stated above, this compound exists as a molecular species in organic solvents (including pure MeOH) but it partially dissociates in the presence of water. In an $MeOH/H_2O$ (1:1) mixture, as used in this study, the conductivity investigations showed that part of the dinuclear compound is undissociated. The observed peak can therefore be attributed to the combination of $[Cp^*_2Mo_2O_5]$ with protons originating from the ammonium buffer. The less abundant and lighter pattern (m/z = 517−533) in this region has 18 fewer m/z units than the previous one and is therefore attributable to a dehydrated form. Probably one of the Cp* protons is involved in the process leading to this species, thereby signaling ESI-MS fragmentation.[27,28]

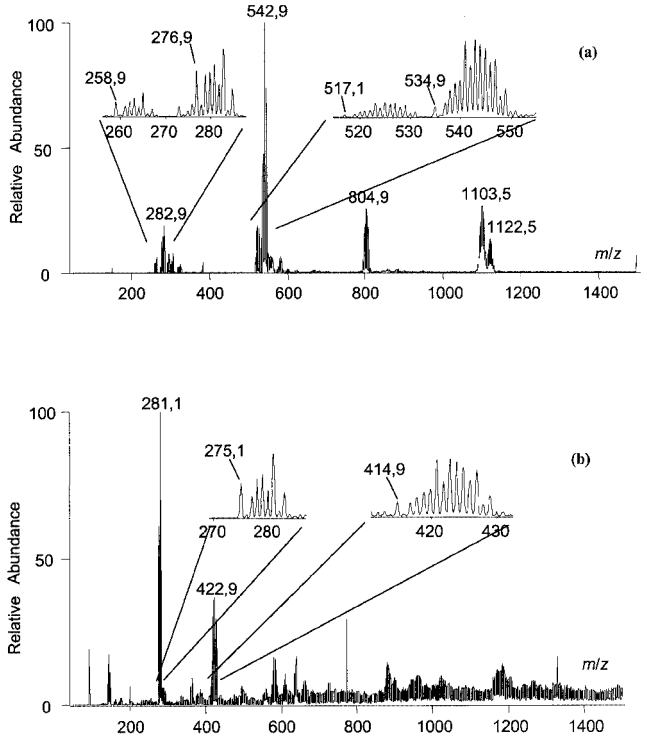

Figure 1. Electrospray mass spectra of a solution of $[Cp^*_2Mo_2O_5]$ (0.1 mM) in H_2O/MeOH (1:1) at pH = 4; heated capillary temperature = 100 °C; (a) positive mode; (b) negative mode; the largest *m/z* peaks are marked in the Figure and the first isotope in each isotopic pattern is marked in the inserts

The isotope patterns at *m/z* = 793−815 and 1090−1117 fit the calculated distributions of $[Cp^*_3Mo_3O_7^+]$ (slope = 1.0005, correlation coefficient R^2 = 0.999) and $[Cp^*_4Mo_4O_{11}H_3^+]$ (slope = 1.008, R^2 = 0.9998), respectively, very well.[29] Thus, both complexes still feature the metal atom in the oxidation state +6. It should be noted that a deviation of a single atomic mass unit (AMU), corresponding to a one-electron reduction process, can easily be distinguished by the isotope distribution fit. For example, curve-fitting of the isotope distribution of a hypothetical $[Cp^*_4Mo_4O_{11}H_4^+]$ to the observed isotope pattern for the tetranuclear species gives a slope of 1.004 but a correlation coefficient R^2 = 0.5451. Of course, the fitting of lower molecular weight molybdenum complexes to the observed patterns is even more sensitive to the assigned composition.

The negative mode spectrum of the same $[Cp^*_2Mo_2O_5]$ solution is given in Figure 1 (b). The major pattern at *m/z* = 275−283 corresponds to the deprotonated mononuclear species $[Cp^*MoO_3^-]$ (left insert). The second major distinguishable pattern (right insert, *m/z* = 415−431) is attributable to a species of formula $[Cp^*Mo_2O_6^-]$: the product of the replacement of one Cp^{*-} group with O^{2-}, a result of ESI-MS fragmentation. The negative mode spectrum also shows a much higher background current, relative to the positive mode spectrum, for *m/z* > 500. For these reasons, all further studies were conducted in the positive ion mode.

Two additional ESI-MS parameters were singled out for further optimization: the temperature of the heated capillary and the heated capillary voltage. Figure 2 (a) shows the ESI-MS spectrum recorded under the same conditions of Figure 2 (a), except that the heated capillary was maintained at 200 °C rather than at 100 °C. The differences between the two spectra confirm that the heated capillary temperature is a decisive factor in ESI-MS studies of our compounds. A comparison between the inserts of Figure 1 (a) and Figure 2 (a) reveals that $[CpMoO_3H_2^+]$ almost completely disappears at high temperatures, while the abundance of a new species with *m/z* = 273−281 (corresponding to $[CpMoO_3H_2^+ - 3\ H]$) − evidently resulting from a fragmentation process − increases. Furthermore, the daughter product with *m/z* = 517−533 in the dinuclear region becomes the preponderant species, while the original isotope pattern of the protonated dinuclear species $[Cp^*_2Mo_2O_5H^+]$ almost completely disappears. In addition,

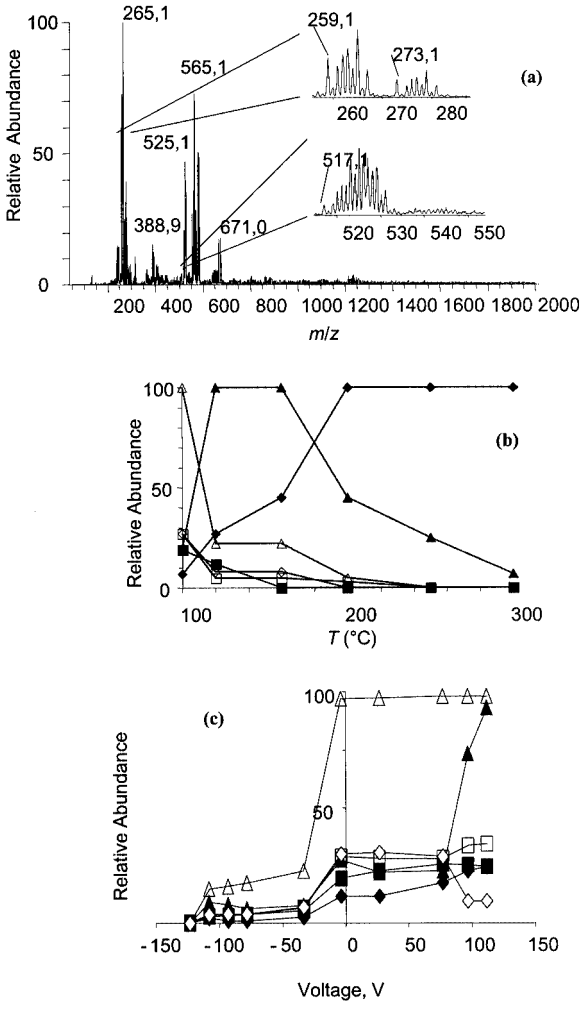

Figure 2. (a) Positive-mode electrospray mass spectra of a solution of $[Cp^*_2Mo_2O_5]$ (0.1 mM) in H_2O/MeOH (1:1) at pH = 4; heated capillary temperature = 200 °C; (b) and (c) evolution of the relative intensity of selected species {black diamonds: $[Cp^*MoO_2^+]$; black squares: $[Cp^*MoO_3H_2^+]$; black triangles: $[Cp^*_2Mo_2O_5H^+ - H_2O]$; white triangles: $[Cp^*_2Mo_2O_5H^+]$; white squares: $[Cp^*_3Mo_3O_7^+]$ species; white diamonds: $[Cp^*_4Mo_4O_{11}H_3^+]$} as a function of the heated capillary temperature (b) and heated capillary voltage (c)

other fragmentation products are also formed in relatively large proportions. Evidently, $[Cp^*_2Mo_2O_5]$ is cleaved at high temperatures.

The temperature dependence demonstrated in Figure 2 (a) is further elaborated upon in Figure 2 (b). The figure shows the dependence of several of the most abundant positive ion peaks as a function of the heated capillary temperature. Peak heights were normalized to the highest peak observed at the given heated capillary temperature. Under increased temperature conditions the abundance of the parent peak of the protonated $[Cp^*_2Mo_2O_5]$ decreases, while the abundance of the secondary peak of the dehydrated moiety goes through a maximum at 120−180 °C and then also decreases. The abundance of the monomeric form $[Cp^*MoO_2^+]$ increases monotonically with temperature, indicating a somewhat surprising thermal stability for this ion, whereas its relative abundance at 100 °C amounts to less than 10% of the dinuclear peak.

The relative abundances of the tri- and tetranuclear molybdenum species decrease steadily with the heated capillary temperature. This decrease suggests that the tri- and tetranuclear molybdenum species originate from the aqueous solution and that they were not generated by condensation reactions in the ESI chamber. Condensation reactions and dehydration should increase at higher temperatures, contrary to the tendency exhibited in Figure 2 (b). We thus believe that these compounds do exist in the solution, although they were not observed before by any other technique. These results directed our subsequent experiments to low source temperatures, set at 100 °C for detector sensitivity reasons.

The capillary voltage value was optimized (+25 V) during the automatic tuning process of our MS in order to give the highest sensitivity for the mass of $[Cp^*_2Mo_2O_5H^+]$. Since prior studies had pointed to the sensitivity of the observed spectra of organometallic complexes to the heated capillary voltage,[30] we carried out a set of tests in order to check the influence of this parameter in our case. The experiments showed that the spectra were not significantly changed as long as the heated capillary voltage remained within the −25 to +100 V range, see Figure 2 (c). It should be pointed out that no reduced molybdenum species were observed even when this potential was set as low as −100 V. Only for more negative cone voltages (< −110 V) did a reduction peak become observable (m/z = 777−799, attributable to $[Cp^*_3Mo_3{}^{V,V,VI}O_6^+]$).

The concentration dependence of the peak intensities for the five major species are shown in Figure 3. The relative abundances of the $[Cp^*MoO_3H_2^+]$ and $[Cp^*MoO_2^+]$ species are virtually concentration-independent, whereas those of all other species, including the dinuclear $[Cp^*_2Mo_2O_5H^+]$, increase with concentration. Given the established equilibrium in MeOH/H_2O solutions of various proportions between the dinuclear $[Cp^*_2Mo_2O_5]$ on one hand, and the separate ions $[Cp^*MoO_2^+]$ and $[Cp^*MoO_3^-]$ on the other, an increase of the relative abundance of dinuclear species with the concentration was to be expected. In principle, the observed increase in relative intensity with concentration for the trinuclear and tetranuclear peaks could be equally well explained by invoking similar solution equilibria. Since we have shown that a water-rich environment favors the spontaneous ionization of $[Cp^*_2Mo_2O_5]$ into $[Cp^*MoO_2^+]$ and $[Cp^*MoO_3^-]$, we propose that the trinuclear species derives from the combination of, for example, $[Cp^*MoO_3^-]$ with two $[Cp^*MoO_2^+]$ ions, as shown in Scheme 1.

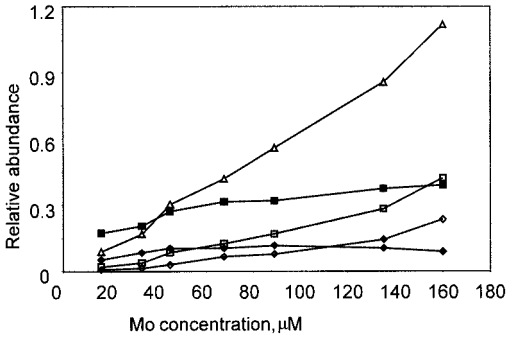

Figure 3. Concentration dependence of the relative intensities of selected species; spectra were recorded under the conditions of Figure 1 (a); black diamonds: $[Cp^*MoO_2^+]$; black squares: $[Cp^*MoO_3H_2^+]$; white triangles: $[Cp^*_2Mo_2O_5H^+]$; white squares: $[Cp^*_3Mo_3O_7^+]$; white diamonds: $[Cp^*_4Mo_4O_{11}H_3^+]$

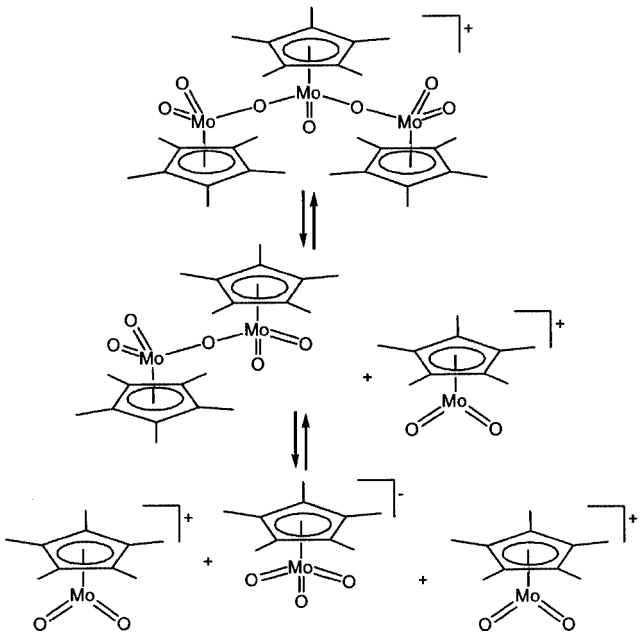

Scheme 1

A similar association process may occur for the tetranuclear species, although a simple breakdown into mononuclear charged components and a tentative structure for the assembled species cannot be as easily imagined as for the trinuclear species. It should further be remarked that these ionic association processes should be favored by the low polarity of the water/methanol (50:50) mixture. In the more polar (80:20) mixture, in which our previous speciation study was conducted,[25] no evidence for the presence of these ions was obtained, although the kinetics and conduc-

tivity may have been insensitive to the presence of small amounts of these species.

The choice of a buffer based on the ammonium cation rather than on other metal cations was dictated by the observation of complicating metal addition processes when the latter were used. For instance, Figure 4 shows the basic set of peaks of the dinuclear species in the presence of 1 M $LiBF_4$ (acidified to pH = 3.3 by acetic acid). Competitive protonation and formation of adducts with metal cations, the latter being preponderant, take place, and both adducts are discerned in the ESI-MS spectrum. The formation of metal ion adducts in preference to protonation in the ESI-MS chamber is a known phenomenon for neutral organometallic molecules.[31,32]

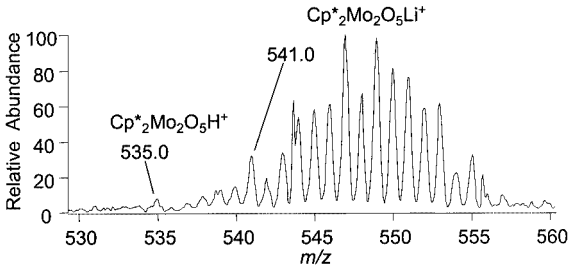

Figure 4. Detailed positive-mode electrospray mass spectra for a 0.1 mM solution of $[Cp^*_2Mo_2O_5]$ in H_2O/MeOH (1:1) in the presence 1 M $LiBF_4$ (pH = 3.3)

In addition to obtaining optimal ESI-MS parameters, two important interim conclusions could be reached on the basis of open-circuit studies of $[Cp^*_2Mo_2O_5]$ in methanol/water/acetate solutions. Firstly, condensation reactions do not occur to a large extent in the ESI chamber; the tri- and tetranuclear molybdenum species appear to be already present in solution. Secondly, reduced molybdenum compounds are not generated to any noticeable extent in the ESI-MS. This condition is a prerequisite for our further on-line electrochemical reduction/ESI-MS studies.

(b) On-Line Electrochemical Reduction/ESI-MS Study

Figure 5 (a) shows the background 3 mV/s voltammogram of an MeOH/H_2O (1:1) solution (acetic buffer, pH = 4) recorded in a regular three-compartment electrochemical cell with a glassy carbon working electrode. Curve (b) shows the voltammogram of a 1 mM solution of $[Cp^*_2Mo_2O_5]$. The reduction wave starts at approximately −0.45 V vs. saturated Ag/AgCl electrode. The current/potential curves at the forward and backward scans nearly coincide and the height of the reduction wave is virtually independent of the scan rate for a fairly wide range of scan rates (3−100 mV/s). The last two observations indicate that the electrochemical reduction of $[Cp^*_2Mo_2O_5]$ is controlled by an interfacial step and it is not diffusion-limited. A slope change at $E = -0.65$ V implies that an additional reduction step is switched on at this potential. It is quite obvious that identification of the electroreduction products solely on the basis of the voltammetric experiment is impossible.

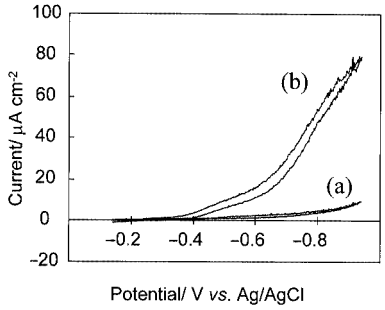

Figure 5. Voltammetry in 0.25 M NH_4Ac in H_2O/MeOH (1:1) at pH = 4 on a GC electrode; scan rate: 3 mV/s; (a) blank solution; (b) 1 mM $[Cp^*_2Mo_2O_5]$

Preparative electrolysis studies at −0.6, −0.7, and −0.8 V with a conventional 10-mm-diameter glassy carbon electrode showed a gradual decrease of the current after prolonged polarization (2 h) due to the formation of a thick oxide film on the electrode surface. This was accompanied by the accumulation of polymeric products in the solution, which increased the turbidity of the solution and could also be detected by ESI-MS studies. We thus preferred to direct our electrochemical studies towards the flow-through configuration because the shorter timescale of the experiment and the constant renewal of the electrolyzed solution insured the absence of contamination from slower secondary reactions.

The electrochemical investigations were therefore pursued in a combined on-line electrochemical cell/ESI-MS experimental setup (Figure 6). The flow configuration and the characteristics of this setup are described in full details elsewhere.[33] Briefly, the feed stream in this cell reaches the sample electrode through the outer annulus of a concentric dual capillary arrangement. The feed stream is split into an outer stream that diverges outwards and washes away the cell solution and an axial stream that flows inward through a 20-μm gap between the glassy carbon sample and the flat end of the dual capillary arrangement. The feed converges into an inner capillary transfer line that leads to the mass spectrometer. We preferred this type of setup over a regular tabular flow cell in order to avoid chemical interference due to the oxidation reactions on the counter-electrode. This configuration also minimizes ohmic potential drops in the cell. Note that, unlike regular flow-through electrochemical detectors that operate under mass-transport-limited conditions, we target a kinetically controlled reaction. Thus, by use of conventional flow-through cells, oxidized compounds generated at the counter-electrode will most probably escape electroreduction on the working electrode and will reach the transfer line to the mass spectrometer. This phenomenon may result either in the appearance of oxidized species in the MS or, even worse, in the occurrence of chemical reactions between the compounds generated at the counter-electrode and the working electrode. The flow cell of Figure 6 assures the confinement of the compounds gen-

erated at the counter-electrode away from the transfer line to the mass spectrometer.

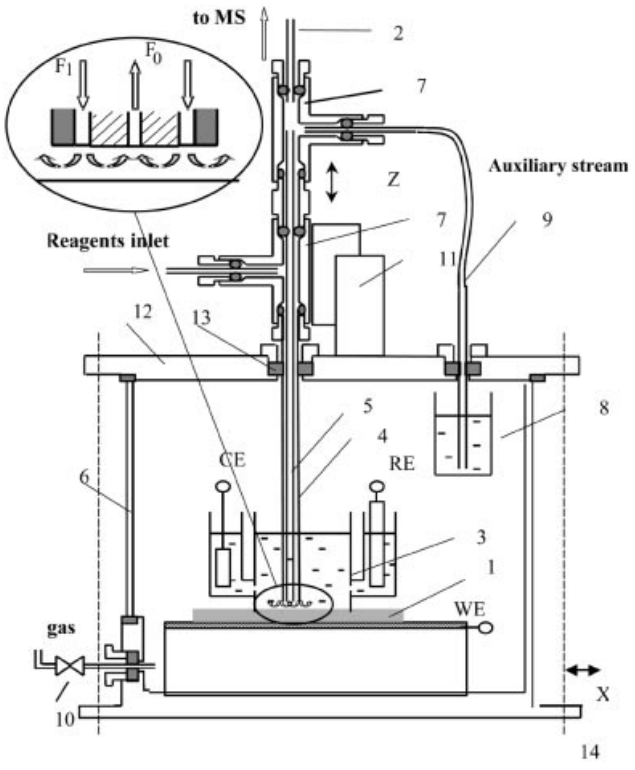

Figure 6. Scheme of the electrochemical cell used in this study; 1: working electrode; 2: transfer line to the ESI/MS; 3: three-compartment electrochemical glass cell; 4: outer capillary; 5: inner capillary; 6: pressure chamber; 7: T-junction; 8: auxiliary fluid beaker; 9: auxiliary capillary; 10: pressure regulator; 11: Z-translation stage; 12: pressure chamber cover; 13: rubber seal; 14: steel rod; insert: a scheme of the miniature flow cell formed at the bottom of the coaxial capillary setup; F_1 is the feed through the annulus of the coaxial capillary setup; F_0 is the product stream to the MS

Mass spectra are continuously recorded during the coupled EC/ESI-MS experiments, and so a three-dimensional domain of signal intensities as a function of *m*/*z* and time is generated. Projection of this space onto an *m*/*z* axis for a given time range gives a time-integrated traditional mass spectrum, while projection onto the time axis for a given *m*/*z* range gives the time evolution of the chosen species. Under potential ramp constraint, a potential-dependent generation or consumption of the specific compounds is obtained.

In order to translate the time-dependent relative abundances into potential-dependent curves it is necessary to measure the lag time in the transfer line from the electrochemical flowcell to the mass spectrometer and to estimate the degree of back-mixing (i.e. signal averaging) in the transfer line. These parameters were determined by application of a potential step to the GC working electrode between −0.35 and −0.9 V. According to the voltammetric curve (b) shown in Figure 5, the Mo species in the solution are exclusively in their oxidized state at $E = -0.35$ V, while reduction processes occur at $E = -0.9$. Figure 7 shows that the application of the potential step sharply decreases the concentration of $[Cp^*_2Mo_2O_5H^+]$. The intensity of the signal starts to decrease after a delay time of ca. 25 s. This seemingly corresponds to the retention time in the transfer line, in agreement with flow calculations. An additional 15-s interval is required to reach the half height of the concentration step change. The deviation of the MS response from a sharp step change is attributable to back-mixing in the transfer line and to the time constant of the ESI interface. Thus, the "lag time" of the instrument is approximately 40 s. The coupled EC/ESI-MS experiment with a continuous potential linear scan were therefore recorded under the quite slow scan rate conditions of 0.5 mV s^{-1}.

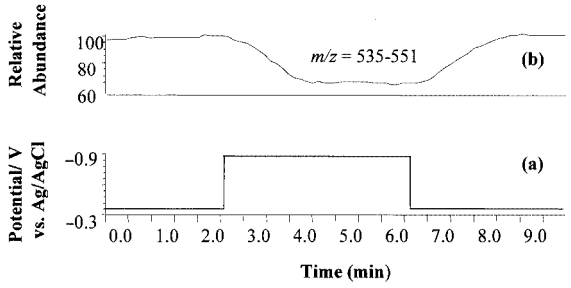

Figure 7. Response of the EC/ESI-MS (positive mode) to a potential step change of the GC electrode; feed stream: $[Cp^*_2Mo_2O_5]$ (1 mM) in 0.25 M NH_4Ac H_2O/MeOH (1:1) at pH = 4; (a) potential step function; (b) time trace of the $[Cp^*_2Mo_2O_5H^+]$ signal intensity, integrated over the given *m*/*z* range

Figure 8 shows the potential-dependent abundance of all major species present in solution under open-circuit conditions {i.e., the mononuclear $[Cp^*MoO_2^+]$ and $[Cp^*MoO_3H_2^+]$, the dinuclear $[Cp^*_2Mo_2O_5H^+]$, the trinuclear $[Cp^*_3Mo_3O_7^+]$ and the tetranuclear $[Cp^*_4Mo_4O_9(OH)_3^+]$; see Figure 1 (a)}, during the electroreduction process. The recorded signal was obtained by summing the relative abundances of all the peaks in each respective *m*/*z* range, covering the entire isotope envelope. The time axis of the product evolution curve was synchronized with the corresponding potential scale by the use of a 40 s delay time based on the potential step-change studies. During the backward, anodic scan, the concentration profiles essentially follow the same pattern as observed in the cathodic scan, indicating that the experiment is not significantly polluted by film-deposition processes. It is to be noted that all species start to be reduced at approximately the same potential. This would seem consistent with the presence of rapid equilibria between the various complexes, as proposed above, and with the selective reduction of only one of these species. However, it cannot be excluded that all the different species, or at least some of them, are reduced independently at approximately the same potential. A clarification of this point needs additional experiments under different concentration and pH conditions, which are in progress and will be reported in due course.

The mass spectrum measured at the switching potential (see Figure 9) reveals a set of new peaks corresponding to the different products of electrochemical reduction. New isotopic patterns corresponding to the formation of reduced

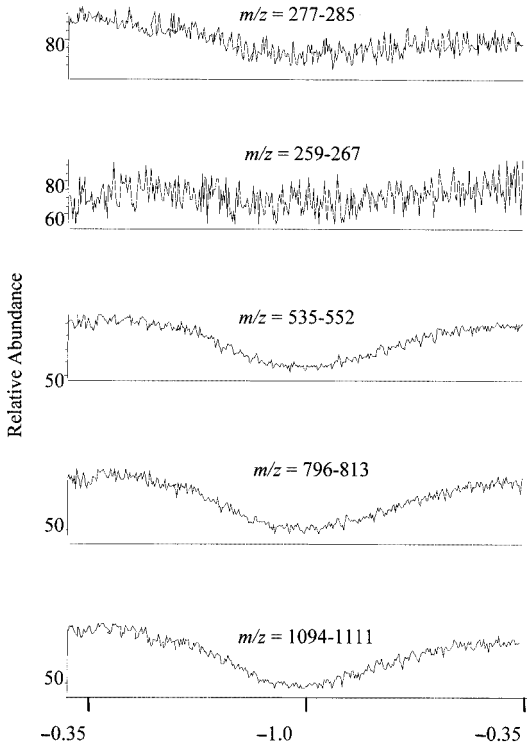

Figure 8. Mass spectra and potential-dependent abundance of the initially present species during a linear potential sweep (scan rate 0.5 mV s^{-1} from −0.35 to −1.0 V and back); experimental conditions are as specified in Figure 7

mononuclear, dinuclear, trinuclear, and tetranuclear species evolved at reduced potentials.

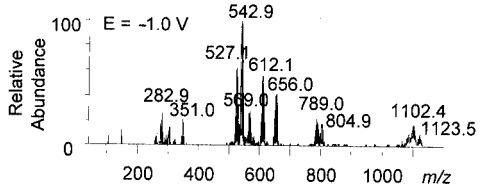

Figure 9. Mass spectrum recorded at $E = -1.0$ V (switching potential) during the EC/ESI-MS study of $[Cp^*_2Mo_2O_5]$; experimental conditions are as specified in Figure 7

The potential-dependence of the MS intensities of the reduced molybdenum species are shown in Figure 10, together with their corresponding MS isotopic patterns and assigned structures. The last are based on the fit of the observed MS isotope patterns to the calculated isotope distributions. It should be noted that, although the molecular weight and Mo nuclearity are unambiguous, the assigned structures are only tentative. Alternative possibilities exist: species $[Cp^*_2Mo_2O_2(OAc)_2^+]$, for instance, may display two terminal oxo and two bridging acetato ligands, or two bridging oxo and two terminal (chelating) acetato ligands, or all ligands may be bridging, as shown in Figure 10. The chosen assignments are based on comparison with related examples from the literature. The closest analogues to the dinuclear complexes are half-sandwich sulfido and alkylsulfido species extensively investigated in the groups of Rakowski-Dubois and Pétillon.[34−36] No previous report of compounds in which the $[Cp^*_2Mo_2^{n+}]$ core is fully coordinated by hard, oxygen-based ligands seems to be available, the exceptions being the starting material $[Cp^*_2Mo_2O_5]$ and the corresponding Mo^V dimer $[Cp^*_2Mo_2O_4]$.[24,37,38] Related trinuclear [Cp*Mo] species of formula $[Cp^*_3Mo_3O_6H_n]^{2+}$ (n = 4, 5, 6), on the other hand, have previously been reported by Bottomley et al.[39] Amongst tetranuclear oxo clusters, the closest relationship is found with a Cp derivative, a red isomer of "$[CpMoO_2]$", the nuclearity of which was based solely on molecular weight determinations.[40] The more stable orange isomer has a dinuclear structure. A more reduced tetranuclear oxo cluster, $[Cp^*_4Mo_4O_7]$, formally a $Mo^{4.5+}$ species, has also previously been described.[41] No indication has been obtained, however, that the latter species is formed under our experimental conditions.

As shown in Figure 10 (central column), the isotopic envelopes of most identified species do not overlap with the other nearby isotopic patterns. An exception is the dinuclear complex $[Cp^*_2Mo_2O_4H^+]$ (m/z = 519−535), which overlaps with another species with m/z = 517−533, a daughter ion obviously deriving from hydrogen loss from the Cp* rings. The voltage-dependent intensity of the $[Cp^*_2Mo_2O_4H^+]$ species is obtained by integration of an m/z region where the overlap with the minor species is minimal (m/z = 532−534). Complex $[Cp^*MoO(OAc)^+]$ (m/z = 302−310) overlaps with another species with one fewer mass unit, indicating fragmentation with loss of hydrogen atoms. The envelope of the reduced trinuclear species is shifted to lower m/z by exactly 16 units from that of its precursor complex $[Cp^*_3Mo_3O_7^+]$, suggesting its formulation as a proton-free hexaoxo species.

The assignment of the chemical formulas for the reduced species is further supported by ion-trap MS^n fragmentation studies, the results being collected in Table 1. All MS^n studies were conducted with isolation widths corresponding to the whole range of the observed isotope patterns. The m/z = 302−310 monoacetate complex shows loss of acetic acid and formation of a methanol adduct in the MS^2. Similarly, the diacetate mononuclear complex (m/z = 345−353) exhibits loss of an acetic acid unit. The low stability of these low-weight mononuclear fragments did not allow further MS^3 fragmentation studies. The assignment of the m/z = 519−535 to a $[Cp^*_2Mo_2O_4H^+]$ species is supported by $MS^2/MS^3/MS^4$ subsequent fragmentations showing a consecutive series of single dehydrations. In addition, an MS^n study of separately synthesized $[Cp^*_2Mo_2O_4]$ revealed an identical fragmentation pathway. The assignment of m/z = 561−577 to a $[Cp^*_2Mo_2O_3(OAc)]$ species is supported by MS^2 fragmentation showing neutral losses of an acetyl fragment or water. The isotope pattern at m/z = 604−620 is assigned to $[Cp^*_2Mo_2O_2(OAc)_2^+]$ on the basis of the acetyl loss and dimer cleavage to give the $[Cp^*MoO_2(OAc)^+]$ and $[Cp^*MoO(OAc)_2^+]$ cationic fragments in the MS^2. The $[Cp^*_2Mo_2O(OAc)_3^+]$ complex (m/z = 647−663) gives rise to three different fragmentations at different collision ener-

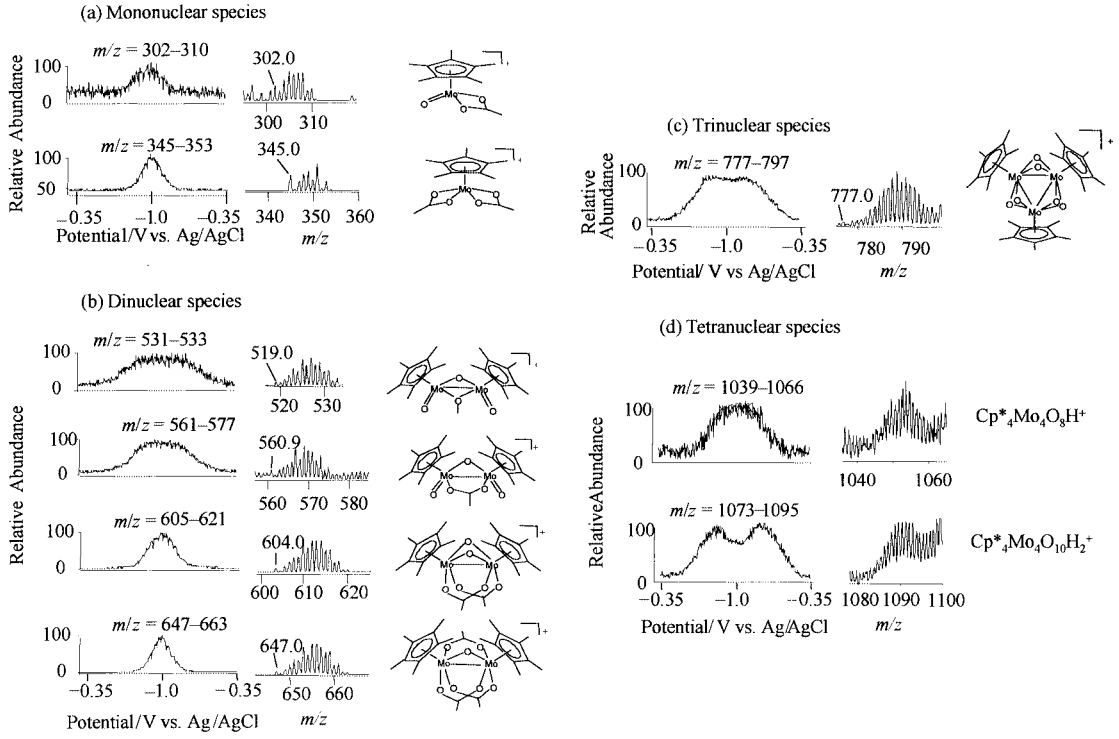

Figure 10. Potential dependence of the relative abundance of selected species generated during the coupled electrochemistry/ESI-MS of $[Cp^*_2Mo_2O_5]$; left: potential-dependent evolution of the integrated signal, the *m/z* range used for signal integration is specified above each curve; center: expanded isotopic pattern; right: proposed chemical structure; experimental conditions are as specified in Figure 7

gies, corresponding to loss of a one and two acetyl groups, and to dimer cleavage to give the mononuclear fragment $[Cp^*Mo(OAc)_2^+]$. Further MS^3 fragmentation of $[Cp^*Mo(OAc)_2^+$ reveals an additional acetyl loss. Finally, MS^4 fragmentation of $[Cp^*Mo(OAc)^+]$ reveals one oxygen atom loss.

The MS^n fragmentation of the trinuclear species is even more complicated. The primary species $[Cp^*_3Mo_3O_6^+]$ (m/z = 777−799) produces four fragments in the MS^2. The first two correspond to loss of $C_5Me_4CH_2$ and $C_5Me_4CH_2 + H_2O$, respectively, the third is a methanol adduct of the second, and the fourth corresponds to $[Cp_2Mo_2O_4^+]$, resulting from the loss of $[Cp^*MoO_2]$. It should be noted that the latter cleavage involves disruption of two oxo bridges and indeed it occurs at much higher collision energy than the first three processes. MS^3 fragmentation of the methanol adduct results in MeOH loss, and a subsequent MS^4 fragmentation reveals four ions corresponding to Cp* loss plus formation of three solvent adducts of the resulting fragment. MS^3 and MS^4 fragmentation of $[Cp^*_2Mo_2O_4^+]$ give rise to subsequent dehydration processes. No MS^n study of the reduced tetranuclear species could be carried out, because of the very low abundance of these peaks.

Table 2 presents the approximate potential values for the appearance of the various reduced species that may be measured in Figure 10. Analysis of these values enabled us to derive a certain number of conclusions: (i) for a given nuclearity, the potential becomes more negative as the oxidation state decreases, as one would expect, (ii) when comparing species of the same formal oxidation state, the dinuclear compounds are always obtained at a less negative potential than the mononuclear ones, while the tetranuclear $[Cp^*_4Mo_4O_8H^+]$ species is obtained at approximately the same potential (−0.52 V) as the dinuclear $[Cp^*_2Mo_2O_4H^+]$ species (−0.48 V), (iii) the latter complex is obtained at a less negative reduction potential than the other Mo^V dinuclear species containing an acetate ligand, and finally (iv) this potential nearly matches the potential at which the peaks of the starting complex start to disappear (Figure 8). The large deviation between the threshold formation potentials and the mid-intensity potential $E_{1/2}$ points to kinetically controlled formation reactions for all of the reduced molybdenum species. This is unfortunate, since it precludes direct evaluation of the corresponding thermodynamic formation parameters for these new compounds.

These combined observations may be interpreted as follows. The mononuclear products are likely to derive from the one-electron reduction of $[Cp^*MoO_2^+]$, affording a neutral radical. At more negative potentials, the latter species may be reduced further, possibly after a protonation stage. At each oxidation state level, two competing processes may occur: namely acetate/hydroxide exchange and dimerization (accompanied by the establishment of a metal−metal bond). For instance, the neutral Mo^V intermediate may dimerize to $[Cp^*_2Mo_2O_4]$, which is then detected by ESI-MS in its protonated form, or it may be protonated and the resulting $[Cp^*MoO(OH)^+]$ species may undergo a hydroxide/acetate exchange to produce the observed

Table 1. Assigned formulas and MS^n studies of the reduction products formed during EC/ESI-MS studies of $[Cp^*_2Mo_2O_5]$

Product of EC reduction	MS^2		MS^3		MS^4	
Loss	Range of isotopic pattern	Loss	Range of isotopic pattern	Loss	Range of isotopic pattern	
$[Cp^*_3Mo_3^{V,V,VI}O_6^+]$	$-C_5Me_4CH_2$	643–665	n.a.[a]	n.a.	n.a.	n.a.
m/z = 777–799						
$-Cp^*-OH$	625–647	n.a.	n.a.	n.a.	n.a.	
$-Cp^*-OH+MeOH$	653–675	$-MeOH$	625–647	$-H_2O$	607–629	
$-C_5Me_4CH_2+2H_2O$	509–531					
$-C_5Me_4CH_2+2H_2O+MeOH$	541–563					
$-C_5Me_4CH_2+H_2O$	490–512					
$[Cp^*_2Mo_2^{IV,IV}O(OAc)_3^+]$	$-OAc-O$	572–588	n.a.	n.a.	n.a.	n.a.
m/z = 647–663						
$-2(OAc)-O$	513–529	n.a.	n.a.	n.a.	n.a.	
$-[Cp^*MoO(OAc)]$	345–353	$-OAc$	286–294	$-O$	270–278	
$[Cp^*_2Mo_2^{IV,V}O_2(OAc)_2^+]$	$-OAc$	542–558	n.a.	n.a.	n.a.	n.a.
m/z = 604–620						
$-[Cp^*MoO(OAc)]$	302–310	n.a.	n.a.	n.a.	n.a.	
$-[Cp^*MoO]$	361–369	n.a.	n.a.	n.a.	n.a.	
$-2(OAc)$	486–502	$-H_2O$	468–484	n.a.	n.a.	
$[Cp^*_2Mo_2^{V,V}O_3(OAc)^+]$	$-OAc$	502–518	n.a.	n.a.	n.a.	n.a.
m/z = 561–577						
$-H_2O$	543–559	n.a.	n.a.	n.a.	n.a.	
$[Cp^*_2Mo_2^{V,V}O_4H^+]$	unclear	360–368	n.a.	n.a.	n.a.	n.a.
m/z = 519–533						
$-H_2O$	501–517	$-H_2O$	483–499	$-H_2O$	465–481	
$[Cp^*Mo^{IV}(OAc)_2^+]$	$-AcOH$	285–293	n.a.	n.a.	n.a.	n.a.
m/z = 345–353						
$[Cp^*Mo^{V}O(OAc)^+]$	$-AcOH+MeOH$	274–282	n.a.	n.a.	n.a.	n.a.
m/z = 302–310						

[a] n.a. = not available

Table 2. Threshold potential (E_{in}) and half-wave potential ($E_{1/2}$) corresponding to the formation of reduced compounds during the EC/ESI-MS study of $[Cp^*_2Mo_2O_5]$ in methanol/water/acetate solutions; experimental conditions are described in the caption of Figure 9

Compound	m/z	E_{in}[a] [V]	$E_{1/2}$ [V]
$[Cp^*_4Mo_4^{V,VI,VI,VI}O_{10}H^+]$	1073–1100	−0.40	−0.47
$[Cp^*_4Mo_4^{V,V,V,V}O_8H^+]$	1040–1067	−0.52	−0.61
$[Cp^*_3Mo_3^{V,V,VI}O_6^+]$	777–800	−0.48	−0.75
$[Cp^*_2Mo_2^{IV,IV}O(OAc)_3^+]$	647–663	−0.78	−0.94
$[Cp^*_2Mo_2^{IV,V}O_2(OAc)_2^+]$	604–620	−0.74	−0.91
$[Cp^*_2Mo_2^{V,V}O_3(OAc)^+]$	561–577	−0.55	−0.81
$[Cp^*_2Mo_2^{V,V}O_4H^+]$	519–533	−0.48	−0.77
$[Cp^*Mo^{IV}(OAc)_2^+]$	345–353	−0.81	−0.94
$[Cp^*Mo^{V}O(OAc)^+]$	302–310	−0.76	−0.92

[a] E_{in} is defined as the potential corresponding to a 100% abundance increase over the background signal. $E_{1/2}$ = potential at which half of the maximum signal intensity is obtained.

$[Cp^*MoO(OAc)^+]$. The driving force of the rapid and irreversible metal–metal bond formation would account for the smaller reducing potential needed to generate an oligonuclear species relative to a mononuclear one at the same oxidation state level. It is also possible, however, that the higher nuclearity products are obtained by direct reduction of the higher nuclearity species present in solution. It can be noted that each one-electron reduction for the mononuclear and dinuclear species is formally accompanied by the replacement of one oxygen atom with an acetate group (corresponding to a mass increase of 43 units). The only exception to this substitution rule is the observation of two different compounds with the $Mo_2^{V,V}$ core and related to each other by the formal replacement of an OH with an acetate group. The spectrum in Figure 9 does not show any mononuclear species with a mass greater than the 345–353 envelope, nor dinuclear species with a mass greater than the 647.0–664.0 envelope. This suggests that no Mo species in oxidation states lower than +4 are produced under the experimental conditions chosen.

The major trinuclear product obtained under reducing conditions is an $Mo_3^{V,V,VI}$ species. On the other hand, the same basic structure was reported for the dicationic $Mo_3^{IV,IV,V}$, $Mo_3^{IV,IV,IV}$, and $Mo_3^{III,IV,IV}$ complexes $[Cp^*_3Mo_3O_6H_n^{2+}]$ (n = 4, 5, 6).[39] Although the isotope envelope simulation quite clearly indicates the nature of the major product, minor amounts of products of further reduction cannot be excluded. We did not observe any signals attributable to dicationic species. It is possible that the reduction potential range and the conditions used in this study do not allow access to the more reduced known trinuclear species, which were in fact previously obtained by zinc reduction of $[Cp^*MoO_2Cl]$ under non-aqueous conditions.[39]

As far as the tetranuclear reduction products are concerned, the $[Cp^*_4Mo_4O_8H]^+$ species may be related to the kinetic isomer previously identified for the Cp system when complex $[CpMoCl_4]$ is hydrolyzed, namely $[Cp_4Mo_4O_8]$.[40]

It is believed that this complex does not contain metal−metal bonds, whereas the dinuclear $[Cp_2Mo_2O_4]$ isomer does.[42] The formation of this tetranuclear compound from precursors that themselves are devoid of metal−metal interactions is therefore to be expected. The mixed-valence $[Cp^*_4Mo_4O_{10}H_2]^+$ species does not have any equivalent in the literature. The shape of the abundance vs. potential curve indicates that a direct reduction to other species, possibly the tetranuclear Mo^V cluster, becomes more favorable at more negative potentials.

As clearly shown by the cone voltage optimization study [Figure 2 (c)], the experimental conditions of the positive-mode electrospray process cannot, by themselves, induce an oxidation state decrease for the analyte. The reduced molybdenum products shown in Figure 10 must therefore originate from the electrochemical reactions in the electrochemical cell. The simple chemical composition of these species and the fact that they contain unfragmented acetate and pentamethylcyclopentadienyl ligands lead us to believe that they are all indeed solution-borne species.

Conclusion

The coupled EC/ESI-MS technique has proven to be a powerful analytical tool for the investigation of complex electrochemical transformations. At least six previously unreported species have been identified from the electroreduction of $[Cp^*_2Mo_2O_5]$, and the potential required for the generation of each one has been assessed. These species may be described as oxo- and/or acetate-stabilized $[Cp^*Mo^{n+}]$, $[Cp^*_2Mo_2^{n+}]$, $[Cp^*_3Mo_3^{n+}]$, and $[Cp^*_4Mo_4^{n+}]$ complexes. These species, as well as analogues with less coordinating anionic ligands, may be expected to result in new aqueous coordination chemistry, catalysis, and electrocatalysis. Indeed, a few dinuclear and trinuclear species related to those observed by this EC/ESI-MS investigation have been synthesized and isolated in one of our laboratories. These investigations are described in separate publications.[43,44]

Experimental Section

General Remarks: The starting compound was prepared by a literature procedure.[24] Unless otherwise stated, all solutions were prepared in H_2O/MeOH (1:1) containing CH_3COONH_4 (0.25 M) and buffered to pH = 4.0 by the addition of CH_3COOH. A lower concentration of MeOH in the spray solution resulted in significant losses of relative abundances. All reagents were purchased from Aldrich. Methanol was purchased from Baker and was of HPLC grade. The water was triple-distilled.

Electrospray Mass Spectrometry: A Finnigan (San Jose, USA) LCQ quadrupole ion trap mass spectrometer, equipped with an electrospray ionization (ESI) interface, was used for data acquisition. ESI was operated either in positive or in negative ion mode. In negative mode the tip of the capillary and the sampling cone were maintained at potentials of −3.5 kV (spray voltage) and −70 V (capillary voltage), respectively. In positive mode the spray voltage was at 3.6 kV and the capillary voltage was 25 V. The source temperature was the subject of a separate study. Mass spectra were acquired by scanning the mass analyzer from m/z = 100 to 2000 with five total microscans. The maximum injection time into the ion trap was 50 ms, and the sample injection flow rate was 5 μL min^{-1}. In all experiments, helium was introduced at an estimated pressure of 1 mTorr to improve the ion trapping efficiency. During MS^n experiments the compounds were isolated in the ion trap with isolation width of isotope pattern and activated by use of increased collision energy.

Electrochemical Investigations: A PARC 273 potentiostat/galvanostat (Princeton, USA) was used. A three-compartment electrochemical cell with a disk glassy-carbon working electrode (Metrohm, Herisau, Switzerland), platinum counter-electrode and Ag/AgCl (satd.) reference electrode (Metrohm) was used for the voltammetric studies.

Coupled Electrochemistry/Electrospray Mass Spectrometry: Figure 6 shows a scheme of the experimental setup used in this study; a detailed description of the electrochemical setup is given elsewhere.[33] The setup comprises a three-compartment electrochemical cell placed in a pressure chamber, a two coaxial capillary set, a micropositioning device, and a mass spectrometer equipped with an electrospray ionization (ESI) interface. The working glassy-carbon electrode (1) was pressed to the bottom opening of a three-compartment electrochemical cell (3). A Pt wire counter-electrode and Ag/AgCl (KCl satd.) reference electrodes were placed in the side compartments of the cell. All reported potentials are given relative to this reference electrode. The electrolyte in the cell was 0.25 M CH_3COONH_4 in H_2O/MeOH (1:1), buffered to pH = 4.0 by CH_3COOH. A $[Cp^*_2Mo_2O_5]$ solution (1 mM) in the same electrolyte was pumped through the annulus of the capillary set to the electrode. A coaxial capillary set (4, 5) was used to deliver the reagent solution to the electrode and to transfer the product stream to the interface of the mass spectrometer through the inner capillary. A syringe pump was used to deliver the feed stream to a T-junction (7) located outside the pressure chamber (6), from which the stream was directed through the annulus between the two capillaries to the electrode. The product stream (F_0) was pumped, following the interaction with the electrode, upward through the inner capillary (4) by the excess pressure in the pressure vessel. All capillaries were fused silica from SGE (Austin, USA). The inner capillary was 25 μm inner diameter, 285 μm outer diameter, 15 cm long. The product stream was diluted with excess methanol delivered from a glass beaker (8). The liquid flow rates and dilution ratio (product stream/methanol) were controlled by setting the pressure in the pressure vessel and choice of capillary length and inner diameter. The cell pressure was 2600 kPa. After mixing with the auxiliary liquid, the sample stream was delivered to the ESI interface of the mass spectrometer by a 30 cm long, 50 μm inner diameter capillary. The flow rate of the product stream was ca. 0.7 μL min^{-1}. The methanol flow in the auxiliary capillary was 14 μL min^{-1}. The reagent flow rate (F_1) was set to 4 μL min^{-1}.

Acknowledgments

R. P. and M. V. thank the CNRS and the Ministry of Research for funding. D. S. thanks the Conseil Régional de Bourgogne for a postdoctoral fellowship. A. D. M. and O. L. acknowledge the financial support of the Israel Science Foundation. J. G. thanks the University of Bourgogne for a visiting professorship. We are grateful to the French Embassy in Israel for an Arc-en-Ciel/Keshet travel grant and to Prof. G. Tsirlina for useful discussions.

[1] M. Yamashita, J. B. Fenn, *J. Phys. Chem.* **1984**, *88*, 4451−4459.
[2] R. E. March, R. J. Hujhes, *Quadrupole Storage Mass Spectrometry in Chemical analysis* (Ed.: J. D. Wiefordner), J. Wiley and Sons, New York, **1989**.
[3] M. L. Vestal, *Mass Spectrom. Rev.* **1983**, *2*, 447−480.
[4] W. Henderson, B. K. Nicholson, L. J. McCaffrey, *Polyhedron* **1998**, *17*, 4291.
[5] G. Wolfbauer, A. M. Bond, D. R. MacFarlane, *J. Chem. Soc., Dalton Trans.* **1999**, 4363−4372.
[6] A. M. Bond, R. Colton, D. G. Humphrey, P. J. Mahon, G. A. Snook, V. Tedesco, J. N. Walter, *Organometallics* **1998**, *17*, 2977−2985.
[7] B. Bittins-Cattaneo, E. Cattaneo, P. Konigshoven, W. Vielstich, in *Electroanalytical Chemistry*, vol. 16 (Ed.: A. J. Bard), Marcel-Dekker, New York − Basel − Hong Kong, **1991**.
[8] X. Xu, W. Lu, R. B. Cole, *Anal. Chem.* **1996**, *68*, 4244−4253.
[9] W. Lu, X. Xu, R. B. Cole, *Anal. Chem.* **1997**, *69*, 2478−2484.
[10] A. M. Bond, R. Colton, A. D'Agostino, A. J. Downard, J. C. Traeger, *Anal. Chem.* **1995**, *67*, 1691−1695.
[11] F. Zhou, G. J. Van Berkel, *Anal. Chem.* **1995**, *67*, 3643−3649.
[12] H. Deng, G. J. Van Berkel, *Anal. Chem.* **1999**, *71*, 4284−4293.
[13] D. K. Walanda, R. C. Burns, G. A. Lawrance, E. I. von Nagy-Felsobuki, *J. Chem. Soc., Dalton Trans.* **1999**, 311−321.
[14] B. Salignac, S. Riedel, A. Dolbecq, F. Secheresse, E. Cadot, *J. Am. Chem. Soc.* **2000**, *122*, 10381−10389.
[15] M. Herberhold, W. Kremnitz, A. Razavi, H. Schöllhorn, U. Thewalt, *Angew. Chem. Int. Ed. Engl.* **1985**, *24*, 601−602.
[16] K. Isobe, S. Kimura, Y. Nakamura, *J. Organomet. Chem.* **1987**, *331*, 221−228.
[17] P. Gomez-Sal, E. de Jesus, P. Royo, A. Vazquez de Miguel, S. Martinez-Carrera, S. Garcia-Blanco, *J. Organomet. Chem.* **1988**, *353*, 191−196.
[18] P. Leoni, M. Pasquali, L. Salsini, C. di Bugno, D. Braga, P. Sabatino, *J. Chem. Soc., Dalton Trans.* **1989**, 155−159.
[19] A. L. Rheingold, J. R. Harper, *J. Organomet. Chem.* **1991**, *403*, 335−344.
[20] J. W. Faller, Y. Ma, *J. Organomet. Chem.* **1988**, *340*, 59−69.
[21] K. Umakoshi, K. Isobe, *J. Organomet. Chem.* **1990**, *395*, 47−53.
[22] J. Sundermeyer, U. Radius, C. Burschka, *Chem. Ber.* **1992**, *125*, 2379−2384.
[23] M. S. Rau, C. M. Kretz, G. L. Geoffroy, A. L. Rheingold, *Organometallics* **1993**, *12*, 3447−3460.
[24] D. Saurenz, F. Demirhan, P. Richard, R. Poli, H. Sitzmann, *Eur. J. Inorg. Chem.* **2002**, 1415−1424.
[25] E. Collange, J. Garcia, R. Poli, *New J. Chem.* **2002**, *26*, 1249−1256.
[26] J. C. Traeger, *Int. J. Mass Spectr.* **2000**, *200*, 387−401.
[27] R. Colton, J. C. Traeger, *Inorg. Chim. Acta* **1992**, *201*, 153−155.
[28] A. M. Bond, R. Colton, J. B. Cooper, J. C. Traeger, J. N. Walter, D. M. Way, *Organometallics* **1994**, *13*, 3434−3441.
[29] M. J. Winter, *Sheffield Chemputer*, http://www.shef.ac.uk/chemistry/chemputer/
[30] W. Henderson, J. S. McIndoe, B. K. Nicholson, P. J. Dyson, *Chem. Commun.* **1996**, 1183.
[31] W. Z. Shou, R. F. Browner, *Anal. Chem.* **1999**, *71*, 3365−3373.
[32] E. C. Kempen, J. S. Brodbelt, *Anal. Chem.* **1999**, *71*, 5493−5500.
[33] A. D. Modestov, S. Srebnik, O. Lev, J. Gun, *Anal. Chem.* **2001**, *73*, 4229−4240.
[34] M. Rakowski DuBois, *Chem. Rev.* **1989**, *89*, 1−9.
[35] M. Rakowski DuBois, *Polyhedron* **1997**, *16*, 3089−3098.
[36] F. Y. Pétillon, P. Schollhammer, J. Talarmin, K. W. Muir, *Coord. Chem. Rev.* **1998**, *178/179*, 203−247.
[37] H. Arzoumanian, A. Baldy, M. Pierrot, M. Petrignani, *J. Organomet. Chem.* **1985**, *294*, 327−331.
[38] E. de Jesus, A. Vazquez de Miguel, P. Royo, A. M. M. Lanfredi, A. Tiripicchio, *J. Chem. Soc., Dalton Trans.* **1990**, 2779−2784.
[39] F. Bottomley, J. Chen, K. F. Preston, R. C. Thompson, *J. Am. Chem. Soc.* **1994**, *116*, 7989−7995.
[40] M. Cousins, M. L. H. Green, *J. Chem. Soc.* **1964**, 1567−1572.
[41] F. Bottomley, V. Sanchez, R. C. Thompson, O. O. Womiloju, Z. Q. Xu, *Can. J. Chem.* **2000**, *78*, 383−394.
[42] C. Couldwell, K. Prout, *Acta Crystallogr., Sect. B* **1978**, *34*, 933−934.
[43] F. Demirhan, J. Gun, O. Lev, A. Modestov, R. Poli, P. Richard, *J. Chem. Soc., Dalton Trans.* **2002**, 2109−2111.
[44] F. Demirhan, P. Richard, R. Poli, *Inorg. Chim. Acta*, in press.

Received June 19, 2002
[I02336]

New Monocyclopentadienyl Complexes of Tantalum(V) and Titanium(IV) with Chelating Pyrimidinethiolate and Oxypyridine Ligands − Molecular Structure of [Cp*$TaCl_3(SC_6H_7N_2)$]

Rosa Fandos,*[a] Carolina Hernández,[a] Antonio Otero,*[b] Ana Rodríguez,[c] María José Ruiz,[a] and Pilar Terreros[d]

Keywords: N ligands / S ligands / Tantalum / Titanium / Cyclopentadienyl ligands

New monocyclopentadienyl species of Ta^V, [Cp*TaL_3(XR)] (L = Cl, Me, X = O, S) bearing 4,6-dimethyl-2-pyrimidinethiolate (SR = $SC_6H_7N_2$) or 3-cyano-4,6-dimethyloxypyridine (OR = $OC_8H_7N_2$) ligands were prepared, namely [Cp*$TaCl_3(SC_6H_7N_2)$] (**1**), [Cp*$TaCl_3(OC_8H_7N_2)$] (**2**), [Cp*$TaMe_3(SC_6H_7N_2)$] (**3**). In addition, a bis(oxypyridine)titanium(IV) complex [Cp*$TiMe_2(OC_8H_7N_2)_2$] was isolated. The X-ray structure analysis of **1** revealed that the thiolate group is bonded to the metal center through the sulfur atom and one of the nitrogen atoms in an η^2-fashion. The reactivity of complex **3** with isocyanides (CNR), R = *t*Bu, Xyl (Xyl = 2,6-dimethylphenyl) was also studied showing differences depending on the nature of R group. The reaction with 2,6-dimethylphenyl isocyanide gives the azatantalacyclobutane complex [Cp*TaMe{XylN=CC(Me_2)NXyl}($SC_6H_7N_2$)] (**5**) as the final product, whereas in the reaction with *tert*-butyl isocyanide the η^2-imine-containing complex [Cp*Ta{*t*BuNC(Me_2)}($SC_6H_7N_2$)] (**6**) is proposed to be formed. The dynamic behavior of [Cp*$TaMe_3(SC_6H_7N_2)$] (**3**) was also studied by variable-temperature ^1H NMR spectroscopy.
(© Wiley-VCH Verlag GmbH & Co. KGaA, 69451 Weinheim, Germany, 2003)

Introduction

Ligand systems with two different donor atoms are attracting increasing interest in the chemistry of metal complexes. Under appropriate conditions, the remaining donor atom can coordinate reversibly to the metal center and eventually block a vacant coordination site.[1] In this field, complexes that incorporate pyridinethiolate and pyrimidinethiolate, as well as their alkoxide analogues, are interesting for their ability to chelate and bridge transition metal atoms, allowing access to both mono- and oligonuclear products. In addition, they contain functional groups that are common in crude oils and nucleic acids. The thiolate complexes are of particular interest in the field of bioinorganic chemistry due to their relevance to the structure, bonding and function of biologically active reaction centers such as nitrogenase or metalothioneins.[2,3]

Thiolate complexes also play an important role in different reactions, such as the desulfurization of organosulfur compounds [4,5] and metal-catalyzed synthetic reactions involving C−S bond cleavage and formation.[6] All of these features, as well as the propensity of sulfur to form M(μ-SR)M′ bridges, has led to the widespread use of sulfur-containing complexes as synthons for multinuclear transition metal complexes.[7]

Alkoxide and aryloxide ligands have been widely used to stabilize high oxidation states of early transition metals[8] and numerous studies have been reported concerning the catalytic activity of their complexes in alkene metathesis and, in particular, in alkene polymerization.[9]

A systematic study of the chemistry of mono- and bis(cyclopentadienyl) complexes of group-4 transition metals bearing chelating pyrimidinethiolate ligands and analogous oxygen derivatives has been carried out by our research group in recent years.[10] The interesting coordination modes and the reactivity observed along with the scarce number of reported examples of this kind of compounds[11] encouraged us to prepare analogous monocyclopentadienyl complexes of group-5 metals. In particular, this paper will focus on the synthesis, structural details and reactivity of

[a] Departamento de Química Inorgánica, Orgánica y Bioquímica, Universidad de Castilla-La Mancha, Facultad de Ciencias del Medio Ambiente
Avda. Carlos III, sn 45071 Toledo, Spain
[b] Departamento de Química Inorgánica, Orgánica y Bioquímica, Universidad de Castilla-La Mancha, Facultad de Químicas, Campus de Ciudad Real, 13071 Ciudad Real, Spain
Fax: (internat.) + 34-926/295318
E-mail: antonio.otero@uclm.es
[c] Departamento de Química Inorgánica, Orgánica y Bioquímica, Universidad de Castilla-La Mancha, ETS Ingenieros Industriales,
Avda. Camilo José Cela, 3, 13071 Ciudad Real, Spain
[d] Instituto de Catálisis y Petroleoquímica, CSIC, Cantoblanco, 28049 Madrid, Spain

new monocyclopentadienyl complexes of tantalum(v) and titanium(iv) bearing chelating pyrimidinethiolate and oxypyridine ligands.

Results and Discussion

The reaction of [Cp*TaCl$_4$] (Cp* = η^5-C$_5$H$_5$) with 4,6-dimethyl-2-mercaptopyrimidine (HSR, R = C$_6$H$_7$N$_2$) in the presence of 1 equiv. of triethylamine proceeds at room temperature in toluene to yield the complex [Cp*TaCl$_3$(SR)] (**1**) [Equation (1)]. Attempts to perform the substitution of a second chlorine atom by a thiolate ligand were made under a wide variety of conditions but no further reaction was observed and in all cases the only isolated compound was **1**.

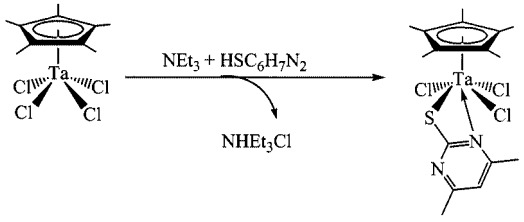

(1)

1

Complex **1** was isolated as an air-sensitive orange solid, soluble in toluene and THF and less soluble in pentane or Et$_2$O. It was characterized by ^{1}H and ^{13}C NMR and IR spectroscopy as well as by elemental analysis (see Exp. Sect.). The ^{1}H and ^{13}C NMR spectra indicate that the thiolate ligand is bonded to the metal atom in a bidentate fashion. For example, two resonances at δ = 1.71 and 2.88 ppm are present in the ^{1}H MNR spectrum for the two nonequivalent methyl groups of the thiolate ligand, in accordance with the proposed η^2-*S*,*N* coordination mode.

Crystals of **1**, suitable for an X-ray crystal structure determination, were obtained by slow diffusion of pentane into a saturated solution of the complex in toluene. Figure 1 shows an ORTEP diagram of the molecule; selected bond lengths and angles are given in Table 1.

The structure consists of discrete molecules separated by van der Waals distances. The tantalum atom is bonded to the cyclopentadienyl ring in an η^5-mode, to three chlorine atoms and to the thiolate ligand in the proposed chelate fashion. In this way, the coordination around the metal atom is pseudo-octahedral, with the tantalum atom 0.59 Å out of the plane defined by the S(1), Cl(1), Cl(2) and Cl(3) atoms. The nitrogen atom of the pyrimidinethiolate ligand is located *trans* to the Cp* group. The Ta(1)−S(1) bond length [2.456(2) Å] is as expected for tantalum(v) thiolate complexes[12] and the Ta(1)−N(1) bond [2.327(5) Å] is also in the normal range for pyridyltantalum(v) complexes.[13] Finally, the Ta(1)−S(1)−C(1) angle [84.6(2)°] is in accordance with others observed in this kind of complexes.[10,11]

When 3-cyano-2-hydroxy-4,6-dimethylpyridine was treated with [Cp*TaCl$_4$] in the presence of Et$_3$N in toluene at room temperature [Equation (2)] complex **2** was isolated

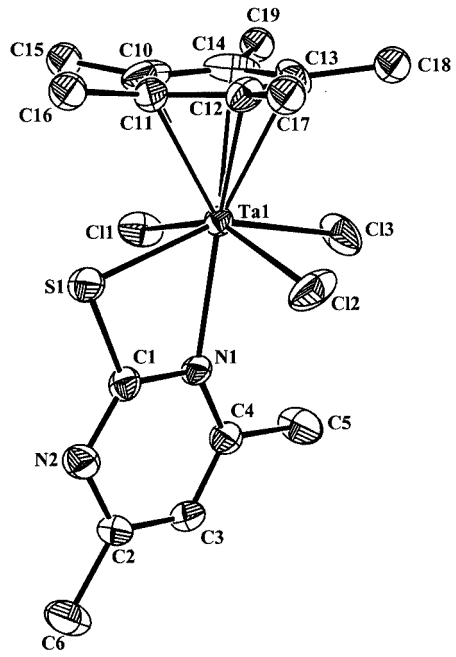

Figure 1. ORTEP drawing of complex **1** with the atomic labeling scheme; hydrogen atoms omitted for clarity; thermal ellipsoids are at the 30% level of probability

Table 1. Bond lengths [Å] and angles [°] for **1**

Ta(1)−N(1)	2.327(5)	N(1)−Ta(1)−Cl(1)	76.2(1)
Ta(1)−Cl(3)	2.393(2)	N(1)−Ta(1)−Cl(2)	76.3(2
Ta(1)−Cl(2)	2.407(2)	N(1)−Ta(1)−Cl(3)	87.6(1)
Ta(1)−Cl(1)	2.407(2)	Cl(2)−Ta(1)−Cl(1)	151.37(8)
Ta(1)−C(14)	2.431(8)	Cl(3)−Ta(1)−Cl(1)	85.4(1)
Ta(1)−C(11)	2.447(7)	Cl(3)−Ta(1)−Cl(2)	85.5(1)
Ta(1)−S(1)	2.456(2)	N(1)−Ta(1)−S(1)	64.3(1)
Ta(1)−C(13)	2.463(8)	Cl(1)−Ta(1)−S(1)	87.87(8)
Ta(1)−C(10)	2.472(8)	Cl(2)−Ta(1)−S(1)	87.49(9)
Ta(1)−C(12)	2.484(7)	Cl(3)−Ta(1)−S(1)	151.96(7)
		C(1)−S(1)−Ta(1)	84.6(2)
		C(1)−N(1)−Ta(1)	99.5(4)
		C(4)−N(1)−Ta(1)	143.8(4)

as a yellow, air-sensitive solid which was sparingly soluble in alkanes but soluble in toluene or THF.

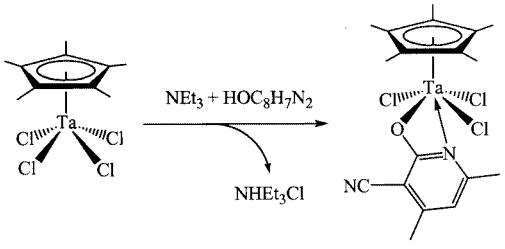

(2)

2

The ^{1}H and ^{13}C NMR spectra for **2** are analogous to those previously described for **1**. For example, the ^{1}H NMR spectrum exhibits two singlet resonances at δ = 1.52 and 2.49 ppm, attributable to the two nonequivalent methyl

groups of the alkoxide ligand. By analogy with the situation for compound **1**, a bidentate coordination mode for the alkoxide ligand is proposed to be present in this complex.

Another general way to synthesize thiolate complexes is to carry out the protonolysis of metal−alkyl bonds with the corresponding thiol. In this way, the reaction of Cp^*TaMe_4 with 2-mercapto-4,6-dimethylpyrimidine at 80 °C in toluene yields $[Cp^*TaMe_3(SR)]$ (**3**) as an orange solid which is soluble in toluene and THF and scarcely soluble in pentane [Equation (3)]. As in the case of the chlorinated complex **1**, all attempts to increase the number of thiolate ligands around the metal atom were unsuccessful.

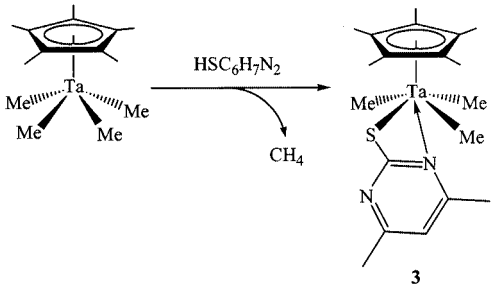

3 (3)

The ^{1}H NMR spectrum of **3** at room temperature shows a broad resonance at δ = 2.43 ppm that integrates for six protons and which is assigned to the methyl groups of the thiolate ligand. The broadness of the peak indicates a fluxional behavior through which both nitrogen atoms interchange their positions in the coordination sphere of the tantalum atom by rotation around the S−C bond (Scheme 1).

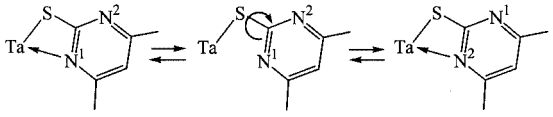

Scheme 1

In order to study this fluxional behavior a variable-temperature (VT) ^{1}H NMR experiment was carried out. At −40 °C the methyl groups are inequivalent and appear as two signals at δ = 2.74 and 2.04 ppm, indicating that rotation around the C−S bond is hindered for the thiolate ligand. When the temperature is raised, the peaks coalesce at −10 °C. The two site-exchange equations[14] and the coalescence temperature of 263 K can be used to estimate a value for $\Delta G^{\neq}$ of 12.0(2) kcal·mol^{-1} for the process. This value is in accordance with that previously found for analogous systems, i.e. $[Cp_2ZrMe(SR)]$ (SR = 4,6-dimethylpyrimidine-2-thiolate).[10a]

Complex **4** was synthesized in a similar way to **3**, by reaction of $[Cp^*TiMe_3]$ with 2 equiv. of 3-cyano-2-hydroxy-4,6-dimethylpyridine in toluene [Equation (4)].

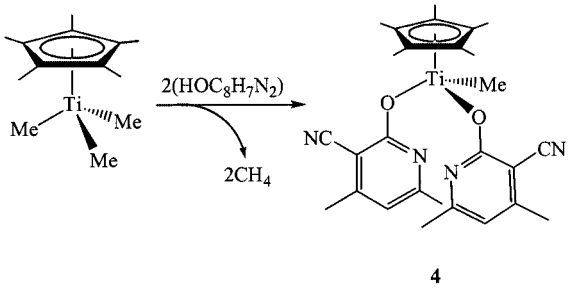

4 (4)

This compound was isolated as a red solid which is soluble in toluene and THF but less soluble in pentane. The ^{1}H NMR spectrum shows a singlet at δ = 1.00 ppm, corresponding to the methyl group bonded to the titanium atom and a further singlet at δ = 1.77 ppm for the Cp* methyl groups. The pyridine ligands give rise to three signals, two of them at δ = 1.71 and 1.82 ppm are assigned to the methyl groups bonded to the pyridine rings, and the other, at δ = 5.46 ppm, corresponds to the aromatic proton. It can be inferred from these results that in complex **4** the two pyridine ligands are in the same chemical environment, and an η^1-*O* coordination is proposed for both ligands.

Finally, the reactivity of **3** toward isocyanide ligands has been considered. Compound **3** reacts readily in toluene at room temperature with 2,6-dimethylphenyl isocyanide in a 1:2 molar ratio to give the azatantalacyclobutane complex **5** containing an iminoacyl fragment (Scheme 2).

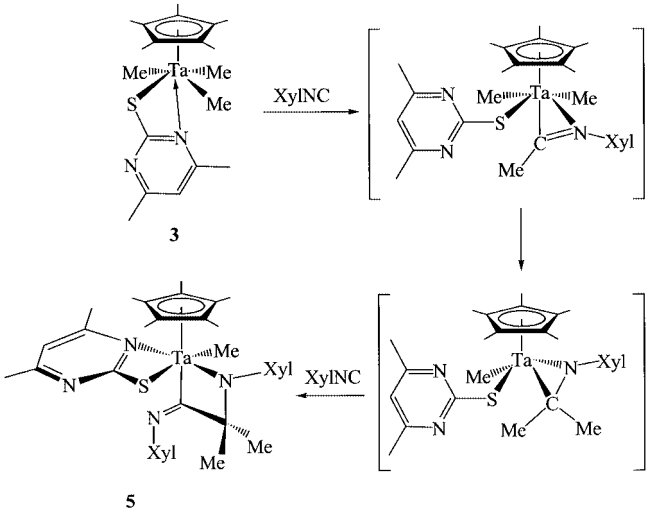

3 **5**

Scheme 2

The ^{1}H NMR spectrum of compound **5** shows a singlet signal at δ = 1.39 ppm which is assigned to the Cp* protons and nine singlet signals between δ = 1.00 and 2.45 ppm, each of them integrating for three protons, corresponding to the methyl groups present in the molecule (see Exp. Sect.).

Furthermore, the ^{13}C NMR spectrum shows, among others, two signals at δ = 230.0 and 86.7 ppm, which we tentatively assign to an iminoacyl carbon atom and to the quaternary carbon atom of the Ta−N−C−C metallacycle.[15]

We propose (see Scheme 2) that, initially, complex **3** reacts with one molar equivalent of xylyl isocyanide by insertion into one Ta−Me bond to form an η^2-iminoacyl-containing complex. A second methyl migration would then occur, forming an η^2-imine-containing species. Finally, the insertion of a second isocyanide molecule into the newly formed Ta−C bond would lead to **5**.

Recently, we reported a mechanism for the reaction of xylyl isocyanide with $[Cp^*TaMe_2(SCH_2CH_2)_2O]$ in which the proposed η^2-imine intermediate was isolated .[16] Attempts to isolate this type of intermediate in the reaction of **3** were unsuccessful.

Furthermore, compound **3** reacts readily with *tert*-butyl isocyanide, at room temperature, in C_6D_6 on an NMR-tube scale, to give the η^2-imine complex **6** as the only detectable compound by ^1H NMR spectroscopy (Scheme 3). Isolation of **6** on a preparative scale with an acceptable level of purity was not possible.

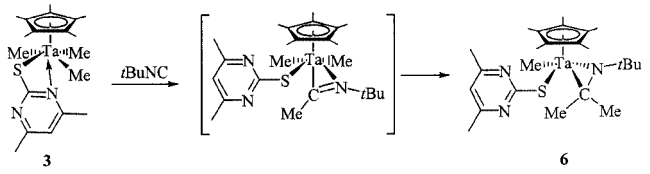

Scheme 3

In contrast to the reactivity observed for complex **3** with xylyl isocyanide, no further reaction was observed when an excess of *tert*-butyl isocyanide was added.

The ^1H and ^{13}C NMR spectroscopic data point to an η^2-coordination of the imine ligand, while the thiolate would act as a monodentate ligand (see Exp. Sect.). The ^1H NMR spectroscopic data exhibit a singlet signal at $\delta = 0.04$ ppm corresponding to the methyl group bonded to the tantalum atom, a singlet at $\delta = 1.31$ ppm integrating for nine protons assignable to the *tert*-butyl group and a broad signal at $\delta = 1.79$ ppm due to the methyl groups of the thiolate ligand, indicating that a fluxional behavior similar to that described for **3** takes place. The methyl groups bonded to the quaternary carbon atom of the imine ligand appear as two singlets at $\delta = 1.66$ and 1.99 ppm, respectively. The ^{13}C NMR spectrum shows, as its outstanding feature, a signal at $\delta = 68.1$ ppm corresponding to the quaternary carbon atom of the imine ligand. The high-field shift of this resonance seems to confirm the η^2-coordination of the imine group.[17]

Conclusion

In this paper we report the synthesis of some new monocyclopentadienyl-containing tantalum(V) and titanium(IV) complexes with chelating pyrimidinethiolate and oxypyridine ligands. These compounds were prepared by halide or methyl displacement. The molecular structure of **1**, as determined by X-ray diffraction studies, shows a pseudo-octahedral geometry around the tantalum atom with the thiolate ligand chelating two coordination positions. This structural situation can be considered to also be present in the related tantalum complexes **2** and **3**, on the basis of spectroscopic data. We have also studied the reactivity of complex **3** with xylyl and *tert*-butyl isocyanides. With the first reagent the azatantalacyclobutane complex **5** was isolated, whereas with the second isocyanide the η^2-imine-containing complex **6** was obtained.

Experimental Section

General Remarks: The preparation and handling of the described compounds was performed with rigorous exclusion of air and moisture under nitrogen using standard vacuum line and Schlenk techniques. All solvents were dried and distilled under nitrogen. The following reagents were prepared by literature procedures: $[Cp^*TaCl_4]$[18] $[Cp^*TaMe_4]$[19] and $[Cp^*TiMe_3]$.[20] The commercially available compounds Cp*H, MeLi in diethyl ether, xylyl isocyanide, *tert*-butyl isocyanide, 2-mercapto-4,6-dimethylpyrimidine and 3-cyano-2-hydroxy-4,6-dimethylpyridine were used as received from Aldrich. ^1H and ^{13}C NMR spectra were recorded with a 200 Mercury Varian Fourier Transform spectrometer. Trace amounts of protonated solvents were used as reference, and chemical shifts are reported in units of ppm relative to $SiMe_4$. IR spectra were recorded in the region 4000−400 cm^{-1} with a Nicolet Magna-IR 550 spectrophotometer as Nujol mulls using PET cells.

$[Cp^*TaCl_3(SC_6H_7N_2)]$ (1): $HSC_6H_7N_2$ (0.136 g, 0.97 mmol) and Et_3N (0.140 mL, 0.97 mmol) were added to a solution of Cp^*TaCl_4 (0.446 g, 0.97 mmol) in 5 mL of toluene. The mixture was stirred at room temperature for 1 h. After filtration, the solid was washed twice with 5 mL of THF. The resulting solution was concentrated to dryness and the solid obtained was washed with diethyl ether to give an orange solid, which was characterized as **1** (0.425 g, 78%). IR (Nujol/PET): $\tilde{\nu} = 1591$ cm^{-1} (s), 1558 (w), 1520 (s), 1342 (m), 1271 (s), 1021 (m), 956 (w), 848 (m). ^1H NMR (200 MHz, C_6D_6): $\delta = 1.71$ (s, 3 H, CH_3), 2.24 (s, 15 H, Cp*), 2.88 (s, 3 H, CH_3), 5.67 (s, 1 H, CH pyrimidine) ppm. $^{13}C\{^1H\}$ NMR (C_6D_6): $\delta = 13.0$ (Cp*), 23.7 (CH_3), 24.8 (CH_3), 119.6 (CH pyrimidine), 130.3 (Cp*), 165.5 ($C-CH_3$), 168.5 (CCH_3), 172.2 (CS) ppm. $C_{16}H_{22}N_2Cl_3STa$ (561.73): calcd. C 34.17, H 3.91, N 4.98; found C 34.17, H 3.90, N 5.09.

$[Cp^*TaCl_3(OC_8H_7N_2)]$ (2): $HOC_8H_7N_2$ (0.517 g, 3.49 mmol) and Et_3N (0.486 mL, 3.49 mmol) were added to a solution of $[Cp^*TaCl_4]$ (1.6 g, 3.49 mmol) in 25 mL of toluene. The mixture was stirred at room temperature for 2 h. After filtration, the resulting solution was concentrated to dryness and the solid obtained was washed with pentane to give a yellow solid, which was characterized as **2** (1.465 g, 74%). IR (Nujol/PET): $\tilde{\nu} = 2216$ cm^{-1} (s), 1666 (w), 1604 (ms), 1551 (s), 1304 (s), 1256 (m), 1026 (w), 651 (w), 570 (s). ^1H NMR (200 MHz, C_6D_6): $\delta = 1.52$ (s, 3 H, CH_3), 2.22 (s, 15 H, Cp*), 2.49 (s, 3 H, CH_3), 5.49 (s, 1 H, CH pyridine) ppm. $^{13}C\{^1H\}$ NMR (C_6D_6): $\delta = 12.6$ (Cp*), 20.1 (CH_3), 22.1 (CH_3), 94.1 (*C*CN), 112.9 (CN), 118.7 (Cp*), 131.9 (CH pyridine), 155.9 (CCH_3), 157.3 (CCH_3), 168.3 (CO) ppm. $C_{18}H_{22}N_2Cl_3OTa$ (569.69): calcd. C 37.95, H 3.89, N 4.92; found C 38.14, H 3.75, N 4.66.

[Cp*TaMe$_3$(SC$_6$H$_7$N$_2$)] (3): Toluene (10 mL) was added to a mixture of Cp*TaMe$_4$ (0.379 g, 1.01 mmol) and HSC$_6$H$_7$N$_2$ (0.141 g, 1.01 mmol). The solution was heated slowly to 80 °C and stirred at this temperature for 1 h. After cooling, the mixture was filtered and the solvent removed. The oil obtained was washed with 10 mL of *n*-pentane to afford an orange solid (0.373 g, 75%) which was characterized as **3**. IR (Nujol/PET): $\tilde{\nu}$ = 1623 cm^{-1} (w), 1580 (s), 1532 (s), 1340 (s), 1274 (s), 1138 (m), 1026 (m) 955 (w) 844 (w), 814 (w). ^{1}H NMR (200 MHz, [D$_8$]toluene): δ = 0.23 (s, 6 H, CH$_3$Ta), 0.34 (s, 3 H, CH$_3$Ta), 2.04 (s, 15 H, Cp*), 2.43 (br. s, 6 H, CH$_3$ pyrimidine), 6.04 (s, 1 H, CH pyrimidine) ppm. ^{13}C{^{1}H} NMR (C$_6$D$_6$): δ = 11.6 (Cp*), 23.7 (CH$_3$, pyrimidine), 45.6 (CH$_3$Ta), 48.7 (CH$_3$Ta), 119.1 (CH pyrimidine), 120.5 (Cp*), 165.8 (*C*CH$_3$), 174.6 (CS) ppm. C$_{19}$H$_{31}$N$_2$STa (500.48): calcd. C 45.60, H 6.24, N 5.60; found C 45.39, H 5.82, N 5.61.

[Cp*TiMe(OC$_8$H$_7$N$_2$)$_2$] (4): Toluene (2 mL) was added to a mixture of [Cp*TiMe$_3$] (0.209 g, 0.92 mmol) and HOC$_8$H$_7$N$_2$ (0.271 g, 1.83 mmol). The solution was stirred at room temperature for 5 h and filtered. By addition of 4 mL of *n*-pentane and cooling to −30 °C a red solid (0.190 g, 42%) was obtained and characterized as **4**. IR (Nujol/PET): $\tilde{\nu}$ = 2218 cm^{-1} (s), 1560 (s), 1504 (s), 1221 (s), 1157 (m), 1098 (s), 783 (ms). ^{1}H NMR (200 MHz, C$_6$D$_6$): δ = 1.00 (s, 3 H, CH$_3$-Ti), 1.71 (s, 6 H, CH$_3$), 1.77 (s, 15 H, Cp*), 1.82 (s, 6 H, CH$_3$), 5.46 (s, 2 H, CH pyridine) ppm. ^{13}C{^{1}H} NMR (C$_6$D$_6$): δ = 11.9 (Cp*), 20.0 (CH$_3$), 20.9 (CH$_3$), 63.8 (CH$_3$Ti), 91.4 (*C*CN), 114.4 (CN), 115.0 (Cp*), 127.4 (CH pyridine), 155.1 (*C*CH$_3$), 157.5 (*C*CH$_3$), 171.0 (CO) ppm. C$_{27}$H$_{32}$N$_4$O$_2$Ti (492.44): calcd. C 65.85, H 6.55, N 11.38; found calcd. C 65.57, H 6.88, N 11.72.

[Cp*TaMe{XylN=CC(Me$_2$)NXyl}(SC$_6$H$_7$N$_2$)] (5): Toluene (5 mL) was added to a mixture of [Cp*TaMe$_3$(SC$_6$H$_7$N$_2$)] (0.132 g, 0.26 mmol) and XylN≡C (0.70 g, 0.53 mmol). The solution was stirred at room temperature for 30 min. After that, the mixture was filtered and the solvent removed. The oil obtained was washed with 5 mL of cool *n*-pentane to afford a yellow solid (0.110 g, 54%) which was characterized as **5**. IR (Nujol/PET): $\tilde{\nu}$ = 1666 cm^{-1} (w), 1633 (m), 1593 (s), 1553 (m). ^{1}H NMR (200 MHz, C$_6$D$_6$): δ = 1.00 (s, 3 H, CH$_3$-Ta), 1.29 (s, 3 H, CH$_3$), 1.39 (s, 15 H, Cp*), 1.44 (s, 3 H, CH$_3$), 1.76 (s, 3 H, CH$_3$), 1.94 (s, 3 H, CH$_3$), 2.11 (s, 3 H, CH$_3$), 2.15 (s, 3 H, CH$_3$), 2.40 (s, 3 H, CH$_3$), 2.45 (s, 3 H, CH$_3$), 5.64 (s, 1 H, CH pyrimidine), 6.57−6.82 (m, 6 H, Xyl) ppm. ^{13}C{^{1}H} NMR (C$_6$D$_6$): δ = 10.8 (Cp*), 19.6, 20.1, 21.8, 22.1, 22.3, 23.5, 23.8, 24.3 (CH$_3$), 39.8 (CH$_3$Ta), 86.7 (*C*Me$_2$), 116.9 (CH pyrimidine), 119.6 (Cp*), 119.6 (CH, Xyl), 125.0 (CH, Xyl), 127.1 (CH, Xyl), 127.9 (CH, Xyl), 128.4 (CH, Xyl), 128.6 (CH, Xyl) 136.4 (*C*CH$_3$, Xyl), 137.0 (*C*CH$_3$, Xyl), 146.9 (*C*N=C), 154.8 (CN), 164.9 (*C*CH$_3$, pyrimidine), 165.8 (*C*CH$_3$, pyrimidine), 176.7 (CS), 230.0 (C=N) ppm. C$_{37}$H$_{49}$N$_4$STa (762.83): calcd. C 58.26, H 6.47, N 7.34; found C 57.80, H 7.34, N 7.61.

[Cp*TaMe{*t*BuNC(Me$_2$)}(SC$_6$H$_7$N$_2$)] (6): *t*BuN≡C (7μL, 0.06 mmol) was added to a solution of Cp*TaMe$_3$(SC$_6$H$_7$N$_2$) (0.031 g, 0.06 mmol) in 0.7 mL of C$_6$D$_6$. The mixture was allowed to react at room temperature in an NMR tube during 10 min to yield the proposed complex **6** as only detectable compound. ^{1}H NMR (200 MHz, C$_6$D$_6$): δ = 0.04 (s, 3 H, CH$_3$Ta), 1.31 (s, 9 H, *t*Bu), 1.62 (s, 15 H, Cp*), 1.66 (s, 3 H, CH$_3$), 1.79 (br, 6 H, CH$_3$), 1.99 (s, 3 H, CH$_3$), 5.79 (s, 1 H, CH pyrimidine) ppm. ^{13}C{^{1}H} NMR (C$_6$D$_6$): δ = 11.4 (Cp*), 23.6 (CH$_3$ pyrimidine), 27.3, 32.8 (*C*H$_3$C=N), 31.5 (*t*Bu), 45.9 (CH$_3$Ta), 62.6 (*C*Me$_3$), 68.1 (*C*Me$_2$), 114.1 (CH pyrimidine), 116.3 (Cp*), 164.40 (*C*CH$_3$), 182.4 (CS) ppm.

Table 2. Crystal data and structure refinement for **1**

Empirical formula	C$_{16}$H$_{22}$Cl$_3$N$_2$STa
Formula mass	561.71
Temperature	293(2) K
Wavelength	0.71073 Å
Crystal system, space group	monoclinic, $P2_1/c$
Unit cell dimensions	a = 13.328(4) Å b = 8.596(3) Å, β = 90.74(3)° c = 17.224(2) Å
Volume	1973.1(9) Å^3
Z, calculated density	4, 1.891 Mg/m^3
Absorption coefficient	6.082 mm^{-1}
F(000)	1088
Crystal size	0.3 × 0.3 × 0.2 mm
θ range for data collection	2.37−27.97°
Limiting indices	$-17 \le h \le 17$, $0 \le k \le 11$, $0 \le l \le 22$
Reflections collected/unique	9175/4747 [R(int) = 0.0920]
Data/restraints/parameters	4747/0/213
Goodness-of-fit on F^2	1.052
Final R indices [$I > 2\sigma(I)$]	$R1$ = 0.0351, $wR2$ = 0.0859
R indices (all data)	$R1$ = 0.0542, $wR2$ = 0.1060
Largest diff. peak and hole	1.297 and −2.295 e Å^{-3}

X-ray Crystallographic Study: The crystallographic data and experimental details are given in Table 2. Crystals of complex **1** suitable for an X-ray diffraction study were obtained by slow diffusion of pentane into a saturated solution of the complex in toluene. A prismatic crystal was selected, sealed in a Lindeman capillary under dry nitrogen and used for data collection. Accurate unit-cell parameters were determined by least-squares refinement of the setting angles of 25 randomly distributed and carefully centered reflections. The data collection was performed with a NONIUS-MACH3 diffractometer equipped with graphite-monochromated Mo-K_α radiation (λ = 0.71073 Å) using an ω/2θ scan technique to a maximum value of 56°. Data were corrected for Lorentz and polarization effects. The structure was solved by direct methods (SIR92)[21] and refined first isotropically by full-matrix least squares using SHELXL-97[22] program and then anisotropically by blocked full-matrix least-squares techniques for all the non-hydrogen atoms. The hydrogen atoms were included in calculated positions and refined as "riding" on their parent carbon atoms. CCDC-189366 contains the supplementary crystallographic data for this paper. These data can be obtained free of charge at www.ccdc.cam.ac.uk/conts/retrieving.html [or from the Cambridge Crystallographic Data Centre, 12 Union Road, Cambridge CB2 1EZ, UK; Fax: (internat.) + 44-1223/336-033; E-mail: deposit@ccdc.cam.ac.uk].

Acknowledgments

The support of this work by the Dirección General de Enseñanza Superior e Investigación Científica (Spain, Grant No. PB 98-0159-C02-01) is gratefully acknowledged.

[1] [1a] P. Jutzi, T. Redeker, B. Neumann, H. G. Stammler, *Organometallics* **1996**, *15*, 4153−4161. [1b] P. Jutzi, T. Heidemann, B. Neumann, H. G. Stammler, *J. Organomet. Chem.* **1994**, *472*, 27−38.
[2] J. R. Dilworth, J. Hu, *Adv. Inorg. Chem.* **1993**, *40*, 411 and references therein.
[3] D. Sellmann, R. Ruf, F. Knoch, M. Moll, *Inorg. Chem.* **1995**, *34*, 4745−4755.

[4] [4a] F. E. Massoth, *Adv. Catal.* **1978**, *27*, 265. [4b] W. L. Orr, *Oil Sand and Oil Shale Chemistry*, Verlag Chemie, Weinheim, **1978**, p. 233. [4c]T. D. Cyr, J. D. Payzant, D. S. Montgomery, O. P. Srauzs, *Org. Geochem.* **1986**, *9*, 139−143. [4d] M. Nishioka, *Energy Fuels* **1988**, *2*, 214−219.

[5] [5a] R. A. Sánchez-Delgado, *J. Mol. Catal.* **1994**, *86*, 287. [5b] H. Kwart, G. C. A. Schuit, B. C. Gates, *J. Catal.* **1980**, *61*, 128−134. [5c] F. Zaera, E. B. Kollin, J. L. Gland, *Surf. Sci.* **1987**, *184*, 75−89. [5d] J. J. Eisch, L. E. Hallenbeck, K. L. Han, *J. Org. Chem.* **1983**, *48*, 2963−2968. [5e] S. Antebi, H. Alper, *Organometallics* **1986**, *5*, 596−598. [5f] R. J. Angelici, *Acc. Chem. Res.* **1988**, *21*, 387−394. [5g] R. J. Angelici, *Coord. Chem. Rev.* **1990**, *105*, 61−76. [5h] J. Chen, R. J. Angelici, *Organometallics* **1992**, *11*, 992−996. [5i] T. B. Rauschfuss, *Prog. Inorg. Chem.* **1991**, *39*, 259.

[6] [6a] H. Okamura, M. Miura, H. Takei, *Tetrahedron Lett.* **1979**, 43−46. [6b] H. Okamura, H. Takei, *Tetrahedron Lett.* **1979**, 3425−3428. [6c] S. Murahashi, M. Yamamura, K. Yanagisawa, N. Mita, K. Kondo, *J. Org. Chem.* **1979**, *44*, 2408−2417. [6d] M. Kosugi, T. Shimizu, T. Migita, *Chem. Lett.* **1978**, 13−14. [6e] R. O. Hutchins, K. Learn, *J. Org. Chem.* **1982**, *48*, 4380−4382. [6f] E. Wender, J. M. Hanna, M. H. Leftin, E. L. Michelotti, K. T. Potts, D. Usifer, *J. Org. Chem.* **1985**, *50*, 1125−1126. [6g] M. Tiecco, L. Testaferri, M. Tingoli, P. Chianelli, E. Wenkert, *Tetrahedron Lett.* **1982**, *23*, 4629−4632. [6h] K. Osakada, T. Yamamoto, A. Yamamoto, *Tetrahedron Lett.* **1987**, *27*, 6321−6324.

[7] D. W. Stephan, T. T. Nadasdi, *Coord. Chem. Rev.* **1996**, *147*, 147−208.

[8]]D. C. Bradley, R. C. Mehrota, A. Singh, I. P. Rothwell, *Alkoxo and Aryloxo Derivatives of Metals*, Academic Press, London, **2001**.

[9] [9a] A. K. Rappe, W. A. Goddard, *J. Am. Chem. Soc.* **1982**, *104*, 448−456. [9b] Z. Cossee, *J. Catal.* **1964**, *3*, 80−88. [9c] S. Doherty, R. J. Errington, A. P. Jarvis, S. Collins, W. Clegg, M. R. J. Elsegood, *Organometallics* **1998**, *17*, 3408−3410. [9d] Q. Wang, R. Quyoum, D. J. Gillis, M.-J. Tudoret, D. Jeremic, B. K. Hunter, M. C. Baird, *Organometallics* **1996**, *15*, 693−703.

[10] [10a] R. Fandos, M. Lanfranchi, A. Otero, M. A. Pellinghelli, M. J. Ruiz, P. Terreros, *Organometallics* **1996**, *15*, 4725−4730. [10b] A. Antiñolo, F. Carrillo-Hermosilla, A. Corrochano, R. Fandos, J. Fernández-Baeza, A. M. Rodríguez, M. J. Ruiz, A. Otero, *Organometallics* **1999**, *18*, 5219−5224.

[11] A. Antiñolo, F. Carrillo-Hermosilla, J. Fernandez-Baeza, A. M. F. de Toro, S. Garcia-Yuste, A. Otero, J. C. Perez-Flores, A. M. Rodriguez, *Inorg. Chim. Acta* **2000**, *300*, 131−137.

[12] [12a] K. Tatsumi, I. Matsubara, Y. Inoue, A. Nakamura, K. Miki, N. Kasai, *J. Am. Chem. Soc.* **1989**, *111*, 7766−7777. [12b] S.-M. Koo, R. Bergero, A. Salifoglou, D. Coucouvanis, *Inorg. Chem.* **1990**, *29*, 4844−4846. [12c] R. R. Schrock, M. Wesolek, A. H. Liu, K. C. Wallace, J. C. Dewan, *Inorg. Chem.* **1988**, *27*, 2050−2054. [12d] K. Tatsumi, Y. Inoue, H. Kawaguchi, M. Koshada, A. Nakamura, R. E. Cramer, W. VanDoorne, G. J. Taogoshi, P. N. Richmann, *Organometallics* **1993**, *12*, 352−364.

[13] S. M. Pugh, D. J. M. Trösch, M. E. G. Skinner, L. H. Gade, P. Mountford, *Organometallics* **2001**, *20*, 3531−3542.

[14] R. J. Abrahams, J. Fisher, P. Loftus, *Introduction to NMR Spectroscopy*, John Wiley and Sons, New York, **1988**.

[15] [15a] M. J. Scott, S. J. Lippard, *Organometallics* **1997**, *16*, 5857−5868. [15b] M. V. Galakov, M. Gómez, G. Jiménez, P. Royo, *Organometallics* **1995**, *14*, 2843−2854.

[16] R. Fandos, C. Hernández, I. López-Solera, A. Otero, A. Rodríguez, M. J. Ruiz, P. Terreros, *Organometallics* **2000**, *19*, 5318−5324.

[17] L. D. Durfee, J. E. Hill, P. E. Fanwick, I. P. Rothwell, *Organometallics* **1990**, *9*, 75−80.

[18] R. J. Burt, J. Chatt, G. J. Leigh, J. H. Teuben, A. Westerhof, *J. Organomet. Chem.* **1977**, *129*, C33−C35.

[19] R. D. Sanner, S. T. Carter, W. J. Burton, *J. Organomet. Chem.* **1982**, *240*, 157−162.

[20] M. Mena, M. A. Pellinghelli, P. Royo, R. Serrano, A. Tiripicchio, *J. Chem. Soc., Chem. Commun.* **1986**, 1118−1119.

[21] A. Altomare, G. Cascarano, C. Giacovazzo, A. Guagliardi, M. C. Burla, G. Polidori, M. Camalli, *J. Appl. Crystallogr.* **1994**, 435.

[22] G. M. Sheldrick, *Program for the Refinement of Crystal Structures from diffraction data*, University of Göttingen, Göttingen, Germany, **1997**.

Received July 24, 2002
[I02414]

Efficient Asymmetric Synthesis of Δ- and Λ-Enantiomers of (Bipyridyl)ruthenium Complexes and Crystallographic Analysis of Δ-Bis(2,2′-bipyridine)(2,2′-bipyridine-4,4′-dicarboxylato)ruthenium: Diastereoselective Homo- and Heterochiral Ion Pairing Revisited

Régis Caspar,[a] Hani Amouri,*[a] Michel Gruselle,[a] Christine Cordier,[b] Bernard Malézieux,[a] Raphäel Duval,[c] and Hubert Leveque[c]

Keywords: Ruthenium / Chiral resolution / Circular dichroism

Optically pure ruthenium complexes of the type Δ- or Λ-[Ru(bpy)$_2$(L–L)][PF$_6$]$_2$ [L–L = cmbpy = 4′-methyl-2,2′-bipyridine-4-carboxylic acid (**3a**, **b**); L–L = dcbpy = 2,2′-bipyridine-4,4′-dicarboxylic acid (**4a**, **b**)] were prepared and fully characterized. The Ru^{II} carboxylate complexes Δ- and Λ-[Ru(bpy)$_2$(dcabpy)] (**5a**, **b**) (dcabpy = 2,2′-bipyridine-4,4′-dicarboxylate) were resolved efficiently by chiral column chromatography and isolated in good yields. The Δ-[Ru(bpy)$_2$(dcabpy)] (**5a**) enantiomer was crystallized and its X-ray molecular structure determined. The enantiomeric nature and the absolute configuration of the tris(bipyridyl)ruthenium complexes were confirmed by NMR and circular dichroism studies. In addition, ion-pairing interactions between Δ-Trisphat (Δ-**1**, D_3 symmetry) and each enantiomer of the (monocarboxylic acid)Ru^{II} complex (**3a** and **3b**, C_1 symmetry) and the dicarboxylic acid complex (**4a** and **4b**, C_2 symmetry) were examined by NMR spectroscopy.

(© Wiley-VCH Verlag GmbH & Co KGaA, 69451 Weinheim, Germany, 2003)

Introduction

Octahedral hexacoordinated ruthenium(II) complexes bearing 2,2′-bipyridine ligands (bpy) have received considerable attention because of their potential use as chiral building blocks for supramolecular assemblies,[1] or as chiral probes for biological molecules (polynucleotides, DNA).[2] In addition, they exhibit photoluminescence and electroluminescence properties, making them promising light-emitting devices.[3] More recently, efforts have been devoted to the study of the stereochemistry of these complexes as a result of the different interactions that may arise when enantiomeric forms (Δ or Λ) interact with a variety of substrates.[4,5a,5b]

We, and others, have been working in the area of stereoselective synthesis of tris(bpy)metal complexes with D_3 symmetry.[5] The determination of their enantiomeric purity by ^{1}H NMR spectroscopy has become an easy and routine task in the presence of the Trisphat anion (**1**) [Trisphat = tris(tetrachlorobenzenediolato)phosphate(v)],[6] which acts as a chiral shift reagent.[7] Further investigations carried out by Lacour have also shown that homochiral association (Δ,Δ) or (Λ,Λ) is favored over heterochiral association (Δ,Λ) in a solvent of low polarity and proceeds with high selectivity.[8] More recently Le Bozec, Lacour, and co-workers also found that homochiral ion-pairing is also favored for the tris(DEAS-bpy)ruthenium complex {DEAS-bpy = 4,4′-bis(diethylaminostyryl)-[2,2′]-bipyridine}.[9] Very recently, Kol and co-workers reported that octahedral mono(eilatin)ruthenium complexes form discrete dimers held by π-stacking interactions in both the solid state and in solution. In contrast to the results outlined above, heterochiral association (Δ,Λ) was found to be strongly favored.[10]

In order to investigate this ion-pairing phenomenon, we decided to prepare the optically pure dicationic (bipyridyl)-Ru^{II} complexes Δ- and Λ-[Ru(bpy)$_2$(cmbpy)][PF$_6$]$_2$ (**3a**, **b**; cmbpy = 4′-methyl-2,2′-bipyridine-4-carboxylic acid) and Δ- and Λ-[Ru(bpy)$_2$(dcbpy)][PF$_6$]$_2$ (**4a**, **b**; dcbpy = 2,2′-bipyridine-4,4′-dicarboxylic acid), with C_1 and C_2 symmetries, respectively. We anticipated that association of our model complexes with the Δ-Trisphat anion of D_3 symmetry should be the ideal probe to discriminate between homochiral and heterochiral ion-pairing association.

[a] Laboratoire de Chimie Inorganique et Matériaux Moléculaires, UMR CNRS 7071, Université Pierre et Marie Curie,
4, place Jussieu, case 42, 75252 Paris Cedex 05, France
Fax: (internat.) + 33-1/44273841
E-mail: amouri@ccr.jussieu.fr
[b] ITODYS, CNRS − UPRES-A 7086, Université Paris 7, Denis Diderot,
1 rue Guy de la Brosse, 75005 Paris, France
[c] Chiralsep,
Parc de la Boissière, 76170 La Frenaye, France

Supporting Information for this article is available on the WWW under http://www.eurjic.org or from the author.

In this paper we report the synthesis and complete characterization of **3a**, **3b**, **4a**, and **4b**. We also report the X-ray crystal structure of the optically pure Ru^{II} dicarboxylate complex Δ-[Ru(bpy)$_2$(dcabpy)] (**5a**; dcabpy = 2,2′-bipyridine-4,4′-dicarboxylate). The solution behavior and NMR studies of these resolved complexes in the presence of Δ-Trisphat are presented and discussed.

Results and Discussion

Synthesis of the (Bipyridyl)ruthenium Complexes 3a, b and 4a, b

The optically pure ruthenium complexes **3a** and **3b** were prepared in a single step by treatment of the resolved ruthenium complexes Δ- and Λ-[Ru(bpy)$_2$py$_2$][dibenzoyltartrate-*O*,*O*′] (**2a**, **b**)[11] with the appropriate chelating ligands in ethylene glycol/H_2O for several hours (Scheme 1). These compounds were obtained as red microcrystalline solids in good yields and were fully characterized (the synthesis of racemic **3** has been reported previously[2f]). The absolute configurations of **3a** and **3b** (Δ and Λ, respectively) were assigned by circular dichroism (see Figure 2).

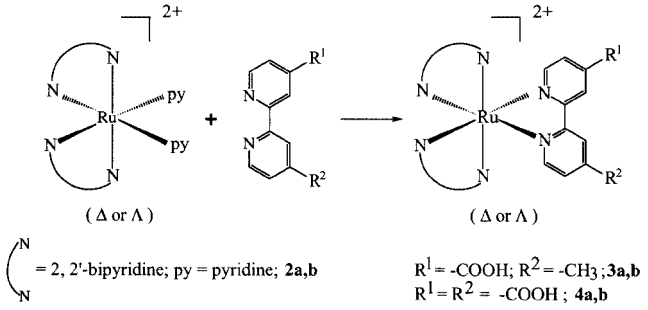

Scheme 1. Preparation of ruthenium complexes **3a**, **3b**, **4a**, and **4b**

The dicarboxylic acid complexes **4a** and **4b** were obtained by two different methods. The first involves direct treatment of **2a** and **2b** with the dcabpy ligand following the synthetic procedure described above. However, several weeks were required to obtain resolved crystals of either **2a** or **2b**. A more convenient method was thus used, involving the preparation of racemic [Ru(bpy)$_2$(dcbpy)][Cl]$_2$ by treatment of Ru(bpy)$_2$Cl$_2$ with dcabpy in a refluxing 1:1 water/methanol mixture.[2g] [Ru(bpy)$_2$(dcbpy)][Cl$_6$]$_2$ was easily resolved using HPLC chromatography,[12] affording initially the related carboxylate derivatives **5a** and **5b** in almost quantitative yields (see Exp. Sect.), which on subsequent protonation and workup gave optically pure **4a** and **4b** (vide infra).

The IR spectra of **5a** and **5b** recorded as KBr disks supported the formation of the Ru^{II} carboxylate species with ν(CO) = 1617 cm^{-1}, and the structure of **5a** was confirmed by X-ray structural analysis.

X-ray Structure of Δ-[Ru(bpy)$_2$(dcabpy)] (5a)

Suitable crystals of **5a** were obtained by slow concentration of a saturated acetonitrile solution. Complex **5a** crystallizes in the chiral C_2 space group. Crystallographic data for **5a** are given in Table 2 (Exp. Sect.) and selected bond lengths and angles are given in Table 1. The structure shows a hexacoordinated Ru^{II} center complexed by one dcabpy and two bpy ligands, and confirms that the functionalized bipyridine ligand has two deprotonated carboxylate groups at the 4 and 4′ positions.

Table 1. Selected interatomic distances [Å] and angles [°] for **5a** (* denotes dihedral angles)

Ru(1)−N(1)	2.072(7)
Ru(1)−N(1′)	2.046(7)
Ru(1)−N(2)	2.067(8)
Ru(1)−N(2′)	2.078(7)
Ru(1)−N(3)	2.060(7)
Ru(1)−N(3′)	2.045(8)
C(7)−O(1)	1.21(1)
C(7)−O(2)	1.25(1)
C(7′)−O(1′)	1.25(1)
C(7′)−O(2′)	1.23(1)
O(1)−C(7)−O(2)	124.7(10)
O(1′)−C(7′)−O(2′)	126.6(8)
(pyridyl ring)−[O(1)−C(7)−O(2)]*	17.2
(pyridyl ring)−[O(1′)−C(7′)−O(2′)]*	14.4

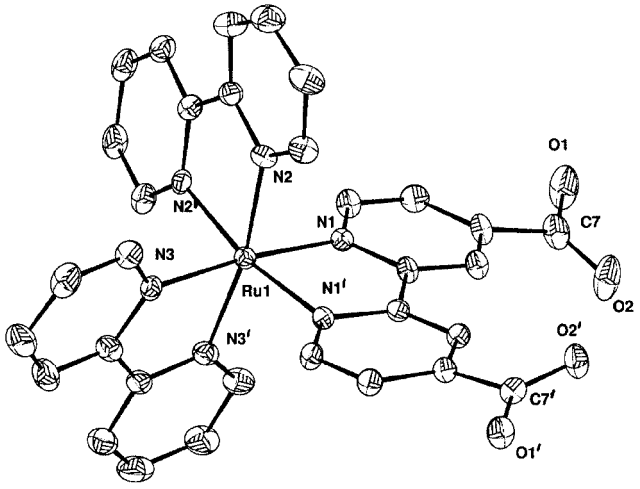

Figure 1. Molecular structure of **5a** with the atom numbering system; hydrogen atoms have been omitted for clarity

Figure 1 shows that the two carboxylate groups of the dcabpy ligand are coplanar with the substituted aromatic rings, suggesting an electronic delocalization throughout the conjugated π-systems. Although there has been a number of structural determinations of tris(bidentate ligand)ruthenium(II) complexes containing polypyridyl ligands,[13−15] the majority of these have involved racemic samples, and only a few structures confirming the absolute configuration of such complexes have been reported. Therefore our example is of interest, especially because several groups are currently interested in the polymetallic assembly involving optically pure ruthenium complexes as individual components.[1c] The absolute configurations of Δ and Λ for **5a** and **5b**, respectively, were also assigned by circular dichroism using the characteristic MLCT absorption band at λ_{max} = 295 nm (Figure 3). The $[\alpha]_D$ values of **5a** and **5b** were re-

corded in aqueous solution with $[\alpha]_D = -951$ ($c = 0.0063$, H_2O) for **5a** and $[\alpha]_D = +961$ ($c = 0.0083$, H_2O) for **5b**.

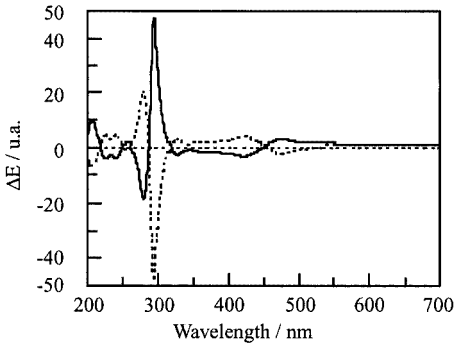

Figure 2. CD curves for **3a** (solid line) and **3b** (dotted line) in acetonitrile

We believe that the basic conditions used in the HPLC resolution (diethylamine/MeOH eluent) resulted in complete deprotonation of the acidic functions and led to the isolation of the deprotonated complexes **5a** and **5b**. The equilibrium between the carboxylate and carboxylic acid forms of the tris(bidentate ligand)ruthenium complexes can be monitored by ^{1}H NMR spectroscopy. Thus, addition of $HBF_4{\cdot}Et_2O$ to a racemic mixture of **5a** and **5b** in D_2O leads to significant changes in the ^{1}H NMR spectrum. For example, the signal corresponding to 3-H and 3′-H shifts downfield by 0.1 ppm. The spectrum of the starting material can be recovered by addition of excess triethylamine. Thus, starting from the pure enantiomers **5a** or **5b**, it is easy to obtain the related carboxylic acid complexes **4a** or **4b**.

Acidification of a solution of **5a** or **5b** in water (pH = 0.5, 1 M H_2SO_4), followed by addition of excess NH_4PF_6, leads to precipitation of **4a** or **4b**. These two enantiomers were characterized by elemental analyses, IR and ^{1}H NMR. It is noteworthy that the ν(CO) vibration in these complexes occurs at 1734 cm^{-1}, shifted by 117 cm^{-1} compared to the carboxylate starting materials. The circular dichroism curves for **4a** and **4b** (Figure 4) were recorded in CH_3CN solution, and show little change compared to those of the related starting carboxylates **5a** and **5b** (Figure 3). The $[\alpha]_D$ value for **4a** is −1058 ($c = 0.0152$, CH_3CN) and for **4b** is +1250 ($c = 0.0104$, CH_3CN).

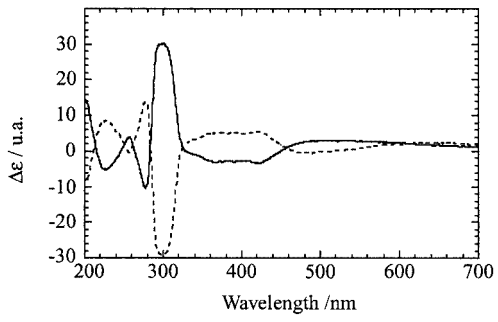

Figure 3. CD curves for **5a** (solid line) and **5b** (dotted line) in acetonitrile

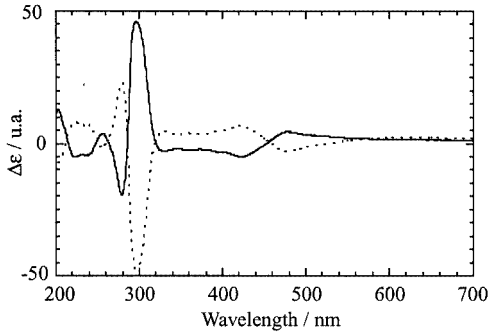

Figure 4. CD curves for **4a** (solid line) and **4b** (dotted line) in acetonitrile

Homo- and Heterochiral Ion-Pairing with Δ-Trisphat (Δ-1)

The determination of the enantiomeric purity of a variety of tris(bidentate ligand)Ru complexes by ^{1}H NMR techniques using the anion Δ-**1** as a chiral shift reagent has become a definitive and accurate method.[6] Thus, addition of Δ-**1** (D_3 symmetry) to D_3-symmetric ruthenium complexes causes a discrimination in the chemical shifts of the two enantiomeric forms. In fact several studies have suggested that the Δ−Δ homochiral ion-pairing interaction between the complex and Δ-**1** is stronger than that of the heterochiral triad based on geometrical criteria.[7,9]

We sought specific interactions between Δ-**1** and the ruthenium complexes of C_2 or C_1 symmetry in the hope that such complexes will act as appropriate probes to highlight this ion-pairing phenomenon; the results of these investigations are presented below.

i) C_2 Symmetry: Δ-Trisphat (Δ-1) and Δ- and Λ-[Ru(bpy)$_2$(dcbpy)][PF$_6$]$_2$ (4a, b)

Sequential addition of up to 5 equiv. of Δ-**1** to a racemic mixture of **4a** and **4b** in CD_2Cl_2/5%CD_3CN (v/v) was monitored by ^{1}H NMR spectroscopy at 293 K. Prior to addition of this chiral shift reagent, the ^{1}H NMR spectrum showed only one set of signals for the two magnetically equivalent enantiomers, in agreement with a C_2-symmetric topology. As shown in Figure 5, a splitting and a progressive chemical shift variation of specific signals are seen on successive addition of 0.5 equiv. aliquots of Δ-**1**. We attribute this result to the formation of a pair of diastereoisomers, **4a**−Δ-**1** and **4b**−Δ-**1**. The signals showing the largest changes in chemical shifts also broaden significantly. In order to discriminate between the two sets of signals ascribed to each diastereoisomeric pair, pure **4a** was added to the initial mixture. Full assignment of the ^{1}H NMR spectrum was achieved using standard 2D experiments (see Exp. Sect. and Supporting Information; see also footnote on the first page of this article).

The chemical shift variation upon addition of Δ-**1** is attributed to a fast exchange process between either Ru^{II} enantiomer (**4a**, **b**) and the ion-pair **4a**−Δ-**1** or **4b**−Δ-**1**, while the broad signals denote a slower dynamic phenomenon. These broad signals are assigned to the homochiral (Δ−Δ) ion-pair and these results therefore suggest that the interac-

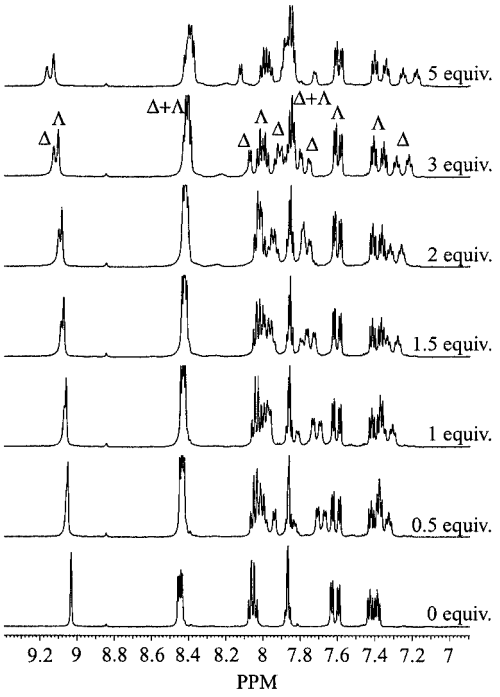

Figure 5. Section of the ^{1}H NMR spectra of racemic **4a**, **b** upon sequential addition of Δ-**1** from 0 to 5 equiv.; the symbols Δ and Λ, on the second trace from top, denote the diastereoisomers **4a**−Δ-**1** and **4b**−Δ-**1**, respectively

tions within the homochiral ion pair are stronger than those involved in the heterochiral ion pair. Moreover, the protons of the homochiral ion-pair exhibit the most pronounced shift of their resonance frequency upon addition of Δ-**1** (Figure 6 and Scheme 2). The resonance signals ascribed to the enantiomer **4a** are strongly spread out either upfield or downfield as a consequence of two concomitant effects; the intimate π-stacking with Δ-**1** and the coulombic attractions between the cationic metal center and the anionic phosphorus atom. The large shifts of the signals are clear evidence of the high vicinity of the octupoles within the homochiral association.

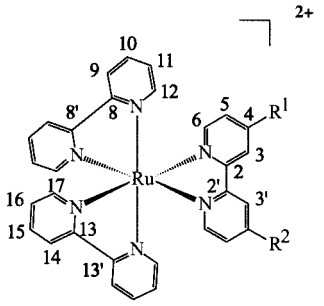

Scheme 2. Atom labelling for the NMR investigations

The heterochiral assembly is less favored, as suggested by the small variation in the chemical shifts of the signals of **4b**. We note that for this Λ−Δ ion-pair, only one C_2-related proton pair is shifted downfield, while the other proton signals remain unchanged or shift slightly upfield (Figure 6). From the ^{1}H NMR spectra, the retention of the twofold symmetry for both diastereoisomeric pairings is postulated. This suggests that in our model complex the pairing of one chiral object either with a homochiral species, or with a mirror-image partner, induces a decrease of symmetry for

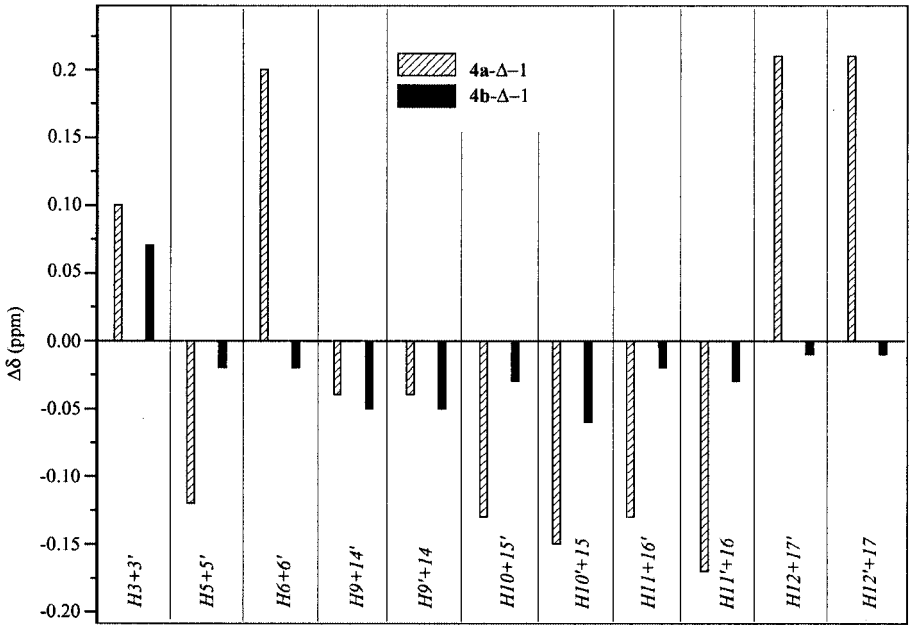

Figure 6. The differences, δ(**4a**−Δ-**1**) − δ(*rac*-**4a**, **b**) (white columns) and δ(**4b**−Δ-**1**) − δ(*rac*-**4a**, **b**) (black columns), point out the effect of Δ-Trisphat on the proton resonances; these values were measured in the presence of 3 equiv. of Δ-**1**

the whole supramolecular assembly i.e. C_2 symmetry in the latter case.

ii) C_1 Symmetry: Δ-Trisphat (Δ-1) and Δ- and Λ-[Ru(bpy)$_2$(cmbpy)][PF$_6$]$_2$ (3a, b)

We anticipated that both the homochiral (**3a**−Δ-**1**) and heterochiral (**3b**−Δ-**1**) ion-pairs should display the same NMR profile (i.e. the same number of signals). To avoid any complex NMR patterns, we studied the behavior of **3a** and **3b** separately in the presence of 4 equiv. of Δ-Trisphat in CD_2Cl_2/5%CD_3CN (v/v), and monitoring was performed by standard ^{1}H NMR techniques (see Exp. Sec. and Supporting Information). Our choice to run only one experiment in the presence of 4 equiv. of Δ-**1** is based on previous results that we obtained for **4a** and **4b**, where maximum separation of the signals of the enantiomers (Δδ) was achieved.

Surprisingly, the ^{1}H NMR spectrum of the homochiral ion-pair **3a**−Δ-**1** displays more signals than that of the heterochiral ion-pair **3b**−Δ-**1** (Figure 7). In the latter case the protons of the unsubstituted bipyridine ligands remain almost unchanged relative to the initial mixture (i.e. without chiral shift reagent) and this suggests that the ion-pairing interactions are weak.

In sharp contrast, the ^{1}H NMR spectrum of **3a**−Δ-**1** displays many signals, consistent with a C_1-symmetric ion-pair. Both the substituted and unsubstituted bipyridine ligands showed distinct signals (see Exp. Sect.) and we suggest this behavior is a result of a strong ion-pairing interaction in the homochiral self assembly **3a**−Δ-**1**. The NMR spectra of all samples remained unchanged over several weeks and we thus conclude that no enantiomeric conversion from **3a** to **3b** (i.e. the conversion from **3a**−Δ-**1** to **3b**−Δ-**1**) occurs. This observation suggests that these ruthenium complexes are configurationally rigid, in agreement with previous reports.[5d]

In summary, our NMR spectroscopic data suggest that the Δ−Δ homochiral ion-pairing interaction is stronger than that of the heterochiral triad. It appears that the initial geometry of the ionic partner is crucial in allowing an intimate association of the ions. The homosymmetry (D_3−D_3) criterion is not the sole defining parameter for the occurrence of ion-pairing; both D_3−C_2 and D_3−C_1 symmetries exhibit stable ion-pairs. These results represent the first investigation of ruthenium complexes with different symmetries.

Concluding Remarks

In this paper we have reported the synthesis of optically pure ruthenium complexes of the type Δ- or Λ-[Ru(bpy)$_2$(L−L)][PF$_6$]$_2$ [L−L = cmbpy = 4′-methyl-2,2′-bipyridine-4-carboxylic acid (**3a**, **b**); L−L = dcbpy = 2,2′-bipyridine-4,4′ dicarboxylic acid (**4a**, **b**)], including the X-ray crystal structure of the (dicarboxylato)ruthenium species Δ-[Ru(bpy)$_2$(dcabpy)] (**5a**). The enantiomeric nature and the absolute configuration of these tris(bidentate ligand)ruthenium complexes were confirmed by NMR and circular dichroism studies. NMR studies of **3a**, **3b**, **4a**, and **4b** in the presence of Δ-Trisphat (Δ-**1**) suggest that strong ion-pairing interactions are taking place, which favor a homochiral association (Δ−Δ), relative to the heterochiral ion pairing (Δ−Λ). We also note that the ^{1}H NMR spectrum of each ion-pair differs for each enantiomer, and depends on whether the cation possesses C_1 or C_2 symmetry. Further investigations are currently in progress with other ruthenium and osmium complexes.

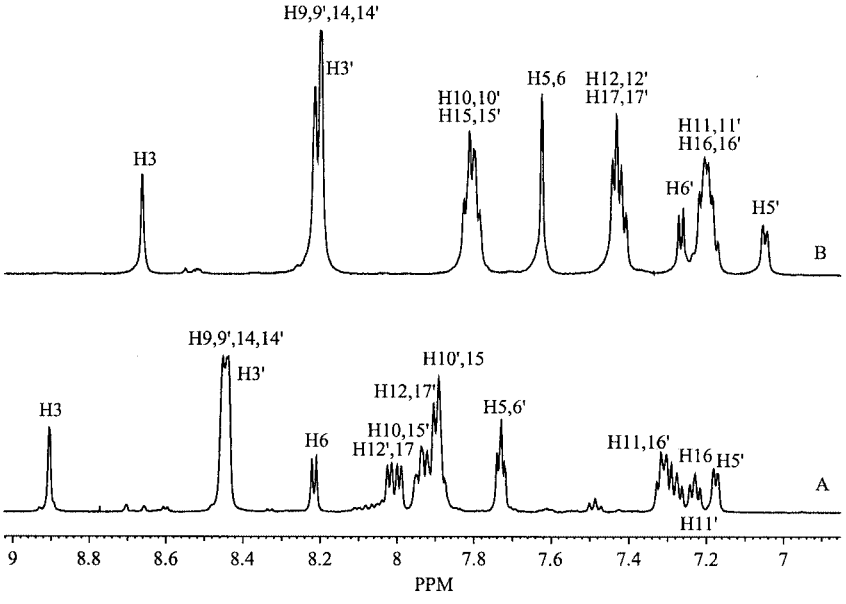

Figure 7. Section of the ^{1}H NMR spectra of **3a**−Δ-**1** (trace A) and **3b**−Δ-**1** (trace B), in the presence of 4 equiv. of Δ-**1**, showing the region of signals of aromatic protons

Experimental Section

General Procedures: All solvents used were reagent grade or better. Deuterated solvents were used as received. Commercially available reagents were used as received. The complexes Δ- and Λ-[Ru^{II}-$(bpy)_2(py)_2$][dibenzoyltartrate-*O*,*O*′],[11] [$Ru^{II}(bpy)_2(Cl)_2$],[16] and *rac*-[$Ru(bpy)_2(cmbpy)][PF_6]_2$ (**3a**,**b**),[2f] were prepared according to literature procedures. The ligand 2,2′-bipyridine-4,4′-dicarboxylate (dcbpy) was purchased from STREM Chemicals and used as received. ^1H NMR spectra were recorded with a Bruker AC-300 spectrometer and with a Bruker DRX-500 spectrometer, equipped with a Silicon Graphics workstation (vide infra). Chemical shifts are reported in ppm downfield from the tetramethylsilane signal and are referenced to the residual hydrogen signal of deuterated solvents (δ = 1.94 ppm, acetonitrile). IR spectra were recorded with a Bio-RAD IR-FT spectrophotometer as KBr disks in the 4000−250 cm^{-1} region. Specific rotations were measured at 20 °C, in a 1-dm cell using the sodium D-line of an Amber AA5 polarimeter. Circular dichroism spectra were measured using a Jasco model J-710 spectropolarimeter. HPLC was carried out using a CHIROSE-(R)C3 chiral column, (CHIRALSEP, La Frenaye, France) 50 mm diameter × 250 mm length, with methanol/diethylamine (100/0.1, v/v), as mobile phase; UV detection 275 nm. For a flow rate of 100 mL/min, retention times of 9.00 min for **5b** and 13.00 min for **5a** were observed. 60 mg of racemic mixture in 4 mL of acetonitrile was injected in each run.

Supporting Information: NMR spectra including complete assignments of the protons and carbon atoms of **3a**, **3b, 4a**, and **4b** (6 figures) are provided (see also footnote on the first page of this article).

Δ- or Λ-[$Ru(bpy)_2(cmbpy)][PF_6]_2$ (3a or 3b): Δ- or Λ-[$Ru^{II}(bpy)_2$-$(py)_2$][dibenzoyltartrate-*O*,*O*′] (390 mg, 419 μmol), cmbpy (220 mg, 1 mmol, 2.38 equiv.), sodium acetate (220 mg, 2.7 mmol, 5.65 equiv.), water (3 mL), and ethylene glycol (13 mL) were heated at 120 °C overnight, and the pH was then adjusted to 1 by addition of concentrated sulfuric acid. Water (30 mL) was added and the mixture was filtered to remove excess free ligand. The product was precipitated by addition of a saturated aqueous solution of NH_4PF_6, and filtration through a fine (porosity 5) glass frit gave a red powder. This was washed with water and dried under vacuum. Yield: 321 mg (85%). Spectroscopic data are similar to those reported for the racemic complexes.[2f]

***rac*-[$Ru(bpy)_2(dcbpy)][PF_6]_2$ (4a, b):** This product was prepared as described in the literature.[2h] Yield: 331 mg (85%). Selected IR data (KBr disk): $\tilde{\nu}$ = 1734 (C=O), 842 (P−F) cm^{-1}. ^1H NMR (300 MHz, CD_3CN): δ = 7.40 (qd, *J* = 5.7, *J*′ = 1.3 Hz, 4 H), 7.68 (dd, *J* = 6.5, *J*′ = 5.7 Hz, 4 H), 7.82 (dd, *J* = 5.7, *J*′ = 1.8 Hz, 2 H), 7.92 (d, *J* = 5.7 Hz, 2 H), 8.08 (qd, *J* = 7.5, *J*′ = 1.3 Hz, 4 H), 8.51 (dd, 4 H, *J* = 7.9, *J*′ = 2.6 Hz, 4 H), 9.11 (d, *J* = 0.9 Hz, 2 H) ppm. $^{13}C\{^1H\}$ NMR (500 MHz, CD_3CN): C (quaternary): δ = 163.97 (C=O), 157.45, 156.53, 156.41, 138.57; =CH: δ = 152.59, 152.49, 151.54, 151.30, 138.09, 137.98, 127.59, 127.52, 127.45, 126.52, 124.17, 123.74, 123.60. $C_{32}H_{24}F_{12}N_6O_4P_2Ru{\cdot}3H_2O$ (1001.66): calcd. C 38.37, H 3.02, N 8.39; found C 38.68, H 3.03, N 8.10.

Δ- or Λ-[$Ru(bpy)_2$ (dcbpy)][$PF_6]_2$ (4a or 4b): These complexes were prepared in a similar fashion to **3a** and **3b** using Δ- or Λ-[Ru^{II}-$(bpy)_2(py)_2$][tartrate] (200 mg 215 μmol), dcbpy (110 mg, 426 μmol, 1.98 equiv.), sodium acetate (110 mg, 1.34 mmol, 6.23 equiv.), water (3 mL), and ethylene glycol (13 mL). The compounds were obtained as purple powders. Yield: 140 mg (67%). Spectroscopic data are similar to those reported for the racemic compound (vide supra).

NMR Studies and Experimental Conditions: NMR samples were prepared by dissolving the solid Ru^{II} complexes in 500 μL of CD_2Cl_2 + 5 vol-% of CD_3CN ($c \approx 10^{-2}$ M for each sample). The spectra were recorded with a Bruker DRX-500 spectrometer, equipped with a Silicon Graphics workstation. A 5-mm broad-band probe with a shielded z-gradient was used. The temperature was monitored with a BCU 05 temperature unit and fixed at 293 K. Data were processed with Silicon Graphics stations using GIFA (version 4.3).[17,18] Proton spectra were obtained in 16 scans of 16 K data points over a 5.12 kHz spectral width. A presaturation (60 dB) of the solvent residual signal was performed. The free induction decays were processed using standard Fourier transformation. COSY 2D NMR spectra in the absolute mode were recorded using the standard pulse sequence with a presaturation (60 dB) of the solvent signal during the relaxation delay. This 2.0-s relaxation delay was introduced between the 48 transients of each increment. 320 FIDs with 2 K data points in F_2 over a 5.12 kHz spectral width were collected. Zero-fillings were added to increase the resolution in F_1. Before 2D Fourier transformation, a sine-bell window function was applied to both dimensions. The transformed data were then symmetrized. For the $^1H-^1H$ dipolar contact analyses, 2D ROESY experiments were preferred because of the molecular weight of the concerned ions for which NOEs are weakly positive or zero. The chosen ROESY sequence[19] introduces trim pulses (180_X, 180_{-X}, ...) used as spinlock to avoid TOCSY effects. The 180° pulses were calibrated for a 20 dB power. These experiments were acquired in the TPPI mode. Solvent signal suppression was achieved by a low power transmitter pulse of presaturation (45 dB) during the relaxation delay. 2D ROESY data were recorded with 2 K points in t_2 over 5.12 kHz and 400 points in t_1. A 2.0-s relaxation delay and a mixing time of 600 ms were used for the 32 scans of each FID. Zero-fillings were added in F_1. Shifted sinebell window functions were applied in both dimensions before the Fourier transformation. Baselines were corrected using a polynomial function if necessary.

Table 2. Crystal data and structure refinement for **5a**

Empirical formula	$C_{32}H_{36}N_6O_{11}Ru$
Formula mass	781.74
Temperature [K]	295
Crystal system	monoclinic
Space group	*C*2
a [Å]	22.772(9)
b [Å]	13.336(4)
c [Å]	17.340(6)
β [°]	137.33(3)
V [$Å^3$]	3569(3)
Z	4
$\rho_{calcd.}$ [$g{\cdot}cm^{-3}$]	1.455
λ (Mo-K_α) [Å]	0.71069
μ [cm^{-1}]	4.92
$R = \Sigma\|\|F_o\| - \|F_c\|\|/\Sigma\|F_o\|$	0.0532
$Rw = [\Sigma w(\|\|F_o\| - \|F_c\|\|)^2/\Sigma wF_o^2]^{1/2}$	0.0615

X-ray Structure Determination: Data for **5a** (Table 2) were collected with an Enraf−Nonius CAD4 diffractometer, Mo-K_α radiation (λ = 0.71069 Å) collection range 2θ = 2−50°, crystal dimensions 0.25 × 0.30 × 0.35 mm. An empirical absorption correction (DIFABS)[20] was applied (T_{min} = 0.89, T_{max} = 1). The structure was solved by direct methods and subsequent difference Fourier syn-

theses, and refined by full-matrix least squares on *F* by using the programs of the PC version of CRYSTALS. All non-hydrogen atoms were refined anisotropically. Hydrogen atoms were located in a difference Fourier map and their coordinates were refined with an overall isotropic thermal parameter. CCDC-174554 (**5a**) contains the supplementary crystallographic data for this paper. These data can be obtained free of charge at www.ccdc.cam.ac.uk/conts/retrieving.html or from the Cambridge Crystallographic Data Centre, 12 Union Road, Cambridge CB2 1EZ, UK [fax: (internat.) + 44-1223/336-033; E-mail: deposit@ccdc.cam.ac.uk].

[1] [1a] U. Knof, A. von Zelewsky, *Angew. Chem. Int. Ed.* **1999**, *38*, 302−322, and references cited therein. [1b] F. R. Keene, *Coord. Chem. Rev.* **1997**, *166*, 121−159. [1c] Md. M. Ali, F. M. MacDonnell, *J. Am. Chem. Soc.* **2000**, *122*, 11527−11528. [1d] K. Okamoto, Y. Matsuoka, N. Wakabayashi, A. Yamagishi, N. Hoshino, *Chem. Commun.* **2002**, 282−283.

[2] [2a] J. K. Barton, *Science* **1986**, *233*, 727−734. [2b] R. Hartshorn, J. K. Barton, *J. Am. Chem. Soc.* **1992**, *114*, 5919−5925. [2c] A. E. Friedman, J.-C. Chambron, J.-P. Sauvage, N. J. Turro, J. K. Barton, *J. Am. Chem. Soc.* **1990**, *112*, 4960−4962. [2d] J. K. Barton, A. T. Danishefsky, J. M. Goldberg, *J. Am. Chem. Soc.* **1984**, *106*, 2172−2176. [2e] C. Hiort, P. Lincoln, B. Nordén, *J. Am. Chem. Soc.* **1993**, *115*, 3448−3454. [2f] B. M. Peek, G. T. Ross, S. W. Edwards, G. J. Meyer, T. J. Meyer, B. W. Erikson, *Int. J. Pept. Protein Res.* **1991**, *38*, 114−123. [2g] T. Shimidzu, T. Iyoda, K. Izaki, *J. Phys. Chem.* **1985**, *89*, 642−645. [2h] E. Terpetschung, H. Szmacinski, H. Malak, J. R. Lakowicz, *Biophys. J.* **1995**, *68*, 342−350.

[3] [3a] H. Dürr, S. Bossman, *Acc. Chem. Res.* **2001**, *34*, 905−917. [3b] H. Rudmann, S. Shimada, M. F. Rubner, *J. Am. Chem. Soc.* **2002**, *124*, 4918−4921. [3c] M. Buda, G. Kalyuzhny, A. J. Bard, *J. Am. Chem. Soc.* **2002**, *124*, 6090−6098.

[4] [4a] A. Shulman, F. P. Dwyer, *Chelating Agents and Metal Chelates* (Eds.: F. P. Dwyer, D. P. Mellor) Academic Press, New York, **1964**, pp. 383−439. [4b]T. J. Rutherford, P. A. Pellegrini, J. Aldrich-Wright, P. C. Junk, F. R. Keene, *Eur. J. Inorg. Chem.* **1998**, 1677−1688 and refs therein. [4c] A. Kirsch-De Mesmaeker, J.-P. Lecomte, J. M. Kelly, *Top. Curr. Chem.* **1996**, *177*, 25−76.

[5] [5a] K. Warnmark, J. A. Thomas, O. Heyke, J.-M. Lehn, *Chem. Commun.* **1996**, 701−702. [5b] K. Warnmark, O. Heyke, J. A. Thomas, J.-M. Lehn, *Chem. Commun.* **1996**, 2603−2604. [5c] F. M. MacDonell, S. Bodige, *Inorg. Chem.* **1996**, *35*, 5758−5759. [5d] S. Bodige, A. S. Torres, D. J. Maloney, D. Tate, G. R. Kinsel, A. K. Walker, F. M. MacDonnell, *J. Am. Chem. Soc.* **1997**, *119*, 10364−10369. [5e] M. Brissard, H. Amouri, M. Gruselle, R. Thouvenot, *C. R. Chim.* **2002**, *5*, 53−58. [5f] D.-R. Ahn, T. W. Kim, J.-I. Hong, *J. Org. Chem.* **2001**, *66*, 5008−5011.

[6] J. Lacour, C. Ginglinger, C. Grivet, G. Bernardinelli, *Angew. Chem. Int. Ed. Engl.* **1997**, *36*, 608−610.

[7] [7a] H. Ratni, J. J. Jodry, J. Lacour, E. P. Kündig, *Organometallics* **2000**, *19*, 3997−3999. [7b] H. Amouri, R. Thouvenot, M. Gruselle, *C. R. Chim.*, **2002**, *5*, 257−262. [7c] M. Brissard, M. Gruselle, B. Malézieux, R. Thouvenot, C. Guyard-Duhayon, O. Convert, *Eur. J. Inorg. Chem.* **2001**, 1745−1751. [7d] H. Amouri, R. Thouvenot, M. Gruselle, B. Malézieux, J. Vaissermann, *Organometallics* **2001**, *20*, 1904−1906.

[8] J. Lacour, S. Torche-Haldimann, J. J. Jodry, C. Ginglinger, F. Favarger, *Chem. Commun.* **1998**, 1733−1734.

[9] O. Maury, J. Lacour, H. Le Bozec, *Eur. J. Inorg. Chem.* **2001**, 201−204.

[10] D. Gut, A. Rudi, J. Kopilov, I. Goldberg, M. Kol, *J. Am. Chem. Soc.* **2002**, *124*, 5449−5456.

[11] X. Hua, A. Von Zelewsky, *Inorg. Chem.* **1995**, *34*, 5791−5797.

[12] D. Kotkar, P. K. Ghosh, *Inorg. Chem.* **1987**, *26*, 208−209.

[13] D. Hesek, Y. Inoue, S. R. L. Everitt, H. Ishida, M. Kunieda, M. G. B. Drew, *Inorg. Chem.* **2000**, *39*, 308−316.

[14] B. Kolp, H. Viebrock, A. Von Zelewsky, D. Abeln, *Inorg. Chem.* **2001**, *40*, 1196−1198.

[15] C. Lodeiro, F. Pina, A. J. Parola, A. Bencini, A. Bianchi, C. Bazzicalupi, S. Ciattini, C. Giorgi, A. Masotti, B. Valtancoli, J. Seixas de Melo, *Inorg. Chem.* **2001**, *40*, 6813−6819.

[16] B. P. Sullivan, D. J. Salmon, T. J. Meyer, *Inorg. Chem.* **1978**, *17*, 3334−3341

[17] M. A. Delsuc, in: *Maximum Entropy and Bayesian Methods* (Ed.: J. Skilling), Kluwer Academic, Dordrecht, **1988**, pp. 285−290.

[18] J. L. Pons, T. E. Malliavin, M. A. Delsuc, *J. Biomol. NMR* **1996**, *8*, 445−452.

[19] T. L. Hwang, A. J. Shaka, *J. Am. Chem. Soc.* **1992**, *114*, 3157−3159.

[20] N. Walker, D. Stuart, *Acta Crystallogr., Sect. A* **1983**, *A39*, 158−166.

Received February 11, 2002
[I02069]

In-situ Energy-Dispersive X-ray Diffraction Studies of Crystal Growth and Compound Conversion Under Solvothermal Conditions

Lars Engelke,*[a] Michael Schaefer,[a] Felix Porsch,[b] and Wolfgang Bensch[a]

Keywords: X-ray diffraction / Cell design / Kinetics / Solvothermal synthesis / Thioantimonates

The results of in-situ energy-dispersive X-ray diffraction under solvothermal conditions performed on isostructural, layered thioantimonates $Mn_2Sb_2S_5$·L (L = amine) demonstrate the great potential of the method. When the synthesis was carried out at low temperatures with L being 1,3-diaminopropane (DAP), two crystalline intermediate phases were detected which then grew and disappeared when product growth started. Surprisingly, when *N*-methyl-1,3-diaminopropane (MDAP) was used, no crystalline intermediates could be detected and the induction time was significantly shorter than for DAP. For reactions up to 100 °C and for higher temperatures with $\alpha < 0.8$ (α is the extent of reaction), the crystallisation is predominantly controlled by nucleation. Further progress of crystallisation ($\alpha > 0.8$) leads to a change of the dominant process and a diffusion-controlled mechanism is observed. During the reaction with diethylenetriamine (DIEN), three crystalline intermediates were detected prior to product growth. The induction time is longer than for the other two compounds. The crystallisation seems to be diffusion-controlled and is faster than for the DAP and MDAP compounds. In a solution of DIEN, the crystalline phases $Mn_2Sb_2S_5$·L (L = DAP or MDAP) are transformed into the DIEN product under solvothermal conditions, and a rigorous analysis of the intensities of the reflections suggests a partial dissolution of the crystalline starting materials followed by crystallisation of the DIEN material.
(© Wiley-VCH Verlag GmbH & Co. KGaA, 69451 Weinheim, Germany, 2003)

Introduction

The synthesis of new and exciting porous materials is directly related to the application of solvo- and hydrothermal techniques. Under these conditions, primary building units like the TO_4 tetrahedra used to prepare zeolites, and organic molecules, which can act as structure-directing agents, are often stable. The final products are formed from these units and/or molecules by heterogeneous multicomponent reactions. Hydrothermal methods are widely applied in the preparation of open framework lattices such as zeolites, zeotypes, and metal-substituted zeolites.[1−4] Such porous materials are of great interest because of their use in a range of molecular recognition applications, as catalysts, absorption materials, and for ion-exchange reactions.[5−7] Due to the large technological potential of porous materials, most experiments are devoted to the preparation of new compounds with new and unprecedented properties. In order to understand solvothermal reactions and their mechanisms and to allow systematic developments of these materials, however, kinetic analyses by in-situ methods are necessary. Since the first study of a zeolite with in-situ energy-dispersive X-ray diffraction using synchrotron radiation (EDXRD) in 1992,[8] several reports of the results of such in-situ experiments have been published[5,9−15] (see also citations in ref.[11]). The in-situ powder diffraction method, as well as the latest developments in the technology required for such challenging experiments, was reviewed very recently by Walton and O'Hare.[16] The direct observation of crystallisation offers several advantages over conventional ex-situ techniques like angular-dispersive X-ray diffraction (ADXRD) and the advantages of in-situ methods are well documented in the literature.[5,11,16] Most of the experiments were performed on oxides and only a few studies were done on sulfides, i.e. on the compounds $(Me_4N)_2Sn_3S_7$·H_2O,[12,17] $(C_7H_{13}N)Mn_{0.25}Ge_{1.75}S_4$·$H_2O$,[18] and $Mn_2Sb_2S_5$·DAP.[19]

It must be kept in mind that the syntheses of chalcogenides or oxide phases under solvothermal conditions are multi-component heterogeneous reactions between liquid and solid components, and the chief difficulty of these reactions is the very large number of possible reaction variables. Changing one of these variables affects the pathway and kinetics of the reactions in ways which are not well understood. A systematic exploration of the effect on the synthesis of changing each variable can be a very time-consuming and inefficient process. In-situ EDXRD is a powerful method that allows the study of crystallisation kinetics under real-time conditions and the effect of altering one variable on crystallisation and product formation can be monitored easily. Furthermore, the occurrence and decay of

[a] Institut für Anorganische Chemie, Universität Kiel,
Otto-Hahn-Platz 6/7, 24098 Kiel, Germany
Fax: (internat.) + 49-431/880-1520
[b] Mineralogisch-Petrologisches Institut, Universität Bonn,
Poppelsdorfer Schloß, 53115 Bonn, Germany
Fax: (internat.) + 49-40/8998-4475

crystalline intermediate phases can be detected and monitored.

During the last few years we have prepared several new chalcogenides under solvothermal conditions.[20−29] The layered thioantimonates(III) $Mn_2Sb_2S_5$·L[20−22] [L = 1,3-diaminopropane (DAP), *N*-methyl-1,3-diaminopropane (MDAP), and diethylenetriamine (DIEN)] are of special interest because they are isostructural and can be prepared in the laboratory as phase-pure products under very similar reaction conditions. Therefore, the Mn−Sb−S−L systems are suitable for the study of the crystallisation kinetics as a function of the amine. The results of conversion experiments should give hints about the kinetic and thermodynamic stability of the different compounds.

In the present contribution we report the results of experiments carried out on the compounds $Mn_2Sb_2S_5$·MDAP and $Mn_2Sb_2S_5$·DIEN. In addition, the results of in-situ studies concerning the stability of the crystalline thioantimonates as well as their conversion are presented.

Results and Discussion

It is well documented that under solvothermal conditions several experimental variables strongly influence the product formation,[12,13,31−33] one of the most critical parameters being the reaction temperature. Bearing in mind that solvothermal crystallisation is a multicomponent heterogeneous reaction, it is clear that changing one parameter will influence other parameters in a way which is not well understood.

Prior to the in-situ EDXRD investigations, it was necessary to conduct the syntheses of $Mn_2Sb_2S_5$·L under dynamic conditions, i.e. stirring the mixtures during the reaction. Ex-situ experiments were performed to determine the stability of the crystalline thioantimonates in basic amine solutions. Interestingly, when diethylenetriamine (DIEN) was added to crystalline $Mn_2Sb_2S_5$·L (L = DAP or MDAP) phase-pure $Mn_2Sb_2S_5$·DIEN was always formed. These results obtained with the ex-situ experiments encouraged us to study the transformation of the crystalline starting materials with the in-situ EDXRD technique.

Studies of the Mn−Sb−S−DAP System

Very recently we reported the results of in-situ EDXRD experiments performed on the system Mn, Sb, S with DAP as amine.[19] The most important results of the experiments can be summarised as follows: The induction time t_0 depends strongly on the reaction temperature and increases from 15 min at 130 °C to about 60 min at 105 °C. The product growth is significantly accelerated at higher temperature. Analysis of the crystallisation kinetics showed that similar effects occur between 105 and 125 °C. The best agreement is obtained with a first-order reaction and/or a phase-boundary-controlled mechanism. With increasing α (α is the extent of reaction) the mechanism changes suggesting consecutive kinetics as the reaction proceeds. At 130 °C and α > 0.75 a three-dimensional, diffusion-controlled process dominates.

One of the surprising results was the observation of a crystalline precursor and a crystalline intermediate phase at reaction temperatures below 105 °C (Figure 1). The preliminary analysis provided evidence for a close correlation between the composition and structure of the intermediate and final products.[19] To trap the precursor and the intermediate, several experiments with different mixtures were conducted to isolate and characterise the two unknown crystalline phases. When a mixture of Mn, S, and DAP was heated to the desired temperature the first unknown phase formed; subsequent addition of antimony led to the product formation. Obviously, the precursor is an antimony-free phase composed of Mn, S, and DAP. Unfortunately, it was not possible to index the diffraction pattern of this precursor, but EDS and elemental analyses yielded an Mn/S/DAP ratio of 2:5:2. The second crystalline intermediate contains Sb, but its nature is still not clear. All attempts to quench the phase failed and it must be concluded that it is converted or destroyed during the cooling procedure and the workup of the mixture. Such a decomposition of a compound which is stable under the synthetic conditions is not surprising and similar observations have been made by other groups who have studied oxide systems by in-situ EDXRD.[13−16]

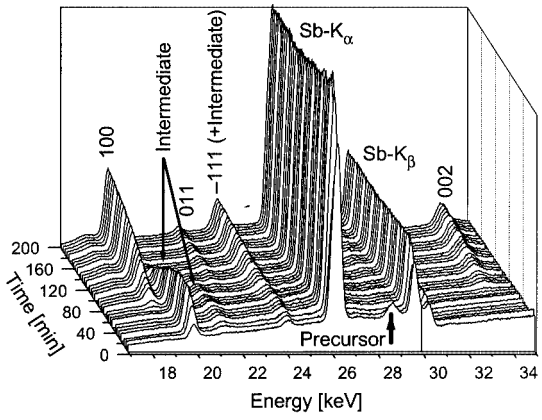

Figure 1. Time-resolved diffraction pattern of $Mn_2Sb_2S_5$·DAP recorded at 105 °C; the most prominent reflections of the two crystalline intermediates are marked; the numbers are reflection indices of the product

In-situ EDXRD Investigations of the Mn−Sb−S−MDAP and Mn−Sb−S−DIEN Systems

The experiments with MDAP and DIEN should show whether product formation with DAP, MDAP, and DIEN is identical or not. By comparing α with time for the three amines it is clear that product growth is significantly faster for MDAP than for DAP over the whole temperature range (see Figure 2). Between 85 and 120 °C the induction time t_0 is significantly shorter for MDAP (see Figure 3). The fastest growth was observed for DIEN but crystallisation needed the longest induction time. The DIEN reaction was therefore investigated in a temperature range from 110 to 170 °C.

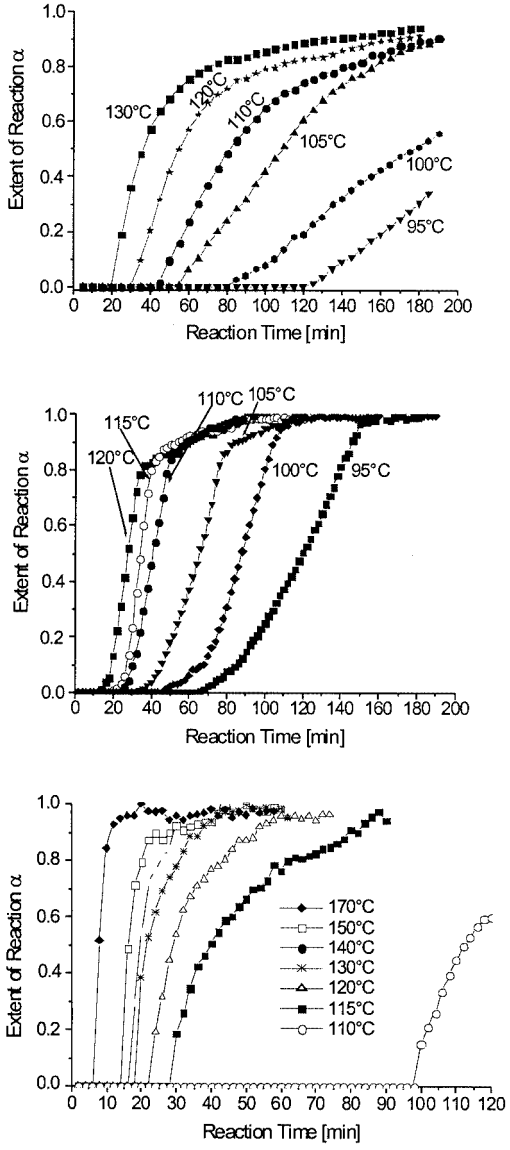

Figure 2. The extent of reaction (α) versus time for the (100) reflection of $Mn_2Sb_2S_5$·DAP (top), $Mn_2Sb_2S_5$·MDAP (centre) and $Mn_2Sb_2S_5$·DIEN (bottom) for different reaction temperatures

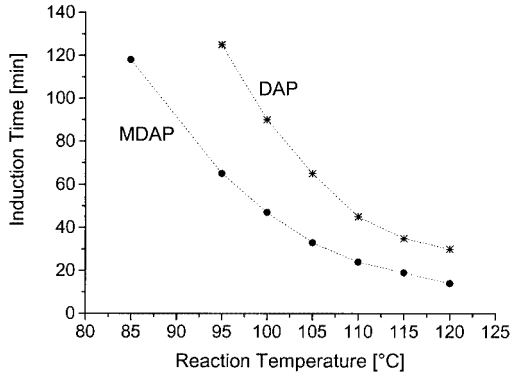

Figure 3. A comparison of the induction times t_0 for $Mn_2Sb_2S_5$·MDAP and $Mn_2Sb_2S_5$·DAP

In contrast to the experiments with DAP, no crystalline intermediate phases could be detected during the reaction with MDAP. All ex-situ and in-situ experiments to generate an analogue of the DAP precursor (see above) were unsuccessful. When using DIEN we observed a different pathway, as shown in Figure 4. First, an antimony-free precursor formed, as in the case of the DAP reaction. After a few minutes, the precursor disappeared, and this was followed by the occurrence of the first, short-lived, crystalline intermediate. A second crystalline compound was then seen which existed for a longer time. Finally, the product reflections of $Mn_2Sb_2S_5$·DIEN appeared.

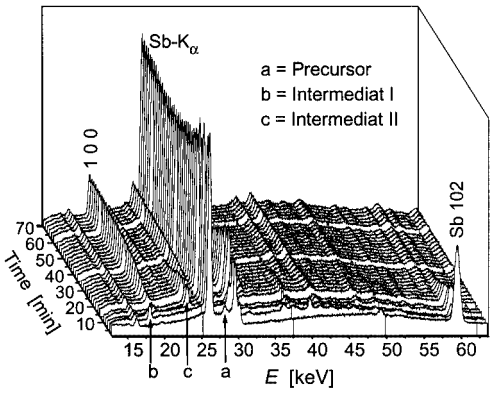

Figure 4. Time-resolved diffraction pattern of $Mn_2Sb_2S_5$·DIEN recorded at 130 °C; the most prominent reflections of the three crystalline intermediates are marked

These results suggest that in the early stages of the reactions, different consecutive and/or parallel mechanisms occur depending on the amine used. Analogous to the examinations of the DAP system,[19] kinetic studies were conducted with MDAP and DIEN. The spectra were collected every 120 s due to fast growth of the crystalline products. The intensity data were normalised with the Sb-K_α resonance and fitted to a theoretical expression relating α and time. The results were compared with expressions applied to solid-state kinetics. The general shapes of such expressions, represented graphically, are well documented.[13,34] The kinetic parameters were obtained by the Avrami−Erofeev expression $\alpha(t) = 1 - \exp[-(kt)^m]$ with α being the extent of reaction, m the reaction exponent and k [s^{-1}] the reaction rate coefficient.[35−37] The expression was then converted into the linear equation $\ln[-\ln(1-\alpha)] = m\cdot\ln(k) + m\cdot\ln(t)$ to analyse the product growth by a so-called Sharp−Hancock plot[34] plotting $\ln[-\ln(1-\alpha)]$ versus $\ln(t)$. Such a plot gives a straight line for that part of the reaction which follows the same mechanism. The reaction exponent m is obtained from the slope of the curve, whilst the rate constant k can be evaluated from the intercept with the y axis. The kinetic data obtained in this way for the MDAP reactions between 95 °C and 120 °C are listed in Table 1. For temperatures up to 100 °C a consistent mechanism was observed, being confirmed by the straight line through the points on the Sharp−Hancock plots (Figure 5, top). At higher temperatures two different regions can be

distinguished, with an inflexion point at $\alpha = 0.8$ (Figure 5, bottom). At $\alpha > 0.8$ a significantly lower reaction exponent m and a higher rate coefficient k were obtained. Due to the long induction times the DIEN data were collected between 110 and 170 °C (Table 2). After induction, the product growth is very fast. For larger α values the straight line in the Sharp−Hancock plots suggests a consistent mechanism.

Table 1. Kinetic data obtained by the analysis with Sharp−Hancock plots for crystallisation of $Mn_2Sb_2S_5$·MDAP; t_0 is the induction time, $t_{0.5}$ is the time when $\alpha = 0.5$

Reaction temp.	t_0 [s]	$t_{0.5}$ [s]	Rate constant k [s^{-1}]	Exponent (order) m
95 °C	3900	3300	$2.60(2)\cdot10^{-4}$	1.96(3)
100 °C	2800	2450	$3.69(7)\cdot10^{-4}$	3.13(6)
105 °C ($\alpha < 0.8$)	2000	1920	$4.40(6)\cdot10^{-4}$	1.97(3)
105 °C ($\alpha > 0.8$)			$7.01(8)\cdot10^{-4}$	1.07(6)
110 °C ($\alpha < 0.8$)	1350	1110	$7.75(5)\cdot10^{-4}$	2.27(4)
110 °C ($\alpha > 0.8$)			$1.36(9)\cdot10^{-3}$	0.78(6)
115 °C ($\alpha < 0.8$)	1100	970	$9.26(8)\cdot10^{-4}$	3.15(6)
115 °C ($\alpha > 0.8$)			$2.13(9)\cdot10^{-3}$	0.55(2)
120 °C ($\alpha < 0.8$)	800	850	$9.95(9)\cdot10^{-4}$	2.18(3)
120 °C ($\alpha > 0.8$)			$2.15(8)\cdot10^{-3}$	0.56(2)

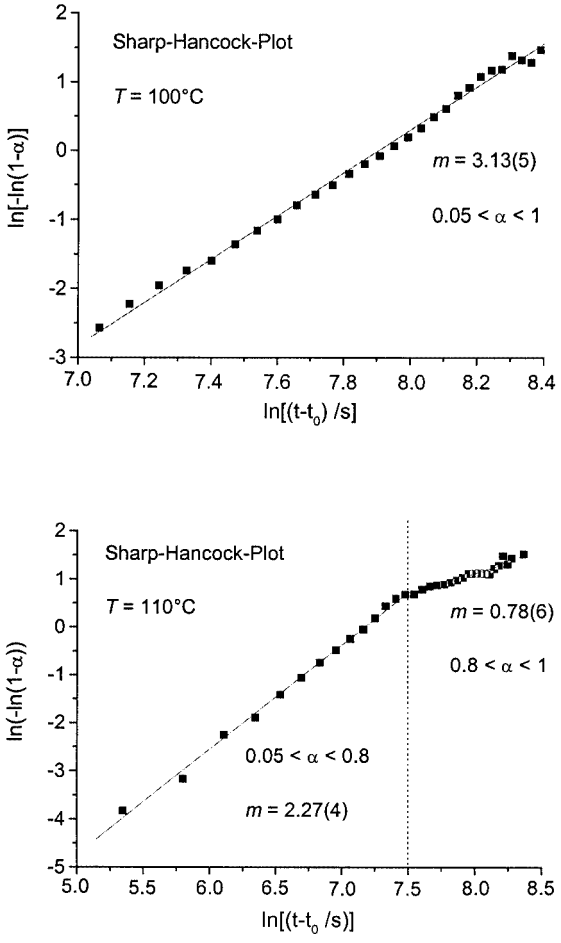

Figure 5. Sharp−Hancock plots of the data obtained for $Mn_2Sb_2S_5$·MDAP at 100 °C and 110 °C; experimental points are the solid squares and the lines represent the fits

Table 2. Kinetic data obtained by the analysis with Sharp−Hancock plots for the crystallisation of $Mn_2Sb_2S_5$·DIEN; t_0 is the induction time, $t_{0.5}$ is the time when $\alpha = 0.5$

Reaction temp.	t_0 [s]	$t_{0.5}$ [s]	Rate constant k [s^{-1}]	Exponent (order) m
110 °C ($\alpha < 0.6$)	5880	840	$7.64\cdot10^{-4}$	0.88(2)
110 °C ($\alpha > 0.6$)			$6.10\cdot10^{-4}$	0.44(2)
115 °C	1680	720	$8.86\cdot10^{-4}$	0.74(1)
120 °C	1320	440	$1.46\cdot10^{-3}$	0.87(2)
130 °C	1080	280	$2.79\cdot10^{-3}$	0.78(3)
140 °C	960	240	$5.38\cdot10^{-3}$	0.51(4)
150 °C	900	120	$7.84\cdot10^{-3}$	0.49(4)
160 °C	580	100	$8.87\cdot10^{-3}$	0.34(4)

To find a correct model for the crystallisation kinetics the data were plotted as $t/t_{0.5}$ versus α, with $t_{0.5}$ being the reaction time at $\alpha = 0.5$. Such a plot allows a direct comparison with the different models under consideration.[38] The different established models were compared with the experimental results (Table 3). For the temperatures up to 100 °C the $Mn_2Sb_2S_5$·MDAP crystallisation is predominately controlled by nucleation (Figure 6, top). This seems also to be the case for the reactions at higher temperatures with $\alpha < 0.8$. For the data with $\alpha > 0.8$ the curves are in reasonable agreement with a diffusion-controlled mechanism (D3) (Figure 6, bottom). It must be emphasised that such analyses are only approximations to the ideal borderline cases of the different models. Nevertheless, the data confirm that the crystallisation kinetics as well as the mechanisms are very different for the amines DAP and MDAP. The formation of $Mn_2Sb_2S_5$·DAP involves the formation and disappearance of two crystalline intermediates, and the crystallisation follows a phase-boundary-controlled mechanism. In contrast, for $Mn_2Sb_2S_5$·MDAP a nucleation-controlled growth without formation of any crystalline intermediate is observed. The proposed models are confirmed by the shapes of the α vs. time curves (Figure 2), which, as predicted by the theoretical models, are sigmoidal for nucleation-controlled mechanisms but not for phase-boundary-controlled models.[13] Interestingly, for the reaction with DIEN, different crystallisation kinetics are observed. Both, the shape of the curves and the $t/t_{0.5}$ data point to a diffusion-controlled mechanism. Due to the high rate constants the time resolution of 120 s is not adequate to determine low α values.

The activation energy of crystallisation was calculated by applying the Arrhenius equation $\ln(k) = \ln(A) - E_a/RT$. From the slope of an $\ln(k)$ versus $1/T$ plot, activation energies E_a of 65(5) kJ/mol (MDAP system) and 73(3) kJ/mol (DIEN system) were obtained. The values are in a range similar to those calculated for the crystallisation of the DAP compound as well as for usual zeolite compounds reported in the literature.[9,39] For the reactions with changing mechanisms the k values for $\alpha < 0.8$ were used.

Table 3. The rate equations for solid-state reactions reported in the literature

Growth model[38]	Rate equation f(α) = kt	m
Diffusion-controlled:		
$D_1(\alpha)$	$\alpha^2 = 0.25\ (t/t_{0.5})$	0.62
$D_2(\alpha)$	$(1-\alpha)\ln(1-\alpha)+\alpha = 0.1534\ (t/t_{0.5})$	0.57
$D_3(\alpha)$ [Jander]	$[1-(1-\alpha)^{1/3}]^2 = 0.0425\ (t/t_{0.5})$	0.54
$D_4(\alpha)$ [Ginstling−Brounshtein]	$1-2\alpha/3-(1-\alpha)^{2/3} = 0.0367\ (t/t_{0.5})$	0.57
Phase-boundary-controlled:		
$R_2(\alpha)$	$1-(1-\alpha)^{1/2} = 0.2929\ (t/t_{0.5})$	1.11
$R_3(\alpha)$	$1-(1-\alpha)^{1/3} = 0.2063\ (t/t_{0.5})$	1.07
First order		
F1(α)	$[-\ln(1-\alpha)] = 0.6931\ (t/t_{0.5})$	1.00
Nucleation [Avrami−Erovéef]:		
A2(α)	$[-\ln(1-\alpha)]^{1/2} = 0.8326\ (t/t_{0.5})$	2.00
A3(α)	$[-\ln(1-\alpha)]^{1/3} = 0.885\ (t/t_{0.5})$	3.00

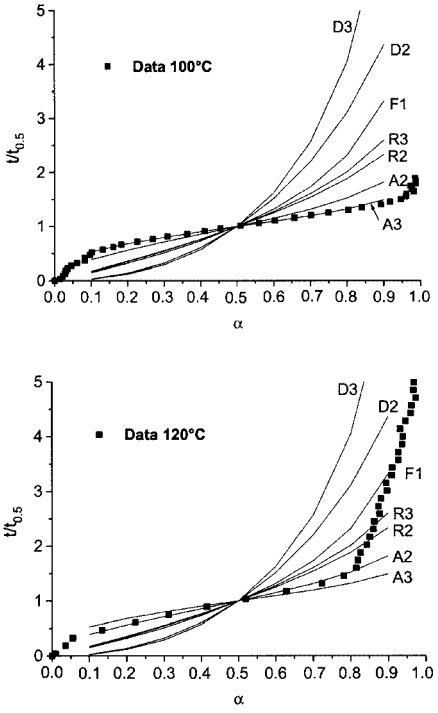

Figure 6. Comparison of the evolution of experimental $t/t_{0.5}$ data (T = 100 and 120 °C) as a function of α (black squares) with different kinetic models for $Mn_2Sb_2S_5$·MDAP; the letters with the numbers are the abbreviations of the different models listed in Table 2

Stability of Crystalline $Mn_2Sb_2S_5$·L Phases

In order to study the competition between the amines during product formation, 1:1 and 3:1 mixtures of two amines were examined and the reactions monitored. At the end of the reactions only one pure product containing only one amine was observed. The DAP/DIEN and MDAP/DIEN mixtures gave pure $Mn_2Sb_2S_5$·DIEN and for both mixtures the three crystalline phases were detected that were also seen using pure DIEN (see above). For DAP/MDAP mixtures the pure MDAP compound was formed, and even after 175 min no reflections of $Mn_2Sb_2S_5$·DAP were visible in the patterns. No hints were found for the appearance of the crystalline intermediate phases that were detected in the Mn−Sb−S−DAP system.

The conversion of the different isostructural phases which was observed with the ex-situ experiments was investigated in situ in the following way: The reactions with the amines DAP or MDAP, which gave the desired crystalline product, were monitored by in-situ EDXRD; after completion, 1 mL of a second amine was added to the product and spectra were recorded after 2 h at different temperatures to monitor possible changes in the starting material caused by the added amine.

After the addition of MDAP to the crystalline $Mn_2Sb_2S_5$·DAP product, no differences in the spectra could be detected even after 2 h at 120 °C (Figure 7). Very different results were obtained, however, when crystalline $Mn_2Sb_2S_5$·L (L = DAP or MDAP) products were treated with DIEN. The reaction between $Mn_2Sb_2S_5$·DAP and DIEN at 120 °C is relatively fast, and after about 45 min only reflections due to $Mn_2Sb_2S_5$·DIEN occurred in the pattern (Figure 8). The peak maximum of the (100) reflection shifts continuously from the position of $Mn_2Sb_2S_5$·DAP (18.74 keV) to that of $Mn_2Sb_2S_5$·DIEN (18.66 keV) as shown in Figure 9. The conversion of the DAP compound to the pure DIEN sample depends on the temperature, and the half-life was extended from about 10 min at 120 °C to 20 min at 110 °C.

Performing the experiments with crystalline $Mn_2Sb_2S_5$·MDAP resulted in the conversion into the DIEN product being slower. At 120 °C the appearance of reflections due to $Mn_2Sb_2S_5$·DIEN started after a few minutes but full conversion was not achieved for a further 2 h. Figure 10 shows the transformation of the MDAP to the DIEN phase. The temperature dependence is more pronounced than for DAP: The half-life has increased from 30 min at 120 °C to 120 min at 100 °C, and the completion requires several hours. These results suggest that $Mn_2Sb_2S_5$·DIEN is the most stable compound, followed by $Mn_2Sb_2S_5$·MDAP and $Mn_2Sb_2S_5$·DAP.

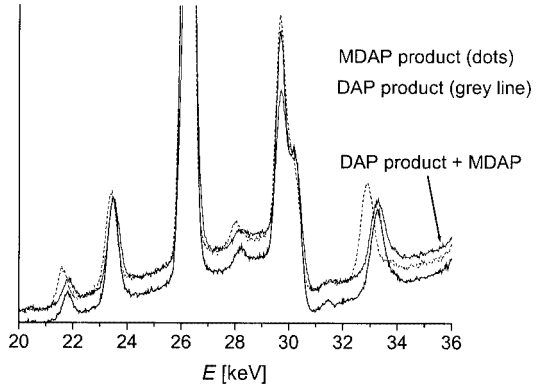

Figure 7. Comparison of the powder patterns of $Mn_2Sb_2S_5$·DAP and $Mn_2Sb_2S_5$·MDAP with the pattern measured after the reaction of $Mn_2Sb_2S_5$·DAP with a solution of MDAP

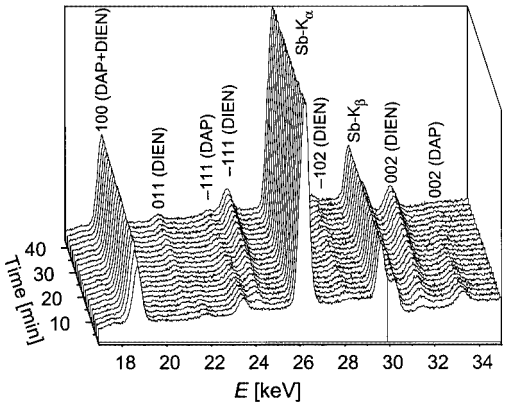

Figure 8. Time-resolved powder patterns collected during the conversion of $Mn_2Sb_2S_5$·DAP on adding DIEN at 120 °C; the indices of the reflections of the two phases are given

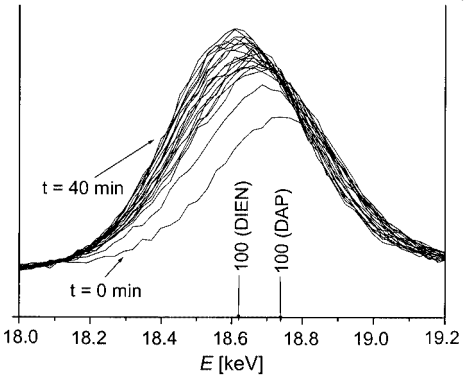

Figure 9. Subsequent shift of the position of the (100) reflection of $Mn_2Sb_2S_5$·DAP after DIEN addition

A quantitative evaluation of the change of MDAP into DIEN of the intensities of the (002) reflections at 100 and 120 °C is shown in Figure 11. Interestingly, the curves of the normalised intensities intersect at $\alpha \approx 0.5$ and several possibilities must be considered to explain this observation: i) direct solid-solid transformation, no amorphous intermediate, no dissolved phases involved in the process;

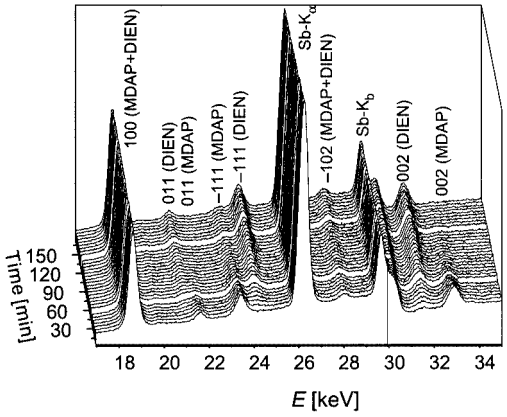

Figure 10. Time-resolved powder patterns collected during the conversion of $Mn_2Sb_2S_5$·MDAP applying DIEN at 120 °C; the indices of the reflections of the two phases are given

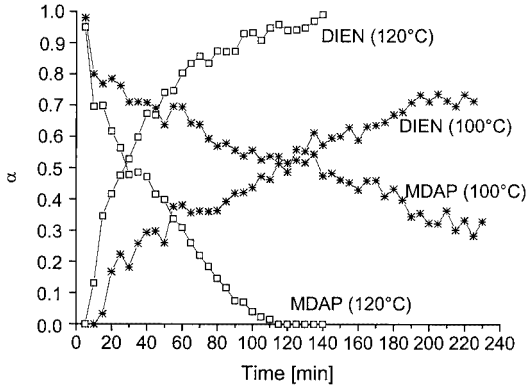

Figure 11. The evolution of the extent of reaction (α) for the (002) reflection of $Mn_2Sb_2S_5$·MDAP during the reaction with a DIEN solution monitored at 100 and 120 °C; note: the lines joining the symbols are only guides

ii) the first compound is completely converted into an amorphous phase, the product nucleates and crystallises subsequently;
iii) the first compound is completely dissolved and the product nucleates and crystallises from the solution;
iv) two completely separate processes for the formation of the first and the second product.

The decrease of the intensities of the DAP and MDAP compounds coincide with the occurrence of the reflections of the DIEN product. Therefore, explanation iv) can be immediately ruled out. Because the curves cross near $\alpha = 0.5$, a solid-solid transformation seems to be plausible, but partial dissolution or amorphisation of the starting material prior to crystallisation of the DIEN product cannot be excluded. A dissolution/amorphisation of a few percent of the DAP/MDAP starting material yields only minute changes in the intensities of the reflections.

It is highly likely that the transformation of the starting material compounds proceeds by one of the two mechanisms ii) or iii). To fully distinguish between these two possibilities other in-situ measurements are necessary. During

the syntheses of aluminophosphates intermediates were detected by in-situ NMR experiments. It is clear, however, that the Mn−Sb−S system is not suitable for such NMR investigations and other techniques such as in-situ Raman spectroscopy or in-situ XAS may provide the information necessary to understand what happens during the transformation of the intermediate into the final product. As demonstrated by Sankar[40,41] and Thomas[42] the combination of in-situ EDXRD and EXAFS is a powerful analytical tool for obtaining the missing information.

Conclusions

Despite the fact that $Mn_2Sb_2S_5$·DIEN, $Mn_2Sb_2S_5$·MDAP, and $Mn_2Sb_2S_5$·DAP are isostructural compounds, the mechanisms of formation are very different. For $Mn_2Sb_2S_5$·DAP crystallisation proceeds via two crystalline intermediates whereas for $Mn_2Sb_2S_5$·MDAP no hints for the formation of such intermediates were found. It is noteworthy that for the DIEN compound three crystalline precursors/intermediates could be detected. In addition, the data provide evidence that the crystallisation kinetics are different for the three compounds. For $Mn_2Sb_2S_5$·DAP, a first-order reaction or phase-boundary mechanism dominates at low temperatures, whereas at higher temperatures and $\alpha > 0.75$ a three-dimensional controlled process (D3) dominates. MDAP nucleation is the rate-limiting step in the low-temperature process and upon increasing the temperature the mechanism changes to D3 when $\alpha > 0.8$. Furthermore, the formation of $Mn_2Sb_2S_5$·MDAP requires shorter induction times than for the DAP analogue. The crystallisation of the DIEN compound proceeds by a diffusion-controlled mechanism after a significantly longer induction time.

The crystalline compounds $Mn_2Sb_2S_5$·DAP and $Mn_2Sb_2S_5$·MDAP are completely converted into the DIEN product suggesting that $Mn_2Sb_2S_5$·DIEN is the thermodynamically most stable compound of the isostructural samples. The difference in the stability between the DAP and MDAP compounds is too small for a transformation of DAP into MDAP. The rigorous analysis of the in-situ EDXRD data for the conversion of MDAP starting material into the DIEN product suggests that a small amount of $Mn_2Sb_2S_5$·MDAP is dissolved, followed by an immediate crystallisation of $Mn_2Sb_2S_5$·DIEN. It must be noted that the amount of the amine applied guarantees a 60-fold excess with respect to the elements Mn/Sb/S.

The results presented here clearly demonstrate that even for isostructural compounds the actual mechanism of formation is very different. Evidently, the amine used determines the mechanism of product crystallisation.

It is well documented that the reactions occurring in the heterogeneous mixture determine what type of compound nucleates and starts to crystallise. Because X-ray diffraction is "blind" with respect to the processes within the so-called induction period, future projects will focus on combined in-situ EXAFS/EDXRD experiments.

Experimental Section

The HASYLAB Beamline F3 receives white synchrotron radiation from a bending magnet with a critical energy of 16 keV and gives a positron beam energy of 4.5 GeV. An energy range from 13.5 to 65 keV can be observed with a maximum at about 20 keV. The diffracted beam is monitored by a nitrogen-cooled solid-state germanium detector. The detector angle was chosen so that all important Bragg reflections could be detected. The *d*-spacing range is given by $E = 6.199/(d \cdot \sin\theta)$. With a detector angle of approximately 1.96° the observable *d*-spacing range is 2.8 to 13.4 Å. Above 26 keV, the energy resolution $\Delta d/d$ is about 10^{-2}. The beam was collimated to 0.2 mm giving the best results.

The investigations were carried out in Teflon-lined autoclaves under autogenous pressure and isothermal conditions similar to those used for the ex-situ investigations in the laboratory. Because common steel autoclaves are not sufficiently permeable for synchrotron radiation, aluminium was used instead. Furthermore, the overall thickness of the wall of the autoclave was reduced from 2.5 mm to 1 mm. At the positions of beam inlet and outlet the wall thickness was machined down to 0.5 mm. The Teflon liner had an internal diameter of 10 mm, wall thickness of 1 mm, height of 94 mm and a capacity of 7 mL. A slightly different set-up for an in-situ cell was described by Evans et al.,[30] the smaller diameter should reduce absorption effects due to the pathway of the beam through the solution.

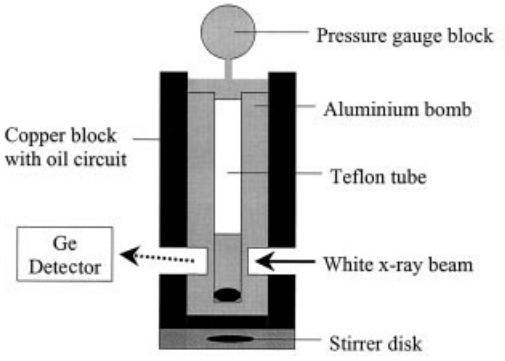

Figure 12. The experimental set-up used for the in-situ EDXRD experiments

The whole experimental set-up is shown in Figure 12 and the entire assembly was constructed according to the requirements of the desk of beamline F3 at HASYLAB in Hamburg. Time-resolved X-ray powder patterns with good counting statistics could be recorded with acquisition times of 300 s. A shorter acquisition time of 120 s was also used to obtain a higher resolution of induction times and reaction courses.

For the syntheses of $Mn_2Sb_2S_5$·L, elemental Mn (27.5 mg; 0.5 mmol), Sb (61.0 mg; 0.5 mmol), and S (40.0 mg; 1.25 mmol) were heated in a 70 % aqueous solution of the amines (2 mL) at temperatures ranging from 85 to 170 °C.

Acknowledgments

We gratefully acknowledge financial support from the State of Schleswig-Holstein, the Deutsche Forschungsgemeinschaft (DFG), and the Fonds der Chemischen Industrie (FCI).

[1] W. S. Sheldrick, M. Wachhold, *Angew. Chem. Int. Ed. Engl.* **1997**, *36*, 206−226.
[2] A. Rabenau, *Angew. Chem. Int. Ed. Engl.* **1985**, *24*, 1026−1040.
[3] M. T. Weller, S. E. Dann, *Curr. Op. Solid State Mater. Sci.* **1998**, *3*, 137−143.
[4] M. E. Davis, R. F. Lobo, *Chem. Mater.* **1992**, *4*, 756−768.
[5] J. M. Thomas, *Angew. Chem. Int. Ed.* **1999**, *38*, 3588−3628.
[6] R. Barrer, *Zeolites and Clay Minerals as Sorbents and Molecular Sieves*, Academic Press, London **1978**.
[7] H. van Bekkum, E. Flanigan, J. Jansen (Eds.), *Introduction to Zeolite Science and Practice*, Elsevier, Amsterdam **1991**.
[8] J. Munn, P. Barnes, D. Hausermann, S. A. Axon, J. Klinowski, *Phase Transitions* **1992**, *39*, 129−134.
[9] A. T. Davies, G. Sankar, C. R. Catlow, S. M. Clark, *J. Phys. Chem. B* **1997**, *101*, 10115−10120.
[10] P. Norby, J. C. Hanson, *Catal. Today* **1998**, *39*, 301−309.
[11] R. J. Francis, D. O'Hare, *J. Chem. Soc., Dalton Trans.* **1998**, 3133−3148.
[12] A. N. Christensen, T. R. Jensen, P. Norby, J. C. Hanson, *Chem. Mater.* **1998**, *10*, 1688−1693.
[13] R. J. Francis, S. O'Brien, A. M. Fogg, P. Halasyamani, D. O'Hare, T. Loiseau, G. Férey, *J. Am. Chem. Soc.* **1999**, *121*, 1002−1015.
[14] S. O'Brien, R. J. Francis, A. M. Fogg, D. O'Hare, N. Okazaki, K. Koruda, *Chem. Mater.* **1999**, *11*, 1822−1832.
[15] R. I. Walton, T. Loiseau, D. O'Hare, G. Férey, *Chem. Mater.* **1999**, *11*, 3201−3209.
[16] R. I. Walton, D. O'Hare, *Chem. Commun.* **2000**, 2283−2291.
[17] R. J. Francis, S. J. Price, J. S. O. Evans, S. O'Brien, D. O'Hare, *Chem. Mater.* **1996**, *8*, 2102−2108.
[18] C. L. Cahill, Y. Ko, J. C. Hanson, K. Tan, J. B. Parise, *Chem. Mater.* **1998**, 1453−1458.
[19] L. Engelke, M. Schaefer, M. Schur, W. Bensch, *Chem. Mater.* **2001**, *13*, 1383−1390.
[20] W. Bensch, M. Schur, *Eur. J. Solid State Inorg. Chem.* **1996**, *33*, 1149−1160.
[21] M. Schur, C. Näther, W. Bensch, *Z. Naturforsch., Teil B* **2001**, *56*, 79−84.
[22] L. Engelke, R. Stähler, M. Schur, C. Näther, W. Bensch, *Z. Anorg. Allg. Chem.*, in preparation.
[23] W. Bensch, M. Schur, *Z. Naturforsch., Teil B* **1997**, *52*, 405−409.
[24] W. Bensch, C. Näther, M. Schur, *Chem. Commun.* **1997**, 1773−1774.
[25] M. Schur, W. Bensch, *Eur. J. Solid State Inorg. Chem.* **1997**, *34*, 457−466.
[26] M. Schur, W. Bensch, *Z. Anorg. Allg. Chem.* **1998**, *624*, 310−314.
[27] F. Wendland, C. Näther, M. Schur, W. Bensch, *Acta Crystallogr., Sect. C* **1998**, *54*, 317−319.
[28] H. Rijnberk, C. Näther, M. Schur, I. Jeß, W. Bensch, *Acta Crystallogr., Sect. C* **1998**, *54*, 920−923.
[29] M. Schur, A. Gruhl, C. Näther, I. Jeß, W. Bensch, *Z. Naturforsch., Teil B* **1999**, *54*, 1524−1528.
[30] J. S. O. Evans, R. J. Francis, D. O'Hare, S. J. Price, S. M. Clark, J. Flaherty, J. Gordon, A. Nield, C. Tang, *Rev. Sci. Instrum.* **1995**, *66*, 2442−2445.
[31] A. M. Fogg, D. O'Hare, *Chem. Mater.* **1999**, *11*, 1771−1775.
[32] J. S. O. Evans, S. Price, H. Wong, D. O'Hare, *J. Am. Chem. Soc.* **1998**, *120*, 10837−10846.
[33] A. K. Cheetham, C. F. Mellot, *Chem. Mater.* **1997**, *9*, 2269−2279.
[34] J. D. Hancock, J. H. Sharp, *J. Am. Ceram. Soc.* **1972**, *55*, 74−76.
[35] M. Avrami, *J. Chem. Phys.* **1939**, *7*, 1103−1112.
[36] M. Avrami, *J. Chem. Phys.* **1940**, *8*, 212−224.
[37] M. Avrami, *J. Chem. Phys.* **1941**, *9*, 177−184.
[38] J. H. Sharp, G. W. Brindley, B. N. N. Achar, *J. Am. Ceram. Soc.* **1966**, *49*, 379−382.
[39] A. Gualtieri, P. Norby, G. Artoli, J. C. Hanson, *Phys. Chem. Miner.* **1997**, *24*, 191−199.
[40] G. Sankar, J. M. Thomas, F. Rey, G. N. Greaves, *J. Chem. Soc., Chem. Commun.* **1995**, 2549−2550.
[41] M. Epple, G. Sankar, J. M. Thomas, *Chem. Mater.* **1997**, *9*, 3127−3131.
[42] J. M. Thomas, *Chem. Eur. J.* **1997**, *3*, 1557−1562.

Received February 22, 2002
[I02089]

Formation of (σ-Alkenyl)- and (μ-Vinylidene)palladium and -platinum Complexes by Oxidative Addition of 4,4-Dichloro-1,1-diphenyl-2-azabuta-1,3-diene − The Molecular Structure of an Unusual Asymmetric (μ-Vinylidene)Pd−Pd Complex

Michael Knorr,*[a] Gérard Schmitt,*[a] Marek M. Kubicki,[b] and Estelle Vigier[b]

Keywords: Palladium / Vinylidene ligands / Platinum / Metal-metal interactions

4,4-Dichloro-1,1-diphenyl-2-azabuta-1,3-diene (**1**) oxidatively adds to $[Pd(PPh_3)_4]$ and $[Pt(C_2H_4)(PPh_3)_2]$ giving rise to the σ-alkenyl complexes *trans*-$[MCl\{[C(Cl)=C(H)–N=CPh_2]\}(PPh_3)_2]$ (**2a**: M = Pd; **2b**: M = Pt). When **1** is treated with $[Pd(PPh_3)_4]$ in a 1:2 ratio in refluxing toluene, the dimetallic μ-vinylidene complex $[(PPh_3)ClPd\{\mu\text{-}[C=C(H)–N=CPh_2]\}PdCl(PPh_3)_2]$ (**3**) is formed. In this fluxional compound, a PPh_3 ligands migrates in a reversible manner between the two Pd centers. Substitution of the PPh_3 ligands of **3** by 2 equiv. of $Ph_2PCH_2PPh_2$ affords the A-frame complex $[ClPd(\mu\text{-}dppm)_2\{\mu\text{-}[C=C(H)–N=CPh_2]\}PdCl]$ (**4**).

(© Wiley-VCH Verlag GmbH & Co. KGaA, 69451 Weinheim, Germany, 2003)

Introduction

Due to the eminent role of palladium in organometallic synthesis and homogenous catalysis, several methods for the formation of palladium−carbon bonds have been developed.[1] Among them, the oxidative addition of alkyl and aryl halides to Pd^0 complexes is common. It has been shown that vinyl chlorides may also oxidatively add to $[Pd(PPh_3)_4]$ giving rise to σ-alkenyl complexes of the type *trans*-$[PdCl\{[C(R)=CR_2]\}(PPh_3)_2]$.[2] In the course of our earlier studies in the field of organic 1,3-dipolar cycloaddition reactions, we prepared the new dichloro vinyl-like compound 4,4-dichloro-1,1-diphenyl-2-azabuta-1,3-diene (**1**).[3,4] This compound exhibits some promising features for coordination to inorganic and/or organometallic units as it bears a conjugated π-system and a potentially reactive C=N double bond. Furthermore, the basic iminium nitrogen atom may act as a potential donor for coordination of further metal centres to assemble (hetero)dimetallic systems. The group-10 late transition metal (Pd, Pt) complexes seem to be particularly good candidates for activation and coordination of this compound. We present here the first application of **1** in the organometallic chemistry of palladium and platinum.

Results and Discussion

Upon heating in toluene at 50 °C, complex **1** oxidatively adds to $[Pd(PPh_3)_4]$ to yield *trans*-$[PdCl\{[C(Cl)=C(H)-N=CPh_2]\}(PPh_3)_2]$ (**2a**) (Scheme 1). The expected

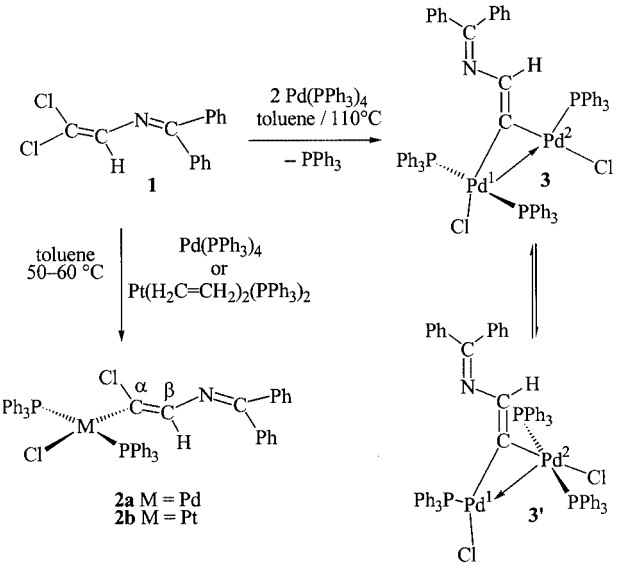

Scheme 1

[‡] Supporting information for this article is available on the WWW under http://www.eurjic.org or from the author.

[a] Laboratoire de Chimie des Matériaux et Interfaces Université de Franche-Comté, Faculté des Sciences et des Techniques
16 Route de Gray, 25030 Besançon Cedex, France
E-mail: michael.knorr@univ-fcomte.fr
[b] Laboratoire de Synthèse et d'Electrosynthèse Organométalliques (UMR, 5632) Université de Bourgogne, Faculté des Sciences et des Techniques
9 Av. A. Savary, 21000 Dijon Cedex, France

Supporting information for this article is available on the WWW under http://www.eurjic.org or from the author.

trans orientation of the two PPh_3 ligands follows from the $^{31}P\{^1H\}$ NMR spectrum, which displays a singlet at δ = 23.6 ppm. In order to obtain an unambiguous assignment of the stereochemistry of **2a**, the Pt analogue *trans*-[PtCl{[C(Cl)=C(H)−N=CPh_2]}$(PPh_3)_2$] (**2b**) was prepared by treating **1** in toluene with [Pt$(C_2H_4)(PPh_3)_2$] at 60 °C. The ^1H NMR spectrum of **2b** indicates that the regioisomer with the hydrogen atom on C-β in the *cis* position relative to the platinum atom is formed exclusively.[5] Since the chemical shifts for the olefinic hydrogen atom of **2a** (δ = 6.21 ppm) and **2b** [δ = 6.19 ppm, $^3J_{cis}$(Pt−H) = 27 Hz] are quite close, we suggest a (*Z*) configuration for these complexes.

When **1** is treated with [Pd$(PPh_3)_4$] in a 1:2 ratio in refluxing toluene, a two-centre, three-fragment oxidative addition of both vinylidene−chloride bonds across two Pd centers occurs affording the dimetallic μ-vinylidene complex [(PPh_3)ClPd{μ-[C=C(H)−N=CPh_2]}PdCl$(PPh_3)_2$] (**3**) in 49% yield {together with small amounts of **2a** and *trans*-[$PdCl_2(PPh_3)_2$]}. Suitable crystals of **3** for an X-ray diffraction study (Figure 1) were grown as red needles from a toluene/heptane solution. Surprisingly, this dimetallic complex possesses two different coordination spheres around each palladium atom; Pd(1) is ligated by P(1), P(2), and Cl(1), and the two Pd^{II} centers are bridged by C(1) in an slightly asymmetric manner [Pd(1)−C(1) 2.031(3), Pd(2)−C(1) 1.910(3) Å]. The close contact between Pd(1) and Pd(2) of 2.6785(3) Å is indicative of the existence of a metal−metal bond,[6,7] therefore Pd(1) may be described as five-coordinate. In contrast, Pd(2) is ligated with Cl(2) and only one phosphane ligand. To achieve the necessary 16-electron count, the metal−metal interaction is best described as a dative Pd1→Pd2 bond.

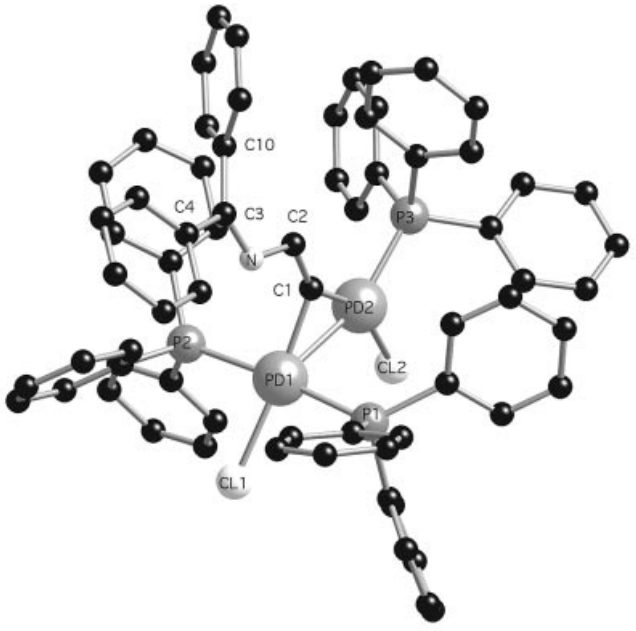

Figure 1. View of the crystal structure of **3**; selected bond lengths [Å] and angles [°]: Pd−Pd 2.6785(3), Pd(1)−P(1) 2.3375(9), Pd(1)−P(2) 2.3430(9), Pd(2)−P(3) 2.2399(9), Pd(1)−C(1) 2.031(3), Pd(2)−C(1) 1.910(3), Pd(1)−Cl(1) 2.3897(9), Pd(2)−Cl(2) 2.3887(9), C(1)−C(2) 1.339(4), N−C(2) 1.407(40), N−C(3) 1.302(4); Cl(1)−Pd(1)−C(1) 173.27(9), P(1)−Pd(1)−P(2) 174.82(3), P(1)−Pd(1)−C(1) 93.74(9), P(2)−Pd(1)−C(1) 91.28(9), P(3)−Pd(2)−C(1) 104.33(10), Pd(2)−C(1)−Pd(1) 85.58(13), C(1)−Pd(1)−Pd(2) 45.32(9), C(1)−Pd(2)−Pd(1) 49.10(10), C(1)−Pd(2)−Cl(2) 155.54(10), C(1)−C(2)−N 121.5(3)

To the best of our knowledge, no related Pd−Pd compound has been structurally characterized to date. However, the overall core structure in **3** is quite similar to that found in a platinum derivative [(PEt_3)BrPt{μ-[C=C(H)−Ph]}PtBr$(PEt_3)_2$].[8] Compound **3** is fluxional in solution, since a very broad singlet resonance at δ = 27.4 ppm is observed in the $^{31}P\{^1H\}$ NMR spectrum at 293 K, which sharpens upon heating to 323 K. At low temperature (223 K), the spectrum consists of distinct triplet and doublet resonances in a 1:2 ratio at δ = 34.0 and 24.8 ppm (see Figure 2). Addition of 2 equiv. of PPh_3 (at 293 K) to a sample of **3** has no influence on the chemical shift or shape of the resonance.

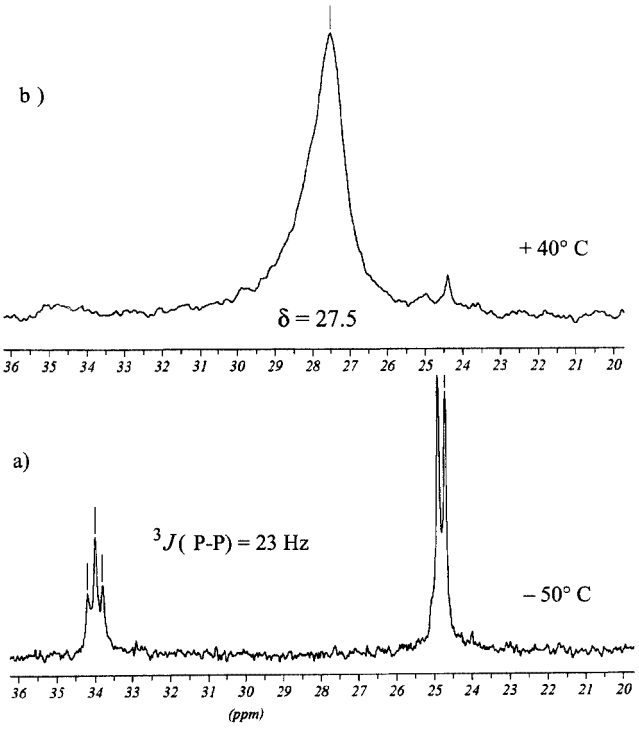

Figure 2. $^{31}P\{^1H\}$ NMR spectrum of **3** recorded in $CDCl_3$ at 223 K (a) and 313 K (b)

This fluxionality may be explained by a nondissociative intramolecular flipping[9a] of one PPh_3 ligand between Pd(1) and Pd(2) with concomitant switching of the vector of the dative bond, resulting in an averaged **3** ⇄ **3′** equilibrium on the NMR time scale. Note that this hypothesis involving the intermediacy of a μ-PPh_3 ligand is supported by the structural characterization of a stable Rh(μ-$PMe_3)_2$Rh complex.[9b,9c] Furthermore, a related reversible and nondissociative migration of a PR_3 ligand has been studied in detail very recently for the dimetallic system [{(η^5-C_5Me_5)Ru}$_2(PR_3)$(μ-H)$_2$].[9d] The ligation of Pd(2) by *just one* PPh_3 ligand is probably due to steric reasons. To avoid steric overcrowding by four bulky PPh_3 ligands in a mutual

trans arrangement on each Pd center, steric repulsion is minimized by dissociation of one of the four PPh_3 ligands, followed by an electronic *quasi* saturation of Pd(2) (up to 16 e^-) by formation of a dative Pd→Pd bond during formation of **3**. This hypothesis is corroborated by the observation that after addition of 2 equiv. of dppm, the three PPh_3 ligands are instantaneously replaced by two diphosphane ligands giving complex **4** quantitatively ($^{31}P\{^1H\}$ NMR monitoring, Scheme 2). As expected for an unsymmetrical dipalladium A-frame complex,[10−12] **4** displays an AA′BB′ pattern in the $^{31}P\{^1H\}$ NMR spectrum centered at δ = 16.3 ppm. This asymmetry may be explained by the coplanar orientation of the μ-azabutadiene unit with the Cl−Pd−C_μ−Pd−Cl array, thus rendering the two Pd environments nonequivalent.

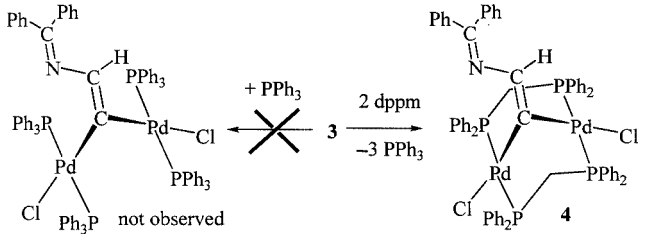

Scheme 2

The potential of **1** and its derivatives as pincer ligands for cyclometallation and carbon−carbon coupling reactions as well for synthesis of other (hetero)dimetallic compounds is currently under investigation.[13]

Experimental Section

General: All reactions were performed in Schlenk-tube flasks under purified nitrogen. Solvents were dried and distilled under nitrogen before use: toluene and heptane from sodium, dichloromethane from P_4O_{10}. The ^1H, $^{31}P\{^1H\}$ NMR, and $^{195}Pt\{^1H\}$ NMR spectra were recorded with a Bruker Avance 300 MHz spectrometer (300.13, 121.49 MHz, and 64.52 MHz for ^1H, ^{31}P, and ^{195}Pt, respectively). Phosphorus chemical shifts are referenced to 85% H_3PO_4 in H_2O with downfield shifts reported as positive. ^{195}Pt chemical shifts are referenced to external K_2PtCl_4 in water with downfield chemical shifts reported as positive. All NMR spectra were recorded in $CDCl_3$.

Preparation of *trans*-[PdCl{[C(Cl)=C(H)−N=CPh$_2$]}(PPh$_3$)$_2$] (2a): Complex **1** (122 mg, 0.44 mmol) was added to a suspension of $[Pd(PPh_3)_4]$ (462 mg, 0.4 mmol) in toluene (15 mL) and the mixture warmed to 50 °C for 5 h. The resulting clear, orange solution was then concentrated to 8 mL, and layered with heptane. After keeping overnight in a refrigerator, **2a** crystallized. The yellow microcrystalline compound was rinsed with hexane (4 mL) and dried in vacuo. Yield: 66% (241 mg). ^1H NMR: δ = 6.21 (s, 1 H, C=CH), 6.49−7.86 (m, 40 H, phenyl) ppm. $^{31}P\{^1H\}$ NMR: δ = 23.6 (s) ppm. $C_{51}H_{41}Cl_2NP_2Pd$ (907.15): calcd. C 67.53, H 4.56, N 1.54; found C 67.98, H 4.56, N 1.90.

Preparation of *trans*-[PtCl{[C(Cl)=C(H)−N=CPh$_2$]}(PPh$_3$)$_2$] (2b): A mixture of $[Pt(C_2H_4)(PPh_3)_2]$ (750 mg, 1 mmol) and **1** (304 mg, 1.1 mmol) in toluene (20 mL) was heated to 60 °C for 14 h. The resulting clear yellowish solution was concentrated to ca. 10 mL and layered with heptane. After keeping at −25 °C, **2b** precipitated as an off-white, air-stable, microcrystalline solid, which was dried in vacuo. Yield: 79% (778 mg). ^1H NMR: δ = 6.19 [s, 1 H, C=CH, $^3J_{cis}$(Pt-H) = 27 Hz], 6.94−7.92 (m, 23 H, phenyl) ppm. $^{31}P\{^1H\}$ NMR: δ = 24.8 (s, $^1J_{Pt,P}$ = 3015 Hz). $^{195}Pt\{^1H\}$ NMR: δ = −2641 (t, $^1J_{Pt,P}$ = 3015 Hz) ppm. $C_{51}H_{41}Cl_2NP_2Pt$ (995.85.): calcd. C 61.51, H 4.15, N 1.41; found C 61.89, H 4.02, N 1.21.

Preparation of [(PPh$_3$)ClPd{μ-[C=C(H)−N=CPh$_2$]}PdCl(PPh$_3$)$_2$] (3): Complex **1** (55 mg, 0.2 mmol) was added to a suspension of $[Pd(PPh_3)_4]$ (462 mg, 0.4 mmol) in toluene (10 mL) and the mixture heated under reflux for 5 h. The solvent was then evaporated and the residue was washed with Et_2O (5 mL). The remaining solid was redissolved in warm toluene and layered with heptane. A mixture of red, air-stable, needle-shaped crystals of **3** and yellow crystals of **2a** and of *trans*-$[PdCl_2(PPh_3)_2]$ co-crystallized; they were separated manually. Yield: 49% (134 mg). ^1H NMR: δ = 6.30 (s, 1 H, C=CH), 6.32−7.98 (m, 55 H, phenyl) ppm. $^{31}P\{^1H\}$ NMR (223 K): δ = 24.8 (d, 2 P, $^3J_{P,P}$ = 23 Hz), 34.0 (t, 1 P, $^3J_{P,P}$ = 23 Hz) ppm. $C_{69}H_{56}Cl_2NP_3Pd_2{\cdot}C_7H_8$ (1367.99): calcd. C 66.73, H 4.72, N 1.02; found C 66.98, H 4.54, N 0.97.

Preparation of [ClPd(μ-dppm)$_2${μ-[C=C(H)−N=CPh$_2$]}PdCl] (4): To a solution of **3** (14 mg, 0.01 mmol) in CH_2Cl_2 (2 mL) was added dppm (8 mg, 0.021 mmol). The resulting orange solution was stirred for a further 10 min, and then the solvent was removed under reduced pressure. The residue was rinsed with Et_2O (2 mL) and than dried to afford orange, air-stable **4** in almost quantitative yield (12 mg). ^1H NMR: δ = 2.55 (m, 2 H, PCH_AP), 3.02 (m, 2 H, PCH_BP), 6.53 (m, 1 H, C=CH), 6.70−7.94 (m, 50 H, phenyl) ppm. $^1H\{^{31}P\}$ NMR: δ = 2.55 (d, 2 H, PCH_AP), 3.02 [d, 2 H, PCH_BP, $J(H_A\text{-}H_B)$ = 12.9 Hz], 6.53 (s, 1 H, C=CH), 6.70−7.94 (m, 50 H, phenyl) ppm. $^{31}P\{^1H\}$ NMR: δ = 16.3 (m, AA′BB′ pattern) ppm. $C_{65}H_{55}Cl_2NP_4Pd_2$ (1257.78): calcd. C 62.07, H 4.41, N 1.12; found C 61.68, H 4.24, N 0.96.

X-ray Crystal Structure Determination of 3·Toluene: A small (0.10 × 0.08 × 0.05 mm) irregularly shaped solvated (toluene) single crystal of **3** was mounted on a Nonius Kappa CCD diffractometer. The unit cell determination and intensity data collection were carried out with Mo-K_α radiation (λ = 0.71073 Å) at 120 K. The measured intensities were reduced with the DENZO program.[14] The structure was solved by both Patterson and direct methods using the routines incorporated in SHELXS-97.[15] The asymmetric unit contains one dinuclear complex and one toluene molecule. The model was further refined with SHELXL-97.[15]

Crystallographic Data: $C_{76}H_{64}Cl_2NP_3Pd_2$ (M = 1367.89): monoclinic, space group $P2_1/n$; a = 16.2461(2), b = 25.3368(3), c = 16.7569(2) Å, β = 108.934(1)°, V = 6524.34(14) Å^3, Z = 4, $\rho_{calcd.}$ = 1.393 g·cm^{-3}, $F(000)$ = 2792; 35364 measured reflections in the scan range 5.4° < 2θ < 61.0°, of which 18823 independent and 9156 observed with $I > 2\sigma(I)$ were used in the structure solution and refinement for 757 parameters; $R1 = \Sigma|F_o - F_c|/\Sigma|F_o|$ = 0.049 [$I > 2\sigma(I)$], $wR2 = [\Sigma w(F_o^2 - F_c^2)^2/\Sigma wF_o^4]^{1/2}$ = 0.101 (all data), S(GoF) = 0.929; anisotropic refinement for non-hydrogen atoms; hydrogen atoms in idealized (riding model) geometries. The highest residual electron-density peak in the differential Fourier map of 0.98 e·Å^{-3} is quasi-symmetrically located between the heavy palladium atoms (1.38 Å from Pd1 and 1.40 Å from Pd2). CCDC-185833 (**3**) contains the supplementary crystallographic data for

this paper. These data can be obtained free of charge at www.ccdc.cam.ac.uk/conts/retrieving.html or from the Cambridge Crystallographic Data Centre, 12 Union Road, Cambridge CB2 1EZ, UK [Fax: (internat.) + 44-1223/336-033; E-mail: deposit@ccdc.cam.ac.uk]. An ORTEP Plot of compound **3** (at the 50% probability level) and the SFC Eurochem 2002 abstract P2-41[13b] are available as Supporting Information.

Acknowledgments

The Ministère de la Recherche et de la Technologie, la Région de Franche-Comté and the CNRS are gratefully thanked for financial support.

[1] *Comprehensive Organometallic Chemistry*, 2nd ed. (Eds.: E. W. Abel, F. G. A. Stone, G. Wilkinson), Pergamon Press, Oxford, New York, **1995**, vol. 6.
[2] P. Fitton, J. E. McKeon, *J. Chem. Soc., Chem. Commun.* **1968**, 4−6.
[3] S. Jacquot, A. Belaissaoui, G. Schmitt, B. Laude, M. M. Kubicki, O. Blacque, *Eur. J. Org. Chem.* **1999**, 1541−1544.
[4] S. Jacquot, G. Schmitt, B. Laude, M. M. Kubicki, O. Blacque, *Eur. J. Org. Chem.* **2000**, 1235−1239.
[5] R. A. Bell, M. M. Chisholm, *Inorg. Chem.* **1977**, *16*, 698−703.
[6] M. Suginome, Y. Kato, N. Takeda, H. Oike, Y. Ito, *Organometallics* **1998**, *17*, 495−497.
[7] [7a] Y. Yamamoto, H. Yamazaki, *Inorg. Chem.* **1986**, *25*, 3327−3329. For a recent review on dinuclear Pd−Pd complexes see: [7b] T. Murahashi, H. Kurosawa, *Coord. Chem. Rev.* **2002**, *231*, 207−228.
[8] E. Baralt, E. A. Boudreaus, J. N. Dernas, P. G. Lenhert, C. M. Lukehart, A. T. McPhail, D. R. McPhail, J. B. M. Junior, L. Sacksteder, W. R. True, *Organometallics* **1989**, *8*, 2417−2430.
[9] [9a] P. Braunstein, N. M. Boag, *Angew. Chem.* **2001**, *113*, 2493−2499; *Angew. Chem. Int. Ed.* **2001**, *40*, 2427−2433. [9b] T. Pechmann, C. D. Brandt, H. Werner, *Angew. Chem.* **2000**, *112*, 4069−4072; *Angew. Chem. Int. Ed.* **2000**, *39*, 3909−3911. For a stable Pd(μ-phosphole)$_2$Pd complex see: [9c] M. Sautier, B. Le Guennic, V. Deborde, L. Toupet, J.-F. Halet, R. Réau, *Angew. Chem.* **2001**, *113*, 234−237; *Angew. Chem. Int. Ed.* **2001**, *40*, 228−231. [9d] Y. Ohki, H. Suzuki, *Angew. Chem.* **2002**, *114*, 3120−3123; *Angew. Chem. Int. Ed.* **2002**, *41*, 2994−2997.
[10] C. Kluwe, J. Müller, J. A. Davies, *J. Organomet. Chem.* **1996**, *526*, 385−387.
[11] A. L. Balch, C. T. Hunt, C. T. Lee, M. M. Olmstead, J. P. Farr, *J. Am. Chem. Soc.* **1981**, *103*, 3764−3772.
[12] X. L. R. Fontaine, S. J. Higgins, B. L. Shaw, *J. Chem. Soc., Dalton Trans.* **1988**, 1179−1184.
[13] [13a] M. Knorr, G. Schmitt, M. M. Kubicki, E. Vigier, *CONCORD-GECOM*, Paris, **2002**, abstract CO 14. [13b] M. Knorr, G. Schmitt, S. Jacquot, M. M. Kubicki, E. Vigier, *SFC EUROCHEM*, Toulouse, **2002**, abstract P 2-41.
[14] Z. Otwinowski, W. Minor, *Methods Enzymol.* **1997**, *276*, 307−326.
[15] G. M. Sheldrick, *SHELXS97* and *SHELXL97*, University of Göttingen, Germany.

Received May 31, 2002
[I02287]

Coordination Modes in a Tridentate NNS (Thiosemicarbazonato)copper(II) System Containing Oxygen-Donor Coligands − Structures of [{Cu(L)(X)}$_2$] (X = Formato, Propionato, Nitrito)

Patricia Gómez-Saiz,[a] Javier García-Tojal,*[a] Aránzazu Mendia,[a] Bruno Donnadieu,[b] Luis Lezama,[c] José Luis Pizarro,[d] Maria Isabel Arriortua,[d] and Teófilo Rojo[c]

Keywords: Copper / Magnetic properties / Stacking interactions / Thiosemicarbazone complexes

Complexes with the formula [{Cu(L)X}$_2$] [X = $HCOO^-$ (**1**), $CH_3CH_2COO^-$ (**2**), NO_2^- (**3**)], where HL = $C_7H_8N_4S$ (pyridine-2-carbaldehyde thiosemicarbazone), have been synthesised and characterised. Single-crystal X-ray diffraction studies show that the structures of these compounds consist of centrosymmetric dimers containing distorted square-pyramidal copper(II) ions. The metal centres are coordinated to the NNS atoms of the tridentate thiosemicarbazonato ligand and one oxygen atom of the X coligand in the basal position. These complexes mainly differ in the atom that occupies the apical position. The structures of compounds **1** and **3** are made up of {$Cu_2(\mu$–SL)$_2$} entities in which the sulfur atom of the tridentate ligand acts as a bridge occupying the apical position. Compound **2** contains a {$Cu_2(\mu$-OX)$_2$} species bridged through the oxygen atoms from both propionato ligands. The results demonstrate the influence of the size of the coligand on the structure of these complexes. Structural and spectroscopic results suggest the presence of relevant ligand-to-metal charge transfers in these compounds. The EPR spectra exhibit rhombic symmetry. Magnetic measurements show antiferromagnetic couplings. The susceptibility data were fitted using the Bleaney–Bowers equation for copper(II) dimers. The J/k values obtained are −4.0, −4.8 and −4.9 K for compounds **1**, **2** and **3**, respectively.
(© Wiley-VCH Verlag GmbH & Co. KGaA, 69451 Weinheim, Germany, 2003)

Introduction

In the last 30 years, thiosemicarbazones and their metal complexes have been extensively studied due to their relevant biological properties.[1] In particular, the copper(II) derivatives of pyridine-2-carbaldehyde thiosemicarbazone (HL = $C_7H_8N_4S$) have drawn much attention (see Scheme 1). This thiosemicarbazone ligand coordinates to the metal ions in both the anionic (L^-) and neutral (HL) forms. The anionic L^- form is usually present in [{Cu(L)X}$_2$] dimers. In these dinuclear compounds, the metal centres can either be bridged through the sulfur enethiolato atom (X = Cl, Br, NCS)[2,3] or the non-thiosemicarbazone coligands[4,5] (X = $CH_3CH_2COO^-$, Scheme 2). In recent work, we have tried to rationalise the structural,

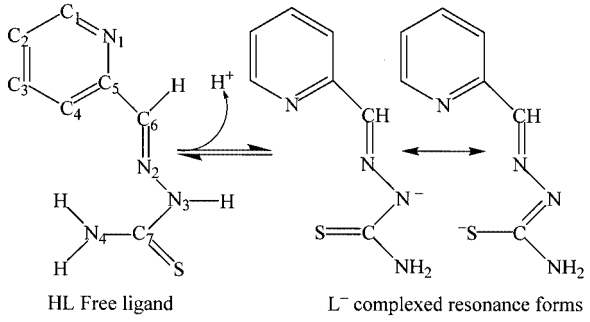

Scheme 1

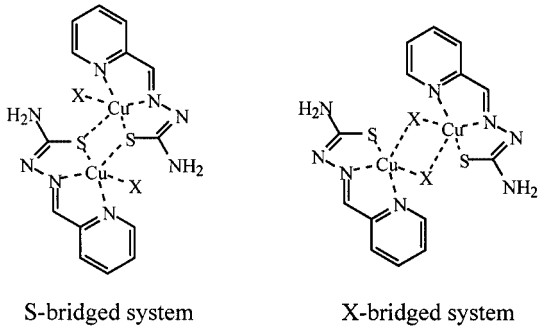

Scheme 2

[a] Departamento de Química, Universidad de Burgos
Plaza Misael Bañuelos s/n, 09001 Burgos, Spain
Fax: (internat.) + 34-947/258831
E-mail: qipgatoj@ubu.es
[b] Laboratoire de Chimie de Coordination du CNRS
205 route de Narbonne, 31077 Toulouse Cedex, France
[c] Departamento de Química Inorgánica, Universidad del País Vasco
Aptdo. 644, 48080 Bilbao, Spain
[d] Departamento de Mineralogía-Petrología, Universidad del País Vasco
Aptdo. 644, 48080 Bilbao, Spain

spectroscopic and magnetic aspects of this system by means of comparative structural studies and approximate molecular orbital calculations.[6] Several structural differences between dinuclear S- and X-bridged complexes have been found. The presence of S-bridges is due to p + sp^2 hybridising of the thiolato sulfur atom. The results suggest that the electron density of the S p_z orbital in the S-bridged systems is less delocalised towards the thiosemicarbazone chain than that of the X-bridged complexes. The formation of complexes with the S-bridge as opposed to the X-bridge depends on the nature of the non-thiosemicarbazone ligands. However, the actual underlying reasons for the formation of S- over X-bridged systems are not clear to date.

In order to evaluate the influence of the size and the type of O-donor coligand in the structure of these compounds, we present the synthesis, crystal structure, spectroscopic and magnetic properties of the [{Cu(L)X}$_2$] [X = $HCOO^-$ (**1**), $CH_3CH_2COO^-$ (**2**), NO_2^- (**3**)] complexes. Approximate molecular orbital calculations of the extended Hückel type have been carried out in order to understand the magnetic features of these systems.

Results and Discussion

The pyridine-2-carbaldehyde thiosemicarbazone (HL) ligand and the [Cu(L)(NO_3)] complex used as starting materials were synthesised according to published methods with slight modifications.[7,8] Elemental analyses are consistent with the proposed stoichiometries. Crystallographic details are given in Table 1.

Discrete quasi-planar [Cu(L)(HCOO)] and [Cu(L)(NO_2)] entities form the crystal structures of compounds **1** and **3**, respectively, linked through the sulfur atom of the thiosemicarbazonato ligand, which leads to dinuclear centrosymmetric [{Cu(L)X}$_2$] species. The molecular structures are shown in Figures 1 and 2. Selected interatomic dimensions are given in Table 2. The copper(II) ions are five-coordinate with two nitrogen atoms and one sulfur atom from the thiosemicarbazonato ligand [Cu−N(1), N(2), S: 2.016(4), 1.976(4), 2.265(2), and 2.025(3), 1.974(3), 2.268(1) Å for **1** and **3**, respectively] and an oxygen atom from one of the formato/nitrito ligands [Cu−O(1) 1.956(4) and 1.964(3) Å] in the basal position. The axial position is occupied by the sulfur atom belonging to the thiosemicarbazonato ligand of

Table 1. Summary of crystallographic data and parameters for **1**, **2** and **3**

	1	**2**	**3**
Empirical formula	$C_{16}H_{16}Cu_2N_8O_4S_2$	$C_{20}H_{24}Cu_2N_8O_4S_2$	$C_{14}H_{14}Cu_2N_{10}O_4S_2$
Formula mass	575.56	631.68	577.56
Crystal size [mm]	0.30 × 0.20 × 0.07	0.15 × 0.10 × 0.07	0.14 × 0.10 × 0.04
System	triclinic	triclinic	triclinic
Space group	$P\bar{1}$	$P\bar{1}$	$P\bar{1}$
a [Å]	7.786(2)	8.687(2)	7.734(1)
b [Å]	8.540(2)	8.723(2)	8.776(1)
c [Å]	8.887(2)	9.273(2)	8.836(1)
α [°]	111.64(3)	108.11(3)	68.23(1)
β [°]	98.78(3)	114.28(3)	95.12(1)
γ [°]	109.75(3)	90.27(3)	68.97(1)
V [Å^3]	496.7(2)	601.6(2)	502.4(1)
Z	1	1	1
F(000)	580	644	580
$\rho_{calcd.}$ [g·cm^{-3}]	1.924	1.743	1.909
μ (Mo-K_α) [mm^{-1}]	2.397	1.987	2.372
T [K]	160(2)	160(2)	298(2)
λ (Mo-K_α) [Å]	0.71073	0.71073	0.71073
Scan type	φ	ω	ω/2θ
2θ range [°]	3.3−52.1	5.5−52.06	2−25
No. measured reflections	3681	5857	1896
Interval h, k, l	±8, ±9, ±9	±10, ±10, ±11	±9, $-9 \le k \le 10$, $0 \le l \le 10$
Unique reflections	1348	2175	1771
R(int)	0.0498	0.0364	0.0326
Refinement method	Full-matrix least squares on F^2		
Data/restraints/parameters	1348/1/158	2175/0/172	1771/0/146
S	1.030	1.182	1.012
w	$1/[\sigma^2(F_o)^2 + (0.0765P)^2]$	$1/[\sigma^2(F_o)^2 + (0.0328P)^2 + 0.864]$	$1/[\sigma^2(F_o)^2 + (0.0283P)^2]$
$R1$ [$I \ge 2\sigma(I)$]	0.0402	0.0317	0.0336
wR 2 [$I \ge 2\sigma(I)$]	0.1008	0.0830	0.0644
$R1$ (all data)	0.0537	0.0364	0.0912
$wR2$ (all data)	0.1089	0.045	0.0753
Largest diff. peak/hole [e Å^{-3}]	0.484, −0.726	0.389, −0.463	0.346, − 0.362

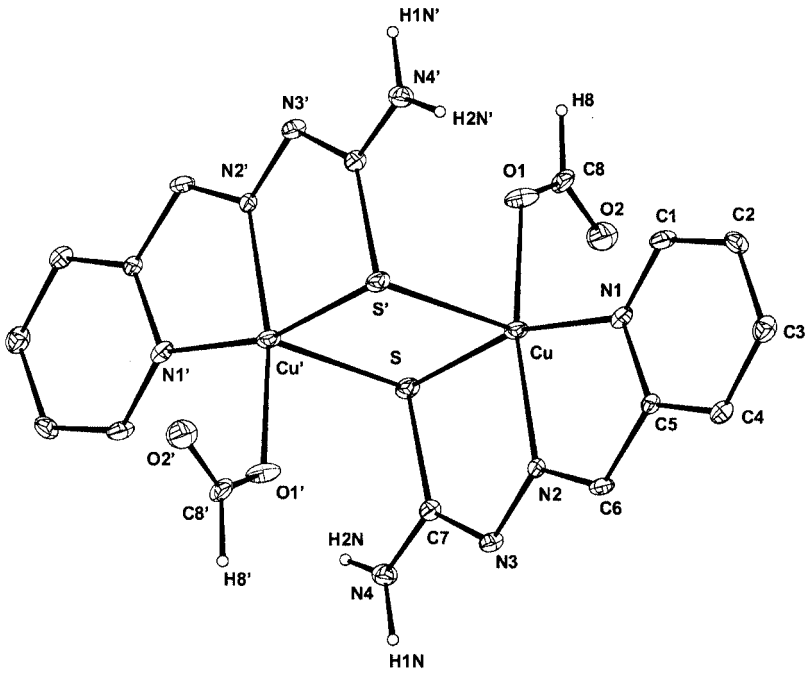

Figure 1. Molecular structure of **1** with thermal ellipsoids at 50% probability level

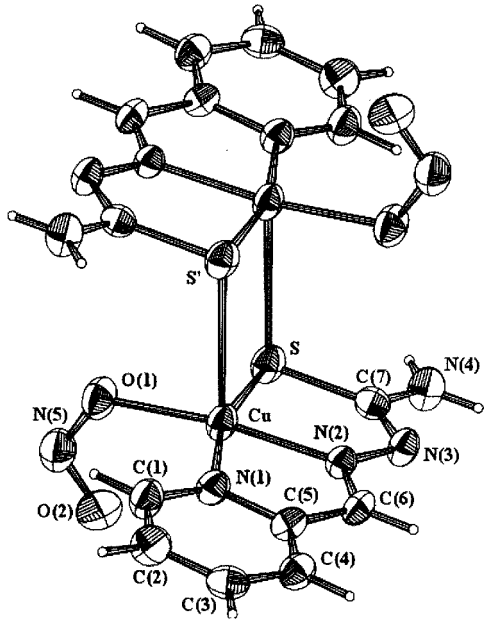

Figure 2. Molecular structure of **3** with thermal ellipsoids at 50% probability level

the adjacent [Cu(L)(X)] entity [Cu−S′ 2.820(2) and 2.918(2) Å for **1** and **3**, respectively]. The intramolecular Cu···Cu′ distance is 3.503(2) Å in **1** and 3.554(1) Å in **3**. The distortion of the coordination polyhedra from square-pyramidal (SP, $\tau = 0$) and trigonal-bipyramidal (TBP, $\tau = 1$) topologies have been analysed.[9] The τ values obtained were 0.06 (**1**) and 0.13 (**3**), which clearly indicates that the environment of the copper(II) ions is close to the SP topology.

The thiosemicarbazonato ligand exhibits high planarity. The dihedral angles formed by the least-squares planes of both the thiosemicarbazone molecules, inside the dimer, are about 2.4 and 1.5° for **1** and **3**, respectively.

The crystal structure of complex **2** consists of centrosymmetric $[\{Cu(L)(CH_3CH_2COO)\}_2]$ entities. A perspective view of the molecular structure is shown in Figure 3. Several distances and angles are shown in Table 2. Each copper(II) ion exhibits a five-coordinate geometry. It is coordinated by two nitrogen atoms and one sulfur atom of the thiosemicarbazonato ligand [Cu−N(1), N(2), S: 2.056(2), 1.966(2), 2.287(1) Å] and the oxygen O(1) atom of the propionato ligand at 1.951(2) Å, in the basal plane. The oxygen atom belonging to the thiosemicarbazonato ligand of the adjacent $[Cu(L)(CH_3CH_2COO)]$ entity [Cu−O(1)′ 2.387(2) Å] occupies the axial position. The intramolecular Cu···Cu′ distance is 3.460(2) Å. The distortion of the coordination polyhedron gives a value of $\tau = 0.19$ characteristic of a geometry close to that of SP.

The thiosemicarbazonato ligand is nearly planar in complex **2**. Both thiosemicarbazone molecules in the dimer are coplanar (dihedral angle about 0.0°).

As can be expected, the longest C−O/N−O bonds inside the coligands involve the O(1) atoms that are linked to the metal ions, for all three of the complexes.

Several hydrogen bonds are established in the lattice of these compounds in which the O(2), N(3) and N(4) atoms are involved (see Table 2). The presence of C−H···S linkages is also remarkable.

It is worth mentioning that the shortest distances between the pyridine plane and the thiosemicarbazone moiety of different molecules are 3.28 [C(3)···C(7)^{iv}], 3.31 [C(5)···N(2)^{iii}] and 3.37 Å [C(3)···C(7)^{v}] for **1**, **2** and **3**, re-

Table 2. Selected bond lengths [Å] and angles [°] for **1**, **2** and **3**

	1	**2**	**3**	
Cu−S	2.265(2)	2.287(1)	2.268(1)	
Cu−N(1)	2.016(4)	2.056(2)	2.025(3)	
Cu−N(2)	1.976(4)	1.966(2)	1.974(3)	
Cu−O(1)	1.956(4)	1.951(2)	1.964(3)	
Cu−S′ /−O(1)′	2.820(2)[i]	2.387(2)[ii]	2.918(2)[iii]	
S−C(7)	1.752(5)	1.735(3)	1.739(4)	
N(2)−C(6)	1.271(7)	1.290(4)	1.285(5)	
N(2)−N(3)	1.367(6)	1.367(3)	1.365(4)	
N(3)−C(7)	1.317(7)	1.330(4)	1.324(5)	
N(4)−C(7)	1.329(7)	1.335(4)	1.333(5)	
N(2)−Cu−O(1)	167.8(2)	173.98(9)	172.2(1)	
S−Cu−N(1)	164.3(1)	162.59(8)	164.40(9)	
Cu−X−Cu′	86.34(5)	105.35(9)	85.5(1)	
Selected coligand bonds				
O(1)−C(8)/O(1)−N(5)	1.238(7)	1.283(4)	1.279(4)	
O(2)−C(8)/O(2)−N(5)	1.220(6)	1.231(4)	1.209(4)	
Closest Cu···Cu distances				
Intramolecular	3.503(2)[i]	3.460(2)[ii]	3.554(1)[iii]	
Intermolecular	5.437(2)[iv]	5.514(2)[iii]	5.573(1)[v]	
Hydrogen bonding contacts A−H···B	A−H [Å]	A···B [Å]	H···B [Å]	A−H···B [°]
1:				
N(4)−H(1n)···N(3)[iii]	0.94(5)	3.203(6)	2.30(6)	161(5)
N(4)−H(2n)···O(2)[vi]	0.94(5)	3.023(6)	2.15(5)	155(5)
C(4)−H(4)···S[vii]	0.93	3.487(5)	2.820(2)	129.5(4)
2:				
N(4)−H(1n)···N(3)[v]	0.88(5)	3.005(5)	2.12(5)	174.5(4)
N(4)−H(2n)···O(2)[viii]	0.73(6)	3.062(5)	2.56(5)	130.7(4)
C(1)−H(1)···S[ix]	0.95	3.452(4)	2.879(1)	119.9(3)
3:				
N(4)−H(41)···N(3)[x]	0.860(3)	3.167(4)	2.320(3)	168.0(3)
N(4)−H(42)···O(2)[ix]	0.860(4)	3.298(5)	2.550(3)	145.9(3)
C(4)−H(4)···S[xi]	0.930(3)	3.514(4)	2.807(1)	133.6(3)
i = $-x$, $-y+1$, $-z+1$	v = $-x$, $-y+1$, $-z$		ix = $-x+1$, $-y$, $-z$	
ii = $-x+1$, $-y$, $-z$	vi = $-x+1$, $-y+1$, $-z+1$		x = $-x$, $-y+1$,$-z-1$	
iii = $-x$, $-y$, $-z$	vii = $-x+1$, $y-1$, z		xi = $x-1$, $y+1$, $-z$	
iv = $-x$, $-y$, $-z+1$	viii = x, $y+1$, z		ii = $-x-1$, $-y+1$, $-z$	

spectively. This suggests the existence of π-π stacking of the slipped packing type[10] as represented in Figure 4. These interactions have been evaluated,[11,12] and the results are shown in Table 3. The coordination of a metal ion to the nitrogen heteroatom of pyridines and other heterocycles enhances the electron-withdrawing effect through its positive charge, and hence the stability of the π-π interaction increases.[13,14] These kinds of interactions have been observed in other thiosemicarbazone systems.[15−18]

Complexation induces conformational changes in the ligand. Atoms N(1) and N(2) are *anti* with respect to the C(5)−C(6) bond in the free ligand;[19] however, they become *syn* after chelation. Furthermore, the N(2) and S atoms are *anti* with respect to the N(3)−C(7) bond in the free ligand[19] and also in the pyridinium $(H_2L)Cl{\cdot}H_2O$ cationic derivative,[20] but they are *syn* in the metal complexes. The C−C and C−N distances are similar to those found in the free ligand and its cationic form, except for the N(3)−C(7) and C(7)−S bond lengths, which are 1.358(4) and 1.698(3) Å, respectively, in the free ligand. This suggests that the double bond character of the N(3)−C(7) and C(7)−S bonds increases and decreases, respectively, in the complexed thiosemicarbazonato ligand. However, bond lengths are often in the range of the experimental error and other structural parameters such as some of the bond angles and non-contact distances are more appropriate to evaluate the anionic vs. neutral character of the ligand upon complexation.[6] The results summarised in Table 4 show that the distances and angles for the title complexes are in good agreement with those expected for compounds con-

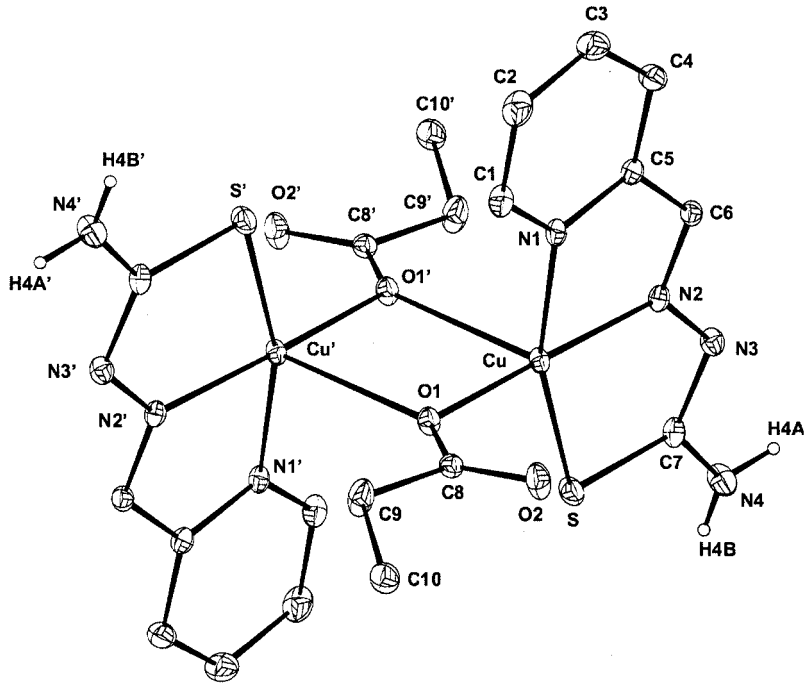

Figure 3. Molecular structure of **2** with thermal ellipsoids at 50% probability level

taining the pyridine-2-carbaldehyde thiosemicarbazone ligand in the anionic form.

The presence of μ-thiolato bridges between the metal centres in the iminothiolato systems such as heterocyclic thiosemicarbazone complexes is unusual,[21] although they have been found in other related thiosemicarbazone compounds.[2,3,17,22−28]

The existence of different infrared absorptions corresponding to the thioamide and pyridine substituents, together with the electron delocalisation through the thiosemicarbazone molecule, make the assignation of the bands in these compounds difficult. The intense bands around 1600 cm^{-1} can be attributed to the $\nu(C{=}N)_{azomethine}$, $\nu(C{=}N)_{pyridine}$ and $\delta(NH_2)$ modes. The strong band at 1525 cm^{-1} in the free ligand has been identified as corresponding to a thioamide I absorption, with high contribution of the $\delta(NH_2)$ and δ(NH) deformation modes. This band undergoes an increase in energy on complexation[29] and its intensity decreases in the compounds containing the deprotonated ligand. The thioamide IV band, which appears at 820 cm^{-1} in the free ligand, is absent in the copper(II) complexes. This is probably due to both a decrease in the double bond character of the C7−S bond and the change in the conformation of the N3−C7 bond on complexation.[3] Other absorptions observed in the 815−830 cm^{-1} region for **2** and **3** have been attributed to the coligand (see below). The bands at ca. 447 cm^{-1} have been assigned to the $\nu(Cu{-}N_{azomethine})$ vibration. These results indicate the presence of the thiosemicarbazonato ligand coordinated to the copper(II) ions through the $N_{pyridine}N_{azomethine}S$ chelating centres.

The very strong bands at 1616 and 1316 cm^{-1} in **1** have been attributed to the ν(C=O) and ν(C−O) absorptions of the formato ligand [the latter overlapped with a thioamide III absorption mainly due to δ(N−H) and ν(C−N) contributions of the thiosemicarbazone]. The Δ value [ν_a(COO) − ν_s(COO) in the free ion] is 300 cm^{-1} for **1**, which is greater than the value of 201 cm^{-1} observed for the ionic formate, in good agreement with the unidentate character of the coligand.[30] Unfortunately, the complexity of the spectrum of compound **2** only allows for the distinction of the strong band at 1603 cm^{-1}, due to the overlapped ν(C=O) and thioamide I absorptions [δ(N−H) and ν(C=N) contributions]. A weak band at 816 cm^{-1} appears in the infrared spectrum of **2** which is also present for the sodium propionate, and can be attributed to ν(C−C) vibration modes of the propionato ligand.

The infrared spectrum of compound **3** shows a shoulder at around 1408 cm^{-1} and two bands at 1125 and 826 cm^{-1}. These bands are attributed to the ν(N=O), ν(N−O) and δ(ONO) absorptions of the nitrito ligand.[31]

The reflectance spectra of the title compounds show bands in the 220−235, 260−270, 360−465 and 590−750 nm regions. These are assigned to $(\pi \rightarrow \pi^*)_{pyridine}$, $(n \rightarrow \pi^*)_{pyridine}$, $(n \rightarrow \pi^*)_{thiosemicarbazone}$, LMCT N/O/S → d and d → d transitions, respectively.[32,33]

The intense absorption observed in the 384−405 nm range is attributed to a S → Cu^{II} charge transfer transition.[3] The absorptions between 430−465 nm may be due to LMCT O/N → Cu^{II} transitions, as were observed in other related compounds.[34]

The maxima observed from the solid samples in the 595−650 nm region are characteristic of d → d transitions for compounds exhibiting a square pyramidal geometry with a $d_{x^2-y^2}$ ground state. These bands show unresolved shoulders obscured by the tails above 700 nm, which can be

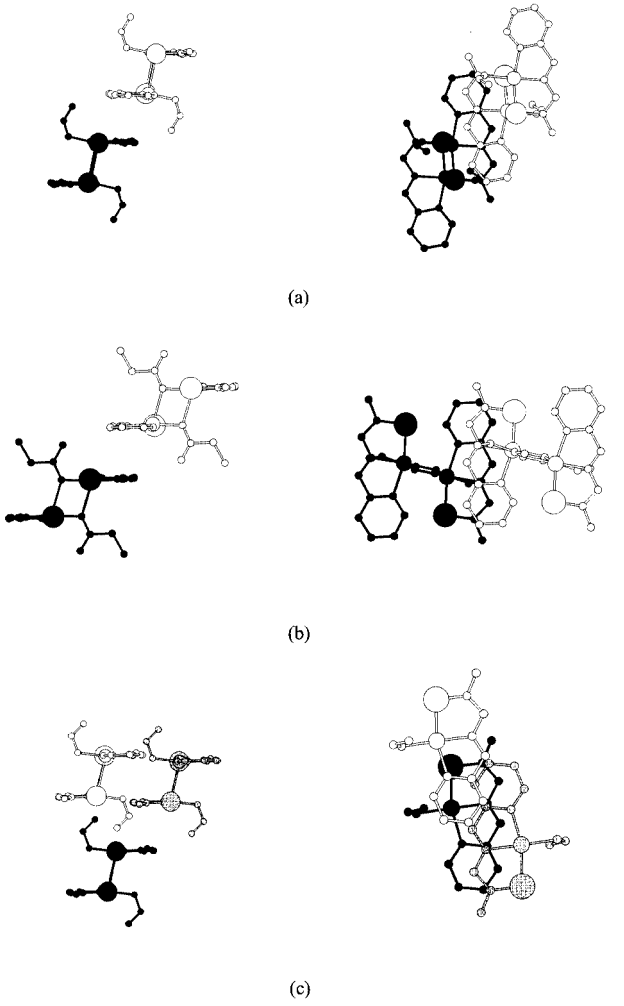

Figure 4. Details of π−π stacking for (a) **1**, (b) **2** and (c) **3**; drawing (c) on the right represents monomeric fragments for a clearer view

Table 3. π−π stacking interactions; the symmetry transformations follow the nomenclature used in Table 2; 1: N(1), C(1), C(2), C(3), C(4), C(5) ring in compound **1**; 2: C(6), N(2), N(3), C(7) set in compound **1**, N(3) is considered as the "centroid"; 3: N(1), C(1), C(2), C(3), C(4), C(5) ring in compound **2**; 4: C(6), N(2), N(3), C(7) set in compound **2**, N(3) is considered as the "centroid"; 5: N(1), C(1), C(2), C(3), C(4), C(5) ring in compound **3**; 6: C(6), N(2), N(3), C(7) set in compound **3**, N(3) is considered as the "centroid"; DC: distance [Å] between the centroids of the sets *i* and *j*; ANG: angle [°] between the least-squares planes; DZ: distance [Å] between the "centroid" of the *j* plane and the least-squares plane of the *i* ring; DZ′: distance [Å] between the centroid of the *i* ring and the least-squares plane of *j*; DXY: distance [Å] between the "centroids" of *i* and *j* projected onto the least-squares plane of *i*; DXY′: distance [Å] between the "centroids" of *i* and *j* projected onto the least-squares plane of *j*; DS: distance [Å] from the centroid of *j* to the nearest hydrogen atom of the *i* ring

i	j	DC	ANG	DZ	DXY	DZ′	DXY′	DS
1	2^{iv}	3.34	1.83	3.31	0.26	3.34	0.18	4.01
3	4^{iii}	3.29	4.40	3.27	0.06	3.17	0.07	3.99
5	5^{xii}	4.10	0.00	3.39	2.26	3.39	2.26	3.52
5	6^{v}	3.42	1.62	3.40	0.37	3.39	0.37	4.04

attributed to a certain amount of distortion of the coordination polyhedra to trigonal bipyramidal, in these compounds.

The three compounds exhibit the same solution spectrum with bands at 280, 317 (sh), 382 and 629 nm (see Exp. Sect.), which is basically the same as that previously described for the acetato[35,36] and the nitrato derivatives.[3,5] This shows that the coligand has been removed from the coordination sphere indicating the possible existence of entities of type $[CuL(H_2O)_3]^+$ in aqueous solution, in good agreement with the close to 1:1 electrolyte character of these compounds in water.

The X-band EPR spectra of polycrystalline samples of the title complexes are shown in Figure 5. They all exhibit rhombic signals. The *g* values obtained are given in Table 5. These values are similar to those observed for other pyridine-2-carbaldehyde thiosemicarbazone derivatives containing copper(II) ions in distorted square-pyramidal topologies, with a $d_{x^2-y^2}$ ground state.[2,3,5,6] The O-bridged dimer is the most rhombic and has the largest value for g_1, which is in good accordance with the differences in the crystal structure.

The plot of the molar susceptibility (χ_m), together with the $\chi_m T$ vs. T curve for **1** is given in Figure 6. The results are very similar to those of complexes **2** and **3**. In all cases, the magnetic measurements obey the Curie−Weiss law at temperatures higher than 50 K. The Weiss temperatures are −2.72 (**1**), −3.29 (**2**) and −3.02 K (**3**). The C_m experimental value is approximately 0.41 $cm^3 \cdot K \cdot mol^{-1}$ and the calculated μ_{eff} values at room temperature are 1.80 BM for all of the compounds. The χ_m values increase with decreasing temperature, reaching a maximum at 5.0 [0.040 $cm^3\ mol^{-1}$ (**1**)], 6.0 [0.033 $cm^3\ mol^{-1}$ (**2**)] and 5.5 [0.033 $cm^3\ mol^{-1}$ (**3**)] K. The $\chi_m T$ value continuously decreases on lowering the temperature indicating the presence of antiferromagnetic interactions in these compounds.

Taking the dimeric nature of these complexes into account, we fitted the susceptibility data using the expression given by Bleaney−Bowers for copper(II) dinuclear compounds [Equation (1)],[37] derived from the Heisenberg isotropic spin Hamiltonian ($H = -2J\ S_1S_2$), for two coupled S = 1/2 ions; where $N\alpha = 60 \times 10^{-6}\ cm^3\ mol^{-1}$ per copper(II) ion, N = Avogadro number, β = Bohr magneton, and k = Boltzmann constant.

$$\chi = \frac{Ng^2\beta^2}{kT}\left(\frac{2}{3+\exp(-2J/kT)}\right) + N\alpha \qquad (1)$$

The best least-squares fit (solid line in Figure 6) is obtained from the parameters J/k = −4.0 K (−2.8 cm^{-1}), −4.8 (−3.3 cm^{-1}) and −4.9 K (−3.4 cm^{-1}). The *g* values are 2.09, 2.10 and 2.09 for the formato, propionato and nitrito complexes, respectively. These *g* values are in good agreement with those obtained from EPR spectroscopy, 2.083 (**1**), 2.091 (**2**) and 2.090 (**3**). Taking into account the structural features, the existence of interdimeric magnetic

Table 4. Selected structural differences between copper(II) complexes containing neutral (HL) and anionic (L^-) pyridine-2-carbaldehyde thiosemicarbazone ligand [Å, °]

Compound	N(2)−N(3)−C(7)	S−C(7)−N(3)	S−C(7)−N(4)	Cu···N(3)	N(2)···C(7)
1	111.6(4)	125.2(4)	117.1(4)	2.98	2.22
2	111.6(2)	125.3(2)	119.3(2)	2.96	2.23
3	111.6(3)	125.2(3)	118.3(3)	2.97	2.23
HL range	116−118	121−122	121−123	2.89−2.90	2.28−2.32
L^- range	109−114	123−127	117−119	2.94−3.00	2.22−2.23

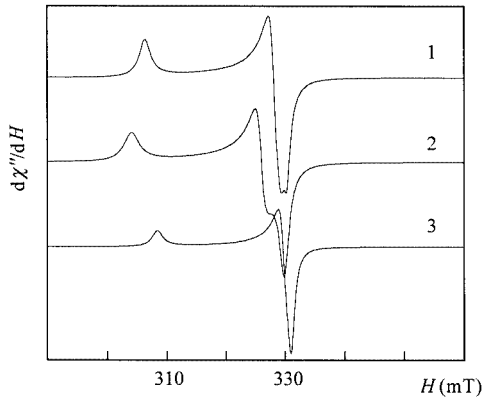

Figure 5. X-band EPR spectra of (a) **1**, (b) **2** and (c) **3** in the solid state at room temp.

Table 5. Experimental EPR spectroscopic parameters

	Temperature	g_1	g_2	g_3
1	room temp.[a]	2.183	2.037	2.029
2	room temp.[a]	2.198	2.050	2.026
3	room temp.[a]	2.186	2.046	2.038

[a] No variation in the g values from room temperature to 100 K.

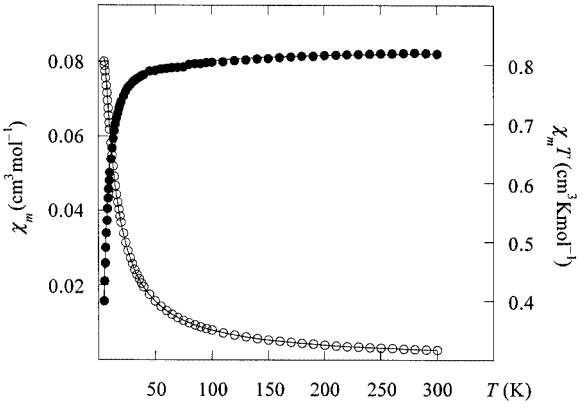

Figure 6. Thermal variation of the molar susceptibility (white circles) and $\chi_m T$ (black circles) for **1**; solid lines represent the best fit

interactions should be considered. However, an improvement in the fit was not observed.

The small values of the magnetic interactions suggest that the exchange propagation direction is in a different plane from that formed by the magnetic $d_{x^2-y^2}$ orbitals. These results are in good agreement with the existence of an intradimer exchange coupling in the Cu_2S_2 (**1**, **3**) and Cu_2O_2 (**2**) units.

It has been proposed[38] that the antiferromagnetic contribution to the magnetic exchange constant J for a dinuclear system with two unpaired electrons is proportional to the square of the energy difference (Δ^2) between the two molecular orbitals constructed from the $d_{x^2-y^2}$ magnetic orbitals. An Extended Hückel molecular orbital (EHMO) analysis has been carried out by means of the CACAO program[39] to give a qualitative explanation for the magnetic behaviour of these complexes. The EHMO calculations have been carried out using the crystallographic coordinates of the compounds followed by reorientation of the molecules to ensure a maximum overlap.[40] The data are given in Table 6. The results show a qualitative agreement between Δ^2 and the values of the exchange constant. Unfortunately, the limitations of the EHMO calculations do not allow a perfect sequence to be obtained for very similar J values (for instance, the value of Δ^2 for **3** should be slightly greater than that in **1**, but the opposite trend is observed).

The results obtained of the influence of the bridge angle and the bridge atom are not consistent with those of idealised dimers.[2,3] One of the factors to be considered is the nature of the terminal coligands placed in the basal plane. In our case, O-donor coligands show the smallest J values. In this sense, it has been established that the less electronegative the donor atom in the basal plane the stronger the induced antiferromagnetic coupling, due to a greater hybridisation of the $d_{x^2-y^2}$ metal orbital towards the bridge.[41,42] On the other hand, the relationship between J and the bridge angle could be clarified for a given X-donor set. Therefore, it seems that angles close to 90° tend to diminish the J value for compounds containing O-donor basal coligands. This is in good agreement with the results previously reported.[2] In any case, several concomitant factors could be involved in the values of the exchange coupling constants for these compounds [Cu···Cu intradimer distance, SP vs. BPT distortions around the copper(II) ion, deviation of the metal ion from the basal plane, deviation of the coligand from the basal plane, Cu−X apical distances, etc.]. The synthesis of new (pyridinecarbaldehyde thiosemicarbazonato)copper(II) complexes could lead to a better

Table 6. Comparison of the J, Δ^2 and bridging distance and angle values for (pyridine-2-carbaldehyde thiosemicarbazonato)copper(II) dinuclear complexes; the atoms are numbered according to the nomenclature used in the present work (*: average value)

Compound	Bridging atom	Cu−S′/ Cu−X′ [Å]	Bridging angle [°]	J [cm^{-1}]	Δ^2 [eV]$^2 \times 10^3$
[{Cu(NO_2)(L)}$_2$]	S	2.918(2)	85.5(1)	−3.4	1.09
[{CuCl(L)}$_2$][2]	S	2.760(2)	87.01(4)	−4.7	11.45
[{CuBr(L)}$_2$][2]	S	2.743(2)	87.12(5)	−4.7	17.42
[{Cu(NCS)(L)}$_2$][3]	S	2.754(5)*	85.9(1)*	−5.1	45.80
[{Cu(HCOO)(L)}$_2$]	S	2.820(2)	86.34(5)	−2.8	1.68
[{Cu(CH_3COO)(L)}$_2$][26]	O	2.427(2)	103.5(1)	−3.1	1.60
[{Cu(CH_3CH_2COO)(L)}$_2$]	O	2.387(2)	105.35(9)	−3.3	1.85

evaluation of the parameters that influence their magnetic behaviour.

Conclusions

The structural features of these compounds suggest that the increment in the size of the coligand is the main factor that leads to an X- vs. an S-bridge in the [{CuX(L)}$_2$] systems. These results may serve to rationalise and predict the interactions of the [Cu(L)(H_2O)$_3$]$^+$ entities with biomolecules present in the physiological medium.

Magnetic susceptibility data indicate the presence of weak intradimer antiferromagnetic interactions in these complexes. This behaviour can be qualitatively described from an EHMO study on real molecules.

Experimental Section

Preparation of the Complexes: Thiosemicarbazide, pyridine-2-carbaldehyde, formic and propionic acids, sodium nitrite and copper(II) nitrate were purchased from Probus, Carlo Erba and Fluka. All the complexes were dried under vacuum. The pyridine-2-carbaldehyde thiosemicarbazone (HL) ligand and the [Cu(L)(NO_3)] complex were synthesised according to published methods with slight modifications.[5,7]

Synthesis of [{Cu(L)(HCOO)}$_2$] (1): Formic acid (0.23 g, 5 mmol) was slowly added to an aqueous solution of Cu(L)(NO_3) (0.152 g, 0.5 mmol). The pH of the solution was adjusted to 5.5 by the addition of NaOH (1 M). After 1 h, a dark green precipitate was filtered off, washed with water and acetone and dried. The yield was 0.105 g (73%). Crystals suitable for X-ray studies were obtained by diffusion of diethyl ether vapours into a solution of **1** in methanol. $C_{16}H_{16}Cu_2N_8O_4S_2$ (575.56): calcd. C 33.4, H 2.8, N 19.5, S 11.1; found C 33.3, H 2.8, N 19.4, S 12.0. Molar conductivity of $5 \cdot 10^{-4}$ M solutions in water (dimethylformamide) at 25 °C: Λ_M = 102 (4) Ω^{-1} cm^2 mol^{-1}. Selected IR bands (KBr): $\tilde{\nu}$ = 3290 (m), 3146 (m), 2829 (w), 1634 (s), 1616 (vs), 1602 (vs), 1585 (m, sh), 1559 (w), 1482 (s), 1444 (vs), 1432 (vs), 1381 (s), 1316 (vs), 1264 (m), 1219 (s), 1166 (vs), 1151 (m, sh), 922 (m), 880 (m), 783 (m), 766 (m), 746 (w), 732 (m), 624 (m, b), 449 (w), 416 (m) cm^{-1}. UV/Vis (reflectance spectrum on solid sample): λ_{max} (ε) = ca. 750 (vb, sh), 608 (vb), 463 (b, sh), 405, 267 (sh), 223 nm; (6×10^{-5} M water solution): λ_{max} (ε) = 628 (150), 382 (9600), 317 (10600), 280 (14600 M^{-1} cm^{-1}) nm.

Synthesis of [{Cu(L)(CH_3CH_2COO)}$_2$] (2): This compound was prepared according to an analogous procedure to that of **1** but replacing formic acid with propionic acid (0.37 g, 5 mmol). The bright green product obtained was filtered off, washed with water and acetone and dried. The yield was 0.137 g (87%). Good-quality green crystals were obtained from the mother liquor after some weeks. $C_{20}H_{24}Cu_2N_8O_4S_2$ (631.68): calcd. C 38.0, H 3.8, N 17.7, S 10.2; found C 37.8, H 3.8, N 17.6, S 9.7. Molar conductivity of $5 \cdot 10^{-4}$ M solutions in water (dimethylformamide) at 25 °C: Λ_M = 75 (2) Ω^{-1} cm^2 mol^{-1}. Selected IR bands (KBr): $\tilde{\nu}$ = 3442 (m), 3290 (m), 3106 (bs), 2974 (m), 1640 (s), 1603 (vs), 1585 (m, sh), 1560 (m), 1485 (m), 1443 (s, sh), 1430 (vs), 1380 (s, b), 1324 (b m), 1271 (s), 1233 (m), 1168 (s), 1153 (s), 931 (w), 880 (m), 816 (w), 764 (w), 738 (m), 630 (m), 449 (w), 415 (w) cm^{-1}. UV/Vis (reflectance spectrum on solid sample): λ_{max} = 649 (vb), 445 (b, sh), 384, 264, ca. 235 (b, sh) nm.

Synthesis of [{Cu(L)(NO_2)}$_2$] (3): Sodium nitrite (0.036 g, 0.5 mmol) was allowed to react with an aqueous solution of Cu(L)(NO_3) (0.152 g, 0.5 mmol). Several drops of NaOH (1 M) were added whilst stirring to reach pH ≈ 7. The green precipitate was filtered off, washed with water and acetone and dried. The yield was 0.105 g (73%). Dark green crystals suitable for X-ray studies were separated from the mother liquor by slow concentration at room temperature. $C_{14}H_{14}Cu_2N_{10}O_4S_2$ (577.56): calcd. C 29.1, H 2.4, N 24.3, S 11.1; found C 28.8, H 2.7, N 23.9, S 10.8. Molar conductivity of $5 \cdot 10^{-4}$ M solutions in water (dimethylformamide) at 25 °C: Λ_M = 123 (15) Ω^{-1} cm^2 mol^{-1}. Selected IR bands (KBr): $\tilde{\nu}$ = 3409 (m), 3280 m, 3148 (m), 2974 (m), 1627 (s), 1604 (s), 1585 (w), 1560 (w), 1482 (s), 1445 (vs), 1434 (vs), 1408 (s, sh), 1391 (vs), 1320 (m), 1268 (m), 1228 (s), 1169 (vs), 1125 (vs), 914 s, 878 (m), 826 (w), 775 (s), 743 (s, b), 732 (m, b), 626 (s), 447 (m), 415 (s) cm^{-1}. UV/Vis (reflectance spectrum on solid sample): λ_{max} = ca. 750 (vb, sh), 593 (vb), 463, 430 (sh), 396 (b), 269, 222 nm.

Physical Measurements: Microanalyses were performed with a LECO CHNS-932 analyser. Conductivity measurements were made with a CRISON 522 conductimeter. Infrared spectra were obtained with samples prepared as KBr pellets in the 400−4000 cm^{-1} region with a Nicolet Impact 410 FTIR spectrophotometer. Reflectance spectra were carried out with a Cary 2415 spectrometer in the range 200−2000 nm. For UV/Vis solution measurements, a Varian UV/Vis/NIR spectrophotometer was employed in the range 200−900 nm. X-band EPR spectra were recorded with a Bruker EMX spectrometer, equipped with a standard Oxford continuous-flow cryostat. Magnetic measurements of powdered samples were carried out in the temperature range 1.8−300 K using a Quantum Design MPMS-7 Squid magnetometer. Diamagnetic corrections were estimated from Pascal tables.

X-ray Crystallographic Studies: Data were collected at low temperature (T = 160 K) with an IPDS STOE diffractometer for **1** and an XCALIBUR-CCD OXFORD DIFFRACTION diffractometer for **2**, both equipped with a Nitrogen Cooler Device, an Enraf-Nonius CAD4 was used for **3**. Graphite-monochromated Mo-K_α radiation (λ = 0.71073 Å) was employed in all cases. Semi-empirical absorption corrections: DIFABS[43] were applied on **1** and **2**, and a φ-scan method[44] on **3**. Structures were solved by Direct Methods using SIR92[45] (**1**, **2**) and (SHELXS-97)[46] (**3**), and refined by least-squares procedures on F^2 with the aid of SHELXL-97,[47] included in the package WinGX.[48] The Atomic Scattering Factors were taken from the International Tables for X-ray Crystallography.[49] All hydrogen atoms were located on difference Fourier maps, and refined by using a riding model with a common isotropic thermal parameter, except the H(1*n*), H(2*n*) hydrogen atoms connected to nitrogen atoms N(4) in **1** and **2**, which were isotropically refined. For the three compounds all non-hydrogen atoms were anisotropically refined. Drawings were performed by using the programs CAMERON[50] and ORTEP32[51] with 50% probability displacement ellipsoids for non-hydrogen atoms. CCDC-187690, -187691 and -187508 for compounds **1**, **2** and **3**, respectively, contain the supplementary crystallographic data for this paper. These data can be obtained free of charge from the Cambridge Crystallographic Data Centre, 12 Union Road, Cambridge CB2 1EZ, UK; Fax: (internat.) + 44-1223/336-033; E-mail: deposit@ccdc.cam.ac.uk.

Acknowledgments

We thank Dr. J. J. Delgado (SCAI, Universidad de Burgos, Spain) for the elemental analyses and Prof. R. Olazcuaga and Dr. F. Guillen (CNRS, Pessac, France) for the reflectance measurements. This work has been carried out with the financial support of the Basque Government (PI99/53). P. G.-S. thanks to the Universidad de Burgos for a Doctoral Fellowship.

[1] [1a] M. J. M. Campbell, *Coord. Chem. Rev.* **1975**, *15*, 279−319. [1b] S. Padhyé, G. B. Kauffman, *Coord. Chem. Rev.* **1985**, *63*, 127−160. [1c] D. X. West, S. B. Padhyé, P. B. Sonawane, *Struct. Bonding* **1991**, *76*, 1−50. [1d] D. X. West, A. E. Liberta, S. B. Padhyé, R. C. Chikate, P. B. Sonawane, A. S. Kumbhar, R. G. Yerande, *Coord. Chem. Rev.* **1993**, *123*, 49−71.
[2] J. García-Tojal, M. K. Urtiaga, R. Cortés, L. Lezama, T. Rojo, M. I. Arriortua, *J. Chem. Soc., Dalton Trans.* **1994**, 2233−2238.
[3] J. García-Tojal, L. Lezama, J. L. Pizarro, M. Insausti, M. I. Arriortua, T. Rojo, *Polyhedron* **1999**, *18*, 3703−3711.
[4] C. F. Bell, C. R. Theocharis, *Acta Crystallogr., Sect. C* **1987**, *43*, 26−29.
[5] A. G. Bingham, H. Bögge, A. Müller, E. W. Ainscough, A. M. Brodie, *J. Chem. Soc., Dalton Trans.* **1987**, 493−499.
[6] J. García-Tojal, T. Rojo, *Polyhedron* **1999**, *18*, 1123−1130, and references therein.
[7] F. E. Anderson, C. J. Duca, J. V. Scudi, *J. Am. Chem. Soc.* **1951**, *73*, 4967−4968.
[8] C. F. Bell, K. A. K. Lott, N Hearn, *Polyhedron* **1987**, *6*, 39−44.
[9] A. W. Addison, T. N. Rao, J. Reedijk, J. van Rijn, G. C. Verschoor, *J. Chem. Soc., Dalton Trans.* **1984**, 1349−1356.
[10] C. Janiak, *J. Chem. Soc., Dalton Trans.* **2000**, 3885−3896.
[11] A. Albert, F. H. Cano, *Cristalografia*, Publicaciones CSIC, Madrid, **1995**.
[12] I. Unamuno, J. M. Gutiérrez-Zorrilla, A. Luque, P. Román, L. Lezama, R. Calvo, T. Rojo, *Inorg. Chem.* **1998**, *37*, 6452−6460.
[13] C. A. Hunter, J. K. M. Sanders, *J. Am. Chem. Soc.* **1990**, *112*, 5525−5534.
[14] F. Cozzi, M. Cinquini, R. Annunziata, J. S. Siegel, *J. Am. Chem. Soc.* **1993**, *115*, 5330−5331.
[15] C.-Y. Duan, B.-M. Wu, T. C. W. Mak, *J. Chem. Soc., Dalton Trans.* **1996**, 3485−3490.
[16] Z.-H. Liu, C.-Y. Duan, J. Hu, X.-Z. You, *Inorg. Chem.* **1999**, *38*, 1719−1724.
[17] H. Cheng, D. Chun-ying, F. Chen-jie, L. Yong-jiang, M. Quing-jin, *J. Chem. Soc., Dalton Trans.* **2000**, 1207−1212.
[18] L. Ze-hua, D. Chun-ying, L. Ji-hui, L. Yong-jiang, M. Yu-hua, Y. Xiao-zeng You, *New. J. Chem.* **2000**, *24*, 1057−1062.
[19] V. N. Byushkin, Y. M. Chumakov, N. M. Samus, I. O. Baka, *Zh. Strukt. Khim.* **1987**, *28*, 140−142.
[20] M. K. Urtiaga, M. I. Arriortua, J. García-Tojal, T. Rojo, *Acta Crystallogr., Sect. C* **1995**, *51*, 2172−2174.
[21] Z. Lu, C. White, A. L. Rheingold, R. H. Crabtree, *Inorg. Chem.* **1993**, *32*, 3991−3994.
[22] G. W. Bushnell, A. Y. M. Tsang, *Can. J. Chem.* **1979**, *57*, 603−607.
[23] M. R. Taylor, J. P. Glusker, E. J. Gabe, J. A. Minkin, *Bioinorg. Chem.* **1974**, *3*, 189.
[24] L. E. Warren, W. E. Hatfield, *Chem. Phys. Lett.* **1970**, *7*, 371.
[25] G. A. Kiosse, V. K. Rotaru, A. V. Ablov, T. I. Malinovskii, N. I. Belichuk, *Russ. J. Inorg. Chem.* **1973**, *18*, 757−758.
[26] E. W. Ainscough, A. M. Brodie, J. D. Ranford, J. M. Waters, K. S. Murray, *Inorg. Chim. Acta* **1992**, *197*, 107−115.
[27] B. Moubaraki, K. S. Murray, J. D. Ranford, X. Wang, Y. Xu, *Chem. Commun.* **1998**, 353−354.
[28] [28a] M-B. Ferrari, G. G. Fava, C. Pelizzi, P. Tarasconi, G. Tosi, *J. Chem. Soc., Dalton Trans.* **1987**, 227−233. [28b] D. Kovala-Demertzi, N. Kourkoumelis, D. X. West, J. Valdés-Martínez, S. Hernández-Ortega, *Eur. J. Inorg. Chem.* **1998**, 861−863. [28c] D. Kovala-Demertzi, N. Kourkoumelis, M. A. Demertzis, J. R. Miller, C. S. Frampton, J. K. Swearingen, D. X. West, *Eur. J. Inorg. Chem.* **2000**, 727−734.
[29] M. C. Jain, R. K. Sharma, P. C. Jain, *J. Inorg. Nucl. Chem.* **1980**, *42*, 1229.
[30] G. B. Deacon, R. J. Phillips, *Coord. Chem. Rev.* **1980**, *33*, 227.
[31] K. Nakamoto, *Infrared and Raman Spectra of Inorganic and Coordination Compounds*, 5th ed., Wiley, New York, **1997**, pp. 50, 60.
[32] E. S. Stern, C. J. Timmons, *Electronic Absorption Spectroscopy in Organic Chemistry*, Edward Arnold, London, **1970**.
[33] D. X. West, M. A. Lockwood, J. N. Albert, A. E. Liberta, *Spectrochim. Acta* **1991**, *49A*, 1809−1816.
[34] D. X. West, Y. Yang, T. L. Klein, K. I. Goldberg, A. E. Liberta, J. Valdés-Martínez, R. A. Toscano, *Polyhedron* **1995**, *14*, 1681−1693.
[35] W. E. Antholine, J. M. Knight, D. H. Petering, *Inorg. Chem.* **1977**, *16*, 569−574.
[36] H. Beraldo, L. Tosi, *Inorg. Chim. Acta* **1986**, *125*, 173−182.
[37] B. Bleaney, K. D. Bowers, *Proc. R. Soc. London, Ser. A.* **1952**, *214*, 451.
[38] P. J. Hay, J. C. Thibeault, R. Hoffmann, *J. Am. Chem. Soc.* **1975**, *97*, 4884−4899.
[39] *CACAO Program, Computer Aided Composition of Atomic Orbitals*, PC version 4.0, July **1994**: C. Mealli, D. M. Proserpio, *J. Chem. Educ.* **1990**, *67*, 399−402.
[40] J. García-Tojal, J. L. Pizarro, L. Lezama, M. I. Arriortua, T. Rojo, *Inorg. Chim. Acta* **1998**, *278*, 150−158.
[41] P. Román, C. Guzmán-Miralles, A. Luque, J. I. Beitia, J. Cano, F. Lloret, M. Julve, S. Alvarez, *Inorg. Chem.* **1996**, *35*, 3741−3751.
[42] J. Cano, P. Alemany, S. Alvarez, M. Verdaguer, E. Ruiz, *Chem. Eur. J.* **1998**, *4*, 476−484.
[43] N. Walker, D. Stuart, *Acta Crystallogr., Sect. A* **1983**, *39*, 158−166.
[44] A. C. T. North, D. C. Phillips, F. S. Mathews, *Acta Crystallogr., Sect. A* **1968**, *24*, 351.
[45] A. Altomare, G. Cascarano, C. Giacovazzo, A. Guagliardi, *J. Appl. Crystallogr.* **1993**, *26*, 343−350.
[46] G. M. Sheldrick, *SHELXS-97, A Program for Crystal Structure Solution*, Univ. of Göttingen, Göttingen, Germany, **1997**.

[47] G. M. Sheldrick, *SHELX97, Programs for Crystal Structure Analysis (Release 97−2)*, Institut für Anorganische Chemie der Universität, Tammanstrasse 4, D-3400 Göttingen, Germany, **1998**.
[48] *WINGX − 1. 63, Integrated System of Windows Programs for the Solution, Refinement and Analysis of Single Crystal X-ray Diffraction Data:* L. Farrugia, *J. Appl. Crystallogr.* **1999**, *32*, 837−838.
[49] *International Tables for X-ray Crystallography*, Kynoch Press, Birmingham, England, **1974**, vol. IV.
[50] D. M. Watkin, L. Pearce, C. K. Prout, *CAMERON, A Molecular Graphics Package*, Chemical Crystallography Laboratory, University of Oxford, England, **1993**.
[51] L. J. Farrugia, *J. Appl. Crystallogr.* **1997**, *30*, 565.

Received June 14, 2002
[I02316]

DNA Cleavage by Copper Complexes of 2- and 3-Clip-Phen Derivatives

Marguerite Pitié,[a] Christophe Boldron,[a] Heinz Gornitzka,[b] Catherine Hemmert,[a] Bruno Donnadieu,[a] and Bernard Meunier*[a]

Keywords: Copper / DNA cleavage / Helical structures / Ligand design / N ligands

The DNA cleavage activity of copper complexes of phenanthroline has been increased by the use of "2-Clip-Phen" and "3-Clip-Phen" ligands containing two phenanthroline entities linked by a serinol bridge. In order to optimize DNA cleavage activity, two series of new Clip-Phen ligands (L) with two phenanthroline residues linked through their C-2 or C-3 carbon atoms by different bridges have been synthesized. The physicochemical properties and the DNA cleavage activities of the corresponding (Clip-Phen)copper complexes were investigated in the presence of a reductant and air. X-ray analyses of single crystals showed that the cupric complexes of Clip-Phen were able adopt dimeric double-helical geometries with L_2Cu_2 stoichiometries in the solid state. These complexes adopt different geometries and stoichiometries in solution, with monomeric LCu species predominant. The compounds with a bridge connected at C-2 are less active as DNA cleavage agents than complexes with the bridge at the C-3 positions. Copper complexes with a bridge containing three methylene units appear to give the best results in DNA cleavage experiments. This activity is increased in the case of 3-Clip-Phen·$CuCl_2$ by the presence of the primary amine function of the serinol bridge. This amine function is probably coordinated to the copper atom in the case of 2-Clip-Phen·$CuCl_2$, decreasing the reactivity toward DNA.
(© Wiley-VCH Verlag GmbH & Co KGaA, 69451 Weinheim, Germany, 2003)

Introduction

1,10-Phenanthroline (Phen) is a well-known motif for the preparation of a large range of strongly chelating ligands for various metal ions. The complexing capability of this easily accessible ligand has been used to develop biomimetic models of metalloenzymes, to design analytical reagents, cleavers, or conformational probes for nucleic acids, or to prepare supramolecules for molecular recognition and self-assembling systems.[1−13]

Redox-active copper complexes of phenanthroline are efficient artificial nucleases.[13−15] This versatile ligand is able to chelate copper ions to give mono- or bis(Phen)-copper complexes in oxidation states +I or +II. These interact efficiently with double-stranded DNA from the minor groove, probably by partial intercalation.[20,21] In the presence of hydrogen peroxide the $(Phen)_2Cu^{I}$ complex mediates single-strand cleavage of double-stranded DNA by oxidative attacks at C-1′ and C-4′ of 2-deoxyribose units.[13,16−18] Hydrogen peroxide can be generated in close proximity to DNA by $(Phen)_2Cu^{II}$ itself in the presence of a reductant and molecular oxygen.

[a] Laboratoire de Chimie de Coordination du CNRS,
205 route de Narbonne, 31077 Toulouse cedex 4, France
Fax: (internat.) + 33-5/61553003
E-mail: bmeunier@lcc-toulouse.fr
[b] Laboratoire d'Hétérochimie Fondamentale et Appliquée (UMR, 5069), Université Paul Sabatier,
118 route de Narbonne, 31062 Toulouse cedex 04, France

$(Phen)_2Cu^{I}$ is significantly more active than $(Phen)Cu^{I}$, but the association constant for the second phenanthroline ligand is only $10^{5.5}$ M^{-1}, too low for biological use at submicromolar concentrations of these complexes.[22] For this reason, we have recently prepared 2- and 3-Clip-Phen derivatives (Scheme 1) containing two Phen ligands linked through their 2′- or 3′-positions by a serinol bridge in order to favor the coordination of two Phen units around the same copper ion.[23,24] The oxidative nuclease activity of the copper complexes of these new ligands was found to be higher than with Phen itself; by a factor of 2 for 2-Clip-Phen, but by a factor of 60 for 3-Clip-Phen. The nuclease activity of 3-Clip-Phen·$CuCl_2$ is due to C-1′, C-4′, and C-5′ deoxyribose oxidations resulting from the cleavage interaction within the DNA minor groove.[25] 3-Clip-Phen·$CuCl_2$ itself appeared to be poorly sequence-selective, but the exogenous amine of its serinol bridge allowed the preparation of a conjugate with an analogue of distamycin (a minor groove binder that interacts selectively with five successive A·T base pairs) that appeared to be a sequence-selective DNA cleaver.[25,26] Conjugates of 2-Clip-Phen with the natural polyamine spermine (a minor groove binder)[27] or intercalators such as acridine derivatives[28] also exhibit enhanced nuclease activity.

Copper complexes of Clip-Phen have high DNA cleavage activity. This activity is preserved (and sometimes enhanced) when conjugated to a variety of vectors, which also retain their previous biological characteristics. This remarkable combination of properties opens wide perspectives for

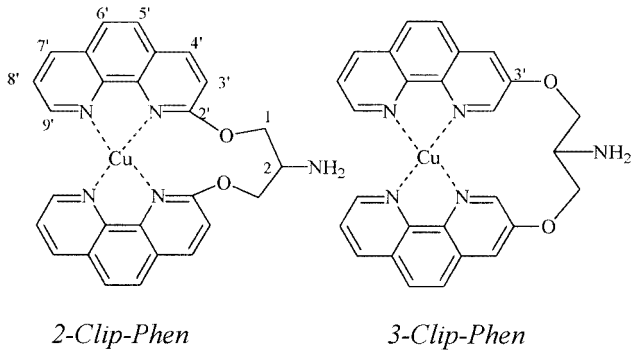

Scheme 1. Structures of 2-Clip-Phen and 3-Clip-Phen; numbering corresponds to NMR assignments; the type of coordination with Cu attempted from the design of the ligands is shown

the use of Clip-phen derivatives. The compounds can be used as biological tools to study DNA structures, as new DNA footprinting agents or as potential antitumoral or antiviral agent mimics of iron bleomycin, a well-known antitumoral drug able to cleave the DNA of cancer cells.[29,30] In this context, Clip-Phen's properties of cell penetration and specificity for DNA might be modulated by the preparation of conjugates incorporating many different vectors.

The serinol bridge included in 2- and 3-Clip-Phen was initially chosen because of a number of different parameters: (i) its length was well adapted to favor "crab-pincer" copper complexes with two Phen entities of the same ligand chelating the same copper atom, (ii) its flexibility allowed the conformational changes that occur during Cu^{I}/Cu^{II} redox cycles, (iii) its amine function facilitated the synthesis of conjugates without modification of the Phen chelating entities, (iv) its C_2 symmetry axis avoided the formation of stereoisomers, and (v) its commercial accessibility. Both 2- and 3-Clip-Phen do, however, contain the same junction bridge even though the steric constraints in their copper complexes are not the same. On the other hand, a comparison of their physicochemical properties needs to be done.

Our interest in improving the efficiency of the Clip-Phen·Cu scission reagents prompted us to synthesize new Clip-Phen ligands with different short bridges between the two Phen entities in order to optimize the linker parameters (Figure 1). The length of the linker between C-2 or C-3 of the two Phen moieties was varied from two to five methylene units (ethyl-, propyl-, butyl-, or pentyl-Clip-Phen derivatives). Larger variations in the linker length were tested in the case of the 3-Clip-Phen series, on the assumption that that these ligands were sterically more constrained than the 2-Clip-Phen ones, in order to produce "crab-pincer" copper complexes. The influence of the primary amine of Clip-Phen on the nuclease activity was also studied, as was that of amide residues such as those included in conjugates with different vectors, by comparison with acetyl-Clip-Phen derivatives. In this work the geometry and the redox activity of these new copper complexes of phenanthroline have been analyzed under conditions similar to those used for DNA cleavage experiments. Determination of their respective DNA cleavage efficiency was performed. This study allows the parameters increasing the DNA cleavage activity of copper complexes of Clip-Phen to be clearly defined and provides information concerning the different types of complexes that can be generated in solution with the same ligand.

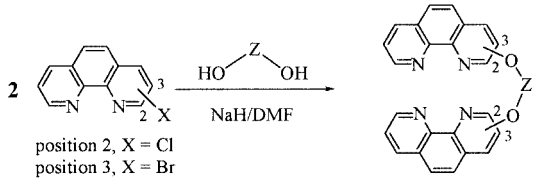

−O−Z−O−	Bridge on C2 of Phen	Bridge on C3 of Phen
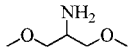	**1** 2-Clip-Phen	**5** 3-Clip-Phen
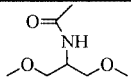	**2** 2-acetyl-Clip-Phen	**6** 3-acetyl-Clip-Phen
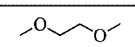	**3** 2-ethyl-Clip-Phen	**7** 3-ethyl-Clip-Phen
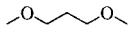	**4** 2-propyl-Clip-Phen	**8** 3-propyl-Clip-Phen
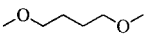	-	**9** 3-butyl-Clip-Phen
	-	**10** 3-pentyl-Clip-Phen

Figure 1. Structure of Clip-Phen derivatives **1**−**10** and general reaction pathways used for the preparation of Clip-Phen ligands

Results and Discussion

Preparation of the Ligands

The compounds **1**, **3**−**5**, and **7**−**10** were prepared by condensation of 1 equiv. of diol and 2 equiv. of halogenated phenanthroline (2-chloro or 3-bromo derivatives). Products substituted on C-2 of phenanthroline were obtained in good yields at 4 °C (70−80%). Products substituted at C-3, however, appeared to be more difficult to be prepared and were only obtained in poor yields (20−30%). As previously observed for the synthesis of 3-Clip-Phen (**5**), the low reactivity of 3-bromophenanthroline towards nucleophilic substitution necessitated a reaction temperature of 55 °C, and a proportion of the 3-BrPhen was lost due to a reduction process, giving back phenanthroline itself.[24] Ligands **2** and **6** were easily obtained by acetylation of 2- and 3-Clip-Phen, respectively (yield ca. 90%).

Characterization of the Copper Complexes

Ligands **1**−**10** were metallated with 1 equiv. of $CuCl_2$ in a DMF/methanol mixture and then precipitated with diethyl ether to produce polycrystalline green materials. We chose to use a copper chloride salt, since other DNA cleavage experiments have been carried out in the presence of NaCl in order to mimic physiological conditions. Analytical data are consistent with the formation of L/Cu^{II} 1:1 complexes,

but the coordination chemistry of the Clip-Phen family of ligands (L) with copper ions appeared to be more complicated than expected.

Crystal Structures

Copper complexes of Clip-Phen derivatives were unfortunately difficult to crystallize, and several attempts with 1 equiv. of different copper salts and various solvents were performed in order to obtain monocrystals of the copper complexes of **1**−**10** suitable for X-ray analysis. After several unsuccessful attempts, it was found to be possible to obtain suitable monocrystals of **1**·$Cu(BF_4)_2$, **3**·$CuCl_2$, **7**·$CuCl_2$, and also **1**·$ZnCl_2$ (Figures 2, 3, 4, and 5, respectively).

The $Cu(BF_4)_2$ complex of 2-Clip-Phen (**1**) crystallized on slow diffusion of CH_2Cl_2 into a solution of the complex, dissolved in a DMF/CH_3OH mixture, as a double-helical structure of general formula bis[(**1**)Cu][BF_4]$_2$ (Figure 2). Table 1 presents selected average bond lengths and angles of this complex. Each copper center shows the same coordination geometry and can be described as a distorted square-planar-pyramidal arrangement around the metal ion with the aliphatic amine and two phenanthroline residues (one from each Clip-Phen derivative ligand of the double helix). The equatorial positions are occupied by the aliphatic amine and three nitrogen atoms of the phenanthroline residues, with similar bond lengths of 2.02−2.05 Å. The axial bond length at 2.18 Å is longer. The phenanthroline nitrogen atom in the α-position to the bridge is equatorial. However, the angles in the crystal structure deviate from ideal values for a square-planar pyramid, although EPR results are in accordance with this geometry (see Exp. Sect. for these EPR values). Accordingly, the geometry could also be described as a distorted trigonal bipyramid with each nitrogen atom of a phenanthroline residue occupying one axial and one equatorial position.

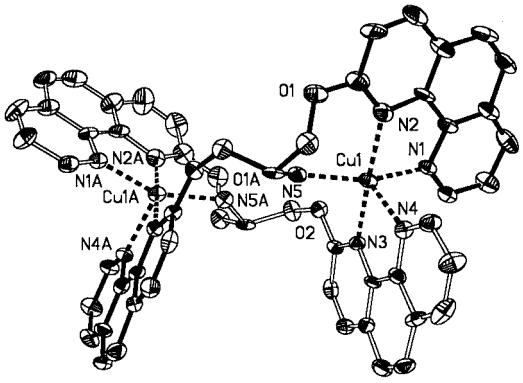

Figure 2. Crystal structure of bis[(**1**)Cu][BF_4]$_2$; hydrogen atoms, non-coordinated counter-ions, and solvent molecules are omitted for clarity

The double-helical motif of copper(II) complexes of Clip-Phen derivatives is also observed in the structures of **3**·$CuCl_2$ and **7**·$CuCl_2$, but with some major differences. The $CuCl_2$ complex of 2-ethyl-Clip-Phen (**3**) crystallizes in aqueous methanol as a double-helical structure of general formula [(**3**)CuCl]$_2$Cl$_2$ (Figure 3). Table 2 presents selected average bond lengths and angles of this complex. The coordination geometries are similar for each metal center and can be described as a distorted trigonal-bipyramidal arrangement with one chloride ion and two phenanthroline residues (one from each 2-ethyl-Clip-Phen ligand of the double-helix) around the copper atom. Each phenanthroline group occupies one axial and one equatorial position. The nitrogen atom in the α-position to the bridge is in an axial position for one phenanthroline residue and equatorial for the other. The third equatorial position is occupied by the chloride ion, with close Cu−Cl distances of 2.27 and 2.32 Å, respectively, for each copper center. Each coordinated chloride ion points in opposite direction of the double helix. The bond lengths between the copper atom and the phenanthroline nitrogen atoms are approximately 2.0 Å. The N−Cu−N angle formed by the nitrogen atoms of one phenanthroline residue and the central atom is smaller than the ideal value of 90° for a trigonal-bipyramid geometry, but the observed values of approximately 80° are typical for copper complexes of phenanthroline.[31] In addition, the axial Cu−N distances are always slightly compressed, consistently with other known trigonal-bipyramidal bis(phenanthroline)Cu^{II} crystal structures.[32]

Table 1. Selected bond lengths [Å] and angles [°] for bis[(**1**)Cu][BF_4]$_2$

Cu−N(1)	2.014(9)
Cu−N(2)	2.051(10)
Cu−N(3)	2.051(8)
Cu−N(4)	2.180(8)
Cu−N(5)	2.005(9)
N(5)−Cu−N(1)	153.6(4)
N(5)−Cu−N(2)	93.0(4)
N(1)−Cu−N(2)	81.7(4)
N(5)−Cu−N(3)	90.2(3)
N(1)−Cu−N(3)	93.7(4)
N(2)−Cu−N(3)	175.0(4)
N(5)−Cu−N(4)	111.6(3)
N(1)−Cu−N(4)	94.7(3)
N(2)−Cu−N(4)	103.7(4)
N(3)−Cu−N(4)	78.7(3)

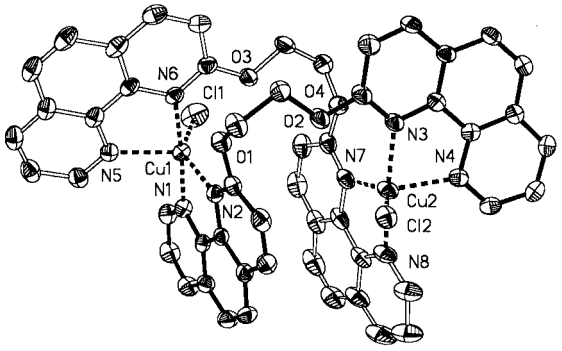

Figure 3. Crystal structure of [(**3**)CuCl]$_2$Cl$_2$; hydrogen atoms, non-coordinated counter-ions, and solvent molecules are omitted for clarity

Table 2. Selected bond lengths [Å] and angles [°] for [(**3**)$CuCl]_2Cl_2$

Cu(1)−N(1)	1.985(5)	Cu(2)−N(3)	1.981(4)
Cu(1)−N(6)	1.987(4)	Cu(2)−N(8)	1.984(5)
Cu(1)−N(5)	2.140(5)	Cu(2)−N(4)	2.139(5)
Cu(1)−N(2)	2.141(5)	Cu(2)−N(7)	2.169(5)
Cu(1)−Cl(1)	2.275(2)	Cu(2)−Cl(2)	2.3229(15)
N(1)−Cu(1)−N(6)	175.17(18)	N(3)−Cu(2)−N(8)	174.13(19)
N(1)−Cu(1)−N(5)	94.70(18)	N(3)−Cu(2)−N(4)	81.00(17)
N(6)−Cu(1)−N(5)	81.03(18)	N(8)−Cu(2)−N(4)	94.27(19)
N(1)−Cu(1)−N(2)	80.44(18)	N(3)−Cu(2)−N(7)	97.31(19)
N(6)−Cu(1)−N(2)	98.98(18)	N(8)−Cu(2)−N(7)	80.5(2)
N(5)−Cu(1)−N(2)	111.57(16)	N(4)−Cu(2)−N(7)	104.74(17)
N(1)−Cu(1)−Cl(1)	92.20(14)	N(3)−Cu(2)−Cl(2)	92.59(14)
N(6)−Cu(1)−Cl(1)	91.16(14)	N(8)−Cu(2)−Cl(2)	92.38(15)
N(5)−Cu(1)−Cl(1)	106.20(13)	N(4)−Cu(2)−Cl(2)	111.42(13)
N(2)−Cu(1)−Cl(1)	141.94(13)	N(7)−Cu(2)−Cl(2)	143.58(12)

Ligands **3** and **7** are isomers differing only in the position of the bridge − at C-2 or C-3 of the phenanthroline group in the cases of **3** and **7**, respectively. Figure 4 provides a view of the $CuCl_2$ complex of 3-ethyl-Clip-Phen (**7**). Because of the poor quality of the very small and weakly diffracting crystals, we were not able to refine the structure satisfactorily. Nevertheless, our model is good enough for discussion of the main features of this complex. Complex **7**·$CuCl_2$ crystallizes in a DMF/methanol (2:1) mixture in the form of a double-helical structure of general formula [(**7**)$CuCl]_2Cl_2$. In the case of [(**7**)$CuCl]_2Cl_2$ − as in that of [(**3**)$CuCl]_2Cl_2$ − the coordination geometries of each copper center are similar and are best described as a distorted trigonal-bipyramidal arrangement with one chloride ion and two phenanthroline residues (one from each ethyl-Clip-Phen ligand of the double-helix) around the copper atom. The main difference is the Cu···Cu distances, 11.00 Å in [(**7**)$CuCl]_2Cl_2$ and 6.48 Å in [(**3**)$CuCl]_2Cl_2$.

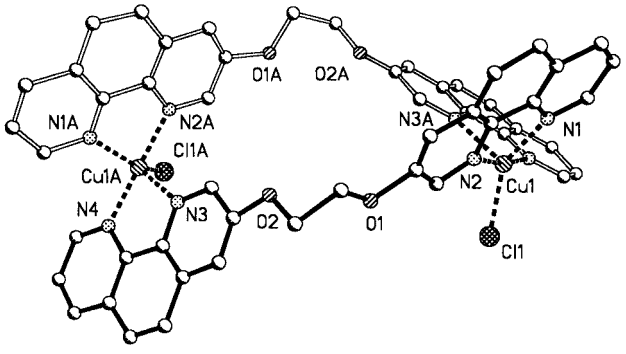

Figure 4. Complex of [(**7**)$CuCl]_2Cl_2$ in the crystalline solid state; hydrogen atoms, non-coordinated counter-ions, and solvent molecules are omitted for clarity

The double-helix units in all L_2Cu_2 copper complexes are chiral, but the three structures are in centrosymmetric space groups, which means that there is a racemic mixture of left- and right-turning helices present in the crystal.

Since copper(II) complexes of Clip-Phen derivatives are difficult to crystallize, we attempted to obtain more information on their geometry through the preparation of the corresponding zinc(II) complexes. We chose Zn^{II} since its coordination behavior and ionic radius are very close to those of Cu^{II} and because it − like Cu^{II} − forms penta- and hexadentate complexes, which could be isostructural to the Cu^{II} ones. Major differences, but also some interesting similarities, could be observed on comparison of the copper and zinc complexes of the same 2-Clip-Phen ligand **1**. Complex **1**·$ZnCl_2$ crystallizes in DMSO as a monomeric structure of general formula (**1**)$ZnCl_2$ (Figure 5). Table 3 presents selected average bond lengths and angles of this complex. The $P\bar{1}$ spatial group is centrosymmetric, in accordance with a racemic mixture in which the two enantiomers exits in the crystal in 1:1 proportions. As would be expected from the ionic radii of the divalent metal ions, the average of the Zn^{II}−N bonds is longer than those involving Cu^{II}. The coordination geometry is again best described as a distorted trigonal-bipyramidal arrangement around the metal atom, and the phenanthroline residue again occupies one axial and one equatorial position. Only one Phen residue of the ligand is coordinated; however; the other positions around the zinc(II) ion are occupied by two chloride ions in equatorial positions and the primary amine of the bridge in an axial one. The differences in geometry between **1**·$Cu(BF_4)_2$ and **1**·$ZnCl_2$ could easily be explained by the exchange of Cu^{II} by Zn^{II} and also the presence of chloride ions, which are better ligands than tetrafluoroborate, but in any case the coordination of the amine of the bridge of 2-Clip-Phen is strong and competes with the coordination of the second Phen residue of the ligand.

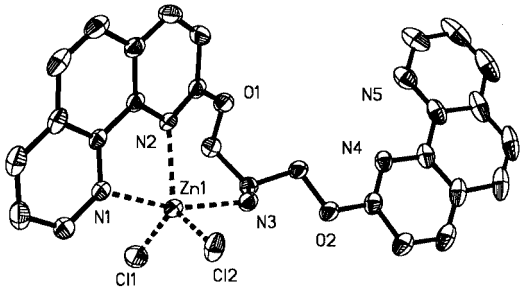

Figure 5. Crystal structure of (**1**)$ZnCl_2$; hydrogen atoms and solvent molecules are omitted for clarity

Mass Analysis

It is remarkable that, although we could legitimately assume that copper(II) complexes of Clip-Phen adopted a double-helical geometry with a copper/ligand stoichiometry of 2:2, these species were particularly difficult to observe by mass spectrometry (Figure 6). Electrospray mass spectra of the different complexes generally reflected a 1:1 copper/ligand stoichiometry. Analyses were conducted in a CH_3OH/H_2O 1:1 mixture, chosen because our DNA cleavages were performed in aqueous solution. High concentrations of $CuCl_2$ complexes (10^{-4} and 10^{-5} M) and different orifice voltages (50, 5, but also 0 V) were tested with the goal of promoting the observation of L_2Cu_2 complexes (see ref.[9]

Table 3. Selected bond lengths [Å] and angles [°] for (**1**)$ZnCl_2$

Zn(1)−N(3)	2.1294(16)
Zn(1)−N(1)	2.1431(16)
Zn(1)−N(2)	2.2645(16)
Zn(1)−Cl(1)	2.2929(6)
Zn(1)−Cl(2)	2.3452(6)
N(3)−Zn(1)−N(1)	161.42(7)
N(3)−Zn(1)−N(2)	88.34(6)
N(1)−Zn(1)−N(2)	75.73(6)
N(3)−Zn(1)−Cl(1)	98.82(5)
N(2)−Zn(1)−Cl(1)	121.81(4)
N(3)−Zn(1)−Cl(2)	88.48(5)
N(1)−Zn(1)−Cl(2)	89.90(5)
N(2)−Zn(1)−Cl(2)	115.77(4)
Cl(1)−Zn(1)−Cl(2)	122.05(2)

and references therein for a discussion about these analytical conditions generally best used in order to promote the detection of double-helical structures by electrospray mass spectrometry). The 1:1 stoichiometry was confirmed by comparison with theoretical isotopic patterns, which could be analyzed unambiguously thanks to the presence of $^{63/65}Cu$ and $^{35/37}Cl$ isotopes, the *m*/*z* values being determined from the spacing between two isotope peaks.

The LCu^+ species was always observed, in agreement with the expected reduction of Cu^{II} in a mass spectrometer.[33] The monocationic species $LCu^{II}Cl$, however, was also clearly observed; LCu^{2+} species only being observed at lower activation voltages. The L_2Cu_2 species with or without chloride ion(s) or different charge states, though, were only observed − and only as minor products − for concentrated solutions with a low orifice voltage. It is reasonable to speculate that the dimeric species are poorly stable in solution and dissociate during analysis, or that they are absent or only present in small quantities in solution and are, in this last case, in equilibrium with monomeric LCu species in solution. No direct evidence for this last hypothesis was obtainable, but it seems reasonable since equilibria between monomeric and dimeric copper complexes of bis(phenanthroline) ligands have been observed previously, during the synthesis of a trefoil knot for example.[34] The geometries of monomeric species are probably similar to those of other previously described pincer-crab bis(phenanthroline)-copper complexes.[32]

It should be noted that different attempts were made to perform ^1H NMR analysis of cuprous complexes of **1**, **2**, **4**, or **5** (obtained by reduction of deaerated solutions of the cupric complexes in DMSO/H_2O mixtures by addition of ascorbate) or zinc complexes of the same ligands. The ^1H NMR spectra showed broader signals at room temperature, sharpening when the temperature increased, consistent with mixtures of species in rapid exchange on the NMR timescale (results not shown). Only the spectra of **1**·$ZnCl_2$ seem to be resolved at room temperature, but these also showed complex signals for the bridge protons, and irradiation experiments also confirmed the presence of different species in solution in this case (see the Exp. Sect. for these NMR spectroscopic data).

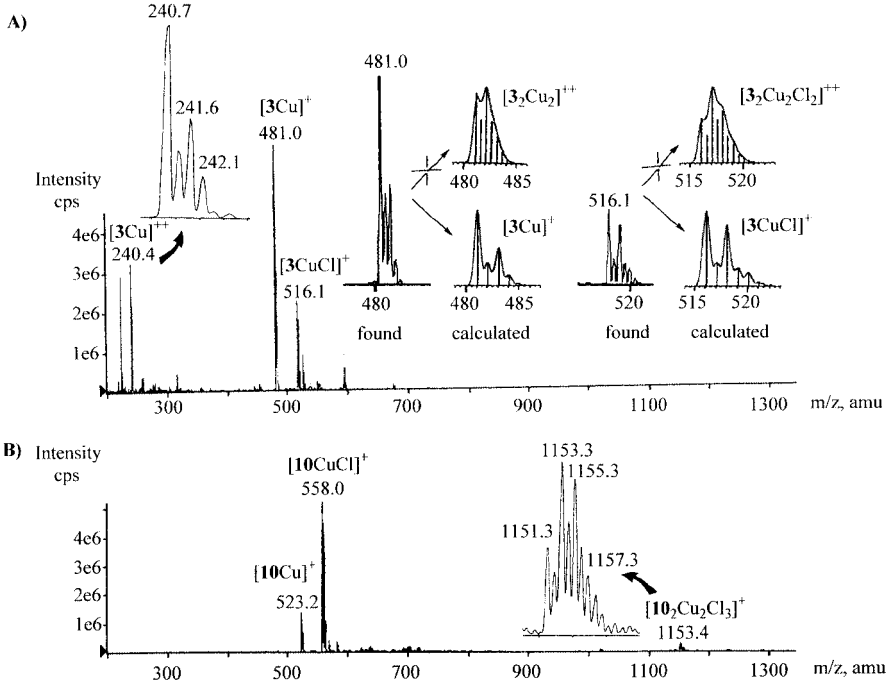

Figure 6. Typical examples of electrospray mass spectra analyses of copper(II) complexes of Clip-Phen derivatives in CH_3OH/H_2O (1:1): A) mass spectrum analysis of 2-ethyl-Clip-Phen·$CuCl_2$ (**3**·$CuCl_2$) (10^{-4} M, orifice voltage = 5 V); B) observation of traces of L_2Cu_2 species in the case of 3-pentyl-Clip-Phen·$CuCl_2$ (**10**·$CuCl_2$) (10^{-4} M, orifice voltage = 0 V)

It cannot be discounted that the copper complexes of Clip-Phen derivatives may adopt different geometries or stoichiometries in solution and that the relative proportions of these species could vary with the concentrations of the complexes (with the monomeric species being favored in dilute solutions, such as those used for DNA cleavage experiments).

As observed in the single-crystal analyses, L_2Cu_2 cupric complexes can form left- and right-turning double-helices. Cuprous and cupric LCu monomeric complexes, however, could form Λ and Δ enantiomers. Separations of these enantiomers have not been performed, but from model studies the two enantiomers probably have different DNA-binding modes. However, such studies are well behind the scope of this paper (for recent studies on DNA interaction with enantiomeric metal complexes, and metal helicates in particular, see refs.[35,36] and references therein).

EPR Data

Copper(II) complexes of the Clip-Phen derivatives were analyzed by electron spin resonance (Table 4). None of the complexes was magnetically sufficiently diluted to yield EPR spectra indicative of the solid-state geometry. X-EPR spectra of these green polycrystalline samples are best described as isotropical signals centered at $g = 2.12-2.14$ (except for **1**·$CuCl_2$ and **10**·$CuCl_2$, for which two g values were observed, reflecting axial symmetry). Superhyperfine coupling to nitrogen was not apparent but hyperfine coupling constants were obtained in DMF/CH_2Cl_2/CH_3OH (2:4:1) and H_2O/$C_2H_6O_2$ (1:2) glasses. Two g values were generally observed, in accordance with an axial symmetry of the g tensor, but different families of complexes could be observed.

The spectrum of the cupric complex of 2-ethyl-Clip-Phen (**3**·$CuCl_2$) was not well resolved in the two types of glasses tested, but the spectra of the cupric complexes of all the other compounds substituted at C-2 of the phenanthroline residues and in which the linker contained three carbon atoms (ligands **1**, **2**, and **4**) were well resolved. They had similar geometries in DMF/CH_2Cl_2/CH_3OH glass, since they exhibited similar EPR spectra consistent with a single configuration for a randomly oriented sample. The g and A values are in agreement with reported cases of trigonal-bipyramidal copper(II) complexes.[32] They exhibit two identifiable magnetic g values, together with the corresponding copper ($I = 3/2$) hyperfine splitting constants. The following values were observed: $g_{\|} = 2.20-2.23$, $A_{\|} = 100-110$ G, $g_{\perp} = 2.01$, $A_{\perp} = 78-90$ G. The parallel or perpendicular attribution of g values did not appear clearly in the spectra but was confirmed by integration of the corresponding signal area, the $g_{\|}$ area being, as expected, roughly twice that of the $g_{\perp}$ one. Crystallographic data obtained previously confirm that the complexes could adopt this trigonal-bipyramidal geometry. The fifth ligand might be a Cl^- or a water molecule, but the primary amine function can also play this role in the particular case of 2-Clip-Phen (**1**).

It is remarkable that these cupric complexes can adopt different geometries and that their geometries change in more polar media, as observed in H_2O/$C_2H_6O_2$ glasses. The resolution of the EPR spectra was poor, probably due to the presence of different conformations, but these spectra indicated that copper complexes of **1**, **2**, and **4** would be able to adopt geometries similar to those of cupric complexes of 3-Clip-Phen in water solution (the solvent used for DNA cleavage experiments).

The cupric complexes of 3-Clip-Phen derivatives **5**−**10** probably have poorer capabilities to change their geometries than the 2-Clip-Phen ones, since the EPR spectra for all these complexes are nearly superimposable in the two media tested. The spectra of **5**−**10**·$CuCl_2$ are consistent with a single configuration for a randomly oriented sample. They were in agreement with classical five- or six-coordinated copper(II) in a square-pyramidal or octahedral geometry with four equatorial ligands in a deformed square-planar geometry.[36] Two identifiable magnetic g values were observed, along with the corresponding copper ($I = 3/2$) hyp-

Taable 4. EPR data of **1**−**10**·$CuCl_2$ complexes

Complex	Solid	DMF/CH_2Cl_2/CH_3OH glass					H_2O/$C_2H_6O_2$ glass		
		$g_{\|}$	$A_{\|}$ (G)	$g_{\perp}$	$A_{\perp}$ (G)	$g_{\|}$	$A_{\|}$ (G)	$g_{\perp}$	$A_{\perp}$ (G)
1·$CuCl_2$	$g_{\|} = 2.14$ $g_{\perp} = 2.09$	2.20	110	2.005	78	2.26	bad resolved	2.07	bad resolved
2·$CuCl_2$	$g_{iso} = 2.14$	2.22	102	2.01	90	2.29	160	2.08	105
3·$CuCl_2$	$g_{iso} = 2.12$	unresolved complex signal					unresolved complex signal		
4·$CuCl_2$	$g_{iso} = 2.12$	2.23	101	2.01	83	2.29	135	2.08	30
5·$CuCl_2$	$g_{iso} = 2.12$	2.26	155	2.07	60	2.28	150	2.07	−
6·$CuCl_2$	$g_{iso} = 2.12$	2.25	155	2.06	−	2.28	155	2.07	−
7·$CuCl_2$	$g_{iso} = 2.12$	2.27	153	2.06	−	2.28	150	2.07	−
8·$CuCl_2$	$g_{iso} = 2.12$	2.26	153	2.06	−	2.28	154	2.08	−
9·$CuCl_2$	$g_{iso} = 2.12$	2.26	166	2.06	−	2.28	150	2.06	−
10·$CuCl_2$	$g_{\|} = 2.12$ $g_{\perp} = 2.06$	2.27	159	2.06	−	2.28	158	2.07	−
$CuCl_2$	$g_1 = 2.24$ $g_2 = 2.18$ $g_3 = 2.04$	2.40	117	2.08	14	2.42	121	2.08	−

erfine splitting constants with the following values: $g_{\|}$ = 2.28, $A_{\|}$ = 150−158 G, $g_{\perp}$ = 2.07; $A_{\perp}$(Cu) was unobservable.

These results indicated that the EPR values of the complexes, and consequently their geometries, depend on the solvent and on the position of the bridge, at C-2 or C-3 of the phenanthroline entity. The length of the bridge, however, or the incorporation of substituents in this linker, in particular in the case of 3-Clip-Phen derivatives, had a limited influence on EPR spectra and probably also on the geometries of the cupric complexes.

Electrochemical Properties

The copper(II/I) redox potentials of the different copper complexes were compared in aqueous solution with KCl as supporting electrolyte, since nucleic acid cleavage experiments are performed in water in the presence of NaCl. The cyclic voltammograms consisted of only one oxidation and one reduction wave in all cases except for that of the copper complex of 3-pentyl-Clip-Phen (**10**·$CuCl_2$), for which the oxidation wave was not observable. As in the case of the EPR analyses, copper complexes of 2- and 3-Clip-Phen derivatives showed different behavior although the results were similar for all 2-Clip-Phen and all 3-Clip-Phen derivatives, respectively. Results are summarized in Table 5. $(Phen)_2CuCl_2$ was also used for comparison. $\Delta Ep = Ep_{ox} - Ep_{red}$ (= separation of its Cu^{II}/Cu^{I} couple) approached the 56/*n* mV separation expected for a reversible one-electron process. This one-electron metal-centered process has been confirmed for this complex previously, but also for 2-Clip-Phen·$CuCl_2$ by coulometry and EPR.[23]

Table 5. Comparison of cyclic voltammetry data for **1**−**10**·$CuCl_2$ complexes (1 mM in water); cyclic voltammetry measurements were carried out at 0.1 V/s with 0.1 M KCl as supporting electrolyte under argon and at room temperature; $\Delta Ep = Ep_{ox} - Ep_{red}$; SCE was used as a reference

	Ep_c [mV/ECS]	Ep_a [mV/ECS]	Ip_c/Ip_a	$E_{1/2}$ [mV/ECS]	ΔEp [mV]
1·$CuCl_2$	−25	+237	0.60	+106	262
2·$CuCl_2$	+34	+297	1.89	+165	263
3·$CuCl_2$	+39	+219	0.84	+129	180
4·$CuCl_2$	+38	+303	0.93	+170	265
5·$CuCl_2$	−76	+157	1.12	+40	233
6·$CuCl_2$	−72	+92	1.50	+10	163
7·$CuCl_2$	−278	+134	6.80	−15	412
8·$CuCl_2$	−110	+93	18.4	+8	203
9·$CuCl_2$	−99	+74	2.36	−12	172
10·$CuCl_2$	−91	–	–	–	–
$(Phen)_2CuCl_2$	−68	+1	0.67	−33	69

The ΔEp separation for copper complexes of 2-Clip-Phen derivatives (**1**−**4**) ranges from 180 to 263 mV and is best described as quasi-reversible. In all cases, the reduction potentials of the copper complexes of 2-Clip-Phen derivatives were shifted to more positive values relative to the Cu^{II}/Cu^{I} couple of $(Phen)_2CuCl_2$, reflecting their more facile reduction and indicating that 2-Clip-Phen ligands stabilized the copper(I) state for their complexes. This phenomenon is well known in the cases of phenanthroline derivatives substituted on their C-2 and C-9 carbon atoms, in the α-position to the chelating nitrogen atom. They are known to stabilize the tetrahedral copper(I) complexes relative to copper(II) complexes, mostly through steric effects that inhibit the pentahedral or octahedral geometries favorable for copper(II).[3,4,7,22,38] In the case of 2-Clip-Phen derivatives only substituted at the C-2 position, however, this phenomenon was less important.

Further bulk electrolysis was performed with 2-Clip-Phen·$CuCl_2$ and **3**·$CuCl_2$, which form dimers in the crystals. This gave an *n* value of 1 for both. The observation of only one wave of oxidation and reduction and the observed *n* value were in accordance with the presence of monomeric species under the conditions used for electrolyses. The absence of two distinct redox states in cyclic voltammograms should not, however, be interpreted as definitive proof of monomeric species in solution, since double-helical dimeric structures can also exhibit a single redox state when both metal centers are strictly equivalent (as previously observed for some other copper dimetallic complexes[8,32,39,40]). Cyclic voltammetry was performed on the electrochemically reduced product, and again only one oxidation and one reduction wave were observed, with small differences in comparison with the cyclic voltammetry data of the oxidized form attributed to geometrical exchanges occurring between the +II and +I oxidation states. This reduced complex was then reoxidized electrochemically, and the cyclic voltammetry of the reoxidized form remained similar to that of the initial copper(II) complex, confirming the quasi-reversibility of the system (results not shown). Finally, it could be noted that the ΔEp increased when the scan rate increased in the case of 2-Clip-Phen·$CuCl_2$, this last result also being in accordance with a slow quasi-reversible system.

Surprisingly, the copper complexes of the 3-Clip-Phen derivatives (**5**−**10**) were only poorly electroactive. More strongly negative reduction potentials were observed than for $(Phen)_2CuCl_2$, which could reflect the greater stabilization of the copper(II) ion in these complexes with 3-Clip-Phen derivative ligands. However, the Cu^{II}/Cu^{I} reduction is quasi-irreversible for cupric complexes of **5**−**9** and seems to be irreversible for **10**·$CuCl_2$. The cupric complex of 3-pentyl-Clip-Phen (**10**) is in fact the most difficult of this series to reduce, but also the most irreversible (and is also the worst DNA cleaver in the 3-Clip-Phen series).

DNA Cleavage Activity

The DNA cleavage activities of the different (Clip-Phen)-copper complexes were compared. Relaxation of supercoiled circular ΦX174 DNA (form I) into relaxed (form II) and linear (form III) forms was used to quantify the relative cleavage efficiencies of the different complexes. Redox activity of the Cu^{II} complexes was initiated by the addition of 5 mM mercaptopropionic acid (MPA) in the presence of air. Control experiments clearly showed the necessity of the presence of copper complexes and a reductant for noticeable DNA cleavage (Table 7). Residual DNA cleavage was

observed in the case of 3-Clip-Phen (**5**) and for its cupric complex (the more active compound) without MPA. This was probably due to buffer impurities.

As previously observed for copper complexes of 2- and 3-Clip-Phen (**1** and **5**), DNA cleavage experiments performed in the presence of different concentrations of complexes showed that all compounds produced single-strand cleavages in DNA, since they transformed form I into form II. Form III resulted from multiple cleavage of form II and appeared only when full cleavage of form I was practically achieved. A smear corresponding to multifragmented DNA was also observed for higher DNA cleavage activities (results not shown).

All complexes were tested under the same experimental conditions (1 μM concentration for a reaction time of 1 h at 37 °C), in order to provide direct comparison of their DNA cleavage efficiencies. To facilitate this analysis, attempts to quantify the number *S* of single-strand cleavages per ΦX174 molecule were carried out according to refs.[41,42] This assumes random cleavage of the DNA target, as previously observed for **1**·$CuCl_2$ and **5**·$CuCl_2$.[25,27] Table 6 indicates that the relative DNA cleavage efficiencies of the different copper complexes were in the following order: **5**·$CuCl_2$ >> **6**·$CuCl_2$ > **8**·$CuCl_2$ > **7**·$CuCl_2$ ≈ **9**·$CuCl_2$ > **4**·$CuCl_2$ > **10**·$CuCl_2$ > **1**·$CuCl_2$ > **2**·$CuCl_2$ > **3**·$CuCl_2$. Comparison of the cleavage patterns of copper complexes of **1** versus **5**, **2** versus **6**, **3** versus **7**, and **4** versus **8** (*S* = 1.2 and 35, 0.8 and 21, 0.7 and 10, 6 and 15, respectively) clearly indicated that, for the same bridge, copper complexes of 3-Clip-Phen derivatives were always more active than their isomers with a junction at C-2 of the phenanthroline.

Differences between 2- and 3-Clip-Phen series also clearly appeared during electrochemical analyses of the different copper complexes (Table 5). All these data suggest that the lower DNA cleavage efficiency of copper complexes of 2-Clip-Phen derivatives might be correlated with their higher stabilization of cuprous species. It can be seen, however, that no correlation between the redox activity and the DNA cleavage efficiency within each series was observed. Other parameters such as steric or electrostatic constraints in the vicinity of the DNA target probably modulate the cleaving activities of the complexes.

The reactivities of the complexes are largely governed by the position of the bridge, at C-2 or C-3 of each phenanthroline residue. However, the length and the nature of this bridge also appeared to be significant for the DNA cleavage activity of these copper complexes. Hence, **4**·$CuCl_2$ of the 2-Clip-Phen series, for example, is a better DNA cleaver than **10**·$CuCl_2$ of the 3-Clip-Phen series.

Effect of the Length of the Bridge on the DNA Cleavage Efficiency

Comparison of cleavage patterns obtained with copper complexes of **3** and **4** on one hand and **7**−**10** on the other allowed the optimal length of the bridge for high DNA cleavage patterns to be determined, since these compounds differed only in the number of methylene units in the bridge.

Table 6 shows that for copper complexes of ethyl (**3**) and propyl (**4**) derivatives of 2-Clip-Phen, a small change due to the addition of one methylene unit to the bridge has a dramatic effect on DNA cleavage efficiency. For 1 μM of **3**·$CuCl_2$, 50% of DNA form I was present after 1 h of reac-

Table 6. Comparison of ΦX174 DNA cleavage efficiency of **1**−**10**·$CuCl_2$ complexes (1 μM in the presence of 5 mM MPA and air for 1 h at 37 °C); *S* corresponds to the average number of single-strand breaks per DNA molecule, assuming a random cleavage of the DNA target by the activated copper complexes

	% Form I	% Form II	% Form III	% Forms (I + II +III)[a]	S
DNA control	85±5	15±5	0	100	0.16±0.05
MPA control	85±5	15±5	0	100	0.16±0.05
$CuCl_2$/MPA	80±5	20±5	0	100	0.22±0.05
1·$CuCl_2$/MPA	30±5	70±5	0	100	1.2±0.2
2·$CuCl_2$/MPA	45±5	55±5	0	100	0.80±0.1
3·$CuCl_2$/MPA	50±5	50±5	0	100	0.70±0.1
4·$CuCl_2$/MPA	1±1	95±5	5±2	100	6±2
5·$CuCl_2$/MPA	0	35±10	65±10	50±10	35±5
6·$CuCl_2$/MPA	0	50±5	50±5	95±5	21±1
7·$CuCl_2$/MPA	0	85±5	15±5	100	10±2
8·$CuCl_2$/MPA	0	70±5	30±5	95±5	15±1
9·$CuCl_2$/MPA	5±2	80±5	15±5	100	10±2
10·$CuCl_2$/MPA	55±5	45±5	2±2	100	2±1
$(Phen)_2CuCl_2$/MPA	40±5	60±5	0	100	0.92±0.1
$(Phen)CuCl_2$/MPA	60±5	40±5	0	100	0.51±0.05
1·$CuCl_2$	80±5	20±5	0	100	0.22±0.05
4·$CuCl_2$	80±5	20±5	0	100	0.22±0.05
5·$CuCl_2$	70±5	30±5	0	100	0.36±0.05
8·$CuCl_2$	70±5	30±5	0	100	0.36±0.05
1/MPA	85±5	15±5	0	100	0.16±0.05
5/MPA	60±5	40±5	0	100	0.51±0.05
1	85±5	15±5	0	100	0.16±0.05
5	70±5	30±5	0	100	0.36±0.05

[a] For values less of 100%, the other part of DNA appeared as a smear on the gel.

tion. With $S = 0.7$, **3**·$CuCl_2$ has a rather poor DNA cleavage activity, just below that of $(Phen)_2$·$CuCl_2$ itself ($S = 0.9$). However, **4**·$CuCl_2$ appeared to be an efficient DNA cleaver under the same experimental conditions, converting nearly all supercoiled DNA not only into form II (95%), but also into form III (5%). With an S value estimated as 6, **4**·$CuCl_2$ appeared to be roughly ten times more active than **3**·$CuCl_2$. It is reasonable to propose that the poor DNA cleavage activity of **3**·$CuCl_2$, with the smallest bridge between the two phenanthroline residues, is due to steric constraints around the copper ion.

For copper complexes of ethyl (**7**), propyl (**8**), butyl (**9**), and pentyl (**10**) derivatives of 3-Clip-Phen ($S = 10$, 15, 10, and 2, respectively), variation by one methylene unit in the bridge had more limited effects. However, better DNA cleavage activity was obtained for **8**·$CuCl_2$, with three methylene units in the bridge, while, for a longer bridge such as in **10**·$CuCl_2$ (with five methylene units), the DNA cleavage efficiency significantly decreased. It is remarkable that 3-Clip-Phen (**5**) has the same bridge length as **8**. Thus, though serinol was chosen for reasons previously described, it also appears to have an optimal length to favor a high level of DNA cleavage activity.

Effect of the Nature of the Bridge on the DNA Cleavage Efficiency

Table 6 indicates that the nuclease activity of the copper complexes is also modulated by the chemical composition of the bridge. Three types of bridges of the previously observed optimized length were studied: unsubstituted ones [copper complexes of 2- and 3-propyl-Clip-Phen (**4** and **8**)], bridges including an amine residue such as in Clip-Phen [copper complexes of 2- and 3-Clip-Phen (**1** and **5**)], and bridges with an acetamido residue mimicking the amide junction used for the vectorization of Clip-Phen [copper complexes of 2- and 3-acetyl-Clip-Phen (**2** and **6**)].

Increases in DNA cleavage activity had previously been observed for copper complexes of conjugates of 2- or 3-Clip-Phen with DNA-binding molecules.[26−28] Acetylation of the amine residue of 2- and 3-Clip-Phen, however, resulted in a decrease in the DNA cleavage efficiency of their copper complexes by roughly 50%. This phenomenon was observed on comparison of the DNA cleavage activities of **1**·$CuCl_2$ and **5**·$CuCl_2$ ($S = 1.2$ and 35, respectively) with those of the corresponding acetylated derivatives **2**·$CuCl_2$ and **6**·$CuCl_2$ ($S = 0.8$ and 21, respectively). This difference was probably due not only to the steric effects of the bulkier amido group on the interaction with the DNA target, but also on the geometry changes during the Cu^I/Cu^{II} redox cycle. While this last proposal is not supported by the electrochemical data (Table 5), the phenomenon is probably enhanced in the case of a complex confined in the vicinity − or, more probably, in the floor − of the DNA minor groove, as suggested by DNA cleavage mechanism studies.[25] However, these phenomena were overcompensated by the increase of DNA affinity in conjugates with DNA binders, resulting in higher nuclease activities.

It is remarkable, though, that the amine on the bridge produced different effects on DNA cleavage for copper complexes of 2-Clip-Phen and 3-Clip-Phen derivatives. This phenomenon was clear on comparison of the DNA cleavage activities of **1**·$CuCl_2$ and **5**·$CuCl_2$ ($S = 1.2$ and 35, respectively) with those of their derivatives without the amine function **4**·$CuCl_2$ and **8**·$CuCl_2$ ($S = 6$ and 15, respectively). These data suggested that the presence of the amine decreased the DNA cleavage activity in the case of 2-Clip-Phen derivatives but increased it in the case of 3-Clip-Phen ones. Since the X-ray structures of the monocrystals of copper and zinc complexes of 2-Clip-Phen indicate that this amine could coordinate the metal ion, it is reasonable to propose that this type of coordination could also occur under DNA cleavage conditions. DNA cleavage results indicated that this coordination has an unfavorable effect on the DNA cleavage activity. However, geometrical constraints did not allow this type of coordination in the case of 3-Clip-Phen. It is reasonable to propose that, in the case of the copper complex of 3-Clip-Phen (**5**), the free amine residue could be protonated under the conditions used for DNA cleavage experiments, generating a cationic species with a higher affinity for the polyanionic DNA target, consequently increasing the DNA cleavage activity.

On the other hand, these last results indicate that the benefit of bridging on the C-2 carbon atom of Phen had previously been greatly underestimated, since data were obtained with the copper complex of 2-Clip-Phen (**1**), with the free primary amine function able to perturb the coordination sphere of the copper ion.

Conclusion

Different bis(phenanthroline) ligands were prepared in order not only to study their copper complexes but also to optimize the DNA cleavage activity of Clip-Phen derivatives. Physicochemical analysis showed that these copper complexes appear to be particularly versatile. As shown by structural analysis, the cupric complexes can adopt double-helical L_2Cu_2 geometries, but this type of geometry seems to be labile. The mass spectra results showed that the presence of monomeric structure L_1Cu_1 in solution could not be discounted. NMR studies showed that the complexes adopt different geometries, existing in equilibrium in solution. EPR analyses indicated that the geometries of the cupric complexes of 2-Clip-Phen derivatives could change with the composition of the solvent employed for their dilution. From electrochemical studies it also appears that all the ligands related to 2-Clip-Phen stabilize Cu^I more than their 3-Clip-Phen counterparts. Copper complexes of this latter ligand family appear to be surprisingly poorly redox-active.

DNA cleavage experiments allowed optimization of the bridge between the two phenanthroline residues of Clip-Phen to provide higher nuclease activity. The compounds with a bridge linked at C-3 were more active DNA cleavers than complexes with the bridge in the C-2 position. A tether length corresponding to three methylene units gave better

DNA cleavage activities, but incorporation of voluminous substituents within the linker could decrease the DNA cleavage efficiency. Surprisingly, the presence of an amine group in the bridge had different effects on DNA cleavage activity for the copper complexes of 2-Clip-Phen and of 3-Clip-Phen, and allowed the proposal that, in the case of 2-Clip-Phen·$CuCl_2$, this amine group could be coordinated to the copper ion under the DNA cleavage conditions.

Experimental Section

General Remarks: 2-Chloro-1,10-phenanthroline,[43] 3-bromo-1,10-phenanthroline,[44] 2-Clip-Phen (**1**),[23] 3-Clip-Phen (**5**),[24] 2-acetyl-Clip-Phen (**2**),[28] 3-propyl-Clip-Phen (**8**),[45] and 2-Clip-Phen·$CuCl_2$ (**1**·$CuCl_2$)[23] were synthesized by literature procedures. Proton NMR spectra were recorded with a Bruker 250 MHz instrument. The ESI-MS spectrometer was a Perkin−Elmer SCIEX API 365 used in positive mode; samples were introduced into the electrospray source with a Havard Apparatus syringe pump. UV/Vis spectra were recorded with a Hewlett Packard 8452A diode array spectrophotometer. EPR spectra were recorded with a Bruker ESP 300 in X Band, with an ER035 M gaussmeter (NMR probe) and an EIP 548 hyperfrequencemeter. Syntheses were monitored by thin layer silica chromatography (Macherey−Nagel Alugram Sil G/UV 254) eluted by CH_2Cl_2/methanol (9:1, v/v) to which 1% of concentrated aqueous ammonia (30%) had been added, and spots were viewed under UV light (violet spots at 254 nm). DMF was dried with 4 Å molecular sieves. Other commercially available reagents and solvents were purchased from standard chemical suppliers and used without further purification.

General Method for the Synthesis of 2-alkyl-Clip-Phen 3 and 4: 2-Chloro-1,10-phenanthroline (200 mg, 0.93 mmol) and the diol (ca. 0.46 mmol of ethylene glycol or 1,3-propanediol) were added to a suspension of sodium hydride (275 mg of a 60% suspension in mineral oil, 6.85 mmol) in 4 mL of dry DMF, cooled by an ice bath. After the mixture had been stirred for 24 h and allowed to warm to room temperature, the crude product was dissolved in 4 mL of ethanol before being precipitated with 40 mL of water. After filtration, the product was precipitated from 15 mL of hot methanol to give 2-alkyl-Clip-Phen.

2,2′-Ethane-1,2-dioxybis(1,10-phenanthroline) (2-ethyl-Clip-Phen, 3): Yield = 146 mg (75%) as white needles. ^{1}H NMR ($CDCl_3$): δ = 5.25 ppm (s, 4 H, 1-H), 7.21 (d, *J* = 8.7 Hz, 2 H, 3′-H), 7. 58 (dd, *J* = 8.1, 4.2 Hz, 2 H, 8′-H), 7.66 and 7.75 (AB, *J* = 8.7 Hz, 4 H, 5′-H and 6′-H), 8.12 (d, *J* = 8.7 Hz, 2 H, 4′-H), 8.23 (dd, *J* = 8.1, 1.8 Hz, 2 H, 7′-H), 9.18 (dd, *J* = 4.2, 1.8 Hz, 2 H, 9′-H). MS (CDI, NH_3): *m*/*z* (%) = 419 (100) [M + 1], 223 (67), 197 (65). UV/Vis (CH_3OH): λ (ε) = 228 nm (73600 $mol^{-1}·cm^{-1}$), 276 (52300), 292 (16400, sh), 316 (4000, sh), 332 (2300), 350 (1500). $C_{26}H_{18}N_4O_2$ (418): calcd. (+ 0.25 H_2O) C 73.86, H 4.41, N 13.25; found C 73.53, H 4.17, N 13.11.

2,2′-Propane-1,3-dioxybis(1,10-phenanthroline) (2-propyl-Clip-Phen, 4): Yield = 157 mg (78%) as a white powder. ^{1}H NMR (CD_2Cl_2): δ = 2.52 ppm (quint, *J* = 6.2 Hz, 2 H, 2-H), 4.93 (t, *J* = 6.2 Hz, 4 H, 1-H), 7.15 (d, *J* = 8.6 Hz, 2 H, 3′-H), 7. 59 (dd, *J* = 8.1, 4.2 Hz, 2 H, 8′-H), 7.68 and 7.76 (AB, *J* = 8.7 Hz, 4 H, 5′-H and 6′-H), 8.13 (d, *J* = 8.6 Hz, 2 H, 4′-H), 8.25 (dd, *J* = 8.1, 1.8 Hz, 2 H, 7′-H), 9.11 (dd, *J* = 4.2, 1.8 Hz, 2 H, 9′-H). MS (CDI, NH_3): *m*/*z* (%) = 433 (100) [M + 1], 235 (5), 197 (6). UV/Vis (CH_3OH): λ (ε) = 228 nm (67700 mol^{-1} cm^{-1}), 276 (48700), 292 (16400, sh), 314 (4400, sh), 332 (2300), 348 (1400). $C_{27}H_{20}N_4O_2$ (432): calcd. (+ 0.75 H_2O) C 72.74, H 4.85, N 12.56; found C 72.83, H 4.57, N 12.40.

General Method for the Synthesis of 3-Alkyl-Clip-Phen 7, 9, and 10: The appropriate diol (ca. 0.77 mmol of ethylene glycol, 1,4-butanediol, or 1,5-pentanediol) was added to a suspension of sodium hydride (156 mg of a 60% suspension in mineral oil, 3.9 mmol) in 7 mL of dry DMF. The mixture was stirred for 1 h at 55 °C, and then cooled to 4 °C with an ice bath. 3-Bromo-1,10-phenanthroline (400 mg, 1.54 mmol) was added, and the mixture was warmed at 55 °C overnight. After return to room temperature, 2 mL of ethanol was added, then 20 mL of water. The precipitate was filtered, dissolved in dichloromethane, and washed with a 5% solution of ammonia. The organic layer was concentrated and the product was crystallized from 3 mL of methanol before being dissolved in dichloromethane and precipitated with hexane to give pure 3-alkyl-Clip-Phen as white powder. *Warning:* The number of NaH equivalents should be optimized according to the intrinsic quality of reagents and solvents (ultrapure quality is preferred).

3,3′-Ethane-1,2-dioxybis(1,10-phenanthroline) (3-ethyl-Clip-Phen, 7): Yield = 74 mg (23%). ^{1}H NMR (CD_2Cl_2): δ = 4.67 ppm (s, 4 H, 1-H), 7.59 (dd, *J* = 4.4, 8.1 Hz, 2 H, 8′-H), 7.69 (d, *J* = 3.0 Hz, 2 H, 4′-H), 7.83 and 7.78 (AB, *J* = 8.9 Hz, 4 H, 5′-H and 6′-H), 8.25 (dd, *J* = 1.8, 8.1 Hz, 2 H, 7′-H), 8.93 (d, *J* = 3.0 Hz, 2 H, 2′-H), 9.09 (dd, *J* = 1.8, 4.4 Hz, 2 H, 9′-H). MS (CDI, NH_3): *m*/*z* (%) = 419 (100) [M + 1]. UV/Vis (CH_3OH): λ (ε) = 240 nm (69500 $mol^{-1}·cm^{-1}$),·272 (51700), 294 (27400, sh), 304 (17100, sh), 314 (8400, sh), 328 (5500), 342 (3600). $C_{26}H_{18}N_4O_2$ (418): calcd. (+ 0.5 CH_2Cl_2) C 69.06, H 4.15, N 12.16; found C 69.08, H 4.05, N 12.34.

3,3′-Butane-1,4-dioxybis(1,10-phenanthroline) (3-butyl-Clip-Phen, 9): Yield = 80 mg (23%). ^{1}H NMR (CD_2Cl_2): δ = 2.20 ppm (m, 4 H, 2-H), 4.30 (t, *J* = 5.4 Hz, 4 H, 1-H), 7.56 (dd, *J* = 4.2, 8.1 Hz, 2 H, 8′-H), 7.58 (d, *J* = 3.0 Hz, 2 H, 4′-H), 7.79 and 7.74 (AB, *J* = 8.9 Hz, 4 H, 5′-H and 6′-H), 8.23 (dd, *J* = 1.8, 8.1 Hz, 2 H, 7′-H), 8.87 (d, *J* = 3.0 Hz, 2 H, 2′-H), 9.08 (dd, *J* = 1.8, 4.2 Hz, 2 H, 9′-H). MS (CDI, NH_3): *m*/*z* (%) = 447 (100) [M + 1]. UV/Vis (CH_3OH): λ (ε) = 242 nm (72600 $mol^{-1}·cm^{-1}$), 272 (48200), 294 (24300, sh), 306 (14500, sh), 314 (7000, sh), 328 (5000), 344 (3300). $C_{28}H_{22}N_4O_2$ (446): calcd. (+ 0.1 CH_2Cl_2) C 74.18, H 4.92, N 12.31; found C 73.84, H 4.33, N 12.18.

3,3′-Pentane-1,5-dioxybis(1,10-phenanthroline) (3-pentyl-Clip-Phen, 10): Yield = 110 mg (31%). ^{1}H NMR (CD_2Cl_2): δ = 1.80 ppm (m, 2 H, 3-H), 1.99 (m, 4 H, 2-H), 4.20 (t, *J* = 6.3 Hz, 4 H, 1-H), 7.51−7.56 (m, 4 H, 4′-H and 8′-H), 7.79 and 7.74 (AB, *J* = 8.9 Hz, 4 H, 5′-H and 6′-H), 8.23 (dd, *J* = 1.8, 8.1 Hz, 2 H, 7′-H), 8.87 (d, *J* = 3.0 Hz, 2 H, 2′-H), 9.08 (dd, *J* = 1.8, 4.2 Hz, 2 H, 9′-H). MS (CDI, NH_3): *m*/*z* (%) = 461 (100) [M + 1]. UV/Vis (CH_3OH): λ (ε) = 240 nm (72400 $mol^{-1}·cm^{-1}$), 272 (51000), 294 (26600, sh), 304 (17000, sh), 314 (92000, sh), 328 (6000), 344 (4200). $C_{29}H_{24}N_4O_2$ (460): calcd. (+ 0.5 CH_2Cl_2 + 1.5 H_2O) C 66.85, H 5.32, N 10.57; found C 67.08, H 5.37, N 10.70.

2-Acetylamino-3,3′-propane-1,3-dioxybis(1,10-phenanthroline) (3-acetyl-Clip-Phen, 6): Acetic anhydride (50 μL, 50 mg, 0.49 mmol) was added to a solution of 3-Clip-Phen (50 mg, 0.11 mmol) in 2 mL of $CHCl_3$. The solution was stirred for 1 h at room temperature, 2 mL of water was then added, and the pH was adjusted to 9 with concentrated aqueous ammonia (30%). The organic layer was separated and washed twice with water, and the solvent was evaporated under vacuum to give **6** as a pale brown foam (50 mg, yield = 92%). ^{1}H NMR (CD_2Cl_2): δ = 2.16 ppm (s, 2 H, CH_3), 4.45 (m, 4 H, 1-H), 4.88 (m, 1 H, 2-H), 6.59 (d, *J* = 8.0 Hz, 1 H, NH), 7.55

(dd, J = 8.0, 4.4 Hz, 2 H, 8′-H), 7. 63 (d, J = 2.8 Hz, 2 H, 4′-H), 7.69 and 7.75 (AB, J = 8.7 Hz, 4 H, 5′-H and 6′-H), 8.19 (dd, J = 8.0, 1.7 Hz, 2 H, 7′-H), 8.90 (d, J = 2.8 Hz, 2 H, 2′-H), 9.11 (dd, J = 4.4, 1.7 Hz, 2 H, 9′-H). MS (CDI, NH_3): m/z (%) = 490 (81) [M + 1], 294 (100), 197 (60). UV/Vis (CH_3OH): λ (ε) = 240 nm (62700 $mol^{-1}\cdot cm^{-1}$), 272 (44500), 294 (22300, sh), 306 (12400, sh), 314 (6100, sh), 328 (4300), 342 (2700). $C_{29}H_{23}N_5O_3$ (489): calcd. (+ 0.4 $CHCl_3$) C 66.40, H 4.37, N 13.20; found C 66.19, H 4.51, N 13.22.

General Preparation of Copper Complexes (8·$CuCl_2$ exempted): $CuCl_2$ (1 equiv., previously dissolved at 58.7 mM concentration in DMF) was added to a solution of ligand (10 mg) in 1 mL of DMF/CH_3OH (1:1). After 1 h at room temperature, the complex was precipitated with 5 mL of diethyl ether overnight at −20 °C and then centrifuged for 10 min at 3000 rpm and washed twice with diethyl ether (2 × 6 mL) before being dried under vacuum.

Preparation of 8·$CuCl_2$: Solubility problems meant that the metallation of 3-propyl-Clip-Phen (**8**) was conducted under more dilute conditions than used for the General Preparation of the other copper complexes. A solution of $CuCl_2$ (23.1 μmol, 1 equiv.) in DMF was added over 2 h, as 5 aliquots of 100 μL, to a solution of 3-propyl-Clip-Phen (**8**, 10 mg, 23.1 μmol) in 23 mL of DMF (1 mM final concentration),. The mixture was stirred overnight and the volume was then reduced to 5 mL. The copper complex was precipitated with diethyl ether and centrifuged, the supernatant was removed, and the precipitate was washed twice with diethyl ether before being dried under vacuum.

2·$CuCl_2$: Treatment of **2** with $CuCl_2$ as described above on a 17.0 μmol scale afforded 11.4 mg (89%) of **2·$CuCl_2$** as a pale green powder. MS (ES, positive mode): m/z = 587 (monocation, M − Cl), 551 (cuprous complex). UV/Vis (H_2O): λ (ε) = 210 nm (59000 $mol^{-1}\cdot cm^{-1}$), 224 (66800), 276 (48400), 336 (2100, sh), 356 (1500, sh), 862 (160). $C_{29}H_{23}Cl_2CuN_5O_3$ (624): calcd. (+ 2.5 H_2O) C 52.07, H 4.21, N 10.47; found C 52.19, H 4.27, N 10.40.

3·$CuCl_2$: Treatment of **3** with $CuCl_2$ on a 23.1 μmol scale afforded 13.6 mg (98%) of **3·$CuCl_2$** as a pale green powder. MS (ES, positive mode): m/z = 516 (monocation, M − Cl), 481 (cuprous complex). UV/Vis (H_2O): λ (ε) = 208 nm (60500 $mol^{-1}\cdot cm^{-1}$), 218 (57300), 274 (38900), 340 (3300, sh), 356 (2600, sh), 825 (120). $C_{26}H_{18}Cl_2CuN_4O_2$ (553): calcd. (+ 2 H_2O) C 53.03, H 3.77, N 9.51; found C 53.11, H 4.20, N 9.48. Green crystals suitable for X-ray analysis were obtained by recrystallization of **3·$CuCl_2$** from hot methanol.

4·$CuCl_2$: Treatment of **4** with $CuCl_2$ on a 19.3 μmol scale afforded 12.2 mg (93%) of **4·$CuCl_2$** as a pale green powder. MS (ES, positive mode): m/z = 530 (monocation, M − Cl), 495 (cuprous complex). UV/Vis (H_2O): λ (ε) = 210 nm (61300 $mol^{-1}\cdot cm^{-1}$), 224 (69000), 274 (51300), 338 (2000, sh), 354 (1400, sh), 855 (160). $C_{27}H_{20}Cl_2CuN_4O_2$ (567): calcd. (+ 3.5 H_2O) C 51.48, H 4.32, N 8.89; found C 51.56, H 4.00, N 9.05.

5·$CuCl_2$: Treatment of **5** with $CuCl_2$ on a 20.3 μmol scale afforded 13.3 mg (93%) of **5·$CuCl_2$** as a green-brown powder. MS (ES, positive mode): m/z = 546 (monocation, M − Cl), 510 (cuprous complex). UV/Vis (H_2O): λ (ε) = 210 nm (51700 mol^{-1} cm^{-1}), 232 (56200), 280 (41100), 318 (10400, sh), 332 (7200, sh), 344 (3400, sh), 702 (70), 955 (40, sh). $C_{27}H_{21}Cl_2CuN_5O_2$ (582): calcd. (+ 4 H_2O) C 49.59, H 4.47, N 10.71; found C 49.64, H 4.10, N 10.85.

6·$CuCl_2$: Treatment of **6** with $CuCl_2$ on a 18.6 μmol scale afforded 11.4 mg (89%) of **6·$CuCl_2$** as a green-brown powder. MS (ES, positive mode): m/z = 587 (monocation, M − Cl), 552 (cuprous complex). UV/Vis (H_2O): λ (ε) = 208 nm (43000 mol^{-1} cm^{-1}), 230 (41900), 282 (31200), 316 (2100, sh), 330 (7400, sh), 344 (4000, sh), 693 (50), 900 (40, sh). $C_{29}H_{23}Cl_2CuN_5O_3$ (624): calcd. (+ 3.5 H_2O) C 50.70, H 4.40, N 10.19; found C 50.80, H 4.05, N 10.22.

7·$CuCl_2$: Treatment of **7** with $CuCl_2$ on a 23.8 μmol scale afforded 10.0 mg (76%) of **7·$CuCl_2$** as a green powder. MS (ES, positive mode): m/z = 516 (monocation, M − Cl), 481 (cuprous complex). UV/Vis (H_2O): λ (ε) = 208 nm (46900 mol^{-1} cm^{-1}), 232 (55700), 245 (50626, sh), 280 (45900), 320 (14700, sh), 332 (10300, sh), 346 (4300, sh), 700 (51). $C_{26}H_{18}Cl_2CuN_4O_2$ (553): calcd. (+ 0.1 H_2O) C 56.30, H 3.31, N 10.10; found C 56.39, H 3.50, N 9.98. Green crystals suitable for X-ray analysis were obtained from a DMF/methanol (2:1) solution of the complex after 3 d at −20 °C.

8·$CuCl_2$: Treatment of **8** with $CuCl_2$ on a 23.1 μmol scale afforded 10.3 mg (76%) of **8·$CuCl_2$** as a green powder. MS (ES, positive mode): m/z = 530 (monocation, M − Cl), 495 (cuprous complex). UV/Vis (H_2O): λ (ε) = 208 nm (49100 $mol^{-1}\cdot cm^{-1}$), 232 (54200), 245 (41900, sh), 280 (41100), 320 (14100, sh), 332 (11900, sh), 346 (4400, sh), 700 (59). $C_{27}H_{20}Cl_2CuN_4O_2$ (567): calcd. (+ 1.3 H_2O) C 54.93, H 3.86, N 9.49; found C 54.87, H 3.56, N 9.27.

9·$CuCl_2$: Treatment of **9** with $CuCl_2$ on a 22.3 μmol scale afforded 10.0 mg (74%) of **9·$CuCl_2$** as a green powder. MS (ES, positive mode): m/z = 544 (monocation, M − Cl), 509 (cuprous complex). UV/Vis (H_2O): λ (ε) = 208 nm (49000 $mol^{-1}\cdot cm^{-1}$), 232 (54600), 245 (43700, sh), 280 (40700), 320 (14100, sh), 332 (11800, sh), 346 (5100, sh), 720 (68). $C_{28}H_{22}Cl_2CuN_4O_2$ (581): calcd. (+ 1.5 H_2O) C 55.32, H 4.14, N 9.22; found C 55.09, H 4.02, N 9.48.

10·$CuCl_2$: Treatment of **10** with $CuCl_2$ on a 21.7 μmol scale afforded 10.3 mg (77%) of **10·$CuCl_2$** as a green powder. MS (ES, positive mode): m/z = 557 (monocation, M − Cl), 523 (cuprous complex). UV/Vis (H_2O): λ (ε) = 208 nm (48200 $mol^{-1}\cdot cm^{-1}$), 232 (50900), 245 (33700, sh), 280 (35900), 320 (12500, sh), 332 (11000, sh), 346 (5300, sh), 740 (71). $C_{29}H_{24}Cl_2CuN_4O_2$ (595): calcd. (+ 1.3 H_2O) C 56.33, H 4.34, N 9.06; found C 56.28, H 4.02, N 9.10.

Preparation of 1·$Cu(BF_4)_2$: $Cu(BF_4)_2\cdot 6\ H_2O$ (26.8 mg, 0.08 mmol) was added to 2-Clip-Phen (**1**, 50.6 mg, 0.11 mmol) dissolved in 600 μL of DMF/CH_3OH. The mixture was stirred for 1 h at room temperature, and green crystals of **1**·$Cu(BF_4)_2$ suitable for X-ray analysis were then obtained by slow diffusion of CH_2Cl_2 into the mixture. MS (ES, positive mode): m/z = 509 (monocharged monomer, **1**·Cu^+, major pick), 529 (monomer, **1**·$Cu^{++}F^-$), 1281 {monocharged dimer, $[(\mathbf{1})_2Cu_2][BF_4]_3$, minor pick}. $C_{27}H_{21}B_2CuF_8N_5O_2$ (685): calcd. (+ 1.5 H_2O) C 45.01, H 3.40, N 9.85; found C 44.91, H 3.38, N 9.60. EPR data: from solid state: $g_\perp$ = 2.09, $g_\parallel$ = 2.2; from a DMF/CH_2Cl_2/CH_3OH (2:4:1) glass (1 mM) at 100 K: $g_\perp$ = 2.09 ($A_\perp$ = 42 G, badly resolved), $g_\parallel$ = 2.24 ($A_\parallel$ = 67 G); from a H_2O/ethylene glycol (1:2) glass (1.1 mM) at 100 K: $g_\perp$ = 2.09, $g_\parallel$ = 2.27 ($A_\parallel$ = 75 G).

Preparation of 1·$ZnCl_2$: Compound **1** (10 mg, 22 μmol) was metallated with 1 equiv. of $ZnCl_2$ (3 mg, 22 μmol) in 0.5 mL of a CH_2Cl_2/CH_3OH (9:1) mixture. After 1 h at room temperature, the solvent was evaporated and the product was dissolved in 0.5 mL of [D_6]DMSO. White crystals suitable for X-ray analysis were obtained, directly in the NMR tube, after 2 d at room temperature. ^1H NMR ([D_6]DMSO): δ = 3.99 ppm (m, 1 H), 4.97 (dd, 2 H, 4.7 Hz and 12 Hz), [3.47 (d, J = 6.2 Hz), 3.99 (s) and 5.40 (br. d): 4 H in slow exchange on the NMR time scale as confirmed by selective irradiation of NMR signals], 7.29 (d, J = 8.7 Hz, 2 H, 3′-H), 7. 82 (dd, J = 7.9, 3.6 Hz, 2 H, 8′-H), 7.92 and 8.00 (AB, 4 H,

J = 8.8 Hz, 5′-H and 6′-H), 8.42 (d, J = 8.7 Hz, 2 H, 4′-H), 8.60 (br. d, 2 H, J = 7.9, 7′-H), 9.19 (br. d, 2 H, J = 3.6, 9′-H).

X-ray Crystallographic Study: Crystal data for all structures are presented in Table 7. Data for bis[(**1**)Cu][BF_4]$_2$ were collected at low temperature with a Stoe-IPDS diffractometer, and data for [(**3**)CuCl]$_2$Cl$_2$, [(**7**)CuCl]$_2$Cl$_2$, and (**1**)ZnCl$_2$ were collected at low temperatures with a Bruker-CCD with Mo-K_α (λ = 0.71073 Å). The structures were solved by direct methods by use of SIR92[46−47] {bis[(**1**)Cu][BF_4]$_2$} or SHELXS-97[48] {[(**3**)CuCl]$_2$Cl$_2$, [(**7**)CuCl]$_2$Cl$_2$, and (**1**)ZnCl$_2$} and refined with all data on F^2 by SHELXL-97.[49] All non-hydrogen atoms were refined anisotropically. The hydrogen atoms of the molecules were geometrically idealized and refined using a riding model. In all cases non-coordinated solvent molecules were refined anisotropically with the help of ADP and distances restraints. The fact that the very small crystals of [(**7**)CuCl]$_2$Cl$_2$ diffracted weakly and the presence of highly disordered solvent molecules do not permit the structure to be discussed in detail. We have limited the discussion to the main features of the complex. [(**7**)CuCl]$_2$Cl$_2$ crystallizes in the monoclinic space group $C2/c$ with the cell parameters: a = 26.020(11), b = 10.363(5), c = 29.498(13) Å and β = 114.20(1)°. Crystallographic data for the structures reported in this paper have been deposited with the Cambridge Crystallographic Data Centre: CCDC-187474 {bis[(**1**)Cu][BF_4]$_2$}, -187475 {[(**3**)CuCl]$_2$Cl$_2$}, -187476 [(**1**)ZnCl$_2$]. Copies of the data can be obtained, free of charge, on application to CCDC, 12 Union Road, Cambridge CB2 1EZ, U.K. [Fax: (internat.) + 44-1223/336-033, E-mail: deposit@ccdc.cam.ac.uk].

Electrochemistry: Electrochemical measurements were carried with a custom-made potentiostat, using the interrupt method to minimize the uncompensated resistance (IR) drop.[50] Electrochemical experiments were performed at room temperature in an air-tight three-electrode cell connected to a vacuum argon/N_2 line. The reference electrode consisted of a saturated calomel electrode (SCE) separated from the solutions by a bridge compartment. The counter-electrode was a spiral of ca. 1 cm^2 apparent surface area, made of Pt wire 8 cm long and 0.5 mm in diameter. Cyclic voltammetry was conducted with a Pt (1 mm) working electrode in the potential range of −600 to +600 mV. The supporting electrolyte was KCl (Prolabo RP, Normapur) and was used as received. All solutions measured were 1 mM in complex and 0.1 M in supporting electrolyte. All experiments were conducted in water under argon. Stock solutions (2 mM) of ligand·$CuCl_2$ were prepared in water.

DNA Cleavage Experiments: The desired complex [4 μM, 5 μL, metallations carried out at 1 mM $CuCl_2$ concentration with 1 equiv. of ligand in DMF/water (1:1) for 4 h at room temperature before dilution of the complex with water to 4 μM] was added to ΦX174 (10 μL, 7 nM, 40 μM in bp) in sodium phosphate buffer (80 mM, pH = 7.2), NaCl (100 mM), and $MgCl_2$ (20 mM). After 30 min at room temperature, cleavage was initiated by addition of an aqueous solution of MPA (5 μL, 20 mM) and samples were incubated for 1 h at 37 °C. A solution of 7.5 μL of 50% (v/v) glycerol/40 mM Tris·Cl buffer (pH = 8)/0.05% bromophenol blue (w/v) was then added and samples were immediately loaded onto agarose gel (0.8%) containing 1 μg/mL of ethidium bromide. Electrophoresis was run at constant current (25 mA for 15 h) in TBE buffer. Bands were located by UV light (254 nm), photographed, and quantified by microdensity. The correction coefficient 1.47 was used for the decreased stainability of form I DNA vs. forms II and III.[41] When only forms I and II were present, the average number of single-strand scissions per DNA phage, S, was considered to be equal to

Table 7. Crystal structure data for bis-[(**1**)Cu][BF_4]$_2$, [(**3**)CuCl]$_2$Cl$_2$, and (**1**)ZnCl$_2$

	bis[(**1**)Cu][BF_4]$_2$	[(**3**)CuCl]$_2$Cl$_2$	(**1**)ZnCl$_2$
Empirical ormula	$[C_{54}H_{40}Cu_2N_{10}O_4][BF_4]_2$, C_3H_7NO, H_2O, 4 CH_4O, 0.8 CH_2Cl_2	$C_{26}H_{18}CuCl_2N_4O_2$· 4.75 H_2O	$C_{27}H_{21}Cl_2N_5O_2Zn$· 3 C_2H_6OS
Formula mass [g·mol^{-1}]	1647.8	638.46	818.14
Temperature [K]	180(2)	173(2)	193(2)
Crystal system	monoclinic	triclinic	triclinic
Space group	$P2/c$	$P\bar{1}$	$P\bar{1}$
a [Å]	11.141(5)	13.3616(10)	8.8789(10)
b [Å]	15.632(5)	14.2053(10)	14.7728(16)
c [Å]	21.496(5)	15.5438(11)	15.2291(16)
α [°]	90	80.81(10)	88.52(2)
β [°]	99.224(5)	87.56(10)	76.15(2)
γ [°]	90	68.48(10)	76.78(2)
Volume [Å^3]	3695(2)	2709.03(3)	1887.2(4)
Z	4	4	2
$D_{calcd.}$ [Mg/m^3]	1.481	1.565	1.440
Abs. coeff. [mm^{-1}]	0.736	1.056	1.004
Crystal size [mm]	0.25 × 0.30 × 0.42	0.05 × 0.1 × 0.6	0.05 × 0.1 × 0.1
F(000)	1666	1314	848
θ range [°]	1.45−24.2	1.33−24.71	1.38−28.28
Reflections collected/R(int)	16839/0.0499	15804/0.0275	19529/0.0832
Completeness to θ (%)	98.6	98.6	99.3
Absortion correction	numerical	semi-empirical	none
Max./min. transmission	0.80/0.41	1.00/0.78	−
Data/restraints/parameters	3306/326/592	9132/704/895	9313/114/489
Goodness-of-fit on F^2	1.486	1.022	1.038
R_1 [$I > 2\sigma(I)$]	0.1052	0.0491	0.0412
$wR2$ (all data)	0.3161	0.1487	0.1144
Largest diff. peak/hole [e·Å^{-3}]	1.058/−0.972	1.065/−0.749	1.096/−0.640

−ln(fraction of form I) according to a Poisson distribution. In case of the presence of the form III, the number of single-strand breaks per ΦX174 DNA molecule was calculated according to the equation: $I + II = \{1 - [S\cdot(2h + 1)/2L]\}^{S/2}$;[41,42] the (I + II) value is the percentage of form I and II, L is the number of DNA base pairs in ΦX174 (5386 bp), and h is the distance between nicks on opposite strands needed to produce a linear molecule. A value h = 16 bp previously proposed in ref.[42] was used since it allowed a good linearity of S as a function of the concentration of copper complexes of Clip-Phen derivatives.

Acknowledgments

The authors thank Catherine Claparols, Alain Mari, and Dominique de Montauzon for mass, magnetic, and electrochemical data, respectively.

[1] J.-M. Lehn, *Supramolecular Chemistry*, VCH, Weinheim, **1995**.
[2] M. Albrecht, *Chem. Rev.* **2001**, *101*, 3457−3497.
[3] V. Amendola, L. Fabbrizzi, P. Pallavicini, *Coord. Chem. Rev.* **2001**, *216/217*, 435−448.
[4] V. Balzani, A. Credi, F. M. Raymo, J. F. Stoddart, *Angew. Chem. Int. Ed.* **2000**, *39*, 3348−3391.
[5] F. M. Mac Donnel, M.-J. Kim, S. Bodige, *Coord. Chem. Rev.* **1999**, *185/186*, 535−549.
[6] K. Matyjaszewski, *Chem. Eur. J.* **1999**, *5*, 3095−3102.
[7] J.-P. Sauvage, *Acc. Chem. Res.* **1998**, *31*, 611−619.
[8] P. L. Boulas, M. Gomez-Kaifer, L. Echegoyen, *Angew. Chem. Int. Ed.* **1998**, *37*, 216−247.
[9] C. Piguet, G. Bernardinelli, G. Hopfgartner, *Chem. Rev.* **1997**, *97*, 2005−2062.
[10] B. Linton, A. D. Hamilton, *Chem. Rev.* **1997**, *97*, 1669−1680.
[11] V. Balzani, A. Juris, M. Venturi, *Chem. Rev.* **1996**, *96*, 759−833.
[12] P. G. Sammes, G. Yahioglu, *Chem. Soc. Rev.* **1994**, 237−334.
[13] D. S. Sigman, A. Mazunder, D. M. Perrin, *Chem. Rev.* **1993**, *93*, 2295−2316.
[14] C.-H. B. Chen, L. Milne, R. Landgraf, D. M. Perrin, D. S. Sigman, *ChemBioChem* **2001**, *2*, 735−740.
[15] B. Meunier (Ed.), *DNA and RNA Cleavers and Chemotherapy of Cancer and Viral Diseases*, Kluwer, Dordrecht, **1996**.
[16] G. Pratviel, J. Bernadou, B. Meunier, *Angew. Chem. Int. Ed. Engl.* **1995**, *34*, 746−769.
[17] D. R. Mc Millin, K. Mc Nett, *Chem. Rev.* **1998**, *98*, 1201−1219.
[18] W. K. Pogozelski, T. D. Tullius, *Chem. Rev.* **1998**, *98*, 1089−1107.
[19] J. Gallagher, C.-H. B. Chen, C. Q. Pan, D. M. Perrin, Y.-M. Cho, D. S. Sigman, *Bioconjugate Chem.* **1996**, *7*, 413−420.
[20] L. E. Marshall, D. R. Graham, K. A Reich, D. S. Sigman, *Biochemistry* **1981**, *20*, 244−250.
[21] J. M. Veal, K. Merchant, R. L. Rill, *Biochemistry* **1991**, *30*, 1132−1140.
[22] B. R. James, R. J. P Williams, *J. Chem. Soc.* **1961**, 2007−2019.
[23] M. Pitié, B. Donnadieu, B. Meunier, *Inorg. Chem.* **1998**, *37*, 3486−3489.
[24] M. Pitié, B. Sudres, B. Meunier, *Chem. Commun.* **1998**, 2597−2598.
[25] M. Pitié, C. J. Burrows, B. Meunier, *Nucleic Acids Res.* **2000**, *28*, 4856−4864.
[26] M. Pitié, J. D. van Horn, D. Brion, C. J. Burrows, B. Meunier, *Bioconjugate Chem.* **2000**, *11*, 892−900.
[27] M. Pitié, B. Meunier, *Bioconjugate Chem.* **1998**, *9*, 604−611.
[28] S. A. Ross, M. Pitié, B. Meunier, *Eur. J. Inorg. Chem.* **1999**, 557.
[29] C. A. Claussen, E. C. Long, *Chem. Rev.* **1999**, *99*, 2797−2816.
[30] M. Burger, *Chem. Rev.* **1998**, *98*, 1153−1169.
[31] P. M. Bush, J. P. Whitehead, C. C. Pink, E. C. Gramm, J. L. Eglin, S. P. Watton, L. E. Pence, *Inorg. Chem.* **2001**, *40*, 1871−1877; and references therein.
[32] Y. Yao, M. W. Perkovic, D. P. Rillema, C. Woods, *Inorg. Chem.* **1992**, *31*, 3956−3962.
[33] M. Satterfield, J. S. Brodbelt, *Inorg. Chem.* **2001**, *40*, 5393−5400.
[34] C. O. Dietrich-Buchecker, J.-P. Sauvage, *Angew. Chem. Int. Ed. Engl.* **1989**, *28*, 189−192.
[35] I. Meistermann, V. Moreno, M. J. Prieto, E. Moldrheim, E. Sletten, S. Khalid, P. M. Rodger, J. C. Peberdy, C. J. Isaac, A. Rodger, M. J. Hannon, *Proc. Natl. Acad. Sci. U. S. A.* **2002**, *99*, 5069−5074.
[36] M. J. Hannon, V. Moreno, M. J. Prieto, E. Moldrheim, E. Sletten, K. J. Sanders, A. Rodger, *Angew. Chem. Int. Ed.* **2001**, *40*, 880−884.
[37] D. A. Bardwell, A. M. W. Cargill Thompson, J. C. Jeffrery, E. E. M. Tilley, M. D. Ward, *J. Chem. Soc., Dalton Trans.* **1995**, 835−841; and reeferences therein.
[38] D. V. Scaltrito, D. W. Thompson, J. A. O'Callaghan, G. J. Meyer, *Coord. Chem. Rev.* **2000**, *208*, 243−266.
[39] M.-T. Youinou, R. Ziessel, J.-M. Lehn, *Inorg. Chem.* **1991**, *30*, 2144−2148.
[40] E. C. Constable, M. J. Hannon, D. A. Tocher, *J. Chem. Soc., Dalton Trans.* **1993**, 1883−1890.
[41] J. Bernadou, G. Pratviel, F. Bennis, M. Girardet, B. Meunier, *Biochemistry* **1989**, *28*, 7268−7275.
[42] D. Freifelder, B. Trumbo, *Biopolymers* **1969**, *7*, 681−693.
[43] J. Lewis, T. D. O'Donoghue, *J. Chem. Soc., Dalton Trans.* **1980**, 736−742.
[44] D. Tzalis, Y. Tor, F. Salvatorre, S. Failla, J. S. Siegel, *Tetrahedron Lett.* **1995**, *36*, 3489−3490.
[45] C. Boldron, M. Pitié, B. Meunier, *Synlett* **2001**, *10*, 1629−1631.
[46] A. Altomare, G. Cascarano, C. Giacovazzo, A. Guagliardi, *J. Appl. Crystallogr.* **1993**, *26*, 343−350.
[47] A. Altomare, M. C. Burla, M. Camalli, M. Cascarano, C. Giacovazzo, A. Guagliardi, A. G. G. Moliterni, G. Polidori, R. Spagna, *J. Appl. Crystallogr.* **1999**, *32*, 115−119.
[48] G.M. Sheldrick, *Acta Crystallogr., Sect. A* **1990**, *46*, 467.
[49] G.M. Sheldrick, *SHELXL-97*, Program for Crystal Structure Refinement, Universität Göttingen, **1997**.
[50] P. Cassoux, R. Dartiguepeyron, C. David, D. de Montauzon, J. B. Tommasino, P.-L. Fabre, *Actual. Chim.* **1994**, *1*, 49.

Received June 17, 2002
[I02317]

Ground Spin State Variation in Carboxylate-Bridged Tetranuclear $[Fe_2Mn_2O_2]^{8+}$ Cores and a Comparison with Their $[Fe_4O_2]^{8+}$ and $[Mn_4O_2]^{8+}$ Congeners

Phalguni Chaudhuri,*[a] Eva Rentschler,[a] Frank Birkelbach,[a] Carsten Krebs,[a] Eckhard Bill,[a] Thomas Weyhermüller,[a] and Ulrich Flörke[b]

Keywords: Oxo ligands / Carboxylate ligands / Iron / Manganese / Magnetic properties / Tetranuclear complexes

Syntheses of ten new tetranuclear complexes containing the $[M_A(\mu_3\text{-}O)_2M_B]^{8+}$ butterfly core [$M_A = M_B = Fe^{III}$ (**1** and **2**), $M_A = M_B = Mn^{III}$ (**3** and **4**) and $M_A = Fe^{III}$, $M_B = Mn^{III}$ (**5**–**10**)] using 1,4,7-trimethyl-1,4,7-triazacyclononane (L) as the capping ligand, salicylaldoximato dianion ($salox^{2-}$) and six different carboxylate anions as bridging ligands, are described. The crystal structures of $[L_2Fe_2(\mu_3\text{-}O)_2(salox)_2(diphenylglycolate)_3Fe_2](ClO_4)$ (**1**), $[L_2Mn_2(\mu_3\text{-}O)_2(salox)_2(diphenylglycolate)_3Mn_2](ClO_4)$ (**3**), $[L_2Fe_2(\mu_3\text{-}O)_2(salox)_2(acetate)_3Mn_2](ClO_4)$ (**5**), $[L_2Fe_2(\mu_3\text{-}O)_2(salox)_2(diphenylglycolate)_3Mn_2](ClO_4)$ (**6**), and $[L_2Fe_2(\mu_3\text{-}O)_2(salox)_2(benzoate)_3Mn_2](ClO_4)$ (**8**) were determined by X-ray crystallography. The complexes are isostructural, with M^{III} ions disposed in a butterfly core where bridging between the M^{III} ions occurs via two μ_3-oxo anions. In complexes **5**, **6** and **8** the "wing-tip" positions of the butterfly are occupied by the LFe^{3+} units, whereas the "body" metal ions are d^4 high-spin Mn^{III} ions. Complexes **1**–**10** have been characterised by variable-temperature (2–290 K) magnetic susceptibility measurements (1 T) and by Mössbauer spectroscopy. A "2*J*" model has been applied to simulate the experimental μ_{eff} vs. *T* plots. Overall exchange interactions are antiferromagnetic in nature. Complexes with the Fe_4O_2 core (**1** and **2**) and the Mn_4O_2 core (**3** and **4**) possess an $S_t = 0$ and $S_t = 3$ ground state, respectively, regardless of the nature of the bridging carboxylate ligand. In contrast, changing the bridging carboxylates in the $[Fe_2Mn_2O_2]$ core from acetate (**5**) to diphenylglycolate (**6**), triphenyl acetate (**7**), benzoate (**8**), chloroacetate (**9**) and propionate (**10**), results in a variation of the ground state from $S_t = 1$ to $S_t = 3$, due to spin frustration of the "body" manganese centres. The spin-correlation diagram for the $Fe_2Mn_2O_2$ butterfly arrangement clearly demonstrates the ground state variation as a function of the ratio of two competing coupling interactions.
(© Wiley-VCH Verlag GmbH & Co. KGaA, 69451 Weinheim, Germany, 2003)

Introduction

Tetranuclear, oxide-bridged metal carboxylate assemblies are relevant to several areas including bioinorganic modelling and magnetochemistry. In the field of iron chemistry, the pursuit of model complexes for the iron proteins has yielded several interesting tetranuclear complexes[1–6] amongst other polynuclear iron complexes with unusual electronic structures.[7] The knowledge that in PSII the site of water oxidation is a tetranuclear manganese aggregate[8] in which four manganese atoms are essential for activity and appear to be in close proximity to one another, has augmented the search for tetranuclear manganese complexes. Thus, tetramanganese butterfly[6,9–12] complexes with the $[Mn_4O_2]^{8+}$ core have emerged as the most intensely studied oxide-bridged carboxylate clusters. Comparatively fewer studies of the butterfly $[Fe_4O_2]^{8+}$ core have been made, and there are relatively few studies of the analogous heterometallic butterfly complexes,[13,14] despite the fact that such studies might be more informative in comparison to those of homometal complexes. New exchange pathways can be expected for heteronuclear complexes,[15–18] where unusual sets of magnetic orbitals can be brought into close proximity.

There are several intriguing features associated with oxo-bridged carboxylate clusters. Firstly, these complexes can have unusual electronic structures and may serve as sources of fundamental information about exchange coupling in multinuclear assemblies. A second general reason to study polynuclear metal complexes is that they may be building blocks for molecular-based magnetic materials.[19] Because of their topology, molecules that have large numbers of unpaired electrons should serve as good starting points for constructing molecular magnetic materials. Even though the pairwise exchange interactions in these complexes are found almost always to be antiferromagnetic, spin frustration[20,21] in the general sense of the term, or more accurately, competing spin interactions, can result in polynuclear complexes having a relatively large number of unpaired

[a] Max-Planck-Institut für Strahlenchemie,
Stiftstraße 34–36, 45470 Mülheim an der Ruhr, Germany
E-mail: Chaudh@mpi-muelheim.mpg.de
[b] Anorganische und Analytische Chemie, Universität Paderborn, 33095 Paderborn, Germany

electrons in their ground states. Although spin frustration is a well-known magnetic phenomenon for extended lattices, its application to the magnetochemistry of discrete polynuclear complexes is not widely recognised. Competing spin interactions may give rise to unpredictable ground state spins and peculiar spin state spectra. Thus, the situation of ground state degeneracy induced by competing spin interactions is worth investigating.

We have been exploring the feasibility of using salicylaldoxime to influence the nuclearity and metal topology of metal carboxylate complexes. Although salicylaldoxime[22] has been known as a metal-chelating agent since 1930, reports on the ligating properties of salicylaldoxime towards trivalent transition metal ions are rare.[23,24] Our approach of using oximes as ligands has yielded several interesting 3d metal complexes with the cores $[M_A(oxime)_3M_B]^{n+}$,[24] $[M^{III}_3(\mu_3\text{-}O)(\mu_2\text{-}OPh)]^{6+}$ (M = Ti, V, Cr, Mn, Fe and Co),[25,26] $[M^{III}_6(\mu_3\text{-}O)_2(\mu_2\text{-}OOCR)_2]^{12+}$ (M = V, Cr, Mn, Fe)[27] and $[(M^{III}_A)_2(\mu_3\text{-}O)_2(M^{III}_B)_2]^{8+}$ ($M_A = M_B = Fe^{III}$;[4] $M_A = Cr^{III}$, $M_B = Fe^{III}$;[13] $M_A = Cr^{III}$, $M_B = Mn^{III}$).[14] In this paper we report the extension of our studies to complexes having tetranuclear cores, and include the preparation and characterisation of $[L_2Fe_4(\mu_3\text{-}O)_2(\mu_2\text{-}OOCC(OH)Ph_2]_3(salox)_2]\text{-}ClO_4$ (**1**), $[L_2Fe_4(\mu_3\text{-}O)_2(\mu_2\text{-}OOCCPh_3)_3(salox)_2]ClO_4$ (**2**), $[L_2Mn_4(\mu_3\text{-}O)_2(\mu_2\text{-}OOCC(OH)Ph_2]_3(salox)_2]ClO_4$ (**3**), $[L_2Mn_4(\mu_3\text{-}O)_2(\mu_2\text{-}OOCCPh_3)_3(salox)_2]ClO_4$ (**4**) and $[L_2Fe_2Mn_2(\mu_3\text{-}O)_2(\mu_2\text{-carboxylate})_3(salox)_2]ClO_4$ (**5**−**10**) [carboxylate = acetate (**5**), benzilate (diphenylglycolate) (**6**), triphenylacetate (**7**), benzoate (**8**), chloroacetate (**9**) and propionate (**10**)], where L is the cyclic amine 1,4,7-trimethyl-1,4,7-triazacyclononane and salox is the dianion of salicylaldoxime (H_2salox). Molecules **1**−**10** contain M^{III} ions disposed in a butterfly $[M_4O_2]^{8+}$ core, where bridging between the M^{III} ions occurs via two μ_3-oxo anions.

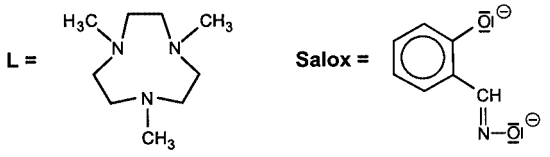

Results

Our previous investigations of the use of solvolysis reactivity of $[LFeCl_3]$[28] in the synthesis of homo- and heteropolynuclear complexes led us to anticipate compounds with a butterfly structure, in which the "body" metal ions differ from the "wing-tip" (Fe^{3+}) ions. The fact that the iron centres remain bonded to the macrocyclic ligand L during the formation of the polynuclear complexes was recognised and subsequently utilised as a synthetic strategy for building $Fe_2(O)_2Mn_2$ cores with Mn^{3+} as the "body" ions. Accordingly, the dark brown solution obtained from manganese(II) chloride, a carboxylic acid, salicylaldehyde oxime and triethylamine in methanol reacted with $[LFeCl_3]$ to afford, after addition of a perchlorate solution, dark brown crystals of $[L_2Fe_2(\mu_3\text{-}O)_2(\mu\text{-carboxylate})_3(salox)_2Mn_2]ClO_4$ in reasonable yield. Complex **5** was prepared by using Mn^{III} acetate.

The IR spectra of the tetranuclear complexes **1**−**10** exhibit, besides ligand and ClO_4 absorptions, a sharp medium-intensity band in the region 670−660 cm^{-1}, probably due to the ν_{asym} vibration of the four modes of the $FeMn_2(\mu_3\text{-}O)$ triangle.[29] The ν(CN) vibration is assigned to the medium-intensity band at ca. 1600 cm^{-1}. One of the characteristics in the IR spectra is a strong carboxyl stretching vibration found in the region 1550−1580 cm^{-1}. The complexes show a strong band, whose intensity is similar to that of ν(COO), at ca. 1090 cm^{-1} (antisymmetric stretch) and a sharp band at ca. 620 cm^{-1} (antisymmetric bend), indicative of uncoordinated perchlorate anions.

Interestingly, the mass spectra of complexes **1**−**7** differ widely. Although the all-iron complexes **1** and **2** show signals due to the respective monocations $[M^+]$ with the expected isotope distributions in the ESI positive mode, the manganese compound **3** does not show the corresponding molecular ion. However, in the case of the mixed-metal complexes **5**−**7**, mass spectrometry in the ESI-positive mode has proved to be a very useful tool for characterisation.

Structures of Complexs 1 and 3

Figure 1 shows a perspective view of the cation of **1**. Although this complex contains an $[Fe_4(\mu\text{-diphenylglycolate})_3(\mu_3\text{-oxo})_2]$ core very similar to that in the previously reported $[Fe_4(\mu\text{-acetato})_3(\mu_3\text{-oxo})_2]$ complex,[4] we have included the description of the structure of **1** in this paper to show that the OH groups of the diphenylglycolate ligands are not coordinated to the oxophilic Fe^{III} centres. It should also be noted that there are very few tetranuclear Fe^{III} complexes with the $[Fe_4O_2]^{8+}$ butterfly core reported

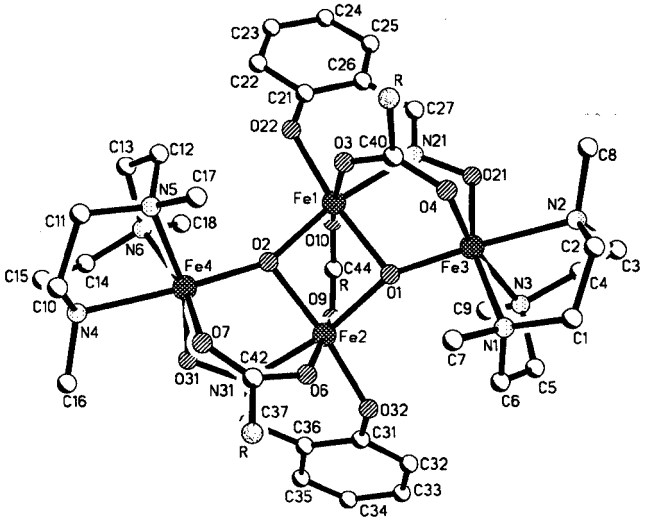

Figure 1. Structure of the monocation of complex **1**; the bridging diphenylglycolate (benzilate) anions are denoted by $RCOO^-$, i.e. "$Ph_2C(OH)$" has been replaced by "R" for clarity

Table 1. Selected bond lengths [Å] and angles [°] for **1**

Fe(1)−O(22)	1.906(7)	Fe(1)−O(2)	1.949(7)
Fe(1)−O(1)	1.988(6)	Fe(1)−O(3)	2.109(6)
Fe(1)−O(10)	2.111(9)	Fe(1)−N(21)	2.115(10)
		Fe(2)−O(32)	1.910(8)
Fe(2)−O(1)	1.949(7)	Fe(2)−O(2)	1.981(7)
Fe(2)−N(31)	2.112(10)	Fe(2)−O(9)	2.130(6)
Fe(2)−O(6)	2.140(7)	Fe(3)−O(1)	1.874(7)
Fe(3)−O(21)	1.926(6)	Fe(3)−O(4)	2.031(10)
Fe(3)−N(3)	2.167(12)	Fe(3)−N(1)	2.204(11)
Fe(3)−N(2)	2.267(11)	Fe(4)−O(2)	1.872(7)
Fe(4)−O(31)	1.928(8)	Fe(4)−O(7)	2.039(8)
Fe(4)−N(6)	2.171(10)	Fe(4)−N(5)	2.217(10)
Fe(4)−N(4)	2.294(10)		
O(22)-Fe(1)−O(2)	104.2(3)	O(22)-Fe(1)−O(1)	172.6(3)
O(2)−Fe(1)−O(1)	83.0(3)	O(22)-Fe(1)−O(3)	87.4(3)
O(2)−Fe(1)−O(3)	96.8(3)	O(1)−Fe(1)−O(3)	90.3(3)
O(22)−Fe(1)−O(10)	84.8(3)	O(2)−Fe(1)−O(10)	94.7(3)
O(1)−Fe(1)−O(10)	96.2(3)	O(3)−Fe(1)−O(10)	167.4(3)
O(22)−Fe(1)−N(21)	85.3(4)	O(2)−Fe(1)−N(21)	169.5(3)
O(1)−Fe(1)−N(21)	87.6(3)	O(3)−Fe(1)−N(21)	88.1(4)
O(10)−Fe(1)−N(21)	81.4(4)	O(22)-Fe(1)−Fe(2)	144.0(3)
O(2)−Fe(1)−Fe(2)	44.1(2)	O(1)−Fe(1)−Fe(2)	43.3(2)
O(3)−Fe(1)−Fe(2)	109.7(2)	O(10)−Fe(1)−Fe(2)	82.2(2)
N(21)−Fe(1)−Fe(2)	125.4(3)	O(32)−Fe(2)−O(1)	104.0(3)
O(32)−Fe(2)−O(2)	172.8(3)	O(1)−Fe(2)−O(2)	33.2(3)
O(32)−Fe(2)−N(31)	86.3(4)	O(1)−Fe(2)−N(31)	166.5(3)
O(2)−Fe(2)−N(31)	86.5(3)	O(32)−Fe(2)−O(9)	83.9(4)
O(1)−Fe(2)−O(9)	92.3(3)	O(2)−Fe(2)−O(9)	95.3(3)
N(31)−Fe(2)−O(9)	79.9(4)	O(32)−Fe(2)−O(6)	88.0(3)
O(1)−Fe(2)−O(6)	99.8(3)	O(2)−Fe(2)−O(6)	91.3(3)
N(31)−Fe(2)−O(6)	89.1(3)	O(9)−Fe(2)−O(6)	166.8(3)
O(32)−Fe(2)−Fe(1)	143.1(2)	O(1)−Fe(2)−Fe(1)	44.4(2)
O(2)−Fe(2)−Fe(1)	43.2(2)	N(31)−Fe(2)−Fe(1)	122.7(2)
O(9)−Fe(2)−Fe(1)	80.0(2)	O(6)−Fe(2)−Fe(1)	112.4(2)
O(1)−Fe(3)−O(21)	96.4(3)	O(1)−Fe(3)−O(4)	97.4(3)
O(21)−Fe(3)−O(4)	92.4(4)	O(1)−Fe(3)−N(3)	96.8(4)
O(21)−Fe(3)−N(3)	92.7(4)	O(4)−Fe(3)−N(3)	164.3(4)
O(1)−Fe(3)−N(4)	100.5(4)	O(21)−Fe(3)−N(1)	162.6(4)
O(4)−Fe(3)−N(1)	89.6(5)	N(3)−Fe(3)−N(1)	81.2(5)
O(1)−Fe(3)−N(2)	176.0(4)	O(21)−Fe(3)−N(2)	85.5(4)
O(4)−Fe(3)−N(2)	86.1(5)	N(3)−Fe(3)−N(2)	79.6(5)
N(1)−Fe(3)−N(2)	77.5(4)	O(2)−Fe(4)−O(31)	95.7(3)
O(2)−Fe(4)−O(7)	98.2(3)	O(31)−Fe(4)−O(7)	91.8(3)
O(2)−Fe(4)−N(6)	96.4(3)	O(31)−Fe(4)−N(6)	95.3(4)
O(7)−Fe(4)−N(6)	163.0(4)	O(2)−Fe(4)−N(5)	100.5(3)
O(31)−Fe(4)−N(5)	163.7(4)	O(7)−Fe(4)−N(5)	87.5(4)
N(6)−Fe(4)−N(5)	81.3(4)	O(2)−Fe(4)−N(4)	176.2(3)
O(31)−Fe(4)−N(4)	86.3(4)	O(7)−Fe(4)−N(4)	85.0(4)
N(6)−Fe(4)−N(4)	80.1(4)	N(5)−Fe(4)−N(4)	77.4(4)
Fe(3)−O(1)−Fe(2)	155.8(4)	Fe(3)−O(1)−Fe(1)	111.7(3)
Fe(2)−O(1)−Fe(1)	92.4(3)	Fe(4)−O(2)−Fe(1)	155.5(4)
Fe(4)−O(2)−Fe(2)	111.8(3)	Fe(1)−O(2)−Fe(2)	92.6(3)
Fe(1)···Fe(2)	2.841(2)	Fe(2)···Fe(3)	3.738(2)
Fe(1)···Fe(3)	3.197(2)	Fe(2)···Fe(4)	3.192(2)
Fe(1)···Fe(4)	3.734(2)	Fe(3)···Fe(4)	6.077(2)

in the literature.[1−6] The metal geometry of the cluster may be described as "butterfly" based on two edge-sharing $Fe_3(\mu_3\text{-O})$ triangular units, with the oxygen atoms O(1) (0.029 Å) and O(2) (0.004 Å) above the corresponding Fe_3 triangles. The Fe(1)···Fe(2) distance [2.841(2) Å] is at the low end of the range (2.829−3.108 Å) observed in other $[Fe_4O_2]$-containing compounds.[1−6] There are three types of independent Fe−O(oxo) distances, ranging from 1.872 to 1.988 Å, the two shortest being Fe(4)−O(2) [1.872(7) Å] and Fe(3)−O(1) [1.874(7) Å].

The dihedral angle between the planes Fe(1)Fe(2)Fe(3)O(1) and Fe(1)Fe(2)Fe(4)O(2) is 145.9°, which is slightly smaller than that in the corresponding acetate complex (153.9°). Selected bond lengths and angles for the $Fe_4(\mu_3\text{-O})_2$ core and for the rest of the cation are given in Table 1.

In addition to the two μ_3-oxo groups, there are three bridging carboxylate groups in the tetranuclear structure originating from the diphenylglycolate ion, one each between iron atom pairs Fe(4)Fe(2), Fe(1)Fe(2) and Fe(1)Fe(3). Additionally two N−O groups of the deprotonated salicylaldoximes are coordinated to iron atom pairs Fe(4)Fe(2) and Fe(3)Fe(1) through their oxygen and nitrogen donor atoms, respectively.

It should be noted that the enolic OH group of diphenylglycolic acid is not coordinated to any iron centre. It seems that the nonplanarity of the $[Fe_4O_2]^{8+}$ unit is a consequence of the bridging carboxylate (diphenylglycolate) groups. Specifically, the carboxylate-bridged iron atoms are apparently "pulled" closer to one another [Fe(1)···Fe(3) = 3.197(2) Å, Fe(2)···Fe(4) = 3.192(2) Å] than those without carboxylate bridging [Fe(1)···Fe(4) = 3.734(2) Å, Fe(2)···Fe(3) = 3.738(2) Å]. Just as there are two long and two short Fe···Fe separations, there are also two long [Fe(1)−O(1) = 1.988(6) Å, Fe(2)−O(2) = 1.981(7) Å] and two short [Fe(2)−O(1) = 1.949(7) Å, Fe(1)−O(2) = 1.949(7) Å] iron−μ_3-oxo bonds in the inner Fe(1)Fe(2)O(1)O(2) core.

Each iron atom is in a distorted octahedral environment, with Fe(1) and Fe(2) having an $FeNO_5$ and Fe(3) and Fe(4) an FeN_3O_3 coordination sphere, respectively. Fe−N and Fe−O bond lengths are typical of high-spin ferric complexes. The Fe−N bonds *trans* to the short Fe−μ_3-O bonds are noticeably longer than those *cis* to them, as observed

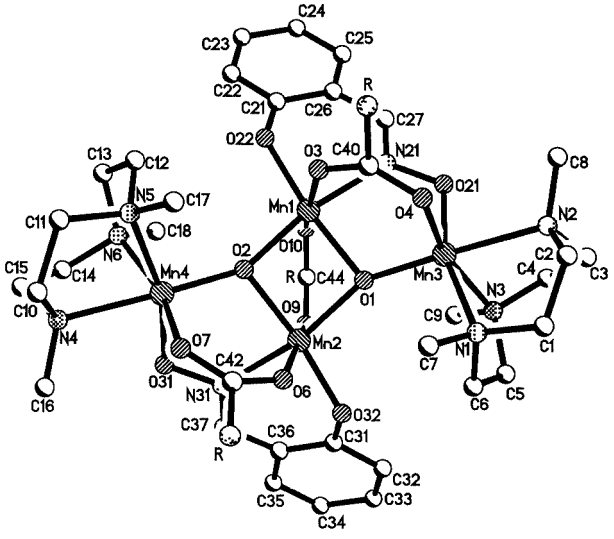

Figure 2. Perspective view of the cation of **3**; "$Ph_2C(OH)$" -units of the bridging diphenylglycolate (benzilate) anions are denoted only by "R" for the sake of clarity

earlier.[4] The structural parameters for **1** lie in the range reported for the other $[Fe_4O_2]^{8+}$ complexes.[1−6]

A perspective view of the cation of complex **3** is shown in Figure 2, and selected structural parameters are listed in Table 2. The cation, like that in **1**, possesses an M_4O_2 core which can be considered as two edge-sharing Mn_3O units, the metal dispositions being a butterfly structure with Mn(1) and Mn(2) occupying the "body" sites and Mn(3) and Mn(4) occupying "wing-tip" sites. Each body-wing-tip and body-body Mn_2 pair is bridged by a carboxylate group of the diphenylglycolate anion in its common *syn*,*syn* binding mode. The μ_3-O atoms O(1) and O(2) on each Mn_3 wing of the butterfly are 0.04 and 0.008 Å, respectively, above their Mn_3 least-squares planes. The dihedral angle between the planes comprising Mn(1)Mn(2)Mn(3)O(1) and Mn(1)Mn(2)Mn(4)O(2) is 145.8°, a value identical with that in the Fe_4O_2 core of **1**. The shortest Mn···Mn contact is 2.844(2) Å, between Mn(1) and Mn(2). The coordination spheres of "wing-tip" [Mn(4) and Mn(3)], and "body" [Mn(1) and Mn(2)] manganese ions are MnN_3O_3 and $MnNO_5$, respectively, in which the distortions along the axes O(3)Mn(1)O(10), O(6)Mn(2)O(9), N(2)Mn(3)O(1) and N(4)Mn(4)O(2) are as expected for Jahn−Teller-distorted high-spin d^4 ions in an octahedral geometry. The Mn−N and Mn−O bond lengths are consistent with a d^4 high-spin electronic configuration for the Mn^{III} centres. The essential features of the structure of the cation of **3** are very similar to those of **1.**

Table 2. Selected bond lengths [Å] and angles [°] for **3**

Mn(1)−O(22)	1.913(8)	Mn(2)−O(32)	1.904(8)
Mn(1)−O(2)	1.961(8)	Mn(2)−O(1)	1.959(8)
Mn(1)−O(1)	1.971(7)	Mn(2)−O(2)	1.966(8)
Mn(1)−O(10)	2.107(9)	Mn(2)−N(31)	2.101(10)
Mn(1)−N(21)	2.109(10)	Mn(2)−O(9)	2.116(9)
Mn(1)−O(3)	2.117(9)	Mn(2)−O(6)	2.125(9)
Mn(3)−O(1)	1.872(8)	Mn(4)−O(2)	1.869(8)
Mn(3)−O(21)	1.938(9)	Mn(4)−O(31)	1.926(8)
Mn(3)−O(4)	2.048(11)	Mn(4)−O(7)	2.048(9)
Mn(3)−N(3)	2.170(13)	Mn(4)−N(6)	2.167(11)
Mn(3)−N(1)	2.198(13)	Mn(4)−N(5)	2.221(11)
Mn(3)−N(2)	2.281(12)	Mn(4)−N(4)	2.267(11)
O(22)−Mn(1)−O(2)	103.9(3)	O(32)−Mn(2)−O(1)	104.5(4)
O(22)−Mn(1)−O(1)	173.0(3)	O(32)−Mn(2)−O(2)	172.4(4)
O(2)−Mn(1)−O(1)	82.9(3)	O(1)−Mn(2)−O(2)	83.1(3)
O(22)−Mn(1)−O(10)	85.1(4)	O(32)−Mn(2)−N(31)	86.0(4)
O(2)−Mn(1)−O(10)	94.8(3)	O(1)−Mn(2)−O(31)	166.0(4)
O(1)−Mn(1)−O(10)	96.5(4)	O(2)−Mn(2)−N(31)	86.5(4)
O(22)−Mn(1)−N(21)	86.1(4)	O(32)−Mn(2)−O(9)	83.8(4)
O(2)−Mn(1)−N(21)	169.1(4)	O(1)−Mn(2)−O(9)	91.6(4)
O(1)−Mn(1)−N(21)	87.4(4)	O(2)−Mn(2)−O(9)	95.5(4)
O(10)−Mn(1)−N(21)	81.5(4)	N(31)−Mn(2)−O(9)	80.2(4)
O(22)−Mn(1)−O(3)	86.4(3)	O(32)−Mn(2)−O(6)	87.6(4)
O(2)−Mn(1)−O(3)	96.8(3)	O(1)−Mn(2)−O(6)	100.6(3)
O(1)−Mn(1)−O(3)	90.9(3)	O(2)−Mn(2)−O(6)	91.6(3)
O(10)−Mn(1)−O(3)	166.9(3)	N(31)−Mn(2)−O(6)	88.9(4)
N(21)−Mn(1)−O(3)	88.1(4)	O(9)−Mn(2)−O(6)	166.5(4)
O(1)−Mn(3)−Mn(1)	34.8(2)	O(2)−Mn(4)−O(31)	95.4(4)
O(21)−Mn(3)−Mn(1)	67.5(3)	O(2)−Mn(4)−O(7)	98.2(3)
O(4)−Mn(3)−Mn(1)	80.4(3)	O(31)−Mn(4)−O(7)	91.7(4)
N(3)−Mn(3)−Mn(1)	117.6(5)	O(2)−Mn(4)−N(6)	96.7(4)
N(1)−Mn(3)−Mn(1)	129.8(4)	O(31)−Mn(4)−N(6)	95.5(4)
N(2)−Mn(3)−Mn(1)	147.3(3)	O(7)−Mn(4)−N(6)	162.7(4)
O(1)−Mn(3)−O(21)	95.9(4)	O(2)−Mn(4)−N(5)	100.7(4)
O(1)−Mn(3)−O(4)	98.6(4)	O(31)−Mn(4)−N(5)	163.8(4)
O(21)−Mn(3)−O(4)	92.7(4)	O(7)−Mn(4)−N(5)	87.7(4)
O(1)−Mn(3)−N(3)	97.8(5)	N(6)−Mn(4)−N(5)	81.0(5)
O(21)−Mn(3)−N(3)	93.0(5)	O(2)−Mn(4)−N(4)	177.3(4)
O(4)−Mn(3)−N(3)	161.9(5)	O(31)−Mn(4)−N(4)	85.5(4)
O(1)−Mn(3)−N(1)	101.1(4)	O(7)−Mn(4)−N(4)	84.3(4)
O(21)−Mn(3)−N(1)	162.5(4)	N(6)−Mn(4)−N(4)	80.7(4)
O(4)−Mn(3)−N(1)	88.5(6)	N(5)−Mn(4)−N(4)	78.4(4)
N(3)−Mn(3)−N(1)	81.1(6)	Mn(3)−O(1)−Mn(2)	154.8(4)
O(1)−Mn(3)−N(2)	177.4(5)	Mn(3)−O(1)−Mn(1)	112.3(4)
O(21)−Mn(3)−N(2)	85.0(4)	Mn(2)−O(1)−Mn(1)	92.7(3)
O(4)−Mn(3)−N(2)	83.7(5)	Mn(4)−O(2)−Mn(1)	154.8(4)
N(3)−Mn(3)−N(2)	79.7(6)	Mn(4)−O(2)−Mn(2)	112.3(4)
N(1)−Mn(3)−N(2)	77.8(5)	Mn(1)−O(2)−Mn(2)	92.8(3)
Mn(1)···Mn(2)	2.844(2)	Mn(2)···Mn(3)	3.738(2)
Mn(1)···Mn(3)	3.191(3)	Mn(2)···Mn(4)	3.186(2)
Mn(1)···Mn(4)	3.737(2)	Mn(3)···Mn(4)	6.070(2)

Structures of Complexes 5, 6 and 8

The molecular geometry and the atom-labelling scheme of the cation of **5** are shown in Figure 3. The structure consists of a discrete monocationic tetranuclear unit having a twofold rotation axis. Selected interatomic distances and angles are listed in Table 3. The cation possesses a "butterfly" $[Fe_2(\mu_3\text{-}O)_2Mn_2]$ core. Mn(1) and Mn(1a) occupy "body" positions, and Fe(1) and Fe(1a) occupy the "wing-tip" positions, with O(1) and O(1a) triply bridging each $FeMn_2$ wing. The structure can thus be considered as two edge-sharing $FeMn_2O$ triangular units with a dihedral angle of 145.1°. In contrast to the Mn_4O_2 complex **3**, O(1) lies significantly out (0.14 Å) of the $FeMn_2$ plane. In addition to the two μ_3-oxo groups, there are three bridging acetate groups in the tetranuclear structure, one each between the metal atom pairs Fe(1)Mn(1), Fe(1a)Mn(1a) and Mn(1)Mn(1a). Additionally, a salicylaldoximate dianion is

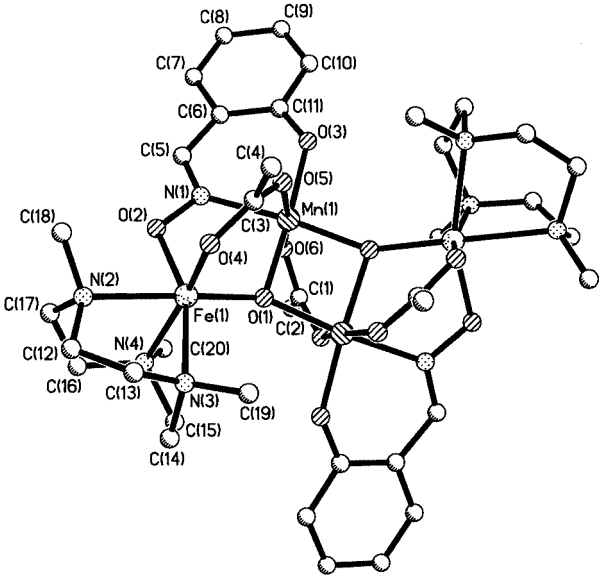

Figure 3. Molecular structure of the heterometal cation of **5**, showing the atom-numbering scheme

Table 3. Selected bond lengths [Å] and angles [°] for **5**

Fe(1)−O(1)	1.8795(13)
Fe(1)−O(2)	1.974(2)
Fe(1)−O(4)	1.989(2)
Fe(1)−N(4)	2.184(2)
Fe(1)−N(3)	2.230(2)
Fe(1)−N(2)	2.279(2)
Mn(1)−O(3)	1.897(2)
Mn(1)−O(1)#1	1.9343(13)
Mn(1)−O(1)	1.9397(14)
Mn(1)−N(1)	2.047(2)
Mn(1)−O(6)	2.160(2)
Mn(1)−O(5)	2.212(2)
O(1)−Fe(1)−O(2)	94.35(6)
O(1)−Fe(1)−O(4)	97.72(6)
O(2)−Fe(1)−O(4)	98.21(7)
O(1)−Fe(1)−N(4)	95.86(7)
O(2)−Fe(1)−N(4)	90.36(7)
O(4)−Fe(1)−N(4)	163.32(7)
O(1)−Fe(1)−N(3)	104.06(6)
O(2)−Fe(1)−N(3)	160.08(6)
O(4)−Fe(1)−N(3)	86.95(7)
N(4)−Fe(1)−N(3)	80.37(8)
O(1)−Fe(1)−N(2)	174.17(7)
O(2)−Fe(1)−N(2)	83.35(6)
O(4)−Fe(1)−N(2)	87.93(7)
N(4)−Fe(1)−N(2)	78.83(7)
N(3)−Fe(1)−N(2)	77.60(7)
O(3)−Mn(1)−O(1)#1	98.03(6)
O(3)−Mn(1)−O(1)	175.73(6)
O(1)#1−Mn(1)−O(1)	84.90(6)
O(3)−Mn(1)−N(1)	87.31(7)
O(1)#1−Mn(1)−N(1)	173.94(6)
O(1)−Mn(1)−N(1)	89.94(6)
O(3)−Mn(1)−O(6)	89.96(7)
O(1)#1−Mn(1)−O(6)	91.35(6)
O(1)−Mn(1)−O(6)	93.09(6)
N(1)−Mn(1)−O(6)	85.76(6)
O(3)−Mn(1)−O(5)	89.86(6)
O(1)#1−Mn(1)−O(5)	95.11(6)
O(1)−Mn(1)−O(5)	86.78(6)
N(1)−Mn(1)−O(5)	87.74(6)
O(6)−Mn(1)−O(5)	173.50(6)
O(3)−Mn(1)−Mn(1)#1	140.19(5)
O(1)#1−Mn(1)−Mn(1)#1	43.57(4)
O(1)−Mn(1)−Mn(1)#1	43.41(4)
N(1)−Mn(1)−Mn(1)#1	130.59(5)
O(6)−Mn(1)−Mn(1)#1	82.49(4)
O(5)−Mn(1)−Mn(1)#1	101.73(4)
Fe(1)−O(1)−Mn(1)#1	152.41(8)
Fe(1)−O(1)−Mn(1)	112.39(7)
Mn(1)#1−O(1)−Mn(1)	93.02(6)
Mn(1)···Mn(1a)	2.811(1)
Mn(1)···Fe(1)	3.174(1)
Fe(1)···Fe(1a)	6.022(1)
Fe(1)···Mn(1a)	3.704(1)

coordinated to Mn(1) through its phenolate oxygen atom O(3) and oxime nitrogen atom N(1), thus making Mn(1) six-coordinate. The X-ray structure clearly shows that the "body" metal ions are Jahn−Teller-distorted, high-spin d^4 Mn^{III} ions; the axially elongated sites are occupied by the carboxylate oxygen atoms of acetate, with Mn(1)−O(6) 2.160(2) Å, Mn(1)−O(5) 2.212(2) Å and O(5)−Mn(1)−O(6) 173.5°. Interestingly, the Mn(1)−O(1) distance [1.940(1) Å] is significantly shorter than the corresponding bond length in the analogous cation of **6**, but is similar to that in **8**.

The coordination geometry of the "wing-tip" ferric ion Fe(1) is distorted octahedral, with three nitrogen atoms from the facially coordinated tridentate macrocyclic amine (L) and three oxygen atoms [O(2) from the deprotonated oxime group, O(4) from the bridging acetate and O(1) from the μ_3-bridging oxo group], resulting in a *fac*-FeN_3O_3 coordination sphere. The Fe(1)−N(2) distance [2.279(2) Å] is significantly longer than the other Fe−N distances, due to the *trans* effect. The Fe−N (average 2.23 Å) and Fe−O (average 1.95 Å) distances are in agreement with a d^5 high-spin electronic configuration for the iron centres. The Fe(1)−μ_3-oxo distance [1.880(1) Å] is, as expected, the shortest amongst the metal−ligand bond lengths. The iron atom Fe(1) is displaced by 0.28 Å from the mean basal plane comprising N(3)N(4)O(2)O(4) toward the apical μ_3-oxygen atom O(1).

The structure of the cation of complex **6** is presented in Figure 4. The cation possesses an $Fe_2^{III}Mn_2^{III}(\mu_3\text{-}O)_2$ core very similar to those present in the Fe_4O_2 (**1**), Mn_4O_2 (**3**) and $Fe_2Mn_2O_2$ (**5** and **8**) core structures. The metal centres are thus disposed in a "butterfly" arrangement based on two edge-sharing $FeMn_2(\mu_3\text{-}O)$ triangular units, with the oxygen atoms O(1) and O(2) slightly above (0.07 Å) and below (0.02 Å) the Mn_2Fe triangle, as depicted below; note that the drawing is not meant to suggest a stepwise assembly process.

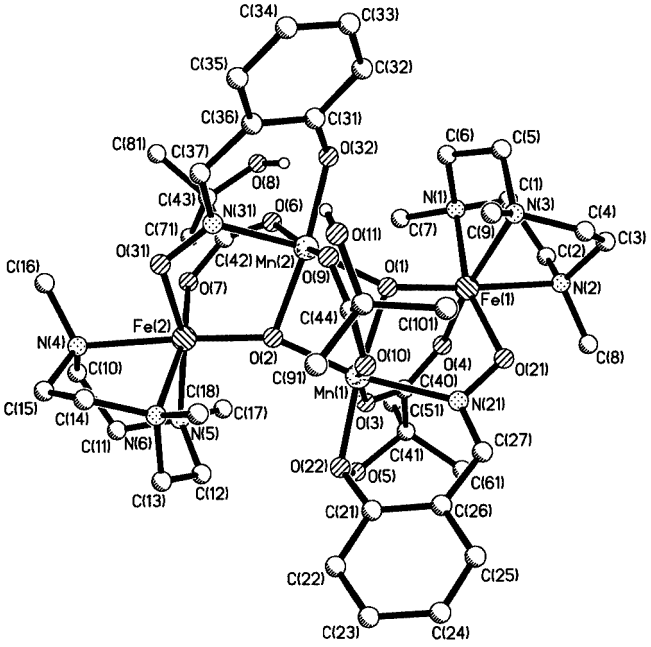

Figure 4. Structure of the tetranuclear monocation of **6**; phenyl rings (Ph) of the bridging diphenylglycolate (benzilate) $Ph_2C(OH)COO^-$ are denoted by C atoms

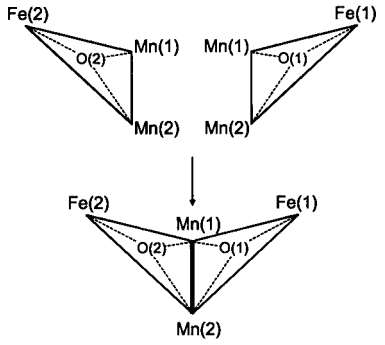

The dispositions of the μ_3-oxo groups are not completely symmetrical, but are consistent with all metal atoms being in the 3+ oxidation state. The dihedral angle between the planes Mn(1)Mn(2)Fe(2) and Mn(1)Mn(2)Fe(1) is 145.9°. Selected bond lengths and angles for the $Fe_2^{III}Mn_2^{III}O_2$ core and for the rest of the cation are given in Table 4. The "body" metal centres [Mn(1) and Mn(2)] show clear evidence of Jahn−Teller distortions, as expected for high-spin octahedral d^4 Mn^{III}, and the axially elongated sites are all occupied by carboxylate oxygen atoms of diphenylglycolic acid [O(3), O(10) for Mn(1) and O(6), O(9) for Mn(2)]. The hydroxy oxygen atoms of $(C_6H_5)_2C(OH)COO^-$ O(8), O(5) and O(11) are not coordinated to any of the metal centres. There are three types of independent Fe−O distances, ranging from 1.863(2) to 2.045(2) Å, with the shortest, as expected, being the Fe−μ_3-oxo distances Fe(1)−O(1) [1.863(2) Å] and Fe(2)−O(2) [1.876(2) Å]. The Fe−N distances *trans* to the μ_3-oxo groups [Fe(1)−N(2) = 2.268(3) Å, Fe(2)−N(4) = 2.270(2) Å] are longer than the other Fe−N distances, due to the *trans* effect. The coordination geometry of the "wing-tip" ferric ions, Fe(1) and Fe(2), is distorted octahedral, with three nitrogen atoms from the facially coordinated tridentate macrocyclic amine (L) and three oxygen atoms [O(31) or O(21) of the deprotonated oxime group, O(4) or O(7) of the bridging carboxylate and O(1) or O(2) of the μ_3-bridging oxo group] resulting in a *fac*-FeN_3O_3 coordination sphere. The Fe−N [average 2.20(6) Å] and Fe−O [average 1.95(6) Å] distances are similar to literature values[28] for high-spin Fe^{III} complexes with this macrocyclic amine. A deviation from the idealised octahedral geometry at the metal centre is found for the ligand L; the N−Fe−N angles range from 77.6 to 81.2°, whereas the O−Fe−O angles fall between 91.7 and 98.2°. The iron ions Fe(1) and Fe(2) are displaced by 0.28 Å from the mean basal planes comprising O(21)O(4)N(3)N(1) and N(5)N(6)O(7)O(31), respectively, toward the apical μ_3-oxygen atoms O(1) and O(2).

The "body" manganese ions, Mn(1) and Mn(2), are bridged by two oxo groups, O(2) and O(1). Each Mn is coordinated to three oxygen atoms [O(1), O(2) and phenolate O(22) or O(32)] and an imine nitrogen atom [N(21) or N(31)] of an oxime group in the basal plane. The carboxylate oxygen atoms O(3)/O(10) or O(6)/O(9) occupy the axially elongated apical positions. The Mn−N and Mn−O bond lengths are consistent with a d^4 high-spin electronic configuration for the Mn^{III} centres. The manganese centres Mn(1) and Mn(2) lie out of the best basal planes comprising Mn(1)N(21)O(22)O(1)O(2) and Mn(2)N(31)O(32)O(1)O(2) by 0.028 Å and 0.09 Å in the direction of the bridging O(3) or O(6), respectively.

The structure of **8**·2CH_3CN is very similar to that of **5** and **6** and hence only the core structure is shown in Fig-

Table 4. Selected bond lengths [Å] and angles [°] for **6**

Mn(1)−O(22)	1.906(2)	Fe(1)−O(1)	1.863(2)
Mn(1)−O(2)	1.930(2)	Fe(1)−O(21)	1.933(2)
Mn(1)−O(1)	1.972(2)	Fe(1)−O(4)	2.041(2)
Mn(1)−O(3)	2.097(2)	Fe(1)−N(3)	2.167(3)
Mn(1)−O(10)	2.103(2)	Fe(1)−N(1)	2.188(2)
Mn(1)−N(21)	2.113(2)	Fe(1)−N(2)	2.268(3)
Mn(1)−Mn(2)	2.8310(6)	Fe(2)−O(2)	1.876(2)
Mn(2)−O(32)	1.907(2)	Fe(2)−O(31)	1.931(2)
Mn(2)−O(1)	1.944(2)	Fe(2)−O(7)	2.045(2)
Mn(2)−O(2)	1.966(2)	Fe(2)−N(6)	2.149(2)
Mn(2)−N(31)	2.098(2)	Fe(2)−N(5)	2.205(2)
Mn(2)−O(9)	2.114(2)	Fe(2)−N(4)	2.270(2)
Mn(2)−O(6)	2.127(2)		
O(22)−Mn(1)−O(2)	103.93(8)	O(1)−Fe(1)−O(21)	95.68(8)
O(22)−Mn(1)−O(1)	172.69(8)	O(1)−Fe(1)−O(4)	97.72(8)
O(2)−Mn(1)−O(1)	83.21(7)	O(21)−Fe(1)−O(4)	93.00(9)
O(22)−Mn(1)−O(3)	86.86(8)	O(1)−Fe(1)−N(3)	96.82(10)
O(2)−Mn(1)−O(3)	96.82(8)	O(21)−Fe(1)−N(3)	92.73(10)
O(1)−Mn(1)−O(3)	90.74(8)	O(4)−Fe(1)−N(3)	163.75(10)
O(22)−Mn(1)−O(10)	85.02(8)	O(1)−Fe(1)−N(1)	100.61(9)
O(2)−Mn(1)−O(10)	95.00(8)	O(21)−Fe(1)−N(1)	163.08(9)
O(1)−Mn(1)−O(10)	96.05(8)		
O(3)−Mn(1)−O(10)	166.98(8)		
O(22)−Mn(1)−N(21)	85.82(9)	O(4)−Fe(1)−N(1)	89.38(10)
O(2)−Mn(1)−N(21)	169.12(8)	N(3)−Fe(1)−N(1)	80.85(11)
O(1)−Mn(1)−N(21)	87.21(8)	O(1)−Fe(1)−N(2)	176.44(9)
O(3)−Mn(1)−N(21)	88.42(8)	O(21)−Fe(1)−N(2)	85.53(9)
O(10)−Mn(1)−N(21)	80.86(9)	O(4)−Fe(1)−N(2)	85.54(10)
O(22)−Mn(1)−Mn(2)	143.91(6)	N(3)−Fe(1)−N(2)	79.77(11)
O(2)−Mn(1)−Mn(2)	43.89(5)	N(1)−Fe(1)−N(2)	77.95(10)
O(1)−Mn(1)−Mn(2)	43.30(5)	O(2)−Fe(2)−O(31)	95.65(8)
O(3)−Mn(1)−Mn(2)	109.38(6)	O(2)−Fe(2)−O(7)	98.24(8)
O(10)−Mn(1)−Mn(2)	83.00(5)	O(31)−Fe(2)−O(7)	91.73(8)
N(21)−Mn(1)−Mn(2)	125.31(6)	O(2)−Fe(2)−N(6)	95.98(8)
O(32)−Mn(2)−O(1)	103.88(8)	O(31)−Fe(2)−N(6)	95.43(8)
O(32)−Mn(2)−O(2)	172.94(8)	O(7)−Fe(2)−N(6)	163.37(8)
O(1)−Mn(2)−O(2)	83.02(7)	O(2)−Fe(2)−N(5)	101.08(8)
O(32)−Mn(2)−N(31)	86.14(9)	O(31)−Fe(2)−N(5)	163.17(8)
O(1)−Mn(2)−N(31)	166.16(8)	O(7)−Fe(2)−N(5)	87.65(8)
O(2)−Mn(2)−N(31)	86.81(8)	O(6)−Fe(2)−N(5)	81.16(9)
O(32)−Mn(2)−O(9)	83.73(8)	O(2)−Fe(2)−N(4)	175.81(8)
O(1)−Mn(2)−O(9)	91.94(8)	O(31)−Fe(2)−N(4)	85.60(8)
O(2)−Mn(2)−O(9)	94.70(8)	O(7)−Fe(2)−N(4)	85.71(8)
N(31)−Mn(2)−O(9)	79.53(8)	N(6)−Fe(2)−N(4)	79.91(9)
O(32)−Mn(2)−O(6)	88.20(8)	N(5)−Fe(2)−N(4)	77.58(8)
O(1)−Mn(2)−O(6)	100.22(7)		
O(2)−Mn(2)−O(6)	92.03(7)	Fe(1)−O(1)−Mn(2)	154.88(10)
N(31)−Mn(2)−O(6)	89.47(8)	Fe(1)−O(1)−Mn(1)	112.26(9)
O(9)−Mn(2)−O(6)	166.74(8)	Mn(2)−O(1)−Mn(1)	92.62(8)
O(32)−Mn(2)−Mn(1)	142.84(6)	Fe(2)−O(2)−Mn(1)	154.95(10)
O(1)−Mn(2)−Mn(1)	44.08(5)	Fe(2)−O(2)−Mn(2)	111.80(9)
O(2)−Mn(2)−Mn(1)	42.90(5)	Mn(1)−O(2)−Mn(2)	93.21(8)
N(31)−Mn(2)−Mn(1)	122.91(6)		
O(9)−Mn(2)−Mn(1)	80.11(5)		
O(6)−Mn(2)−Mn(1)	112.36(5)		
Mn(1)···Mn(2)	2.831(1)	Mn(2)···Fe(1)	3.715(1)
Mn(1)···Fe(1)	3.185(1)	Mn(2)···Fe(2)	3.182(1)
Mn(1)···Fe(2)	3.716(1)	Fe(2)···Fe(1)	6.048(1)

ure 5. Table 5 gives selected bond lengths and angles for **8**. Remarkably, the Mn−O−Mn angles in **5**, **6** and **8** (93°) are nearly identical. On the other hand, the Mn−μ_3-O distances in **8** (average 1.92 Å) are shorter than those in **5** or **6** (average 1.94 Å), although the Fe−μ_3-O distances for **5**, **6** and **8** are nearly identical (average 1.88 Å). This difference in bond lengths presumably has significant effects on the ground state S_t values, as will be shown later.

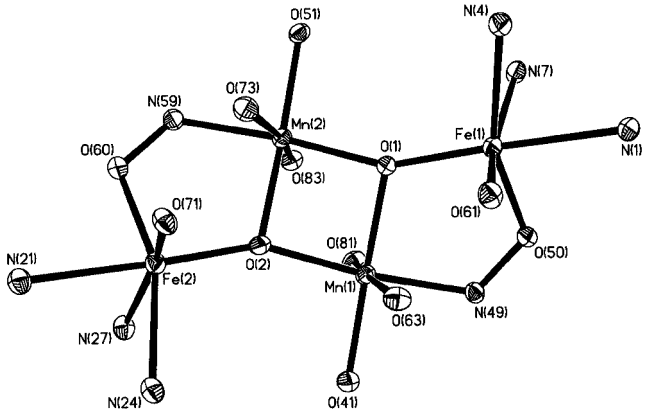

Figure 5. Atom connectivity of the $Fe_2Mn_2O_2$ core in the cation of **8**

Mössbauer Spectroscopy

The Mössbauer spectra of **1** (Figure 6, curve A) and **2** were recorded without an applied field at 80 K. Each spectrum is best fit to two equal-area doublets, whose isomer shifts (δ_{Fe}) and quadrupole splitting (ΔE_Q) values are listed in Table 6. The two doublets imply two Fe sites with different coordination spheres, in agreement with the molecular structure of **1**, and are thus assigned to the "body" and "wing-tip" pairs of Fe^{III} atoms. The isomer shift δ_{Fe} of 0.5 ± 0.05 mm/s is of the magnitude expected for the high-spin ferric state and is close to the values reported for similar compounds.[30] The ΔE_Q values for both sites in **1** and **2** reflect deviations from octahedral geometry, since the valence electron contribution to ΔE_Q is negligible for high-spin Fe^{III}. The two ΔE_Q values are significantly different, and larger than the 0.4−0.7 mm/s range observed for basic iron carboxylates.[31] By comparing the bond lengths for the NO_5 coordination sphere around Fe(1) and Fe(2) with those of the more symmetrical N_3O_3 coordination sphere about Fe(3) and Fe(4), the doublet with $\Delta E_Q \approx 1.37$ mm/s can be assigned to the "body" iron atoms Fe(1) and Fe(2), whereas the inner doublet is assignable to the "wing-tip" iron atoms Fe(3) and Fe(4). This assignment is also corroborated by the Mössbauer data for complexes **5**−**10**.

The powder-state Mössbauer spectrum of **6** at 80 K is displayed in Figure 6, curve B. Essentially similar spectra were obtained for the remaining complexes of the group. The δ_{Fe} and ΔE_Q values for **5**−**10** are listed in Table 6. Mössbauer results indicate a single quadrupole splitting, in accordance with only one type of iron coordination sphere in the solid-state structure, namely the "wing-tip" iron sites Fe(1) and Fe(2). The δ_{Fe} values of ca. 0.45 mm/s are consistent with a d^5 high-spin electron configuration for the iron centres Fe(1) and Fe(2) in complexes **5**−**10**. The isomer shift values are surprisingly constant within these complexes, and indicate that a change in the carboxylate group − with its varying electron-withdrawing power − has little effect upon the s-electron density at the iron nucleus. The ΔE_Q values (0.53−0.61 mm/s) for **5**−**10** lie within the 0.4−0.7 mm/s range found for basic iron carboxylates, and are similar to those for analogous structures with a dis-

Table 5. Selected bond lengths [Å] and angles [°] for **8**

Fe(1)−O(1)	1.892(2)	Mn(1)−O(41)	1.890(2)
Fe(1)−O(50)	1.959(2)	Mn(1)−O(2)	1.927(2)
Fe(1)−O(61)	2.013(2)	Mn(1)−O(1)	1.933(2)
Fe(1)−N(7)	2.190(2)	Mn(1)−N(49)	2.022(2)
Fe(1)−N(4)	2.226(2)	Mn(1)−O(81)	2.187(2)
Fe(1)−N(1)	2.265(2)	Mn(1)−O(63)	2.222(2)
Fe(1)−O(2)	1.895(2)	Mn(1)−Mn(2)	2.8034(6)
Fe(1)−O(60)	1.961(2)	Mn(2)−O(51)	1.890(2)
Fe(1)−O(71)	1.985(2)	Mn(2)−O(1)	1.917(2)
Fe(1)−N(27)	2.196(2)	Mn(2)−O(2)	1.918(2)
Fe(1)−N(24)	2.213(2)	Mn(2)−N(59)	2.010(2)
Fe(1)−N(21)	2.268(2)	Mn(2)−O(83)	2.220(2)
		Mn(2)−O(73)	2.294(2)
O(1)−Fe(1)−O(50)	93.52(8)	O(41)−Mn(1)−O(2)	96.86(8)
O(1)−Fe(1)−O(61)	96.42(7)	O(41)−Mn(1)−O(1)	176.12(8)
O(50)−Fe(1)−O(61)	100.55(8)	O(2)−Mn(1)−O(1)	84.03(7)
O(1)−Fe(1)−N(7)	97.14(8)	O(41)−Mn(1)−N(49)	88.70(8)
O(50)−Fe(1)−N(7)	92.00(8)	O(2)−Mn(1)−N(49)	171.68(8)
O(61)−Fe(1)−N(7)	160.89(8)	O(1)−Mn(1)−N(49)	90.84(8)
O(1)−Fe(1)−N(4)	106.76(8)	O(41)−Mn(1)−O(81)	89.73(8)
O(50)−Fe(1)−N(4)	158.64(8)	O(2)−Mn(1)−O(81)	91.01(7)
O(61)−Fe(1)−N(4)	84.10(8)	O(1)−Mn(1)−O(81)	94.04(7)
N(7)−Fe(1)−N(4)	79.13(8)	N(49)−Mn(1)−O(81)	82.80(8)
O(1)−Fe(1)−N(1)	173.57(8)	O(41)−Mn(1)−O(63)	87.97(7)
O(50)−Fe(1)−N(1)	81.35(8)	O(2)−Mn(1)−O(63)	96.89(7)
O(61)−Fe(1)−N(1)	88.36(8)	O(1)−Mn(1)−O(63)	88.17(7)
N(7)−Fe(1)−N(1)	79.27(8)	N(49)−Mn(1)−O(63)	89.47(8)
N(4)−Fe(1)−N(1)	77.94(8)	O(81)−Mn(1)−O(63)	171.98(7)
O(2)−Fe(2)−O(60)	93.89(8)	O(51)−Mn(2)−O(1)	97.49(7)
O(2)−Fe(2)−O(71)	96.96(8)	O(51)−Mn(2)−O(2)	177.81(8)
O(60)−Fe(2)−O(71)	98.69(8)	O(1)−Mn(2)−O(2)	84.70(7)
O(2)−Fe(2)−N(27)	96.72(8)	O(51)−Mn(2)−N(59)	87.71(8)
O(60)−Fe(2)−N(27)	90.30(8)	O(1)−Mn(2)−N(59)	174.32(8)
O(71)−Fe(2)−N(27)	163.06(8)	O(2)−Mn(2)−N(59)	90.10(8)
O(2)−Fe(2)−N(24)	105.74(8)	O(51)−Mn(2)−O(83)	89.21(7)
O(60)−Fe(2)−N(24)	158.95(8)	O(1)−Mn(2)−O(83)	93.75(7)
O(71)−Fe(2)−N(24)	86.61(8)	O(2)−Mn(2)−O(83)	90.68(7)
N(27)−Fe(2)−N(24)	80.09(8)	N(59)−Mn(2)−O(83)	84.02(8)
O(2)−Fe(2)−N(21)	173.58(8)	O(51)−Mn(2)−O(73)	91.50(7)
O(60)−Fe(2)−N(21)	81.18(8)	O(1)−Mn(2)−O(73)	95.73(7)
O(71)−Fe(2)−N(21)	87.89(8)	O(2)−Mn(2)−O(73)	88.24(7)
N(27)−Fe(2)−N(21)	79.29(8)	N(59)−Mn(2)−O(73)	86.36(8)
N(24)−Fe(2)−N(21)	78.66(8)	O(83)−Mn(2)−O(73)	170.32(7)
Fe(1)−O(1)−Mn(2)	154.22(10)		
Fe(1)−O(1)−Mn(1)	111.25(8)		
Mn(2)−O(1)−Mn(1)	93.49(7)		
Fe(2)−O(2)−Mn(2)	112.25(9)		
Fe(2)−O(2)−Mn(1)	150.98(10)		
Mn(2)−O(2)−Mn(1)	93.64(8)		
Mn(1)···Mn(2)	2.803(1)	Mn(2)···Fe(1)	3.713(2)
Mn(1)···Fe(1)	3.157(2)	Mn(2)···Fe(2)	3.166(2)
Mn(1)···Fe(2)	3.700(2)	Fe(2)···Fe(1)	6.024(2)

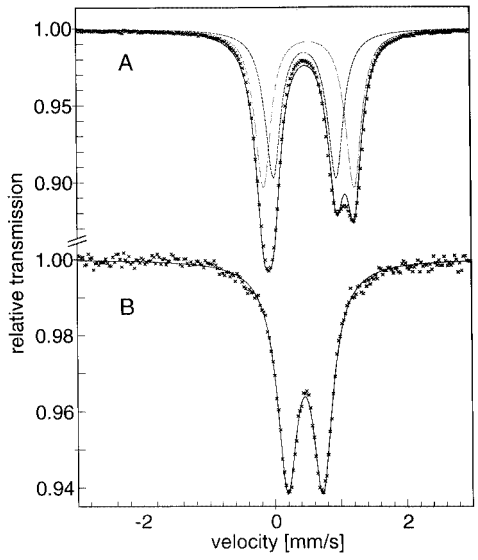

Figure 6. Mössbauer spectra of **1** (A) and **6** (B) at 80 K

Table 6. Mössbauer parameters at 80 K

Complex	δ_{Fe} [mm·s^{-1}][a]	ΔE_Q [mm·s^{-1}]
1	0.47	0.95
	0.53	1.37
2	0.47	0.95
	0.53	1.38
5	0.45	0.61
6	0.46	0.54
7	0.45	0.53
8	0.46	0.58
9	0.46	0.54
10	0.46	0.54

[a] Isomer shift relative to iron foil at room temperature. Typical errors are ±0.01 for δ_{Fe} and ±0.02 for ΔE_Q.

torted octahedral symmetry. Comparison of the Mössbauer data for **5**−**10** with those for **1** and **2** makes it clear that the "wing-tip positions in complexes **5**−**10** are occupied by Fe atoms in all cases, and hence the cyclic amine 1,4,7-trimethyl-1,4,7-triazacyclononane is coordinated to iron centres only.This is confirmed by the X-ray structures of **5**, **6** and **8**.

The remarkable difference in quadrupole splitting of the "wing-tip" and "body" iron sites in complexes **1**, **2** and **6** can be rationalised by comparing the distributions of bond lengths for the different coordination polyhedra. To this end, the iron−ligand bonds were classified into "short" and "long" bonds as sketched in Scheme 1.

It is striking that for the "wing-tip" iron atoms, the three shortest Fe−O bonds lie in a *fac* configuration, whereas for the "body" site, they have a *mer* arrangement. Thus, the "body" site can be regarded as a distorted octahedron with bond compression in the equatorial plane (if the *z* axis is taken in the O3−Fe1−O10 direction). Since large quadrupole splittings of high-spin Fe^{III} ($3d^5$ configuration) are the result of strong anisotropy in the covalent delocalisation of valence electrons, as suggested for the Fe−O−Fe unit in other systems,[32] we infer that the large electric field gradient for the "body" site [Fe(1) of complexes **1** and **2**] originates predominantly from strong covalency of the $d_{x^2-y^2}$ orbital and the resulting anisotropy in the distribution of valence electrons. In contrast, the short bonds in the "wing-tip" sites are distributed in a more balanced manner among the three major axes. In addition, the covalency due to the particularly short Fe4−O2 and Fe2−O2 bonds in compounds **1** and **6**, respectively, appears to be partly compensated for by a pronounced *trans* effect in the opposite bonds. Thus, the covalent delocalisation of 3d electrons seems to be more isotropic, as it affects both e_g orbitals. Since these orbitals, $d_{x^2-y^2}$ and d_{z^2}, have equally strong but opposite contributions to the total electric field gradient, the smaller quadrupole splittings observed for the "wing-tip" iron sites appears to be plausible.

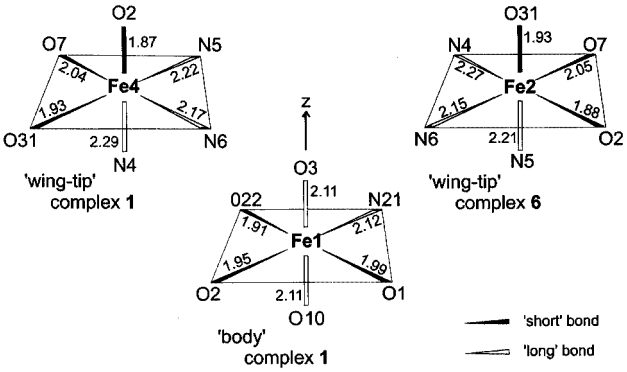

Scheme 1

Magnetic Properties

The magnetic susceptibility data for polycrystalline samples of **1**−**10** were collected in the temperature range 2−290 K in an applied magnetic field of 1 T and are displayed in Figures 7−9 as plots of the effective magnetic moment (μ_{eff}) versus temperature (*T*). Table 7 summarises the intracluster exchange parameters, together with the observed spin ground states, and selected μ_{eff} values for **1**−**10** are listed in Table 8. The solid lines in Figures 7−9 repres-

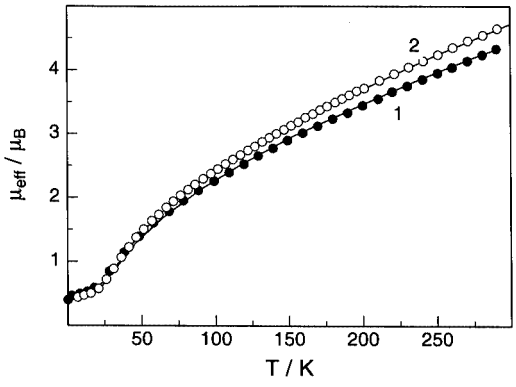

Figure 7. Temperature dependence of the magnetic moments of complexes **1** and **2**; the solid lines represent the best fit of data to the Heisenberg−Dirac−van Vleck model (see text)

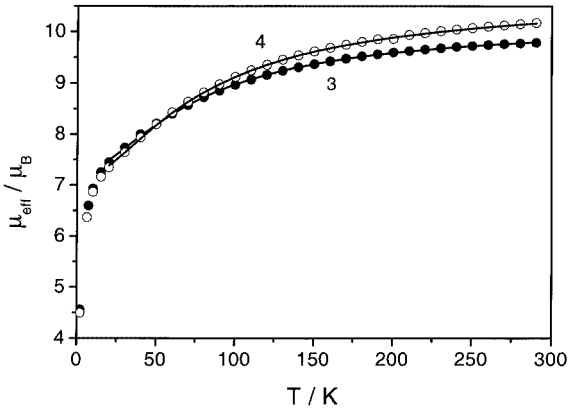

Figure 8. Plots of μ_{eff} vs. T for solid **3** and **4**; the solid lines are the best least-squares fits of the experimental data to the theoretical equation

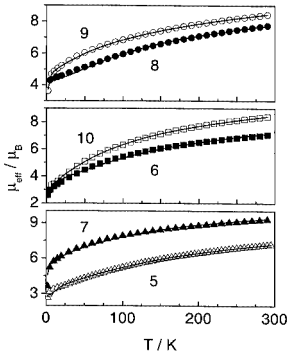

Figure 9. Temperature dependence of the magnetic moment, μ_{eff}, for **5**−**10**; the solid lines represent the simulation with the spin Hamiltonian (see text)

ent the simulations. The model used for the simulations involves two pairwise exchange interactions, J_{wb} for the wing-tip-body and J_{bb} for the body-body interactions. The oxide bridges have been shown to be more important mediators for the exchange interactions than the carboxylate bridges in the structurally related complexes $[Fe_4(\mu_3\text{-}O)_2]^{8+}$,[3,4] $[Mn_4(\mu_3\text{-}O)_2]^{8+}$,[9,35] $[Cr_4(\mu_3\text{-}O)_2]^{8+}$,[33] $[V_4(\mu_3\text{-}O)_2]^{8+}$,[34] $[Cr_2(\mu_3\text{-}O)_2Fe_2]^{8+}$ [13] and $[Cr_2(\mu_3\text{-}O)_2Mn_2]^{8+}$,[14] in which a similar "2J" model is able to adequately describe the magnetic behaviour of the tetranuclear complexes. Consequently, the other conceivable "3J" model has not been considered to avoid overparametrisation.

The resulting spin Hamiltonian used to describe the isotropic exchange interactions is given by

$\hat{H} = -2J_{wb}\ (\hat{S}_1 \bullet \hat{S}_3 + \hat{S}_2 \bullet \hat{S}_3 + \hat{S}_1 \bullet \hat{S}_4 + \hat{S}_2 \bullet \hat{S}_4) - 2J_{bb}(\hat{S}_1 \bullet \hat{S}_2)$

where S_i (i = 1, 2, 3, 4) = $^5/_2$ for **1** and **2**, S_i (i = 1, 2, 3, 4) = 2 for **3** and **4**, and $S_1 = S_2 = 2$; $S_3 = S_4 = {}^5/_2$ for **5**−**10**.

The magnetic moment for **1** and **2** decreases monotonically with decreasing temperature to an essentially diamag-

Table 8. Selected μ_{eff} values as a function of temperature for complexes **1**−**10**

Compound	Complex	μ_{eff}, μ_B (T [K])
1	Fe_4 benzilate	0.56 (2), 1.26 (40), 2.46 (110), 4.32 (290)
2	Fe_4 triphenyl acetate	0.52 (5), 1.30 (40), 2.64 (110), 4.66 (290), 4.76 (300)
3	Mn_4 benzilate	4.56 (2), 6.93 (10), 8.00 (40), 9.07 (110), 9.79 (290)
4	Mn_4 triphenyl acetate	4.50 (2), 6.87 (10), 7.95 (40), 9.27 (110), 10.22 (290)
5	Fe_2Mn_2 acetate	2.67 (2), 3.14 (5), 3.38 (10), 3.49 (15), 4.05 (40), 5.37 (110), 7.13 (290), 7.16 (295)
6	Fe_2Mn_2 benzilate	2.60 (2), 2.98 (5), 3.23 (15), 4.20 (40), 5.58 (110) 7.05 (290)
7	Fe_2Mn_2 triphenyl acetate	3.63 (2), 5.20 (5), 5.95 (15), 6.79 (40), 8.01 (110) 9.27 (290)
8	Fe_2Mn_2 benzoate	3.62 (2), 4.30 (5), 4.44 (10), 4.50 (15), 4.96 (40) 6.10 (110), 7.75 (290)
9	Fe_2Mn_2 chloroacetate	3.63 (2), 5.06 (15), 5.82 (40), 6.97 (110), 8.42 (290)
10	Fe_2Mn_2 propionate	2.72 (2), 3.62 (15), 4.73 (40), 6.49 (110), 8.39 (290)

Table 7. Magnetic parameters for complexes **1**−**10**

Compound	Complex	J_{wb} [cm^{-1}] ($J_{13} = J_{24} = J_{23} = J_{14}$)	J_{bb} [cm^{-1}] (J_{12})	g ($g_1 = g_2 = g_3 = g_4$)	D [cm^{-1}] ($D_1 = D_2 = D_3 = D_4$)	Ground state S_t
1	Fe_4 benzilate	−41.4	0 (fixed)	2.0 (fixed)	−	0
2	Fe_4 triphenyl acetate	−38.2	0 (fixed)	2.0 (fixed)	−	0
3	Mn_4 benzilate	−0.47	−7.73	2.099 (fixed)	0 (fixed)	3
4	Mn_4 triphenyl acetate	−1.63	−6.71	2.215 (fixed)	0 (fixed)	3
5	Fe_2Mn_2 acetate	−25.2	−35.1	2.05 (fixed)	−0.38	1
6	Fe_2Mn_2 benzilate	−22.3	−31.6	2.00 (fixed)	0 (fixed)	1
7	Fe_2Mn_2 triphenyl acetate	−5.5	−10.2	2.00 (fixed)	0 (fixed)	2, 3
8	Fe_2Mn_2 benzoate	−19.4	−28.9	2.09	0	2, 1
9	Fe_2Mn_2 chloroacetate	−10.6	−17.8	2.01 (fixed)	2.07	2
10	Fe_2Mn_2 propionate	−14.4	−19.4	2.13 (fixed)	0 (fixed)	1

netic value of 0.55 μ_B for **1** at 2 K and 0.52 μ_B at 5 K for **2**; the residual nonzero moment is due primarily to an amount of a paramagnetic impurity PI (assumed $S = {}^5/_2$). Thus, the temperature-dependent behaviours of the magnetic moments of **1** and **2** clearly indicate an $S_t = 0$ electronic ground state, in agreement with previous observations[1−6] for other molecules of similar structure. The theoretical van Vleck equation used for simulation of the susceptibility data has been described earlier.[4]

The Zeeman interaction of the high-spin ferric ion in a $^6A_1$ ground state with practically no contribution from orbital angular momentum is isotropic and the observed g values are thus very close to the free-electron spin value of 2.0. Hence, we have used a fixed value of $g = 2.0$ for **1** and **2** during simulation. As the quality of the fit is negligibly dependent on J_{bb},[3,4] we have kept $J_{bb} = 0$. Previous work has shown that J_{bb} cannot be precisely determined from the susceptibility data in the temperature range ca 4−300 K for such complexes, but J_{wb} can be evaluated with reasonable accuracy.[3,4] Additionally, an error-surface plot for **1** as a function of J_{wb} and J_{bb} shows that, while the value of J_{wb} is well determined by the fitting procedure, the value of J_{bb} is not. The best fits are shown as solid lines in Figure 7 and the fitting parameters are $J_{wb} = -41.4$ cm^{-1}, $J_{bb} = 0$ (fixed), $g = 2.0$ (fixed) and PI = 0.008 for **1**, and $J_{wb} = -38.2$ cm^{-1}, $J_{bb} = 0$ (fixed), $g = 2.00$ (fixed) and PI = 0.009 for **2**. The J_{wb} values obtained compare closely with those previously determined by us for the Fe_4 acetate system[4], and also those reported in the literature.[3,6]

The effective magnetic moment of complexes **3** and **4** as a function of temperature is shown in Figure 8. The magnetic moment gradually decreases to 6.93 μ_B at 10 K for **3** and 6.87 μ_B at 10 K for **4**, whereupon the moment falls sharply to 4.56 μ_B for **3** and 4.50 μ_B for **4** by 2 K. Thus, the temperature-dependent behaviours of the magnetic moments of **3** and **4** suggest an $S_t = 3$ ground state. In both cases, only data for temperatures above 20 K were considered in the fit, to avoid complications at low temperature from zero-field splitting. The solid lines in Figure 8 represent the best fits with the following parameters: $J_{wb} = -0.47$ cm^{-1}, $J_{bb} = -7.73$ cm^{-1}, $g = 2.099$ (fixed) and $D = 0$ (fixed) for **3**, and $J_{wb} = -1.63$ cm^{-1}, $J_{bb} = -6.71$ cm^{-1}, $g = 2.215$ (fixed) and $D = 0$ cm^{-1} (fixed) for **4**. Field-dependent magnetisation measurements (not shown) at 2 K up to 6 T also confirm that the ground state for **3** is $S_t = 3$ [simulation with $S = 3.0$ (fixed), $g = 2.02$, $D = 4.13$ cm^{-1}]. The ground state is within 5 cm^{-1} of the first excited state with $S_t = 4$.

We note that the g values employed for the simulation are high for Mn^{III}. Nevertheless, they do not affect our conclusion that **3** and **4** have an $S_t = 3$ ground state. The ground state of $S_t = 3$ has been found for all carboxylate-bridged clusters with an $[Mn_4O_2]^{8+}$ core except one with a quintuply degenerate ground state.[35]

At 295 K the magnetic moment (μ_{eff}/molecule) for **5** is 7.16 μ_B, which is significantly lower than the value of $\mu_{eff} = 10.86$ μ_B expected for an uncoupled system containing two Fe^{III} ($S = {}^5/_2$) and two Mn^{III} ($S = 2$) ions. On lowering the temperature, μ_{eff} decreases monotonically until it reaches a value of $\mu_{eff} = 2.67$ μ_B at 2 K, indicating a ground state of $S_t = 1$ (Figure 9). A full-matrix diagonalisation approach including spin exchange ($-2J\ S_1 \cdot S_2$), Zeeman interactions, and single-ion zero-field interaction (DS_z^2), was employed to fit the data. The solid line in Figure 9 shows the good quality of the fit above $T = 15$ K with the following parameters:

$J_{FeMn} = J_{wb} = -25{\cdot}2$ cm^{-1}; $J_{MnMn} = J_{bb} = -35.1$ cm^{-1}; $D(Mn^{III}) = -0.38$ cm^{-1} and $g = 2.05$ (fixed). As it is difficult, if not impossible, to unambiguously determine the sign of D from powder magnetic susceptibility measurements, one should not put too much weight on the absolute value of D, although inclusion of D as a parameter slightly improved the quality of the fit. We addressed the point of global and local minima by consideration of the two-dimensional contour projection of the error surface. The error surface shows that the fitting procedure has correctly identified the global minimum and we conclude that **5** has an $S_t = 1$ ground state lying 22.3 cm^{-1} below the first excited state with $S_t = 2$. For a system of two high-spin Fe^{III} and two high-spin Mn^{III} ions disposed in a butterfly-type arrangement as found in complexes **5**−**10**, the overall spin degeneracy (900) is distributed over 110 levels with S_t values ranging from 0 to 9.

The effective magnetic moment (μ_{eff}/molecule) for **6** decreases monotonically with decreasing temperature from 7.05 μ_B at 290 K to 2.60 μ_B at 2 K (Figure 9). The two exchange coupling constants, J_{wb} and J_{bb}, were allowed to vary independently in the full-matrix diagonalisation program to optimise the agreement. A good fit was found with the following parameters: $J_{wb} = J_{FeMn} = -22.3$ cm^{-1}, $J_{bb} = J_{MnMn} = -31.6$ cm^{-1}, $g = 2.0$ (fixed) and $D = 0$ (fixed). The ground state of $S_t = 1$ for **6** lies about 14 cm^{-1} below the first excited state with $S_t = 2$.

A steady decrease of the magnetic moment with decreasing temperature is observed for **7**. The value of μ_{eff} at 2 K (3.63 μ_B) clearly indicates a different ground state than that for **5** or **6** with $S_t = 1$. The solid line in Figure 9 shows the good quality of the fit with the following parameters: $J_{wb} = J_{FeMn} = -5.5$ cm^{-1}; $J_{bb} = J_{MnMn} = -10.16$ cm^{-1}; $g = 2.00$ (fixed) and $D = 0$ (fixed). The relative error surface for fitting the magnetic data of **7** as a function of both J_{FeMn} and J_{MnMn}, representing a well-defined global minimum in the parameter space, has allowed us to estimate the error bars on the quoted J_{FeMn} and J_{MnMn} values as approximately ± 0.2 and ± 1.0 cm^{-1}, respectively. The ground state of $S_t = 2$ for **7** obtained from the exchange coupling constants is separated from the first excited state with $S_t = 3$ by an energy gap of only 5 cm^{-1}.

A good fit of the magnetic data for **8** yields $J_{wb} = J_{FeMn} = -19.38$ cm^{-1}, $J_{bb} = J_{MnMn} = -28.91$ cm^{-1}, $g = 2.09$ and $D = 0$ (Figure 9). The ground state of $S_t = 1$ for **8** is not well separated ($\Delta E \approx 1$ cm^{-1}) from the first excited state with $S_t = 2$.

The magnetic behaviour of **9** can be easily interpreted in terms of the competing influence of J_{wb} and J_{bb} upon spin coupling, yielding a ground state of $S_t = 2$. An excellent fit representing a well-defined global minimum for **9,** together

with the experimental magnetic moments, is shown in Figure 9. The parameters used for the least-squares fitting (fit shown as a solid line in Figure 9) are $J_{wb} = J_{FeMn} = -10.6$ cm^{-1}, $J_{bb} = J_{MnMn} = -17.8$ cm^{-1}, $g = 2.01$ (fixed) and $D = 2.07$ cm^{-1} (fixed). The relative error surface calculation has allowed us to estimate the error bars on the J_{FeMn} and J_{MnMn} values as approximately ± 0.6 cm^{-1} and ± 1.5 cm^{-1}, respectively. The relatively large uncertainties in the absolute magnitudes of J_{FeMn} and J_{MnMn} do not affect our conclusion that **9** has an $S_t = 2$ ground state lying 15.8 cm^{-1} below the first excited state of $S_t = 1$.

For **10**, a monotonous decrease of the magnetic moment with decreasing temperature, reaching a value of $\mu_{eff} = 2.72$ μ_B at 2 K, is observed. This clearly indicates a ground state with $S_t > 1$, which is attained by competing antiferromagnetic coupling between the wing-body ($J_{wb} = -14.4$ cm^{-1}) and the body-body ($J_{bb} = -19.4$ cm^{-1}) metal centres. The g value used for the simulation of the experimental data (data shown as squares in Figure 9) is $g = 2.13$. The solid line in Figure 9 is the simulation of the magnetic data with the abovementioned parameters. The evaluated lowest lying state of $S_t = 1$ lies 18 cm^{-1} below the second lowest state with $S_t = 2$.

Discussion

In the preceding section it has been experimentally established that **1** and **2**, with the Fe_4O_2 core, possess an $S_t = 0$ ground state. All thermally populated excited states are effectively only determined by J_{wb}, and the intrinsic character (i.e. antiparallel coupling) of the Fe(2)···Fe(1) interaction, $J_{bb} = J_{12}$, can be totally negated due to spin frustration,[20] making the J_{bb} interaction indeterminate in the $[Fe_4(\mu_3\text{-}O)_2]^{8+}$ core. On the other hand, **3** and **4**, with the Mn_4O_2 core, possess the ground state $S_t = 3$, irrespective of the nature of the bridging carboxylate, as has been found earlier.[9] In contrast, variation of the six bridging carboxylates from acetate (**5**), to benzilate (diphenylglycolate) (**6**), triphenyl acetate (**7**), benzoate (**8**), chloroacetate (**9**), and propionate (**10**), causes changes in the ground states for **5**−**10**, varying from $S_t = 1$ to 3, although the replacement of acetate in **5** by benzilate in **6** or benzoate in **8** has little structural effect within the $[Fe_2Mn_2O_2]^{8+}$ core, as is evident from the X-ray structures. These ground states have been confirmed by the field-dependent (0.5−6.5 T) magnetisation measurements. This indicates that *the "R" groups of the different carboxylic acids (RCOOH) might not be that innocent in mediating exchange interactions, as is commonly taken for granted.* The ground state does not represent the smallest spin state possible for the electronic d^n configuration when both interactions are antiferromagnetic. It is noteworthy in this respect that the ratio of competing coupling pathways, and not so much their absolute magnitudes, determines the electronic structures of these butterfly complexes. The ratio J_{MnMn}/J_{FeMn} varies from 1.39 for **5** (acetate), to 1.42 for **6** (benzilate), 1.85 for **7** (triphenyl acetate), 1.49 for **8** (benzoate), 1.68 for **9** (chloroacetate), and 1.35 for **10** (propionate). Figure 10 gives a selective spin-correlation diagram for the $Fe^{III}_2M^{III}_2(O)_2$ butterfly arrangement in which the energy (in units of J_{wb}) of a spin state denoted by (S_t, S_{Mn}, S_{Fe}) is plotted as a function of J_{bb}/J_{wb}. The correlation diagram clearly demonstrates the ground state variation as a function of the ratio of J_{bb}/J_{wb}, which is also consistent with the experimental findings for the different carboxylate bridging ligands within the heterometallic Fe_2Mn_2 core. As an example, the ground state $S_t = 3$ has component S_{Fe} and S_{Mn} values of 5 and 2, respectively. These values result from different relative orientations of $S_{Fe(3)}$, $S_{Fe(4)}$, $S_{Mn(1)}$, $S_{Mn(2)}$, which is represented below as an overall spin alignment due to spin frustration.

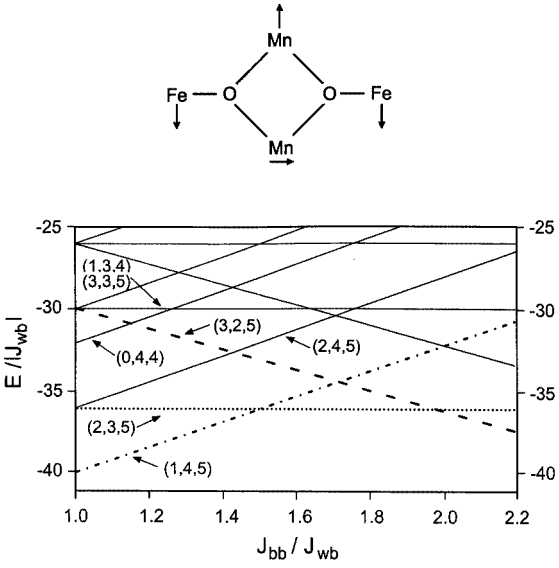

Figure 10. A selected energy-level diagram for the $[Fe_2Mn_2O_2]^{8+}$ core emphasising the ground state variation as a function of the ratio J_{bb}/J_{wb}; spin states are denoted by S_t, S_{Mn} and S_{Fe}, where $S_t = S_{Mn} + S_{Fe}$

Concluding Remarks

The results described in the present paper show that not only homometal tetranuclear metal clusters of Fe^{III} and Mn^{III} with a butterfly disposition, $[M_4(\mu_3\text{-}O)_2]^{8+}$, can be isolated, but also their mixed-metal analogues $[Fe^{III}_2M^{III}_2(\mu_3\text{-}O)_2]^{8+}$ are easily accessible. The tetranuclear cores are amenable to carboxylate bridging ligand variation but the structural parameters show insignificant variation. Although the spin ground states resulting from the exchange interactions within the $[Fe_4O_2]^{8+}$ and $[Mn_4O_2]^{8+}$ cores are little affected by the peripheral carboxylate ligands, variation of the six carboxylates (acetate, benzilate, triphenyl acetate, benzoate, chloroacetate propionate) causes significant changes in the electronic ground state structure ($S_t = 1-3$) of the $[Fe_2Mn_2O_2]^{8+}$ core. As the crystallographic data exclude steric effects as the cause of the ground state variation, the electronic (donor) properties seem to be responsible for the dependence of spin ground states on the nature of the bridging carboxylates. Presum-

Table 9. Crystal data and structure refinement for **1**, **3**, **5**, **6** and **8**

	1	**3**	**5**	**6**	**8**
Empirical formula	$C_{74}H_{85}ClFe_4N_8O_{19}$	$C_{74}H_{85}ClMn_4N_8O_{19}$	$C_{38}H_{61}ClFe_2Mn_2N_8O_{16}$	$C_{74}H_{85}ClFe_2Mn_2N_8O_{19}$	$C_{53}H_{67}ClFe_2Mn_2N_8O_{16}\cdot 2CH_3CN$
Formula mass	1649.35	1645.71	1142.98	1647.53	1411.28
Temperature [K]	293(2)	293(2)	100(2)	100(2)	100(2)
Crystal system	orthorhombic	orthorhombic	tetragonal	orthorhombic	monoclinic
Space group	$Pna2_1$	$Pna2_1$	$P4(1)2(1)2$	$Pna2_1$	$P2_1/n$
Unit cell dimensions [Å]	$a = 16.329(4)$	$a = 16.317(3)$	$a = 11.6230(9)$	$a = 16.144(2)$	$a = 16.0785(6)$
	$b = 18.644(4)$	$b = 18.655(4)$	$b = 11.6230(9)$	$b = 18.396(2)$	$b = 14.6897(5)$
	$c = 25.009(6)$	$c = 25.001(5)$	$c = 35.827(2)$	$c = 24.759(3)$	$c = 27.5133(10)$
	$\alpha = \beta = \gamma = 90°$	$\alpha = \beta = \gamma = 90°$	$\alpha = \beta = \gamma = 90°$	$\alpha = \beta = \gamma = 90°$	$\beta = 106.23°$
Volume [Å^3]; Z	7613.7(3); 4	7610.1(3); 4	4840.0(6); 4	7353(2); 4	6239.3(4); 4
Density (calcd.) [Mg/m^3]	1.439	1.436	1.569	1.488	1.502
Absorpt. coeff. [mm^{-1}]	0.857	0.759	1.227	0.836	0.969
$F(000)$	3432	3416	2368	3424	2928
Crystal size [mm]	$0.40 \times 0.37 \times 0.12$	$0.50 \times 0.45 \times 0.07$	$0.31 \times 0.28 \times 0.12$	$0.42 \times 0.24 \times 0.09$	$0.30 \times 0.25 \times 0.25$
Reflections collected	8991	9056	54594	59215	53728
Independent reflections	8991	8648	9541	20348	14147
Data/restraints/parameters	8972/214/931	8634/321/954	9536/0/316	20331/1/964	14124/0/801
Absolute structure parameter	0.00(3)	−0.01(3)	0.012(12)	−0.016(8)	−
Final $R1$ [$I > 2\sigma(I)$]	0.0770	0.0827	0.0396	0.0439	0.0436
$R2$ (all data)	0.178	0.168	0.0965	0.0961	0.1021

ably, spin coupling through carboxylate is not negligible, in contrast to the prevailing notion. Thus, future low molecular weight structural modelling of metalloproteins is expected to be guided by proper choice of the carboxylate ligands, in order to mimic the amino acids in the biomolecules.

The $[M_4O_2]^{8+}$ tetranuclear cores are structurally incongruent with currently known biological metal sites and hence might be irrelevant from a biological view point. However, being readily prepared and amenable to carboxylate variation, **5**−**10** have proven useful starting points to increase our knowledge on fine-tuning the spin properties of molecular aggregates. This fine-tuning is a result of spin frustration. Both the lowest and the intermediate spin ground states have been observed in the isostructural complexes **5**−**10** which vary only in the nature of their carboxylate bridging ligands. As is seen from Figure 10 "spin-frustration degeneracy" of the ground state leading to unusual electronic properties is expected for the $[Fe_2Mn_2O_2]^{8+}$ core if $J_{bb}/J_{wb} \approx 1.52$ and 2.0.

Experimental Section

General: ***CAUTION:*** Although we experienced no difficulties, the unpredictable behaviour of perchlorate salts necessitates extreme caution in their handling. The complex $LFeCl_3$ was prepared as described previously.[36] All other reagents were used as received. Elemental microanalyses were performed by the microanalytical laboratory Kolbe, Mülheim. Iron and manganese were determined spectrophotometrically by using pyridine-2,6-dicarboxylic acid as described in the literature.[37] Perchlorate ion was determined gravimetrically as tetraphenylarsonium perchlorate. Infrared spectra were measured as KBr disks with a Perkin−Elmer FT-IR spectrometer 2000. The magnetochemical measurements of the powdered samples were performed with a Quantum Design SQUID-Magnetometer, MPMS generally in a field of 1 T. The samples were put in gelatine capsules and the response function was measured four times for each of 32 measured temperature points. Diamagnetic contributions were estimated for each compound by making use of Pascal's constants. The Mössbauer spectrometer worked in the conventional constant-acceleration mode with a ^{57}Co/Rh source. Isomer shifts are given relative to α-Fe at room temperature.

X-ray Crystallography: The crystallographic data for **1**, **3**, **5**, **6** and **8** are summarised in Table 9. Graphite-monochromated Mo-K_α radiation ($\lambda = 0.71073$ Å) was used throughout. X-ray diffraction data were collected with a Siemens R3m/V diffractometer for **1** and **3**. Dark brown single crystals of **5**, **6** and **8** were fixed with perfluoropolyether on glass fibres and mounted on a Siemens SMART diffractometer equipped with a cryogenic nitrogen cold stream, and intensity data were collected at 100(2) K. Final cell constants were obtained from a least-squares fit of the setting angles of several thousand strong reflections. Intensity data were corrected for Lorentz and polarisation effects. An empirical absorption correction by Ψ scans was applied for **1** and **3**; intensity data of **5** and **8** were corrected for absorption using the program SADABS (G. M. Sheldrick, University of Göttingen, **1994**) giving maximum and minimum transmission factors of 0.928 and 0.736 for **5** and 0.853 and 0.768 for **8**. Intensities of **6** were left uncorrected. The Siemens ShelXTL, Vers. 5.0 (Siemens Industrial Automation, Inc., **1994**) software package was used for solution, refinement and artwork of the structures. Neutral atom scattering factors of the program were used. All structures were solved and refined by direct methods and difference Fourier techniques. Non-hydrogen atoms were refined anisotropically and hydrogen atoms were placed at calculated positions and refined as riding atoms with isotropic displacement parameters. A crystallographic twofold axis passes through the central acetate bridge of the complex cation of **5** and the perchlorate anion is disordered since this axis is not coincident with the twofold axis of the ClO_4^- moiety. The disorder was satis-

factorily modelled by refining the complete anion slightly displaced from the axis with an occupation factor of 0.5. A phenyl group of a benzilate ligand in **6** was found to be disordered and therefore a split atom model was used. Two positions of the phenyl ring were refined with occupancies of 0.5 each. CCDC-187680 (**1**), -187681 (**3**), -187705 (**5**), -187706 (**6**) and -187707 (**8**) contain the supplementary crystallographic data for this paper. These data can be obtained free of charge at www.ccdc.cam.ac.uk/conts/retrieving.html [or from the Cambridge Crystallographic Data Centre, 12 Union Road, Cambridge CB2 1EZ, UK; Fax: (internat.) + 44-1223/336-033; E-mail: deposit@ccdc.cam.ac.uk].

Preparation of Complexes: Complexes **1** and **2** were prepared similarly by using a modified procedure for the corresponding acetate-bridged tetranuclear Fe^{III} compound.[4]

$[L_2Fe^{III}_4(salox)_2(\mu_3\text{-}O)_2(Ph_2C(OH)COO)_3]ClO_4$ (1): All operations were carried out under argon. $Fe(ClO_4)_2\cdot 6H_2O$ (0.30 g, 1 mmol), sodium diphenylglycolate (benzilate) (0.50 g, 2 mmol) and salicylaldoxime (0.27 g, 2 mmol) were added to vigorously stirred, degassed methanol (60 mL). The resulting suspension was stirred at room temperature for 1 h to yield a dark violet solution. This solution was charged with a solid sample of $[LFeCl_3]$[36] (0.33 g, 1 mmol), sodium diphenylglycolate (benzilate) (0.75 g, 3 mmol) and triethylamine (1 mL). The suspension was refluxed for 1 h and then filtered to remove some dark solid, identified as $[LFe^{III}(salox)_3Fe^{III}]$ by IR as described earlier.[24b] Sodium perchlorate monohydrate (0.4 g) was added to the filtrate and the red-brown solution was kept in air at ambient temperature. After 1 d, the red-brown crystals were filtered off and air-dried. Yield: 390 mg (47%). $C_{74}H_{85}ClFe_4N_8O_{19}$ (1648.35): calcd. C 53.89, H 5.19, N 6.79, Fe 13.54, ClO_4 6.03; found C 53.9, H 5.1, N 6.8, Fe 13.7, ClO_4 5.8. MS (ESI positive in CH_3CN/H_2O): *m/z* (%) = 1549 (100) $[M]^+$. IR (KBr): $\tilde{\nu}$ = 3472, 1600, 1569, 1157, 700, 669, 648, 638 cm^{-1}.

$[L_2Fe^{III}_4(salox)_2(\mu_3\text{-}O)_2(Ph_3CCOO)_3]ClO_4$ (2): Complex **2** was obtained similarly to complex **1** with sodium triphenylacetate used instead of sodium diphenylglycolate as the carboxylate source. Dark brown crystals were obtained. Yield: 410 mg (42%). $C_{92}H_{97}ClFe_4N_8O_{16}$ (1829.63): calcd. C 60.39, H 5.34, N 6.12, Fe 12.21, ClO_4 5.43; found C 58.4, H 5.4, N 6.0, Fe 12.3, ClO_4 5.5. MS (ESI positive in CH_3CN/H_2O): *m/z* (%) = 1730 (100) $[M]^+$. IR (KBr): $\tilde{\nu}$ = 1594, 1155, 1567, 699, 671, 652, 623 cm^{-1}.

$[L_2Mn^{III}_4(salox)_2(\mu_3\text{-}O)_2(Ph_2C(OH)COO)_3]ClO_4$ (3): Step 1: A suspension of diphenylglycolic acid (0.46 g, 2 mmol) and sodium hydroxide (0.08 g, 2 mmol) in water (30 mL) was stirred vigorously for 15 min. $MnCl_2\cdot 4H_2O$ (0.20 g, 1 mmol) was added and stirring was continued for a further 15 min. The precipitated solid was filtered off, washed thoroughly with water, and dried for 24 h under vacuum. Step 2: A suspension of the dried solid obtained from step 1 and salicylaldoxime (0.27 g, 2 mmol) in methanol (40 mL) containing triethylamine (1 mL) was refluxed in air for 0.5 h to obtain a dark green suspension. The green suspension was charged with $LMnCl_3$ [38] (0.33 g, 1 mmol) under argon and treated with triethylamine (0.5 mL). The resulting suspension was refluxed under argon for 0.5 h and then filtered to remove some green solid (presumably $[Mn(Hsalox)_3]$). Sodium perchlorate monohydrate (0.8 g) was added, and after 1−2 d the dark brown solution yielded deep brown crystals of **3**, which were collected by filtration and air-dried. Yield: 275 g (ca. 33%). $C_{74}H_{85}ClMn_4N_8O_{19}$ (1645.71): calcd. C 54.00, H 5.21, N 6.81, Mn 13.35, ClO_4 6.04; found C 53.8, H 5.1, N 6.8, Mn 13.1, ClO_4 5.9. IR (KBr): $\tilde{\nu}$ = 3472, 1617, 1592, 1574, 1158 cm^{-1}.

$[L_2Mn^{III}_4(salox)_2(\mu_3\text{-}O)_2(Ph_3CCOO)_3]ClO_4$ (4): Complex **4** was prepared similarly to **3** with triphenylacetic acid as the carboxylate source. Deep brown crystals were obtained in moderately good yield (45%). $C_{92}H_{97}ClMn_4N_8O_{16}$ (1825.99): calcd. C 60.51, H 5.35, N 6.14, Mn 12.03, ClO_4 5.45; found C 58.9, H 5.5, N 6.2, Mn 12.2, ClO_4 5.1. MS(ESI positive in CH_3CN): *m/z* (%) = 1727 (80) $[M]^+$, 1484 (100) $[M - L(Mn)(O)]^+$, 1439 (60) $[M - (C_6H_5)_3CCOO]^+$. IR (KBr): $\tilde{\nu}$ = 3441, 1587, 1541, 1152 cm^{-1}. Complex **4** was also prepared using CH_3CN as solvent.

$[L_2Fe^{III}_2(\mu_3\text{-}O)_2(salox)_2(\mu\text{-}OOC\cdot CH_3)_3Mn^{III}_2]ClO_4$ (5): "Basic manganese(III) acetate"[39] (0.27 g, 1 mmol) was added to a vigorously stirred solution of salicylaldoxime (0.135 g, 1 mmol) in methanol (60 mL). The resulting suspension was stirred at room temperature for 0.5 h to yield a dark brown solution which was then charged with a solid sample of $LFeCl_3$ (0.33 g, 1 mmol), sodium acetate (0.24 g, 3.0 mmol) and triethylamine (2 mL). The suspension was refluxed for 1 h and then filtered to remove some green solid (presumably $[Mn(Hsalox)_3]$). Sodium perchlorate monohydrate (0.4 g) was added to the clear solution and the red-brown solution was kept at ambient temperature in a closed vessel. After 12 h, the dark brown crystals were filtered off and air-dried. Yield: 400 mg (70%). $C_{38}H_{61}ClFe_2Mn_2N_8O_{16}$ (1142.98): calcd. C 39.93, H 5.38, N 9.80, Fe 9.77, Mn 9.61, ClO_4 8.70; found C 39.7, H 5.4, N 9.8, Fe 9.9, Mn 9.5, ClO_4 8.9. IR (KBr): $\tilde{\nu}$ = 1594, 1544, 1155, 755, 743, 663 cm^{-1}.

$[L_2Fe^{III}_2(\mu_3\text{-}O)_2(salox)_2(\mu\text{-}OOC\cdot C(OH)Ph_2]_3Mn^{III}_2]ClO_4$ (6): A solution containing $MnCl_2\cdot 4H_2O$ (0.20 g, 1 mmol), salicylaldoxime (0.27 g, 2 mmol) diphenylglycolic acid (0.63 g, 3 mmol) and triethylamine (1 mL) in methanol (60 mL) was heated to reflux for 0.5 h. $LFeCl_3$ (0.33 g, 1 mmol) and sodium diphenylglycolate (0.25 g, 1 mmol) were added to the resulting suspension. The mixture was refluxed for 1 h and then filtered to remove some green solid. The red-brown solution was kept at room temperature following addition of $NaClO_4\cdot H_2O$ (0.8 g). After 24 h, the deep brown crystals were filtered off and air-dried. Yield: 510 mg (ca. 62%). $C_{74}H_{85}ClFe_2Mn_2N_8O_{19}$ (1647.53): calcd. C 53.95, H 5.20, N 6.80, Fe 6.78, Mn 6.67, ClO_4 6.04; found C 53.80, H 5.1, N 6.8, Fe 6.5, Mn 6.4, ClO_4 5.5. MS (ESI positive in CH_3CN): *m/z* (%) = 1547 (100), 1548 (90) $[M]^+$. IR (KBr): $\tilde{\nu}$ = 3742, 1617, 1592, 1540, 1158, 704, 670, 638, 603 cm^{-1}.

$[L_2Fe^{III}_2(\mu_3\text{-}O)_2(salox)_2(\mu\text{-}OOC\cdot CPh_3)_3Mn^{III}_2]ClO_4$ (7), $[L_2Fe^{III}_2(\mu_3\text{-}O)_2(salox)_2(\mu\text{-}OOC\cdot Ph)_3Mn^{III}_2]ClO_4$ (8), $[L_2Fe^{III}_2(\mu_3\text{-}O)_2(salox)_2(\mu\text{-}OOCCH_2Cl)_3Mn^{III}_2]ClO_4$ (9), $[L_2Fe^{III}_2(\mu_3\text{-}O)_2(salox)_2(\mu\text{-}OOC\cdot CH_2CH_3)_3Mn^{III}_2]ClO_4$ (10): Complexes **7**−**10** were prepared according to the same protocol for **6** using triphenylacetic acid (**7**), benzoic acid (**8**), chloroacetic acid (**9**) or propionic acid (**10**) as the bridging carboxylate sources. Red-brown crystals were obtained with yields in the range 40−50%.

7: $C_{92}H_{97}ClFe_2Mn_2N_8O_{16}$ (1827.81): calcd. C 60.45, H 5.35, N 6.13, Fe 6.11, ClO_4 5.44; found C 58.9, H 5.4, N 6.3, Fe 6.0, Mn 6.01, ClO_4 5.8. MS (ESI positive in CH_3CN/H_2O): *m/z* (%) = 1727 (100) $[M]^+$. IR (KBr): $\tilde{\nu}$ = 1591, 1540, 701, 670, 645, 612 cm^{-1}.

8: $C_{53}H_{67}ClFe_2Mn_2N_8O_{16}$ (1329.18): calcd. C 47.89, H 5.08, N 8.43, Fe 8.40, Mn 8.27, ClO_4 7.48; found C 48.1, H 5.0, N 8.5, Fe, 8.4, Mn, 8.2, ClO_4 7.9. IR (KBr): $\tilde{\nu}$ = 1594, 1541, 1157, 738, 723, 663, 636 cm^{-1}.

9: $C_{38}H_{58}Cl_4Fe_2Mn_2N_8O_{16}$ (1246.30): calcd. C 36.62, H 4.69, N 8.99, Fe 8.96, Mn 8.82, ClO_4 8.00; found C 35.0, H 5.0, N 9.0, Fe 9.2, Mn 8.8, ClO_4 8.1. IR (KBr): $\tilde{\nu}$ = 1594, 1543, 1156, 757, 745, 663 cm^{-1}.

10: $C_{41}H_{67}ClFe_2Mn_2N_8O_{16}$ (1185.06): calcd. C 41.55, H 5.70, N 9.46, Fe, 9.43, Mn 9.27, ClO_4 8.39; found C 42.0, H 5.6, N 9.6, Fe 9.1, Mn 9.5, ClO_4 8.4. IR (KBr): $\tilde{\nu}$ = 1592, 1538, 1158, 704, 672, 640, 602 cm^{-1}.

Acknowledgments

This work was initiated in Bochum. Our thanks are due to Mrs. M. Hess, H. Schucht (Mülheim) and M. Winter (Bochum) for their technical assistance. Support from the Max Planck Society and Fonds der Chemischen Industrie is gratefully acknowledged.

[1] V. I. Ponomarev, L. O. Atovmyan, S. A. Bobkova, K. I. Turté, *Dokl. Akad. Nauk. SSSR.* **1984**, *274*, 368.
[2] W. H. Armstrong, M. E. Roth, S. J. Lippard, *J. Am. Chem. Soc.* **1987**, *109*, 6318.
[3] J. M. McCusker, J. B. Vincent, E. A. Schmitt, M. L. Mino, K. Shin, D. K. Coggin, P. M. Hagen, J. C. Huffman, G. Christou, D. N. Hendrickson, *J. Am. Chem. Soc.* **1991**, *113*, 3012.
[4] P. Chaudhuri, M. Winter, P. Fleischhauer, W. Haase, U. Flörke, H.-J. Haupt, *Inorg. Chim. Acta* **1993**, *212*, 241.
[5] L. Wu, M. Pressprich, P. Coppens, M. J. DeMarco, *Acta Crystallogr., Sect. C* **1993**, *49*, 1255.
[6] M. W. Wemple, D. K. Coggin, J. B. Vincent, J. K. McCusker, W. E. Streib, J. C. Huffman, D. N. Hendrickson, G. Christou, *J. Chem. Soc., Dalton Trans.* **1998**, 719.
[7] [7a] K. Wieghardt, K. Pohl, I. Jibril, G. Huttner, *Angew. Chem. Int. Ed. Engl.* **1984**, *23*, 77. [7b] C. Delfs, D. Gatteschi, L. Pardi, R. Sessoli, K. Wieghardt, D. Hanke, *Inorg. Chem.* **1993**, *32*, 3099. [7c] A.-L. Barra, D. Gatteschi, R. Sessoli, *Chem. Eur. J.* **2000**, *6*, 1608.
[8] [8a] V. L. Pecoraro, Ed. *Manganese Redox Enzymes*, VCH Verlagsgesellschaft, Weinheim, **1992**. [8b] H. Sigel, A. Sigel, Ed. *Metal Ions in Biological Systems*, Marcel Dekker, New York, **2000**, vol. 37. [8c] R. H. Holm, E. I. Solomon (Guest Eds.), *Chem. Rev.* **1996**, no. 7.
[9] J. B. Vincent, C. Christmas, H.-R. Chang, Q. Li, P. D. Boyd, J. C. Huffman, D. N. Hendrickson, G. Christou, *J. Am. Chem. Soc.* **1989**, *111*, 2086.
[10] E. Libby, J. K. McCusker, E. A. Schmitt, K. Folting, D. N. Hendrickson, G. Christou, *Inorg. Chem.* **1991**, *30*, 3486.
[11] E. Bouwman, M. A. Bolcar, E. Libby, J. C. Huffman, K. Folting, G. Christou, *Inorg. Chem.* **1992**, *31*, 5185.
[12] M. W. Wemple, H.-L. Tsai, S. Wang, J. B. Claude, W. E. Streib, J. C. Huffman, D. N. Hendrickson, G. Christou, *Inorg. Chem.* **1996**, *35*, 6437.
[13] P. Chaudhuri, M. Winter, P. Fleischhauer, W. Haase, U. Flörke, H.-J. Haupt, *J. Chem. Soc., Chem. Commun.* **1993**, 566.
[14] P. Chaudhuri, F. Birkelbach, M. Winter, V. Staemmler, P. Fleischhauer, W. Haase, U. Flörke, H.-J. Haupt, *J. Chem. Soc., Dalton Trans.* **1994**, 2313.
[15] O. Kahn, *Molecular Magnetism*, VCH Publishers, Weinheim, **1993**.
[16] [16a] F. Birkelbach, U. Flörke, H.-J. Haupt, C. Butzlaff, A. X. Trautwein, K. Wieghardt, P. Chaudhuri, *Inorg. Chem.* **1998**, *37*, 2000. [16b] F. Birkelbach, M. Winter, U. Flörke, H.-J. Haupt, C. Butzlaff, M. Lengen, E. Bill, A. X. Trautwein, K. Wieghardt, P. Chaudhuri, *Inorg. Chem.* **1994**, *33*, 3990. [16c] C. Krebs, M. Winter, T. Weyhermüller, E. Bill, K. Wieghardt, P. Chaudhuri, *J. Chem. Soc., Chem. Commun.* **1995**, 1913. [16d] P. Chaudhuri, M. Winter, P. Fleischhauer, W. Haase, U. Flörke, H.-J. Haupt, *J. Chem. Soc., Chem. Commun.* **1990**, 1728. [16e] C. N. Verani, E. Rentschler, T. Weyhermüller, E. Bill, P. Chaudhuri, *J. Chem. Soc., Dalton Trans.* **2000**, 4263.
[17] A few selected examples: [17a] K. E. Vostrikova, D. Luneau, W. Wernsdorfer, P. Rey, M. Verdagner, *J. Am. Chem. Soc.* **2000**, *122*, 718. [17b] C. Diaz, J. Ribas, R. Costa, J. Tercero, M. S. E. Fallah, X. Solans, M. Forit-Bardia, *Eur. J. Inorg. Chem.* **2000**, 675. [17c] A. Aukauloo, X. Ottenwaelder, R. Ruiz, Y. Journaux, Y. Pei, E. Riviere, M. C. Munoz, *Eur. J. Inorg. Chem.* **2000**, 951. [17d] B. Cervera, R. Ruiz, F. Lloret, M. Julve, J. Faus, C. M. Munoz, Y. Journaux, *Inorg. Chim. Acta* **1999**, *288*, 57. [17e] E. Colacio, J. M. Dominguez-Vera, M. Ghazi, R. Kivekäs, M. Klinga, J. M. Moreno, *Inorg. Chem.* **1998**, *37*, 3040. [17f] S. Mohanta, K. K. Nand, L. K. Thompson, U. Flörke, K. Nag, *Inorg. Chem.* **1998**, *37*, 1465.
[18] [18a] O. Kahn, *Adv. Inorg. Chem.* **1995**, *43*, 179. [18b] K. S. Murray, *Adv. Inorg. Chem.* **1995**, *43*, 261.
[19] [19a] P. D. W. Boyd, Q. Li, J. B. Vincent, K. Folting, H. R. Chang, W. E. Streib, J. C. Huffman, G. Christou, D. N. Hendrickson, *J. Am. Chem. Soc.* **1988**, *110*, 8537. [19b] D. Sessoli, H. L. Tsai, A. R. Schake, S. Wang, J. B. Vincent, K. Folting, D. Gatteschi, G. Christou, D. N. Hendrickson, *J. Am. Chem. Soc.* **1993**, *115*, 1804. [19c] D. Gatteschi, A. Caneschi, L. Pardi, R. Sessoli, *Science* **1994**, *265*, 1054. [19d] S. M. J. Aubin, M. W. Wemple, D. M. Adams, H. L. Tsai, G. Christou, D. N. Hendrickson, *J. Am. Chem. Soc.* **1996**, *118*, 7746. [19e] A. L. Barra, A. Caneschi, A. Cornia, D. Fabrizi de Biani, D. Gatteschi, C. Sanggregorio, R. Sessoli, L. Sorace, *J. Am. Chem. Soc.* **1999**, *121*, 5302. [19f] G. Aromi, S. M. J. Aubin, M. A. Bolcar, G. Christou, H. J. Eppley, K. Folting, D. N. Hendrickson, J. C. Huffman, R. C. Squire, H.-L. Tsai, S. Wang, M. W. Wemple, *Polyhedron* **1998**, *17*, 3005 and references therein. [19g] J. Larinova, M. Gross, M. Pilkington, H. Andres, H. Stoeckli-Evans, H. U. Güdel, S. Decurtins, *Angew. Chem. Int. Ed.* **2000**, 1605. [19h] D. Gatteschi, R. Sessoli, A. Cornia, *Chem. Commun.* **2000**, 725 and references therein.
[20] D. N. Hendrickson, *Research Frontiers in Magnetochemistry* (Ed.: C. J. O'Connor), World Scientific Singapore, **1993**, p. 87.
[21] O. Kahn, *Chem. Phys. Lett.* **1997**, *265*, 109.
[22] F. Ephraim, *Ber. Dtsch. Chem. Ges.* **1930**, *63*, 1928.
[23] [23a] E. Toyota, K. Umakoshi, Y. Yamamoto, *Bull. Chem. Soc. Jpn.* **1995**, *68*, 858. [23b] J. M. Thorpe, R. L. Beddoes, D. Collison, C. D. Garner, M. Helliwell, J. M. Holmes, P. A. Tasker, *Angew. Chem. Int. Ed.* **1999**, *38*, 1119. [23c] S. J. Rettig, A. STorr, J. Trotter, *Acta Crystallogr., Sect. C* **1992**, *48*, 1587. [23d] K. R. Manolov, *Russ. J. Inorg. Chem.* **1967**, *12*, 1431.
[24] [24a] P. Chaudhuri, *Proc. Indian Acad. Sci. (Chem. Sci)* **1999**, *111*, 397. [24b] C. N. Verani, E. Bothe, D. Burdinski, T. Weyhermüller, U. Flörke, P. Chaudhuri, *Eur. J. Inorg. Chem.* **2001**, 2161.
[25] E. Bill, C. Krebs, M. Winter, M. Gerdan, A. X. Trautwein, U. Flörke, H.-J. Haupt, P. Chaudhuri, *Chem. Eur. J.* **1997**, *3*, 193.
[26] P. Chaudhuri, M. Hess, T. Weyhermüller, E. Bill, H.-J. Haupt, U. Flörke, *Inorg. Chem. Commun.* **1998**, *1*, 39.
[27] P. Chaudhuri, M. Hess, E. Rentschler, T. Weyhermüller, U. Flörke, *New J. Chem.* **1998**, 533.
[28] P. Chaudhuri, M. Winter, B. P. C. Della Védova, P. Fleischhauer, W. Haase, U. Flörke, H.-J. Haupt, *Inorg. Chem.* **1991**, *30*, 4777.
[29] R. D. Cannon, R. P. White, *Progr, Inorg. Chem.* **1988**, *36*, 195.
[30] [30a] P. Gütlich, in *Mössbauer Spectroscopy* (Ed.: U. Gonser), Springer-Verlag, Berlin, Heidelberg, New York, **1975**. [30b] N. N. Greenwood, T. C. Gibb, *Mössbauer Spectroscopy*, Chapman and Hall, London, **1971**.
[31] G. J. Long, W. T. Robinson, W. P. Tappmeyer, D. L. Bridges, *J. Chem. Soc., Dalton Trans.* **1973**, 573.
[32] [32a] J. H. Rodriguez, H. Ok, Y.-M. Xia, P. G. Debrunner, B. E. Hinrichs, T. Meyer, N. H. Packard, *J. Phys. Chem.* **1996**, *100*, 6849. [32b] J. H. Rodriguez, Y.-M. Xia, P. G. Debrunner, P. Chaudhuri, K. Wieghardt, *J. Am. Chem. Soc.* **1996**, *118*, 7542.
[33] A. Bino, R. Chayat, E. Pedersen, A. Schneider, *Inorg. Chem.* **1991**, *30*, 856.
[34] S. L. Castro, Z. Sun, C. M. Grant, J. C. Bollinger, D. N. Hendrickson, G. Christou, *J. Am. Chem. Soc.* **1988**, *120*, 2365.
[35] C. Canada-Vilalta, J. C. Huffman, G. Christou, *Polyhedron* **2001**, *20*, 1785.

[36] P. Chaudhuri, M. Winter, K. Wieghardt, S. Gehring, W. Haase, B. Nuber, J. Weiss, *Inorg. Chem.* **1988**, *27*, 1564.
[37] H. Hartkamp, *Z. Anal. Chem.* **1964**, *199*, 183.
[38] K. Wieghardt, U. Bossek, B. Nuber, J. Weiss, J. Bonvoisin, M. Corbella, S. E. Vitols, J. J. Girerd, *J. Am. Chem. Soc.* **1988**, *110*, 7398.
[39] F. A. Cotton, G. Wilkinson, *Advanced Inorganic Chemistry*, 5th ed., John Wiley & Sons, New York, **1988**, p. 704.

Received July 3, 2002
[I02363]

Chiral Complexes of Rh^{I} Containing Binaphthalene-Core P,S-Heterobidentate Ligands − Synthesis, Characterization, and Catalytic Activity in Asymmetric Hydrogenation of α,β-Unsaturated Acids and Esters

Serafino Gladiali,*[a] Fabrizia Grepioni,[a] Serenella Medici,[a] Antonio Zucca,[a] Zoltán Berente,[b] and László Kollár[c]

Keywords: S ligands / P ligands / Rhodium / Asymmetric catalysis / Hydrogenations

The enantiopure complexes **3a** and **3b** $[Rh(NBD)(P,S)]^{+}BF_4^{-}$ [P,S = (*S*)-2-(diphenylphosphanyl)-2′-(methylthio)-1,1′-binaphthalene (**a**); (*S*)-2-(diphenylphosphanyl)-2′-(isopropylthio)-1,1′-binaphthalene (**b**)] have been prepared from $[Rh(NBD)(THF)_2]^{+}BF_4^{-}$ by reaction with a stoichiometric amount of the appropriate P,S-heterobidentate ligand. Single-crystal X-ray analysis of the *S*-methyl derivative shows that the seven-membered chelate ring is locked in a boat-like conformation with the methyl group in the equatorial position. Variable-temperature NMR measurements confirm that this conformation is maintained in solution and that the dynamic behaviour displayed by the complex is due to pseudo-rotation of the diolefin. Complexes **3** have been tested in the asymmetric hydrogenation of α,β-unsaturated acids and esters. Enantioselectivities of up to 60% *ee* have been recorded.
(© Wiley-VCH Verlag GmbH & Co. KGaA, 69451 Weinheim, Germany, 2003)

Introduction

The catalytic activity of transition metal complexes is largely dependent on the structure of the supporting ligands. The nature of the donor atoms is crucial because it affects substantially the electron density at the metal centre as well as the geometric properties of the corresponding complexes.

Owing to the presence of two donors of diverse ligating properties, bidentate P,X-heterodonor ligands, where the chelate coordination of a phosphanyl group (P) is supported by a different heteroatom (X), are sometimes endowed with a peculiar catalytic activity. Within the family of P,X-heterobidentate ligands, the P,S-pair deserves particular attention. When the sulfur atom is in a low oxidation state, as in sulfides, the softness of the S-donor is similar to that of the P-donor in a phosphane. Phosphanyl sulfides can be thus regarded as heterobidentate ligands that differ little in the ligating strength of the two donors. Consequently, such ligands are expected to have a fairly weak hemilabile character and to show a strong propensity towards chelate coordination to the metal atom.[1]

An additional interesting feature of the S-donor of a sulfide group is that upon coordination the S-centre becomes stereogenic. The stereochemistry at the S-binding site depends on the chiral backbone of the ligand and on the steric demand of the alkyl substituent at the S-centre. This results in the formation of diastereomeric complexes featuring either a matching or a mismatching combination of chiral elements; a fact that is expected to have a significant bearing on the use of these ligands in asymmetric catalysis.

Various chiral P,S-heterobidentate ligands have been reported recently. Phosphito sulfide derivatives based on the xylofuranose framework have been used in the Ir-catalysed asymmetric hydrogenation of itaconic acid (51% *ee*).[2] Glucopyranose-substituted phosphanyl sulfides are able to stabilize otherwise elusive Pd^0 complexes.[3]

Bis(phosphinite) ligands with a tetrahydrothiophene backbone have been synthesised and used in rhodium-catalysed enantioselective hydrogenation of methyl acetamidocinnamate. A tridentate coordination of the ligand, forming thioether-bridged dinuclear species, has been proposed.[4]

Novel P,S-bidentate ligands possessing an oxathiane ring condensed onto pulegone[5] or norbornane[6] moieties led to quite good enantioselectivity in the Co-catalysed asymmetric intramolecular Pauson−Khand reaction and in the Pd-catalysed asymmetric allylic substitution reaction, respectively.

Mixed phosphorus/sulfur ligands, where the thioether fragment is flanked by a diarylphosphinito[7] or a diaryl-

[a] Dipartimento di Chimica, Università di Sassari,
Via Vienna 2, 07100 Sassari, Italia
Fax: (internat.) + 39-079/212069, -229559
E-mail: gladiali@uniss.it
[b] Institute of Biochemistry, University of Pécs and Research Group for Chemical Sensors of the Hungarian Academy of Sciences,
P. O. Box 266, 7601 Pécs, Hungary
[c] Department of Inorganic Chemistry, University of Pécs and Research Group for Chemical Sensors of the Hungarian Academy of Sciences,
P. O. Box 266, 7601 Pécs, Hungary

phosphanyl[8] unit supported on chiral 1,2-disubstituted aliphatic backbones, proved to be highly efficient in Pd-catalysed enantioselective allylic substitution and in Rh-catalysed hydrogenation, respectively.

Atropisomeric 1,1′-binaphthyl-templated diphosphanes such as BINAP are among the most efficient chiral ligands for asymmetric hydrogenation. Recently, we reported on the synthesis of BINAPS,[9] a heterobidentate version of BINAP in which one of the two diphenylphosphanyl substituents is replaced by an alkylthio group. BINAPS derivatives performed well in some Pd-catalysed asymmetric reactions, such as allylic alkylation[10] and hydrosilylation,[11] but were less satisfactory in Rh-catalysed processes such as hydroformylation and H-transfer reduction.[11]

We report here on further investigations into the preparation, dynamic behaviour and utilization in enantioselective hydrogenation of such BINAPS-based Rh complexes.

Results and Discussion

The required ligands (*S*)-**1a** and (*S*)-**1b** were synthesised in enantiopure form as reported previously.[11] The preparation of the enantiopure complexes **3a** and **3b** was accomplished as reported in Scheme 1 by treating the rhodium complex $[Rh(NBD)(THF)_2]^+BF_4^-$ (**2**) (NBD = 1,4-norbornadiene) with a stoichiometric amount of (*S*)-**1a** and (*S*)-**1b**, respectively. The required intermediate adduct **2** was prepared in situ from the corresponding chloro-bridged dimer $[Rh(NBD)Cl]_2$ and $AgBF_4$.[12] The isolated yields of the complexes **3a** and **3b** were in the range of 60−70%.

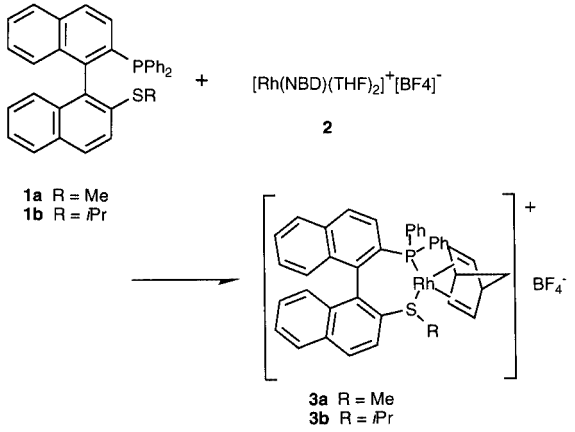

Scheme 1. Synthesis of complexes **3a** and **3b**

The molecular structure of the complex cation **3a** is depicted in Figure 1, together with the labelling scheme.

The Rh atom has a square-planar coordination geometry involving the double bonds of the norbornadiene ligand, the P atom and the stereogenic S-donor. The configuration at the newly created S-stereocentre is (*R*). The Rh−P and Rh−C bond lengths are comparable to those previously observed in $[Rh(NBD)(BINAP)]^+$.[13] The dihedral angle between the two naphthyl ligands (ca. 75°) is comparable to the 74.4° observed in the BINAP complex.

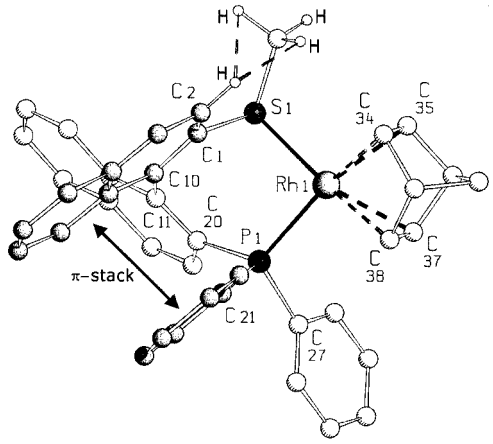

Figure 1. Ball-and-stick representation of the cationic complex in **3a**; selected structural parameters [Å]: Rh(1)−C(34) 2.200(5), Rh(1)−C(35) 2.216(5),Rh(1)−C(37) 2.181(5), Rh(1)−C(38) 2.144(6), Rh(1)−P(1) 3.290(1), Rh(1)−S(1) 2.343(1), P(1)−C(20) 1.838(4), S(1)−C(1) 1.793(4), C(34)−C(35) 1.385(7), C(37)−C(38) 1.356(9); the longest contacts involving H(2) and the H_{Me} atoms are shown by dotted lines; all remaining H atoms omitted for clarity

The H atom bound to C(2) is in close contact with the hydrogen atoms of the methyl group on the S atom; if free reorientation of the methyl group is assumed, the "dynamic" contacts between the H atoms range from 1.84 to 2.46 Å (assuming a normalised distance of 1.08 Å for the $C_{(by)}$−H group). One of the two extremes, with two equivalent $H_{CH}\cdots H_{Me}$ contacts of 2.46 Å, is shown in Figure 1.

Contrary to the BINAP complex, where the seven-membered chelate ring adopts a skew conformation in the solid state,[13] the seven-membered ring in **3a** adopts a boat-like conformation (see Figure 2), with the Rh(1), P(1), C(10), and C(1) atoms constituting the flat part of the boat (maximum deviation from the average plane 0.05 Å). The sulfur and C_{methyl} atom elevations from this plane are 1.21 and 1.28 Å, respectively; thus, the methyl group bound to the sulfur atom is in an equatorial position with respect to the ring.

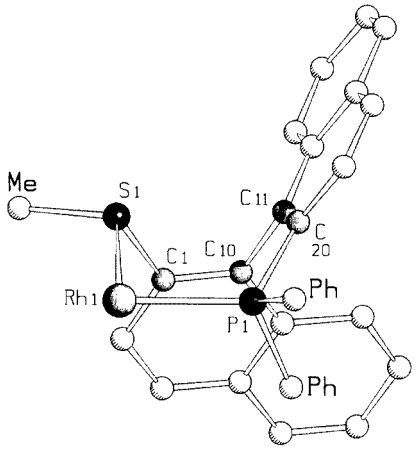

Figure 2. Boat-like conformation adopted by the seven-membered chelate ring in complex cation **3a**

Crystalline **3a** contains a stoichiometric amount of $CHCl_3$ solvent per formula unit. The H atom belonging to the solvent molecule interacts via bifurcated hydrogen bonding of the CH···F type with the BF_4^- anion (see Figure 3). The (C)H···F distances (after normalisation of the C−H distance to the neutron value of 1.08 Å) are 2.26(1) and 2.24(1) Å, and compare well with the shortest CH···F interactions observed for organometallic salts containing BF_4^- or PF_6^- anions.[14]

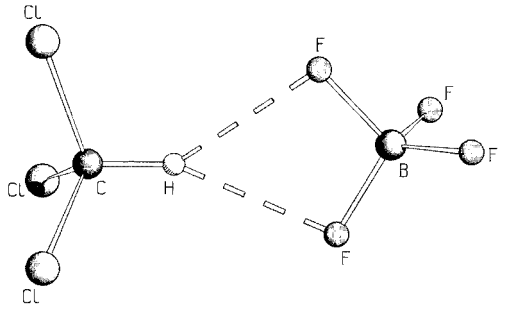

Figure 3. Bifurcated CH···F hydrogen bond interaction between the $CHCl_3$ solvent molecule and BF_4^-

One of the phenyl substituents bound to the phosphorus atom and the portion of the binaphthyl moiety bound to S(1) are arranged in a π-stacking fashion, with an average distance between the two mean planes of ca. 3.5 Å (see Figure 1).

In the ^1H NMR spectrum of **3a** ($CDCl_3$ solution) four lines, each one accounting for two protons, can be observed for the coordinated NBD at 303 K (Figure 4). The signals of the allylic (δ = 4.04 ppm) and the olefinic protons (δ = 4.40 and 4.67 ppm) are broad singlets, while the bridging methylene group resonates as a sharp singlet (δ = 1.50 ppm). When the temperature is lowered to 273 K, the olefinic protons' signal at δ = 4.67 ppm undergoes line broadening, becoming extremely broad at 258 K and practically disappearing at 243 K. The second olefinic signal at δ = 4.40 ppm also broadens, but at lower temperatures [ν(1/2) ≈ 20 Hz at 258 K], and practically disappears at 223 K. The allylic and the methylenic signals at δ = 4.04 and 1.50 ppm, respectively, are still observable even at 223 K [(ν(1/2) ≈ 40 Hz and 25 Hz, respectively]. From the NMR spectroscopic data it is apparent that a dynamic process is occurring in solution which averages the protons of the NBD ligand in the bound state.

The methyl peak appears at δ = 2.59 ppm as a sharp doublet (J = 1.5 Hz). This is due to ^3J(Rh,H) coupling as demonstrated by a selective $^1H\{^{31}P\}$ decoupling. The shape, chemical shift and coupling constant of this signal remain unchanged over the whole temperature range investigated (303−203 K), suggesting that in this interval no dissociation of the S-donor from the metal atom occurs. Irradiation of this peak causes a significant NOE enhancement of the signal at δ = 7.67 ppm which should be attributed to the naphthyl proton on the carbon atom adjacent to the *S*-substituted one. This is consistent with an equatorial location of the *S*-methyl group and confirms that the solid-state structure is preserved in solution.

The pattern of the aromatic protons undergoes some minor variation with temperature, but the isolated peaks remain sharp and the coupling constants are substantially unchanged.

The protons were assigned to the corresponding carbon atoms by a ^1H-^{13}C HSQC experiment. In the ^{13}C NMR spectrum all the carbon signals but those at δ = 81.61, 71.25, and 66.50 ppm show sharp lines. These were assigned to the olefinic and the methylenic carbon atoms of norbornadiene, respectively. Finally, the sharp doublet in the ^{31}P NMR spectrum [^1J(Rh,P) = 161.7 Hz] was not affected by the temperature variation.

The NOESY experiments show that the S−CH_3 group gives cross peaks with both olefinic signals at δ = 4.40 and 4.67 ppm. This tells us that the two vinylic protons of the same double bond of NBD are not averaged and provides further evidence for the equatorial position of the methyl group. If the methyl group were axial, only one of the two protons on the same double bond would give a cross peak (Figure 5).

The NOESY spectra also show close contacts between the naphthyl proton adjacent to the S atom (signal at δ = 7.67 ppm) and the olefinic proton of NBD (signal at δ = 4.67 ppm). Thus, the more deshielded olefinic signal could confidently be assigned to the olefinic proton H^a (H^d) located below the average plane of the chelate ring (Figure 5).

The olefinic protons (signals at δ = 4.40 and 4.67 ppm) also show contacts with the *ortho* protons of the two different phenyl substituents of the PPh_2 unit (signals at δ = 7.38 and 7.41 ppm).

These NMR experiments indicate that the dynamic process the complex experiences in solution results in averaging protons H^a with H^d and protons H^b with H^c (see Figure 5).

Dynamic behaviour of this type has been previously observed in cationic (diolefin)rhodium complexes with bidentate P,S- or P,N-ligands. This has been attributed to a mechanism involving Rh−S[15,16] or Rh−N[16] bond dissociation, followed by rotation around the remaining Rh−P bond and subsequent recombination of the dissociated bond.

Although the S-stereocentre might be labilised more readily than the P-centre, the present NMR evidence indicates that the sulfur atom remains tightly bound to the metal atom throughout. Chemical shift, coupling constant and sharpness of the signal of the *S*-methyl group remain unchanged over the temperature range investigated. No shift of the methyl group towards that of the free ligand is observed; such a shift would be expected if the sulfur donor were displaced from the metal atom. Furthermore, the doublet at δ = 6.01 ppm, regarded as diagnostic of the chelate coordination of the binaphthyl ligand, remains unchanged from 223 to 303 K.

All this evidence indicates that dissociation/inversion processes at the sulfur atom or conformational interconversions of the seven-membered ring do not take place. Instead, it appears that in solution both the chelate coordination of the P,S-ligand and the configurational integrity of

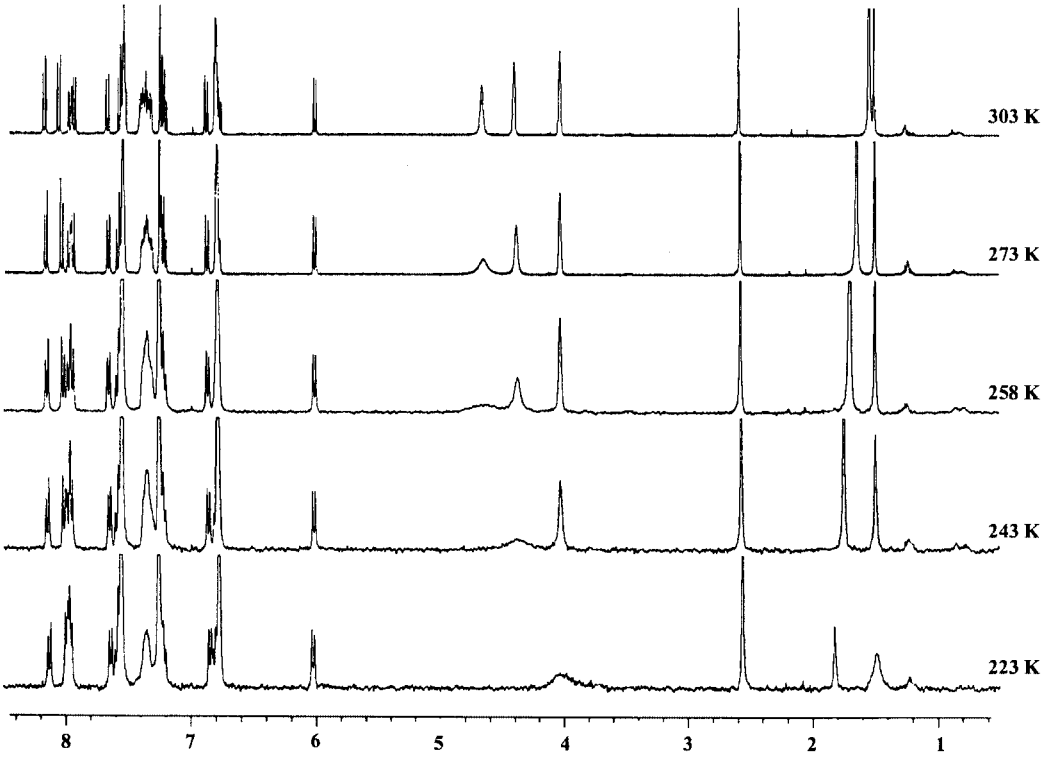

Figure 4. Variable-temperature ^1H NMR spectrum of **3a**

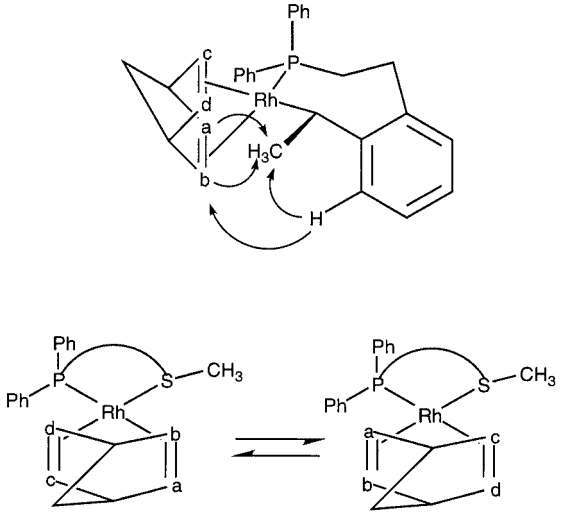

Figure 5. Representation of NOE contacts in **3a**

the S-stereocentre in the bound state are preserved over the temperature range investigated.

An alternative plausible mechanism involves a Barry pseudo-rotation promoted by coordination of a donor at the fifth position of the metal atom. Such a reaction path has been proposed previously for a (1,5-cycloctadiene)Rh complex containing 2-(diphenylphosphanyl)pyridine.[17] However, this possibility was not substantiated as the ^1H NMR spectra registered in $CDCl_3$ after addition of donor solvents such as THF, or in [D_6]acetone, show no significant change with respect to those registered in plain $CDCl_3$.

As it seems even more unlikely that the phosphorus atom is involved in a displacement/recombination process, the observed results should be ascribed to a dynamic process of the diolefin. This should proceed through an olefin pseudo-rotation, prompted by dissociation of one rhodium−olefin bond, followed by rotation through 180° around the remaining Rh−olefin bond and subsequent rebuilding of the chelate coordination of the diolefin. This conclusion fits better the experimental finding that the dynamic behaviour of the NBD protons is far more pronounced than that of the protons of the backbone of the P,S-ligand.

The isopropyl derivative **3b** shows in solution the same dynamic behaviour as **3a** as judged from the similar NMR pattern. The methylenic, allylic and olefinic protons of the norbornadiene ligand give rise to four broad singlets at δ = 1.49, 4.00, 4.48, and 4.61 ppm (2 H each), respectively. The signals of the diastereotopic methyl groups of the isopropyl group appear at δ = 1.18 and 1.28 ppm. The chelating coordination of **1b** is confirmed by the presence of the aromatic doublet at δ = 5.95 ppm.

Asymmetric Hydrogenation of α,β-Unsaturated Acids and Esters

Hydrogenation tests were performed on acrylic acid derivatives **4a**−**4c** (Scheme 2) at room temperature in methanol/benzene (1:1). A slight positive pressure of hydrogen was employed because at 1 bar the reaction was too sluggish. Even so, the catalytic activity of complexes **3a** and **3b** was rather low and fairly long reaction times were required

to attain a satisfactory conversion (Table 1). The two complexes exhibited comparable catalytic activity and both led to products of the same (*R*) configuration, although the methyl derivative **3a** was notably more efficient than the isopropyl counterpart **3b** and in all runs produced much higher *ee*s.

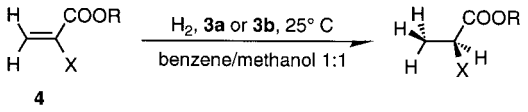

Scheme 2. Asymmetric hydrogenation of α,β-unsaturated carboxylic acids and esters **4a**−**4c**

Under our reaction conditions, the acid **4b** was hydrogenated with 49% *ee* by **3a**. This is basically the same *ee* obtained with the Rh complex with BINAPP′ [2-(Diphenylphosphanyl)-2′-(di-*o*-tolylphosphanyl)-1,1′-binaphthalene] (46% *ee*) and is much higher than the 13% *ee* we obtained with the corresponding Rh complex with BINAP.[18]

The improvement over the chelate diphosphane-based catalysts was more pronounced with the methyl ester **4a** where *ee*s obtained with BINAP (21%) and BINAPP′ (40%)[18] were outperformed by that obtained with complex **3a** (60%). This value is among the highest obtained in Rh-catalysed asymmetric hydrogenation using chiral P,S-heterodonor ligands. It is also close to that reported for the hydrogenation of the acid **4b** with a preformed [(*S*)-(BINAP)Rh(MeOH)$_2$]$^+$ClO$_4^-$ complex (67% *ee*).[19]

Both complexes **3a** and **3b** proved to be effective in hydrogenating dimethyl itaconate (**4c**), leading to high conversions (93 and 94%, respectively). Unfortunately, this activity was not matched by a high selectivity, and *ee*s were decidedly poor both with **3a** and **3b** (8% and 2% *ee*, respectively).

In all these experiments the prevailing enantiomer showed the (*R*) configuration, the same as obtained with (*S*)-BINAP and (*S*)-BINAPP′. Therefore, the stereochemistry of the hydrogenation of these substrates is basically driven by the handedness of the chiral backbone; the stereogenicity at the sulfur plays a minor, albeit cooperative role, in the transfer of the chiral information.

Further work is in progress to determine the effect of a substituent of higher steric demand on the sulfur atom, and whether this situation can be reversed by introducing a bulkier group such as *tert*-butyl on this donor centre.

Experimental Section

General: Some ^{1}H, ^{31}P, and ^{13}C NMR spectra, as well as NOESY measurements (mixing time = 500 ms) were carried out with a Varian VXR-S 300 instrument at 299.9 MHz, 121.4 MHz and 75.4 MHz, respectively. ^{1}H and ^{31}P variable-temperature measurements at 400 MHz and 161.9 MHz, respectively, as well as ^{1}H-^{13}C HSQC experiments were run with a Varian INOVA 400 WB spectrometer using a Highland VT unit. Chemical shifts, given in ppm, are referred to internal TMS (^{1}H and ^{13}C) or external 85% H_3PO_4 (^{31}P); coupling constants are in Hz. The two-dimensional experiments (NOESY and ^{1}H-^{13}C HSQC) were performed using standard pulse sequences. Solvents were dried and distilled under nitrogen before use. All the reactions were performed under argon. [Rh(NBD)Cl]$_2$ was purchased from Strem Chemicals and used without further purification. The ligands, (*S*)-2-(diphenylphosphanyl)-2′-(methylthio)-1,1′-binaphthalene (**1a**) and (*S*)-2-(diphenylphosphanyl)-2′-(isopropylthio)-1,1′-binaphthalene (**1b**), were prepared as previously reported.[11] The *ee*s of the samples from the catalytic runs were determined with a Hewlet Packard 5890A gas chromatograph fitted with a 25-m capillary column coated with diethyl *tert*-butylsilyl-β-cyclodextrin PS 086 (i.d. 0.25 mm), purchased from MEGA (Legnano, Italia), using He as the carrier (head pressure 60 kPa, split ratio 100).

Preparation of [(*S*)-2-(Diphenylphosphanyl)-2′-(methylthio)-1,1′-binaphthalene](2,5-norbornadiene)rhodium(i) Tetrafluoroborate (3a): $AgBF_4$ (39 mg, 0.2 mmol) was added to a solution of [Rh(NBD)Cl]$_2$ (48 mg, 0.1 mmol) in THF (10 mL). After stirring for 1 h, the mixture was filtered through Celite and (*S*)-2-(diphenylphosphanyl)-2′-(methylthio)-1,1′-binaphthalene (100 mg, 0.2 mmol) was added to the resulting yellow solution. A yellow solid precipitated immediately and was recovered by filtration. Yield 107 mg (70%). Crystals of **3a**$CHCl_3$ suitable for X-ray structure determination were obtained by slow concentration of a chloroform solution. ^{1}H NMR ($CDCl_3$ 298 K): δ = 1.50 [br. s, 2 H, CH_2 (NBD)], 2.59 (d, *J* = 1.5 Hz, 3 H, SCH_3), 4.04 [br. s, 2 H, allylic CH (NBD)], 4.40 and 4.67 [br. s, 2 × 2 H, olefinic CH (NBD)], 6.01 (d, *J* = 8.6 Hz, 1 H, Ar), 6.76−6.8 (m, 4 H, Ar), 6.88 (d, *J* = 8.6 Hz, 1 H, Ar), 7.20−7.26 (m, 2 H), 7.30−7.44 (m, 4 H),

Table 1. Asymmetric hydrogenation of α,β-unsaturated acids and esters **4a**−**4c** catalysed by complexes **3a** and **3b** (substrate/catalyst = 100:1)

Substrate.	R	X	Catalyst.	$p(H_2)$ [bar]	*t* [h]	Conversion[a] [%]	*ee*[a] [%]	Conformation
4a	CH_3	$NHCOCH_3$	**3a**	2.6	16	13	60	(*R*)
4b	H	$NHCOCH_3$	**3a**	2.3	16	31	49	(*R*)
4c	CH_3	CH_2COOCH_3	**3a**	1.9	16	93	8	(*R*)
4a	CH_3	$NHCOCH_3$	**3b**	1.9	11	11	27	(*R*)
4b	H	$NHCOCH_3$	**3b**	4.1	16	33	11	(*R*)
4c	CH_3	CH_2COOCH_3	**3b**	4.6	16	94	2	(*R*)

[a] Determined by gas chromatography.

7.51−7.59 (m, 5 H), 7.67 (d, J = 8.1 Hz, 1 H, Ar), 7.94 (d, J = 8.1 Hz, 1 H, Ar), 7.97 (d, J = 8.1 Hz, 1 H, Ar), 8.06 (d, J = 8.9 Hz, 1 H, Ar), 8.18 (d, J = 8.9 Hz, 1 H, Ar) ppm. $^{31}P\{^{1}H\}$ NMR ($CDCl_3$, 298 K): δ = 27.1 [d, ^{1}J(Rh,P) = 161.7 Hz] ppm. $^{13}C\{^{1}H\}$ NMR ($CDCl_3$, 298 K): δ = 15.27 (SCH_3), 52.99 (allylic *C*H, NBD), 66.50 (NBD CH_2), 71.25 (olefinic *C*H, NBD), 81.61 (olefinic *C*H, NBD), 123.30−135.09 (32 C, Ar) ppm.

Preparation of [(*S*)-2-(Diphenylphosphanyl)-2′-(isopropylthio)-1,1′-binaphthalene](2,5-norbornadiene)rhodium(i) Tetrafluoroborate (3b): Compound **3b** was obtained by the procedure described for **3a** except that after the addition of the ligand (*S*)-2-(diphenylphosphanyl)-2′-(isopropylthio)-1,1′-binaphthalene an orange solution was obtained. The solution was stirred for 1 h then concentrated. The orange precipitate formed after addition of pentane was recovered by filtration. Yield 99 mg (62%). ^{1}H NMR ($CDCl_3$, 298 K): δ = 1.18 (d, J = 6.6 Hz, 3 H, CH_3), 1.28 (d, J = 6.6 Hz, 3 H, CH_3), 1.50 [s, 2 H, CH_2 (NBD)], 3.88 (sept, J = 6.6 Hz, 1 H, CH), 4.00 [s, 2 H, allylic CH (NBD)], 4.50 [s, 2 H, olefinic CH (NBD)], 4.6 [s, 2 H, olefinic CH (NBD)], 5.95 (d, J = 8.1 Hz, 1 H, Ar), 6.71−6.80 (m, 4 H, Ar), 6.94 (d, J = 8.4 Hz, 1 H, Ar), 7.21−7.58 (m, 11 H, Ar), 7.73 (d, J = 7.8 Hz, 1 H, Ar), 7.98 (m, 2 H, Ar), 8.14 (d, J = 8.7 Hz, 1 H, Ar), 8.27 (d, J = 8.7 Hz, 1 H, Ar) ppm. $^{31}P\{^{1}H\}$ NMR ($CDCl_3$, 298 K): δ = 26.8 [d, ^{1}J(Rh,P) = 161 Hz] ppm. $[\alpha]_D^{25}$ = −386 (c = 0.5, $CHCl_3$).

X-ray Structural Determination of 3a: X-ray diffraction data for **3a** were collected at 293 K with a Bruker diffractometer (SMART) (Mo-K_α radiation, λ = 0.71073 Å) and corrected for absorption. $C_{41}H_{32}BCl_3F_4PRhS$, M_r = 883.77, triclinic, space group $P\bar{1}$, a = 9.1724(7), b = 10.7757(7), c = 10.9453(8) Å, α = 68.456(2), β = 88.282(2), γ = 72.591(2)°, V = 956.2(1) Å^3, Z = 1, d_c = 1.535 g·cm^{-3}, μ = 0.802 mm^{-1}, F(000) = 446, 11681 reflections measured, refinement on F^2 (8621 independent reflections) for 446 parameters, $wR2$ (on F^2, all data) = 0.0906, $R1$ [on F, $I > 2\sigma(I)$] = 0.0358. The computer program SHELXL-97[20] was used for structure solution and refinement. All non-H atoms were treated anisotropically. The naphthyl moieties were refined as rigid groups. Hydrogen atoms were added in calculated positions and refined riding on their respective C atoms. For all molecular representations the graphic program SCHAKAL99[21] was used. Intermolecular interactions were calculated by means of the program PLATON.[22] CCDC-189656 contains the supplementary crystallographic data for this paper. These data can be obtained free of charge at www.ccdc.cam.ac.uk/conts/retrieving.html or from the Cambridge Crystallographic Data Centre, 12 Union Road, Cambridge CB2 1EZ, UK [Fax: (internat.) + 44-1223/336-033; E-mail: deposit@ccdc.cam.ac.uk].

[1] C. S. Slone, D. A. Weinberger, C. A. Mirkin, "The Transition Metal Coordination Chemistry of Hemilabile Ligands", in: *Progress in Inorganic Chemistry* (Ed.: K. D. Karlin), John Wiley and Sons, New York, **1999**, vol. 48, p. 233.

[2] O. Pàmies, M. Diéguez, G. Net, A. Ruiz, C. Claver, *Organometallics* **2000**, *19*, 1488−1496.

[3] M. Tschoerner, G. Trabesinger, A. Albinati, P. S. Pregosin, *Organometallics* **1997**, *16*, 3447−3453.

[4] E. Hauptman, R. Shapiro, W. Marshall, *Organometallics* **1998**, *17*, 4976−4982.

[5] X. Verdaguer, A. Moyano, M. A. Pericàs, A. Riera, M. A. Maestro, J. Mahía, *J. Am. Chem. Soc.* **2000**, *122*, 10242−10243.

[6] H. Nakano, Y. Okuyama, M. Yanagida, H. Hongo, *J. Org. Chem.* **2001**, *66*, 620−625.

[7] D. A. Evans, K. R. Campos, J. S. Tedrow, F. E. Michael, M. R. Gagné, *J. Org. Chem.* **1999**, *64*, 2994−2995.

[8] E. Hauptmann, P. J. Fagan, W. Marshall, *Organometallics* **1999**, *18*, 2061−2073.

[9] S. Gladiali, A. Dore, D. Fabbri, *Tetrahedron: Asymmetry* **1994**, *5*, 1143−1146.

[10] J. Kang, S. H. Yu, J. I. Kim, H. G. Cho, *Bull. Korean Chem. Soc.* **1995**, *16*, 439−443.

[11] S. Gladiali, S. Medici, G. Pirri, S. Pulacchini, D. Fabbri, *Can. J. Chem.* **2001**, *79*, 670−678.

[12] P. Pertici, F. D'Arata, C. Rosini, *J. Organomet. Chem.* **1996**, *515*, 163−171.

[13] K. Toriumi, T. Ito, H. Takaya, T. Souchi, R. Noyori, *Acta Crystallogr., Sect. B* **1982**, *38*, 807−812.

[14] [14a] F. Grepioni, G. Cojazzi, S. M. Draper, N. Scully, D. Braga, *Organometallics* **1998**, *17*, 296−307. [14b] D. Braga, F. Grepioni, in: *Current Challenges on Large Supramolecular Assemblies* (Ed.: G. Tsoucaris), Kluwer Academic Publishers, Dordrecht, The Netherlands, **1998**, p. 173.

[15] A. Albinati, J. Eckert, P. S. Pregosin, H. Rüegger, R. Salzmann, C. Stössel, *Organometallics* **1997**, *16*, 579−590.

[16] M. Valentini, K. Selvakumar, M. Wörle, P. S. Pregosin, *J. Organomet. Chem.* **1999**, *587*, 244−251.

[17] E. Rotondo, G. Battaglia, C. G. Arena, F. Faraone, *J. Organomet. Chem.* **1991**, *419*, 399−402.

[18] S. Gladiali, A. Dore, D. Fabbri, S. Medici, G. Pirri, S. Pulacchini, *Eur. J. Org. Chem.* **2000**, *3*, 2861−2865.

[19] A. Miyashita, H. Takaya, T. Souchi, R. Noyori, *Tetrahedron* **1984**, *40*, 1245. In a previous work we failed to reproduce this result.

[20] G. M. Sheldrick, *SHELXL-97, Program for Crystal Structure Determination*; University of Göttingen, Göttingen, Germany, **1997**.

[21] E. Keller, *SCHAKAL99, Graphical Representation of Molecular Models*; University of Freiburg, Germany, **1999**.

[22] PLATON: A. L. Spek, *Acta Crystallogr., Sect. A* **1990**, *46*, C31.

Received July 14, 2002
[I02384]

Activation of C−S Bonds in Organosulfur Compounds Containing α,β-Unsaturated Ketone Systems by Carbonylruthenium and -iron Complexes

Cecilio Alvarez-Toledano,[a] Esther Delgado,*[b] Bruno Donnadieu,[c] M. Angeles Gómez,[b] Elisa Hernández,[b] Gema Martín,[b] Fernando Ortega-Jiménez,[a] and Félix Zamora[b]

Keywords: Vinylidene ligands / Clusters / Iron / Carbonyl ligands / Ruthenium

Vinylidenetetraruthenium clusters have been obtained from the reactions between $[Ru_3(CO)_{12}]$ and $[CH_3C(O)CH=C(SCH_3)_2]$ or $[(C_5H_5)Fe\{C_5H_4CH=CHC(O)CH=C(SCH_2CH_2S)\}]$ by cleavage of the S–C sp^2 bonds in these ligands. An excess of $[CH_3C(O)CH=C(SCH_3)_2]$ afforded the dinuclear complex $[Ru_2(CO)_4(\mu\text{-}SCH_3)_2\{\eta^2\text{:}\kappa\text{-}C,O\text{-}C(SCH_3)CHC(O)CH_3\}_2]$, which was then converted into the vinylidene cluster $[Ru_4(CO)_{10}(\mu\text{-}SCH_3)_2\{\mu_4,\eta^3\text{:}\kappa\text{-}C,C,O\text{-}C{=}CHC(O)CH_3\}]$ in the presence of more of the carbonylruthenium complex. However, the carbonyliron complex led to the formation of the dinuclear compounds $[Fe_2(CO)_4(\mu\text{-}SCH_3)_2\{\eta^2\text{:}\kappa\text{-}C,O\text{-}(SCH_3)CHC(O)CH_3\}_2]$ and $[Fe_2(CO)_5\{\mu,\eta^4\text{:}\kappa\text{-}C,O,S,S\text{-}(SCH_2CH_2S)C{=}CHC(O)CH{=}CHC_5H_4\}Fe(C_5H_5)]$. All of the new complexes exhibit a pentametallacycle group as a consequence of the rupture of the S–C bonds, as well as the presence of the C(O)R substituent in these ligands. The compounds have been characterised by analytical and spectroscopic data and the crystal structures of some of them have been solved by X-ray diffraction.

(© Wiley-VCH Verlag GmbH & Co. KGaA, 69451 Weinheim, Germany, 2003)

Introduction

The chemistry of transition metals with organosulfur ligands is being widely developed due to its importance in a variety of applications such as hydrodesulfurisation processes, bioinorganic chemistry and synthetic procedures.[1] The activation of S−C bonds is known in the synthesis of sulfur cluster compounds.[2] We have previously reported[3] that the reaction between $Ru_3(CO)_{12}$ and $S(C{\equiv}CSiMe_3)_2$ affords two compounds $[Ru_3(CO)_9(\mu,\eta^2\text{-}SC{\equiv}CSiMe_3)(\mu_3,\eta^2\text{-}C{\equiv}CSiMe_3)]$ and $[Ru_4(CO)_9(\mu\text{-}CO)_2(\mu_4\text{-}S)(\mu_4,\eta^2\text{-}C(SiMe_3)C(C{\equiv}CSiMe_3)]$ by cleavage of one or two of the S−C bonds in the sulfide ligand.

On the other hand, although clusters containing vinylidene ligands bonded to several metals have been considered as models in processes that imply the formation of hydrocarbons, as far as we know not many homopolynuclear derivatives have been prepared.[4]

Finally, in spite of the use of carbonyliron and -ruthenium compounds containing α,β-unsaturated ketone systems as precursors in organic syntheses,[5] there are few reports on the coordination chemistry of these multifunctional ligands with transition metals.[6]

Taking all of the above into account we are interested in exploring the chemistry of carbonylruthenium and -iron complexes and some organosulfur ligands, which have an α,β-unsaturated ketone group in common, in order to prepare some vinylidene clusters. Here, we report on the preparation of some dinuclear and cluster compounds containing pentametallacycle and thiolate groups. These compounds have been characterised by analytical and spectroscopic data and the structures of some of them have been confirmed by X-ray diffraction.

Results and Discussion

Treatment of $[Ru_3(CO)_{12}]$ and $[CH_3C(O)CH=C(SCH_3)_2]$ (1:1 stoichiometry) in the presence of $ONMe_3$ in toluene at 85 °C afforded the new compound $[Ru_4(CO)_{10}(\mu\text{-}SCH_3)_2\{\mu_4,\eta^3\text{:}\kappa\text{-}C,C,O\text{-}C{=}CHC(O)CH_3\}]$ (**1**) (Scheme 1) which was isolated in 35% yield as orange crystals after purification by column chromatography on silica gel, followed by recrystallisation from hexane at −20 °C. Compound **1** was characterised by analytical and spectroscopic data. The ν(CO) pattern in the carbonyl region is similar to that observed for the vinylidene derivatives $[Ru_4(CO)_{10}(\mu_4,\eta^2\text{-}C{=}CH\textit{i}Pr)(OR)(PPh_2)]$ (R = H, Et).[7] On the other hand, ^1H NMR resonances at δ = 4.50

[a] Instituto de Química-UNAM, Circuito Exterior, Ciudad Universitaria,
Coyoacán,
C. P. 04510, México D. F., México
[b] Departamento de Química Inorgánica, Facultad de Ciencias, Universidad Autónoma de Madrid,
28049 Madrid, Spain
Fax: (internat.) + 34-91/397-4833
E-mail: esther.delgado@uam.es
[c] Service de Cristallochimie, Laboratoire de Chimie de Coordination CNRS,
31077 Toulouse, France

[C(O)CH=C], 2.70 and 2.20 (SCH_3) and 2.00 ppm [$C(O)CH_3$] are shifted in comparison with those of the ligand {δ = 6.02 [C(O)CH=C], 2.46 and 2.43 (SCH_3), 2.18 ppm [$C(O)CH_3$]}. A single-crystal X-ray diffraction study on compound **1** confirmed the formation of a vinylidenetetraruthenium compound by rupture of the two S−C bonds in the ligand. Examples of activation of the S−C bonds in the synthesis of clusters are known. Thus, the thioketene $C_6H_6Me_4C_2S$ derivative in its reaction with $[Os_3Pt(\mu\text{-}H)_2(CO)_{10}(PCy_3)]$ generates a heteronuclear compound bearing a terminal vinylidene ligand[8] and the triosmium cluster $[Os_3(CO)_9(\mu\text{-}H)(\mu\text{-}SPh)\{\mu_3,\eta^2\text{-}(CCH_2CH_2C)\}]$ has been isolated from cyclobutenyl thioether.[2a] We have also previously reported the synthesis of ruthenium clusters by thermolysis of $[Ru_3(CO)_{12}]$ and $S(C{\equiv}CSiMe_3)_2$.[3]

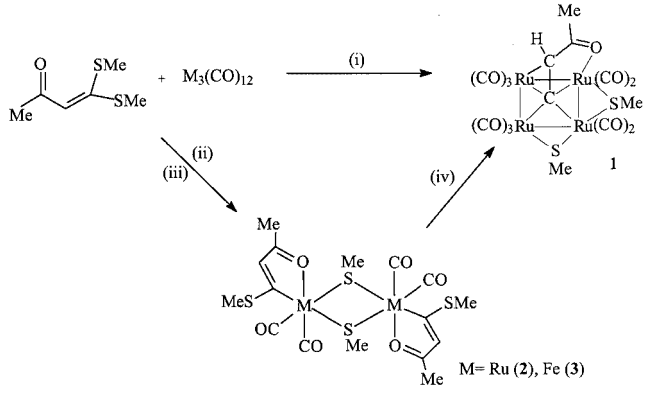

Scheme 1. (i) $ONMe_3$, toluene, 85 °C, 1:1 stoichiometry; (ii) $ONMe_3$, toluene, 85 °C, 3:1 stoichiometry; (iii) $ONMe_3$, THF, room temp., 1:1 stoichiometry; (iv) $[Ru_3(CO)_{12}]$, $ONMe_3$, toluene, 85 °C

Although several clusters with vinylidene ligands have been reported, as far as we know only a few examples of homotetrametallic compounds containing a μ_4-C=CRR′ or μ_4-C=CR_2 group have been described. Compounds $[Ru_4(CO)_{10}(\mu_4,\eta^2\text{-}C{=}CHiPr)(OR)(PPh_2)]$ (R = H, Et),[7] have been obtained in moderate yield by reaction of $[Ru_4(CO)_{11}(PPh_2C{\equiv}CR)]$ in wet THF, while the complexes $[Fe_4(CO)_{12}\{\mu_4,\eta^2\text{-}C{=}C(OMe)R\}]$ (R = OMe, Me)[9a] have been synthesised in high yield by methylation of the anionic clusters $[Fe_4(CO)_{12}\{CC(O)(OMe)\}]^-$ or $[Fe_4(CO)_{12}\{CC(O)(Me)\}]^-$, the former cluster being the precursor for $[Fe_4(CO)_{12}\{\mu_4,\eta^2\text{-}C{=}C(OMe)H\}]$.[9b] The reaction between $[Os_4(CO)_{12}(\mu_3\text{-}S)]$ and PhC≡CH affords the cluster $[Os_4(CO)_{12}(\mu_3\text{-}S)\{\mu_4,\eta^2\text{-}C{=}C(Ph)H\}]$.[9c] The known compound $[Ru_2(CO)_6(\mu\text{-}SCH_3)_2]$[10] was also obtained from this reaction in trace amounts along with compound **1**.

The same reaction, carried out with an excess of the ligand, yielded the new compound $[Ru_2(CO)_4(\mu\text{-}SCH_3)_2\{\eta^2{:}\kappa\text{-}C,O\text{-}C(SCH_3)CHC(O)CH_3\}_2]$ (**2**) in 45% yield. Compound **2** exists as a mixture of two isomers (*syn*/*anti*) in a 20:80 ratio, as determined from ^1H NMR spectroscopic data, that could be separated by chromatography. The major isomer gave suitable crystals for X-ray diffraction studies (Figure 2). The two IR bands observed at 2028, 1970 (*anti*) and 2044, 1988 cm^{-1} (*syn*) are expected for compounds of the type $[Ru(CO)_2L_2]_2$.[11] In the ^1H NMR spectrum, in addition to the resonance corresponding to the CH_3 group [δ = 2.12 (*anti*) and δ = 2.12 ppm (*syn*)], two more signals appear in this region at δ = 2.39 and 2.42 (*anti*), δ = 2.33 and 2.41 ppm (*syn*) that are indicative of the presence of two inequivalent SCH_3 groups. The FAB^+ mass spectrum of compound **2** reveals a molecular ion at *m*/*z* = 638 in agreement with this formulation. Conversion of the dinuclear compound **2** to the cluster **1** occurred on heating the former at 85 °C in toluene (Scheme 1).

The compound $[Ru_4(CO)_{10}(\mu\text{-}SCH_3)_2\{\mu_4,\eta^3{:}\kappa\text{-}C,C,O\text{-}C{=}CHC(O)CH_3\}]$ (**1**) contains two crystallographically independent molecules in the asymmetric unit. The discussion will be limited to only one of these molecules. An ORTEP illustration of compound **1** is given in Figure 1. Selected interatomic distances and angles are shown in Table 1.

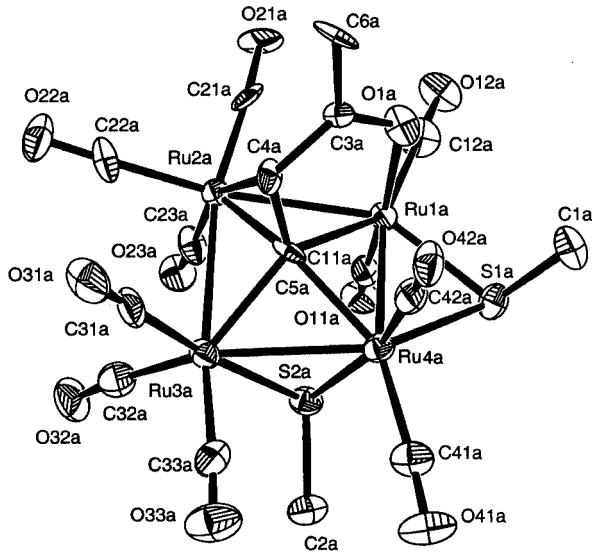

Figure 1. Molecular structure of compound **1**

Table 1. Selected distances [Å] and angles [°] for compound **1**

Ru(1)−Ru(2)	2.8306(14)	Ru(2)−C(5)	2.002(16)
Ru(2)−Ru(3)	2.923(2)	Ru(2)−C(4)	2.206(14)
Ru(1)−Ru(4)	2.7869(19)	Ru(3)−C(5)	2.137(13)
Ru(3)−Ru(4)	2.8009(14)	Ru(1)−C(5)	2.210(13)
Ru(1)−O(1)	2.108(10)	Ru(4)−C(5)	2.135(15)
Ru(1)−S(1)	2.368(4)	O(1)−C(3)	1.281(17)
Ru(3)−S(2)	2.403(4)	C(4)−C(5)	1.43(19)
Ru(4)−S(2)	2.424(4)	C(3)−C(4)	1.45(2)
Ru(4)−Ru(1)−Ru(2)	90.72(5)	C(3)−O(1)−Ru(1)	114.5(8)
Ru(4)−Ru(3)−Ru(2)	88.56(4)	O(1)−C(3)−C(4)	119.0(12)
Ru(1)−Ru(2)−Ru(3)	86.80(5)	C(3)−C(4)−C(5)	115.0(12)
Ru(1)−Ru(4)−Ru(3)	90.08(5)		

The four ruthenium atoms form a distorted rectangular geometry with three similar distances [Ru(1)−Ru(4) 2.7869(19), Ru(1)−Ru(2) 2.8306(14), Ru(3)−Ru(4) 2.8009(14) Å] and one that is slightly longer [Ru(2)−Ru(3) 2.923(2) Å] but still within the normal range found for other ruthenium clusters.[3,12] Although compounds

$[Ru_4(CO)_{10}(\mu_4,\eta^2\text{-}C{=}CH\textit{i}Pr)(OR)(PPh_2)]$ (R = H, Et)[7] and $[Fe_4(CO)_{12}\{\mu_4,\eta^2\text{-}C{=}C(OMe)R\}]$ (R = OMe, Me)[9a] show a butterfly geometry, a rhombus frame has been observed in the compound $[Os_4(CO)_{12}(\mu_3\text{-}S)\{\mu_4,\eta^2\text{-}C{=}C(Ph)H\}]$.[9c]

The breaking of two S−C sp^2 bonds in $[CH_3C(O)CH{=}C(SCH_3)_2]$ affords two methylthiolate ligands that are joined to three Ru atoms of the cluster framework. The remaining vinylidene group is coordinated to the four metal atoms at the C-α atom while the C-β atom is only attached to the Ru(2) atom. It is worth noting that the presence of the $C(O)CH_3$ group as a substituent on the C=CHR ligand allows the formation of a pentametallacycle. The cluster shell is completed by ten terminal carbonyl ligands. Most of the vinylidene tetranuclear cluster show a μ_4-η^2 coordination mode, such as has been observed in compound **1**. However, in the clusters $[Fe_4(CO)_{12}\{\mu_4,\eta^2\text{-}C{=}C(OMe)R\}]$ (R = OMe, Me)[9a] this ligand only acts towards the C-α atom.

The Ru−S distances [2.368(4), 2.335(4), 2.403(4) and 2.424(4) Å] are similar to the values reported for other thiolate-bridged complexes, $[Ru_3(CO)_9(\mu,\eta^2\text{-}SC{\equiv}CSiMe_3)(\mu_3,\eta^2\text{-}C{\equiv}CSiMe_3]$ [2.4353(7) and 2.4337(7) Å][3] and $[Ru_3(CO)_9(\mu\text{-}SEt)(\mu_3,\eta^2\text{-}C{\equiv}CPh)]$ [2.424(2) and 2.4116(2) Å].[13] The C(4)−C(5) distance [1.43(19) Å] for compound **1** is similar to those observed in $[Ru_4(CO)_{10}(\mu_4,\eta^2\text{-}C{=}CH\textit{i}Pr)(OH)(PPh_2)]$ [1.415 Å],[7] $[Ru_5(\mu\text{-}H)(\mu_4\text{-}\eta^2\text{-}C{=}CHPPh_2)(\mu\text{-}PPh_2)(CO)_{13}]$ [1.435(5) Å],[12] $[Ru_3H_2(\mu_3,\eta^2\text{-}C{=}C(CH_3)(C_6H_5)(CO)_9]$[14] [1.379(8) Å], and $[Os_4(CO)_{12}(\mu_3\text{-}S)\{\mu_4,\eta^2\text{-}C{=}C(Ph)H\}]$[9c] [1.446(16) Å]. The C(3)−O(1) distance of 1.281(17) Å is slightly longer than expected for a C=O bond [1.20 Å], which is indicative of the existence of a σ-bond between the oxygen atom of the ketone group and the Ru(1) atom.

This arrangement of the four Ru−Ru bonds is consistent with an electron count of 64 electrons achieved when the two methylthiolate ligands as well as the vinylidene $C{=}CHC(O)CH_3$ group each contribute six electrons.

The molecular structure of the *anti* isomer of $[Ru_2(CO)_4(\mu\text{-}SCH_3)_2\{\eta^2\text{:}\kappa\text{-}\textit{C},\textit{O}\text{-}C(SCH_3)CHC(O)CH_3\}_2]$ (**2**) is illustrated in Figure 2 and selected bond lengths and angles are given in Table 2. Compound **2** crystallises in the space group $P\bar{1}$ and is centrosymmetric. The cleavage of one $C{-}SCH_3$ bond in the disulfide ligand leads to the $C(SCH_3)CHC(O)CH_3$ group that acts as a three-electron donor making a pentaruthenacycle around each Ru atom. Both metal units are linked through two bridging methylthiolate ligands. The intramolecular distance between the ruthenium atoms [3.634(2) Å] suggests that there is no bonding interaction, while the Ru−S distances [2.4599(10) and 2.4352(11) Å] are slightly longer than those observed for compound **1**. The C(12)−Ru−S(1) [177.63(8)°] and C(1)−Ru−S′(1) [168.00(7)°] angles are indicative of a *cis* position for the two CO ligands. The equatorial plane of the octahedron seems to consist of the S(1), S′(1), C(1) and C(12) atoms. The remaining CO ligand and O(1) atom are located in the apical positions. The distances Ru−O(1) [2.1109(18) Å] and O(1)−C(3) [1.270(3) Å] are similar to those reported in the related compounds $[RuCl\{\textit{o}\text{-}C_6H_3CH_3C(O)C_6H_4CH_3\}(CO)(PMe_2Ph)]$,[15] $[RuCl\{\textit{o}\text{-}C_6H_4C(O)C_6H_4CH_3\}(CO)(PPh_3)]$,[16] and $[RuCl\{{=}C(CH_2Ph)OC(O)H\}(P\textit{i}Pr_3)]$.[17]

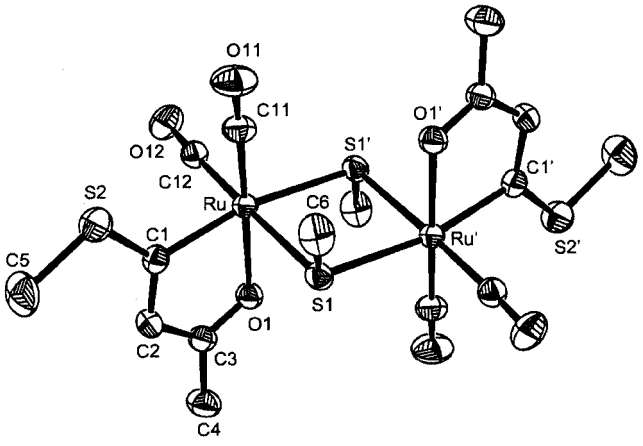

Figure 2. View of the *anti* isomer of compound **2**

Table 2. Selected interatomic distances [Å] and angles [°] for compound **2**

C(1)−C(2)	1.372(4)	C(11)−Ru	1.854(3)
C(1)−Ru	2.055(2)	C(12)−Ru	1.894(3)
C(3)−O(1)	1.270(3)	S(1)−Ru	2.4352(11)
C(2)−C(3)	1.411(4)	Ru−S(1)′1	2.4599(10)
O(1)−Ru	2.1109(18)	Ru−Ru′	3.634(2)
O(1)−C(3)−C(2)	119.9(2)	C(12)−Ru−S(1)	177.63(8)
C(2)−C(1)−Ru	113.16(18)	C(1)−Ru−S(1′)	168.00(7)
C(1)−C(2)−C(3)	115.4(2)	S(1)−Ru−S(1′)	84.13(4)
C(3)−O(1)−Ru	112.77(16)	O(1)−Ru−C(11)	173.24(8)
C(1)−Ru−O(1)	78.57(9)		

We have previously reported[6b] that the reaction of $[Fe_2(CO)_9]$ and $C_6H_5CH{=}CHC(O)CH{=}C(SCH_2CH_2S)$, in diethyl ether at room temperature, affords the compound $[Fe_2(CO)_5\{\mu,\eta^4\text{:}\kappa\text{-}\textit{C},\textit{O},\textit{S},\textit{S}\text{-}(SCH_2CH_2SC{=}CHC(O)CH{=}CHC_6H_5\}]$ by rupture of one S−C bond. On the other hand, taking into account that treatment of $Ru_3(CO)_{12}$ with $[CH_3C(O)CH{=}C(SCH_3)_2]$ yields the new cluster **1**, reported here, we were interested to know whether the use of $[Fe_3(CO)_{12}]$ instead of $[Fe_2(CO)_9]$, in the presence of $ONMe_3$ under mild conditions, leads to an iron cluster by reaction with $[CH_3C(O)CH{=}C(SCH_3)_2]$. Unfortunately, in this case, the reaction carried out by heating in toluene affords the expected vinylidene compound in trace amounts only, with $[Fe_2(CO)_6(\mu\text{-}SCH_3)_2]$ being the main product. However, the dinuclear compound $[Fe_2(CO)_4(\mu\text{-}SCH_3)_2\{\eta^2\text{:}\kappa\text{-}\textit{C},\textit{O}\text{-}C(SCH_3)CHC(O)CH_3\}_2]$ (**3**) was obtained at room temperature in THF in 25% yield (Scheme 1). The spectroscopic data are similar to those shown for compound **2**. In the FAB^+ mass spectrum peaks analogous to those observed in **2** corresponding to the molecular ion and the loss of CO groups were found.

Compound **3** was not converted into a vinylidene cluster on reaction with more carbonyliron compound, showing a

different behaviour from that observed in the analogous ruthenium case.

Following our research interest to synthesize vinylidene derivatives we decided to prepare [(C_5H_5)Fe{C_5H_4CH=CHC(O)CH=C(SCH_2CH_2S)}] (**4**), which is similar to the ligand studied before with an α,β-unsaturated ketone system. The presence of one more C=C bond in the chain as well as the active redox ferrocenyl group could lead to differences in its reactivity. Compound **4** was prepared according to the procedure described in the literature for other analogous compounds[19] and was characterised by analytical and spectroscopic techniques (see Exp. Sect.).

Treatment of [$Ru_3(CO)_{12}$] with [(C_5H_5)Fe{C_5H_4CH=CHC(O)CH=C(SCH_2CH_2S)}] in the presence of $ONMe_3$ in toluene at 85°C afforded the tetraruthenium compound [$Ru_4(CO)_{10}$(μ_4,η^3:κ-*C*,*C*,*O*-(C=CHC(O)CH=CHC_5H_4)Fe(C_5H_5)}] (**5**) (Scheme 2), as was inferred from the presence of the molecular ion peak in the FAB^+ mass spectrum (*m*/*z* = 1041) as well as from the analytical data. The ν(CO) pattern in the carbonyl region is similar to that observed for compound **1** and other related derivatives [$Ru_4(CO)_{10}$(μ_4,η^2-C=CH*i*Pr)(OR)(PPh_2)] (R = H, Et).[7] In the ^{1}H NMR spectrum resonances that appear at δ = 4.07 [C(O)CH=C] and 3.29, 2.42, 2.26 ppm [SCH_2CH_2S] are shifted in comparison with those of the ligand [δ = 6.77 ppm for C(O)CH=C; δ = 3.43, 3.35 ppm for SCH_2CH_2S]. It was found that the same chemical shift occurs as was observed in **1** for the [C(O)CH=C] resonance.

Finally, the reaction carried out between [$Fe_3(CO)_{12}$] and [(C_5H_5)Fe{C_5H_4CH=CHC(O)CH=C(SCH_2CH_2S)}] with $ONMe_3$ in THF at room temperature for 2 h yielded three compounds after chromatographic workup (Scheme 2). The first band, that appeared as traces from the column, gave an orange solid which was identified by IR and ^{1}H NMR spectroscopic data as the known compound [$Fe_2(CO)_6$(μ-SCH_2CH_2S)].[20] The second band afforded the main compound [$Fe(CO)_3${(C_5H_5)Fe{η^4:κ-(*C*=*C*,*C*=*O*)-C_5H_4CH=CHC(O)CH=C(SCH_2CH_2S)}}] (**6**) in 23% yield; its structure was confirmed by X-ray diffraction. A small amount of [$Fe_2(CO)_5$(μ,η^4:κ-*C*,*O*,*S*,*S*-SCH_2CH_2SC=CHC(O)CH=CHC_5H_4}Fe(C_5H_5)] (**7**) was obtained from the third band of the column. We have observed that if the reaction time is increased to 48 h, compound **7** is the main product of this reaction.

Compound **6** is formed by coordination of the $Fe(CO)_3$ fragment towards both the ketone group and the C=C bond of the ligand. The IR spectrum in the carbonyl region is similar to that found in the analogous compound [η^4-{(3*E*)-4-phenyl-1-(1,3-dithiolan-2-ylidene)butene-2-one}$Fe(CO)_3$] recently prepared by us.[6b] The ^{1}H NMR spectrum of compound **6** shows, as a prominent feature, two signals at δ = 5.71 and 3.38 ppm ($^3J_{H,H}$ = 8.7 Hz), corresponding to the protons of the coordinated CH=CHC(O) group which are shifted upfield with respect to the free ligand. A view of compound **6** with the atom numbering scheme is shown in Figure 3. Selected interatomic distances and angles are presented in Table 3. The coordination geometry of Fe(2) can be described as a distorted trigonal bipyramid with the atoms C(20), C(30) of the carbonyl groups and the C(2)−C(3) double bond in the equatorial positions, while the O(1) atom and the C(10) atom of the carbonyl group are located in the apical positions. The ferrocene unit is not affected much by the coordination of the $Fe(CO)_3$ moiety and the distances and angles are in the usual range found in many other ferrocene derivatives. The enone moiety and the 1,3-dithiolane ring shows only slight deviations from the analogous fragment present in [$Fe(CO)_3${η^4-H_5C_6CHCHC(O)CHC(SCH_2CH_2S)}].[6b] The comparison of the Fe−CO distance of the carbonyl group *trans* to the oxygen atom of the enone and the rest of the carbonyl groups suggests a *trans* influence.

Finally, the breaking of only one S−C bond in [(C_5H_5)Fe{(C_5H_4CH=CHC(O)CH=C(SCH_2CH_2S)}] generated [$Fe_2(CO)_5${μ,η^4-SCH_2CH_2SC=CHC(O)CH=CH-C_5H_4}Fe(C_5H_5)] (**7**). The analogous compound [{(3*E*)-4-phenyl-1-(1,3-dithiolan-2-ylidene)butene-2-one}$Fe_2(CO)_5$], whose structure has been confirmed by X-ray diffraction, was formed in a similar manner.[6b] The ν(CO) pattern is similar in both compounds. In the FAB^+ spectrum, a peak observed at *m*/*z* = 609 corresponding to the molecular ion

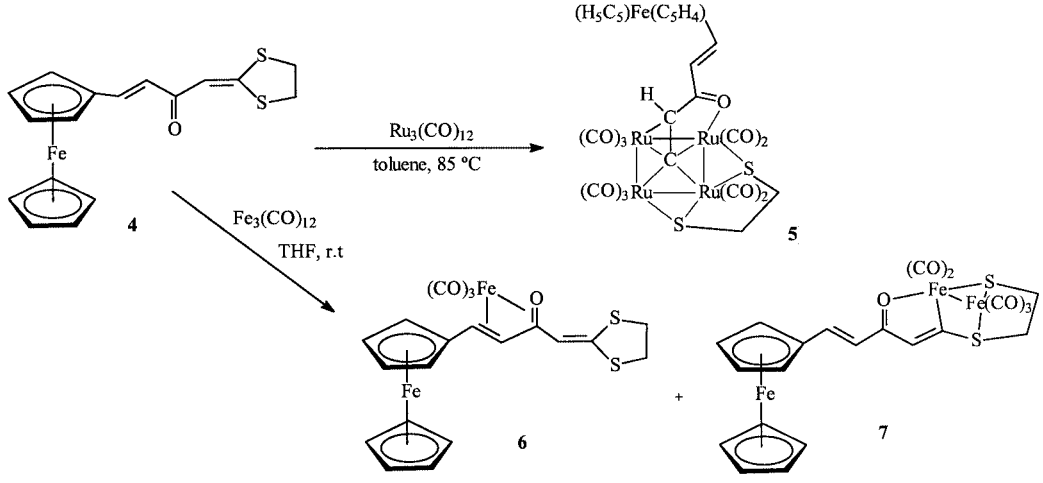

Scheme 2

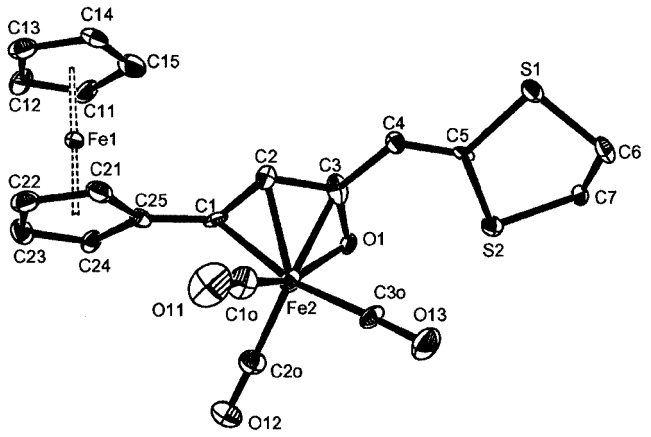

Figure 3. Structure of compound **6**

Table 3. Selected distances [Å] and angles [°] for compound **6**

Fe(1)−Cp(1)	1.632	Fe(2)−C(2)	2.043(10)
Fe(1)−Cp(2)	1.633	Fe(2)−C(3)	2.086(10)
Fe(2)−C(10)	1.742(13)	O(1)−C(3)	1.324(12)
Fe(2)−C(20)	1.805(12)	C(1)−C(2)	1.415(14)
Fe(2)−C(30)	1.799(11)	C(2)−C(3)	1.403(14)
Fe(2)−O(1)	2.036(6)	C(3)−C(4)	1.453(14)
Fe(2)−C(1)	2.162(10)	C(4)−C(5)	1.353(14)
Cp(1)−Fe(1)−Cp(2)	178.26	C(20)−Fe(2)−C(3)	139.3(4)
C(10)−Fe(2)−C(20)	90.7(5)	C(30)−Fe(2)−C(2)	128.8(4)
C(20)−Fe(2)−C(30)	99.2(4)	C(30)−Fe(2)−C(3)	96.2(4)
C(10)−Fe(2)−O(1)	159.8(4)	O(1)−C(3)−C(2)	114.5(8)
C(20)−Fe(2)−O(1)	104.8(4)	O(1)−C(3)−C(4)	121.5(9)
C(30)−Fe(2)−O(1)	90.3(4)	C(4)−C(5)−S(1)	120.7(8)
C(10)−Fe(2)−C(1)	98.2(4)	C(4)−C(5)−S(2)	125.1(7)
C(10)−Fe(2)−C(2)	95.6(4)	C(1)−C(2)−C(3)	118.4(9)
C(10)−Fe(2)−C(3)	122.5(5)	C(2)−C(3)−C(4)	24.0(9)
C(20)−Fe(2)−C(1)	91.4(4)	C(5)−S(1)−C(6)	95.5(5)
C(20)−Fe(2)−C(2)	130.46(12)		

and the analytical data are in agreement with this formulation. The ^{1}H NMR spectrum exhibits two doublet resonances at δ = 7.12 and 6.47 ppm assigned to the uncoordinated double bond, with a value of $^3J_{H,H}$ = 15.7 Hz similar to that observed in compound **5**. Additionally a singlet signal that appears at δ = 2.35 ppm [C(O)CHC] is strongly shifted to a higher field than that observed in the free ligand (δ = 6.79 ppm). The compounds **6** and **7** are obtained in similar yield to those prepared by us using $[Fe_2(CO)_9]$ and analogous ligands.

Conclusion

Compounds $[CH_3C(O)CH{=}C(SCH_3)_2]$ and $[(C_5H_5)Fe\{C_5H_4CH{=}CHC(O)CH{=}C(SCH_2CH_2S)\}]$ act as precursors of vinylidene groups by activation of the two S−C bonds in their reactions with $[Ru_3(CO)_{12}]$ but not with $[Fe_3(CO)_{12}]$. This has allowed the formation of new homonuclear vinylideneruthenium clusters, which is important when one considers the scarcity of literature reports on these complexes.

The cleavage of only one S−C bond from $[CH_3C(O)CH{=}C(SCH_3)_2]$ as well as the presence of the ketone group led to the compounds $[M_2(CO)_4(\mu\text{-}SCH_3)_2\{\eta^2{:}\kappa\text{-}C,O\text{-}C(SCH_3)CHC(O)CH_3\}_2]$ (M = Ru, Fe) containing two metallacycles.

The presence of SCH_2CH_2S instead of two SCH_3 groups in the ligand $[(C_5H_5)Fe\{C_5H_4CH{=}CHC(O)CH{=}C(SCH_2CH_2S)\}]$ seems to drive the formation of the compound $[Fe_2(CO)_5\{\mu,\eta^4\text{-}SCH_2CH_2SC{=}CHC(O)CH{=}CHC_5H_4\}Fe(C_5H_5)]$.

Experimental Section

General Remarks: All reactions were carried out under argon using Schlenk techniques. Solvents were dried according to standard methods. IR spectra were recorded with a Perkin−Elmer 1650 FTIR spectrophotometer using NaCl cells. ^{1}H NMR spectra were recorded with a Bruker AMX-300 instrument in $CDCl_3$. Elemental analyses were performed with a Perkin−Elmer 240-B microanalyser. FAB mass spectra were carried out with a WG AutoSpec spectrometer, using 3-nitrobenzyl alcohol as the matrix. $[CH_3C(O)CH{=}C(SCH_3)_2]$[19] was synthesised according to literature methods.

Synthesis of $[Ru_4(CO)_{10}(\mu\text{-}SCH_3)_2\{\mu_4,\eta^3{:}\kappa\text{-}C,C,O\text{-}C{=}CHC(O)CH_3\}]$ (1): An excess of $ONMe_3$ (0.103 g, 1.38 mmol) was added to a solution of $[Ru_3(CO)_{12}]$ (0.300 g, 0.46 mmol) and $[CH_3C(O)CH{=}C(SCH_3)_2]$. (0.076 g, 0.46 mmol) in toluene (30 mL). The mixture was stirred at 85 °C for 24 h to give an orange-brown solution. The solvent was removed under vacuum, and the residue was chromatographed on silica gel 100. Elution with hexane afforded $[Ru_2(CO)_6(\mu\text{-}SMe)_2]$ in low yield. A second band using *n*-hexane/toluene (4:1) gave compound **1** as the main product (0.136 g, 35% yield). Crystals of **1** were obtained from *n*-hexane at −20 °C. IR (THF): $\tilde{\nu}$ = 2080 (m), 2044 (vs), 2026 (s), 2012 (s), 1986 (m), 1969 (sh), 1955 (w) cm^{-1}. ^{1}H NMR ($CDCl_3$): δ = 4.50 [s, 1 H, C*H*C(O)], 2.70 (s, 3 H, SCH_3), 2.20 (s, 3 H, SCH_3), 2.00 [s, 3 H, C(O)CH_3] ppm. FAB$^+$: *m*/*z* = 846 [M$^+$], 818−566 [M$^+$ − *n* CO, *n* = 1−10]. $C_{16}H_{10}O_{11}Ru_4S_2$ (846.64): calcd. C 22.70, H 1.19; found C 22.83, H 1.44.

Synthesis of $[Ru_2(CO)_4(\mu\text{-}SCH_3)_2\{\eta^2{:}\kappa\text{-}C,O\text{-}C(SCH_3)CHC(O)CH_3\}_2]$ (2): $ONMe_3$ (0.092 g, 1.23 mmol) was added to a solution of $[Ru_3(CO)_{12}]$ (0.250 g, 0.39 mmol) and $[CH_3C(O)CH{=}C(SCH_3)_2]$ (0.200 g, 1.23 mmol) in toluene (30 mL). The mixture was stirred at 85 °C for 24 h. Removal of the solvent and chromatography on silica gel gave the first band of compound **1** in trace amounts, eluted with *n*-hexane/toluene (4:1). A second band using toluene/THF (5:1) afforded $[Ru_2(CO)_4(\mu\text{-}SCH_3)_2\{\eta^2{:}\kappa\text{-}C,O\text{-}C(SCH_3)CHC(O)CH_3\}_2]$ (**2**) as the main product (0.75 g, 45% yield). Crystals of **2** were obtained by diffusion of hexane in THF at 0 °C. IR (toluene): *anti* isomer: $\tilde{\nu}$ = 2028 (s), 1970 (s) cm^{-1}; *syn* isomer: $\tilde{\nu}$ = 2044 (s), 1988 (s) cm^{-1}. ^{1}H NMR ($CDCl_3$): δ = 6.62 [s, 1 H, C*H*C(O)], 2.42 (s, 3 H, SCH_3, *anti* isomer), 2.41 (s, 3 H, SCH_3, *syn* isomer), 2.39 (s, 3 H, SCH_3, *anti* isomer), 2.39 (s, 3 H, SCH_3, *syn* isomer), 2.12 [s, 3 H, C(O)CH_3] ppm. FAB$^+$: *m*/*z* = 638 [M$^+$]. $C_{16}H_{20}O_6Ru_2S_4$ (638.71): calcd. C 30.11, H 3.13; found C 30.73, H 3.31.

Synthesis of $[Fe_2(CO)_4(\mu\text{-}SCH_3)_2\{\eta^2{:}\kappa\text{-}C,O\text{-}C(SCH_3)CH(CO)CH_3\}_2]$ (3): A solution of $[CH_3C(O)CH{=}C(SCH_3)_2]$ (0.068 g, 0.42 mmol) in THF (10 mL) was slowly added to a solution of $[Fe_3(CO)_{12}]$ (0.210 g, 0.42 mmol) and $ONMe_3$ (0.031 g, 0.42 mmol)

in THF. The resulting mixture was stirred at room temperature for 2.5 h. The solvent was then evaporated under vacuum to dryness and the residue chromatographed on silica gel 100. An orange band of $[Fe_2(CO)_6(\mu\text{-}SCH_3)_2]$ (trace) was obtained using *n*-hexane as the eluent. Further elution with *n*-hexane/THF (10:3) yielded a red band. The solvent was removed under vacuum and recrystallisation of the residue in THF/*n*-hexane at −20 °C yielded compound **3** (29 g, 25.9% yield). IR (THF): $\tilde{\nu}$ = 2017 (s), 1969 (s) cm^{-1}. ^1H NMR ($CDCl_3$): δ = 6.69 [s, 1 H, C*H*C(O)], 2.52 (s, 3 H, SCH_3), 2.35 (s, 3 H, SCH_3) 2.08 [s, 3 H, C(O)CH_3] ppm. FAB$^+$: *m*/*z* = 549.0 [M$^+$], 520.0 [M$^+$ − CO], 492.0 [M$^+$ − 2 CO], 436.0 [M$^+$ − 4 CO] ppm. $C_{16}Fe_2H_{20}O_6S_4$ (548.26): calcd. C 35.05; H 3.68; found C 34.88, H 3.62.

Synthesis of [(C$_5$H$_5$)Fe{C$_5$H$_4$CH=CHC(O)CH=C(SCH$_2$CH$_2$S)}] (4): This compound was prepared according to a procedure described for other analogous compounds.[17] Sodium hydroxide (0.125 g, 3.12 mmol) in EtOH (20 mL) was added to a solution of 1-(1,3-dithiolan-2-ylide)acetone (0.500 g, 3.12 mmol) in EtOH (30 mL). After 40 min of stirring, [(C$_5$H$_5$)Fe(C$_5$H$_5$CHO)] (0.067 g, 3.12 mmol) in EtOH (10 mL) was added. The mixture was stirred for 24 h affording a red precipitate. The solid compound was purified by column chromatography using *n*-hexane as the eluent (0.3 g, 27% yield). ^1H NMR ($CDCl_3$): δ = 7.52 [d, $^3J_{H,H}$ = 15.6 Hz, 1 H, *H*C=CHC(O)], 6.79 [s, 1 H, C(O)C*H*C], 6.39 [d, $^3J_{H,H}$ = 15.6 Hz, 1 H, HC=C*H*C(O)], 4.50 (t, $^3J_{H,H}$ = 1.8 Hz, 2 H, C_5H_4), 4.42 (t, $^3J_{H,H}$ = 1.8 Hz, 2 H, C_5H_4), 4.14 (s, 5 H, C_5H_5), 3.43 and 3.35 (m, 4 H, SCH_2CH_2S) ppm. FAB$^+$: *m*/*z* = 356 [M$^+$]. $C_{17}FeH_{16}OS_2$ (356.28): calcd. C 57.31; H 4.53; found C 56.90, H 4.59.

Reaction of Ru$_3$(CO)$_{12}$ and [(C$_5$H$_5$)Fe{C$_5$H$_4$CH=CHC(O)CH=C(SCH$_2$CH$_2$S)}]: The reaction was carried out according to the same procedure as for compound **1**, but leaving the reaction for 48 h. Chromatography on silica gel 100 afforded two compounds. Elution with hexane gave $[Ru_2(CO)_6(\mu\text{-}SCH_2CH_2S)]$ in a small amount, while hexane/toluene (5:3) gave the cherry-coloured compound **5** as the main product (0.100 g, 28% yield). IR (THF): $\tilde{\nu}$ = 2078 (m), 2045 (vs), 2028 (s), 2008 (s), 1974 (m) cm^{-1}. ^1H NMR ($CDCl_3$): δ = 7.30 [d, $^3J_{H,H}$ = 15.5 Hz, 1 H, *CH*CH*C*(O)], 6.13 [d, $^3J_{H,H}$ = 15.5 Hz, 1 H, CH*CHC*(O)], 4.50 (m, 4 H, C_5H_4), 4.10 (s, 5 H, C_5H_5), 4.07 [s, 1 H, C(O)C*H*C], 3.29 (m, 2 H, SCH_2), 2.42 (m, 1 H, SCH_2), 2.26 (m, 1 H, SCH_2) ppm. FAB$^+$: *m*/*z* = 1041 [M$^+$], 985 [M$^+$ − 2 CO], 957 [M$^+$ − 3 CO], 901 [M$^+$ − 5 CO], 873 [M$^+$ − 6 CO], 789 [M$^+$ − 9 CO], 761 [M$^+$ − 10 CO]. $C_{27}FeH_{16}O_{11}Ru_4S_2$ (1040.66): calcd. C 31.16, H 1.55; found C 31.53, H 1.67.

Reaction of Fe$_3$(CO)$_{12}$ and [(C$_5$H$_5$)Fe{C$_5$H$_4$CH=CHC(O)CH=C(SCH$_2$CH$_2$S)}]: A solution of [(C$_5$H$_5$)Fe{C$_5$H$_4$CH=CHC(O)CH=C(SCH$_2$CH$_2$S)}] (0.156 g, 0.44 mmol) in THF (5 mL) was slowly added to a mixture of $[Fe_3(CO)_{12}]$ (0.220 g, 0.44 mmol) and $ONMe_3$ (0.033 g, 0.44 mmol) in the same solvent (15 mL). The resulting mixture was stirred at room temperature for 2 h. Then the solvent was evaporated under vacuum to dryness and the residue chromatographed on silica gel 100. Using *n*-hexane as the eluent, an orange band of $[Fe_2(CO)_6(\mu\text{-}SCH_2CH_2S)]$ (trace) was obtained. Further elution with a mixture of *n*-hexane/toluene (10:1) yielded a red band of **6** (0.050 g, 23.0% yield). Subsequent elution with *n*-hexane/toluene (1:2) gave a red-brown band of compound **7** in trace amounts. Applying the same procedure and increasing the reaction time to 48 h, compound **7** was obtained in a 17.8% yield.

6: IR (THF): $\tilde{\nu}$ = 2052 (s), 1990 (s), 1975 (s), 1604 (w) cm^{-1}. ^1H NMR ($CDCl_3$): δ = 6.72 [s, 1 H, C(O)CHC], 5.71 [d, $^3J_{H,H}$ = 8.7 Hz, 1 H, *CH*CH*C*(O)], 4.42 (s, 1 H, C_5H_4), 4.20 (s, 2 H, C_5H_4), 4.16 (s, 1 H, C_5H_4), 4.13 (s, 5 H, C_5H_5), 3.38 [m, 5 H, SCH_2CH_2S and CHC*H*C(O)] ppm. FAB$^+$: *m*/*z* = 440 [M$^+$ − 2 CO], 412 [M$^+$ − 3 CO], 356 [M$^+$ − Fe − 3 CO]. $Fe_2S_2O_4C_{20}H_{16}$ (495.91): calcd. C 48.42, H 3.25; found C 48.12, H 3.61.

7: IR (THF): $\tilde{\nu}$ = 2052 (s), 2009 (vs), 1991 (s), 1975(sh), 1959 (w), 1946 (sh), 1647 (w) cm^{-1}. ^1H NMR ($CDCl_3$): δ = 7.12 [d, $^3J_{H,H}$ = 15.7 Hz, 1 H, *CH*CH*C*(O)], 6.47 [d, $^3J_{H,H}$ = 15.7 Hz,1 H,CHC*H*C(O)], 4.45 (m, 2 H, C_5H_4), 4.34 (m, 2 H, C_5H_4), 4.15 (s,

Table 4. Crystal data, data collection and structure refinement for the complexes

	1	**2**	**6**
Empirical formula	$C_{16}H_9O_{11}Ru_4S_2$	$C_{16}H_{20}O_6Ru_2S_4$	$C_{20}H_{16}Fe_2O_4S_2$
Formula mass	845.63	638.70	496.15
T [K]	160(2)	180(2)	180(2)
Crystal size [mm]	0.45 × 0.20 × 0.17	0.45 × 0.40 × 0.37	0.20 × 0.15 × 0.06
Colour	orange	orange	dark red
Crystal form	parallelepiped	parallelepiped	platelet
Crystal system	monoclinic	triclinic	monoclinic
Space group	$P2_1$	$P\bar{1}$	$P21/c$
a [Å]	9.680(2)	7.994(2)	6.2660(10)
b [Å]	15.217(3)	8.845(2)	30.673(6)
c [Å]	15.746(3)	8.961(2)	10.125(2)
α [°]	90	76.27(3)	90
β [°]	89.927(2)	69.58(3)	98.10(3)
γ [°]	90	82.62(3)	90
V [Å^3]	2319.4(8)	576.1(2)	1926.6(6)
Z	4	1	4
μ [mm^{-1}]	2.789	1.701	1.747
2θ range [°]	3.3−52.1	3.77−24.41	2.9−48.4
Reflections measured	18095	4381	7916
Reflections unique	8666	1631	2008
R	0.0358	0.0208	0.0863
R_w	0.0429	0.0518	0.1458
Goodness of fit	0.987	1.167	1.082

2 H, C_5H_4), 4.13 (s, 5 H, C_5H_5), 3.14 (m, 1 H, SCH_2CH_2S), 2.35 [s, 1 H, C(O)CHC], 2.20 (m, 3 H, SCH_2CH_2S) ppm. FAB$^+$: m/z = 609 [$M^+ + 1$], 580 [$M^+ - CO$], 552 [$M^+ - 2\ CO$], 524 [$M^+ - 3\ CO$], 496 [$M^+ - 4\ CO$], 468 [$M^+ - 5\ CO$]. $C_{22}Fe_3H_{16}O_6S_2$ (608.02): calcd. C 43.46, H 2.65; found C 42.38, H 2.58.

X-ray Crystallographic Studies: For all the compounds data have been collected at low temperature with an STOE Imaging Plate Diffraction System (IPDS), equipped with an Oxford Cryosystems Cryostream Cooler Device and using a graphite-monochromated Mo-K_α radiation (λ = 0.71073 Å). Crystal data and structure refinement parameters for compounds **1**, **2** and **6** are listed in Table 4. Final unit cell parameters have been obtained by using a least-squares refinement of a set of 5000 well-measured reflections, and crystal decay was monitored during data collection. No significant fluctuations of the intensity were observed. Structures were solved by Direct Methods using SIR92,[20] and subsequent difference Fourier maps refined by least-squares procedures on F^2 by using SHELXL-97[21] included in the package WINGX.[22] Atomic scattering factors were taken from the International Tables for X-ray Crystallography.[23] All hydrogen atoms were located on a difference Fourier map and refined by using a riding model with an isotropic thermal parameter fixed at 20% higher than those of the carbon atoms to which they are connected. For all structures all non-hydrogen atoms were anisotropically refined and in the last cycles of refinement a weighting scheme was applied, where weights have been calculated from the following formula: $w = 1/[\sigma^2(F_o^2) + (aP)^2 + bP]$ where $P = (F_o^2 + 2F_c^2)/3$. Drawings of the molecules were performed using the program ORTEP32[24] with 50% probability displacement ellipsoids for non-hydrogen atoms. The structure of compound **1** has been solved in the monoclinic cell (space group $P2_1$) with $\beta = 90°$ and may be emulated by an orthorhombic system of space group $P2_12_12$, all attempts to solve this structure in this system failed. We observed some characteristic warning signs of the presence of twinning in the data, notably a very low value for $E^2 - 1$ (= 0.63), lower than the expected value of 0.74 for the non-centrosymmetric case. Consequently, **1** was solved in the monoclinic system $P2_1$ by using the following twin law which allows to simultaneously refine general and racemic twinning: TWIN 1.00 0.00 0.00 0.00 − 1.00 0.00 0.00 0.00 − 1.00 −4. Application of this specific instruction led to a stable model which could be refined without any constraints or restraints and converged nicely. CCDC-183656 (**1**), -186787 (**2**), and -186357 (**6**) contain the supplementary crystallographic data for this paper. These data can be obtained free of charge at www.ccdc.cam.ac.uk/conts/retrieving.html [or from the Cambridge Crystallographic Data Centre, 12 Union Road, Cambridge CB2 1EZ, UK; Fax: (internat.) + 44-1223/336-033; E-mail: deposit@ccdc.cam.ac.uk].

Acknowledgments

Financial support was generously provided by the Dirección General de Investigación, Spain (Project BQU 2001/0216).

[1] [1a] R. J. Angelici, *Polyhedron* **1997**, *16*, 3073. [1b] C. Bianchini, A. Meli, *Acc. Chem. Res.* **1998**, *31*, 109. [1c] I. R. Wittall, A. M. McDonagh, M. G. Humphry, M. Samoc, *Adv. Organomet. Chem.* **1998**, *42*, 291. [1d] C. D. Stout, in *Iron Sulfur Proteins* (Ed. T. G. Spiro), John Wiley, New York, **1982**, chapter 3. [1e] W. E. Newton, in *Sulfur: Its Significance for Chemistry, for the Geo-, Bio-, and Cosmosphere and Technology*, Studies in Inorganic Chemistry, Elsevier, Amsterdam, **1984**, vol. 5. [1f] D. Coucouvanis, *Acc. Chem. Res.* **1981**, *14*, 201.

[2] [2a] R. D. Adams, X. Qu, W. Wu, *Organometallics* **1994**, *13*, 1272. [2b] T. M. Räsänen, S. Jääskeläinen, T. A. Takkanen, *J. Organomet. Chem.* **1998**, *554*, 129. [2c] C. Rosenberg, N. Stennou, S. Jeannin, Y. Jeannin, *J. Organomet. Chem.* **1995**, *494*, 17.

[3] M. I. Alcalde, A. J. Carty, Y. Chi, E. Delgado, B. Donnadieu, E. Hernández, K. Dallmann, J. Sánchez-Nieves, *J. Chem. Soc., Dalton Trans.* **2001**, 2502.

[4] [4a] M. I. Bruce, *Chem. Rev.* **1991**, *91*, 197. [4b] M. I. Bruce, *Chem. Rev.* **1998**, *98*, 2797. [4c] A. A. Pasynskii, I. L. Eremenko, S. E. Nefedov, B. I. Kolobkov, A. D. Shaposhnikova, R. A. Stadnitchenko, M. V. Drab, Yu T. Struchkov, A. I. Yanovskii, *New J. Chem.* **1994**, *18*, 69.

[5] [5a] A. C. Reduto dos Rios, I. S. Hegedus, *Organometallics* **1995**, *14*, 1586. [5b] L. S. Hegedeus, R. Inwinkel-Reid, M. Alarid-Sargent, D. Dorak, Y. Saton, *J. Am. Chem. Soc.* **1990**, *112*, 1109. [5c] S. E. Gibson, G. J. Tustin, *J. Chem. Soc., Perkin Trans. 1* **1995**, 2427. [5d] R. S. Tanke, R. H. Crabtree, *Tetrahedron Lett.* **1988**, *29*, 6737. [5e] O. García-Mellado, R. Gutiérrez-Pérez, C. Alvarez-Toledano, R. A. Toscano, A. Cabrera, *Polyhedron* **1997**, *16*, 2979.

[6] [6a] C. Alvarez-Toledano, J. Enríquez, R. A. Toscano, M. Martínez-García, E. Cortés-Cortés, Y. Osornio, O. García, R. Gutiérrez-Pérez, *J. Organomet. Chem.* **1999**, *577*, 38. [6b] F. Ortega-Jiménez, M. C. Ortega-Alfaro, J. G. López-Cortés, R. Gutierrez-Pérez, R. A. Toscano, L. Velasco-Ibarra, E. Peña-Cabrera, C. Alvarez-Toledano, *Organometallics* **2000**, *19*, 4127. [6c] C. Alvarez-Toledano, R. Gutiérrez-Pérez, R. A. Toscano, M. Moya-Cabrera, T. Haquet, M. C. Ortega, A. Cabrera, *Polyhedron* **2001**, *20*, 215.

[7] A. J. Carty, S. A. MacLaughlin, N. J. Taylor, *J. Chem. Soc., Chem. Commun.* **1981**, 476.

[8] R. D. Adams, G. Chen, X. Qu, W. Wu, J. H. Yamamoto, *J. Am. Chem. Soc.* **1992**, *114*, 10977.

[9] [9a] J. S. Bradley, S. Harris, E. W. Hill, M. A. Modrick, *Polyhedron* **1990**, *9*, 1809. [9b] J. S. Bradley, S. Harris, E. W. Hill, *J. Chem. Soc., Dalton Trans.* **1997**, 3139. [9c] R. D. Adams, S. Wang, *Organometallics* **1985**, *4*, 1902.

[10] B. F. G. Johnson, R. D. Johnson, P. L. Josty, J. Lewis, I. G. Williams, *Nature* **1967**, *213*, 901.

[11] [11a] M. V. Ovchinnikov, I. A. Guzei, R. J. Angelici, *Organometallics* **2001**, *20*, 691. [11b] K. Vollhardt, C. Peter, T. W. Weidman, *J. Am. Chem. Soc.* **1983**, *105*, 1676.

[12] M. I. Bruce, M. L. Williams, B. W. Skelton, A. H. White, J. S. Bradley, S. Harris, E. W. Hill, *J. Organomet. Chem.* **1989**, *369*, 393.

[13] S. Jeannin, Y. Jeannin, F. Robert, C. Rosenberg, *Inorg. Chem.* **1994**, *33*, 243.

[14] R. Dodsworth, T. Dutton, B. F. G. Jonhson, J. Lewis, P. R. Raithby, *Acta Crystallogr., Sect. C* **1989**, *45*, 707.

[15] Z. Dauster, R. T. Mawby, C. D. Reynolds, D. R. Saunders, *J. Chem. Soc., Dalton Trans.* **1985**, 1235.

[16] M. F. McGluiggin, L. H. Pignolet, *Inorg. Chem.* **1982**, *21*, 2523.

[17] P. Gonzalez-Herrero, B. Weberndorfer, K. Illg, J. Wolf, H. Werner, *Organometallics* **2001**, *20*, 3672.

[18] A. Thuillier, J. Vialle, *Bull. Soc. Chim. Fr.* **1962**, 2182.

[19] R. B. King, *J. Am. Chem. Soc.* **1963**, *85*, 1584.

[20] A. Altomare, G. Cascarano, G. Giacovazzo, A. Guagliardi, M. C. Burla, G. Polidori, M. Camalli, *J. Appl. Crystallogr.* **1994**, *27*, 435.

[21] G. M. Sheldrick, *SHELXL-97, Program for the refinement of Crystal Structures*, University of Göttingen, Germany, **1998**.

[22] L. J. Farrugia, *J. Appl. Crystallogr.* **1999**, *32*, 837.

[23] *International Tables for X-ray Crystallography*, Kynoch Press, Birmingham, England, **1974**, vol. IV.

[24] L. J. Farrugia, *J. Appl. Crystallogr.* **1997**, *30*, 565.

Received May 23, 2002
[I02285]

EurJIC
European Journal of Inorganic Chemistry

February 2003
Issue 4
Pages 569–776

Papers available ahead of print in Early View at www.interscience.wiley.com

Earliest available Table of Contents:
Automatically, free of charge by e-mail through
www.interscience.wiley.com/alerts

COVER PICTURE

The cover picture shows the X-ray crystal structure of the complex [IrCl(Pigiphos)], where Pigiphos is a unique chiral tridentate ligand containing two ferrocenyl units. Enantiomerically pure triphosphanes are still quite rare and Pigiphos is particularly attractive because of its simple synthesis – one step from commercially available precursors. The study of the coordination chemistry of Pigiphos has shown that it can accomodate metal ions in essentially perfect square-planar geometries (Ni^{II}, Pd^{II}, Ph^{I}). In case of an ocatahedral coordination sphere it can adopt both a facial or an equatorial configuration (Ru^{II}). However, the present [IrCl(Pigiphos)] complex displays a severe deviation from the expected square-planar geometry and shows a dynamic behavior in solution. Synthesis, characterization, and reactivity of this and other Pigiphos complexes of Ir and Rh are presented in the article by P. Barbaro, A. Togni et al. on p. 601 ff.

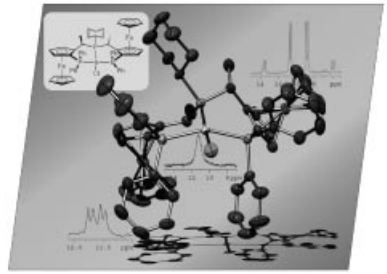

MICROREVIEW

Contents

583 **W.-H. Leung**

Synthesis and Reactivity of Organoimido Complexes of Chromium

Keywords: Chromium / N ligands / Synthesis / Reactivity

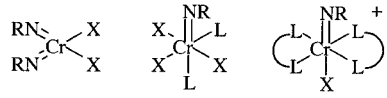

 © WILEY-VCH Verlag GmbH, 69451 Weinheim, Germany, 2003 1434–1948/03/0204–0573 $ 20.00+.50/0

SHORT COMMUNICATION

595 **L. Caron, M. Canipelle, S. Tilloy, H. Bricout, E. Monflier***

Unexpected Effect of Cyclodextrins on Water-Soluble Rhodium Complexes

Keywords: Rhodium / Phosphanes / Biphasic catalysis / Cyclodextrins / Molecular recognition

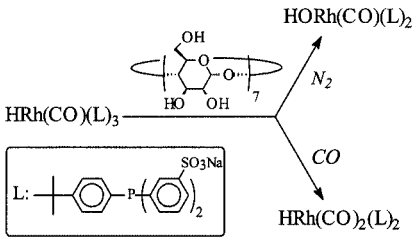

FULL PAPERS

601 **L. Hintermann, M. Perseghini, P. Barbaro,* A. Togni***

Complexes of Rhodium(I) and Iridium(I) with the Chiral Tridentate Phosphane Pigiphos: Structure and Reactivity Studies

Keywords: Ferrocenyl ligands / Phosphanes / Iridium / Rhodium / Chiral ligands

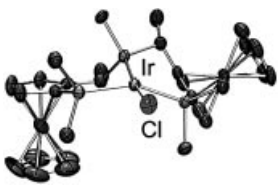

610 **R. Giordano, P. Serp,* P. Kalck, Y. Kihn, J. Schreiber, C. Marhic, J.-L. Duvail**

Preparation of Rhodium Catalysts Supported on Carbon Nanotubes by a Surface Mediated Organometallic Reaction

Keywords: Nanotubes / Rhodium / Supported catalysts / Surface chemistry / Heterogeneous catalysis

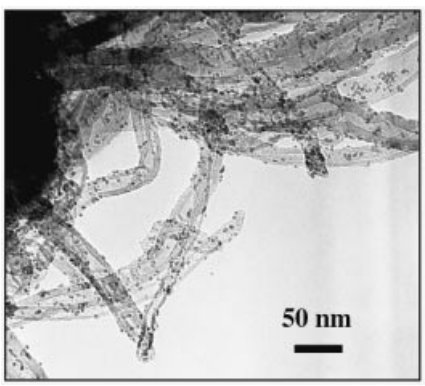

618 **X.-M. Ouyang, B.-L. Fei, T. Okamura, H.-W. Bu, W.-Y. Sun,* W.-X. Tang, N. Ueyama**

Syntheses, Crystal Structures, and Properties of Four Two-Dimensional Network Complexes with Multidentate Bis(Schiff Base) Ligands

Keywords: Schiff bases / Silver / Cobalt / Crystal engineering

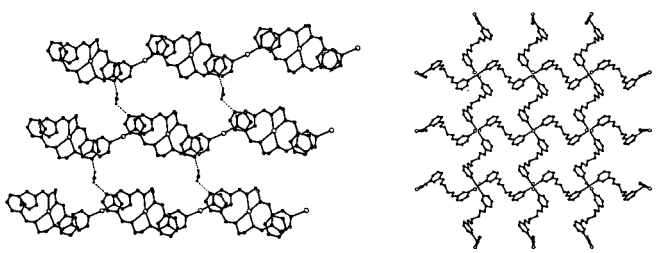

628 **F. Wolff, R. Choukroun,* C. Lorber, B. Donnadieu**

Reactivity of $B(C_6F_5)_3$ with Oxovanadium(V) Complexes VOL_3 (L = OCH_2CF_3, NEt_2): Formation of the Organometallic Vanadium(V) Complex $[VO(\mu\text{-}OCH_2CF_3)(OCH_2CF_3)(C_6F_5)]_2$ and the Lewis Acid Adduct $[(Et_2N)_3VO{\cdot}(C_6F_5)_3]$

Keywords: N ligands / O ligands / Boranes / Structure determination / Vanadium

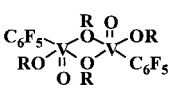

1

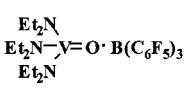

2

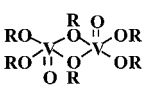

3

633 **C. Poulard, D. Perrey, G. Boni,* E. Vigier, O. Blacue, M. M. Kubicki, C. Moïse**

A Tantalocene Trihydride Containing an Aminoethyl-Functionalised Ligand

Keywords: Cyclopentadienyl ligands / Metallocenes / Hydride ligands / Tantalum

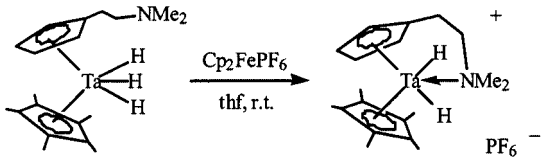

638 **M. Schreuder Goedheijt, T. Nijbacker, A. D. Horton, F. J. J. de Kanter, O. S. Akkerman, F. Bickelhaupt***

Investigations on 1-Metallaindanes

Keywords: Metallacycles / Isomerization / Magnesium / Mercury / Zirconium

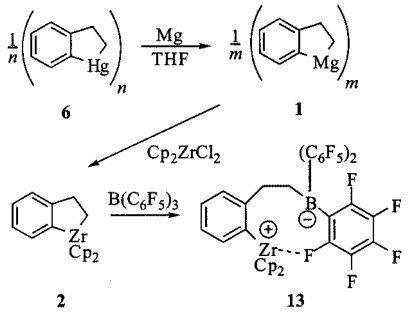

644 **Y. Liu,* J. Cao, J. Zeng, C. Li, Y. Qian, S. Zhang**

A Complex-Based Soft Template Route to PbSe Nanowires

Keywords: Nanostructures / Semiconductors / Luminescence / Carboxylate ligands

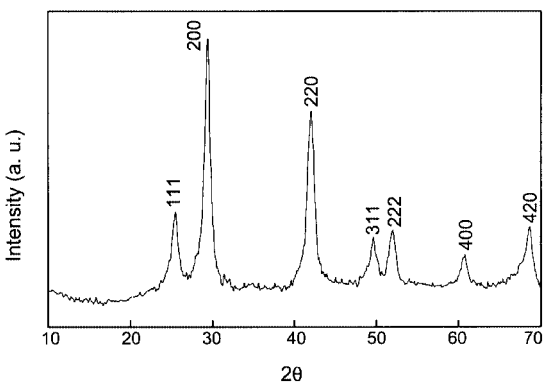

648 **T. M. Kooistra, K. F. W. Hekking, Q. Knijnenburg, B. de Bruin, P. H. M. Budzelaar, R. de Gelder, J. M. M. Smits, A. W. Gal***

Cobalt Chloride Complexes of N_3 and N_4 Donor Ligands

Keywords: Cobalt / N Ligands / Polymerisation

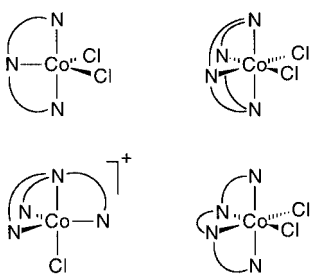

656 **Y. Zhang, P. H. M. Budzelaar, J. M. M. Smits, R. de Gelder, P. R. Hageman, A. W. Gal***

Reactions of *cis*-2,3-Dimethylaziridine, 3-Pyrroline and Pyrrolidine with Me_3Al and Me_3Ga: Adducts and Dimeric Amides

Keywords: Aluminium / Chemical vapour deposition / Gallium / Nitrides

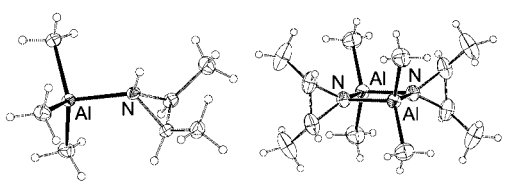

666 **H.-W. Lerner,* S. Scholz, M. Bolte, N. Wiberg, H. Nöth, I. Krossing**

Synthesis and Structures of Alkaline-Earth Metal Supersilanides: tBu$_3$SiMX and tBu$_3$Si−M−SitBu$_3$ (M = Be, Mg; X = Cl, Br)

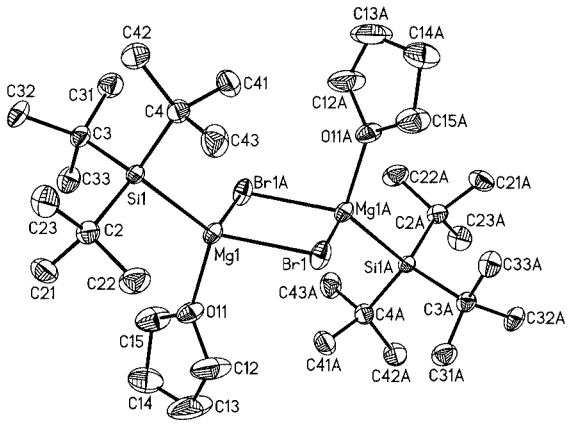

Keywords: Silanes / Beryllium / Magnesium / X-ray structure analysis

671 **K. Flinzner, A. F. Stassen, A. M. Mills, A. L. Spek, J. G. Haasnoot,* J. Reedijk**

The Chelating Ligand 1,3-Bis(pyrazol-1′-yl)propane (Bpp) Enforces a Tetrahedral Geometry in Both Cu^{II} and Cu^{I} Species

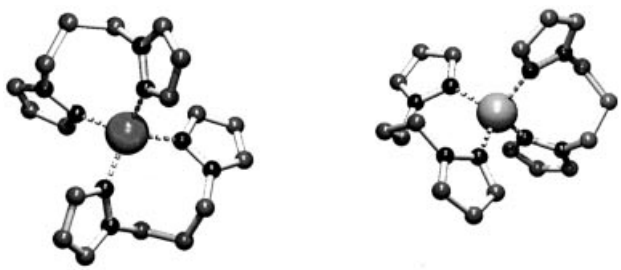

Keywords: N ligands / Copper / Crystal structures / Cyclic voltammetry

678 **A. Sousa-Pedrares,* M. I. Casanova, J. A. García-Vázquez, M. L. Durán, J. Romero, A. Sousa,* J. Silver, P. J. Titler**

Synthesis and X-ray Structures of Tin(IV) and Lead(II) Complexes with Heterocyclic Thiones

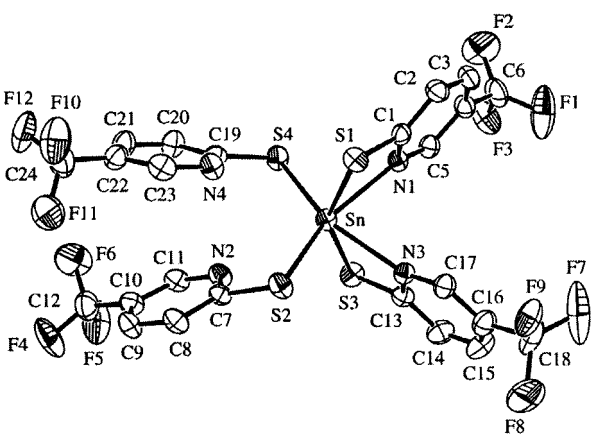

Keywords: Tin / Lead / N ligands / S ligands / Heterocycles

687 **M. Doux, L. Ricard, F. Mathey, P. Le Floch,* N. Mézailles***

Synthesis and Reactivity of the First η^6-Rhodium(I) and η^6-Iridium(I) Complexes of 2,6-Bis-(trimethylsilyl)phosphinines

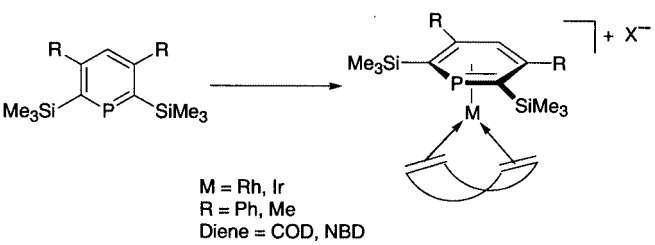

Keywords: Phosphinines / P ligands / Pi interactions / Rhodium / Iridium

699 **M. Bonchio,* O. Bortolini,* V. Conte, A. Sartorel**

Electrospray Behavior of Lacunary Keggin-Type Polyoxotungstates $[XW_{11}O_{39}]^{p-}$ (X = Si, P) − Mass Spectrometric Evidence for a Concentration-Dependent Incorporation of an MO^{n+} ($M = W^{VI}$, Mo^{VI}, V^{V}) Unit into the Polyoxometalate Vacancy

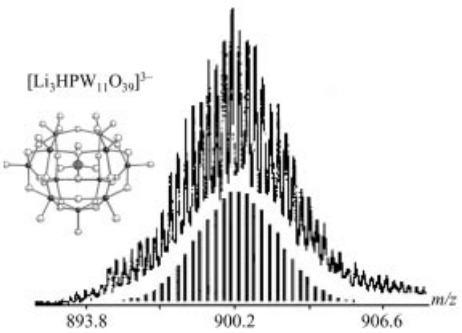

Keywords: Polyoxometalates / Mass spectrometry / Tungsten / Speciation / Lacunary species

705 **E. Lindner,* R. Zong, K. Eichele, U. Weisser, M. Ströbele**

Synthesis and Structure of Redox-Active Heterotetranuclear Molecular Polygons by Self-Assembly of Two Ferrocene-Bridged Bis(pyridines) with Two Transition Metals

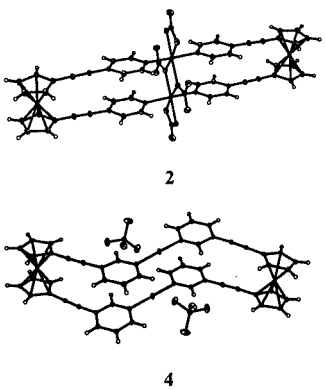

Keywords: Self-assembly / Nanostructures / Metal-metal interactions / N ligands / Nickel / Silver / Palladium

713 **A. H. Velders, A. G. Quiroga, J. G. Haasnoot, J. Reedijk***

Orientation- and Temperature-Dependent Rotational Behavior of Imidazole Ligands (L) in β-$[Ru(azpy)_2(L)_2](PF_6)_2$ Complexes

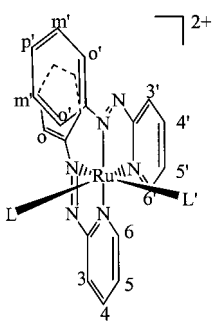

Keywords: Ruthenium / N ligands / NMR spectroscopy / Bioinorganic chemistry

720 **M. Mas-Torrent, S. S. Turner, K. Wurst, J. Vidal-Gancedo, J. Veciana, P. Day,* C. Rovira***

New Molecular Charge-Transfer Salts of TM-TTF and BMDT-TTF with Thiocyanate and Selenocyanate Complex Anions [TMTTF = Tetramethyltetrathiafulvalene; BMDT-TTF = Bis(methylenedithio)tetrathiafulvalene]

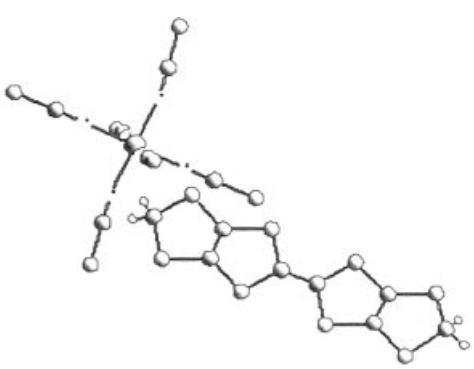

Keywords: Charge transfer / Tetrathiafulvalene / Complex anions / Magnetic properties

726 **P. Yin, Y. Peng, L.-M. Zheng,* S. Gao, X.-Q. Xin**

Syntheses and Structures of Layered Copper(II) Diphosphonates with Mixed Ligands

Keywords: Organic-inorganic hybrid composites / Phosphonates / Copper / N ligands

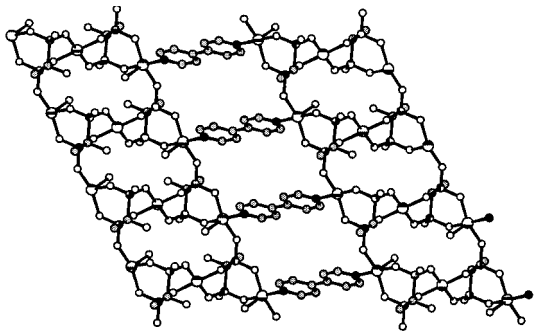

731 **Q.-D. Liu, J.-R. Li,* S. Gao,* B.-Q. Ma, H.-Z. Kou, L. Ouyang, R.-L. Huang, X.-X. Zhang, K.-B. Yu**

Synthesis, Crystal Structures and Magnetism of a Series of Heptanuclear Rare-Earth-Centered Trigonal Prism Clusters

Keywords: Copper / Lanthanides / N ligands / O ligands / Template synthesis / Magnetic properties

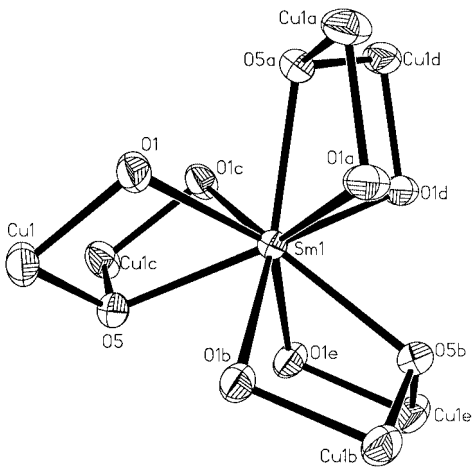

737 **D. Bayot, B. Tinant, B. Mathieu, J.-P. Declercq, M. Devillers***

Spectroscopic and Structural Characterizations of Novel Water-Soluble Peroxo[polyaminocarboxylato bis(*N*-oxido)]niobate(V) Complexes

Keywords: Niobium / Peroxo ligands / N,O ligands / NMR spectroscopy / IR spectroscopy

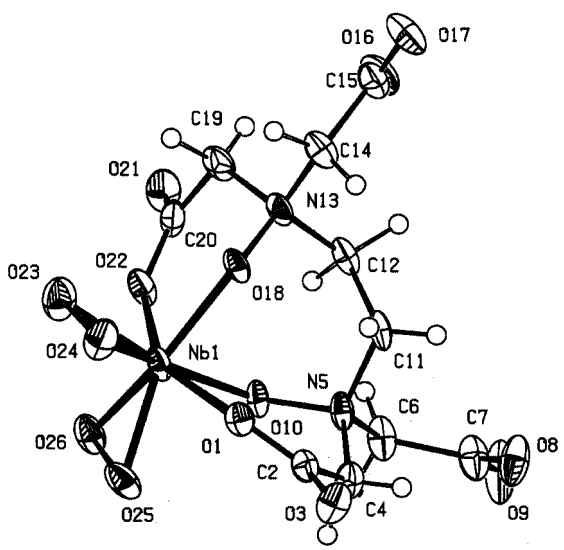

744 **S. Dey, V. K. Jain,* J. Singh, V. Trehan, K. K. Bhasin, B. Varghese**

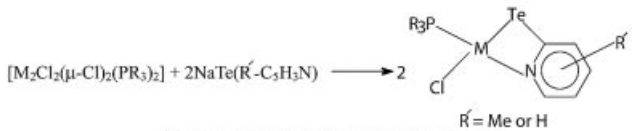

Pyridine- and 3-/6-Methylpyridine-2-tellurolate Complexes of Palladium(II) and Platinum(II)

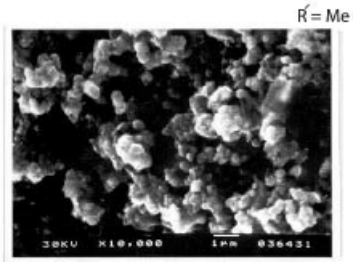

Keywords: Palladium / Platinum / N ligands / Tellurium / NMR spectroscopy

751 **U. Böhme,* B. Günther, B. Rittmeister**

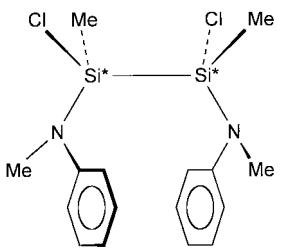

(*R*,*R*) isomer

Selective Synthesis of *N*-Methylanilinooligosilanes

Keywords: Amides / Silanes / Disilanes / Aminosilanes / Stereochemistry

759 **M. Rat, R. A. de Sousa, A. Tomas, Y. Frapart, J.-P. Tuchagues, I. Artaud***

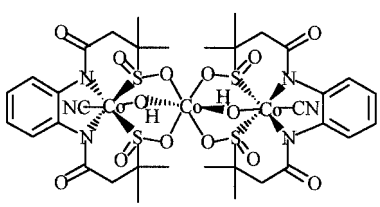

Synthesis, X-ray Structure and Properties of a Trinuclear Mixed-Valence Co^{III}-Co^{II}-Co^{III} Complex with Carboxamido N and Sulfinato S Donors

Keywords: Cobalt / N ligands / S ligands / Enzyme models

766 **A. D. Burrows,* R. W. Harrington, M. F. Mahon, S. J. Teat**

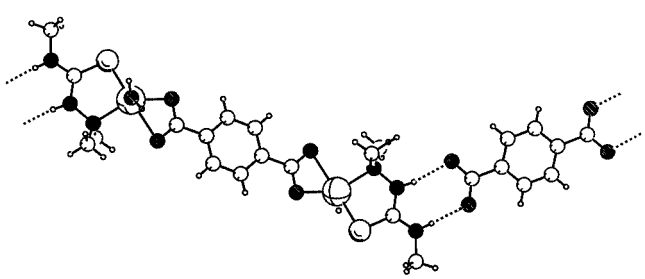

The Influence of Functional Group Orientation on the Structure of Zinc 1,1,4-Trimethylthiosemicarbazide Dicarboxylates: Probing the Limits of Crystal Engineering Strategies

Keywords: Zinc / Carboxylate ligands / Hydrogen bonds / Coordination polymers / Supramolecular chemistry

Synthesis and Reactivity of Organoimido Complexes of Chromium

Wa-Hung Leung[a]

Keywords: Chromium / N ligands / Synthesis / Reactivity

Organoimido groups are excellent spectator ligands for high-valent organometallic compounds due to their strong π-donating capability. Of interest are imidochromium complexes that are used as catalysts for olefin polymerization. This microreview provides an overview of the organometallic chemistry of high-valent imidochromium complexes. Synthetic routes to alkyl- and arylimido complexes of chromium in oxidation states VI–IV will be presented. The reactivity of imidochromium complexes including imido group transfer and cycloaddition will be described. The use of imidochromium complexes as catalysts for regioselective ring opening of epoxides will be discussed.
(© Wiley-VCH Verlag GmbH & Co. KGaA, 69451 Weinheim, Germany, 2003)

1. Introduction

Transition metal imido complexes have attracted much attention because of their proposed intermediacy in the industrially important ammoxidation of propylene,[1] and also due to their applications to organic transformations such as aziridination[2] and aminohydroxylation[3] of olefins, amidation of hydrocarbons,[2b] amination of silyl enol ethers,[4] hydroamination of unsaturated hydrocarbons,[5,6] imine metathesis,[7] and activation of alkane C−H bonds.[8] In addition, because of their high π-donor strength, organoimido groups (NR^{2-}; R = alkyl or aryl) prove to be excellent spectator ligands for high-valent organometallic complexes. Well-defined ring-opening metathesis polymerization[9] and ring-closing metathesis[10] catalysts based on Mo^{VI} imido alkylidene complexes have been developed, while the last decade has witnessed significant progress in the organometallic chemistry of high oxidation state (imido)Cr complexes, due in part to their catalytic activities toward olefin polymerization.[11,12] This microreview reviews the synthesis and reactivity of organoimido complexes of Cr in oxidation states VI−III. General reviews on organoimido complexes of transition metals have also appeared.[13−15]

[a] Department of Chemistry and Open Laboratory of Chirotechnology of the Institute of Molecular Technology for Drug Discovery and Synthesis, The Hong Kong University of Science and Technology,
Clear Water Bay, Kowloon, Hong Kong, China
Fax: (internat.) + 852/2358-1594
E-mail: chleung@ust.hk

2. Synthesis of Imidochromium Complexes

2.1. (Imido)Cr^{VI} Complexes

Nugent synthesized the first (organoimido)Cr^{VI} complex $[Cr(N\mathit{t}Bu)_2(OSiMe_3)_2]$ (**1**) by treatment of $[CrO_2Cl_2]$ with $\mathit{t}BuSiMe_3NH$.[16] Treatment of **1** with BCl_3 afforded the dichloride compound $[Cr(N\mathit{t}Bu)_2Cl_2]$ (**2**).[17] The bis(adamantyl)imido complex $[Cr(NAd)_2Cl_2]$ (Ad = 1-adamantyl) was synthesized similarly, from $[CrO_2Cl_2]$, $Ad(SiMe_3)NH$, and BCl_3,[18] while $[Cr(NR)_2Cl_2]$ reacted with donor ligands L to give monoadducts $[Cr(NR)_2Cl_2(L)]$ [R = tBu,[17] Ad;[18] L = pyridine (py), PMe_2Ph, and tBuNC]. The pyridine adduct $[Cr(N\mathit{t}Bu)_2Br_2(py)]$ (**3**) was also synthesized from **1** and Me_3SiBr in the presence of pyridine.[19] Treatment of **2** either with [Ag(OTf)] (OTf = triflate) or with

Wa-Hung Leung was born in Hong Kong in 1963. He obtained his Ph.D. degree from the University of Hong Kong in 1989 under the supervision of Prof. Chi-Ming Che. He was a Croucher Foundation postdoctoral fellow from 1989 to 1991 and joined Professor Geoffrey Wilkinson's research group in the Department of Chemistry, Imperial College, London, UK. He then joined the faculty of the Chemistry Department, the Hong Kong University of Science and Technology, where he is currently Associate Professor of Chemistry. He has been working in the field of synthetic inorganic and organometallic chemistry, and his research interests include metal−ligand multiple bonds, metal chalcogenide complexes, and organometallic complexes with O-donor ligands.

MICROREVIEWS: This feature introduces the readers to the author's research through a concise overview of the selected topic. Reference to important work from others in the field is included.

Ag(OAc) (OAc = acetate) afforded $[Cr(NtBu)_2(OTf)_2]$ and $[Cr(NtBu)_2(OAc)_2]$, respectively, while treatment of $[Cr(NtBu)_2(OTf)_2]$ with pyridine (py) or 2,2′:6′,2′′-terpyridine (terpy) gave cationic $[Cr(NtBu)_2(py)_2(CF_3SO_3)]^+$ (**4**)[17] or dicationic $[Cr(NtBu)_2(terpy)]^{2+}$ (**5**),[20] respectively. Treatment of **2** with R′$_3$TACN (TACN = 1,4,7-triazacyclononane) or KTp* [Tp* = hydrotris(3,5-dimethylpyrazol-1-yl)borate] afforded $[Cr(NtBu)_2(R'_3TACN)Cl]^+$ (**6**, R = H; **7**, R = Me)[21] and [Tp*Cr(N*t*Bu)$_2$Cl],[22] respectively (Scheme 1).

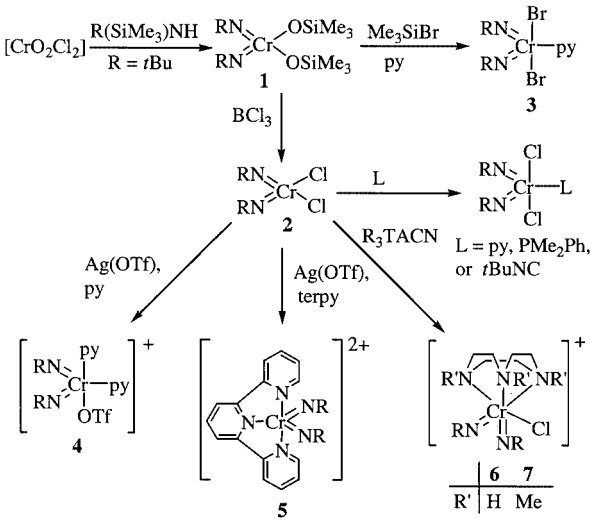

Scheme 1. Synthesis of bis(imido)Cr^{VI} complexes

Compound **2** afforded the bis(aryl oxide) compound $[Cr(NtBu)_2(OC_6H_3iPr_2\text{-}2,6)_2]$ (**8**) on treatment with NaO-$C_6H_3iPr_2$-2,6,[20] and $[Cr(NtBu)_2(NPPh_3)_2]$ on treatment with $LiNPPh_3$,[17] while with *t*BuNHLi it afforded $[Cr(NtBu)_2(NHtBu)_2]$, which was deprotonated with *n*BuLi to give the homoleptic (imido)Cr complex $[Li_2Cr(NtBu)_4]$. NMR spectroscopy suggested that $[Li_2Cr(NtBu)_4]$ has a structure similar to $[Li_2W(NtBu)_4]_2$, with terminal linear imido and bridging bent imido groups.[23]

The bis(arylimido)Cr^{VI} complex $[Cr(NC_6H_3iPr_2\text{-}2,6)_2(NHtBu)Cl]$ was prepared by imido group exchange between **2** and 2,6-$iPr_2C_6H_2NH_2$. Treatment of $[Cr(NC_6H_3iPr_2\text{-}2,6)_2(NHtBu)Cl]$ with BCl_3 afforded $[Cr(NC_6H_3iPr_2\text{-}2,6)_2Cl_2]$ (**9**).[24] Alternatively, $[Cr(NAr)_2Cl_2]$ (**10**, Ar = 2,4,6-$Me_3C_6H_2$; **11**, Ar = 2,6-$Me_2C_6H_3$) were synthesized from **2** and ArNCO through Wittig-like [2 + 2] exchange of imido groups[25] (Scheme 2).

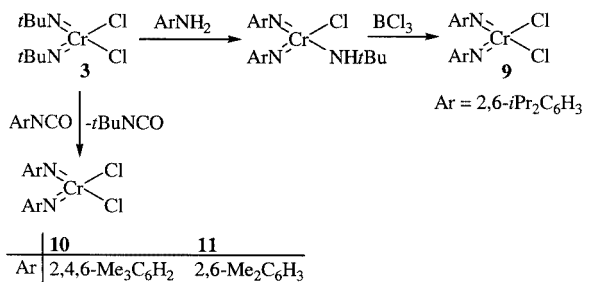

Scheme 2. Synthesis of bis(arylimido)Cr^{VI} complexes

Interestingly, treatment of **2** with 2,6-$iPr_2C_6H_3NCO$ resulted in the formation of the Cr^{V} dimer $[Cr(\mu\text{-}NtBu)(N\text{-}C_6H_3iPr_2\text{-}2,6)Cl]_2$ rather than **9**.[24] Unlike **2**,[17] **3**,[18] and **9**,[26] which all formed monoadducts with donor ligands, **10** reacted with PMe_3 or py to yield six-coordinate $[Cr(NR)_2Cl_2(L)_2]$ (L = py, PMe_3).[25] Treatment of **10** with NaSR afforded the dithiolate compounds $[Cr(NC_6H_3Me_2\text{-}2,4,6)_2(SR)_2]$ (R = C_6F_5, 2,4,6-$Me_3C_6H_2$, 2,4,6-$iPr_3C_6H_2$),[25] while with 4 equiv. of ArNHLi (Ar = 2,4,6-$Me_3C_6H_2$), **10** gave $[Cr(NAr)(NHAr)(\mu\text{-}NAr)_2Li(OEt_2)_2]$ (**13**, Figure 1). The amido group in **12** could not be further deprotonated by *n*BuLi.[27]

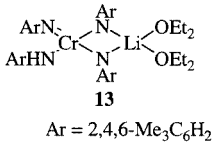

Figure 1. Structure of $[Cr(NAr)(NHAr)(\mu\text{-}NAr)_2Li(OEt_2)_2]$ (Ar = 2,4,6-$Me_3C_6H_2$)

Similarly, treatment of **9** with 2,6-$iPr_2C_6H_3NHLi$ afforded $[Cr(NC_6H_3iPr_2\text{-}2,6)_2(NHC_6H_3iPr_2\text{-}2,6)Cl]$, which also resisted further deprotonation.[26]

(Imido)Cr^{VI} Complexes Containing σ-Alkyl and Related Ligands

$[Cr(NtBu)_2(C_6H_2Me_3\text{-}2,4,6)_2]$ (**14**), the first isolated stable Cr^{VI} σ-aryl complex, was synthesized by alkylation of **1** with 2,4,6-$Me_3C_6H_2MgBr$. Similarly, alkylation of $[Cr(NR)_2Cl_2]$ with Li(fmes) [fmes = 2,4,6-$(CF_3)_3C_6H_2$] yielded $[Cr(NR)_2(fmes)_2]$ (R = *t*Bu, Ad).[18b] X-ray diffraction studies of $[Cr(NR)_2(fmes)_2]$ revealed pseudo-tetrahedral coordination of Cr, complemented by two secondary Cr···F interactions with the *ortho*-CF_3 groups of the fmes ligands. Treatment of **14** with *t*BuNC afforded the η^2-(iminoacyl) complex $[Cr(NtBu)_2(C_6H_2Me_3\text{-}2,4,6)(\eta^2\text{-}tBuN{=}CC_6H_2Me_3\text{-}2,4,6)]$ (**15**, Scheme 3).[28]

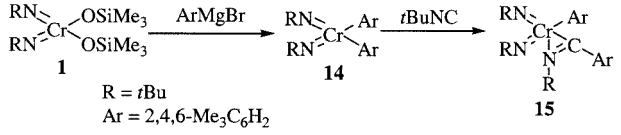

Scheme 3. Synthesis of $[Cr(NtBu)_2(C_6H_2Me_3\text{-}2,4,6)_2]$ and its reaction with *t*BuNC

Treatment of **2** or **3** with Me_3SiCH_2MgCl or $Zn(CH_2SiMe_3)_2$ gave $[Cr(NtBu)_2(CH_2SiMe_3)_2]$, isolated as an oil.[17,19] Alkylation of **3** with *o*-$C_6H_4[(CHSiMe_3)Li(TMEDA)]_2$ (TMEDA = *N*,*N*,*N*′,*N*′-tetramethylethylenediamine) afforded crystalline $[Cr(NtBu)_2\{o\text{-}C_6H_4(CHSiMe_3)_2\}]$ (**16**).[19] Treatment of **3** with $Cp_2Mg(THF)_{2.5}$ (Cp = η^5-C_5H_5) afforded $[CpCr(NtBu)_2Br]$, which could be alkylated to give the monoalkyl compounds $[CpCr(NtBu)_2R]$ (R = Me, CH_2SiMe_3, CH_2CMe_3, CH_2CMe_2Ph).[19] Crystalline $[Cr(NR)_2(CH_2Ph)(\eta^2\text{-}CH_2Ph)]$ (**17**, R = *t*Bu;[29] **18**, R = Ad[18]) were isolated after alkylation of $[Cr(NR)_2Cl_2]$ with $PhCH_2MgCl$ (Scheme 4).

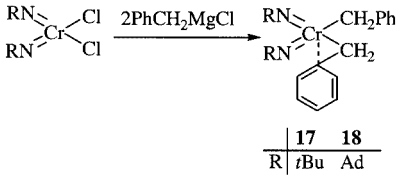

Scheme 4. Synthesis of dibenzylbis(imido)Cr^{VI} complexes

The Cr−C_α and Cr−C_{ipso} distances for the η^2-benzyl ligand in **17** are 207.1(2) and 235.7(2) pm, respectively.[28] The solid-state ^{13}C CP/MAS NMR spectrum of **17** displays two different resonance signals at δ = 157.9 and 124.4 ppm, assigned to the η^1- and η^2-*ipso*-phenyl carbon atoms, respectively.[29] Similarly, the dialkyl compounds $[Cr(NC_6H_3iPr_2\text{-}2,6)_2R_2]$ (R = CH_3, CH_2Ph, CH_2CMe_3)[30] and $[Cr(NC_6H_2Me_3\text{-}2,4,6)_2R_2]$ (R = CH_2Ph, CH_2CMe_3, CH_2CMe_2Ph)[25] have been prepared by alkylation of **9** and **10**, respectively, with RMgCl. In the solid state, $[Cr(NC_6H_3iPr_2\text{-}2,6)_2(CH_2CMe_3)_2]$ (**19**) shows weak α-agostic interactions between Cr and the methylene hydrogen atoms of the neopentyl ligands. Complex **19** reacted with C_6D_6 at room temperature to give $[Cr(NC_6H_3iPr_2\text{-}2,6)_2(CHDCMe_3)(C_6D_5)]$ (**20**) and $CHDCMe_3$, through an (alkylidene)Cr^{VI} intermediate that could be trapped by THF or PMe_3 to form adducts $[Cr(NC_6H_3iPr_2\text{-}2,6)_2(=CHCMe_3)L]$ (L = THF, PMe_3). The conversion of **19** into **20** was found to follow first-order kinetics, suggesting that the rate-determining step is the α-hydrogen elimination of **19** to give the transient three-coordinate alkylidene intermediate, which rapidly reacted with C_6D_6. Neither $[Cr(NC_6H_3iPr_2\text{-}2,6)_2(=CHCMe_3)L]$ nor base-free $[Cr(NC_6H_3iPr_2\text{-}2,6)_2(=CHCMe_3)]$ reacted with simple olefins (Scheme 5).[30]

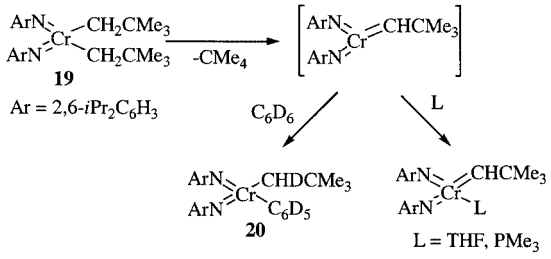

Scheme 5. Synthesis and C−H bond activation by an (alkylidene)Cr^{VI} complex

The (methylidene)(α-phosphonio) complex $[Cr(NtBu)_2Cl\{CH(PPh_3)\}]$ (**21**) was synthesized by transylidation of **2** with $Ph_3P{=}CH_2$. The NMR spectroscopic data for **21** ($\delta_{H\alpha}$ = 11.84 ppm; $\delta_{C\alpha}$ = 200.1 ppm) are characteristic for alkylidene complexes. The high barrier to rotation about the Cr−C bond [$\Delta G^{\ddagger}$(336 K) = 75 kJ·mol^{-1}] for **21** is indicative of the Cr=C double bond character. Treatment of **21** with $Ph_2C{=}C{=}O$ resulted in the nucleophilic attack of Cα on the ketene and the formation of the chromaoxetane $[Cr(NtBu)_2\{\eta^2\text{-}(O,C)\text{-}OC(CHPPh_3)CPh_2\}Cl]$ (**22**, Scheme 6).[31]

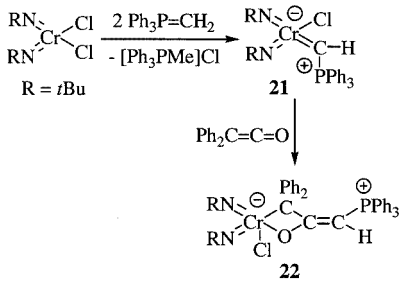

Scheme 6. Synthesis of (methylidene)(phosphanyl)Cr^{VI} complex and its reaction with ketene

Alkylation of $[Cr(NO)(NiPr_2)(O_2CPh)_2]$ with $(2\text{-}MeC_6H_4)_2Mg$ afforded the (imido)(oxo) compound $[Cr(O)(NC_6H_4Me\text{-}2)(NiPr_2)(C_6H_4Me\text{-}2)]$ (**23**), presumably through N−O cleavage in the intermediate $[Cr(NO)(C_6H_4Me\text{-}2)_2(NiPr_2)]$ (Scheme 7).[32]

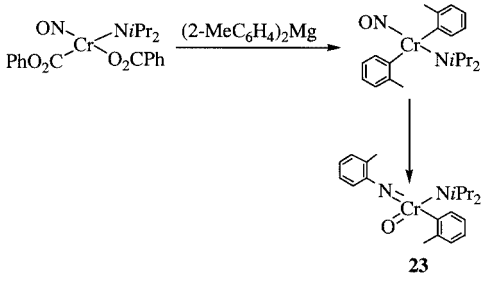

Scheme 7. Isolation of a mono(arylimido)Cr^{VI} complex from the alkylation of a (nitrosyl)Cr complex

2.2. (Imido)Cr^{V} Complexes

Treatment of $[CpCrCl_2]_2$ with $Me_3SiN{=}NSiMe_3$ gave the (silylimido)Cr^{V} complex $[CpCr(\mu\text{-}NSiMe_3)(NSiMe_3)]_2$ (**24**), which reacted with MeOH to yield the parent imido species $[CpCr(NH)(NSiMe_3)]_2$.[33] Reduction of **2** with cobaltocene gave dinuclear $[Cr(\mu\text{-}NtBu)(NtBu)Cl]_2$ (**25**).[17] Similarly, **9** reacted with LiCp or NaCp to give $[Cr(\mu\text{-}NC_6H_2iPr_2\text{-}2,6)(NC_6H_2iPr_2\text{-}2,6)Cl]_2$ (**26**).[26] Both **25** and **26** are diamagnetic, due to spin coupling through the imido bridges or Cr···Cr interaction [the Cr−Cr separation in **26** is 247.5(2) pm[26]].

Treatment of $[CrO_2Cl_2]$ with $(Me_3Si)_2NH$ afforded $[CrO_2\{N(SiMe_3)_2\}_2]$ (**27**), which reacted with pyridine to give the imido-bridged Cr^{V} dimer $[Cr_2(\mu\text{-}NSiMe_3)_2(NSiMe_3)_2(O)_2(py)]$ (**28**, Scheme 8).[34]

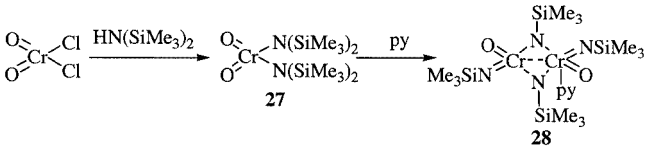

Scheme 8. Synthesis of a dinuclear (imido)(oxo)Cr^{V} complex

Treatment of **27** with *t*BuOH resulted in desilylation of the amido ligands and the formation of the (nitrido)Cr^{VI}

compound [Cr(N)(O*t*Bu)$_3$] (**29**). Complex **29** could also be prepared directly by addition of excess *t*BuOH to a reaction mixture of [NH$_4$]$_2$[Cr$_2$O$_7$], Me$_3$SiCl, HN(SiMe$_3$)$_2$, and Et$_3$N.[35]

Chlorination of **2** afforded mono(imido)Cr^{V} species [Cr(N*t*Bu)Cl$_3$]$_x$, which reacted with Lewis bases to give six-coordinate [Cr(N*t*Bu)Cl$_3$L$_2$] [L = PEt$_2$Ph, THF, py, 0.5DME (DME = 1,2-dimethoxyethane), 0.5bpy (bpy = 2,2′-bipyridine)].[36] Treatment of [Cr(N*t*Bu)Cl$_3$]$_x$ with CtCl in CH$_2$Cl$_2$ gave [Ct][Cr(N*t*Bu)Cl$_4$(H$_2$O)] {[Ct]$^+$ = [*n*Bu$_4$N]$^+$, [PPh$_4$]$^+$, or [N(PPh$_3$)$_2$]$^+$}.[36,37] Treatment of [Cr(N*t*Bu)Cl$_3$(DME)] (**30**) with H$_2$(bpb) [bis(2-pyridinecarboxamido)benzene] or with H$_2$(Busalen) [bis(2,4-di-*tert*-butylsalicylidene)diaminoethane] in the presence of a base afforded [Cr(N*t*Bu)(Busalen)Cl] (**31**)[37] and [Cr(N*t*Bu)(Cl)(bpb)] (**32**),[38] respectively. Treatment of [PPh$_4$][Cr(N*t*Bu)Cl$_4$(H$_2$O)] with Na$_2$(mnt) [mnt^{2-} = 1,2-maleonitriledithiolate(2−)] gave [PPh$_4$][Cr(N*t*Bu)(mnt)$_2$] (**33**)[36b] (Scheme 9), while treatment of **30** with NaO*t*Bu resulted in the isolation of [Cr(O*t*Bu)$_4$] together with [Cr(N*t*Bu)$_2$(O*t*Bu)$_2$], presumably through disproportionation of the trialkoxide intermediate [Cr(N*t*Bu)(OR)$_3$].[36b]

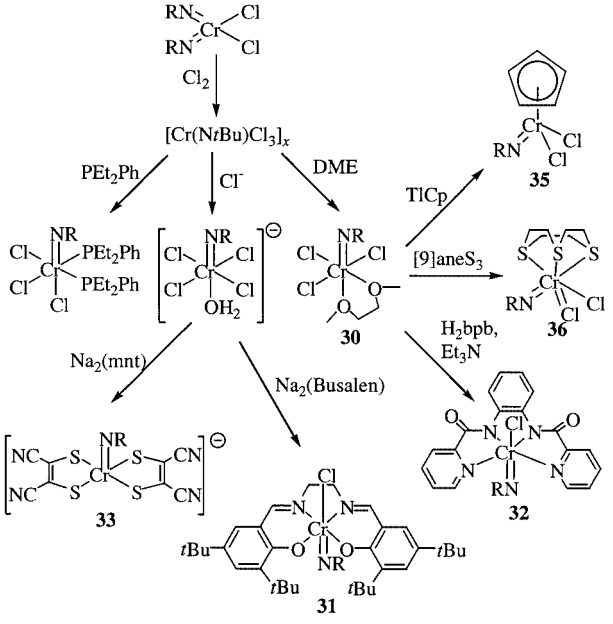

Scheme 9. Synthesis of mono(imido)Cr^{V} complexes

Treatment of **30** with NaL$_{OEt}$ (L$_{OEt^-}$ = [CpCo{P(O)(OEt)$_2$}$_3$]$^-$), TlCp (Cp = η^5-C$_5$H$_5$), or [9]aneS$_3$ gave [L$_{OEt}$Cr(N*t*Bu)Cl$_2$] (**34**), [CpCr(N*t*Bu)Cl$_2$] (**35**),[37] or [([9]ane[S$_3$])Cr(N*t*Bu)Cl$_2$]$^+$ (**36**),[39] respectively. Attempts to prepare (imido)(pentamethylcyclopentadienyl)Cr^{V} complexes from **30** and LiCp* or TlCp* (Cp* = η^5-C$_5$Me$_5$) were unsuccessful. Half-sandwich Cp*Cr^{V} imido complexes [Cp*Cr(NR)(SPh)$_2$] (R = *t*Bu, 2-*i*PrC$_6$H$_4$, 4-MeC$_6$H$_4$, 2-*t*BuC$_6$H$_4$) were prepared from [Cp*CrBr$_2$]$_2$ and Li(RNSPh).[40] Chlorination of [Cp*Cr(NR)(SPh)$_2$] with BCl$_3$ afforded [Cp*Cr(NR)Cl$_2$] (Scheme 10).[27]

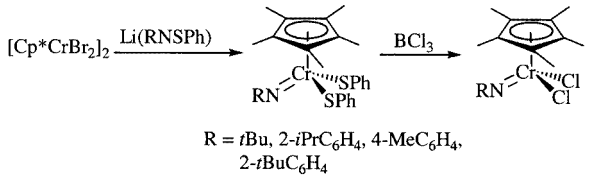

Scheme 10. Synthesis of (imido)Cp*Cr^{V} complexes

2.3. (Imido)Cr^{IV} and -Cr^{III} Complexes

Addition of a solution of Ba(CF$_3$SO$_3$)$_2$ in MeOH to [Cr(DMPE)$_2$(MeCN)Cl][BPh$_4$] [DMPE = 1,2-bis(dimethylphosphanyl)ethane] in MeCN afforded the (ethylimido)Cr^{IV} complex *trans*-[Cr(NEt)Cl(DMPE)$_2$]$^+$ (**37**). In contrast, addition of MeOH to [Cr(DMPE)$_2$(MeCN)Cl][BPh$_4$] in MeCN yielded the bis(ethylideneamido) complex *trans*-[Cr(N=CHMe)$_2$(DMPE)$_2$][BPh$_4$]$_2$ (**38**). It was proposed that the formation of complexes **37** and **38** involved hydride transfer from MeOH or methoxide to the carbon atom of the MeCN ligand (Scheme 11). Reduction of **30** with Na/Hg in the presence of DMPE gave [Cr(N*t*Bu)(DMPE)$_2$Cl]$^+$ (**39**).[36a] Complexes **37**−**39** are diamagnetic and show well-resolved ^{1}H NMR spectra in solution (Scheme 11).[41]

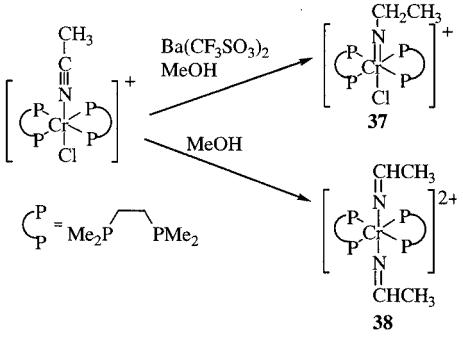

Scheme 11. Reaction between *trans*-[Cr(DMPE)$_2$(MeCN)Cl]$^+$ and MeOH

Heating of the dialkyl compounds [Cr(NC$_6$H$_2$Me$_3$-2,4,6)$_2$R$_2$] (R = CH$_2$Ph, CH$_2$CMe$_3$, CHCMe$_2$Ph) with PMe$_3$ in aromatic solvents afforded dinuclear (imido)Cr^{IV} complex [Cr(μ-NC$_6$H$_2$Me$_3$-2,4,6)(NC$_6$H$_2$Me$_3$-2,4,6)]$_2$.[25] Treatment of **10** with MgEtBr in the presence of PMe$_3$ resulted in the formation of [Cr$_2$(μ-NC$_6$H$_2$Me$_3$-2,4,6)$_2$(NC$_6$H$_2$Me$_3$-2,4,6)$_2$Br$_2$(PMe$_3$)],[25] while reduction of **9** with Mg in the presence of PMe$_3$ afforded [Cr(NC$_6$H$_3$*i*Pr$_2$-2,6)$_2$(PMe$_3$)$_2$] (**40**), which reacted with PhCHN$_2$ to give the diazoalkane compound [Cr(NC$_6$H$_3$*i*Pr$_2$-2,6)$_2$(PMe$_3$)(N$_2$CHPh)] (**41**, Scheme 12).[26]

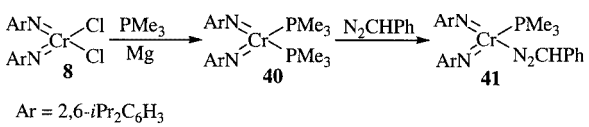

Scheme 12. Preparation of bis(arylimido)Cr^{IV} complexes

The (imido)Cr^{IV} porphyrins [$Cr(NC_6H_4X\text{-}4)(TPP)$] have been prepared from [Cr(TPP)] (TPP = tetraphenylporphyrin dianion) and aryl azides $4\text{-}XC_6H_4N_3$ (X = Me, Cl, I, MeO). Unlike the diamagnetic [Cr(O)(TPP)] and *trans*-$[Cr(NEt)Cl(DMPE)_2]^+$, [$Cr(NC_6H_4X\text{-}4)(TPP)$] are high spin, with measured μ_{eff} values of ca. 2.83 μ_B at 293 K. Treatment of [$Cr(TPP)(NC_6H_4Me\text{-}4)$] with [$V(O)(acac)_2$] (Hacac = 2,4-pentanedione) and [Fe(salen)(MeIm)] [salen = bis(salicylideneiminato)-1,2-diaminoethane, MeIm = 1-methylimidazole] afforded extremely moisture-sensitive imido-bridged dimetallic Cr−V and Cr−Fe species.[42]

The natures of the products of reactions between [Cp*$CrBr_2]_2$ and LiNHR were found to be dependent both upon the reactant used and upon the reaction conditions. Thus, treatment of [Cp*$CrBr_2]_2$ with 2,6-iPr$_2$C$_6$H$_3$NHLi in THF at −78 °C and subsequent rapid workup afforded dinuclear Cr^{III} complex [$(Cp^*Cr)_2(\mu\text{-}Br)(\mu\text{-}NHC_6H_3iPr_2\text{-}2,6)(\mu\text{-}NC_6H_3iPr_2\text{-}2,6)$] (**42**), which has a magnetic moment of 1.12 μ_B per Cr atom. The short Cr−Cr separation in **42** [264.7(5) and 265.1(5) pm)] is indicative of Cr···Cr interaction. On the other hand, addition of [Cp*$CrBr_2]_2$ to ArNHLi in toluene at 0 °C, followed by heating at 60 °C, gave the dinuclear (imido)Cr^{III} complexes [$Cp^*Cr(\mu\text{-}NAr)]_2$ (Ar = 2,6-iPr$_2$C$_6$H$_3$, **43**; 2,4,6-tBu$_3$C$_6$H$_2$, **44**). The Cr−Cr separations in **43** and **44** − of 259.1(1) and 256.4(1) pm, respectively − are indicative of Cr···Cr interaction. In contrast, treatment of [Cp*$CrBr_2]_2$ with $C_6H_{11}NHLi$ (C_6H_{11} = cyclohexyl) in toluene at −78 °C gave the paramagnetic dinuclear (imido)Cr^{IV} complex [$Cp^*CrBr(\mu\text{-}NC_6H_{11})]_2$ (**45**), presumably through 2 III → IV + II disproportionation (Scheme 13).[43]

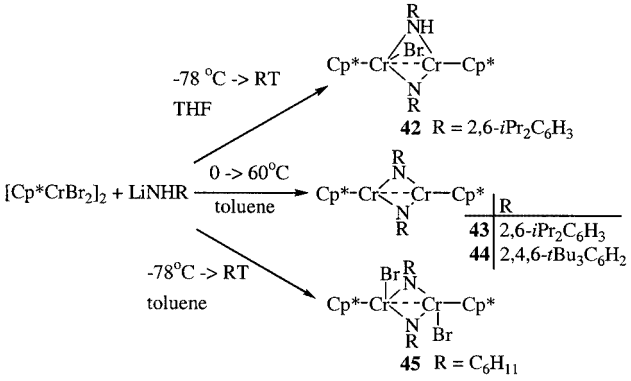

Scheme 13. Reactions of [Cp*$CrBr_2]_2$ with RNHLi

It seems likely that complexes **42**−**45** were formed by dimerization of the "Cp*Cr(NR)" intermediates that could be trapped by donor ligands. Thus, treatment of "Cp*$Cr(NC_6H_3iPr_2\text{-}2,6)$", prepared in situ from [Cp*$CrBr_2]_2$ and 2,6-iPr$_2$C$_6$H$_3$NHLi, with PhC≡CPh gave [Cp*$Cr(NC_6H_3iPr_2\text{-}2,6)(\eta^2\text{-}PhC{\equiv}CPh)$] (**46**). The C−C distance of the acetylene ligand in **46** is fairly long [129.5(5) pm], indicative of C=C double bond character, and so the Cr oxidation state for **46** could be assigned as either III or V. Complex **46** has a measured μ_{eff} of 2.20 μ_B at room temperature and showed an isotropic EPR signal at g = 2.007 with α_N = 3.7 G. In contrast, treatment of "Cp*Cr(NtBu)" (prepared in situ) with PhC≡CPh gave [Cp*CrBr(μ-NHtBu)$_2$Cr(NHtBu)(NtBu)] (**47**, Scheme 14).[43]

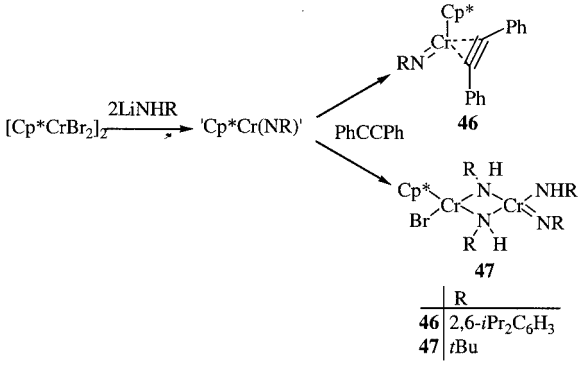

Scheme 14. Trapping of [Cp*Cr(NR)] intermediates by diphenylacetylene

3. Linear versus Bent Binding Modes of Imido Ligands

Imido groups bind to transition metal atoms either in linear or in bent fashion (Scheme 15). In general, linear imido ligands have M−N−C angles greater than 160°, whereas the bond angles for bent ones are less than 150°, although the dividing line between these two binding modes is not clear-cut. In valence bond description terms, the bent imido group − with sp^2-hybridized nitrogen atom − is regarded as a 4e donor (structure **I**). On the other hand, the linear imido group − with sp-hybridized nitrogen atom − can be either a 4e or a 6e donor, depending upon whether there are one or two M−N π bonds (structures **II** and **III**, respectively).[15]

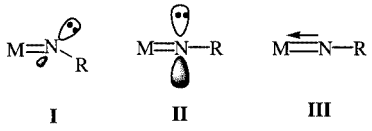

Scheme 15. Valence bond description of linear and bent imido ligands[15]

The bent and linear binding modes for imido ligands have recently been investigated both theoretically[44−49] and experimentally.[50−55] Nitrogen NMR studies indicate that complexes possessing both linear and bent imido groups are fluxional in solution and that the energy barrier to bending of the M−N−C unit is relatively small,[51] consistently with the results of theoretical studies.[32,44,49] It appears that both electronic and steric factors affect the geometry of the imido ligands. Thus, while the observation of one bent imido ligand in [$Mo(NPh)_2(Et_2NCS_2)_2$] [Mo−N−C angle of

139.4(4)°; cf. 169.4(4)° for the linear one] has been interpreted in terms of the 18e rule,[53] the more bulky 2,6-diisopropylphenylimido analogue [Mo($NC_6H_3iPr_2$-2,6)$_2$(Et_2NCS_2)$_2$] possesses essentially linear imido groups [Mo−N−C angle of 169.9(2)°], presumably due to steric effects.[54]

The vast majority of (imido)Cr complexes so far isolated contain essentially linear imido ligands (type **III**). One of the imido ligands in **6** was found to be bent [Cr−N−C(imido) angle = 151.8(4)°], but this bending was attributed to crystal packing rather than electronic effects. It may be noted that both imido groups in the Mo analogue [Mo(TACN)(N*t*Bu)$_2$Cl][ClO_4] are essentially linear [Mo−N−C(imido) angles are 171.1(3) and 161.5(3)°].[22] An example of a strongly bent (imido)Cr complex is **23**, the Cr−N−C(imido) angle of which is 146.2(3)°. The bent Cr−N−C(imido) angle in **23** was explained in terms of π-conflict between the oxo and the imido groups. In order to investigate the origin of the bending of the Cr−N−C(imido) unit in **23**, DFT calculations were performed on a simplified model compound [Cr(NMe)(O)(N-Me_2)Me], which lacks the steric bulk present in **23**. It was found that the DFT-optimized geometry of [Cr(NMe)(O)(NMe_2)Me] satisfactorily reproduced the pertinent structural features in **23**. The calculated Cr−N−C(imido) angle of 149.0° is similar to that found in **23**, suggesting that electronic factors play a significant role in the distortion in **23**.[32]

4. Electrochemistry of (Imido)Cr Complexes

The reduction couples observed in the range of −1.2 to −2.0 V vs. $Cp_2Fe^{+/0}$ for bis(imido)Cr^{VI} complexes have been attributed to metal-centered $Cr^{VI/V}$ reduction. For example, the diaryl compound **14** underwent 1e reduction in THF at $E_{1/2}$ = −1.31 V vs. Ag/AgCl (ca. −1.65 V vs. $Cp_2Fe^{+/0}$).[28] The $Cr^{VI/V}$ couple for the diaryl oxide compound **8** was found at −1.2 V vs. $Cp_2Fe^{+/0}$,[20] which is less negative than that for **14**, indicating that the σ-aryl moiety is a stronger donor than the aryl oxide. As would be expected, the $Cr^{VI/V}$ couple for dicationic **5** has a less negative $Cr^{VI/V}$ potential (−0.74 vs. $Cp_2Fe^{+/0}$).[20] Attempts to isolate bis(imido)Cr^{V} complexes by reduction of **5** or **14** with reducing agents were unsuccessful. For **6**, in addition to the Cr-centered reduction wave at −1.29 V vs. $Cp_2Fe^{+/0}$, a quasi-reversible oxidation couple was observed at 0.86 V and attributed to imido-centered oxidation. A similar oxidation potential (0.99 V) was found for the Mo analogue [Mo(TACN)(N*t*Bu)$_2$Cl]$^+$.[21] Cyclic voltammograms of (imido)Cr^{V} complexes showed irreversible reduction waves that were assigned to $Cr^{V/IV}$ reduction. For example, the $Cr^{V/IV}$ reduction for **31** was found at −0.71 V, which is more negative than that for the oxo analogue [Cr(O)(L)]$^+$ [L = 2,3-dimethyl-*N*,*N*′-bis(salicylidene)butane-2,3-diamine] (0.63 V vs. standard calomel electrode), reflecting the higher donor strength of imide relative to oxo.[37]

5. Reactivity of (Imido)Cr Complexes

5.1. Hydrolysis

(Imido)Cr complexes are generally moisture-sensitive and readily hydrolyze to (oxo)Cr complexes. However, cationic bis(imido)Cr^{VI} complexes **5** and **6** are air-stable and inert to hydrolysis. Treatment of **1** with 1 equiv. of water in diethyl ether afforded the (imido)(oxo) complex [Cr(O)(N*t*Bu)($OSiMe_3$)$_2$], which reacted with PCl_5 to give [Cr(O)(N*t*Bu)Cl_2].[19] Treatment of **2** with [O(Ph_2SiOH)$_2$] in the presence of pyridine gave a dinuclear chromosiloxane complex [{Cr(O)(N*t*Bu)(OPh_2SiO)$_2$}$_2$] (**48**, Figure 2), the oxo group of which was presumably derived from the silanol.[56]

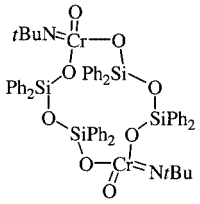

48

Figure 2. Structure of [{Cr(O)(N*t*Bu)(OPh_2SiO)$_2$}$_2$]

Treatment of [Cr(NAr)$_2$(SAr)$_2$] (Ar = 2,4,6-$Me_3C_6H_2$) with PMe_2Ph, followed by workup in the presence of adventitious oxygen, afforded an interesting tetranuclear (imido)(oxo)Cr cluster [Cr_4(μ-O)$_2$(μ-NAr)$_4$(O)$_2$(NAr)$_2$(SAr)$_2$] (**49**, Figure 3) in low yield.[57]

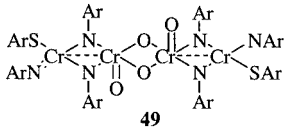

49

Ar = 2,4,6-$Me_3C_6H_2$

Figure 3. Structure of [Cr_4(μ-O)$_2$(μ-NAr)$_4$(O)$_2$(NAr)$_2$(SAr)$_2$] (Ar = 2,4,6-$Me_3C_6H_2$)

5.2. Cycloaddition

The [2 + 2] cycloaddition reactions between imido complexes and doubly bonded X=Y systems, presumably through four-membered metallacyclic intermediates (Scheme 16), are well documented.

Scheme 16. [2 + 2] cycloadditions between M=NR and X=Y

Treatment of **1** with PhCHO afforded the (imido)(oxo)-Cr^{VI} complex [Cr(N*t*Bu)(O)($OSiMe_3$)$_2$] and PhCH=N*t*Bu.[58] While **2** underwent cycloaddition and imido group exchange with aryl isocyanates ArNCO to give [Cr(NAr)$_2$$Cl_2$], no reactions were found between [Cr(NAr)$_2$$Cl_2$] and *t*BuNCO.[25] Treatment of

$[Cr(NtBu)_2\{N(SiMe_3)_2\}_2]$ with *t*BuNCO resulted in isocyanate insertion into the Cr−amide bond to give the *N*,*N*′,*N*′′-tri-*tert*-butylbiureto complex $[Cr(NtBu)_2\{(tBuNCO)_2NtBu\}]$ (**50**, Figure 4) rather than cycloaddition of Cr=N*t*Bu with isocyanate.[59]

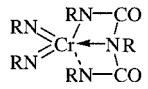

50

R = *t*Bu

Figure 4. Structure of $[Cr(NtBu)_2\{(tBuNCO)_2NtBu\}]$

Treatment of "Cp*Cr($NC_6H_3iPr_2$-2,6)" (prepared in situ) with 2,6-$Me_2C_6H_4NC$ resulted in coupling of the isocyanide with Cr=$NC_6H_3iPr_2$-2,6 and the formation of a Cp*Cr^{III} complex containing an *N*,*N*-bis(2,6-diisopropylphenyl)-4-isopropyl-1-(2,6-xylylamino)naphthaline-2,3-diamido ligand (**51**, Figure 5).[40]

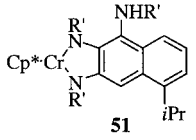

51

R = 2,6-$iPr_2C_6H_3$, R′ = 2,6-$Me_2C_6H_3$

Figure 5. Structure of the product obtained on treatment of "Cp*Cr($NC_6H_3iPr_2$-2,6)" with 2,6-$Me_2C_6H_3NC$

Recent theoretical studies on olefin polymerization with bis(imido)Cr^{VI} catalysts revealed that the [2 + 2] cycloadditions between C=C and Cr=NR double bonds proceed with very low energy barriers. It was suggested that the resulting azachromacycles could be a starting point for further modification of the (alkyl)Cr^{VI} cations in the catalytic cycle.[12]

5.3. Imido Group Transfer

Organoimido complexes are less reactive than acylimido (M=NCOR) and tosylimido ($M=NSO_2R$) complexes toward imido group transfer. (Imido)Cr complexes undergo imido transfer with strong reducing agents such as tertiary phosphanes[20,36b,37,42] and isocyanides.[57,60] Imido transfer from (imido)Cr^{IV}−porphyrin compounds to benzaldehyde, CS_2, and styrene has also been reported,[42] and imido group transfer to phosphanes from (imido)Cr^{V} complexes was found to be catalyzed by light.[36,37] It was noted that the reactivity of (imido)Cr complexes toward imido transfer could be correlated with the electron deficiency at the Cr center.[20] Thus, while no reaction was found between the diaryl oxide compound **8** ($E_{1/2}$ = −1.2 V vs. $Cp_2Fe^{+/0}$) and PMe_3, dicationic **5** ($E_{1/2}$ = −0.74 V vs. $Cp_2Fe^{+/0}$) readily underwent imido transfer with tertiary phosphanes to give phosphanimines. Under pseudo-first-order conditions, the reaction between **5** and PMe_3 was found to follow biphasic kinetics, with $k_{obs1} \propto [PMe_3]$ and $k_{obs2} \propto [PMe_3]^2$. The kinetic data are consistent with a two-step mechanism as shown in Scheme 17.[20]

step 1

$$[Cr(NtBu)_2(terpy)]^{2+} + PMe_3 \xrightarrow{k_2} [Cr(NtBu)(terpy)]^{2+} + tBu{=}PMe_3$$

step 2

$$[Cr(NtBu)(terpy)]^{2+} + PMe_3 \overset{K}{\rightleftharpoons} [Cr(NtBu)(terpy)(PMe_3)]^{2+}$$

$$[Cr(NtBu)(terpy)(PMe_3)]^{2+} + PMe_3 \xrightarrow{k'} Cr(II) + tBuN{=}PMe_3$$

Scheme 17. Proposed mechanism for imido transfer from $[Cr(NtBu)(terpy)]^{2+}$ to PMe_3

For step 1, rate = k_2[Cr][PMe_3]. For step 2, at $K[PMe_3] >> 1$, rate = Kk'[Cr][PMe_3]^2 with $k_3 = kK'$. At 25 °C in acetonitrile solution, $k_2 = 0.48 \pm 0.10$ $M^{-1}\cdot s^{-1}$ and $k_3 = Kk' = 1.44 \pm 0.16$ $M^{-2}\cdot s^{-1}$.[20]

Treatment of $[Cr(NC_6H_2Me_3\text{-}2,4,6)_2(SC_6H_2Me_3\text{-}2,4,6)_2]$ with 2,6-$Me_2C_6H_3NC$ at reflux resulted in the formation of the mono(imido)Cr^{IV} complex $[Cr(NC_6H_2Me_3\text{-}2,4,6)(SC_6H_2Me_3\text{-}2,4,6)_2(CNC_6H_4Me_2\text{-}2,6)_2]$ and the carbodiimide 2,4,6-$Me_3C_6H_2N{=}C{=}NC_6H_3Me_2$-2,6. It seems likely that the imido transfer to the isocyanide occurred through a (η^2-carboimide)Cr intermediate.[57] Treatment of $[Cr(NC_6H_2Me_3\text{-}2,4,6)_2(SC_6F_5)_2]$ with 2,6-$Me_2C_6H_3NC$ resulted in the isolation of *mer*-$[Cr(SC_6F_5)_3(NCC_6H_2Me_2\text{-}2,6)_3]$ and *trans*-$[Cr(SC_6F_5)_2(NCC_6H_2Me_2\text{-}2,6)_4]$, together with other unidentified products.[60] No imido transfer was found between 2,6-$Me_2C_6H_3NC$ and either $[Cr(NC_6H_2iPr_3\text{-}2,4,6)(SC_6H_2Me_3\text{-}2,4,6)_2]$ or $[Mo(NAr)_2(SC_6H_3iPr_2\text{-}2,6)_2]$ (R = 2,4,6-$Me_3C_6H_2$ or 2,6-$iPr_2C_6H_3$), probably because of steric effects.[57][60]

5.4. Addition of Alkyl Group to Imido Ligand

Nugent and Harlow studied the addition of alkyl groups to coordinated imido groups in attempts to model the C−N formation step in ammoxidation of propylene. Thus, treatment of **1** with Ph_2Zn, followed by hydrolysis, afforded organic products including *tert*-butylaniline and biphenyl. It was believed that the former product was formed by the Cr-to-N migration of the phenyl ligand in a mono(phenyl)Cr^{VI} intermediate, whereas the latter product originated from reductive elimination of a diphenylCr^{VI} species.[61] Similarly, the reaction between **1** and benzyl radical, generated from toluene and dibenzyl peroxide, resulted in addition of benzyl radical to the imido nitrogen atom. Upon hydrolysis, *t*BuN=CHPh was produced, along with CO_2, bibenzyl, and methylbiphenyls.[1b] The (amido)Cr^{IV} species $[Cr\{N(C_6H_4\text{-}Me_3\text{-}2,4,6)(4\text{-}tBuC_6H_4)Cl\}_2(\mu\text{-}NC_6H_4Me_3\text{-}2,4,6)Cl]_2$, obtained from the alkylation of **9** with 4-$tBuC_6H_4CH_2MgCl$, has been isolated and characterized structurally.[25] No alkyl group migration was found for the alkylation of **1** with 2,4,6-$Me_3C_6H_2MgBr$, apparently because of the steric bulk of the mesityl group.[28] However, thermal decomposition of $[Cr(NtBu)_2\{C(O)C_6H_2Me_3\text{-}2,4,6\}_2]$, prepared by carbonylation of **14**, yielded 2,4,6-$Me_3C_6H_2C(O)NHtBu$, pre-

sumably through migration of the acyl group to the imido nitrogen atom.[28]

6. Reactions Catalyzed by (Imido)Cr Complexes

6.1. Olefin Polymerization

Chromium catalysts play important roles in the manufacture of polyolefins in industry. To this end, much effort has been devoted to the development of new, well-defined molecular chromium catalysts for olefin polymerization.[62] The catalytic activity of bis(imido)Cr^{VI} complexes and half-sandwich Group-5 CpM(NR) systems, which are isolobal with Group-4 metallocenes, toward olefin polymerization has been investigated.[11] Gibson and co-workers reported that **2** in conjunction with an activator such as MAO (methylaluminoxanes) and Et_2AlCl was capable of polymerization of ethylene to give poly(ethylene)s of high molecular weights with little branching. $[Mo(N\textit{t}Bu)_2Cl_2]$ was found to be a less active polymerization catalyst than the Cr congener.[11a] The dibenzyl compound $[Cr(N\textit{t}Bu)_2(CH_2Ph)_2]$ was able to polymerize ethylene in the presence of boron activators $[PhNMe_2H][B(C_6F_5)_4]$, $[CPh_3][B(C_6F_5)_4]$, and $B(C_6F_5)_3$ to give poly(ethylene)s of high molecular weights.[11c,29] Both $[Cr(NC_6H_4Me_2\text{-}2,6)_2Me_2]$ and $[Mo(NC_6H_4Me_2\text{-}2,6)_2Me_2]$ are active catalysts for polymerization of ethylene in the presence of $B(C_6F_5)_3$.[11c] Treatment of $[Cr(N\textit{t}Bu)_2(CH_2Ph)_2]$ with $[CPh_3][B(C_6F_5)_4]$ afforded an oily cationic species $[Cr(N\textit{t}Bu)_2(\eta^2\text{-}CH_2Ph)]^+$, which reacted with PMe_3 to give the monophosphane adduct. On the other hand, $[Cr(N\textit{t}Bu)_2(CH_2Ph)_2]$ reacted with $[PhNMe_2H][B(C_6F_5)_4]$ to yield a mixture of mono- and bis(dimethylaniline) adducts $[Cr(N\textit{t}Bu)_2(\eta^2\text{-}CH_2Ph)(NMe_2Ph)_n]^+$ (n = 1 or 2). Solutions containing $[Cr(N\textit{t}Bu)_2(\eta^2\text{-}CH_2Ph)]^+$ or $[Cr(N\textit{t}Bu)_2(\eta^2\text{-}CH_2Ph)(NMe_2Ph)_n]^+$ are capable of catalyzing ethylene polymerization in the absence of a co-catalyst.[11c] A recent theoretical study on $[Cr(NR)_2(C_3H_7)(C_2H_4)]^+$ (R = H, *t*Bu) revealed a facile reductive elimination involving β-hydrogen transfer from the alkyl chain, suggesting that the active species for the bis(imido)Cr^{VI}-based catalysts contain Cr in a lower oxidation state.[12b] Recently, Siemeling and co-workers reported that an *ansa*-bis(imido)Cr^{VI} complex $[(NCMe_2CH_2CH_2CMe_2N)Cr(CH_2Ph)(\eta^2\text{-}CH_2Ph)]$ (**52**), prepared from $[Cr(NCMe_2CH_2CH_2CMe_2N)Cl_2]$ and $PhCH_2MgCl$, and complex **17**, were capable of catalyzing polymerization of acrylonitrile in the absence of a co-catalyst to give poly(acrylonitrile)s with high molecular weights. Complexes **17** and **52** also catalyzed the copolymerization of acrylonitrile and methyl methacrylate.[63]

6.2. Ring-Opening of Epoxides and Aziridines

Coordinatively unsaturated imido complexes are good Lewis acid catalysts because of the presence of low-lying vacant metal d-orbitals, their high solubility in organic solvents, and their low tendency to dimerize or oligomerize in organic solvents. In view of this, the use of (imido)metal complexes as Lewis acid catalysts for ring-opening of epoxides and aziridines has been investigated. (Imido)Cr complexes **2** and **30** were capable of catalyzing ring-opening of epoxides[64] and tosylaziridines[65] with Me_3SiN_3 in good yield and with good regioselectivity (Scheme 18).

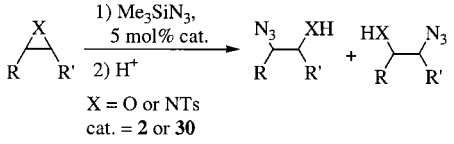

Scheme 18. Ring-opening of epoxides and aziridines catalyzed by (imido)Cr complexes

Treatment of styrene oxide (R = Ph, R′ =H) with Me_3SiN_3 and a catalytic amount of **2** exclusively gave 2-azido-1-phenylethanol, consistent with the Lewis acid mechanism for epoxide ring-opening. The catalytic activity of (imido)-metal complexes was found to decrease in the order **30** > **2** > $[Mo(N\textit{t}Bu)_2Cl_2]$.[64] It is believed that (azido)(imido)Cr complexes are the active intermediates for the Cr-mediated azidolysis of epoxides. Indeed, treatment of **2** with Me_3SiN_3 afforded dinuclear $[Cr(\mu\text{-}N_3)(N\textit{t}Bu)_2Cl]_2$, an active catalyst for epoxide ring-opening.[65] In an attempt to prepare a chiral (imido)Cr complex for asymmetric catalysis, **30** was treated with (*S*,*S*)-DIOP {(*S*,*S*)-4,5-[bis(diphenylphosphanyl)methyl]-2,2-dimethyl-1,3-dioxolane}. Unfortunately, dinuclear $[Cr(N\textit{t}Bu)Cl_3]_2${μ-(*S*,*S*)-DIOP} was isolated rather than mononuclear (*S*,*S*)-DIOP complex.[66] Recently, Sundermeyer and co-workers prepared a chiral Mo^{VI} complex with a C_2-symmetric bidentate diimido ligand $[TADDAMINat]^{4-}$ [TADDAMIN = (4*S*,5*S*)-2,2-dimethyl-α,α,α′,α′-tetraphenyl-1,3-dioxolane-4,5-diylbis(methanamine)]. [Mo(TADDAMINat)Cl_2(DME)] (**53**, Figure 6) has been used as a catalyst for the kinetic resolution of styrene oxide with Me_3SiN_3 and the asymmetric trimethylsilylcyanation of benzaldehyde. The enantioselectivities for the two reactions were 30 and 20% *ee*, respectively.[67]

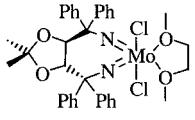

53

Figure 6. Structure of [Mo(TADDAMINat)Cl_2(DME)]

Because of the high affinities of (imido)Cr^{V} complexes for O-donor ligands, **30** and $[Cr(N\textit{t}Bu)Br_3(DME)]$ (**54**) were used to study the regioselectivity of ring-opening of disubstituted epoxides containing benzyloxy groups. Thus, treatment of **30** or **54** with disubstituted epoxide **55** afforded the corresponding 3-halohydrins in good yield and with good selectivity (C-3/C-2 > 49:1). The imido complexes **30** and **54** were also capable of catalyzing regioselective ring-opening of disubstituted epoxides with trimethylsilyl halide. Thus, treatment of epoxide **55** with trimethylsilyl halide in

the presence of a catalytic amount of **30** or **54** afforded the halohydrins with good C-3 selectivity (C-3/C-2 > 18, Scheme 19).[68]

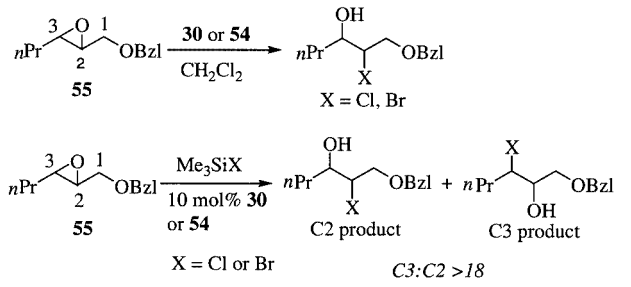

Scheme 19. Cr-mediated regioselective ring-opening of benzyloxy epoxides

The observed C-3 selectivity for the ring-opening of **55** has been explained in terms of Cr chelation (Scheme 20). Nucleophilic attack at C-3 is preferred because of the higher stability of the five-membered metallacycle intermediate relative to the six-membered analogue.[68]

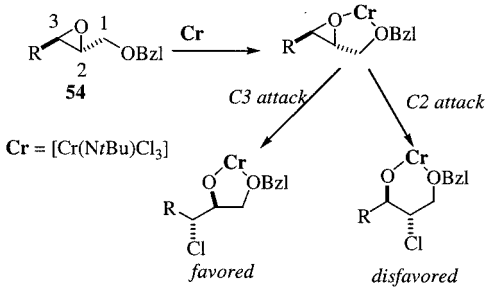

Scheme 20. Proposed mechanism for Cr-catalyzed regioselective ring-opening of disubstituted epoxides

6.3. Cyclopropanation of Olefins

Bis(imido)Cr^{VI} complexes $[Cr(\mu\text{-}NPh)(NPh)Cl_2]_2$ and $[Cr(NAr)_2Cl_2]$ (Ar = 2,6-$Cl_2C_6H_3$ or 2,6-$Br_2C_6H_3$) were found to catalyze cyclopropanation of substituted styrene on treatment with ethyl diazoacetate (EDA, Scheme 21). For example, treatment of styrene with EDA in the presence of ca. 4 mol % of $[Cr(\mu\text{-}NPh)(NPh)Cl_2]_2$ afforded the cyclopropane product in 90% yield with a *cis*/*trans* ratio of 0.65. Treatment of ethyl acrylate with EDA in the presence of the (imido)Cr catalyst afforded both cyclopropane and vinyl C−H insertion products.

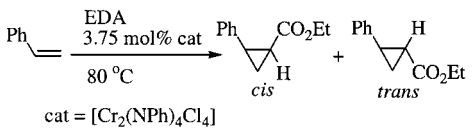

Scheme 21. Cyclopropanation of styrene catalyzed by (imido)Cr complexes

The active intermediate for the Cr-catalyzed cyclopropanation was believed to be a Cr imido carbene species, possibly $[Cr(NPh)_2Cl_2(CHCO_2Et)]$. A competition experiment for the Cr-mediated carbene transfer showed that ethyl acrylate was consumed in preference to styrene, indicative of the nucleophilic character of the (carbene)Cr intermediate.[69]

7. Concluding Remarks

The successes obtained in isolation of stable (imido)Cr^{VI} and -Cr^{V} complexes and their organometallic derivatives demonstrate the significance of organoimido groups as stabilizing spectator ligands for organometallic compounds with highly oxidizing metal centers. In addition, owing to the steric bulk of organoimido ligands, coordinatively unsaturated $M(NR)_2$ and M(NR) complexes that are reactive toward unsaturated organic substrates can readily be synthesized. For example, d^0 Group-6 M(NR) and $M(NR)_2$ complexes have been found to be well-defined catalysts for olefin metathesis and polymerization, and have been used as Lewis acid catalysts for organic transformations. Recently, the imido chemistry has been extended to the right-hand side of the first transition series.[70−74] Notably, a new family of stable imido complexes of Mn in oxidation states VII−V has been synthesized by Danopoulos et al.[52,70] It may therefore be anticipated that compounds of Fe in less common oxidation states, such as Fe^{IV} and Fe^{V}, should be accessible if stabilized by organoimido ligands[72] and would exhibit novel organometallic chemistry.

Acknowledgments

Financial support from the Hong Kong University of Science and Technology, the Hong Kong Research Grants Council, and the Areas of Excellence Scheme established under the University Grants Committee of the Hong Kong Special Administrative Region, China (project no.: AoE-P10-01) is gratefully acknowledged. The author is indebted to the students and co-workers whose names appear in the references.

[1] [1a] D. M.-T. Chan, W. C. Fultz, W. A. Nugent, D. C. Roe, T. H. Tulip, *J. Am. Chem. Soc.* **1985**, *107*, 251−252. [1b] D. M.-T. Chan, W. A. Nugent, *Inorg. Chem.* **1985**, *24*, 1422−1424.
[2] [2a] J. T. Groves, T. Takahashi, *J. Am. Chem. Soc.* **1983**, *105*, 2073−2074. [2b] S.-M. Au, J.-S. Huang, W.-Y. Yu, W.-H. Fung, C.-M. Che, *J. Am. Chem. Soc.* **1999**, *121*, 9120−9132. [2c] S. Minakata, M. Komatsu, in: *Modern Amination Methods* (Ed.: A. Ricci), Wiley-VCH, Weinheim, **2000**, pp. 169−194 and references cited therein. [2d]S. Minakata, T. Ando, M. Nishimura, I. Ryu, M. Komatsu, *Angew. Chem.* **1998**, *110*, 3596−3598; *Angew. Chem. Int. Ed.* **1998**, *37*, 3392−3393. [2e] C.-M. Ho, T.-C. Lau, H.-L. Kwong, W.-T. Wong, *J. Chem. Soc., Dalton Trans.* **1999**, 2411−2413.
[3] G. Li, H.-T. Chang, K. B. Sharpless, *Angew. Chem.* **1996**, *108*, 449−452; *Angew. Chem. Int. Ed. Engl.* **1996**, *35*, 451−454 and references cited therein.
[4] [4a] J. Du Bois, J. Hong, E. M. Carreira, M. W. Day, *J. Am. Chem. Soc.* **1996**, *118*, 915−916. [4b] J. Du Bois, C. S. Tomooka, J. Hong, E. M. Carreira, *J. Am. Chem. Soc.* **1997**, *119*, 3179−3180. [4c] J. Du Bois, C. S. Tomooka, J. Hong, E. M. Carreira, *Acc. Chem. Res.* **1997**, *30*, 364 −372.

[5] E. Haak, I. Bytschkov, S. Doye, *Angew. Chem.* **1999**, *111*, 3584−3586; *Angew. Chem. Int. Ed.* **1999**, *38*, 3389−3391.

[6] [6a] J. S. Johnson, R. G. Bergman, *J. Am. Chem. Soc.* **2001**, *123*, 2923−2924. [6b] B. F. Straub, R. G. Bergman, *Angew. Chem.* **2001**, *113*, 4768−4771; *Angew. Chem. Int. Ed.* **2001**, *40*, 4632−4635.

[7] [7a] K. E. Meyer, P. J. Walsh, R. G. Bergman, *J. Am. Chem. Soc.* **1994**, *116*, 2669−2670. [7b] S. W. Krska, R. L. Zuckerman, R. G. Bergman, *J. Am. Chem. Soc.* **1998**, *120*, 11828−11829. [7c] A. J. Blake, P. E. Collier, S. C. Dunn, W.-S. Li, P. Mountford, O. V. Shishkin, *J. Chem. Soc., Dalton Trans.* **1997**, 1549−1558. [7d] J. M. McInnes, P. M. Mountford, *Chem. Commun.* **1998**, 1669−1670. [7e] G. K. Cantrell, T. Y. Meyer, *Organometallics* **1997**, *16*, 5381−5383. [7f] G. K. Cantrell, T. Y. Meyer, *J. Am. Chem. Soc.* **1998**, *120*, 8035−8042. [7g] J. W. Bruno, X. J. Li, *Organometallics* **2000**, *19*, 4672−4674. [7h] K. R. Birdwhistell, J. Lanza, J. Pasos, *J. Organomet. Chem.* **1999**, *584*, 200−205.

[8] [8a] C. C. Cummins, S. M. Baxter, P. T. Wolczanski, *J. Am. Chem. Soc.* **1988**, *110*, 8731−8733. [8b] C. C. Cummins, C. P. Schaller, G. D. Van Duyne, P. T. Wolczanski, A. W. E. Chan, R. Hoffmann, *J. Am. Chem. Soc.* **1991**, *113*, 2985−2994. [8c] C. P. Schaller, P. T. Wolczanski, *Inorg. Chem.* **1993**, *32*, 131−144. [8d] D. F. Schafer II, P. T. Wolczanski, *J. Am. Chem. Soc.* **1998**, *120*, 4881 −4882.

[9] [9a] R. R. Schrock, *Acc. Chem. Res.* **1990**, *23*, 158−165. [9b] J. Feldman, R. R. Schrock, *Prog. Inorg. Chem.* **1991**, *39*, 2−66.

[10] A. H. Hoveyda, R. R. Schrock, *Chem. Euro J.* **2001**, *7*, 945−950 and references cited therein.

[11] [11a] M. P. Coles, V. C. Gibson, *Polym. Bull.* **1994**, *33*, 529−533. [11b] M. P. Coles, C. I. Dalby, V. C. Gibson, W. Clegg, M. R. J. Elsegood, *Chem. Commun.* **1997**, 1709−1710. [11c] M. P. Coles, C. I. Dalby, V. C. Gibson, I. R. Little, E. L. Marshall, M. H. Ribeiro de Costa, S. Mastroianni, *J. Organomet. Chem.* **1999**, *591*, 78−87.

[12] [12a] V. R. Jensen, K. J. Børve, *Organometallics* **2001**, *20*, 616−626. [12b] V. R. Jensen, K. J. Børve, *Chem. Commun.* **2002**, 542−543.

[13] W. A. Nugent, *Coord. Chem. Rev.* **1980**, *31*, 123−175.

[14] W. A. Nugent, J. M. Mayer, *Metal-Ligand Multiple Bonds*, Wiley-Interscience, New York, **1988**.

[15] D. E. Wigley, *Prog. Inorg. Chem.* **1994**, *42*, 239−482.

[16] W. A. Nugent, R. L. Harlow, *Inorg. Chem.* **1980**, *19*, 777−779.

[17] A. A. Danopoulos, W.-H. Leung, G. Wilkinson, B. Hussain-Bates, M. B. Hursthouse, *Polyhedron* **1990**, *9*, 2625−2634.

[18] [18a] M. P. Coles, V. C. Gibson, W. Clegg, M. R. J. Elsegood, *Polyhedron* **1998**, *17*, 2483−2489. [18b] A. S. Batsanov, K. B. Dillon, V. C. Gibson, J. A. K. Howard, L. J. Sequeira, J. W. Yao, *J. Organomet. Chem.* **2001**, *631*, 181−187.

[19] N. Meijboom, C. J. Schaverien, A. G. Orpen, *Organometallics* **1990**, *9*, 774−782.

[20] W.-H. Leung, M.-C. Wu, T.-C. Lau, W.-T. Wong, *Inorg. Chem.* **1995**, *34*, 4271−4274.

[21] M. C. W. Chan, F.-W. Lee, K.-K. Cheung, C.-M. Che, *J. Chem. Soc., Dalton Trans.* **1999**, 3197−3201.

[22] J. Sundermeyer, J. Putterlik, M. Foth, J. S. Field, N. Ramesar, *Chem. Ber.* **1994**, *127*, 1201−1212.

[23] A. A. Danopoulos, G. Wilkinson, *Polyhedron* **1990**, *9*, 1009−1010.

[24] M. P. Coles, C. I. Dalby, V. C. Gibson, W. Clegg, M. R. J. Elsegood, *Polyhedron* **1995**, *14*, 2455−2459.

[25] A. A. Danopoulos, G. Wilkinson, T. K. N. Sweet, M. B. Hursthouse, *J. Chem. Soc., Dalton Trans.* **1995**, 2111−2123.

[26] K. C. Chew, W. Clegg, M. R. Coles, M. R. J. Elsegood, V. C. Gibson, A. J. P. White, D. J. Williams, *J. Chem. Soc., Dalton Trans.* **1999**, 2633−2639.

[27] A. A. Danopoulos, D. M. Hankin, G. Wilkinson, S. M. Cafferkey, T. K. N. Sweet, M. B. Hursthouse, *Polyhedron* **1997**, *16*, 3879−3892.

[28] A. C. Sullivan, G. Wilkinson, M. Motevalli, M. B. Hursthouse, *J. Chem. Soc., Dalton Trans.* **1988**, 53−60.

[29] M. P. Coles, C. I. Dalby, V. C. Gibson, W. Clegg, M. R. J. Elsegood, *J. Chem. Soc., Chem. Commun.* **1995**, 1709−1710.

[30] M. P. Coles, V. C. Gibson, M. R. J. Elsegood, P. A. Porrelli, *Chem. Commun.* **1996**, 1963−1964.

[31] J. Sundermeyer, K. Weber, H. Pritzkow, *Angew. Chem.* **1993**, *105*, 751; *Angew. Chem. Int. Ed. Engl.* **1993**, *32*, 731−733.

[32] E. W. Jandciu, P. Legzdins, W. S. McNeil, B. O. Patrick, K. M. Smith, *Chem. Commun.* **2000**, 1809−1910.

[33] N. Wiberg, H.-W. Häring, U. Schubert, *Z. Naturforsch., Teil B* **1978**, *33*, 1365−1369.

[34] H.-W. Lam, G. Wilkinson, B. Hussain-Bates, M. B. Hursthouse, *J. Chem. Soc., Dalton Trans.* **1993**, 1477−1482.

[35] H.-T. Chiu, Y.-P. Chen, S.-H. Chuang, J.-S. Jen, G.-H. Lee, S.-M. Peng, *Chem. Commun.* **1996**, 139−140.

[36] [36a] A. A. Danopoulos, B. Hussain-Bates, M. B. Hursthouse, W.-H. Leung, G. Wilkinson, *J. Chem. Soc., Chem. Commun.* **1990**, 1678−1679. [36b] W.-H. Leung, A. A. Danopoulos, G. Wilkinson, B. Hussain-Bates, M. B. Hursthouse, *J. Chem. Soc., Dalton Trans.* **1991**, 2051−2061.

[37] W.-H. Leung, M.-C. Wu, K.-Y. Wong, Y. Wang, *J. Chem. Soc., Dalton Trans.* **1994**, 1659−1663.

[38] C. H. Wang, T.-H. Tang, Y. Wang, *J. Phys. Chem. A* **2000**, *104*, 9566−9572.

[39] W. H. Leung, M. C. Wu, T. Wong, W.-T. Wong, *Inorg. Chim. Acta* **2000**, *304*, 134−136.

[40] D. M. Hankin, A. A. Danopoulos, G. Wilkinson, T. K. N. Sweet, M. B. Hursthouse, *J. Chem. Soc., Dalton Trans.* **1996**, 4063−4069.

[41] A. R. Barron, J. E. Salt, G. Wilkinson, M. Motevalli, M. B. Hursthouse, *J. Chem. Soc., Dalton Trans.* **1987**, 2947−2954.

[42] B. Moubaraki, K. S. Murray, P. J. Nicols, S. Thomson, B. O. West, *Polyhedron* **1994**, *13*, 485−495.

[43] A. A. Danopoulos, G. Wilkinson, T. K. N. Tracy, M. B. Hursthouse, *J. Chem. Soc., Dalton Trans.* **1996**, 271−281.

[44] W. A. Nugent, R. L. Harlow, R. J. McKinney, *J. Am. Chem. Soc.* **1979**, *101*, 7265−7268.

[45] [45a] T. R. Cundari, *J. Am. Chem. Soc.* **1992**, *114*, 7879−7888. [45b] T. R. Cundari, *Chem. Rev.* **2000**, *100*, 807−818.

[46] M. H. Schofield, T. P. Kee, J. T. Anhaus, R. R. Schrock, J. H. Johnson, W. M. Davis, *Inorg. Chem.* **1991**, *30*, 3595−3604.

[47] Z. Lin, M. B. Hall, *Coord. Chem. Rev.* **1993**, *123*, 149−167.

[48] K. A. Jørgensen, *Inorg. Chem.* **1993**, *32*, 1521−1522.

[49] D. W. H. Rankin, H. E. Robertson, A. A. Danopoulos, P. D. Lyne, D. M. P. Mingos, G. Wilkinson, *J. Chem. Soc., Dalton Trans.* **1994**, 1563−1569.

[50] J. P. Le Ny, J. A. Osborn, *Organometallics* **1991**, *10*, 1546−1550.

[51] D. Bradley, S. R. Hodge, J. D. Ruunacles, M. Hughes, J. Mason, R. L. Richards, *J. Chem. Soc., Dalton Trans.* **1992**, 1663−1668.

[52] A. A. Danopoulos, J. C. Green, M. B. Hursthouse, *J. Organomet. Chem.* **1999**, *591*, 36−44.

[53] B. L. Haymore, E. A. Maatta, R. A. D. Wentworth, *J. Am. Chem. Soc.* **1979**, *101*, 2063−2068.

[54] T. A. Coffey, G. D. Forster, G. Hogarth, A. Sella, *Polyhedron* **1993**, *12*, 2741−2743.

[55] V. C. Gibson, E. L. Marshall, C. Redshaw, W. Clegg, M. R. J. Elsegood, *J. Chem. Soc., Dalton Trans.* **1996**, 4197−4199.

[56] [56a] L. King, M. Motevalli, A. C. Sullivan, *J. Chem. Soc., Dalton Trans.* **1999**, 3225−3228. [56b] L. King, M. Motevalli, A. C. Sullivan, *J. Chem. Soc., Dalton Trans.* **2000**, 1357−1361.

[57] A. A. Danopoulos, G. Wilkinson, T. K. N. Sweet, M. B. Hursthouse, *Polyhedron* **1996**, *15*, 873−879.

[58] W. A. Nugent, *Inorg. Chem.* **1983**, *22*, 965−969.

[59] H.-W. Lam, G. Wilkinson, B. Hussain-Bates, M. B. Hursthouse, *J. Chem. Soc., Dalton Trans.* **1993**, 781−788.

[60] A. A. Danopoulos, G. Wilkinson, T. K. N. Sweet, M. B. Hursthouse, *Polyhedron* **1997**, *16*, 2631−2636.

[61] W. A. Nugent, R. L. Harlow, *J. Am. Chem. Soc.* **1980**, *102*, 1759−1760.

[62] [62a] K. H. Theopold, *Eur. J. Inorg. Chem.* **1998**, 15−24. [62b] G. J. P. Britovsek, V. C. Gibson, D. F. Wass, *Angew. Chem.* **1999**, *111*, 448−468; *Angew. Chem. Int. Ed.* **1999**, *38*, 429−447.
[63] U. Siemeling, L. Kölling, A. Stammler, H.-G. Stammler, E. Kaminski, G. Fink, *Chem. Commun.* **2000**, 1177−1178.
[64] W.-H. Leung, E. K. F. Chow, M.-C. Wu, P. W. Y. Kum, L.-L. Yeung, *Tetrahedron Lett.* **1995**, *36*, 107−108.
[65] W.-H. Leung, M.-T. Yu, M.-C. Wu, L.-L. Yeung, *Tetrahedron Lett.* **1996**, *37*, 891−892.
[66] W.-H. Leung, M.-C. Wu, J. L. C. Chim, M. T. Yu, H.-w. Hou, L.-L. Yeung, W.-T. Wong, Y. Wang, *J. Chem. Soc., Dalton Trans.* **1997**, 3525−3529.
[67] E. A. Kretzschmar, J. Kipke, J. Sundermeyer, *Chem. Commun.* **1999**, 2381−2382.
[68] W.-H. Leung, T. K. T. Wong, J. C. H. Wong, L.-L. Yeung, *Synlett* **2000**, 677−679.
[69] D. Jan, F. Simal, A. Demonceau, A. F. Noels, K. A. Rufanov, N. A. Ustynyuk, D. N. Gourevitch, *Tetrahedron Lett.* **1999**, *40*, 5695−5699.
[70] [70a] A. A. Danopoulos, G. Wilkinson, T. Sweet, M. B. Hursthouse, *J. Chem. Soc., Chem. Commun.* **1993**, 495−496. [70b] A. A. Danopoulos, G. Wilkinson, T. K. N. Sweet, M. B. Hursthouse, *J. Chem. Soc., Dalton Trans.* **1994**, 1037−1049. [70c] A. A. Danopoulos, G. Wilkinson, T. K. N. Sweet, M. B. Hursthouse, *J. Chem. Soc., Dalton Trans.* **1995**, 205−216. [70d] A. A. Danopoulos, G. Wilkinson, T. K. N. Sweet, M. B. Hursthouse, *J. Chem. Soc., Dalton Trans.* **1995**, 937−950.
[71] R. A. Eikey, S. I. Khan, M. M. Abu-Omar, *Angew. Chem.* **2002**, *114*, 3743−3747; *Angew. Chem. Int. Ed.* **2002**, *41*, 3592−3595.
[72] A stable terminal (*tert*-butylimido)iron complex has been isolated recently: A. K. Verma, T. N. Nazif, C. Achim, S. C. Lee, *J. Am. Chem. Soc.* **2000**, *122*, 11013−11014.
[73] A terminal (imido)cobalt complex has been isolated recently: D. M. Jenkins, T. A. Betley, J. C. Peters, *J. Am. Chem. Soc.* **2002**, *124*, 11238−11239.
[74] [74a] A terminal (imido)nickel complex has been isolated recently: D. J. Mindiola, G. L. Hillhouse, *J. Am. Chem. Soc.* **2001**, *123*, 4623−4624. [74b] D. J. Mindiola, G. L. Hillhouse, *Chem. Commun.* **2002**, 1840−1841.

Received August 12, 2002
[I02455]

Unexpected Effect of Cyclodextrins on Water-Soluble Rhodium Complexes[‡]

Laurent Caron,[a] Mickael Canipelle,[a] Sébastien Tilloy,[a] Hervé Bricout,[a] and Eric Monflier*[a]

Keywords: Rhodium / Phosphanes / Biphasic catalysis / Cyclodextrins / Molecular recognition

As shown by ^{31}P NMR spectroscopy, addition of β-cyclodextrin or randomly methylated β-cyclodextrin to an aqueous solution of $[HRh(CO)\{P(m\text{-}C_6H_4SO_3Na)_3\}_3]$ has no effect on the organometallic complex. In contrast, $[HRh(CO)\{(p\text{-}t\text{Bu}C_6H_4)P(m\text{-}C_6H_4SO_3Na)_2\}_3]$ can be partially converted in the presence of the same β-cyclodextrin derivatives into the hydroxy complex $[HORh(CO)\{(p\text{-}t\text{Bu}C_6H_4)P(m\text{-}C_6H_4SO_3Na)_2\}_2]$, under nitrogen, or to the hydrido complex $[HRh(CO)_2\{(p\text{-}t\text{Bu}C_6H_4)P(m\text{-}C_6H_4SO_3Na)_2\}_2]$ under carbon monoxide. This remarkable difference of behavior was attributed to the fact that the phosphane $(p\text{-}t\text{Bu}C_6H_4)P(m\text{-}C_6H_4SO_3Na)_2$ forms more stable inclusion complexes with the β-cyclodextrin derivatives than the phosphane $P(m\text{-}C_6H_4SO_3Na)_3$.
(© Wiley-VCH Verlag GmbH & Co. KGaA, 69451 Weinheim, Germany, 2003)

Introduction

In the course of our work on the use of cyclodextrins as mass-transfer promoters in aqueous-phase organometallic catalysis, we found that cyclodextrins (Scheme 1) form inclusion compounds with the water-soluble ligands used to dissolve the catalyst in the aqueous phase.[1,2] We have reported that tris(3-sodiosulfonatophenyl)phosphane [TPPTS; $P(m\text{-}C_6H_4SO_3Na)_3$],[3,4] diphenyl(3-sodiosulfonatophenyl)phosphane [TPPMS; $(C_6H_5)_2P(m\text{-}C_6H_4SO_3Na)$][5,6] and (4-*tert*-butylphenyl)bis(3-sodiosulfonatophenyl)phosphane [*t*BuTPPDS; $(p\text{-}t\text{Bu}C_6H_4)P(m\text{-}C_6H_4SO_3Na)_2$][7] are partially included in the hydrophobic cavity of the β-cyclodextrin derivatives. In the case of TPPMS and *t*BuTPPDS, it was also clearly demonstrated that the group included into the cavity is a non-sulfonated ring of the phosphane.

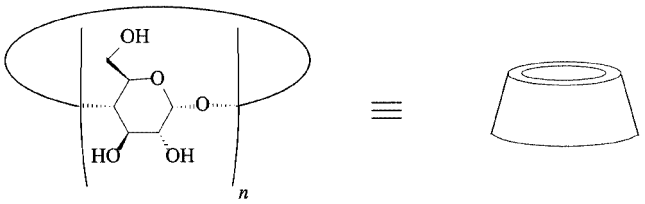

$n = 6$ α-cyclodextrin
$n = 7$ β-cyclodextrin
$n = 8$ γ-cyclodextrin

Scheme 1. Schematic representation of the shape of α-cyclodextrin ($n = 6$), β-cyclodextrin ($n = 7$) and γ-cyclodextrin ($n = 8$); the protons H-3 and H-5 are situated inside the host cavity, whereas protons H-1, H-2 and H-4 point outwards

Although we have assumed that these inclusion complexes can induce a decreased selectivity in the rhodium-catalyzed hydroformylation reaction by modifying the different equilibria between the catalytic species,[8] no spectroscopic evidence of an interaction of cyclodextrins with the catalysts has been obtained until now. In order to correct this, we have studied the influence of β-cyclodextrin (β-CD) or randomly methylated β-cyclodextrin (RAMEB) on two water-soluble, phosphane-modified rhodium hydroformylation catalysts by ^{31}P NMR spectroscopy. The water-soluble phosphanes used for this study were TPPTS and *t*BuTPPDS. These two phosphanes were chosen for their different affinity towards β-CD and RAMEB: the values of the association constants for the TPPTS/β-CD and *t*BuTPPDS/β-CD inclusion complexes were estimated to be 1,200 and 400,000 M^{-1} at 25 °C, respectively.[4,7] In the case of RAMEB, these values are lower and were estimated to be 1,000 and 250,000 M^{-1} at 25 °C for the TPPTS/RAMEB and *t*BuTPPDS/RAMEB inclusion complexes, respectively.[7,8]

Results and Discussion

Initial experiments were conducted with the complex $[HRh(CO)(TPPTS)_3]$ (**1**). As shown in Figure 1, the ^{31}P NMR spectrum of **1** (3 mM) exhibits, besides the minor resonance of the phosphane oxide impurity at $\delta = 35.7$ ppm, a characteristic sharp doublet at $\delta = 44.7$ ppm ($J_{Rh,P} = 156$ Hz).[9,10]

[‡] Cyclodextrins in Aqueous Phase Organometallic Catalysis, 22. Part 21: Ref.[1]

[a] Université d'Artois, Faculté des Sciences Jean Perrin, Rue Jean Souvraz
SP 18−62307 Lens Cédex, France
Fax: (internat.) +33-(0)3/2179-1755
E-mail: monflier@univ-artois.fr

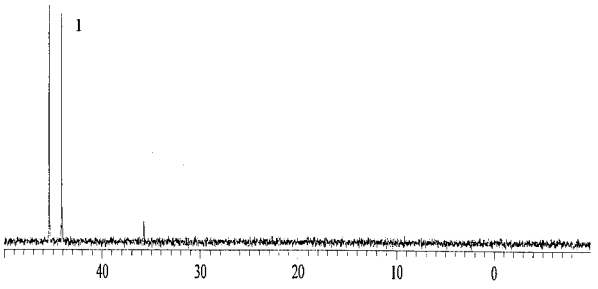

Figure 1. ^{31}P NMR spectrum of **1** (3 mM) at 27 °C in D_2O under nitrogen

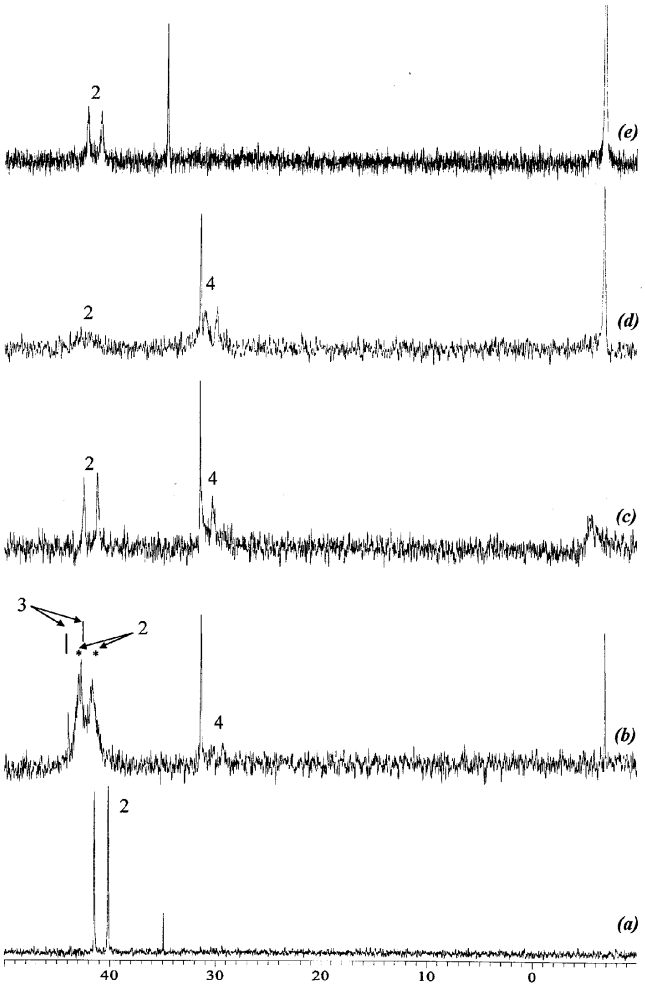

Figure 2. Effect of β-CD on complex **2**: (a) ^{31}P NMR spectrum of **2** (3 mM) in D_2O at 27 °C under nitrogen; (b) after addition of β-CD (9 mM) at 27 °C; (c) after 1 hour at 60 °C and recorded at 60 °C under nitrogen; (d) previous solution allowed to cool to 27 °C and recorded after 1 hour at 27 °C under nitrogen; (e) previous solution after addition of *t*BuTPPDS (9 mM) under 1 bar of hydrogen

When three equivalents of β-CD or RAMEB (9 mM) was added under nitrogen or carbon monoxide to an aqueous solution of **1**, no significant shift of any NMR signal was observed at different temperatures (20, 40 and 60 °C), suggesting that the cyclodextrin derivatives have no effect on the organometallic complex.

In the case of the complex [HRh(CO)(*t*BuTPPDS)$_3$] (**2**), addition of β-CD to the rhodium catalyst solution results in changes in the ^{31}P NMR spectrum. Indeed, the signal of **2** [δ = 40.8 ppm (d, $J_{Rh,P}$ = 155 Hz)] decreases significantly in intensity and three new signals are observed. The first signal at δ = −6.4 ppm is due to the *t*BuTPPDS/β-CD inclusion complex.[7] The second signal at δ = 43.2 ppm (d, $J_{Rh,P}$ = 155 Hz) and the third signal at δ = 30.4 ppm (d, $J_{Rh,P}$ = 131 Hz) were attributed to two new rhodium species **3** and **4** containing less than three phosphanes, as non-coordinated phosphane was observed at δ = −6.4 ppm (see Figure 2a and 2b).

Finally, it must be pointed out that the chemical shift difference for *t*BuTPPDS oxide (δ = 35 ppm without β-CD vs. δ = 31.4 ppm in the presence of β-CD) is due to the formation of an inclusion complex between β-CD and the phosphane oxide.[7]

Interestingly, when an aqueous solution of **2** was heated at 60 °C for one hour under nitrogen and the NMR spectra recorded at this temperature, the intensity of the signal of **4** increased significantly while the signal of **3** disappeared (Figure 2c). When the solution was allowed to cool to room temperature, only the signals of the *t*BuTPPDS/β-CD inclusion complex, **2** and **4** were observed (Figure 2d). The formation of **3** and **4** cannot be due to the temperature increase as no reaction occurred even at high temperature (80 °C) in the absence of cyclodextrins under the same experimental conditions.

As shown in Figure 3, addition of RAMEB to **2** under nitrogen also affects the ^{31}P NMR spectrum. However, only signals of **3** and the RAMEB-phosphane complex appear at room temperature; the formation of **4** requires heating of the complex solution to 60 °C (see Figure 3a−c).

As in the case of the β-CD, complex **3** disappears when the solution is warmed. It should be stressed that the chemical shift of *t*BuTPPDSO/RAMEB complex (δ = 30.1 ppm is lower than that of *t*BuTPPDSO/β-CD complex (δ = 31.4 ppm), probably owing to the affinity difference of phosphane oxide for each cyclodextrin. Interestingly, Figure 3c, 3d and 3e show that the proportion of different species does not change after heating or long reaction time (48 h), confirming that the transformation is complete, although not quantitative. Although the ^{31}P NMR spectra are not presented here, it is worth mentioning that it is possible to achieve the quantitative transformation of **2** into **4** by using a larger amount of RAMEB (20 mM) and high temperature (60 °C). Interestingly, when addition of RAMEB was carried out under carbon monoxide, the signal corresponding to the *t*BuTPPDS/RAMEB inclusion complex was always present but a sharp, new doublet was observed at δ = 37.1 ppm ($J_{Rh,P}$ = 139 Hz) (**5**; Figure 4).

Before discussing the nature of the new rhodium species observed in the presence of cyclodextrins under nitrogen or carbon monoxide, it must be pointed out that addition of methyl-α-D-glucopyranoside or an acyclic oligosaccharide composed of glucopyranose units such as maltose or maltoheptaose to **2** does not modify the NMR spectra of the rhodium complex and no new signal can be observed even

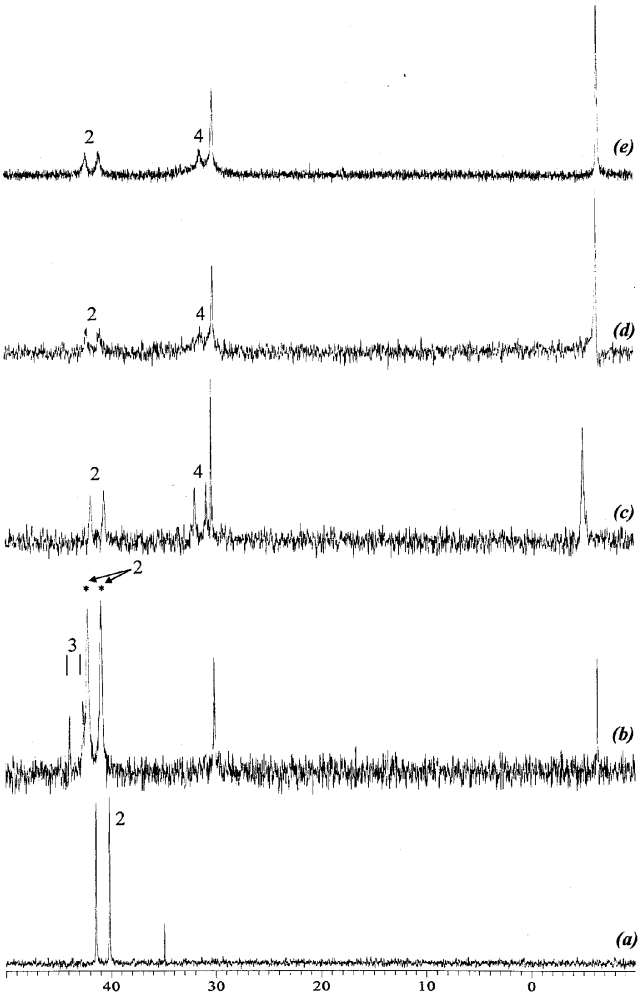

Figure 3. Effect of RAMEB on complex **2** under a nitrogen atmosphere: (a) ^{31}P NMR spectrum of **2** (3 mM) at 27 °C under nitrogen; (b) after addition of RAMEB (9 mM) at 27 °C; (c) after 1 hour at 60 °C and recorded at 60 °C under nitrogen; (d) previous solution allowed to cold to 27 °C and recorded after 1 hour at 27 °C under nitrogen; (e) previous solution recorded after 48 hours at 27 °C under nitrogen

at 40 °C or 60 °C. These experiments prove without a shadow of a doubt that the phenomenon observed with β-CD and RAMEB cannot be attributed to a solvent effect but must be due to the complexing properties of the β-cyclodextrin derivatives. Methyl α-D-glucopyranoside or acyclic oligosaccharides have the same subunits as the cyclodextrins but do not possess a lipophilic cavity that can host an organic group.

The new rhodium species **4** and **5** were identified by comparison of their chemical shift and rhodium-phosphorus coupling constant values with those of known rhodium complexes.[10−15] In particular, we found that the spectroscopic data of **4** (δ = 30.4 ppm, $J_{Rh,P}$ = 131 Hz) are very similar to those of water-soluble hydroxy complexes {[HORh(CO)(TPPTS)$_2$]: δ = 31.8 ppm, $J_{Rh,P}$ = 129 Hz; [HORh(CO){P(C$_6$H$_5$)$_2$[CH$_2$CH(CH$_3$)(CO$_2$Na)]}$_2$]: δ = 27 ppm, $J_{Rh,P}$ = 130 Hz}.[13−5] As reported by Herrmann, the hydroxy complex [HORh(CO)(TPPTS)$_2$] can be obtained from [HRh(CO)(TPPTS)$_3$] by heating an aqueous solution of [HRh(CO)(TPPTS)$_3$] at reflux and can be quantitatively reconverted into [HRh(CO)(TPPTS)$_3$] under an H_2/CO atmosphere in the presence of an excess of TPPTS (Scheme 2).

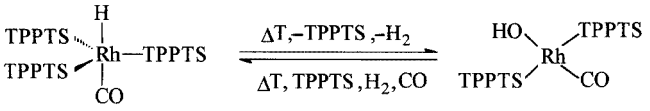

Scheme 2. Equilibrium between [HRh(CO)(TPPTS$_3$] and [HORh(CO)(TPPTS)$_2$] as reported by Herrmann and coworkers[13,14]

Our assignment was fully supported by experiments conducted under H_2 atmosphere and in the presence of an excess of *t*BuTPPDS. Under these experimental conditions complex **4** can be converted into **2** as shown in Figure 2e.

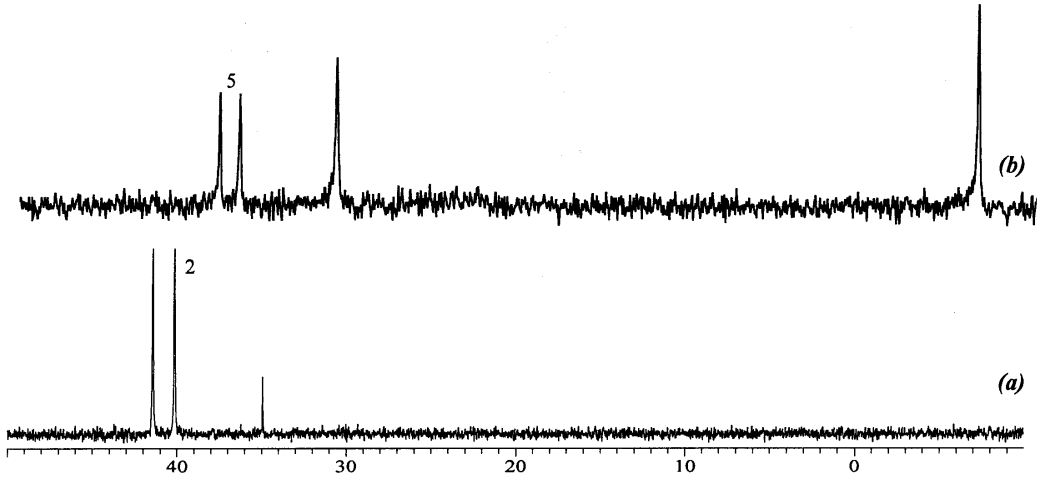

Figure 4. Effect of RAMEB on complex **2** under a carbon monoxide atmosphere: (a) spectrum of **2** (3 mM) in D_2O at 27 °C under carbon monoxide; (b) after addition of RAMEB (9 mM) at 27 °C under carbon monoxide

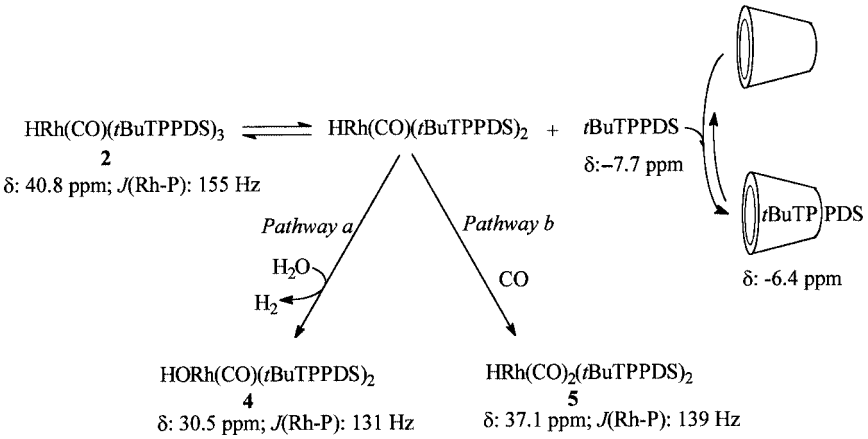

Scheme 3. Proposed mechanism for the formation of **4** and **5** from **2** in the presence of β-cyclodextrin derivatives

With respect to the rhodium species that forms under carbon monoxide, the spectroscopic data (δ = 37.1 ppm, $J_{Rh,P}$ = 139 Hz) are very similar to those of the hydrido complex [HRh(CO)$_2$[P(C$_6$H$_5$)$_3$]$_2$] (δ = 39.9 ppm, $J_{Rh,P}$ = 138 Hz), suggesting strongly that **5** is [HRh(CO)$_2$(*t*-BuTPPDS)$_2$].[16]

From a mechanistic point of view, the formation of an inclusion complex between the water-soluble phosphane and the cyclodextrin is probably the driving force of the reaction leading to the production of **4** (under nitrogen) or **5** (under carbon monoxide). Therefore the trapping of *t*BuTPPDS by the cyclodextrin can promote the dissociation of *t*BuTPPDS from **2** and, consequently, the formation of [HRh(CO)(*t*BuTPPDS)$_2$] as described in Scheme 3.

The complex [HRh(CO)(*t*BuTPPDS)$_2$] or its aqua form [HRh(H$_2$O)(CO)(*t*BuTPPDS)$_2$], either of which could be the unstable species **3**, would react with water (*pathway a* in Scheme 3) or a carbon monoxide molecule (*pathway b* in Scheme 3) to give rise to **4** and **5**, respectively. In the case of TPPTS, the affinity of cyclodextrin for the TPPTS is probably much too weak to observe an effect on the equilibrium described in Scheme 3, and therefore formation of the hydroxy or hydrido dicarbonyl complex is not promoted.

Conclusion

This work has clearly demonstrated that cyclodextrin can promote the formation of new species by trapping the ligand. This phenomenon is all the more important as the molecular recognition between the water-soluble ligand and the cyclodextrin is high. This finding is of interest for the development of transition metal chemistry in water because it could be used to generate easily coordinatively unsaturated organometallic complexes, which are catalytically active species in numerous reactions.

Experimental Section

General Remarks: The ^{31}P NMR spectra (121.49 MHz, referenced to external 85% H$_3$PO$_4$) were recorded on a Bruker DRX instrument. FTIR spectra were recorded on a Bruker IFS 55 spectrophotometer. D$_2$O (99.95% isotopic purity) was obtained from Merck. β-cyclodextrin (β-CD) and randomly methylated β-cyclodextrin (RAMEB) were purchased from Aldrich and dried carefully before use. The RAMEB used is a mixture of methylated-β-cyclodextrins, in which about fourteen of the twenty one hydroxy groups have been methylated. Tris(3-sodiosulfonatophenyl)phosphane [TPPTS; P(*m*-C$_6$H$_4$SO$_3$Na)$_3$] was synthesized as reported by Gärtner et al.[17] The purity of the TPPTS was carefully controlled. In particular, ^{31}P NMR spectroscopy indicated that the product was a mixture of the phosphane (ca. 98%) and its oxide (ca. 2%). The synthesis of (4-*tert*-butylphenyl)bis(3-sodiosulfonatophenyl)phosphane [*t*BuTPPDS; (*p*-*t*BuC$_6$H$_4$)P(*m*-C$_6$H$_4$SO$_3$Na)$_2$] was described in one of our previous publication.[18] The complex [HRh(CO)(TPPTS)$_3$] (**1**) was prepared by a modification of the literature method.[19]

[HRh(CO)(*t*BuTPPDS)$_3$] (2): [Rh(CO)$_2$(acac)] (100 mg) was introduced into a Schlenk tube and a *t*BuTPPDS solution (3.6 eq, 738 mg in 10 mL of degassed water) was added whilst stirring under CO/H$_2$ pressure (2 bar). After 6 hours, the crude reaction mixture was filtered and 20 mL of degassed dimethyl ethylene glycol ether was added to the solution. The pale green precipitate formed was collected by filtration, washed with dimethyl ethylene glycol ether and then dried under oil-pump vacuum: 535 mg, yield: 82%. ^{1}H NMR (300 MHz, D$_2$O, 25 °C): δ = −9.6 (q, $^2J_{H,P}$ = 13.1 Hz, 1 H, H-Rh), 1.26 (s, 27 H, *t*Bu), 7.17 (m, 18 H), 7.48 (br. s, 6 H), 7.67 (m, 12 H) ppm. ^{31}P{^{1}H} NMR (121.49 MHz, D$_2$O, 25 °C): δ = 40.8 (d, $^1J_{P,Rh}$ = 155 Hz, P) ppm. FTIR (KBr): $\tilde{\nu}$ = 2003 cm^{-1} (H-Rh), 1917 (CO).

[1] S. Tilloy, H. Bricout, E. Monflier, *Green Chem.* **2002**, *4*, 188−193.
[2] H. Bricout, L. Caron, D. Bormann, E. Monflier, *Catal. Today* **2001**, *66*, 355−361.
[3] E. Monflier, S. Tilloy, C. Méliet, A. Mortreux, S. Fourmentin, D. Landy, G. Surpateanu, *New J. Chem.* **1999**, *23*, 469−472.
[4] E. Monflier, S. Tilloy, L. Caron, J. M. Wieruszeski, G. Lippens, S. Fourmentin, D. Landy, G. Surpateanu, *J. Inclusion Phenom.* **2000**, *38*, 361−379.
[5] L. Caron, C. Christine, S. Tilloy, E. Monflier, D. Landy, S. Fourmentin, G. Surpateanu, *Supramol. Chem.* **2002**, *14*, 11−20.
[6] M. Canipelle, L. Caron, C. Christine, S. Tilloy, E. Monflier, *Carbohyd. Res.* **2002**, *337*, 281−287.
[7] L. Caron, PhD Dissertation, Univ. of Lille I, France, **2002**.
[8] T. Mathivet, C. Méliet, Y. Castanet, A. Mortreux, L. Caron, S. Tilloy, E. Monflier, *J. Mol. Catal.* **2001**, *176*, 105−116.

[9] I. T. Horvath, R. Kastrup, A. Oswald, E. Mozeleski, *Catalysis Lett.* **1989**, *2*, 85−90.
[10] P. Kalck, M. Dessoudeix, *Coord. Chem. Rev.* **1999**, *190*, 1185−1198.
[11] T. Bartik, B. Bartik, B. E. Hanson, *J. Mol. Catal.* **1994**, *88*, 43−56.
[12] C. Larpent, R. Dabard, H. Patin, *Inorg. Chem.* **1987**, *26*, 2922−2924.
[13] W. A. Herrmann, J. A. Kulpe, J. Kellner, H. Riepl, H. Bahrmann, W. Konkol, *Angew. Chem.* **1990**, *102*, 408−411; *Angew. Chem. Int. Ed. Engl.* **1990**, *29*, 391−393.
[14] W. A. Herrmann, J. A. Kulpe, W. Konkol, H. Bahrmann, *J. Organomet. Chem.* **1990**, *389*, 85−101.
[15] E. Miecznska, A. M. Trzeciak, R. Grzybek, J. J. Ziolkowski, *J. Mol. Catal.* **1998**, *132*, 203−212.
[16] J. M. Brown, L. R. Canning, A. G. Kent, P. J. Sidebottom, *J. Chem. Soc., Chem. Commun.* **1982**, 721−723.
[17] R. Gärtner, B. Cornils, H. Springer, P. Lappe, DE pat. 3235030, **1982**. (*Chem. Abstr.* **1984**, *101*, P55331t).
[18] L. Caron, M. Canipelle, S. Tilloy, H. Bricout, E. Monflier, *Tetrahedron Lett.* **2001**, *42*, 8837−8840.
[19] J. P. Arhancet, M. E. Davis, B. E. Hanson, *J. Catal.* **1990**, *121*, 327−339.

Received September 18, 2002
[I02518]

Complexes of Rhodium(I) and Iridium(I) with the Chiral Tridentate Phosphane Pigiphos: Structure and Reactivity Studies

Lukas Hintermann,[a] Mauro Perseghini,[a] Pierluigi Barbaro,*[b] and Antonio Togni*[a]

Keywords: Ferrocenyl ligands / Phosphanes / Iridium / Rhodium / Chiral ligands

The chiral ferrocenyltriphosphane Pigiphos [bis{(*S*)-1-[(*R*)-2-(diphenylphosphanyl)ferrocenyl]ethyl}cyclohexylphosphane] forms four-coordinate complexes with Ir^I and Rh^I. The tridentate ligand assumes different conformations in the derivatives [Rh(CO)(Pigiphos)]OTf (**4**) and [IrCl(Pigiphos)] (**1b**), the latter also showing a drastic deviation from the square-planar geometry. Reactivity studies have focussed on the more reactive **1b**. The HCl and O_2 adducts have been characterized in solution.

(© Wiley-VCH Verlag GmbH & Co. KGaA, 69451 Weinheim, Germany, 2003)

Introduction

Chiral tridentate phosphanes and their transition metal complexes are rare.[1] We have previously described the chiral tridentate ferrocenylphosphane (*S*,*R*)-Pigiphos = bis{(*S*)-1-[(*R*)-2-(diphenylphosphanyl)ferrocenyl]ethyl}-cyclohexylphosphane (Scheme 1) and its complexes with palladium, nickel and ruthenium.[2] An element of design of Pigiphos is its simple synthetic accessibility (one step from commercially available materials),[2a] thus giving the possibility of varying the steric and electronic properties of the ligand according to a modular approach. Pigiphos forms two six-membered chelate rings when coordinating as a tridentate ligand and is thus best suited for both equatorial and facial arrangements around a transition metal atom, although partial hemilability cannot be excluded.

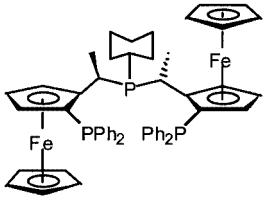

Scheme 1. (*S*,*R*)-Pigiphos

We were able to show that [*fac*-Ru{(*S*,*R*)-Pigiphos}$(CH_3CN)_3$]$(PF_6)_2$ is a catalyst for the enantioselective transfer-hydrogenation of *i*PrOH to acetophenone where *ee* values up to 71.7% could be obtained.[2b] Furthermore, cationic complexes of rhodium(III) and nickel(II) were prepared and their activity as acetalization catalysts was demonstrated.[2c] The synthesis of additional complexes with the unique Pigiphos ligand thus seemed worthwhile in order to explore its coordination chemistry and to find reactive complexes with possible application as catalysts.

The recent findings from our laboratory and from Tani's research group that highly reactive dinuclear iridium(I) complexes with chelating diphosphanes $[Ir_2Cl_2(PP)_2]$ (PP = Josiphos, Xyliphos, BINAP, bpbp) oxidatively add water[3,4] and methanol[4] pointed our attention towards low-valent group-9 species. It seemed that Pigiphos as an electron-rich tridentate ligand should give rise to similar reactivity.

In this paper we describe the synthesis of the reactive mononuclear complexes [RhCl{(*S*,*R*)-Pigiphos}] (**1a**) and [IrCl{(*R*,*S*)-Pigiphos}] (**1b**), and we report on several aspects of their coordination chemistry, including cationic solvento complexes, carbonyl complexes, and their reaction with molecular oxygen. The potential for oxidative addition of small molecules to the iridium(I) complex was investigated. X-ray structures have been determined for **1b** and for [Rh(CO){(*S*,*R*)-Pigiphos}]OTf (**4**)

Results and Discussion

Synthesis and Characterization of the Rh^I and Ir^I Complexes 1, 2, 4

Mononuclear, four-coordinate complexes of the general formula [MX(Pigiphos)]Y were prepared in good yields with M as Rh^I or Ir^I (Scheme 2). The neutral chloro complexes **1a** and **1b** were obtained by a ligand-exchange reaction using $[Rh_2Cl_2(COD)_2]$ or $[Rh_2Cl_2(C_2H_4)_4]$ and

[a] Department of Chemistry, Swiss Federal Institute of Technology,
ETH Hönggerberg, 8093 Zürich, Switzerland
Fax: (internat.) + 41-1/632-1310
E-mail: togni@inorg.chem.ethz.ch
[b] ISSECC − CNR,
Via Jacopo Nardi 39, 50132 Firenze, Italy
E-mail: pigi@fi.cnr.it

$[Ir_2Cl_2(COE)_4]$ (COE = cyclooctene) or $[IrCl(C_2H_4)_4]$, respectively. The cationic derivatives **2a**, **2b** and **4** were obtained by halogen abstraction from the corresponding chloro complexes, using a chloride scavenger.

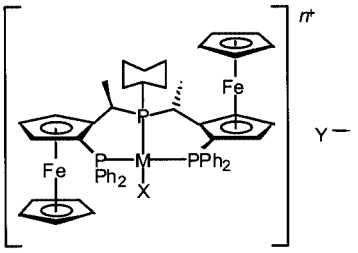

M = Rh, X = Cl, *n* = 0 (**1a**)
M = Ir, X = Cl, *n* = 0 (**1b**)
M = Rh, X = CH_3CN, *n* = 1, Y = PF_6 (**2a**)
M = Ir, X = CH_3CN, *n* = 1, Y = PF_6 (**2b**)
M = Rh, X = CO, *n* = 1, Y = OTf (**4**)

Scheme 2. Sketch of the complexes **1**, **2**, **4**

With the exception of chlorinated solvents, all complexes are fairly stable in solution in deaerated, noncoordinating solvents. The solid-state IR spectra of the acetonitrile and carbonyl adducts [**2a**: ν(C−N) 2317 cm^{-1}; **4**: ν(C−O) 2020 cm^{-1}] show absorptions characteristic of coordinated CH_3CN[5−7] and CO[5,6,8] molecules. The $^{31}P\{^1H\}$ NMR spectroscopic data for the complexes are reported in Table 1, whereas selected ^1H NMR spectroscopic data are reported in the Exp. Sect.

The ^{31}P NMR spectral parameters are consistent with the presence of two diastereotopic ferrocenyl units with $^2J_{P_AP_B}$ coupling constants (from 131.8 to 287.0 Hz) indicative of *trans*-Ph_2P groups in each compound.[9] The complexes are slightly fluxional on the NMR time scale at room temperature, as shown by a moderate broadening of the $^{31}P\{^1H\}$ resonances. However, a slow-motion regime is attained by all compounds to give well-resolved patterns on lowering the temperature to 233−223 K. An analogous ^{31}P NMR behavior has been previously reported for the parent square-planar Pigiphos Pd^{II} and Ni^{II} complexes.[2a] These findings can be attributed to the presence of a conformational equilibrium within the six-membered chelate rings in the complexes. The dynamics of the process have been investigated in detail for complex **1b** (see below). In the rhodium complexes, the trend observed for the $^1J_{RhP}$ coupling constants can be rationalized on the basis of the *trans* influence of the coligands, which decreases in the order CyP ≈ CO > CH_3CN > Cl.[9b,10−12] Indeed, the $^1J_{RhP_A}$ and $^1J_{RhP_B}$ coupling constants of the two *trans*-Ph_2P phosphorus atoms are invariably smaller than the $^1J_{RhP}$ constant for the central CyP phosphorus atom. Consistently, this latter increases in going from **4** (121 Hz) to **2a** (163 Hz), to **1a** (173 Hz) (i.e. from *trans* to CO, CH_3CN, Cl).

The observed ^1H NMR spectral parameters, although in line with two diastereotopic ferrocenyl units, are rather routine and do not deserve any particular comment.

Solid-State Structure of 4

A single-crystal X-ray diffraction analysis carried out on **4** shows that the molecular structure consists of complex

Table 1. $^{31}P\{^1H\}$ NMR data for the Pigiphos complexes

Complex[a]	Compd.	(Cy)P	(Ph)P_A	(Ph)P_B
[(*S*,*R*-Pigiphos]RhCl	**1a**[b]	79.40 (dt) $^2J_{PP}$ = 41.4, $^1J_{PRh}$ = 172.9	17.04 (br. d)	16.48 (br. d)
	1a[c][d]	79.94 (dt) $^2J_{PP}$ = 42.1, $^1J_{PRh}$ = 173.3	17.90 (ddd) $^2J_{P_AP_B}$ = 131.8, $^1J_{P_A}$ = 81.8	17.90 (ddd) $^1J_{P_B}$ = 81.8
[{(*S*,*R*)-Pigiphos}Rh(CH_3CN)]$^+$	**2a**[c]	84.04 (dt) $^2J_{PP}$ = 44.1, $^1J_{PRh}$ = 162.7	24.14 (ddd) $^2J_{P_AP_B}$ = 280.5, $^1J_{P_A}$ = 135.8	19.21 (ddd) $^1J_{P_B}$ = 128.1
[(*S*,*R*)-Pigiphos]Rh(O_2)Cl	**3a**[b]	66.21 (dt) $^2J_{PP}$ = 22.4, $^1J_{PRh}$ = 122.1	16.14 (dt) $^1J_{P_A}$ = 134.8	1.18 (dt) $^1J_{P_B}$ = 134.8
[{(*S*,*R*)-Pigiphos}Rh(CO)]$^+$	**4**[c]	64.23 (ddd) $^2J_{PP_A}$ = 37.1, $^2J_{PP_B}$ = 47.0, $^1J_{PRh}$ = 121.9	21.98 (ddd) $^2J_{P_AP_B}$ = 238.3, $^1J_{P_A}$ = 119.3	15.4 (br. m)
	4[c][e]	63.64 (ddd) $^2J_{PP_A}$ = 34.4, $^2J_{PP_B}$ = 50.3, $^1J_{PRh}$ = 120.4	22.07 (ddd) $^2J_{P_AP_B}$ = 235.8, $^1J_{P_A}$ = 118.7	13.02 (ddd) $^1J_{P_B}$ = 116.5
[(*R*,*S*)-Pigiphos]IrCl	**1b**[f][g]	44.02 (br. t) $^2J_{PP}$ = 26.0	11.3 (br. s) (2P)	
[{(*R*,*S*)-Pigiphos}Ir(CH_3CN)]$^+$	**2b**[f][h]	46.60 (t) $^2J_{PP}$ = 27.0	15.54 (dd) $^2J_{P_AP_B}$ = 287.0	8.51 (dd)
[(*R*,*S*)-Pigiphos]Ir(O_2)Cl	**3b**[f,g]	19.23 (t) $^2J_{PP}$ = 17.2	−20.7 (dd) $^2J_{P_AP_B}$ = 22.4	−34.3 (dd)
[{(*R*,*S*)-Pigiphos}IrClH]$^+$	**5**[b][m]	41.7 (t) $^2J_{PP}$ = 13.4	14.51 (bd) $^2J_{P_AP_B}$ = 328	9.22 (bd)
[(*R*,*S*)-Pigiphos]IrCl_2H	**6**[b,m]	17.04 (t) $^2J_{PP}$ = 17.7	−2.01 (dd) $^2J_{P_AP_B}$ = 400.1	−30.93 (dd)
[(*R*,*S*)-Pigiphos]IrClH_2	**7**[b,f]	15.0 (br. s)	6.53 (dd) $^2J_{PP_A}$ = 20.3, $^2J_{P_AP_B}$ = 347.0	−9.52 (dd) $^2J_{PP_B}$ = 21.0

[a] Chemical shifts in ppm, coupling constants in Hz. 202.47 MHz, 294 K. Abbreviations: s, singlet; d, doublet; t, triplet; m, multiplet; br., broad. [b] C_6D_6. [c] CD_3COCD_3. [d] 233 K. [e] 223 K. [f] 121.5 MHz. [g] [D_8]Toluene. [h] CD_3CN. [m] 101.3 MHz.

cations $[Rh(CO)\{(S,R)\text{-Pigiphos}\}]^+$ and OTf^- anions. An ORTEP view of the cation is shown in Figure 1 while selected bond lengths and angles are reported in Table 2.

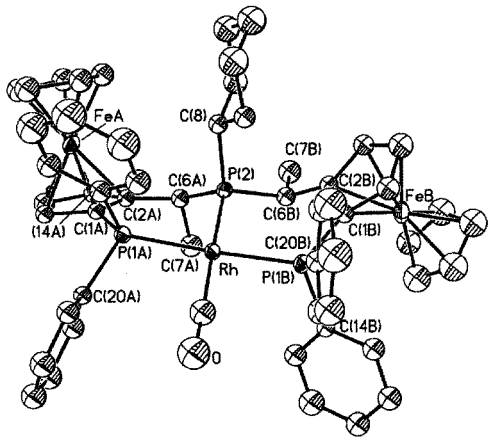

Figure 1. ORTEP drawing of the complex cation $[Rh(CO)\{(S,R)\text{-Pigiphos}\}]^+$ in **4**

The coordination around the metal center is approximately square-planar in which the carbonyl ligand and the CyP P(2) atom are mutually *trans*. The distortions from the idealized geometry are represented by the displacements of the Rh and C(26) atoms from the plane containing the three phosphorus atoms (−0.182 and −0.622 Å, respectively), as well as by the value of the bond angles at the metal (87.4−94.0°). However, considering the best idealized coordination plane of Rh (maximum deviations of the donor atoms 0.152 to −0.179 Å) one can observe that: (i) one of the unsubstituted Cp rings and the two methyl groups lie below this plane, whereas the second Cp ring and the cyclohexyl group are above, (ii) the four phenyl rings are pairwise above and below the plane, thus assuming an overall pseudo-C_2 symmetry, (iii) the couple of "C_2-symmetry-related" phenyl rings, identified by the C(14A) and C(14B) *ipso*-carbon atoms, face an observer lying on the C(26)−P(2) axis. Although both six-membered chelate rings adopt a distorted boat conformation in **4**, their geometry is markedly different. This is shown by the different relative positions of the two methyl groups [cf. the torsion angles C(1B)−C(2B)−C(6B)−C(7B) = −164.8(8)° and C(1A)−C(2A)−C(6A)−C(7A) = 95.7(11)°], as well as by the conformation of the two alkyl side chains [cf. the torsion angles C(1B)−C(2B)−C(6B)−P(2) = 62.7(10)° and C(1A)−C(2A)−C(6A)−P(2) = −26.4(13)°]. Furthermore, the P(1A) phenyl rings are closer to an axial/equatorial arrangement with respect to the coordination plane of Rh than those bonded to P(1B) [cf. the torsion angles C(26)−Rh−P(1A)−C(14A) = 90.3(7)°, C(26)−Rh−P(1A)−C(20A) = −22.3(7)°, C(26)−Rh−P(1B)−C(20B) = −59.1(7)°, C(26)−Rh−P(1B)−C(14B) = 56.7(7)°]. The Rh−C(26)−O angle (178.8°) as well as the C(26)−O (1.134 Å) and Rh−C(1) (1.849 Å) distances are in the range commonly observed for other square-planar (carbonyl)Rh^I complexes.[13,14] The overall conformation of the Pigiphos ligand in **4** closely resembles that already described for the square-planar cation complex $[PdCl\{(S,R)\text{-Pigiphos}\}]^+$.[2a]

Solid-State Structure of 1b·2(C_6H_6)

Compound **1b**·2(C_6H_6) was characterized by X-ray diffraction analysis. Selected bond lengths and angles are reported in Table 3. An ORTEP drawing is depicted in Figure 2.

Table 3. Selected bond lengths [Å] and angles [°] for $[IrCl\{(R,S)\text{-Pigiphos}\}]\cdot 2(C_6H_6)$

Ir−Cl	2.3997(17)	Ir−P(1A)	2.2714(16)
Ir−P(2)	2.2123(17)	Ir−P(1B)	2.2581(18)
Cl−Ir−P(2)	166.79(6)	P(1A)−Ir−P(1B)	154.29(6)
P(1A)−Ir−P(2)	90.73(7)	P(1B)−Ir−P(2)	95.82(7)
Cl−Ir−P(1A)	91.73(7)	Cl−Ir−P(1B)	87.53(7)

The coordination around Ir is approximately square-planar with the chlorine atom and the CyP(2) group *trans* to each other. However, the displacement of the iridium and chlorine atoms above the plane containing the three phosphorus atoms (0.450 and 1.462 Å, respectively) and the bond angles around the metal center (87.50−95.82°) show that the degree of distortion of this complex is larger than for the cation $[Rh(CO)\{(S,R)\text{-Pigiphos}\}]^+$ in **4**. In addition, the overall arrangement of the Pigiphos ligand is markedly different from that observed in **4** and in $[PdCl\{(S,R)\text{-Pigiphos}\}]^+$.[2a] Thus, both methyl groups are below the coordination plane, no pseudo-C_2 symmetry is shown by the phenylphosphanyl groups, and no specific axial/equatorial arrangement is adopted by the phenyl rings [cf. the torsion angles Cl−Ir−P(1B)−C(14B) = 65.7(3)°, Cl−Ir−P(1B)−C(20B) = −53.0(3)°, Cl−Ir−P(1A)−C(14A) = 71.3(3)°, Cl−Ir−P(1A)−C(20A) = −47.1(3)°]. The unusual

Table 2. Selected bond lengths [Å] and angles [°] for the cation $[Rh(CO)\{(S,R)\text{-Pigiphos}\}]^+$ in **4**

Rh-P(1B)	2.302(3)	O−C(26)	1.134(16)
Rh−P(1A)	2.305(3)	Rh−C(26)	1.849(14)
Rh−P(2)	2.318(3)		
C(26)−Rh−P(1B)	86.9(4)	C(26)−Rh−P(2)	170.7(6)
C(26)−Rh−P(1A)	89.9(4)	P(1B)−Rh−P(2)	93.97(11)
P(1B)−Rh−P(1A)	169.45(12)	P(1A)−Rh−P(2)	90.77(11)
Rh−C(26)−O	177.0(6)		
C(1B)−C(2B)−C(6B)−P(2)	62.7(10)	C(1A)−C(2A)−C(6A)−P(2)	−26.4(13)
C(1B)−C(2B)−C(6B)−C(7B)	−164.8(8)	C(1A)−C(2A)−C(6A)−C(7A)	95.7(11)

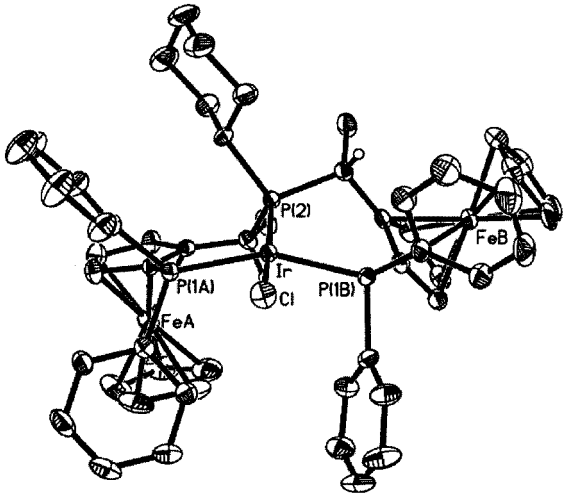

Figure 2. ORTEP view of the complex [IrCl{(*R*,*S*)-Pigiphos}] in **1b**·2(C_6H_6); solvent molecules are omitted for clarity

arrangement of Pigiphos in **1b** is inferred by the different conformation assumed by the two six-membered chelate rings; while the ring incorporating P(1A) can be described as an envelope with five atoms almost lying in a plane [with P(2) out of the plane], the one including P(1B) adopts a distorted boat conformation. It is worth noting that in most of the Josiphos-type ferrocenyldiphosphane complexes the six-membered chelate ring adopts a distorted boat conformation.[3,15,16]

$^{31}P\{^1H\}$ VT NMR Study of Complex 1b

A variable-temperature $^{31}P\{^1H\}$ NMR study was carried out on **1b**. Sections of the $^{31}P\{^1H\}$ NMR spectra of **1b** are shown in Figure 3.

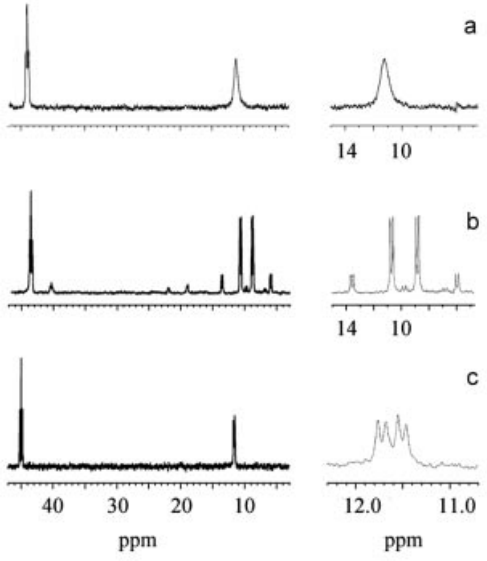

Figure 3. $^{31}P\{^1H\}$ NMR spectra of [IrCl{(*R*,*S*)-Pigiphos}] (**1**) (121.5 MHz, [D_8]toluene): (a) 21 °C, (b) −50 °C and (c) 80 °C

Compared to the parent rhodium complex **1a**, a greater fluxionality is observed for **1b** in room temperature solutions (see Table 1 and Figure 3 a). Indeed, only two resonances are observed at 21 °C, a broad triplet (δ = 44.02 ppm, J = 26 Hz) and a broad singlet (δ = 11.3 ppm), which can be attributed to the central CyP phosphorus atom and to the two terminal Ph_2P atoms, respectively. On lowering the temperature, the latter resonance splits to give a broad ABM spin system, as expected for two diastereotopic diphenylphosphanyl groups. Further cooling causes the signals to sharpen and a second ABM spin system to appear. The spectrum recorded at −50 °C is shown in Figure 3 b. Both sets of resonances (ca. 7:1 ratio, based on ^{31}P NMR integration) show signals characteristic of a central CyP phosphorus atom (major: δ = 43.5 ppm, $^2J_{PP}$ = 25 Hz; minor: δ = 40.3 ppm, $^2J_{PP}$ = 26 Hz) and *trans*-terminal diphenylphosphanyl groups (major: δ = 12.1 and 7.3 ppm, $^2J_{PP}$ = 351 Hz; minor: δ = 8.3 and 20.2 ppm, $^2J_{PP}$ = 358 Hz).[17] According to the solid-state structure, the two spin systems can be attributed to the presence of two isomers of **1b** differing in their conformation − either boat or envelope − of the two six-membered chelate rings. The signals due to the Ph_2P phosphorus atoms are much more differentiated in the minor than in the major isomer (Δδ = 11.9 ppm vs. Δδ = 4.8 ppm). This finding suggests that in the minor isomer the two PPh_2 groups are situated in a quite different chemical environment which results in comparatively unfavorable steric interactions. The observed variable temperature NMR pattern is consistent with an exchange equilibrium between the two isomers, most likely due to a ring-inversion mechanism. Similar ring-inversion processes have been observed previously for six-membered chelate rings in ferrocenyldiphosphane transition metal complexes.[3,15,16] The spectrum recorded at 80 °C is in line with the trend observed at lower temperature. Only one tightly coupled ABM system is found which accounts for the fast interconversion of the two conformers. The spectral parameters (CyP: δ = 44.83 ppm, $^2J_{PP}$ = 8.50 Hz; Ph_2P: δ = 12.02 and 11.19 ppm, $^2J_{PP}$ = 179.9 Hz)[17] indicate that at this temperature the complex attains a time-averaged preferred conformation in which the two terminal phenylphosphanyl groups are located in a similar chemical environment.

Synthesis and Characterization of the (Dioxygen)Rh^{III} and -Ir^{III} Adducts

The (dioxygen)Rh and -Ir adducts **3a** and **3b** were quantitatively obtained by exposure of a C_6H_6 solution of **1a** and **1b** to air, respectively. A color change from orange to yellow (**1a**) or deep red (**1b**) accompanied the O_2 uptake and the solid dioxygen complexes precipitated within a few minutes. The adducts **3** can be treated as formal six-coordinate (peroxo)Rh^{III} and -Ir^{III} complexes obtained by the oxidative addition of O_2 to the Rh^I and Ir^I centers,[18−24] in which an η^2-O_2 ligand is *trans* to the Ph_2P phosphorus atoms. This hypothesis is substantiated by the following experimental observations: (i) the solid-state IR spectra show an absorption characteristic for η^2-O_2 complexes (902 and 829 cm^{-1} ν(O−O) for **3a** and **3b**, respectively);[7,18,19,21−23,25] (ii) no residual paramagnetism is detected by magnetic susceptivity

measurement either in solution or in the solid state; (iii) the MALDI MS analysis carried out under oxygen-free conditions shows peaks consistent with O_2 uptake; (iv) the ^{31}P NMR spectra of **3a** and **3b** show a $^2J_{PP}$ coupling constant (17.2−22.4 Hz, Table 1) indicating a *cis* disposition of the phosphorus atoms and, therefore, a *fac* arrangement of the tridentate ligand; (v) consistent with the increased oxidation state of Rh, the $^1J_{RhP}$ coupling constant of the CyP phosphorus atom (122.1 Hz) in **3a** is smaller than the corresponding constant in the deoxygenated Rh^I complex **1a**;[2c,10,26] (vi) the $^1J_{RhP}$ coupling constant observed for the Ph_2P atoms in **3a** (134.8 Hz) is greater than that observed for the CyP phosphorus atom (122.1 Hz), thus indicating that the two diphenylphosphanyl groups experience a lower *trans* influence, as expected for a *trans*-oxygen donor as compared to a *trans* chloride donor.[12,27,28] The formation of η^2-O_2 complexes by addition of dioxygen to (polydentate phosphane)Rh^I and -Ir^I complexes has a number of precedents in the literature.[7,29−34] It is generally agreed that in the reaction of square-planar d^8 metal complexes with dioxygen to give peroxo adducts, the starting metal complex undergoes a geometrical distortion to allow a better overlap between the metal d orbitals and the π_g* orbital of dioxygen.[20,35,36] The observed *mer*-to-*fac* rearrangement of the Pigiphos ligand accompanying the conversion of **1** to **3** can be explained on this basis.

Oxidative Addition Reactions

The ability of **1b** to react with other small molecules to give the oxidative addition product was examined. In particular, the use of protic reagents with very different acid dissociation constants was investigated.

The reaction with an excess of HBF_4 in benzene solution was monitored by NMR spectroscopy. A quantitative conversion into the complex [IrClH{(*R*,*S*)-Pigiphos}]BF_4 (**5**) was shown and the product was characterized in situ by ^1H and $^{31}P\{^1H\}$ NMR spectroscopy. The value of the $^2J_{PP}$ coupling constant (328 Hz) indicates a *trans* arrangement of the two terminal Ph_2P atoms and, therefore, a *mer* coordination of the tridentate ligand. An apical position can be assigned to the hydride observed in the ^1H NMR spectrum at $\delta = -32.15$ ppm on the basis of the low value of its $^2J_{PH}$ coupling (13.0 Hz).[9]

The reaction of **1b** with HCl gave the complex [$IrCl_2H$\{(*R*,*S*)-Pigiphos\}] (**6**), which was isolated in the solid state and completely characterized in solution by 2D NMR spectroscopy. All resonances were unequivocally attributed by 2D techniques. Once again, the $^{31}P\{^1H\}$ NMR spectroscopic data indicate a *mer* arrangement of the ligand ($^2J_{PP}$ = 440.1 Hz, Table 1). The $^2J_{HP}$ values (16.0 Hz) indicate a *cis* disposition of the hydride ligand [$\delta = -19.48$ (q) ppm] with respect to the phosphorus atoms.[9] An apical position of the hydride ligand can thus be anticipated. It only remained to be seen whether this proton is above or below the coordination plane of the iridium atom. A simple ^1H NOESY measurement addressed this point. The main NOE interactions observed for **6** are represented schematically in Figure 4.

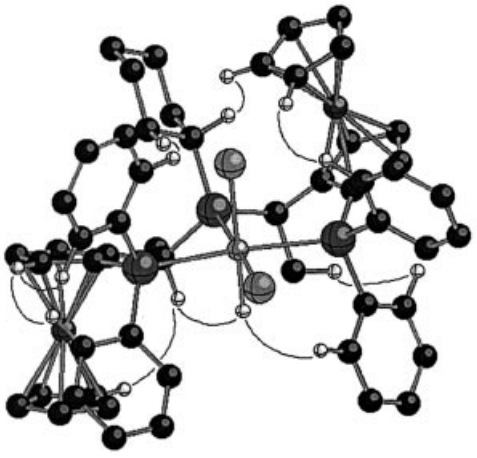

Figure 4. Significant NOEs observed for **6** (C_6D_6, 294 K, 400.13 MHz, drawing generated using the program Ball-and-Stick, see also Figure 5)

The dipolar interaction observed between the hydride atom and one of the α-methyl protons shows the hydride ligand to be located on the side of the plane opposite to that of the cyclohexyl group.

Reaction with methanol did not afford an oxidative addition product. The dihydrido complex [$IrClH_2$\{(*R*,*S*)-Pigiphos\}] (**7**) was obtained and isolated instead. The ^1H NMR spectrum of **7** shows resonances at $\delta = -21.5$ and -7.7 ppm for the two hydride ligands, respectively (see Exp. Sect.). Similar hydride resonances were previously reported for the product from the reaction of [$Ir_2Cl_2(COD)_2$] with tridentate phosphanes in the presence of ethanol/benzene mixtures.[37]

Conclusion

We have shown that Pigiphos behaves as a tridentate ligand with Rh^I and Ir^I forming tetracoordinate complexes. By virtue of a significant distortion of the ideal square-planar geometry, as observed in the solid state and as reflected by the dynamical behavior in solution, the Ir derivative **1b** displays a higher reactivity than **1a** (Rh).

Complex **1b** did not yield OH addition products. This can be explained by the inability of the sterically hindered complex **1b** to generate dinuclear bridged compounds, which seem to stabilize such oxidative addition products. A mononuclear compound would force the lone pairs of the oxygen atom into the electron-rich region of the complex, causing electronic repulsion. The high reactivity of **1b** is now under investigation in order to find possible applications as a catalyst precursor.

Experimental Section

General Remarks: All manipulations were performed under pure nitrogen or argon using standard Schlenk techniques unless other-

wise stated. Freshly distilled solvents were used throughout. Diethyl ether and THF were distilled from Na/benzophenone. Methanol, benzene, toluene, *n*-pentane and *n*-hexane were dried with sodium. CH_3CN was dried with CaH_2. (*S*,*R*)-PPFA and (*R*,*S*)-PPFA,[38] $[RhCl(COD)]_2$,[39] $[RhCl(C_2H_4)_2]_2$,[40] $[RhCl(CO)_2]_2$,[41] and $[IrCl(COE)_2]_2$ [42] were prepared as described previously. The ligands (*S*,*R*)-Pigiphos and (*R*,*S*)-Pigiphos were obtained in better yields (ca. 90%) than previously reported[2a] by using higher concentrations of the starting reagents. All the other chemicals were commercial products of reagent grade and were used as received. All solid compounds were collected on sintered glass frits before being dried in a stream of nitrogen. ^1H, $^{13}C\{^1H\}$ and $^{31}P\{^1H\}$ NMR spectra were recorded with Bruker DPX 250, 300, 400 or Avance DRX-500 spectrometers. ^1H and ^{13}C chemical shifts are relative to tetramethylsilane as external reference or calibrated against solvent resonance. ^{31}P NMR shifts are referenced to external 85% H_3PO_4. The assignments of the signals resulted from ^1H homonuclear decoupling experiments, 2D ^1H COSY and proton-detected ^1H,^{13}C correlations using degassed nonspinning samples. 2D NMR spectra were recorded using pulse sequences suitable for phase-sensitive representations using TPPI. The ^1H,^{13}C correlations[43] were recorded using the standard HMQC sequence with no decoupling during acquisition. Standard pulse sequences were used for ^1H NOESY measurements.[44] Infrared spectra were recorded on Perkin−Elmer Paragon 1000 or 1600 FT-IR spectrometers using samples of KBr or mulled in Nujol between KBr plates. Mass spectrometry was carried out in inert matrices by the Analytical Service of the Organic Chemistry Laboratory, ETH Zürich. Intensities are given as percent relative to the largest peak. Microanalyses were performed by the Microelemental Analysis Service of the Organic Chemistry Laboratory, ETH Zürich. Merck silica gel 60, 230−400 mesh ASTM was used for column chromatography. Thin layer chromatography was performed with Macherey−Nagel Polygram SIL G/UV254 precoated plastic sheets.

[RhCl{(*S*,*R*)-Pigiphos}] (1a). (a): Solid $[Rh_2Cl_2(COD)_2]$ (0.05 g, 0.10 mmol) was added to a solution of (*S*,*R*)-Pigiphos (0.19 g, 0.21 mmol) in absolute ethanol (20 mL). The suspension was refluxed with stirring for 1.5 h causing the precipitation of an orange solid. After cooling the mixture to room temperature, the solid was filtered off and washed with *n*-hexane (20 mL) to give **1a** (0.17 g, 81%) as orange microcrystals. ^1H NMR (C_6D_6, 294 K, 500.13 MHz): δ = 3.69 (quint, $J_{HH} = J_{HP} = 6.9$ Hz, 1 H, C*H*′CH_3), 3.25 (dt, $J_{H,H} = 7.5$, $J_{HP} = 19.4$ Hz, 1 H, C*H*′′CH_3), 1.76 (t, 3 H, CH′C*H*$_3$), 1.80 (dd, $J_{HP} = 4.6$ Hz, 3 H, CH′′C*H*$_3$), 4.60 (s, 1 H, C_5H_3), 4.48 (s, 1 H, C_5H_3), 4.35 (s, 1 H, C_5H_3), 4.30 (s, 1 H, C_5H_3), 4.24 (s, 2 H, C_5H_3), 3.92 (s, 5 H, C_5H_5′), 3.67 (s, 5 H, C_5H_5") ppm. $C_{54}H_{55}ClFe_2P_3Rh$ (1047.01): calcd. C 61.95, H 5.29; found C 61.76, H 5.34. **(b):** Solid $[Rh_2Cl_2(C_2H_4)_4]$ (0.04 g, 0.10 mmol) was added to a solution of (*S*,*R*)-Pigiphos (0.19 g, 0.21 mmol) in benzene (20 mL). After stirring for 2 h at room temperature, the orange solution obtained was concentrated to ca. 10 mL under reduced pressure. Addition of *n*-hexane (10 mL) gave **1a** as an orange solid which was filtered off and washed with *n*-hexane (yield 0.10 g, 48%).

[IrCl{(*R*,*S*)-Pigiphos}] (1b): Solid $[Ir_2Cl_2(COE)_4]$ (COE = cyclooctene) (1.920 g, 2.143 mmol) was added to a solution of (*R*,*S*)-Pigiphos (3.897 g, 4.289 mmol) in THF (15 mL). After stirring for 2 h, the resulting dark brown solution was freed from undissolved material by decantation. Evaporation of the solvent under high vacuum for 3 h at 70 °C gave an orange crystalline mass. This material was triturated with *n*-hexane (30 mL), filtered, washed with *n*-pentane (50 mL) and dried under high vacuum to give 4.584 g of **1b** (94% yield) as a dark yellow powder. ^1H NMR ([D$_8$]toluene, 294 K, 400.13 MHz): δ = 8.15 (br. s, 2 H, *ortho*-Ph), 8.10−8.03 (m, 2 H, *ortho*-Ph), 8.03−7.96 (m, 2 H, *ortho*-Ph), 7.86−7.79 (m, 2 H, *ortho*-Ph), 7.18−6.98 (m, 12 H, Ph), 4.34−4.32 (m, 1 H, C_5H_3), 4.23 (br. s, 1 H, C_5H_3), 4.07−4.05 (m, 1 H, C_5H_3), 4.04−4.02 (m, 1 H, C_5H_3), 4.02−3.99 (m, 2 H, C_5H_3), 3.66 (s, 5 H, C_5H_5′), 3.64−3.59 (m, 1 H, C*H*′CH_3), 3.38 (s, 5 H, C_5H_5"), 3.14 (br. s, 1 H, C*H*"CH_3), 2.75 (br. q, $J = 11.0$ Hz, 1 H, CyH), 2.31−2.21 (m, 1 H, CyH), 1.84−1.75 (m, 1 H, CyH), 1.71−1.63 (m, 1 H, CyH), 1.58 (dd, $J = 7.0$, $J = 5.8$ Hz, 3 H, CH_3′), 1.54 (dd, $J = 4.0$, $J = 3.4$ Hz, 3 H, CH_3′′), 1.45−1.26 (m, 2 H, CyH), 1.23−1.16 (m, 3 H, CyH), 1.10−0.86 (m, 2 H, CyH) ppm. $^{13}C\{^1H\}$ NMR ([D$_8$]toluene, 294 K, 62.9 MHz): δ = 137.4, 137.1, 134.9, 134.4, 129.3, 129.2, 128.2, 126.9, 125.4, 99.8 (1 C, C_5H_3), 93.5 (1 C, C_5H_3), 75.3 (1 C, C_5H_3), 73.3 (1 C, C_5H_3), 70.7 (5C, C_5H_5′), 70.6 (5C, C_5H_5"), 69.2 (1 C, C_5H_3), 68.8 (1 C, C_5H_3), 68.1 (1 C, C_5H_3), 67.3 (1 C, C_5H_3), 38.9, (1 C, *C*HCH_3), 35.3 (1 C, α-CH-Cy), 30.3 (1 C, CH_2), 29.8 (1 C, CH_2), 28.0 (1 C, CH_2), 27.5 (1 C, CH_2), 27.2 (1 C, CH_2), 26.3 (1 C, *C*HCH_3), 23.0 (1 C, CH_3), 15.4 (1 C, CH_3) ppm. MS (MALDI): *m*/*z* (%) = 1101 (100) $[M - Cl]^+$, 1018 (22) $[M - Cl - Cy]^+$, 984 (14) $[M - Cl - FeCp]^+$, 919 (15), 902 (16), 838 (14), 804 (16), 725 (16), 711 (17), 634 (28). $C_{54}H_{55}ClFe_2IrP_3$ (1136.32): calcd. C 57.08, H 4.88, P 8.18; found C 57.34, H 5.02, P 8.44.

[Rh{(*S*,*R*)-Pigiphos}(CH$_3$CN)]PF$_6$ (2a): Solid $TlPF_6$ (0.03 g, 0.08 mmol) was added to a solution of **1a** (0.08 g, 0.08 mmol) in acetonitrile (7 mL) and the mixture was stirred for 10 min. After removal of TlCl by filtration, the orange solution obtained was concentrated to ca. half the volume under reduced pressure. Addition of diethyl ether (10 mL) caused the precipitation of an orange solid, which was separated, washed with diethyl ether (40 mL) and dried in vacuo to give 52 mg of **2a** (55% yield). ^1H NMR (CD_3COCD_3, 294 K, 500.13 MHz): δ = 3.68 (dt, $J_{H,H} = 6.8$, $J_{HP} = 19.3$ Hz, 1 H, C*H*′CH_3), 3.42 (quint, $J_{H,H} = J_{HP} = 7.3$ Hz, 1 H, C*H*"CH_3), 1.88 (dd, $J_{HP} = 13.8$ Hz, 3 H, CH′C*H*$_3$), 2.10 (dd, $J_{HP} = 10.4$ Hz, 3 H, CH"C*H*$_3$), 5.09 (s, 1 H, C_5H_3), 4.82 (s, 1 H, C_5H_3), 4.78 (q, 1 H, C_5H_3), 4.76 (s, 1 H, C_5H_3), 4.73 (t, 1 H, C_5H_3) 4.49 (s, 1 H, C_5H_3), 4.09 (s, 5 H, C_5H_5′), 3.87 (s, 5 H, C_5H_5"), 1.68 (s, 3 H, C*H*$_3$CN) ppm. ^{13}C NMR (CD_3COCD_3, 294 K, 125.76 MHz): δ = 1.82 (s, *C*H$_3$CN, $J_{C,H} = 134.4$ Hz) ppm. IR: $\tilde{\nu}$ = 2317 ν(C−N) cm^{-1}. $C_{56}H_{58}F_6Fe_2NP_4Rh$ (1197.57): calcd. C 56.17, H 4.88; found C 56.24, H 4.87.

[Ir{(*R*,*S*)-Pigiphos}(CH$_3$CN)]PF$_6$ (2b): $TlPF_6$ (0.36 g, 1.02 mmol) was added to a solution of **1b** (1.15 g, 1.01 mmol) in CH_3CN (10 mL). After stirring at room temperature for 4 d, the mixture obtained was filtered. Concentration to dryness yielded an orange resin which crystallized on standing. The solid material was powdered and dried under high vacuum (3 d at 50 °C) affording 1.3 g of **2b** (quantitative yield). ^1H NMR (CD_3CN, 294 K, 300.13 MHz): δ = 8.18−8.04 (m, 4 H, Ph), 7.56−7.37 (m, 11 H, Ph), 7.30−7.23 (m, 3 H, Ph), 6.99−6.90 (m, 2 H, Ph), 4.81 (br. s, 1 H, C_5H_3), 4.56−4.51 (m, 2 H, C_5H_3), 4.51−4.49 (m, 1 H, C_5H_3), 4.47 (br. t, 1 H, C_5H_3), 4.26 (br. s, 1 H, C_5H_3), 3.86 (s, 5 H, C_5H_5′), 3.67 (s, 5 H, C_5H_5"), 3.41 (dd, $J = 11.5$, $J = 6.8$ Hz, 1 H, C*H*′CH_3), 3.33 (dd, $J = 11.5$, $J = 7.7$ Hz, 1 H, C*H*"CH_3), 2.36 (br. q, $J = 11.0$ Hz, 1 H, CyH), 2.28 (br. d, $J = 14.0$ Hz, 1 H, CyH), 1.96 (s, 3 H, C*H*$_3$CN), 1.82 (dd, $J = 11.1$, $J = 7.3$ Hz, 3 H, C*H*$_3$′), 1.65 (dd, $J = 13.5$, $J = 6.9$ Hz, 3 H, C*H*$_3$′′), 1.78−1.56 (m, 3 H, CyH), 1.50 (br. d, $J = 11.0$ Hz, 1 H, CyH), 0.16−1.90 (m, 2 H, CyH), 0.68 (br. q, $J = 13.0$ Hz, 1 H, CyH), 0.50 (br. q, $J = 13.0$ Hz, 1 H, CyH), 0.31 (m, 1 H, CyH) ppm. $^{13}C\{^1H\}$ NMR (CD_3CN, 294 K, 62.9 MHz): δ = 121.3 (br. d, $J_{P,C} = 16.0$ Hz, 1 C, CD_3CN), 100.9 (br. d, $J_{P,C} = 21.0$ Hz 1 C, C_5H_3), 93.4 (dd, $J_{P,C} = 20.0$, $J_{P,C}$ =

5.0 Hz, 1 C, C_5H_3), 75.3 (t, $J_{P,C}$ = 3.0 Hz, 1 C, C_5H_3), 74.1 (t, $J_{P,C}$ = 3.0 Hz, 1 C, C_5H_3), 71.6 (s, 5 H, C_5H_5'), 71.3 (s, 5 H, C_5H_5"), 1.8 (s, 1 C, CH_3CN) ppm. $C_{56}H_{58}F_6Fe_2IrNP_4$ (1286.88): calcd. C 52.27, H 4.54, N 1.09; found C 51.78, H 5.00, N 1.04.

[RhCl(O$_2$){(*S*,*R*)-Pigiphos}] (3a): A solution of **1a** (0.05 g, 0.05 mmol) in benzene (5 mL) was stirred in air for 30 min. During this time, yellow microcrystals of **3a** precipitated. Subsequently, they were filtered off and washed with *n*-hexane. Yield: 47 mg (87%). ^{1}H NMR (C_6D_6, 294 K, 500.13 MHz): δ = 4.72 (dt, $J_{H,H}$ = 6.2, J_{HP} = 12.0 Hz 1 H, C*H*′CH$_3$), 3.61 (quint, 1 H, C*H*"CH$_3$, $J_{H,H}$ = J_{HP} = 5.2 Hz), 1.72 (dd, J_{HP} = 10.5 Hz, 3 H, CH′C*H*$_3$), 1.94 (dd, J_{HP} = 9.2 Hz, 3 H, CH"C*H*$_3$), 4.50 (s, 1 H, C_5H_3), 4.48 (s, 1 H, C_5H_3), 4.35 (s, 1 H, C_5H_3), 4.22 (s, 1 H, C_5H_3), 4.18 (s, 1 H, C_5H_3) 3.74 (s, 1 H, C_5H_3), 3.68 (s, 5 H, C_5H_5'), 3.47 (s, 5 H, C_5H_5") ppm. IR: $\tilde{\nu}$ = 902 ν(O−O) cm^{-1}. $C_{54}H_{55}ClFe_2O_2P_3Rh$ (1079.01): calcd. C 60.11, H 5.14; found C 60.33, H 5.01.

[IrCl(O$_2$){(*R*,*S*)-Pigiphos}] (3b): A solution of **1b** (15 mg, 13.2 μmol) in benzene (3 mL) was stirred in air for 5 min yielding **3** as a red precipitate. ^{1}H NMR ([D$_8$]toluene, 294 K, 300.13 MHz): δ = 8.87−8.73 (br. s, 2 H, *ortho*-Ph), 7.84−7.75 (m, 2 H, *ortho*-Ph), 7.69−7.61 (m, 2 H, *ortho*-Ph), 7.59−7.51 (m, 2 H, *ortho*-Ph), 4.26−4.23 (m, 1 H, C_5H_3), 4.22−4.20 (m, 1 H, C_5H_3), 4.13−4.10 (m, 2 H, C_5H_3), 3.95 (t, *J* = 2.4 Hz, 1 H, C_5H_3), 3.87 (t, *J* = 2.7 Hz, 1 H, C_5H_3), 3.41 (s, 5 H, C_5H_5'), 3.37 (s, 5 H, C_5H_5"), 1.67 (dd, *J* = 11.4, *J* = 7.2 Hz, 3 H, CH$_3$′), 1.45 (dd, *J* = 11.4, *J* = 7.2 Hz, 3 H, CH$_3$′′) ppm. MS (MALDI): *m*/*z* (%) = 1168 (20) [M]$^+$, 1152 (20) [M − O]$^+$, 1136.3 (100) [M − O$_2$]$^+$. IR (KBr): $\tilde{\nu}$ = 829 ν(O−O) cm^{-1}.$C_{54}H_{55}ClFe_2IrO_2P_3$ (1168.32): calcd. C 55.52, H 4.74; found C 55.71, H 4.91.

[Rh(CO){(*S*,*R*)-Pigiphos}]OTf (4): Solid [Rh$_2$Cl$_2$(CO)$_4$] (0.06 g, 0.15 mmol) was added to a solution of (*S*,*R*)-Pigiphos (0.30 g, 0.33 mmol) in acetone (10 mL). Solid AgOTf (0.08 g, 0.33 mmol) was added to the resulting solution and CO was bubbled through it for 10 min. The red solution obtained after filtration was concentrated to ca. half the volume under reduced pressure. Addition of *n*-pentane (15 mL) caused the formation of a red oil which crystallized on standing. The solid was washed with *n*-pentane and dried in vacuo to give 114 mg of **4** (64%). ^{1}H NMR (CD_3COCD_3, 294 K, 500.13 MHz): δ = 3.88 (dt, $J_{H,H}$ = 6.4, J_{HP} = 12.4 Hz, 1 H, C*H*′CH$_3$), 3.59 (quint, $J_{H,H}$ = J_{HP} = 7.4 Hz, 1 H, C*H*"CH$_3$), 1.84 (dd, J_{HP} = 14.1 Hz, 3 H, CH′C*H*$_3$), 2.14 (dd, J_{HP} = 11.0 Hz, 3 H, CH"C*H*$_3$), 5.23 (s, 1 H, C_5H_3), 4.96 (s, 1 H, C_5H_3), 4.90 (q, 1 H, C_5H_3), 4.86 (t, 1 H, C_5H_3), 4.81 (s, 1 H, C_5H_3) 4.56 (s, 1 H, C_5H_3), 4.16 (s, 5 H, C_5H_5'), 3.96 (s, 5 H, C_5H_5") ppm. IR: $\tilde{\nu}$ = 2020 ν(C−O) cm^{-1}. $C_{56}H_{55}F_3Fe_2O_4P_3RhS$ (1188.63): calcd. C 56.59, H 4.66; found C 56.63, H 4.64.

[IrClH{(*R*,*S*)-Pigiphos}]BF$_4$ (5): A solution of HBF_4 in diethyl ether (54%, 2 μL, 14.6 μmol) was added to a solution of **1b** (10 mg, 8.8 μmol) in C_6D_6 (1 mL). An NMR analysis showed a quantitative conversion into **5**. ^{1}H NMR (C_6D_6, 294 K, 250.1 MHz): δ = 5.63 (m, 1 H, C_5H_3), 5.50 (m, 1 H, C_5H_3), 4.38 (m, 1 H, C_5H_3), 4.25 (m, 2 H, C_5H_3), 4.21 (s, 6 H, C_5H_5' + C_5H_3), 3.99 (s, 5 H, C_5H_5"), 2.26 (dd, *J* = 13.5, *J* = 7.5 Hz, 3 H, CH$_3$′), 2.05 (dd, *J* = 13.5, *J* = 7.5 Hz, 3 H, CH$_3$′′), −32.15 (br. q, J_{HP} = 13.0 Hz, 1 H, hydride).

[IrCl$_2$H{(*R*,*S*)-Pigiphos}] (6): A solution of HCl in diethyl ether (1 M, 0.1 mL, 100 μmol) was added to **1b** (46 mg, 40.5 μmol), dissolved in benzene (1 mL). After stirring for 3 h, the solution was concentrated to dryness under high vacuum to yield **6** as a yellow solid. ^{1}H NMR (C_6D_6, 294 K, 400.13 MHz, see Figure 5 for the labeling scheme): δ = 8.77 [m, 2 H, H−C(21B), H−C(25B)], 8.66 [m, 2 H, H−C(15B), H−C(19B)], 8.37 [m, 2 H, H−C(21A), H−C(25A)], 8.20 [m, 2 H, H−C(15A), H−C(19A)], 7.39 [m, 2 H, H−C(22A), H−C(24A)], 7.36 [m, 2 H, H−C(16B), H−C(18B)], 7.31 [m, 2 H, H−C(16A), H−C(18A)], 7.26 [m, 1 H, H−C(23A)], 7.24 [m, 1 H, H−C(17A)], 7.20 [m, 1 H, H−C(17B)], 7.11 [m, 2 H, H−C(22B), H−C(24B)], 7.05 [m, 1 H, H−C(23B)], 4.49 [m, 1 H, H−C(5A)], 4.45 [s, 5 H, H−C(1B′) to C(5B′)], 4.36 [m, 1 H, H−C(3A)], 4.26 [m, 1 H, H−C(5B)], 4.22 [m, 1 H, H−C(4B)], 4.07 [m, 1 H, H−C(4A)], 4.03 [m, 1 H, H−C(8)], 4.02 [m, 1 H, H−C(3B)], 3.41 [m, 1 H, H−C(6A)], 3.36 [s, 5 H, H−C(1A′) to H−C(5A′)], 3.23 [m, 1 H, H−C(6B)], 2.67 (m, 1 H, H$_{eq}$−C(9)], 2.49 (m, 1 H, H$_{eq}$−C(13)], 1.86 [m, 1 H, H−C(12)], 1.74 (m, 1 H, H$_{eq}$−C(10)], 1.73 (m, 1 H, H$_{ax}$−C(13)], 1.71 (m, 1 H, H$_{eq}$−C(11)], 1.59 [m, 1 H, H−C(12)], 1.49 (m, 3 H, Me−C(7A)], 1.44 (m, 1 H, H$_{ax}$−C(10)], 1.22 (m, 1 H, H$_{ax}$−C(11)], 1.08 (m, 3 H, Me−C(7B)], 0.93 (m, 1 H, H$_{ax}$−C(9)], −19.48 (q, J_{PH} = 16.0 Hz, 1 H, hydride) ppm. ^{13}C{^{1}H} NMR (C_6D_6, 294 K, 75.5 MHz, see Figure 5 for the labeling scheme): δ = 137.3 [C(21B), C(25B)], 136.9 [C(21A), C(25A)]; 136.3 [C(15A), C(19A)], 134.4 [C(15B), C(19B)], 129.9 [C(17B)], 129.9 [C(23B)], 129.8 [C(23A)], 129.7 [C(17A)], 127.6 [C(16B), C(18B)], 127.4 [C(22A), C(24A)], 127.3 [C(22B), C(24B)], 126.6 [C(16A), C(18A)], 98.8 [d, $J_{P,C}$ = 19.9 Hz, C(2B)], 94.6 [d, $J_{P,C}$ = 15.4 Hz, C(2A)], 75.9 [C(5A)], 72.4 [C(5B)], 71.6 [5C, C(1B′) to C(5B′)], 71.3 [d, $J_{P,C}$ = 7.6 Hz, C(3B)], 71.0 [5C, C(1A′) to C(5A′)], 69.3 [C(3A)], 68.3 [C(4A)], 68.1 [C(4B)], 67.5 [C(1B)], 35.9 [d, $J_{P,C}$ = 25.3 Hz, C(6A)], 34.6 [d, $J_{P,C}$ = 26.0 Hz, C(8)], 30.5 [d, $J_{P,C}$ = 14.0 Hz, C(9)], 29.7 [C(13)], 27.9 [C(12)], 27.1 [C(10)], 27.1 [C(11)], 24.4 [d, $J_{P,C}$ = 32.6 Hz, C(6B)], 23.3 [C(7B)], 16.6 [C(7A)] ppm. IR (KBr): $\tilde{\nu}$ = 2185 ν(Ir−H) cm^{-1}. MS (FAB): *m*/*z* (%) = 1137.5 (100) [M − Cl]$^+$, 1097.4 (20), 1016.4 (53) [M − Cl − CpFe,]$^+$, 981.5. $C_{54}H_{56}Cl_2Fe_2IrP_3$ (1172.78): calcd. C 55.30, H 4.81; found C 57.63, H 5.61.

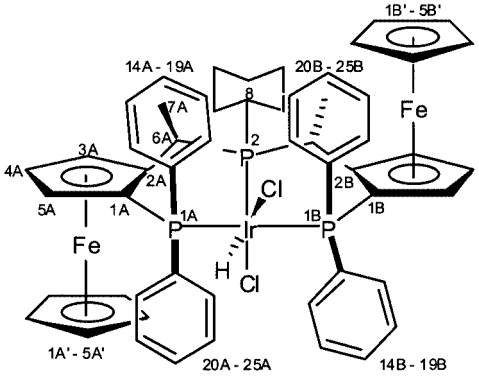

Figure 5. Labeling scheme adopted for the NMR assignment of **6**

[IrClH$_2${(*R*,*S*)-Pigiphos}] (7): A solution of **1b** (34 mg, 29.9 μmol) in benzene/methanol (1:1, v/v; 6 mL) was stirred at room temperature for 11 h. The solvent was evaporated in vacuo and the yellow residue obtained was dissolved in benzene. On addition of *n*-pentane a yellow solid precipitated which was filtered and washed three times with *n*-pentane. Yield: 10 mg (29%). ^{1}H NMR (C_6D_6, 294 K, 300.13 MHz): δ = 4.65 (m, 1 H), 4.58 (m, 1 H), 4.32 (m, 1 H), 4.18 (m, 2 H), 4.10 (m, 1 H), 3.96 (s, 5 H, C_5H_5'), 3.80 (br. *m*, 5 H, C_5H_5"), 3.22 (m, 1 H, C*H*′CH$_3$), 2.56 (br. *m*, 1 H, C*H*"CH$_3$), 1.81 (m, 3 H, CHC*H*$_3$′), 1.78 (m, 3 H, CHC*H*$_3$"), −7.7 (dt, *J* = 123.5, *J* = 16.4, 1 H, hydride), −21.5 (br. m, 1 H, hydride) ppm. MS (FAB): *m*/*z* (%) = 1137.2 (100) [M − Cl]$^+$, 1099.3 (66), 1016.3 (28), 694.7 (13). $C_{54}H_{57}ClFe_2IrP_3$ (1138.33): calcd. C 56.98, H 5.05; found C 56.95, H 5.01.

Table 4. X-ray crystallographic data for compounds **1b** and **4**

	1b	**4**
Empirical formula	C66H55ClFe2IrP3	C56H55F3Fe2O4P3RhS
Formula mass	1280.36	1188.58
Crystal system	orthorhombic	orthorhombic
Space group	*P*212121	*P*212121
a [Å]	9.9347(15)	19.629(6)
b [Å]	21.090(3)	19.713(8)
c [Å]	27.474(4)	13.727(2)
Volume [Å^3]	5756.4(15)	5312(3)
Z	4	4
Density (calculated) [g/cm^3]	1.477	1.486
Absorption coefficient [mm^{-1}]	2.973	1.031
F(000)	2568	2432
Crystal size [mm]	0.82 × 0.26 × 0.12	0.500 × 0.275 × 0.225
θ range [°]	1.22−26.40	2.54−22.47
Index ranges	−12/+12, −26/+26, −25/+34	0/+21, 0/+21, 0/+14
Reflections collected	36365	3844
Independent reflections	11815 [*R*(int) = 0.0486]	3844 [*R*(int) = 0.0000]
Parameters	600	277
Final *R* indices [$I > 2\sigma(I)$]	0.034	0.0515
R indices (all data)	0.074	0.1477
Largest diff. peak and hole [e/Å^3]	1.234 and −1.421	0.716 and −0.557

X-ray Crystallographic Study: Crystals of **1b**·2(C_6H_6) were obtained by slow evaporation of the solvent from concentrated benzene/pentane solutions of **1b** under nitrogen. The X-ray diffraction analysis was performed with exclusion of air with a Siemens CCD SMART area detector system. Selected bond lengths and angles of **1b**·2(C_6H_6) are reported in Table 3. Crystals of **4** suitable for an X-ray diffraction analysis were obtained by recrystallization from acetone/*n*-pentane under a stream of nitrogen. X-ray data were collected at room temperature with an Enraf−Nonius CAD4 diffractometer. Selected bond lengths and angles for **4** are reported in Table 2. A summary of the most important crystal and data collection parameters is given in Table 4 for both compounds. CCDC-186457 (**1b**) and -186458 (**4**) contain the supplementary crystallographic data for this paper. These data can be obtained free of charge at www.ccdc.cam.ac.uk/conts/retrieving.html [or from the Cambridge Crystallographic Data Centre, 12 Union Road, Cambridge CB2 1EZ, UK; Fax: (internat.) + 44-1223/336-033; E-mail: deposit@ccdc.cam.ac.uk].

Acknowledgments

We are grateful to D. Broggini, H. Rüegger and D. Masi for technical assistance. We thank Patrick Dietemann, Laboratorium für Organische Chemie, ETH, for the graphite-assisted laser desorption/ionisation experiments which were performed with a home-built 2-m linear time-of-flight mass spectrometer. Thanks are also due to COST D24 Chemistry Action for financial support.

[1] [1a] F. A. Cotton, B. Hong, *Prog. Inorg. Chem.* **1992**, *40*, 179. [1b] C. R. Johnson, T. Imamoto, *J. Org. Chem.* **1987**, *52*, 2170. [1c] M. J. Burk, R. L. Harlow, *Angew. Chem.* **1990**, *102*, 1511. [1d] M. J. Burk, J. E. Feaster, R. L. Harlow, *Tetrahedron: Asymmetry* **1991**, *2*, 569. [1e] T. R. Ward, L. M. Venanzi, A. Albinati, F. Lianza, T. Gerfin, V. Gramlich, G. M. Ramos Tombo, *Helv. Chim. Acta* **1991**, *74*, 983. [1f] H. Heidel, G. Huttner, L. Zsolnai, *Z. Naturforsch., Teil B* **1995**, *50*, 729. [1g] G. Jia, H. M. Lee, I. D. Williams, *Organometallics* **1996**, *15*, 4235. [1h] Y. Yao, C. J. A. Daley, R. McDonald, S. H. Bergens, *Organometallics* **1997**, *16*, 1890. [1i] H. M. Lee, C. Yang, G. Jia, *J. Organomet. Chem.* **2000**, *601*, 330. [1j] R. B. King, J. Bakos, C. D. Hoff, L. Markó, *J. Org. Chem.* **1979**, *44*, 3095. [1k] H. Heidel, J. Scherer, A. Asam, G. Huttner, O. Walter, L. Zsolnai, *Chem. Ber.* **1995**, *128*, 293.

[2] [2a] P. Barbaro, A. Togni, *Organometallics* **1995**, *14*, 3570. [2b] P. Barbaro, C. Bianchini, A. Togni, *Organometallics* **1997**, *16*, 3004. [2c] P. Barbaro, C. Bianchini, W. Oberhauser, A. Togni, *J. Mol. Cat. A* **1999**, *145*, 139.

[3] R. Dorta, A. Togni, *Organometallics* **1998**, *17*, 3423.

[4] K. Tani, A. Iseki, T. Yamagata, *Angew. Chem. Int. Ed.* **1998**, *37*, 3381.

[5] K. Nakamoto, *Infrared and Raman Spectra of Inorganic and Coordination Compounds*, Wiley, New York, **1986**.

[6] M. Sekine, W. D. Harman, H. Taube, *Inorg. Chem.* **1988**, *27*, 3604.

[7] T. E. Nappier, Jr, D. W. Meek, R. M. Kirchner, J. A. Ibers, *J. Am. Chem. Soc.* **1973**, *95*, 4194.

[8] G. G. Johnston, M. C. Baird, *Organometallics* **1989**, *8*, 1894.

[9] [9a] A. L. Crumbliss, R. J. Topping, "Phosphorus-31 NMR Spectroscopy in Stereochemical Analysis" (Eds.: J. G. Verkade, L. D. Quin), in: *Methods in Stereochemical Analysis 8*, VCH, Weinheim, Germany, **1987**, chapter 15, p. 531. [9b] P. S. Pregosin, R. W. Kunz, in: *^{31}P and ^{13}C NMR of Transition Metal Phosphane Complexes* (Eds.: P. Diehl, E. Fluck, R. Kosfeld), Springer-Verlag, Berlin, **1979**.

[10] D. W. Meek, T. J. Mazanec, *Acc. Chem. Res.* **1981**, *14*, 266.

[11] T. G. Appleton, H. C. Clark, L. E. Manzer, *Coord. Chem. Rev.* **1973**, *10*, 335.

[12] J. G. Verkade, J. A. Mosbo, "Phosphorus-31 NMR Spectroscopy in Stereochemical Analysis" (Eds.: J. G. Verkade, L. D. Quin), in: *Methods in Stereochemical Analysis 8*, VCH, Weinheim, Germany, **1987**, chapter 13, p. 432.

[13] P. R. Sharp, in: *Comprehensive Organometallic Chemistry II* (Eds.: E. W. Abel, F. G. A. Stone, G. Wilkinson), Pergamon, Oxford, U. K., **1995**, vol. 8, chapter 2, p. 138−158.

[14] A. G. Orpen, L. Brammer, F. H. Allen, O. Kennard, D. G. Watson, R. Taylor in *Structure Correlation* (Eds.: H.-B. Bürgi, J. D. Dunitz), VCH, Weinheim, Germany, **1994**, vol. 2, p. 751−857.

[15] A. Togni in: *Organic Synthesis via Organometallics* [OSM5] (Eds.: G. Helmchen, J. Dibo, D. Flubacher, B. Wiese), Vieweg, Braunschweig, **1997**, p. 185−208.

[16] A. Togni, F. Spindler, G. Rihs, N. Zanetti, M. C. Soares, T. Gerfin, V. Gramlich, *Inorg. Chim. Acta* **1984**, *222*, 213.
[17] ABM spin system. Data obtained from computer simulation using the program g NMR ver. 4.1.0, IvorySoft, Cherwell Scientific Publishing, **1995−1999**.
[18] H. Allen, O. Hill, D. G. Tew, "Dioxygen, Superoxide and Peroxide", in: *Comprehensive Coordination Chemistry* (Eds.: G. Wilkinson, R. D. Gillard, J. A. McCleverty), Pergamon Press, Oxford, England, **1987**, vol. 2, p. 315.
[19] L. Vaska, *Acc. Chem. Res.* **1976**, *9*, 175.
[20] M. H. Gubelmann, A. F. Williams, *Struct. Bonding [Berlin]* **1983**, *55*, 1.
[21] *Oxygen Complexes and Oxygen Activation by Transition Metal* (Eds.: A. E. Martell, D. T. Sawyer), Plenum Press, New York, **1988**.
[22] H. Mimoun, "Metal Complexes in Oxidation" in: *Comprehensive Organometallic Chemistry* (Eds.: G. Wilkinson, F. G. A. Stone, E. W. Abel), Pergamon Press, Oxford, England, **1982**, vol. 6.
[23] J. S. Valentine, *Chem. Rev.* **1973**, *73*, 235.
[24] M. Laing, M. J. Nolte, E. Singleton, *J. Chem. Soc., Chem. Commun.* **1975**, 660.
[25] A. Nakamura, Y. Tatsuno, M. Yamamoto, S. Otsuka, *J. Am. Chem. Soc.* **1971**, *93*, 6052.
[26] P. S. Pregosin, L. M. Venanzi, *Chem. Ber.* **1978**, *14*, 276.
[27] C. Eaborn, N. Farrell, J. L. Murphy, A. Pidcock, *J. Chem. Soc., Dalton Trans.* **1976**, 58.
[28] T. H. Brown, P. J. Green, *J. Am. Chem. Soc.* **1970**, *92*, 2359.
[29] C. A. Ghilardi, S. Midollini, S. Moneti, A. Orlandini, G. Scapacci, *J. Chem. Soc., Dalton Trans.* **1992**, 3371.
[30] T. E. Nappier, Jr., D. W. Meek, *J. Am. Chem. Soc.* **1972**, *94*, 306.
[31] T. J. Mazanec, PhD Dissertation, The Ohio State University, Columbus, OH, Dec. **1978**.
[32] J. A. McGinnety, N. C. Payne, J. A. Ibers, *J. Am. Chem. Soc.* **1969**, *91*, 6301.
[33] C. Bianchini, A. Meli, M. Peruzzini, F. Vizza, *J. Am. Chem. Soc.* **1990**, *112*, 6726.
[34] M. J. Nolte, E. Singleton, M. Laing, *J. Am. Chem. Soc.* **1975**, *97*, 6396.
[35] P. Barbaro, C. Bianchini, F. Laschi, S. Midollini, S. Moneti, G. Scapacci, P. Zanello, *Inorg. Chem.* **1994**, *33*, 1622.
[36] S. Sakaki, K. Hori, A. Ohyoshi, *Inorg. Chem.* **1978**, *17*, 3183.
[37] C. Yang, S. M. Socol, D. J. Kountz, D. W. Meek, R. Glaser, *Inorg. Chim. Acta* **1986**, *114*, 119.
[38] T. Hayashi, T. Mise, M. Fukushima, M. Kagotani, N. Nagashima, Y. Hamada, A. Matsumoto, S. Kawakami, M. Konishi, K. Yamamoto, M. Kumada, *Bull. Chem. Soc. Jpn.* **1980**, *53*, 1138.
[39] G. Giordano, R. H. Crabtree, *Inorg. Synth.* **1990**, *28*, 88.
[40] R. Cramer, *Inorg. Synth.* **1990**, *28*, 86.
[41] J. A. McCleverty, G. Wilkinson, *Inorg. Synth.* **1990**, *28*, 84.
[42] A. Van der Ent, A. L. Onderderlinden, *Inorg. Synth.* **1990**, *28*, 92.
[43] M. F. Summers, L. G. Marzilli, A. Bax, *J. Am. Chem. Soc.* **1986**, *108*, 4285.
[44] [44a] V. Sklener, H. Miyashiro, G. Zon, H. T. Miles, A. Bax, *FEBS Lett.* **1986**, *208*, 94. [44b] J. Jeener, B. H. Meier, P. Bachmann, R. R. Ernst, *J. Chem. Phys.* **1979**, *71*, 4546.

Received August 19, 2002
[I02469]

Preparation of Rhodium Catalysts Supported on Carbon Nanotubes by a Surface Mediated Organometallic Reaction

Roberto Giordano,[a] Philippe Serp,*[a] Philippe Kalck,[a] Yolande Kihn,[b] Joachim Schreiber,[c] Christiane Marhic,[c] and Jean-Luc Duvail[c]

Keywords: Nanotubes / Rhodium / Supported catalysts / Surface chemistry / Heterogeneous catalysis

The dimeric complex $[Rh_2Cl_2(CO)_4]$ was grafted to multi-walled carbon nanotubes (MWNTs) previously oxidised with nitric acid and then treated with sodium carbonate to produce carboxylate groups on their outer surface. The grafting mechanism involves bridge-splitting and substitution of -COO for Cl, as evidenced by the presence of NaCl in the samples. A further reduction/decomposition step under dihydrogen at 573 K afforded highly dispersed rhodium nanoparticles (≈1.5–2.5 nm). This novel rhodium-supported carbon material (Rh/MWNT-COONa) was tested as a catalyst for the hydrogenation of *trans*-cinnamaldehyde and the hydroformylation of hex-1-ene in the liquid phase: in both cases it was found to be very selective, toward C=C double-bond hydrogenation and the production of linear and branched aldehydes, respectively. A comparison was made between its catalytic activity and that of rhodium supported on pristine MWNTs and on nitric acid-oxidised MWNTs. We observed that these latter catalysts have larger particle sizes and lower activities, thus confirming the efficiency of our grafting procedure. Moreover, the better results obtained when using MWNT-COONa as support with respect to carboxylate-containing activated carbon also point to the important role played by the mesoporous nature of the carbon nanotube support, which can ameliorate transfer processes.
(© Wiley-VCH Verlag GmbH & Co. KGaA, 69451 Weinheim, Germany, 2003)

Introduction

Carbon materials are attractive supports in heterogeneous catalytic processes owing to their ability to be tailored to meet specific needs. Indeed, activated forms of carbon are currently employed as catalyst supports because of their high surface area, their stability at high temperatures under a nonoxidising atmosphere and the possibility of controlling both their porous structure and the chemical nature of their surface.[1,2] New forms of carbon have appeared during the last decade, showing novel interesting potentialities as supports.[3] Carbon nanofibres, also called graphite nanofibres, and carbon nanotubes, have so far been used successfully and shown to present, as final supported materials, catalytic properties superior to those of catalysts prepared on activated carbon, soot, or graphite.[2] Whilst carbon nanofibres consist of graphite sheets arranged in various orientations along the fibre axis — the most common structure being the one in which the planes are stacked up like a fishbone, with a lot of edges — both single-walled (SWNT)- and multi-walled (MWNT) carbon nanotubes show a concentric wall structure consisting of ordered graphite platelets. The morphology and the size of the above supports, especially since they present huge lengths vs. diameters, can play a significant role in catalytic applications owing to their ability to disperse the active phase. Their electronic properties are also of primary importance,[4] and their mechanical strength makes them resistant in view of recycling. A recent comparison between the interaction of transition metal atoms with carbon nanotube walls and with graphite indicates major differences in bonding sites, magnetic moments and charge-transfer direction.[5]

The most widely used technique to achieve the deposition of metals on the above materials is the incipient wetness impregnation one, in which the purified carrier is impregnated with a solution of the metal precursor, then dried, calcinated and/or reduced so as to obtain metal particles dispersed on the support.[3,6] Several studies have been performed on graphite-nanofibre-supported Fe-Cu,[7] Ni[8] or Pd[9] particles for catalytic hydrogenation. Graphite-nanofibre-supported rhodium catalysts were found to be active in ethene hydroformylation.[10] If we consider the use of carbon nanotubes, several examples are worth mentioning: Cu

[a] Laboratoire de Catalyse, Chimie Fine et Polymères, Ecole Nationale Supérieure des Ingénieurs en Arts Chimiques Et Technologiques,
118 route de Narbonne, 31077 Toulouse Cédex 4, France
Fax: (internat.) +33-5/6288-5600
E-mail: philippe.serp@ensiacet.fr
[b] CEMES-CNRS no. 8011,
2 rue Jeanne Marvig, 31055 Toulouse, France
[c] Institut des Matériaux Jean Rouxel-UMR 6502, Université de Nantes,
2 rue de le Houssinière, BP 32229, 44322 Nantes Cédex 3, France

nanoparticles were synthesised employing SWNTs as a template;[11] Ru/SWNTs[12] and alkali-promoted Ru/MWNTs[13] catalysts were prepared for hydrogenation reactions and for ammonia synthesis, respectively; Pd, Pt, Ag and Au nanoparticles were grown on SWNTs, and their size could be adjusted by changing the metal to carbon ratio;[14] Rh/MWNTs catalysts for propene hydroformylation were prepared by incipient wetness impregnation from benzene solutions of $[RhH(CO)(PPh_3)_3]$ on pristine nanotubes.[15]

Chemical treatment and/or modification of the surface of carbon nanotubes was found to be a useful tool for controlling their hydrophobic or hydrophilic character,[16] and studies carried out in order to accomplish the deposition of metals point to a strong interaction between metal atoms and the groups created by oxidation of the support surface.[17]

Thus, graphite nanofibre-supported iron Fischer–Tropsch catalysts have been prepared by three different methods on HNO_3-treated supports.[18] Important improvements toward the preparation of selective hydrogenation catalysts were achieved by supporting Pt on SWNTs oxidised in dilute HNO_3: the bonding between platinum and the carbon nanotube surface was presumably accomplished by ion-exchange on the carboxylic acid sites so formed.[19] Another example of such reactivity is the replacement of the proton of carboxylic groups with uranyl ions: XPS studies of oxidised nanotubes revealed that their surface is covered by carboxylic, carbonyl and hydroxyl groups, and, in particular, the presence of -COOH groups could be used to initiate nucleation on the support surface, leading to the selective covering of the outer surface by metallic species.[20] A Co/MWNTs system showing a good catalytic activity in dehydrogenation was prepared by oxidising MWNTs in boiling nitric acid prior to impregnation with a cobalt salt, followed by drying, calcination and reduction with H_2.[21]

Bimetallic Ru/Pt and Ru/Sn nanoparticles have been prepared from molecular heterobimetallic carbonyl clusters deposited on MWNTs previously treated with HNO_3.[22] A heterobimetallic precursor was also used to prepare Pt-Ru anode catalysts supported on oxidised and nonoxidised carbon nanofibres, SWNTs and MWNTs.[23] Coordination of Pd on HNO_3-treated carbon nanofibres[24] and of Pt on H_2SO_4/HNO_3-treated MWNTs has also been reported.[25]

A suitable technique to achieve the grafting of metal particles onto carbon nanotubes would therefore consist of functionalising the outer surface of the tubes and then performing a chemical reaction with a metal complex. This was initially accomplished by reacting Vaska's complex $[IrCl(CO)(PPh_3)_2]$ with a HNO_3-oxidised support: the tethering reaction occurs by coordination of iridium to the nanotubes through the oxygen atoms.[26]

Furthermore, a controlled chemical grafting of a metal species to the surface of carbon nanotubes would very likely result in a fine dispersion of metallic particles.

In this paper we describe a new technique that involves the organometallic reaction of the rhodium complex $[Rh_2Cl_2(CO)_4]$ with a modified MWNT surface bearing sodium carboxylate groups, which permits the production of highly dispersed Rh nanoparticles, after a decomposition/reduction step. We also report some preliminary results concerning the catalytic activity of these novel materials either in hydrogenation or hydroformylation reactions. Last but not least, the catalytic activity of these materials is compared to that observed when using rhodium-supported catalysts prepared by reacting $[Rh_2Cl_2(CO)_4]$ with pristine or HNO_3-treated MWNTs, as well as with activated carbon bearing sodium carboxylate groups.

Results and Discussion

Surface Modification of MWNTs

High purity samples of MWNTs were employed for this study (MWNTs 97%, the remaining 3% coming from iron nanoparticles encapsulated within the nanotubes and generated by the catalytic production process).[27] Typical TEM micrographs of this material are shown in Figure 1.

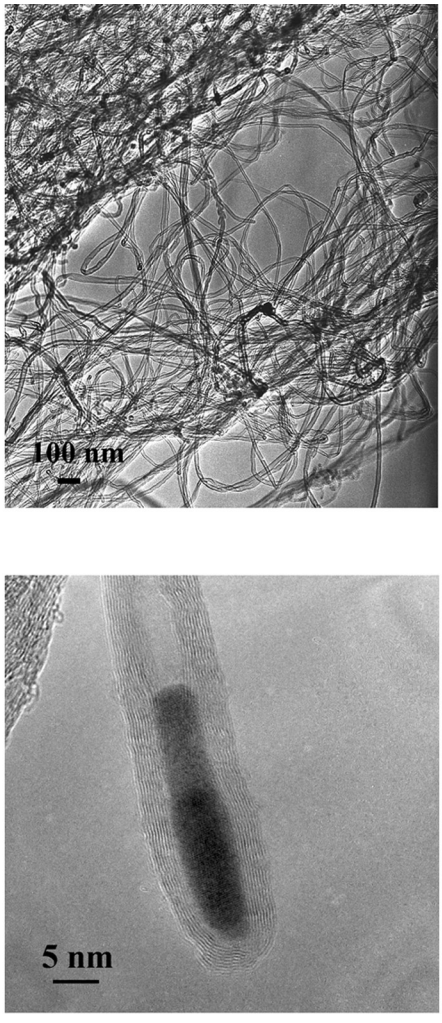

Figure 1. Typical TEM micrographs of pristine MWNTs

It consists of graphene layers (interlayer spacing d_{002} = 0.342 nm) arranged in a roughly parallel way with respect to the tube axis. Mean tube external and internal diameters

are 17 nm and 8 nm, respectively, which corresponds to about 13 walls. These nanotubes are characterised by a length of several micrometers and a specific surface area of about 180 $m^2 \cdot g^{-1}$, with no microporosity. Pores in aggregated MWNTs can be mainly divided into inner hollow cavities of small diameter (3−9 nm) and aggregated pores (15−25 nm) formed by interaction of isolated MWNTs.[28] From TEM observations it appears that one end of the tube is closed by graphene layers, the remaining iron carbide nanoparticles being located either at the tip of the tubes (see Figure 1) or in their inner cavities. Moreover, this material is highly hydrophobic since it does not present oxygen-containing groups, and therefore it should be unsuitable for supporting metallic nanoparticles.[29]

Thus, we envisaged to investigate the effect of chemical surface modifications on the feasibility of the grafting of the complex $[Rh_2Cl_2(CO)_4]$ and on the subsequent nanoparticle formation process by reductive treatment under H_2. Bridge-splitting and replacement reactions of rhodium carbonyl chloride dimer have been known for many years and often involve the use of silver carboxylate salts as reagents.[30] As it is well-known that oxidation of carbon nanotubes with nitric acid mainly generates carboxylic groups on the surface,[17b] we decided to investigate the possibility of synthesising the corresponding sodium carboxylates and hence of producing a true *nanotube salt*. Therefore the surface-mediated organometallic reaction depicted in Scheme 1 would be expected to occur on treatment with the dirhodium precursor, leading to a molecular dispersion of Rh carbonyl species and to a high dispersion of metallic particles after a further decomposition/reduction step (Scheme 1).

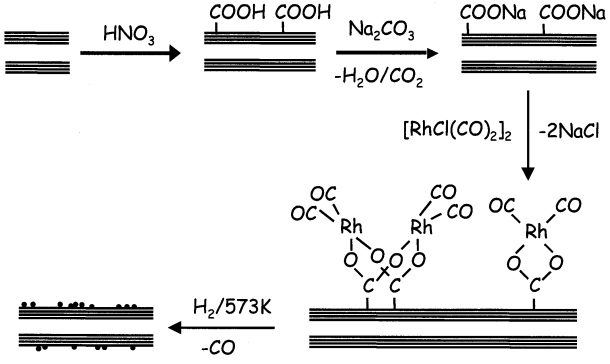

Scheme 1. Surface mediated organometallic reaction between $[Rh_2(\mu\text{-}Cl)_2(CO)_4]$ and MWNT-COONa

From TEM micrographs it appears that the morphology of MWNT-COOH and MWNT-COONa does not differ significantly from that of pristine tubes. Thus, under our experimental conditions the oxidation treatment performed causes only minor damage to the tips of the nanotubes (Figure 2). Raman spectra recorded either on pristine tubes or on oxidised samples clearly indicate that oxidation does not affect the degree of graphitisation of these materials (Figure 3). In both cases the graphite mode G-band and the defect mode D-band possess nearly the same intensities. Furthermore, a slight increase in the surface area is observed in the case of MWNT-COOH (S_{BET} = 200 $m^2 \cdot g^{-1}$).

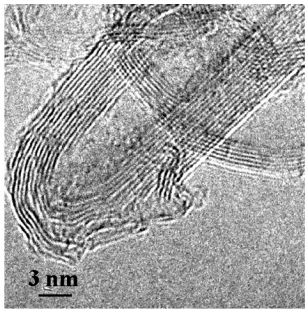

Figure 2. TEM micrograph of HNO_3-treated MWNTs

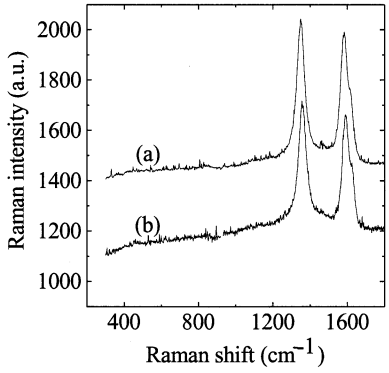

Figure 3. Raman spectra of: (a) pristine MWNTs and (b) MWNT-COOH

In order to examine the carbon environment on the surface, XPS analyses were performed on the different samples; the relevant data are given in Table 1.

Table 1. XPS data obtained from MWNT samples

Sample	Binding Energy[a] (eV)				S[b]	O[b]	C[b]	Na[b]
	530.9	532.1	533.2	534.2				
MWNT	55	45	–	–	0.14	0.81	99.05	–
MWNT-COOH	23	44	24	9	–	3.23	96.77	–
MWNT-COONa	25	49	–	14	–	5.29	93.04	1.67

[a] Values given as % of the total amount. [b] Atomic percentage.

The ratio of total oxygen to total carbon is a measure of the degree of surface oxidation, and reconstruction of the O1s peak gives additional information about the surface oxygen-containing groups. XPS spectra of all the modified MWNT samples show an increase of the oxygen content. The MWNT-COOH sample exhibits functionalities that contribute to the intensity of the O1s peaks located at 530.9 eV, 532.1 eV, 533.2 eV and 534.2 eV, in agreement with published data for activated carbon treated with nitric acid.[31] Hence, this type of treatment significantly increases

the amount of surface carboxylic groups. As for MWNT-COONa, a new peak appears at 535.4 eV, which can be attributed to the sodium carboxylate groups[32] (an XPS analysis performed on a CH_3COONa sample gave a value of 534.9 eV for -COONa). The presence of sodium was confirmed by the Na1s peak at 1071.5 eV.

The formation of sodium carboxylate groups on the outer surface of MWNTs makes this material highly hydrophilic, and it can easily be dispersed in water. Moreover, it is interesting to note that a small amount (ca, 5 mg·L^{-1}) of the so formed MWNT sodium salt is dissolved during washing with water, performed to remove the excess of sodium carbonate.

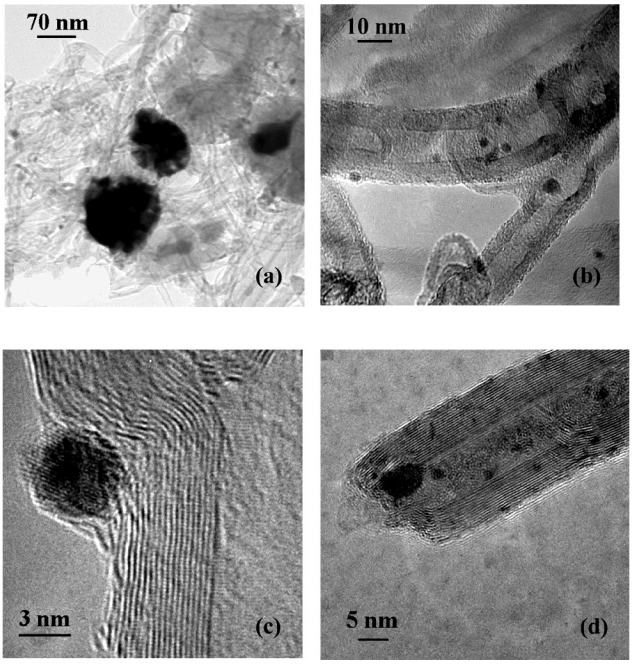

Figure 4. TEM micrographs of: (a) 1%Rh/MWNTs; (b) and (c) 1%Rh/MWNT-COOH; (d) 1%Rh/MWNT-COONa

Rh/MWNTs Catalyst Preparation by $[Rh_2Cl_2(CO)_4]$ Grafting

The grafting procedure described above involves the reaction between toluene solutions of $[Rh_2Cl_2(CO)_4]$ and various supports, namely MWNTs, MWNT-COOH, MWNT-COONa and C*-COONa. It is worth noting that with a loading of Rh equal to 1% w/w, whatever the carbon nanotube support employed, after impregnation and filtration the resulting solution is always colourless, pointing to a complete adsorption of the rhodium complex by some interaction between the complex and the MWNTs. IR spectra of these toluene solutions confirmed the absence of any detectable carbonyl bands due to rhodium species. Moreover, infrared and Raman spectra of all the solid samples obtained via the grafting procedure showed no bands attributable to the carbonyl ligands; this could very likely be due to the low rhodium loading (1−5% w/w), although the possibility of a decarbonylation reaction occurring during the grafting/drying procedure should also be considered. Furthermore, in the case of the reaction between $[Rh_2Cl_2(CO)_4]$ and MWNT-COONa, the observation by X-ray diffraction of the presence of NaCl in the samples coming from decomposition under dihydrogen clearly indicates the occurrence of the carboxylate group mediated grafting of the complex through bridge splitting.

After reductive decomposition at 573 K, careful rinsing with water to remove NaCl, and drying at 383 K under vacuum overnight, all of the samples were examined by TEM (Figure 4 and 5).

In the case of Rh/MWNTs the very large particle size distribution observed (particle size up to 100 nm has been measured) points to a weak interaction between the metal carbonyl precursor and the tube surface, which favours the migration and agglomeration of the rhodium(0) atoms deriving from the decomposition/reduction steps. As for Rh/MWNT-COOH, a better dispersion is obtained (mean particle size 2.5−5 nm), indicating that a reaction has occurred between the -COOH groups and the rhodium complex.

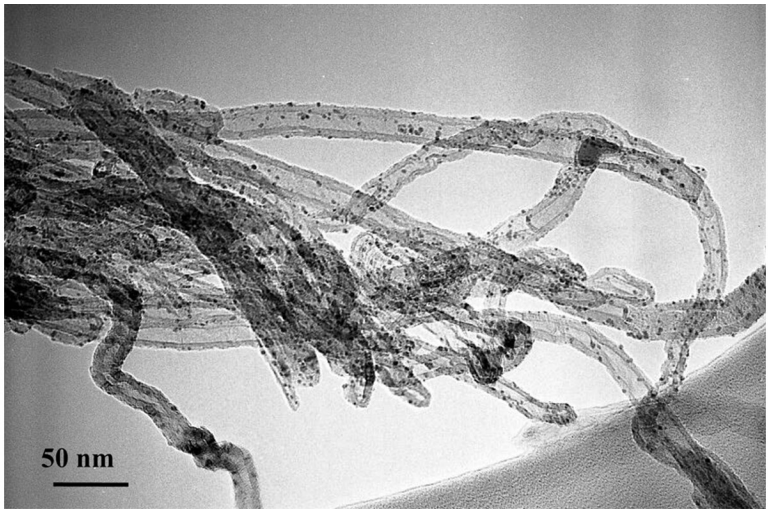

Figure 5. TEM micrographs of 9.5%Rh/MWNT-COONa

However, the results obtained with MWNT-COONa (mean particle size ≈1.5−2.5 nm) clearly show that the grafting to carboxylate groups is more efficient. Indeed, the reaction of surface carboxylate groups with the dirhodium precursor, which gives better results with respect to particle size and dispersion, is expected to be different from that of the carboxylic groups, owing to the higher nucleophilicity of the two oxygen atoms of the anionic -COO^- moiety and to the symmetric distribution of the charge (the hydrogen atom having been removed).

The MWNT sodium salt can hence be considered as a primary ligand that would be prone to react with the dirhodiumchlorocarbonyl dimeric complex to produce rhodium species grafted to the surface via splitting of the Cl bridges. Further decomposition under H_2 affords highly dispersed rhodium-supported particles even with metal loadings up to 9.5% w/w: a mean particle size of 3 nm has been measured in the case of 9.5% Rh/MWNT-COONa, with a very narrow (3 ± 2 nm) particle size distribution (see Figure 5).

Catalytic Experiments

In general, we have investigated liquid-phase catalytic reactions in order to determine whether the peculiar structures of MWNTs, and particularly their high mesoporosity, could improve transfer phenomena with respect to highly microporous activated carbons. Additionally, we were interested in the possibility of comparing surface-mediated organometallic synthesis methods to more classical impregnation techniques involving prior oxidation by nitric acid. Two reactions were studied: the hydrogenation of *trans*-cinnamaldehyde and the hydroformylation of hex-1-ene.

Prior to evaluating the catalytic activity of rhodium-supported catalysts, blank experiments were performed with MWNTs and MWNT-COOH in order to check the possible role of the remaining 3% w/w iron nanoparticles, encapsulated within the nanotubes, in the investigated catalytic systems. For MWNTs no activity was observed either in hydrogenation or in hydroformylation; in the case of MWNT-COOH a 1.7% conversion into hydrocinnamaldehyde was obtained, whilst no hydroformylation product could be detected. Indeed, iron nanoparticles of approx. 5 × 20 nm size, located either at the tip, or in inner cavities, of the nanotubes, are not accessible to the reactants in the case of MWNTs owing to the presence of graphene layers roughly perpendicular to the axis of MWNTs (bamboo-like structure), as shown on Figure 6. As depicted in Figure 2, the nitric acid treatment induces opening of the tip of the tubes, thus making iron particles reachable by the reactants. Since iron-based supported catalysts are known to be active in alkene hydrogenation,[33] it is very likely that the observed activity could actually be due to the presence of zero-valent iron and/or iron carbide particles.

Selective Hydrogenation of *trans*-Cinnamaldehyde

The catalytic results of liquid-phase hydrogenation of *trans*-cinnamaldehyde are depicted in Table 2.

One can observe that, except in the case of Rh/MWNTs, all these catalytic systems selectively afford hydrocinnamaldehyde through C=C double bond hydrogenation, irrespective of the Rh-supported carbon sample employed.

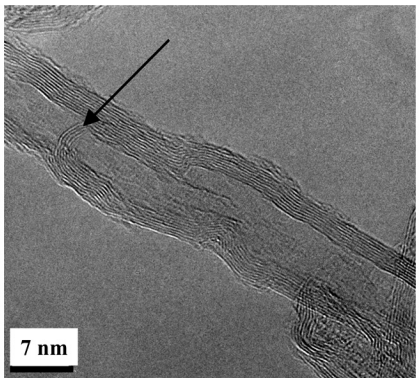

Figure 6. TEM micrograph showing graphene layers closing the inner cavity of a MWNT

Table 2. Catalytic hydrogenation of *trans*-cinnamaldehyde

Catalyst	Conv (%)	Activity[a]	Selectivity[b]
1% Rh/MWNT	–	–	–
1% Rh/MWNT-COOH	5.3	26.8	100.0
1% Rh/MWNT-COONa	15.1	78.2	100.0
9.5% Rh/MWNT-COONa	23.2	11.4	100.0
1% Rh/C*-COONa	4.9	27.1	100.0
5% Pd/C*[c]	62.8	343.3	64.5[d]

[a] In g substrate transformed·g^{-1}_{Rh}·h^{-1} g^{-1}_{Rh}·h^{-1}. [b] % cinnamaldehyde. [c] A commercial 5% w/w Pd/C* (Johnson Matthey) was used for comparison purposes. [d] Hydrocinnamyl alcohol was the other product of the reaction.

The Rh/MWNTs samples, in accordance with TEM micrographs in which very large rhodium aggregates can be observed, possess no catalytic activity. In contrast, Rh/MWNT-COOH and Rh/MWNT-COONa are active and very selective catalysts for hydrocinnamaldehyde formation. If one compares the selectivity data, Rh-supported catalysts are more selective than a commercial Pd/C* catalyst, in that C=C double bond hydrogenation is the only reaction occurring under our experimental conditions.

As far as catalytic activity and conversion are concerned, it appears that the best method to support Rh particles on the MWNTs surface is indeed the grafting of the complex via surface-mediated organometallic synthesis, followed by reduction under H_2. The good performance of the thus-prepared catalysts can hence be attributed to the very small particle size obtained after the decomposition/reduction step and to the high purity of the metallic deposit. Higher conversion together with lower activity values for a 9.5% loading of rhodium on MWNTs could be attributed to the effect of the larger particle size observed. As for mass-transfer limitations, the complete absence of microporosity, together with a relatively high surface area, are crucial to a good catalytic activity. For instance, if we compare the Rh/MWNT-COONa catalyst to Rh/C*-COONa prepared ac-

cording to the same procedure, the former is three times more active.

Hydroformylation of Hex-1-ene

Liquid-phase hydroformylation runs were carried out with hex-1-ene under relatively mild conditions (2 MPa, 353 K) and afforded *n*-heptanal and 2-methylhexanal, together with 2-ethylpentanal. The presence of the last product is due to partial isomerization of the substrate to hex-2-ene, which has been observed in the reaction solutions by GC. Such a reaction pathway was previously observed under more drastic conditions (10 MPa, 423 K) on Rh/C* catalysts,[34] leading to C7 aldehyde, hexane and C7 alcohol formation. The catalytic results are shown in Table 3, and the selectivities to the products obtained are listed in Table 4.

It should be noted that the production of linear and branched aldehydes and a high linear/branched ratio (2.6) occur only with 1% Rh/MWNT-COOH, a sample characterised by large particle sizes and by the acidic character of the support. In this case no ethylpentanal and lower amounts of methylhexanal were detected. The most important feature of our catalytic system is the high conversion and activity values found for 1% Rh/MWNT-COONa and the selectivity of the reaction toward aldehyde formation, thus confirming, as for *trans*-cinnamaldehyde hydrogenation, the efficiency of our grafting method and the advantage of using carbon nanotubes as a support in liquid-phase catalytic reactions.

Table 3. Catalytic hydroformylation of hex-1-ene

Catalyst	Conv. (%)	Activity[a]	n/b ratio[b]
1% Rh/MWNT	–	–	–
1% Rh/MWNT-COOH	52.3	72.9	2.6
1% Rh/MWNT-COONa	75.8	197.6	1.2
9.5% Rh/MWNT-COONa	65.8	11.6	1.2
1%Rh/C*-COONa	66.1	105.6	1.2

[a] In g substrate transformed·g^{-1}_{Rh}·h^{-1} in g^{-1}_{Rh}·h^{-1}. [b] n = linear isomer; b = branched isomer.

Conclusion

Oxidation of the outer surface of multi-walled carbon nanotubes by nitric acid leads to the formation of carboxylic groups that can be used to anchor rhodium carbonyl moieties. Better results are obtained upon conversion of carboxylic into more reactive carboxylate groups. A further reduction step under dihydrogen affords highly dispersed (for instance 1.5−2.5 nm for a 1% w/w loading) rhodium nanoparticles even for rhodium loadings up to 9.5% w/w. These Rh-supported catalysts show interesting performances with respect to liquid-phase hydrogenation and hydroformylation reactions. Additionally, the nature of the MWNT support probably contributes to a better activity, presumably by ameliorating transfer processes with respect to what happens on classical activated carbons.

Experimental Section

General Remarks: Nitric acid (Prolabo, 52.5%), Na_2CO_3·$10H_2O$ (Acros Organics), toluene (Acros Organics, 99%), dioxane (SDS), *trans*-cinnamaldehyde (Aldrich, 98%) and hex-1-ene (Janssen, 97%) were used as received. H_2 and CO (Air Liquide, 99.99998 and 99.99%, respectively) were also used as received. The complex $[Rh_2Cl_2(CO)_4]$ was prepared according to a well established procedure.[36]

Carbon nanotubes were prepared by a catalytic CVD method[27] on an Fe/Al_2O_3 catalyst.[35] Dissolution of the alumina support and some of the iron was performed by acidic treatment (H_2SO_4, 98% Prolabo). Typical characterisation data for this material are given in Table 5.

Surface Modification of MWNTs

A mixture of 5 g of MWNTs in 150 mL of HNO_3 (52.5%) was refluxed for 3 hours at 403 K. Then the mixture was filtered and

Table 4. Product distribution for hex-1-ene hydroformylation (as selectivities, %)

Catalyst	2-Ethyl-pentanal	2-Methyl-hexanal	Heptanal
1% Rh/MWNT	–	–	–
1% Rh/MWNT-COOH	–	27.7	72.3
1% Rh/MWNT-COONa	12.6	39.8	47.6
9.5% Rh/MWNT-COONa	8.1	38.0	53.9
1%Rh/C*-COONa	7.3	37.4	55.3

Table 5. Main characteristics of pristine MWNTs

Internal diameter (nm)	External diameter (nm)	Real density ($g·mL^{-1}$)	Pore diameter (nm)	d_{002} (nm)	S_{BET} ($m^2·g^{-1}$)
8	17	1.95	20	0.342	180

rinsed with deionized water until the pH of the water reached 7. The resulting material was dried overnight at 383 K in a thermostatted oven and crushed to a powder by a ball-milling process for 20 min.[37] This material is named MWNT-COOH.

The preparation of the corresponding nanotube sodium carboxylate salt (MWNT-COONa) was accomplished by treatment of a suspension of 5 g of MWNT-COOH in 100 mL of toluene with 200 mg of $Na_2CO_3 \cdot 10H_2O$ dissolved in 50 mL of H_2O. This suspension was stirred for 15 min, sonicated for 2 hours at 313 K and stirred again for 15 min at room temperature. The resulting mixture was then filtered through a Büchner funnel, and the material washed with deionized water to fully remove the excess of the sodium salt. Drying overnight in a thermostatted oven at 383 K afforded MWNT-COONa. Moreover, a C*-COONa sample was prepared for comparison purposes by the same procedure starting from a commercial activated carbon (Darco-G60, 100 mesh, $S_{BET} = 700\ m^2 \cdot g^{-1}$, Aldrich).

Surface Grafting of $[Rh_2Cl_2(CO)_4]$ and Production of Rh/MWNTs or Rh/C*-COONa: 100 mg of $[Rh_2Cl_2(CO)_4]$ was added to a suspension of 5.29 g of the carbon support in 100 mL of toluene, stirred for 3 hours at 333 K under nitrogen and then sonicated for 2 hours at room temperature. Filtration through a Büchner funnel, washing with *n*-hexane, drying in vacuo and crushing for 20 min resulted in the production of the rhodium grafted material. Activation of the supported complex was done under a continuous flow (250 sccm) of a N_2/H_2 gas mixture (80:20 v/v) for three hours at 573 K, then the samples were washed with water to remove the NaCl formed, dried overnight at 383 K and crushed to powder. The rhodium loading was so fixed at 1% w/w, if not otherwise specified in the text.

Evaluation of Catalyst Activity for trans-Cinnamaldehyde Hydrogenation and Hex-1-ene Hydroformylation: The selective hydrogenation of cinnamaldehyde was carried out at atmospheric pressure in a three-necked flask equipped with a reflux condenser and gas inlet. The mixture containing 100 mg of rhodium-supported catalyst, 2 mL of *trans*-cinnamaldehyde and 50 mL of dioxane was sonicated for 15 min at room temperature prior to each catalytic run; nitrogen gas at room temperature was bubbled through the liquid phase to purge the system, the temperature was raised to 353 K, then dihydrogen gas was let in. Each catalytic run lasted 4 h, during which time samples were taken at regular intervals for analysis.

The hydroformylation of hex-1-ene was performed in an autoclave under the following reaction conditions: 353 K, 2 MPa of CO/H_2 (1:1). A catalyst sample (100 mg) was dispersed in a mixture of 40 mL of toluene and 5 mL of hex-1-ene, sonicated in a Schlenk tube for 15 min and transferred under nitrogen into the autoclave, which was then pressurized and heated. At the end of the catalytic runs (24 h) the resulting mixture was cooled to room temperature, then filtered and analysed.

Analysis of the reaction products, both from hydrogenation and hydroformylation runs, was performed on a Carlo Erba HRGC 5160 gas-chromatograph equipped with a capillary column (DB-5 J&W Scientific, 30 m, i.d. O.32 μm, film O.25 μm); a Perkin−Elmer Q-Mass 910 GC-MS instrument (capillary column DB-1 J&W Scientific, E.I. 70 eV) was used to identify the hydrogenation or hydroformylation products and to confirm the nature of the by-products.

Characterisation of the Materials: TEM observations were made with a Hitachi HF2000 (200 kV) microscope equipped with a field emission gun, a cold cathode and a multiscan camera (Gatan) which allows the recording and manipulation of high-resolution images by means of Digital Micrograph software. The rhodium particle-size distributions were determined on the basis of TEM micrographs. Additional TEM observation were performed on a Phillips CM12 (120 kV voltage) electron microscope.

Raman spectra were recorded on a T64000 Jobin−Yvon spectrometer (4 cm^{-1} resolution) equipped with a Spectra Phisycs $Argon^+$ Laser; samples were excited at $\lambda = 514$ nm. X-ray photoelectron spectra were obtained on a VG ESCALAB MK II spectrometer. The measurements were carried out using unmonochromatized Mg-K_α radiation ($\lambda = 0.989$ nm) under a mean pressure of 6×10^{-11} kPa.

Acknowledgments

Special thanks to Dr B. Richard for technical assistance and to Mr J. Y. Mevellec for his help in Raman studies. We would like to thank also Engelhard-CLAL for a generous loan of $RhCl_3 \cdot 3H_2O$.

[1] F. Rodriguez-Reinoso, *Carbon* **1998**, *36*, 159−175.
[2] E. Auer, A. Freund, J. Pietsch, T. Tacke, *Appl. Catal. A* **1998**, *173*, 259−271.
[3] B. Coq, J. M. Planeix, V. Brotons, *Appl. Catal. A* **1998**, *173*, 175−183.
[4] J. E. Fischer, A. T. Johnson, *Curr. Opin. Solid State Mater. Sci.* **1999**, *4*, 28−33.
[5] M. Menon, A. N. Andriotis, G. E. Froudakis, *Chem. Phys. Lett.* **2000**, *320*, 425−434.
[6] K. P. de Jong, *Curr. Opin. Solid State Mater. Sci.* **1999**, *4*, 55−62.
[7] N. M. Rodriguez, M. Kim, R. T. K. Baker, *J. Phys. Chem.* **1994**, *98*, 13108−13111.
[8] [8a] F. Salman, C. Park, R. T. K. Baker, *Catal. Today* **1999**, *53*, 385−394. [8b] C. Park, R. T. K. Baker, *J. Phys. Chem. B* **1998**, *102*, 5168−5177.
[9] [9a] C. Pham-Huu, N. Keller, L. J. Charbonnière, R. Ziessel, M. J. Ledoux, *Chem. Commun.* **2000**, 1871−1872. [9b] C. Pham-Huu, N. Keller, G. Erhet, L. J. Charbonnière, R. Ziessel, M. J. Ledoux, *J. Mol. Cat.* **2001**, *170*, 155−163.
[10] R. Gao, C. D. Tan, R. T. K. Baker, *Catal. Today* **2001**, *65*, 19−29.
[11] P. Chen, X. Wu, J. Lin, K. L. Tan, *J. Phys. Chem.* **1999**, *103*, 4559−4561.
[12] J. M. Planeix, N. Coustel, B. Coq, V. Brotons, P. S. Kumbhar, R. Dutartre, P. Geneste, P. Bernier, P. M. Ajayan, *J. Am. Chem. Soc.* **1994**, *116*, 7935−7936.
[13] H. Chen, J. Lin, Y. Cai, X. Wang, J. Yi, J. Wang, G. Wei, Y. Lin, D. Liao, *Appl. Surf. Sci.* **2001**, *180*, 328−335.
[14] B. Xue, P. Chen, Q. Hong, J. Lin, K. L. Tan, *J. Mater. Chem.* **2001**, *11*, 2378−2381.
[15] Y. Zhang, H. Zhang, G. Lin, P. Chen, Y. Yuan, K. R. Tsai, *Appl. Cat. A* **1999**, *187*, 213−234.
[16] N. M. Rodriguez, *J. Mater. Res.* **1993**, *8*, 3233−3255.
[17] [17a] S. Nagasawa, M. Yudasaka, K. Hirahara, T. Ichihashi, S. Iijima, *Chem. Phys. Lett.* **2000**, *328*, 374−380. [17b] A. Kuznetsova, I. Popova, J. T. Yates, Jr, M. J. Bronikowski, C. B. Huffman, J. Lin, R. E. Smalley, H. H. Hwu, J. G. Cheu, *J. Am. Chem. Soc.* **2001**, *123*, 10699−10704. [17c] T. Kyotani, S. Nakozaki, W. Xu, A. Tamita, *Carbon* **2001**, *39*, 782−785.
[18] E. van Steen, F. F. Prinsloo, *Catal. Today* **2002**, *71*, 327−334.
[19] V. Lordi, N. Yao, J. Wei, *Chem. Mater.* **2001**, *13*, 733−737.
[20] T. W. Ebbesen, H. Hiura, M. E. Bisher, M. M. J. Treacy, J. L. Shreeve-Keyer, R. C. Haushalter, *Adv. Mater.* **1996**, *8*, 155−157.
[21] Z. Liu, Z. Yuan, W. Zhou, L. Peng, Z. Xu, *Phys. Chem. Chem. Phys.* **2001**, *3*, 2518−2521.
[22] S. Hermans, J. Sloan, D. S. Shephard, B. F. J. Johnson, M. L. H. Green, *Chem. Commun.* **2002**, 276−277.
[23] E. S. Steigerwalt, G. A. Deluga, C. M. Lukehart, *J. Phys. Chem.* **2002**, *106*, 760−766.

[24] B. L. Mojet, M. S. Hoogenraad, A. J. van Dillen, J. W. Geus, D. C. Koningsberger, *J. Chem. Soc., Faraday Trans.* **1997**, *3*, 4371−4375.
[25] W. Li, C. Liang, J. Qiu, W. Zhou, H. Han, Z. Wei, G. Sun, Q. Xin, *Carbon* **2002**, *40*, 791−794.
[26] S. Banerjee, S. S. Wong, *Nano Lett.* **2002**, *2*, 49−53.
[27] P. Serp, R. Feurer, C. Vahlas, P. Kalck, *French Patent* 01−08511, **2001**.
[28] Q. Yang, P. Hou, S. Bai, M. Wang, H. Cheng, *Chem. Phys. Lett.* **2001**, *345*, 18−24.
[29] P. Serp, R. Feurer, Y. Kihn, P. Kalck, J. L. Faria, J. L. Figueiredo, *J. Phys. IV* **2002**, *12*, 24−36.
[30] D. N. Lawson, G. Wilkinson, *J. Chem. Soc. A* **1965**, 1900−1907.
[31] J. L. Figueiredo, M. F. R. Pereira, M. M. A. Freites, J. J. M. Orfao, *Carbon* **1996**, *37*, 1379−1389.
[32] U. Zielke, K. J. Huttinger, W. P. Hoffman, *Carbon* **1996**, *34*, 983−998.
[33] A. Kazusaka, H. Suzuki, I. Toyoshima, *J. Chem. Soc., Chem. Commun.* **1983**, 150−151.
[34] T. A. Kainulainen, M. K. Niemelä, A. O. I. Krause, *J. Mol. Cat.* **1997**, *122*, 39−49.
[35] P. Serp, R. Feurer, C. Vahlas, P. Kalck, *French Patent* 01−13233, **2001**.
[36] P. Serp, R. Feurer, R. Morancho, P. Kalck, *J. Catal.* **1995**, *157*, 294−300.
[37] N. Pierard, A. Fonseca, Z. Konya, I. Willems, G. Van Tendeloo, J. B. Nagy, *Chem. Phys. Lett.* **2001**, *335*, 1−8.

Received June 19, 2002
[I02335]

Syntheses, Crystal Structures, and Properties of Four Two-Dimensional Network Complexes with Multidentate Bis(Schiff Base) Ligands

Xing-Mei Ouyang,[a] Bao-Li Fei,[a] Taka-aki Okamura,[b] Hong-Wei Bu,[a] Wei-Yin Sun,*[a] Wen-Xia Tang,[a] and Norikazu Ueyama[b]

Keywords: Schiff bases / Silver / Cobalt / Crystal engineering

Four novel two-dimensional coordination polymers $[Ag_2(L1)_2](CF_3SO_3)_2{\cdot}H_2O$ (**1**), $[Ag_3(L1)_2](NO_3)_3{\cdot}H_2O$ (**2**), $[Co(L1)_2(SCN)_2]{\cdot}EtOH$ (**3**), and $[Co(L2)_2(SCN)_2]$ (**4**) were obtained by reactions of the bis(Schiff base) ligand 1,2-bis(4′-pyridylmethyleneamino)ethane (L1) with silver(I) trifluoromethanesulfonate, silver(I) nitrate, and cobalt(II) thiocyanate, and 1,2-bis(3′-pyridylmethyleneamino)ethane (L2) with cobalt(II) thiocyanate, respectively. In complex **1**, a 2D network structure was achieved by hydrogen bonding interactions between the two 1D chains, consisting of double-stranded helicates, through solvate water molecules. The 2D network of complex **2** was formed by the coordination to a two-coordinate silver(I) ion instead of hydrogen bonds as in complex **1**. Complex **3** contains molecular square units, which are occupied by disordered ethanol molecules. Complex **4** exhibits a classic square-grid network which is different from that of **3** due to the different terminal pyridyl groups in L1 (4-pyridyl) and L2 (3-pyridyl). These coordination polymers were characterized by X-ray crystallography, electrospray mass spectrometry, cyclic voltammetry and magnetic measurements. The results show a 2D network superstructural diversity by the fine-tuning of construction components.
(© Wiley-VCH Verlag GmbH & Co. KGaA, 69451 Weinheim, Germany, 2003)

Introduction

The construction of polymeric coordination complexes has developed rapidly in recent years owing to their structural topologies and interesting catalytic, electronic, magnetic and spectroscopic properties.[1] The "node-and-spacer" approach has been remarkably successful in constructing predictable network architectures, including zero-dimensional polyhedrons, and infinite one- (1D), two- (2D), and three-dimensional (3D) periodic nets.[2−7] In the case of 2D architectures, one would anticipate that the network would possess an inherent ability to include guest molecules. Square grid,[8] rectangular grid,[9] brick wall,[10] herringbone,[11] and bi-layer[12] networks have been reported and can be generated from commonly available metal moieties and linear "spacer" ligands. The square-grid is a simple and well-known 2D metal-organic network.[13] A series of square-grid networks has been obtained by the reaction of bipy spacer ligands with various transition metal ions such as Cd^{II}, Co^{II}, Ni^{II}, and Zn^{II}, with different crystal packing modes.[14] Other commonly used spacer ligands include cyano[15] and pyrazine moieties[16] and longer analogs of bipy.[17]

Although the node-and-spacer approach exerts significant effects on the construction of the network polymers, it can only successfully be applied to the self-assembly of rigid bidentate ligands and metal moieties. An assembly process containing multidentate ligands is usually very complicated and is influenced by various factors such as solvent system, templates, counterions, valences and the geometric needs of the metal ions and sometimes the ratio between the metal salt and the ligand.[18] Therefore it is still difficult at the present time to design and synthesize supermolecular architectures with predicted structures and properties when the number of donor atoms in the ligands is more than two.

To investigate the influence of the nature of multidentate ligands on the construction of 2D network polymers, the tetradentate bis(Schiff base) ligands 1,2-bis(4′-pyridyl)ethylenediamine (L1) and 1,2-bis(3′-pyridyl)ethylenediamine (L2; Scheme 1) − longer analogs of bipyridine − were em-

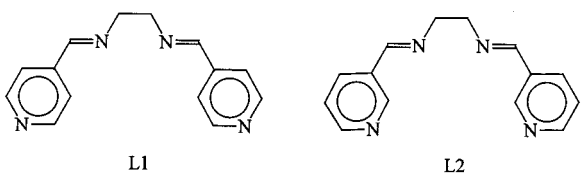

Scheme 1

[a] Coordination Chemistry Institute, State Key Laboratory of Coordination Chemistry, Nanjing University, Nanjing 210093, China
Fax: (internat.) + 86-25/3314502, /3317761
E-mail: sunwy@nju.edu.cn
[b] Department of Macromolecular Science, Graduate School of Science, Osaka University, Toyonaka, Osaka 560-0043, Japan
Supporting information for this article is available on the WWW under http://www.eurjic.org or from the author.

ployed as organic ligands. Self-assembly of these ligands with monovalent silver(I) and divalent cobalt(II) salts as the nodes was carried out.

Schiff bases are an important class of ligands in coordination chemistry and have been studied extensively[19] as they are selective and sensitive toward various metal ions. In our previous work we reported that the assembly of Schiff base ligand L1 with copper(I) salts produced two complexes $[Cu(L1)(CH_3CN)]NO_3$ and $[Cu(L1)(CH_3CN)]ClO_4$ with infinite zigzag chain-like structures;[20] two infinite 2D grid networks were obtained by assembly of reduced L1 ligand, 1,6-bis(4′-pyridyl)-2,5-diazahexane (L), with the same copper(I) salts.[22] This indicates the significant influence of the nature of the ligand on the construction of supramolecular architectures. In this paper, the reaction of L1 with silver(I) salts with different counteranions, is shown to produce two 2D coordination polymers $[Ag_2(L1)_2](CF_3SO_3)_2·H_2O$ (**1**) and $[Ag_3(L1)_2](NO_3)_3·H_2O$ (**2**) containing double-stranded helicates. In addition, the self-assembly of ligands L1 and L2 with $Co(SCN)_2$ produces two different 2D coordination complexes, $[Co(L1)_2](SCN)_2·EtOH$ (**3**) and $[Co(L2)_2](SCN)_2$ (**4**). These coordination complexes were characterized by X-ray crystal diffraction, electrospray mass spectrometry, cyclic voltammetry and magnetic measurements.

Results and Discussion

Crystal Structure Description

Complexes **1** and **2** have the same ligand and metal ion but different anions, while complexes **3** and **4** have different ligands. X-ray crystal structure analyses reveal that complexes **1**−**4** crystallize in different crystal systems with different symmetries, from triclinic to tetragonal. Details of the crystal parameters, data collection and refinement for complexes **1**−**4** are summarized in Table 4, and selected bond lengths and angles with their estimated standard deviations are listed in Table 1.

Table 1. Selected bond lengths [Å] and angles [°] for **1**−**4**

$[Ag_2(L1)_2](CF_3SO_3)_2·H_2O$ (**1**)			
Ag(1)−N(1)	2.337(2)	Ag(1)−N(3)	2.328(2)
Ag(1)−N(2)	2.405(2)	Ag(1)−N(4)	2.387(2)
Ag(2)−N(11)	2.176(2)	Ag(2)−N(31)	2.185(2)
N(1)−Ag(1)−N(2)	75.77(8)	N(2)−Ag(1)−N(3)	125.17(8)
N(1)−Ag(1)−N(3)	135.86(8)	N(2)−Ag(1)−N(4)	129.37(8)
N(1)−Ag(1)−N(4)	125.21(8)	N(3)−Ag(1)−N(4)	74.68(8)
N(11)−Ag(2)−N(31)	171.42(9)		
$[Ag_3(L1)_2](NO_3)_3·H_2O$ (**2**)			
Ag(1)−N(31)	2.331(4)	Ag(1)−N(21)	2.346(3)
Ag(1)−N(41)	2.402(4)	Ag(1)−N(11)	2.407(3)
Ag(2)−N(12)	2.154(4)	Ag(2)−N(42)	2.155(4)
Ag(3)−N(32)	2.147(4)	Ag(3)−N(22)	2.152(4)
N(31)−Ag(1)−N(21)	138.71(13)	N(31)−Ag(1)−N(41)	74.92(12)
N(21)−Ag(1)−N(41)	122.40(12)	N(31)−Ag(1)−N(11)	128.74(12)
N(21)−Ag(1)−N(11)	73.90(11)	N(41)−Ag(1)−N(11)	127.04(13)
N(12)−Ag(2)−N(42)	167.50(17)	N(32)−Ag(3)−N(22)	177.56(18)
$[Co(L1)_2](SCN)_2·EtOH$ (**3**)			
Co(1)−N(1)	2.096(3)	Co(1)−N(2)	2.098(3)
Co(1)−N(12)	2.188(3)	Co(1)−N(22)	2.191(3)
Co(1)−N(32)	2.171(3)	Co(1)−N(42)	2.159(3)
N(1)−Co(1)−N(2)	176.47(12)	N(1)−Co(1)−N(42)	92.43(11)
N(1)−Co(1)−N(32)	91.18(12)	N(1)−Co(1)−N(22)	87.63(11)
N(1)−Co(1)−N(12)	89.13(11)	N(12)−Co(1)−N(22)	89.56(10)
N(42)−Co(1)−N(22)	91.93(10)	N(42)−Co(1)−N(32)	86.54(10)
N(42)−Co(1)−N(12)	177.89(11)	N(32)−Co(1)−N(22)	178.02(10)
N(12)−Co(1)−N(32)	92.01(11)		
$[Co(L2)_2](SCN)_2$ (**4**)			
Co(1)−N(1)	2.051(4)	Co(1)−N(2)	2.053(5)
Co(1)−N(12)	2.1791(15)		
N(1)−Co(1)−N(2)	180.0	N(1)−Co(1)−N(12)	89.92(6)
N(12)−Co(1)−N(12B)	90.0		

Crystallographic analysis indicates that the asymmetric unit of complex **1** consists of two silver(I) ions, two L1 ligands, two $CF_3SO_3^-$ anions and one water molecule, as shown in Figure 1. It is interesting that the Ag^I atoms have two different coordination environments, which is not com-

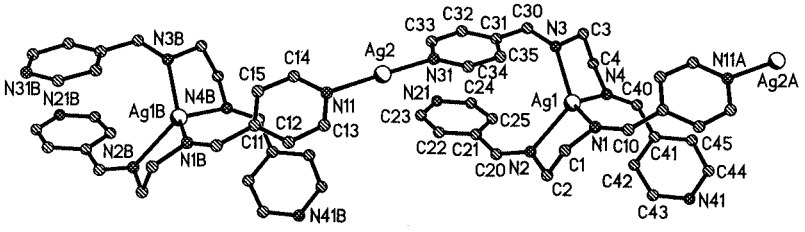

Figure 1. 1D chain structure of $[Ag_2(L1)_2](CF_3SO_3)_2·H_2O$ (**1**) with atom numbering scheme; anions, water molecules, and hydrogen atoms have been omitted for clarity

mon in metal complexes with open-chain bis(Schiff base) ligands. In the previously reported silver(I) complex with a flexible reduced bis(Schiff base) ligand, 1,7-bis(4′-pyridyl)-2,6-diazaheptane, the 2D brick-wall network consists of trigonal and linear silver(I) ions.[21] In complex **1**, four imine N atoms from two different L1 ligands bind to the Ag(1) atom to form a double-stranded helicate. The coordination geometry of the four-coordinate Ag(1) is distorted tetrahedral with N−Ag(1)−N coordination angles ranging from 74.68(8) to 135.86(8)° and an average Ag(1)−N bond length of 2.364(2) Å (Table 1). Similar Ag−N bond lengths have been reported for silver(I) complexes with the same AgN_4 binding site, for example $[Ag(L)]NO_3$ has an average Ag−N bond length of 2.360(3) Å.[22] The double-stranded helicates are further linked to the Ag(2) atom through the coordination of two pyridine N(11) and N(31) atoms, as illustrated in Figure 1. The N(31)−Ag(2)−N(11) angle of 171.42(9)° indicates that the Ag(2) has an almost linear coordination geometry with bond lengths of 2.176(2) and 2.185(2) Å. Therefore, each Ag(1) atom in **1** is coordinated by two different L1 ligands and, in turn, each L1 ligand connects two Ag^I ions. Such a coordination mode generates an infinite chain-like structure (Figure 1). The intermetallic distance between Ag(1) and Ag(2) is 7.39 Å. It has been reported that the bis(Schiff base) ligand obtained from pyridine-2-carbaldehye and 1,2-ethanediamine forms a dinuclear double-stranded helical complex with silver(I) tetrafluoroborate.[23,24] This helical complex shows remarkable differences to ours with respect to the coordination mode, as shown schematically in Scheme 2.

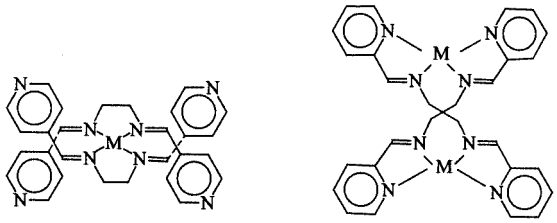

Scheme 2

It is noteworthy that one pyridine unit of each L1 ligand remains uncoordinated in complex **1**. This means that the N_4 donor ligand L1 actually serves as a tridentate ligand when it reacts with silver(I) trifluoromethanesulfonate. A similar phenomenon has been observed in the complex $[Cu(L1)(CH_3CN)]NO_3$ with a zigzag chain-like structure.[20] In this complex, one pyridine unit of the L1 ligand is also free from coordination; instead, one acetonitrile molecule coordinates to the copper center to complete the coordination sphere of the copper(I) ion.[20] The uncoordinated pyridine N atom in complex **1** forms an O−H···N hydrogen bond with a solvate water molecule. Each water molecule forms two such O−H···N hydrogen bonds between the two adjacent chains and links the 1D chains to give a 2D network structure as shown in Figure 2. The $CF_3SO_3^-$ anions located at the vacancy of the 2D network form four C−H···O hydrogen bonds. Each cavity contains two $CF_3SO_3^-$ anions. The hydrogen bonding data are summarized in Table 2.

When the self-assembly of ligand L1 with silver(I) nitrate was carried out under the same conditions as **1**, coordination polymer **2** with a similar 2D network structure was obtained. However, the asymmetric unit of complex **2** contains three Ag^I ions (rather than two as in **1**), two L1 ligands, three NO_3^- anions and one water molecule, as shown in Figure 3. The most important difference between **1** and **2** is that the four N atoms of the L1 ligand all participate in the coordination with silver(I) ions in complex **2**, while in **1** only three of the four N atoms coordinate to Ag (vide supra). The four-coordinate Ag(1) has a distorted tetrahedral geometry with coordination angles ranging from 73.90(11) to 138.71(13)° while Ag(2) [N(12)−Ag(2)−N(42) = 167.50(17)°] and Ag(3) [N(32)−Ag(3)−N(22) = 177.56(18)°] are both two-coordinate with an almost linear geometry in complex **2**. As illustrated in Figure 4, the 1D chains containing double-stranded helicates in **2** are connected by the coordination bonds of two-coordinate silver(I) ions with two pyridine ring N donors from two adjacent chains − instead of O−H···N hydrogen bonds as in complex **1** − into a 2D network structure. The NO_3^- anions located at the voids of the network form nine C−H···O hydrogen bonds as listed in Table 2. Each cavity contains three NO_3^- anions with the solvate water molecules located in the cavity between the two layers.

The different linkage mode from 1D chains to 2D network for complexes **1** and **2** may be explained by the different sizes of the $CF_3SO_3^-$ and NO_3^- anions which occupy the vacancies of the 2D network i.e. the size of the anion controls the vacancy size of the 2D networks. In the case of **1** (with the larger $CF_3SO_3^-$ anion) the vacancy has an Ag(2A)−Ag(2B) distance of 14.98 Å and an O(7A)−O(7B) distance of 14.36 Å (Figure 2), while in the case of **2** with the smaller NO_3^- anion, the corresponding distances are Ag(2)−Ag(2A) = Ag(3)−Ag(3B) = 14.09 Å (Figure 4). The distance between two pyridine N atoms [e.g. N(21B) and N(41A) in Figure 2] linked by one water molecule in complex **1** is 5.22 Å, which is longer than the distance of 4.29 Å between two pyridine N atoms [e.g. N(12) and N(42), N(22) and N(32) in Figure 4] coordinated by the two-coordinate silver(I) ion in complex **2**. This result shows that the counteranions have a large effect on the formation of network structures.

The Schiff-base ligand L1 and its reduced form L react with silver(I) nitrate to form the 2D network complex **2** and the 1D hinged-chain complex $[Ag(L)]NO_3$,[22] respectively. It is interesting that each ligand L1 in **2** has a "C" shape while the shape of L in $[Ag(L)]NO_3$ is "Z" due to the flexibility of the ligands. In addition, the imine N atoms and pyridyl N atoms are coordinated to four-coordinate and two-coordinate silver(I) ions, respectively, in **2** while in the case of $[Ag(L)]NO_3$, each silver(I) ion is coordinated by two

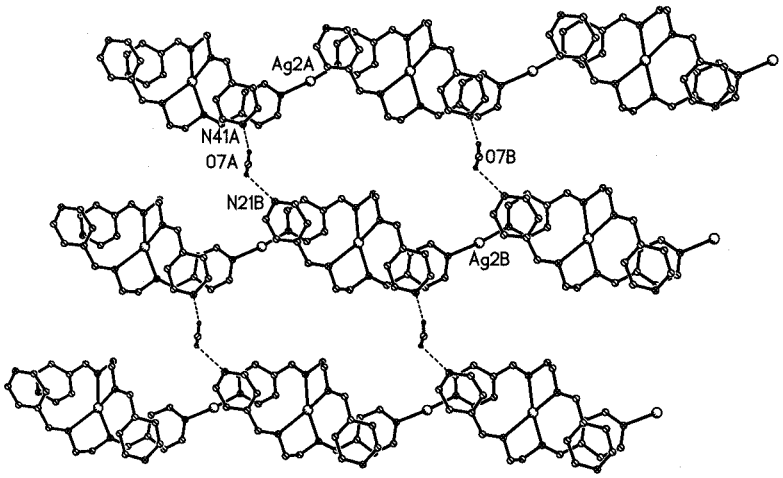

Figure 2. Formation of the 2D network structure of $[Ag_2(L1)_2](CF_3SO_3)_2 \cdot H_2O$ (**1**) from 1D chains linked by O−H···N hydrogen bonds

Table 2. Hydrogen bonds data for the complexes **1**−**3**

D−H···A	Distance of D···A [Å]	Angle of D−H−A [°]
$[Ag_2(L1)_2](CF_3SO_3)_2 \cdot H_2O$ (**1**)		
O(7)−H(29)···N(21)[a]	2.898(7)	113
O(7)−H(30)···N(41)[b]	3.005(7)	161
C(3)−H(5)···O(5)[c]	3.203(4)	125
C(10)−H(9)···O(4)[d]	3.293(4)	152
C(14)−H(12)···O(6)[e]	3.247(4)	130
C(33)−H(21)···O(6)[e]	3.207(4)	139
$[Ag_3(L1)_2](NO_3)_3 \cdot H_2O$ (**2**)		
C(4)−H(7)···O(12)	3.354(9)	137
C(10)−H(9)···O(11)[f]	3.249(7)	141
C(12)−H(10)···O(11)[f]	3.212(7)	130
C(12)−H(10)···O(21)[g]	3.281(6)	132
C(13)−H(11)···O(41)[h]	3.420(11)	154
C(14)−H(12)···O(12)	3.380(7)	161
C(14)−H(12)···O(13)	3.074(7)	124
C(23)−H(16)···O(22)	3.333(8)	171
C(44)−H(27)···O(13)	3.277(8)	137
$[Co(L1)_2](SCN)_2 \cdot EtOH$ (**3**)		
O(1)−H(39)···S(2)	3.480(9)	151
O(2)−H(40)···S(2)[i]	3.421(13)	170
C(13)−H(11)···N(2)	3.146(5)	115
C(23)−H(16)···O(1)	3.110(10)	136
C(23)−H(16)···O(1)[j]	3.415(10)	148
C(25)−H(18)···N(41)[k]	3.482(5)	151
C(44)−H(27)···N(21)[i]	3.325(5)	133

[a] Equivalent atoms generated by $2 - x, 1 - y, 1 - z$. [b] Equivalent atoms generated by $1 - x, 1 - y, -z$. [c] Equivalent atoms generated by $1 + x, y, -1 + z$. [d] Equivalent atoms generated by $x, y, -1 + z$. [e] Equivalent atoms generated by $1 + x, y, z$. [f] Equivalent atoms generated by $x, 1 + y, z$. [g] Equivalent atoms generated by $0.5 + x, 0.5 + y, z$. [h] Equivalent atoms generated by $x, 1 - y, -0.5 + z$. [i] Equivalent atoms generated by $1 - x, -y, z$. [j] Equivalent atoms generated by $1 - x, 1 - y, z$. [k] Equivalent atoms generated by $x, 1 - y, 0.5 + z$.

amine N atoms and two pyridyl N atoms from three different L ligands.[22] This suggests that a subtle change in the organic ligand may cause a large change in the assembly products.

In contrast to monovalent metal ions like Cu^I and Ag^I, which require a tetrahedral or linear coordination geometry, a divalent metal ion such as Co^{II} is usually six-coordinate with an octahedral geometry. After several attempts at reactions between the L1 ligand and Co^{II} salts with different anions, we succeeded in the isolation of a complex with the SCN^- anion, $[Co(L1)_2(SCN)_2] \cdot EtOH$ (**3**). The repeat unit of complex **3** is shown in Figure 5. The coordination sphere of the cobalt(II) ion is defined by four pyridine N donors of four different L1 ligands situated in the equatorial plane and two N donors of SCN^- anions at the axial positions, leading to a slightly distorted octahedral coordination environment. The two linear SCN^- anions are not perpendicular to the equatorial plane and the C(2)−N(2)−Co(1) and C(1)−N(1)−Co(1) angles are 147.3(3) and 161.2(3)°, respectively. The four equatorial Co−N bond lengths range from 2.159(3) to 2.191(3) Å and are longer than those of the two axial Co−N bonds [2.096(3) and 2.098(3) Å] (Table 1). Similar bond lengths and angles have been observed in a Co^{II} complex with the tetradentate Schiff-base ligand 1,3-bis(pyridine-2-carboxaldiamino)propane.[25] Surprisingly, the L1 ligand in **3** serves as a bidentate, not a tetradentate, ligand and connects two Co^{II} ions; the N atoms of the imine group do not participate in the coordination to the Co^{II} ion, as shown in Figure 6. The structure of complex **3** consists of many square units interconnected through L1 bridges into a 2D network. Each square unit is composed of two L1 spacers and two cobalt(II) ions and its cavity is occupied by a disordered ethanol molecule (Figure 6). It is obvious that the sheets of **2** have a corrugated and wavy network structure and are linked by C−H···N hydrogen bonds [Figure S1 (for Supporting Information see footnote on the first page of this article) and Table 2]. The disordered ethanol molecules are disposed between the layers by (ethanol) O−H···S and C−H···O (ethanol) hydrogen bonds (Table 2). Similar to the

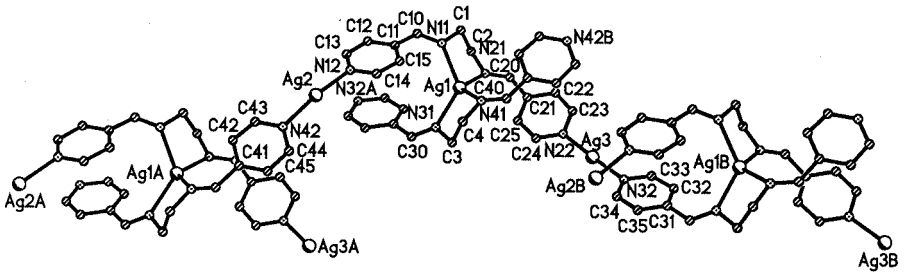

Figure 3. Coordination environment around the silver(I) ions in $[Ag_3(L1)_2](NO_3)_3 \cdot H_2O$ (**2**) with atom numbering scheme, anions, water molecules, and hydrogen atoms have been omitted for clarity

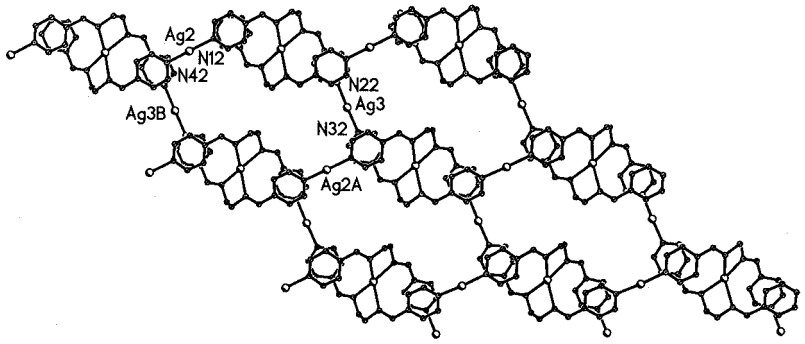

Figure 4. 2D network structure of $[Ag_3(L1)_2](NO_3)_3 \cdot H_2O$ (**2**) formed by coordination bonds

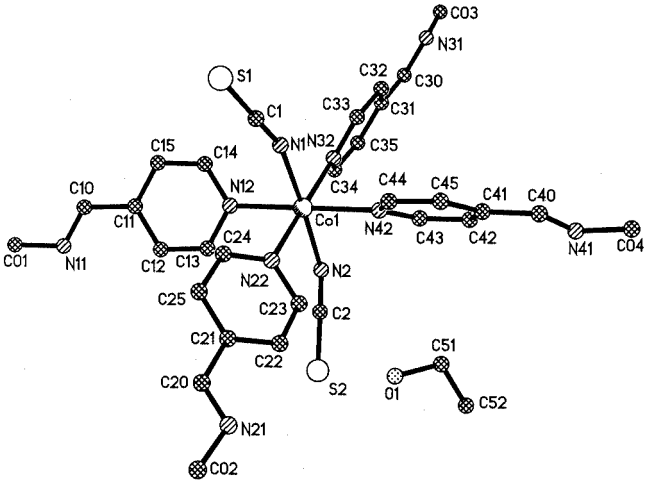

Figure 5. Asymmetric unit structure of complex $[Co(L1)_2](SCN)_2 \cdot EtOH$ (**3**); hydrogen atoms have been omitted for clarity

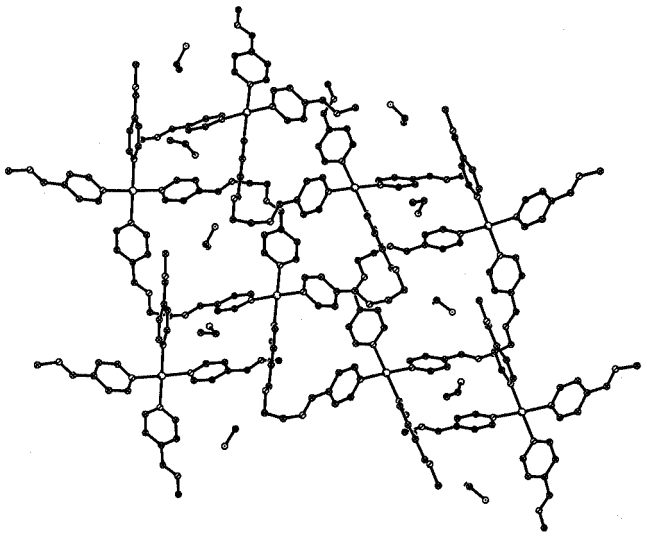

Figure 6. 2D network structure of the complex $[Co(L1)_2(SCN)_2] \cdot EtOH$ (**3**) with ethanol molecules filled in the vacancy of 2D sheet; SCN^- ions have been omitted for clarity

extended analog of bipyridine, a metal-organic framework with larger cavity was constructed by reaction of the ligand L1 with the metal moiety.

In order to compare the structures of complexes obtained by reactions of $Co(SCN)_2$ with different ligands L1 and L2, a crystallographic analysis was carried out for complex **4**. It can be seen from Figure 7 that the coordination mode around the Co^{II} ion in complex **4** is similar to that in complex **3** (Figure 5); the N atoms of the imine groups also remain uncoordinated as in complex **3**. However, two SCN^- anions and the Co^{II} ion are in a line, i.e. the SCN^- anions are perpendicular to the equatorial plane in **4**. In addition, each Co^{II} ion is bridged by four L2 ligands to four adjacent Co^{II} centers, resulting in an infinite 2D square grid with dimensions of 11.34 × 11.34 Å (Figure 8, a), near to the value of 11 Å observed in the 1D ladder complex

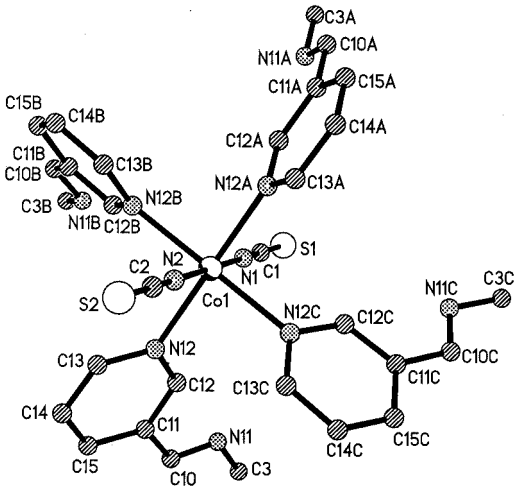

Figure 7. Coordination environment around the Co^{II} ion in the complex $[Co(L2)_2](SCN)_2$ (**4**) with atom numbering scheme; hydrogen atoms have been omitted for clarity

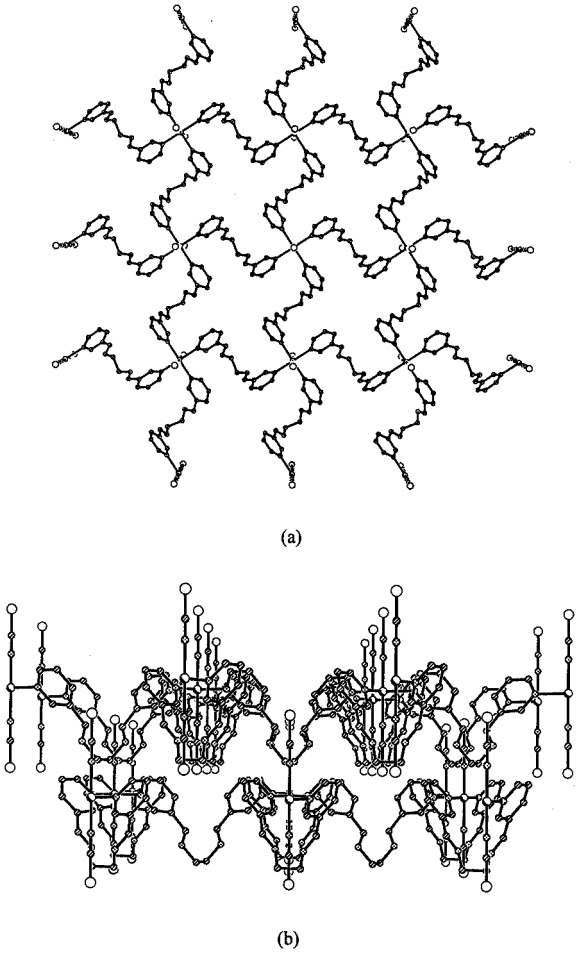

Figure 8. (a) Square-grid network of complex **4**; (b) packing diagram of two sheets in **4**

$[Co(bpy)_{1.5}(NO_3)_2]$.[26] The crystal packing diagram of **4**, shown in Figure 8, b, reveals that the 2D sheets repeat in an ---ABAB--- stacking sequence, with the Co atom of one layer located above the center of the grid of the adjacent layer. As a result, there is no open channel and no solvate molecules are found in complex **4**. Ligand L2 is different from L1 as it contains a 3-pyridyl group instead of a 4-pyridyl group and this change results in a completely different metal-organic framework. These results again demonstrate that the nature of the organic ligand plays an important role in the construction of supramolecular architectures.

Properties

Electrospray mass spectrometry (ES-MS) has recently been proved to be a powerful technique in the characterization of assemblies.[27] However, there are few reports on the application of ES-MS to self-assembled coordination polymers. Using this technique our group has successfully characterized coordination polymers and observed cationic mono-, di-, tri-, and tetranuclear metal species under ES-MS conditions.[22,28] Complexes **1**−**4** were also investigated by ES-MS and the spectroscopic data are summarized in Table 3. The ES-MS spectrum of the 2D coordination polymer **1** in acetonitrile solution is shown in Figure 9, a and gives a clear picture of the different species formed. Four main peaks at m/z = 345.2, 376.7, 583.0, and 615.0 are observed corresponding to the mononuclear species $[Ag(L1)]^+$ $[Ag(L1) + CH_3OH]^+$, $[Ag(L1)_2]^+$, and $[Ag(L1)_2 + CH_3OH]^+$ (methanol was used as the mobile phase), respectively. The other four peaks at 840.7, 872.9, 904.7, and 1162.5 originate from the dinuclear species (Table 3). All these assignments were confirmed by good agreement between the observed and calculated isotopic distributions. Figure 9, b shows a typical example of a comparison between the experimental and calculated isotope distributions for the peak at m/z = 872.9, corresponding to the dinuclear species $[Ag_2(L1)_2(CF_3SO_3) + CH_3OH]^+$. The observation of cationic species in the ES-MS spectrum confirms the coordination of L1 to the Ag^I atom under the ES-MS experimental conditions. Similar mono- and dinuclear species were also observed in the complexes **2**−**4** (Table 3). Observation of a peak at m/z = 715.9, corresponding to the $[Co(L1)_2H(SCN)_2 + C_2H_5OH + H_2O]^+$ species, confirms the presence of an ethanol molecule in complex **3**.

The complexes were further investigated by electrochemistry. The cyclic voltammograms for $[Co(L1)_2(SCN)_2]$·EtOH (**3**) and $[Co(L2)_2(SCN)_2]$ (**4**) are shown in Figure 10. It can be seen that the cobalt(II) complexes exhibit similar electrochemical behavior in the positive potential region. Irreversible anodic peaks were observed at +0.76 V for complex **3** and at +0.80 V for complex **4** vs. Ag/AgCl in acetonitrile. The known (Schiff base)cobalt complexes $[Co(DSALPTP)]_2[CoCl_4]$ [H_2DSALPTP = 1,3-bis(*o*-salicylaldiminophenylthio)propane] and [CoSalmbfn] [Salmbfn = bis(salicylaldehyde)methylene-*p*,*p*′-diphenylene] showed a similar irreversible oxidation of Co^{II} to Co^{III} at 0.75 and 0.80 V vs. Ag/AgCl, respectively.[29−31] The more positive oxidation potential of

Table 3. ES-MS data for complexes **1**−**4**

m/z	Assignment	*m/z*	Assignment
1		**2**	
239.3	$[(L1)H]^+$	239.2	$[(L1)H]^+$
271.2	$[(L1)H+CH_3OH]^+$	271.2	$[(L1)H+CH_3OH]^+$
345.2	$[Ag(L1)]^+$	345.2	$[Ag(L1)]^+$
376.7	$[Ag(L1)+CH_3OH]^+$	566.9	$[Ag_2(L1)(NO_3)+CH_3OH+H_2O]^+$
583.0	$[Ag(L1)_2]^+$	583.0	$[Ag(L1)_2]^+$
615.0	$[Ag(L1)_2+CH_3OH]^+$	615.0	$[Ag(L1)_2+CH_3OH]^+$
840.7	$[Ag_2(L1)_2(CF_3SO_3)]^+$	753.8	$[Ag_2(L1)_2(NO_3)]^+$
872.9	$[Ag_2(L1)_2(CF_3SO_3)+CH_3OH]^+$	785.8	$[Ag_2(L1)_2(NO_3)+CH_3OH]^+$
904.7	$[Ag_2(L1)_2(CF_3SO_3)+2CH_3OH]^+$	818.0	$[Ag_2(L1)_2(NO_3)+2CH_3OH]^+$
1162.5	$[Ag_2(L1)_2(CF_3SO_3)+2CH_3OH+H_2O]^+$		
3		**4**	
239.2	$[(L1)H]^+$	239.3	$[(L2)H]^+$
271.1	$[(L1)H+CH_3OH]^+$	271.2	$[(L2)H+CH_3OH]^+$
386.9	$[Co(L1)SCN+ CH_3OH]^+$	332.7	$[Co_3(L2)(SCN)_4+ H_2O]^{2+}$
562.9	$[Co_2(L1)(SCN)_3 +CH_3OH]^+$	386.9	$[Co(L2)SCN+ CH_3OH]^+$
593.0	$[Co(L1)_2SCN]^+$	579.0	$[Co_2(L2)(SCN)_3+CH_3OH+H_2O]^+$
625.0	$[Co(L1)_2SCN +CH_3OH]^+$	691.9	$[Co(L2)_2H(SCN)_2+CH_3CN]^+$
651.8	$[Co(L1)_2H(SCN)_2]^+$		
684.0	$[Co(L1)_2H(SCN)_2+CH_3OH]^+$		
715.9	$[Co(L1)_2H(SCN)_2 + C_2H_5OH + H_2O]^+$		
768.0	$[Co_2(L1)_2(SCN)_3]^+$		

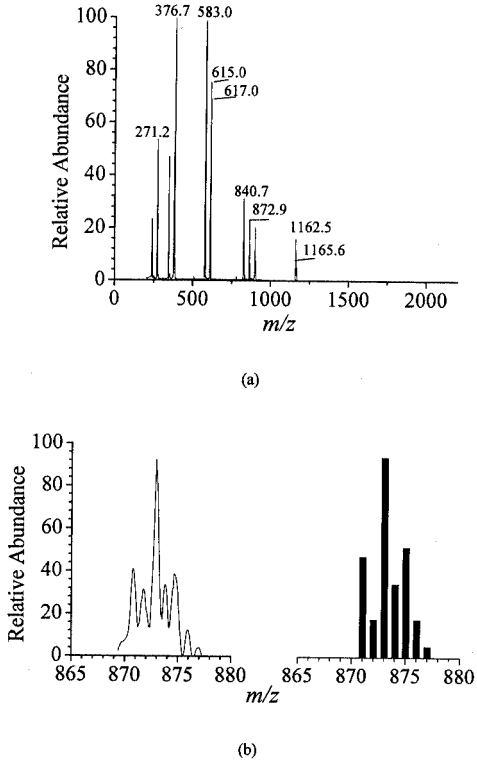

Figure 9. (a) ES mass spectrum of $[Ag_2(L1)_2](CF_3SO_3)_2·H_2O$ (**1**) in acetonitrile solution; (b) observed (traces) and calculated (bars) isotopic distributions for the peak at *m/z* = 872.9

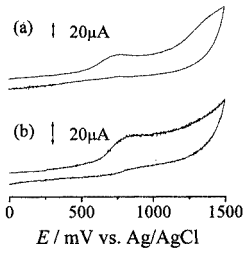

Figure 10. Cyclic voltammograms in acetonitrile with 0.1 M Bu_4NClO_4 as supporting electrolyte: (a) $[Co(L1)_2(SCN)_2]·EtOH$ (**3**); (b) $[Co(L2)_2(SCN)_2]$ (**4**); scan rate = 100 mV/s

complex **4** implies that it is more difficult to oxidize than complex **3** under the electrochemical conditions.

The temperature dependence of the magnetic susceptibility of complexes **3** and **4** was measured in the temperature range 75−300 K. It was found that the effective magnetic moment values for **3** and **4** were 5.05 μ_B and 4.85 μ_B ($\mu_B \approx 9.27\cdot10^{-24}$ J·T^{-1}), respectively, at 300 K. These values are within the expected range (4.3−5.2 μ_B) for isolated d^7 high-spin, six-coordinate Co^{II} complexes.[32] Upon lowering the temperature, the effective magnetic moment gradually decreased to 4.32 μ_B for **3** and 4.20 μ_B for **4**. These results indicate that there are only weak antiferromagnetic interactions between the metal centers due to the large Co···Co separations revealed by the crystal structures.

Table 4. Crystallographic data for complexes **1**−**4**

Complex	**1**	**2**	**3**	**4**
Empirical formula	$C_{30}H_{30}Ag_2F_6N_8O_7S_2$	$C_{28}H_{30}Ag_3N_{11}O_{10}$	$C_{32}H_{34}N_{10}CoOS_{.2}$	$C_{30}H_{28}N_{10}CoS_{.2}$
Molecular weight	1008.48	1004.24	697.74	651.67
Crystal system	triclinic	monoclinic	orthorhombic	tetragonal
Space group	$P\bar{1}$	Cc	*Iba*2	*I*4
a [Å]	11.0577(4)	26.2730(13)	29.5151(8)	11.3350(9)
b [Å]	13.9358(12)	10.1924(3)	12.5454(3)	11.3350(9)
c [Å]	14.3642(10)	14.3278(8)	18.8052(5)	13.0035(7)
α [°]	99.538(3)			
β [°]	109.125(3)	119.5780(10)		
γ [°]	108.798(2)			
V [Å^3]	1886.5(2)	3336.8(3)	6963.2(3)	1670.7(2)
Z	2	4	8	2
$D_{calcd.}$ [g·cm^{-3}]	1.775	1.999	1.331	1.295
μ [mm^{-1}]	1.234	1.817	0.654	0.674
Reflections collected	13716	15008	33548	7535
Independent reflections	8564	6516	7983	1915
R_{int}	0.0241	0.0303	0.0746	0.0738
Obsd. reflections [$I > 2\sigma(I)$]	6482	6201	6466	1750
Parameters refined	502	502	432	103
R (obsd. data)	0.0334	0.0314	0.0549	0.0378
wR (obsd. data)	0.0837[a]	0.0802[b]	0.1002[c]	0.0851[d]
Goodness of fit	1.083	1.043	1.030	1.028
Residuals [e·Å^{-3}]	0.602; −0.721	0.853; −0.691	0.375; −0.321	0.317; −0.238

[a] $\omega = 1/[\sigma^2(F_o)^2 + (0.0478P)^2]$, where $P = (F_o^2 + 2F_c^2)/3$. [b] $\omega = 1/[\sigma^2(F_o)^2 + (0.0537P)^2 + 3.4468P]$, where $P = (F_o^2 + 2F_c^2)/3$. [c] $\omega = 1/[\sigma^2(F_o)^2 + (0.0483P)^2 + 5.7779P]$, where $P = (F_o^2 + 2F_c^2)/3$. [d] $\omega = 1/[\sigma^2(F_o)^2 + (0.0524P)^2]$, where $P = (F_o^2 + 2F_c^2)/3$.

Conclusion

From the structure analysis of 2D networks **1** and **2**, it has been found that the anions play a key role in the construction of coordination polymers. In complex **1**, the large $CF_3SO_3^-$ anion lengthens the distances between the 1D chains, so that the formation of 2D network depends on the O−H···N hydrogen bonds formed between the chains and solvate water molecules. In complex **2**, with the small nitrate anion, a 2D structure is obtained by the coordination interactions between two-coordinate silver(I) ions and 1D chains. In addition variation of the terminal coordination group from 4-pydriyl to 3-pyridyl generates two completely different polymers **3** and **4**. These results indicate that a small change in the organic ligand has a significant effect on the self-assembly products.

The present study shows that the multidentate Schiff-base ligands L1 and L2 can offer a different number of N donors according to the coordination requirement of different transition metal ions. The ligand L1 is tridentate in complex **1** and tetradentate in complex **2**, while in the case of complexes **3** and **4**, both L1 and L2 act as bidentate ligands. This also suggests the complexity of multidentate ligands in the self-assembly process with metal salts.

Experimental Section

General: All commercially available chemicals were of reagent grade and used as received without further purification. L1 was prepared by a method reported previously.[20] Solvents were purified according to standard methods. Samples for C, H, N analyses were dried under vacuum and the analyses were performed with a Perkin−Elmer 240C elemental analyzer at the analysis center of Nanjing University. ^{1}H NMR spectra were measured with a Bruker DRX500 MHz NMR spectrometer at room temperature. Electrospray MS measurements were carried out with an LCQ System (Finnigan MAT, USA) using methanol as mobile phase. Variable-temperature magnetic susceptibilities (75−300 K) of complexes **3** and **4** were measured with a CHAN-2000 Faraday magnetometer. A diamagnetic correction was made with Pascal's constants for all the constituent atoms, and the magnetic moments were calculated by the equation $\mu_{eff} = 2.828(\chi_m)^{1/2}$. Cyclic voltammograms (CVs) were recorded with an EG&G M273 potentiostat/galvanostat system using a platinum working electrode, a platinum wire counter electrode and an Ag/AgCl reference electrode. The CV measurements were carried out in acetonitrile solution containing 0.1 M tetrabutylammonium perchlorate as supporting electrolyte at a scan rate of 100 mV·s^{-1}. Ferrocene was added at the end of the experiment and used as an internal reference.

Preparation of 1,2-Bis(3′-pyridylmethyleneamino)ethane (L2): 1,2-Ethanediamine (0.53 mL, 7.9 mmol) was dissolved in refluxing absolute methanol (30 mL) and pyridine-3-carbaldehyde (1.42 mL, 15.0 mmol) in absolute methanol (30 mL) was added slowly to give a clear yellowish solution. The mixture was refluxed for 3 h and stirred overnight at ambient temperature. The solvents were evaporated to give a yellow solid under reduced pressure. White needle-shaped crystals were obtained by recrystallization of the residue from methanol and deionized water. After washing with diethyl ether and drying under vacuum, 1.52 g of L2 was obtained with a yield of 85%. ES-MS: $m/z = 239.1$ [L2 + H]$^+$. $C_{14}H_{14}N_4$ (238.29): calcd. C 70.56, H 5.92, N 23.51; found C 70.39, H 5.81, N 23.75.

Synthesis of $[Ag_2(L1)_2](CF_3SO_3)_2·H_2O$ (1): All procedures for synthesis and recrystallization were carried out in the dark. A deionized aqueous solution (5 mL) of CF_3SO_3Ag (12.8 mg, 0.05 mmol)

was added dropwise to a stirred solution of L1 (11.9 mg, 0.05 mmol) in acetonitrile (5 mL) at room temperature. After filtration, the clear filtrate was allowed to stand at 5 °C for several days, and colorless crystals were collected (14.1 mg, 56%). Single crystals suitable for X-ray diffraction analysis were obtained by slow concentration of the filtrate at 5 °C. ^{1}H NMR (D_2O, 25 °C): δ = 3.98 (s, 4 H), 5.97 (s, 2 H), 7.81 (d, 4 H), 8.73 (d, 4 H) ppm. $C_{30}H_{30}Ag_2F_6N_8O_7S_2$ (1008.48): calcd. C 35.73, H 3.00, N 11.11; found C 35.77, H 3.05, N 11.05.

Synthesis of $[Ag_3(L1)_2](NO_3)_3·H_2O$ (2): The complex was prepared in a manner similar to that for **1** except that CF_3SO_3Ag was replaced by $AgNO_3$. Light-brown block single crystals were obtained (8.4 mg, 50%). $C_{28}H_{30}Ag_3N_{11}O_{10}$ (1004.24): calcd. C 33.49, H 3.01, N 15.34; found C 33.38, H 3.26, N 15.36.

Synthesis of $[Co(L1)_2(SCN)_2]·EtOH$ (3): This complex was prepared by the layering method. A solution of ligand L1 (11.9 mg, 0.05 mmol) in ethanol (5 mL) was added slowly and carefully to a layer of a solution of $Co(SCN)_2$ (11.5 mg, 0.05 mmol) in ethanol (3 mL) in a tube. Red-orange platelet single crystals suitable for X-ray diffraction analysis were obtained after standing for several days (12.6 mg, 72%). $C_{32}H_{34}CoN_{10}OS_2$ (697.74): calcd. C 55.08, H 4.91, N 20.07; found C 55.02, H 5.00, N 20.28.

Synthesis of $[Co(L2)_2(SCN)_2]$ (4): According to the preparation method of complex **3**, pink column single crystals suitable for X-ray diffraction analysis were obtained by reaction of the ligand L2 with $Co(SCN)_2$; yield 11.1 mg, 68%. $C_{30}H_{28}CoN_{10}S_2$ (651.67): calcd. C 55.29, H 4.33, N 21.49; found C 55.12, H 4.49, N 21.47.

X-ray Crystal Structure Analysis for Complexes 1−4: The intensity data for the complexes **1**−**4** (Table 4) were collected with a Rigaku RAXIS-RAPID Imaging Plate diffractometer at 200 K, using graphite-monochromated Mo-K_α radiation (λ = 0.7107 Å). The structures were solved by direct methods with SIR92[33] and expanded using Fourier techniques.[34] All data were refined anisotropically by the full-matrix least-squares method for non-hydrogen atoms. The hydrogen atom positions were generated geometrically except for those of the water molecules, which were found from difference maps. Disordered NO_3^- anions and ethanol molecules were observed in complex **2** and **3**, respectively, although the data collection was performed at low temperature (200 K). All calculations were carried out with an SGI workstation using the teXsan crystallographic software package of Molecular Structure corporation.[35] CCDC-189685 (**1**), -189686 (**2**), -189687 (**3**), and -189688 (**4**) contain the supplementary crystallographic data for this paper. These data can be obtained free of charge at www.ccdc.cam.ac.uk/conts/retrieving.html [or from the Cambridge Crystallographic Data Centre, 12 Union Road, Cambridge CB2 1EZ, UK; Fax: (internat.) + 44-1223/336-033; E-mail: deposit@ccdc.cam.ac.uk].

Acknowledgments

This work was supported by National Natural Science Foundation of China.

[1] J. L. Atwood, J. Eric D. Davies, D. D. MacNicol, J.-M. Lehn, *Comprehensive Supramolecular Chemistry* **1996**, vol. 6, p. 733−755.
[2] B. F. Abrahams, B. F. Hoskins, R. Robson, *J. Am. Chem. Soc.* **1991**, *113*, 3606−3607.
[3] B. Olenyuk, J. A. Whiteford, A. Fechtenkotter, P. J. Stang, *Nature* **1999**, *398*, 796−799.
[4] A. Muller, E. Krickemeyer, H. Bogge, M. Schmidtmann, F. Peters, *Angew. Chem. Int. Ed.* **1998**, *37*, 3360.
[5] M. J. Zaworotko, *Chem. Soc. Rev.* **1994**, *23*, 283−288.
[6] H. Li, M. Eddaoudi, M. O' Keeffe, O. M. Yaghi, *Nature* **1999**, *402*, 276.
[7] S. Noro, S. Kitagawa, M. Kondo, K. Seki, *Angew. Chem. Int. Ed.* **2000**, *39*, 2081−2084.
[8] [8a] J. Lu, T. Paliwala, S. C. Lim, C. Yu, T. Niu, A. J. Jacobson, *Inorg. Chem.* **1997**, *36*, 923−929. [8b] R. W. Gable, B. F. Hoskins, R. Robson, *J. Chem. Soc., Chem. Commun.* **1990**, 1677−1678.
[9] K. Biradha, M. Fujita, *Chem. Commun.* **2001**, 15−16.
[10] [10a] L. Carlucci, G. Ciani, D. M. Proserpio, *J. Chem. Soc., Dalton Trans.* **1999**, 1799−1804. [10b] Y. B. Dong, M. D. Smith, R. C. Layland, H. C. Zur Loye, *J. Chem. Soc., Dalton Trans.* **2000**, 775−780. [10c] H. J. Choi, M. P. Suh, *J. Am. Chem. Soc.* **1998**, *120*, 10622−10628.
[11] [11a] M. Fujita, Y. J. Kwon, O. Sasaki, K. Yamaguchi, K. Ogura, *J. Am. Chem. Soc.* **1995**, *117*, 7287−7288. [11b] M. A. Withersby, A. J. Blake, N. R. Champness, P. A. Cooke, P. Hubberstey, M. Schroder, *New J. Chem.* **1999**, *23*, 573−575.
[12] [12a] K. N. Power, T. L. Hennigar, M. J. Zaworotko, *New J. Chem.* **1998**, *22*, 177−181. [12b] A. Rujiwatra, C. J. Kepert, M. J. Rosseinsky, *Chem. Commun.* **1999**, 2307−2308.
[13] S. Nishikiori, T. Iwamoto, *Inorg. Chem.* **1986**, *25*, 788−794.
[14] [14a] M. Fujita, Y. J. Kwon, S. Washizu, K. Ogura, *J. Am. Chem. Soc.* **1994**, *116*, 1151−1152. [14b] K. Biradha, K. V. Domasevitch, B. Moulton, C. Seward, M. J. Zaworotko, *Chem. Commun.* **1999**, 1327−1328.
[15] S. Nishikiori, T. Iwamoto, *Bull. Chem. Soc. Jpn.* **1983**, *56*, 3246−3252.
[16] [16a] S. R. Batten, B. F. Hoskins, R. Robson, *New. J. Chem.* **1998**, *22*, 173−175. [16b] B. F. Abrahams, M. J. Hardie, B. F. Hoskins, R. Robson, E. E. Sutherland, *J. Chem. Soc., Chem. Commun.* **1994**, 1049−1050. [16c] L. R. Macgillivray, R. H. Groeneman, J. L. Atwood, *J. Am. Chem. Soc.* **1998**, *120*, 2676−2677.
[17] [17a] T. L. Hennigar, D. C. Macquarrie, P. Losier, R. D. Rogers, M. J. Zaworotko, *Angew. Chem. Int. Ed. Engl.* **1997**, *36*, 972. [17b] Y.-B. Dong, M. D. Smith, H.-C. zur Loye, *Inorg. Chem.* **2000**, *39*, 4927−4935.
[18] [18a] M. Munakata, L. P. Wu, T. Kuroda-Sowa, M. Maekawa, K. Moriwaki, S. Kitagawa, *Inorg. Chem.* **1997**, *36*, 5416. [18b] L. Carlucci, G. Ciani, D. W. Gudenberg, D. M. Prosperpio, A. Siraoni, *Chem. Commun.* **1997**, 631. [18c] S.-I. Noro, M. Kondo, T. Ishii, S. Kitagawa, H. Matsuzaka, *J. Chem. Soc., Dalton Trans.* **1999**, 1569.
[19] G. Singh, Ph. A. Singh, A. K. Sen, K. Singh, S. N. Dubey, R. N. Handa, J. Choi, *Synth. React. Inorg. Met.-Org. Chem.* **2002**, *32*, 171−187.
[20] W.-Y. Sun, B.-L. Fei, T.-A. Okamura, W.-X. Tang, N. Ueyama, *Eur. J. Inorg. Chem.* **2001**, 1855−1861.
[21] B. L. Fei, W. Y. Sun, T.-a. Okamura, W. X. Tang, N. Ueyama, *New J. Chem.* **2001**, *25*, 210−212.
[22] B. L. Fei, W. Y. Sun, K. B. Yu, W. X. Tang, *J. Chem. Soc., Dalton Trans.* **2000**, 805−811.
[23] P. K. Bower, K. A. Porter, A. D. Rae, A. C. Willis, S. B. Wild, *Chem. Commun.* **1998**, 1153−1154.
[24] G. C. van Stein, G. van Koten, K. Vrieze, A. L. Pek, *J. Am. Chem. Soc.* **1984**, *106*, 4486−4492.
[25] A. Jäntti, K. Rissanen, J. Valkonen, *Acta Chem. Scand.* **1998**, *52*, 1010−1016.
[26] P. Losier, M. J. Zaworotko, *Angew. Chem. Int. Ed. Engl.* **1996**, *35*, 2779−2782.
[27] E. Leize, A. V. Dorsselaer, R. Kramer, J.-M. Lehn, *J. Chem. Soc., Chem. Commun.* **1993**, 990−993.
[28] [28a] B. L. Fei, W.-Y. Sun, Y.-A. Zhang, K.-B. Yu, W.-X. Tang, *Inorg. Chim. Acta* **2000**, *306*, 106−111. [28b] W.-Y. Sun, J. Fan, T.-a. Okamura, N. Ueyama, *Inorg. Chem. Commun.* **2000**, *3*, 541−544.

[29] S. Chang, V. V. Karambelkar, R. D. Sommer, A. L. Rheingold, D. P. Goldberg, *Inorg. Chem.* **2002**, *41*, 239−248.
[30] S. Pal, P. Sengupta, S. Ghosh, G. Mukherjee, G. Mostafa, *J. Coord. Chem.* **2002**, *55*, 271−280.
[31] A. Pui, I. Berdan, I. Morgenstern-Badarau, A. Greg, M. Perree-Fauvet, *Inorg. Chim. Acta* **2001**, *320*, 167−171.
[32] M. Mikuriya, K. Nakadera, J.-W. Lim, *Synth. React. Inorg. Met.-Org. Chem.* **2002**, *32*, 117−125.
[33] SIR92: A. Altomare, M. C. Burla, M. Camalli, M. Cascarano, C. Giacovazzo, A. Guagliardi, G. Polidori, *J. Appl. Crystallogr.* **1994**, *27*, 435.
[34] *DIRDIF94:* P. T. Beurskens, G. Admiraal, G. Beurskens, W. P. Bosman, R. de Gelder, R. Israel, J. M. M. Smits, *The DIRFID-94 program system*, Technical Report of the Crystallography Laboratory, University of Nijmegen, The Netherlands, **1994**.
[35] *teXsan:* Crystal Structure Analysis Package, Molecular Structure Corporation, **1999**.

Received July 18, 2002
[I02400]

Reactivity of $B(C_6F_5)_3$ with Oxovanadium(V) Complexes VOL_3 ($L = OCH_2CF_3$, NEt_2): Formation of the Organometallic Vanadium(V) Complex $[VO(\mu\text{-}OCH_2CF_3)(OCH_2CF_3)(C_6F_5)]_2$ and the Lewis Acid Adduct $[(Et_2N)_3VO{\cdot}B(C_6F_5)_3]$

Fabien Wolff,[a] Robert Choukroun,*[a] Christian Lorber,[a] and Bruno Donnadieu[a]

Keywords: N ligands / O ligands / Boranes / Structure determination / Vanadium

Treatment of the oxovanadium(V) complex $[VO(OCH_2CF_3)_3]_2$ (**3**) with the Lewis acid $B(C_6F_5)_3$ leads to aryl/alkoxy group exchange and formation of the unexpected organometallic oxovanadium(V) $[VO(\mu\text{-}OCH_2CF_3)(OCH_2CF_3)(C_6F_5)]_2$ (**1**), while reaction of $B(C_6F_5)_3$ and $[VO(NEt_2)_3]$ produces the Lewis acid adduct $[(Et_2N)_3VO{\cdot}B(C_6F_5)_3]$ (**2**). The crystal structures of **1**, **2** and **3** were determined. ^{51}V NMR chemical shifts for complexes **1**–**3** and $[VO(NEt_2)_3]$ are discussed. A concentration-dependant monomer-dimer equilibrium for **3** is observed in solution.
(© Wiley-VCH Verlag GmbH & Co. KGaA, 69451 Weinheim, Germany, 2003)

Introduction

The reactivity and bonding of tris(pentafluorophenyl)-borane $B(C_6F_5)_3$ to transition metal complexes continues to be a field of intense interest in both fundamental and applied chemistry.[1] The Lewis acid properties of $B(C_6F_5)_3$ influence the reactivity greatly, and C−F···metal interactions or perfluoroaryl/alkyl exchange reactions have been observed.[2] More recently, the reactivity of tris(pentafluorophenyl)borane towards different oxo metal complexes M=O has been investigated and oxo-group adducts isolated, particularly $[(acac)_2VO{\cdot}B(C_6F_5)_3]$.[3] Additionally, a Lewis acid adduct derived from the coordination of an alkylaluminium complex to the terminal oxygen of the oxovanadium(V) complex $[VO(CH_2SiMe_3)_{3-x}(OSiPh_3)_x$ (x = 0−3)] was observed by multinuclear NMR spectroscopy (^{17}O, ^{51}V).[4]

We are interested in vanadium chemistry[5] and, among our recent work, we have identified a C−F···V interaction in vanada(IV)azirine complexes isolated from a new type of reaction between $[VCp_2]$ and the activated nitrile $RC{\equiv}N{\cdot}B(C_6F_5)_3$.[6] We have recently extended our study to the oxovanadium(V) complexes $[VO(NEt_2)_3]$[7] and $[VO(OCH_2CF_3)_3]$,[8] and have found that the reactivity of these complexes is influenced by the substituents L (L = NEt_2, OCH_2CF_3) attached to the vanadium center. In agreement with the ^1H NMR scale that we deduced from the chemical shift measurements of the mixed series $[VOL_2(O\textit{i}Pr)]$ or $[VOL(O\textit{i}Pr)_2]$, the relative Lewis acidity of $[VO(OCH_2CF_3)_3]$ toward $[VO(NEt_2)_3]$ can be inferred.[7−9]

Results and Discussion

Synthesis and Molecular Structures of $[VO(\mu\text{-}OCH_2CF_3)(OCH_2CF_3)(C_6F_5)]_2$ (1) and $[VO(OCH_2CF_3)_3]_2$ (3)

The reaction of $[VO(OCH_2CF_3)_3]_2$ (**3**) in pentane with $B(C_6F_5)_3$ gives the dimeric organometallic complex $[VO(\mu\text{-}OCH_2CF_3)(OCH_2CF_3)(C_6F_5)]_2$ (**1**), as shown in Equation (1). Complex **1** is the second example[10a] of an organometallic oxovanadium(V) to be fully characterized by an X-ray structure determination (Figure 1).

$$[VO(OCH_2CF_3)_3]_2 + 2B(C_6F_5)_3 \longrightarrow [VO(\mu\text{-}OCH_2CF_3)(OCH_2CF_3)(C_6F_5)]_2 \quad \text{(+ unidentified products)} \qquad (1)$$

The formation of this organometallic oxovanadium(V) complex is due to an exchange reaction between the $B(C_6F_5)_3$ and the fluoroalkoxy ligand OCH_2CF_3. Such an exchange is not unique and is already known in zirconium chemistry.[2a−2c] The distance of the vanadium atom to the basal plane O(2), C(11), O(3), O′(2) in **1** is 0.5476(19) Å. The molecular structure establishes that **1** is a complex with a five-coordinate distorted square pyramidal geometry with the three oxygen atoms and the C_{ipso} atom of the perfluorophenyl group occupying the basal site (79.6% on the Berry pseudorotation path between D_{3h} and C_{4v} [11]) for the vanadium center. The V−C distance [2.066(4) Å] is in the expected range for such a bond.[10] In order to compare the

[a] Laboratoire de Chimie de Coordination du CNRS,
205 route de Narbonne, 31077 Toulouse Cedex, France
Fax: (internat.) + 33-5/61553003
E-mail: choukrou@lcc-toulouse.fr

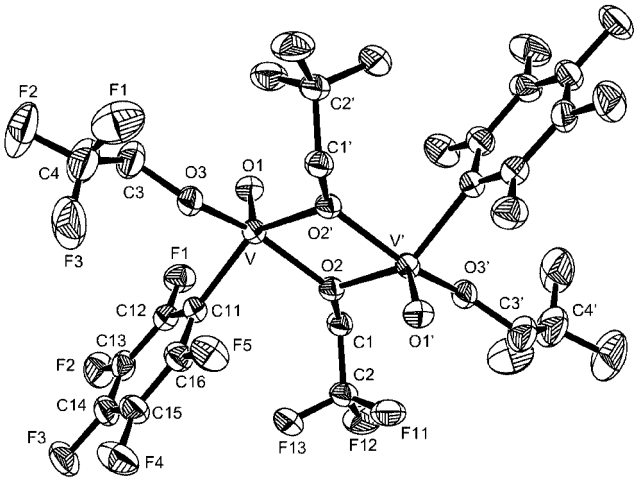

Figure 1. Molecular structure of **1** with selected bond lengths (Å) and angles (°), showing the labeling scheme; hydrogen atoms are omitted for clarity: V−C(11) 2.069(5), V−O(1) 1.569(4), V−O(2) 1.998(3), V−O(2)′ 1.995(3), V−O(3) 1.748(3); O(2)−V−O(2)′ 72.03(15), O(1)−V−O(3) 105.99(18), O(1)−V−C(11) 100.7(2), O(3)−V−C(11) 90.50(18), O(2)−V−C(11) 87.77(17), O(2)′−V−C(11) 141.13(18), V-[O(2)−V′ 107.97(15), V−O(2)−C(1) 126.4(3), V−O(3)−C(3) 134.8(3)

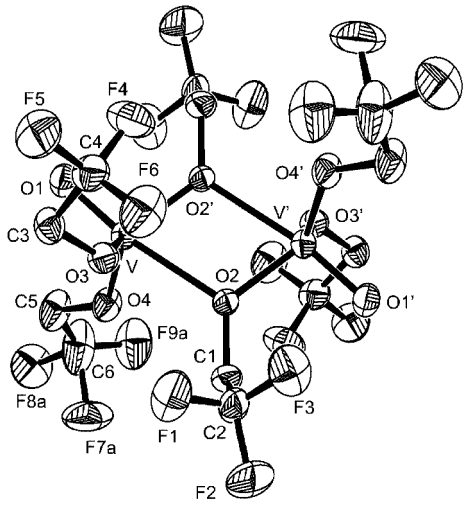

Figure 2. Molecular structure of **3** with selected bond lengths (Å) and angles (°), showing the labeling scheme; hydrogen atoms are omitted for clarity: V−O(1) 1.579(2), V−O(2) 2.297(2), V−O(3) 1.757(2), V−O(4) 1.771(2), V−O′(2) 1.843(2); V−O(2)−V′ 108.85(9), O(2)−V−O(2)′ 71.15(9), O(1)−V−O(2) 170.63(11), O(1)−V−O(2)′ 99.49(11), O(1)−V−O(3) 101.69(12), O(1)−V−O(4) 102.97(12), V−O(2)−C(1) 124.15(19), V′−O(2)−C(1) 126.3(2), V−O(3)−C(3) 131.0(2), V−O(4)−C(5) 129.9(3)

vanadium-oxygen bond lengths with the parent compound, a single-crystal X-ray diffraction study was performed on **3** (Figure 2). The vanadium centre is trigonal bipyramidal, as seen by the larger O(1)−V−O(2) angle of 170.6°, the sum of the O−V−O angles containing O(3), O(4) and O′(2) around the vanadium atom being 348.6° (18.7% on the Berry pseudorotation path[11]).

Both complexes **1** and **3** are centrosymmetric dimers in the solid state. A disymmetrical bridge V−O(R)−V is observed for **3**, and the average V−O bond length is similar to that in **1** (**1**: 1.997 Å (av); **3**: 1.843(2) Å, 2.296(3) Å]. The other V−OR (terminal) and V=O distances around the vanadium atom in **1** and **3** are essentially the same (**1**: 1.748(3) Å, 1.568(3) Å; **3**: 1.757(3) Å and 1.771(3) Å, 1.579(3) Å, respectively).

Although the V−O−C angle of the terminal OR group for **1** (134.8°) is similar to other V−O−C angles observed in different vanadium alkoxides ([$VO(OtBu)_3$]: 139.0° (av),[12] [$V(OiPr)_4]_2$: 126.27°, 134.67°, 140.27°,[13] [$VO(OSiPh_3)_3$]: V−O−Si (av) 155° [14]) the V−O−C angles of **3** are more acute (130.5° (av)), suggesting a poorer p_π-d_π overlap between the oxygen atoms and the vanadium center of **3**. It is worth noting that in a previous work published by one of us, a synthetic route for the preparation of the phenylvanadium(v) complexes [$PhVO(OiPr)_2$] and [PhVOCl(O*i*Pr)] was reported using LiPh or $HgPh_2$ as phenylating agents, although these vanadium complexes are unstable and decompose with time.[15] Attempts to prepare the phenyl analogue [$PhVO(OCH_2CF_3)_2$] by these routes were unsuccessful, in contrast to the easy formation of **1** using $B(C_6F_5)_3$ as an alkylating agent.

Synthesis and Molecular Structure of $[(Et_2N)_3VO{\cdot}B(C_6F_5)_3]$ (2)

Treatment of the more basic complex $[VO(NEt_2)_3]$ with $B(C_6F_5)_3$ gave the oxovanadium Lewis acid adduct compound $[(Et_2N)_3VO{\cdot}B(C_6F_5)_3]$ (**2**) as dark red crystals [Equation (2)].

$$[VO(NEt_2)_3] + B(C_6F_5)_3 \longrightarrow [(Et_2N)_3VO{\cdot}B(C_6F_5)_3] \quad (2)$$

The crystal structure of complex **2** (Figure 3) reveals the coordination of the Lewis acid $B(C_6F_5)_3$ to the V=O moiety. Both vanadium and boron atoms have a pseudo-tetrahedral structure (O−V−N and N−V−N average angles 113.3° and 105.4° respectively; O−B−C and C−B−C average angles 106.6° and 112.3°, respectively). The longer V=O distance of 1.6983(16) Å and the shorter B−O bond length [1.498(3) Å] indicate the reduction in bond order of the V=O moiety and the formation of a boron−oxygen single bond with a nearly linear V−O−B angle of 174.87 (15)°. It is worth noting that: i) the V−O bond length indicates the formation of a single V−O bond {cf. V−O (for terminal OR group) and V=O distances in $[VO(OR)_3]$: 1.753 Å (av), 1.790 Å and 1.595(2) Å and 1.591 Å (av) for R = *t*Bu and Me, respectively};[11] ii) the B−O bond length is shorter than that observed in $F_3B{\cdot}OPPh_3$ [1.516(3) Å][16] (for comparison, in $[(acac)_2VO{\cdot}B(C_6F_5)_3]$,[3a] V=O 1.648(1) Å, B−O 1.527(2) Å, V−O−B 168.9(1)°].

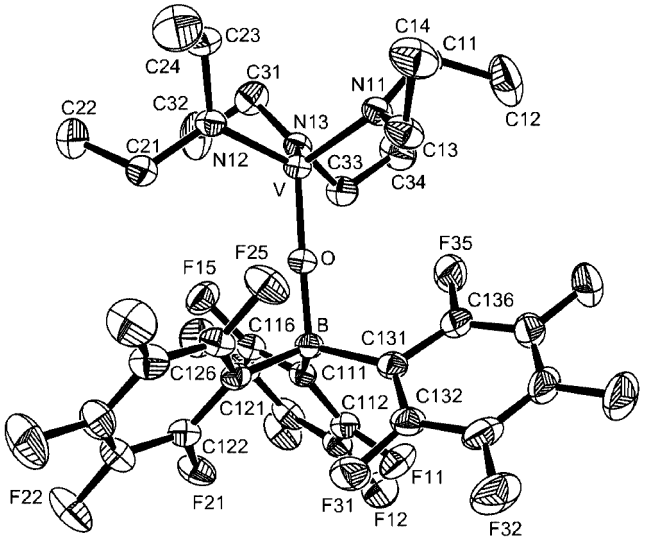

Figure 3. Molecular structure of **2** with selected bond lengths (Å) and angles (°), showing the labeling scheme; hydrogen atoms are omitted for clarity: V−O 1.6983(16), V−N(11) 1.8255(19), V−N(12) 1.8285(19), V−N(13) 1.8211(19), O−B 1.498(3); V−O−B 174.87(15), O−V-(N11) 104.03(9), O−V−N(12) 106.39(9), O−V−N(13) 112.97(8), O−B−C(111) 107.41(19), O−B−C(121) 105.49(18), O−B−C(131) 106.60(18).

^{1}H and ^{51}V NMR Spectroscopy

The ^{1}H NMR spectrum of **1** at room temperature shows a unique quadruplet resonance for the OCH_2CF_3 group (δ = 4.50 ppm), which reflects a rapid exchange of both terminal and bridging OR groups in solution. This persists at low temperature (in [D_8]toluene at −90 °C), indicating that the exchange is extremely rapid.[9] In contrast the ^{1}H NMR spectrum of **3** is concentration dependant, a well-known aspect of the monomer-dimer/polymer behavior in early transition metal alkoxides.[9,17] At low concentration, **3** is monomeric (δ = 4.56 ppm) whereas it dimerizes at higher concentration (δ = 4.95 ppm) showing an equilibrium between both forms in solution (see Exp. Sect.). The upfield shift of the methylene protons observed for **1** (δ = 4.50 ppm) relative to **3** (δ = 4.95 ppm) reflects the difference between an OR group which allows some π-donation and a purely electron-withdrawing σ-group (C_6F_5). The relative overall electron-withdrawing capability of both ligands (OCH_2CF_3 > C_6F_5) was deduced from these chemical shifts. Addition of one equivalent of $B(C_6F_5)_3$ to **1**, and monitoring of the reaction by ^{1}H and ^{19}F NMR spectroscopy for two days, confirmed that vanadium complex remains unchanged.

The ^{51}V NMR spectra for the series **1**, **2**, **3** and [$VO(NEt_2)_3$] were recorded in C_6D_6 solution at two different concentrations (see Exp. Sect.) to ensure that association phenomena do not interfere with the observed chemical shifts. We also verified that the synthesis of **2** gives only one compound in solution. For complex **1**, the preparative solution shows the peak assigned to the formation of **1** (isolated in high yield) and three other minor ^{51}V signals that could not be assigned. The two different ^{51}V NMR signals observed for **3** at low and high concentration (δ = −625 ppm and −570 ppm, respectively) confirm the above ^{1}H NMR results, i.e. a concentration-dependant monomer-dimer equilibrium. The values observed at δ = −481 ppm for the dimer **1** and δ = −570 ppm for dimer **3** show a deshielding effect for **1** due to the replacement of a fluoroalkoxy group with an alkyl perfluorophenyl group as a purely σ-bonding ligand. From the relative overall electron-withdrawing capability of both ligands already pointed out above, the ^{51}V chemical shifts of **1** and **3** follow an "inverse" halogen dependence, i.e. a shielding of the metal in the d^0 configuration upon increasing the electronegativity of the ligands attached to the coordination center.[18−21]

The ^{51}V chemical shifts for [$VO(NEt_2)_3$] and the borane adduct **2** (δ = −205 ppm and +57 ppm, respectively) are puzzling. If we consider that the sp^2 hybridization observed for the planar nitrogen atom of the NEt_2 ligands in **2** is unchanged in [$VO(NEt_2)_3$] before borane coordination (based on recent X-ray diffraction studies of different dialkylamido vanadium(IV) and vanadium(V) complexes recently carried out by our group[22] and others[23]) the observed deshielding shift could be attributed mainly to a decrease in electron density at the vanadium atom when the Lewis acid $B(C_6F_5)_3$ is attached to the oxygen atom. A similar consequence of poorer π-donation from O to V is also observed in the Lewis acid adducts [$VO(CH_2SiMe_3)_{3-x}(OSiPh_3)_x$ (x = 0−3)] with $Al(CH_2SiMe_3)_3$.[4b]

Conclusion

We have demonstrated that the reactivity of the Lewis acid $B(C_6F_5)_3$ with [VOL_3] is modulated by the electronic properties of the ligands L. The reaction with V=O is facilitated by the nucleophilic oxo group when L is an electron-donating dialkylamido group whereas formation of the organometallic complex **1** containing a V−C_6F_5 bond is promoted by an exchange reaction with $B(C_6F_5)_3$ when L is OCH_2CF_3 (an electron-withdrawing group). Potentially, this provides a suitable synthetic route for the development of new organometallic fluoroalkoxy complexes.

Experimental Section

General Remarks: All manipulations were carried out using standard Schlenk line or drybox techniques under an atmosphere of argon. Starting materials were purchased from Aldrich Inc. or Fluka Inc. and used without further purification. Solvents were refluxed and dried over appropriate drying agents under an atmosphere of argon, collected by distillation and stored in a drybox over activated 4-Å molecular sieves. Deuterated solvents were degassed and dried over activated 4-Å molecular sieves. NMR spectroscopic data were recorded using Bruker AMX-400, DPX-300 and AC-200 spectrometers, and referenced internally to residual protonated-solvent (^{1}H) resonances and are reported relative to tetramethylsilane (δ = 0 ppm). ^{19}F NMR (188.298 MHz) spectra were recorded on a Bruker AC-200 spectrometer (reference CF_3CO_2H). The AA′MM′X system in the ^{19}F NMR spectrum of compound **2** was simulated using the MestRe-C sofware package. ^{51}V NMR

(105.17 MHz) spectra were recorded on a Bruker AMX-400 spectrometer (reference $VOCl_3$ in C_6D_6: 9:1). Infrared spectra were prepared as KBr pellets under argon in a glove box and were recorded on a Perkin−Elmer Spectrum GX FT-IR spectrometer. Infrared data are quoted in wavenumbers (cm^{-1}). Elemental analyses were performed at the Laboratoire de Chimie de Coordination (Toulouse, France).

$[VO(NEt_2)_3]$ and **3** were prepared as described previously[7,8] and $B(C_6F_5)_3$ according to the literature.[24] Crystals of **3** were obtained by sublimation under vacuo (10^{-2} Torr) at 40 °C. The ^{51}V NMR spectrum of $[VO(NEt_2)_3]$ (EPR silent) was recorded in C_6D_6 at different ratios (9:1; 1:9) and found at δ = −205 ppm (we note that the value published by Rehder et al. for $[VO(NEt_2)_3]$ at δ = −389 ppm,[20] as a neat liquid, differs notably from our result). **$[VO(OCH_2CF_3)_3]$:** 2 experiments: a) 100 mg and b) 2 mg in 0.6 mL C_6D_6: a) ^1H NMR (C_6D_6): δ = 4.95 (q, $^3J_{H\text{-}F}$ = 8.3 Hz, CH_2) ppm. ^{19}F NMR (C_6D_6): δ = −0.8 (t, $^3J_{F\text{-}H}$ = 8.3 Hz, CF_3) ppm. ^{13}C NMR (C_6D_6): δ = 124.0 ($^1J_{C,F}$ = 279.3 Hz, CF_3), 80.6 ($^2J_{C,F}$ = 36.1 Hz, CH_2) ppm. ^{51}V NMR (C_6D_6): δ = −570. b) ^1H NMR (C_6D_6): δ = 4.55 (q, $^3J_{H\text{-}F}$ = 8.3 Hz, CH_2) ppm. ^{19}F NMR (C_6D_6): δ = −0.2 (t, $^3J_{F\text{-}H}$ = 8.3 Hz, CF_3) ppm. ^{51}V NMR (C_6D_6): δ = −625. $VO(NEt_2)_3$ ppm. ^1H NMR (C_6D_6): δ = 3.74 (q, ^3J = 6.9 Hz, CH_2), 1.25 (t, ^3J = 6.9 Hz, CH_3) ppm. ^{13}C NMR (C_6D_6): δ = 52.7 (CH_2), 16.5 (CH_3) ppm. ^{51}V NMR (C_6D_6): δ = −205 ppm.

$[VO(C_6F_5)(\mu\text{-}OCH_2CF_3)(OCH_2CF_3)]_2$ (1): A solution of $B(C_6F_5)_3$ (281 mg, 0.55 mmol) in pentane (4 mL) was added dropwise to a solution of $[VO(OCH_2CF_3)_3]$ (200 mg, 0.55 mmol) in pentane (3 mL) at room temperature. The reaction mixture was stirred for 2 h at room temperature and then cooled in the freezer overnight. Red crystals were filtered off, washed with pentane and dried under vacuum (152 mg, 64%). ^1H NMR (2 experiments at 5 mg and 60 mg in 0.6 mL C_6D_6 give same δ values): δ = 4.50 (q, $^3J_{H,F}$ = 8.0 Hz, CH_2CF_3). ^{13}C NMR (C_6D_6): δ = 149.2, 146.3, 145.2, 142.2, 138.8, 134.8 (C_6F_5) 123.5 (q, $^1J_{C,F}$ = 279.2 Hz, OCH_2CF_3), 79.4 (q, $^2J_{C,F}$ = 36.2 Hz, OCH_2CF_3) ppm. ^{19}F NMR (C_6D_6): δ = −0.2 (t, $^3J_{F,H}$ = 8.0 Hz, OCH_2CF_3), −40.7 (d, ^3J = 85.6 Hz, *o*-F, C_6F_5), −70.3 (t, ^3J = 11.3 Hz, *p*-F, C_6F_5), −84.2 (br. s, *m*-F, C_6F_5) ppm. ^{51}V NMR (C_6D_6) (2 experiments as for ^1H NMR): δ = −481 ppm. IR (KBr): $\tilde{\nu}$ = 2359 (m), 1636 (w), 1540 (s), 1510 (s), 1466 (m), 1359 (w), 1268 (s, br), 1182 (s, br), 1074 (s, br), 1035 (m, br), 962 (s), 839 (m), 746 (m), 669 (m), 581 (w), 497 (w). $C_{20}H_8F_{22}O_6V_2$: calcd. C 27.80, H 0.93; found C 27.80, H 0.85.The ^1H, ^{11}B and ^{51}V NMR spectra of the filtrate, after workup, show peaks for three minor unidentified species (^1H NMR: δ = 4.09, 3.86, 3.74 ppm. ^{11}B NMR: δ = 42, 27, 25 ppm. ^{51}V: δ = −531, −840, −885 ppm). Some of these high-field resonances could correspond to species where fluorines are attached directly to the vanadium atom.[20]

$[V(NEt_2)_3O{\cdot}B(C_6F_5)_3]$ (2): A solution of $B(C_6F_5)_3$ (362 mg, 0.70 mmol) in pentane (4 mL) was added dropwise to a solution of $[VO(NEt_2)_3]$ (200 mg, 0.70 mmol) in pentane (3 mL) at room temperature. After 4 days at room temperature, dark red crystals were filtered off, washed with pentane and dried under vacuum (122 mg, 22%). In another experiment, a solution of $B(C_6F_5)_3$ (15 mg, 0.03 mmol) in C_6D_6 (0.3 mL) was added to a solution of $[VO(NEt_2)_3]$ (8 mg, 0.03 mmol) in C_6D_6 (0.3 mL). The ^1H and ^{51}V NMR of the solution were identical to those of isolated **2** in the same solvent. ^1H NMR (C_6D_6): δ = 3.59 (q, ^3J = 7.0 Hz, 6 H, CH_2CH_3), 0.62 (t, ^3J = 7.0 Hz, 9 H, CH_2CH_3) ppm. ^{13}C NMR (C_6D_6): δ = 151.2, 147.5, 140.1, 138.5, 136.1 [$B(C_6F_5)_3$], 54.7 (CH_2CH_3), 14.6 (CH_2CH_3) ppm. ^{19}F NMR (C_6D_6): δ = −56.7 (AA′MM′X system, $^3J_{AM} = {}^3J_{A'M'}$ = −24.5, $^5J_{A'M} = {}^5J_{AM'}$ = 9.0 Hz, 2F, *o*-F, $B(C_6F_5)_3$], −82.9 (AA′MM′X system, $^3J_{M'X} = {}^3J_{MX}$ = −20.8 Hz, *p*-F, $B(C_6F_5)_3$], −88.7 (AA′MM′X system, $^3J_{AM} = {}^3J_{A'M'}$ = −24.5, $^5J_{A'M} = {}^5J_{AM'}$ = 9.0, $^4J_{MM'} = \pm$ 3.1 Hz, 2 F, *m*-F, $B(C_6F_5)_3$] ppm. ^{11}B NMR (C_6D_6): δ = 1.2. ^{51}V NMR (C_6D_6): δ = 57 ppm. IR (KBr): $\tilde{\nu}$ = 2983 (m), 2944 (m), 2360 (m), 2341 (m), 1643 (m), 1515 (s), 1458 (s, br), 1374 (m), 1358 (m), 1279 (m), 1182 (w), 1144 (m), 1096 (s, br), 972 (s, br), 909 (w), 848 (w), 793 (m), 771 (m), 738 (w), 676 (m), 626 (m), 613 (w), 574 (w), 478

Table 1. Crystallographic data, data collection and refinement parameters for compounds **1**, **2** and **3**

Compound	**1**	**2**	**3**
Chemical formula	$C_{10}H_4F_{11}O_3V$	$C_{30}H_{30}BF_{15}N_3OV$	$C_6H_6F_9O_4V$
Molecular weight	432.07	795.32	364.05
T (K)	180	180	180
Crystal system	monoclinic	monoclinic	monoclinic
Space group	$P2_1/c$	$P2_1/c$	$P2_1/n$
a (Å)	12.462(5)	10.226(1)	8.4858(8)
b (Å)	12.311(5)	19.575(2)	10.0566(7)
c (Å)	9.250(5)	17.178(2)	14.498(2)
β (deg)	95.175(5)	104.85(1)	92.59(1)
V (Å)	1413.3(11)	3323.6(5)	1235.9(2)
μ (mm^{-1})	0.844	0.413	0.928
Z, $D_{calcd.}$ (g/cm^3),	4, 2.031	4, 1.589	4, 1.956
Measured reflections	8096	26141	6940
Unique reflections	1986	6213	1752
R_{int}	0.0520	0.0575	0.0489
no. of variables	254	466	208
$t_{min.} - t_{max.}$	0.2970−0.7380	0.6080−0.8830	0.3930−0.7920
GOF on F^2	1.069	0.930	1.038
*R*1 [$I > 2\sigma(I)$]	0.0476	0.0386	0.0384
*wR*2 [$I > 2\sigma(I)$]	0.1299	0.0777	0.1085
*R*1 (all data)	0.0580	0.0711	0.0428
*wR*2 (all data)	0.1370	0.0875	0.1126
$\rho_{min.}$ and $\rho_{max.}$, e·Å^{-3}	0.942 and −0.478	0.255 and −0.290	0.399 and −0.354

(w). $C_{30}H_{30}BF_{15}N_3OV$: calcd. C 45.28, H 3.77, N 5.28; found C 45.33, H 3.66, N 5.07).

X-ray Analysis of 1, 2 and 3: Data were collected at low temperature (T = 180 K) for the three compounds, on a IPDS STOE diffractometer equipped with an Oxford Cryosystems Cryostream Cooler Device and using graphite-monochromated Mo-K_α radiation (λ = 0.71073 Å). Final unit-cell parameters were obtained by means of a least-squares refinement of a set of well-defined reflections; crystal decay was monitored during data collection and no significant fluctuations of intensities were observed. The structures were solved by direct methods using SIR92,[25] refined by least-squares procedures on F^2 with the aid of SHELXL-97[26] included in the program package WinGX version 1.63.[27] The atomic scattering factors were taken from the International Tables for X-ray Crystallography.[28] All hydrogens atoms were located on difference Fourier maps and refined using a riding model with an isotropic thermal parameter fixed at 20% higher than those of the carbons atoms to which they are connected. For **3** a disorder was located on the fluorine group: the fluorine atoms were found to be statistically disordered over two distinct orientations with an occupancy ratio of 55/45. Some restraints on interatomic C−F distances and F−C−F angles were imposed in order to reach a reasonable geometry and regularize the motion of the F atoms. For the three compounds all non-hydrogens atoms were refined anisotropically and, in the last cycles of refinement, a weighting scheme was used whose weights were calculated from the following formula: $w = 1/[\sigma^2(F_o^2) + (aP)^2 + bP]$ where $P = (F_o^2 + 2F_c^2)/3$. For all structures the criteria for a satisfactory complete analysis were a ratio of rms shift to standard deviations of less than 0.1 and no significant residual electronic densities in the final differences maps. Drawings of molecules were performed with the program ORTEP32[29] with 50% probability displacement ellipsoids for non-hydrogen atoms. The crystallographic data of **1**, **2** and **3** are summarized in Table 1. CCDC-190469 (**1**) -190470 (**2**) and -190471 (**3**) contain the supplementary crystallographic data for this paper. These data can be obtained free of charge at www.ccdc.cam.ac.uk/conts/retrieving.html [or from the Cambridge Crystallographic Data Center, 12, Union Road, Cambridge CB2 1EZ, UK; fax: (internat.) +44−1223/336−033; E-mail: deposit@ccdc.cam.ac.uk].

[1] [1a] R. L. Halterman, in "*Metallocenes*"; (Eds.: A. Togni; R. L. Halterman);Wiley-VCH: New York, **1998**, vol. 1, chapter 8, p. 455. Some recent contributions: [1b] N. E. Grimmer, N. J. Coville, C. B. De Koning, J. M. Smith, L. M Cook, *J. Organomet. Chem.* **2000**, *616*, 112. [1c] E. J. Thomas, M. D. Rausch, J. C. W. Chien, *Organometallics* **2000**, *19*, 5744. [1d] F. Zhang, Y. Mu, L. Zhao, Y. Zhang, W. Bu, C. Chen, H. Zhai, H. Hong, *J. Organomet. Chem.* **2000**, *613*, 68. For some recent leading references see also: [1e] A. Alt, H. G. Köppl, *Chem. Rev.* **2000**, *100*, 1205. [1f] G. W. Coates, *Chem. Rev.* **2000**, *100*, 1223. [1g] G. G. Hlatky, *Chem. Rev.* **2000**, *100*, 1347. [1h] E. Chen, T. J. Marks, *Chem. Rev.* **2000**, *100*, 1391. [1i] V. C. Britovsek, G. J. P. Gibson, D. F. Wass, *Angew. Chem. Int. Ed.* **1999**, *38*, 428. [1j] W. E. Piers, T. Chivers, *Chem. Soc. Rev.* **1997**, *26*, 345.

[2] [2a] G. J. Pindado, M. Thornton-Pett, M. Bouwkamp, A. Meetsma, B. Hessen, M. Bochmann, *Angew. Chem. Int. Ed. Engl.* **1997**, *36*, 2358. [2b] T. J. Woodman, M. Thornton-Pett, D. L. Hughes, M. Bochmann, *Organometallics* **2001**, *20*, 4080. [2c] R. Gomez, M. L. H. Green, J. L. J. Haggitt, *J. Chem. Soc., Dalton Trans.* **1996**, 939. [2d] J. Klosin, G. R. Roof, E. Y-X. Chen, K. A. Abboud, *Organometallics* **2000**, *19*, 4684. [2e] D. Bellamy, N. G Connelly, O. M. Hicks, A. G. Orpen, *J. Chem. Soc., Dalton Trans.* **1999**, 3185. [2f] V. V. Burlakov, P. Arndt, W. Baumann, A. Spannenberg, U. Rosenthal, A. V. Letov, K. A. Lyssenko, A. A. Korlyukov, L. I. Strunkina, M. Kh. Minacheva, V. B. Shur, *Organometallics* **2001**, *20*, 4072. [2g] G. M. Benedikt, B. L. Goodall, S. Iyer, L. H. McIntosh III, R. Mimna, L. F. Rhodes, *Organometallics* **2001**, *20*, 2565. [2h] N. Kleigrewe, T. Brackemeyer, G. Kehr, R. Frolïch, G. Erker, *Organometallics* **2001**, *20*, 1952. [2i] Y. Sunn, R. E. H. Spence, W. E. Piers, M. Parvez, G. P. A. Yap, *J. Am. Chem. Soc.* **1997**, *119*, 5132.

[3] [3a] J. R. Galsworthy, M. L. H. Green, M. Müller, K. J. Prout, *J. Chem. Soc., Dalton Trans.* **1997**, 1309. [3b] J. R. Galsworthy, J. C. Green, M. L. H. Green, M. J. Müller, *J. Chem. Soc., Dalton Trans.* **1998**, 15. [3c] L. H. Doerrer, J. R. Galsworthy, M. L. H. Green, M. A. Leech, *J. Chem. Soc., Dalton Trans.* **1998**, 2483.

[4] [4a] F. J. Feher, R. L. Blanski, *Organometallics* **1993**, *12*, 958. [4b] F. J. Feher, R. L. Blanski, *J. Am. Chem. Soc.* **1992**, *114*, 5886.

[5] R. Choukroun, C. Lorber, B. Donnadieu, *Organometallics* **2002**, *21*, 1124 and references therein.

[6] R. Choukroun, C. Lorber, B. Donnadieu, *Chem. Eur. J.* **2002**, *8*, 2700.

[7] R. Choukroun, D. Gervais, *Inorg. Chim. Acta* **1978**, *27*, 163.

[8] R. Choukroun, A. Dia, D. Gervais, *Inorg. Chim. Acta* **1979**, *34*, 211.

[9] C. Campbell, S. G. Bott, R. Larsen, W. G. Van der Sluys, *Inorg. Chem.* **1994**, *33*, 4950.

[10] [10a] M. Vivanco, J. Ruiz, C. Floriani, A. Chiesi-Villa, C. Rizzoli, *Organometallics* **1993**, *12*, 1802. [10b] V. J. Murphy, H. Turner, *Organometallics* **1997**, *16*, 2495. [10c] C. P. Gerlach, J. Arnold, *Organometallics* **1996**, *15*, 5260. [10d] P. T. Witte, A. Meetsma, B. Hessen, *J. Am. Chem. Soc.* **1997**, *119*, 10561.

[11] R. R. Holmes, *Prog. Inorg. Chem.* **1984**, *32*, 119.

[12] J. Spandt, I. Brüdgam, H. Hartl, *Z. Anorg. Allg. Chem.* **2000**, *626*, 2125.

[13] R. Kempe, A. Spannenberg, *New Crystal Structures* **1997**, *212*, 485.

[14] F. J. Feher, J. F. Walzer, *Inorg. Chem.* **1991**, *30*, 1689.

[15] R. Choukroun, S. Sabo, *J. Organomet. Chem.* **1979**, *182*, 221.

[16] M. A. Beckett, S. Brassington, S. J. Coles, M. B. Hursthouse, *Inorg. Chem. Communications* **2000**, *3*, 530.

[17] D. C. Bradley, R. C. Mehrotra, D. P. Gaur, *Metal Alkoxides*, Academic Press, **1978**, London, England.

[18] D. D. Devore, J. D. Lichtenhan, F. Takusagawa, E. A. Maatta, *J. Am. Chem. Soc.* **1987**, *109*, 7408.

[19] D. Rehder, *Coordination Chemistry Reviews* **1991**, *110*, 161.

[20] W. Priebsch, D. Rehder, *Inorg. Chem.* **1985**, *24*, 3058.

[21] H. Hagen, C. Bezemer, J. Boersma, H. Kooijman, M. Lutz, A. Spek, G. Van Koten, *Inorg. Chem.* **2000**, *39*, 3970.

[22] [22a] R. Choukroun, P. Moumboko, S. Chevalier, M. Etienne, B. Donnadieu, *Angew. Chem. Int. Ed.* **1998**, *37*, 3169. [22b] C. Lorber, R. Choukroun, B. Donnadieu, *Inorg. Chem.* **2002**, *41*, 4217. [22c] R. Choukroun, F. Wolff, Unpublished results.

[23] C. P. Gerlach, J. Arnold, *Organometallics* **1996**, *15*, 5260.

[24] A. G. Massey, A. J. Park, *J. Organomet. Chem.* **1964**, *21*, 245.

[25] [25a] A. Altomare, G. Cascarano, C. Giacovazzo, A. Guagliardi, *J. Appl. Crystallogr.* **1993**, *26*, 343. [25b] A. Altomare, M. C. Burla, M. Camalli, G. L. Cascarano, C. Giacovazzo, A. Guagliardi, A. G. G. Moliterni, G. Polidori, R. Spagna, *J. Appl. Cryst.* **1999**, *32*, 115.

[26] G. M. Sheldrick, *SHELX97* (Includes SHELXS-97, SHELXL-97, CIFTAB), Institüt für Anorganische Chemie der Universität, Tammanstrasse 4, Göttingen, Germany, **1998**.

[27] L. Farrugia, *J. Appl. Crystallogr.* **1999**, *32*, 837.

[28] International Tables for X-ray Crystallography, vol. IV, Kynoch Press, Birmingham, England, **1974**.

[29] L. Farrugia, *J. Appl. Crystallogr.* **1997**, *30*, 565.

Received July 26, 2002
[I02422]

Formation and Reactivity of a Tantalocene Trihydride Containing an Aminoethyl-Functionalised Ligand

Cyril Poulard,[a] Danièle Perrey,[a] Gilles Boni,*[a] Estelle Vigier,[a] Olivier Blacque,[a] Marek M. Kubicki,[a] and Claude Moïse[a]

Keywords: Cyclopentadienyl ligands / Metallocenes / Hydride ligands / Tantalum

The complex [Cp*{$C_5H_4(CH_2CH_2NMe_2)$}$TaCl_2$] (**1**) was synthesised by reaction of the lithium salt $LiC_5H_4(CH_2CH_2NMe_2)$ with the tantalum compound [Cp*$TaCl_3(PMe_3)$]. Reduction of **1** with $NaAl(H)_2(OCH_2CH_2OMe)_2$ leads to the trihydride derivative [Cp*{$C_5H_4(CH_2CH_2NMe_2)$}TaH_3] (**2**). The oxidation of **2** in THF with ferrocenium ion leads to a cationic dihydride intermediate [Cp*{$C_5H_4(CH_2CH_2NMe_2)$}TaH_2]PF_6 (**3**) with an intramolecular stabilization by the aminoethyl side-chain of the cyclopentadienyl ligand. The hemilabile character of the functionalised cyclopentadienyl ligand was checked by treating **3** with electron-donating ligands (e.g. phosphanes, sulfides, anions); in all cases, no displacement of the amino group was observed. When treated with HBF_4, **2** undergoes a loss of the hydride and the resulting cation can be isolated as a solvento adduct by carrying out the reaction in dimethyl sulfide. Acidolysis of **2** in the presence of an excess of trifluoroacetic acid affords the compound [Cp*{$C_5H_4(CH_2CH_2NHMe_2)$}$TaH(OCOCF_3)_2$](CF_3COO) (**5**). Microanalytical and NMR spectroscopic data for these complexes are given. The X-ray crystal structures are reported for [Cp*{$C_5H_4(CH_2CH_2NMe_2)$}TaH_2]PF_6 (**3**) and [Cp*{$C_5H_4(CH_2CH_2NHMe_2)$}$TaH(OCOCF_3)_2$](CF_3COO) (**5**).

(© Wiley-VCH Verlag GmbH & Co. KGaA, 69451 Weinheim, Germany, 2003)

Introduction

The cyclopentadienyl group has become one of the most important ligands in organo-transition-metal chemistry.[1] Variation in the ring substituents results in important changes in steric and electronic properties of this type of ligands.[2] In the last few years a wide range of functionalised cyclopentadienyl ligands, where a donor group (NR_2, OR, PR_2) is connected to the Cp ring by a suitable spacer, has been investigated.[3] Interest in such organometallic systems lies in the fact that the Cp ring binds strongly to the metal atom, whereas the donor atom interacts only when necessary. This concept of a hemilabile ligand has been used for the stabilisation of reactive intermediates and for catalytic processes.[4]

Following our studies on tantalocene complexes,[5] we have synthesised a new tantalocene dichloride and a trihydride incorporating the aminoethyl-functionalised cyclopentadienyl ligand [$C_5H_4(CH_2CH_2NMe_2)$]. The oxidation behaviour of the trihydride compound has been studied. It undergoes a loss of hydrogen atom upon reaction with ferrocenium ion leading to a cationic dihydride intermediate that is intramolecularly stabilized by the aminoethyl side-chain of the cyclopentadienyl ring.

[a] Laboratoire de Synthèse et d'Electrosynthèse Organométalliques (UMR, 5632), Université de Bourgogne, 2100 Dijon, France

Results and Discussion

Synthesis of [Cp*{$C_5H_4(CH_2CH_2NMe_2)$}$TaCl_2$] (1) and [Cp*{$C_5H_4(CH_2CH_2NMe_2)$}TaH_3] (2)

The synthesis of the tantalocene dichloride **1** was adapted from Bercaw's method[6] as outlined in Scheme 1. Complex **1** is isolated in good yield (80%) as a green solid soluble in halogenated solvents. It displays the eight-line ESR spectrum characteristic of bis(cyclopentadienyl)tantalum(IV) derivatives.

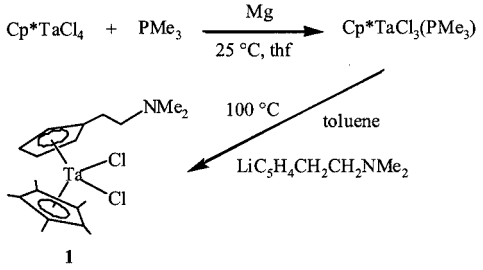

Scheme 1

Treatment of **1** with $NaAl(H)_2(OCH_2CH_2OMe)_2$ in toluene over a period of 3 h affords a red solution which, on hydrolysis, gives the trihydridometallocene **2** (Scheme 2). The ^1H NMR spectrum of **2** has the characteristic pattern of tantalocene trihydride:[7] a doublet ($\delta = -1.24$ ppm) and

a triplet (δ = 0.46 ppm) ($^2J_{H,H}$ = 12.7 Hz) corresponding to the central and lateral hydride ions respectively.

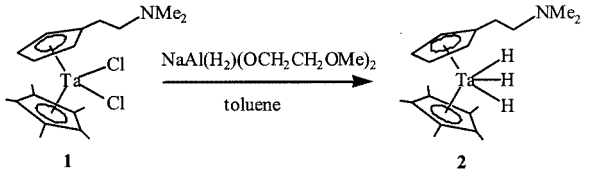

Scheme 2

Formation and Stabilization of the Cationic Dihydride Species "[Cp*{$C_5H_4(CH_2CH_2NMe_2)$}TaH_2]$^+$"

It has been shown by our group that chemical oxidation of tantalocene trihydride [(η^5-tBuC_5H_4)$_2$TaH_3] by ferrocenium ion leads to the formation of the reactive species [(η^5-tBuC_5H_4)$_2$TaH_2]$^+$;[5c] this cationic intermediate can be stabilized and isolated as a solvento adduct when the reaction is carried out in a potentially coordinating solvent like dimethyl sulfide or tetrahydrothiophene. In contrast, when an amine is added to the reaction mixture, no stabilization is observed and no well-defined product could be isolated. In this context, it was interesting to oxidize the trihydride complex **2** and to test the intramolecular stabilization abilities of the pendant aminoethyl chain. Treatment of a THF solution of **2** with 1 equiv. of [Cp_2Fe]PF_6 at room temperature results in the formation of [Cp*{$C_5H_4(CH_2CH_2NMe_2)$}TaH_2]PF_6 (**3**) and ferrocene, while a vigorous gas evolution is observed (Scheme 3).

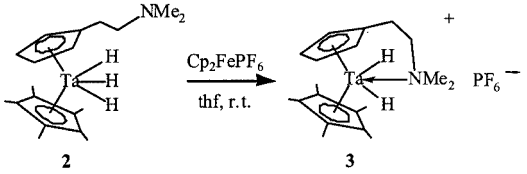

Scheme 3

The ^{1}H and ^{13}C NMR spectroscopic data for **3** show some remarkable differences compared with the data of **2**. The most significant change in the ^{1}H NMR spectra is the low-field shift for the signal of the methylene hydrogen atoms adjacent to the nitrogen atom of the side chain. While for complex **2** this signal is observed at δ = 2.67 ppm, the signal appears at δ = 3.20 ppm for **3**. In addition, the signals for the methyl group at the nitrogen atom are shifted downfield (Δδ = 0.57 ppm with respect to the tantalocene trihydride **2**). Corresponding downfield shifts for the signals of the methylene and methyl groups adjacent to the nitrogen atom are also observed in the ^{13}C NMR spectra. The signal for the NMe_2 group is shifted downfield by 32 ppm for complex **3** (δ = 77.9 ppm) relative to that in **2** (δ = 45.6 ppm). These NMR spectroscopic data agree with the intramolecular coordination of the amino group.[8] Moreover, the ^{1}H NMR spectrum of **3** displays one low-field singlet at δ = 6.71 ppm for the hydrido ligands (the value usually observed for cationic tantalocene species), suggesting their lateral positions and, consequently, the central position of the coordinated amino arm of the side chain. Such a description of the molecular structure of the cation in **3** has been confirmed by an X-ray diffraction study. The crystal structure of **3** is built up of discrete organometallic cations and PF_6 anions. The geometry of the cation is typical of bent tantalocenes (Ta^V, Figure 1). The intramolecular Ta−N bond of 2.430(3) Å observed in the cation corresponds well to the value expected for a single bond between the large metallic centre and the tertiary amine.

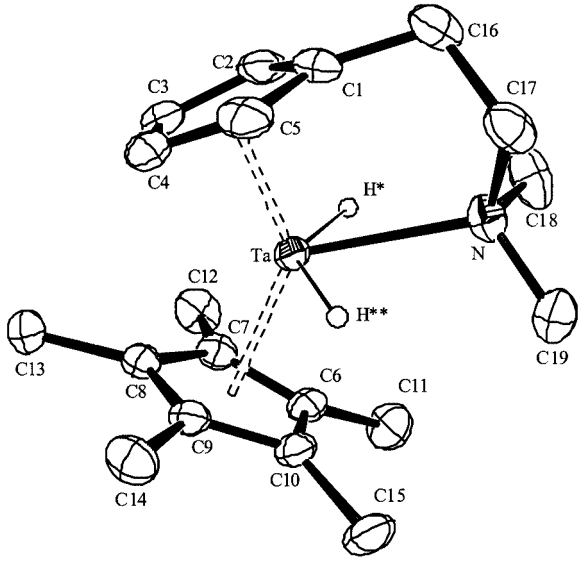

Figure 1. ORTEP drawing (50% probability displacement ellipsoids) of the cation in **3**; selected bond lengths [Å] and angles [°]: Ta−CP1 (geometrical centre of C1...C5 ring) 2.05, Ta−CP2 (geometrical centre of C6...C10 ring) 2.08, Ta−N 2.430(4), Ta−H* 1.71(5), Ta−H** 1.74(6); CP1−Ta−CP2 134.9, CP1−Ta−N 101.2, CP2−Ta−N 123.9, H*−Ta−H** 137(3), H*−Ta−N 67(2), H**−Ta−N 72(2)

In order to check the hemilabile properties of the aminoethyl arm, complex **3** was treated with electron-donating species. When **3** is heated at 80 °C in toluene in the presence of a phosphane (PMe_3, PMe_2Ph, PPh_2H) or a sulfur donor (Me_2S) no reaction occurs and the starting material is recovered. Reactions with anions (BuLi, PPh_2Li) also failed and degradation products were obtained. Thus, the aminoethyl chain coordinates strongly to the tantalum atom and cannot be displaced.

However, an acidolysis-type reaction may generate the cationic species "[Cp*{$C_5H_4(CH_2CH_2NMe_2)$}TaH_2]$^+$".[5c] The addition of 2 equiv. of HBF_4·Et_2O to a dimethyl sulfide solution of **2** results, as expected, in the evolution of dihydrogen and the formation of the dicationic solvento adduct [Cp*{$C_5H_4(CH_2CH_2NHMe_2)$}TaH_2(SMe_2)](BF_4)$_2$ (**4**) (Scheme 4). The ^{1}H NMR spectrum of **4** shows two signals at δ = 5.36 and 5.89 ppm for the cyclopentadienyl protons together with one singlet at δ = 2.38 ppm for the two hydride ions, characteristic of a symmetrical structure. Deprotonation of the ammonium group with several different bases (NEt_3, NaOH, EtONa) was carried out. These reactions give degradation products and the displacement of the di-

methyl sulfide ligand by the amino group could not be studied.

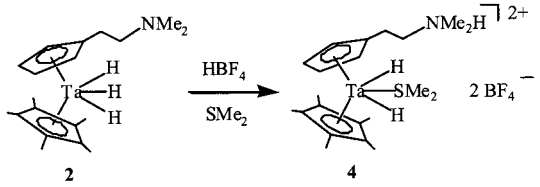

Scheme 4

Reaction of [Cp*{$C_5H_4(CH_2CH_2NMe_2)$}TaH_3] (2) with Carboxylic Acids

Complex **2** reacts rapidly with trifluoroacetic acid (4 equiv.) in toluene at room temperature leading to the protonation of the amino group and the formation of the tantalum(v) dicarboxylate complex **5** as a white solid, with evolution of dihydrogen (Scheme 5).

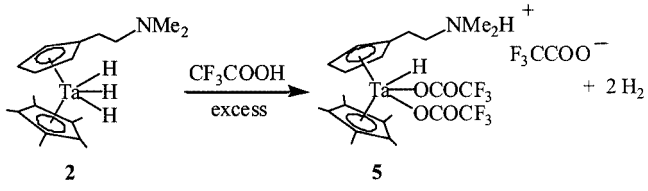

Scheme 5

The loss of two hydrido ligands is accompanied by the monodentate coordination of two carboxylate ions at the tantalum centre. As previously observed for the parent complex [$(\eta^5$-tBu$C_5H_4)_2TaH_3$],[5c] an excess of trifluoroacetic acid does not lead to the trisubstituted derivative. Complex **5** has been characterised by spectroscopic and analytical methods. Four signals are observed for the cyclopentadienyl protons in the ^{1}H NMR spectrum of **5** (δ = 4.99, 5.17, 6.06, 6.24 ppm), indicating an unsymmetrical structure due to the lateral position of the tantalocene hydride. The spectrum also contains a downfield singlet (δ = 12.58 ppm) for the residual hydride ion, consistent with the strong electron-withdrawing properties of the carboxylato ligands. In order to deprotonate the ammonium group, compound **5** was treated with MeLi, EtONa, or Et_3N. All attempts failed and no defined products were formed. X-ray diffraction experiment confirmed the proposed structure of the cation in **5** (Figure 2).

The asymmetric unit of the triclinic ($P\bar{1}$) unit cell of **5** contains one metal-containing cation, one trifluoroacetate anion and two chloroform solvent molecules. There is strong hydrogen bonding[9] between the ammonium end of the substituted cyclopentadienyl ligand and the anion [N···O5 = 2.732(4) Å]. The acetato ligands coordinated to Ta do not seem to participate in secondary interactions. For steric reasons their noncoordinated oxygen atoms (O2 and O4) lie on the less-hindered side of the C1...C5 ring.

Experimental Section

General: All manipulations were carried out under argon using standard Schlenk line techniques and conventional glass vessels. The solvents were dried with suitable reagents and freshly distilled under argon before use. [Cp*$TaCl_4$],[6] Li[$C_5H_4(CH_2CH_2NMe_2)$],[10] and ferrocenium salts[11] were prepared according to literature methods. NMR spectra were recorded with Bruker AC 200 or DRX 300 spectrometers for ^{1}H, ^{13}C, and ^{31}P NMR, with $SiMe_4$ and H_3PO_4 as references. Elemental analyses were performed with an EA 1108 CHNS-O FISONS Instruments apparatus.

[Cp*{$C_5H_4(CH_2CH_2NMe_2)$}$TaCl_2$] (1): Compound **1** was synthesised according to Bercaw's method reported for [Cp*$CpTaCl_2$][6] with minor modifications. [Cp*$TaCl_4$] (4.58 g, 10 mmol) was reduced with magnesium (0.12 g, 5 mmol) in THF

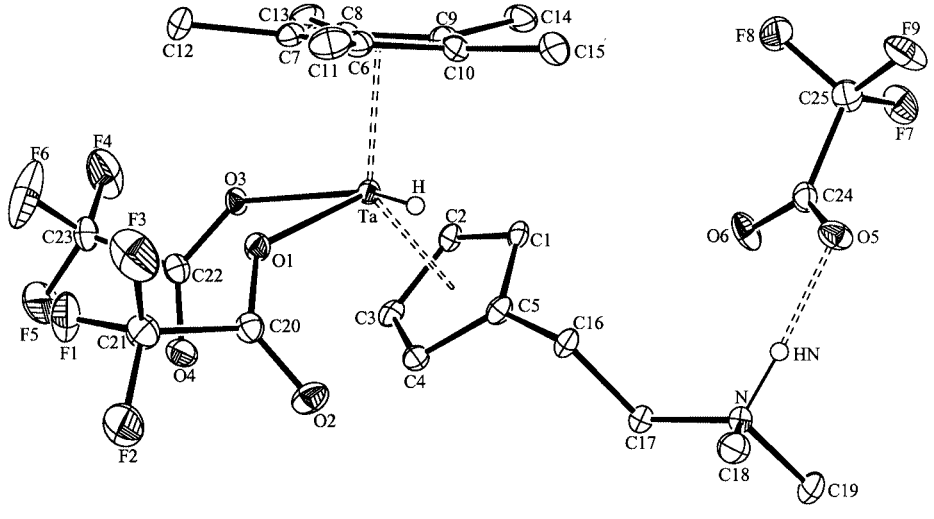

Figure 2. ORTEP drawing (30% probability displacement ellipsoids) of the cation in **5** showing the hydrogen bond between the ammonium group of the Cp ligand and the trifluoroacetate anion; selected bond lengths [Å] and angles [°]: Ta−CP1 (C1...C5 ring) 2.08, Ta−CP2 (C6...C10 ring) 2.095, Ta−H 1.48(4), Ta−O1 2.131(2), Ta−O3 2.162(2), CP1−Ta−CP2 132.8, H−Ta−O1 71(1), H−Ta−O3 143(1), O1−Ta−O3 72.2(1), N−HN 1.02(4), HN···O5 1.74(4), N···O5 2.732(4), N−HN···O5 166

(50 mL) in the presence of PMe_3 (0.76 g, 10 mmol). Removal of the solvent afforded a red residue which was treated with $Li[C_5H_4(CH_2CH_2NMe_2)]$ (1.43 g, 10 mmol) in toluene (50 mL) at 100 °C. After 12 h of stirring, extraction and crystallisation from acetone afforded the green paramagnetic product **1** (4.20 g, 80% yield). $C_{19}H_{29}Cl_2NTa$ (523.3): calcd. C 43.61, H 5.59, N 2.68; found C 44.16, H 5.74, N 2.47. The ESR spectrum in toluene showed an eight-line spectrum: g_{iso} = 1.9336; $A_{Ta,iso}$ = 103.54 G.

[Cp*{$C_5H_4CH_2CH_2NMe_2$)}TaH_3] (2): Complex **1** (2.62 g, 5 mmol) was reduced by $NaAlH_2(OCH_2CH_2OMe)_2$ (5 mL, 2 M in toluene, 10 mmol) in toluene (50 mL) at 0 °C. After 3 h of stirring, the brown-red solution was hydrolysed slowly with degassed water (10 mL). The organic layer was decanted and extracted. Evaporation of the solvent, followed by washing with pentane gave complex **2** (1.48 g, 65% yield). ^{1}H NMR (200 MHz, C_6D_6, 25 °C): δ = −1.24 (d, J = 12.7 Hz, 2 H), 0.46 (t, J = 12.7 Hz, 1 H), 1.99 (s, 15 H, Cp*), 2.06 (s, 6 H, NMe_2), 2.39 (t, J = 6.8 Hz, 2 H, CH_2), 2.67 (t, J = 6.8 Hz, 2 H, CH_2N), 4.53 (t, J = 2.4 Hz, 2 H, C_5H_4), 4.80 (t, J = 2.4 Hz, 2 H, C_5H_4) ppm. $^{13}C\{^1H\}$ NMR (50 MHz, C_6D_6, 25 °C): δ = 12.8 (CH_3 of Cp*), 29.3 (CH_2), 45.6 (NMe_2), 62.2 (CH_2N), 88.7 (ring C), 89.1 (ring C), 102.8 (ring Cp*), 113.8 (ring C) ppm. $C_{19}H_{32}NTa$ (455.42): calcd. C 50.11, H 7.08, N 3.08; found C 49.69, H 6.79, N 3.35.

[Cp*($C_5H_4CH_2CH_2NMe_2$)TaH_2][PF_6] (3): A solution of **2** (0.10 g, 0.22 mmol) in THF (10 mL) was treated at room temperature with $[Cp_2Fe][PF_6]$ (0.08 g, 0.22 mmol). The solution was stirred for an additional 0.5 h. During this time, a white precipitate formed; it was filtered off and washed with pentane. The crude reaction product was crystallised from chloroform (0.12 g, 90% yield). ^{1}H NMR (200 MHz, $CDCl_3$, 25 °C): δ = 2.11 (s, 15 H, Cp*), 2.56 (t, J = 2.6 Hz, 2 H, CH_2), 2.63 (s, 6 H, NMe_2), 3.20 (t, J = 2.6 Hz, 2 H, CH_2-N), 4.14 (t, J = 2.6 Hz, 2 H, C_5H_4), 6.71 (s, 2 H, Ta−H), 7.14 (t, J = 2.6 Hz, 2 H, C_5H_4) ppm. $^{13}C\{^1H\}$ NMR (50 MHz, $CDCl_3$, 25 °C): δ = 12.3 (CH_3 of Cp*), 24.1 (CH_2), 58.7 (CH_2), 77.9 (NMe_2), 93.3 (ring C), 100.2 (ring C), 111.6 (ring Cp*), 126.3 (ring C) ppm. $^{31}P\{^1H\}$ NMR (80 MHz, $CDCl_3$, 25 °C): δ = −153.8 (sept, J = 712 Hz) ppm. $C_{19}H_{31}F_6NPTa$ (599.38): calcd. C 38.07, H 5.21, N 2.34; found C 38.08, H 5.30, N 2.56.

[Cp*($C_5H_4CH_2CH_2NHMe_2$)TaH_2SMe_2][BF_4)$_2$ (4): A solution of **2** (0.105 g, 0.23 mmol) in dimethyl sulfide (10 mL) was treated at room temperature with 0.1 mL of HBF_4·Et_2O (54 wt% in Et_2O); the solution was stirred for an additional 0.5 h. After evaporation of the solvents, the crude solid was washed with diethyl ether and the complex was recrystallised from chloroform/pentane (2:1). Yield: 0.127 g (80%). ^{1}H NMR (200 MHz, $CDCl_3$, 25 °C): δ = 2.19 (s, 15 H, Cp*), 2.38 (s, 2 H, TaH), 2.70 (s, 6 H, SMe_2 or NMe_2),

Table 1. Crystallographic data for [Cp*{$C_5H_4(CH_2CH_2NMe_2)$}TaH_2]PF_6 (**3**) and [Cp*{$C_5H_4(CH_2CH_2NHMe_2)$}-$TaH(OCOCF_3)_2$](CF_3COO) (**5**)

Compound	**3**	**5**
Colour	colourless	pale yellow
Shape	prism	irregular
Size [mm]	0.15 × 0.12 × 0.08	0.20 × 0.13 × 0.10
Empirical formula	$C_{19}H_{31}F_6NPTa$	$C_{27}H_{33}Cl_6F_9NO_6Ta$
Formula mass	599.37	1032.19
Crystal system	triclinic	triclinic
Space group	$P\bar{1}$ (2)	$P\bar{1}$ (2)
T [K]	293	120
a [Å]	8.7546(7)	12.2794(2)
b [Å]	10.4533(10)	12.6826(2)
c [Å]	13.0578(8)	13.7804(3)
α [°]	73.150(6)	68.159(1)
β [°]	72.048(5)	72.982(1)
γ [°]	86.452(7)	87.595(1)
V [Å^3]	1087.50(15)	1899.39(6)
Z	2	2
$D_{calcd.}$ [g·cm^{-3}]	1.830	1.805
μ (Mo-$K_α$) [Mm^{-1}]	5.182	3.399
λ (Mo-$K_α$) [Å]	0.71073	0.71073
F(000)	588	1012
θ range [°]	4.8; 18.6	1.018; 30.508
hkl ranges	−10; 0/ −13; 12/ −16; 15	−17; 17/ −17; 17/ −18; 15
Collected reflections, Unique reflections, Measured reflections, R_{int}	4699, 4401, 4122, 0.0112	13088, 9731, 7660, 0.0338
Reflections/parameters/restraints	4401/268/0	9731/459/0
Goodness-of-fit on F^2	1.086	0.999
$R(F)$, $Rw(F^2)$[a] [$I > 2σ(I)$]	0.0246, 0.0647	0.0417, 0.0709
$R(F)$, $Rw(F^2)$[a] (all data)	0.0279, 0.0661	0.0664, 0.0778
w:[b] a, b	0.0421, 0.8624	0.0268, 0.0000
$ρ_{max}$, $ρ_{min}$ [e·Å^{-3}]	0.409, −1.526	0.982, −1.673

[a] $R(F) = Σ||F_o| - |F_c||/Σ|F_o|$, $Rw(F^2) = [Σw(F_o^2 - F_c^2)^2/Σ[w(F_o^2)^2]^{1/2}$. [b] $w = 1/[σ^2(F_o^2) + (aP)^2 + bP]$ with $P = (F_o^2 + 2F_c^2)/3$.

2.95 (m, 2 H, CH_2), 3.11 (s, 6 H, NMe_2 or SMe_2), 3.52 (m, 2 H, CH_2), 5.36 (t, J = 2.5 Hz, 2 H, C_5H_4), 5.89 (t, J = 2.5 Hz, 2 H, C_5H_4) ppm. $C_{21}H_{38}B_2F_8NSTa$ (691.16): calcd. C 36.49, H 5.54, N 2.03; found C 35.98, H 1.71, N 5.45.

[Cp*($C_5H_4CH_2CH_2NHMe_2$)TaH($OCOCF_3$)$_2$][CF_3COO] (5): A toluene (20 mL) solution of **2** (2.28 g, 5 mmol) was treated at room temperature with an excess of trifluoroacetic acid (0.176 g, 2 mmol). The colourless solution turned pale yellow, and gas evolution was observed. The solution was stirred for an additional 30 min, and the volatiles were then removed in vacuo. Recrystallisation from chloroform gave white crystals (3.17 g, 80% yield). ^{1}H NMR (300 MHz, $CDCl_3$, 25 °C): δ = 2.10 (s, 15 H, Cp*), 2.82 (d, J = 23.5 Hz, 6 H, NMe_2), 3.23 (m, 2 H, CH_2), 3.89 (m, 2 H, CH_2), 4.99 (br. s, 1 H, C_5H_4), 5.17 (br. s, 1 H, C_5H_4), 6.06 (br. s, 1 H, C_5H_4), 6.24 (br. s, 1 H, C_5H_4), 12.58 (s, 2 H, TaH), 13.20 (s, 1 H, $HNMe_2$) ppm. $C_{25}H_{31}F_9NO_6Ta$ (793.46): calcd. C 37.84, H 3.94, N 1.77; found C 37.89, H 4.19, N 2.07.

X-ray Structure Analyses: Crystals of **3** and **5** suitable for X-ray studies were grown from acetone and chloroform solutions, respectively. The intensities were measured at room temperature (298 K) for **3** with an Enraf Nonius CAD4 and at 120 K for **5** with a Nonius Kappa CCD diffractometer with Mo-K_α radiation (λ = 0.71073 Å). The measured intensities were reduced with MolEN of Enraf Nonius[12] for **3** and with the DENZO program[13] for **5**. The structures were solved by direct methods and Patterson syntheses with SHELXS-97. All models were further refined with full-matrix least-squares methods (SHELXL-97) based on $|F^2|$.[14] All non-hydrogen atoms were refined with anisotropic thermal parameters. The hydrido ligands in both structures as well as the hydrogen atom of the ammonium group in **5** were located from difference Fourier maps and refined isotropically. Other hydrogen atoms were included in calculated positions and refined with a riding model. Crystallographic data and refinement parameters are gathered in Table 1. CCDC-190157 (**3**) and -190158 (**5**) contain the supplementary crystallographic data for this paper. These data can be obtained free of charge at www.ccdc.cam.ac.uk/conts/retrieving.html [or from the Cambridge Crystallographic Data Centre, 12 Union Road, Cambridge CB2 1EZ, UK; Fax: (internat.) + 44-1223/336-033; E-mail: deposit@ccdc.cam.ac.uk].

[1] C. Janiak, H. Schumann, *Adv. Organomet. Chem.* **1991**, *33*, 291−393.
[2] [2a] J. Okuda, *Top. Curr. Chem.* **1991**, *160*, 97−145. [2b] N. J. Coville, K. E. du Plooy, W. Pickl, *Coord. Chem. Rev.* **1992**, *116*, 1−267.
[3] [3a] U. Seimeling, *Chem. Rev.* **2000**, *100*, 1495−1526. [3b] H. Butenschön, *Chem. Rev.* **2000**, *100*, 1527−1564. [3c] P. Jutzi, U. Siemeling, *J. Organomet. Chem.* **1995**, *500*, 175−185. [3d] P. Jutzi, T. Redeker, *Eur. J. Inorg. Chem.* **1998**, 663−674. [3e] C. Müller, D. Vos, P. Jutzi, *J. Organomet. Chem.* **2000**, *600*, 127−143.
[4] [4a] E. Lindner, S. Pautz, M. Haustein, *Coord. Chem. Rev.* **1996**, *155*, 145−162. [4b] M. Enders, G. Kohl, H. Pritzkow, *J. Organomet. Chem.* **2001**, *622*, 66−73.
[5] [5a] V. I. Bakhmutov, E. V. V. Vorontsov, E. V. Bakhmutova, G. Boni, C. Moïse, *Inorg. Chem.* **1999**, *38*, 1121−1125. [5b] S. Sabo-Etienne, B. Chaudret, H. A. el Makarim, J.-C. Barthelat, J.-P. Daudey, C. Moise, J.-C. Leblanc, *J. Am. Chem. Soc.* **1994**, *116*, 9335−9336. [5c] P. Sauvageot, A. Sadorge, B. Nuber, M. M. Kubicki, J. C. Leblanc, C. Moïse, *Organometallics* **1999**, *18*, 2133−2138.
[6] V. C. Gibson, J. E. Bercaw, W. J. Burton Jr., R. D. Sanner, *Organometallics* **1986**, *5*, 976−979.
[7] M. L. H. Green, J. A. McCleverty, L. Pratt, G. Wilkinson, *J. Chem. Soc.* **1961**, 4854−4859.
[8] P. Jutzi, M. O. Kirsten, B. Neumann, H.-G. Stammler, *Organometallics* **1994**, *13*, 3854−3861.
[9] [9a] A. A. Khan, W. H. Baur, *Acta Crystallogr., Sect. B* **1972**, *28*, 683−693. [9b] I. D. Brown, D. Altermatt, *Acta Crystallogr., Sect. B* **1985**, *41*, 244−247.
[10] [10a] B. B. Kaul, B. Noll, S. Renshaw, M. Rakowski DuBois, *Organometallics* **1997**, *16*, 1604−1611. [10b] P. C. McGowan, C. E. Hart, B. Donnadieu, R. Poilblanc, *J. Organomet. Chem.* **1997**, *528*, 191−194.
[11] N. G. Connelly, W. E. Geiger, *Chem. Rev.* **1996**, *96*, 877−910.
[12] C. K. Fair, *MolEN*, Enraf−Nonius, Delft, Netherlands, **1990**.
[13] Z. Otwinowski, W. Minor, *Methods Enzymol.* **1997**, *276*, 307−326.
[14] G. M. Sheldrick, *SHELXS-97* and *SHELXL-97*, University of Göttingen, Germany **1997**.

Received September 16, 2002
[I02522]

Investigations on 1-Metallaindanes

Marcel Schreuder Goedheijt,[a] Tom Nijbacker,[b] Andrew D. Horton,[c] Franciscus J. J. de Kanter,[b] Otto S. Akkerman,[b] and Friedrich Bickelhaupt*[b]

Keywords: Metallacycles / Isomerization / Magnesium / Mercury / Zirconium

1-Mercuraindane (**6**) was prepared in three steps from 1-bromo-2-(2-bromoethyl)benzene (**3**) and converted into 1-magnesaindane (**1**) by reaction with magnesium. In solution, **6** was observed to occur in a remarkable dimer/trimer equilibrium, whereas **1** forms a dimer. From **1** and dichlorozirconocene, the 1-zirconaindane **2** was obtained, which reacted with $B(C_6F_5)_3$ to form the adduct **13**. According to spectroscopic data, **13** is formed by attack of the β-methylene carbon atom at the boron atom and has a zwitterionic structure with weak interactions between the zirconium ion and one of the *ortho*-fluorine atoms.

(© Wiley-VCH Verlag GmbH & Co. KGaA, 69451 Weinheim, Germany, 2003)

Introduction

Cyclic diorganylmagnesium compounds[1] often show interesting structural features.[2,3] One aspect is the relatively large C−Mg−C bond angle, which for normal diorganylmagnesium compounds of the general type R_2MgL_2 (L = ligand, mostly an ether) is around 120−130°. This leads to considerable strain if the two R groups are connected such that magnesium is incorporated into a small ring. As the carbon−magnesium bonds undergo a rapid exchange in ethereal solution, the strained monomers can easily escape from this situation and thus tend to form more stable dimers or higher aggregates in which the large bond angle can be accommodated free of strain; sometimes an equilibrium between two oligomers is established. For the sake of simplicity, the oligomers are indicated by the names of the *monomeric* parent units where appropriate; furthermore, magnesium is assumed to be tetracoordinate including two solvent molecules,[1−3] which in the present case is THF. We have previously reported the investigation of a number of such cyclic diorganylmagnesium compounds,[3,4] and wanted to extend this study to 1-magnesaindane (**1**) (Scheme 1).

A further reason for our interest in **1** was that it is a difunctional organomagnesium compound and as such is attractive for the preparation of other metallacycles such as the corresponding 1-zirconaindane **2**, which is potentially of interest as a precursor of a new class of single-site olefin polymerization catalysts.[5−7]

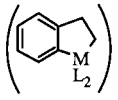

1: ML_2 = Mg ·2 THF
2: ML_2 = $ZrCp_2$

Scheme 1

Results and Discussion

Synthesis of Magnesaindane (1)

In order to obtain **1** in pure form, we decided to prepare it by transmetalation of the corresponding cyclic organomercury compound **6** with metallic magnesium, as shown in Scheme 2. For this purpose, the dibromide **3** was converted into **4**, which is the known[8] di-Grignard reagent corresponding to the diorganylmagnesium **1**. In an attempt to obtain **6** from **4** directly, we treated **4** with 1 mol-equiv. of mercury dibromide but, according to the ^{199}Hg NMR spectrum, a mixture of organomercury compounds was formed which could not be separated. However, **6** was obtained by reduction[9] of the corresponding organomercury halide **5** with stannous chloride in the presence of base. Reaction of **6** with metallic magnesium in THF furnished **1**, which was characterized spectroscopically by its ^1H and ^{13}C NMR spectrum (see Exp. Sect.) and chemically by reaction with deuterium oxide which gave [D_2]ethylbenzene (**7**) exclusively.

[a] Diosynth bv,
Postbus 20, 5340 BH Oss, The Netherlands
[b] Scheikundig Laboratorium, Vrije Universiteit,
De Boelelaan 1083, 1081 HV Amsterdam, The Netherlands
Fax: (internat.) + 31-20/444-7488
E-mail: bicklhpt@chem.vu.nl
[c] Shell Research and Technology Centre,
Badhuisweg 3, 1031 CM Amsterdam, The Netherlands

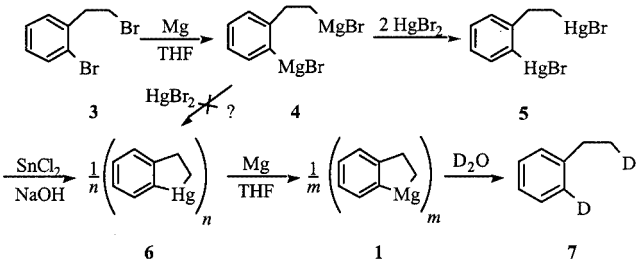

Scheme 2

Structure of 1-Mercuraindane (6)

Although initially **6** was only of interest as an intermediate for the preparation of **1**, it showed spectral features which led to a closer investigation. The ^{13}C NMR spectrum of pure **6** in $CDCl_3$ shows evidence for the occurrence of two species **6a** and **6b**, presumably differing in their degree of oligomerization. For instance, four methylene carbon resonances were observed (δ = 41.5 and 39.7 ppm for **6a**; δ = 41.7 and 38.4 ppm for **6b**) as well as eight resonances of aromatic carbon atoms and two of ^{199}Hg (δ = −273.2 ppm for **6a**; δ = −305.5 ppm for **6b**). The signal integral ratio of the benzylic methylene protons of **6a** and **6b** in the ^1H NMR spectrum was found to be concentration-dependent, which suggests an equilibrium between them in solution (Scheme 3). From ^1H NMR spectroscopic data (Table 1), the equilibrium constant at room temperature was determined. As, according to HRMS spectroscopy, **6** has a dimeric structure (m/z = 610.0642) in the gas phase, one of the species involved in solution is presumably a dimer. Assuming a dimer/trimer equilibrium, the equilibrium constant was found to be in the range of $K = 0.4 \pm 0.2$ L·mol^{-1}.

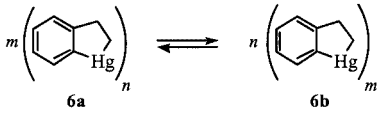

Scheme 3

Table 1. Data on the equilibrium of **6** at room temperature [in 0.5 mL of $CDCl_3$ at room temperature; determined from the ratio of the benzylic protons at δ = 3.36 ppm (**6a**) and 2.95 ppm (**6b**)]

6[a]	[**6a**][b]	[**6b**][b]	K[c]
1.5	$8.8\cdot10^{-3}$	$5.8\cdot10^{-4}$	0.49
4.1	$2.4\cdot10^{-2}$	$2.8\cdot10^{-3}$	0.57
9.1	$5.2\cdot10^{-2}$	$7.6\cdot10^{-3}$	0.41
13.5	$7.6\cdot10^{-2}$	$1.2\cdot10^{-2}$	0.33
17.8	$1.0\cdot10^{-1}$	$1.7\cdot10^{-2}$	0.30
21.5	$1.2\cdot10^{-1}$	$2.1\cdot10^{-2}$	0.26
25.4	$1.4\cdot10^{-1}$	$2.7\cdot10^{-2}$	0.24
31.0	$1.7\cdot10^{-1}$	$3.3\cdot10^{-2}$	0.22

[a] In mg. [b] In mol·L^{-1} (**6a** as dimer, **6b** as trimer). [c] In L·mol^{-1}.

A dimer/trimer equilibrium is plausible since, in hypothetical monomeric **6**, the C−Hg−C angle would deviate too much from the ideal value of 180°, making the ensuing ring strain prohibitive. This is less so for a dimeric species **6a**, while a trimeric species **6b** is strain-free as concluded from CPK model studies. Species higher than a trimer are not formed since oligomerization is entropically unfavorable.

The establishment of such an equilibrium is unexpected because, in contrast to the kinetically highly labile carbon−magnesium bond, the carbon−mercury bond is usually stable under ordinary conditions. Redistribution reactions of bifunctional organomercury compounds have been reported, but only in the presence of a catalyst such as $AlCl_3$ [10] or an organomercury halide (RHgX).[10,11] For example, an equimolar mixture of Me_2Hg and Et_2Hg gives a random distribution of the three possible alkylmercury compounds, Me_2Hg, Et_2Hg and MeEtHg, upon standing at room temperature in the presence of $AlCl_3$, but after removal of the catalyst, MeEtHg can be distilled at 127 °C and is stable for months at room temperature.[10] The presence of an organomercury halide, such as **5**, as an impurity, which might act as a catalyst, was excluded by a negative halide test performed by evaporation of the solvent from a sample followed by treatment with HNO_3 and $AgNO_3$; a precipitate of AgCl was not observed.

To confirm the occurrence of an equilibrium for **6** and to estimate the exchange rates between both species, the magnetization-transfer NMR technique[12] was applied between 25 and 95 °C. Below 83 °C, no transfer was observed, which indicates that the establishment of the equilibrium is relatively slow at these temperatures. At 83 °C and 95 °C, the (pseudo-first-order) rates obtained for the equilibrium 3 **6a** $\rightleftarrows$ 2 **6b** were in the range of 0.1−1 s^{-1}. Thus, the exchange between the two oligomers is rather fast, and even at room temperature, one can estimate that it will be sufficient to allow establishment of the equilibrium. However, it is a remarkable process, and it remains unclear whether it is caused by inherent structural features or by some kind of undetected catalyst present in the system. Compound **6a** is probably dimeric (vide supra) and CPK models show that, of the two possible structures, **6a′** is less strained than **6a′′** due to the presence of the aryl−Hg−aryl arrangement in the latter (Scheme 4).

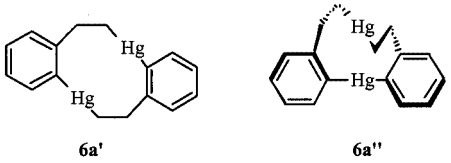

Scheme 4

Structure of 1 in Solution

The appreciable solubility of **1** in THF (ca. 0.1 M at room temperature) allowed investigations concerning its structure in solution. The degree of association was determined by the stationary isothermal distillation method,[13] which fur-

nished a concentration-independent degree of association of 2.08 (see Table 2).

Table 2. Degree of association of **1** in THF solution at 301 K[13]

[Mg][a]	S_{th}[b]	S_a[c]	i[d]
1.24	0.052	0.028	1.84
2.42	0.101	0.045	2.26
3.53	0.148	0.068	2.15
4.57	0.192	0.092	2.08
5.55	0.233	0.117	1.99
6.49	0.272	0.126	2.16

[a] [Mg] = Formal concentration of magnesium in mmol·g^{-1}. [b] S_{th} = Theoretical rate of evaporation (in mm·h^{-1}) = [Mg]·S_S, where S_S (in mm·h^{-1}·mmol^{-1}·L) = standard rate of evaporation found by calibration of the apparatus with triphenylmethane, S_S (301 K) = 0.0119 mm·h^{-1}·mmol^{-1}·L. [c] S_a = Apparent rate of evaporation in mm·h^{-1}. [d] Association number $i = S_{th}/S_a$.

The structure of two benzomagnesacycloalkanes in solution has been investigated by Freijee et al., who determined the degree of association in solution of the 1-magnesatetralin **8** and the tetrahydrobenzomagnesepin **9** (Scheme 5).[4] It was established that **8** was involved in a monomer/dimer equilibrium as its concentration-dependent degree of association was 1.26−1.49 in THF solution at room temperature, whereas the higher homologue **9** was completely monomeric. It was assumed that the higher ring strain in monomeric **8** (about 46 kJ·mol^{-1}) than in **9** (about 11 kJ·mol^{-1}) is largely responsible for the observed difference.

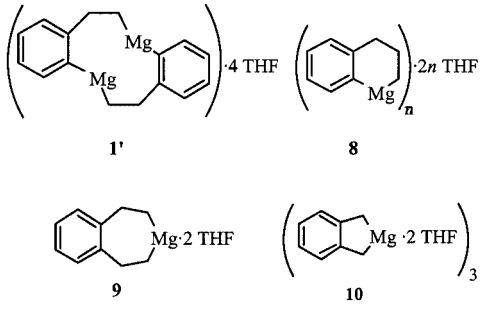

Scheme 5

The fact that **1** is completely dimeric in THF solution at room temperature is in line with the results obtained from **8** and **9** since ring strain in the hypothetical monomer of **1**, with magnesium in a five-membered ring, will be even higher than in monomeric **8**. As the trimer of **1** is not observed, we assume that entropy protects the system from further oligomerization as is also the case for other cyclic organomagnesium compounds.[3,4,14,15] Note, however, that the results presented so far pertain to the situation in solution where an equilibrium can be established; in the solid state, the degree of oligomerization may be different. Thus, Lappert et al. reported the crystal structure of 2-magnesaindane (**10**), the regioisomer of **1**, which turns out to be a trimer with a central fifteen-membered ring.[16] Unfortunately, data on the degree of oligomerization of **10** in solution are not available.

In analogy to other magnesacycles,[1−3] one may safely assume that the dimeric **1** has a ten-membered ring structure. As both the magnesium atom and the benzene ring prefer large bond angles (≥ 120°), the structure of **1′** as shown in Scheme 5 (which is analogous to **6a′**, Scheme 4), is suggested to be energetically more favorable than the alternative arrangement **1′′** (analogous to **6a"**) in which a C(Ar)−Mg−C(Ar) unit is present which probably would cause a higher ring strain in the molecule, as discussed for **6a**.

1,1-Dicyclopentadienyl-1-zirconaindane (2)

Having **1** available, it appeared to be an attractive starting material for the preparation of the 1-zirconaindane **2** which has previously been obtained by thermolysis of diphenylzirconocene in the presence of ethene.[17] It has been shown that the reaction of **11**, the 2-zircona analogue of **2**, with $B(C_6F_5)_3$ furnished the intramolecular ion pair **12** (Scheme 6).[5] It was therefore of interest to investigate the reaction of **2** with $B(C_6F_5)_3$ in order to generate the zwitterionic complex **13**. Study of the effect of anion−cation bonding interactions in **13** on the reactivity of unsaturated molecules was expected to improve our understanding of the factors influencing the activity of cationic metallocene catalysts in olefin polymerization.[18−22]

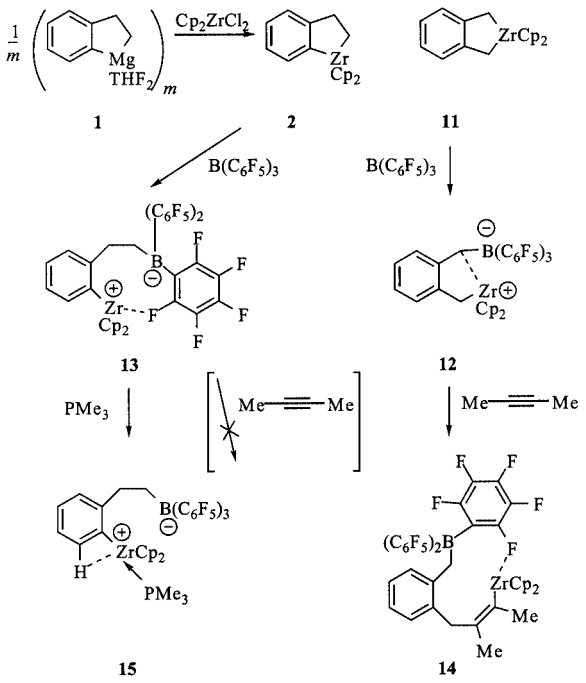

Scheme 6

Compound **2** was treated with 1 equiv. of $B(C_6F_5)_3$ in bromobenzene at −30 °C, and the product was isolated as a pale yellow powder in 81% yield by precipitation with *n*-pentane. Elemental analysis confirmed the composition of **13**. The ^{1}H NMR spectrum in $C_2D_2Cl_4$ shows a broad trip-

let signal at δ = 2.30 ppm which was assigned to the methylene protons next to the borate group; in the ^{13}C NMR spectrum, a signal at δ = 178.2 ppm indicates that the Zr−C(Ar) bond is still intact. Furthermore, the ^{19}F NMR spectrum ($C_2D_2Cl_4$, −25 °C) shows three resonances at δ = −134.8 (*o*-F), −160.1 (*p*-F), and −165.0 ppm (*m*-F). These data are in line with the presence of a tetracoordinate, negatively charged boron substituent[5] $[RB(C_6F_5)_3]^-$ in **13**. The presence of an anion−cation bonding interaction is indicated by the large value of Δδ(*m*,*p*-F) = 4.9 (Scheme 6).[23]

Solutions of **13** in tetrachloroethane are stable at room temperature for several hours. We ascribe this stabilization to intramolecular coordination of an *ortho*-fluoro substituent of one of the C_6F_5 groups to zirconium, as shown. This assumption was confirmed by variable-temperature ^{19}F NMR experiments in C_6D_5Br/[D_8]toluene. At −60 °C, the ^{19}F NMR spectrum shows eight resonances (Table 3) as expected when one of the C_6F_5 groups is coordinating to the zirconium atom and hence becomes rigid and unsymmetrical. One fluorine resonance is shielded to δ = −180.2 ppm, more than 50 ppm from the region typical for an *ortho*-fluorine nucleus in an $[RB(C_6F_5)_3]^-$ anion. A similar shielding (to δ = −190.3 ppm at −88 °C) was observed for one of the *ortho*-fluorine nuclei in the zirconoxyborane $Cp^*_2ZrOB(C_6F_5)_3$ in which the C−F···Zr interaction was proven by X-ray analysis;[24] more recently, a number of zwitterionic complexes with similar Zr···F bonding interactions have been spectroscopically and structurally characterized.[6,7] The ^{19}F resonances of **13** broaden above −50 °C, and at room temperature, only the initial three ^{19}F resonances are discernible. Note that, presumably for steric reasons, such a Zr···F interaction does not occur in **12**; instead, the X-ray structure reveals an interaction between the zirconium atom and the methylene group carrying the borate substituent.[5]

Table 3. ^{19}F NMR chemical shifts of **12** {in C_6D_5Br/[D_8]toluene at −60 °C (283.23 MHz; ref. $CF_3C_6H_5$ in C_6D_6: δ = −64 ppm)}

	F(2)[a]	F(3)[b]	F(4)[b]	F(5)[b]	F(6)[b]
Ring A	−180.2	−155.6	−156.3	−161.8	−123.3
Ring B, C	−131.5	−162.6	−157.5	−162.6	−131.5

[a] Fluorine positions are numbered clockwise, starting from the boron-substituted position.

The reactivity of **13** contrasts sharply with that of the related complex **12**. Whilst **12** inserts 2-butyne to furnish **14** (Scheme 6) and shows moderate catalytic activity in the polymerization of ethylene (about 20−40 times less active than simple cationic Group-4 catalysts[18,19]), **13** is inactive in both types of reactions. This may be partly due to the low intrinsic reactivity of the metal−aryl bond towards insertion as compared to metal−alkyl bonds.[25] Additionally, the fluorine−zirconium interaction in **13** (which is absent in **12**) hinders coordination of the substrate. Nevertheless, the fluorine−zirconium interaction in **13** is not strong enough to resist cleavage by PMe_3 in CD_2Cl_4 with formation of **15**. The yellow color of **13** disappeared, and **15** was isolated as an off-white solid in 96% yield by precipitation with *n*-pentane. The structure of **15** was assigned on the basis of the ^1H and ^{19}F NMR spectra. In particular, the small value of Δδ(*m*,*p*-F) = 3.0 ppm is consistent with the donor having displaced the anion−cation bonding interaction;[23] an aromatic proton signal at δ = 4.48 ppm strongly suggests an agostic Zr···H interaction.[26]

Conclusion

1-Magnesaindane (**1**) was obtained via the corresponding 1-mercuraindane (**6**) and found to occur as a dimeric ten-membered ring species in THF solution; in line with the behavior of other magnesacycles, this is due to an interplay between ring strain and entropy. In contrast, intermediate **6** forms a dimer/trimer equilibrium, which is remarkable as, at room temperature and in the absence of a catalyst, diorganomercury compounds usually do not establish equilibria by exchanging ligands.

The 1-zirconaindane **2** was obtained from **1** and dichlorozirconocene. It reacts with $B(C_6F_5)_3$ to form the adduct **13** which, according to spectroscopic data, has a zwitterionic structure with transannular interactions between the zirconium atom and one of the *ortho*-fluorine atoms. Although this interaction may contribute to the inertness towards insertion of the zirconium−aryl bond in **13**, it is kinetically unstable at room temperature and is easily cleaved by the Lewis base trimethylphoshane, which coordinates to the zirconium atom with formation of **15**.

Experimental Section

General: All manipulations involving organometallic compounds were carried out in fully sealed glassware using standard high vacuum techniques. Solvents were dried by distillation from liquid Na/K alloy after predrying with NaOH. Magnesium was sublimed twice before use. NMR spectra were measured with a Bruker AC 200 spectrometer (^1H NMR: 200 MHz. ^{13}C NMR: 50.3 MHz), a Varian VXR-300 spectrpmeter (^1H NMR: 300 MHz. ^{13}C NMR: 75.4 MHz, ^{31}P NMR: 121.6 MHz. ^{19}F NMR: 283.23 MHz), or a Bruker MSL 400 spectrometer (^1H NMR: 400.1 MHz. ^{199}Hg NMR: 71.6 MHz). GCMS analyses were performed with an HP 5890 GC/5970 MS combination, operating at 70 eV and equipped with a Chrompack BP1 (QSGE) 50 m/0.25 mm column. HRMS measurements were performed with a Finnigan MAT 90 mass spectrometer under EI conditions using a direct introducing interface for the introduction of air- and moisture-sensitive compounds. Elemental analyses were carried out at the Microanalytical Laboratory, Rijksuniversiteit Groningen, The Netherlands.

1-(Bromomercurio)-2-[2-(bromomercurio)ethyl]benzene (5): In a Schlenk vessel, 1-bromo-2-(2-bromoethyl)benzene (**3**)[8] (3.17 g, 12 mmol) in 20 mL of THF was slowly added during 5 h to a stirred suspension of magnesium (1.54 g, 64 mmol) in 60 mL of THF at room temperature. After the addition was complete, an

aliquot was hydrolyzed. Titration (HCl, EDTA)[27] showed an Mg^{2+}/OH^- ratio of 1.1:1 and 78% yield of 1-(bromomagnesio)-2-[2-(bromomagnesio)ethyl]benzene. Subsequently, mercury bromide (8.70 g, 24.2 mmol) in 30 mL of THF was added and the solution was stirred overnight, after which a grey suspension was obtained. After hydrolysis, the resulting suspension was filtered and the residue was washed twice with THF and H_2O and subsequently dried in vacuo to give **5** as a white powder. Yield: 6.0 g (75% based on **3**). ^{1}H NMR (200 MHz, [D$_6$]DMSO, ref. [D$_5$]DMSO: δ = 2.50 ppm; NOESY): δ = 7.47 (m, 1 H, 4-H), 7.30 (m, 1 H, 7-H), 7.21 (m, 2 H, 5,6-H), 3.00 (t, $^3J_{H,H}$ = 7.5 Hz, 2 H, $ArCH_2$), 2.06 (t, $^3J_{H,H}$ = 7.5 Hz, 2 H, CH_2Hg) ppm. ^{13}C NMR (50.3 MHz, [D$_6$]DMSO, ref. [D$_6$]DMSO: δ = 39.5 ppm): δ = 154.0 (br. s, C-1), 149.9 (s, C-2), 136.4 (dd, $^1J_{C,H}$ = 161.9, $^3J_{C,H}$ = 5.6 Hz, C-6), 128.1 (dd, $^1J_{C,H}$ = 159.6, $^3J_{C,H}$ = 7.8 Hz, C-4 or -5), 127.8 (dd, $^1J_{C,H}$ = 156.0, $^3J_{C,H}$ = 5.8 Hz, C-3), 125.5 (dd, $^1J_{C,H}$ = 159.6, $^3J_{C,H}$ = 7.0 Hz, C-4 or -5), 38.8 (t, $^1J_{C,H}$ = 126.1 Hz, $ArCH_2$), 35.2 (bt, $^1J_{C,H}$ = 139.8 Hz, CH_2Hg) ppm. ^{199}Hg NMR (71.6 MHz, DMSO, ref. Me_2Hg = 0): δ = −1107, −1231 ppm.

1-Mercuraindane (6): A solution of $SnCl_2{\cdot}2H_2O$ (5.42 g, 24 mmol) in 120 mL of 20% aqueous NaOH was slowly added over 5 h to a suspension of **5** (8.0 g, 12 mmol) in a mixture of 120 mL of 10% aqueous NaOH and 24 mL of $CHCl_3$ at room temperature.[9] After the addition was complete, a grey precipitate (Hg) was filtered off and the residue was extracted twice with $CHCl_3$. The combined organic phases were dried with $MgSO_4$ and the solvents evaporated to give **6** as a light-grey solid (3.46 g, 95%). **6:** M.p. 71 °C. HRMS: ($^{12}C_{16}H_{16}{}^{200}Hg^{202}Hg$): calcd. 610.0642; found 610.0642. C_8H_8Hg (304.74): calcd.C 31.53, H 2.65; found C 31.91, H 2.69. **6a:** ^{1}H NMR (200 MHz, $CDCl_3$, ref. $CHCl_3$: δ = 7.22 ppm): δ = 7.30−7.16 (m, 4 H, ArH), 3.36 (m, 2 H, $ArCH_2$), 1.73 (m, 2 H, CH_2Hg) ppm. ^{13}C NMR (50.3 MHz, $CDCl_3$, ref. $CDCl_3$: δ = 76.8 ppm): δ = 180.1, C-7a), 153.2 (s, C-3a), 136.7 (dd, $^1J_{C,H}$ = 158, $^3J_{C,H}$ = 7 Hz, C-3), 130.4 (dd, $^1J_{C,H}$ = 156, $^3J_{C,H}$ = 6 Hz, C-6), 127.7 (dd, $^1J_{C,H}$ = 159, $^3J_{C,H}$ = 7 Hz, C-5), 125.5 (dd, $^1J_{C,H}$ = 159, $^3J_{C,H}$ = 7 Hz, C-4), 41.5 (t, $^1J_{C,H}$ = 131 Hz, C-3), 39.7 (t, $^1J_{C,H}$ = 125.5 Hz, C-2) ppm. ^{199}Hg NMR (71.6 MHz, $CDCl_3$, ref. Me_2Hg: δ = 0): δ = −237.2 ppm. **6b:** Due to the lower concentration of **6b** and to partial overlap of its NMR signals with those of **6a**, not all signals could be identified. ^{1}H NMR (200 MHz, $CDCl_3$, ref. $CHCl_3$: δ = 7.22 ppm): δ = 7.30−7.16 (undiscernible from those of **6a**, ArH), 2.95 (m, $ArCH_2$), 1.7 (shoulder on signal of **6a**, CH_2Hg) ppm. ^{13}C NMR (50.3 MHz, $CDCl_3$, ref. $CDCl_3$: δ = 76.8 ppm): δ = 178.8, C-7a), 154.5 (C-3a), 136.9 (C-3), 129.2 (C-6), 128.4 (C-5), 125.8 (C-4), 41.7 (C-3), 38.7 (C-2) ppm. ^{199}Hg NMR (71.6 MHz, $CDCl_3$, ref. Me_2Hg: δ = 0): δ = −305.5. ppm.

1-Magnesaindane (1): Compound **6** (1.78 g, 5.9 mmol) and magnesium (2.5 g, 103 mmol) in 70 mL of THF were stirred for 4 d at 70 °C. A brown solution and a fine black precipitate were obtained. The excess magnesium and the black precipitate were removed by careful decantation. Crystallization by cooling a saturated THF solution gave **1** as colorless needles (4.1 mmol, 70% based on **6**; determined by titration[27]). Attempts to obtain crystals suitable for an X-ray crystal structure determination were not successful. ^{1}H NMR (400 MHz, [D$_8$]THF, ref. [D$_7$]THF: δ = 1.75 ppm): δ = 7.71 (d, $^3J_{H,H}$ = 6.4 Hz, 1 H), 6.73−6.86 (m, 3 H), 3.06 (t, $^3J_{H,H}$ = 7.2 Hz, 2 H, $ArCH_2$), 0.02 (t, $^3J_{H,H}$ = 7.2 Hz, 2 H, CH_2Mg) ppm. ^{13}C NMR (50.3 MHz, ref. [D$_8$]THF = 67.4): δ = 168.7 (bs), 167.2 (bs), 142.2 (d, $^1J_{C,H}$ = 149.3 Hz), 125.4 (d, $^1J_{C,H}$ = 154.5 Hz), 124.9 (d, $^1J_{C,H}$ = 150.3 Hz), 122.2 (d, $^1J_{C,H}$ = 153.6 Hz), 43.3 (t, $^1J_{C,H}$ = 119.3 Hz, C-3), 17.6 (t, $^1J_{C,H}$ = 108.6 Hz, C-2) ppm.

Reaction of 1 with Deuterium Oxide: An excess of D_2O was added at room temperature to a solution of **1** (about 0.1 mmol) in THF. Diethyl ether and water were added and the organic layer was dried ($MgSO_4$). By GCMS, only [D$_2$]ethylbenzene (**7**) was observed. GCMS: *m*/*z* (%) = 108 (100) $[M]^+$, 107 (18), 106 (6), 105 (7), 104 (6), 103 (2).

Formation of Zwitterion 13: The known complex **2**[17] was obtained from the reaction of **1** with Cp_2ZrCl_2. To a mixture of **2** (53.4 mg, 0.16 mmol) and $B(C_6F_5)_3$ (84.0 mg, 0.16 mmol), 1 mL of C_6H_5Br was added at −30 °C. Addition of 3 mL of *n*-pentane gave a light yellow microcrystalline solid. The supernatant was pipetted off and the precipitate was washed twice with *n*-pentane (3 mL) and dried at 25 °C in the glovebox (1 h) to yield **13** (108.9 mg, 81%) as a pale yellow solid. ^{1}H NMR (300 MHz, $C_2D_2Cl_4$, ref. C_2DHCl_4: δ = 5.91 ppm; −25 °C): δ = 6.83 (m, 3 H, ArH), 6.40 (s, 10 H, Cp), 6.32 (d, $^3J_{H,H}$ = 5.6 Hz, 1 H, ArH), 2.70 (bt, $^3J_{H,H}$ = 7.5 Hz, 2 H, $ArCH_2$), 2.30 (bm, 2 H, CH_2B) ppm. ^{13}C NMR (75.43 MHz, $C_2D_2Cl_4$, ref. $C_2D_2Cl_4$: δ = 74.35; −25 °C, cation signals only; those of the anion part were too broad for identification): δ = 178.2 (CZr), 152.2, 138.7, 129.4, 125.3, 124.8 (d, $^1J_{C,H}$ = 157.9 Hz), 116.5 (d, $^1J_{C,H}$ = 170.6 Hz, Cp), 37.8 (t, $^1J_{C,H}$ = 126.5 Hz, $ArCH_2$), 14.6 (CH_2B) ppm. ^{19}F NMR (283.23 MHz, $C_2D_2Cl_4$, ref. $CF_3C_6H_5$ in C_6D_6: δ = −64; −25 °C): δ = −134.8 (*o*-F), −160.1 (*p*-F), −165.0 (*m*-F) ppm. $C_{36}H_{18}F_{15}Zr$ (826.73): calcd. C 51.62, H 2.17; found C 52.02, H 2.37.

Reaction of 13 with PMe_3. Formation of Adduct 15: PMe_3 was added (0.046 mmol, 4.8 μL) to a solution of **13** (38.5 mg, 0.046 mmol) in 0.5 mL of $C_2D_2Cl_4$ and an immediate color change from yellow to almost colorless was observed. After addition of 1 mL of *n*-pentane, a light yellow precipitate was obtained, which was filtered off and washed twice with *n*-pentane (2 mL). Evaporation of the *n*-pentane solution in the glovebox gave **15** as an off-white solid (40.2 mg, 96%). ^{1}H NMR (300 MHz, $C_2D_2Cl_4$, ref. C_2DHCl_4: δ = 5.91; −25 °C): δ = 7.09 (d, $^3J_{H,H}$ = 7.1 Hz, 1 H, ArH), 6.92 (m, 2 H, ArH), 5.53 (s, 10 H, Cp), 4.48 (dd, $^3J_{H,H}$ = 10.4, $^4J_{H,H}$ = 7.0 Hz, 1 H, ArH···Zr), 2.06 (m, 2 H, $ArCH_2$), 1.35 (d, $^2J_{P,H}$ = 7.4 Hz, 9 H, PMe_3), 1.06 (m, 2 H, CH_2B) ppm. ^{19}F NMR (283.23 MHz, $C_2D_2Cl_4$, ref. $CF_3C_6H_5$ in C_6D_6: δ = −64 ppm; −25 °C): δ = −131.9 (*o*-F), −163.0 (*p*-F), −166.0 (*m*-F) ppm. ^{31}P{H} NMR (121.6 MHz, $C_2D_2Cl_4$, ref. PPh_3: δ = −6.0 ppm): δ = −15.8 ppm.

Acknowledgments

The investigations were supported by Shell International Chemicals B. V.

[1] F. Bickelhaupt in *Grignard Reagents, New Developments* (Ed.: H. G. Richey, Jr.), Wiley, Chichester, **2000**, chapter 11.
[2] H. L. Uhm in *Handbook of Grignard Reagents* (Ed.: G. S. Silverman, P. E. Rakita), Marcel Dekker, New York, **1996**, chapter 9.
[3] F. Bickelhaupt in *Grignard Reagents, New Developments* (Ed.: H. G. Richey, Jr.), Wiley, Chichester, **2000**, chapter 9.
[4] F. M. J. Freijee, G. Schat, O. S. Akkerman, F. Bickelhaupt, *J. Organomet. Chem.* **1982**, *240*, 217−227, and references cited therein.
[5] J. Karl, G. Erker, R. Fröhlich, F. Zippel, F. Bickelhaupt, M. Schreuder Goedheijt, O. S. Akkerman, P. Binger, J. Stannek, *Angew. Chem.* **1997**, *109*, 2914−2917; *Angew. Chem. Int. Ed. Eng. l* **1997**, *36*, 2771−2774.
[6] M. Dahlmann, G. Erker, M. Nissinen, R. Fröhlich, *J. Am. Chem. Soc.* **1999**, *121*, 2820−2828.
[7] N. Kleigrewe, T. Brackemeyer, G. Kehr, R. Fröhlich, G. Erker, *Organometallics* **2001**, *20*, 1952−1955.

[8] H. Gilman, O. L. Marrs, *J. Org. Chem.* **1965**, *30*, 325−328.
[9] H. Sawatzky, G. F. Wright, *Can. J. Chem.* **1958**, *36*, 1555−1569.
[10] G. Calingaert, H. Soroos, V. Hnizda, *J. Am. Chem. Soc.* **1940**, *62*, 1107−1110.
[11] H. B. Charman, E. D. Hughes, C. Ingold, *J. Chem. Soc.* **1959**, 2523−2530.
[12] J. J. Led, H. Gesmar, *J. Magn. Reson.* **1982**, *49*, 444−463.
[13] A. Van Vulpen, J. Coops, *Recl. Trav. Chim. Pays-Bas* **1966**, *85*, 203−215.
[14] H. C. Holtkamp, C. Blomberg, F. Bickelhaupt, *J. Organomet. Chem.* **1969**, *19*, 279−285.
[15] F. Bickelhaupt, *Angew. Chem.* **1987**, *99*, 1020−1035; *Angew. Chem. Int. Ed. Engl.* **1987**, *26*, 990.
[16] M. F. Lappert, T. R. Martin, C. L. Raston, B. W. Skelton, A. H. White, *J. Chem. Soc., Dalton Trans.* **1982**, 1959−1964.
[17] G. Erker, K. Kropp, *J. Am. Chem. Soc.* **1979**, *101*, 3659−3660.
[18] M. Bochmann, *Angew. Chem.* **1992**, *104*, 1206−1207; *Angew. Chem. Int. Ed. Engl.* **1992**, *31*, 1181−1182.
[19] J. L. Kiplinger, T. G. Richmond, C. E. Osterberg, *Chem. Rev.* **1994**, *94*, 373−431.
[20] X. Yang, C. L. Stern, T. J. Marks, *J. Am. Chem. Soc.* **1994**, *116*, 10015−10032.
[21] L. Lia, X. Yang, A. Ishihara, T. J. Marks, *Organometallics* **1995**, *14*, 3135−3137.
[22] B. Temme, G. Erker, J. Karl, H. Luftmann, R. Fröhlich, S. Kotila, *Angew. Chem.* **1995**, *107*, 1867−1869; *Angew. Chem. Int. Ed. Engl.* **1995**, *34*, 1755−1757.
[23] A. D. Horton, J. de With, A. J. van der Linden, H. van de Weg, *Organometallics* **1996**, *15*, 2672−2674.
[24] A. R. Siedle, R. A. Newmark, W. M. Lamanna, *Organometallics* **1993**, *24*, 1491−1492.
[25] S. L. Borkowsky, R. F. Jordan, G. D. Hinch, *Organometallics* **1991**, *10*, 1268−1274.
[26] G. G. Hlatky, H. W. Turner, R. R. Eckman, *J. Am. Chem. Soc.* **1989**, *111*, 2728−2729.
[27] A. D. Vreugdenhil, C. Blomberg, *Recl. Trav. Chim. Pays Bas* **1963**, *83*, 453−460.

Received September 18, 2002
[I02526]

A Complex-Based Soft Template Route to PbSe Nanowires

Yuanfang Liu,*[a,b] Jinbo Cao,[a] Jinghui Zeng,[a] Cun Li,[a] Yitai Qian,[a] and Shuyuan Zhang[c]

Keywords: Nanostructures / Semiconductors / Luminescence / Carboxylate ligands

PbSe nanowires with an average size of 8 × 350 nm were synthesized by the reaction of $Pb(NO_3)_2$ and Se powder at 60 °C under ambient pressure. A mixture of arachidic acid (AA, n-$C_{19}H_{39}COOH$) and octadecylamine (ODA), which could form a complex with Pb^{2+}, was employed as a soft template to control the morphology of the resultant PbSe nanowires. The products were characterized by X-ray powder diffraction (XRD), X-ray photoelectron spectroscopy (XPS), and transmission electron microscopy. The photoluminescence (PL) spectrum of the PbSe nanowires is presented.
(© Wiley-VCH Verlag GmbH & Co. KGaA, 69451 Weinheim, Germany, 2003)

Introduction

Nanomaterials often display optical, electronic, and structural properties different from those of their bulk counterparts. Nanoparticles may adopt various shapes, which play a critical role in determining their basic properties.[1] To obtain a nanomaterial of a particular shape a variety of synthetic methods are needed not only to prepare the starting material but also to manipulate such materials to give desirable nanostructures.

One-dimensional (1D) nanostructures, such as nanorods, nanowires, and nanotubes, which serve as building blocks for many novel functional materials, are currently the focus of considerable interest.[2] So far, several significant synthetic methods, which include hard templates[3] (such as porous anodic alumina and carbon nanotubes), soft templates[4] (such as liquids and polymers), and hydrothermal routes[5] have been employed to prepare 1D nanostructures.

The study of PbSe 1D nanostructures is meaningful since PbSe can be used in IR sensors,[6] solar cells and infrared detectors,[7] and chemical sensors,[8] and is an important semiconductor owing to its large Bohr exciton radius, which can result in a strong confinement of the electron-hole pair.[9] However, there are only a few examples of the preparation of 1D PbSe nanostructures. These include: (i) synthesis of PbSe nanowires with an average size of 18 nm × 3 μm by the reaction of $PbCl_2$ and Se in ethylenediamine with KBH_4 as the reducing agent,[10] (ii) preparation in a monolayer of rod-like PbSe nanocrystals with a size of 10 × 100 nm,[3] and (iii) synthesis of PbSe nanorods with an average size of 60 × 700 nm through ultrasonic and γ-irradiation techniques in ethylenediamine.[11]

Soft templates have been demonstrated to be a very effective method for controlling the shapes of materials. Soft templates include liquid crystals,[12] monolayers,[13] polymers,[1] and surfactants.[14]

In this work, we obtained PbSe nanowires with an average size of 8 × 350 nm from a $CHCl_3$ solution of the surfactants arachidic acid (AA, n-$C_{19}H_{39}COOH$) and octadecylamine (ODA).

Results and Discussion

The XRD pattern of the PbSe nanowires isolated is shown in Figure 1. All peaks in Figure 1 could be indexed

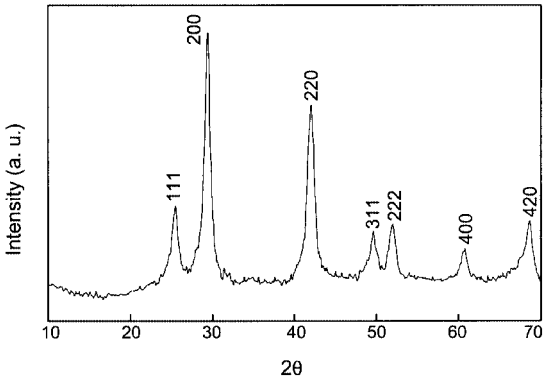

Figure 1. XRD pattern of prepared PbSe nanowires from AA/ODA (1:2)

[a] Department of Chemistry, University of Science and Technology of China,
Hefei, Anhui 230026, People's Republic of China
E-mail: liuyf1589@yahoo.com
[b] Department of Chemistry, Oklahoma State University, Stillwater, OK 74078-3071, USA
[c] Structure Research Laboratory, University of Science and Technology of China,
Hefei, Anhui 230026, People's Republic of China

as cubic PbSe. The calculated cell constant, a = 6.128 Å, is consistent with the reported value (a = 6.124 Å, JCPDS Card No.6-354). No peaks characteristic of impurities were observed. Given that the Debye−Scherrer calculations are approximate and more accurate for spherical particles, and that the PbSe has a curved nanowire morphology, the calculated average size of PbSe nanowires relies only on the TEM results.

XPS was further applied to determine the purity and composition of the product. The survey spectrum of PbSe nanowires is typical, and higher-resolution spectra of the Pb and Se regions of PbSe are shown in Figure 2. The survey spectrum of PbSe shows the presence of Pb and Se from the nanowires, and C and O from the surface of the material and from absorbed gaseous molecules. The strong peak observed in the Pb region at 137.2 eV is assigned to the (4f) Pb binding energy; the peak in the Se energy region is detected at 53.2 eV and is attributed to (3d) Se. No other peaks in the survey spectrum of PbSe were obvious. The (4f) Pb and (3d) Se peak areas quantified the content of Pb and Se and gave the atomic ratio of Pb to Se as 1:0.92, which is close to the literature value of 1:0.91.[10] Elemental analysis shows the atomic ratio of Pb/Se to be 1.003. This value is close to the stoichiometric ratio of PbSe (1) and the XRD results but is slightly different from that obtained by XPS. This is because XRD and elemental analysis are bulk-phase analyses while XPS gives only surface composition analysis. For nanoparticles, it is a common phenomenon, that surface composition is different from the corresponding bulk material, which is caused by the dangling bonds existing on the surface and segregation of a particular element to the surface of nanoparticles.[15,16]

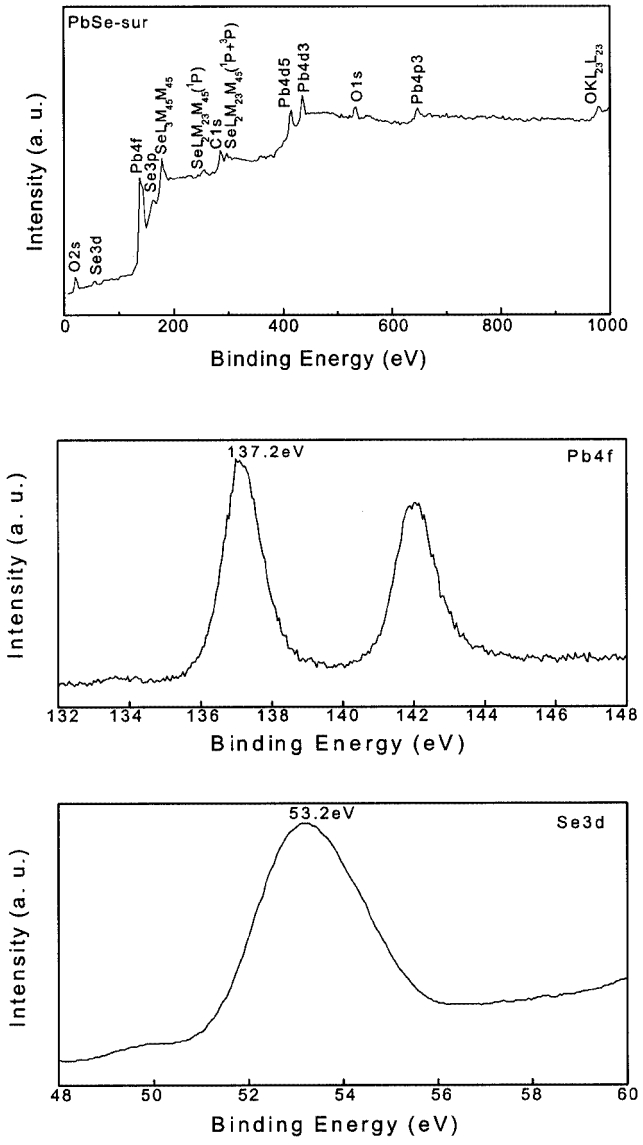

Figure 2. XPS analysis of as prepared PbSe nanowires from AA/ODA (1:2)

The morphology and size of the PbSe product were investigated by TEM, and the results are shown in Figure 3. The curved PbSe nanowires cross and overlap each other to form a net-like structure, and their average size is 8 × 350 nm (Figure 3, a). ED images of PbSe nanowires, shown in Figure 3, b, confirmed that the product is highly crystalline.

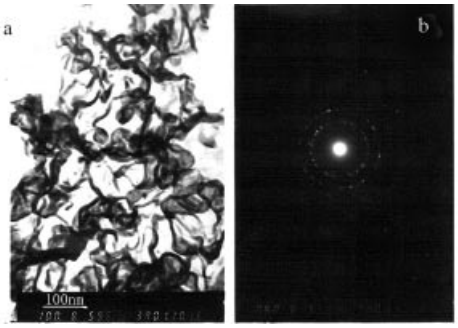

Figure 3. TEM and ED images of as prepared product from AA/ODA (1:2); (a) TEM of PbSe nanowires, (b) ED image of PbSe nanowires

To examine the quantum-confined effect of the product, the room-temperature photoluminescence (PL) spectrum of the PbSe nanowires, which were dispersed in alcohol, was recorded. To avoid the possible interference of trace AA and ODA, an alcohol solution of AA and ODA in a 2:1 ratio was used as reference. Figure 4 depicts the photoluminescence (PL) emission spectrum of the PbSe nanowires. Under photoluminescence excitation at 280 nm, the emitting peak is located at 359 nm with a 40 nm blue-shift compared with Guha's report.[9] The characteristic blue-shift of the PL spectrum of PbSe nanowires is attributed to their small diameter and larger aspect ratio.[17]

During formation of the PbSe nanowires, surfactants AA and ODA, in their various ratios, play an important role. When there is no surfactant and other conditions are identical, the PbSe obtained is a spherical nanoparticle. Mixtures of AA and ODA in varying ratios (0:1, 1:5, 1:1, 2:1, 5:1, and 1:0) were applied successively as a soft template keeping other conditions identical with those when AA/ODA = 1:2. The XRD patterns of the resultant products indicated that PbSe could indeed be formed in the mixtures of AA

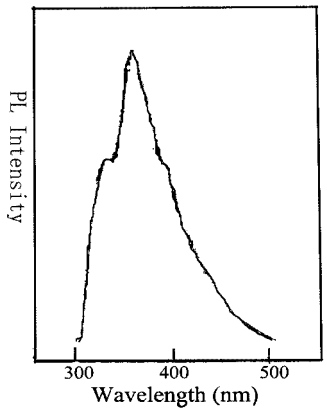

Figure 4. Photoluminescence (PL) spectrum of PbSe nanowires from AA/ODA (1:2)

and ODA. TEM images show the product yield of nanowires is clearly affected by the ratios of AA and ODA. When AA/ODA = 0:1, 1:5, 1:1, 2:1, or 5:1, nanorods and nanoparticles or hollow spheres consisting of nanoparticles are produced instead of nanowires. When the ratio of AA/ODA = 1:0, PbSe nanowires and a small amount of nanorods and nanoparticles are formed.

As regards the shape formation mechanism of PbSe nanowires, mixtures of AA and ODA have been employed before to prepare monolayers, which acted as a soft template to control the morphology of PbS and PbSe.[13] The shape of the PbS obtained is equilateral-triangular while that of PbSe is equilateral-triangular and rod-like. These results differ from those obtained in our experiments; presumably due to the different behavior and structure of AA/ODA as a solid-state monolayer compared to those of AA/ODA as a solution. In our experiment, the basicity of ODA which could promote conversion of RCOOH (AA) to $RCOO^-$.

It has been reported that Pb^{2+} can react with $RCOO^-$ to form lead carboxylate complexes with, for example, a three-dimensional polymer structure, a chain structure, or as monomers and dimers.[18,19] It can be concluded, therefore, that $RCOO^-$ in AA may act as a bidentate ligand to react with Pb^{2+} to form relatively stable complexes. According to the following experimental results, a three-dimensional polymer or chain structure was formed when $Pb(CH_3COO)_2$ reacted with AA in the presence of ODA. Lead carboxylate complexes of general formula $[Pb(C_{19}H_{39}COO)_2]_n$ were prepared as described in the Exp. Sect. IR spectroscopy indicates that the product has a similar IR spectrum to that of AA, except that the peaks at 1707.4 cm^{-1} [ν(C=O)], 2917.2 cm^{-1}, and 2848.8 cm^{-1} [ν(OH)] disappear, and new peaks at 1598.7 cm^{-1} [$\nu_{asym}(COO^-)$] and 1361 cm^{-1} [$\nu_{sym}(COO^-)$] appear. The values of $\nu_{asym}(COO^-)$ and $\nu_{sym}(COO^-)$ in the Pb^{2+}−AA complex are close to those in the Pb^{2+}−citric acid complex, which has a chain structure and bidentate carboxylic groups.[20] However, MALDI-TOF-MS results indicate no polymer was formed when the AA/ODA ratio was 0:1, 1:5, 1:1, 2:1, or 5:1. The MS of the Pb^{2+} complex formed when AA/ODA = 1:2, is as follows: calcd. for $\{[Pb(C_{19}H_{39}COO)_2]_{395}Na_2\}^{2+}$ 327738, found 327736.7; additional peaks: calcd. for $\{[Pb(C_{19}H_{39}COO)_2]_{10}Na_2\}^{2+}$ 8342, found 8344; calcd. for $[Pb(C_{19}H_{39}COO)_2Na_2]^{2+}$ 875.6, found 877.5.

All the above results confirm the formation of polymers of the Pb^{2+}−AA complex. From both literature reports[18,19] and these results, such $[Pb(C_{19}H_{39}COO)_2]_n$ systems may have a three-dimensional polymeric structure or a curved chain structure. In solution, Se^{2-}, which is produced in hydrazine,[21] attacks the complex. This attack can disrupt the bonds between the Pb and O atoms and promote gradual bond formation between Pb and Se. In the event of Pb−O bond cleavage, the Pb centre is ligated to Se and net-like PbSe nanowires are formed. Clearly, other carboxylic acids may be used as a soft template to prepare 1D nanomaterials. For example, Jiang et al.[2] prepared Ag nanowires with oleic acid as a soft template; Brase et al.[22] observed $BaSO_4$ nanowires in aqueous polymer solution, and pointed out that for nanowire formation, the polymer must have a high percentage of carboxy groups; Benton et al.[23] produced $BaSO_4$ nanofibers from polymaleate-based macromolecules with a high content of maleic acid as a modifier. All these results agree with our soft-template mechanism.

Efforts have also been made to prepare PbS 1D nanostructures with S replacing Se under identical conditions to those for the PbSe nanowires. The product obtained is a PbS nanorod. However, the nanorods are short and product yield is low. This result may be due to the different radii and coordination properties of S^{2-} and Se^{2-}.

Conclusion

In summary, a complex-based soft-template method has been developed to prepare PbSe nanowires in a mixture of AA and ODA at 60 °C under ambient atmosphere. The ratio of surfactants has a crucial influence on the rate of production of the PbSe nanowires. The optimum ratio of AA and ODA for preparing PbSe nanowires is 1:2. PbSe nanowires are formed because Pb^{2+} can react with AA to produce polymers of a Pb^{2+}−AA complex, which acts as a soft template. The soft-template mechanism provides a good example of the use of surfactants in the synthesis of 1D nanostructures. It is possible to replace AA by other carboxylic acid as a soft template for certain inorganic systems. The PL spectra of the PbSe nanowires show a strong confinement effect.

Experimental Section

General: Elemental analyses were carried out by gravimetric analysis combined with atomic emission spectroscopy using a Perkin−Elmer/6500 ICP-AES instrument. Microanalysis of C and H was carried out with a Perkin−Elmer 240C elemental analyzer. ^1H NMR spectra were recorded with a Bruker AM-200 spectrometer. MALDI-TOF-MS was performed with a Bruker Beflex III

mass spectrometer equipped with 1.25-m linear and 2.7-m reflection flight tubes and a 337-nm nitrogen laser. Angiotensin I (1269.5 Da) and adrenocorticotropic hormone (2466.7 Da) were used as external standards. The experiment was done at an accelerating potential of 20 kV. Sample solutions were prepared by dissolution of polymer, matrix (5-chlorosalicylic acid), and cationizing agent (CF_3COONa) in acetone. Typically, mixtures of 1.0 mL of a polymer solution (10 mg/ml) and 9.0 mL of a matrix solution (8.89 mg/ml) containing a cationizing agent (1.11 mg/ml) were prepared. Immediately after mixing, 1.0 μL portions of solution were deposited with a calibrated pipette onto the dimples of the sample slide and gently dried under air at room temperature. The plate was inserted into the apparatus under high vacuum (about 10^{-5} Pa). The X-ray powder diffraction (XRD) analysis was carried out with a Japan Rigaku D/max-γA X-ray diffractometer with graphite-monochromatized Cu-K_α radiation ($\lambda = 1.54178$ Å). X-ray photoelectron spectra (XPS) were collected with an ESCALAB MK II X-ray photoelectron spectrometer, using a monomochromatized Mg-K_α radiation as the X-ray excitation source. The binding energies are referenced to the (1s) C binding energy (284.6 eV) of the carbonaceous contaminant of the sample. Transmission electron microscopy (TEM) images were taken with a Hitachi H-800 transmission electron microscope. Infrared analyses were performed with KBr discs with a Magna IR-750 FT spectrometer in the range 400−4000 cm^{-1} at room temperature. Luminescence spectra were recorded with a Hitachi 850-fluorescence spectrophotometer.

Synthesis of PbSe Nanowires: In a typical procedure, AA and ODA in a 1:2 molar ratio (0.001 mol of AA and 0.002 mol of ODA) were dissolved in 100 mL of chloroform to form colloidal solutions of surfactants whilst stirring at 60 °C. A solution of 20 mL of absolute ethanol solution and 0.002 mol of $Pb(OAc)_2$ was added to the surfactants. A red solution of 0.002 mol of Se, 10 mL of 85% hydrazine, and 40 mL of absolute alcohol was added to the surfactant/metal salt mixture drop by drop to give an immediate black precipitate. After stirring at 60 °C for 0.5 h and standing for 1 h, the precipitate was filtered, and then washed successively with chloroform, absolute ethanol, and distilled water. Finally, the black product was dried under vacuum at 60 °C for 4 h.

Synthesis of the Lead Carboxylate Polymer: Similar to the preparation of PbSe nanowires, 0.001 mol of AA and 0.002 mol of ODA were dissolved in 100 mL of chloroform stirred at 60 °C to form a colloidal solution. A solution of 20 mL of absolute ethanol solution and 0.002 mol of $Pb(OAc)_2$ was added and after stirring at 60 °C for 0.5 h and standing for 1 h, the resultant white precipitate was filtered, then washed with chloroform, absolute ethanol, and distilled water. Finally, the white product was dried under vacuum at 60 °C for 4 h. ICP-AES for $[Pb(C_{19}H_{39}COO)_2]_n$: calcd. C 57.91, H 9.40, Pb 24.98; found C 57.58, H 9.82, Pb 24.88. ^1H NMR (C_6D_6): δ = 0.9 [3 H, $CH_3(CH_2)_{18}COO^-$], 1.27 [32 H, CH_3-$(CH_2)_{16}CH_2CH_2COO^-$], 1.65 [2 H, $CH_3(CH_2)_{16}CH_2CH_2COO^-$], 2.35 [2 H, $CH_3(CH_2)_{16}CH_2CH_2COO^-$] ppm. MALDI-TOF-MS: m/z = 344332.5, calcd. for $\{[Pb(C_{19}H_{39}COO)_2]_{415}Na_2\}^{2+}$ 344330; additional peaks at m/z = 322762.5, calcd. for $\{[Pb(C_{19}H_{39}COO)_2]_{389}Na_2\}^{2+}$ 322760.4 and m/z = 8344, calcd. for $\{[Pb(C_{19}H_{39}COO)_2]_{10}Na_2\}^{2+}$ = 8342.

Acknowledgments

We acknowledge the National Natural Science Research of China (No. 20071028).

[1] J. H. Zhan, X. G. Yang, D. W. Wang, S. D. Li, Y. Xie, Y. N. Xia, Y. T. Qian, *Adv. Mater.* **2000**, *12*, 1348−1351.
[2] P. D. Yang, C. M. Lieber, *Science* **1996**, *273*, 1836−1840.
[3] H. Dai, W. Wong, E. Y. Z. Lu, S. S. Fan, C. M. Lieber, *Nature* **1995**, *375*, 769−772.
[4] X. C. Jiang, Y. Xie, J. Lu, L. Y. Zhu, W. He, Y. T. Qian, *Chem. Mater.* **2001**, *13*, 1213−1218.
[5] Y. F. Liu, J. H. Zeng, W. X. Zhang, W. C. Yu, Y. T. Qian, J. B. Cao, W. Q. Zhang, *J. Mater. Res.* **2001**, *16*, 3361−3365.
[6] X. F. Liu, M. D. Zhang, *Int. J. Infrared Millimeter Waves* **2000**, *21*, 1697−1701.
[7] P. A. Kondas, *Report ARFSD-TD-92024*, **1993**.
[8] J. N. Zemel, *J. Franklin Inst.* **1973**, *296*, 475−483.
[9] S. Guha, V. J. Leppert, S. H. Risbud, I. Kang, *Solid State Commun.* **1998**, *105*, 695−699.
[10] W. Z. Wang, Y. Gen, Y. T. Qian, M. R. Ji, X. M. Liu, *Adv. Mater.* **1998**, *10*, 1479−1481.
[11] M. Chen, Y. Xie, J. C. Lu, L. J. Zhu, Y. T. Qian, *J. Mater. Chem.* **2001**, *11*, 518−520.
[12] X. C. Jiang, Y. Xie, J. Lu, L. Y. Zhu, W. He, Y. T. Qian, *J. Mater. Chem.* **2001**, *11*, 1775−1777.
[13] [13a] J. Yang, J. H. Fender, T. C. Jao, T. Laurion, *Microsc. Res. Tech.* **1994**, *27*, 402−411. [13b] J. Yang, J. H. Fender, *J. Phys. Chem.* **1995**, *99*, 5505−5511.
[14] N. W. Zheng, Q. S. Wu, Y. P. Ding, Y. D. Li, *Chem. Lett.* **2000**, 638−639.
[15] C. J. Lu, A. X. Kuang, G. Guang, *J. Appl. Phys.* **1996**, *81*, 202−206.
[16] H. Y. Lee, N. H. Goo, W. T. Jeong, K. S. Lee, *J. Alloys Compd.* **2000**, *313*, 258−262.
[17] B. M. I. van der Zande, L. Pages, R. A. M. Hikmet, A. van Blaaderen, *J. Phys. Chem. B* **1999**, *103*, 5761−5767.
[18] R. G. Bryant, V. P. Chacko, M. C. Etter, *Inorg. Chem.* **1984**, *23*, 3580−3584.
[19] P. G. Harrison, A. T. Steel, *J. Organomet. Chem.* **1982**, *239*, 105−113.
[20] M. Kourgiantakis, M. Matzapetakis, C. P. Raptopoulou, A. Terzis, A. Salifoglou, *Inorg. Chim. Acta* **2000**, *297*, 134−138.
[21] Y. F. Liu, J. H. Zeng, C. Li, J. B. Cao, Y. Y. Wang, Y. T. Qian, *Mater. Res. Bull.*, in press.
[22] I. E. Brase, United States Patent, no. 4,898,677, **1990**.
[23] W. J. Benton, I. R. Collins, I. M. Grimsey, G. M. Parkinson, S. A. Roger, *Faraday Discuss.* **1993**, *95*, 281−297.

Received May 3, 2002
[I02228]

Cobalt Chloride Complexes of N_3 and N_4 Donor Ligands

T. Martijn Kooistra,[a] Koen F. W. Hekking,[a] Quinten Knijnenburg,[a] Bas de Bruin,[a] Peter H. M. Budzelaar,[a] René de Gelder,[a] Jan M. M. Smits,[a] and Anton W. Gal*[a]

Keywords: Cobalt / N Ligands / Polymerisation

A number of cobalt(II) chloride complexes of pyridine/amine N_3 and N_4 donors have been prepared and structurally characterised. Even though they are paramagnetic, assignment of the ^{1}H NMR signals was possible in several cases. With the exception of tpa, which formed a cationic monochloride complex, all new complexes have *cis*-coordinated chlorides. Nevertheless, only the relatively rigid pyp ligands gave rise to (low) ethene polymerisation activity on activation with MAO.

(© Wiley-VCH Verlag GmbH & Co. KGaA, 69451 Weinheim, Germany, 2003)

Introduction

Cobalt complexes with nitrogen donor ligands have been used to mimic biological systems such as vitamin B-12 coenzyme.[1] They are also of interest in the context of dioxygen activation at transition metals.[2] Recently they have attracted attention as precatalysts for olefin polymerisation.[3] Typically, the precatalysts are the cobalt(II) chloride complexes of diiminepyridine (dip) ligands (see Figure 1). Structural characterisation of these complexes requires X-ray analysis because the paramagnetic Co^{II} centre complicates NMR studies. In the hope of obtaining some insight into the optimal coordination geometries for olefin polymerisation, we decided to study a range of flexible pyridine/amine complexes and compare these with the more rigid dip complexes. The ligands are of the picolylamine type and are multidentate, with amine (N_{am}) and pyridine (N_{py}) nitrogens (Figure 1).[4]

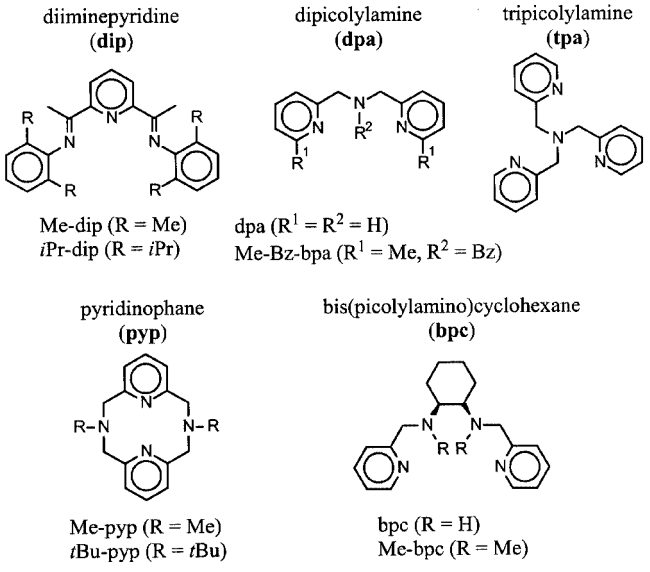

Figure 1. Pyridine/amine ligands used in this work; the dip ligand has been included for comparison

For polymerisation the two chlorides must be converted into an alkyl chain and a vacant coordination site *cis* to it. In five-coordinate complexes of dpa-type N_3 ligands, the small bite angles of the two five-membered chelate rings should disfavour equatorial coordination of all three nitrogens in a trigonal-bipyramidal coordination geometry; this leaves the *fac* and *mer* arrangements shown in Figure 2, both of which have a *cis* orientation of the remaining coordination sites (for the more rigid dip ligands, only the *mer* arrangement is accessible). Of the N_4 ligands, pyp is the least flexible one. In practice, it strongly prefers a *cis*-octahedral coordination geometry (Figure 2),[5] although other arrangements have been observed.[6,7] Six-coordinate complexes of tpa will also have a *cis*-octahedral structure; in addition, this ligands supports five-coordination, usually with an apical N_{am} donor (Figure 2). Finally, bpc-type ligands have been observed in three distinct coordination geometries shown in Figure 2: planar ("N4"), symmetric *cis*-octahedral ("N2/N2") and asymmetric *cis*-octahedral ("N3/N"). The different coordination geometries possible for the N_3 and N_4 donors also result in different patterns of N_{am} and N_{py} donors *trans* to the two sites potentially involved in polymerisation.

Results and Discussion

Synthesis

The N_3 and N_4 ligands used have all been reported previously.[8] Their $CoCl_2$ complexes were easily obtained by reaction with $CoCl_2 \cdot 6H_2O$ in the appropriate solvent.

[a] Toernooiveld 1, 6525 ED Nijmegen, The Netherlands
E-mail: gal@sci.kun.nl

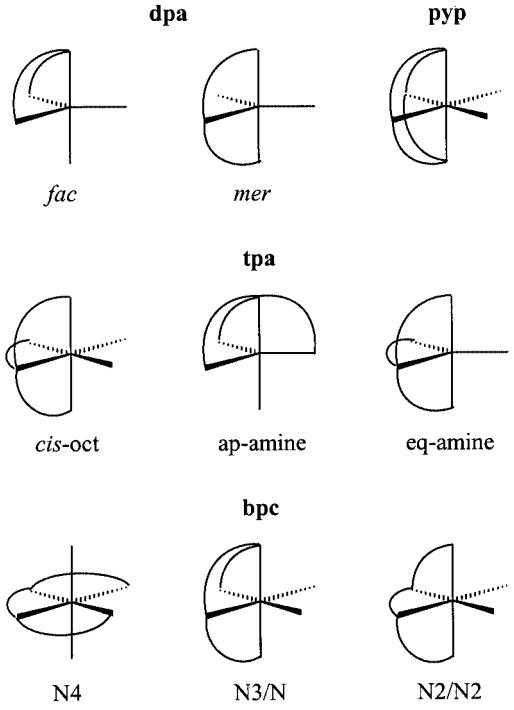

Figure 2. Coordination geometries of N_3 and N_4 ligands

Whereas most of the complexes are air stable, [(bpc)$CoCl_2$] (**5**) proved very sensitive to air and water. This complex was therefore synthesised by reaction of the ligand with dry $CoCl_2$ in anhydrous acetonitrile. The related complex [(Me-bpc)$CoCl_2$] (**6**) decomposes only very slowly in the presence of air and water.

Crystal Structures of N_4-Ligand Complexes

[(tpa)CoCl]$_2$$CoCl_4$

We expected to prepare an octahedral complex from tpa and $CoCl_2 \cdot 6H_2O$. However, X-ray analysis showed that the five-coordinate cation [(tpa)CoCl]$^+$ (**1**$^+$) had formed (Figure 3), with $CoCl_4^{2-}$ as the counterion. The unit cell contains two crystallographically independent cations **1**$^+$. Each of these has an almost C_3-symmetric trigonal-bipyramidal coordination geometry with N_{am} and Cl^- at the two axial positions. The Co^{II} centre is displaced approximately 0.5 Å from the equatorial N_3 plane in the direction of the chloride.

The structure of **1**$^+$ is very similar to that of the dicationic complex [(tpa)Co(MeCN)]$^{2+}$ (**2**) reported by Karlin.[9] The Co−N_{py} distances of **1**$^+$ and **2**$^{2+}$ are identical within experimental error. The Co−N_{am} distance for **1**$^+$ is longer than that for **2**$^{2+}$, as expected on the basis of the larger *trans*-influence of Cl^- compared to acetonitrile.

The structures of [(*t*Bu-pyp)$CoCl_2$] (**3**)[5d] and [(Me-pyp)-$CoCl_2$] (**4**)[5a] have been reported before. Both have a *cis*-octahedral coordination; the steric bulk of the *t*Bu substituents in **3** forces the ligand to twist, lowering the symmetry from C_{2v} (as observed in **4**) to C_2.

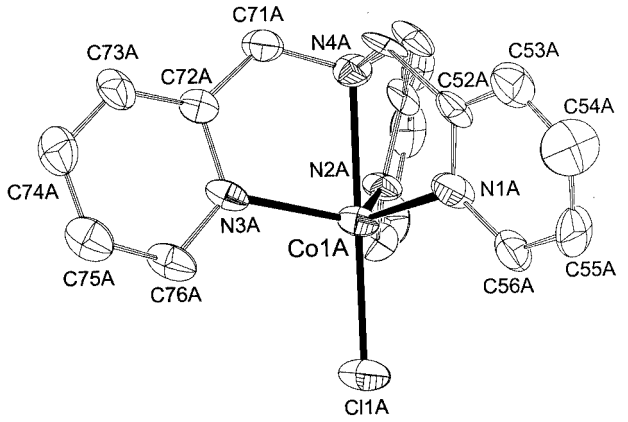

Figure 3. X-ray structure of one of the two independent cations **1**$^+$; selected bond lengths [Å] and angles [°]: Co1A−N1A 2.028(15), Co1A−N2A 2.038(14), Co1A−N3A 2.055(14), Co1A−N4A 2.240(14), Co1A−Cl1A 2.284(5), N1A−Co1A−N4A 76.3(6), N2A−Co1A−N4A 78.8(5), N3A−Co1A−N4A 76.7(5); corresponding values for the second cation: Co1B−N1B 2.072(15), Co1B−N2B 2.075(16), Co1B−N3B 2.055(14), Co1B−N4B 2.229(15), Co1B−Cl1B 2.280(6), N1B−Co1B−N4B 77.9(6), N2B−Co1B−N4B 76.2(6), N3B−Co1B−N4B 77.1(5); corresponding values for [(tpa)Co(MeCN)]$^{2+}$ (ref.[9]): Co−N1 2.041(3), Co−N2 2.037(3), Co−N3 2.053(3), Co−N4 2.177(3), Co−N5 2.046(3), N1−Co−N4 79.1(1), N2−Co−N4 78.9(1), N3−Co−N4 78.7(1)

[(bpc)$CoCl_2$] (5) and [(Me-bpc)$CoCl_2$] (6)

Both bpc complexes adopt a C_2-symmetric, *cis*-octahedral N2/N2 geometry (Figure 4). These two are the first examples of bis(picolylamino)ethylenediamine $CoCl_2$ complexes to be characterised by an X-ray structure determination. The structure of [(bpc)$CrCl_2$]$^+$ (an analogue of **5**) has been reported.[10] In addition, several metal dichloride com-

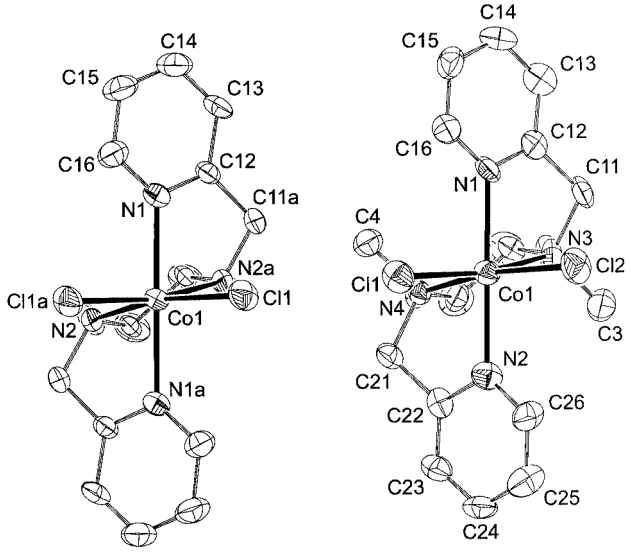

Figure 4. X-ray structures of **5** and **6**; selected bond lengths [Å] and angles [°] for **5**: Co1−N1 2.187(4), Co1−N2 2.205(4), Co1−Cl1 2.4187(14), N1−Co1−N1a 170.1(2), N2−Co1−N2a 79.8(2), Cl1−Co1−Cl1a 98.24(8) (atoms labeled a symmetry-related by $-x$, y, 1/2 − z); corresponding values for **6**: Co−N1 2.147(8), Co−N2 2.134(9), Co−N3 2.255(9), Co−N4 2.236(7), Co−Cl1 2.436(3), Co−Cl2 2.435(3), N1−Co−N2 173.1(4), N3−Co−N4 78.7(3), Cl1−Co−Cl2 98.24(13)

plexes of bis(picolylamino)ethylenediamine ligands lacking the cyclohexane ring have been structurally characterised.[11] A number of bpc and Me-bpc complexes of cobalt with counterions other than chloride have also been reported; all of these contain Co^{III}. Remarkably, all previously reported bpc cobalt complexes have the N3/N coordination geometry,[12] whereas the three Me-bpc cobalt complexes reported so far all have the N2/N2 arrangement.[13] Considering the wider class of bis(picolyl)ethylenediamine cobalt complexes, there are only a few examples of the N2/N2 arrangement: these include the more highly substituted system **A**[14] and the atypical, oxalato-bridged dimer **B**.[15]

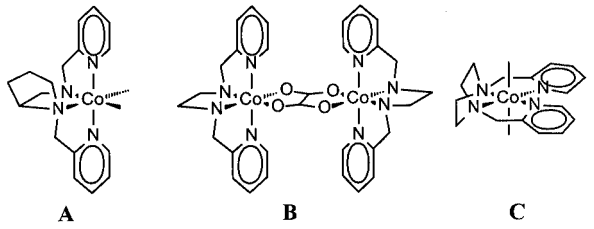

Judging from these examples, the N3/N arrangement is preferred over N2/N2 by only a small margin; substituents at the backbone may cause increased steric hindrance at the "planar" N_{am} and so promote the more extensive folding of the N2/N2 geometry. The N2/N2 geometry found in the oxalato-bridged dimer might be caused by steric hindrance between the monomer units in the N3/N geometry. Finally, only a single example of the N4 arrangement has ever been reported,[16] and in that case (**C**, above) the geometry is probably enforced by the rigid ligand backbone.

Returning to our $CoCl_2$ complexes, it seems remarkable that even bpc adopts the N2/N2 structure here. We believe that the larger size of Co^{II} (compared to Co^{III}) disfavours formation of the N3/N structure and hence is responsible for shifting the balance towards N2/N2.

In contrast to **3**, where the two enantiomeric conformations of the ligand are only slightly different and will interconvert in solution, the chiral geometry in **5** and **6** is locked through the coordination of the two pyridyl groups. On going from **5** to **6**, the introduction of the N_{am} methyl substituent results in a longer $Co-N_{am}$ distance, which is compensated for by a strengthening of the $Co-N_{py}$ interaction. In addition, the two pyridyl fragments become more nearly orthogonal (angle between planes: 121° and 104°, respectively). The rather similar Co−Cl distances in complexes **3**−**6** indicate that the *trans*-influence of N_{am} and N_{py} on the chlorides is similar.

Crystal Structures of N_3-Ligand Complexes

[(Me−Bz−dpa)$CoCl_2$] (7)

Complex **7** (Figure 5) has a pseudo trigonal-bipyramidal coordination geometry, with the two axial positions occupied by the two N_{py} atoms. The rather similar crystal structure of [(Me-dpa)$NiBr_2$] has previously been reported.[17]

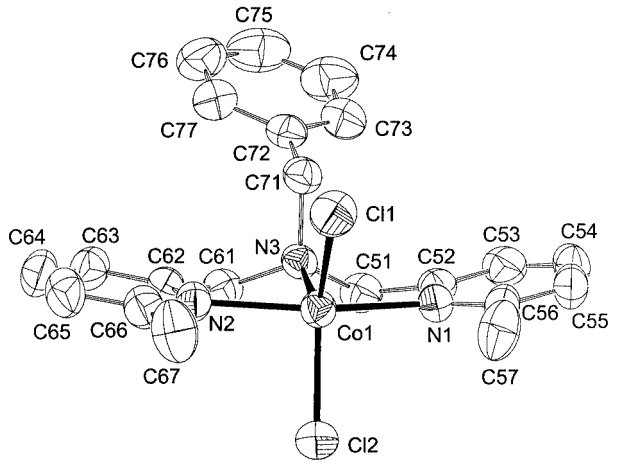

Figure 5. X-ray structure of **7**; selected bond lengths [Å] and angles [°]: Co−N1 2.178(2), Co−N2 2.182(2), Co−N3 2.124(2), Co−Cl1 2.2999(9), Co−Cl2 2.2784(9), N1−Co−N2 157.98(10), N3−Co−Cl1 111.33(6), N3−Co−Cl2 114.24(6), Cl1−Co−Cl2 134.41(4); corresponding values for (Me-dpa)$NiBr_2$ (ref.[17]): Ni−N1 2.042(10), Ni−N2 2.050(11), Ni−N3 2.007(14), Ni−Br1 2.473(3), Ni−Br2 2.494(3), N1−Ni−N2 163.6(5), N3−Ni−Br1 112.1(6), N3−Ni−Br2 98.7(5), Br1−Ni−Br2 149.2(1)

[(Me-dip)$CoCl_2$] (8)

Complex **8** (Figure 6) has a trigonal-bipyramidal geometry in the solid state, like its Fe analogue[18] and dpa complex **7**. In contrast, the $CoCl_2$ and $FeCl_2$ complexes of the isopropyl-substituted dip ligand have structures which are more nearly square pyramidal.[19] Apparently, the bulkier aryl groups promote this kind of distortion; a similar effect has been observed in a series of β-diiminate complexes.[20] In both dpa and dip complexes, the equatorial nitrogen is closer to the metal centre than the axial nitrogens. This effect is most pronounced for the dip complex, possibly due to geometric constraints of the ligand backbone.

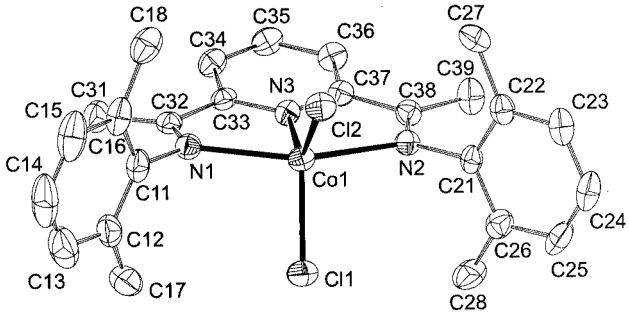

Figure 6. X-ray structure of **8**; selected bond lengths [Å] and angles [°]: Co−N1 2.247(2), Co−N2 2.265(2), Co−N3 2.0371(19), Co−Cl1 2.2578(7), Co−Cl2 2.2730(7), N1−Co−N2 150.42(7), N3−Co−Cl1 119.90(6), N3−Co−Cl2 127.14(6), Cl1−Co−Cl2 112.92(3); corresponding values for Fe analogue (ref.[18]): Fe−N1 2.271(6), Fe−N2 2.266(5), Fe−N3 2.110(6), Fe−Cl1 2.312(2), Fe−Cl2 2.278(2), N1−Fe−N2 145.5(2), N3−Fe−Cl1 118.9(2), N3−Fe−Cl2 131.3(2), Cl1−Fe−Cl2 109.9(1)

Five versus Six Coordination

The present work shows examples of both five- and six-coordinate structures. It seems that the ligand has a large influence on the preference for five- or six-coordination. The N_3 donor complexes **7** and **8** are naturally five-coordinate, but even the cobalt chloride complex of tpa prefers an ionic five-coordinate structure ($\mathbf{1}^+$). Five-coordination must be very favourable over six-coordination here (compared to pyp and bpc ligands) since even if a large excess of ligand is used, one-third of the cobalt is found as the counterion $[CoCl_4]^{2-}$ and free ligand remains. When NH_4PF_6 is then added to the reaction mixture, all cobalt is complexed by the ligand and the (presumably also five-coordinate) complex [**1**]PF_6 can be isolated. The other N_4 complexes all seem to prefer six-coordinate structures, although for complex **6** five-coordination in solution cannot be completely ruled out (see NMR section below). For **4** the coordination behaviour in solution has been described in the literature.[5a] Conductivity studies performed by Krüger showed that one chloride is exchanged for a coordinated solvent molecule in methanol, but only partial dissociation of one chloride takes place in acetonitrile. Although acetonitrile is generally considered to be a better ligand than methanol, methanol is very well suited for the solvation of chloride anions. This may be the driving force in the dissociation of chloride from **4**. The NMR spectrum of **3** shows a similar solvent dependence and suggests that this complex can also undergo chloride substitution in methanol. Clearly, complexes of pyp and bpc prefer six-coordination, although a chloride can sometimes be displaced by a polar solvent molecule. It is possible that five-coordination only occurs when the ligand can easily accommodate a trigonal-bipyramidal arrangement.

EPR Measurements

Six-coordinate [(*t*Bu-pyp)$CoCl_2$] (**3**) and five-coordinate [(Me-Bz-dpa)$CoCl_2$] (**7**) both have very broad X-band EPR spectra in the range $g = 2-6$, characteristic of high-spin ($S = 3/2$) cobalt(II) species with a large zero-field splitting ($D >> h\nu$). The EPR spectrum of **3** is shown in Figure 7.

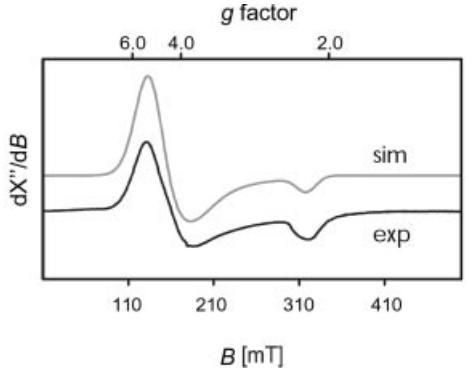

Figure 7. Experimental and simulated X-band EPR spectrum of **3**; experimental spectra in acetone/MeOH (2:3) at 6 K, 9.64 GHz. (attn. 55 dB, mod. 10 G)

Complex **3** reveals a nearly axial spectrum with no resolved hyperfine couplings, whereas the spectrum of **7** is rhombic and reveals hyperfine coupling with the cobalt nucleus at one of the *g*-tensors (Co, $I = 7/2$, 102 G). The apparent symmetry from the EPR spectra seems to correlate well with the cobalt coordination environments seen in the X-ray structures. The approximate real g values and *E*/*D* rhombicity factors derived from simulation of the experimental EPR spectra are $g_{11} = 2.17$, $g_{22} = g_{33} = 2.30$, $E/D = 0$ for complex **3** and $g_{11} = 2.03$, $g_{22} = 2.05$, $g_{33} = 2.20$, $E/D = 0.17$ for complex **7**. Apart from establishing the spin-state ($S = 3/2$) and the apparent coordination environment symmetry, these very broad EPR spectra are not very informative.

NMR Analysis

A complete interpretation of the paramagnetic ^1H NMR spectrum of $[(tpa)Co(CH_3CN)]^{2+}$ is presented in the report of Karlin,[9] and this helped us to assign all the peaks in the spectrum of $[(tpa)CoCl]^+$ ($\mathbf{1}^+$) on the basis of peak positions, linewidths and integrals. The signals from pyridine-H3, -H4, and -H5 are distinctly sharper than those of pyridine-H6 and the methylene protons. This seems to be the case for most pyridine-amine cobalt complexes studied here. Because the NMR shifts of [**1**]PF_6 and [**1**]$_2CoCl_4$ are identical, the same trigonal bipyramidal structure is assumed for both. Unfortunately, we did not succeed in growing X-ray quality crystals of [(dpa)$CoCl_2$] (**9**). However, its spectrum shows enough of a similarity to that of $[(tpa)CoCl]^+$ to allow a complete interpretation. For (Me−Bz−dpa)$CoCl_2$ (**7**), however, the extra signals from the benzyl substituent complicate the NMR spectrum too much to allow unambiguous assignments. Also, we observed no signals for the pyridine-H3 and -H5 protons between $\delta = 40$ and 60 ppm, although this is the most consistent feature of our NMR spectra. Since paramagnetic spectra are very sensitive to the environment at the metal centre, the large differences between the spectra of **7** and **9** may mean that these complexes do not have the same geometry. One possibility would be a switch to *fac* coordination of the dpa ligand in **9**. This would be inconsistent with the *decreased* tendency towards folding of bpc over Me-bpc discussed earlier. However, the two dpa complexes of Co that have been structurally characterised both have *fac*-coordinated dpa ligands.[21]

The ^1H NMR spectrum of [(bpc)$CoCl_2$] (**5**) could not be fully assigned, because all signals (apart from the NH) have approximately the same intensity and no distinct pattern could be discovered. The number of signals, however, agrees with the symmetrical structure observed in the solid state. [(Me-bpc)$CoCl_2$] (**6**) was never obtained as a single compound. A mixture of two products in a ratio of 10:6 or 10:4 was formed in the reaction of the ligand with $CoCl_2$ in CH_2Cl_2 and CH_3CN, respectively. ^1H NMR spectroscopy shows that *both* products produce twelve paramagnetic signals, the number expected for a symmetrically coordinated ligand (i.e. N4 or N2/N2, but *not* N3/N). Slow evaporation of an NMR sample resulted in crystallisation of one of the

products. This is probably the major product of the reaction, because both the crystal structure and the NMR spectrum resemble those of **5**, while the spectrum of the minor product shows no obvious similarities to that of **5**. Since the minor product also has a symmetrical ligand, one possibility would be the N4 structure, although this seems unlikely given that Co^{II} should have an even larger aversion to this arrangement than Co^{III}. Another possibility is that it is a cationic five-coordinate complex like $[(tpa)CoCl]^+$. A distinction between these two possibilities cannot be made at this stage. We were not able to obtain a ^{13}C NMR spectrum for any of the paramagnetic complexes.

Ethene Polymerisation

All the complexes except **8** were tested for polymerisation activity by treating them with 100 equivalents of MAO in chlorobenzene under an ethene atmosphere (7 and 35 bar). Most complexes did not exhibit any polymerisation activity at all, but pyp complexes **3** and **4** produced some polymer. The *tert*-butyl-substituted complex was particularly interesting as it remained active for a very long time (35 hours), resulting in an activity of 70 $g \cdot mol^{-1} \cdot h^{-1} \cdot bar^{-1}$. This is a factor of 7000 less than the reported cobalt-dip system under optimised conditions.[3a,3b] GPC analysis of the polymer formed at 35 bar showed that, besides a small amount of high molecular weight polyethene, the bulk of the "polymer" had a molecular weight of approximately 1000. It was difficult to optimise the pyp system because the complex seemed to decompose when a fresh batch of MAO was used for the polymerisation experiments.

It has been suggested that the dip-cobalt and -iron complexes used by Brookhart and Gibson polymerise ethene to high molecular weight polyethene because the large aryl substituents prevent associative displacement of the growing polymer chain. $[(Me\text{-}Bz\text{-}dpa)CoCl_2]$ (**7**) has nearly the same cobalt environment as precatalyst **8**, but lacks the steric bulk above and below the active site on cobalt. Indeed, **7** is not active in ethene polymerisation (nor is **9**). If this were caused by rapid chain transfer, formation of dimers would be expected. The fact that no ethene consumption was observed indicates that the lack of steric bulk is not the only obstruction for the reactivity of our N_3 complexes. Rather, it seems likely that the electronic properties of the ligand are also important. For example, $[(dip)CoCl_2]$ is apparently activated by reduction to a low-spin Co^{I} species, although the nature of the actual active species is still unclear.[22] Our pyridine-amine ligands are much weaker π-acceptors than dip ligands and are unlikely to stabilize the Co^{I} oxidation state, let alone induce the switch to a low-spin configuration. The main problem here is could be the *formation* of the active species, rather than the activity it would have once formed.

Conclusions

Analytically pure paramagnetic cobalt(II) complexes were easily synthesised by the reaction of $Co^{II}Cl_2$ with the appropriate N_3 or N_4 ligand. Most complexes are air-stable for at least a couple of days. Different modes of coordination became apparent from the obtained crystal structures. These were correlated with the ^1H NMR spectra of the complexes and helped in their interpretation. Variation of the solvent in the NMR experiments was informative for the behaviour in solution of the pyp complexes. The pyp ligands seemed to promote six-coordination, since even when a chloride dissociates in solution, a solvent molecule occupies the free coordination site. In contrast, tpa appears to favour five-coordination. The bpc complexes **5** and **6** are both six-coordinate in the solid state, but for **6** formation of a five-coordinate complex in solution cannot be excluded. Only two of the pyridine/amine complexes prepared (**3** and **4**) showed (low) activity in ethene polymerisation.

Experimental Section

General: All procedures were carried out under N_2 using standard Schlenk techniques unless specified otherwise. Acetonitrile, THF, dichloromethane and diethyl ether were distilled under nitrogen. Ethanol and methanol were deoxygenated by bubbling a stream of N_2 through the solvent for 15 minutes. For the synthesis of **5** and **6**, $CoCl_2 \cdot 6H_2O$ was dried for 4 hours at 150 °C before use. Ligands were prepared according to literature procedures.[8] All other chemicals are commercially available and were used without further purification. NMR measurements were performed on Bruker DPX200, AMX400, and AMX500 spectrometers. X-band EPR spectra were recorded on a Bruker ER 220 spectrometer. Samples were measured in acetone/MeOH (2:3) at 6−10 K. Simulations were performed with the program WEPR (F. Neese, University of Konstanz). Chemical shifts are listed in ppm with TMS as external reference (δ = 0 ppm). NMR signals for the NH protons of paramagnetic complexes were never observed. FAB^+- and ESI^+-MS spectra were recorded on a Finnigan MAT 900XL instrument.

$[(tpa)CoCl]_2[CoCl_4]$ ($[1]_2[CoCl_4]$): $CoCl_2 \cdot 6H_2O$ (205 mg, 0.86 mmol) was added to a solution of tpa (248 mg, 0.86 mmol; 1.0 equiv.) in 20 mL of ethanol. A blue solid precipitated almost immediately. After stirring for 1 hour at room temperature, the mixture was filtered. The solid was washed with diethyl ether and dried in vacuo; yield 0.19 g (66%). Crystals suitable for X-ray diffraction were grown by vapour diffusion of THF into a saturated acetonitrile solution. The blue product is air-stable as a solid and in solution. $C_{36}H_{36}Cl_6Co_3N_8$ (970.25): calcd C 44.56, H 3.74, N 11.55; found C 44.41, H 3.79, N 11.47. ^1H NMR (200 MHz, 298 K, ppm) CD_3OD: δ = 130.1 (3 H, py-*H6*), 108.0 (6 H, NCH_2), 58.2 (3 H, py-*H5*), 49.2 (3 H, py-*H3*), −1.7 (3 H, py-*H4*). CD_3CN: δ = 134.3 (3 H, py-*H6*), 107.3 (6 H, NCH_2), 60.8 (3 H, py-*H5*), 46.2 (3 H, py-*H3*), −3.5 (3 H, py-*H4*). FAB-MS: *m/z* = 803 $[(tpa)_2Co_2Cl_3]^+$, 384 $[M]^+$, 349 $[M - Cl]^+$, 291 $[M - CH_3Py]^+$, 256 $[M - Cl, - CH_3Py]^+$. ESI-MS: *m/z* = 384 $[M]^+$, 349 $[M - Cl]^+$.

$[(tpa)CoCl]PF_6$ ($[1]PF_6$): $CoCl_2 \cdot 6H_2O$ (330 mg, 1.39 mmol) was added to a solution of tpa (424 mg, 1.46 mmol; 1.05 equiv) in 25 mL of methanol. After addition of NH_4PF_6 (1.2 g, 7.2 mmol, 5.2 equiv.) a green microcrystalline solid precipitated. This solid was filtered off, washed three times with diethyl ether and dried under vacuum; yield 676 mg (92%). The product is air-stable as a solid and in solution. $C_{18}H_{18}ClCoF_6N_4P$ (529.72): calcd C 40.81, H 3.43, N 10.58; found C 40.64, H 3.42, N 10.44. ^1H NMR (200 MHz, 298 K, ppm): CD_3OD δ = 129.8 (3 H, py-*H6*), 107.6 (6 H, NCH_2),

57.91 (3 H, py-*H5*), 49.1 (3 H, py-*H3*), −1.44 (3 H, py-*H4*). CD_3CN: δ = 134.4 (3 H, py-*H6*), 107.1 (6 H, NCH_2), 60.8 (3 H, py-*H5*), 46.2 (3 H, py-*H3*), −3.6 (3 H, py-*H4*).

[(*t*Bu-pyp)$CoCl_2$] (3):[5d] $CoCl_2·6H_2O$ (172 mg, 0.72 mmol) was added to a warm solution (40 °C) of *t*Bu-pyp (256 mg, 0.72 mmol; 1.00 equiv.) in 35 mL of THF. After refluxing for 30 min a light-blue solid precipitated. The mixture was cooled to room temperature and filtered. The residue was washed twice with small portions of THF and dried under vacuum; yield 275 mg (79%). $C_{22}H_{32}Cl_2CoN_4$ (483.26): calcd C 54.78, H 6.69, N 11.62; found C 54.66, H 7.78, N 11.55. ^{1}H NMR (200 MHz, 298 K, ppm) CD_2Cl_2: δ = 81.4 (4 H, py-*H3*), 26.2 (2 H, py-*H4*), 3.1 (?), −9.4 (4 H, NCH_2), −35.8 (4 H, NCH_2), −43.5, −76.3 (*t*Bu?). CD_3OD: δ = 73.8 (4 H, py-*H3*), 28.3 (4 H, NCH_2), 18.8 (2 H, py-*H4*), −4.7 (4 H, NCH_2), −38.6 (*t*Bu). FAB-MS: *m*/*z* = 446 [M − Cl]$^+$, 411 [M − 2Cl]$^+$, 353 [M − 2Cl, − *t*BuH]$^+$.

[(Me-pyp)$CoCl_2$]·H_2O (4·H_2O): This compound was synthesised according to a literature procedure.[5a] ^{1}H NMR (200 MHz, 298 K, ppm) CD_2Cl_2: δ = 48.0 (4 H, NCH_2), 46.4 (4 H, py-*H3*), 24.0 (6 H, NCH_3), 14.2 (4 H, NCH_2), 7.2 (2 H, py-*H4*). CD_3OD: δ = 117.7 (6 H, NCH_3), 88.8 (4 H, NCH_2), 46.9 (4 H, py-*H3*), 31.5 (4 H, NCH_2).

[(bpc)$CoCl_2$] (5): A solution of dried $CoCl_2$ (106 mg, 0.82 mmol) in 10 mL of CH_3CN was added to a solution of bpc (239 mg, 0.81 mmol; 0.99 equiv.) in 7 mL of CH_3CN. The mixture immediately turned bright red. Evaporation of the solvent yielded a bright pink compound, which was washed twice with THF and dried under vacuum; yield 237 mg (68%). Single crystals suitable for X-ray diffraction were grown from a saturated CD_3CN solution. The product is highly air-sensitive as a solid and in solution. ^{1}H NMR (200 MHz, CD_3CN, 298 K, ppm): δ = 195.1 (2 H), 88.9 (2 H), 52.4 (2 H), 26.0 (2 H), 22.0 (4 H), 16.2 (2 H), 9.2 (2 H), 5.6 (2 H), 4.2 (2 H), 0.4 (2 H).

[(Me-bpc)$CoCl_2$] (6): Dried $CoCl_2$ (115 mg, 0.88 mmol) was added to a solution of Me-bpc (296 mg, 0.91 mmol; 1.03 equiv.) in 12 mL of CH_3CN. A purple solid precipitated immediately. After 2 hours the mixture was filtered and the dark pink residue was dried in vacuo; yield 244 mg (61%). Additional product precipitated from the mother liquor on standing at −20 °C. Crystals suitable for X-ray diffraction were obtained by slow evaporation of a CD_2Cl_2 solution. The product is air-stable as a solid and in solution, although it is very poorly soluble in most organic solvents. $C_{20}H_{28}Cl_2CoN_4$ (454.31): calcd C 52.88, H 6.21, N 12.33; found C 51.66, H 6.22, N 12.00. ^{1}H NMR (500 MHz, CD_2Cl_2, 298 K, ppm): δ = 164.9 (2H), 104.3 (2H), 102.6 (1.2 H), 89.4 (1.2 H), 83.0 (3.6 H, NCH_3), 61.1 (6 H, NCH_3), 51.8 (2 H), 47.5 (1.2 H), 29.7 (1.2 H), 24.7 (1.2 H), 24.4 (1.2 H), 23.9 (2H), 21.8 (0.8 H), 21.1 (2 H), 20.5 (2 H), 18.6 (2 H), 17.4 (1.2 H), 15.9 (1.2 H), 9.3 (1.2 H), 8.1 (2 H), 6.6 (2 H), 5.8 (2 H), 3.3 (1.2 H), −16.93 (2 H). FAB-MS: *m*/*z* = 418 [M − Cl]$^+$, 383 [M − 2Cl]$^+$.

[(Me-Bz-dpa)$CoCl_2$] (7): A solution of $CoCl_2·6H_2O$ (88 mg, 0.37 mmol) in 10 mL of acetonitrile was added to a solution of Me-Bz-dpa (111 mg, 0.35 mmol; 0.95 equiv.) in 5 mL of acetonitrile. The colour of the mixture immediately changed to blue/purple. After stirring for 7 hours at room temperature the volume was reduced by half under reduced pressure and a purple precipitate formed. The solid was collected by filtration, washed three times with diethyl ether and dried under vacuum; yield 85 mg (54%). The purple product is air-stable as a solid and in solution. Crystals of **7** suitable for X-ray diffraction were obtained by slow evaporation of an acetonitrile solution. **7**·CH_3CN, $C_{23}H_{26}Cl_2CoN_4$ (488.32): calcd C 56.57, H 5.37, N 11.47; found C 56.48, H 5.32, N 11.41. ^{1}H NMR (200 MHz, CD_3CN, 298 K, ppm): δ = 152.0 (2 H), 28.0 (2H), 15.6 (2 H), 14.6 (2 H), 14.2 (2 H), 12.1 (2 H), 7.7 (1 H, bz-*p*), −12.0 (2 H), −61.1 (6 H, py-CH_3). FAB-MS: *m*/*z* = 446 [M]$^+$, 411 [M − Cl]$^+$.

[(Me-dip)$CoCl_2$] (8):[3a] Me-dip (564 mg, 1.53 mmol) and $CoCl_2·6H_2O$ (363 mg, 1.53 mmol, 1.00 equiv.) were dissolved in 40 mL of THF. A colour change could be observed almost immediately and a green solid precipitated. After stirring for an additional hour at room temperature, this solid was filtered off, washed with THF (2×) and hexane (2×), and recrystallised from a layered methanol/hexane (1:1) solution, giving 266 mg (0.53 mmol, 35%) of the product as green air-stable crystals. ^{1}H NMR (200 MHz, 298 K, ppm) CD_2Cl_2: δ = 112.0 (2 H, py-*H3*), 36.1 (1 H, py-*H4*), 6.1 (4 H, Ar-*Hm*), −1.2 (6 H, N=C*Me*), −12.1 (2 H, Ar-*Hp*), −28.2 (12 H, Ar-*Me*). CD_3OD: δ = 111.9 (2 H, py-*H3*), 36.2 (1 H, py-*H4*), 6.2 (4 H, Ar-*Hm*), −1.1 (6 H, N=C*Me*), −12.0 (2 H, Ar-*Hp*), −28.1 (12 H, Ar-*Me*). FAB-MS: *m*/*z* = 463 [M − Cl]$^+$.

[(dpa)$CoCl_2$] (9): A solution of $CoCl_2·6H_2O$ (136 mg, 0.57 mmol) in 5 mL of ethanol was added to a solution of dpa (102 mg, 0.52 mmol; 0.91 equiv.) in 5 mL of ethanol. The colour of the mixture changed from light purple to dark-blue after stirring for 5 minutes at room temperature. After stirring for 16 hours at room temperature, the product was precipitated by adding diethyl ether. The mixture was filtered and the residue washed with diethyl ether and dried in vacuo; yield 73 mg (42%). The purple product is air-stable as a solid, however it decomposed in solution after being exposed to air for one day. ^{1}H NMR (200 MHz, 298 K, ppm) CD_3CN: δ = 126.1 (2 H, py-*H6*), 120.8 (2 H, NCH_2), 113.5 (2 H, NCH_2), 55.9 (2 H, py-*H5*), 44.0 (2 H, py-*H3*), −1.1 (2 H, py-*H4*). CD_2Cl_2: δ = 127.0 (2 H, py-*H6*), 113.6 (2 H, NCH_2), 110.3 (2 H, NCH_2), 55.7 (2 H, py-*H5*), 44.6 (2 H, py-*H3*), −0.80 (2 H, py-*H4*). $CDCl_3$: δ = 126.4 (2 H, py-*H6*), 112.9 (4 H, NCH_2), 55.1 (2 H, py-*H5*), 45.2 (2 H, py-*H3*), −0.7 (2 H, py-*H4*). FAB-MS: *m*/*z* = 293 [M − Cl]$^+$, 258 [M − 2Cl]$^+$.

Polymerisation Experiments: Chlorobenzene was distilled from a small amount of sodium. MAO was purchased as a solution in toluene (4.96% Al) and used as such. Polymerisation reactions under 7 bar of ethene were performed in a glass autoclave; reactions under 35 bar of ethene were done in a steel vessel (Hastelloy C).

A suspension of 33 μmol of the precatalyst in 10 mL of chlorobenzene was transferred under nitrogen into a 100 mL autoclave. Under nitrogen-flow 2 mL of MAO (100 equiv.) was transferred into a steel tube connected to the top of the pressure vessel. The complete system was put under ethylene pressure (7 or 35 bar), the MAO was added to the reaction mixture and the autoclave was closed. When ethylene consumption had stopped, or after about 6 hours if no reaction was observed, the autoclave was opened and the reaction mixture was neutralised by adding a mixture of methanol and aqueous HCl (5:1). The mixture was filtered and the polyethylene − if formed − was washed several times with methanol and dried under vacuum.

X-ray Structure Determinations: Single crystals were mounted in air on glass fibres. Intensity data were collected at room temperature on an Enraf−Nonius CAD4 diffractometer. Unit cell dimensions were determined from the angular setting of a limited number of reference reflections. Intensity data were corrected for Lorentz and polarisation effects, and for absorption using a semi-empirical ψ-scan correction.[23] Structures were solved by the program system DIRDIF[24] using the program PATTY[25] to locate all non-hydrogen atoms and refined with standard methods (refinement against

F^2 of all reflections) using SHELXL-97.[26] All non-hydrogen atoms were refined anisotropically; hydrogens were placed at calculated positions and refined isotropically in a riding mode, unless otherwise noted. Geometrical calculations (PLATON[27]) revealed neither unusual geometric features, nor unusual short intermolecular contacts, no higher symmetry and no (further) solvent-accessible areas. Details of the data collection and structure determinations are collected in Table 1.

CCDC-186122−186127 contain the supplementary crystallographic data for this paper. These data can be obtained free of charge at www.ccdc.cam.ac.uk/conts/retrieving.html [or from the Cambridge Crystallographic Data Centre, 12, Union Road, Cambridge CB2 1EZ, UK; Fax: (internat.) +44−1223/336-033; E-mail: deposit@ccdc.cam.ac.uk].

Notes on Individual Structures

[1]$_2$[CoCl$_4$]: One molecule of water and one molecule of acetonitrile were located and refined (hydrogen atoms for the water molecule were not included in the refinement). Hydrogen atoms were placed at calculated positions and were subsequently refined freely. Some anisotropic thermal displacement parameters showed physically unacceptable values when determined using default least-squares refinement parameters. The SQUEEZE procedure[27] was used to account for the residual electron density in a solvent area of 50 Å^3, resulting in a total electron count for this void of 44 electrons in the unit cell. This electron density should probably also be attributed to water molecules. Next the DIFABS procedure[28] was used, lowering the anisotropic *R*-value from 8.3% to 7.9%, resulting in considerably improved anisotropic thermal displacement parameters. The DELU and SIMU options still had to be applied to all atoms, however, and the ISOR option specifically to N2A, C51A, C55A, C62A, C51B, C65B, C72B, C76B, and O1.

5: One molecule of acetonitrile was located and refined. The refinement was hampered by the severe deterioration of the crystal during the data collection. A correction of almost 50% for crystal decay was necessary during the data reduction process.

6: One molecule of water was located and refined; hydrogen atoms for this water molecule were not included in the refinement. Based solely on donor-acceptor distances hydrogen bonds could probably be formed between O1 and Cl1 and between O1 and Cl2.

Table 1. Details of crystal structure determinations

Compound	[**1**]$_2$[CoCl$_4$]	**5**	**6**	**7**	**8**
Crystal colour	dark green	transparent red-brown	transparent purple-red	purple	green
Crystal shape	regular fragment	very irregular fragment	rather regular fragment	regular fragment	small, regular fragment
Crystal size [mm	0.24×0.18×0.15	0.52×0.48×0.28	0.29×0.17×0.10	0.42×0.24×0.12	0.13×0.11×0.08
Empirical formula	$C_{19}H_{20.5}Cl_3Co_{1.5}N_{4.5}O_{0.5}$	$C_{22}H_{30}Cl_2CoN_6$	$C_{20}H_{30}Cl_2CoN_4O$	$C_{23}H_{26}Cl_2CoN_4$	$C_{26}H_{31}Cl_2CoN_3O$
Molecular weight	514.64	508.35	472.31	488.31	531.37
Temperature [K]	293(2)	298(2)	293(2)	293(2)	150(2)
Crystal system, space group	Monoclinic, *Cc*	Monoclinic, *C*2/*c*	Orthorhombic, *Pna*2$_1$	Monoclinic, *P*2$_1$/*c*	Monoclinic, *P*2$_1$/*n*
Unit cell det. #, θ range	15, 6.504···11.817	25, 19.293···22.715	25, 11.961···14.468	25, 10.488···20.064	13258, 1.830···25.350
a [Å]	12.095(3)	12.9525(6)	16.3169(11)	8.9564(12)	14.1667(12)
b [Å]	27.587(9)	12.1804(10)	14.7110(10)	20.817(5)	14.6541(8)
c [Å]	14.074(3)	16.3098(10)	8.8110(6)	13.1776(19)	13.1684(11)
α [°]	90	90	90	90	90
β [°]	93.967(17)	103.698(4)	90	106.227(10)	109.558(4)
γ [°]	90	90	90	90	90
Volume [Å^3]	4685(2)	2499.9(3)	2115.0(2)	2359.0(7)	2576.0(3)
Z, d_{calc} [g·cm^{-3}]	8, 1.459	4, 1.351	4, 1.483	4, 1.375	4, 1.370[a]
Abs. coeff. [mm^{-1}	1.432	0.921	1.083	0.971	0.897[a]
Scan	ω	ω/2θ	ω/2θ	ω/2θ	Area det. θ, ω
F(000)	2092	1060	988	1012	1108[a]
θ range [°]	2.78···23.25	2.57···27.46	2.85···27.46	2.56···25.61	1.83···25.35
Index ranges	$0 \le h \le 13$ $-30 \le k \le 0$ $-15 \le l \le 15$	$-16 \le h \le 0$ $0 \le k \le 15$ $-20 \le l \le 21$	$0 \le h \le 21$ $0 \le k \le 19$ $0 \le l \le 11$	$0 \le h \le 10$ $0 \le k \le 25$ $-16 \le l \le 15$	$-17 \le h \le 15$ $-17 \le k \le 16$ $-15 \le l \le 12$
Collected/unique [R_{int}]	3546/3546	2985/2863 [0.0320]	2576/2576	4722/4431 [0.0242]	13258/4707 [0.0501]
Observed [$I_o > 2\sigma(I_o)$]	1888	2210	1314	3067	3265
Abs struct par	0.02(4)		0.00(5)		
DIFABS used?	yes	no	no	no	no
Relat. transm. fact.	1.052···0.962	1.051···0.916	1.021···0.965	1.069···0.961	
Data/restraints/pars	3546/531/515	2863/0/142	2576/1/250	4431/0/375	4707/0/286
Goodness−of−fit on F^2	1.004	1.332	1.053	1.084	0.960
SHELXL-97 wt pars	0.0692	0.2000	0.0361, 1.3080	0.0403, 0.6266	0.0402
*R*1, *wR*2 [$I > 2\sigma(I)$]	0.0733, 0.1365	0.0995, 0.2789	0.0705, 0.1074	0.0405, 0.0846	0.0400, 0.0802
*R*1, *wR*2 (all data)	0.1635, 0.1608	0.1207, 0.3140	0.1700, 0.1331	0.0741, 0.0963	0.0689, 0.0869
Diff. peak, hole [e·Å^{-3}]	0.629, −0.537	2.084, −1.124	0.402, −0.501	0.278, −0.224	0.309, −0.371

[a] Excluding contents of a "void" of 165 Å^3; see text for details.

7: One molecule of acetonitrile was located and refined. Hydrogen atoms were refined freely.

8: Calculations[27] showed a void of 165 Å^3, containing 32 electrons, resulting in a large volume of about 35 Å^3 per atom. Hexane and methanol were used in the synthetic route but no reasonable guess could be made about the nature of the solvent moiety or moieties present, nor was it possible to assign any physically meaningful parameters to the electron density. Therefore the SQUEEZE procedure was applied to account for this electron density. As a consequence this electron density could not be taken into account while calculating the physical·molecular properties as given in Table 1.

Acknowledgments

We thank Dr. E. J. Reijerse for recording the EPR spectra of **3** and **7**.

[1] See e.g.: [1a] Y. Murakami, J.-I. Kikuchi, Y. Hisaeda, O. Hayashida, *Chem. Rev.* **1996**, *96*, 721. [1b] J. Halpern, in: *Chemistry and Significance of Vitamin B_{12} Model Systems* (Ed.: D. Dolphin); John Wiley: New York, **1982**; vol. 1, p. 501.

[2] See e.g.: C. Bianchini, R. W. Zoellner, *Adv. Inorg. Chem.* **1997**, *44*, 263.

[3] [3a] B. L. Small, M. Brookhart, A. M. A. Bennett, *J. Am. Chem. Soc.* **1998**, *120*, 4049−4050. [3b] G. J. P. Britovsek, V. C. Gibson, B. S. Kimberley, P. J. Maddox, S. J. McTavish, G. A. Solan, A. J. P. White, D. J. Williams, *Chem. Commun.* **1998**, 849−850. [3c] B. L. Small, M. Brookhart, *J. Am. Chem. Soc.* **1998**, *120*, 7143−7144. [3d] G. J. P. Britovsek, M. Bruce, V. C. Gibson, B. S. Kimberley, P. J. Maddox, S. Mastroianni, S. J. McTavish, C. Redshaw, G. A. Solan, S. Strömberg, A. J. P. White, D. J. Williams, *J. Am. Chem. Soc.* **1999**, *121*, 8728−8740. [3e] G. J. P. Britovsek, S. Mastroianni, G. A. Solan, S. P. D. Baugh, C. Redshaw, V. C. Gibson, A. J. P. White, D. J. Williams, M. R. J. Elsegood, *Chem. Eur. J.* **2000**, *6*, 2221−2231.

[4] Me-dip = 2,6-bis[1-(2,6-dimethylphenylimino)ethyl]pyridine; *i*Pr-dip = 2,6-bis[1-(2,6-diisopropylphenylimino)ethyl]pyridine; dpa = *N*,*N*-bis(2-pyridylmethyl)amine; Me-Bz-dpa = *N*-benzyl-*N*,*N*-bis[(6-methyl)pyrid-2-ylmethyl)]amine; tpa = *N*,*N*,*N*-tris(2-pyridylmethyl)amine; Me-pyp = 2,11-dimethyl-2,11-diaza[3,3]-(2,6)pyridinophane; *t*Bu-pyp = 2,11-di-*tert*-butyl-2,11-diaza[3,3](2,6)pyridinophane; bpc = *trans*-*N*,*N*′-bis(2-pyridylmethyl)cyclohexane-1,2-diamine; Me-bpc = *trans*-*N*,*N*′-dimethyl-*N*,*N*′-bis(2-pyridylmethyl)cyclohexane-1,2-diamine

[5] [5a] H.-J. Krüger, *Chem. Ber.* **1995**, *128*, 531. [5b] C.-M. Che, Z.-Y. Li, K.-Y. Wong, C.-K. Poon, T. C. W. Mak, S.-M. Peng, *Polyhedron* **1994**, *13*, 771. [5c] Y. Yamamoto, Y. Hata, Y. Shimura, *Chem. Lett.* **1981**, 1559−1560. [5d] S. P. Meneghetti, P. J. Lutz, J. Fischer, J. Kress, *Polyhedron* **2001**, *20*, 2705.

[6] For an example of eight-coordinate Co, see: W. O. Koch, J. T. Kaiser, H.-J. Krüger, *Chem. Commun.* **1997**, 2237.

[7] For κ^3-coordinated pyridinophane ligands, see: [7a] H. Kelm, H.-J. Krüger, *Eur. J. Inorg. Chem.* **1998**, 1381. [7b] S. P. Meneghetti, P. J. Lutz, J. Kress, *Organometallics* **2001**, *20*, 5050. [7c] T. Sciarone, J. Hoogboom, P. P. J. Schlebos, P. H. M. Budzelaar, R. De Gelder, J. M. M. Smits, A. W. Gal, *Eur. J. Inorg. Chem.* **2002**, 457.

[8] [8a] Me-dip, *i*Pr-dip: ref.[3d] [8b]dpa: H. Nagao, N. Komeda, M. Mukaida, M. Suzuki, K. Tanaka, *Inorg. Chem.* **1996**, *35*, 6809. [8c] Me-Bz-dpa: B. De Bruin, J. A. Brands, J. J. J. M. Donners, M. P. J. Donners, R. De Gelder, J. M. M. Smits, A. W. Gal, A. L. Spek, *Chem. Eur. J.* **1999**, *5*, 2921. [8d] tpa: F. Højland, H. Toftlund, S. Yde-Andersen, *Acta Chem. Scand., Ser. A* **1983**, *37*, 251. [8e] Me-pyp: F. Bottino, M. de Grazia, P. Finocchario, F. R. Frinczek, A. Mamo, S. Pappalardo, *J. Org. Chem.* **1988**, *53*, 3521. [8f] *t*Bu-pyp: ref.[5b] [8g] bpc: M. A. Heinrichs, D. J. Hodgson, K. Michelsen, E. Pedersen, *Inorg. Chem.* **1984**, *23*, 3174. [8h] Me-bpc: J. Glerup, P. A. Goodson, A. Hazall, R. Hazall, D. J. Hodgson, C. J. McKanzie, K. Michelsen, U. Rychlewska, H. Toftlund, *Inorg. Chem.* **1994**, *33*, 4105.

[9] A. Nanthakumar, S. Fox, N. N. Murthy, K. D. Karlin, *J. Am. Chem. Soc.* **1997**, *119*, 3898.

[10] Y. Yamamoto, Y. Hata, Y. Shimura, *Chem. Lett.* **1981**, 1559.

[11] Cr: [11a] Y. Hata, Y. Yamamoto, Y. Shimura, *Bull. Chem. Soc. Jpn.* **1981**, *54*, 1255; Fe: [11b] N. Arulsamy, D. J. Hodgson, J. Glerup, *Inorg. Chim. Acta* **1993**, *209*, 61. [11c] Y. Mekmouche, S. Menage, C. Toia-Duboc, M. Fontecave, J.-B. Galey, C. Lebrun, J. Pecaut, *Angew. Chem. Int. Ed.* **2001**, *40*, 949. [11d] P. Mialane, J.-J. Girerd, J. Guilhem, L. Tchertanov, *Inorg. Chim. Acta* **2000**, *298*, 38. [11e] J. Simaan, S. Poussereau, G. Blondin, J.-J. Girerd, D. Defaye, C. Philouze, J. Guilhem, L. Tchertanov, *Inorg. Chim. Acta* **2000**, *299*, 221. [11f] B. Rieger, A. S. Abu-Surrah, R. Fawzi, M. Steiman, *J. Organomet. Chem.* **1995**, *497*, 73; Cu: [11g] C. Ng, M. Sabat, C. L. Fraser, *Inorg. Chem.* **1999**, *38*, 5545.

[12] [12a] M. A. Cox, T. J. Goodwin, P. Jones, P. A. Williams, F. S. Stephens, R. S. Vagg, *Inorg. Chim. Acta* **1987**, *127*, 49. [12b] E. F. Birse, M. A. Cox, P. A. Williams, F. S. Stephens, R. S. Vagg, *Inorg. Chim. Acta* **1988**, *148*, 45. [12c] E. F. Birse, P. A. Williams, F. S. Stephens, R. S. Vagg, *Inorg. Chim. Acta* **1988**, *148*, 63. [12d] J. A. Chambers, T. J. Goodwin, P. A. Williams, F. S. Stephens, R. S. Vagg, *J. Coord. Chem.* **1988**, *17*, 277. [12e] M. A. Anderson, E. F. Birse, M. J. E. Hewlins, J. P. G. Richards, F. S. Stephens, R. S. Vagg, P. A. Williams, *Inorg. Chem.* **1991**, *30*, 3774. [12f] P. D. Newman, F. S. Stephens, R. S. Vagg, P. A. Williams, *Inorg. Chim. Acta* **1993**, *204*, 257.

[13] [13a] P. Leverett, J. Petherick, P. A. Williams, R. S. Vagg, *J. Coord. Chem.* **1996**, *37*, 195. [13b] R. R. Fenton, F. S. Stephens, R. S. Vagg, P. A. Williams, *Inorg. Chim. Acta* **1991**, *182*, 67. [13c] R. R. Fenton, F. S. Stephens, R. S. Vagg, P. A. Williams, *Inorg. Chim. Acta* **1995**, *236*, 109.

[14] R. R. Fenton, F. S. Stephens, R. S. Vagg, P. A. Williams, *Inorg. Chim. Acta* **1992**, *197*, 233.

[15] J. Glerup, P. A. Goodson, D. J. Hodgson, K. Michelson, *Inorg. Chem.* **1995**, *34*, 6255.

[16] J. Ratilainen, K. Airola, R. Frohlich, M. Nieger, K. Rissanen, *Polyhedron* **1999**, *18*, 2265.

[17] J. Rogers, R. A. Jacobson, *J. Chem. Soc. (A)* **1970**, 1826.

[18] $FeCl_2$ complex of 2,4,6-trimethylphenyl-substituted dip ligand: see ref.[3d]

[19] [19a] (*i*Pr-dip)$CoCl_2$: ref.[3d] [19b] (*i*Pr-dip)$FeCl_2$: refs.[3a,3b]

[20] P. H. M. Budzelaar, A. B. Van Oort, A. G. Orpen, *Eur. J. Inorg. Chem.* **1998**, 1485.

[21] [21a] T. Ama, K.-I. Okamoto, T. Yonemura, H. Kawaguchi, Y. Ogasawara, T. Yasui, *Chem. Lett.* **1996**, 29. [21b] R. M. Hartshorn, S. G. Telfer, *J. Chem. Soc., Dalton Trans.* **2000**, 2801.

[22] [22a] V. C. Gibson, M. Humphries, K. Tellmann, D. Wass, A. J. P. White, D. J. Williams, *Chem. Commun.* **2001**, 2252. [22b] T. M. Kooistra, Q. Knijnenburg, J. M. M. Smits, A. D. Horton, P. H. M. Budzelaar, A. W. Gal, *Angew. Chem. Int. Ed.* **2001**, *40*, 4719.

[23] A. C. T. North, D. C. Philips, F. S. Mathews, *Acta Crystallogr., Sect. A* **1968**, *24*, 351.

[24] P. T. Beurskens, G. Beurskens, W. P. Bosman, R. de Gelder, S. García-Granda, R. O. Gould, R. Israël, J. M. M. Smits, *DIRDIF-96. A computer program system for crystal structure determination by Patterson methods and direct methods applied to difference structure factors*, Crystallography Laboratory, University of Nijmegen: The Netherlands, **1996**.

[25] P. T. Beurskens, G. Beurskens, M. Strumpel, C. E. Nordman, in: *Patterson and Pattersons* (Eds.: J. P. Glusker, B. K. Patterson, M. Rossi); Clarendon Press: Oxford, **1987**; p. 356.

[26] G. M. Sheldrick, *SHELXL-97. Program for the refinement of crystal structures*; University of Göttingen: Germany, **1997**.

[27] [27a] A. L. Spek, *Acta Crystallogr., Sect. A* **1990**, *46*, C34. [27b] A. L. Spek, *PLATON-93. Program for display and analysis of crystal and molecular structures*; University of Utrecht: The Netherlands, **1995**.

[28] N. Walker, D. Stuart, *Acta Crystallogr., Sect. A* **1983**, *39*, 158.

Received June 6, 2002
[I02298]

Reactions of *cis*-2,3-Dimethylaziridine, 3-Pyrroline and Pyrrolidine with Me_3Al and Me_3Ga: Adducts and Dimeric Amides

Yuankui Zhang,[a,c] Peter H. M. Budzelaar,[a] Jan M. M. Smits,[a] René de Gelder,[a] Paul R. Hageman,[b] and Anton W. Gal*[a]

Keywords: Aluminium / Chemical vapour deposition / Gallium / Nitrides

The reactions of Me_3Al and Me_3Ga with *cis*-2,3-dimethylaziridine (**1**-H), 3-pyrroline (**2**-H) and pyrrolidine (**3**-H) have been investigated. At room temperature, monomeric adducts [Me_3M·LH] are obtained (M = Al, Ga; L = **1**–**3**). [Me_3Al·**1**-H] is the first example of a structurally characterized adduct of an aziridine and a group 13 metal. On heating in mesitylene, all adducts except [Me_3Ga·**2**-H] evolve methane to form the corresponding amides; the Ga complexes require somewhat higher temperatures for this reaction. In contrast to the unsubstituted aziridine derivatives (which are *trimers*), dimethylaziridine amides Me_2M-**1** are *dimers*, as shown by X-ray crystallography. NMR spectroscopic data suggest the occurrence of a *cis*-*trans* equilibrium for these dimers in solution. For the pyrroline and pyrrolidine derivatives, the X-ray structures suggested large changes in the C–C and C–N bond lengths on formation of the adducts and amides. However, DFT calculations reveal that these changes are artefacts, and that the real bond length changes are fairly modest.

(© Wiley-VCH Verlag GmbH & Co. KGaA, 69451 Weinheim, Germany, 2003)

Introduction

Compounds containing both a group 13 (Al, Ga) atom and nitrogen are of considerable interest, owing to their potential use as single-source precursors for the fabrication of aluminium/gallium nitrides. Two common types of single-source precursors are trialkylmetal−amine adducts **A** and their alkane elimination products **B**. A drawback of adducts **A** is that they dissociate relatively easily into their trialkylmetal and amine components. Amides **B** do not suffer from this problem, but they are invariably associated (into dimers or higher) and thus have a reduced volatility (Scheme 1).

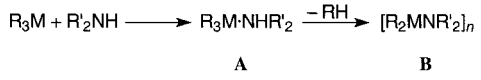

Scheme 1

Despite these disadvantages, both types of compounds have been studied for their potential as MOCVD precursors. Aluminium amides and imides have been studied extensively,[1] and several Me_3Al−secondary amine adducts have been reported.[2] Gallium amides have been synthesized by hydrocarbon or salt elimination reactions[3] or by other means.[4] Several metallacyclic aluminium and gallium nitrogen compounds have also been reported.[5]

We were interested in preparing aluminium/gallium adducts or amides in which the amide could easily lose its hydrocarbon fragment through some kind of elimination reaction, potentially providing lower decomposition temperatures and/or reduced carbon contamination of the nitride formed. We chose the aziridinyl and 3-pyrrolinyl fragments, which should easily eliminate an alkene or a diene, respectively, as represented schematically in Scheme 2.

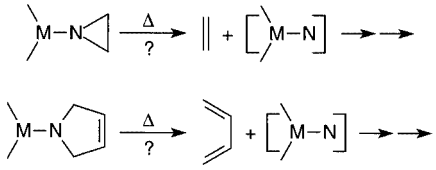

Scheme 2

Amides derived from the parent aziridine and Me_3Al[5b] and GaH_3 [23] have been reported. These have trimeric structures, however, and hence a vapour pressure too low for convenient MOCVD usage. We have studied the reactions of Me_3Al and Me_3Ga with *cis*-2,3-dimethylaziridine **1**-H, in the hope of obtaining more volatile amides. No Al

[a] Department of Inorganic Chemistry, University of Nijmegen, Toernooiveld 1, 6525 ED Nijmegen, The Netherlands
E-mail: gal@sci.kun.nl
[b] Department of Experimental Solid State Physics III, University of Nijmegen,
Toernooiveld 1, 6525 ED Nijmegen, The Netherlands
E-mail: paulh@sci.kun.nl
[c] Schuit Institute of Catalysis, Eindhoven University of Technology,
P. O. Box 513, 5600MB Eindhoven, The Netherland

or Ga derivatives of 3-pyrroline (**2**-H) have yet been reported. Derivatives of the (presumably more stable) pyrrolidine (**3**-H) have been included here for comparison. Since **2**-H is expensive and the synthesis of the pure compound is cumbersome, we have also used a commercially available mixture of **2**-H and **3**-H (Scheme 3).

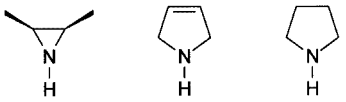

1-H **2**-H **3**-H

Scheme 3

Results and Discussion

Aziridine Adducts [Me_3M·1-H]

Treatment of Me_3M (M = Al, Ga) with dimethylaziridine in mesitylene at room temperature cleanly afforded the 1:1 Lewis acid-base adducts [Me_3M·**1**-H]. No further reaction to afford the amides occurred under these conditions. This is somewhat surprising, since Stucky reported that the reaction between Me_3Al and unsubstituted aziridine produced the amide $[Me_2AlNC_2H_4]_3$ directly, without formation of a detectable adduct ("solvated intermediate").[5b] Also, Trotter described the formation of $[H_2GaNC_2H_4]_3$ from GaH_3·NMe_3 and aziridine at room temperature, again without a detectable intermediate.[23] In our case, considerable heating (95 °C for Al, 155 °C for Ga) was required to induce methane elimination. It may be that the methyl substituents on the aziridine ring reduce its reactivity: in the adduct (see below), the amine proton is *cis* to the aziridine methyls, and is thus shielded by these groups as well as the bulky Me_3Al moiety. Another explanation might be that elimination is slower in the mesitylene solvent we use than in the neat aziridine employed by Stucky and Trotter.

As far as we are aware, [Me_3Al·**1**-H] is the first structurally characterized adduct of an aziridine with a group 13 metal (Al−Tl). Figure 1 shows the structure of the complex. The Me_3Al group is located *trans* to the aziridine methyl groups. The C−N ring bonds [1.493(3) Å av] appear to be slightly elongated with respect to those observed for unsubstituted aziridine [1.467(3) av.][15] and *cis*-2-methyl-3-phenylaziridine (1.475 av., no errors given),[16] whereas the differences in C−C bond lengths are small [1.472(2) vs. 1.462(3) and 1.486, respectively]. The most notable changes in the ^1H NMR spectrum on formation of the adduct are a low-field shift of the NH proton ($\Delta\delta$ = 0.33 ppm) and a high-field shift of the aziridine methyl groups ($\Delta\delta$ = −0.64 ppm).

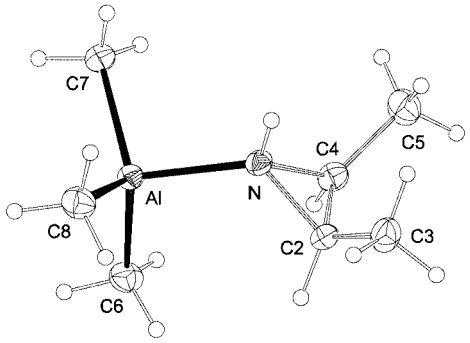

Figure 1. Molecular structure and atom numbering scheme for [Me_3Al·**1**-H]; selected bond lengths (Å): Al−C6 1.975(2), Al−C7 1.981(2), Al−C8 1.976(2), Al−N 1.977(2), N−C4 1.490(3), N−C2 1.495(2), C2−C4 1.472(3)

Aziridine Amides [Me_2M·**1**]$_2$

On heating in solution, the Al and Ga adducts both eliminate methane to give [Me_2Al·**1**]$_2$ and [Me_2Ga·**1**]$_2$, respectively. The amides, which are isostructural, crystallize as centrosymmetric dimers with a planar M_2N_2 ring; the aziridinyl and MMe_2 planes are nearly perpendicular to the M_2N_2 plane. Figure 2 shows the structure of the Al derivative. The bond lengths within the aziridinyl groups are virtually indistinguishable from those of adduct [Me_3Al·**1**-H]. These dimeric structures should be contrasted with the *trimeric* structures of the unsubstituted aziridinyl derivatives reported by Stucky,[5b] Trotter[23] and Müller,[5c] in which the six-membered M_3N_3 rings are markedly twisted. It seems likely that the added bulk of the methyl substituents in **1** is responsible for the lower degree of association, as it would result in steric hindrance between these methyl groups and the MMe_2 unit *cis* to it in any trimeric ring structure. Indeed, increased steric hindrance at aluminium instead of at the aziridine also results in the formation of dimers, as illustrated by the structure of $[(BH_4)_2AlNC_2H_4]_2$.[17]

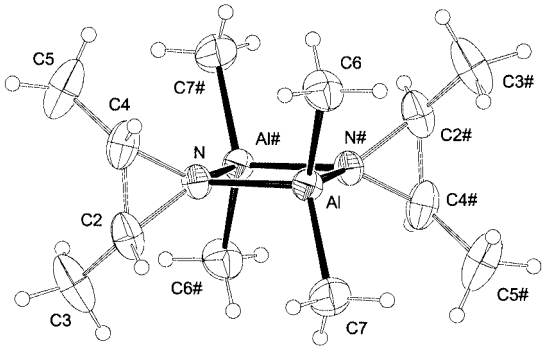

Figure 2. Molecular structure and atom numbering scheme for [Me_2Al-**1**]$_2$; selected bond lengths (Å): Al−C6 1.951(2), Al−C7 1.951(2), Al−N 1.938(2), Al−N# 1.929(2), N1−C4 1.489(2), N−C2 1.493(3), C2−C4 1.467(4); for the isostructural Ga complex: Ga−C6 1.955(8), Ga−C7 1.953(7), Ga−N 1.986(6), Ga−N# 2.000(5), N−C2 1.48(1), N−C4 1.49(1), C2−C4 1.47(1); # indicates symmetry-related atoms (−*x*, 1−*y*, 1−*z*)

In the solid state, both amides have a *trans* arrangement of the aziridine moieties (structure **C**). In solution, we see two sets of signals for the aziridine CH and CH_3 groups in a roughly 1:1 ratio; this is particularly clear in the ^{13}C spectra [the CH_3(M) signals are broad and do not show a clear splitting]. This might indicate a dimer−trimer equilibrium, but in view of the concentration independence of this phe-

nomenon a more logical explanation would be a *cis-trans* equilibrium (e.g. **C** ⇄ **D**), apparently slow on the NMR timescale (Scheme 4).

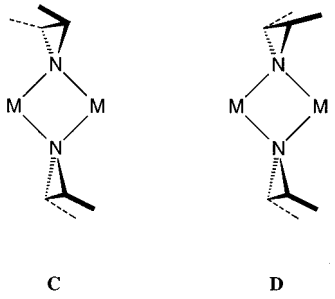

Scheme 4

Pyrroline and Pyrrolidine Adducts, [Me_3M·2-H] and [Me_3M·3-H]

Treatment of Me_3M with **2**-H and **3**-H at room temperature in toluene afforded the 1:1 Lewis acid-base adducts [Me_3M·**2**-H] and [Me_3M·**3**-H]. No further reaction to afford the amides occurred under these conditions. A peak due to the NH group was observed in each ^1H NMR spectrum. Compared with those of free **2**-H and Me_3Al, the most notable changes in the ^1H NMR spectrum on formation of the adduct are a low-field shift of the NH proton ($\Delta\delta = 0.90$ ppm) and a high-field shift of the methyl groups of Me_3Al ($\Delta\delta = -0.17$ ppm). If a 2:1 mixture of **2-H** and **3**-H is used, the two adducts co-crystallize in approximately the same ratio as was present in solution. The crystal structures both of pure [Me_3Al·**2**-H] and of the [Me_3Al·**2-H**]/[Me_3Al·**3**-H] mixture were determined, and show only minor differences in bond lengths. Remarkably, pure [Me_3Al·**3**-H] and [Me_3Ga·**3**-H] crystallize in space groups different from those found for [Me_3Al·**2**-H] and the co-crystal. However, the molecular conformations are fairly similar for all these compounds. Figure 3 shows the structures of [Me_3Al·**2**-H] and [Me_3Al·**3**-H]. [Me_3Al·**3**-H] has been prepared before, by Krannich.[2a]

Pyrroline and Pyrrolidine Amides, [Me_2M-2]$_2$ and [Me_2M-3]$_2$

On heating in solution, the pyrroline and pyrrolidine adducts eliminate methane to give dimeric amides. Pyrroline appears to be a bit more reactive, and the Ga compounds require heating to higher temperatures than the Al compounds. Complex [Me_2Ga-**2**]$_2$ could not be prepared in this way, because disproportionation of the 3-pyrroline (to pyrrole, pyrrolidine and possibly 2-pyrroline) occurred at the temperature required for reaction. The other amides crystallize as dimers with planar or near-planar M_2N_2 rings, as shown in Figure 4 for [Me_2Al-**2**]$_2$ and in Figure 5 for [Me_2Ga-**3**]$_2$.

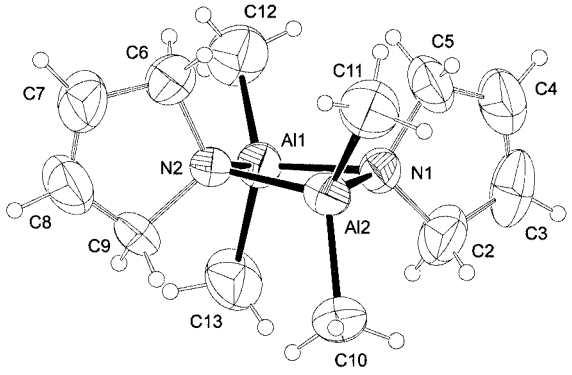

Figure 4. Structure of [Me_2Al-**2**]$_2$; selected bond lengths (Å): Al1−C12 1.94(2), Al1−C13 2.00(1), Al1−N1 1.98(1), Al1−N2 1.92(1), Al2−C10 1.93(1), Al2−C11 1.98(2), Al2−N1 1.94(1), Al2−N2 1.94(1), N1−C2 1.46(2), N1−C5 1.51(2), C3−C4 1.33(2), N2−C6 1.50(1), N2−C9 1.52(1), C7−C8 1.27(2)

Bond Length Changes Associated with Adduct and Amide Formation

The availability of several X-ray structures of adducts and amides makes it tempting to evaluate the bond length changes accompanying formation of these adducts and amides. One should, however, be careful in doing this for two reasons:

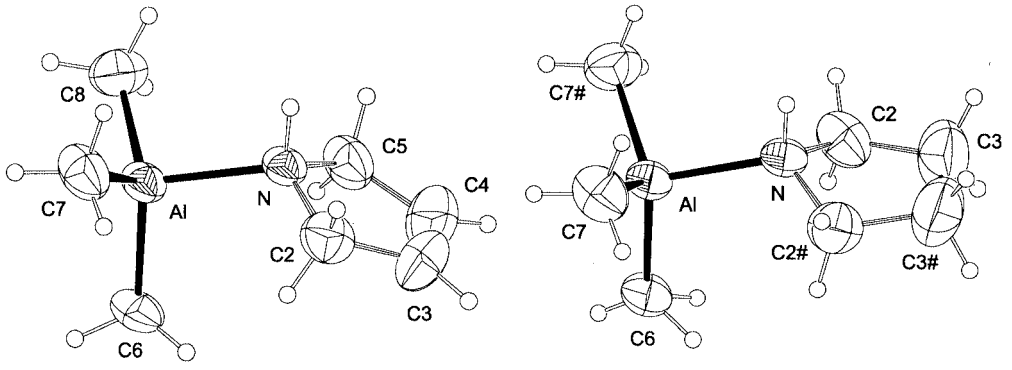

Figure 3. Structures of [Me_3Al·**2**-H] (left) and [Me_3Al·**3**-H] (right); selected bond lengths (Å) for [Me_3Al·**2**-H]: Al−C6 1.984(3), Al−C7 1.966(5), Al−C8 1.963(4), Al−N 1.999(3), N−C2 1.485(5), N−C5 1.495(5), C3−C4 1.264(8); for [Me_3Al·**3**-H]: Al−C6 1.977(4), Al−C7 1.967(3), Al−N 1.997(3), N−C2 1.468(4), C3−C3# 1.48(1) where # indicates symmetry−related atoms (x, 1/2−y, z); for [Me_3Ga·**3**-H] (refined in $P21$, i.e. not isostructural with [Me_3Al·**3**-H]): Ga−C6 2.00(1), Ga−C7 2.07(4), Ga−C8 1.91(4), Ga−N 2.11(1), N−C2 1.57(5), N−C5 1.38(5), C3−C4 1.53(3)

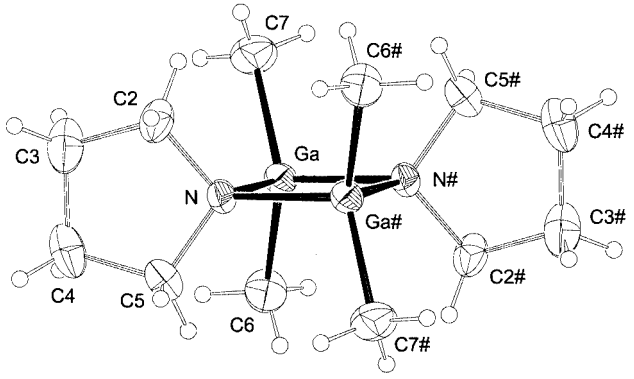

Figure 5. Structure of $[Me_2Ga\text{-}\mathbf{3}]_2$; selected bond lengths (Å): Ga−C7 1.969(6), Ga−C6 1.978(7), Ga−N# 2.017(5), Ga−N 2.028(5), N−C5 1.468(8), N−C2 1.482(7), C3−C4 1.512(12)

1. Bond length changes would be expected to be of the order of a few hundredths of an Å (i.e., not much larger than the error margins of X-ray structure determinations).
2. Many structures probably suffer from nonresolvable disorder problems, as we show further on. We find that the C−C and C−N bond lengths both of pyrrolines and of pyrrolidines often refine to unrealistically small values (see below). It is not clear a priori how strongly the other bond lengths in the molecule will be affected by such disorder problems.

To address these issues, we carried out geometry optimizations at the B3LYP/6-31G* level for all relevant Al species. The advantage of such theoretical results is that the *random* errors in bond lengths are much smaller (typically ≈ 0.001 Å) than found in X-ray structures. There are still significant *systematic* errors, but these should not strongly affect the bond length *changes* we are interested in. We first discuss the theoretical results (Table 1) and then compare them to the X-ray data (Table 2, Table 3).

For pyrrolidines and pyrrolines, complexation to $AlMe_3$ results in an elongation of the C−N bonds by about 0.02−0.03 Å. The adjacent C−C bonds are shortened by a much smaller amount (ca. 0.01 Å), and the distal C−C bond is not affected significantly. The same effects can be observed in the dimeric amides, and are even more pronounced there. For aziridine and dimethylaziridine, we find much smaller changes in the C−N and C−C bond lengths (≈ 0.01 Å at most). We tentatively interpret this as follows. The changes in C−N bond lengths for pyrrolidine and pyrroline derivatives are due to the changes in hybridization of the nitrogen atom, which becomes closer to sp^3 and hence uses a larger *p*-contribution for the C−N bonds. For the aziridines, however, the composition of the N hybrids used for forming the C−N bonds is nearly "fixed" by the small

Table 1. Calculated bond length changes (Å; B3LYP/6-31G*) on formation of Al adducts and amides

	$[Me_3Al\cdot\mathbf{L}H]$				$[Me_2Al\mathbf{L}]_2$			
L	Al−C	C−N	C1−C2	C2−C3	Al−C	C−N	C1−C2	C2−C3
Aziridine	+.022	+.008	−.003	n/a	+.005	+.002	−.003	n/a
1	+.024	+.010	−.001	+.002	(*trans*) +.009	+.005	−.004	0
					(*cis*) +.009	+.006	−.004	0
2	+.023	+.027	0	−.001	+.008	+.045	−.011	−.025
3	+.024	+.022	−.005	0	+.010	+.020	−.007	−.001

Table 2. Reference bond lengths (Å) for ligands **1**-H−**3**-H (Calculated for free Me_3Al: Al−C = 1.975 Å.)

Ligand	$C_\alpha-N$	$C_\alpha-C_\beta$	$C_\beta-C_\beta$
Aziridine[15]	1.463(2), 1.464(2), 1.469(2), 1.470(2), 1.465(2), 1.468(2)	1.463(2), 1.465(2), 1.459(1)	
Av:	1.467	1.462	
Calcd. (aziridine):	1.473 1.477[15]	1.485 1.487[15]	
Calcd. (**1**-H):	1.480	1.491	
Pyrrolines[16]	1.470, 1.477, 1.462, 1.469	1.498, 1.534, 1.505, 1.509	1.279, 1.313
Av:	1.470	1.512	1.296
Calcd. (**2**-H)	1.483	1.515	1.333
Pyrrolidines[17]	1.494, 1.513	1.480, 1.523	1.448
Av:	1.504	1.502	1.448
Calcd. (**3**-H)	1.466	1.544	1.558

Table 3. Observed and calculated bond lengths (Å) for adducts and amides

Ligand	Complex	M−C	M−N	N−C_α	C_α−C_β	C_β−C_β
Aziridine	[Me_3Al·**1**-H] X-ray	1.975(2), 1.981(2), 1.976(2)	1.977(2)	1.490(3), 1.495(2)	1.472(3)	
	[Me_3Al·**1**-H] calcd.	1.997−2.001	2.081	1.490	1.490	
	[Me_2AlAz]$_3$ [5b]	1.96(2), 1.98(2), 1.94(2)	1.91(2), 1.94(1), 1.88(2)	1.41(2), 1.48(2), 1.52(2)	1.46(3), 1.46(3)	
	[H_2GaAz]$_3$ [23]	n/a	1.93(1), 1.99(2), 1.99(2)	1.49(3), 1.50(3), 1.53(4), 1.67(4)	1.51(4), 1.60(5)	
	[Me_2Al-**1**]$_2$ X-ray	1.951(2)	1.938(2)	1.489(2), 1.493(3)	1.467(4)	
	[Me_2Ga-**1**]$_2$ X-ray	1.955(8), 1.953(7)	1.986(6)	1.48(1), 1.49(1)	1.47(1)	
	[Me_2Al-**1**]$_2$ calcd. (*trans*)	1.983−1.984	1.974−1.988	1.485	1.487	
Pyrroline	[Me_3Al·**2**-H] X-ray	1.984(3), 1.966(5), 1.963(4)	1.999(3)	1.485(5), 1.495(5)	1.441(8), 1.489(8)	1.264(8)
	[Me_3Al·**2**-H] calcd.	1.997−1.998	2.107	1.505	1.510	1.333
	[Me_2Al-**2**]$_2$ X-ray	1.94(2), 2.00(1), 1.93(1), 1.98(2)	1.98(1), 1.92(1), 1.94(1), 1.94(1)	1.46(2), 1.50(1), 1.51(2), 1.52(1)	1.37(2), 1.38(2), 1.40(2), 1.42(2)	1.27(2), 1.33(2)
	[Me_2Al-**2**]$_2$ calcd.	1.983	2.001−2.008	1.503	1.508	1.332
Pyrrolidine	[Me_3Al·**3**-H] X-ray	1.977(4), 1.967(3)	1.997(3)	1.468(4)	1.512(6)	1.48(1)
	Me_3Ga·**3**-H] X-ray	2.00(1), 2.07(4), 1.91(4)	2.11(1)	1.38(5), 1.57(5)	1.47(6), 1.52(5)	1.53(3)
	[Me_3Al·**3**-H] calcd.	1.998−1.999	2.106	1.493	1.544	1.557
	[Me_2Ga-**3**]$_2$ X-ray	1.969(6), 1.978(7)	2.017(5), 2.028(5)	1.468(8), 1.482(7)	1.50(1), 1.52(1)	1.51(1)
	[***3***$_2$-Al-**3**]$_2$ X-ray[24]	n/a	1.958(2), 1.967(2)	1.494(3), 1.500(3)	1.528(4), 1.531(4)	1.526(4)
	[Me_2Al-**3**]$_2$ calcd.	1.984−1.986	2.002−2.004	1.505, 1.507, 1.515, 1.515	1.529, 1.530, 1.538, 1.541	1.533, 1.533

CNC angle, so adduct or amide formation have little effect there. In agreement with this interpretation, the Al−C bonds of Me_3Al become longer on adduct formation by about 0.023 Å, *independent* of the nature of the amine.

To compare experimentally determined and calculated bond length changes, we need accurate reference bond lengths for our ligands. The structure of aziridine has been determined accurately.[18] For pyrroline, however, the only crystallographic data available is for two derivatives containing π-acceptor substituents at nitrogen.[19] The only available "non-disordered" X-ray structure for pyrrolidine available to date concerns a molecule intercalated in an aluminophosphate.[20] Relevant data are collected in Table 2. For pyrroline and in particular for pyrrolidine, the reported Cβ−Cβ bond lengths are too short. This indicates that these reference structures are already affected by some kind of disorder, which − in particular for the pyrrolidine intercalate − is unsurprising. Therefore, use of these reference bond lengths to assess bond length changes expected to be only a few hundredth of an Å is probably useless.

If we now compare the calculated and observed bond lengths for the adducts and amides (Table 3), we see that observed ring bond lengths are in general shorter, and in several cases − in particular for pyrrolidines and pyrrolines − *much* shorter. Several differences exceed the X-ray error limits, are larger than expected for any systematic errors in the B3LYP/6-31G* results, and are large enough to indicate unrealistic "observed" bond lengths (i.e., more than about 0.05 Å too short). A large in-plane libration amplitude for the whole ring might contribute for free pyrrolidine, but probably not for the adducts and amides. It thus seems likely that there are unresolved disorder problems in several of the structures.

Pyrrolidine rings are invariably puckered. The calculated puckering amplitudes[21] (Table 4) are consistently larger than the observed ones. This suggests the presence of disorder in the *orientation* of the puckering: any such disorder would result in a more nearly planar ring[22] as well as too short C−C and/or C−N bonds.

Table 4. Ring-puckering amplitudes for pyrroline and pyrrolidine rings

Compound	Ring puckering amplitude
C_4H_6N-NO X-ray[19a]	≈ 0
C_4H_6N-SSCTe(I)(C_4H_8) X-ray[19b]	≈ 0
2-H calcd.	0.156
[Me_3Al·**2**-H] X-ray	0.086
[Me_3Al· **2**-H] calcd.	0.198
[Me_2Al-**2**]$_2$ X-ray	≈0/0.133
[Me_2Al-**2**]$_2$ calcd.	0.226
3-H X-ray[17]	0.290
3-H calcd.	0.429
[Me_3Al·**3**-H] X-ray	0.292
Me_3Ga·**3**-H] X-ray	0.329
[Me_3Al·**3**-H] calcd.	0.367
[Me_2Ga-**3**]$_2$ X-ray	0.398
[***3***$_2$Al***3***]$_2$ X-ray[24]	0.374/0.384
[Me_2Al-**3**]$_2$ calcd.	0.421

Pyrroline rings have a near-planar $CH_2CH{=}CHCH_2$ fragment, but the ring may be folded somewhat along the $CH_2{-}CH_2$ line to produce an envelope-type conformation. Calculations predict that this happens both in free pyrroline and in its adduct and amide. Folding in the X-ray structure of adduct [Me_3Al·**2**-H] is smaller than predicted by calculations; the X-ray structure of amide [Me_2Al-**2**]$_2$ has two inequivalent rings, one of which is planar, while the other is distinctly folded. It seems likely that the potential for folding the ring is very flat, so that the actual structures are to a large degree determined by packing forces. Therefore, disordered structures can also be expected for pyrroline derivatives.

Clearly, in the presence of such disorder problems, little meaning can be attached even to those C−C and C−N bond lengths that look "reasonable". We thus conclude that a comparison of bond length changes on the basis of X-ray structures would be meaningless.

Decomposition Studies

All amides were tested under a variety of flow rates and substrate (Si) temperatures (up to 800 °C) in various configurations of a simplified MOCVD set-up. In several cases, dark-coloured deposits were observed. However, X-ray analysis of these deposits never gave any evidence for the formation of crystalline nitrides. We therefore decided to study the stability of the amides by DSC measurements.

The aziridine amides $[Me_2Al\text{-}\mathbf{1}]_2$ and $[Me_2Ga\text{-}\mathbf{1}]_2$ show an endothermic effect at their melting points (≈ 100 °C), a broad exotherm at 330−430 °C (Al) or 390−450 °C (Ga), and a very sharp endotherm at 450 °C (Al) or 470 °C (Ga). $[Me_2Al\text{-}\mathbf{2}]_2$ shows an endotherm at the melting point (≈ 64 °C) and a weak exotherm at 240−260 °C, followed by a sharp and large endotherm at 275 °C. Neither $[Me_2Al\text{-}\mathbf{3}]_2$ nor $[Me_2Ga\text{-}\mathbf{3}]_2$ show any such sharp endotherms up to the maximum temperature investigated (640 °C); weak effects were seen around 230 °C (ex), 300 °C (ex) and 330 °C (end) for Al, and around 300 °C (ex/end) for Ga. It thus appears that derivatives of **1** and **2** indeed undergo some kind of decomposition at a significantly lower temperature than those of saturated analogue **3**. However, we have not yet ascertained the nature of this decomposition.

Conclusions

The introduction of methyl substituents on aziridine has significant implications for its reaction behaviour with Me_3Al and Me_3Ga. In the first place, amide formation was slowed down so much that the amine *adducts* could be isolated and (for M = Al) crystallized. Secondly, the degree of association of the amides is reduced from 3 to 2, which might increase their volatility enough to allow their usage as MOCVD single-source precursors, although we have not yet been able to grow crystalline nitrides from them. Finally, the presence of the methyl groups allows observation of what are probably the *cis* and *trans* isomers of the amide dimer.

Adducts and amides for pyrroline and pyrrolidine could also be isolated. Comparison of calculated and observed bond lengths in the heterocyclic rings shows that the changes associated with complexation and amide formation are quite modest, and are completely swamped by random errors and hidden disorder in the X-ray structures.

Experimental Section

General Procedures: All manipulations of air- and moisture-sensitive compounds were performed under dry nitrogen by standard glove box and Schlenk techniques. Mesitylene, toluene and hexane were distilled over sodium/benzophenone under an atmosphere of nitrogen prior to use. *cis*-2,3-Dimethylaziridine (**1**-H) was prepared by the published procedure[6] and dried over KOH and distilled prior to use. 3-Pyrroline (**2**-H, 97% pure), pyrrolidine (**3**-H) and a 2:1 **2**-H/**3**-H mixture were purchased from Aldrich. Yields of crude adducts and amides (i.e. after evaporation of the solvent, as described below) were essentially quantitative (>95%) except for that of $[Me_2Ga\text{-}\mathbf{2}]_2$. Yields after crystallization were much lower (typically 10−25%) due to the high solubility of most complexes in the solvents used. ^1H and ^{13}C NMR spectroscopic data were collected for about 0.3 M C_6D_6 solutions at room temperature on Bruker DPX 200 and DPX 300 spectrometers. Elemental analyses were performed by the Analytical Laboratory of the Industriepark Kaiserau (Haus Heidbruch), 51789 Lindlar, Germany. Melting points were obtained with a Büchi B-545 melting point apparatus in silicon grease-sealed capillaries and are uncorrected. DSC measurements were performed on a Perkin−Elmer DSC7. In a glove box, samples (approximately 1.5 mg) were encapsulated in a 30μL sample vessel. This copper vessel fits closely into a stainless steel holder capable of withstanding 150 bar. DSC measurements covered the range of 30 °C to 650 °C, with a scanning rate of 20 °C/min.

Synthesis

[Me_3Al·1-H]: Compound **1**-H (3.5 mmol) was added slowly (0.5 h) at room temperature to a stirred solution of Me_3Al (0.25 g, 3.5 mmol) in mesitylene (4 mL) in a glove-box. After the reaction was complete, the Schlenk tube was taken out of the glove-box and the solvent was removed in vacuo at about 45 °C. The product, a white solid powder, was crystallized from toluene/hexane at about −20 °C. M.p. 75.7 °C. ^1H NMR: δ = −0.47 (s, 9 H, CH_3Al), 0.33 (d, 6 H, CH_3C), 0.87 (s, 1 H, N*H*), 1.81 (m, 2 H, C*H*) ppm. ^{13}C NMR: δ = −9.1 (br, *C*H_3Al), 11.1 (*C*H_3C), 34.7 (*C*H) ppm. $C_7H_{18}NAl$ (143.21): calcd. C 58.77, H 12.58, N 9.79, Al 18.86 found C 59.00, H 12.88, N 9.56, Al 18.56..

[Me_3Ga·1-H]: This compound was obtained in the same way as [Me_3Al·**1**-H], with Me_3Ga instead of Me_3Al. However, we did not succeed in crystallizing it. M.p. 45.7 °C. ^1H NMR: δ = −0.17 (s, 9 H, CH_3Ga), 0.40 (d, 6 H, CH_3C), 0.84 (s, 1 H, N*H*), 1.68 (m, 2 H, C*H*) ppm. ^{13}C NMR: δ = −6.3 (br, *C*H_3Ga), 11.5 (*C*H_3C), 33.4 (*C*H) ppm . $C_7H_{18}NGa$ (185.95): calcd. C 45.22, H 9.76, N 7.53, Ga 37.49; found C 44.98, H 9.52, N 7.48, Ga 37.26.

[Me_2Al-1]$_2$: *cis*-2,3-Dimethylaziridine (13.1 mmol) was added slowly (0.5 h) at room temperature to a stirred solution of Me_3Al (0.94 g, 13.1 mmol) in mesitylene (6 mL) in a glove-box. During the mixing, the solution warmed spontaneously. After it had cooled down to room temperature, the Schlenk tube was taken out of the glove-box. The solution was heated to 95 °C for 1 h, during which period evolution of gas (methane) was visible. After the solution had cooled, volatiles were removed in vacuo at 60 °C. The product, a white solid powder, was crystallized from toluene/hexane at about −20 °C. M.p. 94.7 °C. ^1H NMR: δ = −0.58 (s, 12 H, CH_3Al), 0.93−0.97 (m, 12 H, CH_3C), 2.04−2.09 (m, 4 H, C*H*) ppm. ^{13}C NMR: δ = −9.5 (br, *C*H_3Al), 14.2, 14.3 (*C*H_3C), 36.0, 36.4 (*C*H) ppm. $C_{12}H_{24}N_2Al_2$ (254.33): calcd. C 56.72, H 11.02, N 11.02, Al 21.24; found C 56.40, H 10.99, N 10.77, Al 21.47.

[Me_2Ga-1]$_2$: This compound was obtained in the same way as [Me_2Al-**1**]$_2$ (with Me_3Ga instead of Me_3Al), except that the solution was heated to 155 °C instead of 95 °C. The light-yellow product was crystallized from toluene/hexane at about −20 °C. M.p. 101.5 °C. ^1H NMR: δ = −0.22 (s, 12 H, CH_3Ga), 0.94−0.95 (m,

12 H, CH_3C), 1.89−1.95 (m, 4 H, CH) ppm. ^{13}C NMR: δ = −7.1 (*C*H_3Ga), 14.7, 14.8 (*C*H_3C), 34.3, 34.9 (*C*H) ppm. $C_{12}H_{24}N_2Ga_2$ (339.81): calcd. C 42.44, H 8.25, N 8.25, Ga 41.06; found C 42.30, H 8.23, N 8.27, Ga 40.92.

[Me_3Al·2-H]: Compound **2**-H (4 mmol) was added slowly (0.5 h) at room temperature to a stirred solution of Me_3Al (289 mg, 4 mmol) in toluene (1.0 mL) in a glove-box. After the reaction was complete, the Schlenk tube was taken out of the glove-box and put it in a refrigerator at about −20 °C for crystallization to take place. The formed crystals were transparent and light yellow. M.p. 65.5 °C. ^{1}H NMR: δ = −0.54 (s, 9 H, CH_3Al), 1. 86, (s, 1 H, NH), 3.51, (br. s, 4 H, CH_2), 5.44, (br. s, 2 H, CH) ppm. ^{13}C NMR: δ = −11.2 (*C*H_3Al), 55.4 (*C*H_2), 128.9 (*C*H) ppm. C_7H_{16}NAl (141.19): calcd. C 59.60, H 11.34, N 9.93, Al 19.13; found C 59.80, H 11.20, N 10.11, Al 19.32.

[Me_2Al-2]$_2$: Compound **2**-H (10 mmol) was added slowly (0.5 h) at room temperature to a stirred solution of Me_3Al (0.72 g, 10 mmol) in mesitylene (5 mL) in a glove-box. During the mixing, the solution warmed spontaneously. After it had cooled down to room temperature, the Schlenk tube was taken out of the glove-box. The solution was heated to 90 °C for 30 min, during which period evolution of gas (methane) was visible. After cooling the solution, volatiles were removed in vacuo at 40 °C. The transparent white product was crystallized from toluene/hexane at about −20 °C. M.p. 64.1 °C. ^{1}H NMR: δ = −0.53 (s, 12 H, CH_3Al), 3.51, (br. s, 8 H, CH_2), 5.43, (br. s, 4 H, CH) ppm. ^{13}C NMR: δ = −11.4 (*C*H_3Al), 55.4 (*C*H_2), 128.8 (*C*H) ppm. $C_{12}H_{24}N_2Al_2$ (250.30): calcd. C 57.63, H 9.60, N 11.20, Al 21.58; found C 57.33, H 9.58, N 10.98, Al 21.53.

[Me_3Al·3-H]: This compound was obtained in the same way as [Me_3Al·**2**-H], with use of **3**-H instead of **2**-H. The formed crystal was transparent and light yellow. M.p. 70.1 °C. ^{1}H NMR: δ = −0.52 (s, 9 H, CH_3Al), 0.89−0.96, (m, 4 H, β-CH_2), 1. 42, (s, 1 H, NH), 2.16−2.19 (m, 4 H, α-CH_2) ppm. ^{13}C NMR: δ = −9.6 (br, *C*H_3Al), 24.7 (β-*C*H_2), 46.4 (α-*C*H_2) ppm. C_7H_{18}NAl (143.21): calcd. C 58.77, H 12.58, N 9.79, Al 18.86; found C 58.44, H 12.42, N 9.67, Al 19.08.

[Me_2Al-3]$_2$: This compound was obtained in the same way as [Me_2Al-**2**]$_2$ (with use of **3**-H instead of **2**-H), except that the solution was heated at 125 °C for 1.5 h instead of at 90 °C for 30 min. The product was a light-white power. However, we did not succeed in crystallizing it. M.p. 59.3 °C. ^{1}H NMR: δ = −0.59 (s, 12 H, CH_3Al), 1.29−1.35, (m, 8 H, β-CH_2), 2.57−2.63 (m, 8 H, α-CH_2) ppm. ^{13}C NMR: δ = −11.9 (br, *C*H_3Al), 25.1 (β-*C*H_2), 49.7 (α-*C*H_2) ppm. $C_{12}H_{28}N_2Al_2$ (254.33): calcd. C 56.72, H 11.02, N 11.02, Al 21.24; found C 56.54, H 10.86, N 10.99, Al 20.98

Mixture (Cocrystal) of [Me_3Al·2-H] and [Me_3Al·3-H]: This compound was obtained in the same way as [Me_3Al·**2**-H], with the use of a 2:1 mixture of **2**-H/**3**-H. The product, a light-white solid powder, was crystallized from toluene/hexane at about −20 °C. M.p. 59.1 °C. ^{1}H and ^{13}C NMR spectra corresponded to a 2:1 mixture of [Me_3Al·**2**-H] and [Me_3Al·**3**-H] (see data given above). An NMR spectrum of a fragment of a large single crystal showed the same ratio of **2**-H/**3**-H as in the bulk mixture, demonstrating that the two compounds cocrystallize. Anal; found C 59.46, H 11.36, N 10.09, Al 19.31.

Mixture (Cocrystal) of [Me_2Al-2]$_2$ and [Me_2Al-3]$_2$: This compound was obtained in the same way as [Me_2Al-**2**]$_2$ (with the use of a 2:1 mixture of **2**-H/**3**-H), except that the solution was heated at 130 °C for 3 h instead of at 90 °C for 30 min. The product, a transparent light-white powder, was crystallized from toluene/hexane at about −20 °C. M.p. 65.8 °C. The ^{1}H and ^{13}C NMR spectra recorded at room temperature corresponded to a 2:1 mixture of [Me_2Al-**2**]$_2$ and [Me_2Al-**3**]$_2$ (see data given above) and did not show separate peaks for a mixed dimer. We do not know whether this means that the mixed dimer does not form or that exchange is rapid on the NMR timescale. Anal; found C 57.40, H 9.61, N 10.97, Al 21.72.

[Me_3Ga·2-H]: This compound was obtained in the same way as [Me_3Al·**2**-H], with the use of Me_3Ga instead of Me_3Al. The formed crystals were transparent light white. M.p. 35.5 °C. ^{1}H NMR: δ = −0.23 (s, 9 H, CH_3Ga), 1.51, (s, 1 H, NH), 2.96, (br. s, 4 H, CH_2), 5.05, (br. s, 2 H, CH) ppm. ^{13}C NMR: δ = −6.8 (*C*H_3Ga), 53.6 (*C*H_2), 126.8 (*C*H) ppm. C_7H_{16}NGa (183.93): calcd. C 45.71, H 8.77, N 7.62, Ga 37.91; found C 45.61, H 8.82, N 7.79, Ga 38.07.

Attempted Synthesis of [Me_2Ga-2]$_2$: Treatment of Me_3Ga with **2**-H to form [Me_2Ga-**2**]$_2$ was carried out similarly to that of Me_3Al with **2**-H. Heating to 155 °C was required for reaction. After evaporation of the solvent, a yellow-brown powder was left. ^{1}H NMR did not show any peaks attributable to the (protonated or deprotonated) pyrrolinyl group in the δ = 4 to 6 ppm range. Instead, broad singlets at δ = 6.29 and 6.85 ppm and several multiplets in the 0.9−2.8 ppm range were observed, which suggested that disproportionation to pyrrole and pyrrolidine and possibly isomerization to 2-pyrroline had occurred. No further attempts were made to separate or purify the products.

[Me_3Ga·3-H]: This compound was obtained in the same way as [Me_3Al·**3**-H] (with the use of Me_3Ga instead of Me_3Al). The formed crystal was cloudy and colourless. M.p. 48.3 °C (ref.[5e] 47 °C). ^{1}H NMR: δ = −0.18 (s, 9 H, CH_3Ga), 0.90−0.97, (m, 4 H, β-CH_2), 1. 15, (s, 1 H, NH), 2.12−2.15 (m, 4 H, α-CH_2) ppm. ^{13}C NMR: δ = −6.8 (br, *C*H_3Ga), 24.84 (s, β-*C*H_2), 46.7 (α-*C*H_2) ppm. C_7H_{18}NGa (185.95): calcd. C 45.25, H 9.69, N 7.54, Ga 37.53; found C 45.11, H 9.60, N 7.69, Ga 37.27.

[Me_2Ga-3]$_2$: This compound was obtained in the same way as [Me_2Al-**3**]$_2$ (with the use of Me_3Ga instead of Me_3Al), except that the solution was heated at 170 °C for 2.5 h instead of at 125 °C for 1.5 h. The product, a white solid, was crystallized from toluene at about −20 °C. M.p. 65.8 °C (ref.[5d], 74−75 °C; 64−67 °C[5a]). ^{1}H NMR: δ = −0.28 (s, 12 H, CH_3Ga), 1.29−1.36, (m, 8 H, β-CH_2), 2.59−2.65 (m, 8 H, α-CH_2) ppm. ^{13}C NMR: δ = −10.2 (*C*H-Ga), 24.9 (β-*C*H_2), 51.6 (α-*C*H_2) ppm. $C_{12}H_{28}N_2Ga_2$ (339.81): calcd. C 42.44, H 8.25, N 8.25, Ga 41.06; found C 42.27, H 8.06, N 8.34, Ga 40.87.

X-ray Crystal Structure Determinations

General: Crystals of these Al and Ga complexes were generally found to be soft. The crystal fragments sampled were cut from larger crystals, resulting in irregular shapes. Both factors may have contributed to the generally poor quality of the X-ray structure determinations (see below). Crystals were mounted in thin-walled glass capillaries under Ar. Data were collected on an Enraf−Nonius CAD4 diffractometer by use of graphite-monochromated Mo-K_α radiation (0.71073 Å). Details of all structure determinations are collected in Table 5 and Table 6. Since the glass capillaries prevented accurate description of the crystal shape, semi-empirical absorption corrections from ψ-scans[7] were applied. Structures were solved by use of the PATTY option[8] of the DIRDIF program system.[9] Refinements were carried out with the SHELXL-97 package.[10] All refinements were full-matrix, least-squares on *F*2. All non-hydrogen atoms were refined with anisotropic temperature factors. The hydrogen atoms were placed at cal-

culated positions, and refined isotropically in riding mode, unless noted otherwise (see below). Geometrical calculations[11] revealed neither unusual geometric features, nor unusual short intermolecular contacts. The calculations revealed no higher symmetry and no solvent-accessible areas. The structure drawings in Figure 1−5 show 30% thermal ellipsoids. Crystallographic data (excluding structure factors) for the structures reported in this paper have been deposited with the Cambridge Crystallographic Data Centre as supplementary publications nos. CCDC-187355 to -187364. Copies of the data can be obtained free of charge on application to CCDC, 12 Union Road, Cambridge CB2 1EZ, UK [Fax: (internat.) + 44-1223/336-033; E-mail: deposit@ccdc.cam.ac.uk].

Notes on Individual Structures

[Me_3Al·1-H]: 1-H was refined freely.

[Me_3Al·2-H]: All hydrogen atoms refined freely.

[Me_3Al·2-H]/[Me_3Al·3-H] Cocrystal: 1-H was refined freely. The crystal structure determination was hampered by the poor crystal quality and more than average decay (up to 15%). No reliable data could be collected above 22° (resolution 0.95 Å).

[Me_3Al·3-H]: To test the presence of the mirror plane, a full least-squares refinement was performed in space group *P*21. Although the *R* factor was lower (0.0589), the standard deviations in bond angles and distances were significantly higher. Moreover, a statistical analysis of the intensities favours a centrosymmetric space group.

[Me_3Ga·3-H]: The crystal structure determination was hampered by the very poor crystal quality. No reliable data could be collected above 22° (resolution 0.95 Å). Because the semiempirical absorption correction by itself was not adequate, presumably due to the poor quality of the data and hence of the ψ-scans, an additional absorption correction was applied by use of the DIFABS procedure.[12] Even then it was necessary to use the ISOR option for N1 in the least-squares refinement to provide physically acceptable anisotropic thermal displacement parameters.

[Me_2Al-2]$_2$: The crystal structure determination was hampered by the extremely poor crystal quality. No reliable data could be collected above 21° (resolution 0.99 Å).

[Me_2Al-2]$_2$/[Me_2Al-3]$_2$ Cocrystal: The crystal structure determination was hampered by the very poor crystal quality. No reliable data could be collected above 23° (resolution 0.91 Å).

Calculations

All calculations were carried out with the GAMESS-UK package[13] by use of the B3LYP hybrid density functional[14] and the

Table 5. Details of crystal structure determinations for [Me_3Al·**1**-H], [Me_2Al-**1**]$_2$, [Me_2Ga-**1**]$_2$,[Me_3Al·**2**-H] and [Me_2Al-**2**]$_2$/[Me_2Al-**3**]$_2$

Compound	[Me_3Al·**1**-H]	[Me_2Al-**1**]$_2$	[Me_2Ga-**1**]$_2$	[Me_3Al·**2**-H]	[Me_2Al-**2**]$_2$/[Me_2Al-**3**]$_2$
Crystal colour	transparent cloudy white	transparent cloudy colourless	transparent cloudy white	transparent light yellow	transparent colourless
Crystal shape	rough fragment	rough fragment	rough platelet	rough fragment	very large, very irregular fragment
Crystal size, mm	0.25 × 0.23 × 0.10	0.33 × 0.21 × 0.18	0.31 × 0.29 × 0.08	0.54 × 0.36 × 0.28	1.20 × 0.70 × 0.36
Empirical formula	$C_7H_{18}AlN$	$C_{14}H_{28}Al_2N_2$	$C_{14}H_{28}Ga_2N_2$	$C_7H_{16}AlN$	$C_{14}H_{24}Al_2N_2$
Molecular mass	143.20	254.32	339.80	141.19	250.29
Temperature, K	148(2)	293(2)	293(2)	293(2)	293(2)
Crystal system,	orthorhombic,	triclinic,	triclinic,	monoclinic,	monoclinic,
Space group	*Pcab*	$P\bar{1}$	$P\bar{1}$	$P2_1/c$	$C2/m$
Unit cell det. #,	10982,	25,	25,	22,	23,
θ range	2.100−25.290	10.293−14.897	10.235−14.595	10.273−13.602	10.437−13.217
a, Å	8.3271(2)	7.2341(5)	7.2343(10)	6.2786(5)	14.049(3)
b, Å	19.4095(6)	7.7648(7)	7.7407(9)	9.3098(17)	9.069(4)
c, Å	12.5463(4)	8.7149(11)	8.710(2)	17.0244(18)	7.2797(17)
α, °	90	71.784(8)	71.684(16)	90	90
β, °	90	73.353(10)	73.488(19)	92.354(10)	120.56(2)
γ, °	90	65.969(7)	66.410(11)	90	90
Volume, Å^3	2027.79(10)	417.48(7)	417.26(14)	994.3(2)	798.8(4)
Z, $d_{calcd.}$ (g·cm^{-3})	8, 0.938	1, 1.012	1, 1.352	4, 0.943	2, 1.041
Abs. coeff., mm^{-1}	0.134	0.156	3.210	0.136	0.163
Scan	area det. φ, ω	ω/2θ	ω/2θ	ω/2θ	ω
F(000)	640	140	176	312	272
θ range, °	2.10···25.29	2.95−27.47	3.12−27.47	2.39−27.48	4.49−23.00
Index ranges	$-9 \le h \le 10$	$-9 \le h \le 9$	$-9 \le h \le 0$	$0 \le h \le 8$	$-13 \le h \le 15$
	$-23 \le k \le 23$	$-10 \le k \le 10$	$-10 \le k \le 9$	$-12 \le k \le 0$	$-9 \le k \le 9$
	$-14 \le l \le 15$	$-11 \le l \le 11$	$-11 \le l \le 10$	$-22 \le l \le 22$	$-8 \le l \le 0$
Collected/unique	10982/1839	3834/1917	2068/1918	2481/2276	1197/592
[$R_{int.}$]	[0.0631]	[0.0383]	[0.0558]	[0.1073]	[0.1396]
Observed [$I_o > 2\sigma(I_o)$]	1276	1454	1092	1200	327
DIFABS?, abs. struct. par.	no	no	no	no	no
Relat. transm. fact.		1.057−0.953	1.547−0.841	1.657−0.820	1.244−0.841
Data/restraints/pars.	1839/0/91	1917/0/77	1918/0/77	2276/0/85	592/0/46
Goodness-of-fit on F^2	1.047	1.050	1.050	1.079	1.109
SHELXL-97 wt. pars.	0.0507, 0.5441	0.0661, 0.0509	0.0592, 0.5977	0.1341, 0.1512	0.1348, 0.0000
*R*1, *wR*2 [$I > 2\sigma(I)$]	0.0421, 0.1004	0.0444, 0.1154	0.0696, 0.1235	0.0860, 0.2217	0.0915, 0.2277
*R*1, *wR*2 (all data)	0.0737, 0.1121	0.0650, 0.1255	0.1516, 0.1492	0.1511, 0.2619	0.1441, 0.2668
Diff. peak, hole (e· Å^{-3})	0.195, −0.179	0.305, −0.118	0.677, −0.697	0.470, −0.310	0.241, −0.238

Table 6. Details of crystal structure determinations for [Me_3Al·**2**-H]/[Me_3Al·**3**-H], [Me_3Al·**3**-H], [Me_3Ga·**3**-H], and [Me_2Al-**2**]$_2$,[Me_2Ga-**3**]$_2$

Compound	[Me_3Al·**2**-H] / [Me_3Al·**3**-H]	[Me_3Al·**3**-H]	Me_3Ga·**3**-H]	[Me_2Al-**2**]$_2$	[Me_2Ga-**3**]$_2$
Crystal colour	transparent yellow	transparent cloudy light yellow	transparent cloudy colourless	transparent cloudy colourless	transparent colourless
Crystal shape	rough platelet	irregular fragment	rough fragment	large irregular fragment	rough fragment
Crystal size, mm	0.50 × 0.28 × 0.10	0.53 × 0.42 × 0.35	0.46 × 0.33 × 0.23	0.90 × 0.59 × 0.40	0.46 × 0.35 × 0.25
Empirical formula	$C_7H_{16}AlN$	$C_7H_{18}AlN$	$C_7H_{18}GaN$	C_1 **2**-$H_{24}Al_2N_2$	C_1 **2**-$H_{28}Ga_2N_2$
Molecular weight	141.19	143.20	185.94	250.29	339.80
Temperature, K	293(2)	293(2)	293(2)	293(2)	293(2)
Crystal system,	monoclinic,	monoclinic,	monoclinic,	monoclinic,	monoclinic,
Space group	$P2_1/c$	$P2_1/m$	$P2_1$	$P2_1/c$	$P2_1/n$
Unit cell det. #,	25,	23,	24,	25,	25,
θ range	9.366−11.407	10.216−11.722	10.311−13.707	10.260−13.630	10.252−14.419
a, Å	6.2765(9)	6.3054(6)	6.3484(8)	8.4774(12)	7.6440(7)
b, Å	9.3588(16)	11.0728(10)	11.0264(16)	8.4981(12)	8.5036(7)
c, Å	16.982(3)	7.6501(15)	7.6364(19)	22.453(3)	12.8894(11)
α, °	90	90	90	90	90
β, °	92.411(19)	107.423(9)	107.838(15)	100.035(14)	106.773(12)
γ, °	90	90	90	90	90
Volume, Å^3	996.6(3)	509.61(12)	508.86(16)	1592.8(4)	802.19(13)
Z, $d_{calcd.}$ (g·cm^{-3})	4, 0.941	2, 0.933	2, 1.214	4, 1.044	2, 1.407
Abs. coeff., mm^{-1}	0.136	0.134	2.638	0.163	3.340
Scan	ω/2θ	ω/2θ	ω	ω/2θ	ω
F(000)	312	160	196	544	352
θ range, °	3.24−22.00	2.79−27.46	4.11−21.95	2.57−20.99	3.62−27.44
Index ranges	$-6 \le h \le 6$	$0 \le h \le 8$	$-6 \le h \le 6$	$-8 \le h \le 8$	$-9 \le h \le 0$
	$0 \le k \le 9$	$0 \le k \le 14$	$-11 \le k \le 0$	$-8 \le k \le 0$	$-11 \le k \le 0$
	$-17 \le l \le 0$	$-9 \le l \le 9$	$-8 \le l \le 0$	$-22 \le l \le 0$	$-16 \le l \le 16$
Collected/unique	1266/1217	1334/1228	710/655	1747/1693	1951/1820
[$R_{int.}$]	[0.0668]	[0.0481]	[0.0555]	[0.1036]	[0.0336]
Observed [$I_o > 2\sigma(I_o)$]	547	650	447	822	1125
DIFABS?, abs. struct. par.	no	no	yes, −0.15(16)	no	no
Relat. Transm. fact.	1.164−0.883	1.089−0.923	1.192−0.878	1.527−0.854	1.298−0.803
Data/restraints/pars.	1217/0/89	1228/0/52	655/7/85	1693/0/149	1820/0/75
Goodness-of-fit on F^2	1.013	1.032	1.126	1.072	1.091
SHELXL-97 wt. pars.	0.0774, 0.0000	0.1010, 0.0192	0.0409, 0.6351	0.1657, 5.7380	0.0925, 0.0517
*R*1, *wR*2 [$I > 2\sigma(I)$]	0.0706, 0.1417	0.0630, 0.1626	0.0514, 0.0978	0.1064, 0.2917	0.0617, 0.1425
*R*1, *wR*2 (all data)	0.1840, 0.1799	0.1230, 0.1937	0.1018, 0.1174	0.1955, 0.3624	0.1167, 0.1657
Diff. Peak, hole (e· Å^{-3})	0.204, −0.211	0.263, −0.160	0.300, −0.351	0.292, −0.304	1.198, −0.731

6-31G* basis set.[15] All structures were fully optimized without symmetry constraints.

Acknowledgments

This work was supported by the Research Institute for Materials (RIM), University of Nijmegen (KUN). We also thank Mr. B. Thijs for his helpful discussions on the synthesis of **1**-H, and Mr. H.L. van der Linden for assisting in construction of the simplified MOCVD set-up.

[1] [1a] F. C. Sauls, L. V. Interrante, *Coord. Chem. Rev.* **1993**, *128*, 193. [1b] J. Pinkas, T. Wang, R. A. Jacobson, J. G. Verkade, *Inorg. Chem.* **1994**, *33*, 4202. [1c] J. Pinkas, T. Wang, R. A. Jacobson, J. G. Verkade, *Inorg. Chem.* **1994**, *33*, 5244. [1d] C. Jones, G. A. Koutsantonis, C. L. Raston, *Polyhedron* **1993**, *12*, 1829. [1e] D. C. Bradley, *Polyhedron* **1994**, *13*, 1111. [1f] A. C. Jones, *J. Cryst. Growth* **1993**, *129*, 728. [1g] D. C. Bertolet, H. Liu, J. W. Rogers Jr., *J. Appl. Phys.* **1994**, *75*, 5385. [1h] J. F. Janik, E. N. Duesler, R. T. Paine, *J. Organomet. Chem.* **1997**, *539*, 19. [1i] D. C. Bradley, I. S. Harding, I. A. Maia, M. Motevalli, *J. Chem. Soc., Dalton Trans.* **1997**, 2969. [1j] D. A. Neumayer, J. G. Ekerdt, *Chem. Mater.* **1996**, *8*, 9. [1k] T. D. Getman, G. W. Franklin, *Comments Inorg. Chem.* **1995**, *17*, 79.

[2] [2a] C. J. Thomas, L. K. Krannich, C. L. Watkins, *Polyhedron* **1993**, *12*, 389. [2b] C. H. Hendrickson, D. Duffy, D. P. Eyman, *Inorg. Chem.* **1968**, *7*, 1047. [2c] M. Taghiof, D. G. Hendershot, M. Barber, J. P. Oliver, *J. Organomet. Chem.* **1992**, *431*, 271.

[3] [3a] J. T. Park, Y. Kim, J. Kim, K. Kim, Y. Kim, *Organometallics* **1992**, *11*, 3320. [3b] K. M. Waggoner, P. P. Power, *J. Am. Chem. Soc.* **1991**, *113*, 3385. [3c] B. Sen, G. L. White, *J. Inorg. Nucl. Chem.* **1973**, *35*, 2207. [3d] O. T. Beachley Jr., C. Bueno, M. R. Churchill, R. B. Hallock, R. G. Simmons, *Inorg. Chem.* **1981**, *20*, 2423. [3e] O. T. Beachley Jr., M. J. Noble, M. R. Churchill, C. H. Lake, *Organometallics* **1992**, *11*, 1051. [3f] B. Lee, W. T. Pennington, G. H. Robinson, *Inorg. Chim. Acta* **1991**, *190*, 173. [3g] J. J. Byers, B. Lee, W. T. Pennington, G. H. Robinson, *Polyhedron* **1992**, *11*, 967. [3h] D. C. Bradley, H. M. Dawes, M. B. Hursthouse, L. M. Smith, M. Thornton-Pett, *Polyhedron* **1990**, *9*, 343. [3i] D. A. Atwood, R. A. Jones, A. H. Cowley, S. G. Bott, J. L. Atwood, *J. Organomet. Chem.* **1992**, *434*, 143. [3j] D. A. Atwood, V. O. Atwood, D. F. Carriker, A. H. Cowley, F. P. Gabai, R. A. Jones, M. R. Bond, C. J. Carrano, *J. Organomet. Chem.* **1993**, *463*, 29. [3k] D. A. Atwood, R. A. Jones, A. H. Cowley, S. G. Bott, J. L. Atwood, *Polyhedron* **1991**, *10*, 1897. [3l] S. T. Barry, D. S. Richeson, *J. Organomet. Chem.* **1996**, *510*, 103.

[4] [4a] O. T. Beachley, Jr., T. L. Royster, Jr., J. R. Arhar, A. L. Rheingold, *Organometallics* **1993**, *12*, 1976. [4b] O. T. Beachley

Jr., D. B. Rosenblum, M. R. Churchill, C. H. Lake, L. M. Toomey, *Organometallics* **1996**, *15*, 3653. [4c] W. R. Nutt, K. J. Murry, J. M. Gulick, J. D. Odom, Y. Ding, L. Lebioda, *Oganometallics* **1996**, *15*, 1728.

[5] [5a] A. STorr, B. S. Thomas, *J. Chem. Soc.* **1971**, 3850. [5b] J. L. Atwood, G. D. Stucky, *J. Am. Chem. Soc.* **1970**, *92*, 285. [5c] J. Müller, K. Margiolis, K. Dehnicke, *J. Organomet. Chem.* **1972**, *46*, 219. [5d] S. J. Schauer, C. H. Lake, C. L. Watkins, L. K. Krannich, D. H. Powell, *J. Organomet. Chem.* **1997**, *549*, 31. [5e] S. J. Schauer, C. L. Watkins, L. K. Krannich, R. B. Gala, E. N. Gundy, C. B. Lagrone, *Polyhedron* **1995**, *14*, 3505.

[6] [6a] G. Lamaty, A. Sovade, *Bull. Soc. Chim.* **1974**, 2149. [6b] G. Lamaty, A. Delbord, W. Werner, *Ann. Chem.* **1969**, *726*, 77.

[7] A. C. T. North, D. C. Philips, F. S. Mathews, *Acta Crystallogr., Sect. A* **1968**, *24*, 351.

[8] P. T. Beurskens, G. Beurskens, M. Strumpel, C. E. Nordman *in "Patterson and Pattersons"*; (Eds.: J. P. Glusker, B. K. Patterson, M. Rossi); Clarendon Press: Oxford, **1987**; p. 356.

[9] P. T. Beurskens, G. Beurskens, W. P. Bosman, R. de Gelder, S. García-Granda, R. O. Gould, R. Israël, J. M. M. Smits, DIRDIF-96. A computer program system for crystal structure determination by Patterson methods and direct methods applied to difference structure factors; Crystallography Laboratory, University of Nijmegen: The Netherlands, **1996**.

[10] G. M. Sheldrick, SHELXL-97. Program for the refinement of crystal structures; University of Göttingen: Germany, **1997**.

[11] [11a] A. L. Spek, *Acta Crystallogr., Sect. A* **1990**, *46*, C34. [11b] A. L. Spek, PLATON-93. Program for display and analysis of crystal and molecular structures; University of Utrecht: The Netherlands, **1995**.

[12] N. Walker, D. Stuart, *Acta Crystallogr., Sect. A* **1983**, *39*, 158.

[13] GAMESS-UK is a package of ab initio programs written by M. F. Guest, J. H. van Lenthe, J. Kendrick, K. Schoffel, and P. Sherwood, with contributions from R. D. Amos, R. J. Buenker, H. J. J. van Dam, M. Dupuis, N. C. Handy, I. H. Hillier, P. J. Knowles, V. Bonacic-Koutecky, W. von Niessen, R. J. Harrison, A. P. Rendell, V. R. Saunders, A. J. Stone, D. J. Tozer, and A. H. de Vries. The package is derived from the original GAMESS code by M. Dupuis, D. Spangler, J. Wendoloski, NRCC Software Catalog, Vol. 1, Program No. QG01 (GAMESS), **1980**.

[14] [14a] A. D. Becke, *J. Chem. Phys.* **1993**, *98*, 5648. [14b] C. Lee, W. Yang, R. G. Parr, *Phys. Rev.* **1988**, B37, 785. [14c] B. Miehlich, A. Savin, H. Stoll, H. Preuss, *Chem. Phys. Lett.* **1989**, *157*, 200.

[15] [15a] R. Ditchfield, W. J. Hehre, J. A. Pople, *J. Chem. Phys.* **1971**, *54*, 724. [15b] W. J. Hehre, R. Ditchfield, J. A. Pople, *J. Chem. Phys.* **1972**, *56*, 2257. [15c] P. C. Hariharan, J. A. Pople, *Mol. Phys.* **1974**, *27*, 209. [15d] M. S. Gordon, *Chem. Phys. Lett.* **1980**, *76*, 163. [15e] P. C. Hariharan, J. A. Pople, *Theor. Chim. Acta* **1973**, *28*, 213.

[16] A. Galindo, L. Orea, F. D. Gnecco, R. G. Enríquez, R. A. Toscano, W. F. Reynolds, *Tetrahedron: Asymmetry* **1997**, *8*, 2877.

[17] K. N. Semenenko, E. B. Lobkovskii, B. L. Tarnopolskii, M. A. Simonov, *Zh. Strukt. Khim.* **1976**, *17*, 1076.

[18] N. W. Mitzel, J. Riede, C. Kiener, *Angew. Chem. Int. Ed. Engl.* **1997**, *36*, 2215.

[19] [19a] V. Garcia-Montalvo, A. Marcelo-Polo, R. Montaya, R. A. Toscano, S. Hernandez-Ortega, R. Cea-Olivares, *J. Organomet. Chem.* **2001**, *623*, 74. [19b] T. Ohwada, M. Miura, H. Tanaka, S. Sakamoto, K. Yamaguchi, H. Ikeda, S. Inagaki, *J. Am. Chem. Soc.* **2001**, *123*, 10164.

[20] [20a] J. B. Parise, C. S. Day, *Acta Crystallogr., Sect. C* **1985**, *41*, 515. [20b] J. B. Parise, *Stud. Surf. Sci. Catal.* **1985**, *24*, 271.

[21] D. Cremer, J. A. Pople, *J. Am. Chem. Soc.* **1975**, *97*, 1354.

[22] A similar type of disorder is observed in many coordinated THF molecules, for which the C3−C4 bond is often too short.

[23] [23a] W. Harrison, A. Storr, J. Trotter, *J. Chem. Soc., Chem. Commun.* **1971**, 1101. [23b] W. Harrison, A. Storr, J. Trotter, *J. Chem. Soc., Dalton Trans.* **1972**, 1554.

[24] M. M. Andrianarison, M. C. Ellerby, I. B. Gorrell, P. B. Hitchcock, J. D. Smith, D. R. Stanley, *J. Chem. Soc., Dalton Trans.* **1996**, 211.

Received June 14, 2002
[I02326]

Synthesis and Structures of Alkaline-Earth Metal Supersilanides: tBu$_3$SiMX and tBu$_3$Si−M−SitBu$_3$ (M = Be, Mg; X = Cl, Br)

Hans-Wolfram Lerner,*[a] Stefan Scholz,[a] Michael Bolte,[b][‡] Nils Wiberg,[c] Heinrich Nöth,[c][‡] and Ingo Krossing[c][‡]

Keywords: Silanes / Beryllium / Magnesium / X-ray structure analysis

The alkaline-earth metal silanides, (tBu$_3$Si)$_2$Be and (tBu$_3$Si)$_2$Mg, have been synthesized from the reaction of the sodium silanide tBu$_3$SiNa with BeCl$_2$ in Bu$_2$O and MgBr$_2$ in THF. The bissupersilylmagnesium THF adduct [(tBu$_3$Si)$_2$Mg(THF)$_2$] reacts with GaBr$_3$ in benzene at ambient temperature to form tBu$_3$SiGaBr$_2$ and tBu$_3$SiMgBr(THF). The structures of bissupersilyl silanides, (tBu$_3$Si)$_2$Be and (tBu$_3$Si)$_2$Mg(THF)$_2$, and the Grignard analogue, tBu$_3$SiMgBr(THF), have been determined by X-ray structure analysis.

(© Wiley-VCH Verlag GmbH & Co. KGaA, 69451 Weinheim, Germany, 2003)

Introduction

Silyl anions, which are conveniently accessible from silyl halides, are important and versatile organometallic reagents in synthesis. Various details of their molecular structures have, however, still not been fully elucidated and are therefore the subject of current investigations.[1] The best-studied class of silyl anions are the alkali metal silanides that feature monomeric,[2,3] dimeric,[2,3] and polymeric[4] arrangements as molecular units. Alkali metal silanides have not only become interesting for their molecular structures but have also attracted recent attention due to their synthetic utility. More recently, alkali metal tri-*tert*-butylsilanides (supersilanides), tBu$_3$SiM, have been used for the synthesis of new main group element clusters and compounds with elements in low coordination states. Accordingly, the reaction of sodium supersilanide with thallium(III) chloride produces the supersilylated thallium clusters [(tBu$_3$Si)$_6$Tl$_6$Cl$_2$] and [(tBu$_3$Si)$_4$Tl$_3$Cl],[5] and with [(Me$_3$Si)$_2$N]$_2$Sn leads to the tristannaallene, (tBu$_3$Si)$_2$Sn=Sn=Sn(SitBu$_3$)$_2$.[6]

In contrast to the well-established silanides with alkali metals, only a few alkaline-earth metal silanides are known. Information regarding the structure and reactivity of these molecules is thus still rather limited.[1,7]

We have therefore become interested in the synthesis of alkaline-earth metal silanides, tBu$_3$SiMX and tBu$_3$Si−M−SitBu$_3$, and in their respective structures.

Results and Discussion

Synthesis

Several routes to silyl anions are known. In this study of the synthesis of alkaline-earth metal supersilanides only the metathesis of MX$_2$ (M = Be, X = Cl; M = Mg, X = Br) with sodium supersilanide, tBu$_3$SiNa, has been employed. We expected that the Grignard analogous compound, tBu$_3$SiMX, should be produced by reaction of MX$_2$ with one equivalent of tBu$_3$SiNa, and that tBu$_3$Si−M−SitBu$_3$ should be obtained upon elimination of MX$_2$ from two molecules of tBu$_3$SiMX.

$$n\ t\mathrm{Bu_3SiNa} + n\ \mathrm{MX_2} \xrightarrow[-\,n\,\mathrm{NaX}]{} \underset{\mathbf{1}}{(t\mathrm{Bu_3SiMX})_n} \xrightarrow[-\,0.5\,n\,\mathrm{MX_2}]{} \underset{\mathbf{2}}{0.5\ n\ t\mathrm{Bu_3Si\text{-}M\text{-}Si}t\mathrm{Bu_3}} \quad (1)$$

1a: M = Be, X = Cl
1b: M = Mg, X = Br
2a: M = Be
2b: M = Mg

The compounds tBu$_3$Si−M−SitBu$_3$ (M = Be, Mg) were indeed formed by the addition of two equivalents of tBu$_3$SiNa to BeCl$_2$ in dibutyl ether or to a tetrahydrofuran solution of MgBr$_2$. The Grignard analogous compound, tBu$_3$SiMgBr, was prepared by mixing tetrahydrofuran solutions of MgBr$_2$ and tBu$_3$SiNa in a 1:1 molar ratio at −78 °C, but no crystals suitable for X-ray crystallography could be obtained from this solution. While tBu$_3$SiMgBr(THF)$_n$ was transformed in a similar manner to the

[a] Institut für Anorganische Chemie, Johann Wolfgang Goethe-Universität Frankfurt am Main,
Marie-Curie-Straße 11, 60439 Frankfurt am Main, Germany
Fax: (internat.) +49−(0)69/798-29260
E-mail: lerner@chemie.uni-frankfurt.de.
[b] Institut für Organische Chemie, Johann Wolfgang Goethe-Universität Frankfurt am Main
Marie-Curie-Straße 11, 60439 Frankfurt am Main, Germany
[c] Department für Chemie der Universität München,
Butenandtstr. 5−13 (Haus D), 81377 München, Germany
[‡] X-ray structure analysis.

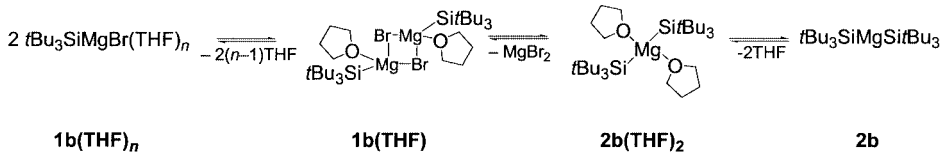

(2)

related hypersilyl compound $(Me_3Si)_3SiMgBr(THF)_2$[8] in non-donor solvents, as indicated in Equation (2), obtaining X-ray quality crystals from $tBu_3SiMgBr$ was very difficult.-

Tetrahydrofuran molecules could be eliminated by heating the solid adduct $(tBu_3Si)_2Mg(THF)_2$ in vacuo. From the resulting residue, uncomplexed $(tBu_3Si)_2Mg$ could be recovered quantitatively. When two equivalents of sodium supersilanide reacted with $BeCl_2$ in dibutyl ether only donor free $(tBu_3Si)_2Be$ was formed. The use of one equivalent of sodium supersilanide led to oligomeric $(tBu_3SiBeCl)_n$ which shows broad signals in the ^1H and ^{29}Si NMR spectrum.

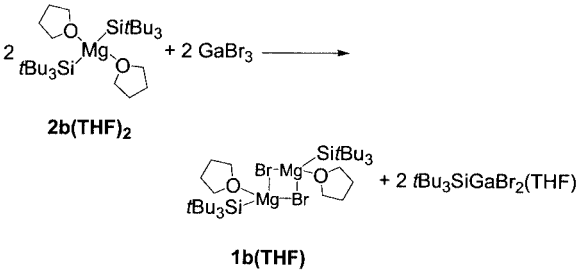

(3)

$GaBr_3$ reacts with $(tBu_3Si)_2Mg(THF)_2$ in benzene at ambient temperature to give the Grignard analogous compound, $tBu_3SiMgBr(THF)$, and $tBu_3SiGaBr_2(THF)$. X-ray quality crystals of $tBu_3SiMgBr(THF)$ were grown from this benzene solution.

Reactivity

The supersilylated silanides of magnesium and beryllium are extremely sensitive to air and moisture. When a solution of $(tBu_3Si)_2Mg(THF)_2$ in benzene is treated with a small amount of water, the Mg^{2+} cation is substituted cleanly by two protons. When exposed to air, oxidation of $(tBu_3Si)_2Mg(THF)_2$ proceeds with the formation of superdisilane, $tBu_3Si-SitBu_3$, and $(tBu_3SiO)_2Mg$. Nucleophilic substitution reactions of alkali metal supersilanides with element halides EX_n often occur with the reduction of E and the formation of E–E bonds. As reported previously, the reaction of $tBu_3SiNa(THF)_2$ with ECl_3 (E = P, As) leads surprisingly to the sodium disupersilyltriphosphenide, $tBu_3Si(Na)P-P=PSitBu_3$, and the disupersilyltriarsenide, $tBu_3Si(Na)As-As=AsSitBu_3$, as shown in Equation (4).[9]

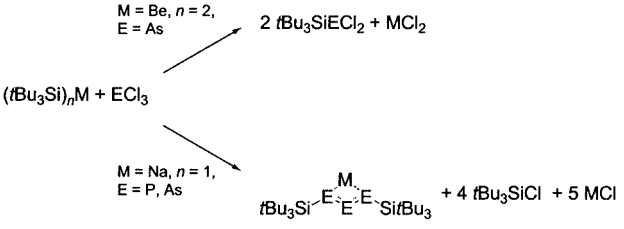

(4)

This result demonstrates the high reduction potential of alkali metal supersilanides. On the other hand, $(tBu_3Si)_2Be$ reacts with $AsCl_3$ to produce $tBu_3SiAsCl_2$ in high yield.

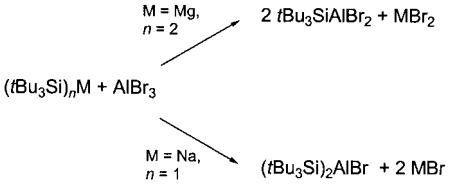

(5)

We have reported that the reaction of sodium supersilanide with triel halides, EX_3, does not depend on the starting material ratio (1:1 or 2:1) and always produces the disupersilylated compounds, $(tBu_3Si)_2EX$.[10] However, the reactions between $(tBu_3Si)_2Mg(THF)_2$ and EBr_3 (E = Al, Ga) take a different course, as depicted in Equations (3) and (5), and only the monosupersilylated compounds tBu_3SiEBr_2 (E = Al, Ga) are formed. $tBu_3SiAlBr_2$ could be isolated as its $MgBr_2$ adduct[10] and $tBu_3SiGaBr_2$ as its THF adduct.

Structures

Figure 1 shows the molecular structure of **2a**. Similar to the isoelectronic compound $(tBu_3Si)_2Zn$,[11] the Si–Be–Si unit is perfectly linear. The alkaline-earth metal silanide **2a** crystallizes in the triclinic space group $P\bar{1}$. The Be–Si distance of 2.1930(10) Å in the donor-free silanide **2a** is a little longer than the sum of the atomic radii (2.10 Å).[12]

The crystal structure of **2b(THF)$_2$** is shown in Figure 2; selected bond lengths and angles are listed in Table 1. X-ray-quality crystals of **2b(THF)$_2$** (orthorhombic, *Pbca*) were

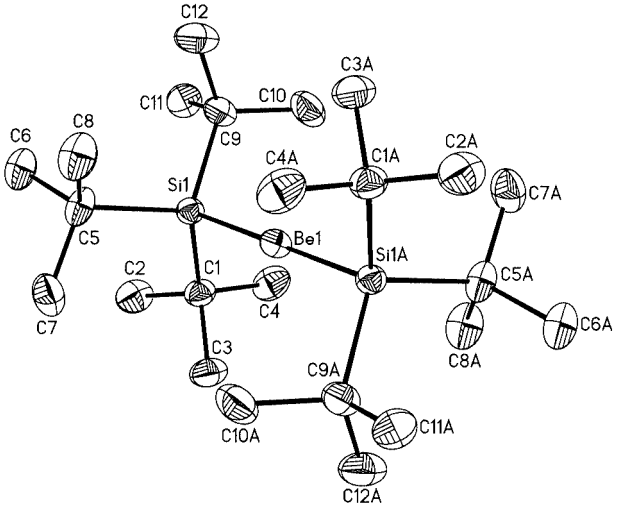

Figure 1. Thermal ellipsoid plot of **2a** showing the atom numbering scheme. The displacement ellipsoids are drawn at the 50% probability level

grown from pentane. Its Si−Mg−Si unit deviates from linearity [bond angle Si(1)−Mg−Si(2) = 132.82(4)°], due to interactions between Mg and two O atoms from tetrahydrofuran molecules. The distance between the Mg and Si atom is 2.777(2) Å. This distance is characteristic of a Mg−Si bond (sum of the atomic radii: 2.77 Å),[12] but is longer than in $(Me_3Si)_2Mg{\cdot}TMEDA$,[13] $(Me_3Si)_2Mg{\cdot}TMDAP$,[14] and $(Me_3Si)_2Mg{\cdot}DME$.[15]

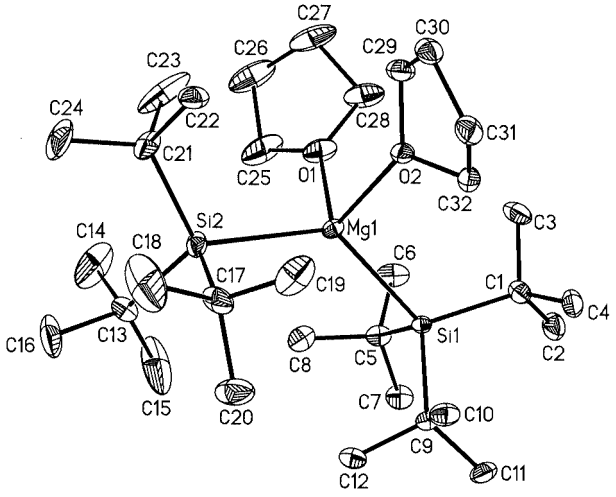

Figure 2. Thermal ellipsoid plot of **2b(THF)$_2$** showing the atom numbering scheme. The displacement ellipsoids are drawn at the 50% probability level

Table 1. Selected bond lengths (average) [Å] and angles (average) [°] for **1b(THF)**, **2a**, and **2b(THF)$_2$**

	1b(THF)	**2a**	**2b(THF)$_2$**
M−Si	2.6075(11)	2.1930(10)	2.777(2)
C−C	1.543(4)	1.540(5)	1.531(12)
Si−C	1.963(3)	1.952(3)	1.973(7)
Mg−O	2.040(2)	−	2.153(2)
Si−M−Si	−	180	132.82(4)
C−Si−M	108.97(9)	107.34(10)	111.5(4)

Complex **1b(THF)** crystallizes with a molecule of benzene in the monoclinic space group *C*2/*c*, as shown in Figure 3. The central framework of the Grignard analogous compound **1b(THF)** forms a planar four-membered ring. The corners of this ring are alternately occupied by Mg and Br atoms [angle of **1b(THF)**: Br−Mg−Br 98.2(2)°, Mg−Si−Mg 81.4(2)°]. Apart from these two Br atoms, the Mg atom is surrounded by one Si atom and one molecule of tetrahydrofuran. Contrary to the Mg center in **1b(THF)**, the Mg atoms in $(Me_3Si)MgBr{\cdot}TMEDA$[13] and $(Me_3Si)_2Mg{\cdot}MeN(CH_2CH_2NMe_2)_2$[14] are pentacoordinate. Complex **1b(THF)** features two Mg−Si contacts with a Mg−Si distance of 2.6075(11) Å. However, the Mg−Si distances in **1b(THF)** are significantly shorter than in **2b(THF)$_2$**. The Mg−Br bond in **1b(THF)** has a length of 2.5929(9) Å. This distance is characteristic of a Mg−Br bond (sum of the ionic radii: 2.53 Å).[12]

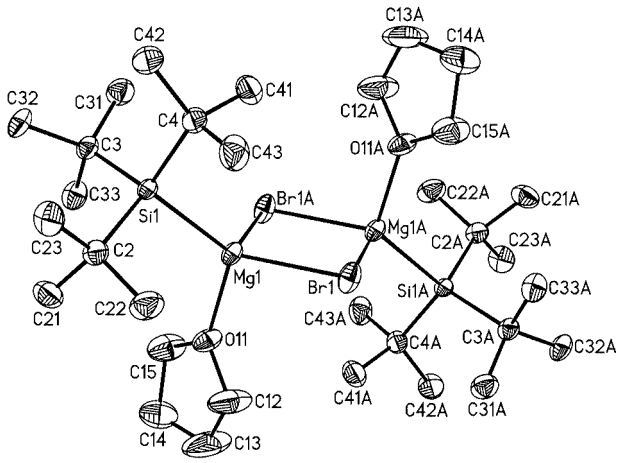

Figure 3. Thermal ellipsoid plot of **1b(THF)** showing the atom numbering scheme. The displacement ellipsoids are drawn at the 50% probability level

The disupersilylmagnesium compound **2b(THF)$_2$** shows an C−Si−C angle smaller than 110° [107.81(13)°], indicating a negatively polarized Si atom.[11]

Experimental Section

General Procedures: All experiments were carried out under dry argon or nitrogen with strict exclusion of air and moisture using standard Schlenk techniques. tBu$_3$SiNa[2] was prepared according to literature procedures. The solvents (benzene, heptane, toluene, tetrahydrofuran) were distilled from sodium/benzophenone prior to use.

The NMR spectra were recorded on a Jeol GSX 270 (^{1}H/^{13}C/^{29}Si: 270.17/67.94/53.67 MHz), a Jeol EX 400 (^{1}H/^{13}C/^{29}Si: 399.78/100.53/79.31 MHz), a Bruker AM 250 (^{1}H/^{13}C: 250.133/62.896 MHz), a Bruker DPX 250 (^{1}H/^{13}C/^{29}Si: 250.130/62.895/49.69 MHz) or a Bruker AMX 400 (^{1}H/^{29}Si: 400.130 MHz/79.495 MHz) spectrometer. The ^{29}Si NMR spectra were recorded using the INEPT pulse sequence with empirically optimized parameters for polarization transfer from the tBu substituents.

Caution! In view of the extreme toxicity of beryllium compounds, all experimental work was carried out in a well-ventilated fume cupboard used exclusively for this work. Any spillage of the beryllium solutions was washed out immediately. Established procedures for handling dangerous materials were followed rigorously in all phases of the synthetic work and measurements.

Synthesis of tBu$_3$SiBeCl [1a]: A solution of tBu$_3$SiNa(THF)$_n$ (0.146 g, 0.40 mmol) in 10 mL of tetrahydrofuran was added to a solution of $BeCl_2$ (0.093 g, 1.16 mmol) in 5 mL of tetrahydrofuran at ambient temperature. After concentrating the solution to 5 mL, **1a** was obtained as an air- and moisture-sensitive precipitate at −25 °C. Yield: 0. 101 g of **1a** (80%). ^{1}H NMR (C_6D_6, internal TMS): δ = 1.105 (s, 27 H, tBu$_3$Si) ppm. ^{13}C{^{1}H} NMR (C_6D_6, internal TMS): δ = 22.3 (s, *C*Me$_3$), 30.7 (s, C*Me$_3$*) ppm. ^{29}Si{^{1}H} NMR (C_6D_6, internal TMS): δ = 6.5 (s, SitBu$_3$) ppm.

Synthesis of tBu$_3$SiMgBr(THF)$_n$ [1b(THF)$_n$]: A solution of tBu$_3$SiNa(THF)$_n$ (0.792 g, 2.16 mmol) in 1.8 mL of tetrahydrofuran was added to a cooled solution (−78 °C) of $MgBr_2(THF)_4$ (0.403 g, 2.10 mmol) in 20 mL of tetrahydrofuran. After allowing the mix-

ture to attain ambient temperature and concentrating the solution to 10 mL, **1b(THF)$_n$** was obtained at −25 °C as air- and moisture-sensitive, colorless crystals. Yield: 0.482 g (0.82 mmol) of **1b(THF)$_n$** (39%). Decomposition at 144 °C. ^{1}H NMR ([D$_8$]THF internal TMS): δ = 1.056 (s, 27 H, *t*Bu$_3$Si) ppm. ^{13}C{^{1}H} NMR ([D$_8$]THF internal TMS): δ = 24.0 (s, *C*Me$_3$), 33.6 (s, C*Me$_3$*) ppm. ^{29}Si{^{1}H} NMR ([D$_8$]THF external TMS): δ = 26.4 (s, Si*t*Bu$_3$) ppm.

Remark: **1b(THF)$_n$** dissolved in [D$_6$]benzene transforms into **2b(THF)$_2$** (by ^{1}H and ^{29}Si NMR spectroscopy).

Synthesis of (*t*Bu$_3$Si)$_2$Be (2a): A slurry of BeCl$_2$ (0.154 g, 1.93 mmol) and *t*Bu$_3$SiNa(Bu$_2$O)$_2$ (1.40 g, 3.80 mmol) in 10 mL of heptane was stirred for two days at ambient temperature. The reaction mixture became colorless. The solid that formed was removed by filtration. Colorless crystals of **2a** were grown from the filtrate at −25 °C. Yield: 0.632 g (1.55 mmol) of **2a** (80%). m.p. 208−210 °C. ^{1}H NMR (C$_6$D$_6$, internal TMS): δ = 1.250 (s, 54 H, *t*Bu$_3$Si) ppm. ^{29}Si{^{1}H} NMR (C$_6$D$_6$, external TMS): δ = 6.9 (s, Si*t*Bu$_3$) ppm. X-ray structure analysis: see Figure 1.

Synthesis of (*t*Bu$_3$Si)$_2$Mg(THF)$_2$ [2b(THF)$_2$]: A solution of *t*Bu$_3$SiNa(THF)$_n$ (2.64 g, 7.20 mmol) in 6 mL of tetrahydrofuran was added to a cooled solution (−78 °C) of MgBr$_2$(THF)$_4$ (1.718 g, 3.63 mmol) in 20 mL of tetrahydrofuran. After allowing the mixture to attain ambient temperature, the solvent was removed in vacuo. The remaining residue was treated with 20 mL of heptane. After filtrating the insoluble material and concentrating the filtrate to 10 mL, **2b(THF)$_2$** was obtained at −25 °C as air- and moisture-sensitive colorless crystals, which were suitable for X-ray diffraction analysis (Figure 2). Yield: 1.402 g (2.48 mmol) of **2b(THF)$_2$** (68%). decomposition 116 °C. ^{1}H NMR (C$_6$D$_6$, internal TMS): δ = 1.328 (s, 54 H, *t*Bu$_3$Si), 1.269 (m, 8 H, CH$_2$), 3.566 (m, 8 H, OCH$_2$) ppm. ^{13}C{^{1}H} NMR (C$_6$D$_6$, internal TMS): δ = 24.1 (s, *C*Me$_3$), 33.5 (s, C*Me$_3$*), 24.7 (CH$_2$), 68.3 (OCH$_2$) ppm. ^{29}Si{^{1}H} NMR (C$_6$D$_6$, external TMS): δ = 31.2 (s, Si*t*Bu$_3$) ppm. C$_{32}$H$_{70}$Si$_2$O$_2$Mg (567.38): calcd. C 67.79, H 12.45; found C 62.15, H 11.40.

According to the ^{1}H and ^{29}Si NMR spectra solvent-free (*t*Bu$_3$Si)$_2$Mg was obtained quantitatively after (*t*Bu$_3$Si)$_2$Mg(THF)$_2$ (0.040 g, 0.07 mmol) was heated to 80 °C for 2 h in high vacuo. ^{1}H NMR (C$_6$D$_6$, internal TMS): δ = 1.380 (s, 54 H, *t*Bu$_3$Si) ppm. ^{29}Si{^{1}H} NMR (C$_6$D$_6$, external TMS): δ = 38.0 (s, Si*t*Bu$_3$) ppm.

Reaction of (*t*Bu$_3$Si)$_2$Be [2a] with AsCl$_3$: A solution of (*t*Bu$_3$Si)$_2$Be (0.054 g, 0.13 mmol) in 2 mL of heptane was added to a cooled solution (−78 °C) of AsCl$_3$ (0.42 g, 2.90 mmol) in 20 mL of tetrahydrofuran. After allowing the mixture to attain ambient temperature, all volatile compounds were removed in vacuo. The remaining residue was treated with 10 mL of heptane. After filtrating the insoluble material and removing the solvent in vacuo, *t*Bu$_3$SiAsCl$_2$ remained as an air- and moisture-sensitive colorless oil. Yield: 0.061 g (0.176 mmol) of *t*Bu$_3$SiAsCl$_2$ (68%). ^{1}H NMR

Table 2. Crystallographic data and further details of the structure determination of **1b(THF)**, **2a**, and **2b(THF)$_2$**

	1b(THF)	**2a**	**2b(THF)$_2$**
Formula	$C_{38}H_{76}Br_2Mg_2O_2Si_2$	$C_{24}H_{54}BeSi_2$	$C_{32}H_{70}MgO_2Si_2$
Molecular weight [g/mol]	829.61	407.86	567.73
Temperature [K]	173	158	153
Wave length [Å]	Mo-K_α, 0.71073	Mo-K_α, 0.71073	Mo-K_α, 0.71073
Crystal system	Monoclinic	Triclinic	Orthorhombic
Space group	*C*2/*c*	$P\bar{1}$	*Pbca*
Z	4	2	8
Cell parameters			
a [Å]	12.3504(9)	8.631(4)	15.583(6)
b [Å]	12.624(1)	11.871(4)	17.162(8)
c [Å]	29.853 (2)	14.942(6)	22.433(13)
α [°]	90	74.03(2)	90
β [°]	98.958(6)	87.64(2)	90
γ [°]	90	73.377(15)	90
Volume [Å^3]	4597.7(7)	1409.2(9)	7336.6(6)
Calculated density [Mg/m^3]	1.199	0.961	1.027
Absorption coeff. [mm^{-1}]	1.870	0.132	0.138
F(000)	1768	460	2544
crystal dimensions [mm^3]	0.4 × 0.3 × 0.2	0.3 × 0.2 × 0.07	0.3 × 03 × 0.2
$2\theta_{max}$ [°]	55.9	54.0	55.0
Index ranges	$-15 \le h \le 15$, $-15 \le k \le 15$, $-34 \le l \le 36$	$-10 \le h \le 10$, $-15 \le k \le 10$, $-19 \le l \le 19$	$-17 \le h \le 12$, $-7 \le k \le 22$, $-35 \le l \le 35$
Measured reflections	27623	8066	19444
Independent reflections	4700	4358	7363
R_{int}	0.0470	0.0379	0.0408
Reflections with $I > 2\sigma(I)$	3910	2911	4048
Data /Restraints/Parameter	4700/0/209	3610/0/265	4967/0/405
Weighting scheme *x*/*y*	0.0588/7.931	0.0292/1.2655	0.028/12.656
GooF	1.071	1.133	1.126
*R*1 [$I > 2\sigma(I)$]	0.0567	0.0502	0.0595
*wR*2 [$I > 2\sigma(I)$][a]	0.1027	0.1084	0.1221
*wR*2	0.1089	0.1336	0.1593
Difference electron density [e/Å^3]	0.862	0.543	0.357

[a] $w = 1/[\sigma^2(F_o^2) + (x \cdot P)^2 + y \cdot P]$; $P = (F_o^2 + 2F_c^2)/3$.

(C_6D_6, internal TMS): δ = 1.166 (s, 27 H, tBu$_3$Si) ppm. $^{13}C\{^1H\}$ NMR (C_6D_6, internal TMS): δ = 26.5 (s, CMe_3), 30.7 (s, CMe_3) ppm. $^{29}Si\{^1H\}$ NMR (C_6D_6, external TMS): δ = 23.0 (s, SitBu$_3$) ppm.

Reaction of (tBu$_3$Si)$_2$Mg(THF)$_2$ [2b(THF)$_2$] with GaBr$_3$: GaBr$_3$ (0.085 g, 0.274 mmol) was added to a solution of **2b(THF)$_2$** (0.150 g, 0.264 mmol) in 1.2 mL of C_6D_6. Colorless crystals of **1b(THF)**, tBu$_3$SiMgBr(THF)$_2$, grew from this benzene solution within one week at ambient temperature. These crystals were suitable for X-ray diffraction analysis (Figure 3). Yield: 0.084 g (0.194 mmol) of **1b(THF)** (73%). For NMR of **1b(THF)** see above. For the reaction of (tBu$_3$Si)$_2$Mg(THF)$_2$ (**2b**) with AlBr$_3$ see ref.[10]

The ^1H, ^{13}C, and ^{29}Si NMR spectra of the remaining benzene solution showed only the signals of tBu$_3$SiGaBr$_2$(THF).[10] After removing the solvent in vacuo, colorless tBu$_3$SiGaBr$_2$(THF) was obtained as a solid. ^1H NMR (C_6D_6, internal TMS): δ = 1.29 (s, 27 H, tBu$_3$Si), 1.42 (m, 8 H, CH_2), 3.62 (m, 8 H, OCH_2) ppm. $^{13}C\{^1H\}$ NMR (C_6D_6, internal TMS): δ = 25.6 (s, CMe_3), 31.7 (s, CMe_3), 25.0 (CH_2), 68.2 (OCH_2) ppm. $^{29}Si\{^1H\}$ NMR (C_6D_6, external TMS): δ = 47.7 (s, SitBu$_3$) ppm.

Oxidation of (tBu$_3$Si)$_2$Mg(THF)$_2$ [2b(THF)$_2$]: N_2O (0.104 g, 0.61 mmol) was condensed into a solution of (tBu$_3$Si)$_2$Mg(THF)$_2$ (0.017 g, 0.027 mmol) in 1 mL of benzene. The supersiloxide (tBu$_3$SiO)$_2$Mg and N_2 were formed in quantitative yield (by ^1H, ^{13}C, and ^{29}Si NMR spectroscopy). Compound **2b** (0.2 mmol/1 mL of C_6D_6) reacts with dry air, forming superdisilane, tBu$_3$SiSitBu$_3$,[10] and (tBu$_3$SiO)$_2$Mg: ^1H NMR (C_6D_6, internal TMS): δ = 1.146 (s, 54 H, tBu$_3$Si) ppm. $^{13}C\{^1H\}$ NMR (C_6D_6, internal TMS): δ = 22.1 (s, CMe_3), 30.8 (s, CMe_3) ppm. $^{29}Si\{^1H\}$ NMR (C_6D_6, external TMS): δ = −9.4 (s, SitBu$_3$) ppm.

X-ray Structure Determination: Data Collection (Table 2): Siemens CCD three-circle diffractometer, graphite-monochromated Mo-K_α radiation; empirical absorption correction using SADABS,[16] structure solution by direct methods,[17] structure refinement: full-matrix least-squares on F^2 with SHELXL-97.[17] Hydrogen atoms were placed at ideal positions and refined with fixed isotropic displacement parameters using a riding model. CCDC-192308 (**1b**), CCDC 192306 (**2a**), and CCDC-192307 (**2b**) contain the supplementary crystallographic data for this paper. These data can be obtained free of charge at www.ccdc.cam.ac.uk/conts/retrieving.html [or from the Cambridge Crystallographic Data Centre, 12, Union Road, Cambridge CB2 1EZ, UK; Fax: (internat.) +44-1223/336-033; E-mail: deposit@ccdc.cam.ac.uk].

Acknowledgments

We are grateful to Professor M. Wagner, University of Frankfurt, for his generous support and to the University of Frankfurt for funding.

[1] P. D. Lickiss, C. M. Smith, *Coord. Chem. Rev.* **1995**, *145*, 75−124.
[2] N. Wiberg, K. Amelunxen, H.-W. Lerner, H. Schuster, H. Nöth, I. Krossing, M. Schmidt-Amelunxen, T. Seifert, *J. Organomet. Chem.* **1997**, *542*, 1−18.
[3] K. W. Klinkhammer, *Chem. Eur. J.* **1997**, *3*, 1418−1441.
[4] H.-W. Lerner, S. Scholz, M. Bolte, *Z. Anorg. Allg. Chem.* **2001**, *627*, 1638−1642.
[5] N. Wiberg, T. Blank, H.-W. Lerner, D. Fenske, G. Linti, *Angew. Chem.* **2001**, *113*, 1275−1278, *Angew. Chem. Int. Ed.* **2001**, *40*, 1232−1235.
[6] N. Wiberg, H.-W. Lerner, S.-K. Vasisht, S. Wagner, K. Karaghiosoff, H. Nöth, W. Ponikwar, *Eur. J. Inorg. Chem.* **1999**, 1211−1218.
[7] R. Goddard, C. Krüger, N. A. Ramadan, A. Ritter, *Angew. Chem.* **1995**, *107*, 1107−1109, *Angew. Chem. Int. Ed. Engl.* **1995**, *34*, 1030−1032.
[8] J. D. Farwell, M. F. Lappert, C. Marschner, C. Strissel, D. Tilley, *J. Organomet. Chem.* **2000**, *603*, 185−188.
[9] N. Wiberg, A. Wörner, H.-W. Lerner, K. Karaghiosoff, D. Fenske, G. Baum, A. Dransfeld, P. von Ragué Schleyer, *Eur. J. Inorg. Chem.* **1998**, 833−841.
[10] N. Wiberg, K. Amelunxen, H.-W. Lerner, H. Schuster, H. Nöth, J. Knizek, I. Krossing, *Z. Naturforschung, Teil B* **1998**, *53*, 333−348.
[11] N. Wiberg, K. Amelunxen, H.-W. Lerner, H. Nöth, A. Appel, J. Knizek, K. Polborn, *Z. Anorg. Allg. Chem.* **1997**, *623*, 1861−1870.
[12] Holleman-Wiberg, *Lehrbuch der Anorganischen Chemie*, 101. Ed., de Gruyter, Berlin **1995**, p. XXXVI.
[13] D. W. Goebel Jr., J. L. Hencher, J. P. Oliver, *Organometallics* **1983**, *2*, 746−750.
[14] L. Rösch, J. Pickardt, S. Imme, U. Börner, *Z. Naturforschung, Teil B* **1986**, *41*, 1523−1526.
[15] A. R. Claggett, W. H. Ilsley, T. J. Anderson, M. D. Glick, J. P. Oliver, *J. Am. Chem. Soc.* **1977**, *99*, 1797−1801.
[16] G. M. Sheldrick, *SADABS*, a Program for Empirical Absorption Correction of Area Detector Data; University of Göttingen, Germany, **1996**.
[17] G. M. Sheldrick, *Acta Crystallogr., Sect. A* **1990**, *46*, 467−473.
[18] G. M. Sheldrick, *SHELXL-97*, A Program for the Refinement of Crystal Structures; University of Göttingen, Germany, **1997**.

Received September 3, 2002
[I02305]

The Chelating Ligand 1,3-Bis(pyrazol-1′-yl)propane (Bpp) Enforces a Tetrahedral Geometry in Both Cu^{II} and Cu^{I} Species

Kristel Flinzner,[a] Arno F. Stassen,[a] Allison M. Mills,[b] Anthony L. Spek,[b] Jaap G. Haasnoot,*[a] and Jan Reedijk[a]

Keywords: N ligands / Copper / Crystal structures / Cyclic voltammetry

The ligand 1,3-bis(pyrazol-1′-yl)propane (bpp) has been prepared by reacting 1,3-dichloropropane with two equivalents of pyrazole. After reaction of bpp with copper(II) tetrafluoroborate, three different compounds were obtained, two with Cu^{II} and one with Cu^{I} as cation, depending on the preparative method. The formation of single crystals of these compounds was only observed when 1-(3-chloropropyl)pyrazole (ppc) was present in the solution. The single-crystal X-ray structures of $[Cu(bpp)_2](BF_4)_2$ and $[Cu(bpp)_2](BF_4)$ show that bpp acts as a didentate chelating ligand to form an uncommon eight-atom chelate ring with the copper ion. Two polymorphs of the Cu^{II} complex were characterized. In each of them, the metal atoms possess a distorted tetrahedral geometry. In the copper(I) complex the metal center is present in a less-distorted tetrahedral coordination sphere. The spectroscopic properties of the compounds are in agreement with the structural data. Cyclic voltammetry measurements showed a redox wave at 0.92 V vs. Ag/AgCl.
(© Wiley-VCH Verlag GmbH & Co. KGaA, 69451 Weinheim, Germany, 2003)

Introduction

Didentate ligands may either form chelates or bridges between two different metal ions depending on the number of atoms between the donor atoms. However, they frequently form chelates, coordinating to one metal ion in a chelate ring.[1] Chelate rings of different sizes have been the subject of intensive research in the past. For instance, five- to thirteen-membered rings are formed with 2,2′-bipyridine,[2] bis(2-benzimidazolyl)ethanes,[3,4] bis(2-benzimidazolyl)propanes[3,5,6] 1,3-bis(pyrazol-1′-yl)propane and derivatives[7] and 1,8-bis(3,5-dimethyl-1-pyrazolyl)-3,6-dithiaoctane.[8] Five-membered chelate rings are generally the most stable.[9]

The metal ion used also influences the stability of a complex. Although Cu^{I} is very unstable in protic solutions with respect to disproportionation [2 $Cu^{+}(aq) \rightarrow Cu^{2+}(aq) + Cu^{0}(s)$],[1] the Cu^{I} ion can be stabilized by coordination with ligands having a π-acceptor character.

Generally, Cu^{I} ions in coordination complexes have a (distorted) tetrahedral geometry. A few examples are complexes formed with bipyridine derivatives,[10] thiocyanate,[11] adiponitriles,[12] pyridines[13,14] and indole-containing ligands.[15] In rare cases, Cu^{I} can have other coordination environments, including linear,[1] trigonal,[1] and trigonal pyramidal.[16]

[a] Leiden Institute of Chemistry, Gorlaeus Laboratories, Leiden University
P. O. Box 9502, 2300 RA Leiden, The Netherlands
[b] Bijvoet Center for Biomolecular Research, Vakgroep Kristalen Structuurchemie, Utrecht University
Padualaan 8, 3584 CH Utrecht, The Netherlands
E-mail: haasnoot@chem.leidenuniv.nl

Cu^{II} ions in coordination complexes display several geometries; (distorted) octahedral,[17–19] distorted trigonal bipyramidal,[10] square pyramidal,[11] (distorted) square-planar[8,20] and (distorted) tetrahedral[4,5] complexes have been observed. However, because of the influence of the Jahn–Teller effect square-planar-based geometries are usually preferred[1] by four-coordinate Cu^{II}. Steric constraints are known to generate tetrahedral geometries. Coordination complexes of Cu^{II} and Cu^{I} sharing the same molecular formula and (distorted) tetrahedral geometry are therefore very rare. The previously reported[21] Cu^{II} and Cu^{I} compounds formed with the ligand 2,2′-bis(2-imidazolyl)biphenyl are examples of such complexes.

In this paper, Cu^{II} and Cu^{I} complexes with 1,3-bis(pyrazol-1′-yl)propane (bpp) that display similar (distorted) tetrahedral geometries are described. In these complexes, the bpp ligands act as didentate chelating ligands to form uncommon eight-atom chelate rings. In earlier work[7] metal complexes with the general formula $[M(bpp)X_2]$ (M = Cu^{2+}, Zn^{2+} or Co^{2+} and X = Cl^{-} or NO_3^{-}) have been reported.

The complexes described in this paper are the first containing two bpp ligands coordinated to one metal center. The best single crystals were grown from solutions of 1,3-bis(pyrazol-1′-yl)propane and Cu^{II} tetrafluoroborate, in which an excess of 1-(3-chloropropyl)pyrazole (ppc) was also present.

Two red polymorphic forms of the compound $[Cu(bpp)_2](BF_4)_2$ were obtained: orthorhombic α-$[Cu(bpp)_2](BF_4)_2$ (**1**) crystallized from ethanol, and triclinic β-$[Cu(bpp)_2](BF_4)_2$ (**2**) crystallized from methanol. In addi-

tion, the light yellow Cu^{I} complex $[Cu(bpp)_2](BF_4)$ (**3**) was isolated. This complex also formed from Cu^{II} tetrafluoroborate, upon standing, by auto-reduction.

The X-ray crystal structures of the two forms of $[Cu(bpp)_2](BF_4)_2$ and $[Cu(bpp)_2](BF_4)$ will be presented and discussed. Furthermore, the spectroscopic properties of $[Cu(bpp)_2](BF_4)$, and spectroscopic and magnetic properties of $[Cu(bpp)_2](BF_4)_2$ will be presented. Finally, the results of cyclic voltammetry measurements performed with $[Cu(bpp)_2](BF_4)_2$ will be discussed.

Results and Discussion

General Complex Synthesis

When crystallization attempts were performed with the ligand ppc, complexes containing the ligand bpp, which was present as a contamination in ppc, were isolated instead. These experiments were repeated using different Cu:bpp ratios and ppc in a large excess. In each case, independent of the Cu:bpp ratio, complexes in which Cu and bpp are present in a 1:2 ratio were formed. When crystallizations were performed without ppc, red solids formed which were shown by elemental analysis also to possess a Cu:bpp ratio of 1:2, as for the complexes formed in the presence of ppc. However, no single crystals could be obtained when ppc was not present in the solution. A possible reason for this is that ppc keeps the bpp complexes in solution longer, thus allowing slower crystallization and therefore the growth of high-quality single crystals. This theory is supported by the fact that the copper(I) complex $[Cu(bpp)_2](BF_4)$ does not form at all without the presence of ppc. Because the complex does not spend enough time in solution, formation by slow auto-reduction does not take place.

Molecular Structures of α-$[Cu(bpp)_2](BF_4)_2$ (1) and β-$[Cu(bpp)_2](BF_4)_2$ (2)

The Cu^{II} complex $[Cu(bpp)_2](BF_4)_2$ crystallizes in two polymorphs: orthorhombic α-$[Cu(bpp)_2](BF_4)_2$ (**1**), formed in ethanol, and triclinic β-$[Cu(bpp)_2](BF_4)_2$ (**2**), formed in methanol. The formation of **1** and **2** in different solvents is probably caused by a solvent effect. The presence of both polymorphs in the preparations is unlikely because several crystals were used for structure determination and each time only one polymorph was observed. Selected geometric parameters for **1** and **2** are listed in Table 1 and 2, respectively. The asymmetric unit of **1** contains one unique quarter of a cation with D_2 symmetry (Figure 1). In **2**, three independent cations are present in the asymmetric unit, all of which adopt similar conformations with approximate (noncrystallographic) D_2 symmetry (Figure 2). The cations in both structures are oriented such that one of their (pseudo) C_2-axes is parallel to a short a axis [**1**: a = 7.9532(1) Å; **2**: a = 7.9557(15) Å]. Translation-related cations are stacked into columns along the [100] direction (Figure 3). These columns, separated by the (disordered) BF_4^- anions, are arranged in different patterns in the two polymorphs. In **1**, all of the cations are parallel with their three C_2-axes aligned with the three cell axes, as required by the orthorhombic symmetry (Figure 4). In the triclinic polymorph **2**, the cations centered by Cu(2) and Cu(3) are nearly parallel and together with the BF_4^- anions they form two-column-wide layers within which the packing is similar to that in **1**. Columns of Cu(1)-centered cations, rotated by approximately 60° (about [100]) with respect to the other cations, fit efficiently between these layers (Figure 5). The higher calculated density of **2** (1.590 g cm^{-3}) in comparison to that of **1** (1.563 g cm^{-3}) reflects its more compact packing.

Table 1. Selected bond lengths (Å) and bond angles (°) in α-$[Cu(bpp)_2](BF_4)_2$ (**1**) and $[Cu(bpp)_2](BF_4)$ (**3**)

α-$[Cu(bpp)_2](BF_4)_2$ Bond lengths (Å)		$[Cu(bpp)_2](BF_4)$ Bond lengths (Å)	
Cu(1)−N(2)	1.948(3)	Cu(1)−N(2)	2.0344(15)
		Cu(1)−N(4)	2.0207(15)
		Cu(1)−N(6)	2.0246(15)
		Cu(1)−N(8)	2.0458(15)
Bond angles (°)		**Bond angles (°)**	
N(2)−Cu(1)−N(2)a	107.71(13)	N(2)−Cu(1)−N(4)	113.00(6)
N(2)−Cu(1)−N(2)b	127.20(13)	N(2)−Cu(1)−N(6)	106.91(6)
N(2)−Cu(1)−N(2)c	95.23(13)	N(2)−Cu(1)−N(8)	103.33(6)
		N(4)−Cu(1)−N(6)	114.18(6)
		N(4)−Cu(1)−N(8)	107.65(6)
		N(6)−Cu(1)−N(8)	111.26(6)

Table 2. Selected bond lengths (Å) and bond angles (°) in β-$[Cu(bpp)_2](BF_4)_2$ (**2**)

Bond lengths (Å)		Bond angles (°)	
		Residue 1	
Cu(1)−N(2)	1.973(3)	N(2)−Cu(1)−N(4)	104.49(11)
Cu(1)−N(4)	1.982(3)	N(6)−Cu(1)−N(8)	104.32(10)
Cu(1)−N(6)	1.975(3)	N(2)−Cu(1)−N(8)	135.66(10)
Cu(1)−N(8)	1.981(3)	N(4)−Cu(1)−N(6)	135.65(11)
		N(2)−Cu(1)−N(6)	91.34(10)
		N(4)−Cu(1)−N(8)	92.80(10)
		Residue 2	
Cu(2)−N(10)	1.961(3)	N(10)−Cu(2)−N(12)	105.58(11)
Cu(2)−N(12)	1.957(3)	N(14)−Cu(2)−N(16)	105.08(11)
Cu(2)−N(14)	1.967(3)	N(10)−Cu(2)−N(14)	134.25(11)
Cu(2)−N(16)	1.963(3)	N(12)−Cu(2)−N(16)	130.34(11)
		N(10)−Cu(2)−N(16)	93.96(10)
		N(12)−Cu(2)−N(14)	93.16(11)
		Residue 3	
Cu(3)−N(18)	1.959(2)	N(18)−Cu(3)−N(20)	105.76(10)
Cu(3)−N(20)	1.966(3)	N(22)−Cu(3)−N(24)	105.61(11)
Cu(3)−N(22)	1.963(3)	N(18)−Cu(3)−N(22)	130.47(10)
Cu(3)−N(24)	1.967(3)	N(20)−Cu(3)−N(24)	132.15(11)
		N(18)−Cu(3)−N(24)	94.24(10)
		N(20)−Cu(3)−N(22)	93.71(10)

As shown in Figure 1 and 2, the Cu^{II} ions in both structures are each coordinated to two didentate bpp ligands via the N2 atoms of the pyrazole rings [**1**: Cu−N 1.948(3) Å; **2**: Cu−N 1.957(3)−1.982(3) Å], forming eight-membered

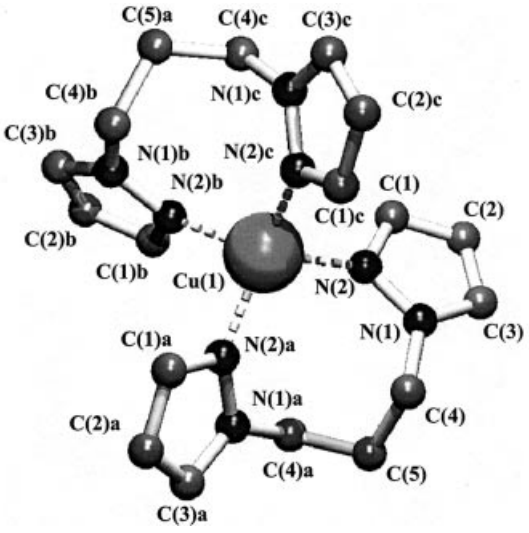

Figure 1. PLATON/POVRAY representation[27,28] of the molecular structure of the cation in α-$[Cu(bpp)_2](BF_4)_2$ (**1**); hydrogen atoms and counterions have been omitted for clarity

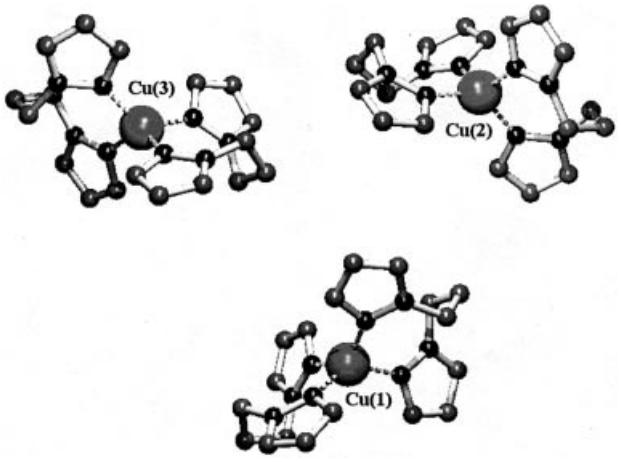

Figure 2. PLATON/POVRAY representation[27,28] of the molecular structure of the three independent cations in β-$[Cu(bpp)_2](BF_4)_2$ (**2**); hydrogen atoms and counterions have been omitted for clarity

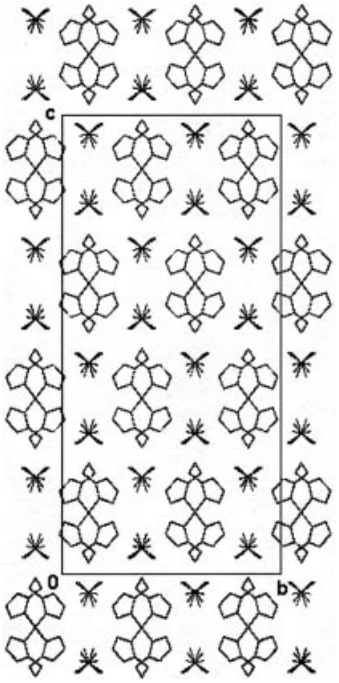

Figure 4. PLATON/POVRAY representation[27,28] of the crystal packing of α-$[Cu(bpp)_2](BF_4)_2$ (**1**), seen in a view down the *a* axis

chelate rings. The coordination geometry at the metal centers is distorted tetrahedral. Although the ligand bite angles are close to 109° [**1**: N−Cu−N 107.71(13)°; **2**: N−Cu−N 104.32(10)−105.76(10)°], the other N−Cu−N angles deviate by up to 18° (**1**) or 27° (**2**) from the ideal tetrahedral value. The dihedral angles between the N−Cu−N planes of the chelate rings in each complex cation [**1**: 66.8(2)°; **2**: 57.05(15)−62.30(15)°] also indicate a flattening of the CuN_4 tetrahedrons for which a value of 90° would be expected.

Molecular Structure of $[Cu(bpp)_2](BF_4)$ (3)

In the crystal structure of the Cu^I complex $[Cu(bpp)_2](BF_4)$ (**3**), the asymmetric unit contains one inde-

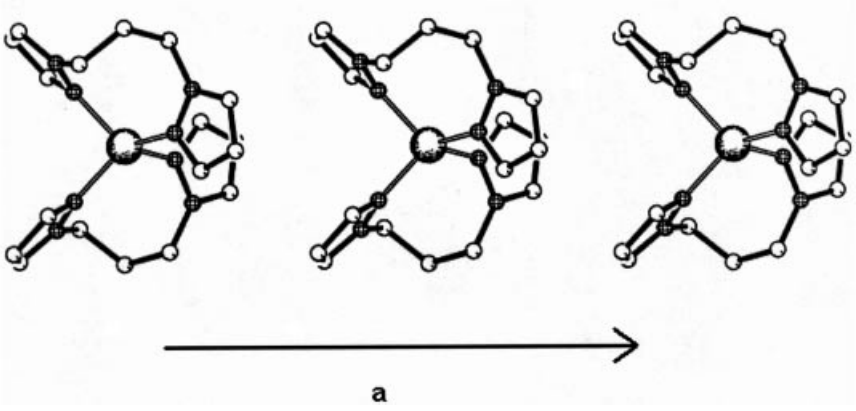

Figure 3. PLATON/POVRAY representation[27,28] of translation-related cations stacked into columns parallel to the *a* axis, in α-$[Cu(bpp)_2](BF_4)_2$ (**1**) and β-$[Cu(bpp)_2](BF_4)_2$ (**2**)

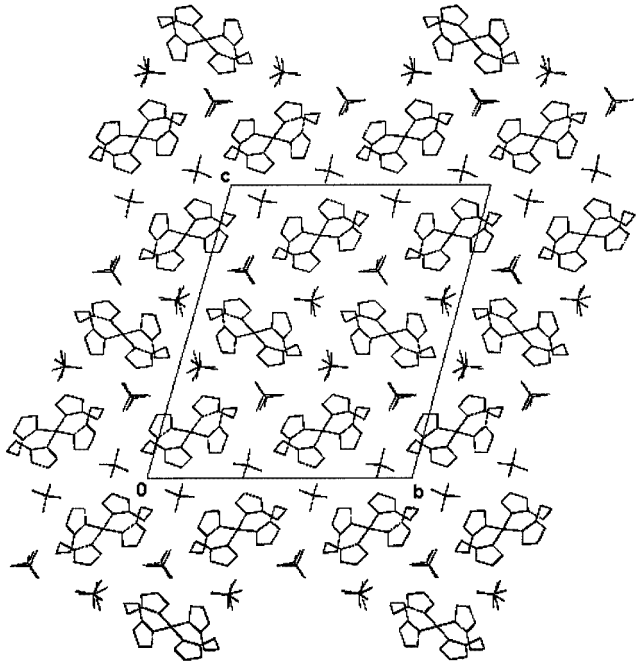

Figure 5. PLATON/POVRAY representation[27,28] of the crystal packing of β-[Cu(bpp)$_2$](BF$_4$)$_2$ (**2**), seen in a view down the *a* axis

pendent cation possessing (noncrystallographic) S_4-based symmetry, as shown in Figure 6. The relevant geometric parameters for **3** are given in Table 1. The Cu^{I} ion of **3** is coordinated to two bpp ligands, but at Cu−N distances of 2.0207(15)−2.0458(15) Å which, as expected, are longer than those found in the Cu^{II} complex. Similar Cu^{I}−N [2.029(6)−2.053(6) Å] and Cu^{II}−N [1.941(9)−1.977(8) Å] bond lengths have been reported for the nearly tetrahedral complexes [CuL$_2$](ClO$_4$) and [CuL$_2$](ClO$_4$)$_2$ [L = 2,2′-bis(2-imidazolyl)biphenyl].[21] In **3**, The Cu-centered coordination environment is a slightly distorted tetrahedron; the N−Cu−N angles range from 103.33(6)−114.18(6)°, and the dihedral angle between the N−Cu−N planes of the chelate rings is 89.58(9)°.

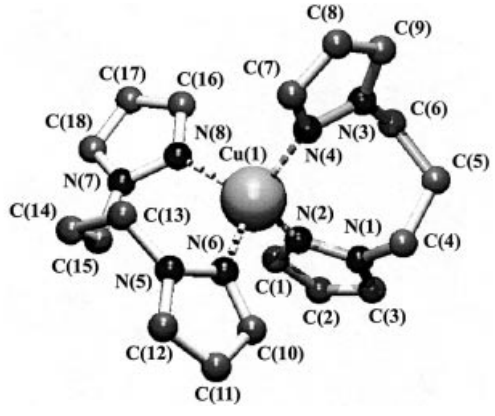

Figure 6. PLATON/POVRAY representation[27,28] of the molecular structure of the cation in [Cu(bpp)$_2$](BF$_4$) (**3**); hydrogen atoms and counterions have been omitted for clarity

Spectroscopic and Magnetic Properties

Ligand field spectra have been recorded for both [Cu(bpp)$_2$](BF$_4$)$_2$ and [Cu(bpp)$_2$](BF$_4$) in the solid state. The spectrum of α-[Cu(bpp)$_2$](BF$_4$)$_2$ (**1**) consists of broad signals at 39.2 × 10^3 cm^{-1} and 22.7 × 10^3 cm^{-1}, which are attributed to LMCT transitions. In the spectrum of β-[Cu(bpp)$_2$](BF$_4$)$_2$ (**2**), these signals are present at 40.2 × 10^3 cm^{-1} and 21.5 × 10^3 cm^{-1}. Furthermore, in the spectrum of **1** a weak signal is present at 14.5 × 10^3 cm^{-1}, in the normal range for d-d transitions in slightly distorted tetrahedrally coordinated Cu^{II} complexes.[7,22] This signal is not visible in the spectrum of **2**, where the LMCT transition dominates.

The diffuse reflectance spectrum of [Cu(bpp)$_2$](BF$_4$) consists of one broad signal at 37.9 × 10^3 cm^{-1}, with a shoulder at 25.0 × 10^3 cm^{-1}, which is ascribed to MLCT transitions. No d-d transition signals are present, as is expected for Cu^{I}.

The X-band EPR spectra of a polycrystalline powder of α-[Cu(bpp)$_2$](BF$_4$)$_2$ (**1**) were recorded at room temperature and 77 K. The resolution did not improve upon cooling to 77 K. The spectra show an axial $S = 1/2$ signal with g values that are normal for Cu^{II} in a slightly distorted tetrahedral environment: $g_{\perp} = 2.11$, $g_{//} = 2.32$ and $A_{//} = 13.0$ mT.[7] The spectrum of α-[Cu(bpp)$_2$](BF$_4$)$_2$ in a frozen solution of ethanol was also recorded. This spectrum shows g values that are similar to the g values of the powder spectra, which indicates that the complex is stable in solution. The same spectra were recorded for β-[Cu(bpp)$_2$](BF$_4$)$_2$ (**2**). These spectra show an axial $S = 1/2$ signal with $g_{\perp} = 2.13$, $g_{//} = 2.38$ and $A_{//} = 12.0$ mT.

Magnetic susceptibility measurements were also performed on [Cu(bpp)$_2$](BF$_4$)$_2$ to detect any possible magnetic exchange. A plot of χ^{-1} vs. T fits a straight line through zero, with a value of the Curie constant C of 0.44 cm^3·K·mol^{-1}, which corresponds to a μ_{eff} of 1.88.

Cyclic Voltammetry

The cyclic voltammogram of [Cu(bpp)$_2$](BF$_4$)$_2$ (Figure 7) shows an irreversible wave at 0.92 V vs. Ag/AgCl, ascribed to the couple Cu^{II}/Cu^{I} (E_{pc} at 0.83 V, E_{pa} at 1.01 V). At scan rates between 30−80 mV/s, $I_{pc}/I_{pa} = 1$ and $I_p/v^{1/2}$ is independent of v, but at higher and lower scan rates this reversibility is lost. In the Cu^{II} and Cu^{I} complexes with the ligand 2,2′-bis(2-imidazolyl)biphenyl mentioned above,[21] the Cu^{II}/Cu^{I} reduction wave occurs at 0.08 V vs. SCE (−0.052 V vs. Ag/AgCl) in acetonitrile.[23] Upon comparison, the reduction of [Cu(bpp)$_2$]$^{2+}$ to [Cu(bpp)$_2$]$^{+}$ takes place at an unusually high potential, confirming the high stability of the Cu^{I} complex [Cu(bpp)$_2$](BF$_4$), and also explaining the easy reduction of the Cu^{II} species in ethanol solution. Such a stabilisation of Cu^{I} by π-donor ligands such as azoles is well known. After reduction of Cu^{I} to Cu(0) at $E_{pc} = -0.55$ V, a stripping peak appears at $E_{pa} = -0.28$ V, as a result of the deposition of Cu(0) on the electrode surface. The Cu^{II}/Cu^{I} reduction wave becomes less prominent at scan rates higher and lower than 60 mV/s.

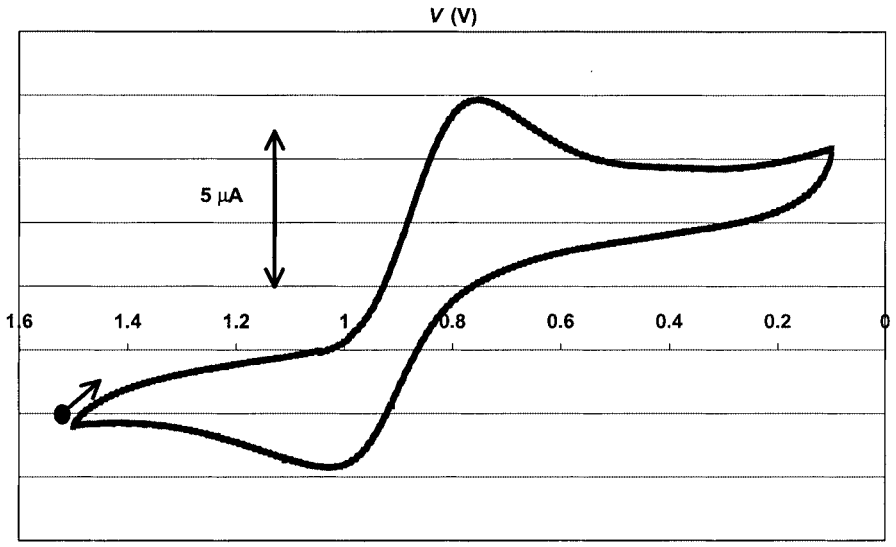

Figure 7. Cyclic voltammogram of $[Cu(bpp)_2](BF_4)_2$, in acetonitrile (10^{-3} M) at a scan rate of 60 mV/s

Conclusion

The ligand 1,3-bis(pyrazol-1′-yl)propane (bpp) has been synthesized from 1,3-dichloropropane and pyrazole. Attempts to obtain coordination complexes of bpp with both Cu^{II} and Cu^{I} succeeded. The complexes that were obtained are the first to contain copper ions surrounded by two — rather than only one — bpp ligands forming eight-atom chelate rings with the metal ion.[7] The best single crystals were grown from solutions of 1,3-bis(pyrazol-1′-yl)propane and Cu^{II} tetrafluoroborate, in which an excess of 1-(3-chloropropyl)pyrazole (ppc) was also present. A possible reason for this behavior is that the complexes stay in solution longer when ppc is present. The slower crystal growth yields higher quality single crystals. All attempts to obtain crystalline Cu^{II} complexes with only ppc were unsuccessful. The Cu^{II} ions in the two polymorphs of the $[Cu(bpp)_2](BF_4)_2$ complex are surrounded by a distorted tetrahedral coordination environment. This is remarkable because Cu^{II} has a strong preference for a square-planar geometry when it is surrounded by four monodentate ligands or two didentate ligands.[1] Tetrahedral geometries are much more common for Cu^{I} than for Cu^{II}. When the Cu^{II} complexes were found to be stable in a distorted tetrahedral geometry, it was expected that a tetrahedral Cu^{I} complex should also be stable, as is indeed the case. However, this complex was not expected to form from a Cu^{II} solution. The large redox potential for the copper ion in the complexes (0.92 V vs. Ag/AgCl) indicates the stability of the Cu^{I} complex.

Experimental Section

General Remarks

^{1}H NMR spectra were obtained with a Bruker 300 MHz spectrometer. X-band powder EPR spectra were obtained with a Jeol RE2x electron spin resonance spectrometer using DPPH (g = 2.0036) as a standard. FTIR spectra were obtained with a Perkin−Elmer Paragon 1000 FTIR spectrophotometer equipped with a Golden Gate ATR device, using the diffuse reflectance technique (4000−300 cm^{-1}, res. 4 cm^{-1}). Magnetic susceptibility measurements (2−300 K) were carried out using a Quantum Design MPMS-5 5T SQUID magnetometer (measurements carried out at 1000 Gauss). Data were corrected for the magnetization of the sample holder and for the sample diamagnetism, which was estimated from the Pascal constants.[24] Cyclic voltammetry measurements were performed with an Autolab PGSTAT 10 cyclic voltammeter, using a Pt working electrode, a Pt auxiliary electrode and a Ag/AgCl reference electrode in acetonitrile (10^{-3} M), with tetrabutylammonium hexafluorophosphate as electrolyte, at a scan rate of 60 mV/s. C, H, N determinations were performed with a Perkin−Elmer 2400 Series II analyzer.

Synthesis of the Ligands

1,3-Bis(pyrazol-1′-yl)propane (bpp; Figure 8) was prepared by adding 0.2 mol (13.6 g) of pyrazole and 0.4 mol (45.2 g) of 1,3-dichloropropane dissolved in 80 mL of toluene to a solution of 0.1 mol (4 g) of sodium hydroxide in 80 mL of water. After addition of 0.2 g of tetrabutylammonium bromide to increase the rate of charge transfer between the layers, the solution was refluxed at 100 °C for four days. The two layers were separated and the water layer was extracted with dichloromethane. All organic layers were combined, then dried with magnesium sulfate, and filtered. After evaporation of the solvents, the product was obtained as a yellow oil. The yield was 17% (2.99 g). ^{1}H NMR (300 MHz, $[D_6]$DMSO): δ = 7.70(d, a), 6.23 (dd, b), 7.44 (d, c), 4.07 (t, d), 2.17 (q, e).

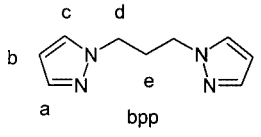

Figure 8. The ligand bpp

Table 3. Crystallographic data for α-$[Cu(bpp)_2](BF_4)_2$, β-$[Cu(bpp)_2](BF_4)_2$ and $[Cu(bpp)_2](BF_4)$

	α-$[Cu(bpp)_2](BF_4)_2$	β-$[Cu(bpp)_2](BF_4)_2$	$[Cu(bpp)_2](BF_4)$
Formula	$C_{18}H_{24}B_2CuF_8N_8$	$C_{18}H_{24}B_2CuF_8N_8$	$C_{18}H_{24}BF_4CuN_8$
Molecular weight	589.61	589.61	502.80
Crystal system	Orthorhombic	Triclinic	Monoclinic
Space group	Fddd (No. 70)	$P\bar{1}$ (No. 2)	$P2_1/c$ (No. 14)
a (Å)	7.9532(1)	7.9557(15)	9.6773(2)
b (Å)	17.0680(3)	20.485(4)	23.9139(4)
c (Å)	36.9087(8)	23.835(4)	9.5287(1)
α (°)		74.406(16)	
β (°)		81.178(15)	90.4560(10)
γ (°)		89.381(14)	
V (Å^3)	5010.18(15)	3695.3(12)	2205.08(6)
Z	8	6	4
D_{calc} (g·cm^{-3})	1.563	1.590	1.515
μ (Mo-K_α) (mm^{-1})	0.955	0.972	1.047
F(000)	2392	1794	1032
Crystal size (mm)	0.06 × 0.12 × 0.21	0.09 × 0.30 × 0.45	0.09 × 0.15 × 0.30
T (K)	150	150	150
λ (Å)	Mo-K_α 0.71073	Mo-K_α 0.71073	Mo-K_α 0.71073
θ range (°)	2.2 to 27.5	1.5 to 27.5	1.7 to 26.0
Data collected	14882	44203	15999
Data unique	1448	16786	4243
Data observed [$I > 2\sigma(I)$]	1167	12647	3624
R_{int}	0.046	0.051	0.032
No. of parameters	123	1160	289
No. of restraints	84	566	0
R(F), [$I > 2\sigma(I)$]	0.0548	0.0466	0.0280
ωR(F^2)	0.1470	0.1041	0.0706
S	1.03	1.08	1.04
$\Delta\rho_{min}$, $\Delta\rho_{max}$ (e·Å^{-3})	−0.41, 0.88	−0.52, 0.70	−0.35, 0.25

1-(3-Chloropropyl)pyrazole (ppc) was prepared using the same procedure, but in this case only 0.1 mol (6.8 g) of pyrazole was added to the reaction mixture.

Synthesis of the Complexes

α-$[Cu(bpp)_2](BF_4)_2$ (1): This complex was obtained by adding a solution of 1.0 mmol (0.31 g) of $Cu(BF_4)_2{\cdot}4H_2O$ in 8 mL of ethanol to a solution of 1.0 mmol (0.15 g) of ppc and 0.1 mmol (0.02 g) of bpp in 8 mL ethanol. The compound crystallized from the green solution as red plates that were isolated by filtration and dried for several hours in air. $C_{18}H_{24}B_2CuF_8N_8$ (589.6): calcd. C 36.7, H 4.1, N 19.0; found C 36.7, H 4.3, N 19.0.

β-$[Cu(bpp)_2](BF_4)_2$ (2): This complex was obtained by adding a solution of 1.0 mmol (0.31 g) of $Cu(BF_4)_2{\cdot}4H_2O$ in 3 mL of methanol to a solution of 1.0 mmol (0.15 g) of ppc and 0.1 mmol (0.02 g) of bpp in 3 mL of methanol. The compound crystallized from the green solution as red plates that were isolated by filtration and dried for several hours in air. $C_{18}H_{24}B_2CuF_8N_8$ (589.6): calcd. C 36.7, H 4.1, N 19.0; found C 36.5, H 4.0, N 18.5.

$[Cu(bpp)_2](BF_4)$ (3): This complex was obtained by adding a solution of 1.0 mmol (0.31 g) of $Cu(BF_4)_2{\cdot}4H_2O$ in 12 mL of ethanol to a solution of 10.5 mmol (2.16 g) of ppc and 3.0 mmol (0.54 g) of bpp in 12 mL of ethanol. The resulting solution was heated to boiling and immediately filtered. After two weeks, colorless blocks crystallized from the green solution and these were isolated by filtration, then dried for several hours in air. $C_{18}H_{24}BCuF_4N_8$ (502.8): calcd. C 43.0, H 4.8, N 22.3; found C 42.7, H 5.0, N 22.5.

X-ray Crystallographic Study: Intensity data for each of the structures were collected on a Nonius KappaCCD diffractometer with rotating anode (Mo-K_α, λ = 0.71073 Å) at 150 K. Correction for absorption was considered unnecessary in all cases. The structures were solved by automated Patterson methods using DIRDIF99,[25] and refined on F^2 by least-squares procedures using SHELXL-97.[26] Structure validation and molecular graphics preparation were performed with the PLATON package.[27]

The BF_4^- anion in **1**, and four of the six independent anions in **2**, are disordered over two sets of atomic positions. All non-hydrogen atoms were refined with anisotropic displacement parameters, but the displacement parameters of the disordered atoms, as well as the ligand alkyl C atoms in complex **1**, were restrained to be approximately isotropic. Hydrogen atoms were constrained to idealized geometries and allowed to ride on their carrier atoms with an isotropic displacement parameter related to the equivalent displacement parameter of their carrier atoms. The BF_4^- anions were restrained to approximately tetrahedral geometries. Crystal data and further details of the data collections are given in Table 3.

CCDC-184550 (**1**), -184551 (**2**), and -184552 (**3**) contain the supplementary crystallographic data for this paper. These data can be obtained free of charge at www.ccdc.cam.ac.uk/conts/retrieving.html (or from the CCDC, 12 Union Road, Cambridge CB2 1EZ, UK; Fax: (internat.) +44-1223/336-033; E-mail: deposit@ccdc.cam.ac.uk).

Acknowledgments

The work described in this paper has been supported by the Leiden University Study Group WFMO and has been performed under

the auspices of the Graduate Research School HRSMC, a joint activity of Leiden University and the two Universities in Amsterdam. This work has also been supported in part (A. L. S. & A. M. M.) by the Netherlands Foundation of Chemical Research (CW) with financial aid from the Netherlands Organization for Scientific Research (NWO). We are indebted to Jos van Brussel for performing the elemental analyses, to Annemarieke Schuitema for assistance with the EPR measurements and to Martijn Mulder and Elisabeth Bouwman for their help with the cyclic voltammetry measurements.

[1] N. N. Greenwood, A. Earnshaw, *Chemistry of the Elements*, second ed., Butterworth-Heinemann: Oxford, **1997**.
[2] J. Foley, S. Tyagi, B. J. Hathaway, *J. Chem. Soc., Dalton Trans.* **1984**, 1−5.
[3] G. A. v. Albada, W. J. J. Smeets, N. Veldman, A. L. Spek, J. Reedijk, *Inorg. Chim. Acta* **1999**, *290*, 105−112.
[4] V. Broughton, G. Bernardinelli, A. F. Williams, *Inorg. Chim. Acta* **1998**, *275−276*, 279−288.
[5] G. A. v. Albada, W. J. J. Smeets, A. L. Spek, J. Reedijk, *Inorg. Chim. Acta* **1999**, *288*, 220−225.
[6] G. Bernardinelli, A. Kuebel-Pollak, S. Ruettimann, A. F. Williams, *Chimia 46* **1992**, 155−158.
[7] A. M. Schuitema, M. Engelen, I. A. Koval, S. Gorter, W. L. Driessen, J. Reedijk, *Inorg. Chim. Acta* **2001**, *324*, 57−64.
[8] W. G. Haanstra, W. A. J. W. v. d. Donk, W. L. Driessen, J. Reedijk, J. S. Wood, M. G. B. Drew, *J. Chem. Soc., Dalton Trans.* **1990**, 3123−3128.
[9] D. F. Shriver, P. W. Atkins, C. H. Langford, *Inorganic Chemistry*, Oxford University Press, Oxford, **1994**.
[10] P. J. Burke, K. Henrick, D. R. McMillin, *Inorg. Chem.* **1982**, *21*, 1881−1886.
[11] K. Nieminen, *Acta Chem. Scand., Ser. A* **1981**, *35*, 753−757.
[12] Y. Kinoshita, I. Matsubara, T. Higuchi, Y. Saito, *Bull. Chem. Soc. Jpn.* **1959**, *32*, 1221−1226.
[13] K. Nilsson, Å. Oskarsson, *Acta Crystallogr., Sect. A* **1981**, *37*, C227.
[14] K. Nilsson, Å. Oskarsson, *Acta Chem. Scand., Ser. A* **1982**, *36*, 605−610.
[15] Y. Shimazaki, H. Yokoyama, O. Yamauchi, *Angew. Chem. Int. Ed.* **1999**, *38*, 2401−2403.
[16] M. T. Miller, P. K. Gantzel, T. B. Karpishin, *J. Am. Chem. Soc.* **1999**, *121*, 4292−4293.
[17] G. Ivarsson, *Acta Chem. Scand.* **1973**, *27*, 3523−3530.
[18] M. E. Quiroz-Castro, G. A. v. Albada, I. Mutikainen, U. Turpeinen, J. Reedijk, *Inorg. Chim. Acta* **2000**, *297*, 129−133.
[19] D. L. McFadden, A. T. McPhail, C. D. Garner, F. E. Mabbs, *J. Chem. Soc., Dalton Trans.* **1976**, 47−52.
[20] P. F. Kelly, A. M. Z. Slawin, K. W. Waring, *J. Chem. Soc., Dalton Trans.* **1997**, 2853−2854.
[21] S. Knapp, T. P. Keenan, X. Zhang, R. Fikar, J. A. Potenza, H. J. Shugar, *J. Am. Chem. Soc.* **1987**, *109*, 1882.
[22] B. J. Hathaway, in *Comprehensive Coordination Chemistry* (Eds.: G. Wilkinson, R. D. Gillard, J. A. E. McCleverty), Pergamon, Oxford, **1987**, *5*.
[23] P. Zanello, in *Stereochemistry of Organometallic and Inorganic Compounds* (Ed.: I. Bernal), Elsevier Science Publishers: Amsterdam, **1990**, *4*.
[24] I. M. Kolthoff, P. J. Elving *Treatise on Analytical Chemistry*, New York, **1963**, *4*.
[25] P. T. Beurskens, G. Admiraal, G. Beurskens, W. P. Bosman, S. Garcia-Granda, R. O. Gould, J. M. M. Smits, C. Smykalla *The DIRDIF program system, Technical report of the Crystallography Laboratory* University of Nijmegen, The Netherlands, **1992**.
[26] G. M. Sheldrick *SHELXL-97. Program for the Refinement of Crystal Structures* University of Göttingen, Germany, **1997**.
[27] A. L. Spek *PLATON, A multi-purpose crystallographic tool*, Utrecht University, The Netherlands, **2000**. Internet: http://www.cryst.chem.uu.nl/platon
[28] C. Carson *POVRAY, rendering engine for Windows*, **1996−1999**.

Received June 12, 2002
[I02310]

Synthesis and X-ray Structures of Tin(IV) and Lead(II) Complexes with Heterocyclic Thiones

Antonio Sousa-Pedrares,*[a] María I. Casanova,[a] José A. García-Vázquez,[a] María L. Durán,[a] Jaime Romero,[a] Antonio Sousa,*[a] Jack Silver,[b] and Philip J. Titler[b]

Keywords: Tin / Lead / N ligands / S ligands / Heterocycles

Tin(IV) and lead(II) complexes of 3-(trifluoromethyl)pyridine-2-thione (3-CF_3-pySH) and 5-(trifluoromethyl)pyridine-2-thione (5-CF_3-pySH) have been synthesised. The compounds [Sn(3-CF_3-pyS)$_4$] (1), [Sn(5-CF_3-pyS)$_4$] (2), [Pb(3-CF_3-pyS)$_2$] (3), and [Pb(5-CF_3-pyS)$_2$] (4) were obtained by addition of the appropriate ligand to a methanol solution of tin(II) chloride or lead acetate in the presence of triethylamine. The complex [Sn(5-CF_3-pyS)$_4$] was also prepared by electrochemical oxidation of a tin anode in a cell containing an acetonitrile solution of the ligand 5-(trifluoromethyl)pyridine-2-thione. The X-ray crystal structure of [Sn(3-CF_3-pyS)$_4$] reveals a dodecahedral coordination geometry around Sn^{IV}, with the four thionate ligands acting in a bidentate (N,S) manner. [Sn(5-CF_3-pyS)$_4$] also consists of monomeric neutral molecules with the tin(IV) atom in an octahedral geometry with two bidentate (N,S) ligands and two monodentate S ligands. The molecular structure of [Pb(3-CF_3-pyS)$_2$] shows the metal in a five-coordinate geometry with the stereochemically active lead(II) lone pair in an equatorial position of a trigonal bipyramid. Spectroscopic data for the complexes (IR, NMR, FAB, and Mössbauer spectra) are discussed and related to the structural information.
(© Wiley-VCH Verlag GmbH & Co. KGaA, 69451 Weinheim, Germany, 2003)

Introduction

Much of the interest in metal-sulfur chemistry results from the potential relevance of the resulting compounds to active sites in metalloenzymes and also to their ability to adopt various nuclearities of significant structural complexity.[1−3] However, in comparison with the coordination chemistry of transition metals, the chemistry of the main group metals with sulfur ligands remains much less developed.[4] In many cases, the interaction of toxic metals with biological systems involves bonding of the metal to the sulfydryl groups present in enzymes. Hence, an insight into the chemistry of main group thiolate compounds is important in terms of understanding the aforementioned interaction and for the design of detoxifying agents.[5,6] The generally poor solubility of group 14 metal/thiolate compounds makes it difficult to structurally characterise these systems and, for this reason, there is a lack of compounds whose structures have been determined by X-ray diffraction. Zubieta has determined the structures of [Sn(2-SC_5H_4N)$_4$][7] and [Sn(2-SC_5H_4N-3-$SiMe_3$)$_4$].[8] Curiously, while [Sn(2-SC_5H_4N)$_4$] has a distorted octahedral structure, the structure of [Sn(2-SC_5H_4N-3-$SiMe_3$)$_4$] is dodecahedral. This suggests that the nature and location of the substituents in the heterocyclic ring are important in determining the structure of the compound isolated. As a result of our continued interest in the coordination chemistry of thionate ligands, we decided to study the influence of the nature and location of substituents in the heterocyclic ring on the structure of the corresponding complexes. In particular, the work described here encompasses the synthesis and characterisation of tin(IV) and lead(II) complexes with 3-(trifluoromethyl)- and 5-(trifluoromethyl)pyridine-2-thionato ligands.

[a] Departamento de Química Inorgánica,
Universidad de Santiago de Compostela,
15782 Santiago de Compostela, Spain
[b] School of Chemical and Life Sciences, University of Greenwich,
Wellington St, Woolwich, London, SE18 6PF, UK

Results and Discussion

The reactions of 3-(trifluoromethyl)- and 5-(trifluoromethyl)pyridine-2-thione with $SnCl_2$ in methanol in the presence of triethylamine produce compounds whose microanalytical data correspond to SnL_4. On going from the tin precursor to the product, the metal atom is oxidised and so one possible reaction mechanism involves the formation of an initial tin(II) compound, which is subsequently oxidised in solution to tin(IV) in accordance with the following equations:

$$SnCl_2 + 2\ Et_3N + 2\ (R\text{-}pySH) \rightarrow [Sn(R\text{-}pyS)_2] + 2\ HEt_3NCl$$

$$[Sn(R\text{-}pyS)_2] + 2\ (R\text{-}pySH) \rightarrow [Sn(R\text{-}pyS)_4] + H_2$$

It is well-known that the electrochemical procedure for the synthesis of metal complexes produces compounds in which the metal is in a low oxidation state. For this reason,

we tried to ascertain whether tin(II) compounds with these ligands could be obtained using such a procedure. With this aim in mind, a solution of 5-(trifluoromethyl)pyridine-2-thione in acetonitrile was electrolysed using a tin plate as the anode. Once more, the microanalytical data and the X-ray structure (vide infra) for the resulting compound were consistent with the composition [Sn(5-CF_3-pyS)$_4$]. The electrochemical process has an efficiency value near to 0.5 mol·F^{-1} (E_f = 0.49). This means that the anode oxidation leads initially to a tin(II) species, which is then further oxidised to [SnL_4] in accordance with the following reaction sequence:

Cathode: 2 (5-CF_3pySH) + 2 e^- → 2 (5-CF_3pyS^-) + H_2

Anode: 2 (5-CF_3pyS^-) + Sn → [Sn(5-CF_3pyS)$_2$] + 2 e^-

[Sn(5-CF_3pyS)$_2$] + 2 (5-CF_3pySH) → [Sn(5-CF_3pyS)$_4$] + H_2

This behaviour has been observed in the synthesis of other Sn^{IV} complexes by electrochemical procedures.[9]

The lead(II) complexes were obtained in reasonable yields by stirring the corresponding ligand and lead acetate in solution in methanol in the presence of triethylamine. The formation of these lead complexes is believed to follow a similar scheme to that described above for [Sn(3-CF_3-pyS)$_4$]. However, in this case, the further oxidation step does not occur and the complexes have the general formula [PbL_2].

$Pb(CH_3COO)_2$ + 2 [Et_3N+ (R-pySH)] → [Pb(R-pyS)$_2$] + 2 HEt_3NCH_3COO

Crystallographic Studies

Structure of [Sn(3-CF_3-pyS)$_4$] (1)

Figure 1 shows the ORTEP drawing of the structure of [Sn(3-CF_3-pyS)$_4$] along with the numbering system used.

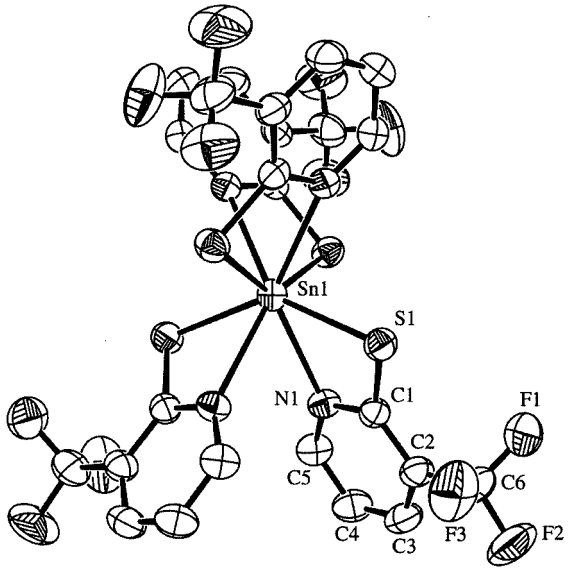

Figure 1. Molecular structure of [Sn(3-CF_3-pyS)$_4$]

The relevant bond lengths and bond angles are listed in Table 1.

The structure of **1** shows the tin atom to be coordinated by four bidentate (N,S) ligands. In this arrangement the metal atom is in an eight-coordinate environment. Comparison of the parameters found with values for the corresponding ideal geometry with the same coordination number shows that, in this case, the geometry is closer to a dodecahedron than to an antiprism.

The distortion of the dodecahedral geometry with regard to the regular geometry can be understood if we consider the regular dodecahedron as being the result of the interpenetration of two regular tetrahedra (Figure 2). In the complex under discussion, the four sulfur atoms are situated at the vertices of a distorted tetrahedron and the nitrogen atoms in the vertices of another distorted tetrahedron in an alternating manner.[10]

The main cause of distortion is the small bite of the chelate angle N−Sn−S at 61.72(5)°. Another factor that contributes to the distortion is the difference between the bond lengths Sn−N and Sn−S, which are 2.556(2) and 2.4935(8) Å, respectively. This causes the tetrahedron formed by the nitrogen atoms to be more distorted than the one formed by the sulfur atoms. In the tetrahedron formed by the sulfur atoms the values of the S−Sn−S angles are 97.322(12) and 138.17(3)°, while the N−Sn−N angles are 67.45(10) and 133.77(6)°, i.e. further from the theoretical value expected for a regular tetrahedron.

The four Sn−S bond lengths [2.4935(8) Å] are not very different from those found in other tin complexes with four-membered chelate rings such as, for example, [Sn(S_2CNEt_2)$_4$][11] and [Sn(S_2CNMe)$_4$],[12] or in the complex of tin with trisilylpyridine-2-thionate, [Sn(3-Me_3Si-pyS)$_4$], where the tin atom is also eight-coordinate in a dodecahedral geometry [average value 2.496(4) Å].[8]

The values of the Sn−N bond lengths are similar to those found in [Sn(3-Me_3Si-pyS)$_4$], average value 2.56(1) Å, but longer than the values found in [Sn(5-CF_3-pyS)$_4$], vide infra, where the tin atom is in a six-coordinate environment.

The pyridine rings are essentially planar and the S(1) atom lies approximately on the plane of the pyridine ring to which it is bound (maximum deviation 0.028 Å). The average S−C and C−N bond lengths [1.768(17) and 1.345(16) Å, respectively] are intermediate between the values found in free pyridine-2-thione [1.695(2) Å, 1.356(3) Å, respectively][13] and those in bis(3-*tert*-butyldimethylsilyl)-2-pyridyldisulfide[14] [average C−S: 1.794(3) Å; average N−C: 1.330(5) Å], suggesting that the ligand is coordinating in a way that is closer to the pyridine-2-thionato form than to the thione form.

Structure of [Sn(5-CF_3-pyS)$_4$] (2)

Figure 3 shows the ORTEP drawing of the structure of [Sn(5-CF_3-pyS)$_4$] along with the numbering system used. The relevant bond lengths and bond angles are listed in Table 2.

The geometry of [Sn(5-CF_3-pyS)$_4$] can be described as a severely distorted octahedron, with the tin atom coordin-

Table 1. Selected bond lengths [Å] and angles [°] for complex [Sn(3-CF_3-pyS)$_4$]

Sn(1)−S(1)	2.4935(8)	N(1)−C(1)	1.339(3)
Sn(1)−N(1)	2.556(2)	N(1)−C(5)	1.331(3)
S(1)−C(1)	1.742(3)		
S(1)−Sn(1)−S(1)#1[a]	97.322(12)	S(1)#2−Sn(1)−N(1)#1	83.10(5)
S(1)−Sn(1)−S(1)#2	97.322(12)	S(1)#2−Sn(1)−N(1)#2	61.72(5)
S(1)−Sn(1)−S(1)#3	138.17(3)	S(1)#3−Sn(1)−N(1)	83.10(5)
S(1)#1−Sn(1)−S(1)#2	138.17(3)	S(1)#3−Sn(1)−N(1)#1	79.01(5)
S(1)#1−Sn(1)−S(1)#3	97.322(12)	S(1)#3−Sn(1)−N(1)#2	141.67(5)
S(1)#2−Sn(1)−S(1)#3	97.322(12)	N(1)−Sn(1)−N(1)#1	133.77(6)
S(1)#2−Sn(1)−N(1)#3	79.01(5)	N(1)−Sn(1)−N(1)#2	133.77(6)
S(1)#3−Sn(1)−N(1)#3	61.72(5)	N(1)−Sn(1)−N(1)#3	67.45(10)
S(1)−Sn(1)−N(1)	61.72(5)	N(1)#1−Sn(1)−N(1)#2	67.45(10)
S(1)−Sn(1)−N(1)#1	141.67(5)	N(1)#1−Sn(1)−N(1)#3	133.77(6)
S(1)−Sn(1)−N(1)#2	79.01(5)	N(1)#2−Sn(1)−N(1)#3	133.77(6)
S(1)−Sn(1)−N(1)#3	83.10(5)	C(1)−S(1)−Sn(1)	88.41(9)
S(1)#1−Sn(1)−N(1)	79.01(5)	C(1)−N(1)−C(5)	120.1(2)
S(1)#1−Sn(1)−N(1)#1	61.72(5)	C(1)−N(1)−Sn(1)	95.76(16)
S(1)#1−Sn(1)−N(1)#2	83.10(5)	C(5)−N(1)−Sn(1)	143.6(2)
S(1)#1−Sn(1)−N(1)#3	141.67(5)	N(1)−C(1)−S(1)	113.79(19)
S(1)#2−Sn(1)−N(1)	141.67(5)		

[a] Symmetry transformations used to generate equivalent atoms. #1: $-y + 1/4$, $x + 1/4$, $-z + 1/4$, #2: $y - 1/4$, $-x + 1/4$, $-z + 1/4$, #3: $-x$, $-y + 1/2$, z.

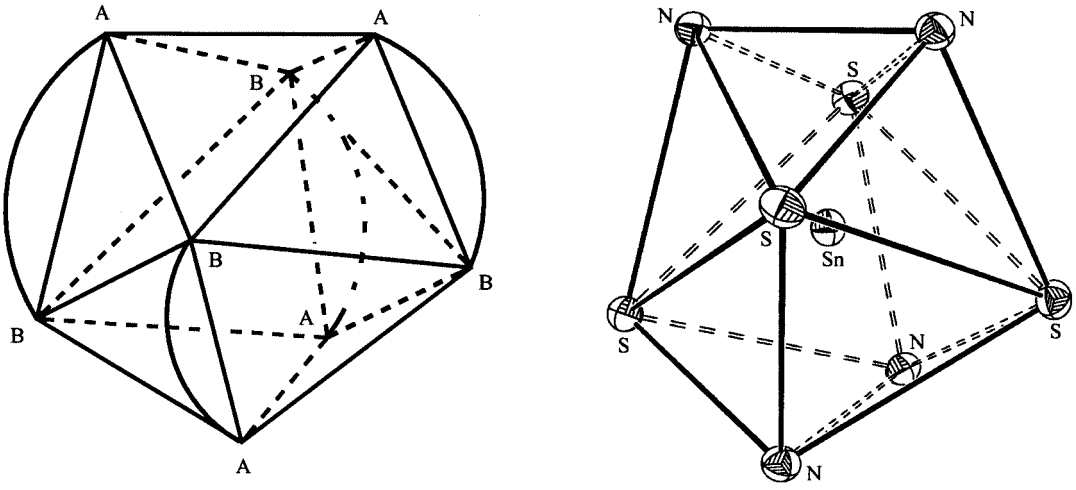

Figure 2. (left) View of the regular dodecahedral structure for a complex of the type [M(AB)$_4$]; (right) view of the coordination polyhedron for the complex [Sn(3-CF_3-pyS)$_4$]

ated to two monodentate S thionato ligands and two bidentate (N,S) ligands.

The arrangement of the ligands is such that the sulfur atoms of the two monodentate thionate ligands are in a *cis* disposition with respect to one another and the sulfur atoms of the two bidentate ligands are in a *trans* disposition. The main cause of the distortion is the small bite of the bidentate thionato ligands [N−Sn−S angles of 64.6(9)° and 64.9(9)°]. This situation causes the angles defined by the two *trans* atoms and the tin atom [S(1)−Sn(1)−S(3) = 149.47(9), N(1)−Sn(1)−S(2) = 149.54(5), and N(3)−Sn(1)−S(4) = 148.02(5)°] to be very different from the expected values of 180° and, consequently, the angles formed by the tin and two *cis* atoms are also significantly different from 90° [64.09(9)−122.38(4)°].

The Sn−S distances are all slightly different and depend on whether the sulfur atom is provided by the bidentate ligand [2.4942(13) and 2.4921(13) Å] or by the monodentate ligand [2.4573(14) and 2.4618(13) Å]. The longest Sn−S distance is slightly shorter than those found in the tin complex with pyridine-2-thionate [Sn(pyS)$_4$][7] [average value 2.512(2) Å] but is very similar to those found in [Sn(3-CF_3-pyS)$_4$]. The distances between the tin atom and the sulfur atoms of the monodentate ligands [2.4573(14) and 2.4618(13) Å] are slightly shorter than those of [Sn(pyS)$_4$] [average value 2.469(2) Å].

The Sn−N bond lengths [2.384(4)−2.371(4) Å] are longer than the corresponding distances found in [Sn(pyS)$_4$] [2.332(5)−2.324(5) Å] but are shorter than those observed in the aforementioned eight-coordinate [Sn(3-CF_3-pyS)$_4$].

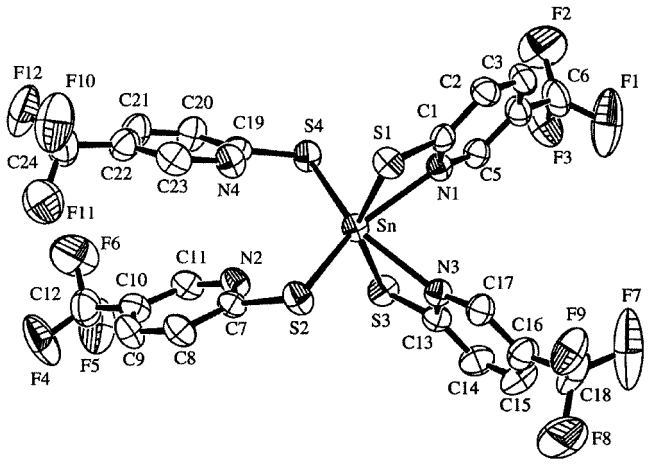

Figure 3. Molecular structure of [Sn(5-CF_3-pyS)$_4$]

Table 2. Selected bond lengths [Å] and angles [°] for complex [Sn(5-CF_3-pyS)$_4$]

Sn(1)−S(1)	2.4942(13)	S(4)−C(19)	1.751(5)
Sn(1)−S(2)	2.4573(14)	N(1)−C(1)	1.341(6)
Sn(1)−S(3)	2.4921(13)	N(1)−C(5)	1.335(6)
Sn(1)−S(4)	2.4618(13)	N(2)−C(7)	1.332(6)
Sn(1)−N(1)	2.384(4)	N(2)−C(11)	1.326(7)
Sn(1)−N(3)	2.371(4)	N(3)−C(13)	1.343(6)
S(1)−C(1)	1.744(5)	N(3)−C(17)	1.343(6)
S(2)−C(7)	1.754(5)	N(4)−C(19)	1.326(6)
S(3)−C(13)	1.740(5)	N(4)−C(23)	1.325(7)
S(1)−Sn(1)−S(2)	92.25(4)	C(7)−S(2)−Sn(1)	100.8(2)
S(1)−Sn(1)−S(3)	148.02(5)	C(13)−S(3)−Sn(1)	84.3(2)
S(1)−Sn(1)−S(4)	101.47(5)	C(19)−S(4)−Sn(1)	101.3(2)
S(2)−Sn(1)−S(3)	102.27(5)	C(1)−N(1)−C(5)	119.4(4)
S(2)−Sn(1)−S(4)	122.38(4)	C(1)−N(1)−Sn(1)	98.1(3)
S(3)−Sn(1)−S(4)	94.59(5)	C(5)−N(1)−Sn(1)	142.5(3)
S(1)−Sn(1)−N(1)	64.09(9)	C(7)−N(2)−C(11)	117.0(4)
S(2)−Sn(1)−N(1)	149.47(9)	C(13)−N(3)−C(17)	119.7(4)
S(3)−Sn(1)−N(1)	91.03(10)	C(13)−N(3)−Sn(1)	98.5(3)
S(4)−Sn(1)−N(1)	83.06(9)	C(17)−N(3)−Sn(1)	141.8(3)
S(1)−Sn(1)−N(3)	89.45(9)	C(19)−N(4)−C(23)	117.5(4)
S(2)−Sn(1)−N(3)	84.97(10)	N(1)−C(1)−S(1)	113.6(3)
S(3)−Sn(1)−N(3)	64.06(9)	N(2)−C(7)−S(2)	117.2(3)
S(4)−Sn(1)−N(3)	149.54(10)	N(3)−C(13)−S(3)	113.1(3)
N(1)−Sn(1)−N(3)	76.28(13)	N(4)−C(19)−S(4)	117.9(4)
C(1)−S(1)−Sn(1)	84.2(2)		

This change in Sn−N bond length could be due to a change in the coordination number from six to eight.

The C−S bond lengths of the coordinated ligand range from 1.744(5) to 1.740(5) Å with an average value of 1.742 Å for the chelating ligands and 1.754(5)−1.751(5) Å for the monodentate ligands. Both distances are similar to those found in [Sn(3-CF_3-pyS)$_4$]. The C−N and C−C bond lengths of the ligands are as one would expect and do not warrant further discussion.

Each of the ligands is planar within experimental error, with the sulfur atoms of the bidentate ligands lying practically in the plane of the pyridine ring to which they are bound [by 0.032 Å for S(1) and 0.031 Å for S(3)]. In the case of the monodentate ligands the sulfur atoms lie out of the pyridine plane [by 0.082 Å for S(2) and 0.095 Å for S(4)].

It is worth noting that although compounds **1** and **2** have the same composition [SnL_4], their molecular structures are quite different. In the case of **1**, all of the ligands behave in a bidentate (S,N) manner and the Sn is in an eight-coordinate dodecahedral environment [SnS_4N_4]. Compound **2**, on the other hand, has two ligands that behave in a bidentate (S,N) way and another two that act in a monodentate S manner to give a six-coordinate octahedral geometry [SnS_4N_2] around the metal atom. The remarkable feature of this arrangement is that the more crowded structure is provided by the more sterically demanding ligand, 3-CF_3-pySH.

Structure of [Pb(3-CF_3-pyS)$_2$] (3)

The molecular structure of [Pb(3-CF_3-pyS)$_2$] is shown in Figure 4 together with the atom-labelling scheme. Selected bond lengths and angles are given in Table 3. The structure consists of discrete molecules without interactions between neighbours and with the lead atom coordinated by two bidentate (N,S) anionic 3-(trifluoromethyl)pyridine-2-thionato ligands. On the assumption that the lone pair on the lead atom is symmetrically placed with respect to the nitrogen and sulfur atoms, a value of 0.84 can be calculated for τ.[15] In this situation the environment around the lead atom is best described as a pseudo-trigonal bipyramid with a 16% distortion towards a square pyramid. In this case the nitro-

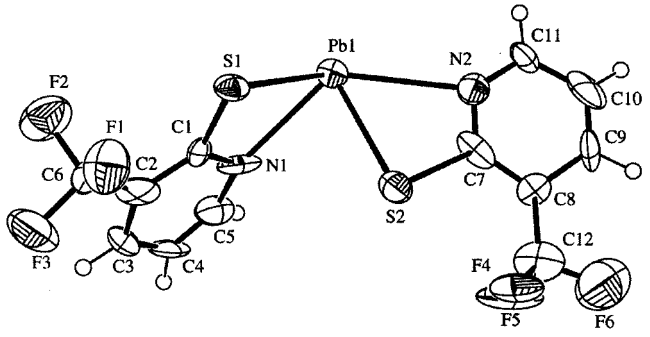

Figure 4. Molecular structure of [Pb(3-CF_3-pyS)$_2$]

Table 3. Selected bond lengths [Å] and angles [°] for complex [Pb(3-CF_3-pyS)$_4$]

Pb(1)−S(1)	2.883(11)	S(2)−C(7)	1.81(4)
Pb(1)−S(2)	2.707(11)	N(1)−C(1)	1.42(5)
Pb(1)−N(1)	2.59(3)	N(1)−C(5)	1.33(5)
Pb(1)−N(2)	2.79(3)	N(2)−C(7)	1.23(5)
S(1)−C(1)	1.72(3)	N(2)−C(11)	1.30(5)
N(1)−Pb(1)−S(1)	57.8(7)	C(1)−N(1)−C(5)	115(4)
S(2)−Pb(1)−N(2)	55.8(8)	C(1)−N(1)−Pb(1)	102.4(19)
S(1)−Pb(1)−N(2)	125.0(9)	C(5)−N(1)−Pb(1)	143(3)
S(2)−Pb(1)−N(1)	75.3(7)	C(7)−N(2)−C(11)	121(4)
S(1)−Pb(1)−S(2)	86.4(3)	C(7)−N(2)−Pb(1)	98(3)
N(1)−Pb(1)−N(2)	129.0(10)	C(11)−N(2)−Pb(1)	136(3)
C(1)−S(1)−Pb(1)	84.2(14)	N(1)−C(1)−S(1)	115(3)
C(7)−S(2)−Pb(1)	88.3(16)	N(2)−C(7)−S(2)	115(3)

gen atoms are in axial positions and the sulfur atoms and the lone pair in equatorial positions. This geometry is highly distorted with S−Pb−S and N−Pb−N bond angles of 86.4(3)° and 129.0(10)°, respectively. The bond angles between the axial nitrogen and sulfur atoms of the equatorial plane are in the range 55.8(8)−125.0(9)°, which is significantly different from the theoretical 90° for an ideal geometry. The main sources of distortion are the small value of the bond angle of the chelate ring [N−Pb−S = 55.8(8) and 57.8(7)°] and the effect of the active lone pair of the lead atom. The values of the bond angles among axial and equatorial positions, or in other words the angles S−Pb−N between atoms corresponding to different thionato ligands, are 75.3(7) and 125.0(9)°, again significantly different to the expected value of 90°.

The Pb−S bond lengths [2.883(1) and 2.707(11) Å] are longer than the Pb−S axial distance (2.696 Å) found in bis[6-(diethylcarbamoyl)-1-hydroxy-2(1*H*)-pyridine-2-thionato-*O*,*S*)lead(II)],[16] but are very close to the values of 2.737(7) and 2.782(8) Å in the trinuclear complex [Pb_3(3-$SiMe_3$-pyS)$_6$].[8]

Two different Pb−N bond lengths are observed in the compound [Pb(3-CF_3-pyS)$_2$]. The longest bond (2.793 Å) is similar to the distances observed for [Pb_3(3-$SiMe_3$-pyS)$_6$] [2.81(3) and 2.89(3) Å]. The other Pb−N bond length is significantly shorter at 2.59(3) Å, but is similar to the value of 2.59 Å found in other lead complexes with pyridine ligands.[17]

The structure of this compound differs markedly from that of [Pb(3-$SiMe_3$-pyS)$_2$], which shows a trinuclear structure with pentacoordinate metal atoms: two of the metals are coordinated by two nitrogen and three sulfur atoms in a distorted trigonal pyramidal environment and the third metal by the sulfur and nitrogen atoms of the two chelating ligands in a square pyramidal arrangement with the lead atom at the apex. Note that [Pb(3-$SiMe_3$-pyS)$_2$] has the more associated structure, despite the fact that contains a $SiMe_3$ group, which is considerably more bulky than the CF_3 group. Hence, in these cases steric hindrance is not a factor that determines the degree of association.

The pyridine rings of the ligands are essentially planar but the sulfur atoms lie out of the plane of the pyridine ring to which they are bound [by 0.077 Å for S(1) and 0.076 Å for S(2)]. The interplanar angle between these two ligands is 65.98°. The C−S bond lengths for the two ligands are also very different [C(1)−S(1) = 1.72(3) Å and 1.81(4) Å] but the average value of 1.765(4) Å is similar to those found in the complexes described above.

Spectroscopic Data

IR Spectra

The IR spectra of the complexes do not show bands assignable to ν(N−H), which in the free ligands appear at 3175 cm^{-1}. This suggests that deprotonation of the NH group has occurred during the synthesis and therefore that the ligand is coordinated in the thionato form. This conclusion is supported by the shift to smaller wavenumbers of the strong bands for ν(C=C) and ν(C=N), which appear at 1604−1545 and 1570−1512 cm^{-1} in the free ligands, on going from the free ligands to the complexes. In addition, the bands attributable to the ring breathing vibration at ca. 1000 and 630 cm^{-1} and the bands due to the C−H bending vibration at ca. 770 and 750 cm^{-1} are shifted to higher frequencies with respect to the free ligand. These shifts provide evidence that the nitrogen atom is bound to the metal atom.

NMR Spectra

The ^{1}H NMR spectra of the complexes do not show a signal for the NH proton, which appears as a broad singlet between δ = 13.0 and 14.0 ppm in the spectrum of the free ligand, thus demonstrating that in the complexes the ligands are deprotonated. The signals of all the hydrogen atoms of the pyridine ring are shifted to lower-field values in the complexes relative to the same signals in the spectra of the free ligands. The main change observed is the low-field shift of the signal due to the proton *ortho* to the nitrogen atom of the pyridine ring (δ = 9.18−8.14 ppm), demonstrating the coordination of the ligands to the metal atoms through the pyridine nitrogen.

It should be noted that in the case of [Sn(5-CF_3-pyS)$_4$], if the structure observed in the solid state is maintained in solution, two different types of ligands should be observed in the NMR spectrum. In particular, two different signals should be observed in the ^{1}H NMR spectrum for the proton *ortho* to the pyridine rings, two signals for C^2 and C^6 in the ^{13}C NMR spectrum, and two signals in the ^{19}F NMR spectrum. However, at room temperature only one signal is observed for each of these nuclei. This shows that the compound has a fluxional behaviour in solution. In order to investigate this possibility further, the spectrum was acquired at different temperatures down to −55 °C. Unfortunately, the spectrum does not change, showing that the fluxional exchange is too fast even at the lowest temperature compatible with the solvent used.

It is well-known that ^{119}Sn NMR spectroscopy is very sensitive to changes in the coordination number of tin(IV)[7] and can be used to determine the denticity of the ligands. The ^{119}Sn NMR spectrum of **2** in CD_3Cl at room temperature consists of a singlet at δ_{Sn} = −500.5 ppm. This value is similar to that of the hexacoordinate tin(IV) complex [Sn(pyS)$_4$], which also has a distorted octahedral [SnN_2S_4] environment with two ligands acting as monodentate S-bonded systems and another two as bidentate N,S bonded ligands.[7] The ^{119}Sn NMR spectrum of complex **1** shows a signal at δ_{Sn} = −662.6 ppm. The shift observed with respect to **2** is consistent with an increase in the coordination number from six to eight on going from **2** to **1**, and shows that the solid-state environment of **1** is maintained in solution.

Mass Spectra

The tin and lead complexes were also characterised by mass spectrometry using the positive ion FAB technique (*m*/*z*) in 3-nitrobenzyl alcohol (NBA) as matrix. The FAB spectrum of [Sn(3-CF_3-pyS)$_4$] shows the molecular ion

at m/z = 831, as well as peaks due to the fragments [Sn(3-CF_3-pyS)$_3$], [Sn(3-CF_3-pyS)$_2$], and [Sn(3-CF_3-pyS)] at m/z = 654, 475, and 298, produced by the loss of one, two, and three thionate ligands, respectively. The spectrum of the compound [Sn(5-CF_3-pyS)$_4$] does not show the molecular ion peak, but does show peaks associated with [Sn(5-CF_3-pyS)$_3$], [Sn(5-CF_3-pyS)$_2$], and [Sn(5-CF_3-pyS)] at m/z = 654 (100%), 475, and 298, respectively.

The FAB mass spectra of the lead compounds, [Pb(RpyS)$_2$] show, in all cases, the molecular ion peak at m/z = 563 along with a peak at m/z = 385, which is associated with [Pb(RpyS)] formed by loss of one thionate ligand. This evidence, together with the fact that the ^{19}F NMR spectra of both compounds are very similar, shows that [Pb(5-CF_3-pyS)$_2$] is a monomer with a structure similar to that of [Pb(3-CF_3-pyS)$_2$].

Mössbauer Spectroscopy

The ^{119}Sn Mössbauer data for compounds **1** and **2** appear in Table 4.

Table 4. ^{119}Sn Mössbauer Spectroscopic data recorded at 78 K

Compound[a]	δ [mm·s^{-1}]	ΔE_Q [mm·s^{-1}]	Γ[a] [mm·s^{-1}]
[Sn(3-CF_3-pyS)$_4$] (**1**)	0.93(1)	1.12(2)	1.16(3)
[Sn(5-CF_3-pyS)$_4$] (**2**)	0.98(1)	0.84(3)	1.14(6)

[a] Full width at half-mean height.

The *isomer shift* (δ) values are dependant on the *s*-electron density at the tin nucleus relative to a reference standard ($BaSnO_3$). As the *s*-electron density at the tin nucleus is measured relative to that in the valence shell of the atom, then factors that affect the latter must also affect the former. Therefore *p*-electron shielding and the polarity of the tin-ligand bonds,[18,19] together with their number, will affect δ.[20]

Clearly compound **1** has the smallest δ value, in keeping with the fact that it has eight ligands and these are relatively far from the Sn atom compared to those of compound **2**. Hence we would expect the environment to be "more ionic" and hence less s-electron density on the tin atom. The coordination number or stereochemistry at the tin also affects the δ value. When the coordination number of the tin atom increases, the concomitant increased involvement of the metal *5d* orbitals for bonding leads to a reduction in the *5s* electron density at the tin nucleus.[20,21]

The *quadrupole splitting* (ΔE_Q) arises from the interaction of the tin nucleus with the electric field gradient (EFG). If the tin atom has a perfectly symmetrical electronic environment ("cubic") then there is no EFG and only a single line is observed in the Mössbauer spectrum (as for $SnMe_4$).[21] Any deviation from a cubic electronic environment results in a doublet spectrum. As the EFG is the second derivative of the potential, its magnitude is inversely related to the cube of the distance of the charge from the nucleus. Therefore electron density on the Sn atom makes a larger contribution to ΔE_Q than that in the tin-ligand bonds. These latter are more important than charges on neighbouring atoms or ions.

Compound **1** has a ΔE_Q value of 1.12(2) mm·s^{-1} which is larger than that obtained for compound **2**. This means that the EFG in **1** is larger than that of **2**. This is in keeping with the distortion of the dodecahedral arrangement found in the structure of **1** and most probably arises from the imbalance of the electron density in the tin−ligand bonds, though the different polarity induced by the nitrogen and sulfur ligands must also play a role.

Compound **2** has a ΔE_Q value of 0.84(3) mm·s^{-1} which, although small, is substantial for an octahedral electronic environment. A perfect octahedral site would be expected to have zero splitting in a cubic structure. In this case it is in keeping with a highly distorted octahedral environment and is thus very compatible with the structure of compound **2**. It should be noted that these two Mössbauer spectra have low recoil-free fractions and hence were collected at 78 K only, whereas the crystal structures of **1** and **2** were recorded at room temperature. However at the very least it is shown here that the structures do not become symmetrical upon cooling to 78 K, and that in fact the Mössbauer spectra recorded at 78 K may reflect the room temperature structures.

Conclusions

The results discussed in this paper show that the structures of complexes of tin(IV) and lead(II) with derivatives of pyridine-2-thione depend on the nature and location of the substituents on the heterocyclic ring. Indeed, while [Sn(5-CF_3-pyS)$_4$] has an [SnN_2S_4] octahedral geometry around the metal atom, the structure of [Sn(3-CF_3-pyS)$_4$] shows the tin atom in an [SnN_4S_4] dodecahedral environment. On the other hand, while [Pb(3-CF_3-pyS)$_2$] and [Pb(5-CF_3-pyS)$_2$] are mononuclear compounds with the lead atom in a trigonal bipyramidal environment, [Pb(3-$SiMe_3$-pyS)$_2$] has a trimeric molecular structure. It appears that the factor responsible for this different behaviour is not of a steric nature, as the most sterically demanding ligands produce the structures with the higher coordination numbers. Further work is required to clarify this interesting phenomenon.

Experimental Section

Microanalysis were performed using a Carlo−Erba EA1108 microanalyser. Infrared spectra were recorded as compressed KBr discs by using an IR-FT Mattson model CYGNUS-100. Electron impact (EI) and fast atom bombardment (FAB) mass spectra were recorded on Hewlett−Packard HP5988A and Micromass Autospec spectrometers, respectively, with 3-nitrobenzyl alcohol as the matrix for the FAB spectra. ^{1}H and ^{13}C NMR spectra were recorded on a Bruker AMX300 using $CDCl_3$ as solvent and TMS as internal reference. ^{119}Sn NMR spectra were recorded on a Bruker AMX500 spectrometer using $CDCl_3$ as solvent and saturated $SnMe_4$ as a secondary reference. ^{19}F NMR spectra were recorded on a Bruker AMX300 spectrometer and referenced to $CFCl_3$. All Mössbauer

spectra were recorded at 78 K, with a ^{119m}Sn 23.875 keV γ source (370MBq, 10 mCi $CaSnO_3$ matrix, Wissel GmbH) mounted on the previously reported experimental setup.[22] All thiones and metal salts were commercial products and were used without further purification.

Preparations

All the complexes were prepared by reaction of a methanolic solution of the corresponding thione and triethylamine with a solution of the tin(II) or lead(II) salts in the same solvent. Tetrakis[5-(trifluoromethyl)pyridine-2-thiolato]tin(IV) was also prepared using an electrochemical procedure.[23]

[Sn(3-CF_3-pyS)$_4$] (1): $SnCl_2{\cdot}2H_2O$ (0.189 g, 0.84 mmol) was added to a solution of 3-(trifluoromethyl)pyridine-2-thione (0.30 g, 1.67 mmol) and dry triethylamine (0.25 mL, 1.84 mmol) in methanol (20 mL) with constant stirring at room temperature. The solution was evaporated to dryness and the solid was recrystallised from diethyl ether. Yield 38% (0.132 g). $C_{24}H_{12}F_{12}N_4S_4Sn$ (831.4): calcd. C 34.7, H 1.4, N 6.7; found C 34.8, H 1.2, N 6.8. IR (KBr): $\tilde{\nu}$ = 1584, 1563, 1485 cm^{-1} [ν(C=C), ν(C=N)py]. FAB MS: *m*/*z* (%) = 831.6 (1.1) [SnL_4], 654.0 (100) [SnL_3], 475 (9.5) [SnL_2], 298 (27.4) [SnL]. ^{1}H NMR ($CDCl_3$, 300 MHz): δ = 8.15 (d, 1 H, py-H^6), 7.78 (d, 1 H, py-H^5), 7.01 (dt, 1 H, py-H^4) ppm. ^{13}C NMR ($CDCl_3$, 300 MHz): δ = 163.1 (py-C^2), 124.6 (py-C^3), 136.0 (py-C^4), 121.0 (py-C^5), 147.2 (py-C^6), 116.4 (CF_3) ppm. ^{19}F NMR ($CDCl_3$, 300 MHz): δ = −65.3 ppm. ^{119}Sn NMR ($CDCl_3$, 500 MHz): δ = −662.6 ppm.

[Sn(5-CF_3-pyS)$_4$] (2): (a) $SnCl_2{\cdot}2H_2O$ (0.189 g, 0.84 mmol) was added to a solution of 5-(trifluoromethyl)pyridine-2-thione (0.30 g, 1.67 mmol) and triethylamine (0.25 mL, 1.84 mmol) in methanol (20 mL) with constant stirring at room temperature. The reaction mixture was stirred for 4 hours and the resulting yellow solid was filtered off, washed with a small amount of diethyl ether, and dried under vacuum. Yield 47% (0.163 g). $C_{24}H_{12}F_{12}N_4S_4Sn$ (831.4): calcd. C 34.7, H 1.4, N 6.7, S 15.4; found C 34.9, H 1.5, N 6.7, S 15.3.

(b) A solution of 5-(trifluoromethyl)pyridine-2-thione (0.267 g, 1.49 mmol) in acetonitrile containing 20 mg of tetraethylammonium perchlorate was electrolysed using a tin rod as the anode and a platinum wire as the cathode. A current of 10 mA was applied during two hours, dissolving 43.39 mg of metal (E_f = 0.49 mol·F^{-1}). At the end of the electrolytic process the solution was evaporated to dryness and the solid recrystallised from diethyl ether. Yield 69% (0.213 g). $C_{24}H_{12}F_{12}N_4S_4Sn$ (831.4): calcd. C 34.7, H 1.4, N 6.7; found C 34.5, H 1.4, N 6.6. IR (KBr): $\tilde{\nu}$ = 1590, 1540, 1455 cm^{-1} [ν(C=C), ν(C=N)py]. FAB MS: *m*/*z* (%) = 654.0 (100) [SnL_3], 475 (3.5) [SnL_2], 298 (49.7) [SnL]. ^{1}H NMR ($CDCl_3$, 300 MHz): δ = 9.18 (m, 1 H, py-H^6), 8.51 (m, 1 H, py-H^4), 7.79 (m, 1 H, py-H^3) ppm. ^{13}C NMR ($CDCl_3$, 300 MHz): δ = 167.9 (py-C^2), 128.6 (py-C^3), 134.6 (py-C^4), 125.0 (py-C^5), 142.4 (py-C^6), 121.4 (CF_3) ppm. ^{19}F NMR ($CDCl_3$, 300 MHz): δ = −62.7 ppm. ^{119}Sn NMR ($CDCl_3$, 500 MHz): δ = −500.5 ppm.

[Pb(3-CF_3-pyS)$_2$] (3): $Pb(OAc)_2{\cdot}3H_2O$ (0.21 g, 0.55 mmol) was added to a solution of 3-(trifluoromethyl)pyridine-2-thione (0.20 g, 1.11 mmol) and triethylamine (0.17 mL, 1.23 mmol) in methanol (20 mL) with constant stirring at room temperature. The reaction mixture was stirred for 5 hours and the resulting yellow precipitate was filtered off, washed with diethyl ether, and dried under vacuum. The product was recrystallised from diethyl ether. Yield 62% (0.195 g). $C_{12}H_6F_6N_2PbS_2$ (563.5): calcd. C 25.6, H 1.1, N 5.0; found C 25.3, H 1.0, N 4.8. IR (KBr): $\tilde{\nu}$ = 1583, 1558, 1442, 1402 cm^{-1} [ν(C=C), ν(C=N)py]. FAB MS: *m*/*z* (%) = 563.8 (4.4) [PbL_2], 385.8 (29.3) [PbL]. ^{1}H NMR ($CDCl_3$, 300 MHz): δ = 8.75 (d, 1 H, py-H^6), 8.09 (dd, 1 H, py-H^5), 7.23 (dt, 1 H, py-H^4) ppm. ^{13}C NMR ($CDCl_3$, 300 MHz): δ = 169.9 (py-C^2), 128.0 (py-C^3), 134.6 (py-C^4), 121.7 (py-C^5), 148.4 (py-C^6), 115.6 (CF_3) ppm. ^{19}F NMR ($CDCl_3$, 300 MHz): δ = −48.8 ppm.

[Pb(5-CF_3-pyS)$_2$] (4): $Pb(OAc)_2{\cdot}3H_2O$ (0.21 g, 0.55 mmol) was added to a solution of 5-(trifluoromethyl)pyridine-2-thione (0.20 g, 1.11 mmol) and triethylamine (0.17 mL, 1.23 mmol) in methanol (20 mL) with constant stirring at room temperature. The reaction mixture was stirred for 5 hours and the resulting yellow precipitate was filtered off, washed with diethyl ether, and dried under vacuum. Yield 18% (0.057 g). $C_{12}H_6F_6N_2PbS_2$ (563.5): calcd. C 25.6, H 1.1, N 5.0; found C 25.6, H 1.2, N 5.2. IR (KBr): $\tilde{\nu}$ = 1603, 1547, 1460 cm^{-1} [ν(C=C), ν(C=N)py]. FAB MS: *m*/*z* (%) = 563.8 (0.5) [PbL_2], 385.8 (38.1) [PbL]. ^{1}H NMR ([D$_6$]DMSO, 300 MHz): δ = 8.38 (d, 1 H, py-H^6), 7.46 (dd, 1 H, py-H^4), 6.87 (dd, 1 H, py-H^3) ppm. ^{13}C NMR ($CDCl_3$, 300 MHz): δ = 176.9 (py-C^2), 131.9 (py-C^4), 130.3 (py-C^5), 142.1 (py-C^6), 117.6 (CF_3) ppm. ^{19}F NMR ($CDCl_3$, 300 MHz): δ = −56.2 ppm.

In the cases of compounds **1**, **2**, and **3**, X-ray quality crystals were obtained from saturated solutions of the complexes by slow evaporation of the solvents at room temperature.

X-ray Crystal Structure Determinations

Data Collection and Processing: X-ray data were collected on a Smart-CCD-1000 Bruker diffractometer for **1** and on an Enraf−Nonius CAD4 diffractometer for **2** and **3**: both fitted with graphite monochromated Mo-K_α radiation (λ = 0.71073 Å). The data were collected at 293 K for all structures. The ω-scan technique was employed to measure intensities in all crystals up to a maximum Bragg angle of 26.37° for **1**, 24.97° for **2**, and 28.04° for **3**. Decomposition of the crystals did not occur during data collection. Corrections were applied for Lorentz and polarisation effects and for absorption (μ = 1.195 mm^{-1} for **1**, 1.223 mm^{-1} for **2**, and 11.683 mm^{-1} for **3**).[24] A total of 14630 reflections for **1**, 4014 for **2**, and 3652 for **3** were collected, of which 1569 reflections in **1**, 3829 in **2**, and 3585 in **3** were unique [R_{int} = 0.0362 (**1**), 0.0148 (**2**), 0.0766 (**3**)] and, of these, 1261 (**1**), 3829 (**2**), and 1515 (**3**) satisfied the $I > 2\sigma(I)$ criterion of observability and were used in the subsequent analysis.

Structure Analysis and Refinement: The structures were solved by direct methods and missing atoms were located in the difference Fourier map and included in subsequent refinement cycles. The structures were refined by full-matrix least-squares refinement on F^2, using anisotropic displacement parameters for all non-hydrogen atoms. In all cases, hydrogen atoms were included using a riding model with C−H distances of 0.93−0.97 Å and fixed isotropic thermal parameters, except for **2**, where hydrogen atoms were located in the difference Fourier map and refined isotropically. A weighting scheme of the form $\omega = 1/\sigma^2(F)$ was introduced and the refinement proceeded smoothly to convergence with a maximum δ/σ = 0.000 when R = 0.0270, R_w = 0.0597 and GOF = 1.092 (goodness-of-fit) for 102 variables for **1**, maximum δ/σ = 0.001 when R = 0.0306, R_w = 0.0861 and GOF = 1.045 for 491 variables for **2** and δ/σ = 0.001 when R = 0.1145, R_w = 0.2843 and GOF = 1.049 for 208 variables for **3**. The residual analysis of the variance showed no special features and the maximum and minimum residual electron density peaks in the final difference map were, respectively, +0.24 and −0.23 e·$Å^{-3}$ in **1**, +0.64 and −0.45 e·$Å^{-3}$ in **2**, and +4.84 and −4.40 e·$Å^{-3}$ in **3**.

Table 5. Crystal data and experimental details for **1**, **2** and **3**

	1	**2**	**3**
Empirical formula	$C_6H_3F_3NSSn_{0.25}$	$C_{24}H_{12}F_{12}N_4S_4Sn$	$C_{12}H_6F_6N_2PbS_2$
Molecular weight	207.83	831.30	563.50
Temperature [K]	293(2)	293(2)	293(2)
Wavelength [Å]	0.71073	0.71073	0.71073
Crystal System	Tetragonal	Triclinic	Monoclinic
Space group	*I* 4(1)/a	*P* −1	*C* 2/c
a [Å]	13.7103(18)	11.9010(10)	27.45(5)
b [Å]	13.7103(18)	12.554(2)	4.458(1)
c [Å]	16.418(3)	12.794(2)	24.325(6)
α [deg]	90	99.910(10)	90
β [deg]	90	117.080(10)	91.90(6)
γ [deg]	90	107.770(10)	90
Cell volume [Å^3]	3086.1(8)	1507.7(4)	2975(6)
Z	4	2	8
D_c [Mg·m^{-3}]	1.789	1.831	2.516
λ(Mo-K_α) [mm^{-1}]	1.195	1.223	11.683
Crystal size [mm]	0.49 × 0.38 × 0.30	0.40 × 0.25 × 0.18	0.32 × 0.32 × 0.08
θ limits [deg]	1.94−26.37	1.83−24.97	4.41−28.04
Collected reflections	14630	4014	3652
Unique reflections	1569 [R_{int} = 0.0362]	3829 [R_{int} = 0.0148]	3585 [R_{int} = 0.0766]
Observed reflections [$F_o > 2\sigma(F_o)$]	1261	3829	1515
Parameters	102	491	208
Goodness of fit on F^2	1.092	1.045	1.049
$R1(F)$[a]	0.0270	0.0306	0.1145
$wR2(F^2)$[b]	0.0597	0.0861	0.2843
Largest difference peak and hole [e·Å^{-3}]	0.24 and −0.23	0.64 and −0.45	4.84 and −4.40

[a] $R1 = [|F_o| - |F_c|]/|F_o|$. [b] $wR2 = [(F_o^2 - F_c^2)/(F_o^2)^2]^{1/2}$ where $w = 1/[\sigma^2(F_o^2) + (aP)^2 + bP]$ and $P = (F_o^2 + 2F_c^2)/3$.

The crystallographic programs in SHELX97[25] were used for the structure solutions and refinement. Atomic scattering factors and anomalous-dispersion corrections for all atoms were taken from the International Tables for X-ray Crystallography.[26] Crystallographic data for these compounds are given in Table 5. Ortep3[27] drawings with the numbering scheme used are shown in Figures 1, 3, and 4.

CCDC-186656 (**1**), -186658 (**2**), and -186657 (**3**) contain the supplementary crystallographic data for this paper. These data can be obtained free of charge at www.ccdc.cam.ac.uk/conts/retrieving.html [or from the Cambridge Crystallographic Data Centre, 12, Union Road, Cambridge CB2 1EZ, UK; Fax: (internat.) +44-1223/336-033; E-mail: deposit@ccdc.cam.ac.uk].

Acknowledgments

We thank the Xunta de Galicia (PGIDT00PXI20305PR) for financial support. One of us (A. S.-P.) thanks Ministerio de Educación y Cultura (Spain) for a doctoral grant.

[1] E. S. Raper, *Coord. Chem. Rev.* **1985**, *61*, 115−184; E. S. Raper, *Coord. Chem. Rev.* **1996**, *153*, 199−255; E. S. Raper, *Coord. Chem. Rev.* **1997**, *165*, 475−567.
[2] B. Krebs, G. Henkel, *Angew. Chem. Int. Ed. Engl.* **1991**, *30*, 769−788.
[3] [3a] I. G. Dance, *Polyhedron* **1986**, *5*, 1037−1104. [3b] P. G. Blower, J. R. Dilworth, *Coord. Chem. Rev.* **1987**, *76*, 121−185. [3c] J. R. Dilworth, J. Hu, *Adv. Inorg. Chem.* **1993**, *40*, 411−459.
[4] E. J. Fernández, M. B. Hurthouse, M. Laguna, R. Terrota, *J. Organomet. Chem.* **1999**, *574*, 207−212; S. R. Foley, G. P. A. Yap, D. S. Richeson, *J. Chem. Soc., Dalton Trans.* **2000**, 1663−1668; R. Jurkschat, V. Pieper, S. Seemeyer, M. Schurmanm, M. Biesmans, I. Verbruggen, R. Willem, *Organometallics* **2001**, *20*, 868−880; D. Dakternieks, K. Jurkschat, R. Tozer, J. Hook, E. R. S. Tickink, *Organometallics* **1997**, *16*, 3696−3706.
[5] E. Block, G. Ofori-Okai, J. Zubieta, *J. Am. Chem. Soc.* **1989**, *111*, 2327−2329.
[6] M. M. Jones, *Met. Ions Biol. Syst.* **1983**, *16*, 47−83.
[7] L. C. Damude, P. A. W. Dean, V. Masivannman, R. S. Srivastava, J. J. Vitali, *Can. J. Chem.* **1990**, *68*, 1323−1331.
[8] E. Block, G. Ofori-Okai, H. Hang, J. Wu, J. Zubieta, *Inorg. Chim. Acta* **1991**, *190*, 5−6.
[9] E. Labisbal, A. de Blas, J. A. García-Vázquez, J. Romero, M. L. Durán, A. Sousa, N. A. Bailey, D. E. Fenton, P. B. Leeson, R. V. Parish, *Polyhedron* **1992**, *11*, 227−233; E. Labisbal, J. A. García-Vázquez, J. Romero, A. Sousa, A. Castiñeiras, C. Maichle-Mössmer, U. Russo, *Inorg. Chim. Acta* **1994**, *223*, 87−92.
[10] S. W. Ng, C. Wei, V. G. K. Das, T. C. W. Mak, *J. Organomet. Chem.* **1987**, *334*, 295−305.
[11] C. S. Harreld, E. O. Schlemper, *Acta Crystallogr., Sect. B* **1971**, *27*, 1964−1969.
[12] J. Potenza, R. J. Johnson, D. Mastropaolo, *Acta Crystallogr., Sect. B* **1976**, *32*, 941−943.
[13] B. R. Penfold, *Acta Crystallogr.* **1953**, *6*, 707−713.
[14] J. A. García-Vázquez, J. Romero, A. Sousa-Pedrares, M. L. Louro, A. Sousa, J. Zubieta, *J. Chem. Soc., Dalton Trans.* **2000**, 559−567.
[15] A. W Addison, T. N. Rao, J. Reedijk, J. Van Rijn, G. N. Verschoor, *J. Chem. Dalton Trans.* **1984**, 1349−1356.
[16] K. Abu-Dari, T. B. Karpinshin, K. N. Raymond, *Inorg. Chem.* **1993**, *32*, 3052−3055.
[17] N. A. Bailey, D. E. Fenton, I. T. Jackson, R. Moody, C. R. de Barbarin, *J. Chem. Soc., Chem. Commum.* **1983**, 1463−1465; L. M. Engelhardt, J. M. Patrick, C. R. Whitaker, A. H. White. *Aust. J. Chem.* **1987**, *40*, 2107−2114.
[18] R. V. Parish, *Prog. Inorg. Chem.* **1972**, *15*, 101.
[19] P. A. Flinn, in: *Mössbauer Isomer Shifts* (Eds.: G. K. Shenoy, T. E. Wagner), Elsevier, North-Holland, **1978**, pp. 593−616.

[20] J. Silver, in: *Solid State Organometallic Chemistry: Methods and Applications* (Eds.: M. Gielen, R Willem, B. Wrackmeyer), John Wiley and Sons Ltd, **1999**, pp. 279−396.
[21] R. V. Parish, R. H. Platt, *Inorg. Chim. Acta* **1970**, *4*, 65.
[22] J. Ovenstone, P. J. Titler, R. Withnall, J. Silver, *J. Phys. Chem. B* **2001**, *105*, 7170−7177.
[23] J. A. García-Vázquez, J. Romero, A. Sousa, *Coord. Chem. Rev.* **1999**, *193−195*, 691.
[24] N. Walker, D. Stuart, *Acta Crystallogr., Sect. A* **1983**, *39*, 158−166.
[25] *SHELX97* [Includes SHELXS-97, SHELXL-97, CIFTAB] − Programs for Crystal Structure Analysis (Release 97−2). G. M. Sheldrick, Institüt für Anorganische Chemie der Universität, Tammanstrasse 4, 3400 Göttingen, Germany, **1998**.
[26] International Tables for Crystallography, Volume C (Ed.: A. J. C. Wilson), Kluwer Academic Publishers, Dordrecht, The Netherlands, **1995**.
[27] ORTEP3 for Windows: L. J. Farrugia, *J. Appl. Crystallogr.* **1997**, *30*, 565.

Received June 25, 2002
[I02349]

Synthesis and Reactivity of the First η^6-Rhodium(I) and η^6-Iridium(I) Complexes of 2,6-Bis(trimethylsilyl)phosphinines

Marjolaine Doux,[a] Louis Ricard,[a] François Mathey,[a] Pascal Le Floch,*[a] and Nicolas Mézailles*[a]

Keywords: Phosphinines / P ligands / Pi interactions / Rhodium / Iridium

It has been shown that 2 equiv. of 2,3,5,6-tetraphenylphosphinine (**2**) react with $[Rh(COD)_2][BF_4]$ to yield the bis(η^1-phosphinine)Rh^I complex **6**, whose X-ray crystal structure is presented. On the other hand, 2,6-bis(trimethylsilyl)phosphinines **4** and **5** react with Rh^+ and Ir^+ precursors to yield the first (η^6-phosphinine)Rh^I and -Ir^I complexes **7**–**10**, and **11**–**12**, respectively. The X-ray crystal structure of complex **8** is presented. Reaction of these η^6-phosphinine complexes with water or ethanol yields the first (η^5-phosphacyclohexadienyl)Rh^I and -Ir^I complexes **13**–**17**, resulting from the formal 1,1-addition of RO^- and H^+. DFT calculations comparing isoelectronic (η^6-phosphinine)- and (η^6-benzene)Fe^0 and -Rh^I complexes allows the rationalization of the large difference in reactivity of these complexes.
(© Wiley-VCH Verlag GmbH & Co. KGaA, 69451 Weinheim, Germany, 2003)

Introduction

The coordination chemistry of phosphinines has been studied for many years now. These ligands usually bind to electron-rich metal centers through the lone pair on the phosphorus atom.[1] Comparatively, fewer η^6 complexes have been synthesized with these ligands. The sandwich bis-η^6 complexes were usually synthesized by co-condensation techniques between the ligand (in large excess) and the vaporized metal(0) (Ti, V, Cr, Ho).[2] The Group-6 mono-η^6 complexes were synthesized either by starting with an η^1-coordinated phosphinine, or by a phosphinine bearing two bulky groups at the *ortho* positions.[3] The only Group-7 η^6 complex was obtained by photolysis of a mixed (carbonyl)(η^1-phosphinine) complex.[4] For Group 8, the zerovalent Fe complexes were obtained by Zenneck et al. in the mid 1990s,[5] and very recently we reported on the syntheses of [(η^6-phosphinine)RuCp*] complexes.[6] Most interestingly, [(η^6-phosphinine)Fe(COD)] complexes were found to be active in the cyclotrimerization of alkynes and in the synthesis of pyridine derivatives.[5a]

The [(η^6-arene)Rh]$^+$ complexes have been known for more than 30 years now and were first synthesized by Haines et al. in 1969.[7] Since then, a number of [(η^6-arene)Rh(L)(L′)]$^+$ have been isolated.[8] Among them, the zwitterionic complex [(η^6-$PhBPh_3$)Rh(COD)] appeared to be a versatile and effective catalyst for a number of carbonylation reactions[9] and for the silylformylation of alkynes.[10] More recently, analogous [(η^6-benzene)Ir]$^+$ complexes were obtained by Oro et al. on reduction of an [(η^6-benzene)$Ir(H)_2$]$^+$ complex by ethylene.[11]

Therefore, we were interested in developing a method leading to the first η^6-phosphinine complexes with Group-9 metal centers. We now wish to report on the syntheses of the [(η^6-phosphinine)M]$^+$ (M = Rh, Ir) complexes, and present DFT calculations comparing the isoelectronic (phosphinine)- and (benzene)Fe^0 and -Rh^I derivatives. Studies on their reactivity, leading to the first (η^5-phosphacyclohexadienyl)Rh^I and -Ir^I complexes are also presented.

Results and Discussion

The syntheses of (phosphinine)Fe^0 complexes relies on the co-condensation of Fe^0 with phosphinine and COD. Obviously, this method can not be duplicated to yield the

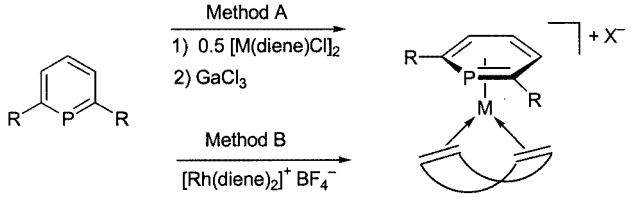

Scheme 1

[a] Laboratoire "Héteroéléments et Coordination", UMR CNRS 7653, Ecole Polytechnique,
91128 Palaiseau Cedex, France
Supporting information for this article is available on the WWW under http://www.eurjic.org or from the author.

desired isoelectronic Rh^I and Ir^I complexes. Two different methods were thus devised. The first one, Method A, relies on the chloride abstraction of $[M(diene)Cl]_2$ (M = Rh, Ir; diene = COD, NBD) by $GaCl_3$ at low temperatures, followed by the coordination of the phosphinine. It is hoped that the phosphinine adopts a η^6-coordination mode. Method B relies on the classical displacement of one diene ligand from the $[Rh(diene)_2][BF_4]$ (diene = COD, NBD) precursor by phosphinine (Scheme 1).

Moreover, since the η^1 complexes are usually favored, it was necessary to study the different factors that lead to the η^6 complexes, namely the nature of the metal precursor and the substitution pattern of the ligand. In order to test the importance of this second factor, we chose four different phosphinines, **2**−**5**. Among these, two had not been previously reported (**2**−**3**) [Equation (1)].

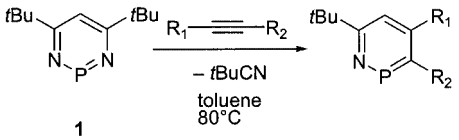

(1)

	2	3	4	5
R_1	Ph	Ph	Me	Ph
R_2	Ph	Ph	$SiMe_3$	$SiMe_3$
R_3	Ph	H	Me	Ph
R_4	Ph	$SiMe_3$	$SiMe_3$	$SiMe_3$

The phosphinines were synthesized according to the method developed several years ago in our laboratories.[12] This method relies on the high reactivity of the 1,3,2-diazaphosphinine **1** with alkynes. In a first step, **1** reacts with 1 equiv. of the first alkyne in a [4+2]/retro [4+2] sequence to produce a 1,2-monoazaphosphinine, which is not isolated, but whose complete formation is checked by ^{31}P NMR spectroscopy. This intermediate then reacts with the second alkyne, at higher temperature, in another [4+2]/retro [4+2] sequence to yield the desired phosphinine. The phosphinines are then easily purified by column chromatography. Phosphinines **2** and **3**, which are white solids, were fully characterized by usual NMR spectroscopic techniques and elemental analysis.

A first series of experiments showed that the 2,6-diphenyl derivatives only led to the formation of the bis(η^1) complex, irrespective of the method or the number of equivalents of phosphinine used, as indicated by ^{31}P NMR spectroscopy [Equation (2)]. Thus, 2 equiv. of the 2,3,5,6-tetraphenyl derivative **2** reacts with $[Rh(COD)_2]^+$ to quantitatively yield complex **6**.

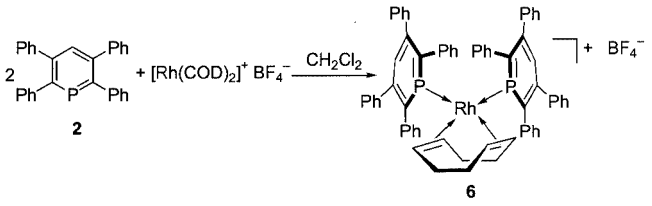

(2)

This complex was fully characterized by usual NMR techniques as well as by elemental analysis. In the ^{31}P NMR spectrum, the complex is characterized by a doublet at δ = 175 ppm (coordination chemical shift $\Delta\delta$ = −33 ppm) and a large coupling constant $^1J_{Rh,P}$ of 166.5 Hz, clearly indicating the η^1-coordination mode.[1] This coordination mode was confirmed by the crystal structure analysis of **6**. An ORTEP drawing of **6** is presented in Figure 1, along with selected bond lengths and angles. As expected, the structure reveals a square-planar geometry around the rhodium center. The Rh−P bond lengths are 2.281 and 2.301 Å, and are typical, as are the C=C bond lengths within the ring (1.386−1.410 Å). The two C−P−C internal angles of the phosphinine ligands are 106.4 and 107.0°, and fall in the usual range for coordinated phosphinine. The C=C bond lengths of the COD moiety [1.353(7) and 1.388(7) Å] compare with those in the isoelectronic Fe^0 complex.[5a]

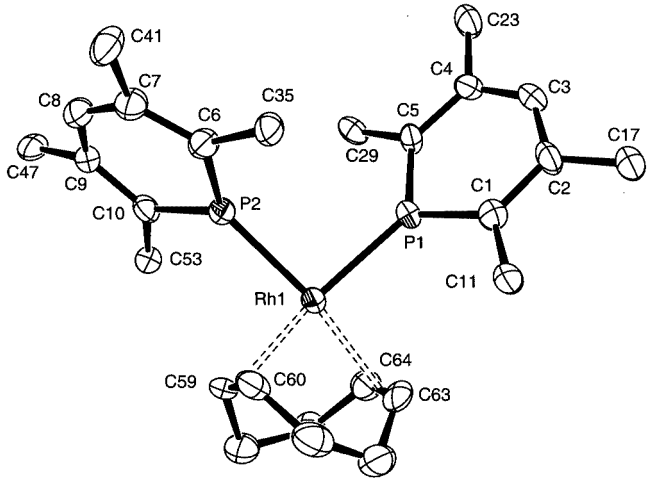

Figure 1. ORTEP view of complex **6**; ellipsoids are scaled to enclose 50% of the electron density; phenyl groups have been omitted for clarity; selected bond lengths [Å] and angles [°]; numbering is arbitrary and differs from the ones used in NMR spectra: Rh1−P1 2.301(1), P1−C1 1.738(5), P1−C5 1.738(5), C1−C2 1.407(6), C2−C3 1.386(7), C3−C4 1.391(7), C4−C5 1.410(6), Rh1−P2 2.281(1), P2−C6 1.721(5), P2−C10 1.740(5), C6−C7 1.397(7), C7−C8 1.388(7), C8−C9 1.396(7), C9−C10 1.405(6), C63−C64 1.353(7), C59−C60 1.388(7); C5−P1−C1 106.4(2), C6−P2−C10 107.0(2)

When a bulkier trimethylsilyl group replaces one phenyl group, such as in **3**, a different outcome is observed. In fact, the two methods yield different products. Method A leads to a mixture of two η^1 complexes as can be seen by ^{31}P

NMR spectroscopy, corresponding to different stereoisomers formed as a result of the bulkiness of the ligand which probably precludes their free rotation [Equation (3)].

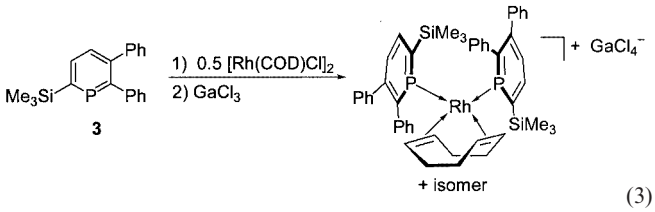

(3)

However, when **3** was treated with $[Rh(COD)_2][BF_4]$ at room temperature for 4 h, the desired η^6 complex was formed [Equation (4)] as the major product (about 60% by ^{1}H NMR spectroscopy). The signal for the complex appears as a doublet which is strongly shifted to a higher field (δ = 84 ppm, $\Delta\delta$ = −124 ppm, $^1J_{Rh,P}$ = 6 Hz). The very small coupling constant between the phosphinine and the rhodium center is also very indicative of this type of coordination. Nevertheless, a mixture of the above-mentioned η^1 complexes (sets of doublets at $\delta \approx$ 190 ppm, $^1J_{Rh,P} \approx$ 160 Hz) was also formed during the reaction (about 40% by ^{1}H NMR spectroscopy).

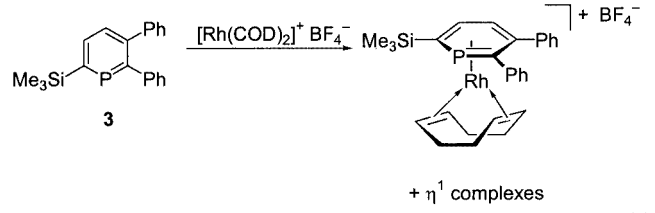

(4)

Unfortunately, due to the large amount of by-products, the isolation of the pure η^6 complex was not achieved. In a third attempt, 2,6-bis(trimethylsilyl) derivatives were used. The two different methods depicted above led to the desired η^6 complexes [Equation (5)]. It appears then that two very bulky groups are needed to favor η^6-versus η^1 coordination. As can be seen with the syntheses of complexes **11** and **12**, this approach can be successfully extended to the Ir derivatives.

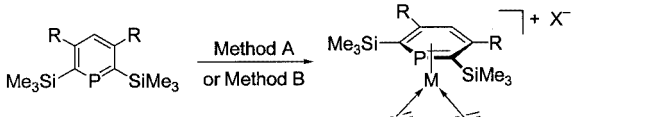

	4	5
R	Me	Ph

	7	8	9	10	11	12
M	Rh	Rh	Rh	Rh	Ir	Ir
R	Me	Ph	Me	Ph	Me	Ph
diene	COD	COD	NBD	NBD	COD	COD

(5)

As can be predicted, the first method is faster and the reaction is completed between −78 °C and room temperature, whereas the second method requires a few hours of heating at 40 °C. The main NMR spectroscopic characteristics of the ligands and of these six complexes are summarized in Table 1.

As can be seen from the data, all the complexes are characterized by a strong shift of the signals in the ^{31}P NMR spectra ($\Delta\delta$ ranges from −150 to about −200 ppm). Unlike the η^1 coordination of phosphinines to Rh ($^1J_{Rh,P} \approx$ 160 Hz), the signals for complexes **7** and **8** appear as weakly coupled (small Rh-P coupling constant of 7.6 and 9.1 Hz, respectively), or as singlets for **9** and **10**. The signals for the iridium complexes **11** and **12** appear as singlets but at a much higher field than the Rh analogs ($\Delta\delta \approx$ −50 ppm). The strong shift of the signal for 4-H in the ^{1}H NMR spectra is also indicative of the η^6-coordination mode. This ranges from δ = 5.7 ppm in **7** to δ = 6.7 ppm in **9** (compared with δ = 7.1 ppm for **4**). In the ^{13}C NMR spectra, the most significant change on η^6-coordination is indicated by the chemical shift of the C-4 signal. In the Rh complexes, it appears as a doublet of doublets with $^3J_{C,P}$ of about 10 Hz (compared with $^3J_{C,P}$ = 20 Hz in the free ligand) and $^1J_{C,Rh}$ of about 2 Hz. The same $^3J_{C,P}$ value is observed in the Ir complexes **11** and **12**. The π coordination of the phosphinine was confirmed by two X-ray crystal analyses. Yellow crystals of **7** and **8** were obtained by slow diffusion of hexane into a CH_2Cl_2 solution of the complex. As the two structures are very similar, only the ORTEP plot of complex **8** is shown in Figure 2, together with selected bond lengths and bond angles. The ORTEP plot of complex **7** can be found in the Supporting Information (see footnote on the first page of this article).

The bonds between P and Rh are rather long [2.464(1) Å] compared with 2.279 and 2.304 Å in **6**. It should be noted that the bond between Rh and C3 (2.188 Å) is much shorter, by more than 0.18 Å, than the bonds between the rhodium atom and the other carbon atoms. Note that the atoms labeled C3 in the different crystal structures are named C-4 in the NMR discussions. A close inspection of the C−C bond lengths in these two complexes shows that what can be perceived as a minor change (Me or Ph substituents) can induce significant changes in the complexes. There are two long [C1−C2 (1.414 Å) and C4−C5 (1.420 Å)] bonds and two short [C2−C3 (1.409 Å) and C3−C4 (1.392 Å)] bonds in **7** (R = Me). The reverse is seen in **8** (R = Ph). The aromaticity of the phosphinine ring does not seem to be significantly perturbed by the coordination to the Rh center, as indicated by the typical bond lengths and angles. These values compare with those found in non-strained macrocycles recently synthesized.[13]

A study of the reactivity of the series of six η^6-phosphinine complexes was undertaken. First, the stability of the complexes towards water and ethanol was tested. All of the complexes were quantitatively converted, within minutes at room temperature and with 5 equiv. of water or ethanol, to the previously unknown (η^5-phosphacyclohexadienyl)rhodium and -iridium complexes (Scheme 2). As all the com-

Table 1. NMR characteristics of ligands and complexes, in $CDCl_3$ unless otherwise stated

	^{31}P NMR		^{1}H NMR		^{13}C NMR					
	δ	$^{1}J_{P,Rh}$	$\delta_{4\text{-H}}$	$^{4}J_{H,P}$	$\delta_{C\text{-}2,6}$	$^{1}J_{C,P}/^{1}J_{C,Rh}$	$\delta_{C\text{-}3,5}$	$^{2}J_{C,P}/^{1}J_{C,Rh}$	$\delta_{C\text{-}4}$	$^{3}J_{C,P}/^{1}J_{C,Rh}$
4	265.0	–	7.1	0	164.0	84.1	150.4	11.0	133.9	22.8
5[a]	269.4	–	7.3	0	166.5	89.1	154.9	10.8	133.4	21.3
7	101.4	7.6	5.9	0	134.5	76.5/1.7	131.5	2.8/1.7	97.1	8.6/3.2
8	103.2	9.1	5.7	1.3	141.1	104.5/0	137.9	0/0	94.1	10.4/3.5
9	107.7	0	6.7	0	130.3	101.2/3.0	127.9	3.2/0	101.5	12.9/2.3
10	116.6	0	6.6	1.5	132.2	104.6/2.3	133.2	5.7/2.3	100.7	12.0/2.3
11[b]	60.4	–	6.0	0	123.7	102.1	127.7	5.4	90.7	10.3
12[b]	58.1	–	6.0	0	[c]	[c]	[c]	[c]	[c]	[c]

[a] In C_6D_6. [b] In CD_2Cl_2. [c] Hydrolyzed during ^{13}C NMR recording.

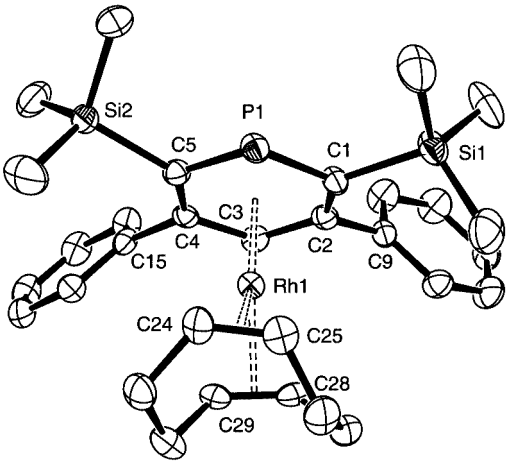

Figure 2. ORTEP view of complex **8**; ellipsoids are scaled to enclose 50% of the electron density; selected bond lengths [Å] and angles [°]; numbering is arbitrary and differs from the ones used in NMR spectra: Rh1–P1 2.464(1), Rh1–C1 2.388(4), Rh1–C2 2.366(4), Rh1–C3 2.188(4), Rh1–C4 2.325(4), Rh1–C5 2.437(4), P1–C1 1.777(4), P1–C5 1.772(5), C1–C2 1.389(6), C2–C3 1.427(6), C3–C4 1.431(6), C4–C5 1.392(6), Si1–C1 1.920(4), Si1–C6 1.858(6), Si1–C7 1.863(6), Si1–C8 1.861(6), C24–C25 1.402(7), C28–C29 1.400(7); C5–P1–C1 105.8(2), P1–C1–Si1 114.0(2), P1–C5–Si2 112.3(2)

plexes behave similarly, only three were fully characterized in their reaction with water, and two in their reaction with ethanol.

The most significant NMR spectroscopic data of the complexes **13**–**17** are collected in Table 2. In the ^{31}P NMR spectra of complexes **13** and **14**, the signals for both complexes appear as singlets at $\delta \approx -19.8$ and -16.2 ppm, respectively, despite the coordination to an Rh center. The reaction of **8** with ethanol yields complex **16** which displays a signal at a lower field ($\delta = -8.5$ ppm). The same trend is observed with the Ir complexes. For all of these complexes, when ^{31}P NMR spectroscopy is coupled with ^{1}H NMR spectroscopy, the singlets split into doublets, with very large $^{1}J_{H,P}$ coupling constants of 586 Hz (**13**) and 626 Hz (**17**). This proves the $R_2P(OR)H$ structure. When the ^{1}H NMR characteristics of these complexes are compared with the starting η^6-phosphinine complexes, it should be noted that the signal for 4-H is not significantly perturbed, showing that C-4 is still attached to the Rh center. This is also observed in the ^{13}C NMR spectra. In fact, the signals for C-4 and C-3,5 are only slightly shifted: $\delta = 91.8$ ppm and 125.9 ppm, respectively, in **13**, compared with $\delta = 97.1$ and 131.5 ppm, respectively, in **7**. However, the signal for C-2,6 is very significantly shifted in the new complexes: $\delta_{C\text{-}2,6}$ ranges from $\delta = 134.5$ ppm in **7** to $\delta = 69.7$ ppm in **13**. These data suggest the proposed new η^5-coordination mode. The crystal structures of **14**, **15** and **17** confirm this coordination mode. Suitable crystals were obtained by slow diffusion of hexane into THF solutions of the complexes. ORTEP views of **14** and **17** are presented in Figures 3 and 4, together with selected bond lengths and angles. The ORTEP view of complex **15** is very similar to that of **14**, and can be found in the Supporting Information.

From the three structures it can be seen that the phosphorus atom adopts a pyramid-type configuration. The η^5 coordination of the carbon part of the ring is also apparent. The presence of an $O-GaCl_3$ bond in **14** and **15** can be rationalized by the reaction of the transient P–OH with $GaCl_4^-$, which releases HCl [Equation (6)]. A similar type

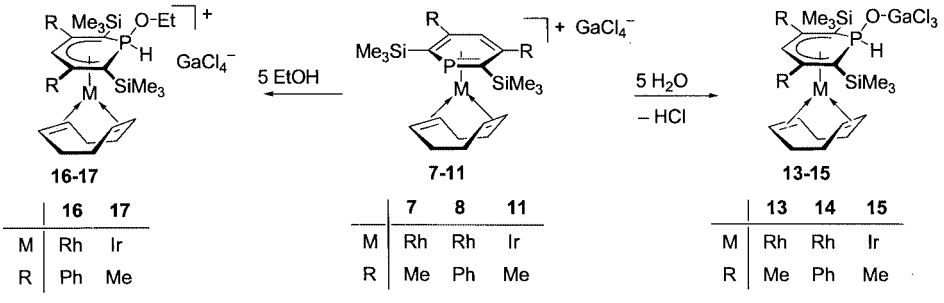

	16	17
M	Rh	Ir
R	Ph	Me

	7	8	11
M	Rh	Rh	Ir
R	Me	Ph	Me

	13	14	15
M	Rh	Rh	Ir
R	Me	Ph	Me

Scheme 2

Table 2. NMR characteristics of complexes **13**−**17**, in $CDCl_3$

	^{31}P	^{1}H						^{13}C			
	δ	$\delta_{4\text{-H}}$	$^4J_{H,P}$	δ_{PH}	$^1J_{H,P}$	$\delta_{C\text{-}2,6}$	$J_{C,P}/J_{C,Rh}$	$\delta_{C\text{-}3,5}$	$J_{C,P}/J_{C,Rh}$	$\delta_{C\text{-}4}$	$J_{C,P}/J_{C,Rh}$
13	−19.8	5.04	2.7	6.69	586	69.7	59.4/3.6	125.9	3.6/3.6	91.8	29.0/3.6
14	−15.3	5.43	3.2	7.13	584	67.5	51.1/0	129.0	4.6/4.6	92.9	25.4/2.7
15	−5.8	5.9	3.2	6.77	590	51.5	broad	112.0	5.7	98.6	27.6
16	−8.5	5.77	3.0	7.25	621	63.8	42.7/3.0	133.1	2.9/2.9	92.0	22.7/3.5
17	−1.8	6.42	1.6	6.90	626	48.0	45.6	114.5	4.8	98.9	30.3

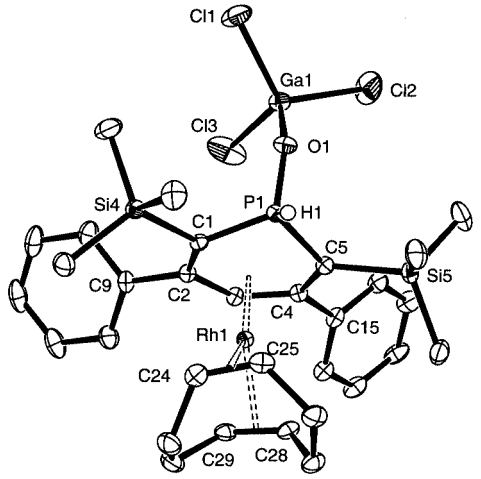

Figure 3. ORTEP view of complex **14**; ellipsoids are scaled to enclose 50% of the electron density; selected bond lengths [Å] and angles [°]; numbering is arbitrary and differs from the ones used in NMR spectra: Rh1−P1 2.7959(7), Rh1−C1 2.312(2), Rh1−C2 2.285(2), Rh1−C3 2.246(2), Rh1−C4 2.357(2), Rh1−C5 2.442(2), P1−C1 1.759(2), P1−C5 1.756(2), P1−O1 1.542(2), C1−C2 1.433(3), C2−C3 1.417(3), C3−C4 1.442(3), C4−C5 1.413(3), C24−C25 1.407(3), C28−C29 1.411(3); C5−P1−C1 107.0(1)

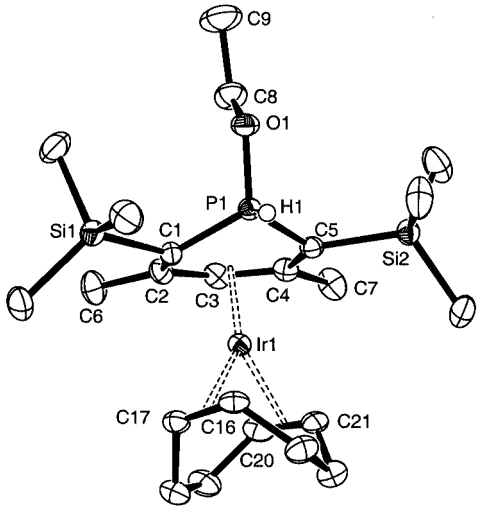

Figure 4. ORTEP view of complex **17**; ellipsoids are scaled to enclose 50% of the electron density; selected bond lengths [Å] and angles [°]; numbering is arbitrary and differs from the ones used in NMR spectra: Ir1−P1 2.755(1), Ir1−C1 2.242(3), Ir1−C2 2.265(3), Ir1−C3 2.262(3), Ir1−C4 2.250(3), Ir1−C5 2.362(3), P1−C1 1.751(3), P1−C5 1.735(3), P1−O1 1.592(2), C1−C2 1.447(4), C2−C3 1.410(4), C3−C4 1.428(4), C4−C5 1.441(4), C16−C17 1.430(4), C20−C21 1.408(5); C5−P1−C1 106.4(2)

of reactivity has been observed between a [CpFe(η^6-phosphinine)][$AlCl_4^-$] complex and water.[14]

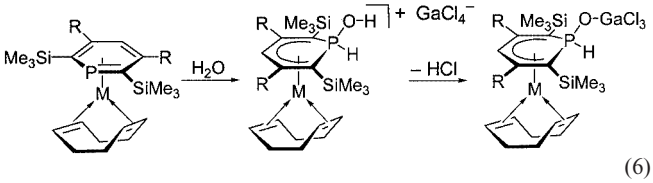

(6)

Apart from these features, the C−C and Rh−C bond lengths are very similar to those of the η^6 complexes. In the final products, a formal 1,1-addition of water or methanol takes place at the phosphorus atom. The mechanism most likely involves the reaction of the nucleophile at the electropositive phosphorus center, followed by the reaction of the electrophile. This type of mechanism has been reported by Dimroth in 1983 for the syntheses of tricarbonyl[η^5-(1λ^5-phosphinine)]metal(0) complexes (metal = Group-6 metal).[15]

Having tested the reactivity of the complexes towards protic sources, we then investigated the ease with which the diene moiety can be displaced. This factor is a prerequisite for the catalytic behavior of these complexes. Unfortunately, the reaction of the η^6 complexes with four-electron donor ligands, such as bipy or dppe, or even two-electron donor ligands, such as phosphanes, only led to the displacement of the phosphinine moiety within a few hours. In fact, this behavior is not unprecedented, and Valderrama et al. noted in 1982 that the arene ring in [Rh(C_6Me_6)($CO)_2$][PF_6] was very labile.[8g] It is not only displaced by bipy (instantaneously) but also by acetone or acetonitrile. In 2000, Werner et al. synthesized various [(η^6-arene)Rh(P*i*Pr$_3$)(η^2-COE)]$^+$ complexes with electron-rich and electron-poor arenes. They showed that both the alkene and the arene were displaced by ligands such as alkynes.[8m] Therefore, we tried to hydrogenate the diene moiety of these complexes under various pressures of H_2 in the presence of two-electron donors, hoping that hydrogenation would be faster than displacement of the phosphinine. Unfortunately, the typical solvent in which hydrogenation is fast (MeOH), destroys the η^6 coordination of the phosphinine, as shown above. In other solvents, the hydrogenation was not fast enough and displacement of the phosphinine always occurred.

The high sensitivity of the above-mentioned complexes towards nucleophilic attack prompted us to theoretically investigate, by DFT, the nature of the interaction between the

phosphinine ligand and the metal fragment. Considering the important difference in stability between cationic Group-9 complexes and their isoelectronic neutral iron(0) complexes synthesized by Zenneck et al., we extended our investigation to the η^6-Fe^0 species. Furthermore, in order to draw a comparison between phosphinines and arenes, the corresponding benzene derivatives were also studied. Therefore, a series of four complexes was studied: the $[Rh(\eta^6\text{-arene})(C_2H_4)_2]^+$ cationic species **I** (arene = C_6H_6) and **II** (arene = C_5H_5P), and the neutral species $[Fe(\eta^6\text{-arene})(C_2H_4)_2]$ **III** (arene = C_6H_6) and **IV** (arene = C_5H_5P) (Scheme 3).

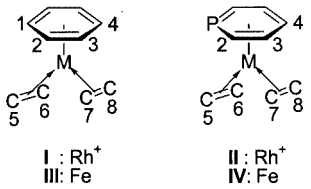

Scheme 3

All the geometric parameters of the calculated structures **I**−**IV** are summarized in Table 3.

Table 3. Calculated geometries and binding energies *D*e (non-ZPE-corrected) of complexes **I**−**IV**

	I[a]	**II**[a]	**III**[a]	**IV**[a]
P1−C2		1.781		1.776
C1−C2	1.421		1.418	
C2−C3	1.402	1.396	1.405	1.399
C3−C4		1.423		1.417
P1—M		2.617		2.481
C1—M	2.365		2.135	
C2—M	2.444	2.474	2.166	2.217
C3—M		2.431		2.173
C4—M		2.329		2.135
C5−C6	1.402	1.399	1.406	1.402
C7−C8		1.400		1.403
M−C5	2.179	2.197	2.071	2.091
M−C7		2.197		2.086
*D*e (ring)	55.86	57.21	57.17	60.55
*D*e (C5−C6)	60.60	61.19	48.12	45.24
*D*e (C7−C8)		58.44		46.39

[a] Binding energies are expressed in kcal/mol.

A first remark concerns the overall geometries of the calculated complexes that are analogous to that of the experimental structure. In each case, the D_2 (phosphinine complexes) and C_{2v} (benzene complexes) symmetries correspond to a minimum on the potential energy surface. Some discrepancies can be noted between the experimental and theoretical structures in the case of the (phosphinine)Fe and -Rh complexes; however, as mentioned above in the discussion of experimental structures of complexes **7** and **8**, the difference in the substitution pattern of the ring plays a very important role. Note that the nature of the olefin most likely plays a role in these distortions. The same can be said of the benzene complexes. Apart from this, all the coordinated ligands show a slightly inverse boat conformation (as noted in the structures of **7**−**9**). This distortion had already been observed in $[Rh(\eta^6\text{-arene})(olefin)L]$ complexes (L = 2e-donor ligand).

The most significant information is given by the NBO analysis,[16] which reveals that in rhodium complexes **I** and **II**, the arene ligands are electronically deficient (see Table 4). Thus, the sum of the NBO charges at the ligand reveals that +0.340 e has been transferred to the metallic fragment in **I**, and +0.423 e in the case of the phosphinine complex **II**. Most significant is the fact that in the coordinated phosphinine ligand, the phosphorus atom now bears a more important positive charge of +0.825, vs. +0.658 in the free ligand (calculated at the same level of theory). This simple comparison accounts for the higher reactivity of these η^6-ligated phosphinines towards nucleophilic attack. The NBO analysis also reveals that the Rh atom is more positively charged in the benzene complex **I** (+0.404) than in **II** (+0.274). In line with experimental observations (e.g. stability towards hydrolysis), the charge distribution pattern of the phosphinine ring is not significantly perturbed by coordination to the zero-valent $[Fe(C_2H_4)_2]$ fragment, and the NBO charges compare with those calculated for the free ligand. Thus, in complex **IV** the phosphorus atom bears a charge of +0.685, and the sum of the charges on all the atoms of the ring is close to zero (+0.035). Note that in **III** and **IV** a significant amount of electron-density has now been delocalized on the ethylene ligands, as shown by the sum of the charges (−0.204 in **III** and −0.160 in **IV**).

Interestingly, bond dissociation energies indicate that, although the bond strength of the ethylene ligands are quite similar in both types of complexes, benzene and phosphinine are more firmly bound to Fe in **III** and **IV**, than to Rh in **I** and **II**. This correlates very well with the experimental observations that shows that substitution of the ethylene ligands can occur in the case of Fe^0 complexes, but competes with that of the arene group in cationic Rh^I complexes. The bond dissociation energies are reported in Table 3. These data suggest that the contribution of the benzene and phosphinine ligands is nearly equivalent in these two types of complexes.

Therefore, to gain a deeper understanding of the arene−metal interactions in these complexes, a CDA analysis of **I**−**IV** was undertaken.[17] This method developed by Frenking and co-workers already proved to be a powerful tool in analyzing donor−acceptor interactions in terms of the common Dewar−Chatt−Duncansson (DCD) model concepts. The results given by the CDA analysis are summarized in Table 5. We did not limit our investigation to the arene ligands, and the analysis of the ethylene−metal interaction was also carried out. Care was taken to differentiate between the ethylene ligands in the phosphinine complexes **II** and **IV**, for obvious symmetry reasons.

A first important point concerns the residual term (Δ), which is important in analyzing the donor−acceptor interaction. In all cases, the values calculated are small and compare with those already reported in the literature for various ligands that were described following the DCD model. These values were found to be comparable for the ethylene

Table 4. Calculated NBO charge distribution for complexes **I**−**IV**

	I[a]	**II**[a]	**III**[a]	**IV**[a]
qP		0.825		0.685
qC1	−0.244		−0.258	
qC2	−0.230	−0.593	−0.247	−0.622
qC3		−0.227		−0.245
qC4		−0.236		−0.256
Σq_{ring}	0.340	0.423	0.080	0.035
qM	0.404	0.274	0.124	0.125
qC5 (P)[a]	−0.435 (1.445)	−0.421 (1.436)	−0.495 (1.410)	−0.491 (1.437)
qC7 (P)[a]		−0.432 (1.451)		−0.492 (1.428)
$\Sigma q_{olefin\ (C5-C6)}$	0.256	0.165	−0.204	−0.074
$\Sigma q_{olefin\ (C7-C8)}$		0.138		−0.086

[a] Wiberg bond indices.

Table 5. Results of the charge decomposition analysis of complexes **I**−**IV**

	I	II	III	IV
Arene ring:				
d[a]	0.649	0.759	0.912	1.062
b[b]	0.121	0.161	0.386	0.398
d/b	5.364	4.714	2.363	2.669
$b/(d + b)$	15.71%	17.5%	29.73%	27.26%
r[c]	−0.592	−0.613	−0.563	−0.540
$\Delta \cong$[d]	−0.009	−0.015	−0.029	−0.058
C-5=C-6, C-7=C-8:				
d	0.430	0.452, 0.385	0.508	0.500, 0.495
b	0.268	0.257, 0.241	0.342	0.331, 0.333
d/b	1.604	1.759, 1.597	1.485	1.510, 1.480
$B(d/d + b)$	38.39%	36.25%, 38.50%	40.23%	39.83%, 40.22%
r	−0.377	−0.376	−0.380	−0.403, −0.387
Δ	−0.013	−0.016	−0.014	−0.015, −0.014

[a] d = donation. [b] b = back donation. [c] r = repulsion. [d] Δ = residual.

ligands in all the complexes studied; however, they were found to be higher for the two arene ligands in the iron complexes. This is consistent with the finding that the π-accepting capacity of both arenes is enhanced in the zero-valent iron complexes **III** and **IV**. As can be seen in Table 4, the $b/(b + d)$ ratio increases by about 10% on going from the rhodium to the iron complexes. Consequently, one may propose that an increase in the back donation (b) would increase covalency, and hence a larger absolute value for this residual term results. On examining the d/b and $b/(b + d)$ ratios, one can assume that in both types of complexes, the arenes essentially behave as π-donors, the percentage of π-acceptance [given by the $b/(d + b)$ ratio] does not exceed 29.73%. It also appears that absolute values of donation (d) are slightly greater in the case of the phosphinine complexes, but care must be taken since it should be emphasized that the absolute values of d and b are not important, only their ratios are relevant. In view of these results, it is obvious that the contribution of the phosphinine and benzene groups to the electronic exchange in the complex are relatively similar. On the other hand, the contribution of the ethylene ligands also appears to be comparable in both types of complexes, as shown by the $b/(d + b)$ ratio, which ranges from 36.25 to 40.23%, and the corresponding Wiberg bond indices, which vary from 1.41 to 1.45.

In conclusion, we have devised two different methods that allowed us to synthesize the first (η^6-phosphinine)Rh^I and -Ir^I complexes. The first studies of the reactivity of these complexes with ethanol or water quantitatively yielded the first (η^5-phosphacyclohexadienyl)Rh^I and -Ir^I complexes, which resulted from the formal 1,1-addition of RO^-, followed by H^+. DFT calculations allowed us to rationalize the large differences in reactivity between the (η^6-phosphinine or benzene)rhodium cationic complexes and the isoelectronic Fe^0 complexes. A study on the chemical reactivity of these complexes is underway in our laboratories.

Experimental Section

General: All reactions were routinely performed under argon or nitrogen by using Schlenk and glove-box techniques and dry deoxygenated solvents. Dry THF and hexane were obtained by distillation from Na/benzophenone, and dry $CDCl_3$ from P_2O_5. CD_2Cl_2 was dried and stored, like $CDCl_3$, overn 4 Å Linde molecular sieves. Nuclear magnetic resonance spectra were recorded with a

Bruker AC-200 SY spectrometer operating at 300.0 MHz for ^{1}H, 75.5 MHz for ^{13}C and 121.5 MHz for ^{31}P. Solvent peaks were used as internal references relative to Me_4Si for ^{1}H and ^{13}C chemical shifts (ppm); ^{31}P chemical shifts were relative to a 85% H_3PO_4 external reference. Coupling constants are given in Hz. The following abbreviations are used: s = singlet, d = doublet, t = triplet, m = multiplet, quint = quintuplet, v = virtual. IR data were collected with a Perkin−Elmer 297 spectrometer. Mass spectra were obtained at 70 eV with an HP 5989B spectrometer coupled to an HP 5980 chromatograph by the direct inlet method. Elemental analyses were performed by the "Service d'analyse du CNRS", at Gif sur Yvette, France. Diazaphosphinine **1**,[12a] phosphinines **4**,[18] **5**,[12a] $[Rh(COD)Cl]_2$,[19] $[Rh(NBD)Cl]_2$,[20] $[Ir(COD)Cl]_2$,[21] $[Rh(COD)_2][BF_4]$[8b,22] were prepared according to reported procedures.

Synthesis of 2,3,5,6-Tetraphenylphosphinine (2): 5 equiv. of diphenylacetylene (1.78 g, 10.0 mmol) were added to a solution of **1** (0.42 g, 2.0 mmol) in 8 mL of toluene. The mixture was then heated at 130 °C for 12 h. The completion of the reaction was checked by ^{31}P NMR spectroscopy. The solution was then cooled to room temperature, and the title product purified by column chromatography on silica gel. Excess diphenylacetylene was eluted first with hexane, and phosphinine **2** was then eluted with a mixture of hexane/toluene (80:20). Yield 55%, 440 mg. ^{1}H NMR (300 MHz, $CDCl_3$, 298 K): δ = 7.26−7.40 (m, 20 H, CH of Ph), 7.70 (d, $^4J_{H,P}$ = 3.6, 1 H, 4-H) ppm. ^{13}C NMR (75.5 MHz, $CDCl_3$, 298 K): δ = 127.5−130.9 (m, CH of Ph), 137.4 (d, $^3J_{C,P}$ = 12.5, C-4), 142.4 (d, $^2J_{C,P}$ = 24.5, C-α of Ph), 142.5 (s, C-α of Ph), 145.8 (d, $^2J_{C,P}$ = 10.9, C-3,5), 169.6 (d, $^1J_{C,P}$ = 54.8, C-2,6) ppm. ^{31}P NMR (121.5 MHz, $CDCl_3$, 298 K): δ = 206.0 (s) ppm. $C_{29}H_{21}P$ (400.45): calcd. C 86.98, H 5.29; found C 86.97, H 5.44.

Synthesis of 5,6-Diphenyl-2-(trimethylsilyl)phosphinine (3): 1 equiv. of (trimethylsilyl)acetylene (0.20 g, 2.0 mmol) was added to a solution of **1** (0.42 g, 2.0 mmol) in 8 mL of toluene. The mixture was then heated at 60 °C for 12 h. The complete formation of the monoazaphosphinine was observed by ^{31}P NMR spectroscopy. 3 equiv. of diphenylacetylene (1.07 g, 6.0 mmol) were then added to the mixture, and the mixture was heated at 130 °C for 16 h. The solution was then cooled to room temperature and the title product purified by column chromatography. Excess diphenylacetylene was eluted first with hexane, and phosphinine **3** was then eluted with a mixture of hexane/toluene (80:20). **3** was recovered as a white solid after solvent evaporation. Yield 75%, 480 mg. ^{1}H NMR (300 MHz, $CDCl_3$, 298 K): δ = 0.32 (d, $^4J_{H,P}$ = 0.8, 9 H, $SiMe_3$), 7.02−7.16 (m, 10 H, CH of Ph), 7.45 (dd, $^4J_{H,P}$ = 3.0, $^2J_{H,H}$ = 8.1, 1 H, 4-H), 8.03 (dd, $^3J_{H,P}$ = 10.6, $^2J_{H,H}$ = 8.1, 1 H, 3-H) ppm. ^{13}C NMR (75.5 MHz, $CDCl_3$, 298 K): δ = 0.6 (d, $^3J_{C,P}$ = 5.7, $SiMe_3$), 127.2−131.3 (m, CH of Ph), 137.9 (d, $^3J_{C,P}$ = 12.5, C-4), 142.8 (s, C-α of Ph), 143.4 (d, $^2J_{C,P}$ = 23.6, C-α of Ph), 146.4 (d, $^2J_{C,P}$ = 10.3, C-3,5), 170.0 (d, $^1J_{C,P}$ = 62.3, C-2), 170.7 (d, $^1J_{C,P}$ = 77.1, C-6) ppm. ^{31}P NMR (121.5 MHz, $CDCl_3$, 298 K): δ = 232.7 (s) ppm. $C_{20}H_{21}PSi$ (320.44): calcd. C 74.96, H 6.61; found C 75.27, H 6.25.

Synthesis of Complex 6: Phosphinine **2** (240 mg, 0.6 mmol) and $[Rh(COD)_2][BF_4]$ (121 mg, 0.3 mmol) were weighed in air and then placed under nitrogen in a Schlenk flask. CH_2Cl_2 (10 mL) was then added by syringe into the mixture, which was stirred for 2 h at 40 °C. The solvent was then evaporated under vacuum and the COD extracted with 2 mL of hexane. The solid was then dried under vacuum to yield pure **6** as a yellow powder. Yield 95%, 313 mg. ^{1}H NMR (300 MHz, $CDCl_3$, 298 K): δ = 1.97−2.01 (m, Σ*J* = 13, 8 H, CH_2 of COD), 4.00 (m, Σ*J* = 13, 4 H, CH of COD), 6.92−7.26 (m, 20 H, CH of C_6H_5), 7.50 (AXX′, vt, $\Sigma J_{H,P}$ = 7.5, 1 H, 4-H) ppm. ^{13}C NMR (75.5 MHz, $CDCl_3$, 298 K): δ = 25.8 (s, CH_2 of COD), 70.0 (s, CH of COD), 127.8 (s, CH of Ph), 128.3 (s, CH of Ph), 128.5 (s, CH of Ph), 128.6 (s, CH of Ph), 129.5 (s, CH of Ph), 132.2 (s, CH of Ph), 134.9 (AXX′, vt, $\Sigma J_{C,P}$ = 23, C-4), 138.9 (m, C-α of Ph), 140.5 (t, $^1J_{C,P}$ = 2.3, C-2,6), 150.5 (m, C of Ph) 161.5 (m, C-3,5) ppm. ^{31}P NMR (121.5 MHz, CD_2Cl_2, 298 K): δ = 175.15 (d, $^1J_{P,Rh}$ = 166.5) ppm. $C_{66}H_{54}P_2RhBF_4$ (1098.81): calcd. C 72.14, H 4.95; found C 72.43, H 5.15.

Synthesis of the η^6-Phosphinine Complexes. Method A: A solution of $GaCl_3$ (63.4 mg, 0.36 mmol) in CH_2Cl_2 was added by cannula into a mixture of $[M(diene)Cl]_2$ (0.15 mmol) and phosphinine (0.3 mmol) in CH_2Cl_2 at −78 °C. The resulting mixture was then stirred for 30 min at room temperature. The solid was then precipitated with hexane, filtered, and dried under vacuum yielding the title complex. **Method B:** CH_2Cl_2 (10 mL) was added to a mixture of $[Rh(diene)_2][BF_4]$ (0.3 mmol) and phosphinine (0.3 mmol). The solution was heated at 40 °C until the reaction was complete, as shown by ^{31}P NMR spectroscopy. After evaporation of the solvent under vacuum, the solid was washed with hexane and dried to yield the title complex.

Synthesis of Complex 7: 3,5-Dimethyl-2,6-bis(trimethylsilyl)phosphinine (**4**) (80 mg, 0.3 mmol) was used with Method A {$[Rh(COD)Cl]_2$ (74 mg, 0.15 mmol)} and Method B {$[Rh(COD)_2][BF_4]$ (121 mg, 0.3 mmol)}. Method A: yield 87%, 180 mg; Method B: yield 66%, 112 mg. Slow diffusion of hexane into a THF solution of the complex yielded X-ray quality crystals. ^{1}H NMR (300 MHz, $CDCl_3$, 298 K): δ = 0.49 (s, 18 H, $SiCH_3$), 2.20−2.28 (m, 8 H, CH_2 of COD), 2.64 (s, 6 H, CH_3), 4.70 (s, 4 H, CH of COD), 5.92 (s, 1 H, 4-H) ppm. ^{13}C NMR (75.5 MHz, $CDCl_3$, 298 K): δ = 1.2 (d, $^3J_{C,P}$ = 16.8, $SiCH_3$), 24.4 (s, CH_3), 32.0 (s, CH_2 of COD), 83.3 (d, $^1J_{C,Rh}$ = 11.6, CH of COD), 97.1 (dd, $^3J_{P,C}$ = 8.6, $^1J_{C,Rh}$ = 3.2, C-4), 131.5 (dd, $^2J_{C,P}$ = 2.8, $^1J_{C,Rh}$ = 1.7, C-3,5), 134.5 (dd, $^1J_{C,P}$ = 76.5, $^1J_{C,Rh}$ = 1.7, C-2,6) ppm. ^{31}P NMR (121.5 MHz, $CDCl_3$, 298 K): δ = 101.42 (d, $^1J_{Rh,P}$ = 7.6) ppm. $C_{21}H_{37}BF_4PRhSi_2$ (566.37): calcd. C 44.53, H 6.58; found C 44.02, H 6.18.

Synthesis of Complex 8: 3,5-Diphenyl-2,6-bis(trimethylsilyl)phosphinine (**5**) (118 mg, 0.3 mmol) was used with Method A {$[Rh(COD)Cl]_2$ (74 mg, 0.15 mmol)} and Method B {$[Rh(COD)_2][BF_4]$ (122 mg, 0.3 mmol)}. Method A: yield 77%, 188 mg; Method B: yield 69%, 143 mg. Slow diffusion of hexane into a THF solution of the complex yielded yellow crystals suitable for X-ray analysis. ^{1}H NMR (300 MHz, $CDCl_3$, 298 K): δ = 0.26 (s, 18 H, $SiCH_3$), 2.34−2.37 (m, 4 H, CH_2 of COD), 2.39−2.53 (m, 4 H, CH_2 of COD), 4.85 (s, 4 H, CH of COD), 5.72 (d, $^4J_{H,P}$ = 1.3, 1 H, 4-H, 7.51−7.57 (m, 10 H, CH of Ph) ppm. ^{13}C NMR (75.5 MHz, $CDCl_3$, 298 K): δ = 2.2 (dd, $^3J_{C,P}$ = 9.8, $^3J_{C,Rh}$ = 2.3, $SiCH_3$), 32.1 (s, CH_2 of COD), 84.8 (d, $^1J_{C,Rh}$ = 11.5, CH of COD), 94.1 (dd, $^3J_{C,P}$ = 10.4, $^1J_{C,Rh}$ = 3.5, C-4), 129.5−136.8 (s, Ph), 137.9 (s, C-3,5), 141.1 (d, $^1J_{C,P}$ = 104.5, C-2,6) ppm. ^{31}P NMR (121.5 MHz, $CDCl_3$, 298 K): δ = 103.16 (d, $^1J_{Rh,P}$ = 9.1) ppm. $C_{31}H_{41}Cl_4GaPRhSi_2$ (815.24): calcd. C 45.67, H 5.07; found C 45.23, H 4.76.

Synthesis of Complex 9: 3,5-Dimethyl-2,6-bis(trimethylsilyl)phosphinine (**4**) (80 mg, 0.3 mmol) was used with Method A {$[Rh(NBD)Cl]_2$ (69 mg, 0.15 mmol)} and Method B {$[Rh(NBD)_2][BF_4]$ (112 mg, 0.3 mmol)}. Beige solid. Method A: yield 58%, 117 mg; Method B: yield 75%, 124 mg. ^{1}H NMR (300 MHz, $CDCl_3$, 298 K): δ = 0.46 (s, 18 H, $SiCH_3$), 1.34 (s, 2 H, CH_2 of NBD), 2.57 (s, 6 H, CH_3), 3.58 (s, 2 H, CH of NBD), 4.12

(m, ΣJ = 7.3, 4 H, CH of NBD), 6.68 (s, 1 H, 4-H) ppm. ^{13}C NMR (75.5 MHz, $CDCl_3$, 298 K): δ = 1.3 (d, $^3J_{C,P}$ = 9.7, $SiCH_3$), 24.7 (s, CH_3), 47.1 (d, $^2J_{C,Rh}$ = 2, CH of NBD), 48.3 (d, $^1J_{C,Rh}$ = 8.8, CH of NBD), 60.1 (d, $^3J_{C,Rh}$ = 4, CH_2 of NBD), 101.5 (dd, $^3J_{C,P}$ = 12.9, $^1J_{C,Rh}$ = 2.3, C-4), 127.9 (d, $^1J_{C,Rh}$ = 3.2, C-3,5), 130.3 (dd, $^1J_{C,P}$ = 101.2, $^1J_{C,Rh}$ = 3.0, C-2,6) ppm. ^{31}P NMR (121.5 MHz, $CDCl_3$, 298 K): δ = 107.77 ppm. $C_{20}H_{33}BF_4PRhSi_2$ (550.33): calcd. C 43.65, H 6.04; found C 42.27, H 5.75.

Synthesis of Complex 10: 3,5-Diphenyl-2,6-bis(trimethylsilyl)phosphinine (**5**) (118 mg, 0.3 mmol) was used with Method A {$[Rh(NBD)Cl]_2$ (69.1 mg, 0.15 mmol)} and Method B {$[Rh(NBD)_2][BF_4]$ (112 mg, 0.3 mmol)}. Brown solid. Method A: yield 62%, 148 mg; Method B: yield 71%, 144 mg. ^{1}H NMR (300 MHz, $CDCl_3$, 298 K): δ = 0.18 (d, $^4J_{H,P}$ = 1.7, 18 H, $SiCH_3$), 1.49 (t, $^3J_{H,H}$ = 1.7, 2 H, CH_2 of NBD), 3.76 (t, $^3J_{H,H}$ = 1.7, 2 H, CH of NBD), 4.44 (m, ΣJ = 10, 4 H, CH of NBD), 6.6 (d, $^4J_{H,P}$ = 1.5, 1 H, 4-H), 7.35−7.52 (m, 10 H, CH of Ph) ppm. ^{13}C NMR (75.5 MHz, $CDCl_3$, 298 K): δ = 2.3 (dd, $^3J_{C,P}$ = 9.3, $^3J_{C,Rh}$ = 3.1, $SiCH_3$), 46.9 (d, $^2J_{C,Rh}$ = 1.7, CH of NBD), 49.2 (d, $^1J_{C,Rh}$ = 8.7, CH of NBD), 61.1 (d, $^3J_{C,Rh}$ = 6.8, CH_2 of NBD), 100.7 (dd, $^3J_{C,P}$ = 12, $^1J_{C,Rh}$ = 2.3, C-4), 129.3−130.5 (s, Ph), 132.2 (d, $^1J_{C,P}$ = 104.6, $^1J_{C,Rh}$ = 2.3, C-2,6), 133.2 (dd, $^1J_{C,P}$ = 5.7, $^1J_{C,Rh}$ = 2.3, C-3,5) ppm. ^{31}P NMR (121.5 MHz, $CDCl_3$, 298 K): δ = 116.57 ppm. $C_{30}H_{37}Cl_4GaPRhSi_2$ (799.20): calcd. C 45.09, H 4.67; found C 44.71, H 4.34.

Synthesis of Complex 11: 3,5-Dimethyl-2,6-bis(trimethylsilyl)phosphinine (**4**) (80 mg, 0.3 mmol) was used with Method A {$[Ir(COD)Cl]_2$ (101 mg, 0.15 mmol)}. Beige solid. Method A: yield 84%, 197 mg. ^{1}H NMR (300 MHz, $CDCl_3$, 298 K): δ = 0.46 (s, 18 H, $SiCH_3$), 2.15−2.18 (m, 8 H, CH_2 of COD), 2.69 (s, 3 H, CH_3), 4.55 (s, 4 H, CH of COD), 6.0 (s, 1 H, 4-H) ppm. ^{13}C NMR (75.5 MHz, CD_2Cl_2, 298 K): δ = 0.5 (d, $^3J_{P,C}$ = 9.7, $SiCH_3$), 23.4 (d, $^3J_{P,C}$ = 2.4, CH_3), 32.8 (s, CH_2 of COD), 67.8 (s, CH of COD), 90.7 (d, $^3J_{P,C}$ = 10.3, C-4), 123.7 (d, $^1J_{P,C}$ = 102.1, C-2,6), 127.7 (d, $^2J_{P,C}$ = 5.4, C-3,5) ppm. ^{31}P NMR (121.5 MHz, CD_2Cl_2, 298 K): δ = 60.45 ppm. $C_{21}H_{37}Cl_4GaIrPSi_2$ (780.41): calcd. C 32.32, H 4.78; found C 31.95, H 4.31.

Synthesis of Complex 12: 3,5-Diphenyl-2,6-bis(trimethylsilyl)phosphinine (**5**) (118 mg, 0.3 mmol) was used with Method A {$[Ir(COD)Cl]_2$ (101 mg, 0.15 mmol)}. Brown solid. Method A: yield 79%, 215 mg. ^{1}H NMR (300 MHz, CD_2Cl_2, 298 K): δ = 0.15 (s, 18 H, TMS), 2.17−2.21 (m, 8 H, CH_2 of COD), 4.70 (s, 4 H, CH of COD), 6.01(s, 1 H, 4-H), 7.34−7.48 (s, 10 H, H of Ph) ppm. ^{31}P NMR (121.5 MHz, CD_2Cl_2, 298 K): δ = 58.09 ppm.

Reactivity with H_2O: The same procedure was used for all the complexes: 5 equiv. of water were added to a CH_2Cl_2 solution of the complex. The solution instantaneously turned pale yellow and the ^{31}P NMR spectra showed the formation of a unique product. The solution was then concentrated to dryness and the title complex was obtained as a yellow solid. Yield 100%.

Synthesis of Complex 13: Complex **7** (70 mg, 0.1 mmol) was used. Yield 100%, 67 mg. Slow diffusion of hexane into a CH_2Cl_2 solution of the complex yielded X-ray quality crystals. ^{1}H NMR (300 MHz, $CDCl_3$, 298 K): δ = 0.46 (s, 18 H, $SiCH_3$), 2.06 (d, $J_{H,H}$ = 8.5, 4 H, CH_2 COD), 2.28 (s, 3 H, CH_3), 2.38 (d, $J_{H,H}$ = 14.8, 4 H, CH_2 of COD), 4.12 (s, 4 H, CH of COD), 5.04 (d, $^4J_{H,P}$ = 2.7, 1 H, 4-H), 6.69 (d, $^1J_{H,P}$ = 586, 1 H, PH) ppm. ^{13}C NMR (75.5 MHz, $CDCl_3$, 298 K): δ = 1.3 (m, $SiCH_3$), 24.23 (d, $^3J_{C,P}$ = 10.8, CH_3), 32.3 (s, CH_2 of COD), 69.7 (dd, $^1J_{C,P}$ = 59.4, $^1J_{C,Rh}$ = 3.6, C-2,6), 75.0 (d, $^1J_{C,Rh}$ = 12.5, CH of COD), 91.8 (dd, $^3J_{C,P}$ = 29,$^1J_{C,Rh}$ = 3.6, C-4), 125.9 (t, $^1J_{C,Rh}$ = $^3J_{C,P}$ = 3.6, C-3,5) ppm. ^{31}P NMR (121.5 MHz, $CDCl_3$, 298 K): δ = −19.81 (d, $^1J_{P,H}$ = 586) ppm. $C_{21}H_{38}Cl_3GaOPRhSi_2$ (672.66): calcd. C 37.50, H 5.69; found C 37.21, H 5.25.

Synthesis of Complex 14: Complex **8** (73 mg, 0.09 mmol) was used. Yield 100%, 71 mg. ^{1}H NMR (300 MHz, CD_2Cl_2, 298 K): δ = 0.20 (s, 18 H, $SiMe_3$), 2.16−2.45 (m, 8 H, CH_2 of COD), 4.48 (s, 4 H, CH of COD), 5.53 (d, $^4J_{H,P}$ = 3.4, 1 H, 4-H), 7.13 (d, $^1J_{H,P}$ = 581.2, 1 H, PH), 7.18−7.48 (m, 10 H, CH of Ph) ppm. ^{13}C NMR (75.5 MHz, CD_2Cl_2, 298 K): δ = 1.4 (d, $^3J_{C,P}$ = 3.0, $SiMe_3$), 31.5 (s, CH_2 of COD), 69.0 (dd, $^1J_{C,P}$ = 53.5, $^1J_{C,Rh}$ = 53.5, C-2,6), 75.9 (d, $^1J_{C,Rh}$ = 12.2, CH_2 of COD), 94.3 (dd, $^3J_{C,P}$ = 25.7, $^1J_{C,Rh}$ = 3.1, C-4), 128.5−129.7 (s, CH of Ph), 130.3 (t, $^1J_{C,Rh}$ = $^2J_{C,P}$ = 3.0, C-3), 139.7 (d, $^3J_{C,P}$ = 11.3, C-α of Ph) ppm. ^{31}P NMR (121.5 MHz, CD_2Cl_2, 298 K): δ = −15.31 (d, $^1J_{P,H}$ = 581.2) ppm. $C_{31}H_{42}Cl_3GaOPRhSi_2$ (796.80): calcd. C 46.73, H 5.31; found C 46.32, H 4.97.

Synthesis of Complex 15: Complex **11** (100 mg, 0.13 mmol) was used. Yield 100%, 99 mg. ^{1}H NMR (300 MHz, CD_2Cl_2, 298 K): δ = 0.39 (s, 18 H, $SiCH_3$), 1.96−2.22 (m, 8 H, CH_2 COD), 2.24 (s, 3 H, CH_3), 2.93 (d, $J_{H,H}$ = 14.8, 4 H, CH_2 of COD), 4.12 (s, 4 H, CH of COD), 5.99 (d, $^4J_{H,P}$ = 3.2, 1 H, 4-H), 6.77 (d, $^1J_{H,P}$ = 582.4, 1 H, PH) ppm. ^{13}C NMR (75.5 MHz, $CDCl_3$, 298 K): δ = 1.2 (d, $^3J_{C,P}$ = 3.4, $SiCH_3$), 22.7 (d, $^3J_{C,P}$ = 8.6, CH_3), 33.0 (s, CH_2 of COD), 51.5 (m, C-2,6), 58.6 (s, CH of COD), 98.6 (m, C-4), 112.0 (t, $^3J_{C,P}$ = 5.7, C-3,5) ppm. ^{31}P NMR (121.5 MHz, CD_2Cl_2, 298 K): δ = −5.79 (d, $^1J_{P,H}$ = 582.4) ppm. $C_{21}H_{38}Cl_3GaIrOPSi_2$ (761.97): calcd. C 33.10, H 5.03; found C 32.88, H 4.65.

Reactivity with Ethanol: The same procedure was used for all the complexes: 5 equiv. of ethanol were added to a CH_2Cl_2 solution of the complex (100 mg). The solution instantaneously turned pale yellow and the ^{31}P NMR spectra showed the formation of a unique product. The solution was then concentrated to dryness and the title complex was obtained as a yellow solid. Yield 100%.

Synthesis of Complex 16: Complex **8** (73 mg, 0.09 mmol) was used. Yield 100%, 77.4 mg. ^{1}H NMR (300 MHz, $CDCl_3$, 298 K): δ = 0.20 (s, 18 H, $SiCH_3$), 1.39 (t, $^3J_{H,H}$ = 6.9, 3 H, CH_3 of EtO), 2.28 (d, J = 8.8, 4 H, CH_2 of COD), 2.31−2.49 (m, 4 H, CH_2 of COD), 3.75 (dq, $^3J_{H,P}$ = 14.9, $^3J_{H,H}$ = 6.9, 2 H, CH_2 of EtO), 4.63 (s, 4 H, CH of COD), 5.77 (d, $^4J_{H,P}$ = 3.0, 1 H, 4-H), 7.25 (d, $^4J_{H,P}$ = 621, 1 H, PH), 7.35−7.38 (m, 4 H, CH of Ph), 7.49−7.50 (m, 6 H, H of Ph) ppm. ^{13}C NMR (75.5 MHz, $CDCl_3$, 298 K): δ = 1.3 (m, $SiCH_3$), 15.0 (s, CH_3), 30.3 (s, CH_2 of COD), 62.2 (d, $^2J_{C,P}$ = 6.8, CH_2), 63.8 (dd, $^1J_{C,P}$ = 42.7, $^1J_{C,Rh}$ = 3, C-2,6), 79.0 (d, $^1J_{C,Rh}$ = 12.3, CH of COD), 92.0 (d, $^4J_{C,P}$ = 22.7, $^1J_{C,Rh}$ = 3.5, C-4), 129.4−129.6 (s, Ph), 133.1 (t, $^1J_{C,Rh}$ = $^3J_{C,P}$ = 2.9, C-3,5), 138.6 (d, $^2J_{C,P}$ = 11.9, Ph) ppm. ^{31}P NMR (121.5 MHz, $CDCl_3$, 298 K): δ = −8.51 (d, $^1J_{P,H}$ = 621) ppm. $C_{33}H_{47}Cl_4GaOPRhSi_2$ (861.31): calcd. C 46.02, H 5.50; found C 45.71, H 5.19.

Synthesis of Complex 17: Complex **11** (100 mg, 0.13 mmol) was used. Yield 100%, 107 mg. ^{1}H NMR (300 MHz, $CDCl_3$, 298 K): δ = 0.41 (s, 18 H, $SiCH_3$), 1.24 (t, $^3J_{H,H}$ = 7, 3 H, CH_3), 2.13−2.16 (m, 8 H, CH_2 of COD), 2.41 (s, 3 H, CH_3), 3.49 (dq, $^3J_{H,P}$ = 15.2, $^3J_{H,H}$ = 7.1, 2 H, CH_2), 4.08 (s, 4 H, CH of COD), 6.42 (d, $^4J_{H,P}$ = 1.6, 1 H, 4-H), 6.90 (d, $^1J_{H,P}$ = 626, 1 H, PH) ppm. ^{13}C NMR (75.5 MHz, $CDCl_3$, 298 K): δ = 1.3 (s, $SiCH_3$), 16.3 (s, CH_3), 23.2 (d, $^3J_{C,P}$ = 9.4, CH_3), 33.3 (s, CH_2 of COD), 48.0 (d, $^1J_{C,P}$ = 45.6, C-2,6), 61.3 (s, CH of COD), 63,5 (d, $^2J_{P,C}$ = 6.5, CH_2), 98.9 (d, $^3J_{P,C}$ = 30.3, C-4), 114.5 (d, $^2J_{P,C}$ = 4.8, C-3,5) ppm. ^{31}P NMR (121.5 MHz, $CDCl_3$, 298 K): δ = −1,82 (d, $^1J_{P,H}$ = 626) ppm. $C_{23}H_{43}Cl_4GaIrOPSi_2$ (826.48): calcd. C 33.42, H 5.24; found C 33.08, H 4.83.

Theoretical Methods: The geometries of complexes **I**−**IV** were optimized using the gradient-corrected density functional theory (DFT), using Becke's three-parameter hybrid method B3LYP.[16] The basis set used is identical to that used by Frenking and coworkers in many studies.[17] The basis set, which is known as "Basis Set II", incorporates the Hay and Wadt small-core relativistic effective core potential and double-ζ valence basis set (441/2111/*N*1) (N = 4, 3, 2 for first, second, and third transition metal rows, respectively) for transition metals, in conjunction with all-electron 6-31G(d) basis sets for the main-group elements, H, C, and P.[25] All optimized structures reported here have only positive eigenvalues of the Hessian matrix, i.e. they are minima on the potential energy surface. The charge distribution in the optimized structures was calculated with the NBO partitioning scheme. Inspection of the arenes (benzene or phosphinine) and ethylene−metal fragment donor−acceptor interactions was performed using the charge-decomposition analysis (CDA).[26] In the CDA method, the molecular orbitals (canonical, natural, or Kohn−Sham) of the complex are expressed in terms of MOs of appropriately chosen fragments. In the cases studied, the Kohn−Sham orbitals of the B3LYP/II calculations are formed in the CDA procedure as a linear combination of the MOs of the arene and those of the remaining fragment [M(C_2H_4)$_2$] (positively charged for M = Rh and neutral for M = Fe). The same approach was used for the analysis of the ethylene ligand, [M(arene)(C_2H_4)] (positively charged for M = Rh and neutral for M = Fe) being considered as the second fragment. In both cases, the arene and ethylene ligands, as well as the considered fragments were computed in the geometry of the complex. The orbital contributions are divided into four parts: (i) the mixing of the occupied MOs of the ligand and the unoccupied MOs of the metal fragment; this value (noted *d*) represents the donation ligand → [metal fragment]; (ii) the mixing of the unoccupied MOs of the ligand and the occupied MOs of the metal fragment; this value (noted *b*) accounts for the back donation [metal fragment] → ligand; (iii) the mixing of the occupied MOs of the ligand and the occupied MOs of the metal fragment; this term (noted <*r*>), which describes the repulsive polarization ligand ⇄ [metal fragment], is negative because electronic charge is removed from the overlapping area of the occupied orbitals; (iv) the residual term (Δ), which results from the mixing of the unoccupied MOs of the two respective fragments; usually, this term is very close to zero for closed-shell interactions. This value constitutes an important probe in determining whether the bonding studied can really be classified as a donor−acceptor interaction following the Dewar−Chatt−Duncansson model. Important deviations from Δ = 0 imply that the bond studied is more conventionally described as a normal covalent bond between two open-shell fragments. A more detailed presentation of the CDA method and the interpretation of the results can be found in the literature. CDA calculations were performed with the program CDA version 2.1. More details about the method and a discussion of its applications and results can be found in the literature. These calculations were performed with the Gaussian-98 program.[27]

X-ray Structure Determinations: Crystals of complexes **6**−**8**, **14**, **15**, **17** suitable for X-ray diffraction were obtained by slow diffusion of hexane into a dichloromethane solution of the complexes. Data were collected with a Nonius Kappa CCD diffractometer, using an Mo-K_α (λ = 0.71070 Å) X-ray source and a graphite monochromator. Experimental details are described in Tables 6 and 7. The crystal structures were solved using SIR 97[28] and SHELXL-97.[29] ORTEP drawings were made using ORTEP III for Windows.[30]

Table 6. Details of X-ray structure determinations

	6	**8**
Crystal color/shape	orange/plate	yellow/cube
Crystal size [mm]	0.18 × 0.16 × 0.12	0.16 × 0.16 × 0.16
Empirical formula	$C_{67}H_{56}Cl_6GaP_2Rh$	$C_{31}H_{41}Cl_4GaPRhSi_2$
Formula mass	1308.39	815.22
Temperature [K]	150.0(10)	150.0(10)
Radiation (graphite monochromator)	Mo-K_α	Mo-K_α
Wavelength [Å]	0.71069	0.71069
Crystal system	monoclinic	monoclinic
Space group	*P*21/*n*	*Cc*
a [Å]	14.348(5)	21.309(9)
b [Å]	17.724(5)	11.185(5)
c [Å]	47.681(5)	30.250(5)
β [°]	94.120(5)	90.446(6)
V [Å^3]	12094(6)	7210(5)
Z, calcd. density [g·cm^{-3}]	8, 1.437	8, 1.502
Absorption coefficient [cm^{-1}]	1.077	1.633
$2\Theta_{max}$ [°]	25.03	27.45
F(000)	5328	3312
Index ranges *h*,*k*,*l*	−16/17, −21/21, −56/31	−26/27, −13/14, −39/38
Refl.collected/independent	38747/19776	25079/14757
Refl. used	13955	13036
(R_{int})	0.0378	0.0569
Absorption correction	0.8297 min, 0.8816 max	0.7802 min, 0.7802 max
Parameters refined	1385	757
Reflection/parameter ratio	10	17
Final *R*1, *wR*2 [$I > 2\sigma(I)$]	0.0561, 0.1657	0.0368, 0.0906
Goodness-of-fit on F^2	1.040	1.001
Diff. peak/hole [e·Å^{-3}]	1.034(0.093)/−1.371(0.093)	1.199(083)/−0.738(083)
Flack parameter	−	−0.002(8)

Table 7. Details of X-ray structure determinations

	14	**17**
Crystal color	yellow	colorless
Crystal shape	plate	needle
Crystal size [mm]	0.22 × 0.22 × 0.09	0.20 × 0.16 × 0.16
Empirical formula	$C_{32}H_{44}Cl_5GaOPRhSi_2$	$C_{23}H_{43}Cl_4GaIrOPSi_2$
Formula mass	881.70	826.44
Temperature [K]	150.0(10)	150.0(10)
Radiation (graphite monochromator)	Mo-K_α	Mo-K_α
Wavelength [Å]	0.71069	0.71069
Crystal system	monoclinic	monoclinic
Space group	$P2_1/n$	$P2_1/n$
a [Å]	8.371(5)	13.421(5)
b [Å]	25.173(5)	14.379(5)
c [Å]	17.777(5)	17.895(5)
β [°]	91.970(5)	110.090(5)
V [Å^3]	3744(3)	3243.3(19)
Z, calcd. density [g·cm^{-3}]	4, 1.564	4, 1.693
Absorption coefficient [cm^{-1}]	1.649	5.398
$2\Theta_{max}$ [°]	30.01	30.01
F(000)	1792	1628
Index ranges h,k,l	−11/11, −33/35, −24/24	−18/18, −20/18, −24/25
Refl.collected/independent	19140/10843	16753/9447
Refl. used	9382	7817
(R_{int})	0.0177	0.0228
Absorption correction	0.7130 min., 0.8657 max.	0.4115 min., 0.4788 max.
Parameters refined	382	307
Reflection/parameter ratio	24	25
Final $R1$, $wR2$ [$I > 2\sigma(I)$]	0.0332, 0.1238	0.0293, 0.0765
Goodness-of-fit on F^2	0.943	1.023
Diff. peak/hole [e·Å^{-3}]	0.800(106)/−1.008(106)	1.692(127)/−1.328(127)

Compound **6** and **14** each contain a highly disordered CH_2Cl_2 molecule. They were accounted for by using the Platon SQUEEZE function. The structure of compound **6** calls for an additional comment. Both $GaCl_4$ anions present in the asymmetric unit appear to be disordered. When average positions are used, $R1$ converges to about 7.9%. The anion labeled GA1 has fewer problems than the second one, and the disorder could not be refined. For the anion labeled GA2, a model consisting of a major site, accounting for 70% of the electron-density, and a minor site (30% at GA2A) was refined. This model implies that the neighboring CH_2Cl_2 solvate is similarly disordered; not taking this into account results in apparent contacts of about 1.4 Å between the chlorine atoms of GA2A and the H atoms of the solvate. Compound **7** is twinned, twin operator [1 0 0 0 −1 0 0 0 −1], BASF = 0.41. CCDC-188543 (**6**), -188544 (**7**), -188545 (**8**), -188546 (**14**), -188547 (**15**), and -188548 (**17**) contain the supplementary crystallographic data for this paper. These data can be obtained free of charge at www.ccdc.cam.ac.uk/conts/retrieving.html [or from the Cambridge Crystallographic Data Centre, 12 Union Road, Cambridge CB2 1EZ, UK; Fax: (internat.) + 44-1223/336-033; E-mail: deposit@ccdc.cam.ac.uk].

Supporting Information Available: ORTEP drawings of complexes **7** and **15** (see footnote on the first page of this article).

Acknowledgments

The authors thank the CNRS and the Ecole Polytechnique for supporting this work.

[1] For a recent review: N. Mézailles, F. Mathey, P. Le Floch, *Prog. Inorg. Chem.* **2001**, *49*, 455−550.
[2] [2a] Ti: P. L. Arnold, F. G. N. Cloke, K. Khan, P. Scott, *J. Organomet. Chem.* **1997**, *528*, 77−81. [2b] V: C. Elschenbroich, M. Nowotny, B. Metz, W. Massa, J. Graulich, K. Biehler, W. Sauer, *Angew. Chem. Int. Ed. Engl.* **1991**, *30*, 547−550, *Angew. Chem.* **1991**, *103*, 601−604. [2c] Cr: C. Elschenbroich, F. Bär, E. Bilger, D. Mahrwald, M. Nowotny, B. Metz, *Organometallics* **1993**, *12*, 3373−3378. [2d] Ho: P. L. Arnold, F. G. N. Cloke, P. B. Hitchcock, *Chem. Commun.* **1997**, 481−482.
[3] [3a] H. Vahrenkamp, H. Nöth, *Chem. Ber.* **1972**, *105*, 1148−1157. [3b] J. Deberitz, H. Nöth, *Chem. Ber.* **1973**, *106*, 2222−2226. [3c] K. C. Nainan, C. T. Sears, *J. Organomet. Chem.* **1978**, *148*, C31−C34.
[4] [4a] F. Nief, C. Charrier, F. Mathey, M. Simalty, *J. Organomet. Chem.* **1980**, *187*, 277−285. [4b] J. Fisher, A. De Cian, F. Nief, *Acta Crystallogr., Sect. B* **1979**, *35*, 1686−1695.
[5] [5a] F. Knoch, F. Kremer, U. Schmidt, U. Zenneck, P. Le Floch, F. Mathey, *Organometallics* **1996**, *15*, 2713−2719. [5b] D. Böhm, H. Geiger, F. Knoch, S. Kummer, P. Le Floch, F. Mathey, U. Schmidt, U. Zenneck, *Phosphorus, Sulfur Silicon* **1996**, *109/110*, 173−176. [5c] P. Le Floch, F. Knoch, F. Kremer, F. Mathey, J. Scholz, W. Scholz, K.-H. Thiele, U. Zenneck, *Eur. J. Inorg. Chem.* **1998**, 119−126.
[6] N. Mézailles, L. Ricard, P. Le Floch, F. Mathey, *Organometallics* **2001**, *20*, 3304−3307.
[7] M. J. Nolte, G. Gafner, L. M. Haines, *J. Chem. Soc., Chem. Commun.* **1969**, 1406−1407.
[8] [8a] R. R. Schrock, J. A. Osborn, *Inorg. Chem.* **1970**, *9*, 2339−2343. [8b] R. R. Schrock, J. A. Osborn, *J. Am. Chem. Soc.* **1971**, *93*, 3089−3091. [8c] M. Green, T.A. Kuc, *J. Chem. Soc., Dalton Trans.* **1972**, 832−839. [8d] M. Green, G. J. Parker, *J. Chem. Soc., Dalton Trans.* **1974**, 333−343. [8e] R. Uson, L. A. Oro, C. Foces-Foces, F. Cano, A. Vegas, M. Valderrama, *J. Organomet. Chem.* **1981**, *215*, 241−253. [8f] R. Uson, L. A. Oro, C. Foces-Foces, F. Cano, H. Garcia-Blanco, M. Valderrama, *J. Organomet. Chem.* **1982**, *229*, 293−304. [8g] M. Valderrama, L.

A. Oro, *Can. J. Chem.* **1982**, *60*, 1044−1047. [8h] R. R. Burch, E. L. Muetterties, V. W. day, *Organometallics* **1982**, *1*, 188−197. [8i] M. Valderrama, M. Scotti, R. Ganz, L. A. Oro, F. J. Lahoz, C. Foces-Foces, F. H. Cano, *J. Organomet. Chem.* **1985**, *288*, 97−107. [8j] E. Bittersmann, K. Hildebrand, A. Cervilla, P. Lahuerta, *J. Organomet. Chem.* **1985**, *287*, 255−263. [8k] J. R. Bleeke, A. J. Donaldson, *Organometallics.* **1988**, *7*, 1588−1596. [8l] M. A. Esteruelas, L. A. Oro, *Coord, Chem. Rev.* **1999**, *195*, 557−618. [8m] H. Werner, G. Canepa, K. Ilg, J. Wolf, *Organometallics.* **2000**, *19*, 4756−4766.

[9] [9a] I. Amer, H. Alper, *J. Am. Chem. Soc.* **1990**, *112*, 3674−3676. [9b] J. Q. Zhou, H. Alper, *J. Chem. Soc., Chem. Commun.* **1991**, 233−234. [9c] H. Alper, J. Q. Zhou, *J. Org. Chem.* **1992**, *57*, 3729−3731. [9d] J. Q. Zhou, H. Alper, *J. Org. Chem.* **1992**, *57*, 3328−3331. [9e] J. Q. Zhou, H. Alper, *J. Chem. Soc., Chem. Commun.* **1993**, 316−317. [9f] K. Totland, H. Alper, *J. Org. Chem.* **1993**, *58*, 3326−3329. [9g] C. M. Crudden, H. Alper, *J. Org. Chem.* **1994**, *59*, 3091−3097.

[10] [10a] J. Q. Zhou, H. Alper, *Organometallics* **1994**, *13*, 1586−1591. [10b] F. Monteil, I. Matsuda, H. Alper, *J. Am. Chem. Soc.* **1995**, *117*, 4419−4420. [10c] J. Q. Zhou, G. Facey, B. R. James, H. Alper, *Organometallics* **1996**, *15*, 2496−2503.

[11] [11a] F. Torres, E. Sola, M. Martin, J. A. Lopez, F. J. Lahoz, L. A. Oro, *J. Am. Chem. Soc.* **1999**, *121*, 10632−10633. [11b] F. Torres, E. Sola, M. Martin, C. Ochs, G. Picazo, J. A. Lopez, F. J. Lahoz, L. A. Oro, *Organometallics* **2001**, *20*, 2716−2724.

[12] [12a] N. Avarvari, P. Le Floch, F. Mathey, *J. Am. Chem. Soc.* **1996**, *118*, 11978−11979. [12b] N. Avarvari, P. Le Floch, L. Ricard, F. Mathey, *Organometallics* **1997**, *16*, 4089−4098.

[13] N. Avarvari, N. Maigrot, L. Ricard, F. Mathey, P. Le Floch, *Chem. Eur. J.* **1999**, *5*, 2109−2118.

[14] F. Nief, J. Fischer, *Organometallics* **1986**, *5*, 877−883.

[15] K. Dimroth, H. Kaletsch, *J. Organomet. Chem.* **1983**, *247*, 271−285.

[16] A. E. Reed, L. A. Curtiss, F. Weinhold, *Chem. Rev.* **1988**, *88*, 899−926.

[17] See for example: G. Frenking, N. Fröhlich, *Chem. Rev.* **2000**, *100*, 717−774.

[18] L. Cataldo, S. Choua, T. Berclaz, M. Goeffroy, N. Mézailles, L. Ricard, F. Mathey, P. Le Floch, *J. Am. Chem. Soc.* **2001**, *123*, 6654−6661.

[19] G. Giordano, R. H. Crabtree, *Inorg. Synth.* **1990**, *28*, 88−90.

[20] E. W. Abel, M. A. Bennett, G. Wilkinson, *J. Chem. Soc.* **1959**, 3178.

[21] J. L. Herde, J. C. Lambert, C. V. Senoff, *Inorg. Synth.* **1974**, *15*, 18−20.

[22] [22a] M. Green, T. A. Tuc, S. H. Taylor, *J. Chem. Soc., Chem. Commun.* **1970**, 1553−1554. [22b] R. R. Schrock, J. A. Osborn, *J. Am. Chem. Soc.* **1971**, *93*, 3089−3090.

[23] [23a] A. D. Becke, *Phys. Rev. A* **1988**, *38*, 3098−3100. [23b] C. Lee, W. Yang, R.G. Parr, *Phys. Rev.* **1988**, *B41*, 785−789. [23c] A.D. Becke, *J. Chem. Phys.* **1993**, *98*, 5648−5652. [23d] D. J. Stevens, F. J. Devlin, C. F. Chablowski, M. J. Frisch, *J. Phys. Chem.* **1994**, *80*, 11623−11627.

[24] G. Frenking, I. Antes, M. Böhme, S. Dapprich, A. W. Ehlers, V. Jonas, A. Neuhaus, M. Otto, R. Stegmann, A. Veldkamp, S. F. Vyboishchikov, *Reviews in Computational Chemistry* (Eds.: K. B. Lipkowitz, D. B. Boyd), VCH, New York, **1996**, vol. 8, pp. 63−144.

[25] P. J. Hay, W. R. Wadt, *J. Chem. Phys.* **1985**, *82*, 299−310.

[26] S. Dapprich, G. Frenking, *CDA* 2.1, Marburg, **1995**. The program is available on-line: ftp://chemie.uni-marburg.de (/pub/cda).

[27] M. J. Frisch, G. W. Trucks, H. B. Schlegel, G. E. Scuseria, M. A. Robb, J. R. Cheeseman, V. G. Zakrzewski, Jr. J. A. Montgomery, R. E. Stratmann, J. C. Burant, S. Dapprich, J. M. Millam, A. D. Daniels, K. N. Kudin, M. C. Strain, O. Farkas, J. Tomasi, V. Barone, M. Cossi, R. Cammi, B. Mennucci, C. Pomelli, C. Adamo, S. Clifford, J. Ochterski, G. A. Petersson, P. Y. Ayala, Q. Cui, K. Morokuma, D. K. Malick, A. D. Rabuck, K. Raghavachari, J. B. Foresman, J. Cioslowski, J. V. Ortiz, A. G. Baboul, B. B. Stefanov, G. Liu, A. Liashenko, P. Piskorz, I. Komaromi, R. Gomperts, R. L. Martin, D. J. Fox, T. Keith, M. A. Al-Laham, C. Y. Peng, A. Nanayakkara, M. Challacombe, P. M. W. Gill, B. Johnson, W.Chen, M. W. Wong, J. L. Andres, C. Gonzalez, M. Head-Gordon, E. S. Replogle, J. A. Pople, *Gaussian 98*, Revision A-11, Gaussian, Inc., Pittsburgh PA, **1998**.

[28] A. Altomare, M. C. Burla, M. Camalli, G. Cascarano, C. Giacovazzo, A. Guagliardi, A. G. G. Moliterni, G. Polidori, R. Spagna, *SIR97, an integrated package of computer programs for the solution and refinement of crystal structures using single crystal data*.

[29] G. M. Sheldrick, *SHELXL-97*, Universität Göttingen, Göttingen, Germany, **1997**.

[30] Louis J. Farrugia, *ORTEP-3*, Department of Chemistry, University of Glasgow.

Received June 28, 2002
[I02356]

Electrospray Behavior of Lacunary Keggin-Type Polyoxotungstates $[XW_{11}O_{39}]^{p-}$ (X = Si, P): Mass Spectrometric Evidence for a Concentration-Dependent Incorporation of an MO^{n+} ($M = W^{VI}$, Mo^{VI}, V^{V}) Unit into the Polyoxometalate Vacancy

Marcella Bonchio,*[a] Olga Bortolini,*[b] Valeria Conte,[c] and Andrea Sartorel[a]

Keywords: Polyoxometalates / Mass spectrometry / Tungsten / Speciation / Lacunary species

ESI-MS analysis provides a straightforward tool for the solution characterization of highly charged mono-lacunary Keggin-type polyoxotungstates α-$[XW_{11}O_{39}]^{p-}$ (X = Si, P; p = 8, 7). Doubly and triply charged quasi-molecular ion peaks were identified on the basis of both the theoretical simulation of the isotopic cluster distributions and the fragmentation modes observed with MS/MS technique. This approach allows the characterization of the inorganic polyanions transferred into the gas-phase with associated alkali metal cations (Li^+, Na^+). Indeed, the ESI-MS spectrum was found to be dependent on the counterion nature and on the initial concentration of the polyoxotungstate. While lithium salts at millimolar concentration represent the best choice for the analytical protocol, upon dilution the inorganic structure rearranges to a saturated Keggin dodecametalate complex. This phenomenon is induced by the electrospray ionization process and was exploited to produce gas-phase ions of monosubstituted species formed through incorporation of molybdenum and vanadium into the polyoxotungstate framework.
(© Wiley-VCH Verlag GmbH & Co. KGaA, 69451 Weinheim, Germany, 2003)

Introduction

Polyoxometalates (POM), are discrete metal−oxygen clusters of early transition metals in their highest oxidation state.[1] Their chemistry, dictated by their remarkable structural and electronic properties, is the subject of an intense interdisciplinary research activity in some major scientific areas, namely catalysis, materials science and medicine.[1−3]

An efficient approach to the synthesis of new polyoxometalate architectures is mainly based on lacunary POMs, i.e. species with defect structures.[1−3] Due to the presence of a structural "vacancy", lacunary species possess a reactive nucleophilic polyoxygenated site that can be readily functionalized, and because of this they have been used to provide (i) highly robust, all-inorganic ligands for catalytically active hetero-transition metal nuclei;[4,5] (ii) linking building units for the preparation of nanosized aggregates;[6,7] (iii) inorganic rigid templates that can be derivatized with organic or organometallic residues.[8−10]

The study of such reactive intermediates in terms of their intricate assembly equilibria, solution speciation and stability both in aqueous and in organic media is relevant to the success of the synthetic strategies mentioned above and therefore is receiving considerable attention.[11,12] In this respect, heteronuclear NMR spectroscopy has been the technique of choice to investigate the solution speciation and to identify the products. The main drawbacks inherent to such a technique are, however, the low sensitivity and the difficulties in structural assignments.[13,14]

Recently, electrospray mass spectrometry (ESI-MS) has been successfully employed for the inspection of different polynuclear metal complexes equilibrating in solution.[15,16] In these studies, ESI-MS has emerged as an effective tool for the investigation of rapidly exchanging systems, and has proved to be a powerful diagnostic alternative to NMR spectroscopy.[15−17]

ESI-MS has been underused in the analysis of polyoxoanion solutions, even though the soft ESI-mode allows the transfer of even large inorganic polyanions from solution to the gas phase.[18−20] In contrast, the Fast Atom Bombardment (FAB) ionization mode has been used very often for the characterization of POMs, providing information on their molecular mass and elemental composition. Such a technique, however, leads to extensive cationization and fragmentation of the POMs, and the necessary use of a matrix support often interferes with their solution chemistry.[21−24]

[a] ITM-CNR Sezione di Padova Dipartimento di Chimica Organica, Università di Padova
Via Marzolo 1, 35131, Padova, Italy
Fax: (internat.) + 39-049/827-5239
E-mail: marcella.bonchio@unipd.it
[b] Dipartimento di Chimica, Università di Ferrara,
Via Borsari 46, 44100 Ferrara, Italy
[c] Dipartimento di Scienze e Tecnologie Chimiche, Università di Roma Tor Vergata,
Via Della Ricerca Scientifica, 00133 Roma, Italy

We describe here the straightforward ESI-MS analysis of aqueous solutions containing lacunary Keggin-type polyoxotungstates with general formula α-$[XW_{11}O_{39}]^{p-}$. The present paper indicates a rapid and efficient protocol for the solution characterization of these polyanions based on: (i) the simultaneous examination of the multiply charged ions generated from the polyelectrolyte; (ii) the theoretical simulation of the isotopic cluster distributions determined experimentally for such ions; (iii) the use of the tandem mass spectrometric technique[25] to evaluate the fragmentation modes of the complex. Our results also include the new observation that the electrospray behavior of the inorganic polyanion depends on the nature of the alkali metal counterion and on the polyelectrolyte concentration. Thus, lithium salts at millimolar concentrations were found to be the best choice for the analytical protocol, allowing a fast and unambiguous solution characterization of the polyanion in agreement with the NMR results.

Results and Discussion

Monovacant Keggin-type polyoxotungstates with formula α-$[XW_{11}O_{39}]^{p-}$ (X = P, Si) were readily prepared by stoichiometric acidification of $[WO_4]^{2-}$ in the presence of $[HPO_4]^-$ or $[SiO_3]^{2-}$ (Scheme 1, path a).[26] The defect nature and the purity of the polyoxotungstate formed in solution, obtained as lithium or sodium salt by ion-exchange chromatography, was checked by ^{29}Si, ^{31}P and ^{183}W NMR spectroscopy, this latter analysis giving a clean six-signal spectrum (C_s symmetry) in agreement with literature data.[26]

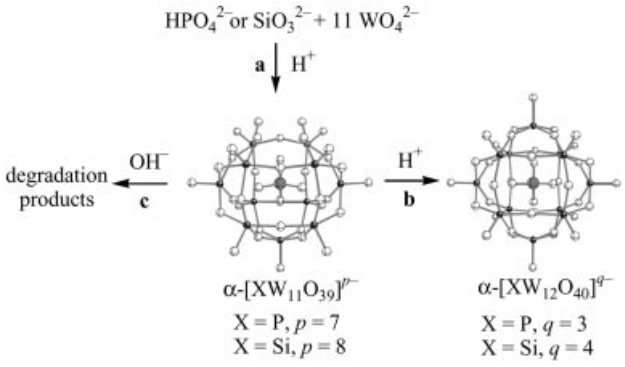

Scheme 1. Synthesis and hydrolytic stability of mono-lacunary α-Keggin polyoxotungstates with formula α-$[XW_{11}O_{39}]^{p-}$ (X = P, Si)

The solution integrity of the lacunary complex is pH-dependent: reconstitution of the T_d-symmetric, complete Keggin structure, α-$[XW_{12}O_{40}]^{q-}$, occurs readily upon further acidification (Scheme 1, path b), while addition of base leads to a progressive degradation of the structure producing lower order aggregates and eventually re-forming the original monomeric reagents (Scheme 1, path c).[1] The pH stability of the analyte is an important parameter to evaluate before the ESI-MS experiments. In fact, the electrospray process of aqueous solutions is known to produce a marked acidity increase in the nebulized droplets formed under ESI positive-ion mode, while, under ESI negative-ion mode, a considerable pH increase is obtained.[27]

Table 1 presents the negative-ion ESI-MS data collected for the lacunary polyoxotungstates α-$[PW_{11}O_{39}]^{7-}$ (Entries 1−5) and α-$[SiW_{11}O_{39}]^{8-}$ (Entries 6, 7), using water/methanol (1:1) as the mobile phase. In the case of α-$[PW_{11}O_{39}]^{7-}$, the electrospray behavior of both the lithium and sodium derivatives has been analyzed under analogous conditions (see Exp. Sect.). Table 1 also includes the results obtained for the reference monomer Li_2WO_4 (Entries 8, 9).

As a general feature, at millimolar concentrations the mass spectrum of the heteropolyanion is dominated by two peaks corresponding to the doubly and triply charged molecular ions (vide infra). Other ionic species, ascribable to an ES-induced decomposition, can be identified as the monocharged ions $[HWO_4]^-$, $[LiW_6O_{19}]^-$ and the analogous $[NaW_6O_{19}]^-$, observed at m/z = 249, 1415, 1431, respectively.

Both the charge state and the molecular composition of all the ions detected in the mass spectra have been assigned through examination of the experimental isotopic cluster distributions. This approach is exemplified in Figure 1 for the doubly and triply charged molecular species derived from $Li_7PW_{11}O_{39}$. In the mass spectrum of the latter (Table 1, Entry 1), the base peak is found at m/z = 1353 and features a double-charge signature with an isotopic separation of ca. 0.50 m/z units (Figure 1, part a), while the other diagnostic ion peak is found at m/z = 900 and displays the isotopic envelope spaced by ca. 0.33 m/z units, i.e. a triple charge (Figure 1, part b). Theoretical simulation of both the observed isotopic patterns allows the assignment the pertinent molecular formula, $[Li_4PW_{11}O_{39}^{3-} + H^+]^{2-}$ and $[Li_3PW_{11}O_{39}^{4-} + H^+]^{3-}$, with the highest peak of the calculated isotopic distributions located at m/z = 1353.00 and 899.67, respectively.

Such results indicate that the lithium salt $Li_7PW_{11}O_{39}$ is a suitable precursor for the ESI-MS analysis of the lacunary polyanion since both Li^+-for-H^+ exchange (cationization) and fragmentation are observed only to a small extent (see Table 1, Entry 1).

A more complicated spectrum is obtained in the case of the sodium salt (Table 1, Entry 4), whose ESI behavior shows a high degree of cationization and the formation of the non-lacunary derivative, indicated by peaks for $[NaPW_{12}O_{40}]^{2-}$ at m/z = 1450 and $[PW_{12}O_{40}]^{3-}$ at m/z = 959 with an overall relative intensity of 14%.

The first point at issue is very well represented in Figure 2, which shows the expanded spectrum of the sodium salt in the m/z range from 1340 to 1410. The simulated isotopic distributions agree with the presence of at least four doubly charged molecular ions whose compositions differ by the number of sodium and/or proton countercations as indicated by the general formula $[Na_xH_yPW_{11}O_{39}]^{2-}$.

The second aspect of the problem is the ESI-induced production of the W_{12}-containing species by inclusion of a formal WO^{4+} unit into the W_{11} precursor. Such a phenomenon may be ascribed to an intrinsic weakness of the vacant

Table 1. Counterion (Li^+, Na^+) and concentration effect on the ESI-MS data collected for lacunary polyoxotungstates α-$[XW_{11}O_{39}]^{p-}$ (X = P, Si) and for the monomeric precursor Li_2WO_4

Entry	Precursor (mM)	Ions m/z[a] (%)	Identification
1	$Li_7PW_{11}O_{39}$ (2)	1353 (100)	$[Li_4HPW_{11}O_{39}]^{2-}$
		900 (55)	$[Li_3HPW_{11}O_{39}]^{3-}$
		1415 (30)	$[LiW_6O_{19}]^-$
		249 (62)	$[HWO_4]^-$
2	$Li_7PW_{11}O_{39}$ (0.2)	1353 (25)	$[Li_4HPW_{11}O_{39}]^{2-}$
		900 (55)	$[Li_3HPW_{11}O_{39}]^{3-}$
		1415 (15)	$[LiW_6O_{19}]^-$
		959 (2)	$[PW_{12}O_{40}]^{3-}$
		249 (100)	$[HWO_4]^-$
3	$Li_7PW_{11}O_{39}$ (0.02)	1353 (5)	$[Li_4HPW_{11}O_{39}]^{2-}$
		900 (15)	$[Li_3HPW_{11}O_{39}]^{3-}$
		1442 (8)	$[LiPW_{12}O_{40}]^{2-}$
		959 (100)	$[PW_{12}O_{40}]^{3-}$
		249 (30)	$[HWO_4]^-$
4	$Na_7PW_{11}O_{39}$ (2)	1352−1396 (53)	$[Na_xH_yPW_{11}O_{39}]^{2-}$ [b]
		923−908 (100)	$[Na_xH_yPW_{11}O_{39}]^{3-}$ [c]
		1431 (42)	$[NaW_6O_{19}]^-$
		1450 (3)	$[NaPW_{12}O_{40}]^{2-}$
		959 (11)	$[PW_{12}O_{40}]^{3-}$
		249 (30)	$[HWO_4]^-$
5	$Na_7PW_{11}O_{39}$ (0.02)	1352−1396 (80)	$[Na_xH_yPW_{11}O_{39}]^{2-}$ [b]
		923−908 (10)	$[Na_xH_yPW_{11}O_{39}]^{3-}$ [c]
		1450 (45)	$[NaPW_{12}O_{40}]^{2-}$
		959 (100)	$[PW_{12}O_{40}]^{3-}$
		249 (32)	$[HWO_4]^-$
6	$Li_8SiW_{11}O_{39}$ (2)	1358 (100)	$[Li_6SiW_{11}O_{39}]^{2-}$
		903 (5)	$[Li_5SiW_{11}O_{39}]^{3-}$
		1444 (5)	$[Li_2SiW_{12}O_{40}]^{2-}$
		960 (25)	$[LiSiW_{12}O_{40}]^{3-}$
		1415 (25)	$[LiW_6O_{19}]^-$
7	$Na_8SiW_{11}O_{39}$ (2)[d]	1396 (40)	$[Na_5HSiW_{11}O_{39}]^{2-}$
		1407 (40)	$[Na_6SiW_{11}O_{39}]^{2-}$
		930 (100)	$[Na_5SiW_{11}O_{39}]^{3-}$
		1460 (30)	$[Na_2SiW_{12}O_{40}]^{2-}$
		958 (50)	$[HSiW_{12}O_{40}]^{3-}$
		966 (20)	$[NaSiW_{12}O_{40}]^{3-}$
		1431 (n.d)[d]	$[NaW_6O_{19}]^-$
8	Li_2WO_4 (2)	249 (100)	$[HWO_4]^-$
9	Li_2WO_4 (0.02)	249 (50)	$[HWO_4]^-$
		704 (100)	$[W_6O_{19}]^{2-}$
		1409(40)	$[HW_6O_{19}]^-$

[a] m/z values refer to the highest peak of the ion clusters. [b] % includes contribution of $[Na_5PW_{11}O_{39}]^{2-}$ (m/z = 1396), $[Na_4HPW_{11}O_{39}]^{2-}$ (m/z = 1385), $[Na_2H_3PW_{11}O_{39}]^{2-}$ (m/z = 1363), $[NaH_4PW_{11}O_{39}]^{2-}$ (m/z = 1352), see Figure 2. [c] % includes contribution of $[Na_4PW_{11}O_{39}]^{3-}$ (m/z = 923), $[Na_3HPW_{11}O_{39}]^{3-}$ (m/z = 916) and $[Na_2H_2PW_{11}O_{39}]^{3-}$ (m/z = 908). [d] Ions ascribable to potassium-containing species were also observed: $[Na_xK_ySiW_{11}O_{39}]^{2-}$ (m/z = 1415−1447) and $[NaK_4SiW_{11}O_{39}]^{3-}$ (m/z = 952).

polyoxometalate structure as its sodium salt. The importance of the nature of the countercation in determining the solution behavior of polyoxometalates in terms of their stability, spectroscopic response, selectivity of reactions and reaction rates has been documented in several literature reports.[26,28−31] In particular, the lithium form of the lacunary tungstophosphate anion has been indicated as the precursor of choice for high temperature hydrothermal synthesis due to its peculiar stability.[32,33] The ESI-MS results support this latter observation.

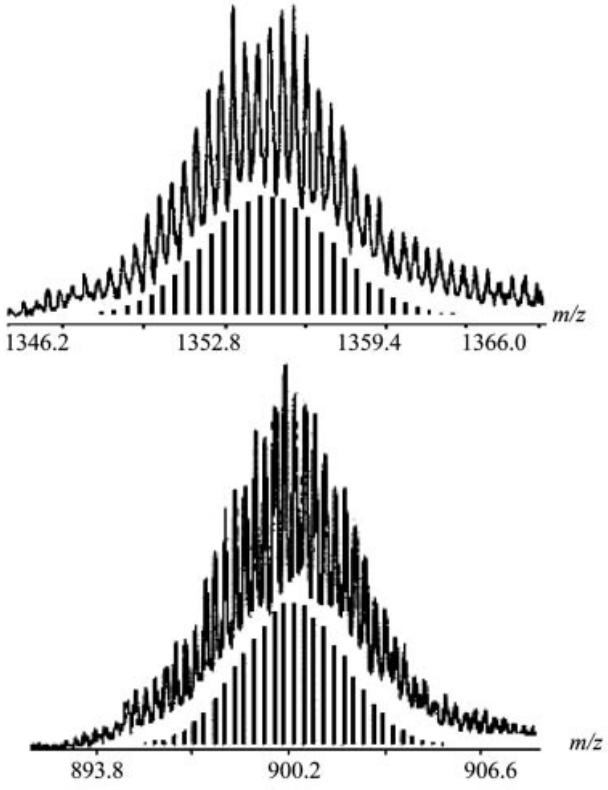

Figure 1. Experimental and calculated isotopic distribution for ion $[Li_4HPW_{11}O_{39}]^{2-}$ (m/z = 1353) and ion $[Li_3HPW_{11}O_{39}]^{3-}$ (m/z = 900)

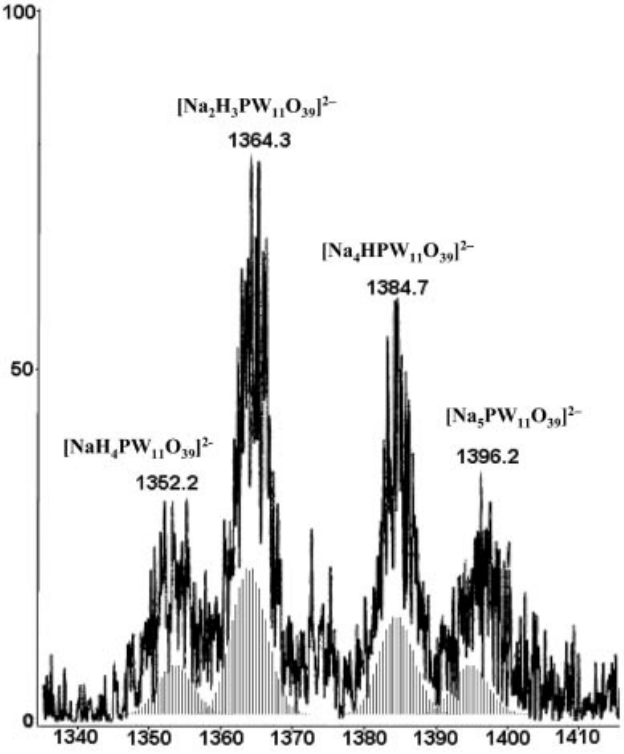

Figure 2. Experimental and calculated isotopic distributions of ions with general formula $[Na_xH_yPW_{11}O_{39}]^{2-}$ (m/z = 1352−1396)

In the negative-ion mode ESI-MS spectrum of the undecatungstosilicate species α-$[Li_8SiW_{11}O_{39}]$ (Table 1, Entry 6), the quasi-molecular ion peaks ($[Li_6SiW_{11}O_{39}]^{2-}$ at m/z = 1358 and $[Li_5SiW_{11}O_{39}]^{3-}$ at m/z = 903) are observed together with a 30% total intensity of the W_{12} anion ($[Li_2SiW_{12}O_{40}]^{2-}$ at m/z = 1444 and $[LiSiW_{12}O_{40}]^{3-}$ at m/z = 960). This evidence is consistent with the limited pH stability range registered in aqueous solution for this lacunary species.[1] The sodium salt (Table 1, Entry 7) again shows a more complicated spectrum.

The Collision Induced Dissociation (CID) of both saturated and lacunary derivatives has been analyzed for tungstophosphate anions as their lithium salts. MS/MS experiments performed on the doubly and triply charged precursors show the multiple loss of WO_3 fragments and oxygen atoms to yield di- or trivacant structures (W_{10}- or W_9-containing anions, respectively; Table 2). This behavior is known to dominate the gas-phase fragmentation of polyoxotungstates as generally observed under FAB-MS conditions.[21–24] As expected, due to the stability of the saturated complex, MS/MS experiments on the W_{12} species require high CID energy conditions of up to 3 V.

In order to optimize the ESI-MS protocol for these highly charged inorganic complexes, the spectra were recorded at different analyte concentrations (Table 1). Surprisingly, the spray of dilute solutions (initial polyanion concentration $\leq 10^{-5}$ M) yields different mass spectra. In particular, starting with the vacant W_{11} polyanion as its lithium or sodium salt (Table 1, Entries 3, 5), the peak corresponding to the saturated W_{12} anion becomes the dominant one. These results are in contrast to the NMR characterization of the species and with the ESI results achieved at higher concentrations. This ESI-MS behavior can be conveniently monitored by progressive dilution of the initially sprayed POM solution ($[Li_7PW_{11}O_{39}]_0 = 2 \times 10^{-3}$ M) with the mobile phase. The spectra recorded at different time intervals (Figure 3) show the evolution of the original W_{11} anion (ion peaks at m/z = 900 and 1353) to the W_{12} species (ion peaks at m/z = 959 and 1442).

The origin of the phenomenon can be discussed on the basis of the following control experiments: (i) the spray of an equimolar solution (2×10^{-3} M) of Li_2WO_4 and $Li_7PW_{11}O_{39}$ yields peaks ascribable only to the two reagents, with no trace of the W_{12} anion, thus indicating that no solution reaction is taking place under the conditions adopted; (ii) when these two ions are isolated within the instrument ion-trap, no gas-phase reaction is again observed; (iii) an aggregation process is also detected when sub-millimolar Li_2WO_4 solutions are sprayed (Table 1, Entries 8, 9), producing the hexatungstate complex, revealed as its dianion $[W_6O_{19}]^{2-}$ at m/z = 704 or in its monoprotonated form at m/z = 1409. This latter result is of particular interest in the study of the nucleation of polyoxometalate structures.

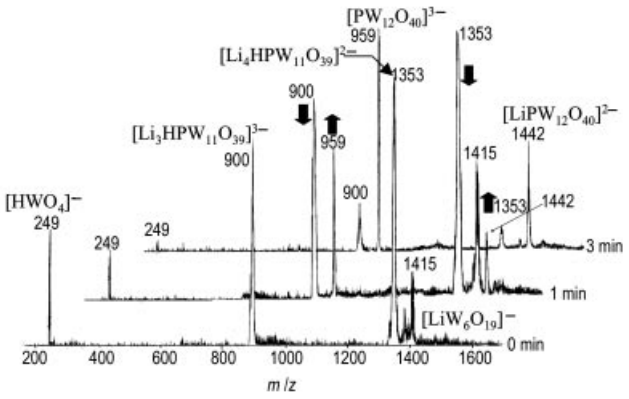

Figure 3. Evolution of the ESI-MS spectrum with time collected for α-$[Li_7PW_{11}O_{39}]$ (initial concentration of 2×10^{-3} M) upon progressive dilution

Considering the ESI process and the generation of POM-based gas-phase ions, the observed changes of ion charge and structure can be ascribed to the relief of coulombic stress as solvent is removed upon the transfer of the ions from the charged droplets to the gas phase.[27]

This might well be the driving force for the ESI-induced polyoxometalate aggregation in the incipient gas phase, producing species with lower charge or with a reduced charge density. However, the opportunity to detect structural rearrangement of the charged analytes should be related both to the composition and to the time of residency of the species within the charged droplets generated by the ESI process. It is then conceivable that at particularly high polyelectrolyte concentration the rapid droplet fission allows the minimization and eventual suppression of any side reactions.[34]

As the reconstitution of the W_{12} structure occurs very efficiently for the undecatungstate complex sprayed at sub-millimolar concentration, a set of experiments was designed to detect the inclusion of a hetero-transition metal based MO^{n+} unit within the lacunary site, under analogous ESI-

Table 2. MS/MS fragment ions of precursor ions **I** originating from lithium salts of mono-lacunary (W_{11}) and saturated (W_{12}) polyoxotungstophospate anions under ESI-MS conditions

I (m/z)[a]	Fragment ions (m/z)[a]	Lost fragments
$[Li_4HPW_{11}O_{39}]^{2-}$ (1353)	$[Li_3PW_{10}O_{35}]^{2-}$ (1225)	**I** − WO_3 − LiOH
$[Li_3HPW_{11}O_{39}]^{3-}$(900)	$[Li_3PW_{10}O_{35}]^{2-}$ (1225), $[Li_2HPW_9O_{32}]^{2-}$ (1106)	**I** − WO_3 − OH, **I** − 2 WO_3 − OLi
$[LiPW_{12}O_{40}]^{2-}$ (1442)	$[W_{11}O_{34}]^{2-}$ (1283), $[PW_{12}O_{40}]^{3-}$ (959)	**I** − PWO_6 − Li, **I** − Li
$[PW_{12}O_{40}]^{3-}$ (959)	$[PW_9O_{26}]^{3-}$ (701)[b]	**I** − 3 WO_3 − 5 O

[a] m/z values refer to the highest peak of the ion clusters. [b] Assigned according to the literature.[19]

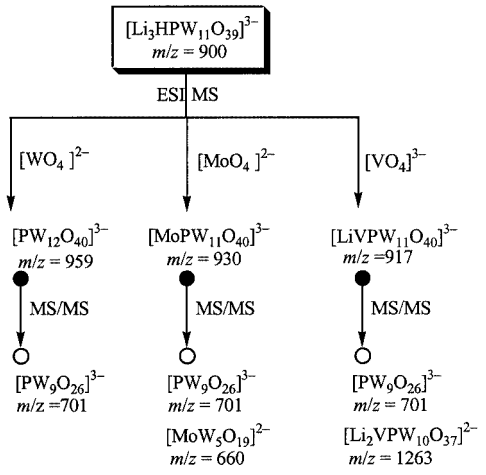

Scheme 2. Formation of the triply charged ions (*m*/*z*) in the ESI-MS spectrum of α-$[Li_7PW_{11}O_{39}]$ collected at sub-millimolar concentration (10^{-5} M) in the presence of stoichiometric $[MoO_4]^{2-}$ or $[VO_4]^{3-}$, showing the evolution to a dodecametalate structure as confirmed also by tandem MS/MS experiments

MS conditions (Scheme 2). To this aim, a solution of $Li_7PW_{11}O_{39}$ (10^{-5} M) was sprayed in the presence of equimolar amounts of molybdate and vanadate anions. Inspection of the triply charged *m*/*z* region (Scheme 2) gives a clear indication that the monosubstituted Keggin species forms by incorporation of either an Mo^{VI} or a V^{V} atom within the polyoxotungstate structure, yielding ion peaks at *m*/*z* = 930 ($[MoPW_{11}O_{40}]^{3-}$) and 917 ($[LiVPW_{11}O_{40}]^{3-}$).[35] This process competes, however, with the production of the dodecatungstate anion, by far the main process emerging in all the recorded spectra, where the ion peak at *m*/*z* = 959 appears always as the most intense one.[35] MS/MS experiments performed on the resulting $[Li_nMPW_{11}O_{40}]^{3-}$ (M = V^{V}, Mo^{VI}; *n* = 0, 1) anions yield fragments that are consistent with the expected Keggin structure (the peak at *m*/*z* = 701, identified as $[PW_9O_{26}]^{3-}$, is common to all the three dodecametallate structures)[19] and monosubstitution with the hetero-transition metal (see the lacunary fragments incorporating vanadium or molybdenum in Scheme 2).

The ESI-induced metalation of the lacunary undecatungstate establishes a new route to the gas-phase detection of the Mo and V monosubstituted species whose hydrolytic instability hampers the synthetic protocol.[36,37] As a matter of fact, the direct hydrothermal metalation (H_2O, 150 °C) of the lacunary precursor (2×10^{-3} M) in the presence of stoichiometric amounts of tungstate, molybdate or vanadate anions, in the first two cases does not lead to products, while in the latter case the disubstituted complex is formed. This conclusion has been reached by ESI-MS analysis of the reaction mixtures, showing, for the vanadium-containing system, the replacement of the reagent signals with two new ion peaks at *m*/*z* = 873 and 1313, attributed to $[LiHPV_2W_{10}O_{40}]^{3-}$ and $[Li_2HPV_2W_{10}O_{40}]^{2-}$, respectively.[38]

Conclusion

This study highlights the use of ESI-MS to address the solution structure of polyoxometalates. The results collected delineate a precise protocol for the straightforward characterization of highly charged mono-vacant undecatungsto complexes, thus providing a convenient alternative to heteronuclear NMR spectroscopy. Although extreme care is required to correlate the ESI-MS data with the content of the original solution, it has been shown that the ESI technique allows the isolation of discrete ion-paired structures whose stoichiometry, composition and gas-phase reactivity can be readily defined. Both the role of the counterion on the gas-phase transfer of polyoxometalate-based ion-pairs and the effect of the polyelectrolyte concentration in promoting an ESI-induced aggregation process are fundamental aspects that need further clarification.

Experimental Section

Materials: Monovacant Keggin-type polyoxotungstates with formula α-$[XW_{11}O_{39}]^{p-}$ (X = P, Si) were prepared by literature procedures[26] and characterized in solution by heteronuclear NMR spectroscopy as follows: **α-$[Li_7PW_{11}O_{39}]$:** ^{31}P NMR (162.00 MHz, D_2O, H_3PO_4 85%): δ = −11.2 ppm. ^{183}W NMR (16.67 MHz, H_2O, Na_2WO_4): δ = −98.0 (2 W), −98.6 (2 W), −103.3 (2 W), −121.0 (1 W), −132.0 (2 W) −151.8 (2 W) ppm. **α-$[Na_7PW_{11}O_{39}]$:** ^{183}W NMR (16.67 MHz, H_2O, Na_2WO_4): δ = −99.0 (2 W), −103.9 (2 W), −110.7 (2 W), −118.6 (1 W), −134.0 (2 W) −154.8 (2 W) ppm. **α-$[Na_8SiW_{11}O_{39}]$:** ^{29}Si NMR (79.50 MHz, D_2O, TMS): δ = −84.5 ppm. ^{183}W NMR (16.67 MHz, H_2O, Na_2WO_4): δ = −100.9 (2 W), −116.4 (2 W), −121.5 (1 W), −128.4 (2 W), −143.2 (2 W) −176.5 (2 W) ppm. **α-$[Li_8SiW_{11}O_{39}]$:** ^{183}W NMR (16.67 MHz, H_2O, Na_2WO_4): δ = −106.7 (2 W), −108.7 (2 W), −122.0 (2 W), −123.1 (1 W) −144.9 (2 W) −175.1 (2 W) ppm. All other reagents were obtained from commercial sources and used as received. HPLC grade solvents were generally used. Cation-exchange chromatography was performed on Amberlite IR 120 resin.

Methods: NMR spectra were obtained with a Bruker Avance DRX 400 instrument, equipped with a standard (^{31}P-^{109}Ag) 10-mm broadband probe which could be tuned below its specifications. Hydrothermal syntheses were performed in a closed reactor (HPR-1000/10S, Milestone) equipped with temperature and pressure control units and irradiated inside the cavity of an MW Ethos-1600 labstation (Milestone). ESI-MS full-scan mass spectra were performed with a Mariner Time-of-Flight Mass Spectrometer (Perspective Biosystem) and with a Finnigan LCQ instrument, obtaining comparable results. The *m*/*z* values refer to the highest peak of the ion clusters. All experiments were performed in negative mode by direct infusion with a syringe pump. Standard experimental conditions given for the LCQ instrument were as follows: sample concentration (10^{-3} to 10^{-5} M), mobile phase (H_2O/CH_3OH, 1:1) flow rate 8 μL min^{-1}, nebulizing gas N_2: 40 units flow rate, spray voltage −4.00 kV, capillary voltage −25 V, capillary temperature 150 °C, tube lenses offset, 30 V. The parameters related to octupoles and detector were those achieved by the automatic setup procedure. The tuning of the spray parameters i.e. flow rate (3−13 μL min^{-1}), nebulizing gas (20−70 units flow rate), negative spray voltage (2−4.50 kV), negative capillary voltage (3−28 V) and capillary temperature (70−160 °C) was investigated and did not

affect the spectra. The collision-induced decomposition of selected ions was obtained by applying a supplementary radio frequency voltage (tickling voltage) to the end-cap electrodes of the ion-trap in Finnigan LCQ instrument (resonance activation).

Hydrothermal Synthesis: α-$[Li_7PW_{11}O_{39}]$ (60 μmol) was dissolved in water (30 mL). The solution was then divided into three portions (10 mL each), in the presence of a stoichiometric amount of Li_2WO_4 (reaction 1), Na_2MoO_4 (reaction 2) or Na_3VO_4 (reaction 3). The reaction mixtures were then placed in three closed units of the multi-section microwave reactor system (HPR-1000/10S) inside the Microwave labstation and irradiated (ν = 2.45 GHz) according to the following parameters: initial power 300 W; initial time 4 min; $T_{max.}$ = 150 °C, final power 150 W, reaction time 5 min. ESI-MS analysis was used to monitor the reaction outcome. Reaction 1: MS (ESI-LCQ): *m/z* (%) = 249 (90) $[HWO_4]^-$, 900 (53) $[Li_3HPW_{11}O_{39}]^{3-}$, 1353 (100) $[Li_4HPW_{11}O_{39}]^{2-}$, 1415 (50) $[LiW_6O_{19}]^-$. Reaction 2: MS (ESI-LCQ): *m/z* (%) = 163 (100) $[HMoO_4]^-$, 249 (75) $[HWO_4]^-$, 900 (48) $[Li_3HPW_{11}O_{39}]^{3-}$, 1353 (70) $[Li_4HPW_{11}O_{39}]^{2-}$, 1415 (40) $[LiW_6O_{19}]^-$. Reaction 3: MS (ESI-LCQ): *m/z* (%) = 249 (100) $[HWO_4]^-$, 873 (45) $[LiHPV_2W_{10}O_{40}]^{3-}$, 959 (15) $[PW_{12}O_{40}]^{3-}$, 1313 (50) $[Li_2HPV_2W_{10}O_{40}]^{2-}$, 1324 (48) $[NaLi_2PV_2W_{10}O_{40}]^{2-}$, 1415 (10) $[LiW_6O_{19}]^-$.

Acknowledgments

We thank Prof. A. Bagno for valuable help in heteronuclear NMR characterization of polyoxotungstates. Technical assistance from "Servizio di Spettrometria di Massa del CNR, Area di Ricerca, Padova" is also gratefully acknowledged. CNR and MURST are acknowledged for financial support.

[1] M. T. Pope, *Heteropoly and Isopoly Oxometalates*, Springer, New York, NY, **1983**, vol. 1.
[2] *Polyoxometalates: From Platonic Solids to Anti Retroviral Activity* (Eds.: M. T. Pope, A. Müller), Kluwer, Dordrecht, **1994**.
[3] Polyoxometalates: *Chem. Rev.* **1998**, *98*, 1−390 (Ed.: C. L. Hill).
[4] M. T. Pope, A. Müller, *Angew. Chem.* **1991**, *103*, 56−70; *Angew. Chem. Int. Ed. Engl.* **1991**, *30*, 34−48.
[5] C. L. Hill, C. M. Prosser-McCartha, *Coord. Chem. Rev.* **1995**, *143*, 407−455.
[6] A. Muller, P. Kogerler, *Coord. Chem. Rev.* **1999**, *182*, 3−17.
[7] A. Muller, P. Kogerler, C. Kuhlmann, *Chem. Commun.* **1999**, 1347−1358.
[8] P. Gouzerh, A. Proust, *Chem. Rev.* **1998**, *98*, 77−111.
[9] P. Gouzerh, R. Villanneau, R. Delmont, A. Proust, *Chem. Eur. J.* **2000**, *6*, 1184−1192.
[10] C. R. Mayer, I. Fournier, R. Thouvenot, *Chem. Eur. J.* **2000**, *6*, 105−110.
[11] G. S. Kim, H. Zeng, D. VanDerveer, C. L. Hill, *Angew. Chem.* **1999**, *111*, 3413−3416; *Angew. Chem. Int. Ed. Eng.* **1999**, *38*, 3205−3207.
[12] N. Belai, M. Sadakane, M. T. Pope, *J. Am. Chem. Soc.* **2001**, *123*, 2087−2088.
[13] A. Bagno, M. Bonchio, *Chem. Phys. Lett.* **2000**, *317*, 123−128.
[14] A. Bagno, M. Bonchio, *Eur. J. Inorg. Chem.* **2002**, 1475−1483.
[15] M. Bonchio, G. Licini, G. Modena, S. Moro, O. Bortolini, P. Traldi, W. A. Nugent, *Chem. Commun.* **1997**, 869−870.
[16] M. Bonchio, G. Licini, G. Modena, O. Bortolini, S. Moro, W. A. Nugent, *J. Am. Chem. Soc.* **1999**, *121*, 6258−6268.
[17] O. Bortolini, V. Conte, F. Di Furia, S. Moro, *Eur. J. Inorg. Chem.* **1998**, 1193−1197.
[18] J. Le Quan Tuoi, E. Muller, *Rapid Commun. Mass Spectrom.* **1994**, *8*, 692−694.
[19] T. Lau, J. Wang, R. Guevremont, K. W. M. Siu, *J. Chem. Soc., Chem. Commun.* **1995**, 877−878.
[20] M. J. Deery, O. W. Howarth, K. R. Jennings, *J. Chem. Soc., Dalton Trans.* **1997**, 4783−4788.
[21] R. G. Finke, M. W. Droege, J. C. Cook, K. S. Suslick, *J. Am. Chem. Soc.* **1984**, *106*, 5750−5751.
[22] K. S. Suslick, J. C. Cook, B. Rapko, M. W. Droege, R. G. Finke, *Inorg. Chem.* **1986**, *25*, 241−243.
[23] S. H. Wasfi, C. E. Costello, A. L. Rheingold, B. S. Haggerty, *Inorg. Chem.* **1991**, *30*, 1788−1792.
[24] A. Trovarelli, R. G. Finke, *Inorg. Chem.* **1993**, *32*, 6034−6039.
[25] *Mass spectrometry/Mass spectrometry: Techniques and Applications of Tandem Mass Spectrometry* (Eds.: K. L. Busch, G. L. Glish, S. A. McLuckey), VCH, New York, **1988**.
[26] C. Brévard, R. Schimpf, G. Tourné, C. M. Tourné, *J. Am. Chem. Soc.* **1983**, *105*, 7059−7063.
[27] *Electrospray Ionization Mass Spectrometry: Fundamentals, Instrumentation and Applications* (Eds: R. B. Cole), J. Wiley & Sons, Inc., New York, **1997**.
[28] J. F. Kirby, L. C. W. Baker, *Inorg. Chem.* **1998**, *37*, 5537−5543 and references therein.
[29] I. A. Weinstock, *Chem. Rev.* **1998**, *98*, 113−170.
[30] K-Chan Kim, M. T. Pope, *J. Am. Chem. Soc.* **1999**, *121*, 8512−8517.
[31] V. A. Grigoriev, C. L. Hill, I. A. Weinstock, *J. Am. Chem. Soc.* **2000**, *122*, 3544−3545.
[32] X. Wei, R. E. Bachman, M. T. Pope, *J. Am. Chem. Soc.* **1998**, *120*, 10248−10253.
[33] A. Bagno, M. Bonchio, A. Sartorel, G. Scorrano, *Eur. J. Inorg. Chem.* **2000**, 17−20.
[34] Tuning of the spray parameters, in the range indicated, did not affect the spectra: flow rate (3−13 μL min^{-1}), nebulizing gas (20−70 units flow rate), negative spray voltage (2−4.50 kV), negative capillary voltage (3−28 V), capillary temperature (70−160 °C).
[35] Doubly charged ions relative to monosubstituted polyoxotungstates were also revealed for molybdenum at *m/z* = 1399 ($[LiMoPW_{11}O_{40}]^{2-}$) and for vanadium at *m/z* = 1379 ($[Li_2VPW_{11}O_{40}]^{2-}$). Incorporation of vanadium was also confirmed by detection of an ion peak at *m/z* = 686 attributed to $[VPW_{11}O_{40}]^{4-}$. In all spectra the base peak was found at *m/z* = 959 $[PW_{12}O_{40}]^{3-}$.
[36] [36a] D. P. Smith, M. T. Pope, *Inorg. Chem.* **1973**, *12*, 331−336. [36b] J. J. Altenau, M. T. Pope, *Inorg. Chem.* **1975**, *14*, 417−421.
[37] P. J. Domaille, *J. Am. Chem. Soc.* **1984**, *106*, 7677−7687.
[38] The hydrolytic instability of the mono-substituted species $[PVW_{10}O_{40}]^{4-}$ gradually converting in solution into the disubstituted anion $[PV_2W_{10}O_{40}]^{5-}$ has been reported.[36]

Received July 2, 2002
[I02361]

Synthesis and Structure of Redox-Active Heterotetranuclear Molecular Polygons by Self-Assembly of Two Ferrocene-Bridged Bis(pyridines) with Two Transition Metals[‡]

Ekkehard Lindner,*[a] Ruifa Zong,[a] Klaus Eichele,[a] Ulrike Weisser,[a] and Markus Ströbele[a]

Keywords: Self-assembly / Nanostructures / Metal-metal interactions / N ligands / Nickel / Silver / Palladium

The macrocyclic complexes $[(\eta^5\text{-}C_5H_4C_2\text{-}4\text{-}py)_2Fe]_2Ni_2(NO_3)_4$ (**2**), $[(\eta^5\text{-}C_5H_4C_2\text{-}3\text{-}py)_2Fe]_2Ag_2(ClO_4)_2$ (**4**), and $[(\eta^5\text{-}C_5H_4C_2\text{-}3\text{-}py)_2Fe]_2Pd_2Cl_4$ (**5**) were obtained by reaction of $[Ni(H_2O)_6](NO_3)_2$, $AgClO_4$, and $PdCl_2(COD)$ with the ligands $(\eta^5\text{-}C_5H_4C_2\text{-}4\text{-}py)_2Fe$ (**1**) and $(\eta^5\text{-}C_5H_4C_2\text{-}3\text{-}py)_2Fe$ (**3**), respectively, under high dilution conditions (Scheme 1). The molecular motifs of **2**, **4**, and **5** were studied by single-crystal X-ray structural investigations. Elemental analyses and ^1H NMR and IR spectra were also used to confirm the structures. Compound **2** represents an unsymmetric paddlewheel, in which the centers of the four Cp rings define a nearly ideal rectangle with dimensions of 20.2 × 3.3 Å. In principle, macrocycles **4** and **5** can also be described as rectangles, however, due to the 3-positioned nitrogen donors with deformed edges (17.4 × 3.3 Å for **4**). In contrast to the offset packing of the molecules in **2**, the macrocycles in the crystal of **4** are aligned, with trapped acetonitrile molecules in between. The intra- and intermolecular Ag–Ag distances are 3.50 and 3.79 Å, respectively. Cyclovoltammetric studies reveal chemically reversible ferrocene-based redox reactions of **1**–**4**. Although no electronic communication was observed between the two identical ferrocene units, a weak through-bond electronic interaction between ferrocene and nickel, or silver, was established. In **2** a weak antiferromagnetic interaction between the nickel atoms was also found.

(© Wiley-VCH Verlag GmbH & Co. KGaA, 69451 Weinheim, Germany, 2003)

Introduction

A great number of bis(pyridine)-functionalized ligands with different angles between their binding sites have been rationally designed, synthesized, and treated with transition metal complexes to obtain two-dimensional macrocyclic molecular assemblies, such as molecular squares, triangles, and other polygons.[1,2] With the increasing multitude of motifs self-assembled from these nitrogen-functionalized building blocks, a library of such supramolecular architectures has been set up.[3] Stang and Fujita have made a huge contribution to this field, although they have mainly employed pre-constructed *cis*-ML_2 (M = Pd/Pt) units.[1–4] Both metals are electrochemically and magnetically inert. Hence, it is desirable to make accessible molecular polygons and polyhedra with magnetic and redox-active centers.[1,5] Although 1,1′-bis(diphenylphosphanyl)ferrocene (dppf) has been used to obtain redox-active molecular squares, the *syn*-dppf conformer is not part of the backbone.[1,6] A structurally characterized molecular square containing an *anti*-1,1′-ferrocenedicarboxylate moiety in its backbone was recently reported by Cotton et al.[4,5] Compared to systems assembled from non-ferrocene bridges, its electrochemical properties are rather unusual. The preparation of self-assembled structures that contain functionalized sites capable of showing interesting electronic, magnetic, and optical properties is still a big challenge.[1]

Linked metallocenes, in particular those with extended conjugated spacers, are redox-active and good candidates for the investigation of through-bond electronic communication.[7] Ideal models consist of two or more identical metallocene units as spectators.[7,8] It has been demonstrated that acetylene-bridged ferrocenes show third-order non-linear optical properties.[9] Furthermore, systems incorporating paramagnetic transition metal ions are good candidates for novel molecular-based magnetic materials.[10,11] Dinuclear molecules based on dinickel, dicopper, and dimanganese cores, with different magnetic coupling patterns, have drawn much attention in the last decade.[12–14] Here, we present the synthesis and structure of three redox-active tetranuclear supramolecular rectangles **2**, **4**, and **5**, each bearing two ferrocene subunits and two nickel(II), silver(I), and palladium(II) atoms, respectively, in their backbone.

[‡] Preparation, Properties, and Reactions of Metal-Containing Heterocycles, 109. Part 108: Ref.[17]

[a] Institut für Anorganische Chemie der Unversität Tübingen, Auf der Morgenstelle 18, 72076 Tübingen, Germany
Fax: (internat.) + 49-(0)7071/295306
E-mail: ekkehard.lindner@uni-tuebingen.de

Results and Discussion

Syntheses of the Macrocycles 2, 4, and 5

The macrocyclic motifs **2**, **4**, and **5** were obtained in 92−95% yields by mixing a solution of the nitrogen donor ligands 1,1′-bis(4- and 3-pyridylethynyl)ferrocene **1**[15] and **3**[15] in dichloromethane with a solution of $[Ni(OH_2)_6](NO_3)_2$, $AgClO_4$, or $PdCl_2(COD)$ in methanol, acetonitrile, or dichloromethane, respectively, under high-dilution conditions[16] at room temperature (Scheme 1). Elemental analyses are satisfactory and consistent with their proposed structures. While the red silver compound **4** is at least slightly soluble in polar organic media like acetonitrile, the red nickel complex **2** shows only a very low solubility in methanol and acetonitrile. Macrocycle **5** is insoluble in these solvents, but slightly soluble in dichloromethane and DMF. Complex **2** decomposes in DMF and DMSO.

Crystal Structures of 2, 4, and 5

To obtain detailed information about the structures of the nickel(II)-, silver(I)-, and palladium(II)-containing macrocyclic complexes **2**, **4**, and **5**, X-ray structural investigations were performed. Selected distances and angles are summarized in Tables 1 and 2, respectively, and the corresponding ORTEP plots with atom labeling are depicted in Figures 1 and 2. Both compounds **2** and **4** crystallize in the triclinic space group $P\bar{1}$ and each molecule has a center of symmetry. They crystallize with three CH_2Cl_2 and two CH_3CN solvent molecules, respectively.

Table 1. Selected distances [Å] and angles [°] for **2**·3CH_2Cl_2

Ni1−O1	2.081(2)	Ni1−Ni1A	3.39
Ni1−O1A	2.112(2)	Cp1 (cent.)−Cp2 (cent.)	3.31
Ni1−O4	2.120(2)	Fe1−Fe1A	20.18
Ni1−O5	2.079(2)	Cp1 (cent.)−Cp2A (cent.)	20.24
Ni1−N1	2.058(2)	Fe1−Ni1	10.20
Ni1−N2A	2.058(2)	Fe1−Ni1A	10.25
O2−H41A	2.49	O6−H41B	2.42
O3−H40B	2.55		
N1−Ni1−O1	91.58(9)	N2A−Ni1−O5	89.97(9)
N1−Ni1−O1A	92.42(9)	O1−Ni1−O4	115.06(9)
N1−Ni1−O4	89.37(9)	O1−Ni1−O1A	72.22(9)
N1−Ni1−O5	88.28(9)	O5−Ni1−O4	61.40(10)
N2A−Ni1−O1	90.00(9)	O5−Ni1−O1A	111.33(9)
N2A−Ni1−O1A	90.70(9)	N1−Ni1−N2A	176.81(9)
N2A−Ni1−O4	87.45(9)	Ni1−O1−Ni1A	107.79(9)

Both nickel atoms in **2** are octahedrally coordinated by two nitrogen and four oxygen donor functions, forming a *trans*-N_2O_4 coordination sphere. The two *trans*-located nitrogen atoms are equidistant from the nickel atom (2.05 Å), while the four Ni−O bonds have lengths of between 2.08

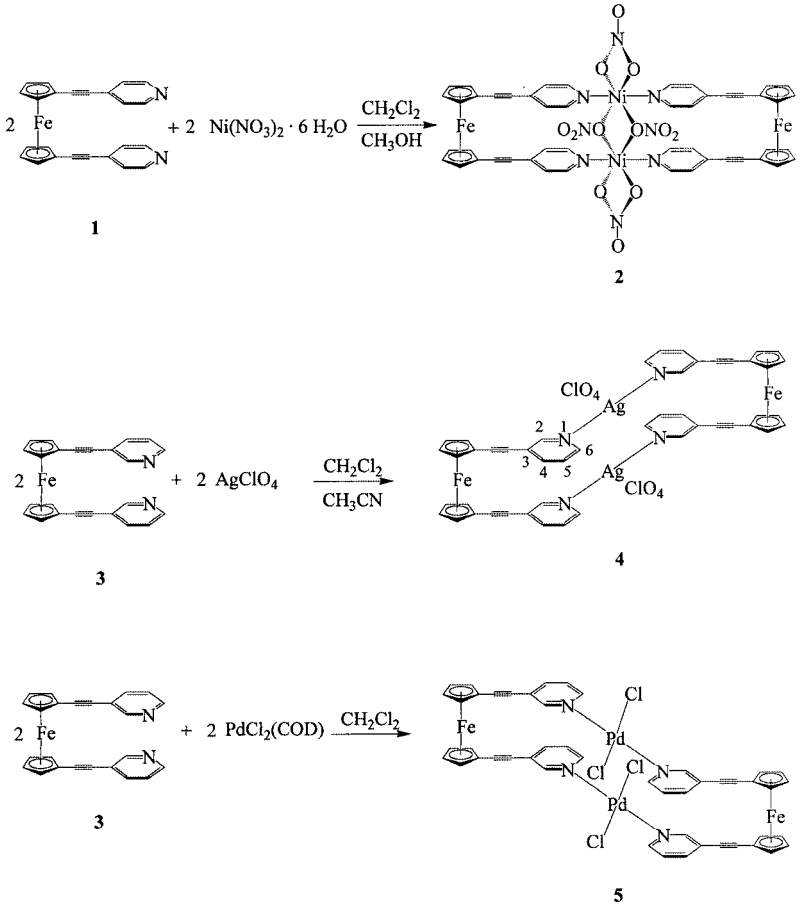

Scheme 1

Table 2. Selected distances [Å] and angles [°] for **4**·2 CH_3CN

Ag1−O1	2.791(2)	Ag1−Ag1A	3.50
Ag1−O1A	3.743(2)	Cp1 (cent.)−Cp2 (cent.)	3.31
Ag1−N1	2.179(2)	Fe1−Fe1A	17.34
Ag1−N2A	2.170(2)	Cp1 (cent.)−Cp2A (cent.)	17.42
Ag1−N3B	2.891(2)	Fe1−Ag1	8.65
Ag1−N3A	2.705(2)	Fe1−Ag1A	9.03
O1−Cl	1.433(2)	Ag1−Ag1 (intermolecular)	3.79
O2−Cl	1.434(2)	O3−Cl	1.434(2)
O4−Cl	1.435(2)		
Cp−py (dihedral)	6.12(4)	py−py (dihedral)	6.17(4)
	13.10(3)	N1−Ag1−N2A	178.1(1)

and 2.12 Å. However, the nickel-centered angles of the octahedron vary between 61 and 115°, indicating a considerably distorted geometry around the nickel atom.

Complex **2** is constructed of a dinickel core with two bridging ligands **1** [μ-η^1:η^1-**1**-*N*,*N*′] and four nitrate counterions. The nitrate ions are coordinated in two different modes to the nickel centers. Two of them function as μ_2-bridging ligands, whereas the other two are η^2-chelated. Within a ligand **1** in complex **2**, the N−N distance of 3.49 Å is significantly shorter than the corresponding average distance of 3.96 Å in the free ligand **1**,[17] in which the repulsion of the nitrogen lone pairs has to be considered.

Concerning the dinickel core, the structure of **2** can be designated as an unsymmetric paddlewheel consisting of the coordinated nitrate ions and two moieties of ligand **1**. The

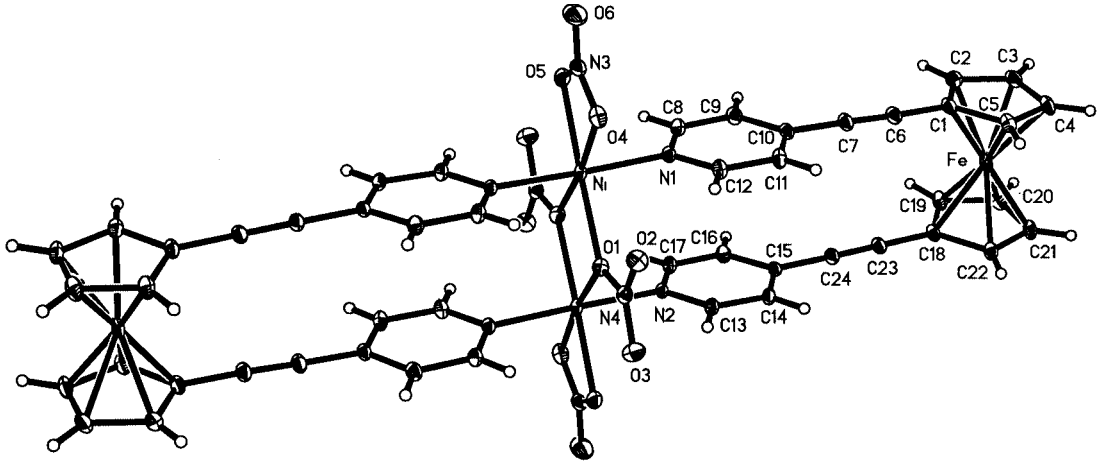

Figure 1. Molecular structure of **2**; ORTEP plot with thermal ellipsoids at 20% probability; solvent molecules are omitted for clarity; for bond lengths and angles see Table 1

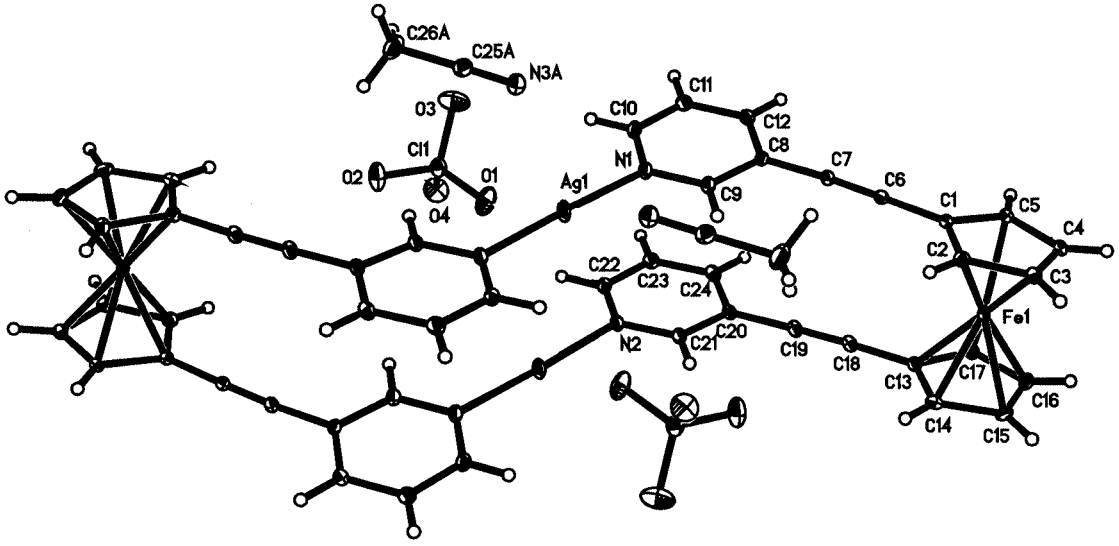

Figure 2. Molecular structure of **4**; ORTEP plot with thermal ellipsoids at 20% probability; for bond lengths and angles see Table 2

whole structure has the shape of a molecular rectangle in which the four Cp rings occupy the vertices, whereas the four metal atoms are located in the middle of the edges. The lengths of the edges are 3.31 and 20.24 Å, calculated from the center points of the cyclopentadienyl rings. Both nickel and iron atoms are separated by a distance of 3.39 and 20.18 Å, respectively. In this molecule the four metal atoms lie in a plane, creating almost a regular rhombus with lengths of 10.20 (Fe−Ni) and 10.25 Å (Fe−NiA) and angles of 19° (Ni−Fe−NiA) and 161° (Fe−Ni−FeA). One of the most important structural features of **2** is the coplanarity of the entire inorganic entity (nickel atoms and all four nitrates). The ferrocene units are positioned above and below this plane. In the solid state, molecules of **2** are offset positioned and separated by two crystallographically different kinds of dichloromethane molecules (Figure 3). Dichloromethane molecules of each kind are oriented head-to-head. Weak contacts (shown by dotted lines in Figure 3) between the solvent molecules and the macrocycles are found, as indicated by the non-bonding distances of 2.42, 2.49, and 2.55 Å for H(41B)−O(2), H(41A)−O(6), and H(40B)−O(3), respectively.

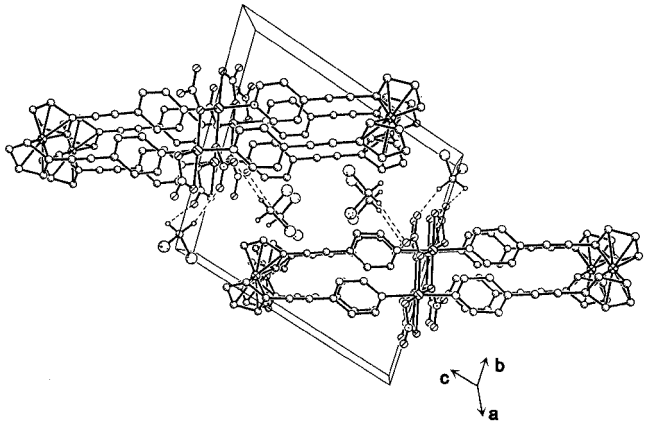

Figure 3. Molecular packing of **2** showing the head-to-head orientation of dichloromethane molecules, the offset arrangement of **2**, and the weak H···O contacts (dotted lines); aromatic protons are omitted for clarity

Due to the 3-position of the nitrogen donors in ligand **3**, the structure of the cation in **4** is somewhat different from that of **2**. The former forms a distorted rectangle defined by the central points of the four cyclopentadienyl rings (Figure 2). If a connecting line is drawn between these points, one pyridine ring is located in front of and the other one behind this line. The dimensions of the rectangle are 17.42 × 3.31 Å. All four transition metals (two silver and two iron atoms) lie in a plane and the Fe−Fe and Ag−Ag distances are 17.34 and 3.50 Å, respectively. The heteroatom distances (Ag−Fe) are 8.65 and 9.03 Å. Similar to complex **2**, the silver atom in **4** is nearly equidistant from the two coordinated pyridine N atoms [2.170(2) and 2.179(2) Å]. Only a slight deviation from a linear N−Ag−N arrangement is observed (178.1°). The two CpC_2py arms on each side of the macrocycle are not oriented exactly parallel, deviations with respect to Cp/py and py/py are 6.1/13.1 and 6.2°, respectively.

In the crystals of **4** (Figure 4), both perchlorate anions are positioned on opposite sides of the rectangular plane, but are not coordinated to silver(I). The macrocycles of **4** are layered and acetonitrile is located between these rectangular molecules. The molecules of **4** are held together along the *a* axis by interactions between the bifurcated acetonitrile molecules and the macrocycles as indicated by the remarkably short Ag−N distances of 2.705(2) and 2.891(2) Å compared to the corresponding sum of the van der Waals radii. The inter- (Ag_2N_2) and intramolecular (Ag_2O_2) planes deviate by an angle of 17.5°. Contrary to the offset packing of macrocycle **2**, the cationic macrocycle **4** is aligned along the *a* axis with intra- and intermolecular Ag−Ag distances of 3.50 and 3.79 Å, respectively.

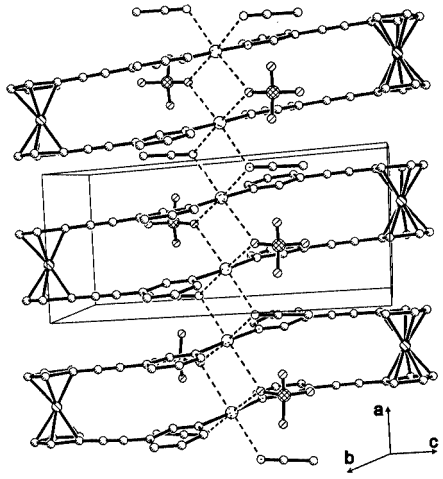

Figure 4. Molecular packing of **4** along the *a* axis presenting the parallel alignment of the silver ions and the other components as well as the weak Ag···O and Ag···N contacts (dotted lines); protons are omitted for clarity

Due to the low quality of the crystal of **5**, only a brief description is given.[18,19] The molecular structure of **5** is similar to that of **4**, and also has a center of symmetry. Each palladium atom is additionally coordinated by two *trans*-positioned chloride ions with $PdCl_2$ units about 45° to the pyridine rings.

^{1}H NMR and IR Spectroscopic Characterization of the Macrocycles 2, 4, and 5

Because of the low solubility only ^{1}H NMR spectra of the macrocycles **4** and **5** could be recorded; the nickel(II) complex **2** is paramagnetic. Upon complexation of ligand **3** to silver(I) (**4**) and palladium(II) (**5**) a slight downfield shift of the pyridine proton signals is observed. While only the resonance at δ = 7.05 ppm, which is assigned to 5-H of the pyridine ring in **3** (numbering scheme is given in Scheme 1), is markedly downfield shifted to δ = 7.20 ppm in the disilver complex **4**, all other protons of this entity remain unchanged. In the ^{1}H NMR spectrum of **5** the protons (2-H and 6-H) adjacent to the nitrogen atom give rise to a re-

markable downfield shift of 0.18 and 0.31 ppm, respectively. On the other hand, notable upfield shifts of 0.27 and 0.31 ppm are observed for 4-H and 5-H. The AA′XX′ pattern for the cyclopentadienyl rings in the spectra of **4** and **5** remains unchanged.

In the FT-IR spectra of **2**, **4**, and **5** the absorptions for the C=N and C≡C stretching vibrations are shifted (12−16 and 2−5 cm^{-1}, respectively) to somewhat higher wavenumbers relative to the free ligands **1** and **3**. This is consistent with the coordination of transition metals to nitrogen. Intense bands at 1289/1218 and 1095/1050 cm^{-1} are assigned to the stretching vibrations of the nitrate and perchlorate anions, respectively.

Electrochemical Investigation of 1−4

The redox properties of compounds **1**−**4** were investigated in acetonitrile; cyclic voltammetric data are listed in Table 3. The low solubility of the palladium complex **5** prevents any studies of its electrochemical behavior. Although the ferrocene-based redox reactions of **1**−**4** are chemically reversible in each case, their electrochemistry is somewhat different. While ligand **3** shows a diffusion-controlled one-electron transfer reaction, the response of ligand **1** is diffusion-controlled and dependent on the rate of electron transfer. Isomeric ligands **1** and **3** show different redox potentials, at 318 and 283 mV relative to that of ferrocene/ferrocenium, respectively. They are more difficult to oxidize than the unsubstituted parent ferrocene, which is due to the electron-withdrawing nature of the substituents on the Cp rings. However, the difference of 35 mV between **1** and **3** indicates the influence of the charge distribution on the transfer of this effect. Although both ferrocene subunits of complex **2** are oxidized at the same potential, it reveals a 32 mV positive shift relative to ligand **1**. This finding demonstrates a successful electron transfer from ferrocene to the nickel atoms, but no communication between the two ferrocene units.

Table 3. Cyclic voltammetric responses of compounds **1**−**4** in acetonitrile

Compound	$E_{1/2}$ [mV]	ΔE [mV]	i_{pa}/i_{pc}
Ferrocene	0	69	1.00
1	318	63	0.99
2	350	60	1.16[a]
3	283	71	0.96
4	273	70	1.04

[a] A background correction was not carried out because of the adsorption nature of this complex.

Compared to ligand **3** a negative shift of 10 mV was established for the disilver complex **4**. This effect is usually not expected and is probably due to the weak σ-electron acceptor and strong π-donor capabilities of silver(I).[20] As a result of this back bonding and/or the charge distribution

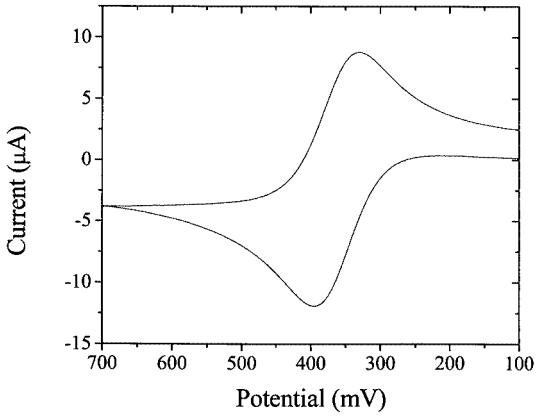

Figure 5. Cyclic voltammogram of **4** in acetonitrile/0.1 M tetrabutylammonium hexafluorophosphate; concentration of **4**: $1 \cdot 10^{-4}$ M, scan rate of 100 mV/s

order the ferrocene moieties are easily oxidized. Figure 5 shows the cyclic voltammogram of complex **4**, the electrochemical response of which is diffusion-controlled, whereas that of the dinickel complex **2** is more complicated due to its adsorption character.

For a possible electronic communication between the two ferrocene units the intramolecular iron−iron distances (**2**: 2.0 nm; **4**: 1.7 nm) are of importance. Because of the well-separated ferrocene building blocks the coulombic interaction (through-space electronic coupling) is negligible. On the other hand, the alignment of the molecular orbitals[21] and the extent of conjugation[7] could be a reason for through-bond electronic communication, as was observed in a conjugated alkyne-bridged rhenium(II) complex.[22] In spite of these favorable preconditions no electronic communication was found in complexes **2** and **4**.

Magnetic Investigation of Complex 2

The magnetic properties of the dinickel complex **2** were studied at 10 T in the temperature range between 300 and 5 K. Experimental data obtained for the molar susceptibility and the calculated effective magnetic moment are plotted in Figure 6. The general isotropic spin-Hamiltonian expression for the symmetrical dinickel compound is $\mathbf{H} = -J\mathbf{S_A}\cdot\mathbf{S_B}$ ($S_A = S_B = 1$), where J is the coupling constant between the two nickel(II) atoms. Although no maximum for χ_M in Figure 6 is found in the selected temperature range, a non-linear fit of the experimental data for the susceptibility per nickel dimer using published expressions[23] yields the following values: $g = 2.22 \pm 0.01$, $J = -17.37 \pm 0.24$ cm^{-1}, $D = 7.87 \pm 0.17$ cm^{-1}, and $p = 17.6 \pm 0.1\%$. The g value is reasonable for octahedrally coordinated nickel(II),[13] and the coupling constant reveals a weak, intramolecular, antiferromagnetic interaction between the nickel(II) atoms. This coupling for the bis(μ-oxo)-bridged dinickel(II) complex **2** (Ni−Ni distance of 3.39 Å) is more significant than that observed for other dinickel complexes in which two bridges consisting of two or more atoms are present and both nickel units are separated by distances of between 4.16 and 4.32 Å,[13] although it is cle-

arly weaker than that of cyano-bridged dinickel complexes.[12] Complex **2** also contains an uncoupled paramagnetic impurity which is a chain-like polymer or oligomer[24] which is formed even under high-dilution conditions. This could not be separated from **2** because both entities show very low solubility. The agreement factor $R = 9.8 \cdot 10^{-5}$ shows that the curve is well fitted.

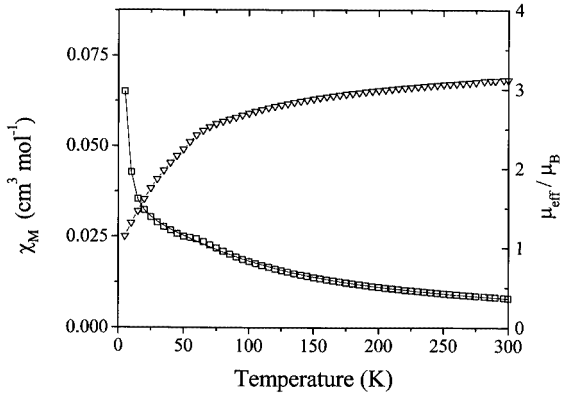

Figure 6. Temperature dependence of the magnetic susceptibility (squares, left scale) and effective magnetic moment (triangles, right scale) of **2**; the solid lines represent the best-fit curves

Conclusion

Functionalized heterotetranuclear regular and distorted rectangles bearing two redox-active ferrocene subunits and a pair of transition metal atoms each were made accessible by coordination-driven spontaneous self-assembly. Although silver is considerably bigger than nickel the separation between the two equal transition metal atoms in the dimetallic Ag_2 and Ni_2 cores is rather similar (3.50 vs. 3.39 Å). This behavior is mainly controlled by the kind of ligands employed (**1** or **3**). Due to the different positions of the nitrogen atoms in ligands **1** and **3**, the molecular structure of **2** is an ideal rectangle, whereas **4** and **5** are deformed rectangles. No long-range through-bond electronic communication was established in the macrocyclic complexes **2** and **4**. Two factors should mainly be responsible for this observation: (i) both ferrocene building blocks are separated by a distance of more than 1.7 nm, and are thus too far away to communicate, and (ii) the Ni_2 and Ag_2 cores fail to transmit the Cp−C≡C−py conjugation.[25] However, a weak influence of the Ni^{II} and Ag^{I} atoms on the redox potential of the ferrocene units has been established through the conjugated bonds in spite of a separation of 1 nm. In the case of the nickel(II) complex **2**, a weak antiferromagnetic interaction between the intramolecularly arranged nickel(II) atoms was found.

Experimental Section

General Remarks: All reactions and manipulations were carried out under argon by use of standard Schlenk techniques except otherwise noted. Acetonitrile and dichloromethane were dried with calcium hydride and distilled, degassed, and stored under argon. FT-IR data were obtained with a Bruker IFS 48 FT-IR spectrometer. The EI mass spectrum of ligand **3** was recorded with a Finnigan TSQ 70 (200°C) instrument. ^1H and $^{13}C\{^1H\}$ NMR spectra were recorded at 25 °C with a Bruker DRX 250 spectrometer operating at 250.13 and 62.90 MHz, respectively. ^1H and ^{13}C NMR chemical shifts are referenced to partially deuterated and deuterated solvent peaks, and are reported relative to TMS. Elemental analyses were carried out with an Elementar Vario EL analyzer. All electrochemical experiments were performed with a Bioanalytical CV-50W Voltammetric Analyzer (BAS, West Lafayette, IN, USA) controlled by a standard 80486 personal computer (control program version 2.0). For electroanalytical experiments a Metrohm platinum-tip electrode (Filderstadt, Germany) was applied as working electrode. The counter electrode was a platinum wire of 1 mm in diameter. A single-unit Haber-Luggin Ag^+/Ag double reference electrode was used. The resulting potential values are referenced to Ag/Ag^+ (0.01 M in CH_3CN/0.1 M Bu_4NPF_6). Ferrocene was used as an external standard. Its potential of 102.5 mV was determined by separate cyclic voltammetric experiments in the respective solvent, and all potentials in the present paper are reported relative to the fc/fc^+ standard. For cyclic voltammetry, a glass-tight full-glass three-electrode cell was used; its assembly for the experiments has been described previously.[26] The cell was purged with argon before it was filled with the electrolyte. Background curves were recorded before adding the substrate to the solution. These were later subtracted from the experimental data of the samples (excluding complex **2**). The automatic BAS CV-50 W *iR*-drop compensation facility was used for all experiments. Magnetic susceptibility of a powdered sample packed in a capsule was measured using a SQUID Quantum Design MPMS magnetometer at 10000 Gauss over the temperature range 5−300 K. All data were corrected for sample-holder contribution. The diamagnetism of the sample and paramagnetism of nickel(II) were represented by a parameter in the non-linear fit equation. This parameter was found to be $(5.4 \pm 1.4) \times 10^{-4}$ emu/mol. Compounds **1**,[15] **3**,[15] and $[PdCl_2(COD)]$[27] were synthesized according to literature methods. $AgClO_4$ and $Ni(NO_3)_2 \cdot 6H_2O$, were used as received without further treatment.

Complex 2: Solutions of nickel(II) nitrate hexahydrate (74 mg, 0.25 mmol) in methanol (50 mL) and of ligand **1**[15] (98 mg, 0.25 mmol) in dichloromethane (50 mL) were simultaneously added dropwise to a stirred mixture of dichloromethane and methanol (50/50 mL) within 4 h at room temperature. The resulting red mixture was stirred for 20 h at the same temperature. Then, the solvents were removed under vacuum. The red residue was washed with methanol (2 mL) and dichloromethane (5 mL) and dried in vacuo for 15 h. Yield 136 mg (92%), red solid, m.p. > 270°C. FT-IR (KBr, cm^{-1}): $\tilde{\nu}$ = 2207 s (C≡C), 1611 vs (C=N), 1289 s (NO_3^-), 1218 sh (NO_3^-). $C_{48}H_{32}Fe_2N_8Ni_2O_{12} \cdot 0.5CH_2Cl_2$ (1184.37): calcd. C 49.18, H 2.81, N 9.46; found C 49.12 H, 2.88 N 9.25.

Ligand 3: This ligand was prepared by a published method,[15] and further purified by recrystallization from dichloromethane and acetonitrile. Red crystals, m.p. 195°C. ^1H NMR (CD_2Cl_2, ppm): δ = 8.50 (dd, $^4J_{H,H}$ = 2.20, $^5J_{H,H}$ = 0.82 Hz, 4 H, 2-H, C_5H_4N), 8.35 (dd, $^3J_{H,H}$ = 4.87, $^4J_{H,H}$ = 1.73 Hz, 4 H, 6-H, C_5H_4N), 7.63 (ddd, $^3J_{H,H}$ = 7.91, $^4J_{H,H}$ = 1.92, $^4J_{H,H}$ = 1.92 Hz, 4 H, 4-H, C_5H_4N), 7.05 (ddd, $^3J_{H,H}$ = 7.91, $^4J_{H,H}$ = 4.87, $^5J_{H,H}$ = 0.82 Hz, 4 H, 5-H, C_5H_4N), 4.50 (m,[28] 8 H, C_4H_4C), 4.29 (m,[29] 8 H, C_4H_4C). $^{13}C\{^1H\}$ NMR (CD_2Cl_2, ppm): δ = 152.17 (C-2), 148.23 (C-6), 138.11 (C-4), 123.24 (C-5), 121.10 (C-3), 90.55, 83.79 (C≡C), 73.38,

71.41 (C_4H_4C), 66.96 (C_4H_4C). MS (EI); *m/z*: 388.0 [M^+]. IR (KBr, cm^{-1}): $\tilde{\nu}$ = 2206 s (C≡C), 1581 w (C=N). $C_{24}H_{16}FeN_2 \cdot 0.05CH_2Cl_2$ (392.50): calcd. C 73.60, H 4.13, N 7.14; found C 73.44, H 4.18, N 6.98.

Complex 4: Solutions of ligand **3** (42 mg, 0.108 mmol) in a mixture of acetonitrile/dichloromethane (25/2 mL) and of silver(I) perchlorate (23.5 mg, 0.114 mmol) in acetonitrile (20 mL) were simultaneously added dropwise to stirred dichloromethane (20 mL) at room temperature during a period of 2 h. After the addition, the mixture was stirred for 24 h at the same temperature followed by the removal of solvents under vacuum. The precipitate was filtered (P3) and washed with dichloromethane (3 mL) and finally dried in vacuo. ***WARNING:*** *This perchlorate complex is hazardous because of the possibility of explosion! Compound* ***4*** *exploded at about 220 °C during the measurement of the melting point! Special care should therefore be taken and only very small amounts of the sample should be handled!* Yield 64.5 mg (94%), red powder, m.p. > 220°C (*explosive!*). ^{1}H NMR (CD_3CN, ppm): δ = 8.49 (dd, $^4J_{H,H}$ = 2.20, $^5J_{H,H}$ = 0.71 Hz, 4 H, 2-H, C_5H_4N), 8.41 (dd, $^3J_{H,H}$ = 4.94, $^4J_{H,H}$ = 1.57 Hz, 4 H, 6-H, C_5H_4N), 7.64 (ddd, $^3J_{H,H}$ = 7.98, $^4J_{H,H}$ = 1.88, $^4J_{H,H}$ = 1.88 Hz, 4 H, 4-H, C_5H_4N), 7.20 (ddd, $^3J_{H,H}$ = 7.98, $^4J_{H,H}$ = 4.94, $^5J_{H,H}$ = 0.71 Hz, 4 H, 5-H, C_5H_4N), 4.50 (m,[28] 8 H, C_4H_4C), 4.29 (m,[29] 8 H, C_4H_4C). IR (KBr, cm^{-1}): $\tilde{\nu}$ = 2211 m (C≡C), 1593 w (C=N), 1095 vs, 1050 s (ClO_4^-). $C_{48}H_{32}Ag_2Cl_2Fe_2N_4O_8 \cdot CH_3CN \cdot 0.5\ CH_2Cl_2$ (1274.66): calcd. C 47.59, H 2.85, N 5.49; found C 47.30, H 2.83, N 5.30.

Complex 5: Solutions of ligand **3** (77 mg, 0.2 mmol) in dichloromethane (50 mL) and of [$PdCl_2$(COD)] (57 mg, 0.2 mmol) in dichloromethane (50 mL) were simultaneously added dropwise to stirred dichloromethane (50 mL) at room temperature during a period of 1 h. After the addition, the mixture was stirred for 20 h at the same temperature followed by the removal of solvents under vacuum. The precipitate was filtered and washed with dichloromethane (3 mL) and finally dried in vacuo. Yield 107 mg (95%), red powder, m.p. > 270 °C. ^{1}H NMR (CD_2Cl_2, ppm): δ = 8.68 (d, $^4J_{H,H}$ = 2.51 Hz, 4 H, 2-H, C_5H_4N), 8.66 (dd, $^3J_{H,H}$ = 6.08, $^4J_{H,H}$ = 1.30 Hz, 4 H, 6-H, C_5H_4N), 7.36 (ddd, $^3J_{H,H}$ = 7.96, $^4J_{H,H}$ = 1.90, $^4J_{H,H}$ = 1.90 Hz, 4 H, 4-H, C_5H_4N), 6.74 (ddd, $^3J_{H,H}$ = 7.96, $^4J_{H,H}$ = 6.08, $^5J_{H,H}$ = 0.67 Hz, 4 H, 5-H, C_5H_4N), 4.55 (m,[28] 8 H, C_4H_4C), 4.30 (m,[29] 8 H, C_4H_4C). IR (KBr, cm^{-1}): $\tilde{\nu}$ = 2209 s (C≡C), 1596 w (C=N), 1095 vs, 1050 s (ClO_4^-). $C_{48}H_{32}Cl_4Fe_2N_4Pd_2$ (1131.15): calcd. C 50.97, H 2.85, Cl 12.54, N 4.95; found C 50.58, H 2.68, Cl 12.57, N 4.83.

X-ray Crystallographic Study: Crystallographic and data collection information as well as a description of the structural analyses and refinements for complexes **2** and **4** are summarized in Table 4. Single crystals of **2** were obtained by slow diffusion of a solution of ligand **1** in dichloromethane into a solution of nickel(II) nitrate hexahydrate in methanol.[30] Suitable single crystals of **4** were obtained by slow diffusion of a solution of ligand **3** in dichloromethane into a solution of silver(I) perchlorate in acetonitrile. Crystals of **5** were obtained by slow diffusion of a [$PdCl_2$(COD)] solution

Table 4. Crystal data and structure refinement for **2** and **4**

	2·3CH_2Cl_2	**4**·2CH_3CN
Empirical formula	$C_{51}H_{38}Cl_6Fe_2N_8Ni_2O_{12}$	$C_{52}H_{38}Ag_2Cl_2Fe_2N_6O_8$
Formula mass	1396.72	1273.22
Crystal system	triclinic	triclinic
Space group	$P\bar{1}$	$P\bar{1}$
a [Å]	8.0907(17)	7.0579(8)
b [Å]	13.424(2)	10.5149(10)
c [Å]	13.955(2)	16.5415(15)
α [°]	71.455(9)	75.829(7)
β [°]	75.946(11)	85.663(9)
γ [°]	75.045(14)	85.196(8)
V [Å^3]	1366.7(4)	1184.1(2)
Z	1	1
$d_{calcd.}$ [g·cm^{-3}]	1.697	1.785
Temperature [K]	173(2)	173(2)
F(000)	706	636
Crystal size [mm]	0.1×0.4×0.4	0.1×0.8×0.2
Wavelength [Å]	0.71073	0.71073
θ limits [°]	2.55 to 27.49	2.00 to 27.50
hkl ranges	$-10 \le h \le 8$	$-9 \le h \le 9$
	$-16 \le k \le 16$	$-13 \le k \le 13$
	$-17 \le l \le 18$	$-21 \le l \le 21$
Reflections collected	11739	10851
Reflections unique	6214 (R_{int} = 0.0255)	5426 (R_{int} = 0.0189)
Completeness to θ = max.	99.0%	99.7%
Absorption correction	empirical	empirical
Max. and min. transmission	0.3614 and 0.2643	0.5151 and 0.3983
Refinement method	full-matrix least-squares on F^2	full-matrix least-squares on F^2
Data/restraints/parameters	6214/0/380	5426/0/327
Goodness of fit on F^2	1.021	1.072
Final *R* indices [$I > 2\sigma(I)$][a]	$R1$ = 0.0425, wR_2 = 0.1115	$R1$ = 0.0236, wR_2 = 0.0613
R indices (all data)	$R1$ = 0.0561, wR_2 = 0.1189	$R1$ = 0.0272, wR_2 = 0.0630
Extinction coefficient	0.0024	0.0082(4)
Largest diff. peak and hole [e·Å^{-3}]	1.175 and −0.696	0.520 and −0.500

[a] $R_1 = ||F_o| - |F_c||/|F_o|$; $wR_2 = \{[w(F_o^2 - F_c^2)^2]/[w(F_o^2)^2]\}^{0.5}$.

in dichloromethane into a dichloromethane solution of ligand **3** at room temperature. Each crystal was fixed on a glass fiber using perfluoropolyether RS 3000 and transferred to a Siemens P4 diffractometer (**2**, **4**) or a Stoe IPDS diffractometer (**5**) equipped with a graphite-monochromated Mo-K_α radiation unit. The lattice constants for both macrocycles **2** and **4** were determined by 50 precisely centered high-angle reflections. Intensities were collected by the ω-scan technique. An empirical absorption correction was performed in each case. The structures of **2** and **4** were solved by direct methods with SHELXTL V5.1 (NT version)[31] and refined by least-squares methods with the same program, with anisotropic thermal parameters for all non-hydrogen atoms. All hydrogen atoms were located in calculated positions (riding mode). In **2**, one of the dichloromethane molecules (near the corner of the unit cell in Figure 3) is disordered about the center of inversion. The largest peak and hole in the last difference synthesis were 1.175/−0.696 (**2**), and 0.520/−0.500 (**4**) e·Å^{-3}, respectively. The structure of **5** was solved by direct methods with SHELXS.[32] CCDC-190120 (**2**) and -190121 (**4**) contain the supplementary crystallographic data for this paper. These data can be obtained free of charge at www.ccdc.cam.ac.uk/conts/retrieving.html [or from the Cambridge Crystallographic Data Center, 12 Union Road, Cambridge CB2 1EZ, UK; Fax: (internat.) + 44-1223/336-033; E-mail: deposit@ccdc.cam.ac.uk].

Acknowledgments

Support of this research by the Deutsche Forschungsgemeinschaft and the Fonds der Chemischen Industrie is gratefully acknowledged. Degussa AG is thanked for supplying starting materials. We thank Prof. B. Speiser and Prof. H.-J. Meyer for their helpful discussions and suggestions.

[1] S. Leininger, B. Olenyuk, P. J. Stang, *Chem. Rev.* **2000**, *100*, 853−908.
[2] M. Fujita, *Chem. Soc. Rev.* **1998**, *27*, 417−425.
[3] B. Olenyuk, A. Fechtenkötter, P. J. Stang, *J. Chem. Soc., Dalton Trans.* **1998**, 1707−1728.
[4] F. A. Cotton, C. Lin, C. A. Murillo, *Inorg. Chem.* **2001**, *40*, 478−484.
[5] F. A. Cotton, L. M. Daniels, C. Lin, C. A. Murillo, *J. Am. Chem. Soc.* **1999**, *121*, 4538−4539.
[6] P. J. Stang, B. Olenyuk, J. Fan, A. M. Arif, *Organometallics* **1996**, *15*, 904−908.
[7] S. Barlow, D. O'Hare, *Chem. Rev.* **1997**, *97*, 637−669.
[8] F. Barriere, N. Camire, W. E. Geiger, U. T. Mueller-Westerhoff, R. Sanders, *J. Am. Chem. Soc.* **2002**, *124*, 7262−7263.
[9] Z. Yuan, G. Stringer, I. R. Jobe, D. Kreller, K. Scott, L. Koch, N. J. Taylor, T. B. Marder, *J. Organomet. Chem.* **1993**, *452*, 115−120.
[10] M. Pilkington, S. Decurtins, *Chimia* **2001**, *55*, 1014−1016.
[11] J. C. Noveron, M. S. Lah, R. E. Del Sesto, A. M. Arif, J. S. Miller, P. J. Stang, *J. Am. Chem. Soc.* **2002**, *124*, 6613−6625.
[12] A. Rodriguez-Fortea, P. Alemany, S. Alvarez, E. Ruiz, A. Scuiller, C. Decroix, V. Marvaud, J. Vaissermann, M. Verdaguer, I. Rosenman, M. Julve, *Inorg. Chem.* **2001**, *40*, 5868−5877.
[13] M. Conrad, F. Meyer, A. Jacobi, P. Kircher, P. Rutsch, L. Zsolnai, *Inorg. Chem.* **1999**, *38*, 4559−4566.
[14] D. Volkmer, A. Hörstmann, K. Griesar, W. Haase, B. Krebs, *Inorg. Chem.* **1996**, *35*, 1132−1135.
[15] E. Lindner, R. F. Zong, K. Eichele, *Phosphorus, Sulfur Silicon* **2001**, *169*, 219−222.
[16] P. Knops, N. Sendhoff, H.-B. Mekelburger, F. Vögtle, *High Dilution Reactions − New Synthetic Applications: Topics in Current Chemistry* (Eds.: E. Weber, F. Vögtle), Springer, Heidelberg, **1992**.
[17] E. Lindner, R. F. Zong, K. Eichele, M. Ströbele, *J. Organomet. Chem.* **2002**, *660*, 78−84.
[18] Complex **5**, monoclinic, space group $P2_1/c$, molecular formula: $C_{48}H_{32}Cl_4Fe_2N_4Pd_2$, formula weight: 1131.08, a = 6.7738(14), b = 13.508(3), c = 24.351(5) Å, β = 96.73(3)°, V = 2212.7(8) Å^3, and Z = 2.
[19] R. F. Zong, Dissertation, University of Tübingen, Germany **2002**.
[20] A. N. Khlobystov, A. J. Blake, N. R. Champness, D. A. Lemenovskii, A. G. Majouga, N. V. Zyk, M. Schröder, *Coord. Chem. Rev.* **2001**, *222*, 155−192.
[21] J. V. Ortega, B. Hong, S. Ghosal, J. C. Hemminger, B. Breedlove, C. P. Kubiak, *Inorg. Chem.* **1999**, *38*, 5102−5112.
[22] M. Brady, W. Q. Weng, J. A. Gladysz, *J. Chem. Soc., Chem. Commun.* **1994**, 2655−2666.
[23] D. Volkmer, A. Hörstmann, K. Griesar, W. Haase, B. Krebs, *Inorg. Chem.* **1996**, *35*, 1132−1135.
[24] W. M. Xue, F. E. Kühn, E. Herdtweck, Q. C. Li, *Eur. J. Inorg. Chem.* **2001**, 213−221.
[25] O. Lavastre, J. Plass, P. Bachmann, S. Guesmi, C. Moinet, P. H. Dixneuf, *Organometallics* **1997**, *16*, 184−189.
[26] S. Dümmling, E. Eichhorn, S. Schneider, B. Speiser, M. Würde, *Curr. Sep.* **1996**, *15*, 53−56.
[27] D. Drew, J. R. Doyle, *Inorg. Synth.* **1990**, *28*, 346−349.
[28] m: low-field part of an AA′XX′ pattern, $N = |^3J_{H,H} + {}^5J_{H,H}|$.
[29] m: high-field part of an AA′XX′ pattern, $N = |^3J_{H,H} + {}^5J_{H,H}|$.
[30] V. Jullien, M. W. Hosseini, J. -M. Planeix, A. D. Cian, *J. Organomet. Chem.* **2002**, *634/644*, 376−380.
[31] G. M. Sheldrick, *SHELXTL V5.03, Program for crystal structure refinement*, University of Göttingen, Germany **1995**.
[32] G. M. Sheldrick, *Acta Crystallogr., Sect. A* **1995**, *51*, 33−38. *SHELXS V5.03 program for crystal structure solution*, University of Göttingen, Germany).

Received July 24, 2002
[I02413]

Orientation- and Temperature-Dependent Rotational Behavior of Imidazole Ligands (L) in β-$[Ru(azpy)_2(L)_2](PF_6)_2$ Complexes

Aldrik H. Velders,[a][‡] Adoracion Gomez Quiroga,[a][‡‡] Jaap G. Haasnoot,[a] and Jan Reedijk*[a]

Keywords: Ruthenium / N ligands / NMR spectroscopy / Bioinorganic chemistry

The synthesis and characterization of the *cis* bifunctional coordinated ruthenium(II) complexes β-$[Ru(azpy)_2(MeIm)_2](PF_6)_2$ (β-MeIm) and β-$[Ru(azpy)_2(MeBim)_2](PF_6)_2$ (β-MeBim) (azpy = 2-phenylazopyridine, MeIm = 1-methylimidazole and MeBim = 1-methylbenzimidazole) is reported. In β-MeIm the two MeIm ligands can both freely rotate around the Ru–N axes on the NMR timescale. In β-MeBim the two MeBim ligands appear restricted in their rotation around the Ru–N axes, which becomes slow on the NMR timescale at low temperatures. In contrast to the analogous complexes α-$[Ru(azpy)_2(MeBim)_2](PF_6)_2$ and *cis*-$[Ru(bpy)_2(MeBim)_2](PF_6)_2$, only one atropisomer is observed for the two MeBim ligands in β-MeBim. The orientation of the MeBim ligands appears to correspond to an HT isomer which is similar to the orientation of the MeBim ligands in the most abundant atropisomer found in the related α-$[Ru(azpy)_2(MeBim)_2](PF_6)_2$. A stacking interaction between the phenyl ring of one azpy and one MeBim ligand is likely to stabilize the observed atropisomer of β-MeBim, and is such that the rotation of the phenyl ring of one of the two azpy ligands is restricted. At very low temperatures this rotation, or flipping of the phenyl ring between two identical positions, is in the slow-exchange range on the NMR timescale.

(© Wiley-VCH Verlag GmbH & Co KGaA, 69451 Weinheim, Germany, 2003)

Introduction

Dichlorobis(azpy)ruthenium(II) isomers [azpy = 2-(phenylazo)pyridine] have gained interest because of the very different cytotoxicity they exhibit against a series of tumor cell lines, α-$[Ru(azpy)_2(Cl)_2]$ being very cytotoxic and β-$[Ru(azpy)_2(Cl)_2]$ only moderately so.[1] In a similar manner to platinum antitumor compounds, ruthenium complexes are thought to exhibit their cytotoxic activity through their coordination to biological target molecules like proteins or DNA.[2] Therefore, the differences in cytotoxicity found for the isomeric $[Ru(azpy)_2Cl_2]$ complexes might be very useful in the search for a structure-activity relationship (SAR) of antitumor-active ruthenium complexes. From steric aspects derived from the crystal structures[3,4] of α- and β-$[Ru(azpy)_2(Cl)_2]$ and *cis*-$[Ru(bpy)_2(Cl)_2]$, it was suggested that the potential *cis* binding sites in these three complexes are least accessible in the β isomer.[1,5] All three *cis*-$[Ru(LL')_2]$ moieties (LL′ = bpy or azpy) bind only monofunctionally to guanine derivatives.[5–7] Due to the absence of a C_2 axis, the β isomer has actually two different binding sites (see Figure 1), which both appear to be accessible for the binding of an oxopurine ligand; however, the bifunctional coordination of non-tethered purines appears impossible for this isomer.

Previously,[5,8,9] it has been described that the study of the coordination of ruthenium complexes to the lopsided heterocyclic ligand 1-methylbenzimidazole, MeBim, can provide information about the (steric) possibilities of a complex to bind in a *cis* bis(configuration) to the purines of DNA. In the present paper the binding of the lopsided imidazoles (L) 1-methylimidazole (MeIm) and MeBim (see Figure 2) to β-$[Ru(azpy)_2(NO_3)_2]$ is described and their ro-

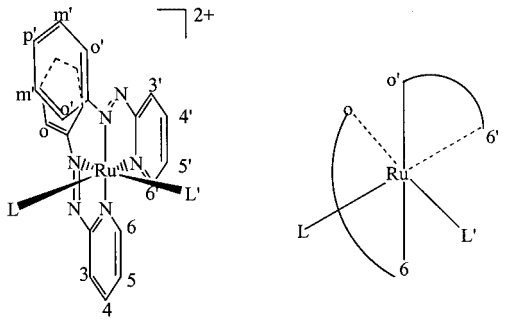

Figure 1. Structural (left) and schematic (right) representation of β-$[Ru(azpy)_2(L)_2](PF_6)_2$ and the used proton numbering scheme

[a] Leiden Institute of Chemistry, Gorlaeus Laboratories, Leiden University,
P. O. Box 9502, 2300 RA Leiden, The Netherlands
[‡] Current address: Molteni Farmaceutici, S.S.
67 Loc. Granatieri, 50018 Scandicci, Florence, Italy
[‡‡] Current address: Departamento de Química Inorgánica, Universidad Autonoma de Madrid,
Cantoblanco, 28049 Madrid, Spain

Supporting information for this article is available on the WWW under http://www.ejic.com or from the author.

tational behavior discussed. The results are compared with those obtained for the analogous bpy complexes *cis*-[Ru(bpy)$_2$(L)$_2$](PF$_6$)$_2$,[8,9] and the isomeric α complexes α-[Ru(azpy)$_2$(L)$_2$](PF$_6$)$_2$.[5,10]

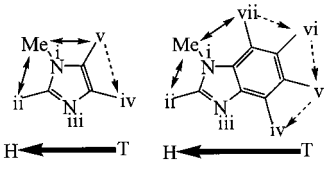

Figure 2. Structural representation, proton numbering scheme, NOE (solid arrows) and COSY (dashed arrows) connectivities of methylimidazole (MeIm, left) and methylbenzimidazole (MeBim, right); the bold arrows (bottom) represent the head-tail axis of the imidazole ligands, as will be used in the schematic drawings in Figures 4 and 9

Results and Discussion

The α- and β-isomers are generally accepted to be the most stable isomers of the bis(azpy)ruthenium(II) complexes.[11−13] However, in solution these two complexes can isomerize, as in fact is observed in the reaction of the isomeric complexes α- and β-[Ru(azpy)$_2$(NO$_3$)$_2$] with guanine derivatives under refluxing conditions in water.[5−7] In the synthesis of bis(adducts) of the type α-[Ru(azpy)$_2$(L)$_2$](PF$_6$)$_2$ no evidence for isomerisation has been found;[5,10] in the present synthesis of the β-isomer bis(adducts), no isomerized compounds were observed either. Apparently, once fully coordinated with nitrogen ligands the α- and β-bis(azpy)ruthenium complexes are stable to isomerisation, even under refluxing conditions in acetone/water.

Similar to the ^{1}H NMR spectra of the analogous complexes α-[Ru(azpy)$_2$(MeIm)$_2$](PF$_6$)$_2$ [5,10] and *cis*-[Ru(bpy)$_2$(MeIm)$_2$](PF$_6$)$_2$,[8,9] the β-MeIm complex shows a ^{1}H NMR spectrum with sharp signals, suggesting that the MeIm ligands are rotating rapidly on the NMR timescale (Figure 3). Also analogous to the bpy and α-azpy systems, the β-MeBim complex shows mainly broad peaks at room temperature, suggesting that the MeBim ligands are rotating at an intermediate speed on the NMR timescale. The possible

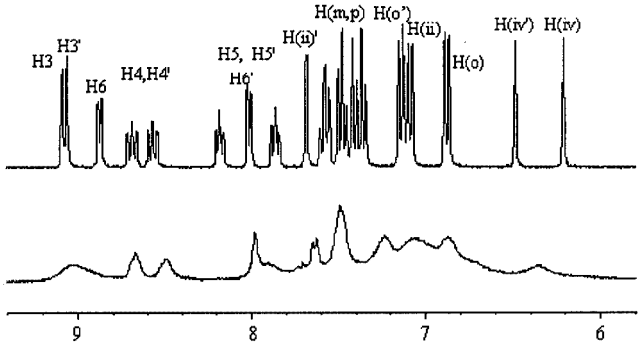

Figure 3. ^{1}H NMR spectra (δ scale in ppm) of the complexes β-MeIm (top) and β-MeBim (lower spectrum) in [D$_6$]acetone, at 25 °C; assignments are indicated in the figure

presence of rotameric structures in the β-MeBim complex requires a short introduction, which is given below.

For two *cis*-coordinated lopsided ligands on the ruthenium ion, the corresponding atoms can be on the same side (head-to-head, HH), or on opposite sides (head-to-tail, HT) of the ligand−metal−ligand plane.[14] As a lopsided ligand prefers not to orient in the same plane as another ligand,[15] four staggered orientations are possible. In a *cis* bifunctional octahedrally coordinated complex 16 possible atropisomers can be drawn.[5] It can be reasonably assumed that the bicyclic ligands will prefer an orientation with the longitudinal axis parallel to each other, and not orthogonal, therefore only the eight atropisomers depicted in Figure 4 have to be taken into account when identifying the atropisomers. In the complex *cis*-[Ru(bpy)$_2$(L)$_2$](PF$_6$)$_2$] the orientation of the imidazole ligands above the bpy ring system is not observed, diminishing the number of possible atropisomers.[8,9] The other four atropisomers, R5−R8, are not observed, the steric hindrance of the bpy rings most likely preventing the orientation of an MeBim unit above its ring system. It appears, however, that such an orientation cannot be excluded in α-[Ru(azpy)$_2$(L)$_2$](PF$_6$)$_2$ complexes.[5,10] The identification of the observed rotamers for bis(azpy)ruthenium complexes therefore requires a detailed investigation and consideration of all the eight atropisomers R1−R8. Most convenient for the identification of atropisomers in the α-[Ru(azpy)$_2$(MeBim)$_2$](PF$_6$)$_2$ system[5,10] is the fact that the C_2 symmetry in the α-[Ru(azpy)$_2$] moiety reduces the number of different rotamers from eight to six. Furthermore, four of the HT rotamers have C_2 symmetry, resulting in the two azpy and the two MeBim ligands being indistinguishable by ^{1}H NMR spectroscopy, which proves the presence of the HT isomers already from a 1D ^{1}H NMR spectrum. Due to the lack of C_2 symmetry in the β-[Ru(azpy)$_2$] moiety, all the eight atropisomers are different from each other, and each of them is expected to give different proton resonances for both azpy and both imidazole ligands.

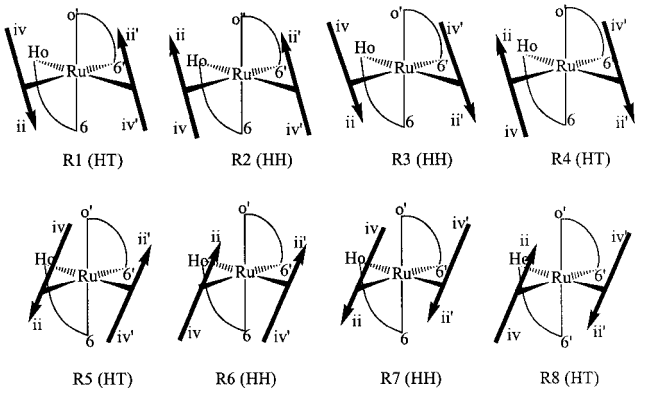

Figure 4. Schematic representation of eight theoretically possible rotameric structures of β-[Ru(azpy)$_2$(MeBim)$_2$](PF$_6$)$_2$

β-[Ru(azpy)$_2$(MeIm)$_2$](PF$_6$)$_2$ (β-MeIm)

The ^{1}H NMR spectrum of β-MeIm at room temperature is shown in Figure 3. In the aromatic region, 20 resonances

are found, several of which overlap with other signals. With the use of COSY and NOESY data the complete assignment of all resonances has been done (Figure 3 and Table 1). One doublet and two triplet peaks with double intensity in the high-field region can immediately be attributed to the azpy *ortho* [H(*o*)], and *meta* [H(*m*)] protons of the phenyl ring, respectively, after which a COSY spectrum reveals the triplet at δ = 7.55 ppm to be attributed to H(*p*). The MeIm peaks were assigned starting from an NOESY spectrum in which the Me(i) resonances show interaction with the parent H(ii) as well as the H(v) proton resonances; the latter also shows a cross peak with H(iv). From a COSY spectrum, the four signals of the pyridine part of the azpy ligands could be correlated; on the basis of the ^3J coupling, the doublets at δ = 8.8 and 7.9 ppm were assigned to the H6 and H6′ resonances (≈ 6 Hz), whilst the doublet at δ = 9.0 ppm (≈ 9 Hz) was assigned to the two overlapping H3 and H3′ resonances. The peak assignment was further confirmed by the (weak) NOE cross-peaks observed between the H6 and the H6′ resonances, and the H(*o*) and H(*o*′) signals, as would be expected for the β-isomer.[5,7,16]

Table 1. Selection of ^{1}H NMR spectroscopic data (chemical shifts) of β-[Ru(azpy)$_2$(MeIm)$_2$](PF$_6$)$_2$, β-MeIm, and β-[Ru(azpy)$_2$(MeBim)$_2$](PF$_6$)$_2$, β-MeBim, in [D$_6$]acetone at room temp. and at −95 °C, respectively

	H3	H6	H3′	H6′	H(ii)	H(iv)	H(ii′)	H(iv′)
β-MeIm	9.08	8.87	9.08	8.02	7.08	6.21	7.69	6.49
β-MeBim	9.35	7.82	9.35	8.87	8.02	5.3	7.76	6.35

On the basis of only the inter-azpy NOE interactions, it is impossible to attribute one of the two sets of pyridine- or one of the two sets of phenyl-ring proton resonances to a specific azpy ligand. Whereas the interligand NOE peaks of H6 with H(*o*) in a (non-C_2-symmetric) bis(adduct) of the α-isomer allow to distinguish between the azpy moieties, this is not the case for the β-isomer.[5,16] As the H6′ is oriented just above the pyridine ring of the other azpy ligand (Figure 5) a relatively strong shielding of this proton resonance is expected with respect to the H6 proton, and therefore the high-field doublet with a ^3J coupling of 6 Hz has been attributed to the H6′ proton, whilst the low-field doublet with a coupling of 6 Hz is assigned to H6. The

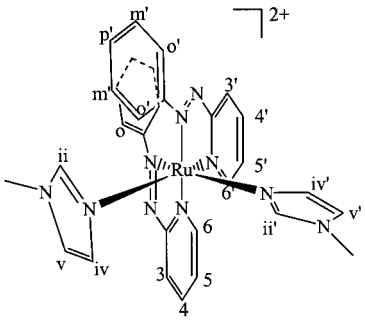

Figure 5. Structural representation and proton numbering scheme of β-[Ru(azpy)$_2$(MeIm)$_2$](PF$_6$)$_2$ (β-MeIm)

resonances of the two phenyl ring systems have been assigned on the basis of the interligand azpy-MeIm NOE interactions (vide infra).

The ^{1}H NMR spectrum of β-MeIm (Figure 3) shows two sets of azpy and two sets of imidazole signals. In theory, such a spectrum can either represent a complex in which both the MeIm ligands are rotating rapidly on the NMR timescale, or it can represent one of the eight atropisomers depicted in Figure 4. As the MeBim ligands in this complex show rotational behavior at room temp. (vide infra) it is reasonable to assume the smaller MeIm ligands do so, too. Upon lowering the temperature to −95 °C, the ^{1}H NMR spectrum of β-MeIm does not change significantly, indicating that at lower temperatures the MeIm ligands are still rotating rapidly on the NMR timescale. In the study with the *cis*-[Ru(bpy)$_2$(L)$_2$]$^{2+}$ [8,9] and α-[Ru(azpy)$_2$(L)$_2$]$^{2+}$ complexes[5,10] it is pointed out that the didentate heterocycles are spectator ligands, with the protons closest to the coordination sites functioning as probe protons that can be used to monitor the orientation and/or the rotation of the monodentate imidazole ligands L. The present results indicate that the H6/H6′ and the H(*o*)/H(*o*′) protons of the azpy ligand can also function as probe protons to monitor the orientation and rotational behavior of the *cis* bis(coordinated) ligands L. The NOESY spectrum of β-MeIm (Figure 6) shows that the azpy H6 proton interacts with the H(ii) and H(iv) protons of both MeIm ligands. These NOE peaks indicate that the MeIm ligands are rotating around their Ru−N axes on the NMR timescale, and this is further confirmed by the cross peaks between the two MeIm ligands: H(ii)-H(ii′), H(ii)−H(iv′), H(iv)−H(ii′) and H(ii)−H(iv′). The 2D ^{1}H NMR spectroscopic data clearly confirm, therefore, that the MeIm ligands are indeed rotating (fast) around their Ru−N(iii) axes.

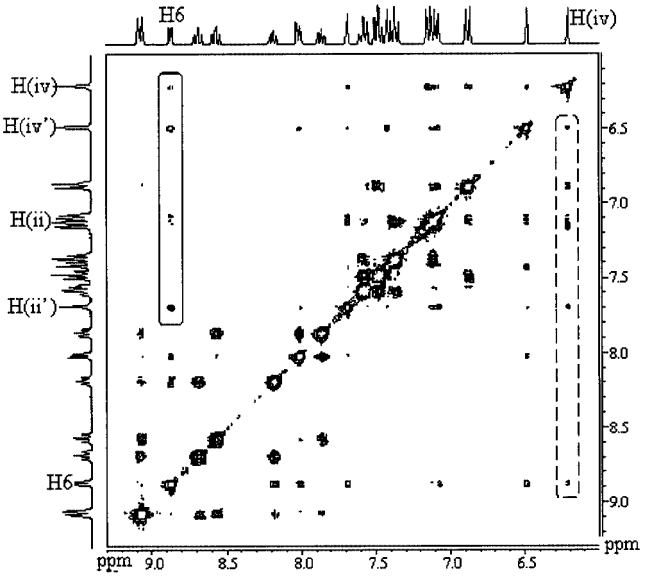

Figure 6. NOESY spectrum of β-[Ru(azpy)$_2$(MeIm)$_2$](PF$_6$)$_2$, in [D$_6$]acetone at 25 °C; the highlighted areas indicate the NOE cross peaks of the H6 (solid rectangle) and H(iv) (dashed rectangle) resonances

β-[Ru(azpy)$_2$(MeBim)$_2$](PF$_6$)$_2$ (β-MeBim)

Variable-Temperature ^{1}H NMR Behavior

At room temperature broad peaks are observed in the ^{1}H NMR spectrum of β-MeBim (Figure 3). These are characteristic of a complex with different rotamers that are exchanging with each other on the NMR timescale. In the ^{1}H NMR spectrum of β-MeBim at higher temperatures, no (complete) sharpening of the signals is observed. On lowering the temperature, on the other hand, a sharp set of signals is observed (Figure 7). All the azpy protons resonances can be assigned from the COSY and NOESY spectra in a similar way to β-MeIm. The identification of the rotamers was made from the 2D NOE data and by evaluating the (de)shielding effects of the ligands on the other proton resonances; the rotational aspects of the ligands at different temperatures were determined from the ROESY data.

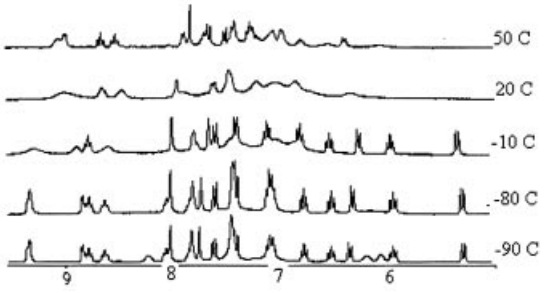

Figure 7. ^{1}H NMR spectra (δ scale in ppm) of β-[Ru(azpy)$_2$(MeBim)$_2$](PF$_6$)$_2$ at different temperatures; assignment of resonances in the low temperature spectrum is given in Table 1

Analogous to the discussion of the MeIm complex, for β-MeBim a theoretical total of 24 resonance signals in the aromatic region for the two azpy ligands and the two MeBim ligands could indicate the presence in solution of only one symmetric atropisomer, in slow exchange on the NMR timescale, or on the other hand it could indicate the average of a rotational system which is in fast exchange on the NMR timescale. For β-MeBim the ^{1}H NMR spectrum at room temperature shows broad peaks, suggesting that the presence of different atropisomers could possibly be observed at lower temperatures. The results obtained with the α-[Ru(azpy)$_2$(MeBim)$_2$]$^{2+}$ complex explicitly demonstrate[5,10] that one should take great care in interpreting the ^{1}H NMR spectroscopic data of rotational complexes, as a set of signals can indicate a system which has no rotating ligands on the NMR timescale, but can also indicate a system with fast moving ligands, which can freeze out into different atropisomers upon lowering the temperature. Furthermore, the sets of signals belonging to these "atropisomers" in slow exchange can sometimes represent the average signal of more possible atropisomers.[5,10] For β-MeBim, the spectrum at −95 °C is shown to represent one specific atropisomer (see next section), but the VT ^{1}H NMR spectroscopic data show one particular feature that should be treated in more detail. This regards the rotational behavior of the phenyl ring of one of the two azpy ligands, which, due to interaction with the lopsided ligands, becomes slow on the NMR timescale in the low-temperature region.

Orientations of the Two MeBim Ligands in β-MeBim

The orientation of the MeBim ligands in β-MeBim as observed at low temperatures was determined from the NOE data. As pointed out for the MeIm complex β-MeIm, the H(*o*) and H6 protons of the azpy ligands are found close to the imidazole ligands, and NOE interactions are most useful for determining the orientation of the MeBim ligands. Unfortunately, the H(*o*) resonances are very broad at the recording temperature and no NOE cross-peaks are observed. The most important NOE cross peaks observed for β-MeBim (Figure 8) are the H6−H(iv′) and the weak cross peaks between the H(ii) and H(iv′) resonances and H(iv) and H(ii′) resonances. These three cross peaks point to a conformer in which the imidazole H(ii) protons of both the benzimidazole ligands are oriented above the aza binding of their *fac*-coordinated azpy ligands (R5 in Figure 4; see Note added in proof). The six-membered ring of the MeBim ligand [H(iv)] is oriented in a face-to-face manner with the pyridine of the *mer*-coordinated azpy ligand, whilst the other MeBim ligand [H(iv′)] has its six-membered ring face-to-face with the phenyl ring of the *mer*-oriented azpy ligand. This HT atropisomer is different from the two HT atropisomers found for the *cis*-[Ru(bpy)$_2$(MeBim)$_2$](PF$_6$)$_2$ system[8,9] in which none of the rotamers has the lopsided part of a MeBim ligand oriented above the didentate ligand. Interestingly, this rotamer is very similar to the most abundant (HT) atropisomer observed in the related α complex.[5,10]

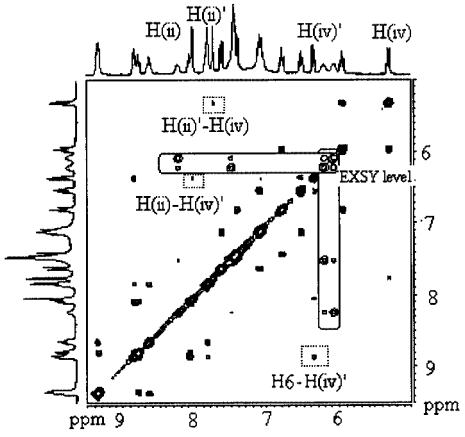

Figure 8. ROESY spectrum of β-[Ru(azpy)$_2$(MeBim)$_2$](PF$_6$)$_2$ (β-MeBim) in [D$_6$]acetone at −95 °C; NOE cross peaks are highlighted in the dotted areas (see Note added in proof)

It is most likely that the bulky, rotating phenyl rings of the two azpy ligands prevent the MeBim ligand from orienting in the direction of the two aromatic rings of the two azpy ligands (R1−R4).The orientation of the MeBim′ li-

gand with the six-membered ring above the azpy ligand is also not expected due to severe steric clashes (R7, R8). For the same reason atropisomer R6 is likely to be sterically disfavored. The remaining atropisomer, R5, has the MeBim ligands oriented in such a way that the imidazole ring protons are oriented close to the aza bond of the azpy ligands. Besides the steric effects preferring this orientation, an electronic effect is possibly also stabilizing the orientations of the MeBim ligands. Marzilli et al.[17] have pointed out that the orientation of imidazole ligands can partly be determined by the electrostatic interaction between the relatively positive NCHN δ^+ site of the imidazole ring with partly negative ligands like chloride ions. In β-MeBim there might be two such interactions between the imidazole ring of both MeBim ligands and the aza bond of the respectively *fac*-oriented azpy ligands.

In summary, taking into account that, for symmetry reasons the two HH rotamers in α-[Ru(azpy)$_2$(MeBim)$_2$](PF$_6$)$_2$ each represent two (identical) atropisomers, seven out of the eight possible orientations of the two MeBim ligands shown in Figure 4 are observed.[5,10] The isomeric complex β-MeBim, however, shows only one stable atropisomer, i.e. the HT isomer R5 (Figure 4).

From the discussion of the possible orientation of the non-tethered MeBim ligands in β-MeBim, it is concluded that only one stable atropisomer is to be expected. For the investigation of atropisomers in *cis*-[Ru(bpy)$_2$(L)$_2$](PF$_6$)$_2$ complexes, the mdbz ligand [bis(1-methyl-2-benzimidazolyl)-ethane] has been used to prepare the complex *cis*-[Ru(bpy)$_2$(mdbz)](PF$_6$)$_2$. In this mdbz complex, the two MeBim moieties are oriented as in the R1 atropisomer (A in the previous paper)[9] but are tethered, and therefore rotation of the imidazole ligands around the Ru−N axes cannot be expected and is indeed not observed. On reaction of β-[Ru(azpy)$_2$(NO$_3$)$_2$] with mdbz, however, no β-[Ru(azpy)$_2$(mdbz)](PF$_6$)$_2$ could be obtained at all. From a space-filling model of β-[Ru(azpy)$_2$(mdbz)](PF$_6$)$_2$, and from Figure 4, it is clear that the didentate ligand mdbz cannot coordinate in a bifunctional mode to the β-bis(azpy) isomer in such a way as to adopt the HT atropisomer R5, as the imidazole moieties in the R5 orientation are too distant. On the other hand, to adopt the HT orientation from atropisomer R1, one phenyl ring of the mdbz should be coordinated wedged in between the pyridine rings of the two azpy ligands. The "tail" part of the mdbz in β-[Ru(azpy)$_2$(mdbz)](PF$_6$)$_2$ should be wedged in between the phenyl rings of the two azpy ligands. In particular, the phenyl rings of the two azpy ligands are prevent the second benzimidazole moiety of the mdbz from coordinating to the ruthenium ion. (See the Supporting Information where the hypothetical structure of β-[Ru(azpy)$_2$(mdbz)](PF$_6$)$_2$ is drawn schematically.) This indicates that the (main) HT conformation in which the benzimidazole ligands coordinate to the *cis*-[Ru(bpy)$_2$] is not possible for the β-[Ru(azpy)$_2$] complex, and confirms the mdbz to be a good model ligand for an HT interaction in which the imidazole sites of the MeBim ligands are pointing towards each other.

(De)Shielding Effects

Because of the different (de)shielding effects caused by the different orientations of the MeBim ligands, the probe protons shift characteristically, as is nicely illustrated for the three main atropisomers found[5,10] in α-[Ru(azpy)$_2$(MeBim)$_2$](PF$_6$)$_2$ and the three atropisomers observed[8,9] in *cis*-[Ru(bpy)$_2$(MeBim)$_2$](PF$_6$)$_2$. In β-MeBim only one atropisomer is observed, and therefore the relative shifts of the probe protons in different atropisomers cannot be discussed. However, a few remarkable proton resonances do require further discussion.

The most upfield-shifted aromatic proton signal appears to be the H(iv) resonance at δ = 5.30 ppm. In the free ligand the H(iv) proton resonance is observed at δ = 7.6 ppm, and in the *cis*-[Ru(bpy)$_2$(MeBim)$_2$](PF$_6$)$_2$ complex at δ = 7.1−7.2 ppm for the atropisomer R2/R3 and R4 (atropisomers B and C, respectively, as mentioned in the corresponding previous publications).[8,9] In the α-[Ru(azpy)$_2$(MeBim)$_2$](PF$_6$)$_2$ complex the most upfield-shifted H(iv) resonance signals are at δ = 6.1 and 6.2 ppm,[5,10] and belong to the least abundant atropisomer R6/R7. The exceptional upfield shift of H(iv) in β-MeBim can be nicely explained by the strong shielding effect of the proximate phenyl ring of the azpy ligand (see Figure 9).

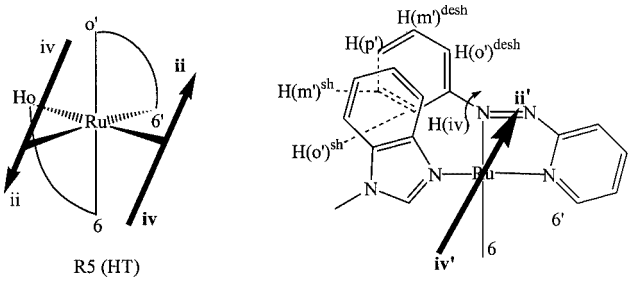

Figure 9. Schematic representation of the atropisomer R5 of β-MeBim (left) and projection along the MeBim′−Ru axis (right); the overlap and consequential mutual shielding effects of the six-membered rings of the azpy phenyl group and the MeBim ligand is visualized

It is most likely that some kind of stacking interaction is present, with H(iv) oriented just above the slowly flipping phenyl ring, which most of the time is oriented parallel and face-to-face with the MeBim six-membered ring. Consecutively, the two phenyl ring H(*o*) protons, once having become inequivalent due to the slow rotation of the ring around the C−N axis, are, in turn, expected to shift characteristically due to the shielding effect of the six-membered ring of the MeBim ligand. In fact, one resonance [δ = 6.1 ppm, H(*o*)^{sh}] is shifted strongly upfield whilst the other is deshielded [δ = 8.3 ppm, H(*o*)^{desh}] and shifted downfield. The H(*m*′) protons show a similar effect {δ = 6.3 [H(*m*′)^{sh}] and 7.6 ppm [H(*m*′)^{desh}]}, albeit with a frequency difference, $\Delta\nu$, less extreme than observed for the H(*o*) resonances (660 and 390 Hz, respectively).

From Figure 9 the mutual shielding effect of the azpy phenyl ring and the MeBim six-membered ring is evident. The H(*o*′)^{sh} signal is assigned to the proton which is oriented just above the shielding cone of the MeBim six-mem-

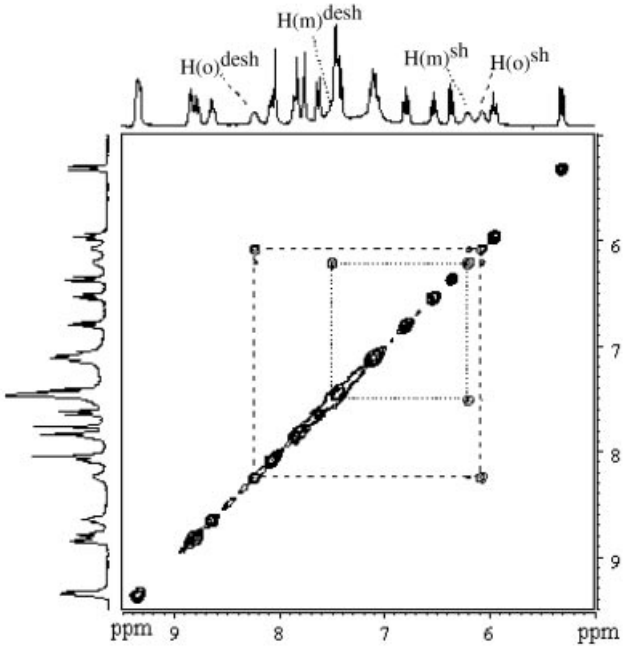

Figure 10. EXSY level of the ROESY spectrum of β-MeBim in [D$_6$]acetone at −95 °C; the H(*o′*) and H(*m′*) exchange peaks are indicated with dashed and dotted lines, respectively

bered ring, whilst the H(*o′*)^{desh} signal is attributed to the other H(*o′*) proton. NOE cross peaks between H(*o′*) and H(iv) would unambiguously confirm this orientation; however, none are observed. At −95 °C the phenyl ring is still flipping as can be concluded from the cross peaks observed in the EXSY level of a ROESY spectrum (Figure 10). The H(*o′*) resonance is too broad to detect any NOE interaction. However, all assignments and conclusions agree well with the results of the analogous 1,2-dimethylimidazole complex, in which the phenyl ring is rotating even more slowly on the NMR timescale than in the analogous MeBim complex, and the signals of the phenyl ring protons are sharper.[18]

Exchange Mechanism

The kinetics of exchanging systems can be studied by 1D and/or 2D NMR spectroscopic techniques. At higher temperatures a broadening of signals is observed for β-MeBim which might be due to rotational behavior of the MeBim ligands. The broadening of the peaks is not the result of interchanging rotamers present at low temperatures. The energy input upon increasing the temperature might allow the interconversion of the atropisomers R5 into (one of the) other atropisomers. In the highly symmetric system *cis*-[Ru(bpy)$_2$(4Pic)$_2$](PF$_6$)$_2$, in which the four rotamers present are all identical,[19] the thermodynamic parameters of the rotation of a heterocyclic six-ring ligand, 4-picoline, could be determined. The phenyl ring rotation in complex β-MeBim is observed to be relatively independent from the other rotational processes in the temperature range between −95 °C and −50 °C. However, close to the temperatures where the coalescence of the H(*o′*)^{desh} and H(*o′*)^{sh}, and the H(*m′*)^{desh} and H(*m′*)^{sh} signals are expected, the other signals of β-MeBim are also broadening, indicating that another rotational process is occurring. Besides the fact that the coalescence temperature of the phenyl ring protons is difficult to observe because of overlap with other signals, the occurrence of other dynamic processes in the same temperature region severely complicates the calculation of the thermodynamic parameters.

Conclusion

The synthesis and characterization of the bifunctional coordinated ruthenium(II) complexes β-[Ru(azpy)$_2$(L)$_2$](PF$_6$)$_2$ provides detailed information of the steric properties of the β-[Ru(azpy)$_2$] moiety. Both MeIm ligands in β-MeIm can rotate freely on the NMR timescale at all recording temperatures. The MeBim ligands in β-MeBim, in contrast to MeBim in the analogous complexes α-[Ru(azpy)$_2$(MeBim)$_2$](PF$_6$)$_2$ and *cis*-[Ru(bpy)$_2$(MeBim)$_2$](PF$_6$)$_2$, do not orient in different ways on the ruthenium ion at low recording temperatures, and only one atropisomer is observed. By using NMR techniques, including COSY and NOESY, the complete structural characterization of the conformation has been carried out, and the MeBim ligands appear to be oriented in an HT orientation similar to that found in the isomeric complex α-[Ru(azpy)$_2$(MeBim)$_2$](PF$_6$)$_2$. An interesting observation is that the steric hindrance of the MeBim ligands is such that the rotation of the phenyl rings of one of the two azpy ligands is hindered. At very low temperatures the rotation is just at slow exchange on the NMR timescale, causing all five phenyl-ring protons to become inequivalent. This stacking interaction probably stabilizes the observed atropisomer.

The results for α-[Ru(azpy)$_2$(MeBim)$_2$](PF$_6$)$_2$ and β-[Ru(azpy)$_2$(MeBim)$_2$](PF$_6$)$_2$ might indicate that the cytotoxic effect of the α-[Ru(azpy)$_2$Cl$_2$] complex is not due to a (static) interaction with the DNA bases in an HT configuration, which is observed in the main atropisomer of all three complexes. The antitumor drug cisplatin coordinates in a *cis* bis(mode) to two neighboring guanine units in DNA, with the guanine units oriented in an HH conformation.[20] In the complex β-MeBim, neither of the two MeBim ligands appears to rotate around its Ru−N(iii) axis on the NMR timescale. The 1D and 2D VT ^{1}H NMR studies on complexes of the type *cis*-[Ru(Xpy)$_2$(L)$_2$]$^{2+}$ (with Xpy being a didentate ligand like bpy or azpy, and L an imidazole ligand) confirm clearly that complexes of the type *cis*-[Ru(Xpy)$_2$(L)$_2$]$^{2+}$ are sterically borderline cases in which bifunctional coordination of lopsided heterocycles depends on relatively small differences in the ligands or in their mutual orientations. The 1D and 2D VT ^{1}H NMR study presented here is an elaborate, but informative, method for determining such small differences in the steric properties of complexes of the type *cis*-[Ru(Xpy)$_2$]$^{2+}$. Whether the coordination and/or fluxional properties of heterocyclic ligands to *cis*-[Ru(Xpy)$_2$]$^{2+}$-type ruthenium complexes is indeed crucial for the biological activity of the complexes is a sub-

ject that should be investigated further with other *cis*-[Ru(Xpy)$_2$]$^{2+}$ complexes, as well as with in vitro DNA binding studies.

The current data prove that coordination of heterocyclic bicyclic ligands to bpy and azpy complexes differs significantly. The β-[Ru(azpy)$_2$]$^{2+}$ moiety is sterically less versatile than the *cis*-[Ru(bpy)$_2$]$^{2+}$ and α-[Ru(azpy)$_2$]$^{2+}$ moieties. Therefore, the β isomer, which is biologically not as active as the α isomer, shows a relatively reduced affinity regarding coordination to the heterocyclic ligands. Besides the orientation of DNA bases to platinum complexes, also the (ligand) rotational properties are accepted to be important factors influencing the antitumor properties.[20] If these differences in orientational and rotational behavior can indeed explain the differences in biological activity of *cis*-dichlororuthenium complexes, then a systematic, extensive investigation of a series of complexes of the type *cis*-[Ru(Xpy)$_2$] is of paramount importance.

Experimental Section

Materials and Physical Measurements: 1-Methylimidazole (MeIm, Aldrich) and 1-methylbenzimidazole (MeBim, Sigma) were used without further purification. Hydrated $RuCl_3$ was used as received from Johnson Matthey; azpy and β-[Ru(azpy)$_2$(Cl)$_2$]·$CHCl_3$ were prepared according to literature procedures.[11] For the purification of β-Ru(azpy)$_2$(MeBim)$_2$](PF$_6$)$_2$ neutral aluminum oxide (Alumina Woelm N Super I) was used. The complex β-[Ru(azpy)$_2$-(NO$_3$)$_2$]·$CHCl_3$ was prepared as described elsewhere.[5,7] NMR measurements were performed as described before[8,9] at 300.13 MHz with a Bruker 300 MHz DPX spectrometer, equipped with a Bruker B-VT1000 variable-temperature unit. Concentrations were in the 0.01 M region or below.

Syntheses

β-Ru(azpy)$_2$(MeIm)$_2$](PF$_6$)$_2$ (β-MeIm): β-[Ru(azpy)$_2$(NO$_3$)$_2$]·$CHCl_3$ (0.15 g, 0.21 mmol) was dissolved in a mixture of 10 mL of water and 4 mL of acetone and stirred at room temperature for 24 h. After addition of an excess of 1-methylimidazole (0.78 g, 9 mmol), the solution was refluxed for 3 h, and after addition of NH_4PF_6, β-MeIm was isolated by filtration. Recrystallization from ethanol/water, and from acetone/diethyl ether resulted in a purple microcrystalline material. Yield 0.10 g (54%). $C_{30}H_{30}F_{12}N_{10}P_2Ru$ (921.63): calcd. C 39.10, H 3.28, N 15.2; found C 38.5, H 3.18, N 14.7.

β-Ru(azpy)$_2$(MeBim)$_2$](PF$_6$)$_2$ (β-MeBim): β-[Ru(azpy)$_2$(NO$_3$)$_2$]·$CHCl_3$ (0.15 g, 0.21 mmol) was dissolved in a mixture of 10 mL of water and 4 mL of acetone and stirred at room temperature for 24 h. An excess of 1-methylbenzimidazole (1.19 g., 9 mmol) was added and the solute was refluxed for 3 h. The solid isolated after addition of NH_4PF_6 was recrystallized from ethanol/water and further purified by column chromatography with acetone/methanol (99:1) as eluent. Yield 0.060 g. (42%).^{1}H NMR spectroscopic data indicate the presence of a co-crystallized acetone molecule. $C_{38}H_{34}F_{12}N_{10}P_2Ru$·$(CH_3)_2CO$ (1079.83): calcd. C 45.6, H 3.73, N 12.9; found C 45.8, H 3.79, N 12.6.

Supporting Information: Schematic representation of the α and β isomers of Ru(azpy)$_2$L$_2$ species is given in Figure S1 (see also footnote on the first page of this article). A representation of the mdbz ligand and a hypothetical orientation of the mdbz ligand on the β-[Ru(azpy)$_2$] is given in Figures S2 and S3. The steric hindrance of the two phenyl rings of the two azpy ligands prevents the coordination of one of the MeBim moieties to the ruthenium ion.

Acknowledgments

One of the authors (J. R.) is indebted to Johnson−Matthey (Reading, UK) for their generous loan of $RuCl_3$·$3H_2O$. The support and sponsorship concerted by COST Action D8/0017/97 (Chemistry of Metals in Medicine) is kindly acknowledged. This research has also been financially supported by the Council for Chemical Sciences of the Netherlands Organisation for Scientific Research (CW-NWO). One of the authors (A. G. Q.) wants to thank the CICYT Spain (SAF00-0029).

Note added in proof (December 16, 2002): The assignment to this atropisomer is further confirmed by the observation of (very) weak NOE cross peaks from both H(ii) and H(ii)′ with the (overlapping) H3 and H3′ proton resonances (not visible in the present Figure 8).

[1] A. H. Velders, H. Kooijman, A. L. Spek, J. G. Haasnoot, D. de Vos, J. Reedijk, *Inorg. Chem.* **2000**, *39*, 2966−2967.
[2] M. J. Clarke, F. Zhu, D. R. Frasca, *Chem. Rev.* **1999**, *99*, 2511−34.
[3] A. Seal, S. Ray, *Acta Crystallogr., Sect. C* **1984**, *40*, 929−32.
[4] D. S. Eggleston, K. A. Goldsby, D. J. Hodgson, T. J. Meyer, *Inorg. Chem.* **1985**, *24*, 4573−80.
[5] A. H. Velders, PhD Thesis, Leiden University, The Netherlands, **2000**.
[6] A. C. G. Hotze, A. H. Velders, F. Ugozzoli, M. Biagini-Cingi, A. M. Manotti-Lanfredi, J. G. Haasnoot, J. Reedijk, *Inorg. Chem.* **2000**, *39*, 3838−3844.
[7] A. H. Velders, K. van der Schilden, A. C. G. Hotze, J. Reedijk, F. Ugozzoli, M. Biagini-Cingi, A. M. Manotti-Lanfredi, to be published.
[8] A. H. Velders, A. C. G. Hotze, J. G. Haasnoot, J. Reedijk, *Inorg. Chem.* **1999**, *38*, 2762−2763.
[9] A. H. Velders, A. C. G. Hotze, G. A. van Albada, J. G. Haasnoot, J. Reedijk, *Inorg. Chem.* **2000**, *39*, 4073−4080.
[10] A. H. Velders, A. C. G. Hotze, J. Reedijk, to be published.
[11] R. A. Krause, K. Krause, *Inorg. Chem.* **1980**, *19*, 2600−3.
[12] S. Goswami, A. R. Chakravarty, A. Chakravorty, *Inorg. Chem.* **1981**, *20*, 2246−50.
[13] T. Bao, K. Krause, R. A. Krause, *Inorg. Chem.* **1988**, *27*, 759−61.
[14] L. G. Marzilli, P. A. Marzilli, E. Alessio, *Pure Appl. Chem.* **1998**, *70*, 961−68.
[15] S. E. Sherman, D. Gibson, A. H. J. Wang, S. J. Lippard, *J. Am. Chem. Soc.* **1988**, *110*, 7368−81.
[16] A. H. Velders, A. C. G. Hotze, K. van der Schilden, J. Reedijk, H. Kooijman, A. L. Spek, to be published.
[17] L. G. Marzilli, M. Iwamoto, E. Alessio, L. Hansen, M. Calligaris, *J. Am. Chem. Soc.* **1994**, *116*, 815−16.
[18] A. H. Velders, A. G. Quiroga, unpublished results.
[19] A. H. Velders, C. Massera, F. Ugozzoli, M. Biagini-Cingi, A. M. Manotti-Lanfredi, J. G. Haasnoot, J. Reedijk, *Eur. J. Inorg. Chem.* **2002**, 193−198.
[20] S. O. Ano, Z. Kuklenyik, L. G. Marzilli, in *Cisplatin − Chemistry and Biochemistry of a Leading Anticancer Drug* (Ed.: B. Lippert), Verlag Helvetica Chimica Acta, Zürich, Wiley-VCH, Weinheim, **1999**.

Received August 5, 2002
[I02441]

New Molecular Charge-Transfer Salts of TM-TTF and BMDT-TTF with Thiocyanate and Selenocyanate Complex Anions [TMTTF = Tetramethyltetrathiafulvalene; BMDT-TTF = Bis(methylenedithio)tetrathiafulvalene]

Marta Mas-Torrent,[a] Scott S. Turner,[b] Klaus Wurst,[c] José Vidal-Gancedo,[a] Jaume Veciana,[a] Peter Day,*[b] and Concepció Rovira*[a]

Keywords: Charge transfer / Tetrathiafulvalene / Complex anions / Magnetic properties

Three new charge-transfer salts of tetrathiafulvalene (TTF)-based donors with thiocyanato- or selenocyanato-metal complex anions have been synthesised. The salts isolated were $[BMDT\text{-}TTF]_4[Cr(NCS)_6]$ (**1**), $[TM\text{-}TTF]_4[Cr(NCS)_6]\cdot 2CH_3CN$ (**2**) and $[TM\text{-}TTF]_4[Cr(NCSe)_6]\cdot 2CH_3CN$ (**3**) [BMDT-TTF = bis-(methylenedithio)tetrathiafulvalene and TM-TTF = tetramethyltetrathiafulvalene]. Single crystals of compound **1** crystallise in the monoclinic $C2/c$ space group with a = 37.286(3), b = 10.0539(6), c = 21.069(2) Å, β = 124.348(4)°, V = 6520.9(9) Å^3 and Z = 4. Compound **3** was also suitable for an X-ray diffraction study, however the anionic part, $[Cr(NCSe)_6]^-$ was highly disordered and the best solution gave a final R factor of 16.4%. A solution was found for the monoclinic space group $C2/m$ with a = 13.787(3), b = 19.507(3), c = 14.735(5) Å, β = 102.90(3)°, V = 3862.9(17) Å^3 and Z = 2. For compound **1** there are several S···S close atomic contacts between the donors and acceptors, but there is no discernible magnetic exchange between ions. Such an interaction was previously observed in related salts such as $[TTF][Cr(NCS)_4(phenanthroline)_2]$ and $[donor][M(NCS)_4(isoquinoline)_2]$ [M = Cr, Fe and donor = TTF, BEDT-TTF or TM-TTF (tetramethyltetrathiafulvalene)]. Compounds **1** to **3** are all paramagnetic semiconductors in which the magnetic susceptibility is dominated by the Cr-containing anions. The structure-function relationship, along with a comparison with related compounds, indicates that there is no long-range magnetic order because there are no π-stacking interactions between donor and acceptor; these types of interactions are seen in all of the bulk magnets of this type in which the donor spin is magnetically coupled to the anion.
(© Wiley-VCH Verlag GmbH & Co. KGaA, 69451 Weinheim, Germany, 2003)

Introduction

With the discovery of metallic properties in molecular organic compounds,[1] large efforts have been devoted to the development of new organic conductors based on π-electron donors. Tetrathiafulvalene (TTF) and its analogues have to date provided the largest number of organic metals and superconductors.[2] Until relatively recently interest in this class of compounds was focused on their transport properties, whereas current synthetic efforts are aimed towards bringing together combinations of physical properties. Since the majority of TTF-based salts consist of discrete layers of cationic and anionic components, it should be possible to prepare new molecular-based materials in which electrical, optical and magnetic properties can coexist, by including different properties into the different layers. Components with magnetic properties can be introduced by anionic complexes with paramagnetic centres.[3−8] Of special interest to us is to establish electrical transport, even superconductivity, in a crystal lattice containing localised magnetic moments.[3,4] With the aim of obtaining salts with long-range magnetic ordering, together with conductivity properties, some research groups have been using bimetallic complexes as counterions to the TTF-based molecule.[4,5b] Some of us recently embarked on a different approach that consists of promoting strong interactions between the cationic and anionic sub-lattices so the electronic systems in the different networks can be coupled to achieve interesting magnetic properties.[7] For example, we prepared a range of TTF-based salts with strong donor-acceptor interactions and subsequently long-range ferrimagnetic order.[7] This was achieved by using anions of the type $[Cr(NCS)_4(N\text{-donor})_x]^-$, where N-donor = 1,10′-phenanthroline (x = 1)

[a] Institut de Ciència de Materials de Barcelona (CSIC), Campus Universitari de Bellaterra,
08193 Bellaterra, Catalunya, Spain,
Fax: (internat.) +34-93/580-5729
E-mail: cun@icmab.es
[b] The Royal Institution of Great Britain, Davy-Faraday Research Laboratory,
21 Albemarle Street, London, W1S 4BS, UK
Fax: (internat.) + 44-(0)20/7629-3569
E-mail: profpday@msn.com
[c] Institut für Allgemeine, Anorganische und Theoretische Chemie, Univ. Innsbruck,
Innrain 52a, 6020 Innsbruck, Austria
E-mail: Klaus.Wurst@uibk.ac.at

or isoquinoline ($x = 2$). The anions were designed to provide the opportunity for both π-stacking and close S···S contacts between the anion containing localised magnetic moments and the radical donor; the resulting ferrimagnetic compounds display both of these interactions. The question still remains, however, as to what role each of these interactions plays in promoting long-range magnetic ordering. Looking at this point we prepared salts using hexathiocyanato complexes, which can only have short S···S contacts between anions and cations. No magnetic order was observed.[8] However, the empirical conclusion that S···S contacts are less important than π-stacking for magnetic exchange interactions was preliminary, since other factors, such as the angle of overlap of S···S short contacts and the donor charge could, of course, be significant in promoting certain physical properties.

The purpose of the present work is to continue building a range of similar compounds for our investigation into the origin of the bulk ferrimagnetism found in this family of salts. We report on the synthesis and characterisation of novel charge-transfer salts based on TM-TTF (tetramethyltetrathiafulvalene) and BMDT-TTF [bis(methylenedithio)tetrathiafulvalene] with paramagnetic anions that can only provide S···S or S···Se interactions.[9]

Results and Discussion

Synthesis

The salts described here were synthesised by electrocrystallisation in conventional H-shaped electrocrystallisation cells with Pt electrodes. Black needle-shaped crystals of $[BMDT\text{-}TTF]_4[Cr(NCS)_6]$ (**1**) were obtained with BMDT-TTF as donor and $[C_9H_8N][Cr(NCS)_4(C_9H_7N)_2]$ [(C_9H_7N) = quinoline] as electrolyte in CH_2Cl_2 solution. The fact that the quinoline ligand is not present can only be explained by a ligand exchange during the electrocrystallisation due to the lability of the quinoline.[9] The isostructural salts $[TM\text{-}TTF]_4[Cr(NCS)_6]\cdot 2CH_3CN$ (**2**) and $[TM\text{-}TTF]_4[Cr(NCSe)_6]\cdot 2CH_3CN$ (**3**) were synthesised with TM-TTF as donor and the anions $[(C_2H_5)_4N]_3[Cr(NCS)_6]$ and $[(C_2H_5)_4N]_3[Cr(NCSe)_6]$, respectively, as electrolytes in a mixture of dichloromethane and acetonitrile.

Table 1. The collection and crystal-structure parameters for **1** and **3**

Compound	**1**	**3**
Chem. formula	$C_{38}H_{16}CrN_6S_{38}$	$C_{50}H_{54}CrN_8S_{16}Se_6$
a (Å)	37.286(3)	13.787(3)
b (Å)	10.0539(6)	19.507(3)
c (Å)	21.069(2)	14.735(5)
α (°)	90.00	90.0
β (°)	124.348(4)	102.90(3)
γ (°)	90.00	90.0
V (Å^3)	6520.9(9)	3862.9(17)
Z	4	2
Molecular weight	1826.85	1805.73
Crystal system	Monoclinic	Monoclinic
Space group	$C2/c$	C2/m
T (K)	223(2)	223(2)
Reflections [$I > 2\sigma(I)$]	2549	1234
$\rho_{calcd.}$ (g cm^{-3})	1.861	1.552
μ (mm^{-1})	1.433	3.444
R (F_0)	0.0371	0.1639
Rw (F_0^2)	0.0731	0.4066

Description of Crystal Structures

The collection data and crystal parameters for compounds **1** and **3** are given in Table 1. A standard ORTEP[13] diagram of the asymmetric unit of compound **1**, showing the atom numbering scheme and atoms as 50% thermal ellipsoids, is shown in Figure 1.

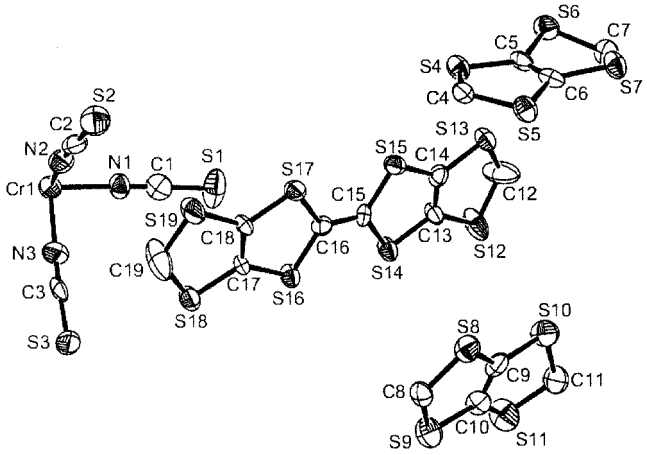

Figure 1. An ORTEP[13] diagram of the asymmetric unit of **1**, showing the atom numbering scheme and atoms as 50% thermal ellipsoids; the hydrogen atoms have been removed for clarity

As with many charge-transfer salts based on TTF-like donors the overall structure consists of alternating layers of cations and anions, as shown in Figure 2.

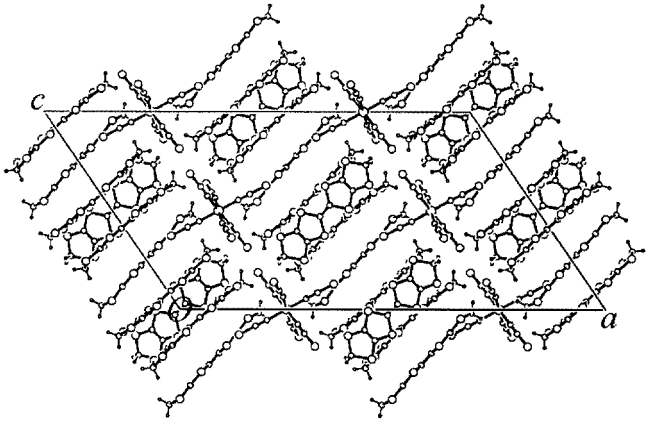

Figure 2. Unit cell diagram showing the overall molecular packing arrangement for **1**

Furthermore, in this salt the cationic BMDT-TTF layers are interpenetrated by two NCS ligands per anion. The packing arrangement for the donor molecules within each cationic layer in Figure 3 can be described in terms of two

types of rows. Row A, as marked in Figure 3, consists of a face-to-face BMDT-TTF dimer that alternates with a single donor molecule arranged perpendicular to the dimer. Row B, which lies between each type-A row, consists of single BMDT-TTF molecules that lie parallel to the dimers of row A, but are translated along the crystallographic *b* axis with respect to the dimers.

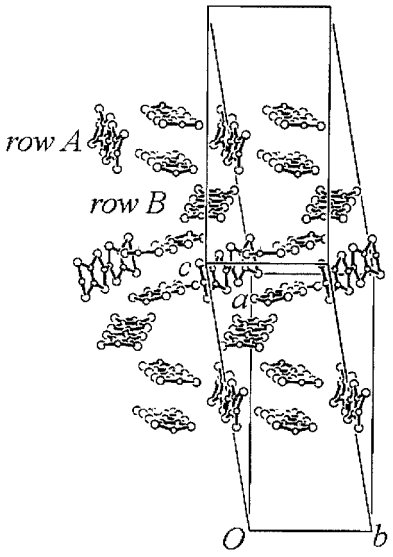

Figure 3. Packing motif of BMDT-TTF donors in compound **1**; the labels for rows A and B are described in the text

Furthermore, in successive instances of row A, the C=C central bonds of the donors are twisted by an angle of approximately 31° with respect to each other. Any close S···S intermolecular contacts are almost all in rows of type A and for the inter-dimer distances these range from 3.38 Å (S12···S6) to 3.50 Å (S15···S16). Between molecules of a dimer and the neighbouring perpendicular BMDT-TTF molecule in the same row they range from 3.43 Å (S14···S17) to 3.56 Å (S13···S4). There are only two close atomic contacts between rows A and B of 3.50 Å (S19···S10) and 3.57 Å (S17···S10). In addition there are a few atomic S···S contacts between the anions and cations even though an NCS ligand (with terminal S1) penetrates the cation layer. Each of these contacts is close to the sum of the van de Waals radii of two sulfur atoms, with values of 3.55, 3.57 and 3.60 Å for contacts S18···S3, S19···S2 and S7···S3, respectively. There are no significant atomic contacts between the anions, as the shortest distance between the terminal S atoms on neighbouring Cr complexes is just 4.06 Å.

For compound **3** the structure could only be refined to an *R* factor of 16%, mainly due to one-dimensional disorder of the anion layers and therefore this structure will not be discussed in detail. Nevertheless, the donor molecules are well ordered and are stacked along the *a* axis with intermolecular S···S distances of between 3.65 and 3.81 Å (Figure 4). The donor molecules between neighbouring stacks along the *c* axis have alternate distances due to the insertion of NCSe ligands. A simplified layout showing only Cr and Se atoms of the anionic layer, parallel to the crystallographic *ab* plane, is shown in Figure 5. The $CrSe_6$ units with filled bonds form a regular anionic sheet, although in this refinement all the positions have an occupancy factor of 0.5 except for the overlying Se(1) atoms along the *b* axis, which have a factor of 1.0. The one-dimensional disorder is caused by displacement of the regular layer with a half-lattice constant along the *a* direction.

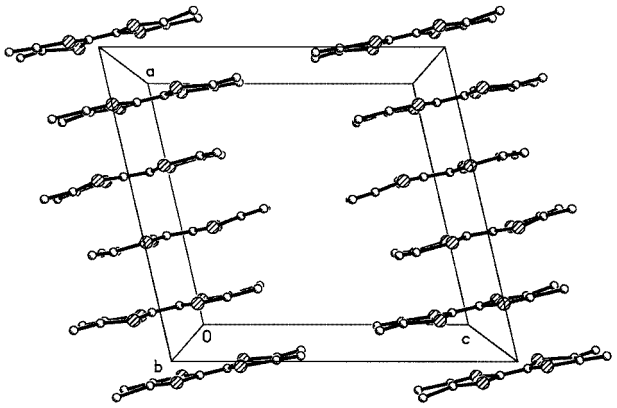

Figure 4. Packing motif of TM-TTF donors in compound **2** and **3**

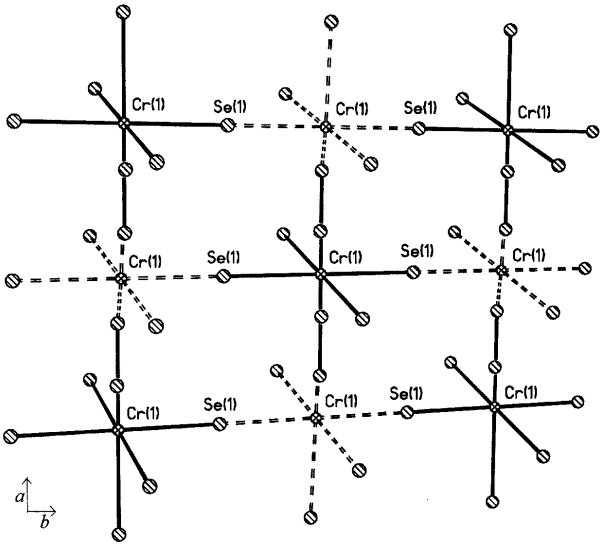

Figure 5. Two overlying $Cr(NCSe)_6^{3-}$ sheets showing one-dimensional disorder (see text)

Compound **2** crystallises in the same space group with nearly identical coordinates for all atoms and a similar one-dimensional disorder. The *R* value is about 18.5%, with unit cell parameters $a = 13.806(7)$, $b = 19.41(1)$, $c = 14.63(1)$ Å, $\beta = 103.03(4)°$ and $V = 3818.7(4)$ Å^3 at 223 K

Electrical Transport and Magnetic Properties

The conductivity behaviour for compound **1** was measured from 300 to 120 K. This compound shows a semiconducting behaviour with a modest room temperature conductivity (σ_{300K}) of 4×10^{-3} S cm^{-1} and an Arrhenius-like behaviour on decreasing the temperature with an activation energy (E_a) of 0.1 eV. For compound **2**, due to the crystal

morphology (elongated hexagonal plates), we were able to measure the electrical transport in three mutually perpendicular directions, although because of the small crystal size only two probe measurements were possible. For all three directions a plot of ln(resistance) vs. 1/T gave a straight line, i.e the Arrhenius behaviour of a semiconductor. Perpendicular to the plane of the plate $\sigma_{300K} = 2.26 \times 10^{-3}$ S cm^{-1} and $E_a = 0.05$ eV; in the plane of the plate, across the long direction of the elongated hexagon $\sigma_{300K} = 3.07 \times 10^{-3}$ S cm^{-1} and $E_a = 0.04$ eV; in the plane of the plate across the shorter direction $\sigma_{300K} = 6.02 \times 10^{-3}$ S cm^{-1} and $E_a = 0.04$ eV. For compound **3** it was only possible to measure along the needles long axis by standard four-probe methods and although a large σ_{300K} of 454.1 S cm^{-1} was found, the variation with temperature indicated semiconducting behaviour, with $E_a = 0.06$ eV (Figure 6).

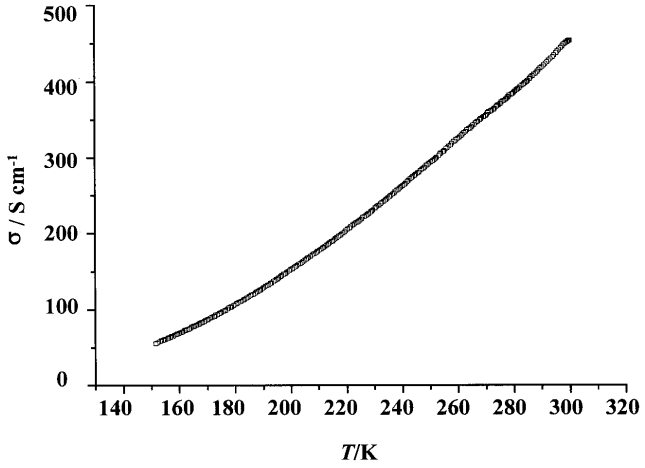

Figure 6. Plot of conductivity vs. temperature for compound **3**

The magnetic properties of **1** resemble a paramagnetic material in which the magnetic susceptibility is dominated by the metal complex. A plot of susceptibility vs. temperature was fitted well to the Curie−Weiss law and gave a Curie constant C of 2.49 emu K mol^{-1} and a small negative Weiss constant of $\theta = -1.1$ K. For compound **2** a similar fit gave C = 2.10 emu K mol^{-1} and $\theta = -0.05$ K; for compound **3** the values are C = 1.94 emu K mol^{-1} and $\theta = -0.28$ K. All of the salts gave a Curie constant greater than expected for a Cr^{III} spin 3/2 centre alone, for which a value of 1.875 emu K mol^{-1} is expected, indicating that the donor radical contributes to the measured susceptibility to some extent. The salts each show small negative Weiss values, which indicate that they all have a small number of short range antiferromagnetic interactions.

Spectroscopic Properties

The mixed-valence character of compounds **1**−**3** was confirmed by the presence of the characteristic broad A band in the IR and NIR-visible spectra, corresponding to the mixed-valence states of low-dimensional conducting organic solids, centred at 3300, 2400 and 2350 cm^{-1}, respectively.[14]

Since the size of the crystals for compound **1** was suitable, the degree of ionicity of the donor could be studied by Raman reflection spectrometry. It has been reported previously that there is an approximately linear dependence between the donor charge and the Raman-active C=C stretching frequencies in salts of the electron-donor molecule BEDT-TTF.[15] Raman spectra of the BMDT-TTF neutral donor shows two bands at 1501.9 and 1549.7 cm^{-1} in the C=C stretching region, while in salt **1** we can observe one band at 1438.6 cm^{-1}. Fitting this data to the equations used for BEDT-TTF, for salt **1** the donor charge was found to be 0.75, which is in agreement with the compound stoichiometry found by single crystal X-ray diffraction and elemental analysis. The Raman data further show that the charge is the same for each of the donor molecules, rather than being distributed unevenly.

EPR Spectroscopy

The EPR spectrum of **1** was carried out on a microcrystalline sample. One unique broad signal with a *g* factor of 2.0134 and a linewidth of 320 G was observed. Since no discrete signals were seen for the cation and anion this indicates that there is some electronic interaction between the spins of the different sites. The temperature dependence of the EPR signal for compound **1** was studied down to 108 K but no significant changes in its parameters were observed, revealing that there are no electronic phase-transitions down to this temperature. Compounds **2** and **3** both display a narrow EPR signal of 7.5 G with a *g* factor of 2.0076, which is consistent with the radical donor alone, and also show a very broad signal arising from the Cr^{III} spin, with a *g* factor of 1.8455. This shows that there are no electronic interactions between the anion and the radical donor. In order to examine the paramagnetic contribution of the donor network separately, the temperature dependence of the narrow signal was observed down to 4 K. The dependence of the double integral of this signal with temperature follows the Curie−Weiss law, with the rest of the signal parameters not changing to any significant extent.

Conclusions

We have described three new charge-transfer salts, including their synthesis and characterisation by magnetic susceptibility, electrical transport and spectroscopic measurements. One of the salts, $[BMDT\text{-}TTF]_4[Cr(NCS)_6]$ (**1**), was well characterised by single crystal X-ray diffraction. The remaining two compounds were found to be $[TM\text{-}TTF]_4[Cr(NCS)_6]\cdot 2CH_3CN$ and $[TM\text{-}TTF]_4[Cr(NCSe)_6]\cdot 2CH_3CN$. As observed in the crystal structure of **1** the only close atomic contacts between the anion and cation components are close S···S contacts at distances below the sum of the van de Waals radii of two sulfur atoms. It must also be assumed that the TM-TTF salts have either no anion to cation contacts or, more likely, they are also only those between chalcogenides. As a result each of the salts is a paramagnetic semiconductor, since there is no magnetic ex-

change between donor and acceptor molecules. Unlike the related salts based on $[Cr(NCS)_4$phenanthroline$]^-$ or $[Cr(NCS)_4(isoquinoline)_2]^-$ anions, which show magnetic exchange, the new salts have no mechanism for anion to cation π-stacking. At present we and others have made several salts, with different stoichiometries,[16] which only have close S···S or S···Se contacts between ions, and none of them show long range-magnetic order. Other salts have been made with other close contacts between ions, such as those involving halogens[17] or hydrogen bonding,[18] but so far only our approach with π-stacking has resulted in bulk magnetic materials with TTF-based donor-to-acceptor magnetic exchange. Therefore, our further efforts in this area will focus on the synthesis of TTF-based salts containing paramagnetic anions with aromatic ligands that can increase π-stacking interactions between the ions in an effort to increase magnetic critical temperatures beyond the current highest value of 8.9 K.

Experimental Section

Synthesis

The synthesis of BMDT-TTF was carried out as described previously.[10] TM-TTF was synthesised by a Wittig-type coupling with triethylamine as reported in the literature.[11] $[C_9H_8N][Cr(NCS)_4(C_9H_7N)_2]$, where C_9H_7N is quinoline, was prepared as described previously for the isoquinoline derivative,[7a] by a ligand-exchange reaction with Reinecke's salt, $NH_4[Cr(NCS)_4(NH_3)_2]$, on adding the corresponding nitrogen donor ligand and refluxing in ethanol overnight. $[(C_2H_5)_4N]_3[Cr(NCS)_6]$ and $[(C_2H_5)_4N]_3[Cr(NCSe)_6]$ were prepared by the published methods.[12]

Electrocrystallisation

The charge-transfer salts were synthesised by electrochemical crystallisation from freshly distilled dichloromethane or acetonitrile solutions (see below for details) in conventional H-shaped electrochemical cells with Pt electrodes at a constant temperature of 295(2) K over one week and at a constant current of 1 μA.

A suspension of $[C_9H_8N][Cr(NCS)_4(C_9H_7N)_2]$ (80 mg) in 50 mL of dichloromethane was prepared and, whilst stirring, 18-crown-6-ether was added slowly until the anion dissolved completely. Solid BMDT-TTF (10 mg) was placed on the anode arm and the remainder of the cell was filled with the solution of the Cr complex (total cell volume 60 mL). Black needle-shaped crystals suitable for X-ray diffraction were obtained and found to be $[BMDT\text{-}TTF]_4[Cr(NCS)_6]$ (**1**).

The compound $[(C_2H_5)_4N]_3[Cr(NCS)_6]$ or $[(C_2H_5)_4N]_3[Cr(NCSe)_6]$ (6 mg) was dissolved in 12 mL of a mixture of dichloromethane and acetonitrile (2:1 v/v). TM-TTF (3 mg) was placed in the anode compartment of the electrochemical cell and the remainder was filled with the solution of the anion (total cell volume 15 mL). The product salts are characterised as black elongated hexagonal plates of $[TM\text{-}TTF]_4[Cr(NCS)_6]$ $2CH_3CN$ (**2**) and thin dark needles of $[TM\text{-}TTF]_4[Cr(NCSe)_6]\cdot 2CH_3CN$ (**3**).

Physical Measurements

The magnetic measurements of polycrystalline and randomly orientated samples of **1**−**3**, held in gelatine capsules inside a plastic tube, were measured using a Quantum Design MPMS7 SQUID magnetometer. The core diamagnetism was estimated for each of the salts by using Pascal's constants.

Conductivity measurements were performed on an Oxford Instruments Maglab System 2000 with an electrical properties (EP) probe. Gold wires (0.0025 mm) were attached directly to the crystals using Au conductive paste, and then connected to the EP probe with an eight-pin integrated circuit plug, allowing simultaneous measurement of two samples by four-electrode techniques.

EPR spectra were obtained with a Bruker X-band ESP 300E spectrometer, equipped with a rectangular cavity, operating in the T102 mode. Spectra were recorded in the 2−400 K range using a Bruker variable-temperature unit and an Oxford Instruments EPR-900 cryostat, a field frequency lock ER 033M system and an NMR gaussmeter ER 035M.

Transmission spectra were measured for finely ground samples as a KBr pellet (about 1 wt.%) with a Nicolet 5ZDX interferometer with Fourier transform (400−4400 cm^{-1}) or a Varian Cary 5 spectrometer (3330−20000 cm^{-1}). The Raman spectrum of **1** was measured at room temperature on a Renishaw Ramascope System 1000 using a He-Ne laser (632.8 nm), a CCD detector, a slit width of 10 μm and a 10% neutral density filter.

X-ray diffraction data were collected at 223 K, on a Nonius Kappa CCD diffractometer with monochromatic Mo-K_α (λ = 0.71073 Å) radiation. Data were collected via φ and ω multiscans and reduced with the program DENZO-SMN without absorption correction. For compounds **2** and **3** several crystals were checked and four or five measurements were made with the best of them. Nevertheless, the refinement of the structures was not good due to one-dimensional disorder of the anionic lattice. This resulted in diffuse stripes being seen in the broad reflections of the diffraction images, which means that some diffuse scattering is included in the diffraction. Further problems with one-dimensional disorder lie in the variability of the diffraction, which usually produces extinction of some of the reflections and hence a change in the Bravais lattice could occur. Since the disorder only exists in the anionic part, the donor molecules are well ordered and the packing can be well established.

CCDC-179735 (**1**) and CCDC-179736 (**3**) contain the supplementary crystallographic data for this paper. These data can be obtained free of charge at www.ccdc.cam.ac.uk/conts/retrieving.html [or from the Cambridge Crystallographic Data Centre, 12, Union Road, Cambridge CB2 1EZ, UK; fax: (internat.) +44-1223/336-033; E-mail: deposit@ccdc.cam.ac.uk].

Acknowledgments

This work was supported by grants from the EC [TMR, ERBFMRX-CT980181], COST action D14/0003/99, DGI-Spain [BQU2000−1157], and Generalitat de Catalunya (2001SGR-00362). The work at the Royal Institution was supported by the UK Engineering and Physical Sciences Research Council. We thank Prof. R. Clark and Dr. S. Firth of University College London (UK) for access to the Ramascope.

[1] J. P. Ferraris, D. O. Cowan, V. Walatka, J. H. Perlstein, *J. Am. Chem. Soc.* **1973**, *95*, 948.

[2] J. M Williams, J. R. Ferraro, R. J. Thorn, K. D. Carlson, U. Geiser, H. H. Wang, A. M. Kini and M-H. Whangbo, *Organic Superconductors (Including Fullerenes): Synthesis, Structure, Properties, and Theory*, Prentice Hall, Englewood Cliffs, New Jersey, **1992**.

[3] [3a] A. W. Graham, M. Kurmoo, P. Day, *J. Chem. Soc., Chem. Commun.* **1995**, 2061. [3b] M. Kurmoo, A. W. Graham, P. Day, S. J. Coles, M. B. Hursthouse, J. L. Caufield, J. Singleton, F. L. Pratt, W. Hayes, L. Ducasse, P. Guionneau, *J. Am. Chem. Soc.* **1995**, *117*, 12209.
[4] E. Coronado, J. R. Galán-Mascarós, C. J. Goméz-García, V. Laukhin, *Nature* **2000**, *408*, 447.
[5] [5a] M. Kurmoo, P. Day, P. Guionneau, G. Bravic, D. Chasseau, L. Ducasse, M. L. Allan, I. D. Marsden, R. H. Friend, *Inorg. Chem.* **1996**, *35*, 4719. [5b] E. Coronado, J. R. Galán-Mascarós, C. Jiménez-Sainz, C. J Gómez-García, *Adv. Mater. Opt. Electron* **1998**, *8*, 61. [5c] H. Kobayashi, T. Naito, A. Sato, K. Kawano, A. Kobayashi, H. Tanaka, T. Saito, M. Tokumoto, L. Brossard, P. Cassoux, *Mol. Cryst. Liq. Cryst. Sci. Technol., Sect. A* **1996**, *284*, 61. [5d] C. J. Kepert, M. Kurmoo, M. R. Truter, P. Day, *J. Chem. Soc., Dalton Trans.* **1997**, 607. [5e] P. LeMagueres, L. Ouahab, N. Conan, D. J. Gómez-García, P. Delhaes, J. Even, M. Bertault, *Solid State Commun.* **1996**, *97*, 27.
[6] [6a] L. Martín, S. S. Turner, P. Day, F. E. Mabbs, E. J. L McInnes, *Chem. Commun.* **1997**, 1367. [6b] S. S. Turner, P. Day, D. E. Hibbs, K. M. Abdul Malik, M. B. Hursthouse, S. Teat, E. J. MacLean, L. Martin, S. A. French, *Inorg. Chem.* **1999**, *38*, 3543.
[7] [7a] S. S. Turner, C. Michaut, S. Durot, P. Day, T. Gelbrich, M. B. Hurtshouse, *J. Chem. Soc., Dalton Trans.* **2000**, 905. [7b] S. S. Turner, D. Le Pevelen, P. Day, K. Prout, *J. Chem. Soc., Dalton Trans.* **2000**, 2739.
[8] S. S. Turner, P. Day, T. Gelbrich, M. B. Hursthouse, *J. Solid State Chem.* **2001**, *159*, 385.
[9] Partial sections of this work have been published previously as a conference proceeding: M. Mas-Torrent, S. S. Turner, K. Wurst, J. Vidal-Gancedo, J. Veciana, C. Rovira, P. Day, *Synth. Met.* **2001**, *120*, 799.
[10] Kato, Y. Sasaki, H. Kobayashi, *Chem. Lett.* **1984**, 993.
[11] [11a] K. Bechgaard, D. Cowan, A. N. Bloch, L. Henriksen, *J. Org. Chem.* **1975**, *40*, 746. [11b] L.-Y. Chiang, P. Shu, D. Holt, D. Cowan, *J. Org. Chem.* **1983**, *48*, 4713. [11c] N. C. Gonella, M. P. Cava, *J. Org. Chem.* **1978**, *43*, 369. [11d] J. Llacay, I. Mata, E. Molins, J. Veciana, C. Rovira, *Adv. Mater.* **1998**, *4*, 330.
[12] A. Sabatini, I. Bertini, *Inorg. Chem.* **1965**, *4*, 959.
[13] [13a] C. K. Johnson, *ORTEP*, Report ORNL-5138, Oak Ridge National Laboratory, Oak Ridge, TN **1976**. [13b] L. J. Farrugia, *J. Appl. Cryst.* **1997**, *30*, 565.
[14] J. B. Torrance, B. W. Scott, F. B. Kaufman, P. E. Seiden, *Phys. Rev. B* **1979**, *19*, 730.
[15] H. H. Wang, J. R. Ferraro, J. M. Williams, U. Geiser, J. A. Schlueter, *J. Chem. Soc., Chem. Commun.* **1994**, 1893.
[16] S. S. Turner, D. Le. Pevelen, P. Day, K. Prout, *J. Sol. State Chem.* in press for publication in special issue devoted to Molecular Metals.
[17] D. Thoyon, K. Okabe, T. Imakubo, S. Golhen, A. Miyazaki, T. Enoki, L. Ouahab, *Mol. Cryst. & Liq. Cryst.*, in press.
[18] L. Martin, S. S. Turner, P. Day, P. Guionneau, J. K. Howard, D. E. Hibbs, M. E. Light, M. B. Hursthouse, M. Uruichi, K. Yakushi, *Inorg. Chem.* **2001**, *40*, 1363.

Received August 1, 2002
[102443]

Syntheses and Structures of Layered Copper(II) Diphosphonates with Mixed Ligands

Ping Yin,[a] Yang Peng,[a] Li-Min Zheng,*[a,b] Song Gao,[b] and Xin-Quan Xin[a]

Keywords: Organic-inorganic hybrid composites / Phosphonates / Copper / N ligands

This paper describes the syntheses and crystal structures of two new copper(II) diphosphonates with mixed ligands: $[Cu_3(hedpH)_2(4,4'\text{-bipy})(H_2O)_2]\cdot 2H_2O$ (**1**) and $[Cu_3(hedpH)_2(4,4'\text{-azpy})(H_2O)_2]\cdot 1.6H_2O$ (**2**) (hedp = 1-hydroxyethylidenediphosphonate, 4,4′-bipy = 4,4′-bipyridine, 4,4′-azpy = 4,4′-azobispyridine). Both adopt a two-dimensional layer structure containing neutral ladder-like chains of $\{Cu_3(hedpH)_2(H_2O)_2\}_n$ linked by 4,4′-bipy or 4,4′-azpy ligands. The adjacent layers are held together by strong hydrogen bonds, thus generating a three-dimensional network with rectangular shaped channels. The lattice water is found in these channels. The magnetic properties of compounds **1** and **2** have also been investigated.

(© Wiley-VCH Verlag GmbH & Co. KGaA, 69451 Weinheim, Germany, 2003)

Introduction

Research on metal phosphonates is undergoing rapid expansion because of their potential applications in the areas of sorption, ion exchange, catalysis, sensors, and nonlinear optics.[1−5] Many efforts have been devoted to the exploration of metal phosphonate materials with new structure types, especially open-framework structures.[6−10] Among the metal phosphonates reported so far, the number of copper phosphonates is still limited. Most of them were prepared by direct reactions of copper salts and phosphonic acids.[11−16] By introducing a second organic ligand, a few copper phosphonates with mixed ligands have been synthesised, including a dodecanuclear cage compound containing 3,5-dimethylpyrazole.[17−19] We are interested in both the structures and magnetic properties of copper diphosphonates based on 1-hydroxyethylidenediphosphonate [hedp, $CH_3C(OH)(PO_3)_2^{4-}$], and a series of compounds have been obtained using a template approach.[20] In order to construct open-framework structures of Cu-hedp compounds, we tried to introduce a second bridging ligand into the system, and compound $[Cu_4(hedp)_2(pz)(H_2O)_4]$, with a three-dimensional structure, was prepared successfully.[21] This compound also shows interesting metamagnetic properties. In this paper we report the syntheses and structures of two new layered copper phosphonates containing 4,4′-bipyridine (4,4′-bipy) or 4,4′-azobispyridine (4,4′-azpy) ligands.

[a] State Key Laboratory of Coordination Chemistry, Coordination Chemistry Institute, Nanjing University, Nanjing 210093, P. R. China
Fax: (internat.) + 86-25/3314502
E-mail: lmzheng@netra.nju.edu.cn
[b] State Key Laboratory of Rare Earth Materials and Applications, Peking University, Beijing 100871, P. R. China

Results and Discussion

Crystal Structures of 1−2

The structures of $[Cu_3(hedpH)_2(4,4'\text{-bipy})(H_2O)_2]\cdot 2H_2O$ (**1**) and $[Cu_3(hedpH)_2(4,4'\text{-azpy})(H_2O)_2]\cdot 1.6H_2O$ (**2**) were determined by X-ray crystallography. Crystallographic and refinement details are listed in Table 3, with selected bond lengths and angles in Table 1 for **1** and Table 2 for **2**. The fundamental building unit of **1** is shown in Figure 1, with the atomic labeling scheme. Apparently, there are two types

Table 1. Selected bond lengths [Å] and angles [deg] for **1**

Cu(1)−O(1)[a]	1.922(4)	Cu(1)−O(4)	1.970(4)
Cu(2)−O(3B)	1.915(3)	Cu(2)−O(2)	1.949(3)
Cu(2)−O(5)	2.004(3)	Cu(2)−N(1)	2.025(6)
Cu(2)−O(1w)	2.191(4)	Cu(2)−N(1′)	2.037(6)
P(1)−O(1)	1.507(4)	P(1)−O(2)	1.527(3)
P(1)−O(3)	1.514(4)	P(2)−O(4)	1.501(4)
P(2)−O(5)	1.519(3)	P(2)−O(6)	1.562(4)
O(1)−Cu(1)−O(4)	92.66(16)	O(3B)−Cu(2)−O(2)	158.76(16)
O(3B)−Cu(2)−O(5)	88.35(14)	O(2)−Cu(2)−O(5)	92.61(14)
O(3B)−Cu(2)−N(1)	89.0(3)	O(2)−Cu(2)−N(1)	87.3(3)
O(5)−Cu(2)−N(1)	172.3(3)	O(3B)−Cu(2)−O(1w)	103.19(16)
O(2)−Cu(2)−O(1w)	97.82(15)	O(5)−Cu(2)−O(1w)	95.97(16)
N(1)−Cu(2)−O(1w)	91.6(3)	P(1)−O(1)−Cu(1)	128.2(2)
P(1)−O(2)−Cu(2)	129.1(2)	P(1)−O(3)−Cu(2C)	140.0(2)
P(2)−O(4)−Cu(1)	125.1(2)	P(2)−O(5)−Cu(2)	130.9(2)
C(3)−N(1)−Cu(2)	122.9(4)	C(7)−N(1)−Cu(2)	120.0(4)

[a] Symmetry code: A, $-x + 1, -y, -z$; B, $x - 1, y, z$; C, $x + 1, y, z$.

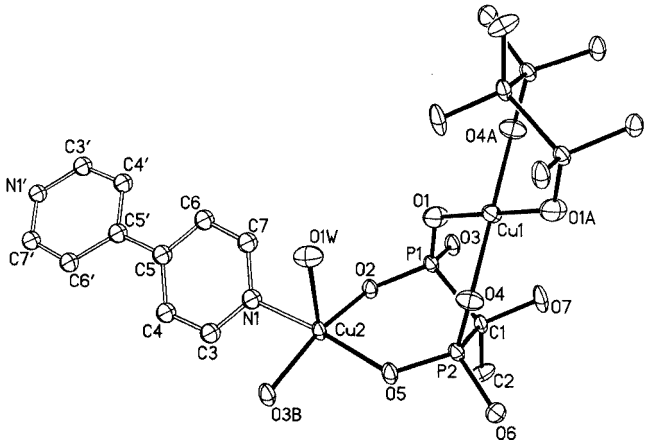

Figure 1. Building unit of **1** with the atomic labeling scheme (50% probability)

of copper atoms. The Cu(1) atom, sitting at an inversion center, has a square-planar environment. The four coordination sites are provided by two pairs of oxygens [O(1), O(4)] from two equivalent $hedpH^{3-}$ ligands. The Cu(2) atom resides in a general position, and bears a distorted square-pyramidal coordination geometry. The basal positions are filled with three phosphonate oxygens from two $hedpH^{3-}$ groups and one nitrogen atom from a 4,4′-bipyridine ligand. The largest deviation of the basal plane, defined by O(2), O(5), O(3B), and N(1), is 0.112(7) Å at O(3B). The Cu(2) atom lies out of this plane by 0.243(3) Å. The apical position is occupied by O(1w) from the water molecule. The Cu−O bond lengths are similar to those in other copper phosphonates, although the Cu(2)−O(1w) distance is slightly longer [2.192(4) Å]. The Cu(2)−N(1) bond length [av. 2.031(6) Å] is in agreement with that in $[\{Cu(dmp)(MeCN)\}_2(\mu\text{-}4,4'\text{-bipy})]^{2+}$ [2.070(4) Å].[22]

Each $hedpH^{3-}$ group in **1** serves as a bis-chelating ligand, and bridges the Cu(1) and Cu(2) atoms using four of its six phosphonate oxygens. One of the remaining two oxygen atoms, O(3), is further linked to the equivalent Cu(2) atom, forming an infinite chain along the [100] direction (Figure 2). The O(6) atom is protonated [P(2)−O(6) 1.562(4) Å]. The ladder-like chains are connected by 4,4′-bipy ligands, forming a zigzag layer in the (101) plane (Figures 2 and 3). These layers are held together by strong interlayer hydrogen bonds between the phosphonate ligands. The shortest inter-layer O···O distances are 2.594(5) and 2.757(5) Å for O(6)···O(7)^{i} and O(7)···O(5)^{ii}, respectively (symmetry code: i, $-x+1$, $-y+2$, $-z$; ii, $x+1$, y, z). Hence, a three-dimensional open network structure is constructed with rectangular channels generated along the *a* axis. The lattice water resides in these channels (Figure 3).

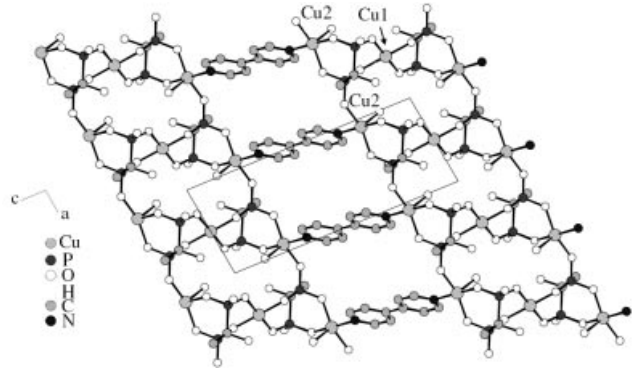

Figure 2. One layer of structure **1** viewed along the *b* axis; all the H atoms and half of the disordered 4,4′-bipy are omitted for clarity

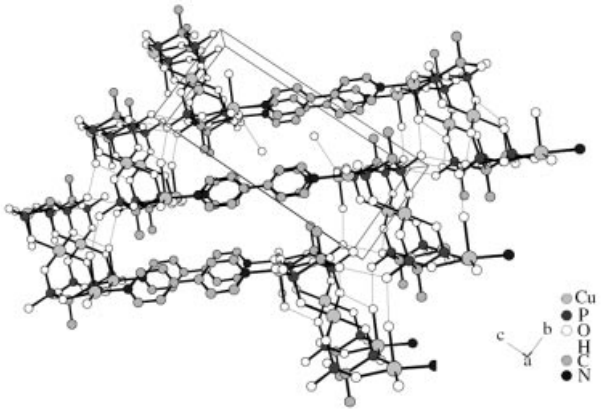

Figure 3. Structure of **1** packed along the *a* axis; all the H atoms and half of the disordered 4,4′-bipy are omitted for clarity

The structure of compound **2** is analogous to that of **1**, except that 4,4′-bipy is replaced by a longer bi-functional ligand 4,4′-azpy (Figure 4, Table 2). It also has a layer structure in which the ladder-like chains of $\{Cu_3(hedpH)_2(H_2O)_2\}$ are connected by 4,4′-azpy (Figure 5). As the ligand is arranged approximately along the [001] direction, the *c* axis in **2** (16.071 Å) is longer than that in **1** (15.469 Å). Strong interlayer hydrogen bonds are also observed.

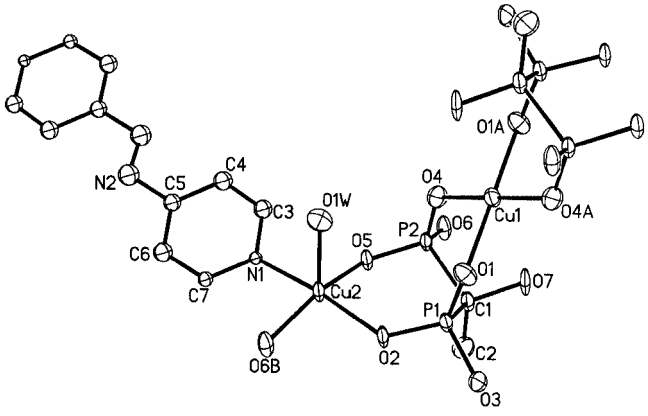

Figure 4. Building unit of **2** with the atomic labeling scheme (50% probability); all the H atoms and half of the disordered 4,4′-azpy are omitted for clarity

The layer structures of compounds **1** and **2** are different from that of $[Cu_4(hedp)_2(pz)(H_2O)_4]$,[21] where a three-dimensional open-framework structure is observed. Although all three contain similar layers built up from $\{Cu_3(hedp)_2(H_2O)_2\}$ double chains and bifunctional organic linkages, the contacts between the layers are completely different. In compounds **1** and **2**, it is mainly the hydrogen bonds between the phosphonate or hydroxy oxy-

Table 2. Selected bond lengths [Å] and angles [deg] for **2**

Cu(1)−O(4)[a]	1.930(3)	Cu(1)−O(1)	1.964(3)
Cu(2)−O(6B)	1.916(3)	Cu(2)−O(5)	1.936(3)
Cu(2)−O(2)	2.022(3)	Cu(2)−N(1)	2.059(5)
Cu(2)−O(1w)	2.195(4)	Cu(2)−N(1X)	2.065(6)
P(1)−O(1)	1.502(4)	P(1)−O(2)	1.505(3)
P(1)−O(3)	1.569(3)	P(2)−O(4)	1.508(4)
P(2)−O(5)	1.525(3)	P(2)−O(6)	1.507(3)
O(4)−Cu(1)−O(1A)	87.05(15)	O(6B)−Cu(2)−O(5)	159.16(15)
O(6B)−Cu(2)−O(2)	88.46(13)	O(5)−Cu(2)−O(2)	92.09(13)
O(6B)−Cu(2)−N(1)	89.0(2)	O(5)−Cu(2)−N(1)	87.1(2)
O(2)−Cu(2)−N(1)	170.7(2)	O(6B)−Cu(2)−O(1w)	102.12(15)
O(5)−Cu(2)−O(1w)	98.56(14)	O(2)−Cu(2)−O(1w)	95.62(14)
N(1)−Cu(2)−O(1w)	93.7(2)	P(1)−O(1)−Cu(1)	125.0(2)
P(1)−O(2)−Cu(2)	130.5(2)	P(2)−O(6)−Cu(2C)	140.0(2)
P(2)−O(4)−Cu(1)	127.9(2)	P(2)−O(5)−Cu(2)	129.6(2)
C(7)−N(1)−Cu(2)	123.3(4)	C(3)−N(1)−Cu(2)	118.3(4)

[a] Symmetry code: A, $-x + 1$, $-y + 1$, $-z + 1$; B, $x - 1$, y, z; C, $x + 1$, y, z.

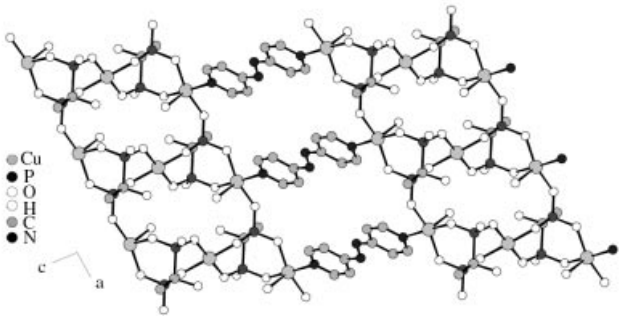

Figure 5. One layer of structure **2** viewed along the *b* axis; all the H atoms and half of the disordered 4,4′-azpy are omitted for clarity

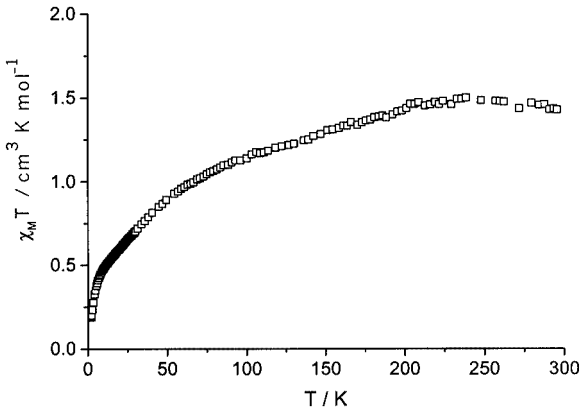

Figure 6. The $\chi_M T$ vs. T plot for **1**

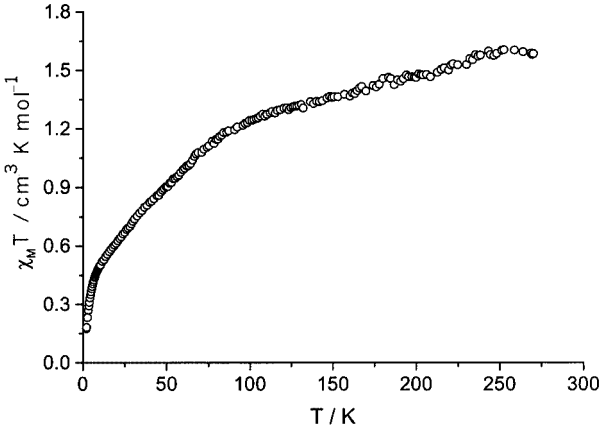

Figure 7. The $\chi_M T$ vs. T plot for **2**

gens of the $\{Cu_3(hedp)_2(H_2O)_2\}$ chains that connect the layers into a supramolecular network. In compound $[Cu_4(hedp)_2(pz)(H_2O)_4]$, however, the $\{Cu_3(hedp)_2(H_2O)_2\}$ chains from the neighboring layers are linked by CuO_4 units through corner-sharing of CPO_3 tetrahedra and CuO_4 planes, forming a unique open-framework structure. This structure can also be viewed as being composed of $\{Cu_4(hedp)_2(H_2O)_2\}$ layers and pz linkages. Furthermore, the phosphonate oxygens in compound $[Cu_4(hedp)_2(pz)(H_2O)_4]$ are all deprotonated, while in compounds **1** and **2** one oxygen is protonated in order to balance the overall charges and to stabilize the lattice through interlayer hydrogen bonds.

Magnetic Properties

Figure 6 shows the temperature-dependent magnetic susceptibility for **1** in the form of a $\chi_m T$ vs. T plot. The effective magnetic moment at 295 K, calculated from $\mu_{eff} = 2.828(\chi_m T)^{1/2}$, is 3.38 μ_B per Cu_3, in agreement with the calculated value (3.00 μ_B) for three isolated spin 1/2 nuclei. Upon cooling, $\chi_m T$ decreases continuously, and more steeply below 10 K towards zero, indicating a dominant antiferromagnetic interaction. The magnetic behavior of **2** is very similar to that of **1** (Figure 7).

Both compounds **1** and **2** have a layer structure made up of $\{Cu_3(hedp)_2(H_2O)_2\}$ chains and organic linkages. Between the layers, the magnetic interactions are very weak because the shortest Cu···Cu distance is 7.009 Å. The exchange coupling within the layer can be propagated either through the organic bridging ligand or through the O−P−O units. Considering that the Cu···Cu distances through the 4,4′-bipyridine and 4,4′-azobispyridine ligands are 11.165 (for **1**) and 13.087 Å (for **2**), the bulk magnetic behavior should be mainly attributed to the $\{Cu_3(hedp)_2(H_2O)_2\}$ chain. Within the double chain, the Cu(1)···Cu(2) distance through the O−P−O bridge is ca. 4.8 Å, and the Cu(2)···Cu(2) distance is ca. 6.2 Å (Figure 2). The exchange between Cu(1) and Cu(2) should be more efficient. The susceptibility data were thus analyzed by an expression based on a topological 1D ferrimagnet model.[23] This theoretical fitting was, however, unsuccessful. It is worth noting that, for a homometallic chain like $\{Cu_3(hedp)_2(H_2O)_2\}$, the odd number of magnetic centers should result in a ferrimagnetic behavior within the chain. The overall antiferromagnetic interactions observed in compounds **1** and **2** could be due to the dominant antiferromagnetic exchange couplings between the chains through the organic linkages and/or space at low temperature.

Conclusion

Two new copper(II) diphosphonates $[Cu_3(hedpH)_2(4,4'\text{-bipy})(H_2O)_2]\cdot 2H_2O$ (**1**) and $[Cu_3(hedpH)_2(4,4'\text{-azpy})(H_2O)_2]\cdot 1.6H_2O$ (**2**) have been reported in this paper. Their structures are two-dimensional with strong inter-layer hydrogen-bond interactions. Within the layer, the ladder-like chains of $\{Cu_3(hedpH)_2(H_2O)_2\}_n$ are linked by 4,4′-bipy or 4,4′-azpy ligands. The magnetic studies show that both compounds exhibit dominant antiferromagnetic interactions. The results demonstrate that novel metal phosphonates may be anticipated by combining with second organic ligands.

Experimental Section

Materials and Methods: The 50% aqueous solution of 1-hydroxyethylidenediphosphonic acid ($hedpH_4$) was purchased from Nanjing Shuguang Chemical Factory. All other starting materials were reagent grade and used as purchased. The elemental analyses were performed with a PE 240C elemental analyzer. The infrared spectra were recorded on a Nicolet 170SX FT-IR spectrometer with pressed KBr pellets. Thermal analyses were performed in nitrogen in the temperature range 20−600 °C with a heating rate of 5 °C/min on a TGA-DTA V1.1B TA Inst 2100. Variable-temperature magnetic susceptibility data were obtained on polycrystalline samples (27.9 mg for **1**, 27.5 mg for **2**) from 2 to ca. 300 K in a magnetic field of 10 kOe after zero-field cooling using a MagLab System 2000 magnetometer. Diamagnetic corrections were estimated from Pascal's constants.[24]

Synthesis of $[Cu_3(hedpH)_2(4,4'\text{-bipy})(H_2O)_2]\cdot 2H_2O$ (1): A mixture of $Cu(NO_3)_2\cdot 3H_2O$ (1 mmol, 0.2450 g), 4,4′-bipy (1 mmol, 0.1543 g), 50% $hedpH_4$ (2.5 mmol, 1 cm^3), 1 M NaOH (6 cm^3), and water (2 cm^3) with a pH of approximately 3 was transferred to a Teflon-lined autoclave (25 cm^3) and kept at 165 °C for 48 h. After slow cooling, blue plate-like crystals were obtained together with some yellow flocculent material. The blue crystals were isolated and their purity judged by a powder X-ray diffraction measurement. These crystals were further used for the structural determination and the physical property measurements. Yield: 22% based on Cu. $C_{14}H_{26}Cu_3N_2O_{18}P_4$: calcd. (found) C 20.73 (20.38), H 3.28 (3.18), N 2.85 (3.40). IR (KBr): $\tilde{\nu}$ = 3654 m, 3573 m, 3414 m, 3078 m, 2760 m, 1634 m, 1611 m, 1492 m, 1414 m, 1227 m, 1166 s, 1131 s, 1039 s, 940 s, 821 m, 674 m, 572 m, 444 m cm^{-1}.

When a molar ratio of Cu/4,4′-bipy/hedp/Na was 1:1:1.25:2 (pH ≈ 3), a similar hydrothermal reaction at 140 °C led to the same compound with a higher yield (58%). Thermal analysis of **1** showed two decomposition steps between 20 and 180 °C. The total observed weight loss (8.45%) is in agreement with the theoretical value (8.74%) for the removal of two lattices plus two coordinated water molecules.

Synthesis of $[Cu_3(hedpH)_2(4,4'\text{-azpy})(H_2O)_2]\cdot 1.6H_2O$ (2): A mixture of $Cu(NO_3)_2\cdot 3H_2O$ (1 mmol, 0.2440 g), 4,4′-azpy (1.1 mmol, 0.2081 g), 50% $hedpH_4$ (1.25 mmol, 0.5 cm^3), 1 M NaOH (2 cm^3), and water (6 cm^3) with a pH of approximately 3 was transferred to a Teflon-lined autoclave (25 cm^3) and kept at 140 °C for 48 h. After slow cooling, green crystals appeared as a single phase. Yield: 78% based on Cu. $C_{14}H_{27.2}Cu_3N_4O_{17.6}P_4$: calcd. (found) C 20.64 (19.81), H 3.19 (3.21), N 6.60 (6.61). IR (KBr): $\tilde{\nu}$ = 3575 m, 3413 m, 3093 m, 2771 m, 1605 m, 1484 w, 1421 m, 1166 s, 1130 s, 1039 s, 940 s, 827 m, 675 m, 574 s, 419 m cm^{-1}. Compound **2** can be obtained at pH = 1.6−3.6 with a Cu:hedp molar ratio of 1:2.5. Thermal analysis of **2** revealed that the total weight loss (7.14%) in the temperature range 30−160 °C corresponds to the release of 3.6 H_2O molecules (7.64%).

Crystallographic Studies: Single crystals of dimensions 0.30 × 0.30 × 0.20 mm for **1** and 0.40 × 0.05 × 0.05 mm for **2** were used for structure determinations (Table 3). Data corrections for compound **1** were made at room temperature on an Enraf−Nonius CAD-4 diffractometer equipped with graphite-monochromatized Mo-K_α radiation (λ = 0.71073 Å), operating in ω-2θ scanning mode. The unit cell parameters were obtained by least-squares refinement of 25 well-centred reflections. Intensity data were collected in the θ range 1.33−24.97°. Corrections for Lorentz and polarizaton factors were applied to the intensity values.

Table 3. Crystallographic data for **1**−**2**

Compound	**1**	**2**
Empirical formula	$C_{14}H_{26}Cu_3N_2O_{18}P_4$	$C_{14}H_{27.2}Cu_3N_4O_{17.6}P_4$
*F*w	824.87	847.7
Space group	$P\bar{1}$	$P\bar{1}$
a [Å]	6.2250(12)	6.2097(9)
b [Å]	7.0090(14)	7.0149(10)
c [Å]	15.469(3)	16.081(3)
α [deg]	90.73(3)	99.085(3)
β [deg]	97.41(3)	94.852(3)
γ [deg]	98.39(3)	97.937(3)
V [Å^3]	661.8(2)	681.02
Z	1	1
D [g·cm^{-3}]	2.070	2.062
μ(Mo-*Kα*) [cm^{-1}]	27.17	26.44
R_1, $wR_2[I > 2\sigma(I)]$[a]	0.0331, 0.1046	0.0484, 0.1366
R_1, wR_2(all data)[a]	0.0399, 0.1327	0.0547, 0.1467

[a] $R_1 = \Sigma||F_o| - |F_c||/\Sigma|F_o|$. $wR_2=[\Sigma w(F_o^2 - F_c^2)^2/\Sigma w(F_o^2)^2]^{1/2}$.

Data corrections for compound **2** were made at room temperature on a Bruker SMART APEX CCD diffractometer equipped with graphite-monochromatized Mo-K_α radiation (λ=0.71073 Å). A hemisphere of data was collected in the θ range 3.03−25.02° using a narrow-frame method with scan widths of 0.30° in ω and an exposure time of 20 s/frame. The data were integrated using the Siemens SAINT program,[25] with the intensities corrected for Lorentz factors, polarization, air absorption, and absorption due to variation in the path length through the detector faceplate. An empirical absorption correction was applied for both compounds.

The structures were solved by direct methods and refined on F^2 by a full-matrix least-squares procedure using SHELXL 97.[26] All the non-hydrogen atoms were refined anisotropically except the O atom of lattice water and the C and N atoms of 4,4′-bipy (for **1**) and 4,4′-azpy (for **2**). The latter are disordered and were refined isotropically. Hydrogen atoms were either put in calculated positions or found by Fourier syntheses, and were refined isotropically. The H atoms of lattice water were not located in either compound. In the final Fourier-difference map of **2** the deepest hole was −0.737 e·Å^3 and the highest peak 1.994 e·Å^3 [located near C(6); 1.729 Å]. The X-ray fluorescence spectrum measurement excludes the possible presence of Cl.

CCDC-184721 (**1**) and CCDC-184722 (**2**) contain the supplementary crystallographic data for this paper. These data can be obtained free of charge at www.ccdc.cam.ac.uk/conts/retrieving.html [or

from the Cambridge Crystallographic Data Centre, 12, Union Road, Cambridge CB2 1EZ, UK; Fax: (internat.) +44-1223/336-033; E-mail: deposit@ccdc.cam.ac.uk].

Acknowledgments

Support from the National Natural Science Foundation of China, Natural Science Foundation of Jiangsu Province and the Analysis Center of Nanjing University is gratefully acknowledged. The authors also thank Dr. J. D. Korp for valuable discussions, Mr. H.-Q. Wang and Mr. Y.-J. Liu for crystal data collection.

[1] G. Cao, H. Hong, T. E. Mallouk, *Acc. Chem. Res.* **1992**, *25*, 420.
[2] G. Alberti, U. Constantino, M. Casciola, R. Vivani, *Adv. Mater.* **1996**, *8*, 291.
[3] J. L. Snover, H. Byrd, E. P. Suponeva, E. Vicenzi, M. E. Thompson, *Chem. Mater.* **1996**, *8*, 1490.
[4] G. Huan, J. W. Johnson, A. J. Jacobson, J. S. Merola, *J. Solid State Chem.* **1990**, *89*, 220.
[5] G. Alberti, *Comprehensive Supramolecular Chemistry* (Ed.: J. M. Lehn); Pergamon, Elsevier Science, Ltd.: Oxford, U. K., **1996**, vol. 7.
[6] A. Clearfield, *Progress in Inorganic Chemistry* (Ed.: K. D. Karlin); John Wiley & Sons, Inc. New York, **1998**, vol. 47, pp. 371−510.
[7] K. Maeda, J. Akimoto, Y. Kiyozumi, F. Mizukami, *Angew. Chem. Int. Ed. Engl.* **1995**, *34*, 1199.
[8] V. Soghomonian, Q. Chen, R. C. Haushalter, J. Zubieta, *Angew. Chem. Int. Ed. Engl.* **1995**, *34*, 223.
[9] D. L. Lohse, S. C. Sevov, *Angew. Chem. Int. Ed. Engl.* **1997**, *36*, 1619.
[10] C. Serre, G. Ferey, *Inorg. Chem.* **1999**, *38*, 5370.
[11] D. M. Poojary, B. Zhang, A. Clearfield, *J. Am. Chem. Soc.* **1997**, *119*, 12550.
[12] D. M. Poojary, B. Zhang, P. Bellinghausen, A. Clearfield, *Inorg. Chem.* **1996**, *35*, 4942.
[13] Y. Zhang, A. Clearfield, *Inorg. Chem.* **1992**, *31*, 2821.
[14] J. Le Bideau, B. Bujoli, A. Jouanneaux, C. Payen, P. Palvadeau, J. Rouxel, *Inorg. Chem.* **1993**, *32*, 4617.
[15] J. Le Bideau, C. Payen, P. Palvadeau, B. Bujoli, *Inorg. Chem.* **1994**, *33*, 4885.
[16] M. Riou-Cavellec, M. Sanselme, N. Guillou, G. Ferey, *Inorg. Chem.* **2001**, *40*, 723.
[17] F. Cecconi, C. A. Ghilardi, P. A. L. Luis, S. Midollini, A. Orlandini, D. Dakternieks, A. Duthie, S. Dominguez, E. Berti, V. Vacca, *J. Chem. Soc., Dalton Trans.* **2001**, 211.
[18] R. C. Finn, J. Zubieta, *J. Chem. Soc., Dalton Trans.* **2000**, 1821.
[19] V. Chandrasekhar, S. Kingsley, *Angew. Chem. Int. Ed.* **2000**, *39*, 2320.
[20] L.-M. Zheng, H.-H. Song, X.-Q. Xin, *Comments, Inorg. Chem.* **2000**, *22*, 129.
[21] P. Yin, L.-M. Zheng, S. Gao, X.-Q. Xin, *Chem. Commun.* **2001**, 2346.
[22] A. J. Blake, S. J. Hill, P. Hubbersttey, J. Stroud, *J. Chem. Soc., Dalton Trans.* **1998**, 909.
[23] M. Drillon, E. Coronado, M. Belaiche, R. L. Carlin, *J. Appl. Phys.* **1988**, *63*, 3551.
[24] O. Kahn, *Molecular Magnetism*, VCH Publishers, Inc., New York, **1993**.
[25] SAINT, *Program for Data Extraction and Reduction*, Siemens Analytical X-ray Instruments, Madison, WI 53719, **1994−1996**.
[26] SHELXTL (*version 5.0) Reference Manual*, Siemens Industrial Automation, Analytical Instrumentation, Madison, WI, **1995**.

Received August 2, 2002
[I02444]

Synthesis, Crystal Structures and Magnetism of a Series of Heptanuclear Rare-Earth-Centered Trigonal Prism Clusters

Qin-De Liu,[a] Jun-Ran Li,*[a] Song Gao,*[a] Bao-Qing Ma,[a] Hui-Zhong Kou,[a] Liang Ouyang,[a] Rui-Li Huang,[b] Xi-Xiang Zhang,[c] and Kai-Bei Yu[d]

Keywords: Copper / Lanthanides / N ligands / O ligands / Template synthesis / Magnetic properties

A series of heptanuclear rare-earth-centered trigonal prism clusters $[LnCu_6(\mu\text{-}OH)_3(HL)_2(L)_4]\cdot(ClO_4)_2\cdot 25H_2O$ (Ln = La–Ho and Y; H_2L = iminodiacetic acid) was synthesized and their crystal structures were determined by X-ray diffraction. The rare-earth center and the copper ions are bridged by three μ_3-OH and six μ_2-O moieties from the carboxyl groups of six different ligands. The rare earth ion is nine-coordinate and the coordination polyhedron is an unusual, highly symmetrical tricapped trigonal prism (C_{3h}). The cluster has an interesting, highly symmetrical eclipsed structure (C_{3h}) which utilizes the central rare earth cation as a template. The temperature-dependence of the magnetic susceptibility of the cluster series was investigated and was found to vary with the central rare-earth ions. The magnitude of the antiferromagnetic interaction constants J between Cu^{2+} ions in $[LaCu_6]$ and $[YCu_6]$ were compared and estimated to be –24 cm^{-1} and –7 cm^{-1}, respectively, indicating a significant effect of the central diamagnetic ions.
(© Wiley-VCH Verlag GmbH & Co. KGaA, 69451 Weinheim, Germany, 2003)

Introduction

Heteronuclear transition-metal and rare-earth mixed complexes are of great interest due to their interesting structures and magnetic properties.[1−9] These compounds are very important in understanding the nature of magnetic exchange interactions between rare-earth and transition-metal ions. Potential applications can be found for them in magnetic materials.[2−8] However, previous magnetic investigations of these complexes have mostly focused on the nature of Gd−Cu coupling. Up until now, reports on Ln−Cu complexes other than those of Gd have been rather scarce.[6,10−13] Whereas magnetostructural correlations have been established in some transition-metal complexes,[14−21] little is known about the same correlation in polynuclear complexes containing both rare-earth and transition-metal ions.

Host-guest interactions have proven to be of paramount importance for the template synthesis of large magnetic clusters,[22−25] and one expects to learn more on how the guests influence the magnetic coupling in the clusters. Schröder and co-workers reported some heteronuclear complexes obtained by template assembly of metal aggregates using imino-carboxylate ligands.[26] In that work, a tetradentate ligand was used to synthesize complexes that containd various metal ions as templates. Recently we reported the structures and magnetic properties of $[LaCu_6]$ and $[TbCu_6]$ clusters.[13] As an extension of that work, a series of heptanuclear lanthanide-centered trigonal prism clusters $[LnCu_6(\mu\text{-}OH)_3(HL)_2(L)_4]\cdot(ClO_4)_2\cdot 25H_2O$ (Ln = Ce−Gd, Dy−Ho and Y; H_2L = iminodiacetic acid), were obtained at a considerably higher pH value (approx. 6.0), and their magnetic behaviors were studied in the context of their structures.

Results and Discussion

IR Spectra

Using $[GdCu_6]$ as an example, the IR resonances of the carboxylate moiety, ν_{as}(OCO) and ν_s(OCO), in free (H_2L) and coordinated (HL) ligands were compared. After coordination to the metal centers, the ν_{as}(OCO) absorption was found to have blue-shifted 45 cm^{-1}, from a value of 1583cm^{-1} to 1628 cm^{-1}; the ν_s(OCO) absorption at 1397cm^{-1} shifted 35 cm^{-1} up to 1432 cm^{-1}, and 19 cm^{-1}

[a] State Key Laboratory of Rare Earth Materials Chemistry and Applications, PKU-HKU Joint Laboratory on Rare Earth Materials and Bioinorganic Chemistry, College of Chemistry and Molecular Engineering,
Peking University, Beijing 100871, China
E-mail: lijunran@pku.edu.cn; gaosong@pku.edu.cn
[b] Department of Chemistry, Iowa State University, USA
[c] Department of Physics, The Hong Kong University of Science and Technology,
Clear Water Bay, Kowloon, Hong Kong
[d] Chengdu Center for Analysis and Measurement, Academia Sinica,
Chengdu 610041, China

down to 1378 cm^{-1}. This shows that the two carboxyl groups of the ligand bound to the metal ions have two coordination modes.[26] The value of ν_s(C−N) in the complex shifted 92 cm^{-1} down to 1118 cm^{-1}. These results indicate that the carboxyl groups and the N atom of the ligand are all coordinated to metal ions. The IR spectra of the other [$LnCu_6$] complexes are very similar to that of [$GdCu_6$].

Thermal Analysis

The thermal behavior of all eleven complexes is similar. For example, the crystalline compound [$GdCu_6$] begins to lose part of its crystal lattice water molecules at a surprisingly low temperature (around 30 °C), and the water-loss rate reaches a maximum at ca 56 °C. The complex loses a total of nine water molecules in the temperature range 30.0−60.0 °C (loss of weight found: 8.1%; loss of weight calculated based on the loss of nine water molecules: 8.0%). The thermal analysis results are in accordance with the elemental analysis results for all eleven complexes. Elemental analysis data are given in Table 1.

Table 1. Elemental analysis data

	Calcd. (found)		
	C (%)	H (%)	N (%)
$C_{24}H_{67}Cl_2Cu_6LaN_6O_{51}$	15.61 (15.27)	3.66 (3.45)	4.55 (4.57)
$C_{24}H_{67}CeCl_2Cu_6N_6O_{51}$	15.60 (15.67)	3.65 (3.60)	4.55 (4.53)
$C_{24}H_{67}Cl_2Cu_6N_6O_{51}Pr$	15.59 (15.67)	3.65 (3.70)	4.55 (4.62)
$C_{24}H_{67}Cl_2Cu_6N_6NdO_{51}$	15.56 (15.83)	3.65 (3.84)	4.54 (4.53)
$C_{24}H_{67}Cl_2Cu_6N_6O_{51}Sm$	15.51 (15.89)	3.63 (3.58)	4.52 (4.56)
$C_{24}H_{67}Cl_2Cu_6EuN_6O_{51}$	15.50 (15.57)	3.63 (3.53)	4.52 (4.57)
$C_{24}H_{67}Cl_2Cu_6GdN_6O_{51}$	15.45 (15.53)	3.62 (3.61)	4.51 (4.70)
$C_{24}H_{67}Cl_2Cu_6N_6O_{51}Tb$	15.44 (15.00)	3.62 (3.21)	4.50 (4.32)
$C_{24}H_{67}Cl_2Cu_6DyN_6O_{51}$	15.41 (15.49)	3.61 (3.56)	4.49 (4.48)
$C_{24}H_{67}Cl_2Cu_6HoN_6O_{51}$	15.39 (15.42)	3.61 (3.67)	4.49 (4.71)
$C_{24}H_{67}Cl_2Cu_6N_6O_{51}Y$	16.04 (16.36)	3.76 (3.71)	4.68 (4.90)

Description of Structures

X-ray diffraction analyses indicate that these complexes are isomorphous. Among them the crystal structures of the [$LaCu_6$] and [$TbCu_6$] complexes have been reported.[13] As a typical example, the structural features of [$SmCu_6$] will be discussed briefly. Figure 1 shows an ORTEP view of this complex. The Sm^{3+} ion is nine-coordinate and the coordination polyhedron can be described as a tricapped trigonal prism, which is highly symmetrical. The observed geometries of nine-coordinate lanthanide ions are usually asymmetrical monocapped square antiprism[28,29] or distorted tricapped trigonal prism.[30−32] This kind of highly symmetrical coordination polyhedron (C_{3h}) is very unusual among 4f-3d and 4f coordination compounds. The Cu^{2+} ions in the complex are all five-coordinate, exhibiting a distorted tetragonal pyramidal geometry. Crystal data, details of data collection, and refinement are listed in Table 2. Crystal cell parameters of all the complexes are listed in Table 3 and important bond lengths and angles are given in Table 4.

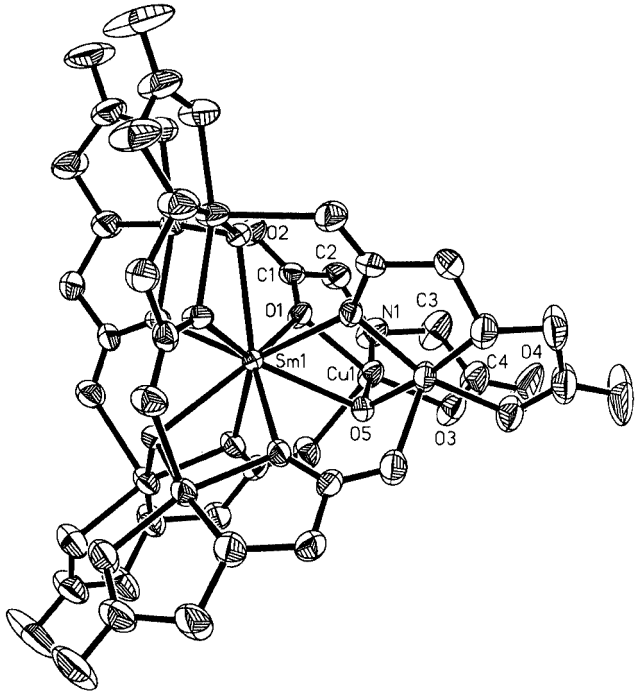

Figure 1. An ORTEP drawing of [$SmCu_6$]

The [$SmCu_6$] cluster consists of two parallel layers, with each layer being composed of three Cu^{2+}ions and three L's. The six Cu^{2+} ions form a trigonal prism (C_{3h}) with the Sm^{3+} ion located in the center (Figure 2). The Sm^{3+} ion lying between two layers is bridged to the six Cu^{2+} ions by three μ_3-OH groups and six μ_2-O atoms from six L's. Therefore, the two layers are connected by the nine-coordinate Sm^{3+} ion and three μ_3-OH groups. Each μ_3-OH is coordinated to the Sm^{3+} ion and two Cu^{2+} ions, one from each layer.

The structural features of the eleven complexes are practically the same, except that the volumes of the crystal cells are slightly different. This result shows that almost all the rare earth ions (except for Er, Tm, Yb, and Lu) can be centered in this type of [$LnCu_6$] complex. Crystals of these complexes were obtained at relatively high pH (approx. 6). Therefore, it can be considered that these complexes were assembled using a rare-earth cation as the template, and the process is also affected by the μ_3-bridged hydroxyl groups yielded from the slow hydrolysis of the rare earth ions while the pH value of the reaction mixture was adjusted with aqueous ammonia. From their crystal cell parameters (Table 3), we can see that the size of the trigonal prism cage formed by Cu^{2+} ions does not change much in the presence of different rare earth ions. This indicates that the radius of the template cation should be limited to within a certain range. Our failure to obtain complexes of Er, Tm, Yb and Lu similar to [$SmCu_6$] may be explained by the fact that the

Table 2 Crystallographic data for [$SmCu_6$] [$GdCu_6$] [$HoCu_6$] and [YCu_6]; space group $P6_3/m$

Empirical formula	$C_{24}H_{85}Cl_2Cu_6N_6O_{60}Sm$	$C_{24}H_{85}Cl_2Cu_6GdN_6O_{60}$	$C_{24}Cl_2Cu_6H_{85}HoN_6O_{60}$	$C_{24}H_{85}Cl_2Cu_6N_6O_{60}Y$
Color	blue	blue	blue	blue
Crystal size (mm)	0.25 × 0.23 × 0.17	0.48 × 0.38 × 0.30	0.30 × 0.30 × 0.20	0.31 × 0.25 × 0.19
Crystal system	Hexagonal	Hexagonal	Hexagonal	Hexagonal
Space group	$P6_3/m$	$P6_3/m$	$P6_3/m$	$P6_3/m$
a (Å)	12.6126(7)	12.6157(15)	12.587(2)	12.5840(18)
b (Å)	12.6126(7)	12.6157(15)	12.587(2)	12.5840(18)
c (Å)	24.4445(13)	24.415(6)	24.354(5)	24.415(5)
α (°)	90	90	90	90
β (°)	90	90	90	90
γ (°)	120	120	120	120
V (Å^3)	3367.6(3)	3365.2(10)	3341.5(10)	3348.3(10)
Z	2	2	2	2
M	2020.47	2027.36	2035.05	1959.02
D_c (g cm^{-3})	1.993	2.001	2.023	1.973
Absorption coefficient (mm^{-1})	2.931	3.039	3.246	2.940
F(000)	2042	2046	2052	1996
λ (Å) (Mo-K_α)	0.71073	0.71073	0.71073	0.71073
Monochromator	Graphite	Graphite	Graphite	Graphite
θ range for data collection (°)	1.67−28.33	2.04-25.00	2.05-25.01	3.64-25.00
Index range h; k; l	−11 to 16	0 to 14	0 to 12	0 to 14
	−16 to 15	−14 to 1	0 to 12	−12 to 0
	−32 to 32	0 to 29	0 to 28	−28 to 29
Reflections collected	23747	4587	2192	3909
Independent reflections	2870 (R_{int} = 7.78%)	2019 (R_{int} = 3.75%)	1919 (R_{int} = 6.55%)	2009 (R_{int} = 1.82%)
Observed reflections	2137 [$I > 2\sigma(I)$]	1519 [$I > 2\sigma(I)$]	1370 [$I > 2\sigma(I)$]	1787 [$I > 2\sigma(I)$]
Number of parameters refined	181	168	182	182
Final R	0.0588	0.0467	0.0487	0.0611
Final wR	0.1585	0.1246	0.1280	0.1676
Goodness-of-fit on F^2	1.055	0.966	1.038	1.040

Table 3. Crystal cell parameters of the [$LnCu_6$] complexes; space group $P6_3/m$

Complex	Color	Crystal system	a (Å)	b (Å)	c (Å)	α (°)	β (°)	γ (°)
[$LaCu_6$]	blue	hexagonal	12.6425(14)	12.6425(14)	24.541(5)	90	90	120
[$CeCu_6$]	blue	hexagonal	12.672(2)	12.672(2)	24.563(5)	90	90	120
[$PrCu_6$]	blue	hexagonal	12.677(2)	12.677(2)	24.538(5)	90	90	120
[$NdCu_6$]	blue	hexagonal	12.666(2)	12.666(2)	24.607(5)	90	90	120
[$SmCu_6$]	blue	hexagonal	12.6126(7)	12.6126(7)	24.445(13)	90	90	120
[$EuCu_6$]	blue	hexagonal	12.663(5)	12.663(5)	24.538(9)	90	90	120
[$GdCu_6$]	blue	hexagonal	12.6157(15)	12.6157(15)	24.415(6)	90	90	120
[$TbCu_6$]	blue	hexagonal	12.5802(9)	12.5802(9)	24.285(4)	90	90	120
[$DyCu_6$]	blue	hexagonal	12.619(8)	12.619(8)	24.454(5)	90	90	120
[$HoCu_6$]	blue	hexagonal	12.587(2)	12.587(2)	24.354(5)	90	90	120
[YCu_6]	blue	hexagonal	12.584(2)	12.584(2)	24.415(4)	90	90	120

radii of these ions are too small for them to be stably centered in the cage.

Magnetic Properties

The temperature dependence of the magnetic susceptibilities (χ_M) and of $\chi_M T$ for [$LaCu_6$], [$PrCu_6$], [$NdCu_6$], [$GdCu_6$], [$TbCu_6$], [$DyCu_6$], [$HoCu_6$], and [YCu_6] are shown in Figure 3 and Figure 4. The M···M (M = Ln or Cu) distances in some [$LnCu_6$] clusters are listed in Table 5.

It can be seen that the complexes exhibit different overall magnetic behaviors which seem to be dependent upon the different central rare earth ions within the [$LnCu_6$] complexes, even though all these complexes are isomorphous. Our previous results tells us that the magnetic interactions between the Cu^{2+} ions are antiferromagnetic in [$LaCu_6$], and there is a ferromagnetic coupling between the Tb^{3+} and Cu^{2+} ions in [$TbCu_6$].[13] The magnetic behavior of [$GdCu_6$], which shows an obvious ferromagnetic coupling between the Gd^{3+} and Cu^{2+} ions, is similar to that of [$TbCu_6$]. Referring to the structural data in Table 5, the M···M separations in [$GdCu_6$] are all very similar to those in [$TbCu_6$] (with a general difference of ca 0.01 Å). This may be an explanation for their similar magnetic behavior. For [$DyCu_6$], [$HoCu_6$], [$NdCu_6$], and [$PrCu_6$], the nature of the magnetic interactions between the Ln^{3+} and Cu^{2+} ions cannot be definitively defined because the magnetic behavior of these systems can be affected by many factors, such as the Ln−Ln, Cu−Cu, and Ln−Cu interactions, the

Table 4. Selected bond lengths (Å) and angles (deg) for [$SmCu_6$], [$GdCu_6$], [$HoCu_6$] and [YCu_6][a]

	[$SmCu_6$]	[$GdCu_6$]	[$HoCu_6$]	[YCu_6]
Ln−O1	2.464(4)	2.457(4)	2.421(7)	2.425(4)
Ln−O5	2.495(6)	2.489(6)	2.445(11)	2.438(6)
Cu−O1	1.973(4)	1.980(4)	1.977(8)	1.977(4)
Cu−O3	1.933(5)	1.940(5)	1.937((9)	1.939(4)
Cu−O5	1.933(3)	1.935(3)	1.935(6)	1.935(3)
Cu−N	1.961(6)	1.970(6)	1.958(10)	1.980(6)
Cu−O2A	2.310(5)	2.294(5)	2.278(9)	2.279(4)
O1−Ln−O1A	75.8(2)	75.48(17)	76.0(3)	75.57(15)
O1−Ln−O1C	89.6(2)	90.1(2)	89.4(4)	89.9(2)
O1−Ln−O1E	138.43(8)	138.61(8)	138.36(14)	138.57(7)
O1−Ln−O5	65.66(14)	66.11(13)	66.3(2)	66.11(14)
O1−Ln−O5B	72.89(15)	72.59(14)	72.2(3)	72.55(14)
O1−Ln−O5A	134.94(11)	134.76(11)	135.13(19)	134.82(10)
O5−Ln−O5B	120.000(1)	120.000(1)	120.010(4)	120.000(1)
O1−Cu−N	85.5(2)	85.2(2)	85.5(4)	85.8(2)
O1−Cu−O3	163.7(2)	163.8(2)	163.8(4)	163.74(19)
O1−Cu−O5	87.0(2)	87.1(2)	85.7(4)	85.4(2)
O1−Cu−O2A	94.8(2)	94.76(18)	94.9(3)	94.79(17)
O3−Cu−N	85.0(2)	85.4(2)	85.6(4)	85.2(2)
O3−Cu−O5	101.7(2)	101.4(2)	102.5(4)	102.7(2)
O3−Cu−O2A	98.8(2)	98.8(2)	99.0(4)	99.00(19)
O5−Cu−N	172.0(3)	171.9(3)	171.1(5)	170.9(3)
O5−Cu−O2A	91.4(2)	91.0(2)	90.4(4)	91.6(2)
N−Cu−O2A	91.8(2)	92.2(3)	92.1(5)	91.5(2)
Cu−O1−Ln	102.3(2)	102.07(18)	102.6(3)	102.62(16)
Cu−O5−Ln	102.5(2)	102.30(19)	103.1(4)	103.5(2)
Cu−O5−CuC	119.4(3)	118.8(3)	117.3(5)	118.4(3)

[a] Symmetry transformations used to generate equivalent atoms: A $-y+1, x-y+1, z$; B $-x+y, -x+1, z$; C $x, y, -z+1/2$; D $-y+1, x-y+1, -z+1/2$; E $-x+y, -x+1, -z+1/2$

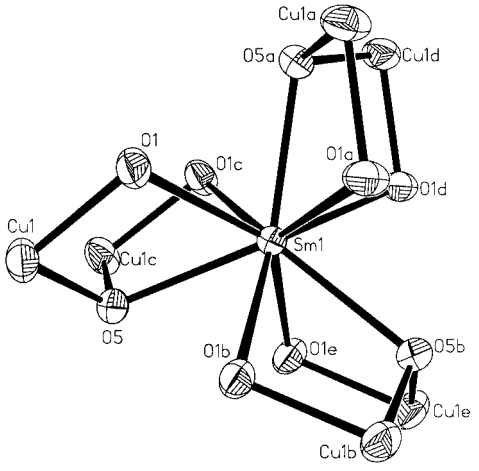

Figure 2. The trigonal prism cage formed by six Cu^{2+} and the bridges among Sm^{3+} and six Cu^{2+} (O5, O5C, O5E are from the three μ_3-OH; O1, O1A−O1E are from carboxyl groups of the six ligands)

ligand-field effects of the Ln^{3+} ion, and field saturation effects.

Figure 4 indicates that the interactions between the Cu^{2+} ions in [$LaCu_6$] and [YCu_6] are all antiferromagnetic in nature. However, the magnitudes of these antiferromagnetic interactions are different, and the J values are evaluated to

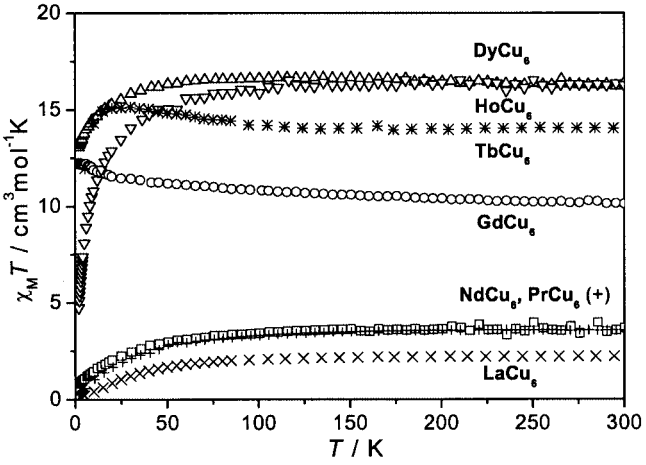

Figure 3. Plot of the magnetic susceptibilities (χ_M) and the $\chi_M T$ product vs. T for [$LaCu_6$], [$PrCu_6$], [$NdCu_6$], [$GdCu_6$], [$TbCu_6$], [$DyCu_6$], [$HoCu_6$]

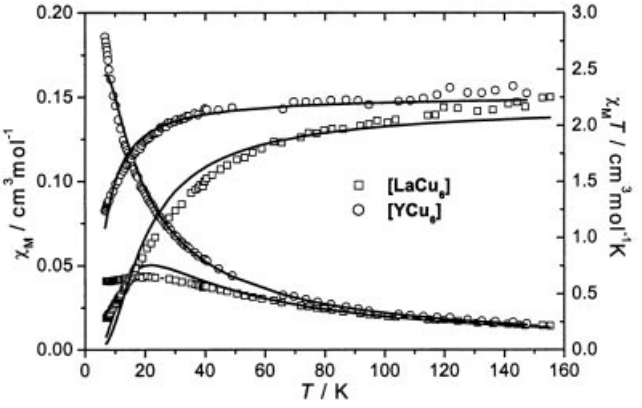

Figure 4. Plot of the magnetic susceptibilities (χ_M) and the $\chi_M T$ product vs. T for [$LaCu_6$] and [YCu_6]; solid lines show the best fit of the data

be $-24\ cm^{-1}$ and $-7\ cm^{-1}$ for [$LaCu_6$] and [YCu_6], respectively, using the same approach as previously[13] ($R = \Sigma(\chi_M T^{cal} - \chi_M T^{obs})^2/\Sigma(\chi_M T^{obs})^2 = 7.4 \times 10^{-3}$, and 9.7×10^{-4} for [$LaCu_6$] and [YCu_6], respectively). The difference in the J values shows the significant impact of the central diamagnetic ions, La^{3+} and Y^{3+}. Upon substitution of La^{3+} ion with Y^{3+} ion, the Cu···Cu distances decrease from 5.325 Å, 3.383 Å and 6.309 Å to 5.231 Å, 3.324 Å and 6.197 Å, the Ln···Cu distance deceases from 3.509 Å to 3.447 Å, and the Cu···O···Cu angle decreases from 120.7° to 118.4°. Therefore, the shorter ionic radius of Y^{3+} (1.075 Å), with respect to that of La^{3+} (1.216 Å), leads to a decrease in the size of the cage composed from the Cu^{2+} ions. The fact that the J value is larger in [$LaCu_6$] than in [YCu_6] reveals a dependency of J on the Cu···Cu separation and the Cu···O···Cu angle: smaller Cu···Cu separations and Cu···O···Cu angles lead to weaker antiferromagnetic exchange-coupling interactions between the Cu^{2+} ions for the systems in this paper. This result is consistent with the conclusion drawn previously,[17] showing that the direct overlap of metal orbitals plays a minor role, since it would enhance

Table 5. Selected M···M distances (Å) and Cu−O−Cu angles (deg)

	Cu···Cu (intra-layer)	Cu···Cu (inter-layer)	Ln···Cu	Cu−O−Cu
[$LaCu_6$]	5.325	3.383, 6.309	3.509	120.7
[$SmCu_6$]	5.271	3.337, 6.238	3.470	119.4
[$GdCu_6$]	5.258	3.331, 6.225	3.463	118.8
[$TbCu_6$]	5.245	3.319, 6.207	3.453	118.1
[$HoCu_6$]	5.233	3.304, 6.189	3.444	117.3
[YCu_6]	5.231	3.324, 6.197	3.447	118.4

antiferromagnetic coupling at shorter Cu···Cu separations. The encapsulated Ln^{3+} ion in the cage has a tuning effect on the magnetism of the core: the magnetic behavior is related to the ionic radius of the guest rare earth ion, which determines the exact geometry of the bridging ligands.

Conclusion

A series of highly symmetrical heptanuclear trigonal prism clusters, [$LnCu_6$], was assembled using rare earth cations as templates. The process is also affected by the μ_3-bridged hydroxyl groups. It was also shown that different central rare-earth ions in the cage significantly influence the magnetic behavior of these complexes.

Experimental Section

Physical Measurements: Elemental analysis was performed on a German Elementar Vario EL instrument. IR spectra were measured as KBr pellets with a Nicolet Magna-IR 750 spectrometer at 295 K. Thermal analyses were performed on a Du Pont 1090B thermal analyzer. Magnetic measurements were performed on a SQUID and an Oxford MagLab2000 System in the temperature range 2−300 K. Diamagnetic corrections were estimated on the basis of Pascal's constants. All starting materials were analytical reagents from Beijing Reagent Co. Sodium iminodiacetate (Na_2L) was obtained by the direct reaction of iminodiacetic acid with sodium hydroxide in an aqueous solution.

Preparations

$LnCu_6C_{24}H_{85}N_6Cl_2O_{60}$ (Ln =La−Ho and Y): All heptanuclear complexes (La−Ho,Y) were synthesized by first mixing copper perchlorate, the rare earth perchlorate and sodium iminodiacetate (1:1:1 mol ratio) in 10 cm^3 water under vigorous stirring, then carefully adjusting the pH value to about 6 with aqueous ammonia. The reaction mixture was left to stand at room temperature. After two days, deep-blue hexagonal prism crystals of $LnCu_6C_{24}H_{85}N_6Cl_2O_{60}$ (Ln = La−Ho and Y) were obtained and collected, with yields of ca 20%. Previous to the elemental analyses, the loosely bound waters of crystallization were eliminated by keeping the products at 60 °C until constant weights were reached. The results of elemental analysis are listed in Table 1. Similar crystals of the compounds with Ln = Er, Tm, Yb or Lu could not be obtained.

X-ray Crystallographic Study: All single-crystal X-ray experiments were performed on a Nonius CAD4 or Kappa CCD, or a Siemens P4 four-circle diffractometer. For example, with [$GdCu_6$], a crystal of dimensions 0.48 × 0.38 × 0.30 mm was mounted in a thin-walled capillary for the structure determination. Intensity data were collected on a Siemens P4 diffractometer with Mo-K_α radiation in the ω-scan mode. Lattice parameter were obtained from a least-squares refinement of 36 reflections in the range $6.22° \leq 2\theta \leq 33.14°$ and 2019 independent reflections were collected. Empirical absorption corrections were applied using the XPRED program. The structure was determined by direct methods and difference-Fourier syntheses, and refined by full-matrix least-squares using Siemens SHELXTL/PC system. The proton of the HL ligand in the complexes is assumed to have statistical distribution.

CCDC-135918 ($C_{24}H_{85}Cl_2Cu_6GdN_6O_{60}$), -135919 ($C_{24}H_{85}Cl_2Cu_6N_6O_{60}Sm$), -136464 ($C_{24}H_{85}Cl_2Cu_6HoN_6O_{60}$), and -170527 ($C_{24}H_{85}Cl_2Cu_6N_6O_{60}Y$) contain the supplementary crystallographic data for this paper. These data can be obtained free of charge at www.ccdc.cam.ac.uk/conts/retrieving.html [or from the Cambridge Crystallographic Data Centre, 12, Union Road, Cambridge CB2 1EZ, UK; fax: (internat.) +44-1223/336-033; E-mail: deposit@ccdc.cam.ac.uk].

Acknowledgments

This work was partly supported by the State Key Project of Fundamental Research (G1998061305), the National Science Fund for Distinguished Young Scholars (20125104) and NSFC (20023005), the Research Fund for the Doctoral Program of Higher Education (20010001020), and the Excellent Young Teachers Fund of MOE, P. R. C.

[1] A. J. Blake, V. A. Cherepeno, A. A. Dunlop, C. M. Grant, P. E. Y. Milne, J. M. Rawson, R. E. P. Winpenny, *J. Chem. Soc., Dalton Trans.* **1994**, 2719−2727.
[2] M. Andruh, I. Ramade, E. Codjovi, O. Guiliou, O. Kahn, J. C. Trombe, *J. Am. Chem. Soc.* **1993**, *115*, 1822−1829.
[3] R. Georges, O. Kahn, O. Guiliou, *Phys. Rev.* **1994**, *B49*, 3235−3242.
[4] M. Andruh, E. Bakalbassis, O. Kahn, J. C. Trombe, P. Porcher, *Inorg. Chem.* **1993**, *32*, 1616−1622.
[5] C. Benelli, A. Caneschi, D. Gatteschi, O. Guillou, L. Pardi, *J. Magn. Magn. Mater.* **1990**, *83*, 522−524.
[6] C. Benelli, A. Caneschi, D. Gatteschi, O. Guillou, L. Pardi, *Inorg. Chem.* **1990**, *29*, 1750−1755.
[7] A. Bencini, C. Benelli, A. Caneschi, A. Dei, D. Gatteschi, *Inorg. Chem.* **1986**, *25*, 572−575.
[8] A. Bencini, C. Benelli, A. Caneschi, R. L. Carlin, A. Dei, D. Gatteschi, *J. Am. Chem. Soc.* **1985**, *107*, 8128−8136.
[9] S. W. Keller, V. A. Carson, D. Sandford, F. Stenzel, A. M. Stacy, G. H. Kwei, M. Alario-Franco, *J. Am. Chem. Soc.* **1994**, *116*, 8070−8076.
[10] J. P. Costes, F. Dahan, A. Dupuis, J. P. Laurent, *Chem. Eur. J.* **1998**, *4*, 1616−1620.
[11] O. Kahn, O. Guillou, R. L. Oushoorn, M. Drillon, P. Rabu, K. Boubekeur, P. Batail, *New J. Chem.* **1995**, *19*, 655−660.

[12] M. L. Kahn, C. Mathoniere, O. Kahn, *Inorg. Chem.* **1999**, *38*, 3692−3697.
[13] Q. D. Liu, S. Gao, J. R. Li, Q. Z. Zhou, K. B. Yu, B. Q. Ma, S. W. Zhang, X. X. Zhang, T. Z. Jin, *Inorg. Chem.* **2000**, *39*, 2488−2492.
[14] R. D. Willet, D. Gatteschi, O. Kahn, *Magneto-structural Correlations in Exchange Coupled Systems*; NATO ASI Series; D. Reidel Publishing Company: Dordrecht, Holland, **1985**.
[15] H. Weihe, H. U. Güdel, *J. Am. Chem. Soc.* **1997**, *119*, 6539−6543.
[16] O. Waldmann, J. Schülein, A. Koch, P. Müller, I. Bernt, R. W. Saalfrank, H. P. Andres, H. U. Güdel, P. Allenspach, *Inorg. Chem.* **1999**, *38*, 5879−5886.
[17] G. L. Abbati, A. Cornia, A. C. Fabretti, W. Malavasi, L. Schenetti, A. Caneschi, D. Gatteschi, *Inorg. Chem.* **1997**, *36*, 6443−6446.
[18] H. Weihe, H. U. Güdel, *J. Am. Chem. Soc.* **1997**, *119*, 6539−6543.
[19] F. Le Gall, F. F. de Biani, A. Caneschi, P. Cinelli, A. Cornia, A. C. Fabretti, D. Gatteschi, *Inorg. Chim. Acta* **1997**, *262*, 123−132.
[20] B. Pilawa, R. Desquiotz, M. T. Kelemen, M. Weickenmeier, A. Geisselmann, *J. Magn. Magn. Mater.* **1998**, *177−181*, 748−749.
[21] A. Cornia, M. Affronte, A. G. M. Jansen, G. L. Abbati, D. Gatteschi, *Angew. Chem. Int. Ed.* **1999**, *38*, 2264−2266.
[22] T. L. Jorris, M. Kozik, L. C. W. Baker, *Inorg. Chem.* **1990**, *29*, 4584−4586.
[23] A. Müller, M. Penk, R. Rohlfing, E. Krickemeyer, J. Döring, *Angew. Chem. Int. Ed. Engl.* **1990**, *29*, 926−927.
[24] A. Caneschi, A. Cornia, S. J. Lippard, *Angew. Chem. Int. Ed. Engl.* **1995**, *34*, 467−469.
[25] A. Caneschi, A. Cornia, A. C. Fabretti, S. Foner, D. Gatteschi, R. Grandi, L. Schenetti, *Chem. Eur. J.* **1996**, *2*, 1379−1387.
[26] D. M. J. Doble, C. H. Benison, A. J. Blake, D. Fenske, M. S. Jachson, R. D. Kay, W. S. Li, M. Schröder, *Angew. Chem. Int. Ed.* **1999**, *38*, 1915−1918.
[27] K. Nakamoto, *Infrared Spectra of Inorganic and Coordination Compound*, 4th Ed., John Wiley & Sons Inc., New York, **1986**, 258.
[28] A. Bouayad, C. Brouca-Cabarrecq, J. C. Trombe, *Inorg. Chim. Acta* **1992**, *195*, 193−201.
[29] S. M. Bowen, E. N. Duesler, R. T. Paine, *Inorg. Chim. Acta* **1982**, *61*, 155−166.
[30] J. G. Mao, L. Song, J. S. Huang, *J. Chem. Crystallog.* **1998**, *28*, 475−479.
[31] J. G. Mao, L. Song, J. S. Huang, *Chin. J. Struc. Chem.* **1999**, *18*, 4−8.
[32] L. J. Radonovich, M. D. Glick, *Inorg. Chem.* **1971**, *10*, 1463−1468.

Received June 21, 2002
[I02334]

Spectroscopic and Structural Characterizations of Novel Water-Soluble Peroxo[polyaminocarboxylato bis(*N*-oxido)]niobate(v) Complexes

Daisy Bayot,[a] Bernard Tinant,[b] Benoît Mathieu,[b] Jean-Paul Declercq,[b] and Michel Devillers*[a]

Keywords: Niobium / Peroxo ligands / N,O ligands / NMR spectroscopy / IR spectroscopy

New water-soluble peroxo complexes of niobium(v) with polyaminocarboxylic acids (PAC) have been prepared and characterized by IR and NMR (^{1}H, ^{13}C, ^{15}N) spectroscopy, as well as by thermal analysis. The synthesis in presence of excess H_2O_2 leads to the oxidation of the nitrogen atoms of the PAC ligand into *N*-oxide groups. The compounds obtained correspond to the general formula $(A^I)_3[Nb(O_2)_2(LO_2)]\cdot xH_2O\cdot yH_2O_2$ [$A^I = NH_4^+$ or $CN_3H_6^+$ (gu) and L = edta, pdta] in which H_4LO_2 refers to the bis(*N*-oxide) derivative of the PAC ligand. The crystal structures of the guanidinium derivatives of the (edta)- and (pdta)Nb complexes have been determined, both showing an eight-coordinate Nb atom with two bidentate peroxo ligands and a quadridentate PAC bis(*N*-oxido) ligand, resulting in a distorted dodecahedral geometry. The structure of the guanidinium derivative of the edta bis(*N*-oxido) ligand is also described.
(© Wiley-VCH Verlag GmbH & Co. KGaA, 69451 Weinheim, Germany, 2003)

Introduction

Because multimetallic Nb-based oxides generate great interest as potential heterogeneous catalysts for several highly challenging industrial processes, like alkane oxidation or ammoxidation,[1−4] fundamental research on Nb coordination compounds that could be used as molecular precursors for the preparation of such catalysts, is definitely welcome. In particular, the aqueous chemistry of niobium is restricted to very few available precursors, some of them being poorly defined from the point of view of composition and molecular structure. Because peroxoniobium compounds are soluble in water, they are adequate candidates for that purpose. Several such complexes have already been described in the literature; they correspond either to homoleptic tetraperoxoniobates of general formula $(A^I)_3[Nb(O_2)_4]$ [$A^I = Na^+$, K^+, Rb^+, Cs^+, NH_4^+, and $CN_3H_6^+$ (guanidinium, gu^+)][5−7] or to heteroleptic carboxylato(peroxo) compounds such as $(A^I)_3[Nb(O_2)_3(L)]\cdot nH_2O$ ($A^I = K^+$ or NH_4^+ and L = tartrate, citrate, *o*-phenanthroline),[8−10] $(A^I)_3[Nb(O_2)_2(C_2O_4)_2]\cdot H_2O$ ($A^I = NH_4^+$ or $CN_3H_6^+$)[9,11] and $K[Nb(O_2)_2(L)_2]\cdot 3H_2O$ (L = 8-hydroxyquinolinate).[12] As far as the peroxo(polyaminocarboxylato) compounds are concerned, only a few studies have been reported and they are essentially restricted to the edta(peroxo) compound and its solution chemistry.[13,14] A bis(aqua)edta complex of Nb^{IV}, $[Nb(edta)(H_2O)_2]\cdot 2H_2O$, has also been described.[15]

Within the framework of the preparation of oxide materials, we have already reported on the use of carboxylato and carboxylato(peroxo)Nb complexes in the preparation of silica-dispersed Nb-Mo-O phases, by association with analogous Mo compounds.[9] The present work dedicates particular attention to new water-soluble peroxo(polyaminocarboxylato)Nb^V compounds corresponding to the general formula $(A^I)_3[Nb(O_2)_2(LO_2)]\cdot nH_2O\cdot nH_2O_2$ [$A^I = NH_4^+$ or guanidinium ($CN_3H_6^+$)]. Two different PAC ligands (L) have been selected: ethylenediaminetetraacetic acid (H_4edta) and propylenediaminetetraacetic acid (H_4pdta). There is so far only one report of *N*-oxide derivatives of polyaminocarboxylato complexes with some alkaline-earth and transition metal ions.[16] The present paper reports for the first time crystal structures of such compounds.

Results and Discussion

General Comments on the Synthetic Procedures

The peroxo(polyaminocarboxylato)Nb^V complexes were prepared by replacing peroxo groups by a PAC ligand of the tetraperoxoniobate anion $[Nb(O_2)_4]^{3-}$, formed in situ. The syntheses were adapted from the procedure used by Vuletic et al.[13] to obtain the ammonium edta(peroxo) complex. These syntheses were carried out in the presence of

[a] Unité de Chimie des Matériaux Inorganiques et Organiques
Place Louis Pasteur 1/3, 1348 Louvain-la-Neuve, Belgium
[b] Unité de Chimie Structurale et des Mécanismes Réactionnels,
Université Catholique de Louvain,
Place Louis Pasteur 1/3, 1348 Louvain-la-Neuve, Belgium
Fax: (internat.) + 32-10/472330
E-mail: devillers@chim.ucl.ac.be

Table 1. Infrared data (in cm^{-1}) for compounds **1**, **2a**, and **3** (s = strong, m = medium, w = weak)

Compound	ν(O−O)	ν_s[Nb(O_2)]	ν_{as}[Nb(O_2)]	ν_{as}(COO)	ν_s(COO)	ν(N−O)
1	870m	646w	558m	1619s	1443s	904m
	855m				1391s	
2a	872m	642m	554m	1622s	1446s	905m
	857m				1376s	
3	875m	634w	544m	1674s	1401s	898m
	860m			1609s	1373s	

excess hydrogen peroxide, which led to the direct formation of the *N*-oxide derivative of the PAC ligand. The PAC bis(*N*-oxido) ligands, H_4edtaO_2, and H_4pdtaO_2, were synthesized separately according to the procedure of Porter et al.[17] The peroxo(PAC)Nb^V complexes were also prepared starting from the pre-isolated reactants $(A^I)_3[Nb(O_2)_4]$ and $H_4LO_2{\cdot}nH_2O$ (with $A^I = NH_4^+$, gu^+ and L = edta, pdta) in aqueous media. Both synthetic pathways were shown to lead to the same compounds.

IR Spectroscopy

Table 1 lists the infrared bands assigned to the side-bonded peroxo ligands, the *N*-oxide groups and some representative vibrational modes of the coordinated PAC ligands for compounds **1**, **2a**, and **3**.

In addition to the bands arising from the PAC ligands, the IR spectra of the complexes systematically show two ν(O−O) bands of medium intensity in the range 855−875 cm^{-1}, assigned to a diperoxo species.[9,18] Other bands due to the presence of coordinated peroxo ligands also arise at ca. 550 and 650 cm^{-1} and correspond to ν_{as}[Nb(O_2)] and ν_s[Nb(O_2)], respectively. The asymmetric stretching frequency of the carboxylato groups bound to the niobium atom occurs in the spectra of the edta and pdta compounds as a broad band near 1600−1650 cm^{-1}. Coordination of the metal atom by these carboxylato groups is evidenced by the broadening of this ν_{as}(COO) band and by its significant shift in comparison with the free acid [ν_{as}(COO) at ca. 1700 cm^{-1}]. Finally, oxidation of the nitrogen atoms of the PAC ligand during the syntheses (excess H_2O_2 medium) is evidenced by the presence, in all IR spectra, of the ν(N−O) band at ca. 900 cm^{-1}. In the corresponding bis(*N*-oxide) derivative of the free ligand, $H_4edtaO_2{\cdot}1/2H_2O$ (**4a**) and $H_4pdtaO_2{\cdot}H_2O$ (**5**), this band appears at 890 and 909 cm^{-1}, respectively.

NMR Spectroscopy

Table 2 lists the ^{13}C and ^{15}N resonance lines occurring from compounds **1**, **3**, **4a**, **5**, and also from the commercial PAC ligands. The results obtained for the guanidinium edta compound **2a** are not reported because they are very similar to those obtained for the ammonium derivative.

Table 2. ^{13}C and ^{15}N NMR chemical shifts (δ, in ppm) for compounds **1**, **3**, **4a**, **5**, and commercial PAC ligands

Compound	^{13}C NMR[a]	^{15}N NMR[a]
1	57.4, 64.9, 70.8, 168.4, 169.9	121.2
3	19.3, 54.8, 66.6, 67.9, 168.8, 171.3	72.1, 128.1
4a/NaOD[b]	59.7, 67.5, 170.6	114.9
5/NaOD[b]	19.1, 64.9, 66.6, 171.4	123.6
H_4edta/NaOD[b]	50.9, 57.5, 176.9	38.5
H_4pdta/NaOD[b]	23.0, 53.2, 58.9, 179.3	53.1

[a] In D_2O. [b] H_4L and H_4LO_2 compounds are not soluble in D_2O at room temp. and were solubilized by adding an excess of NaOD.

Just like the IR spectra, the ^{15}N NMR spectra of the prepared complexes reveal the oxidation of the nitrogen atoms in the PAC ligand. The ^{15}N NMR spectrum of compound **1** displays one single line at δ = 121.2 ppm arising from the two identical nitrogen atoms in the ligand. This particularly high ^{15}N chemical shift confirms the formation of *N*-oxide groups by comparison with the values obtained for the species H_4edta and $H_4edtaO_2{\cdot}1/2H_2O$ (**4a**) (δ = 38.5 and 114.9 ppm, respectively). A similar effect of *N*-oxidation on ^{15}N chemical shifts was observed by Hadden et al. in alkaloid compounds.[19] In the ^{15}N NMR analysis of compound **3**, resonances occurring at δ = 72.1 and 128.1 ppm are assigned to the nitrogen atoms of the guanidinium counterions and the oxidized pdta ligand, respectively. In free H_4pdta and $H_4pdtaO_2{\cdot}H_2O$ (**5**), the related lines occur at δ = 53.1 and 123.6 ppm, respectively.

Information on the coordination mode of the bis(*N*-oxido) ligand is provided by ^{13}C NMR spectroscopy. The ^{13}C NMR spectrum of the anion $[Nb(O_2)_2(edtaO_2)]^{3-}$ shows three lines at δ = 57.4, 64.9, and 70.8 ppm, arising from the CH_2 groups of the edta ligand. These carbon atoms are clearly influenced by the complexation process. Whereas all four CH_2 moieties of the acetate groups occur as one single peak in the free ligand (δ = 50.9 ppm), they undergo a significant variation in chemical shift and are differentiated in the complex (δ = 57.4 and 64.9 ppm). Moreover, the CH_2 groups of the *N*-bound ethylene moiety are not differentiated (they appear as a single line as in H_4edta) but they are shifted from δ = 57.5 ppm in the free ligand to δ = 70.8 ppm in the complex. A similar value is observed for these carbon atoms in the free edta bis(*N*-oxido) ligand (**4a**;

δ = 67.5 ppm). This result confirms the presence of N−O groups in the complexed ligand. The signal corresponding to the quaternary carbon atoms of the carboxylato groups in the complex appears as two resonance signals rather than the single line found for the free ligand. The presence of two lines at δ = 168.4 and 169.9 ppm in the ^{13}C NMR spectrum implies that two carboxylato groups are coordinated to Nb and the other two remain free. The complete analysis of the ^{13}C NMR spectrum of compound **1** allows us to determine the coordination mode of the ligand to the niobium atom; the edta bis(*N*-oxide) is quadridentate, the four binding atoms being oxygen atoms of two of the carboxylate groups (each placed on a different N atom) and two *N*-oxide groups. A similar analysis based on the ^{13}C NMR spectrum obtained for compound **3** leads to the same conclusion about the coordination mode of the pdta bis(*N*-oxido) ligand.

X-ray Crystal Structures

The asymmetric part of the unit cell of **2b** consists of two $[Nb(O_2)_2(edtaO_2)]^{3-}$ anions, six guanidinium cations, six water molecules, and two hydrogen peroxide molecules. In **3**, only one half of the $[Nb(O_2)_2(pdtaO_2)]^{3-}$ entity is observed in the asymmetric part of the unit cell as a consequence of a crystallographic twofold axis passing through the Nb atom, the central carbon atom of the PAC ligand (C10) and the C and N atoms belonging to one guanidinium ion. In **4b**, only one half of the molecule is observed in the asymmetric part of the unit cell. Crystallographic data for **2b**, **3**, and **4b** are given in Table 4 and selected bond lengths for **2b** and **3** in Table 3.

Table 3. Selected bond lengths and maximum deviations from mean peroxo plane [Å] for both anionic moieties of **2b** and **3**

	2b		**3**
	Anion 1	Anion 2	
Distances			
Nb−O (carboxylate)	2.155(5)	2.147(5)	2.162(2)
	2.154(5)	2.140(5)	
Nb−O (*N*-oxide)	2.089(4)	2.087(5)	2.119(2)
	2.083(5)	2.074(4)	
Nb−O (peroxo)	1.966(5)	1.982(4)	1.973(2)
	1.968(5)	1.979(5)	1.988(2)
	1.977(5)	1.972(5)	
	1.992(5)	1.990(5)	
O−O (peroxo)	1.478(7)	1.485(7)	1.488(3)
	1.483(7)	1.475(7)	
N−O (*N*-oxide)	1.411(7)	1.414(7)	
	1.416(7)	1.407(7)	1.419(2)
Maximum deviation from mean plane through four O (peroxo)			
O (peroxo)	0.04	0.03	0.060
O (*N*-oxide)	2.72	2.75	2.75
	2.69	2.66	
O (carboxylate)	1.64	1.65	1.65
	1.78	1.78	
Nb	1.10	1.17	1.16

The crystal structures of complexes **2b** and **3** are similar in many ways. The bis(*N*-oxido) ligands, $edtaO_2$ and $pdtaO_2$, wrap around the Nb atom, essentially in the same manner. The quadridentate coordination mode of these ligands, deduced from the NMR analysis, is confirmed and, for each anion, coordination is completed by two bidentate peroxo groups. From this it is seen that the niobium atom exhibits an eightfold coordination as observed in all (peroxo)Nb compounds described so far in the literature.[5,6,9−12] Figures 1 and 2 show the molecular structure of the $[Nb(O_2)_2(edtaO_2)]^{3-}$ and $[Nb(O_2)_2(pdtaO_2)]^{3-}$ anions, respectively. The coordination polyhedron observed in both cases is identical to those reported for dioxalatodiperoxoNb^V compounds with different counterions.[9,11] The question of whether eightfold coordinated atoms display dodecahedral (DD) or square-antiprismatic (SAP) config-

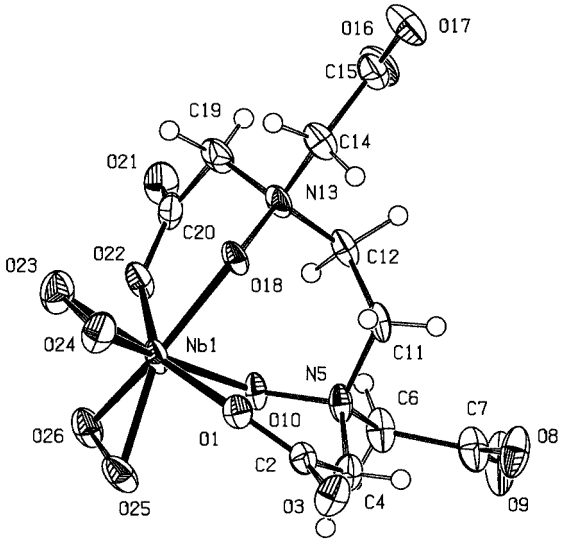

Figure 1. ORTEP plot of $[Nb(O_2)_2(edtaO_2)]^{3-}$ (50% probability)[24]

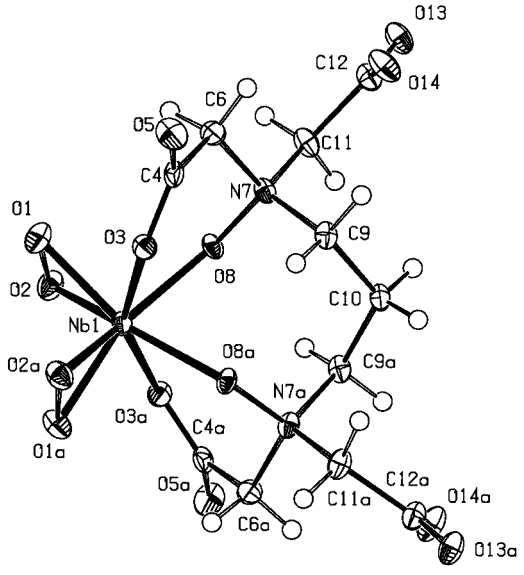

Figure 2. ORTEP plot of the molecular anion of $[Nb(O_2)_2(pdtaO_2)]^{3-}$ (50% probability)[24]

urations is not an obvious one to answer, and has been addressed from a theoretical point of view in the literature.[20] In relation to the fact that the energy balance between DD and SAP is very sensitive to small differences in electronic or steric effects, the obtention of intermediate configurations between them has also been discussed.[21] Theoretical considerations confirmed that "small-bite" ligands like O_2^{2-} definitely prefer the dodecahedral geometry,[20] as is observed in all peroxoniobate complexes described so far. In the present cases, the polyhedron may be described as a triangular dodecahedron that is rather distorted on one side. As indicated in Table 3, for the three anionic moieties encountered in these compounds, the four oxygen atoms of the peroxo groups are coplanar within experimental error. The maximum deviation from the best mean plane through these four O atoms is less than 0.06 Å. On the opposite side of the polyhedron, the four oxygen atoms of the PAC ligand are not coplanar. In all three anions described above, the oxygen atoms of the two carboxylate and the two *N*-oxide groups are observed with quite similar distances from the mean plane, of about 1.7 Å and 2.7 Å, respectively (see Table 3).

The mean Nb−O (*N*-oxide) bond length is 2.090(4) Å, a value which is larger than that observed in the related (hydroxyimino)niobium complex $(PPh_4)[Nb(hida)_2]$.[22] The other coordination distances are in the range of the values already reported.[6,9−11,22] The mean value for the Nb−O (carboxylato) distances is 2.152(5) Å and is slightly larger than the average of the sixteen values reported in the literature (2.095 Å). The Nb−O (peroxo) and (O−O) mean distances are 1.979(5) and 1.482(7) Å, respectively, and compare very well with the reported Nb−O distances (average over 36 values is 2.000 Å) and O−O distances (average over 14 values is 1.495 Å).[6,9−11,22] It is worth noting that, for both Nb complexes, the N−O (*N*-oxide) bond lengths range from 1.407(7) to 1.419(2) Å with a mean value of 1.413(5) Å. As expected, this value is slightly larger than the N−O distance observed in the free ligand [1.398(2) Å]. Moreover, as illustrated in Figure 3, which shows the molecular structure of the $[edtaO_2]^{4-}$ anion, there is a significant change of ligand conformation upon chelation. In the free anion, the N−O bands that are related by a symmetry center are in an "*anti*" orientation, pointing in opposite directions.

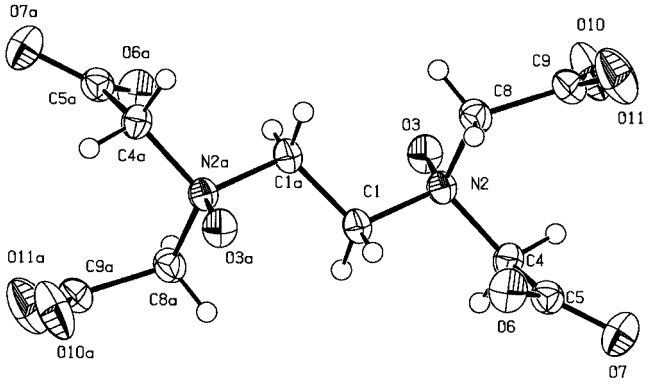

Figure 3. ORTEP plot of the molecular anion of $[edtaO_2]^{4-}$ (50% probability)[24]

For **2a**, the co-crystallized water and hydrogen peroxide molecules are involved in an intricate hydrogen bond network as illustrated in Figure 4. All the H-donors of the carboxylato groups and of the NH_2 groups of the guanidinium counterions participate in the network. There is no co-crystallized solvent molecule in crystals of **3** and **4b** but, in both structures, all carboxylate, peroxo, and amine groups are hydrogen-bonded.

Thermal Analyses

After dehydration, compound **1** undergoes a three-step degradation into Nb_2O_5 up to a final decomposition tem-

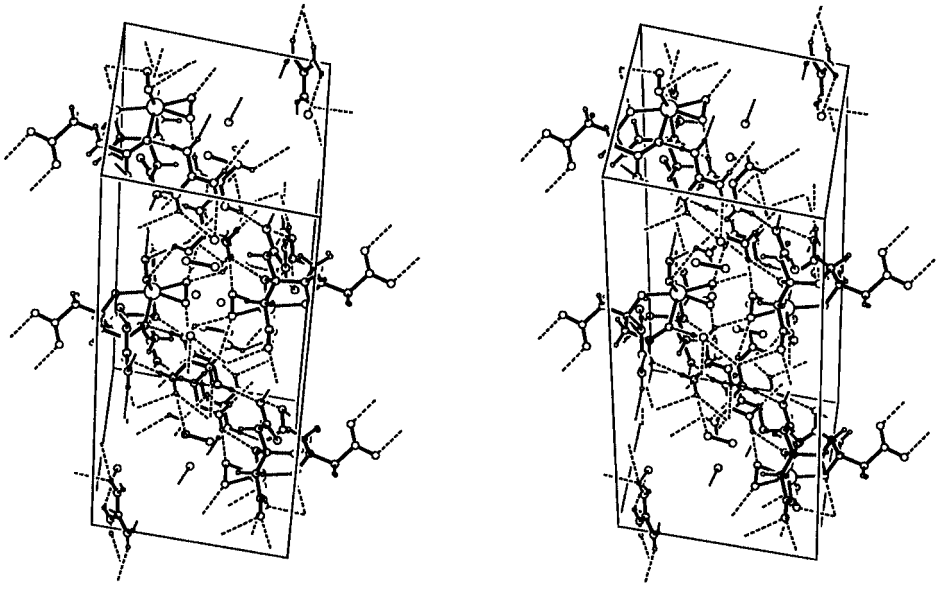

Figure 4. Stereoscopic view of the unit cell of **2b** showing the hydrogen bond network

perature of 620 °C. The thermal behavior of the guanidinium compounds **2a** and **3** is quite similar but their thermograms display an additional step, probably due to the counterion itself. The thermogravimetric analyses of the two edta(peroxo) compounds (**1** and **2a**) are illustrated in Figure 5.

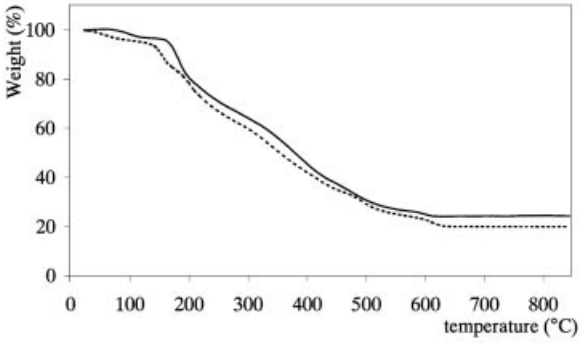

Figure 5. Thermogravimetric analyses of **1** (straight line) and **2a** (dashed line) in air (10 °C/min)

Conclusion

New niobium(v) complexes with *N*-oxide derivatives of polyaminocarboxylic acids have been prepared and characterized from the structural and spectroscopic point of view. Because these compounds exhibit a high solubility in water, they are ideal as precursors for Nb-based materials. The structures reported here are the first ones describing metal complexes with *N*-oxide derivatives of PAC ligands. The one-step synthesis of such compounds in the presence of hydrogen peroxide or their formation from the pre-isolated PAC (*N*-oxide)s opens new perspectives towards the obtention of PAC-type complexes with hard cations which, like Nb^{5+}, display a higher affinity towards oxygen than towards nitrogen.

Experimental Section

General: Ethylenediaminetetraacetic acid, H_4edta (Fluka), propylenediaminetetraacetic acid, H_4pdta (Fluka), and guanidinium carbonate, $(gu)_2CO_3$ (Aldrich), were commercial products and used as received. Niobic acid, $Nb_2O_5{\cdot}nH_2O$ was supplied by CBMM (Brazil). Hydrogen peroxide, H_2O_2 (35 wt-%, Acros), aqueous ammonia (25 wt-%), ethanol, and acetic acid were used without purification. Elemental analyses (C, H, N) were carried out at the University College of London. IR spectra in the 4000−400 cm^{-1} range were recorded with an FTS-135 Bio-RAD spectrometer, using KBr pellets containing ca 1 wt-% of the powder. ^1H, ^{13}C, and ^{15}N NMR spectra were measured in D_2O at 500, 125, and 50 MHz, respectively, with a Bruker Avance 500 MHz spectrometer equipped with a broad-band inverse probe. ^{15}N NMR spectra were recorded using the HMBC pulse sequence with a mixing time of 100 ms. Chemical shifts are expressed in ppm and are referenced to TMS for ^1H and ^{13}C (δ = 0 ppm) or nitromethane for ^{15}N (δ = 375 ppm).

$(NH_4)_3[Nb(O_2)_2(edtaO_2)]{\cdot}H_2O{\cdot}H_2O_2$ (1): A slurry of niobic acid (1 g, 6.36 mmol) in distilled water (20 mL) was treated with a 35 wt-% solution of H_2O_2 (20 mL) and ammonia (6 mL of a 25 wt-% solution). The cloudy solution was stirred for a few hours. When the solid was totally dissolved, H_4edta (1.86 g, 6.36 mmol) was added gradually, reaching pH = 5−5.5. The pale yellow solution was then gently heated for 10 min (T = 60 °C) and the solvents evaporated to a final volume of 20 mL under reduced pressure. The addition of ethanol (100 mL) yielded a white solid that was filtered off, washed with ethanol, and air-dried. Yield: 2.09 g (56%). $C_{10}H_{28}N_5NbO_{17}$ (583.16): calcd. C 20.57, H 4.80, N 12.00; found C 20.51, H 4.78, N 11.97. ^1H NMR (500 MHz, D_2O): δ = 3.88 (d, J = 16.5 Hz, 2 H), 4.06 (d, J = 16.0 Hz, 2 H), 4.37 (d, J = 16.5 Hz, 2 H), 4.42 (d, J = 14.0 Hz, 2 H), 4.76 (d, J = 13.5 Hz, 2 H), 5.04 (d, J = 16.5 Hz, 2 H) ppm. ^{13}C (125 MHz, D_2O) and ^{15}N (50 MHz, D_2O) NMR: see Table 2.

$(gu)_3[Nb(O_2)_2(edtaO_2)]{\cdot}2H_2O$ (2a): This guanidinium compound was prepared according to the same procedure as used for the ammonium derivative **1** but replacing ammonia by guanidinium carbonate, $(gu)_2CO_3$ (1.72 g, 9.55 mmol). The complex was isolated as a crystalline light-yellow solid. Yield: 2.78 g (63%). $C_{13}H_{34}N_{11}NbO_{16}$ (693.16): calcd. C 22.50, H 4.90, N 22.21; found C 22.36, H 5.02, N 22.03. The slow concentration at 5 °C of an aqueous concentrated solution yielded after several days small crystals suitable for structure determination by single-crystal X-ray diffraction and similar to compound **2a**, but containing additional water and hydrogen peroxide molecules $\{(gu)_3[Nb(O_2)_2(edtaO_2)]{\cdot}3H_2O{\cdot}H_2O_2$, **2b**$\}$.

$(gu)_3[Nb(O_2)_2(pdtaO_2)]$ (3): A slurry of niobic acid (1 g, 6.36 mmol) in distilled water (50 mL) was treated with a 35 wt-% solution of H_2O_2 (50 mL) and $(gu)_2CO_3$ (1.72 g, 9.55 mmol). When the solid was totally dissolved, H_4pdta (1.95 g, 6.36 mmol) was added, reaching pH = 6. The pale yellow solution was then gently heated for 10 min (T = 60 °C) and the solvents evaporated to a final volume of 50 mL under reduced pressure. Addition of ethanol (100 mL) produced, after a few minutes, a pale yellow crystalline solid that was filtered off, washed with ethanol, and air-dried. Yield: 3.01 g (71%). $C_{14}H_{32}N_{11}NbO_{14}$ (671.18): calcd. C 25.03, H 4.77, N 22.94; found C 25.20, H 4.69, N 22.76. ^1H NMR (500 MHz, D_2O): δ = 2.2−2.3 (m, 2 H), 3.94 (d, J = 16.5 Hz, 2 H), 3.99 (d, J = 13.0 Hz, 2 H), 4.19 (d, J = 16.5 Hz, 2 H), 4.83 (d, J = 13.0 Hz, 2 H), 4.86 (d, J = 16.5 Hz, 2 H) ppm. ^{13}C (125 MHz, D_2O) and ^{15}N (50 MHz, D_2O) NMR: see Table 2. The slow concentration at room temperature of an aqueous concentrated solution yielded after several days small yellow crystals of compound **3**.

$H_4edtaO_2{\cdot}1/2\ H_2O$ (4a): H_4edta (2 g, 6.84 mmol) was dispersed in glacial acetic acid (100 mL) and 35 wt-% solution of H_2O_2 (50 mL). The suspension was stirred for 72 h at room temperature. The white solid was then filtered off, washed with water and ethanol and finally air-dried. Yield: 1.81 g (79%). $C_{10}H_{16}N_2O_{10}{\cdot}1/2H_2O$ (333.25): calcd. C 36.00, H 5.10, N 8.40; found C 36.19, H 4.91, N 8.27. ^1H NMR (500 MHz, D_2O): δ = 4.09 (d, J = 15.5 Hz, 4 H), 4.19 (s, 4 H), 4.37 (d, J = 15.5 Hz, 4 H), 4.70 (s, H_2O) ppm. ^{13}C (125 MHz, D_2O) and ^{15}N (50 MHz, D_2O) NMR: see Table 2. Crystallization of a guanidinium derivative of the edta bis(*N*-oxido) ligand was obtained after neutralizing the carboxylic groups by guanidinium carbonate; **4a** (1 g, 3 mmol) was dissolved in distilled water (10 mL) and the addition of $(gu)_2CO_3$ (2.16 g, 12 mmol) yielded a clear solution that was allowed to concentrate at room temperature. After several days, large crystals of $(gu)_4edtaO_2$ (**4b**) had formed. $C_{14}H_{36}N_{14}O_{10}$ (560.57): calcd. C 29.98, H 6.07, N 34.98; found C 30.40, H 6.22, N 35.40.

$H_4pdtaO_2{\cdot}H_2O$ (5): This compound was prepared according to the same procedure as used for the edta derivative but replacing H_4edta

Table 4. Crystallographic data and structure refinement parameters for **2b**, **3**, and **4b**

	2b	**3**	**4b**
Empirical formula	$C_{26}H_{76}N_{22}Nb_2O_{38}$	$C_{14}H_{32}N_{11}NbO_{14}$	$C_{14}H_{36}N_{14}O_{10}$
Formula mass	1490.9	671.2	560.6
Temperature [K]	100(2)	100(2)	293(2)
Crystal system, space group	triclinic, $P\bar{1}$	Monoclinic, $C2/c$	Monoclinic, $P2_1/c$
Unit cell dimensions			
a [Å]	11.233(4)	12.093(3)	10.670(4)
b [Å]	11.430(4)	19.206(5)	8.305(3)
c [Å]	23.220(8)	12.115(3)	14.454(5)
α [°]	101.01(3)	90	90
β [°]	102.07(3)	110.84(2)	91.84(2)
γ [°]	94.01(3)	90	90
V [Å^3]	2843(2)	2630(1)	1280(2)
Z	2	4	2
$D_{calcd.}$ [g·cm^{-3}]	1.75	1.71	1.45
Absorption coefficient [mm^{-1}]	0.526	0.545	0.122
F(000)	1532	1380	596
Crystal size [mm]	0.36 × 0.32 × 0.30	0.4 × 0.32 × 0.18	0.30 × 0.30 × 0.25
θ range for data collection [°]	3.5−23.2	3.5−27.5	2.8−26.4
Index range	$-12 \geq h \geq 8$ $-12 \geq k \geq 9$ $-24 \geq l \geq 25$	$-15 \geq h \geq 15$ $-24 \geq k \geq 24$ $-15 \geq l \geq 15$	$-13 \geq h \geq 13$ $-10 \geq k \geq 10$ $-18 \geq l \geq 18$
Reflections collected/unique	47090/7021	8094/2998	19424/2540
R_{int}	0.055	0.064	0.057
Data/restraints/parameters	7021/0/867	2998/0/185	2540/0/228
R_1, wR_2 [$I > 2\sigma(I)$]	0.068, 0.173 [6452]	0.038, 0.101 [2696]	0.054, 0.126 [2384]
R_1, wR_2 (all data)	0.072, 0.177	0.042, 0.102	0.055, 0.128
Goodness-of-fit on F^2	1.093	1.148	1.177
Larg. res. peak [e/Å^3]	2.67/−2.11	0.73/−0.62	0.51/−0.43

by H_4pdta (2 g, 6.53 mmol). Yield: 1.68 g (72%). $C_{11}H_{20}N_2O_{10}\cdot H_2O$ (356.25): calcd. C 37.05, H 5.61, N 7.86; found C 37.10, H 5.71, N 7.81. ^{1}H NMR (500 MHz, D_2O): δ = 2.41−2.51 (m, 2 H), 4.10 (t, J = 7.0 Hz, 4 H), 4.39 (d, J = 16.0 Hz, 4 H), 4.46 (d, J = 16.0 Hz, 4 H) ppm. ^{13}C (125 MHz, D_2O) and ^{15}N (50 MHz, D_2O) NMR: see Table 2.

X-ray Crystallography: The X-ray intensity data were measured at 100 K with an MAR345 image plate using Mo-K_α (λ = 0.71069 Å) radiation. Selected crystals of **2b** and **3** were mounted in inert oil and transferred to the cold gas stream for flash cooling. Data of **4b** were collected at room temperature. Crystal data and data collection parameters are summarized in Table 4. The unit cell parameters were refined using all the collected spots after the integration process. The three structures were solved by direct methods and refined by full-matrix least-squares on F^2 using SHELXL-97.[23] All the non-hydrogen atoms were refined anisotropically. For **2b** and **3**, the hydrogen atoms were calculated with AFIX and included in the refinement with a common isotropic temperature factor. The H atoms of the carboxylic groups, the water and hydrogen peroxide molecules were not localized. For **4b**, the H atoms were localized by Fourier difference synthesis. In compound **2b**, the asymmetric part of the unit cell concsists of two complex units related to each other by a pseudo translation symmetry. There is only one half of the ligand molecule and two guanidinium cations in the asymmetric part of the unit cell of **4b**; the midpoint of the central C1−C1a bond corresponds to a crystallographic center of symmetry. The details of the refinement and the final R indices are presented in Table 4. In **2b** and **3**, the largest peak in the final Fourier difference synthesis is located near an Nb atom. CCDC-187664 (**2b**), -187665 (**3**), and -192609 (**4b**) contain the supplementary crystallographic data for this paper. These data can be obtained free of charge at www.ccdc.cam.ac.uk/conts/retrieving.html or from the Cambridge Crystallographic Data Centre, 12 Union Road, Cambridge CB2 1EZ, UK [Fax: (internat.) + 44-1223/336-033; E-mail: deposit@ccdc.cam.ac.uk].

Acknowledgments

The authors thank the Belgian National Fund for Scientific Research (FNRS) for the Research fellowship allotted to D. B. and financial support. They also thank the CBMM company (Brazil) for supplying the niobic acid.

[1] [1a] K. Ruth, R. Burch, R. Kieffer, *J. Catal.* **1998**, 16−26. [1b] K. Ruth, R. Burch, R. Kieffer, *J. Catal.* **1998**, 27−39.
[2] Y. Mimura, K. Ohyachi, I. Matsuura, *Stud. Surf. Sci. Catal.* **1999**, *21*, 69−74.
[3] M. Aouine, J. L. Dubois, J. M. M. Millet, *Chem. Commun.* **2001**, 1180−1181.
[4] S. A. Holmes, J. Al-Saeedi, V. V. Guliants, P. Boolchand, D. Georgiev, U. Hackler, E. Sobkow, *Catal. Today* **2001**, 403−409.
[5] L. C. Passoni, M. R. H. Siddiqui, A. Steiner, I. N. Kozhevnikov, *J. Mol. Catal. A* **2000**, *153*, 103−108.
[6] G. Mathern, R. Weiss, *Acta Crystallogr., Sect. B* **1971**, *27*, 1598−1609.
[7] R. N. Shchelokov, E. N. Traggeim, M. A. Michnik, *Russ. J. Inorg. Chem.* **1971**, *16*, 211−213.
[8] A. C. Dengel, W. P. Griffith, *Polyhedron* **1989**, *8*, 1371−1377.
[9] D. Bayot, B. Tinant, M. Devillers, *Catal. Today*, in press.
[10] G. Mathern, R. Weiss, *Acta Crystallogr., Sect. B* **1971**, *27*, 1582−1597.
[11] G. Mathern, R. Weiss, *Acta Crystallogr., Sect. B* **1971**, *27*, 1572−1581.

[12] V. de Oliveira, R. Aguilar da Silva San Gil, E. R. Lachter, *Polyhedron* **2001**, *20*, 2647−2649.
[13] N. Vuletic, E. Prcic, *Z. Anorg. Allg. Chem.* **1979**, *450*, 67−69.
[14] M. J. Kim, E. Matijevic, *J. Am. Ceram. Soc.* **1994**, *77*, 1950−1953.
[15] B-L. Ooi, Q. Xu, T. Shibahara, *Inorg. Chim. Acta* **1998**, *274*, 103−107.
[16] L. E. Freyer, Ph. D. Dissertation, University of Texas, **1975**.
[17] D. B. Porter, M. de Haro Rodriguez, P. P. Conesa, *Afinidad* **1976**, 489−495.
[18] R. N. Shchelokov, E. N. Traggeim, M. A. Michnik, M. Petrov, *Russ. J. Inorg. Chem.* **1972**, *17*, 1270−1272.
[19] C. E. Hadden, B. D. Kaluzny, R. H. Robins, G. E. Martin, *Magn. Reson. Chem.* **1999**, *37*, 325−327.
[20] J. K. Burdett, R. Hoffmann, R. C. Fay, *Inorg. Chem.* **1978**, *17*, 2553−2568.
[21] S. J. Lippard, B. J. Russ, *Inorg. Chem.* **1968**, *7*, 1686−1688.
[22] P. D. Smith, S. M. Harben, R. L. Beddoes, M. Helliwell, D. Collison, C. D. Garner, *J. Chem. Soc., Dalton Trans.* **1997**, 685−691.
[23] G. M. Sheldrick, *SHELX-97* and *SHELXL-97, Program for crystal structure refinement*, University of Göttingen, Germany, **1997**.
[24] A. L. Spek, *PLATON Molecular Geometry Program*, University of Utrecht, The Netherlands, **1998**.

Received June 25, 2002
[I02345]

Pyridine- and 3-/6-Methylpyridine-2-tellurolate Complexes of Palladium(II) and Platinum(II)

Sandip Dey,[a] Vimal K. Jain,*[a] Jaspreet Singh,[b] Veena Trehan,[b] Kuldip K. Bhasin,[b] and Babu Varghese[c]

Keywords: Palladium / Platinum / N ligands / Tellurium / NMR spectroscopy

The reaction of py_2Te_2 or $(3\text{-}MeC_5H_3N)_2Te_2$ with Na_2PdCl_4 in methanol yields an insoluble brown complex, $[PdCl(TeNC_5H_3R)]_n$ (R = H or Me). Several reactions of $pyTe^-$, $(3\text{-}MeC_5H_3N)Te^-$, or $(6\text{-}MeC_5H_3N)Te^-$ with various palladium(II) and platinum(II) complexes have been carried out. Complexes of the types $[MCl(Te\text{–}N)(PR_3)]$, $[Pt(Te\text{–}N)_2(dppe)]$, $[Pt(Te\text{–}N)_2(PPh_3)_2]$, and $[Pt_2(\mu\text{-}Te\text{–}N)_2(dppe)_2][BPh_4]_2$ [M = Pd or Pt; Te–N = pyTe, (3- or 6-MeC_5H_3N)Te] have been prepared and characterized by elemental analyses, UV/Vis, IR, and NMR (^1H, ^{31}P, ^{195}Pt) spectroscopy. The complexes $[MCl(Te\text{–}N)(PR_3)]$ show irreversible oxidation and reduction by CV in DMF. The molecular structure of $[PdCl\{Te(3\text{-}MeC_5H_3N)\}(PPh_3)]$ (**2c**) has been established by single-crystal X-ray diffraction analysis. The palladium atom is bound to the chelating 3-methylpyridinetellurolate ligand, a chlorine atom and a PPh_3 ligand. The pyrolysis of $[PdCl\{Te(3\text{-}MeC_5H_3N)\}(PR_3)]$ (PR_3 = PEt_3 or PPh_3) at 340 °C yields PdTe.

(© Wiley-VCH Verlag GmbH & Co. KGaA, 69451 Weinheim, Germany, 2003)

Introduction

The synthesis and characterization of metal chalcogenolates continues to be an area of considerable interest. Their emerging applications as single-source precursors for a low-temperature preparation of solid-state chalcogenide materials has further accelerated work in this area.[1–4] The area of metal chalcogenolates has been dominated by molecules containing the M–SR linkage.[5] In most cases, these molecules have been isolated as non-volatile insoluble (or sparingly soluble) polymers, thus making them inconvenient precursors for the preparation of metal chalcogenides. To suppress polymerization, several strategies have been explored. These include use of (a) a strongly coordinating ligand, such as tertiary phosphanes,[6,7] (b) a sterically demanding chalcogenolate ion,[8] (c) internally functionalized small-bite ligands.[9–13] One of the families of the latter class of ligands is the pyridine-2-chalcogenolate ion **I**. While the ligand chemistry of $C_5H_4NO^-$ [14] and $C_5H_4NS^-$ [15] has been well documented, the coordination chemistry of the pyridine-2-selenolate ion has been explored only recently by us[11,16] and others.[17–21] In contrast, metal complexes with pyridine-2-tellurolate are virtually non-existent, although py_2Te_2 has been known for some time.[22,23] Possibly, a rather tedious preparation ("difficult to reproduce"[22]) of py_2Te_2, the precursor for $C_5H_4NTe^-$, appears to be a limiting factor for its use as a ligand.

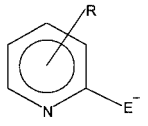

I

(E = O, S, Se, Te; R = H or Me)

Group-10 metal chalcogenides (M_xE_y; M = Pd or Pt; E = S, Se, Te) have found several applications in catalysis[24] (PdTe supported on carbon is employed industrially) and in the electronic industry.[25,26] Besides their wide structural diversity[5] and relevance in catalysis,[9,27,28] platinum-group metal chalcogenolates offer an attractive possibility of serving as precursors for the synthesis of metal chalcogenides.[12,29] In continuation of our program on the molecular design of platinum-group metal precursors, we have now synthesized bis(2-pyridyl) and bis(methyl-substituted 2-pyridyl) ditelluride, and have investigated the chemistry of their palladium and platinum complexes.

[a] Novel Materials and Structural Chemistry Division, Bhabha Atomic Research Centre,
Mumbai 400085, India
E-mail: jainvk@apsara.barc.ernet.in
[b] Department of Chemistry, Panjab University,
Chandigarh 160014, India
[c] RSIC, Indian Institute of Technology,
Chennai 600036, India

Results and Discussion

Synthesis and NMR Spectroscopic Data

A methanolic solution of Na_2PdCl_4 was treated with py_2Te_2 or $(3\text{-}MeC_5H_3N)_2Te_2$ at room temperature to give a brown insoluble product, $[PdCl\{Te(3\text{-}RC_5H_3N)\}]_n$ [R = H (**1a**) or Me (**1b**)]. The IR spectrum of **1b** exhibits a band at 281 cm^{-1} which is assigned to the terminal ν_{Pd-Cl} stretching. On treatment with tertiary phosphanes, the mononuclear complexes $[MCl\{Te(3\text{-}MeC_5H_3N)\}(PR_3)]$ are obtained. The latter complexes and their platinum analogues can readily be prepared by the reaction of $[M_2Cl_2(\mu\text{-}Cl)_2(PR_3)_2]$ with 2 equiv. of $NaTe(RC_5H_3N)$ (R = H, 3-Me, or 6-Me) [(Scheme 1), prepared by the cleavage of the Te−Te bond in bis(2-pyridyl) ditelluride with $NaBH_4$ in methanol]. The reaction exclusively gives $[MCl\{Te(RC_5H_3N)\}(PR_3)]$ (**2**).

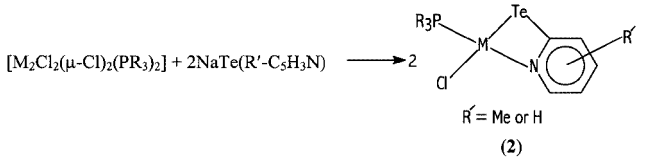

(2)

(M = Pd or Pt; PR_3 = PEt_3, $PnPr_3$, PMe_2Ph, $PMePh_2$, PPh_3, $Ptol_3$, PPh_2py)

Scheme 1

Similar reactions with pyO^- afford 2-pyridinolate-bridged dinuclear complexes, $[M_2Cl_2(\mu\text{-}OC_5H_4N)_2(PR_3)_2]$,[30] while in the reactions with pyS^-, both mono- and dinuclear complexes $[MCl(SC_5H_4N)(PR_3)]$ and $[M_2Cl_2(\mu\text{-}SC_5H_4N)_2(PR_3)_2]$ are formed, depending on the nature of the phosphane ligand.[31−35] In solution a dimer ⇄ monomer equilibrium is established, which is shifted to either side by subtle energetic factors. The reactions with $C_5H_4NSe^-$ preferentially yield mononuclear complexes, $[MCl(SeC_5H_4N)(PR_3)]$. However, dinuclear species are formed in small concentration (ca. 5%) in certain cases when trialkylphosphanes are used.[11] Clearly, as the Pd−E

Table 1. $^{31}P\{^1H\}$ and ^1H NMR spectroscopic data for the 2-pyridine- and methyl-2-pyridinetellurolate complexes of palladium(II) and platinum(II)

Complex	$^{31}P\{^1H\}$ NMR (δ)	^1H NMR (δ)
$[PdCl\{Te(3\text{-}MeC_5H_3N)\}(PEt_3)]$[a]	33.2	1.23 [dt, J(d) = 17.4, J(t) = 7.6 Hz, PCH_2CH_3]; 1.88 (dq), 10.6 (d), 7.6 (q, PCH_2); 6.98 (m, 5-H); 7.47 (d, J = 7.6 Hz, 4-H); 8.19 (br, 6-H)
$[PdCl\{Te(3\text{-}MeC_5H_3N)\}(PMePh_2)]$[a]	17.8	2.27 (d, J = 11.4 Hz, PMe); 6.99 (m, 5-H); 7.46−7.51 (m, 4-H + C_6H_5); 7.72−7.79 (m, C_6H_5); 8.29 (br, 6-H)
$[PdCl\{Te(3\text{-}MeC_5H_3N)\}(PPh_3)]$[a]	29.8	7.05 (m, 5-H); 7.50−7.54 (m, 4-H + C_6H_5); 7.74−7.78 (m, C_6H_5); 8.45 (br, 6-H)
$[PdCl\{Te(3\text{-}MeC_5H_3N)\}(Ptol_3)]$[a]	27.8	2.38 (s, tol-*Me*); 7.00 (m, 5-H); 7.30 (m, C_6H_4); 7.51 (d, J = 7.6 Hz, 4-H); 7.64 (dd, J = 8 Hz, J = 11.6 Hz, C_6H_4); 8.42 (br, 6-H)
$[PdCl\{Te(3\text{-}MeC_5H_3N)\}(PPh_2py)]$[a]	30.1	6.99 (m, 5-H); 7.50 (m, 4-H + C_6H_5, C_5H_4N); 7.83 (br, C_6H_5 + C_5H_4N); 8.38 (br, 6-H); 8.83 (br, 6-H, pyP)
$[PdCl(TeC_5H_4N)(PMePh_2)]$[a]	17.6	2.33 (d, J = 11 Hz, PMe), 7.05 (br), 7.33−7.64 (br, m); 7.80 (br), 8.40 (br) (Ph + C_5H_4)
$[PtCl\{Te(3\text{-}MeC_5H_3N)\}(PnPr_3)]$[a]	−9.3 ^1J(Pt-P) = 3575 Hz	1.05 (t, J = 7.2 Hz, PCH_2CH_2Me); 1.64−1.88 (m, PCH_2CH_2); 7.10 (t, J = 5.7 Hz, 5-H); 7.49 (d, J = 7.5 Hz, 4-H); 8.34 [br, ^3J(Pt-H) = 41 Hz, 6-H]
$[PtCl\{Te(3\text{-}MeC_5H_3N)\}(PMe_2Ph)]$[b]	−26.0 ^1J(Pt-P) = 3605 Hz	1.93 [d, J = 11 Hz, ^3J(Pt-H) = 37 Hz, PMe_2]; 2.01 (s, MeC_5H_3N); 6.92 (m, 5-H); 7.27 (d, J = 7.1 Hz, 4-H); 7.45 (m, C_6H_5); 7.69−7.77 (m, C_6H_5); 8.44 [br, ^3J(Pt-H) = 37 Hz, 6-H].
$[PtCl\{Te(3\text{-}MeC_5H_3N)\}(PMePh_2)]$[b]	−10.4 ^1J(Pt-P) = 3699 Hz	1.97 (s, MeC_5H_3N); 2.25 [d, J = 11.1 Hz, ^3J(Pt-H) = 33 Hz, P*Me*]; 6.93 (m, 5-H); 7.27 (d, J = 7 Hz, 4-H); 7.43 (m, C_6H_5); 7.66−7.73 (m, C_6H_5); 8.51 [br, ^3J(Pt-H) = 41 Hz, 6-H]
$[PtCl(TeC_5H_4N)(PMePh_2)]$[a]	−2.6 ^1J(Pt-P) = 3814 Hz	2.34 [d, J = 11 Hz, ^3J(Pt-H) = 36 Hz, PMe]; 6.61 (m), 7.22 (m), 7.45 (m), 7.76 (m), 8.00 (m), 8.20 (m) (Ph + C_5H_4)
$[Pt\{Te(3\text{-}MeC_5H_3N)\}_2(dppe)]$[b]	44.8 ^1J(Pt-P) = 2947 Hz	2.08 (s, MeC_5H_3N); 2.02 (m, CH_2CH_2); 6.57 (dd, J = 5 Hz, J = 7 Hz, 5-H); 6.77 (d, 7.5 Hz, 4-H); 7.27−7.37 (m, C_6H_5); 7.56 (d, J = 5 Hz, 6-H); 7.71−7.77 (m, C_6H_5)
$[Pt\{Te(6\text{-}MeC_5H_3N)\}_2(dppe)]$[b]	46.8 ^1J(Pt-P) = 2900 Hz	2.05 (s, MeC_5H_3N); 2.09 (m, CH_2CH_2); 6.48 (d, J = 7.4 Hz, 3-H); 6.61 (t, J = 7.5 Hz, 4-H); 7.27−7.36 (m, Ph); 7.69−7.76 (m, Ph, 5-H)
$[Pt_2\{Te(3\text{-}MeC_5H_3N)\}_2(dppe)_2][BPh_4]_2$[b]	37.1 ^1J(Pt-P) = 2944 Hz, 42.1 ^1J(Pt-P) = 3259 Hz	2.02 (s, MeC_5H_3N); 1.85−2.00 (m, CH_2CH_2); 6.55 (m, 5-H); 6.73−6.88 (m), 7.31 (br), 7.47−7.60 (m) [C_6H_5 + 4-H, 6-H]
$[Pt\{Te(3\text{-}MeC_5H_3N)\}_2(PPh_3)_2]$[b]	6.6 ^1J(Pt-P) = 3725 Hz −4.5 (PPh_3)	2.15 (s, MeC_5H_3N); 6.65 (br, 5-H); 7.10 (br, 4-H); 7.35 (m), 7.80 (m) (C_6H_5); 8.20 (br, 6-H)

[a] Recorded in $[D_6]$acetone; methyl resonance of the $3\text{-}MeC_5H_3N$ merged in the multiplet of $[D_6]$acetone. [b] Recorded in $CDCl_3$.

distance (Pd−O ≈ 2.10 Å; Pd−S ≈ 2.28 Å; Pd−Se ≈ 2.45 Å; Pd−Te ≈ 2.55 Å) increases with increasing size of the chalcogen atom, the Pd−N interaction of these small-bite ligands with a single metal center is facilitated.

The reaction of $PtCl_2$(dppe) with 2 equiv. of NaTe(3-MeC_5H_3N) yields the yellow mononuclear complex [Pt{Te(3-MeC_5H_3N)}$_2$(dppe)]. The NMR spectroscopic data (^{1}H, ^{31}P, and ^{195}Pt) are consistent with several organochalcogenolates, *cis*-[Pt(ER)$_2$(P−P)].[6,7,11−13] The reaction, performed in a 1:1 ratio in the presence of $NaBPh_4$, gives a cationic complex [Pt$_2$\{Te(3-MeC_5H_3N)\}$_2$(dppe)$_2$][BPh_4]$_2$. The ^{31}P and ^{195}Pt NMR spectra show two sets of resonances and doublets of doublets, respectively; a pattern which can be attributed to the non-equivalence of the phosphorus nuclei of the P−P ligand. Similar spectral features have been reported for [Pt$_2$(μ-$SeCH_2CH_2NMe_2$)$_2$(dppe)$_2$]$^{2+}$ [13] for which the existence of an asymmetric M−Se bridge has been suggested.

Treatment of $PtCl_2(PPh_3)_2$ with 2 equiv. of NaTe(3-MeC_5H_3N) affords [Pt{Te(3-MeC_5H_3N)}$_2$(PPh_3)$_2$]. The ^{31}P NMR spectrum of the complex exhibits a resonance at δ = 6.6 ppm, with ^1J(Pt−P) = 3725 Hz, together with a signal which is assigned to PPh_3 (δ = −4.5 ppm) (Table 1). A dynamic equilibrium between free PPh_3 and [M(EC_5H_4N)$_2$(PPh_3)] (M = Pd or Pt; E = S or Se)[11,16] has been reported earlier.

The ^{1}H NMR spectra of **2** show characteristic resonances for the ligand protons. The 6-H proton signal for the (3-MeC_5H_3N)Te ligand in the platinum complexes is flanked by ^{195}Pt satellites with ^3J(Pt-H) ≈ 40 Hz. The ^{31}P NMR spectra of these complexes display a single resonance indicating the formation of only one isomer. The magnitude of ^1J(^{195}Pt-^{31}P) in the platinum complexes suggests that the phosphane ligand is *trans* to the nitrogen atom of the chelating 2-pyridinetellurolate ligands,[11−13] and this is confirmed by the X-ray structural analysis. The ^{195}Pt NMR spectra (Table 2) show a doublet due to coupling with the single phosphorus nucleus. The ^{195}Pt resonance is considerably shielded relative to the signal for the corresponding 2-pyridineselenolate complexes.[11]

Table 2. ^{195}Pt{^{1}H} NMR spectra of the 2-pyridinetellurolates of platinum(II)

Complex	^{195}Pt NMR (δ)
[PtCl{Te(3-MeC_5H_3N)}(P*n*Pr_3)]	−4347 [d, ^1J(Pt-P) = 3580 Hz]
[PtCl{Te(3-MeC_5H_3N)}(PMe_2Ph)]	−4312 [d, ^1J(Pt-P) = 3634 Hz]
[PtCl{Te(3-MeC_5H_3N)}($PMePh_2$)]	−4314 [d, ^1J(Pt-P) = 3690 Hz]
[PtCl(TeC_5H_4N)($PMePh_2$)]	−3830 [d, ^1J(Pt-P) = 3820 Hz]
[Pt{Te(3-MeC_5H_3N)}$_2$(dppe)]	−5311 [t, ^1J(Pt-P) = 2952 Hz]
[Pt$_2$\{Te(3-MeC_5H_3N)\}$_2$(dppe)$_2$]-[BPh_4]$_2$	−4843 [dd, ^1J(Pt-P) = 2962 Hz]

UV/Vis Spectroscopy

All these complexes are deeply colored crystalline solids. The UV/Vis spectra (Table 3) in dichloromethane show a well-separated relatively weak broad band in the visible region, and this is responsible for the deep colors observed for these complexes. The platinum complexes have an absorbance band at higher energies than that of the corresponding palladium analogues. For both the series of complexes (Pd or Pt), this band is hypsochromically shifted with increasing donor strength of the phosphane ligand. The DFT calculations of [MCl($TeCH_2CH_2NMe_2$)(PR_3)] (M = Pd or Pt) reveal a metal-mediated charge-transfer between coordinated ligands. The highest occupied molecular orbital (HOMO) is predominantly centered on the tellurolate ligand, whereas the lowest unoccupied molecular orbital (LUMO) is delocalized over the system, with significant phosphane contributions. The low-energy electronic transitions between the frontier orbitals give rise to the colors.[35]

Table 3. UV/Vis data for the 2-pyridinechalcogenolate complexes of [MCl{E(3-MeC_5H_3N)}(PR_3)] (M = Pd^{II} and Pt^{II}; E = Se, Te) in CH_2Cl_2

Complex	λ_{max}[a] [nm]
[PdCl{Te(3-MeC_5H_3N)}(PEt_3)] (**2a**)	283 (13860), 371 (3280), 567 (190)
[PdCl{Te(3-MeC_5H_3N)}($PMePh_2$)] (**2b**)	294 (16560), 377 (4670), 595 (240)
[PdCl{Te(3-MeC_5H_3N)}(PPh_3)] (**2c**)	277 (16930), 297 (15710), 380 (4400), 614 (210)
[PdCl{Te(3-MeC_5H_3N)}($Ptol_3$)] (**2d**)	299 (15040), 381 (4660), 609 (210)
[PdCl(TeC_5H_4N)($PMePh_2$)] (**2f**)	293 (sh, 13170), 373 (4200), 570 (320)
[PtCl{Te(3-MeC_5H_3N)}(P*n*Pr_3)] (**3a**)	286 (sh, 7420), 402 (1880)
[PtCl{Te(3-MeC_5H_3N)}(PMe_2Ph)] (**3b**)	285 (6430), 313 (sh, 3940), 404 (1342)
[PtCl{Te(3-MeC_5H_3N)}($PMePh_2$)] (**3c**)	286 (sh, 8090), 316 (3950), 408 (1760)
[PdCl(SeC_5H_4N)(P*n*Pr_3)][b]	293 (26070), 475 (89)
[PtCl(SeC_5H_4N)(P*n*Pr_3)][b]	282 (7350), 376 (1480)

[a] Wavelengths λ_{max} at the absorbance maxima in nm, molar extinction coefficients ε in M^{-1} cm^{-1}. [b] Prepared according to ref.[11]

Cyclic Voltammetry

The complexes show irreversible oxidation and reduction in DMF/0.01 M Et_4NClO_4 (Table 4). The lower oxidation potential of the Pt/Te system indicates that the HOMO (Te) is destabilized relative to that of the corresponding Pd/Te system. Such behavior has been reported for [MCl($TeCH_2CH_2NMe_2$)(PR_3)] complexes.[35] It was difficult to oxidize the 2-pyridineselenolates [MCl(SeC_5H_4N)(PR_3)] (high oxidation potential values).

Structure of [PdCl{Te(3-MeC_5H_3N)}(PPh_3)] (2c)

The molecular structure of [PdCl{Te(3-MeC_5H_3N)}(PPh_3)] (**2c**) was established by single-crystal X-ray diffrac-

Table 4. Electrochemical data

Complex	E_{pa} (ox)[a]	E_{pc} (red)[a]
[PdCl{Te(3-MeC_5H_3N)}(PEt_3)] (**2a**)	0.46	−2.13
[PdCl{Te(3-MeC_5H_3N)}($PMePh_2$)] (**2b**)	0.40	−1.78
[PtCl{Te(3-MeC_5H_3N)}(PMe_2Ph)] (**3b**)	0.36	−2.26
[PtCl{Te(3-MeC_5H_3N)}($PMePh_2$)] (**3c**)	0.39	−2.30
[PdCl(SeC_5H_4N)(P*n*Pr_3)][b]	0.98	−1.98
[PtCl(SeC_5H_4N)(P*n*Pr_3)]	0.80	−1.63

[a] Scan rate 100 $mV \cdot s^{-1}$, peak potentials for irreversible processes in V vs. $FeCp_2/FeCp_2^+$. [b] Measurement in DMF/Et_4NClO_4.

tion analysis. The ORTEP[36] plot with the atomic numbering scheme is shown in Figure 1, and the selected bond lengths and angles are given in Table 5. The molecule consists of a distorted square-planar palladium atom that is bound to the chelating 3-methyl-2-pyridinetellurolate ligand, a chlorine atom and a PPh_3 ligand. The neutral donors (N, P) are mutually *trans*, and as a consequence the chloride ion and the Te atom adopt a *trans* arrangement, a configuration that has been reported previously for selenolate and tellurolate complexes, [MCl(E−N)(PR_3)] (M = Pd or Pt; E−N = $SeCH_2CH_2NMe_2$, $TeCH_2CH_2NMe_2$).[12,13,35] The square plane of the palladium atom (defined by the N, Cl, P, Te atoms), the four-membered chelate ring [Pd, N, C(5), Te], and the pyridine ring are almost coplanar, with the interplanar angles varying between 3.68 and 6.68°. The Te atom lies 0.1 Å out of the plane defined by the Pd, N, Cl, and P atoms.

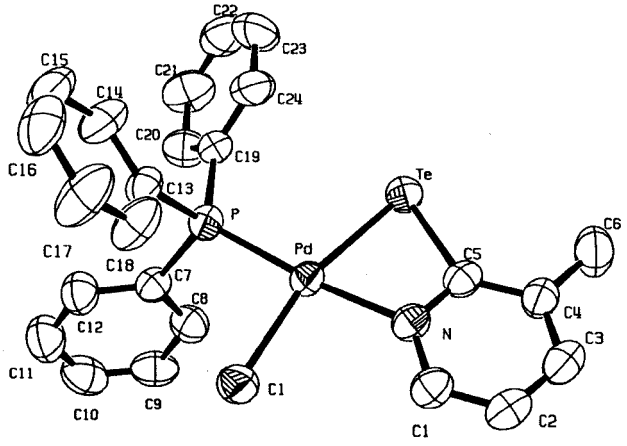

Figure 1. Molecular structure of [PdCl{Te(3-MeC_5H_3N)}(PPh_3)] (**2c**) with the atomic numbering scheme

Table 5. Selected bond lengths [Å] and angles [°] for [PdCl{Te(3-MeC_5H_3N)}(PPh_3)] (**2c**)

Pd−Te	2.5606(8)	Te−C(5)	2.118(5)
Pd−N	2.085(4)	N−C(1)	1.337(7)
Pd−Cl	2.3620(16)	N−C(5)	1.330(7)
Pd−P	2.2420(15)	P−C(av)	1.821
N−Pd−P	173.76(13)	Pd−Te−C(5)	72.71(15)
N−Pd−Cl	94.17(13)	Te−C(5)−N	106.1(4)
P−Pd−Cl	92.07(5)	Te−C(5)−C(4)	131.1(4)
N−Pd−Te	73.18(12)	C(7)−P−C(13)	107.1(3)
P−Pd−Te	100.67(4)	C(7)−P−C(19)	104.0(3)
Cl−Pd−Te	165.21(4)	C(13)−P−C(19)	103.0(3)

The various angles around the Pd atom differ significantly from [PdCl($TeCH_2CH_2NMe_2$)(PR_3)] (PR_3 = P*n*Pr_3, $PMePh_2$),[35] owing to the small bite of the four-membered (3-MeC_5H_3N)Te moiety. The Pd−Te distanceis slightly longer [2.5606(8) Å] than that observed for [PdCl($TeCH_2CH_2NMe_2$)(PR_3)] [PR_3 = P*n*Pr_3 2.5095(8) and $PMePh_2$ 2.5156(6) Å],[35] while the Pd−N distance [2.085(4) Å] is shorter than that reported for [PdCl($TeCH_2CH_2NMe_2$)(PR_3)].[35] These distances, as well as the Pd−Cl, Pd−P and Te−C bond lengths are not unusual.[33−35,37−40]

Thermal Behavior

Thermogravimetric analysis of [PdCl{Te(3-MeC_5H_3N)}(PPh_3)] (**2c**) was carried out under a dynamic argon pressure. The TG curve shows a one-step decomposition (290°C), leading to the formation of PdTe as inferred from the calculated weight loss. In order to prepare large quantities of the telluride, a substantial amount (100−350 mg) of the complexes (**2a**, **2c**) was heated in a furnace at 340°C for 2 h under a dynamic dry argon pressure. The weight loss and XRD pattern (Figure 2) of the residue obtained after decomposition in each case matches the product obtained from TG. The XRD patterns (Figure 2) of all these samples are in agreement with the standard pattern of PdTe[41] [analysis of the prepared PdTe: sample from **2a**: C 1.8, H < 0.2, N < 0.2; sample from **2c**: C < 0.2, H < 0.2, N < 0.2 (detection limit 0.2%)]. The scanning electron micrographs

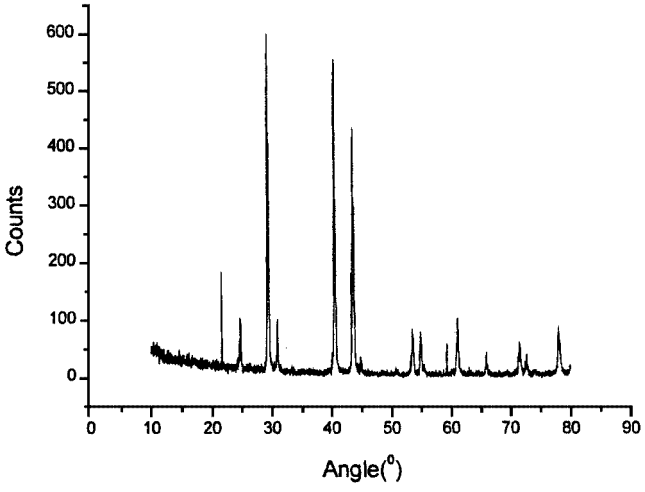

Figure 2. XRD pattern of PdTe obtained from [PdCl{Te(3-MeC_5H_3N)}(PPh_3)]

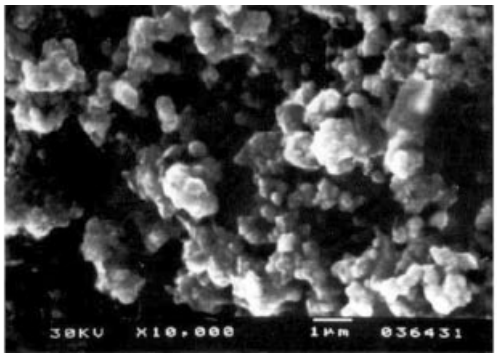

Figure 3. SEM picture of PdTe obtained from [PdCl{Te(3-MeC_5H_3N)}(PPh_3)]

(Figure 3) of PdTe obtained from **2c** taken at different resolutions show large aggregates of microcrystals.

Experimental Section

General: The complexes Na_2PdCl_4, $[PtCl_2(PPh_3)_2]$, $[M_2Cl_2(\mu\text{-}Cl)_2(PR_3)_2]$ (M = Pd or Pt; PR_3 = PEt_3, $PnPr_3$, PMe_2Ph, $PMePh_2$, PPh_3), $[PtCl_2(dppe)]$,[42] py_2Te_2,[43a] (3-/6-$MeC_5H_3N)_2Te_2$,[43b] and the methyl-substituted 2-bromopyridines[44] were prepared according to literature methods. The phosphanes were obtained from Strem Chemicals (USA). All reactions were carried out under nitrogen, in dry and distilled analytical grade solvents. Microanalyses were carried out in the Analytical Chemistry Division of B.A.R.C. ^1H, $^{31}P\{^1H\}$, $^{125}Te\{^1H\}$, and $^{195}Pt\{^1H\}$ NMR spectra were recorded with a Bruker DPX-300 NMR spectrometer, operating at 300, 121.49, 94.86, and 64.52 MHz, respectively. Chemical shifts are relative to the internal chloroform peak (δ = 7.26 ppm) for ^1H, external 85% H_3PO_4 for ^{31}P, $Te(dtc)_2$ (dtc = Et_2NCS_2) for ^{125}Te, and $Na_2[PtCl_6]$ in D_2O for ^{195}Pt. A 90° pulse was used in every case. The IR spectra were recorded as Nujol mulls between CsI plates with a Bomen MB-102 FT-IR spectrometer. UV/Vis absorbance spectra were recorded with a JASCO V-530 spectrometer using quartz cuvettes with a diameter of 1 cm. Cyclic voltammetry was carried out at a scan rate of 100 $mV \cdot s^{-1}$ in DMF/0.01 M Et_4NClO_4, using a three-electrode configuration (glassy carbon electrode, platinum counter electrode, calomel reference electrode) and an Ecochemie potentiostat 100 with autolab software. The ferrocene/ferrocenium couple served as the external reference. Mass spectra were recorded with a VG-705 11-250J spectrometer at RSIC, Panjab University, Chandigarh. Thermogravimetric analysis (TGA) was carried out using a Setaram 92-16-18 instrument calibrated with $CaC_2O_4 \cdot H_2O$. The TG curves were recorded at a heating rate of 10 $°C \cdot min^{-1}$ under a flow of argon. X-ray powder diffraction was measured using Cu-K_α radiation. SEM photographs were taken using a JEOL JSM-T330A instrument.

Preparations

Preparation of Bis(3- and 6-methyl-2-pyridyl) Ditelluride: Sodium borohydride (4.0 g, 108 mmol) was added slowly under a flow of nitrogen to a suspension of tellurium powder (9.65 g, 76 mmol) in 2-ethoxyethanol. The resulting colorless solution was refluxed for 30 min and then cooled to room temperature; 3- or 6-methyl-substituted 2-bromopyridine (13.07 g, 76 mmol) was added and the resulting solution was refluxed until all the 2-bromopyridine was consumed (48−96 h). The progress of the reaction was monitored by TLC. The nitrogen flow was stopped and the mixture was subjected to oxidation in air. The solvent was removed under vacuum and the crude residue was washed with water, and extracted with diethyl ether (4 × 100 mL). The extract was dried with anhydrous sodium sulfate and the solvent removed using a rotary evaporator, leaving the crude ditelluride. This was purified by column chromatography (silica gel; hexane/ethyl acetate, 10:1).

Bis(3-methyl-2-pyridyl) Ditelluride {[(3-$MeC_5H_3N)Te]_2$}: Yield 52%, m.p. 125−128°C. $C_{12}H_{12}N_2Te_2$ (439.4): calcd. C 32.8, H 2.7, N 6.4; found C 32.6, H 2.42, N 6.18. UV/Vis (CH_2Cl_2): λ_{max} (ε) = 297 (3260), 346 (sh, 1340), 412 (510) nm. ^1H NMR ($CDCl_3$): δ = 2.41 (s, Me), 6.96 (dd, *J* = 3.2, 5.0 Hz, 5-H), 7.25 (d, *J* = 4.6 Hz, 4-H); 8.20 (dd, *J* = 0.8, 3.5 Hz, 6-H) ppm. $^{13}C\{^1H\}$ NMR ($CDCl_3$): δ = 24.4 (s, Me), 122.1 (C-4), 134.9 (C-5), 137.8 (C-2), 140.7 (C-3), 148.3 (C-6) ppm. $^{125}Te\{^1H\}$ NMR ($CDCl_3$): δ = −382.7 ppm. IR (KBr): $\tilde{\nu}$ = 3060, 2960, 2920, 1580, 1540, 1430, 1120, 1090, 1020, 840, 780, 660, 540 cm^{-1}. MS (EI): *m*/*z* (%) = 440 (7.33) [M (^{130}Te)]$^+$, 314 (14.51) [M − Te]$^+$, 216 (1.47) [M − MeC_5H_3NTe], 183 (76.62) [M − Te_2H]$^+$, 92 (100) [M − CH_3pyTe_2]$^+$.

Bis(6-methyl-2-pyridyl) Ditelluride: Yield 24%, m.p. 55−56°C. $C_{12}H_{12}N_2Te_2$ (439.4): calcd. C 32.8, H 2.7, N 6.4; found C 32.21, H 2.52, N 6.18. UV/Vis (CH_2Cl_2): λ_{max} (ε) = 292 (sh, 8110), 386 (850) nm. ^1H NMR ($CDCl_3$): δ = 2.50 (s, Me), 6.85 (d, *J* = 5.0 Hz, 3-H), 7.25 (t, *J* = 5.0 Hz, 4-H), 7.84 (d, *J* = 5.0 Hz, 5-H) ppm. $^{13}C\{^1H\}$ NMR ($CDCl_3$) δ = 24.2 (s, Me), 121.0 (C-4), 128.0 (C-5), 134.9 (C-2), 137.0 (C-3), 158.9 (C-6) ppm. $^{125}Te\{^1H\}$ NMR ($CDCl_3$): δ = −426.4 ppm. IR (KBr): $\tilde{\nu}$ = 3042, 2916, 1571, 1429, 1376, 1242, 1163, 1083, 988, 826, 781, 655, 545 cm^{-1}. MS (EI): *m*/*z* (%) = 444 (5.5) [M (^{130}Te)]$^+$, 314 (6.5) [M − Te]$^+$, 216 (0.6) [M − MeC_5H_3NTe], 183 (30.9) [M − Te_2H]$^+$, 92 (100) [M − CH_3pyTe_2]$^+$.

[PdCl{Te(3-MeC_5H_3N)}]$_n$ (1b): A methanolic solution (10 mL) of Na_2PdCl_4 (342 mg, 1.16 mmol) was added to a methanolic solution (20 mL) of (3-$MeC_5H_3N)_2Te_2$ (256 mg, 0.58 mmol) while stirring at room temperature, whereupon a brown precipitate formed. Stirring was continued for 3 h. The brown precipitate was filtered, washed with methanol, water, acetone, and diethyl ether and dried in vacuo (yield: 235 mg, 56%). Complex **1a** was also prepared in a similar manner.

[PdCl{Te(3-MeC_5H_3N)}(PEt_3)] (2a): An acetone suspension (20 mL) of $[Pd_2Cl_2(\mu\text{-}Cl)_2(PEt_3)_2]$ (108 mg, 0.18 mmol) was added to a freshly prepared methanolic solution (5 mL) of NaTe(3-MeC_5H_3N) [prepared from (3-$MeC_5H_3N)_2Te_2$ (82 mg, 0.19 mmol) and $NaBH_4$ (15 mg, 0.39 mmol)], and the mixture was stirred for 4 h at room temperature. The solvents were evaporated in vacuo and the residue was extracted with acetone (3 × 8 mL). The solution was passed through a Florisil column. The blue solution was concentrated to 3 mL, a few drops of hexane were added, and the solution was kept at −5°C in a freezer giving blue-violet crystals (130 mg, 74%). Similarly, other palladium (**2b**, **2c**, **2f**) and platinum (**3a**−**3d**) complexes were prepared. The most important data are summarized in Table 6.

[PdCl{Te(3-MeC_5H_3N)}($Ptol_3$)] (2d): Solid $Ptol_3$ (tol = 4-MeC_6H_4) (26 mg, 0.09 mmol) was added to an acetone suspension (20 mL) of **1** (30 mg, 0.08 mmol), and the mixture was stirred for 1 h. The green solution was dried in vacuo and the residue was washed with hexane, diethyl ether and recrystallized from acetone/hexane to yield green crystals (38 mg, 68%). The complexes **2c** and **2e** were prepared in an analogous manner.

Table 6. Physical and analytical data for 3-methyl- and 6-methyl-2-pyridinetellurolate complexes of Pd^{II} and Pt^{II}

Complex	Color	Recrystallization solvent (yield [%])	M.p. [°C]	Analysis: found (calcd.) C	H	N
$[PdCl(TeC_5H_4N)]_n$ (**1a**)	brown		164 (dec.)	17.0 (17.3)	1.2 (1.2)	4.1 (4.0)
$[PdCl\{Te(3\text{-}MeC_5H_3N)\}]_n$ (**1b**)	brown		185 (dec.)	18.6 (19.9)	1.3 (1.7)	3.6 (3.9)
$[PdCl\{Te(3\text{-}MeC_5H_3N)\}(PEt_3]$ (**2a**)	blue-violet	hexane (74)	116	30.5 (30.1)	4.2 (4.4)	2.8 (2.9)
$[PdCl\{Te(3\text{-}MeC_5H_3N)\}(PMePh_2)]$ (**2b**)	blue	acetone/hexane (72)	163	40.6 (40.7)	3.3 (3.4)	2.4 (2.5)
$[PdCl\{Te(3\text{-}MeC_5H_3N)\}(PPh_3)]$ (**2c**)	green	acetone (76)	150	45.4 (46.2)	3.2 (3.4)	2.3 (2.2)
$[PdCl\{Te(3\text{-}MeC_5H_3N)\}(P(tol)_3]$ (**2d**)	green	acetone/hexane (68)	167	48.6 (48.7)	3.7 (4.1)	2.2 (2.1)
$[PdCl\{Te(3\text{-}MeC_5H_3N)\}(PPh_2py)]$ (**2e**)	green	acetone (60)	78	45.0 (44.2)	3.0 (3.2)	4.8 (4.5)
$[PdCl(TeC_5H_4N)(PMePh_2)]$ (**2f**)	green	acetone/hexane (56)	102	38.9 (39.5)	3.3 (3.1)	2.8 (2.6)
$[PtCl\{Te(3\text{-}MeC_5H_3N)\}(P\textit{n}Pr_3]$ (**3a**)	orange-red	hexane (66)	98	29.5 (29.5)	4.2 (4.5)	2.2 (2.3)
$[PtCl\{Te(3\text{-}MeC_5H_3N)\}(PMe_2Ph)]$ (**3b**)	red	diethyl ether/hexane (58)	124	28.8 (28.6)	2.7 (2.9)	2.3 (2.4)
$[PtCl\{Te(3\text{-}MeC_5H_3N)\}(PMePh_2)]$ (**3c**)	red	acetone (62)	187	35.1 (35.1)	2.6 (2.9)	2.1 (2.2)
$[PtCl(TeC_5H_4N)(PMePh_2)]$ (**3d**)	brown	acetone/hexane (52)	166	(34.0)	(2.7)	(2.2)
$[Pt\{Te(3\text{-}MeC_5H_3N)\}_2(dppe)]$ (**4a**)	yellow	CH_2Cl_2/hexane (64)	192	45.0 (44.2)	3.2 (3.5)	2.8 (2.7)
$[Pt\{Te(6\text{-}MeC_5H_3N)_2(dppe)]$ (**4b**)	yellow	acetone/hexane (56)	167	43.4 (44.2)	3.2 (3.5)	2.4 (2.7)
$[Pt\{Te(3\text{-}MeC_5H_3N)\}_2(PPh_3)_2]$ (**5**)	yellow	acetone/benzene (42)	168	49.3 (49.8)	2.5 (3.6)	2.1 (2.4)
$[Pt_2\{Te(3\text{-}MeC_5H_3N)\}_2(dppe)_2][BPh_4]_2$ (**6**)	yellow	acetone (60)	213	59.5 (59.4)	4.2 (4.4)	1.4 (1.2)

$[Pt\{Te(3\text{-}MeC_5H_3N)\}_2(dppe)]$ (4a): This compound was prepared analogously to **2a** by using $[PtCl_2(dppe)]$ (110 mg, 0.17 mmol) and $NaTe(3\text{-}MeC_5H_3N)$ [prepared from $(3\text{-}MeC_5H_3N)_2Te_2$ (73 mg, 0.17 mmol) and $NaBH_4$ (13 mg, 0.34 mmol)]. The yellow residue was recrystallized from a CH_2Cl_2/hexane mixture (yield: 109 mg, 64%). Complex **4b** was prepared in a similar manner.

$[Pt\{Te(3\text{-}MeC_5H_3N)\}_2(PPh_3)_2]$ (5): A benzene suspension of $[PtCl_2(PPh_3)_2]$ (154 mg, 0.19 mmol) was added to a freshly prepared methanolic solution (5 mL) of $NaTe(3\text{-}MeC_5H_3N)$ [prepared from $(3\text{-}MeC_5H_3N)_2Te_2$ (85 mg, 0.19 mmol) and $NaBH_4$ (15 mg, 0.39 mmol)], and the yellow-orange mixture was stirred for 4 h. The solvents were evaporated in vacuo and the residue was washed thoroughly with hexane, diethyl ether, and acetone and then extracted with benzene (3 × 8 mL). The solution was passed through a Florisil column and concentrated to 5 mL, a few drops of acetone were added, and the solution was kept at −5°C in a freezer, giving a yellow powder (95 mg, 42%).

$[Pt_2\{Te(3\text{-}MeC_5H_3N)\}_2(dppe)_2][BPh_4]_2$ (6): An acetone suspension (20 mL) of $[PCl_2(dppe)]$ (203 mg, 0.31 mmol) was added to a freshly prepared methanolic solution (5 mL) of $NaTe(3\text{-}MeC_5H_3N)$ [prepared from $(3\text{-}MeC_5H_3N)_2Te_2$ (68 mg, 0.16 mmol) and $NaBH_4$ (12 mg, 0.32 mmol)], while stirring. After 2 h, an acetone solution (8 mL) of $NaBPh_4$ (107 mg, 0.31 mmol) was added, while stirring was continued for 3 h. The solvents were evaporated under vacuum. The yellow residue was extracted with acetone (3 × 8 mL) and passed through a Florisil column. The solution was concentrated to 5 mL and yellow crystals were obtained (207 mg, 60%).

Crystallography: X-ray data on dark green crystals of $[PdCl\{Te(3\text{-}MeC_5H_3N)\}(PPh_3)]$ (**2c**) were collected at room temperature with an Enraf−Nonius CAD-4 diffractometer using graphite-monochromated Mo-K_α radiation (λ = 0.71073 Å), employing the ω-2θ scan technique. Crystal data are given in Table 7. The unit cell parameters were determined from 25 reflections measured by random search routine and indexed by the method of short vectors followed by least-squares refinement. The intensity data were corrected for Lorentz polarization and absorption effects. The structure was solved using the SHELXS86[45] and refined using the SHELXL97[46] computer programs. The non-hydrogen atoms were refined anisotropically. CCDC-181928 contains the supplementary crystallographic data for this paper. These data can be obtained free of charge at www.ccdc.cam.ac.uk/conts/retrieving.html or from the Cambridge Crystallographic Data Centre, 12 Union Road, Cambridge CB2 1EZ, UK [Fax: (internat.) + 44-1223/336-033; E-mail: deposit@ccdc.cam.ac.uk].

Table 7. Crystallographic and structure refinement details for $[PdCl\{Te(3\text{-}MeC_5H_3N)\}(PPh_3)]$ (**2c**)

Empirical formula	$C_{24}H_{21}ClNPPdTe$
Formula mass	623.84
Crystal size [mm]	0.3×0.3×0.2
T [K]	293(2)
λ [Å]	0.71073
Crystal system	monoclinic
Space group	$P2_1/n$
Unit cell dimensions	
a [Å]	8.607(2)
b [Å]	11.088(3)
c [Å]	24.552(5)
β [°]	98.83(2)
V [Å^3]	2315.4(9)
$\rho_{calcd.}$ [Mg·m^{-3}]	1.790
Z	4
μ [mm^{-1}]	2.231
θ for data collection/°	2.02 to 24.96
Reflections collected/unique	4349/4059 [R_{int} = 0.03−0.01]
Refinement method	Full-matrix least-squares on F^2
Absorption correction	ψ scan
Data/restraints/parameters	4059/0/263
Goodness of fit on F^2	1.104
Final $R1$, wR_2 indices	0.0376, 0.0955
R_1, wR_2 (all data)	0.0563, 0.1265
Largest diff peak and hole [e·Å^{-3}]	0.944 and −1.058

Acknowledgments

We thank Dr. J. P. Mittal and Dr. P. Raj for encouragement of this work. We are grateful to Dr. M. Sudersan, Head, Analytical Chemistry Division, for providing microanalyses of the complexes. We are thankful to Mr. S. Nath of RC&CD and Mr. A. Satpati of ACD for recording the UV/Vis spectra and cyclic voltammograms.

[1] M. Bochmann, *Chem. Vap. Deposition* **1996**, *2*, 85.
[2] H. B. Singh, N. Sudha, *Polyhedron* **1996**, *15*, 745.
[3] M. A. Mallik, P. O'Brien, D. J. Otway, *Phosphorus, Sulfur Silicon* **1998**, *136−138*, 431.
[4] [4a] Proceedings of the 9th International Conference on II-VI compounds, Kyoto, Japan **1999**. [4b] *J. Cryst. Growth* **2000**, 214/215.
[5] [5a] I. G. Dance, *Polyhedron* **1986**, *5*, 1037. [5b] P. J. Blower, J. R. Dilworth, *Coord. Chem. Rev.* **1987**, *76*, 121.
[6] V. K. Jain, S. Kannan, R. J. Butcher, J. P. Jaisinski, *J. Chem. Soc., Dalton Trans.* **1993**, 1509.
[7] A. Singhal, V. K. Jain, B. Varghese, E. R. T. Tiekink, *Inorg. Chim. Acta* **1999**, *285*, 190.
[8] [8a] A. L. Seligson, J. Arnold, *J. Am. Chem. Soc.* **1993**, *115*, 8214. [8b] J. Arnold, *Prog. Inorg. Chem.* **1995**, *43*, 353.
[9] J. R. Dilworth, N. Wheatley, *Coord. Chem. Rev.* **2000**, *199*, 89.
[10] [10a] M. Capdevila, W. Clegg, P. Gonzalez Duarte, B. Hanis, I. Mira, J. Sola, I. C. Taylor, *J. Chem. Soc., Dalton Trans.* **1992**, 2817. [10b] M. A. Ciriano, J. J. Perez-Torrente, L. A. Oro, A. Tiripicchio, M. J. Tiripicchio-Camellini, *J. Chem. Soc., Dalton Trans.* **1991**, 225.
[11] S. Narayan, V. K. Jain, B. Varghese, *J. Chem. Soc., Dalton Trans.* **1998**, 2359.
[12] S. Dey, V. K. Jain, S. Chaudhury, A. Knoedler, F. Lissner, W. Kaim, *J. Chem. Soc., Dalton Trans.* **2001**, 723.
[13] S. Dey, V. K. Jain, A. Knoedler, W. Kaim, S. Zalis, *Eur. J. Inorg. Chem.* **2001**, 2965.
[14] J. M. Rawson, R. E. P. Winpenny, *Coord. Chem. Rev.* **1995**, *139*, 313.
[15] [15a] E. S. Raper, *Coord. Chem. Rev.* **1996**, *153*, 199. [15b] E. S. Raper, *Coord. Chem. Rev.* **1997**, *165*, 475.
[16] V. K. Jain, S. Narayan, *Trans. Met. Chem.* **1999**, *24*, 409.
[17] Y. Cheng, T. J. Emge, J. G. Brennan, *Inorg. Chem.* **1994**, *33*, 3711.
[18] [18a] Y. Cheng, T. J. Emge, J. G. Brennan, *Inorg. Chem.* **1996**, *35*, 342. [18b] Y. Cheng, T. J. Emge, J. G. Brennan, *Inorg. Chem.* **1996**, *35*, 7339.
[19] C. O. Kienitz, C. Thone, P. G. Jones, *Inorg. Chem.* **1996**, *35*, 3990.
[20] N. Chopra, L. C. Damude, P. A. W. Dean, J. J. Vittal, *Can. J. Chem.* **1996**, *74*, 2095.
[21] J. Laube, S. Jager, C. Thone, *Eur. J. Inorg. Chem.* **2001**, 1983.
[22] F. P. Colonna, G. Distefano, V. Galasso, K. J. Irgolic, G. C. Pappalardo, L. Pope, *J. Chem. Soc., Perkin Trans. 2.* **1981**, 281.
[23] L. Engman, M. P. Cava, *Organometallics* **1981**, *1*, 470.
[24] [24a] L. Y. Chiang, J. W. Swirczewski, R. Kastrup, C. S. Hsu, R. B. Upasani, *J. Am. Chem. Soc.* **1991**, *113*, 6574. [24b] M. Misono, N. Nojiri, *Appl. Catal.* **1990**, *64*, 1.
[25] T. Yamamoto, Jpn. Pat. 61215661, **1986**; *Chem. Abstr.* **1987**, *106*, 87694h.
[26] T. Oota, K. Yoshoka, T. Kyama, S. Mori, Jpn. Pat. 07205548, **1995**; *Chem. Abstr.* **1995**, *123*, 325855j.
[27] W. D. Jones, M. R. Chim, *J. Am. Chem. Soc.* **1994**, *116*, 198.
[28] J. Real, M. Pages, A. Polo, J. F. Pinella, A. Alvarez-Larena, *Chem. Commun.* **1999**, 277.
[29] A. Singhal, V. K. Jain, R. Misra, B. Varghese, *J. Mater. Chem.* **2000**, 1121.
[30] V. K. Jain, *Trans. Met. Chem.* **1996**, *21*, 494.
[31] N. Nakatsu, Y. Nakamura, K. Matsumoto, S. Ooi, *Inorg. Chim. Acta* **1992**, *196*, 81.
[32] J. H. Yamamoto, W. Yoshida, C. M. Jensen, *Inorg. Chem.* **1991**, *30*, 1353.
[33] G. P. A. Yap, C. M. Jensen, *Inorg. Chem.* **1992**, *31*, 4823.
[34] M. Gupta, R. E. Cramer, K. Ho, C. Pettersen, S. Mishina, J. Belli, C. M. Jensen, *Inorg. Chem.* **1995**, *34*, 60.
[35] S. Dey, V. K. Jain, A. Knoedler, A. Klein, W. Kaim, S. Zalis, *Inorg. Chem.* **2002**, *41*, 2864.
[36] C. K. Johnson, *ORTEPII-A*, FORTRAN Thermal Ellipsoid Plot program for crystal structure illustrations, ORNL-5138, **1976**.
[37] V. K. Jain, S. Kannan, R. Bohra, *Polyhedron* **1992**, *11*, 1551.
[38] A. K. Singh, V. Srivastava, S. K. Dhingra, J. E. Drake, J. H. Bailey, *Acta Crystallogr., Sect. C* **1992**, *48*, 655.
[39] E. M. Padilla, J. A. Golen, P. N. Richmann, C. M. Jensen, *Polyhedron* **1991**, *10*, 1343.
[40] D. M. Giolando, T. B. Rauchfuss, A. L. Rheingold, *Inorg. Chem.* **1987**, *26*, 1636.
[41] Powder diffraction File No. 29-971, compiled by JPCDS, International Centre for Diffraction Data USA, **1986**.
[42] F. R. Hertley, *The Chemistry of Platinum, Palladium*, John Wiley & Sons, New York, **1973**.
[43] [43a] S. J. Dunne, L. A. Summer, E. I. Nagy-Fesobuki, *J. Heterocycl. Chem.* **1993**, *30*, 409. [43b] K. K. Bhasin, V. K. Jain, H. Kumar, J. Singh, *Synth. Commun.*, in press.
[44] L. C. Craig, *J. Am. Chem. Soc.* **1934**, *56*, 231.
[45] G. M. Sheldrick, *SHELXS86, Program for crystal structure determination*, University of Göttingen, **1986**.
[46] G. M. Sheldrick, *SHELXL97, Program for refinement of crystal structures*, University of Göttingen, Germany, **1997**.

Received June 25, 2002
[I02350]

Selective Synthesis of *N*-Methylanilinooligosilanes

Uwe Böhme,*[a] Betty Günther,[a] and Ben Rittmeister[a]

Keywords: Amides / Silanes / Disilanes / Aminosilanes / Stereochemistry

Defined crystalline amino-substituted organosilanes were prepared by reaction of *N*-methylaniline with 1,1,2,2-tetrachloro-1,2-dimethyldisilane. It is possible to selectively prepare mono-, di-, and triaminodisilanes depending on the reactant ratio. The X-ray structure analyses of 1,2-dichloro-1,2-dimethyl-1,2-bis(*N*-methylanilino)disilane (**2**), 1-chloro-1,2-dimethyl-1,2,2-tris(*N*-methylanilino)disilane (**3**), and 1,2-dimethyl-1,1,2,2-tetrakis(*N*-methylanilino)disilane (**4**) were performed. The absolute structure of **2** was determined by crystallographic methods. Compound **2** is a useful reagent for preparing a variety of other aminoorganodisilanes like $[Me(PhMeN)_2Si]_2$ (**4**), $[FMe(PhMeN)Si]_2$ (**12**), [(PhCC)-Me(PhMeN)Si]$_2$ (**13**), $[(p\text{-}MeC_6H_4)Me(PhMeN)Si]_2$ (**14**), and $[(PhCH_2)Me(PhMeN)Si]_2$ (**15**). Other chloroorganooligosilanes also react with *N*-methylaniline to give PhMeN[Si-$Me_2]_2Cl$ (**5**), PhMeN$[SiMe_2]_2$NMePh (**6**), Cl$[SiMe_2]_3$NMePh (**7**), PhMeN$[SiMe_2]_3$NMePh (**8**), Cl$[SiMe_2]_4$NMePh (**9**), MeClSi[Si(NMePh)ClMe]$_2$ (**10**), and MeSi[Si(NMePh)-ClMe]$_3$ (**11**).

(© Wiley-VCH Verlag GmbH & Co. KGaA, 69451 Weinheim, Germany, 2003)

Introduction

Functionally substituted di- and oligosilanes are valuable building blocks for preparing organopolysilanes and silicon-containing materials.[1] A good method for preparing such compounds is the reductive coupling of chloroorganosilanes with alkaline metals[2] and subsequent cleavage of aromatic substituents with gaseous hydrogen chloride and $AlCl_3$[3] or trifluoromethylsulfonic acid.[4] The preparation of chloro(methyl)oligosilanes by halogen/methyl exchange using Me_3SiCl and $AlCl_3$ is another frequently used method.[5]

The reductive coupling of chloro(diethylamino)organosilanes is a convenient new way to prepare functionalized oligosilanes. The diethylamino group in the resulting oligosilanes can be replaced, under very mild conditions, by various reagents such as alcohols or hydrogen chloride. A number of amino(chloro)organooligosilanes have been prepared, but these are often oils and it is very difficult to separate pure compounds from the mixture of liquid products.[6,7] Some X-ray structures of amino(organo)oligosilanes without chlorine substituents are known.[8] Until now very little structural data on amino(chloro)organooligosilanes has been available.[9]

We have developed reliable synthetic pathways to a variety of crystalline amino(chloro)methyloligosilanes. A number of different aromatic diorganoamines were tested for their reactivity with 1,1,2,2-tetrachloro-1,2-dimethyldisilane.[9] The large flat aromatic groups should help to obtain crystalline products. The products obtained with *N*-methylaniline are soluble in aprotic organic solvents and are extremely crystalline.

Results and Discussion

The reaction of *N*-methylaniline with 1,1,2,2-tetrachloro-1,2-dimethyldisilane in the presence of excess NEt_3 gives mono-, di-, and triaminodisilanes depending on the reactant ratio. 1,1,2-Trichloro-2-(*N*-methylanilino)-1,2-dimethyldisilane (**1**) was obtained as a colorless oil. According to the ^{29}Si NMR spectrum, the product contains about 20% impurities, which were identified as **2** and 1,1,2,2-tetrachloro-1,2-dimethyldisilane. Because of these impurities we did not use this compound in further reactions. 1,2-Dichloro-1,2-bis(*N*-methylanilino)-1,2-dimethyldisilane (**2**) was isolated as an ivory-colored solid. The crude product contains traces of **3** and was recrystallized from a pentane/diethyl ether mixture (5:1); **3** was synthesized by the same experimental procedure and obtained as a white crystalline solid (Scheme 1).

The ^{29}Si NMR spectra of **2**, **3**, and **4** have some interesting features. The tetraamide **4** shows one signal at $\delta = -7.53$ ppm for the spectroscopically equivalent silicon atoms; **3** has two chemically and spectroscopically different silicon atoms. The (*R*) and (*S*) isomers have identical signals in the spectrum. Thus, two signals with an intensity ratio of 1:1 are observed at $\delta = -7.94$ and 6.27 ppm. The silicon atoms in **2** are chemically equivalent, and chiral. Two signals are expected, one for the racemate [(*R*,*R*) and (*S*,*S*) isomer] and one for the *meso* form and there are indeed two such signals at $\delta = 3.66$ and 1.37 ppm. The intensity ratio

[a] Technische Universität Bergakademie Freiberg, Institut für Anorganische Chemie,
Leipziger Straße 29, 09596 Freiberg, Germany
E-mail: uwe.boehme@chemie.tu-freiberg.de

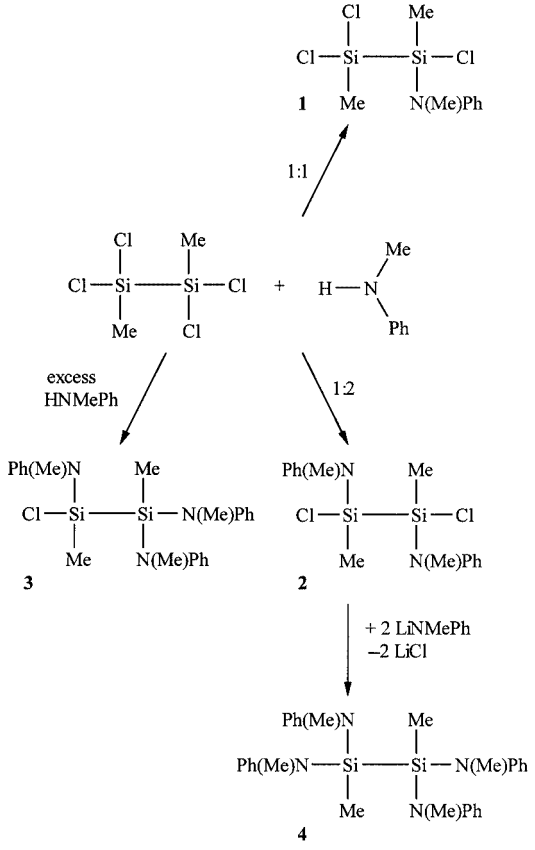

Scheme 1

of the two signals is always between 5:1 and 6:1. We assume that the main product is the racemate. It is rather unusual that one isomer is formed preferentially over another. Investigations concerning the isomerization of diastereomers of $(FArMeSi)_2$ have shown that a *rac*/*meso* mixture of 1:1 was obtained during the preparation process.[10] Detailed experiments regarding the isomerization processes of this compound have shown that the enrichment of the *meso* form proceeds by crystallization-induced asymmetric transformation (AT).[11]

We investigated the quantitative composition of the crude product of **2** by in situ NMR spectroscopy and found a relative intensity ratio of 5.5:1. In further experiments, we used NMR spectroscopy to monitor the course of the reaction for several weeks. We prepared two reaction batches, one with pentane and the other with DME as the solvent. In both experiments, we found no substantial change in the relative product composition! The relative product ratio was always between 5.5:1 and 6:1. Furthermore, samples of **2** can be dissolved and recrystallized without change in the composition of the diastereomers. In summary, we found no evidence for a crystallization-induced asymmetric transformation of **2**.

Quantum chemical calculations on the diastereomers of **2** show that the *rac* form has a substantially lower total energy. The energy difference between the (*R*,*R*) and the *meso* form is 18 kJ/mol at the B3LYP/6-31G* level of theory.[12] This suggests a preferred formation of the racemate during the synthesis of **2**.

In order to explore further the available range of *N*-methylanilinosilanes, we treated different oligomeric chloro(organo)silanes with *N*-methylaniline. It was possible to selectively obtain mono- and disubstituted aminosilanes (**5**, **7** and **6**, **8**) from $Cl[SiMe_2]_nCl$. The reactivity of the homologous α,ω-dichlorooligosilanes decreases with increasing chain length. Therefore, the tetrasilane $Cl[SiMe_2]_4Cl$ gave only the monosubstituted product $Cl[SiMe_2]_4NMePh$ (**9**). The branched chlorosilanes $MeClSi(SiCl_2Me)_2$ and $MeSi(SiCl_2Me)_3$ were prepared by disproportionation of 1,1,2,2-tetrachloro-1,2-dimethyldisilane.[13] The reaction of these compounds with *N*-methylaniline in different stoichiometric ratios gave product mixtures. We succeeded in obtaining defined reaction products only when an excess of *N*-methylaniline was used. One chlorine atom remains at each silicon atom and the products formed under these conditions were characterized as $MeClSi[Si(NMePh)ClMe]_2$ (**10**) and $MeSi[Si(NMePh)ClMe]_3$ (**11**). It was not possible to replace all the chlorine atoms in these chlorine-rich organosilanes with the *N*-methylanilido group. Although, it might be possible to replace the last chlorine atoms when using the corresponding lithium amide. The compounds **5**−**11** were characterized by NMR spectroscopy (see Exp. Sect.).

The reactivity of **2** and **3** was investigated: 1-chloro-1,2-dimethyl-1,2,2-tris(*N*-methylanilino)disilane (**3**) is rather inert with respect to nucleophilic reagents. The compound does not react with diorganoamines, such as $HNEt_2$ and Grignard reagents. The treatment of **3** with alkyllithium compounds yields mainly unchanged starting material. Aside from this, small amounts of reaction products were detected by NMR spectroscopy. It was not possible to isolate pure compounds by recrystallization of the product mixtures. ^{29}Si NMR spectroscopy identified one of the compounds in these mixtures as 1,2-dimethyl-1,1,2,2-tetrakis(*N*-methylanilino)disilane (**4**), which was also synthesized by an alternative method, see below; **4** was formed in these reactions, probably by transamination with the strong nucleophilic alkyllithium compound. The alkyllithium compound might form in situ lithium *N*-methylanilide which reacts with **3**.

In contrast to **3**, 1,2-dichloro-1,2-dimethyl-1,2-bis(*N*-methylanilino)disilane (**2**) reacts with nucleophiles with the substitution of both chlorine atoms in a straightforward reaction (see Scheme 2). It was possible to prepare a variety of derivatives with different nucleophiles, such as lithium amides (**4**), zinc fluoride (**12**), alkynyllithium compounds (**13**), and Grignard reagents (**14** and **15**; see Scheme 2). Since the *N*-methylanilino group remains unaffected in these reactions, it acts as a valuable protecting group.

1,2-Difluoro-1,2-dimethyl-1,2-bis(*N*-methylanilino)-disilane (**12**) was prepared by the reaction of excess of ZnF_2 with **2**. The reaction between the dissolved amino(chloro)silane and the solid zinc fluoride took about 6 d. The progress of the reaction was monitored by NMR spectroscopy. A mixture of ClMe(PhMeN)SiSi(NMePh)MeF and

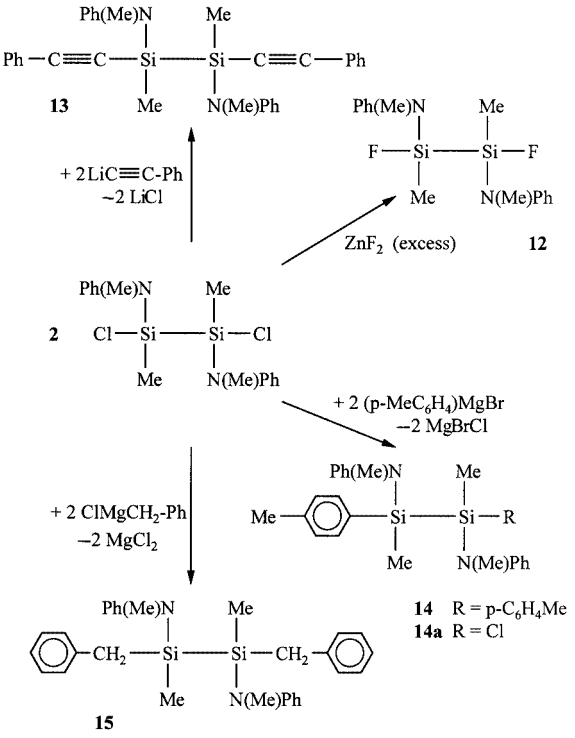

Scheme 2

$[FMe(PhMeN)Si]_2$ (**12**) was formed during the first 48 h. This mixture slowly converted to **12** in the presence of excess ZnF_2. Signals for the diastereomers of **12** (*rac* and *meso*) were observed in the reaction mixture but only one diastereomer was obtained after the workup procedure. This suggests that the solubility for both diastereomers is very different. It might also be caused by crystallization-induced asymmetric transformation.

$[(p\text{-}MeC_6H_4)Me(PhMeN)Si]_2$ (**14**) was obtained as a mixture with the monosubstituted product $(p\text{-}MeC_6H_4)$-Me(PhMeN)SiSi(NMePh)MeCl (**14a**) (ratio **14**/**14a** = 2:1). The reaction of **2** with excess *p*-tolylmagnesium bromide gave a slightly different product ratio of 2.2:1, but this synthesis did not enable pure **14** to be obtained. The compounds $[(PhCC)Me(PhMeN)Si]_2$ (**13**), $[(p\text{-}MeC_6H_4)$-$Me(PhMeN)Si]_2$ (**14**), and $[(PhCH_2)Me(PhMeN)Si]_2$ (**15**) were obtained as a mixture of diastereomers. Integration of the MeSi signals in the ^1H NMR spectra provides the relative ratio of *rac*/*meso* isomers; **13** and **15** have a ratio of about 1:1, and **14** a ratio of 1.5:1. This means that the substitution reactions with the organometallic reagents are not stereoselective.

Crystal and Molecular Structures

The solid-state structures of **2**−**4** were determined from the data obtained by X-ray diffraction. Details of the structure determinations and refinement are summarized in Table 3. The X-ray structure analyses confirm the structures of the compounds **2**−**4** as proposed in Scheme 1; **3** crystallizes in the space group $P2_1/n$ as a racemate and **4** crystallizes in the space group $P2_1/a$; **2** was obtained as separated pure enantiomorphic crystals that crystallize in the noncentrosymmetric space group $C222_1$. The structure of one crystalline modification was determined. Only the half-molecule, ClSi(NMePh)Me, is found in the asymmetric unit, so the unit cell only contains four molecules. The second part of the molecule is generated by symmetry elements. Three times more reflections were collected than normally necessary for an orthorhombic space group, in order to determine the absolute configuration through the anomalous scattering effect. Refinement of the Flack enantiopole parameter led to a value of ca. 0, thus confirming the absolute structure of the crystal.[14] The molecular structure of **2** is shown in Figure 1. The silicon atom has an (*R*) configuration. The fact that both silicon atoms have the same configuration means that, in the crystal under examination, the molecules have an (*R*,*R*) configuration. There are a number of chiral silicon compounds reported in the literature.[15,16] Diastereomers have mainly been prepared with one chiral silicon atom and one chiral organic group such as the (−)-menthoxy group. Only one diastereomeric dichlorodisilane with two chiral silicon atoms was found in the Cambridge Crystallographic Database.[17] The value of optical rotation was estimated to be $\alpha = 377°$ (20 °C, 302 nm, *n*-pentane) from a randomly chosen crystal of **2**.

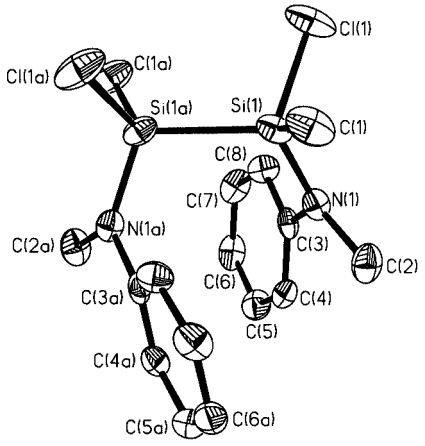

Figure 1. Molecular structure of 1,2-dichloro-1,2-dimethyl-1,2-bis(*N*-methylanilino)disilane (**2**) with 50% thermal ellipsoids; hydrogen atoms are omitted for clarity

The compounds **2** (Figure 1), **3** (Figure 2), and **4** (Figure 3) are homologous amino(methyl)disilanes with an increasing number of *N*-methylanilino groups bonded to the silicon atoms. The increasing degree of substitution with *N*-methylanilino groups causes some changes in the molecular structure of these three compounds. The silicon−silicon bond length is 2.375 Å in **4**, which is an increase in length from that seen in **2**. The Si−N bonds in **4** (1.754 Å, average value) are also longer than those in **2** (1.718 Å) and **3** (1.740 Å). The Si−C bond is slightly shorter in **2** than it is in **3** and **4**. The torsion angle C−Si−Si−C has similar values for **2** (141.9°) and **3** (−130.4°);[18] **4** has a *transoid* conformation around this torsion angle which is 173.6°. All bond lengths are in the normal range for covalent bonds, the silicon

Table 1. Selected bond lengths [Å] and bond angles [°]

1,2-Dichloro-1,2-dimethyl-1,2-bis(*N*-methylanilino)disilane (**2**)			
Si(1)−Si(1a)	2.341(1)	N(1)−Si(1)−Cl(1)	111.88(8)
Si(1)−Cl(1)	2.097(1)	N(1)−Si(1)−Si(1a)	109.34(6)
Si(1)−N(1)	1.718(2)	Cl(1)−Si(1)−Si(1a)	104.41(4)
Si(1)−C(1)	1.845(3)	C(1a)−Si(1a)−Si1−C1	141.9(1)
1-Chloro-1,2-dimethyl-1,2,2-tris(*N*-methylanilino)disilane (**3**)			
Si(1)−Si(2)	2.3726(6)	N(1)−Si(1)−Si(2)	109.04(6)
Si(1)−N(1)	1.751(2)	N(2)−Si(1)−Si(2)	109.26(6)
Si(1)−N(2)	1.736(2)	N(3)−Si(2)−Si(1)	114.42(6)
Si(2)−N(3)	1.732(2)	Cl(1)−Si(2)−Si(1)	104.84(3)
Si(2)−Cl(1)	2.1068(7)	C(1)−Si(1)−Si(2)−C(2)	−130.4(1)
Si(1)−C(1)	1.894(2)		
Si(2)−C(2)	1.859(2)		
1,2-Dimethyl-1,1,2,2-tetrakis(*N*-methylanilino)disilane (**4**)			
Si(1)−Si(2)	2.375(1)	N(1)−Si(1)−Si(2)	115.80(9)
Si(1)−N(1)	1.755(2)	N(2)−Si(1)−Si(2)	102.92(8)
Si(1)−N(2)	1.761(3)	N(3)−Si(2)−Si(1)	113.22(8)
Si(2)−N(3)	1.749(2)	N(4)−Si(2)−Si(1)	101.98(9)
Si(2)−N(4)	1.752(2)	C(1)−Si(1)−Si(2)	111.2(1)
Si(1)−C(1)	1.868(3)	C(2)−Si(2)−Si(1)	114.2(1)
Si(2)−C(2)	1.864(3)	C(1)−Si(1)−Si(2)−C(2)	173.6(2)

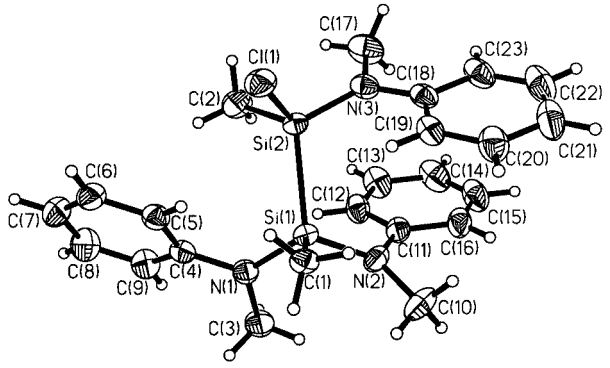

Figure 2. Molecular structure of 1-chloro-1,2-dimethyl-1,2,2-tris(*N*-methylanilino)disilane (**3**) with 50% thermal ellipsoids

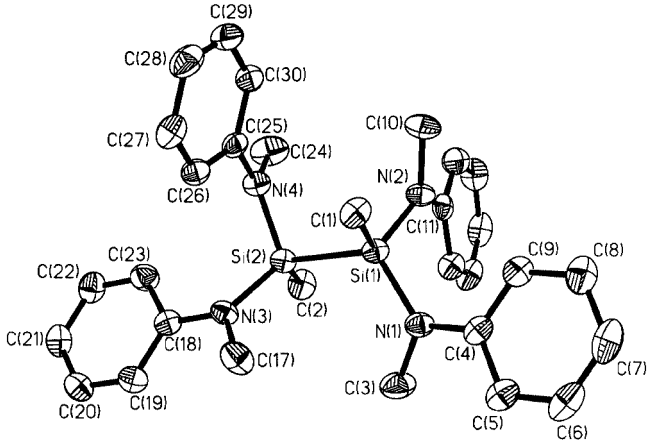

Figure 3. Molecular structure of 1,2-dimethyl-1,1,2,2-tetrakis(*N*-methylanilino)disilane (**4**) with 50% thermal ellipsoids; hydrogen atoms are omitted for clarity

atoms are tetrahedrally coordinated and no significant intermolecular interactions are observed.

Conclusions

The ease of preparing a variety of structurally different linear and branched chloro(methyl)(*N*-methylanilino)oligosilanes was demonstrated throughout this work. We were able to show that the *N*-methylanilino group is a highly useful substituent for chloro(organo)silanes in two respects. First, it is possible to obtain crystalline amino(organo)disilanes with this substituent. Second, the *N*-methylanilino group acts as a protecting group in further substitution reactions. With this strategy we were able to prepare a variety of amino(organo)disilanes starting from 1,2-dichloro-1,2-dimethyl-1,2-bis(*N*-methylanilino)disilane (**2**).

Experimental Section

General: All preparative work and handling of the samples was carried out under Ar using dry glassware and dry solvents. Pentane was freshly distilled from $LiAlH_4$. Triethylamine was refluxed over sodium/benzophenone until the color of the solution was violet, then freshly distilled prior to use. Zinc fluoride was dried 6 h in vacuo to remove all traces of moisture. Commercially available *N*-methylaniline was distilled prior to use from KOH pellets. 1,1,2,2-Tetrachloro-1,2-dimethyldisilane was prepared according to a well-known procedure.[19] Melting points were recorded in capillary tubes and are uncorrected. NMR spectra were recorded with a Bruker DPX 400 with $SiMe_4$ (TMS) as internal standard at 25 °C with 400.13 MHz for ^{1}H NMR, 100.62 MHz for ^{13}C NMR, and 79.49 MHz for ^{29}Si NMR spectroscopy. Signals are noted as s (singlet), d (doublet), t (triplet), q (quadruplet), m (multiplet), and dd (doublet, doublet). The Si-Si coupling constants have been calculated from the shift differences of the Si satellites in the ^{29}Si NMR spectrum. Elemental analyses were performed with a CHN-O-RAPID (Hanau). The carbon content values were lower than expected due to the formation of silicon carbide. GC-MS spectra were obtained with a 70 eV Hewlett Packard 5890 Series II/5971 Series GC/MS system.

1,1,2-Trichloro-1,2-dimethyl-2-(*N*-methylanilino)disilane (1): *N*-methylaniline (2.4 g, 23 mmol) was added to a solution of 1,1,2,2-tetrachloro-1,2-dimethyldisilane (5.2 g, 23 mmol) and triethylamine (4.7 g, 46 mmol) in pentane (200 mL). The mixture was stirred for 140 h at room temperature. A white precipitate formed after a few hours. The resulting suspension was filtered to remove the resulting Et_3NHCl. The solvent was removed in vacuo and the resulting oily product was dried in vacuo. The purity of the product was 80%, estimated by ^{29}Si NMR spectroscopy. About 15% 1,2-dichloro-1,2-dimethyl-1,2-bis(*N*-methylanilino)disilane (**2**) and 5% 1,1,2,2-tetrachloro-1,2-dimethyldisilane were detected as impurities. NMR ($CDCl_3$, 25 °C, TMS): ^{1}H: δ = 0.65 ppm (s, 3 H, MeSiClN), 0.77 (s, 3 H, $MeSiCl_2$), 3.07 (s, 3 H, MeN), 6.4−7.48 (m, 5 H, Ph). ^{13}C: δ = 1.29 ppm ($MeSiCl_2$), 6.61 (MeSiClN), 37.84 (MeN), 123.40, 123.85, 129.30 (*o*-, *m*-, *p*-Ph), 148.52 (*i*-Ph). ^{29}Si: δ = −0.6 ppm (MeSiClN), 21.4 ($MeSiCl_2$).

1,2-Dichloro-1,2-dimethyl-1,2-bis(*N*-methylanilino)disilane (2): Triethylamine (14 mL, 10.1 g, 100 mmol) was added to a solution of 1,1,2,2-tetrachloro-1,2-dimethyldisilane (6.0 g, 26 mmol) in pentane (150 mL). *N*-Methylaniline (5.7 mL, 5.6 g, 52 mmol) was mixed

with pentane (60 mL) and added dropwise over a period of 1 h to the reaction mixture. The reaction mixture became warm, and a voluminous white precipitate formed. The suspension was stirred at room temperature for 10 h, and then the precipitate consisting of Et_3NHCl was removed by filtration. The volume of the filtrate was reduced in vacuo to ca. 100 mL and left overnight at 5 °C. A white precipitate formed that consisted mainly of Et_3NHCl. The precipitate was removed by filtration and the filtrate was concentrated to give **2** (6.4 g , 67% yield) as a crystalline product. The crude product contained traces of **3** and was recrystallized from a pentane/diethyl ether (5:1) mixture. Ivory-colored crystals (5.9 g, 61.5%) resulted with m.p. 38 °C. $[\alpha]_\lambda$ = 377° (0.165 g/100 mL *n*-pentane, 20 °C, 302 nm). NMR ($CDCl_3$, 25 °C, TMS): ^{1}H: δ = 0.51 ppm (s, SiMe, *meso*), 0.77 (s, SiMe, *rac*), 2.67 (s, NMe, *rac*), 3.0 (s, NMe, *meso*), 6.83−7.23 (m, Ph). ^{13}C: δ = 3.08 ppm (SiMe, *meso*), 3.57 (SiMe, *rac*), 36.43 (NMe, *rac*), 37.86 (NMe, *meso*), 120.95, 122.19, 123.01, 123.10, 128.83, 129.0, 148.99, 149.18 (Ph). ^{29}Si: δ = 3.66 ppm (*rac*), 1.37 (*meso*). MS: *m*/*z* = 368 [M^+], 262 [M^+ − NMePh], 184 (98) [M^+ − NMePh − HCl], 149 (100%) [Si(NMePh)Me^+]. $C_{16}H_{22}Cl_2N_2Si_2$ (369.45): calcd. C 52.02, H 6.00, N 7.58; found calcd. C 51.89, H 6.08, N 7.54.

1-Chloro-1,2-dimethyl-1,2,2-tris(*N*-methylanilino)disilane (3): To synthesize compound **3**, the same approach was applied as described for **2** using 1,1,2,2-tetrachloro-1,2-dimethyldisilane (5.47 g, 24 mmol), triethylamine (16.7 mL, 12.1 g, 120 mmol) and *N*-methylaniline (13 mL, 12.8 g, 120 mmol). White crystals (7.6 g, 72% yield), m.p. 76 °C. NMR ($CDCl_3$, 25 °C, TMS): ^{1}H: δ = 0.33 ppm (s, 3 H, SiMe), 0.72 (s, 3 H, SiMe), 2.52 (s, 3 H, NMe), 2.57 (s, 3 H, NMe), 2.91 (s, 3 H, NMe), 6.72−7.27 (m, 18 H, Ph). ^{13}C: δ = 1.47, 4.71 ppm (SiMe); 30.72, 34.50, 36.50 (NMe); 112.41, 117.09, 117.25, 118.67, 119.51, 120.06, 120.87, 121.07, 121.54, 128.57, 128.64, 128.83, 149.57, 149.66, 149.79 (Ph). ^{29}Si: δ = −7.94 ppm [SiMe(NMePh)$_2$], 6.27 [SiMe(NMePh)Cl], $^1J_{Si\text{-}Si}$ = 152 Hz. MS: *m*/*z* = 439 [M^+], 255 (100%) [Si(NMePh)$_2$$Me^+$], 226 [PhSi(NMePh)$Me^+$], 184 [ClSi(NMePh)$Me^+$]. $C_{23}H_{30}ClN_3Si_2$ (440.14): calcd. C 62.76, H 6.87, N 9.55; found calcd. C 62.24, H 7.53, N 9.24.

1,2-Dimethyl-1,1,2,2-tetrakis(*N*-methylanilino)disilane (4): A solution of lithium *N*-methylanilide (1.2 g, 10.3 mmol) in diethyl ether (20 mL) was added to a solution of 1,2-dichloro-1,2-dimethyl-1,2-bis(*N*-methylanilino)disilane (1.4 g, 3.7 mmol) at 0 °C. A white precipitate was formed after 4 h. The solution was stirred for an additional 24 h at room temperature. Afterwards, the solvent was removed completely in vacuo. The remaining oily residue was extracted with diethyl ether and the resulting suspension was filtered. The solvent was partially removed in vacuo and the remaining solution was cooled to 5 °C to yield the product as a white crystalline solid. The product contained crystals that were suitable for X-ray structure analysis. Yield: 1.08 g (57.2%), m.p. 116−118 °C NMR ($CDCl_3$, 25 °C, TMS): ^{1}H: δ = 0.48 ppm (s, 6 H), 2.74 (s, 12 H), 7.11−7.16 (m, 20 H). ^{13}C: δ = 2.31 ppm (MeSi), 36.09 (MeN), 119.18, 120.30, 129.19 (*o*-, *m*-, *p*-Ph), 150.4 (*i*-Ph). ^{29}Si: δ = −7.53 ppm. $C_{30}H_{38}N_4Si_2$ (510.54): calcd. C 70.52, H 7.50, N 10.98; found calcd. C 70.15, H 7.38, N 9.95.

1-Chloro-1,1,2,2-tetramethyl-2-(*N*-methylanilino)disilane (5) and 1,1,2,2-Tetramethyl-1,2-bis(*N*-methylanilino)disilane (6): A solution of *N*-methylaniline (15.0 g, 140 mmol) in pentane (50 mL) was added dropwise to a solution of 1,2-dichloro-1,1,2,2-tetramethyldisilane (8.5 g, 45 mmol) and triethylamine (14.2 g, 140 mmol) in pentane (100 mL). A voluminous white precipitate formed during this procedure. The suspension was stirred at reflux temperature for 28 h and for a further 60 h at room temperature. The suspension was then filtered, the solvent was removed in vacuo and the remaining residue was distilled under high vacuum to give **5** and **6** in separated fractions. 1st fraction, b.p. (0.025 Torr) 56−59 °C, 1-chloro-1,1,2,2-tetramethyl-2-(*N*-methylanilino)disilane (**5**); 2nd fraction, b.p. (0.025 Torr) 66−70 °C, 1-chloro-1,1,2,2-tetramethyl-2-(*N*-methylanilino)disilane (**5**); 3rd fraction, b.p. (0.025 Torr) 129−137 °C, 1,1,2,2-tetramethyl-1,2-bis(*N*-methylanilino)disilane (**6**). Compound **5**: Colorless oil, fractions 1 and 2 together are 3.6 g (31.1% yield, 98% purity). NMR ($CDCl_3$, 25 °C, TMS): ^{1}H: δ = 0.40 ppm (s, 6 H, MeSiN), 0.46 (s, 6 H, MeSiCl), 2.93 (s, 3 H, MeN), 6.81−7.21 (m, 5 H, Ph). ^{13}C: δ = −0.30 ppm (MeSiCl), 2.95 (MeSiN), 35.81 (MeN), 117.85, 119.24, 128.86 (*o*-, *p*-, *m*-Ph), 150.98 (*i*-Ph). ^{29}Si: δ = −1.9 ppm (SiN), 20.9 (SiCl); $^1J_{Si\text{-}Si}$ = 106 Hz. Compound **6**: Pale yellow oil, yield: 3.8 g (25.7% yield, 87% purity). The product contains 13% of **5**. NMR ($CDCl_3$, 25 °C, TMS): ^{1}H: δ = 0.34 ppm (s, 12 H, MeSi), 2.72 (s, 6 H, MeN), 6.71−7.16 (m, 10 H, Ph). ^{13}C: δ = 1.07 ppm (MeSi), 34.99 (MeN), 116.65, 117.99, 128.59 (*o*-, *p*-, *m*-Ph), 151.09 (*i*-Ph). ^{29}Si: δ = −1.9 ppm. MS: 164 (100%) [$Me_2SiNMePh^+$], 59 [Me_2SiH^+], 222 [$Me_4Si_2NMePh^+$], 328 [M^+].

General Procedure for Preparing the Chloro(methyl)oligosilanes 7−11: An excess of triethylamine (1.5 mol per mol of reactive chlorine) was added to a solution of the chloro(methyl)oligosilane (5 mmol) in 100 mL of pentane. The stoichiometric amount of *N*-methylaniline (see Table 2) was mixed with pentane and added dropwise to the reaction mixture. A voluminous white precipitate of triethylammonium chloride was formed. The suspension was stirred at room temperature for at least 10 h. The solvent and the excess triethylamine was distilled off at reduced pressure. The remaining solid was extracted with pentane and filtered. The solvent

Table 2. Reaction products of oligomeric chloro(methyl)oligosilanes with *N*-methylaniline in the presence of excess triethylamine

Chlorosilane	Ratio chlorosilane/HNMePh	Product
$Cl_2Si(Me)SiMeCl_2$	1:1	$Cl_2MeSiSi(NMePh)ClMe$ (**1**)
$Cl_2Si(M)eSiMeCl_2$	1:2	$[ClMe(PhMeN)Si]_2$ (**2**)
$Cl_2Si(Me)SiMeCl_2$	1:5−6	$ClMe(PhMeN)SiSi(NMePh)_2Me$ (**3**)
$Cl[SiMe_2]_2Cl$	1:1	$PhMeN[SiMe_2]_2Cl$ (**5**)
$Cl[SiMe_2]_2Cl$	1:2	$PhMeN[SiMe_2]_2NMePh$ (**6**)
$Cl[SiMe_2]_3Cl$	1:1	$Cl[SiMe_2]_3NMePh$ (**7**)
$Cl[SiMe_2]_3Cl$	1:2	$PhMeN[SiMe_2]_3NMePh$ (**8**)
$Cl[SiMe_2]_4Cl$	1:2	$Cl[SiMe_2]_4NMePh$ (**9**)
$MeClSi(SiCl_2Me)_2$	excess HNMePh	$MeClSi[Si(NMePh)ClMe]_2$ (**10**)
$MeSi(SiCl_2Me)_3$	excess HNMePh	$MeSi[Si(NMePh)ClMe]_3$ (**11**)

was partially removed from the filtrate in a vacuum and the concentrated solution was left for several days at 5 °C; **9**, **10**, and **11** formed a white precipitate which was isolated by filtration and dried in vacuo; **7** and **8** did not crystallize and were therefore purified by vacuum distillation.

Cl[SiMe$_2$]$_3$NMePh (7): Colorless oil, yield: 340 mg (22%), b.p.$_{0.01Torr}$ 97 °C. NMR ($CDCl_3$, 25 °C, TMS): ^{1}H: δ = 0.16 ppm (s, 6 H, (PhMeNSiMe$_2$Si*Me*$_2$), 0.28 (s, 6 H, (PhMeNSi*Me*$_2$SiMe$_2$), 0.59 (s, 6 H,ClSi*Me*$_2$), 2.79 (s, 6 H, Ph*Me*N), 6.83−7.24 (m, 5 H, Ph). ^{13}C: δ = −1.6 ppm (PhMeNSiMe$_2$Si*Me*$_2$), 0.8 (PhMeNSi*Me*$_2$-SiMe$_2$), 5.2 (ClSi*Me*$_2$), 37.3 (Ph*Me*N), 119.2.120.1.127.9, 149.8 (Ph). ^{29}Si: δ = 25.9 ppm, 2.4, −45.2.

PhMeN[SiMe$_2$]$_3$NMePh (8): Yellow oil, yield: 600 mg (31%), b.p.$_{0.01Torr}$ 128 °C. NMR ($CDCl_3$, 25 °C, TMS): ^{1}H: δ = 0.16 ppm [s, 6 H, (PhMeNSiMe$_2$)$_2$Si*Me*$_2$], 0.28 [s, 12 H, (PhMeNSi*Me*$_2$)$_2$-SiMe$_2$], 2.82 (s, 6 H, Ph*Me*N), 6.76−7.19 (m, 10 H, Ph). ^{13}C: δ = −3.8 ppm [(PhMeNSiMe$_2$)$_2$Si*Me*$_2$], 0.7 [(PhMeNSi*Me*$_2$)$_2$SiMe$_2$], 35.6 (Ph*Me*N), 117.1, 118.1.128.6, 151.3 (Ph). ^{29}Si: δ = 3.0 ppm, −47.6; $^1J_{Si\text{-}Si}$ = 80 Hz.

Cl[SiMe$_2$]$_4$NMePh (9): Pale yellow oil, yield: 880 mg (47%). NMR ($CDCl_3$, 25 °C, TMS): ^{1}H: δ = 0.23 ppm (s, 6 H, Si*Me*$_2$SiMe$_2$N-MePh), 0.34 (s, 6 H, ClSiMe$_2$Si*Me*$_2$), 0.42 (s, 6 H, Si*Me*$_2$NMePh), 0.61 (s, 6 H, ClSi*Me*$_2$), 2.92 (s, 3 H, N*Me*Ph), 6.96−7.31 (m, 5 H, Ph). ^{13}C: δ = 2.3 ppm (Si*Me*$_2$SiMe$_2$NMePh), 3.4 (ClSiMe$_2$Si*Me*$_2$), 3.9 (Si*Me*$_2$NMePh), 6.1 (ClSi*Me*$_2$), 36.3 (N*Me*Ph), 118.3, 122.4, 123.3, 148.7 (Ph). ^{29}Si: δ = 26.4, 3.3, −41.3, −43.9 ppm.

MeClSi[Si(NMePh)ClMe]$_2$ (10): Yellow oil, yield: 510 mg (23%). NMR ($CDCl_3$, 25 °C, TMS): ^{1}H: δ = 0.37 ppm {s, 6 H, MeClSi[Si-(NMePh)Cl*Me*]$_2$}, 0.58 {s, 3 H, *Me*ClSi[Si(NMePh)ClMe]$_2$}, 2.73, 2.74, 2.82, 2.86, {s, 6 H, MeClSi[Si(N*Me*Ph)ClMe]$_2$}, 6.54−7.09 (m, 10 H, Ph). ^{13}C: δ = −0.8 ppm {*Me*ClSi[Si(NMePh)ClMe]$_2$}, 6.3 {MeClSi[Si(NMePh)Cl*Me*]$_2$}, 36.9, 37.1, 37.7, 37.9 {MeClSi[Si(N*Me*Ph)ClMe]$_2$, diastereomers}, 122.9, 123.6, 128.6, 128.7, 129.1, 129.3, 149.2 (Ph, diastereomers). ^{29}Si: δ = −4.3 ppm, 3.0; $^1J_{Si\text{-}Si}$ = 58 Hz.

MeSi[Si(NMePh)ClMe]$_3$ (11): Yellow oil, yield: 2.17 g (73%). NMR ($CDCl_3$, 25 °C, TMS): ^{1}H: δ = 0.64 ppm, 0.5 {s, 9 H, MeSi-[Si(NMePh)Cl*Me*]$_3$, diastereomers}, 0.50 {s, 3 H, *Me*Si[Si-(NMePh)ClMe]$_3$, diastereomers}, 2.93, 2.96.2.97.3.01 {s, 9 H, MeSi[Si(N*Me*Ph)ClMe]$_3$, diastereomers} 6.99-7.26 (m, 15 H, Ph). ^{13}C: δ = −7.6 ppm, −7.4 {*Me*Si[Si(NMePh)ClMe]$_3$, diastereomers}, 5.2, 5.5 {MeSi[Si(NMePh)Cl*Me*]$_3$, diastereomers}, 38.1, 38.4, 38.7, 38.8 {MeSi[Si(N*Me*Ph)ClMe]$_3$, diastereomers}, 122.2, 122.5, 122.8.122.9, 123.0, 123.4, 128.9, 129.0, 148.8, 148.9, (Ph, diastereomers). ^{29}Si: δ = −73.3 ppm, −72.9, 12.45, 12.62, 12.76, 12.80 ($^1J_{Si\text{-}Si}$ = 88 Hz, diastereomers).

1,2-Difluoro-1,2-dimethyl-1,2-bis(*N*-methylanilino)disilane (12): A suspension of 1,2-dichloro-1,2-dimethyl-1,2-bis(*N*-methylanilino)-disilane (**2**) (3.9 g, 10.6 mmol) and zinc fluoride (11.4 g, 110 mmol) in DME (50 mL) was stirred for 150 h at room temperature. Afterwards, the solvent was removed under reduced pressure. The remaining oily residue was extracted with pentane, filtered, and cooled to 5 °C. A white crystalline solid was formed. The product was isolated by filtration, washed with pentane, and dried in vacuo to yield 2.55 g (71.5%) white crystalline powder with m.p. 89−90 °C. NMR ($CDCl_3$, 25 °C, TMS): ^{1}H: δ = 0.48 ppm (dd, 6 H, MeSi, $^3J_{H\text{-}F}$ = 3 Hz), 2.44 (d, 6 H, MeN), 6.72−7.23 (10 H, Ph). ^{13}C: δ = 0.43 ppm (MeSi), 43.13 (MeN), 118.16, 20.88, 128.88 (*o*-, *m*-, *p*-Ph), 149.41 (*i*-Ph). ^{29}Si: δ = 2.45 ppm (dd, $^1J_{Si\text{-}F}$ = 326, $^2J_{Si\text{-}F}$ = 63 Hz). $C_{16}H_{22}F_2N_2Si_2$ (336.54): calcd. C 57.10, H 6.59, N 8.32; found C 57.71, H 6.98, N 7.96.

1,2-Dimethyl-1,2-bis(*N*-methylanilino)-1,2-bis(phenylethynyl)-disilane (13): A solution of lithium phenylacetylide (0.17 g, 17.0 mmol) in diethyl ether (30 mL) was added dropwise to a solution of 1,2-dichloro-1,2-dimethyl-1,2-bis(*N*-methylanilino)disilane (**2**) (3.15 g, 8.5 mmol) in DME (80 mL) at 0 °C. A white precipitate formed immediately. The suspension was stirred for an additional 24 h. The solvent was then removed under reduced pressure. The remaining oily residue was extracted with pentane, filtered and the clear filtrate was stored in the refrigerator. The cooling of the solution led to a phase separation. The solvent was removed completely in vacuo and the product was isolated as a pale yellow oil, yield: 2.72 g (64%). NMR ($CDCl_3$, 395 K, TMS) ^{1}H: δ = 0.65 ppm, 0.72 (6 H, MeSi, *rac*/*meso* = 1:1), 2.73, 2.90 (6 H, MeN, *rac*, *meso*); 6.76−7.47 (m, 10 H, Ph). ^{13}C: δ = 0.43 ppm (MeSi), 35.2, 35.7 (MeN, *rac*, *meso*), 91.3, 91.6 (SiC*C*Ph, *rac*, *meso*), 109.2 (Si*C*CPh), 116.7, 117.0, 128.1, 128.2, 128.48, 128.53, 128.6, 128.7, 131.8 (*o*-, *m*-, *p*-Ph, *rac*, *meso*), 122.2 (*i*-CC*Ph*), 150.0 (*i*-PhN). ^{29}Si: δ = −25.78, −25.82 ppm (*rac*, *meso*).

1,2-Dimethyl-1,2-bis(*N*-methylanilino)-1,2-bis(*p*-tolyl)disilane (14) and 1-Chloro-1,2-dimethyl-1,2-bis(*N*-methylanilino)-2-(*p*-tolyl)disilane (14a): A solution of *p*-tolylmagnesium bromide (3.6 g, 18.6 mmol) in THF (20 mL) was added slowly to a solution of 1,2-dichloro-1,2-dimethyl-1,2-bis(*N*-methylanilino)disilane (**2**) (3.4 g, 9.3 mmol) in DME (60 mL) at 0 °C. The resulting mixture was stirred for 24 h at room temperature. The solvent was removed completely in vacuo. The residue was extracted with a pentane/DME mixture (3:1). The resulting suspension was filtered and the solvent was partially removed in vacuo. The addition of a small amount diethyl ether and cooling to −16 °C gave a white precipitate, which was isolated by filtration and dried in vacuo. The product consisted of a mixture of **14** and **14a** in a product ratio of 2:1. It was not possible to separate both products by fractional crystallization. 1,2-Dimethyl-1,2-bis(*N*-methylanilino)-1,2-bis(*p*-tolyl)disilane (**14**): ^{29}Si NMR ($CDCl_3$, 25 °C, TMS): δ = −7.7 ppm, −7.5 (*rac*/*meso* = 1.5:1). 1-Chloro-1,2-dimethyl-1,2-bis(*N*-methylanilino)-2-(*p*-tolyl)disilane (**14a**): ^{29}Si NMR ($CDCl_3$, 25 °C, TMS): δ = −9.6 ppm (MeSiTolN), 8.5 (MeSiClN); $^1J_{Si\text{-}Si}$ = 20 Hz (only one diastereomer was detected).

1,2-Dibenzyl-1,2-dimethyl-1,2-bis(*N*-methylanilino)disilane (15): A solution of benzylmagnesium chloride (3.2 g, 21.2 mmol) in diethyl ether (17 mL) was added dropwise to a solution of 1,2-dichloro-1,2-dimethyl-1,2-bis(*N*-methylanilino)disilane (**2**) (3.9 g, 10.6 mmol) in DME (80 mL) at 0 °C. The solution was stirred for an additional 24 h. Afterwards, the solvent was removed under reduced pressure. The remaining residue was extracted with pentane, filtered and the solvent was partially removed in vacuo. Storage of the concentrated solution at −16 °C yielded a white precipitate which was separated by filtration, washed with cold pentane and dried in vacuo; yield: 1.8 g (35.4%), m.p. 98−100 °C. NMR ($CDCl_3$, 25 °C, TMS): ^{1}H: δ = 0.17 ppm, 0.25 (6 H, MeSi, *rac*/*meso* = 1:1), 2.10, 2.13, 2.64, 2.67 (4 H, CH_2Ph, *rac*, *meso*), 2.45, 2.54 (6 H, MeN, *rac*, *meso*), 6.68−7.21 (m, 10 H, Ph). ^{13}C: δ = −1.8 ppm, −1.4 (MeSi, *rac*, *meso*), 27.1, 27.5 (CH_2, *rac*, *meso*), 35.6 (MeN), 117.3, 117.5, 128.07, 128.12, 128.52, 128.58 (*o*-, *m*-, *p*-CH_2*Ph*, *rac*, *meso*), 118.6, 124.3, 128.8 (*o*-, *m*-, *p*-*Ph*N), 138.6 (*i*-CH_2*Ph*), 151.0 (*i*-PhN). ^{29}Si: δ = −3.4 ppm, −4.3 (*rac*, *meso*). $C_{30}H_{36}N_2Si_2$ (480.80): calcd. C 74.94, H 7.55, N 5.83; found C 74.35, H 7.48, N 5.46.

X-ray Crystal Structure Determinations: Suitable single crystals were mounted on glass fibers under paraffin oil and transferred to the diffractometer. Diffraction measurements were made with an Enraf−Nonius CAD-4 diffractometer. Further details on crystal data and structure determination are summarized in Table 3.

Table 3. Crystal data and structure refinement for compounds **2**, **3**, and **4**

	2	**3**	**4**
Empirical formula	$C_{16}H_{22}Cl_2N_2Si_2$	$C_{23}H_{30}ClN_3Si_2$	$C_{30}H_{38}N_4Si_2$
Formula mass	369.44	440.13	510.82
Temperature [K]	172(2)	208(2)	193(2)
Wavelength [Å]	0.71073	1.54178	1.54178
Crystal system	orthorhombic	monoclinic	monoclinic
Space group	$C222_1$	$P21/n$	$P21/a$
Unit cell dimensions			
a [Å]	9.273(2)	12.597(1)	12.222(2)
b [Å]	15.090(3)	13.863(1)	13.641(2)
c [Å]	13.322(3)	13.394(1)	17.588(3)
β [°]	90	90.05(1)	109.32(1)
Volume [Å^3]	1864.1(7)	2339.0(3)	2767.1(8)
Z	4	4	4
Calculated density [mg·m^{-3}]	1.316	1.250	1.226
Absorption coefficient [mm^{-1}]	0.475	2.529	1.352
F(000)	776	936	1096
Crystal size [mm]	0.7 × 0.3 × 0.3	0.6 × 0.5 × 0.3	0.6 × 0.5 × 0.5 mm
θ range for data collection [°]	2.58−27.98	4.59−74.88	2.66−75.49
Limiting indices	$-12 \le h \le 12$, $-19 \le k \le 19$, $-17 \le l \le 9$	$-15 \le h \le 15$, $-17 \le k \le 0$, $-16 \le l \le 0$	$-15 \le h \le 14$, $-17 \le k \le 6$, $0 \le l \le 22$
Reflections collected/unique	6984/2256 [R(int) = 0.0535]	5015/4809 [R(int) = 0.0179]	8632/5665 [R(int) = 0.0715]
Completeness to θ [°]	27.98/100.0%	74.88/100.0%	75.49/98.9%
Absorption correction	none	empirical	none
Max./min. transmission	−	0.999/0.647	−
Refinement method		Full-matrix least-squares on F^2	
Data/restraints/parameters	2256/0/102	4809/0/267	5665/0/331
Goodness-of-fit on F^2	1.006	1.056	1.062
Final R indices [$I > 2\sigma(I)$]	$R1$ = 0.0376, $wR2$ = 0.0656	$R1$ = 0.0431, $wR2$ = 0.1214	$R1$ = 0.0572, $wR2$ = 0.1324
R indices (all data)	$R1$ = 0.0648, $wR2$ = 0.0723	$R1$ = 0.0454, $wR2$ = 0.1235	$R1$ = 0.0888, $wR2$ = 0.1481
Absolute structure parameter	−0.08(9)	−	−
Largest diff. peak/hole [e·Å^3]	0.245/−0.206	0.369/−0.496	0.532/−0.322

CCDC-116146 (**2**), -111583 (**3**), and -144275 (**4**) contain the supplementary crystallographic data for this paper. These data can be obtained free of charge at www.ccdc.cam.ac.uk/conts/retrieving.html [or from the Cambridge Crystallographic Data Centre, 12 Union Road, Cambridge CB2 1EZ, UK; Fax: (internat.) + 44-1223/336-033; E-mail: deposit@ccdc.cam.ac.uk].

Acknowledgments

Financial support for this work from the Deutsche Forschungsgemeinschaft and the Fonds der Chemischen Industrie is gratefully acknowledged.

[1] [1a] R. J. P. Corriu, *Angew. Chem.* **2000**, *112*, 1432−1455; *Angew. Chem. Int. Ed.* **2000**, *39*, 1376−1398. [1b] F. Aldinger, M. Weinmann, J. Bill, *Pure Appl. Chem.* **1998**, *70*, 439. [1c] M. Gastreich, C. M. Marian, H. Jüngermann, M. Jansen, *Eur. J. Inorg. Chem.* **1999**, 75. [1d] R. Richter, G. Roewer, U. Boehme, K. Busch, F. Babonneau, H.-P. Martin, E. Mueller, *Appl. Organomet. Chem.* **1997**, *11*, 71.

[2] [2a] R. West, in: *Organopolysilanes* (Eds.: G. Wilkinson, E. W. Abel, F. G. A. Stone), **1995**, vol. 2, p. 96. [2b]R. D. Miller, J. Michl, *Chem. Rev.* **1989**, *89*, 1359.

[3] [3a] K. Hassler, W. Köll, *J. Organomet. Chem.* **1997**, *540*, 113. [3b] K. Schenzel, K. Hassler, *Spectrochim. Acta* **1994**, *50A*, 127−138. [3c] H. Stüger, P. Lassacher, *J. Organomet. Chem.* **1993**, *450*, 79. [3d] E. Hengge, W. Kalchauer, F. Schrank, *Monatsh. Chem.* **1986**, *117*, 1399. [3e] F. K. Mitter, G. I. Pollhammer, E. Hengge, *J. Organomet. Chem.* **1986**, *314*, 1. [3f] E. Hengge, D. Kovar, *J. Organomet. Chem.* **1977**, *125*, C29.

[4] [4a] W. Uhlig, *J. Prakt. Chem.* **2000**, *342*, 132. [4b] W. Uhlig, *Chem. Ber.* **1996**, *129*, 733. [4c] W. Uhlig, *Chem. Ber.* **1992**, *125*, 47.

[5] [5a] P. K. Jenkner, E. Hengge, *J. Organomet. Chem.* **1992**, *430*, 259. [5b] K. Hassler, *Monatsh. Chem.* **1986**, *117*, 613.

[6] [6a] U. Herzog, K. Trommer, G. Roewer, *J. Organomet. Chem.* **1998**, *552*, 99. [6b] K. Trommer, U. Herzog, G. Roewer, *J. Prakt. Chem./Chem.-Ztg.* **1997**, *339*, 637.

[7] [7a] A. Kawachi, K. Tamao, *J. Am. Chem. Soc.* **2000**, *122*, 1919. [7b] A. Kawachi, K. Tamao, *J. Organomet. Chem.* **2000**, *601*, 259.

[8] [8a] C. Ackerhans, B. Räke, R. Krätzner, P. Müller, H. W. Roesky, I. Usón, *Eur. J. Inorg. Chem.* **2000**, 827. [8b] J. Heinicke, S. Mantey, A. Oprea, M. K. Kindermann, P. G. Jones, *Heteroatom Chem.* **1999**, *10*, 605. [8c] M. Veith, A. Rammo, S. Faber, B. Schillo, *Pure Appl. Chem.* **1999**, *71*, 401. [8d] I. Rietz, E. Popowski, H. Reinke, M. Michalik, *J. Organomet. Chem.* **1998**, *556*, 67. [8e] Th. Schlosser, A. Sladek, W. Hiller, H. Schmidbaur, *Z. Naturforsch., Teil B* **1994**, *49*, 1247.

[9] U. Böhme, B. Günther, B. Rittmeister, *Inorg. Chem. Commun.* **2000**, *3*, 428.

[10] K. A. Trankler, D. S. Wyman, J. Y. Corey, E. E. Katz, *Organometallics* **2000**, *19*, 2408.

[11] K. A. Trankler, D. S. Wyman, J. Y. Corey, E. E. Katz, N. P. Rath, *Organometallics* **2001**, *20*, 5139.

[12] Total energies of **2** at the B3LYP/6-31G* level of theory: (*R*,*R*) form $E = -2232.01515442$ H, *meso* form $E = -2232.00828043$ H.
[13] [13a] U. Herzog, R. Richter, E. Brendler, G. Roewer, *J. Organomet. Chem.* **1996**, *507*, 221. [13b] R. Richter, G. Roewer, U. Böhme, K. Busch, F. Babonneau, H. P. Martin, E. Müller, *Appl. Organomet. Chem.* **1997**, *11*, 71.
[14] H. Flack, *Acta Crystallogr., Sect. A* **1983**, *39*, 876.
[15] R. J. P. Corriu, C. Guerin, J. J. E. Moreau, in: *The Chemistry of Organic Silicon Compounds*, (Eds.: S. Patai, Z. Rappoport), John Wiley & Sons, Chichester, **1989**, p. 305 and references cited therein.
[16] [16a] R. Tacke, S. A. Wagner, in: *The Chemistry of Organic Silicon Compounds*, part 3 (Eds.: S. Patai, Z. Rappoport), John Wiley & Sons, Chichester, **1998**, p. 2363. [16b] R. Tacke, S. Brakmann, M. Kropfgans, C. Strohmann, F. Wuttke, G. Lambrecht, E. Mutschler, P. Proksch, H.-M. Schiebel, L. Witte, in: *Frontiers of Organosilicon Chemistry* (Eds: A. R. Bassindale, P. P. Gaspar), The Royal Society of Chemistry, Cambridge **1991**, p. 218. [16c]A. Kawachi, H. Maeda, K. Mitsudo, K. Tamao, *Organometallics* **1999**, *18*, 4530.
[17] *meso*-1,2-Dichloro-1,2-dimethyl-1,2-diphenylsilane: A. Sekiguchi, I. Maruki, H. Sakurai, *J. Am. Chem. Soc.* **1993**, *115*, 1993.
[18] The negative sign of the torsion angle can be ignored in this context, since it only describes the clockwise or anticlockwise twist about the three connected bonds.
[19] R. Z. Lehnert, *Z. Anorg. Allg. Chem.* **1990**, *591*, 209.

Received July 3, 2002
[I02362]

Synthesis, X-ray Structure and Properties of a Trinuclear Mixed-Valence Co^{III}-Co^{II}-Co^{III} Complex with Carboxamido N and Sulfinato S Donors

Mathieu Rat,[a] Rodolphe Alves de Sousa,[a] Alain Tomas,[b] Yves Frapart,[a] Jean-Pierre Tuchagues,[c] and Isabelle Artaud*[a]

Keywords: Cobalt / N ligands / S ligands / Enzyme models

Air oxidation of the six-coordinate $(Et_4N)_2[Co(N_2S_2)(CN)(CH_3CN)]$ complex derived from *N*,*N*′-(3-mercapto-3-methylbutyryl)-*o*-phenylenediamine results in the formation of the trinuclear mixed-valence complex $(Et_4N)_4\{Co^{II}[Co^{III}\{N_2(SO_2)_2\}(CN)(OH)]_2\}$ (**3**) where the thiolates have been oxidized to sulfinates. Its X-ray structure reveals a linear arrangement of cobalt ions with bridging hydroxides and sulfinates. All cobalt ions are in a distorted octahedral environment. The mixed-valence nature of this complex has been demonstrated by temperature-dependent magnetic susceptibility measurements and by EPR spectroscopy both in the solid state and in solution. These data are in agreement with a high-spin Co^{II}. The IR spectrum shows the typical vibrations of cyanide and sulfinate at 2130 cm^{-1} (ν_{CN}), 1175 ($\nu_{as/SO2}$) and 1030 cm^{-1} ($\nu_{s/SO2}$). Trapping of Co^{II} by chelex chromatography after treatment with aqueous HCl, or " in situ" in aqueous solution, yields six-coordinate low-spin complexes with two different axial ligands $Na_3[Co\{N_2(SO_2)_2\}(CN)(Cl)]$ (**5a**) and $(Et_4N)_2[Co\{N_2(SO_2)_2\}(CN)(H_2O)]$ (**5b**). The pK_a of the bound water molecule was estimated as 10.1 by pH-metric titration. While **3** and **5a** were inactive toward acetonitrile hydration, **5b** catalyzes acetamide formation at 50 °C and pH 4.7 and 7 with low efficiency.

(© Wiley-VCH Verlag GmbH & Co. KGaA, 69451 Weinheim, Germany, 2003)

Introduction

Nitrile hydratases (NHases) are at the centre of the industrial production of acrylamide. These bacterial enzymes, which catalyze the hydration of nitriles to amides, contain either a non-heme iron(III) or a non-corrinoid cobalt(III) centre. The crystal structure of a Co-type NHase produced from a *Pseudonocardia thermophila* species at 1.8 Å resolution has been reported recently.[1] The ligands to the cobalt atom are two peptide amide nitrogens and three sulfurs from cysteines. The two cysteines in the mean-plane *trans* to the amide nitrogens are oxidized to cysteine-sulfinic and cysteine-sulfenic acids. The apical ligands are one cysteine thiolate and a water molecule. As previously suggested,[2] the cobalt environment is very similar to the iron environment revealed by the X-ray structure of *Rhodococcus* Fe-type NHase crystallised in its NO inactivated form.[3] In this case, NO replaces H_2O as the sixth axial ligand. These results clearly show that the post-translational cysteine oxidations are general among NHases irrespective of whether they contain iron or cobalt at their active site

Most of the cobalt NHase mimics reported so far contain thiolates as sulfur donors; a few contain sulfinates and/or sulfenates.[4−7] One six-coordinate Co^{III} complex with two thiolato S-donors includes CN^- which can be replaced by H_2O at the sixth site.[4a] Most of the complexes containing oxidized thiolates as sulfur donors are six-coordinate and do not have a labile ligand that might be exchanged with H_2O or HO^-. Only one complex containing a sulfinate ligand is five-coordinate and has an open coordination site,[5] but the presence of an apical sulfinate prevents binding of any exogenous ligand at this open coordination site. Recently, we have prepared square planar $(Et_4N)[Co^{III}(N_2S_2)]$ complexes[7,8] containing, similarly to NHase, two carboxamido nitrogens *trans* to two thiolates, and we have described the conversion of the *S*-bound thiolates to *S*-bound sulfinates in the presence of *tert*-butyl isocyanide.[7] The resulting six-coordinate complex $(Et_4N)[Co^{III}(N_2(SO_2)_2](CN\textit{t}Bu)_2]$ has two isocyanide ligands tightly ligated to the cobalt centre. All attempts to exchange one isocyanide with another axial ligand have failed. This contrasts with the behaviour of the precursor square planar Co^{III} complex which has only a low affinity for isocyanide. In this report we show that this $[Co^{III}(N_2S_2)]$ complex interacts with cyanide yielding a six-coordinate complex with apically bonded cy-

[a] Laboratoire de Chimie et Biochimie Toxicologiques et Pharmacologiques, Université René Descartes, UMR 8601 CNRS,
45 rue des Sts Pères 75270 Paris cedex O6 France
Fax: (internat.) +33-1/42868387
E-mail: artaud@biomedicale.univ-paris5.fr
[b] Laboratoire de Cristallographie et de RMN biologiques UMR 8015, Faculté de Pharmacie,
4 Rue de l'observatoire, 75270 Paris cedex 06 France
[c] Laboratoire de Chimie de Coordination, UPR CNRS 8241, 205 route de Narbonne, 31077 Toulouse Cedex 04 France

anide and solvent molecule. Air oxidation of this complex affords a trinuclear Co^{III}-Co^{II}-Co^{III} species which has been crystallographically and spectroscopically characterised. The ligands at the Co^{III} centre are two nitrogens *trans* to two *S*-bound sulfinates in the mean plane and one cyanide and one hydroxide in the axial positions. Finally we describe its reactivity in solution and show that Co^{II} can be removed, yielding a six-coordinate Co^{III} complex.

Results and Discussion

The synthesis and spectroscopic characterisation of the square planar $(Et_4N)[Co^{III}(N_2S_2)]$ complex **1** (Scheme 1) has been described previously.[7] Its interaction with CN^- was monitored by UV/Vis spectroscopy under argon. While the electronic spectrum of complex **1** in acetonitrile exhibits an absorption at 695 nm, addition of a CH_3CN solution of Et_4NCN results in the progressive disappearance of this band and appearance of a new one at 820 nm. The conversion is complete after addition of one equivalent of CN^- per Co^{III} centre. Complex **2a** prepared in deaerated DMF and isolated by precipitation with diethyl ether corresponds to the formula $(Et_4N)_2[Co^{III}(N_2S_2)(CN)(DMF)]$. Its ^1H NMR spectrum in $[D_7]$DMF exhibits only signals between $\delta = 0$ and 10 ppm, indicating that **2** is a six-coordinate low spin Co^{III} complex. The non-equivalence of the CH_3 groups and of the CH_2 protons on either side of the N_2S_2 plane is in agreement with the binding of only one axial cyanide. The sixth position is occupied by a DMF molecule whose methyl resonances are clearly different from those of the free solvent. In the IR spectrum (KBr pellet), the ν_{CN} and ν_{CO} stretching bands corresponding to the axial CN^- and DMF are located at 2080 cm^{-1} and 1670 cm^{-1} respectively. In contrast to a related $[Co^{III}(N_2S_2)]$ complex with two aliphatic carboxamido N donors,[9] addition of cyanide in excess does not result in the formation of a dicyanide species. Consequently, whereas complex **1** can bind two isocyanide molecules, complex **2** binds only one cyanide ion and a solvent molecule such as DMF yielding, in both cases, a six-coordinate low spin Co^{III} complex.

Slow air oxidation of an acetonitrile solution of complex **1** with one equivalent of Et_4NCN (yielding **2b** with CH_3CN at the sixth site, Scheme 1) results in the precipitation of an orange powder, which was collected by filtration. Vapour diffusion of diethyl ether into a highly diluted CH_3CN solution of this species afforded crystals of complex **3** suitable for X-ray analysis. The crystal structure of complex **3** shown in Figure 1 reveals the formation of a linear tetra-

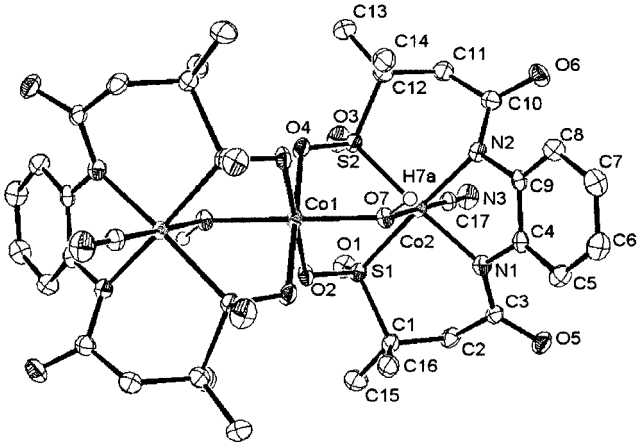

Figure 1. ORTEP picture of the anionic complex **3** $\{Co[Co\{N_2(SO_2)_2\}(CN)(OH)]_2\}^{4-}$ with atom labelling (40% probability level of displacement ellipsoids); the H atoms, the water molecule and Et_4N^+ are omitted for clarity

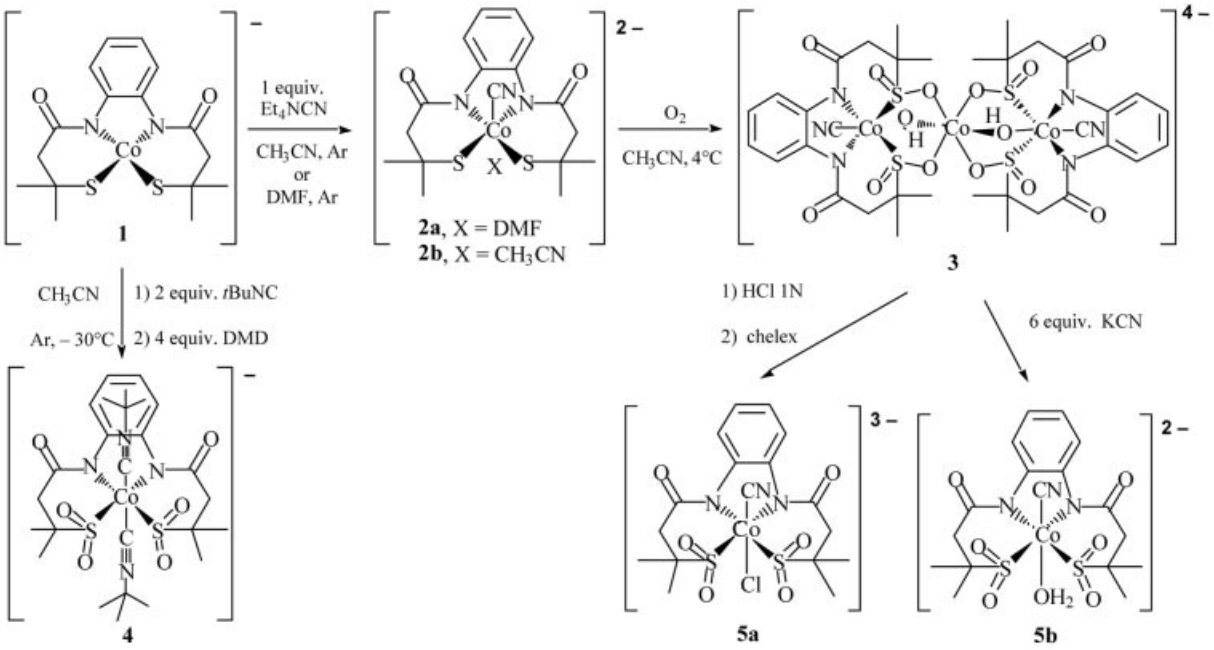

Scheme 1. Synthesis of the complexes

Table 1. Crystallographic data from the X-ray diffraction of **3**

Empirical formula	$C_{34}H_{42}Co_3N_6O_{14}S_4{\cdot}4C_8H_{20}N{\cdot}6H_2O$
Molecular mass	1692.90
Crystal System	Monoclinic
Space	*C*2/*c*
a[Å]	28.598(2)
b [Å]	12.9144(7)
c [Å]	22.916(2)
α [°]	90
β [°]	100.81 (1)
V [$Å^3$]	8313.2(11)
Z	4
F(000)	
3620	
$D_{calcd.}$ [$g.cm^{-3}$]	1.353
λ (Mo-K_α) [mm^{-1}]	0.8
Temperature (K)	100
Index ranges	$-34 < h < 34$
	$-14 < k < 14$
	$-27 < l < 27$
Observed data [$I > 2.0\ \sigma(I)$]	5531
No. of reflns. Collected	29402
No. of unique reflns	7020
θ limits [°]	2.4, 25.0
R_{int}	0.078
Data/restraints/parameters	7020/7/499
*R*1, *wR*2 [$I > 2\sigma(I)$]	0.0589, 0.1509
*R*1, *wR*2 (all data)	0.0738, 0.1616
$\Delta\delta_{min}/\Delta\delta_{max.}$ [$e{\cdot}Å^{-3}$]	−0.59/1.32
GOF	1.08

Table 2. Selected bond lengths [Å] and angles [°] for **3** ($C_{34}H_{42}Co_3N_6O_{14}S_4{\cdot}4C_8H_{20}N{\cdot}6H_2O$)

Co1−O2	2.130(3)	Co1−O7	2.015(3)
Co1−O4	2.118(3)		
Co2−S1	2.1968(12)	Co2−S2	2.2102(10)
Co2−O7	1.940(3)	Co2−S2	2.2102(10)
Co2−N1	2.002(3)	Co2−C17	1.876(4)
Co2−N2	1.980(4)		
S1−O1	1.461(3)	C1−C16	1.532(6)
S1−O2	1.490(3)	C1−C2	1.526(6)
S1−C1	1.838(4)	C1−C15	1.529(6)
S2−O3	1.448(4)	C2−C3	1.502(6)
S2−C12	1.834(5)	C4−C5	1.404(6)
S2−O4a	1.495(3)	C4−C9	1.397(5)
O5−C3	1.264(5)	C5−C6	1.388(7)
O6−C10	1.251(6)	C6−C7	1.381(7)
C7−C8	1.389(7)	C8−C9	1.387(6)
C10−C11	1.516(6)	C11−C12	1.537(7)
C12−C14	1.534(6)	C12−C13	1.531(6)
N1−C44	1.404(5)	N1−C3	1.339(5)
N2−C99	1.425(5)	N2−C10	1.339(5)
N3−C17	1.155(6)		
O2−Co1−O4	91.57(10)	O2−Co1−O7	84.24(10)
O4−Co1−O7	94.38(10)		
N1−Co2−C17	90.53(15)	N2−Co2−C17	90.02(15)
S1−Co2−S2	88.62(4)	S1−Co2−O7	87.27(8)
S1−Co2−N1	95.18(11)	N1−Co2−N2	82.11(14)
S1−Co2−C17	91.49(12)	S2−Co2−O7	87.78(8)
S2−Co2−N2	94.03(10)	S2−Co2−C17	91.94(12)
O7−Co2−N1	89.84(12)	O7−Co2−N2	91.23(12)

anionic trinuclear complex in which the thiolates of the tetradentate ligand have been oxidized to sulfinates. For crystal data of **3** see also Table 1. All three Co centres are in distorted coordination environments. The distortion from ideal octahedral geometry for each cobalt atom is due to restrictions imposed by the ligand, as evidenced by the bite angles [O(2)−Co(1)−O(7): 84.2°, O(4)−Co(1)−O(7): 85.6° and O(2)−Co(1)−O(4): 91.6° for Co(1) and N(1)−Co(2)−N(2): 82.1(1)° for Co(2)]. The terminal Co atoms are related by an inversion centre occupied by the central Co(1) atom. Each outer Co is surrounded by two carboxamido-N and two sulfinato-S donors, *trans* to the nitrogens in the equatorial plane, and by one cyanide and one hydroxide at the axial coordination sites [Co(2)−O(7)−Co(1): 116.2(1)°]. Co(2) lies 0.037(1) Å out of the best least-squares plane defined by S(1), S(2), N(1) and N(2) [maximum deviation of −0.008(1) Å for S(2)]. The Co(1)−Co(2) distance is 3.359 Å. The sulfinates and the hydroxide bridge the terminal and central cobalt ions, the latter being coordinated to the two bridging hydroxides and four oxygens from the four bridging sulfinates. Selected bond angles and distances are listed in Table 2. The Co-N distances are equivalent to those determined for complex **4**[7] (Scheme 1) and related complexes,[4−6] and for the Co-NHase active site.[1] They are in agreement with cobalt coordination to deprotonated amide nitrogens. The sulfur-to-Co bond lengths are about 0.025 Å shorter than in complex **4**.[7] O-coordination of the sulfinates to the central Co atom differentiates the two S−O bonds. The sulfur distances to the bonded oxygen atoms [S(1)−O(2), 1.488(3) Å; S(2)−O(4), 1.493(9) Å] are significantly longer than those to the non-coordinated oxygen atoms [S(1)−O(1) 1.4621 Å; S(2)−O(3) 1.4488 Å). The Co(1)−O(2)−S(1)−Co(2) and Co(1)−O(4)−S(2)−Co(2) bridges are slightly twisted with torsion angles of −0.4(2)° and +2.9(2)°, respectively. The Co(2)−CN and C−N distances fall within the range so far determined for other mono- or dicyanide Co^{III} complexes containing carboxamido nitrogens and pyridine nitrogens[10] or thiolates.[11]

The stoichiometry of four Et_4N cations per trinuclear cobalt cluster and the charge balance suggest a Co^{III}-Co^{II}-Co^{III} distribution of oxidation states. This hypothesis is supported by the length of the Co−OH bonds: as expected from the larger ionic radius of Co^{II} compared to Co^{III},[12] the Co(1)−O(7) bond length is noticeably longer than the Co(2)−O(7) one. Furthermore the *N*-amidate- bonded Co(2) centre is expected to be Co^{III} as in complex **4**.[7] Interestingly, the Co^{III}(2)−O(7) distance (1.94 Å) is shorter than the corresponding Co-O distance (2.58 Å) reported for Co-NHase.[1] This result supports the proposal of the Japanese group[1] that a water molecule, rather than a hydroxide ion, is coordinated to the Co centre of NHase.

In the CSD database,[13] we found few trinuclear cobalt complexes with a Co^{III}-Co^{II}-Co^{III} arrangement where the central Co^{II} is octahedrally coordinated to six oxygens.[14] Complex **3** is the first example of such a trinuclear complex containing bridging sulfinato groups.

Further characterisation of the trinuclear complex **3** has been performed both in the solid state and in solution.

Infrared Spectroscopy

Thiolate to sulfinate oxidation results in a shift of the ν_{CN} band from 2080 cm^{-1} in **2** to 2130 cm^{-1} in **3**. As previously discussed,[7] this shows that the cyanide is a weaker π-acceptor and a stronger σ-donor ligand in **3** than in **2**. In addition, comparison of the IR spectra of complexes **3** and **4** shows a decrease of the $\nu_{as}(SO_2)$ and $\nu_s(SO_2)$ from 1210 and 1070 cm^{-1} (**4**) to 1175 and 1030 cm^{-1} (**3**). This shift to lower energy associated with the shorter C−S distances found in the structure of **3** shows that the metal-to-ligand back donation is stronger in the N_2S_2 mean plane of **3** than in **4**.

Magnetic Properties

The temperature dependence of the magnetic susceptibility in the 300−2 K range is shown in Figure 2. The room temperature effective magnetic moment (μ_{eff} = 4.73 BM) lies in the 4.40−5.00 BM range corresponding to one high-spin cobalt(II) (S = 3/2).[15] It decreases slowly to 3.99 BM at 20 K and then drops to 3.63 BM at 4 K. This behaviour may be understood as arising from the combined effects of orbital degeneracy and zero-field splitting (ZFS). These magnetic data are very similar to those previously reported

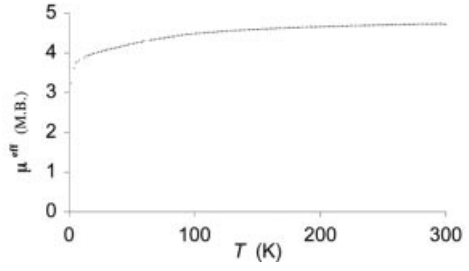

Figure 2. Temperature dependence of the effective magnetic moment for complex **3**

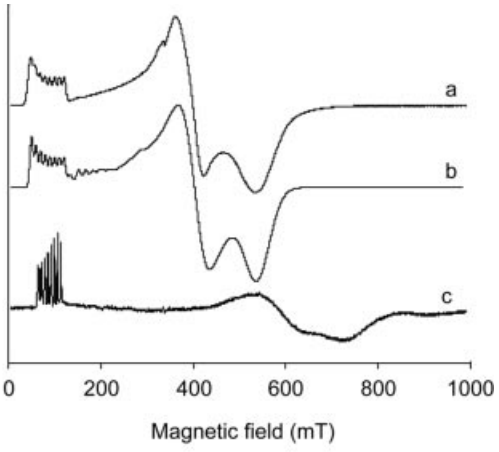

Figure 3. X-band EPR spectra of **3** at 10 K in the polycrystalline state (a) and in methanol solution (c); **3b**) simulation of spectrum **3a** using the Xsophe software package (g_x^{eff}=1.26, g_y^{eff}=1.71, g_z^{eff}= 7.91 and A_z = 10 mT, and linewidths Θ_x = 20.2 mT, Θ_Θ = 31.3 mT, Θ_Θ = 15.1 mT); experimental conditions: microwave frequency: 9.45 GHz, modulation frequency 100 kHz, modulation amplitude 1 mT, microwave power 20 mW

for a sulfito-bridged trinuclear cobalt complex,[14b] and confirm that complex **3** is in the mixed valence state Co^{III}(S = 0)-Co^{II}(S = 3/2)-Co^{III}(S = 0) as suggested by the X-ray structural analysis.

EPR Spectroscopy

The EPR spectrum of compound **3** as a polycrystalline powder recorded at 10 K is shown in Figure 3, part a. The simulation (Figure 3, part b) yields the effective *g* values g_x^{eff}=1.26, g_y^{eff}=1.71, g_z^{eff}=7.91 and a hyperfine splitting value A_z of 10 mT, which are characteristic of a single S = 3/2 Co^{II} ion. The eight-line hyperfine structure observed at g_z is due to the coupling between the electronic spin and the nuclear spin of Co^{II} (I = 7/2). The g^{eff} values can be analysed on the basis of the spin hamiltonian for an S = 3/2 centre:

$$\hat{H}_{eff} = \mu_b \vec{S}\,\bar{g}\,\vec{B} + D[\hat{S}^2_z - 1/3\,S(S+1) + E/D(\hat{S}^2_x - \hat{S}^2_y)] + \vec{S}\,\bar{A}\,\vec{I} \quad (1)$$

μ_b is the Bohr magneton, $\vec{B}$ is the external magnetic field, $\bar{g}$ the electronic tensor, $\bar{A}$ the hyperfine coupling tensor, and I the nuclear spin quantum number. *D* and *E*/*D* correspond to the zero-field splitting and rhombicity parameters, respectively. Such *g* values are due to a large axial distortion giving rise to a large zero-field splitting (10 $cm^{-1} \leq D \leq 30\ cm^{-1}$) and a large rhombicity ($E/D \geq 0.27$).[16,17] Finally, the EPR spectra of compound **3** in solution (*g* = 7.55, 1.15 and 0.9 in MeOH) (Figure 3, part c) and in the solid state (Figure 3, part a) are very similar. Therefore the same Co^{II} (S = 3/2, I = 7/2) formalism can be used to analyze the spectrum of compound **3** in solution. The signals broaden with temperature, and disappear above 30 K as expected for high-spin Co^{II} complex for which electron spin-lattice relaxation is very fast. It is very likely that the trinuclear structure determined in the solid state is retained in solution.

^{1}H NMR Spectroscopy

Complex **3** is paramagnetic as evidenced by its ^{1}H NMR spectrum in D_2O which extends over 70 ppm. The assignment of only six resonances to the $N_2(SO_2)_2$ ligand is consistent with the presence of an inversion centre in the overall structure and with the absence of a symmetry plane for the terminal Co^{III} centres. Consequently, the two signals at δ = −41 and +11.6 ppm were attributed to the methyl groups on the basis of the integration ratios. The four remaining signals, each accounting for two protons, were not assigned.

The purpose of the investigation reported below was to find proper conditions for removing the Co^{II} cation with the aim of recovering a six-coordinate Co^{III} mononuclear complex. In a first experiment, the trinuclear complex was treated with an excess of aqueous HCl solution and the resulting complex **5a** (Scheme 1) was purified over chelex chromatography, to retain the cobalt(II), and isolated as a powder after lyophilization. The characteristics of complex **5a** are consistent with the formation of a six-coordinate

Co^{III} complex with both cyanide and chloride axial ligands: (i) electrospray mass ionization (ESI^-) exhibits two peaks at 565.85 and 507.93 corresponding to the mass of the $\{(Na)_2[Co^{III}\{N_2(SO_2)_2\}(CN)(Cl)]\}^-$ and $\{(Na)[Co^{III}\{N_2(SO_2)_2\}(CN)]\}^-$ anions, respectively; (ii) elemental analysis corresponds to the formula $C_{19}H_{20}ClN_3O_6S_2Na_3Co\cdot 3NaCl\cdot 2H_2O$; (iii) IR spectroscopy shows a ν_{CN} vibration located at 2130 cm^{-1}; (iv) ^1H NMR spectroscopy is consistent with a low-spin six-coordinate Co^{III} with two different axial ligands. As expected, the methyl protons on both sides of the mean plane are non-equivalent, as are the protons of the CH_2 groups.

Using the same procedure, the corresponding aquo or hydroxo complex **5b** (Scheme1) was prepared upon stirring an aqueous (H_2O or D_2O) solution of **3** with chelex. However, **5b** could not be isolated in the solid state since it was destroyed during the lyophilisation step; it was characterised "in situ" in solution after filtration. Its ^1H NMR spectrum in D_2O is characteristic of a low-spin mononuclear Co^{III} species with two different axial ligands (CN^-/H_2O or CN^-/HO^-). The pK_a of the bound water molecule was determined by pH-metry. Titration of **5b** ($2.7\ 10^{-4}$ M) with aqueous HCl (10^{-3} M) reveals two acidic functions with pK_a values of 10.1 and 6.5 (Figure 4, part b). The former is attributed to the bound water in $[Co^{III}\{N_2(SO_2)_2\}(CN)(H_2O)]^{2-}$ and the latter to a bound HNC in $[Co^{III}\{N_2(SO_2)_2\}(HNC)(H_2O)]^-$. None of these p$K_a$ values can correspond to an amide coordinated in its protonated tautomer iminol form, since in complex **4**, which has two *tert*-butyl isocyanides at the axial sites, no protonation site was identified upon acidic titration (Figure 4, part a).

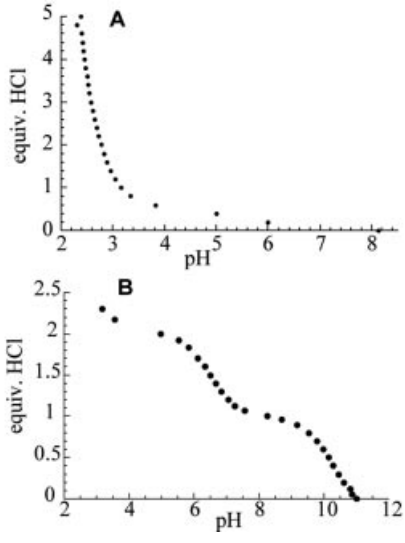

Figure 4. pH-metric titration of complex **4** a) and complex **5b** b) with aqueous HCl

A more efficient way for preparing a more concentrated solution of **5b** "in situ" is to trap the Co^{II} cation with cyanide as $K_3[Co(CN)_6]$. This reaction was monitored by ^1H NMR spectroscopy. Progressive addition of six equivalents of KCN to a D_2O solution of **3** resulted in the formation of a low-spin species identical to **5b**. Finally the reactivity of complexes **3**, **5a**, **5b** (prepared as mentioned previously) was assayed toward acetonitrile hydration in buffered solution at pH 4.7, 7.3 and 10.3. The amide conversion was estimated by ^1H NMR spectroscopy after lyophilisation and dissolution of the residue in [D_6]DMSO. While the trinuclear and chloro complexes were inactive, amide formation corresponding to 7 and 14 turnovers of complex **5b** was determined after 24 h at 50 °C at pH 4.7 and 7, respectively. The catalyst was destroyed at higher pH. Under the same conditions, formation of amide was not detected either in the absence of complex **5b** or in the presence of the unique $K_3[Co(CN)_6]$ species. Two other mimics of NHase catalyze acetonitrile hydration with low efficiency (Scheme 2): a dithiolato hydroxo Co^{III} complex, $[Co(PyPS)(OH)]^{2-}$, prepared by Mascharak et al.[4a] and a di-sulfenato Co^{III} complex, $[Co\{N_2(SO)_2\}(t\text{BuNC})_2]^-$, described by Chottard et al.[6b] These two complexes, as well as **5b**, reproduce some of the structural features characteristic of the Co-NHase active site but not all of them. Accordingly, the presence of both a sulfenate and an aquo or hydroxo ligand seems to be required for a high activity.

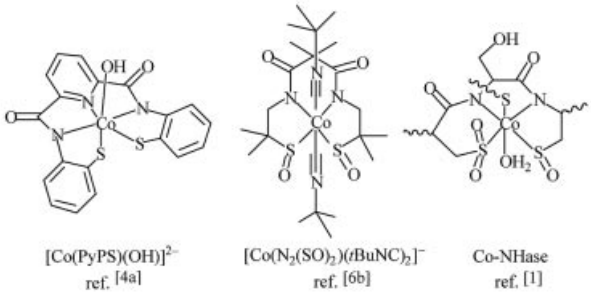

Scheme 2. Schematic drawing of the two previously reported mimics of Co-NHase activity and of the Co-NHase active site

Conclusion

This work describes the first example of thiolate to sulfinate oxidation in a six-coordinate Co^{III} complex whose apical sites are occupied by a cyanide and a labile solvent molecule. This oxidation results in the formation of a new trinuclear mixed valence Co^{III}-Co^{II}-Co^{III} complex with bridging sulfinates which has been characterised both in the solid state and in solution. The terminal Co^{III} ions retain the environment of the starting Co^{III} compound but with S-bonded sulfinates and a hydroxide replacing the solvent molecule in the sixth coordination position. The high-spin Co^{II} is held by interactions with the six oxygens of the bridging hydroxides and sulfinates. The central Co^{II} ion is easily trapped by chelating agents, yielding the first example of a six-coordinate low-spin $[Co^{III}\{N_2(SO_2)_2\}(CN)(H_2O)](Et_4N)_2$ complex including an exchangeable coordination site able to bind Cl^-. Preliminary experiments show that the aquo complex catalyzes hydration of acetonitrile, although with a low efficiency.

Experimental Section

Complex 2: Et_4NCN (14.8 mg, 0.095 mmol) in deaerated CH_3CN was added to a deaerated DMF solution of $(Et_4N)[Co(N_2S_2)]$ **1** (50 mg, 0.095 mmol, 1 mL). The resulting brown mixture was stirred at room temp. for 5 min. Cooling to −20 °C and addition of cold Et_2O afforded complex **2** as a brown powder. The solid was dried under vacuum and stored in a glovebox. (35 mg, 45%). $C_{36}H_{67}CoN_6O_3S_2{\cdot}CH_3CN{\cdot}2H_2O$ (832.10): calcd. C 54.85, H 8.96, N 11.78; found C 55.06, H 9.36, N 11.99. UV/Vis (CH_3CN): λ_{max} (ε, $M^{-1}cm^{-1}$) = 232 (24000), 259 (21800), 470 (1100), 822 (800) nm. IR (KBr): $\tilde{\nu}$ = 2080 (ν_{CN}), 1620 (ν_{CO} DMF), 1545 (ν_{CO}) cm^{-1}. ^1H NMR (250 MHz, [D_7]DMF, 300 K): δ = 1.16 (s, 24 H, Me Et_4N), 1.25 (s, 6 H, Me), 1.43 (s, 6 H, Me), 2.23 (d, J = 12 Hz, 2 H, CH_2,), 2.66 (s, 3 H, Me DMF), 2.82 (s, 3 H, Me DMF), 2.98 (s,16 H, CH_2 Et_4N), 3.42 (d, J = 12 Hz, 2 H, CH_2), 6.36 (dd, 2 H, H_{ar}), 7.90 (s, HCO DMF), 8.52 (dd, 2 H, H_{ar}) ppm. MS (FAB^-): m/z (%) = 395 (100) $[Co(N_2S_2)]^-$.

Complex 3: Et_4NCN (60 mg, 0.4 mmol) was added to a CH_3CN solution of $(Et_4N)[Co(N_2S_2)]$ **1** (200 mg, 0.4 mmol, 4 mL). The resulting brown mixture was stirred under a dioxygen atmosphere at 4 °C for a week. An orange precipitate was collected (95 mg, 41%), washed with Et_2O and dried under vacuum. $C_{66}H_{122}Co_3N_{10}O_{14}S_4{\cdot}6H_2O{\cdot}CH_3CN$ (1733.97): calcd. C 47.10, H 7.96, N 8.89; found C 46.94, H 8.02, N 8.83. UV/Vis (H_2O): λ_{max} (ε, $M^{-1}cm^{-1}$) = 252 (33800), 279 (44300), 300 (sh), 460 (1400) nm. IR (KBr): $\tilde{\nu}$ = 2130 (ν_{CN}), 1540 (ν_{CO}), 1175 and 1030 (ν_{SO2}) cm^{-1}. ^1H NMR (250 MHz, D_2O): δ = 27 (2 H), 22 (2 H), 11.7 (6 H), 3.33 (32 H, CH_2 Et_4N), 1.55 (2 H), 1.50 (s, 48 H, Me Et_4N) −8 (2 H), −42.2 (6 H) ppm. MS(ESI^- in MeOH): m/z (%) = 242.5 (100) $[Co\{N_2(SO_2)_2\}(CN)]^{2-}$.

Complex 5a: A batch of **3** (50 mg, 0.029 mmol) was dissolved in 10 mL of 1 N HCl and stirred for 15 min. After lyophilisation, the residue was dissolved in methanol and loaded onto a Chelex 100 resin column. The first pink band eluted with methanol was collected. Addition of Et_2O afforded complex **5a** as a pink powder (20 mg, 42%) upon cooling. $C_{17}H_{20}CoN_3Na_3O_6S_2Cl{\cdot}3NaCl{\cdot}3H_2O$ (819.22): calcd. C 24.92, H 3.20, N 5.13; found C 25.18, H 3.27, N 5.22. UV/Vis (H_2O): λ_{max} (ε, $M^{-1}cm^{-1}$) = 250 (36700), 281 (51700), 302 (42800), 470 (1400) nm. IR (KBr): $\tilde{\nu}$ = 2130 (ν_{CN}), 1535 (ν_{CO}), 1175 and 1060 (ν_{SO2}) cm^{-1}. ^1H NMR (250 MHz, D_2O): δ = 1.30 (s, 6 H, Me), 1.42 (s, 6 H, Me), 2.43 (d, J = 17 Hz, 2 H CH_2), 2.91 (d, J = 17 Hz, 2 H, CH_2), 6.90 (dd, 2 H, H_{ar}), 7.42 (dd, 2 H, H_{ar}) ppm. MS (ESI^- in MeOH): m/z (%) = 507.93 (100) $\{(Na)[Co\{N_2(SO_2)_2\}(CN)]\}^-$, 565.83 (25) $\{(Na)_2[Co\{N_2(SO_2)_2\}(CN)(Cl)]\}^-$.

Crystal Structure Determination of 3: A brown crystal with dimensions 0.6 × 0.6 × 0.3 mm^3 was stuck on a glass fibre and mounted on a Stoe IPDS Imaging Plate Diffraction System (IPDS) equipped with an Oxford Cryosystems Cooler Device.[18] The final unit cell parameters were obtained by the least-squares refinement of 5000 reflections. Only statistical fluctuations were observed in the intensity monitors over the course of the data collection. Crystal data and data collection parameters are listed in Table 1. Corrections for Lorentz and polarisation effects were applied. The structure was solved by direct methods using SHELXS-97.[19] Refinement, based on F^2, was carried out by full-matrix least-squares with anisotropic thermal parameters for all non-hydrogen atoms using SHELXL-97.[20] All hydrogen atoms were located on a difference Fourier map and refined as riding models with isotropic parameters constrained to be 1.2-times the Ueq of the carrier atom. Least-squares refinements were carried out by minimising the function $\Sigma w(F_o^2 - F_c^2)^2$, where F_o and F_c are the observed and calculated structure factors. The weighting scheme used in the last refinement was $w = 1/[\sigma^2(F_o^2) + (aP)^2 + bP]$ where $P = (F_o^2 + 2F_c^2)/3$. Models reached convergence with $R1 = \Sigma(||F_o| - |F_c||)/\Sigma(|F_o|)$ and $wR2 = \{\Sigma w(F_o^2 - F_c^2)^2/\Sigma w (F_o^2)^2\}^{1/2}$, having the values listed in Table 1. ORTEP-II was used to produced molecular graphics.[21] Fractional atomic coordinates, anisotropic thermal parameters for non-hydrogen atoms and atomic coordinates for H atoms have been deposited with the Cambridge Crystallographic Data Centre.
CCDC-182354 contains the supplementary crystallographic data for this paper. These data can be obtained free of charge at www.ccdc.cam.ac.uk/conts/retrieving.html [or from the Cambridge Crystallographic Data Centre, 12, Union Road, Cambridge CB2 1EZ, UK; Fax: (internat.) +44−1223/336−033; E-mail: deposit@ccdc.cam.ac.uk].

Complex 5b: A D_2O solution of complex **3** (1.7 mg in 1 mL) was stirred with chelex (10 mg) resulting in the formation of **5b**. The supernatant was analysed by ^1H NMR spectroscopy. ^1H NMR (250 MHz, D_2O): δ = 1.34 (s, 3 H, Me), 1.46 (s, 3 H, Me), 2.48 (d, J = 17 Hz, 2 H, CH_2), 2.95 (d, J = 17 Hz, 2 H, CH_2), 6.95 (m, 2 H_{ar}), 7.78 (m, 2 H_{ar}) ppm.

pH-metric Titration of Complex 5b: 5 mL of an aqueous solution of complex **3** (3.5 mg) was stirred at room temp. with chelex (50 mg) for 3 hours. After filtration the resin was washed with water (2.5 mL) and the filtrate (**5b**: 2.7 10^{-4} M) was titrated with HCl (10^{-3} M).

Catalytic Assays: 50 μL of an aqueous solution of KCN (1.8 M, 90 μmoL) was added to 950 μL of an aqueous solution of **3** (26 mg, 15 μmoL) yielding a 3 10^{-3} M solution of **5b**. 100 μL was withdrawn and added to a mixture of 500 μL of a 0.1 M buffered solution (acetate pH 4.7, Hepes pH 7.3 and carbonate pH 10.3) and CH_3CN (100 μL). The mixture was heated to 50 °C for 48 H. After cooling and lyophilization, the residue was dissolved in [D_6]DMSO in the presence of trimethoxybenzene as an internal standard. The filtrate was analysed by ^1H NMR spectroscopy.

Acknowledgments

This work was supported by the European Commission TMR-NOHEMIP research network N° ERBFMRXCT98-0174.

[1] A. Miyanaga, S. Fushinobu, K. Ito, T. Wakagi, *Biochem. Biophys. Res. Commun.* **2001**, *288*, 1169−1174.
[2] B. A. Brennan, G. Alms, M. J. Nelson, L. T. Durney, R. C. Scarrow, *J. Am. Chem. Soc.* **1996**, *118*, 9194−9195.
[3] S. Nagashima, M. Nakasako, N. Dohmae, M. Tsujimura, K. Takio, M. Odaka, M. Yohda, N. Kamiya, I. Endo, *Nature Struct. Biol.* **1998**, *5*, 347−351.
[4] [4a] J. C. Noveron, M. M. Olmstead, P. K. Mascharak, *J. Am. Chem. Soc.* **1999**, *121*, 3553−3554. [4b] L. A. Tyler, J. C. Noveron, M. M. Olmstead, P. K. Mascharak, *Inorg. Chem.* **2000**, *39*, 357−362. [4c] L. A. Tyler, M. M. Olmstead, P. K. Mascharak, *Inorg. Chem.* **2001**, *40*, 5408−5414.
[5] I. Kung, D. Schweitzer, J. Shearer, W. D. Taylor, H. L. Jackson, S. L. Ovell, J. A. Kovacs, *J. Am. Chem. Soc.* **2000**, *122*, 8299−8300.
[6] [6a] L. Heinrich, Y. Li, J. Vaisssermann, J. C. Chottard, *Eur. J. Inorg. Chem.* **2001**, 1407−1409. [6b] L. Heinrich, A. Mary-Verla, Y. Li, J. Vaisssermann, J. C. Chottard, *Eur. J. Inorg. Chem.* **2001**, 2203−2206.
[7] M. Rat, R. Alves de Sousa, J. Vaissermann, P. Leduc, D. Mansuy, I. Artaud, *J. Inorg. Biochem.* **2001**, *84*, 207−213.
[8] S. Chatel, M. Rat, S. Dijols, P. Leduc, J. P. Tuchagues, D. Mansuy, I. Artaud, *J. Inorg. Biochem.* **2000**, *80*, 239−246.

[9] L. Heinrich, Y. Li, K. Provost, A. Michalowicz, J. Vaissermann, J. C. Chottard, *Inorg. Chim. Acta* **2001**, *318*, 117−126.
[10] S. Dutta, U. Beckmann, E. Bill, T. Weyhermüller, K. Wieghardt, *Inorg. Chem.* **2000**, *39*, 3355−3364.
[11] L. A. Tyler, M. M. Olmstead, P. K. Mascharak, *Inorg. Chim. Acta* **2001**, *321*, 135−141.
[12] R. D. Shannon, *Acta Crystallogr., Sect. A* **1976**, *32*, 751−767.
[13] F. H. Allen, O. Kennard, 3D Search and Reasearch Using the Cambridge Data Base, Chemical Design Automation News, **1993**, *8*, 31−37.
[14] [14a] D. A. House, V. McKee, P. Steel, *Inorg. Chem.* **1986**, *25*, 4884−4889. [14b] C. Fukuhara, E. Asato, T. Shimoji, K. Katsura, M. Mori, K. Matsumoto, S. Ooi, *J. Chem. Soc., Dalton Trans.* **1987**, 1305−1311. [14c] A. Golobic, B. Stefane, S. Polanc, *Polyhedron* **1999**, *18*, 36661−3668.
[15] B. N. Figgis, *Nature (London)* **1958**, 182, 1568−1570.
[16] L. Banci, A. Bencini, C. Benelli, D. Gatteschi, C. Zanchini, *Struct. Bonding (Berlin)* **1982**, *52*, 37−67.
[17] A. Bencini, C. Benelli, D. Gatteschi, C. Zanchini, *Inorg. Chem.* **1983**, *22*, 2123−2126.
[18] Stoe and Cie (1996) IPDS Manual. Version 2.75. Stoe and Cie, Darmstadt, Germany.
[19] G. M. Sheldrick, *SHELXS−97, Program for Crystal structure solution*, University of Göttingen, Germany, **1997**.
[20] G. M. Sheldrick, *SHELXL-97, Program for Crystal structure refinement*, University of Göttingen, Germany, **1997**.
[21] C. K. Johnson, *ORTEPII*, Report ORNL-5138, Oak Ridge National Laboratory, TN, **1976.**

Received July 18, 2002
[I02398]

The Influence of Functional Group Orientation on the Structure of Zinc 1,1,4-Trimethylthiosemicarbazide Dicarboxylates: Probing the Limits of Crystal Engineering Strategies

Andrew D. Burrows,*[a] Ross W. Harrington,[a] Mary F. Mahon,[a] and Simon J. Teat[b]

Keywords: Zinc / Carboxylate ligands / Hydrogen bonds / Coordination polymers / Supramolecular chemistry

The reaction of $[Zn(tmtsc)_2](NO_3)_2$ [tmtsc = 1,1,4-trimethylthiosemicarbazide, $MeNHC(S)NHNMe_2$] with a range of sodium dicarboxylates has been shown to lie on the borderline between commonly used crystal engineering strategies. The products exhibit a wide range of structural diversity with the main driving force being the relative orientation of the carboxylate groups. Thus, fumarate leads to the hydrogen-bonded aggregate $[Zn(tmtsc)_2(OH_2)][fumarate]$ (**2**) in which cations and anions are linked by hydrogen bond donor-donor acceptor-acceptor (DD:AA) interactions, whereas isophthalate and (+)-camphorate lead to coordination polymers [Zn(tmtsc)(μ-isophthalate)] (**3a**) and [Zn(tmtsc)(μ-camphorate)] (**4**) with the metal centres linked by bridging dicarboxylate ligands. In the case of isophthalate, a hydrated product [Zn(tmtsc)(μ-isophthalate)]·H_2O (**3b**) was also characterised, although microanalysis and powder X-ray diffraction revealed this to be a minor product. Incorporation of water was shown to lead to a change in carboxylate coordination mode from η^1 in **3a** to η^2 in **3b**. Use of terephthalate leads to the compound $[\{Zn(tmtsc)(OH_2)\}_2(\mu\text{-terephthalate})]$-[terephthalate]·$2H_2O$ (**5**), in which half of the terephthalates bridge metal centres, to form dimers, and the remainder link the dimeric cations through DD:AA hydrogen bond interactions. Homophthalate leads to discrete dimers $[Zn(tmtsc)(\mu\text{-homophthalate})]_2$ (**6**), whereas acetylenedicarboxylate yields the unexpected compound $[Zn(tmtsc)_2(OH_2)][O_2CCH{=}CC(O)N(Me)C(=NNMe_2)S]_2{\cdot}H_2O$ (**7**) in which the dicarboxylate has reacted with tmtsc to give a 2-hydrazono-4-oxo-1,3-thiazolidineacetate, which is subsequently trapped in the solid state by DD:AA hydrogen bonding interactions with $[Zn(tmtsc)_2(OH_2)]^{2+}$. All products were characterised by single crystal X-ray crystallography, and the representational nature of these crystal structures to the bulk materials was confirmed by microanalysis and powder diffraction.
(© Wiley-VCH Verlag GmbH & Co. KGaA, 69451 Weinheim, Germany, 2003)

Introduction

Progress in the field of crystal engineering has largely arisen as a result of the identification and use of *supramolecular synthons*[1] − small units within molecules that are anticipated to interact with each other in a predictable manner. There are currently two main strategies adopted in crystal engineering, in which these supramolecular synthons are based either on metal-ligand interactions[2] or, alternatively, on intermolecular interactions such as hydrogen bonds,[3] and recently there have been reports using both of these approaches together.[4] We are particularly interested in the competitive interplay between the two strategies, and as a consequence have focussed our attention on systems in which both types of aggregation are possible.

As part of this study, we have shown that $[Zn(thiourea)_4]^{2+}$ cations react with dicarboxylates by displacing thiourea ligands to give polymers or dimers in which the zinc centres are linked by bridging dicarboxylates.[5,6] In contrast, under similar conditions $[M(tsc)_2]^{2+}$ (M = Zn, Ni; tsc = thiosemicarbazide) cations give ionic structures of the type $[M(tsc)_2][dicarboxylate]$ in which the cations and anions are linked together into tapes by hydrogen bonds.[5,7] Hence, changing the ligands on the metal centre from uni- to bidentate has been shown to alter the mode of supramolecular assembly and consequently the type of structure formed.

In this paper we report on the reactions of $[Zn(tmtsc)_2]^{2+}$ [tmtsc = 1,1,4-trimethylthiosemicarbazide, $MeNHC(S)NHNMe_2$] with a range of dicarboxylates. The presence of the tertiary amine group in the tmtsc ligand was expected to increase its lability relative to tsc,[8] and therefore enhance the possibility of ligand displacement from the metal coordination sphere. This has been borne out and, in contrast to the reactions with $[Zn(thiourea)_4]^{2+}$ or $[M(tsc)_2]^{2+}$, reactions with $[Zn(tmtsc)_2]^{2+}$ give a wide variety of structural types, with that observed from a particular reaction depending on the relative orientation of the carboxylate groups within the anion.

[a] Department of Chemistry, University of Bath, Claverton Down, Bath BA2 7AY, UK
E-mail: a.d.burrows@bath.ac.uk
[b] CLRC Daresbury Laboratory, Daresbury, Warrington WA4 4AD, UK

Results and Discussion

Synthesis

The complex $[Zn(tmtsc)_2](NO_3)_2$ was prepared from the reaction of zinc(II) nitrate with tmtsc in ethanol. Recrystallisation of the product from water gave single crystals of $[Zn(tmtsc)_2(OH_2)_2](NO_3)_2$ (**1**), the identity of which was confirmed crystallographically. Selected bond lengths and angles for **1** are given in Table 1.

Table 1. Selected bond lengths (Å) and angles (°) for compounds **1**, **3a**, **3b** and **6**

[a]	**1**	**3a**	**3b**	**6**
Zn(1)−S	2.4186(5)	2.327(2)	2.3267(9)	2.3814(7)
Zn(1)−N(1)	2.2513(15)	2.098(5)	2.195(2)	2.162(2)
Zn(1)−O(1)	2.1224(14)	1.933(4)	2.078(2)	2.0165(16)
Zn(1)−O(2)			2.334(2)	2.540(2)
Zn(1)−O(3′)		1.930(4)	2.343(2)	2.2823(19)
Zn(1)−O(4′)			2.056(2)	2.054(2)
N(1)−Zn(1)−S	81.76(4)	86.66(14)	84.09(6)	84.15(6)
O(1)−Zn(1)−O′ [b]		116.13(17)	103.61(8)	137.90(8)

[a] Primed atoms generated by symmetry transformations $-x + {}^3/_2$, $y-{}^1/_2$, $z + {}^1/_2$ (**3a**), $-x + 1$, $y-{}^1/_2$, $-z + {}^1/_2$ (**3b**) and $-x + 1$, $-y + 1$, $-z$ (**6**). [b] O′ = O(3)′ for **3a**; O′ = O(4)′ for **3b** and **6**.

Reaction of $[Zn(tmtsc)_2](NO_3)_2$, in aqueous solution, with sodium salts of fumaric, (+)-camphoric, terephthalic, homophthalic and acetylenedicarboxylic acids gave compounds $[Zn(tmtsc)_2(OH_2)]$[fumarate] (**2**), [Zn(tmtsc)(μ-(+)camphorate)] (**4**), $[\{Zn(tmtsc)(OH_2)\}_2$(μ-terephthalate)][terephthalate]·$2H_2O$ (**5**), [Zn(tmtsc)(μ-homophthalate)]$_2$ (**6**) and $[Zn(tmtsc)_2(OH_2)][O_2CCH{=}CC(O)N(Me)C(=NNMe_2)S]_2{\cdot}H_2O$ (**7**), as the only isolated compounds in good yield. The analogous reaction with isophthalate gave two compounds, [Zn(tmtsc)(μ-isophthalate)] (**3a**) and [Zn(tmtsc)(μ-isophthalate)]·H_2O (**3b**), with the anhydrous complex **3a** the major product. The empirical formulae of compounds **2**, **3a**, **4**, **5**, **6** and **7** were confirmed by microanalyses, and the structures of all the compounds were determined by single crystal X-ray analyses. A comparison of the experimental powder diffraction data with that simulated from the single-crystal data confirmed that the crystal structures are representative of the bulk materials, with the experimental data for isophthalate consistent with **3a**. The dicarboxylates used are illustrated in Scheme 1.

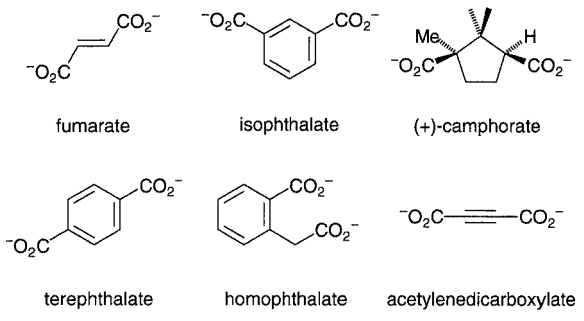

Scheme 1. Structures of the dicarboxylates used

Supramolecular Structures of 2−7

The crystal structure of compound **2** consists of $[Zn(tmtsc)_2(OH_2)]^{2+}$ cations and fumarate anions. The coordination geometry around the zinc centre is distorted square pyramidal ($\tau = 0.39$),[9] with mutually *trans* tmtsc ligands. Selected bond lengths and angles are given in Table 2, and hydrogen bonding parameters are given in Table 3. Two hydrogen bonds between the parallel NH

Table 2. Selected bond lengths (Å) and angles (°) for compounds **2** and **7**

	2	**7**
Zn(1)−S(1)	2.3127(8)	2.3425(8)
Zn(1)−S(2)	2.3073(8)	2.3319(8)
Zn(1)−N(1)	2.306(2)	2.240(2)
Zn(1)−N(4)	2.280(2)	2.239(2)
Zn(1)−O(w)[a]	1.986(2)	1.993(2)
S(1)−Zn(1)−S(2)	141.34(3)	143.74(3)
N(1)−Zn(1)−N(4)	164.60(7)	168.84(7)
N(1)−Zn(1)−S(1)	82.25(5)	82.38(5)
N(4)−Zn(1)−S(2)	82.68(5)	81.99(5)
O(w)−Zn(1)−N(1)	97.15(7)	95.40(7)
O(w)−Zn(1)−N(4)	98.23(7)	95.75(7)
O(w)−Zn(1)−S(1)	108.10(6)	102.55(5)
O(w)−Zn(1)−S(2)	110.56(6)	113.69(6)

[a] O(w) = O(5) for **2**, O(w) = O(7) for **7**.

Table 3. Hydrogen bond lengths (Å) and angles (°) for compounds **2**−**7**

		d(D···A)/Å	*d*(H···A)/Å	∢(DH···A)/°
2	N(2)−H(2)···O(1)	2.803(2)	1.94(2)	173(2)
	N(3)−H(3)···O(2)	2.730(2)	1.86(2)	172(2)
	N(5)−H(5)···O(3)	2.831(3)	1.95(2)	177(3)
	N(6)−H(6)···O(4)	2.731(3)	1.87(2)	176(3)
	O(5)−H(5A)···O(4)	2.649(2)	1.82(2)	170(2)
	O(5)−H(5B)···O(2)	2.588(2)	1.71(2)	172(4)
3a	N(2)−H(2)···O(2)	2.765(6)	2.01(6)	142(5)
	N(3)−H(3)···O(2)	2.909(7)	2.19(6)	138(5)
3b	N(3)−H(3)···O(3)	2.793(3)	2.10(3)	146(3)
	N(2)−H(2)···O(5)	2.869(3)	2.08(3)	171(3)
	O(5)−H(5A)···O(2)	2.890(4)	2.15(4)	163(4)
	O(5)−H(5B)···O(1)	2.877(3)	2.13(4)	163(4)
4	N(2)−H(2)···O(2)	2.758(4)	1.91(2)	167(3)
	N(3)−H(3)···O(8)	2.907(4)	2.16(2)	141(3)
	N(5)−H(5)···O(4)	2.747(4)	1.89(3)	164(4)
	N(6)−H(6)···O(5)	2.892(4)	2.13(3)	144(4)
5	N(2)−H(2)···O(1)	2.871(2)	2.00(2)	170(2)
	N(3)−H(3)···O(2)	2.779(2)	1.91(2)	179(2)
	O(5)−H(5A)···O(6)	2.654(3)	1.80(3)	173(3)
	O(5)−H(5B)···O(3)	2.665(3)	1.79(2)	173(4)
	O(6)−H(6A)···O(1)	2.854(3)	2.01(2)	166(3)
	O(6)−H(6B)···O(4)	2.812(3)	2.07(3)	145(4)
6	N(2)−H(2)···O(2)	2.790(3)	1.94(2)	159(3)
	N(3)−H(3)···O(2)	2.982(3)	2.19(2)	151(3)
7	N(2)−H(2)···O(2)	2.676(2)	1.79(2)	173(2)
	N(3)−H(3)···O(1)	2.901(2)	2.03(2)	179(2)
	N(5)−H(5)···O(4)	2.651(2)	1.77(2)	177(2)
	N(6)−H(6)···O(5)	2.831(2)	1.95(2)	171(2)
	O(7)−H(7A)···O(1)	2.640(2)	1.78(2)	170(3)
	O(7)−H(7B)···O(8)	2.640(2)	1.81(2)	165(2)
	O(8)−H(8A)···O(5)	2.697(3)	1.83(2)	169(3)
	O(8)−H(8B)···N(12)	3.034(3)	2.20(3)	159(5)

groups on the tmtsc ligands and the two oxygen atoms of the carboxylate groups serve to link the cations and anions together into tapes (Figure 1). These hydrogen bond donor-donor acceptor-acceptor (DD:AA) interactions are similar to those observed in $[Zn(tsc)_2(OH_2)_2][terephthalate]\cdot 2H_2O$[5] and in nickel thiosemicarbazide dicarboxylates[7] [graph set[10] $R_2^2(8)$]. The cation···anion tapes in **2** are linked into sheets by O−H···O hydrogen bonds from the aqua ligands in a neighbouring plane to carboxylate oxygen atoms. Since the aqua ligands within each tape are all orientated in the same direction, these O−H···O hydrogen bonds ensure that the sheets exist as bilayers, with weaker C−H···O interactions linking these bilayers into the gross structure. Similar DD:AA interactions were observed between the tmtsc ligands and the nitrate anions in the structure of **1**. However, a mismatch in both the charge and shape of the ions guarantees that the DD:AA interactions do not lead to tape formation in the nitrate − instead, discrete $[Zn(tmtsc)_2(OH_2)_2](NO_3)_2$ units are linked only by O−H···O hydrogen bonds.

The crystal structures of compounds **3a** and **3b** reveal that, in contrast to **2**, both compounds are coordination polymers with isophthalates bridging between metal centres (Figure 2). In both structures each zinc(II) centre is coordinated to a tmtsc ligand and two isophthalate ligands; in **3b** included water molecules are also present in the lattice. Selected bond lengths and angles for both **3a** and **3b** are given in Table 1 and hydrogen bonding parameters are given in Table 3.

The coordination geometry around the zinc centre in compound **3a** is distorted tetrahedral with the carboxylates η^1-coordinated (Figure 2, top), as observed in [Zn(thiourea)$_2$(μ-dicarboxylate)] polymers.[6] Coordination of the carboxylates prevents the formation of DD:AA interactions, although hydrogen bonding is still present, linking the chains through two N−H···O interactions from the NH groups to a single carboxylate oxygen atom [graph set $R_2^1(6)$].

The presence of the lattice water molecule in compound **3b** leads to differences in the manner in which the chains are linked together (Figure 2, bottom). One of the NH groups hydrogen bonds to a carboxylate oxygen atom, whereas the other forms an N−H···O hydrogen bond to the included water molecule. Two O−H···O hydrogen bonds from the water to carboxylate oxygen atoms complete the hydrogen bonding, with one of these leading to the formation of $R_3^3(10)$ rings. Significant π−π interactions are also present, with the shortest C···C distance between isophthalate rings being 3.45 Å. In order to accommodate the hydrogen bonding in **3b** there is a change in the metal coordination geometry relative to that in **3a**, with both carboxylate groups unsymmetrically η^2-coordinated, thus affording distorted octahedral geometry at the metal centre. Consequently the longer Zn−O distances have been reduced from 2.838(5)

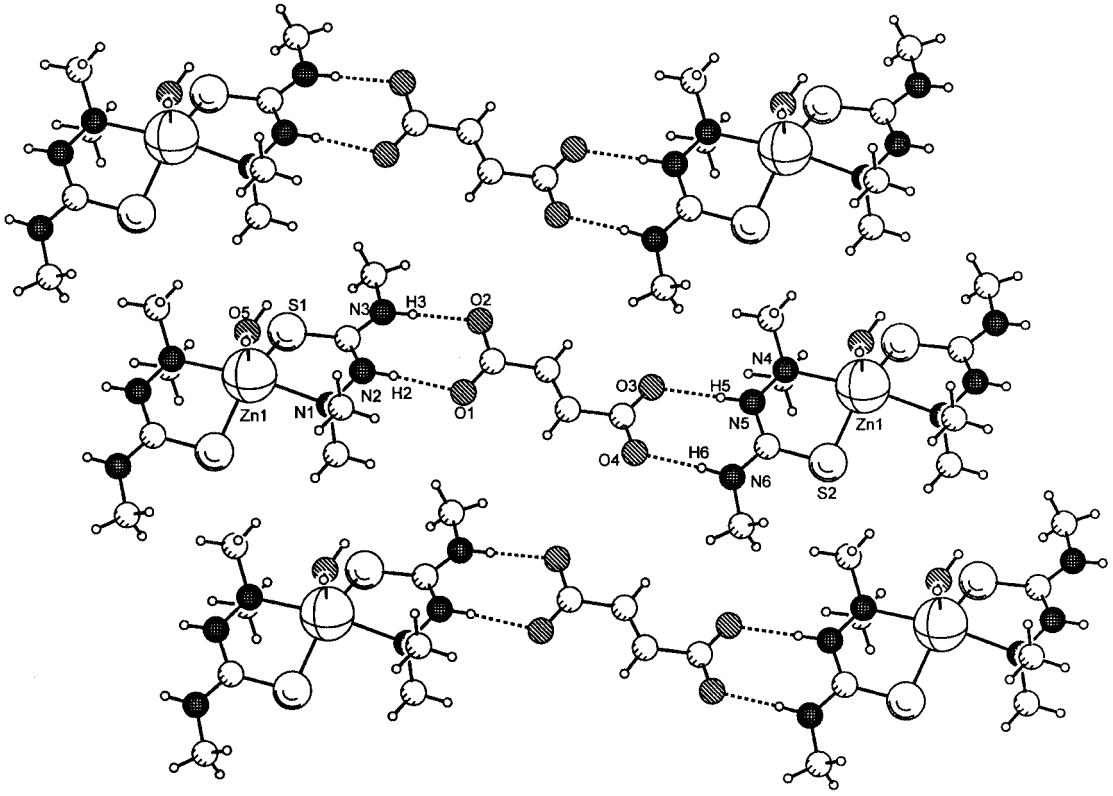

Figure 1. The solid state structure of $[Zn(tmtsc)_2(OH_2)][fumarate]$ (**2**)

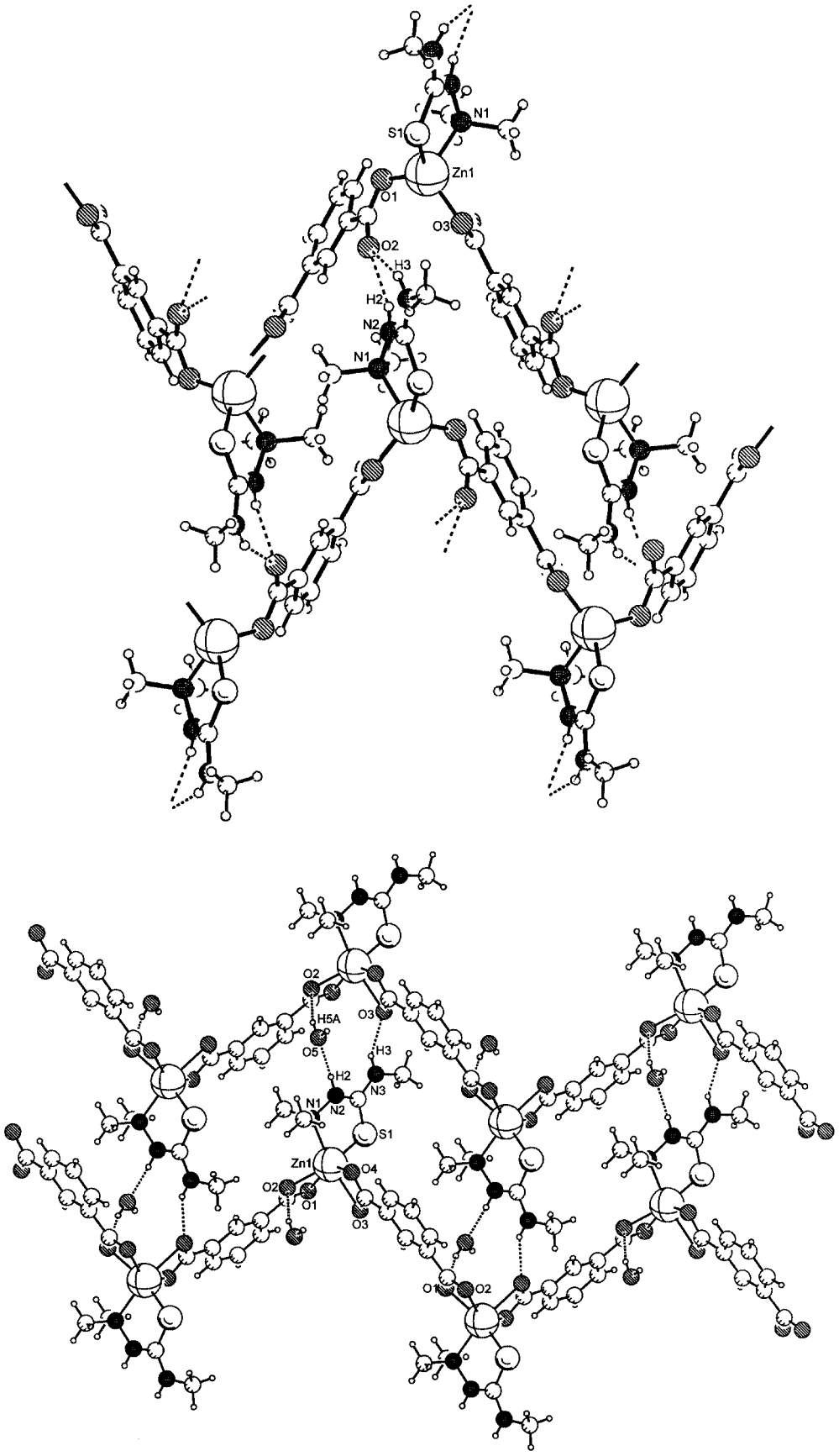

Figure 2. The solid state structures of (top) [Zn(tmtsc)(μ-isophthalate)] (**3a**) and (bottom) [Zn(tmtsc)(μ-isophthalate)]·H_2O (**3b**)

and 3.071(4) Å in **3a** to 2.334(2) and 2.343(2) Å in **3b** on incorporation of the water. The increase in coordination number has little effect on the Zn−S distance, but leads to a significant increase in the Zn−N bond length and a reduction of the tmtsc bite angle (Table 1).

Compound **4**, incorporating the (+)-camphorate dianion, also exists as a coordination polymer, with the (+)-camphorates linking the zinc centres. The asymmetric unit of this compound contains two independent Zn(tmtsc) groups and two independent (+)-camphorates. Both zinc centres are five-coordinate, with one carboxylate group bound η^1 and the other η^2. Selected bond lengths and angles are given in Table 4 and hydrogen bonding parameters are given in Table 3. The two independent (+)-camphorate dianions differ in that one contains two η^1-carboxylates whereas the other contains two η^2-carboxylates.

The structure of **4** differs from those for **3a** and **3b** by virtue of the manner in which the coordination polymers interact with each other. In **4** this is through two N−H···O hydrogen bonds from each of the tmtsc ligands, with the acceptors being oxygen atoms on separate carboxylate groups (Figure 3). One of these oxygen atoms is non-coordinated [O(2) or O(4)] whereas the other forms the longer Zn−O bond of an η^2-carboxylate [O(5) or O(8)]. This hydrogen bonding pattern is facilitated by a change in conformation of the tmtsc ligand. A rotation of 180° around the C−N(amino) bond means that the two NH groups within each ligand are no longer orientated in the same direction. Such a conformational change has been observed previously in the structure of *cis*-[Ni(4-Et-tsc)$_2$][terephthalate],[11] although in the nickel complex the *cis* orientation of the ligands results in the formation of a new DD face which is involved in hydrogen bonding. This does not happen for **4** however, and the loss of potential secondary interactions is compensated by the formation of four strong hydrogen bonds.

Table 4. Selected bond lengths (Å) and angles (°) for compound **4**

Zn(1)−S(1)	2.3564(8)
Zn(1)−N(1)	2.169(2)
Zn(1)−O(1)	1.968(2)
Zn(1)−O(8)′ [a]	2.081(2)
Zn(1)−O(7)′	2.254(2)
Zn(2)−S(2)	2.3494(9)
Zn(2)−N(4)	2.163(3)
Zn(2)−O(5)	2.124(3)
Zn(2)−O(6)	2.251(2)
Zn(2)−O(3)	1.978(2)
N(1)−Zn(1)−S(1)	83.48(7)
O(1)−Zn(1)−O(8)′	128.68(9)
N(4)−Zn(2)−S(2)	83.93(7)
O(3)−Zn(2)−O(5)	130.73(10)

[a] Primed atoms generated by symmetry transformation *x*, *y*, *z* − 1.

The crystal structure of compound **5** consists of [{Zn(tmtsc)(OH$_2$)}$_2$(μ-terephthalate)]$^{2+}$ cations, terephthalate anions and included water molecules. The geometry around the zinc centres in **5** is distorted square pyramidal ($\tau = 0.36$[9]), with the carboxylate unsymmetrically coordin-

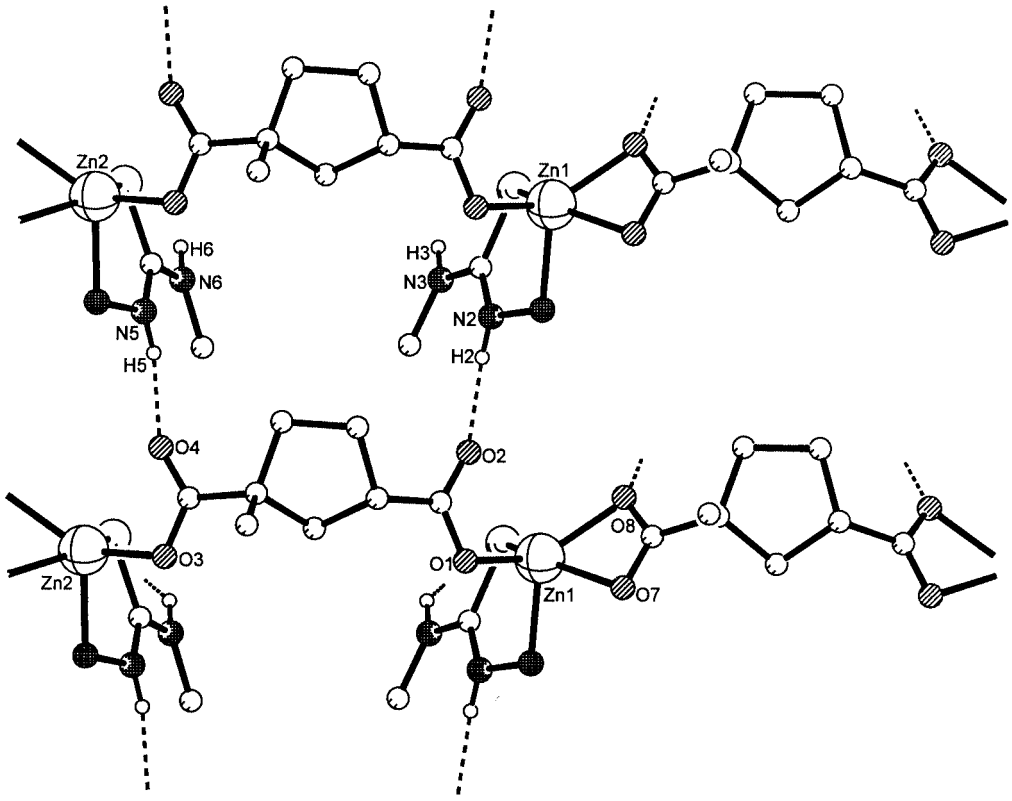

Figure 3. The solid state structure of [Zn(tmtsc)(μ-(+)camphorate)] (**4**), with all carbon-bound hydrogen atoms omitted for clarity

ated. Selected bond lengths and angles are given in Table 5 and hydrogen bonding parameters are given in Table 3. The cation in **5** can be regarded in hydrogen bonding terms as an "expanded" $[Zn(tmtsc)_2]^{2+}$ cation, since both contain the same number and relative orientation of NH groups. The cations and anions in **5** interact through two hydrogen bonds in a similar DD:AA manner to that observed in **2**, which overall serves to link the ions into tapes (Figure 4). These tapes are connected into sheets by hydrogen bonding to water molecules, although, in contrast to **2**, these involve both water included within the lattice and coordinated water ligands from tapes above and below the sheets. Since each cation contains two axial coordinated water molecules, pointing in opposite directions, the sheets are all linked in the same manner, which contrasts with the bilayers observed in **2**. The structure of **5** can be regarded as intermediate between those of **2** and **3**, as half the dicarboxylates link the metal centres together through coordinative bonds while the remaining half link the metal centres through hydrogen bonds to the coordinated tmtsc ligands. Despite the importance of dicarboxylates in crystal engineering this is, to the best of our knowledge, the first occasion a structure has been observed in which the anion fulfils both discrete coordination and hydrogen bonding roles.

Table 5. Selected bond lengths (Å) and angles (°) for compound **5**

Zn(1)−S(1)	2.3036(7)
Zn(1)−N(1)	2.119(2)
Zn(1)−O(3)	2.289(2)
Zn(1)−O(4)	2.005(2)
Zn(1)−O(5)	1.993(2)
N(1)−Zn(1)−S(1)	86.55(5)
O(3)−Zn(1)−O(4)	60.62(8)
N(1)−Zn(1)−O(4)	137.87(9)
S(1)−Zn(1)−O(3)	159.58(7)
O(5)−Zn(1)−O(4)	106.94(9)
O(5)−Zn(1)−O(3)	90.68(8)
O(5)−Zn(1)−N(1)	103.89(8)
O(5)−Zn(1)−S(1)	109.56(6)

The crystal structure of compound **6** consists of discrete $[Zn(tmtsc)(\mu\text{-homophthalate})]_2$ molecules (Figure 5), in which the two zinc centres are crystallographically equivalent, related through an inversion centre. Selected bond lengths and angles are given in Table 2, and hydrogen bonding parameters are given in Table 3. Each carboxylate group is unsymmetrically η^2-coordinated, though the Zn(1)−O(2) distance is long [2.540(2) Å]. This oxygen atom is involved in N−H···O hydrogen bonding (see below). The distorted octahedral coordination geometry around the metal centres is similar to that observed in **3b**. The dimeric structure of **6**

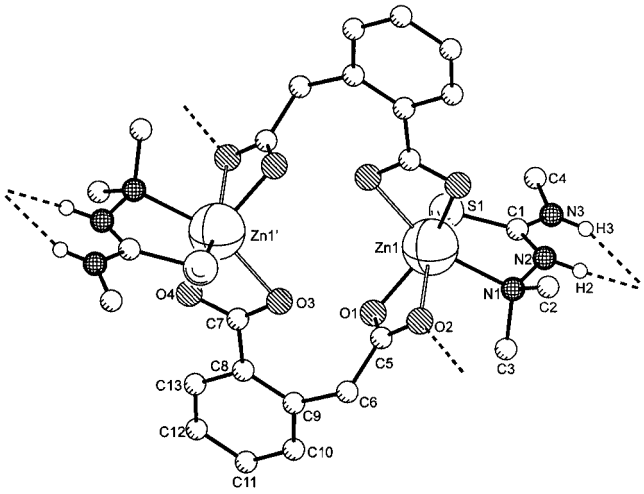

Figure 5. The molecular structure of $[Zn(tmtsc)(\mu\text{-homophthalate})]_2$ (**6**), with all carbon-bound hydrogen atoms omitted for clarity

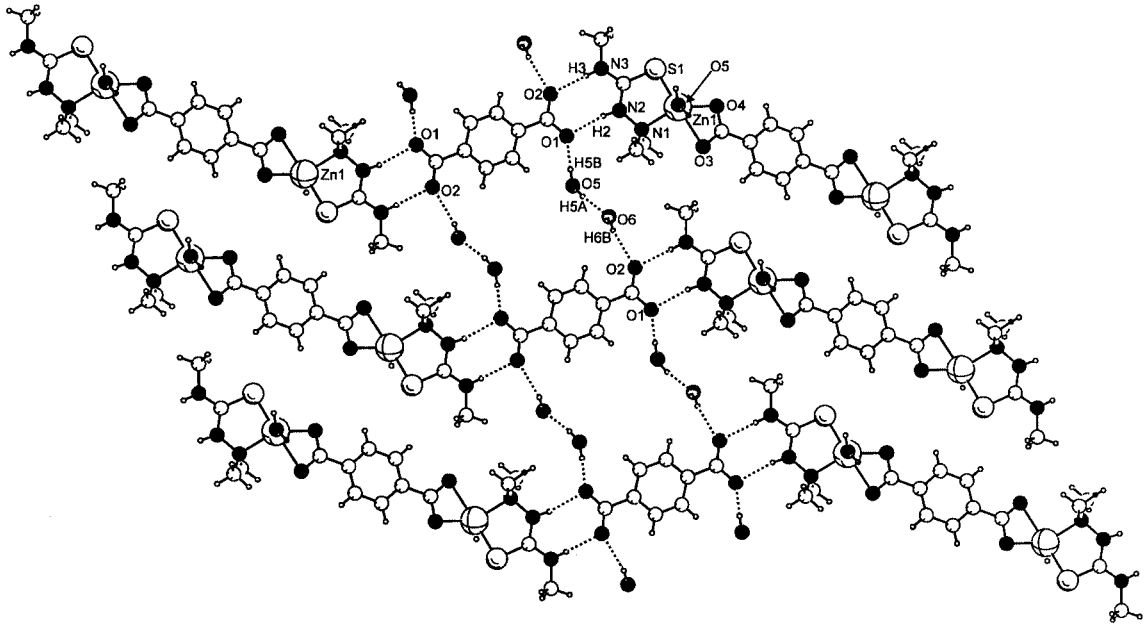

Figure 4. The solid state structure of $[\{Zn(tmtsc)(OH_2)\}_2(\mu\text{-terephthalate})][terephthalate]\cdot 2H_2O$ (**5**)

is similar to that previously observed in $[Zn\{SC(NH_2)_2\}_2(\mu\text{-homophthalate})]_2$ [6] strongly suggesting that dimer formation is driven by the relative orientation of the carboxylate groups in the homophthalate dianion. In contrast to **6**, $[Zn\{SC(NH_2)_2\}_2(\mu\text{-homophthalate})]_2$ contains η^1-coordinated carboxylate groups, with non-bonded Zn−O distances of 2.86(3) and 3.05(3) Å. The distances across the ring in **6**, as represented by the O(2)···O(2′) and O(3)···O(3′) separations, are 5.9 and 3.9 Å respectively, hence the dimers are somewhat flattened relative to those present in $[Zn\{SC(NH_2)_2\}_2(\mu\text{-homophthalate})]_2$ (O···O 5.3 and 4.9 Å).

Molecules of **6** are linked in the solid state through two N−H···O hydrogen bonds to a single carboxylate oxygen atom O(2), in an analogous manner to **3a** [graph set $R_2^1(6)$]. Each molecule provides hydrogen bond donors in one dimension and hydrogen bond acceptors in a second, as shown schematically in Figure 6 (top). These interactions therefore serve to link the molecules into sheets (Figure 6, bottom). Despite the presence of carboxylate oxygen atoms which are not involved in hydrogen bonding, there are no hydrogen bond interactions linking the sheets together.

The reaction between $[Zn(tmtsc)_2](NO_3)_2$ and acetylenedicarboxylate does not give a compound in which the dicarboxylate is incorporated, either as a ligand or as a hydrogen bonded anion. Instead, a reaction (Scheme 2) between acetylenedicarboxylate and a tmtsc molecule occurs to give a

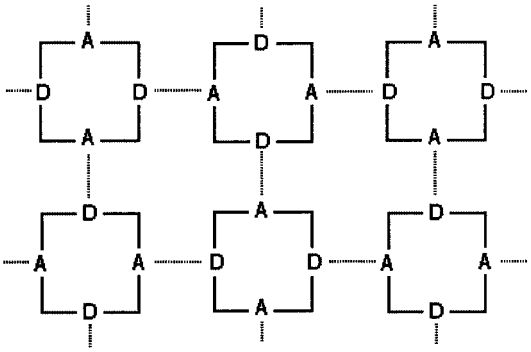

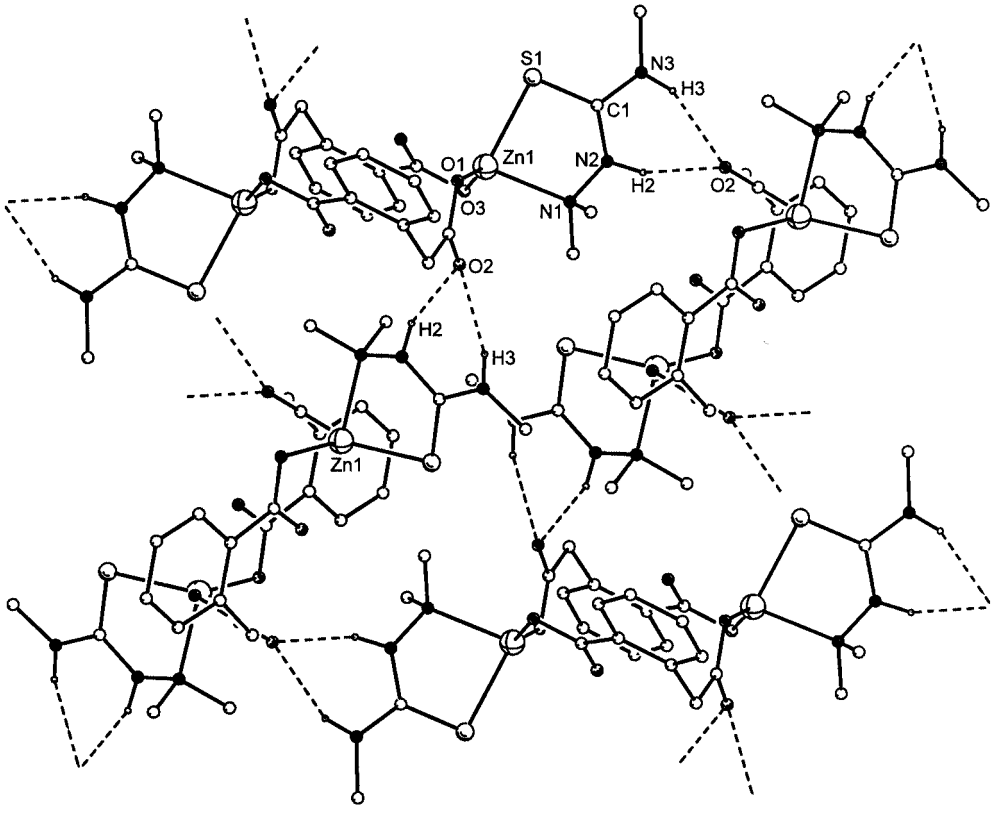

Figure 6. Intermolecular interactions present in $[Zn(tmtsc)(\mu\text{-homophthalate})]_2$ (**6**); (top) schematic representation of hydrogen bonded sheets; (bottom) part of the extended structure, with all carbon-bound hydrogen atoms omitted for clarity

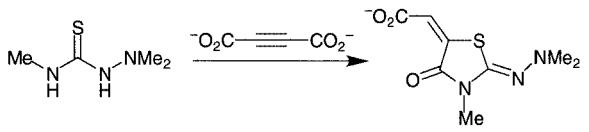

Scheme 2. Conversion of 1,1,4-trimethylthiosemicarbazide into the anion observed in compound **7**

2-hydrazono-4-oxo-1,3-thiazolidineacetate, which is itself incorporated into the structure as the anion. Thus the identity of **7**, as determined by the crystal structure, is $[Zn(tmtsc)_2(OH_2)][O_2CCH{=}CC(O)N(Me)C(=NNMe_2)S]_2{\cdot}H_2O$ (Figure 7). The $[Zn(tmtsc)_2(OH_2)]^{2+}$ cation has a distorted square pyramidal geometry ($\tau = 0.41$[9]) with the tmtsc ligands mutually *trans* as in **2** and **5**. Selected bond lengths and angles are given in Table 2, with hydrogen bond parameters given in Table 3. Reactions between thiosemicarbazides and acetylenedicarboxylic acid giving similar products have been reported previously,[12] and the observation of such a reaction here provides evidence of the lability of the tmtsc ligand on zinc, as is also evident from the structures of **3**−**6**.

The heterocyclic anion contains a carboxylate group, and these oxygen atoms are involved in DD:AA hydrogen bonds with the parallel NH groups of the tmtsc ligands. Thus the principal hydrogen bonding motif in **7** is the same as that in both **2** and **5**. However, the presence of only one carboxylate group per anion means that extended cation···anion tapes cannot be formed, and instead the available interactions afford only [cation][anion]$_2$ units as observed for **1**. These units are linked together into the gross structure of **7** *via* hydrogen bonds involving the coordinated and included water molecules, where the former acts as a hydrogen bond donor to both a carboxylate oxygen atom and the included water, and the latter acts as a hydrogen bond donor to a carboxylate oxygen atom and a nitrogen atom.

Discussion

Compounds **2**−**7** were all isolated in good yield as the sole products from the reactions between $[Zn(tmtsc)_2](NO_3)_2$ and a dicarboxylate under identical conditions. There is a wide structural diversity in the products ranging from coordination polymers (**3a**, **3b**, **4**) to hydrogen-bonded ionic aggregates (**2**) via an intermediate structure (**5**) in which half the anions are coordinated. This diversity confirms the initial premise concerning the lability of tmtsc lying between those of tsc and thiourea. The metal coordination number varies from 4 to 6, and is not a major factor in determining the supramolecular structure − this is witnessed by the zinc centres in the coordination polymers **3a**, **3b** and **4** having coordination numbers of 4, 6 and 5 respectively. The products observed are also not affected by changes in the stoichiometry of $[Zn(tmtsc)_2](NO_3)_2$ and dicarboxylate used in the reaction, nor do differences appear to be related to the basicity of the dicarboxylates or the pH of the reaction mixture. However, it is possible to rationalise the structural differences on the basis of the dicarboxylate shape, specifically the relative orientation of the two carboxylate groups.

Yaghi, O′Keeffe and co-workers have recently described the geometry of dicarboxylates in terms of three angles, θ, ψ and φ, and used these angular parameters to help in the design and preparation of porous metal-organic frameworks with predictable structures.[13] Starting from the planar terephthalate anion, θ represents bending in the centre of the anion with the two carboxylates remaining coplanar, ψ represents bending of the carboxylates towards each other, and φ represents the relative twisting of the planes of the carboxylate groups. For terephthalate and fumarate in the structures of **5** and **2**, θ and ψ are 180° and φ is close to zero, as the carboxylate groups are almost coplanar and orientated in opposite directions. These compounds consist of ionic structures based on cation···anion tapes, held together by DD:AA hydrogen bond interactions. This is consistent with previous structures containing these anions,[5,7] though the formation of **5**, in which half of the terephthalates are coordinated giving "extended" $[\{Zn(tmtsc)(OH_2)\}_2(\mu\text{-terephthalate})]^{2+}$ cations is somewhat unexpected, as the nickel compound $[Ni(tmtsc)_2(OH_2)_2]$[terephthalate] readily forms in a comparative reaction. The presence of the extended cation in **5** does prevent unfavourable interactions between the methyl groups on neighbouring tapes that would occur if simple $[Zn(tmtsc)_2]^{2+}$ cations were incorporated in the orientation

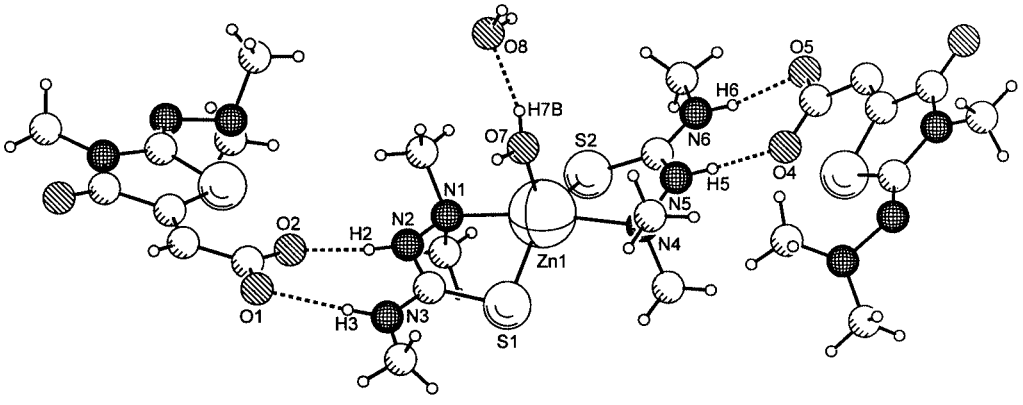

Figure 7. Part of the solid state structure of $[Zn(tmtsc)_2(OH_2)][O_2CCH{=}CC(O)N(Me)C(=NNMe_2)S]_2{\cdot}H_2O$ (**7**)

adopted. Despite possessing the same angular parameters, terephthalate and fumarate differ in the distance between the carboxylate groups and the fact that for fumarate these are not co-linear, there being a lateral displacement of 1.07 Å.

While isophthalate and camphorate are structurally very different, it is noteworthy that each possesses one of the angular parameters − θ for isophthalate and φ for camphorate − that has been reduced from the 180° value for terephthalate to 120°, and both of these dicarboxylates form coordination polymers with Zn(tmtsc) centres. While the carboxylate orientations in **3a**, **3b** and **4** do not preclude hydrogen bonded structures, they may reduce their likelihood since there are more limited ways in which the resultant zig-zag tapes would be able to pack.

The structures of **6** and $[Zn\{SC(NH_2)_2\}_2(\mu\text{-homophthalate})]_2$ reflect a clear propensity for homophthalate to form dimers, despite the dicarboxylates in these complexes adopting different coordination modes. In the $[Zn\{SC(NH_2)_2\}_2]^{2+}$ system this tendency is particularly marked since homophthalate is the only dicarboxylate out of 13 structurally characterised compounds not to form a coordination polymer. A search of the CSD[14] reveals no examples of homophthalate coordination polymers, and it is noticeable that dimerisation of Mo_2 units has also been observed with this dicarboxylate.[15]

The reaction between $[Zn(tmtsc)_2](NO_3)_2$ and acetylenedicarboxylate gave an unexpected product in **7**. The coupling reaction between tmtsc and acetylenedicarboxylate has generated a 2-hydrazono-4-oxo-1,3-thiazolidineacetate anion, and the structure of **7** illustrates the potential for trapping reaction products in hydrogen bonded networks through the use of species containing complementary hydrogen bonding groups.

Four of the seven carboxylate-containing structures reported in this paper contain water, either as a ligand (**2**), included in the lattice (**3b**), or both (**5** and **7**). The tmtsc ligand has only two hydrogen bond donors whereas a carboxylate group can accept four or even more hydrogen bonds. Therefore use of tmtsc as a ligand in these systems leads to a relative deficiency of hydrogen bond donors in the gross structure which can be overcome by inclusion of water. This solvent inclusion also affords greater flexibility in the relative orientations of hydrogen bonding groups.

Conclusions

In this paper we have demonstrated that a deceptively simple series of compounds − those resulting from the reaction between $[Zn(tmtsc)_2]^{2+}$ and a dicarboxylate − have widely differing structures, with the relative orientation of the carboxylate groups a major factor in determining the type of structure formed. The variety of structural types obtained from this reaction series contrasts with the products observed from analogous reactions using thiourea or thiosemicarbazide complexes. Thiourea is invariably displaced from $[Zn\{SC(NH_2)_2\}_4]^{2+}$ leading to coordination polymers or cyclic oligomers, all containing tetrahedral zinc centres, whereas thiosemicarbazide is generally retained on the metal leading to structures in which the ions are only associated through hydrogen bonds. The tmtsc ligand lies between these two extremes confirming our initial premise concerning its lability, and this places $[Zn(tmtsc)_2]^{2+}$ on the borderline between the two main strategies currently employed in crystal engineering. These observations are important in helping to define the limits of the different crystal engineering strategies.

Experimental Section

Microanalyses were carried out by Mr. Alan Carver (University of Bath Microanalytical Service). 1,1,4-Trimethylthiosemicarbazide (tmtsc) was prepared from the reaction of *N*,*N*-dimethylhydrazine with methyl isothiocyanate in diethyl ether.[16] Sodium dicarboxylates were either purchased from commercial sources and used directly (fumarate and terephthalate) or prepared from the appropriate dicarboxylic acid and either sodium hydroxide or sodium hydrogen carbonate.

Synthesis of $[Zn(tmtsc)_2](NO_3)_2$: 1,1,4-Trimethylthiosemicarbazide (0.448 g, 3.36 mmol) in ethanol (10 cm^3) was added to zinc nitrate hexahydrate (0.500 g, 1.68 mmol) in ethanol (10 cm^3) and the solution stirred for 1 h. The volume of the solution was reduced to 5 cm^3 in vacuo, and the colourless crystals that precipitated overnight were separated by filtration. Yield 0.75 g (98%). On recrystallisation from water, crystals of $[Zn(tmtsc)_2(OH_2)_2](NO_3)_2$ (**1**) were obtained.

Synthesis of 2: Aqueous solutions of sodium fumarate (35 mg, 0.22 mmol) and $[Zn(tmtsc)_2](NO_3)_2$ (100 mg, 0.22 mmol) were mixed. After approximately 24 hours colourless crystals formed, and these were isolated by filtration. Yield 80 mg (79%). $C_{12}H_{26}N_6O_5S_2Zn$ (463.9): calcd. C 31.1, N 18.1, H 5.65; found C 31.3, N 18.1, H 5.71.

Synthesis of 3a and 3b: As for **2** using sodium isophthalate (53 mg, 0.25 mmol) and $[Zn(tmtsc)_2](NO_3)_2$ (115 mg, 0.25 mmol). Yield 81 mg (88%). $C_{12}H_{15}N_3O_4SZn$ (362.7): calcd. C 39.7, N 11.6, H 4.17; found C 39.6, N 11.5, H 4.22

Synthesis of 4: As for **2** using sodium (1*R*,3*S*)-(+)-camphorate (54 mg, 0.22 mmol) and $[Zn(tmtsc)_2](NO_3)_2$ (100 mg, 0.22 mmol). Yield 56 mg (64%). $C_{14}H_{25}N_3O_4SZn$ (396.8) calcd. C 42.4, N 10.6, H 6.35; found C 42.1, N 10.6, H 6.28.

Synthesis of 5: As for **2** using sodium terephthalate (46 mg, 0.22 mmol) and $[Zn(tmtsc)_2](NO_3)_2$ (100 mg, 0.22 mmol). Yield 63 mg (72%). $C_{24}H_{38}N_6O_{12}S_2Zn_2$ (797.5): calcd. C 36.2, N 10.5, H 4.80; found C 36.5, N 10.4, H 4.79.

Synthesis of 6: As for **2** using sodium homophthalate (49 mg, 0.22 mmol) and $[Zn(tmtsc)_2](NO_3)_2$ (100 mg, 0.22 mmol). Yield 59 mg (71%). $C_{26}H_{34}N_6O_8S_2Zn_2$ (753.5): calcd. C 41.5, N 11.2, H 4.55; found C 41.2, N 10.9, H 4.48.

Synthesis of 7: As for **2** using sodium acetylenedicarboxylate (35 mg, 0.22 mmol) and $[Zn(tmtsc)_2](NO_3)_2$ (100 mg, 0.22 mmol). Yellow crystals. Yield 74 mg (82% based on tmtsc).

Table 6. Crystallographic data for complexes **1**, **2**, **3a**, **3b**, **4**, **5**, **6** and **7**

	1	**2**	**3a**	**3b**	**4**	**5**	**6**	**7**
Formula	$C_8H_{26}N_8O_8S_2Zn$	$C_{12}H_{26}N_6O_5S_2Zn$	$C_{12}H_{15}N_3O_4SZn$	$C_{12}H_{17}N_3O_5SZn$	$C_{14}H_{25}N_3O_4SZn$	$C_{12}H_{19}N_3O_6SZn$	$C_{13}H_{17}N_3O_4SZn$	$C_{24}H_{46}N_{12}O_8S_4Zn$
M_r	491.86	463.88	362.70	380.72	396.80	398.73	376.73	824.34
T / K	170(2)	293(2)	150(2)	293(2)	100(2)	293(2)	150(2)	293(2)
Crystal size/mm	0.25 × 0.15 × 0.15	0.30 × 0.20 × 0.20	0.05 × 0.04 × 0.02	0.17 × 0.15 × 0.15	0.30 × 0.13 × 0.10	0.20 × 0.20 × 0.20	0.30 × 0.13 × 0.10	0.23 × 0.20 × 0.20
Crystal system	monoclinic	triclinic	orthorhombic	monoclinic	monoclinic	triclinic	monoclinic	triclinic
Space group	$P2_1/c$	$P\bar{1}$	$Pna2_1$	$P2_1/c$	$C2$	$P\bar{1}$	$P2_1/c$	$P\bar{1}$
a/ Å	9.6360(3)	8.122(1)	15.716(2)	8.488(1)	26.6250(4)	7.397(1)	9.6890(2)	9.623(2)
b/ Å	12.4200(4)	8.364(1)	11.792(2)	14.444(2)	7.5350(1)	9.384(1)	12.2920(3)	11.844(2)
c/ Å	9.8170(3)	16.247(6)	7.603(1)	13.675(2)	18.6840(4)	12.085(2)	13.2240(3)	17.848(5)
α/°	90	97.11(2)	90	90	90	98.90(1)	90	102.56(1)
β/°	118.4370(16)	101.98(1)	90	104.92(1)	103.7490(7)	90.80(2)	94.835(1)	102.69(1)
γ /°	90	103.200(9)	90	90	90	99.40(1)	90	92.467(10)
U/ Å	1033.13(6)	1034.0(4)	1409.0(3)	1620.0(4)	3640.97(11)	817.0(2)	1569.34(6)	1928.2(7)
Z	2	2	4	4	8	2	4	2
$d_{calcd.}$/g cm^{-3}	1.555	1.490	1.710	1.561	1.448	1.621	1.594	1.420
μ/mm^{-1}	1.442	1.423	1.910	1.670	1.485	1.664	1.718	0.912
θ_{min}, θ_{max}	2.91, 27.49	2.54, 24.97	2.10, 29.33	2.09, 24.98	3.59, 27.49	2.23, 24.98	3.59, 27.48	2.18, 24.97
Reflections collected	12570	4023	13734	3201	27784	3229	37834	7485
Independent reflections	2369	3618	3894	2840	8071	2857	3580	6764
R_{int}	0.0385	0.0117	0.1073	0.0167	0.0430	0.0119	0.0959	0.0095
No. parameters, restraints	144, 5	257, 6	189, 3	219, 0	447, 5	235, 6	210, 2	486, 8
Final R_1, wR_2 [$I > 2\sigma(I)$]	0.0287, 0.0955	0.0280, 0.0736	0.0667, 0.1473	0.0298, 0.0747	0.0375, 0.0842	0.0272, 0.0841	0.0332, 0.0893	0.0312, 0.0850
R_1, wR_2 (all data)	0.0368, 0.1056	0.0346, 0.0764	0.0852, 0.1530	0.0423, 0.0781	0.0468, 0.0884	0.0363, 0.0899	0.0476, 0.1018	0.0409, 0.0894

$C_{24}H_{46}N_{12}O_8S_4Zn$ (824.3): calcd. C 35.0, N 20.4, H 5.62; found C 34.7, N 20.1, H 5.59.

The syntheses of **2**–**7** were repeated on a smaller scale in more dilute solutions in order to obtain crystals of suitable quality for the single-crystal X-ray analyses.

For compounds **2**, **3b**, **5** and **7**, data were collected on an Enraf–Nonius CAD4 automatic four-circle diffractometer and for compounds **1**, **4** and **6** data were collected on a Nonius Kappa CCD diffractometer, in all cases using Mo-K_α radiation (graphite monochromated) with λ = 0.71069 Å for **2**, **3b**, **5** and **7** and 0.71070 Å for **1**, **4** and **6**. Due to small crystal size, data for compound **3a** were collected at Station 9.8 at the SRS, Daresbury using synchrotron radiation (silicon 111 monochromated) with λ = 0.68980 Å. Crystallographic data are presented in Table 6. Lorentz and polarisation corrections were applied in all analyses and extinction coefficients were applied for compounds **2**, **3a**, **3b** and **4**. Absorption corrections (SORTAV[17]) were applied to the data for **1**, **4** and **6**. The structures were solved by direct methods (SHELXS-86[18] or SHELXS-97) with full-matrix least-squares (SHELXL-97[19]) refinement based on F^2. Non-hydrogen atoms were treated anisotropically. Hydrogen atoms were refined in calculated positions where relevant on carbon atoms, whereas the NH and OH hydrogen atoms were located and refined at a fixed distance of 0.89 Å from the parent atom throughout. CCDC 191738–191745 contain the supplementary crystallographic data for this paper. These data can be obtained free of charge at www.ccdc.cam.ac.uk/conts/retrieving.html [or from the Cambridge Crystallographic Data Centre, 12 Union Road, Cambridge CB2 1EZ, UK; fax: (internat.) +44–1223/336–033; Email: deposit@ccdc.cam.ac.uk].

Acknowledgments

The EPSRC is thanked for financial support.

[1] V. R. Thalladi, B. S. Goud, V. J. Hoy, F. H. Allen, J. A. K. Howard, G. R. Desiraju, *Chem. Commun.* **1996**, 401–402.
[2] R. Robson, *J. Chem. Soc., Dalton Trans.* **2000**, 3735–3744; B. Moulton, M. J. Zaworotko, *Chem. Rev.* **2001**, *101*, 1629–1658; A. J. Blake, N. R. Champness, P. Hubberstey, W. S. Li, M. A. Withersby, M. Schröder, *Coord. Chem. Rev.* **1999**, *183*, 117–138; M. Eddaoudi, D. B. Moler, H. Li, B. Chen, T. M. Reineke, M. O′Keeffe, O. M. Yaghi, *Acc. Chem. Res.* **2001**, *34*, 319–330; O. R. Evans, W. Lin, *Chem. Mater.* **2001**, *13*, 2705–2712; M.-L. Tong, S.-L. Zheng, X.-M. Chen, *Chem. Commun.* **1999**, 561–562.
[3] V. A. Russell, C. C. Evans, W. Li, M. D. Ward, *Science* **1997**, *276*, 575–579; D. G. Kurth, K. M. Fromm, J.-M. Lehn, *Eur. J. Inorg. Chem.* **2001**, 1523–1526; D. Braga, L. Maini, F. Paganelli, E. Tagliavini, S. Casolari, F. Grepioni, *J. Organomet. Chem.* **2001**, *637*, 609–615; S. B. Copp, K. T. Holman, J. O. S. Sangster, S. Subramanian, M. J. Zaworotko, *J. Chem. Soc., Dalton Trans.* **1995**, 2233–2243; A. D. Burrows, C.-W. Chan, M. M. Chowdhry, J. E. McGrady, D. M. P. Mingos, *Chem. Soc. Rev.* **1995**, *24*, 329–339; G. R. Desiraju, *Chem. Commun.* **1997**, 1475–1482.
[4] C. B. Aakeröy, A. M. Beatty, K. R. Lorimer, *J. Chem. Soc., Dalton Trans.* **2000**, 3869–3872; T. J. Prior, M. J. Rosseinsky, *Chem. Commun.* **2001**, 1222–1223.
[5] A. D. Burrows, S. Menzer, D. M. P. Mingos, A. J. P. White, D. J. Williams, *J. Chem. Soc., Dalton Trans.* **1997**, 4237–4240.
[6] A. D. Burrows, R. W. Harrington, M. F. Mahon, C. E. Price, *J. Chem. Soc., Dalton Trans.* **2000**, 3845–3854.
[7] A. D. Burrows, D. M. P. Mingos, A. J. P. White, D. J. Williams, *Chem. Commun.* **1996**, 97–99; M. T. Allen, A. D. Burrows, M. F. Mahon, *J. Chem. Soc., Dalton Trans.* **1999**, 215–221.
[8] A. D. Burrows, M. D. Coleman, M. F. Mahon, *Polyhedron* **1999**, *18*, 2665–2671.
[9] A. W. Addison, T. N. Rao, J. Reedijk, J. van Rijn, G. C. Verschoor, *J. Chem. Soc., Dalton Trans.* **1984**, 1349–1356.
[10] J. Bernstein, R. E. Davis, L. Shimoni, N.-L. Chang, *Angew. Chem. Int. Ed. Engl.* **1995**, *34*, 1555–1573, *Angew. Chem.* **1995**, *107*, 1687–1706.

[11] A. D. Burrows, R. W. Harrington, M. F. Mahon, *CrystEngComm* **2000**, 12.
[12] V. Y. Kauss, É. É. Liepin'sh, I. Y. Kalvin'sh, É. Lukevits, *Chem. Heterocycl. Compd.* **1990**, 103.
[13] M. Eddaoudi, J. Kim, D. Vodak, A. Sudik, J. Wachter, M. O'Keeffe, O. M. Yaghi, *Proc. Natl. Acad. Sci. USA* **2002**, *99*, 4900−4904.
[14] F. H. Allen, O. Kennard, *Chem. Des. Automat. News* **1993**, *8*, 31−37.
[15] F. A. Cotton, C. Lin, C. A. Murillo, *Inorg. Chem.* **2001**, *40*, 472−477.
[16] K. A. Jensen, U. Anthoni, B. Kägi, C. Larsen, C. T. Pedersen, *Acta Chem. Scand.* **1968**, *22*, 1.
[17] R. H. Blessing, *Acta Crystallogr., Sect. A* **1995**, *51*, 33−38; R. H. Blessing, *J. Appl. Crystallogr.* **1997**, *30*, 421−426.
[18] G. M. Sheldrick, *Acta Crystallogr., Sect. A* **1990**, *46*, 467−473.
[19] G. M. Sheldrick, *SHELXL-97, Computer Program for Crystal Structure Refinement*, University of Göttingen, **1997**.

Received August 15, 2002
[I02462]

EurJIC
European Journal of Inorganic Chemistry

March 2003
Issue 5
Pages 777–1012

Papers available ahead of print in Early View at www.interscience.wiley.com

Earliest available Table of Contents:
Automatically, free of charge by e-mail through
www.interscience.wiley.com/alerts

COVER PICTURE

The cover picture shows yellow crystals and red melt of tellurium(II) dimethanethiolate, $Te(SCH_3)_2$, together with its molecular structure in the solid state and the light-induced deposition of elemental tellurium on glass, from a solution of $Te(SCH_3)_2$. In the solid state, $Te(SCH_3)_2$ exhibits a *cis* conformation of the methyl groups with respect to the TeS_2 plane, an unprecedented case for nonfunctionalized organotrichalcogenides. For $Te(SR)_2$ (R = Me, Et, *i*Pr, *t*Bu) Te–S bonding and Te···S intermolecular distances are correlated, as are ^{125}Te NMR chemical shifts and the ionization energies of the corresponding thiols. Results are rationalized in terms of σ- and π-type $n_p(S)$-σ*(Te–S) orbital interactions. Details are presented in the article by H. Fleischer et al. on p. 815ff.

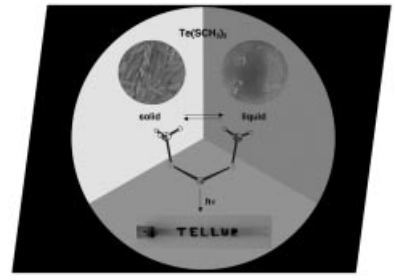

MICROREVIEW

Contents

791 **R. Kempe**

The Strained η^2-N_{Amido}–$N_{Pyridine}$ Coordination of Aminopyridinato Ligands

Keywords: N ligands / Catalysis / Coordination modes / Lanthanides / Transition metals

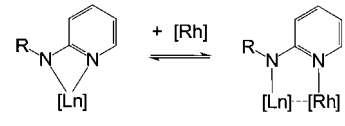

 © 2003 WILEY-VCH Verlag GmbH & Co. KGaA, 69451 Weinheim 1434–1948/03/0305–0781 $ 20.00+.50/0

SHORT COMMUNICATIONS

805 **D. Armspach,* D. Matt,* F. Peruch,* P. Lutz***

Cyclodextrin-Encapsulated Iron Catalysts for the Polymerization of Ethylene

Keywords: Cyclodextrins / Polymerization / Iron / N ligands / Cavitands

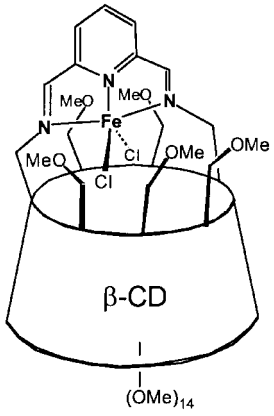

810 **J.-F. Li, S.-P. Huang,* L.-H. Weng, D.-S. Liu***

Ti^{IV} Complexes with Novel, Chiral, Tridentate Amido-Amidinate or Monoanionic, Didentate Amidinate Ligands

Keywords: Titanium / N ligands / Coordination modes / Rearrangement / Elimination

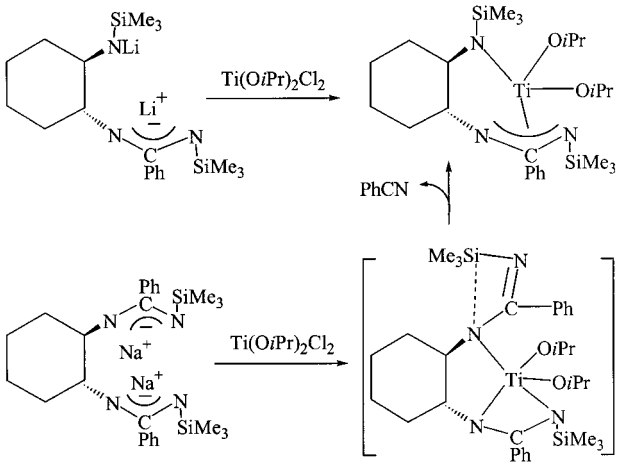

FULL PAPERS

815 **H. Fleischer,* N. W. Mitzel, D. Schollmeyer**

Tellurium(II) Dialkanethiolates: $n_p(S)$-σ*(Te−S′) Orbital Interactions Determine the ^{125}Te NMR Chemical Shift, and the Molecular and Crystal Structure

Keywords: NMR spectroscopy / Noncovalent interactions / Solid-state structures / Sulfur / Tellurium

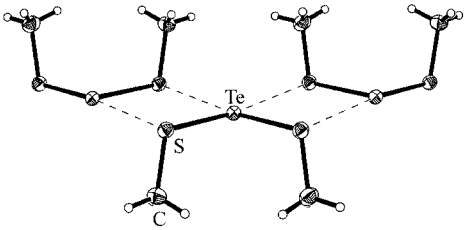

822 **R. W. Saalfrank,* B. Demleitner, H. Glaser, H. Maid, S. Reihs, W. Bauer, M. Maluenga, F. Hampel, M. Teichert, H. Krautscheid**

Synthesis of Tetrahemispheraplexes with Ammonium, Alkylammonium or Alkaline Metal Ions as Exohedral Guests via Self-Assembly or Guest Exchange

Keywords: Cage compounds / Supramolecular chemistry / Magnesium / Host-guest chemistry

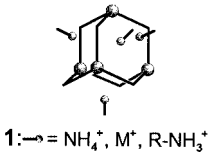

830 **H. P. Dijkstra, M. Q. Slagt, A. McDonald, C. A. Kruithof, R. Kreiter, A. M. Mills, M. Lutz, A. L. Spek, W. Klopper, G. P. M. van Klink, G. van Koten***

para-Functionalized NCN-Pincer Palladium(II) Complexes: Synthesis, Catalysis and DFT Calculations

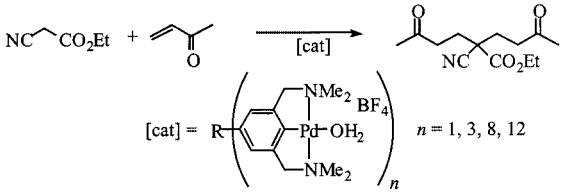

Keywords: Density functional calculations / Homogeneous catalysis / Substituent effects / Supported catalysts / Synthesis design

839 **M. P. Feth,* A. Klein,* H. Bertagnolli**

Investigation of the Ligand Exchange Behavior of Square-Planar Nickel(II) Complexes by X-ray Absorption Spectroscopy and X-ray Diffraction

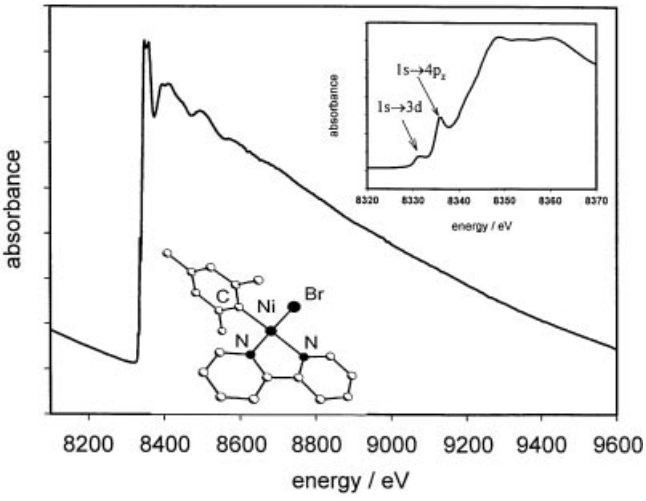

Keywords: Nickel / Ligand exchange / EXAFS spectroscopy / XANES / X-ray diffraction

853 **H.-F. Klein,* R. Beck, U. Flörke, H.-J. Haupt**

Regiospecific Cyclometalation of Diphenyl(2-substituted phenyl)phosphane with Methyltetrakis(trimethylphosphane)cobalt(I)

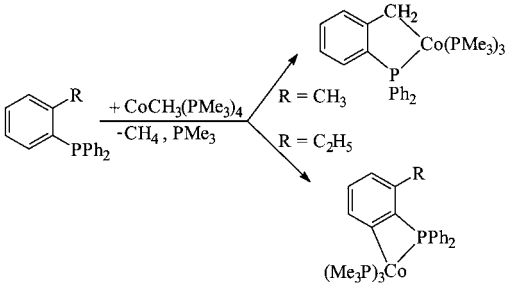

Keywords: Orthometalation / Cobalt / Coordination chemistry / Structure elucidation / Steric control

863 **S. Mukherjee, T. Weyhermüller, E. Bothe, K. Wieghardt, P. Chaudhuri***

Single-Atom *O*-Bridged Urea in a Dinickel(II) Complex together with Ni^{II}_4, Cu^{II}_2 and Cu^{II}_4 Complexes of a Pentadentate Phenol-Containing Schiff Base with (O,N,O,N,O)-Donor Atoms

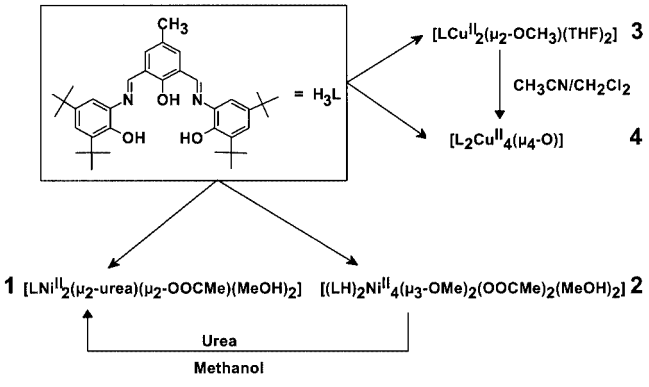

Keywords: N,O ligands / Nickel / Copper / Magnetic properties / Radicals / Electrochemistry

876 **S. Hartmann, R. F. Winter,* B. M. Brunner, B. Sarkar, A. Knödler, I. Hartenbach**

(Allenylidene)ruthenium Complexes with Redox-Active Substituents and Ligands

Keywords: Electrochemistry / Sandwich complexes / Ruthenium / Spectroelectrochemistry

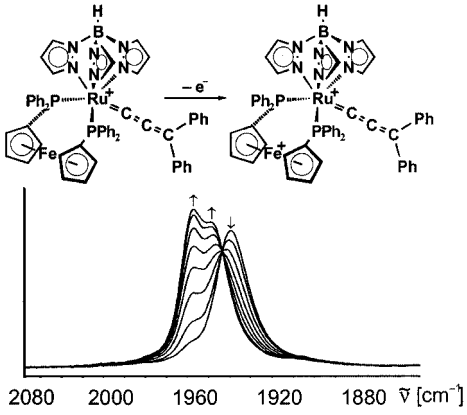

892 **L. Cavallo, H. Jacobsen***

Manganese-Salen Complexes as Oxygen-Transfer Agents in Catalytic Epoxidations − A Density Functional Study of Mechanistic Aspects

Keywords: Density functional calculations / Epoxidation / Manganese / N,O ligands / Radicals

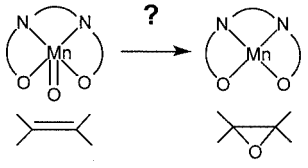

903 **D. Sellmann,* K. P. Peters, R. M. Molina, F. W. Heinemann**

A Dinuclear Iron Complex with Two Cofacial [FeS_4] Cores Linked by Covalent Ligand Periphery Clamps and Dissociable Thiolate Bridges

Keywords: Iron / S ligands / Bridging ligands / Enzyme models

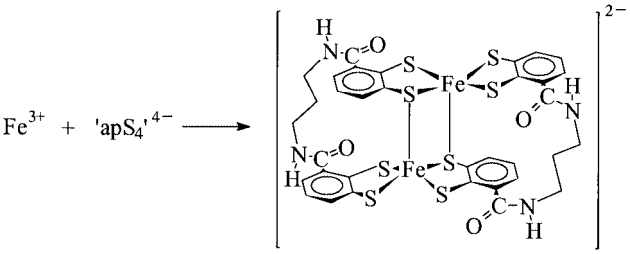

908 **M. Vennat, P. Herson, J.-M. Brégeault,* G. B. Shul'pin**

Vanadium-Catalysed Aerobic Cleavage of C−C Bonds in Substituted Cyclohexanones To Afford Carboxylic Acids: Two Model Complexes with Tetrahedral Geometry around Vanadium(V)

Keywords: Catalysis / Oxidation / Dioxygen / Oxo ligands / Vanadium

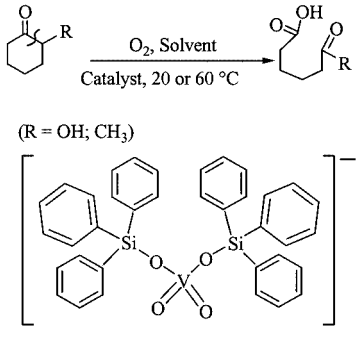

918 **P. Bergamini,* V. Bertolasi, M. Cattabriga, V. Ferretti, U. Loprieno, N. Mantovani, L. Marvelli**

Template Synthesis of Chiral Vicinal Diphosphinites as Their Pt^{II} and Pd^{II} Complexes

Keywords: Template synthesis / Ligand design / P ligands / Platinum / Palladium

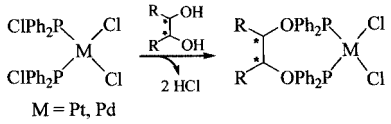

926 **A. T. Trifonov, T. P. Spaniol, J. Okuda***

Di- and Trivalent Ytterbium Complexes Containing Linked Amino- and Amidocyclopentadienyl Ligands

Keywords: Ytterbium / Chelates / Metallocenes / Cyclopentadienyl ligands

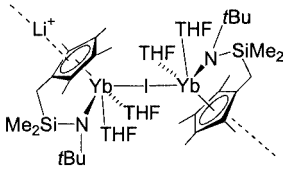

936 **T. Meyer-Friedrichsen, H. Wong, M. H. Prosenc, J. Heck***

Vinylogue Mono- and Bimetallic Cationic Sesquifulvalene and Monohydro Sesquifulvalene Complexes for Second Harmonic Generation

Keywords: Sesquifulvalene / Ruthenium / X-ray structure determination / Hyper-Rayleigh Scattering (HRS) / Second harmonic generation (SHG)

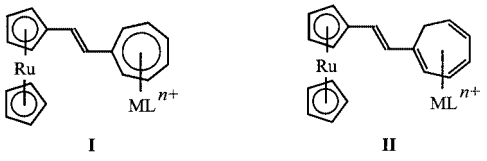

947 **W. Huang, S. Gou,* H. Qian, D. Hu, S. Chantrapromma, H.-K. Fun, Q. Meng**

Macrocyclic, Dinuclear Zinc(II)-Directed Self-Assembly with Pyridine, 2,2′-Bipyridine and 2-Methylquinoline: μ^2-OH Bridging Bi-Macrocyclic Complexes and Hydrogen-Bond-Supported Donor-Acceptor Complexes

Keywords: N,O ligands / Macrocycles / Zinc / Self-assembly / Structure elucidation / Hydrogen bonds

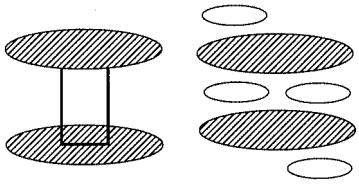

955 **A. Harriman,* M. Hissler, A. Khatyr, R. Ziessel**

The Photophysical Properties of Hybrid Metal Complexes Containing both 2,2′-Bipyridine and 2,2′:6′,2′′-Terpyridine Units

Keywords: Luminescence / Photophysics / Molecular electronics / Energy transfer

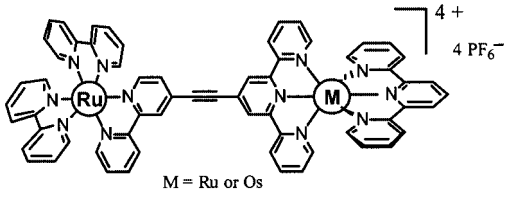

960 **A. Maraval, K. Owsianik, D. Arquier, A. Igau,* Y. Coppel, B. Donnadieu, M. Zablocka, J.-P. Majoral***

Dynamic Behavior of an *N*-Metalated β-Enaminoimine Complex − Preparation of *N*-Phosphanylenamine and β-Enaminoimine Derivatives

Keywords: N ligands / NMR spectroscopy / Imines / Zirconium / Metallocenes / Transmetalation

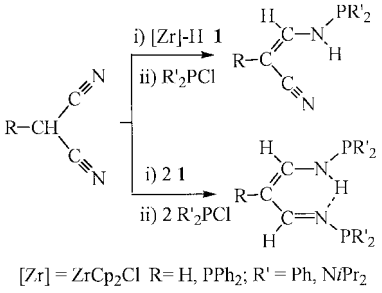

969 **G. K. Patra, I. Goldberg***

Syntheses and Crystal Structures of Copper and Silver Complexes with New Imine Ligands − Air-Stable, Photoluminescent $Cu^{I}N_4$ Chromophores

Keywords: N ligands / Copper / Silver / Luminescence / Electrochemistry

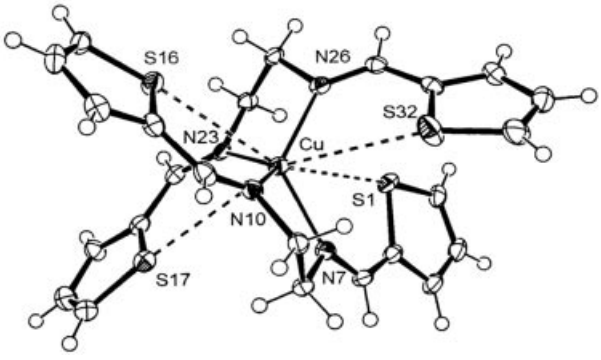

978 **V. M. Ugalde-Saldivar, M. E. Sosa-Torres, I. González***

The Reactivity of an Iron(II)/Iron(III) System with Polyamine Ligands in Ethanol: An Electrochemical Study

Keywords: Iron / N ligands / Electrochemistry / Oxidative dehydrogenation / Disproportionation

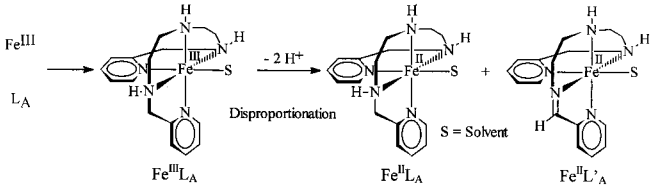

988 **C. S. Campos-Fernández, J. R. Galán-Mascarós,* B. W. Smucker, K. R. Dunbar***

Synthesis, X-ray Studies and Magnetic Properties of Dinuclear Ni^{II} and Cu^{II} Complexes Bridged by the Azo-2,2′-bipyridine Ligand

Keywords: Magnetic properties / Azo compounds / Nickel / Copper

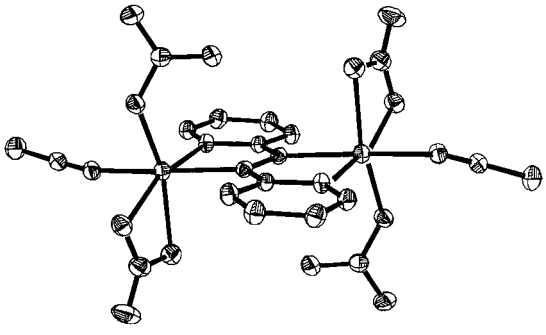

995 **P. Paredes, D. Miguel, F. Villafañe***

Synthesis of (η^3-Allyl)bromodicarbonylbis(pyrazole)molybdenum(II) and Reactivity towards [Au(acac)PPh_3]: Structure and Dynamic Behavior of the Monometallic Pyrazole and Heterometallic Pyrazolate Complexes

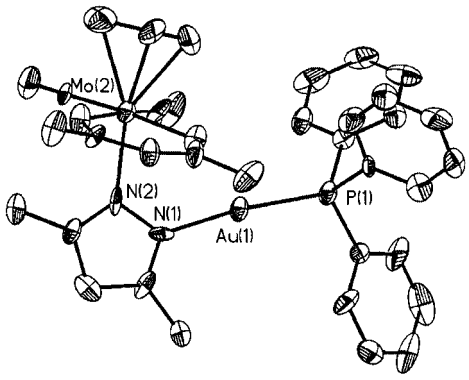

Keywords: Molybdenum / Gold / Heterometallic complexes / N ligands / Fluxionality

1005 **T. K. Maji, G. Mostafa, J. M. Clemente-Juan, J. Ribas,* F. Lloret, K. Okamoto, N. Ray Chaudhuri***

Synthesis, Crystal Structure and Magneto-Structural Correlation of an Unusual Thiocyanato-bridged Nickel(II) Compound, [Ni(μ-NCS)-(dpt)(NCS)]$_2$[Ni(μ-NCS)(dpt)(NCS)]$_4$ [dpt = bis(3-aminopropyl)amine]

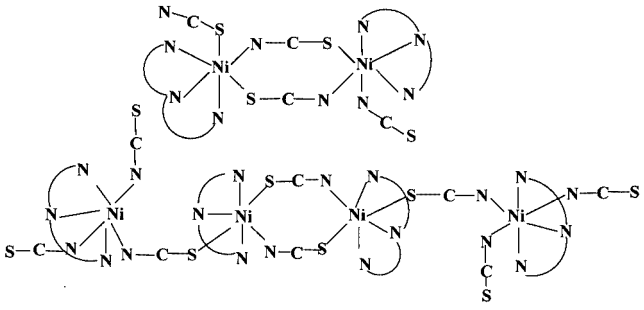

Keywords: Nickel / Bridging ligands / S ligands / Magnetic properties / N ligands

The Strained η^2-N_{Amido}−$N_{Pyridine}$ Coordination of Aminopyridinato Ligands

Rhett Kempe*[a,b][‡]

Dedicated to Prof. Dr. Uwe Rosenthal

Keywords: N ligands / Catalysis / Coordination modes / Lanthanides / Transition metals

This review gives an account of the syntheses and structures of group-3 (including lanthanides), -4 and -5 metal complexes stabilised by strained η^2-coordinated aminopyridinato ligands. Reactivity studies and catalytic applications of the coordination compounds are discussed.

(© Wiley-VCH Verlag GmbH & Co. KGaA, 69451 Weinheim, Germany, 2003)

Introduction

General Remarks

Considerable efforts are being expended in organometallic chemistry on modifying the reactivity of metal−carbon bonds through choice of appropriate coligands. The information thus obtained is now being extensively used in, for example, homogeneous catalysis.[1] Coligands such as the cyclopentadienyl (Cp) fragment and phosphanes (Scheme 1) have hitherto played the dominant role as anionic and neutral donor functions, respectively.[2]

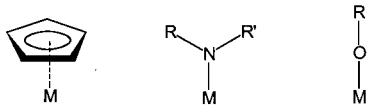

Scheme 1. The three most important ligand types for the stabilisation of early transition metal ions in medium to high oxidation states (R, R′ = alkyl, aryl or silyl)

In addition to these classic examples for the control of complex reactivity, exhaustive efforts over the last decade have been devoted to the development of novel ligands. As well as Cp ligands (Scheme 1, left), alkoxy (right) and amido ligands[3] (centre) have proven to be suitable for the stabilisation of early, electron-poor transition metal ions in medium to high oxidation states. Of these two alternatives, the amido ligand is especially interesting since it offers a

[a] Fachbereich Chemie, University of Oldenburg,
P. O. Box 2503, 26111 Oldenburg, Germany
E-mail: kempe@uni-oldenburg.de
[b] Institut für Organische Katalyseforschung Rostock,
Buchbinderstraße 5−6, 18055 Rostock, Germany
[‡] New address: Lehrstuhl für Anorganische Chemie II,
Universität Bayreuth,
95440 Bayreuth, Germany
E-mail: kempe@uni-bayreuth.de

Rhett Kempe was born in Dresden in 1964. He studied chemistry at the Universität Leipzig including research stays in Jena (Prof. D. Walther) and Stuttgart (Prof. H.-G. von Schnering) and received his PhD degree (organonickel chemistry) under the supervision of Prof. J. Sieler (1989). During a DAAD postdoctoral research fellowship at MIT (1992/1993) with Prof. R. R. Schrock he became interested in N_2 activation. After a period at the MPI für Kohlenforschung in Mülheim (1993/1994) he began to study for his habilitation in the Max-Planck-Gesellschaft Group "Complex Catalysis" led by Prof. U. Rosenthal. The habilitation (metal−amido chemistry) followed at the Universität Rostock in 1998. He worked as a group leader in the Institut für Organische Katalyseforschung Rostock (IfOK) for two years and moved in 2000/2001 as a visiting scientist to the University of Melbourne (Prof. R. Robson's group). He became a Professor of Inorganic Chemistry at the University of Oldenburg in 2001 and was appointed to a Chair of Inorganic Chemistry at the University of Bayreuth in 2002. His research interests include the development of novel catalyst systems and he is working at the interface between coordination chemistry and homogeneous catalysis. He is an author of more than 170 publications and was awarded the Karl-Winnacker-Stipendium (1998) and the Heisenberg-Stipendium (2000).

MICROREVIEWS: This feature introduces the readers to the authors' research through a concise overview of the selected topic. Reference to important work from others in the field is included.

greater variety in ligand and complex design because of the possibility for double substitution at the donor atom.

The foundations of amido transition metal chemistry were laid in the 1960s and 1970s and are associated with names such as Bürger, Wannagat, Bradley, and Lappert. The motivation for these investigations was mainly the exploration of the reactivity of metal−amido bonds in comparison to the metal−carbon bond. Disappointingly, the metal−amido bond is kinetically inert and thermodynamically more stable than the corresponding metal−carbon bond, and thus synthetically far less interesting. Today in metal−amido chemistry the stable metal−amido bond is exploited to produce well-defined reaction centres in transition metal complexes. In this way the reactivity of the resulting compounds can be specifically tailored.[4]

Aminopyridinato ligands (Scheme 2) are an important class of amido ligands and are derived from deprotonated 2-aminopyridines.[5]

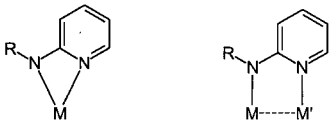

Scheme 2. Binding modes of aminopyridinato ligands (R = alkyl, aryl or silyl; M = transition metal, M′ = late transition metal)

They are interesting due to the flexibility of their binding modes. This microreview encompasses the early transition metal coordination chemistry of aminopyridinato ligands as well as the reactivity of their complexes.

Di- and Multimetallic Compounds

In addition to early transition metal coordination chemistry, deprotonated 2-aminopyridine ligands have been used to stabilise di- and multimetallic compounds (Scheme 3).[6]

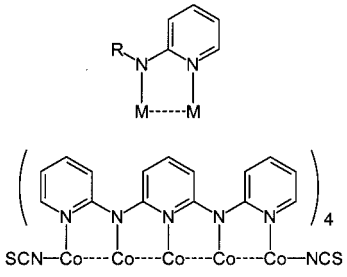

Scheme 3. Dimetallic complexes (top) and an example of a multinuclear cobalt compound (bottom) stabilised by deprotonated 2-aminopyridine ligands (R = H, alkyl or aryl; M = Ag, Cd, Co, Cr, Cu, Ir, Mo, Ni, Os, Pd, Pt, Rh, Ru, W and Zn)

Such complexes have been extensively described for Co,[7] Cr,[8] Cu,[7a,7b,9], Mo,[8a,10] Ni,[7e,9b,11] Rh,[12] and Ru[12i,13] and are known for Ag,[9e,9i,14] Cd,[15] Ir,[16] Os,[17] Pd,[18] Pt,[18] W,[8a,10d,19] and Zn.[9e,20]

Cluster Chemistry

The syntheses and reactivities of Ru[21] and Os[22] cluster compounds coordinated by deprotonated 2-aminopyridines (Scheme 4) have been reported.

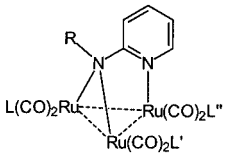

Scheme 4. Examples of cluster compounds stabilised by deprotonated 2-aminopyridines (R = H, alkyl or aryl, L, L′, L′′ = additional ligand, for instance CO, PPh_3 or alkyne)

Main-Group Metal Complexes

The structural variety of aminopyridinato main-group metal complexes[23,60] makes their coordination chemistry a fascinating field and must be mentioned in any discussion of such ligands. This chemistry, as well as that of the multimetallic and cluster compounds, are not reviewed in this article.

Early Work and Contributions to the Renaissance of (Amido)metal Chemistry

The first strained η^2-coordinated aminopyridinato complex (Scheme 2, left) was published by Cotton et al.,[24] and only a few compounds[9e,25,26] had been investigated prior to 1996. The first early transition metal complex, a vanadium compound, was published by Gambarotta et al. in 1991.[26] Four years later, aminopyridinato ligands started to become extensively used to stabilise early transition metal ions in medium or high oxidation states. These studies can be seen in the context of the renaissance of metal−amido chemistry[4] which was initiated by the search for alternatives to the well-known Cp ligands. An interest in these systems soon grew due to the unique chemistry of these ligands, which is mainly a result of the close proximity of the amido and pyridine functions. In addition, these ligands may be easily derivatised to fine-tune metal complex reactivity.

Lanthanide Chemistry Including Sc and Y

The steric bulk of aminopyridinato ligands is rather small in comparison to the related cyclopentadienyl ligands[27] and the closely related silyl-substituted amidinates.[28,29] Therefore the chemistry of aminopyridinato ligands differs dramatically from these two types in cases such as group-3 or lanthanide chemistry where steric bulk is important for the stabilisation of reactive transition metal complexes.[30]

Simple Aminopyridinato Ligands and Their Transfer Reactions

The reactions of deprotonated aminopyridines such as **1** (Scheme 5) with lanthanide trihalides gave the ate complexes such as **2**.[31] Monochloro compounds were formed

if 2 equiv. of cyclopentadienyl ligands[32] or silyl-substituted amidinates[33,28,29] were used instead of **1**.

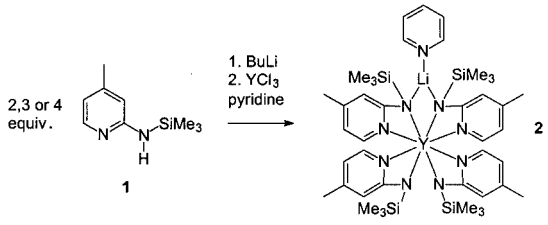

Scheme 5. Synthesis of extensively N-coordinated ate complexes

Compound **2** can be considered as a sterically demanding lithium amide and was thus expected to react with transition metal chlorides. The reaction with $ZrCl_4$ and [(cod)$PdCl_2$] (COD = 1,5-cyclooctadiene) afforded the aminopyridinato complexes **4** and **5**, respectively (Scheme 6). The isolation of **3**, a Y−Zr dimetallic complex, indicates that such reactions proceed via heterodimetallic intermediates. Complex **5** is a rare example of a homoleptic (amido)-palladium compound.[34] In addition to the ligand transfer method, **5** was also synthesised by a salt elimination reaction at low temperature in THF (THF = tetrahydrofuran).[31] Since lanthanide ate complexes react with late metal chlorides, such salt metathesis reactions might be the key to the synthesis of heterodimetallic compounds combining lanthanides and group-8 to -10 metals. The ligand transfer reaction must be avoided in order to stabilise intermediates such as **3**.

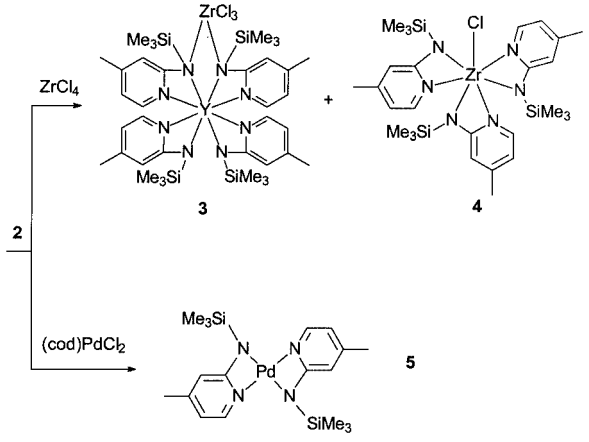

Scheme 6. Ligand transfer reactions

Bis(aminopyridinato) Ligand Complexes

Some of the limitations of simple aminopyridinato ligands can be overcome by using bis(aminopyridinato) ligands such as deprotonated **6**.

Reaction of bis(lithiated) **6** (generated in situ) with $LnCl_3$ gave different products depending on the size of the lanthanide ion. For Ln = Y and Sm, the monochloro complexes **7** and **8** were formed (Scheme 7). These could be further functionalised with $LiCH(SiMe_3)_2$, $(C_4H_9)_4NBH_4$ and $NaBH_4$ to give the corresponding bis[$CH(SiMe_3)_2$] and bis(BH_4) ate complexes.[35] Similar reactions as used to synthesise **7** and **8** afforded **9** and **10** for the larger Nd and La ions (Scheme 7). The aminopyridinato ate complex **10** was investigated as an initiator in the ring opening polymerisation of ε-caprolactone and δ-valerolactone, with particular interest focusing on the relationship between the monomer/initiator ratio and the molecular weight of the polyester, as well as the production of high molecular weight products. In both cases an almost linear relationship between the monomer/initiator ratio and the molecular weight was observed.[35] The high efficiency of the system was shown by carrying out the polymerisation in neat ε-caprolactone at room temperature. A solid polyester block (300000 g/mol, M_w/M_n = 2.3) was formed after 3 min. Ring-opening polymerisation of lactones is a useful method to produce biodegradable aliphatic polyesters,[36] and well-defined polymers of this type have possible applications as surgical sutures and in drug delivery systems.[37] The production of polymers with a well-defined molecular weight as well as a narrow molecular weight distribution is needed for such applications, since the polymer decomposition process depends on the length of the polymer chains.

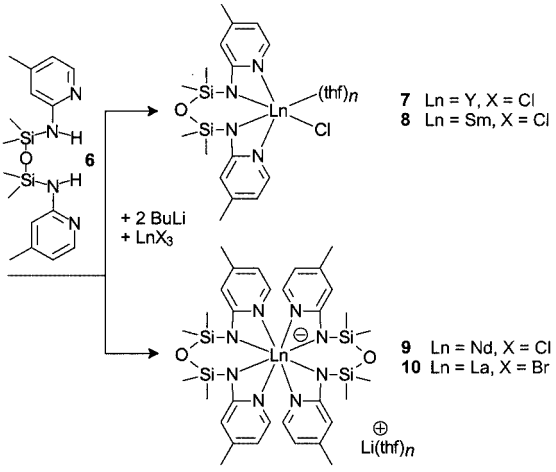

Scheme 7. Synthesis of bis(aminopyridinato) complexes

The reaction of **9** with [(cod)$RhCl]_2$ and $[(C_2H_4)_2RhCl]_2$ gave rise to the dimetallic compounds **11** and **12**, respectively (Scheme 8).[38] Both compounds are rare examples of early late heterobimetallics (ELHB) in which lanthanides and group-9 metals are combined. Investigations of the nature of the interactions between the two metals are underway.[39] The very short distance between Nd and Rh in **12** is consistent with a direct metal−metal bond, the only other example being the Lu−Ru bond in $[Cp_2(THF)Lu-RuCp(CO)_2]$ [2.955(2) Å].[40]

The reaction of **9** or **10** with [(dme)$NiCl_2$] and [(cod)$PtCl_2$] (DME = dimethoxyethane) gave the dimeric nickel complex **13** and a mononuclear platinum complex **14** (Scheme 9).[41] Both compounds are rare examples of late metal amido complexes.

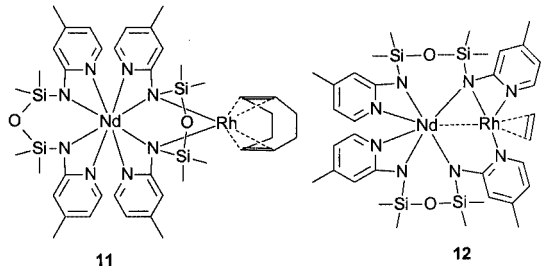

Scheme 8. Nd−Rh dimetallic complexes; Nd−Rh distances are 3.2283(15) Å for **11** and 2.9744(15) Å for **12**

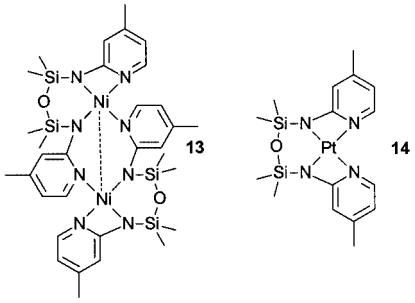

Scheme 9. Synthesis of **13** and **14** by ligand transfer

The mechanism shown in Scheme 10 was proposed for the synthesis of **14**. The neodymium ate complex **9** reacts with [(cod)$PtCl_2$] and the heterodimetallic intermediate **17** is formed. Transient **17** decomposes to give **14** and **15**. In addition to **14**, the monochloro complex **15** and LiCl were also isolated as by-products.

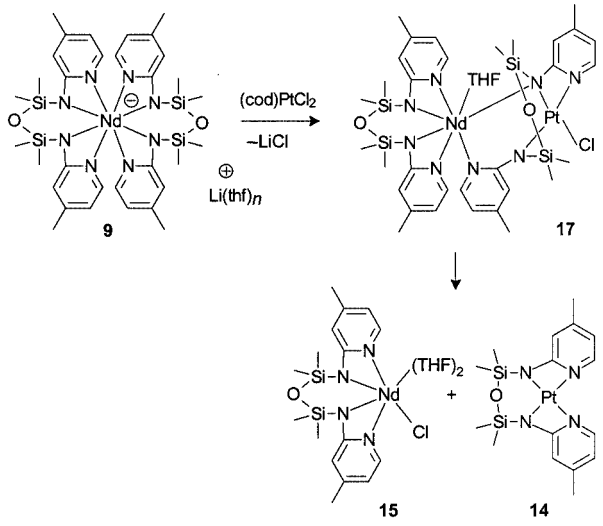

Scheme 10. Proposed mechanism for the formation of **14**

The reaction of **9** with [(cod)PdClMe][42] afforded the dimetallic compound **18** which can be considered as a model compound for the intermediate **17**. If **9** or **10** were treated with [(cod)$PdCl_2$] the formation of Pd black was observed. Ligand transfer also gave the tetrameric copper complex **19** (Scheme 11).

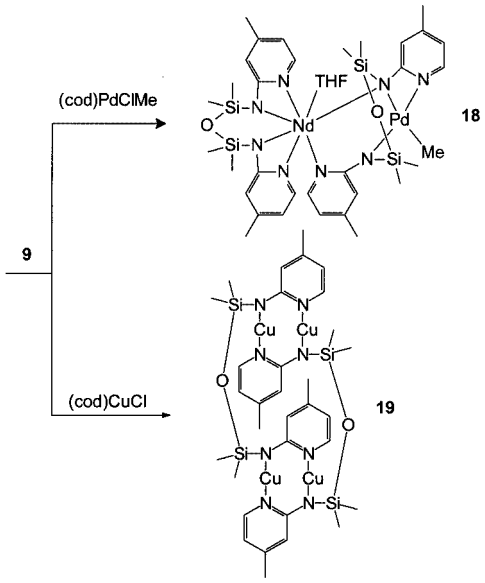

Scheme 11. Synthesis of **18** and **19**

The compounds **13**, **14** and **19** are rare examples of group-10 and -11 amido complexes.[43,44] Activation of **13** with $EtAlCl_2$ (Al/Ni = 150) in hexane at room temperature generated an efficient ethylene oligomerisation catalyst. The obtained oligoethylenes contained mainly internal double bonds (Schulz−Flory distribution, TOF = 2400 h^{-1}). When $Et_3Al_2Cl_3$ was used as a co-catalyst and CH_2Cl_2 as the solvent, highly branched oligomers with a very narrow molecular weight distribution [M_n = 230 g/mol (relative to polystyrene standards), M_w/M_n = 1.14] were produced. According to NMR investigations, the oligomers are identical with results recently published by Sen et al. The catalyst system based on **13** has significantly higher activity.[45]

The ligand transfer reactions that led to **5**, **13**, **14** and **19** can be explained in terms of modification of the reactivity of the corresponding lithium amides by coordination at the lanthanide centres. Thus, the reduction potential is lowered but the lithium amides are still active enough to react with transition metal chlorides. Unstable Ln−Ni, Ln−Pt and Ln−Cu heterodimetallic complexes can be assumed as intermediates in the ligand transfer reactions. These intermediates are important for the formation of the polycyclic and multinuclear structures of the resulting complexes such as **13** and **19**.

Bis(aminopyridinato) ligands are useful to prepare heterodimetallic compounds with metal−metal distances smaller then 3 Å. The nature of possible interactions between the lanthanides and the group-9 or -10 metals is not yet clear. Unfortunately, the synthesis of ate complexes using deprotonated **6** is limited to larger Ln ions, and the ligand transfer could only be avoided for selected examples of group-9 and -10 metals. Ligand variations might be the key to overcome these restrictions, as was shown by the recent use of (aminopyridinato)(Cp) ligands.[46]

Titanium, Zirconium and Hafnium

Titanium and Zirconium Complexes that Contain Alkyl-, Aryl- and Silyl-Substituted Ap (Ap = Aminopyridinato) Ligands

The exploration of group-4 metal coordination chemistry of selected aminopyridinato ligands began in 1996.[47,48] The investigators were interested in replacing Cp ligands with special amido-type ligands and studying the reactivities of the resulting complexes. It was emphasised that traditional synthesis protocols such as salt metathesis failed in the case of titanium. For instance, the lithiation of the preligand **20** with BuLi and subsequent reaction with $TiCl_4$ or $[TiCl_4(THF)_2]$ afforded **21** in only very low yield (Scheme 12).

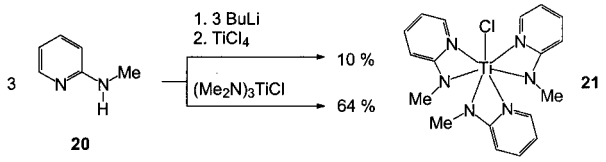

Scheme 12. Synthesis of **21** by salt metathesis and amine elimination

The poor yield was thought to be due to reduction of the titanium centre by the lithiated Ap ligands. Two solutions were found, namely "direct synthesis" (Scheme 13) and amine elimination (Scheme 12). Direct synthesis involves treatment of an alkyl- or aryl-substituted aminopyridine (for instance **22**) with $TiCl_4$ in either boiling toluene or without solvent at temperatures above 100 °C.

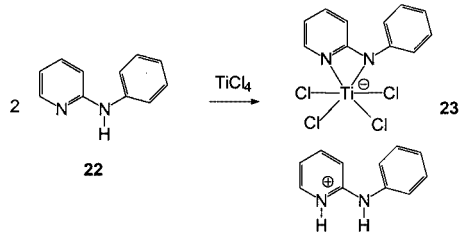

Scheme 13. "Direct synthesis": reaction of an aminopyridine with $TiCl_4$

Amine elimination has been useful for the synthesis of many titanium complexes. The reaction of **1**, **20** and **22** with $(Me_2N)_3TiCl$[49] or $(Me_2N)_2TiCl_2$ [49] afforded **21**, **24**, **25**, **26**[48] and **27**.[50] Reaction of **20** with $(Me_2N)_4Ti$ gave **28**.[51]

Compound **27** showed very high[52] activities for the polymerisation of propene and 1-butene if activated with MAO, triisobutylaluminium/$B(C_6F_5)_3$ or ethylaluminium sesquichloride.[50] Remarkably the corresponding zirconium complex **30** (Scheme 15) was inactive. Compound **30** is accessible by amine elimination starting from $[(Et_2N)_2Zr(THF)_2Cl_2]$[53] and **29**.

The use of in situ-generated mixed (amido)(chloro)zirconium complexes instead of the well-defined starting material $(Et_2N)_2Zr(THF)_2Cl_2$ leads to by-products such as **31**.[54] Besides amine elimination and salt metathesis, "direct synthesis" has proven to be efficient for the synthesis of zirconium complexes. In situ lithiation of **1** and subsequent reaction with $ZrCl_4$ gave **32**.[55] The propeller-like arrangement of the three Ap ligands in **32** provides a sterically well-protected reactive pocket. This allows the stabilisation of a variety of alkyl-,[55] aryl-,[55,56] alkynyl-[55,57] and butadiynylzirconium[58] complexes (Scheme 16).

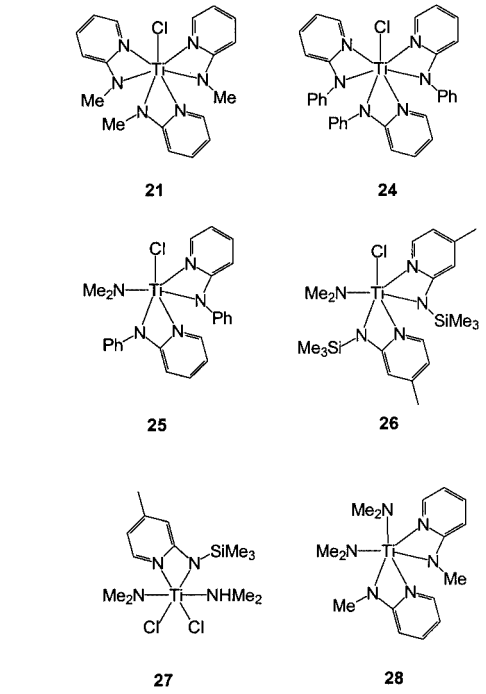

Scheme 14. Ap titanium complexes by amine elimination starting from $(Me_2N)_3TiCl$, $(Me_2N)_2TiCl_2$ and $(Me_2N)_4Ti$

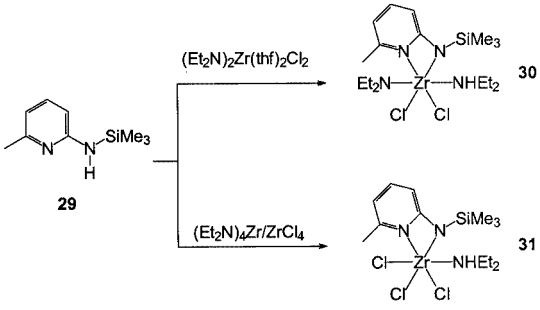

Scheme 15. Synthesis of **30** and **31**

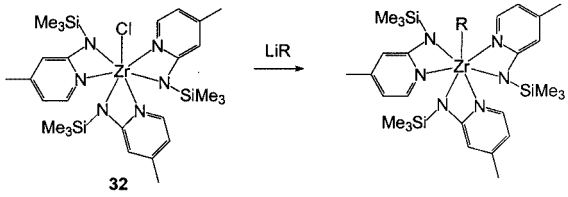

Scheme 16. Synthesis of alkyl-, aryl-, alkynyl- and butadiynylzirconium complexes [R = Me (**33**), Ph (**34**), C≡CPh (**35**), C≡CSiMe$_3$ (**36**), C≡CC≡CSiMe$_3$ (**37**)]

Better control of the zirconium/ligand stoichiometry and structures of bis(aminopyridinato) complexes is possible by introduction of sterically demanding alkyl substituents (e.g. adamantyl) on the ligands. Scott et al. reported the synthesis and structure of bis(Ap)zirconium complexes by salt metathesis, amine and alkyl elimination reactions (Scheme 17).[59]

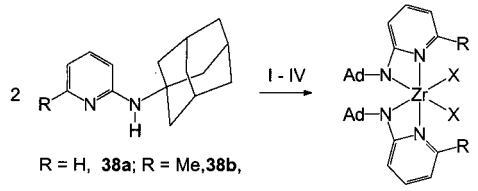

Scheme 17. Synthesis of bis(aminopyridinato)zirconium complexes [I: 2 BuLi, $ZrCl_4$; II: $(Me_2N)_4Zr$; III: $(PhCH_2)_4Zr$; IV: (*tert*-butyl$CH_2)_4Zr$; **39a/39b** R = H/Me, X = Cl; **40a/40b** R = H/Me, X = NMe_2; **41a/41b** R = H/Me, X = CH_2Ph; **42a/42b** R = H/Me, X = CH_2-*tert*-butyl]

The activation of **39a** with MAO afforded a catalyst that showed moderate[52] activity in ethylene polymerisation. A bis(aminopyridinato) complex of zirconium has been described previously. Polamo et al. reported the "direct synthesis" of **43** by treating **22** with $ZrCl_4$.[60] A similar reaction of **22** with $HfCl_4$ gave the homoleptic complex **4** (Scheme 18).[61] This work shows that the "direct synthesis" is not a consistent method and does not allow control of the metal/ligand stoichiometry.

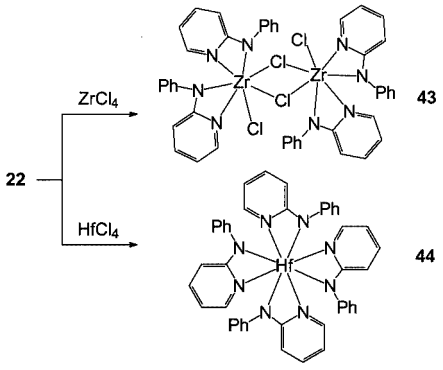

Scheme 18. Synthesis of **43** and **44**

Bis(aminopyridinato)titanium Complexes

As mentioned above (see group-3 and lanthanide chemistry) two aminopyridine moieties may be easily connected and this leads to better tuned reactive sites of the corresponding transition metal complexes. The reaction of the siloxane-bridged bis(aminopyridine) **6**, **45** and **46** with $(Me_2N)_3TiCl$ yielded mixed (amido)(chloro) complexes **47**−**49** (Scheme 19).[62]

Olefin polymerisation studies of **47**−**49** have been carried out. Activation of the complexes with MAO gave rise to low[52] activities in ethylene polymerisation and no activity was observed for higher olefins. Structural studies of the precatalysts showed planar coordination of the bis(aminopyridinato) ligands and the ligands thus "cut" the complexes into two parts. This results in a separation of the coordination site of the growing alkyl chain and the coordination site for olefins during the polymerisation process. Such a separation leads to a high insertion barrier and a correspondingly slow polymerisation process. In addition to siloxane bridges, a ferrocene moiety was also introduced as a connector.[63] The reaction of **50** with $(Me_2N)_4Ti$ and $(Me_2N)_3TiCl$ afforded the heterodimetallic complexes **51** and **52** (Scheme 20).

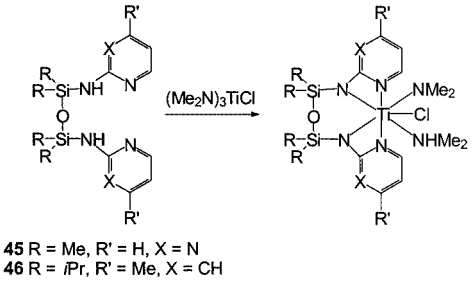

Scheme 19. Synthesis of the bis(aminopyridinato)titanium complexes **47** (R = Me, R′ = Me, X = CH), **48** (R = Me, R′ = H, X = N) and **49** (R = *i*Pr, R′ = Me, X = CH)

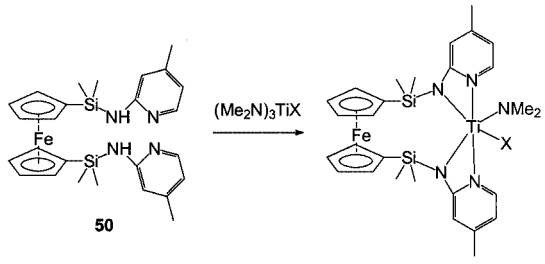

Scheme 20. Synthesis of heterodimetallic complexes **51** (X = NMe_2) and **52** (X = Cl)

Ligand/Substrate Communication

Ligand/substrate communication (steric repulsion between a ligand core and an ancillary coordinated substrate as well as electronic interactions of both via the metal centre) is a fundamental component of all metal-mediated transformation reactions, especially catalysis. While the design of a reactive metal centre is well understood in many cases,[1] understanding of the opposite influence, how substrate binding changes the coordination mode of a certain ligand core, is poor. Owing to the high flexibility of the binding modes of aminopyridinato ligands, their corresponding metal complexes may act as model systems to study ligand substrate communication because the ligands are sensitive to the steric and electronic requirements of the ancillary coordinated substrates. Comparison of the σ-butadiynylzirconium complex **37** with the dimethylamido compound **53** and the *ansa*-(aminopyridinato)titanium complexes accommodating dimethylamido (**54**) and ε-caprolactamato moieties (**55**) shows how the flexible Ap ligands can meet substrate requirements.[58] Molecular structures of the aforementioned compounds are shown in Scheme 21.

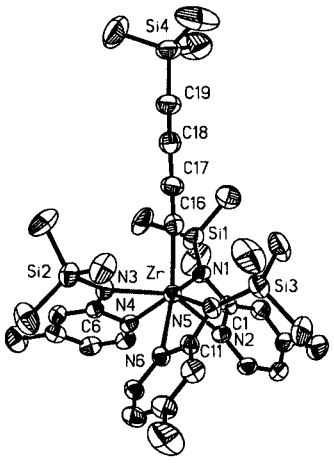

37

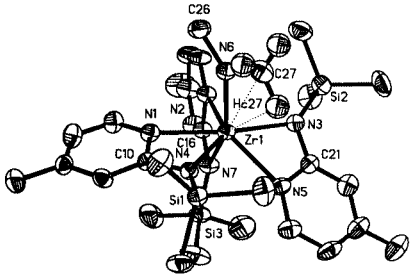

53

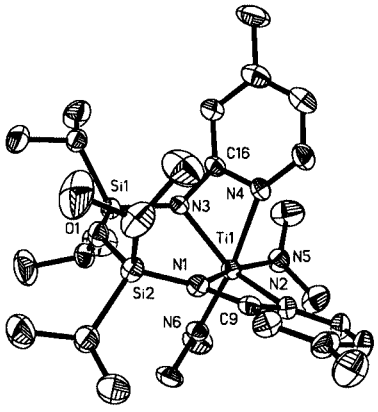

54

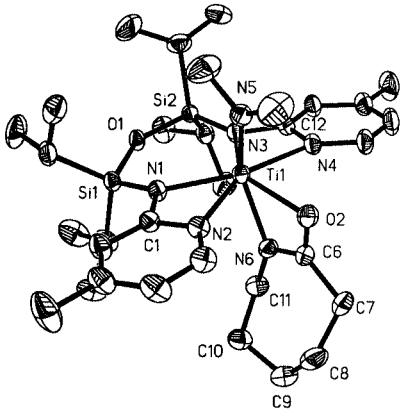

55

Scheme 21. Crystal structures of **37**, **53**, **54** and **55**

The propeller-like arrangement of the three aminopyridinato ligands in **37** may cause a kinetic stabilisation. The zirconium−carbon bond is sterically shielded by the three bulky trimethylsilyl groups of the ligands. This coordination mode seems to be favoured with regard to electronic considerations and is accomplished as long as the steric demand of the ancillary coordinated substrate does not dictate a rearrangement. If the substrate is sterically demanding like the dimethylamido moiety (see complex **53**), the aminopyridinato-coordinated metal centre easily alters its coordination mode. This alteration is facilitated by the extraordinary flexibility of the ligand system. It opens up a large coordination site to provide sufficient space even for an agostic interaction of the methyl group of the dimethylamido moiety. Such an interaction is proposed as an intermediate in the early transition metal catalysed aminomethylation of non-activated olefins.[64] An adaptation of the coordination mode of the ligand core can also be observed by comparing **54** and **55**. Compound **54** is a six-coordinate complex, and in order to achieve an octahedral coordination geometry the aminopyridinato ligand must become twisted. Thus, two different binding modes of the ligand core can be observed. The coordination number must be raised from six to seven to bind the caprolactamato ligand, and the pyridine moiety situated "out of plane" in **54** is turned "in the plane" in **55** to offer the additional coordination site. The ligand thus becomes planar. In addition to the geometric rearrangement, the binding mode of the formerly "out-of-plane" ligand arm is switched to the delocalised form[65] (almost equal Ti−N bond lengths). Steric and electronic changes are necessary to meet the requirements of the caprolactamato moiety.

The Vanadium Triad

Niobium and Tantalum Complexes and Their Application in Polymerisation Reactions

The first well-characterised early transition metal aminopyridinato complex was reported by Gambarotta et al.[26] The reaction of $[(tmeda)_2VCl_2]$ (tmeda = tetramethylethylenediamine) with in situ lithiated **20** gave **56** (Scheme 22).

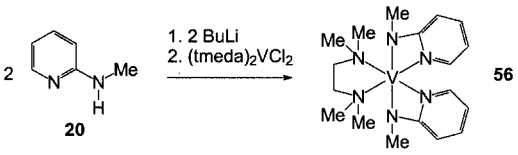

Scheme 22. Synthesis of **56**

A more detailed investigation of the group-5 metal coordination chemistry was started by Polamo et al. He applied the "direct synthesis" method to prepare a variety of niobium and tantalum complexes in high oxidation states (Scheme 23).[60,66−68]

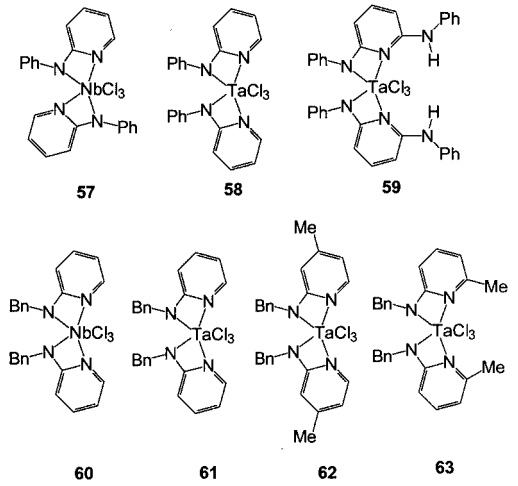

Scheme 23. Trichloro complexes of Nb and Ta prepared by "direct synthesis"

The syntheses of **57**−**59** were carried out in toluene and the compounds **60**−**63** were generated "solvent-free" using molten preligands (aminopyridines) as solvent. All compounds have been characterised by X-ray crystallography and adopt a pentagonal-bipyramidal molecular structure in the solid state. Very high[52] ethylene polymerisation activities were observed for **59** and **61** if the complexes were activated with MAO.[69] The catalyst system based on **61** gave up to 5000 $kg_{PE}/(mol_{Ta}h)$ and that based on **59** up to 23900 $kg_{PE}/(mol_{Ta}h)$. Experiments were carried out for 7 min, with longer polymerisation times leading to dramatically reduced activities. While the exact nature of the catalysts is not known, some analogy to group-4 metallocene chemistry can be drawn,[70] and mechanistic studies on high oxidation state (alkyne)bis(aminopyridinato)niobium complexes underline this analogy.[71] Treatment of $[(dme)NbCl_3(PhC{\equiv}CSiMe_3)]$[72] with 3 equiv. of in situ lithiated **1** gave the orange-red alkylniobium complex **64** (Scheme 24). The niobacyclopropene ring in **64** is extremely stable and does not react with ketones, styrene oxide, alkynes and olefins. This converses the high reactivity for the (alkyne)metallocene complexes of the titanium triad.[73]

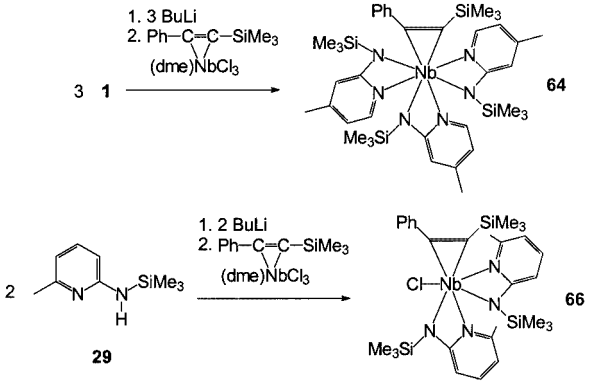

Scheme 24. (Alkyne)niobium complexes

Complexes containing two amido ligands are accessible by using the sterically more demanding deprotonated **29** (Scheme 24). The otherwise analogous reaction (first line in Scheme 24) led to **66**. NMR spectra of **66** indicated a dynamic behaviour which could be explained by alkyne rotation, with the barrier to rotation being $\Delta G^{\neq} = 80$ kJ/mol. The reaction of **66** with MeLi led to **67**, a methyl complex where the methyl group could be partially abstracted by $B(C_6F_5)_3$ (Scheme 25).

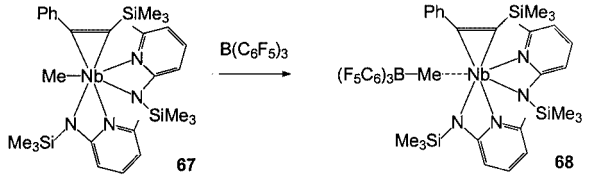

Scheme 25. Partial abstraction of a methyl group by $B(C_6F_5)_3$

Complex **68** is a zwitterionic compound and a single component ethylene polymerisation catalyst. The partial abstraction of the methyl group and the structural parameters of **68** are similar to what has been observed for group-4 metallocenes.[74] Thus, an analogy in terms of the generation of ethylene polymerisation catalysts can be drawn between high oxidation state group-5 metal Ap compounds and group-4 metallocenes. The synthetic procedure described in Scheme 24 could also be used to synthesise the niobium alkyne **69**.[75] Complex **69** polymerised acetylene without the formation of benzene as a by-product. The first metal complex of a tris(aminopyridinato) ligand (**70**) was reported by Gade et al.[76] Complexes of such ligands are rarely described (see **69**, **70** and **71** in Scheme 26).

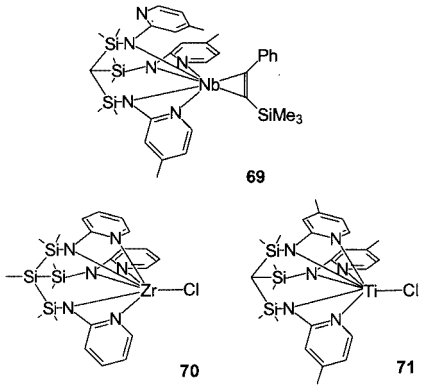

Scheme 26. Complexes stabilised by tris(aminopyridinato) ligands

Complex **71** was synthesised by amine elimination. Owing to the steric crowding in **69**, one of the three pyridine moieties does not coordinate to the niobium centre, in contrast to the hexadentate coordination of **71**. Tris(aminopyridinato) ligands are variable in their denticity, a phenomenon which is characteristic of many Ap compounds during substrate binding and release, but seldom observed in molecular structures determined by X-ray crystallography.

Low Oxidation State Chemistry

Oxidative addition of C−X bonds (X = N, P, O, S, halogen) performed by transition metal complexes is an area of research which is of interest not only from a fundamental point of view, but also because of the many possible applications of such reactions. Aminopyridinato ligands can either stabilise reactive group-5 metal complexes in low oxidation states or be involved in bond cleavage processes. Compound **56** (Scheme 22) is an example of a group-5 complex in a low oxidation state. The reaction which led to **56** proceeded as expected and no C−X bond activation was observed. C−N bond cleavage took place if $(tmeda)_3Nb_2Cl_5$ was treated with the lithium salt of **72** (Scheme 27).[77]

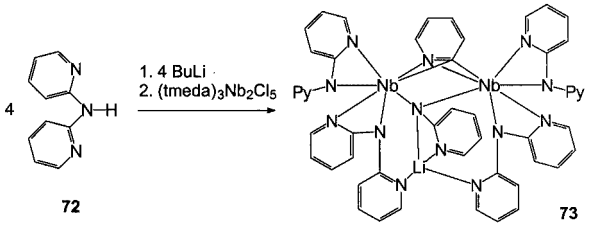

Scheme 27. C−N bond cleavage of an aminopyridinato moiety

The reaction of "$VCl_2{\cdot}n$THF" [generated in situ by the reduction of $VCl_3(THF)_3$ with $NaB(C_2H_5)_3H$] and lithiated **72** yielded **74** if a mixture of THF and toluene was used as solvent at reflux temperature. A similar reaction carried out in THF at 0 °C gave **76**. C−Cl bond cleavage was observed during the reaction of **76** with CH_2Cl_2. Compound **75** was the product of this transformation (Scheme 28).[78]

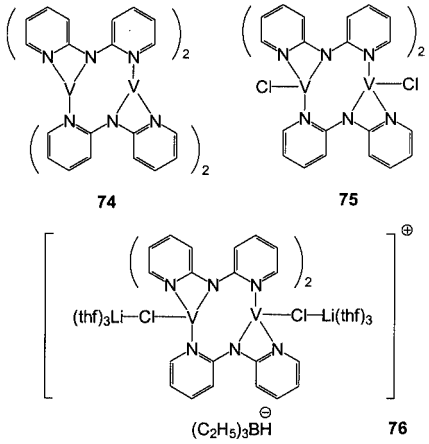

Scheme 28. Products of the reaction of "$VCl_2{\cdot}n$THF" with lithiated **72**

Complexes shown in Scheme 27 and Scheme 28 are dinuclear compounds. Deprotonated **72** acts as a tridentate ligand and its linear arrangement of the three N donor functions does not stabilise mononuclear complexes. A mononuclear homoleptic tris(aminopyridinato)vanadium complex was synthesised from lithiated **1** (in situ) and $[VCl_3(THF)_3]$ (Scheme 29).[79]

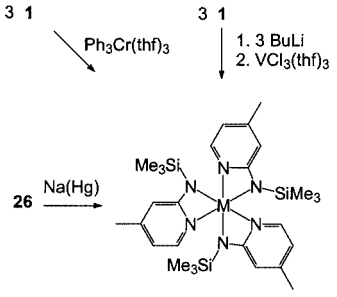

Scheme 29. Mononuclear tris(aminopyridinato)M^{III} complexes (**77**: M = V; **78**: M = Ti; **79**: M = Cr)

Compound **79** is a rare example of an aminopyridinato group-6 metal complex in which the Ap ligands coordinate in a strained η^2-fashion.[25,80]

Conclusions and Outlook

Aminopyridinato ligands can coordinate a variety of early transition metal complexes in the strained η^2-fashion. This binding mode initiates a special reactivity. Thus, it has become possible to stabilise heterodinuclear compounds with unusual metal−metal combinations including short metal−metal distances as well as highly active olefin polymerisation catalysts. The exploration of the catalytic and stoichiometric reactivity of many of the complexes synthesised so far was started only recently and a lot of exiting "chemistry" can be expected in the near future, covering

fields like small molecule activation, homogenous catalysis and the synthesis and reactivity of multinuclear complexes.

Acknowledgments

Financial support of our own work from the Deutsche Forschungsgemeinschaft (KE, 756/2-1, KE 756/3-1), the Fonds der Chemischen Industrie, the Max-Planck-Gesellschaft, the Karl-Winnacker-Stiftung, the IfOK Rostock, and the Carl von Ossietzky Universität Oldenburg is gratefully acknowledged. I would like to thank the group members who were working on the "Ap project": Beate Friedrich, Anke Spannenberg, Markus Oberthür, Gerhard Hillebrand, Simon Brenner, Henrik Noss, Thomas Schareina, Torsten Irrgang and Yvonne Jüttke.

[1] B. Cornils, W. A. Herrmann, *Applied Homogenous Catalysis with Organometallic Compounds*, VCH Verlagsgesellschaft, Weinheim, **1996**.

[2] C. Elschenbroich, A. Salzer, *Organometallchemie*, Teubner, Stuttgart, **1993**.

[3] M. F. Lappert, P. P. Power, A. R. Sanger, R. C. Srivastava, *Metal and Metalloid Amides*, Ellis Norwood Ltd., Chichester, **1980**.

[4] R. Kempe, *Angew. Chem.* **2000**, *112*, 478−504; *Angew. Chem. Int. Ed.* **2000**, *39*, 468−493.

[5] Examples of the polymorphism of aminopyridines: [5a] J. E. Johnson, R. A. Jacobson, *Acta Crystallogr., Sect. B* **1973**, *29*, 1669−1674. [5b] G. J. Pyrka, A. A. Pinkerton, *Acta Crystallogr., Sect. C* **1992**, *48*, 91−94. [5c] H. Schödel, C. Näther, H. Bock, F. Butenschön, *Acta Crystallogr., Sect. B* **1996**, *52*, 842−853. Reviews: [5d] T. Kottke, D. Stalke, *Chem. Ber./Recueil* **1997**, *130*, 1365−1374. [5e] T. Clark (Ed.), *Highlights in Computational Chemistry*, Springer, Heidelberg, **2001**.

[6] F. A. Cotton, R. A. Walton, *Multiple Bonds Between Metal Atoms*, John Wiley and Sons, New York, **1982**.

[7] [7a] F. A. Cotton, C. A. Murillo, X. Wang, *Inorg. Chem. Commun.* **1998**, *1*, 281−283. [7b] S.-M. Peng, Y.-N. Lin, *Acta Crystallogr., Sect. C* **1986**, *42*, 1725−1731. [7c] R. Clerac, F. A. Cotton, K. R. Dunbar, T. Lu, C. A. Murillo, X. Wang, *J. Am. Chem. Soc.* **2000**, *122*, 2272−2278. [7d] E.-C. Yang, M.-C. Cheng, M.-S. Tsai, S.-M. Peng, *J. Chem. Soc., Chem. Commun.* **1994**, 2377−2378. [7e] S.-J. Shieh, C.-C. Chou, G.-H. Lee, C.-C. Wang, S.-M. Peng, *Angew. Chem. Int. Ed. Engl.* **1997**, *36*, 56−59. [7f] F. A. Cotton, L. M. Daniels, G. T. Jordan IV, *Chem. Commun.* **1997**, 421−422. [7g] F. A. Cotton, L. M. Daniels, G. T. Jordan IV, C. A. Murillo, *J. Am. Chem. Soc.* **1997**, *119*, 10377−10381;

[8] [8a] F. A. Cotton, R. H. Niswander, J. C. Sekutowski, *Inorg. Chem.* **1978**, *17*, 3541−3545. [8b] F. A. Cotton, L. M. Daniels, T. Lu, C. A. Murillo, X. Wang, *J. Chem. Soc., Dalton Trans.* **1999**, 517−518. [8c] Y.-H. Chen, C.-C. Lee, C.-C. Wang, G.-H. Lee, S.-Y. Lai, F.-Y. Li, C.-Y. Mou, S.-M. Peng, *Chem. Commun.* **1999**, 1667−1668. [8d] H.-C. Chang, J.-T. Li, C.-C. Wang, T.-W. Lin, H.-C. Lee, G.-H. Lee, S.-M. Peng, *Eur. J. Inorg. Chem.* **1999**, 1243−1251. [8e] F. A. Cotton, L. M. Daniels, C. A. Murillo, X. Wang, *Chem. Commun.* **1999**, 2461−2462. [8f] R. Clerac, F. A. Cotton, L. M. Daniels, K. R. Dunbar, C. A. Murillo, I. Pascual, *Inorg. Chem.* **2000**, *39*, 752−756. [8g] R. Clerac, F. A. Cotton, L. M. Daniels, K. R. Dunbar, C. A. Murillo, I. Pascual, *Inorg. Chem.* **2000**, *39*, 748−751. [8h] F. A. Cotton, L. M. Daniels, C. A. Murillo, I. Pascual, *Inorg. Chem. Commun.* **1998**, *1*, 1−3. [8i] F. A. Cotton, L. M. Daniels, C. A. Murillo, I. Pascual, H.-C. Zhou, *J. Am. Chem. Soc.* **1999**, *121*, 6856−6861. [8j] F. A. Cotton, L. M. Daniels, C. A. Murillo, X. Wang, *Chem. Commun.* **1998**, 39−40. [8k] F. A. Cotton, L. M. Daniels, C. A. Murillo, I. Pascual, *J. Am. Chem. Soc.* **1997**, *119*, 10223−10224. [8l] J. J. H. Edema, S. Gambarotta, A. Meetsma, F. van Bolhuis, A. L. Spek, W. J. J. Smeets, *Inorg. Chem.* **1990**, *29*, 2147−2153. [8m] J. J. H. Edema, S. Gambarotta, A. Meetsma, A. L. Spek, W. J. J. Smeets, M. Y. Chiang, *J. Chem. Soc., Dalton Trans.* **1993**, 789−797.

[9] [9a] J. Y. Lu, B. R. Cabrera, R.-J. Wang, J. Li, *Inorg. Chem.* **1998**, *37*, 4480−4481. [9b] S.-M. Peng, C.-H. Lai, *J. Chin. Chem. Soc. (Taipei)* **1988**, *35*, 325−336. [9c] L.-P. Wu, P. Field, T. Morrissey, C. Murphy, P. Nagle, B. Hathaway, C. Simmons, P. Thornton, *J. Chem. Soc., Dalton Trans.* **1990**, 3835−3846. [9d] M.-S. Tsai, S.-M. Peng, *J. Chem. Soc., Chem. Commun.* **1991**, 514−515. [9e] L. M. Engelhardt, G. E. Jacobsen, W. C. Patalinghug, B. W. Skelton, C. L. Raston, A. H. White, *J. Chem. Soc., Dalton Trans.* **1991**, 2859−2868. [9f] H. Aghabozorg, S. Gambarotta, C. Bensimon, *J. Sci. I. R. Iran* **1994**, *5*, 158−162. [9g] G. J. Pyrka, M. El-Mekki, A. A. Pinkerton, *J. Chem. Soc., Chem. Commun.* **1991**, 84−84. [9h] H.-Y. Cheng, P.-H. Cheng, C.-F. Lee, S.-M. Peng, *Inorg. Chim. Acta* **1991**, *181*, 145−147. [9i] C.-F. Lee, S.-M. Peng, *J. Chin. Chem. Soc. (Taipei)* **1991**, *38*, 559−564. [9j] J. Poitras, A. L. Beauchamp, *Can. J. Chem.* **1994**, *72*, 2339−2347. [9k] G. A. van Albada, I. Mutikainen, U. Turpeinen, J. Reedijk, *Eur. J. Inorg. Chem.* **1998**, 547−549. [9l] S. W. Lee, W. C. Trogler, *Inorg. Chem.* **1990**, *29*, 1659−1662. [9m] W. Kaim, S. Kohlmann, J. Jordanov, D. Fenske, *Z. Anorg. Allg. Chem.* **1991**, *598/599*, 217−234. [9n] C.-K. Chan, C.-X. Guo, K.-K. Cheung, D. Li, C.-M. Che, *J. Chem. Soc., Dalton Trans.* **1994**, 3677−3682.

[10] [10a] F. A. Cotton, D. G. Lay, M. Millar, *Inorg. Chem.* **1978**, *17*, 186−188. [10b] A. Dossing, S. Larsen, A. van Lelieveld, R. M. Bruun, *Acta Chem. Scand.* **1999**, *53*, 230−234. [10c] M.-C. Suen, Y.-Y. Wu, J.-D. Chen, T.-C. Keng, J.-C. Wang, *Inorg. Chim. Acta* **1999**, *288*, 82−89. [10d] A. R. Chakravarty, F. A. Cotton, E. S. Shamshoum, *Inorg. Chem.* **1984**, *23*, 4216−4221. [10e] F. Allaire, A. L. Beauchamp, *Inorg. Chim. Acta* **1989**, *156*, 241−249. [10f] F. A. Cotton, W. H. Ilsley, W. Kaim, *Inorg. Chem.* **1979**, *18*, 2717−2719. [10g] M. Mintert, W. S. Sheldrick, *Chem. Ber.* **1996**, *129*, 683−689.

[11] [11a] C.-C. Wang, W.-C. Lo, C.-C. Chou, G.-H. Lee, J.-M. Chen, S.-M. Peng, *Inorg. Chem.* **1998**, *37*, 4059−4065. [11b] S.-Y. Lai, T.-W. Lin, Y.-H. Chen, C.-C. Wang, G.-H. Lee, M. Yang, M. Leung, S.-M. Peng, *J. Am. Chem. Soc.* **1999**, *121*, 250−251. [11c] R. Clerac, F. A. Cotton, K. R. Dunbar, C. A. Murillo, I. Pascual, X. Wang, *Inorg. Chem.* **1999**, *38*, 2655−2657. [11d] S. Aduldecha, B. Hathaway, *J. Chem. Soc., Dalton Trans.* **1991**, 993−998. [11e] N. A. Bailey, T. A. James, J. A. McCleverty, E. D. McKenzie, R. D. Moore, J. M. Worthington, *J. Chem. Soc., Chem. Commun.* **1972**, 681−682. [11f] N. A. Bailey, E. D. McKenzie, J. M. Worthington, *Inorg. Chim. Acta* **1980**, *46*, 145−153. [11g] G. Sanchez, F. Ruiz, J. Garcia, M. C. Ramirez de Arellano, G. Lopez, *Helv. Chim. Acta* **1997**, *80*, 2477−2485.

[12] [12a] L. A. Oro, M. A. Ciriano, B. E. Villarroya, A. Tiripicchio, F. J. Lahoz, *J. Chem. Soc., Chem. Commun.* **1984**, 521−522. [12b] L. A. Oro, M. A. Ciriano, B. E. Villarroya, A. Tiripicchio, F. J. Lahoz, *J. Chem. Soc., Dalton Trans.* **1985**, 1891−1898. [12c] A. M. M. Lanfredi, A. Tiripicchio, R. Uson, L. A. Oro, M. A. Ciriano, B. E. Villaroya, *Inorg. Chim. Acta* **1984**, *88*, L9−L10. [12d] A. Tiripicchio, F. J. Lahoz, L. A. Oro, M. A. Ciriano, B. E. Villarroya, *Inorg. Chim. Acta* **1986**, *111*, L1−L3. [12e] F. J. Lahoz, F. Viguri, M. A. Ciriano, L. A. Oro, C. Foces-Foces, F. H. Cano, *Inorg. Chim. Acta* **1987**, *128*, 119−125. [12f] J. L. Bear, C.-L. Yao, L. -M. Liu, F. J. Capdevielle, J. D. Korp, T. A. Albright, S. -K. Kang, K. M. Kadish, *Inorg. Chem.* **1989**, *28*, 1254−1262. [12g] L. Lu-Mei, J. L. Bear, *Sci. China, Ser. B (Engl.)* **1990**, *33*, 513−522. [12h] C. -L. Yao, K. H. Park, A. R. Khokhar, M. -J. Jun, J. L. Bear, *Inorg. Chem.* **1990**, *29*, 4033−4039. [12i] J.-T. Sheu, C.-C. Lin, I. Chao, C.-C. Wang, S.-M. Peng, *Chem. Commun.* **1996**, 315−316.

[13] [13a] A. R. Chakravarty, F. A. Cotton, D. A. Tocher, *Inorg. Chem.* **1984**, *23*, 4030−4033. [13b] A. R. Chakravarty, F. A. Cotton, D. A. Tocher, *Inorg. Chem.* **1985**, *24*, 172−177. [13c] A. R. Chakravarty, F. A. Cotton, L. R. Falvello, *Inorg. Chem.* **1986**,

25, 214–219. [13d] A. R. Chakravarty, F. A. Cotton, *Inorg. Chim. Acta* **1986**, *113*, 19–26. [13e] H. J. McCarthy, D. A. Tocher, *Polyhedron* **1992**, *11*, 13–20. [13f] Y. Li, B. Han, K. M. Kadish, J. L. Bear, *Inorg. Chem.* **1993**, *32*, 4175–4176. [13g] J. L. Bear, Y. Li, B. Han, E. Van Caemelbecke, K. M. Kadish, *Inorg. Chem.* **1997**, *36*, 5449–5456. [13h] F. A. Cotton, A. Yokochi, *Inorg. Chem.* **1998**, *37*, 2723–2728. [13i] J. L. Bear, Y. Li, B. Han, E. Van Caemelbecke, K. M. Kadish, *Inorg. Chem.* **1996**, *35*, 3053–3055. [13j] F. A. Cotton, A. Yokochi, *Inorg. Chem.* **1997**, *36*, 567–570. [13k] W. S. Sheldrick, M. Mintert, *Inorg. Chim. Acta* **1994**, *219*, 23–29. [13l] M. Mintert, W. S. Sheldrick, *J. Chem. Soc., Dalton Trans.* **1995**, 2663–2669. [13m] M. Mintert, W. S. Sheldrick, *Inorg. Chim. Acta* **1995**, *236*, 13–20.

[14] [14a] J.-P. Charland, A. L. Beauchamp, *J. Crystallogr. Spectrosc. Res.* **1985**, *15*, 581–601. [14b] J. Beck, M. Reitz, *Z. Naturforsch., Teil B* **1997**, *52*, 604–608.

[15] S. Cabaleiro, E. Vazquez-Lopez, J. Castro, J. A. Garcia-Vazquez, J. Romero, A. Sousa, *Inorg. Chim. Acta* **1999**, *294*, 87–94.

[16] N. Kanematsu, M. Ebihara, T. Kawamura, *Inorg. Chim. Acta* **1999**, *292*, 244–248.

[17] A. R. Chakravarty, F. A. Cotton, D. A. Tocher, *Inorg. Chem.* **1984**, *23*, 4693–4697.

[18] B. Oskui, M. Mintert, W. S. Sheldrick, *Inorg. Chim. Acta* **1999**, *287*, 72–81.

[19] F. A. Cotton, L. R. Falvello, W. Wang, *Inorg. Chim. Acta* **1997**, *261*, 77–81.

[20] C.-F. Lee, K.-F. Chin, S.-M. Peng, C.-M. Che, *J. Chem. Soc., Dalton Trans.* **1993**, 467.

[21] [21a] P. Nombel, N. Lugan, B. Donnadieu, G. Lavigne, *Organometallics* **1999**, *18*, 187–196. [21b] J. A. Cabeza, L. A. Oro, A. Tiripicchio, M. Tiripicchio Camellini, *J. Chem. Soc., Dalton Trans.* **1988**, 1437–1444. [21c] P. L. Andreu, J. A. Cabeza, V. Riera, Y. Jeannin, D. Miguel, *J. Chem. Soc., Dalton Trans.* **1990**, 2201–2206. [21d] P. L. Andreu, J. A. Cabeza, V. Riera, C. Bois, Y. Jeannin, *J. Organomet. Chem.* **1990**, *384*, C25–C28. [21e] P. L. Andreu, J. A. Cabeza, V. Riera, C. Bois, Y. Jeannin, *J. Chem. Soc., Dalton Trans.* **1990**, 3347–3353. [21f] P. L. Andreu, J. A. Cabeza, A. Llamazares, V. Riera, S. Garcia-Granda, J. F. Van der Maelen, *J. Organomet. Chem.* **1992**, *434*, 123–132. [21g] P. L. Andreu, J. A. Cabeza, M. A. Pellinghelli, V. Riera, A. Tiripicchio, *Inorg. Chem.* **1991**, *30*, 4611–4616. [21h] P. L. Andreu, J. A. Cabeza, A. Llamazares, V. Riera, C. Bois, Y. Jeannin, *J. Organomet. Chem.* **1991**, *420*, 431–442. [21i] J. A. Cabeza, J. M. Fernandez-Colinas, S. Garcia-Granda, A. Llamazares, F. Lopez-Ortiz, V. Riera, J. F. Van der Maelen, *Organometallics* **1994**, *13*, 426–428. [21j] J. A. Cabeza, I. del Rio, J. M. Fernandez-Colinas, A. Llamazares, V. Riera, *J. Organomet. Chem.* **1995**, *494*, 169–177. [21k] J. A. Cabeza, I. del Rio, V. Riera, S. Garcia-Granda, S. B. Sanni, *Organometallics* **1997**, *16*, 1743–1748. [21l] J. A. Cabeza, A. Llamazares, V. Riera, P. Briard, L. Ouahab, *J. Organomet. Chem.* **1994**, *480*, 205–212. [21m] J. A. Cabeza, I. del Rio, V. Reira, F. Grepioni, *Organometallics* **1997**, *16*, 812–815. [21n] N. Lugan, F. Laurent, G. Lavigne, T. P. Newcomb, E. W. Liimatta, J.-J. Bonnet, *J. Am. Chem. Soc.* **1990**, *112*, 8607–8609. [21o] N. Lugan, F. Laurent, G. Lavigne, T. P. Newcomb, E. W. Liimatta, J.-J. Bonnet, *Organometallics* **1992**, *11*, 1351–1363. [21p] J. A. Cabeza, S. Garcia-Granda, A. Llamazares, V. Riera, J. F. van der Maelen, *Organometallics* **1993**, *12*, 157–163. [21q] J. A. Cabeza, S. Garcia-Granda, A. Llamazares, V. Riera, J. F. Van der Maelen, *Organometallics* **1993**, *12*, 2973–2979. [21r] J. A. Cabeza, A. Llamazares, V. Riera, S. Triki, L. Ouahab, *Organometallics* **1992**, *11*, 3334–3339. [21s] P. Briard, J. A. Cabeza, A. Llamazares, L. Ouahab, V. Riera, *Organometallics* **1993**, *12*, 1006–1008. [21t] J. A. Cabeza, R. J. Franco, A. Llamazares, V. Riera, E. Perez-Carreno, J. F. Van der Maelen, *Organometallics* **1994**, *13*, 55–59. [21u] J. A. Cabeza, J. M. Fernandez-Colinas, A. Llamazares, V. Riera, S. Garcia-Granda, J. F. Van der Maelen, *Organometallics* **1994**, *13*, 4352–4359. [21v] S. Alvarez, P. Briard, J. A. Cabeza, I. del Rio, J. M. Fernandez-Colinas, F. Mulla, L. Ouahab, V. Riera, *Organometallics* **1994**, *13*, 4360–4366. [21w] P. Nombel, N. Lugan, F. Mulla, G. Lavigne, *Organometallics* **1994**, *13*, 4673–4675. [21x] J. A. Cabeza, I. del Rio, A. Llamazares, V. Riera, S. Garcia-Granda, J. F. Van der Maelen, *Inorg. Chem.* **1995**, *34*, 1620–1623. [21y] J. A. Cabeza, I. del Rio, V. Riera, F. Grepioni, *Organometallics* **1995**, *14*, 3124–3126.

[22] [22a] A. J. Deeming, R. Peters, M. B. Hursthouse, J. D. J. Backer-Dirks, *J. Chem. Soc., Dalton Trans.* **1982**, 1205–1211. [22b] K. Burgess, B. F. G. Johnson, J. Lewis, P. R. Raithby, *J. Chem. Soc., Dalton Trans.* **1983**, 1661–1665. [22c] F.-S. Kong, W.-T. Wong, *J. Chem. Soc., Dalton Trans.* **1997**, 1237–1241. [22d] Y.-K. Au, K.-K. Cheung, W.-T. Wong, *Inorg. Chim. Acta* **1995**, *238*, 193–195.

[23] [23a] D. Barr, W. Clegg, R. E. Mulvey, R. Snaith, *J. Chem. Soc., Chem. Commun.* **1984**, 469–470. [23b] D. Barr, W. Clegg, R. E. Mulvey, R. Snaith, *J. Chem. Soc., Chem. Commun.* **1984**, 700–701. [23c] A. M. Arif, D. C. Bradley, D. M. Frigo, M. B. Hursthouse, B. Hussain, *J. Chem. Soc., Chem. Commun.* **1985**, 783–784. [23d] A. M. Arif, D. C. Bradley, H. Dawes, D. M. Frigo, M. B. Hursthouse, B. Hussain, *J. Chem. Soc., Dalton Trans.* **1987**, 2159–2164. [23e] G. B. Deacon, S. J. Faulks, B. M. Gatehouse, A. J. Jozsa, *Inorg. Chim. Acta* **1977**, *21*, L1–L2. [23f] L. M. Engelhardt, G. E. Jacobsen, P. C. Junk, C. L. Raston, B. W. Skelton, A. H. White, *J. Chem. Soc., Dalton Trans.* **1988**, 1011–1020. [23g] C. L. Raston, B. W. Skelton, V.-A. Tolhurst, A. H. White, *Polyhedron* **1998**, *17*, 935–942. [23h] Q. Zhao, H.-S. Sun, W.-Z. Chen, Y.-J. Liu, X.-Z. You, *J. Organomet. Chem.* **1998**, *556*, 159–163. [23i] K. W. Henderson, R. E. Mulvey, W. Clegg, P. A. O'Neil, *Polyhedron* **1993**, *12*, 2535–2538. [23j] J. Ashenhurst, L. Brancaleon, S. Gao, W. Liu, H. Schmider, S. Wang, G. Wu, Q. G. Wu, *Organometallics* **1998**, *17*, 5334–5241. [23k] P. C. Andrews, D. R. Baker, R. E. Mulvey, W. Clegg, P. A. O'Neil, *Polyhedron* **1991**, *10*, 1839–1841. [23l] D. K. Kennepohl, H.-G. Schmidt, M. Noltemeyer, H. W. Roesky, *Z. Naturforsch., Teil B* **1992**, *47*, 5–8. [23m] S. Hadjikakou, M. A. Demertzis, J. R. Miller, D. Kovala-Demertzi, *J. Chem. Soc., Dalton Trans.* **1999**, 663–666. [23n] L. M. Engelhardt, G. E. Jacobsen, P. C. Junk, C. L. Raston, A. H. White, *J. Chem. Soc., Chem. Commun.* **1990**, 89–91. [23o] P. C. Andrews, W. Clegg, R. E. Mulvey, *Angew. Chem.* **1990**, *102*, 1480–1481; *Angew. Chem. Int. Ed. Engl.* **1990**, *29*, 1440–1441. [23p] K. W. Henderson, R. E. Mulvey, W. Clegg, P. A. O'Neil, *J. Organomet. Chem.* **1992**, *439*, 237–250. [23q] W. Liu, A. Hassan, S. Wang, *Organometallics* **1997**, *16*, 4257–4259. [23r] N. Feeder, R. Snaith, A. E. H. Wheatley, *Eur. J. Inorg. Chem.* **1998**, 879–883. [23s] R. Kempe, A. Spannenberg, S. Brenner, *Z. Kristallogr.* **1996**, *211*, 567–568. [23t] L. M. Engelhardt, M. G. Gardiner, C. Jones, P. C. Junk, C. L. Raston, A. H. White, *J. Chem. Soc., Dalton Trans.* **1996**, 3053–3057. [23u] H. Gornitzka, D. Stalke, *Eur. J. Inorg. Chem.* **1998**, 311–317. [23v] D. K. Kennepohl, A. A. Pinkerton, Y. F. Lee, R. G. Cavell, *Inorg. Chem.* **1990**, *29*, 5088–5096. [23w] Y. Zhou, D. S. Richeson, *Organometallics* **1995**, *14*, 3558–3561.

[24] A. R. Chakravarty, F. A. Cotton, E. S. Shamshoum, *Inorg. Chim. Acta* **1984**, *86*, 5–11.

[25] M. J. Calhorda, M. A. A. F. de C. T. Carrondo, R. G. da Costa, A. R. Dias, M. T. L. S. Duarte, M. B. Hursthouse, *J. Organomet. Chem.* **1987**, *320*, 53–62.

[26] J. J. H. Edema, S. Gambarotta, A. Meetsma, A. L. Spek, N. Veldman, *Inorg. Chem.* **1991**, *30*, 2062–2066.

[27] [27a] T. J. Kealy, P. L. Pauson, *Nature* **1951**, *168*, 1039. [27b] G. Wilkinson, M. Rosenblum, M. C. Whiting, R. B. Woodward, *J. Am. Chem. Soc.* **1952**, *74*, 2125–2126. [27c] E. O. Fischer, W. Pfab, *Z. Naturforsch., Teil B* **1952**, *7*, 377–379.

[28] D. Fenske, E. Hartmann, K. Dehnicke, *Z. Naturforsch., Teil B* **1988**, *43*, 1611–1615.

[29] H. W. Roesky, B. Meller, M. Noltemeyer, H.-G. Schmidt, U. Scholz, G. M. Sheldrick, *Chem. Ber.* **1988**, *121*, 1403–1406.

[30] R. Kempe, H. Noss, T. Irrgang, *J. Organomet. Chem.* **2002**, *647*, 12−20.
[31] A. Spannenberg, P. Arndt, R. Kempe, *Angew. Chem.* **1998**, *110*, 824−827; *Angew. Chem. Int. Ed.* **1998**, *37*, 832−835.
[32] [32a] H. Schumann, *Angew. Chem.* **1984**, *96*, 475−493; *Angew. Chem. Int. Ed. Engl.* **1984**, *23*, 474−492. [32b] W. J. Evans, *Adv. Organomet. Chem.* **1985**, *24*, 131−177. [32c] W. J. Evans, *Polyhedron* **1987**, *6*, 803−835. [32d] R. D. Köhn, G. Kociok-Köhn, H. Schumann in *Encyclopedia of Inorganic Chemistry* (Ed.: R. B. King), John Wiley & Sons, New York, **1994**. [32e]C. J. Schaverien, *Adv. Organomet. Chem.* **1994**, *36*, 283−362. [32f] H. Schumann, J. A. Meese-Marktscheffel, L. Esser, *Chem. Rev.* **1995**, *95*, 865−986.
[33] F. T. Edelmann, *J. Alloys Compd.* **1994**, *207/208*, 182−188.
[34] [34a] M. D. Fryzuk, C. D. Montgomery, *Coord. Chem. Rev.* **1989**, *95*, 1−40. [34b] J. V. Cuevas, G. Garcia-Herbosa, A. Muñoz, S. Garcia-Granda, D. Miguel, *Organometallics* **1997**, *16*, 2220−2222. [34c] M. S. Driver, J. F. Hartwig, *J. Am. Chem. Soc.* **1996**, *118*, 4206−4207. [34d] M. S. Driver, J. F. Hartwig, *J. Am. Chem. Soc.* **1995**, *117*, 4708−4709. [34e] L. A. Villanueva, K. A. Abboud, J. M. Boncella, *Organometallics* **1994**, *13*, 3921−3931. [34f] J. M. Boncella, L. A. Villanueva, *J. Organomet. Chem.* **1994**, *465*, 297−304. [34g] J. Ruiz, M. T. Martinez, C. Vincente, G. Garcia, G. López, P. A. Chaloner, P. B. Hitchcock, *Organometallics* **1993**, *12*, 4321−4326. [34h] P. Espinet, M. Y. Alonso, G. Garcia-Herbosa, J. M. Ramos, Y. Jeannin, M. Philoche-Levisalles, *Inorg. Chem.* **1992**, *31*, 2501−2507. [34i] A. L. Seligson, R. L. Cowan, W. C. Trogler, *Inorg. Chem.* **1991**, *30*, 3371−3381.
[35] H. Noss, M. Oberthür, C. Fischer, W. P. Kretschmer, R. Kempe, *Eur. J. Inorg. Chem.* **1999**, 2283−2288.
[36] A. Löfgren, A.-C. Albertsson, P. Dubois, R. Jerome, *J. Macromol. Sci., Rev. Macromol. Chem. Phys.* **1995**, *C35*, 379−418.
[37] [37a] M. Hayakawa, M. Mitani, T. Yamada, T. Mukaiyama, *Macromol. Chem. Phys.* **1997**, *198*, 1305−1317. [37b] J. Zhang, Z. Gan, Z. Zhong, X. Jing, *Polymer International* **1998**, *45*, 60−66.
[38] A. Spannenberg, M. Oberthür, H. Noss, A. Tillack, P. Arndt, R. Kempe, *Angew. Chem.* **1998**, *110*, 2190−2192; *Angew. Chem. Int. Ed.* **1998**, *37*, 2079−2082.
[39] H. Noss, R. Kempe, T. Irrgang, W. Baumann, A. Schluz, *Inorg. Chim. Acta*, in press.
[40] I. P. Beletskaya, A. Z. Voskoboynikov, E. B. Chuklanova, N. I. Kirillova, A. K. Shestakova, I. N. Parshina, A. I. Gusev, G. K.-I. Magomedov, *J. Am. Chem. Soc.* **1993**, *115*, 3156−3166.
[41] R. Kempe, H. Noss, H. Fuhrmann, *Chem. Eur. J.* **2001**, *7*, 1630−1636.
[42] R. E. Rülke, J. M. Ernsting, A. L. Spek, C. J. Elsevier, P. W. N. M. van Leeuwen, K. Vrieze, *Inorg. Chem.* **1993**, *32*, 5769−5778.
[43] Examples of nickel amido complexes: [43a] D. C. Bradley, M. B. Hursthouse, R. J. Smallwood, A. J. Welch, *J. Chem. Soc., Chem. Commun.* **1972**, 872−873. [43b] M. D. Fryzuk, P. A. MacNeil, *J. Am. Chem. Soc.* **1981**, *103*, 3592−3593. [43c] M. D. Fryzuk, P. A. MacNeil, S. J. Reettig, A. S. Secco, J. Trotter, *Organometallics* **1982**, *1*, 918−930.) [43d] H. Hope, M. M. Olmstead, B. D. Murry, *J. Am. Chem. Soc.* **1985**, *107*, 712−713. [43e] R. A. Barlett, H. Cheng, P. P. Power, *Angew. Chem.* **1989**, *101*, 325−327; *Angew. Chem. Int. Ed. Engl.* **1989**, *28*, 316−318. [43f] P. T. Matsunaga, C. R. Hess, G. L. Hillhouse, *J. Am. Chem. Soc.* **1994**, *116*, 3665−3666. [43g] K. Koo, G. L. Hillhouse, *Organometallics* **1995**, *14*, 4421−4423. [43h] D. D. VanderLende, K. A. Abboud, J. M. Boncella, *Inorg. Chem.* **1995**, *34*, 5319−5376. [43i] P. L. Holland, R. A. Andersen, R. G. Bergman, *J. Am. Chem. Soc.* **1996**, *118*, 1092−1104; P. L. Holland, R. A. Andersen, R. G. Bergman, J. Huang, S. P. Nolan, *J. Am. Chem. Soc.* **1997**, *119*, 12800−12814.
[44] Examples of copper amido complexes: [44a] L.-P. Wu, P. Field, T. Morrissey, C. Murphy, P. Nagle, B. Hathaway, C. Simmons, P. Thornton, *J. Chem. Soc., Dalton Trans.* **1990**, 3835−3840. [44b] K. Dehnicke, *Chem.-Ztg.* **1990**, *114*, 295−304. [44c] S. Maier, W. Hiller, J. Strähle, C. Ergezinger, K. Dehnicke, *Z. Naturforsch., Teil B* **1988**, *43*, 1628−1632. [44d] J. Beck, J. Strähle, *Angew. Chem.* **1985**, *97*, 325−327; *Angew. Chem. Int. Ed. Engl.* **1985**, *24*, 409−410.
[45] J. S. Kim, J. H. Pawlow, L. M. Wojcinski II, S. Murtuza, S. Kacker, A. Sen, *J. Am. Chem. Soc.* **1998**, *120*, 1932−1933.
[46] One example is the connection of a Cp moiety with an aminopyridinato function: M. S. Hill, P. B. Hitchcock, *Angew. Chem.* **2001**, *113*, 4213−4216; *Angew. Chem. Int. Ed.* **2001**, *40*, 4089−4092.
[47] M. Polamo, M. Leskela, *Acta Crystallogr., Sect. C* **1996**, *52*, 2975−2977.
[48] R. Kempe, P. Arndt, *Inorg. Chem.* **1996**, *35*, 2644−2649.
[49] E. Benzing, K. Kornicker, *Chem. Ber.* **1961**, *94*, 2263−2267.
[50] H. Fuhrmann, S. Brenner, P. Arndt, R. Kempe, *Inorg. Chem.* **1996**, *35*, 6742−6745.
[51] R. Kempe, *Z. Kristallogr. NCS* **1997**, *212*, 477−478.
[52] G. J. P. Britovsek, V. C. Gibson, D. F. Wass, *Angew. Chem.* **1999**, *111*, 448−468; *Angew. Chem. Int. Ed.* **1999**, *38*, 428−447.
[53] S. Brenner, R. Kempe, P. Arndt, *Z. Anorg. Allg. Chem.* **1995**, *621*, 2021−2024.
[54] R. Kempe, A. Spannenberg, S. Brenner, *Z. Kristallogr.* **1996**, *211*, 497−498.
[55] R. Kempe, S. Brenner, P. Arndt, *Organometallics* **1996**, *15*, 1071−1074.
[56] R. Kempe, A. Spannenberg, S. Brenner, *Z. Kristallogr.* **1996**, *211*, 499−500.
[57] R. Kempe, A. Spannenberg, S. Brenner, *Z. Kristallogr.* **1996**, *211*, 569−570.
[58] M. Oberthür, G. Hillebrand, P. Arndt, R. Kempe, *Chem. Ber./Recueil* **1997**, *130*, 789−794.
[59] C. Morton, P. O'Shaughnessy, P. Scott, *Chem. Commun.* **2000**, 2099−2100.
[60] M. Polamo, M. Leskelä, *J. Chem. Soc., Dalton Trans.* **1996**, 4345−4349.
[61] M. Polamo, M. Leskelä, *Acta Chem. Scand.* **1997**, *51*, 69−72.
[62] [62a] M. Oberthür, P. Arndt, R. Kempe, *Chem. Ber.* **1996**, *129*, 1087−1091. [62b] R. Kempe, M. Oberthür, G. Hillebrand, A. Spannenberg, H. Fuhrmann, *Polimery* **1998**, *43*, 96−103. [62c] R. Kempe, M. Oberthür, A. Spannenberg, *Z. Kristallogr. NCS* **1997**, *212*, 481−482.
[63] A. Spannenberg, P. Arndt, M. Oberthür, R. Kempe, *Z. Anorg. Allg. Chem.* **1997**, *623*, 389−393.
[64] D. Steinborn, R. Taube, *Z. Chem.* **1986**, *26*, 349−359. D. Steinborn, B. Thies, I. Wagner, R. Taube, *Z. Chem.* **1989**, *29*, 333−334. W. A. Nugent, D. W. Ovenall, S. J. Holmes, *Organometallics* **1983**, *2*, 161−162.
[65] The anionic function of the aminopyridinato ligand is not localised at the amino nitrogen atom.
[66] M. Polamo, *Acta Crystallog. Sect. C* **1996**, *52*, 2977−2980.
[67] M. Polamo, M. Leskelä, *Acta Chem. Scand.* **1997**, *51*, 449−454.
[68] M. Polamo, M. Leskelä, *Acta Chem. Scand.* **1997**, *51*, 709−713.
[69] K. Hakala, B. Lofgren, M. Polamo, M. Lesela, *Macromol. Rapid. Commun.* **1997**, *18*, 635−638.
[70] [70a] H.-H. Brintzinger, D Fischer, R. Mülhaupt, B Rieger, R. Waymouth, *Angew. Chem.* **1995**, *107*, 1255−1282; *Angew. Chem. Int. Ed. Engl.* **1995**, *34*, 1143−1170. [70b] M. Aulbach, F. Küber, *Chem. Unserer Zeit* **1994**, *28*, 197−208. [70c] P. C. Möhring, N. J. Coville, *J. Organomet. Chem.* **1994**, *479*, 1−29.
[71] A. Spannenberg, H. Fuhrmann, P. Arndt, W. Baumann, R. Kempe, *Angew. Chem.* **1998**, *110*, 3565−3567; *Angew. Chem. Int. Ed.* **1998**, *37*, 3363−3365.
[72] J. B. Hartung, S. F. Pedersen, *Organometallics* **1990**, *9*, 1414−1417.
[73] [73a] A. Ohff, S. Pulst, C. Lefeber, N. Peulecke, P. Arndt, V. V. Burlakov, U. Rosenthal, *Synlett* **1996**, 111−118. [73b] U. Rosenthal, P.-M. Pellny, F. G. Kirchbauer, V. V. Burlakov, *Acc. Chem. Res.* **2000**, *33*, 119−129.
[74] [74a] M. Bochmann, S. J. Lancaster, M. B. Hursthouse, K. M. Abdul Malik, *Organometallics* **1994**, *13*, 2235−2243. [74b] R.

Gomez, M. L. H. Green, J. L. Haggitt, *J. Chem. Soc., Chem. Commun.* **1994**, 2607−2608. [74c] R. Gomez, M. L. H. Green, J. L. Haggitt, *J. Chem. Soc., Chem. Commun.* **1996**, 939−946. [74d] X. Yang, C. L. Stern, T. J. Marks, *J. Am. Chem. Soc.* **1991**, *113*, 3623−3626. [74e] X. Yang, C. L. Stern, T. J. Marks, *J. Am. Chem. Soc.* **1994**, *116*, 10015−10031. [74f] R. E. von H. Spence, J. D. Parks, W. E. Piers, M.-A. MacDonald, M. J. Zaworotko, S. J. Rettig, *Angew. Chem.* **1995**, *107*, 1337−1339; *Angew. Chem. Int. Ed. Engl.* **1995**, *34*, 1230−1232.

[75] G. Hillebrand, A. Spannenberg, P. Arndt, R. Kempe, *Organometallics* **1997**, *16*, 5585−5588.

[76] B. Findeisen, M. Schubart, L. H. Gade, F. Möller, I. Scowen, M. McPartlin, *J. Chem. Soc., Dalton Trans.* **1996**, 125−132.

[77] M. Tayebani, S. Gambarotta, G. Yap, *Organometallics* **1998**, *17*, 3639−3641.

[78] F. A. Cotton, L. M. Daniels, C. A. Murillo, H.-C. Zhou, *Inorg. Chem. Acta* **2000**, *305*, 69−74.

[79] A. Spannenberg, A. Tillack, P. Arndt, R. Kirmse, R. Kempe, *Polyhedron* **1998**, *17*, 845−850.

[80] [80a] M. Polamo, *Acta Crystallogr., Sect. C* **1996**, *52*, 2980−2982. [80b] H. K. Lee, Y.-L. Wong, Z.-Y. Zhou, Z.-Y. Zhang, D. K. P. Ng, T. C. W. Mak, *J. Chem. Soc., Dalton Trans.* **2000**, 539−544.

Received March 1, 2002
[I02109]

Cyclodextrin-Encapsulated Iron Catalysts for the Polymerization of Ethylene

Dominique Armspach,*[a] Dominique Matt,*[a] Frédéric Peruch,*[b] and Pierre Lutz*[b]

Keywords: Cyclodextrins / Polymerization / Iron / N ligands / Cavitands

The synthesis and characterization of dichloroiron(II) complexes of tridentate nitrogen ligands based on 2,6-bis(imino)-pyridine-capped α- and β-cyclodextrin derivatives are described and their propensity to act as ethylene polymerization catalysts reported.

(© Wiley-VCH Verlag GmbH & Co. KGaA, 69451 Weinheim, Germany, 2003)

Introduction

Although dominated by the very active Group 4 metallocenes catalysts for a long time,[1] the field of catalytic polymerization has recently been rejuvenated by Brookhart[2] and Gibson's seminal works[3,4] on the use of late transition metal complexes in olefin polymerization. Beside systems containing the α-diimine ligand framework,[5] nitrogen-containing tridentate complexes of iron and cobalt based on the 2,6-bis(iminoaryl)pyridine fragment are amongst the most studied because of their ability to promote the formation of linear polyethylene very efficiently.[6] Steric bulk control around the metal center is a prerequisite not only for forming the neutral trigonal-pyramidal MCl_2 catalyst precursor at the expense of the inactive octahedral cationic $[(N,N,N)_2Fe]^{2+}$ complex,[7] but also for tuning the molecular weight of the polymer produced.[4] So far, the control of the steric environment at the metal has been achieved by changing the size of the aryl (Ar) and imino carbon (R) substituents of the 2,6-bis(iminoaryl)pyridine moiety. An alternative would be to encapsulate the metal fragment in molecular cavities of various sizes. Here we describe the synthesis of methylated α- and β-cyclodextrin (CD) derivatives[8] rigidly capped with a 2,6-bis(imino)pyridyl fragment and the activity of their iron complexes in ethylene polymerization.

Results and Discussion

The ligands **4a** and **4b** used in this study were prepared by condensing 2,6-diformylpyridine with diamines **3a**[9] and **3b**, respectively (Scheme 1). The latter was synthesized in two steps from the known dimesylate **1**[10] according to a procedure adapted from that used for preparing diamine **3a**. The cyclisation of both diamines proceeded smoothly in dilute MeCN solution in the presence of molecular sieves (4 Å) with only small amounts of oligomeric material being produced during the reaction. The latter was removed by simple recrystallisation from $CHCl_3$/pentane so that the pure capped CDs **4a** and **4b** could be obtained in 46 and 64% yields, respectively. As shown by ^1H NMR and ^{13}C NMR spectroscopy, the C_2 symmetry of diamine **3a** is retained upon cyclisation. In addition, it is unlikely that the macrocyclic structures of both **4a** and **4b** are strongly distorted by the presence of the relatively short and rigid capping unit as the signals of the anomeric protons all fall in a narrow chemical shift region ($\Delta\delta < 0.17$ ppm).[9] This observation was confirmed by a single-crystal X-ray diffraction study on ligand **4a** (Figure 1). The structure of the latter reveals an almost perfectly round shape for the C_2-symmetrical CD framework, with all the glucose units in the standard $^4C_1$ conformation. Interestingly, the atoms of the bridging unit lie almost in the same plane, the N(1)−C(27)−C(28)−N(2) torsion angle being 4.5°. This particular feature is a result of the presence of a single water molecule located in the middle of the cavity, which is hydrogen-bonded to two opposing imine nitrogen atoms. A distance of 3.00(2) Å can be calculated between the imine nitrogen N(1)/N(1A) atoms and the encapsulated water oxygen O_w, while the N(1)−O_w−N(1A) angle has a value of 106.5°. In keeping with the C_2 symmetry of the ligand, the plane defined by the water and the 2,6-diformylpyridyl atoms is perpendicular to the average plane defined by the six glucosidic O-4 atoms. Clearly, the three nitrogen atoms are well positioned to coordinate a metal fragment inside the CD cavity. As expected, treatment of ligands **4a/4b** with $FeCl_2$ afforded the desired complexes **5a/5b** in good yields. Both compounds could be univocally identified by mic-

[a] Laboratoire de Chimie Inorganique Moléculaire, Université Louis Pasteur, UMR 7513 CNRS,
1 rue Blaise Pascal, 67008 Strasbourg Cedex, France
E-mail: darmspach@chimie.u-strasbg.fr
dmatt@chimie.u-strasbg.fr
[b] Institut Charles Sadron, UPR CNRS 22,
6 rue Boussingault, 67083 Strasbourg Cedex, France

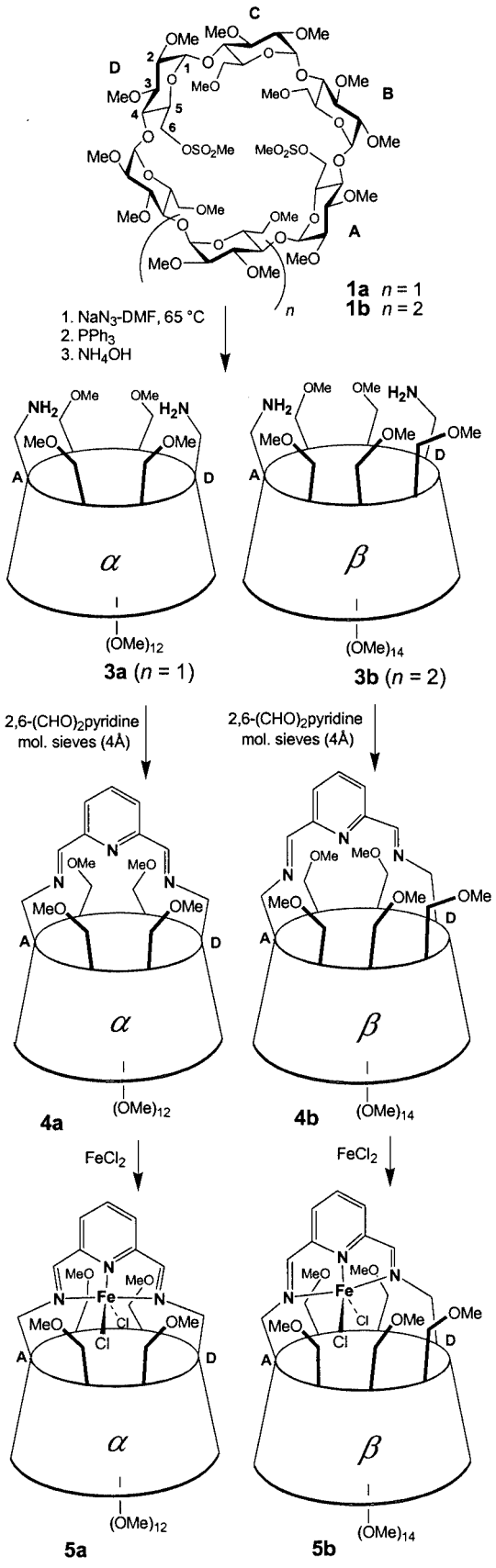

Scheme 1. Synthesis of the iron complexes **5a** and **5b**

roanalysis and FAB-MS measurements, the latter showing an intense peak for the $[M-Cl]^+$ ion in each case. ^{1}H NMR spectroscopy also proved to be useful even though both complexes are paramagnetic. In particular, the C_2 symmetry of **5a** could be confirmed by the presence of eight signals of equal intensity, corresponding to 16 CD methoxy groups, in its ^{1}H NMR spectrum. Although similar Fe^{II}-aldimines are reported to be green-brown,[4] **5a/5b** turned out to be deep blue. This difference in color probably results from the fact that the coordinating unit no longer consists of a 2,6-bis(imino*aryl*)pyridine fragment but, for the first time, of a 2,6-bis(imino*alkyl*)pyridine one. We anticipated that the **5a/5b**-promoted ethylene polymerization might be influenced by this modification, which undoubtedly alters the electronic nature of the Fe^{II} complexes.

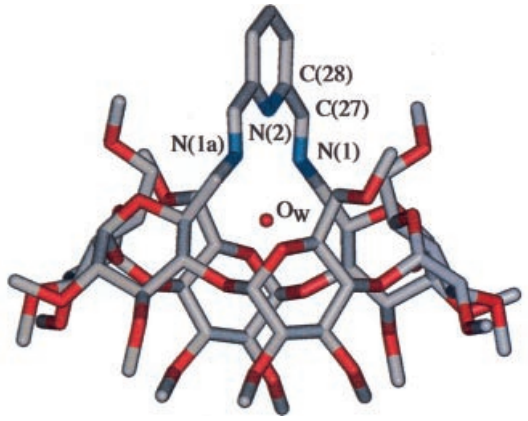

Figure 1. Molecular structure of ligand **5a** (sticks); "O_w" stands for the oxygen atom of the entrapped water molecule

The results of ethylene polymerization are collected in Table 1. Procatalyst **5a**, after activation with a large excess of MAO (methylaluminoxane), proved to be almost inactive. With a maximum TOF value of 125 h^{-1}, **5b**, which possesses a larger cavity, is much more active and produces linear polyethylene, as expected. However, **5b** is still about 1000 times less active than the comparable iron-aldimine system **6**.[3] The presence of a CD cavity tightly wrapped around the metal center may inhibit the chain growing process to the extent that the small α-CD host does not allow any polymerization at all even if **5a** is activated by MAO, as revealed by the change of color from blue to orange. Moreover, **5b** requires larger amounts of MAO than usual to reach the maximum activity (Al/Fe > 2000 equiv.), which means that access to the metal center by MAO may be also hindered to a certain extent. It is also possible that the numerous primary face ether oxygen atoms interact unfavorably with the MAO-generated iron(III) cationic active species,[11] thus reducing the overall rate of polymerization. In terms of molecular weight, melting temperatures and crystallinity, the polyethylene generated by **5b** compares well

Table 1. Results of ethylene polymerization runs using precatalysts **5a** and **5b**

Run	Precatalyst (μmol)	Activator[a] (mmol/equiv.)	T (°C)	T (h)	Yield (mg)	TOF[b] (mol/mol·h)	T_f (°C)	χ_c	M_n (g·mol^{-1})	M_w (g·mol^{-1})	IP
1[c]	**5a** (7.0)	MAO (2.8/400)	25	23	Traces	–	–	–	–	–	–
2[c]	**5a** (7.0)	MAO (7.0/1000)	35	30	1	<1	–	–	–	–	–
3[c]	**5b** (6.8)	MAO (6.8/1000)	20	30	70	12	71.4, 105.6, 124.8	0.76	1700	15300	9.0
4[c]	**5b** (6.8)	MAO (6.8/1000)	40	30	210	37	75.3, 105.5, 124.7	0.79	1970	22300	11.3
5[c]	**5b** (6.8)	MAO (13.6/2000)	40	30	710	125	65.8, 104.1, 123.2	0.72	1460	12800	8.7
6[d]	**5b** (3.7)	MAO (7.4/2000)	40	30	140	25	74.0, 108.0, 126.4	0.77	1150	27300	23.8

[a] For runs 1–5, commercial MAO (in toluene); for run 6, solid MAO (see Exp. Sect.). [b] Turnover frequency, mol of converted ethene/mol of catalyst/h. [c] High pressure reactor conditions: toluene solvent (20 mL), P_{Eth} = 6 bar. [d] High pressure reactor conditions: toluene solvent (15 mL), P_{Eth} = 6 bar.

with that obtained with the classical system **6**. Clearly, the β-CD cavity in **5b** provides adequate steric protection of the active site for the polymer chain to reach an appreciable length, although at the expense of activity.

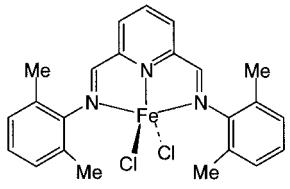

6

We have demonstrated that encapsulation of the metal center in molecular cavities like cyclodextrins is a viable alternative to the active site steric protection provided by substituted aryl rings in 2,6-bis(imino)pyridyl-based ethylene polymerization catalysts. The activity and the potential of the latter may be further improved by using large capped calixarenes, which contain only a limited number of oxygen atoms and provide plenty of space for the chain growth to take place. Investigation of these alternative systems is currently underway.

Experimental Section

General: All manipulations were performed under dry nitrogen using purified solvents. Pyridine dicarboxaldehyde,[12] dimesylate **1**,[10] and diamine **3a**[9] were synthesized according to literature procedures. MAO 10-wt% (Aldrich) was used either as received or as a white powder which was obtained after evaporation of the solvent (60 °C, 3 h). This treatment reduces the amount of residual trimethylaluminium to ca. 3%. The synthesis of compound **3b** starts with the preparation of intermediate **2b**.

Diazide 2b: Dry sodium azide (0.550 g, 8.50 mmol) was added to a solution of **1** (0.650 g, 0.42 mmol) in dry DMF (75 mL). The reaction mixture was stirred under N_2 at 65 °C for 18 h, cooled to room temperature, and then poured into ice-water (200 mL). The aqueous solution was extracted with diethyl ether (4 × 100 mL) and the organic extract washed with water (200 mL) before being dried ($MgSO_4$) and the solvents evaporated to dryness to afford **2** (0.610 g, 100%) as a colorless solid. m.p. 188–190 °C. ^{1}H NMR (200.1 MHz, $CDCl_3$): δ = 3.38 (s, 9 H, CH_3O-6), 3.40 (s, 6 H, CH_3O-6), 3.50 (s, 3 H, OCH_3), 3.51 (s, 9 H, OCH_3), 3.52 (s, 9 H, OCH_3), 3.63 (s, 12 H, OCH_3), 3.64 (s, 3 H, OCH_3), 3.65 (s, 3 H, OCH_3), 3.66 (s, 3 H, OCH_3), 3.15–3.98 (42 H, H-2, H-3, H-4, H-5, H-6), 5.06 (d, ^3J = 3.9 Hz, 1 H, H-1), 5.07 (d, ^3J = 4.1 Hz, 1 H, H-1), 5.12 (d, ^3J = 3.7 Hz, 5 H, H-1) ppm. ^{13}C{^{1}H} NMR (50.3 MHz, $CDCl_3$, 25 °C): δ = 51.9 [×2] (CH_2N_3), 58.3 [×3], 58.4, 58.5 [×2], 58.6, 58.8 [×5], 61.1 [×3], 61.2 and 61.4 [×3] (OCH_3), 70.6, 70.7 [×2], and 70.8 [×4] (C-5), 70.9, 71.2, and 71.5 [×3] (C-6^{B,C,E,F,G}), 80.0 [×4], 80.1 [×2], 81.3 [×3], 81.5, 81.6 [×5], 81.8 [×4], and 81.9 [×2] (C-2, C-3, C-4), 98.2 [×2], 98.8, 98.9, 99.0, and 99.1 [×2] (C-1) ppm. $C_{61}H_{106}N_6O_{33}$ (1451.54): calcd. C 50.48, H 7.36, N 5.79; found C 50.75, H 7.54, N 5.57.

Diamine 3b: Triphenylphosphane (0.610 g, 2.32 mmol) was added to a solution of diazide **2** (0.550 g, 0.39 mmol) in dioxane (6 mL) under N_2. The clear solution was stirred for 1 h at room temperature before adding conc. aqueous NH_4OH solution (1.6 mL) dropwise. After overnight stirring, the reaction mixture was poured into water (200 mL) and the pH of the resulting suspension adjusted to 4 with HCl before being extracted with toluene (5 × 50 mL). The aqueous phase was then made alkaline by adding 2 M NaOH (50 mL) and the compound subsequently extracted with CH_2Cl_2 (5 × 50 mL). The CH_2Cl_2 extract was dried ($MgSO_4$) before being evaporated to dryness. Recrystallisation from heptane afforded **3b** (0.46 g, 84%) as colorless fluffy solid. ^{1}H NMR (200.1 MHz, $CDCl_3$): δ = 1.56 (br. s, 4 H, NH_2), 3.37 (s, 9 H, CH_3O-6), 3.38 (s, 6 H, CH_3O-6), 3.49 (s, 6 H, OCH_3), 3.50 (s, 9 H, OCH_3), 3.53 (s, 6 H, OCH_3), 3.58 (s, 3 H, OCH_3), 3.62 (s, 3 H, OCH_3), 3.63 (s, 3 H, OCH_3), 3.64 (s, 6 H, OCH_3), 3.65 (s, 3 H, OCH_3), 3.67 (s, 3 H, OCH_3), 3.02–3.90 (42 H, H-2, H-3, H-4, H-5, H-6), 5.04–5.11 (5 H, H-1), 5.19 (d, ^3J = 3.7 Hz, 2 H, H-1) ppm. ^{13}C{^{1}H} NMR (50.3 MHz, $CDCl_3$, 25 °C): δ = 42.3 and 42.4 (CH_3N), 57.7, 57.9 [×2], 58.0, 58.2, 58.7 [×3], 58.8 [×2], 58.9 [×2], 60.7 [×2], 61.2 [×2], 61.3 and 61.4 [×2] (OCH_3), 66.7 [×2], 70.9 [×2], and 71.2 (C-6^{B,C,E,F,G}), 70.9 [×5] and 71.3 [×2] (C-5), 79.4, 79.5, 80.1, 80.3 [×3], 80.5, 81.4 [×4], 81.5 [×5], 81.6 [×2], 81.7, 82.4 and 82.8 (C-2, C-3, C-4), 98.4 [×2], 98.6, 98.8 [×2], and 99.2 [×2] (C-1) ppm. $C_{61}H_{110}N_2O_{33}·2H_2O$ (1399.55 + 36.03): calcd. C 51.04, H 8.00, N 1.95; found C 51.16, H 8.03, N 1.85.

Ligand 4a: A solution of diamine **3a** (1.000 g, 0.84 mmol) in CH_3CN (50 mL) and a solution of 2,6-diformylpyridine (0.113 g, 0.84 mmol) in CH_3CN (50 mL) were added simultaneously to a vigorously stirred suspension of molecular sieves (4 Å) in CH_3CN (20 mL) in 1 h at room temperature. The reaction mixture was then

stirred for 1 h at room temperature before being filtered through Celite. Removal of the solvent in vacuo afforded a colorless solid which was recrystallized from $CHCl_3$/pentane to afford pure **4a** (0.500 g, 46%) as a colorless solid. m.p. 200 °C (dec.). ^{1}H NMR (200.1 MHz, $CDCl_3$): δ = 3.03 (s, 6 H, CH_3O-6), 3.18 (s, 6 H, CH_3O-6), 3.44 (s, 6 H, OCH_3), 3.48 (s, 6 H, OCH_3), 3.51 (s, 6 H, OCH_3), 3.64 (s, 12 H, OCH_3), 3.71 (s, 6 H, OCH_3), 2.88−4.77 (36 H, H-2, H-3, H-4, H-5, H-6), 4.95 (d, ^3J = 3.4 Hz, 2 H, H-1), 5.00 (d, ^3J = 3.2 Hz, 2 H, H-1), 5.09 (d, ^3J = 3.4 Hz, 2 H, H-1), 7.51 (d, ^3J = 7.3 Hz, 2 H, H_{pyr}-3,5), 7.96 (t, ^3J = 7.6 Hz, 1 H, H_{pyr}-4), 8.41 (br. m, 2 H, CH=N) ppm. ^{13}C{^{1}H} NMR (50.3 MHz, $CDCl_3$, 25 °C): δ = 57.3, 57.6, 58.0, 58.8, 61.5, 61.8 [×2] and 62.0 (OCH_3), 62.8 (CH_2N), 70.1 and 70.8 (C-6^{B,C,E,F}), 70.3, 70.6 and 72.5 (C-5), 80.4, 81.2 [×2], 81.8, 82.0, 82.5 [×2], 82.6 and 85.3 (C-2, C-3, C-4), 99.2, 99.7 and 100.1 (C-1), 125.9 (C_{pyr}-3,5), 137.9 (C_{pyr}-4), 153.2 (C_{pyr}-2,6), 159.8 (C=N) ppm. MS (FAB): *m*/*z* (%) = 1294.6 (95) [M^+ + H], 1316.6 (25) [M^+ + Na]. $C_{59}H_{95}N_3O_{28}$ (1294.43): calcd. C 54.75, H 7.40, N 3.25; found C 54.71, H 7.69, N 3.14.

Ligand 4b: The previously described procedure was used to prepare **4b** from diamine **3b** (0.450 g, 0.32 mmol) and 2,6-diformylpyridine (0.044 g, 0.32 mmol). Addition of pentane to a solution of crude **4b** in $CHCl_3$ resulted in the precipitation of higher oligomers that were eliminated by filtration. The filtrate was then evaporated to dryness to afford pure **4b** as a colorless amorphous solid (0.300 g, 64%). m.p. 200 °C (dec.). ^{1}H NMR (200.1 MHz, $CDCl_3$): δ = 3.04 (s, 3 H, OCH_3), 3.10 (s, 3 H, OCH_3), 3.30 (s, 6 H, OCH_3), 3.31 (s, 3 H, OCH_3), 3.44 (s, 3 H, OCH_3), 3.47 (s, 9 H, OCH_3), 3.49 (s, 3 H, OCH_3), 3.53 (s, 3 H, OCH_3), 3.58 (s, 3 H, OCH_3), 3.63 (s, 9 H, OCH_3), 3.65 (s, 3 H, OCH_3), 3.67 (s, 3 H, OCH_3), 3.68 (s, 3 H, OCH_3), 3.74 (s, 3 H, OCH_3), 2.85−4.73 (42 H, H-2, H-3, H-4, H-5, H-6), 4.90 (d, ^3J = 3.7 Hz, 1 H, H-1), 4.97 (d, ^3J = 3.4 Hz, 1 H, H-1), 5.02 (d, ^3J = 3.7 Hz, 1 H, H-1), 5.05 (d, ^3J = 3.7 Hz, 2 H, H-1), 5.17 (d, ^3J = 3.9 Hz, 2 H, H-1), 7.51 (d, ^3J = 6.4 Hz, 1 H, H_{pyr}-3 or H_{pyr}-5), 7.62 (t, ^3J = 7.6 Hz, 1 H, H_{pyr}-4), 7.99 (d, ^3J = 6.6 Hz, 1 H, H_{pyr}-3 or H_{pyr}-5), 8.49 (br. s, 2 H, CH=N) ppm. ^{13}C{^{1}H} NMR (50.3 MHz, $CDCl_3$, 25 °C): δ = 57.2, 57.3, 58.0, 58.1 [×3], 58.4 [×2], 58.8 [×3], 59.3, 60.0, 60.6, 60.7, 61.6 [×3], 61.7, 61.9 and 62.0 (OCH_3), 64.9 [×2] (CH_2N), 69.4, 70.1 [×2], and 70.5 [×2] (C-6^{B,C,E,F,G}), 70.2, 70.5, 70.7 [×2], 71.0, 71.3 and 73.6 (C-5), 80.9 [×2], 81.0, 81.2 [×2], 81.3, 81.4 [×3], 81.7 [×2], 81.8 [×2], 81.9, 82.0 [×2], 82.2, 82.4, 82.9, 83.0 and 83.1 (C-2, C-3, C-4), 98.4, 98.6, 99.1, 99.3, 99.6, 99.8 and 100.2 (C-1), 121.7 and 125.0 (C_{pyr}-3,5), 136.9 (C_{pyr}-4), 152.7 and 155.3 (C_{pyr}-2,6), 159.4 and 164.5 (C=N) ppm. $C_{68}H_{111}N_3O_{33}$ (1498.64): calcd. C 54.50, H 7.47, N 2.80; found C 54.62, H 7.70, N 2.71.

Complex 5a: A solution of **4a** (0.400 g, 0.31 mmol) in degassed *n*-butanol (3 mL) was added dropwise to a solution of anhydrous $FeCl_2$ (0.039 g, 0.31 mmol) in *n*-butanol (5 mL) at 80 °C. The resulting blue solution was stirred at 80 °C for 30 min before being cooled to room temperature. The reaction mixture was evaporated almost to dryness whereupon diisopropyl ether (30 mL) was added to precipitate the product as a blue powder, which was subsequently filtered, washed with diethyl ether (3 × 10 mL), and dried to afford 0.280 g of **4** (64%). ^{1}H NMR (400.1 MHz, $CDCl_3$, 25 °C): δ = −44 to +32 (44 H, H-1, H-2, H-3, H-4, H-5, H-6, C*H*=N), −10.19 (6 H, OCH_3), −7.81 (6 H, OCH_3), 1.36 (6 H, OCH_3), 3.88 (6 H, OCH_3), 4.68 (6 H, OCH_3), 6.23 (6 H, OCH_3), 8.98 (6 H, OCH_3), 9.27 (6 H, OCH_3), 46.87 (1 H, H_{pyr}-4), 66.95 (2 H, H_{pyr}-3,5) ppm. MS (FAB): *m*/*z* (%) = 1387.7 (100) [M^+ − Cl]. $C_{59}H_{95}Cl_2FeN_3O_{28}$ (1421.17): calcd. C 49.86, H 6.74, N 2.96; found C 49.76, H 6.64, N 2.81.

Complex 5b: The previously described procedure was used to prepare **5b** from ligand **4b** (0.260 g, 0.17 mmol) and anhydrous $FeCl_2$ (0.022 g, 0.17 mmol) in 5 mL of degassed *n*-butanol. Complex **5b** was obtained as a blue microcrystalline solid in 61% yield (0.170 g). ^{1}H NMR (400.1 MHz, $CDCl_3$, 25 °C): δ = −43.4 to +50.7 (51 H, H-1, H-2, H-3, H-4, H-5, H-6, C*H*=N), −15.24 (3 H, OCH_3), −0.98 (3 H, OCH_3), −0.80 (3 H, OCH_3), 0.14 (3 H, OCH_3), 0.24 (3 H, OCH_3), 0.38 (3 H, OCH_3), 0.78 (3 H, OCH_3), 1.24 (3 H, OCH_3), 1.32 (3 H, OCH_3), 1.42 (3 H, OCH_3), 2.37 (3 H, OCH_3), 3.71 (3 H, OCH_3), 4.67 (3 H, OCH_3), 4.85 (3 H, OCH_3), 5.45 (3 H, OCH_3), 6.38 (3 H, OCH_3), 8.56 (3 H, OCH_3), 9.41 (3 H, OCH_3), 13.03 (3 H, OCH_3), 44.96 (1 H, H_{pyr}-4), 54.15 (1 H, H_{pyr}-3 or H_{pyr}-5), 62.33 (1 H, H_{pyr}-3 or H_{pyr}-5) ppm. MS (FAB): *m*/*z* (%) = 1623.7 (70) [M^+], 1588.7 (100) [M^+ − Cl]. $C_{68}H_{111}Cl_2FeN_3O_{33}$ (1625.39): calcd. C 50.25, H 6.88, N 2.59; found C 50.46, H 7.06, N 2.56.

Crystal Data for 4a: $C_{59}H_{95}N_3O_{28}{\cdot}H_2O{\cdot}5CHCl_3$, M_r = 1909.32, orthorhombic, space group $P2_12_12$, a = 25.3628(2), b =18.2041(3), c = 9.6156(6) Å, V = 4439.6(3) Å^3, Z = 2 (the ligand has crystallographic C_2 symmetry), ρ = 1.43 g·cm^{-3}, Mo-K_α radiation (λ = 0.71073 Å), μ = 0.321 mm^{-1}. Data were collected on a Kappa CCD Enraf−Nonius system at 173 K. The structure was solved by direct methods and refined on F_0^2 by full-matrix least-squares. All non-hydrogen atoms were refined anisotropically. The absolute structure was determined by refining Flack's x parameter. $R1$ = 0.065 and $\omega R2$ = 0.075 for 3478 data with $I > 3\sigma(I)$.
CCDC-192556 contains the supplementary crystallographic data for this paper. These data can be obtained free of charge at www.ccdc.cam.ac.uk/conts/retrieving.html [or from the Cambridge Crystallographic Data Centre, 12, Union Road, Cambridge CB2 1EZ, UK; Fax: (internat.) +44−1223/336−033; E-mail: deposit@ccdc.cam.ac.uk].

Polymerization Procedure: The polymerization reactions were carried out in a Büchi miniclave (200 mL). In a typical procedure, a Schlenk flask was charged with the complex (7 mmol) and toluene (10 mL). The solution was injected into the autoclave together with additional toluene (10 mL) whereupon MAO was introduced. The autoclave was then pressurized with ethene. After completion of the reaction (see reaction conditions in Table 1), acidified ethanol (30 mL) was added to the reaction mixture. Further precipitation was achieved by adding more ethanol. The white polymer was dried under vacuum at 50 °C for 12 h.

Acknowledgments

The authors thank Mrs. S. Zehnacker (Strasbourg) for DSC measurements, and Prof. H. Cramail and E. Ibarboure (Laboratoire de Chimie des Polymères Organiques de Bordeaux) for HT SEC measurements. We also thank the University Louis Pasteur for financial support (projet exceptionnel 2001).

[1] H. G. Alt, A. Köppl, *Chem. Rev.* **2000**, *100*, 1205−1222.
[2] B. L. Small, M. Brookhart, A. M. A. Bennet, *J. Am. Chem. Soc.* **1998**, *120*, 4049−4050.
[3] G. J. P. Britovsek, V. C. Gibson, B. S. Kimberley, P. J. Maddox, S. J. McTavish, G. A. Solan, A. J. P. White, D. J. Williams, *Chem. Commun.* **1998**, 849−850.
[4] G. J. P. Britovsek, M. Bruce, V. C. Gibson, B. S. Kimberley, P. J. Maddox, S. Mastroianni, S. J. McTavish, C. Redshaw, G. A. Solan, S. Strömberg, A. J. P. White, D. J. Williams, *J. Am. Chem. Soc.* **1999**, *121*, 8728−8740.

[5] S. Plentz-Meneghetti, J. P. Kress, P. Lutz, *Macromol. Chem. Phys.* **2000**, *201*, 1823−1832.
[6] S. D. Ittel, L. K. Johnson, M. Brookhart, *Chem. Rev.* **2000**, *100*, 1169−1203.
[7] B. De Bruin, E. Bill, E. Bothe, T. Weyhermüller, K. Wieghardt, *Inorg. Chem.* **2000**, *39*, 2936−2947.
[8] CD derivatives have already been used successfully in non-metal-catalysed polymerisations. See for example: H. Ritter, M. Tabatabai, *Prog. Polym. Sci.* **2002**, *27*, 1713−1720.
[9] D. Armspach, D. Matt, *Inorg. Chem.* **2001**, *40*, 3505−3509.
[10] Z. Chen, J. S. Bradshaw, Y.-F. Shen, Y. Habata, M. L. Lee, *J. Org. Chem.* **1997**, *62*, 8529−8534.
[11] G. J. P. Britovsek, G. K. B. Clentsmith, V. C. Gibson, D. M. L. Goodgame, S. J. McTavish, Q. A. Pankhurst, *Catal. Commun.* **2002**, *3*, 207−211.
[12] N. W. Alcock, R. G. Kingston, P. Moore, C. Pierpoint, *J. Chem. Soc., Dalton Trans.* **1984**, 1937−1948.

Received October 18, 2002
[I02585]

Ti^{IV} Complexes with Novel, Chiral, Tridentate Amido-Amidinate or Monoanionic, Didentate Amidinate Ligands

Jian-Feng Li,[a] Shu-Ping Huang,*[a] Lin-Hong Weng,[b] and Dian-Sheng Liu*[a]

Keywords: Titanium / N ligands / Coordination modes / Rearrangement / Elimination

Reaction of LiL or a new type of dianionic ligand Li_2L (**2**) {H_2L = (1*R*,2*R*)-(−)-1-[N(H)C(Ph)N(SiMe$_3$)]-2-[N(H)SiMe$_3$]-C_6H_{10}} with $TiCl_2(OiPr)_2$ yielded the novel complexes [TiCl(L)(O*i*Pr)$_2$] (**1**) and [Ti(L)(O*i*Pr)$_2$] (**3**), respectively. Treatment of Na_2L' {H_2L' = (1*R*,2*R*)-(−)-1,2-[N(H)C(Ph)N-(SiMe$_3$)]$_2C_6H_{10}$} with $Ti(OiPr)_2Cl_2$ unexpectedly gave **3** via a unusual rearrangement/elimination reaction; The structure of complex **3** shows both an η^3-π bond and σ-bonds to the central metal. This is a new coordination model and is obtained for the first time for this type of amido-amidinate complex.

(© Wiley-VCH Verlag GmbH & Co. KGaA, 69451 Weinheim, Germany, 2003)

There has been an intense interest in organometallic complexes with amidinate ligands as these ligands have proven to be very versatile due to the ease of adapting their properties to the steric and electronic requirements of the metal centre simply by changing the substitution at the terminal nitrogen atoms.[1,2] For group 4 transition metals, amidinates have been used as ancillary ligands in olefin polymerization catalysis.[3,4] Recently, several groups have reported the introduction of an additional electron-donor amine or pyridine functionality thus forming six-electron-donor, three-coordinate ligands that are close analogues of Cp ligands.[5−9] This system may be sub-divided into models **A**−**C** (see Scheme 1): (**A**) a mixed ligand with the amine group and amidinate attached to the central metal via η^3-π and σ bonds {e.g. Ge[$C_6H_{11}NC(CMe_3)NC_6H_{11}]_2$};[10] (**B**) a linked amido-amidinate ligand with the tertiary amine functionality as a pendant group on the amidinate framework and the nitrogen of the amine bonding through a lone pair of electrons {e.g. [Al{N(SiMe$_3$)C(Ph)N(CH$_2$)$_3$NMe$_2$}Cl$_2$];[9] (**C**) a linked amido-amidinate ligand but with η^3-π- and σ-bonds both to the central metal — a new type of ligand that we have developed.

Recently, we reported a fully characterized chiral amidinate ligand of type **B** (LiL) {HL = (1*R*,2*R*)-(−)-1-[N(H)C(Ph)N(SiMe$_3$)]-2-[N(H)SiMe$_3$]C_6H_{10}} containing a pendant amine group.[11−13] To apply our preceding work in transition element chemistry and explore the ligand geometry and bonding modes, we report here the synthesis of

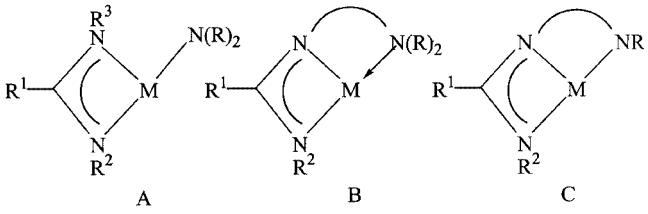

Scheme 1. Three ligand models

[TiCl(L)(O*i*Pr)$_2$] (**1**) from LiL, and, for the first time, a new, chiral, dianionic tridentate amido-amidinate ligand (Li_2L; **2**), similar to type **C** and its corresponding titanium compound [Ti(L)(O*i*Pr)$_2$] (**3**). The crystallographic studies and comparison of the complexes **1** and **3** show several noteworthy features.

Treatment of LiL with one equivalent of $TiCl_2(OiPr)_2$ gave the mixed-ligand monochloride complex [TiCl(L)(O-*i*Pr)$_2$] (**1**; Scheme 2). A second deprotonation of LiL with *n*BuLi gave white crystals of Li_2L (**2**) in high yield (80%). Reaction of **2** with $TiCl_2(OiPr)_2$ afforded yellow, crystalline [Ti(L)(O*i*Pr)$_2$] (**3**), in marked contrast to the didentate amidinate product **1**.

Interestingly, treatment of Na_2L' {H_2L' = [(1*R*,2*R*)-(−)-1,2-[N(H)C(Ph)N(SiMe$_3$)]$_2C_6H_{10}$]} (derived from the lithium compound by reaction with *t*BuNa and synthesized in a manner analogous to that employed for the preparation of benzamidinates[6,9,11]) with $TiCl_2(OiPr)_2$ also gave compound **3**, probably via an unusual rearrangement/elimination reaction (Scheme 3)[14] that is actually the reverse reaction of the addition reaction. A similar reaction was reported by Richeson in which the treatment of two equivalents of Li[N(SiMe$_3$)C(*t*Bu)N(SiMe$_3$)] with $SnCl_2$ or $GeCl_2$ gave mixed amido-amidinate complexes of type **A** and loss

[a] School of Chemistry and Chemical Engineering, The Shanxi University,
Shanxi 030006, China
Fax: (internat.) +86-351/7018091
E-mail: dsliu@sxu.edu.cn
[b] Department of Chemistry, The Fudan University,
Shanghai, China

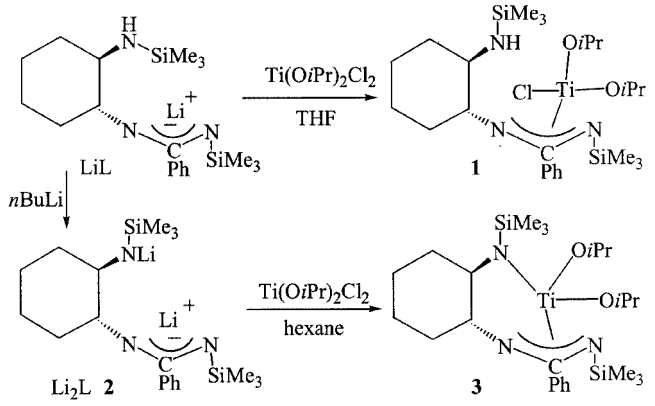

Scheme 2. Synthesis of complexes **1**−**3**

of *t*BuCN.[15] Their investigation showed that the lithium reagent rearranges to form the amido complex, with a 1,3 trimethylsilyl group migration and elimination of *t*BuCN, upon dissolution in Et_2O, prior to reaction with the metal chloride. In our case, from the ^1H and ^{13}C NMR spectroscopic data of [Na_2L'] there was no such rearrangement/elimination in hexane, and treatment of [Li_2L'] with $ZrCl_4$ gave a linked bis(amidinate) complex [$Zr(L')Cl_2(THF)$] without loss of PhCN (as confirmed by X-ray diffraction).[16] Thus, treatment of [Na_2L'] with $TiCl_2(OiPr)_2$ is likely to proceed via a transition state such as intermediate **I** in Scheme 3, and then lead directly to an amido-amidinate titanium complex of type **C** by an intramolecular rearrangement/elimination of $SiMe_3$/PhCN. The driving force for this reaction might be the steric effects of the isopropoxy groups attached to the Ti atom.

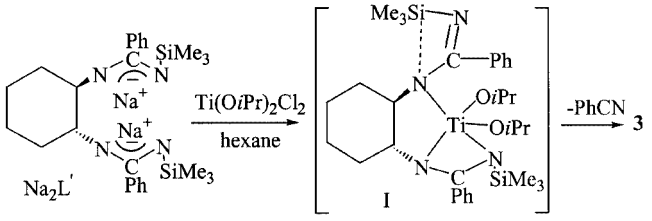

Scheme 3. Reaction of [Na_2L'] with $TiCl_2(OiPr)_2$

The structures of complexes **1**−**3** were determined by X-ray diffraction and elemental analysis; ^1H and ^{13}C NMR spectroscopy also gave satisfactory results. The molecular structure of **1** is shown in Figure 1. The ligand is doubly coordinated to the central metal atom with Ti−N bond lengths of 2.128(3) and 2.078(4) Å. The benzamidinate ligands form four-membered rings that are almost coplanar with the titanium atom [torsion angle N(5)−C(10)−N(6)−Ti(1) = 9.27°]. The dihedral angle between the benzyl moiety and N5−N6−Ti1 is almost vertical (95.4°), with the two isopropyl groups placed above/below the N5−N6−Ti1 plane.

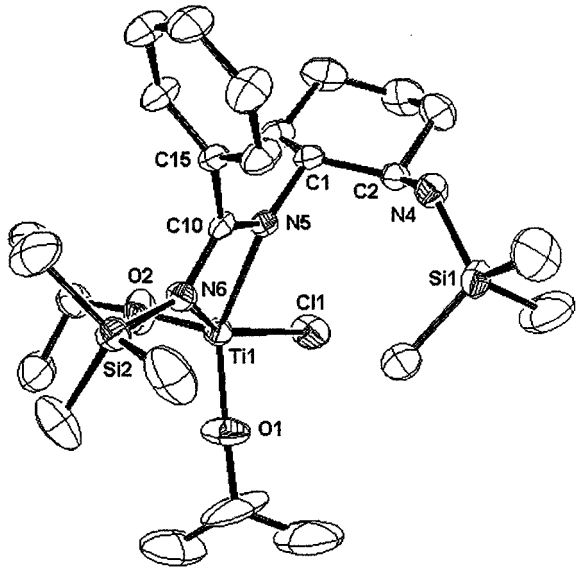

Figure 1. ORTEP view of **1** with thermal ellipsoids at 50% probability level (for one of the two independent molecules in the unit cell); all hydrogen omitted for clarity; selected bond lengths (Å) and angles (deg): N5−Ti1 2.128(3), N6−Ti1 2.078(4), C10−Ti1 2.521(4); N5−C10−N6 112.7(4), N5−Ti1−N6 63.51(13), N5−C1−C2 110.5(3), C1−C2−N4 111.8(4), C1−N5−Ti1 143.1(3)

The molecular structure of **2** is shown in Figure 2. Dimeric aggregation is observed and built around a nearly planar Li_4 ring. However, the coordination number of the Li atoms is different — two are four-coordinate and the other two are three- and two-coordinate — and the Li−Li distances range from 2.415(13) to 2.641(13) Å. Two of the five-membered Li−N−C−C−N rings adopt an envelope conformation.

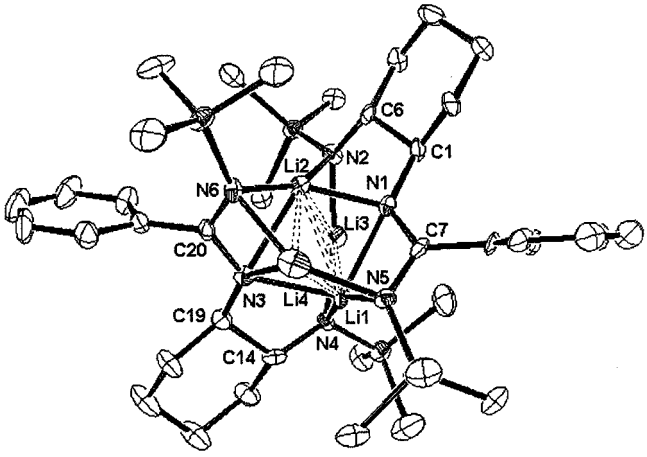

Figure 2. ORTEP view of **2** with thermal ellipsoids at 30% probability level; all hydrogen atoms omitted for clarity; selected bond lengths (Å) and angles (deg): Li1−N1 2.225(10), Li1−N4 1.982(10), Li1−N5 2.039(10), Li1−N3 2.133(9); N1−C7−N5 117.6(5), N6−C20−N3 116.0(5)

The crystal structure determination of **3** confirmed the tridentate nature and the chelating bonding mode of the

linked amido-amidinate ligand (Figure 3). The ligand adopts an approximately meridional coordination mode with the amidinate attached to the metal in an η^3-fashion [two Ti−N bonds of 2.087(2) and 2.127(3) Å; Ti−C = 2.492(3) Å] and the amido group by a σ-bond [Ti−N = 1.972(2) Å], a distinct difference from complexes of type **B**, which have a coordinated lone pair of electrons and obvious differences in bond lengths.[8]

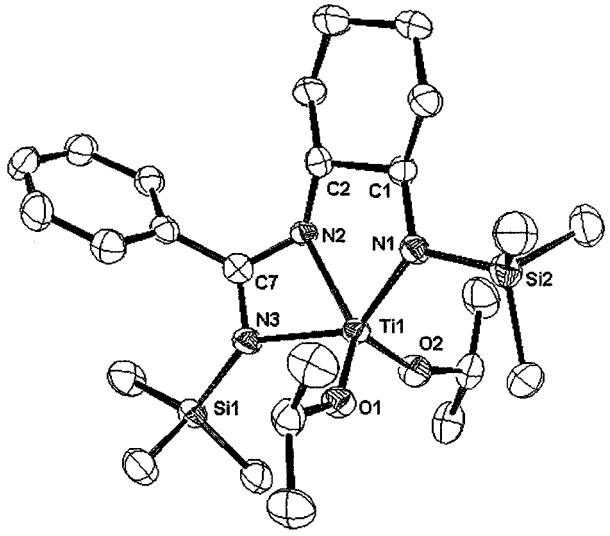

Figure 3. ORTEP view of **3** with thermal ellipsoids at 50% probability level; all hydrogen omitted for clarity; selected bond lengths (Å) and angles (deg): N1−Ti1 1.972(2), N2−Ti1 2.087(2), N3−Ti1 2.127(3), Ti1−C7 2.492(3); C2−C1−N1 108.9(2), C1−C2−N2 103.0(2), C2−N2−Ti1 116.79(18), N2−C7−N3 111.1(3), O1−Ti1−O2 108.82(10)

A comparison of the geometry in **3** with the parent complex **1** shows that the ligand responds to the tethering in the following way: The titanium atom in **3** links to N1 and N2 forming a five-membered ring and thus gives a rigid, bicyclic core with the cyclohexane. This behavior restricts the angles C2−C1−N1 [108.9(2)°] and C1−C2−N2 [103.0(2)°] [the same angles in **1** are 111.8(4) and 110.5(3)°]. As a result of this coordination sphere, the C2−N2−Ti1 angle [116.79(18)°] in **3** is dramatically smaller than the C1−N5−Ti1 angle in **1** [143.1(3)°]. The bond between Ti and the pendant amido group also greatly weakens the *trans* nature of the ligand, with the N1−C1−C2−N2 torsion angle in **3** being −42.68 (1)° [62.71(42)° in **1**].

Experimental Section

General: All manipulations were carried out under argon, using standard high-vacuum, Schlenk techniques. Deuterated solvents (C_6D_6, $CDCl_3$) were dried over Na/K alloy and vacuum transferred before use. Hexane, Et_2O and THF were distilled from over Na or Na/K alloy before use; chlorinated solvents were distilled from over activated molecular sieves (3 Å) or CaH_2. Benzonitrile was redistilled and dried over activated molecular sieves (4 Å) before use. ^{1}H (300 MHz) and ^{13}C (75.47 MHz) NMR spectra were recorded on a Bruker DRX-300 spectrometer at ambient temperature. Element analyses were performed by the Analysis Center of Shanxi University.

Preparation of [(1*R*,2*R*)-(−)-1-{NC(Ph)N(SiMe$_3$)}-2-{N(H)SiMe$_3$}-C$_6$H$_{10}$][TiCl(O*i*Pr)$_2$]: White solid $TiCl_2(OiPr)_2$ (0.28 g, 1.12 mmol) was added at −78 °C to a solution of LiL (0.41 g, 1.12 mmol) in 20 mL of THF. The mixture was warmed to room temperature slowly and stirred for 12 h. Subsequently, the solvent was removed in vacuo and the residual yellow solid was extracted with hexane (15 mL). The extract was concentrated to ca. 5 mL and cooled to −10 °C for two days, yielding 0.49 g (79%) of pale-yellow, crystalline **1**. ^{1}H NMR ($CDCl_3$): δ = −0.12 [s, 9 H, NSi(C*H*$_3$)$_3$], 0.06 [s, 9 H, NSi(C*H*$_3$)$_3$], 0.72 (m, 1 H, C*H*), 0.92 (m, 1 H, C*H*), 1.33 (m, 12 H, 2 × OCHC$_2$*H*$_6$), 1.48 (m, 2H C*H*), 1.57 (m, 2 H, C*H*), 1.77 (m, 1 H, C*H*), 2.18 (m, 1 H, C*H*), 2.53 (m, 1 H, C*H*), 3.17 (m, 1 H, C*H*), 4.81 (m, 2 H, 2 × OC*H*C$_2$H$_6$), 7.19 (m, 2 H, Ph), 7.39 (m, 3 H, Ph) ppm. ^{13}C NMR ($CDCl_3$): δ = 2.4 [s, (*C*H$_3$)$_3$], 2.5 [s, (*C*H$_3$)$_3$], 26.4 (s, OCH*C*$_2$H$_6$), 26.5 (s, OCH*C*$_2$H$_6$), 33.9 (s, NCC*C*), 38.9 (s, NCC*C*), 54.8 (s, NC*C*), 66.8 (s, CN), 78.2 (s, CN), 83.4 (s, O*C*HC$_2$H$_6$), 83.6 (s, O*C*HC$_2$H$_6$), 129.2 (s, *C*$_5$H$_5$), 130.0 (s, *C*$_5$H$_5$), 136.0 (s, *C*C$_5$H$_5$), 181.2 (s, *C*Ph) ppm. $C_{25}H_{48}ClN_3O_2Si_2Ti$ (562.19): calcd. C 53.41, H 8.61, N 7.47; found C 53.45, H 8.68, N 7.28.

Preparation of Li$_2$L (2): *n*BuLi (2.98 mL, 2.22 M in hexane) was added carefully to a solution of LiL (2.436 g, 6.63 mmol) in hexane (50 mL) by syringe at 0 °C. The mixture was warmed to ambient temperature slowly and stirred overnight. The clear, pale-yellow solution was concentrated to ca. 15 mL, to give colorless, pillar-like, crystalline **2** (1.98 g, 80%). ^{1}H NMR ([D$_6$]benzene): δ = 0.06 [s, 9 H, NSi(C*H*$_3$)$_3$], 0.59 [s, 9 H, NSi(C*H*$_3$)$_3$], 0.85 (m, 1 H, C*H*),1.19 (m, 1 H, C*H*), 1.44 (m, 4 H, C*H*), 1.65 (m, 1 H, C*H*), 1.90 (m, 1 H, C*H*), 3.08 (m, 1 H, C*H*), 3.30 (m, 1 H, C*H*), 7.22 (m, 2 H, Ph), 7.43 (m, 3 H, Ph) ppm. ^{13}C NMR ([D$_6$]benzene): δ = 2.8 [s, (*C*H$_3$)$_3$], 5.3 [s, (*C*H$_3$)$_3$], 26.3 (s, NCC*C*), 27.1 (s, NCC*C*), 35.1 (s, NC*C*), 40.6 (s, NC*C*), 65.1 (s, CN), 67.5 (s, CN), 128.1−128.7 (m, *C*$_5$H$_5$), 141.5 (s, *C*C$_5$H$_5$), 180.4 (s, *C*Ph) ppm. $C_{19}H_{33}Li_2N_3Si_2$ (373.55): calcd. C 61.09, H 8.90, N 11.25; found C 61.23, H 9.11, N 11.01.

Preparation of [(1*R*,2*R*)-(−)-1-{NC(Ph)N(SiMe$_3$)}-2-(NSiMe$_3$)-C$_6$H$_{10}$][Ti(O*i*Pr)$_2$]: $TiCl_2(OiPr)_2$ (0.28 g, 1.17 mmol) was added at 0 °C to a solution of Li_2L (**2**; 0.44 g, 1.17 mmol) in 25 mL of hexane. The mixture was warmed to room temperature and stirred overnight. Then, the yellow solution was filtered and reduced to ca.10 mL. Cooling to −20 °C for 5 days yielded 0.47 g (76%) of yellow crystalline **3**. ^{1}H NMR ($CDCl_3$): δ = −0.12 [s, 9 H, NSi(C*H*$_3$)$_3$], 0.24 [s, 9 H, NSi(C*H*$_3$)$_3$], 0.98 (m, 2 H, C*H*), 1.33 (m, 12 H, 2×OCHC$_2$*H*$_6$), 1.57 (m, 4 H, C*H*), 1.80 (m, 1 H, C*H*), 1.96 (m, 1 H, C*H*), 2.81 (m, 1 H, C*H*), 3.57 (m, 1 H, C*H*), 4.66 (m, 2 H, 2 × OC*H*C$_2$H$_6$), 7.28 (m, 2 H, Ph), 7.40 (m, 3 H, Ph) ppm. ^{13}C NMR ($CDCl_3$): δ = 2.1 [s, (*C*H$_3$)$_3$], 4.3 [s, (*C*H$_3$)$_3$], 25.3 (s, NCC*C*), 26.2 (s, NCC*C*), 27.0 (s, OCH(*C*H$_3$)CH$_3$], 27.1 (s, OCH(CH$_3$)*C*H$_3$], 27.5 (s, OCH(*C*H$_3$)CH$_3$], 27.6 (s, OCH(*C*H$_3$)CH$_3$], 34.7 (s, NC*C*), 36.4 (s, NC*C*), 71.0 (s, CN), 71.3 (s, CN), 76.1 (s, O*C*HC$_2$H$_6$), 76.7 (s, O*C*HC$_2$H$_6$), 137.4 (s, *C*C$_5$H$_5$), 178.4 (s, *C*Ph) ppm. $C_{25}H_{47}N_3O_2Si_2Ti$ (525.74): calcd. C 57.12, H 9.01, N 7.99; found C 57.30, H 9.23, N 7.63.

Crystal Structure Analysis of 1−3: Bruker SMART APEX diffractometer/CCD area detector, Mo-K_α radiation (λ = 0.71073 Å). Crystal data for **1**: $C_{25}H_{48}ClN_3O_2Si_2Ti$, M = 562.19, orthorhombic, space group $P2_12_12_1$, a = 11.1529(15) Å, b = 13.5196(18) Å, c = 43.770(6) Å, α = 90.00°, V = 6599.7(15) Å^3, Z = 8, $D_{calcd.}$ = 1.130 g/cm^3, T = 180(2) K, scan type ω, μ = 0.436 mm^{-1}, 27252 measured reflections, 11565 independent reflections (R_{int} =

0.0475), refinement on F^2, R_1 [$F^2 > 2\sigma(F^2)$] = 0.0587, ωR_2 = 0.1294.

Crystal data for **2**: $C_{38}H_{66}Li_4N_6Si_4$, M = 747.09, orthorhombic, space group $P2_12_12_1$, a = 13.136(3) Å, b = 18.020(4) Å, c = 19.569(5) Å, α = 90.00°, V = 4632(2) Å^3, Z = 4, $D_{calcd.}$ = 1.071 g/cm^3, T = 180(2) K, scan type ω, μ = 0.159 mm^{-1}, 16612 measured reflections, 7566 independent reflections (R_{int} = 0.0945), refinement on F^2, R_1 [$F^2 > 2\sigma(F^2)$] = 0.0688, ωR_2 = 0.0942.

Crystal data for **3**: $C_{25}H_{47}N_3O_2Si_2Ti$, M = 525.74, orthorhombic, space group $P2_12_12_1$, a = 10.566(2), b = 13.500(3), c = 21.385(4) Å, α = 90.00°, V = 3050.1(10) Å^3, Z = 4, $D_{calcd.}$ = 1.145 g/cm^3, T = 193(2) K, scan type ω, μ = 0.383 mm^{-1}, 12610 measured reflections, 5313 independent reflections (R_{int} = 0.0363), refinement on F^2, R_1 [$F^2 > 2\sigma(F^2)$] = 0.0482, ωR_2 = 0.0888.

CCDC-183020 (**1**), -191953 (**2**) and -191954 (**3**) contain the supplementary crystallographic data for this paper. These data can be obtained free of charge at www.ccdc.cam.ac.uk/conts/retrieving.html [or from the Cambridge Crystallographic Data Centre, 12, Union Road, Cambridge CB2 1EZ, UK; fax: (internat.) +44-1223/336-033; E-mail: deposit@ccdc.cam.ac.uk].

Acknowledgments

We thank the Natural Science Foundation of China (20171030 and 29872024, D.-S. L.) and the Science Foundation of ShanXi province, China (20011008, D.-S. L.).

[1] For a general review, see: J. Barker, M. Kilner, *Coord. Chem. Rev.* **1994**, *133*, 219−300.
[2] F. T. Edelmann, *Coord. Chem. Rev.* **1994**, *137*, 403−481.
[3] J. C. Flores, J. C. W. Chien, M. D. Rausch, *Organometallics* **1995**, *14*, 1827−1833.
[4] A. Littke, N. Sleiman, C. Bensimon, D. S. Richeson, *Organometallics* **1998**, *17*, 446−451.
[5] M. P. Coles, D. C. Swenson, R. F. Jordan, V. G. Young, Jr., *Organometallics* **1997**, *16*, 5183−5194.
[6] M. J. R. Brandsma, E. A. C. Brussee, B. Hessen, J. H. Teuben, *Eur. J. Inorg. Chem.* **1998**, 1867−1870.
[7] K. Kincaid, C. P. Gerlach, G. R. Giesbrecht, J. Hagadorn, G. D. Whitener, A. Shafir, J. Arnold, *Organometallics* **1999**, *18*, 5360−5366.
[8] S. Bambirra, M. J. R. Brandsma, E. A. C. Brussee, A. Meetsma, B. Hessen, J. H. Teuben, *Organometallics* **2000**, *19*, 3197−3204.
[9] D. Doyle, Y. K. Gun′Ko, P. B. Hitchcock, M. F. Lappert, *J. Chem. Soc., Dalton Trans.* **2002**, 4093−4097.
[10] S. R. Foley, C. Bensimon, D. S. Richeson, *J. Am. Chem. Soc.* **1997**, *119*, 10359−10363.
[11] J.-F. Li, L.-H. Weng, X.-H. Wei, D.-S. Liu, *J. Chem. Soc., Dalton Trans.* **2002**, *07*, 1401−1405.
[12] J.-F. Li, L.-H. Weng, S.-P. Huang, H.-B. Tong, D.-S. Liu, *Acta Crystallogr. Sect. E* **2002**, *58*, o1078−1080.
[13] J.-F. Li, L.-H. Weng, S.-P. Huang, H.-B. Tong, D.-S. Liu, *Acta Crystallogr. Sect. E* **2002**, *58*, m510−512.
[14] $TiCl_2(OiPr)_2$ (0.19 g, 0.82 mmol) was added at 0 °C to a solution of Na_2L' (0.42 g, 0.82 mmol) in 20 mL of hexane. The mixture was warmed to room temperature and stirred for 48 h. Subsequently, the yellow solution was filtered and reduced to ca. 10 mL. Cooling to −20 °C for seven days yielded 0.32 g (74%) of yellow crystalline **3**.
[15] S. R. Foley, Y. Zhou, G. P. A. Yap, D. S. Richeson, *Inorg. Chem.* **2000**, *39*, 924−929.
[16] Unpublished work. Crystal data deposited at Cambridge Crystallographic Data Centre as CCDC-173962.

Received October ö21, 2002
[I02578]

Tellurium(II) Dialkanethiolates: $n_p(S)$-σ*(Te−S′) Orbital Interactions Determine the ^{125}Te NMR Chemical Shift, and the Molecular and Crystal Structure

Holger Fleischer,*[a] Norbert W. Mitzel,[b] and Dieter Schollmeyer[c]

Keywords: NMR spectroscopy / Noncovalent interactions / Solid-state structures / Sulfur / Tellurium

Tellurium(II) dimethanethiolate, $Te(SMe)_2$, and tellurium(II) diethanethiolate, $Te(SEt)_2$, were synthesized by reaction of TeO_2 and $Te(OiPr)_4$ with HSMe and HSEt, respectively. In the solid state, $Te(SMe)_2$ exhibits a *cis*-conformation of the methyl groups with respect to the TeS_2 plane – an unprecedented situation for nonfunctionalized organotrichalcogenides – whereas $Te(SEt)_2$ shows a *trans*-conformation. Ab initio calculations performed for $Te(SMe)_2$ and $Te(SEt)_2$ show that the *cis*- and *trans*-conformers represent minima on the potential energy surface and are stabilized by intramolecular π-type n(S)-σ*(Te–S′) orbital interactions. In the solid state, the molecules of each compound are associated through two centrosymmetric Te_2S_2 units with two of their neighbors, resulting in tetracoordinate Te atoms with distorted trapezoidal configurations. While the intermolecular Te···S distance increases in the sequence R = Me < Et < *i*Pr < *t*Bu, the length of the covalent Te–S bond decreases in the same order, a result attributed to intermolecular σ-type $n_p(S)$-σ*(Te–S′) orbital interactions. The ^{125}Te NMR chemical shift of $Te(SR)_2$ largely depends on R (R = Me, Et, *i*Pr, *t*Bu) and shows a nearly linear correlation with the first ionization energy of the corresponding thiol HSR. Ab initio calculations of the ^{125}Te NMR shifts for the model compound $Te(SH)_2$ (C_2 symmetry) reveal that it also depends strongly on the HSTeS torsion angle. These results can be explained by a model in which π-type $n_p(S)$-σ*(Te–S′) and $n_p(Te)$-σ*(S–H) orbital interactions determine the paramagnetic shielding of the tellurium nucleus.

(© Wiley-VCH Verlag GmbH & Co. KGaA, 69451 Weinheim, Germany, 2003)

Introduction

In nearly every case known so far, noncyclic diorganotrichalcogenides, $RE^1E^2E^3R$ (see Scheme 1), exhibit a helical structure, as is the case in hexagonal selenium or tellurium, i.e. both R groups are *trans* with respect to the $E^1E^2E^3$ plane.[1−5] Spectroscopic and quantum chemical investigations have clearly demonstrated that trisulfane, HSSSH, can exist as both the *cis*- and *trans*-conformer. Due to the small steric demand of the hydrogen atoms, their energies differ by only 1 kJ·mol^{-1} in favor of the *trans*-conformer.[6,7]

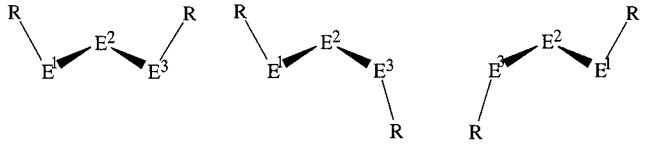

Scheme 1. Structural formulae of the organotrichalcogenides with *cis*- (left) and two enantiomeric *trans*- (middle and right) conformations (R = organic group, E^1, E^2, E^3 = S, Se, Te)

Tellurium(II) dithiolates, $Te(SR)_2$, are thermally and photochemically unstable with respect to decomposition to elemental tellurium and disulfide, RSSR, but their kinetic stability depends very much on R.[3,8] This class of compounds is thus a source of elemental tellurium, whose release and deposition on surfaces can be controlled by thermal energy and irradiation. Recent ab initio studies have shown that the kinetic stability is due to the conformation of the CSTeS unit, which, in turn, is likely to be a consequence of π-type $n_p(S^1)$-σ*(Te−S^2) orbital interactions.[8] The motivation of the present research was to synthesize sterically noncrowded tellurium(II) dithiolates, $Te(SR)_2$, and to investigate their stability, physical properties and structural features.

Results and Discussion

Synthesis

$Te(SMe)_2$ and $Te(SEt)_2$ were prepared by reductive elimination from Te^{IV} compounds according to Equations (1) and (2):

[a] Institut für Anorganische Chemie und Analytische Chemie, Johannes Gutenberg Universität Mainz,
Duesbergweg 10−14, 55099 Mainz, Germany
Fax: (internat.) + 49-(0)6131/3923351
E-mail: fleische@mail.uni-mainz.de
[b] Institut für Anorganische und Analytische Chemie, Westfälische Wilhelms-Universität Münster
48149 Münster, Germany
[c] Institut für Organische Chemie, Johannes Gutenberg Universität Mainz
Duesbergweg 10−14, 55099 Mainz, Germany

$$TeO_2 + 4\ MeSH \rightarrow Te(SMe)_2 + (SMe)_2 + 2\ H_2O \quad (1)$$

$$Te(O\mathit{i}Pr)_4 + 4\ EtSH \rightarrow Te(SEt)_2 + (SEt)_2 + 4\ HO\mathit{i}Pr \quad (2)$$

Both compounds form yellow crystals giving dark red liquids on melting. They are stable towards air and water, but, like other tellurium(II) dithiolates,[4] are thermodynamically unstable towards decomposition to Te and the respective disulfides. They are kinetically much less stable than $Te(S\mathit{i}Pr)_2$ and $Te(S\mathit{t}Bu)_2$ and, within a few hours, the walls of glass flasks containing one of the compounds at room temperature are covered by a thin, mirror-like film of tellurium. $Te(SMe)_2$ and $Te(SEt)_2$ are also very sensitive to light, and in order to minimize decomposition the compounds were kept in the dark at −40 °C.

Like $Te(S\mathit{i}Pr)_2$ and $Te(S\mathit{t}Bu)_2$, $Te(SMe)_2$ and $Te(SEt)_2$ exchange their thiolate ligands with thiols and other tellurium(II) dithiolates.[4] On the other hand, cryoscopic measurements hint at $Te(SMe)_2$ being monomeric in cyclohexane solution, which means that intermolecular associations are rather weak (vide infra).

NMR Spectroscopy

In contrast to the compounds $Te(OR)_4$, whose ^{125}Te NMR chemical shifts vary only slightly with R, $\delta[^{125}Te(SR)_2]$ depends strongly on R, as can be seen from the data given in Table 1. A major influence of inductive electronic effects or of through-space shielding of the groups R on $\delta(^{125}Te)$ can hence be excluded, since in these cases, the four ligands in $Te(OR)_4$ should have a stronger effect than the two ligands in $Te(SR)_2$. Thus, $\delta[^{125}Te(SR)_2]$ must largely be determined by stereoelectronic effects and should therefore depend on the C−S−Te−S torsion angle. Indeed, ab initio NMR calculations performed in the present study for the model compound $Te(SH)_2$ (C_2 symmetry) revealed a strong dependence of $\delta(^{125}Te)$ on τ(H−S−Te−S), while $\delta[^{125}Te(OH)_4]$ (C_2 symmetry) varies only slightly with $\tau(HO^{eq}TeO^{eq})$ (see Figure 1 and Table 2). For $Te(SH)_2$, the shielding of the ^{125}Te nucleus is at its maximum, i.e. $\delta(^{125}Te)$ is a minimum, if τ(H−S−Te−S) = 90°.[12] Figure 2 shows the nearly linear correlation between $\delta[^{125}Te(SR)_2]$ and the first ionization energy of the corresponding thiol. A theoretical model for these results is presented in terms of natural orbitals and their interaction;[12,13] the relevant data are given in Table 2. The chemical shift of the heavier elements is mainly determined by the paramagnetic contribution to the nuclear shielding, σ_p. In terms of the MO concept, σ_p is proportional to the reciprocal of the energy difference, ΔE, between the highest occupied and the lowest unoccupied MO to which the AOs of the atom considered make a substantial contribution.[14] Hence, the bigger ΔE, the smaller is σ_p and the more the signal is shifted to high field. In terms of localized natural bond orbitals (NBO), the HOMO is mainly represented by the n_p(Te) orbital and the LUMO by the symmetric combination of both σ*(Te−S) orbitals. Nevertheless, a second-order perturbation analysis revealed significant n_p(Te)-σ*(S−H) and n_p(S)-σ*(Te−S′) orbital interactions. According to second-order perturbation theory, the energy of n_p(Te), and thus of the HOMO, is lowered and the energy of σ*(Te−S), and thus of the LUMO, is raised by these interactions. The data given in Table 2 confirm that E_{HOMO} correlates with $E[n_p(Te)\text{-}\sigma^*(S-H)]$ and E_{LUMO} with $E[n_p(S)\text{-}\sigma^*(Te-S')]$. Hence, the energies of HOMO and LUMO also show a strong dependence on τ(HSTeS) and support the model that their difference is essential for $\delta(^{125}Te)$. With Koopman's theorem,[15] the dependence of $\delta(^{125}Te)$ on the first ionization energy of the corresponding thiol can be rationalized. According to this theorem, the first ionization energy of a molecule is equal to the negative energy of its HOMO, i.e. n_{3p}(S) in the case of the thiols. Second-order perturbation theory predicts an increased $n_p(S)\text{-}\sigma^*(Te-S')$ interaction if $E[n_{3p}(S)]$ is raised and hence IE(HSR) is lowered. This has the effect that E_{LUMO} and ΔE are increased and thus $\delta(^{125}Te)$ is decreased, in accordance with the results presented in Figure 1 and 2.[16]

Table 1. ^{125}Te NMR chemical shifts of tellurium(II) dialkanethiolates and tellurium(IV) tetraalkoxides, calculated values are given in parentheses[9]

	R = Me	R = Et	R = *i*Pr	R = *t*Bu
$Te(SR)_2$	1419 (1376) [a]	1184 (1319)[a]	1026 [b]	907 (883) [a,b]
$Te(OR)_4$	1519 (792) [a] [c]	1503 [d]	1538 [c]	–

[a] Calculated value for conformer with C_2 symmetry. [b] Value from reference.[4] [c] Value from reference.[10] [d] Value from reference.[11]

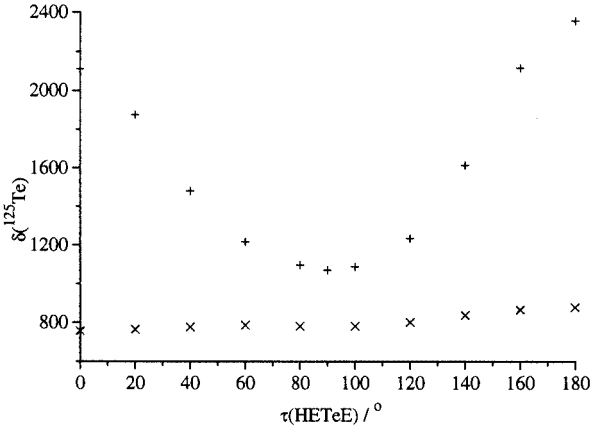

Figure 1. HF/3−21G(d) calculated ^{125}Te NMR chemical shifts of $Te(SH)_2$ (+, C_2 symmetry, MP2/LANL2DZP optimized geometry) and $Te(OH)_4$ (*x*, C_2 symmetry, MP2/LANL2DZP optimized geometry) vs. the H−E−Te−E torsion angle (E = S for $Te(SH)_2$ and $E = O^{eq}$ for $Te(OH)_4$)[9]

The temperature dependence of $\delta(^{125}Te)$ of $Te(SMe)_2$ and $Te(S\mathit{t}Bu)_2$, which is presented in Table 3, can also be interpreted in terms of this model. A rise in temperature will lead to an increased torsional vibration around the Te−S bonds. Since electronic energy and $\delta[^{125}Te(SR)_2]$ exhibit minima for values of τ(X−S−Te−S) close to 90° (X = H, C; see Figure 1 and Figure 6 (b) further down. See also ref.[4]), thermally induced torsional vibrations will increasingly populate angles outside 90° and hence cause an increase in $\delta(^{125}Te)$.

Table 2. Physical data of the model compound $Te(SH)_2$ (C_2 symmetry) as a function of τ(HSTeS)

τ(HS^{1}TeS^2)[a]	Te−S	δ(^{125}Te)	E_{rel}	E_{HOMO}	E_{LUMO}	ΔE	E_1 [b]	E_2 [c]
0	246.0	2112	73.8	−0.29780	0.03080	0.32860	0	0
20	244.7	1876	59.6	−0.30077	0.03690	0.33767	−	17.2
40	242.5	1480	32.0	−0.30875	0.04351	0.35226	10.0	38.5
60	240.9	1217	10.5	−0.32111	0.05373	0.37484	17.9	64.4
80	240.2	1096	0.1	−0.33300	0.05565	0.38865	22.7	80.8
90	240.2	1070	0	−0.33409	0.05611	0.39020	22.9	82.5
100	240.4	1088	3.3	−0.33043	0.05631	0.38674	21.4	79.1
120	241.4	1235	17.8	−0.31659	0.04830	0.36489	14.7	59.9
140	242.9	1615	36.7	−0.30418	0.03560	0.33978	6.9	33.9
160	244.1	2117	53.1	−0.29734	0.02607	0.32341	−	14.3
180	244.6	2358	60.2	−0.29534	0.02299	0.31833	0	0

[a] E_{rel}, E_1 and E_2 in kJ·mol^{-1}, E_{HOMO}, E_{LUMO} and ΔE in Hartree, δ(^{125}Te) relative to $TeMe_2$, Te−S in pm. [b] E_1 is the second order energy for the n_p(Te)-σ*(S−H) orbital interaction in an NBO basis. n_p(Te) also interacts with ry_d(S), but the energy of this interaction is nearly independent of τ(HS^{1}TeS^2) and varies between 10.5 and 12.5 kJ·mol^{-1}. [c] E_2 is the second order energy for the n_p(S)-σ*(Te−S′) orbital interaction in an NBO basis.

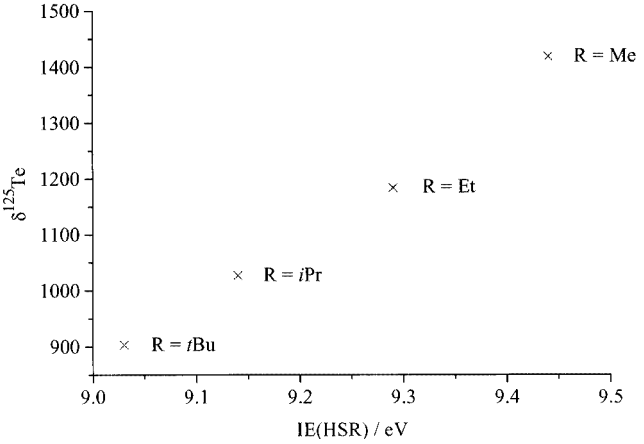

Figure 2. Experimental ^{125}Te NMR chemical shifts of $Te(SR)_2$ vs. first ionization energy of HSR (R = Me, Et, *i*Pr, *t*Bu)

Table 3. ^{125}Te NMR chemical shift of $Te(SMe)_2$ and $Te(StBu)_2$ at different temperatures

T /K	223	243	263	283	298
δ[^{125}Te(SMe)$_2$]	1395	1402	1410	1417	1423
δ[^{125}Te(S*t*Bu)$_2$]	881	885	890	896	901

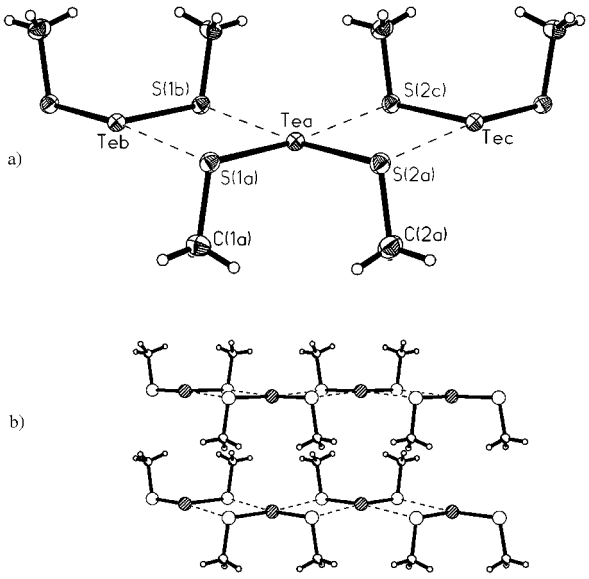

Figure 3. (a) Molecular structure and intermolecular association of *cis*-$Te(SMe)_2$ in the solid state; displacement ellipsoids are at the 50% probability level; (b) packing of chains of [*cis*-$Te(SMe)_2$]$_n$ in the solid state

Molecular and Crystal Structures

The single crystal X-ray structure of $Te(SMe)_2$ (see Figure 3, a) shows this compound to exhibit a *cis*-conformation in the solid state. It is thus different from $Te(SEt)_2$ (see Figure 4, a), $Te(SiPr)_2$, $Te(StBu)_2$ and the isovalence electronic compound $S(OCH_3)_2$, which crystallize as *trans*-conformers.[4,17] Since the energy differences between *cis*- and *trans*-conformers are similar for $Te(SMe)_2$ and $Te(SEt)_2$ (vide infra), packing effects in the crystal are seen to stabilize the *cis*-conformer in one and the *trans*-conformer in the other case. Each $Te(SMe)_2$ and each $Te(SEt)_2$ molecule forms two Te···S bonds to each of its two nearest neighbors, leading to $(TeS_2)_n$ chains in which each Te atom exhibits a distorted trapezoidal coordination (see Figure 3 and 4). In $Te(SEt)_2$, neighboring molecules in these chains exhibit enantiomeric *trans*-conformations. The average intermolecular Te···S distances and the Te−S bond lengths in $Te(SR)_2$ (R = Me, Et, *i*Pr, *t*Bu) correlate with each other, as can be seen in Figure 5: the shorter the intermolecular Te···S distances are, the longer the Te−S bonds become. This corresponds to the correlation of S−S bond lengths with intramolecular S···S distances in 6a-thiathiophthene derivatives.[18] Comparison of the MP2/LANL2DZP optimized structural parameters of monomeric *cis*-$Te(SMe)_2$ with the middle unit of [*cis*-$Te(SMe)_2]_3$ also reveals that Te···S interactions increase the Te−S bond lengths and narrow the S−Te−S angle (see Table 4). This structure correlation leads to the assumption that a σ*(Te−S) orbital is involved

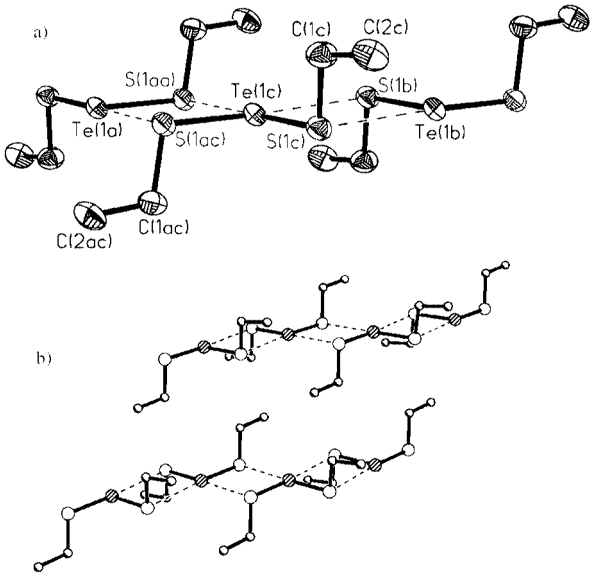

Figure 4. (a) Molecular structure and intermolecular association of $Te(SEt)_2$ in the solid state; displacement ellipsoids are at the 50% probability level; (b) packing of chains of $[trans\text{-}Te(SEt)_2]_n$ in the solid state; hydrogen atoms are omitted for clarity

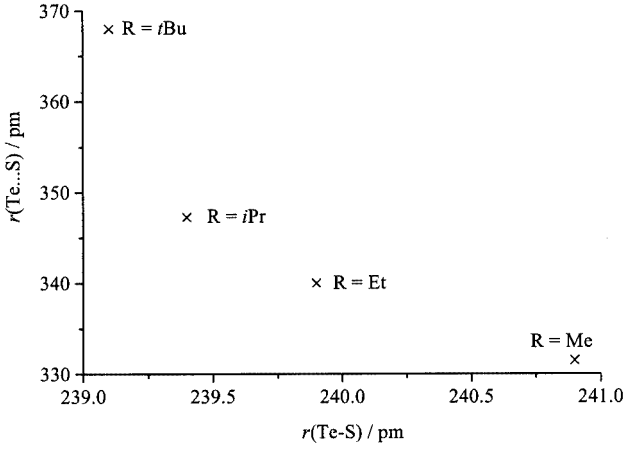

Figure 5. Intermolecular Te···S distances vs. Te−S bond lengths in the solid state structures of $Te(SR)_2$ (R = Me, Et, *i*Pr, *t*Bu); data for $Te(SiPr)_2$ and $Te(StBu)_2$ are taken from reference[4]

in the formation of the Te···S bond. An analysis of the bonding situation in the $Te(SMe)_2$ trimer in terms of natural bond orbitals shows that apart from π-type intramolecular $n_p(S)$-σ*(Te−S′) interactions (69 kJ·mol^{-1}), σ-type intermolecular $n_p(S)$-σ*(Te−S′) interactions (61 kJ·mol^{-1}) are also present. While the former are important for the Te−S bonds, the latter are essential for the Te···S interaction. These σ-type intermolecular $n_p(S)$-σ*(Te−S′) interactions explain the lengthening of the Te−S bond (transfer of electron density into an antibonding orbital) as well as the narrowing of the S−Te−S angle (reduced intramolecular repulsion of the S atoms).

Ab initio Thermochemistry

There are several constitutional isomers of $Te(SMe)_2$, some of which are given in Scheme 2 together with their calculated (MP2/LANL2DZP) relative standard enthalpies. Each of these isomers represents a minimum on the potential energy surface. The *trans*-conformers are given for isomers A and B. In isomers D and E, the Te−C and S−C bond vectors are nearly orthogonal to each other. Isomer A exhibits the lowest standard enthalpy of the entire group, hence $Te(SMe)_2$ is not only the kinetically favored product of the reaction of Te^{IV} compounds with HSMe, but is also thermodynamically more stable than the other constitutional isomers. Isomers A and B, which contain only divalent chalcogen atoms, are more stable than C−E, where one tetravalent chalcogen atom is present. Among the latter, E, which possesses a tetravalent Te atom, is more stable than C and D, which contain tetravalent S atoms. Regarding the relative stabilities of A and B, a comparison with ab initio calculations of the constitutional isomers of HSOSH is of interest.[19] Due to the larger energy of the O−H bond com-

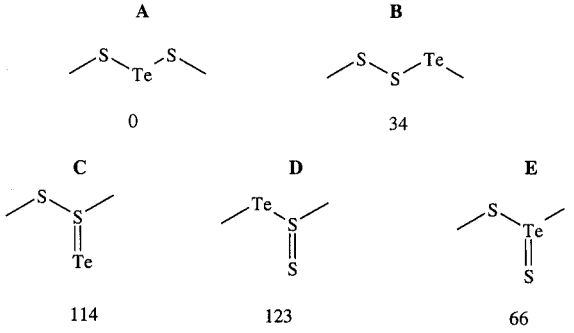

Scheme 2. Different constitutional isomers of $Te(SMe)_2$ (A) and their MP2/LANL2DZP calculated relative standard enthalpies, ΔH^{298} (kJ·mol^{-1})

Table 4. Selected parameters from ab initio optimized and solid-state structures of $Te(SMe)_2$ and $Te(SEt)_2$

	XRD		ab initio		
	$Te(SMe)_2$	$Te(SEt)_2$	$Te(SMe)_2$ [a]	$[Te(SMe)_2]_3$ [b]	$Te(SEt)_2$ [c]
Te−S/pm	240.6(1)/241.2(1)	239.9(1)	239.3	241.3	239.4
Te···S/pm	328.1(1)/334.8(1)	340.0(1)		348.5	
S−C/pm	181.3(4)/181.7(4)	182.8(5)	183.5	183.4	184.1
S−Te−S/°	98.9(1)	98.7(1)	103.4	99.4	100.2
Te−S−C/°	104.0(2)/103.5(1)	104.6(2)	102.9	102.5	101.9
τ_1/°	85.1(2)	80.6(2)	86.4	91.2	76.1
τ_2/°	−86.3(2)	80.6(2)	−86.4	−91.2	76.1

[a] C_s symmetry. [b] All three $Te(SMe)_2$ with C_s symmetry, only parameters for the middle unit are given. [c] C_2 symmetry.

pared to that of the S−H bond, the HOSSH isomer is significantly more stable than the HSOSH form. For $Te(SMe)_2$, an analogous case is assumed regarding the energies of the S−C and the Te−C bond.

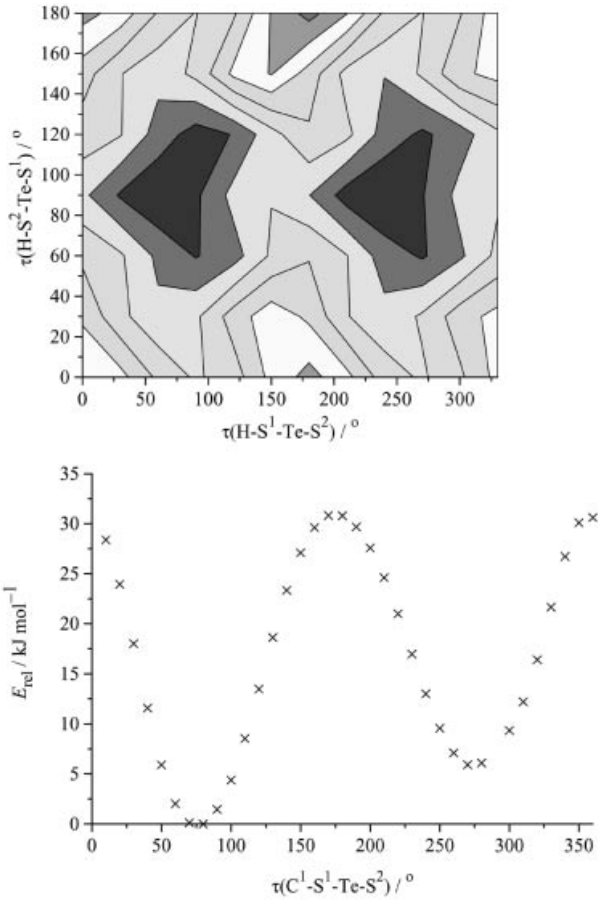

Figure 6. (a) MP2/LANL2DZP electronic energy of $Te(SH)_2$ as a function of both STeSH torsion angles; dark regions correspond to low energies and light regions to high energies; (b) MP2/LANL2DZP electronic energy of $Te(SMe)_2$ as a function of the $C^1-S^1-Te-S^2$ torsion angle; the $C^2-S^2-Te-S^1$ torsion angle was optimized freely and adopted values between 75 and 90°

As can be seen from Figure 6, part a, the model compound $Te(SH)_2$ forms stable *cis*- and *trans*-conformers. The electronic energy of *trans*-$Te(SH)_2$ [left minimum in Figure 6, part a)] is only about 1 kJ·mol^{-1} smaller than that of *cis*-$Te(SH)_2$. The C_{2v} symmetric conformation with $H-S^1-Te-S^2 = H-S^2-Te-S^1 = 180°$ represents a second-order saddle point on the potential energy surface.

Ab initio studies revealed that $Te(SMe)_2$ and $Te(SEt)_2$ also form stable *cis*- and *trans*-conformers. The electronic energies of *trans*-$Te(SMe)_2$ and *trans*-$Te(SEt)_2$ are lower than those of *cis*-$Te(SMe)_2$ and *cis*-$Te(SEt)_2$ by 6 and 5 kJ·mol^{-1}, respectively. The potential energy of $Te(SMe)_2$ as a function of one C−S−Te−S torsion angle is depicted in Figure 6, part b). The barrier between *cis*- and *trans*-$Te(SMe)_2$ amounts to about 30 kJ·mol^{-1} and should thus allow for a rapid interconversion of the two conformers at ambient temperatures.

Conclusion

Characteristic structural and ^{125}Te NMR spectroscopic features of tellurium(II) dialkanethiolates, $Te(SR)_2$, can be explained by intra- and intermolecular $n_p(S)$-σ*(Te−S′) orbital interactions. Since this orbital interaction varies significantly with the C−S−Te−S- torsion angle, the ^{125}Te NMR chemical shift of $Te(SR)_2$ shows a strong dependence on the molecular conformation. While intramolecular $n_p(S)$-σ*(Te−S′) interactions are responsible for molecular conformations, intermolecular $n_p(S)$-σ*(Te−S′) interactions play an essential role in determining the structure in the solid state. Since the orbital energies depend on the ligand, the electronic features of the tellurium atom in $Te(SR)_2$, and hence the reactivity of the compound, can be controlled by changing the nature of the alkyl group R.

Experimental Section

General Procedures: All procedures were carried out under an inert gas atmosphere or in vacuo. Solvents were purified according to standard procedures. If possible, exposure of $Te(SMe)_2$ and $Te(SEt)_2$ to daylight was avoided. Due to their thermal instability, both compounds were stored at −40 °C.

NMR: Bruker DRX 400. IR: Mattson Galaxy 2030 FTIR, resolution 4 cm^{-1}. MS: Finnigan MAT 8230. CHS analysis: Elemental Vario EL2.

$Te(SCH_3)_2$: Liquid methanethiol ($HSCH_3$; 20 mL; ρ(0 °C) = 0.87 g·mL^{-1}, 0.36 mol) was slowly transferred in the gas phase with a stream of argon into an ice-cooled suspension of tellurium dioxide (14.30 g, 89.6 mmol) in methanol (100 mL) and hydrochloric acid (0.5 mL, 37%). During the course of the reaction, the suspension at first became yellow before turning black due to precipitation of elemental tellurium. Subsequently, the solvent and all volatile reaction products were removed from the reaction mixture by low temperature distillation under reduced pressure. The crude product was extracted with petroleum ether several times and, from the combined extracts, yellow crystals of $Te(SCH_3)_2$ precipitated at −40 °C. Yield: 13.92 g (70.5%). M.p. 5 °C. $C_2H_6S_2Te$ (221.79): calcd. C 10.83, H 2.73, S 28.91; found C 10.37, H 2.35, S 27.63. MS(70 eV, EI): *m/z* (%) = 223.6 (36.4) [M^+], 176.7 (27.2) [$TeSCH_3^+$], 93.9 (100.0) [$H_3CSSCH_3^+$] ppm. ^1H NMR (400.000 MHz, C_6D_6, 25 °C, TMS): δ = 2.86 ppm. $^{13}C\{^1H\}$ NMR (100.577 MHz, C_6D_6, 25 °C, TMS): δ = 22.7 ppm. $^{125}Te\{^1H\}$ NMR (126.387 MHz, C_6D_6, 25 °C, $Te(CH_3)_2$]: δ = 1419 ppm. IR (liq., CsI): $\tilde{\nu}$ = 2981 [s, $\nu_s(CH_3)$], 2908 [vs, $\nu_{as}(CH_3)$], 2836 [m, $\nu(CH_3)$], 2815 (s, 1st overtone of 1419), 1419 [vs, $\delta(CH_3)$], 1303 [vs, $\delta(CH_3)$], 950 [vs, $\rho(CH_3)$], 688 [m, $\nu_{as}(S-C)$], 351 [s, $\nu_{as}(TeS_2)$], 331 [s, $\nu_s(TeS_2)$] cm^{-1}.

$Te(SCH_2CH_3)_2$: Tellurium(IV) tetraisopropoxide [$Te(OiPr)_4$; 1.18 g, 3.2 mmol) dissolved in petroleum ether (10 mL) was slowly added to a stirred solution of ethanethiol ($HSCH_2CH_3$; 0.82 g, 13.2 mmol) in petroleum ether (10 mL) at −78 °C. During this procedure the initally colorless solution turned yellow. Subsequently, the solvent and all volatile compounds were distilled in vacuo and the remaining yellow solid was dissolved in petroleum ether. From this solution yellow crystals of $Te(SCH_2CH_3)_2$ precipitated at −40 °C which were dried in vacuo. Yield: 0.76 g (95.0%). M. p. 18−20 °C. $C_4H_{10}S_2Te$ (249.84): calcd. C 19.23, H 4.03, S 25.66; found C 19.25, H 4.01, S 25.57. MS (70 eV, EI): *m/z* (%) = 251.9 (58.8)

Table 5. Crystal data for $Te(SMe)_2$ and $Te(SEt)_2$

[a]	$Te(SMe)_2$	$Te(SEt)_2$
Empirical formula	$C_2H_6S_2Te$	$C_4H_{10}S_2Te$
FW/g mol^{-1}	221.79	249.84
Crystal system	triclinic	monoclinic
Space group	$P\bar{1}$	$C2/c$
Z	2	4
Temperature/K	133(2)	193
$\rho_{calcd.}$/g cm^{-3}	2.382	1.99
μ/mm^{-1}	5.337[b]	3.97[c]
$F(000)$	204	472
Crystal size	0.40 × 0.20 × 0.20 mm	0.05 × 0.26 × 1.00 mm
θ-range	2.56 to 35.02°	2.8 to 28.3°
Limiting indices	$-8 \le h \le 8$	$-15 \le h \le 17$
	$-12 \le k \le 12$	$-11 \le k \le 10$
	$-13 \le l \le 13$	$-11 \le l \le 8$
a/Å	5.2828(5)	13.2228(4)
b/Å	7.480(1)	8.9408(3)
c/Å	8.256(1)	8.4005(3)
α/deg	105.12(1)	90.0
β/deg	90.19(1)	122.909(2)
γ/deg	100.51(1)	90.00
V/Å^3	309.21(8)	833.77(6)
Reflections measured	5408	8130
Unique reflections	2705	1026
Refl. $\|F\| > 4\sigma(F)$	2705	996
R [$\|F\| > 4\sigma(F)$][d]	0.0491	0.0355
Goodness-of-fit on F^2	1.108	1.074
Largest diff. peak and hole	7.10 and −3.12 e·Å^{-3} [e]	2.26 and −1.00 e·Å^{-3}

[a] Mo-K_α radiation with $\lambda = 0.71069$ Å was used. [b] Absorption correction with DELABS.[20] [c] Absorption correction with MULABS.[21] [d] $R = \Sigma \, ||F_o| - |F_c|| / \Sigma \, |F_o|$. [e] Maximum and minimum are 86 pm and 79 pm, respectively, away from the Te atom.

[M^+], 188.9 (19.1) [$TeSEt^+$], 159.8 (20.0) [TeS^+], 122.0 (29.2) [$EtSSEt^+$]. ^{1}H NMR (400.000 MHz, C_6D_6, 25 °C, TMS): δ = 1.14 (t, $^3J_{H,H}$ = 7.3 Hz, 3 H, CH_3), 2.85 (q, $^3J_{H,H}$ = 7.3 Hz, 2 H, CH_2) ppm. $^{13}C\{^1H\}$ NMR (100.577 MHz, C_6D_6, 25 °C, TMS): δ = 17.7 (CH_3), 32.4 (CH_2) ppm. $^{125}Te\{^1H\}$ NMR (126.387 MHz, C_6D_6, 25 °C, $Te(CH_3)_2$]: δ = 1184 ppm. IR (liq., CsI): $\tilde{\nu}$ = 2962 [vs, $\nu_s(CH_3)$], 2955 [vs, $\nu_s(CH_3)$], 2919 [vs, $\nu_{as}(CH_2)$], 2862 [s, $\nu_{as}(CH_3)$], 2821 [m, $\nu_s(CH_2)$], 1445 [vs, $\delta_{as}(CH_3)$], 1420 [s, $\delta(CH_2)$], 1371 [vs, $\delta_s(CH_3)$], 1268 (sh), 1248 [vs, $\delta(CH_2)$], 1116 (sh), 1099 (s), 1045 [s, $\rho(CH_3)$], 1024 (s), 966 (s), 758 [s, $\rho(CH_3)$], 657 (w), 638 [m, ν(S−C)], 539 (w), 515 (w), 392 [m, δ(S−C)], 361 [s, ν_{as}(Te−S)], 329 [s, ν_s(Te−S)], 263 (m) cm^{-1}.

Crystal Structure Determination: Diffraction experiments for $Te(SMe)_2$ were performed on a Nonius-Turbo-CAD4 diffractometer. Its crystal structure was solved by direct methods and structural refinement against F^2 (SHELXTL 5.01).[22]

Diffraction experiments for $Te(SEt)_2$ were performed on a BRUKER Nonius CCD diffractometer. Its crystal structure was solved by direct methods and structural refinement was F^2 (SHELXL 97).[23] Details of the crystal structure determination of $Te(SMe)_2$ and $Te(SEt)_2$, as well as their crystal data, are given in Table 5.

CCDC-170962 and CCDC-191964 contain the supplementary crystallographic data for this paper. These data can be obtained free of charge via www.ccdc.cam.ac.uk/conts/retrieving.html (or from the Cambridge Crystallographic Data Centre,12 Union Road, Cambridge CB2 1EZ, UK; fax: (+44)1223−336−033; or E-mail: deposit@ccdc.cam.ac.uk).

Theoretical Methods: Quantum chemical ab initio investigations were performed with the Gaussian 94 and Gaussian 98 program packages.[24,25] Optimization of molecular geometries, calculation of vibrational frequencies and an analysis of the electronic structure in terms of natural orbitals [12,13] was performed at the MP2 level, with an effective core double-zeta valence basis set,[26] augmented by appropriate polarization functions for Te, S (with exponents according to Höllwarth et al. [27]), and C (exponent 0.75), the basis set being designated as LANL2DZP. Applied symmetry restrictions are given in the text. Calculated vibrational frequencies, scaled by a factor 0.96, were used to assign the IR signals. NMR shielding tensors were calculated according to the GIAO method[28] by using density functional theory (B3LYP) [29] and the IGLO-II basis set,[30] together with an MP2/LANL2DZP optimized molecular geometry.

Acknowledgments

We thank Prof. Dr. M. Kaupp (Universität Würzburg) for his support concerning the calculation of NMR shifts.

[1] Out of 34 solid-state molecular structures with noncyclic $CE^1E^2E^3C$ units found in the Cambridge crystallographic data base, $S(S_2COCH_3)$ and $Se(S_2COCH_3)$ are the only examples exhibiting a *cis*-conformation (see ref.[2]).

[2] N. J. Brøndmo, S. Esper Ås, S. Husebye, *Acta Chem. Scand., Ser. A* **1975**, *29*, 93−104.

[3] R. E. Allan, H. Gornitzka, J. Kärcher, M. A. Paver, M.-A. Rennie, C. A. Russell, P. R. Raithby, D. Stalke, A. Steiner, D. W. Wright, *J. Chem. Soc., Dalton Trans.* **1996**, 1727−1730.

[4] H. Fleischer, S. Stauf, D. Schollmeyer, *Inorg. Chem.* **1999**, *38*, 3725−3729.

[5] H. Fleischer, D. Schollmeyer, *Angew. Chem.* **2000**, *112*, 3840−3842; *Angew. Chem. Int. Ed.* **2000**, *39*, 3705−3706.

[6] R. Steudel, *Angew. Chem.* **1975**, *87*, 683−692; *Angew. Chem. Int. Ed. Engl.* **1975**, *14*, 655−664.
[7] M. Liedtke, A. H. Saleck, K. M. T. Yamada, G. Winnewisser, D. Cremer, E. Kraka, A. Dolgner, J. Hahn, S. Dobos, *J. Phys. Chem.* **1993**, *97*, 11204−11210.
[8] H. Fleischer, D. Schollmeyer, *Inorg. Chem.* **2002**, *41*, 4739−4747.
[9] Since no relativistic effects were included in the calculation of the nuclear shielding constants, there are considerable differences between calculated and experimental ^{125}Te NMR chemical shifts. It was previously shown (Y. Ruiz-Morales, G. Schreckenbach, T. Ziegler, *J. Phys. Chem. A* **1997**, *101*, 4121−4127) that calculations neglecting the spin-orbit-induced contributions to nuclear shielding still give ^{125}Te chemical shifts which are in good agreement with experimental values. In the present case, the experimentally observed trends of $\delta[^{125}Te(SR)_2]$ with R are at least well reproduced.
[10] H. Fleischer, D. Schollmeyer, *Inorg. Chem.* **2001**, *40*, 324−328.
[11] D. B. Denney, D. Z. Denney, P. J. Hammond, Y. F. Hsu, *J. Am. Chem. Soc.* **1981**, *103*, 2340−2347.
[12] A. E. Reed, R. B. Weinstock, F. Weinhold, *J. Chem. Phys.* **1985**, *83*, 735−746.
[13] A. E. Reed, L. A. Curtiss, F. Weinhold, *Chem. Rev.* **1988**, *88*, 899−926.
[14] R. K. Harris, *Nuclear Magnetic Resonance − A Physicochemical View*, Longman Scientific & Technical, Harlow, **1986**.
[15] T. A. Koopmans, *Physica* **1934**, *1*, 104−113.
[16] It is assumed that the differences in ionization energies and thus in $E[n_p(S)]$ between various thiols are reflected in different $E[n_p(S)]$ values for the corresponding tellurium(II) dithiolates.
[17] J. Buschmann, P. Luger, R. Koritsanszky, H. Schmidt, R. Steudel, *J. Phys. Chem.* **1992**, *96*, 9243−9250.
[18] H.-B. Bürgi, *Angew. Chem.* **1975**, *87*, 461−496; *Angew. Chem. Int. Ed. Engl.* **1975**, *14*, 460−
[19] R. Steudel, Y. Drozdova, R. H. Hertwig, W. Koch, *J. Phys. Chem.* **1995**, *99*, 5319−5324.
[20] A. L. Spek, *Acta Crystallogr., Sect. A* **1990**, *46*, C-34.
[21] R. Blessing, *Acta Crystallogr., Sect. A* **1995**, *51*, 33−38.
[22] SHELXTL PC version 5.01, Siemens Analytical X-ray Instruments, Inc., Madison, WI, **1994**.
[23] G. M. Sheldrick, SHELXL-97, *Program for crystal structure refinement*, Universität Göttingen, Göttingen (Germany), **1996**.
[24] Gaussian 94, Revision E.1, M. J. Frisch, G. W. Trucks, H. B. Schlegel, P. M. W. Gill, B. G. Johnson, M. A. Robb, J. R. Cheeseman, T. Keith, G. A. Petersson, J. A. Montgomery, K. Raghavachari, M. A. Al-Laham, V. G. Zakrzewski, J. V. Ortiz, J. B. Foresman, J. Cioslowski, B. B. Stefanov, A. Nanayakkara, M. Challacombe, C. Y. Peng, P. Y. Ayala, W. Chen, M. W. Wong, J. L. Andres, E. S. Replogle, R. Gomperts, R. L. Martin, D. J. Fox, J. S. Binkley, D. J. Defrees, J. Baker, J. P. Stewart, M. Head-Gordon, C. Gonzalez, J. A. Pople, Gaussian, Inc., Pittsburgh PA, **1995**.
[25] Gaussian 98, Revision A.6, M. J. Frisch, G. W. Trucks, H. B. Schlegel, G. E. Scuseria, M. A. Robb, J. R. Cheeseman, V. G. Zakrzewski, J. A. Montgomery, Jr., R. E. Stratmann, J. C. Burant, S. Dapprich, J. M. Millam, A. D. Daniels, K. N. Kudin, M. C. Strain, O. Farkas, J. Tomasi, V. Barone, M. Cossi, R. Cammi, B. Mennucci, C. Pomelli, C. Adamo, S. Clifford, J. Ochterski, G. A. Petersson, P. Y. Ayala, Q. Cui, K. Morokuma, D. K. Malick, A. D. Rabuck, K. Raghavachari, J. B. Foresman, J. Cioslowski, J. V. Ortiz, B. B. Stefanov, G. Liu, A. Liashenko, P. Piskorz, I. Komaromi, R. Gomperts, R. L. Martin, D. J. Fox, T. Keith, M. A. Al-Laham, C. Y. Peng, A. Nanayakkara, C. Gonzalez, M. Challacombe, P. M. W. Gill, B. Johnson, W. Chen, M. W. Wong, J. L. Andres, C. Gonzalez, M. Head-Gordon, E. S. Replogle, and J. A. Pople, Gaussian, Inc., Pittsburgh PA, **1998**.
[26] W. R. Wadt, P. J. Hay, *J. Chem. Phys.* **1985**, *82*, 284−298.
[27] A. Höllwarth, M. Böhme, S. Dapprich, A. W. Ehlers, A. Gobbi, V. Jonas, K. F. Köhler, R. Stegmann, A. Veldkamp, G. Frenking, *Chem. Phys. Lett.* **1993**, *208*, 237−240.
[28] K. Wolinski, J. F. Hinton, P. Pulay, *J. Am. Chem. Soc.* **1992**, *112*, 8251−8260.
[29] A. D. Becke, *J. Chem. Phys.* **1993**, *98*, 5648−5652.
[30] W. Kutzelnigg, U. Fleischer, M. Schindler, *NMR-Basic Principles and Progress*, Vol. 23, Springer-Verlag, Heidelberg, **1990**.

Received August 20, 2002
[I02470]

Synthesis of Tetrahemispheraplexes with Ammonium, Alkylammonium or Alkaline Metal Ions as Exohedral Guests via Self-Assembly or Guest Exchange[‡]

Rolf W. Saalfrank,*[a] Bernhard Demleitner,[a] Horst Glaser,[a] Harald Maid,[a] Stefan Reihs,[a] Walter Bauer,[a] Monica Maluenga,[a] Frank Hampel,[a] Markus Teichert,[b] and Harald Krautscheid[c]

Dedicated to Prof. Dr. Horst Kisch on the occasion of his 60th birthday

Keywords: Cage compounds / Supramolecular chemistry / Magnesium / Host-guest chemistry

To study the interplay between the steric demand of the guest and the space available at the host, we have prepared the tetraammonium complexes $\{(NH_4)_4 \cap [Mg_4(L^{1/2})_6]\}$ **1**, tetrakis(methylammonium) complexes $\{(Me\text{-}NH_3)_4 \cap [Mg_4(L^{1/2})_6]\}$ **2**, tetrakis(ethylammonium) complex $\{(Et\text{-}NH_3)_4 \cap [Mg_4(L^1)_6]\}$ **3**, and mixed sodium tris(ethylammonium) complex $\{Na(Et\text{-}NH_3)_3 \cap [Mg_4(L^2)_6]\}$ **4**. The tetrahemispheraplexes **1**–**4** were available in one-pot syntheses. The tetrakis(alkylammonium) clusters $\{(R^1\text{–}NH_3)_4 \cap [Mg_4(L^1)_6]\}$ **5** and the mixed diammonium-bis(*p*-methoxybenzylammonium) cluster $\{(NH_4)_2(R^2\text{–}NH_3)_2 \cap [Mg_4(L^1)_6]\}$ **6**, however, were prepared by exchange of the ammonium ions of **1a** by alkylammonium ions. Similarly, exchange of the four ammonium ions of **1b** by alkaline metal cations afforded the tetraalkaline metal tetrahemispheraplexes $\{M_4 \cap [Mg_4(L^2)_6]\}$ **7**.

(© Wiley-VCH Verlag GmbH & Co. KGaA, 69451 Weinheim, Germany, 2003)

Introduction

Following the considerable progress made towards predicting ordered supramolecular assemblies on the basis of coordinative metal/ligand bonds,[1] great attention is being paid to the role guest molecules play in the self-assembly of metal/ligand clusters. The inner voids of supramolecular metal/ligand cages are possible sites for encapsulated anionic,[2] electronically neutral[3] and cationic species.[4] Kinetic data for the equilibria of guest exchange reactions have been determined.[5] In special cases, the nature of the encapsulated guest was shown to be the crucial factor for the nuclearity of the compound formed.[6] However, there are far fewer examples of host/guest interactions at the surface of supramolecular coordination polygons.[7–9] The synthesis of novel tetrahemispheraplexes that contain alkylammonium and alkaline-metal cations has been achieved by an advanced one-pot procedure or by host/guest exchange reactions and is subject of this paper.

[‡] Chelate complexes (metalla-coronates), 24. Part 23: Ref.[16]
[a] Institut für Organische Chemie der Universität Erlangen-Nürnberg,
Henkestrasse 42, 91054 Erlangen, Germany
Fax: (internat.) + 49-(0)9131/852−1165
E-mail: saalfrank@chemie.uni-erlangen.de
[b] Institut für Anorganische Chemie der Universität Göttingen, Göttingen, Germany
[c] Institut für Anorganische Chemie der Universität Leipzig, Leipzig, Germany

Results and Discussion

One-Pot Syntheses of Tetraammonium Complexes 1 and Tetrakis(methylammonium) Complexes 2

We have previously reported the gram-scale synthesis of tetraammonium tetramagnesium chelate complexes $\{(NH_4)_4 \cap [Mg_4(L^{1/2})_6]\}$ **1a**,**b** in high yields by deprotonation of dialkyl malonates with methyllithium in tetrahydrofuran, subsequent addition of magnesium chloride and oxalyl chloride followed by workup with aqueous ammonium chloride solution (Scheme 1).[8] The doubly bidentate bridging ligands $(L^{1/2})^{2-}$ (R = Me, Et) are formally obtained by template coupling of two malonate monoanions with oxalyl chloride and spontaneous double deprotonation of the bisenol intermediates. Replacement of the aqueous ammonium chloride solution of this one-pot reaction by a solution of methylammonium chloride yielded the corresponding tetrahemispheraplexes $\{(Me\text{−}NH_3)_4 \cap [Mg_4(L^{1/2})_6]\}$ **2a,b** (Scheme 1).

The NMR spectra of the tetrahemispheraplexes **1** and **2** are surprisingly simple. For example, despite there being four stereogenic metal centers and six C_2-symmetric ligands, the ^{13}C NMR spectrum of **2a** displays only six signals, representing the atropisomeric ligands, and only one for the four exohedrally bonded methylammonium ions. The low number of signals is explained by approximate molecular T symmetry of **2a** (characterised by three C_2 and four C_3 axes). To further support the proposed structure of

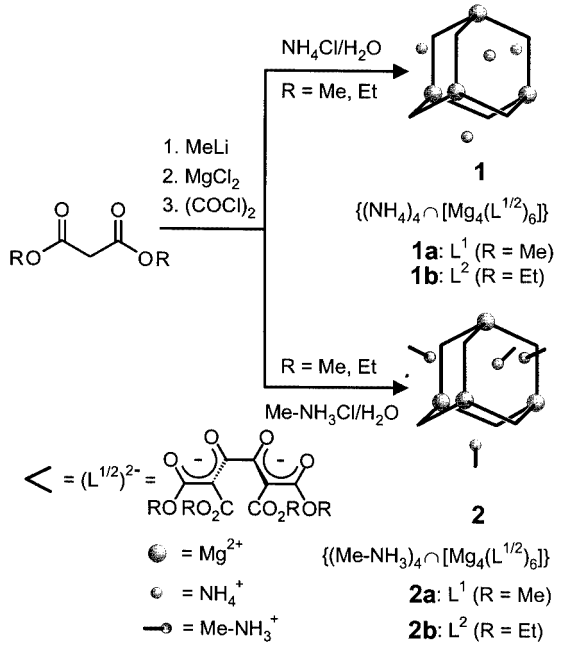

Scheme 1. Synthesis of tetraammonium tetrahemispheraplexes **1** and tetrakis(methylammonium) tetrahemispheraplexes **2**

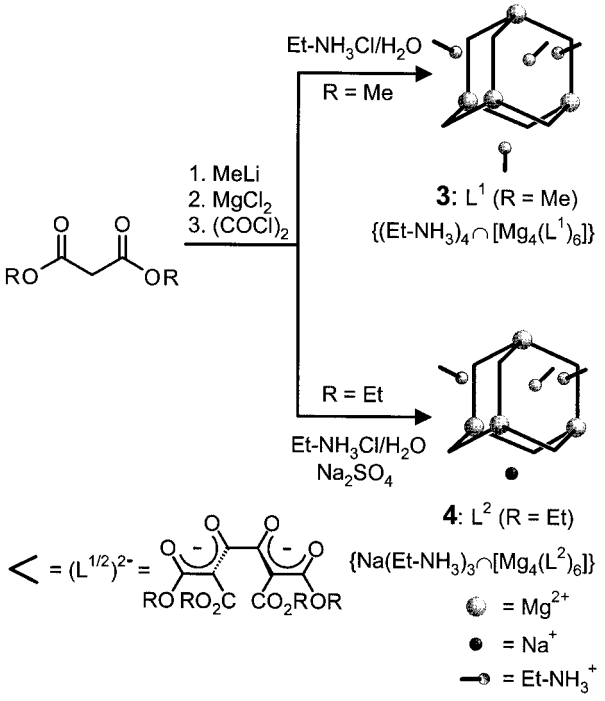

Scheme 2. Synthesis of tetrakis(ethylammonium) tetrahemispheraplex **3** and mixed sodium tris(ethylammonium) tetrahemispheraplex **4**

2a, we carried out a single crystal X-ray structure determination.[11−13] According to this analysis, **2a** crystallises in the monoclinic space group $P2_1/c$ with four molecules per unit cell. The four magnesium cations of the tetraanionic core $[Mg_4(L^1)_6]^{4-}$of tetrahemispheraplex **2a** frame the corners of an idealised tetrahedron and are linked along each of the six edges by doubly bidentate tetramethyl-2,3-dioxobutane-1,1,4,4-tetracarboxylato(2^-) bridges. Consequently, each of the four magnesium ions is octahedrally coordinated by six oxygen donors. Charge compensation of $[Mg_4(L^1)_6]^{4-}$ is achieved by a set of four methylammonium counterions, which are hydrogen bonded to the oxygen donors of the triangular faces of the tetraanionic core to give **2a**. The crystals of **2a** consist of a racemic mixture of homochiral stereoisomers with (Δ,Δ,Δ,Δ)-*fac* or (Λ,Λ,Λ,Λ)-*fac* configuration at the magnesium centers and with six atropisomeric ligands each, twisted clockwise or counter-clockwise.

One-Pot Synthesis of Tetrakis(ethylammonium) Complex 3 and Mixed Sodium Tris(ethylammonium) Complex 4

To study the effect of the steric demand of the ligands $(L^{1/2})^{2-}$ (R = Me, Et) on the packing density at the surfaces of the tetraanionic $[Mg_4(L^{1/2})_6]^{4-}$ cores, unlike the synthesis of **2**, an aqueous *ethyl*ammonium instead of an *methyl*ammonium chloride solution was used for workup. Starting from *dimethyl* malonate, tetrakis(ethylammonium) complex $\{(Et-NH_3)_4\cap[Mg_4(L^1)_6]\}$ **3** was formed, whereas sodium tris(ethylammonium) complex $\{Na(Et-NH_3)_3\cap[Mg_4(L^2)_6]\}$ **4** was isolated with *diethyl* malonate as starting material and the reaction mixture dried over sodium sulfate (Scheme 2).

The NMR spectra of **3**, as with **1** and **2**, originate from the molecular T symmetry of the tetrahemispheraplex in solution. However, the ^1H and ^{13}C NMR spectra of **4** were more complex. Two signals in the ^{13}C NMR spectrum confirm magnetically equivalent exohedral ethylammonium guests. Integration of the ^1H NMR signals provide an ethylammonium-to-ligand ratio of 1:2, indicating that only three of the four triangular faces of the compound are occupied by ethylammonium ions. Compared to the higher symmetric analogue **3**, the ^{13}C NMR spectrum of C_3-symmetric **4** displayed a total of 32 signals due to two sets of three C_1-symmetric ligands $(L^2)^{2-}$ (R = Et). The structure proposed for **4** is further supported by a single crystal X-ray structure determination,[11−13] which shows that $\{Na(Et-NH_3)_3\cap[Mg_4(L^2)_6]\}\cdot 2H_2O$ **4** crystallises in the monoclinic space group $P2_1/n$ with four molecules per unit cell. The crystals of **4** consist of a racemic mixture of homochiral stereoisomers with a (Δ,Δ,Δ,Δ)-*fac* or (Λ,Λ,Λ,Λ)-*fac* configuration at the metal centers and with two sets of three atropisomeric ligands each, twisted clockwise or counter-clockwise. Unlike to the tetrahedral core $[Mg_4(L^1)_6]^{4-}$ of **2a**, in **4** the $[Mg_4(L^2)_6]^{4-}$ framework is stretched along the C_3 axis. This results in an overall trigonal pyramidal scaffold for **4**. Each of the three isosceles triangular faces of the pyramid are occupied by one ethylammonium ion hydrogen bonded to three oxygen donors of the adjacent ligands. Charge compensation of the resulting $\{(Et-NH_3)_3\cap[Mg_4(L^2)_6]\}^-$ framework is achieved by the sterically less demanding sodium ion, which is coordinated by two carbonyl oxygen donors of each of the three ligands,

establishing the basic equilateral triangle. The sodium coordination sphere is completed by two water molecules. Remarkably, one water molecule is located *in* the void and the other one *outside* the trigonal pyramid (Figure 1).[10]

Exchange of Ammonium Ions of 1a,b by Alkylammonium Ions to give the Tetrakis(alkylammonium) Clusters 5 and the Mixed Diammonium-bis(*p*-methoxybenzylammonium) Cluster 6

To tune the physical and chemical properties of the spherical surface of $\{(NH_4)_4 \cap [Mg_4(L^1)_6]\}$ **1a** we extended the *direct method* described above by replacing the four ammonium ions with *n*-alkylammonium ions. The exchange of the ammonium ions in **1a** (R = Me) for *n*-alkylammonium ions to form the tetrakis(alkylammonium) tetrahemispheraplexes $\{(R^1-NH_3)_4 \cap [Mg_4(L^1)_6]\}$ **5** is achieved by addition of *n*-alkylamines R^1-NH_2 in excess. Ammonia is liberated during this exchange process.[9,14] The NMR spectra of **5** are consistent with the predicted structures (see the Exp. section for data).

However, when **1a** (R = Me) was allowed to react with an excess of bulky *p*-methoxybenzylamine R^2-NH_2, only two ammonium ions were exchanged by *p*-methoxybenzylammonium groups to give diammonium bis(*p*-methoxybenzylammonium) tetrahemispheraplex $\{(NH_4)_2(R^2-NH_3)_2 \cap [Mg_4(L^1)_6]\}$ **6** (Scheme 3).

The ^1H and ^{13}C NMR spectra of **6** were rather complex. Six signals in the ^{13}C NMR spectrum confirmed magnetically equivalent exohedral *p*-methoxybenzylammonium guests. Integration of the ^1H NMR signals provided a *p*-methoxybenzylammonium-to-ligand ratio of 1:3, indicating that only two of the four triangular faces of **6** are occupied by *p*-methoxybenzylammonium ions. Whereas the ^{13}C NMR spectrum for the *T*-symmetric precursor **1a** shows six signals, that of the C_2 symmetric core of **6** displays 36 signals. In **6**, the ligands are subdivided into four types: two different C_2-symmetric ligands and two sets of two identical C_1-symmetric ligands. Accordingly, thirteen discrete singlets are expected, representing the methoxy groups of the ligands and the guests; twelve (two signals are superimposed) were recorded.

A single crystal X-ray structure determination of **6**[11−13,15] is consistent with the proposal that **6** crystallises in the monoclinic space group *P*2/*c* with four molecules per unit cell. A common feature of **1a**, **5** and **6** is the tetrahedral module $[Mg_4(L^1)_6]^{4-}$. However, they differ markedly due to their exohedral guests. In **6**, charge compensation is achieved by two ammonium and two *p*-methoxybenzylammonium counterions, which are hydrogen-bonded to the

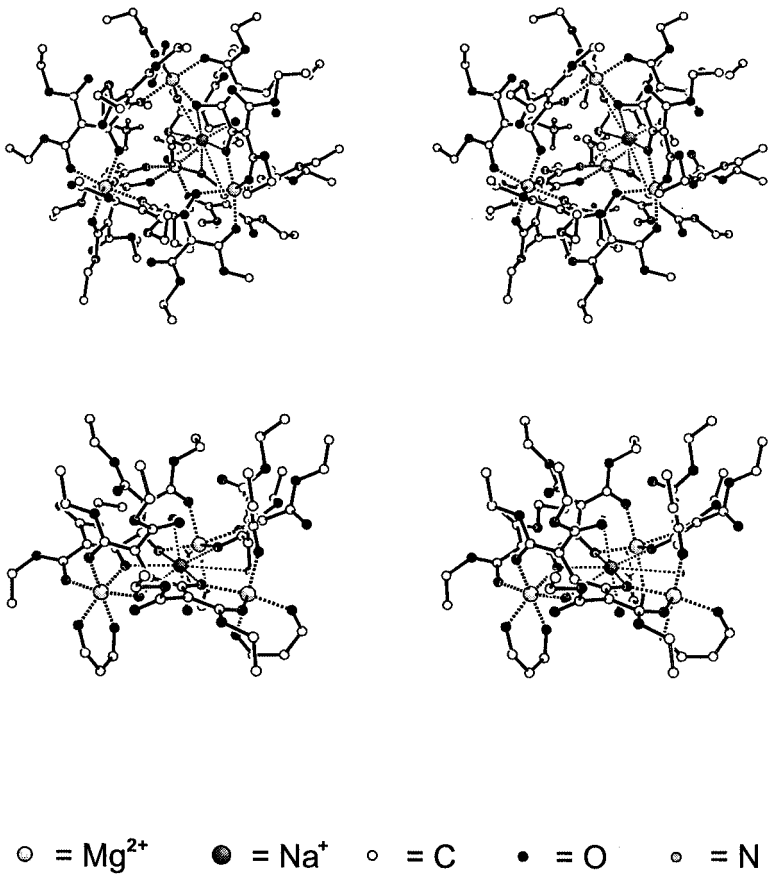

Figure 1. (Stereo view): Top: Structure of $\{Na(Et-NH_3)_3 \cap [Mg_4(L^2)_6]\}$ **4** (L^2: R = Et) in the crystal. Bottom: Selected tetrahedral face highlighting its metalla-coronate character. Solvent molecules and hydrogen atoms except ammonium hydrogens are not depicted for clarity

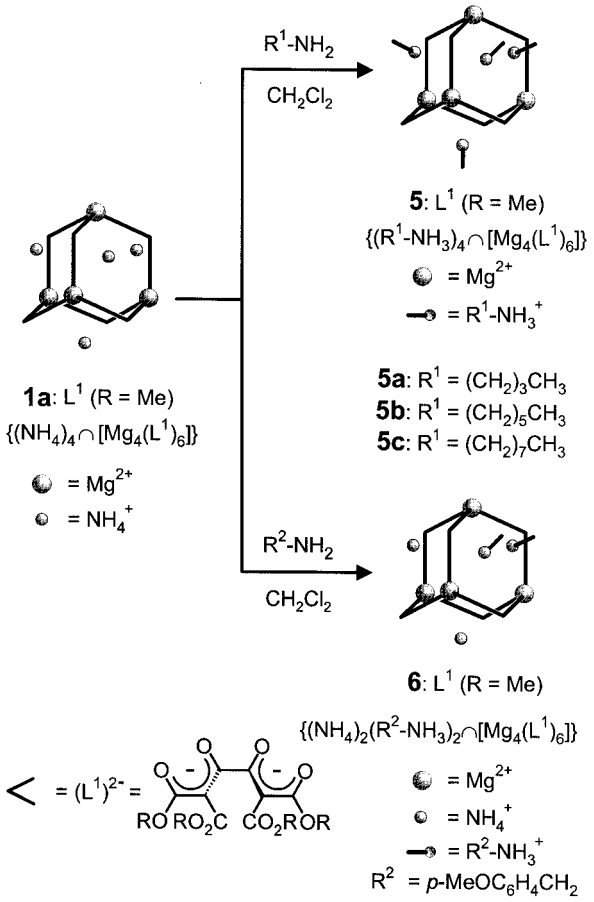

Scheme 3. Ammonium ion exchange of **1a**: Synthesis of tetrakis(alkylammonium) tetrahemispheraplexes **5** and diammonium-bis(*p*-methoxybenzylammonium) tetrahemispheraplex **6**

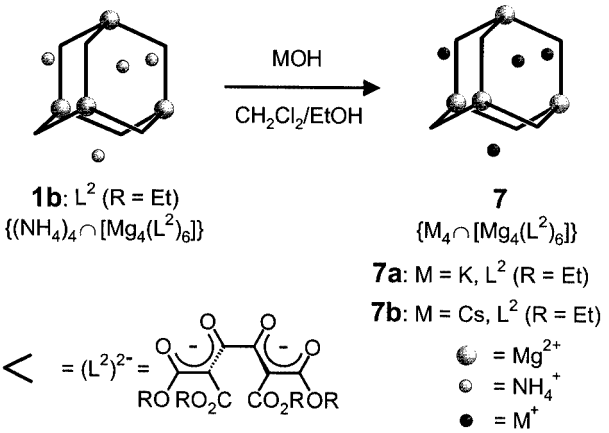

Scheme 4. Ammonium ion exchange of **1b**: Synthesis of tetraalkaline metal tetrahemispheraplexes **7**

oxygen donors of the ligands of the triangular faces (Figure 2).[10]

Exchange of the Four Ammonium Ions of 1b by Alkaline Cations to Give the Tetraalkaline Metal Complexes 7

Reaction of a solution of tetraammonium tetrahemispheraplex **1b** in dichloromethane with a solution of potassium or caesium hydroxide in dichloromethane/ethanol afforded the alkaline metal complexes $\{M_4 \cap [Mg_4(L^2)_6]\}$ **7** [(M = K, Cs; L^2 (R = Et)] in excellent yields (Scheme 4).

The NMR spectra of the tetrahemispheraplexes $\{M_4 \cap [Mg_4(L^2)_6]\}$ **7a**,**b** are principally identical to those of **1b**, except for the missing ^{1}H NMR signals characteristic of the ammonium protons of **1b**. According to a single crystal X-ray structure determination, $\{K_4 \cap [Mg_4(L^2)_6]\} \cdot 4H_2O$ **7a** crystallises in the monoclinic space group $P2_1$ with two molecules per unit cell.[11–13] Charge compensation of the tetrahedral $[Mg_4(L^2)_6]^{4-}$ core is achieved by a set of four potassium counterions. The idealised structure of **7a** consists of four fused [15]metalla-crown-6 systems that encapsulate one potassium cation, each (Figure 3, top).[10] However, careful consideration revealed different coordination spheres at the potassium ions. Remarkably, the coordination number at the most symmetrically ligated potassium cation is eight. Its coordination sphere is composed of six carbonyl oxygen donors, one oxygen donor of a water molecule at the periphery and one oxygen donor of a water molecule encapsulated in the void of the tetrahedron (Figure 3, bottom). As with **1b**, the crystals of **7a** consist of a racemic mixture of homochiral stereoisomers.

Conclusions

The present study has shown that the space available at the surface of the self-assembled tetrahedral tetraanionic cores $[Mg_4(L^{1/2})_6]\}^{4-}$ depends on the steric demand of the ligands $(L^{1/2})^{2-}$. Whereas $[Mg_4(L^1)_6]\}^{4-}$ (L^1: R = Me) is able to host four Et–NH_3^+ cations, the more crowded $[Mg_4(L^2)_6]\}^{4-}$ (L^2: R = Et) is apt to only host four of the smaller NH_4^+-, Me–NH_3^+- or alkaline metal cations. However, tetrahemispheraplexes of $[Mg_4(L^2)_6]\}^{4-}$ (L^2: R = Et) with Et–NH_3^+ are conceivable in combination with the smaller Na^+ cation, and of $[Mg_4(L^1)_6]\}^{4-}$ (L^1: R = Me) with *p*-$MeOC_6H_4CH_2$–NH_3^+ together with NH_4^+ cations. In $\{(NH_4)_4 \cap [Mg_4(L^2)_6]\}$ **1b** the four ammonium ions could be exchanged by potassium or caesium ions.

Experimental Section

General Methods: NMR spectra were recorded on a JEOL EX 400 and on a JEOL ALPHA 500 in $CDCl_3$ solutions. The residual solvent signal (δ = 7.27 ppm) was used as an internal standard. IR spectra were performed on a Bruker IFS 25 spectrometer. Elemental analyses were carried out on an EA 1110 CHNS-Microautomat.

Materials: All reagents and solvents employed were commercially available, high-grade purity materials (Fluka, Aldrich), used as supplied.

General Procedure. Direct Synthesis: A methyllithium solution (18.75 mL, 1.6 M in diethyl ether, 30 mmol) diluted with dry THF (10 mL) was added dropwise to a solution of dialkyl malonate (30 mmol) in dry THF (50 mL) (N_2, −78 °C) over 30 min. After stirring for 1 h, $MgCl_2$ (2.86 g, 30.0 mmol) was added and 1 h later a solution of oxalyl chloride (0.95 g, 7.5 mmol) in dry THF (20 mL)

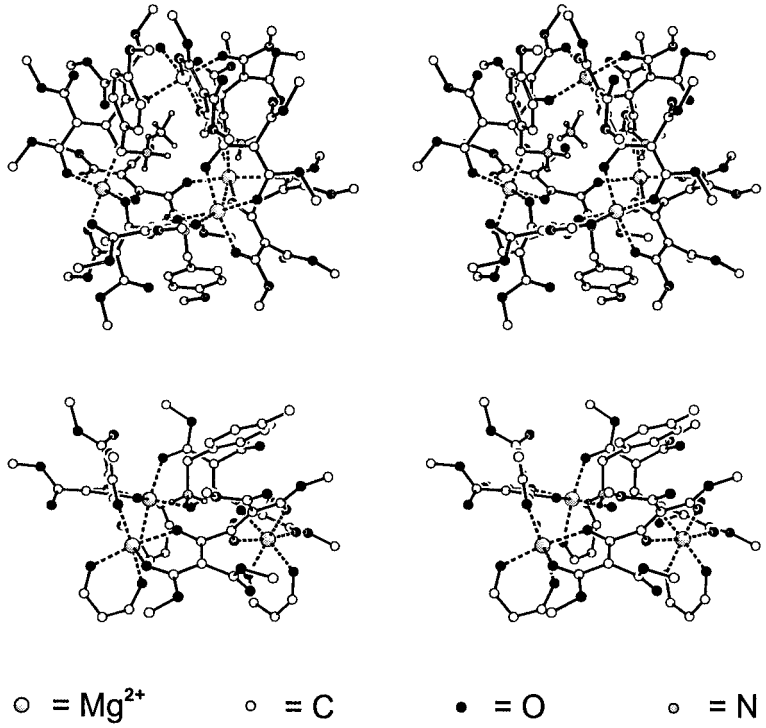

Figure 2. (Stereo view): Top: Structure of $\{(NH_4)_2(R^2-NH_3)_2\cap[Mg_4(L^1)_6]\}$ **6** (L^1: R = Me; R^2 = *p*-$MeOC_6H_4CH_2$) in the crystal. Bottom: Selected tetrahedral face hosting *p*-methoxybenzylammonium. Solvent molecules and hydrogen atoms except ammonium hydrogens are not depicted for clarity

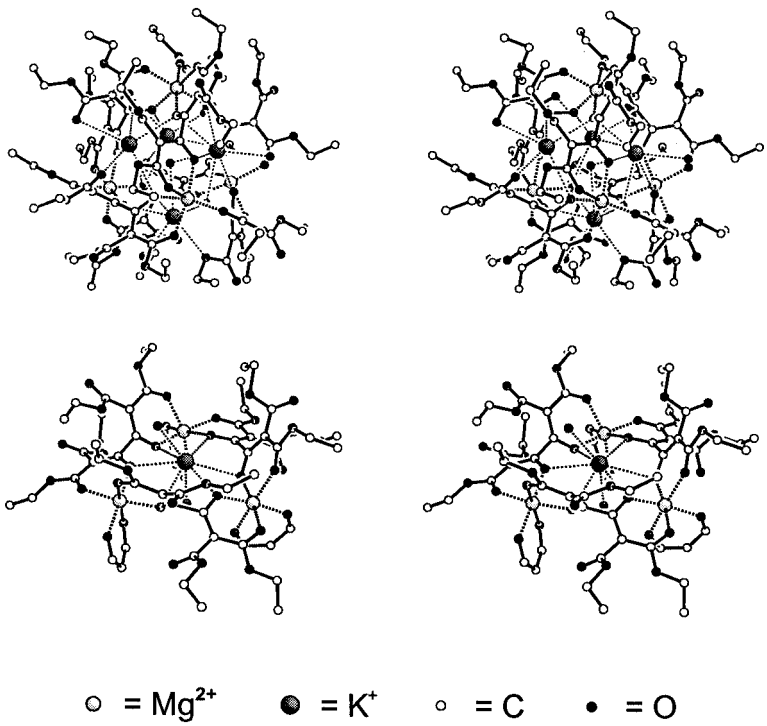

Figure 3. (Stereo view): Top: Structure of $\{K_4\cap[Mg_4(L^2)_6]\}$ **7a** (L^2: R = Et) in the crystal. Bottom: Selected tetrahedral face highlighting its metalla-coronate character. Solvent molecules and hydrogen atoms are not depicted for clarity

was added dropwise into the suspension within 2 h. The mixture was then allowed to warm to 20 °C during 18 h and the resulting yellow solution treated for 5 min with 10% aqueous alkyl ammonium chloride (50 mL). The two layers present were separated, the aqueous layer was extracted three times with chloroform (50 mL), and the combined organic phases were dried over anhydrous sodium sulfate. The solvent was removed in vacuo and the remaining yellow oil was diluted in chloroform (5 mL). The reaction product was crystallised by addition of isohexane (50 mL).

Compound 1a: Yield: 2.23 g (86%) colourless powder; m.p. 181 °C (decomp.). ^{1}H NMR (400 MHz, $CDCl_3$): δ = 3.57, 3.78 (each s, 72 H, 24 OCH_3), 7.30 ppm (br. s, 16 H, 4 NH_4^+). ^{13}C NMR (100.5 MHz, $CDCl_3$): δ = 51.39, 52.05 (24 OCH_3), 94.29 (12 =C), 167.97, 170.82 (24 C=O, ester), 184.25 ppm (12 C=O, keto). IR ($CHBr_3$): $\tilde{\nu}$ = 3180 (NH), 1680 (C=O), 1630 cm^{-1} (C=C). $C_{72}H_{88}Mg_4N_4O_{60}$ (2066.71): calcd. C 41.84, H 4.29, N 2.71; found C 41.29, H 4.63, N 2.66.

Compound 1b: See ref.[8]

Compound 2a: Yield: 1.80 g (68%) colourless microcrystals; m.p. 161 °C (decomp.). ^{1}H NMR (400 MHz, $CDCl_3$): δ = 2.20 (s, 12 H, 4 CH_3), 3.55, 3.81 (each s, 72 H, 24 OCH_3), 8.09 ppm (br. s, 12 H, 4 NH_3^+). ^{13}C NMR (100.5 MHz, $CDCl_3$): δ = 25.92 (4 CH_3), 51.26, 52.26 (24 OCH_3), 94.56 (12 =C), 167.30, 170.88 (24 C=O, ester), 184.34 ppm (12C=O, keto). IR ($CHBr_3$): $\tilde{\nu}$ = 1710 (C=O), 1640 cm^{-1} (C=C). $C_{76}H_{96}Mg_4N_4O_{60}$ (2122.82): calcd. C 43.00, H 4.56, N 2.64; found C 42.64, H 4.68, N 2.43.

Compound 2b: Yield: 1.65 g (54%) colourless powder; m.p. 202 °C (decomp.). ^{1}H NMR (400 MHz, $CDCl_3$): δ = 1.15, 1.27 (each t, *J* = 7.08 Hz, 72 H, 24 CH_3), 2.25 (br. s, 12 H, 4 NCH_3), 3.95, 4.06, 4.18, 4.29 (each m, 48 H, 24 $OCH^{A/B}$), 8.16 ppm (br. s, 12 H, 4 NH_3^+). ^{13}C NMR (100.5 MHz, $CDCl_3$): δ = 14.03, 14.08 (24 CH_3), 26.00 (4 NCH_3), 59.76, 60.73 (24 OCH_2), 95.40 (12 =C), 166.71, 170.59 (24 C=O, ester), 184.24 ppm (12 C=O, keto). IR ($CHBr_3$): $\tilde{\nu}$ = 1700 (C=O), 1640 cm^{-1} (C=C). $C_{100}H_{144}Mg_4N_4O_{60}$ (2459.46): calcd. C 48.84, H 5.90, N 2.28; found C 48.94, H 5.90, N 2.23.

Compound 3: Yield: 1.25 g (46%) colourless powder; m.p. 182 °C (decomp.). ^{1}H NMR (400 MHz, $CDCl_3$): δ = 0.89 (t, *J* = 7.08 Hz, 12 H, 4 CH_3), 2.65, 2.82 (each br. m, 8 H, 4 $NCH^{A/B}$), 3.56, 3.78 (each s, 72 H, 36 OCH_3), 7.67 ppm (br. s, 12 H, 4 NH_3^+). ^{13}C NMR (100.5 MHz, $CDCl_3$): δ = 11.80 (4 CH_3), 36.50 (4 NCH_2), 51.26, 52.01 (24 OCH_3), 95.15 (12 =C), 167.39, 170.80 (24 C=O, ester), 184.56 ppm (12 C=O, keto). IR ($CHBr_3$): $\tilde{\nu}$ = 1730 (C=O), 1650 cm^{-1} (C=C). $C_{80}H_{104}Mg_4N_4O_{60}$ (2178.95): calcd. C 44.10, H 4.81, N 2.57; found C 42.84, H 4.64, N 1.80.

Compound 4: Yield: 2.83 g (91%) colourless prisms, from dichloromethane/isohexane; m.p. 186 °C (decomp.). ^{1}H NMR (400 MHz, $CDCl_3$): δ = 0.92 (t, *J* = 7.4 Hz, 9 H, 3 CH_3), 1.08−1.27 (m, 72 H, 24 CH_3), 2.61, 2.81 (each br. m, 6 H, 3 $NCH^{A/B}$), 3.85−4.31 (m, 48 H, 24 OCH_2), 7.50 ppm (br. s, 9 H, 3 NH_3^+). ^{13}C NMR (100.5 MHz, $CDCl_3$): δ = 11.91 (3 CH_3), 13.67, 13.83, 13.93, 13.98, 14.19, 14.22, 14.36, two superimposed signals (24 CH_3), 36.12 (3 NCH_2), 59.74, 59.88, 60.09, 60.12, 60.20, 60.42, 60.55, 60.60 (24 OCH_2), 94.38, 94.91, 95.09, 95.59 (12 =C), 167.07, 167.27, 167.56, 168.99, 170.34, 170.58, 170.76, two superimposed signals (24 C=O, ester), 184.54, 184.74, 185.23, 185.67 ppm (12 C=O, keto); When the NMR spectra of C_3-symmetric **4** were carried out in $CD_3CN/CDCl_3$ instead of $CDCl_3$ alone, the spectra of **4** revealed molecular *T* symmetry due to the core $[Mg_4(L^2)_6]^{4-}$. This is explained by fast exchange of Na^+ and $[H_3NC_2H_5]^+$. ^{1}H NMR (400 MHz, $CDCl_3/CD_3CN$): δ = 0.92 (t, *J* = 7.4 Hz, 9 H, 3 CH_3); 1.13, 1.22 (t, *J* = 7.1 Hz, 72 H, 24 CH_3); 2.22, 2.70 (each br. s, 6 H, 3 CH_2); 3.88, 3.99, 4.09, 4.17 (each m, 48 H, 24 OCH_2); 7.51 (br. s, 9 H, 3 NH_3^+) ppm. ^{13}C NMR (100.5 MHz, $CDCl_3/CD_3CN$): δ = 12.26 (3 CH_3); 14.26, 14.48 (24 CH_3); 36.75 (3 NCH_2); 60.45, 61.06 (24 OCH_2); 95.71 (12 =C); 167.95, 171.28 (24 C=O, ester); 185.56 (12 C=O, keto). IR ($CHBr_3$): $\tilde{\nu}$ = 1700 (C=O), 1640 cm^{-1} (C=C). $C_{102}H_{144}Mg_4N_3NaO_{60}$ (2492.47): calcd. C 49.15, H 5.82, N 1.69; found C 48.09, H 6.02, N 1.60.

General Procedure. Ammonium/Alkylammonium Cation-Exchange: A solution of the corresponding primary amine (5 mmol, 1 mmol for **6**) in dichloromethane (5 mL) was added dropwise to a solution of the corresponding tetrahemispheraplex **1a** (1.03 g, 0.5 mmol) in dichloromethane (50 mL) over 5 min. The mixture was then stirred for 20 min (5 min for **6**) at 0 °C. Subsequently, the volatile components were removed in vacuo and the resulting colourless solid was washed three times with hexane (30 mL), dried and crystallised from dichloromethane/diethyl ether.

Compound 5a: Yield: 0.49 g (43%) colourless powder; m.p. 186 °C (decomp.). ^{1}H NMR (400 MHz, $CDCl_3$): δ = 0.65 (t, *J* = 7.1 Hz, 12 H, 4 CH_3), 0.93, 1.30 (each m, 16 H, 8 CH_2), 2.47, 2.73 (each br. m, 8 H, 4 $NCH^{A/B}$), 3.56, 3.79 (each s, 72 H, 24 CH_3), 7.68 ppm (br. s, 12 H, 4 NH_3^+). ^{13}C NMR (100.5 MHz, $CDCl_3$): δ = 12.89 (4 CH_3), 20.00, 28.18 (8 CH_2), 41.58 (4 NCH_2), 51.15, 51.93 (24 OCH_3), 95.36 (12 =C), 167.16, 170.78 (24 C=O, ester), 184.38 ppm (12 C=O, keto). IR ($CHBr_3$): $\tilde{\nu}$ = 1720 (C=O), 1650 cm^{-1} (C=C). $C_{88}H_{120}Mg_4N_4O_{60}$ (2291.17): calcd. C 46.13, H 5.28, N 2.45; found C 46.06, H 5.56, N 2.51.

Compound 5b: Yield: 0.47 g (49%) colourless powder; m.p. 194 °C (decomp.). ^{1}H NMR (400 MHz, $CDCl_3$): δ = 0.79 (t, *J* = 7.3 Hz, 12 H, 4 CH_3), 0.89, 0.98, 1.12, 1.30 (each m, 32 H, 16 CH_2), 2.45, 2.74 (each br. m, 8 H, 4 $NCH^{A/B}$), 3.55, 3.78 (each s, 72 H, 24 CH_3), 7.70 ppm (br. s, 12 H, 4 NH_3^+). ^{13}C NMR (100.5 MHz, $CDCl_3$): δ = 13.88 (4 CH_3), 22.06, 25.99, 26.34, 30.61 (16 CH_2), 41.50 (4 NCH_2), 51.16, 51.95 (24 OCH_3), 95.26 (12 =C), 167.18, 170.78 (24 C=O, ester), 184.30 ppm (12 C=O, keto). IR ($CHBr_3$): $\tilde{\nu}$ = 1725 (C=O), 1640 cm^{-1} (C=C). $C_{96}H_{136}Mg_4N_4O_{60}$ (2403.36): calcd. C 47.98, H 5.70, N 2.33; found C 48.07, H 6.13, N 2.22.

Compound 5c: Yield: 0.48 g (38%) colourless powder; m.p. 187 °C (decomp.). ^{1}H NMR (400 MHz, $CDCl_3$): δ = 0.86 (t, *J* = 7.1 Hz, 12 H, 4 CH_3), 0.98, 1.00, 1.13, 1.15, 1.24, 1.26 (each m, 48 H, 24 CH_2), 2.45, 2.73 (each br. m, 8 H, 4 $NCH^{A/B}$), 3.55, 3.78 (each s, 72 H, 24 CH_3), 7.69 ppm (br. s, 12 H, 4 NH_3^+). ^{13}C NMR (100.5 MHz, $CDCl_3$): δ = 14.12 (4 CH_3), 22.51, 26.25, 26.89, 28.59, 28.99, 31.86 (24 CH_2), 41.56 (4 NCH_2), 51.21, 51.98 (24 OCH_3), 95.35 (12 =C), 167.22, 170.82 (24 C=O, ester), 184.36 ppm (12 C=O, keto). IR ($CHBr_3$): $\tilde{\nu}$ = 1720 (C=O), 1645 cm^{-1} (C=C). $C_{104}H_{152}Mg_4N_4O_{60}$ (2515.57): calcd. C 49.66, H 6.09, N 2.23; found C 49.26, H 6.54, N 2.41.

Compound 6: Yield: 0.73 g (63%) colourless microcrystals; m.p. 182 °C (decomp.). ^{1}H NMR (400 MHz, $CDCl_3$): δ = 3.43, 3.50, 3.51, 3.55, 3.56, 3.64, 3.67, 3.71, 3.72, 3.77, 3.79, 3.87, two times two superimposed signals (each s, 80 H, 26 OCH_3, 2 CH^A), 4.06 (br. m, 2 H, 2 CH^B, the corresponding H^A was identified by HETCOR), 6.55 (d, *J* = 8.6 Hz, 4 H, Ar-H), 6.96 (d, *J* = 8.6 Hz, 4 H, 4 Ar-H), 7.03 (br. s, 8 H, 2 NH_4^+), 8.05 (br. s, 6 H, 2 NH_3^+). ^{13}C NMR (100.5 MHz, $CDCl_3$): δ = 43.66 (2 CH_2), 50.47, 50.86, 51.29, 51.32, 51.62, 51.70, 51.75, 51.98, 52.09, three times two superimposed signals (24 OCH_3), 54.86 (2 OCH_3), 94.05, 94.32, 94.45, 95.22, 95.25, two superimposed signals (12 =C), 113.56 (4 Ar-CH), 124.41 (2 Ar-C), 131.05 (4 Ar-CH), 159.71 (2 Ar-C), 166.18, 166.73, 166.99, 168.09, 169.54, 169.58, 170.35, 170.39, 170.67, 170.87, 170.93, 171.09 (24 C=O, ester), 183.83, 184.10, 184.22, 184.36, 185.33, 185.44 (12 C=O, keto); When the NMR spectra of C_2-symmetric **6** were recorded in $CD_3CN/CDCl_3$ instead of $CDCl_3$ alone, the spectra of **6** revealed molecular *T* symmetry due to the core $[Mg_4(L^1)_6]^{4-}$. This is explained by fast exchange of $[NH_4]^+$ and $[H_3NCH_2C_6H_4OMe]^+$. At lower temperatures, the NMR signals characteristic of C_2-symmetric **6** reappeared. ^{1}H NMR (500 MHz, $CDCl_3/CD_3CN$): δ = 3.44 (s, 36 H, 12 CH_3);

Table 1. Details of X-ray structure determinations

	2a	**4**	**6**	**7a**
Empirical formula	$C_{76}H_{96}Mg_4N_4O_{60}$ · 6 $CHCl_3$	$C_{102}H_{144}Mg_4N_3NaO_{60}$ · 2 H_2O · CH_2Cl_2	$C_{88}H_{104}Mg_4N_4O_{62}$ · 6 $CHCl_3$	$C_{96}H_{120}K_4Mg_4O_{60}$ · 4 H_2O
Molecular mass	2839.08	2613.39	3023.28	2555.59
Crystal size [mm]	0.70 × 0.65 × 0.30	0.35 × 0.35 × 0.30	0.40 × 0.35 × 0.15	0.30 × 0.30 × 0.25
Crystal system	monoclinic	monoclinic	monoclinic	monoclinic
Space group	$P2_1/c$	$P2_1/n$	$C2/c$	$P2_1$
T [K]	133(2)	173(2)	200(2)	173(2)
a [Å]	14.763(3)	20.9857(2)	22.412(6)	15.6360(2)
b [Å]	29.130(6)	22.9751(2)	19.277(4)	15.6507(3)
c [Å]	28.872(6)	26.6598(3)	29.950(9)	26.1277(4)
α [°]				
β [°]	90.15	98.8370(10)	90.97(3)	93.4160(10)
γ [°]				
V [Å^3]	12420(4)	12701.4(2)	12938(6)	6382.46(18)
Z	4	4	4	2
$P_{calcd.}$ [Mg·m^{-3}]	1.519	1.367	1.552	1.330
θ range [°]	1.70 to 25.00	2.19 to 24.42	3.87 to 24.00	1.30 to 24.10
reflections collected	187866	38797	24503	18804
independent reflections	21582	20881	10011	18804
parameters	1873	1576	845	1513
final $R1$ [$I > 2\sigma(I)$]	0.0541	0.0666	0.0967	0.0611
$wR2$ (all data)	0.1304	0.2017	0.2934	0.1761
largest residuals [e·Å^{-3}]	0.966/−0.772	0.988/−0.667	0.960/−1.365	1.348/−0.596

3.73 (s, 6 H, 2 CH_3); 3.74 (s, 38 H, 12 CH_3, 2 CH^B); 3.99 (br. s, 2 H, 2 CH^A); 6.65 (d, J = 8.5 Hz 4 H, Ar-H); 6.98 (d, J = 8.5 Hz, 4 H, 4 Ar-H; 7.00 (br. s, 8 H, 2 NH_4^+); 7.94 (br. s, 6 H, 2 NH_3^+).^{13}C NMR (125.7 MHz, $CDCl_3/CD_3CN$): δ = 44.16 (2 CH_2); 51.60, 52.38 (24 OCH_3); 55.60 (2 OCH_3); 95.69 (12 =C); 114.62 (4 Ar-CH); 125.10 (2 Ar-C); 131.64 (4 Ar-CH); 160.61 (2 Ar-C); 168.21, 171.68 (24 C=O, ester); 185.60 (12 C=O, keto). ^{13}C NMR (125.7 MHz, $CD_3CN/CDCl_3$): δ = 44.16 (2 CH_2), 51.60, 52.38 (24 OCH_3), 55.60 (2 OCH_3), 95.69 (12 =C), 114.61 (2 Ar-C), 125.10 (4 Ar-CH), 131.64 (4 Ar-CH), 160.61 (2 Ar-C), 168.21, 171.68 (24 C=O, ester), 185.60 (12 C=O, keto). IR ($CHBr_3$): $\tilde{\nu}$ = 1710 (C=O), 1640 cm^{-1} (C=C). $C_{88}H_{104}Mg_4N_4O_{62}$ (2307.01): calcd. C 45.82, H 4.54, N 2.43; found C 46.25, H 4.71, N 2.41.

General Procedure. Ammonium/Alkali Cation-Exchange: A solution of potassium hydroxide or caesium hydroxide hydrate (1.7 mmol) in a dichloromethane/ethanol mixture (1:1, 12 mL) was added dropwise to a solution of tetrahemispheraplex **1b** (0.96 g, 0.4 mmol) in dichloromethane (12 mL) over a period of 10 min. The mixture was stirred for 48 h at room temperature and concentrated to ca. 10 mL. The products were then obtained by addition of a mixture of diethyl ether/hexane (1:1, 100 mL), filtered off, washed three times with hexane and dried in vacuo.

Compound 7a: Yield: 0.94 g (94%) colourless microcrystals; m.p. >250 °C (decomp.). ^{1}H NMR (400 MHz, $CDCl_3$): δ = 0.94, 0.98 (each t, J = 7.0 Hz, 72 H, 24 CH_3), 3.55, 3.78, 4.11, 4.24 (each m, 48 H, 24 $OCH^{A/B}$). ^{13}C NMR (100.5 MHz, $CDCl_3$): δ = 13.79, 14.02 (24 CH_3), 60.01, 60.23 (24 OCH_2), 93.99 (12 =C), 166.61, 170.14 (24 C=O, ester), 185.38 ppm (12 C=O, keto). IR ($CHBr_3$): $\tilde{\nu}$ = 1640 (C=O), 1480 cm^{-1} (C=C). $C_{96}H_{120}K_4Mg_4O_{60}$ (2487.60): calcd. C 46.35, H 4.86; found C 45.32, H 5.23.

Compound 7b: Yield: 1.03 g (91%) colourless microcrystals; m.p. 224 °C (decomp.). ^{1}H NMR (400 MHz, $CDCl_3$): δ = 1.17, 1.21 (each t, J = 7.2 Hz, 72 H, 24 CH_3), 3.93, 3.98, 4.05, 4.14 (each m, 48 H, 24 $CH^{A/B}$). ^{13}C NMR (100.5 MHz, $CDCl_3$): δ = 13.90, 14.14 (24 CH_3), 60.03, 60.24 (24 OCH_2), 94.00 (12 =C), 168.88, 170.14 (24 C=O, ester), 185.30 ppm (12 C=O, keto). IR ($CHBr_3$): $\tilde{\nu}$ = 1640 (C=O), 1480 cm^{-1} (C=C). $C_{96}H_{120}Cs_4Mg_4O_{60}$ (2862.82): calcd. C 40.28, H 4.22; found C 41.57, H 4.41.

Acknowledgments

This work was supported by the Deutsche Forschungsgemeinschaft (Sa, 276/25-1, SFB 583, GK 312), the Bayerisches Langzeitprogrammm *Neue Werkstoffe* and the Fonds der Chemischen Industrie. H. G. thanks the Freistaat Bayern for a scholarship.

[1] Recent reviews: F. Hof, S. L. Craig, C. Nuckolls, J. Rebek, Jr., *Angew. Chem.* **2002**, *114*, 1556−1578; *Angew. Chem. Int. Ed.* **2002**, *41*, 1488−1508; B. J. Holliday, C. A. Mirkin, *Angew. Chem.* **2001**, *113*, 2076−2097; *Angew. Chem. Int. Ed.* **2001**, *40*, 2022−2043; S. Leininger, B. Olenyuk, P. J. Stang, *Chem. Rev.* **2000**, *100*, 853−908; R. W. Saalfrank, B. Demleitner, in *Transition Metals in Supramolecular Chemistry* (Ed.: J. P. Sauvage), Wiley-VCH, Weinheim, **1999**, p. 1−51; E. Uller, B. Demleitner, I. Bernt, R. W. Saalfrank, in *Structure and Bonding* (Ed.: M. Fujita), Springer, Berlin, **2000**, vol. *96*, p. 149−175; D. L. Caulder, K. N. Raymond, *Acc. Chem. Res.* **1999**, *32*, 975−982; J. L. Atwood, L. R. MacGillivray, *Angew. Chem.* **1999**, *111*, 1080−1096; *Angew. Chem. Int. Ed.* **1999**, *38*, 1018−1033; M. Fujita, *Chem. Soc. Rev.* **1998**, *27*, 417−425; C. J. Jones, *Chem. Soc. Rev.* **1998**, *27*, 289−299; D. Philp, J. F. Stoddart, *Angew. Chem.* **1996**, *108*, 1242−1286; *Angew. Chem. Int. Ed. Engl.* **1996**, *35*, 1154−1196; P. N. W. Baxter, in *Comprehensive Supramolecular Chemistry* (Ed.: J.-M. Lehn), Pergamon, Oxford, **1996**, vol. 9, p. 165−211; E. C. Constable, in *Comprehensive Supramolecular Chemistry* (Ed.: J.-M. Lehn), Pergamon, Oxford, **1996**, vol. 9, p. 213−252; J.-C. Chambron, C. Dietrich-Buchecker, J.-P. Sauvage, in *Comprehensive Supramolecular Chemistry* (Ed.: J.-M. Lehn), Pergamon, Oxford, **1996**, vol. 9, p. 43−83; C. Piguet, G. Bernardinelli, G. Hopfgartner, *Chem. Rev.* **1997**, *97*, 2005−2062; R. W. Saalfrank, B. Demleitner, N. Löw, S. Trummer, S. Kareth, *Molecular Crystals and Liquid Crystals* **2001**, *356*, 71−90; D. W. Johnson, K. N. Raymond, *Supramol. Chem.* **2001**, *13*, 639−659; M. Ziegler, J. L. Brumaghim, K. N. Raymond, *Angew. Chem.* **2000**, *112*, 4285−4287;

Angew. Chem. Int. Ed. **2000**, *39*, 4119−4121; G. F. Swiegers, T. J. Malefetse, *Coordination Chemistry Rev.* **2002**, *225*, 91−121; M. D. Ward, J. A. McCleverty, J. C. Jeffery, *Coord. Chem. Rev.* **2001**, *222*, 251−272.

[2] B. Hasenknopf, J.-M. Lehn, B. O. Kneisel, G. Baum, D. Fenske, *Angew. Chem.* **1996**, *108*, 1987−1990; *Angew. Chem. Int. Ed. Engl.* **1996**, *35*, 1838−1840; J. S. Fleming, K. L. V. Mann, C.-A. Carraz, E. Psillakis, J. C. Jeffery, J. A. McCleverty, M. D. Ward, *Angew. Chem.* **1998**, *110*, 1315−1318; *Angew. Chem. Int. Ed.* **1998**, *37*, 1279−1281; S. Mann, G. Huttner, L. Zsolnai, K. Heinze, *Angew. Chem.* **1996**, *108*, 2983−2984; *Angew. Chem. Int. Ed. Engl.* **1996**, *35*, 2808−2809.

[3] N. Fujita, K. Biradha, M. Fujita, S. Sakamoto, K. Yamaguchi, *Angew. Chem.* **2001**, *113*, 1768−1771; *Angew. Chem. Int. Ed.* **2001**, *40*, 1718−1721; K. Umemoto, H. Tsukui, T. Kusukawa, K. Biradha, M. Fujita, *Angew. Chem.* **2001**, *113*, 2690−2692; *Angew. Chem. Int. Ed.* **2001**, *40*, 2620−2622; A. Ikeda, M. Yoshimura, H. Udzu, C. Fukuhara, S. Shinkai, *J. Am. Chem. Soc.* **1999**, *121*, 4296−4297.

[4] R. W. Saalfrank, R. Burak, A. Breit, D. Stalke, R. Herbst-Irmer, J. Daub, M. Porsch, E. Bill, M. Müther, A. X. Trautwein, *Angew. Chem.* **1994**, *106*, 1697−1699; *Angew. Chem. Int. Ed. Engl.* **1994**, *33*, 1621−1623; D. L. Caulder, R. E. Powers, T. N. Parac, K. N. Raymond, *Angew. Chem.* **1998**, *110*, 1940−1943; *Angew. Chem. Int. Ed.* **1998**, *37*, 1840−1843.

[5] D. W. Johnson, K. N. Raymond, *Inorg. Chem.* **2001**, *40*, 5157−5161.

[6] S. Hiraoka, M. Fujita, *J. Am. Chem. Soc.* **1999**, *121*, 10239−10240; M. Scherer, D. L. Caulder, D. W. Johnson, K. N. Raymond, *Angew. Chem.* **1999**, *111*, 1690−1694; *Angew. Chem. Int. Ed.* **1999**, *38*, 1588−1592.

[7] R. W. Saalfrank, B. Hörner, D. Stalke, J. Salbeck, *Angew. Chem.* **1993**, *105*, 1223−1225; *Angew. Chem. Int. Ed. Engl.* **1993**, *32*, 1179−1182; T. Beissel, R. E. Powers, K. N. Raymond, *Angew. Chem.* **1996**, *108*, 1166−1168; *Angew. Chem. Int. Ed. Engl.* **1996**, *35*, 1084−1086.

[8] R. W. Saalfrank, A. Stark, M. Bremer, H.-U. Hummel, *Angew. Chem.* **1990**, *102*, 292−295; *Angew. Chem. Int. Ed. Engl.* **1990**, *29*, 311−314; R. W. Saalfrank, A. Stark, K. Peters, H. G. von Schnering, *Angew. Chem.* **1988**, *100*, 878−880; *Angew. Chem. Int. Ed. Engl.* **1988**, *27*, 851−853.

[9] R. W. Saalfrank, R. Burak, S. Reihs, N. Löw, F. Hampel, H.-D. Stachel, J. Lentmair, K. Peters, E.-M. Peters, H. G. v. Schnering, *Angew. Chem.* **1995**, *107*, 1085−1087; *Angew. Chem. Int. Ed. Engl.* **1995**, *34*, 993−995.

[10] To facilitate comparison of structures of **4**, **6**, and **7a** (Figures 1−3), identical projections are presented.

[11] Single crystal X-ray structure analyses: Details for crystal data, data collection and refinement are given in Table 1. X-ray data for **2a** were collected on a Stoe−Siemens−Huber Vierkreisdiffraktometer, for **4** and **7a** on a Nonius Kappa CCD area detector, and for **6** on a Stoe IPDS using Mo-K_α radiation (λ = 0.71073 Å). Semiempirical absorption corrections were employed. The structures were solved by direct methods with SHELXS-97[12] and refined with full-matrix least-squares against F^2 with SHELXL-97[12] (**2a**, **4** and **7a**) and SHELXL-93[12] (**6**).

[12] G. M. Sheldrick, *SHELXS-97*, *Program for the solution of Crystal Structures,* **1997**, University of Göttingen, Germany; G. M. Sheldrick, *SHELXL-93/97*, *Program for the Refinement of Crystal Structures,* **1993/97**, University of Göttingen, Germany.

[13] CCDC-185489 (**2a**), CCDC-185404 (**4**), CCDC-186843 (**6**)[15] and CCDC-185405 (**7a**) contain the supplementary crystallographic data for this paper. These data can be obtained free of charge via www.ccdc.cam.uk/conts/retrieving.html (or from the Cambridge Crystallographic Data Centre, 12 Union Road, Cambridge CB2 1EZ, UK; Fax: +44 1223−336−033; or E-mail: deposit@ccdc.cam.ac.uk).

[14] Because of the low boiling points of methyl- and ethylamine it is more convenient to use the procedure as described for **2a,b** and **3**.

[15] Compound **6** features polymorphism. For supplementary data see CCDC-186844.

[16] R. W. Saalfrank, I. Bernt, F. Hampel, F. W. Heinemann, M. Schmidtmann, A. Müller, *Polyhedron*, in press.

Received August 21, 2002
[I02474]

para-Functionalized NCN-Pincer Palladium(II) Complexes: Synthesis, Catalysis and DFT Calculations

Harm P. Dijkstra,[a] Martijn Q. Slagt,[a] Aidan McDonald,[a] Cornelis A. Kruithof,[a] Robert Kreiter,[a] Allison M. Mills,[b] Martin Lutz,[b] Anthony L. Spek,[b][‡] Wim Klopper,[c][‡‡] Gerard P. M. van Klink,[a] and Gerard van Koten*[a]

Keywords: Density functional calculations / Homogeneous catalysis / Substituent effects / Supported catalysts / Synthesis design

Several *para*-substituted NCN-pincer palladium(II) complexes (**1a**–**g** and **6a**–**g**) {NCN = $[C_6H_3(CH_2NMe_2)_2$-2,6$]^-$, *para* = 4-position} have been prepared and the electronic influences of the *para* substituents were studied in catalysis as well as by DFT calculations (B3LYP/LANL2DZ). From DFT calculations, it was found that the *para* substituent exerts only a minor effect on the partial charge, investigated by means of the Mulliken population analysis, at the palladium(II) center. Also, when the *para*-functionalized, cationic NCN–Pd^{II} complexes **6a**–**g** were applied as Lewis acid catalysts in the double Michael reaction between methyl vinyl ketone and ethyl α-cyanoacetate, only small differences in the activities of the various catalysts were observed. These results, when translated to immobilized multipincer catalysts, imply that various *para* functionalities can be used for immobilization of the pincer–metal complexes without affecting the catalytic activity of the individual sites. The application of a number of shape-persistent nanosize $(NCN–Pd^{II})_n$ complexes (**7**, $n = 3$; **8**, $n = 3$; **9**, $n = 8$; **10**, $n = 12$) as homogeneous catalysts in the same Michael reaction, confirmed this expectation. For complexes **7**, **8** and **9**, the catalytic activity per Pd^{II} center was found to be the same as for the monopincer analogs. Only dodecakis(NCN–Pd^{II}) complex **10** showed an almost threefold enhancement in catalytic activity per Pd^{II} center, which is ascribed to the high catalyst concentration at the periphery of this material.
(© Wiley-VCH Verlag GmbH & Co. KGaA, 69451 Weinheim, Germany, 2003)

Introduction

Metalated pincer complexes (see Figure 1) have been successfully applied as homogeneous catalysts in organic transformations.[1] Advantageous to the pincer system is the ease of alteration of several functionalities, allowing fine-tuning of these pincer complexes for the desired application.[2] The donor substituents Y can be varied easily, giving access to NCN- (Y = NR'_2), PCP- (Y = PR'_2) and SCS-type (Y = SR′) pincer ligands. As a result, metal centers such as palladium, platinum, nickel, iridium, ruthenium and rhodium can nowadays be introduced into the various pincer ligands thereby allowing application of pincer catalysts in a broad range of catalytic reactions.[2] Furthermore, chirality can be introduced into the pincer catalysts by the benzylic substituent R′′ and/or the donor group Y, opening the possibility for asymmetric catalysis.[3] In addition, the electronic as well as the steric environment of the metal center can be fine-tuned by variation of the substituent Y and/or the R′ groups attached to Y. A recent study illustrated the influence of the donor substituent Y on the catalytic activity of cationic YCY−Pd^{II} complexes in a double Michael reaction.[4] It was found that NCN-type catalysts were superior to SCS- and PCP-type catalysts, while also small effects on the catalytic activity were observed when different types of N-donor groups were used. Finally, the *para* substituent R (Figure 1) can also be used to influence the electron density at the metal center. An illustrative example of the *para* substituent influence on the reactivity of a pincer−metal catalyst was reported by Van de Kuil et al., in which various *para*-substituted NCN−Ni^{II} catalysts were studied in the Kharasch addition reaction.[1d,5] Electron-donating and -withdrawing substituents were found to have a significant effect on the Ni^{II}/Ni^{III} oxidation potential, the crucial step in the catalytic cycle of the Kharasch addition.

[a] Debye Institute, Department of Metal-Mediated Synthesis, Utrecht University,
Padualaan 8, 3584 CH Utrecht
Fax: (internat.) + 31-30/2523615
E-mail: g.vankoten@chem.uu.nl
[b] Bijvoet Center for Biomolecular Research, Department of Crystal and Structural Chemistry, Utrecht University,
Padualaan 8, 3584 CH Utrecht
E-mail: a.l.spek@chem.uu.nl
[c] Debye Institute, Department of Theoretical Chemistry, Utrecht University,
Padualaan 14, 3584 CH Utrecht, The Netherlands
E-mail: w.m.klopper@chem.uu.nl
[‡] Correspondence pertaining to crystallographic studies should be addressed to this author.
[‡‡] Correspondence pertaining to theoretical studies should be addressed to this author.

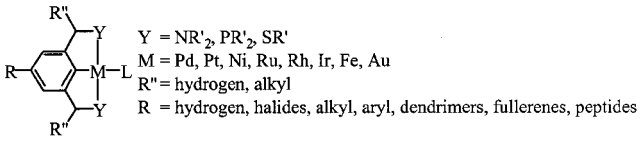

Figure 1. The metalated pincer system

Immobilization of pincer catalysts on soluble or solid supports in order to prepare recyclable catalysts has been intensively studied in recent years.[1e,6] It was demonstrated that the *para* position (R, Figure 1) is excellent for anchoring these pincer complexes to support materials. In particular, we studied shape-persistent multi(YCY−metal) complexes as homogeneous catalysts as well as their application in a nanofiltration membrane reactor in order to enhance total turnover numbers of the catalysts by recycling.[4,7,8] In this field of research, it is desirable to be able to use diverse functionalities at the *para* position of the pincer complex for anchoring purposes. In order to estimate beforehand any uncontrolled influences by these functionalities on the catalytic properties of the pincer−metal moieties, we set out to study the electronic influence of *para* substituents on the catalytic activity of pincer systems in organic transformations. Since (NCN−Pd^{II}) complexes were already found to be very active as homogeneous Lewis acid catalysts in the double Michael reaction between methyl vinyl ketone (MVK) and ethyl α-cyanoacetate[4] and because the conditions nicely meet the requirements for the commercially available nanofiltration membranes,[9] we decided to use this reaction for our catalyst screening. A number of *para*-functionalized, cationic NCN−Pd^{II} complexes [Figure 2, X = $OH_2(BF_4)$] were prepared and applied as Lewis acid catalysts in the double Michael reaction. We also performed density functional theory (DFT) calculations on these systems in order to gain insight in the electronic influence of the *para* substituent on the Pd^{II} center. Furthermore, palladated shape-persistent multi(NCN-pincer) complexes, in which the pincer moiety is anchored to the various supports by different *para* functionalities, were also included in this study.

Results and Discussion

Synthesis of *para*-Substituted NCN−Pd^{II} Complexes

para-Substituted NCN-pincer complexes **1a**−**g** were selected for this study (Figure 2). Complexes **1a** (X = Br),[10] **1b** (X = Br)[11] and **1g** (X = Cl)[12] were prepared according

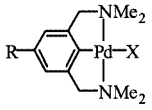

	1a	1b	1c	1d	1e	1f	1g
R	H	NO_2	NMe_2	C(O)Me	OCH_2Ph	Ph	$SiMe_3$

Figure 2. A series of *para*-substituted NCN-pincer palladium(II) complexes

to literature procedures. Palladium(II) complex **1c** (X = Br) was prepared in two steps (Scheme 1). Treatment of *para*-amino pincer derivative **2**[13] with formaldehyde and formic acid, yielded the desired ligand **3c** in 62% yield. Treatment of **3c** with $Pd_2(dba)_3$·$CHCl_3$ in benzene, afforded NCN−palladium(II) complex **1c** (Scheme 1). The *para*-acetyl-substituted NCN-pincer complex **1d** (X = Br) was prepared according to the same palladation procedure, starting from the previously prepared ligand precursor **3d**[13] (Scheme 1).

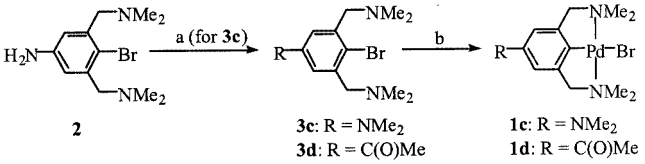

Scheme 1. a) Formaldehyde, formic acid, room temp., 3 h; b) [$Pd_2(dba)_3$]·$CHCl_3$, C_6H_6, room temp., 18 h

para-Benzyloxy pincer complex **1e** (X = I) was synthesized according to a procedure recently developed for the synthesis of nanosize multipincer complexes.[7b] Treatment of a mixture of the *para*-(*tert*-butyldimethylsilyl)-protected phenolic pincer **4**, benzyl bromide, potassium carbonate and 18-crown-6 with tetrabutylammonium fluoride in acetone, resulted in the formation of **1e** in 80% yield (Scheme 2). Note that the metal ion is already present during the introduction step of the *para* substituent, showing the versatility and strength of the pincer system.[14]

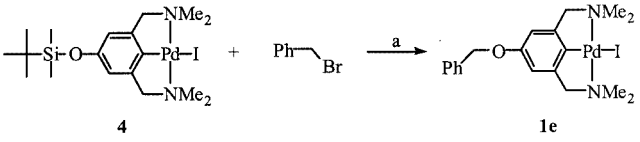

Scheme 2. a) Bu_4NF, K_2CO_3, 18-crown-6, acetone, room temp., 18 h

para-Phenyl pincer complex **1f** (X = Cl) was synthesized from *para*-phenyl-substituted NCN ligand precursor **5**[15] by a lithiation/transpalladation procedure (Scheme 3), affording **1f** in 83% yield.

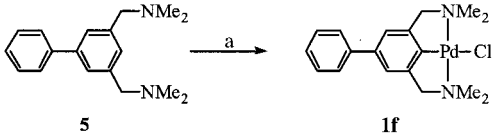

Scheme 3. a) *n*BuLi, hexanes, −80 °C → room temp., 4 h, followed by [$PdCl_2$(cod)], Et_2O, room temp., 2 h

Noteworthy is that three different methods were used to arrive at *para*-substituted NCN−Pd^{II} complexes: i) an oxidative addition reaction (**1a**−**1d**), ii) a lithiation/transmetalation reaction (**1f** and **1g**), and iii) the introduction of the *para* substituent with the metal ion already present in the pincer ligand (**1e**). These examples illustrate the wide variety of reactions which can be used to prepare functionalized pincer−metal complexes. Especially for the synthesis of multi(YCY−metal) complexes, having a variety of

methods available to construct the multimetallic material is considered of great importance.[4,7]

The neutral NCN−Pd^{II} complexes **1a**−**g** were readily converted into the corresponding cationic species **6a**−**g**, the Lewis acid catalyst precursors for the double Michael reaction, by treatment with silver tetrafluoroborate in wet acetone (Scheme 4).[16]

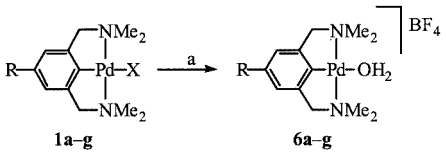

1a–g **6a–g**

Scheme 4. a) $AgBF_4$, wet acetone, room temp., 1 h

Crystals suitable for X-ray crystal structure determination were obtained for neutral NCN−palladium complexes **1c** and **1d** [Figure 3, parts a) and b), respectively]. The molecular structures comprise square-planar palladium(II) centers ligated by a terdentate η^3-coordinating NCN ligand and a bromine ligand *trans* to the aryl ring of the pincer ligand. Table 1 summarizes a number of representative interatomic bond lengths and angles of **1c** and **1d**. The crystal structure of **1d** contains two independent molecules, of which only one is shown in Figure 3. The two molecules differ only slightly in the conformation of the acetyl substituent with respect to the pincer−palladium fragment. In both **1c** and **1d**, the *para* substituents are almost in the same plane with the pincer aryl ring, as can be concluded from the dihedral angles given in Table 1. This coplanarity is commonly observed in the crystal structures of molecules containing an Me_2N−aryl or MeC(O)−aryl moiety.[17] Furthermore, as indicated by the small differences in the Pd−Br distances [**1b**: Pd−Br = 2.5516(3) Å],[11] the different *para* substituents have only minor influences on the electron density of the palladium center.

Density Functional Theory (DFT) Calculations

To further investigate the electronic influences of the *para* substituents on the Lewis acidity of the palladium(II) center, DFT calculations were performed on cationic catalyst precursors **6a**−**g**. Recently, similar calculations on substituted

Table 1. Interatomic distancess [Å] and angles [°] of **1c** and **1d**

1c		**1d**[a]	
Bond lengths:			
Pd1-C1	1.921(2)	Pd1A−C1A	1.911(5)
Pd1−Br1	2.5565(3)	Pd1A−Br1A	2.5636(7)
Pd1−N1	2.119(2)	Pd1A−N1A	2.121(4)
Pd1−N2	2.1171(19)	Pd1A−N2A	2.120(4)
C4−N3	1.387(3)	C6A−C7A	1.499(7)
Bond angles:			
C1−Pd1−Br1	176.99(7)	C1A−Pd1A−Br1A	172.98(15)
C1−Pd1−N1	80.32(9)	C1A−Pd1A−N1A	82.02(19)
C1−Pd1−N2	81.16(9)	C1A−Pd1A−N2A	81.98(18)
N1−Pd1−N2	161.45(7)	N1A−Pd1A−N2A	161.80(16)
Dihedral Angles:			
C14−N3−C4−C5	179.6(2)	C5A−C6A−C7A−O1A	167.6(5)

[a] Only the values for one of the two independent molecules are given.

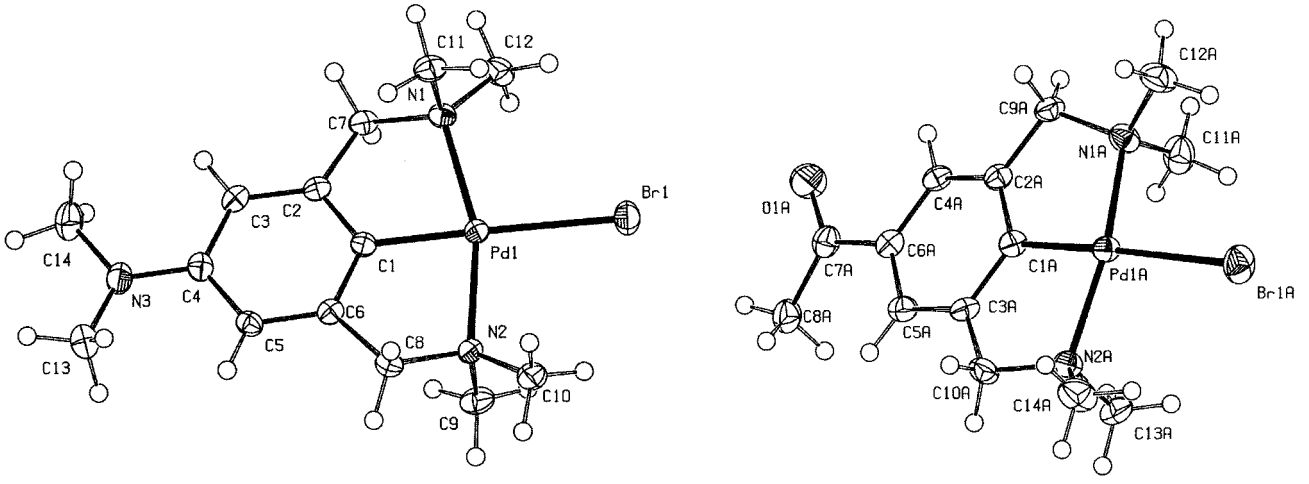

Figure 3. Crystal structures of *para*-substituted NCNPdBr complexes; ORTEP 50% displacement ellipsoids; a) (left): Me_2N−NCNPdBr (**1c**); b) (right): one of the two independent molecules of MeC(O)−NCNPdBr (**1d**)

Table 2. Selected data obtained from DFT calculation with **6a**−**g**, $[R-NCN-Pd(OH_2)]^+$

p-R	Compound	Charge Pd [e][a]	Pd−OH_2 [Å]	Pd−C_{ipso} [Å]	σ_p [b]
H	**6a**	0.187	2.286	1.942	0
NO_2	**6b**	0.217	2.273	1.938	0.778
NMe_2	**6c**	0.171	2.293	1.940	−0.83
C(O)Me	**6d**	0.195	2.281	1.939	0.502
OCH_2Ph	**6e**	0.183	2.286	1.941	−0.42
Ph	**6f**	0.179	2.286	1.940	−0.01
$SiMe_3$	**6g**	0.183	2.285	1.941	−0.07

[a] By means of Mulliken population analysis. [b] Hammett parameters for the various *para*-substituents obtained from Exner.[20]

NCN−Pt^{II} complexes demonstrated that the calculated structures correlated well with the experimental observations.[11b] In addition, the calculated Mulliken charge at the Pt^{II} centers showed a linear relationship with the chemical shifts of the Pt nuclei in the ^{195}Pt NMR spectra of the various complexes as well as with the σ_p Hammett parameter of the various *para* substituents.[11b] The DFT method B3LYP/LANL2DZ[18] as implemented in Gaussian 98[19] was used to calculate the partial charge, by means of Mulliken population analysis, at the palladium(II) centers of *para*-substituted catalyst precursors **6a**−**g**. Table 2 summarizes a number of selected data which were obtained from these calculations and also displays the Hammett parameter (σ_p) of the various *para* substituents.

Both from the Mulliken charge at the Pd^{II} centers and from the Pd−OH_2 and Pd−C_{ipso}(aryl) distances, it becomes clear that the *para* substituent R has only a minor electronic influence on the palladium(II) center, and thus on its Lewis acidity. Nevertheless, the complexes with the highest Mulliken charge at the Pd^{II} center (**6b** and **6d**, most electron-withdrawing substituents) have the shortest calculated Pd−O distances, while complex **6c** (most electron-donating substituent) possessing the lowest Mulliken charge at the Pd^{II} center displays the largest Pd−O distance (Table 2). In addition, plotting the Hammett parameter (σ_p) against the calculated Mulliken charge at the Pd^{II} centers of **6a**−**g**, clearly demonstrates the expected trend (Figure 4). Although, the linear fit is rather poor (in particular **6b** shows a significant deviation), this result indicates that DFT calculations can be used to predict the relative electronic influence of substituents on catalytically active metal centers.

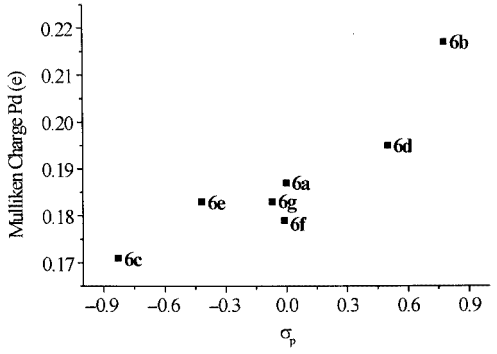

Figure 4. Linear relationship between Hammett parameter (σ_p) of the *para* substituents and Mulliken charge at the Pd centers

Catalysis Using *para*-Substituted NCN−Pd^{II} Catalysts

Cationic NCN−Pd^{II}−aqua complexes **6a**−**g** were applied as homogeneous Lewis acid catalysts in the double Michael reaction between methyl vinyl ketone (MVK) and ethyl α-cyanoacetate (Scheme 5). The results are summarized in Table 3.[21] In all cases 0.5 mol % [Pd^{II}] centers was used. From the $k_{obsd.}$ found for the various catalysts, it is apparent once again that the *para* substituents exert only a small influence on the catalytic activity of the Pd^{II} centers for this particular reaction. Only **6c** (R = Me_2N, Table 3) displays a significantly lower activity in this reaction as compared to the other catalysts.

Table 3. Catalytic results of **6a**−**g** in the double Michael reaction

Catalyst	*p*-R	$k_{obsd.}$ [$\times 10^{-4}$ s^{-1}][a]	$t_{1/2}$ [min][b]
6a	H	2.8	41
6b	NO_2	2.2	53
6c	NMe_2	1.3	89
6d	C(O)Me	2.3	50
6e	OCH_2Ph	2.4	48
6f	Ph	2.7	43
6g	$SiMe_3$	2.6	44

[a] Determined by ^1H NMR spectroscopy by comparison of the integration of the α-CH_2 protons of ethyl α-cyanoacetate to the combined integration of the ethyl ester CH_2 protons of the reactant and product. First-order reactions CN (CN = ethyl α-cyanoacetate); rate constant *k* was determined by plotting $-\ln([CN]/[CN]_0)$ versus time [s]. [b] $t_{1/2} = \ln 2/(k \times 60)$.

Comparison of the experimentally obtained catalytic data with the theoretical data reveals that there is no linear relationship between the observed rate constants ($k_{obsd.}$, Table 3) and the calculated Mulliken charges at the Pd^{II} centers of **6a**−**g** (Table 2). Plotting the Hammett σ_p parameters of the various *para* substituents against the log-

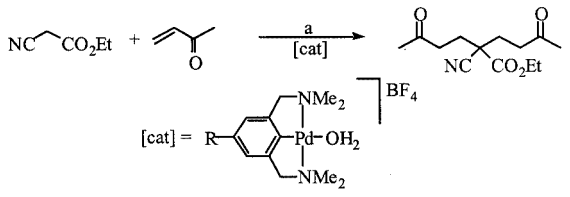

Scheme 5. Double Michael reaction between MVK and ethyl α-cyanoacetate; a) iPr_2NEt (10 mol %), [cat] (0.5 mol %), CH_2Cl_2, room temp.

($k_{obsd.}$) values of **6a**−**g** resulted in a curved function passing through a maximum (Figure 5). This type of behavior has previously been observed for reactions in which a reversible step is followed by an irreversible step.[22] Apparently, the *para* substituents alter the relative magnitude of the rate constants of the individual mechanistic steps and thus change the rate-determining step. In the double Michael reaction, a reversible step − deprotonation of the α-CH_2 group of ethyl α-cyanoacetate − is followed by an irreversible step − the 1,4-addition of the ethyl α-cyanoacetate anion to MVK. Thus, changing the *para* substituent from an electron-withdrawing to an electron-donating group can shift the rate-determining step from the deprotonation step to the nucleophilic 1,4-addition step. From the catalytic data presented in Table 3, it seems that the *p*-NMe_2 substituent has the largest influence, as the activity of **6c** was found to be considerably lower than that of the other catalytic species. Further research to elucidate this change in the rate-determining step is currently under investigation.

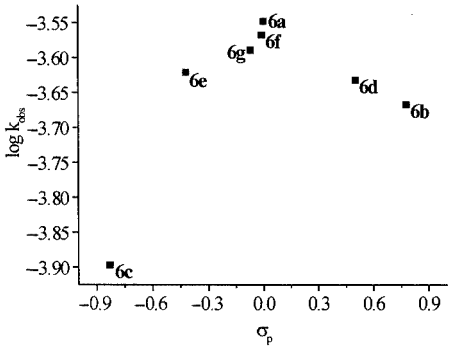

Figure 5. Hammett σ_p parameter versus log($k_{obsd.}$) of **6a**−**g**

Catalysis Using Multi(NCN−Pd^{II}) Catalysts

Previously, we reported the synthesis of shape-persistent multi(NCN−Pd^{II}) catalyst precursors **7**−**10** (Figure 6).[23] These complexes were also applied as homogeneous catalysts in the double Michael reaction between MVK and ethyl α-cyanoacetate (Scheme 5). The catalytic results are

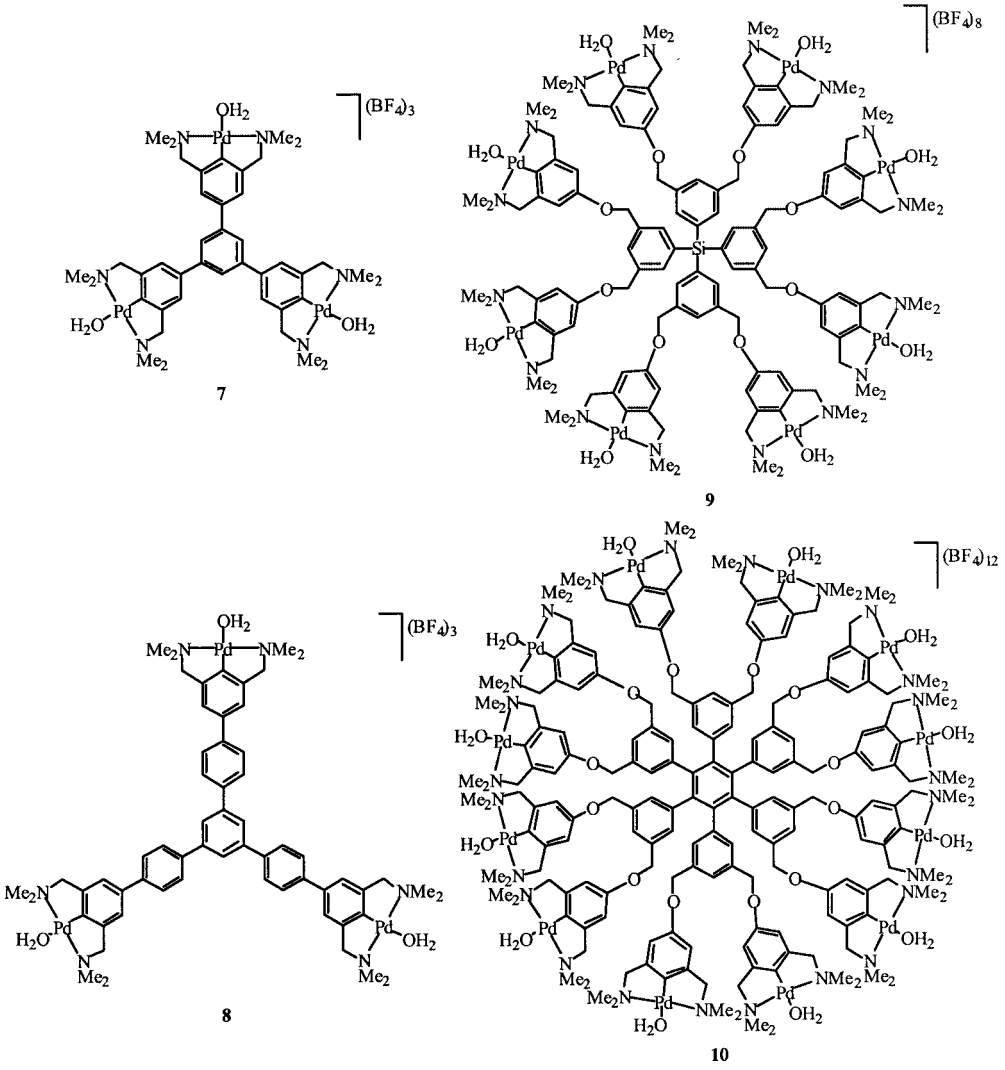

Figure 6. Shape-persistent homogeneous Lewis acid catalysts

Table 4. Catalytic activities of **7**−**10** in the double Michael reaction

Catalyst	$k_{obsd.}$ [$\times 10^{-4}$ s^{-1}][a]	$t_{1/2}$ [min][b]
7	2.3	50
8	2.6	44
9	2.1	55
10	8.1	14

[a] Determined by ^{1}H NMR spectroscopy by comparison of the integration of the α-CH_2 protons of ethyl α-cyanoacetate to the combined integration of the ethyl ester CH_2 protons of the reactant and product. First-order reactions CN (CN = ethyl α-cyanoacetate); rate constant k was determined by plotting $-\ln[CN/[CN]_0)$ versus time [s]. [b] $t_{1/2} = \ln 2/(k \times 60)$.

summarized in Table 4. In all cases, 0.5 mol % [Pd^{II}] centers was used and the $k_{obsd.}$ values for the various multimetallic systems were determined per palladium(II) center.

The catalysis results obtained for the tris(NCN−Pd^{II}) catalyst **7** (Table 4) were reported previously.[4] Compared to the catalytic activity of the reference monometallic catalyst **6a** (R = H, Table 3), it becomes clear that the catalytic activities per palladium(II) center for multi(NCN−Pd^{II}) catalysts **7**−**9** (Table 4) are similar, indicating that all palladium(II) centers in **7**−**9** act as independent catalytic sites. This is an important result; it implies an efficient use of all catalytic sites during catalysis. In addition, it once again underlines that the (Lewis acid) catalytic activity depends little on the *para* functionality of the pincer moiety, which is in agreement with the results obtained for the monometallic *para*-substituted NCN−Pd^{II} catalysts (Table 3). Interestingly, the dodecakis(NCN−Pd^{II}) catalyst **10** shows an almost threefold increase in catalytic activity per Pd^{II} center (Table 4) as compared to reference **6a** (R = H, Table 3). This increase in catalytic activity does not originate from the influence of the *para* substituent, since no increase in catalytic activity was observed for **6e** (R = OCH_2Ph, Table 3) and **9** (Table 4), both possessing the same *para* substituent as **10**. Molecular modeling studies of the isostructural platinum analogs of **9** and **10**,[7b] respectively, already indicated that on average the metal sites are in closer proximity to each other in the case of **10**, suggesting cooperative effects between the Pd^{II} centers during catalysis. Another possible explanation is that large aggregates of **10**, induced by the polar organometallic periphery, assemble in solution, resulting in the formation of polar micro-environments and thereby enhancing the catalytic transformations. This aggregate formation would be more difficult for **9** due to its spherical geometry.

Conclusions

A series of *para*-substituted NCN−Pd^{II} complexes was synthesized and the electronic influence of the *para* substituents on the Lewis-acidic palladium(II) centers was investigated by means of catalysis and DFT calculations. The application of these complexes as homogeneous Lewis acid catalysts in the double Michael reaction between MVK and ethyl α-cyanoacetate, clearly showed that in general the *para* substituents only slightly affect the catalytic activity of the Pd^{II} centers. Only the use of the *para*-(dimethylamino) substituent (**6c**) resulted in a considerable decrease in the catalytic activity. These results were confirmed by DFT calculations, which revealed that the *para* substituents have only minor influences on the partial charge (expressed by the Mulliken population) and thus on the Lewis acidity of the palladium(II) centers. In addition, several shape-persistent multi(NCN−Pd^{II}) complexes were applied as Lewis acid catalysts in the double Michael reaction. The catalysis results of **7**−**9** showed that all catalytic sites act as independent catalysts; the activities per Pd^{II} center were similar to the activities found for the mononuclear catalysts. Surprisingly, the dodecakis(NCN−Pd^{II}) system **10** exhibited a threefold increase in catalytic activity, probably due to cooperativity between metalated pincer groups at the periphery of **10**. Retention measurements with the isostructural platinum analogs of **7**−**10** in a nanofiltration membrane reactor have already shown that these shape-persistent complexes are very efficiently retained by nanofiltration membranes.[7b] Currently, these shape-persistent nanosize complexes are being further explored as homogeneous catalysts in a nanofiltration membrane reactor under continuously operating conditions.

Experimental Section

General: Solvents were purified and dried according to standard procedures, stored under nitrogen and freshly distilled prior to use. NMR solvents were purchased and used without further purification. Compounds **1a**,[10] **1b**,[11] **1g**,[12] **2**,[1d] **3d**,[5] **4**,[7b] **5**,[15] **6a**,[16] and [$PdCl_2$(cod)][24] were prepared according to literature procedures. All other reagents were purchased and used without further purification. NMR spectra were recorded with a Varian 300 spectrometer (^{1}H NMR: 300.1 MHz. ^{13}C NMR: 75.5 MHz. ^{31}P NMR: 121.5 MHz) or a Varian Gemini 200 spectrometer (^{1}H NMR: 200.1 MHz. ^{13}C NMR: 50.3 MHz. ^{31}P NMR: 81.0 MHz). Microanalyses were determined by Dornis and Kolbe, Mikroanalytisches Laboratorium, Mülheim a. d. Ruhr, Germany.

3c: Arylamine **2** (0.20 g, 0.68 mmol) was dissolved in a mixture of formaldehyde (10 mL) and formic acid (10 mL) and this mixture was stirred at room temperature for 3 h. Subsequently, 1 M NaOH (aq) was added to this solution until pH = 11 was reached. The aqueous layer was extracted with CH_2Cl_2 (3 × 20 mL) and the combined organic layers were dried with $MgSO_4$. After evaporation of all volatiles, hexanes (20 mL) were added and the resulting mixture was filtered and the solvents were evaporated to dryness, leaving a slightly brown solid. This product was used without further purification. Yield: 0.13 g (62%). ^{1}H NMR ($CDCl_3$, 200 MHz): δ = 2.30 (s, 12 H, NCH_3), 2.95 (s, 6 H, *p*-NCH_3), 3.50 (s, 4 H, CH_2), 6.74 (s, 2 H, Ar*H*) ppm. ^{13}C NMR ($CDCl_3$, 75 MHz): δ = 40.95, 45.98, 64.49, 114.15, 123.66, 138.77, 149.59 ppm.

1c: [Pd_2(dba)$_3$]·$CHCl_3$ (0.33 g, 0.32 mmol) in benzene (10 mL) was added to a solution of **3c** (0.20 g, 0.64 mmol) in benzene (10 mL) and this solution was stirred at room temperature for 3 h. Subsequently, all volatiles were evaporated, CH_2Cl_2 (15 mL) was added and the resulting solution was filtered through Celite. The Celite layer was washed with CH_2Cl_2 (2 × 5 mL). The combined filtrates

were concentrated to ca. 5 mL and upon addition of Et_2O (10 mL) the product precipitated from the yellow solution. Light-brown crystals suitable for a crystal structure determination were obtained by slow diffusion of pentane into a concentrated solution of **1c** in CH_2Cl_2. Yield: 0.13 g (50%). ^1H NMR ($CDCl_3$, 200 MHz): δ = 2.86 (s, 6 H, *p*-NCH_3), 2.96 (s, 12 H, NCH_3), 3.95 (s, 4 H, CH_2), 6.26 (s, 2 H, Ar*H*) ppm. ^{13}C NMR ($CDCl_3$, 75 MHz): δ = 41.55, 53.96, 75.05, 105.28, 144.53, 145.67, 149.53 ppm. $C_{14}H_{24}BrN_3Pd$ (420.69): calcd. C 39.97, H 5.75, N 9.99; found C 39.78, H 5.67, N 9.92.

1d: Synthesis as described for **1c**, using **3d** (0.20 g, 0.64 mmol) and $Pd_2(dba)_3{\cdot}CHCl_3$ (0.33 g, 0.32 mmol) in benzene (10 mL). Orange/brown crystals of **1d** suitable for a crystal structure determination were obtained by slow concentration in air of a concentrated solution of **1d** in CH_2Cl_2. Yield: 0.18 g (67%). ^1H NMR ($CDCl_3$, 200 MHz): δ = 2.52 [s, 3 H, C(O)CH_3], 2.99 (s, 12 H, NCH_3), 4.05 (s, 4 H, NCH_2), 7.41 (s, 2 H, Ar*H*) ppm. ^{13}C NMR ($CDCl_3$, 75 MHz): δ = 26.80, 54.09, 74.66, 120.22, 134.75, 145.45, 197.92 ppm. $C_{14}H_{21}BrN_2OPd$ (419.66): calcd. C 40.07, H 5.04, N 6.68; found C 40.26, H 5.11, N 6.56.

1e: Tetrabutylammonium fluoride (1 M in THF) (0.54 mL, 0.54 mmol) was added to a mixture of **4** (0.30 g, 0.54 mmol), benzyl bromide (0.10 mL, 0.83 mmol), K_2CO_3 (0.38 g, 2.7 mmol) and 18-crown-6 (13 mg, 0.05 mmol) in acetone (15 mL). This mixture was stirred at room temperature for 5 h. Subsequently, all volatiles were evaporated, CH_2Cl_2 (15 mL) was added and the resulting mixture was filtered. The filtrate was reduced to 5 mL and upon addition of Et_2O (10 mL) the product precipitated as an off-white solid. Slow diffusion of Et_2O into a concentrated solution of **1e** in CH_2Cl_2, afforded analytically pure **1e** as a white powder. Yield: 0.17 g (59%). ^1H NMR ($CDCl_3$, 300 MHz): δ = 2.98 (s, 12 H, NCH_3), 3.97 (s, 4 H, NCH_2), 4.98 (s, 2 H, OCH_2), 6.49 (s, 2 H, Ar*H*), 7.30−7.42 (m, 5 H, Ar*H*) ppm. ^{13}C NMR ($CDCl_3$, 75 MHz): δ = 54.01, 73.66, 74.80, 107.25, 127.65, 128.22, 128.84, 137.32, 145.86, 157.48 ppm. $C_{19}H_{25}IN_2OPd$ (530.74): calcd. C 43.00, H 4.75, N 5.28; found C 43.15, H 4.80, N 5.24.

1f: *n*BuLi (2.3 mL, 3.7 mmol) was added to a solution of **5** (1.0 g, 3.7 mmol) in dry hexanes (20 mL) at −80 °C. After the addition was completed, the temperature was allowed to rise to room temperature and stirring was continued for 4 h. Subsequently, this solution was added to a suspension of [$PdCl_2$(cod)] (1.1 g, 3.7 mmol) in Et_2O at room temperature and the resulting mixture was stirred for an additional 3 h. The solvents were evaporated to dryness and the residue was extracted with CH_2Cl_2 (10 mL). The organic layer was filtered through Celite and the filtrate was reduced to ca. 3 mL. Addition of Et_2O resulted in the formation of a white precipitate which was collected and dried in vacuo. Analytically pure **1f** was obtained by slow diffusion of Et_2O into a concentrated solution of **1f** in CH_2Cl_2, affording colorless needles of **1f**. Yield: 1.2 g (78%). ^1H NMR ($CDCl_3$, 200 MHz): δ = 2.97 (s, 12 H, NCH_3), 4.05 (s, 4 H, NCH_2), 7.00 (s, 2 H, Ar*H*), 7.30−7.51 (m, 5 H, Ar*H*) ppm. ^{13}C NMR ($CDCl_3$, 75 MHz): δ = 53.38 (C_{ipso} signal not observed), 75.03, 119.00, 127.16, 128.99, 138.51, 141.84, 145.65, 156.09 ppm. $C_{18}H_{23}ClN_2Pd$ (409.27): calcd. C 52.83, H 5.66, N 6.84; found C 52.65, H 5.75, N 6.73.

General Procedure for the Synthesis of 6a−g: $AgBF_4$ (97.3 mg, 0.50 mmol) in wet acetone (1 mL) was added to a solution of **1a−g** (0.50 mmol) in acetone (10 mL) and the resulting solution was stirred at room temperature for 1 h. The mixture was filtered through Celite and the filtrate was concentrated to ca. 3 mL. Upon slow addition of Et_2O (5 mL), the product precipitated as an off-white solid. After isolation, the product was analyzed by ^1H NMR spectroscopy and immediately used in the catalytic experiments.

6a:[16] Yield: 0.17 g (86%). ^1H NMR ([D_6]acetone, 300 MHz): δ = 2.87 (s, 12 H, NCH_3), 4.11 (s, 4 H, NCH_2), 6.84 (d, $^3J_{H,H}$ = 7.5 Hz, 2 H, Ar*H*), 7.02 (t, $^3J_{H,H}$ = 7.5 Hz, 1 H, Ar*H*) ppm. ^{13}C NMR ([D_6]acetone, 75 MHz): δ = 51.72, 73.32, 120.42, 125.48, 145.68, 150.49 ppm.

6b: Yield: 0.17 g (78%). ^1H NMR ([D_6]acetone, 300 MHz): δ = 2.92 (s, 12 H, NCH_3), 4.34 (s, 4 H, NCH_2), 7.79 (s, 2 H, Ar*H*) ppm. ^{13}C NMR ([D_6]acetone, 75 MHz): δ = 51.93, 73.08, 115.81, 146.80, 146.90, 161.97 ppm.

6c: Yield: 0.15 g (67%). ^1H NMR ([D_6]acetone, 200 MHz): δ = 2.81 (s, 6 H, *p*-NCH_3), 2.83 (s, 12 H, NCH_3), 4.08 (s, 4 H, NCH_2), 6.38 (s, 2 H, Ar*H*) ppm.

6d: Yield: 0.21 g (93%). ^1H NMR ([D_6]acetone, 300 MHz): δ = 2.49 [s, 3 H, C(O)CH_3], 2.94 (s, 12 H, NCH_3), 4.22 (s, 4 H, NCH_2), 7.50 (s, 2 H, Ar*H*) ppm. ^{13}C NMR ([D_6]acetone, 75 MHz): δ = 26.02, 52.42, 73.66, 120.42, 135.78, 146.80, 162.29, 197.02 ppm.

6e: Yield: 0.24 g (95%). ^1H NMR ([D_6]acetone, 300 MHz): δ = 2.85 (s, 12 H, NCH_3), 4.13 (s, 4 H, NCH_2), 5.04 (s, 2 H, OCH_2), 6.63 (s, 2 H, Ar*H*), 7.32−7.46 (m, 5 H, Ar*H*) ppm. ^{13}C NMR ([D_6]acetone, 75 MHz): δ = 52.01, 70.13, 73.49, 107.80, 127.71, 127.95, 128.61, 137.83, 146.11, 158.28 ppm.

6f: Yield: 0.22 g (93%). ^1H NMR ([D_6]acetone, 300 MHz): δ = 2.89 (s, 12 H, NCH_3), 4.25 (s, 4 H, NCH_2), 7.18 (s, 2 H, Ar*H*), 7.29−7.60 (m, 5 H, Ar*H*) ppm. ^{13}C NMR ([D_6]acetone, 75 MHz): δ = 51.93, 73.45, 119.29, 129.06, 126.94, 127.24, 139.08, 141.54, 146.13, 150.31 ppm.

6g: Yield: 0.22 g (91%). ^1H NMR ([D_6]acetone, 200 MHz): δ = 0.21 (s, 9 H, SiCH_3), 2.85 (s, 12 H, NCH_3), 4.16 (s, 4 H, NCH_2), 7.03 (s, 2 H, Ar*H*) ppm. ^{13}C NMR ([D_6]acetone, 75 MHz): δ = −1.48, 51.84, 73.45, 125.07, 136.92, 145.30, 152.75 ppm.

Catalysis in the Double Michael Reaction Between MVK and Ethyl α-Cyanoacetate. A Typical Experiment. Ethyl α-cyanoacetate (0.17 mL, 1.6 mmol), methyl vinyl ketone (0.40 mL, 4.8 mmol), ethyldiisopropylamine (28 μL, 0.16 mmol) and **6a** (3.2 mg, 8 μmol, 0.5 mol % [Pd]) were mixed in CH_2Cl_2 (5 mL) and stirred at room temperature. The reaction mixture was sampled (100 μL) at regular intervals and the samples worked up by evaporating solvent and methyl vinyl ketone with a gentle stream of nitrogen. The conversions were determined by ^1H NMR spectroscopy. Conversions obtained were confirmed by GC analysis of the reaction mixture. In all cases, the product was isolated by bulb-to-bulb distillation. For all reactions, yields were found to be between 85 and 100%.

Crystal Structure Determinations: Intensities were measured with a Nonius KappaCCD diffractometer with rotating anode (Mo-K_α, λ = 0.71073 Å) at a temperature of 150 K. The structure was solved with automated Patterson methods using the program DIRDIF97,[25] and refined with the program SHELXL-97[26] against F^2 of all reflections up to a resolution of $(\sin/\lambda)_{max}$ = 0.65 $Å^{-1}$. Non-hydrogen atoms were refined freely with anisotropic displacement parameters. Hydrogen atoms were refined as rigid groups. The drawings, structure calculations, and checking for higher symmetry was performed with the program PLATON.[27]

Compound 1c: $C_{14}H_{24}BrN_3Pd$, M = 420.67, orange plate, 0.24 × 0.24 × 0.09 mm, monoclinic, $P2_1/c$ (no. 14), a = 9.1973(1) Å, b = 11.1707(2) Å, c = 16.4736(3) Å, β = 108.3990(8)°, V = 1605.98(4) $Å^3$, Z = 4, ρ = 1.740 g cm^{-3}. The absorption correction was per-

formed with PLATON[27] (routine DELABS, μ = 3.64 mm^{-1}, 0.49−0.72 transmission). 17563 measured reflections, 3671 unique reflections (R_{int} = 0.0508), 2999 observed reflections [$I > 2\sigma(I)$]. 178 refined parameters, 0 restraints. *R* (obsd. refl.): *R*1 = 0.0254, *wR*2 = 0.0517. *R* (all data): *R*1 = 0.0387, *wR*2 = 0.0549. *S* = 1.039. CCDC-187019 contains the supplementary crystallographic data for this paper. These data can be obtained free of charge at www.ccdc.cam.ac.uk/conts/retrieving.html [or from the Cambridge Crystallographic Data Centre, 12 Union Road, Cambridge CB2 1EZ, UK; Fax: (internat.) + 44-1223/336-033; E-mail: deposit@ccdc.cam.ac.uk].

Compound 1d: $C_{14}H_{21}BrN_2OPd$, *M* = 419.64, yellow plate, 0.12 × 0.12 × 0.05 mm, monoclinic, $P2_1/c$ (no. 14), *a* = 17.1168(3) Å, *b* = 15.1078(3) Å, *c* = 12.4777(3) Å, β = 107.1925(12)°, *V* = 3082.52(11) $Å^3$, *Z* = 8, ρ = 1.808 g cm^{-3}. The absorption correction was performed with PLATON[27] (routine MULABS, μ = 3.79 mm^{-1}, 0.68−0.82 transmission). 26887 measured reflections, 7047 unique reflections (R_{int} = 0.0729), 5091 observed reflections [$I > 2\sigma(I)$]. 353 refined parameters, 0 restraints. *R* (obsd. refl.): *R*1 = 0.0456, *wR*2 = 0.0931. *R* (all data): *R*1 = 0.0748, *wR*2 = 0.1034. *S* = 1.012. CCDC-187020 contains the supplementary crystallographic data for this paper. These data can be obtained free of charge at www.ccdc.cam.ac.uk/conts/retrieving.html [or from the Cambridge Crystallographic Data Centre, 12 Union Road, Cambridge CB2 1EZ, UK; Fax: (internat.) + 44-1223/336-033; E-mail: deposit@ccdc.cam.ac.uk].

Acknowledgments

This work was supported by the Council for Chemical Sciences of the Netherlands Organization for Scientific Research (CW/NWO) and the Dutch Technology Foundation (STW).

[1] For representative examples see: [1a] M. Gupta, C. Hagen, R. J. Flesher, W. C. Kaska, C. M. Jensen, *Chem. Commun.* **1996**, 2083−2084. [1b] P. Dani, T. Karlen, R. A. Gossage, S. Gladiali, G. van Koten, *Angew. Chem. Int. Ed.* **2000**, *39*, 743−745; *Angew. Chem.* **2000**, *112*, 759−761. [1c] M. Ohff, A. Ohff, M. E. van der Boom, D. Milstein, *J. Am. Chem. Soc.* **1997**, *119*, 11687−11688. [1d] L. A. van de Kuil, D. M. Grove, R. A. Gossage, J. W. Zwikker, L. W. Jenneskens, W. Drenth, G. van Koten, *Organometallics* **1997**, *16*, 4985−4994. [1e] D. E. Bergbreiter, P. L. Osburn, Y.-S. Liu, *J. Am. Chem. Soc.* **1999**, *121*, 9531−9538. [1f] A. S. Gruber, D. Zim, G. Ebeling, A. L. Monteiro, J. Dupont, *Org. Lett.* **2000**, *2*, 1287−1290. [1g] C. Granel, Ph. Dubois, R. Jérôme, Ph. Teyssié, *Macromolecules* **1996**, *29*, 8576−8582.

[2] For a review about pincer−metal(d^8) chemistry see; M. Albrecht, G. van Koten, *Angew. Chem. Int. Ed.* **2001**, *40*, 3750−3781; *Angew. Chem.* **2001**, *113*, 3866−3898.

[3] [3a] F. Gorla, A. Togni, L. M. Venanzi, A. Albinati, F. Lianza, *Organometallics* **1994**, *13*, 1607−1616. [3b] J. M. Longmire, X. Zhang, M. Shang, *Organometallics* **1998**, *17*, 4374−4379. [3c] M. A. Stark, G. Jones, C. J. Richards, *Organometallics* **2000**, *19*, 1282−1291. [3d] Y. Motoyama, H. Narusawa, H. Nishiyama, *Chem. Commun.* **1999**, 131−132. [3e] S. E. Denmark, R. A. Stavenger, A.-M. Faucher, J. P. Edwards, *J. Org. Chem.* **1997**, *62*, 3375−3385. [3f] L. A. van de Kuil, Y. S. J. Veldhuizen, D. M. Grove, J. W. Zwikker, L. W. Jenneskens, W. Drenth, W. J. J. Smeets, A. L. Spek, G. van Koten, *Recl. Trav. Chim. Pays-Bas* **1994**, *113*, 267−277. [3g] M. Albrecht, B. M. Kocks, A. L. Spek, G. van Koten, *J. Organomet. Chem.* **2001**, *624*, 271−286. [3h] B. S. Williams, P. Dani, M. Lutz, A. L. Spek, G. van Koten, *Helv. Chim. Acta* **2001**, *84*, 3519−3530.

[4] H. P. Dijkstra, M. D. Meijer, J. Patel, R. Kreiter, G. P. M. van Klink, M. Lutz, A. L. Spek, A. J. Canty, G. van Koten, *Organometallics* **2001**, *20*, 3159−3168.

[5] L. A. van de Kuil, H. Luitjes, D. M. Grove, J. W. Zwikker, J. G. M. van der Linden, A. M. Roelofsen, L. W. Jenneskens, W. Drenth, G. van Koten, *Organometallics* **1994**, *13*, 468−477.

[6] [6a] J. W. J. Knapen, A. W. van der Made, J. C. de Wilde, P. W. N. M. van Leeuwen, P. Wijkens, D. M. Grove, G. van Koten, *Nature* **1994**, *372*, 659−663. [6b] A. W. Kleij, R. A. Gossage, R. J. M. Klein Gebbink, E. J. Reyerse, N. Brinkmann, U. Kragl, M. Lutz, A. L. Spek, G. van Koten, *J. Am. Chem. Soc.* **2000**, *122*, 12112−12124. [6c] M. Albrecht, N. J. Hovestad, J. Boersma, G. van Koten, *Chem. Eur. J.* **2001**, *7*, 1289−1294. [6d] P. J. Davies, D. M. Grove, G. van Koten, *Organometallics* **1997**, *16*, 800−802. [6e] M. Albrecht, R. A. Gossage, M. Lutz, A. L. Spek, G. van Koten, *Chem. Eur. J.* **2000**, *6*, 1431−1445. [6f] M. D. Meijer, N. Ronde, D. Vogt, G. P. M. van Klink, G. van Koten, *Organometallics* **2001**, *20*, 3993−4000. [6g] L. A. van de Kuil, D. M. Grove, J. W. Zwikker, L. W. Jenneskens, W. Drenth, G. van Koten, *Chem. Mater.* **1994**, *6*, 1675−1683. [6h] C. Patmamanoharan, P. Wijkens, D. M. Grove, A. P. Philipse, *Langmuir* **1996**, *12*, 4372−4377.

[7] [7a] H. P. Dijkstra, P. Steenwinkel, D. M. Grove, M. Lutz, A. L. Spek, G. van Koten, *Angew. Chem. Int. Ed.* **1999**, *38*, 2186−2188; *Angew. Chem.* **1999**, *111*, 2321−2324. [7b] H. P. Dijkstra, C. A. Kruithof, N. Ronde, R. van de Coevering, D. J. Ramón, D. Vogt, G. P. M. van Klink, G. van Koten, *J. Org. Chem.*, in press, manuscript available on the world wide web: http://pubs3.acs.org/acs/journals. [7c] H. P. Dijkstra, M. Albrecht, G. van Koten, *Chem. Commun.* **2002**, 126−127.

[8] For an overview on homogeneous catalyst recycling using ultra- and nanofiltration membranes see: H. P. Dijkstra, G. P. M. van Klink, G. van Koten, *Acc. Chem. Res.* **2002**, *35*, 798−810.

[9] See ref.[7b] SelRo-nanofiltration membranes (MPF-60: MWCO = 400 Dalton; MPF-50: MWCO = 700 Dalton) were purchased from Koch Membrane Systems Inc., Düsseldorf, Germany; further product information can be found at http://www.kochmembrane.com.

[10] P. L. Alsters, P. J. Baesjou, M. D. Janssen, H. Kooijman, A. Sicherer-Roetman, A. L. Spek, G. van Koten, *Organometallics* **1992**, *11*, 4124−4135.

[11] [11a] M. Q. Slagt, R. J. M. Klein Gebbink, G. van Koten, *J. Chem. Soc., Dalton Trans.* **2002**, 2591−2592. [11b] M. Q. Slagt, G. Rodríguez, R. J. M. Klein Gebbink, W. Klopper, M. Lutz, A. L. Spek, G. van Koten, submitted.

[12] A. W. Kleij, H. Kleijn, J. T. B. H. Jastrzebski, A. L. Spek, G. van Koten, *Organometallics* **1999**, *18*, 277−285.

[13] For the synthesis of **2** and **3d**, see ref.[1d] and ref.[5], respectively.

[14] G. Rodríguez, M. Albrecht, J. Schoenmaker, A. Ford, M. Lutz, A. L. Spek, G. van Koten, *J. Am. Chem. Soc.* **2002**, *124*, 5127−5138.

[15] P. Steenwinkel, S. L. James, D. M. Grove, N. Veldman, A. L. Spek, G. van Koten, *Chem. Eur. J.* **1996**, *2*, 1440−1445.

[16] D. M. Grove, G. van Koten, J. N. Louwen, J. G. Noltes, A. L. Spek, H. J. C. J. Ubbels, *J. Am. Chem. Soc.* **1982**, *104*, 6609−6616.

[17] This information can be obtained from the Cambridge Structural Database: F. H. Allen, O. Kennard, *Chem. Des. Autom. News* **1993**, *8*, 1 and 31.

[18] The DFT-B3LYP/LANL2DZ method uses density functional theory combined with effective core potentials. The basis set used for palladium is the Los Alamos National Laboratory set (LANL) for effective core potentials (ECP) of double ζ type, consisting of a small core ECP with 3s and 3p orbitals in the valence space. The functional form used is the B3LYP, and the relativistic correlations for heavy atoms are considered in the ECP.

[19] M. J. Frisch, G. W. Trucks, H. B. Schlegel, G. E. Scuseria, M. A. Robb, J. R. Cheeseman, V. G. Zakrzewski, J. A. Montgomery Jr., R. E. Stratmann, J. C. Burant, S. Dapprich, J. M. Millam, A. D. Daniels, K. N. Kudin, M. C. Strain, O. Farkas, J. Tomasi, V. Barone, M. Cossi, R. Cammi, B. Mennucci, C. Po-

melli, C. Adamo, S. Clifford, J. Ochterski, G. A. Petersson, P. Y. Ayala, Q. Cui, K. Morokuma, D. K. Malick, A. D. Rabuck, K. Raghavachari, J. B. Foresman, J. Cioslowski, J. V. Ortiz, A. G. Baboul, B. B. Stefanov, G. Liu, A. Liashenko, P. Piskorz, I. Komaromi, R. Gomperts, R. L. Martin, D. J. Fox, T. Keith, M. A. Al-Laham, C. Y. Peng, A. Nanayakkara, C. Gonzalez, M. Challacombe, P. M. W. Gill, B. Johnson, W. Chen, M. W. Wong, J. L. Andres, C. Gonzalez, M. Head-Gordon, E. S. Replogle, J. A. Pople, *Gaussian 98*, Revision A.7, Gaussian, Inc., Pittsburgh PA, **1998**.

[20] O. Exner, *Correlation Analysis of Chemical Data*, Plenum Press, New York, **1998**.

[21] The catalytic results obtained for **6a** were previously published; see ref.[4]

[22] J. Shorter in *Correlation Analysis in Organic Chemistry: an Introduction to the Linear Free-energy Relationships*, Clarendon Press, Oxford, **1973**.

[23] For the synthesis of **7**, see ref.[4] For the synthesis of **8**−**10**, see ref.[7b]

[24] D. Drew, J. R. Doyle, A. G. Shaver, *Inorg. Synth.* **1972**, *13*, 47.

[25] P. T. Beurskens, G. Admiraal, G. Beurskens, W. P. Bosman, S. Garcia-Granda, R. O. Gould, J. M. M. Smits, C. Smykalla, *The DIRDIF97 program system*, Technical Report of the Crystallography Laboratory, University of Nijmegen, The Netherlands, **1997**.

[26] G. M. Sheldrick, *SHELXL-97, Program for crystal structure refinement*, University of Göttingen, Germany, **1997**.

[27] A. L. Spek, *PLATON, A multipurpose crystallographic tool*, Utrecht University, The Netherlands, **2002**.

Received September 16, 2002
[I02523]

Investigation of the Ligand Exchange Behavior of Square-Planar Nickel(II) Complexes by X-ray Absorption Spectroscopy and X-ray Diffraction

Martin P. Feth,*[a] Axel Klein,*[b] and Helmut Bertagnolli[a]

Keywords: Nickel / Ligand exchange / EXAFS spectroscopy / XANES / X-ray diffraction

The local structure of nickel and bromine in three square-planar nickel(II) complexes [(2,2′-bipyridyl)(bromo)(mesityl)-nickel(II)] (**1**), [(bromo)(*N*,*N*-diisopropyl-1,2-ethanediimine)-(mesityl)nickel(II)] (**2**), [(bromo)(mesityl)bis(triphenylphosphane)nickel(II) (**3**)] and their ligand exchange behavior towards several solvents has been determined by means of X-ray Absorption Near Edge Spectroscopy (XANES), Extended X-ray Absorption Fine Structure Spectroscopy (EXAFS), X-ray Diffraction (XRD), multinuclear NMR and UV/Vis spectroscopy. Several square-planar and octahedral nickel(II) complexes were prepared and spectroscopically characterized as reference compounds. The exchange behavior strongly depends on the nature of the incoming donor ligand (solvent molecule). In some cases the substitution of one or more ligands was accompanied by conservation of the square-planar geometry. In other solvents the geometry changed from square-planar to octahedral. The structural information obtained is important to the further development of such nickel(II) complexes as catalysts for various applications.
(© Wiley-VCH Verlag GmbH & Co. KGaA, 69451 Weinheim, Germany, 2003)

Introduction

Organonickel(II) complexes are widely used in organometallic catalysis. One of the first benchmarks was the (phosphane)nickel complexes used in the Shell Higher Olefin Process (SHOP)[1−7] (Scheme 1).

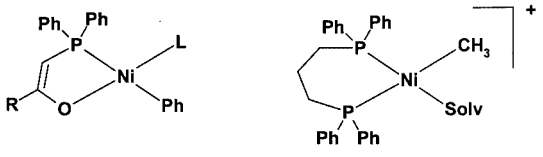

Scheme 1. Nickel catalysts for the oligomerization of olefins in the Shell Higher Olefin Process (SHOP) (**A**)[2−5] (left) or for copolymerization of ethene with CO (**B**)[6,7] (right)

A crucial requirement for these two systems to act as catalysts is that they contain a labile ligand (L or Solv) − as exhibited by the highly reactive catalysts for olefin polymerization developed over the last decade, mainly by Brookhart [1,2,8−14]. The active catalyst species are prepared from dialkylnickel precursor complexes as shown in Scheme 2.

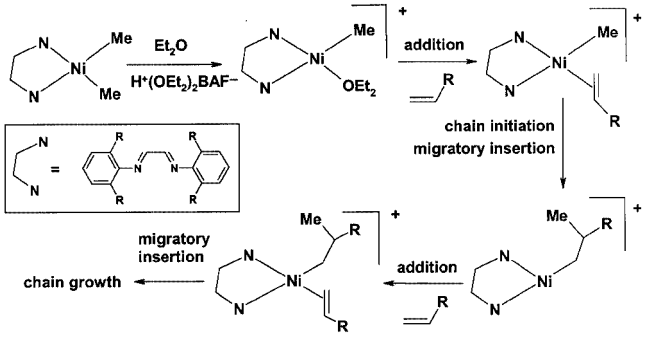

Scheme 2. (α-Diimine)nickel complexes (diimine = 1,4-diazabutadiene) as catalysts for the polymerization of olefins;[2] preparation of the active catalyst species (top) and elemental steps in polymerization catalysis (bottom); BAF = perfluorinated tetraarylborates

Recently, we have investigated organonickel complexes of the type [(diimine)Ni(R)X] (R = alkyl or aryl; X = Cl or Br) to develop an alternative route to catalytically active species. We originally intended to abstract X by the addition of silver salts or related reagents; however, in polar solvents the complexes already showed a considerable degree of dissociation into the ionic species $[(diimine)Ni(R)(Solv)]^+$ and X^-, depending on X, the polarity of the solvent and the bulkiness of the R group [2,8,9,11−13]. With X = Cl the complexes are more inert towards X-dissociation but are very sensitive to hydrolysis. Complexes with X = Br are much more reactive towards dissociation but are quite inert towards water. Alkyl derivatives (R = alkyl) are very reactive to both dissociation and water whereas aryl complexes are relatively stable.[15,16] Dissociation can be enormously accel-

[a] Institut für Physikalische Chemie, Universität Stuttgart, Pfaffenwaldring 55, 70550 Stuttgart
Fax: (internat.) + 49-711/685-4443
E-mail: m.feth@ipc.uni-stuttgart.de
[b] Institut für Anorganische Chemie, Universität Stuttgart, Pfaffenwaldring 55, 70550 Stuttgart
Fax: (internat.) + 49-711/685-4165
E-mail: aklein@iac.uni-stuttgart.de
Supporting information for this article is available on the WWW under http://www.eurjic.org or from the author.

erated by electrochemical reduction of the starting complexes. The rapid loss of Br^- after reduction to the radical anionic species $[(diimine)Ni(R)Br]^{\cdot -}$ can only be slowed to a measurable rate for the very bulky mesityl group and at quite low temperatures.[17−20] The dissociation reactions yield species which should be quite reactive in the catalytic polymerization of olefins. However, we first wanted to examine in detail the structural aspects of these ligand exchange reactions (X^- to Solv) and to determine whether, in these media, further ligand exchange reactions occur that would lead to the replacement of the diimine ligand. To our astonishment this question has never been investigated thoroughly in mechanistic studies of olefin polymerization or related reactions.[1,6,7,9,11,21] In the nonpolar media used for the reactions and the applied excesses of ligand there is no need to consider ligand loss. However, if the reactions are to be extended to highly polar solvents with donor capabilities, or the ligand appears to be the "cost-determining step" and should not be used in excess, the partial or total loss of the chelate ligand (here the diimine) has to be considered, since it might influence the catalytic mechanism. We therefore investigated the ligand exchange reactions of the complexes [(diimine)Ni(Mes)Br] and also *trans*-$[(PPh_3)_2Ni(Mes)Br]$. The latter is not only the starting complex for the preparation of the *cis*-configured diimine complexes but shows the same dissociation lability and has been the subject of a related kinetic study.[22] Also it was previously used to catalyze the co-dimerization of butadiene and ethylene.[23] The combination of the bulky R group and the good leaving group Br^- renders these systems very suitable for a detailed mechanistic study since the timescale of the reactions lie in the range of minutes to hours. From the available diimine complexes we have chosen two different types: 2,2′-bipyridine (bpy), a classical aromatic diimine ligand, and *N*,*N*-diisopropyl-1,4-diazabutadiene (*i*Pr-DAB), a "Brookhart"-type ligand (see Scheme 2) developed some five decades ago.[24−27] in addition to the standard spectroscopic techniques (multinuclear NMR or UV/Vis absorption spectroscopy) we have made great use of EXAFS spectroscopy to investigate the ligand exchange reactions. For studies were crystalline samples are not available or of isotropic (X-ray amorphous) media like solutions, or powders, EXAFS is a powerful tool to elucidate the coordination sphere of such catalytically relevant species.[28−31] We used EXAFS spectroscopy at the nickel *K*-edge as well as on the bromine *K*-edge to investigate ligand exchange reactions in these complexes in solution as well as on separately prepared and isolated samples of possible intermediates. Molecular structures determined by XRD from single crystals helped to adjust reasonable fitting models. Investigation of the XANES region of an X-ray absorption spectra is also a powerful tool for the determination of the geometry of the first coordination shell and the oxidation state of an absorbing atom.[32,33] Emphasis can be given to the so-called pre-edge peaks (short: pre-peaks), which are related to electric dipole transitions from inner shells to unfilled bound states, e.g. 1s → 3d. These pre-peaks are very sensitive to geometrical changes in the first coordination shell of the absorbing atom. The symmetry of the first shell determines if certain pre-peaks appear in the spectrum or are symmetrically forbidden. For the square-planar Ni^{II} complexes the XANES investigations focus on the pre-peaks assigned to the 1s → 3d and 1s → $4p_z$ transitions.[34,35]

Results and Discussion

UV/Vis Absorption and Multinuclear NMR Spectroscopy in Solution

The bright colors of the compounds under investigation can be used to monitor their reactions. The complexes [(diimine)Ni(Mes)Br] show characteristic solvatochromic absorptions in the visible region[18,21,36,37] and dissolving them in non- to moderately coordinating solvents, such as toluene, CH_2Cl_2, THF, acetone, propylene carbonate (PC) and *N*,*N*-dimethylformamide (DMF), leads only to the expected solvatochromic shift. Solutions with pyridine or acetonitrile as solvent, however, show markedly blue-shifted absorption maxima within a few seconds {as shown for [(bpy)Ni(Mes)Br] in Figure 1}. These rapid reactions are followed by slower ones and the observed absorption bands were again shifted to higher energies. For the reaction of [(bpy)Ni(Mes)Br] in MeCN the rate of the first reaction was determined as $k = 0.324(6)\ M^{-1}\ s^{-1}$, assuming a first-order mechanism. We assign this to the dissociation of the bromide ligand and substitution by MeCN. The second reaction is much slower [$k = 0.0041(3)\ M^{-1}\ s^{-1}$] and is assigned to the replacement of the chelate ligand. This is deduced from the corresponding reaction in pyridine solution, where the rate constant is comparable [$k = 0.0029(3)\ M^{-1}\ s^{-1}$] and the resulting absorptions are coincident with those of the pyridine complex $[(py)_3NiMes]^+$ (see Exp. Sect.).

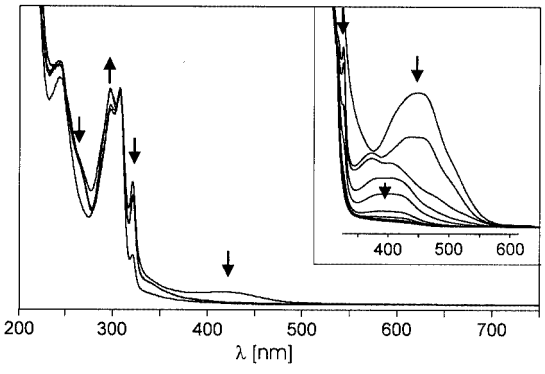

Figure 1. UV/Vis absorption spectra of [(bpy)Ni(Mes)Br] in acetonitrile (MeCN), immediately after dissolution and 3, 4.5 and 21 h later; insert: 20 s, 60 s, 180 s, 360 s, 540 s, and 720 s after dissolution

^1H NMR spectroscopy gives no sign of (partial) dissociation of the chelate ligand in the first minutes after dissolving, thus supporting the assumed reaction sequence. Subsequently, several reaction products appear that cannot be assigned unambiguously. After a prolonged reaction (several days) only in the case of pyridine we could clearly identify $[(py)_3Ni(Mes)]^+$ and the free ligand. In MeCN

numerous soluble products are found, along with insoluble green material.

The complex $[(PPh_3)_2Ni(Mes)Br]$ exhibits, in solvents such as toluene, CH_2Cl_2 or acetone, a solvent-invariant, weak long-wavelength absorption band with a maximum around 450 nm.[22] In pyridine solution a reaction occurs that can be monitored by a decrease of this band and the appearance of the blue-shifted maximum at around 410 nm. After this relatively fast reaction [$k(1) = 0.284(9)$ м$^{-1}$ s^{-1}], a second slower reaction follows with $k(2) = 0.0061(5)$ м$^{-1}$ s^{-1}. The reactions were confirmed by ^{1}H and ^{31}P NMR spectroscopy as identical to those of the diimine complexes.[11]. The ^{31}P NMR signal at $\delta = 20.2$ ppm for the starting complex is replaced by a singlet at $\delta = 27$ ppm that can be assigned to *trans*-$[(PPh_3)_2Ni(Mes)(py)]^+$ (see Exp. Sect.). Finally, after 36 h, only free PPh_3 ($\delta = -5$ ppm) is detected in solution. The ^{1}H NMR spectrum confirms the formation of $[(py)_3Ni(Mes)]^+$. In THF solution the reaction seems to stop after the first sequence and the resulting ^{31}P signal at $\delta = 29$ ppm is assigned to the solvent-coordinated species $[(PPh_3)_2Ni(Mes)(THF)]^+$. For a ligand-exchange reaction using thiocyanate (SCN^-) Martinez and Muller derived a two-term rate law, with $k_s = 5.2 \pm 0.6 \times 10^{-2}$ mol^{-1} s^{-1}, for the exchange of bromide versus the acetone solvent and $k_{an} = 3.0 \pm 0.4 \times 10^{-1}$ mol^{-1} s^{-1} for the subsequent replacement of acetone by SCN^-. On varying R in $[(PPh_3)_2Ni(R)Br]$ from C_6H_4Cl to C_6Cl_5 the k_{an} value lies in the range 43 to 6.6×10^{-4} with mesityl occupying an intermediate position.[22] Our experiments (see also EXAFS) confirm that even weakly coordinating solvents such as acetone or THF can replace bromide to form $[(PPh_3)_2Ni(Mes)(Solv)]^+$, which is in sharp contrast to the behavior of [(bpy)Ni(Mes)Br]. This is due to the strong *trans* effect of the mesityl ligand. Since our substitution reactions on $[(PPh_3)_2Ni(Mes)Br]$ were performed in neat pyridine or other media that are potential ligands, we fitted our kinetic data according to a first-order rate law, thus deviating from the established two-term rate law.[22] Our $k(1)$ value agrees excellently with the k_{an} measured by Martinez and Muller, indicating that SCN^- and pyridine are of comparable σ-donor capability. In acetonitrile the first rapid reaction leads to a green solution. Inspection of the absorption spectrum shows weak long-wavelength absorptions at 1228 nm (8143 cm^{-1}; $\varepsilon = 40$ м$^{-1}$·cm^{-1}) and 630 nm (15873 cm^{-1}; $\varepsilon = 160$ м$^{-1}$·cm^{-1}; with a shoulder at 681 nm). The latter is responsible for the observed green color. In the UV region, shoulders at 431 nm (23202 cm^{-1}) and 419 nm (23877 cm^{-1}) are discernible and the spectrum is dominated by an intense band at 267 nm (37450 cm^{-1}; $\varepsilon = 23000$ м$^{-1}$cm^{-1}). The long-wavelength bands are quite weak and typical for ligand field transitions of nickel(II) complexes.[38,39] We assume a tetrahedral coordination of the ligands in $[(PPh_3)_2Ni(Mes)(MeCN)]^+$, the product of the first substitution reaction. An octahedral coordination was excluded because of the bulkiness of the Mes and PPh_3 ligands. The corresponding absorptions were assigned to $\nu_1 = {}^3T_2(F) \rightarrow {}^3T_1(F)$; $\nu_2 = {}^3A_2(F) \rightarrow {}^3T_1(F)$ and $\nu_3 = {}^3T_1(P) \rightarrow {}^3T_1(F)$. Such transitions are usually more intense than those of octahedral species and exhibit splitting due to spin-orbit coupling. The ^{31}P NMR spectra of such green solutions show the presence of a singlet at $\delta = 21.7$ ppm. In addition, two further singlets at $\delta = 20.3$ ppm (starting complex) and $\delta = 19.3$ ppm (1/20 intensity of the $\delta = 21.7$ ppm signal) are observed whereas free PPh_3 is not found. The ^{1}H NMR spectra confirm the presence of several species, but line broadening precludes further assignments.. Apart from different degrees of substitution, an equilibrium between tetrahedral and square-planar conformations of an individual species might account for the complicated behavior, as has been described for $[(PEtPh_2)_2NiBr_2]$.[40,41] As tetrahedral nickel(II) species should be paramagnetic ($S = 1$), which might explain the poor NMR spectroscopic data, an ESR investigation of these species is planned.

Structural Studies on the [(bpy)Ni(Mes)Br] System

Crystal Structure

The crystal structure of [(bpy)Ni(Mes)Br]·THF (Figure 2) shows two very similar, but independent, molecules in the unit cell. Both structures exhibit the expected square-planar environment of the nickel atoms, with only slight tetrahedral distortions [N(11)−Ni(1)−N(12) towards C(11)−Ni(1)−Br(1) of 8.6° or 12.1°, respectively].

The bond lengths of **1** and **2** are very similar and lie in the expected range.[17,42,43] However, while the interplanar angle between the two pyridine moieties is negligible for **1** (1.9°) it is appreciable for **2** (10.5°). A further distortion for **2** concerns the C(21)−Ni(2)−N(22) angle of 170.4(3), which deviates markedly from the idealized 180°. For **1** we found 176.2(3)°. Both molecules are similar to the recently described dimesityl complex $[(bpy)Ni(Mes)_2]$.[17] The distortion of the coordination plane in $[(bpy)Ni(Mes)_2]$ is very much like that in **2** (12.4°) whereas the pyridine interplanar angle (3.2°) is close to that of **1**. Many other molecular parameters are very similar for these three structures, with the notable exception of the Ni−N distance *trans* to the Br ligand, which is markedly shorter than the others in agreement with the expected *trans* influence.

XANES Investigations

In the XANES spectra of the square-planar Ni^{II} at the Ni *K*-edge complexes two pre-edge peaks can be observed [Figure 3 (a)]. The pre-peak at about 8333 eV can be assigned to a $1s \rightarrow 3d$ electron transition, while the second peak, which occurs at about 8337 eV, is due to a $1s \rightarrow 4p_z$ transition.[34,35] In octahedral Ni^{II} complexes the $1s \rightarrow 3d$ transition as well as the $1s \rightarrow 4p_z$ transition are forbidden; however, the small orbital mixing by lower symmetry gives some probability for the $1s \rightarrow 3d$ transition. Thus, in octahedral complexes the $1s \rightarrow 4p_z$ pre-peak at 8337 eV is absent and the $1s \rightarrow 3d$ pre-peak shows a much smaller intensity than in square-planar complexes [34,35,44]. Therefore octahedral and square-planar complexes can be distinguished by the presence or absence of the $1s \rightarrow 4p_z$ transition.

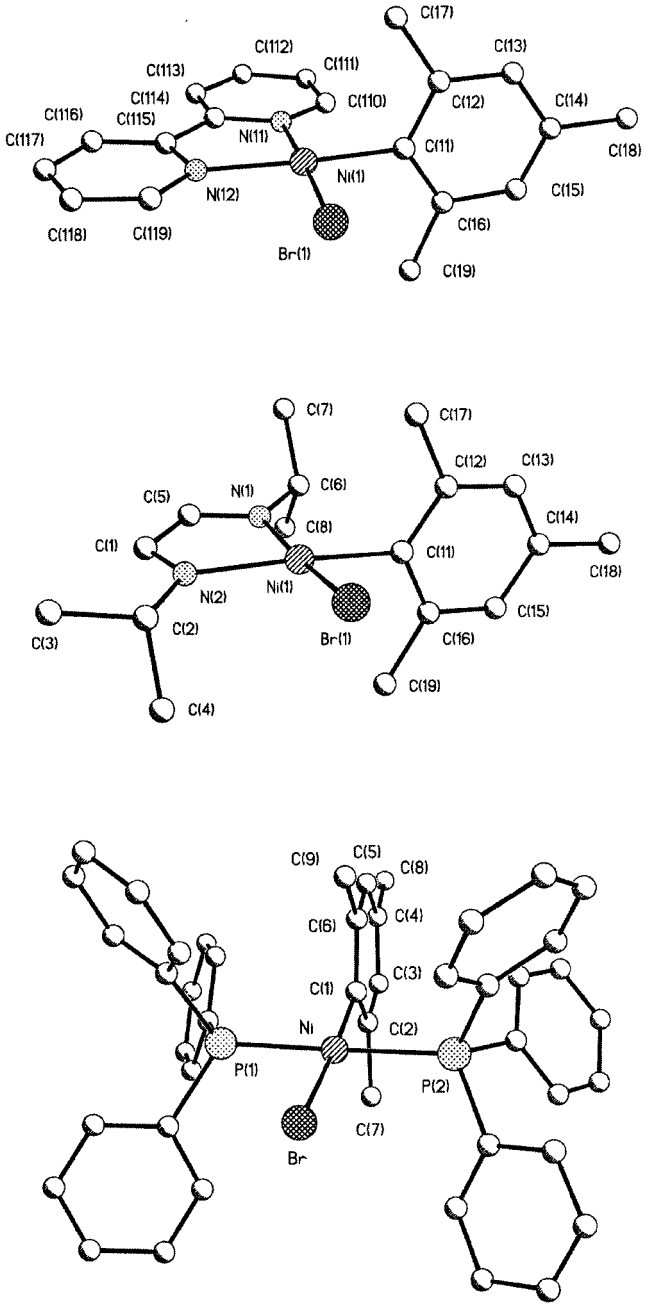

Figure 2. Molecular structure of the investigated Ni^{II} complexes: [(bpy)Ni(Mes)Br] (**1**) (top), [(*i*Pr-DAB)Ni(Mes)Br] (**2**) (center) and $[(PPh_3)_2Ni(Mes)Br]$ (**3**) (bottom)

In Figure 3 (a) the pre-edge and XANES region at the Ni *K*-edge of the solid complex **1** is shown in comparison with its solutions in pyridine and acetonitrile. As an octahedral reference compound the XANES spectra of $[(1,10\text{-phenanthroline})_2NiBr_2]$ is also shown. In the pure, solid square-planar complex (solid line) the typical two pre-peaks for the $1s \rightarrow 3d$ and $1s \rightarrow 4p_z$ transitions are clearly visible. The solution in pyridine (dotted line) also shows these two pre-peaks; thus the local structure around the Ni atoms remains in a square-planar geometry. The XANES spectra of the dissolved complex **1** in THF, collidine, or acetone also reveal retention of the square-planar geometry.

In contrast to the pyridine solution the XANES region of **1** in acetonitrile solution shows only the weak pre-peak of the $1s \rightarrow 3d$ transition, similar to the XANES region of the octahedral reference complex $[(phen)_2NiBr_2]$. This clearly hints that the complex has changed from a square-planar to an octahedral structure. The same behavior was observed for other nitriles (benzonitrile or butyronitrile), in alcohols, e.g. methanol in Figure 3 (b), and a mixture of acetone and water (molar ratio 1:1.23).

Figure 3 (b) the XANES region of [(bpy)Ni(Mes)(OMe)] shows two pre-peaks, indicating a square-planar geometry. This compound was obtained from the reaction of [(bpy)-Ni(Mes)Br] with sodium methoxide in THF (see Exp. Sect.). The same species was observed upon prolonged reaction of [(bpy)Ni(Mes)Br] in methoxide solutions. Retention of the square-planar geometry, even in the presence of a large excess of methoxide, indicates that formation of the octahedral species requires the acid protons of the solvent. Presumably the loss of the shielding mesityl ligand is the crucial step.

Figure 3 (c) shows the XANES spectra of the solid products of [(bpy)Ni(Mes)Br] in several linear primary and secondary alcohols after 16 h reaction. In methanol only the $1s \rightarrow 3d$ transition can be seen; thus, it can be concluded that the Ni^{II} complex has completely changed its geometry from square-planar to octahedral. In other alcohols after the same reaction time, the $1s \rightarrow 4p_z$ transition is still observable, but the signal is significantly weaker than that of the pure complex. This can be explained by a mixture of square-planar and octahedral species in the investigated reaction products. The highest $1s \rightarrow 4p_z$ signal is observed in 2-butanol and the signal decreases in the sequence 2-butanol, 2-propanol, 1-propanol, ethanol and methanol. Thus, the reaction rate decreases with increasing carbon-chain length and is higher in primary alcohols. This is also in agreement with the sequence of the acidity constants of the corresponding alcohols.[45–47]

EXAFS Investigations

The obtained structural parameters of the system [(bpy)-Ni(Mes)Br] system, determined by EXAFS at the Ni *K*- and Br *K*-edge, are summarized in Table 1. Table 2 presents results from the EXAFS fitting procedure of several octahedral and square-planar reference compounds, also measured at the Ni *K*- and Br *K*-edge.

Figure 4 shows the k^3-weighted experimental and Fourier-transformed (FT) EXAFS function of the solid complex **1** in comparison with its solutions in THF and pyridine at the Ni *K*-edge.

The fit of the Ni *K*-edge EXAFS spectrum of the solid complex was performed with three different coordination shells. The first shell at about 1.9 Å consists of the two coordinating nitrogen atoms of the bipyridine ligand and the carbon atom of the mesityl ligand. Because of the similar distances of these backscatterers [XRD: $r(Ni-C_{Mes})$ = 1.896 Å, $r(Ni-N_{bpy,1})$ = 1.896 Å, $r(Ni-N_{bpy,2})$ = 1.984 Å], they cannot be fitted separately and thus were fitted as one

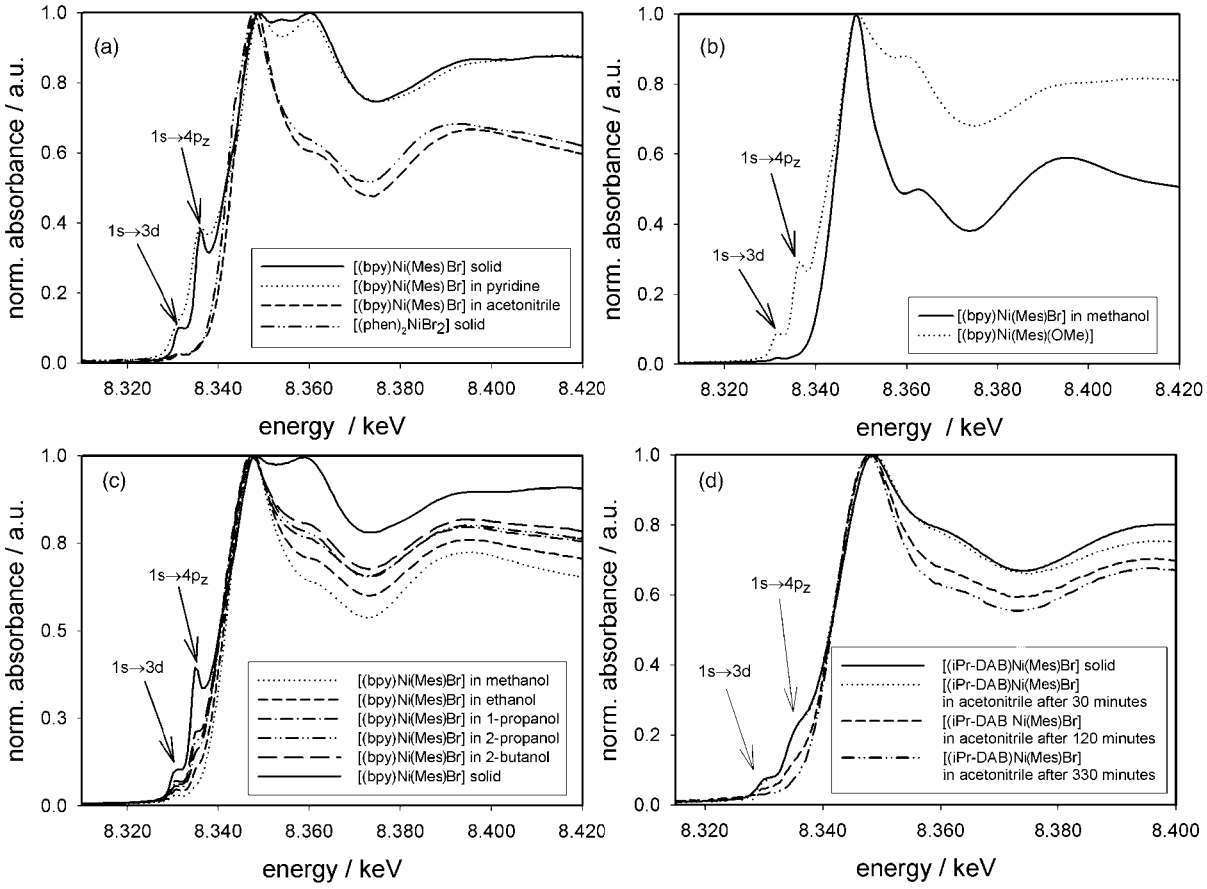

Figure 3. (a) Comparison of the Ni *K*-edge XANES regions of solid [(bpy)Ni(Mes)Br] and its solutions in pyridine and acetonitrile with solid $[(phen)_2NiBr_2]$; (b) comparison of the Ni *K*-edge XANES regions of the solid products of [(bpy)Ni(Mes)Br] in methanol after 48 h reaction with [(bpy)Ni(Mes)Br] + MeONa in THF; (c) comparison of the Ni *K*-edge XANES regions of the solid products of [(bpy)Ni-(Mes)Br] in methanol, ethanol, 1-propanol, 2-propanol and 2-butanol after 16 h reaction; (d) comparison of the Ni *K*-edge XANES regions of solid [(*i*Pr-DAB)Ni(Mes)Br] and its solution in acetonitrile over time

shell with nitrogen amplitude- and phase-functions. The determined distance of 1.92 Å as well as the coordination number of 3.1 is in good agreement with the average value of 1.93 Å known from XRD. The bromine backscatterer was found at 2.30 Å with a coordination number of 1.0. These values are in very good agreement with those found from the Br *K*-edge EXAFS spectrum [N = 0.9, r(Ni−Br) = 2.30 Å] and from the single-crystal XRD experiment (2.30 Å). The third coordination shell was fitted with carbon backscatterers and led to an Ni−C distance of 2.81 Å and a coordination number of 5.6. Possible candidates for these carbon backscatterers are the C(12) and C(16) atom of the mesityl ligand and the C(114), C(115) and C(110) atoms of the bipyridine ligand. This is also in agreement with the relatively high Debye−Waller factor of this shell (σ = 0.110 Å), which is a consequence of the distance distribution of the backscatterers from 2.77 to 2.91 Å. As the observed coordination numbers of the fitted three shells are in good agreement with the expected values, multiple scattering does not seem to play a significant role. Therefore the definition of multiple scattering units is unnecessary.

As can be seen from Figure 4 (a and b), there are only negligible differences between the spectra of the solid complex and its solution in THF. The Ni *K*-edge EXAFS spectra of [(bpy)Ni(Mes)Br] solutions in acetone, THF, or collidine yielded almost identical structural parameters to those found for the solid complex (Table 1). Thus, in these solvents, the complex does not undergo structural changes. This is consistent with observations from the Ni XANES region. In pyridine, however, upon dissolving the initial red complex the solution immediately turned yellow. Fourier-transform of the experimental EXAFS spectrum of the pyridine solution [Figure 4 (b)] shows, in comparison with the solid complex, a higher intensity for the peak at about 1.9 Å and the loss of bromine atom signal at ca. 2.3 Å. Fitting the EXAFS function revealed an increase in the coordination number of the first coordination shell from 3 to 4, with an average distance of 1.88 Å. Bromine backscatterers did not contribute to the EXAFS function. As the XANES region of the pyridine solution shows the typical pre-peaks for a square-planar geometry around the Ni atoms, it can be concluded that the bromine atom has been substituted in an associative process by a pyridine solvent molecule. To determine whether the bipyridine ligand has also been replaced by pyridine, several pyridine derivatives of [(bpy)Ni(Mes)Br] have been synthesized and characterized by EXAFS, and ^{1}H and ^{13}C NMR spectroscopy. The results of the EXAFS experiments on these reference compounds at the Ni *K*- and Br *K*-edge are reported

Table 1. Structural parameters of solid [(bpy)Ni(Mes)Br] and its reaction products in various solvents, determined from Ni *K*- and Br *K*-edge EXAFS spectra [absorber A, backscatterer Bs, A−Bs distance *r*, coordination number *N*, Debye-Waller factor σ with calculated deviation, shift of the energy threshold energy ΔE_0 and the fit-index *R* (AFAC = 0.8)]

	A−Bs	*r* [Å]	N	σ [Å]	ΔE_0 [eV]	*k*-range [Å^{-1}] fit-index
Pure	Ni−C/N	1.92 ± 0.02	3.1 ± 0.3	0.081 ± 0.008	28.0	3.60−14.90
EXAFS in the solid state	Ni−Br	2.30 ± 0.02	1.0 ± 0.2	0.062 ± 0.011		21.8
	Ni−C	2.81 ± 0.03	5.6 ± 1.7	0.110 ± 0.030		
	Br−Ni	2.30 ± 0.02	0.9 ± 0.1	0.060 ± 0.006	14.5	3.60−11.30
						23.5
THF	Ni−C/N	1.90 ± 0.02	2.7 ± 0.3	0.073 ± 0.008	28.2	3.60−13.90
EXAFS in solution	Ni−Br	2.29 ± 0.02	1.1 ± 0.2	0.065 ± 0.010		21.9
	Ni−C	2.81 ± 0.03	5.5 ± 1.7	0.110 ± 0.030		
Acetone	Ni−C/N	1.92 ± 0.02	2.8 ± 0.3	0.067 ± 0.007	26.6	3.70−12.00
EXAFS in solution	Ni−Br	2.31 ± 0.02	1.1 ± 0.2	0.059 ± 0.009		21.9
	Ni−C	2.84 ± 0.03	3.9 ± 1.1	0.077 ± 0.023		
Collidine	Ni−C/N	1.90 ± 0.02	3.2 ± 0.3	0.095 ± 0.008	28.1	3.80−12.00
EXAFS in solution	Ni−Br	2.29 ± 0.02	0.8 ± 0.1	0.067 ± 0.010		22.9
	Ni−C	2.82 ± 0.03	4.6 ± 1.4	0.112 ± 0.030		
Pyridine	Ni−C/N	1.90 ± 0.02	3.8 ± 0.3	0.072 ± 0.007	28.0	3.80−15.00
EXAFS in solution	Ni−C	2.82 ± 0.03	5.0 ± 1.5	0.087 ± 0.026		21.9
Acetonitrile	Ni−N	2.06 ± 0.02	6.1 ± 0.6	0.077 ± 0.007	23.5	3.38−14.00
Solid product after 3 h reaction,	Ni−C	2.24 ± 0.03	2.7 ± 0.4	0.091 ± 0.014		23.6
EXAFS in the solid state	Ni−C	2.84 ± 0.03	3.5 ± 1.1	0.110 ± 0.033		
	Ni−Ni	3.05 ± 0.03	2.1 ± 0.6	0.099 ± 0.026		
Butyronitrile	Ni−N	2.08 ± 0.02	6.4 ± 0.7	0.063 ± 0.007	21.8	3.47−11.00
Solid product after 12 h reaction,						41.9
EXAFS in the solid state						
Benzonitrile	Ni−N	2.07 ± 0.02	6.3 ± 0.7	0.074 ± 0.007	24.5	3.47−11.00
Solid product after 12 h reaction,						44.0
EXAFS in the solid state						
Methanol	Ni−O	2.06 ± 0.02	6.4 ± 0.3	0.071 ± 0.007	20.7	3.30−12.90
Solid product after 48 h reaction,	Ni−C	2.95 ± 0.03	6.2 ± 1.5	0.071 ± 0.023		31.6
Solid state EXAFS	Ni−Ni	3.09 ± 0.03	3.5 ± 1.5	0.077 ± 0.023		
H_2O/acetone (1:1.23)	Ni−O	2.05 ± 0.02	6.4 ± 0.3	0.087 ± 0.007	23.8	3.56−12.49
solid product after 12 h reaction,	Ni−Ni	3.07 ± 0.03	1.9 ± 1.5	0.081 ± 0.023		33.9
EXAFS in the solid state						
Pure	Ni−C/N	1.93	3			
Single crystal XRD[17]	Ni−Br	2.30	1			
	Ni−C	2.85	5			
$C_{31}H_{52}C_{l4}N_4Ni_4O_{15}$	Ni−O	2.07	6			
Methanol	Ni−Ni	3.09	3			
Single crystal XRD[48]						
$[Ni(NCCH_3)_6][SbF_6]$	Ni−N	2.08	6			
Single crystal XRD[50]	Ni−C	2.23	2			
	Ni−C	2.46	4			
	Ni−Ni	2.92	4			

in Table 2. Comparison of the experimental EXAFS functions in Figure 4 (c and d) shows that the complex in pyridine solution is not identical to [(bpy)Ni(Mes)(py)]NO_3, but exhibits a very similar spectrum to $[(py)_3$Ni(Mes)]Br. In [(bpy)Ni(Mes)(py)] two different Ni−C_{Mes}/N and Ni−N distances for the first coordination sphere were observed at 1.93 Å (*N* = 3.1) and 2.11 Å (*N* = 1.4), possibly due to the rigidity of the bipyridine ligand, which endeavors to keep a chelate bite angle of 82−83°. In $[(py)_3$Ni(Mes)]Br the first coordination sphere was fitted, as well as the pyridine solution, with only one shell at 1.90 Å (*N* = 4.2). In $[(py)_2$Ni(Mes)Br] the Ni−C_{Mes}/*N* distance of 1.88 Å (*N* = 3.2) agrees with those found in $[(py)_3$Ni(Mes)]Br and the pyridine solution. The quite long Ni−Br−distance in $[(py)_2$Ni(Mes)Br] of 2.40 Å is a consequence of a *trans* orientation of the mesityl and the bromide ligand.

In agreement with the other spectroscopic results we conclude that, in pyridine, [(bpy)Ni(Mes)Br] undergoes a ligand exchange reaction in which the bromide and bipyridine ligands are replaced, but the geometry of the first coordination shell around the nickel atom remains square-planar. The stability of [(bpy)Ni(Mes)Br] in collidine is due to the bulky nature of both the collidine and mesityl ligands, which prevents associative substitution.

Table 2. Structural parameters of solid reference Ni^{II} complexes determined from Ni *K*- and Br *K*-edge EXAFS spectra; [absorber A, backscatterer Bs, A−Bs distance *r*, coordination number *N*, Debye-Waller factor σ with calculated deviation, shift of the energy threshold energy ΔE_0 and the fit-index *R* (AFAC = 0.8)]

	A−Bs	*r* [Å]	N	σ [Å]	ΔE_0 [eV]	*k*-range [$Å^{-1}$] fit-index
[(bpy)Ni(Mes)(py)]NO_3	Ni−C/N	1.93 ± 0.02	3.1 ± 0.3	0.074 ± 0.008	27.8	3.70−13.50
EXAFS in the solid state	Ni−N	2.11 ± 0.02	1.4 ± 0.2	0.063 ± 0.011		38.9
	Ni−C	2.86 ± 0.03	4.9 ± 2.0	0.110 ± 0.030		
[$(py)_2$Ni(Mes)Br]	Ni−C/N	1.88 ± 0.02	3.2 ± 0.3	0.075 ± 0.008	28.9	3.40−11.50
EXAFS in the solid state	Ni−Br	2.40 ± 0.02	1.0 ± 0.2	0.076 ± 0.011		26.1
	Ni−C	2.80 ± 0.03	6.4 ± 2.0	0.099 ± 0.030		
	Br−Ni	2.39 ± 0.02	1.1 ± 0.1	0.081 ± 0.007	21.0	3.90−12.50
						32.3
[$(py)_3$Ni(Mes)]Br	Ni−C/N	1.90 ± 0.02	4.2 ± 0.3	0.072 ± 0.008	28.0	3.70−15.10
EXAFS in the solid state	Ni−C	2.82 ± 0.03	5.0 ± 1.5	0.087 ± 0.011		31.3
[(bpy)Ni(Mes)(MeO)]	Ni−C/N/O	1.89 ± 0.02	3.9 ± 0.3	0.070 ± 0.007	25.8	3.70−12.00
EXAFS in the solid state	Ni−C	2.82 ± 0.03	4.1 ± 1.2	0.080 ± 0.024		37.6
[$(phen)_2NiBr_2$][a]	Ni−N	2.05 ± 0.02	4.5 ± 0.5	0.068 ± 0.007	27.7	4.10−12.50
EXAFS in the solid state	Ni−Br	2.50 ± 0.03	2.1 ± 0.5	0.104 ± 0.011		43.4
	Br−Ni	2.49 ± 0.03	0.9 ± 0.1	0.063 ± 0.007	28.6	4.10−11.30
						56.6
$Ni(OH)_2$	Ni−O	2.07 ± 0.02	6.0	0.068 ± 0.007	23.5	3.70−13.50
EXAFS in the solid state	Ni−Ni	3.12 ± 0.03	6.0	0.077 ± 0.023		37.2
$Ni(OH)_2$	Ni−O	2.12	6			
powder ND[49]	Ni−Ni	3.13	6			

[a] phen = 1,10-phenanthroline.

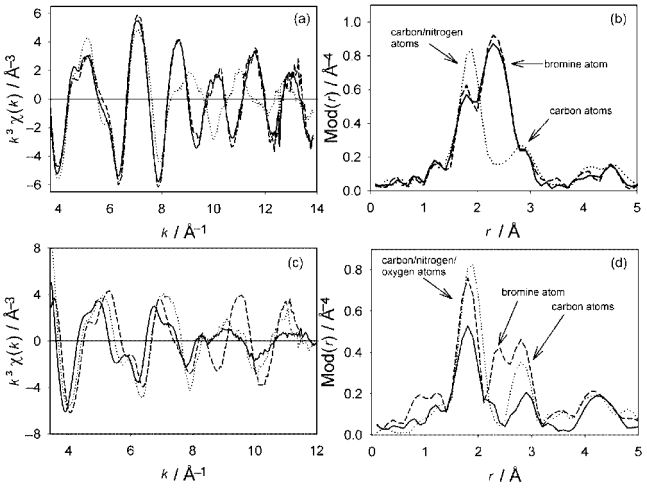

Figure 4. Comparison of the experimental $k^3\ \chi(k)$ functions (a) and their Fourier transforms (b) of solid [(bpy)Ni(Mes)Br] (solid line) with its solutions in THF (dashed line) or pyridine (dotted line) (Ni *K*-edge); comparison of the experimental $k^3\ \chi(k)$ functions (c) and their Fourier transforms (d) of solid [(bpy)Ni(Mes)(py)]NO_3 (solid line), [$(py)_3$Ni(Mes)]Br (dotted line) with solid [$(py)_2$Ni-(Mes)Br] (dashed line) (Ni *K*-edge)

From the XANES spectra it is evident that, in nitriles, alcohols and mixtures of acetone and water, the complex changes from square-planar to octahedral. The solubility of the complex in nitriles and alcohols is sufficient to carry out XANES experiments in transmission mode. For EXAFS investigations, however, the quality of the spectra obtained in solution was not satisfactory. Therefore the reaction mixtures were concentrated to dryness and the EXAFS measurements performed on the solid reaction products. In all the above-mentioned cases an octahedral coordination of the Ni atom was confirmed by EXAFS.

The distance of the first coordination shell from the metal ion is in all cases higher than in the square-planar complexes and consistent with the $Ni-N_{Phen}$ distance of 2.05 Å found in the octahedral reference compound [(1,10-phenanthroline)$_2$NiBr$_2$] (see Table 2).

Figure 5 shows the EXAFS spectra and the Fourier transforms of the products of the reaction of **1** in methanol after 2 or 48 h reaction, respectively, measured at the Ni *K*-edge [Figure 5 (a and b)] and Br *K*-edge [Figure 5 (c and d)]. The bromine FT-EXAFS spectrum of the product after 2 h of reaction in methanol [Figure 5 (b)] still shows a significant, but weak, contribution of nickel backscatterers to the signal. The fit of the EXAFS function led to a coordination number of 0.3, thus revealing that the reaction product after 2 h is still a mixture of bromide-containing square-planar and octahedral species. The EXAFS spectrum at the Ni *K*-edge of the product after 48 h reaction in methanol [Figure 5 (a)] was fitted with three coordination shells. The first coordination shell was fitted with oxygen backscatterers at 2.06 Å and proved the sixfold coordination of the nickel atom ($N = 6.5 \pm 0.6$). The very intense signal at about 3 Å in the FT EXAFS spectrum [Figure 5 (b)] is due to C backscatterers at 2.95 Å ($N = 6.2$) and Ni backscatterers at 3.09 Å ($N = 3.5$). These structural parameters fit the reported crystal structure of a (methanol)Ni^{II} complex.[48] In addition to the EXAFS investigations, the ^{1}H NMR spectrum of the [D_6]acetone extract of the prod-

uct obtained after 48 h showed the presence of uncoordinated bipyridine and mesitylene. Thus, in methanol, complete ligand exchange of all ligands (bromide, bipyridine and mesityl) against methanol molecules has taken place. That the Ni atoms in the methanolic product are only surrounded by oxygen atoms can be shown by comparison of the EXAFS spectra of solid $Ni(OH)_2$ with the product. In $Ni(OH)_2$ the Ni atoms are surrounded by six oxygen atoms at a similar distance (2.07 Å), as in the methanolic product. Furthermore, $Ni(OH)_2$ reveals an Ni−Ni distance (3.12 Å) that is almost identical with the one found in the methanolic product. The EXAFS spectrum and the FT of $Ni(OH)_2$ have been added to Figure 5 (a and b). The intensity of the first signal in the FT of both compounds is almost identical, which can be correlated with the same number and type of backscatterers in these compounds. The signal of the Ni backscatterers at 3.12 Å in $Ni(OH)_2$ is higher due to the higher coordination number of 6 in $Ni(OH)_2$.[49]

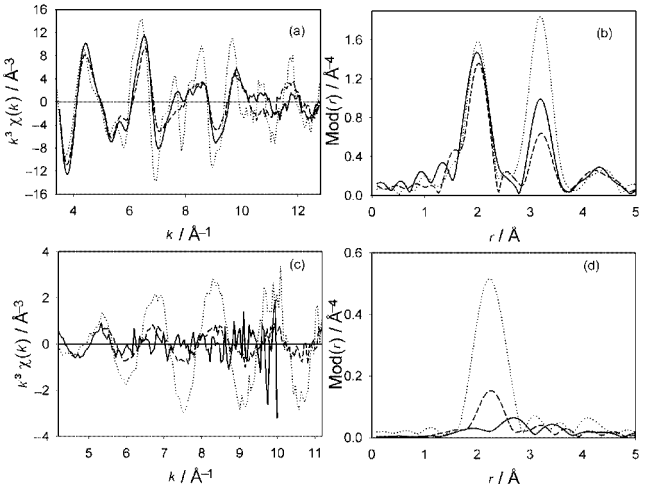

Figure 5. Comparison of the experimental k^3 $\chi(k)$ functions (a) and their Fourier transforms (b) of the isolated solid product of [(bpy)Ni(Mes)Br] in methanol after 2 h reaction (dashed line) and after 48 h reaction (solid line) with solid $Ni(OH)_2$ (dotted line) (Ni *K*-edge); comparison of the experimental k^3 $\chi(k)$ functions (c) and their Fourier transforms (d) of solid [(bpy)Ni(Mes)Br] (dotted line) with the isolated solid products of [(bpy)Ni(Mes)Br] in methanol after 2 h reaction (dashed line) and after 48 h reaction (solid line) (Br *K*-edge)

In the EXAFS function of the solid product of [(bpy)Ni(Mes)Br] in acetonitrile after 3 h reaction [Figure 6 (a)] the contribution of Ni backscatterers was similar to that of the product of the methanol solution. The structural parameters determined from the Ni *K*-edge EXAFS spectrum agree quite well to the acetonitrile complex $[Ni(CH_3CN)_6]SbF_6$,[50] in which the acetonitrile molecules have a bridging position between the Ni atoms. ^1H NMR experiments on the acetonitrile product have proved the splitting of the bpy and the mesityl ligand (as mesitylene), the latter seems to be a pre-requisite to the formation of octahedral species.

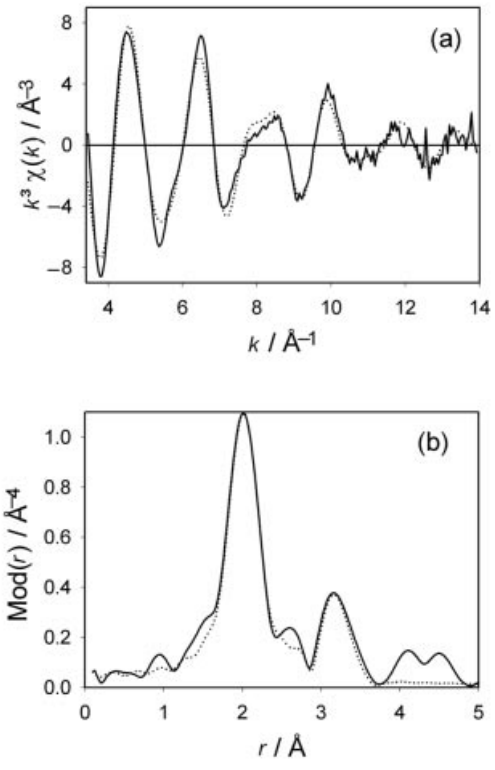

Figure 6. Experimental (solid line) and calculated (dotted line) k^3 $\chi(k)$ function (a) and their Fourier transform (b) of the isolated solid product of [(bpy)Ni(Mes)Br] acetonitrile after 3 h reaction (Ni *K*-edge)

Structural Studies on the [(*i*Pr-DAB)Ni(Mes)Br] System

Crystal Structure

In the crystal structure of [(*i*Pr-DAB)Ni(Mes)Br] (Figure 2) no intermolecular interactions other than van der Waals were found. The structure was solved with a disorder on one of the two isopropyl substituents. The two positions were found to be occupied in a 60:40% ratio. However, this has no impact on the square-planar coordination sphere of the nickel atom. Deviation towards the tetrahedron is only 9.3° and the angle C(11)−Ni(1)−N(2) deviates by 6.6° from the ideal 180°, thus resembling the less distorted molecule 1 of [(bpy)Ni(Mes)Br]·THF. The *trans* influence has a marked effect on the Ni−N bond lengths as Ni−N *trans* to the strong donor mesityl is about 100 pm longer than *trans* to Br. As expected, to reduce the inter-ligand interactions the isopropyl substituents point away from the coordination sphere.[51−53] Nevertheless, they might also shield the nickel center, along with the methyl substituents of the mesityl ligand,[17] as the distances of the two groups from the Ni atom are similar, ca. 3.5 Å and ca. 3.1 Å, respectively.

XANES Investigations

In Figure 3 (d) the XANES spectra of solid [(*i*Pr-DAB)-Ni(Mes)Br] and its solution in acetonitrile in dependence

of time are shown. The spectrum of the solid complex shows the typical two pre-peaks for square-planar Ni^{II} complexes. The acetonitrile solution after 30 min reaction also shows these two pre-peaks, which means that most of the Ni atoms have retained their square-planar geometry. After 120 min, the signal of the $1s \rightarrow 4p_z$ transition is significantly weaker, strongly indicating a change from square-planar to octahedral for the Ni atoms. After 330 min, the signal of the $1s \rightarrow 4p_z$ transition has vanished. Obviously, the geometry change was completed within 330 min, which is in good agreement with the rate constants determined by UV/Vis in the acetonitrile solution of [(bpy)Ni(Mes)Br].

EXAFS Investigations

The structural parameters of the [(*i*Pr-DAB)Ni(Mes)Br] system determined from the Ni *K*-edge and Br *K*-edge are summarized in Table 3. The obtained structural data of the pure, solid complex are in good agreement with those found from the single-crystal analysis. The experimental and calculated EXAFS functions and the FT (Ni *K*-edge) of the pure, solid complex can be seen in Figure 7 (a and b). To examine if [(*i*Pr-DAB)Ni(Mes)Br] shows a similar ligand exchange behavior to [(bpy)Ni(Mes)Br], a solution of the complex in acetonitrile was monitored by EXAFS spectroscopy. Because of the low solubility of the complex in acetonitrile the spectra were of low quality. Therefore the EXAFS functions were fitted with only one coordination shell, in the *k*-range of 2.8−8 $Å^{-1}$ [Figure 7 (c)], and showed that the coordination number of the first coordination shell increased from 3.1 nitrogen backscatterers after 30 min to 6.0 nitrogen backscatterers after 330 min. The determined average distance of 2.13 Å for the first coordination shell after 330 min is 0.07 Å higher than in the solid product of [(bpy)Ni(Mes)Br] in acetonitrile due to a higher mobility of the coordinated solvent molecules in the liquid state. From these experiments there is no evidence of an additional shielding of the nickel atom by the *i*Pr-DAB ligand compared to bpy.

Structural Studies on the $[(PPh_3)_2Ni(Mes)Br]$ System

Crystal Structure

As with the two diimine complexes the crystal structure of $[(PPh_3)_2Ni(Mes)Br]$ (Figure 2) reveals no significant intermolecular interaction. The coordination plane is nearly perfect, with only the Br ligand being slightly bent (by 3.8°) so that the Br−Ni−C1 angle is 176.2°. Concurrently, the angle P(1)−Ni−P(2) of 183.95° is larger than the ideal 180°. The mesityl ligand is oriented perfectly orthogonal to the coordination plane in contrast to the diimine complexes where tilt angles around 70° are found for the mesityl ligand. The molecular structure is thus similar to that of the related molecule $[(PMe_3)_2Ni(Ph)Br]$.[54] The Ni−P distances [2.214(2) Å and 2.202(2) Å] and the Ni−C(1) distance

Table 3. Structural parameters of solid [(*i*Pr-DAB)Ni(Mes)Br] and its solution in acetonitrile as determined from Ni *K*- and Br *K*-edge EXAFS spectra [absorber A, backscatterer Bs, A−Bs distance *r*, coordination number *N*, Debye-Waller factor σ with calculated deviation, shift of the energy threshold energy ΔE_0 and the fit-index *R* (AFAC = 0.8)]

	A−Bs	*r* [Å]	N	σ [Å]	ΔE_0 [eV]	*k*-range [$Å^{-1}$] fit-index
Pure	Ni−C/N	1.96 ± 0.02	3.1 ± 0.3	0.089 ± 0.008	29.9	3.70−11.50
Solid state EXAFS	Ni−Br	2.31 ± 0.02	0.8 ± 0.2	0.085 ± 0.011		28.3
	Ni−C	2.69 ± 0.03	4.2 ± 1.3	0.062 ± 0.030		
	Br−Ni	2.30 ± 0.02	0.9 ± 0.1	0.060 ± 0.007	17.4	3.90−12.00
						27.2
After 30 min reaction	Ni−N	2.11 ± 0.02	3.1 ± 0.3	0.097 ± 0.010	15.7	3.00−8.00
						28.3
After 60 min reaction	Ni−N	2.16 ± 0.02	3.6 ± 0.4	0.097 ± 0.010	13.5	3.00−8.00
						28.3
After 90 min reaction	Ni−N	2.15 ± 0.02	4.4 ± 0.4	0.097 ± 0.010	15.5	3.00−8.00
						28.3
After 150 min reaction	Ni−N	2.14 ± 0.02	4.9 ± 0.5	0.097 ± 0.010	16.7	3.00−8.00
						28.3
After 180 min reaction	Ni−N	2.14 ± 0.02	5.1 ± 0.5	0.097 ± 0.010	16.1	3.00−8.00
						28.3
After 210 min reaction	Ni−N	2.13 ± 0.02	5.3 ± 0.5	0.097 ± 0.010	17.7	3.00−8.00
						28.3
After 300 min reaction	Ni−N	2.14 ± 0.02	5.7 ± 0.6	0.097 ± 0.010	18.3	3.00−8.00
						28.3
After 330 min reaction	Ni−N	2.13 ± 0.02	6.0 ± 0.6	0.097 ± 0.010	18.7	3.00−8.00
						28.3
Pure	Ni−C/N	1.94	3			
Single-crystal XRD	Ni−Br	2.31	1			
	Ni−C	2.71	2			

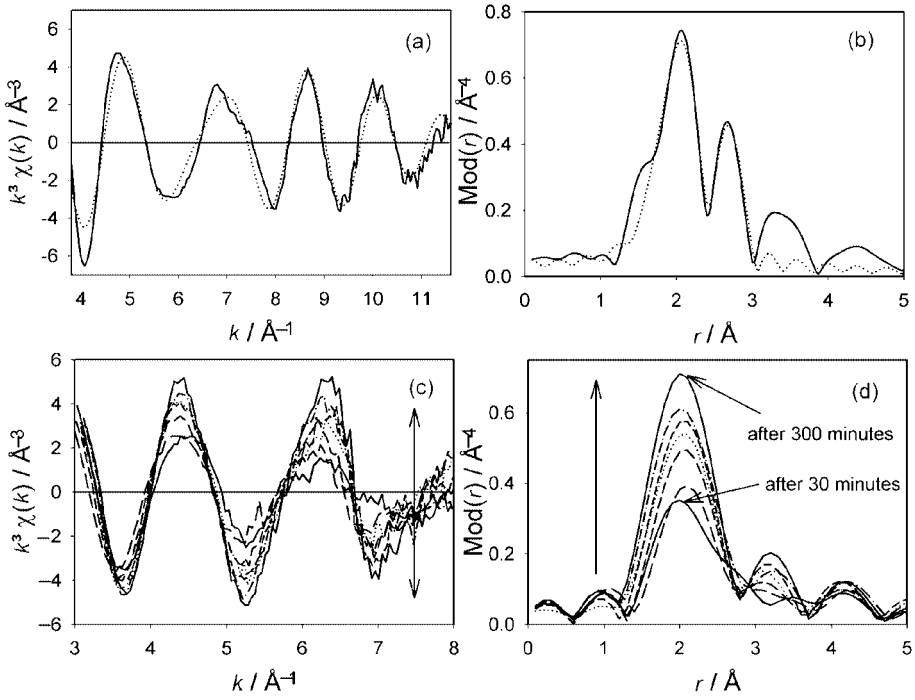

Figure 7. Comparison of the experimental $k^3\,\chi(k)$ functions (a) and their Fourier transforms (b) of [(*i*Pr-DAB)Ni(Mes)Br] in acetonitrile in dependence of time (after 30, 60, 120, 180, 240 and 300 min); experimental (solid line) and calculated (dotted line) $k^3\,\chi(k)$ functions (a) and their Fourier transforms (b) of solid [(*i*Pr-DAB)Ni(Mes)Br] (Ni *K*-edge)

[1.891(6) Å] in the latter are slightly shorter than can be explained by the bulkiness of the PPh_3 ligand. A marked difference lies in the orientation of the PR_3 ligands. The *trans*-oriented PPh_3 ligands show a nearly eclipsed conformation, whereas the PMe_3 ligands are staggered. Viewing the PPh_3 complex along an axis that parallels P(1)−Ni−P(2) one can see a graphite-like interaction of each one of the phenyl substituents with the nickel-bound mesityl ligand. This interaction might account for the eclipsed conformation, which probably leads to the steric repulsion of the phosphane ligands.

XANES Investigations

The XANES spectra of solid $[(PPh_3)_2Ni(Mes)Br]$ and its solid products formed by dissolving in acetonitrile, pyridine and collidine are shown in Figure 8. In all cases the 1s → $4p_z$ transition is clearly visible, identifying the complex and its solution products as square-planar. The 1s → 3d transition in all investigated complexes was very weak.

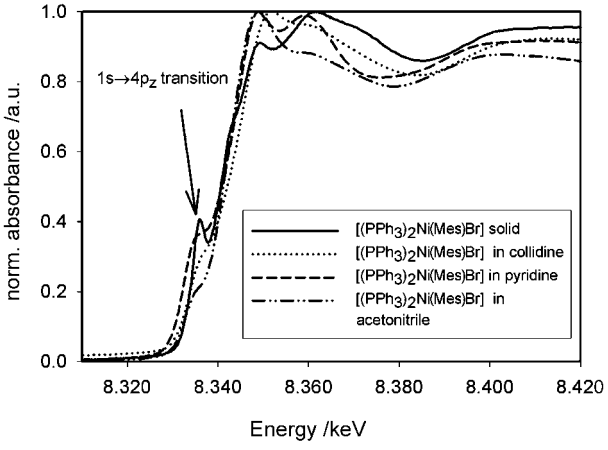

Figure 8. Comparison of the Ni *K*-edge XANES regions of solid $[(PPh_3)_2Ni(Mes)Br]$ with the solid products formed after 3 h in pyridine, collidine and acetonitrile

EXAFS Investigations

The solid $[(PPh_3)_2Ni(Mes)Br]$ was investigated at Ni *K*- and Br *K*-edge. The obtained structural parameters are summarized in Table 4. To fit the EXAFS function at the Ni *K*-edge three coordination shells were necessary. The determined values for the Ni−C_{Mes}, Ni−P and Ni−Br distances, as well as the coordination numbers of each shell, are in good agreement with the single-crystal experiment. EXAFS experiments on the solid products of $[(PPh_3)_2Ni(Mes)Br]$ in acetonitrile, pyridine and collidine after 3 h reaction are shown in Figure 9 (a and b). In all cases Br backscatterers did not contribute to the EXAFS functions. In contrast to the [(bpy)Ni(Mes)Br] and [(*i*Pr-DAB)Ni(Mes)Br] systems no geometrical change towards octahedral was observed in acetonitrile or THF solution. In the solid products of $[(PPh_3)_2Ni(Mes)Br]$ in acetonitrile or THF the coordination number of the first coordination shell is in total 4 (2 C/N + 2 P or 2 C/O + 2 P). The preservation of

Table 4. Structural parameters of solid $[(PPh_3)_2Ni(Mes)Br]$ and its reaction products in THF, acetonitrile, pyridine, or collidine determined from Ni *K*- and Br *K*-edge EXAFS spectra [absorber A, backscatterer Bs, A−Bs distance *r*, coordination number *N*, Debye-Waller factor σ with calculated deviation, shift of the energy threshold energy ΔE_0 and the fit-index *R* (AFAC = 0.8)]

	A−Bs	*r* [Å]	N	σ [Å]	ΔE_0 [eV]	*k*-range [Å^{-1}] fit-index
Pure	Ni−C	1.92 ± 0.02	1.1 ± 0.1	0.077 ± 0.007	25.0	3.50− 13.52
EXAFS in the solid state	Ni−P	2.23 ± 0.02	2.3 ± 0.3	0.081 ± 0.008		22.6
	Ni−Br	2.36 ± 0.02	1.1 ± 0.2	0.074 ± 0.011		
	Br−Ni	2.37 ± 0.02	1.0 ± 0.1	0.065 ± 0.007	16.0	3.90−15.00
						28.3
THF	Ni−C	1.91 ± 0.02	1.3 ± 0.1	0.081 ± 0.008	27.8	3.71−11.30
EXAFS in solution	Ni−O	2.07 ± 0.02	1.2 ± 0.2	0.055 ± 0.008		29.7
	Ni−P	2.21 ± 0.02	2.1 ± 0.2	0.089 ± 0.024		
Acetonitrile	Ni−C/N	1.98 ± 0.02	1.8 ± 0.2	0.089 ± 0.009	27.6	3.60−14.97
EXAFS in solution	Ni−P	2.25 ± 0.02	1.7 ± 0.3	0.063 ± 0.011		25.6
Pyridine	Ni−C/N	1.97 ± 0.02	3.1 ± 0.3	0.081 ± 0.008	24.0	3.50−11.00
EXAFS in the solid state	Ni−P	2.23 ± 0.02	0.9 ± 0.1	0.077 ± 0.011		23.3
	Ni−C	2.88 ± 0.03	6.0 ± 1.8	0.114 ± 0.034		
Collidine	Ni−C/N	1.91 ± 0.02	2.0 ± 0.2	0.050 ± 0.005	26.0	3.50−12.30
EXAFS in the solid state	Ni−P	2.22 ± 0.02	1.7 ± 0.3	0.081 ± 0.012		18.8
	Ni−C	2.80 ± 0.03	3.7 ± 1.0	0.089 ± 0.027		
Pure	Ni−C	1.91	1			
Single crystal XRD	Ni−P	2.24	2			
	Ni−Br	2.37	1			

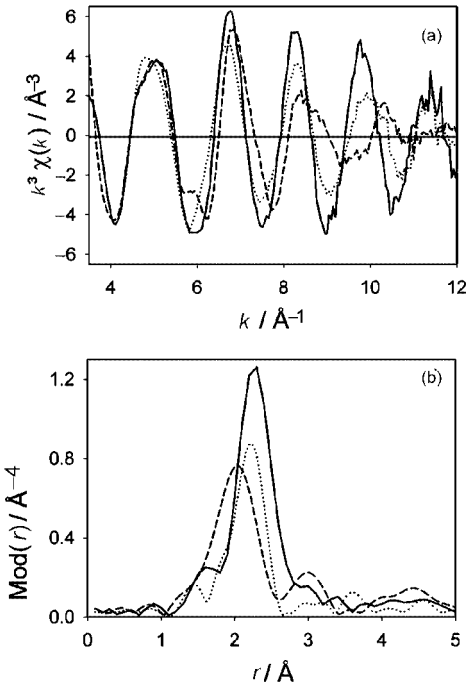

Figure 9. Comparison of the experimental $k^3\,\chi(k)$ functions (a) and their Fourier transforms (b) of solid $[(PPh_3)_2Ni(Mes)Br]$ (solid line) with the solid products of $[(PPh_3)_2Ni(Mes)Br]$ in acetonitrile (dotted line) or pyridine (dashed line)

the square-planar geometry can again be explained by the shielding mesityl ligand that prevents the formation of octahedral species. However, as to why in acetonitrile or THF solution the mesityl ligand is not split off as observed for the diimine complexes we can so far only speculate. Perhaps the steric hindrance of the bulky triphenylphosphane ligands prevents the hydrolysis reaction. Abstraction of the bromide ligand was also observed in the product obtained from the collidine solution. The $Ni-C_{Mes}/N_{Col}$ distance, however, is 0.07 Å shorter than in the acetonitrile product, since collidine is a better σ-donor ligand than acetonitrile.

It is noteworthy that [(bpy)Ni(Mes)Br] is stable in collidine solution, whereas for $[(PPh_3)_2Ni(Mes)Br]$ substitution of the bromide ligand was observed. Obviously, the bromide is a better leaving group in $[(PPh_3)_2Ni(Mes)Br]$ than in [(bpy)Ni(Mes)Br]. In pyridine solution the bromide ligand is replaced by the solvent as in the above-mentioned cases. Furthermore, substitution of one of the triphenylphosphane ligands was concluded from the increase in coordination number in the carbon/nitrogen shell from 1.2 in the pure complex to 3.1 in the pyridine solution and the decrease in the phosphorus coordination from 2.3 to 0.9.

Conclusion

A combined spectroscopic (multinuclear NMR, absorption) and structural investigation using XRD, XANES and EXAFS was successfully applied to monitor the ligand exchange behavior of three square-planar mesitylnickel(II) complexes, *cis*-[(diimine)Ni(Mes)Br] (diimine = 2,2′-bipyridine or *N*,*N*-diisopropyl-1,2-ethanediimine), and *trans*-$[(PPh_3)_2Ni(Mes)Br]$. The chosen system with bromide as the leaving ligand, the mesityl ligand as a strong donor and effective shielding group, as well as the *cis* (diimine ligands) and *trans* (PPh_3) variation of the complexes conformation has allowed us to draw some important conclusions.

The replacement of bromide is strongly accelerated when oriented *trans* to the strong donor ligand mesityl, which can be observed from the rapid splitting off of bromide from *trans*-[$(PPh_3)_2$Ni(Mes)Br] in weakly coordinating solvents such as acetone or THF in which the diimine complexes are stable. While further ligand exchange has never been reported for such complexes we have found that upon prolonged reaction times the diimine ligands or PPh_3 were also replaced by the solvent molecules, which is of great importance regarding the catalytic activity of such molecules. The rates of these reaction are smaller by orders of magnitude but this has to be viewed against the backdrop of long-term stability. In protic media such as alcohols the mesityl ligand is split off and, after the loss of this shielding group, octahedral nickel species are formed. Interestingly this is also valid for nitriles. The change in geometry from square-planar to octahedral can be readily monitored by XANES. Since the formation of such saturated octahedral species is concomitant with the breakdown of catalytic activity a successfully operating catalyst system has to contain a stable shielding unit. In the successfully applied systems by Brookhart and others this is provided by the diimine ligand, e.g. bulky R-DAB ligands with R = 2-6-dialkylated aryl substituents. However, we found that the diimine ligands can also be cleaved. Therefore, new long-term stable systems need to take account of the potential loss of the diimine ligand. In further studies we aim to develop catalytic systems with such long-term stability and apply them under real catalytic conditions.

Experimental Section

Preparations: All preparations were carried out under argon. The synthesis of the complexes [$(PPh_3)_2$Ni(Mes)Br] and [(bpy)Ni(Mes)Br] has been recently described.[17] All solvents were obtained from commercial sources and used as received. The alcohols and acetonitrile used were anhydrous. The other solvents were of spectroscopic grade.

Synthesis of [(*i*Pr-DAB)Ni(Mes)Br]: *i*Pr-DAB (250 mg, 1.78 mmol) was added to a vigorously stirred suspension of [$(PPh_3)_2$Ni(Mes)Br] (250 mg, 0.32 mmol) in 500 mL of *n*-pentane. After a few minutes, the yellow solid dissolved and at the same time a violet voluminous solid precipitated. After stirring for 4 h, the solid was filtered off, washed with pentane, recrystallized from CH_2Cl_2/*n*-heptane (1:8) and dried in vacuo to yield dark violet microcrystals. Yield: 112 mg (82%). $C_{17}H_{27}BrN_2Ni$ (398.03): calcd. C 57.07, H 6.59, N 31.60; found C 56.55, H 6.29, N 32.09. ^{1}H NMR ([D$_6$]acetone): δ = 8.55 (s, 1 H, H_{imine}), 8.43 (s, 1 H, H_{imine}), 6.42 (s, 2 H, *m*-H), 3.26 (m, 2 H, HC*i*Pr), 2.97 (s, 6 H, *o*-CH_3), 2.21 (s, 3 H, *p*-CH_3), 2.03 (d, 12 H, H_3C*i*Pr) ppm.

Synthesis of [(bpy)Ni(Mes)(OMe)]: Fine-cut sodium (100 mg, 4.35 mmol) was added to a mixture of 50 mL of THF and 10 mL of methanol. After all of the sodium had dissolved and reacted, [(bpy)Ni(Mes)Br] (400 mg, 0.97 mmol) was added to this solution. The red color of the starting material immediately turned to violet. After stirring for 3 h, the reaction solvents were evaporated to dryness and the residue extracted with 5 × 10 mL of CH_2Cl_2. The resultant Bordeaux colored solution was carefully filtered and then concentrated to dryness. Recrystallization from CH_2Cl_2/*n*-heptane (1:1) gave red-violet microcrystals. Yield: 290 mg (82%). $C_{20}H_{22}N_2NiO$ (365.12): calcd. C 65.79, H 6.07, N 7.67; found C 65.55, H 6.02, N 7.59. ^{1}H NMR ([D$_6$]acetone): δ = 9.0 [s (broad), 1 H, bpy-6], 8.31 (d, 1 H, bpy-3), 8.20 (d, 1 H, bpy-3′), 8.20 (dt, 1 H, bpy-4), 8.04 (dt, 1 H, bpy-4′), 7.71 (ddd, 1 H, bpy-5), 7.56 [s (broad), 1 H, bpy-6′), 7.21 (ddd, 1 H, bpy-5′), 6.57 (s, 2 H, *m*-H), 3.28 (s, 3 H, OCH_3), 3.07 (s, 6 H, *o*-CH_3), 2.20 (s, 3 H, *p*-CH_3) ppm. ^{13}C NMR ([D$_6$]acetone): δ = 156.4, 153.1, 151.5, 148.4, 148.3, 143.5, 139.6, 137.7, 127.3, 126.5, 132.8, 126.1, 122.4, 121.35, 69.1 (OCH_3), 25.8 (*o*-CH_3), 20.8 (*p*-CH_3) ppm.

Synthesis of [(bpy)Ni(Mes)(py)](NO$_3$): [(bpy)Ni(Mes)Br] (203 mg, 0.49 mmol) was dissolved in a mixture of 50 mL of acetone/acetonitrile (3:1) and thallium nitrate ($TlNO_3$) (133 mg, 0.5 mmol) and pyridine (40 mg, 0.5 mmol) were added to the red solution. $TlNO_3$ slowly dissolved while the reaction proceeded. After 5 h of stirring, the solution was orange-yellow and a greenish precipitate had formed that was carefully filtered off, and the filtrate was then concentrated to dryness. After washing the residue with 5 × 10 mL of diethyl ether, a bright yellow amorphous solid was obtained. Yield: 209 mg (90%). $C_{24}H_{24}N_4NiO_3$ (475.19): calcd. C 60.66, H 5.09, N 11.79; found C 60.36, H 5.01, N 11.68%. Due to the insolubility of the compound in common organic solvents no NMR spectra were obtained.

Synthesis of [(py)$_3$Ni(Mes)]Br: [(bpy)Ni(Mes)Br] (240 mg, 0.58 mmol) was dissolved in pyridine (30 mL) and stirred for 24 h. The volume was then reduced to 1/3 and *n*-octane (30 mL) added. The resultant yellow solution was stored at −30 °C overnight during which time a microcrystalline solid precipitated. After filtration, this solid was washed with *n*-pentane. Yield: 192 mg (67%). From the mother liquor further yellow material was isolated. However, this turned out to be a mixture of products. $C_{24}H_{26}BrN_3Ni$ (495.1): calcd. C 58.22, H 5.29, N 8.49; found C 58.18, H 5.21, N 8.44. ^{1}H NMR ([D$_6$]acetone): δ = 8.91 (d, 4 H, py-2,6), 8.18 (d, 2 H, py-2,6), 7.75 (t, 2 H, py-4), 7.46 (t, 1 H, py-4), 7.32 (dd, 4 H, py-3,5), 7.00 (dd, 2 H, py-3,5), 6.41 (d, 2 H, *m*-H), 3.45 (s, 6 H, *o*-CH_3), 2.21 (s, 3 H, *p*-CH_3) ppm. UV/Vis (pyridine): λ = 420 nm (ε = 320 M^{-1} cm^{-1}), 396 (sh, 320), 363 (1000), 323 (sh, 710).

Synthesis of *trans*-[(py)$_2$Ni(Mes)Br]: [$(PPh_3)_2$Ni(Mes)Br] (180 mg, 0.23 mmol) was dissolved in toluene (20 mL) and pyridine (80 mg, 1 mmol) was added to this red solution. After a few minutes, when the solution had turned yellow, the volume was reduced to 1/2. During storing of the solution at −20 °C overnight, yellow microcrystals had formed. Filtration and subsequent washing with *n*-pentane yielded a first crop (46 mg, 48%). The material that was further isolated from the mother liquor turned out to be a mixture including compounds of higher and lower degrees of substitution. $C_{14}H_{21}BrN_2Ni$ (416): calcd. C 54.86, H 5.09, N 6.73; found C 54.81, H 5.06, N 6.70. ^{1}H NMR ([D$_6$]acetone): δ = 8.96 (d, 4 H, py-2,6), 7.68 (t, 2 H, py-4), 7.20 (dd, 4 H, py-3,5), 6.33 (s, 2 H, *m*-H), 3.44 (s, 6 H, *o*-CH_3), 2.16 (s, 3 H, *p*-CH_3) ppm.

Synthesis of [(phen)$_2$NiBr$_2$]: [$NiBr_2$] (236 mg, 1.08 mmol) was added to DMF (10 mL) and dissolved on heating to 100 °C. Upon addition of 1,10-phenanthroline (390 mg, 2.16 mmol), the initially brownish solution turned green. On cooling to ambient temperature, a green solid precipitated that was collected by filtration, washed with diethyl ether and recrystallized from ethanol/diethyl ether (4:1). Yield: 562 mg (90%). $C_{24}H_{16}Br_2N_4Ni$ (578.93): calcd. C 49.79, H 2.79, N 9.68; found C 49.63, H 2.71, N 9.61. UV/Vis (MeCN): λ = 1055 nm (ε = 61 M^{-1} cm^{-1}), 631 nm (82), 326 (1040), 268 (26600), 226 (17860).

XANES and EXAFS Measurements: XANES and EXAFS measurements were performed at beamlines X1.1 (RÖMO II) and E4 at the Hamburger Synchrotronstrahlungslabor des Deutschen Elektronensynchrotrons (HASYLAB at DESY, Hamburg, Germany), at beamline 2−3 at the Stanford Synchrotron Radiation Laboratory (SSRL) at SLAC (Stanford, USA) and at beamline KMC-2 at the Berliner Elektronenspeicherring-Gesellschaft für Synchrotronstrahlung m.b.H. (BESSY II, Berlin, Germany). For measurements at the Ni *K*-edge (8332.8 eV) an Si(111) double crystal monochromator was used and at the Br *K*-edge (13474.0 eV) a Si(311) double crystal monochromator was used at SSRL and at DESY respectively. At BESSY a SiGe(220) double crystal (0.5% Ge/cm) monochromator was used for the nickel and the bromine *K*-edge. The synchrotron beam current was between 80 and 100 mA at HASYLAB (positron energy 4.45 GeV), between 100 and 250 mA at BESSY (electron energy 1.7 GeV) and between 80 and 100 mA at the SSRL (electron energy 1.7 GeV). The tilt of the second monochromator crystal was set to 40% harmonic rejection. The energy resolution was estimated to be about 0.7−1.0 eV for the Ni *K*-edge and 4.0 eV for the Br *K*-edge. Energy calibration was performed with the corresponding metal foils in the case of nickel, and with lead metal foil (Pb L_{III}-edge) in the case of bromine. The spectra were collected under ambient conditions at 25 °C in transmission mode with ion chambers. All ion chambers were filled with nitrogen for measurements at the Ni *K*-edge, and the second and third chamber filled with argon for measurements at the Br *K*-edge. The solid-state samples were embedded in a polyethylene matrix and pressed into pellets. Solutions of the complexes were measured in a specially designed transmission sample cell for liquids. The concentration of all samples was adjusted to yield an absorption jump of $\mu \approx 1.5$. Data evaluation started with removal of the background absorption from the experimental absorption spectrum by subtraction of a Victoreen-type polynomial. The background-subtracted spectrum was then convoluted with a series of increasingly broader Gauss functions and the common intersection point of the convoluted spectra was taken as energy E_0.[55,56] To determine the smooth part of the spectrum, corrected for pre-edge absorption, a piecewise polynomial was adjusted in such a way that the low-*R* components of the resulting Fourier transform were minimal. After division of the background subtracted spectrum by its smooth part, the photon energy was converted into photoelectron wave numbers *k*. The resulting EXAFS function was weighted with k^3. Data analysis in *k* space was performed according to the curved wave multiple scattering formalism of the program EXCURV92 with XALPHA phase- and amplitude-functions.[57] The mean free path of the scattered electrons was calculated from the imaginary part of the potential (VPI was set to −4.00) and an overall energy shift (ΔE_0) was assumed. The Amplitude Reduction Factor (AFAC) was set to a value of 0.8 in the case of both the Ni *K*-edge and Br *K*-edge.

NMR and UV/Vis Spectroscopy: ^{1}H, ^{13}C and ^{31}P NMR spectra were recorded with a Bruker AC 250 spectrometer. UV/Vis absorption spectra were recorded with a Bruins Instruments Omega 10 spectrometer. Kinetic data were fitted using a monoexponential decay assuming a first-order mechanism.

X-ray Crystallography: For compounds **1**−**3** data collection was performed at $T = 173(2)$ K with a Siemens P4 diffractometer using Mo-K_α radiation ($\lambda = 0.71073$ Å). The structures were solved by the Patterson method using the SHELXTL-PLUS package [58] and refinement was carried out with SHELXL-97 employing full-matrix least-squares methods on F^2 [59] with $F_o^2 \geq 3\sigma(F_o^2)$. Empirical absorption ($\psi$ scans) correction was performed for all three complexes. All non-hydrogen atoms were treated anisotropically, and hydrogen atoms were included by using appropriate riding models. CCDC-194378, -194379 and -194380 contain the supplementary crystallographic data for this paper. These data can be obtained free of charge at www.ccdc.cam.ac.uk/conts/retrieving.html [or from the Cambridge Crystallographic Data Centre, 12 Union Road, Cambridge CB2 1EZ, UK; Fax: (internat.) + 44-1223/336-033; E-mail: deposit@ccdc.cam.ac.uk].

Acknowledgments

We thank HASYLAB at DESY (Hamburg, Germany), the SSRL at SLAC (Stanford, USA) and BESSY (Berlin, Germany) for providing synchrotron radiation. The SSRL is operated by the U.S. Department of Energy, Office of Basic Energy Science. The authors would like to also thank Prof. Dr. Alexei Erko and Dr. Martin Fieber-Erdmann (BESSY GmbH, Berlin, Germany) for support during the beam times.

[1] S. Mecking, A. Held, F. M. Bauers, *Angew. Chem. Int. Ed.* **2002**, *41*, 544.
[2] S. D. Ittel, L. K. Johnson, M. Brookhart, *Chem. Rev.* **2000**, *100*, 1169.
[3] W. Keim, R. P. Schulz, *J. Mol. Catal.* **1994**, *92*, 21.
[4] W. Keim, A. Behr, B. Limbacker, C. Krüger, *Angew. Chem. Int. Ed. Engl.* **1983**, *22*, 503.
[5] K. Nomura, *Recent Res. Dev. Pure Appl. Chem.* **1998**, *2*, 473.
[6] C. S. Shultz, J. M. De Simone, M. Brookhart, *J. Am. Chem. Soc.* **2001**, *123*, 9172.
[7] C. S. Shultz, J. M. De Simone, M. Brookhart, *Organometallics* **2001**, *20*, 16.
[8] C. M. Killian, L. K. Johnson, M. Brookhart, *Organometallics* **1997**, *16*, 2005.
[9] S. Mecking, L. K. Johnson, L. Wang, M. Brookhart, *J. Am. Chem. Soc.* **1998**, *120*, 888.
[10] A. M. LaPointe, M. Brookhart, *Organometallics* **2001**, *17*, 1530.
[11] A. Michalak, T. Ziegler, *Organometallics* **2001**, *20*, 1521.
[12] S. Mecking, *Angew. Chem. Int. Ed.* **2001**, *40*, 534.
[13] A. Held, S. Mecking, *Chem. Eur. J.* **2000**, *6*, 4623.
[14] G. J. P. Britovsek, V. C. Gibson, D. F. Wass, *Angew. Chem. Int. Ed.* **1999**, *38*, 428.
[15] T. Yamamoto, M. Abla, *J. Organomet. Chem.* **1997**, *535*, 209.
[16] T. Yamamoto, S. Wakabayashi, K. Osakada, *J. Organomet. Chem.* **1992**, *428*, 223.
[17] A. Klein, *Z. Anorg. Allg. Chem.* **2001**, *627*, 645.
[18] A. Klein, M. P. Feth, H. Bertagnolli, S. Zális, manuscript in preparation.
[19] Y. H. Budnikova, J. Perichon, D. G. Yakhvarov, Y. M. Kargin, O. G. Sinyashin, *J. Organomet. Chem.* **2001**, *630*, 185.
[20] Y. H. Budnikova, O. E. Petrukhina, Y. M. Kargin, O. G. Sinyashin, *Zh. Obshch. Khim.* **1996**, *66*, 605.
[21] T. Yamamoto, A. Yamamoto, S. Ikeda, *J. Am. Chem. Soc.* **1971**, *93*, 3350.
[22] M. Martinez, G. Muller, *J. Chem. Soc., Dalton Trans.* **1989**, 1669.
[23] N. Kawata, K. Maruya, T. Mizoroki, A. Ozaki, *Bull. Chem. Soc. Jpn.* **1974**, *47*, 2003.
[24] H. Bock, H. Tom Dieck, *Angew. Chem.* **1966**, *78*, 549.
[25] D. J. Stufkens, *Coord. Chem. Rev.* **1990**, *104*, 39.
[26] R. W. Balk, T. L. Snoeck, D. J. Stufkens, A. Oskam, *Inorg. Chem.* **1980**, *19*, 3015.
[27] G. van Koten, K. Vrieze, *Adv. Organomet. Chem.* **1982**, *21*, 151.
[28] H. Bertagnolli, T. S. Ertel, *Angew. Chem. Int. Ed. Engl.* **1994**, *33*, 45.
[29] G. Kickelbick, U. Reinöhl, T. S. Ertel, H. Bertagnolli, K. Matyajaszewski, *The Copper Catalyst in Atom Transfer Radical Polymerizations: Structural Observations Controlled/Living Radical Polymerization* (Ed.: K. Matyaszewski), American Chemical Society, Washington, DC, **2000**, p. 211.

[30] E. Lindner, F. Auer, A. Baumann, P. Wegner, H. A. Mayer, H. Bertagnolli, U. Reinöhl, T. S. Ertel, A. Weber, *J. Mol. Catal. A* **2000**, *157*, 97.
[31] G. Kickelbick, U. Reinöhl, T. S. Ertel, A. Weber, H. Bertagnolli, K. Matyjaszewski, *Inorg. Chem.* **2001**, *40*, 6.
[32] F. Wong, F. W. Lytle, R. P. Messmer, D. H. Maylotte, *Phys. Rev.* **1984**, *B30*, 5596.
[33] A. Biaconi, *Springer Proc. Phys.* **1984**, *2*, 167.
[34] G. J. Colpas, M. J. Maroney, C. Bagyinka, M. Kumar, W. S. Willis, S. L. Suib, N. Baidya, P. K. Mascharak, *Inorg. Chem.* **1991**, *30*, 920.
[35] M. W. Renner, L. R. Furenlid, K. M. Barkigia, J. Fajer, *J. Phys. IV Fr.* **1997**, *7*, C2-661.
[36] A. Arcas, P. Royo, *Inorg. Chim. Acta* **1978**, *31*, 97.
[37] T. R. Miller, I. G. Dance, *J. Am. Chem. Soc.* **1973**, *95*, 6970.
[38] L. Sacconi, *Transit. Metal Chem.* **1968**, *4*, 199.
[39] D. Nicholls, "Nickel" in *Comprehensive Inorganic Chemsitry*, Pergamon Press, Oxford, **1973**, vol.3, p. 1109.
[40] R. H. Holm, M. J. O'Conner, *Inorg. Chem.* **1971**, *14*, 241.
[41] R. G. Hayter, F. S. Humiec, *Inorg. Chem.* **1965**, *4*, 1701.
[42] H. Weiss, F. Hampel, W. Donaubauer, M. A. Grundl, J. W. Bats, A. S. K. Hashmi, S. Schindler, *Organometallics* **2001**, *20*, 1713.
[43] P. T. Matsunaga, G. L. Hillhouse, *J. Am. Chem. Soc.* **1993**, *115*, 2075.
[44] M. Sato, Y. Fujii, T. Yamamura, S. Yano, *Bull. Chem. Soc. Jpn.* **1994**, *67*, 1954.
[45] R. Oritz, J. Borrás, L. Perelló, H. Jimenez, *Monatsh. Chem.* **1986**, *117*, 443.
[46] J. Mollin, Z. Pavelek, A. Schneiderova, J. Vicar, V. Simanek, J. Lasovsky, *Coll. Czech. Chem. Commmun.* **1983**, *48*, 2156.
[47] pK_a (methanol, 25 °C) = 15.32; pK_a (ethanol, H_2O, 90% molar content, 25 °C) = 16.29; pK_a (1-propanol, H_2O, 90% molar content, 25 °C) = 16.78; pK_a (2-propanol, H_2O, 90% molar content, 25 °C) = 17.97
[48] A. J. Blake, E. K. Brechin, A. Codron, R. O. Gould, C. M. Grant, S. Parsons, J. M. Rawson, R. E. P. Winpenny, *J. Chem. Soc., Chem. Commun.* **1983**, 1995.
[49] A. Szytula, A. Murasik, M. Balanda, *Phys. stat. sol. (b)* **1971**, *43*, 125.
[50] I. Leban, D. Gantar, B. Frlec, D. R. Russell, J. H. Holloway, *Acta Crystallogr., Sect. C* **1987**, *43*, 1888.
[51] H.-D. Hausen, K. Krogmann, *Z. Anorg. Allg. Chem.* **1972**, *389*, 247.
[52] S. Hasenzahl, H.-D. Hausen, W. Kaim, *Chem. Eur. J.* **1995**, *1*, 95.
[53] V. De Felice, P. Ganis, A. Vitagliano, G. Valle, *Inorg. Chim. Acta* **1988**, *144*, 57.
[54] H.-F. Klein, A. Bickelhaupt, M. Lemke, H. Sun, A. Brand, T. Jung, C. Röhr, U. Flörke, H. J. Haupt, *Organometallics* **1997**, *16*, 668.
[55] T. S. Ertel, H. Bertagnolli, S. Hückmann, U. Kolb, D. Peter, *Appl. Spectrosc.* **1992**, *46*, 690.
[56] M. Newville, P. Livins, Y. Yakoby, J. J. Rehr, E. A. Stern, *Phys. Rev. B* **1993**, *47*, 14126.
[57] S. J. Gurman, N. Binsted, I. Ross, *J. Phys. C* **1986**, *19*, 1845.
[58] G. M. Sheldrick, *SHELXTL-PLUS: An Integrated System for Solving, Refining and Displaying Crystal Structures from Diffraction Data*; Siemens Analytical X-ray Instruments Inc., Madison, WI, **1989**.
[59] G. M. Sheldrick, *SHELXL-97: A program for Crystal Structure Determination*; Universität Göttingen, Göttingen, **1997**.

Received July 11, 2002
[I02382]

Regiospecific Cyclometalation of Diphenyl(2-substituted phenyl)phosphane with Methyltetrakis(trimethylphosphane)cobalt(I)

Hans-Friedrich Klein,*[a] Robert Beck,[a] Ulrich Flörke,[b] and Hans-Jürgen Haupt[b]

Keywords: Orthometalation / Cobalt / Coordination chemistry / Structure elucidation / Steric control

The pre-chelate molecules 2-(diphenylphosphanyl)-*N*,*N*-dimethylaniline, [2-(diphenylphosphanyl)benzyl]dimethylamine, 1-(diphenylphosphanyl)-2-ethylbenzene, 1-(diphenylphosphanyl)-2-isopropylbenzene, and 2-(diphenylphosphanyl)benzonitrile, in a reaction with [CoMe(PMe_3)$_4$], eliminate methane to afford the selectively 6-*ortho*-metalated complexes **1**–**5** that contain four-membered metallacycles. The molecular structure of **3** shows a tbp-coordinated cobalt atom, with axial C and PMe_3 donor groups. Metalation in the aliphatic side-chain occurs with 2-(diphenylphosphanyl)toluene, giving complex **6** that contains a five-membered metallacycle. Benzyldiphenylphosphane is selectively *ortho*-metalated in the benzyl group, affording **7**. As shown by the molecular structures, complex **7** is a true ligand isomer of **6**. Substitution of a trimethylphosphane group in compounds **4** and **6** by ethene gives the pentacoordinate complexes **8** and **9**, respectively. The ethene ligand is π-coordinated in the equatorial plane of a trigonal bipyramid. Under 1 bar of CO, complex **6** forms monocarbonyl complex **10**. Carbonylation of complexes **3** and **4** proceeds by insertion of CO into the Co–C bond under ring expansion, affording the aroylcobalt complexes **11** and **12**, respectively. Complex **6** reacts with iodomethane in an oxidative substitution reaction yielding a structurally characterized octahedral complex *mer*-**13**, which eliminates a methyl group in THF at 20 °C to form a pentacoordinate cobalt(II) complex **14**. Complex **3** oxidatively adds iodomethane in a stereoselective *cis* addition to give the cobalt(III) complex *mer*-**15**, which retains its four-membered metallacycle and the $CoCH_3$ group.

(© Wiley-VCH Verlag GmbH & Co. KGaA, 69451 Weinheim, Germany, 2003)

Introduction

Cyclometalation reactions are among the oldest C−H-activation processes, and those involving phenylphosphanes are well known in electron-rich complexes of the late transition metals.[1] In many cases cyclometalation has been shown to be a reversible reaction involving an oxidative-addition and a reductive-elimination step (Scheme 1).

A residual methylmetal function can utilize the new hydrido ligand in an alternative reductive elimination reaction and can also stabilize three-membered Zr−N−C rings.[2] With [CoMe(PMe_3)$_4$], the subsequent elimination of methane, which proceeds at −70 °C, renders the formation of a metallacycle practically irreversible, since methane does not react in the same manner as dihydrogen at 20 °C in a hydrogenolytic cleavage reaction.[3] Given a selective course of such cyclometalation reactions, we do not expect the kinetically favored product complex to undergo equilibration of possible isomers. We have recently found an unusually high selectivity in the reaction of [CoMe(PMe_3)$_4$] with 2-(diphenylphosphanyl)-*N*,*N*-dimethylaniline,[4] and report here on our investigation of substituent effects on the selectivity of cyclometalation reactions. Our strategy was firstly to generate gradual steric and electronic changes in the vicinity of the anchoring PPh_2 group in order to favor attack at the available four sites in the unsubstituted phenyl groups, and secondly to provide 2-substituents that would favor an attack at the side-chain. Investigation of molecular structures with respect to ring size and bite-angle of chelating ligands are warranted because these parameters have

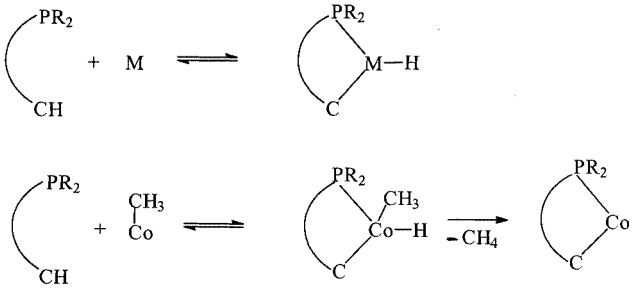

Scheme 1. Reversible and irreversible cyclometalation reactions

[a] Eduard-Zintl-Institut für Anorganische und Physikalische Chemie, Technische Universität Darmstadt
Petersenstr. 18, 64287 Darmstadt, Germany
Fax: (internat.) + 49-6151/16-4173
E-mail: hfklein@hrz2.hrz.tu-darmstadt.de
[b] Anorganische und Analytische Chemie der Universität Paderborn,
Warburger Straße, 33098 Paderborn, Germany

been shown in homogeneous catalysis to be among the most sensitive steering devices within the metal coordination sphere.[5]

Results and Discussion

a) The $ArNMe_2 \rightarrow ArCH_2NMe_2 \rightarrow ArCH_2Me \rightarrow ArCHMe_2$ Line

A side-chain in one of the six *ortho* positions of triphenylphosphane containing an N-donor function and activated aliphatic C−H bonds was provided in the pre-chelate molecules 2-(diphenylphosphanyl)-*N*,*N*-dimethylaniline, [2-(diphenylphosphanyl)benzyl]dimethylamine, 1-(diphenylphosphanyl)-2-ethylbenzene, and 1-(diphenylphosphanyl)-2-isopropylbenzene. Reactions with $[CoMe(PMe_3)_4]$ proceeded at −70 °C in THF [Equation (1)], and afforded the selectively *ortho*-metalated complexes **1**,[4] and **2**−**4**.

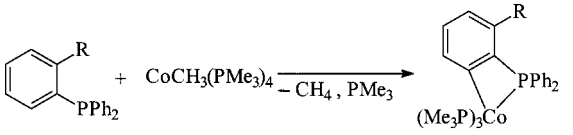

(1)

1: R = NMe_2
2: R = CH_2NMe_2
3: R = CH_2CH_3
4: R = $CH(CH_3)_2$
5: R = CN

The ^{31}P NMR spectra at 233 K most clearly show three resonances with chemical shifts and a coupling pattern which are characteristic of an *ortho*-metalated tris(trimethylphosphane)cobalt complex.[3] As no other signals are detected, the absence of possible isomers in solution (< ca. 2%) is demonstrated in all four compounds.

The dominant feature in the molecular structure of **3** is a four-membered cobaltacycle (Figure 1), in which the chelating ligand spans the C-axial and P-equatorial positions of a trigonal bipyramid. The small bite-angle [C12−Co−P1 = 71.02(15)°], which falls just outside the range of Rh and Ir complexes (67−69°),[6] causes bending between the axial positions [C12−Co−P4 = 166.25(15)°]. Bond lengths and angles do not substantially deviate from those in the unsubstituted molecule.[3]

b) The $ArNMe_2 \rightarrow ArCH_2Me \rightarrow ArCN$ Line

Electron-donating dimethylamino and ethyl groups were replaced by the strong electron-accepting cyano group. However, reaction of $[CoMe(PMe_3)_4]$ with 2-(diphenylphosphanyl)benzonitrile followed the same route as in Equation (1), affording **5** as a single *ortho*-metalated isomer. The ^{31}P NMR spectrum at 233 K closely resembles those of **1**−**4**. Thus, there is little chance for the electronic steering of the *ortho*-metalation reaction.

c) The $ArOH \rightarrow ArNH_2 \rightarrow ArCH_3$ Line

The isoelectronic donor functions of the pre-chelate systems in 2-(diphenylphosphanyl)phenol or 2-(diphenylphosphanyl)aniline were compared with the P,C-donor group in 2-(diphenylphosphanyl)toluene. Reaction of this type of weak C−H acid with $[CoMe(PMe_3)_4]$ at −70 °C produces methane [Equation (2)].

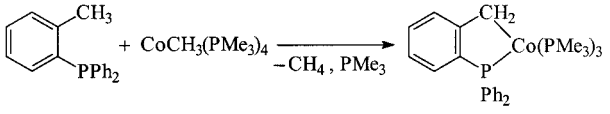

(2)

6

From a red-brown solution in pentane, complex **6** is obtained as black prismatic crystals. In the ^1H NMR spectrum at 296 K, a broad resonance at δ = 1.80 ppm (2 H) containing multiple phosphorus coupling is assigned to a $CoCH_2$ group. Doublet and pseudotriplet PCH_3 resonances with intensity ratios of 1:2 also indicate little ligand mobility. Complex **6** remains pentacoordinate, which differs from the rapidly exchanging trimethylphosphane from [P,O]-chelate and [P,N]-chelate systems on the NMR time scale. However, the ^{31}P NMR chemical shifts at 233 K are found in similar positions to those of the [P,N] and [P,O] complexes, and are in no way related to those in complexes **1**−**4**.

Therefore, a selective attack appears to be directed at the *ortho*-methyl group to form a five-membered metallacycle, which is known to form with platinum.[7] The molecular structure (Figure 2) is entirely consistent with the configuration of **6** derived from the solution data. A cobalt atom is centered in a trigonal bipyramid with axial CH_2 and PMe_3 groups and a five-membered metallacycle occupying C-axial and P-equatorial positions with a narrow bite-angle [C10−Co−P1 = 77.77(17)°] and considerable ring bending

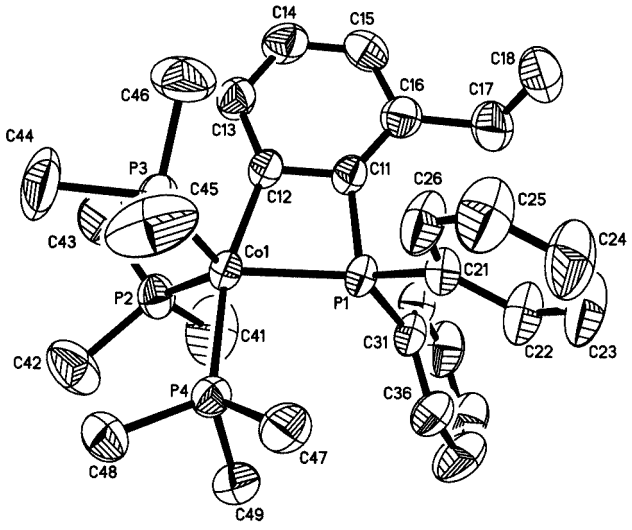

Figure 1. Molecular structure of **3** (ORTEP plot with hydrogen atoms omitted); selected bond lengths [Å] and angles [°]: Co−C12 1.984(5), Co−P1 2.2103(14), Co−P2 2.1639(17), Co−P3 2.1691(17), Co−P4 2.1857(17), P1−C11 1.796(6), C11−C12 1.401(7); C12−Co−P1 71.02(15), C12−Co−P2 90.96(16), C12−Co−P3 90.89(15), C12−Co−P4 166.25(15), P1−Co−P2 119.25(7), P1−Co−P3 121.97(7), P1−Co−P4 95.23(6), P2−Co−P3 115.56(7), P2−Co−P4 95.79(7), P3−Co−P4 96.95(7)

(sum of internal angles = 518.8°). The Co−C10 distance [2.080(5) Å] is within the range of Co−C(sp^3) bonds (2.03−2.15 Å),[8] and Co−P distances are typical and appear unaffected by the *trans* influence of the distant CH_2 group. We note here an unexpected and complete switching of the cyclometalation reaction on changing from a 2-methyl to a 2-ethyl group.

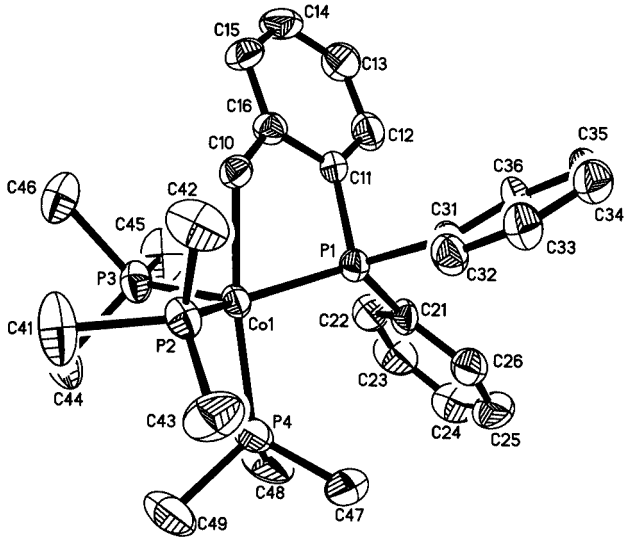

Figure 2. Molecular structure of **6** (ORTEP plot with hydrogen atoms omitted); selected bond lengths [Å] and angles [°]: Co−C10 2.080(5), Co−P1 2.1646(18), Co−P2 2.206(2), Co−P3 2.186(2), Co−P4 2.180(2), P1−C11 1.827(7), C10−C16 1.494(8), C11−C16 1.399(8); C10−Co−P1 77.77(17), C10−Co−P2 87.15(17), C10−Co−P3 88.10(18), C10−Co−P4 172.48(18), P1−Co−P2 132.14(8), P1−Co−P3 114.22(8), P1−Co−P4 95.86(7), P2−Co−P3 110.29(7), P2−Co−P4 94.36(8), P3−Co−P4 98.26(8)

Formation of a five-membered cobaltacycle with reversed ring positions of $Co(PMe_3)_3$ and PPh_2 groups can be expected from a reaction of $[CoMe(PMe_3)_4]$ with benzyldiphenylphosphane [Equation (3)].

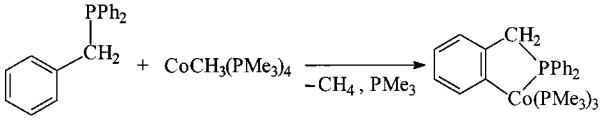

(3)

7

When the reactants are combined at −70 °C, the color changes to red-brown and the evolution of gas commences. Eventually, red crystals of **7**, which are air-sensitive and decompose under argon above 75 °C, were obtained from pentane. The ^{31}P NMR spectrum contains a doublet of triplets (δ = 63 ppm, PPh_2) and two doublets of doublets (δ = −4 and 22 ppm, PMe_3), with couplings that suggest a five-membered cobaltacycle in the C(axial)/P(equatorial) positions of a trigonal bipyramid. The expected configuration is observed in the molecular structure of **7** (Figure 3).

All bond lengths in **7** are similar to those in the ligand isomer **6** (Figure 2). In particular, the distance [Co−C11 = 2.011(4) Å] falls in the range reported for Co−C(sp^2) bonds

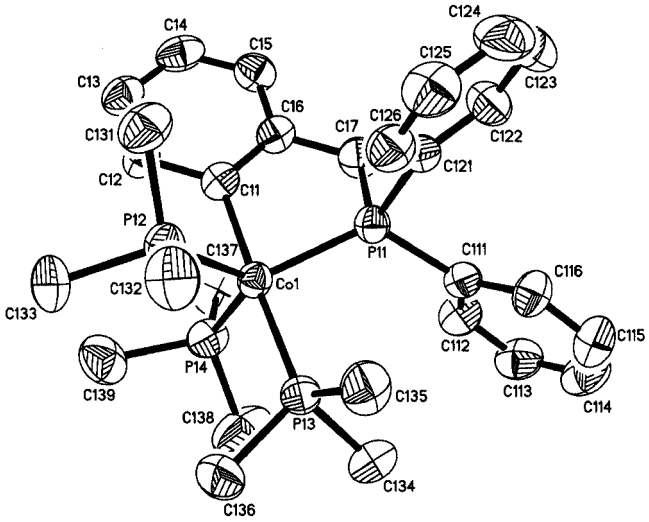

Figure 3. Molecular structure of **7** (molecule A) (ORTEP plot with hydrogen atoms omitted); selected bond lengths [Å] and angles [°]: Co−C11 2.011(4), Co−P11 2.1625(12), Co−P12 2.2197(13), Co−P13 2.1994(12), Co−P14 2.1833(13), P11−C17 1.830(4), C16−C17 1.501(5), C11−C16 1.415(6); C11−Co−P11 83.08(12), C11−Co−P12 88.51(12), C11−Co−P13 177.17(12), C11−Co−P14 84.22(12), P11−Co−P12 120.47(5), P11−Co−P13 94.83(5), P11−Co−P14 119.37(5), P12−Co−P13 94.21(5), P12−Co−P14 118.13(5), P13−Co−P14 95.19(5), Co−C11−C16 120.6(3), C11−C16−C17 118.0(4), C16−C17−P11 106.2(3)

(1.97−2.01 Å).[8,9] The approximation to an ideal tbp geometry is better in **7**, and the sum of the internal angles in the cobaltacycle (532.7°) is closer to planarity (540°) than in **6** (518.8°).

d) Reactions with Ethene

π-Olefin coordination in aryl(trimethylphosphane)cobalt(I) complexes is an expected phenomenon.[4] The steric limitations of pentacoordination will be modified by the angular strain of the four- and five-membered metallacycles on the preferred equatorial binding site. A spontaneous substitution reaction is not feasible with complex **4**. When complex **4** is kept at 100 °C for 3 h under vacuum, a vacant coordination site is formed by dissociation of 1 mol-equiv. of trimethylphosphane that is necessary for subsequent coordination of olefin to occur [Equation (4)].

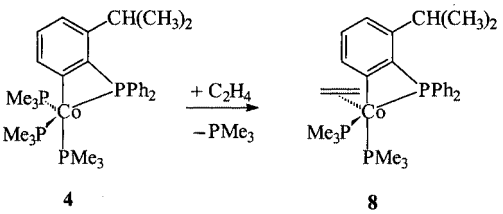

(4)

4 **8**

On dissolution of **4** in diethyl ether under 1 bar of ethene, complex **8** is obtained as orange crystals. In the ^{31}P NMR spectrum of **8**, three doublets of doublets are seen at δ = −12, 9, and 17 ppm. These signals are in the same region as those of a four-membered cobaltacycle, as expected from the data of compounds **1**−**5**.

When heated under argon, decomposition of **8** occurs with the release of ethene, and no alteration of the four-membered metallacycle is indicated (IR) prior to the deposition of cobalt.

Without thermal pretreatment of complex **6**, which contains a five-membered cobaltacycle, substitution of trimethylphosphane by ethene occurs [Equation (5)].

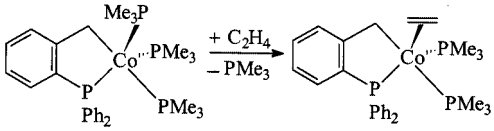

6 **9** (5)

The orange-yellow needles of **9** (from pentane, decomp. > 87 °C) exhibit a better thermal stability than π-ethene complexes containing five-membered cobaltacycles with (P,N) and (P,O) ligands,[4,10] which are isoelectronic. From the ^{31}P NMR spectrum, the doublet of doublets pattern, with characteristic shifts at δ = 66, 18, and 11 ppm, indicates that the π-ethene ligand occupies an equatorial position.

e) Reactions with Carbon Monoxide

Carbonylated methylcobalt(I) compounds, $[CoCH_3(CO)(PMe_3)_3]$ or $[Co(CH_3CO)(CO)_2(PMe_3)_2]$,[11] are unreactive towards diphenyl(2-substituted phenyl)phosphanes and do not undergo a cyclometalation reaction of the proscribed type. However, CO ligands are smoothly introduced into metallacyclic product complexes. In solution under 1 bar of CO at 20 °C, **6** forms the monocarbonyl complex **10** [Equation (6)].

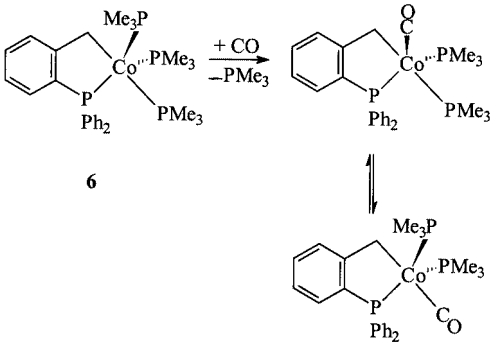

6 **10** (6)

The dark-red crystals of **10** are thermally more stable (by 30 K) and less air-sensitive than those of complexes containing five-membered cobaltacycles with (P,N) and (P,O) ligands.[4,10] The ^{31}P NMR spectra in THF solutions show mixtures of isomers, with couplings consistent with a tbp configuration where a terminal carbonyl ligand resides either in an axial or in an equatorial position. In toluene solutions, only the isomer with the CO ligand in the axial position is observed.

When carbonylation reactions of complexes **3** and **4**, which contain four-membered cobaltacycles, take place under the same conditions, monosubstitution is accompanied by insertion of CO into the Co–C bond under ring expansion [Equation (7)], thus affording the aroylcobalt complexes **11** and **12**, respectively.

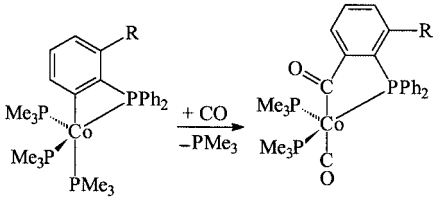

3, 4 **11**: R = C_2H_5 **12**: R = $CH(CH_3)_2$ (7)

The lustrous red crystals of **11** and **12** have narrow melting ranges (**11**: 152–153 °C; **12**: 161–162 °C) and melt without decomposing. The IR spectra contain two conspicuous new bands which are assigned to the terminal carbonyl ligand and to the benzoylcobalt group [**11**: $\tilde{\nu}$ = 1913 (C≡O), 1542 cm^{-1} (C=O); **12**: $\tilde{\nu}$ = 1906 (C≡O), 1513 cm^{-1} (C=O)].

In the ^{31}P NMR spectra, the ring expansion causes a low-field shift of the chelating phosphorus resonance by 85 ppm, which appears as a triplet by coupling to two equatorial trimethylphosphane groups. The observed doublet and triplet pattern is only compatible with the acyl and carbonyl ligands arranged in the axial positions.

f) Reactions with Iodomethane

Complex **6** reacts with excess iodomethane in diethyl ether by dissociation and quaternization of a trimethylphosphane [Equation (8)], thus undergoing an oxidative substitution reaction.

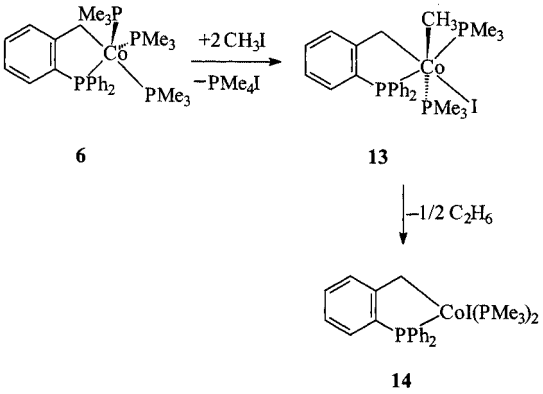

6 **13** **14** (8)

All volatile materials were removed in vacuo as soon as the precipitation of white tetramethylphosphonium iodide began. Extraction of the remaining solid with diethyl ether at 20 °C and cooling of the red-brown solution gave a moderate yield of short orange rods. Complex **13** is air-stable, but decomposes above 82 °C. In tetrahydrofuran at 20 °C,

spontaneous evolution of ethane transforms hexacoordinate **13** into the pentacoordinate cobalt(II) complex **14** [Equation (8)]. More conveniently, **14** is obtained by performing the synthesis in THF.

A $^{31}P\{^{1}H\}$ NMR spectrum of **13** in [D_8]THF at 213 K shows three multiplet signals, suggesting three P-donor functions in an octahedral coordination geometry, but allows no clear distinction between the *mer* and *fac* configurations. The molecular structure of *mer*-**13** was revealed by a single-crystal X-ray diffraction analysis (Figure 4).

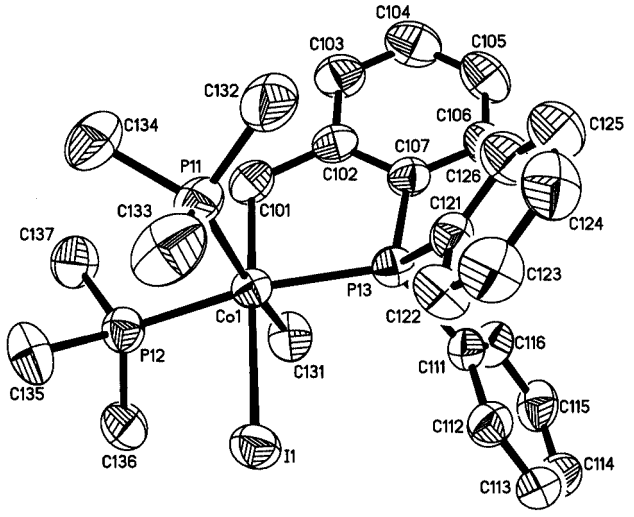

Figure 4. Molecular structure of *mer*-**13** (ORTEP plot with hydrogen atoms omitted); selected bond lengths [Å] and angles [°]: Co−C101 2.016(5), Co−C131 2.053(5), Co−I 2.7250(9), Co−P11 2.2749(17), Co−P12 2.2581(19), Co−P13 2.2301(18), C101−C102 1.515(8), C102−C107 1.386(8), P13−C107 1.818(5); C101−Co−P13 86.89(18), C101−Co−I 178.47(17), C101−Co−P12 94.70(18), P11−Co−P12 95.82(7), P11−Co−P13 98.31(6), P12−Co−P13 165.85(6), C107−P13−Co 102.8(2), P13−C107−C102 112.4(4), C101−C102−C107 122.3(5), Co−C101−C102 114.9(4)

The iodide ion and one of the trimethylphosphane ligands are coplanar with the cobaltacycle, while the other trimethylphosphane ligand and the $CoCH_3$ group are below and above the plane. While the Co−P and Co−C bond lengths are as expected, the Co−I bond is slightly elongated by the benzylic CH_2−Co interaction in *trans* position.

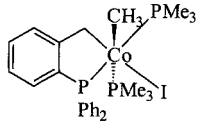

mer-**13**

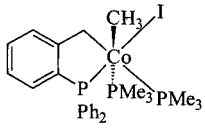

fac-**13**

As the *trans* influences along Me_3P−Co−CH_3 would be very similar to that of Me_3P−Co−CH_3 in the *fac* configuration, *mer*-**13** would appear to be the product of a *cis* addition under kinetic control. However, when compared with **6**, the chelate bite angle [C101−Co−P13 = 86.89(13)°] is augmented by 10°, while the Co−C bond is shortened by 6.5 pm. The sum of the internal angles is 539.3°, indicating considerable relaxation of the metallacycle towards planarity. These differences could make *mer*-**13** the thermodynamically most stable isomer. Eventually, *mer*-**13** is metastable with respect to a C−C-coupling reaction forming **14**.

Although the molecular geometry of **14** has not been clarified due to poor crystal quality and broad and overlapping NMR signals, the magnetic moment (μ_{eff}/μ_B = 1.93) is as expected for a tbp configuration of cobalt (d^7).[13−15]

Under the same conditions, **3** oxidatively adds iodomethane after substitution and quaternization of a trimethylphosphane group [Equation (9)].

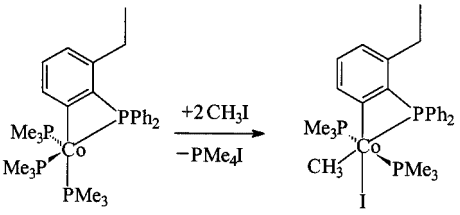

3 **15** (9)

The dark-red crystals of **15** melt at 115−116 °C under argon, and are stable for more than 1 d in air at 20 °C. The IR spectrum resembles that of **3**, except for an additional band [$\tilde{\nu}$ = 1165 cm^{-1} ($CoCH_3$)]. The ^{31}P NMR spectrum at 213 K shows a triplet resonance at δ = −32 ppm, characteristic of a PPh_2 group in a four-membered cobaltacycle, and a doublet at δ = 10 ppm containing a typical *cis* coupling (^2J = 23 Hz). The observed pattern is consistent with two isochronic trimethylphosphane ^{31}P nuclei in *trans* positions, and a meridional arrangement of the three P-donor atoms which appears to result from a regioselective *cis* addition of iodomethane.[3] At variance with the spontaneous transformation of *mer*-**13** [Equation (8)], solutions of **15** in THF at 20 °C remain stable for at least 1 d.

While cobalt(I) compounds containing five-membered metallacycles in a reaction with iodomethane undergo oxidative substitution, followed by reductive elimination of ethane, those containing four-membered cobaltacycles attain the cobalt(III) state without a subsequent C−C-coupling reaction. In both transformations the endocyclic Co−C bonds remain unaffected.

Conclusion

The reactivity in irreversible cyclometalation processes with [$CoMe(PMe_3)_4$] appears to be controlled by a high electron density on the metal atom, and is lost in the presence of a single strongly π-accepting ligand, e.g. in $CoMe(CO)(PMe_3)_3$. The observed selectivity, which is based on the orientation of the C−H bonds that are in the proximity of the metal atom, is sterically controlled by the preferred substrate conformation. The usual fan-type conformation of a triphenylphosphane ligand is most effectively distorted by a 2-substituent, whereby the substituted phenyl group is rotated in such a way that only this particular *ortho*-CH group closes in on the metal atom (Scheme 2) and the four-

membered cobaltacycle is formed. Thus, a sterically hindered rotation of an aryl group renders the cyclometalation reaction regiospecific.

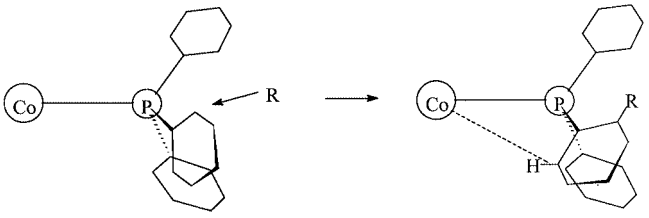

Scheme 2. Sterically controlled proximity conformation

A five-membered cobaltacycle is formed as the preferred ring size, by activation of a benzylic C−H bond only in the absence of steric strain. In a monosubstituted triphenylphosphane steric crowding is significant as the substituents are changed from 2-methyl to the 2-ethyl substituents. Once formed, the five-membered cobaltacycle does not insert a CO ligand in a process that accompanies carbonylation of complexes with four-membered cobaltacycles. Neither metallacycle shows insertion of a π-ethene ligand.

While cobalt(I) compounds containing five-membered metallacycles in a reaction with iodomethane undergo oxidative substitution, followed by reductive elimination of ethane, those containing four-membered cobaltacycles attain the cobalt(III) state without a subsequent C−C-coupling reaction. In both transformations the endocyclic Co−C bonds remain unaffected.

Experimental Section

General Procedures and Materials: All air-sensitive and volatile materials were handled using standard vacuum techniques and were kept under argon. Microanalyses: Kolbe Microanalytical Laboratory, Mülheim/Ruhr, FRG. Melting points/decomposition temperatures: Sealed capillaries, uncorrected values. Chemicals (Merck/Schuchardt) were used as purchased. Literature methods were applied for the preparation of 2-(diphenylphosphanyl)-*N*,*N*-dimethylaniline,[16] [2-(diphenylphosphanyl)benzyl]dimethylamine,[17] 1-(diphenylphosphanyl)-2-ethylbenzene, 1-(diphenylphosphanyl)-2-isopropylbenzene,[18] 2-(diphenylphosphanyl)benzonitrile,[19] 2-(diphenylphosphanyl)toluene,[20] benzyldiphenylphosphane,[21] and [CoMe(PMe$_3$)$_4$].[11] IR: Nujol mulls between KBr discs, Bruker spectrophotometer type FRA 106. ^{1}H and ^{13}C NMR spectra (300 MHz and 75 MHz, respectively) were recorded with a Bruker ARX-300 spectrometer, ^{31}P NMR spectra (81 MHz) with a Bruker AM-200 instrument. ^{13}C and ^{31}P resonances were obtained with proton decoupling. Magnetic susceptibility data were obtained by the Faraday method using a Cahn D 200 torsion balance (Bruker) at 1.5 Tesla.

[3-(Dimethylamino)-2-(diphenylphosphanyl)phenyl-*C^I*,*P*]tris(trimethylphosphane)cobalt (1): 2-(Diphenylphosphanyl)-*N*,*N*-dimethylaniline (549 mg, 1.79 mmol) in 50 mL of diethyl ether was combined at −70 °C with [CoMe(PMe$_3$)$_4$] (680 mg, 1.79 mmol) in 30 mL of diethyl ether. The reaction was accompanied by the evolution of a gas. After the solution had warmed up, the red-brown mixture was kept at 20 °C for 16 h. The volatiles were removed in vacuo, the solid residue was extracted with 80 mL of pentane, and the solution cooled to 4 °C, affording dark-red rectangular crystals of **1**. Yield 270 mg (85%); m.p. 112−114 °C (dec.). ^{1}H NMR (300 MHz, [D$_8$]THF, 296 K): δ = 1.02 [d, ^2J(PH) = 5.6 Hz, 9 H, PCH$_3$], 1.23 [s (br), 18 H, PCH$_3$], 2.13 (s, 6 H, NCH$_3$), 5.90−6.23 (m, 3 H, CH), 7.22−7.24 (m, 6 H, CH), 7.75−7.79 (m, 4 H, CH) ppm. ^{13}C NMR (75.4 MHz, [D$_8$]THF, 296 K): δ = 22.2−22.7 (m, PCH$_3$), 23.3 (m, PCH$_3$), 43.3 (s, NCH$_3$), 109.3 (s, CH), 125.9 [d, ^3J(PC) = 3.1 Hz, CH], 126.0 (s, CH), 126.3 [d, ^3J(PC) = 5.6 Hz, CH], 126.9 (s, CH), 133.2 [d, ^2J(PC) = 7.6 Hz, CH], 133.3 [d, ^2J(PC) = 7.6 Hz, CH], 139.1 [d, ^2J(PC) = 9.2 Hz, CH], 171.3 (m, CoC) ppm. ^{31}P NMR (81 MHz, [D$_8$]THF, 233 K): δ = −24 [dt, ^2J(PP) = 89 and 68 Hz, 1 P, PPh$_2$], −4 [dd, ^2J(PP) = 89 and 68 Hz, 2 P, PCH$_3$], 22 [dt, ^2J(PP) = 68 and 47 Hz, 1 P, PCH$_3$] ppm. $C_{29}H_{46}CoNP_4$ (591.5): calcd. C 58.89, H 7.84, N 2.37, P 20.95; found C 58.92, H 7.82, N 2.27, P 20.83.

{3-[(Dimethylamino)methyl]-2-(diphenylphosphanyl)phenyl-*C^I*,*P*}tris(trimethylphosphane)cobalt (2): [2-(Diphenylphosphanyl)benzyl-]dimethylamine (608 mg, 1.90 mmol) in 50 mL of diethyl ether was combined at −70 °C with [CoMe(PMe$_3$)$_4$] (720 mg, 1.90 mmol) in 30 mL of diethyl ether. The reaction was accompanied by the evolution of a gas. After keeping the red-brown mixture at 20 °C for 16 h, the volatiles were removed in vacuo and the solid residue was extracted with two 70-mL portions of pentane. When the solution was kept at −27 °C, dark-red crystals of **2** were obtained. Yield 967 mg (84%); m.p. 107−109 °C (dec.). ^{1}H NMR (300 MHz, [D$_8$]THF, 296 K): δ = 0.90 [d, ^2J(PH) = 6.2 Hz, 9 H, PCH$_3$], 1.28 [s (br), 18 H, PCH$_3$], 1.73 (s, 6 H, NCH$_3$), 2.78 (s, 2 H, NCH$_2$), 6.68−6.77 (m, 3 H, CH), 7.24−7.26 (m, 6 H, CH), 7.72−7.78 (m, 4 H, CH) ppm. ^{13}C NMR (75.4 MHz, [D$_8$]THF, 296 K): δ = 22.1−22.5 (m, PCH$_3$), 23.3 [d, ^1J(PC) = 20.1 Hz, PCH$_3$], 27.3 (s, NCH$_3$), 58.1 (s, NCH$_2$), 118.5 [d, ^3J(PC) = 3.1 Hz, CH], 126.4 (s, CH), 126.5 [d, ^3J(PC) = 5.6 Hz, CH], 126.9 (s, CH), 134.8 (s, CH), 135.6 [d, ^2J(PC) = 7.6 Hz, CH], 135.7 [d, ^2J(PC) = 7.6 Hz, CH], 138.1 [d, ^2J(PC) = 9.2 Hz, C], 151.1 [d, ^2J(PC) = 10.7 Hz, C], 1511.5 [d, ^2J(PC) = 10.7 Hz, C], 169.9 (m, CoC) ppm. ^{31}P NMR (81 MHz, [D$_8$]THF, 233 K): δ = −26 [dt, ^2J(PP) = 89 and 70 Hz, 1 P, PPh$_2$], −4 [dd, ^2J(PP) = 89 and 48 Hz, 2 P, PCH$_3$], 21 [dt, ^2J(PP) = 70 and 48 Hz, 1 P, PCH$_3$] ppm. $C_{30}H_{48}CoNP_4$ (605.5): calcd. C 59.50, H 7.99, N 2.31, P 20.46; found C 59.36, H 8.10, N 2.18, P 20.38.

[2-(Diphenylphosphanyl)-3-ethylphenyl-*C^I*,*P*]tris(trimethylphosphane)cobalt (3): 1-(Diphenylphosphanyl)-2-ethylbenzene (590 mg, 2.03 mmol) in 50 mL of THF was combined at −70 °C with [CoMe(PMe$_3$)$_4$] (770 mg, 2.03 mmol) in 30 mL of THF. As the solution warmed up, the slow evolution of a gas was observed. After keeping the dark-red mixture at 20 °C for 16 h, the volatiles were removed in vacuo and the solid residue was extracted with two 50-mL portions of pentane. Reduction of the volume to 60 mL and keeping of the red solution at 4 °C afforded dark-red rectangular crystals of **3**, which were suitable for X-ray diffraction. Yield 809 mg (69%); m.p. 120−121 °C. ^{1}H NMR (300 MHz, [D$_8$]THF, 296 K): δ = 0.53 (t, ^3J = 7.5 Hz, 3 H, CCH$_3$), 1.09 [d, ^2J(PH) = 6.3 Hz, 9 H, PCH$_3$], 1.25 [t′, |^2J(PH) + ^4J(PH)| = 4.5 Hz, 18 H, PCH$_3$], 2.43 (q, ^3J = 7.5 Hz, 2 H, CH$_2$), 6.29 (d, ^3J = 6.4 Hz, 1 H, CH), 6.67 (t, ^3J = 7.1 Hz, 1 H, CH), 6.73 (m, 1 H, CH), 7.21−7.27 (m, 6 H, CH), 7.72−7.80 (m, 4 H, CH) ppm. ^{13}C NMR (75.4 MHz, [D$_8$]THF, 296 K): δ = 22.1 (s, CH$_3$), 22.1−22.9 (m, PCH$_3$), 23.7 (s, CH$_2$), 117.9 [d, ^2J(PC) = 11.5 Hz, CH], 126.9 (s, CH), 128.6 [d, ^3J(PC) = 9.0 Hz, CH], 129.3 [d, ^4J(PC) = 3.1 Hz, CH], 130.1 [d, ^1J(PC) = 15.1 Hz, CH], 131.5 [d, ^2J(PC) = 12.3 Hz, CH], 137.9 [d, ^2J(PC) = 10.5 Hz, CH], 138.2 (s, C), 145.5 (m, C), 171.5 (m, CoC) ppm. ^{31}P NMR (81 MHz, [D$_8$]THF, 233 K): δ = −26 [dt, ^2J(PP) =

87 and 69 Hz, 1 P, PPh_2], −4 [dd, ^2J(PP) = 87 and 47 Hz, 2 P, PCH_3], 21 [dt, ^2J(PP) = 69 and 47 Hz, 1 P, PCH_3] ppm. $C_{29}H_{45}CoP_4$ (576.5): calcd. C 60.42, H 7.87, P 21.49; found C 60.51, H 8.13, P 21.19.

[2-(Diphenylphosphanyl)-3-isopropylphenyl-*C*^{1},*P*]tris(trimethylphosphane)cobalt (4): 1-(Diphenylphosphanyl)-2-isopropylbenzene (732 mg, 2.40 mmol) in 50 mL of THF was combined at −70 °C with [$CoMe(PMe_3)_4$] (910 mg, 2.40 mmol) in 50 mL of THF. After the solution had warmed up, the dark-red mixture was kept at 20 °C for 16 h. The volatiles were removed in vacuo and the solid residue was extracted with two 80-mL portions of pentane. When the solution was kept at 4 °C, dark-red rectangular crystals of **4** were obtained. Yield 1040 mg (73%); m.p. 95−98 °C. ^{1}H NMR (300 MHz, [D_8]THF, 296 K): δ = 0.61 [d, ^3J = 6.8 Hz, 6 H, $C(CH_3)_2$], 1.08 [d, ^2J(PH) = 6.3 Hz, 9 H, PCH_3], 1.25 [t′, $|^2J(PH) + {}^4J(PH)|$ = 4.4 Hz, 18 H, PCH_3], 2.52 (sept, ^3J = 6.8 Hz, 1 H, CH), 6.34 (d, ^3J = 7.2 Hz, 1 H, CH), 6.66 (t, ^3J = 7.2 Hz, 1 H, CH), 6.72 (m, 1 H, CH), 7.24−7.26 (m, 6 H, CH), 7.75−7.82 (m, 4 H, CH) ppm. ^{13}C NMR (75.4 MHz, [D_8]THF, 296 K): δ = 21.2 (s, CH_3), 22.5−22.6 (m, PCH_3), 27.9 (s, CH), 114.8 (s, CH), 126.5 [d, ^2J(PC) = 8.5 Hz, CH], 126.9 (s, CH), 131.7 [d, ^3J(PC) = 13.2 Hz, CH], 135.2 (s, CH), 135.4 [d, ^1J(PC) = 16.6 Hz, CH], 138.2 (m, C), 138.4 (s, CH), 140.4 (s, C), 171.2 (m, CoC) ppm. ^{31}P NMR (81 MHz, [D_8]THF, 233 K): δ = −26 [dt, ^2J(PP) = 87 and 71 Hz, 1 P, PPh_2], −4 [dd, ^2J(PP) = 87 and 47 Hz, 2 P, PCH_3], 21 [dt, ^2J(PP) = 71 and 47 Hz, 1 P, PCH_3] ppm. $C_{30}H_{47}CoP_4$ (590.5): calcd. C 61.02, H 8.02, P 20.98; found C 61.35, H 8.37, P 20.54.

[3-Cyano-2-(diphenylphosphanyl)phenyl-*C*^{1},*P*]tris(trimethylphosphane)cobalt (5): 2-(Diphenylphosphanyl)benzonitrile (486 mg, 1.69 mmol) in 50 mL of THF was combined with [$CoMe(PMe_3)_4$] (640 mg, 1.69 mmol) in 50 mL of THF, at −70 °C. After the solution had warmed up, the dark-brown mixture was stirred at 20 °C for 16 h. The volatiles were then removed in vacuo. The solid residue was extracted with two 80-mL portions of pentane. At 4 °C, black needles of **5** were obtained. Yield 408 mg (42%); m.p. 114−116 °C (dec.). IR (Nujol): $\tilde{\nu}$ = 2209 cm^{-1} (C≡N). ^{1}H NMR (300 MHz, [D_8]THF, 296 K): δ = 1.11 [d, ^2J(PH) = 6.6 Hz, 9 H, PCH_3], 1.30 [t′, $|^2J(PH) + {}^4J(PH)|$ = 4.5 Hz, 18 H, PCH_3], 6.66 (d, ^3J = 4.7 Hz, 1 H, CH), 6.68 (d, ^3J = 8.2 Hz, 1 H, CH), 7.01 (m, 1 H, CH), 7.24−7.30 (m, 6 H, CH), 7.80−7.86 (m, 4 H, CH) ppm. ^{13}C NMR (75.4 MHz, [D_8]THF, 296 K): δ = 21.8 (m, PCH_3), 22.3 (m, PCH_3), 119.3 [m, *C*(CN)], 121.7, 125.5 (s, CH), 126.4 [d, ^2J(PC) = 7.7 Hz, CH], 127.4 (s, CH), 132.4 [d, ^2J(PC) = 13.5 Hz, CH], 134.2, 136.5 (s, CH), 138.8 (s, C), 139.6 (m, C), 169.9 (m, CoC) ppm. ^{31}P NMR (81 MHz, [D_8]THF, 233 K): δ = −26 [dt, ^2J(PP) = 89 and 73 Hz, 1 P, PPh_2], −4 [dd, ^2J(PP) = 89 and 50 Hz, 2 P, PCH_3], 21 [dt, ^2J(PP) = 73 and 50 Hz, 1 P, PCH_3] ppm. $C_{28}H_{41}CoNP_4$ (574.5): calcd. C 58.54, H 7.19, N 2.44, P 21.57; found C 58.41, H 7.48, N 2.41, P 21.51.

[2-(Diphenylphosphanyl)tolyl-*C*,*P*]tris(trimethylphosphane)cobalt (6). Method a): 2-(Diphenylphosphanyl)toluene (616 mg, 2.23 mmol) and $CoCl(PMe_3)_3$ (720 mg, 2.23 mmol) in 40 mL of THF were combined at −70 °C with 1.6 M MeLi in diethyl ether (1.4 mL, 2.23 mmol), whilst stirring. The dark-green mixture turned red-brown. After the solution had warmed up, and after stirring at 20 °C for 30 min, the volatiles were removed in vacuo and the solid residue was extracted with two 80-mL portions of diethyl ether. Removal of the solvent afforded a dark-brown solid of **6**. Raw yield 928 mg (74%). **Method b):** 2-(Diphenylphosphanyl)-toluene (489 mg, 1.77 mmol) in 50 mL of THF was combined with [$CoMe(PMe_3)_4$] (670 mg, 1.77 mmol) in 50 mL of THF, at −70 °C. As the solution warmed up, the mixture turned red-brown and was stirred at 20 °C for 16 h. The volatiles were removed in vacuo, and the solid residue was extracted with three 80-mL portions of pentane. At 4 °C, black crystals of **6**, which were suitable for X-ray diffraction, were obtained. Yield 806 mg (81%); m.p. 124−126 °C (dec.). ^{1}H NMR (300 MHz, [D_8]THF, 296 K): δ = 0.93 [d, ^2J(PH) = 6.5 Hz, 9 H, PCH_3], 1.19 [t′, $|^2J(PH) + {}^4J(PH)|$ = 4.3 Hz, 18 H, PCH_3], 1.80 [m (br), 2 H, $CoCH_2$], 6.71 (t, ^3J = 7.2 Hz, 1 H, CH), 6.80 (tt, ^3J = 7.2, ^4J = 1.4 Hz, 1 H, CH), 6.92 (d, ^3J = 7.2 Hz, 1 H, CH), 7.08 (t, ^3J = 6.3 Hz, 1 H, CH), 7.22−7.24 (m, 6 H, CH), 7.56−7.65 (m, 4 H, CH) ppm. ^{13}C NMR (75.4 MHz, [D_8]THF, 296 K): δ = 21.1−22.9 (m, PCH_3), 24.8 (m, $CoCH_2$), 108.2 (m, C), 117.3 (m, CH), 120.4 (s, CH), 122.9 [d, ^2J(PC) = 13.0 Hz, CH], 125.1 (s, CH), 125.9 [d, ^4J(PC) = 3.1 Hz, CH], 130.1 [d, ^1J(PC) = 15.1 Hz, CH], 131.5 [d, ^2J(PC) = 12.3 Hz, CH], 137.9 [d, ^2J(PC) = 13.1 Hz, CH], 126.4 [d, ^1J(PC) = 22.4 Hz, C], 130.2 (s, CH), 132.6[d, ^2J(PC) = 12.3 Hz, C], 141.2 (m, C) ppm. ^{31}P NMR (81 MHz, [D_8]THF, 233 K): δ = −4 [dd, ^2J(PP) = 94 and 44 Hz, 2 P, PCH_3], 22 [dd, ^2J(PP) = 50 and 44 Hz, 1 P, PCH_3], 58 [dt, ^2J(PP) = 94 and 50 Hz, 1 P, P Ph_2] ppm. $C_{28}H_{43}CoP_4$ (562.5): calcd. C 59.79, H 7.71, P 22.03; found C 59.97, H 7.30, P 22.08.

[2-(Diphenylphosphanyl)benzyl-*C*^{2},*P*]tris(trimethylphosphane)cobalt (7): Benzyldiphenylphosphane (679 mg, 2.45 mmol) in 50 mL of THF was combined with [$CoMe(PMe_3)_4$] (930 mg, 2.45 mmol) in 50 mL of THF, at −70 °C. The color of the solution changed from brown to deep-red. After the solution had warmed up, the mixture was stirred at 20 °C for 4 h. The volatiles were then removed in vacuo to give a light-red solid. This was dissolved in 50 mL of diethyl ether and crystallized at 4 °C to give red cubes of **7**, which were suitable for X-ray diffraction. Yield 856 mg (62%); m.p. 75−77 °C (dec.). ^{1}H NMR (300 MHz, [D_8]THF, 296 K): δ = 0.97 [d, ^2J(PH) = 6.3 Hz, 9 H, PCH_3], 1.16 [t′, $|^2J(PH) + {}^4J(PH)|$ = 4.6 Hz, 18 H, PCH_3], 1.80 [d, ^2J(PH) = 8.2 Hz, 2 H, PCH_2], 6.49 (m, 2 H, CH), 6.70 (m, 1 H, CH), 7.19−7.25 (m, 6 H, CH), 7.42 (m, 1 H, CH), 7.56−7.62 (m, 4 H, CH) ppm. ^{13}C NMR (75.4 MHz, [D_8]THF, 296 K): δ = 23.4 [d, ^1J(PC) = 20.8 Hz, PCH_3], 23.9 [dd, ^1J(PC) = 12.6, ^3J(PC) = 6.4 Hz, PCH_3], 50.4 [d, ^1J(PC) = 27.1, ^3J(PC) = 8.7 Hz, PCH_2], 119.9 (s, CH), 121.6 (s, CH), 121.9 (s, CH), 127.5 [d, ^3J(PC) = 8.0 Hz, CH], 127.6 (s, CH), 132.8 [d, ^2J(PC) = 11.6 Hz, CH], 141.6 (m, C), 143.6 (m, C), 144.6 (s, CH), 171.6 (m, CoC) ppm. ^{31}P NMR (81 MHz, [D_8]THF, 233 K): δ = −4 [dd, ^2J(PP) = 104 and 54 Hz, 2 P, PCH_3], 22 [dd, ^2J(PP) = 54 and 51 Hz, 1 P, PCH_3], 63 [dt, ^2J(PP) = 104 and 51 Hz, 1 P, PPh_2] ppm. $C_{28}H_{43}CoP_4$ (562.5): calcd. C 59.79, H 7.71, P 22.03; found C 59.63, H 7.79, P 22.12.

[2-(Diphenylphosphanyl)-3-isopropylphenyl-*C*^{1},*P*](ethene)bis(trimethylphosphane)cobalt (8): A sample of **4** (610 mg, 1.03 mmol) was heated in vacuo at 100 °C for 3 h. It was then dissolved in 70 mL of diethyl ether at 20 °C, and was stirred under 1 bar of ethene for 3 h. The volatiles were removed in vacuo and the solid residue was extracted with two 50-mL portions of pentane. Crystallization at 4 °C afforded orange crystals of **8**, together with the dark crystals of **4**. After mechanical separation the yield was 185 mg (33%); m.p. 105−107 °C (dec.). ^{1}H NMR (300 MHz, [D_8]THF, 296 K): δ = 0.85 [d, ^2J(PH) = 5.8 Hz, 9 H, PCH_3], 0.97 (d, ^3J = 6.9 Hz, 6 H, CCH_3), 1.01 [d, ^2J(PH) = 5.9 Hz, 9 H, PCH_3], 1.51 (m, 1 H, =CH_2), 1.88 (m, 2 H, =CH_2), 2.35 (m, 1 H, =CH_2), 2.46 (sept, ^3J = 6.9 Hz, 1 H, C*H*CH_3), 6.42 (t, ^4J = 2.4 Hz, CH), 6.45 (t, ^4J = 2.2 Hz, CH), 6.72 (dt, ^3J = 7.5, ^4J = 1.8 Hz, 1 H, CH), 7.26−7.28 (m, 3 H, CH), 7.38 −7.41 (m, 3 H, CH), 7.64−7.70 (m, 2 H, CH), 7.94−8.00 (m, 2 H, CH) ppm. ^{13}C NMR (75.4 MHz, [D_8]THF, 296 K): δ = 16.4 [d, ^1J(PC) = 22.7 Hz, PCH_3], 18.9 [d, ^1J(PC) = 18.4 Hz, PCH_3], 20.9 (s, CH*C*H_3), 28.5 [d, ^3J(PC) =

4.5 Hz, *C*HCH$_3$], 31.4 [d, ^2J(PC) = 16.1 Hz, =CH$_2$], 37.1 [d, ^2J(PC) = 15.5 Hz, =CH$_2$], 116.2 [d, ^3J(PC) = 6.1 Hz, CH], 126.6 [d, ^3J(PC) = 8.2 Hz, CH], 127.4 [d, ^2J(PC) = 12.6 Hz, C], 128.9 (s, CH), 131.4 [d, ^2J(PC) = 11.1 Hz, CH], 132. 1 [d, ^2J(PC) = 112.3 Hz, CH], 136.1 [d, ^1J(PC) = 15.9 Hz, C], 138.2 (s, C), 141.7 (s, C) ppm. ^{31}P NMR (81 MHz, [D$_8$]THF, 193 K): δ = −21 [dd, ^2J(PP) = 49 and 56 Hz, 1 P, PPh$_2$], 9 [dd, ^2J(PP) = 49 and 33 Hz, 1 P, PCH$_3$], 17 [dd, ^2J(PP) = 33 and 56 Hz, 1 P, PCH$_3$] ppm. $C_{29}H_{42}CoP_3$ (542.5): calcd. C 64.21, H 7.80, P 17.13; found C 63.85, H 7.90, P 17.15.

[2-(Diphenylphosphanyl)tolyl-*C*,*P*](ethene)bis(trimethylphosphane)cobalt (9): A sample of **6** (820 mg, 1.45 mmol) in 50 mL of diethyl ether was stirred under 1 bar of ethene for 1 h. A light-red solution formed. The volatiles were removed in vacuo and the solid residue was extracted with three 50-mL portions of pentane. Crystallization at 4 °C afforded orange needles of **9**. Yield 584 mg (78%); m.p. 87−89 °C (dec.). ^{1}H NMR (300 MHz, [D$_8$]THF, 296 K): δ = 0.71 [d, ^2J(PH) = 6.1 Hz, 9 H, PCH$_3$], 1.21 [d, ^2J(PH) = 5.4 Hz, 9 H, PCH$_3$], 1.65 (m, 2 H, =CH$_2$), 1.97 (m, 2 H, =CH$_2$), 6.82 (m, 1 H, CH), 6.90 (m, 2 H, CH), 7.14 (t, ^3J = 6.5 Hz, 1 H, CH), 7.32−7.36 (m, 6 H, CH), 7.45 (m, 2 H, CH), 8.02−8.04 (m, 2 H, CH) ppm. ^{13}C NMR (75.4 MHz, [D$_8$]THF, 296 K): δ = 16.9 [d, ^1J(PC) = 18.4 Hz, PCH$_3$], 19.7[d, ^1J(PC) = 16.6 Hz, PCH$_3$], 31.7 (m, CoCH$_2$), 38.7 [d, ^2J(PC) = 16.5 Hz, = CH$_2$], 39.8 [d, ^2J(PC) = 20.5 Hz, =CH$_2$], 121.9 [d, ^4J(PC) = 4.9 Hz, CH], 124.9 [d, ^2J(PC) = 11.0 Hz, CH], 127.3 [d, ^3J(PC) = 8.4 Hz, CH], 127.5 [d, ^3J(PC) = 8.3 Hz, CH], 127.6 [d, ^3J(PC) = 7.2 Hz, CH], 128.2 [d, ^1J(PC) = 22.0 Hz, CH], 133.2 [d, ^2J(PC) = 10.5 Hz, CH], 134. 1 [d, ^2J(PC) = 11.6 Hz, CH], 141.1 [d, ^1J(PC) = 20.9 Hz, C], 162.1 (s, C).) ppm. ^{31}P NMR (81 MHz, [D$_8$]THF, 233 K): δ = 11 [dd, ^2J(PP) = 40 and 25 Hz, 1 P, PCH$_3$], 18 [dd, ^2J(PP) = 25 and 38 Hz, 1 P, PCH$_3$], 66 [dd, ^2J(PP) = 40 and 38 Hz, 1 P, PPh$_2$] ppm. $C_{27}H_{38}CoP_3$ (514.5): calcd. C 63.04, H 7.45, P 18.06; found C 63.12, H 7.07, P 18.72.

(Carbonyl)[2-(diphenylphosphanyl)tolyl-*C*,*P*]bis(trimethylphosphane)cobalt (10): A sample of **6** (590 mg, 1.05 mmol) in 30 mL of THF was stirred under 1 bar of CO for 30 min. A light-red solution formed. The volatiles were removed in vacuo and the solid residue was extracted with 50 mL of pentane. Crystallization at 4 °C afforded red crystals of **10**, which were suitable for X-ray diffraction. Yield 410 mg (76%); m.p. 132−135 °C (dec.). IR (Nujol): $\tilde{\nu}$ = 1894 cm^{-1} (C≡O$_{ax}$), 1850 cm^{-1} (C≡O$_{eq}$). ^{1}H NMR (300 MHz, [D$_8$]THF, 296 K): C≡O$_{ax}$ isomer (88%): δ = 1.00 [t′, $|^2J$(PH) + ^4J(PH)| = 6.2 Hz, 18 H, PCH$_3$], 2.09 (m, 2 H, CoCH$_2$), 6.84 (t, ^3J = 7.3 Hz, 1 H, CH), 7.02 (m, 2 H, CH), 7.18 (d, ^3J = 6.9 Hz, 1 H, CH), 7.26−7.31 (m, 6 H, CH), 7.43−7.47 (m, 4 H, CH); C≡O$_{eq}$ isomer (12%): δ = 0.86 [d, ^2J(PH) = 7.3 Hz, 18 H, PCH$_3$], 1.29 [d, ^2J(PH) = 7.5 Hz, 18 H, PCH$_3$], 2.35 (m, 2 H, CoCH$_2$), 6.95−7.62 (m, 14 H, CH) ppm. ^{13}C NMR (75.4 MHz, [D$_8$]THF, 296 K): C≡O$_{ax}$ isomer (88%): δ = 20.1 (s, PCH$_3$), 24.0 (m, CoCH$_2$), 124.1 [d, ^3J(PC) = 4.6 Hz, CH], 127.4 (s, CH), 127.4 [d, ^1J(PC) = 16.4 Hz, CH], 128.5 [d, ^2J(PC) = 8.3 Hz, CH], 128.8 (s, CH), 129.9 (s, CH), 133.1 [d, ^2J(PC) = 12.3 Hz, CH], 140.1 (s, C) ppm. ^{31}P NMR (81 MHz, [D$_8$]THF, 233 K): CO$_{ax}$ isomer (88%): δ = 6 [d, ^2J(PP) = 98 Hz, 2 P, PCH$_3$], 73 [t, ^2J(PP) = 98 Hz, 1 P, PPh$_2$]; CO$_{eq}$ isomer (12%): δ = −1 [dd, ^2J(PP) = 82 and 38 Hz, 1 P, PCH$_3$], 25 [dd, ^2J(PP) = 38 and 51 Hz, 1 P, PCH$_3$], 67 [dd, ^2J(PP) = 82 and 51 Hz, PPh$_2$] ppm. $C_{26}H_{34}CoOP_3$ (514.4): calcd. C 60.71, H 6.66, P 18.06; found C 60.94, H 7.45, P 17.62.

(Carbonyl)[2-(diphenylphosphanyl)-3-ethylbenzoyl-*C*,*P*]bis(trimethylphosphane)cobalt (11): A sample of **3** (580 mg, 1.01 mmol) in 50 mL of THF was stirred under 1 bar of CO for 30 min. A light-red solution formed. The volatiles were removed in vacuo and the solid residue was extracted with two 50-mL portions of pentane. Crystallization at 4 °C afforded dark red plates of **11**. Yield 475 mg (85%); m.p. 152−153 °C. IR (Nujol): $\tilde{\nu}$ = 1913 cm^{-1} (C≡O). ^{1}H NMR (300 MHz, [D$_8$]THF, 296 K): δ = 0.52 (t, ^3J = 7.5 Hz, 3 H, CH$_3$), 1.09 [t′, $|^2J$(PH) + ^4J(PH)| = 7.2 Hz, 18 H, PCH$_3$], 2.43 (q, ^3J = 7.5 Hz, 2 H, CH$_2$), 7.26−7.40 (m, 9 H, CH), 7.54−7.61 (m, 4 H, CH) ppm. ^{13}C NMR (75.4 MHz, [D$_8$]THF, 296 K): δ = 17.2 (s, PCH$_3$), 18.2 (m, PCH$_3$), 19.9 (s, CH$_3$), 26.7 (s, CH$_2$), 47.5 (s, CH), 55.9 (s, CH$_2$), 117.6 [d, ^1J(PC) = 21.2 Hz, CH], 126.9 (s, CH), 128.6 [d, ^2J(PC) = 9.0 Hz, CH], 129.3 [d, ^3J(PC) = 3.1 Hz, CH], 128.8 (s, CH), 130.1 [d, ^1J(PC) = 15.1 Hz, CH], 130.4 (s, CH), 137.8 (s, C), 138.2 (s, C), 145.5 (s, C), 157.7 (s, C) ppm. ^{31}P NMR (81 MHz, [D$_8$]THF, 193 K): δ = 9 [d, ^2J(PP) = 81 Hz, 2 P, PCH$_3$], 84 [t, ^2J(PP) = 81 Hz, 1 P, PPh$_2$] ppm. $C_{28}H_{36}CoO_2P_3$ (556.4): calcd. C 60.44, H 6.52, P 16.70; found C 60.40, H 6.72, P 16.53.

(Carbonyl)[2-(diphenylphosphanyl)-3-isopropylbenzoyl-*C*,*P*]bis(trimethylphosphane)cobalt (12): A sample of **4** (750 mg, 1.27 mmol) in 50 mL of THF was stirred under 1 bar of CO for 3 h. A light-red solution formed. The volatiles were removed in vacuo and the solid residue was extracted with two 50-mL portions of pentane. Crystallization at 4 °C afforded dark-red crystals of **12**. Yield 572 mg (79%); m.p. 161−162 °C. IR (Nujol): $\tilde{\nu}$ = 1906 cm^{-1} (C≡O). ^{1}H NMR (300 MHz, [D$_8$]THF, 296 K): δ = 0.65 [d, ^3J = 6.7 Hz, 6 H, C(CH$_3$)$_2$], 1.05 [t′, $|^2J$(PH) + ^4J(PH)| = 7.3 Hz, 18 H, PCH$_3$], 3.04 (sept, ^3J = 6.7 Hz, 1 H, CH), 7.30−7.39 (m, 9 H, CH), 7.58−7.65 (m, 4 H, CH) ppm. ^{13}C NMR (75.4 MHz, [D$_8$]THF, 296 K): δ = 21.7 (s, CH$_3$), 18.2 [dt, ^1J(PC) = 12.6, ^3J(PC) = 4.2 Hz, PCH$_3$], 30.9 (s, CH), 117.6 (s, CH), 117.9 (s, CH), 126.9 [d, ^2J(PC) = 8.9 Hz, CH], 127.2 (s, CH), 130.2 (s, CH), 130.5 [d, ^3J(PC) = 12.2 Hz, CH], 137.6 (s, C), 137.9 (s, C), 138.3 (m, C), 150.3 (s, C) ppm. ^{31}P NMR (81 MHz, [D$_8$]THF, 233 K): δ = 8 [d, ^2J(PP) = 79 Hz, 2 P, PCH$_3$], 85 [t, ^2J(PP) = 79 Hz, 1 P, PPh$_2$] ppm. $C_{29}H_{38}CoO_2P_3$ (570.5): calcd. C 61.06, H 6.71, P 16.29; found C 61.05, H 6.86, P 16.21.

***mer-cis*-[2-(Diphenylphosphanyl)tolyl-*C*,*P*](iodo)(methyl)bis(trimethylphosphane)cobalt (13):** A sample of **6** (810 mg, 1.44 mmol) in 50 mL of diethyl ether at −70 °C was combined with a slight excess of iodomethane (552 mg, 3.89 mmol). The mixture was allowed to warm to 20 °C, after which it turned brown and deposited an off-white solid of tetramethylphosphonium iodide (IR). After 4 h, the solid was removed by filtering. Crystallization at 4 °C afforded orange crystals of **13**·0.5OEt$_2$, which were suitable for X-ray diffraction. Yield 440 mg (46%); m.p. 82−84 °C (dec.). ^{1}H NMR (300 MHz, [D$_8$]THF, 296 K): δ = 0.53 (m, 3 H, CoCH$_3$), 0.95 [s (br), 18 H, PCH$_3$], 1.12 (m, 2 H, CoCH$_2$), 6.56 (m, 1 H, CH), 7.05 (m, 2 H, CH), 7.31−7.74 (m, 11 H, CH) ppm. ^{31}P NMR (81 MHz, [D$_8$]THF, 213 K): δ = −11 (m, 1 P, PCH$_3$), −1 (m, 1 P, PCH$_3$), 10 (m, 1 P, PPh$_2$) ppm. $C_{28}H_{42}CoIO_{0.5}P_3$ (665.4): calcd. C 50.54, H 6.36, P 13.96; found C 50.40, H 6.64, P 14.21.

[2-(Diphenylphosphanyl)tolyl-*C*,*P*](iodo)bis(trimethylphosphane)cobalt (14): A sample of **6** (760 mg, 1.35 mmol) in 60 mL of THF was combined with iodomethane (192 mg, 1.35 mmol). After 4 h, a slight precipitate of tetramethylphosphonium iodide formed, which was filtered off. The filtrate was concentrated to dryness. Extraction with three 80-mL portions of diethyl ether and cooling to 4 °C afforded black crystals of **14**. Yield 780 mg (94%); m.p. 157−159 °C (dec.). Magnetic moment: μ_{eff} = 1.93 μ_B. $C_{25}H_{34}CoIP_3$ (613.3): calcd. C 48.96, H 5.59, P 15.15; found C 48.62, H 5.88, P 15.25.

***mer-trans*-[2-(Diphenylphosphanyl)-3-ethylphenyl-*C*^{1},*P*](iodo)(methyl)bis(trimethylphosphane)cobalt (15):** A sample of **3** (870 mg,

Table 1. Crystal data for compounds **3**, **6**, **7**, and **13**

	3	**6**	**7**	**13**
Empirical formula	$C_{29}H_{45}CoP_4$	$C_{28}H_{43}CoP_4$	$C_{28}H_{43}CoP_4$	$C_{26}H_{37}CoIOP_3$ 0.5 Et_2O
Formula mass	576.5	562.4	562.4	665.4
Crystal size [mm]	0.38 × 0.25 × 0.16	0.38 × 0.25 × 0.12	0.50 × 0.40 × 0.22	0.44 × 0.20 × 0.19
Crystal system	orthorhombic	orthorhombic	monoclinic	triclinic
Space group	*Pbca*	*Pbca*	$P2_1/n$	$P\bar{1}$
a [Å]	9.060(1)	9.8127(16)	15.231(2)	10.492(2)
b [Å]	18.069(2)	18.7719(19)	24.516(4)	14.450(2)
c [Å]	38.641(6)	32.408(7)	16.201(3)	20.882(3)
α [°]	90	90	90	87.92(1)
β [°]	90	90	101.38(1)	75.56(1)
γ [°]	90	90	90	87.99(1)
V [Å^3]	6325.7(14)	5969.6(17)	5930.6(17)	3062.8(8)
Z	8	8	8	4
$D_{calcd.}$ [g/cm^3]	1.211	1.252	1.260	1.443
μ(Mo-K_α) [mm^{-1}]	0.760	0.804	0.809	1.741
Temperature [K]	293(2)	293(2)	293(2)	293(2)
Data coll. range [°]	4.2 ≤ 2Θ ≤ 54	4.5 ≤ 2Θ ≤ 55	5.1 ≤ 2Θ ≤ 54	4.8 ≤ 2Θ ≤ 55
h	$-1 \le h \le 11$	$0 \le h \le 12$	$-1 \le h \le 19$	$-1 \le h \le 13$
k	$-23 \le k \le 1$	$-1 \le k \le 24$	$-31 \le k \le 1$	$-18 \le k \le 18$
l	$-1 \le l \le 49$	$-42 \le l \le 1$	$-20 \le l \le 20$	$-26 \le l \le 27$
No. reflect. measured	8431	7506	15074	16375
No. unique data	6891 [R_{int} = 0.0587]	6859 [R_{int} = 0.0667]	12931 [R_{int} = 0.0441]	14074[R_{int} = 0.030]
Parameters	318	307	569	605
GoF on F^2	1.017	0.937	1.003	0.978
*R*1 [$I \ge 2\sigma(I)$]	0.0573	0.0586	0.0555	0.0459
*wR*2 (all data)	0.1754	0.1735	0.1307	0.1182

1.51 mmol) in 50 mL of diethyl ether at −70 °C was combined with iodomethane (514 mg, 3.62 mmol). The mixture was allowed to warm to 20 °C, after which it turned red and deposited solid tetramethylphosphonium iodide. After 3 h, the solid was removed by filtering. From the filtrate, dark-red crystals of **15** were obtained at −27 °C. Yield 504 mg (52%); m.p. 115−116 °C. ^{1}H NMR (300 MHz, [D$_8$]THF, 296 K): δ = 0.52 (t, ^3J = 7.5 Hz, 3 H, CH_3), 0.54 (m, 3 H, $CoCH_3$), 1.03 [s (br), 18 H, PCH_3], 2.43 (q, ^3J = 7.5 Hz, 2 H, CH_2), 5.81−7.77 (m, 13 H, CH) ppm. ^{31}P NMR (81 MHz, [D$_8$]THF, 213 K): δ = −32 [t, ^2J(PP) = 23 Hz, 1 P, PPh_2], 10 [d, ^2J(PP) = 23 Hz, 2 P, PCH_3] ppm. $C_{27}H_{39}CoIP_3$ (642.4): calcd. C 50.48, H 6.12, P 14.47; found C 50.24, H 5.72, P 14.54.

Crystal Structure Analyses: Crystal data are presented in Table 1. Data collection: **3**: A crystal was sealed under argon in a glass capillary and mounted on a Bruker AXS P4 diffractometer. Intensities were collected (ω-scans) using graphite-monochromated Mo-K_α radiation; Lp correction and absorption correction based on ψ-scans were applied. The structure was solved by direct and conventional Fourier methods. All non-hydrogen atoms were treated anisotropically, hydrogen atoms were treated with a riding model in idealized positions. **6**: Crystal mounting, data collection, structure solution, and refinement as for **3**. **7**: Crystal mounting, data collection, structure solution, and refinement as for **3**. Two independent molecules per asymmetric unit. **13**·0.5OEt_2: Crystal mounting, data collection, structure solution, and refinement as for **3**. Two independent molecules per asymmetric unit. CCDC-184438 (**3**), -184439 (**6**), -184440 (**7**), and -184441 (**13**) contain the supplementary crystallographic data for this paper. These data can be obtained free of charge at www.ccdc.cam.ac.uk/conts/retrieving.html [or from the Cambridge Crystallographic Data Centre, 12 Union Road, Cambridge CB2 1EZ, UK; Fax: (internat.) + 44-1223/336-033; E-mail: deposit@ccdc.cam.ac.uk].

Acknowledgments

Financial support for this work by Fonds der Chemischen Industrie is gratefully acknowledged.

[1] [1a] R. W. Hilts, R. A. Franchuk, M. Cowie, *Organometallics* **1991**, *10*, 1297−1304. [1b] C. Tejel, M. A. Ciriano, L. A. Oro, M. Bordonaba, C. Graiff, A. Tiripicchio, A. Burini, *Organometallics* **2000**, *19*, 3115−3119.
[2] [2a] R. F. Jordan, A. S. Guram, *Organometallics* **1990**, *9*, 2116−2123. [2b] G. G. Hlatky, H. W. Turner, R. R. Eckman, *J. Am. Chem. Soc.* **1989**, *11*, 2728−2729.
[3] H.-F. Klein, S. Schneider, M. He, U. Flörke, H.-J. Haupt, *Eur. J. Inorg. Chem.* **2000**, 2295−2301.
[4] H.-F. Klein, R. Beck, U. Flörke, H.-J. Haupt, *Eur. J. Inorg. Chem.* **2003**, 240−248.
[5] P. W. N. M. van Leeuwen, P. C. J. Kamer, J. N. H. Reek, P. Dierkes, *Chem. Rev.* **2000**, *100*, 2741−2769.
[6] [6a] M. A. Bennett, S. K. Bhargava, M. Ke, A. C. Willis, *J. Chem. Soc., Dalton Trans.* **2000**, 3537−3545. [6b] K. von Deuten, L. Dahlenburg, *Cryst. Struct. Commun.* **1980**, *9*, 421. [6c] G. del Piero, G. Perego, A. Zazzetta, M. Cesari, *Cryst. Struct. Commun.* **1974**, *3*, 7235.
[7] [7a] A. J. Cheney, B. L Shaw, *J. Chem. Soc., Dalton Trans.* **1972**, 754−763. [7b] A. J. Cheney, B. L Shaw, *J. Chem. Soc., Dalton Trans.* **1972**, 860−865.
[8] A. G. Orpen, L. Brammer, F. H. Allen, O. Kennard, D. G. Watson, R. Taylor, *J. Chem. Soc., Dalton Trans.* **1989**, S1−S83.
[9] [9a] H.-F. Klein, E. Auer, T. Jung, C. Röhr, *Organometallics* **1995**, *14*, 2725−2732. [9b] I. Ya. Levitin, M. V. Tsikalova, V. I. Bakhmutov, A. I. Yanovsky, Yu. T. Stuchkov, M. E. Vol'pin, *J. Organomet. Chem.* **1987**, *330*, 161−178. [9c] P. L. Choo, A. M. Mulichak, R. W. Jones, J. W. Bacon, V. B. Pett, D. Zacharias, *Inorg. Chim. Acta* **1990**, *171*, 183−192.

[10] H.-F. Klein, U. Lemke, M. Lemke, A. Brand, *Organometallics* **1998**, *17*, 4196−4201.
[11] H.-F. Klein, H. H. Karsch, *Chem. Ber.* **1975**, *108*, 944−954.
[12] H.-F. Klein, H. H. Karsch, *Chem. Ber.* **1976**, *109*, 1453−1464.
[13] V. Galamb, G. Palyi, R. Boese, R. Schmid, *Organometallics* **1987**, *6*, 861−867.
[14] H.-F. Klein, X. Li, U. Flörke, H.-J. Haupt, *Z. Naturforsch., Teil B* **2000**, *55*, 707−717.
[15] M. Bressan, P. Rigo, *Inorg. Chem.* **1975**, *14*, 38−42.
[16] L. Horner, G. Simons, *Phosphorus Sulfur* **1983**, *15*, 165−176.
[17] T. B. Rauchfuss, F. T. Patino, D. M. Roundhill, *Inorg. Chem.* **1975**, *14*, 652−656.
[18] G. P. Schiemenz, A. Kaack, *Liebigs Ann. Chem. Soc.* **1973**, 1480−1493.
[19] M. Hingst, M. Tepper, O. Stelzer, *Eur. J. Inorg. Chem.* **1998**, 73−82.
[20] S. O. Grim, A. W. Yankowsky, *Phosphorus Sulfur* **1977**, *3*, 191−195.
[21] V. D. Bianco, S. Doronzo, *Inorg. Synth.* **1976**, *16*, 155−161.

Received July 15, 2002
[I02386]

Single-Atom *O*-Bridged Urea in a Dinickel(II) Complex together with Ni_4^{II}, Cu_2^{II} and Cu_4^{II} Complexes of a Pentadentate Phenol-Containing Schiff Base with (O,N,O,N,O)-Donor Atoms

Soumen Mukherjee,[a] Thomas Weyhermüller,[a] Eberhard Bothe,[a] Karl Wieghardt,[a] and Phalguni Chaudhuri*[a]

Keywords: N,O ligands / Nickel / Copper / Magnetic properties / Radicals / Electrochemistry

A pentadentate phenol-containing ligand (H_3L) with N_2O_3 donor atoms yields Ni_2^{II} (**1**), Ni_4^{II} (**2**), Cu_2^{II} (**3**) and Cu_4^{II} (**4**) complexes, which have been structurally characterized by X-ray diffraction. Complex **1** contains a single-atom *O*-bridged urea. The compounds were characterized by IR, UV/Vis, mass spectrometry, electrochemistry and variable-temperature (2–295 K) magnetic susceptibility measurements. Analysis of the susceptibility data shows antiferromagnetic interactions between the metal centers indicating a diamagnetic ground state for complexes **1**, **3** and **4**, whereas complex **2**, a tetranuclear Ni^{II} cubane, has a complicated low-lying magnetic structure with a non-diamagnetic ground state. A plot of *J* vs. Ni–O–Ni angles for all structurally characterized Ni_4O_4 cubane cores, including **2**, irrespective of their symmetry exhibits a large variation of *J* values within a small range of Ni–O–Ni angles. The electrochemistry of all complexes was investigated in detail and the ligand-centered oxidation to a radical-ligand is inferred from the occurrence of oxidation processes at potentials which are similar.

(© Wiley-VCH Verlag GmbH & Co. KGaA, 69451 Weinheim, Germany, 2003)

Introduction

Polynuclear metal complexes are of current interest to chemists owing to their relevance to metallobiochemistry,[1] materials science[2] and theoretical chemistry.[3] Particular interest has been directed towards the exchange phenomena in di- and polynuclear complexes of nickel(II) and copper(II), in which studies, particularly of the latter, have led to essential insights into magnetostructural correlations.

Since the first report by Robson[4] in 1970 of a dinucleating Schiff-base ligand obtained by condensation of 2,6-diformyl-4-methylphenol with 2-aminophenol, many examples of similar compartmental ligands have been reported.[5] The dinucleating ability of these ligands stems from the readiness of the phenol to deprotonate and bridge two metal ions. Recently, we have reported trinuclear and tetranuclear complexes with the ligands derived from the condensation of 2,6-diformyl-4-methylphenol and selected diamines or hydroxylamines, which yield heteronuclear complexes of the type $M_AM_BM_C$ [6] and $M_AM_BM_BM_A$.[7]

In another field of coordination chemistry, interest in phenol-containing ligands was sparked and fueled by the discovery that tyrosyl radicals, derived from oxidation of the amino acid tyrosine, play an important role in a rapidly growing number of oxygen-dependent enzymatic radical catalysis reactions.[8] Since then chemists have attempted to model tyrosine by phenolate ligands.[9,10]

It has already been reported[10] that *tert*-butyl substituents at the *ortho* and *para* positions of the phenolates facilitate one-electron oxidation to the corresponding phenoxyl radicals, because these substituents decrease the oxidation potential of the phenolates and provide enough steric bulk to suppress bimolecular decay reactions of the generated phenoxyl radicals. Accordingly, we report here the synthesis and characterization of dinuclear and tetranuclear complexes of Ni^{II} and Cu^{II} ions with the Schiff-base ligand H_3LtBu derived from the (1+2) condensation of 2,6-diformyl-4-methylphenol and 6-amino-2,4-di-*tert*-butylphenol. A few square-planar dinickel(II) and dicopper(II) complexes have already been described by Robson,[4] but no structural data are available for these complexes, except one with the composition $[LCo^{II}Co^{III}(OH)(CH_3COO)]_2$.[11]

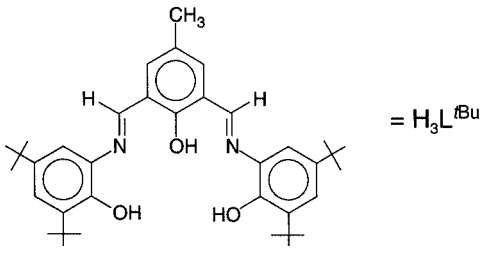

Scheme 1 shows the complexes of the ligand H_3LtBu prepared, along with their labels. Compounds **5**–**8** will not be described in this paper but in a subsequent one, and are

[a] Max-Planck-Institut für Strahlenchemie, Stiftstrasse 34–36, 45470 Mülheim an der Ruhr, Germany
E-mail: Chaudh@mpi-muelheim.mpg.de

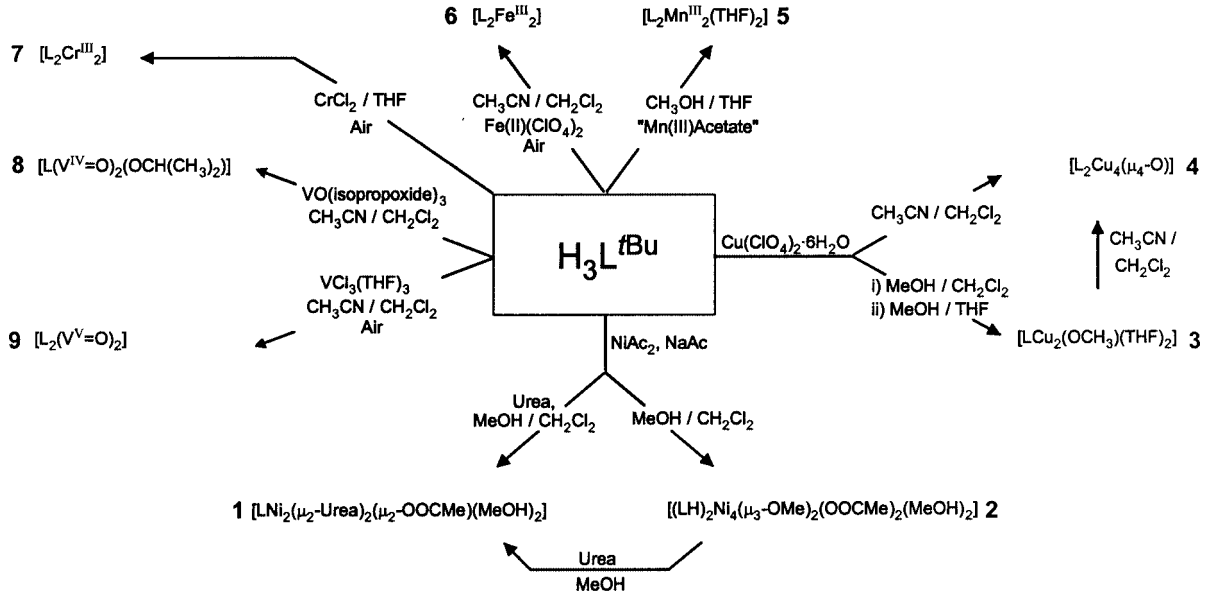

Scheme 1

mentioned here only to exemplify the diversified ligating properties of H_3LtBu. For the sake of simplicity the ligand will be denoted as H_3L without the suffix *t*Bu. We report here a dinuclear nickel(II) complex **1** with a bridging urea through a single-atom *O*-bridging of the carbonyl oxygen, as a model for a binding mode of the substrate urea in the nickel-dependent hydrolase enzyme urease (E.C. 3.5.1.5),[12−13] which is present in bacteria, fungi and higher plants, and catalyzes the hydrolysis of urea to ammonia and carbon dioxide.

$$H_2N\text{-}\underset{\underset{O}{\|}}{C}\text{-}NH_2 \xrightarrow[H_2O]{\text{urease}} 2\,NH_3 + CO_2$$

Several dinuclear nickel(II) complexes with urea[14] have been reported as models for possible binding modes of urea in urease. But none of the complexes reported so far, except one,[15] contain a carbonyl single-atom bridging urea.

Results and Discussion

When nickel acetate and H_3L are allowed to react in the presence of sodium acetate with a slight excess of urea in methanol, complex **1** is obtained. In the absence of urea, the tetranuclear complex **2** is obtained. Complex **2** can also be transformed into **1** by adding urea to the red solution of **2** in methanol (Scheme 1). Formation of **1** from **2** implies that the driving force for formation of **1** lies in the strong tendency of urea to bind to the dinickel center embedded in the dinucleating ligand L^{3-}. The solid-state FTIR spectrum of complex **1** exhibits a shift in the carbonyl stretching frequency of urea from 1690 to 1670 cm^{-1} upon coordination to the dinickel center. Mass spectrometry in the EI mode indicates unambiguously the presence of urea and an acetate ion in **1**. In the ESI positive mass spectrum of **1** a peak with an abundance of 100% is observed centered around m/z = 743, corresponding to $[LNi_2(OOCCH_3)]^+$, with the expected isotope pattern. The EI mass spectrum does not provide much useful information regarding the tetranuclear nature of **2**. It exhibits signals around m/z = 714−720 (100%) with the expected isotope pattern for a dinickel compound, clearly indicating the presence of $[LNi_2(OCH_3)]^+$ in the gas phase.

The electronic spectra of **1** and **2** show intense π-π* transitions below 480 nm, attributable to the ligand, as judged by their high absorption coefficients and comparison with the spectrum of the ligand Additionally, there are three broad, weak transitions in the visible-near IR region at 779, 858 and 1284 nm for **1**, indicating that the nickel ions are in an octahedral environment in solution as well as in the solid state (X-ray structure). Interestingly only one broad absorption is observed in the range 800−1300 nm for **2**.

The reaction of copper perchlorate and the Schiff-base ligand afforded either **3** or **4**, depending on the solvent system, in relatively high yield. In the absence of protic solvents, complex **3**, a methoxy-bridged dicopper(II) species, is transformed easily into **4** — a μ_4-oxo-tetracopper(II) complex — in the presence of the solvent mixture CH_3CN/CH_2Cl_2 (Scheme 1) indicating the stability of **4**. Adventitious water in the solvent serves as a source of the μ_4-oxo ligand. Selected IR data for complexes **3** and **4** are given in the Exp. Sect. The sharp peaks in the solid state FTIR spectrum due to ν(OH) of the ligand LH_3 occur at $\tilde{\nu}$ = 3523, 3492 and 3348 cm^{-1}. These bands are missing in **3** and **4**, indicating that the phenol character of the ligand has been lost upon complexation. For **4** a sharp band of medium intensity at 510 cm^{-1} is associated with the $\nu_{Cu\text{-}O}$ vibration in the Cu_4O core. Support for this assignment is obtained by comparison with the vibrational spectrum of **3**, which exhibits, similar to that for **4**, two sharp bands of medium intensity at 564 and 539 cm^{-1} attributable to ν(Cu−O) vibrations for bonds to the phenolate groups. These three bands are missing in the spectrum of the free ligand. In the

EI mass spectrum of **3** a molecular peak at $m/z = 724$, with an abundance of 100%, corresponding to the $LCu_2(OCH_3)$ species is observed. Additionally, a clear indication of the presence of THF in **3** is found at $m/z = 72$. Mass spectrometry in the EI mode has been proved to be very useful for **4**, for which the molecular peak at $m/z = 1404$, with the expected isotope pattern, confirms the presence of $[L_2Cu_4(O)]$. The electronic spectra of **3** and **4** in CH_2Cl_2 display four intense bands in the 600−200 nm region attributed to the Schiff-base ligand.

Single Crystal X-ray Diffraction Studies

Molecular Structure of 1

The structure of **1** (Figure 1, Table 1) shows the formation of a dinickel(II) complex with a bridging urea through

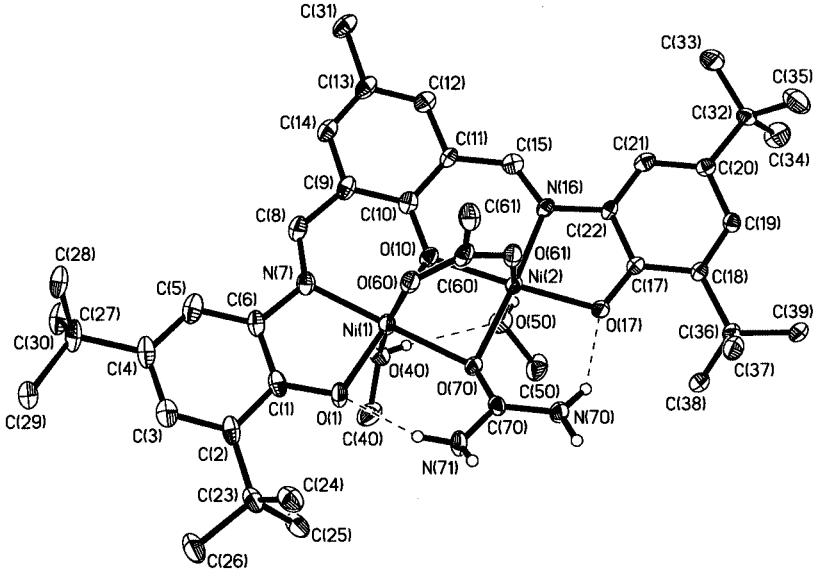

Figure 1. An ORTEP drawing of the neutral molecule **1**, $[LNi^{II}_2(NH_2CONH_2)(OOCCH_3)(CH_3OH)_2]\cdot 4.5CH_3OH$

Table 1. Crystallographic data for $[LNi^{II}_2(NH_2CONH)_2(O_2CMe)(MeOH)_2]\cdot 4.5MeOH$ (**1**), $[(LH)_2Ni^{II}_4(OMe)_2(O_2CMe)_2(MeOH)_2]\cdot 3CH_2Cl_2$ (**2**) and $[L_2Cu^{II}_4(\mu_4\text{-}O)\cdot 3.3CH_2Cl_2\cdot 0.7CH_3CN$ (**4**)

	Ni^{II}_2 (urea) **1**	Ni^{II}_4 **2**	$Cu^{II}_4(\mu_4\text{-}O)$ **4**
Empirical formula	$C_{42}H_{62}N_4Ni_2O_8\cdot 4.5CH_3OH$	$C_{82}H_{116}N_4Ni_4O_{14}\cdot 3CH_2Cl_2$	$C_{74}H_{94}Cu_4N_4O_7\cdot 3.3CH_2Cl_2\cdot 0.7CH_3CN$
Molecular weight	1012.57	1871.41	1715.56
Temperature	100(2) K	100(2) K	100(2) K
Wavelength (Mo-K_α)	0.71073 Å	0.71073 Å	0.71073 Å
Crystal System	Triclinic	Triclinic	Triclinic
Space group	$P\bar{1}$	$P\bar{1}$	$P\bar{1}$
Unit cell dimensions	$a = 12.099(2)$ Å	$a = 19.9102(12)$ Å	$a = 16.4678(9)$ Å
	$b = 12.128(2)$ Å	$b = 21.545(2)$ Å	$b = 17.2675(12)$ Å
	$c = 18.800(3)$ Å	$c = 22.076(2)$ Å	$c = 17.3208(12)$ Å
	$\alpha = 95.90(2)°$	$\alpha = 80.45(2)°$	$\alpha = 106.03(1)°$
	$\beta = 104.16(2)°$	$\beta = 80.88(2)°$	$\beta = 112.14(1)°$
	$\gamma = 91.48(2)°$	$\gamma = 83.43(2)°$	$\gamma = 102.71(1)°$
Volume (Å^3); Z	2656.9(8); 2	9182.7(13); 4	4083.9(5); 2
Density (calc.) Mg/m^3	1.266	1.354	1.395
Absorp. coeff. (mm^{-1})	0.769	1.043	1.298
$F(000)$	1086	3944	1785
Crystal size (mm)	0.20 × 0.19 × 0.10	0.18 × 0.10 × 0.09	0.33 × 0.24 × 0.15
θ range for data collect.	1.69 to 23.27°	3.13 to 22.50°	2.87 to 30.0°
Reflections collected	18237	57320	49175
Independent reflect.	7534 [R(int.) = 0.1014]	23751 [R(int.) = 0.0845]	23491 [R(int.) = 0.0452]
Absorpt. correction	Gaussian, face indexed	Gaussian, face indexed	not measured
Data/restraints/param.	7524/25/672	23751/112/2033	23356/166/964
Goodness-of-fit on F^2	0.877	1.051	1.019
Final R indices [$I > 2\sigma(I)$]	$R_1 = 0.0508$	$R_1 = 0.0837$	$R_1 = 0.0569$
	$wR_2 = 0.0971$	$wR_2 = 0.1851$	$wR_2 = 0.1434$
R indices (all data)	$R_1 = 0.1113$	$R_1 = 0.1412$	$R_1 = 0.0803$
	$wR_2 = 0.1134$	$wR_2 = 0.2173$	$wR_2 = 0.1602$

the carbonyl oxygen. Ni(1) and Ni(2) are additionally bridged by a phenolate oxygen [O(10)] and an acetate ion. Each nickel is in a distorted octahedral NO_5 environment, and is equatorially bound to the NO_3 donor set [Ni−N: av. 1.975 Å; Ni−O: av. 2.01 Å], with axial interactions to a carboxylic *O*-donor of a bridging $MeCO_2^-$ group [Ni−O: av. 2.09 Å] and a methanol *O*-donor [Ni−O: 2.165, 2.159 Å] trans to the $MeCO_2^-$ group. The hydrogen atoms of the hydroxy group in MeOH and the urea molecules were located from a difference map and are shown as circles of arbitrary radii in Figure 1. The hydrogen atoms on the NH_2 groups of urea enter into hydrogen bonding with the phenolate oxygens O(1) and O(17), with O(1)···N(71) and O(17)···N(70) distances of 2.784 and 2.813 Å, respectively, thus making urea presumably not susceptible to alcoholysis (see later). The intramolecular hydrogen bonds between the methanol molecules *cis*-ligated to two different nickel(II) ions [O(40)···O(50) 2.928 Å] are shown as dotted lines. The Ni(1)···Ni(2) distance of 2.966(1) Å in **2** is significantly shorter than those observed in comparable complexes.[14−15] The bridging Ni−O(urea) distances [2.080(3) and 2.065(3) Å] are significantly shorter than those in the only other single-atom *O*-bridged urea compound [Ni−O(urea): 2.158(3) Å].[15] The Ni−O(urea) bond lengths for compounds containing non-bridging urea lie within the range 2.05−2.13 Å.[14] The Ni(1)−O(70)−Ni(2) angle at the bridging urea is 91.4(1)°, whereas the phenoxide bridging angle Ni(1)−O(10)−Ni(2) is significantly greater [97.1(2)°].

Table 2. Selected bond lengths (Å) and angles (deg) for $[LNi^{II}_2(NH_2CONH_2)(OOCCH_3)(CH_3OH)_2]\cdot 4.5CH_3OH$ (**1**)

Ni(1)−O(1)	1.954(3)	O(1)−Ni(1)−N(7)	84.7(2)
Ni(1)−N(7)	1.971(4)	O(1)−Ni(1)−O(10)	175.4(2)
Ni(1)−O(10)	1.971(3)	N(7)−Ni(1)−O(10)	93.2(2)
Ni(1)−O(70)	2.080(3)	O(1)−Ni(1)−O(70)	97.52(13)
Ni(1)−O(60)	2.089(4)	N(7)−Ni(1)−O(70)	176.4(2)
Ni(1)−O(40)	2.165(4)	O(10)−Ni(1)−O(70)	84.38(13)
Ni(1)−Ni(2)	2.9656(11)	O(1)−Ni(1)−O(60)	95.39(14)
Ni(2)−O(17)	1.967(3)	N(7)−Ni(1)−O(60)	93.0(2)
Ni(2)−N(16)	1.978(4)	O(10)−Ni(1)−O(60)	88.84(14)
Ni(2)−O(10)	1.986(3)	O(70)−Ni(1)−O(60)	89.59(14)
Ni(2)−O(70)	2.065(3)	O(1)−Ni(1)−O(40)	94.6(2)
Ni(2)−O(61)	2.088(4)	N(7)−Ni(1)−O(40)	92.0(2)
Ni(2)−O(50)	2.159(4)	O(10)−Ni(1)−O(40)	81.33(14)
		O(70)−Ni(1)−O(40)	85.09(14)
		O(60)−Ni(1)−O(40)	169.22(13)
O(17)−Ni(2)−N(16)	84.6(2)	O(70)−C(70)	1.285(6)
O(17)−Ni(2)−O(10)	174.54(14)	N(70)−C(70)	1.323(7)
N(16)−Ni(2)−O(10)	91.6(2)	N(71)−C(70)	1.312(6)
O(17)−Ni(2)−O(70)	99.33(13)	Ni(1)···Ni(2)	2.966(1)
N(16)−Ni(2)−O(70)	175.7(2)		
O(10)−Ni(2)−O(70)	84.39(13)		
O(17)−Ni(2)−O(61)	94.20(14)		
N(16)−Ni(2)−O(61)	94.2(2)		
O(10)−Ni(2)−O(61)	89.96(13)		
O(70)−Ni(2)−O(61)	87.25(14)		
O(17)−Ni(2)−O(50)	92.8(2)		
N(16)−Ni(2)−O(50)	95.1(2)		
O(10)−Ni(2)−O(50)	83.7(2)		
O(70)−Ni(2)−O(50)	83.08(14)		
O(61)−Ni(2)−O(50)	168.89(13)		

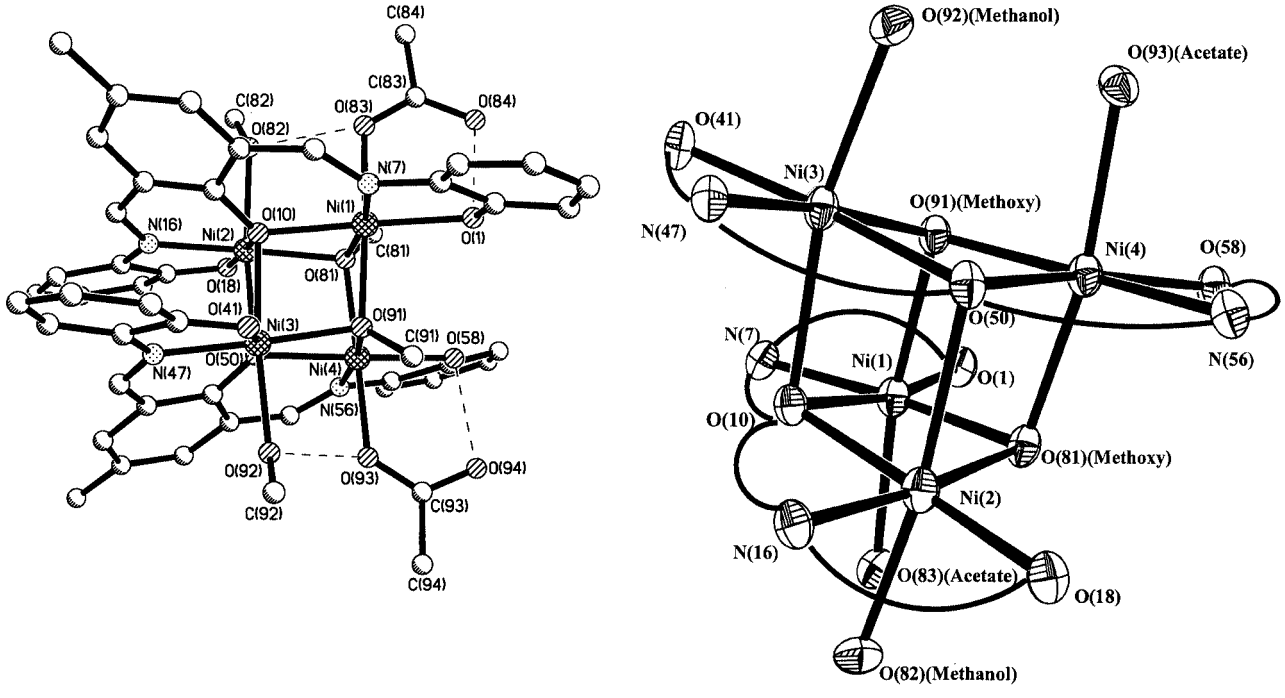

Figure 2. (a) Molecular structure of **2**, $[(LH)_2Ni^{II}_4(OCH_3)_2(OOCCH_3)_2(CH_3OH)_2]\cdot 3CH_2Cl_2$; (b) a view of **2** highlighting the Ni_4O_4 cubane core; the pentadentate ligand L is denoted only by the donor atoms joined by the curved lines

Relevant bond lengths and angles are summarized in Table 2.

Molecular Structure of 2

The crystal structure of **2** is shown in Figure 2, with selected bond lengths and angles provided in Table 3. The molecule is based on a roughly cubic Ni_4O_4 [16] unit, consisting of two interpenetrating tetrahedra, one of four nickel atoms and one of four μ_3-oxygen atoms originating from the cresol phenolate [O(10), O(50)] part of the ancillary ligand L and methoxide groups [O(81), O(91)]. Each Ni^{II} is in a distorted octahedral environment with an NO_5 donor set. For Ni(1) and Ni(4) a peripheral ligation is provided by a monodentate acetate ion, whereas for Ni(2) and Ni(3) a methanol molecule [O(82) and O(92), respectively] completes the sixth coordination position. The ancillary Schiff-base ligands are present in their monoprotonated form HL and are protonated at O(1) and O(58), forming hydrogen bonds with O(84) and O(94) of the acetate ions, respectively [O(1)···O(84): 2.426 Å; O(58)···O(94): 2.449 Å]. Although it was not possible to locate all the hydrogen atoms in the structure, the intramolecular contacts between the oxygen atoms of the methanol molecules [O(82) and O(92)] and the oxygen atoms of the acetate groups [O(83) and O(93), respectively] of 2.657 Å and 2.684 Å, can be interpreted as hydrogen bonds. The Ni−O−Ni angles vary between 94.4(2) and 102.2(3)°. The Ni···Ni distances on different cubic faces are also different, the shortest being Ni(1)···Ni(2) (3.047 Å) and the longest Ni(2)···Ni(3) (3.227 Å). Average Ni−N and Ni−O bond lengths of 1.99 and 2.10 Å, respectively, lie well within the range of reported values for the corresponding bond lengths of the tetranuclear cubane-like Ni^{II}.[16] No substantial differences in bond lengths and angles are found between the two crystallographically independent molecules.

Table 3. Selected bond lengths (Å) and angles (deg) for $[(LH)_2Ni^{II}_4(OCH_3)_2(OOC{\cdot}CH_3)_2(CH_3OH)_2]{\cdot}3CH_2Cl_2$ (**2**)

Ni(1)−N(7)	1.988(7)	N(7)−Ni(1)−O(91)	100.1(3)
Ni(1)−O(91)	2.050(6)	N(7)−Ni(1)−O(81)	170.6(3)
Ni(1)−O(81)	2.052(6)	O(91)−Ni(1)−O(81)	80.9(2)
Ni(1)−O(10)	2.081(6)	N(7)−Ni81)−O(10)	88.5(3)
Ni(1)−O(1)	2.089(6)	O(91)−Ni(1)−O(10)	82.3(2)
Ni(1)−O(83)	2.112(6)	O(81)−Ni(1)−O(10)	82.4(2)
Ni(2)−O(18)	1.970(6)	N(7)−Ni(1)−O(1)	80.9(3)
Ni(2)−N(16)	1.984(7)	O(91)−Ni(1)−O(1)	93.7(2)
Ni(2)−O(81)	2.024(6)	O(81)−Ni(1)−O(1)	108.4(2)
Ni(2)−O(10)	2.049(6)	O(10)−Ni(1)−O(1)	167.9(2)
Ni(2)−O(82)	2.123(6)	N(7)−Ni(1)−O(83)	90.5(3)
Ni(2)−O(50)	2.229(6)	O(91)−Ni(1)−O(83)	169.3(2)
Ni(3)−O(41)	1.970(6)	O(81)−Ni(1)−O(83)	88.4(2)
Ni(3)−N(47)	1.994(7)	O(10)−Ni(1)−O(83)	96.4(2)
Ni(3)−O(91)	2.052(6)	O(1)−Ni(1)−O(83)	89.6(2)
Ni(3)−O(50)	2.054(6)	O(18)−Ni(2)−N(16)	83.8(3)
Ni(3)−O(92)	2.109(6)	O(18)−Ni(2)−O(81)	101.3(2)
Ni(3)−O(10)	2.219(6)	N(16)−Ni(2)−O(81)	174.3(3)
Ni(4)−N(56)	1.979(7)	O(18)−Ni(2)−O(10)	174.3(2)
Ni(4)−O(91)	2.042(6)	N(16)−Ni(2)−O(10)	90.9(3)
Ni(4)−O(81)	2.055(6)	O(81)−Ni(2)−O(10)	83.9(2)
Ni(4)−O(50)	2.069(6)	O(18)−Ni(2)−O(82)	96.4(3)
Ni(4)−O(93)	2.092(7)	N(16)−Ni(2)−O(82)	88.6(3)
Ni(4)−O(58)	2.126(6)	O(81)−Ni(2)−O(82)	93.2(2)
		O(10)−Ni(2)−O(82)	85.5(2)
O(41)−Ni(3)−N(47)	83.5(3)	O(18)−Ni(2)−O(50)	96.9(2)
O(41)−Ni(3)−O(91)	103.7(2)	N(16)−Ni(2)−O(50)	96.9(3)
N(47)−Ni(3)−O(91)	172.1(3)	O(81)−Ni(2)−O(50)	80.2(2)
O(41)−Ni(3)−O(50)	173.7(2)	O(10)−Ni(2)−O(50)	81.8(2)
N(47)−Ni(3)−O(50)	90.6(3)	O(82)−Ni(2)−O(50)	166.1(2)
O(91)−Ni(3)−O(50)	82.2(2)		
O(41)−Ni(3)−O(92)	94.5(3)	Ni(2)−O(10)−Ni(3)	98.1(2)
N(47)−Ni(3)−O(92)	89.5(3)	Ni(1)−O(10)−Ni(3)	95.8(2)
O(91)−Ni(3)−O(92)	93.3(2)	Ni(2)−O(81)−Ni(1)	96.8(2)
O(50)−Ni(3)−O(92)	87.5(2)	Ni(2)−O(81)−Ni(4)	101.3(2)
O(41)−Ni(3)−O(10)	96.8(2)	Ni(1)−O(81)−Ni(4)	98.1(3)
N(47)−Ni(3)−O(10)	97.0(3)	Ni(4)−O(91)−Ni(1)	98.6(3)
O(91)−Ni(3)−O(10)	78.9(2)	Ni(4)−O(91)−Ni(3)	97.5(2)
O(50)−Ni(3)−O(10)	81.9(2)	Ni(1)−O(91)−Ni(3)	102.2(3)
O(92)−Ni(3)−O(10)	167.6(2)	Ni(3)−O(50)−Ni(4)	96.5(2)
N(56)−Ni(4)−O(91)	171.3(3)	Ni(3)−O(50)−Ni(2)	97.7(2)
N(56)−Ni(4)−O(81)	99.8(3)	Ni(4)−O(50)−Ni(2)	94.4(2)
O(91)−Ni(4)−O(81)	81.0(2)	Ni(2)−O(10)−Ni(1)	95.1(2)
N(56)−Ni(4)−O(50)	89.4(3)		
O(91)−Ni(4)−O(50)	82.0(2)	Ni(1)···Ni(2)	3.047
O(81)−Ni(4)−O(50)	83.4(2)	Ni(3)···Ni(4)	3.077
N(56)−Ni(4)−O(93)	89.8(3)	Ni(1)···Ni(3)	3.191
		Ni(2)···Ni(4)	3.155
O(91)−Ni(4)−O(93)	89.0(2)	Ni(1)···Ni(4)	3.102
O(81)−Ni(4)−O(93)	169.9(2)	Ni(2)···Ni(3)	3.227
O(50)−Ni(4)−O(93)	93.7(2)		
N(56)−Ni(4)−O(58)	80.2(3)		
O(91)−Ni(4)−O(58)	108.5(2)		
O(81)−Ni(4)−O(58)	94.0(2)		
O(50)−Ni(4)−O(58)	168.7(2)		
O(93)−Ni(4)−O(58)	90.7(2)		

Molecular Structure of 3

Although the analytical and spectroscopic data show the presence of a dinuclear Cu_2 core as the smallest unit in **3**, an X-ray analysis was undertaken to remove any doubts regarding the connectivity. Unfortunately, crystals of **3**

Table 4. Selected bond lengths (Å) and angles (deg) for $[LCu^{II}_2(OCH_3)(THF)_2]{\cdot}2THF$ (**3**)

Cu(1)−O(1)	1.899(6)	Cu(2)−O(17)	1.880(7)
Cu(1)−O(40)	1.911(6)	Cu(2)−O(40)	1.905(6)
Cu(1)−N(7)	1.915(8)	Cu(2)−N(16)	1.931(8)
Cu(1)−O(10)	1.948(6)	Cu(2)−O(10)	1.952(7)
Cu(1)−O(60)		Cu(2)−O(50)	
Cu(1)−O(10)−Cu(2)	99.38(31)		
Cu(1)−O(40)−Cu(2)	102.43(31)		
O(1)−Cu(1)−O(10)	173.32(27)		
O(40)−Cu(1)−N(7)	170.28(28)		
O(1)−Cu(1)−O(40)	100.83(26)		
O(1)−Cu(1)−N(7)	86.78(29)		
O(40)−Cu(1)−O(10)	78.49(27)		
O(10)−Cu(1)−N(7)	93.25(30)		
O(40)−Cu(2)−O(10)	78.55(27)		
O(40)−Cu(2)−N(16)	167.77(30)		
O(40)−Cu(2)−O(17)	101.62(29)		
O(10)−Cu(2)−N(16)	92.48(33)		
O(10)−Cu(2)−O(17)	172.80(28)		
N(16)−Cu(2)−O(17)	86.24(34)		
Cu(1)···Cu(2)	2.974(2)		

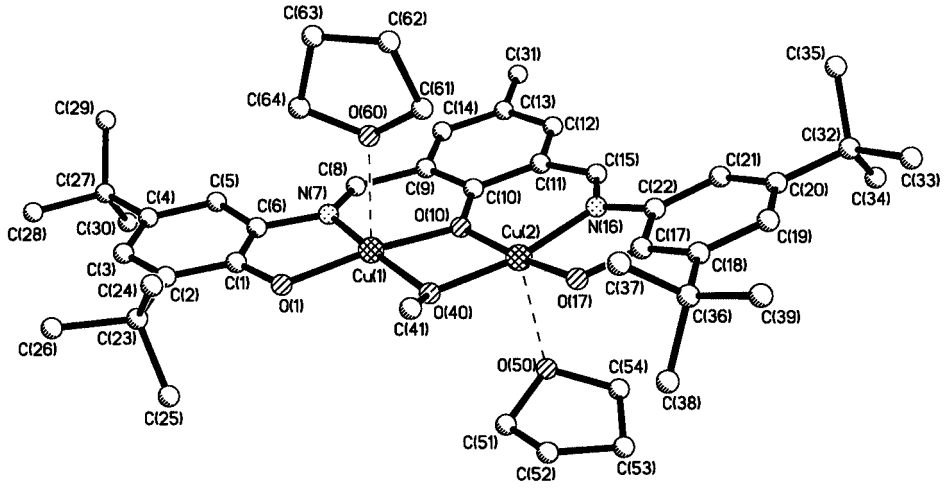

Figure 3. A perspective view of the neutral complex $[LCu_2(OCH_3)(THF)_2]$ **3**

$[C_{46}H_{66}N_2O_6Cu_2 \cdot 2THF$, monoclinic, space group $P2_1/n$, $a = 11.7459(12)$, $b = 30.236(3)$, $c = 15.640(2)$ Å, $\beta = 110.19(3)°$, $V = 5213.2$ Å^3, $T = 100(2)$ K, final $R = 0.092$ for 5150 independent reflections] diffract X-rays very weakly. In spite of the high R factor and large standard deviations, the crystal structure analysis of **3** confirmed its dinuclear structure. Because of its unacceptable quality, we are refraining from publishing the crystal data in detail. Selected bond lengths and angles are given in Table 4. The crystal structure reveals that the copper atoms are doubly bridged by the phenoxo and by a methoxide group (Figure 3). The pentacoordination of copper atoms is achieved by a tetrahydrofuran oxygen with Cu(1)−O(60) and Cu(2)−O(50) distances of 2.444 Å and 2.566 Å, respectively, which are oriented *trans* to each other in the dicopper complex. The coordination polyhedron for the copper centers is a distorted square pyramid with O(1)N(7)O(10)O(40) for Cu(1) and O(10)N(16)O(17)O(40) for Cu(2) forming the equatorial planes, where Cu(1) and Cu(2) are located 0.102 Å and 0.134 Å, respectively, out of the equatorial planes. The ring Cu(1)O(10)Cu(2)O(40) is not planar, the dihedral angle being 12.7°. The distances Cu−N and Cu−O are in the ranges reported for comparable complexes.[17]

Molecular Structure of 4

The molecular structure of **4** is shown in Figure 4. Selected interatomic distances and bond angles are listed in Table 5. Compound **4** consists of four copper(II) ions

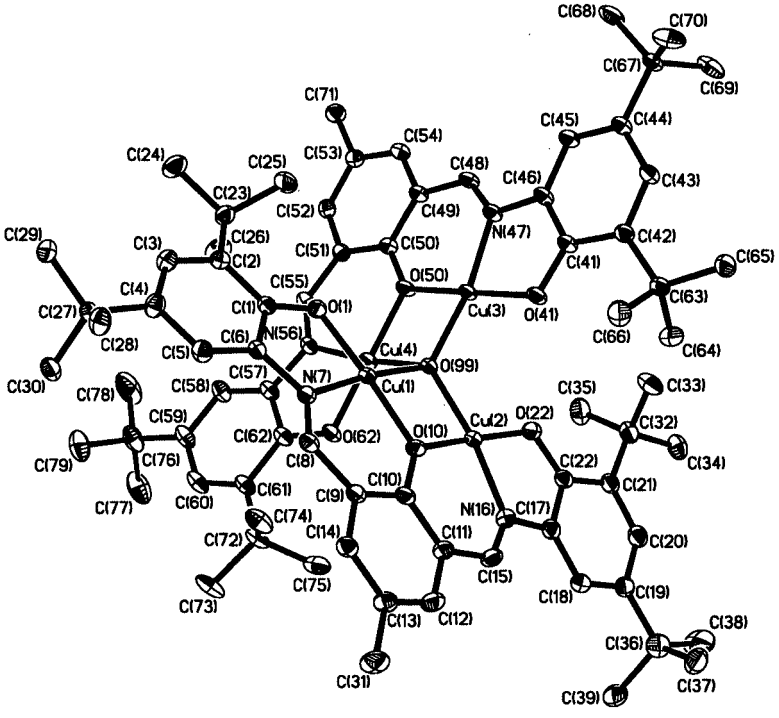

Figure 4. Molecular structure of $[L_2Cu_4(\mu_4\text{-}O)]$ **4**

Table 5. Selected interatomic distances (Å) and angles (deg) for $[L_2Cu^{II}(\mu_4\text{-}O)]\cdot 3.3CH_2Cl_2\cdot 0.7CH_3CN$ (**4**)

Cu(1)−O(1)	1.903(2)	O(1)−Cu(1)−N(7)	86.44(10)
Cu(1)−N(7)	1.919(3)	O(1)−Cu(1)−O(10)	175.87(9)
Cu(1)−O(10	1.925(2)	N(7)−Cu(1)−O(10)	93.86(10)
Cu(1)−O(99)	1.953(2)	O(1)−Cu(1)−O(99)	99.59(9)
Cu(2)−O(22)	1.897(2)	N(7)−Cu(1)−O(99)	173.77(10)
Cu(2)−O(99)	1.915(2)	O(10)−Cu(1)−O(99)	80.02(9)
Cu(2)−N(16)	1.927(3)	O(1)−Cu(1)−Cu(4)	71.26(7)
Cu(2)−O(10)	1.956(2)	N(7)−Cu(1)−Cu(4)	137.58(7)
Cu(3)−O(41)	1.897(2)	O(10)−Cu(1)−Cu(4)	106.01(7)
Cu(3)−O(99)	1.915(2)	O(99)−Cu(1)−Cu(4)	44.71(6)
Cu(3)−N(47)	1.932(2)	O(1)−Cu(1)−Cu(2)	138.52(7)
Cu(3)−O(50)	1.950(2)	N(7)−Cu(1)−Cu(2)	134.27(8)
Cu(4)−O(62)	1.891(2)	O(10)−Cu(1)−Cu(2)	40.64(6)
Cu(4)−N(56)	1.916(3)	O(99)−Cu(1)−Cu(2)	39.53(6)
Cu(4)−O(50)	1.920(2)	Cu(4)−Cu(1)−Cu(2)	71.43(2)
Cu(4)−O(99)	1.942(2)	O(22)−Cu(2)−O(99)	102.40(9)
		O(22)−Cu(2)−N(16)	86.48(11)
Cu(2)−O(99)−Cu(3)	122.37(11)	O(99)−Cu(2)−N(16)	170.27(10)
Cu(2)−O(99)−Cu(4)	120.30(11)	O(22)−Cu(2)−O(10)	174.81(9)
Cu(3)−O(99)−Cu(4)	99.58(9)	O(99)−Cu(2)−O(10)	80.20(9)
Cu(2)−O(99)−Cu(1)	99.98(9)	N(16)−Cu(2)−O(10)	91.26(10)
Cu(3)−O(99)−Cu(1)	121.07(11)	O(22)−Cu(2)−Cu(1)	142.89(7)
Cu(4)−O(99)−Cu(1)	90.23(8)	O(99)−Cu(2)−Cu(1)	40.49(6)
Cu(4)−O(50)−Cu(3)	99.12(9)	N(16)−Cu(2)−Cu(1)	130.53(8)
Cu(1)−O(10)−Cu(2)	99.49(9)	O(10)−Cu(2)−Cu(1)	39.86(6)
		O(41)−Cu(3)−O(99)	101.94(9)
Cu(1)···Cu(4)	2.760(1)	O(41)−Cu(3)−N(47)	86.63(10)
Cu(1)···Cu(2)	2.963(1)	O(99)−Cu(3)−N(47)	169.95(10)
Cu(3)···Cu(4)	2.945(1)	O(41)−Cu(3)−O(50)	174.51(10)
Cu(1)···Cu(3)	3.368(1)	O(99)−Cu(3)−O(50)	80.61(9)
Cu(2)···Cu(4)	3.345(1)	N(47)−Cu(3)−O(50)	91.31(10)
Cu(2)···Cu(3)	3.356(1)	O(41)−Cu(3)−Cu(4)	142.25(6)
		O(99)−Cu(3)−Cu(4)	40.54(6)
		N(47)−Cu(3)−Cu(4)	131.12(8)
		O(50)−Cu(3)−Cu(4)	40.07(6)
		O(62)−Cu(4)−N(56)	87.16(10)
		O(62)−Cu(4)−N(50)	178.00(9)
		N(56)−Cu(4)−O(50)	94.35(10)
		O(62)−Cu(4)−O(99)	97.66(9)
		N(56)−Cu(4)−O(99)	172.05(10)
		O(50)−Cu(4)−O(99)	80.69(9)
		O(62)−Cu(4)−Cu(1)	131.72(8)
		N(56)−Cu(4)−Cu(1)	104.47(6)
		O(50)−Cu(4)−Cu(1)	45.06(6)
		O(99)−Cu(4)−Cu(1)	137.53(7)
		O(62)−Cu(4)−Cu(3)	134.87(8)
		N(56)−Cu(4)−Cu(3)	40.81(6)
		O(50)−Cu(4)−Cu(3)	39.88(6)
		O(99)−Cu(4)−Cu(3)	72.29(2)

bridged by a central μ_4-oxygen atom in an approximately tetrahedral environment. The phenolate oxygen atoms O(10) and O(50) of the cresol part of the ligand bridge two copper centers, resulting in very similar Cu(1)−O(10)−Cu(2) and Cu(3)−O(50)−Cu(4) angles of 99.49(9)° and 99.12(9)°, respectively. Each copper center is coordinated by three oxygen atoms and one nitrogen atom, with the bond lengths ranging from 1.891(2) to 1.953(2) Å. There are considerable deviations of the geometry of the copper center from the ideal square plane, as indicated by the basal plane angles (Table 5), although each CuO_3N portion is essentially planar. The dihedral angles between the Cu(1)/Cu(2) planes, and between the Cu(3)/Cu(4) planes are 8.5° and 3.2°, respectively. The two $Cu_2O_4N_2$ dinuclear units are nearly perpendicular, as evidenced by the dihedral angle of 75.2° between the Cu(1)O(10)Cu(2)O(99) and Cu(3)O(50)-Cu(4)O(99) planes.

The copper tetrahedron around the μ_4-oxygen O(99) is distorted, as the bond angles Cu−O(99)−Cu range from 122.37(1)° for Cu(2)−O(99)−Cu(3) to 90.23(8) for Cu(4)−O(99)−Cu(1), the smallest among the six angles at O(99). Perhaps as a consequence, the Cu(2)···Cu(3) distance of 3.356 Å is substantially longer than that of Cu(4)···Cu(1) (2.759 Å). The remaining Cu···Cu distances are Cu(1)···Cu(2) (2.963 Å), Cu(1)···Cu(3) (3.368 Å), Cu(2)···Cu(4) (3.345 Å) and Cu(3)···Cu(4) (2.945 Å). These differences can be explained by the steric forces of the chelating ligand L^{3-}, which contracts the Cu(1)−O(99)−Cu(4) angle with a concomitant expansion of the opposite angle Cu(2)−O(99)−Cu(3). Examples of tetranuclear copper(II) complexes with a μ_4-O kernel are abundant,[18−20] but all of them involve bridging ligands like halides or carboxylates between the edges of the tetrahedron. Compound **4** without any such bridging ligand is an exception. Figure 5 highlights the core structure for greater clarity and to emphasize the unique structure of the $Cu_4(\mu_4\text{-}O)$ unit present in **4**.

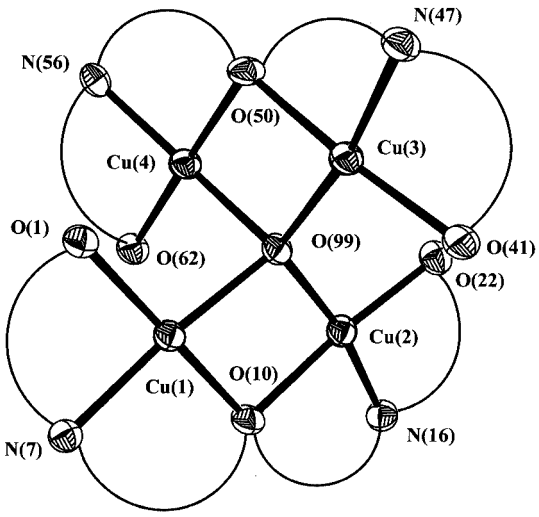

Figure 5. The atom connectivity in the core of complex **4**

Magnetic Susceptibility Studies

Magnetic susceptibility data for polycrystalline samples of complexes **1**−**4** were collected in the temperature range 2−290 K in an applied magnetic field of 1 T to characterize the nature and magnitude of the exchange interaction propagated by the bridging ligands. We use the Heisenberg spin-Hamiltonian in the form $H = -2JS_AS_B$ for an isotropic exchange coupling, with $S_{Ni} = 1$ for **1** and **2** and $S_{Cu} = 1/2$ for **3** and **4**. The experimental magnetic data were simulated using a least-squares fitting computer program[21] with a full-matrix diagonalization of exchange coupling, Zeeman splitting, and axial single-ion zero-field interactions [DS_z^2], if necessary. The susceptibility data were cor-

rected for diamagnetism (Pascal corrections), temperature-independent paramagnetism (TIP) and the presence of paramagnetic monomer impurities (P) in the following way: $\chi_{calc} = (1 - P)\chi + \chi_{TIP} + P\chi_{mono}$. The experimental data are displayed in Figure 6 as the effective magnetic moment (μ_{eff}) versus temperature (T). The solid lines in the figure represent the simulations.

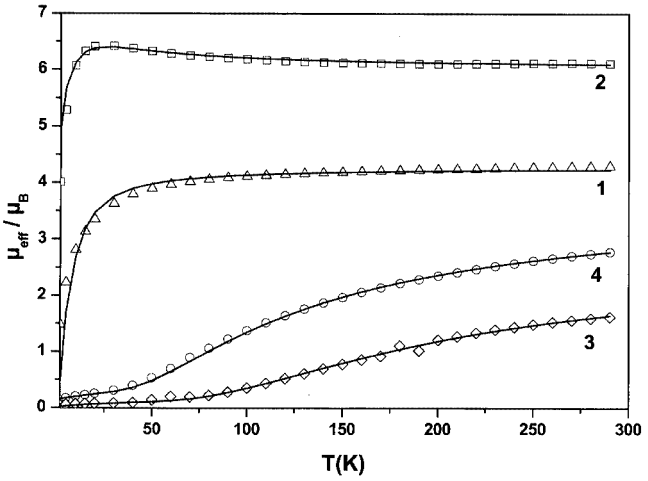

Figure 6. Plots of μ_{eff} vs. T for solid **1**, **2**, **3** and **4**; the solid lines represent the best fit of the data to the exchange coupling models

The magnetic moment μ_{eff}/molecule for **1** of 4.280 μ_B ($\chi_M \cdot T$ = 2.291 cm^3·K·mol^{-1}) at 290 K decreases monotonically with decreasing temperature until it reaches a value of 1.474 μ_B ($\chi_M \cdot T$ = 0.2717 cm^3·K·mol^{-1}) at 2 K; this temperature dependence of μ_{eff} is a clear indication of an antiferromagnetic exchange coupling between two paramagnetic centers Ni^{II} (S_{Ni} = 1) with a resulting diamagnetic ground state. Using only D (i.e. J = 0), a fit of poor quality with unusually large D was obtained and hence discarded. Attempts to fit the data using both D and J yield physically meaningless D values. For example, a good fit (not shown) was obtained with the following parameters: J = −2.6 cm^{-1}, D = +27.1 cm^{-1}, g = 2.13, P = 0.005. As the zero-field splitting D is unusually large for a six-coordinate Ni^{II} ion, this solution was also discarded. Finally, the solid line in Figure 6 represents the best fit with the following parameters: J = −3.5 cm^{-1}, $g_1 = g_2$ = 2.137, P = 0.005. The quality of the fit (Figure 6) is insensitive to D varying between 0 and 5 cm^{-1}.

For **2**, the effective magnetic moment of 6.08 μ_B ($\chi_M \cdot T$ = 4.629 cm^3·K·mol^{-1}) at 290 K increases monotonically with decreasing temperature reaching a broad maximum at 20−30 K with μ_{eff} = 6.39 μ_B ($\chi_M \cdot T$ = 5.1073 cm^3·K·mol^{-1}). Below 20 K, μ_{eff} starts to decrease reaching a value of 3.99 μ_B ($\chi_M \cdot T$ = 1.992 cm^3·K·mol^{-1}) at 2 K (Figure 6); it is clear that the magnetic properties of **2** are dominated by a ferromagnetic exchange interaction between four $^3A_2$ nickel(II) ions as propagated by bridging phenoxides and methoxides. The structural parameters of **2** strongly suggest a lower symmetry than T_d (idealized D_{2d}) for the molecule. The magnetic analyses were carried out using either a two-J or three-J model based on the diagram shown in Scheme 2.

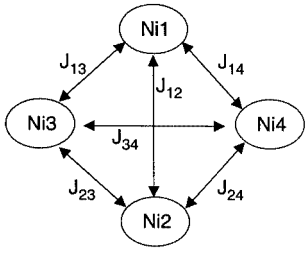

Scheme 2

The data were fit initially by using a higher symmetry model, i.e. $J_{12} = J_{34}$ and $J_{13} = J_{14} = J_{24} = J_{23}$, which yielded a good fit (not shown) with $J_{12} = J_{34}$ = +1.5 cm^{-1}, $J_{13} = J_{14} = J_{24} = J_{23}$ = +0.25 cm^{-1}, g = 2.133, D = 14.8 cm^{-1}. We discarded this solution as the zero-field splitting D is unusually large for a six-coordinate $^3A_2$ Ni^{II} ion.[22] We therefore fitted the data with three different exchange parameters, which also corroborate with three different types of faces present in the Ni_4O_4 cubane core of **2**. The best fit parameters are: $J_{12} = J_{34}$ = +0.47 cm^{-1}, $J_{13} = J_{24}$ = +4.25 cm^{-1}, $J_{14} = J_{23}$ = −1.45 cm^{-1}, g = 2.122 and D = 0 (fixed). The most important parameter in the magnetostructural correlation of the Ni_4O_4 cubane cores has been described in the literature[16] to be the averaged Ni−O−Ni angle of a cubane face. A ferromagnetic exchange interaction is observed when this angle is close to orthogonality. On the other hand, Ni−O−Ni angles in the vicinity of, and larger than, 99° lead to an antiferromagnetic interaction. Thus, the strongest ferromagnetic coupling, $J_{13} = J_{24}$ = +4.25 cm^{-1}, should be associated with the average Ni(1)−O−Ni(3) angle of 99.0°, which is not in agreement with the magnetostructural correlation reported in the literature.[16] This suggested that a better fitting model should be used. We therefore fitted the data by again using three different exchange parameters, but with the following constraints: J_{12}, J_{13} and $J_{14} = J_{24} = J_{23} = J_{34}$, as three different ranges of average Ni−O−Ni angles of 96°, 97−98° and 99° are present in **2**. The best fit obtained with the parameter set J_{12} = +8.0 cm^{-1}, $J_{14} = J_{24} = J_{23} = J_{34}$ = +0.9 cm^{-1}, J_{13} = −3.95 cm^{-1}, g = 2.120, D = 0 (fixed) is shown as a solid line in Figure 6. The differences and nature of the signs of the exchange parameters are in full agreement with the Ni−O−Ni angle correlation and support the three-J model used, which takes into account the reduced symmetry of the cubane core observed in the X-ray structure of **2**. Thus, these results for **2** predict a switch from ferromagnetic to antiferromagnetic coupling only for Ni−O−Ni angles above 98°.

Recently it has been demonstrated[16i] that the major contributor to the superexchange constants observed in $[Ni_4(OR)_4]^{4+}$ cubanes is the Ni−O−Ni angle. Accordingly, a linear correlation between J and the Ni−O−Ni angle has

been reported.[16i,16m] We have also plotted the observed J values for **2** and other structurally characterized $[Ni_4(OR)_4]^{4+}$ cubanes against average Ni−O−Ni angles (Figure 7). The solid line drawn as a guide for the eyes shows a fairly good correlation between J and these angles. This guide allows us to notice that the antiferromagnetic interactions ($-J$) fall fairly well on the correlated line with respect to Ni−O−Ni angles. In contrast, the positive J values scatter appreciably. This is not surprising considering the high tolerance attached in general to the positive J values (ferromagnetic interactions) evaluated through simulation of the susceptibility data.

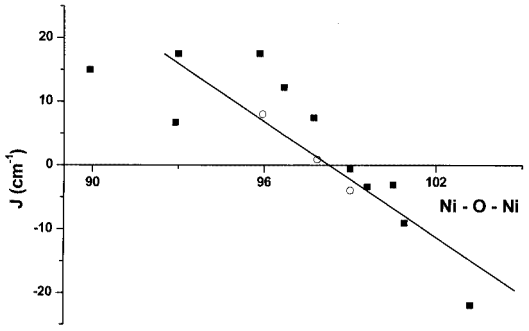

Figure 7. A plot of average Ni−O−Ni angles vs. the exchange interactions (J); closed circles are literature data and open circles are from this work; the solid line is drawn only as a guide

The non-zero magnetic moment of 3.99 μ_B at 2 K and the broad maximum with μ_{eff} = 6.39 μ_B at 20−30 K indicate that **2** has a complicated low-lying magnetic structure with a non-diamagnetic ground state smaller than the spin state of S_t = 4 expected for a ferromagnetically coupled tetranuclear nickel(II) moiety (S_{Ni} = 1). The ground state can be determined by examining the magnetization of the compound at low temperatures as a function of the applied magnetic fields. We have performed magnetization measurements at applied magnetic fields of 1, 4 and 7 T. The field-dependent magnetizations as a function of temperature, and their simulations, are depicted in Figure 8. It is clear from Figure 8 that the saturated magnetization value reaches a value of approximately 3.035 in the temperature range 2.0−2.8 K at the highest field of 7 T. The simulated parameters are: J_{12} = +8.0 cm^{-1}, J_{13} = −3.95 cm^{-1}, J_{14} = J_{24} = J_{23} = J_{34} = +0.60 cm^{-1}, g = 2.12, $|D|$ = 3.0 cm^{-1}. These values agree well with those from the susceptibility measurements. As J_{12}, J_{13} and D are of similar magnitude, it is not possible to calculate the ground state in the form of an S_t value; S is not a good quantum number to describe the ground state, but rather M_S.

Variable-temperature magnetic data for **3** exhibit a steady decrease of μ_{eff} from 1.634 μ_B (χ_M·T = 0.3338 cm^3·K·mol^{-1}) at 290 K to 0.049 μ_B (χ_M·T = 0.03 × 10^{-3} cm^3·K·mol^{-1}) at 2 K, which is indicative of very strong intramolecular antiferromagnetic coupling. The experimental data were simulated with the parameter set J = −192.1 cm^{-1}, g = 2.055, TIP = 30 × 10^{-6}, P = 0 and is shown in Figure 6. The major factor controlling the exchange interactions in hydroxy-, alkoxy- and phenoxy-bridged copper(II) is the Cu−O−Cu bridge angle.[20,23] The average Cu−O−Cu bridge angle of 100.9° for **3** would result in an approximate J value of −250 cm^{-1} according to the empirical equation reported in the literature and it deviates appreciably from the experimentally determined value of −192 cm^{-1} for **3**. A possible reason for the weak exchange coupling in **3** may be the deviation from co-planarity within the central Cu_2O_2 ring. It seems plausible that the methoxide ion, with shorter Cu(1)−O(40) (1.911 Å) and Cu(2)−O(40) (1.905 Å) distances and a larger Cu(1)−O(40)−Cu(2) angle (102.43°) than those with the phenoxide ion, provides a better pathway for antiferromagnetic exchange coupling.[17]

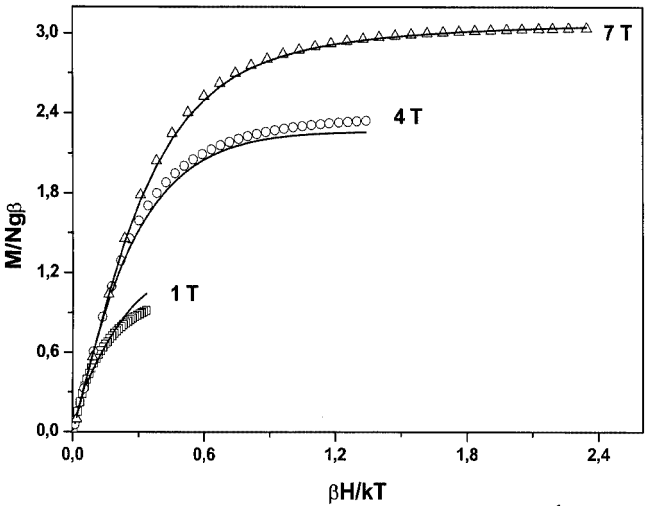

Figure 8. The field-dependent magnetizations of **2** as a function of temperature and their simulations; see text for the parameters

The effective magnetic moment μ_{eff}/molecule for **4** of 2.768 μ_B (χ_M·T = 0.9582 cm^3·K·mol^{-1}) at 290 K decreases monotonically with decreasing temperature until it reaches a value of 0.133 μ_B (χ_M·T = 0.0022 cm^3·K·mol^{-1}) at 2 K, indicating dominant antiferromagnetic interactions between four $^2B_2$ copper(II) ions; the data clearly show an S_t = 0 ground state for **4**.

Two different exchange pathways are possible for **4**: Cu-phenoxo-Cu and Cu-μ_4-oxo-Cu. Scheme 3 shows the connection of the copper centers through the phenoxo and the oxo groups.

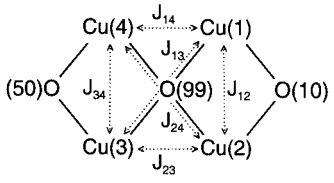

Scheme 3

As the Cu(3)/Cu(4) and Cu(2)/Cu(1) pairs are bridged by both phenoxo and oxo groups and the Cu(4)/Cu(1), Cu(2)/Cu(3), Cu(2)/Cu(4) and Cu(1)/Cu(3) pairs only through the oxo group, O(99), the experimental magnetic data were analyzed as a first approximation with a three-J model: J_{12} = J_{34}, J_{14} = J_{23} and J_{24} = J_{13}. In this model we have neglected the differences in the Cu−O−Cu angles. A very good fit

(not shown) was obtained with the following parameters: $J_{12} = J_{34} = -86.3$ cm^{-1}, $J_{14} = J_{23} = +40.8$ cm^{-1} and $J_{24} = J_{13} = -86.1$ cm^{-1}, $g = 1.976$, $D = 0$ (fixed), $P = 0.007$ and TIP $= 240 \times 10^{-6}$ which imply that the spin exchange is dominated by antiparallel coupling in **4**. The low g value and the positive coupling constants for both J_{14} and J_{23}, which represent the couplings between the copper centers with the angles Cu(4)−O(99)−Cu(1) (90.23°) and Cu(2)−O(99)−Cu(3) (122.37°), however, suggest that a better fitting model should be used. The data were consequently fitted to a more accurate model, again using a three-J model but with a different constraint based on the three ranges of Cu−O−Cu angles, 90.2, 99.12−99.98° and 120.30−122.37°. Thus, the following correlations between the six coupling constants depicted in Scheme 3 were used to fit the experimental data: $J_{12} = J_{34}$, $J_{23} = J_{24} = J_{13}$ and J_{14}. The fit shown in Figure 6 was obtained with $J_{12} = J_{34} = -122.3$ cm^{-1}, $J_{23} = J_{24} = J_{13} = -90.0$ cm^{-1} and $J_{14} = 0$, $g = 2.088$, $P = 0.003$, TIP $= 240 \times 10^{-6}$ and $D = 0$ (fixed). The susceptibility data consistent with this data set were found to be relatively insensitive to J_{14}, but very sensitive to J_{12} and J_{23}; J_{14} values lying in the range −20 to +20 cm^{-1} have no influence on the quality of simulation.

For copper(II) centers bridged by a ligand oxygen atom (oxo, hydroxo, alkoxo, phenoxo, etc.), a linear relationship of exchange coupling J with the average Cu−O−Cu angles in the Cu_2O_2 ring has been reported.[17,20,23] We note that although a J_{12} value of −122 cm^{-1} assigned to an angle of 99.5° does not deviate significantly from the reported linear relationship, the J_{23} value of −90.0 cm^{-1} deviates remarkably. This is not very surprising as the electronic structures of the μ-OR and μ_4-O groups are clearly different. J_{14} is nondeterminant for **4** within the measured temperature range 2−290 K.

Electrochemistry

Electrochemical voltammetric measurements (cyclic voltammetry, CV, and square-wave voltammetry, SQW) were performed with the complexes in CH_2Cl_2 solutions containing 0.1 M $TBAPF_6$. The copper(II) complexes **3** and **4** show very similar behavior. They exhibit an oxidation wave at +0.490 and +0.530 V, vs. Fc^+/Fc for **3** and **4**, respectively. The waves have a reversible appearance, although the peaks in CV and SQW are broad; the peak separation of the oxidative and reductive peaks in the CVs is relatively high (0.110 V even at low scan rates) and in SQW shoulders on the forward and reverse peaks are discernible. This leads us to assume that each of the complexes is oxidized at two different sites with redox potentials that differ somewhat in less than 0.1 V. Since a copper(II) oxidation is not feasible at such low potentials, we assign these redox processes to ligand-centered oxidation yielding two phenoxyl radicals in each complex.

The nickel(II) complexes **1** and **2** are oxidized in a similar potential range. There are waves at +0.470 (**1**) and +0.440 V (**2**), which are preceded by broad peaks (with shoulders in the SQW) at +0.270 V for **1** and +0.153 V for **2**. Additionally, with increasing scan rate the oxidation and re-reduction peaks in the CV were found to split into two components. We assign this more complex behavior to an involvement of the nickel(II) ion in the redox processes leading to radical through oxidation. Ligand-centered oxidation to a radical is inferred from the occurrence of oxidation processes at potentials that are similar, irrespective of the nature of the central metal ion. Involvement of central nickel ions in oxidation processes of radical complexes was documented earlier in detail,[24] including digital simulations of complex cyclic voltammograms.

Concluding Remarks

That single-atom *O*-bridging of urea in a dinuclear nickel(II) complex can be achieved with suitably designed ligands has been demonstrated by isolation of **1**. Unfortunately, **1** is not able to catalyze the ethanolysis of urea [conditions: 1 mmol of **1** and 50 mmol of urea in ethanol (10 mL) was refluxed at 80 °C for 14 hours, which was then worked up for the GC analysis] to form ethyl carbamate presumably because of the hydrogen bonding network involving urea in **1**, which is also maintained in solution. Due to the presence of a stable hydrogen-bonded structure in solution, there is no possibility of intramolecular OH^- delivery to the π*-orbital of urea, as has been proposed for the mechanism of action of urease.[13e,15] It is noteworthy that the bond lengths within the coordinated urea,[14] bridging or nonbridging, are very similar, in contrast to the compound which exhibits catalytic activity.[14g] In the latter compound two different C−N bond lengths — 1.348(4) and 1.303(4) Å — are observed within the coordinated urea.

Complex **2** contains the low-symmetry cubane core $[Ni_4(\mu_3\text{-phenoxide})_2(\mu_3\text{-methoxide})_2]^{4+}$ with differing Ni···Ni distances and Ni−O−Ni angles, resulting in three types of Ni_2O_2 faces. The observation of three discrete exchange parameters for **2** is consistent with the lower symmetry of the cubane than that of all others but one[16m] reported in the literature.[16] Figure 7, a plot of J vs. Ni−O−Ni angles for all structurally characterized Ni_4O_4 cubane cores, irrespective of their symmetry, exhibits a large variation of J values within a small span of Ni−O−Ni angles (90−103°). This figure also indicates that the symmetry of the cubane core has a profound effect on the magnetostructural correlation. It is likely that other structural parameters like Ni···Ni and Ni−O distances take the upper hand in the magnetostructural correlation for the low-symmetry cubane core. Thus, more such distorted cubane-type Ni^{II} complexes are needed to resolve this open question.

Complex **3** containing a (μ-methoxo)(μ-phenoxo)dicopper(II) unit belongs to a ubiquitous class of coordination complexes of copper(II). It is pertinent at this point to compare the magnetic properties of **3** with these related dicopper(II) complexes. Regardless of the coordination geometry of the copper centers — square planar, square pyramidal or trigonal bipyramidal — all complexes with a $Cu^{II}_2(\mu\text{-OPh})(\mu\text{-OCH}_3)$ core as in **3** are antiferromagnetic and show relatively moderate to strong spin coupling with values ran-

ging from −47 to −315 cm^{-1}. These observations extend over eight compounds,[17] in which it has been demonstrated that the $Cu(d_z^2)-O-Cu(d_z^2)$ pathway would yield weaker antiferromagnetic coupling than in related $Cu(d_{x^2-y^2})-O-Cu(d_{x^2-y^2})$ systems. The $-J$ values for six of these compounds lie in the range 150−224 cm^{-1}. The evaluated J value of −192 cm^{-1} for **1** falls at the upper end of the observed range and is in agreement with the paramagnetic copper(II) centers with $(d_{x^2-y^2})^1$ magnetic orbitals. The sum of the angles around the phenoxo-oxygen, O(10), is 357.7°, a planar phenoxo group capable of transmitting spin exchange effectively.

Complex **4**, $[L_2Cu_4(\mu_4\text{-}O)]$, is the first example of a (μ_4-oxo)tetranuclear copper(II) complex without any bridging ligand between the tetrahedral edges. In accordance with the three averaged Cu−O−Cu angles of 90°, 99.5° and 121.3°, a three-J model was used to analyze the magnetic data. It is interesting to note that an exchange coupling constant J_{14} corresponding to the Cu−O−Cu angle of 90° could not be evaluated.

Experimental Section

Materials and Physical Measurements: Reagent or analytical grade materials were obtained from commercial suppliers and used without further purification, except those for electrochemical measurements. Elemental analyses (C, H N) were performed by the Microanalytical Laboratory Dornis & Kolbe, Mülheim, Germany. Fourier transform infrared spectroscopy on KBr pellets was performed on a Perkin−Elmer 2000 FT-IR instrument. Electronic absorption spectra in solution were measured on a Perkin−Elmer Lambda 19 spectrophotometer. Magnetic susceptibilities of *powdered samples* were recorded on a SQUID magnetometer in the temperature range 2−295 K with an applied field of 1 T. Experimental susceptibility data were corrected for the underlying diamagnetism using Pascal's constants and for the TIP contributions. Cyclic voltammetric and coulometric measurements were performed on EG&G equipment (potentiostat/galvanostat model 273A). Mass spectra were obtained with either a Finnigan MAT 8200 (electron ionization, EIMS) or a MAT 95 (electrospray ESI-MS) instrument. A Bruker DRX 400 instrument was used for NMR spectra. Instrumental conditions for liquid chromatography are as follows: Shimadzu SPD-10 AV, Nucleodur-5-C_{18} Sel 220 column, UV-280 nm, eluent = CH_3CN (0.8 mL/min), room temperature, sample size 5 μL, recorder 0.5 cm/min.

H_3LtBu: 6-Amino-2,4-di-*tert*-butylphenol (4.4 g; 20 mmol) was added to a solution of 2,6-diformyl-4-methylphenol (1.6 g, 10 mmol) in methanol (70 mL), and the resulting solution was refluxed for 1 h, during which the color changed to deep red, and a yellow microcrystalline solid precipitated out. The solution was cooled, filtered and the solid was washed with cold methanol, and air-dried. Yield: 5.1 g (ca. 90%). The purity of the ligand was checked by liquid chromatography: Retention time of 13.2 min for the eluent CH_3CN with a rate of 0.8 mL/min. EI-MS: m/z = 570. ^1H NMR ($CDCl_3$): δ = 8.94, 7.26 (6 H, aromatic), 7.12 (2 H, −CH=N-), 2.38 (3 H, CH_3), 1.43 (18 H, tBu), 1.32 (18 H, tBu) ppm. IR (KBr disk): $\tilde{\nu}$ = 3523 cm^{-1}, 3492, 3348w, 2954, 2868s, 1625m, 1580m, 1482s, 1456s, 1361s, 1250s, 987s, 960s, 867m. *For the sake of simplicity the ligand is denoted by H_3L without the suffix tBu.* UV/Vis (CH_2Cl_2): λ_{max} (ε) = 270 nm (18600 $M^{-1}\cdot cm^{-1}$), 306 (17700), 401 (21800). UV/Vis [CH_2Cl_2 in the presence of eight equivalents of $(Bu_4N)OCH_3$]: λ_{max} (ε) = 300 nm (sh), 350 (sh), 496 (13900 $M^{-1}\cdot cm^{-1}$).

$[LNi^{II}_2(NH_2CONH_2)(OAc)(MeOH)_2]\cdot 4.5CH_3OH$ (1): $Ni(CH_3COO)_2\cdot 4H_2O$ (0.24 g; 1 mmol), CH_3COONa (0.16 g, 2 mmol) and urea (0.18 g, 3 mmol) were dissolved in methanol, and a solution of the ligand H_3L (0.28 g, 0.5 mmol) in dichloromethane (30 mL) was added. The resulting solution was refluxed for 15 min and filtered to remove any solid particles. The solution was allowed to evaporate slowly at ambient temperature to yield orange-red crystals. Yield: 0.24 g (60%). $C_{46.5}H_{80}N_4Ni_2O_{12.5}$ (1012.54): calcd. C 55.16, H 7.91, N 5.53, Ni 11.59; found C 55.8, H 7.4, N 6.0, Ni 11.7. MS-ESI pos. (in CH_2Cl_2): m/z = 743.5 $[M - (NH_2CONH_2)(CH_3OH)_2]^+$ (100%). EI-MS indicates the presence of both acetate and urea. IR (KBr disk): $\tilde{\nu}$ = 3586w cm^{-1}, 3382m, 3139m, 2950s, 2965m, 1670m, 1654m, 1568s, 1469s, 1444s, 1410s, 1250s, 1159m, 831m. UV/Vis (CH_2Cl_2): λ_{max} (ε) = 329 nm (14770 $M^{-1}\cdot cm^{-1}$), 464 (16900), 779 (19), 858 (27), 1284 (ca. 12).
Compound **1** can also be obtained from **2** by addition of urea and refluxing the resulting solution.

$[(LH)_2Ni^{II}_4(OMe)_2(OAc)_2(MeOH)_2]\cdot 3CH_2Cl_2$ (2): A solution of methanol (15 mL) containing $Ni(CH_3COO)_2\cdot 4H_2O$ (0.24 g, 1 mmol) and CH_3COONa (0.24 g, 3 mmol) was added to a solution of the ligand H_3L (0.28 g, 0.5 mmol) in dichloromethane (30 mL). The resulting solution was refluxed for 15 min, then cooled and filtered. On reduction of the volume of the filtrate orange-red microcrystals separated out. X-ray quality crystals were obtained by recrystallization from a dichloromethane/methanol mixture. Yield: 0.19 g (47%). $C_{82}H_{116}N_4Ni_4O_{14}$ (1616.60): calcd. C 60.92, H 7.23, N 3.47, Ni 14.52; found C 58.9, H 7.0, N 3.2, Ni 13.1. EI-MS: m/z = 714−720 (100) $[LNi_2(OCH_3)^+]$. IR (KBr disk): $\tilde{\nu}$ = 3440br cm^{-1}, 2955s, 1624s, 1552m, 1477s, 1446s, 1410s, 1259s, 1039s, 805m. UV/Vis (CH_2Cl_2): λ_{max} (ε): 331 nm (40300 $M^{-1}\cdot cm^{-1}$), 405 (32300), 474 (40600), 917 (26).

$[LCu^{II}_2(OCH_3)(THF)_2]\cdot 2THF$ (3): H_3L (0.29 g, 0.5 mmol), $Cu(ClO_4)_2\cdot 6H_2O$ (0.37 g, 1 mmol) and NEt_3 (0.3 mL) were added to a methanol/dichloromethane (1:3) solvent mixture, and the resultant solution refluxed for 0.5 h. The deep-red solution yielded an orange-red microcrystalline solid on slow evaporation of the solvent at ambient temperature. Yield: 0.13 g (70%). $C_{38}H_{50}Cu_2N_2O_4$ (725.92): calcd. C 62.87, H 6.94, N 3.86, Cu 17.51; found C 63.1, H 6.9, N 3.8, Cu 17.4. X-ray quality crystals were obtained by recrystallization with a THF/CH_3OH solvent mixture. EI-MS: m/z = 726 (100) $[LCu_2(OCH_3)]$; a clear indication of the presence of THF. IR (KBr disk): $\tilde{\nu}$ = 2954s cm^{-1}, 2867m, 2816w, 1597m, 1557m, 1474s, 1445s, 1256s, 1159s, 1077m, 830m. UV/Vis (CH_2Cl_2): λ_{max} (ε): 486 nm (17100 $M^{-1}\cdot cm^{-1}$).

$[L_2Cu^{II}_4(\mu_4\text{-}O)]\cdot 3.3CH_2Cl_2\cdot 0.7CH_3CN$ (4): A solution of the ligand H_3L (0.29 g; 0.5 mmol) $Cu(ClO_4)_2\cdot 6H_2O$ (0.37 g; 1 mmol) and NEt_3 (0.3 mL) in acetonitrile/dichloromethane (1:3) was refluxed for 0.5 h and then kept at room temperature to allow the separation of an orange-red microcrystalline substance, which was recrystallized from a CH_3CN/CH_2Cl_2 mixture to yield X-ray quality crystals. Yield: 0.21 g (60%). $C_{74}H_{94}Cu_4N_4O_7$ (1405.76): calcd. C 63.23, H 6.74, N 3.99, Cu 18.08; found C 62.4, H 6.9, N 4.0, Cu 17.8. EI-MS: m/z = 1402 $[M^+]$. IR (KBr disk): $\tilde{\nu}$ = 2952s cm^{-1}, 2904s, 2867m, 1593m, 1557m, 1467s, 1445s, 1409m, 1360m, 1317m, 1254s, 1200m, 1159s, 1077m, 829m, 564m, 539m, 510m. UV/Vis (CH_2Cl_2): λ_{max} (ε): 484 nm (35700 $M^{-1}\cdot cm^{-1}$), ca. 680sh (ca. 430).

Compound **4** can also be obtained by refluxing **3** in CH_3CN/CH_2Cl_2 for 0.5 h.

X-ray Crystallographic Data Collection and Refinement of the Structures: A single crystal of **1** (orange-red), **2** (red), **3** (orange-red) or **4** (orange-red) was coated with perfluoropolyether, mounted on a glass fiber and placed in a Kappa-CCD diffractometer equipped with a cold nitrogen stream at 100 K. Graphite-monochromated Mo-K_α radiation (λ = 0.71073 Å) was used. Crystallographic data of the compounds **1**, **2** and **4** are listed in Table 1. Cell constants were obtained from a least-squares fit of the diffraction angles of several thousand strong reflections. Intensity data were corrected for Lorentz and polarization effects. The data sets of **1** and **2** were corrected for absorption, whereas the intensities of **4** were left uncorrected. The Siemens ShelXTL software package (G. M. Sheldrick, Universität Göttingen) was used for solution, refinement and artwork of the structures; the neutral atom scattering factors of the program were used. All structures were solved and refined by direct methods and difference-Fourier techniques. Non-hydrogen atoms were refined anisotropically, and hydrogen atoms were placed at calculated positions and refined as riding atoms with isotropic displacement parameters.

CCDC-191305 (**1**), -191306 (**2**), and -191307 (**4**) contain the supplementary crystallographic data for this paper. These data can be obtained free of charge at www.ccdc.cam.ac.uk/conts/retrieving.html [or from the Cambridge Crystallographic Data Centre, 12, Union Road, Cambridge CB2 1EZ, UK; Fax: (internat.) +44-1223/336-033; E-mail: deposit@ccdc.cam.ac.uk].

Acknowledgments

Financial support from the DFG (Grant: Priority program Ch111/2−1), the Max-Planck Society and Fonds der Chemischen Industrie is gratefully acknowledged. Thanks are due to Mrs. H. Schucht, Mrs. P. Höfer and Mr. A. Göbels for skilful technical assistance.

[1] For selected examples see: [1a] *Bioinorganic Chemistry of Copper* (Eds.: K. D. Karlin, Z. Tyeklar), Chapman & Hall, New York **1993**. [1b] *Manganese Redox Enzymes* (Ed.: V. L. Pecoraro), VCH Publishers, Weinheim **1992**. [1c] *Multicopper Oxidases* (Ed.: A. Messerschmidt), World Scientific, Singapore **1977**. [1d] T. N. Sorrell, *Tetrahedron* **1989**, *40*, 3. [1e] N. Kitajima, W. B. Tolman, *Progr, Inorg. Chem.* **1995**, *43*, 419. [1f] J. Du Bois, T. J. Mizoguchi, S. J. Lippard, *Coord. Chem. Rev.* **2000**, *200−202*, 443. [1g] V. Mahadevan, R. J. M. Klein Gebbink, T. D. P. Stack, *Curr. Opin. Chem. Biol.* **2000**, *4*, 228. [1h] L. Que, Jr., W. Tolman, *Angew. Chem.* **2002**, *114*, 1160; *Angew. Chem. Int. Ed.* **2002**, *41*, 1114.

[2] See for example: "*Journal of Solid State Chemistry''*, Vol. 159, No. 2, July 2001 − a tribute to Olivier Kahn.

[3] C. Desplanches, E. Ruiz, A. Rodriguez-Fortea, S. Alvarez, *J. Am. Chem. Soc.* **2000**, *124*, 5197 and references therein.

[4] [4a] R. Robson, *J. Inorg. Nucl. Chem. Lett.* **1970**, *6*, 125. [4b] R. Robson, *Aust. J. Chem.* **1970**, *23*, 2217. [4c] A. M. Bond, M. Haga, I. S. Creece, R. Robson, J. C. Wilson, *Inorg. Chem.* **1988**, *27*, 712. [4d] A. M. Bond, M. Haga, I. S. Creece, R. Robson, J. C. Wilson, *Inorg. Chem.* **1989**, *28*, 559.

[5] H. Okawa, H. Furutachi, D. E. Fenton, *Coord. Chem. Rev.* **1998**, *174*, 51 and references therein.

[6] [6a] C. N. Verani, T. Weyhermüller, E. Rentschler, E. Bill, P. Chaudhuri, *Chem. Commun.* **1998**, 2475. [6b] C. N. Verani, E. Rentschler, T. Weyhermüller, E. Bill, P. Chaudhuri, *J. Chem. Soc., Dalton Trans.* **2000**, 4263.

[7] C. Krebs, M. Winter, T. Weyhermüller, E. Bill, K. Wieghardt, P. Chaudhuri, *J. Chem. Soc., Chem. Commun.* **1995**, 1913.

[8] [8a] *Chem. Rev.* **1996**, *96*, No. 7. Guest Editors, R. H. Holm, E. I. Solomon. [8b] *Metal Ions in Biological Systems* (Eds.: H. Sigel, A. Sigel), Marcel-Dekker, New York, 1994, Vol. 30. [8c] G. T. Babcock, M. Espe, C. Hoganson, N. Lydakis-Simantiris, J. McCracken, W. Shi, S. Styring, C. Tommas, K. Warncke, *Acta Chem. Scand.* **1997**, *51*, 533. [8d] M. M. Fontecave, J. L. Pierre, *Bull. Soc. Chim. Fr.* **1996**, *133*, 653. [8e] D. P. Goldberg, S. J. Lippard, *Adv. Chem. Ser.* **1995**, *246*, 59. [8f] J. Stubbe, W. A. van der Donk, *Chem. Rev.* **1998**, *98*, 705.

[9] For example: [9a] J. A. Halfen, B. A. Jazdzewski, S. Mahapatra, L. M. Berreau, E. C. Wilkinson, L. Que, Jr., W. B. Tolman, *J. Am. Chem. Soc.* **1997**, *119*, 8217. [9b] Y. Wang, T. D. P. Stack, *J. Am. Chem. Soc.* **1996**, *118*, 13097. [9c] D. Zurita, I. Gautier-Luneau, S. Menage, J. L. Pierre, E. Saint-Aman, *J. Biol. Inorg. Chem.* **1997**, *2*, 46. [9d] E. Bill, J. Müller, T. Weyhermüller, K. Wieghardt, *Inorg. Chem.* **1999**, *38*, 5795 and references therein. [9e] M. A. Halcrow, L. M. Lindy Chia, X. Liu, E. J. L. McInnes, L. J. Yellowlees, F. E. Mabbs, I. J. Scowen, M. McPartlin, J. E. Davies, *J. Chem. Soc., Dalton Trans.* **1999**, 1753. [9f] S. Itoh, S. Takayama, R. Arakawa, A. Furuta, M. Komatsu, A. Ishida, S. Takamuku, S. Fukuzumi, *Inorg. Chem.* **1997**, *36*, 1407. [9g] K. Yamato, T. Inada, M. Doe, A. Ichimura, T. Takui, Y. Kojima, T. Kikunaga, S. Nakamura, N. Yanagihara, T. Onaka, S. Yano, *Bull. Chem. Soc. Jpn.* **2000**, *73*, 903. [9h] Y. Shimazaki, S. Huth, A. Odani, O. Yamauchi, *Angew. Chem. Int. Ed.* **2000**, *112*, 1666. [9i] M. Vaidyanathan, M. Palaniandavar, *Proc. Indian Acad. Sci. (Chem. Sci)* **2000**, *112*, 223. [9j] C. N. Verani, E. Bothe, D. Burdinski, T. Weyhermüller, U. Flörke, P. Chaudhuri, *Eur. J. Inorg. Chem.* **2001**, 2161.

[10] P. Chaudhuri, K. Wieghardt, *Progr. Inorg. Chem.* (Ed.: K. D. Karlin) **2002**, *50*, 151.

[11] B. F. Hoskins, R. Robson, D. Vince, *J. Chem. Soc., Chem. Commun.* **1973**, 392.

[12] R. K. Andrews, R. L. Blakeley, B. Zerner, in *The Bioinorganic Chemistry of Nickel* (Ed.: J. R. Lancaster), VCH, New York 1988.

[13] [13a] E. Jabri, M. B. Carr, R. P. Hausinger, P. A. Karplus, *Science* **1995**, *268*, 998. [13b] M. A. Pearson, L. O. Michel, R. P. Hausinger, P. A. Karplus, *Biochemistry* **1997**, *36*, 8164. [13c] S. Benini, W. R. Rypniewski, K. S. Wilson, S. Ciurli, S. Mangani, *J. Biol. Inorg. Chem.* **1998**, *3*, 268. [13d] S. Benini, W. R. Rypniewski, K. S. Wilson, S. Miletti, S. Ciurli, S. Mangani, *Structure* **1999**, *7*, 205. [13e] S. Ciurli, S. Benini, W. R. Rypniewski, K. S. Wilson, S. Miletti, S. Mangani, *Coord. Chem. Rev.* **1999**, *190−192*, 331.

[14] [14a] H. E. Wages, K. L. Taft, S. J. Lippard, *Inorg. Chem.* **1993**, *32*, 4985. [14b] Y. Hosokawa, H. Yamane, Y. Nakao, K. Matsumoto, S. Takamizawa, W. Mori, S. Suzuki, *Chem. Lett.* **1997**, 891. [14c] M. Arnold, D. A. Brown, O. Deeg, W. Errington, W. Haase, K. Herlihy, T. J. Kemp, H. Nimir, R. Werner, *Inorg. Chem.* **1998**, *37*, 2920. [14d] T. Koga, H. Furutachi, T. Nakamura, N. Fukita, M. Ohba, K. Takahashi, H. Okawa, *Inorg. Chem.* **1998**, *37*, 989. [14e] F. Meyer, H. Pritzkow, *Chem. Commun.* **1998**, 1555. [14f] F. Meyer, E. Kaifer, P. Kircher, K. Heinze, H. Pritzkow, *Chem. Eur. J.* **1999**, *5*, 1617. [14g] K. Yamaguchi, S. Koshino, F. Akagi, M. Suzuki, A. Uehara, S. Suzuki, *J. Am. Chem. Soc.* **1997**, *119*, 5752. [14h] H. Yamane, Y. Nakao, S. Kawabe, Y. Xie, N. Kanehisa, Y. Kai, M. Kinoshita, W. Mori, Y. Hayashi, *Bull. Chem. Soc. Jpn.* **2001**, *74*, 2107.

[15] A. M. Barrios, S. J. Lippard, *J. Am. Chem. Soc.* **2000**, *122*, 9172.

[16] [16a] K. E. Andrew, A. B. Blake, *J. Chem. Soc. A* **1969**, 1456. [16b] B. Aurivillius, *Acta Chem. Scand., Ser. A* **1977**, *31*, 501. [16c] J. A. Bertrand, C. Marabella, D. G. Vanderveer, *Inorg. Chim. Acta* **1978**, *26*, 113. [16d] W. L. Gladfelter, M. W. Lynch, W. P. Schaefer, D. N. Hendrickson, H. B. Gray, *Inorg. Chem.* **1981**, *20*, 2390. [16e] K. Bizilj, S. G. Hardin, B. F. Hoskins, P. J. Oliver, E. R. T. Tiekink, G. Winter, *Aust. J. Chem.* **1986**, *39*, 1035. [16f] L. Ballester, E. Coronado, A. Gutiérrez, A. Monge, M. F. Perpinán, E. Pinilla, T. Rico, *Inorg. Chem.* **1992**, *31*, 2053. [16g] A. J. Atkins, A. J. Blake, M. Schröder, *J. Chem. Soc., Chem. Commun.* **1993**, 1662. [16h] A. J. Blake, E. K. Brechin, A. Codron, R. O. Gould, C. M. Grant, S. Parsons, J. M. Rawson, R. E. P. Winpenny, *J. Chem. Soc., Chem. Commun.* **1995**,

1983. [16i] M. A. Halcrow, J.-S. Sun, J. C. Huffman, G. Christou, *Inorg. Chem.* **1995**, *34*, 4167. [16j] M. S. E. Fallah, E. Rentschler, A. Caneschi, D. Gatteschi, *Inorg. Chim. Acta* **1996**, *247*, 231. [16k] A. Escuer, M. Font-Bardiá, S. B. Kumar, X. Solans, R. Vicente, *Polyhedron* **1999**, *18*, 909. [16l] M. L. Tong, H. K. Lee, S.-L. Zheng, X.-M. Chen, *Chem. Lett.* **1999**, 1087. [16m] J. M. Clemente-Juan, B. Chansou, B. Donnadieu, J.-P. Tuchagues, *Inorg. Chem.* **2000**, *39*, 5515.

[17] For selected examples see: [17a] K. D. Karlin, A. Farooq, J. C. Hayes, B. I. Cohen, T. M. Rowe, E. Sinn, J. Zubieta, *Inorg. Chem.* **1987**, *26*, 1271. [17b] M. Sakamoto, S. Itose, T. Ishimori, N. Matsumoto, H. Okawa, S. Kida, *J. Chem. Soc., Dalton Trans.* **1989**, 2083. [17c] K. J. Oberhausen, J. F. Richardson, R. M. Buchanan, J. K. McCusker, D. N. Hendrickson, J.-M. Latour, *Inorg. Chem.* **1991**, *30*, 1357. [17d] S. S. Tandon, L. K. Thompson, J. N. Bridson, M. Bubenik, *Inorg. Chem.* **1993**, *32*, 4621. [17e] P. Cheng, D. Liao, S. Yan, J. Cui, Z. Jiang, G. Wang, *Helv. Chim. Acta* **1997**, *80*, 213. [17f] P. Amudha, M. Kandaswamy, L. Govindasamy, D. Velmurugan, *Inorg. Chem.* **1998**, *37*, 4486. [17g] P. Dalgaard, A. Hazell, C. J. McKenzie, B. Moubaraki, K. S. Murray, *Polyhedron* **2000**, *19*, 1909.

[18] [18a] J. A. Bertrand, J. A. Kelly, *J. Am. Chem. Soc.* **1966**, *88*, 4746. [18b] J. A. Bertrand, *Inorg. Chem.* **1967**, *6*, 495.

[19] [19a] H. Bock, H. tom Dieck, H. Pyttlik, M. Schnöller, *Z. Anorg. Allg. Chem.* **1968**, *357*, 54. [19b] B. T. Kilbourn, J. D. Dunitz, *Inorg. Chim. Acta* **1967**, *1*, 209. [19c] F. S. Keij, J. G. Haasnoot, A. J. Oosterling, J. Reedijk, C. J. O'Connor, J. H. Zang, A. L. Spek, *Inorg. Chim. Acta* **1991**, *181*, 185. [19d] H. M. Haendler, *Acta Crystallogr., Sect. C* **1990**, *46*, 2054. [19e] R. E. Norman, N. J. Rose, R. E. Stenkamp, *Acta Crystallogr., Sect. C* **1989**, *45*, 1707. [19f] S. Brownstein, N. F. Han, E. Gabe, F. Leer, *Can. J. Chem.* **1989**, *67*, 551. [19g] J. T. Guy, Jr., J. C. Cooper, R. D. Gillardi, J. L. Flippen-Anderson, C. F. George, Jr., *Inorg. Chem.* **1988**, *27*, 635. [19h] M. R. Churchill, F. J. Rotella, *Inorg. Chem.* **1979**, *18*, 853. [19i] R. C. Dickinson, F. T. Helm, W. A. Baker, Jr., T. D. Black, W. H. Watson, Jr., *Inorg. Chem.* **1977**, *16*, 1530 and references therein. [19j] J. J. de Boer, D. Bright, J. N. Helle, *Acta Crystallogr., Sect. B* **1972**, *28*, 3436. [19k] S. Teipel, K. Griesar, W. Haase, B. Krebs, *Inorg. Chem.* **1994**, *33*, 456. [19l] L. Chen, S. R. Breeze, R. J. Rousseau, S. Wang, L. K. Thompson, *Inorg. Chem.* **1995**, *34*, 454. [19m] S. R. Breeze, S. Wang, L. Chen, *J. Chem. Soc., Dalton Trans.* **1996**, 1341. [19n] A. M. Atria, A. Vega, M. Contreras, J. Valenzuela, E. Spodine, *Inorg. Chem.* **1999**, *38*, 5681.

[20] J. Reim, K. Griesar, W. Haase, B. Krebs, *J. Chem. Soc., Dalton Trans.* **1995**, 2649.

[21] F. Birkelbach, C. Krebs, V. Staemmler, unpublished, Bochum, Germany, **1997**.

[22] S. A. Marshall, A. R. Reinberg, *J. Appl. Phys.* **1960**, *31*, 3365.

[23] [23a] V. H. Crawford, H. W. Richardson, J. R. Wasson, D. H. Hodgson, W. E. Hatfield, *Inorg. Chem.* **1976**, *15*, 2107. [23b] L. Merz, W. Haase, *J. Chem. Soc., Dalton Trans.* **1980**, 875. [23c] L. K. Thompson, S. K. Mandal, S. S. Tandon, J. N. Bridson, M. K. Park, *Inorg. Chem.* **1996**, *35*, 3117 and references cited therein.

[24] P. Chaudhuri, C. N. Verani, E. Bill, E. Bothe, T. Weyhermüller, K. Wieghardt, *J. Am. Chem. Soc.* **2001**, *123*, 2213.

Received August 16, 2002
[I02463]

(Allenylidene)ruthenium Complexes with Redox-Active Substituents and Ligands

Stephan Hartmann,[a] Rainer F. Winter,*[a] Birgit M. Brunner,[a] Biprajit Sarkar,[a] Axel Knödler,[a][‡] and Ingo Hartenbach[a][‡]

Keywords: Electrochemistry / Sandwich complexes / Ruthenium / Spectroelectrochemistry

We describe the allenylidene complexes $[TpL_2Ru{=}C{=}C{=}CPhR]^+ SbF_6^-$ [Tp = $HB(pz)_3^-$, L_2 = 2 PPh_3 or 1,1′-bis(diphenylphosphanyl)ferrocene (dppf), R = Ph or ferrocenyl] and their spectroscopic and electrochemical characteristics. Three of these compounds possess redox-active, ferrocene-based substituents or ligands – that are oxidized at lower potentials than the ruthenium center itself – attached either to the terminal carbon atom of the allenylidene ligand or to the ruthenium atom. The Fc/Ph-substituted complexes **3a** and **3b** provide unique examples of hindered rotation of the allenylidene substituent around the M=C bond. For **3a** (L_2 = 2 PPh_3), two isomers differing in the orientation of the vertically aligned, unsymmetrically substituted allenylidene ligand are discernible even at 388 K. The dppf-substituted congener **3b** has the allenylidene ligand in a horizontal orientation and exhibits a rotational barrier, as determined by dynamic ^{31}P NMR spectroscopy, of $\Delta G^{\neq}$ = 47 kJ/mol at T_C = 238 K. The changes in the spectroscopic and electrochemical properties upon replacement of the PPh_3 by a dppf ligand and the Ph by an Fc moiety can be explained in terms of the bonding within these systems. These effects are attenuated when the ferrocene-based redox tags are oxidized, as shown by IR and UV/Vis spectroelectrochemistry. Thus, infrared spectroelectrochemistry reveals a blue shift of the allenylidene stretch upon oxidation of the dppf ligand, while oxidation of the ferrocene covalently linked to the unsaturated C_3 ligand has the opposite effect. Oxidation of the ruthenium atom influences the bonding within the unsaturated ligand more profoundly. Results from IR spectroelectrochemistry point to a vinylidene structure in the Ru^{III} state. Reduction enhances the contribution of alkynyl-type resonance forms to the overall bonding description, as also shown by IR spectroelectrochemistry. For the ferrocenyl-substituted allenylidene complexes, oxidation and reduction result in bleaching of the intense optical low-energy absorption band attributed to a ferrocenyl-to-allenylidene charge-transfer process. The EPR spectra of the paramagnetic reduced forms of these complexes also indicate spin delocalization into the aryl substituents attached to the allenylidene ligand. The complexes Tp(dppf)RuCl and $[Tp(dppf)Ru{=}C{=}C{=}CPh_2]^+ SbF_6^-$ were also characterized by X-ray crystallography.

(© Wiley-VCH Verlag GmbH & Co. KGaA, 69451 Weinheim, Germany, 2003)

Introduction

In connection with our interest in the reactivity of primary butatrienylidene intermediates *trans*-$[Cl(L_2)_2Ru{=}C{=}C{=}C{=}CH_2]^+$ (L_2 = chelating diphosphane ligand) we have established new routes to heteroatom-substituted allenylidene complexes *trans*-$[Cl(L_2)_2Ru{=}C{=}C{=}C(ER_n)(R')]^+$, in part with unprecedented (ER_n = SR, SeR) substitution patterns.[1,2] These rely either on the regioselective addition of protic nucleophiles to the terminal C=C double bond of the unsaturated ligand or on the regioselective addition of aprotic, allyl-substituted nucleophiles to carbon atom C-γ. In this latter case, the initial addition is followed by a Cope-type rearrangement of the resulting 3-heterohexa-1,5-diene moiety.[1−4] The former approach had also been employed by Bruce and others in the synthesis of amino-substituted allenylidene complexes $[Cp(PPh_3)_2Ru{=}C{=}C{=}C(NR_2)(CH_3)]^+$ [5,6] and the related alkoxy-substituted iron derivative $[Cp^*(dppe)Fe{=}C{=}C{=}C(OCH_3)(CH_3)]^+$.[7] Characteristic attributes of allenylidene complexes include: (i) the asymmetric valence band known as the "allenylidene stretch", giving rise to highly intense absorption bands in their infrared spectra, (ii) low-field signals for the carbon atoms of the unsaturated ligands in their ^{13}C NMR spectra,[4,8] and (iii) their optical spectra, which feature two bands in the visible region. The band at lower energy is due to the forbidden HOMO → LUMO transition and so is only weak, while that at higher energy is much more intense and represents the allowed transition from the lower lying second-highest occupied molecular orbital HOMO-1. Systematic studies on the complexes *trans*-$[Cl(L_2)_2Ru{=}C{=}C{=}C(ER_n)(R')]^+$ revealed that their spectroscopic and electrochemical properties critically depend on the substituent ER_n (ER_n = NR_2, SR, SeR, aryl) and the diphosphane ligands L_2. Replacement of amino substituents NR_2 by the less potent π-donors SR, SeR, or aryl groups induces a systematic red shift of the electronic and infrared absorption bands and a low-field shift of the resonance signals of the

[a] Institut für Anorganische Chemie der Universität Stuttgart, Pfaffenwaldring 55, 70569 Stuttgart, Germany
E-mail: winter@iac.uni-stuttgart.de
[‡] X-ray structure determination

metal-bound carbon atom C-α and the carbon atom C-β adjacent to it.[1,2] Electrochemical investigations by cyclic voltammetry revealed a cathodic displacement of the half-wave potentials of the reduction and, albeit only to a minor degree, of the oxidation potentials upon substitution of NR_2 by SR, SeR, or aryl moieties. Broadly similar effects are observed when the π-acidity of the diphosphane chelate ligands is decreased. This mirrors the push-pull characteristics of these complexes, with the $ClRu(L_2)_2^+$ moiety acting as the donor and the allenylidene unit as the acceptor. One remarkable difference between the effects concomitant with ligand and substituent replacement is their effect on the redox potentials: replacement of the π-acidic ligands dppe and dppm by the more basic depe facilitates oxidation by more than 300 mV but leaves the reduction potential essentially unchanged. This has been taken as an indication of a ruthenium-based oxidation but a largely allenylidene-based reduction. Spectroelectrochemical experiments, monitoring the spectroscopic changes associated with bulk electrolysis by IR, UV/Vis, and EPR techniques, and results from quantum mechanical calculations strongly support this view.[1,4,9−11]

We have now turned our attention to allenylidene complexes with either an additional redox-active moiety attached to the C_3 ligand or a redox-active diphosphane ligand. These were chosen such that they would undergo reversible electron transfer at lower potentials than the parent allenylidene complex itself. This was to allow examination of the effect of variation of the electron density at each of these sites *within the same basic system*, without the need for additional ligand or substituent replacement. Since structural perturbations of the metallabutatriene chromophore associated with electron transfer at a peripheral site would be expected to be reasonably limited, the results from such studies should reflect the effects of changes in the electron density at these sites more truly than any substitution. In this respect, ferrocenyl-based systems are ideal candidates, as they are known to undergo facile and reversible oxidation at substantially lower potentials than the $Ru^{II/III}$ couple. We have already reported on the ferrocenyl-substituted allenylidene complexes *trans*-$[Cl(dppm)_2Ru{=}C{=}C{=}C(NMe_2)(C_2H_4Fc)]^+$ [Fc = $(\eta^5\text{-}C_5H_4)Fe(\eta^5\text{-}C_5H_5)$][12] and *trans*-$[Cl(dppm)_2Ru{=}C{=}C{=}C(SeFc)(C_2H_4CH{=}CH_2)]^+$.[2] In the amino-substituted complex the insulating ethylene spacer separating the allenylidene chromophore from the redox-active ferrocenyl unit prevents effective conjugation between these entities. The spectroscopic changes associated with ferrocene oxidation are therefore small. In the seleno-substituted allenylidene complex, the redox-active group is directly attached to the heteroatom. Electron transfer from this site induces more substantial spectroscopic changes, with a red shift of the IR frequency by 10 cm^{-1}. Here we present our results on a different class of allenylidene complexes based on $TpRuL_2$ units, as pioneered by Puerta and Hill [Tp = $HB(pz)_3^-$, tris(pyrazolyl)borate].[13−15] These complexes offer the opportunity to introduce ferrocene-based redox tags either into the allenylidene ligand or into the diphosphane chelate ligand − or into both − while maintaining the same overall structure. We compare our results for these systems with those for the corresponding "parent" diphenylallenylidene complex $[Tp(PPh_3)_2Ru{=}C{=}C{=}CPh_2]^+$, which lacks any additional redox-active moiety, as a reference system.[13]

Results and Discussion

Synthesis, Molecular Structures, and Spectroscopic Properties

The synthesis of allenylidene complexes containing the $[TpRuL_2]$ moiety is straightforward and follows the method elaborated by Hill and co-workers.[13] Treatment of a CH_2Cl_2 solution of $[TpRuL_2Cl]$ (L_2 = 2 PPh_3: **1a**; L_2 = dppf: **1b**) with the appropriate propargylic alcohol PhR(OH)CC≡CH [R = Ph, Fc; Fc = $(\eta^5\text{-}C_5H_4)Fe(\eta^5\text{-}C_5H_5)$] in the presence of $AgSbF_6$ gave the corresponding cationic allenylidene complexes $[TpL_2Ru{=}C{=}C{=}CRPh]^+$ (**2a**−**3b**) in good to reasonable yields and as intensely purple-colored, microcrystalline solids (Scheme 1). In the course of these syntheses we obtained single crystals of [Tp(dppf)RuCl] and the corresponding diphenyl-substituted allenylidene complex $[Tp(dppf)Ru{=}C{=}C{=}CPh_2]^+$ (**2b**). Their molecular structures in the solid state were established by X-ray crystallography and are presented in Figures 1−3, while selected bond parameters are provided in Tables 1 and 2.

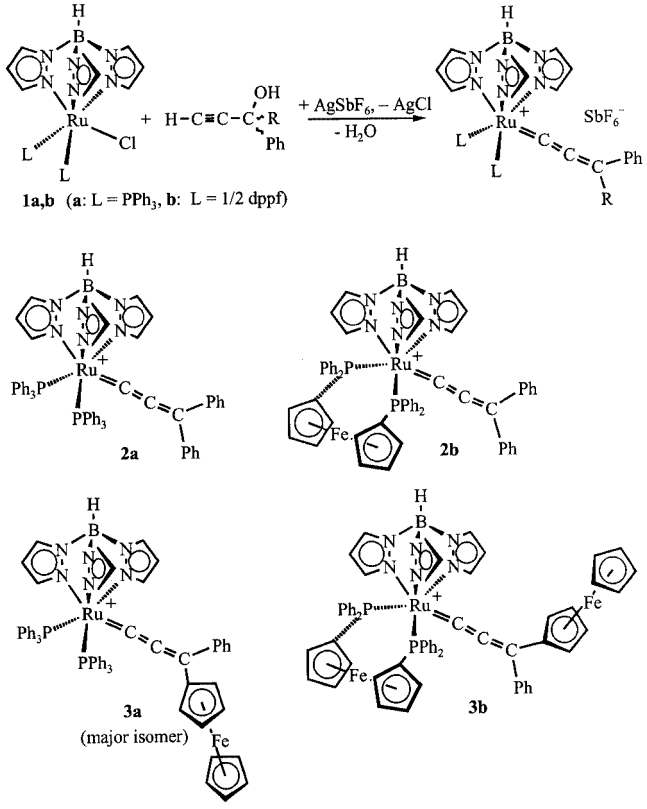

Scheme 1

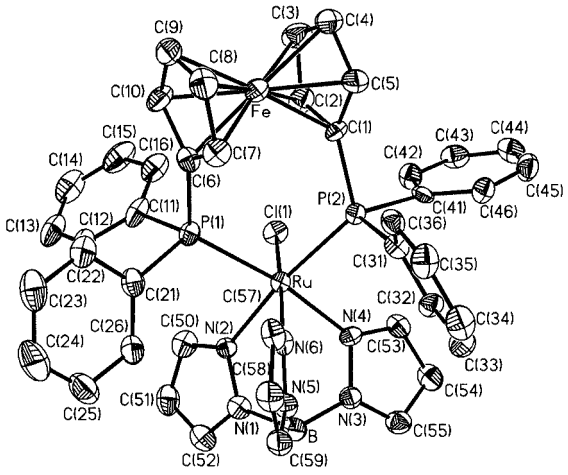

Figure 1. Structure of [Tp(dppf)RuCl] in the solid state

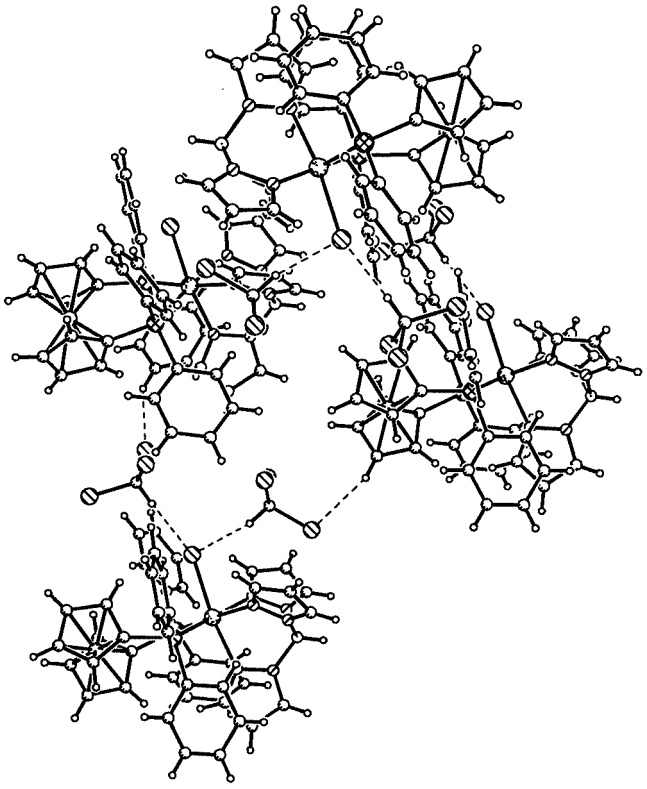

Figure 2. Intermolecular contacts between the chloride ligand and the solvate molecules of [Tp(dppf)RuCl]

[Tp(dppf)RuCl] (**1b**) crystallizes as a bis(solvate) from chloroform, and a plot of its structure is presented as Figure 1. Complex **1b** displays bond parameters (Table 1) very similar to those of the PPh_3-substituted congener.[17] The P(1)−Ru−P(2) bite angle of the chelating dppf ligand is only slightly smaller than the P−Ru−P angle in the other complex [99.23(6) against 101.9(1)°] and induces a compression of the opposite angle N(2)−Ru−N(4) to 81.9(2)°. All other angles between *cis*-disposed ligands are in the 85.0−93.8° range, while mutually *trans*-disposed ligands make angles of approximately 171° at the metal atom.

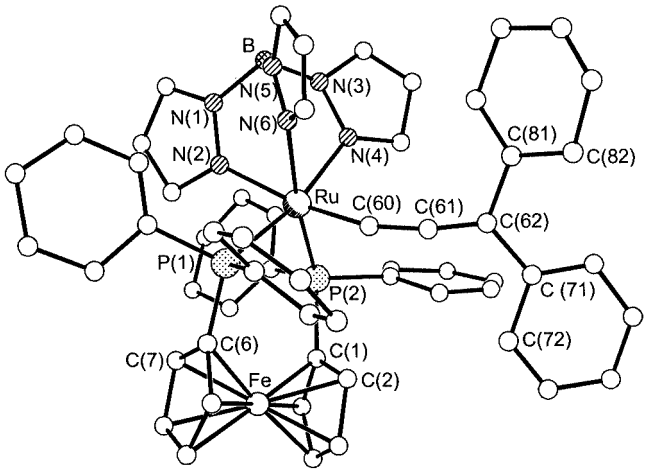

Figure 3. Structure of $[Tp(dppf)Ru{=}C{=}C{=}CPh_2]^+$ in the solid state

Table 1. Selected bond lengths [Å] and bond angles [°] for [Tp(dppf)RuCl] (**1b**)

Ru−N(2)	2.144(5)	N(4)−Ru−N(2)	81.86(19)
Ru−N(4)	2.144(5)	N(6)−Ru−N(2)	87.57(19)
Ru−N(6)	2.099(5)	N(6)−Ru−N(4)	87.60(19)
Ru−P(1)	2.3503(16)	N(2)−Ru−P(1)	89.70(14)
Ru−P(2)	2.3362(16)	N(6)−Ru−P(1)	89.34(15)
Ru−Cl(1)	2.4200(16)	N(4)−Ru−P(1)	171.13(14)
Fe−C(1)	2.001(6)	N(4)−Ru−P(2)	89.27(14)
Fe−C(2)	2.018(7)	N(6)−Ru−P(2)	93.59(14)
Fe−C(3)	2.063(7)	N(2)−Ru−P(2)	171.00(14)
Fe−C(4)	2.084(7)	P(2)−Ru−P(1)	99.23(6)
Fe−C(5)	2.052(7)	P(1)−Ru−Cl	93.83(6)
Fe−C(6)	2.009(6)	P(2)−Ru−Cl	93.28(6)
Fe−C(7)	2.013(7)	N(2)−Ru−Cl	84.98(14)
Fe−C(8)	2.061(7)	N(4)−Ru−Cl	88.15(14)
Fe−C(9)	2.061(7)	N(6)−Ru−Cl	171.87(14)
Fe−C(10)	2.032(7)	P(2)−Ru−P(1)	99.23(6)
P(1)−C(6)	1.835(6)	P(1)−Ru−Cl	93.83(6)
P(1)−C(11)	1.850(7)	P(2)−Ru−Cl	93.28(6)
P(2)−C(1)	1.807(6)		
P(2)−C(31)	1.823(6)		
P(2)−C(41)	1.862(6)		

Table 2. Selected bond lengths [Å] and bond angles [°] for $[Tp(dppf)Ru(=C=C=CPh_2)]\ SbF_6$ (**2b**)

Ru−P(1)	2.416(9)	P(1)−Ru−P(2)	99.1(3)
Ru−P(2)	2.376(11)	P(1)−Ru−C(60)	94.7(11)
Ru−N(2)	2.16(3)	P(2)−Ru−C(60)	92.1(11)
Ru−N(4)	2.18(3)	N(2)−Ru−N(4)	84.8(10)
Ru−N(6)	2.20(3)	N(2)−Ru−N(6)	85.5(10)
Ru−C(60)	1.88(4)	N(4)−Ru−N(6)	81.8(11)
C(60)−C(61)	1.32(5)	P(1)−Ru−N(2)	89.3(7)
C(61)−C(62)	1.26(5)	P(1)−Ru−N(4)	169.2(8)
C(61)−C(71)	1.46(5)	P(1)−Ru−N(6)	88.8(8)
C(61)−C(81)	1.52(5)	P(2)−Ru−N(2)	95.2(7)
		P(2)−Ru−N(4)	90.5(8)
		P(2)−Ru−N(6)	172.2(8)
		Ru−C(60)−C(61)	168(3)
		C(60)−C61)−C(62)	168(4)

The close similarity between [Tp(dppf)RuCl] and [Tp(PPh_3)$_2$RuCl] is also evident from the essentially identical Ru−P and Ru−Cl bond lengths in these two complexes [2.336(2), 2.350(2) and 2.420(2) against 2.332(3), 2.349(3) and 2.409(3) Å]. As is often observed for complexes of the Tp ligand,[13,18,19] the nitrogen atom *trans* to the chloride ligand is closer to the metal center than those opposite to the π-accepting phosphane ligands. Both the cyclopentadienyl (Cp) rings of the dppf ligand are essentially planar, and the phosphorus atoms are situated in the plane of the ring to which they are attached. The ring centroids and the Fe atom make an angle of 178.2°, while the two rings adopt a staggered conformation and are rotated by 38° with respect to one another. The packing in the crystal lattice is stabilized by several inter- and intramolecular hydrogen bonds involving the solvate molecules, the chloride ligand, some nitrogen atoms of the pyrazolyl rings, and one hydrogen atom of each phenyl ring, as well as one of the Cp-hydrogen atoms of the dppf ligand. Intramolecular hydrogen bonds of 2.528 and 2.663 Å are observed between the *ortho*-hydrogen atom attached to C(26) and the nitrogen atoms N(1) and N(2). A similar contact is found for H(32a) − the hydrogen atom at C(32) − and N(4) (2.677 Å). The chloride ligand forms a pair of contacts to one of the *ortho*-hydrogen atoms of each of the adjacent phenyl rings, with a fairly short bond of 2.590 Å to H(42) and a weaker contact of 2.871 Å to H(16) on the other phenyl ring. The chloride ligand also forms strong intermolecular contacts to the protons of the two cocrystallized $CHCl_3$ solvate molecules, as evidenced by H···Cl distances of 2.393 and 2.423 Å. The solute molecules are additionally fixed through weaker interactions to hydrogen atoms on the aromatic substituents. Thus, one chloroform molecule makes a contact of 2.834 Å to one of the phenyl protons, while the other is 2.792 Å away from H(8a) at the 3-position of one of the Cp rings of the dppf ligand. Additional weaker interactions are observed between the other chlorine atoms of the cocrystallized solvent molecules and hydrogen atoms H(13) [3.292 Å to Cl(5), 3.249 Å to Cl(7)], H(14) [3.247 Å to Cl(2), 3.289 Å to Cl(4)], and H(43) [3.274 Å to Cl(3)] on the phenyl rings as well as to H(9) [3.175 Å to Cl(6)] on the Cp ring. The H-bridges resulting from the stronger intermolecular H···Cl contacts are shown in Figure 2.

The diphenylallenylidene complexes **2a** and **2b**, including the solid-state structure of compound **2a**, have already been reported by Hill.[13] We were able to obtain single crystals of the dppf-substituted congener **2b**, but these gave a data set of only poor quality, preventing meaningful discussion of bond lengths and angles within the allenylidene chain. We only note that, as in the chloro precursors **1a** and **1b**, the Ru−P bond lengths and the P−Ru−P angles are nearly identical for both allenylidene complexes [2.376(11) and 2.416(9) against 2.3779(7) and 2.4327(11) Å as well as 99.1(3) against 101.11 (3)°]. We also note that the terminal CPh_2 group of the allenylidene ligand lies approximately in the mirror plane of the molecule [the torsional angle N(2)−Ru−C(62)−C(81) is 18.5°] and roughly bisects the P−Ru−P angle. This orientation has been termed vertical. A plot of the structure is provided as Figure 3, while the most pertinent bond parameters are collected in Table 2.

Complexes **2a** and **2b** and their Fc-substituted congeners **3a** and **3b** have very similar spectroscopic characteristics in their IR and NMR spectra. These are compared in Table 3. Samples (as KBr pellets) display the C=C=C stretch of the unsaturated ligand as a very intense band at 1946 cm^{-1} for **3a** and at 1941 cm^{-1} for **3b**, which are some 5 cm^{-1} higher in energy than in the diphenyl-substituted complexes **2a** and **2b** (see also Table 3). Replacement of the dppf by the less basic PPh_3 ligands induces a blue shift of similar size. The observed effects, albeit small, match previous observations that the presence of a weaker π-donor at the terminal carbon atom C-γ (phenyl versus ferrocenyl) or of a more basic metal center at the opposite end of the metallabutatriene chain (the dppf versus two PPh_3 ligands) shifts the IR absorption of the allenylidene ligand to lower energies. This has been explained in terms of a larger contribution from the alkynyl-type resonance form **II** as opposed to the genuine cumulenylidene-type resonance form **I** (Scheme 2) when the metal center is more electron-rich and the substituents at C-γ are less able to support a positive charge adjacent to them.[1,2,4,20,21] In the light of the stability of the ferrocenylmethylene carbenium ion[22] the ferrocenyl substituent may be expected to stabilize the alternative alkynyl resonance form **III**, as indicated in Scheme 2, in line with the results from IR spectroscopy. We note here that Le Bozec et al. arrived at a similar conclusion in their study of [(C_6Me_6)-Cl(PMe_3)Ru=C=C=C(Ph)(Fc)]$^+$ PF_6^-, closely related to **3a** and **3b**.[23] The ^{13}C NMR spectra also bear witness to this notion. Comparison of the relevant data for the pairs of complexes **2a/3a** and **2b/3b** reveals that replacement of a phenyl by the more strongly electron-donating ferrocenyl substituent shifts the resonance signals of the carbon atoms of the allenylidene ligand to higher field by ca. 30, 25, and 8 ppm. The largest shift is observed for the metal-coordinated carbon atom C-α, while the terminal carbon atom C-γ − where the actual substitution occurs − is influenced least. The sign and relative magnitude of the observed effects agree well with results from previous studies on the allenylidene complexes *trans*-[Cl(L_2)$_2$Ru=C=C=C(ER_n)(R′)]$^+$ (ER_n = NR_2, SR, SeR, aryl, R′ = alkyl).[1,4,24]

The triphenylphosphane-substituted complex **3a** was found to exist as two isomers, as shown by the two sets of resonance signals for the carbon atoms of the cumulenylidene ligand. These are observed at δ = 287.0, 184.3, and 168.2 ppm for the major isomer and δ = 282.8, 180.5 and 169.1 ppm for the minor counterpart, and point to hindered rotation of the allenylidene ligand around the Ru=C bond. Each isomer exhibits a singlet resonance signal in the ^{31}P NMR spectrum. We therefore conclude that the plane of the terminal CR_2 unit of the allenylidene ligand runs parallel to the molecular symmetry plane and bisects the P−Ru−P angle, an orientation that has been termed vertical.[25] Scheme 3 offers a Newman-type projection along the Ru=C=C=C axis. The isomers differ in which of the Ph or the Fc substituents points toward the Tp and the

Table 3. Selected spectroscopic data for complexes **2a**−**3b**

Compd.	^{31}P NMR: δ [ppm]	^{13}C NMR: δ [ppm] C-α	C-β	C-γ	IR (KBr): $\tilde{\nu}$(C=C=C) [cm^{-1}]	UV/Vis: λ_{max} [nm] (log ε)[a] HOMO-1 → LUMO	HOMO → LUMO
2a	36.6	316.6	208.9	160.9	1941	527 (4.217)	907 (2.820)
2b	30.2	316.2	208.3	161.3	1936	522 (4.204)	902 (2.763)
3a	40.8[b]	287.0[b]	184.3[b]	168.2[b]	1946	538 (4.061)	—[d]
	40.5[c]	282.8[c]	180.5[c]	169.1[c]			
3b	29.9	283.7	180.6	167.9	1941	540 (4.190)	—[d]

[a] In CH_2Cl_2. [b] Data for major isomer. [c] Data for minor isomer. [d] Obscured by an intense ILCT band (see text).

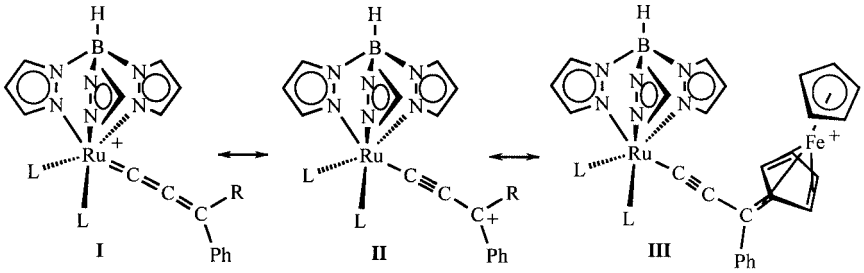

Scheme 2

phosphane ligands. We propose that the major isomer has the less bulky phenyl substituent oriented toward the PPh_3 ligands. By integration of the ^{31}P NMR resonance signals the isomeric distribution was established as 4:1. Unfortunately, we have not yet succeeded in growing X-ray quality crystals of this complex to support this view. We note, however, that both $[Tp(PPh_3)_2Ru{=}C{=}C{=}CPh_2]^+$ PF_6^- (**2a**) and its dppf analogue **2b** (vide supra) crystallize with the allenylidene ligand in just this orientation.[13]

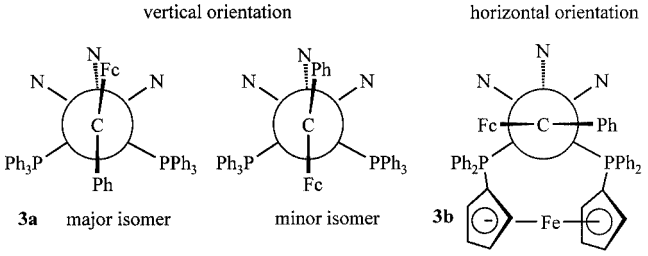

Scheme 3

To the best of our knowledge, complex **3a** represents the first instance of an allenylidene complex in which the energy barrier to rotation of the allenylidene moiety is so high as to allow observation of two different rotamers at ambient temperature. Hindered rotations around M=C double bonds have, however, been noted in the related vinylidene complexes $\{M\}{=}C{=}CR_2$.[26−28] Experimentally measured energy barriers are usually of the order of 30−57 kJ/mol and depend on the substituents on the vinylidene ligand and the coordination environment at the metal center. More recent examples include ruthenium complexes of the tripodal $CH_3C(\eta^5\text{-}C_5H_4)(CH_2PPh_2)_2$ ligand, which coordinates the metal ion through its Cp ring and the two pendant phosphane side-arms ($\Delta G^{\neq} \approx 33$ kJ/mol for secondary vinylidene ligands and 44 kJ/mol for tertiary ones),[29] the dinuclear bis(vinylidene) manganese complex $[(\eta^5\text{-}C_5H_4Me)(dmpe)Mn{=}C{=}C(Ph)C(Ph){=}C{=}Mn(dmpe)(\eta^5\text{-}C_5H_4Me)]^{2+}$ ($\Delta G^{\neq} = 56.7$ kJ/mol),[30] and the cycloheptatrienylmolybdenum complex $[(\eta^7\text{-}C_7H_7)(dppe)Mo{=}C{=}CH_2]^+$ (dppe = $Ph_2PC_2H_4PPh_2$; $\Delta G^{\neq} = 51.9$ kJ/mol).[31] The highest activation energy for vinylidene rotation of which we are aware has been observed for the rhenium complexes $[(\eta^5\text{-}C_5H_5)(NO)(PPh_3)Re{=}C{=}CPhMe]^+$ and $[(\eta^5\text{-}C_5H_5)(NO)(PPh_3)Re{=}C{=}CH_2]^+$ ($\Delta G^{\neq} = 77.9$ kJ/mol).[32] The butyl/methyl-substituted vinylidene complex $[(\eta^7\text{-}C_7H_7)(dppe)Mo{=}C{=}C(C_4H_9)(CH_3)]^+$ displays separate resonance signals for the two different rotamers at 348 K.[31] The rotational barriers are usually thought of as being more steric than electronic in origin. Calculations on (vinylidene)-metal complexes indicate that the intrinsic (electronic) energy difference between the vertical and horizontal rotamers amounts to no more than 10−20 kJ/mol.[25,33] The energy barrier interconnecting them is thus expected to be fairly low. In view of the further remoteness of the terminal methylene group from the metal−ligand array it is therefore not surprising that allenylidene complexes present even lower rotational barriers than their vinylidene counterparts, and so the observation of a truly significant rotational barrier in an allenylidene ligand is quite unusual. This prompted us to study the dynamic behavior of **3a** in 1,2-$D_2C_2Cl_4$ solution by ^{31}P NMR spectroscopy. Upon warming there was a very slight shift of the two singlet resonance signals, but no broadening was observed up to 388 K, at which point **3a** decomposed.

The sterically less hindered complex **3b** exhibits one sharp singlet in its room-temperature ^{31}P NMR spectrum.

When a solution in CD_2Cl_2 is cooled, this signal starts to broaden at 258 K. At 233 K, splitting into two equally intense, broad signals is observed, and at even lower temperatures the four resonance lines of a well-resolved AB spectrum are seen. The coupling constant − 30.65 Hz at 213 K − is typical of *cis*-disposed phosphane ligands (Figure 4). These findings would place the free energy of activation for rotation of the allenylidene ligand at 47 kJ/mol at the coalescence temperature of 238 K. They also indicate a horizontal orientation of the allenylidene ligand with the substituents on the terminal carbon atom orthogonal to the symmetry plane of the [TpRuL$_2$] moiety. This is in sharp contrast to the vertical arrangement proposed for the bis(triphenylphosphane)-substituted counterpart **3a**. In the absence of X-ray data we can only speculate that in the vertical orientation the substituents on the terminal carbon atom would each approach the ferrocenyl backbone of the dppf ligand such that the horizontal orientation would be preferred on steric grounds (see Scheme 3).

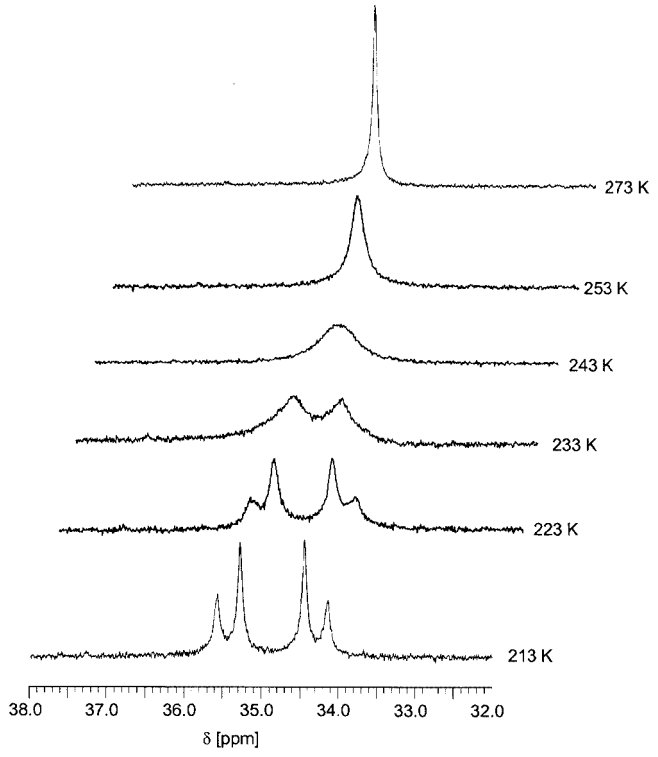

Figure 4. Dynamic ^{31}P NMR spectroscopy of compound **3b** in CD_2Cl_2 solution

In the visible range the electronic spectra of the intensely colored complexes **2a** and **3a** are each dominated by a strong absorption band, at 527 (**2a**) or 522 nm (**2b**) in CH_2Cl_2 solution. This band is only very slightly solvatochromic, shifting to somewhat higher energies in the more polar solvent CH_3CN. For related allenylidene complexes of the *trans*-[Cl(L$_2$)$_2$Ru] moiety, this absorption band has been assigned to an allowed transition from the metal-based second highest molecular orbital HOMO-1 to the LUMO, which is delocalized over the allenylidene ligand. This accounts for the strong Metal-to-Ligand Charge-Transfer (MLCT) character of this band.[4] This assignment also seems to be valid here, since a much weaker absorption at considerably lower energies (907 nm in **2a** and at 902 nm in **2b**) was observed for the forbidden HOMO → LUMO transition. With reference to the *trans*-[Cl(dppm)$_2$Ru]-derived complexes, the HOMO should also be dominated by the metal unit and have appreciable MLCT character as well. As found for the HOMO-1 → LUMO transition, it exhibits negative solvatochromism of a magnitude comparable to that of the main absorption band. We note that replacement of the *trans*-[Cl(L$_2$)$_2$Ru] moiety by [TpRuL$_2$] apparently results in a somewhat smaller energy gap between the two highest occupied levels and the LUMO. This is inferred by comparison of the data for **2a** and **2b** with those for the related complex *trans*-[Cl(dppm)$_2$Ru=C=C=CPh$_2$]$^+$, which has its absorption maxima at 506 and 817 nm. The data also point to a slightly larger energy gap between the two highest occupied levels for the [TpRuL$_2$]-derived complexes. The energy difference between the HOMO-1 → LUMO and the HOMO → LUMO transitions thus amounts to 1.01 eV for **2a** and 0.98 eV for **2b**, as compared to 0.93 eV for *trans*-[Cl(dppm)$_2$Ru=C=C=CPh$_2$]$^+$.

In the ferrocenyl-substituted complexes **3a** and **3b** the intense HOMO-1 → LUMO transition band is shifted to somewhat lower energies, as in the diphenyl-substituted analogues (λ_{max} = 538 nm for **3a**, 540 nm for **3b**, see Table 3). At even lower energies another very intense, broad band is found at 723 (**3a**) and 713 (**3b**) nm, tailing far into the near IR region and burying the HOMO → LUMO band. Again, a slight negative solvatochromism is noted when spectra in CH_2Cl_2 and CH_3CN are compared. This band has no counterpart in **2a** and **2b** and is consequently attributed to a ferrocenyl-to-ligand MLCT charge transfer absorption. If the ferrocenyl substituent and the cumulenic carbon atoms are regarded as belonging to the same chromophore, this band may also be termed an Intraligand Charge Tranfer (ILCT) band, the charge density being shifted between two different sites within the same basic ligand. Irrespective of the exact interpretation, the presence of this additional band points to effective conjugation between the ferrocenyl substituent and the allenylidene chromophore. As discussed later, the above assignment is strongly supported by our results from UV/Vis spectroelectrochemical investigations on the ferrocenyl-based one-electron oxidation.

Spectra of the dppf-substituted complexes **2b** and **3b** are compared in Figure 5. The ferrocene-based absorption of the dppf ligand could not be located, since it is obscured by the much more intense, broad HOMO-1 → LUMO transition. All complexes presented here display another intense band at 350−356 nm (log ε ≈ 4). This feature seems to be characteristic of aryl-substituted allenylidene complexes and so is tentatively assigned to ILCT excitation from the arene substituent(s) to the metallacumulene chromophore. Absorptions at even higher energies in the UV region arise from the n → π* and π → π* transitions of the aryl-substituted phosphane ligands.[34]

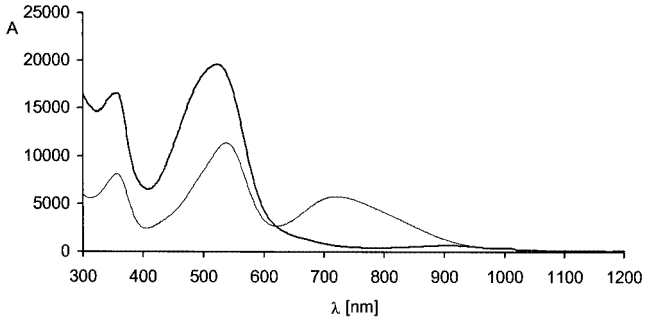

Figure 5. Optical spectra of complexes **2b** and **3b** in CH_2Cl_2

Electrochemistry

Electrochemical studies on the allenylidene complexes *trans*-$[Cl(L)_2Ru{=}C{=}C{=}C(ER_n)(R')]^+$ have shown that each of these complexes undergoes a one-electron oxidation and a one-electron reduction.[1,4] By combining electrochemical and spectroscopic methods we have been able to characterize the oxidation as a primarily metal-based process (i.e., the $Ru^{II/III}$ couple) and the reduction as ligand-based, the latter assignment being confirmed by EPR and IR spectroscopy on their reduced forms. The reduction of the diphenyl-substituted complex *trans*-$[Cl(dppe)_2Ru{=}C{=}C{=}CPh_2]^+$ (**4**), related to **2a**, has meanwhile been investigated by Touchard and co-workers. These authors arrived at essentially the same conclusions and also corroborated the reduction site by exploring the chemical reactivity of the corresponding neutral radical.[35] In that particular compound, a second, irreversible one-electron reduction was observed at a potential −1.10 V lower than the first reversible reduction process. The PPh_3-substituted diphenylallenylidene complex **2a** exhibits essentially identical electrochemical behavior (Figure 6, bottom trace). The one-electron oxidation appears to be only partially reversible under ambient conditions but a meaningful analysis of the degree of chemical reversibility is precluded by its proximity to the anodic discharge limit of the electrolyte solution. Cooling to −78 °C renders the voltammetric wave chemically reversible even at low sweep rates and allowed us to determine its half-wave potential as +1.05 V against the internal ferrocene/ferrocenium standard (Table 4). As with the dppm-substituted complex **4**, two consecutive one-electron reductions are observed. While the first reduction at $E_{1/2}$ = −1.00 V is chemically reversible under ambient conditions, the second reduction is not, and requires cooling to allow detection of the associated anodic return peak. Even so, only partial chemical reversibility could be achieved. It was, however, still possible to determine the half-wave potential of this redox couple as −2.05 V. We note that these potentials are very similar to those of *trans*-$[Cl(dppe)_2Ru{=}C{=}C{=}CPh_2]^+$.[35] This further corroborates our previous finding that − given the same allenylidene ligand − the reduction potentials are virtually independent of the electron density on the metal, a further indication of the ligand-centered nature of this process.[4]

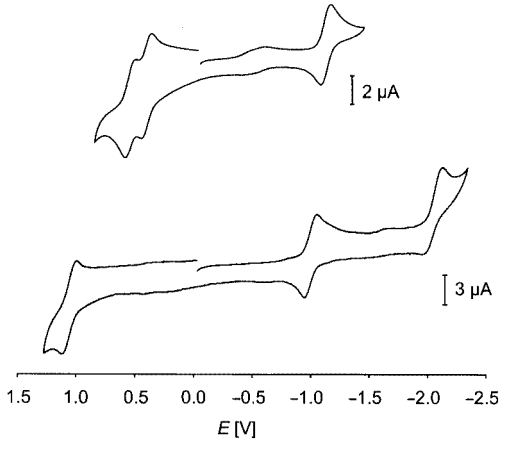

Figure 6. Cyclic voltammograms of complexes **2a** (CH_2Cl_2, 215 K, v = 0.1 V/s, bottom trace) and **3b** (CH_2Cl_2, 298 K, v = 0.1 V/s, top trace)

The analogous compound **2b** contains an electroactive dppf ligand, which would be expected to oxidize at considerably lower potential than the L_nRu^{II} entity. Thus, **2b** displays a reversible one-electron wave at +0.485 V, more than 550 mV more negative than the $Ru^{II/III}$ couple of the PPh_3-substituted congener **2a**. No further anodic processes could be observed within the accessible potential window. During our studies on the ferrocenylethyl-substituted aminoallenylidene complex *trans*-$[Cl(dppm)_2Ru{=}C{=}C{=}C(NMe_2)(C_2H_4Fc)]^+$ we noticed that the $Ru^{II/III}$ couple is shifted anodically by ca. 60 mV relative to closely related complexes upon oxidation of the electroactive ferrocenyl moiety.[12] In that particular example, the observed shift largely reflects the increased electrostatic repulsion between the positively charged centers. A much larger effect is to be expected in **2b**, in which the electroactive ferrocenyl moiety is directly linked to the metal ion. Given the proximity of the $Ru^{II/III}$ process to the anodic discharge limit of the solvent in complex **2a**, it is thus not surprising that it lies outside the accessible potential range in the case of **2b**. The first reduction of this complex is again a fully reversible one-electron process, occurring at almost the same potential as in **2a** (−1.01 V), but no further reduction was observed in this solvent. Complex **3a** has the electroactive ferrocenyl substituent attached to the terminal carbon atom of the allenylidene ligand and gives rise to a reversible one-electron wave at $E_{1/2}$ = +0.36 V. As was the case for **2a**, the ruthenium-based oxidation is again shifted outside the potential window of the electrolyte solution. While this precludes us from quantifying the potential shift of the $Ru^{II/III}$ couple induced by ferrocene oxidation, it nevertheless provides further evidence for effective conjugation between the ferrocene substituent and the cumulenic system, as already inferred from the optical data. Complexes **2a** and **3a** also offer the opportunity to assess the effect on the reduction potentials of replacement of a phenyl by a more strongly donating ferrocene substituent on the terminal carbon atom of the allenylidene ligand. Given the allenylidene-centered nature of the reduction processes, one would expect a cathodic shift of the (+/0) and the (0/−) couples. This is indeed the case. The two reductions for **3a** are observed at potentials 160

Table 4. Electrochemical data for complexes **2a**−**3b**

Complex	Solvent	$E_{1/2}$[a] [$Ru^{II/III}$]	$E_{1/2}$ (dppf)[a]	$E_{1/2}$ (Fc/Fc^+)[a]	$E_{1/2}$ (+/0)[a]	$E_{1/2}$ (0/−)[a]
2a	CH_2Cl_2	+ 1.05 (158)	n. a.	n. a.	−1.00 (138)	−2.05 (192)
	DMF	n. d.	n. d.	n. a.	−0.83 (78)	−2.02[b]
2b	CH_2Cl_2	n. d.	+0.485 (142)	n. a.	−1.01 (134)	n. d.
	DMF	n. d.	n. d.	n. a.	−0.83 (72)	−2.00[b]
3a	CH_2Cl_2	n. d.	n. a.	+0.36 (138)	−1.16 (146)	−2.375[b]
	DMF	n. d.	n. a.	n. d.	−0.99 (80)	−2.16[b]
3b	CH_2Cl_2	n. d.	+0.51 (144)	+0.37 (142)	−1.165 (136)	n. d.
	DMF	n. d.	n. d.	n. d.	−1.00 (78)	−2.13[b]

[a] $E_{1/2}$ values (in V) are calibrated against the internal Fc/Fc^+ standard, ΔE_p values (in mV) are given in brackets. [b] Peak potential of an irreversible process. n. d. = not detected; n. a. = not applicable.

and ca. 320 mV more negative than in its congener **2a**. Despite all efforts, no return peak for the second reduction of **3a** was observed. The reported shift of the (0/−) potential is therefore based on the respective positions of the forward peaks and provides only a qualitative measure.[36]

Lastly, complex **3b** contains both secondary redox sites employed in this study, the dppf ligand on the metal and the ferrocenyl substituent on the terminal carbon atom C-γ. Consequently, two reversible one-electron waves at potentials considerably more negative than those of the $Ru^{II/III}$ couple of **2a** are observed in the cyclic voltammogram of this complex (Figure 6, top trace). The half-wave potentials were determined as +0.37 and +0.51 V relative to the ferrocene/ferrocenium standard. Comparisons with those of **2b** and **3a** argue for an assignment of the less anodic wave to the oxidation of the allenylidene-bound ferrocene moiety and the other one to that of the dppf ligand on the metal ion. Further evidence for this comes from spectroelectrochemical experiments, as detailed below. Paralleling the situation in compounds **2a** and **3a**, the reversible reduction of **3b** is shifted cathodically by 155 mV relative to the diphenyl-substituted **2b**, which again reflects the higher electron density on the allenylidene ligand. No second reduction was observed for **3b** in CH_2Cl_2/Bu_4NPF_6 solution. In order to assess the potential shifts induced on the second reduction by the presence of the ferrocenyl substituent, we also recorded voltammograms in DMF/Bu_4NPF_6 solution. Thanks to its superior cathodic window we were now able to observe this process for all compounds, albeit as an irreversible event. The data in Table 5 show that in this solvent the effect of substitution of one phenyl by a ferrocenyl substituent is probably very similar for both reductions, although the irreversible nature of the second process only allows for a qualitative statement.[36] No useful data, however, could be obtained for any of the oxidations in the DMF solvent.

The voltammetric data for all compounds under study are listed in Table 4. The peak potential splittings significantly exceed the predicted theoretical values of 59 mV at 298 K and 39 mV at 195 K.[36] This effect is largely due to uncompensated resistance of the electrolyte solution, as shown by the nearly identical peak-to-peak separations of the internal ferrocene standard, which is thought to represent an ideal Nernstian redox system, and the much less distorted responses in the more conducting DMF/NBu_4PF_6 electrolyte.

Spectroelectrochemistry

a) Oxidation

We now address the question of how electron transfer from the secondary electroactive moieties attached either to the ruthenium or to the terminal carbon atom of the allenylidene ligand affects the spectroscopic properties of these complexes. As may be inferred from the above discussion, a combination of bulk electrolysis with infrared spectroscopy in an optically transparent thin-layer electrolysis (OTTLE) cell provides the most sensitive tool with which to examine bonding changes accompanying oxidation within the metallacumulene chromophore. The PPh_3-ligated diphenylallenylidene complex **2a** does not contain any additional redox-active moiety and thus serves as a benchmark system for elucidating the spectral changes concomitant with oxidation of the $[\{Ru\}=C=C=C(R)(Ph)]^+$ system itself. It is thus discussed first.

Upon oxidation with IR monitoring, the strong C=C=C stretch of the allenylidene ligand vanishes and is replaced by a weaker absorption at 1587 cm^{-1}. This new band is best accommodated by the vinylidene resonance forms **IV** and **V** (Scheme 4). Both place the unpaired spin on the internal carbon atom C-β of the allenylidene ligand. At a first approximation, one may expect that the electron lost upon oxidation should originate from the HOMO orbital. According to recent DFT calculations on the parent cumulenylidene complexes of the $Cr(CO)_5$ entity,[4,37] and also our own work on the amino-substituted model complex *trans*-$[Cl(PH_3)_4Ru=C=C=C\{N(CH_3)_2\}(CH_3)]^+$,[4] this orbital is mainly composed of the ligand *trans* to the allenylidene ligand, the metal atom, and carbon atom C-β. Spin density calculations performed on *trans*-$[Cl(PH_3)_4Ru=C=C=C(ER_n)(CH_3)]^{2+}$ [ER_n = $O(CH_3)$, $S(CH_3)$, $Se(CH_3)$, CH_3] show that the orbital composition of the HOMO orbital faithfully translates into spin densities in the oxidized form. The mesomeric structures **IV** and **V** agree with these considerations.

Vinylidene complexes of ruthenium are characterized by a fairly intense IR band at around 1690−1580 cm^{-1}.[38] The literature shows a clear trend toward lower energy absorp-

Table 5. Spectroscopic data for complexes **2a**−**3b** in different oxidation states

Compound[a]	IR: $\tilde{\nu}$(B−H), (C=C) or (C=C=C) [cm^{-1}]	UV/Vis: λ [nm] (log ε)
2a [Ru^{II}]	2489 (w) (BH), 1945 (vs)	354 (4.225), 525 (4.284), 909 (2.833)
2a$^+$ [Ru^{III}]	2521 (w) (BH), 1587 (s)	411 (4.282), 491 (4.288), 830 (3.200)
2a$^-$	2469 (w), 1969 (m), 1959 (m)	350 (4.342), 400 (3.879), 480 (3.865), 534 (3.865), 812 (2.531)
2b [Fe^{II} (dppf), Ru^{II}]	2487 (w),1939 (vs), 1573 (m), 1588 (m)	348 (3.995), 361 (sh), 526 (4.201), 901 (2.852)
2b$^+$ [Fe^{III} (dppf), Ru^{II}]	2513 (w), 1957 (vs), 1948 (vs)	351 (4.060), 369 (4.211), 530 (4.044), 850 (2.903)
2b^{2+} [Fe^{III} (dppf), Ru^{III}]	not detected	387 (4.090), 513 (3.949), 728 (3.083)
2b$^-$	2473 (w), 1966 (m), 1956 (m)	351 (4.156), 405 (3.760), 452 (3.680), 530 (5.735), 630 (sh, 3.057), 847 (2.813)
3a [Fe^{II} (Fc), Ru^{II}]	2488 (w), 1948 (vs)	356 (3.903), 538 (4.061), 723 (3.756)
3a$^+$ [Fe^{III} (Fc), Ru^{II}]	2506 (w), 1924 (s)	298 (4.097), 353 (3.863), 544 (4.000)
3a^{2+} [Fe^{III} (Fc), Ru^{III}]	2514 (w), 1507 (s)	not detected
3a$^-$	2463 (w), 1969 (s)	340 (3.929), 410(sh), 451 (3.813), 544 (3.744), 693 (2.653)
3b [Fe^{II} (Fc), Fe^{II} (dppf), Ru^{II}]	2488 (w), 1945 (vs)	353 (4.279), 538 (4.290), 713 (4.112)
3b$^+$ [Fe^{III} (Fc), Fe^{II} (dppf), Ru^{II}]	2506 (w), 1916 (m)	353 (4.250), 540 (4.228), 701 (3.919)
3b^{2+} [Fe^{III} (Fc), Fe^{III} (dppf), Ru^{II}]	2488 (w), 1945 (s), 1912 (m)	315 (4.228), 353 (4.243), 475 (sh), 548 (4.225), 685 (3.829)
3b^{3+} [Fe^{III} (Fc), Fe^{III} (dppf), Ru^{III}]	2519 (w), 1524 (s)	368 (4.188), 468 (4.215), 557 (3.914), 702 (4.047)
3b$^-$	2470 (w), 1963 (m)	343 (4.270), 413 (3.941), 456 (4.072), 549 (4.005), 865 (2.771)

[a] All data in $C_2H_4Cl_2$/0.25 M Bu_4NPF_6 at room temperature.

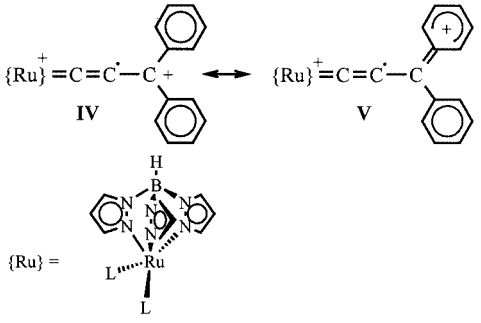

Scheme 4

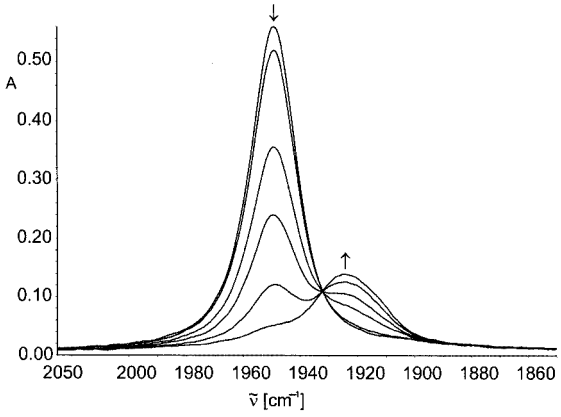

Figure 7. IR spectroelectrochemistry of complex **3a** (1,2-$Cl_2C_2H_4$, 298 K); oxidation of the ferrocenyl substituent attached to the allenylidene ligand

tions for acceptor-substituted vinylidene ligands. This is demonstrated by the complexes $[Cp(PPh_3)_2Ru{=}C{=}C(Ph)(R)]^+$ [$\tilde{\nu}$(C=C) = 1675 cm^{-1} for R = C_7H_7, 1655 cm^{-1} for R = CH_2Ph, 1638 cm^{-1} for R = I or Br, and 1585 cm^{-1} for R = NNPh).[39−42] The IR band observed for the oxidized form of complex **2a** is at the low-energy border of this regime. In contrast to all other (vinylidene)ruthenium complexes so far reported it has the metal atom in a formal +III oxidation state, which may account for its fairly low energy. In any case, it is clear that ruthenium oxidation induces major bonding changes within the metallacumulene chromophore.

In complex **3a**, oxidation involves the ferrocenyl moiety at the terminal carbon atom of the allenylidene ligand. This allows us to examine the effect of decreased electron density at this site on the position of the IR band directly. As shown in Figure 7, electrolysis at a potential positive to the anodic wave of the ferrocenyl substituent induces a red shift of the allenylidene band by ca. 20 cm^{-1} to a value of 1924 cm^{-1}, together with an appreciable decrease in absorptivity. Subsequent reduction restores the original spectrum in nearly quantitative optical yield, showing that the smaller absorptivity is not an artifact of partial decomposition. In the dipositive, monooxidized form, the unsaturated C_3 ligand bridges two positively charged entities. This should reduce the change in dipole moment during this vibration and decrease the absorptivity of this band. The same reasoning has been employed in explaining the considerably lower intensity of the allenylidene stretch in neutral allenylidene complexes as opposed to cationic ones, a situation qualitatively equivalent to the case here.[43]

The dppf-substituted complex **2b** has its additional electroactive moiety at exactly the opposite end of the metallacumulene chromophore. It provides a study case for the effect on the position of the IR band of diminished electron density on the metal. Here, oxidation results in the disappearance of the original IR band and the simultaneous growth of a pair of closely spaced, equally intense bands at 1957 and 1948 cm^{-1}, a blue shift relative to the Ru^{II}/Fe^{II} precursor of an average of 15 cm^{-1} (Figure 8). The observation of a pair of bands instead of just one is most probably the result of Fermi coupling of the asymmetric C=C=C valence stretch with an overtone or a combination mode of other vibrational mode(s) of closely related energies. Although too weak to be detected by themselves, they gain intensity through coupling to the intense C=C=C stretch of the unsaturated ligand, which then causes the additional band. Similar observations have been made for the reduced forms of complexes **2a** and **2b** (vide infra). Notably, such apparent splitting of the valence stretch is observed only in certain oxidation states. Generally speaking, Fermi coupling is only encountered when there is a good energy match between the two underlying fundamentals. It is reasonable to assume that electron transfer alters the energy of at least one of the vibrational modes involved in this coupling, which would explain why such an effect may be observable in one oxidation state but not in another. Paul, Lapinte, and co-workers have very recently reported on such oxidation-state-dependent Fermi coupling between C≡C and, presumably, C−C≡ modes[44] for alkynyl complexes $[Cp^*(dppe)Fe-C\equiv C-C_6H_4R\text{-}4]^{n+}$ (n = 0, 1, $Fe^{II,III}$).[45,46] Similar coupling between the C≡N stretch and the C≡N−C bending modes of the isocyanide ligands in the triruthenium clusters $[Ru_3(NCR)_3(\mu^3\text{-}O)(\mu\text{-}CH_3COO)_6]^{n-}$ (n = 0, 1) has recently been described by Kubiak et al.[47] Since the band energy of the fundamental coupling with the C=C=C valence stretch is unknown, we adopt the center of the Fermi doublet as the energy of the unperturbed C=C=C stretch (and also of the other mode), but this is only an approximation. The alternative explanation of there being two distinct conformers with appreciably different $\tilde{\nu}$(C=C=C) values cannot be discounted, but seems much less likely. No splitting of this band is observed for complexes **3a** or **3b**, in which such rotamers are known to exist and, from NMR spectroscopy (vide supra), not to interconvert on the IR timescale. We also note that oxidation at the [Tp(dppf)Ru] site results in a net increase of absorptivity. This can be explained well by the above reasoning, since the charge difference between the two sites bridged by the cumulenic chain, and hence the change in dipole moment associated with the asymmetric C=C=C stretch, is now enhanced.

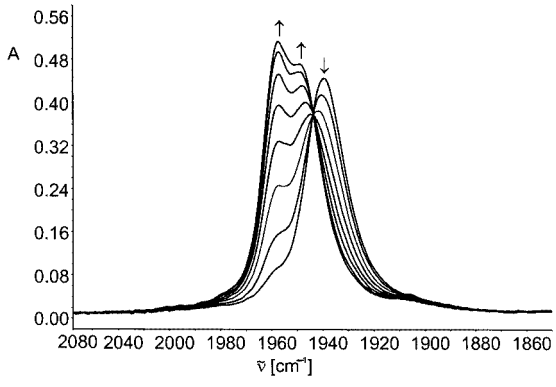

Figure 8. IR spectroelectrochemistry of complex **2b** (1,2-$Cl_2C_2H_4$, 298 K); effect of oxidation of the ferrocene moiety of the dppf ligand

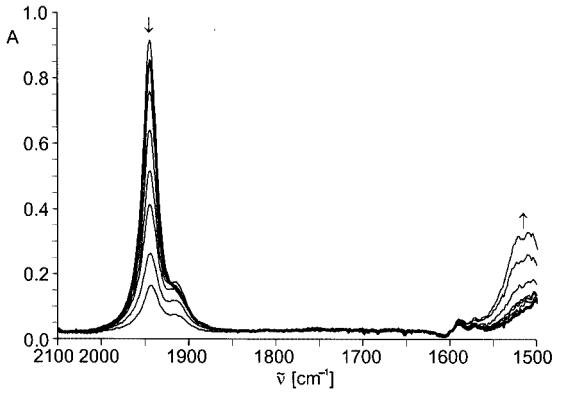

Figure 9. IR spectroelectrochemistry of complex **3b** (1,2-$Cl_2C_2H_4$, 298 K); spectral changes concomitant with ruthenium oxidation

Complex **3b**, which features both types of secondary redox centers, constitutes the most demanding case under study, since it poses the question of which ferrocenyl entity is oxidized first. We have already pointed out that the measured redox potentials favor the first oxidation as involving the ferrocenyl substituent attached to the allenylidene ligand. IR spectroelectrochemistry provides compelling evidence for this assignment. During the first oxidation the C=C=C valence stretch at 1945 cm^{-1} is replaced by a significantly less intense absorption band at 1916 cm^{-1}. The second oxidation occurs at the dppf ligand and shifts the IR band back to exactly its original position. This shows that − at least in terms of IR spectroscopy − the effects of one-electron oxidation of the electroactive moieties positioned at opposite ends of the allenylidene ligand exactly cancel each other. Both oxidized species display a high degree of chemical stability even on the longer timescales of spectroelectrochemical investigations. After bulk electrolysis following the first and second oxidation the starting material was recovered in ca. 95 and 92% optical yields, respectively.

Despite being obscured by the rising background current of the supporting electrolyte in cyclic voltammetry experiments, it still proved possible to examine the ruthenium-centered oxidation of complexes **3a** and **3b** under thin layer spectroelectrochemistry conditions. The results are very similar to those obtained for complex **2a**: the IR bands in the region typical of the C=C=C stretch of the cumulenic ligand vanish and are replaced by new absorptions at 1507 ($\mathbf{3a}^{2+}$) or 1524 cm^{-1} ($\mathbf{3b}^{3+}$), again pointing to a vinylidene structure (see Figure 9). We also note a significant red shift of the vinylidene band relative to the oxidized Ru^{III} form

of **2a** as the electron density of these complexes decreases further.

Electrolysis under UV/Vis monitoring conditions revealed the effects on the optical spectra of complexes **2b**, **3a**, and **3b** of electron transfer from the secondary redox sites. Spectral changes induced by oxidation of the dppf ligand in **2b** are rather small, the most prominent effects being a blue shift of the HOMO → LUMO band by 775 cm^{-1} and the development of a former shoulder at 361 nm into a distinct band located at 369 nm, while the main absorption band at 526 nm remains virtually unchanged. The most likely explanation is provided by reference to our earlier work on amino-substituted allenylidene complexes of the *trans*-[Cl(dppm)$_2$Ru] fragment.[48] Here we found that the electron density on the phosphane ligands was quite small for both occupied frontier levels, and this may also hold for the mixed Tp/diphosphane complexes described here. Our experimental observations can then be accommodated by the assumption that the HOMO level has some contribution from the phosphane ligands while there is only a negligible one to the lower-lying HOMO-1 orbital. For complexes **3a** and **3b**, oxidation of the ferrocene moiety would be expected to have a much more profound effect on the UV/Vis spectra, since the ferrocene moiety now constitutes an integral part of the chromophore. Bulk electrolysis of **3a** at a potential more positive than the first anodic wave indeed causes a bleaching of the intense low-energy absorption band at 723 nm (Figure 10), this finding lending further support to our assignment of this band as resulting from charge transfer from the ferrocene donor to the allenylidene acceptor moieties within this chromophore. As the ferrocene moiety is oxidized, no such transition is possible any longer. Further changes are a slight red shift of the prominent absorption band by some 200 cm^{-1} and an absorptivity decrease of the third prominent feature near 355 nm, accompanied by a slight shift to higher energies. The direction of the shift of the former band is as would be anticipated on the basis of our results on heteroatom-substituted allenylidene complexes *trans*-[Cl(dppm)$_2$Ru=C=C=C(ER$_n$)(R′)]$^+$, but its magnitude is again fairly small. Nearly identical observations were made during the first anodic step of compound **3b**, featuring both kinds of secondary redox centers (Table 5). This reconfirms our previous assignment that it is the ferrocene moiety at the allenylidene ligand that is oxidized first. The second oxidation of this compound causes only a slight blue shift of the lower energy band, along with a further decrease in absorptivity.

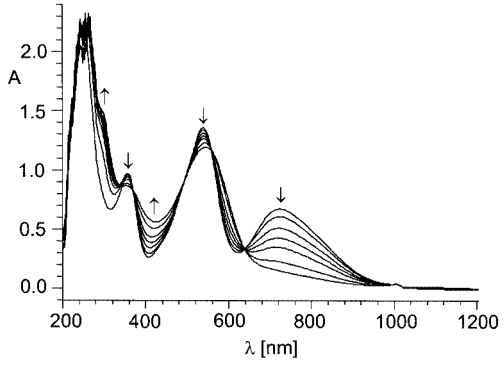

Figure 10. UV/Vis spectroelectrochemistry of complex **3a** (1,2-$Cl_2C_2H_4$, 298 K); oxidation of the ferrocenyl substituent attached to the allenylidene ligand

For complexes **2a**, **2b**, and **3b** we were even able to monitor the spectral changes accompanying oxidation at the ruthenium center. For **2a** and **2b** the effects are very similar. As an example, Figure 11 displays the spectroscopic traces during the second oxidation of **2b**. The HOMO → LUMO and HOMO-1 → LUMO bands experience shifts to higher energies, by 1050 and 1300 cm^{-1} (**2a**) or 625 cm^{-1} for the HOMO-1 → LUMO transition in **2b**. In this latter compound there is no distinct band for the excitation from the HOMO level but only a broad absorption at ca. 700 nm. As the oxidation proceeds, an intense band develops at 411 nm (**2a**) or 351 nm (**2b**). Since only one band in the 350−600-nm region is observed for the Ru^{III} forms of allenylidene complexes of the ClRu(dppm)$_2$ entity, we assume that the additional band (probably the one at higher energy) arises from ligand-to-metal charge transfer from the Tp ligand to Ru^{III}. The fully oxidized form of complex **3b** differs from the other two in that its spectrum, in terms of band positions, is surprisingly similar to that of the Ru^{II}/Fe^{II}(Fc)/Fe^{II}(dppf) starting material. The intensities of the band near 700 and the one near 550 nm, however, are just the opposite of what they were in the beginning, the band at lower energy now being very strong and the one at higher energy being rather weak. At present we have no plausible explanation for this pattern, but note that it seems to be associated with the ferrocenium moiety at the allenylidene ligand. This follows from comparison of the spectra of **2b**$^{2+}$ and **3b**$^{3+}$. Another intense band at 468 nm may again arise from a LMCT transition from the Tp ligand to Ru^{III}.

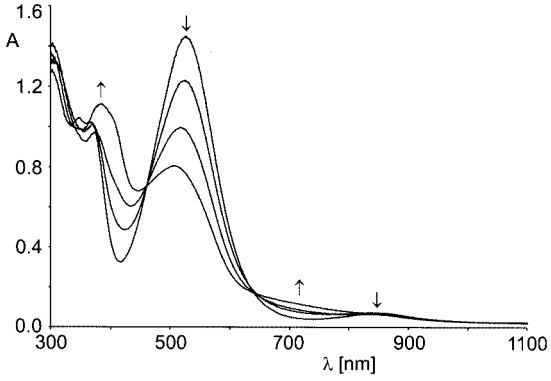

Figure 11. UV/Vis spectroelectrochemistry of complex **2b** (1,2-$Cl_2C_2H_4$, 298 K); effect of oxidation of the ferrocene moiety of the dppf ligand

b) Reduction

It has already been mentioned that the reduction of allenylidene complexes mainly involves the allenylidene ligand. From the shift of the IR band upon reduction of the SR and SeR substituted complexes *trans*-[Cl(dppm)$_2$Ru=C=C=C(ER)(R′)]$^+$ and the coupling pattern of the unpaired

electron in their reduced forms, we have concluded that the unpaired spin mainly resides on the terminal carbon atom.[1,2] Touchard and co-workers have recently presented convincing evidence that this is also true for the reduced form of the diphenyl-substituted *trans*-$[Cl(dppe)_2Ru{=}C{=}C{=}CPh_2]^+$, closely related to the complexes discussed here.[35] DFT calculations on variously substituted model complexes *trans*-$[Cl(PH_3)_4Ru{=}C{=}C{=}C(ER_n)(CH_3)]^+$ [ER_n = $N(CH_3)_2$, $O(CH_3)$, $S(CH_3)$, $Se(CH_3)$, CH_3], which we will detail elsewhere, have broadly confirmed these conclusions but also indicate considerable spin density on the metal-bound carbon atom C-α. This in turn fully agrees with the orbital composition of the LUMO as established by quantum mechanical calculations[4,9−11,37] and the well established regiochemistry of nucleophilic addition to the allenylidene ligand.[8,49] The reversible nature of the first reduction for each of the complexes presented here provided us with the opportunity also to examine the spectral changes accompanying this process. Again, we expected the most revealing results to come from IR spectroelectrochemistry. Since none of the appended secondary redox sites can be reduced, the results are very similar for all complexes. Figure 12 displays the spectral traces recorded during the reduction of complex **2b** as a representative example. In each case we observe a blue shift of the C=C=C band by some 20 wavenumbers, along with an appreciable decrease in intensity. We again confirmed that this was not caused by decomposition of the reduced species, back-electrolysis in each case restoring the original spectrum in optical yields of more than 95%. We note that two IR bands spaced by ca. 10 cm^{-1} were observed for the reduced forms of complexes **2a** and **2b**, while there was only one for complexes **3a** and **3b**. The average shift, however, is almost constant within the entire series and amounts to ca. 20 cm^{-1}. While all the mesomeric structures depicted in Scheme 5 place the unpaired spin either on the carbon atom C-α or on C-γ, we note that **VI** accounts for the high-energy shift of the IR band. Relevant data are listed in Table 5.

In UV/Vis spectroelectrochemical experiments, reduction was observed to change the intensities of the original absorption bands rather than their positions. Representative examples are provided in Figures 13 and 14, while the corresponding data are listed in Table 5. This somewhat unexpected result points to a nearly parallel energy shift of all frontier orbitals involved in the electronic transitions upon reduction. The lower absorptivities may originate from partial loss of the charge-transfer character of these bands as the electron-accepting propensity of the allenylidene ligand is diminished. We note that the main absorption band originating from the HOMO-1 → LUMO transition seemingly splits into two individual bands, which remain unresolved for complex **2b** but are clearly resolved for all other complexes, the energy difference increasing in the order **2b** < **2a** < **3a** ≈ **3b**. Another striking observation is the complete loss of the ferrocenyl-to-ligand (or intraligand) charge-transfer absorption for the ferrocenyl-substituted complexes **3a** and **3b**, while a weak band identical to that seen for the HOMO → LUMO transition in the reduced forms of complexes **2a** and **2b** is now observed for **3b** (Table 5). Des-

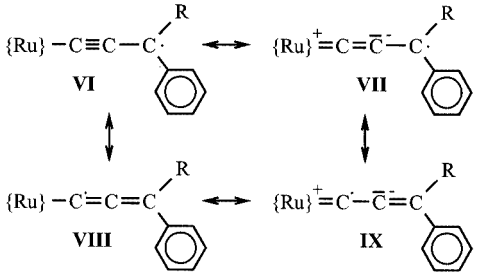

Scheme 5

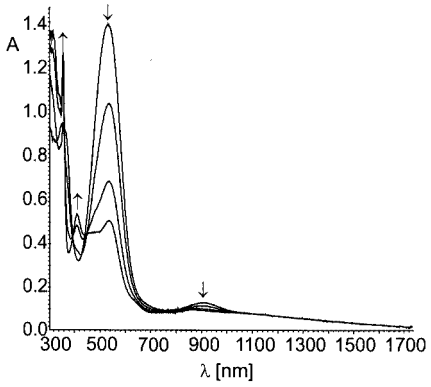

Figure 13. UV/Vis spectroelectrochemistry of complex **2b** (1,2-$Cl_2C_2H_4$, 298 K); spectral changes accompanying reduction

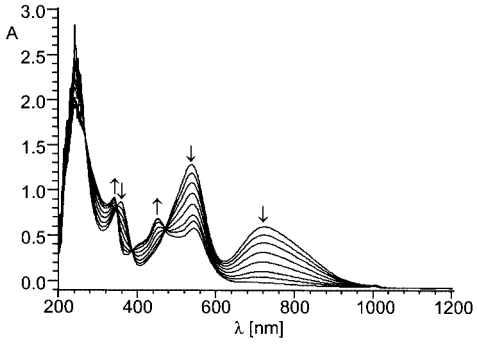

Figure 14. UV/Vis spectroelectrochemistry of complex **3a** (1,2-$Cl_2C_2H_4$, 298 K); spectral changes accompanying reduction

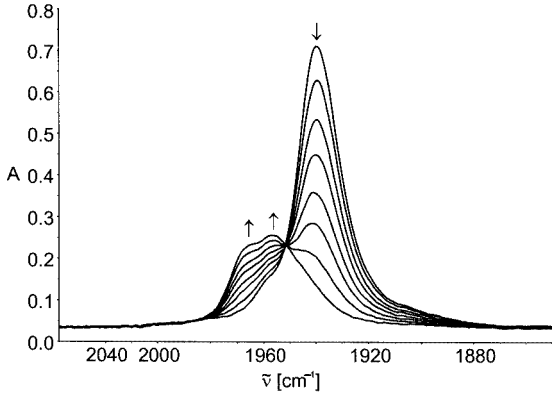

Figure 12. IR spectroelectrochemistry of complex **2b** (1,2-$Cl_2C_2H_4$, 298 K); spectral changes accompanying reduction

pite their loss of intensity, the transition bands in the visible region are still quite strong and obscure the expected ferrocenyl-based absorptions. A new band at 400−410 nm was observed for all complexes and cannot conclusively be assigned at present. Another feature common to all reduced forms is an intense absorption at ca. 350 nm. Bands of this type are familiar for aryl-substituted methyl radicals of the type $Ar_nCR_{3-n}^{\cdot}$, which are characterized by sharp, intense absorptions at 325−360 nm.[50−53] This argues for efficient incorporation of the aryl substituents into the Ru=C=C=C(R)(R′) chromophore and the relevance of resonance forms **VI** and **VII**, which both place the unpaired spin on the carbon atom adjacent to the aromatic rings.

More evidence for spin delocalization into the aromatic substituents was provided by EPR spectroscopy. The reduced forms of complexes **2a** and **2b**, frozen in a 1,2-$Cl_2C_2H_4$ glass at 4 K, display slightly broadened isotropic signals at *g*-values typical of organic paramagnetic species (i.e., close to the free electron value of 2.0023; Table 6). For **3a** and **3b**, however, the spectra were of the rhombic type, with small but clearly detectable *g*-value anisotropies indicating some transition metal contribution, most probably from the ^{57}Fe nucleus of the Fc substituent. Such coupling also prevails in liquid solution, as is evident from a satellite doublet with a signal splitting of 22.3 G (Figure 15; ^{57}Fe has a nuclear spin of 1/2 and a natural abundance of 2.15%). No further resolution of the EPR signal was obtained, however. This is in sharp contrast to observations made by Rigaut, Dixneuf, and co-workers and in our own laboratory on the reduced forms of allenylidene complexes bearing the *trans*-[Cl(L$_2$)$_2$Ru] fragment (L$_2$ = dppm, dppe). These display resolved couplings to the hydrogen atoms on the substituents bonded to the allenylidene ligand and the phosphane P atoms coordinated to the metal ion.[1−3,5] In the mixed Tp/phosphane complexes described here, coupling to the arene protons, the two magnetically different sets of nitrogen atoms of the Tp ligand, and the phosphane P atoms would therefore be expected. It is possible that the larger number of magnetically independent nuclei together with some participation by a metal atom give rise to strongly overlapping resonance lines that cannot be resolved. It is quite revealing to note that the resonance signals are significantly broadened relative to the analogous complexes of the *trans*-[Cl(dppm)$_2$Ru] entity.

Table 6. EPR data for the reduced forms of complexes **2a**−**3b**

	4 K g_{iso} or g_{xx}, g_{yy}, g_{zz} (g_{av})[a]	298 K g_{iso} (A{^{57}Fe})
2a	2.0027	2.0018 (−)
2b	2.0027	2.0030 (−)
3a	2.0228, 2.0094, 2.0011 (2.0111)	2.0108 (22.3 G)
3b	2.0215, 2.0111, 2.0016 (2.0114)	2.0110 (22.3 G)

[a] $g_{av} = \{1/3\ (g_{xx}^2 + g_{yy}^2 + g_{zz}^2)\}^{1/2}$.

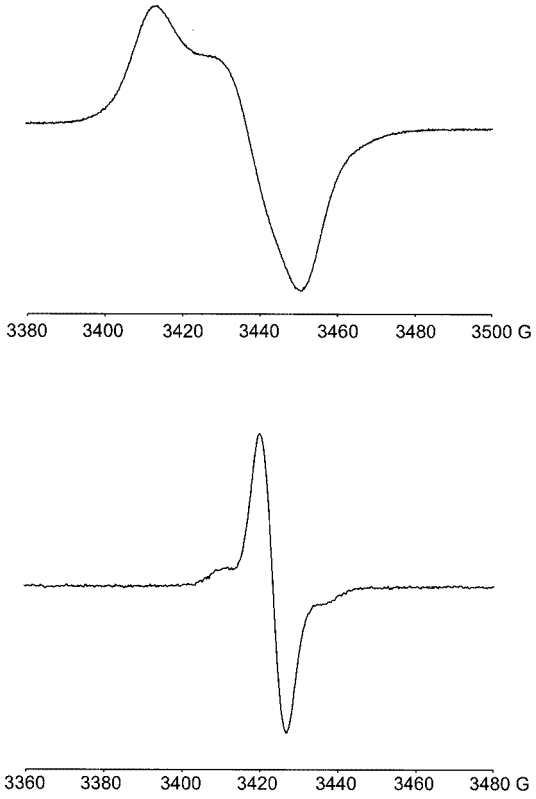

Figure 15. EPR spectra of the reduced form of complex **3a** in (a) a 1,2-$Cl_2C_2H_4$ glass at 4 K (top trace) or (b) in 1,2-$Cl_2C_2H_4$ solution at 300 K (bottom trace)

c) The IR Frequency of the B−H Stretch

The position of the B−H stretch in infrared spectra has been recognized as an indicator for the coordination mode of the Tp ligand (i.e., κ^3 versus κ^2 coordination).[54,55] It has, however, only very recently been realized that the frequency of this band also corresponds to the electron density on the metal ion to which it is coordinated and, more specifically, to its oxidation state. Thus, O'Hare and co-workers have just published a series of mixed-sandwich complexes containing both the Cp and the Tp ligand or the 3,5-dimethyl derivative thereof, several of them in the adjacent M^{II} and M^{III} oxidation states (M = V, Cr, Co, Ni).[55] In all these cases oxidation of the metal atom was found to induce a shift of the B−H band to higher energies, though of a strongly varying magnitude (7−72 cm^{-1}). We have made the same observations with the complexes reported here. As the data for complexes **2a** and **3b** show (see Table 5), oxidation at the ruthenium atom increases the energy of the B−H stretch by about 30 cm^{-1} while the decreasing electron density on the ruthenium atom by oxidation at the dppf ligand has a somewhat smaller effect of some 25 cm^{-1} (**2b**). Ferrocene oxidation at the allenylidene ligand also shifts the B−H band to higher energy (**3a**). Likewise, the reduced forms of these allenylidene complexes display their B−H band at some 15−25 cm^{-1} lower energy, although this process mainly involves the organic ligand. Thus, variation of the B−H stretch with the oxidation state

of the metal atom or that of any redox-active ancillary ligand bonded to it seems to be a quite general result and we expect additional examples of such behavior as more redox pairs of this type are characterized.

Conclusions

We have investigated allenylidene complexes $[TpL_2Ru{=}C{=}C{=}C(Ph)(R)]^+$. Substitution of dppf by less strongly donating PPh_3 ligands or of the phenyl by a ferrocenyl substituent shifts the IR and electronic absorption bands to lower energies, in line with previous results on complexes based on the *trans*-$[Cl(dppm)_2Ru]$ moiety. Oxidation of ferrocene-based redox sites attached either to the metal atom (L_2 = dppf: **2b**, **3b**) or to the allenylidene ligand (R = Fc: **3a** and **3b**) strongly attenuates these effects. The same holds for reduction, which mainly involves a ligand-centered, delocalized orbital. These studies also show that aromatic substituents at the allenylidene ligand are efficiently incorporated into the chromophoric system. Thus, the Fc-substituted complexes **3a** and **3b** display an intense, low-energy absorption band attributable to charge transfer from the ferrocenyl substituent to the allenylidene ligand. Oxidation of the Fc moiety and reduction both cause bleaching of this feature. EPR studies on the reduced forms of **3a** and **3b** reveal coupling of the unpaired spin with the ^{57}Fe nucleus of the ferrocenyl substituent. In their IR spectra some of the oxidized or reduced forms display an apparent splitting of the allenylidene band. This is interpreted in terms of Fermi coupling between the C=C=C fundamental and an overtone or combination of (an)other vibration(s).

Cyclic voltammetry studies reveal that both types of ferrocene-based redox systems are oxidized at much lower potential than the ruthenium center. Although the $Ru^{II/III}$ process lies outside the anodic window of the supporting electrolyte solution in voltammetric studies, it was still possible to perform this oxidation under thin layer conditions in an OTTLE cell. This latter oxidation induces more substantial bonding changes within the cumulenylidene system. Results from IR spectroelectrochemistry point to a vinylidene resonance structure for the Ru^{III} forms of these complexes. The frequency of the B−H stretch of the Tp ligand is also sensitive to the overall oxidation state of the molecule. Oxidation of any of the ferrocene entities or the ruthenium shifts this band to higher energies, while a red shift is observed upon reduction.

The unsymmetrically substituted allenylidene complexes $[TpL_2Ru{=}C{=}C{=}C(Ph)(Fc)]^+$ (**3a** and **3b**) are dynamic in solution, due to an energy barrier to rotation around the Ru=C bond. Two isomeric forms differing in the relative positions of the Fc and the Ph substituents are discernible for the PPh_3-substituted congener **3a** up to 388 K in 1,2-$D_2C_2Cl_4$, at which point this compound decomposes. The observation of just one singlet resonance for each isomer by ^{31}P NMR spectroscopy argues for a vertical orientation of the allenylidene ligand. This is in agreement with the crystallographically determined structures for **2a** and **2b**, the latter presented here.[13] For the dppf-substituted **3b**, however, splitting of the singlet ^{31}P NMR resonance into a well-resolved AB quadruplet is observed upon cooling in CD_2Cl_2, pointing to a horizontal alignment of the allenylidene ligand. The energy barrier for allenylidene rotation is determined as 47 kJ/mol at the coalescence temperature of 238 K.

Experimental Section

General: All manipulations were performed by standard Schlenk techniques under argon. CH_2Cl_2 and 1,2-$Cl_2C_2H_4$ were distilled from CaH_2 and stored over molecular sieves (4 Å). All solvents were deoxygenated by at least three freeze-pump-thaw cycles and saturation with argon prior to use. Benzoylferrocene, [Tp(dppf)RuCl], $[TpRu(PPh_3)_2Cl]$, and $[TpL_2Ru{=}C{=}C{=}CPh_2]^+$ (L_2 = 2 PPh_3, dppf) were obtained by literature methods.[13,18,56,57] Electrochemistry and spectroelectrochemistry were performed as described in an earlier publication.[4] All experiments were performed in the presence of 0.2 M Bu_4NPF_6 as the supporting electrolyte and the given potentials are referenced to the ferrocene/ferrocenium couple, set as 0.00 V. This scale can be related to saturated calomel electrode (SCE) conditions by adding +0.46 V for CH_2Cl_2 and +0.45 V for DMF solutions.[58] NMR: Bruker AC 250. IR: Elmer Paragon 1000 PC. UV/Vis: Omega 10 from Bruins Instruments or J&M TIDAS diode array UV/Vis/NIR spectrometer equipped with a fiber-optic cable and operated with the SCAN 2017 and SPECTRALYS software packages. Electrochemistry: EG&G potentiostat 273 A, BAS glassy carbon working electrode (Ø, 3 mm), Pt wire as counter-electrode and Ag wire as pseudo-reference electrode, potential calibration by addition of ferrocene or decamethylferrocene as internal standard. EPR: Bruker ESP 300, HP frequency counter 5350 B, Bruker NMR gaussmeter ER 035 M, continuous flow cryostat ESR 900 from Oxford Instruments for low-temperature work.

1-Ferrocenyl-1-phenylprop-2-yn-1-ol Trimethylsilyl Ether: *n*BuLi (4.6 mL of a 2.5 M solution in *n*-hexane) was added to trimethylsilylacetylene (1.6 mL, 1.11 g, 11.2 mmol) in degassed THF (250 mL). The clear, colorless solution was allowed to warm to room temperature, and benzoylferrocene (2.32 g, 8 mmol) was added. The resulting solution was stirred for 20 h, whereupon the color visibly brightened to orange. It was hydrolyzed with 5 mL of distilled water and the organic phase was taken to dryness. The brownish residue was taken up in dichloromethane, washed with several portions of a 5% solution of Na_2CO_3, and dried with $MgSO_4$, and the solvent was removed in vacuo. The product was purified by column chromatography on neutral alumina with *n*-hexane/Et_2O (3:1, v/v) as the eluent. Slow evaporation of the solvents deposited orange crystals (1.67 g, 4.3 mmol, 54%).

1-Ferrocenyl-1-phenylprop-2-yn-1-ol: Finely ground KOH (1.68 g, 30 mmol) was dissolved in MeOH, and the silyl ether (1.165 g, 3 mmol) was added. The orange solution was kept under a gentle reflux for 18 h and the solvent was then distilled off. The residue was hydrolyzed in water and carefully acidified with dilute HCl, and the product was extracted with Et_2O. The organic phase was washed with water and dried with $MgSO_4$, and the solvent was removed in vacuo, which deposited the pure product as orange crystals (0.81 g, 2.6 mmol, 85%).

$[Tp(PPh_3)_2Ru{=}C{=}C{=}CPh_2]^+$ SbF_6^- (2a): UV/Vis (CH_3CN): λ_{max} (ε) = 359 (10500), 527 (16500), 901 nm (710 M^{-1} cm^{-1}); (CH_2Cl_2): λ_{max} (ε) = 356 (13000), 527 (16000), 907 nm (660 M^{-1} cm^{-1}).

[Tp(dppf)Ru=C=C=CPh$_2$]$^+$ SbF$_6^-$ (2b): UV/Vis (CH_3CN): λ_{max} (ε) = 346 (11000), 520 (13000), 901 nm (350 M^{-1} cm^{-1}); (CH_2Cl_2): λ_{max} (ε) = 356 (16500), 522 (19600), 902 nm (580 M^{-1} cm^{-1}).

[Tp(PPh$_3$)$_2$Ru=C=C=CFcPh]$^+$ SbF$_6^-$ (3a): Compound **1a** (250 mg, 0.286 mmol), 1-ferrocenyl-1-phenylprop-2-yn-1-ol (260 mg, 0.82 mmol), and $AgSbF_6$ (190 mg, 0.55 mmol) were mixed in THF (10 mL) in a Schlenk flask and stirred in the dark at ambient temperature for 40 min, whereupon an intense purple color developed. THF was removed in vacuo and the solid residue was extracted with CH_2Cl_2 (15 mL). Filtration through a fine frit covered with Celite (10 cm) and silica (5 cm), with use of small portions of CH_2Cl_2, removed the AgCl. The solid residue obtained after the solvent had been pumped off, was subjected to column chromatography on silica (Merck 60) with CH_2Cl_2/CH_3CN (10:1,v/v) as the eluent. The first, orange band contained the excess propargylic alcohol, while the second, purple-black zone was slightly impure product. Further purification was performed by three successive reprecipitations from CH_2Cl_2/hexanes. After drying in vacuo, spectroscopically pure product (251 mg, 0.183 mmol, 64%) was obtained. Data for the major isomer: ^{1}H NMR (CD_2Cl_2): δ = 4.28 (s, 5 H, C_5H_5), 4.81, 5.05 (each t, $^3J_{H,H}$ = 2.0 Hz, 2 H, Cp_{subst}), 5.58 [t, $^3J_{H,H}$ = 2.3 Hz, 1 H, 4-H(pz)], 5.69 [d, $^3J_{H,H}$ = 2.3 Hz, 1 H, 3-H(pz)], 5.72 [t, $^3J_{H,H}$ = 2.3 Hz, 2 H, 4-H(pz)], 6.31 [d, $^3J_{H,H}$ = 2.3 Hz, 2 H, 3-H(pz)], 6.85−8.03 (several m, 36 H, 2 PPh_3, Ph, HB), 7.66 [d, $^3J_{H,H}$ = 2.3 Hz, 2 H, 5-H(pz)], 7.85 [d, $^3J_{H,H}$ = 2.3 Hz, 1 H, 5-H(pz)] ppm. ^{13}C{^{1}H} NMR (62.9 MHz, CD_2Cl_2): δ = 71.6 (C_{ipso}, Fc), 73.2 (C_5H_5), 74.5, 78.3 (C-2−5, Cp_{sub}), 105.7, 106.5 [br., C-4(pz)], 125.5−134.5 (several m, 2 PPh_3, Ph), 136.5, 137.0 (br., C-5(pz)], 144.9 (C_{ipso}, Ph), 145.3, 147.0 (C-3(pz)], 168.2 (t, $^4J_{P,C}$ = 1.6 Hz, C-γ), 184.3 (t, $^3J_{P,C}$ = 1.5 Hz, C-β), 287.0 [t, J_{PC} = 18.2 Hz, C-α] ppm. ^{31}P{^{1}H} NMR (101.3 MHz, CD_2Cl_2): δ = 40.8 (s) ppm. IR (KBr): $\tilde{\nu}$ = 1946 (vs, C=C=C), 1458 (s, Fc), 1436 (s, Ph), 1382 (m, Ph), 1309 (m, Ph), 1049 (m, Ph), 749 (m, Ph), 699 (s, Ph), 658 cm^{-1} (SbF_6). UV/Vis (CH_3CN): λ_{max} (ε) = 355 (3600), 534 (5200), 719 (2650 M^{-1} cm^{-1}); 825 nm (sh); (CH_2Cl_2): λ_{max} (ε) = 356 (8000), 538 (11500), 724 nm (5700 M^{-1} cm^{-1}). $C_{64}H_{54}BF_6FeN_6P_2RuSb$ (1372.59): calcd. C 56.00, H 3.97, N 6.12; found C 55.78, H 4.20, N 5.61.

[Tp(dppf)Ru=C=C=CFcPh]$^+$ SbF$_6^-$ (3b): This compound was prepared analogously to the method described for the synthesis and purification of compound **3a**. The product (289 mg, 74.7%) was obtained from **1b** (250 mg, 0.276 mmol), 1-ferrocenyl-1-phenylprop-2-yn-1-ol (0.26 g, 0.82 mmol), and $AgSbF_6$ (190 mg, 0.55 mmol). ^{1}H NMR (CD_2Cl_2): δ = 4.22 (s, 5 H, C_5H_5), 4.67, 4.76 [each br., 4 H, 2,3-H(dppf)], 5.05, 5.12 (each t, $^3J_{H,H}$ = 2.1 Hz, 2 H, Cp_{subst}), 5.39 [t, $^3J_{H,H}$ = 1.9 Hz, 2 H, 4-H(pz)], 5.93 [t, $^3J_{H,H}$ = 2.2 Hz, 1 H, 4-H(pz)], 6.33 [d, $^3J_{H,H}$ = 2.2 Hz, 1 H, 3-H(pz)], 6.39 [d, $^3J_{H,H}$ = 1.9 Hz, 2 H, 3-H(pz)], 6.42−8.20 (several m, 26 H, 2 PPh_2, Ph, HB), 7.64 [d, $^3J_{H,H}$ = 2.2 Hz, 1 H, 5-H(pz)], 7.81 [d, $^3J_{H,H}$ = 1.9 Hz, 2 H, 5-H(pz)] ppm. ^{13}C{^{1}H} NMR (62.9 MHz, CD_2Cl_2): δ = 70.6 (C_{ipso}, Fc), 73.3 [t, $^2J_{P,C}$ = 3.6 Hz, C-2/5(dppf)], 73.59 [C_{ipso}(dppf)], 73.63 (C_5H_5), 73.9 (Cp_{sub}), 74.6 [t, $^3J_{P,C}$ = 2.9 Hz, C-3/4(dppf), 79.0 (Cp_{sub}), 106.0, 106.5 [C-4(pz)], 128.0−133.5 (several m, 2 PPh_2, Ph), 135.4, 137.3 [br., C-5(pz)], 144.0 (t, $^5J_{P,C}$ = 0.7 Hz, C_{ipso}, Ph), 144.8 [t, $^3J_{P,C}$ = 1.1 Hz, C-3(pz)], 147.3 (t, $^3J_{P,C}$ = 1.5 Hz), 167.9 (t, $^4J_{P,C}$ = 1.5 Hz, C-γ), 180.6 (br., C-β), 283.7 [t, J_{PC} = 18.2 Hz, C-α] ppm. ^{31}P{^{1}H} NMR (101.3 MHz, CD_2Cl_2): δ = 29.9 (s) ppm. IR (KBr): $\tilde{\nu}$ = 1941 (vs, C=C=C), 1457 (s, Fc), 1435 (s, Ph), 1395 (m, Ph), 1382 (m, Ph), 1309 (m, Ph), 1049 (m, Ph), 749 (m, Ph), 697 (s, Ph), 658 (SbF_6) cm^{-1}. UV/Vis (CH_3CN): λ_{max} (ε) = 348 (14000), 534 (15500), 709 (10000), 1030 nm (800 M^{-1} cm^{-1}); (CH_2Cl_2): λ_{max} (ε) = 350 (16500), 540 (19500), 712 (13000), 1030 nm (2000 M^{-1} cm^{-1}). $C_{62}H_{52}BF_6Fe_2N_6P_2RuSb$ (1402.40): calcd. C 53.10, H 3.73, N 5.99; found C 52.32, H 3.85, N 5.54.

Table 7. Crystallographic data for [TpRu(dppf)Cl]·2$CHCl_3$ and [Tp(dppf)RuC_3Ph_2]$^+$ SbF_6^-

	[TpRu(dppf)Cl]·2$CHCl_3$	[Tp(dppf)RuC_3Ph_2]$^+$ SbF_6^-
Empirical formula	$C_{45}H_{40}BCl_7FeN_6P_2Ru$	$C_{58}H_{48}BF_6FeN_6P_2RuSb$
Formula mass	1142.65	1294.44
Temperature [K]	173(2)	293(2)
Wavelength [Å]	0.71073	0.71073
Crystal system	monoclinic	orthorhombic
Space group	$P2_1/n$	Pbca
a [Å]	13.977(3)	21.9546(14)
b [Å]	17.287(4)	27.959(3)
c [Å]	19.645(4)	22.152(2)
β [°]	91.85(3)	90
V [Å^3]	4744.1(16)	13597(2)
Z	4	8
Density (calculated) [Mg/m^3]	1.600	1.265
Absorption coefficient [mm^{-1}]	1.127	0.924
F(000)	2304	5184
Crystal size [mm]	0.3 × 0.25 × 0.15	0.25 × 0.07 × 0.07
θ range for data collection [°]	1.57 to 29.03.	1.96 to 19.04
Index ranges for data collection	$0 \le h \le 19$, $-14 \le k \le 23$, $-22 \le l \le 26$	$-18 \le h \le 20$, $-25 \le k \le 25$, $-18 \le l \le 19$
No. of reflections measured	12760	15729
No. of independent reflections	8069 [R(int) = 0.0526]	4616
Refinement method	full-matrix least-squares on F^2	full-matrix least-squares on F^2
Data/restraints/parameters	12373/0/573	4616/0/360
Goodness-of-fit on F^2	1.288	1.522
Final R indices [$I > 4\sigma(I)$]	$R1$ = 0.0757, $wR2$ = 0.1829	$R1$ = 0.156, $wR2$ = 0.4112
R indices (all data)	$R1$ = 0.1269, $wR2$ = 0.2218	$R1$ = 0.2473, $wR2$ = 0.4528
Largest diff. peak/hole [e·Å^{-3}]	2.10/−2.34	1.648/−1.863

X-ray Crystallography: Crystals of complex **1b** were grown by slow concentration of a saturated solution in $CHCl_3$ while those of **2b** were obtained by cooling a solution in a THF/Et_2O mixture to −15 °C. Experimental details regarding the X-ray structure solutions are provided in Table 7. The structures were solved by direct methods, least-squares refinement, and Fourier techniques. Structure solution and refinement were performed with SHELXTL.[59] CCDC-192092 (**2b**) and -192093 (**1b**) contain the supplementary crystallographic data for this paper. These data can be obtained free of charge at www.ccdc.cam.ac.uk/conts/retrieving.html [or from the Cambridge Crystallographic Data Centre, 12 Union Road, Cambridge CB2 1EZ, UK; Fax: (internat.) + 44-1223/336-033; E-mail: deposit@ccdc.cam.ac.uk].

Acknowledgments

We are grateful to the Volkswagenstiftung for financial support within their program on intra- and intermolecular electron transfer. We also wish to acknowledge Johnson & Matthey Company for a generous loan of $RuCl_3$ hydrate.

[1] R. F. Winter, *Eur. J. Inorg. Chem.* **1999**, 2121−2126.
[2] S. Hartmann, R. F. Winter, T. Scheiring, M. Wanner, *J. Organomet. Chem.* **2001**, *637−639*, 240.
[3] R. F. Winter, *Organometallics* **1997**, *16*, 4248−4250.
[4] R. F. Winter, K.-W. Klinkhammer, S. Záliš, *Organometallics* **2001**, *20*, 1317−1333.
[5] M. I. Bruce, P. Hinterding, P. J. Low, B. W. Skelton, A. H. White, *Chem. Commun.* **1996**, 1009−1010.
[6] M. I. Bruce, P. Hinterding, P. J. Low, B. W. Skelton, A. H. White, *J. Chem. Soc., Dalton Trans.* **1998**, 467−473.
[7] V. Guillaume, P. Thominot, F. Coat, A. Mari, C. Lapinte, *J. Organomet. Chem.* **1998**, *565*, 75−80.
[8] M. I. Bruce, *Chem. Rev.* **1998**, *98*, 2797−2858.
[9] V. Cadierno, M. P. Gamasa, J. Gimeno, M. González-Cueva, E. Lastra, J. Borge, S. García-Granda, E. Pérez-Carreño, *Organometallics* **1996**, *15*, 2137−2147.
[10] M. A. Esteruelas, A. V. Gómez, A. M. López, J. Modrego, E. Oñate, *Organometallics* **1997**, *16*, 5826−5835.
[11] M. Baya, P. Crochet, M. A. Esteruelas, E. Gutiérrez-Puebla, A. M. López, J. Modrego, E. Oñate, N. Vela, *Organometallics* **2000**, *19*, 2585−2596.
[12] R. F. Winter, *Chem. Commun.* **1998**, 2209−2210.
[13] B. Buriez, I. D. Burns, A. F. Hill, A. J. P. White, D. J. Williams, J. D. E. T. Wilton-Ely, *Organometallics* **1999**, *18*, 1504−1516.
[14] B. Buriez, D. J. Cook, K. J. Harlow, A. F. Hill, T. Welton, A. J. P. White, D. J. Williams, J. D. E. T. Wilton-Ely, *J. Organomet. Chem.* **1999**, 264−267.
[15] K. J. Harlow, A. F. Hill, T. Welton, *J. Chem. Soc., Dalton Trans.* **1999**, 1911−1912.
[16] M. A. J. Tenorio, M. J. Tenorio, M. C. Puerta, P. Valerga, *Organometallic* **1997**, *16*, 5528−5535.
[17] N. W. Alcock, I. D. Burns, K. S. Claire, A. F. Hill, *Inorg. Chem.* **1992**, *31*, 2906−2908.
[18] C. Slugovc, V. N. Sapunov, P. Wiede, K. Mereiter, R. Schmid, K. Kirchner, *J. Chem. Soc., Dalton Trans.* **1997**, 4209−4216.
[19] S. Pavlik, C. Gemel, C. Slugovc, K. Mereiter, R. Schmid, K. Kirchner, *J. Organomet. Chem.* **2001**, *617−618*, 301−310.
[20] M. Tamm, T. Jentzsch, W. Werncke, *Organometallics* **1997**, *16*, 1418−1422.
[21] M. Tamm, A. Grzegorzewski, I. Brüdgam, H. Hartl, *J. Chem. Soc., Dalton Trans.* **1998**, 3523−3528.
[22] A. Z. Kreindlin, F. M. Dolgushin, A. I. Yanovsky, Z. A. Kerzina, P. V. Petrovskii, M. I. Rybinskaya, *J. Organomet. Chem.* **2000**, *616*, 106−111.
[23] D. Pilette, K. Ouzzine, H. Le Bozec, P. H. Dixneuf, C. E. F. Rickard, W. R. Roper, *Organometallics* **1992**, *11*, 809−817.
[24] D. Touchard, N. Pirio, P. H. Dixneuf, *Organometallics* **1995**, *14*, 4920−4928.
[25] N. M. Kostic, R. F. Fenske, *Organometallics* **1982**, *1*, 974−982.
[26] G. Consiglio, F. Bangerter, C. Darpin, *Organometallics* **1984**, *3*, 1448−1450.
[27] G. Consiglio, F. Morandini, *Inorg. Chim. Acta* **1987**, *127*, 79−85.
[28] M. P. Gamasa, J. Gimeno, E. Lastra, B. M. Martín, A. Anillo, A. Tiripicchio, *Organometallics* **1992**, *11*, 1373−1381.
[29] K. Urtel, A. Frick, G. Huttner, L. Zsolnai, P. Kircher, P. Rutsch, E. Kaifer, A. Jacobi, *Eur. J. Inorg. Chem.* **2000**, 33−50.
[30] D. Unseld, V. V. Krivykh, K. Heinze, F. Wild, G. Artus, H. Schmalle, H. Berke, *Organometallics* **1999**, *18*, 1525−1541.
[31] R. L. Beddoes, C. Bitchon, R. W. Grime, A. Ricalton, M. W. Whiteley, *J. Chem. Soc., Dalton Trans.* **1995**, 2873−2883.
[32] A. Wong, J. A. Gladysz, *J. Am. Chem. Soc.* **1982**, *104*, 4948−4950.
[33] B. E. R. Schilling, R. Hoffmann, D. L. Lichtenberger, *J. Am. Chem. Soc.* **1979**, *101*, 585.
[34] H. Goetz, F. Nerdel, K.-H. Wiechel, *Justus Liebigs Ann. Chem.* **1963**, *665*, 1−14.
[35] S. Rigaut, O. Maury, D. Touchard, P. H. Dixneuf, *Chem. Commun.* **2001**, 373−374.
[36] R. S. Nicholson, I. Shain, *Anal. Chem.* **1964**, *36*, 706−723.
[37] [37a] N. Re, A. Sgamellotti, C. Floriani, *Organometallics* **2000**, *19*, 1115−1122. [37b] A. Marrone, N. Re, *Organometallics* **2002**, *21*, 3562−3571.
[38] M. I. Bruce, *Chem. Rev.* **1991**, *91*, 107−257.
[39] M. I. Bruce, M. G. Humphrey, G. A. Koutsantonis, M. J. Liddell, *J. Organomet. Chem.* **1987**, *326*, 247−256.
[40] M. I. Bruce, G. A. Koutsantonis, M. J. Liddell, B. K. Nicholson, *J. Organomet. Chem.* **1987**, *320*, 217−227.
[41] M. I. Bruce, M. G. Humphrey, M. J. Liddell, *J. Organomet. Chem.* **1987**, *321*, 91−102.
[42] M. I. Bruce, M. G. Humphrey, *Aust. J. Chem.* **1989**, *42*, 1067−1075.
[43] K. J. Harlow, A. F. Hill, J. D. E. T. Wilton-Ely, *J. Chem. Soc., Dalton Trans.* **1999**, 285−291.
[44] R. M. Badger, *J. Chem. Phys.* **1937**, *5*, 178.
[45] R. Denis, L. Toupet, F. Paul, C. Lapinte, *Organometallics* **2000**, *19*, 4240−4251.
[46] F. Paul, J.-Y. Mevellec, C. Lapinte, *J. Chem. Soc., Dalton Trans.* **2002**, 1783−1790.
[47] I. S. Zavarine, C. P. Kubiak, T. Yamaguchi, K.-i. Ota, T. Matsui, T. Ito, *Inorg. Chem.* **2000**, *39*, 2696−2698.
[48] R. F. Winter, S. Hartmann, S. Zalis, K.-W. Klinkhammer, to be submitted to *J. Chem. Soc., Dalton Trans.*
[49] V. Cadierno, M. P. Gamasa, J. Gimeno, *Eur. J. Inorg. Chem.* **2001**, 571−591.
[50] A. Bromberg, D. Meisel, *J. Phys. Chem.* **1985**, *89*, 2507−2513.
[51] J. L. Faria, S. Steenken, *J. Phys. Chem.* **1993**, *97*, 1924−1930.
[52] M. B. Jones, V. M. Maloney, M. S. Platz, *J. Am. Chem. Soc.* **1992**, *114*, 2163−2169.
[53] D. Weir, *J. Phys. Chem.* **1990**, *94*, 5870−5875.
[54] M. Akita, K. Ohta, Y. Takahashi, S. Hikichi, Y. Moro-Oka, *Organometallics* **1997**, *16*, 4121−2128.
[55] T. J. Bunker, A. R. Cowley, D. O′Hare, *Organometallics* **2002**, *21*, 3123−3138.
[56] J. Tirouflet, R. Dabard, E. Laviron, *Bull. Chem. Soc. Fr.* **1963**, 1655.
[57] G. W. Gokel, I. K. Ugi, *J. Chem. Educ.* **1972**, *49*, 294.
[58] N. G. Connelly, W. E. Geiger, *Chem. Rev.* **1996**, *96*, 877−910.
[59] G. M. Sheldrick, Institut für Anorganische Chemie der Universität, Tammanstraße 4: Göttingen, **1997**.

Received August 26, 2002
[I02487]

Manganese-Salen Complexes as Oxygen-Transfer Agents in Catalytic Epoxidations − A Density Functional Study of Mechanistic Aspects

Luigi Cavallo[a] and Heiko Jacobsen*[b]

Keywords: Density functional calculations / Epoxidation / Manganese / N,O ligands / Radicals

The mechanism of the Jacobsen–Katsuki epoxidation has been investigated by application of density functional theory; the results of a series of calculations for simplified model systems of different spin states are presented. In the chosen computational approach, the epoxidation of ethylene with a cationic five-coordinate model catalyst is predicted to occur through a radical intermediate, similarly to the reaction mechanism calculated for the corresponding neutral six-coordinate species. Although the radical intermediate shows a small energetic preference for the quintet state over the triplet state, the computed reaction profile does not suggest that two-state reactivity involving spin change plays a major role during the oxygen-transfer step. Comparative orbital analysis of the cationic and the neutral complexes elucidates the role of a ligand *trans* to the oxo group. A π-donor *trans* to the forming OR^- ligand in the radical intermediate causes a relative destabilization of a possible quintet occupation, thus conferring spin rigidity to the six-coordinate species derived from the neutral catalyst. A reaction pathway resulting in rotational collapse might involve a spin-crossing process. The ligand framework of the tetra-chelating N,O ligand in the radical intermediate exhibits a considerable amount of ligand folding.

(© Wiley-VCH Verlag GmbH & Co. KGaA, 69451 Weinheim, Germany, 2003)

Introduction

Transition metal-catalyzed oxidations play a vital role not only in preparative organic chemistry, but also in biochemical transformations.[1] We mention as one prominent example that manganese is part of the active site in photosystem II,[2] and that the role of metal oxo species in water oxidation and O_2-formation has been convincingly demonstrated.[3,4] For synthetic purposes, cationic Mn^{III}-salen complexes were introduced as effective catalysts for the epoxidation of olefins by Kochi in 1986.[5] Katsuki[6] and Jacobsen[7] designed chiral manganese catalysts, which also allowed for enantioselective epoxidations, by modifying the backbone of the salen ligand. The Jacobsen−Katsuki reaction is currently recognized as one of the most practical methods for the epoxidation of alkenes.[8,9] Jacobsen's catalyst **1** is effective for virtually every class of conjugated olefins, and industrial production of the catalyst on a ton scale has become possible.[10] New developments in catalytic epoxidation with Mn^{III}-salen complexes include the use of ionic liquids, which allow the homogenous chiral catalyst to be immobilized, recovered, and recycled and so enhance the activity of the system.[11]

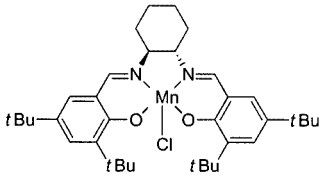

1

The mechanistic scheme commonly proposed for this oxygen-transfer reaction consists of a two-step catalytic cycle (Scheme 1).[8,9,12] Oxygen is transferred from a terminal oxidant to the Mn^{III}-salen catalyst, generating an intermediate Mn^{V} oxo complex, which in the second step carries the activated oxygen to the olefinic double bond.

The existence of a Mn^{V} oxo intermediate, first postulated by Kochi and co-workers,[5] was confirmed by electrospray tandem mass spectrometry by Feichtinger and Plattner.[13] In a recent study, these authors used the same technique to elucidate the mechanism of oxygen transfer to the Mn^{III}-salen complex in great detail,[14] identifying a dimeric μ-

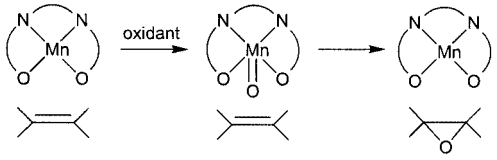

Scheme 1

[a] Department of Chemistry, Università di Salerno
Via Salvador Allende, Baronissi (SA) 84081, Italy
[b] KemKom
1864 Burfield Avenue, Ottawa, Ontario, K1J 6T1, Canada
E-mail: jacobsen@kemkom.com

Supporting information for this article is available on the WWW under http://www.eurjic.org or from the author.

oxo-bridged species acting as reservoir species, and for the first time investigating the coordination chemistry of the terminal oxidant iodosylbenzene with regard to the Mn(salen) system. It should be mentioned that related Mn^{V}-oxo complexes have also been detected in solution by Groves and co-workers, who applied rapid-mixing stopped-flow spectrophotometry.[15]

Keenly debated is the second step in the epoxidation reaction, over which a controversy has erupted in the literature (Scheme 2).[16]

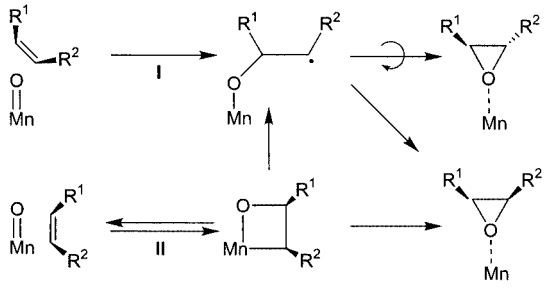

Scheme 2

Since the stereochemistry is determined by the way in which oxygen is delivered to the olefin, detailed knowledge of this step provides the basis for understanding and tuning of the enantioselectivity of the reaction. Both pathway **I**, in which the first attack of the olefin occurs at the oxo center only, and pathway **II**, which proceeds via a manganoxetane, are subjects of discussion. Experimental evidence has been put forward both for the existence of radical intermediates[17] and for the formation of metallacycles.[18] In contrast to direct routes, which should give rise to *cis* epoxides, rotational collapse from the radical intermediate would afford the *trans* product (Scheme 2). This mechanism provides an explanation for the experimentally observed *cis*/*trans* isomerization in the epoxidation of conjugated alkenes.

With regard to the origin of the enantioselectivity, it is generally assumed that it is dominated by steric interactions between the chiral Mn(salen) complex and the two prochiral faces of the olefin. However, it has to be borne in mind that electronic effects, in particular the nature of the substituents in positions 5,5′, also have a strong influence.

Jacobsen developed a mechanistic basis for the electronic effects on enantioselectivity,[19] which assumes the formation of a radical intermediate as the first step in oxygen transfer. Enantioselectivity is tied to the position of the transition state along the reaction coordinate, which can in turn be tuned by electronic variation of the salen ligand system. In connection with the synthesis of optically active α-hydroxy carbonyl compounds, Fell and Adam also showed that the preferentially reacting enantiomer is determined by electronic effects, whereas steric interactions are responsible for the observed stereochemical preference in the double bond epoxidation.[20] When hydroxy group directivity is utilized during the course of the diastereoselective epoxidation,[21] Adam and co-workers conclude that reactions through a metallacycle intermediate and through a direct three-centered transition state both constitute viable reaction mechanisms.[22] Metallacycles have also been discussed by Katsuki and co-workers.[23]

Recently, various density functional (DF) calculations focusing on Mn^{V}-oxo species and their role in olefin epoxidation have appeared. Most of these studies deal with systems **3** or $\mathbf{3}^{+}$, derived from the Mn^{III}-salen model complexes **2** or $\mathbf{2}^{+}$, respectively.

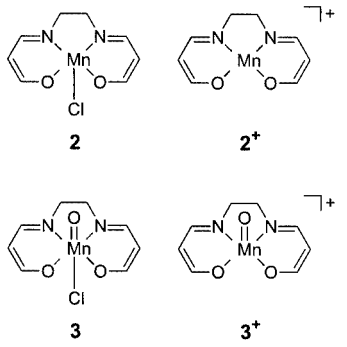

2 $\mathbf{2}^{+}$

3 $\mathbf{3}^{+}$

Strassner and Houk[24] have reported the results of hybrid-DF[25] calculations with the B3LYP functional[26] on the geometries and multiplicities of the systems described above, and discuss their implications for stereoselectivity. By the same methodology, Svensson and co-workers[27] studied the epoxidation of ethylene with catalyst $\mathbf{3}^{+}$. They suggest that the reaction begins with alkene attack on the triplet surface, followed by a spin change to the quintet surface, which affords the quintet epoxide product without a barrier. On the triplet surface it was possible to localize a radical intermediate, whereas on the quintet surface the reaction proceeds from the first, very early, transition state directly to the final products without any other intermediates or transition states. The point at which the spin-crossing occurs determines the stereochemistry of the reaction; only if the spin change takes place after the formation of the radical intermediate does *cis*-*trans* isomerization become possible. The mechanism of the Jacobsen−Katsuki epoxidation is thus explained in terms of two-state reactivity,[28] which has evolved as a new concept in organometallic chemistry.[29] Although reactions that undergo spin inversion have recently been observed in the gas phase,[30] two-state reactivity in the condensed phase has not yet been shown to occur, but "offers a conceptually attractive explanation for these experimental findings that are difficult to understand by any other existing concepts."[29]

We have investigated a similar reaction profile for olefin epoxidation with catalyst **3**,[31] by applying BP86 DF calculations.[32] Contrary to the results obtained by Svensson and co-workers, our calculations for the reaction profile for ethylene epoxidation with **3** indicate that the reaction occurs on the triplet surface, and is likely to involve radical intermediates. The reaction profile on the quintet surface, for which both a radical intermediate and transition states

for C−O bond formation could be localized, is generally higher in energy than that of the triplet surface, and spin inversion does not seem to be a likely process. Both studies on system **3** and **3**$^+$, however, concur on the fact that formation of a metallacycle during the epoxidation is not likely to occur.

One of the differences between the two mechanistic models described above is the presence of a free coordination site versus an occupied one *trans* to the oxo group. The coordination chemistry of Mn salen complexes and effects of axial ligation have recently been investigated by electrospray tandem mass spectrometry in combination with hybrid DF calculations.[33] This study shows that the presence of a *trans* ligand has a significant influence not only on the coordination geometry of the salen framework, but also on the relative energies of different spin states. Similar observations have also been made by Strassner and Houk.[24]

A further difference between our previous study and the contribution by Svensson and co-workers is the choice of computational methodology. Although it has been convincingly demonstrated that DF theory in general constitutes a powerful tool for the prediction of structures and energetics in transition metal chemistry[34] with an accuracy of the gradient corrected method similar to, or better than, standard correlated methods,[35] systematic studies investigating the performance of different functionals for certain problems in transition metal chemistry have only recently begun to appear.[36,37] When it comes to manganese complexes related to the problem at hand, successful applications both of the B3LYP[38] and of the BP86[39] functionals have been demonstrated in the literature. However, it was recently shown by high-level ab initio calculations [coupled cluster CCSD(T)] that a computational procedure based on the BP86 density functional generates numerical results significantly more reliable than those obtained by a B3LYP approach for the Mn-catalyzed epoxidation reactions.[40]

Given the importance of the Jacobsen−Katsuki epoxidation, we decided to reinvestigate the oxidation of ethylene with catalyst **2**$^+$ by means of BP86-DF calculations. This study complements our previous investigations on the corresponding neutral system **2**.[31] Comparison between the energy profiles for the neutral and cationic active species should allow insights on the role of the axial ligand to be obtained. Questions to be addressed include the existence of possible oxametallacyclic intermediates, as well as a possible precoordination of the olefinic double bond. Furthermore, the coordination geometry of the tetra-chelating N,O ligand is investigated, and the possibility of spin inversion is discussed in connection with the geometries of radical intermediates and of transition states. Moreover, since there are some discrepancies between the chemical pictures obtained by the different DF approaches, we believe it is also worthwhile to investigate the energy profile for the cationic system **2**$^+$ with the BP86 functional. We believe that a critical comparison between different computational approaches should allow further details on the mechanism of this relevant reaction to be gained.

Results and Discussion

Electronic Structures of Mn(salen) Model Compounds: (Supporting information including optimized geometries and final bonding energies available, see also footnote on the first page of this article).The qualitative molecular orbital diagram for a d^4-ML_4 complex[41] suggests that, for the square planar compound **2**$^+$, triplet and quintet configurations − corresponding to total spin density values of 2α, *S2*, and 4α, *S4*, respectively − have to be considered. Our nomenclature was chosen to reflect the spin density, and should not be mistaken with spin states or $<S^2>$ values. We calculated an energetic difference of 67 kJ/mol, in favor of the quintet state, between the *S2* and *S4* geometries in **2**$^+$. A singlet ground state can be achieved if the metal d orbitals adopt the familiar two-below-three pattern of a tetrahedral ligand field. The *S0*−**2**$^+$ molecule, however, which is consequently strongly distorted toward a tetrahedral geometry, is 147 kJ/mol higher in energy than *S4*−**2**$^+$. This coordination mode of the core ligand is not considered any further. Complex **2**$^+$ thus possesses an electronic structure similar to that of **2**, for which the energetic difference between the *S4* and *S2* geometries amounts to 38 kJ/mol,[31] *S4*−**2** again being more stable. These results are in agreement with EPR spectroscopic studies of the Mn(salen) complex **1** in CH_2Cl_2 at 77 K performed by Talsi and coworkers,[42] which reveal the presence of manganese species with spin states S = 2. Recent EPR studies by Campbell and co-workers[43] confirm these findings.

For the active species involved in oxygen transfer, the cationic Mn^V complex **3**$^+$, we calculate the *S0* state to be most stable, with a triplet *S2*−**3**$^+$ 27 kJ/mol higher in energy, and a quintet *S4*−**3**$^+$ 101 kJ/mol less stable than the ground state. For the corresponding hexacoordinate compound **3**, on the other hand, the two states *S0* and *S2* are at virtually the same energy level, with a marginal preference for the singlet. In addition, the quintet state *S4*−**3** is only 45 kJ/mol higher in energy than the *S0* local minimum geometry. The molecular orbital diagram for the Mn^V-oxo species **3** and **3**$^+$, presented in Figure 1, offers an explanation for this observation.

The energy level schemes are derived from the corresponding singlet geometries. For **3**$^+$, the HOMO is dominated by contributions from a Mn-$d_{x^2-y^2}$ orbital, whereas the LUMO and LUMO+1 are metal-based, derived from the orbitals d_{xz} and d_{yz}. However, the last two orbitals are strongly antibonding with respect to the p orbitals of the oxo ligand. They are therefore raised in energy relative to the HOMO, and the resulting rather large HOMO/LUMO gap energetically stabilizes the singlet state. The degeneracy of the LUMO and LUMO+1 is lifted, due to orbital contributions from the tetra-chelating ligand. For the HOMO of **3**, we have substantial antibonding interaction between the Mn-$d_{x^2-y^2}$ orbital and occupied p orbitals of the Cl^- ligand. This interaction causes an energetic destabilization of the HOMO. As a consequence, the HOMO/LUMO gap is lowered, in favor of a triplet configuration. This orbital interaction provides a first hint as to how an additional π-

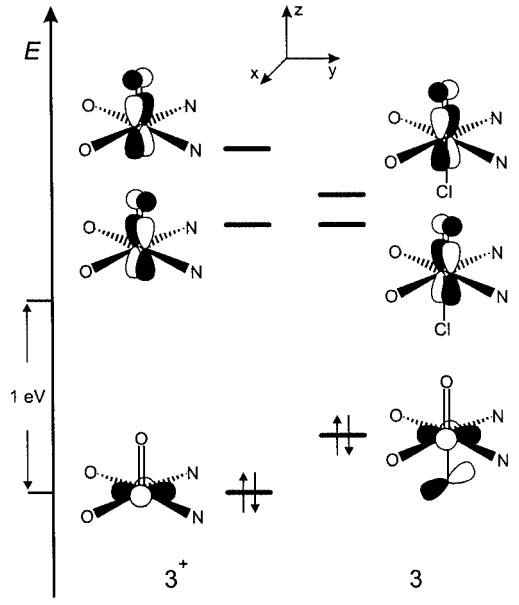

Figure 1. Frontier orbital diagram for Mn^V oxo complexes $\mathbf{3}^+$ and **3**

donor *trans* to the oxo ligand might exert an influence on the oxygen-transfer process.

Table 1 compares the relative energies of different spin state geometries of $\mathbf{2}^+$, **2**, $\mathbf{3}^+$, and **3** with the results of the two B3LYP studies by Strassner and Houk[24] and by Svensson and co-workers,[27] as well as with the recent study of Abashkin and co-workers.[40] This comparison focuses on technical aspects of the calculations, and the results in Table 1 are organized according to basis set quality into three groups. Group **I** refers to calculation utilizing a triple-ζ basis for Mn, and a double-ζ basis plus polarization for the remaining atoms. In group **II**, a double-ζ basis is used and polarization functions are added for Mn, Cl, O, and N, whereas group **III** essentially refers to double-ζ basis set calculations.

Table 1. Relative energies (kJ/mol)[a] of complexes $\mathbf{2}^+$, **2**, $\mathbf{3}^+$, **3** for different spin densities

[a]		$\mathbf{2}^+$		**2**		$\mathbf{3}^+$			**3**		
		S2	*S4*	*S2*	*S4*	*S0*	*S2*	*S4*	*S0*	*S2*	*S4*
I	BP86[b]	67	0	38	0	0	27	101	0	1	45
	B3LYP[c]	113	0	82	0	0	15	47	43	0	8
II	BP86[d].	–	–	–	–	0	53	141	0	25	72
	B3LYP[d]	–	–	–	–	–	–	–	39	5	0
III	B3LYP[e]	–	–	–	–	7	0	21	–	–	–
	B3LYP[f]	–	–	–	–	6	0	11	–	–	–

[a] Literature values have been converted. [b] Values for **2** and **3** from ref.[31] [c] 6−31G* (HCNOCl)/TZ(Mn) basis, ref.[24] [d] DZVP basis for Mn, Cl, N O, DZ basis for C, H; ref.[40] [e] DZ basis, ref.[40] [f] (14s,11p,6d) primitive basis augmented by two p and one diffuse d function contracted to [6s,5p,3d] for Mn, DZ basis for ligands, ref.[27]

Referring to group **I**, for the two cationic species and for **2,** our calculations are in qualitative agreement with the data reported by Strassner and Houk.[24] In particular, both sets of calculations predict the same energetic ranking for the Mn^{III} and Mn^V species, and indicate that the addition of the π-donating Cl^- ligand reduces the energy gap between the *S2* and *S4* states by about 30 kJ/mol. The reason is again to be found in the antibonding contributions from p orbitals of the Cl^- ligand, which destabilize only three of the four singly occupied metal d orbitals, rendering triplet occupation more stable for **2** than for $\mathbf{2}^+$. One difference between the BP86 and B3LYP functionals is the fact that the hybrid method, which contains an admixture of pure Hartree−Fock exchange, energetically favors the *S4* spin states. Thus, in cases in which *S4* is the ground state, such as **2** and $\mathbf{2}^+$, the energy difference between the *S4* and *S2* geometries is higher, by about 45 kJ/mol, for the B3LYP calculation than for BP86 results. On the other hand and for the same reason, *S4*−$\mathbf{3}^+$ is energetically more disfavored in the BP86 calculation, by 54 kJ/mol.

A major discrepancy is found for compound **3**. As discussed above, the BP86 calculations predict a singlet and a triplet geometry at almost the same energy. In contrast, the B3LYP method results in a triplet ground state, with the quintet close by in energy, and the singlet significantly higher.

A reason for this discrepancy may be found if group **II** data are included in the discussion. For $\mathbf{3}^+$ and **3** we find that the results of the BP86 calculations of Abashkin and co-workers[40] follow the same qualitative trend as our current and previous results. However, the energy differences between different spin states are significantly different. For **3** in particular, Abashkin and co-workers predict a singlet state, clearly favored over a triplet state, as ground state, whereas our calculations indicated that a singlet and a triplet state are essentially at the same energy level, well separated from a quintet state. This might be a first indication of the importance of an extended basis set for calculations on the type of molecules under investigation, describing the metal center on a triple-ζ basis, and including polarization functions for all atoms. Comparing B3LYP calculations of group **I** and **II**, we again find qualitative agreement. Triplet and quintet states are close in energy, whereas the singlet state is significantly higher in energy. However, Strassner and Houk find a triplet state at lowest energy, the quintet being 8 kJ/mol higher, whereas Abashkin and co-workers find the triplet to be 5 kJ/mol higher than the quintet, the latter now being the ground state. This again might be an indication for significant basis set influences.

Abashkin and co-workers have also addressed the comparison between the BP86 and the B3LYP approaches.[40] We recall that for **3** the two approaches provide qualitatively different results, the relative energy rankings being $S0 \approx S2 < S4$ for BP86 and $S0 > S2 \approx S4$ for B3LYP. In addition to DFT calculations, Abashkin and co-workers performed high level ab initio calculations, and the results for **3**, obtained from coupled cluster CCSD(T) calculations, are in line with BP86, but not with B3LYP. This study suggests that for this type of molecules the pure BP86 functional provides a more appropriate and a more suitable approach than the popular B3LYP hybrid functional.

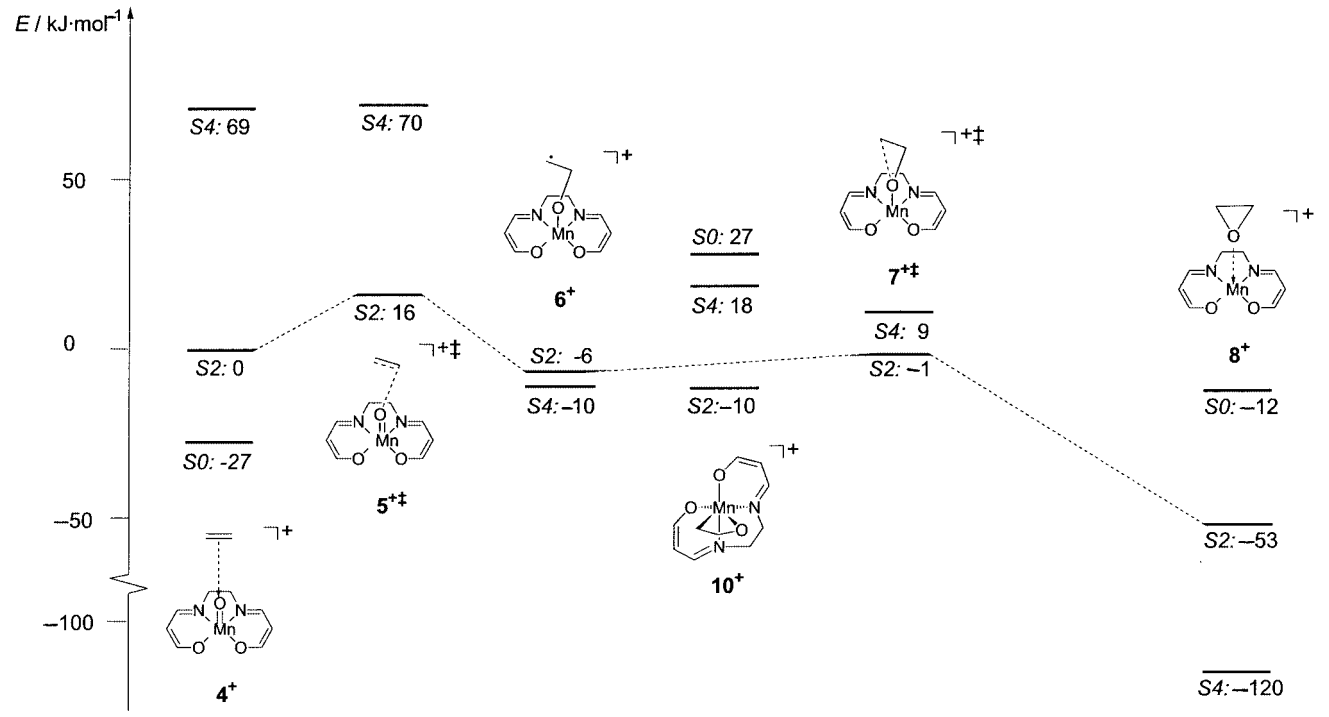

Figure 2. Energy profile for the epoxidation reaction

Finally, turning to group **III**, we find that the two sets of B3LYP calculations are in good qualitative agreement. However, B3LYP calculations without inclusion of polarization functions are significantly different from the B3LYP result for group **I**. This comparison again underlines the importance of an extended basis set for calculations on the type of molecules under investigation.

The importance of basis sets is further evident when the DZVP-BP86 results of Abashkin and co-workers for complex **2** are considered. The authors find a triplet state at lowest energy, a quintet state being 5 kJ/mol higher, whereas our previous BP86 results report the triplet as 38 kJ/mol above the quintet.

The Reaction Profile for Oxygen Transfer: The calculated energy profile for epoxide formation with the model catalyst $\mathbf{3}^+$ is displayed in Figure 2.

Relative energies for reactants, intermediates, transition states, and final products are reported for the *S0*, *S2*, and *S4* energy hypersurfaces. We comment on each of the single steps in more detail below.

The Reference System $\mathbf{4}^+$: In our reference system, the incoming olefin approaches the manganese catalyst from the site of the oxo ligand, and forms a weakly bonded adduct. In this complex, the distances between the olefinic C atoms and the Mn=O function amount to 300 and 320 pm, respectively. The system *S2*−$\mathbf{4}^+$ is set at 0 kJ/mol on the energy scale, and the energies of all other species are then given relative to *S2*−$\mathbf{4}^+$. It is worth mentioning that the relative energies of the different spin states *S0*, *S2*, and *S4* are in essence identical to those obtained for the free oxo cation $\mathbf{3}^+$ (compare Table 1). We chose this aggregate as reference state over the completely separated molecules (C_2H_4 + $\mathbf{3}^+$), since some of the computational errors involved in determining the energetics of bond-forming reactions, especially those stemming from basis set superposition effects,[44] are reduced in such a combined approach.

The First Transition State $\mathbf{5}^{+\ddagger}$: On the *S2* energy hypersurface, the energy of the $\mathbf{5}^{+\ddagger}$ structure lies 16 kJ/mol above the reference state *S2*−$\mathbf{4}^+$, indicating that the first C−O bond formation does not represent much of an energetic barrier. The distance d_{C-O} amounts to 189 pm, similar to that calculated for the corresponding structure *S2*−$\mathbf{5}^{\ddagger}$.[31] The Mn−O bond is 169 pm, significantly elongated compared to that in *S2*−$\mathbf{3}^+$ (d_{Mn-O} = 161 pm). The values of spin density at the Mn center and the terminal C atom of the olefinic substrate amount to 2.4 α and 0.5 β, respectively, indicating that the epoxidation reaction is initialized by a one-electron reduction process. From both the electronic and the geometric structures of *S2*−$\mathbf{5}^{+\ddagger}$ it can be concluded that *S2*−$\mathbf{5}^{+\ddagger}$ has to be classified as a late, or product-like, transition state on the triplet surface. This observation, together with an orbital analysis for the radical intermediate presented in the next section, also rules out the existence of an energetically low-lying *S0*−$\mathbf{5}^{+\ddagger}$ geometry. A different situation is found when the process is assumed to take place on the quintet surface. The *S4*−$\mathbf{5}^{+\ddagger}$ state is already reached when the bond-forming C-atom is about 240 pm away from the oxo center, and is only marginally higher in energy than *S4*−$\mathbf{4}^+$. Also, the electronic situation more closely resembles that of the reactant system, with spin density mostly located at the metal center and at the oxo ligand. In this case the reaction occurs through an early transition state, as already noted by Svensson and coworkers.[27]

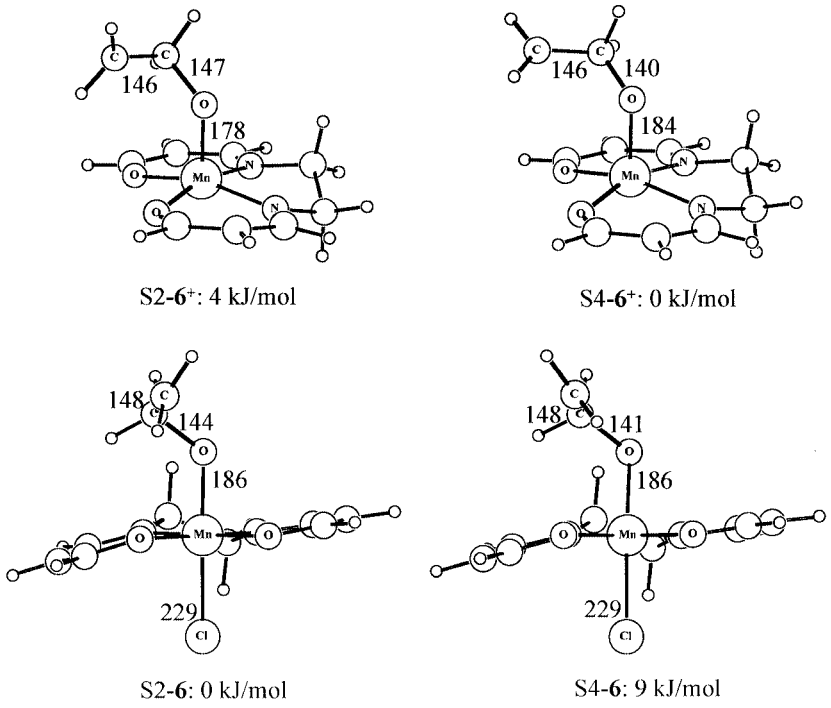

Figure 3. Optimized structures and relative energies for *S2* and *S4* geometries of $\mathbf{6}^+$ and **6**

The Radical Intermediate $\mathbf{6}^+$: Figure 3 compares the geometries and relative energies of the radical intermediates *S2*−$\mathbf{6}^+$ and *S4*−$\mathbf{6}^+$ with those of the corresponding neutral systems *S2*−**6** and *S4*−**6**.

A few important differences deserve more detailed discussion. Firstly, we note that the Mn−O distances in the cationic systems are between 8 and 2 pm shorter than those found for the system with the Cl ligand *trans* to the oxo group, pointing to a *trans* influence of the additional π-donor ligand. We also see that both chloro species *S2*−**6** and *S4*−**6** have the same Mn−O separation, whereas the triplet geometry shows significantly shorter Mn−O distances for the cationic complexes $\mathbf{6}^+$. Secondly, we observe that the coordination geometry of the quintet species is substantially different from that of the triplet systems. In the latter, the original orientation of the olefin is preserved, whereas in the former we see that the terminal CH_2 group is rotated by 90°. Thirdly, for the cationic system $\mathbf{6}^+$ we calculate a small energetic preference for the *S4* state (of 4 kJ/mol), whereas for the neutral system **6** the *S2* state is more stable by 9 kJ/mol.

A qualitative analysis of the frontier Kohn-Sham orbitals corresponding to the α spin density for the *S2* geometries provides a rationale for the above observations. The highest occupied orbital 1a and the lowest unoccupied orbitals 2a for system $\mathbf{6}^+$ and **6** are presented in Figure 4.

For the formal Mn^{IV} species, these orbitals are mainly Mn-based d orbitals, undergoing antibonding interaction with the $-OC_2H_5$ ligand. For **6**, we see that the interplay of the p-Cl and d-Mn orbitals adds additional antibonding character. A promotion of one electron into orbital 2a, resulting in an electronic quintet state, is thus disfavored for

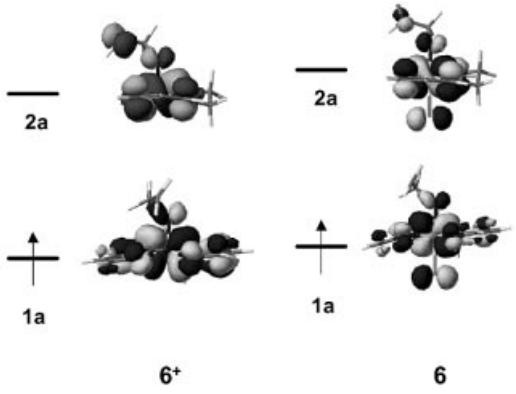

Figure 4. Frontier orbitals for the Mn^{IV} complexes $\mathbf{6}^+$ and **6**

6 by an increase in the repulsive Mn−Cl interaction. This argument suggests that the role of the π-donor in the *trans* position is a relative destabilization of a possible quintet occupation, thus conferring spin rigidity to the six-coordinate species derived from the neutral catalyst **2**. In our previous study we calculated that *S2*−**6** is energetically favored over *S4*−**6** by 9 kJ/mol. We also see that the orbital 2a has large contributions from the p orbitals of the terminal CH_2 group, which interact with the formerly oxo ligand in an antibonding fashion. As a consequence, when this molecular orbital becomes occupied, the terminal CH_2 group twists to relieve this destabilizing interaction. As mentioned before, the *S4* geometries both for **6** and for $\mathbf{6}^+$ do indeed exhibit this structural characteristic.

Another important feature observed in Figure 3 is the folded geometry of the tetra-chelating N,O ligand. This arrangement has been identified as one of the key points in

the mechanism of enantioselectivity[45] and we return to a more detailed analysis of this structural feature at a later point.

The Second Transition State $7^{+\ddagger}$: On the *S2* surface, the transition state $\mathbf{7}^{+\ddagger}$ for the formation of the second C−O bond is only 9 kJ/mol higher in energy than the triplet intermediate (Figure 2). The long length of the newly forming C−O bond classifies *S2*−$\mathbf{7}^{+\ddagger}$ as an early transition state. Product formation from the radical intermediate thus occurs without much of an energetic barrier. In comparison with *S2*−$\mathbf{7}^{+\ddagger}$, the transition state *S4*−$\mathbf{7}^{+\ddagger}$ is 10 kJ/mol higher in energy. The characteristic mode receives a strong contribution from the CH_2-twist required for ring closure to form the epoxide.

The Epoxide Adduct 8^+: Characteristic bond lengths and bonding energies for epoxide complexes $\mathbf{8}^+$ are compiled in Table 2.

Table 2. Bond lengths (pm) and bond energies (kJ/mol) for Mn^{III} epoxide complexes $\mathbf{8}^+$

	d_{Mn-O}	BE
S0−$\mathbf{8}^+$	198	123
S2−$\mathbf{8}^+$	199	85
S4−$\mathbf{8}^+$	223	85

We see that the forming epoxide is only loosely bound to the metal centers, the coordination geometries and relative energies of which resemble those of the Mn^{III} precursor models $\mathbf{2}^+$. Only the *S0* complex is somewhat more strongly stabilized, relative to the *S2* and *S4* systems. The most stable complex is therefore *S4*−$\mathbf{8}^+$, followed by *S2*−$\mathbf{8}^+$, 67 kJ/mol higher in energy. If the cationic complexes considered here are the true catalytically active species, a spin change during the course of the epoxidation reaction might indeed occur in the reaction sequence. On the other hand, it is worth mentioning that the energetic difference between the corresponding chloro complexes *S4*−**8** and *S2*−**8** only amounts to 4 kJ/mol, in favor of the quintet state.[31] As we have already argued in this context, catalytic cycles based on Mn complexes derived from the hexacoordinate model system **3** are likely to take place as spin-conserving reactions.

As mentioned before, the resulting epoxides are only loosely bonded to the metal center. Furthermore, we should keep in mind that our calculations are performed on isolated systems in the gas phase, and we can expect that solvent effects should substantially stabilize the coordinatively unsaturated cation $\mathbf{2}^+$, thus further reducing the bond energy of the epoxide ligand. If in addition we take into account unfavorable coordination entropy, for which at room temperature a $T\Delta S$ contribution between 40 and 50 kJ/mol can be estimated,[46] we conclude that product liberation is not a critical step in the catalytic cycle.

The Transition State $9^{+\ddagger}$ for Synchronous Attack: So far, we have considered the epoxidation reaction as a sequence of two consecutive C−O bond-formation steps. Alternatively, one might think of a concerted mechanism that involves an epoxide-like transition state $\mathbf{9}^{+\ddagger}$ (Scheme 3).

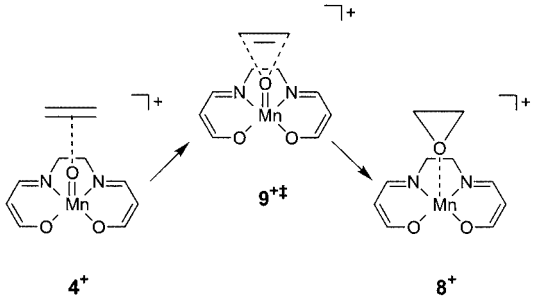

Scheme 3

Such a mechanism, however, although consistent with certain experimental findings,[22] does not offer a simple explanation for the observed *cis*/*trans* isomerization that frequently occurs in the epoxidation reaction. For our model reaction we have localized the corresponding structures both on the triplet and on the quintet surfaces. Compared to the reference system, structures *S2*−$\mathbf{9}^{+\ddagger}$ and *S4*−$\mathbf{9}^{+\ddagger}$ are 32 and 74 kJ/mol higher in energy, respectively. This implies that, on the *S2* surface, the concerted mechanism is kinetically disfavored relative to the stepwise reaction by 16 kJ/mol. Even in the *S4* case the stepwise reaction is favored by 4 kJ/mol.

Ligand Folding: As noted above in the context of the radical intermediate $\mathbf{6}^+$, the tetra-chelating N,O model ligand shows significant deviations from a planar structure, and has a folded geometry, as shown in Figure 3. We now discuss ligand folding for the representative geometries of the oxomanganese species $\mathbf{3}^+$ and **3**, as well as of the radical intermediates $\mathbf{6}^+$ and **6**, including the corresponding structures **3s** and **6s** of a Mn(salen) complex.[31]

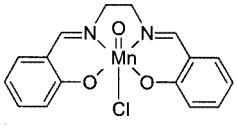

3s

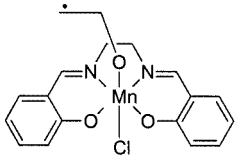

6s

Ligand folding is discussed in connection with the bent angles φ_{up} and φ_{down}, and the distance of pyramidalization, d_P. A bent angle φ is defined as $\varphi = 180° - \angle(Mn-X_{NO}-X_R)$, the angle $\angle(Mn-X_{NO}-X_R)$ being that measured between the metal center, the midpoint of adjacent N,O heteroatoms (X_{NO}), and the midpoint of the six-

membered ring containing the metal and the N,O heteroatoms (X_R, Scheme 4).

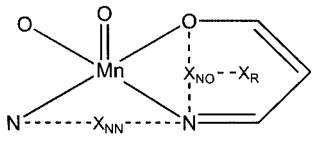

Scheme 4

The angle φ_{up} indicates the part of the tetra-chelating N,O ligand being bent towards the oxo or towards the ethoxy ligand, whereas φ_{down} characterizes the part of the tetra-chelating N,O ligand bent towards the free coordination site or towards the chlorine ligand. Furthermore, the distance of pyramidalization d_P is defined as the separation between the metal atom and the $O-X_{NN}-O$ plane, X_{NN} being the midpoint between the two N atoms. A value of d_P close to zero indicates that the metal essentially lies within the O,N,N,O coordination plane. The values for the folding angles and for the distance d_P are collected in Table 3.

Table 3. Relevant angles (°) φ_{up}, φ_{down} and distance of pyramidalization (pm) d_P for cationic (this work) and neutral (from data of ref.[31]) Mn complexes

	S2			S4		
	φ_{up}	φ_{down}	d_P	φ_{up}	φ_{down}	d_P
3$^+$	18	8	42	7	2	22
3	19	17	11	3	13	4
3s	10	16	0	10	17	1
6$^+$	20	5	29	18	3	31
6	8	16	0	8	15	0
6s	8	15	0	8	15	0

The folded ligand geometries as shown in Figure 3 are characterized by bent angles φ being 10° or larger, and by d_P being essentially zero. Inspection of the values reported in Table 3 indicates that highly bent angles φ are found in all cases, with the single exception of *S4*−**3**$^+$. For the cationic molecules, however, the metal atom is considerably shifted out of the O,N,N,O coordination plane with values of d_P of between 20 and 45 pm. The cationic molecules do not display the folded geometry as shown in Figure 3, and they probably also do not posses the ability to form a chiral pocket, needed for transfer of enantioselectivity.[45] On the other hand, the neutral systems under consideration display φ and d_P values indicative of a folded ligand geometry. In particular, we note that similar structures are observed for the salen ligand in the radical intermediate **6s** and for the model ligand in complex **6**. It has recently been suggested that the degree of ligand folding is determined by the nature of the axial ligand in Mn(salen) complexes, which in turn has implications for the reaction rate of epoxidation reactions.[47]

Structural Alternatives: We briefly discuss two further complex geometries that might be of importance: namely a metallacycle **10**$^+$ and an olefin complex of the Mn^V-oxo species, **11**$^+$. Representative structures are displayed in Figure 5.

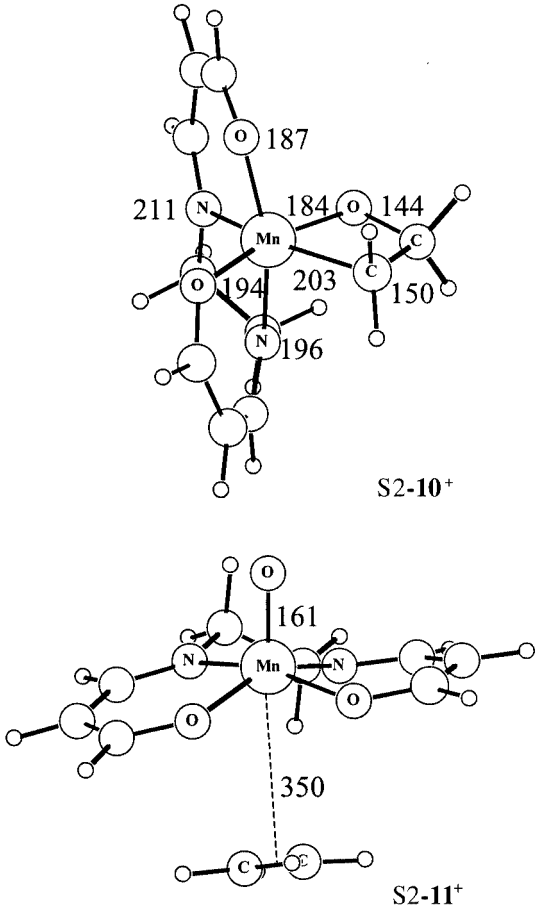

Figure 5. Representative *S2* geometries for a possible manganaoxetane **10**$^+$ (above), and an Mn^V-oxo olefin adduct **11**$^+$ (below)

Metallacyclic Intermediates: The possibility that metallacycles might be viable intermediates in the epoxidation reaction, and might play a key role in the mechanism of enantioselectivity, has been the subject of a vivid debate in the literature.[17] Indeed, one of the first models of the chirality transfer deduced from calculations uses a manganoxetane as a key intermediate.[48] We have already mentioned that the orbital analysis for structures **6**$^+$ points to the possible existence of metallacyclic intermediates. We were able to locate local minima corresponding to such a species on the *S0*, *S2*, and *S4* hypersurfaces, their relative energies being given in Figure 2. Interestingly, the structure *S2*−**10**$^+$ is energetically even slightly more stable than the radical intermediate. Its geometry is displayed in Figure 5. The Mn−O distance of the four-membered ring is about 6 pm longer than *S2*−**6**$^+$, but still within the calculated range for other Mn−O bonds. The Mn−C bond is 203 pm long, substantially shorter than the Mn−C separations in the radical intermediates (around 230 pm). The Mn center possesses a pseudo-octahedral coordination geometry, with a significantly elongated Mn−N bond *trans* to the oxacycle. The formation of the oxacycle is favored since the Mn center in **6**$^+$ is coordinatively unsaturated. Indeed, a seven-coordin-

ated manganaoxetane **10** is 104 kJ/mol higher in energy than the radical intermediate **6**.[31] Although structure $\mathbf{10}^+$ might be an alternative for an intermediate local minimum geometry, it is not likely to play a major role in product formation. We calculated that formation of $\mathbf{8}^+$ starting from $\mathbf{10}^+$, rather than $\mathbf{6}^+$, is associated with an activation barrier of about 35 kJ/mol. This result is in agreement with a recent study that made use of electrospray ionization in combination with tandem mass spectrometric techniques.[49] It was found that the presence of axial ligands decreases the stability and thus enhances the reactivity of the Mn=O moiety. In the cationic system, the manganaoxetane $\mathbf{10}^+$ is an energetically favorable intermediate in comparison with the radical intermediate $\mathbf{6}^+$, but possesses a higher activation barrier towards product formation, and thus a reduced reactivity. In contrast, systems with axial ligands do not possess energetically favorable, metallacyclic resting intermediates.[31]

Olefin Pre-Coordination: Since the catalytic model system $\mathbf{3}^+$ is coordinatively unsaturated, one might consider the possibility that the olefinic substrate coordinates to the metal center before the oxygen transfer occurs. We investigated possible complexes of this type on the S0, *S2*, and *S4* surfaces, and found in all cases that the olefin is only weakly bound. A representative geometry $S2-\mathbf{11}^+$ is shown in Figure 5. The distance between the olefin and the metal center amounts to about 350 pm, and the relative energy is only 4 kJ/mol lower than the one calculated for the reference system $S2-\mathbf{4}^+$. The pre-coordination of an olefin can thus be excluded as a vital step in the epoxidation reaction. This conclusion is in agreement with the results of the recent electrospray tandem mass spectrometric study by Plattner and co-workers, who, in a suitable experimental set-up, did not find any indication of pre-coordination of the substrate as prerequisite for oxidation.[33]

Comparison with d^0 Metal Oxo and Peroxo Species: In this final section we present a brief comparison with related theoretical work on oxygen-transfer reactions involving transition metal complexes. Olefin epoxidations mediated by transition metal oxo complexes in high oxidation states, especially those catalyzed by Herrmann-type complexes $[ReO(O_2)_2CH_3]$ and Mimoun-type complexes $[MoO(O_2)_2(OPR_3)]$, have recently generated much interest among experimentalists and theoreticians alike, and Rösch's[50] and Deubel and Frenking's[51] groups have presented detailed theoretical mechanistic studies. The interested reader will also find extensive references to the literature in these computational contributions. Unlike in this work, the olefin attacks an oxygen center in a *concerted* fashion. The preferred site of initial attack is a peroxo ligand, giving rise to *spiro* oxygen in the transition state. Using charge decomposition analysis, Deubel and Frenking[51a] have characterized the electronic nature of the initial attack in terms of classical donor-acceptor interactions, in which the d^0 metal oxo and peroxo species attack the olefin in an electrophilic manner. For the Mn(salen) systems, charge analysis based on Voronoi deformation densities suggests a similar electronic picture. However, the characteristic feature of the transition states $\mathbf{5}^+$ and **5** is a build-up of spin density at the terminal carbon atom. This process is essentially responsible for the locally asymmetric attack of the olefin at the oxo center, which further determines the geometric features of the transition state necessary for chirality transfer.[45] Consistently with our findings, Deubel and Frenking conclude that olefin precoordination at the metal center does not apparently play a role in Mo^{IV}-catalyzed epoxidation reactions,[51c] the reaction profile in both cases being determined by direct oxygen attack of the olefin.

Conclusion

The main results of this study are summarized in the following points. By our computational approach, the epoxidation of ethylene with the cationic five-coordinate model catalyst $\mathbf{3}^+$ is predicted to occur through a radical intermediate, similarly to the reaction mechanism calculated for the corresponding neutral six-coordinate species **3**. In contrast to the reaction profile for **3**, we do not find a clear preference for the *S2* state throughout the whole process. The radical intermediate $\mathbf{6}^+$ shows a small energetic preference for the quintet state over the triplet state. However, contrary to previous studies,[27] we were able to locate a radical intermediate as a local minimum structure on the *S4* hypersurface. On inspection of the computed reaction profile, it seems unlikely that two-state reactivity involving spin change might play a major role in the oxygen-transfer step. Comparative orbital analysis of the cationic and the neutral complexes provides an explanation as to how the ligand *trans* to the oxo group confers spin rigidity to the catalytic systems. However, the different coordination geometries of models $\mathbf{6}^+$ and **6** on the *S2* and *S4* surfaces, respectively, indicate that spin change might indeed be of importance to epoxide formation. Whereas in the *S2* species the two carbon centers of the olefinic substrate are still in π-conjugation, the terminal methylene group in the *S4* complexes is rotated by 90°. This points to the possibility that the pathway of rotational collapse might involve a spin-crossing process. Metallacyclic intermediates might occur during the epoxidation reaction mediated by cationic complexes. However, these complexes constitute resting states, and are likely to display a reduced reactivity towards epoxide formation, in comparison with radical intermediates. Pre-coordination of an olefin is likely to be excluded as a vital step in the epoxidation reaction

This and our previous studies[31] strongly suggest that the crucial step to enantioselectivity is the transition state of the first carbon-oxygen formation. From this assumption, and from the results obtained so far, we have already developed a model that explains the enantioselectivity in the Mn(salen)-catalyzed epoxidation of olefins.[9,19,45] Nevertheless, one has to keep in mind the fact that solvent effects as well as the presence of auxiliary ligands are likely to influence the course of the epoxidation reaction. In addition, reaction profiles in which other Mn^{IV} species are involved in the epoxidation reaction have recently been addressed in

the literature,[52] and deserve further computational attention. Recent theoretical studies[53] have demonstrated a general interest in mechanistic aspects of transition metal-mediated reactions resulting in the formation of three-membered ring systems, and recent experimental work[54,55] illustrates the ongoing discussion of the mechanistic aspects of enantioselective epoxidation reactions. In particular, the contribution by Adam and co-workers experimentally addresses the question of whether radical or cationic intermediates are present in the Mn(salen)-catalyzed epoxidation, and attributes counterion effects to computationally assessed ligand-dependent reaction profiles.[55] It is to be hoped that this study will prove to be helpful in supporting such studies, and will provide further impetus for future work, experimentally as well as theoretically.

Computational Details

Spin-polarized calculations were performed with the ADF program package, version 2.3.0.[56] The local exchange-correlation potential of Vosko and co-workers[57] was augmented self-consistently by Becke's exchange gradient-correction and Perdew's correlation gradient-correction (BP86).[32] The ADF basis set IV (triple-ζ STO plus one additional 4*p* function) was used for Mn, whereas basis set III (double-ζ STO plus one polarization function) was employed for the remaining atoms. These basis sets imply the use of the frozen core approximation, in which only the *n*- and $(n + 1)$-valence orbitals are treated explicitly in a self-consistent manner.[58] The numerical integration scheme developed by te Velde[59] was used, and the grid was chosen such that representative test integrals were evaluated with an accuracy of at least four significant digits. Analytical gradients were calculated by the method described by Versluis.[60] Transition states were first traced by a synchronous linear transit method, and then refined by establishing one negative frequency in the spectrum of the approximate Hessian used to construct geometry updates. The validity of this approach has been demonstrated in the literature.[61]

Acknowledgments

Support from the Italian MURST (L.C.), and access to the computational facilities of the Rechenzentrum der Universität Zürich (H.J.) are gratefully acknowledged. L.C. thanks the CIMCF of the Università Federico II of Napoli for technical support. The constructive comments of one of our referees are highly appreciated.

[1] All articles in, *Struct. Bond.* **2000**, *97*.
[2] [2a] R. J. Debus, *Biochim. Biophys. Acta* **1992**, *1102*, 269−352. [2b] V. K. Yachandra, K. Sauer, M. P. Klein, *Chem. Rev.* **1996**, *96*, 2927−2950.
[3] J. Limburg, J. S. Vrettos, L. M. Liable-Sands, A. L. Rheingold, R. H. Crabtree, G. W. Brudvig, *Science* **1999**, *108*, 1524−1527.
[4] [4a] M. R. A. Blomberg, P. E. M. Siegbahn, S. Styring, G. T. Babcock, B. Åckermark, P. Korall, *J. Am. Chem. Soc.* **1997**, *119*, 8285−8292. [4b] P. E. M. Siegbahn, *Inorg. Chem.* **2000**, *39*, 2923−2935.
[5] K. Srinivasan, P. Michaud, J. K. Kochi, *J. Am. Chem. Soc.* **1986**, *108*, 2309−2320.
[6] R. Irie, K. Noda, Y. Ito, N. Matsumoto, T. Katsuki, *Tetrahedron Lett.* **1990**, *21*, 7345−7348.
[7] [7a] W. Zhang, J. L. Loebach, S. R. Wilson, E. N. Jacobsen, *J. Am. Chem. Soc.* **1990**, *112*, 2801−2803. [7b] E. N. Jacobsen, W. Zhang, M. L. Güler, *J. Am. Chem. Soc.* **1991**, *113*, 6703−6704. [7c] E. N. Jacobsen, W. Zhang, A. R. Muci, J. R. Ecker, L. Deng, *J. Am. Chem. Soc.* **1991**, *113*, 7063−7064.
[8] [8a] T. Katsuki, *Coord. Chem. Rev.* **1995**, *140*, 189−214. [8b] T. Katsuki, *J. Mol. Cat. A* **1996**, *113*, 87−107.
[9] [9a] E. N. Jacobsen, in *Catalytic Asymmetric Synthesis* (Ed.: I. Ojima,), VCH Verlagsgesellschaft, Weinheim, **1993**, chapter 4.2. [9b] E. N. Jacobsen, in *Comprehensive Organometallic Chemistry II, Vol. 12* (Eds: G. Wilkinson, F. G. A. Stone, E. W. Abel, L. S. Hegedus), Pergamon, New York, **1995**, chapter 11.1.
[10] J. F. Larrow, E. N. Jacobsen, Y. Gao, Y. Hong, X. Nie, C. M. Zepp, *J. Org. Chem.* **1994**, *59*, 1939−1942.
[11] C. E. Song, E. J. Roh, *Chem. Commun.* **2000**, 837−838.
[12] C. T. Dalton, K. M. Ryan, V. M. Wall, C. Bousquet, D. G. Gilheany, *Top. Catal.* **1998**, *5*, 75−91.
[13] D. Feichtinger, D. A. Plattner, *Angew. Chem.* **1997**, *109*, 1796; *Angew. Chem. Int. Ed. Engl.* **1997**, *36*, 1718−1719.
[14] D. Feichtinger, D. A. Plattner, *J. Chem. Soc., Perkin Trans. 2* **2000**, 1023−1028.
[15] [15a] J. T. Groves, J. Lee, S. S. Marla, *J. Am. Chem. Soc.* **1997**, *119*, 6269−6273. [15b] N. Jin, J. T. Groves, *J. Am. Chem. Soc.* **1999**, *121*, 2923−2924.
[16] T. Linker, *Angew. Chem.* **1997**, *109*, 2150−2152; *Angew. Chem. Int. Ed. Engl.* **1997**, *36*, 2060−2062.
[17] N. S. Finney, P. J. Pospisil, S. Chang, M. Palucki, R. G. Konsler, K. B. Hansen, E. N. Jacobsen, *Angew. Chem.* **1997**, *109*, 1798; *Angew. Chem. Int. Ed. Engl.* **1997**, *36*, 1720−1723.
[18] C. Linde, M. Arnold, P.-O. Norrby, B. Åckermark, *Angew. Chem.* **1997**, *109*, 1802−1803; *Angew. Chem. Int. Ed. Engl.* **1997**, *36*, 1723−1725.
[19] M. Palucki, N. S. Finney, P. J. Pospisil, M. L Güler, T. Ishida, E. N. Jacobsen, *J. Am. Chem. Soc.* **1998**, *120*, 948−954.
[20] W. Adam, R. T. Fell, V. R. Stegemann, C. R. Saha-Möller, *J. Am. Chem. Soc.* **1998**, *120*, 708−714.
[21] W. Adam, T. Wirth, *Acc. Chem. Res.* **1999**, *32*, 703−710.
[22] W. Adam, V. R. Stegemann, C. R. Saha-Möller, *J. Am. Chem. Soc.* **1999**, *121*, 1879−1882.
[23] T. Hamada, T. Fukuda, H. Imanishi, T. Katsuki, *Tetrahedron* **1996**, *52*, 515−530.
[24] T. Strassner, K. N. Houk, *Org. Lett.* **1999**, *1*, 419−421.
[25] [25a] A. D. Becke, *J. Chem. Phys.* **1993**, *98* 1372−1377. [25b] A. D. Becke, *J. Chem. Phys.* **1993**, *98* 5648−5652.
[26] P. J. Stephens, F. J. Devlin, C. F. Chabalowski, M. J. Frisch, *J. Phys. Chem.* **1994**, *98*; 11623−11627.
[27] C. Linde, B. Åckermark, P.-O. Norrby, M. Svensson, *J. Am. Chem. Soc.* **1999**, *121*, 5083−5084.
[28] S. Shaik, M. Filatov, D. Schröder, H. Schwarz, *Chem. Eur. J.* **1998**, *4*, 193−199.
[29] D. Schröder, S. Shaik, H. Schwarz, *Acc. Chem. Res.* **2000**, *33*, 139−145.
[30] D. Plattner, *Angew. Chem.* **1999**, *111*, 86−90; *Angew. Chem. Int. Ed.* **1999**, *38*, 82−86.
[31] L. Cavallo, H. Jacobsen, *Angew. Chem.* **2000**, *112*, 602−604; *Angew. Chem. Int. Ed.* **2000**, *39*, 589−592.
[32] [32a] A. D. Becke, *Phys. Rev. A* **1988**, *38*, 3098−3100. [32b] J. P. Perdew, *Phys. Rev. B* **1986**, *33*, 8822−8824.
[33] D. A. Plattner, D. Feichtinger, J. El-Bahraoui, O. Wiest, *Int. J. Mass Spectrom.* **2000**, *195*/*196*, 351−362.
[34] [34a] T. Ziegler, *Chem. Rev.* **1991**, *91*, 651−667. [34b] T. Ziegler, *Can. J. Chem.* **1995**, *73*, 743−761.
[35] L. A. Eriksson, L. G. M. Pettersson, P. E. M. Siegbahn, U. Wahlgren, *J. Chem. Phys.* **1995**, *102*, 872−878.
[36] [36a] S. Yanagisawa, T. Tsuneda, K. Hirao, *J. Chem. Phys.* **2000**,

112, 545−553. [36b] S. Yanagisawa, T. Tsuneda, K. Hirao, *J. Comput. Chem.* **2001**, *22*, 1995−2009.
[37] C. J. Barden, J. C. Rienstra-Kiracofe, H. F. Schaefer, *J. Chem. Phys.* **2000**, *113*, 690−700.
[38] P. E. M. Siegbahn, M. R. A. Blomberg, *Chem. Rev.* **2000**, *100*, 421−437.
[39] [39a] X. G. Zhao, W. H. Richardson, J.-L. Chen, J. Li, L. Noodleman, H.-L. Tsai, D. N. Hendrickson, *Inorg. Chem.* **1997**, *36*, 1198−1217. [39b] J. Li, C. L. Fisher, R. Konecny, D. Bashford, L. Noodleman, *Inorg. Chem.* **1999**, *38*, 929−939.
[40] Y. G. Abashkin, J. R. Collins, S. K. Burt, *Inorg. Chem.* **2001**, *40*, 4040−4048.
[41] T. A. Albright, J. K. Burdett, M.-H. Whangboo, *Orbital Interactions in Chemistry*; John Wiley & Sons: New York, **1985**, chapter 16.4.
[42] [42a] K. P. Bryliakov, D. E. Babushkin, E. P. Talsi, *Mendeleev Commun.* **1999**, 29−32. [42b] K. P. Bryliakov, D. E. Babushkin, E. P. Talsi, *Mendeleev Commun.* **2000**, 1−2A. [42c] K. P Bryliakov, D. E. Babushkin, E. P. Talsi, *J. Mol. Cat. A* **2000**, *158*, 19−35.
[43] K. A. Campbell, M. R. Lashley, J. K. Wyatt, M. H. Nantz, R. D. Britt, *J. Am. Chem. Soc.* **2001**, *123*, 5710−5719.
[44] F. B. van Duijneveldt, J. C. G. M. van Duijneveldt-van de Rijdt, J. H. van Lenthe, *Chem. Rev.* **1994**, *94*, 1873−1895.
[45] H. Jacobsen, L. Cavallo, *Chem. Eur. J.* **2001**, *7*, 800−807.
[46] P. Margl, L. Deng, T. Ziegler, *Organometallics* **1998**, *17*, 933−946.
[47] J. El-Bahraoui, O. Wiest, D. Feichtinger, D. A. Plattner, *Angew. Chem.* **2001**, *113*, 2131−2134; *Angew. Chem. Int. Ed.* **2001**, *40*, 2073−2076.
[48] P.-O. Norrby, C. Linde, B. Åckermark, *J. Am. Chem. Soc.* **1995**, *117*, 11035−11036.
[49] D. Feichtinger, D. A. Plattner, *Chem. Eur. J.* **2001**, *7*, 591−599.
[50] [50a] P. Gisdakis, S. Antonczak, Köstlmeier, W. A. Herrmann, N. Rösch, *Angew. Chem.* **1998**, *110*, 2333−2336; *Angew. Chem. Int. Ed.* **1998**, *37*, 2211−2214. [50b] I. V. Yudanov, C. Di Valentin, P. Gisdakis P, N. Rösch, *J. Mol. Cat. A* **2000**, *158*, 189−197. [50c] P. Gisdakis, I. V. Yudanov, N. Rösch, *Inorg. Chem.* **2001**, *40*, 3755−3765.
[51] [51a] D. V. Deubel, G. Frenking, H. M. Senn, J. Sundermeyer, *Chem. Commun.* **2000**, 2469−2470. [51b] D. V. Deubel, J. Sundermeyer, G. Frenking, *Inorg. Chem.* **2000**, *39*, 2314−2320. [51c] D. V. Deubel, J. Sundermeyer, G. Frenking, *J. Am. Chem. Soc.* **2000**, *122*, 10101−10108. [51d] D. V. Deubel, J. Sundermeyer, G. Frenking, *Eur. J. Inorg. Chem.* **2001**, 1819−1827.
[52] W. Adam, C. Mock-Knoblauch, C. R. Saha-Möller, M. Herderich, *J. Am. Chem. Soc.* **2000**, *122*, 9685−9691.
[53] [53a] T. Ikeno, I. Iwakura, T. Yamada, *Bull. Chem. Soc. Jpn.* **2001**, *74*, 2151−2160. [53b] T. Ikeno, I. Iwakura, S. Yabushita, T. Yamada, *Org. Lett.* **2002**, *4*, 517−520.
[54] C. Linde, N. Koliaï, P.-O. Norrby, B. Åckermark, *Chem. Eur. J.* **2002**, *8*, 2568−2573.
[55] W. Adam, K. J. Roschmann, C. Sahu-Möller, D. Seebach, *J. Am. Chem. Soc.* **2002**, *124*, 5068−5073.
[56] C. Fonseca Guerra, J. G. Snijders, G. te Velde, E. J. Baerends, *Theor. Chem. Acc.* **1998**, *99*, 391−403.
[57] S. H. Vosko, L. Wilk, M. Nusair, *Can. J. Phys.* **1980**, *58*, 1200−1211.
[58] E. J. Baerends, D. E. Ellis, P. Ros, *Chem. Phys.* **1973**, *2*, 41−51.
[59] G. te Velde, E. J. Baerends, *J. Comput. Phys.* **1992**, *99*, 84−98.
[60] L. Versluis, T. Ziegler, *J. Chem. Phys.* **1988**, *88*, 322−328.
[61] [61a] J. C. W. Lohrenz, T. Woo, T. Ziegler, *J. Am. Chem. Soc.* **1995**, *117*, 12793−12800. [61b] L. Cavallo, *J. Am. Chem. Soc.* **1999**, *121*, 4238−4241. [61c] M. Cheong, R. Schmid, T. Ziegler, *Organometallics* **2000**, *19*, 1973−1982. [61d] M. Solà, L. Cavallo, *J. Am. Chem. Soc.* **2001**, *123*, 12294−12302.

Received June 6, 2002
[I02301]

A Dinuclear Iron Complex with Two Cofacial [FeS_4] Cores Linked by Covalent Ligand Periphery Clamps and Dissociable Thiolate Bridges

Dieter Sellmann,*[a] Kai P. Peters,[a] Raquel Montón Molina,[a] and Frank W. Heinemann[a]

Dedicated to Professor Dr. Horst Kisch on the occasion of his 60th birthday

Keywords: Iron / S ligands / Bridging ligands / Enzyme models

As part of a long-term study of dinuclear iron complexes with sulfur-rich coordination spheres and cofacial, sterically variable binding sites for molecules relevant to nitrogenase, the complex $(AsPh_4)_2$ [{Fe('apS_4')}$_2$] (**5**) was synthesized and completely characterized ['apS_4'$^{4-}$ = 1,3-bis(2,3-dimercaptobenzamido)propane(4–)]. Complex **5** contains two cofacial [$Fe^{III}(S_2C_6H_4R)_2]^-$ units linked by [Fe–S–Fe] thiolate bridges and two peripheral propanediamide ligand backbones that are located on opposite sides of the molecular anion and prevent the complete separation of the two [FeS_4] cores of **5** if the Fe–S–Fe bridges dissociate. No marked differences were found in the molecular parameters, spectroscopic, magnetic and electrochemical properties of the [Fe_2S_8] cores in the anion of **5** and the parent complex [{$Fe(S_2C_6H_4)_2$}$_2]^{2-}$.

(© Wiley-VCH Verlag GmbH & Co. KGaA, 69451 Weinheim, Germany, 2003)

Introduction

Iron in sulfur-rich coordination spheres is the characteristic feature of the polynuclear FeMo, FeV or FeFe cofactors of nitrogenases.[1] Interaction of N_2 with these cofactors to give metal-sulfur N_2 complexes is considered to be the primary step of N_2 fixation, and the prevalence of iron in all three types of cofactors supports current hypotheses that the resulting metal−sulfur N_2 complexes are species in which N_2 acts as a bridge between at least two [$Fe(S_n)$] sites held together by the other metal−sulfur bonds of the cofactor and, in addition, the surrounding enzyme protein.[2] Low molecular weight analogues are unknown despite a prolonged search for complexes capable of modeling both structural (metal sulfur sites) and functional (binding N_2) aspects of nitrogenase cofactors.[2]

Complex fragments such as [Fe('N_HS_4')] and [Fe('pyS_4')] (Scheme 1) have been shown to bind and activate or stabilize many molecules relevant to nitrogenase, such as CO, NO, N_2H_2, N_2H_4, and NH_3, though not yet N_2.[2f,3]

To enforce the binding of N_2 to such fragments we initiated work[4] on complexes (type **A**) that contain two [$Fe(S_n)$] sites held together by bridges (potentially modeling the enzyme protein); the [Fe('pyS_4')] fragments favor the low-spin state of Fe^{II}, which in turn favors the binding of nitrogenase relevant molecules,[5] and the bulky [Fe('pyS_4')] fragments plus the spacers protect the vacant sites at the iron centers.

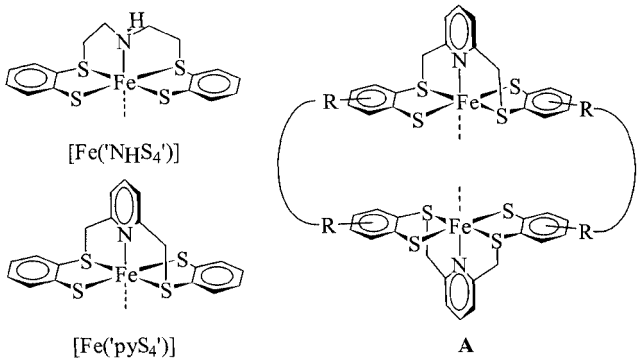

Scheme 1. Known complex fragments and the ultimate target molecule **A**

Such a synthetic challenge requires the complexation of iron by benzene dithiolate ligands, the formation of the [Fe('pyS_4')] fragments, and the connection of two such fragments by bridges between benzene rings. The essential cofacial arrangement of the [$Fe(S_4)$] units and the regioselective formation of the py$(CH_2)_2$ bridge mean that all reaction steps have to be stereoselective.

To obtain cofacial dinuclear iron benzene ditholate complexes we used our previous results on iron complexes of 2,3-dimercaptobenzoic acid,[4] methods developed by Hahn et al. for bridging 2,3-dimercaptobenzoic acid units by α,ω-

[‡] Transition Metal Complexes with Sulfur Ligands, Part 157. Part 156: D. Sellmann, D. C. F. Blum, F. W. Heinemann, J. Sutter, *Eur. J. Inorg. Chem.*, in press.

[a] Institut für Anorganische Chemie der Universität Erlangen-Nürnberg,
Egerlandstraße 1, 91058 Erlangen, Germany
Fax: (internat.) + 49-(0)9131/852-7367
E-mail: sellmann@anorganik.chemie.uni-erlangen.de

diamines,[6] and the fact that Fe^{III} ions and benzene dithiolate give dinuclear $[\{Fe(S_2C_6H_4)_2\}_2]^{2-}$ anions.[7]

Herein we report the synthesis and properties of the novel Fe^{III} complex $(AsPh_4)_2[\{Fe(`apS_4')\}_2]$ (**5**) where 'apS_4'$^{4-}$ denotes a ligand in which two 1,2-benzenedithiolate units are connected by a 1,3-dicarboxamido propane bridge.

Results and Discussion

Scheme 2 summarizes the multi-step procedure leading to the target complex **5**.

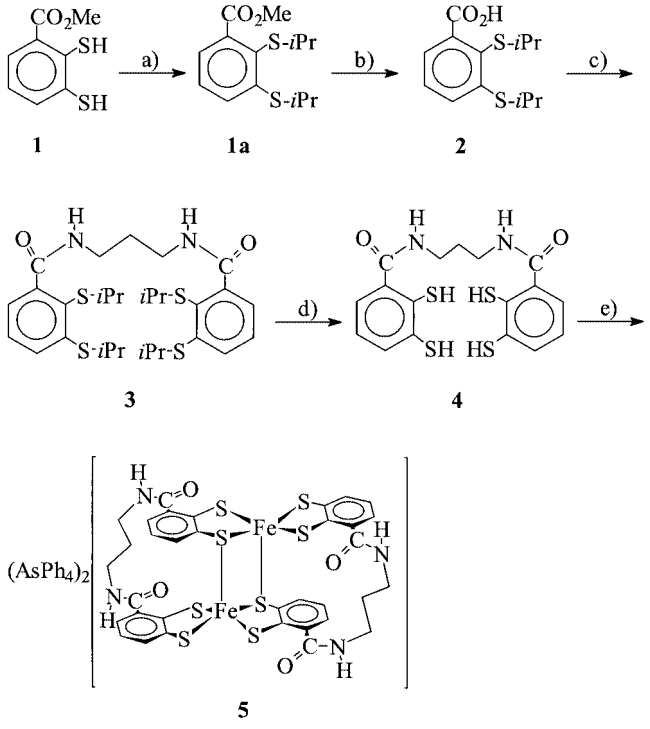

Scheme 2. Synthesis of $(AsPh_4)_2[\{Fe(`apS_4')\}_2]$ (**5**) (a) + 2NaOMe, + 2*i*PrBr, MeOH, 20 h reflux; (b) (1) + $NaOH_{exc.}$, THF/H_2O, 44 h reflux, (2) HCl/H_2O; (c) (1) + $SOCl_{2\ exc.}$, (2) + 0.51, 3-diaminopropane, THF; (d) (1) + 10Na, + $5C_{10}H_8$, THF, (2) HCl, H_2O; (e) (1) + 4LiOMe, + $FeCl_3{\cdot}6H_2O$, MeOH, (2) + $AsPh_4Cl$.

The synthesis of the tetrathiol 'apS_4'-H_4 (**4**) followed the method of Hahn et al. for related compounds.[6] The starting material was the 2,3-dimercaptobenzoic acid methyl ester **1** ('CO_2Me-S_2'-H_2)[4a] in which the thiol functions were protected by isopropyl groups to give **1a**. Ester hydrolysis yielded the acid **2** which was treated with $SOCl_2$ to give the corresponding carboxylic acid chloride. Subsequent reaction with 1,3-diaminopropane yielded the diamide **3**. Deprotection of the thioether functions with sodium naphthalenide and subsequent acidification gave the tetrathiol **4** which was isolated as a white powder in pure form.

Coordination of the tetraanion of **4** to Fe^{III} centers was achieved by deprotonating **4** with equivalent amounts of LiOMe and subsequent reaction with $FeCl_3{\cdot}6H_2O$ in boiling MeOH. A dark violet solution resulted, from which $(AsPh_4)_2[\{Fe(`apS_4')\}_2]$ (**5**) precipitated after addition of $AsPh_4Cl$.

As the X-ray structure analysis of **5** showed, the tendency of the $[Fe^{III}(benzenedithiolate)_2]^{1-}$ units to dimerize via [Fe−S−Fe] bridges,[8] and the steric constraints and electronic effects resulting from the carboxamido substituents were successfully used to obtain the required diastereoisomer. MeOH was employed as solvent because its boiling point favors the formation of dinuclear instead of polynuclear (polymeric) species.

Compounds **1**, **1a**, **2**, **3**, and **4** are moderately to very soluble in organic solvents such as CH_2Cl_2, $CHCl_3$, THF, and DMF. Complex **5** is soluble in DMF and MeCN. All compounds were characterized by elemental analyses and spectroscopic methods.

The molecular structure of **5**·2MeOH, determined by X-ray analysis, is depicted in Figure 1, and Table 1 lists selected distances and angles.

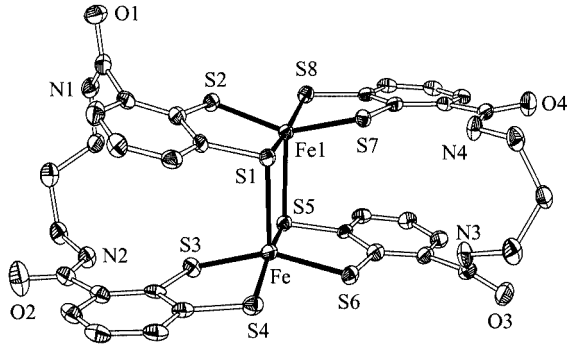

Figure 1. Molecular structure of the anion of $(AsPh_4)_2[\{Fe(`apS_4')\}_2]{\cdot}2MeOH$ (**5**·2MeOH) (50% probability ellipsoids; H atoms omitted)

Table 1. Selected distances [pm] and angles [°] of $(AsPh_4)_2[\{Fe(`apS_4')\}_2]{\cdot}2MeOH$ (**5**·2MeOH)

Distances		Angles	
Fe1−S1	222.9(2)	S8−Fe1−S1	168.55(5)
Fe1−S2	222.7(2)	S2−Fe1−S1	89.93(5)
Fe1−S7	222.4(2)	S1−Fe1−S5	95.19(5)
Fe1−S8	221.6(2)	S5−Fe2−S1	96.02(5)
Fe1−S5	248.4(2)	S4−Fe2−S5	166.21(5)
Fe2−S1	245.5(2)	S5−Fe2−S6	89.01(5)
Fe2−S3	222.9(2)		
Fe2−S4	220.8(2)		
Fe2−S5	222.8(2)		
Fe2−S6	223.1(2)		

The anion of **5**·2MeOH contains two $[FeS_4]$ units linked via two Fe−S−Fe bridges such that five-coordinate Fe centers with distorted square-pyramidal coordination result. In addition, the two $[FeS_4]$ units are connected by two peripheral propanediamide bridges between the benzene rings. These propanediamide bridges are located at opposite sides of the anion, which exhibits pseudo-C_i symmetry.

The bond lengths and angles within the $[Fe_2S_8]$ core are practically identical to those found in $(NEt_4)_2[\{Fe(S_2C_6H_4)_2\}_2]$[8a](**6**) and $(NBu_4)_2[\{Fe(S_2C_6H_3Me)_2\}_2]$[8b](**7**).

This indicates that the peripheral propanediamide bridges exert no steric strain on the [Fe_2S_8] core. For example, the average Fe−S distance within the [$Fe(S_2C_6H_3R)_2$] units amounts to 222 pm in **5** as well as in the nonbridged dinuclear species **6** and **7**. The distances between the iron centers and the (bridging) apical thiolate donors are significantly longer, by ca. 25 pm in **5**, as has also been found in **6** and **7**.

The propanediamide bridges could influence the overall structure of **5**·2MeOH in several ways. The apical thiolate donors S(1) and S(5) forming the bridges between the two iron centers occupy ring positions *meta* to the carboxamide substituents. Consequently, the carboxamide substituents could have an electron-withdrawing influence upon the thiolate donors, which is expected to be larger for the *ortho*-standing thiolate donors, disfavoring the formation of Fe−S−Fe bridges. The structure of **5**·2MeOH further shows that the carboxamide groups can adopt configurations that are in-plane with, or orthogonal to, the benzene rings. This indicates that the carboxamide substituents can rotate around the plane of the benzene ring such that, upon dissociation of the [Fe−S−Fe] bridges, the [Fe(benzenedithiolate)$_2$] fragments can separate to permit the insertion of small molecules between the iron centers, as in $(NBu_4)_2[\mu\text{-}N_2H_4\{Fe(S_2C_6H_4)_2\}_2]$.[9] Rotation of the carboxamide substituents around the benzene rings was corroborated by the X-ray structure determination of solvent-free **5**. In this structure, all carboxamido substituents adopt a skewed conformation with regard to the benzene rings. All other distances and angles are similar to those of **5**·2MeOH. Reduction of dinuclear $[\{Fe^{III}(S_2C_6H_4)_2\}_2]^{2-}$ is also known to give mononuclear $[Fe^{II}(S_2C_6H_4)_2]^{2-}$.[7]

The anion of **5** and the parent $[\{Fe^{III}(S_2C_6H_4)_2\}_2]^{2-}$ anion exhibit similar spectroscopic, magnetic and electrochemical properties. Both anions are paramagnetic with μ_{eff} = 2.4 μ_B for **5** and μ_{eff} = 2.3 μ_B for **6**,[8c] which is indicative of two low-spin Fe^{III} centers and partial antiferromagnetic coupling through the thiolate bridges.

The ^{1}H NMR spectrum of **5** in [D_6]DMSO exhibits paramagnetically shifted signals between δ = 8 and −45 ppm that could not be assigned, with the exception of the $AsPh_4^+$ signal at δ = 7.8 ppm. In the mass spectrum, only the $AsPh_4^+$ ion could be detected.

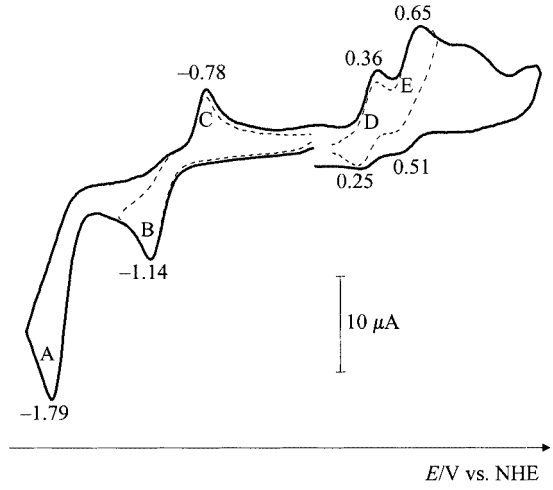

Figure 2. Cyclic voltammogram of **5** in MeCN (10^{-3} M, 10^{-1} M NBu_4PF_6, v = 0.10 V s^{-1})

The UV/Vis spectrum of **5** shows absorptions at 314, 364, and 512 nm while that of **7** exhibits absorptions at 315, 370, and 526 nm. The cyclic voltammogram of **5** in MeCN shows five redox waves (see Figure 2). The anodic waves D and E appear to be quasi-reversible, while waves A−C are regarded as irreversible. However, the redox waves B and C resemble the quasi-reversible redox wave of **6** in DMSO at −0.99 V (vs. NHE) assigned to the redox couple $[\{Fe^{III}(S_2C_6H_4)_2\}_2]^{2-/3-}$.[8c] Correspondingly, the waves B and C may be assigned tentatively to the redox couple $[\{Fe(\text{`}apS_4\text{'})\}_2]^{2-/3-}$.

Conclusion

In the search for dinuclear iron complexes with cofacial [FeS_4] cores as potential precursors for subsequent alkylation reactions yielding cofacial [Fe(‘pyS_4’)] fragments held together by ligand periphery clamps, $(AsPh_4)_2[\{Fe(\text{`}apS_4\text{'})\}_2]$ (**5**) was synthesized and characterized. Structural, magnetic, spectroscopic and electrochemical properties of the anion of **5** are similar to those of the parent anion $[\{Fe(S_2C_6H_4)_2\}_2]^{2-}$ (**6**). In contrast to **6** the peripheral ligand bridges of **5** prevent complete separation of the [$Fe(S_2C_6H_3R)_2$] entities if the [Fe−S−Fe] thiolate bridges dissociate. In addition, the structure of **5** differs from that of the dinuclear Ni complexes with similar benzenedithiolate-based tetrathiol ligands reported recently by Hahn et al.[6d] These Ni complexes, synthesized in the search for helicates, exhibit coplanar [$M(S_4)$] cores arranged in a stair-like manner.

Current experiments aim to introduce, stereoselectively, α,α′-bismethylenpyridine bridges to transform **5** into the target species **A**.

Experimental Section

General Methods: Unless noted otherwise, all reactions and operations were carried out under nitrogen using standard Schlenk techniques. Solvents were dried and distilled before use. As far as possible, reactions were monitored by IR or NMR spectroscopy. Spectra were recorded on the following instruments: IR (KBr discs or CaF_2 cuvettes, solvent bands were compensated): Perkin−Elmer 16PC FTIR. NMR: JEOL-JNM-GX 270 with the protio-solvent signal used as an internal reference. Spectra were recorded at 25 °C. Mass spectra: JEOL MSTATION 700 spectrometer. Elemental analysis: Carlo Erba EA 1106 or 1108 analyzer. Magnetic susceptibility: Johnson Matthey susceptibility balance. UV/Vis: Shimadzu UV-3101 PC. Solutions were 10^{-4} M in DMF. Cyclic voltammetry was performed with a Radiometer Copenhagen IMT 102 electrochemical interface using a three-electrode cell with a glassy carbon (Radiometer Copenhagen EDI) working electrode and Pt reference and counter electrodes. Solutions were 10^{-3} M in MeCN; $NBu_4[PF_6]$ (10^{-1} M) was used as the supporting electrolyte. Potentials were referenced to the normal hydrogen electrode (NHE) using Fc/Fc^+ as internal standard ($E^+_{Fc/Fc}$ = 0.4 V vs. NHE).[10] ‘CO_2Me-

S_2'-H_2 (**1**) (2,3-dimercaptobenzoic acid methyl ester) was prepared as described in the literature.[4a]

'CO_2Me-S_2'-*i*Pr_2 (1a): LiOMe (50 mmol, 50 mL of a 1 M solution in MeOH) and isopropyl bromide (5.87 mL, 62.5 mmol) were added to a light yellow solution of 'CO_2Me-S_2'-H_2 (5.01 g, 25.0 mmol) in MeOH (120 mL) and the resultant lemon yellow solution heated under reflux for 20 h. After evaporation of the solvent, CH_2Cl_2 (120 mL) was added to the residue and the resulting suspension stirred for 2 h and then filtered. The filtrate was evaporated to give a brown oil that was identified by NMR spectroscopy as 'CO_2Me-S_2'-*i*Pr_2 and was used for the synthesis of 'CO_2H-S_2'-*i*Pr_2 (**2**) without further purification. Yield: 7 g (**1a**) (100%). ^{1}H NMR ($CDCl_3$, 269.72 MHz): δ = 1.20 [d, $^3J_{H,H}$ = 6.7 Hz, 6 H, $CH(CH_3)_2$], 1.37 [d, $^3J_{H,H}$ = 6.7 Hz, 6 H, $CH(CH_3)_2$], 3.50 [m, 2 H, $CH(CH_3)_2$], 3.89 (s, 6 H, CO_2CH_3), 7.26 (m, 3 H, C_6H_3) ppm. MS (FD$^+$, CH_2Cl_2): *m*/*z* = 284 ['CO_2Me-S_2'-*i*Pr_2]$^+$.

'CO_2H-S_2'-*i*Pr_2 (2): NaOH (0.115 mmol, 115 mL of a 1 M solution in H_2O) was added to a solution of 'CO_2Me-S_2'-*i*Pr_2 (**1a**) (6.825 g, 0.024 mol) in THF (120 mL). The mixture was heated under reflux for 29 h, then reduced in volume to about 120 mL and heated for a further 15 h. The resulting pale pink solution was filtered. Concentrated hydrochloric acid (12 mL) was added to the filtrate and the light yellow solid that precipitated was separated, washed with water to pH = 7 and dried in vacuo. Yield: 5.66 g (**2**) (87%). ^{1}H NMR ($CDCl_3$, 269.72 MHz): δ = 1.27 [d, $^3J_{H,H}$ = 6.6 Hz, 6 H, $CH(CH_3)_2$], 1.38 [d, $^3J_{H,H}$ = 6.6 Hz, 6 H, $CH(CH_3)_2$], 3.52 [m, 2 H, $CH(CH_3)_2$], 7.41 (m, 2 H, C_6H_3), 7.87 (vdd, 1 H, C_6H_3), 11.75 (br, 1 H, COO*H*) ppm. ^{13}C{^{1}H} NMR ($CDCl_3$, 67.83 MHz): δ = 22.6, 22.8 [$CH(CH_3)_2$], 36.5, 41.2 [$CH(CH_3)_2$], 127.9, 129.3, 129.8, 130.3, 136.5, 146.4 (C_6H_3), 169.1 (CO_2H) ppm. IR (KBr): $\tilde{\nu}$ = 2966 (br, O−H), 1704 cm^{-1} (s, C=O). MS (FD$^+$, acetone): *m*/*z* = 270 ['CO_2H-S_2'-*i*Pr_2]$^+$. $C_{13}H_{18}O_2S_2$ (270.42): calcd. C 57.74, H 6.71, S 23.72; found C 57.49, H 6.99, S 23.90.

'apS$_4$'-*i*Pr_4 (3): $SOCl_2$ (8.5 mL) was added to solid 'CO_2H-S_2'-*i*Pr_2 (**2**) (4.815 g, 0.018 mol) and heated to 60 °C until no further gas evolution was detected. Excess $SOCl_2$ was removed in vacuo; the brown oily residue obtained was dissolved in THF (30 mL) and a solution of 1,3-diaminopropane (0.745 mL, 0.009 mol) and NEt_3 (4.98 mL, 0.036 mol) in THF (20 mL) was added dropwise at 0 °C. The resulting yellow suspension was stirred at room temperature for 15 h, poured into ice water (600 mL) and stirred for a further 1 h. The mixture was extracted with Et_2O (800 mL). The Et_2O phase was dried over Na_2SO_4, filtered and evaporated. The foam-like solid thus obtained was washed with warm pentane which was decanted. The residue was dried in vacuo yielding, again, a yellow foam-like solid material. Yield: 4.6 g (**3**) (88%). ^{1}H NMR ($CDCl_3$, 269.72 MHz): δ = 1.19 (d, $^3J_{H,H}$ = 6.7 Hz, 12 H, $CHCH_3$), 1.36 [d, $^3J_{H,H}$ = 6.7 Hz, 12 H, $CH(CH_3)_2$], 1.87 (m, 2 H, NCH_2CH_2), 3.46 (m, 4 H, NCH_2CH_2), 3.60 [m, 4 H, $CH(CH_3)_2$], 6.95 (br, 2 H, N*H*), 7.26 (m, 6 H, C_6H_3) ppm. ^{13}C{^{1}H} NMR ($CDCl_3$, 67.83 MHz): δ = 22.7, 23.2 [$CH(CH_3)_2$], 29.9 ($NHCH_2CH_2$), 36.0, 36.8 [$CH(CH_3)_2$], 40.5 (NCH_2CH_2), 124.6, 127.6, 128.8, 129.1, 143.8, 145.8 (C_6H_3), 169.5 (*C*ONH) ppm. IR (KBr): $\tilde{\nu}$ = 3289 (s, N−H), 1636 (s, C=O), 1522 cm^{-1} (s, N−H). MS (FD$^+$, Et_2O): *m*/*z* = 578 ['apS$_4$'-*i*Pr_4]$^+$. $C_{29}H_{42}N_2O_2S_4$ (578.93): calcd. C 60.17, H 7.31, N 4.84, S 22.16; found C 60.27, H 7.70, N 4.58, S 21.92.

'apS$_4$'-H$_4$ (4): Small pieces of sodium (0.9 g, 39 mmol) were added to a solution of 'apS$_4$'-*i*Pr_4 (**3**) (2.25 g, 3.9 mmol) and naphthalene (2.52 g, 19.5 mmol) in THF (200 mL). After stirring the resulting green suspension for 16 h at room temperature, MeOH (15 mL) was added cautiously. All solvents were evaporated and H_2O (150 mL) was added to the yellow residue to give a yellow emulsion that was washed with Et_2O (450 mL), and the yellow aqueous phase was separated, filtered, and acidified slowly with concentrated hydrochloric acid (12 mL) at 0 °C. A white precipitate formed which after stirring at room temperature for 15 min was separated, washed with H_2O (60 mL) and dried in vacuo. Yield: 1.3 g (**4**) (81%). ^{1}H NMR ([D$_8$]THF, 269.72 MHz): δ = 1.87 (m, 2 H, NCH_2CH_2), 3.47 (m, 4 H, NCH_2CH_2), 7.01 (vt, 2 H, C_6H_3), 7.33 (vd, 2 H, C_6H_3), 7.40 (vd, 2 H, C_6H_3), 7.94 (br, 2 H, N*H*) ppm. ^{13}C{^{1}H} NMR ([D$_8$]THF, 67.83 MHz): δ = 29.5 ($NHCH_2CH_2$), 36.7 (NCH_2CH_2), 124.2, 125.1, 131.3, 132.7, 133.0, 134.6 (C_6H_3), 169.2 (*C*ONH) ppm. IR (KBr): $\tilde{\nu}$ = 3280 (m, N−H), 2526 (w, S−H), 1628 (s, C=O), 1534 cm^{-1} (s, N−H). MS (FD$^+$, THF): *m*/*z* = 411 ['apS$_4$'-H$_4$]$^+$. $C_{17}H_{18}N_2O_2S_4$ (410.61): calcd. C 49.73, H 4.42, N 6.82, S 31.24; found C 50.32, H 4.66, N 6.85, S 30.79.

(AsPh$_4$)$_2$[{Fe('apS$_4$')}$_2$] (5): A solution of $FeCl_3$·$6H_2O$ (230 mg, 0.85 mmol) in MeOH (10 mL) was added to a solution of 'apS$_4$'-H$_4$ (**4**) (349 mg, 0.85 mmol) and LiOMe (3.40 mmol, 3.40 mL of a 1 M solution in MeOH) in MeOH (25 mL). The resulting purple solution was heated under reflux for 2 h. After removal of the solvent, the resultant black−violet residue was dissolved in MeOH (30 mL) to give a black violet solution that was filtered and combined with a solution of $AsPh_4Cl$·H_2O (1.23 g, 2.49 mmol) in MeOH (25 mL). Violet microcrystals precipitated and were separated, washed with MeOH (20 mL) and dried in vacuo. Yield: 395 mg (**5**) (55%). ^{1}H NMR ([D$_6$]DMSO, 269.72 MHz): δ = 7.8 [br, 40 H, As(C_6H_5)$_4^+$] ppm. IR (KBr): $\tilde{\nu}$ = 3273 (m, N−H), 1640 (s, C=O), 1540 cm^{-1} (s, N−H). MS (FD$^+$, DMF): *m*/*z* = 383 [$AsPh_4$]$^+$; magnetic susceptibility: μ_{eff} = 2.4 μ_B. UV/Vis (DMF, 10^{-4} M): λ = 314 (22068), 364 (21139), and 512 (11464) nm (cm^2 mol^{-1}). $C_{82}H_{68}As_2Fe_2N_4O_4S_8$ (1691.54): calcd. C 58.22, H 4.05, N 3.31, S 15.17; found C 58.27, H 4.22, N 3.36, S 15.05.

X-ray Structure Analyses of (AsPh$_4$)$_2$[{Fe('apS$_4$')}$_2$]·2MeOH (5·2MeOH) and (AsPh$_4$)$_2$[{Fe('apS$_4$')}$_2$] (5): Single crystals were obtained by the following procedures. (AsPh$_4$)$_2$[{Fe('apS$_4$')}$_2$]·2MeOH (**5**·2MeOH): A solution of 'apS$_4$'-H_2 (44 mg, 0.11 mmol), LiOMe (0.43 mmol, 0.43 mL of a 1 M solution in MeOH) and $FeCl_3$·$6H_2O$ (29 mg, 0.11 mmol) in MeOH (20 mL) was heated under reflux for 2 h. After cooling to room temperature the resulting black−violet solution was filtered and layered with a solution of $AsPh_4Cl$ (115 mg, 0.28 mmol) in MeOH (25 mL). Black blocks of (AsPh$_4$)$_2$[{Fe('apS$_4$')}$_2$]·2MeOH (**5**·2MeOH) formed that were separated after one week. $C_{84}H_{76}As_2Fe_2N_4O_6S_8$ (1755.63): calcd. C 57.47, H 4.36, N 3.19, S 14.61; found C 57.87, H 4.47, N 3.29, S 14.24.

(AsPh$_4$)$_2$[{Fe('apS$_4$')}$_2$] (**5**): A concentrated and filtered solution of **5** in DMF was layered with the same amount of THF. Black rhombs of (AsPh$_4$)$_2$[{Fe('apS$_4$')}$_2$] (**5**) formed that were separated after 2 months.

Suitable single crystals were embedded in protective perfluoro polyalkyl ether oil. Intensity data were collected at 100 K on a Nonius KappaCCD diffractometer using Mo-K_α radiation (λ = 71.073 pm, graphite monochromator) (Table 2). Data were corrected for Lorentz and polarization effects and a numerical absorption correction for **5**·2MeOH and a semi-empirical absorption correction from equivalent reflections for **5** were applied. The structures were solved by direct methods, and full-matrix least-squares refinement was carried out on F^2 (SHELXTL NT 5.10).[11] All non-hydrogen atoms were refined anisotropically. The positions of the hydrogen atoms were taken from the difference Fourier maps and refined

Table 2. Selected crystallographic data for $(AsPh_4)_2[\{Fe(`apS_4')\}_2]\cdot 2MeOH$ (**5**·2MeOH) and $(AsPh_4)_2[\{Fe(`apS_4')\}_2]$ (**5**)[12]

Complex	**5**·2MeOH	**5**
Formula	$C_{84}H_{76}As_2Fe_2N_4O_6S_8$	$C_{82}H_{68}As_2Fe_2N_4O_4S_8$
M_r [g mol^{-1}]	1755.51	1691.42
T [K]	100	100
Crystal size [mm]	0.46 × 0.11 × 0.05	0.17 × 0.14 × 0.06
F(000)	1804	1732
Crystal system	triclinic	monoclinic
Space group	$P\bar{1}$	$P2_1/c$
a [pm]	1027.9 (1)	1188.34(5)
b [pm]	1634.8 (2)	1342.41(7)
c [pm]	2407.5 (3)	2240.5(1)
α [°]	106.126 (8)	90
β [°]	94.494 (8)	96.539(4)
γ [°]	96.871 (8)	90
V [nm^3]	3.8320 (8)	3.5509(3)
Z	2	2
$\rho_{calcd.}$ [g cm^{-3}]	1.521	1.582
μ [mm^{-1}]	1.512	1.626
θ range [°]	3.52−26.37	3.43−27.50
Measured refl.	56034	32373
Unique refl.	15548	8089
$R_{int.}$	0.0795	0.1296
Observed refl.	11204	4817
σ criterion	$F_0 \geq 4.0\ \sigma(F)$	$F_0 \geq 4.0\ \sigma(F)$
Refl. parameters	950	562
Abs. correct. $T_{min.}/T_{max.}$	0.506/0.899	0.748/0.912
R_1 [$F_o \geq 4.0\ \sigma(F)$]	0.0556	0.0560
wR_2 (all data)	0.1446	0.1214

with a fixed common isotropic displacement parameter. In accordance with the elemental analysis, the crystal structure of **5**·2MeOH contains two MeOH solvate molecules per unit. One MeOH molecule is disordered. The non-hydrogen atoms of the disordered solvate molecule were refined only isotropically and no hydrogen atoms were taken into account.

Acknowledgments

Financial support by the Deutsche Forschungsgemeinschaft (SFB, 583) and the Fonds der Chemischen Industrie is gratefully acknowledged.

[1] [1a] J. B. Howard, D. C. Rees, *Chem. Rev.* **1996**, *96*, 2965−2982. [1b] R. R. Eady, *Chem. Rev.* **1996**, *96*, 3013−3030. [1c] B. K. Burgess, D. J. Lowe, *Chem. Rev.* **1996**, *96*, 2983−3012. [1d] D. C. Rees, J. B. Howard, *Curr. Opin. Chem. Biol.* **2000**, *4*, 559−566.

[2] [2a] M. D. Fryzuk, S. A. Johnson, *Coord. Chem. Rev.* **2000**, *200−202*, 379−409. [2b] H. Deng, R. Hoffmann, *Angew. Chem.* **1993**, *105*, 1125−1128; *Angew. Chem. Int. Ed. Engl.* **1993**, *32*, 1062−1065. [2c] I. G. Dance, *J. Biol. Inorg. Chem.* **1996**, *1*, 581−586. [2d] K. K. Stavrev, M. C. Zerner, *Chem. Eur. J.* **1996**, *2*, 83−87. [2e] D. Sellmann, J. Sutter, *J. Biol. Inorg. Chem.* **1996**, *1*, 587−593. [2f] D. Sellmann, A. Fürsattel, J. Sutter, *Coord. Chem. Rev.* **2000**, *200−202*, 545−561.

[3] [3a] D. Sellmann, J. Sutter, *Acc. Chem. Res.* **1997**, *30*, 460−469. [3b] D. Sellmann, N. Blum, F. W. Heinemann, B. A. Hess, *Chem. Eur. J.* **2001**, *7*, 1874−1880.

[4] [4a] D. Sellmann, T. Becker, F. Knoch, *Chem. Ber.* **1996**, *119*, 509−519. [4b] K. P. Peters, PhD Dissertation, Universität Erlangen-Nürnberg, **2000**.

[5] [5a] D. Sellmann, J. Utz, N. Blum, F. W. Heinemann, *Coord. Chem. Rev.* **1999**, *190−192*, 607−627. [5b] D. Sellmann, N. Blum, F. W. Heinemann, *Z. Naturforsch., B: Chem. Sci.* **2001**, *56*, 581−588.

[6] [6a] F. E. Hahn, W. W. Seidel, *Angew. Chem.* **1995**, *107*, 2938−2941; *Angew. Chem. Int. Ed. Engl.* **1995**, *34*, 2700−2703. [6b] W. W. Seidel, F. E. Hahn, T. Lügger, *Inorg. Chem.* **1998**, *37*, 6587−6596. [6c] W. W. Seidel, F. E. Hahn, *J. Chem. Soc., Dalton Trans.* **1999**, 2237−2241. [6d] H. V. Huynh, C. Schulze-Isfort, W. W. Seidel, T. Lügger, R. Fröhlich, O. Kataeva, F. E. Hahn, *Chem. Eur. J.* **2002**, *8*, 1327−1335.

[7] D. Sellmann, U. Kleine-Kleffmann, L. Zapf, G. Huttner, L. Zsolnai, *J. Organomet. Chem.* **1984**, *263*, 321−331.

[8] [8a] B. S. Kang, L. H. Weng, D. X. Wu, F. Wang, Z. Guo, L. R. Huang, Z. Y. Huang, H. Q. Liu, *Inorg. Chem.* **1988**, *27*, 1128−1130. [8b] D. T. Sawyer, G. S. Srivatsa, M. E. Bodini, W. P. Schaefer, R. M. Wing, *J. Am. Chem. Soc.* **1986**, *108*, 936−942. [8c] D. Sellmann, M. Geck, M. Moll, *J. Am. Chem. Soc.* **1991**, *113*, 5259−5264.

[9] [9a] D. Sellmann, H. Friedrich, F. Knoch, *Z. Naturforsch., B: Chem. Sci.* **1994**, *49*, 660−664. [9b] D. Sellmann, P. Kreutzer, G. Huttner, A. Frank, *Z. Naturforsch., Teil B* **1978**, *33*, 1341−1346.

[10] [10a] H. M. Koepp, H. Wendt, H. Strehlow, *Z. Elektrochem.* **1960**, *64*, 483−491. [10b] G. Gritzner, J. Kuta, *Pure Appl. Chem.* **1984**, *56*, 461−466.

[11] SHELXTL 5.10 *Bruker AXS*, Inc., Madison, WI, USA, **1998**.

[12] CCDC-188177 (**5**·2MeOH) and CCDC-188178 (**5**) contain the supplementary crystallographic data for this paper. These data can be obtained free of charge at www.ccdc.cam.ac.uk/conts/retrieving.html [or from the Cambridge Crystallographic Data Centre, 12 Union Road, Cambridge CB2 1EZ, UK; Fax: (internat.) +44−1223/336−033; E-mail: deposit@ccdc.cam.ac.uk].

Received July 3, 2002
[I02358]

Vanadium-Catalysed Aerobic Cleavage of C−C Bonds in Substituted Cyclohexanones To Afford Carboxylic Acids: Two Model Complexes with Tetrahedral Geometry around Vanadium(V)

Maxence Vennat,[a] Patrick Herson,[b] Jean-Marie Brégeault,*[a] and Georgiy B. Shul'pin[c]

Keywords: Catalysis / Oxidation / Dioxygen / Oxo ligands / Vanadium

Two monosilanol/disilanol derivatives were synthesised by treatment of Ph_3SiOH or $Ph_2Si(OH)_2$ with $[nBu_4N]VO_3$ (**3**) in ethanol solution. The mononuclear anionic dioxo vanadium(V) species $[\{Ph_3SiO\}_2VO_2]^-$ (**4**) and the dinuclear complex anion $[\{Ph_2SiO_2VO_2\}_2]^{2-}$ (**5**) thus obtained are unusual and novel model compounds with ≡Si–O–V(O)$_2$O linkages characterised by single-crystal X-ray diffraction. The catalytic activities of these *tert*-butylammonium complexes, together with those of the simple vanadium derivatives **3** and **5**, of the vanadyl precursors $VOSO_4{\cdot}5H_2O$ (**1**) and $[VO(acac)_2]$ (**2**), and also of "$H_6[PMo_9V_3O_{40}]{\cdot}aq$", were tested for aerobic C–C bond cleavage in 2-hydroxycyclohexanone and 2-methylcyclohexanone. Monomeric vanadium species show the same chemistry as the polyoxometalate but with lower yields of acids or keto acids, and so the redox and acid properties of HPA-*n* (n = 3, 4) are better tuned. Mechanisms for these oxidation reaction, including electron transfer from a substrate coordinated to vanadium, are proposed.
(© Wiley-VCH Verlag GmbH & Co. KGaA, 69451 Weinheim, Germany, 2003)

Introduction

Vanadium(V) oxoalkoxides such as $[VO(OEt)_3]$ or heteropolyacids containing vanadium(V) ions with common formula $H_{3+n}[PMo_{12-n}V_nO_{40}]{\cdot}xH_2O$ (denoted HPA-*n*, where n = 1, 2, 3 etc.) have been proposed as precursors for the catalytic oxidation of α-ketols and ketones by dioxygen.[1−4] It has also been demonstrated that aqueous solutions of HPA-*n* are multicomponent systems: the higher the value of *n*, the more complex the system. These solutions contain a great number of polyanions, positional isomers of these, as well as monomeric metallo species such as *cis*-dioxo $[VO_2]^+$ (pervanadyl moieties) in equilibrium with lacunary heteropolyanion.[5] The ^{31}P NMR spectrum of "aqueous $H_6[PMo_9V_3O_{40}]$", for example, attests to the existence of several species containing P, Mo and V (Figure 1).

Preparations of HPA-*n* obtained by diethyl ether extraction[6] or by an oxo-peroxo route[7] give EPR signals attributable to $[VO]^{2+}$ species, as do catalytic systems with vanadium(V) oxoalkoxides. At low pH (<2), heteropolyanion solutions contain a solvated *cis*-dioxo cation $[VO_2(H_2O)_4]^+$, usually written as $[VO_2]^+$.[8,9] This is considered to be one of the catalytically active species.[5] Such complexity makes mechanistic studies very difficult. Moreover, in aerobic ketone oxidations, HPA-*n* species are active not only as redox systems but also play a very important role as Brønsted acids for the enolisation process.[3,10] To the best of our

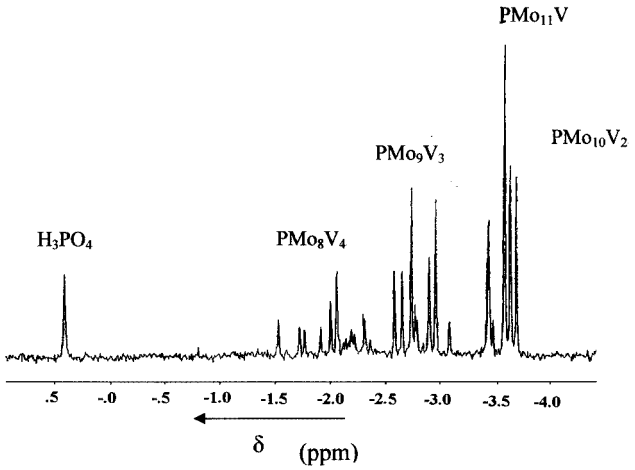

Figure 1. ^{31}P NMR spectrum of "$H_6[PMo_9V_3O_{40}]$" (1 mol·dm^{-3}; pH 0.8) prepared by treatment of $MoO_3.xH_2O$, V_2O_5 and H_3PO_4 with H_2O_2 at room temperature (the identification is supported by solutions and solids prepared with $2 \leqslant n \leqslant 10$ − see ref.[5,7,47]

[a] Systèmes Interfaciaux à l'Echelle Nanométrique, Université Pierre et Marie Curie/CNRS,
case 196, 4 place Jussieu, 75252 Paris cedex 05, France
Fax: (internat.) + 331/44275536
E-mail: bregeaul@ccr.jussieu.fr
[b] Chimie Inorganique et Matériaux Moléculaires, Université Pierre et Marie Curie/CNRS,
case 42, 4 place Jussieu, 75252 Paris cedex 05, France
Fax: (internat.) + 331/44273841
E-mail: herson@ccr.jussieu.fr
[c] Semenov Institute of Chemical Physics, Russian Academy of Sciences, ul. Kosygina, dom 4, Moscow 119991, Russia
Fax: (internat.) + 7-095/1376130
E-mail: shulpin@chph.ras.ru

knowledge there is no iono-covalent crystal structure containing the pervanadyl cation $[VO_2(H_2O)_4]^+$.

In this work we have prepared and characterised two novel dioxovanadium(v) complexes with two organosilanolato ligands. As other catalyst precursors we have also used simple vanadium(v) and vanadium(iv) derivatives, mainly mononuclear compounds, which − unlike HPA-*n* − are not strong acids. Naturally, it was very interesting to study the influence of acids on the oxidation reactions. We hoped that combinations of simple vanadium complexes with added acids would provide models of catalytically active systems based on various V-containing HPA-*n* species. Work on the use of these complexes in homogeneous catalytic systems (oxidation of 2-hydroxycyclohexanone and 2-methylcyclohexanone) with other precursors and comparison of conversions and selectivities with those obtained with HPA-*n* has made us refine our previous mechanism.[3] The novel four-coordinate complexes should open perspectives for incorporation of oxovanadium catalysts into polymeric materials.[11] Organosilanols model the hydroxy groups that lie on silica surfaces,[12] and the complexes synthesised can be regarded as models for metal oxides supported on silica surfaces.[13]

oxo species $[n\mathrm{Bu_4N}][\{Ph_3SiO\}_2VO_2]$ (**4a**) or a dinuclear complex $[n\mathrm{Bu_4N}]_2[\{Ph_2SiO_2VO_2\}_2]$ (**5a**), respectively, in fair to nearly quantitative yields. Formulae of the anions of both complexes are presented in Scheme 1.

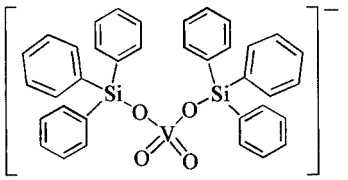

Anion of compounds **4a** and **4b**

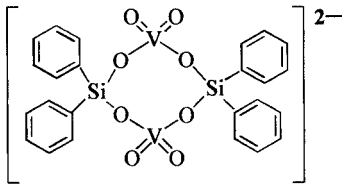

Anion of compound **5a**

Scheme 1

Results and Discussion

As catalyst precursors we used simple derivatives of vanadium(iv), such as $VOSO_4{\cdot}5H_2O$ (**1**) and $[VO(acac)_2]$ (**2**), as well as vanadium(v) derivatives in the form of tetrabutylammonium salts: $[n\mathrm{Bu_4N}]VO_3$ (**3**) and two pervanadyl complexes, $[n\mathrm{Bu_4N}][\{Ph_3SiO\}_2VO_2]$ (**4a**) and $[n\mathrm{Bu_4N}]_2[\{Ph_2SiO_2VO_2\}_2]$ (**5a**).

Synthesis of New Vanadium Pre-Catalysts

Only a few examples of mono- and dioxovanadium(v) complexes derived from silanols or disilanols have been described in the literature.[13,14] Compounds $(Ph_3SiO)_3VO$[15−19] and $[(t\mathrm{Bu})_2Si(O)_2VOCl]_3$ [20] have been structurally characterised. The latter contains a twelve-membered ring, $\{VOSiO\}_3$, in which the vanadium and silicon atoms exist in distorted tetrahedral coordinations. Trisilanols such as $R_7Si_7O_9(OH)_3$ [R = cyclopentyl, cyclohexyl (cy), phenyl, etc.] are known to react with $VOCl_3$, $VO(O\text{-}n\mathrm{Pr})_3$ or $VO(CH_2SiMe_3)_3$ to afford mixtures of the monomeric and dimeric vanadium(v) silsesquioxanes $[(cy)_7Si_7O_{12}VO]$ and $[(cy)_7Si_7O_{12}VO]_2$.[13,18,21] An anionic dioxo complex $(H_2NEt_2)_2[\{Ph_2SiO_2VO_2\}_2]$ was prepared in low yield (29%)[22] from diphenylsilanediol and vanadium(v) dialkylamides, $VO(NEt_2)_3$.

We focused our initial efforts on synthesising oxo-peroxo species and in this paper *cis*-dioxoanionic complexes by undemanding reactions, with the goal of using them to generate catalytic intermediates with the $[VO_2]^+$ group for carbon−carbon bond cleavage in α-hydroxy ketones, cycloalkanones, etc. with dioxygen. Treatment of Ph_3SiOH or $Ph_2Si(OH)_2$ with compound **3**, dissolved in ROH (R = Me, Et), resulted in the formation of a mononuclear anionic di-

The new vanadium-siloxane complexes were fully characterised by elemental analysis, vibrational spectroscopy and room-temperature single-crystal X-ray diffraction studies. Crystals of $[PPh_4][\{Ph_3SiO\}_2VO_2]$ (**4b**; the $n\mathrm{Bu_4N}$ cation was replaced by PPh_4 to prepare crystals for X-ray analysis) and of **5a** present novel anionic structures, shown in Figures 2 and 3. Selected bond lengths and angles are listed in Table 1 and 2.

Solid-State Structure of the Mononuclear Complex $[PPh_4][\{Ph_3SiO\}_2VO_2]$ (4b)

Compound **4b** consists of tetraphenylphosphonium cations and monomeric vanadosiloxane anions. There is one independent anionic species in the asymmetric unit, loosely connected through a series of phenyl ring interactions. The crystal packing is determined by van der Waals forces, the closest C···C approach being 3.6 Å, greater than the sum of the van der Waals radii. The geometry at vanadium(v) is a tetrahedral coordination unusual for mononuclear complexes (Figure 2), with the oxygen atoms of the Ph_3SiO ligands occupying two sites and two terminal oxygen atoms occupying the remaining sites. The VO_2 arrangement is no doubt favoured (as in some other d^0 systems) because this allows better $O_{p\pi} \rightarrow M_{d\pi}$ bonding than a linear arrangement would. The characteristic lengths in **4b** are similar to those observed in **5a** (vide infra); the VO bond lengths to the terminal oxygens are 1.621(3) and 1.607(3) Å to O(1) and O(2), respectively; this suggests a bond order approaching two for the V=O linkages in the VO_2 group. The average V−O(Si) bond length is 1.8145 Å. The Si−O bond lengths are similar to those found in the parent siloxane rings.[23−26]

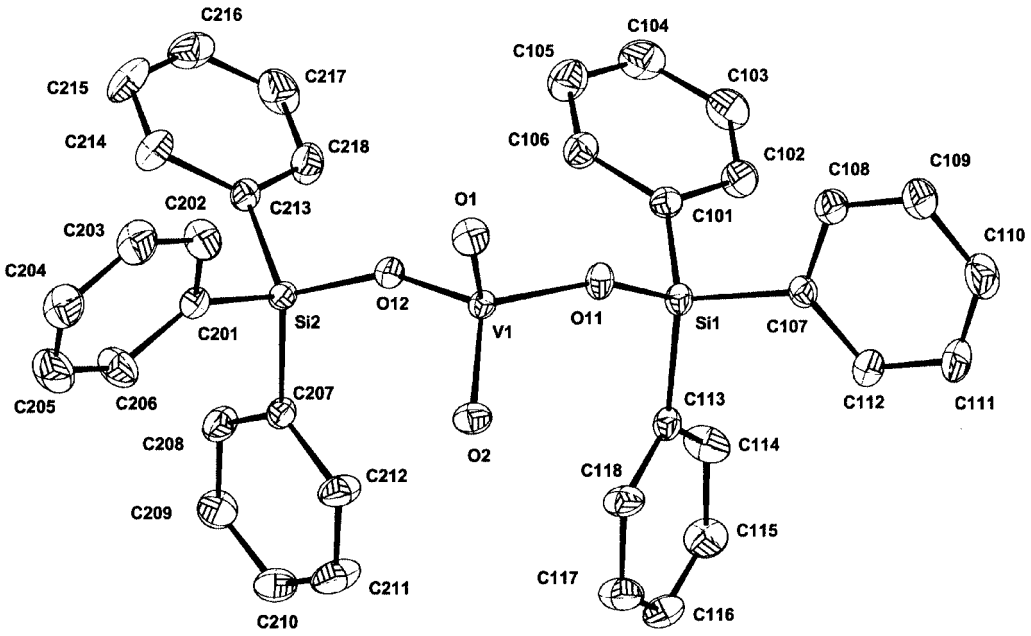

Figure 2. CAMERON representation[61] (ellipsoids at 30% probability level) of $[\{Ph_3SiO\}_2VO_2]^-$, showing the atom-labelling scheme (H atoms omitted for clarity)

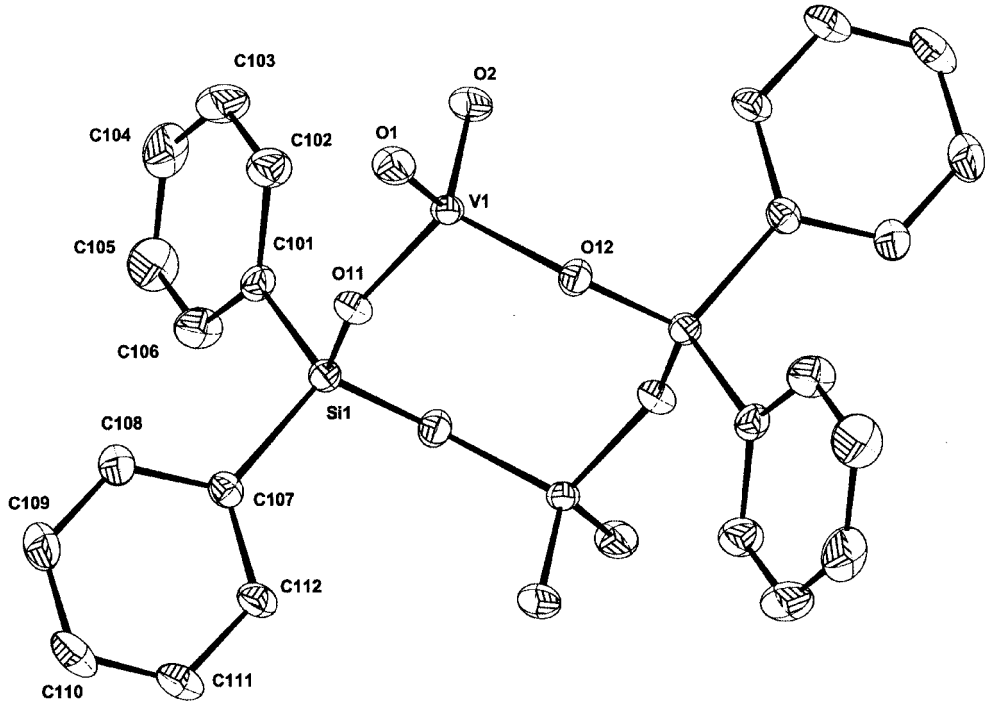

Figure 3. CAMERON representation[61] (ellipsoids at 30% probability level) of $[\{Ph_2SiO_2VO_2\}_2]^{2-}$, showing the atom-labelling scheme (H atoms omitted for clarity)

Table 1. Selected bond lengths [Å] and angles [°] for **4b**

Bond length		Bond angle	
V(1)−O(1)	1.621(3)	O(1)−V(1)−O(2)	108.4(2)
V(1)−O(2)	1.607(3)	O(1)−V(1)−O(11)	109.5(2)
V(1)−O(11)	1.815(3)	O(2)−V(1)−O(11)	110.8(2)
V(1)−O(12)	1.814(3)	O(1)−V(1)−O(12)	109.7(2)
Si(1)−O(11)	1.612(3)	O(2)−V(1)−O(12)	110.6(2)
Si(1)−C(101)	1.853(5)	O(11)−V(1)−O(12)	107.8(2)
Si(1)−C(107)	1.869(5)		
Si(1)−C(113)	1.865(5)		
Si(2)−O(12)	1.601(3)		
Si(2)−C(201)	1.864(5)		
Si(2)−C(207)	1.865(5)		
Si(2)−C(213)	1.862(5)		

Table 2. Selected bond lengths [Å] and angles [°] for **5a**

Bond length		Bond angle	
V(1)−O(1)	1.613(3)	O(1)−V(1)−O(2)	109.0(2)
V(1)−O(2)	1.619(3)	O(1)−V(1)−O(11)	108.9(2)
V(1)−O(11)	1.817(3)	O(2)−V(1)−O(11)	111.5(2)
V(1)−O(12)	1.807(3)	O(1)−V(1)−O(12)	108.2(2)
Si(1)−O(11)	1.613(4)	O(2)−V(1)−O(12)	109.3(2)
Si(1)−O(12′)	1.618(3)	O(11)−V(1)−O(12)	109.9(2)
Si(1)−C(101)	1.872(5)		
Si(1)−C(107)	1.872(5)		

The Si(1)O(11)V(1)O(12)Si(2) moiety in **4b** is almost planar, the largest deviation from the least-squares plane being 0.17 Å for V(1). The angle between the O(1)V(1)O(2) and Si(1)V(1)Si(2) planes is 88.7°. In the siloxane $(Ph_2SiO)_4$ the $\{Si-O\}_4$ ring is somewhat closer to planarity, the maximum deviation from the root-mean square plane being 0.1 Å.[24]

In **4b**, the V−O−Si bond angles are 151.4(2)° and 146.7(2)°. The formation of the tetrahedral VO_2 species was recently evaluated by a theoretical study of the extended Hückel (EH) type, this species being excluded in the cases of SiO_2, TiO_2 and γ-Al_2O_3.[27] To the best of our knowledge, no monomeric tetrahedral vanadium(v) species containing oxo organic ligands has yet been observed in aqueous solution, and such tetrahedral units are also not common for dioxovanadium(v) moieties in the solid state: only distorted square-pyramidal,[28] trigonal-bipyramidal[29] and octahedral[30] geometries have recently been characterised with *cis*-dioxo groups,[28−30] but tetrahedral species exist in some chains of inorganic vanadates. With large metal cations such as Ba^{2+}, the structures adopted by dinegative metavanadates, MV_2O_6, contains chains of vertex-shared VO_4 tetrahedra.[31,32] This structural motif is typically found in orthovanadates such as $LiMnVO_4$[33] and $LnVO_4$.[34] The $[V_4O_{12}]^{4-}$ ion has a cyclic tetrametaphosphate-like structure with an O*t*-V-O*t* angle of only 102.3(1)°,[35] the three others being 111°, while $[V_5O_{14}]^{3-}$ is pentanuclear with O−V−O angles ranging from 107.6(4) to 112.7(3)°.[36] In **4b**, the tetraphenyl phosphonium cations are well behaved and have the expected dimensions.

Solid-State Structure of the Dinuclear Complex $[nBu_4N]_2[\{Ph_2SiO_2VO_2\}_2]$ (5a)

Compound **5a** consists of discrete dimeric anions and tetrabutylammonium cations. The complex possesses crystallographic site symmetry $\bar{1}$, and there is one half of the complex anion per crystallographically independent unit. The anionic moiety has two vanadium(v) atoms bridged by two diphenylsiloxy ligands to form an eight-membered ring, "$\{VOSiO\}_2$", in an extended chair conformation. In addition, each vanadium is bonded to two terminal oxygen atoms. For a side view of the anion showing the conformation of the ring, see Figure 3. The O(1) and O(2) bond lengths to V(1) are 1.613(3) and 1.619(3) Å, respectively; these correspond to V=O linkages in compound **4b**. Similar V=O bond lengths are found for the trigonal-bipyramidal environment of $[VO_2(pic)(HMPA)]$, with 1.600(5) and 1.606(5) Å,[37] and for $[nBu_4][VO_2(pca)_2]$ (pcaH = pyrazine-2-carboxylic acid), for which the vanadium is found to have an octahedral coordination geometry with two terminal oxo ligands in the *cis* positions [d(V=O) ≈ 1.620(1) and 1.634(1) Å].[38]

The V−O(Si) bond lengths of 1.817(3) and of 1.807(3) Å are short in comparison with the chelate ligand V−O(C) bond lengths of 1.990(1) and 1.996(1) Å found in the pyrazine-2-carboxylato complex.[38] We consider that the V−O(Si) distances in **4b** and in **5a** indicate very strong bonds. The Si−O and Si−C bond lengths are in good agreement with values found in other cyclotetrasiloxanes[23−26] and in **4b** (vide supra).

The tetrahedral geometry around vanadium is evidenced by an average O−V−O bond angle of 109.5°. Again, four-coordination is not very common for inorganic anionic dinuclear V^V complexes; another typical dioxovanadium(v) salt that has been found to have a tetrahedral structure with chains is KVO_3.[39] The average V−O−Si bond angle in **5a** − of 144.1(2)° − is smaller than those found in **4b** and similar to the values of 145° found for the Si−O−Si angle in $[(Me_2SiO)_4]$,[40] but significantly smaller than those found for the previously reported tetrasiloxane compounds (ca. 159.5°),[23−26] also with a puckered eight-membered ring, and for V−O−V in $[V_4O_{12}]^{4-}$ [158.2(2)°].[35] The O−Si−O angle of 111.5(2)°, the C−Si−C of 108.1(2)° and the O−Si−C angles (mean ca. 109.3°) are close to the expected values commonly found for tetrahedral geometry in cyclic siloxanes;[23−26] this may indicate that no strain is involved in bridging the nearly 4.4 Å V···V distance. The closest C···C approach being 3.7 Å, the crystal packing must be determined by van der Waals forces .

Main Features of Vibrational Studies of Synthesised Complexes

The infrared spectra of the complexes are consistent with the deprotonation of the silanol functionalities in the complexes. They show features similar to those observed for

other mono- or dinuclear pervanadyl species;[41] in addition a band at 1588 cm^{-1} may be assigned as ν(C−C) of the phenyl ring,[42,43] and a very sharp band at 1113 for **4a** and 1117 cm^{-1} for **5a** is due to an in-plane deformation of the phenyl ring δ(C−H), with some ν(Si−C) character. Consistently with the structural data (vide supra) and the existence of short V=O bonds, there are strong ν(V=O) bands at ca. 939 and 927 cm^{-1} (sh.) for **4a**, and at 941 and 925 cm^{-1} for **5a**; peaks observed in the two above regions for previous $[VO_2]^+$ complexes are assigned to ν_{as} and ν_s modes of the VO_2 group, respectively.[44] A maximum at 925 cm^{-1} for **5a** and a shoulder (**4a**) are tentatively attributed to Si−O(V) stretching. Si−C stretches appear at ca. 743 cm^{-1} for both compounds. In the Raman spectra, comparison of the ν(V=O) at 943 cm^{-1} for solid **4a** with the maximum at 935 cm^{-1} (**4a** in methanol), together with other unattributed maxima, suggests that the overall structure of the pervanadyl complex **4a** is conserved in methanol at room temperature, as would be expected for a compound originally prepared in methanol or ethanol.

Catalytic Oxidative Cleavage of α-Ketols (α-Hydroxy Ketones)

For the oxidation of 2-hydroxycyclohexanone (**6**) we used simple vanadium derivatives **1**, **2** and **3**, the synthesised compounds **4a** and **5a**, and also "$H_6[PMo_9V_3O_{40}]\cdot 11H_2O$" (HPA-3). Methanol was employed as solvent and the reactions were carried out at two temperatures, 20 and 60 °C (Table 3). The main product was adipic acid (Scheme 2), and the concentration of this compound was measured after esterification by addition of ethereal diazomethane. The course of the reaction was followed by dioxygen consumption, monitored by a gas burette system, and by GC analysis. Dioxygen uptake was observed in the reactions catalysed by mononuclear complexes, with moderate conversion even at room temperature (Table 3, entries 1, 3, 5). An induction period was only found in the case of $[VO(acac)_2]$. During this period the active catalyst precursor probably changes; this transformation may be de-coordination of one of the acac ligands strongly bound to vanadium.

Higher degrees of conversion were obtained at 60 °C (entries 2, 4, 6). It can be seen that mono-oxovanadium(IV) complexes and polyoxovanadium(V) species are moderately active but the selectivity is rather low. Thus, oxidation catalysed by VO_3^- results in the formation of undesired products (cyclohexanedione in a yield ≤ 20%, dimethyl pentanedioate, butanedioate etc.). Catalysis by **4a** or **5a**, and especially by HPA-3, favours the formation of dimethyl adipate. It should be noted that the oxidative cleavage of 2-hydroxycyclohexanone[45] to produce adipic acid, as well as of various substituted α-hydroxy ketones,[4] does not require the presence of a strong Brønsted acid and occurs with both mononuclear vanadium(IV) and (V) species; $[VOCl_3]$/MeCN/O_2 systems give only α-diketones.[46]

Recently the "HPA-3/O_2/MeOH" system has been successfully used in the oxidative cleavage at room temperature of (1*S*,2*S*,5*S*)-2-hydroxypinan-3-one (**7a**) and its (1*R*,2*R*,5*R*) enantiomer **7b** (see Scheme 2). The diastereoselective formation of the esters of 3-acetyl-2,2-dimethylcyclobutaneacetic acid (methyl esters of the *cis*-pinonic acids) was observed, with 100% conversion and high diastereoselectivity (99:1 for 1*S*,3*S*:1*S*,3*R* and 1*R*,3*R*:1*R*,3*S*, respectively).[4] As found in this work, compound **4a** does not catalyse the oxidative transformations of **7** at all at room temperature. We assume that steric hindrance is a crucial factor governing the activity of complex **4a**; the bulkiness of the three C_6H_5 groups on Si(1) and Si(2) (Figure 2) and the methyl group of the 2-hydroxypinan-3-one may prevent the interaction of the VO_2 group with the α-hydroxy group of **7**. The inactivity of **4a** in reaction with **7** is in agreement with the assumption that only relatively small mononuclear *cis*-dioxo species are responsible for the catalytic activity. It seems that the HPA-3 anion is also too bulky and that direct coordination of this anion with **7** is sterically restricted. However, the dissociation of HPA-3 to produce, inter alia, a small reactive species such as $[VO_2]^+$ would explain the high efficiency of HPA-3 in the oxidative transformation of sterically hindered **7**.

Table 3. Oxidation of 2-hydroxycyclohexanone (**6**) to adipic acid (Scheme 2)

Entry[a]	Catalyst precursor	*T* (°C)	Conversion (%)[b]	Yield (%)[c]
1	$VOSO_4\cdot 5H_2O$ (**1**)	20	46	26
2		60	95	56
3	$[VO(acac)_2]$ (**2**)	20	42	43
4		60	96	51
5	$[nBu_4N]VO_3$ (**3**)	20	40	39
6		60	77	30
7	**4a**	20	77	61
8		60	100	60
9	**5a**	20	72	66
10		60	100	71
11	HPA-3	60	100	90

[a] Conditions: vanadium complex, 0.076 mmol; 2-hydroxycyclohexanone, 7.6 mmol; methanol, 5 mL; dioxygen, 0.1 MPa; reaction time 24 h. [b] Conversion is percentage of the substrate consumed. [c] Yield (%) is (mmol of dimethyl adipate per mmol of the substrate)×100 (determined after addition of ethereal diazomethane).

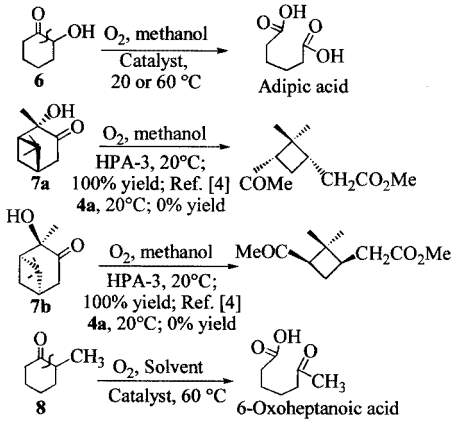

Scheme 2

Catalytic Oxidative Cleavage of 2-Methylcyclohexanone (8)

Unlike 2-hydroxycyclohexanone, 2-methylcyclohexanone is not oxidised in methanol by the V^V-based catalytic systems without an induction period if there is no Brønsted acid present in the reaction solution (Table 4, entries 6 and 8). None of the quaternary ammonium salts of HPA-*n* was active in these oxidations (not shown here) and only the heteropolyacids HPA-*n*, which are known to be strong acids, catalyse C−C bond cleavage (entries 10 and 11). However, these results with alkylammonium may be ambiguous, because these salts are not only less acidic but also less efficient oxidants (change of redox potentials and stabilisation of the $[VO_2]^+$ moieties in the Keggin unit). Addition of only 2−10 equivalents (relative to one vanadium) of *para*-toluenesulfonic acid (PTSA) to the reaction solutions containing catalyst precursors **3** or **4a** results in the formation of 6-oxoheptanoic acid in the form of its methyl ester (see Scheme 2; Table 4, entries 7 and 9). However, it should be noted that the yields for all mononuclear dioxo catalysts are lower than those of HPA-*n* (n = 4 or 3; see entries 10 and 11, respectively). Hence, the redox and acid properties of HPA-3 and mixed valence HPA-4 [$[V^{IV}/V^V]$ are better tuned than those of the mononuclear species. In the case of the "**4a**/O_2/MeOH" system at 60 °C in the absence of added acid, Ph_3SiOMe was formed and characterised by GC-MS (see Exp. Sect.). We conclude that even without addition of strong acid the Ph_3SiO ligands in **4a** are partly replaced to generate oxohydroxo- and/or alkoxo-anionic or neutral vanadium(v) species. As 2-hydroxypinan-3-one is not oxidised by this system at 20 °C, probably due to the bulkiness of this molecule and of **4a** (see above), it is certain that this catalyst precursor does not decompose with formation of small mononuclear species at room temperature (vide supra: vibrational studies).

It is noteworthy that vanadyl precursors (entries 1 and 3) exhibit some activity even in the absence of an acid. Dioxygen consumption has an induction period during which the acac ligand is replaced by other ligands. Addition of 10 equivalents of PTSA increases the yield only in the case of **2** (entry 4). Replacement of PTSA by trifluoromethanesulfonic acid gives the highest yield (entry 5). The addition of either PTSA or CF_3SO_3H (entries 4 and 5) results in O_2 uptake without an induction period. The "$VOSO_4 \cdot 5H_2O$/MeOH/O_2" system gives a blue solution, which turns green immediately after the addition of 2-methylcyclohexanone (**8**). This change in colour is apparently due to the formation of a complex between vanadium-containing species and **8**.

We also investigated the oxidation of **8** in acetonitrile, which is aprotic, although residual water cannot be excluded. It turned out that, in the absence of any other additives, catalyst precursor **3** induces slow consumption of molecular oxygen (Figure 4, curve 1). The oxidation occurs with auto-acceleration after an induction period (ca. 4 hours) during which the colour of the reaction solution changes from very pale yellow to intense orange-yellow. Addition of acetic acid (≈ 4 equivalents relative to **3**) accelerates the reaction insignificantly, the induction period remaining the same (curve 3, see Figure 4). The reaction also proceeds very similarly (curve 4, see Figure 4) in the presence of a chelating amino acid (pyrazine-2-carboxylic acid, PCA) that has been shown to accelerate V-catalysed oxygenations with hydrogen peroxide or air dramatically.[38] Addition of PTSA (only 2 equivalents) considerably increases the rate, and the induction period is eliminated (curve 2; see Figure 4). If 4 equivalents of PCA are added

Table 4. Oxidation of 2-methylcyclohexanone (**8**) to 6-oxoheptanoic acid (Scheme 2)

Entry[a]	Catalyst	[PTSA]/[V]	Conversion (%)[b]	Yield (%)[c]
1	$VOSO_4 \cdot 5H_2O$ (**1**)	0	34	26
2		10	41	21
3	$[VO(acac)_2]$ (**2**)	0	20	18
4		10	66	34
5		10[d]	100	50
6	$[nBu_4N]VO_3$ (**3**)	0	0	0
7		10	48	25
8	**4a**	0	0	0
9		2	50	40
10	HPA-4 ($V^{IV}V^V$)	0	100	90
11	HPA-3[e]	0	99	97

[a] Conditions: vanadium complex, 0.076 mmol; 2-methylcyclohexanone, 7.6 mmol; methanol, 5 mL; dioxygen, 0.1 Mpa; reaction temperature 60 °C; reaction time 24 h. [b] See corresponding footnotes to Table 3. [c] See corresponding footnotes to Table 3. [d] The catalytic species was prepared by the reaction between CF_3SO_3H and $[VO(acac)_2]$ (ratio 1.1) in methanol at 60 °C during 8 h. [e] Reaction in water; reaction time 8 h.

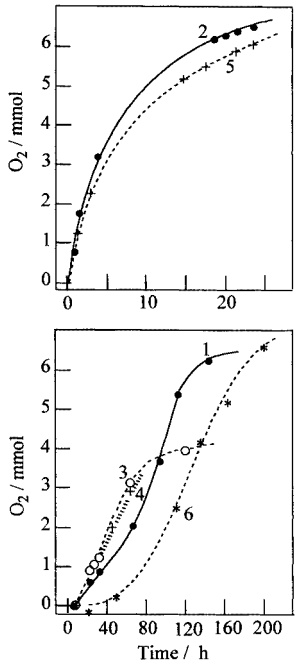

Figure 4. Consumption of O_2 in reaction of 2-methylcyclohexanone (7.6 mmol) in MeCN (total volume of reaction solution 6 mL), catalysed by $[nBu_4N]VO_3$ (0.076 mmol) at 63 °C without additives (curve 1) and with PTSA (0.155 mmol) (2), CH_3COOH (0.32 mmol) (3), PCA (0.306 mmol) (4), PTSA (0.155 mmol) + PCA (0.306 mmol) (5), and pyridine (0.755 mmol) (6)

to the same mixture the oxidation proceeds at practically the same rate (curve 5). It may thus be concluded that acids accelerate the oxidation of **8**, the rate of this reaction rising significantly on going from weak acids to strong ones. When pyridine is added, there is a long induction period (curve 6; see Figure 4), a reduced initial rate and a reduction in the yield of keto acid ($\leq 15\%$).

A study of immobilised $[VO_2]^+/[VO]^{2+}$ on several perfluorinated supports with highly acidic and noncoordinating groups such as $-SO_3^-H^+$ has been presented.[11] This system produces highly selective C−C bond cleavage and low-leaching catalysts; mononuclear vanadium(V/IV) moieties are the most likely active species interacting with SO_3^- groups.[11,47]

On the Mechanism of the Oxidative Cleavage of C−C Bonds

On the basis of our results and others in the literature we propose a mechanism as depicted in Scheme 3 for C−C bond cleavage of 2-hydroxycyclohexanone. This scheme represents a formally closed catalytic cycle, although it is likely that other steps occur and that the equilibria are more complex. The reaction begins with the formation of a catalytically active oxovanadium(V) species **9**, depicted as $[VO_2]^+X^-$, this species containing additional ligands such as coordinated water or organic solvent. Species **9** coordinates to the α-ketol monoanion through its hydroxy oxygen to produce complex **10**. One-electron and proton transfers from the carbon atom to the vanadium moieties give rise to the formation of complex **11**. Naturally, the proton transfer occurs not intramolecularly as schematically depicted as step 2, but through deprotonation and protonation with participation of the solvent, substrate or water (the latter is present at relatively low concentrations in all reaction solutions). The one-electron transfer from the electron-rich organic moiety to the V^V-oxo part of the complex produces species **11**, which contains the organic part of the complex σ, *n*-coordinated to V^{IV}. There is an unpaired electron on the organic ligand, and one of the mesomeric forms of **11** would be a carbon-centred radical. In the presence of molecular oxygen species, **11** would react rapidly with O_2. Indeed, it is well known[48] that carbon-centred radicals add to oxygen molecules in a very fast reaction (Scheme 3).

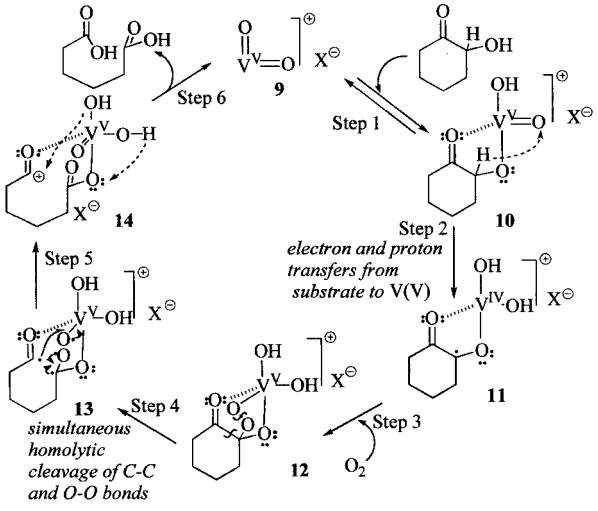

Scheme 3

$$R^{\cdot} + O_2 \rightarrow ROO^{\cdot}$$

It is reasonable to assume that the peroxyl radical formed after addition of O_2 to the carbon atom in **11** would add to the V^{IV} ion of the same complex to form V^V peroxo derivative **12**. In this step, radical ROO· oxidises V^{IV} to V^V. An example of the direct formation of a vanadium(V) peroxo complex in the reaction between a vanadyl(IV) complex and molecular oxygen was recently described.[49]

$$2\,[V^{IV}(=O)(OH)]^+ + O_2 \leftrightarrows [V^V(=O)_2]^+ + [V^V(=O)(O_2)]^+ + H_2O$$

Vanadium(IV) oxo complexes can also be reoxidised by the usual four-electron overall oxidation process shown below.

$$4\,[V^{IV}(=O)]^{2+} + 2\,H_2O + O_2 \leftrightarrows 4\,[V^V(=O)_2]^+ + 4\,H^+$$

Vanadium(V) oxo and peroxo complexes have been reported to hydroxylate aromatic compounds in the presence of acids or/and under light irradiation.[50,51] The mechanism of this oxidation appears to include an electron-transfer step.

Vanadium(V) peroxo complexes are unstable and can decompose by homolytic fission of O−O bonds.[52,53] In our case, we propose that homolytic C−C bond cleavage in **12** occurs simultaneously, possibly through a six-membered transition state. Structure **13** represents one of the species on the reaction coordinate for this electron redistribution. As a result we obtain structure **14** with an acylium cation, which could explain the formation of adipaldehyde and lactones.[45] Addition of hydroxy anion (or methoxy anion when methanol is used as a solvent) gives rise to the formation of adipic acid (or its methyl ester) in Step 6. The hydroxy anion from the V^V species in Scheme 3 is used only conventionally to close the catalytic cycle.

An alternative is that in the interaction between **11** and O_2 the latter adds to the two carbon atoms to produce an endoperoxide species **15** (Scheme 4). It can be seen that this process is also accompanied by the oxidation of V^{IV} to V^V. The simultaneous fission of C−C and O−O bonds in **15** gives adipic acid directly coordinated to vanadium(V) (**16**).

A similar mechanism has previously been proposed for oxidative C−C bond cleavage in acetylacetonate ligand coordinated to palladium(II) to afford acetate.[48,54] In this case the reaction proceeds smoothly at room temperature under irradiation by visible light. Another ligand, *ortho*-metallated azobenzene, coordinated to Pd^{II} plays the role of an "antenna", absorbing light energy necessary for electron transfer from the acac ligand to the palladium centre. It

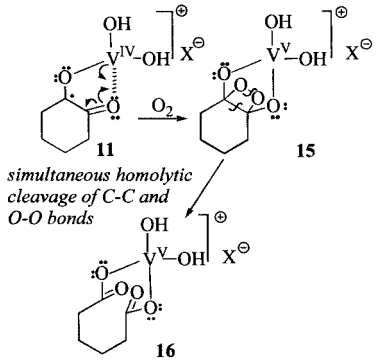

Scheme 4

should be noted that such a mechanism is related to that of C−C bond cleavage in substituted phenols and catechols under the action of O_2 and catalysed by non-heme iron dioxygenase enzymes.[48,55] For example, gentisate 1,2-dioxygenase induces the ring cleavage shown in Scheme 5, and so the oxidative systems described in this paper can be regarded as models of dioxygenases.

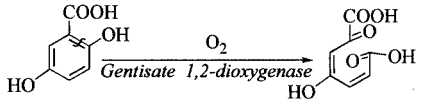

Scheme 5

For the oxidation of 2-methylcyclohexanone, direct σ-coordination of the substrate with vanadium-containing catalytically active species is unlikely. However (see above), this compound could react in the enol form, since addition of weak or, especially, strong acids (see Figure 4) dramatically accelerates the oxidation. The reaction starts with the coordination of the enol species to produce species **17** (Scheme 6). Subsequent electron transfer and dioxygen addition give rise to species **19** or/and **20**. After the cleavage of the C−C and O−O bonds, 6-oxoheptanoic acid is formed.

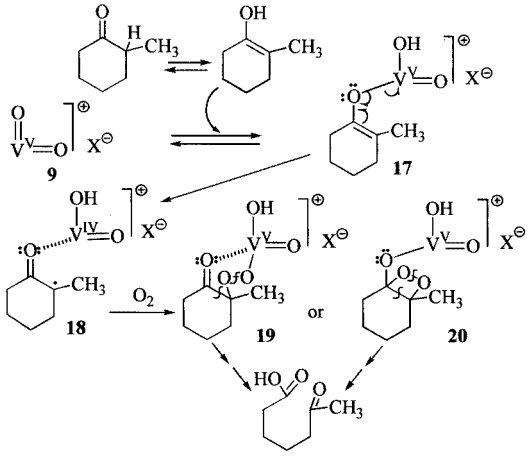

Scheme 6

Conclusion

Despite the advantage of the use of air or dioxygen as the oxidant, there are relatively few known methods that use homogeneous catalysts under very mild conditions. It has been demonstrated here that C−C bond cleavage can be performed efficiently in the presence of dioxygen with simple vanadium-containing precursors or catalysts. Novel anionic vanadium(V) complexes $[n\mathrm{Bu_4N}][\{Ph_3SiO\}_2VO_2]$ (**4a**) and $[n\mathrm{Bu_4N}]_2[\{Ph_2SiO_2VO_2\}_2]$ (**5a**) have been synthesised and used as models of catalytic homogeneous systems in order to generate $[VO_2]^+$ moieties.

Comparison of the activities of substituted heteropolyacids $H_{3+n}[PMo_{12-n}V_nO_{40}]\cdot aq.$, HPA-*n*, with these pervanadyl precursors and other vanadyl complexes with different substrates has caused us to refine our previous mechanism involving mononuclear vanadium(IV) and (V) oxo species and substrate coordination to these $[VO_2]^+$ species.[3] HPA-*n* species are practical and highly efficient reagents for vanadium-based catalysts because their counterions are H_3O^+; they are reversible oxidants, capable of undergoing repeated cycles of reduction and of re-oxidation with dioxygen. Moreover, they can readily be formed from inexpensive reagents: V_2O_5, MoO_3, H_3PO_4 and H_2O_2.[7] We believe that these results can help understanding of systems based on the $[VO_2]^+/[VO]^{2+}$ couple or on modified HPA-*n* species for *linear alkane and cyclohexane oxidation under study in our group*. These systems also give oxygenated intermediates (keto acids, α,ω-diacids, alcohols, ketones, *etc*.) and will be further developed.

Experimental Section

Synthesis

$[n\mathrm{Bu_4N}][\{Ph_3SiO\}_2VO_2]$ (4a): $[n\mathrm{Bu_4N}]VO_3$ [56] (0.68 g; 2 mmol) in ethanol (5 mL) was added to a solution of Ph_3SiOH (1.1 g; 4 mmol) in the same solvent (10 mL). After addition of aqueous ammonia (1.25 M; 3.2 mL), the solution was slowly stirred for 45 min. The white precipitate was isolated by filtration, and then washed with diethyl ether and dried over P_4O_{10} (yield 50−70%). $C_{52}H_{66}NO_4Si_2V$ (876.22): calcd. C 71.28, H 7.59, N 1.60, Si 6.41, V 5.81; found C 71.47, H 7.55, N 1.63, Si 5.58, V 5.40. The structure shows disorder of the tetrabutylammonium cations, but the tetraphenylphosphonium salt gave crystals suitable for an X-ray diffraction study.

$[Ph_4P][\{Ph_3SiO\}_2VO_2]$ (4b): This salt was prepared by dissolving **4a** (0.90 g; 1 mmol) in methanol (10 mL). The complex anion was then precipitated by slow addition of an aqueous solution (10 mL) of PPh_4Cl (0.42 g; 1 mmol). The white solid was isolated by filtration, washed with diethyl ether and then dried in air (yield 95%). $C_{60}H_{50}O_4PSi_2V$ (973.15): calcd. C 74.05, H 5.18, P 3.18, Si 5.77, V 5.23; found C 73.52, H 5.07, P 2.35, Si 5.40, V 5.09.

$[n\mathrm{Bu_4N}]_2[\{Ph_2SiO_2VO_2\}_2]$ (5a): $[n\mathrm{Bu_4N}]VO_3$ [56] (1.36 g; 4 mmol) in ethanol (10 mL) was added to a solution of $Ph_2Si(OH)_2$ (0.86 g; 4 mmol) in the same solvent (10 mL). After 45 min the white precipitate was filtered off, washed with diethyl ether and then dried over P_4O_{10} (yield 50−75%). $C_{56}H_{92}N_2O_8Si_2V_2$ (1079.42): calcd. C 62.31, H 8.59, N 2.59, Si 5.20, V 9.44; found C 62.29, H 8.76, N 2.61, Si 5.30, V 9.38.

"$H_6[PMo_9V_3O_{40}]\cdot 11H_2O$": The heteropolyacids "HPA-3" were prepared by described procedures.[7] $PMo_9V_3O_{51}H_{28}$ (1891.45): calcd. P 1.64, Mo 45.65; V 8.08; found P 1.70, Mo 45.50, V 7.75. Solid HPA-*n* species and their aqueous solutions are multicomponent systems: they contain several polyanions, positional isomers of these, $[VO_2]^+$ and often traces of V^{IV}. The identification is supported by solutions prepared with $2 \leqslant n \leqslant 10$ (see refs.[5,7,47]). Incomplete Keggin species or lacunary HPA-*n* are also formed and only equilibrium exchange-average resonances are observed.

Structure Determinations

Single crystals of **4b** and **5a** were grown from solutions in methanol at room temperature.

$[Ph_4P][\{Ph_3SiO\}_2VO_2]$ (4b): $C_{60}H_{50}O_4PSi_2V$, M_r = 973.14, monoclinic, space group $P2_1/n$ (no. 14); a = 2233.7(4), b = 1118.5(3), c = 2268.2(7) pm, β = 118.59(2)°, V = 4.976 (2) nm^3, Z = 4, $\rho_{calcd.}$ = 1.30 Mg·m^{-3}, $F(000)$ = 2034, λ = 71.069 pm, T = 293 K, μ (Mo-K_α) = 0.317 mm^{-1}, crystal dimensions 0.2 × 0.3 × 0.5 mm^3, $2 \leq 2\theta \leq 50°$, 9487 measured reflections, 8729 were unique; 614 parameters refined in full-matrix, R_1 = 0.046 with 3730 reflections [$I > 3\sigma(I)$], wR_2 = 0.054, $w \neq 1$ [weighting scheme of the form $w = w'[1-(||F_o| - |F_c||) / 6\sigma(Fo))^2]^2$ with $w' = 1/\Sigma_r A_r T_r(X)$ with coefficients 3.55, −0.579 and 2.62 for a Chebyshev series for which X = Fc/Fc(max)].[57] Min./max. residual electron density − 250/320 e nm^{-3}.

$[n Bu_4N]_2[\{Ph_2SiO_2VO_2\}_2]$ (5a): $C_{56}H_{92}N_2O_8Si_2V_2$, M_r = 1079.42, monoclinic, space group $P2_1/n$ (no.14); a = 1207.2(2), b = 1567.8(2), c = 1778.6(2) pm, β = 114.28(1)°, V = 3.068 (2) nm^3, Z = 2, $\rho_{calcd.}$ = 1.17 Mg·m^{-3}, $F(000)$ = 1167, λ = 71.069 pm, T = 293 K, μ (Mo-K_α) = 0.379 mm^{-1}, crystal dimensions 0.1 × 0.3 × 0.4 mm^3, $2 \leq 2\theta \leq 50°$, 5896 measured reflections, 5388 were unique; 317 parameters refined in full-matrix, R_1 = 0.047 with 2386 reflections [$I > 3\sigma(I)$], wR_2 = 0.056, $w \neq 1$ (weighting scheme of the form $w = w'\{1-[(||F_o| - |F_c||)/6\sigma(Fo)]^2\}^2$ with w' = 1/$\Sigma_r A_r T_r(X)$ with coefficients 3.16, 0.109 and 2.29 for a Chebyshev series for which X = Fc/Fc(max)).[57] Min./max. residual electron density −290/300 e nm^{-3}. The data were collected on a Enraf−Nonius CAD4 four-circle diffractometer (ω-2θ scans). All measurements were made at room temperature; two standard reflections showed no significant variation in intensity. Corrections were made for Lorentzian and polarisation effects; an extinction correction was also applied;[58] an empirical absorption correction on the basis of Ψ scan data was introduced. The structures were solved by direct methods (SHELX-86 program)[59] and subsequent Fourier difference techniques. All non-hydrogen atoms were refined anisotropically. All hydrogen atoms were found on difference Fourier maps; their positions were not refined and they were given one overall isotropic thermal parameter. Refinements were carried out by minimising the function $\Sigma w(|F_o| - |F_c|)^2$, where F_o and F_c are the observed and calculated structure factors (program CRYSTALS).[60]

CCDC-167421 (**4b**) and CCDC-167420 (**5a**) contain the supplementary crystallographic data for this paper. These data can be obtained free of charge at www.ccdc.cam.ac.uk/conts/retrieving.html [or from the Cambridge Crystallographic Data Centre, 12, Union Road, Cambridge CB2 1EZ, UK; Fax: (internat.) +44−1223/336−033; E-mail: deposit@ccdc.cam.ac.uk].

General

The solvents were purified by standard procedures and distilled under nitrogen.[62] Triphenyl silanol, Ph_3SiOH and diphenylsilanediol $Ph_2Si(OH)_2$ are commercial products; they were purified by fractional crystallisation. 2-Hydroxycyclohexanone (**6**), (1*S*, 2*S*, 5*S*)-2-hydroxypinane-3-one (**7a**), its (1*R*,2*R*,5*R*) enantiomer **7b**, and 2-methylcyclohexanone (**8**), were better than 99% pure by GC and NMR analysis; they were used without further purification. ^{1}H and ^{13}C NMR spectra were recorded at ambient temperature, on a Fourier transform apparatus (Bruker WP200), using $CDCl_3$ as solvent.

The ^{31}P NMR spectra were recorded with 10 mm o.d. tubes on a Bruker WM 250 apparatus operating at 101.2 MHz. From these NMR measurements it was found that the HPA-*n* precursors ($n \geq 2$) are not pure heteropolyacids: they contains a certain fraction of HPA-1, HPA-2, −3 and −4 with several isomers and excess H_3PO_4. We were unable to prepare a 99% pure isomer.

Raman spectra were recorded at room temperature with a Jobin−Yvon U1000 spectrometer with a resolution of 4 cm^{-1}. Solid samples of the complexes were mounted on a disk rotating at about 1000 rpm in order to avoid decomposition and/or photoreduction by the laser beam (excitation line, 514.5 nm of an Ar^+ laser; source power 30−50 mW; scanning time ca. 2 h). Solutions (0.1 M) of the mononuclear complex **4a** were studied. IR spectra (resolution: 2 cm^{-1}) were measured in a Fourier transform apparatus (Bruker Vector 22) in Nujol suspension either between two caesium bromide plates or in KBr pellets. Elemental analyses (C, H, N, Si, V) were carried out at the Service Central d'Analyses CNRS, Lyon.

Oxidation of 6, 7a or b, or 8 by Dioxygen in the Presence of a Vanadium Precursor

Typical experiments were performed in an all-glass reactor vessel (40 mL) attached to a vacuum line, with a manometer and a gas inlet. This was charged with the vanadium precursor (0.076 mmol V), the solvent (5 mL) and the substrate (ca. 7.6 mmol), and the mixture was stirred magnetically under O_2 for 24 h at 60 °C. Dioxygen uptake was determined by use of a gas burette system. The mixture was cooled and analysed by GC (OV 1701). An aliquot portion (usually 1 mL) including a standard (methyl heptanoate or naphthalene) was esterified by addition of ethereal diazomethane to the crude mixture or after removal of the vanadium on active charcoal (GC-MS experiments). Products were identified by GC-MS.

The GC-MS analyses were performed on a TRACE GC 2000 gas chromatograph (50 m capillary column) interfaced with a mass selective detector (RTX5-MS). ^{1}H and ^{13}C NMR spectra and MS (70 eV or CI, NH_3) data correspond to our previous findings[45] or to literature references.

Acknowledgments

G. B. Shul'pin expresses his gratitude to the Pierre and Marie Curie University in Paris for an Invited Professorship. We thank Dr. J. S. Lomas for constructive discussions and for correcting the manuscript.

[1] J.-M. Brégeault, B. El Ali, J. Mercier, J. Martin, C. Martin, *C. R. Acad. Sci. Paris, Série II* **1988**, *307*, 2011−2014.
[2] J.-M. Brégeault, F. Launay, A. Atlamsani, *C. R. Acad. Sci. Paris, Série IIc, Chimie* **2001**, *4*, 11−21; and references therein.
[3] J.-M. Brégeault, B. El Ali, J. Mercier, J. Martin, C. Martin, O. Mohammedi, *Stud. Surf. Sci. Catal.* **1990**, *55*, 205−212.
[4] L. El Aakel, F. Launay, A. Atlamsani, J.-M. Brégeault, *Chem. Commun.* **2001**, 2218−2219.

[5] I. V. Kozhevnikov, *Chem. Rev.* **1998**, *98*, 171−198.
[6] G. A. Tsigdinos, C. J. Hallada, *Inorg. Chem.* **1968**, *7*, 437−441.
[7] A. Atlamsani, M. Ziyad, J.-M. Brégeault, *J. Chim. Phys.* **1995**, *92*, 1344−1364.
[8] C. F. Baess, R. E. Mesmer, *Hydrolysis of Cations*, Wiley, New York, **1976**.
[9] G. A. Pozarnsky, A. V. Mc. Cornick, *Chem. Mater.* **1994**, *6*, 380−385.
[10] J. Toullec, In *The Chemistry of Enols* (Ed.: Z. Rappoport), Wiley, New York, **1990**, p. 323.
[11] F. Launay, M. Vennat, L. El Aakel, A. Atlamsani, E. Duprey, J.-M. Brégeault, *4th World Congress on Oxidation Catalysis-Extended Abstracts*, Berlin/Potsdam, Sept. 16−21, **2001**. p. 321−326.
[12] J.-Y. Piquemal, J.-M. Manoli, P. Beaunier, A. Ensuque, P. Tougne, A.-P. Legrand, J.-M. Brégeault, *Microporous and Mesoporous Material* **1999**, *29*, 291−304.
[13] R. Murugavel, A. Voigt, M. Ganapati Walawalkar, H. W. Roesky, *Chem. Rev.* **1996**, *96*, [2205−2236.
[14] L. King, A. C. Sullivan, *Coord. Chem. Rev.* **1999**, *189*, 19−57.
[15] N. F. Orlov, B. N. Dolgov, M. G. Voronkov, *Dokl. Akad. Nauk. SSSR* **1958**, *122*, 246−249.
[16] M. M. Chamberlain, G. A. Jabs, B. B. Wayland, *J. Org. Chem.* **1962**, *27*, 3321−3323.
[17] S. Sekiguchi, A. Kurihara, *Bull. Chem. Soc. Jpn.* **1969**, *42*, 1453−1454.
[18] F. J. Feher, J. F. Walzer, *Inorg. Chem.* **1991**, *30*, 1689−1694.
[19] F. J. Feher, R. L. Blanski, *Organometallics* **1993**, *12*, 958−963.
[20] H. J. Gosink, H. W. Roesky, M. Noltemeyer, H. G. Schmidt, C. Freire-Erdbrügger, G. M. Sheldrick, *Chem. Ber.* **1993**, *126*, 279−283.
[21] N. Das, H. Eckert, M. Hu, I. E. Wachs, J. F. Walzer, F. J. Feher, *J. Phys. Chem.* **1993**, *97*, 8240−8243.
[22] N. M. Rutherford, PhD Dissertation, Univ. of California, Berkeley (USA), **1987**.
[23] M. A. Hossain, M. B. Hursthouse, K. M. A. Malik, *Acta Crystallogr., Sect. B* **1979**, *35*, 522−524.
[24] D. Braga, G. Zanotti, *Acta Crystallogr., Sect. B* **1980**, *36*, 950−953.
[25] Y. E. Ovchinnikov, V. E. Shklover, Y. T. Struchkov, V. V. Dement′ev, T. M. Frunze, *Metalloorg. Khim.* **1988**, *1*, 1117−1120.
[26] J. Janczak, R. Kubiak, *Acta Crystallogr., Sect. C* **1992**, *48*, 1299−1301.
[27] M. L. Ferreira, M. Volpe, *J. Mol. Catal. A: Chemical* **2000**, *164*, 281−290.
[28] V. Vergopoulos, W. Priebsch, M. Fritzche, D. Rehder, *Inorg. Chem.* **1993**, *32*, 1844−1849.
[29] G. Asgedom, A. Sreedhara, J. Kivikovski, E. Kolehmainen, C. P. Rao, *J. Chem. Soc., Dalton Trans.* **1996**, 93−97.
[30] D. C. Crans, A. D. Keramidas, M. Mahroof-Tahir, O. P. Anderson, M. M. Miller, *Inorg. Chem.* **1996**, *35*, 3599−3606.
[31] T. Yao, Y. Oka, N. Yamamoto, *Inorg. Chim. Acta* **1995**, *238*, 165−168.
[32] S. Launay, J. Thoret, *C. R. Acad. Sci. Paris, Série D* **1973**, *277*, 541−543.
[33] M. Sato, S. Kano, S. Tamaki, M. Misawa, Y. Shirakawa, M. Ohashi, *J. Mater. Chem.* **1996**, *6*, 1191−1194.
[34] D. F. Mullica, E. L. Sappenfield, M. M. Abraham, B. C. Chakoumakos, L. A. Boatner, *Inorg. Chim. Acta* **1996**, *248*, 85−88.
[35] P. Román, A. San José, A. Luque, J. M. Gutiérrez-Zorrilla, *Inorg. Chem.* **1993**, *32*, 775−776.
[36] V. W. Day, W. G. Klemperer, O. M. Yaghi, *J. Am. Chem. Soc.* **1989**, *111*, 4518−4519.
[37] H. Mimoun, L. Saussine, E. Daire, M. Postel, J. Fischer, R. Weiss, *J. Am. Chem. Soc.* **1983**, *105*, 3101−3110.
[38] G. Süss-Fink, S. Stanislas, G. B. Shul′pin, G. V. Nizova, H. Stoeckli-Evans, A. Neels, C. Bobillier, S. Claude, *J. Chem. Soc., Dalton Trans.* **1999**, 3169−3175.
[39] H. T. Evans, *Z. Krist.* **1960**, *114*, 257; *CA* **1961**, *55*, 1135.
[40] H. Oberhammer, W. Zeil, G. Fogarasi, *J. Mol. Struct.* **1973**, *18*, 309−318.
[41] M. R. Maurya, S. Khurana, W. Zhang, D. Rehder, *Eur. J. Inorg. Chem.* **2002**, 1749−1760.
[42] J.-Y. Piquemal, C. Bois, J.-M. Brégeault, *Chem. Commun.* **1997**, 473−474.
[43] R. G. J. Miller, H. A. Willis, *Infrared Structural Correlation Tables*, Heyden and Son Ltd., London, **1969**, Table 9.
[44] M. Biagoli, L. Strinna-Erre, G. Micera, A. Panzanelli, M. Zema, *Inorg. Chim. Acta* **2000**, *310*, 1−9.
[45] A. Atlamsani, J.-M. Brégeault, M. Ziyad, *J. Org. Chem.* **1993**, *58*, 5663−5665.
[46] M. Kirihara, Y. Ochiai, S. Takizawa, H. Takahata, H. Nemoto, *Chem. Commun.* **1999**, 1387−1388.
[47] L. El Aakel, F. Launay, J.-M. Brégeault, A. Atlamsani, *to be submitted*.
[48] A. E. Shilov, G. B. Shul′pin, *Activation and Catalytic Reactions of Saturated Hydrocarbons in the Presence of Metal Complexes*, Kluwer Academic Publishers, Dordrecht, **2000**.
[49] M. Kosugi, S. Hikichi, M. Akita, Y. Moro-oka, *J. Chem. Soc., Dalton Trans.* **1999**, 1369−1371.
[50] M. M. Kats, G. B. Shul′pin, *Bull. Acad. Sci. USSR, Div. Chem. Sci.* **1990**, *39*, 2233.
[51] D. Attanasio, L. Suber, G. B. Shul′pin, *Bull. Acad. Sci. USSR, Div. Chem. Sci.* **1992**, *41*, 1502−1504.
[52] G. B. Shul′pin, M. C. Guerreiro, U. Schuchardt, *Tetrahedron* **1996**, *52*, 13051−13062.
[53] G. B. Shul′pin, Y. N. Kozlov, G. V. Nizova, G. Süss-Fink, S. Stanislas, A. Kitaygorodskiy, V. S. Kulikova, *J. Chem. Soc., Perkin Trans.* **2001**, *2*, 1351−1371.
[54] J. Vicente, A. Arcas, D. Bautista, G. B. Shul′pin, *J. Chem. Soc., Dalton Trans.* **1994**, 1505−1509.
[55] G. Lin, G. Reid, T. D. H. Bugg, *J. Am. Chem. Soc.* **2001**, *123*, 5030−5039.
[56] V. W. Day, W. G. Klemperer, A. Yagasaki, *Chem. Lett.* **1990**, 1267−1270.
[57] R. J. Carruthers, D. J. Watkin, *Acta Crystallogr.* **1979**, A35, 698−699.
[58] A. C. Larson, In *Crystallographic Computing* (Eds: F. R. Ahmed, S. R. Hall, C. P. Huber), Munksgaard, Copenhagen, **1970**, p. 291−294.
[59] G. M. Sheldrick, SHELXS-86, *Program for the Solution of Crystal Structures*, Universität Göttingen, **1985**.
[60] D. J. Watkin, C. K. Prout, R. J. Carruthers, P. Betteridge, CRYSTALS, *An Advanced Crystallographic Program System*, **1996**, Chemical Crystallography Laboratory, University of Oxford.
[61] D. J. Watkin, C. K. Prout, L. J. Pearce, CAMERON, **1996**, Chemical Crystallography Laboratory, University of Oxford.
[62] D. D. Perrin, W. L. F. Amnarengo, D. R. Perrin, *Purification of Laboratory Chemicals, 3rd ed.,* Pergamon Press, Oxford, U. K., **1988**.

Received July 27, 2002
[I02419]

Template Synthesis of Chiral Vicinal Diphosphinites as Their Pt^{II} and Pd^{II} Complexes

Paola Bergamini,*[a] Valerio Bertolasi,[a] Michela Cattabriga,[a] Valeria Ferretti,[a] Urania Loprieno,[a] Nicoletta Mantovani,[a] and Lorenza Marvelli[a]

Keywords: Template synthesis / Ligand design / P ligands / Platinum / Palladium

The metal-templated synthesis of a few examples of vicinal diphenylphosphinites is accomplished when the corresponding vicinal diols react with the diphenylchlorophosphane complexes *cis*-$[MCl_2(PPh_2Cl)_2]$ (M = Pt, Pd) in anhydrous THF. This process is proposed as a new synthetic route for Pt^{II} and Pd^{II} complexes of the new ligands 1,2-bis(diphenylphosphinito)butane, 2,3-bis(diphenylphosphinito)butane, and 2,3-bis(diphenylphosphinito)diisopropyl-L-tartrate, containing seven-membered chelate rings including stereogenic carbons. The new chiral phosphane-phosphinite (*R*)-3-(diphenylphosphanyl)-2-(diphenylphosphinito)propanol has also been obtained as a Pt^{II} six-membered chelate. The X-ray crystal structure of some of the described complexes and NMR evidence of the possibility of removing the ligands from the metal are reported.

(© Wiley-VCH Verlag GmbH & Co. KGaA, 69451 Weinheim, Germany, 2003)

Introduction

Chiral diphosphinites are a well-documented alternative to chiral diphosphanes as ligands for metal ions to give metal complexes that can be exploited in various processes with the double function of catalysts and asymmetry inductors.[1] Particular attention has been given to vicinal diphosphinites whose coordination gives a seven-membered chelate ring similar in size to the successful DIOP-Rh system.[2]

Several examples of chiral diphosphinites obtained by the functionalization of diols belonging to the natural chiral pool have been reported.[3] In particular Rajan-Babu et al. have described asymmetric diphosphinites obtained by the functionalization of sugars and have shown that it is possible to drive some enantioselective hydrogenations to one product or to the other depending on the hydroxy groups selected for the transformation into phosphinites.[4]

Despite the interest of diphosphinites for catalysis, the synthesis of those deriving from low-weight vicinal diols has not been described, with the sole exception of bis(diphenylphosphinite)ethane,[5] observed in 1999 in solution but not isolated.

The apparent lack of attention paid to the simplest vicinal diphosphinites could be due to the known moisture and oxygen sensitivity[6] reported for some members of this group of ligands, which makes their use in catalysis not very convenient and their synthesis quite puzzling.

[a] Dipartimento di Chimica dell'Università di Ferrara, via L. Borsari 46, 44100 Ferrara. Italy
Fax: (internat.) +39−0532/240-709
E-mail: bgp@unife.it

In fact our attempts to prepare 1,2- and 2,3-bis(diphenylphosphinite)butane by the classical route (Scheme 1) − reaction of the corresponding diols with PPh_2Cl − gave **1** and **2** as impure products in low yield.

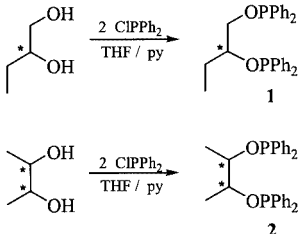

Scheme 1

Nevertheless, when we succeeded in obtaining a few square-planar Pt^{II} and Pd^{II} complexes from crude **1** and **2**, we noticed that the stability of such molecules is greatly enhanced by the coordination. We therefore reasoned that it should be possible to design a general alternative synthetic route for diphenylphosphinites where they could be built inside the coordination sphere of metal ions (metal template synthesis).

In this paper we compare two synthetic pathways to platinum and palladium dichloride complexes of **1** and **2**: in the first one **1** and **2** are prepared in solution as free ligands and then coordinated to the metal by substitution of COD in $[MCl_2(1,5\text{-COD})]$ (M = Pt, Pd); in the second, the reaction of the diphenylchlorophosphane complexes *cis*-$[MCl_2(PPh_2Cl)_2]$ (**3a**, M = Pt; **3b**, M = Pd) with 1,2- or 2,3-butanediol leads to the same complexes in a shorter time and with higher yield and purity.

This "metal-template" synthesis can be extended to more functionalised ligands, and we also report NMR evidence of the possibility of removing these ligands from the metal exploiting the sequestrating action of CN^- on Pt and Pd.

Results and Discussion

Generation of the Diphosphinites 1 and 2 in Solution and Their Coordination to Pt and Pd

The diphosphinites **1** and **2** can be obtained from the reaction of 1,2- and 2,3-butanediol[7] respectively with two equivalents of PPh_2Cl in THF or pyridine (see Exp. Sect.). The reactions were followed by ^{31}P NMR spectroscopy and it was observed that, in both cases, PPh_2Cl (δ = 82.5 ppm) is completely consumed in about 60 min to give the required product (two singlets at δ = 115.7 and 111.5 ppm for **1** and one singlet at δ = 112.2 ppm for **2**) together with a few phosphorus-containing side products.

The major drawback of this direct preparation of **1** and **2** is that impure products were obtained even under carefully controlled conditions. The ^{31}P NMR spectrum of the reaction mixture showed the presence of side products generated both by phosphorus oxidation and by PPh_2Cl decomposition due probably to traces of water contained in the reacting liquid diols.

All attempts to improve the purity of **1** and **2** obtained by this route using chromatographic techniques led to further decomposition. The instability of free phosphinites has been observed before.[6] Nevertheless, the addition of $[MCl_2(1,5\text{-COD})]$ (M = Pt, Pd) to a THF solution containing crude **1** or **2** leads to the precipitation of their platinum (**1a** and **2a**) and palladium (**1b** and **2b**) dichloride complexes in pure form (Scheme 2).

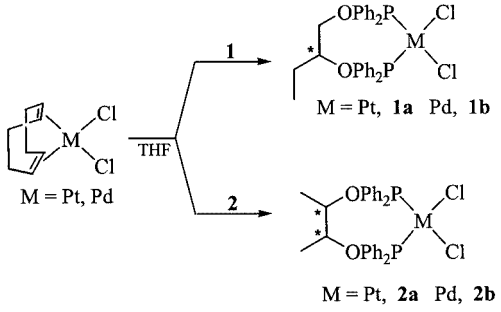

Scheme 2

The ^{31}P NMR spectrum of **1a** shows two doublets with satellites at δ = 90.2 and 89.3 ppm indicating that each phosphorus is coupled to platinum ($^1J_{P,Pt}$ = 4045 and 3994 Hz, typical values for phosphorus *trans* to chloride[8]) and to the other phosphorus ($^2J_{P,P}$ = 12 Hz). The corresponding palladium complex **1b** also shows a doublet of doublets at δ = 119.1 and 118.4 ppm ($^2J_{P,P}$ = 35.7 Hz).

Both **2a** and **2b** show a singlet (with satellites for **2a**, $^1J_{P,Pt}$ = 4021 Hz) in the ^{31}P NMR spectrum due to the equivalence of the two phosphorus atoms in these complexes.

While **1** and **2** undergo rapid decomposition in solution in the presence of traces of oxygen and/or water, solutions of **1a**, **1b**, **2a**, or **2b** in pure chloroform or in $CHCl_3$/acetone do not show any sign of decomposition (by ^{31}P NMR spectroscopy) even in the presence of oxygen and/or water after five days: these observations indicate that coordination to Pt^{II} or Pd^{II} dramatically reduces the susceptibility of phosphinites to oxidation and hydrolysis.

Template Synthesis of 1 and 2

In an attempt to design a more convenient route to diphosphinites we considered that, because the major reason for the interest in these compounds is the use of their complexes with metal ions in catalysis, it should be advantageous to produce them inside the coordination sphere of metal ions of catalytic value, thus obtaining the metal complexes directly. Pt^{II} and Pd^{II} complexes appeared to be convenient models for this synthetic approach. The metal-templated synthesis we carried out is described in Scheme 3.

Treatment of $[MCl_2(1,5\text{-COD})]$ (M = Pt, Pd) with two equivalents of PPh_2Cl in carefully dried THF gives *cis*-$[MCl_2(PPh_2Cl)_2]$ **3a** (M = Pt) and **3b** (M = Pd), which have been described before.[9]

We found that the coordinated chlorophosphane in **3a** and **3b** is still able to react with hydroxy groups. In fact, the reaction of **3a** or **3b** with 1,2- or 2,3-butanediol gave **1a**, **1b**, **2a**, and **2b** which precipitated as pure products in high yields, with elimination of HCl in solution.

Complexes **1a** and **2b** gave crystals suitable for an X-ray crystal-structure determination.

X-ray Crystal Structures of 1a and 2b

ORTEP[10] views of the structure of **1a** and **2b** are shown in Figures 1 and 2, respectively. Selected bond lengths and angles are reported in Table 1. Both complexes present a slightly distorted square-planar geometry, with the metal centre bonded to two chlorides and to two phosphorus atoms belonging to the diphosphinite ligand. The coordination of **1** or **2** to the metal leads to the formation of a seven-membered ring with a boat conformation. The nature of the metallic centre does not significantly affect the bond angles and lengths in the coordination sphere.

A few examples of X-ray crystal structures of diphosphinito complexes have been reported before. For example, both *fac*-$[ReBr(CO)_3(L{-}L)]$ and *fac*-$[ReH(CO)_3(L{-}L)]$ [L−L = 1,2-bis(diphenylphosphinito)ethane] contain seven-membered $ReP_2O_2C_2$ rings with a twisted chair conformation.[5]

Removal of 1 from Its Pt and Pd Complexes

The sequestrating action of cyanide for platinum(II) is well-known.[11] When **1a** was dissolved in $CDCl_3$ and treated with 4.5 equiv. of soluble $(Bu_4N)CN$, the ^{31}P NMR spectrum showed that, in the first step, both the platinum-coordinated chlorides are replaced by cyanide within 5−10 minutes. Further observations show that the diphosphinite **1** is progressively replaced by cyanide and after 30−40 mi-

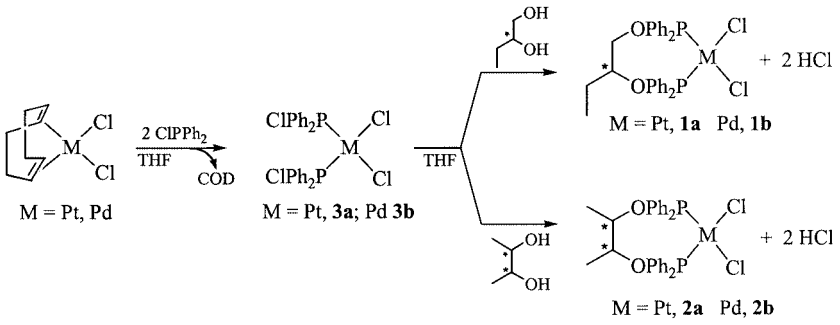

Scheme 3

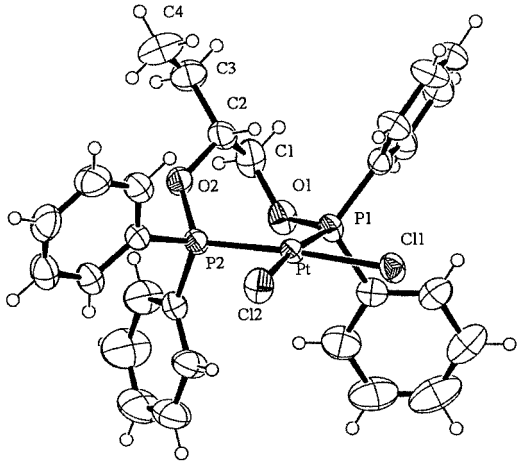

Figure 1. ORTEP[10] view of complex **1a** showing the thermal ellipsoids at the 40% probability level

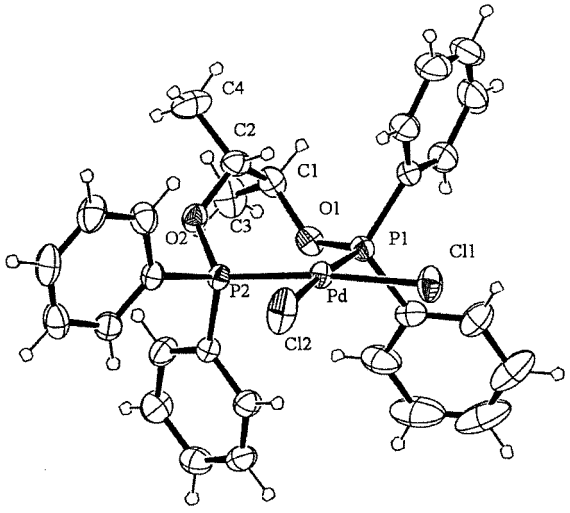

Figure 2. ORTEP[10] view of complex **2b** showing the thermal ellipsoids at the 40% probability level

Table 1. Selected bond lengths [Å] and angles [°] for compounds **1a** and **2b**

1a		**2b**	
Pt−Cl1	2.354(1)	Pd−Cl1	2.352(1)
Pt−Cl2	2.354(1)	Pd−Cl2	2.334(1)
Pt−P1	2.221(1)	Pd−P1	2.235(1)
Pt−P2	2.224(1)	Pd−P2	2.237(1)
P1−O1	1.604(3)	P1−O1	1.608(2)
P2−O2	1.601(2)	P2−O2	1.611(2)
O1−C1	1.463(5)	O1−C1	1.451(3)
O2−C2	1.446(4)	O2−C2	1.442(3)
C1−C2	1.503(6)	C1−C2	1.520(3)
Cl1−Pt−Cl2	88.33(3)	Cl1−Pd−Cl2	92.23(2)
Cl1−Pt−P1	86.64(3)	Cl1−Pd−P1	85.74(2)
Cl1−Pt−P2	176.09(3)	Cl1−Pd−P2	173.74(2)
Cl2−Pt−P1	172.94(4)	Cl2−Pd−P1	175.27(3)
Cl2−Pt−P2	91.47(3)	Cl2−Pd−P2	88.64(2)
P1−Pt−P2	93.22(3)	P1−Pd−P2	92.92(2)

nutes the free ligand **1** is the only phosphorus-containing product.

The addition of a small quantity of $[PdCl_2(1,5\text{-COD})]$ to this solution gives the immediate formation of **1b** (Scheme 4), indicating that the shift of **1** from platinum to palladium can be obtained by the addition of cyanide. An analogous experiment showed that the reverse process of ligand transfer from palladium (**1b**) to platinum is also easily achievable.

Template Synthesis of the New Diphosphinite 4 on Platinum

In an attempt to extend the applicability of our template synthesis of phosphinites to more functionalised ligands, we tried the addition of (+)-diisopropyl L-tartrate to the intermediate $[Pt(PPh_2Cl)_2Cl_2]$ (**3a**) preformed in situ in THF. After 18 hours the formation of the optically active complex **4a*** was complete (Scheme 5).

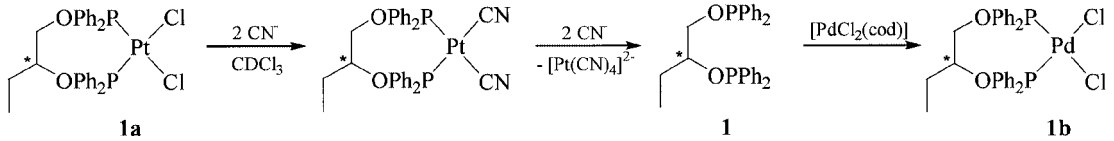

Scheme 4

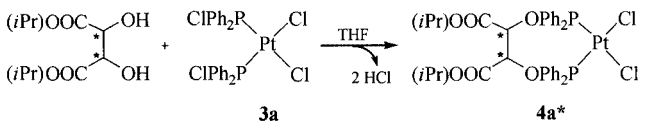

3a **4a***

Scheme 5

This complex was isolated and fully characterised (see Exp. Sect.). The ^{31}P NMR spectrum shows a singlet for the two equivalent phosphorus atoms at $\delta = 94.7$ ppm, in the typical downfield range of diphenylphosphinites, with satellites due to the Pt coupling ($^1J_{P,Pt} = 4003$ Hz).

The optical rotation of **4a*** was measured in $CHCl_3$ ($[\alpha]_D^{25} = -10.6$ ($c = 0.5$, $CHCl_3$). This result confirms the expectation that optically active complexes are obtained when a diol bearing a stereogenic carbon is used in an optically active form, due to the fact that the diol reaction with **3a** or **3b** does not involve the chiral carbon.

Template Synthesis of the New Phosphane-phosphinite-ol 5 on Platinum

The optically active phosphane-diol (*R*)-**I** (Scheme 6) can be obtained in two steps from the commercial precursor (*R*)-2,2-dimethyl-1,3-dioxolane-4-methanol *p*-toluenesulfonate through a known procedure.[12]

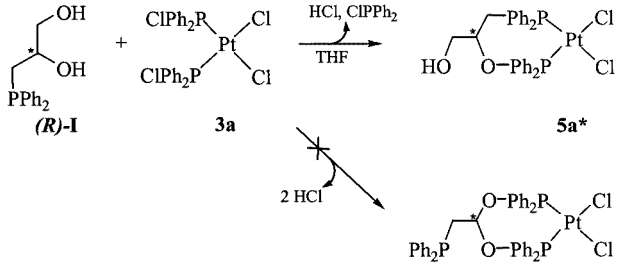

Scheme 6

When (*R*)-**I** is added to a solution of $[Pt(PPh_2Cl)_2Cl_2]$ (**3a**) its phosphinic group replaces the less nucleophilic PPh_2Cl and the *C(2)*hydroxy group reacts with the remaining coordinated PPh_2Cl (Scheme 6). The driving force of this process is probably the formation of a thermodynamically stable six-membered chelate ring. Complex **5a*** is recovered as the only platinum-containing species.

The identity of **5a***, determined by elemental and spectroscopic analysis, was confirmed by X-ray crystal structure (see below) and its optical rotation was measured (see Exp. Sect.). The ^{31}P NMR spectrum of **5a*** shows two doublets with satellites, one at $\delta = 84.7$ ppm, typical of a coordinate phosphinite, while the coordinated phosphinic P resonates at $\delta = -0.4$ ppm: each phosphorus is coupled to platinum ($^1J_{P,Pt} = 3858$ and 3482 Hz, respectively) and to the other phosphorus ($^2J_{P,P} = 17.7$ Hz).

It is noteworthy that **5a*** contains the new ligand (*R*)-3-(diphenylphosphanyl)-2-(diphenylphosphinito)propanol (**5**), whose direct synthesis would not be possible without protection of the *C(3)*-hydroxy group. Not many examples of phosphane-phosphinites have been reported,[13] and **5** is a rare example of this class of ligand with *C*-chirality.

It should also be noted that the reaction of **3a** with both the OH groups of (*R*)-**I** would give a potentially tridentate phosphane-diphosphinite ligand acting in only a bidentate manner; no evidence of this process was observed.

The deplatinization of **5a*** with CN^- in solution ($CDCl_3$) allowed the observation of a ^{31}P NMR spectrum consistent with that expected for the free ligand **5** – a doublet at $\delta = 111$ ppm, typical for a $ROPPh_2$ group, and a second doublet in the phosphinic range ($\delta = -23$ ppm), each coupled to the other with a $^4J_{P,P}$ coupling constant of 7 Hz.

X-ray Crystal Structure of 5a*

The recrystallisation of **5a*** from CH_2Cl_2 and diethyl ether gave crystals whose X-ray structure is shown in Figure 3. Selected bond lengths and angles are given in Table 2.

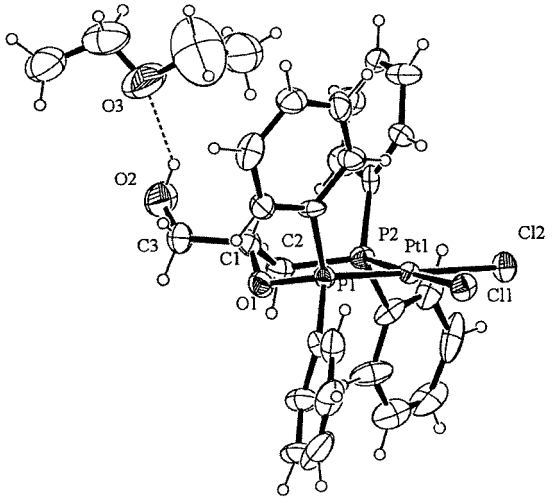

Figure 3. ORTEP[10] view of complex **5a*** linked by hydrogen bonds to a solvent molecule of diethyl ether showing the thermal ellipsoids at the 40% probability level.

Table 2. Selected bond lengths [Å] and angles [°] for compound **5a***

5a*			
Pt1–Cl1	2.352(4)	Cl1–Pt1–Cl2	89.3(1)
Pt1–Cl2	2.364(5)	Cl1–Pt1–P1	87.4(2)
Pt1–P1	2.209(5)	Cl1–Pt1–P2	177.1(2)
Pt1–P2	2.239(5)	Cl2–Pt1–P1	176.6(2)
P1–O1	1.60(1)	Cl2–Pt1–P2	88.0(2)
P2–C2	1.81(2)	P1–Pt1–P2	95.2(1)
C1–O1	1.44(2)		
C1–C2	1.49(2)		
C1–C3	1.52(2)		
C3–O2	1.38(2)		
Hydrogen bond			
O2–H2	0.82		
O3···H2	2.10		
O2···O3	2.78(2)		
O2–H2···O3	140		

The complex displays a slightly distorted square-planar geometry. The Pt1−P1−P2−C1−C2−O1 six-membered ring assumes a half-chair conformation with the C1 atom in the *R* configuration, as determined by the Flack parameter [−0.02(4)] calculated after the least-square refinement. The molecular packing forms channels which include molecules of diethyl ether linked by means of an O2−H···O3 hydrogen bond [O2···O3 = 2.78(2) Å] to the hydroxyl group of the complex.

Hydrolysis of 3a and 3b

The above-described synthesis of diphenylphosphinites on Pt or Pd must be carried out in water-free conditions as we observed that, in the presence of even small quantities of water, competitive hydrolysis of the intermediate complexes **3a** and **3b** prevents the formation of the diphosphinite complexes.

We found that the addition of water to a THF solution of **3a** (Scheme 7) produces a mixture of complex [$PtCl_2(PPh_2OH)_2$] (**6**; δ = 71.1 ppm, $^1J_{P,Pt}$ = 4065 Hz) and of another species, **7**, whose ^{31}P NMR spectrum shows a singlet with satellites at δ = 50.5 ppm ($^1J_{P,Pt}$ = 4090 Hz).

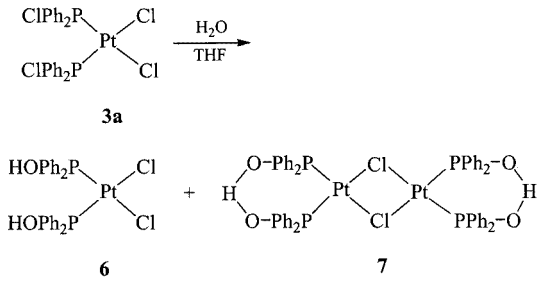

Scheme 7

Recrystallisation of the mixture from THF and diethyl ether gave crystals of **7**, which has been identified before[9] on the basis of its NMR spectroscopic data. The X-ray crystal structure (Figure 4) showed that **7** is the dimeric neutral species [Pt(μ-Cl)($Ph_2POHOPPh_2$)]$_2$ with bridging chloride ligands and terminal PPh_2OH and PPh_2O moieties connected by hydrogen bonds. Although the hydrolysis of **3a** has been studied in detail in the past,[9] the structure of **7** has not been reported before.

In a similar way, the presence of water converts the palladium species **3b** into another species whose ^{31}P NMR spectrum is a singlet at δ = 78.1 ppm, coincident with the signal reported for the palladium analogue of **7** [Pd(μ-Cl)($Ph_2POHOPPh_2$)]$_2$.[9c]

X-ray Crystal Structure of 7

Crystals of **7** were obtained from THF and diethyl ether and its X-ray structure is shown in Figure 4. Selected bond lengths and angles are given in Table 3.

The complex is essentially planar and displays a C_s symmetry. The molecule is characterized by two strong hydrogen bonds O1−H···O2 and O4−H···O3 with very short

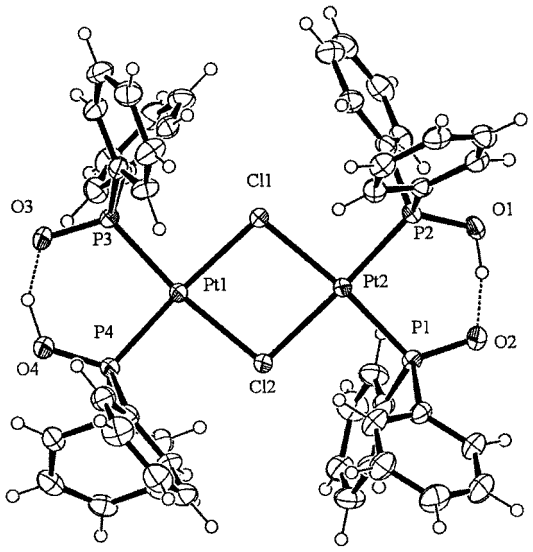

Figure 4. ORTEP[10] view of complex **7** showing the thermal ellipsoids at the 40% probability level

Table 3. Selected bond lengths [Å] and angles [°] for compound **7**

7			
Pt1−Cl1	2.430(1)	Cl1−Pt1−Cl2	81.76(4)
Pt1−Cl2	2.420(1)	Cl1−Pt1−P3	91.17(4)
Pt1−P3	2.237(1)	Cl1−Pt1−P4	172.25(5)
Pt1−P4	2.229(1)	Cl2−Pt1−P3	172.27(4)
Pt2−Cl1	2.413(1)	Cl2−Pt1−P4	93.89(4)
Pt2−Cl2	2.415(1)	P3−Pt1−P4	93.49(5)
Pt2−P1	2.227(1)	Cl1−Pt2−Cl2	82.21(4)
Pt2−P2	2.227(1)	Cl1−Pt2−P1	172.84(4)
P1−O2	1.550(4)	Cl1−Pt2−P2	93.71(4)
P2−O1	1.544(4)	Cl2−Pt2−P1	91.54(5)
P3−O3	1.544(4)	Cl2−Pt2−P2	175.28(5)
P4−O4	1.540(4)	P1−Pt2−P2	92.67(5)
		Pt1−Cl1−Pt2	97.63(4)
		Pt1−Cl2−Pt2	97.84(4)
Hydrogen bonds			
O1−H	0.99(6)	O4−H	1.10(6)
O2···H	1.44(6)	O3···H	1.39(6)
O1···O2	2.415(6)	O3···O4	2.404(5)
O1−H···O2	165(5)	O4−H···O3	149(5)

O···O distances [O1···O2 = 2.415(6) Å and O4···O3 = 2.404(5) Å]. They belong to the $(O-H\cdots O)^-$ class of negative-charge-assisted H-bonds [(−)CAHB][14] where the negative charge is shared between two oxygens. Accordingly, all the P−O bonds are of similar lengths [in the range 1.540(4)−1.550(4) Å], and are significantly longer than the P=O distances [1.48−1.50 Å][15] between phosphorus and neutral oxygen.

Conclusions

The experiments described in this paper show that vicinal diphosphinites can be obtained in the metal-chelate sta-

bilised form, starting from the corresponding 1,2-diols, whose stereochemistry is retained in the process.

We are now investigating the possibility to extend this preparative method to asymmetric complexes of other metals (e.g. Rh or Ru) and of other groups of ligands (e.g. amidophosphane-phosphinites and aminophosphane-phosphinites[16]) relevant to asymmetric catalysis.

Experimental Section

All reactions and manipulations were routinely performed under a dry nitrogen atmosphere by using standard Schlenk-tube techniques. Tetrahydrofuran was doubly distilled from over $LiAlH_4$, while diethyl ether was purified by distillation from over sodium/benzophenone. Dichloromethane and methanol were purified by distillation from calcium hydride. Pyridine was distilled and stored over KOH. $CDCl_3$, used as solvent for the NMR spectra, was dried over molecular sieves (4 Å). PPh_2Cl (d = 1.23 g·mL^{-1}) was purified just prior to use by distillation under nitrogen. All the other solvents and chemicals were reagent grade and, unless otherwise stated, were used as received from commercial suppliers. Infrared spectra were obtained in CsI, using a Nicolet 510 P FT-IR (4000−200 cm^{-1}) spectrometer. ^{1}H and ^{31}P NMR spectra (always ^{1}H decoupled) were recorded on Bruker AC200 spectrometers operating at 200.13 MHz (^{1}H) and 81.01 MHz (^{31}P). Peak positions are given in ppm relative to tetramethylsilane (^{1}H) and to external 85% H_3PO_4 (^{31}P). Elemental analyses (C, H, N) were performed using a Carlo Erba model 1106 elemental analyser. Optical rotations were obtained on a Perkin−Elmer 241 at 25 °C.

Literature methods were used for the preparation of [$PtCl_2$(1,5-COD)][17] and [$PdCl_2$(1,5-COD)].[18]

The diol *R*-**I** was prepared in two steps from commercial *p*-toluenesulfonate of (*R*)-2,2-dimethyl-1,3-dioxolane-4-methanol by the reported procedure.[12]

Synthesis of Pt and Pd Complexes of Ligands 1 and 2

Synthesis of 1a. Method a: A THF (5 mL) solution of 1,2-butanediol (117 mg, 1.3 mmol) was prepared in a Schlenk flask equipped with a dropping funnel and cooled to 0 °C (ice bath). The dropping funnel was charged with THF (5 mL), PPh_2Cl (0.57 mL, 3.2 mmol), pyridine (3 mL), and the mixture was added dropwise to the diol solution whilst stirring. After the addition of a few drops, white pyridinium chloride started to precipitate. After the end of the addition, the reaction mixture was kept stirring at 0 °C for an hour, then the white solid was filtered off under nitrogen on celite, giving a colourless solution whose ^{31}P NMR analysis showed the presence of a main species consistent with **1** [^{31}P NMR (81.01 MHz, $CDCl_3$, 25 °C): P_a 115.7(s), P_b 111.5 (s) ppm] together with small amount of other unidentified species.
The volume of this solution was reduced to 20 mL by addition of THF and solid [$PtCl_2$(1,5-COD)] (500 mg, 1.3 mmol) was added at room temperature. The reaction mixture was stirred for 1 h at room temperature; during this period the product precipitated as a white solid, which was then filtered and washed with diethyl ether (390 mg, 41%).

Method b: A solution of PPh_2Cl (100 μL, 0.56 mmol) in 5 mL of THF was added dropwise whilst stirring to a solution of [$PtCl_2$(1,5-COD)] (100 mg, 0.27 mmol) in THF (10 mL) placed in a Schlenk flask at room temperature. The immediate formation of the dichlorophosphane complex **3a** was unambiguously confirmed by ^{31}P NMR spectroscopy (δ = 73.4 ppm, $^1J_{PPt}$ = 4069 Hz[9]). The addition of 1,2-butanediol (24 μL, 0.27 mmol) gave a colourless mixture, and within 10 minutes **1a** began to separate as a white microcrystalline precipitate. Slow addition of diethyl ether completed the precipitation. The solid product was filtered off, washed with diethyl ether, and dried under vacuum (130 mg, 67%). $C_{28}H_{28}Cl_2O_2P_2Pt$: calcd. C 46.4, H 3.9%; found C 46.6, H 4.0%. IR: ν_a(Pt−Cl) 317; ν_s(Pt−Cl) 293 cm^{-1}. ^{1}H NMR (200 MHz, $CDCl_3$, 25 °C): δ = 0.7 (t, $^3J_{H,H}$ = 7 Hz, 3 H, -C*H*$_3$), 1.7−1.4 (m, 2 H, -C*H*$_2$Me), 3.8−4.2 (m, 2 H, -C*H*$_2$OP), 4.4 (m, 1 H, -C*H*OP), 7.0−8.0 (m, 20 H, Ph) ppm. ^{31}P NMR (81.01 MHz, $CDCl_3$, 25 °C): δ = P_a 90.2 (d, $^1J_{PtP}$ = 4045 Hz,), P_b 89.3 (d, $^1J_{PtP}$ = 3994 Hz) ppm, $^2J_{PaPb}$ = 12 Hz.
Recrystallization of the crude product from dichloromethane/ethanol gave crystals suitable for an X-ray diffraction study.

Synthesis of 2a. Method a: A solution of ligand **2** was prepared from 2,3-butanediol (117 mg, 1.3 mmol), following the method described above for **1**. The ^{31}P NMR analysis showed the presence of a signal consistent with **2** [^{31}P NMR (81.01 MHz, $CDCl_3$, 25 °C): δ =112.2 (s) ppm].
[$PtCl_2$(1,5-COD)] (500 mg, 1.3 mmol) was added to this solution and the procedure described above for **1a** (method a) was followed. The workup gave **2a** as white crystals. (352 mg, 38%).

Method b: Complex **2a** was obtained as a white solid (137 mg, 70%) following the procedure described above for **1a** (method b), based on 100 mg of [$PtCl_2$(1,5-COD)] (0.27 mmol) and replacing 1,2-butanediol with 2,3-butanediol. $C_{28}H_{28}Cl_2O_2P_2Pt$: calcd. C 46.38, H 3.89%; found C 46.43, H 3.90%. IR: ν_a(Pt−Cl) 321; ν_s(Pt−Cl) 295 cm^{-1}. ^{1}H NMR (200 MHz, $CDCl_3$, 25 °C): δ = 1.2 (d, $^3J_{H,H}$ = 6.1 Hz, 6 H, -C*H*$_3$), 4.6 (m, 2 H, -C*H*OP), δ = 7.0−8.0 (m, 20 H, Ph) ppm. ^{31}P NMR (81.01 MHz, $CDCl_3$, 25 °C): δ = 90.4 ppm (s, $^1J_{PtP}$ = 4021 Hz).

Synthesis of 1b. Method a: The diphosphinite **1** was generated in THF (20 mL) from 1,2-butanediol (153 mg, 1.7 mmol), PPh_2Cl (0.64 mL, 3.5 mmol), and pyridine (3 mL) as described above for **1a**. Solid [$PdCl_2$(1,5-COD)] (495 mg, 1.7 mmol) was then added at room temperature with vigorous stirring. Within a few minutes, **1b** precipitated as a yellow solid. The crude product was filtered and washed with diethyl ether (572 mg, 53%). Recrystallization from dichloromethane/ethanol gave yellow crystals.

Method b: The intermediate complex **3b** was prepared in situ by adding a solution of PPh_2Cl (314 μL, 1.75 mmol) in 5 mL of THF dropwise to a second solution of [$PdCl_2$(1,5-COD)] (250 mg, 0.87 mmol) in THF (20 mL). When the complete formation of **3b** was confirmed by ^{31}P NMR spectroscopy (δ = 96 ppm), 1,2-butanediol (81 mg, 0.9 mmol) was added to give a pale yellow mixture. Within a few minutes **1b** began to precipitate as a yellow solid. Slow addition of diethyl ether completed the precipitation. The solid product was filtered off, washed with diethyl ether, and dried under vacuum. (409 mg, 74%). $C_{28}H_{28}Cl_2O_2P_2Pd$: calcd. C 52.85, H 4.44%; found C 53.02, H 4.58%. IR: ν_a(Pd−Cl) 315; ν_s(Pd−Cl) 290 cm^{-1}. ^{1}H NMR (200 MHz, $CDCl_3$, 25 °C): δ = 0.7 (t, $^3J_{H,H}$ = 6.1 Hz, 3 H, -C*H*$_3$), 1.7 (m, 2 H, -C*H*$_2$Me,), 4.1 (m, 2 H, -C*H*$_2$OP); 4.4 (m, 1 H, -C*H*OP), 7.0−8.0 (m, 20 H, Ph) ppm. ^{31}P NMR (81.01 MHz, $CDCl_3$, 25 °C): δ = P_a 119.1 (d), P_b 118.4 (d) ppm, $^2J_{PaPb}$ = 35.7 Hz.

Synthesis of 2b. Method a: Complex **2b** was prepared as a yellow crystalline solid (227 mg, 51%) from [$PdCl_2$(1,5-COD)] (200 mg, 0.7 mmol) and a solution where ligand **2** was generated from 2,3-butandiol (72 mg, 0.8 mmol) following the procedure described above for **1b**.

Method b: Complex **2b** was obtained also following the procedure described above for **1b** (method b), using 2,3-butanediol. Yield 74%. $C_{28}H_{28}Cl_2O_2P_2Pd$: calcd. C 52.85, H 4.44%; found C 52.31, H 4.57%. IR: ν_a(Pd−Cl) 311; ν_s(Pd−Cl) 299 cm^{-1}. ^1H NMR (200 MHz, $CDCl_3$, 25 °C): δ = 1.2 (d, $^3J_{H,H}$ = 6.1 Hz, 6 H, -CH_3), 4.5 (m, 2 H, -C*H*OP), 7.3−8.0 (m, 20 H, Ph) ppm. ^{31}P NMR (81.01 MHz, $CDCl_3$, 25 °C): δ = 118.5 (s) ppm.

Template Synthesis of Other Diphosphinites on Pt^{II}

Synthesis of 4a*: The intermediate complex $[PtCl_2(PPh_2Cl)_2]$ (**3a**; 1.1 mmol) was formed in THF and checked by NMR spectroscopy as described for the previous reactions.
(+)-Diisopropyl L-tartrate (232 μL, 1.1 mmol) dissolved in THF (5 mL) was then added to the reaction mixture. After 18 h the complete formation of **4a*** was detected by ^{31}P NMR spectroscopy. This solution was reduced to a volume of 5 mL and the product was precipitated with *n*-pentane, washed with the same solvent and dried under vacuum (716 mg, 75%). $C_{34}H_{36}Cl_2O_6P_2Pt$: calcd. C 47.00, H 4.15%; found C 47.30, H 4.10%. IR: ν(CO) 1745; ν_a(Pt−Cl) 302; ν_s(Pt−Cl) 292 cm^{-1}. ^1H NMR (200 MHz, $CDCl_3$, 25 °C): δ = 1.1 (dd, $^3J_{H,H}$ = 6 Hz, 12 H, -OCH(CH_3)$_2$], 4.7 (septet, $^3J_{H,H}$ = 6 Hz, 2H, −OC*H*(CH_3)$_2$], 5.2 (m, 2 H, -C*H*OP), 7.2−8.0 (m, 20 H, Ph) ppm. ^{31}P NMR (81.01 MHz, $CDCl_3$, 25 °C): δ = 94.7 (s, $^1J_{PtP}$ = 4003 Hz) ppm. $[\alpha]_D^{25}$ = −10.6 (*c* = 0.5, $CHCl_3$).

Synthesis of Complex 5a*: The intermediate complex $[PtCl_2(PPh_2Cl)_2]$ (**3a**; 0.77 mmol) was formed in THF and checked by NMR spectroscopy as described for the previous reactions. A solution of the phosphane-diol *R*-**I** (200 mg 0.77 mmol) in 5 mL of THF was then added to the reaction mixture and within 10 minutes a white solid began to precipitate. The addition of diethyl ether completed the precipitation of **5a***, which was filtered off, washed with diethyl ether and dried under vacuum. (404 mg, 74%). $C_{27}H_{26}Cl_2O_2P_2Pt{\cdot}C_2H_{10}O$: calcd. C 47.48, H 4.59%; found C 47.55, H 4.68%. IR: ν(OH) 3450; ν_a(Pt−Cl) 306; ν_s(Pt−Cl) 291 cm^{-1}. ^1H NMR (200 MHz, $CDCl_3$, 25 °C): δ = 1.2 (t, 6 H,), 2.6 (m, 2 H, -CH_2P), 3.5 (m, 7 H, OH + Et_2O + CH_2OH), 3.9 (m, 1 H, -C*H*OP), 7.5 (m, 20 H, Ph) ppm. ^{31}P NMR (81.01 MHz, $CDCl_3$, 25 °C): δ = P_a 84.7 (d, $^1J_{PtP}$ = 3858 Hz,), P_b −0.4 (d, $^1J_{PtP}$ = 3482 Hz) ppm, $^2J_{PaPb}$ = 17.7 Hz. $[\alpha]_D^{25}$ = +40.0 (*c* = 0.25, $CHCl_3$).

NMR Experiments

Hydrolysis of 3a and 3b: A solution of PPh_2Cl (300 μL, 1.67 mmol) in dry THF (20 mL) was added dropwise in 15 min to a second solution of $[PtCl_2(1,5\text{-COD})]$ (308 mg, 0.82 mmol) in 30 mL of THF containing 30 μL of water. The mixture was stirred at room temperature. The ^{31}P NMR analysis of an aliquot after two hours showed the formation of **3a** and **6** [δ = 71.1 ppm (s, $^1J_{PtP}$ = 4065 Hz)] in an approximate 1:1 ratio, which increased with time. After 18 h, the signal of **3a** had disappeared and **6** and **7** [δ = 50.5 ppm/s, $^1J_{PtP}$ = 4090 Hz)] were observed in a 2:1 ratio.
At this point, a reduction of the solution volume and the slow addition of diethyl ether induced the separation of a small amount of white crystals whose X-ray structure was determined.

In a similar way, when water (2 equiv.) was added to the palladium complex **3b**, generated in THF from PPh_2Cl (150 μL, 0.83 mmol) and $[PdCl_2(1,5\text{-COD})]$ (117 mg, 0.41 mmol), the ^{31}P NMR showed a mixture of species, the most abundant of which was represented by a singlet at δ = 78.1 ppm {$[Pd(\mu\text{-}Cl)(Ph_2POHOPPh_2)]_2$[9c]}.

Removal and Transfer of Ligand 1

$(Bu_4N)CN$ (4.5 equiv.; 33 mg, 0.121 mmol) was added to a $CDCl_3$ solution (0.8 mL) of **1a** (15 mg, 0.027 mmol) in a 5-mm screw-cap NMR tube. The progress of the reaction was monitored by ^{31}P NMR spectroscopy: within the time necessary for NMR acquisition the substitution of both the chlorides in **1a** with two cyanides was completed (P_a δ = 100.9 ppm, d, $^1J_{PPt}$ = 2815 Hz and P_b δ = 99.5 ppm, d, $^1J_{PPt}$ = 2834, $^2J_{PP}$ 19.6 Hz). The following decomposition of this dicyanide derivative into $[Pt(CN)_4]^{2-}$ and free ligand **1** occurred in about 30 minutes as denoted by the observation of the signals of **1** [δ = P_a 115.7 (s), P_b 111.5 (s) ppm] exclusively.
At this point, the addition of $[PdCl_2(COD)]$ (8.5 mg, 0.03 mmol) to the same NMR tube showed the immediate appearance of the signals of **1b**.

An analogous multi-step transmetallation process was performed by addition of an excess of solid $(Bu_4N)CN$ to a solution of the palladium complex **1b** (15 mg, 0.02 mmol) in 0.8 mL of $CDCl_3$, followed by $[PtCl_2(1,5\text{-COD})]$ (11 mg, 0.03 mmol). The final ^{31}P NMR spectrum showed the phosphinito-platinum complex **1a** to be the only phosphorus-containing species.

Removal of Ligand 5 from Platinum Complex 5a*

A sample of complex **5a*** (10 mg, 0.014 mmol) was dissolved in $CDCl_3$ and a ^{31}P NMR spectrum recorded. Solid $(Bu_4N)CN$ was progressively added to this solution. After the first addition of two equivalents (7.5 mg), a ^{31}P NMR spectrum consistent with the cyanide analogue of complex **5a*** was detected (dd, δ = 92 and −4.4 ppm, $^1J_{PPt}$ = 2716 and $^1J_{PPt}$ = 2398 Hz respectively, $^2J_{PP}$ = 25.6 Hz). Further addition of a large excess of $(Bu_4N)CN$ (5 equiv., 20 mg) produced the appearance of a new pattern showing two coupled doublets (δ = 111 and −23 ppm, $^4J_{PP}$ = 7 Hz), as expected for the phosphane-phosphinite-ol **5**.

X-ray Crystal Structure of 1a, 2b, 5a*, and 7: The crystal data were collected using a Nonius Kappa CCD diffractometer with graphite monochromatized Mo-K_α radiation and corrected for Lorentz, polarization and absorption (SORTAV)[19] effects. The structures were solved by direct and Fourier methods (SIR92)[20] and refined on F^2 (SHELXL-97)[21] using full-matrix least-squares with all non-H atoms anisotropic and hydrogen atoms at calculated positions, riding on their carrier atoms.

1a: $C_{28}H_{28}Cl_2O_2P_2Pt$, *M* = 724.43, *T* = 295 K, monoclinic, space group $P2_1/n$, *a* = 8.9098(2), *b* = 17.8502(4), *c* = 18.1605(4) Å, β = 103.749(1)°, *U* = 2805.5(1) Å^3, *Z* = 4, D_c = 1.715 g·cm^{-3}, μ = 53.269 cm^{-1}. Collected reflections = 18446 (θ ≤ 30°), unique reflections = 8130, R_{int} = 0.031, observed reflections = 6311 [$I \geq 2\sigma(I)$]. Final *R* (observed reflections) = 0.0335, R_w (all reflections) = 0.0659.

2b: $C_{28}H_{28}Cl_2O_2P_2Pd$, *M* = 635.74, *T* = 295 K, monoclinic, space group $P2_1/n$, *a* = 9.2571(2), *b* = 15.4091(3), *c* = 19.7280(4) Å, β = 90.248(1)°, *U* = 2814.0(1) Å^3, *Z* = 4, D_c = 1.501 g·cm^{-3}, μ = 9.865 cm^{-1}. Collected reflections = 18078 (θ ≤ 30°), unique reflections = 8135, R_{int} = 0.036, observed reflections = 6188 [$I \geq 2\sigma(I)$]. Final *R* (observed reflections) = 0.0347, R_w (all reflections) = 0.0845.

5a*: $C_{27}H_{26}Cl_2O_2P_2Pt{\cdot}C_4H_{10}O$, *M* = 784.53, *T* = 295 K, orthorhombic, space group $P2_12_12_1$, *a* = 8.0995(1), *b* = 18.0184(3), *c* = 21.9803(4) Å, *U* = 3207.8(1) Å^3, *Z* = 4, D_c = 1.624 g·cm^{-3}, μ = 46.702 cm^{-1}. Collected reflections = 16288 (θ ≤ 27°), unique reflections = 4850, R_{int} = 0.049, observed reflections = 4057 [$I \geq 2\sigma(I)$]. Flack parameter[22] = −0.02(4). Final *R* (observed reflections) = 0.0428, R_w (all reflections) = 0.1102.

7: $C_{48}H_{42}Cl_2O_4P_4Pt_2$, *M* = 1267.78, *T* = 150 K, triclinic, space group $P\bar{1}$, *a* = 11.9217(2), *b* = 13.3152(2), *c* = 16.1860(4) Å, α = 94.6411(7), β = 99.4177(7), γ = 115.3400(7)°, *U* = 2257.78(8) Å^3,

$Z = 2$, $D_c = 1.865\ g{\cdot}cm^{-3}$, $\mu = 64.935\ cm^{-1}$. Collected reflections = 28569 ($\theta \leq 28°$), unique reflections = 10307, R_{int} = 0.056, observed reflections = 8727 [$I \geq 2\sigma(I)$]. Both the hydrogens forming intramolecular hydrogen bonds O1−H···O2 and O4−H···O3 were refined isotropically. Final R (observed reflections) = 0.0362, R_w (all reflections) = 0.0928.

CCDC-189474, 189475, 189476, 189477 contain the supplementary crystallographic data for this paper. These data can be obtained free of charge at http://www.ccdc.cam.ac.uk/conts/retrieving.html [or from the Cambridge Crystallographic Data Centre, 12 Union Road, Cambridge CB2 1EZ, UK; fax: (internat.) +44−1223/336-033; Email:deposit@ccdc.cam.ac.uk].

[1] [1a] G. Zhu, X. Zhang, *J. Org. Chem.* **1998**, *63*, 3133−3136. [1b] N. Derrien, C. B. Dousson, S. M. Roberts, U. Berens, M. J. Burk, M. Ohff, *Tetrahedron: Asymmetry* **1999**, *10*, 3341−3352. [1c] V. I. Tararov, R. Kadyrov, T. H. Riemeier, J. Holz, A. Börner, *Tetrahedron: Asymmetry* **1999**, *10*, 4009−4015.

[2] H. Brunner, W. Zettlmeier, *Handbook of Enantioselective Catalysis with Transition Metal Compounds*, Vol I, VCH, Weinheim, **1993**.

[3] [3a] R. Selke, H. Pracejus, *J. Mol. Cat.* **1986**, *37*, 213−225. [3b] R. Selke, *J. Organomet. Chem.* **1989**, *370*, 241−248. [3c] R. Selke, *J. Organomet. Chem.* **1989**, *370*, 249−256. [3d] R. Selke, A. Kumar, G. Oehme, J. P. Roque, M. Schwarze, *Angew. Chem. Int. Ed. Engl.* **1994**, *33*, 2197−2199. [3e] Y. Chen, X. Li, S. Tong, M. C. K. Choi, A. S. C. Chan, *Tetrahedron Letters* **1999**, *40*, 957−960.

[4] [4a] T. V. RajanBabu, T. A. Ayers, A. L. Casalnuovo, *J. Am. Chem. Soc.* **1994**, *116*, 4101−4102. [4b] T. V. RajanBabu, T. A. Ayers, G. A. Halliday, K. K. You, J. C. Calabrese, *J. Org. Chem.* **1997**, *62*, 6012−6028. [4c] S. Shin, T. V. RajanBabu, *Org. Lett.* **1999**, *1*, 1229−1232. [4d] T. V. RajanBabu, Y. Yan, *J. Org. Chem.* **2000**, *65*, 900−906.

[5] [5a] S. Bolaño, J. Bravo, R. Carballo, S. Garcia-Fontan, U. Abram, E. M. Vasquez-Lopez, *Polyhedron* **1999**, *18*, 1431−1436. [5b] S. Bolaño, J. Bravo, S. Garcia-Fontan, *Inorg. Chim. Acta* **2001**, *315*, 81−87.

[6] T. H. Johnson, D. K. Pretzer, S. Thomen, V. J. K. Chaffin, G. Rangarajan, *J. Org. Chem.* **1979**, *44*, 1878−1879.

[7] Both 1,2 and 2,3-butanediol were used in racemic form.

[8] P. S. Pregosin, R. W. Kunz, *^{31}P and ^{13}C NMR of Transition Metal Phosphane Complexes*, Spriger-Verlag ed., **1979**, p. 25.

[9] [9a] K. R. Dixon, A. D. Rathray, *Can. J. Chem.* **1971**, *49*, 3997−4004. [9b] D. E. Berry, K. A. Beveridge, G. W. Bushnell, K. R. Dixon, *Can. J. Chem.* **1985**, *63*, 2949−2957. [9c] E. H. Wong, F. C. Bradley, *Inorg. Chem.* **1981**, *20*, 2333−2335.

[10] C. K. Johnson, *ORTEP II*, Report ORNL-5138, Oak Ridge National Laboratory, Oak Ridge, TN, **1976**.

[11] J. J. Pesek, W. R. Mason, *Inorg. Chem.* **1983**, *22*, 2958−2959.

[12] [12a] W. J. Kerr, G. G. Kirk, D. Middlemiss, *J. Organomet. Chem.* **1996**, *519*, 93−101. [12b] H. Brunner, H. Leyerer, *J. Organomet. Chem.* **1987**, *334*, 369−376. [12c] H. Brunner, T. Rückert, *Monatshefte für Chemie* **1998**, *129*, 339−354.

[13] [13a] S. O. Grim, W. L. Briggs, R. C. Barth, C. A. Tolman, J. P. Jesson, *Inorg. Chem.* **1974**, *13*, 1095−1100. [13b] D. Moulin, S. Bago, C. Bauduin, C. Darcel, S. Jugé, *Tetrahedron: Asymmetry* **2000**, *11*, 3939−3956.

[14] P. Gilli, V. Bertolasi, V. Ferretti, G. Gilli, *J. Am. Chem. Soc.* **1994**, *116*, 909−915.

[15] [15a] G. Annibale, P. Bergamini, V. Bertolasi, E. Besco, M. Cattabriga, R. Rossi, *Inorg. Chim. Acta* **2002**, *333*, 116−123. [15b] N. J. Goodwin, W. Henderson, B. K. Nicholson, *Inorg. Chim. Acta* **2002**, *335*, 113−118.

[16] [16a] C. Pasquier, S. Naili, A. Mortreux, F. Agbossou, L. Pelinski, J. Brocard, J. Eilers, I. Reiners, V. Peper, J. Martens, *Organometallics* **2000**, *19*, 5723−5732. [16b] E. A. Broger, W. Burkart, M. Henning, M. Scalone, R. Schmid, *Tetrahedron: Asymmetry* **1998**, *9*, 4043−4054. [16c] H. J. Kreuzfeld, C. Döbler, *J. Mol. Cat.* **1998**, *136*, 105−110. [16d] H. J. Kreuzfeld, C. Döbler, U. Schmidt, H. W. Krause, *Tetrahedron: Asymmetry* **1996**, *7*, 1011−1018. [16e] D. Moulin, C. Darcel, S. Jugé, *Tetrahedron: Asymmetry* **1999**, *10*, 4729−4743.

[17] J. X. Mc Dermott, J. F. White, G. M. Whitesides, *J. Am. Chem. Soc.* **1976**, *98*, 6521−6528.

[18] D. Drew, J. R. Doyle, *Inorg. Synth.* **1972**, *13*, 47−55.

[19] R. H. Blessing, *Acta Crystallogr., Sect. A* **1995**, *51*, 33−38.

[20] *SIR92:* A. Altomare, G. Cascarano, C. Giacovazzo, A. Guagliardi, M. C. Burla, G. Polidori, M. Camalli, *J. Appl. Crystallogr.* **1994**, *27*, 435−436.

[21] G. M. Sheldrick, SHELX-97, *Program for Crystal Structure Refinement*, University of Göttingen, Germany, **1997**.

[22] H. D. Flack, *Acta Crystallogr., Sect. A* **1983**, *39*, 876−881.

Received July 30, 2002
[I02340]

Di- and Trivalent Ytterbium Complexes Containing Linked Amino- and Amidocyclopentadienyl Ligands

Alexander T. Trifonov,[a] Thomas P. Spaniol,[a] and Jun Okuda*[a]

Keywords: Ytterbium / Chelates / Metallocenes / Cyclopentadienyl ligands

Reactions of the aminocyclopentadienes $(C_5Me_4H)SiMe_2NHR$ (R = Et, allyl, *n*Pr, *t*Bu) with $[YbI_2(THF)_2]$ in the presence of two equivalents of potassium 1,2-diphenylethenide in THF at room temperature gave the diamagnetic half-sandwich complexes $[Yb(\eta^5\text{-}C_5Me_4SiMe_2NHR)L_n(\mu\text{-}I)]_2$ (L = THF, *n* = 2, L = DME, *n* = 1). The *tert*-butylamido derivative $[Yb(\eta^5\text{-}C_5Me_4SiMe_2NHtBu)(THF)_2(\mu\text{-}I)]_2$ was characterized by X-ray structural analysis as a dinuclear complex containing a nonchelating aminocyclopentadienyl ligand. Deprotonation of the aminocyclopentadiene $(C_5H_4tBu)SiMe_2NHtBu$ with two equivalents of potassium 1,2-diphenylethenide in THF, followed by reaction with $[YbI_2(THF)_2]$ at 60 °C, gave the trivalent ytterbium ate complex $[K(DME)][Yb\{(\eta^5{:}\eta^1\text{-}C_5H_3tBu\text{-}3)SiMe_2NtBu\}_2]$. A single crystal X-ray diffraction study of this complex shows polymeric chains consisting of trivalent ytterbocene units with two chelating amidocyclopentadienyl ligands coordinated to potassium ions. Metalation of the aminoindene $(C_9H_7)SiMe_2NHtBu$ under the same conditions and treatment with $[YbI_2(THF)_2]$ in THF at ambient temperature resulted in the formation of the divalent ytterbocene complex $[Yb\{\eta^5\text{-}(1\text{-}C_9H_6)SiMe_2NHtBu\}_2(THF)_2]$. The reaction of ytterbium naphthalenide $[Yb(C_{10}H_8)(THF)_2]$ with one equivalent of $(C_9H_7)SiMe_2NHtBu$ afforded the bis(indenyl) compound which was isolated as its 2,2′-bipyridyl adduct $[Yb\{\eta^5\text{-}(1\text{-}C_9H_6)SiMe_2NHtBu\}_2(bipy)]$. It was shown by single-crystal structural analysis to exhibit a bent metallocene structure with noncoordinating amino side-chains. The reaction of $(C_5Me_4H)CH_2SiMe_2NHtBu$, which contains a longer CH_2SiMe_2 bridge, with $[Yb(C_{10}H_8)(THF)_2]$ gave the complex $[Li_{0.5}][Yb(\mu\text{-}\eta^5{:}\eta^1\text{-}C_5Me_4CH_2SiMe_2NtBu)(THF)_2(\mu\text{-}I)_{0.5}]$. Single crystal X-ray structure analysis revealed the presence of polymeric chains consisting of dinuclear iodo-bridged $[Yb(\eta^5{:}\eta^1\text{-}C_5Me_4CH_2SiMe_2NtBu)]$ units with a chelating linked amidocyclopentadienyl ligand, intermolecularly bridged by lithium ions. The lithium ions are bonded in an η^5-manner to both units, forming a lithocene structure. When $YbCl_3$ was reacted with $Li_2[(C_5H_3tBu\text{-}3)SiMe_2NCH_2CH_2X]$ (X = NMe_2, OMe), heterobimetallic complexes $Li[Yb\{(\eta^5{:}\eta^1\text{-}C_5H_3tBu\text{-}3)SiMe_2NCH_2CH_2X\}_2]$ with a helical metallocene structure were isolated. The single crystal structure analysis of one of the three possible diastereomers of $Li\{Yb[(\eta^5{:}\eta^1\text{-}C_5H_3tBu\text{-}3)SiMe_2NCH_2CH_2NMe_2]_2\}$, viz. the thermodynamically stable (*R*,*R*)/(*S*,*S*) epimer was performed. When $YbCl_3$ was reacted with one equivalent of $Li_2[(C_5H_3tBu\text{-}3)SiMe_2NCH_2CH_2NMe_2]$ and reduced "in situ" with one equivalent of sodium 1,2-diphenylethenide in THF, the ytterbium(II) metallocene complex $[Li(THF)]_2[Yb\{(\eta^5\text{-}C_5H_3tBu\text{-}3)\text{-}SiMe_2NH(CH_2CH_2NMe_2)\}_2(\mu\text{-}Cl)_2]$ was isolated, which exhibits a structure with the two amino functions coordinating to the lithium ions and the chloro ligands bridging both the lithium and ytterbium centers.

(© Wiley-VCH Verlag GmbH & Co. KGaA, 69451 Weinheim, Germany, 2003)

Introduction

In contrast to the organometallic chemistry of divalent samarium,[1] that of divalent ytterbium is less developed.[2] In the context of developing lanthanide complexes supported by a linked amidocyclopentadienyl ligand,[3] we have started to explore the synthetic access to complexes of divalent ytterbium. Ytterbium(II) is diamagnetic, thus amenable to NMR spectroscopy, and its large ionic radius (1.02 Å, coordination number 6[4]) should allow coordination of the $SiMe_2$-linked amidocyclopentadienyl ligand for the larger lanthanides.[5] The tendency of divalent ytterbium complexes to undergo facile ligand-exchange reactions in solution to form homoleptic derivatives[6] makes linked amidocyclopentadienyl ligands an attractive ligand system that provides access to half-sandwich-type ytterbium(II) derivatives.[2c] We describe here our attempts at coordinating a linked amidocyclopentadienyl ligand to a divalent ytterbium center. During the course of our work, Hou et al. have independently reported the synthesis of linked anilidocyclopentadienyl lanthanide(II) complexes $[Ln(\eta^5{:}\eta^1\text{-}C_5Me_4SiMe_2NPh)(THF)_n]$ (Ln = Sm, Yb, *n* = 0−3) and $[Yb(\eta^5{:}\eta^1\text{-}C_5Me_4SiMe_2NPh)(THF)]_2$ by the amine elimination reaction of $[Ln\{N(SiMe_3)_2\}_2(THF)_2]$ and $(C_5Me_4H)SiMe_2NHPh$.[7]

Results and Discussion

In order to prepare complexes of divalent ytterbium containing a linked amidocyclopentadienyl ligand, the meta-

[a] Institut für Anorganische Chemie und Analytische Chemie, Universität Mainz,
Duesbergweg 10−14, 55099 Mainz, Germany

thesis of the dilithium derivatives $Li_2(C_5Me_4SiMe_2NtBu)$ and $Li_2[(C_5H_3tBu\text{-}3)SiMe_2NCH_2CH_2NMe_2]$ with $[YbI_2(THF)_2]$ in THF or toluene was first explored, but no tractable products could be isolated. Moreover, all attempts to prepare dipotassium derivatives of the ligand system,[8] for example by exchange reaction of the dilithium derivatives with two equivalents of KO*t*Bu in hexane or toluene, were also unsuccessful. The complete double metalation of the aminocyclopentadienes $(C_5Me_4H)SiMe_2NHR$ (R = Et, allyl, *n*Pr, *t*Bu) was achieved by reaction with two equivalents of potassium 1,2-diphenylethenide in THF at room temperature, as indicated by the disappearance of the characteristic color of the radical anion $[PhCHCHPh]^{\cdot -}$ upon addition of the aminocyclopentadiene. When these "in-situ" prepared dipotassium derivatives were reacted with $[YbI_2(THF)_2]$ in THF, the half-sandwich iodide complexes $[Yb(\eta^5\text{-}C_5Me_4SiMe_2NHR)L_n(\mu\text{-}I)]_2$ (**1**, R = *t*Bu, L = THF, *n* = 2; **2**, R = *n*Pr, L = THF, *n* = 2; **3,** R = Et, L = DME, *n* = 1; **4,** R = allyl, L = DME, *n* = 1) were obtained in good yields as yellow to orange crystals, after filtration and recrystallization from THF/hexane or DME.

The diamagnetic[9] complexes **1**–**4** are soluble in THF, DME, and pyridine, but insoluble in aliphatic and aromatic hydrocarbons. Bright-yellow crystals of **1** suitable for X-ray diffraction analysis were obtained by cooling a concentrated THF/hexane solution to 0 °C. An ORTEP diagram of the structure of **1** is shown in Figure 1. The crystal and structure refinement data are compiled in Table 1. The crystal structure determination revealed **1** to be a centrosymmetric iodo-bridged dimer with *trans*-disposed aminocyclopentadienyl ligands, similar to the structure adopted by its pentamethylcyclopentadienyl analogue $[Yb(\eta^5\text{-}C_5Me_5)(THF)_2(\mu\text{-}I)]_2$.[10] Each ytterbium center is coordinated to an η^5-cyclopentadienyl ring, two bridging iodides and two THF ligands. The pendant amino groups are not coordinated. The value of the Yb-Cp_{Cent} distance in **1** [2.412(6) Å]

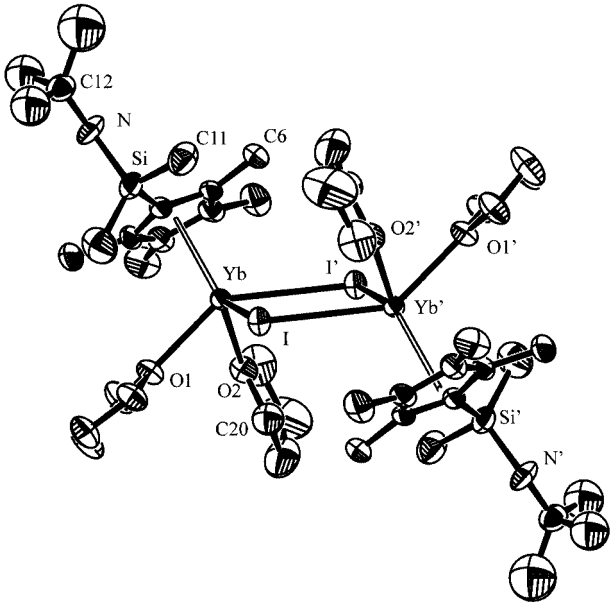

Figure 1. ORTEP drawing and numbering scheme of the molecular structure of **1** with thermal ellipsoids drawn at the 30% probability level; hydrogen atoms are omitted for the sake of clarity; selected bond lengths (Å) and bond angles (°): Yb–O2 2.434(5), Yb–O1 2.486(4), Yb-C2 2.664(6), Yb–C3 2.680(6), Yb–C1 2.681(7), Yb–C4 2.722(6), Yb–C5 2.723(7), Yb–Cp_{cent} 2.412(6), Yb–I 3.0985(5), Yb–I′ 3.3008(5); O2–Yb–O1 75.3(2), O2–Yb–I 116.9(1), O1–Yb–I 88.1(1), O2–Yb–I′ 77.5(1), O1–Yb–I′ 140.8(1), I–Yb–I′ 79.69(1)

Table 1. Crystallographic and refinement parameters for complexes **1**, **5**, and **7**

Compound	**1**	**5**	**7**
Chemical formula	$C_{23}H_{43}INO_2SiYb$	$C_{34}H_{64}KN_2O_2Si_2Yb$	$C_{40}H_{52}N_4Si_2Yb$
M [g mol^{-1}]	693.61	801.19	818.08
Crystal system	triclinic	orthorhombic	orthorhombic
Space group	$P\bar{1}$ (No. 2)	*Pccn* (No. 56)	$P2_12_12_1$ (No.19)
Crystal size [mm]	0.65 × 0.55 ×0.53	1.10 × 0.70 × 0.29	0.88 × 0.62 × 0.48
a [Å]	9.1196(4)	9.5770(7)	12.586(1)
b [Å]	10.6554(9)	19.1900(10)	17.388(1)
c [Å]	15.370(1)	22.372(2)	18.831(2)
α [deg]	92.542(6)	90	90
β [deg]	105.143(4)	90	90
γ [deg]	99.724(5)	90	90
V [Å^3]	1414.8(2)	4111.6(5)	4121.1(6)
Z	2	4	4
$\rho_{calcd.}$ [g cm^{-3}]	1.628	1.294	1.319
F(000)	682	1660	1672
μ(Mo-K_α) [mm^{-1}]	4.455	2.462	2.358
T [K]	296(2)	296(2)	293(2)
2θ range [°]	3–28	3–28	3–29.5
N, N_0	8082, 6765	7922, 4935	39793, 10827
$R_{int.}$	0.0319	0.0419	0.0359
No. of parameters	263	206	410
GOF	0.856	1.001	1.067
R, R_w (observed data)	0.0393, 0.1110	0.0560, 0.1261	0.0337, 0.0827
R,R_w (all data)	0.0581, 0.1241	0.1322, 0.1538	0.0446, 0.0885

is very close to that previously observed for the related complex $[Yb(\eta^5\text{-}C_5Me_5)(THF)_2(\mu\text{-}I)]_2$,[10] but somewhat shorter than the comparable distance in the mononuclear complex $[Yb\{\eta^5{:}\eta^1\text{-}C_5H_3(CH_2CH_2NMe_2)_2\}I(THF)_2]$.[11] The Yb−O bond lengths fall into the range normally observed for derivatives of divalent ytterbium.[12] Significant differences in the Yb−I and Yb−I′ bond lengths have been found for **1** [3.0985(5) and 3.3008(5) Å respectively]. The shorter Yb−I distance is similar to the values previously observed for related dimeric Yb^{II} complexes,[10,13] but the Yb−I′ distance appears to be very long. The I−Yb−I′ bond angle in **1** is significantly smaller than that in the C_5Me_5 analogue.[10] The structures of (cyclopentadienyl)-iodo complexes of divalent ytterbium are known to be influenced by the nature of both the η^5-bonded carbocyclic ligands and the Lewis base: some of them are dimeric $\{[Yb(\eta^5\text{-}C_5Me_5)L_2(\mu\text{-}I)]_2$ (L = THF, DME)[10]$\}$, while others are monomeric in the solid state ($[Yb(\eta^5\text{-}C_9H_7)I(DME)]$,[6a] $[Yb\{\eta^5{:}\eta^1\text{-}C_5H_3(CH_2CH_2NMe_2)_2\}I(THF)_2]$[11]).

The ^1H and ^{13}C NMR spectra of **1**−**4** in [D$_5$]pyridine at room temperature indicate complete dissociation of the THF or DME molecules, as their signals appear at the positions of the free ligands. All signals of the aminocyclopentadienyl ligands give rise to two sets of signals. The nearly constant intensity ratio for all pairs of signals of a given complex varies with the amino substituent: for **1** the signals are of approximately equal intensities, while for the complexes **2**−**4** the ratios are in the range of 1:2.0−2.6. This finding can be explained by the partial dissociation of the dimeric complex $[Yb(\eta^5\text{-}C_5Me_4SiMe_2NHR)L_2(\mu\text{-}I)]_2$ in pyridine into mononuclear species $[Yb(\eta^5\text{-}C_5Me_4SiMe_2NHR)I(py)_3]$ (Scheme 1). This behavior is in agreement with the unsymmetric structure of the Yb_2I_2 core in the crystal structure of **1**. Absorption bands in the region of 3370−3390 cm^{-1} in the IR spectra of the complexes **1**−**4** indicate the presence of NH groups. Since *trans*-stilbene has been isolated from the reaction mixtures in almost quantitative yield, THF can regarded as the only source for the proton abstraction.

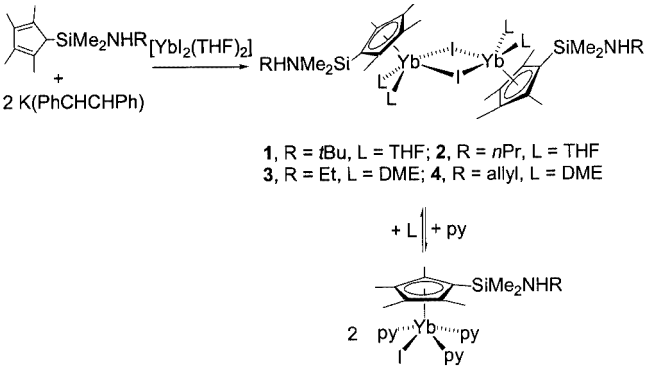

Scheme 1

Temperature was found to have an important influence on the above-mentioned complexation reaction, giving different types of products (Scheme 2). When the aminocyclopentadiene $(C_5H_4tBu)SiMe_2NHtBu$ was deprotonated with two equivalents of potassium 1,2-diphenylethenide in THF and then reacted with $[YbI_2(THF)_2]$ at 60 °C, an ate complex of trivalent ytterbium $[K(DME)][Yb\{(\eta^5{:}\eta^1\text{-}C_5H_3tBu\text{-}3)SiMe_2NtBu\}_2]$ (**5**) was obtained as orange, paramagnetic crystals after recrystallization from DME. The absence of any absorption bands for the NH group in the IR spectrum of **5** indicates coordination of the amido group to the ytterbium atom.

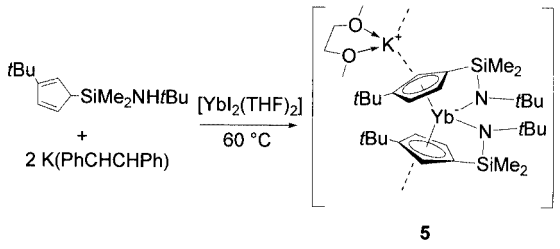

Scheme 2

Orange crystals of **5** suitable for X-ray diffraction analysis were obtained by slow diffusion of hexane into the DME solution at room temperature. An ORTEP diagram of the structure is shown in Figure 2. The compound crystallizes in a polymeric chain structure; crystal structure and refinement data are compiled in Table 1. X-ray diffraction study of **5** shows a polymeric chain consisting of anionic ytterbium(III) metallocene units bridged by $[K(DME)]^+$ ions. The Yb^{III} center is coordinated to two chelating amidocyclopentadienyl ligands to form an anionic metallocene unit with both pendant amido groups coordinated to the ytterbium. The thermodynamically favored (*R*,*R*)/(*S*,*S*) diastereomer is observed. The Yb−C bond lengths in **5** are remarkably scattered [2.571(7) for Yb−C(1) to 2.963(8) Å for Yb−C(3)]. The bond lengths Yb−C(1), Yb−C(2),

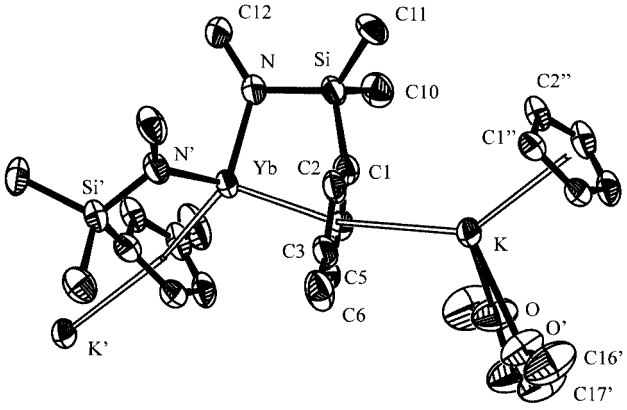

Figure 2. ORTEP drawing and numbering scheme of the molecular structure of **5** with thermal ellipsoids drawn at the 30% probability level; hydrogen atoms as well as the methyl carbon atoms of the *t*Bu groups are omitted for the sake of clarity; selected bond lengths (Å) and bond angles (°): Yb−N 2.237(6), Yb−N′ 2.237(6), Yb−C1 2.571(7), Yb−C5 2.673(7), Yb−C2 2.689(8), Yb−C4 2.908(7), Yb−C3 2.963(8), K−O 2.766(6), K−O′ 2.766(6), K−C1 3.083(7), K−C2 3.062(8), K−C3 3.148(7), K−C5 3.183(7), K−C4 3.225(8), C1−C5 1.39(1), C1−C2 1.42(1), C2−C3 1.40(1), C3−C4 1.38(1), C4−C5 1.40(1); N−Yb−N′ 106.6(3), Cp_{cent1}−Yb−Cp_{cent2} 114.5(3)

Yb−C(5) are slightly longer than those in the Yb^{III} complex $[Yb(\eta^5{:}\eta^1\text{-}C_5Me_4SiMe_2N\textit{t}Bu)(THF)(\mu\text{-}H)]_2$ [3c] and are similar to the values of Yb−C bonds in other bis(cyclopentadienyl)ytterbium(III) complexes.[14] The Yb−C(3) and Yb−C(4) distances are extremely long indicating a significant ring slippage toward η^3-bonding. Such an approach to η^3-coordination is well documented for fluorenyl complexes of the lanthanides.[15] This bonding situation can be explained by the strain resulting from the repulsion of the bulky *t*Bu groups in the cyclopentadienyl ring and those of the amido group. The $Cp_{Cent1}-Yb-Cp_{Cent2}$ bond angle in **5** [114(1)°] is smaller than the values previously described for bis(cyclopentadienyl) complexes of trivalent ytterbium, which normally fall into the range 127−143°.[14,16] The Yb−N distance in **5** is very close to that previously reported for $[Yb(\eta^5{:}\eta^1\text{-}C_5Me_4SiMe_2N\textit{t}Bu)(THF)(\mu\text{-}H)]_2$ [3c] and is similar to values observed for the Yb^{II} complexes $[Yb(\eta^5{:}\eta^1\text{-}C_5Me_4SiMe_2NPh)(THF)]_n$ and $[Yb(\eta^5{:}\eta^1\text{-}C_5Me_4SiMe_2NPh)(THF)]_2$,[7a] accounting for the difference of ionic radii of Yb^{II} and Yb^{III}.[4] The potassium ion is coordinated to one molecule of DME. The potassium-ring distances are in the range of 3.083(7)−3.225(8) Å and are slightly longer than those reported for $[K(py)_2](C_5Me_5)$[17a] and $K[C_5H_4(SiMe_3)]$.[17b] This finding may indicate a more pronounced ionic interaction of the potassium ions with the metallocene ate units. The oxidation of Yb^{II} to Yb^{III} at elevated temperature cannot be satisfactorily explained at this time. We believe, however, that the stability of the bis(chelate) is higher for the monoanionic Yb^{III} species than for the dianionic Yb^{II} complex.

Metalation of the aminoindene $(C_9H_7)SiMe_2N\textit{H}tBu$ under the same conditions and treatment with $[YbI_2(THF)_2]$ in THF at ambient temperature resulted in the Yb^{II} compound $[Yb\{\eta^5\text{-}(1\text{-}C_9H_6)SiMe_2N\textit{H}tBu\}_2(THF)_2]$ (**6**; Scheme 3). Complex **6** was isolated as highly sensitive ruby-red crystals, soluble in THF, DME and aromatic hydrocarbons but insoluble in hexane.

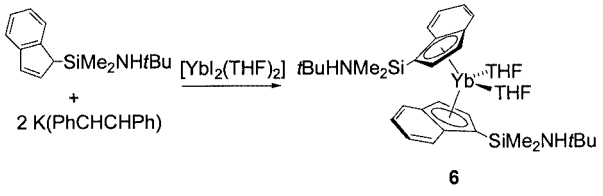

Scheme 3

In the ^1H NMR spectrum of **6** in $[D_6]$benzene the methyl protons of the $SiMe_2$ groups appear as two singlets. The signals in each pair are of equal intensities and the ratio of intensities of the couples is 3:2. The *t*Bu protons are recorded as two singlets in the same ratio as the sets of the $SiMe_2$ protons. All indenyl protons are inequivalent due to the planar chirality, giving rise to six signals. The fact that signals corresponding to the THF molecules are somewhat broadened and high-field shifted (δ = 1.25 and 3.05 ppm for β- and α-CH_2) confirms their coordination to the ytterbium atom in benzene solution. The ^1H and ^{13}C NMR spectra of **6** apparently reflect the presence of rotational isomers in solution, as has previously been reported for the indenyl-derived ytterbocenes $[Yb\{\eta^5\text{-}(C_9H_6\text{-}1\text{-}SiHR_2\text{-}2\text{-}R')\}_2(L)_2]$ (R = Me, Ph, R′ = donor ligand).[18]

Ytterbium naphthalenide $[Yb(C_{10}H_8)(THF)_2]$[19a] has been shown to be a convenient precursor for the synthesis of various types of both di- and trivalent organoytterbium compounds.[19] The reactions of $[Yb(C_{10}H_8)(THF)_2]$ with aminocyclopentadienes $(C_5Me_4H)SiMe_2NHR$ (R = Me, Et, allyl, *n*Pr, *i*Pr, *t*Bu) and $(C_5H_5\textit{t}Bu)SiMe_2N\textit{H}tBu$ in THF or DME at room temperature result in the isolation of yellow-orange powders (Scheme 4). These compounds are diamagnetic, corresponding to the Yb^{II} oxidation state; ^1H, ^{13}C NMR and IR spectra show the presence of the aminocyclopentadiene ligands in deprotonated form. However microanalysis failed to give reproducible data and all attempts to obtain samples suitable for X-ray crystal structure analysis failed. Reaction of one equivalent of $(C_9H_7)SiMe_2N\textit{H}tBu$ with $[Yb(C_{10}H_8)(THF)_2]$ resulted in the ytterbocene $[Yb\{\eta^5\text{-}(1\text{-}C_9H_6)SiMe_2N\textit{H}tBu\}_2(THF)_2]$ which was isolated in crystalline form as a complex with 2,2′-bipyridyl $[Yb\{\eta^5\text{-}(1\text{-}C_9H_6)SiMe_2N\textit{H}tBu\}_2(bipy)]$ (**7**). Complex **7** is soluble in THF, DME and pyridine, sparingly soluble in toluene and insoluble in hexane.

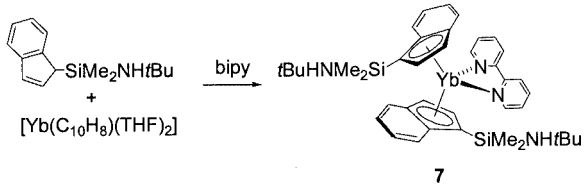

Scheme 4

Black crystals suitable for X-ray diffraction analysis were obtained by slow evaporation of a THF/toluene/hexane solution at room temperature. An ORTEP diagram of the structure of **7** is shown in Figure 3. The crystal and structure refinement data are compiled in Table 1. Single-crystal structural analysis shows that complex **7** adopts a bent metallocene structure with noncoordinating amino side chains and one coordinated 2,2′-bipyridyl ligand. The average value of the Yb−C bond lengths is 2.72 Å. The $Yb-Ind_{Cent}$ bond lengths are 2.440(8) and 2.449(11) Å, and are similar to values for other bis(indenyl) complexes of divalent ytterbium.[20] The bond angle $Ind_{cent}-Yb-Ind_{cent}$ in **7** is slightly larger [132(1)°] than those in complexes $[Yb(\eta^5\text{-}C_9H_7)_2(THF)_2]$ [128.6[20a] and 129.31(5)[20b]] probably due to a lower steric strain resulting from the coordination of a planar 2,2′-bipyridyl ligand instead of two THF molecules. The Yb−N distances [2.454(3) and 2.476(4) Å] are close to those reported for the complex $[YbI(bipy)_2(DME)_2]$.[21]

In the ^1H NMR spectra of **7** in $[D_8]$THF the protons of the $SiMe_2$ groups give rise to four singlets of equal intensity, the *t*Bu protons are recorded as two singlets (1:1 ratio) and the indenyl protons appear as a complex set of six multiplets of different intensities (12 protons together). The bipyridyl protons are observed as a set of eight significantly broadened signals of different intensities.[22] This is probably due to the exchange of bipyridyl by THF within the

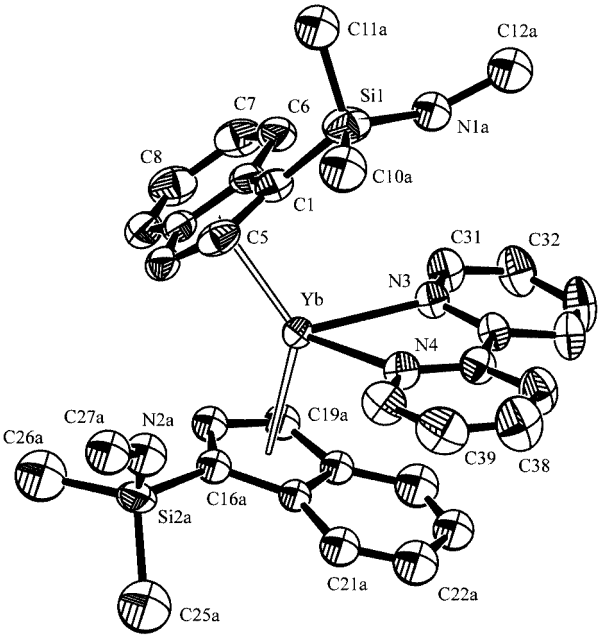

Figure 3. ORTEP drawing and numbering scheme of the molecular structure of **7** with thermal ellipsoids drawn at the 30% probability level; hydrogen atoms as well as the methyl carbon atoms of the *t*Bu groups are omitted for the sake of clarity; for the distorted groups, only one of the two split positions are shown; selected bond lengths (Å) and bond angles (°): Yb-Ind_{cent} 2.440(8), 2.45(1), Yb−C1 2.760(4), Yb−C2 2.755(4), Y−C3 2.722(4), Y−C4 2.680(4), Y−C5 2.695(4), Y−C16A 2.71(1), Y−C17A 2.77(1), Y−C18A 2.79(1), Y−C19A 2.69(1), Y−C20A 2.69(1), Yb−N3 2.454(3), Yb−N4 2.476(4); Ind_{cent}−Yb−Ind_{cent} 132.1(3), N3−Yb−N4 66.1(1)

coordination sphere of ytterbium. The ^1H and ^{13}C NMR spectra of **7** display nonequivalence of the indenyl ligands as a consequence of either chirality or the presence of two rotational isomers in the [D_8]THF solution.

The reaction of $(C_5Me_4H)CH_2SiMe_2NHtBu$[23] with $[Yb(C_{10}H_8)(THF)_2]$ was carried out in THF. Cooling of the THF/hexane mixture at 0 °C produced yellow crystals of the composition $[Li_{0.5}][Yb(\mu\text{-}\eta^5{:}\eta^1\text{-}C_5Me_4CH_2SiMe_2N tBu)(THF)_2(\mu\text{-}I)_{0.5}]$ (**8**; Scheme 5). $[Yb(C_{10}H_8)(THF)_2]$ has been shown to contain an admixture of LiI,[19] and the reaction in the presence of LiI gave complex **8**. It is soluble in THF and DME and insoluble in aromatic and aliphatic hydrocarbons. In the ^1H NMR spectrum of **8** in [D_5]pyridine the protons of the $SiMe_2$, *t*Bu, and CH_2 groups appear as singlets, and the methyl groups of the C_5Me_4 ring give rise to two singlets. The chemical shifts of the signals of the α- and β-methylene protons of THF

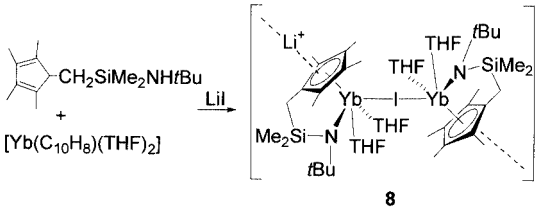

Scheme 5

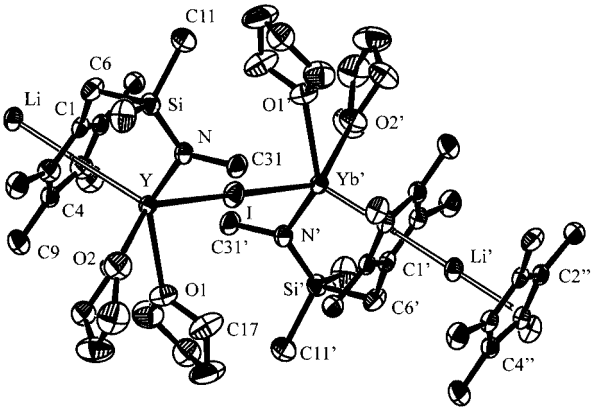

Figure 4. ORTEP drawing and numbering scheme of the molecular structure of **8** with thermal ellipsoids drawn at the 30% probability level; hydrogen atoms as well as the methyl carbon atoms of the *t*Bu groups are omitted for the sake of clarity; selected bond lengths (Å) and bond angles (°): Yb−Cp_{cent} 2.45(3), Yb−C1 2.697(3), Yb−C2 2.713(3), Yb−C3 2.770(3), Yb−C4 2.775(3), Yb−C5 2.740(3), Yb−N 2.356(3), Yb−O1 2.559(3), Yb−O2 2.545(3), Yb−I 3.295(1), Li−C1 2.292(3), Li−C2 2.275(3), Li−C3 2.255(3), Li−C4 2.251(4), Li−C5 2.265(3); Cp_{cent}−Yb−I 106.1(1), Cp_{cent}−Yb−N 104.4(1), Cp_{cent}−Yb−O1 118.8(1), Cp_{cent}−Yb−O2 104.8(1)

molecules and their well-resolved structure indicate THF dissociation in pyridine solution.

Yellow crystals suitable for X-ray diffraction analysis were obtained by recrystallization of **8** from a THF/hexane mixture at 0 °C. An ORTEP diagram of the structure of **8** is shown in Figure 4. The compound crystallizes in a polymeric chain structure; crystal and structure refinement data are compiled in Table 2. Complex **8** exhibits the unusual

Table 2. Crystallographic and refinement parameters for complexes **8** and **9**

Compound	**8**	**9**
Chemical formula	$C_{24}H_{45}I_{0.5}Li_{0.5}NO_2SiYb$	$C_{30}H_{56}LiN_4Si_2Yb$
M [g mol^{-1}]	647.66	708.95
Crystal system	triclinic	monoclinic
Space group	$P\bar{1}$ (No. 2)	$C2/c$ (No. 15)
Crystal size [mm]	0.74 × 0.13 × 0.09	0.55 × 0.53 × 0.45
a [Å]	10.589(4)	11.5816(9)
b [Å]	11.877((5)	16.327(1)
c [Å]	12.316(5)	18.393(2)
α [deg]	85.990(6)	90
β [deg]	66.808(6)	94.207(7)
γ [deg]	87.279(6)	90
V [Å^3]	1420(1)	3468.6(5)
Z	2	4
$\rho_{calcd.}$ [g cm^{-3}]	1.515	1.358
$F(000)$	648	1460
μ(Mo-K_α) [mm^{-1}]	3.897	2.789
T [K]	296(2)	296(2)
2θ range [°]	3−29	3−29
N, N_0	12826, 6838	9641, 4590
$R_{int.}$	0.0247	0.0252
No. of parameters	387	221
GOF	0.987	1.055
R, R_w (observed data)	0.0273, 0.0634	0.0364, 0.0852
R,R_w (all data)	0.0344, 0.0660	0.0516, 0.0904

structure of an "inverted" sandwich complex. The Yb^{II} ion is coordinated to the linked amidocyclopentadienyl group, the bridging iodo, and two THF ligands, giving a distorted square-pyramidal coordination geometry. The iodine atom bridges two ytterbium atoms of the neighboring molecules, while the lithium ions connect the cyclopentadienyl ligands, forming zigzag chains. Both the ytterbium and lithium ions are symmetrically η^5-bonded to the tetramethylcyclopentadienyl ligand. The average Yb−C bond length in **9** is slightly longer than those in complexes $[Yb(\eta^5\text{-}C_5Me_5)I(L)_n]_2$ [10] and $[Yb(\eta^5{:}\eta^1\text{-}C_5Me_4SiMe_2NPh)(THF)]_2$.[7a] The Li−C contacts are similar to those found in lithium complexes of substituted η^5-cyclopentadienyls.[24] The Yb−N bond length in **8** [2.356(3) Å] is close to that in $[Yb(\eta^5{:}\eta^1\text{-}C_5Me_4SiMe_2NPh)(THF)]_2$.[7a] The Yb−I bond length [3.295(1) Å] is slightly longer than the value reported for the monomeric complex $[Yb\{\eta^5{:}\eta^1{:}\eta^1\text{-}C_5H_3(CH_2CH_2NMe_2)_2\}I(THF)_2]$[11] and significantly longer than that in the dimeric complexes $[Yb(\eta^5\text{-}C_5Me_5)I(L)_n]_2$ [10] and $[Yb\{C(SiMe_3)_3\}I(OEt_2)]_2$.[13]

Recently we have shown that reactions of yttrium and lutetium chlorides with dilithium derivatives of tridentate amidocyclopentadienyl ligands result in the formation of chiral lanthanocene complexes with a unique heterobimetallic core.[25] Ytterbium trichloride reacted with $Li_2[(C_5H_3t\text{Bu-}3)SiMe_2NCH_2CH_2X]$ (X = NMe_2, OMe) in THF or DME regardless of the reagent ratio, solvent, and the isolation method, to give heterobimetallic complexes $Li[Yb\{\eta^5{:}\eta^1\text{-}C_5H_3t\text{Bu-}3)SiMe_2NCH_2CH_2X\}_2]$ (X = NMe_2, **9**; OMe, **10**) with a helical metallocene structure (Scheme 6). Complexes **9** and **10** are soluble in THF, DME and toluene and have been characterized by IR spectroscopy as well as microanalysis.

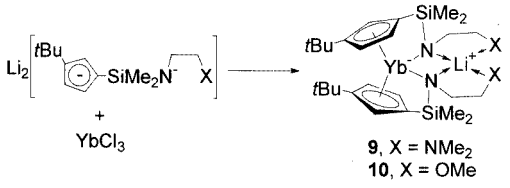

Scheme 6

Yellow crystals of **9** suitable for X-ray diffraction analysis were obtained by recrystallization from toluene at −30 °C. An ORTEP diagram of the structure of **9** is shown in Figure 5. The crystal and structure refinement data are compiled in Table 2. The single crystal structure analysis of one of the three possible diastereomers of **9**, viz. the thermodynamically stable (*R*,*R*) or (*S*,*S*) epimer, was performed and confirmed the bent metallocene structure with C_2-symmetry, similar to that described for a related yttrium complex.[25a] The *t*Bu substituents on the two cyclopentadienyl ligands are oriented *trans* to each other. The ytterbium atom is coordinated by two linked amidocyclopentadienyl ligands, forming a distorted tetrahedral coordination environment. The average value of Yb−C distances is similar to those in bis(cyclopentadienyl) derivatives of trivalent ytterbium,[16] and slightly longer than that in complex

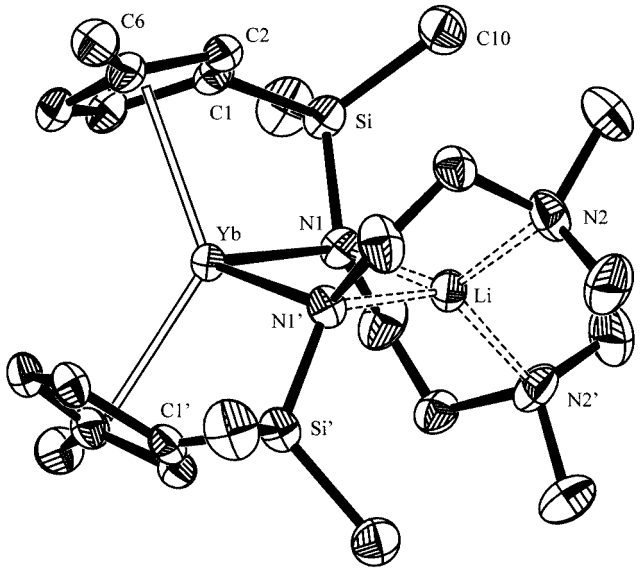

Figure 5. ORTEP drawing and numbering scheme of the molecular structure of **9** with thermal ellipsoids drawn at the 30% probability level; hydrogen atoms as well as the methyl carbon atoms of the *t*Bu groups are omitted for the sake of clarity; selected bond lengths (Å) and bond angles (°): Yb−N1 2.279(3), Yb−C1 2.535(4), Yb−C2 2.672(4), Yb−C3 2.818(4), Yb−C4 2.713(4), Yb−C5 2.548(4), Li−N1 2.193(7), Li−N2 2.124(7); Cp_{cent}−Yb−Cp_{cent} 127.8(1), N1−Yb−N1′ 92.1(2), Li−N1−Yb 85.6(2), N2−Li−N2′ 111.6(5), N1−Li−N2 89.3(2)

$[Yb(\eta^5{:}\eta^1\text{-}C_5Me_4SiMe_2Nt\text{Bu})(THF)(\mu\text{-}H)]_2$.[3c] The scattering of Yb−C bond lengths [2.534(4)−2.818(4) Å] is somewhat higher than those in complexes (*R*,*R*)-, (*R*,*S*)-$Li[Y\{(\eta^5{:}\eta^1\text{-}C_5H_3t\text{Bu-}3)SiMe_2NCH_2CH_2NMe_2\}_2]$[25a] and $[Yb(\eta^5{:}\eta^1\text{-}C_5Me_4SiMe_2Nt\text{Bu})(THF)(\mu\text{-}H)]_2$.[3c] The Yb−C bond lengths distal to the silicon bridge [C(3), C(4)] are longer than the distances for the proximal carbon atoms [C(1), C(2), C(5)]. The Yb−N bond length [2.279(3) Å] is substantially longer than that in $[Yb(\eta^5{:}\eta^1\text{-}C_5Me_4SiMe_2Nt\text{Bu})(THF)(\mu\text{-}H)]_2$,[3c] while the Li−N bond lengths are similar to the corresponding values in related yttrium complexes.[25a] The Cp_{cent}−Yb−Cp_{cent} bond angle (127.8(1)°] in **9** is slightly less than the Cp_{cent}−Y−Cp_{cent} bond angle in (*R*,*R*)-$Li[Y(\eta^5{:}\eta^1\text{-}C_5H_3t\text{Bu-}3)SiMe_2NCH_2CH_2NMe_2]_2$.[25]

Reduction of **9** and **10** with potassium metal or sodium 1,2-diphenylethenide gave a mixture of inseparable products, while reduction of $YbCl_3$ and $Li_2[(C_5H_3t\text{Bu-}3)SiMe_2NCH_2CH_2NMe_2]$ (1:1 molar ratio) prepared "in situ" with one equivalent of sodium 1,2-diphenylethenide in THF resulted in an ate complex of divalent ytterbium $[Li(THF)]_2[Yb\{(\eta^5\text{-}C_5H_3t\text{Bu-}3)SiMe_2N(H)CH_2CH_2NMe_2\}_2(\mu\text{-}Cl)_2]$ (**11**), isolated as bright-red crystals in 46% yield. (Scheme 7).

Complex **11** is soluble in THF and pyridine, sparingly soluble in toluene and in hexane. According to NMR spectroscopy **11** was found to be diamagnetic, indicating the divalency of the ytterbium atom. The ^1H NMR and IR spectroscopic data of **11** suggest the presence of protonated amino groups. This indicates that reduction of the Yb^{III} species by sodium 1,2-diphenylethenide occurs together

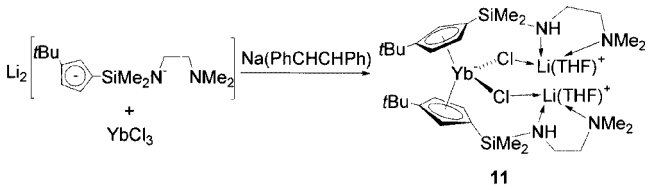

11

Scheme 7

with protonation of the amido groups. THF molecules seem the most likely source for proton abstraction because *trans*-stilbene was isolated from the reaction mixture in nearly quantitative yield. In the ^{1}H NMR spectrum of **11** in [D_8]toluene at 20 °C, the methyl protons on the silicon atom are observed as two singlets, while the protons of both methylene groups of the CH_2CH_2 bridge appear as broad signals. The protons of the *t*Bu and dimethylamino groups also give rise to two singlets. The significantly broadened signals of both α- and β-methylene protons of THF are shifted to higher field than those of free THF. At −60 °C the ^{1}H NMR spectrum shows four singlets for the protons of the $SiMe_2$ groups. The signal of the methylene group $SiNC\mathit{H}_2$ splits into two singlets, and the methylene protons of the $C\mathit{H}_2NMe_2$ group appear as four broad multiplets. Despite the poor crystal quality, a preliminary X-ray crystal structure determination confirmed the connectivity in **11**.[26] Furthermore, the divalent oxidation state of the ytterbium atom could be inferred from the Yb−C distances, ranging from 2.70(2) Å to 2.87(2) Å [Yb−C(Cp)$_{av.}$= 2.78 Å]. In the trivalent ytterbium metallocene **9**, the corresponding values range from 2.535(4) Å to 2.814(4) [Yb−C(Cp)$_{av.}$= 2.657 Å]. The Yb−Cl distances in **11** were found to be 2.753(5) Å and 2.774(6) Å. The unusual bent metallocene structure includes a pseudo-tetrahedrally coordinated Yb^{II} center, bonded to two η^5-*tert*-butylcyclopentadienyl rings and two chloro ligands. Each of the amino functions coordinates a [Li(THF)]$^+$ moiety which is linked to the ytterbium center via a bridging chloride ligand.

Conclusion

The attempts to prepare divalent ytterbium complexes with an $SiMe_2$-linked amidocyclopentadienyl ligand by metathesis of their dipotassium salts with [$YbI_2(THF)_2$] in THF or DME resulted in the formation of dimeric iodo (**1**−**4**) or metallocene-type (**6**) complexes with noncoordinating amino groups. Forcing conditions allow coordination of the amino functions, but the resulting Yb^{III} metallocene ate complexes **5** contain oxidized ytterbium centers. Treatment of the naphthalene ytterbium complex with amino-substituted indene or reduction of the Yb^{III} ate complexes gave the metallocene complexes **7** and **11**. The ligand $(C_5Me_4CH_2SiMe_2N\mathit{t}Bu)^{2-}$ allowed the isolation of the Yb^{II} ate complex **8** which contains a chelating linked amidocyclopentadienyl ligand. Our results are in contrast to the smooth complexation of the anilido ligand $(C_5Me_4SiMe_2NPh)^{2-}$ at divalent ytterbium centers as reported by Hou et al.[7] The coordination of the amidocyclopentadienyl ligands at the large divalent ytterbium center apparently requires electron-withdrawing amido substituents, whereas the sterically bulky *tert*-butyl group appears to severely hinder the chelation reaction.

Experimental Section

General: All experiments were performed under argon using standard Schlenk or glove-box techniques. Solvents were purified, dried, and condensed in vacuo prior to use. ^{1}H, ^{13}C, and ^{29}Si NMR: Bruker DRX 400; all spectra were obtained at 25 °C. Elemental analyses: Microanalytical laboratory of this department.

[Yb(η^5-$C_5Me_4SiMe_2NH\mathit{t}Bu$)(THF)$_2$(μ-I)]$_2$ (1): A solution of $(C_5Me_4H)SiMe_2NH\mathit{t}Bu$ (0.298 g, 1.19 mmol) in THF (5 mL) was added at room temperature to a solution of potassium 1,2-diphenylethenide, prepared in situ from *trans*-stilbene (0.430 g, 2.38 mmol) and potassium (0.093 g, 2.38 mmol) in THF (35 mL). The reaction mixture was stirred for 3 h, then slowly treated with [$YbI_2(THF)_2$] (0.679 g, 1.19 mmol) at room temperature with vigorous stirring. The reaction mixture was left stirring overnight. The brownish-yellow reaction mixture was filtered, THF was evaporated in vacuo, and the dark-yellow residue was heated at 60 °C in vacuo for 3 h to sublime off stilbene. The solid residue was recrystallized from the THF/hexane mixture at 0 °C. The mother liquor was decanted from the bright-yellow crystals which were dried in vacuo to afford 0.620 g (76%) of **1**. ^{1}H NMR ([D_5]pyridine): δ = 0.34, 0.62 (s, 2 × 6 H, $SiCH_3$), 0.71, 1.15 (s, 2 × 1 H, NH), 1.17, 1.32 [s, 2 × 9 H, $C(CH_3)_3$], 1.61 (m, 2 × 8 H, β-CH_2, THF), 1.92, 2.07, 2.12, 2.21 [s, 4 × 6 H, $C_5(CH_3)_4$], 3.65 (m, 2 × 8 H, α-CH_2, THF) ppm. ^{13}C{^{1}H} NMR ([D_5]pyridine): δ = 7.3, 7.7 (Si$\mathit{C}H_3$), 12.4, 12.8 (ring $\mathit{C}H_3$), 15.9, 16.3 (ring $\mathit{C}H_3$), 26.8 (β-CH_2, THF), 34.8, 35.1 [$C(\mathit{C}H_3)_3$], 51.0 [$\mathit{C}(CH_3)_3$, 68.9 (α-CH_2, THF), 106.2 (ring C attached to $SiMe_2$), 122.3, 126.1 (ring C) ppm. IR (KBr): $\tilde{\nu}$ = 3382 w, 2964 s, 2921 s, 2858 s, 1622 m, 1592 m, 1443 m, 1379 m, 1256 s, 1216 m, 1043 s, 984 m, 832 s, 800 s, 644 m cm^{-1}. $C_{46}H_{88}I_2N_2O_4Si_2Yb_2$ (1387.2): calcd. C 39.82, H 6.34, N 2.02; found C 39.39, H 6.47, N 2.30.

[Yb(η^5-$C_5Me_4SiMe_2NHCH_2CH_2CH_3$)(THF)$_2$(μ-I)]$_2$ (2): A solution of $(C_5Me_4H)SiMe_2NHCH_2CH_2CH_3$ (0.322 g, 1.36 mmol) in THF (5 mL) was added at room temperature to a solution of potassium 1,2-diphenylethenide, prepared in situ from *trans*-stilbene (0.489 g, 2.72 mmol) and potassium (0.106 g, 2.72 mmol) in THF (35 mL). The reaction mixture was stirred for 3 h, then slowly treated with [$YbI_2(THF)_2$] (0.780 g, 1.36 mmol) at room temperature with vigorous stirring. The reaction mixture was left stirring overnight. The brownish-yellow reaction mixture was filtered, THF was evaporated in vacuo, and the dark-yellow residue was heated at 60 °C in vacuo for 3 h to sublime off stilbene. The solid residue was recrystallized from DME at 0 °C. The mother liquor was decanted from the yellow crystals which were dried in vacuo to afford 0.670 g (79%) of **2**. ^{1}H NMR ([D_5]pyridine): δ = 0.41, 0.52 (s, 2 × 6 H, $SiCH_3$), 0.78, 1.17 (m, 2 × 1 H, NH), 0.95 (m, 2 × 3 H, $NCH_2CH_2C\mathit{H}_3$), 1.50 (m, 2 × 2 H, $NCH_2C\mathit{H}_2CH_3$), 1.62 (s, 2 × 8 H, β-CH_2, THF), 2.03, 2.06, 2.18, 2.24 (s, 4 × 6 H, $C_5(CH_3)_4$], 2.88 (m, 2 × 2 H, $NC\mathit{H}_2$), 3.65 (s, 2 × 8 H, α-CH_2, THF) ppm. ^{13}C{^{1}H} NMR ([D_5]pyridine): δ = 3.4, 3.9 (Si$\mathit{C}H_3$), 12.4, 12.7 (ring $\mathit{C}H_3$), 15.2, 15.6 (ring $\mathit{C}H_3$), 26.5 (β-CH_2, THF), 28.9 ($CH_2CH_2\mathit{C}H_3$), 45.4 ($CH_2\mathit{C}H_2CH_3$), 46.4 ($\mathit{C}H_2CH_2CH_3$), 68.5 (α-CH_2, THF), 106.4 (ring C attached to $SiMe_2$), 118.1, 121.0 (ring

C) ppm. IR (KBr): $\tilde{\nu}$ = 3378 w, 2969 s, 2918 s, 2860 s, 1642 m, 1582 m, 1449 m, 1379 m, 1250 s, 1116 m, 1043 s, 984 m, 832 s, 810 s, 646m cm^{-1}. $C_{44}H_{84}I_2N_2O_4Si_2Yb_2$ (1360.6): calcd. C 38.84, H 6.17, N 2.05; found C 38.99, H 6.11, N 2.49.

[Yb(η^5-$C_5Me_4SiMe_2NHCH_2CH_3$)(DME)(μ-I)]$_2$ (3): A solution of $(C_5Me_4H)SiMe_2NHCH_2CH_3$ (0.412 g, 1.84 mmol) in THF (5 mL) was added at room temperature to a solution of potassium 1,2-diphenylethenide, prepared in situ from *trans*-stilbene (0.665 g, 3.69 mmol) and potassium (0.144 g, 3.69 mmol) in THF (30 mL). The reaction mixture was stirred for 3 h, then slowly treated with $[YbI_2(THF)_2]$ (1.050 g, 1.83 mmol) at room temperature with vigorous stirring. The reaction mixture was left stirring overnight. The resulting dark-orange reaction mixture was filtered, THF was evaporated in vacuo, and the brown residue was heated at 60 °C in vacuo for 2 h to sublime off stilbene. The solid residue was recrystallized from DME/hexane mixture at 0 °C. The mother liquor was decanted from the orange crystals which were dried in vacuo to afford 0.640 g (59%) of **3**. ^{1}H NMR ([D$_5$]pyridine): δ = 0.40, 0.52 (s, 2 × 6 H, $SiCH_3$), 0.92, 1.07 (m, 2 × 1 H, NH), 1.19 (m, 2 × 3 H, NCH_2CH_3), 2.01, 2.03, 2.08, 2.16 [s, 4 × 6 H, $C_5(CH_3)_4$], 2.94 (m, 2 × 2 H, NCH_2CH_3) 3.26 (s, 2 × 6 H, OCH_3, DME), 3.49 (s, 2 × 4 H, OCH_2CH_2O, DME) ppm. ^{13}C{^{1}H} NMR ([D$_5$]pyridine): δ = 4.5, 4.9 ($SiCH_3$), 11.2, 11.7 (ring CH_3), 14.9, 15.3 (ring CH_3), 35.0, 35.6 (NCH_2CH_3), 48.1, 48.9 (NCH_2), 59.8 (OCH_3, DME), 73.3 (OCH_2, DME), 107.3 (ring C attached to $SiMe_2$), 124.2, 128.7 (ring C) ppm. IR (KBr): $\tilde{\nu}$ = 3383 w, 2963 s, 2916 s, 2860 s, 1449 m, 1385 m, 1319 m, 1249 s, 1104 s, 1058 s, 1020 s, 981 m, 917 m, 825 s, 789 s, 698 m, 636w cm^{-1}. $C_{34}H_{68}I_2N_2O_4Si_2Yb_2$ (1224.5): calcd. C 33.34, H 5.55, N 2.28; found C 33.71, H 5.21, N 2.27.

[Yb(η^5-$C_5Me_4SiMe_2NHCH_2CH{=}CH_2$)(DME)(μ-I)]$_2$ (4): A solution of $(C_5Me_4H)SiMe_2NHCH_2CH{=}CH_2$ (0.300 g, 1.27 mmol) in THF (5 mL) was added at room temperature to a solution of potassium 1,2-diphenylethenide, prepared in situ from *trans*-stilbene (0.457 g, 2.53 mmol) and potassium (0.099 g, 2.54 mmol) in THF (30 mL). The reaction mixture was stirred for 3 h, then slowly treated with $[YbI_2(THF)_2]$ (0.720 g, 1.26 mmol) at room temperature with vigorous stirring. The reaction mixture was left stirring overnight. The brownish-red reaction mixture was filtered, THF was evaporated in vacuo, and the brown residue was heated at 60 °C in vacuo for 2 h to sublime off stilbene. The solid residue was recrystallized from DME/hexane mixture at 0 °C. The mother liquor was decanted from the orange crystals which were dried in vacuo to afford 0.500 g (66%) of **4**. ^{1}H NMR ([D$_5$]pyridine): δ = 0.39, 0.54 (s, 2 × 6 H, $SiCH_3$), 1.10, 1.60 (br. s, 2 × 2 H, NH), 2.01, 2.05, 2.23, 2.32 [s, 4 × 6 H, $C_5(CH_3)_4$], 3.31 (s, 2 × 6 H, OCH_3, DME), 3.49 (s, 2 × 4 H, OCH_2CH_2O, DME), 3.54, 3.56 (m, 2 × 2 H, NCH_2CH), 5.08, 5.29 (m, 2 × 2 H, $CH{=}CH_2$), 6.04−6.11 (m, 2 × 1 H, $CH_2CH{=}CH_2$) ppm. ^{13}C{^{1}H} NMR ([D$_5$]pyridine): δ = 3.4, 3.9 ($SiCH_3$), 12.3, 12.6 (ring CH_3), 15.2, 15.4 (ring CH_3), 46.2, 46.9 (NCH_2), 59.3 (OCH_3, DME), 72.8 (OCH_2, DME), 106.4, 110.2 (ring C attached to $SiMe_2$), 113.5, 114.7 ($CH{=}CH_2$), 121.3, 123.7 (ring C), 141.8, 142.9 ($CH{=}CH_2$) ppm. IR (KBr): $\tilde{\nu}$ = 3384 w, 2984 s, 2914 s, 2857 s, 1634 m, 1574 m, 1450 m, 1252 s, 1045 s, 986 m, 950 m, 832 s, 798 s, 695 m, 645m cm^{-1}. $C_{36}H_{68}I_2N_2O_2Si_2Yb_2$ (1248.5): calcd. C 34.63, H 5.48, N 2.30; found C 34.56, H 5.67, N 2.38.

[K(DME)][Yb{(η^5:η^1-C_5H_3*t*Bu-3)$SiMe_2N$*t*Bu}$_2$] (5): A solution of $(C_5H_4$*t*Bu)$SiMe_2NH$*t*Bu (0.700 g, 2.78 mmol) in THF (5 mL) was added to a solution of potassium 1,2-diphenylethenide, prepared in situ from *trans*-stilbene (1.000 g, 5.55 mmol) and potassium (0.216 g, 5.55 mmol) in THF (30 mL) at room temperature and stirred for 3 h. $[YbI_2(THF)_2]$ (1.580 g, 2.78 mmol) was slowly added at room temperature with vigorous stirring. The reaction mixture was stirred for 3 h at room temperature and at 60 °C for 6 h. The dark orange solution was filtered, THF was evaporated in vacuo, and the brown residue was heated to 60 °C in vacuo for 2 h to remove stilbene (by sublimation). The residue was redissolved in 20 mL of DME and recrystallized by slow condensation of hexane into the DME solution at room temperature. The mother liquor was decanted from the orange crystals which were washed with hexane and dried in vacuo to give 0.850 g (77%) of **5**. IR (KBr): $\tilde{\nu}$ = 2970 s, 2902 s, 2869 s, 1460 m, 1358 m, 1257 s, 1158 s, 1097 s, 1010 s, 838 s, 723 m, 525 m, 433m cm^{-1}. $C_{34}H_{64}KN_2O_2Si_2Yb$ (801.2): calcd. C 50.97, H 7.98, N 3.49; found C 51.24, H 8.03, N 3.68.

[Yb{η^5-(1-C_9H_6)$SiMe_2NH$*t*Bu}$_2$(THF)$_2$] (6): A solution of $(C_9H_7)SiMe_2NH$*t*Bu (0.500 g, 2.04 mmol) in THF (5 mL) was added at room temperature to a solution of potassium 1,2-diphenylethenide, prepared in situ from *trans*-stilbene (0.730 g, 4.05 mmol) and potassium (0.159 g, 4.06 mmol) in THF (30 mL). The reaction mixture was stirred for 3 h, then slowly treated with $[YbI_2(THF)_2]$ (1.160 g, 2.03 mmol) at room temperature with vigorous stirring. The reaction mixture was left stirring overnight. The dark red reaction mixture was filtered, THF was evaporated in vacuo, and the brown residue was heated to 60 °C in vacuo for 4 h (to sublime off stilbene). The solid residue was recrystallized from toluene at −30 °C. The mother liquor was decanted from the red crystals which were dried in vacuo to afford 0.370 g (46%) of **6**. ^{1}H NMR ([D$_6$]benzene): δ = 0.28, 0.39, 0.73, 0.86 (s, 4 × 3 H, $SiCH_3$), 0.81, 1.00 (br. s, 2 × 1 H, NH), 1.12, 1.16 [s, 2 × 9 H, $C(CH_3)_3$], 1.25 (br. s, 2 × 4 H, β-CH_2 THF), 3.05 (br. s, 2 × 4 H, α-CH_2 THF), 6.37, 6.81, 7.04, 7.40, 7.70, 7.88 (m, 2 × 6 H, C_9H_6) ppm. ^{13}C{^{1}H} NMR (101 MHz, [D$_8$]THF): δ = 1.2 ($SiCH_3$), 23.3 (β-CH_2, THF), 31.1 [$C(CH_3)_3$], 47.1 [$C(CH_3)_3$], 65.2 (α-CH_2, THF), 95.2 (ring C attached to $SiMe_2$), 100.2, 114.9, 115.7, 117.8, 120.6, 124.8, 129.3, 132.6 (C_9H_6) ppm. IR (Nujol): $\tilde{\nu}$ = 3382 w, 1322 m, 1222 s, 1154 m, 1025 s, 966 w, 839 s, 764 s, 717 s, 642 w cm^{-1}. $C_{38}H_{60}N_2O_2Si_2Yb$ (806.1): calcd. C 56.61, H 7.58, N 3.47; found C 55.80, H 6.97, N 3.08.

[Yb{η^5-(1-C_9H_6)$SiMe_2NH$*t*Bu}$_2$(bipy)] (7): A solution of $(C_9H_7)SiMe_2NH$*t*Bu (0.548 g, 2.23 mmol) in THF (5 mL) was added to a suspension of $[Yb(C_{10}H_8)(THF)_2]$ (1.000 g, 2.24 mmol) in THF (35 mL) at room temperature with vigorous stirring and the reaction mixture was left standing overnight. The solution was filtered and THF was evaporated in vacuo. The brown residue was washed with hexane to remove naphthalene and redissolved in THF (20 mL). A solution of 2,2′-bipyridyl (0.690 g, 4.48 mmol) in toluene (5 mL) and hexane (3 mL) was added. Slow evaporation of the solvents at room temperature resulted in the precipitation of black crystals. The mother liquor was decanted and the crystals were washed with cold hexane and dried in vacuo to give 0.610 g (67%) of **7**. ^{1}H NMR ([D$_8$]THF): δ = 0.11, 0.21, 0.53, 0.55 (s, 4 × 3 H, $SiCH_3$), 0.62, 1.21 (br. s, 2 × 1 H, NH), 0.92, 1.09 [s, 2 × 9 H, $C(CH_3)_3$], 5.93, 6.36, 6.43, 6.61, 6.95, 7.15 (m, together 12 H, C_9H_6), 7.84, 7.90, 8.02, 8.19, 8.24, 8.39, 8.43, 8.59 (br. s, together 8 H, bipy) ppm. ^{13}C{^{1}H} NMR ([D$_8$]THF): δ = 2.2, 2.6, 2.9, 3.0 ($SiCH_3$), 32.8, 33.0 [$C(CH_3)_3$], 48.6, 48.9 [$C(CH_3)_3$], 97.7, 98.3 (C-1, C_9H_6), 101.8, 102.3 (C-3, C_9H_6), 116.5, 116.7, 117.0, 117.3 (C-6, C-7, C_9H_6), 120, 120.3 (C-5, C_9H_6), 121.6, 121.9 (C-8, C_9H_6), 124.1, 124.6 (C-2, C_9H_6), 129.6, 130.2 (C-4, C_9H_6), 132.2, 135.5 (C-9, C_9H_6), 128.2 (bipy), 136.1 (bipy), 138.0 (bipy), 148.1 (bipy), 153.7 (bipy) ppm. IR (KBr): $\tilde{\nu}$ = 3384 w, 3065 m, 2962 s, 1582 m, 1455 m, 1378 m, 1226 m, 1019 s, 849 m, 759 s, 716 m, 621 w, 450 w cm^{-1}. $C_{40}H_{52}N_4Si_2Yb$ (818.1): calcd. C 58.72, H 6.41, N 6.84; found C 58.80, H 6.39, N 7.63.

[$Li_{0.5}$][Yb(μ−$η^5$: $η^1$-$C_5Me_4CH_2SiMe_2NtBu$)$(THF)_2$(μ-I)$_{0.5}$] (8): A solution of $(C_5Me_4H)CH_2SiMe_2NHtBu$ (0.667 g, 2.51 mmol) in THF (5 mL) was added to a suspension of $[Yb(C_{10}H_8)(THF)_2]$ (1.120 g, 2.51 mmol) in THF (25 mL) at room temperature and the reaction mixture was stirred for 8 h. The brown reaction mixture was filtered, THF was evaporated in vacuo, and the residue extracted with hexane (2 × 20 mL) to remove naphthalene. The resulting solid was recrystallized from a THF/hexane mixture at 0 °C. The mother liquor was decanted and the yellow crystals were dried in vacuo to yield 0.310 g (19%) of **8**. ^{1}H NMR ([D_5]pyridine): δ = 0.73 (s, 6 H, $SiCH_3$), 1.52 [s, 9 H, $C(CH_3)_3$], 1.60 (m, 8 H, β-CH_2, THF), 1.73, 2.10 [s, 6 H, $C_5(CH_3)_4$], 2.37 (s, 2 H, CH_2), 3.64 (m, 8 H, α-CH_2, THF) ppm. $^{13}C\{^1H\}$ NMR ([D_5]pyridine): δ = 10.6 ($SiCH_3$), 12.4, 12.9 (ring CH_3), 20.6 (CH_2), 26.5 (β-CH_2, THF), 36.0 [$C(CH_3)_3$], 54.3 [$C(CH_3)_3$], 68.5 (α-CH_2, THF), 109.7, 109.9 (ring C), 137.2 (ring C attached to CH_2) ppm. IR (KBr): $\tilde{\nu}$ = 2927 s, 2854 s, 1461 m, 1377 m, 1236 w, 1187 w, 1058 s, 1022 m, 987 m, 832 m, 733 w cm^{-1}. $C_{24}H_{45}I_{0.5}Li_{0.5}NO_2SiYb$ (647.7): calcd. C 44.51, H 7.00, N 2.16; found C 44.86, H 7.75, N 2.26.

Li[Yb{(η^5:η^1-C_5H_3tBu-3)$SiMe_2NCH_2CH_2NMe_2$}$_2$] (9): Solid $Li_2(C_5H_3tBuSiMe_2NCH_2CH_2NMe_2)$ (0.670 g, 2.41 mmol) was slowly added at room temperature to a suspension of $YbCl_3$ (0.670 g, 2.40 mmol) in THF (50 mL) with vigorous stirring and the reaction mixture was stirred for a further 18 h. The resulting orange solution was filtered, THF was removed in vacuo, and the crude product was extracted with toluene (2 × 20 mL). LiCl was filtered off and the volume of the solution was reduced to 10 mL. After crystallization at −30 °C for 48 h, the mother liquor was decanted off from the yellow crystals which were dried in vacuo at room temperature to afford 0.530 g (62%) of **9**. IR (KBr): $\tilde{\nu}$ = 2995 s, 2826 m, 2783 m, 1458 m, 1360 m, 1244 s, 1176 m, 1094 s, 1020 s, 952 m, 800 s, 653 w cm^{-1}. $C_{30}H_{56}LiN_4Si_2Yb$ (708.9): calcd. C 50.85, H 7.90, N 7.90; found C 50.34, H 7.76, N 8.11.

Li{Yb[(η^5:η^1-C_5H_3tBu-3)$SiMe_2NCH_2CH_2OMe$]$_2$} (10): Solid $Li_2(C_5H_3tBuSiMe_2NCH_2CH_2OMe)$ (1.150 g, 4.33 mmol) was slowly added at room temperature to a suspension of $YbCl_3$ (1.170 g, 4.34 mmol) in DME (40 mL) under vigorous stirring and the reaction mixture was left stirring overnight. The yellow solution was filtered and the volume of the filtrate was then reduced to 10 mL. After crystallization at 0 °C for 3 days, the mother liquor was decanted from the yellow crystals which were dried in vacuo at room temperature to afford 1.010 g (71%) of **10** as yellow crystals. IR (KBr): $\tilde{\nu}$ = 2949 s, 2898 m, 2819 m, 1459 m, 1359 m, 1239 s, 1176 m, 1075 s, 935 m, 819 s, 763 s, 719 s, 571 m, 426 w cm^{-1}. $C_{28}H_{50}LiN_2O_2Si_2Yb$ (682.4): calcd. C 49.28, H 7.32, N 4.10; found C 48.88, H 7.24, N 4.23.

[Li(THF)]$_2$[Yb{(η^5-C_5H_3tBu-3)$SiMe_2NHCH_2CH_2NMe_2$}$_2$(μ-Cl)$_2$] (11): Solid $Li_2(C_5H_3tBuSiMe_2NCH_2CH_2NMe_2)$ (0.878 g, 3.15 mmol) was slowly added at room temperature to a suspension of $YbCl_3$ (0.882 g, 3.15 mmol) in THF (40 mL) under vigorous stirring and the reaction mixture was stirred overnight. The resulting orange solution was cooled to 0 °C and treated with a solution of sodium 1,2-diphenylethenide, prepared from *trans*-stilbene (0.567 g, 3.15 mmol) and sodium (0.072 g, 3.15 mmol) in THF (30 mL). The reaction mixture was allowed to warm to room temperature and stirred overnight. After filtration, THF was removed in vacuo and the resulting crude product was recrystallized from THF/hexane at −30 °C. The bright red crystals were dried in vacuo to give 1.350 g (46%) of **11**. ^{1}H NMR ([D_8]toluene): δ = 0.11, 0.48 (s, 6 H, $SiCH_3$), 0.87, 1.75 (m, 1 H, NH), 1.48 (br. s, 8 H, β-CH_2, THF), 1.53 (br. s, 4 H, $SiNCH_2CH_2N$), 1.64 [s, 18 H, $C(CH_3)_3$], 1.97 [s, 6 H, $N(CH_3)_2$], 2.29 (br. s, 4 H, NCH_2CH_2N), 3.60 (br. s, 8 H, α-CH_2, THF), 6.06, 6.13, 6.72 (s, 2 H, ring H) ppm. $^{13}C\{^1H\}$ NMR ([D_8]toluene): δ = −2.1, 1.5 ($SiCH_3$), 25.3 (β-CH_2, THF), 31.9 [$C(CH_3)_3$],32.6 [$C(CH_3)_3$, 38.8 [$N(CH_3)_2$], 44.4 ($SiNCH_2$), 61.8 (CH_2NMe_2), 67.3 (α-CH_2, THF), 109.2 (ring C attached to $SiMe_2$), 113.8, 113.1 (ring C), 137.1 (ring C attached to *tBu*) ppm. IR (KBr): $\tilde{\nu}$ = 3380 w, 3050 w, 2960 s, 2826 m, 2783 m, 1458 m, 1360 m, 1240 s, 1176 m, 1050 s, 1090 s, 1024 s, 962 m, 800 s cm^{-1}. $C_{38}H_{74}Cl_2Li_2N_4O_2Si_2Yb$ (933.0): calcd. C 48.91, H 7.93, N 6.00; found C 48.39, H 8.27, Yb 6.42.

X-ray Structure Determination of 1, 5, 7, 8, and 9: The crystal and structure refinement data are listed in Table 1 and 2. Data for **1**, **5**, **8** and **9** were collected on an Enraf−Nonius CAD-4 diffractometer (graphite monochromator, Mo-K_α radiation, λ = 0.71073 Å). Data corrections were carried out using the program WINGX[27a] in the program system WinGX.[27b] Data for **7** were collected on a Bruker AXS diffractometer with area detector. Data correction was carried out using the program system SAINT.[27c] All structures were solved by direct methods using SHELXS-86[27d] and difference Fourier syntheses. All independent reflections were used in the refinement against all F_o^2 data using the program SHELXL-97.[27e] All non-hydrogen atoms were refined with anisotropic thermal parameters; the hydrogen atoms were included in calculated positions. Crystallographic data (excluding structure factors) for the structures reported in this paper have been deposited with the Cambridge Crystallographic Data Centre as supplementary publication no. CCDC-195744 (**1**), CCDC-195745 (**5**), CCDC-195746 (**7**), CCDC-195747 (**8**), and CCDC-195748 (**9**). Copies of the data can be obtained free of charge on application to CCDC, 12 Union Road, Cambridge CB2 1EZ, UK [Fax: (internat.) + 44-1223/336-033; E-mail: deposit@ccdc.cam.ac.uk].

Acknowledgments

Financial support by the Fonds der Chemischen Industrie and the Deutsche Forschungsgemeinschaft is gratefully acknowledged. A.A.T. thanks the Alexander von Humboldt Foundation for a research fellowship. The authors thank Ms. S. Stauf for recording the crystallographic data of compound **7**.

[1] W. J. Evans, *Polyhedron* **1987**, *6*, 803−835.
[2] [2a] H. Schumann, J. A. Meese-Marktscheffel, L. Esser, *Chem. Rev.* **1995**, *95*, 865−986. [2b] F. T. Edelmann, In *Comprehensive Organometallic Chemistry II*; (Eds.: E. W. Abel, F. G. A.Stone, G. Wilkinson); Pergamon Press: London, **1995**, Vol. 4, pp 11−212. [2c] S. Arndt, J. Okuda, *Chem. Rev.* **2002**, *102*, 1953−1976.
[3] [3a] K. C. Hultzsch, T. P. Spaniol, J. Okuda, *Angew. Chem.* **1999**, *38*, 227−230. [3b] K. C. Hultzsch, P. Voth, K. Beckerle, T. P. Spaniol, J. Okuda, *Organometallics* **2000**, *19*, 228−243. [3c] S. Arndt, P. Voth, T. P. Spaniol, J. Okuda, *Organometallics* **2000**, *19*, 4690−4700. [3d] S. Arndt, T. P. Spaniol, J. Okuda, *Eur. J. Inorg. Chem.* **2001**, 73−75. [3e] S. Arndt, A. A. Trifonov, T. P. Spaniol, J. Okuda, M. Kitamura, T. Takahashi, *J. Organomet. Chem.* **2002**, *647*, 158−166.
[4] R. D. Shannon, *Acta Crystallogr., Sect. A* **1976**, *32*, 751−757.
[5] S. Tian, V. M. Arredondo, C. L. Stern, T. J. Marks, *Organometallics* **1999**, *18*, 2568−2570.
[6] [6a] G. Heckman, M. Niemeyer, *J. Am. Chem. Soc.* **2000**, *122*, 4227−4228. [6b] A. A. Trifonov, E. N. Kirillov, S. Dechert, H. Schumann, M. N. Bochkarev, *Eur. J. Inorg. Chem.* **2001**, 3055−3058.
[7] [7a] Z. Hou, T. Koizumi, M. Nishiura, Y. Wakatsuki, *Organometallics* **2001**, *20*, 3323−3328. [7b] Z. Hou, Y. Wakatsuki, *J. Organomet. Chem.* **2002**, *647*, 61−70.

[8] W. P. Schaefer, W. D. Cotter, J. E. Bercaw, *Acta Crystallogr., Sect. C* **1993**, *49*, 1489−1492.
[9] W. J. Evans, M. A. Hozbor, *J. Organomet. Chem.* **1987**, *326*, 299−312.
[10] S. P. Constantine, G. M. De Lima, P. B. Hitchcock, J. M. Keates, G. A. Lawless, *Chem. Commun.* **1996**, 2421−2422.
[11] I. L. Fedushkin, S. Dechert, H. Schumann, *Organometallics* **2000**, *19*, 4066−4076.
[12] M. N. Bochkarev, L. N. Zakharov, C. S. Kalinina, *Organoderivatives of Rare Earth Elements*, Kluwer Academic Publishers, Dordrecht, **1995**.
[13] C. Eaborn, P. B. Hitchcock, K. Izod, J. D. Smith, *J. Am. Chem. Soc.* **1994**, *116*, 12071−12072.
[14] [14a] E. C. Baker, L. D. Brown, K. N. Raymond, *Inorg. Chem.* **1975**, *14*, 1376−1379. [14b] J. M. Boncella, T. Don Tilley, R. A. Andersen, *J. Chem. Soc., Chem. Commun.* **1984**, 710−712. [14c] W. J. Evans, R. Dominguez, T. P. Hanusa, *Organometallics* **1986**, *5*, 263−270. [14d] H. Yasuda, H. Yamamoto, K. Yokota, A. Nakamura, *Chem. Lett.* **1989**, 1309−1312. [14e] X. Z. Zhou, Z. Huang, R. Cai, L. Zhang, L. Zhang, *Organometallics* **1999**, *18*, 4128−4133.
[15] [15a] W. J. Evans, T. S. Gummersheimer, T. J. Boyle, J. W. Ziller, *Organometallics* **1994**, *13*, 1281−1284. [15b] M. H. Lee, J.-W. Hwang, Y. Kim, J. Kim, Y. Han, Y. Do, *Organometallics* **1999**, *18*, 5124−5129. [15c] A. A. Trifonov, E. N. Kirillov, S. Dechert, H. Schumann, M. N. Bochkarev, *Eur. J. Inorg. Chem.* **2001**, 2509−2514.
[16] [16a] T. D. Tilley, R. A. Andersen, A. Zalkin, *Inorg. Chem.* **1983**, *22*, 856−859. [16b] L. Shi, H. Ma, Y. Yn, Z. Ye, *J. Organomet. Chem.* **1988**, *339*, 277−282. [16c] P. B. Hitchcock, M. F. Lappert, S. Prashar, *J. Organomet. Chem.* **2000**, *613*, 105−110.
[17] [17a] G. Rabe, H. W. Roesky, D. Stalke, F. Pauer, G. M. Sheldrick, *J. Organomet. Chem.* **1991**, *403*, 11−19. [17b] P. Jutzi, W. Leffers, B. Hampel, S. Pohl, W. Saak, *Angew. Chem. Int. Edit. Engl.* **1987**, *26*, 583−589.
[18] M. G. Klimpel, W. A. Herrmann, R. Anwander, *Organometallics* **2000**, *19*, 4666−4668.
[19] [19a] M. N. Bochkarev, A. A. Trifonov, E. A. Fedorova, N. S. Emelyanova, T. A. Basalgina, G. S. Kalinina, G. A. Razuvaev, *J. Organomet. Chem.* **1989**, *372*, 217−224. [19b] A. A. Trifonov, E. N. Kirillov, A. Fischer, F. T. Edelmann, M. N. Bochkarev, *Chem. Commun.* **1999**, 2203−2204.
[20] [20a] J. Z. Jin, Z. S. Jin, W. Q. Chen, Y. Zhang, *Chinese J. Struct. Chem. (Jiegou Huaxue)* **1993**, *12*, 241−245. [20b] A. A. Trifonov, E. N. Kirllov, M. N. Bochkarev, S. Dechert, H. Schumann, unpublished results.
[21] T. V. Petrovskaya, I. L. Fedushkin, V. I. Nevodchikov, M. N. Bochkarev, N. V. Borodina, I. L. Eremenko, S. E. Nefedov, *Russ. Chem. Bull.* **1998**, *47*, 2271−2273.
[22] S. Castelano, H. Guenthler, S. Ebersole, *J. Phys. Chem.* **1965**, *19*, 4166−4176.
[23] A. A. Trifonov, T. P. Spaniol, J. Okuda, *Organometallics* **2001**, *20*, 4869−4874.
[24] [24a] M. F. Lappert, A. Singh, L. M. Engelhardt, A. H. White, *J. Organomet. Chem.* **1984**, *262*, 271−278. [24b] P. Jutzi, E. Schulter, C. Krueger, S. Pohl, *Angew. Chem.* **1983**, *95*, 1015−1016. [24c] P. Jutzi, E. Schulter, S. Pohl, W. Saak, *Chem. Ber.* **1985**, *118*, 1959−1967.
[25] [25a] K. C. Hultzsch, T. P. Spaniol, J. Okuda, *Organometallics* **1997**, *16*, 4845−4856. [25b] K. C. Hultzsch, T. P. Spaniol, J. Okuda, *Organometallics* **1998**, *17*, 485−488. [25c] M. C. Hill, P. B. Hitchcock, *Angew. Chem.* **2001**, *113*, 4213−4216.
[26] Crystallographic parameters of **11**: $C_{38}H_{74}Cl_2Li_2N_4O_2Si_2Yb$, a = 11.161(1) Å, b = 20.535(2) Å, c = 21.986(2) Å, orthorhombic, tentative space group $P2_12_12_1$ (No. 19), data collection at 296(2) K, 7420 data, 6940 independent data ($R_{int.}$ = 0.0933), R = 0.0804, R_w = 0.1994 (observed data).
[27] [27a] K. Harms, S. Wocadlo, XCAD4, University of Marburg, Germany, **1995**. [27b] L. J. Farrugia, *WinGX − An Integrated System of Windows Programs for the Solution, Refinement and Analysis of Single-Crystal X-ray Diffraction Data, J. Appl. Cryst.* **1999**, *32*, 837−838. [27c] Siemens. *ASTRO, SAINT and SADABS. Data Collection and Processing Software for the SMART System.* Siemens Analytical X-ray Instruments Inc., Madison, Wisconsin, USA, **1996**. [27d] G. M. Sheldrick, SHELXS-86, Program for the Refinement of Crystal Structures; University of Göttingen, Germany, **1986**. [27e] G. M. Sheldrick, SHELXL-97, Program for the Refinement of Crystal Structures; University of Göttingen, Germany, **1997**.

Received August 9, 2002
[I02449]

Vinylogue Mono- and Bimetallic Cationic Sesquifulvalene and Monohydro Sesquifulvalene Complexes for Second Harmonic Generation

Timo Meyer-Friedrichsen,[a,b] Hans Wong,[a,c] Marc H. Prosenc,[a] and Jürgen Heck*[a]

Dedicated to Prof. Dr. Dieter Fenske on the occasion of his 60th birthday

Keywords: Sesquifulvalene / Ruthenium / X-ray structure determination / Hyper-Rayleigh Scattering (HRS) / Second harmonic generation (SHG)

The donor-acceptor complexes with a vinylogue monohydro sesquifulvalene and sesquifulvalene backbone of the type $[(\eta^5\text{-}C_5H_5)Ru\{\mu\text{-}(\eta^5\text{-}C_5H_4)C_2H_2(\eta^6\text{-}C_7H_7)\}ML](PF_6)_n$ [n = 0: ML = none (**1**), $Cr(CO)_3$ (**2**); n = 1: ML = $Ru(\eta^5\text{-}C_5H_5)$ (**3a**), $Ru(\eta^5\text{-}C_5Me_5)$ (**3b**)] and $[(\eta^5\text{-}C_5H_5)Ru\{\mu\text{-}(\eta^5\text{-}C_5H_4)C_2H_2(\eta^7\text{-}C_7H_6)\}ML](PF_6)_n$ [n = 1: ML = none (**4**), $Cr(CO)_3$ (**5**); n = 2: ML = $Ru(\eta^5\text{-}C_5H_5)$ (**6a**), $Ru(\eta^5\text{-}C_5Me_5)$ (**6b**)], respectively, have been synthesised, and spectroscopically and structurally characterised. A charge-shift correlation was carried out by means of ^1H NMR spectroscopic studies and an increased ground-state donor-acceptor interaction in the order **5** < **6b** < **4** < **6a** was found. The corresponding donor-acceptor interaction in **3a** and **3b** varies by an insignificant amount. Hyper-Rayleigh scattering (HRS) was applied to determine the first hyperpolarisability β of the mono- and dicationic complexes **3a**–**6b**. The β values obtained for the cationic sesquifulvalene complexes **4**–**6b** are among the largest ever measured for ruthenocenyl containing complexes due to a strong resonance enhancement: the sesquifulvalene complexes **4**–**6a**, **6b** show first hyperpolarisabilities which range between 360 and 700×10^{-30} esu, whereas β for the monohydrosesquifulvalene complexes are considerably lower (75 and 162×10^{-30} esu). For the latter complexes the first hyperpolarisability doubles on going from $Ru(\eta^5\text{-}C_5Me_5)$ (**3b**) to $Ru(\eta^5\text{-}C_5H_5)$ (**3a**) in the acceptor unit.

(© Wiley-VCH Verlag GmbH & Co. KGaA, 69451 Weinheim, Germany, 2003)

Introduction

In our studies on mono- and dinuclear sesquifulvalene-type complexes[1] directed to nonlinear optical (NLO) properties of organometallic complexes[2] we have found that cationic ferrocenyl based sesquifulvalene complexes often reveal fluorescence[1c–1e] due to two-photon absorption (TPF)[3] in the hyper-Rayleigh scattering (HRS) experiments, with 1064 nm as the fundamental wavelength. Ruthenocenyl containing sesquifulvalene derivatives are different in that they do not show any TPF in comparable HRS studies, which allows for a reliable determination of the first hyperpolarisability β, a measure of the molecular capability for second harmonic generation (SHG).[2] In order to obtain a better understanding of the donor-acceptor interaction in sesquifulvalene-type complexes, directed to NLO properties, we investigated the ruthenocenyl based conegeners in more detail.[4,5] In this work we focussed our interest on the vinylogue sesquifulvalene complexes (**I**) varying the electron-withdrawing force of the tropylium moiety as the electron acceptor (Figure 1). In addition, the cationic monohydro sesquifulvalene complexes **II** are synthesized and investigated, since the coordinated π-bonding system of

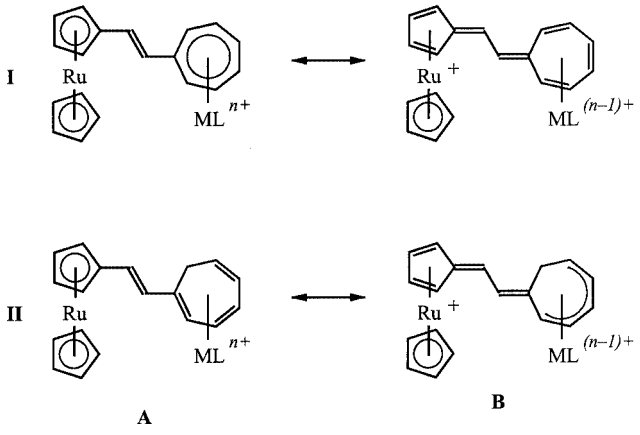

Figure 1. Vinylogue mono- and dinuclear sesquifulvalene (**I**) and monohydro sesquifulvalene (**II**) complexes (**I**: n = 1, ML = none, $Cr(CO)_3$; n = 2, ML = $Ru(\eta^5\text{-}C_5R_5)$, R = H, Me. **II**: n = 1, ML = $Ru(\eta^5\text{-}C_5R_5)$, R = H, Me)

[a] Institut für Anorganische und Angewandte Chemie, Universität Hamburg, Martin-Luther-King-Platz 6, 20146 Hamburg, Germany
Fax: (internat) + 49-40/42838-6945
E-mail: juergen.heck@chemie.uni-hamburg.de
[b] Bayer AG Leverkusen, Werk Uerdingen, Rheinuferstraße 7–9, 47829 Krefeld, Germany
[c] 45–47 Hillwood Road, Hillwood Mansion, 12/F, Flat B, Kowloon, Hong Kong, China

the cationic acceptor moiety is assumed to be electronically coupled to the ruthenocenyl donor. For both types of complexes the bonding situation can be described in two mesomeric forms, which differ between a bisaromatic (**I**, **A**) and cross-conjugated form (**I**, **B**) and an aromatic-homoaromatic (**II**, **A**) and cross-conjugated-dienyl (**II**, **B**) form, respectively.

Former investigations on the archetype sesquifulvalene complexes[4,5a] illustrate an increasing SHG effect by reinforced donor-acceptor interaction in the electronic ground state, which is shown by means of NMR spectroscopic data as well as structural data. In terms of a valence bond picture a growing donor-acceptor interaction may be described as an increasing contribution of the cross-conjugated mesomeric form (**B**) to the electronic ground state (Figure 1).

The extension of our NLO studies on organometallic dipolar cationic donor-acceptor complexes to monohydro sesquifulvalene complexes was motivated by the concept that a transition from a homoaromatic to a conjugated-dienyl form (**II**) demands less energy than the loss of aromaticity as shown for the mesomeric forms of **I**. Additionally, mono cationic η^6-cycloheptatriene complexes are expected to be more stable than the corresponding dicationic η^7-cycloheptatrienylium complexes, due to the less electrophilic nature.

Results and Discussion

Synthesis: The cationic dinuclear vinylogue sesquifulvalene and monohydro sesquifulvalene complexes are readily prepared by starting with a Wittig−Horner−Wadsworth−Emmons (WHWE) reaction of the (cyclohepta-1,3,5-trienyl-1-methyl)diethylphosphonate[1d] with *n*BuLi, and formyl ruthenocene[6] (Scheme 1, see a), yielding the mononuclear, monohydro sesquifulvalene complex **1**. The coordination of the neutral unit $Cr(CO)_3$ (Scheme 1, see b) and the cationic half-sandwich moiety $Ru(\eta^5\text{-}C_5R_5)$ (Scheme 1, see c) to the cycloheptatriene ring yields the uncharged and charged dinuclear monohydro sesquifulvalene complexes **2** [ML = $Cr(CO)_3$] and **3** [ML = $Ru(\eta^5\text{-}C_5H_5)$: **3a**; ML = $Ru(\eta^5\text{-}C_5Me_5)$: **3b**], respectively. Hydride abstraction with $[Ph_3C]PF_6$ transforms **1** into the monocationic sesquifulvalene-type complex **4** (Scheme 1, see d), whereas the corresponding reaction with **2** leads to the monocationic, dinuclear sesquifulvalene complex **5** [ML = $Cr(CO)_3$] (Scheme 1, see e). The dicationic complexes **6** [ML = $Ru(\eta^5\text{-}C_5H_5)$: **6a**; ML = $Ru(\eta^5\text{-}C_5Me_5)$: **6b**] are achieved by addition of $[Ru(\eta^5\text{-}C_5R_5)(MeCN)_3]^+$ (R = H, Me) (Scheme 1, see f) to **4**.

The cationic products are complexes that are orange (**3a, 3b**) to dark-red in colour (**4−6a**, **6b**), indicating an increased electronic interaction in the cationic state compared to the neutral monohydro sesquifulvalene starting complex **1,** which has light yellow crystals. The monocationic and dicationic complexes are very soluble in CH_2Cl_2 and $MeNO_2$, respectively. Solutions of **1**, **2**, **3a**, **3b**, **6a** and **6b** are moderately inert in air, whereas **4** and **5** are sensitive to moisture.

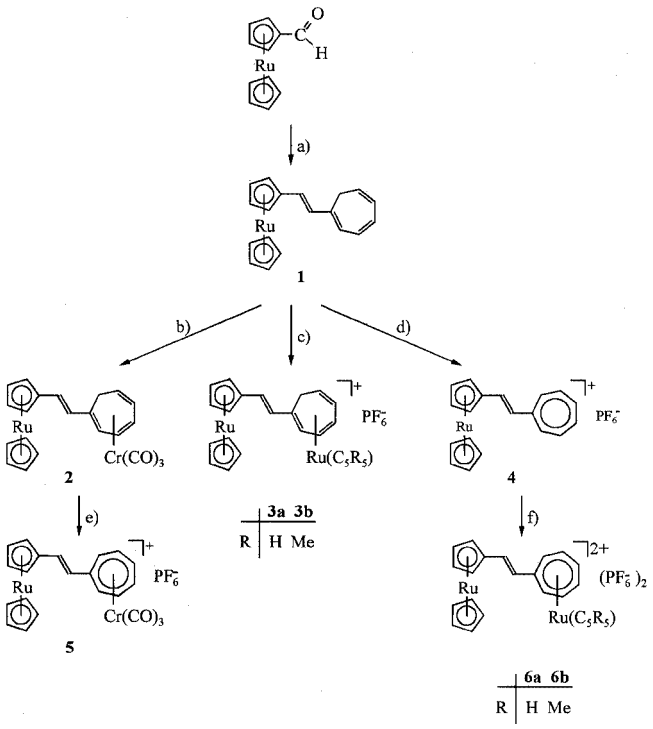

Scheme 1. Synthesis of the mono- and dinuclear monohydro sesquifulvalene and sesquifulvalene type complexes **3a** − **6b**: a) THF; *n*BuLi. $C_7H_7CH_2P(O)(OEt)_2$; b) THF, $Cr(CO)_3(EtCN)_3$; c) CH_2Cl_2, $[Ru(\eta^5\text{-}C_5R_5)(MeCN)_3]PF_6$ (R = H, Me); d) CH_2Cl_2, $[CPh_3]PF_6$; f) CH_2Cl_2 $[Ru(\eta^5\text{-}C_5R_5)(MeCN)_3]PF_6$ (R = H, Me).

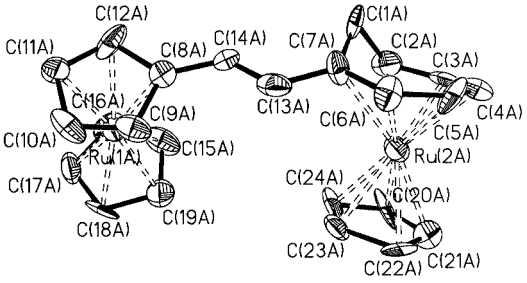

Figure 2. Molecular structure of $[(\eta^5\text{-}C_5H_5)Ru\{\mu\text{-}(\eta^5\text{-}C_5H_4)C_2H_2(\eta^6\text{-}C_7H_7)\}Ru(\eta^5\text{-}C_5H_5)]PF_6$ (**3a**) (50% ellipsoids, only one of the two independent complex cations is shown, the hydrogen atoms and the counterion are omitted for clarity).

X-ray Structure Determination: Suitable crystals for X-ray structure analysis were obtained by gas phase diffusion of Et_2O in concentrated solutions of the complexes in CH_2Cl_2 (**3a**, **3b**) and $MeNO_2$ (**6a**). Complex **3a** crystallises as twins. However, the twinning law could not be determined and thus reflexes had to be excluded by hand with F(obsd.) ≥ 4 F(calcd.) mostly from the *hk*3, *hk*6, etc. planes. In addition a superstructure was found, in which the *a*-axis was tripled resulting in six independent molecules per asymmetric unit. We circumvented the superstructure problem by solving and refining the structure by standard methods using the smaller unit cell. The dinuclear, monocationic monohydro sesquifulvalene complex **3a** crystallises in the monoclinic space group $P2_1/c$, whereas the pentamethylated derivative **3b** crystallises in a triclinic space group $P\bar{1}$. For

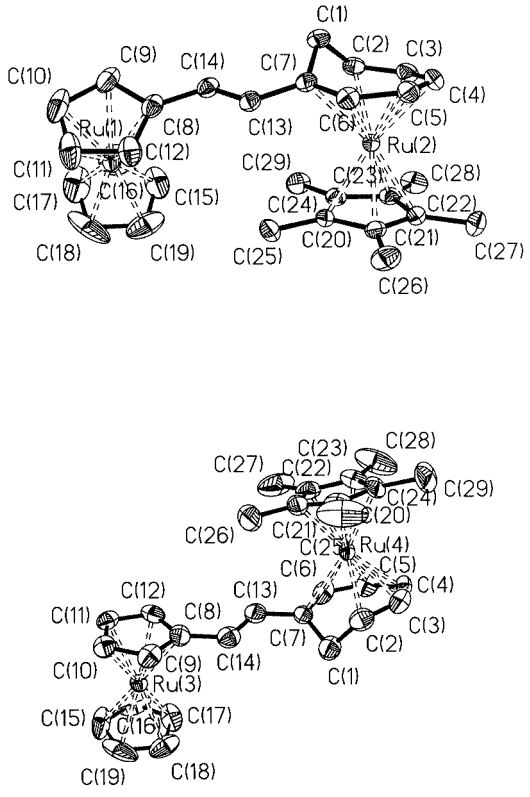

Figure 3. Molecular structures of $[\eta^5\text{-}C_5H_5)Ru\{\mu\text{-}(\eta^5\text{-}C_5H_4)C_2H_2(\eta^6\text{-}C_7H_7)\}Ru(\eta^5\text{-}C_5Me_5)]PF_6$ (**3b**). The *cisoid* (top) and *transoid* (bottom) conformers are shown (50% ellipsoids, the hydrogen atoms, the solvent molecules and counterions are omitted for clarity).

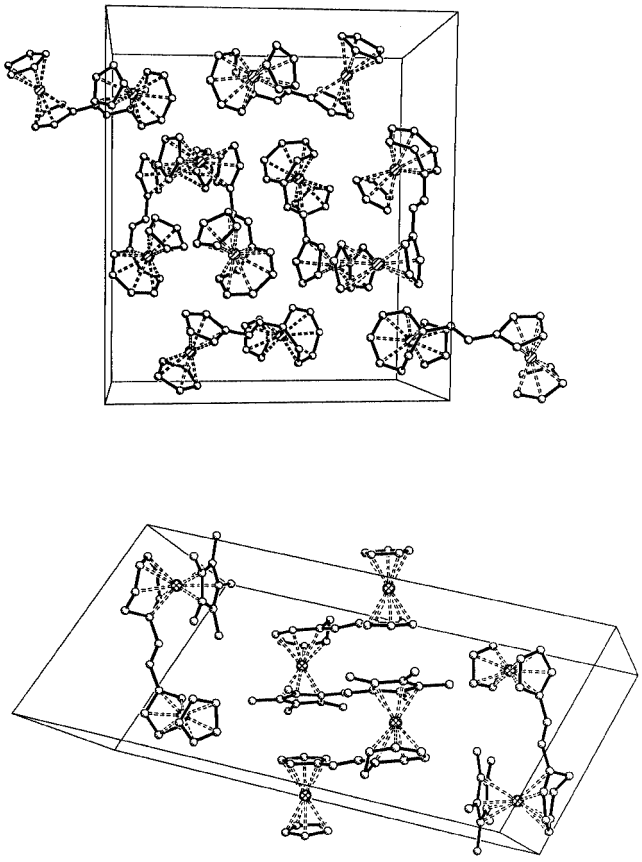

Figure 4. Unit cells of **3a** (top) and **3b** (bottom), illustrating the pairwise arrangements of the two planar chiral enantiomers in pairs (the counterions and solvent molecules are omitted for clarity).

both compounds two independent molecules within the asymmetric unit are found (Figure 2, Figure 3). Since **3a** and **3b** are planar-chiral compounds due to the coordination of the cycloheptatriene ring to a metal centre and its monosubstitution in the proximal position with respect to the sp^3 carbon atom C1, the single crystals are racemic mixtures of both enantiomers. Additionally, for **3b** the solvent molecules $MeNO_2$ and CH_2Cl_2 co-crystallise in a ratio of 2:1. The cations of **3a** and **3b** posses an *E*-configuration, and the sp^3 carbon atom C1 of the seven-membered ring occupies a *trans*-position relative to the hydrogen atom of the neighbouring CH group of the vinyl bridge, which is sterically less demanding. Whereas the monohydro sesquifulvalene cations of **3a** only adopt a *cisoid* conformation in the crystal, the cations of **3b** are packed in a *transoid* and in a *cisoid* conformation (Figure 2, Figure 3, Figure 4). The *transoid* conformation is unprecedented, since all known expanded sesquifulvalene complexes crystallise in a *cisoid* conformation[1] in contrast to the archetype dinuclear sesquifulvalene complexes with directly linked five- and seven-membered rings, which only demonstrate a *transoid* conformation due to steric repulsion.[1a−1c,5a] The *cisoid* complexes of **3a** and **3b** demonstrate a relatively large tilt angle of 47 and 38.1°, respectively, between the best plane of the substituted five-membered ring of the donor moiety and the best plane of the cycloheptatriene ligand defined by the carbon atoms C2−C7; the corresponding tilt angle in the *transoid* conformation only amounts to 20.8°.

The bond lengths and angles of the ruthenocenyl donor moiety are quite similar to those of other ruthenocene derivatives.[6,7]

The cycloheptatriene ligand of the acceptor terminus in **3a** and **3b** adopts a flat boat conformation with a steep bow for the endocyclic methylene group that deflects about 60° from the best plane defined by C2−C7. Similar structural features are known from other cycloheptatriene complexes although with corresponding angles below 50°.[8] The bridging unit C7−C13−C14−C8 does not show any significant deviation from expected bond lengths of sp^2-sp^2 carbon-carbon single and double bonds, indicating only a subtle charge delocalisation in the crystalline state. It is concluded from the bond elongation of more than 10 pm between Ru2 and C7, that a weak donor-acceptor charge equilisation still occurs. This bond elongation indicates electronic communication between the electron donating and accepting termini, which has been found in archetype sesquifulvalene complexes.[1e,5a] Thus, by means of structural data, the electronic ground state of the monohydro sesquifulvalene complexes **3a** and **3b** in the solid state is properly described by the mesomeric form **II**, **A** in Figure 1.

The X-ray structure analysis of the dinuclear dicationic vinylogue sesquifulvalene complex **6a** rendered more diffi-

Table 1. Crystallographic data of $[(\eta^5\text{-}C_5H_5)Ru\{\mu\text{-}(\eta^5\text{-}C_5H_4)C_2H_2(\eta^6\text{-}C_7H_7)\}Ru(\eta^5\text{-}C_5H_5)]PF_6$ (**3a**), $[(\eta^5\text{-}C_5H_5)Ru\{\mu\text{-}(\eta^5\text{-}C_5H_4)C_2H_2(\eta^6\text{-}C_7H_7)\}Ru(\eta^5\text{-}C_5Me_5)]PF_6$ (**3b**) and $[(\eta^5\text{-}C_5H_5)Ru\{\mu\text{-}(\eta^5\text{-}C_5H_4)C_2H_2(\eta^7\text{-}C_7H_6)\}Ru(\eta^5\text{-}C_5H_5)](PF_6)_2$ (**6a**)

	3a	**3b**	**6a**
Empirical formula	$C_{48}H_{46}F_{12}P_2Ru_4$	$C_{29}H_{33}F_6$ P $Ru_2 \times 1/3(CH_3NO_2) \times 2/3$ (CH_2Cl_2)	$C_{24}H_{22}F_{12}P_2Ru_2 \times (CH_3NO_2)$
Formula mass	1317.07	805.95	863.54
T [K]	153(2)	173(2)	173(2)
λ [pm]	71.073	71.073	71.073
Crystal system	monoclinic	triclinic	triclinic
Space group	$P2_1/c$	$P\bar{1}$	$P\bar{1}$
a [pm]	1955.0(17)	1174.8(1)	1060.9(2)
b [pm]	1733.5(15)	1179.6(1)	1385.0(1)
c [pm]	1423.2(12)	2379.7(1)	1070.6(2)
α [°]		82.73(1)	80.57(1)
β [°]	96.704(8)	75.81(1)	83.36(1)
γ [°]		75.37(1)	69.29(1)
V [10^6 pm^3]	4790(7)	3057.7(4)	1448.6(4)
Z	8	4	2
$\rho_{calcd.}$ [Mg/m^3]	1.826	1.751	1.980
μ [mm^{-1}]	1.384	1.219	1.257
F (000)	2592	1611	848
Crystal size [mm^3]	0.1 × 0.2 × 0.2	0.6 × 0.4 × 0.3	0.4 × 0.4 × 0.2
Scan range [°]	1.57−25.00	0.88−39.14	1.59−28.73
Index range	$-23 \le h \le 23$	$-15 \le h \le 16$	$-14 \le h \le 11$
	$-20 \le k \le 20$	$-16 \le k \le 11$	$-18 \le k \le 15$
	$-16 \le l \le 16$	$-31 \le l \le 32$	$-14 \le l \le 12$
Reflections measured	43430	20954	10006
Reflections unique	8120	14884	7063
Rint	0.3217	0.0156	0.0246
Parameters	575	787	445
Reflections $I > 4\ \sigma(I)$	8120[c]	12716	5517
GoF[a]	0.989	1.032	1.030
$R1/wR2$ ($I > 2\sigma(I)$)[b]	0.1127/0.2312	0.0375/0.0886	0.0436/0.1052
$R1/wR2$ (all data)[b]	0.1981/0.2701	0.0469/0.0946	0.0637/0.1153
Resd. min/max. [e-/ Å^3]	−1.453/1.402	−0.819/1.296	−0.957/1.167

[a] GoF (goodness of fit) = $[\Sigma w(F_o^2 - F_c^2)^2 In - p]^{1/2}$ (n = numbers of reflections, p = numbers of parameters). [b] $R1 = \Sigma||F_o| - |F_c|| / \Sigma|F_o|$; $wR2 = [\Sigma w(F_o^2 - F_c^2)^2/\Sigma w(F_o^2)^2]^{1/2}$. [c] For refinement all unique reflections were used.

culties due to a disorder in the vinylene bridge (Figure 5), which is commonly observed in vinylogue sesquifulvalene complexes.[1a,1c,1d,9] The best structural solution was obtained by assuming two different molecules in the ratio 3:1. To separate the atoms of the sesquifulvalene ligand restrictions were necessary, which do not allow a more detailed discussion. Nevertheless, the short carbon-carbon bond C13−C14 [132.1(7) pm] differs distinctly from the carbon-carbon bond C8−C14 [145.3(6) pm) and C7−C13 [144.9(6) p], clearly indicating a carbon-carbon double and single bond, respectively.

The structure data of the cyclopentadienyl-ruthenium moieties in **6a** greatly resemble the data of other CpRu units in Ru sandwich compounds (vide supra and ref.[7]). It is worthwhile noting that − as for **3a** and **3b** − the bond length between the Ru2 atom and the bridge-head carbon atom C7 is elongated by more than 10 pm compared with the other Ru−C bond lengths of the $Ru(\eta^7\text{-}C_7H_6)$ moiety.

Spectroscopic Studies: Considering the two different mesomeric forms depicted in Figure 1, it becomes evident that an increasing contribution of the mesomeric form **B** to the ground state of the complexes under study results in a decrease of the bond order of the carbon-carbon bond C13−C14. Hence, spectroscopic properties based on the C,C bond order should be sensitive probes for the examination of the donor-acceptor interaction.[10]

One indicative probe for the C13−C14 bond order is the energy of the C,C stretching vibration of the carbon-carbon bond C13−C14,[10] which differs only marginally for the cycloheptatriene derivatives but the decrease is more pronounced for the tropylium congeners in the order **5** > **6b** > **4** > **6a** (Table 3). Although the energy of the C,C stretching vibration is still representative of a C=C bond, a distinct charge delocalisation can be stated for the electronic ground state of **6a,** in particular, the amount of which can be taken as a measure of the donor-acceptor interaction. From the energy of the stretching mode of the C,C double bond one can conclude that the donor-acceptor interaction is weakest for **1**−**3** and **5**, and strongest for **6a**, in this series.

This result is in excellent agreement with the NMR spectroscopic data. One NMR probe for the C13−C14 bond order is the *trans* ^{1}H-^{1}H coupling constant of the bridging vinyl group.[10−12] For a real carbon-carbon double bond a *trans*-$^3J(H_\alpha - H_\beta)$ coupling constant of about 16 Hz is expected according to weak donor-acceptor interaction. With increasing charge delocalisation the C13−C14 bond order decreases and hence the ^{1}H-^{1}H coupling constant too;[10] a C,C single bond causes coupling constants of about at least

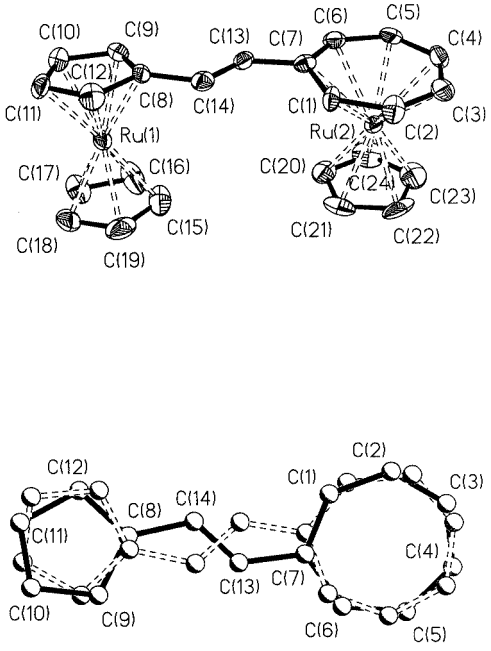

Figure 5. Molecular structure of $[\eta^5\text{-}C_5H_5)Ru\{\mu\text{-}(\eta^5\text{-}C_5H_4)C_2H_2(\eta^7\text{-}C_7H_6)\}Ru(\eta^5\text{-}C_5H_5)](PF_6)_2$ (**6a**) (50% ellipsoids, the hydrogen atoms and counterions are omitted for clarity). The drawing at the bottom demonstrates the disorder of the vinylogue sesquifulvalene ligand.

10 Hz. Whereas for the neutral and monocationic monohydro sesquifulvalene complexes **1**, **2**, **3a**, **3b** the $^3J(H_\alpha-H_\beta)$ only varies between 15.8 and 15.6 Hz, indicating a more or less unchanged carbon-carbon double bond, the corresponding coupling constants of the vinylogue sesquifulvalene complexes decrease from 16 Hz for **5** to 15.4 Hz for **4** and **6b** and drops to 13.4 Hz for **6a** (Table 3).

Another NMR probe for donor-acceptor interactions in cationic NLO chromophores under study is the charge-shift correlation of Ru sandwich complexes. A linear dependence between the shift of the cyclopentadienyl proton signals and the charge per sandwich complex in $[(\eta^5\text{-}C_5H_5)Ru(\eta^n\text{-}C_nH_n)]^{m+}$ ($n = 5$, $m = 0$; $n = 6$, $m = 1$; $n = 7$, $m = 2$) is found, which allows the calculation of the actual charge for a sandwich complex containing a $(\eta^5\text{-}C_5H_5)Ru$ unit, when the shift of the signal of the cyclopentadienyl protons is known.[5a,5b] The singlet of the unsubstituted cyclopentadienyl ligand of the metallocene donor and of the $Ru(\eta^5\text{-}C_5H_5)$ unit of the acceptor is taken as the monitoring signal. The corresponding NMR shifts are listed in Table 3, and clearly indicate an increasing positive charge on the metallocene terminus in the order **5** < **6b** < **4** < **6a** for the tropylium derivatives. For **6a** a positive charge of +0.61 is calculated for the ruthenocenyl donor in the ground state which is in good harmony with the diminishing positive charge on the acceptor to +1.44 with respect to the positive charge of +2.0 in $[(\eta^5\text{-}C_5H_5)Ru(\eta^5\text{-}C_7H_7)]^{2+}$ (Table 3). It is worth noting for the studies concerning the $^1H_\alpha$-$^1H_\beta$ coupling constants that the change of the donor-acceptor interaction in this series of complexes is the largest on going from complex **6b** (or, **5**) to **6a**, which is in agreement with the IR spectroscopic studies.

Table 2. Selected interatomic distances [pm] and angles [°] of $[(\eta^5\text{-}C_5H_5)Ru\{\mu\text{-}(\eta^5\text{-}C_5H_4)C_2H_2(\eta^6\text{-}C_7H_7)\}Ru(\eta^5\text{-}C_5H_5)]PF_6$ (**3a**), $[(\eta^5\text{-}C_5H_5)Ru\{\mu\text{-}(\eta^5\text{-}C_5H_4)C_2H_2(\eta^6\text{-}C_7H_7)\}Ru(\eta^5\text{-}C_5Me_5)]PF_6$ (**3b**) and $[(\eta^5\text{-}C_5H_5)Ru\{\mu\text{-}(\eta^5\text{-}C_5H_4)C_2H_2(\eta^7\text{-}C_7H_6)\}Ru(\eta^5\text{-}C_5H_5)](PF_6)_2$ (**6a**).

	3a[a]	**3b** (*cisoid*)	**3b** (*transoid*)	**6a**
C8−C9	148(2)	143.8(5)	140.1(6)	143.0(10)
C9−C10	140(3)	142.1(6)	140.4(6)	141.9(4)
C10−C11	151(3)	141.7(7)	141.5(6)	141.9(4)
C11−C12	141(3)	143.1(5)	142.4(6)	141.9(4)
C12−C8	150(3)	143.2(5)	144.7(6)	143.0(10)
C7−C1	157(3)	151.6(4)	148.5(5)	141.7(10)
C1−C2	159(3)	150.7(4)	148.2(6)	140.9(2)
C2−C3	142(3)	139.4(5)	136.8(6)	140.9(2
C3−C4	144(3)	142.6(5)	139.0(6)	140.9(2
C4−C5	141(3)	142.5(5)	142.2(6)	140.9(2
C5−C6	140(3)	143.3(5)	143.3(6)	140.9(2
C6−C7	153(2)	140.1(4)	145.1(6)	141.7(10)
Ru1−C8	229.7(18)	220.1(3)	220.1(4)	215.2(5)
Ru1−C9	221.2(19)	216.7(4)	219.7(4)	215.9(6)
Ru1−C10	224(2)	217.6(4)	219.1(4)	220.0(6)
Ru1−C11	222(2)	218.0(4)	217.8(4)	218.5(6)
Ru1−C12	222(2)	219.2(4)	217.8(4)	216.5(7)
Ru2−C1	305(2)	292.7(4)	293.4(4)	224.4(6)
Ru2−C2	232(2)	227.4(3)	228.5(4)	222.7(7)
Ru2−C3	202.2(17)	218.8(3)	219.7(4)	224.5(7)
Ru2−C4	225.1(19)	222.2(3)	222.3(4)	224.4(7)
Ru2−C5	226(2)	221.5(3)	220.6(4)	224.9(8)
Ru2−C6	227.0(17)	221.2(3)	222.0(4)	227.4(6)
Ru2−C7	245(2)	238.1(3)	239.2(3)	238.7(5)
C7−C13	147(3)	145.8(4)	146.8(5)	144.9(6)
C13−C14	136(3)	134.3(4)	131.1(6)	132.1(7)
C14−C8	146(2)	145.4(5)	147.5(6)	145.3(6)
$[(C_5H_4)]$(C2−C7] [°]	47	38.1(1)	20.8(2)	28.5
[C7,C1,C2]-[C2,C3,C6,C7] [°]	56.8	60.8(3)	61.0(4)	

[a] **3a** crystallises with two different molecules (A and B) within the unit cell. In this table only the data for one molecule (A) is given (see Figure 2). The corresponding data for molecule B are equal to A within the margin of error.

UV/Vis spectroscopic studies were performed with solutions of different polarity such as dichloromethane and nitromethane, to elucidate solvatochromism which gives an indication of the dipole change $\Delta\mu$ between the ground and the excited state,[13] and is thus relevant for the static first hyperpolarisability β_0 according to the two-level approximation.[14]

The electronic excitation spectra of the vinylogue sesquifulvalene complexes **4**−**6a**, **6b** exhibit two intense absorption bands in the visible or near UV region (Figure 6, Table 4). As outlined earlier for metallocene containing donor-acceptor complexes,[1e,5a,12] the high-energy absorption band is assigned to a donor(ligand)−acceptor charge-transfer (D_L-A CT) transition whereas the low energy band is caused by a donor(metal)-acceptor charge-transfer (D_M-A CT) transition. In accordance with other cationic sesquifulvalene donor-acceptor complexes the energy of the D_M-A CT transitions increase when the acceptor unit A changes in the order $(C_7H_6)^+ < [(\eta^7\text{-}C_7H_6)Ru(\eta^5\text{-}C_5H_5)]^{2+} < [(\eta^7\text{-}C_7H_6)Ru(\eta^5\text{-}C_5Me_5)]^{2+} < [(\eta^7\text{-}C_7H_6)Cr(CO)_3]^+$ [1e,5] The

Table 3. Selected IR- and NMR spectroscopic data of the vinylogue sesquifulvalene and monohydro sesquifulvalene complexes $[(\eta^5\text{-}C_5H_5)Ru\{\mu\text{-}(\eta^5\text{-}C_5H_4)C_2H_2A]^{n+}$

A	n		IR[a] $\tilde{\nu}$ (C=C) (cm^{-1})	^{1}H NMR[b] $\delta(C_5H_5)$[c] (ppm)	Charge[d][e]	$\delta(C_5H_5)$[f] (ppm)	Charge[e][g]	$\delta(H_\alpha)$ (ppm)	$\delta(H_\beta)$ (ppm)	$^3J(H_\alpha H_\beta)$ (Hz)	^{13}C NMR[b] $\delta(C_5H_5)$[c] (ppm)	$\delta(C_5H_5)$[f] (ppm)
$(C_7H_7)\}$	0	**1**	1622							15.8		
$(\eta^6\text{-}C_7H_7)\}Cr(CO)_3$	0	**2**	1619							15.6		
$(\eta^6\text{-}C_7H_7)\}Ru(\eta^5\text{-}C_5H_5)$	1	**3a**	1624	4.61	+ 0.06	5.35	+ 0.90	6.87	6.40	15.9	72.9	85.3
$(\eta^6\text{-}C_7H_7)\}Ru(\eta^5\text{-}C_5Me_5)$	1	**3b**	1619	4.66	+ 0.11			6.89	6.25	15.8	72.5	
$(C_7H_6)\}$	1	**4**	1603	4.78	+ 0.24			8.18	6.78	15.4	74.8	
$(\eta^7\text{-}C_7H_6)\}Cr(CO)_3$	1	**5**	1624	4.65	+ 0.10			7.63	6.81	16.0	73.3	
$(\eta^7\text{-}C_7H_6)\}Ru(\eta^5\text{-}C_5H_5)^+$	2	**6a**	1599	5.11	+ 0.61	5.86	+ 1.44	7.55	5.92	13.4	81.9	88.2
$(\eta^7\text{-}C_7H_6)\}Ru(\eta^5\text{-}C_5Me_5)^+$	2	**6b**	1609	4.75	+ 0.21			7.98	6.77	15.4	73.9	

[a] KBr pills. [b] CD_3NO_2 solutions. [c] Unsubstituted Cp ligand of the ruthenocenyl donor unit. [d] Charge on the donor unit. [e] Calculated from the charge-shift correlation in ref.[5b] [f] Unsubstituted Cp ligand of the acceptor unit **A**. [g] Charge on the acceptor unit.

Table 4. UV/Vis data of the vinylogue sesquifulvalene and monohydro sesquifulvalene complexes of $[(\eta^5\text{-}C_5H_5)Ru\{\mu\text{-}(\eta^5\text{-}C_5H_4)C_2H_4A]^{n+}$ and their first hyperpolarisability β determined by HRS.

A	n		λ_{max} (nm) D_L-A CT CH_2Cl_2 (ε)[a]	$MeNO_2$ (ε)[a]	$\Delta\tilde{\nu}$ (cm^{-1})	λ_{max} (nm) D_M-A CT CH_2Cl_2 (ε)[a]	$MeNO_2$ (ε)[a]	$\Delta\tilde{\nu}$ (cm^{-1})	β[b]	β_0[b][c]
$(\eta^6\text{-}C_7H_7)\}Ru(\eta^5\text{-}C_5H_5)$	1	**3a**	–	–		423 (10490)	404 (9410)	−1112(2)	162[d]	50
$(\eta^6\text{-}C_7H_7)\}Ru(\eta^5\text{-}C_5Me_5)$	1	**3b**	–	–		424 (11460)	409 (10225)	−865(2)	75[d] (87)[e]	23 (30)
$(C_7H_6)\}$	1	**4**	480 (16265)	470 (12036)	−443(2)	640 (22559)	600 (16427)	−1042(2)	362[d] (649)[e]	105[f] (120)[f]
$(\eta^7\text{-}C_7H_6)\}Cr(CO)_3$	1	**5**	384 (8730)	< 370	–	533 (8375)	490 (7155)	−1611(2)	497[e]	59[f]
$(\eta^7\text{-}C_7H_6)\}Ru(\eta^5\text{-}C_5H_5)$	2	**6a**	> 400 (sh) (10760)	400	–	600 (sh)	560 (4975)	−1190(2)	358[e]	28[f]
$(\eta^7\text{-}C_7H_6)\}Ru(\eta^5\text{-}C_5Me_5)$	2	**6b**	438 (sh)	409 (10580)	−1619(2)	594 (sh)	541 (9280)	−1649(2)	701[e]	17[f]

[a] $M^{-1}cm^{-1}$. [b] Given as units of 10^{-30} esu; as a reference *p*-nitroaniline was used: $\beta(CH_2Cl_2) = 21.6 \times 10^{-30}$ esu,[22] $\beta(MeNO_2) = 34.6 \times 10^{-30}$ esu.[23] [c] Calculated from $\beta_0 = \beta(HRS)\ [(1 - 4\lambda^2_{max}/\lambda^2)(1 - \lambda^2_{max}/\lambda^2)]$.[14] [d] In CH_2Cl_2. [e] In $MeNO_2$. [f] The D_M-A CT transition was taken into account for the calculation of β_0.

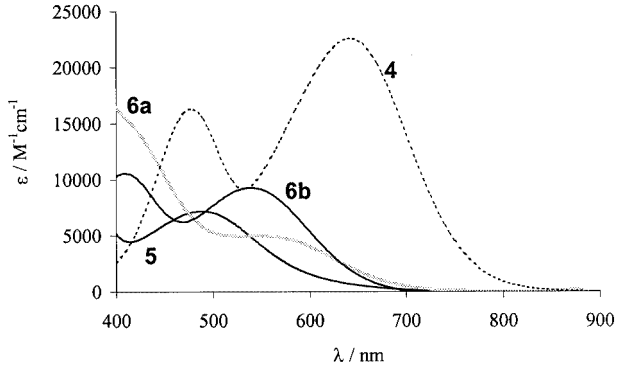

Figure 6. UV/Vis spectra of the vinylogue sesquifulvalene complexes $[(\eta^5\text{-}C_5H_5)Ru\{\mu\text{-}(\eta^5\text{-}C_5H_4)C_2H_2(\eta^7\text{-}C_7H_6)\}ML](PF_6)_n$ [n = 1, ML = none (**4**), $Cr(CO)_3$ (**5**); n = 2, ML = $Ru(\eta^5\text{-}C_5R_5)$, R = H (**6a**), Me (**6b**)] obtained from $MeNO_2$ solutions.

extraordinary low-energy shift of the D_M-A CT band of the mononuclear complex **4** compared with the dinuclear species may be explained by the formation of additional molecular orbitals (MO) upon coordination of a metal-ligand fragment to the tropylium unit, thus forming occupied bonding MOs which would be lower in energy, and empty anti-bonding MOs which would be higher in energy compared with the orbitals of the initially uncoordinated tropylium moiety.

The monohydro sesquifulvalene complexes **3a** and **3b** only reveal one intense absorption band with a λ_{max} between 400 and 430 nm (Figure 7). Since the energetically lower lying absorption bands in metallocene containing donor-acceptor complexes are generally explained as a D_M-A CT transition, the low-lying absorption band for **3a** (λ_{max} = 423 nm) and **3b** (λ_{max} = 424 nm) is also assigned to a D_M-A CT transition.

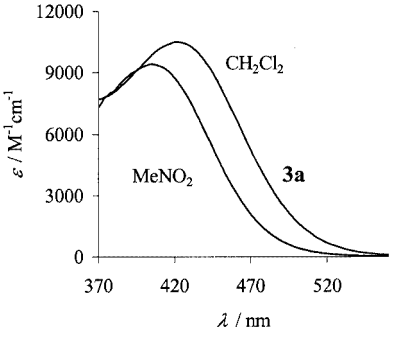

Figure 7. UV/Vis spectra of the vinylogue monohydro sesquifulvalene complex $[(\eta^5\text{-}C_5H_5)Ru\{\mu\text{-}(\eta^5\text{-}C_5H_4)C_2H_2(\eta^6\text{-}C_7H_7)\}Ru(\eta^5\text{-}C_5H_5)]PF_6$ (**3a**) obtained from CH_2Cl_2 and $MeNO_2$ solutions indicating the hypsochromic shift of λ_{max} by increasing solvent polarity.

All of the above mentioned absorption bands undergo considerable negative solvatochromism i.e. hypsochromic shift, with increasing solvent polarity indicating a more localized positive charge in the ground state than in the excited state, or even an inversion of the polarity upon excitation. The extent of the solvatochromism of both of the absorption bands for **4**−**6a**, **6b** is comparable, indicating a similar change in polarity for both of the CT transitions. Therefore, both CT transitions should contribute considerably to the first hyperpolarisability. The situation is different for **3a** and **3b,** which only reveal one absorption band close to the second harmonic generation. The cut off of the absorption bands around 500 nm warrants a reliable calculation of β_0 for **3a** and **3b**.

NLO Measurements: The low-lying excited states of the sesquifulvalene complexes under study, their facile polarisability as indicated by their strong solvatochromism, and the assignment of the HOMOs and LUMOs to the donor and acceptor orbitals, respectively, make these types of complexes very promising for the second harmonic generation. The cationic nature of the sesquifulvalene complexes requires the hyper-Rayleigh scattering (HRS)[15] as the only method for determining the first hyperpolarisability β, which can be regarded as the molecular capability of doubling the frequency of incoming light. However, a draw-back of the HRS method may be fluorescence due to two-photon absorption.[16−18] Since the realisation of the problem of multiphoton absorption induced fluorescence concerning the determination of the first hyperpolarisability, several techniques have been investigated to overcome this problem. These include long wavelength measurements,[10,19,20] time resolved HRS[19] measurement of the two-photon fluorescence spectrum to abstract the fluorescence contribution to the HRS signal,[21] and, just recently, a high-frequency demodulating technique to suppress the multiphoton fluorescence contribution to the HRS signal.[16] A "low cost" check for the two-photon fluorescence was recently described,[1d,1e] and uses bandpass filters with peak transmittance at different wavelengths, which are introduced in front of the photomultiplier of the HRS set-up. The broad fluorescence signal, which yields the emission maximum at λ/2 of the fundamental wavelength, is easily discerned from the narrow second harmonic signal at λ/2.

In the course of this study no fluorescence was observed (Figure 8). Therefore, for all dipolar mono- and dicationic complexes under study the first hyperpolarisability β was determined by means of HRS (Table 4).

Since the wavelengths of the absorption bands are in close proximity to the wavelength of the SHG signal, the obtained β values are strongly resonance enhanced and are therefore corrected by the dispersion term of the two-level model.[14] It has to be emphasised that the β_0 values for **4**, **5**, **6a** and **6b** are not very reliable, since only the low-energy D_M-A CT transition was taken into account for calculating β_0; the high energy D_L-A CT transition will also contribute to the first hyperpolarisability as indicated by the strong solvatochromism of both CT transitions. However, it is worth noting that the first hyperpolarisability for **4** decreases by almost a factor of two on going from a $MeNO_2$ solution to the less polar CH_2Cl_2 solution, although λ_{max} of the D_L-A CT transition is shifted closer to λ(SHG) for CH_2Cl_2 solutions than for $MeNO_2$ solutions. The opposite is true for the D_M-A CT transition. This behaviour points to larger contributions of the D_M-A CT transition to the β values than the D_L-A CT transition.

The HRS-determined first hyperpolarisability of the vinylogue mono- and dicationic sesquifulvalene complexes **4**, **5**, **6a**, and **6b** (Table 4) belong to the largest values ever obtained for ruthenocenyl containing dipolar NLO chromophores,[24] in particular, when the relatively small molecular mass is taken into account, which is often used as a figure of merit. However, it has to be realized that the first hyperpolarisabilities are strongly resonance enhanced by different contributions of D_L-A CT and D_M-A CT transitions. Therefore, no correlation between the β values of **4**, **5**, **6a** and **6b** and their ground-state donor-acceptor interaction as demonstrated by IR- and NMR spectroscopy, can be stated, although the strongest SHG effect may be expected for **6a** taking into account the ground state donor-acceptor interaction. This can only be proven when λ(SHG) is beyond the cut-off of λ(D_M-A CT).

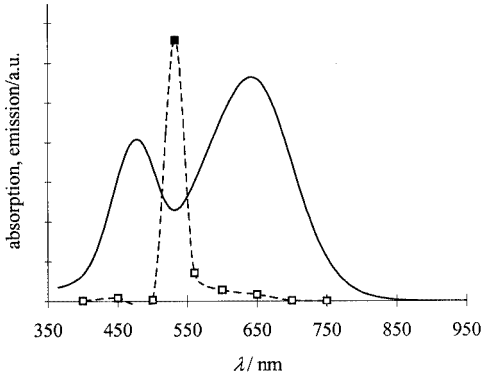

Figure 8. Representative UV/Vis absorption spectrum for vinylogue sesquifulvalene complexes $[(\eta^5\text{-}C_5H_5)Ru\{\mu\text{-}(\eta^5\text{-}C_5H_4)C_2H_2(\eta^7\text{-}C_7H_6)\}ML]PF_6$ (ML: = none: **4**) obtained from CH_2Cl_2 solution (solid line) and the corresponding scattered spectrum obtained from HRS studies (dotted line) indicating only the SHG signal (a.u. = arbitrary units)

In contrast the cut-off of the absorption band of the D_M-A CT transition of **3a** and **3b** is below λ(SHG), and thus allows a reliable determination of the first hyperpolarisability β, which doubles on going from **3b** (ML = Ru(η^5-C_5Me_5); β = 75 × 10^{-30} esu) to **3a** (ML = Ru(η^5-C_5H_5); β = 162 × 10^{-30}esu). This also holds for the β_0 values, since λ_{max} of **3a** and **3b** is almost identical, and is in excellent agreement with the findings from archetype dinuclear sesquifulvalene complexes which also demonstrate a doubling or almost doubling of β and β_0 values when the metal-ligand fragment on the acceptor site is changed from Ru(η^5-C_5Me_5) to Ru(η^5-C_5H_5).[4,5a] The reason for the lack of correlation between the ground-state spectroscopic data and the SHG effect for **3a** and **3b** remains unclear for the time being, and may reflect that the nature of the ground state *and* the excited state determine the SHG effect.

Conclusion

In contrast to ferrocenyl derivatives of vinylogue sesquifulvalene complexes the ruthenocenyl congeners do not show fluorescence, which can be caused by a two photon absorption in HRS experiments with a fundamental wavelength of 1064 nm.[1d,1e] The obtained β values are the highest ever measured for ruthenocenyl containing donor-acceptor NLO chromophores and in particular when they are correlated to the molecular mass of corresponding complexes. However, these β values are strongly resonance enhanced by an energetically low-lying D_M-A CT transition and an energetically higher lying D_L-A CT transition. The different contributions to the resonance enhancement prevent a rationalisation of the NLO property, i.e. the capability of frequency doubling by electronic ground state properties. This is for example the bond order in the olefinic linker between the donor and the acceptor, which can be characterised by the energy of the C=C stretching mode in IR-spectroscopy and $^3J(^1H\text{-}^1H)$ coupling constants between the protons of this double bond. The situation changes for the monohydro sesquifulvalene complexes, which reveal one electronic absorption band with λ_{max} considerably smaller than λ(SHG) and a cut off at about 500 nm. Reliable values for the first hyperpolarisability β have been determined and thus reasonable β_0 values can be calculated. These data confirm the results obtained for dinuclear archetype sesquifulvalene complexes: the first hyperpolarisability is roughly doubled on going from [Ru(η^5-C_5Me_5)]$^+$ to [Ru(η^5-C_5H_5)]$^+$ complex fragments on the acceptor site.

Experimental Section

Manipulations were carried out under a dry nitrogen atmosphere using standard Schlenk techniques. Solvents were saturated with nitrogen, and diethyl ether (Et_2O), tetrahydrofuran (THF), *n*-hexane and toluene were freshly distilled from the appropriate alkali metal or metal alloy. Dichloromethane (CH_2Cl_2) and nitromethane ($MeNO_2$) were dried over calcium hydride. NMR: Varian Gemini 200 BB; Bruker AM 360; measured at 295 K rel. TMS. UV/Vis: Perkin−Elmer Model 554. IR: KBr pills, FT-IR, Perkin−Elmer Model 325. MS: Finnigan MAT 311 A (EI-MS). Elemental analyses: CHN−O-Rapid (Zentrale Elementanalytik, Fachbereich Chemie, Universität Hamburg), Fa. Heraeus. Tropylium hexafluorophosphate (**7**),[25] formyl ruthenocene,[6] triphenylcarbenium hexafluorophosphate/tetrafluoroborate,[26] (tricarbonyl)(trispropionitrile)chromium(0),[27] (trisacetonitrile)(η^5-cyclopentadienyl)-ruthenium(II) hexafluorophosphate,[28] (trisacetonitrile)(η^5-pentamethylcyclopentadienyl)ruthenium(II) hexafluorophosphate,[29] (cyloheptа-1,3,5-trienyl-1-methyl)diethylphosphonate[1d] were synthesised according to literature procedures.

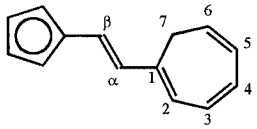

***E*-(1-Ruthenocenyl)(2-cyclohepta-1′,3′,5′-trien-1′-yl)ethene (1), Method A:** A solution of Li*n*Bu in hexane (0.73 mL, 1.6 M in *n*-hexane) was added to a stirred solution of (cyclohepta-1,3,5-trien-1-ylmethyl)(diethyl)phosphonate (270 mg, 1.1 mmol) in THF (20 mL) at −78 °C. The reaction mixture was allowed to warm to room temperature. After 30 min of stirring at ambient temperature the reaction mixture was cooled to −78 °C, and formyl ruthenocene (250 mg, 0.96 mmol) dissolved in THF (10 mL) was added dropwise. After warming to room temperature the solvent was evaporated to dryness. The residue was extracted with *n*-hexane and purified by column chromatography (SiO_2, *n*-hexane/Et_2O, 1:1). Isolation of the yellow band yielded 300 mg (90%) of **1** as a light yellow crystalline powder.

Method B (phase-transfer catalysis): A mixture of an aqueous solution of sodium hydroxide (50%, 30 mL), benzene (30 mL), a catalytic amount of [*n*Bu$_4$N]Br (32 mg, 0.1 mmol), formyl ruthenocene (310 mg, 1.2 mmol) and (cyclohepta-1,3,5-trien-1-yl-methyl)(diethyl)phosphonate (420 mg, 1.7 mmol) was stirred under reflux for 16 h. The progress of the reaction was monitored by TLC. The reaction mixture was extracted by Et_2O, the organic layer dried with $MgSO_4$ and, subsequently, evaporated to dryness. The isolation of the product occurred as described for Method A. Yield (**1**): 198 mg (48%). ^{1}H NMR ($CDCl_3$): δ = 2.60 (d, *J* = 7.2 Hz, 2 H, H-7), 4.52 (s, 5 H, C_5H_5), 4.59 (t, *J* = 1.8 Hz, 2 H, C_5H_4), 4.81 (t, *J* = 1.8 Hz, 2 H, C_5H_4), 5.41 (m, 1 H, H-6), 6.13 (d, *J* = 4.8 Hz, 1 H, H-2), 6.21 (dd, *J* = 9.2, 5.0 Hz, 1 H, H-5), 6.41 (d, *J* = 15.8 Hz, 1 H, CH=C*H*), 6.53 (d, *J* = 15.8 Hz, 1 H, C*H*=CH), 6.54 (m, 2 H, H-3, H-4), ppm. MS(EI): *m/z* (%) = 260 (67) [M$^+$ − 88], 232(100) [$C_{10}H_{10}Ru^+$], 167 (56) [C_5H_5Ru]. $C_{19}H_{18}Ru$ (347.4): calcd. C 65.69, H 5.22; found C 65.52, H 5.55.

***E*-(1-Ruthenocenyl-2-[(tricarbonyl)(η^6-cyclohepta-1′,3′,5′-trien-1′-yl)chromium]ethene (2):** A solution of **1** (90 mg, 0.26 mmol) and $Cr(CO)_3(EtCN)_3$ (78 mg, 0.26 mmol) in THF (20 mL) was stirred overnight at room temperature. The reaction solvent was evaporated in vacuo and the residue extracted with toluene. The toluene extract was filtered and product **2** was precipitated after addition of hexane and cooling to −18 °C. Yield (**2**): 110 mg (88.5%) of a red-violet microcrystalline material. ^{1}H NMR (C_6D_6): δ = 1.07 (m, 1 H, H-7$_{exo}$), 2.62 (m, 2 H, H-7$_{endo}$, H-6), 4.21 (d, *J* = 7.0 Hz, 1 H, H-2), 4.41 (t, *J* = 7.2 Hz, 1 H, H-5), 4.57 (s, 5 H, C_5H_5), 4.67 (s, 2 H, C_5H_4), 4.79 (s, 2 H, C_5H_4), 5.05 (t, *J* = 7.7 Hz, 1 H, H-3), 5.19 (t, *J* = 7.4 Hz, 1 H, H-4), 5.86 (d, *J* = 15.8 Hz, 1 H, CH=C*H*), 6.21 (d, *J* = 15.6 Hz, 1 H, C*H*=CH) ppm. ^{13}C NMR (C_6D_6): δ = 23.0 (C-7), 53.2 (C-6), 68.7 (C_5H_4), 70.7 (C_5H_4), 72.0 (C_5H_5),

75.9 [$C_q(C_5H_4)$], 86.9 (C-1), 96.2 (C-3), 97.5 (C-4), 98.8 (C-2), 100.4 (C-5), 127.5 (C=C), 127.6 (C=C), 232.3 (CO) ppm. IR (KBr): $\tilde{\nu}$ = 1950 (ν_{CO}), 1898 (ν_{CO}), 1883 (ν_{CO}), 1849 (ν_{CO}), 1618 ($\nu_{C=C}$). UV/Vis (CH_2Cl_2): λ_{max} (ε) = 436 (7320), 560 (sh) (1160) nm ($M^{-1}\cdot cm^{-1}$). MS (EI): *m/z* (%) = 484 (10) [M^+], 400 (60) [M^+ − 3CO], 347 (100) [M^+ − H-Cr(CO)$_3$. $C_{22}H_{18}O_3CrRu$ (483.5): C 54.66, H 3.75; found C 54.40, H 3.72.

[*E*-(1-Ruthenocenyl-2-{(η^5-cyclopentadienyl)(η^6-cyclohepta-1′,3′,5′-trien-1′-yl)ruthenium}ethene] Hexafluorophosphate (3a): A solution of **1** (171 mg, 0.49 mmol) and [(η^5-C_5H_5)Ru(MeCN)$_3$]PF_6 (213 mg, 0.49 mmol) in CH_2Cl_2 (20 mL) was stirred at ambient temperature. The progress of the reaction was monitored by TLC. When **1** could not be detected any longer (after three days), the product **3a** was precipitated by addition of Et_2O. A recrystallisation was performed by redissolution of crude **3a** and precipitation by slow gas phase diffusion of Et_2O. Yield (**3a**): 170 mg (53%) of orange-coloured microcrystalline material. ^{1}H NMR (CD_3NO_2): δ = 1.28 (dd, *J* = 13.7, 4.9 Hz, 1 H, H-7$_{exo}$), 3.46 (dd, *J* = 13.7, 9.4 Hz, 1 H, H-7$_{endo}$), 4.15 (m, 1 H, H-6), 4.16 (s, 5 H, C_5H_5), 4.75 (t, *J* = 1.8 Hz, C_5H_4), 4.93 (m, 1 H, C_5H_4), 5.07 (m, 1 H, C_5H_4), 5.35 (s, 5 H, C_5H_5), 5.67 (m, 2 H, H-4, H-5), 6.40 (d, *J* = 15.9 Hz, 1 H, H$_\beta$), 6.51 (m, 2 H, H-2, H-3), 6.87 (d, *J* = 15.9 Hz, 1 H, H$_\alpha$) ppm. ^{13}C NMR (CD_3NO_2): δ = 22.6 (C-7), 30.0 (C-6), 56.6 (C-1), 69.8 (C_5H_4), 71.9 (C_5H_4), 72.9 (C_5H_5) 73.0 (C_5H_4), 73.1 (C_5H_4), 85.3 (C_5H_5), 87.2 [$C_q(C_5H_4)$], 89.0, 91.1 (C-4, C-5), 93.8, 95.8 (C-2, C-3), 126.9 (C_β), 135.2 (C_α) ppm. IR (KBr): $\tilde{\nu}$ = 3115, 3058, 2991, 1624 ($\nu_{C=C}$), 1506, 1416, 1101, 834 ($\nu_{P\text{-}F}$), 557 cm^{-1}. UV/Vis (CH_2Cl_2): λ_{max} (ε) = 423 (10490) nm ($M^{-1}cm^{-1}$), (CH_3NO_2): λ_{max} (ε) = 404 (9410) nm ($M^{-1}cm^{-1}$). $C_{24}H_{23}F_6PRu_2$ (658.6): C 43.77, H 3.52; found C 43.16, H 3.68.

[*E*-(1-Ruthenocenyl-2-{(η^5-pentamethylcyclopentadienyl)(η^6-cyclohepta-1′,3′,5′-trien-1′-yl)ruthenium(II)}ethene] Hexafluorophosphate (3b): A solution of **1** (120 mg, 0.35 mmol) and [η^5-C_5Me_5)Ru(MeCN)$_3$]PF_6 (227 mg, 0.35 mmol) in CH_2Cl_2 (15 mL) was stirred at ambient temperature. The reaction and workup procedure were analogous to that of the synthesis of **3a**. Yield (**3b**): 125 mg (49%) orange-coloured prisms. ^{1}H NMR (CD_3NO_2): δ = 1.24 (dd, *J* = 12.8, 3.5 Hz, 1 H, H-7$_{exo}$) 1.88 (s, 15 H, C_5Me_5), 3.40 (m, 2 H, H-6, H-7$_{endo}$), 4.66 (s, 5 H, C_5H_5), 4.76 (m, 2 H, C_5H_4), 4.93 (m, 1 H, C_5H_4), 5.07 (m, 1 H, C_5H_4), 5.11 (m, 1 H, H-5), 5.18 (dd, *J* = 4.3, 2.6 Hz, 1 H, H-4), 6.18 (m, 2 H, H-2, H-3), 6.25 (d, *J* = 15.8 Hz, 1 H, H$_\beta$), 6.89 (d, *J* = 15.8 Hz, 1 H, H$_\alpha$) ppm. ^{13}C NMR (CD_3NO_2): δ = 10.2 (C_5Me_5), 23.6 (C-7), 35.7 (C-6), 57.8 (C-1), 69.6 (C_5H_4), 71.7 (C_5H_4), 72.5 (C_5H_5), 72.7 (C_5H_4), 72.8 (C_5H_4), 88.2 [$C_q(C_5H_4)$], 94.2 (C-4), 94.7 (C-2 or C-3), 95.4 (C-5), 97.6 (C-2 or C-3), 99.4 (C_5Me_5), 126.8 (C_β), 136.0 (C_α) ppm. IR (KBr): $\tilde{\nu}$ = 2913, 2860, 1619 ($\nu_{C=C}$), 1381, 838 ($\nu_{P\text{-}F}$). UV/Vis (CH_2Cl_2): λ_{max} (ε) = 424 (11460) nm ($M^{-1}\cdot cm^{-1}$), (CH_3NO_2): λ_{max} (ε) 409 (10225) nm ($M^{-1}\cdot cm^{-1}$). ($C_{29}H_{33}PF_6Ru_2$)1/2(CH_2Cl_2)1/2(CH_3NO_2) (801.7): C 44.95, H 4.46, N 0.87; found C 44.62, H 4.39, N 1.07.

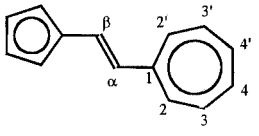

[*E*-1-Ruthenocenyl-2-(cycloheptatrienylium-1′-yl)ethene] Hexafluorophosphate (4): A solution of [Ph_3C]PF_6 (538 mg, 1.38 mmol) in CH_2Cl_2 (10 mL) was added to a stirred solution of **1** (480 mg, 1.38 mmol) in CH_2Cl_2 (20 mL). After stirring for 30 min the product **4** was precipitated by dilution with Et_2O. Recrystallisation was performed by gas phase diffusion of Et_2O into a concentrated CH_2Cl_2 solution of **4**. Yield: 0.52 g (77%) of a blue-violet crystalline powder. ^{1}H NMR (200 MHz, $CDCl_3$): δ = 4.78 (s, 5 H, C_5H_5), 5.24 (s, 4 H, C_5H_4), 6.78 (d, *J* = 15 Hz, 1 H, H$_\beta$), 8.18 (d, *J* = 15 Hz, 1 H, H$_\alpha$,), 8.04−8.23 (m, 4 H, C_7H_6), 8.30−8.35 (d, 2 H, C_7H_6) ppm. ^{13}C NMR (50 MHz, CD_3NO_2): δ = 73.5 (C_5H_4), 74.8 (C_5H_4), 77.7 (C_5H_4), 125.0 (C_β), 147.6 (C_7H_6), 148.6 (C_7H_6), 149.3 (C_7H_6), 152.3 C_α), ppm UV/Vis (CH_2Cl_2): λ_{max} (ε) = 480 (16270), 640 (22560) nm (M^{-1} cm^{-1}); (CH_3NO_2): λ_{max} (ε) = 470 (12040), 600 (16430) nm (M^{-1} cm^{-1}). MS (FAB): *m/z* (%) = 347 (78%) [M^+ − PF_6]. $C_{19}H_{17}F_6PRu$ (492.0): C 46.34, H 3.48; found C 45.86, H 3.74.

[*E*-1-Ruthenocenyl-2-{(tricarbonyl)(η^7-cycloheptatrienylium-1-yl)-chromium}ethene] Hexafluorophosphate (5): A solution of [Ph_3C]PF_6 (90 mg, 0.23 mmol) in CH_2Cl_2 (10 mL) was added to a solution of **2** (110 mg, 0.23 mmol) in CH_2Cl_2 (20 mL) at 0 °C. After stirring for 30 min the reaction solution was diluted by addition of Et_2O. The precipitation was filtered off and recrystallised by a gas-phase diffusion of Et_2O into a concentrated solution of **5** in $MeNO_2$. Yield (**5**): 70 mg (48.5%) dark red needles. ^{1}H NMR (CD_3NO_2): δ = 4.65 (s, 5 H, C_5H_5), 4.88 (s, 2 H, C_5H_4), 5.13 (s, 2 H, C_5H_4), 6.48 (d, *J* = 9.3 Hz, 2 H, H-2,2′), 6.52 (m, 2 H, H-4,4′),6.80 (m, 2 H, H-3,3′),6.81 (d, *J* = 16.0 Hz, 1 H, H$_\beta$), 7.63 (d, *J* = 16.0 Hz, 1 H, H$_\alpha$) ppm. ^{13}C NMR (CD_3NO_2): δ = 71. 8 (C_5H_4), 73.3 (C_5H_5), 74.3 (C_5H_4), 85.6 [$C_q(C_5H_4)$], 100.4 (C-2,2′),104.7 (C-4,4′),106.0 (C-3,3′),121.5 (C_β), 126.8 (C-1), 142.7 (C_α), 223.4 (CO) ppm. IR (KBr): $\tilde{\nu}$ = 3083, 2064 (ν_{CO}), 2012 (ν_{CO}), 1624 ($\nu_{C=C}$), 1546, 839 ($\nu_{P\text{-}F}$). UV/Vis (CH_2Cl_2): λ_{max} (ε) = 384 (8730), 532 (8375) nm ($M^{-1}cm^{-1}$), (CH_3NO_2): λ_{max} (ε) = 490 (7155) nm ($M^{-1}\cdot cm^{-1}$); ($C_{22}H_{17}O_3CrRuPF_6$) 1/2 (CH_3NO_2) (627.4): C 41.01, H 2.83, N: 1.06; found C 40.42, H 3.09, N 0.68.

[*E*-1-Ruthenocenyl-2-{(η^5-cyclopentadienyl)(η^7-cyclohepta-trienylium-1′-yl)ruthenium(II)}ethene] Bishexafluorophosphate (6a): A solution of **4** (340 mg, 0.7 mmol) and [(η^5-C_5H_5)Ru(MeCN)$_3$]PF_6 (300 mg, 0.7 mmol) in CH_2Cl_2 (40 mL) was stirred overnight at ambient temperature. The precipitated product was filtered off, washed with CH_2Cl_2 and recrystallised from $MeNO_2$/Et_2O. Yield (**6a**): 470 mg (84%) red crystals. ^{1}H NMR (CD_3NO_2): δ = 5.11 (s, 5 H, C_5H_5), 5.38 (t, *J* = 1.8 Hz, 2 H, C_5H_4), 5.83 (t, *J* = 1.8 Hz, 2 H, C_5H_4), 5.86 (s, 5 H, C_5H_5), 5.92 (d, *J* = 13.4 Hz, 1 H, H$_\beta$), 6.09 (d, *J* = 9.2 Hz, 2 H, H-2,2′), 6.47 (m, 2 H, H-3,3′), 7.21 (dd, *J* = 5.4, 2.6 Hz, 2 H, H-4,4′), 7.55 (d, *J* = 13.4 Hz, 1 H, H$_\alpha$) ppm. ^{13}C NMR (CD_3NO_2): δ = 70.5 (C-2,2′), 79.6 (C_5H_4), 81.9 (C_5H_5), 87.2 (C_5H_4), 88.2 (C_5H_5), 96.5 [$C_q(C_5H_4)$], 97.5 (C-3,3′), 99.7 (C-4,4′), 117.4 (C_α), 121.6 (C_β), 138.1 (C-1) ppm. IR (KBr): $\tilde{\nu}$ = 3121, 1599 ($\nu_{C=C}$), 1541, 1493, 1418, 835 ($\nu_{P\text{-}F}$). UV/Vis (CH_2Cl_2): λ_{max} (ε) = 400, 600 (sh) nm, (CH_3NO_2): λ_{max} (ε) = 400 (10760), 560 (4975) nm ($M^{-1}\cdot cm^{-1}$). $C_{24}H_{22}Ru_2P_2F_{12}$ (802.5): C 35.92, H 2.76; found C 35.45, H 2.86.

[*E*-1-Ruthenocenyl-2-{η^5-pentamethylcyclopentadienyl)(η^7-cycloheptatrienylium-1′-yl)ruthenium(II)}ethene] Bishexafluorophosphate (6b): The synthesis of **6b** was performed strictly analogously to **6a**. Quantities used: **4** (50 mg, 0.1 mmol), [(η^5-C_5Me_5)Ru(MeCN)$_3$]PF_6 (51 mg, 0.1 mmol), CH_2Cl_2 (10 mL). Yield (**6b**): 64 mg (73%) dark red needles.- ^{1}H NMR (CD_3NO_2): δ = 2.13 (s, 15 H, C_5Me_5), 4.75 (s, 5 H, C_5H_5), 5.05 (t, *J* = 1.7 Hz, 2 H, C_5H_4), 5.24 (t, *J* = 1.7 Hz, 2 H, C_5H_4), 6.77 (d, *J* = 15.4 Hz, 1 H, H$_\beta$), 7.20 (m, 2 H, H-3,3′), 7.23 (d, *J* = 8.6 Hz, 2 H, H-2,2′), 7.33 (dd, *J* = 5.5, 3.6 Hz, 2 H, H-4,4′), 7.98 (d, *J* = 15.4 Hz, 1 H, H$_\alpha$), ppm. ^{13}C NMR (CD_3NO_2): δ = 10.7 (C_5Me_5), 72.7 (C_5H_4), 73.9 (C_5H_5), 76.0 (C_5H_4), 86.1 [$C_q(C_5H_4)$], 99.1 (C-2,2′), 104.9 (C-3,3′), 105.5 (C-4,4′), 110.3 (C_5Me_5), 116.7 (C_β), 128.6 (C-1), 152.6 (C_α) ppm. IR (KBr): $\tilde{\nu}$ = 3071, 1609 ($\nu_{C=C}$), 1539, 1418, 839 ($\nu_{P\text{-}F}$). UV/Vis (CH_2Cl_2): λ_{max}

(ε) = 438, 594 nm, (CH_3NO_2): λ_{max} (ε) = 409 (10580), 541 (9280) nm ($M^{-1}\cdot cm^{-1}$); ($C_{29}H_{32}Ru_2P_2F_{12}$) 2/3 ($CH_3NO_2$) (914.7): C 38.92, H 3.75, N 1.02 found C 39.29, H 3.75, N 1.48.

X-ray Structure Determination: Crystals suitable for an X-ray structure determination were obtained by gas phase diffusion of Et_2O into a CH_2Cl_2 solution of **3a**, **3b** and into an $MeNO_2$ solution of **6a.** Complex **3b** crystallised with CH_2Cl_2 and $MeNO_2$ molecules. During the isolation of the crystalline product of **3b** it was dissolved once in $MeNO_2$, which may explain the co-crystallisation of $MeNO_2$ molecules. The data were collected with a four-circle diffractometer (**3b**, and **6a**: Hilger and Watts, Mo-K_α; **3a**: Siemens aix, Mo-K_α). All structures were resolved by direct methods (SHELXS-86).[30] Refinement on F^2 was carried out by full-matrix least-squares techniques (SHELXL-93, SHELXL-97).[31,32] All non-hydrogen atoms were refined with anisotropic thermal parameters. The hydrogen atoms were refined by the riding-model method with fixed isotropic thermal parameter related by a factor of 1.2 to the value of the equivalent isotropic parameter of their carrier atoms. Weights are optimised in the final refinement cycles.

CCDC-195475 (**3a**) CCCDC-195474 (**3b**) and CCDC-195453 (**6a**) contain the supplementary crystallographic data for this paper. These data can be obtained free of charge at www.ccdc.cam.ac.uk/conts/retrieving.html [or from the Cambridge Crystallographic Data Centre, 12, Union Road, Cambridge CB2 1EZ, UK; Fax: (internat.) +44−1223/336−033; E-mail: deposit@ccdc.cam.ac.uk].

HRS Measurements of the First Hyperpolarisabilities: Hyper-Rayleigh scattering measurements were performed with a pulsed Nd:YAG laser at a wavelength of λ = 1064 nm. For the experimental setup see ref.[15b] Solutions of the complexes in CH_2Cl_2 and $MeNO_2$ with concentrations in the range of 10^{-4} to 10^{-6} M were used with *p*-nitroaniline as a reference [$\beta(CH_2Cl_2) = 21.6 \times 10^{-30}$ esu,[22] $\beta(MeNO_2) = 34.6 \times 10^{-30}$ esu].[23] Fluorescence checks were made by replacing the interference filter in front of the photomultiplier tube with filters that have transmittances at 400, 450, 500, 560, 600 and 700 nm.[4]

Acknowledgments

This work was supported by the Deutsche Forschungsgemeinschaft (DFG, HE 1309/3), by the European Community (COST D4/003/94, TMR FMRX-CT98−0166) and by the Fonds der Chemischen Industrie. We thank the DEGUSSA AG for a donation of $RuCl_3$ and Sartorius GmbH for a donation of microfilters.

[1] [1a] U. Behrens, H. Brussaard, U. Hagenau, J. Heck, E. Hendrickx, J. Körnich, J. G. M. van der Linden, A. Persoons, A. L. Spek, N. Velman, B. Voss, H. Wong, *Chem. Eur. J.* **1996**, *2*, 98−103. [1b] M. Tamm, T. Bannenberg, K. Baum, R. Fröhlich, T. Steiner, T. Meyer-Friedrichsen, J. Heck, *Eur. J. Inorg. Chem.* **2000**, 1161−1169. [1c] J. Heck, S. Dabek, T. Meyer-Friedrichsen, H. Wong, *Coord. Chem. Rev.* **1999**, *190−192*, 1217−1254. [1d] H. Wong, T. Meyer-Friedrichsen, T. Farrell, Ch. Mecker, J. Heck, *Eur. J. Inorg. Chem.* **2000**, 631−646. [1e] T. Meyer-Friedrichsen, C. Mecker, M. H. Prosenc, J. Heck, *Eur. J. Inorg. Chem.* **2002**, 239−248.

[2] [2a] D. J. Williams, *Angew. Chem.* **1984**, *96*, 637−651; *Angew. Chem. Int. Ed. Engl.* **1984**, *23*, 690−703. [2b] R. W. Boyd in: *Nonlinear Optics*, Academic Press, Inc, **1992**. [2c] G. H. Wagnière in: *Linear and Nonlinear Optical Properties of Molecules*, VCH Verlagsgesellschaft, Weinheim, **1993**. [2d] P. N. Prasad, D. J. Williams in: *Nonlinear Optical Effects In Molecules & Polymers*, John Wiley & Sons, New York, **1991**. [2e]H. S. Nalwa, *Appl. Organomet. Chem.* **1991**, *5*, 349−377. [2f] T. J. Marks, M. A. Ratner, *Angew. Chem.* **1995**, *107*, 167−187; *Angew. Chem. Int. Ed. Engl.* **1995**, *34*, 155−174. [2g] N. J. Long, *Angew. Chem.* **1995**, *107*, 37−56; *Angew. Chem. Int. Ed. Engl.* **1995**, *34*, 21−38. [2h] S. Maiorana, A. Pagagni, E. Licandro, A. Persoons, K. Clay, S. Houbrechts, W. Porzio, *Gaz. Chim. Ital.* **1995**, *125*, 377−379. [2i] H. S. Nalwa, S. Miyata (Ed.) in: *Nonlinear Optics of Organic Molecules and Polymers*, CRC Press**,** New York, **1997**. [2j]K. Meerholz, *Angew. Chem.* **1997**, *109*, 981−985; *Angew. Chem. Int. Ed. Engl.* **1997**, *36*, 945−949. [2k] T. Verbiest, S. Houbrechts, M. Kaurann, K. Clays, A. Persoons, *J. Mater. Chem.* **1997**, *7 (11)*, 2175−2189. [2l] I. R. Whittall, A. M. McDonagh, M. G. Humphrey, M. Samoc, *Adv. Organomet. Chem.* **1998**, *42*, 291−362. [2m] B. J. Coe, *Chem. Eur. J.* **1999**, *5*, 2464−2471. [2n] M. Kaurann, T. Verbiest, A. Persoons, *J. Nonl. Opt. Phys. Mater.* **1999**, *2*, 171−189. [2o] G. G. A. Balavoine, J.-C. Daran, G. Iftime, P. G. Lacroix, E. Manoury, J. A. Delaire, I. Maltey-Fanton, K. Nakatani, S. Di Bella, *Organometallics* **1999**, *18*, 21−29. [2p] O. Briel, K. Sünkel, I. Krossing, H. Nöth, E. Schmälzlin, K. Meerholz, C. Bräuchle, W. Beck, *Eur. J. Inorg. Chem.* **1999**, 483−490. [2q] H. Le Bozec, T. Renouard, *Eur. J. Inorg. Chem.* **2000**, 229−239; J. A. Delaire, K. Nakatani, *Chem. Rev.* **2000**, *100*, 1817−1845. [2r] J. A. Mata, E. Peris, I. Asselberghs, R. Van Boxel, A. Persoons, *New. J. Chem.* **2001**, 1043−1046. [2s] M. Malaun, R. Kowallick, A. M. McDonagh, M. Marcaccio, R. L. Paul, I. Asselberghs, K. Clays, A. Persoons, B. Bildstein, C. Fiorini, J.-M. Nunzi, M. D. Ward, J. A. McCleverty, *J. Chem. Soc., Dalton Trans.* **2001**, 3025−3038.

[3] E. Schmälzlin, U. Bitterer, H. Langhals, C. Bräuchle, K. Meerholz, *Chem. Phys.* **1999**, *245*, 73−78; T. Wakebe, E. van Keuren, *Jpn. J. Appl. Phys.* **1999**, *38*, 3556−3561.

[4] T. Meyer-Friedrichsen, Dissertation, University of Hamburg, **1999**.

[5] [5a] T. Meyer-Friedrichsen, M. H. Prosenc, J. Heck, manuscript in preparation. [5b] The ^1H NMR signals of the Ru(η^5-C_5H_5) units are found at δ = 4.56 [Ru(η^5-C_5H_5)$_2$], 5.45 [Ru(η^5-C_5H_5)](η^6-C_6H_6)PF_6 and 6.37 {[Ru(η^5-C_5H_5)](η^7-C_7H_7)PF_6}$_2$ ppm (200 MHz, CD_3NO_2, rel. TMS). These shifts demonstrate a linear correlation with the charge of the corresponding complex cation, which obeys the equation δ[Ru(η^5-C_5H_5)] = 0.905 × *m* + 4.56 (*m* = charge of the sandwich complex; correlation coefficient *r* = 1.000); by means of this equation the actual charges of the donor and/or acceptor moieties of the complexes under study can be calculated from the shift of the Cp signal of the Ru(η^5-C_5H_5) unit.

[6] R. Sanders, U. T. Mueller-Westerhoff, *J. Organomet. Chem.* **1996**, *512*, 219−224.

[7] P. Seiler, J. D. Dunitz, *Acta Crystallogr., Sect. B* **1980**, *36*, 2946−2950.

[8] J. D. Dunitz, P. Pauling, *Helv. Chim. Acta* **1960**, *43*, 2188−2197, F. J. Hadley, T. M. Gilbert, R. D. Rogers, *J. Organomet. Chem.* **1993**, *455*, 107−113.

[9] S. Dabek, Dissertation, University of Hamburg, **2001**.

[10] T. Farrell, A. R. Manning, G. Mitchell, J. Heck, T. Meyer-Friedrichsen, M. Malessa, C. Wittenburg, M. H. Prosenc, D. Cunningham, P. McArdle, *Eur. J. Inorg. Chem.* **2002**, 1677−1686.

[11] [11a] T. Farrell, T. Meyer-Friedrichsen, J. Heck, A. R. Manning, *Organometallics* **2000**, *19*, 3410−3419. [11b] T. Farrell, A. R. Manning, T. C. Murphy, T. Meyer-Friedrichsen, J. Heck, I. Asselberghs, A. Persoons, *Eur. J. Inorg. Chem.* **2001**, 2365−2375; T. Farrell, T. Meyer-Freidrichsen, M. Malessa, Ch. Wittenburg, J. Heck, A. R. Manning, *J. Organomet. Chem.* **2001**, *625*, 32−39;

[12] S. Barlow, S. R. Marder, *Chem. Commun.* **2000**, 1555−1562.

[13] P. Suppan, N. Ghoneim, in Solvatochromism, Paston Press, LTD, Norfolk, **1997**; N. Mataga, T. Kubota, Molecular Interactions and Electronic Spectra; Marcel Dekker; New York, **1970**, chapter 8.

[14] [14a] L. Oudar, D. S. Chemla, *Chem. Phys.* **1977**, *66*, 2664−2668. [14b] E. Hendrickx, K. Clays, A. Persoons, C. Dehu, J. L.

Brédas, *J. Am. Chem. Soc.* **1995**, *117*, 3547−3555. [14c] S. Barlow, H. E. Bunting, C. Ringham, J. C. Green, G. U. Bublitz, S. G. Boxer, J. W. Perry, S. R. Marder, *J. Am. Chem. Soc.* **1999**, *121*, 3715−3723.
[15] [15a] R. W. Terhune, P. D. Maker, C. M. Savage, *Phys. Rev. Lett.* **1962**, *8*, 404−406. [15b] K. Clays, A. Persoons, *Rev. Sci. Instrum.* **1992**, *63*, 3285−3289.
[16] K. Clays, E. Hendrickx, T. Verbiest, A. Persoons, *Adv. Mater.* **1998**, *10*, 643−655; G. Olbrechts, T. Munters, K. Clays, A. Persoons, O.-K. Kim, L.-S. Choi, *Opt. Mat.* **1999**, *12*, 222−224.
[17] J. J. Wolff, R. Wortmann, *Adv. Phys. Org. Chem.* **1999**, *32*, 121−217.
[18] S. Stadler, G. Bourhill, C. Bräuchle, *J. Phys. Chem.* **1996**, *100*, 6927−6934.
[19] S. Stadler, R. Dietrich, G. Bourhill, C. Bräuchle, *Optics Letts.* **1996**, *21*, 251−253.
[20] M. A. Pauley, C. H. Wang, *Rev. Sci. Instrum.* **1999**, *70*, 1277−1284.
[21] N. W. Song, T.-I. Kang, S. C. Jeung, S.-J. Joan, B. R. Cho, D. Kim, *Chem. Phys. Lett.* **1996**, *261*, 307−312; O. K. Song, J. N. Woodford, C. H. Wang, *J. Phys. Chem. A.* **1997**, *101*, 3222−3226.
[22] C. Dehu, F. Meyers, E. Hendrickx, K. Clays, A. Persoons, J. Brédas, *J. Am. Chem. Soc.* **1995**, *117*, 10127−10128.
[23] T. Verbiest, K. Clays, C. Samyn, J. Wolff, D. Reinhoudt, A. Persoons, *J. Am. Chem. Soc.* **1994**, *116*, 9320−9323.
[24] [24a] L.-T. Cheng, W. Tam, G. R. Meredith, *Mol. Cryst. Liq. Cryst.* **1990**, *187*, 137−153. [24b] J. C. Calabrese, C.-T. Cheng, J. C. Green, S. R. Marder, W. Tam, *J. Am. Chem. Soc.* **1991**, *113*, 7227−7232.
[25] K. Conrow, *Organic Synthesis, Coll. Vol. V*, p. 1138.
[26] G. A. Olah, J. J. Svoboda, J. A. Olah, *Synthesis* **1972**, 544.
[27] G. J. Kubas, *Inorg. Chem.* **1983**, *22*, 692−694.
[28] T. P. Gill, K. R. Mann, *Organometallics* **1982**, *1*, 485−488.
[29] B. Steinmetz, W. A. Schenk, *Organometallis* **1999**, *18*, 943−946; P. J. Fagan, M. D. Ward, J. C. Calabrese, *J. Am. Chem. Soc.* **1989**, *111*, 1698−1719.
[30] G. M. Sheldrick, SHELXS-86 program for crystal structure determination, University of Göttingen, Germany, **1986**.
[31] G. M. Sheldrick, SHELXL-93 *program for crystal structure refinement*, University of Göttingen, Germany, **1993**.
[32] G. M. Sheldrick, SHELXL-97, *program for crystal structure refinement*, University of Göttingen, Germany, **1997**.

Received August 9, 2002
[I02450]

Macrocyclic, Dinuclear Zinc(II)-Directed Self-Assembly with Pyridine, 2,2′-Bipyridine and 2-Methylquinoline: μ^2-OH Bridging Bi-Macrocyclic Complexes and Hydrogen-Bond-Supported Donor-Acceptor Complexes

Wei Huang,[a] Shaohua Gou,*[a] Huifen Qian,[b] Dahua Hu,[a] Suchada Chantrapromma,[c] Hoong-Kun Fun,[c] and Qingjin Meng[a]

Keywords: N,O ligands / Macrocycles / Zinc / Self-assembly / Structure elucidation / Hydrogen bonds

Two macrocyclic dinuclear zinc(II) complexes (**1a** and **1b**) have been self-assembled in the presence of pyridine and 2,2′-bipyridine, respectively, to form μ^2-OH-bridged bimacrocycles with a Zn_4O_4 cavity through coordination bonding. The X-ray structural analysis reveals that both compounds {**2a**: $[Zn_4L^a{}_2(OH)_2]_2(ClO_4)_2$; **2b**: $[Zn_4L^b{}_2(OH)_2]_2(ClO_4)_2$} have an open-mouthed sandwich-like structure with π–π interactions between parts of two phenyl rings to strengthen two hydroxyl groups connecting the metal atoms in the same direction of the macrocycle. Furthermore, nonclassical C–H···Cl intermolecular interactions have been observed in the crystal of **2b**. In addition, the reaction of **1a** with quinoline derivatives has yielded novel hydrogen-bond-supported donor-acceptor complexes {**3a**: $[Zn_2L^a(H_2O)_2(C_{10}H_9N)_2](ClO_4)_2$}. The crystallographic study of the complex containing 2-methylquinoline indicates that two 2-methylquinoline molecules are linked to two coordinating water molecules above and below the macrocyclic framework through O–H···N hydrogen bonds. The 2-methylquinoline plane interacts in a face-to-face fashion with the phenyl ring of adjacent macrocyclic frameworks, forming an ordered arrangement where one macrocycle and two 2-methylquinolines are arrayed alternately with almost the same separation. The interplanar distance mentioned before is ca. 3.6 Å.
(© Wiley-VCH Verlag GmbH & Co. KGaA, 69451 Weinheim, Germany, 2003)

Introduction

Metal-directed self-assembly has been actively investigated in recent years because such a phenomenon offers a new and effective way for the construction of organized structures. The known application of this category of self-assembly is mainly focused on the combination of naked or decorated mononuclear metal species with well-designed organic ligands, leading to the production of metal-ligand frameworks with specific structural topologies.[1] Self-assembly involving dinuclear macrocyclic components has rarely been reported[2] since the first homodinuclear macrocyclic complexes were synthesized by template condensation in the early 1970s and a subsequent systematic study of their modeling of metallobiosites.[3]

The coordination behavior of the metal atoms in these complexes plays a key role in controlling the assembly pattern: metal ions with a defined coordination geometry (e.g. square planar, tetrahedral, pyramidal, and octahedral configurations) have to be specifically chosen and/or deliberately modified as building blocks to realize the anticipated assembly; the effect of noncovalent interactions such as hydrogen bonding, aromatic π−π stacking and charge-transfer interactions should also be taken into account.[4]

We recently reported two infinite molecular ladder polymers composed of a macrocyclic component (**1**) (Scheme 1) with 4,4′-bipyridine, in which two adjacent zinc(II) ions, pre-positioned in the macrocyclic backbone, have been linked by 4,4′-bipyridine ligands via coordinating bonds, together with the change of the coordination configuration of the metal atom from a five-coordinate pyramid to a six-coordinate octahedron (Scheme 2, a).[5] To further study the effect of the dinuclear zinc(II) macrocyclic component in self-assembly, some other mono- and bifunctional aromatic ligands have been utilized instead of 4,4′-bipyridine with the expectation of obtaining a novel type of supramolecular compounds or coordination polymers with special structural topologies. When 4-aminopyridine or pyridine-4-carboxylic acid is allowed to react with **1**, molecular ladder elements are obtained (Scheme 2, b and c).[6] We report here two kinds of new complexes obtained by the reaction of macrocyclic component **1** with pyridine, 2,2′-pyridine and quinoline derivatives. Unlike the reaction with 4,4′-bipyrid-

[a] State Key Laboratory of Coordination Chemistry, Nanjing University,
Nanjing 210093, China
Fax: (internat.) + 86-25/3314502
E-mail: sgou@nju.edu.cn
[b] College of Sciences, Nanjing University of Technology,
Nanjing 210009, China
[c] X-ray Crystallography Unit, School of Physics, Universiti Sains Malaysia,
11800 USM, Penang, Malaysia

ine (1-D molecular ladder polymers bridged by M−N coordinating bonds), sandwich-like structures (**2**) are formed where **1** moieties are connected by two μ^2-OH groups via bridging zinc atoms in the presence of pyridine or 2,2′-bipyridine ligands (Scheme 2, c). When a quinoline derivative is involved, an infinite one-dimensional hydrogen-bond-supported donor-acceptor polymer is obtained where no coordinating interaction exists between layers (Scheme 2, d).

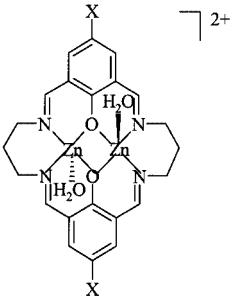

$[Zn_2L(H_2O)_2]^{2+}$ (**1**) L^a: X = Me, L^b: X = Cl

Scheme 1. Macrocyclic units **1** used as building blocks

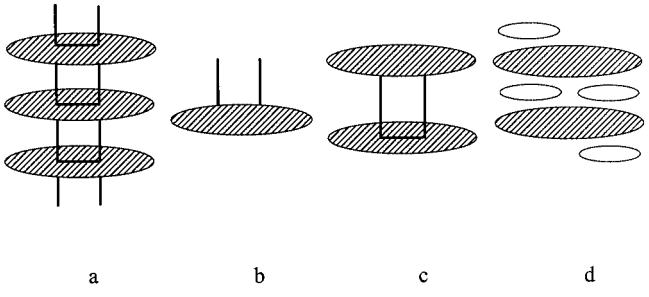

a b c d

Scheme 2. (a) A molecular ladder with macrocyclic platforms; (b) a molecular ladder element with a macrocyclic base; (c) a wheel-like structural unit; (d) a donor-π-acceptor structural pattern

Results and Discussion

Preparations and Characterization

The syntheses of **2a** and **2b** and **3a** and **3b** are shown in Schemes 3 and 4, respectively. The preparation is a simple one-step reaction that gives the products in high yields. In the process of preparing **2**, however, we were surprised to find that irrespective of whether pyridine or 2,2′-pyridine was used, the same products were obtained (spectral characterization and microanalyses). It seems that pyridine and 2,2′-pyridine serve as bases in the formation of **2a** and **2b**, and that these bases are necessary to assist hydrolysis at the zinc(II) cations, which acts as a Lewis acid under the conditions of the experiments.

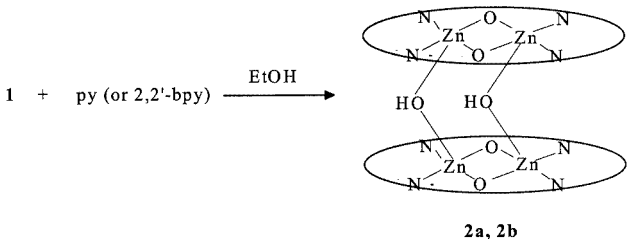

2a, 2b

Scheme 3. Synthesis of complexes **2a** and **2b**

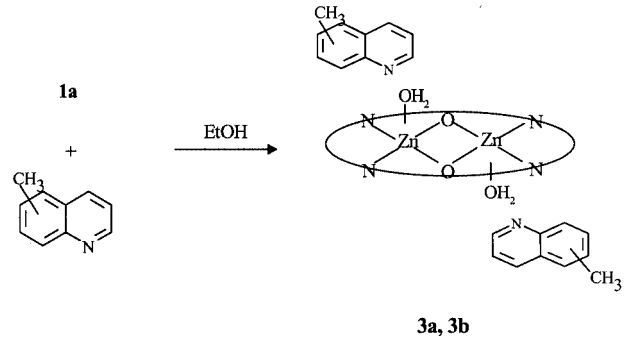

3a, 3b

Scheme 4. Synthesis of compounds **3a** and **3b**

Related infrared and mass spectroscopic data of all compounds indicate the existence of macrocyclic skeletons together with perchlorate anions. In addition, strong broad bands for the O−H stretching vibration of the bridging hydroxyl groups are observed at 3512 cm^{-1} for **2a** and 3533 cm^{-1} for **2b**. The hydrogen atoms belonging to the macrocyclic rings are also observed in the ^1H NMR spectra of **2a** and **2b**, although the nature of the self-assembly products can only be clearly determined from the ^1H NMR spectra of **3a** and **3b**, which demonstrate the presence of hydrogen atoms linking to quinoline rings apart from the macrocycle. However, this routine spectroscopic analysis could not provide the detailed information necessary to determine the structures of the products here.

Structural Description of $\{[Zn_4L^a{}_2(OH)_2]_2(ClO_4)_2(H_2O)_2\cdot CH_3OH\}$ (2a) and $\{[Zn_4L^b{}_2(OH)_2](ClO_4)_2(H_2O)_2C_2H_5OH\}$ (2b)

The X-ray structural analysis of **2a** and **2b** shows that both compounds have a unique open-mouthed sandwich-like structure consisting of two macrocyclic covers with two bridging OH groups in the middle (Figure 1). There are two crystallographically independent $[Zn_4L^a{}_2(OH)_2]^{2+}$ (see Scheme 1) ions per asymmetric unit in **2a** with one methanol, two water molecules, and four perchlorate anions noncoordinating. The structure of **2b** has only one crystallographically independent $[Zn_4L^b{}_2(OH)_2]^{2+}$ moiety in the asymmetric cell; one ethanol, two water molecules as well as two perchlorate anions are free from coordination and located in the lattice. The change of the substituted functional group leads to a modification of the crystal system and space group from monoclinic ($P2_1/c$) in **2a** to triclinic

($P\bar{1}$) in **2b**. In complexes **2a** and **2b**, all metal atoms have similar pyramidal configurations where each zinc(II) atom is situated slightly above the base plane composed of two imine nitrogen atoms and two phenolic oxygen atoms, with the axial position occupied by one OH group. Each macrocyclic framework is folded to fit the requirement of two Zn−OH−Zn bond angles [**2a**: 133.6(3)°, 137.8(3)°; **2b**: 133.3(3)°, 141.8(3)°]. In each subunit of one molecule, one part of one ring is nearly parallel to its counterpart in the other one (with a dihedral angle of 9.1° in **2a** and 0.2° in **2b**), while the other parts of the two rings are bent in the opposite position to a certain degree (with a dihedral angle of 42.8° in **2a** and 56.5° in **2b**). The geometric data of the two compounds with respect to the hydroxyl groups are given in Table 1; the average Zn−O (bridging OH) distances are 1.946 Å for **2a** and 1.933 Å for **2b**.

Although the two compounds have similar molecular structures, they have different packing in their crystals (Figure 2) because of the different substituted groups in their macrocyclic backbones. In **2a** there seems to be no intermolecular interactions, whereas in the crystal structure of **2b**, two adjacent chlorine atoms on benzene rings of two different macrocyclic frameworks and their α-positioned hydrogen atoms in phenyl rings are involved in nonclassical C−H···Cl intermolecular interactions in an end-to-end fashion. Thus a 1-D chain structure is formed with the assistance of eight-membered ring structures containing two C−H···Cl H-bonds. There have been a few reports on C−H···X hydrogen bonds in organic and organometallic compounds (where X can be covalently bound atoms or anions),[7] but whether chlorine atoms can be H-bonding acceptors or not is still controversial.[8] Alhough the existence of C−H···Cl hydrogen bonds is questioned, a statistical survey on more than one hundred crystal structures containing structural patterns similar to that in **2b** showed that this kind of intermolecular interaction is not uncommon, and molecular orbital calculations on the energetics of this structural pattern supported the qualitative observation as well.[9] The length of the C−H···Cl intermolecular interactions in our compound agrees well with those reported previously, except that the intermolecular Cl···Cl distances are slightly longer.[10] Thus it is proposed that the different packing in **2a** and **2b** arises from the different substituted groups on the phenyl rings.

It is interesting to observe that each structure shows a rectangular Zn_4 array containing a rigid Zn_4O_4 cavity in both compounds (Figure 3). This arrangement is similar to that reported by Asato et. al in which a tetranuclear zinc(II) complex was synthesized by a template condensation.[11] The related geometric data are listed in Table 2. The cavity is so small that neither solvent molecules nor perchlorate anions can be hosted. In contrast to the situation with 4,4′-bipyridine, pyridine ligands could not be bound to the zinc(II) atoms on the macrocyclic platform to yield a six-coordinate geometry via π−π interactions of the pyridine rings. The reason for this may be that single Zn−N(pyridine) bonds would be freely rotating and therefore they could not be fixed onto the macrocycle due to the spatial repulsion.

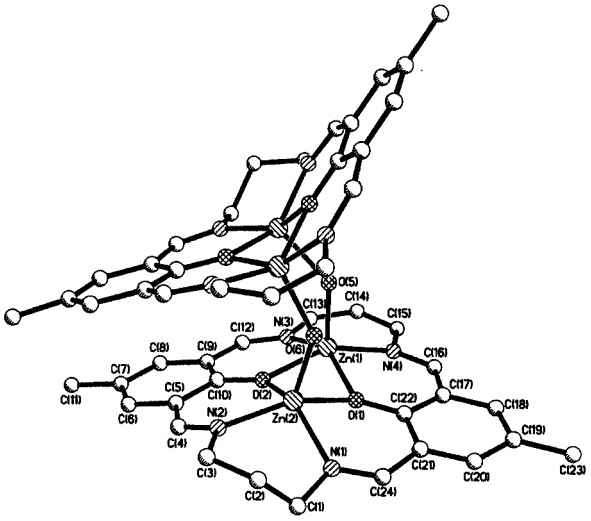

2a

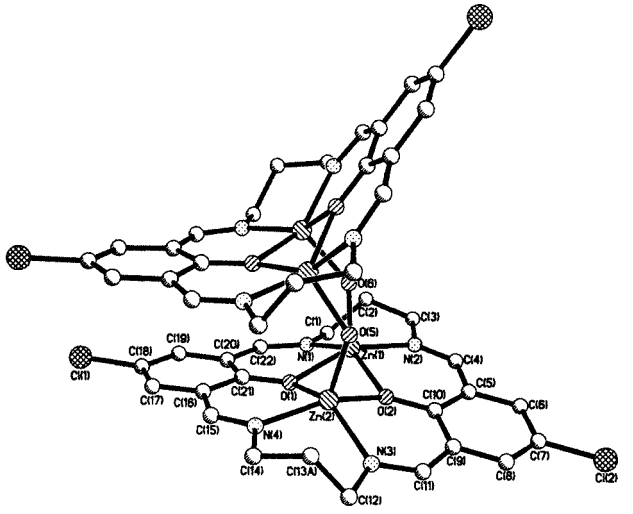

2b

Figure 1. Ball-and-stick representation of the structures of complex cations from **2a** and **2b**; only one of the two tetranuclear clusters from **2a** is shown as they are very similar

This means that monofunctional aromatic ligands cannot take the place of the 4,4′-bipyridine ligands, which are framed with the assistance of the macrocyclic skeleton. It is likely that the absence of 2,2′-bipyridine from the macrocyclic framework is also due to the steric hindrance between aromatic rings. Therefore, in the above two cases, small-sized hydroxyl groups from the solution function as bridges to link two macrocyclic species by coordinating to zinc(II) atoms. Regarding the five-coordinate geometry of zinc(II) atoms in **2**, our prior and current research[2,12] indicates that five-coordinate configuration is preferred if linear monofunctional or bifunctional nonaromatic ligands are used. However, unlike **2**, these nonaromatic ligands will occupy the axial position of the pyramid around the two zinc(II)

Table 1. Selected bond lengths [Å] and angles [°] in **2a** and **2b**; only those associated with bridging OH groups are listed

2a

Zn(1)−O(5)	1.961(5)	Zn(2)−O(6)	1.925(6)
Zn(3)−O(5)	1.948(5)	Zn(4)−O(6)	1.964(6)
Zn(5)−O(11)	1.933(5)	Zn(6)−O(12)	1.933(6)
Zn(7)−O(11)	1.928(5)	Zn(8)−O(12)	1.934(6)
O(5)−Zn(1)−N(3)	109.6(3)	O(5)−Zn(1)−N(4)	105.9(3)
O(5)−Zn(1)−O(1)	100.7(2)	O(5)−Zn(1)−O(2)	97.1(2)
O(6)−Zn(2)−N(1)	107.2(3)	O(6)−Zn(2)−N(2)	111.5(3)
O(6)−Zn(2)−O(1)	96.7(2)	O(6)−Zn(2)−O(2)	110.6(2)
O(5)−Zn(3)−N(7)	114.9(3)	O(5)−Zn(3)−N(8)	106.2(3)
O(5)−Zn(3)−O(3)	93.9(2)	O(5)−Zn(3)−O(4)	105.6(2)
O(6)−Zn(4)−N(5)	107.0(3)	O(6)−Zn(4)−N(6)	110.3(4)
O(6)−Zn(4)−O(3)	107.5(2)	O(6)−Zn(4)−O(4)	98.2(2)
O(11)−Zn(5)−N(9)	101.2(2)	O(11)−Zn(5)−N(10)	112.5(2)
O(11)−Zn(5)−O(7)	96.9(2)	O(11)−Zn(5)−O(8)	113.7(2)
O(12)−Zn(6)−N(11)	108.4(3)	O(12)−Zn(6)−N(12)	103.1(3)
O(12)−Zn(6)−O(7)	105.4(2)	O(12)−Zn(6)−O(8)	99.7(2)
O(11)−Zn(7)−N(13)	109.0(3)	O(11)−Zn(7)−N(14)	99.2(2)
O(11)−Zn(7)−O(9)	112.7(2)	O(11)−Zn(7)−O(10)	99.5(2)
O(12)−Zn(8)−N(15)	114.1(3)	O(12)−Zn(8)−N(16)	101.2(2)
O(12)−Zn(8)−O(9)	100.6(2)	O(12)−Zn(8)−O(10)	106.8(2)

2b

Zn(1)−O(6)	1.942(5)	Zn(2)−O(5)	1.956(5)
Zn(3)−O(5)	1.950(5)	Zn(4)−O(6)	1.937(5)
O(6)−Zn(1)−N(1)	108.8(2)	O(6)−Zn(1)−O(2)	105.0(2)
O(6)−Zn(1)−N(2)	103.1(2)	O(6)−Zn(1)−O(1)	96.8(2)
O(5)−Zn(2)−N(3)	105.5(3)	O(5)−Zn(2)−O(1)	112.8(2)
O(5)−Zn(2)−N(4)	106.7(2)	O(5)−Zn(2)−O(2)	98.8(2)
O(5)−Zn(3)−N(7)	107.4(2)	O(5)−Zn(3)−N(8)	105.6(2)
O(5)−Zn(3)−O(3)	105.9(2)	O(5)−Zn(3)−O(4)	101.8(2)
O(6)−Zn(4)−N(5)	102.6(2)	O(6)−Zn(4)−N(6)	111.6(2)
O(6)−Zn(4)−O(3)	99.4(2)	O(6)−Zn(4)−O(4)	106.2(2)

atoms in a *trans* position of the macrocycle to decrease steric repulsion. It should be noted that there is a π−π interaction between parts of two rings in **2**; this is believed to strengthen two hydroxyl groups connecting the metal atoms in the same direction of the macrocycle.

Structural Description of $\{[Zn_2L^a(H_2O)_2(C_{10}H_9N)_2](ClO_4)_2\}$ (3a)

A single crystal X-ray diffraction study confirmed that the coordination geometry about the two metal atoms in compound **3a** is the same as that in **1**, with two water molecules occupying two apical positions at the opposite side of the macrocyclic plane like **3b** (Figure 4), although the position of the substituted methyl group is different in **3a** and **3b**. There are two crystallographically independent half molecules $[Zn_2L^a(H_2O)_2(C_{10}H_9N)]^{2+}$ in the asymmetric unit, each half molecule being related to another half by a centre of symmetry, giving a total of two molecules in the unit cell. The main bond lengths and angles of complex **3a** are given in Table 3. The zinc(II) atom is situated slightly above the N_2O_2 plane and each metal may be considered as distorted square pyramidal. It has also been clearly observed that two nitrogen atoms from two 2-methylquinoline molecules are linked to two coordinating water molecules above and below the macrocyclic framework, through hydrogen bonds. The resulting two N···H−O hydrogen bonds are the same with N···H, H−O, and N···O lengths of 1.865 Å, 0.809 Å, and 2.663 Å, respectively, and an N···H−O angle of 169.13°. It is very interesting to note that two hydrogen-bonded quinoline rings are found in an almost parallel position to the phenyl ring in the macrocyclic plane (with a dihedral angle of 6.3°). Moreover, they lie in a face-to-face fashion with the adjacent macrocyclic frameworks on their other side. The two quinoline rings situated between two macrocycles are strictly coplanar to each other (with a di-

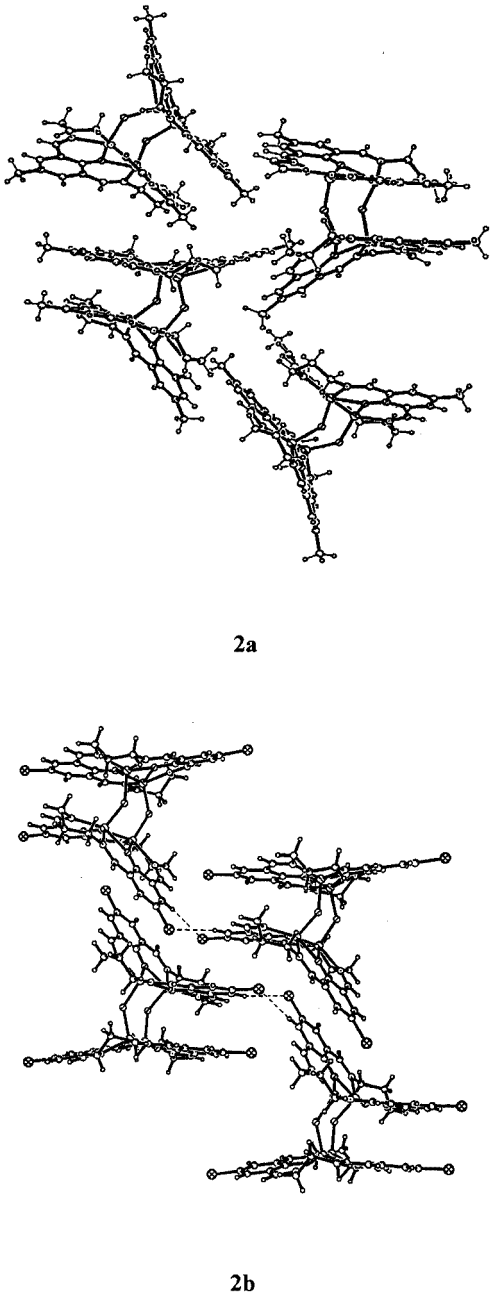

2a

2b

Figure 2. Views of molecular packing in crystals of **2a** (top) and **2b** (bottom); solvent molecules and perchlorate anions have been omitted

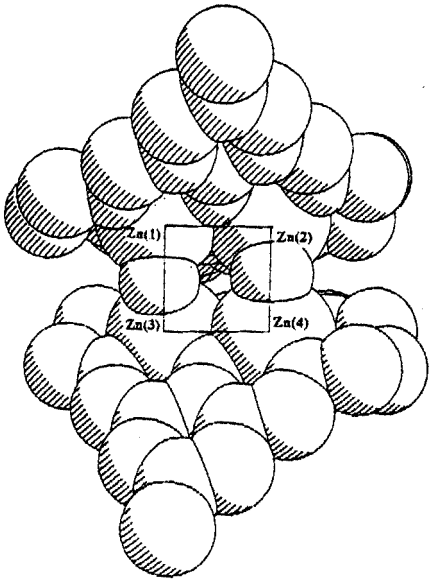

Figure 3. Space-filling view of the Zn_4 array in **2a**; hydrogen atoms are omitted for clarity

Table 2. Geometric dimensions [Å, deg] of the Zn_4 array in **2a** and **2b**

2a			
Zn(1)−Zn(2)	3.133	Zn(5)−Zn(6)	3.128
Zn(3)−Zn(4)	3.126	Zn(7)−Zn(8)	3.100
Zn(1)−Zn(3)	3.593	Zn(5)−Zn(7)	3.514
Zn(2)−Zn(4)	3.628	Zn(6)−Zn(8)	3.561
Zn(2)−Zn(1)−Zn(3)	84.7	Zn(6)−Zn(5)−Zn(7)	93.1
Zn(1)−Zn(2)−Zn(4)	92.6	Zn(5)−Zn(6)−Zn(8)	83.9
Zn(1)−Zn(3)−Zn(4)	93.4	Zn(5)−Zn(7)−Zn(8)	85.1
Zn(2)−Zn(4)−Zn(3)	84.3	Zn(6)−Zn(8)−Zn(7)	92.7
2b			
Zn(1)−Zn(2)	3.145		
Zn(3)−Zn(4)	3.162		
Zn(1)−Zn(3)	3.665		
Zn(2)−Zn(4)	3.586		
Zn(2)−Zn(1)−Zn(3)	84.5		
Zn(1)−Zn(2)−Zn(4)	85.6		
Zn(1)−Zn(3)−Zn(4)	92.4		
Zn(2)−Zn(4)−Zn(3)	94.2		

hedral angle of 0.0°), forming an ordered arrangement where one macrocycle and two 2-methylquinolines are alternately arrayed (Figure 5). The separations between the macrocyclic and quinoline rings are all about 3.6 Å. It is proposed that π−π interactions are present between quinoline and phenyl species in the macrocyclic skeleton, where the electron-rich quinoline moiety (uncoordinated) acts as a donor and the electron-poor phenyl species (owing to the coordination of the macrocyclic ligand) as acceptors. It is suggested that both the π−π interactions and the H-bonding interactions dominate such a stacking structure.

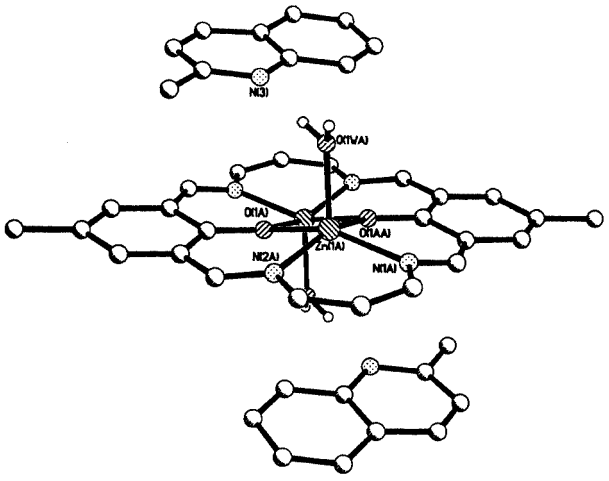

Figure 4. Ball-and-stick representation of the structure of one of the centrosymmetric complex cations from **3a**; only one of the two dinuclear clusters is shown as they are very similar

Our previous studies show that the coordinating water molecules on two sides of the macrocyclic framework can be replaced by a ligand if linear inorganic ligands or organic alkyl ligands are allowed to react with **1**.[12] However, based on the results of **2**, monofunctional aromatic ligands such as pyridine cannot be bonded to the metal atom of **1** at the vertical direction only by one-end coordination bonding, nor can the bidentate chelating ligand 2,2′-bipyridine. This may arise from the spatial repulsion between the macrocycle and the aromatic ring. Such a repulsion could be overcome, however, to permit coordination if extra forces are introduced such as hydrogen bonding or π−π interactions to support the system.[5,6] While in compound **3a** 2-methylquinoline cannot be coordinated directly to the zinc(II) atoms because of its further steric repulsion, it instead adopts a parallel way of interacting with its neighboring macrocyclic plane via π−π forces while, at the same time, forming a hydrogen bond with one macrocyclic unit. The electron transfer from the conjugated system of the macrocycle to the central zinc(II) atom upon coordination assists in forming this kind of arrangement. To the best of our knowledge, **3a** and **3b** are unprecedented examples where a macrocyclic dinuclear metal component serves as an acceptor to produce donor-acceptor compounds sustained by hydrogen bonds.

In recent years, progress in the study of the aggregation of molecular building blocks by self-assembly has risen dramatically, and several studies indicate that the results of self-assembly and the topology of metal-ligand frameworks are mainly upon the application of specific center metal atoms and well-built organic ligands.[13] In our series of experiments, the effect of the coordination geometry of the zinc atom in **1** has been investigated. Based on these and previous results, it is suggested that the coordination behavior of

Table 3. Main bond lengths [Å] and angles [deg] in **3a**

Zn(1A)−O(1WA)	2.007	H(2WA)···N(3)	1.865
O(1WA)−Zn(1A)−N(1A)	105.08(16)	O(1WA)−Zn(1A)−O(1A)	102.65(14)
O(1WA)−Zn(1A)−N(2A)	101.05(16)	O(1WA)−Zn(1A)−O(1AA)	99.27(13)
O(1WA)−H(2WA)···N(3)	169.11(10)		

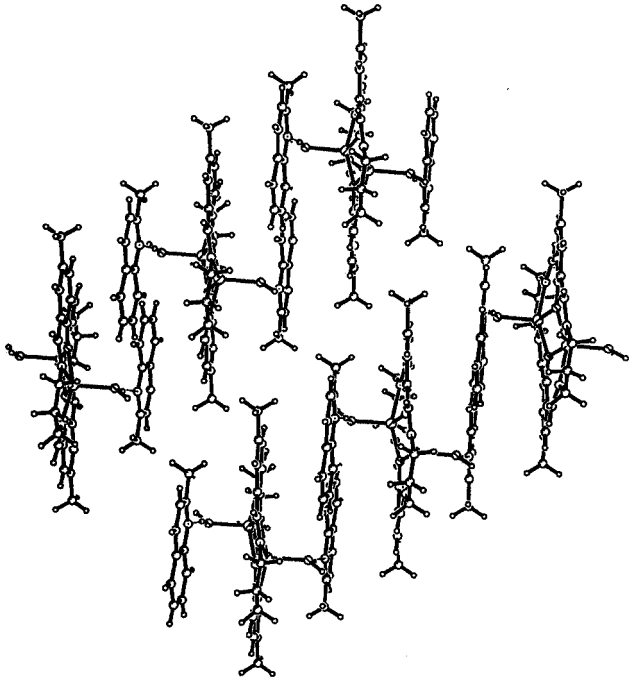

Figure 5. Packing view of **3a** along the *c*-axis; perchlorate anions have been omitted

the metal atom plays an important role in the assembly pattern of **1** with aromatic building blocks.

Experimental Section

Materials and General Methods: The perchlorate salts of **1a** and **1b** were prepared in the same manner as reported previously.[12] All other solvents and chemicals were of analytical grade and used without further purification.

Elemental analyses were measured with a Perkin−Elmer 1400C analyser. Infrared spectra (4000−400 cm^{-1}) were recorded on a Nicolet FT-IR 170X spectrophotometer. ^1H NMR spectra were obtained on a Bruker 500 MHz NMR spectrometer. Electrospray ionization (ES) mass spectra were performed in CH_3CN/CH_3OH on a Finnigan MAT SSQ 710 mass spectrometer in a scan range 300−1200 amu.

Caution! *Although no problem was encountered in all our experiments, transition metal perchlorates are potentially explosive and should be handled in small quantities.*

Preparation

2a: Pyridine (0.08 g, 1 mmol) was added to a solution of **1a** perchlorate (0.37 g, 0.5 mmol) in ethanol (30 cm^3). The solution was refluxed for 1 h, and then cooled to room temperature. Yellow crystal products were obtained, which were washed with a small amount of ethanol and dried in a vacuum. Yield 0.29 g (87%); Elemental analyses: $[C_{48}H_{52}N_8O_4Zn_4(OH)_2](ClO_4)_2(C_2H_5OH)(H_2O)_2$ (M = 1381.53): calcd. C 44.04, H 4.58, N 8.22; found C 44.16, H 4.81, N 8.21%. IR (KBr): $\tilde{\nu}$ [cm^{-1}]: 3512 s (O−H), 1641 s (C=N), 1088 vs and 623 s (ClO_4^-). ES-MS: m/z = 632 $[(Zn_2C_{24}H_{26}N_4O_2)(ClO_4)]^+$ (100%). ^1H NMR (500 MHz, D_2O, 25 °C, TMS) [ppm]: δ = 2.15 (m, 8 H, CH_2), 2.30 (s, 12 H, CH_3), 4.05 (t, 16 H, CH_2), 7.44 (s, 8 H, phenyl), 8.36 (s, 8 H, HC=N).

2b: This preparation is similar to that of **2a**, except that **1b** perchlorate (0.37 g, 0.5 mmol) and 2,2′-bipyridine (0.16 g, 1 mmol) were used. Yield 0.29 g (84%); Elemental analyses: $[C_{44}H_{40}N_8O_4Cl_4Zn_4(OH)_2](ClO_4)_2(C_2H_5OH)(H_2O)_2$ (M = 1463.20): calcd. C 37.76, H 3.58, N 7.66; found C 37.51, H 3.36, N 7.43%. IR (KBr): $\tilde{\nu}$ [cm^{-1}]: 3533 s (O−H), 1643 s (C=N), 1083 vs and 623 s (ClO_4^-). ES-MS: m/z = 337 $\{[(Zn_2C_{22}H_{20}Cl_2N_4O_2)(HClO_4)]^{2+}\}/2$ (100%). ^1H NMR (500 MHz, D_2O, 25 °C, TMS) [ppm]: δ = 2.16 (m, 8 H, CH_2), 4.05 (t, 16 H, CH_2), 7.64 (s, 8 H, phenyl), 8.36 (s, 8 H, HC=N).

3a: 2-Methylquinoline (0.14 g, 1 mmol) was added to an ethanol solution (30 cm^3) of **1a** perchlorate (0.37 g, 0.5 mmol). The solution was refluxed for 1 h and then cooled to room temperature. The yellow precipitate was filtered, washed with a small amount of ethanol, and dried in vacuum. Yield 0.45 g (88%); Elemental analyses: $[C_{24}H_{26}N_4O_2Zn_2(H_2O)_2(C_{10}H_9N)_2](ClO_4)_2$ (M = 1054.56): calcd. C 50.11, H 4.59, N 7.97; found C 50.28, H 4.64, N 7.86%. IR (KBr): $\tilde{\nu}$ [cm^{-1}]: 3377 s (O−H), 1640 s (C=N), 1087 vs and 625 s (ClO_4^-). ES-MS: m/z = 591 $[ZnNaHLClO_4]^+$ (100%). ^1H NMR (500 MHz, D_2O, 25 °C, TMS) [ppm]: δ = 2.26 (m, 4 H, CH_2), 2.43(s, 6 H, CH_3), 2.89 (s, 6 H, CH_3 of quinoline ring), 4.14 (t, 8 H, CH_2), 7.57 (s, 4 H, phenyl), 7.68−8.12 (m, 8 H, quinoline ring), 8.48 (s, 4 H, HC=N), 8.55 (m, 4 H, quinoline ring).

3b: The preparation is analogous to **3a** except that that 8-methylquinoline (0.14 g, 1 mmol) was employed. Yield: 0.46 g (90%). Elemental analyses: $[C_{24}H_{26}N_4O_2Zn_2(H_2O)_2(C_{10}H_9N)_2](ClO_4)_2$ (M = 1054.56): calcd. C 50.11, H 4.59, N 7.97; found: C 50.44, H 4.73, N 8.21. IR (KBr): $\tilde{\nu}$ [cm^{-1}]: 3375 s (O−H), 1641 (C=N), 1087 vs and 624 s (ClO_4^-). Es-ms: m/z = 591 $[ZnNaHLClO_4]^+$ (100). ^1H NMR (500 MHz, D_2O, 25 °C, TMS) [ppm]: δ = 2.25 (m, 4 H, CH_2), 2.41 (s, 6 H, CH_3), 2.84 (s, 6 H, CH_3 of quinoline ring), 4.16 (t, 8 H, CH_2), 7.55 (s, 4 H, phenyl), 7.65−8.10 (m, 8 H, quinoline ring), 8.46 (s, 4 H, HC=N), 8.55 (m, 4 H, quinoline ring).

Crystallography

Single crystals of all compounds suitable for X-ray diffraction measurements were grown from their ethanol/methanol solutions. The molecular structure of **3b** has been reported elsewhere where only 8-methylquinoline was used to assemble **1a**.[14] Because crystals of **2a**, **2b**, and **3a** are very unstable in the absence of their mother liquors, their single-crystal samples were covered in glue before measurements. Reflection data for three crystals were measured by a Bruker SMART 1K CCD diffractometer system at 293(2) K by using graphite monochromated Mo-K_α radiation (λ =

Table 4. Summary of crystal data of **2a**, **2b**, and **3a**

Compound	**2a**	**2b**	**3a**
Chem. formula	$C_{99}H_{118}Cl_4N_{16}O_{32}Zn_8$	$C_{45}H_{48}Cl_6N_8O_{17}Zn_4$	$C_{44}H_{48}Cl_2N_6O_{12}Zn_2$
M	2708.85	1447.09	1054.52
Crystal system	Monoclinic	Triclinic	Triclinic
Space group	*P 21/c*	$P\bar{1}$	$P\bar{1}$
a [Å]	26.5214(4)	13.47870(10)	8.8057(1)
b [Å]	23.4111(3)	15.6702(2)	12.4797(3)
c [Å]	17.8921(2) A	17.3503(3)	21.6900(5)
α [deg]	90.00	63.6995(7)	91.704(1)
β [deg]	103.6923(7)	78.0460(8)	95.942(1)
γ [deg]	90.00	71.3850(9)	102.874(1)
V [Å^3]	10793.4(2)	3104.08(7)	2307.74(8)
Z	4	2	2
D_{calcd} [g·cm^{-3}]	1.667	1.548	1.520
μ [mm^{-1}]	1.933	1.853	1.224
F(000)	5552	1464	1092
Crystal size [mm]	0.34 × 0.18 × 0.14	0.48 × 0.38 × 0.32	0.40 × 0.20 × 0.14
2θ range for data collection	5.46 to 57.98	5.38 to 56.64	1.90 to 56.60
no. of reflns meads, unique	76717, 27472	22352, 14835	16497, 10859
no. of reflns with [$I > 2\sigma(I)$]	9912	6215	4592
max., min. transmission	0.7736, 0.5594	0.5885, 0.4699	0.8473, 0.6403
*R*1, *wR*2 [$I > 2\sigma(I)$]	0.0921, 0.1690	0.0765, 0.2074	0.0638, 0.1502
*R*1, *wR*2 [all data]	0.2581, 0.2313	0.1671, 0.2458	0.1547, 0.1788
Goodness of fit on F^2	0.954	0.902	0.855
|ρ, max, min [e·Å^{-3}]	0.989, −0.684	0.823, −0.754	0.859, −0.826

0.71073 Å). The data were collected by using SMART and reduced with the program SAINT.[15] Empirical absorption correction was done by using the SADABS program.[16] All structures were solved by direct methods and refined by least-squares method on F^2_{obs} with the SHELXTL-PC software package.[17] All non-H atoms, except the oxygen atoms from two perchlorate ions and solvent molecules in **2b**, were refined anisotropically. The hydrogen atom positions were fixed geometrically and allowed to ride on the attached atoms. One middle carbon atom of the 1,3-diaminopropane in one macrocyclic unit in **2b** was found to be disordered over two sites, with an occupancy of 0.48(3) and 0.52(3) for C-13. Crystal data and structural refinement for three compounds are listed in Table 4.

CCDC-140749 (**2a**), -140750 (**2b**), and -157365 (**3a**) contain the supplementary crystallographic data for this paper. These data can be obtained free of charge at www.ccdc.cam.ac.uk/conts/retrieving.html [or from the Cambridge Crystallographic Data Centre, 12, Union Road, Cambridge CB2 1EZ, UK; Fax: (internat.) + 44-1223/336-033; E-mail: deposit@ccdc.cam.ac.uk].

Acknowledgments

We would like to thank Jiangsu Science & Technology Department (BK2001031) and the Third World Academy of Sciences (TWAS) for the financial support. This work is also partly funded by the National Natural Science Foundation of China (project 20271026). W. H. is grateful to Nanjing University Talent Development Foundation.

[1] [1a] R. Robson, B. F. Abrahams, S. R. Batten, R. W. Gable, B. F. Hoskins, J. Liu, *Supramolecular Architecture*, ACS, Washington, DC, **1992**, chapter 19. [1b] S. R. Batten, R. Robson, *Angew. Chem.* **1998**, *110*, 1558−1595; *Angew. Chem. Int. Ed.* **1998**, *37*, 1460−1494. [1c] H. Li, M. Eddaoudi, M. O'Keeffe, O. M. Yaghi, *Nature* **1999**, *402*, 276−279. [1d] P. J. Stang, B. Olenyuk, *Acc. Chem. Res.* **1997**, *30*, 502−518. [1e] M. J. Zawotko, *Nature* **1999**, *402*, 242−243. [1f] M. Fujita, *Chem. Soc. Rev.* **1998**, *27*, 417−423.

[2] In our current experiments, reaction of **1b** with sodium formate results in the generation of a polymer of a binuclear zinc(II) complex bridged by formate anions in an end-to-end fashion. The structure is similar to that of a binuclear nickel(II) complex of ligand **1a** except that pyramidal configurations are present around the zinc(II) atoms in our compound: [2a] W. Huang, D. Hu, S. Gou, S. Chantrapromma, H.-K. Fun, Y. Xu, Q. Meng, *Inorg. Chim. Acta* **2003**, *342*, 9−15. [2b] A. Asokan, B. Varghese, A. Caneschi, P. T. Manoharan, *Inorg. Chem.* **1998**, *37*, 228−232.

[3] [3a] N. H. Pilkington, R. Robson, *Aust. J. Chem.* **1970**, *23*, 2226−2232. [3b] P. A. Vigato, S. Tamburini, D. E. Fenton, *Coord. Chem. Rev.* **1990**, *106*, 25−170. [3c] J. D. Lamb, R. M. Izatt, J. J. Christensen, D. J. Eatough, in: *Coordination Chemistry of Macrocyclic Compounds*, (Ed.: G. A. Melson), Plenum Press: New York, **1979**, p. 145. [3d] D. E. Fenton, H. Okawa, *Perspectives on Bioinorganic Chemistry*, JAI Press: London, **1993**, vol. 2, p. 81.

[4] [4a] M. T. Casey, M. McCann, M. Devereux, M. Curran, C. Cardin, M. Convery, V. Quillet, C. Harding, *J. Chem. Soc., Chem. Commun.* **1994**, 2643−2645. [4b] D. S. Lawrence, T. Jiang, M. Levett, *Chem. Rev.* **1995**, *95*, 2229−2260.

[5] W. Huang, S. Gou, D. Hu, S. Chantrapromma, H.-K. Fun, Q. Meng, *Inorg. Chem.* **2001**, *40*, 1712−1715.

[6] W. Huang, S. Gou, D. Hu, S. Chantrapromma, H.-K. Fun, Q. Meng, *Inorg. Chem.* **2002**, *41*, 864−868.

[7] [7a] R. Taylor, O. Kennard, *J. Am. Chem. Soc.* **1982**, *104*, 5063−5070. [7b] Z. Berkovitch-Yellin, L. Leiserowitz, *Acta Crystallogr., Sect. B* **1984**, *40*, 159−161. [7c] T. Steiner, *Chem. Commun.* **1997**, 727−734. [7d] F. A. Cotton, L. M. Daniels, G. T. Jordon IV, C. A. Murillo, *Chem. Commun.* **1997**, 1673−1674. [7e] T. Spaniel, H. Görls, J. Scholz, *Angew. Chem.* **1998**, *110*, 1962−1966; *Angew. Chem. Int. Ed.* **1998**, *37*, 1862−1865.

[8] [8a] U. Koch, P. L. A. Popelier, *J. Phys. Chem.* **1995**, *99*, 9747−9952. [8b] G. R. Desiraju, *Acc. Chem. Res.* **1996**, *29*, 441−449.

[9] O. Navon, J. Bernstein, V. Khodorkovsky, *Angew. Chem.* **1997**, *109*, 640−642; *Angew. Chem. Int. Ed. Engl.* **1997**, *36*, 601−603.
[10] Two nonclassical C−H···Cl hydrogen bonds in **2b** are C−H 0.930, H···Cl 2.890, C···Cl 3.798 Å, with an angle of 165.6°; C−H 0.930, H···Cl 2.840, C···Cl 3.761 Å, with an angle of 170.8°, a little shorter than the sum of van der Waals radii of chlorine and hydrogen atoms (Cl = 1.75, H = 1.2 Å), and the intermolecular Cl···Cl distance is 4.10 Å.
[11] E. Asato, H. Kawahashi, M. Mikuriya, *J. Chem. Soc., Dalton Trans.* **1995**, 3897−3904.
[12] [12a] H. Adams, N. A. Bailey, P. Bertrand, O. R. Cecilia, D. E. Fenton, S. Gou, *J. Chem. Soc., Dalton Trans.* **1995**, 275−279. [12b] W. Huang, S. Gou, D. Hu, Y. Xu, S. Chantrapromma, Q. Meng, *J. Mol. Struct.* **2001**, *561*, 121−129.
[13] [13a] S. Leininger, B. Olenyuk, P. J. Stang, *Chem. Rev.* **2000**, *100*, 853−907. [13b] M. J. Zaworotko, *Chem. Commun.* **2001**, 1−9. [13c] B. J. Holliday, C. A. Mirkin, *Angew. Chem.* **2001**, *113*, 2076−2097; *Angew. Chem. Int. Ed.* **2001**, *40*, 2022−2043. [13d] F. A. Cotton, C. Lin, C. A. Murillo, *Accounts of Chemical Research* **2001**, *34*, 759−771. [13e] B. Moulton, M. J. Zaworotko, *Chem. Rev.* **2001**, *101*, 1629−1658;
[14] J. Fang, W. Huang, S. Chantrapromma, S. S. S. Raj, I. A. Razak, H.-K. Fun, S. Gou, H. Wang, *Acta Crystalogr. Sect. C* **2000**, *56*, 1429−1430.
[15] Siemens, *SMART* and *SAINT. Area Detector Control and Integration Software*, Siemens Analytical X-ray Systems, Inc., Madison, Wisconsin, USA, **1996**.
[16] G. M. Sheldrick, *SADABS, Program for Empirical Absorption Correction of Area Dectector Data*, University of Göttingen, Germany, **1996**.
[17] G. M. Sheldrick, *SHELXTL V5.1, Software Reference Manual*, Bruker AXS, Inc., Madison, Wisconsin, USA, **1997**.

Received August 21, 2002
[I02473]

The Photophysical Properties of Hybrid Metal Complexes Containing both 2,2′-Bipyridine and 2,2′:6′,2′′-Terpyridine Units

Anthony Harriman,*[a] Muriel Hissler,[b] Abderrahim Khatyr,[b] and Raymond Ziessel[b]

Keywords: Luminescence / Photophysics / Molecular electronics / Energy transfer

Stepwise cross-coupling reactions between functionalized metallo synthons and bipyridine- or terpyridine-based building blocks afford novel photoactive, hybrid complexes bearing multiple chromophores that function separately or cooperatively according to the nature of the coordinated metal cations.
(© Wiley-VCH Verlag GmbH & Co. KGaA, 69451 Weinheim, Germany, 2003)

Introduction

Many (polypyridine)ruthenium(II) complexes possess photophysical and electrochemical properties suitable for the putative construction of luminescent sensors and/or photoactive molecular-scale devices.[1−3] A large number of mono- and multinuclear complexes are now known, notably built around 2,2′-bipyridine (bpy), 1,10-phenanthroline (phen), or 2,2′:6′,2′′-terpyridine (terpy) ligands, and have been used for various applications.[4−6] The terpy-based ligands are especially useful for the design of linear multicomponent systems but, because of its very short-lived triplet excited state, the parent $[Ru(terpy)_2]^{2+}$ complex has found little use in photoactive devices.[7] Different strategies have been devised[8] for prolonging the triplet lifetime of $[Ru(terpy)_2]^{2+}$, and dinuclear derivatives have been identified that exhibit reasonable emission yields in deoxygenated solution at 20 °C.[9,10] The most successful approach for prolonging the triplet lifetime of $[Ru(terpy)_2]^{2+}$ involves direct attachment of an alkynylene group at the 4′-position of the coordinated terpy ligand.[11] We now show that this strategy can be used to generate hybrid metal complexes containing Ru(terpy) and Ru(bpy) metallo terminals linked by a single ethynylene group. The resultant dinuclear complex exhibits photophysical properties suggestive of a highly delocalized triplet state.

[a] Department of Chemistry, Bedson Building, University of Newcastle,
Newcastle upon Tyne NE1 7RU, United Kingdom
Fax: (internat.) + 44-191/222-8660
E-mail: anthony.harriman@ncl.ac.uk
[b] Laboratoire de Chimie Moléculaire, Ecole Européenne de Chimie, Polymères et Matériaux, Université Louis Pasteur, UMR 7008,
25 rue Becquerel, 67087 Strasbourg Cedex 02, France
E-mail: ziessel@chimie.u-strasbg.fr

Results and Discussion

The target complex **RBTR**, together with appropriate reference complexes **RBT** and **RTB**, could not be prepared from the free **BT** ligand[12] by conventional synthetic protocols, but was accessible by iterative Sonogashira-type coupling reactions starting from the relevant metallo synthon, as shown in Figure 1. These cross-coupling reactions proceed smoothly under mild conditions in the presence of a catalytic amount of $[Pd(PPh_3)_4]$ and acetonitrile. It is noteworthy that **RBTR** could be constructed either from the **RTB** or **RBT** precursors, while the mixed **RBTO** species was only obtained from the **RBT** metallo synthon. Interestingly, during the first step (a), when the leaving group (Br) is grafted onto the ruthenium complex the rate of the cross-coupling reaction is significantly enhanced due to the pronounced electron-withdrawing effect of the metal center. However, no major difference in reactivity was observed during cross-coupling of the ethynylene-grafted Ru(bpy) complex with either the bromo- or triflate-substituted terpy fragments (step c). The tripartite complex **RBTZ** was prepared from **RBT** using a slight excess of zinc(II) perchlorate. All compounds were isolated by column chromatography and characterized by FT-IR, ES mass, ^1H and ^{13}C NMR spectra, and elemental analyses. These compounds are stable and reasonably soluble in polar organic solvents. All compounds were studied as their hexafluorophosphate salts in deoxygenated acetonitrile and the chemical structures are depicted in Figure 1.

The photophysical properties recorded for the mononuclear reference compounds were as expected for ethynylene-substituted (polypyridine)ruthenium(II) complexes (Table 1). In particular, each compound shows a pronounced metal-to-ligand charge-transfer (MLCT) absorption transition (λ_{max}) in the region 450−500 nm, for which the molar absorption coefficient (ε_{MLCT}) at the band maximum is reminiscent of related mononuclear com-

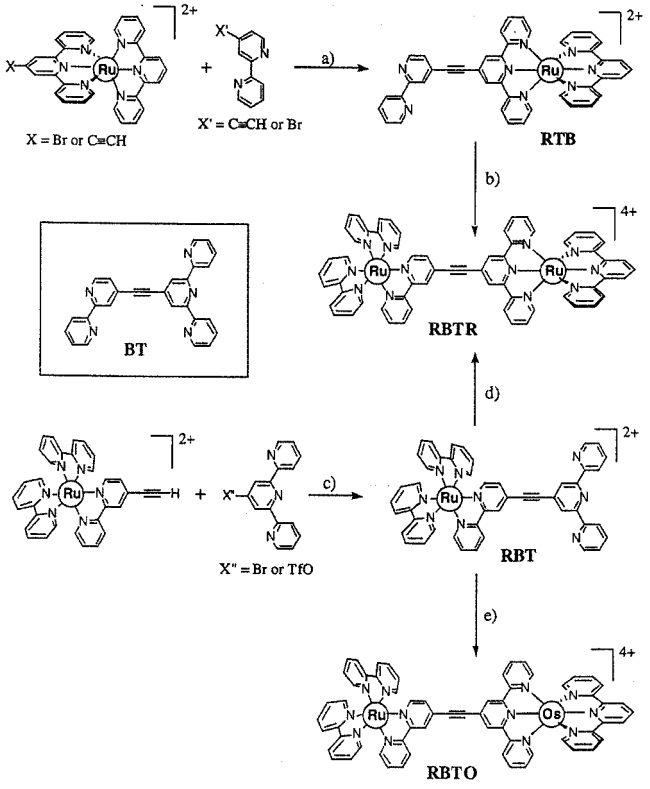

Figure 1. Reaction sequence used to prepare the various metal complexes studied in this work: (a) X = Br, X′ = C≡CH, $[Pd^0(PPh_3)_4]$ (6 mol %), C_6H_6, *i*Pr_2NH, CH_3CN, 80 °C, 15 h, 48%; X = C≡CH, X′ = Br, $[Pd^0(PPh_3)_4]$ (6 mol %), C_6H_6, *i*Pr_2NH, CH_3CN, 90 °C, 4 d, 49%; (b) $[Ru(bpy)_2Cl_2]\cdot 2H_2O$, EtOH/$H_2O$, 80 °C, 12 h, 69%; (c) $[Pd^0(PPh_3)_4]$ (6 mol %), C_6H_6, *i*Pr_2NH, CH_3CN, 80 °C, 18 h for X′′ = Br, 58% or 12 h for X′′ = OTf, 53%; (d) [Ru(terpy)(DMSO)Cl_2], $AgBF_4$ (2 equiv.), CH_3OH, 80 °C, 1 d, 56%; (e) [Os(terpy)$(O)_2$(OH)](NO_3), H_2O, THF, hydrazine, 45 °C, 12 h, 44%; counteranions (PF_6^-) omitted for clarity

plexes.[13,14] Luminescence is readily detected at 20 °C and, by reference to other (polypyridine)ruthenium(II) complexes,[7] can be assigned to emission from the (nominally) triplet excited MLCT state. Luminescence maxima (λ_{lum}), quantum yields (Φ_{lum}), and lifetimes (τ_{lum}) are similar to those recorded earlier for ethynylene-substituted complexes formed from bpy or terpy ligands in deoxygenated acetonitrile. In all cases, the corrected luminescence excitation spectrum agrees well with the absorption spectrum recorded over the range 250−600 nm and emission decay profiles are well described by a mono-exponential fit.

There are two important points to note from these experimental data. First, emission from the Ru(bpy) unit is much more pronounced and longer-lived than that from the corresponding Ru(terpy) fragment. Such behavior is normal and has been attributed to mixing between MLCT triplet and metal-centered states that promotes nonradiative deactivation in Ru(terpy) systems.[15] Second, the luminescence maximum found for the Ru(terpy) unit is red-shifted by ca. 30 nm with respect to that of the Ru(bpy) fragment, suggesting that the latter possesses the higher triplet energy. In fact, the individual luminescence profiles are readily analyzed in terms of a spectral curve-fitting routine[15] that permits accurate calculation of the triplet energies (E_T). This analysis confirms that the triplet state associated with the Ru(terpy) unit lies at lower energy (Table 1) but indicates that the energy gap between these two triplets is rather small ($\Delta E_T = 1100\ cm^{-1} \approx 5\ k_BT$). The same analysis allows calculation of the reorganization energy (λ_T) that accompanies deactivation of the MLCT triplet state and the Huang−Rhys factor (*S*). It can be seen that both values are substantially higher for **RBT** than for **RTB**, indicating that the former undergoes a more significant geometry change upon excitation to the triplet state.[7]

Table 1. Photophysical properties recorded for the various metal complexes in deoxygenated acetonitrile at 20 °C

Property	**RBT**	**RTB**	**RBTO**[a]	**RBTZ**	**RBTR**
λ_{MLCT} [nm][b]	461	490	505	475	506
ε_{MLCT} [$M^{-1}\cdot cm^{-1}$][c]	14,400	24,900	13,900	25,100	35,200
λ_{LUM} [nm][d]	650	680	735	670	705
τ_{LUM} [ns][e]	710	75	380	1,080	350
Φ_{LUM}[e]	0.046	0.001	0.0100	0.060	0.006
E_T [cm^{-1}][f]	16,500	15,400	14,670	16,300	15,320
λ_T [cm^{-1}][f]	1,250	850	1,000	1,450	1,180
S[f]	0.95	0.60	0.70	0.98	0.85

[a] Photophysical properties refer to the osmium-based chromophore. [b] ±2 nm. [c] ±5%. [d] ±5 nm. [e] ±8%. [f] Derived from spectral curve fitting analyses.

Photophysical properties recorded for the corresponding Os(terpy) fragment in the **RBTO** complex are also given in Table 1 and indicate that the triplet state localized on this chromophore lies at significantly lower energy. These measurements were made following laser excitation at 646 nm, where only the Os(terpy) fragment absorbs. The derived values appear to be in reasonable agreement with measurements made for related Os(terpy)-based systems except that the triplet lifetime is rather long. This is probably due to extended electron delocalization at the triplet level.

In fact, the mixed-metal hybrid complex **RBTO** displays a clear indication of intramolecular triplet energy transfer. Thus, the emission spectrum recorded in deoxygenated acetonitrile at 20 °C is characteristic of emission from an Os(terpy) fragment,[16] the peak being at 735 nm, and is independent of excitation wavelength. The corrected excitation spectrum is in excellent agreement with the absorption spectrum recorded across the entire visible range. There is no obvious emission from the Ru(bpy) fragment following excitation around 460 nm, where the latter is the dominant chromophore, and the emission decay profile, recorded after excitation with a 10-ns laser pulse at 460 nm, follows first-order kinetics at all wavelengths. The average triplet lifetime recorded for the Os(terpy) fragment following laser excitation at 460 nm is 410±25 ns, which is similar to that recorded after direct excitation of the Os(terpy) fragment at 646 nm ($\tau_T = 380\pm20$ ns). There is a reasonable thermodynamic driving force for intramolecular energy transfer from the Ru(bpy) unit to the appended Os(terpy) fragment ($\Delta E_T = 1830\ cm^{-1}$).

Excitation of **RBTO** with a sub-ps laser pulse at 460 nm causes a biphasic bleaching of the Os(terpy) chromophore at 500 nm (Figure 2). Approximately 40% of this bleaching occurs within the laser pulse and can be attributed to direct absorption by the Os(terpy) fragment. The remainder bleaches on a time scale of several tens of ps, corresponding to a first-order process of $7\pm2\times10^{10}$ s^{-1}, which is assigned to intramolecular triplet energy transfer from the Ru(bpy) unit. This rate is similar to those observed for other ethynylene-bridged Ru−Os systems.[16]

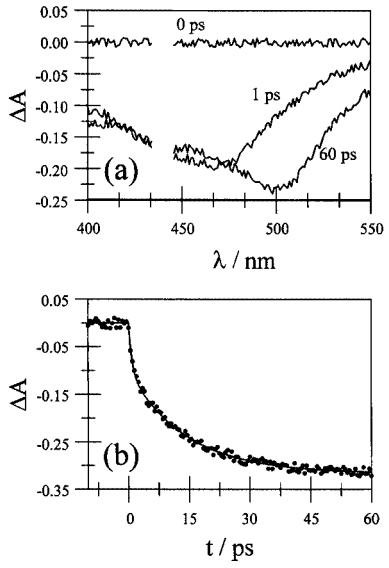

Figure 2. (a) Differential transient absorption spectra recorded at various delay times for **RBTO** in deoxygenated acetonitrile at 20 °C; the excitation source was a sub-ps laser pulse at 460 nm; (b) kinetic trace recorded at 500 nm for the experiment described in (a) above; the solid points refer to the experimental data while the line drawn through the points corresponds to a fit to a two-exponential growth process having time constants of 0.8 (38%) and 14 (62%) ps, respectively

It is normal practice to consider that intramolecular triplet energy transfer in such systems might occur by either the Dexter electron-exchange[17] or the Förster dipole-dipole[18] mechanisms, or by a combination of both processes. Using spectroscopic data collected for **RBT** and the Os(terpy) fragment present in **RBTO**, the Förster spectral overlap integral (J_F) for energy transfer along the molecular axis in **RBTO** was calculated[18] to be 2.8×10^{-14} $mmol^{-1}$ cm^6. Using this latter value in conjunction with the photophysical properties recorded for **RBT**, the rate constant for dipole-dipole energy transfer in **RBTO** is calculated to be ca. 10^8 s^{-1}, for random orientations of the two terminals. Although fast, this rate is well below the experimental value. As such, we conclude that the dominant mechanism for triplet energy transfer in **RBTO** involves through-bond electron exchange.

Assuming energy transfer occurs by electron exchange and that the Franck−Condon factor ($FC = 1.5\times10^{-4}$ cm) can be determined[15] from emission spectra recorded for the relevant subunits, it is possible to calculate the electronic coupling matrix element (V_{DA}) for this system by application of the Fermi−Golden rule[19] [Equation (1)]. The derived value ($V_{DA} = 6$ cm^{-1}) is in keeping with earlier observations.[20] These findings can be used to argue that the mixed-metal hybrid complex **RBTO** comprises two separate chromophores and that, in terms of photophysics, it can be regarded as a closely-spaced molecular dyad. The long triplet lifetime found for the Os(terpy) fragment might indicate that the ethynylene group possesses increased electron density at the MLCT triplet level.

$$k_D = \frac{2\pi}{\hbar}|V_{DA}|^2 FC \quad (1)$$

The photophysical properties of the tripartite complex **RBTZ** (Table 1) can be understood in terms of the coordinated zinc(II) cation extending the degree of electron delocalization over the bridging ligand. Thus, binding of zinc(II) cations to the vacant terpy ligand will lower the LUMO energy of the bridging ligand.[20] This has the effect of increasing blending between orbitals on the bpy and terpy ligands, thereby favoring electron delocalization at the triplet level. The effect is apparent from the red-shifted absorption and emission spectra and from the prolonged triplet lifetime found for **RBTZ** relative to **RBT**. There is a slight decrease in triplet energy (E_T) but a more substantial increase in the reorganization energy (λ_T). The latter effect is characteristic of increased electron delocalization.[7]

Understanding the photophysical properties of the dinuclear hybrid complex **RBTR** is more demanding and it is unclear if this system behaves as two closely coupled but separate units or as a single giant supermolecule. The absorption spectrum (Figure 3) contains indications of MLCT transitions associated with both Ru(bpy) ($\lambda_{MLCT} \approx 450$ nm) and Ru(terpy) ($\lambda_{MLCT} \approx 500$ nm) fragments, together with ligand-centered transitions around 300 nm. This spectrum is in reasonable agreement with a superposition of spectra recorded for **RBT** and **RTB**.[21] The emission spectrum recorded at 20 °C, which is centered around 705 nm, differs markedly from that recorded for a 1:1 molar mixture of **RBT** and **RTB** (Figure 3). This spectrum is independent of excitation wavelength, the corrected excitation spectrum agrees well with the absorption spectrum recorded across the entire visible region, and the emission decay profile follows exponential kinetics, regardless of excitation or detection wavelengths, following excitation with a 10-ns laser pulse. The average emission lifetime in deoxygenated acetonitrile is 350 ns while the luminescence quantum yield is 0.006. These values, except for the triplet lifetime, are more in keeping with **RTB** than **RBT** (Table 1).

The emission spectrum recorded for **RBTR** at room temperature was analyzed[15] as above to give a value for the triplet energy (E_T) that is closely similar to that derived for **RTB** (Table 1). The hybrid compound, however, gave an increased reorganization energy (λ_T) and a larger Huang−Rhys factor (S) than that found for the relevant mononuclear complex **RTB**. In fact, these derived values lie between those observed for **RBT** and **RTB**. Given the small triplet energy gap between these latter two complexes, the

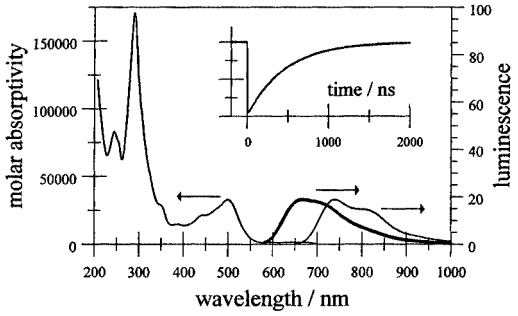

Figure 3. Absorption and emission spectra recorded for **RBTR** in deoxygenated acetonitrile at 20 °C; also shown (solid curve) is the emission spectrum recorded for a 1:1 molar mixture of **RBT** and **RTB** under identical conditions; the excitation wavelength for emission studies was 480 nm; the insert shows the luminescence decay profile recorded at 700 nm

emission spectrum recorded for **RBTR** might be considered to comprise an equilibrium mixture of the two triplets associated with the mononuclear terminal complexes. Taking ΔE_T to be 1100 cm^{-1}, the equilibrium mixture of triplet states would be completely dominated (i.e. 99.6%) by the triplet associated with **RTB**. Allowing for the difference in emission quantum yields found for these terminals, it can be concluded that the luminescence spectrum of the hybrid complex would contain a major contribution (i.e. 85%) from **RTB** and a minor portion (i.e. 15%) from **RBT**. Spectral analysis shows that this is not the case and, instead, the emission spectrum appears to be that of a single chromophore. It is also evident that the decay kinetics recorded at all wavelengths are best fitted by a single-exponential analysis. There is no rapidly decaying component in the kinetic traces; based on the spectral parameters derived for **RBT** and **RTB**, and taking V_{DA} to be 6 cm^{-1}, we would expect triplet energy transfer from **RBT** to **RTB** to occur on a time scale of ca. 30 ps. There is no obvious indication of intramolecular triplet energy transfer on this time scale; the inference being that **RBTR** behaves as a single giant emitter.

A similar conclusion is reached from analysis of the transient absorption spectrum recorded after laser excitation of **RBTR** at 460 nm (Figure 4). Thus, the differential absorption spectrum recorded for **RBTR** in deoxygenated acetonitrile differs markedly from those recorded for the reference compounds under identical conditions. There is strong absorption in the near IR region and bleaching in the MLCT region, especially around where the Ru(terpy) subunit is expected to absorb. This latter observation indicates that the triplet state is primarily of MLCT character and is not a π,π^* state localized on the polytopic ligand. The near-IR differential absorption bands appear as two distinct peaks. Whilst the lower-energy peak centered around 900 nm has some resemblance to the near-IR peak seen for **RTB** the higher-energy peak centered around 650 nm is not apparent in the spectra recorded for either **RTB** or **RBT** (Figure 5). The signal decays by first-order kinetics, with an averaged lifetime of 350±15 ns, at all monitoring wavelengths. Examination of the spectrum on very short time scales indicates that the signal evolves over a few ps but does not undergo any obvious changes in profile that might be consistent with intramolecular triplet energy transfer from **RBT** to **RTB** units. Again, the conclusion is that, at the triplet level, **RBTR** behaves more like a single chromophore than a closely-coupled admixture of two discrete MLCT triplet states.

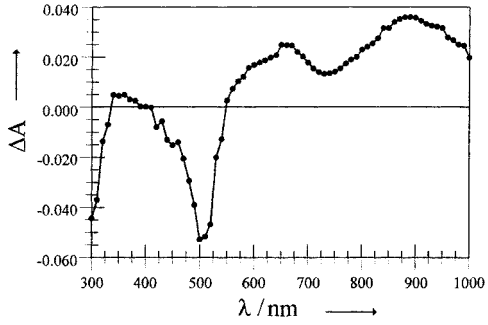

Figure 4. Differential absorption spectrum recorded for **RBTR** in deoxygenated acetonitrile at 20 °C after excitation at 460 nm with a 10-ns laser pulse; the spectrum was recorded 50 ns after excitation

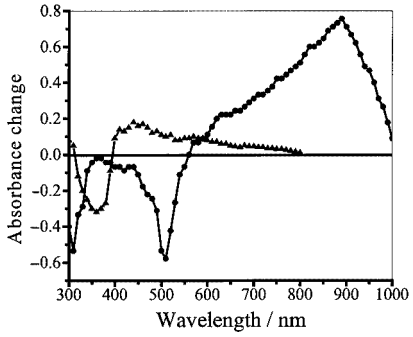

Figure 5. Transient absorption spectra recorded for **RBT** (black triangle) and **RTB** (black circle) in deoxygenated acetonitrile solution following excitation with a 10-ns laser pulse at 460 nm

Conclusion

In summary, the hybrid **BT** ligand introduced here can give rise to several distinct triplet states upon coordination of a metal cation. Either chelate can be capped with a suitable metallo fragment to produce **RBT** or **RTB**, where the lowest-energy, triplet excited state is of MLCT character and is localized on the capped terminal. Coordinating zinc(II) cations to the vacant terpy-based terminal in **RBT** gives rise to the tripartite, mixed-metal complex **RBTZ**, where the triplet state is of MLCT character but is more extensively delocalized than in **RBT**. The mixed-metal complex **RBTO** displays rapid intramolecular triplet energy transfer and the lowest-energy triplet is clearly localized on the Os(terpy) unit. For **RBTR**, the two terminals are of comparable energy, both in terms of redox chemistry and excitation energies, and it appears that the lowest-energy triplet excited state is extensively delocalized.

Experimental Section

Synthesis of RTB: Acetonitrile (4 mL), diisopropylamine (1.5 mL), and $[Pd(PPh_3)_4]$ (6 mol %, 0.008 g, 0.006 mmol) − a catalyst precursor − were added consecutively to a stirred solution containing $[Ru(terpy)(4'\text{-ethynyl-terpy})](PF_6)_2$[22] (0.080 g, 0.090 mmol) and 5-bromo-bpy[23] (0.022 g, 0.090 mmol) in Ar-degassed benzene (10 mL). After heating at 90 °C for 4 d, KPF_6 (0.034 g, 0.18 mmol) was added and the solvent removed under vacuum. The deep-red material was washed with water under centrifugation and the resultant solid was purified by flash chromatography on silica gel, first with a mixture of acetonitrile/water (0−10%) as eluent and secondly with a mixture of acetonitrile/water (0−10%) having a gradient of a saturated aqueous solution of KNO_3 as eluent. Metathesis of the anion was ensured using an excess of KPF_6 in an acetone/water mixture. The solid sample was collected, washed with diethyl ether and dried under vacuum. Yield 0.046 (48%). ^{1}H NMR ([D$_6$]acetone): δ = 9.11−9.01 ppm (m, 3 lines, 4 H), 8.91 (t, ^3J = 7.3 Hz, 4 H), 8.69 (s, 1 H), 8.53 (t, ^3J = 7.9 Hz, 3 H), 8.18 (d, ^3J = 12.8 Hz, 1 H), 8.04 (q, ^3J = 14.0 Hz, 4 H, ^3J = 7.1 Hz), 7.77 (d, ^3J = 5.4 Hz, 2 H), 7.65 (d, ^3J = 5.2 Hz, 2 H), 7.31 (q, ^3J = 6.1 Hz, 4 H), 6.98 (d, ^3J = 7.0 Hz, 1 H), 6.43 (d, ^3J = 12.8 Hz, 1 H), 6.89 (d, ^3J = 7.0 Hz, 1 H). ES-MS (acetone): *m*/*z* = 890.6 [M − PF_6, calcd. 890.8], 372.6 [(M − 2 PF_6)/2, calcd. 372.9]. $C_{42}H_{28}F_{12}N_8P_2Ru$ (1035.74): calcd. C 48.71, H 2.72, 10.82; found C 48.56, H 2.42, N 10.51.

Selected Data for RBTR: ES/MS (acetone): *m*/*z* = 724.9 [(M − 2 PF_6)/2, calcd. 724.6], 434.9 [(M − 3 PF_6)/3, calcd. 434.7], 290.0 [(M − 4 PF_6)/4, calcd. 289.8]. $C_{62}H_{44}F_{24}N_{12}P_4Ru_2{\cdot}CH_3CN$ (1739.12 + 41.05): calcd. C 43.18, H 2.66, 10.23; found C 43.26, H 2.72, N 10.38.

Selected Data for RBTO: ES/MS (acetone): *m*/*z* = 769.5 [(M − 2 PF_6)/2, calcd. 769.2], 464.5 [(M − 3 PF_6)/3, calcd. 464.4], 312.5 [(M − 4 PF_6)/4, calcd. 312.1]. $C_{62}H_{44}F_{24}N_{12}OsP_4Ru$ (1828.24): calcd. C 40.73, H 2.43, 9.19; found C 40.42, H 2.17, N 9.00.

Photophysical Studies Absorption spectra were recorded with a Hitachi U3310 spectrophotometer and emission was monitored with a Hitachi F4500 spectrophotometer. All emission spectra were fully corrected using a correction curve compiled by reference to a standard lamp. Luminescence lifetimes were measured with a Spex tau-3 time-resolved emission spectrometer. All luminescence studies were made at 20 °C using deoxygenated acetonitrile solutions. Transient absorption studies were made by laser flash photolysis using a frequency-doubled Nd-YAG laser as pump for a coumarin dye laser emitting at 460 nm. For direct excitation into the Os(terpy) chromophore at 646 nm the frequency-doubled output from the Nd-YAG laser was Raman shifted with ethanol. In each case, the pulse width was either 10 ns or 25 ps according to the needs of the experiment. Improved time resolution was achieved with a mode-locked, Nd-YAG pumped dye laser operating with Rhodamine 6G (FWHM = 350 fs). Output from the dye laser was focussed into water and the excitation pulse was isolated with a narrow-bandpass filter centered at 460 nm.

Acknowledgments

We thank the University of Newcastle, EPSRC, ECMP, and CNRS for their financial support.

[1] A. Mayer, S. Neuenhofer, *Angew. Chem. Int. Ed. Engl.* **1994**, *33*, 1044; L. Fabbrizzi, A. Poggi, *Chem. Soc. Rev.* **1995**, 197; A. P. De Silva, H. Q. N. Gunaratne, T. Gunnlaugsson, A. J. M. Huxley, C. P. McCoy, J. T. Rademacher, T. E. Rice, *Chem. Rev.* **1997**, *97*, 1515; L. Prodi, F. Bolletta, M. Montalti, N. Zaccheroni, *Coord. Chem. Rev.* **2000**, *205*, 59; P. Bühlmann, E. Pretsch, E. Bakker, *Chem. Rev.* **1998**, *98*, 1593; P. D. Beer, *Acc. Chem. Res.* **1998**, *31*, 71; R. Bergonzi, L. Fabbrizzi, M. Licchelli, C. Mangano, *Coord. Chem. Rev.* **1998**, *170*, 31.

[2] [2a] *Fluorescent Chemosensors for Ion and Molecule Recognition* (Ed.: A. W. Czarnik), ACS, Washington, DC **1992**. [2b] *Chemosensors for Ion and Molecule Recognition* (Eds.: J.-P. Desvergne, A. W. Czarnik), NATO ASI Series, Kluwer Academic Press, Dordrecht, **1997**.

[3] C. Joachim, J. K. Gimzewski, A. Aviram, *Nature* **2000**, *408*, 541.

[4] J.-P. Sauvage, J.-P. Collin, J.-C. Chambron, S. Guillerez, C. Coudret, V. Balzani, F. Barigelletti, L. De Cola, L. Flamigni, *Chem. Rev.* **1994**, *94*, 993; V. Balzani, A. Juris, M. Venturi, S. Campagna, S Serroni, *Chem. Rev.* **1996**, *96*, 759; P. F. H. Scwab, M. D. Levin, J. Michl, *Chem. Rev.* **1999**, *99*, 1863.

[5] L. De Cola, P. Belzer, *Coord. Chem. Rev.* **1998**, *177*, 301.

[6] F. Barigelletti, L. Flamigni, *Chem. Soc. Rev.* **2000**, *29*, 1.

[7] A. Harriman, R. Ziessel, *Chem. Commun.* **1996**, 1707; R. Ziessel, M. Hissler, A. El-ghayoury, A. Harriman, *Coord. Chem. Rev.* **1998**, *178−180*, 1251.

[8] A. A. Bhuiyan, J. R. Kincaid, *Inorg. Chem.* **1998**, *37*, 2525; M. T. Indelli, C. A. Bignozzi, F. Scandola, J.-P. Collin, *Inorg. Chem.* **1998**, *37*, 6084.

[9] A. C. Benniston, A. Harriman, V. Grosshenny, R. Ziessel, *New. J. Chem.* **1997**, *21*, 405.

[10] E. C. Constable, C. E. Housecroft, E. R. Schofield, S. Encinas, N. Armaroli, F. Barigelletti, L. Flamigni, E. Figgemeier, J. G. Vos, *Chem. Commun.* **1999**, 869.

[11] A. C. Benniston, V. Grosshenny, A. Harriman, R. Ziessel, *Angew. Chem. Int. Ed. Engl.* **1994**, *33*, 1884.

[12] V. Grosshenny, F. M. Romero, R. Ziessel, *J. Org. Chem.* **1997**, *62*, 1491.

[13] K. Nakamaru, *Bull. Chem. Soc. Jpn.* **1982**, *55*, 1639.

[14] C. Creutz, M. Chou, T. L. Netzel, M. Okumura, N. Sutin, *J. Am. Chem. Soc.* **1980**, *102*, 1309.

[15] V. Grosshenny, A. Harriman, F. M. Romero, R. Ziessel, *J. Phys. Chem.* **1996**, *100*, 17472.

[16] V. Grosshenny, A. Harriman, R. Ziessel, *Angew. Chem. Int. Ed. Engl.* **1995**, *34*, 1100.

[17] D. L. Dexter, *J. Chem. Phys.* **1953**, *21*, 836.

[18] T. H. Förster, *Discuss. Faraday Soc.* **1959**, *27*, 7.

[19] Z. Murtaza, D. K. Graff, A. P. Zipp, L. A. Worl, W. E. Jones Jr., W. D. Bates, T. J. Meyer, *J. Phys. Chem.* **1994**, *98*, 10504.

[20] A. El-ghayoury, A. Harriman, A. Khatyr, R. Ziessel, *Angew. Chem. Int. Ed.* **2000**, *39*, 185.

[21] A. Harriman, R. Ziessel, *Coord. Chem. Rev.* **1998**, *171*, 331.

[22] M. Hissler, R. Ziessel, *New J. Chem.* **1997**, *21*, 843.

[23] F. M. Romero, R. Ziessel, *Terahedron. Lett.* **1995**, *36*, 6471.

Received September 20, 2002
[I02532]

Dynamic Behavior of an *N*-Metalated β-Enaminoimine Complex − Preparation of *N*-Phosphanylenamine and β-Enaminoimine Derivatives

Alexandrine Maraval,[a] Krzysztof Owsianik,[b] Damien Arquier,[a] Alain Igau,*[a] Yannick Coppel,[a] Bruno Donnadieu,[a] Maria Zablocka,[b] and Jean-Pierre Majoral*[a]

Keywords: N ligands / NMR spectroscopy / Imines / Zirconium / Metallocenes / Transmetalation

Variable-temperature NMR spectroscopy of the β-enaminoimine complex **2** showed a dynamic process which was attributed to an internal fluxional aldimido *N*-zirconated π-linear/σ-bent structure. Such an internal rearrangement has been previously proposed to occur in these systems but never observed. We have prepared a variety of (*N*-phosphanyl-β-enamino)imine ligands using the hydrozirconation/transmetalation reaction of malonodinitrile compounds $RCH(CN)_2$ (R = H, PPh_2). In addition to their potential uses in coordination chemistry, these systems are good tools for the study of intramolecular hydrogen bonding. The X-ray crystal structure of **14** at 180 K shows an unsymmetrical system with the N(H) proton localized on one of the two chelating nitrogen atoms, consistent with the existence in solution of a low barrier proton transfer process with a double-well potential.

(© Wiley-VCH Verlag GmbH & Co. KGaA, 69451 Weinheim, Germany, 2003)

Introduction

β-Enaminoimine derivatives have been intensively studied as members of the family of polymethine merocyanines, a fundamental group of organic dyes with a wide variety of uses. [1] Related compounds of the type **A**, also called β-diimine systems, described as "formal" six-membered rings with a chelating μ^2-H proton bridged to the nitrogen atoms, have been successfully used as ligands in coordination chemistry.[2]

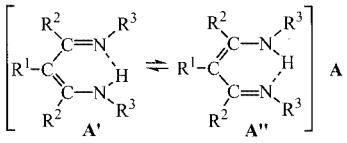

Recently, we described the synthesis of the β-enaminoimine compound **2**, with a transition metal fragment bonded to the nitrogen atoms (**A**: $R^1 = R^2 = H$, $R^3 = ZrCp_2Cl$).[3] In addition to the dynamic NMR behaviour of the *N*-zirconated β-enaminoimine **2**, we present herein the preparation of *N*-phosphanylenamine derivatives and describe the formation of unsymmetrical (*N*-phosphanyl-β-enamino)imine compounds according to a hydrozirconation/transmetalation reaction sequence. We also report an X-ray crystal structure of a β-enaminoimine compound containing an unsymmetrical intramolecular hydrogen bond.

[a] Laboratoire de Chimie de Coordination, CNRS,
205 route de Narbonne, 31077 Toulouse Cedex, France
Fax: (internat.) + 33-5/61553003
E-mail: majoral@lcc-toulouse.fr
igau@lcc-toulouse.fr
[b] Polish Academy of Sciences, Centre of Molecular and Macromolecular Studies,
Sienkiewicza 112, 90-363 Lodz, Poland

Supporting information for this article is available on the WWW under http://www.eurjic.org or from the author.

Dynamic Behavior of the *N*-Zirconated β-Enaminoimine Complex 2

Results

The *N*-metalated β-enaminoimine compound **2** was prepared by the addition of 2 equiv. of **1** to malonodinitrile in the presence of a catalytic amount of MeI (Scheme 1).[3]

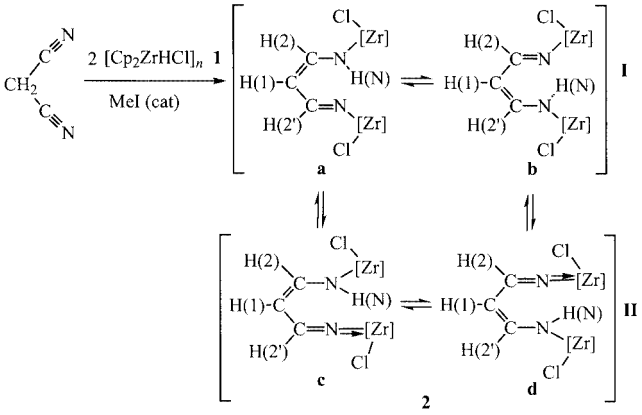

Scheme 1. Description of the different conformers of the (*N*-zircona-β-enamino)imine derivative **2** at 193 K; [Zr] = $ZrCp_2$

At 293 K, 1D ^{1}H and ^{13}C NMR spectra show only one set of signals for the two CH(2/2′)−N aldimine groups, indicative of a process that rapidly interconverts the hydrogen atoms H(2) and H(2′) on the NMR time scale. An excitation-sculpted singly selective 1D TOCSY (Figure 1)[4] allows the assignment of the signal of the H(N) proton bridged by the two nitrogen atoms of the β-enaminoimine skeleton at δ = 7.10 ppm.[5]. It was clear from this experiment that the H(N) proton was involved in an exchange having a rate in the intermediate range on the NMR time scale. The NMR spectra exhibit two singlets for the Cp groups at δ = 6.35 and 6.53 ppm (^{1}H NMR, 10 H each) and δ = 116.6 and 114.5 ppm (^{13}C NMR). Lowering of the temperature from 293 to 193 K leads to a splitting of the H(N) and H(2/2′) protons, suggesting the presence of at least two conformers (Figure 1).

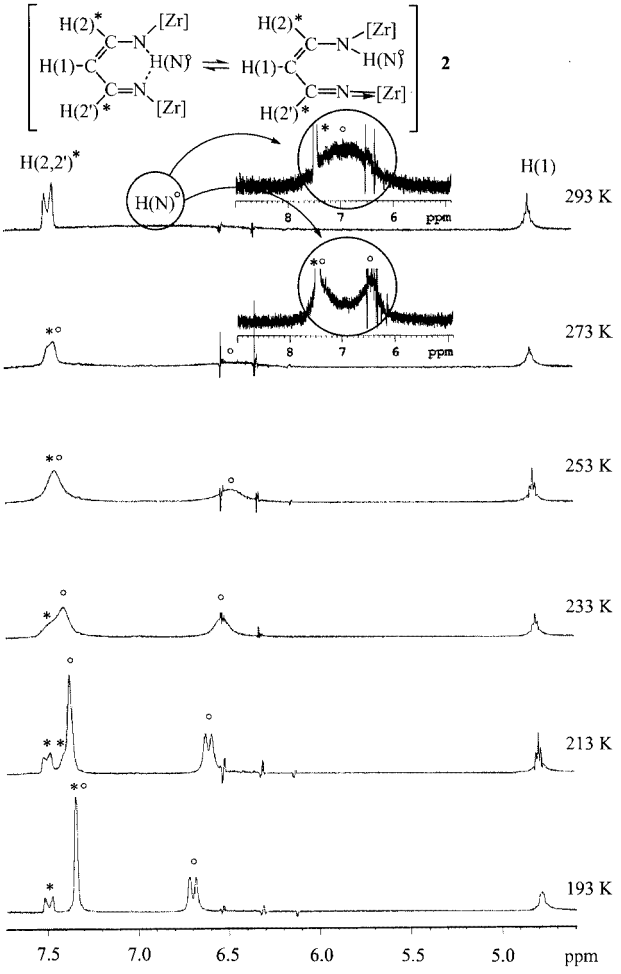

Figure 1. 1D selective TOCSY of **2** at variable temperature with excitation of H(1) (the corresponding symmetric Lewis structures are omitted for clarity); mixing time = 60 ms; [Zr] = $ZrCp_2Cl$

At 193 K the ^{1}H NMR spectrum of the CH(2/2′)−N−H(N) moiety of one of the two conformers shows a doublet of doublets at δ = 7.49 ppm [H(2/2′)] and a doublet at δ = 6.70 ppm [H(N)], with coupling constants of $^3J_{H(2/2')\text{-}H(1)}$ = 5.5 Hz and $^3J_{H(2/2')\text{-}H(N)}$ = 13.0 Hz. The ^{13}C NMR spectrum displays a peak at δ = 157.6 ppm, assigned to the aldimine carbon atom CH(2/2′). Signals due to the H(2/2′) and H(N) protons of the other conformer accidentally overlap (^{1}H at 193 K: δ = 7.34 ppm), and the outer lines of the doublets are thus no longer visible. Consequently, it was not possible to determine the different coupling constants. The ^{13}C NMR spectrum exhibits a peak at δ = 158.4 ppm [CH(2/2′)−N group]. Note that the methine CH(1) group resonances [δ = 4.78 ppm − broad peak (^{1}H); δ = 93.7 ppm (^{13}C)] and the Cp signals of **I** and **II** cannot be differentiated. The NMR spectroscopic assignments have been unambiguously confirmed by 2D NMR experiments at 193 K (gs-DQFCOSY, gs-HMQC). Note that line broadening was observed for the Cp groups, but no splitting of the signals was detected on decreasing the temperature. Exchange between the two conformers **I** and **II** was definitively established by 1D GROESY experiments (Scheme 1, Figure 2).[8]

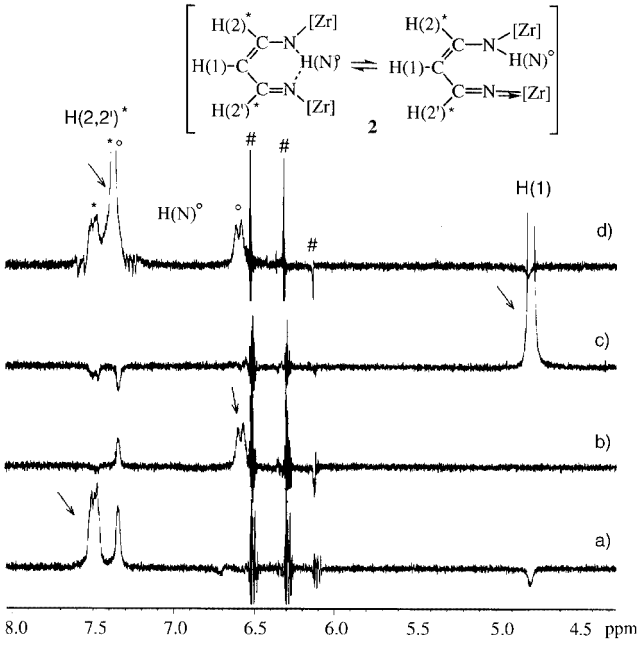

Figure 2. 1D GROESY of **2** at 193 K (the corresponding symmetric Lewis structures are omitted for clarity) with selective excitation of the site indicated by the arrow →; mixing time = 200 ms; lines denoted by # are residual signals of the Cp protons; [Zr] = $ZrCp_2Cl$

The 1D GROESY spectrum obtained on irradiation of the H(2/2′) protons of the conformer with δ = 7.49 ppm displays an exchange peak with the H(2/2′) protons of the other conformer (δ = 7.34 ppm) and an ROE enhancement (spatial proximity) with H(1) (Figure 2, a). Irradiation of the H(N) proton of the conformer with δ = 6.70 ppm gives only a positive exchange peak with the H(N) protons of the other conformer (δ = 7.34 ppm) (Figure 2, b). Finally, irradiation of the H(1) protons only gives rise to ROE enhancements with the H(2/2′) protons of conformers **I** and **II** (Figure 2, c). The GROESY spectrum obtained on irradiation of the signal at δ = 7.34 ppm follows from the experiments a), b), and c) in Figure 2 and definitively demonstrated the overlapping H(2/2′) and N(H) protons for one

conformer: in addition to an ROE enhancement with H(1), an exchange peak with the H(2/2′) protons (δ = 7.49 ppm) and with the N(H) proton (δ = 6.70 ppm) of the other conformer is also observed. The chemical shift equivalence of the H(2) and H(2′) protons in **I** and **II** is accommodated by a rapid tautomeric conversion of **a** and **b** for **I** and **c** and **d** for **II**. From the results of the dynamic NMR spectra, **2** appears to behave as a rather unconventional β-enaminoimine system. At low temperature, it is likely that we have been able to "freeze out" a dynamic process involving a fluxional structure from which each form identified is in a fast tautomeric equilibrium, namely **a** and **b** for **I** and **c** and **d** for **II**.

Discussion

The bis(*N*-zirconated) β-enaminoimine complex **2** contains the vinamidine moiety N−C−C−C−N and an *N*-metalated alkylideneamido arrangement, two types of substructures which may undergo fluxional processes.

It has been reported that β-enaminoimine derivatives with N−C−C−C−N core atoms may exist in three different configurations: "*trans-trans*", "*trans-cis*", and "*cis-cis*" [Equation (1)]. The tautomeric and conformational equilibria of these products have been found to be substituent-, solvent-, and temperature-dependent.[9]

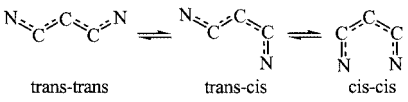

(1)

In CD_2Cl_2 at 193 K, the coupling constant of $^3J_{H(2/2')\text{-}H(1)}$ = 5.5 Hz observed for one of the conformers indicates the presence of the *cis-cis* form.[10] At 293 K the time-averaged $^3J_{H(2/2')\text{-}H(1)}$ coupling constant of 5.7 Hz implies that the second conformer exhibits the same *cis-cis* configuration for the vinamidine moiety. Moreover, the same ^{13}C NMR chemical shift observed for the CH(1) methine group indicates that the geometry around this carbon atom is retained in **I** and **II**.[11] Finally, the ROE enhancement observed for the H(1) and H(2/2′) protons of one of the conformers confirms the proximity of these protons. These NMR spectroscopic data establish conformers **I** and **II** as having a *cis-cis* configuration. Therefore, the dynamic NMR behavior observed for the *N*-zirconated β-enaminoimine complex **2** does not involve the core atoms of the β-enaminoimine system; the *cis-cis* rigidity about the N−C−C−C−N skeleton is maintained throughout the observed fluxional process.

Starting from the Lewis structure **I** for **2** (Scheme 1), two intramolecular dynamic processes may be proposed to rationalize the results of the low-temperature NMR spectra : i) rotation of the $ZrCp_2Cl$ fragments about the Zr−N bond and/or ii) a fluxional π-linear/σ-bent process involving the *N*-metalated alkylideneamido moieties in the plane containing the β-enaminoimine system −N(H)−$(CH)_2$−CH=N−.

Simple close-contact calculations carried out on complex **2**[12] revealed severe intramolecular nonbonded contacts between the Cp ring hydrogen atoms of the two metal fragments and between the Cp ring hydrogen atoms and the hydrogen atom of the H−C−N moiety of the β-iminoenamine skeleton. Because of these steric constraints, the magnitude of the rotation of the $ZrCp_2Cl$ fragments about the Zr−N bonds is limited, and therefore only a restricted rotation is observed for **2**. In metallocene complexes, restricted rotation about the bond between a metal ion and a planar amido/ketimide nitrogen atom is assumed to have a very low activation barrier; to the best of our knowledge no restricted rotation processes in such complexes has been "frozen out" by variable-temperature NMR experiments.[13,14c]

16-Electron d^0 group-4 metallocene complexes of the type Cp_2MRR' (M = Ti, Zr, Hf) have one vacant orbital available for conjugative interaction with lone pairs or π-systems at adjacent σ-bonded ligands R, R′.[15] Even though Cp_2M-N π-interactions are not maximized in group-4 amido[13] and ketimide[14] metallocene complexes, π-overlap between the LUMO of the metal fragment and the nitrogen lone pair has been commonly observed. Erker and co-workers have reported that aldimido [RCH=N−$ZrCp_2Cl$] complexes have a substantial Zr−N π-character. This was unambiguously demonstrated by an X-ray structure analysis of **B** (R = Ph), which showed a nearly linear Zr−N=CHPh unit (Zr−N−C 170.5(5)°].[15a,15b] In solution, the linear heteroallene-type structural unit in **B** (R = Ph) is of high stereochemical persistence and rigidity, and the geometric isomerization (*E*)/(*Z*) could be effected neither thermally nor photochemically. Moreover, the hydrozirconation of nitriles using the Schwartz reagent $[Cp_2ZrHCl]_n$ led to the corresponding zirconocene ketimide complexes with a *syn* stereochemistry; the metal-bound chlorine atom and the hydrogen atom of the aldimine function are positioned *syn* to the linear Zr−N−C moiety.

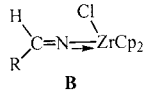

B

It is likely that, at room temperature, we are observing the results of the two rapid dynamic processes which involve: i) restricted rotation about the Zr−N bonds and ii) the σ-bound (**I**) and π-bound-like (**II**) *N*-zirconated conformers of the β-enaminoimine compound **2** (Scheme 1). Consistent with the studies reported in the literature, the two sets of Cp resonances observed for **2** at room temperature may be the result of restricted rotation about the Zr−N bonds, with a molecular geometry which places the chlorine atoms of the zirconocene fragments Cp_2ZrCl *syn* to the hydrogen atom of the HCN subunits. It is reasonable to propose that lowering of the temperature has the effect of "freezing out" the *N*-σ-bent-zirconated β-enaminoimine form **I** and linearising the Zr−N=C units to form the heteroallene system **II** (Scheme 1).[16] This internal fluxional *N*-zirconated π-linear/σ-bent structure [Equation (2)] was previously proposed to occur in these systems but until now

it has not been observed in coordinatively unsaturated *N*-metalated alkylideneamido complexes.

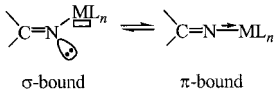

(2)

On the basis of variable-temperature ^{1}H NMR experiments, the activation barrier of the observed dynamic process attributed to the transition between bent (**I**) and linear (**II**) conformers in **2** has been calculated as $\Delta G^{\ddagger} = 13$ kcal/mol.[17]

Preparation of *N*-Phosphanylenamine and (*N*-Phosphanyl-β-enamino)imine Ligands

The next step in the preparation of β-enaminoimine ligands starting from malonodinitrile was to probe the monohydrozirconation/transmetalation reaction process. Treatment of $CH_2(CN)_2$ with 1 equiv. of the Schwartz reagent $[Cp_2Zr(H)Cl]_n$ (**1**), followed by addition of $(i\mathrm{Pr}_2N)_2PCl$ (**3**) led to the formation of the *N*-phosphanylenamine compound **4** in 66% isolated yield (Scheme 2).

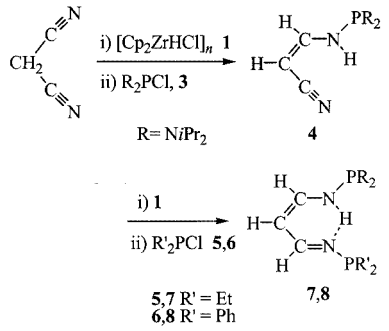

Scheme 2. Selective monohydrozirconation/transmetalation reactions of malonodinitrile and the β-nitriloeneamine compound **4**

This compound was identified by its spectroscopic properties which included strong absorptions in the IR spectrum at 1600 and 2194 cm^{-1} assigned to the C=N and C≡N stretches, respectively. The ^{31}P NMR spectrum of **4** displays a singlet at δ = 87.1 ppm. In addition to signals due to the isopropyl group, ^{1}H and ^{13}C NMR spectra display signals in the region expected for a CH= vinylic group geminal to an electron-withdrawing group [δ = 3.74 (^{1}H) and 66.1 (^{13}C) ppm] and a CH−N< enamine fragment [δ = 6.53 (^{1}H) and 150.8 (^{13}C) ppm]. The broad signal at δ = 5.30 ppm in the ^{1}H NMR is typical of an NH secondary amine. The NMR spectroscopic data establish **4** as an (*N*-phosphanyl-β-enamino)nitrile. Another hydrozirconation/transmetalation reaction on the enamine compound **4** using **1** and R′$_2$PCl [R′ = Et (**5**), Ph (**6**)] gave the expected unsymmetrical (*N*-phosphanyl-β-enamino)imine derivatives **7** and **8**, respectively (Scheme 2). IR spectra indicate the disappearance of the ν(C≡N) band in **4** and the appearance of an absorption in the region expected for the C=N functionality in β-enaminoimine systems [ν(C≡N): 1625 cm^{-1} (**7**), 1621 cm^{-1} (**8**)]. The ^{31}P NMR spectra of **7** and **8** display two singlets at δ = 53.3, 87.1 (**7**) ppm and 64.8, 89.3 (**8**) ppm. Signals in both ^{1}H and ^{13}C NMR spectra are consistent with CH=N aldimine groups [**7**: δ = 7.62 (^{1}H, overlapped) ppm, δ = 156.1, 159.8 (^{13}C) ppm; **8**: δ = 7.39, 7.91 (^{1}H) ppm, δ = 150.5, 164.5 (^{13}C) ppm] and the central methine CH fragments [**7**: δ = 4.87 (^{1}H) and δ = 97.6 (^{13}C) ppm; **8**: δ = 4.89 (^{1}H) and δ = 97.8 (^{13}C) ppm] in the β-diimine derivatives **7** and **8**. The ^{13}C NMR chemical shifts of the central methine CH fragments and the upfield shift of the broad NH signal [δ = 5.30 (**4**), 10.54 (**7**), 10.84 (**8**) ppm] in the ^{1}H NMR spectra establish **7** and **8** as having a *cis-cis* configuration, with a hydrogen-bonded chelate form in a β-diimine compound.

It is noteworthy that hydrozirconation of succinonitrile and glutaronitrile using **1** (1 and 2 equiv.) followed by an exchange reaction with Ph_2PX (X = Cl, Br, CN) led to the formation of insoluble polymeric products.

Under the same experimental conditions as those used for $CH_2(CN)_2$, the phosphanylmalononitrile **9** undergoes the same "one pot" mono- and dihydrozirconation/transmetalation reaction sequence(Scheme 3). Addition of 1 equiv. of **1** to **9** followed by addition of a stoichiometric amount of R_2PCl (**3**, **6**) to the resulting mixture affords the corresponding *N*-phosphanylenamine compounds **10** and **11**, respectively (Scheme 3).

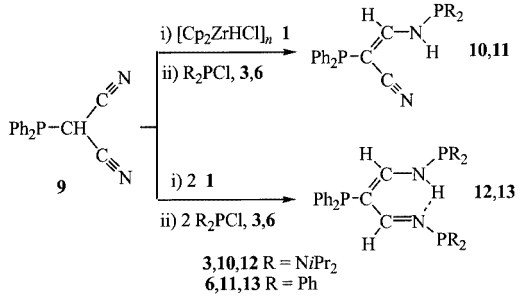

Scheme 3. Mono-and dihydrozirconation/transmetalation reactions of the phosphanylmalonodinitrile compound **9**

The IR spectra of **10** and **11** display both C=N and C≡N stretches. The parent ion peak $[M + 1]^+$ detected in the mass spectrum of **11** is in agreement with the general formula $[C_3H_2N_2(PPh_2)_2]$. The ^{31}P NMR spectra of **10** and **11** display two singlets at δ = 8.0, 85.2 and δ = −1.6, 55.1 ppm, respectively. ^{1}H and ^{13}C NMR spectra exhibit (besides the chemical shifts corresponding to the protons and carbon atoms of the phosphanyl substituents) signals in the region expected for a CH−N< enamine fragment [**10**: δ = 7.58 (^{1}H) and δ = 159.1 (^{13}C) ppm; **11**: δ = 7.75 (^{1}H) and δ = 163.7 (^{13}C) ppm]. The broad signal at δ = 5.90 (**10**) and 8.18 (**11**) ppm in the ^{1}H NMR spectra corresponds to the NH secondary amine. The NMR spectroscopic data establish an (*N*-phosphanyl-β-enamino)nitrile skeleton in **10** and **11**.

Reaction of **9** with 2 equiv. of **1** and addition of 2 equiv. of R_2PCl (**3**, **6**) allowed isolation of the corresponding *N*-phosphanyl-β-diimines **12** and **13**, respectively (Scheme 3). The parent ion $[M + 1]^+$ detected in the mass spectrum of **13** was in agreement with the general formula $[C_3H_3N_2(PPh_2)_3]$. Infrared spectra show absorptions at 1633 cm^{-1} (**12**) and 1635 cm^{-1} (**13**) assigned to the C=N stretch of the enaminoimine fragment. In addition to signals corresponding to the phosphanyl substituents, ^1H and ^{13}C NMR spectra of **12** and **13** show the presence of the β-diimine NC(H)CC(H)N skeleton. The chemical shifts in both ^1H [δ = 7.90 (**12**) and 8.35 (**13**) ppm] and ^{13}C [δ = 161.3 (**12**) and 166.9 (**13**) ppm] NMR spectra are consistent with the CH=N aldimine and with the central methine PC fragments the signals of which appear at δ = 99.9 (**12**) and 103.4 (**13**) ppm in the ^{13}C NMR spectrum, respectively. The NMR spectroscopic data (^{13}P, ^1H, and ^{13}C) indicate symmetric ligand environments, which is consistent with a rapid tautomeric interconversion. Addition of **1** to the (*N*-phosphanyl-β-enamino)nitrile **10**, followed by a substitution reaction with Me_2PCl (**15**), gave the corresponding unsymmetrical β-enaminoimine derivative **16** in 84% yield (Scheme 4).

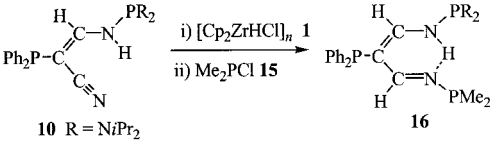

Scheme 4. Monohydrozirconation/transmetalation reactions of the phosphanyl-β-nitriloeneamine compound **10**

The ^{31}P NMR spectrum of **16** displays three singlets at δ = −4.6 (PPh), 40.6 (PMe), and 86.3 ($PNiPr_2$) ppm. Both CH=N aldimine groups exhibit characteristic NMR signals at δ = 7.91 and 8.29 (^1H) ppm and δ = 160.7 and 166.5 (^{13}C) ppm. The ^{13}C NMR chemical shift of the central methine CP fragment (δ = 100.5 ppm) and the upfield shift of the broad NH signal in the ^1H NMR spectrum (δ = 11.39 ppm) establish **16** as having a "*cis-cis*" configuration, with a hydrogen-bonded chelate form in a β-enaminoimine compound.

X-ray Crystal Structure of 14

To confirm the spectroscopic assignments and to have a better insight into the molecular structure of the (*N*-phosphanyl-β-enamino)imine species prepared, an X-ray diffraction study was carried out on the phosphane sulfide product **14** obtained after addition of elemental sulfur to **13** (Figure 3, Table 1).

The crystal structure of **14**, recorded at 180 K, shows discrete molecular units which do not display the C_{2v} symmetry previously observed in compound **A** [$R^1 = R^2 = H$, $R^3 = P(S)Ph_2$].[3,18] All atoms in **14** except those of the phenyl groups and the sulfur atoms S1 and S3 lie in the same plane with a maximum deviation of 0.0046 Å. The

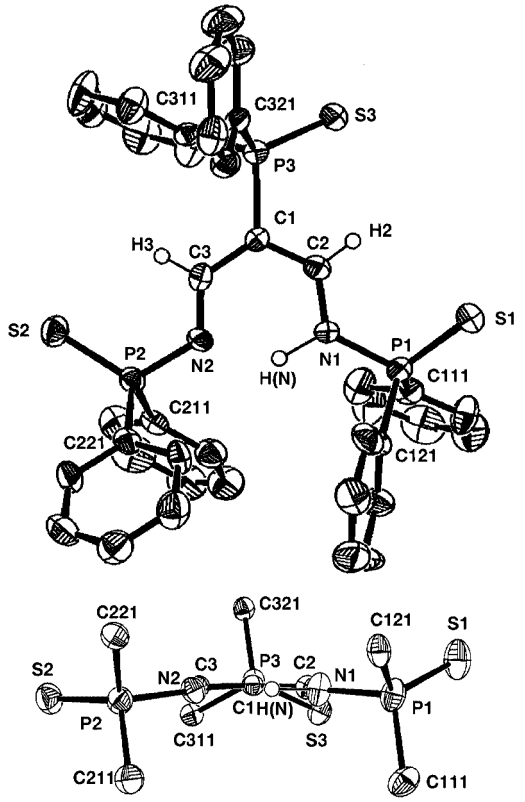

Figure 3. Two views of the molecular geometry of $Ph_2P(S)C[CHNP(S)Ph_2]_2(\mu\text{-}H)$ (**14**) as determined by X-ray diffraction

Table 1. Selected bond lengths [Å] and angles [°] for **14**

C(1)−C(2)	1.378(7)	C(1)−C(3)	1.424(7)
C(1)−P(3)	1.801(5)	C(2)−N(1)	1.351(6)
C(3)−N(2)	1.298(6)	N(1)−P(1)	1.696(5)
N(2)−P(2)	1.691(5)	P(1)−S(1)	1.926(2)
P(2)−S(2)	1.935(2)	P(3)−S(3)	1.953(2)
C(2)−C(1)−C(3)	121.0(5)	P−C(2)−N(2)	168.5(2)
C(1)−C(2)−N(1)	124.0(5)	C(1)−C(3)−N(2)	124.4(5)
P(3)−C(1)−C(2)	116.1(4)	P(3)−C(1)−C(3)	122.9(4)
C(2)−N(1)−P(1)	126.0(4)	C(2)−N(2)−P(2)	121.3(4)

presence of the N1−H1···N2 intramolecular hydrogen bond, with an N···N distance of 2.66 Å[19] and an N−H···N angle of 137°, may be responsible for the planarity of the system, together with some degree of charge delocalization. The C2−N1 [1.351(6) Å] and C3−N2 [1.298(6) Å] distances are close to the values reported for C=C−NH− and $C(sp^2)$−C=N− fragments respectively, and are representative of single and double bond lengths in such systems.[20,21] The thiophosphoryl groups $-P(S)Ph_2$ in **14** showed the expected typical structural parameters.[22]

The X-ray data recorded at 180 K showed that the β-enaminoimine compound **14** possesses an unsymmetrical intramolecular hydrogen H(N) bond with two different nitrogen chelating atoms, N1 and N2, in the solid state. However, in solution it behaves as a symmetric compound, consistent with the occurrence of a very fast tautomeric proton

exchange equilibrium. These observations can be rationalized if it is assumed that **14** possesses a low-barrier hydrogen bond with a double-well potential. This is in agreement with the mechanism of proton transfer in malonaldehyde recently proposed by Silvi and co-workers,[23] involving a two-step reaction with a concerted charge transfer from one bond to another within the planar framework of the aldehyde. This description may also be applied to the analogous β-enaminoimine systems.[24]

Conclusion

In conclusion, we have demonstrated that the bis(*N*-zirconated) β-enaminoimine system **2** shows a dynamic NMR behavior which may be reasonably attributed to a σ-bent/π-linear fluxional structure. Complex **2** is the ideal synthon to prepare unsymmetrical β-enaminoimine derivatives following the hydrozirconation/transmetalation reaction sequence. Starting with the phosphanylmalononitrile $Ph_2P-CH(CN)_2$ and using an identical reaction process, (*N*-phosphanyl-β-enamino)imine derivatives have been prepared and characterized. These compounds will be further investigated as ligands in coordination complexes.

The X-ray crystal structure of **14** at 180 K shows an unsymmetrical system, with the N(H) proton localized on one of the two chelating nitrogen atoms. This solid-state structural analysis is consistent with the existence in solution of a rapidly interconverting pair of tautomers[25] with a low-barrier proton transfer process corresponding to a double-well potential. The β-enaminoimine compounds described in this paper represent a good model for the study of intramolecular hydrogen bonding.

Experimental Section

General Remarks: All manipulations were performed under argon in a vacuum line using standard Schlenk techniques. Solvents were freshly distilled from dark purple solutions of sodium/benzophenone ketyl (THF and toluene), lithium aluminum hydride (pentane), or CaH_2 (CH_2Cl_2). Deuterated NMR solvents were treated with $LiAlH_4$ ([D_8]toluene, C_6D_6, [D_8]THF) and CaH_2 (CD_2Cl_2), distilled, and stored under argon. Nuclear magnetic resonance (NMR) spectra were recorded at 25 °C with Bruker AMX-400, AM-250, AC-200, and AC-80 Fourier transform spectrometers. Chemical shifts are given downfield relative to Me_4Si (^1H, ^{13}C) or H_3PO_4 (^{31}P), respectively. ^{13}C NMR assignments were confirmed by inverse gradient δ^1H-$\delta^{13}C\{^{13}C,^{31}P\}$ HMQC and ^{31}P-^1H NMR experiments. Elemental and mass spectral analyses (obtained using a Nermag R10-10H) were performed by the analytical service of the Laboratoire de Chimie de Coordination (LCC) of the CNRS. $(i\mathrm{Pr}_2\mathrm{N})_2\mathrm{PCl}$[26] and $[Cp_2Zr(H)Cl]_n$[27] were prepared according to literature procedures. Ph_2PCl (Aldrich), Me_2PCl (Strem), Et_2PCl (Strem), MeI (Aldrich), and $CH_2(CN)_2$ (Aldrich) were purchased and used without further purification.

Preparation of 2: A solution of $CH_2(CN)_2$ (0.100 g, 1.514 mmol) in CH_2Cl_2 (5 mL) was added to a suspension of $[Cp_2Zr(H)Cl]_n$ (0.781 g, 3.028 mmol) in CH_2Cl_2 (3 mL) at −30 °C. The reaction mixture was stirred for 30 min at room temperature and then cooled to −50 °C, at which temperature MeI (0.188 μL, 3028 mmol) in CH_2Cl_2 (5 mL) was slowly added. The solution was then stirred for an additional 2 h at room temperature. Removal of the solvent in vacuo gave **2** as an orange solid. ^1H and ^{13}C NMR recorded at 293 K: ^1H NMR (CD_2Cl_2): δ = 4.84 (br, 1 H, CH), 6.35 (s, 10 H, Cp), 6.53 (s, 10 H, Cp), 7.10 (br., 1 H, NH), 7.48 (dd, $J_{H(2)-H(1)}$ = 5.8, $J_{H(2)-H(N)}$ = 12.6 Hz, CHN) ppm. $^{13}C\{^1H\}$ NMR (CD_2Cl_2): δ = 97.9 (s, CH), 114.5, 116.6 (s, Cp), 157.6 (s, CHN) ppm. ^1H and ^{13}C NMR of conformers **I** and **II** recorded at 193 K: ^1H NMR (CD_2Cl_2): δ = 4.78 (br, 1 H, CH), 6.30 (s, 10 H, Cp), 6.52 (s, 10 H, Cp), 6.70 [d, $J_{H(2)-H(N)}$ = 13.0 Hz, NH), 7.49 (dd, $J_{H(2)-H(1)}$ = 5.5, $J_{H(2)-H(N)}$ = 13.0 Hz, CHN) ppm. $^{13}C\{^1H\}$ NMR (CD_2Cl_2): δ = 97.9 (s, CH), 114.8, 117.0 (s, Cp), 157.6 (s, CHN) ppm. ^1H NMR (CD_2Cl_2): δ = 4.78 (br, 1 H, CH), 6.30 (s, 10 H, Cp), 6.52 (s, 10 H, Cp), 7.34 (br, CHN and NH) ppm. $^{13}C\{^1H\}$ NMR (CD_2Cl_2): δ = 97.9 (s, CH), 114.8, 117.0 (s, Cp), 158.4 (s, CHN) ppm.

Preparation of 4: A suspension of $[Cp_2ZrHCl]_n$ (0.600 g, 2.327 mmol) in CH_2Cl_2 (3 mL) was added to a solution of malonodinitrile (2.327 mmol, 0.154 g) in CH_2Cl_2 (10 mL) at −40 °C. and the reaction mixture was allowed to warm slowly to room temperature. As soon as the reaction mixture turned clear, $(i\mathrm{Pr}_2\mathrm{N})_2\mathrm{PCl}$ (0.619 mg, 2.327 mmol) in CH_2Cl_2 (2 mL) was added and the solution was stirred for 1 h at room temperature. Removal of the solvent in vacuo gave a yellow solid residue which was extracted with cold pentane (10 mL). After filtration, the volatiles were evaporated and **4** was obtained as a yellow powder. Yield: 66% (457 mg). $^{31}P\{^1H\}$ NMR (C_6D_6): δ = 87.1 (s) ppm. ^1H NMR (C_6D_6): δ = 1.03 (d, $^3J_{H,H}$ = 6.7 Hz, 24 H, CH_3), 3.24 (d sept, $^3J_{H,H}$ = 6.7, $^3J_{HP}$ = 11.8 Hz, 4 H, $CHCH_3$), 3.74 (d, $^3J_{H,H}$ = 8.1 Hz, 1 H, CHCN), 5.30 (br. d, $^3J_{H,H}$ = 15.0 Hz, 1 H, NH), 6.53 (ddd, $^3J_{HP}$ = $^3J_{H,H}$ = 8.1, $^3J_{H,H}$ = 15.0 Hz, 1 H, CHNH) ppm. ^{13}C NMR (C_6D_6): δ = 24.0 (d, $^3J_{PC}$ = 7.2 Hz, CH_3), 24.6 (d, $^3J_{PC}$ = 7.2 Hz, CH_3), 45.9 (d, $^2J_{PC}$ = 12.8 Hz, $CHCH_3$), 66.1 (d, $^2J_{PC}$ = 7.5 Hz, CHCN), 118.8 (s, CN), 150.8 (d, $^2J_{PC}$ = 27.7 Hz, CHNH) ppm. FT-IR (KBr): $\tilde{\nu}$ = 1600 (C=N), 2194 (C≡N) cm^{-1}. $C_{15}H_{31}N_4P$ (298.47): calcd. C 60.36, H 10.47, N 18.77; found C 60.48, H 10.28, N 18.56.

Typical Procedure for the Synthesis of Compounds 7 and 8: Compound **4** (0.215 g, 0.721 mmol) in CH_2Cl_2 (2 mL) was added to a suspension of $[Cp_2ZrHCl]_n$ (0.186 g, 0.721 mmol) in CH_2Cl_2 (2 mL) at −40 °C. The resulting mixture was stirred and allowed to warm slowly to room temperature. As soon as the solution turned clear, Et_2PCl (0.90 mg, 0.721 mmol) in CH_2Cl_2 (1 mL) was added. The mixture was stirred for 15 min at room temperature and then concentrated to dryness. The volatiles were removed to give **7** as an orange powder. Yield: 78% (218 mg). **7**: $^{31}P\{^1H\}$ NMR (C_6D_6): δ = 64.8 (s, PEt_2), 89.3 (s, $PN\mathrm{i}Pr_2$) ppm. ^1H NMR (C_6D_6): δ = 0.99 (t, $^3J_{H,H}$ = 7.6 Hz, 3 H, CH_2CH_3), 1.05 (t, $^3J_{H,H}$ = 7.6 Hz, 3 H, CH_2CH_3), 1.16 (d, $^3J_{H,H}$ = 6.7 Hz, 12 H, $CHCH_3$), 1.19 (d, $^3J_{H,H}$ = 6.7 Hz, 12 H, $CHCH_3$), 3.50 (d sept, $^3J_{H,H}$ = 6.7, $^3J_{HP}$ = 11.0 Hz, 4 H, $CHCH_3$), 4.87 (dd, $^3J_{H,H}$ = $^3J_{H,H}$ = 5.9 Hz, 1 H, CH), 7.55−7.74 (m, 2 H, CHN), 10.54 (br. m, 1 H, NH) ppm. ^{13}C NMR (C_6D_6): δ = 9.5 (d, $^2J_{PC}$ = 14.5 Hz, CH_2CH_3), 24.6 (d, $^3J_{PC}$ = 7.5 Hz, $CHCH_3$), 24.8 (d, $^3J_{PC}$ = 7.5 Hz, $CHCH_3$), 25.0 (d, $^2J_{PC}$ = 12.3 Hz, CH_2CH_3), 46.3 (d, $^2J_{PC}$ = 12.5 Hz, $CHCH_3$), 97.6 (dd, $^3J_{PC}$ = $^3J_{PC}$ = 13.6 Hz, CH), 156.1 (d, $^2J_{PC}$ = 37.3 Hz, $CHNPN\mathrm{i}Pr$), 159.8 (d, $^2J_{PC}$ = 27.4 Hz, CHNPEt) ppm. FT-IR (KBr): $\tilde{\nu}$ = 1625 (C=N) cm^{-1}. $C_{19}H_{42}N_4P_2$ (388.59): calcd. C 58.72, H 10.89, N 14.42; found C 58.89, H 11.61, N 14.29. **8** [**1** (0.233 g), **4** (0.270 g), **6** (0.199 g)] isolated as an orange-yellow powder. Yield: 87% (0.380 g). $^{31}P\{^1H\}$ NMR (C_6D_6): δ = 53.3 (s,

PPh_2), 84.5 (s, $PNiPr_2$) ppm. ^1H NMR (C_6D_6): δ = 1.05 (d, $^3J_{H,H}$ = 6.7 Hz, 12 H, $CHCH_3$), 1.09 (d, $^3J_{H,H}$ = 6.7 Hz, 12 H, $CHCH_3$), 3·32 (dsept, $^3J_{H,H}$ = 6.7, $^3J_{HP}$ = 11.0 Hz, 4 H, $CHCH_3$), 4.89 (dddd, $^3J_{H,H}$ = $^3J_{H,H}$ = 6.7, $^4J_{HP(Ph)}$ = 4.9, $^4J_{HP(NiPr)}$ = 1.5 Hz, 1 H, CH), 7.41−7.60 (m, 10 H, Ph), 7.82−7.96 (m, 2 H, CHN), 10.84 (br. d, $^2J_{HP}$ = 9.9 Hz, 1 H, NH) ppm. ^{13}C NMR (C_6D_6): δ = 24.5 (d, $^3J_{PC}$ = 7.3 Hz, CH_3), 24.7 (d, $^3J_{PC}$ = 7.3 Hz, CH_3), 46.4 (d, $^2J_{C,P}$ = 12.3 Hz, *C*HCH_3), 97.8 (dd, $^3J_{C,P(Ph)}$ = 10.7, $^3J_{C,P(NiPr)}$ = 13.4 Hz, CH), 128.9 (d, $^3J_{C,P}$ = 7.0 Hz, *m*-Ph), 129.5 (s, *p*-Ph), 132.0 (d, $^2J_{C,P}$ = 20.7 Hz, *o*-Ph), 141.6 (d, $^1J_{C,P}$ = 16.6 Hz, *i*-Ph), 150.5 (d, $^2J_{C,P}$ = 33.2 Hz, *C*HNPPh), 164.5 (d, $^2J_{PC}$ = 15.1 Hz, $CHNPNiPr_2$) ppm. FT-IR (KBr): $\tilde{\nu}$ = 1621 (C=N) cm^{-1}. $C_{27}H_{42}N_4P_2$ (484.67): calcd. C 66.91, H 8.73, N 11.56; found C 67.15, H 8.66, N 11.39.

Preparation of 9: $CH_2(CN)_2$ (0.480 g, 0.076 mmol) in THF (5 mL) was added slowly to a solution of LDA (0.779 g, 0.0726 mmol) in THF (25 mL) at 0 °C. The mixture was stirred at 0 °C for 1 h, then Ph_2PCl (1.600 g, 0.076 mmol) in THF (5 mL) was added dropwise. The mixture was slowly warmed to room temperature over 1 h, filtered, and the solvent was evaporated. The resulting solid residue was washed with Et_2O (2 × 20 mL). The volatiles were removed in a vacuum line over 5 h at 80 °C to give **9** as a yellow-brown solid.Yield: 95% (1.514 g). M.p. 83−84 °C. $^{31}P\{^1H\}$ NMR ([D_8]THF): δ = −5.9 ppm. ^1H NMR ([D_8]THF): δ = 7.18−7.50 (m, 10 H, Ph) ppm. ^{13}C NMR ([D_8]THF): δ = 7.9 (d, $^1J_{C,P}$ = 5.8 Hz, PC), 127.4 (s, *p*-Ph), 127.9 (d, $^3J_{C,P}$ = 6.2 Hz, *m*-Ph), 128.4 (d, $^2J_{C,P}$ = 21.1 Hz, CN), 132.5 (d, $^2J_{C,P}$ = 19.4 Hz, *o*-Ph), 142.2 (d, $^1J_{C,P}$ = 11.2 Hz, *i*-Ph) ppm. FT-IR (KBr): $\tilde{\nu}$ = 2189 (C≡N) cm^{-1}.

Preparation of 10: A solution of **9** (0.262 g, 1.046 mmol) in THF (2 mL) was added to a suspension of $[Cp_2ZrHCl]_n$ (0.270 g, 1.046 mmol) in THF (2 mL) at −40 °C. The resulting mixture was stirred and allowed to warm slowly to room temperature. As soon as the reaction mixture turned clear, $(iPr_2N)_2PCl$ (0.278 mg, 1.046 mmol) in THF (2 mL) was added. The solution was stirred for 30 min at room temperature and the solvent was then removed. The resulting solid residue was extracted with pentane (20 mL) and filtered. The volatiles were removed and **10** was obtained as a yellow-orange solid. Yield: 55% (277 mg). $^{31}P\{^1H\}$ NMR (C_6D_6): δ = −8.0 (PPh_2), 85.2 ($PNiPr_2$) ppm. ^1H NMR (C_6D_6): δ = 1.01 (d, $^3J_{H,H}$ = 6.7 Hz, 12 H, CH_3), 1.05 (d, $^3J_{H,H}$ = 6.7 Hz, 12 H, CH_3), 3.23 (d sept, $^3J_{H,H}$ = 6.7, $^3J_{HP}$ = 11.6 Hz, 4 H, *C*HCH_3), 5.95 (br. dd, $^3J_{H,H}$ = 2.0, $^3J_{HP}$ = 15.6 Hz, 1 H, NH), 7.00−7.28 (m, 5 H, Ph), 7.58 (ddd, $^3J_{H,H}$ = 7.1, $^3J_{HP(PPh2)}$ = 15.6, $^3J_{HP(PNiPr)}$ = 9.5 Hz, 1 H, C*H*NH), 7.65−7.77 (m, 5 H, Ph) ppm. ^{13}C NMR (C_6D_6): δ = 24.4 (d, $^3J_{PC}$ = 8.2 Hz, CH_3), 24.7 (d, $^3J_{PC}$ = 8.2 Hz, CH_3), 46.2 (d, $^2J_{PC}$ = 12.3 Hz, *C*HCH_3), 76.3 (dd, $^1J_{PC}$ = 16.0, $^3J_{PC}$ = 5.8 Hz, PC), 129.2 (s, *p*-Ph), 129.3 (s, *m*-Ph), 133.5 (d, $^1J_{C,P}$ = 20.0 Hz, *o*-Ph), 139.0 (d, $^1J_{C,P}$ = 5.8 Hz, *i*-Ph), 159.1 (dd, $^2J_{C,P}$ = 21.1, $^2J_{C,P}$ = 67.3 Hz, PCCH) ppm. FT-IR (KBr): $\tilde{\nu}$ = 1619 (C=N), 2195 (C≡N) cm^{-1}. $C_{27}H_{40}N_4P_2$ (482.65): calcd. C 67.19, H 8.35, N 11.61; found C 67.35, H 8.12, N 11.45.

Preparation of 11: A solution of **9** (340 mg, 1.356 mmol) in THF (2 mL) was added to a suspension of $[Cp_2ZrHCl]_n$ (250 mg, 1.356 mmol) in THF (2 mL) at −40 °C. The resulting mixture was stirred and allowed to warm slowly to room temperature. As soon as the solution turned clear (ca. 20 min), Ph_2PCl (300 mg, 1.356 mmol) in THF (2 mL) was added. The resulting mixture was stirred at room temperature for 30 min and then concentrated to dryness. The solid residue was extracted with CH_2Cl_2/pentane (1:5, 20 mL) and filtered. The volatiles were removed to give **11** as a white solid. Yield: 66% (391 mg). M.p. 155−156 °C. $^{31}P\{^1H\}$ NMR (C_6D_6): δ = −1.6 ($CPPh_2$), 55.1 ($NPPh_2$) ppm. ^1H NMR (C_6D_6): δ = 7.28−7.65 (m, 20 H, Ph), 7.75 (ddd, $^3J_{H,H}$ = 14.5, $^3J_{HP(NPPh2)}$ = 10.3, $^3J_{HP(C,PPh2)}$ = 9.5 Hz, 1 H, C*H*NH), 8.18 (dd, $^3J_{H,H}$ = 4.0, $^2J_{Hp}$ = 14.5 Hz, 1 H, NH) ppm. ^{13}C NMR (C_6D_6): δ = 80.0 (dd, $^1J_{C,P}$ = 17.6, $^3J_{C,P}$ = 10.4 Hz, PC), 118.4 (d, $^2J_{C,P}$ = 5.0 Hz, CN), 130.3 (d, $^3J_{C,P}$ = 6.9 Hz, *m*-Ph), 130.6 (d, $^3J_{C,P}$ = 6.9 Hz, *m*-Ph), 131.6 (s, *p*-Ph), 133.6 (d, $^2J_{C,P}$ = 19.9 Hz, *o*-Ph), 134.6 (d, $^2J_{C,P}$ = 19.9 Hz, *o*-Ph), 139.9 (d, $^1J_{C,P}$ = 16.1 Hz, *i*-Ph), 140.1 (d, $^1J_{C,P}$ = 16.2 Hz, *i*-Ph), 163.7 (dd, $^2J_{C,P(C,PPh2)}$ = 70.0, $^2J_{C,P(NPPh)}$ = 37.5 Hz, *C*HNP) ppm. FT-IR (KBr): $\tilde{\nu}$ = 1642 (C=N), 2202 (C≡N) cm^{-1}. MS (DCI/CH_4): *m*/*z* = 437 $[M + H]^+$. $C_{27}H_{22}N_2P_2$ (436.45): calcd. C 74.30, H 5.08, N 6.42; found C 74.45, H 4.94, N 6.32.

Typical Procedure for the Synthesis of Compounds 12 and 13: A solution of **9** (0.270 g, 1.078 mmol) in THF (2 mL) was added to a suspension of $[Cp_2ZrHCl]_n$ (0.556 g, 2.156 mmol) in THF (3 mL) at −40 °C. The resulting mixture was stirred and slowly warmed to room temperature. As soon as the reaction mixture turned clear (ca. 30 min), $(iPr_2N)_2PCl$ (0.574 mg, 2.156 mmol) in THF (2 mL) was added. After stirring for 4 h, the solution was concentrated to dryness. The resulting solid residue was extracted with CH_2Cl_2/pentane (1:4, 30 mL) and filtered. The volatiles were evaporated to give **16** as a yellow solid. Yield 67% (516 mg).

Data for 12: $^{31}P\{^1H\}$ NMR (C_6D_6): δ = −1.8 (PPh_2), 86.2 ($PNiPr_2$) ppm. ^1H NMR (C_6D_6): δ = 1.02 (d, $^3J_{H,H}$ = 6.6 Hz, 24 H, CH_3), 1.21 (d, $^3J_{H,H}$ = 6.6 Hz, 24 H, CH_3), 3.54 (dsept, $^3J_{H,H}$ = 6.6, $^3J_{HP}$ = 12.3 Hz, 8 H, C*H*CH_3), 6.90−7.58 (m, 10 H, Ph), 7.90 (ddd, $^3J_{H,H}$ = 7.3, $^3J_{HP(PPh)}$ = 7.3, $^3J_{HP(PniPr)}$ = 18.0 Hz, 2 H, C*H*NH), 10.35 (br. m, 1 H, NH) ppm. ^{13}C NMR (C_6D_6): δ = 24.4 (d, $^3J_{C,P}$ = 7.0 Hz, CH_3), 24.8 (d, $^3J_{C,P}$ = 7.0 Hz, CH_3), 47.9 (d, $^2J_{PC}$ = 13.1 Hz, $CHCH_3$), 99.9 (dd, $^1J_{PC}$ = $^3J_{PC}$ = 9.3 Hz, PC), 128.1 (s, *p*-Ph), 128.7 (d, $^3J_{C,P}$ = 5.5 Hz, *m*-Ph), 133.0 (d, $^2J_{C,P}$ = 17.6 Hz, *o*-Ph), 141.0 (d, $^1J_{C,P}$ = 11.4 Hz, *i*-Ph), 161.3 (dd, $^2J_{C,P(PPh2)}$ = 36.1, $^2J_{HP(PNiPr)}$ = 20.6 Hz, CHNP) ppm. FT-IR (KBr): $\tilde{\nu}$ = 1633 (C=N) cm^{-1}. $C_{39}H_{69}N_6P_3$ (715.05): calcd. C 65.51, H 9.72, N 11.75; found C 65.72, H 9.65, N 11.68.

Data for 13: Yield: 54% (229 mg). M.p. 126−127 °C (dec). $^{31}P\{^1H\}$ NMR (C_6D_6): δ = −3.6 ($CPPh_2$), 54.9 ($NPPh_2$) ppm. ^1H NMR (C_6D_6): δ = 7.00−8.15 (m, 30 H, Ph), 8.35 (ddd, $^3J_{H,H}$ = $^3J_{HP(C,PPh)}$ = 6.1, $^3J_{HP(NPPh)}$ = 16.9 Hz, 2 H, C*H*NH), 12.55 (tt, $^3J_{H,H}$ = $^3J_{HP(NPPh)}$ = 6.1 Hz, 1 H, NH) ppm. ^{13}C NMR (C_6D_6): δ = 103.4 (dt, $^1J_{C,P(CPPh)}$ = 6.3, $^3J_{C,P(NPPh)}$ = 10.3 Hz, PC), 128.4 (s, *p*-NPPh), 128.9 (d, $^3J_{C,P}$ = 5.1 Hz, *m*-CPPh), 129.0 (d, $^3J_{C,P}$ = 6.7 Hz, *m*-NPPh), 129.5 (s, *p*-CPPh), 132.2 (d, $^2J_{C,P}$ = 20.6 Hz, *o*-

Table 2. Crystallographic data for **14**

Empirical formula	$C_{39}H_{33}N_2P_3S_3$
Formula mass	718.76
Temperature	180(2) K
Wavelength	0.71073 Å
Crystal system, space group	monoclinic, $P2_1/c$
Unit cell dimensions	a = 14.804(5) Å
	b = 12.238(5) Å
	c = 20.169(5) Å
	β = 93.710(5)°
Volume	3646(2) $Å^3$
Z, calculated density	4, 1.309 mg/m^3
Absorption coefficient	0.366 mm^{-1}
F(000)	1496
Final R indices [$I > 2\sigma(I)$]	$R1$ = 0.0524, $wR2$ = 0.0638
R indices (all data)	$R1$ = 0.1710, $wR2$ = 0.0901
Largest diff. peak and hole	0.279 and −0.315 e $Å^{-3}$

NPPh), 133.0 (d, $^2J_{C,P}$ = 18.6 Hz, *o*-CPPh), 139.8 (d, $^1J_{C,P}$ = 10.1 Hz, *i*-CPPh), 140.3 (d, $^1J_{C,P}$ = 13.1 Hz, *i*-NPPh), 166.9 (dd, $^2J_{C,P(C,PPh)}$ = 34.5, $^2J_{HP(NPPh)}$ = 25.5 Hz, CHNP) ppm. FT-IR (KBr): $\tilde{\nu}$ = 1635 (C=N) cm^{-1}. MS (DCI/CH_4): *m*/*z* = 623 [M + H]$^+$. $C_{39}H_{33}N_2P_3$ (622.63): calcd. C 75.23, H 5.34, N 4.50; found C 75.41, H 5.23, N 4.33.

Preparation of 14: Treatment of **13** (362 mg, 0.581 mmol) in CH_2Cl_2 (8 mL) with an excess of sulfur at room temperature for 12 h afforded **14**, which was purified by column chromatography (silica gel, pentane/ethyl acetate, 1:4, R_f = 0.49). The product crystallized from toluene as colorless crystals. Yield: 81% (338 mg). M.p. 185−186 °C. $^{31}P\{^1H\}$ NMR (400 MHz, 233 K, [D_8]toluene): δ = 43.5 [CP(S)Ph_2], 63.2 [NP(S)Ph_2] ppm. ^1H NMR (400 MHz, 233 K, [D_8]toluene): δ = 7.46−8.04 (m, 30 H, Ph), 9.59 (ddd, $^3J_{H,H}$ = 5.8, $^3J_{HP(NPPh)}$ = 8.5, $^3J_{HP(C,PPh)}$ = 23.5 Hz, 2 H, C*H*NH), 13.59 (tt, $^3J_{H,H}$ = 5.8, $^2J_{HP(NPPh)}$ = 5.0 Hz, 1 H, NH) ppm. ^{13}C NMR (C_6D_6): δ = 102.8 (dt, $^1J_{C,P(C,PPh)}$ = 97.1, $^3J_{C,P(NPPh)}$ = 14.0 Hz, PC), 128.7 (d, $^3J_{C,P}$ = 13.8 Hz, *m*-Ph), 129.3 (s, *p*-Ph), 131.0 (d, $^2J_{C,P}$ = 11.5 Hz, *o*-Ph), 134.4 (d, $^1J_{C,P}$ = 96.0 Hz, *i*-Ph), 164.4 (d, $^2J_{C,P}$ = 19.7 Hz, *C*HNP) ppm. FT-IR (KBr): $\tilde{\nu}$(C=N) 1596 cm^{-1}. MS (DCI/CH_4): *m*/*z* = 719 [M + H]$^+$. $C_{39}H_{33}N_2P_3S_3$ (718.65): calcd. C 65.18, H 4.63, N 3.90; found C 65.05, H 4.45, N 3.79.

Preparation of 16: A solution of **10** (0.351 g, 0.729 mmol) in CH_2Cl_2 (2 mL) was added to a suspension of $[Cp_2ZrHCl]_n$ (0.556 g, 2.156 mmol) in CH_2Cl_2 (2 mL) at −40 °C. The resulting mixture was stirred and slowly warmed to room temperature. As soon as the reaction mixture turned clear (ca. 20 min), Me_2PCl (0.070 g, 0.729 mmol) in CH_2Cl_2 (2 mL) was added. After stirring for 15 min, the solution was concentrated to dryness. The resulting solid residue was extracted with pentane (30 mL) and filtered. The volatiles were removed to give **16** as a yellow solid. Yield: 84% (0.334 g). $^{31}P\{^1H\}$ NMR (C_6D_6): δ = −4.6 (PPh_2), 40.6 (PMe_2), 86.3 (PN*i*Pr_2) ppm. ^1H NMR (C_6D_6): δ = 1.06 (d, $^2J_{H,H}$ = 4.5 Hz, 6 H, PCH_3), 1.09 (d, $^3J_{H,H}$ = 6.5 Hz, 12 H, CH_3), 1.14 (d, $^3J_{H,H}$ = 6.5 Hz, 12 H, CH_3), 3.41 (dsept, $^3J_{H,H}$ = 6.5, $^3J_{HP}$ = 11.3 Hz, 4 H, C*H*CH_3), 6.86−7.72 (m, 10 H, Ph), 7.91 (m, 1 H, C*H*NPN*i*Pr), 8.29 (m, 1 H, C*H*NPMe), 11.39 (br. m, 1 H, NH) ppm. ^{13}C NMR (C_6D_6): δ = 18.9 (d, $^1J_{C,P}$ = 17.0 Hz, CH_3), 24.6 (d, $^3J_{C,P}$ = 8.4 Hz, CH_3), 24.7 (d, $^3J_{C,P}$ = 8.4 Hz, CH_3), 46.4 (d, $^2J_{C,P}$ = 12.8 Hz, *C*HCH_3), 100.5 (d, $^3J_{C,P}$ = 9.2 Hz, PC), 129.1 (s, *p*-Ph), 129.2 (d, $^3J_{C,P}$ = 8.0 Hz, *m*-Ph), 133.2 (d, $^2J_{C,P}$ = 17.6 Hz, *o*-Ph), 140.7 (d, $^1J_{C,P}$ = 10.9 Hz, *i*-Ph), 160.7 (dd, $^2J_{C,P(PPh2)}$ = 34.6, $^2J_{C,P(PNiPr)}$ = 28.8 Hz, CHNPN*i*Pr), 166.5 (dd, $^2J_{C,P(PPh)}$ = 35.0, $^2J_{C,P(PMe)}$ = 18.9 Hz, CHNPMe) ppm. FT-IR (KBr): $\tilde{\nu}$ = 1593 (C=N) cm^{-1}. $C_{29}H_{47}N_4P_3$ (544.71): calcd. C 63.94, H 8.70, N 10.28; found C 63.92, H 8.56, N 10.35.

X-ray Analysis of 14: Single crystals of **14** were obtained from toluene. Data (Table 2) were collected at 180 K with an IPDS STOE diffractometer equipped with an Oxford Cryosystems Cryostream Cooler Device using graphite-monochromated Mo-K_α radiation (λ = 0.71073 Å). The final unit cell parameters were obtained by means of a least-squares refinement performed on a set of 5000 strong reflections. No significant intensity fluctuations were observed during the data collection, indicating crystal decay was minimal. The structure was solved by Direct Methods using SIR92,[28] and refined by means of least-squares procedures on F^2 using SHELXL-97.[29] Atomic scattering factors were taken from the International Tables for X-ray Crystallography.[30] All hydrogen atoms were located in a difference Fourier map, and, with the exception of H(N), were refined using a riding model with an isotropic thermal parameter fixed at 20% greater than those of the carbon atoms to which they are connected. H(N), the hydrogen atom connected to N(1), was refined isotropically. All non-hydrogen atoms were refined anisotropically, and the weighting scheme $w = 1/[\sigma^2(F_o^2) + (aP)^2 + bP]$, where $P = (F_o^2 + 2F_c^2)/3$, was used in the last cycles of refinement. Molecular graphics were produced using ZORTEP,[31] with non-hydrogen atoms drawn at the 50% probability level. CCDC-196233 contains the supplementary crystallographic data for this paper. These data can be obtained free of charge at www.ccdc.cam.ac.uk/conts/retrieving.html [or from the Cambridge Crystallographic Data Centre, 12 Union Road, Cambridge CB2 1EZ, UK; Fax: (internat.) + 44-1223/336-033; E-mail: deposit@ccdc.cam.ac.uk].

Acknowledgments

Financial support of this work by the CNRS, France, is gratefully acknowledged. This work was completed with the support of the European Associate Laboratory financed by the CNRS (France) and the Polish Committee for Scientific Research (KBN grant no. 3TO9A03619, Poland).

[1] [1a] N. Tyutyulkov, J. Fabian, A. Melhorn, F. Dietz, A. Tadjer, *Polymethine Dyes, Structure and Properties*, St Kliment Ohridski University Press, Sofia, **1991**. [1b] A. D. Kachkovski, "Polymethine Dyes", in: *Kirk-Othmer Encyclopedia of Chemical Technology*; 4th ed., John Wiley & Sons, New York, **1996**, vol. 19, pp. 1004−1030.

[2] For some recent examples see: [2a] N. Burford, P. J. Ragogna, K. N. Robertson, T. S. Cameron, *J. Am. Chem. Soc.* **2002**, *124*, 382−383. [2b] S. B. Cortright, J. N. Johnston Parsons, *Angew. Chem.* **2002**, *114*, 355−358; *Angew. Chem. Int. Ed.* **2002**, *41*, 345−348. [2c] A. M. Neculai, H. W. Roesky, D. Neculai, J. Magull, *Organometallics* **2001**, *20*, 5501−5503. [2d] P. J. Bailey, S. T. Liddle, C. A. Morrison, S. Parsons, *Angew. Chem.* **2001**, *113*, 4595−4598; *Angew. Chem. Int. Ed.* **2001**, *40*, 4463−4466. [2e] J. M. Smith, R. J. Lachicotte, K. A. Pittard, T. R. Cundari, G. Lukat-Rodgers, K. R. Rodgers, P. L. Holland, *J. Am. Chem. Soc.* **2001**, *123*, 9222−9223. [2f] V. C. Gibson, J. A. Segal, A. J. P. White, D. J. Williams, *J. Am. Chem. Soc.* **2000**, *122*, 7120−7121. [2g] C. Cui, H. W. Roesky, H. Hao, H.-G. Schmidt, M. Noltemeyer, *Angew. Chem.* **2000**, *112*, 1885−1887; *Angew. Chem. Int. Ed.* **2000**, *39*, 1815−1817. [2h] S. K. Bertilsson, L. Tedenborg, D. A. Alonso, P. G. Andersson, *Organometallics* **1999**, *18*, 1281−1286.

[3] A. Maraval, D. Arquier, A. Igau, Y. Coppel, B. Donnadieu, J. P. Majoral, *Organometallics* **2001**, *20*, 1716−1718.

[4] The selective Gaussian−shaped pulse was applied at the central methine proton: T. Fäcke, S. Berger, *J. Magn. Reson. A* **1995**, *113*, 257−259. A 1D TOCSY experiment was employed in order to identify the H(N) proton whose signal overlaps with that of the Cp groups.

[5] Note that the NH(N) proton resonance occurred at a considerably higher field than in previously reported β-enaminoimine systems,[3,6] possibly due to the presence of the zirconated metal fragment bonded to the nitrogen atoms.[7]

[6] See this work and: P. H. M. Budzelaar, N. N. P. Moonen, R. de Gelder, J. M. M. Smits, A. W. Gal, *Eur. J. Inorg. Chem.* **2000**, 753−769.

[7] [7a] P. J. Walsh, A. M. Baranger, R. G. Bergman, *J. Am. Chem. Soc.* **1992**, *114*, 1708−1719. [7b] P. J. Walsh, J. Hollander, R. G. Bergman, *J. Am. Chem. Soc.* **1988**, *110*, 8729−8731.

[8] The 1D GROESY experiment is a combination of the DPFGSE sequence; see: [8a] K. Stott, J. Stonehouse, J. Keeler, T.-L. Hwang, A.-J. Shaka, *J. Am. Chem. Soc.* **1995**, *117*, 4199−4200 and the TROESY spin-lock, see: [8b] T. L. Hwang, A. J. Shaka, *J. Magn. Reson. B* **1993**, *102*, 155−165.

[9] [9a] R. Knorr, A. Weiß, *Chem. Ber.* **1982**, *115*, 139−160. [9b] H. H. Limbach, W. Seiffert, *Tetrahedron Lett.* **1972**, 371−374.

[9c] K. Feldmann, E. Daltrozzo, G. Scheibe, *Z. Naturforsch., Teil B* **1967**, *22*, 722−731.

[10] For the "*cis-cis*" configuration, $^3J_{H(2)-H(1)} < 7$ Hz. For the "*trans-trans*" configuration, $^3J_{H(2)-H(1)} > 10$ Hz; see: [10a] C. Jutz, A. F. Kirschner, R.-M. Wagner, *Chem. Ber.* **1977**, *110*, 1259. [10b] R. Knorr, A. Weiß, H. Polzer, *Tetrahedron Lett.* **1977**, 459. [10c] C. L. Honeybourne, G. A. Webb, *Chem. Commun.* **1968**, 739−740.

[11] ^{13}C NMR [CH(1)]: For the *cis-cis* configuration, 130 ppm < δ < 150 ppm. For the *trans-trans* configuration 90 ppm < δ < 110 ppm; see ref.[11]

[12] Simple close-contact calculations were carried out on complex **2** (**I**) using standard $Cp_2Zr(Cl)$ fragment parameters and the β-enaminoimine skeleton $-N(H)-(CH)_2-CH=N-$ from the X-ray crystal structure of **1**. The Cambridge Structural Database was used to determine the mean Zr−N bond lengths in amido (2.15 Å) and ketimide (2.04 Å) zirconocene complexes (note that from the CSD, group-4 metallocene amido complexes exhibit a planar nitrogen atom with a Cp_2M-N-C angle from 135 to 150° and zirconocene ketimide complexes contain C−N−Zr angle values from 164 to 178°). On varying the C−N−Zr angle value from 120 to 180° in **2** (**I**), rotation around the Zr−N bond revealed that: i) van der Waals contacts between Cp ring hydrogen atoms and the hydrogen atom of the H−C=N fragment are observed up to a C−N−Zr angle value of 150°, ii) van der Waals contacts between the Cp ring hydrogen atoms of the two Cp_2ClZr metal moieties are not observed for a C−N−Zr angle lower than 130° in the amido and ketimide subunits. For a good discussion of orbital constraints and symmetry requirements of the bent metallocene derivatives, see: J. W. Lauher, R. Hoffmann, *J. Am. Chem. Soc.* **1976**, *98*, 1729.

[13] See for example: G. L. Hillhouse, A. R. Bulls, B. D. Santarsiero, J. E. Bercaw, *Organometallics* **1988**, *7*, 1309−1312.

[14] [14a] G. Erker, W. Frömberg, J. L. Atwood, W. E. Hunter, *Angew. Chem.* **1984**, *96*, 72−73; *Angew. Chem. Int. Ed. Engl.* **1984**, *23*, 68−69. [14b] W. Frömberg, G. Erker, *J. Organomet. Chem.* **1985**, *280*, 343−354. [14c] G. Erker, W. Frömberg, C. Krüger, E. Raabe, *J. Am. Chem. Soc.* **1988**, *110*, 2400−2405. See also for the X-ray structures of (alkylideneamido)zirconocene complexes: [14d] D. R. Armstrong, K. W. Henderson, I. Little, C. Jenny, A. R. Kennedy, A. E. McKeown, R. E. Mulvey, *Organometallics* **2000**, *19*, 4369−4375. [14e] U. Segerer, S. Blaurock, J. Sieler, E. Hey-Hawkins, *Organometallics* **1999**, *18*, 2838−2842.

[15] [15a] G. Erker, W. Frömberg, R. Benn, R. Mynott, K. Angermund, C. Krüger, *Organometallics* **1989**, *8*, 911−920. [15b] G. Erker, *Angew. Chem.* **1989**, *101*, 411−417; *Angew. Chem. Int. Ed. Engl.* **1989**, *28*, 397−412.

[16] Alternative structures for **2** which involve the formation of dimers, trimers, or oligomers with the zirconated metal fragment cannot be totally ruled out, but it is highly unlikely as it will prevent any fluxional process within the alkylideneamido subunit.

[17] Rate constants were derived from band-shape analysis using the software MEXICO (available from A. D. Bain, Department of Chemistry, McMaster University, Hamilton, Ontario, Canada). NMR parameters were optimized to match the simulated and the experimental data. Activation parameters were determined by a standard Eyring analysis.

[18] The X-ray crystallographic investigation of **A** [$R^1 = R^2 = H$, $R^3 = P(S)Ph_2$] at 293 K revealed two "half-hydrogen" atoms in the N···N region of the molecule, similar to what might be obtained by the superposition of one half molecule of **A′** on one half molecule of **A′′**.

[19] The observed nitrogen−nitrogen separation [N1−N2 = 2.657(6) Å] is smaller than the sum of the nitrogen van der Waals radii (3.10 Å); see: A. Bondi, *J. Chem. Phys.* **1964**, *68*, 441. R. C. Weast, *Handbook of Chemistry and Physics*, CRC, Boca Raton, FL, **1974**.

[20] [20a] M. Stender, R. J. Wright, B. E. Eichler, J. Prust, M. M. Olmstead, H. W. Roesky, P. P. Power, *J. Chem. Soc., Dalton Trans.* **2001**, 3465−3469. [20b] R. M. Claramunt, D. Sanz, S. H. Alarcon, M. P. Torralba, J. Elguero, C. Foces-Foces, M. Pietrzak, U. Langer, H. Limbach, *Angew. Chem.* **2001**, *113*, 434−437; *Angew. Chem. Int. Ed.* **2001**, *40*, 420−423. [20c] F. H. Allen, O. Kennard, D. G. Watson, L. Brammer, A. G. Orpen, R. Taylor, *J. Chem. Soc., Perkin. Trans. 2* **1987**, S1. [20d] S. Brownstein, E. J. Gabe, L. Prasad, *Can. J. Chem.* **1983**, *61*, 1410−1413.

[21] A. G. Orpen, L. Brammer, F. H. Allen, O. Kennard, D. G. Watson, R. Taylor, in: *Structure Correlation* (Eds.: H.-B. Bürgi, J. D. Dunitz), VCH, Weinheim, **1994**, vol. 2, pp. 770−774.

[22] See for example: [22a] V. Cadierno, M. Zablocka, B. Donnadieu, A. Igau, J. P. Majoral, A. Skowronska, *J. Am. Chem. Soc.* **1999**, *121*, 11086−11092. [22b] Y. Miquel, A. Igau, B. Donnadieu, J. P. Majoral, L. Dupuis, N. Pirio, P. Meunier, *Chem. Commun.* **1997**, 279−280.

[23] X. Krokidis, V. Goncalves, A. Savin, B. Silvi, *J. Phys. Chem. A.* **1998**, *26*, 5065−5073.

[24] The representation of β-enaminoimine systems as a symmetrically hydrogen-bonded structure, earlier described as an aromatic six-π-electron system, should be excluded for these compounds; see: [24a] P. Goldstein, K. N. Trueblood, *Acta Crystallogr.* **1967**, *23*, 148−156. [24b] J. E. Parks, R. H. Holm, *Inorg. Chem.* **1968**, *7*, 1408−1416.

[25] A very low activation barrier has to be assumed for the tautomeric process in β-enaminoimine derivatives.

[26] R. B. King, P. M. Sundaram, *J. Org. Chem.* **1984**, *49*, 1784−1789.

[27] [27a] S. L. Buchwald, S. J. LaMaire, R. B. Nielsen, B. T. Watson, S. M. King, *Org. Synth* **1993**, *71*, 77. [27b] S. L. Buchwald, S. J. LaMaire, R. B. Nielsen, B. T. Watson, S. M. King, *Tetrahedron Lett.* **1987**, *28*, 3895−3898.

[28] SIR92, a Program for Automatic Solution of Crystal Structures by Direct Methods: A. Altomare, G. Cascarano, G. Giacovazzo, A. Guargliardi, M. C. Burla, G. Polidori, M. Camalli, *J. Appl. Crystallogr.* **1994**, *27*, 435−440.

[29] G. M. Sheldrick, *SHELXTL-97* (includes *SHELXS-97, SHELXL-97, CIFTAB*), Programs for Crystal Structure Analysis (Release 97-2), Institut für Anorganische Chemie der Universität, Tammanstrasse 4, 3400 Göttingen, Germany, **1998**; *SHELXS-97* and *SHELXL-97* are both included in the package *WinGX* version 1.63 (*WINGX-1.63, Integrated System of Windows Programs for the Solution, Refinement and Analysis of Single Crystal X-ray Diffraction Data*): L. Farrugia, *J. Appl. Crystallogr.* **1999**, *32*, 837−838].

[30] *International Tables for X-ray Crystallography*, Kynoch Press, Birmingham, England, **1974**, vol. IV.

[31] L. Zolnaï, *ZORTEP, Graphical Program for X-ray Structure Analysis*, University of Heidelberg, Heidelberg, Germany, **1998**.

Received March 19, 2002
[I02144]

Syntheses and Crystal Structures of Copper and Silver Complexes with New Imine Ligands − Air-Stable, Photoluminescent Cu^IN_4 Chromophores

Goutam Kumar Patra[a] and Israel Goldberg*[a]

Keywords: N ligands / Copper / Silver / Luminescence / Electrochemistry

A series of new imine ligands [**1** ($C_{12}H_{12}N_2S_2$), **2** ($C_{12}H_{12}N_2S_2$), **3** ($C_{24}H_{18}N_4S_2$), and **5** ($C_{30}H_{27}N_7$)] have been synthesized (**1** and **2** are structural isomers). Cu^I and Ag^I complexes of the nonconjugated dithiophene-diimine ligands **1**, **2** and the tripodal imine-amine ligand **5** have also been prepared and thoroughly characterized by spectroscopic techniques as well as by X-ray diffraction. In cyclic voltammetry at a glassy carbon milli electrode in anhydrous dichloromethane under dry N_2, the corresponding Cu^I complexes [**6** ($2C_{12}H_{12}N_2S_2{\cdot}CuClO_4$), **7** ($2C_{12}H_{12}N_2S_2{\cdot}CuClO_4$), and **12** ($C_{30}H_{27}N_7{\cdot}CuClO_4$)] show quasi-reversible $Cu^{II/I}$ couples with high redox potentials (1.001 V for **6**, 0.958 V for **7**, and 0.692 V for **12**, vs. Ag/AgCl). This indicates that the π-acid ligands **1**, **2**, and **5** preferentially stabilize copper(I) over copper(II). The Cu^IN_4 chromophores in the complexes **6**, **7**, and **12** display photoluminescence in dichloromethane at room temperature. The related silver complexes of the same three ligands **10** ($2C_{12}H_{12}N_2S_2{\cdot}AgClO_4$), **11** ($2C_{12}H_{12}N_2S_2{\cdot}AgClO_4$), and **13** [$C_{30}H_{27}N_7{\cdot}Ag(CH_3CN)ClO_4$] reveal similar structural features but lack specific photophysical properties.

(© Wiley-VCH Verlag GmbH & Co. KGaA, 69451 Weinheim, Germany, 2003)

Introduction

Metal complexes of N-donor ligands are of considerable current interest because they catalyze many organic transformations,[1] including the cyclization of 1,2-allene derivatives,[2] the asymmetric cyclization reaction of isocyanoacetic acid or isocyanomethyl toluenesulfonate with aldehydes,[3] asymmetric intramolecular carbene C−H insertion reactions[4] and the enantioselective addition of allyltin reagents to aldehydes.[5,6] Further interest is in photoluminescent complexes of copper(I). The photophysics of compounds derived from 1,10-phenanthroline species, which contain the Cu^IN_4 chromophore, is well established.[7−9] However, materials based on other ligands with N-donor atoms are less abundant in the literature.[10−12] In this context we have synthesized a series of new nonconjugated diimine and imine-amine nitrogen donor ligands (**1**−**5**) and attempted the formulation and thorough spectral and structural characterization of their complexes with Cu^I, as well as with the related Ag^I ion. The linear ligands **1**−**4** also contain peripheral thiophene substituents, which may have some unique effect on the photophysical properties of the anticipated Cu^IN_4 chromophores, depending on the proximity of the sulfur atoms (although they are considered to be weak nucleophiles) to the complexation site. Another variant of this study involves transition metal complexes with tetradentate tripodal Schiff-base ligands, due to their diverse structural and physical properties, as well as their possible application as magnetic imaging agents and models of metalloenzymes such as superoxide dismutases.[13,14] Correspondingly, Cu^I and Ag^I complexes with the tripodal ligand **5** were prepared and characterized. The Cu^I complex of **5** is also photoluminescent.

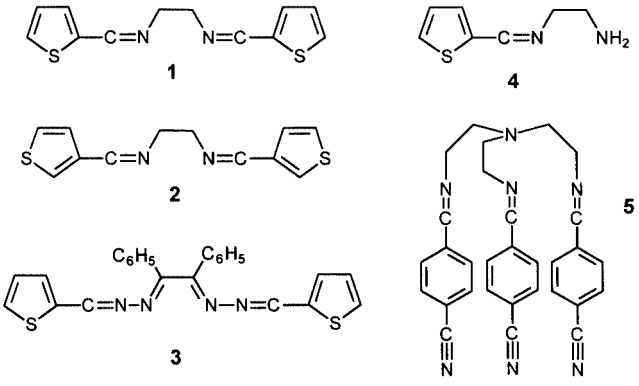

Herein we report the detailed structures and preliminary photophysical properties of three new Cu^IN_4 chromophores derived from ligands **1**, **2**, and **5**; chemical spectral and structural data are provided for the Ag^I complexes of these ligands as well. The bulky ligand **3** does not form stable complexes with these metal ions, while the asymmetric ligand **4** yields a stable structure only with divalent copper ions.

[a] School of Chemistry, Sackler Faculty of Exact Sciences, Tel Aviv University
69978 Ramat Aviv, Tel Aviv, Israel
E-mail: goldberg@post.tau.ac.il

Results and Discussion

Synthesis and Structure

Compounds **1** and **2** were synthesized by condensing ethylenediamine with 2-thiophenecarboxaldehyde or 3-thiophenecarboxaldehyde, respectively. These compounds are flexible about the central C−C bond. A 1:2 condensation reaction of benzil dihydrazone with 2-thiophenecarboxaldehyde yields a bulkier ligand **3**, which is considerably more rigid. The molecular structures of **2** and **3** are shown in Figure 1. Ligand **2** is located in the crystal on an axis of twofold rotational symmetry, the torsion angle about the central C−C bond that connects the two equivalent parts of the molecule being 70.6(3)°. The inner nitrogen atoms are exposed to the surrounding species, and provide excellent sites for metal ion binding. The N−C−C−N torsion angle about the central bond in **3** is 49.6(2)°. The nitrogen atoms are involved in partly delocalized π-electron systems

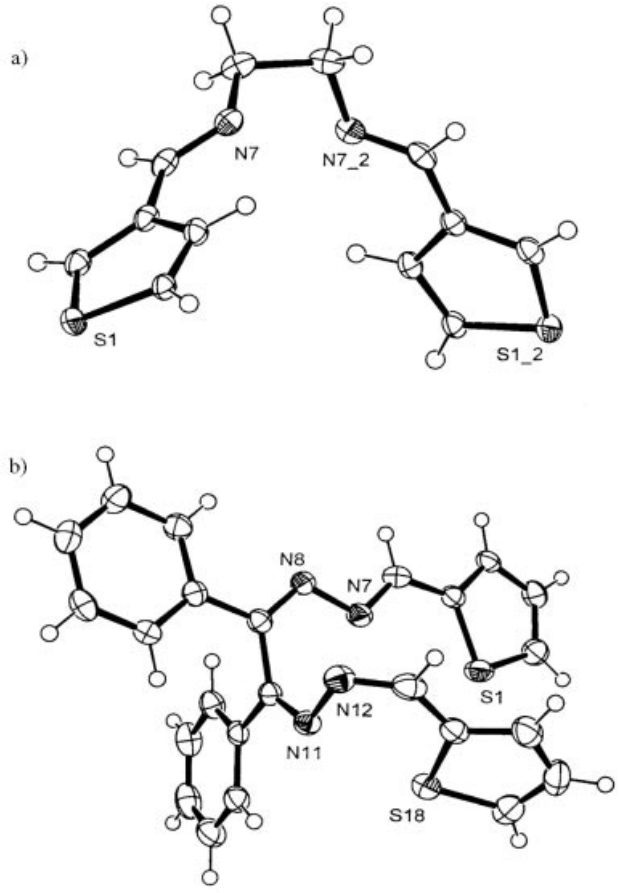

Figure 1. Molecular structures of (a) ligand **2** (located on a twofold symmetry axis), and (b) ligand **3**; the heteroatoms are indicated by darkened circles and are labeled; 50% probability thermal ellipsoids at 110 K are shown

(one part of the molecule is nearly planar; Figure 1), and therefore are less-effective donor sites for complex formation.

In this work we have been able to synthesize and crystallize stable Cu^I and Ag^I complexes of **1** and **2**, but no metal ion complexes of **3** could be obtained. The copper(I) derivatives were prepared by treating ligands **1** and **2** with $[Cu(CH_3CN)_4]ClO_4$ in anhydrous methanol under argon in a 1:2 metal/ligand ratio. The resulting bright orange-yellow solids $[Cu(\mathbf{1})_2](ClO_4)$ (**6**) and $[Cu(\mathbf{2})_2](ClO_4)$ (**7**) are extremely stable in air both in the solid state and in solution (CH_3OH and CH_2Cl_2). The observed structures of the cat-

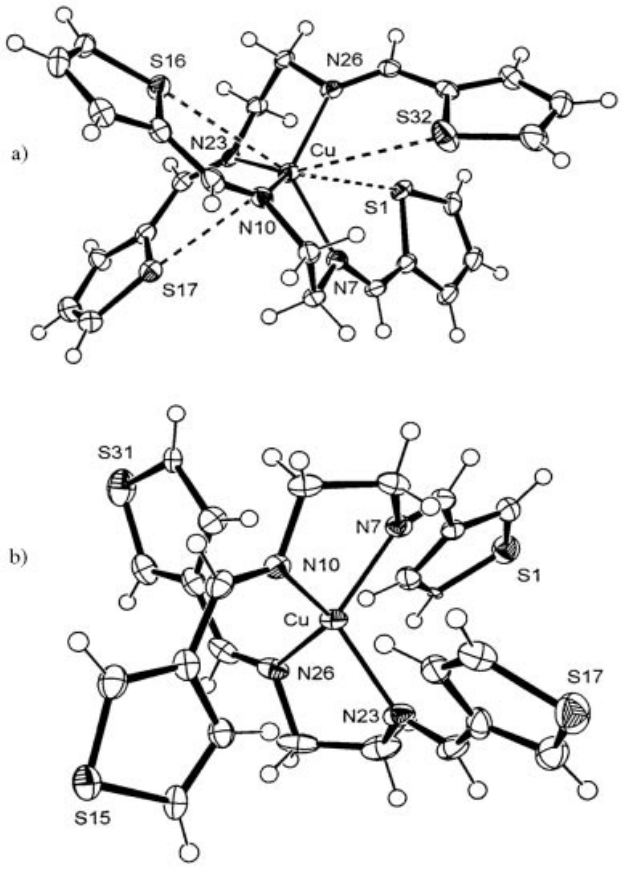

Figure 2. Complexes of Cu^I with (a) ligand **1**, and (b) ligand **2**; note in (a) the additional attractive interactions of the metal ion with the inward turning sulfur sites (dotted lines); in this and the following structural illustration the counterions and solvent moieties are omitted for clarity

ionic species in **6** and **7** are illustrated in Figure 2. The high propensity of the copper ion to form tetrahedrally structured complexes determines the 1:2 stoichiometry of the metal/ligand reaction. In **6** and **7** the Cu−N bond lengths within the Cu^IN_4 chromophore are in the range 2.004−2.111(2) and 2.039−2.071(3) Å, respectively. However, in **6** all the S-atom sites of the 2-thiophene substituents are oriented towards, and weakly interact with, the central metal ion; the corresponding Cu···S distances range from 3.24 to 3.60 Å (Figure 2, a). Such interactions are not possible in the 3-thiophene derivative **7**. As a result the thiophene rings in this structure (as well as in the related complexes described below) tend to exhibit twofold orientational disorder about the C−C bond through which they are connected to the central part of the ligand. The Cu^IN_4 moieties are distorted tetrahedra with two N−Cu−N

angles near 85° (which involve nitrogen atoms from the same ligand) and four N−Cu−N angles greater than 115° (for N atoms of the two different ligands).

The corresponding $[Cu(\mathbf{1})_2](ClO_4)_2$ complex with divalent copper, of a deep-green color, is stable in CH_3OH or CH_3CN only for a few minutes, and could not be characterized. An alternative reaction of **1** with $Cu(CF_3SO_3)_2$ yielded a somewhat more stable product, $[Cu(\mathbf{1})_2](CF_3SO_3)_2$ (**8**), which is stable in air, and in solution in CH_3OH or CH_3CN, for about 2−3 h. However, upon slow recrystallization from the solution mixture the ligand framework in **8** is partially hydrolyzed, transforming after about 8 h to a different species of composition $[Cu(\mathbf{4})_2](CF_3SO_3)_2$ (**9**) characterized by a light pink color.[15] In situ partial hydrolysis of a diimine ligand within the coordination sphere of copper is rare. No stable complexes of ligand **2** with Cu^{II} ions could be obtained under similar experimental conditions. The structure of the $[Cu(\mathbf{4})_2]^{2+}$ cation in **9** is depicted in Figure 3. It shows a nearly square-planar complex with the metal ion located on a center of inversion, with Cu−N distances of 1.997(2) and 2.038(2) Å and N−Cu−N bond angles between the *cis*-related nitrogen sites of 83.40(6)° within the ligand and 96.60(6)° between the two ligands.

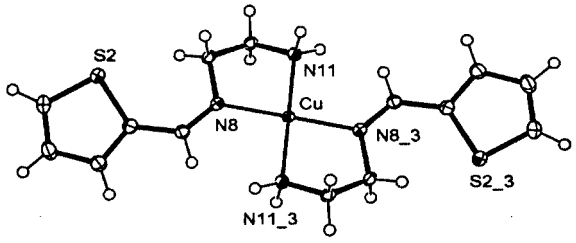

Figure 3. Molecular structure of the square-planar complex **9** of Cu^{II}, the metal ion being located in the crystal on a crystallographic center of inversion

The structures of the respective Ag^I complexes of **1** and **2** {$[Ag(\mathbf{1})_2](ClO_4)$ (**10**) and $[Ag(\mathbf{2})_2](ClO_4)$ (**11**)} are shown in Figure 4. They were prepared readily by treating the ligands with $Ag(ClO_4)$ at room temperature. These two 1:2 metal/ligand complexes are stable in the solid state for about two weeks, and in solution (MeOH or MeCN) for at least 12 h. Their structures have a distorted tetrahedral geometry similar to that observed for the corresponding copper(I) derivatives.

The coordination parameters are: (a) in **10**, Ag−N bond lengths of 2.293−2.298(3) Å, N−Ag−N bond angles within the same ligand of nearly 76°, and involving two different ligands greater than 120°; (b) in **11**, the corresponding values are 2.273−2.353(3) Å, 76−77° and greater than 118°, respectively. In **10**, the silver ions are also approached, in a convergent manner, by the four thiophene S-sites at an Ag···S distance range of 3.22−3.37 Å. The latter may represent additional weakly attractive interactions between the metal ion and the ligand species.

Ligand **5** is a 1:3 condensate of tris(2-aminoethyl)amine (tren) and 4-cyanobenzaldehyde. It contains an amino nitrogen atom, as well as three imino N-donors, and may act

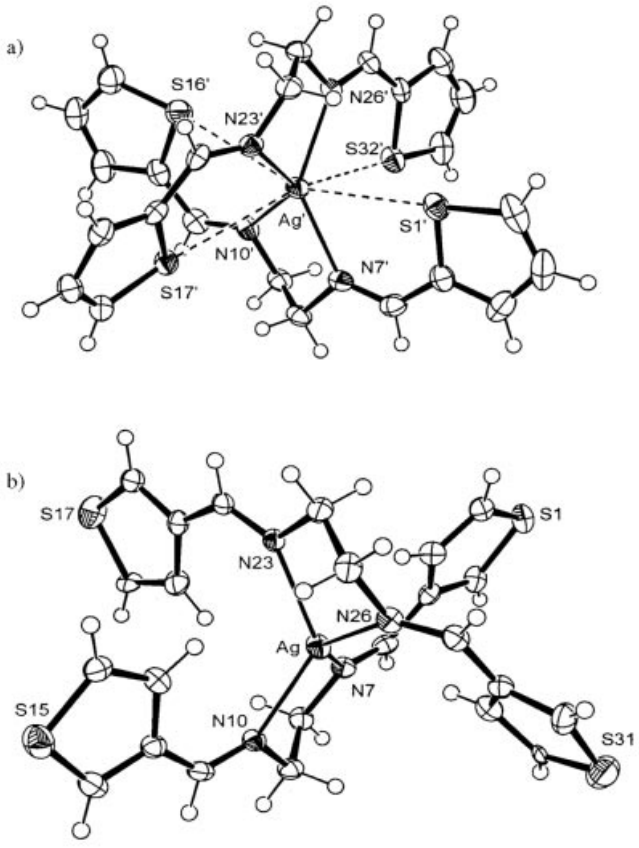

Figure 4. Structures of complexes of Ag^I with (a) ligand **1**, and (b) ligand **2**; note in (a) the additional attractive interactions of the metal ion with the inward turning sulfur sites (dotted lines), as in the corresponding Cu^I complex shown in Figure 2a

as a tetradentate ligand of adjustable conformation. Correspondingly, in complexation reactions with Cu^I and Ag^I one molecule of **5** should function as two molecules of **1** or **2**. The yellow-reddish Cu^I complex $[Cu(\mathbf{5})](ClO_4)$ (**12**) was obtained by treating **5** with $[Cu(CH_3CN)_4]ClO_4$ in equimolar proportions in methanol under argon. Complex **12** is also fairly stable in air, both in the solid state and in solution. A similar reaction of **5** with $Ag(ClO_4)$ in acetonitrile at room temperature yielded $[Ag(\mathbf{5})(CH_3CN)](ClO_4)$ (**13**). The molecular structures of the two complexes are illustrated in Figure 5.

Indeed, complex **12** has a tripodal structure with the Cu^I cation trapped inside the ligand by internal coordination to the four N-donor sites. The Cu−N(imino) distances are within the range 2.000−2.008(2) Å, while the Cu−N(amino) bond length is 2.206(2) Å. The geometry of the Cu^IN_4 moiety in this structure resembles a trigonal pyramid with the amino nitrogen atom at its apex. The Cu^IN_4 chromophore with a trigonal-pyramidal geometry around the metal ion is not common.[16] The N(imino)−Cu−N(amino) bond angles are constrained by the proximity of the two nitrogen sites to low values within the range 84.6−85.3(1)°, while the geometrically less constrained N(imino)−Cu−N(imino) bond angles in the base of the pyramid are characterized by larger values of be-

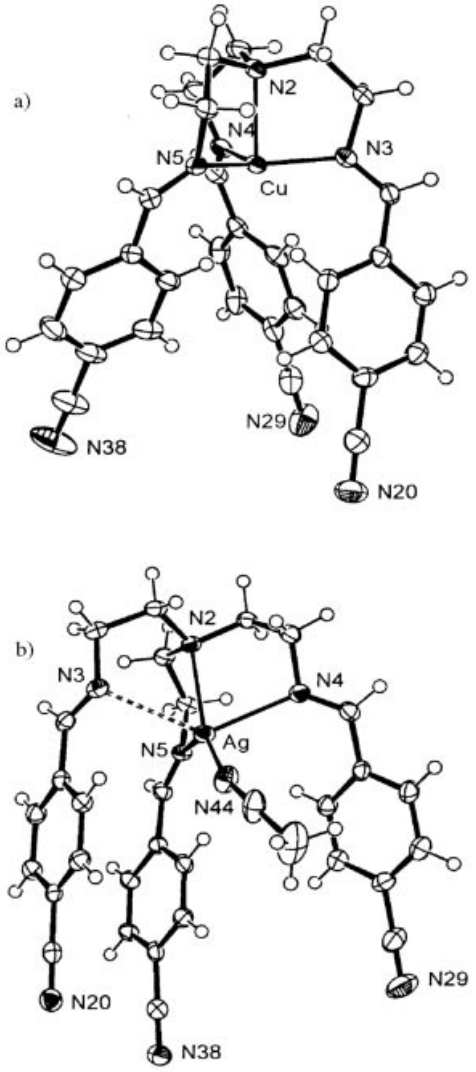

Figure 5. Structures of the tripodal complexes of ligand **5** with (a) Cu^I and (b) Ag^I; the Cu^IN_4 moiety in (a) is characterized by a trigonal-pyramidal geometry; the coordination geometry around the silver ion in (b) is affected by the additional coordinated acetonitrile ligand

tween 116.6 and 121.4(1)°. The geometry of the corresponding silver complex **13** is disrupted by coordination of one acetonitrile ligand which coordinates to the metal ion with an Ag−N distance of 2.211(3) Å. The latter also coordinates strongly to three N-atom donor sites of the ligand at 2.315−2.461(2) Å, and more weakly to the fourth (imino) nitrogen at 2.763(2) Å.

IR and NMR Characterization

Ligands **1** and **2** exhibit strong IR absorption bands at 1635 and 1641 cm^{-1}, respectively, for the ν(C=N) stretching vibration. On coordination with Cu^I this band shifts to much lower energies (1611 and 1614 cm^{-1} for **6** and **7**, respectively). In case of the Ag^I complexes **10** and **11**, however, this band appears at 1631 and 1640 cm^{-1}, respectively. For the ligand **5** and its Cu^I and Ag^I complexes, **12** and **13**, this ν(C=N) stretching vibration appears at 1642, 1635, and 1633 cm^{-1}, respectively, and the ν(C≡N) stretching vibrations appear at 2221, 2228, and 2226 cm^{-1}, respectively. Complexes **6**, **7**, **10**, **11**, **12**, and **13** give characteristic well-resolved bands around 1088, 1080, 1085, 1081, 1090, and 1091 cm^{-1}, respectively, for the noncoordinated ν(ClO_4^-) vibrations.[17]

The ^1H and ^{13}C NMR spectra of the ligands **1**, **2**, and **5** in $CDCl_3$ consist of sharp and well-resolved signals for each of the organic groupings present. The Cu^I and Ag^I complexes **6**, **7** and **10**, **11** show almost the same pattern as the ligand in their ^1H NMR spectra in $(CD_3)_2SO$. While the ^1H NMR spectrum of **13** shows the same pattern as that of the ligand, the ^1H NMR spectrum of **12** shows different chemical shifts. In case of the ligand **5** and its Ag^I complex **13** all the phenylic protons appear at the same position (δ = 7.67 ppm for ligand **5** and δ = 7.93 ppm for the Ag^I complex **13**) but for the Cu^I complex **12** they appear at two different positions (δ = 8.07 and 7.46 ppm). In the EI mass spectra ligands **1** and **2** show exactly the same type of fragmentation pattern.

Electrochemistry

The redox behavior of the Cu^I complexes **6**, **7**, and **12** has been examined by cyclic voltammetry in dichloromethane at a glassy carbon working electrode under dry N_2 (Figure 6). Quasi-reversible oxidative voltammograms attributed to the $Cu^{II/I}$ couple were observed with half-wave potential ($E_{1/2}$) values of 1.001, 0.958 and 0.692 V vs. Ag/AgCl, 1 M KCl for **6**, **7**, and **12**, respectively. The couple is more reversible in the case of **6** and **7** than for **12**. The peak-to-peak (ΔE_p) separation values for this couple are 190, 205, and 310 mV for **6**, **7**, and **12**, respectively, at a scan rate of 50 $mV \cdot s^{-1}$ and these values increase when the scan rate is increased. The higher potential of this couple in **6** and **7** than in **12** indicates that the Cu^I complexes **6** and **7** are more stable than **12**; this has been observed experimentally: a dichloromethane solution of **6** or **7** is stable in air

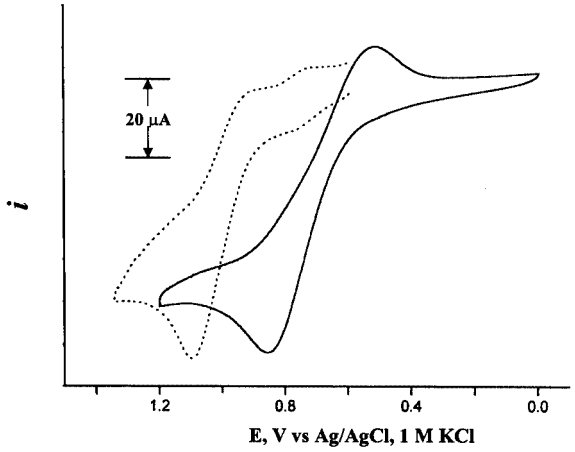

Figure 6. Cyclic voltammograms of **6** (broken line) and **12** (full line) [approximately 10^{-3} M in dichloromethane, 0.2 M Bu_4NClO_4] at a glassy carbon electrode, scan rate 50 $mV \cdot s^{-1}$

for at least 10 d, whereas a solution of **12** is stable only for about 3−4 d. The $Cu^{II/I}$ potential in the $Cu^{I}N_4$ chromophore increases with the π-acidity of the ligand and the extent of tetrahedral distortion in the corresponding copper(II) species.[18] The π-acidity of ligands **1** and **2** is larger than that of **5**. In this context, it should be mentioned that, to the best of our knowledge, the highest potential for the $Cu^{II/I}$ couple so far reported in a $Cu^{I}N_4$ chromophore is 1.55 V vs. SCE.[8]

UV/Vis and Photophysical Data

There is a difference in the absorption spectra of the ligands **1** and **2** in dichloromethane. While ligand **1** shows two charge-transfer bands at 284 and 261 nm with intensities (ε) of 24975 and 28160 $M^{-1}cm^{-1}$, respectively, ligand **2** shows only one charge-transfer band at 250 nm (ε = 31 945). These intra-ligand charge-transfer bands appear at 282 and 266 nm for the Cu^{I} complex **6** and at 254 nm for **7**. In addition to these bands, **6** shows two metal-to-ligand charge-transfer (MLCT) bands at 415 (ε = 2480) and 345 nm (ε = 8785). These two MLCT bands appear at 410 (ε = 2405) and 347 nm (ε = 7250) for complex **7**. The deep green color of copper(II) complexes of the ligand **1** and pale pink color of the copper(II) complex of ligand **4** are due to the d-d transition band at 613 nm (ε = 215) and 587 nm (ε = 150), respectively. Ligand **5** shows an intra-ligand charge-transfer band at 255 nm (ε = 38 120) in dichloromethane. This band appears at 251 nm (ε = 30 730) for its copper(I) complex **12** and at 248 nm (ε = 26 500, in CH_3CN) for its silver(I) complex **13**. The copper(I) complex shows an MLCT band at 379 nm (ε = 2526).

Ligands **1**, **2**, and **5** are not photoluminescent in dichloromethane. Upon excitation at 350 nm (MLCT envelope) in dichloromethane at room temperature both complexes **6** and **7** yield a single, structureless, broad emission band with maxima at 445 and 456 nm, respectively, with quantum yields (φ) of $2.9\cdot10^{-4}$ and $7.2\cdot10^{-5}$ (against quinine sulfate[19] in 0.1 N H_2SO_4; Figure 7), respectively. In complex **6** all the four S-atoms are directed towards the metal ion, so the metal coordination sphere is sterically more hindered. This may be the reason for the larger quantum yield (φ) of **6** than **7**. The chemical nature, the size and the position of the substituents in the ligand can affect the geometry of the excited state, which influences the emission properties.[9] It has been found for 2,9-disubstituted phenanthroline derivatives that the Cu^{I} geometry is stabilized by enforcing a tetrahedral geometry that inhibits the flattened square-planar coordination geometry in the Cu^{II} state formed upon excitation.[20]

On excitation at 380 nm (MLCT band), complex **12** exhibits a single structureless broad emission band with a maximum at 505 nm and a quantum yield (φ) of $5.8\cdot10^{-5}$ (against quinine sulfate[19] in 0.1 N H_2SO_4; Figure 7). The photophysical properties of the $Cu^{I}N_4$ chromophore have been analysed mainly for complexes of Cu^{I} with derivatives of 1,10-phenanthroline.[9] These complexes are of the bis-type in which all the nitrogen donor atoms are essentially of the same type. Complex **12** is only the second known example of a photoluminescent $Cu^{I}N_4$ chromophore where the nitrogen donor atoms are of the imino as well as the amino type, and come from the same ligand. The only photoluminescent $Cu^{I}N_4$ chromophore of this type known so far has been reported recently.[12]

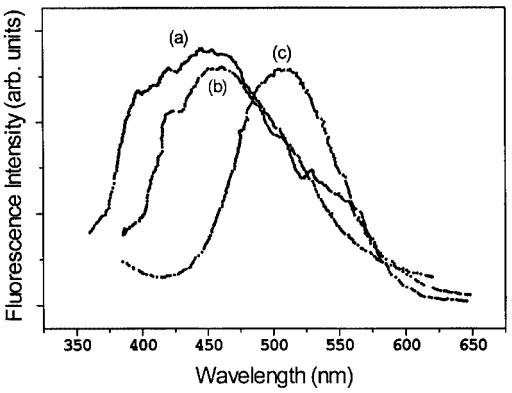

Figure 7. Emission spectra of (a) **6**, (b) **7**, and (c) **12** at room temperature in dichloromethane; excitation wavelength is 350 nm for **6** and **7**, 380 nm for **12**; absorbances for **6**, **7**, and **12** are 0.68, 0.73, and 0.80, respectively

Conclusions

In a search for new metal ion complexes with interesting features, we have synthesized a series of copper(I) and silver(I) compounds with targeted diimine and tripodal ligands, and examined their structural, photophysical, and electrochemical properties. The copper(I) complexes are of particular interest here, as they reveal a more unique photophysical behavior. The emission quantum yield (φ) of complex **6** at room temperature in dichloromethane was found to be four to five times larger than that of complexes **7** and **12**. The $Cu^{II/I}$ redox potential values of all three compounds are rather high, indicating that the copper(I) state is much more stable than the corresponding copper(II) state.

Experimental Section

General Procedures: The complex $[Cu(CH_3CN)_4]ClO_4$ was synthesized by a reported procedure.[21] All other reagents were procured commercially. Copper was estimated gravimetrically as CuSCN. Microanalyses were performed with Perkin−Elmer 2400II elemental analyzer and CE instruments. Melting points were determined by an electrothermal IA9000 series digital melting point apparatus and are uncorrected. IR spectra (KBr disc) were recorded with a Nicolet Magna-IR spectrophotometer (Series II), UV/Vis spectra with a Shimadzu UV-160A spectrophotometer, ^1H and ^{13}C NMR spectra with a Bruker DPX200 spectrometer and EI (electron impact) mass spectra with a VG Autospec M-250 instrument. Cyclic voltammetry was performed at room temperature at a planar glassy carbon milli electrode using μ-Autolab II with GPES software, version 4.8.5 (EcoChemie, The Netherlands) in purified and anhydrous dichloromethane under dry nitrogen with a conventional three-electrode configuration. Under the experimental condi-

tions employed here, the ferrocene/ferrocenium couple appears at 0.42 V vs. Ag/AgCl in 1 M KCl with a ΔE_p of 110 mV at a scan rate of 50 mV·s^{-1} (Figure 6). The photophysical studies were performed in air with a Shimadzu RF-540 spectrofluorophotometer.

Ligand 1: Distilled ethylenediamine (1 mL, 15 mmol) and freshly distilled 2-thiophenecarboxaldehyde (2.80 mL, 30 mmol) were refluxed in 60 mL of anhydrous methanol for 6 h. On evaporating the solvent a light yellow solid was obtained, which on recrystallization from *n*-hexane gave colorless needles suitable for X-ray analysis. Yield: 2.98 g (80%); m.p. 91−93 °C. $C_{12}H_{12}N_2S_2$ (248.36): calcd. C 58.01, H 4.87, N 11.28, S 25.83; found C 58.05, H 4.83, N 11.32, S 25.87. EI-MS: *m*/*z* (%) = 248.1 (20) [M$^+$], 124 (55) [M$^+$/2]. FTIR (KBr): $\tilde{\nu}$ = 507 (m), 577 (m), 648 (w), 715 (vs), 792 (vs), 841 (s), 860 (s), 955 (s), 1051 (s, split), 1192 (m), 1235 (vs), 1284 (s), 1326 (m), 1430 (s), 1635(vs), 2848 (wb), 2908 (wb), 3099 (s) cm^{-1}. ^{1}H NMR (200 MHz, $CDCl_3$, TMS): δ = 8.35 (s, 2 H), 7.35 (d, *J* = 4 Hz, 2 H), 7.27 (d, *J* = 4 Hz, 2 H), 7.04 (dd, *J* = 2 and 4 Hz, 2 H), 3.91 (s, methylene, 4 H) ppm. ^{13}C NMR (200 MHz, $CDCl_3$, TMS): δ = 155.96, 142.27 (quaternary), 130.46, 128.70, 127.27, 60.92 ppm. UV/Vis (CH_2Cl_2): λ_{max} (ε) = 284 (24975), 261 nm (28160 M^{-1}·cm^{-1}).

Ligand 2: This compound was prepared by following a similar procedure starting with distilled ethylenediamine (1 mL, 15 mmol) and freshly distilled 3-thiophenecarboxaldehyde (2.63 mL 30 mmol) to obtain shiny white crystals, suitable for X-ray analysis. Yield: 2.66 g (71%); m.p. 97 °C. $C_{12}H_{12}N_2S_2$ (248.36): calcd. C 58.01, H 4.87, N 11.28, S 25.83; found C 58.08, H 4.91, N 11.27, S 25.90. EI-MS: *m*/*z* (%) = 248.1 [M$^+$] (20), 124 [M$^+$/2] (55). FTIR (KBr): $\tilde{\nu}$ = 575 (m), 625 (s), 717 (m), 789 (vs), 828 (s), 878 (m), 902 (m), 1021 (vs), 1070 (m), 1160 (s, split), 1240 (vs), 1291 (s), 1346 (w), 1354 (m), 1426 (m), 1458 (s), 1641 (vs), 2844 (wb), 3049 (m, split), 3091 (s) cm^{-1}. ^{1}H NMR (200 MHz, $CDCl_3$, TMS): δ = 8.28 (s, 2 H), 7.57 (d, *J* = 4 Hz, 2 H), 7.51 (d, *J* = 4 Hz, 2 H), 7.30 (dd, *J* = 2 and 4 Hz, 2 H), 3.90 (s, methylene, 4 H) ppm. ^{13}C NMR (200 MHz, $CDCl_3$, TMS): δ = 156.98, 140.32 (quaternary), 128.44, 126.30, 125.66, 61.57 ppm. UV/Vis (CH_2Cl_2): λ_{max} (ε) = 250 nm (31945 M^{-1}·cm^{-1}).

Ligand 3: Benzil dihydrazone (1.87 g, 7.85 mmol), synthesized by a reported procedure,[22] was dissolved in 50 mL of anhydrous methanol. To this solution, freshly distilled 2-thiophenecarboxaldehyde (1.47 mL, 15.70 mmol) was added. The resulting yellowish mixture was refluxed for 6 h, maintaining dry conditions. Then it was slowly cooled to room temperature to yield a yellowish crystalline solid, which was filtered off and dried in air. Crystals suitable for X-ray analysis were obtained by slow concentration of an acetonitrile solution. Yield 2.15 g (64%); m.p. 159−160 °C. $C_{24}H_{18}N_4S_2$ (426.54): calcd. C 67.56, H 4.26, N 13.14, S 15.05; found C 67.58, H 4.29, N 13.19, S 14.99. FTIR (KBr): $\tilde{\nu}$ = 525(m), 596 (m), 610 (m), 685 (vs), 712 (vs), 764 (vs, split), 835 (w), 919 (m), 1050 (s), 1074 (m), 1175 (m), 1212 (s), 1237 (m, split), 1299 (w), 1326 (m), 1424 (vs), 1445 (s), 1490 (s), 1605 (vs), 2840 (wb), 2917 (w), 3105(s) cm^{-1}. ^{1}H NMR (200 MHz, $CDCl_3$, TMS): δ = 8.65 (s, 2 H), 8.05−7.99 (m, 6 H), 7.97−7.90 (m, 6 H), 7.30 (d, 2 H), 7.10 (d, 2 H), 6.96 (dd, 2 H) ppm. ^{13}C NMR (200 MHz, $CDCl_3$, TMS): δ = 164.86 (quaternary), 162.40 (quaternary), 155.65, 148.31, 139.22 (quaternary), 134.19, 133.50, 131.75, 128.80, 127.22 ppm. UV/Vis (CH_2Cl_2): λ_{max} (ε) = 328 (35 600), 276 (28 690), 257 nm (26845 M^{-1}·cm^{-1}). EI-MS: *m*/*z* (%) = 426.1 [M$^+$] (15).

[Cu(1)$_2$]ClO$_4$ (6): Solid $[Cu(CH_3CN)_4]ClO_4$ (0.165 g, 0.5 mmol) was added to 30 mL of an anhydrous, degassed methanol solution of **1** (0.25 g, 1 mmol) under argon, and stirred for 1 h maintaining dry conditions. An orange-yellow compound precipitated. This was filtered off, washed with 2 mL of methanol and dried in vacuo over fused $CaCl_2$. Yield: 0.18 g (55%). Single crystals were grown by diffusion of *n*-hexane into a concentrated dichloromethane solution of the complex. $C_{24}H_{24}ClCuN_4O_4S_4$ (659.70): calcd. C 43.67, H 3.67, Cu 9.63, N 8.49, S 19.45; found C 43.62, H 3.73, Cu 9.69, N 8.46, S 19.49. FTIR (KBr): $\tilde{\nu}$ = 625 (m), 641 (w), 722 (m, split), 853 (w), 1088 (vs), 1108 (vs), 1187 (m), 1234 (s), 1288 (s), 1321 (m), 1435 (s), 1611 (vs), 2850 (wb), 2910 (m), 3099 (s) cm^{-1}. ^{1}H NMR [200 MHz, $(CD_3)_2SO$, TMS]: δ = 8.68 (s, 4 H), 7.52 (d, *J* = 4 Hz, 4 H), 7.27 (d, *J* = 4 Hz, 4 H), 7.05 (dd, *J* = 2 and 4 Hz, 4 H), 4.17 (s, methylene, 8 H) ppm. UV/Vis (CH_2Cl_2): λ_{max} (ε) = 415 sh (2480), 345 sh (8785), 282 (22080), 266 nm (31250 M^{-1}·cm^{-1}).

[Cu(2)$_2$]ClO$_4$ (7): This complex was prepared similarly by treating $[Cu(CH_3CN)_4]ClO_4$ (0.165 g, 0.5 mmol) with **2** (0.25 g, 1 mmol) in 50 mL of anhydrous methanol under argon. Yield: 0.16 g (48%). Single crystals were grown by direct diffusion of *n*-hexane into a dichloromethane solution of the complex. $C_{24}H_{24}ClCuN_4O_4S_4$ (659.70): calcd. C 43.67, H 3.67, Cu 9.63, N 8.49, S 19.45; found C 43.69, H 3.74, Cu 9.74, N 8.44, S 19.47. FTIR (KBr): $\tilde{\nu}$ = 628 (m), 722 (m, split), 787 (m), 832 (s), 910 (w), 1080 (vs), 1105 (vs), 1161 (m), 1236 (m), 1326 (w), 1371 (w), 1462 (s), 1614 (vs), 3096 (s) cm^{-1}. ^{1}H NMR [200 MHz, $(CD_3)_2SO$, TMS]: δ = 8.42 (s, 4 H), 7.76 (br., 4 H), 7.55 (br., 4 H), 7.05 (br. 4 H), 4.08 (s, methylene, 8 H) ppm. UV/Vis (CH_3OH): λ_{max} (ε) = 410 sh (2405), 347 sh (7250), 254 nm (34320 M^{-1}·cm^{-1}).

[Cu(1)$_2$](CF$_3$SO$_3$)$_2$ (8): Ligand **1** (0.25 g, 1 mmol) was dissolved in 20 mL of acetonitrile. To this colorless solution 5 mL of an acetonitrile solution of $Cu(CF_3SO_3)_2$ (0.18 g, 0.5 mmol) was added dropwise with constant stirring. The solution turned bottle green. Diethyl ether was then added dropwise to this solution until precipitation occurred. The reaction mixture was kept in a refrigerator for 10 min. The green precipitate was then filtered off, washed with diethyl ether, and dried in air. Yield: 0.44 g (51%). $C_{26}H_{24}CuF_6N_4O_6S_6$ (858.12): calcd. C 36.36, H 2.82, Cu 7.40, N 6.53, S 22.42; found C 36.41, H 2.85, Cu 7.47, N 6.49, S 22.48. FTIR (KBr): $\tilde{\nu}$ = 528 (w), 535 (m), 641 (s), 736 (s), 867 (m), 1118 (m), 1211 (m), 1268 (vs, split), 1338 (m), 1418 (s), 1621 (vs), 2912 (wb), 3095 (m) cm^{-1}. UV/Vis (CH_3CN): λ_{max} (ε) = 613 (215), 287 (34225), 264 nm (35075 M^{-1}·cm^{-1}).

[Cu(4)$_2$](CF$_3$SO$_3$)$_2$ (9): Complex **8** (0.43 g, 0.5 mmol) was dissolved in 15 mL of acetonitrile. To this solution 10 mL of diethyl ether was added. This green solution was kept in the refrigerator for 8 h. Light pink colored crystals, suitable for X-ray analysis were deposited. These were filtered and dried in vacuo over fused $CaCl_2$. Yield: 0.095 g (28%). $C_{16}H_{20}CuF_6N_4O_6S_4$ (670.14): calcd. C 28.66, H 3.01, Cu 9.48, N 8.36, S 19.14; found C 28.72, H 2.95, Cu 9.43, N 8.42, S 19.18. FTIR (KBr): $\tilde{\nu}$ = 515 (m), 576 (m), 635 (s), 755 (m), 1042 (vs, split), 1112 (m), 1170 (vs), 1265 (vs, split), 1486 (m), 1625 (vs), 2895 (w), 3305 (vb) cm^{-1}. UV/Vis (CH_3CN): λ_{max} (ε) = 587 (150), 281 (28470), 269 nm (28750 M^{-1}·cm^{-1}).

[Ag(1)$_2$](ClO$_4$) (10): Ligand **1** (0.25 g, 1 mmol) was dissolved in 15 mL of methanol. To this solution 5 mL of a methanol solution of $AgClO_4$ (0.105 g, 0.5 mmol) was added dropwise with constant stirring, causing an off-white solid to precipitate. It was kept in air for 1 h, then filtered off, washed with 2 mL of methanol and dried in vacuo over fused $CaCl_2$. Yield: 0.19 g (54%). Single crystals suitable for X-ray analysis were grown by slow concentration of an acetonitrile solution. The compound crystallizes with half a molecule of the acetonitrile solvent. $C_{24}H_{24}AgClN_4O_4S_4$ (704.03): calcd. C 40.92, H 3.44, N 7.96, S 18.22; found C 40.95, H 3.39, N 10.89,

S 18.26. FTIR (KBr): $\tilde{\nu}$ = 505 (m), 581 (w), 623 (s), 715 (vs), 842 (s), 951 (m), 1085 (vs, split), 1217 (m), 1285 (m), 1326 (w), 1430 (s), 1459 (m), 1631 (vs), 2861 (wb), 3100 (m) cm^{-1}. ^1H NMR [200 MHz, $(CD_3)_2SO$, TMS]: δ = 8.83 (s, 4 H), 7.74 (d, J = 4 Hz, 4 H), 7.61 (d, J = 4 Hz, 4 H), 7.14 (dd, J = 2 and 4 Hz, 4 H), 4.06 (s, methylene, 8 H) ppm. UV/Vis (CH_3CN): λ_{max} (ε) = 281 (28385), 260 nm (32155 $M^{-1}\cdot cm^{-1}$).

[Ag(2)$_2$](ClO$_4$) (11): Silver perchlorate (0.105 g, 0.5 mmol) was added to a solution of **2** (0.25 g, 1 mmol) in 20 mL of methanol. The reaction mixture was stirred at room temperature for 1 h. A light yellow compound precipitated. This was filtered off, washed with a few drops of methanol and dried in vacuo over fused $CaCl_2$. Yield: 0.16 g (46%). Single crystals suitable for X-ray analysis were grown by slow evaporation of the methanol solution of the complex. $C_{24}H_{24}AgClN_4O_4S_4$ (704.03): calcd. C 40.92, H 3.44, N 7.96, S 18.22; found C 40.97, H 3.48, N 7.91, S 18.28. FTIR (KBr): $\tilde{\nu}$ = 579 (w), 625 (vs), 715 (w), 790 (vs), 867 (m, split), 951 (m), 1081 (vs, split), 1237 (m), 1291 (s), 1346 (m), 1407 (m), 1457 (s), 1522 (m), 1640 (vs), 2843 (wb), 2904 (w), 3098 (m) cm^{-1}. ^1H NMR [200 MHz, $(CD_3)_2SO$, TMS]: δ = 8.68 (s, 4 H), 8.15 (d, J = 4 Hz, 4 H), 7.73 (d, J = 4 Hz, 4 H), 7.63 (dd, J = 2 and 4 Hz, 4 H), 3.94 (s, methylene, 8 H) ppm. UV/Vis (CH_3CN): λ_{max} (ε) = 248 nm (37535 $M^{-1}\cdot cm^{-1}$).

Ligand 5: 4-Cyanobenzaldehyde (3.93 g, 30 mmol) was dissolved in 150 mL of anhydrous methanol. To this solution distilled tris(2-aminoethyl)amine (1.5 mL, 10 mmol) was added dropwise. The re-

Table 1. Crystal and experimental data related to the structural analyses

Compound	**2**[a]	**3**	**6**[b]	**7**[b]	**9**[c]
Empirical formula	$C_{12}H_{12}N_2S_2$	$C_{24}H_{18}N_4S_2$	$2C_{12}H_{12}N_2S_2\cdot CuClO_4$	$2C_{12}H_{12}N_2S_2\cdot CuClO_4$	$2C_7H_{10}N_2S\cdot Cu(CF_3SO_3)_2$
Formula mass	248.36	426.54	659.70	659.70	670.14
Crystallization solvent	−	−	−	−	−
Crystal system	monoclinic	monoclinic	monoclinic	monoclinic	monoclinic
Space group	$C2/c$	$P2_1/c$	$P2_1/c$	$P2_1/n$	$P2_1/c$
a [Å]	22.0020(9)	11.2690(3)	23.3760(2)	17.7670(2)	13.0240(2)
b [Å]	5.4920(3)	7.5640(2)	14.1940(2)	17.3330(1)	10.2440(2)
c [Å]	10.3350(4)	24.4540(8)	17.7390(4)	17.8660(2)	10.1090(4)
α [°]	90	90	90	90	90
β [°]	100.836(3)	91.429(1)	111.005(5)	91.412(4)	111.150(1)
γ [°]	90	90	90	90	90
V [Å^3]	1226.6(1)	2083.7(1)	5494.7(2)	5500.3(1)	1257.9(1)
Z	4	4	8	8	2
μ(Mo-K_α) [mm^{-1}]	0.41	0.27	1.23	1.23	1.29
T [K]	110	110	110	110	110
D_c [$g\cdot cm^{-3}$]	1.345	1.360	1.595	1.593	1.769
$2\theta_{max}$ [°]	56.5	55.0	55.8	55.8	56.4
No. unique reflections	1457	4703	12630	12868	2985
No. reflections ($I > 2\sigma$)	1192	2733	8664	9930	2524
No. refined parameters	73	271	685	918	169
$R1$ ($I > 2\sigma$)	0.037	0.053	0.042	0.049	0.030
$R1$ (all data)	0.049	0.116	0.082	0.070	0.040
$wR2$ (all data)	0.101	0.142	0.103	0.145	0.079
$\|\Delta\rho\|_{max}$ [$e\cdot Å^{-3}$]	0.36	0.39	0.57	1.08	0.41

Compound	**10**[b]	**11**[b]	**12**	**13**
Empirical formula	$2C_{12}H_{12}N_2S_2\cdot AgClO_4$	$2C_{12}H_{12}N_2S_2\cdot AgClO_4$	$C_{30}H_{27}N_7\cdot CuClO_4$	$C_{30}H_{27}N_7\cdot Ag(C_2H_3N)ClO_4$
Formula mass	724.56	704.03	726.69	754.49
Crystallization solvent	$1/2C_2H_3N$		$C_2H_3N + 1/2C_4H_{10}O$	$1/2C_2H_3N$
Crystal system	monoclinic	monoclinic	triclinic	monoclinic
Space group	$P2_1$	$P2_1/c$	$P\bar{1}$	$C2/c$
a [Å]	12.9450(1)	23.0490(2)	12.1820(2)	15.3070(2)
b [Å]	14.5890(2)	14.3170(2)	12.4590(2)	20.0510(3)
c [Å]	16.9380(2)	18.2170(2)	12.6410(4)	22.6490(5)
α [°]	90	90	84.618(1)	90
β [°]	110.281(1)	107.011(1)	78.889(1)	104.893(1)
γ [°]	90	90	65.524(1)	90
V [Å^3]	3000.5(1)	5748.5(1)	1713.2(1)	6717.9(2)
Z	4	8	2	8
μ(Mo-K_α) [mm^{-1}]	1.08	1.12	0.77	0.73
T [K]	110	110	110	110
D_c [$g\cdot cm^{-3}$]	1.60	1.627	1.409	1.492
$2\theta_{max}$ [°]	55.9	55.8	55.0	56.5
No. unique reflections	7283	13665	7581	8032
No. reflections ($I > 2\sigma$)	6780	9261	5405	5668
No. refined parameters	721	685	443	439
$R1$ ($I > 2\sigma$)	0.031	0.051	0.051	0.041
$R1$ (all data)	0.036	0.097	0.084	0.075
$wR2$ (all data)	0.072	0.114	0.137	0.107
$\|\Delta\rho\|_{max}$ [$e\cdot Å^{-3}$]	0.77	0.86	0.71	0.76

[a] Molecules are located on symmetry axes of twofold rotation. [b] The crystallographic asymmetric unit contains two independent moieties of the complex. [c] The metal complex is located on centers of inversion.

action mixture was refluxed for 8 h maintaining dry conditions. Then, it was transferred into a beaker and left in the air overnight. A yellowish solid precipitated. This was filtered off, washed with 5 mL of methanol, dried in the air, and then recrystallized from acetonitrile. Yield: 3.2 g (66%); m.p. 135−137 °C. $C_{30}H_{27}N_7$ (485.27): calcd. C 74.19, H 5.61, N 20.20; found C 74.26, H 5.66, N 20.14. EI-MS: *m/z* (%) = 486.2 [MH^+] (30). FTIR (KBr): $\tilde{\nu}$ = 553 (s), 646 (m), 834 (vs), 927 (m), 1023 (m), 1067 (vs), 1158 (w), 1221 (w), 1287 (m), 1375 (s), 1440 (m), 1503 (m), 1642 (vs), 2221 (vs), 2841 (wb), 3428 (vb) cm^{-1}. ^1H NMR (200 MHz, $CDCl_3$, TMS): δ = 8.19 (s, 3 H), 7.67 (m, 12 H), 3.74 (t, methylene, 6 H), 2.97 (t, methylene, 6 H) ppm. ^{13}C NMR (200 MHz, $CDCl_3$, TMS): δ = 159.73, 139.86 (quaternary), 132.31, 128.26, 118.30 (quaternary), 113.79 (quaternary), 60.08, 55.20 ppm. UV/Vis (CH_2Cl_2): λ_{max} (ε) = 255 nm (38120 $M^{-1}\cdot cm^{-1}$).

[Cu(5)]ClO_4 (12): Complex **5** (0.243 g, 0.5 mmol) was dissolved in 35 mL of anhydrous methanol by warming. Argon was purged through the solution and it was then cooled to room temperature. After 15 min, solid [$Cu(CH_3CN)_4$]ClO_4 (0.165 g, 0.50 mmol) was added to the degassed methanol solution. The reaction mixture was stirred at room temperature under argon for 1 h, maintaining dry conditions. A reddish yellow compound precipitated. This was filtered off, washed with 2 mL of methanol, and dried in vacuo over fused $CaCl_2$. Yield: 0.148 g (46%). Single crystals were grown by direct diffusion of diethyl ether into a concentrated acetonitrile solution of the complex. The compound crystallizes with one molecule of acetonitrile and half a molecule of diethyl ether. $C_{30}H_{27}ClCuN_7O_4$ (648.58): calcd. C 55.53, H 4.20, Cu 9.80, N 15.11; found C 55.61, H 4.25, Cu 9.91, N 15.08. FTIR (KBr): $\tilde{\nu}$ = 556 (s), 624 (s), 829 (s), 890 (m), 1090 (vs, split), 1286 (m), 1390 (w), 1460 (m), 1635 (vs), 2228 (vs), 2858 (wb), 3449 (vb) cm^{-1}. ^1H NMR [200 MHz, $(CD_3)_2SO$, TMS]: δ = 8.75 (s, 3 H), 8.07 (d, 6 H), 7.46 (d, 6 H), 3.88 (s, methylene, 6 H), 3.12 (s, methylene, 6 H) ppm. UV/Vis (CH_2Cl_2): λ_{max} (ε) = 379 (2526), 251 nm (30730 $M^{-1}\cdot cm^{-1}$).

[Ag(5)(CH_3CN)]ClO_4 (13): Silver perchlorate (0.105 g, 0.5 mmol) was added to a solution of **5** (0.243 g, 0.5 mmol) in 25 mL of acetonitrile. The reaction mixture was stirred at room temperature for 1 h and was then kept in a refrigerator for 24 h. Large colorless blocks, which were suitable for X-ray analysis, separated. They were filtered off, washed with a few drops of methanol, and dried in vacuo over fused $CaCl_2$. Yield 0.155 g (42%). One molecule of the acetonitrile solvent was found coordinated to the silver ion (another noncoordinated acetonitrile was found included in the lattice with partial occupancy). $C_{32}H_{30}AgClN_8O_4$ (733.79): calcd. C 52.34 H 4.12, N 15.27; found C 52.60, H 4.10, N 15.32. FTIR (KBr): $\tilde{\nu}$ = 552 (s), 623 (s), 833 (s), 927 (m), 972 (w), 1091 (vs, split), 1220 (w), 1288 (m), 1374 (m), 1505 (m), 1563 (w), 1633 (vs), 2226 (vs), 2842 (wb), 3442 (vb) cm^{-1}. ^1H NMR [200 MHz, $(CD_3)_2SO$, TMS]: δ = 8.61 (s, 3 H), 7.93 (m, 12 H), 3.81 (br., methylene, 6 H), 2.98 (br., methylene, 6 H), 2.07 (s, 3 H) ppm. UV/Vis (CH_3CN): λ_{max} (ε) = 248 nm (26500 $M^{-1}\cdot cm^{-1}$). ***Caution:*** Perchlorates are potentially explosive and should not be prepared and stored in large amounts.

Crystallography: The diffraction measurements were carried out with a Nonius KappaCCD diffractometer, using graphite-monochromated Mo-K_α radiation (λ = 0.7107 Å). Crystalline samples of the analyzed compounds were covered with a thin layer of light oil and freeze-cooled to 110 K in order to minimize solvent escape (if present), structural disorder (particularly of the anions) and thermal motion effects, and to increase the precision of the results. The crystal and experimental data for all the compounds are summarized in Table 1. The structures were solved by direct (SHELXS-86, SIR-92, SIR-97)[23,24] and Patterson methods (DIRDIF-96),[25] and refined by full-matrix least squares on F^2 (SHELXL-97).[26] Intensity data of the silver-containing structures were corrected for absorption effects. All non-hydrogen atoms were refined anisotropically. The hydrogen atoms were located in idealized positions, and were refined using a riding model with fixed thermal parameters [U_{ij} = 1.2·U_{ij}(eq.) of the atom to which they are bonded]. CCDC-188495 to -188503 for compounds **2**, **3**, **6**, **7**, **9**, **10**, **11**, **12**, and **13**, respectively, contain the supplementary crystallographic data for this paper. These data can be obtained free of charge at www.ccdc.cam.ac.uk/conts/retrieving.html [or from the Cambridge Crystallographic Data Center, 12 Union Road, Cambridge CB2 1EZ, UK; Fax: (internat.) + 44-1223/336033; E-mail: deposit@ccdc.cam.ac.uk].

Acknowledgments

The authors thank the Israeli Science Foundation for support of this work.

[1] C. E. Housecroft, *Coord. Chem. Rev.* **1994**, *131*, 1−43.
[2] [2a] J. A. Marshall, K. G. Pinney, *J. Org. Chem.* **1993**, *58*, 7180−7184. [2b] J. A. Marshall, C. A. Sehon, *J. Org. Chem.* **1995**, *60*, 5966−5968. [2c] J. A. Marshall, M. A. Wolf, E. M. Wallace, *J. Org. Chem.* **1997**, *62*, 367−371.
[3] [3a] T. Hayashi, Y. Uozumi, A. Yamazaki, M. Sawamura, H. Hamashima, Y. Ito, *Tetrahedron Lett.* **1991**, *32*, 2799−2802. [3b] M. Sawamura, H. Hamashima, Y. Ito, *J. Org. Chem.* **1990**, *55*, 5935−5936.
[4] K. Burgess, H.-J. Lim, A. M. Porte, G. A. Sulikowski, *Angew. Chem. Int. Ed. Engl.* **1996**, *35*, 220−222.
[5] A. Yanagisawa, H. Nakashima, A. Ishiba, H. Yamamoto, *J. Am. Chem. Soc.* **1996**, *118*, 4723−4724.
[6] A. Yanagisawa, Y. Matsumoto, H. Nakashima, K. Asakawa, H. Yamamoto, *J. Am. Chem. Soc.* **1997**, *119*, 9319−9320.
[7] M. K. Eggleston, D. R. McMillan, K. S. Koenig, A. J. Pallenberg, *Inorg. Chem.* **1997**, *36*, 172−176.
[8] M. T. Miller, P. T. Gantzel, T. B. Karpishin, *Angew. Chem. Int. Ed.* **1998**, *37*, 1556−1558.
[9] N. Armaroli, *Chem. Soc. Rev.* **2001**, *30*, 113−124.
[10] S. Chowdhury, G. K. Patra, M. G. B. Drew, N. Chattopadhyay, D. Datta, *J. Chem. Soc., Dalton Trans.* **2000**, 235−237.
[11] E. C. Riesgo, Y.-Z. Hu, R. P. Thummel, D. V. Scaltrito, G. J. Meyer, *Inorg. Chem.* **2001**, *40*, 3413−3422.
[12] S. Panja, S. Chowdhury, M. G. B. Drew, D. Datta, *Inorg. Chem. Commun.* **2002**, *5*, 304−307.
[13] [13a] A. Deroche, I. Morgensteen-Badarau, M. Cesario, J. Guilhem, B. Kieta, L. Nadjo, C. H. Levin, *J. Am. Chem. Soc.* **1996**, *118*, 4567−4573. [13b] S. H. Gou, X. Z. You, K. B. Yu, *Inorg. Chem.* **1983**, *32*, 1883−1887. [13c] P. G. Sim, E. Sinn, *J. Am. Chem. Soc.* **1981**, *103*, 241−243.
[14] I. Morgensteen-Badarau, F. Lanbert, A. Deroche, M. Cesario, M. Cesario, J. Guilhem, B. Kieta, L. Nadjo, *Inorg. Chim. Acta* **1998**, *275−276*, 234−241.
[15] Ligand **4** is a 1:1 condensate of 2-thiophenecarboxaldehyde and ethylenediamine. If it is allowed to stand in solution for more than 48 h, however, we obtain only the bis(ethylenediamine)Cu^{II} complex [$Cu(en)_2$]$(CF_3SO_3)_2$.
[16] V. Vrabel, J. Garaj, J. Sivy, D. Oktavec, *Acta Crystallogr., Sect. C* **1999**, *55*, 1381−1383.
[17] K. Nakamato, in: *Infrared and Raman Spectra of Inorganic and Coordination Compounds*, 4 th ed., Wiley, New York, **1986**, section II.8.

[18] G. K. Patra, S. Samajdar, D. Datta, *J. Chem. Soc., Dalton Trans.* **2000**, 1555−1558.
[19] [19a] J. N. Demas, G. A. Crosby, *J. Phys. Chem.* **1971**, *75*, 991−1024. [19b] S. R. Meech, D. J. Phillips, *J. Photochem.* **1983**, *23*, 193−217.
[20] M. T. Miller, P. K. Gantzel, T. B. Karpishin, *Inorg. Chem.* **1998**, *37*, 2285−2290.
[21] P. Hemmerich, C. Sigwart, *Experientia* **1963**, *19*, 488−489.
[22] D. H. Busch, J. C. Bailor, *J. Am. Chem. Soc.* **1956**, *78*, 1137−1142.
[23] *SHELXS-86*; G. M. Sheldrick, *Acta Crystallogr., Sect. A* **1990**, *46*, 467−473.
[24] *SIR-92* and *SIR-97*: A. Altomare, M. C. Burla, M. Camalli, M. Cascarano, C. Giacovazzo, A. Guagliardi, G. Polidori, *J. Appl. Crystallogr.* **1994**, *27*, 435−436.
[25] P. T. Beurskens, G, Admiraal, G. Beurskens, W. P. Bosman, S. Garcia-Granda, R. O. Gould, J. M. M. Smits, C. Smykalla, *The DIRDIF-96 Program System*, Technical Report of the Crystallography Laboratory, University of Nijmegen, The Netherlands, **1996**.
[26] G. M. Sheldrick. *SHELXL-97, Program for the Refinement of Crystal Structures from Diffraction Data*, University of Göttingen, Germany, **1997**.

Received July 12, 2002
[I02383]

The Reactivity of an Iron(II)/Iron(III) System with Polyamine Ligands in Ethanol: An Electrochemical Study

Víctor M. Ugalde-Saldivar,[a] Martha E. Sosa-Torres,[a] and Ignacio González*[b]

Keywords: Iron / N ligands / Electrochemistry / Oxidative dehydrogenation / Disproportionation

The pentadentate ligand picdien [L_A; 1,9-bis(2′-pyridyl)-2,5,8-triazanonane)] and $[Fe(DMSO)_6](NO_3)_3$ produce the hexacoordinate coordination compound $[FeL'_B]^{2+}$ after reaction in ethanol. This compound shows a change in the oxidation state of Fe^{III} to Fe^{II} as well as an increase in the denticity of the starting ligand L_A. The new ligand L'_B {1,9-bis(2′-pyridyl)-5-[(ethoxy-2′-pyridyl)methyl]-2,5,8-triazanon-1-ene} has an imine carbon–nitrogen double bond. This study provides evidence for the nature of the intermediate species during the formation of $[FeL'_B](BPh_4)_2$. A systematic study was performed based on the evolution of the voltammograms observed after the addition of ligand (L_A, L_B) or base (LiOEt) to Fe^{III}, Fe^{II} solutions or stoichiometric metal-ligand mixtures (L_B is L'_B without the imine group). The stability of FeL_A^{3+} and FeL_A^{2+} species in acidic media and under nitrogen atmosphere was confirmed. The reactivity of FeL_B^{3+} and FeL_A^{3+} systems was found to be very similar, and the reduction products were found to be Fe^{II} species with simultaneous ligand oxidation, which, in both cases, produces an imine double bond, giving rise to an intramolecular redox reaction. The following disproportionation equation describes the general form of this process: $2\,FeL^{3+} \leftrightharpoons FeL^{2+} + FeL'^{2+} + 2\,H^+$. The oxidation was verified by the double bond formation in L_A and L_B giving rise to L'_A and L'_B as can be seen in the general equation: $R^1–CH_2–NH–R^2 \leftrightharpoons R^1–CH=N–R^2 + 2\,H^+ + 2e^-$. The disproportionation reaction for FeL_A^{3+} and FeL_B^{3+} species depends on the acidity level of the media: this reaction cannot be verified in acidic media, while neutral and slightly basic media favour formation of the Fe^{II} species with L'_A and L'_B.

(© Wiley-VCH Verlag GmbH & Co. KGaA, 69451 Weinheim, Germany, 2003)

Introduction

Oxidative dehydrogenation reactions of alcohols and amines are of great interest in biochemistry (e.g., alcohol dehydrogenase enzymes, galactose oxidase, amine oxidase) as well as in systems related to the protein degradation that contributes to aging. In addition, this type of reaction is of great importance in combustion cell operation. The nature of the products obtained in these reactions and the rates of their formation may vary depending on the reaction conditions, and are particularly strongly influenced by the presence of metallic ions. In the above-mentioned biochemical processes, the Zn^{II} is present in the active site of alcohol dehydrogenase enzyme, whereas Cu^{II} is found in galactose oxidase[1] and amine oxidase.[2] The Fe^{II} of metal-catalyzed oxidation (MCO) systems contributes to enzyme deterioration through dehydrogenation.[3] Amine oxidation may give rise to different products (including nitriles, nitro species and carbonylic compounds formed by insertion of highly reactive imine species formed during oxidation). The oxidation of amines and alcohols coordinated to metallic centers leads to quantitative formation of dehydrogenated products.[4] The nature of the metallic center plays a dominant role since the route followed by imine formation depends on it. Metallic ions available in high oxidation states govern the formation of compounds through radicals in a concerted two-electron reaction, with subsequent loss of two protons, as in the reaction of compounds of Ru^{II} [5–7] and Os^{II} [8,9] with ethylenediamine. When the metallic ion cannot reach high oxidation states, the reaction takes place only in the presence of strong oxidants, as in the reactions with compounds of Ni^{II} [10,11] and Cu^{II}.[12]

In the particular case of iron, most oxidation products of amines and coordinated polyamines are coordination compounds containing imines, and in some cases the final product is stable.[13] There are very few reports on this kind of compounds in which the ligand not only oxidizes, but also increases its size during the process of final compound formation.[14] Despite vast numbers of reports on electrochemical characterization in oxidative dehydrogenation reactions of coordination compounds with polyamines, almost none of them prove the stability of the coordination compounds formed during dissolution.[15,16]

[a] División de Estudios de Posgrado, Departamento de Química Inorgánica, edificio "B", Facultad de Química, UNAM, Cd. Universitaria, 04510 México, D. F. (México)
Fax: (internat.) + 52-55/56162010
E-mail: vmus@servidor.unam.mx
[b] Universidad Autónoma Metropolitana-Iztapalapa; Departamento de Química,
Apartado postal 55-534; C. P. 09340, México D. F. (México)
Fax: (internat.) + 52-55/58044666
E-mail: igm@xanum.uam.mx

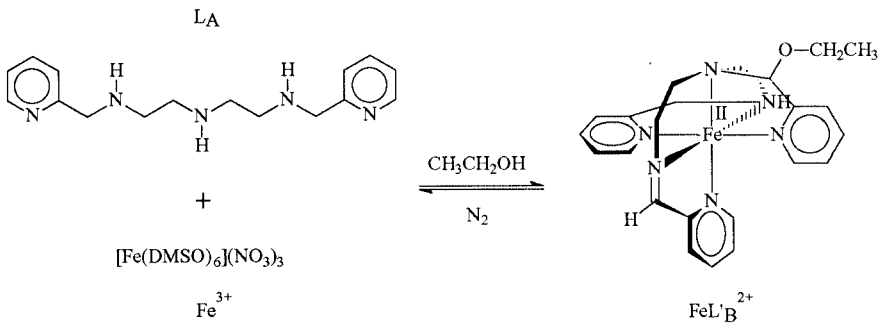

(1a)

Reports on Fe^{III} systems with polyamine ligands published by Morgenstern−Baradau et al.,[13] provide proof of an Fe^{III} system with a tripyridine ligand (TPAA) in which an internal redox reaction proceeds between the metallic ion and the ligand. However, the evidence reported to prove this process is the synthesis of three compounds: two Fe^{II} compounds with TPAA (reduced ligand) and one Fe^{II} compound with $(py)_3$tren (TPAA-oxidized ligand). The compounds were obtained by different procedures from previously isolated starting materials. The evidence presented in the study of possible intermediates formed during the reaction, whether in dissolved or solid form, was inconclusive and in others papers their presence is demonstrated using analytical techniques.[17,18] Few publications address iron(III) and iron(II) compounds with the particular case of pentadentate ligands. The high reactivity of iron(III) in this system produces oxidation reactions between the metallic ion and the coordinated ligand. An interesting example of this reactivity occurs between iron(III) and the ligand L_A {L_A=1,9-bis(2′-pyridyl)-2,5,8-triazanonane)}, in ethanol. When they are mixed in stoichiometric quantities, a reaction occurs whose final product is a coordination compound with a new hexadentate ligand (L'_B). A previous work describes synthesis of the compound in detail and the crystal structure of the final product.[14] An explanation for the unexpected formation of this compound is shown in the following reaction. In the general reaction [Equation (1a)], an electron exchange occurs between Fe^{III} and L_A to stabilize an iron(II) compound, and a new ligand (L'_B), which, besides having a double bond, (oxidation product) includes an additional pyridine ring forming a potentially hexadentate compound $[FeL'_B](BPh_4)_2$. In this work we describe the key steps of the redox reaction and analyze the electrochemical properties of the species formed in solution during this process.

The following equation summarizes the synthesis of the iron(II) compounds using the ligand L_A in the reaction conditions described (ethanol, 70 °C, N_2).

$$Fe^{III} + L_A \leftrightarrows Fe^{II}L'_B \quad (1b)$$

With:
L_A = 1,9-bis(2′-pyridyl)-2,5,8-triazanonane
L_B = 1,9-bis(2′-pyridyl)-5-[(ethoxy)(2′′-pyridyl)methyl]-2,5,8-triazanonane
L'_B = 1,9-bis(2′-pyridyl)-5-[(ethoxy)(2′′-pyridyl)methyl]-2,5,8-triazanon-1-ene

In the proposed reaction [Equation (1)], clarification of the final product of the redox process between the metallic ion and the ligand can be achieved using electrochemical techniques. The characteristics of the intermediates formed in the iron(III)-L_A reaction demand a complete study of dissolved species supported by electrochemical techniques. We performed a systematic evaluation using cyclic voltammetry to elucidate the complicated steps occurring during development of the global reaction described in Equation (1b).

Results and Discussion

Because the reaction in Equation (1) is so complex, it is difficult to perform a direct electrochemical study of the reaction mixture. We therefore proposed electrochemical characterization of the following mixtures: a) L_A·3HCl and $[Fe(DMSO)_6](NO_3)_3$, b) equimolar mixtures of L_A·3HCl and $[Fe(DMSO)_6](NO_3)_3$ and L_A·3HCl and $FeCl_2$, c) neutralization of a stoichiometric mixture of L_A·3HCl with $[Fe(DMSO)_6](NO_3)_3$, d) an equimolar mixture of L_B and $FeCl_2$, and e) an equimolar mixture of L_B and $[Fe(DMSO)_6](NO_3)_3$.

A half-wave potential ($E_{1/2}$) of 0.504 V vs. AgCl/Ag was obtained from the voltammogram of a ferrocene solution, and this was considered the reference system in all the voltammograms discussed below, according to IUPAC convention.[19]

a) Electrochemistry of a Mixture of L_A·3HCl and $[Fe(DMSO)_6](NO_3)_3$

L_A·3HCl (15.73 μmol) was dissolved in 5 mL of electrolyte support (0.1 M LiCl in ethanol) and the voltammograms were obtained at 100 mV·s^{-1} in the potential interval established by the electroactivity domain. Figure 1 (see a) shows a typical voltammogram for L_A·3HCl (3.145×10^{-3} M) obtained on a platinum electrode. When the potential scan was initiated in the negative direction, L_A·3HCl presented three well-defined reduction signals (I_C, II_C and III_C), and when the potential scan was reversed, three less-defined oxidation signals (I_A, II_A and III_A). When the potential scan was reversed after each cathodic peak, the corresponding anodic peak was well defined (not shown). We

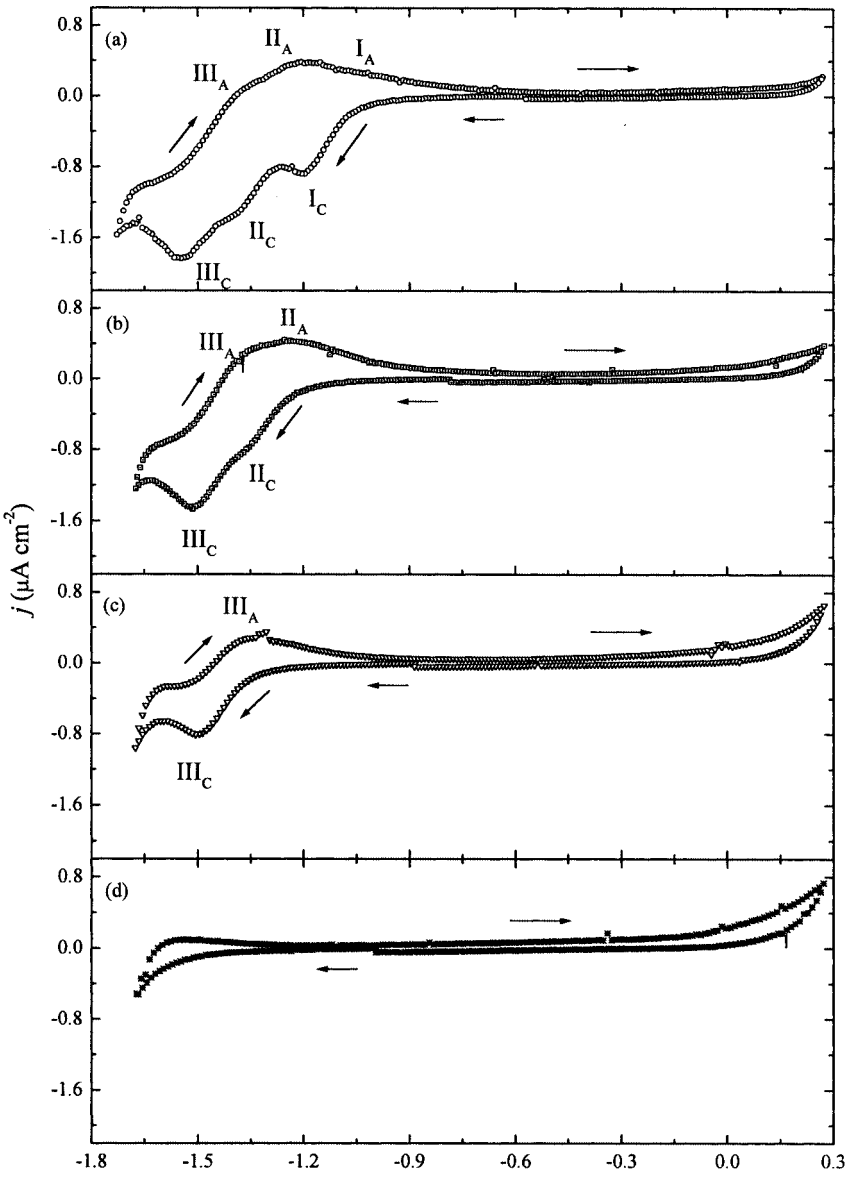

Figure 1. Typical cyclic voltammograms obtained for 15.73 μmol L_A·3HCl in 5 mL of ethanolic 0.1 M LiCl solution at 100 mV s^{-1} on a Pt electrode; the potential scan was initiated in the negative direction from $E_{j=0}$; the voltammograms were obtained after the addition of different quantities of lithium ethoxide: (a) −o− 0.0; (b) −□−15.72; (c) −▽− 31.45 and (d) −■− 47.17 μmol

propose as a preliminary hypothesis that the reductions are due to protons from the hydrochlorides located at the secondary amines of the ligand. To test this, we gradually added aliquots of a 0.524 M solution of LiOEt to 5 mL of a 3.145×10^{-3} M solution of L_A·3HCl. Figure 1 shows the voltammograms obtained when the potential scan was initiated in the negative direction for the L_A·3HCl solution and following several additions of LiEtO.

With the first additions of the LiEtO (15 and 30 μL, 15.72 and 31.45 μmol), the signal I_C decreased until it disappeared. The calculated equivalents added in 30 μL (15.72 μmol) coincide with neutralization of the first acid equivalent in the ligand (Figure 1, b). This observation was repeated for signals II_C and III_C with aliquot volumes of 60 and 90 μL (31.45 and 47.17 μmol), respectively (Figure 1, c and d, respectively). After the intensity of the cathodic peaks had diminished, the corresponding anodic peak was better defined (see Figure 1, c). Thus, we effectively proved that the signals observed correspond to the acidic protons of the ligand. We can thereby explain each of the reductions observed based on the following general electrochemical reaction:

$$H_nL_A^{3+} + e^- \leftrightarrows 1/2\ H_{2(g)} + H_{n-1}L_A^{2+} \quad \text{for } 1 \le n \le 3 \tag{2}$$

This equation confirms that the reduction signals are related to the acidic protons attached to the ligand. In addition, Figure 1 establishes that the neutral ligand is not elec-

troactive as testified by the absence of signals in the voltammogram corresponding to the addition of 90 μL (Figure 1, d). Equation (2) summarizes the different chemical and electrochemical steps and also the different chemical nature of the involved species [i.e. $H_{2(g)}$], and thus is not a reversible process. The difference of the anodic and cathodic peak potential and anodic−cathodic peak current ratio for each peak supports this fact.

An electrochemical study of a 10^{-3} M solution of iron(III) salt $[Fe(DMSO)_6](NO_3)_3$, used for synthesizing the final compound, was performed. A typical voltammogram of a reversible system was obtained, with one cathodic and anodic peak observed (not shown). We analyzed the half-sum of the peak potentials $[(Ep_C + Ep_A)/2]$ as a function of the logarithm of the scan rate (log v_B), observing a constant behavior, in this way the half-wave potential of Fe^{III}/Fe^{II} ($E_{1/2} = -0.546$ V vs. Fc^+/Fc) was obtained. The predominant Fe^{III} species in solution undergoes an electrochemical reaction as shown in the following equation:

$$Fe^{III} + 1e^- \leftrightharpoons Fe^{II}\ (E_{1/2} = -0.546\ \text{V vs. } Fc^+/Fc) \quad (3)$$

b) Electrochemistry of an Equimolecular Mixture of L_A·3HCl and $[Fe(DMSO)_6](NO_3)_3$ and L_A·3HCl and $FeCl_2$

Based on the independent assignment of signals detected for the ligand and iron(III) salt, we proceeded with an electrochemical study with an equimolar mixture of L_A·3HCl and $[Fe(DMSO)_6](NO_3)_3$ (5 μmol) at a concentration of 10^{-3} M in 5 mL of electrolyte support. Voltammograms were obtained initiating the potential scan in the positive direction and then in the negative direction while maintaining the same experimental conditions as for the previous experiments. Figure 2, curve a shows a voltammogram obtained for this solution when the potential scan was initiated in the positive direction; in the direct scan no oxidation signal was observed. In the reversed scan two reduction signals were observed (I''_C, II''_C) with cathodic peak potentials (Ep_C) of −0.540 and −1.126 V vs. Fc^+/Fc, respectively. The value of the current of the peak associated with I''_C is approximately one third that for II''_C. When the negative switching potential was reached ($E_{-\lambda} = -1.725$ V vs. Fc^+/Fc) and the potential scan was performed in the reverse direction, two oxidation signals were observed (II''_A, I''_A) with potential anodic peak values (Ep_A) of −0.913 and −0.401 V vs. Fc^+/Fc, respectively.

The signals I''_C and I''_A appear in the potential zone near the half-wave potential of the Fe^{III}/Fe^{II} system and for this reason we studied the half sum of the peak potentials $(Ep_C + Ep_A)/2$ as a function of the logarithm of the scan rate (log v_B). We observed a constant behavior for the $(Ep_C + Ep_A)/2$ value with $E_{1/2} = -0.470$ V vs. Fc^+/Fc. In this case, ΔEp_{A-C} (0.138 V) and the voltammetry function show a similar behavior to that of the Fe^{III}/Fe^{II} system.

The information obtained from the Fe^{III}/Fe^{II} system in the absence and presence of ligand L_A establishes that the kinetic electron-transfer behavior for both cases is similar, therefore the difference in $E_{1/2}$ is attributable to the formation of the Fe^{III} complex with L_A. Comparison of the voltammograms of the ligand alone (Figure 1, a) and in the presence of Fe^{III} (Figure 2, a) substantiate this assumption, since three initial reduction signals for the ligand are not observed. The initial complexing reaction could explain the formation of the proposed complex according to the following equation:

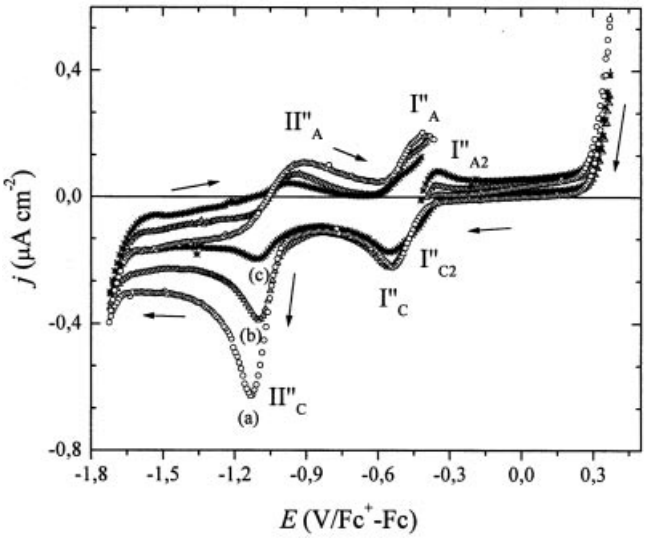

Figure 2. Typical cyclic voltammograms obtained for an equimolar mixture of L_A·3HCl and $[Fe(DMSO)_6](NO_3)_3$ (10^{-3} M) in ethanolic 0.1 M LiCl solution on a Pt electrode at 100 mV s^{-1}; the scan potential was initiated in the positive direction from $E_{j=0}$; the voltammograms were obtained after the addition of different quantities of lithium ethoxide: (a) −o− 0.0; (b) −Δ− 6.0 and (c) −■− 12.0 μmol

$$Fe^{3+} + H_3L_A^{3+} \leftrightharpoons FeL_A^{3+} + 3\,H^+ \quad (4)$$

According to Equation (4), these signals indicate formation of the coordination compound between Fe^{III} and L_A as formation of the FeL_A^{3+} compound increases the acidity of the protons localized in the ligand, producing a strong acid in solution with a concentration three times that of the compound, explaining the appearance of peak II''_C in Figure 2 (a). The new species in solution (FeL_A^{3+}) undergoes an electrochemical reduction reaction (I''_C) described by the following equation:

$$FeL_A^{3+} + 1e^- \leftrightharpoons FeL_A^{2+}$$
$$E_{1/2} = -0.470\ \text{V vs. } Fc^+/Fc \quad (5)$$

As a consequence, the electrochemical reaction for signal II''_C occurs according to the following equation:

$$H^+ + e^- \leftrightharpoons 1/2\ H_{2(g)}$$
$$E_{1/2} = -1.020\ \text{V vs. } Fc^+/Fc \quad (6)$$

The proton reduction [Equation (6)] is not reversible under the experimental conditions considered here despite the fact that it is not associated to L_A ligand. The voltammetric parameters of peak $II''_C-II''_A$ support this conclusion.

Although we still have to confirm that the species formed at the electrode following the reduction is the compound FeL_A^{2+}, we can determine that the difference in half-wave potentials for the Fe^{III}/Fe^{II} system in the absence and presence of L_A is 0.076 V. The shift toward more positive potentials is probably due to the fact that the complex of L_A with Fe^{II} has a greater stability constant than with Fe^{III}. This effect in the Fe^{III}/Fe^{II} system has been described previously when varying the ligand π acceptor and analyzing the effects on $E_{1/2}$ in different compounds.[20] A shift in the half-wave potential for this system can explain whether this is the effect of the ligand in the compound. The presence of strong π-acceptors in the ligand (two pyridine rings) allows the central metal ion to resist a greater electron density due to the cooperative effect of this type of ligand. Therefore, we expect coordination compounds with lower oxidation states to have greater formation constants (K_f). According to the Nernst law, we can predict a new half-wave potential for a system in which both species of the redox pair form stable coordination compounds [Equation (7)]

$$FeL_A^{3+} + 1e^- \cdots FeL_A^{2+}$$

$$E'_{1/2} = E^\circ_{1/2} - 0.058 \log\left[\frac{K_f^{Fe^{III}L_A}}{K_f^{Fe^{II}L_A}}\right] \quad (7)$$

Where $E^\circ_{1/2}$ corresponds to the conditional half-wave potential for the Fe^{III}/Fe^{II} redox pair in 0.1 M lithium chloride and in the absence of the ligand (L_A). Thus the values of $E_{1/2}$ for Fe^{III}/Fe^{II} and FeL_A^{III}/FeL_A^{II} allow us to determine the following equation.

$$\frac{K_f^{Fe^{III}L_A}}{K_f^{Fe^{II}L_A}} = 10^{0.95}$$

Under our experimental conditions (room temperature, ethanol, N_2 atmosphere), the compound FeL_A^{3+} is stable in solution. Nevertheless, the different methods used in attempting to separate out the solid product were unsuccessful.

Equation (5) proposes that the complex FeL_A^{2+} generated electrochemically is stable in solution and, therefore, it is important to use a mixture of L_A·3HCl with an Fe^{II} salt in this study in order to corroborate the presence of this complex.

As electrochemical proof of the formation of the FeL_A^{2+} complex, voltammograms were performed on a solution containing an equimolar mixture of $FeCl_2$ and L_A·3HCl (10^{-3} M; voltammograms not shown). As in Figure 2, curve a, we observed the same number of signals with very similar peak potentials; this confirms the stability of the FeL_A^{2+} species in solution. This conclusion is very important since there are no reports of coordination compounds of Fe^{III} and Fe^{II} with L_A and this could represent a feasible alternative for studying such compounds. The chemical structure of this compound (availability at the sixth position) lets us consider this redox pair for use in catalytic processes in homogeneous phase.

c) Electrochemistry of the Neutralization of an Equimolar mixture of L_A·3HCl with $[Fe(DMSO)_6](NO_3)_3$

During the synthesis reaction, L_A·3HCl is neutralized. We therefore performed a group of experiments with 5 mL of an equimolar metal-ligand mixture at 10^{-3} M (5 μmol) to which was added successive quantities of a 0.10 M LiOEt solution. Figure 2 shows the voltammograms for the initial mixture and after adding 60 and 120 μL (6 and 12 μmol) of LiOEt; in all cases the scan potential was initiated in the positive direction. When the base is added to the solution, the intensity of the reduction signals I''_C and II''_C decreases with increasing amounts of added base, with a greater decrease for the signal II''_C (Figure 2, b and c). We also observe an oxidation signal (I''_{A2}) corresponding to the formation of a new species in solution with an anodic peak potential of −0.351 V vs. Fc^+/Fc. The current values for some signals change as the quantity of added base increases. The oxidation signal I''_{A2} increases while the signals $I''_C-I''_A$, corresponding to the FeL_A^{3+}/FeL_A^{2+} pair, decrease. The changes in the current values for signal II''_C are explained by consumption of the H^+ species during neutralization. The peak-potential value of signal I''_{A2} is more positive than for the FeL_A^{3+}/FeL_A^{2+} system, and for this reason the new signal I''_{A2} suggests formation of a new iron complex with a more positive redox potential under the new acidic conditions. The voltammogram obtained in the absence of added LiEtO shows no oxidation signals of Fe^{II} in the potential interval −0.35 to 1.00 V vs. Fc^+/Fc (Figure 2, a), confirming that only Fe^{III} is present initially in solution as the species FeL_A^{3+}.

Since the study was carried out under an inert atmosphere in the absence of oxygen and only the compounds FeL_A^{3+} and LiCl in ethanol were present in solution, we propose that the ligand L_A is responsible for the reduction via an intramolecular redox reaction. The formation of imines (oxidation) in coordination compounds with this type of ligand has been described in the literature, with a subsequent reduction of the different metal ions, for example cobalt,[21] copper,[17] iron,[13,15,22] nickel,[10,23−27] osmium,[8,9,28−31] platinum[32] and ruthenium.[5−7,16,33−45] To explain this global process we must consider the following:

a) Oxidation of the ligand is a process requiring two electrons. The following equation expresses the general form of the reaction:

$$R^1-CH_2-NH-R^2 \leftrightarrows R^1-CH=N-R^2 + 2\,H^+ + 2e^-$$
$$L_A \leftrightarrows L'_A + 2H^+ + 2e^- \quad (8)$$

b) The reduction of the Fe^{III} species is a single-electron process described by the reaction below:

$$Fe^{III} + 1e^- \leftrightarrows Fe^{II} \quad (9)$$

c) The reaction explaining the overall neutralization process must consider that the FeL_A^{3+} species contains the oxidant (Fe^{III}) and the reductant (L_A). The stoichiometry of the reaction is 2:1 (Fe^{III}:L_A) such that the general form of the intramolecular redox reaction can be represented by the following equation:

$$2\ FeL_A^{3+} \leftrightarrows FeL_A^{2+} + FeL'_A{}^{2+} + 2\ H^+ \quad (10)$$

The above equation describes a disproportionation reaction that is similar to that reported previously,[46,47] and justifies the observed changes, demonstrating that the equilibrium shifts to favour formation of the Fe^{II} species as the H^+ concentration decreases (neutralization). It also explains the transformation of the Fe^{III} species to give rise to two new Fe^{II} species. To confirm this mechanism, we added a slight excess of LiOEt (18 μmol) relative to the initial H^+ concentration (15 μmol) and performed voltammograms under the same conditions as before. The initial scan of the voltammogram obtained in the negative direction (Figure 3, a) shows no reduction signals in the interval −0.40 to −1.00 V vs. Fc^+/Fc. The inverse scan shows only two signals, one for oxidation I''_{A2} and the other for reduction I''_{C2}. The absence of reduction signals in the initial scan confirms the hypothesis proposed in Equation (10) for the quantitative transformation of the initial FeL_A^{3+}. When the voltammogram is performed initiating the potential scan in the positive direction (not shown), two signals were also observed

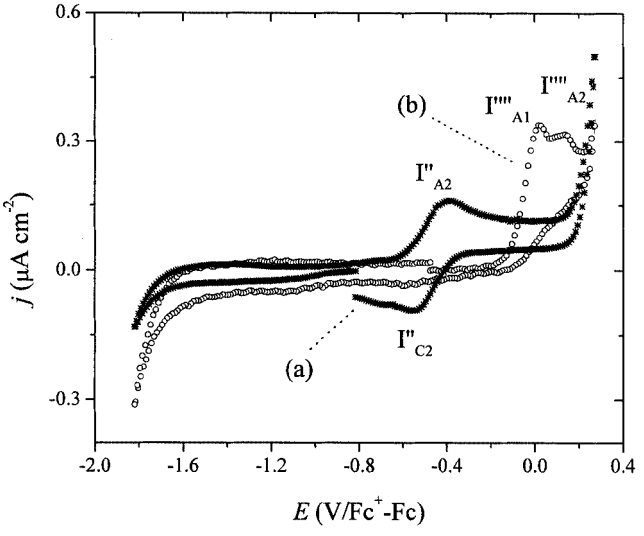

Figure 3. Typical cyclic voltammograms obtained in 5 mL of ethanolic 0.1 M LiCl solution on a Pt electrode at 100 mV s^{-1}; the voltammograms were obtained when the scan potential was initiated from $E_{j=0}$ for different solutions: (a) −■− a mixture of 5 μmol of L_A·3HCl, 5 μmol of $[Fe(DMSO)_6](NO_3)_3$ and 18 μmol of LiEtO (the scan potential was initiated in the negative direction), and (b) −o− 10^{-3} M of $[FeL'_B](BPh_4)_2$ (the scan potential was initiated in the positive direction)

(I''_{A2}, I''_{C2}) as in Figure 3 (a). A comparison of Figure 3 (a) and Figure 2, curve b−c, demonstrates that, under these conditions, only the Fe^{II} complex is present in solution.

We can therefore conclude that the decrease in the intensity of signal II''_C is due to neutralization of the protons formed as products of the complexation reaction. The simultaneous disappearance of the Fe^{III} reduction signal and the appearance of oxidation signals prove that the compound FeL_A^{3+} is chemically transformed into two new Fe^{II} species through a redox process in solution. The redox pair responsible for signals I''_A and I''_C is FeL_A^{3+}/FeL_A^{2+}, and the electrochemical process is described by Equation (5). The signals I''_{A2} and I''_{C2} are explained by the formation of the new species, $FeL'_A{}^{2+}$, through the electrochemical oxidation process described in the following equation:

$$FeL'_A{}^{2+} \leftrightarrows FeL'_A{}^{3+} + 1e^-\ E_{1/2} = -0.365\ \text{V vs. } Fc^+/Fc \quad (11)$$

In the new species, $FeL'_A{}^{2+}$, L'_A represents oxidized picdien (containing an imine group). According to Equation (5) and (11), the half-wave potential for the redox pairs resulting from the disproportionation are very close in value. This explains the breadth of the signal and the observation of a single peak for both species FeL_A^{2+} and $FeL'_A{}^{2+}$ in the voltammogram of Figure 3 (a).

Thereby, the increase in half-wave potential observed for the final product $FeL'_A{}^{2+}$ results principally from an increase in the π-acceptor character of the new ligand (L'_A), giving a conjugated double bond π system between the imine and the pyridine ring. We thus conclude that FeL_A^{3+} is the precursor to $FeL'_A{}^{2+}$ produced by a disproportionation reaction [Equation (10)], favoured at neutral and slightly alkaline pH where the compound $FeL'_A{}^{2+}$ is thermodynamically favored.

To prove that $FeL'_A{}^{2+}$ indeed corresponds to the coordination compound of $FeL'_B{}^{2+}$ (L'_B = oxidized form of ligand L_B), we performed an additional experiment. Figure 3, curve b shows the voltammogram of 5 μmol of $[FeL'_B](BPh_4)_2$ dissolved in 5 mL of electrolyte support; $[FeL'_B](BPh_4)_2$ is the final product isolated in the original synthesis. When the potential scan was initiated in the positive direction, two irreversible oxidation signals, I''''_{A1} and I''''_{A2}, appeared with peak-potential values of 0.075 and 0.158 V vs. Fc^+/Fc, respectively. There is a huge difference between this voltammogram and the one obtained for the neutralized mixture of Fe^{III}-L_A (Figure 3, a), establishing that the $FeL'_A{}^{3+}/FeL'_A{}^{2+}$ system is far from being the final product isolated in the $[FeL'_B](BPh_4)_2$ synthesis process and should be considered an intermediate under the general reaction [Equation (1)].

The end product of the synthesis displays a very different electrochemical behaviour and the voltammograms of the neutralized mixture evolve a wide variety of signals over time which are extremely difficult to explain. Therefore, we used an analogous system to complement our studies in the hope of reproducing this electrochemical behaviour. We proceeded to characterize the Fe^{III}/Fe^{II} system electrochemically with a ligand similar in characteristics to that obtained as the major product of the reaction, in this case ligand L_B, (see Scheme 1).

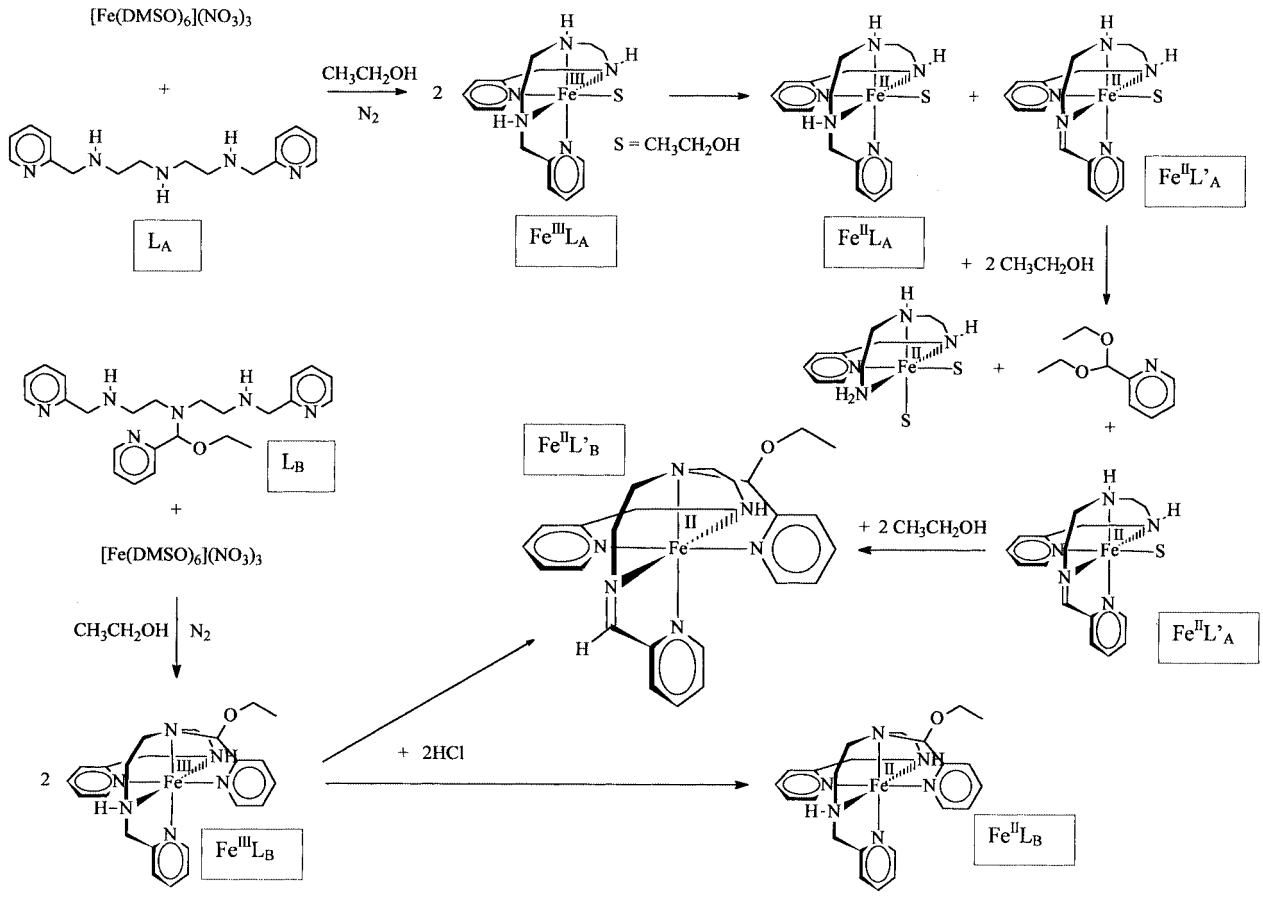

Scheme 1

Synthesis of the ligand L_B begins with formation of the ketal of 2-pyridinecarboxylaldehide in situ followed by addition of the neutral ligand L_A in ethanol to form the compound L_B. This synthetic strategy shows that L_B has a similar reactivity with Fe^{III} as that discussed up to now for Fe^{III} and L_A. We describe the details of these experiments below. Unlike the previous experiments with $L_A \cdot 3HCl$, the new ligand L_B was used in its neutral form.

d) Electrochemistry of an Equimolar Mixture of L_B and $FeCl_2$

We performed a cyclic voltammetric study using 5 mL of a 3×10^{-3} M $FeCl_2$ solution (15 μmol) in electrolyte support to which 250 μL of a 0.06 M L_B (15 μmol) solution was added. The cyclic voltammogram (not shown) obtained when the potential scan was initiated in the positive direction showed a reversible redox system with $E_{1/2} = -0.409$ V vs. Fc^+/Fc. Voltammograms for the mixture were performed initiating the potential scan in the negative direction; none of the voltammograms show a reduction signal for any Fe^{III}-containing species at the start of recording (−0.500 to −1.100 V). In this case the reversible redox system is assigned to the complex FeL_B^{2+} formed in solution. The new species in solution follows the electrochemical reaction described below:

$$FeL'_B{}^{2+} \leftrightharpoons FeL'_B{}^{3+} + 1e^- \quad (12)$$
$$E_{1/2} = -0.409 \text{ V vs. } Fc^+/Fc$$

The FeL_B^{2+} species is stable under the experimental conditions and no change in the oxidation state of the initial Fe^{II} species in solution is observed. The half-wave potential difference between the Fe^{III}/Fe^{II} and FeL_B^{3+}/FeL_B^{2+} systems produces a value of 0.121 V, with the FeL_B^{3+}/FeL_B^{2+} system potential shifting toward more positive values. Nonetheless, the electrochemical behavior of the new system does not explain the signals observed for the compound $[FeL_B](BPh_4)_2$ (Figura 3, b), and for this reason we carried out further experiments with L_B and Fe^{III}.

e) Electrochemistry of an Equimolar Mixture of $[Fe(DMSO)_6](NO_3)_3$ and L_B

The electrochemical study was carried out with an equimolar mixture of $[Fe(DMSO)_6](NO_3)_3$ and L_B (5 mmol) in 5 mL of electrolyte support. Voltammograms were obtained beginning the potential scan in the negative direction (Figure 4, a) and then in the positive direction (Figure 4, b). The signals assigned to the system FeL_B^{3+}/FeL_B^{2+}, ($I'_{A3}-I'_{C3}$) present a half-wave potential of −0.428 V vs. Fc^+/Fc.

When the potential scan is initiated in the positive direction (Figure 4, b), unlike the previous recording, an oxidation signal, I'_{A3}, was observed indicating the presence of an

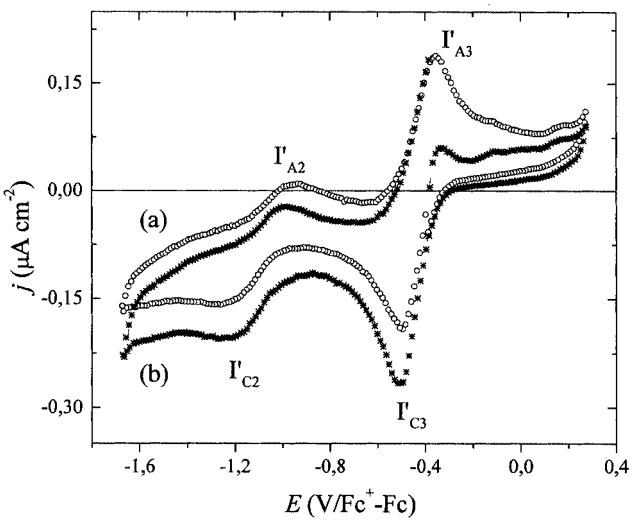

Figure 4. Typical cyclic voltammograms obtained for a fresh equimolar mixture of $[Fe(DMSO)_6](NO_3)_3$ and L_B, (10^{-3} M) in ethanolic 0.1 M LiCl solution on a Pt electrode at 100 mV s^{-1}; the potential was initiated from $E_{j=0}$ in different directions: (a) −o− negative direction and (b) −■− positive direction.

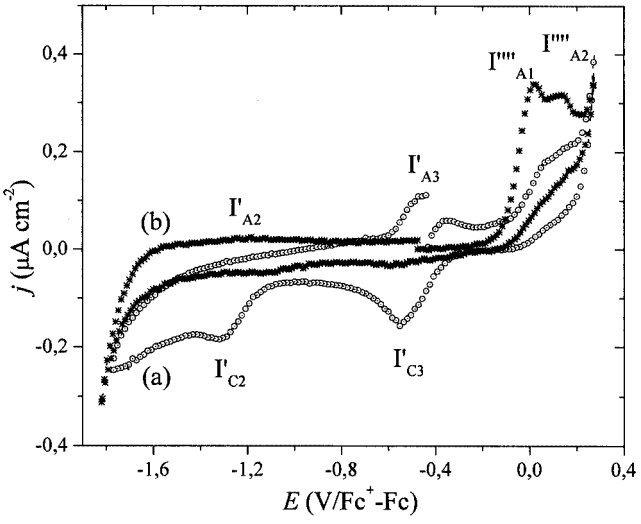

Figure 5. Typical cyclic voltammograms obtained in ethanolic 0.1 M LiCl solution on a Pt electrode at 100 mV s^{-1}; the scan potential was initiated in the positive direction from $E_{j=0}$; the voltammograms were obtained for different solutions: (a) −o− mixture of L_B and $[Fe(DMSO)_6](NO_3)_3$ (10^{-3} M each one), 12 h further mixing and (b) −■− 10^{-3} M $[FeL'_B][B(Ph)_4]_2$

Fe^{II} species in solution. In addition, a reduction signal (I'_{C2}) was present at a peak potential of −1.246 V, with its corresponding oxidation signal I'_{A2} at −0.976 V. The presence of an Fe^{II} species is more obvious (signal I'_{A3}). Although it is not clearly observed, we propose the existence of additional oxidation signals within the −0.10 to 0.2 V potential interval.

These observations and the proposal of Equation (10) suggest that the FeL_B^{3+} species undergoes a similar disproportionation reaction as the FeL_A^{3+} species, involving an oxidation of the ligand L_B with a simultaneous reduction of Fe^{III} to Fe^{II}. The equation below describes this disproportionation.

$$2FeL_B^{3+} \leftrightharpoons FeL_B^{2+} + FeL'_B{}^{2+} + 2H^+ \quad (13)$$

In this case L_B' represents the oxidized ligand (imine), and the species H^+, appearing as a product of the reaction, explains the reduction signal (I'_{C2}) at −1.246 V. A decrease of the Fe^{III} reduction signal along with the presence of oxidation signals demonstrates that the compound FeL_B^{3+} is chemically transformed into two new Fe^{II} species by a redox process in solution. The electrochemical reaction for the redox pair FeL_B^{3+}/FeL_B^{2+} occurs according to Equation (12).

For the Fe^{III}-L_B system, the variation in the concentration of species in solution over time determines the evolution of the voltammograms. To study these variations, an electrochemical study was performed 12 hours after preparing the mixture, initiating the potential scan in the positive direction (Figure 5, a). The recording shows the oxidation signal I'_{A3} and two new oxidation signals, I''''_{A1} and I''''_{A2}, at peak-potential values of 0.075 and 0.158 V vs. Fc^+/Fc (Figure 5, a). When the cycle was complete, the signals described coincided with those described previously in Figure 4. The reduction signal I'_{C2} at −1.246 V increased its current over time while the signal corresponding to the FeL_B^{3+}/FeL_B^{2+} system decreased. These observations confirm the reaction proposed in Equation (13) and, in this particular case, the products of the disproportionation reaction have very different electrochemical properties. It is therefore possible to distinguish the two Fe^{II} species formed. For the FeL_B^{2+} species, the half-wave potential is −0.428 V vs. Fc^+/Fc. The signals with Ep_A = 0.075 and Ep_A = 0.158 V vs. Fc^+/Fc are assigned to the $FeL'_B{}^{2+}$ species. To prove this, this voltammogram was compared with the one shown in Figure 3 (b), where the signals assigned to the complex ion $FeL'_B{}^{2+}$ (Figure 5, b) coincide sufficiently well with the peak-potential values of the isolated product $[FeL'_B](BPh_4)_2$.

We have thus shown that the reactivity of ligands L_A and L_B in the presence of Fe^{II} and Fe^{III} is very similar, and that for Fe^{III} an intramolecular reaction occurs involving a redox process in solution between the ligand and the metal. Scheme 1 shows the key steps proposed for the formation of $[FeL'_B](BPh_4)_2$ based on the stability of the species demonstrated in this work.

Conclusions

A systematic study based on evolution of voltammograms following addition of ligand (L_A, L_B) or base (LiOEt) to solutions containing Fe^{III}, Fe^{II} or stoichiometric metal-ligand mixtures was performed. This study provides evidence for the nature of the intermediate species in the process of formation of $[FeL'_B](BPh_4)_2$. An intramolecular redox process between Fe^{III} and the ligand is demonstrated when the cyclic voltammograms are initiated in the null current potential and by comparing voltammograms when the po-

tential scan is initiated in both positive and negative directions.

The stability of the FeL_A^{3+} and FeL_A^{2+} species in acidic media and under nitrogen atmosphere was confirmed. Since no prior evidence exists of solid state compounds existing with the complex ions mentioned here, the electrochemical technique used herein to demonstrate their existence and stability is fundamental.

The reactivity of the systems FeL_B^{3+} and FeL_A^{3+} was shown to be very similar and the products of the reduction are Fe^{II} species with simultaneous oxidation of the ligand, which, in both cases, produces the formation of an imine double bond, giving rise to an intramolecular redox reaction. The following equation describes the general form of this process.

$$2\ FeL^{3+} \leftrightarrows FeL^{2+} + FeL'^{2+} + 2\ H^+$$

The oxidation is verified by formation of the double bond in L_A and L_B giving rise to L_A' and L_B' as explained by the general equation below.

$$R^1{-}CH_2{-}NH{-}R^2 \leftrightarrows R^1{-}CH{=}N{-}R^2 + 2\ H^+ + 2\ e^-$$

The reduction revealed by the change in oxidation state from Fe^{III} to Fe^{II} due to a single-electron process establishes the proportion of metal to ligand at 2:1 to complete the exchange and thus justify the presence of two different Fe^{II} species. For L_B the compounds identified show very different electrochemical behaviors.

The disproportionation reaction depends on the acidity level of the reaction medium. When this medium is acidic, the disproportionation of the FeL_A^{2+} and FeL_B^{2+} species cannot be verified, while neutral and slightly basic media favor formation of the Fe^{II} species with L'_A and L'_B.

Experimental Section

Synthesis of $[FeL'_B](BPh_4)_2$

The reaction was carried out as described in a previous paper.[14] 20% product yield. $C_{72}H_{70}B_2FeN_6O$: calcd. C 77.71, H 6.34, N 7.55; found C 77.21, H 6.55, N 7.39.

Synthesis of Ligand L_B: This reaction was carried out by mixing three equivalents of lithium hydroxide in ethanol with one equivalent of the ligand trihydrochloride ($L_A{\cdot}3HCl$). After neutralization, one equivalent of 2-pyridylcarboxaldehyde was added while maintaining the reaction mixture temperature at 60−70 °C for one hour. Thin-layer chromatography was performed for the mixture, eluting with methanol/chloroform/hexane (1:5:3), to verify that the aldehyde had reacted completely.

Electrochemistry: 0.10 M LiCl dissolved in absolute ethanol was used as electrolyte support in the electrochemical studies. A Pt disc (0.0314 cm^2) was used as the working electrode, a Pt wire as the auxiliary electrode and $KCl_{(sat)}/AgCl_{(S)}/Ag$ was used as the reference electrode. The working electrode (Pt) was polished with alumina assuring the absence of surface residues. All voltammograms were initiated from the null current potential ($E_{j=0}$) and the scan was initiated in both positive and negative potential directions. In order to report the potentials used according to IUPAC convention,[19] voltammograms were obtained for approximately 10^{-3} M ferrocene (Fc) in electrolyte support. For the working conditions, the electroactive domain was between −1.726 and 0.274 V vs. Fc^+/Fc.

Acknowledgments

The authors are very grateful to financial support to the DGAPA-UNAM IN117200 and to CONACyT 4292-E. VMUS thanks to CONACyT for the PhD scholarship.

[1] G. A. Hamilton, P. K. Adolf, J. de Jersey, G. C. DuBois, G. R. Dyrkacz, J. Libby, *J. Am. Chem. Soc.* **1978**, *10*, 1899−1912.
[2] J. P. Klinman, *Chem. Rev.* **1996**, *96*, 2541−2561.
[3] E. Stadtman, *Science* **1992**, *257*, 1220.
[4] R. F. Keene, *Coord. Chem. Rev.* **1999**, *187*, 121−149.
[5] B. C. Lane, J. E. Lester, F. Basolo, *J. Chem. Soc., Chem. Commun.* **1971**, 1618−1619.
[6] D. F. Mahoney, J. K. Beattie, *Inorg. Chem.* **1973**, *12*, 2561−2565.
[7] P. Bernhard, D. J. Bull, H. B. Büri, P. Osvath, A. Roselli, A. S. Sargeson, *Inorg. Chem.* **1997**, *36*, 2804−2815.
[8] F. P. Dwyer, J. W. Hogart, *J. Am. Chem. Soc.* **1955**, *77*, 6152−6154.
[9] F. P. Dwyer, J. W. Hogart, *J. Am. Chem. Soc.* **1953**, *75*, 1008−1009.
[10] E. K. Barefield, D. H. Bush, *Inorg. Chem.* **1971**, *10*, 108−114.
[11] V. L. Goedken, D. H. Bush, *Inorg. Chem.* **1971**, *10*, 2679−2682.
[12] N. F. Curtis, *Coord. Chem. Rev.* **1968**, *3*, 3.
[13] I. Morgenstern-Baradau, F. Lambert, J. P. Renault, M. Cesario, J. D. Marechal, F. Maseras, *Inorg. Chim. Acta* **2000**, *297*, 338−350.
[14] V. M. Ugalde-Saldívar, M. E. Sosa-Torres, L. A. Ortiz-Frade, S. Bernès, H. Höpfl, *J. Chem. Soc., Dalton Trans.* **2001**, 3099−3107.
[15] F. R. Keene, D. J. Salmon, T. J. Meyer, *J. Am. Chem. Soc.* **1976**, *98*, 1884−1889.
[16] M. Goto, M. Takeshita, N. Kanda, T. Sakai, V. L. Goedken, *Inorg. Chem.* **1985**, *24*, 582−587.
[17] D. C. Olson, J. Vasilevskis, *Inorg. Chem.* **1971**, *10*, 463−470.
[18] M. J. Ridd, D. J. Gakowski, G. E. Sneddon, F. R. Keene, *J. Chem. Soc., Dalton. Trans.* **1992**, 1949−1956.
[19] G. Gritzner, J. Küta, *Pure Appl. Chem.* **1984**, *4*, 462.
[20] P. N. Howker, M. V. Twigg, *Comprehensive in Inorganic Chemistry* **1981**, 44.1, 1179.
[21] C. J. Raleigh, A. E. Martell, *Inorg. Chem.* **1985**, *24*, 142−148.
[22] V. L. Goedken, *J. Chem. Soc., Chem. Commun.* **1972**, 207−208.
[23] E. K. Barefield, M. T. Mocella, *J. Am. Chem. Soc.* **1975**, *97*, 4238−4246.
[24] P. Morliere, L. K. Patterson, *Inorg. Chem.* **1982**, *21*, 1833−1837.
[25] P. Maruthamuthu, L. K. Patterson, G. Ferraudi, *Inorg. Chem.* **1978**, *17*, 3157−3163.
[26] M. Jaacobi, D. Meyerstein, J. Lilie, *Inorg. Chem.* **1979**, *18*, 429−433.
[27] N. F. Curtis, *J. Chem. Soc. A.* **1971**, 2834−2838.
[28] P. A. Lay, A. M. Sargeson, *Inorg. Chim. Acta* **1992**, *198*, 449−459.
[29] P. A. Lay, A. M. Sargeson, B. W. Skelton, A. H. White, *J. Am. Chem. Soc.* **1982**, *104*, 6161−6164.
[30] P. A. Lay, *PhD thesis*, Australian National University, **1981**.
[31] F. R. Keene, P. A. Lay, G. E. Sneddon, G. W. Whebell, *Aust. J. Chem.* **1993**, *46*, 1763−1774.
[32] F. Schwarz, H. Schöllhorn, U. Thewalt, B. Lippert, *J. Chem. Soc., Chem. Commun.* **1990**, 1282−1284.
[33] W. R. Mc Whinnie, J. D. Miller, J. B. Watts, D. Y. Wadden, *J. Chem. Soc., Chem. Commun.* **1971**, 629−630.
[34] D. F. Mahoney, J. K. Beattie, *Inorg. Chem.* **1973**, *12*, 2561−2565.

[35] S. E. Diamond, G. M. Tom, H. Taube, *J. Am. Chem. Soc.* **1975**, *97*, 2661−2664.
[36] K. Y. Wong, C. M. Che, C. K. Li, W. H. Chiu, Z. Y. Zhou, T. C. W. Mak, *J. Chem. Soc., Chem. Commun.* **1992**, 754−756.
[37] M. J. Ridd, F. R. Keene, *J. Am. Chem. Soc.* **1981**, *103*, 5733−5746.
[38] F. R. Keene, M. J. Ridd, M. R. Snow, *J. Am. Chem. Soc.* **1983**, *105*, 7075−7081.
[39] P. A. Adcock, F. R. Keene, R. E. Smhyte, M. R. Snow, *Inorg. Chem.* **1984**, *23*, 2336−2343.
[40] G. W. Whebell, F. R. Keene, *Aust. J. Chem.* **1986**, *39*, 2027−2035.
[41] V. E. Alvarez, R. J. Allen, T. Matsubara, P. C. Ford, *J. Am. Chem. Soc.* **1974**, *96*, 7686−7692.
[42] J. D. K. Miller, J. B. Watts, D. Y. Waddan, *Inorg. Chim. Acta* **1975**, *12*, 267−272.
[43] G. M. Brown, T. R. Weaver, F. R. Keene, T. J. Meyer, *Inorg. Chem.* **1976**, *15*, 190−196.
[44] Y. B. Hoshino, F. Okuyama, A. Nanba, K. Shimizu, G. P. Sato, *Bull. Chem. Soc. Jpn.* **1992**, *65*, 876−881.
[45] P. Bernhard, D. B. Bull, H. B. Burgi, P. Osvath, A. Raselli, A. M. Sargeson, *Inorg. Chem.* **1997**, *36*, 2804−2815.
[46] C. E. Li, P. Krumholz, *Inorg. Chem.* **1974**, *13*, 519−524.
[47] S. E. Diamond, G. M. Tom, H. Taube, *J. Am. Chem. Soc.* **1975**, *97*, 2661−2664.

Received July 16, 2002
[I02389]

Synthesis, X-ray Studies and Magnetic Properties of Dinuclear Ni^{II} and Cu^{II} Complexes Bridged by the Azo-2,2′-bipyridine Ligand

Cristian S. Campos-Fernández,[a] José R. Galán-Mascarós,*[b] Bradley W. Smucker,[a] and Kim R. Dunbar*[a]

Keywords: Magnetic properties / Azo compounds / Nickel / Copper

Two new paramagnetic transition metal complexes that contain the bridging ligand azo-2,2′-bipyridine (abpy) have been prepared and characterized by X-ray crystallography and magnetic susceptibility measurements. The compound $[Ni_2(\mu\text{-abpy})(CH_3CN)_2(NO_3)_4]\cdot 2CH_3CN$ (**1**·2CH_3CN) crystallizes in the triclinic space group $P\bar{1}$ with a = 8.290(5) Å, b = 8.343(5) Å, c = 11.180(5) Å, α = 105.36(3)°, β = 94.39(3)°, γ = 107.56(3)°, V = 700.5(7) Å^3 and Z = 1. The related salt $[Cu_2(\mu\text{-abpy})(CH_3CN)_8][BF_4]_4$ (**2**) crystallizes in the triclinic space group $P\bar{1}$ with a = 10.240(2) Å, b = 10.597(2) Å, c = 10.712(2) Å, α = 64.23(3)°, β = 78.21(3)°, γ = 78.57(3)°, V = 1026.7(3) Å^3 and Z = 1. Solutions of **2** eventually produce the polymeric Cu^I compound $\{[Cu(\mu\text{-abpy})][BF_4]\}_\infty$ (**3**) which was also crystallographically characterized: monoclinic space group $P2_1/n$, with a = 9.295(2) Å, b = 9.541(2) Å, c = 13.486(3) Å, β = 91.58(3)°, V = 1195.5(4) Å^3 and Z = 4. The magnetic properties of these dinuclear paramagnetic complexes have been studied in detail, and have provided an opportunity for probing the ability of this ligand to mediate magnetic exchange interactions between paramagnetic metal centers. Compound **1** exhibits antiferromagnetic exchange interactions (J = −7.5 cm^{-1}) whereas the magnetic interactions in compound **2** were found to be negligible.

(© Wiley-VCH Verlag GmbH & Co. KGaA, 69451 Weinheim, Germany, 2003)

Introduction

The redox and spin-state properties of transition metal complexes render them attractive candidates for applications in many areas including molecular electronics, information recording, and catalysis.[1−3] One approach for the preparation of metal compounds with enhanced properties is to use organic ligands that engage in π-interactions with metal ions. In our quest for such ligands to use in assemblies of paramagnetic metal ions, we recently prepared families of transition metal complexes based on the nitrogen heterocyclic ligands 3,6-bis(2-pyridyl)-1,2,4,5-tetrazine (bptz)[4,5] and 1,4,5,8,9,11-hexaazatriphenylene (HAT).[6] By controlling parameters such as the identity of the anions in reactions of metal cations with bptz, for example, we have demonstrated that one can deliberately prepare different cyclic oligomers, such as molecular squares[4,6] or molecular pentagons.[5] Despite the interesting supramolecular aspects of this work, our main goal, namely to induce magnetic interactions between the paramagnetic metal ions in these molecules, was not achieved. This is primarily due to the fact that the bptz and HAT bridging ligands position the metal centers at greater distances than is reasonable for the observation of strong magnetic coupling. In considering this problem, we turned to the azo-2,2′-bypyridine (abpy) ligand (Figure 1) which offers several obvious advantages over the previous ligands, one of which is the fact that it is possible to prepare the one-electron reduction species $abpy^{-\cdot}$ to use as a radical bridging ligand. It is well-known that the use of a paramagnetic bridge is advantageous for improving magnetic superexchange between metal centers,[7−19] but we reasoned that even the diamagnetic neutral form of abpy may allow for magnetic interactions due to the short distances between metal ions afforded by the azo bridging group. Monomeric and dimeric complexes of this ligand with 3d metals have been reported,[20] although their magnetic properties have only been briefly described for several monomeric complexes and for the dimers $[(\mu\text{-abpy})Co_2Cl_4]$ and $[(\mu\text{-abpy})Co_2(hfacac)_4]$ [hfacac = bis(hexafluoroacetylacetonate)].[21,22] We postulated that the shorter path could give rise to stronger magnetic interactions between spin carriers than the previously mentioned polynitrogen ligands, which require a four-atom separation between metals. There is, in fact, evidence that the abpy ligand allows for electronic communication between metals,[23−25] as illustrated by the redox behavior of the compound [(bpy)Ru(μ-abpy)Ru-

[a] Department of Chemistry, Texas A&M University,
P. O. Box 30012, College Station, Texas 77842-3012, USA
Fax: (internat.) + 1-979/845-7177
E-mail: dunbar@mail.chem.tamu.edu
[b] Instituto de Ciencia Molecular, Universidad de Valencia,
Dr. Moliner, 50, Burjassot 46100, Spain
Fax: (internat.) + 34-96/386-4859
E-mail: jose.r.galan@uv.es

(bpy)][PF_6]$_4$ which exhibits a comproportionation constant K_c of more than 10^8. This value corresponds to a class III delocalized system on the Robin and Day scale.[26]

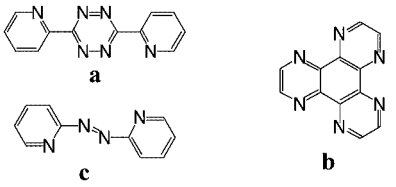

Figure 1. Scheme of the polynitrogen ligands: (a) 3,6-bis(2-pyridyl)-1,2,4,5-tetrazine (bptz); (b) 1,4,5,8,9,11-hexaazatriphenylene (HAT); (c) azo-2,2′-bipyridine (abpy)

With all the aforementioned premises in mind, we embarked on a study of the nature of azo-2,2′-bypyridine (abpy) as a bridge between magnetic ions of the first row transition metals. Three compounds were isolated and characterized in this work, namely two magnetic dinuclear compounds of Ni^{II} and Cu^{II}, and a diamagnetic Cu^{I} polymer.

Results and Discussion

Syntheses

The reactions between Ni^{II} and Cu^{II} ions with abpy proceed instantaneously in acetonitrile to afford the products [Ni_2(abpy)(CH_3CN)$_2$(NO_3)$_4$] (**1**) and [Cu_2(abpy)(CH_3CN)$_8$][BF_4]$_4$ (**2**) in good yields. In marked contrast to previous reports, which concluded that a large activation barrier exists for the coordination of a second metal center after the first metal is bound,[17] the formation of the dinuclear species is facile in these cases. Crystals of [Ni_2(abpy)(CH_3CN)$_2$(NO_3)$_4$] were obtained by slow vapor-diffusion of diethyl ether into the reaction mixture, whereas crystals of [Cu_2(abpy)(CH_3CN)$_8$][BF_4]$_4$ (**2**) were obtained by saturating the solution with diethyl ether and chilling it to −10 °C. The Cu^{II} compound [Cu_2(abpy)(CH_3CN)$_8$][BF_4]$_4$ (**2**) eventually decomposes to the Cu^{I} polymer {[Cu(abpy)][BF_4]$_2$}$_\infty$ (**3**) over a period of several months in toluene/acetonitrile. The identity of the reducing agent is unknown.

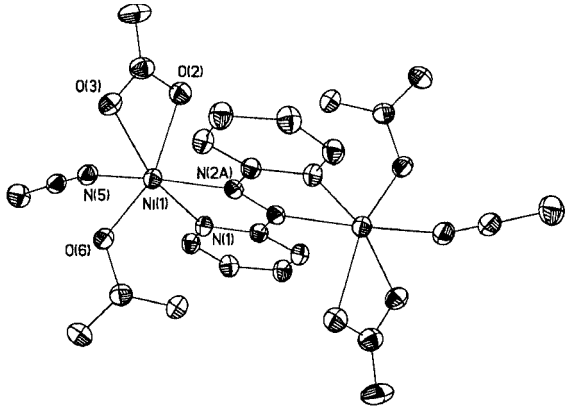

Figure 2. Thermal ellipsoid diagram (50% probability) for the dimer [Ni_2(abpy)(CH_3CN)$_2$(NO_3)$_4$] (**1**)

Electrochemical Studies

The cyclic voltammogram of **1** in acetonitrile exhibits two oxidation features at $E_{p,a}$ = +0.62V and $E_{p,a}$ = +0.4V, with no associated return waves. In addition, there are three reversible reductions located at $E_{1/2}$ = −0.10 V, $E_{1/2}$ = −0.4 V and at $E_{1/2}$ = −0.9 V. The dinuclear Cu^{II} compound **2** also exhibits a rich electrochemistry with an irreversible oxidation located at $E_{p,a}$ = +1.10 V, a reversible oxidation at $E_{1/2}$ = +0.65 V, and two reversible reductions at $E_{1/2}$ = +0.40 V and $E_{1/2}$ = 0.0 V. The fact that these reductions occur at positive potentials vs. Ag/AgCl explains why the formation of **3** is so facile.

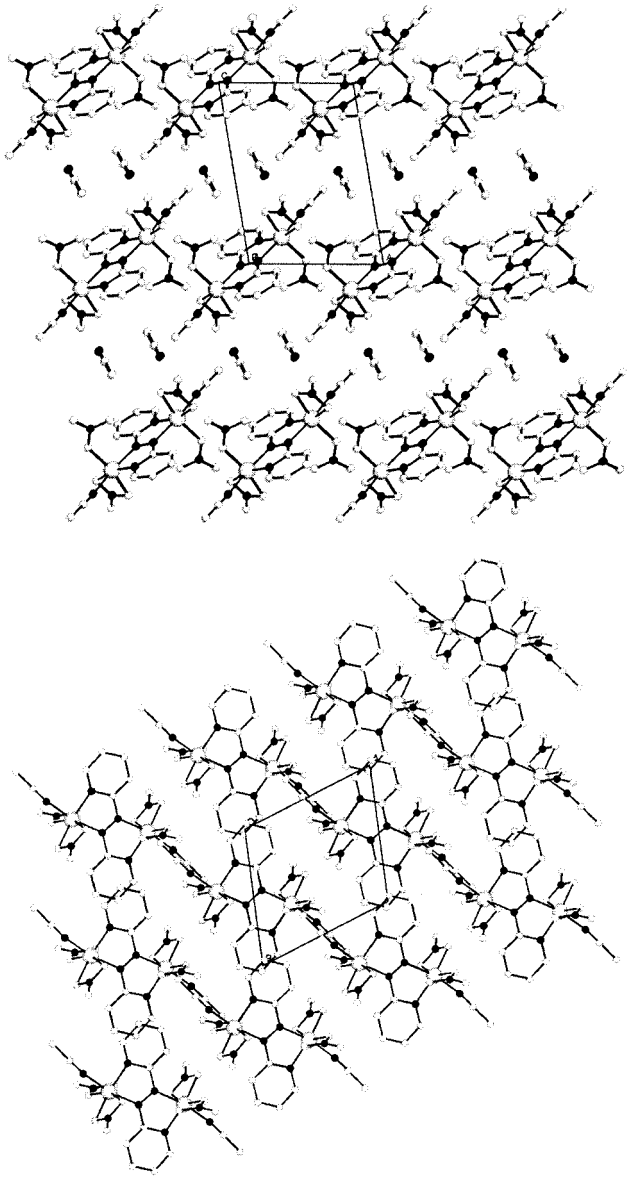

Figure 3. Projection of the packing diagram for [Ni_2(abpy)(CH_3CN)$_2$(NO_3)$_4$]·2CH_3CN (**1**·2CH_3CN) on the *ac* plane (top) and on the *bc* plane (bottom)

X-ray Crystallographic Studies

[Ni$_2$(abpy)(CH$_3$CN)$_2$(NO$_3$)$_4$]·2CH$_3$CN (1)

Crystals of [Ni$_2$(abpy)(CH$_3$CN)$_2$(NO$_3$)$_4$]·2CH$_3$CN (**1**·2CH$_3$CN) contain Ni^{II} ions in a distorted octahedral geometry (Figure 2). Each Ni center is coordinated to two [NO$_3$]$^-$ ligands — one of which acts as a bidentate ligand — as well as to an acetonitrile molecule and the bridging abpy ligand. The distortion from perfect octahedral geometry is most likely a consequence of the small bite angle of the chelating nitrate anion, which leads to an acute O−Ni−O angle of 61.43(8)° and Ni−O distances of 2.125(2) and 2.105(2) Å. The shortest Ni−L bond is with the monodentate nitrate ligand [1.990(2) Å]. The Ni−N distance to the acetonitrile ligand is 2.044(2) Å, which is essentially the same as the distance in the homoleptic solvated cation [Ni(CH$_3$CN)$_6$]$^{2+}$. The Ni−N(azo) interaction is the longest of the three Ni−N interactions [Ni(1)−N(2) = 2.121 (2) Å]. The angles within the coordination sphere also provide some helpful insight into the distortion of the ligand environment of this compound. The angle between the pyridyl and the acetonitrile ligand is close to the ideal value for an octahedron [N(5)−Ni(1)−N(1) = 93.80(2)°]. The binding angle of abpy [N(1)−Ni(1)−N(2) = 76.45(9)°] is very close to the values observed for bptz in [Ni$_2$(bptz)(CH$_3$CN)$_8$][ClO$_4$]$_4$,[4] which contains a bridging interaction involving N atoms from a pyridyl nitrogen and the tetrazine ring to give an N−Ni−N angle of 78.10 (3)°. The two Ni atoms are 4.942 Å apart, which is much shorter than the corresponding distance of 6.904 Å in [Ni$_2$(bptz)(CH$_3$CN)$_8$][ClO$_4$]$_4$. An important feature to note in the structure of **1** is the elongation of the N=N bond in the bridging abpy ligand by 0.025 Å [N(2)−N(2#) = 1.271(4) Å) relative to the corresponding distance in free abpy (1.246 Å).[27] This lengthening is indicative of π back-donation from the Ni^{II} centers into the empty π* (abpy) orbitals. This effect has been noted for a complex of abpy with Cu^I as well.[27]

In terms of intermolecular interactions, the Ni$_2$ molecules form pseudo-tetragonal layers in the *ab* plane, with solvent molecules occupying the interstices (Figure 3). There are no short contacts between the molecules, with the Ni···Ni intermolecular contacts being greater than 6 Å.

[Cu$_2$(abpy)(CH$_3$CN)$_8$][BF$_4$]$_4$ (2)

The structure of [Cu$_2$(abpy)(CH$_3$CN)$_8$][BF$_4$]$_4$ (**2**) contains the tetracationic Cu$_2$ unit, [Cu$_2$(abpy)(CH$_3$CN)$_8$]$^{4+}$, since the Cu^{II} centers are coordinated only by neutral ligands. The Cu^{II} centers exhibit a typical axial Jahn−Teller distortion, with the elongated axis oriented along the azo and acetonitrile interactions [azo: Cu(1)−N(1) 2.401(4) Å and CH$_3$CN: Cu(1)−N(12) 2.313(5) Å] (Figure 4). The other four coordination sites are filled by three acetonitrile molecules at an average Cu(1)−N distance of 2.01(5) Å, and the pyridyl ring [Cu(1)−N(2) 2.040(5) Å]. The L−Cu−L angles are distorted from the ideal octahedral values, with N(1)−Cu(1)−N(13) and N(1)−Cu(1)−N(2) being 107.0(2)° and 71.5(2)°, respectively. As noted for the Ni analogue, the longer N=N distance in the azo group [1.277 (1) Å] is indicative of π back-donation. The Cu^{II} centers are separated by a distance of 5.408 Å, which is longer that the corresponding value in the Ni^{II} compound; this situation is a consequence of the Jahn−Teller distortion.

In the Cu^{II} structure, the 3D arrangement is best described as consisting of mixed anion-cation layers in the *ab* plane separated by [BF$_4$]$^-$ anions (Figure 5). In this structure, the presence of the anions increases the intermolecular distances, with all Cu···Cu intermolecular distances being longer than 8 Å.

{[Cu(abpy)][BF$_4$]}$_\infty$ (3)

The Cu^I species,{[Cu(abpy)][BF$_4$]}$_\infty$ (**3**) is a 1-D polymer consisting of Cu^I ions connected along the *a* axis (Figure 6). The Cu^I centers exhibit a distorted tetrahedral geometry

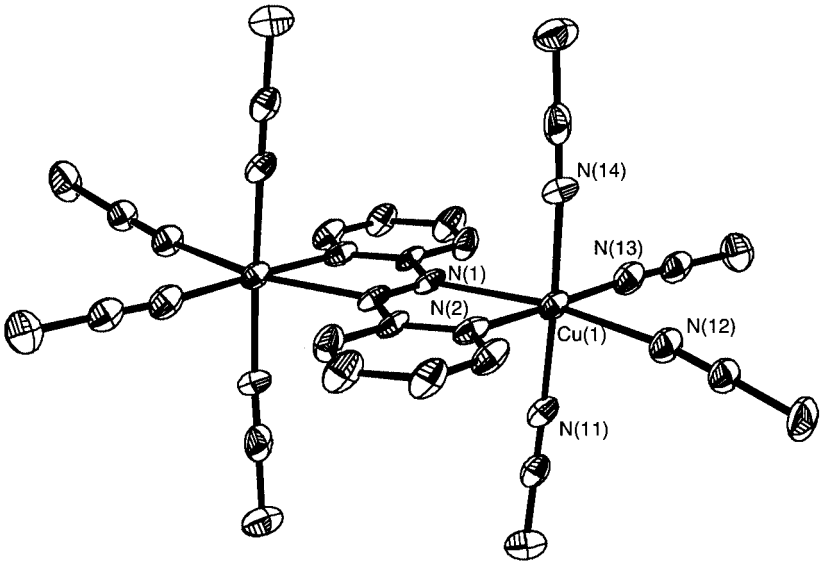

Figure 4. Thermal ellipsoid diagram (50% probability) for the dimer [Cu$_2$(abpy)(CH$_3$CN)$_8$]$^{4+}$ (**2**)

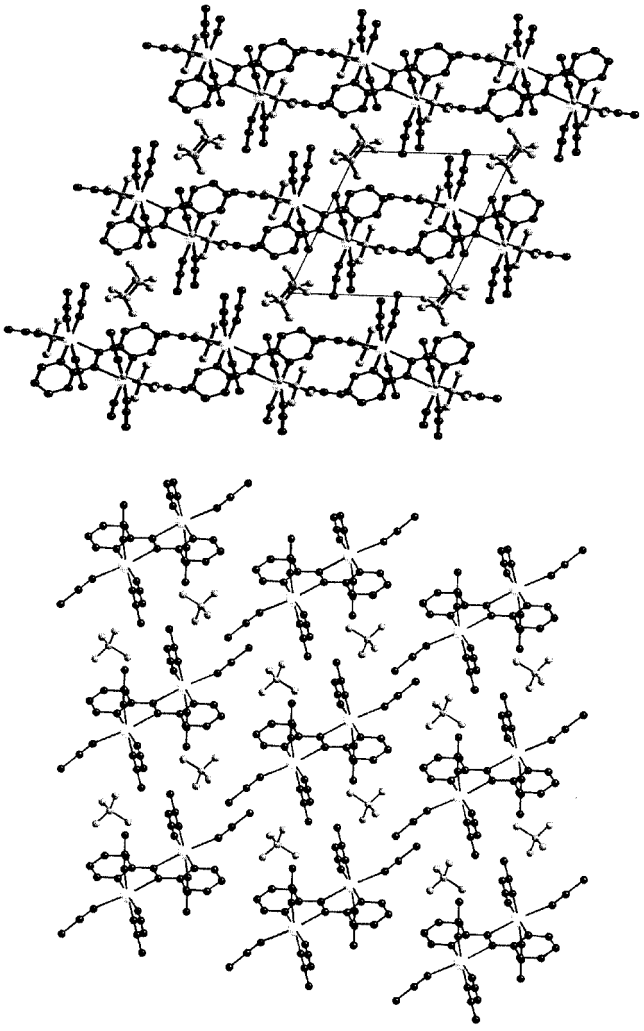

Figure 5. Projection of the packing diagram for $[Cu_2(abpy)(CH_3CN)_8][BF_4]_4$ (**2**) on the *bc* plane (top) and of the structure of one of the layers (bottom)

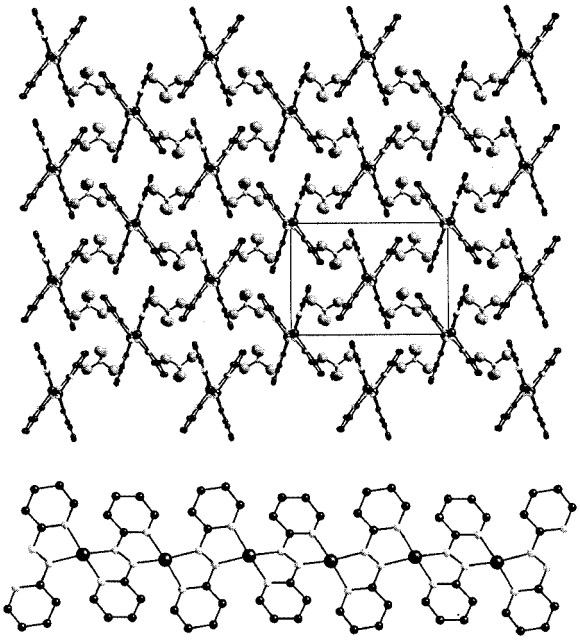

Figure 6. Projection of the packing diagram for $\{[Cu(abpy)][BF_4]\}_\infty$ (**3**) on the *bc* plane (top) and of the structure of one of the chains perpendicular to the *bc* plane (bottom)

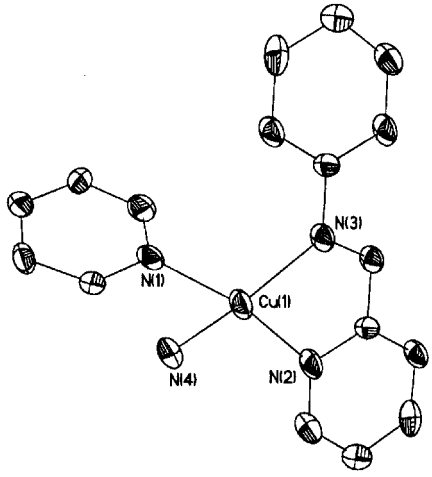

Figure 7. Thermal ellipsoid diagram (50% probability) for the monomeric building block of the $\{[Cu(abpy)]\}_\infty$ chain

(Figure 7), with the main distortions being observed due to the bite angles of the abpy ligand: N(1)−Cu(1)−N(4) = 77.7 (3)°, and N(2)−Cu(1)−N(3) = 79.4 (3)°. These angles are far from the ideal 109.5° for a tetrahedral geometry. The N(3)−N(3#) distance of 1.29(2) Å indicates that the azo group is obviously involved in appreciable π back-donation from the Cu^I, as expected for an electron-rich d^{10} center. The N=N distance is 0.054 Å longer in this compound than in free abpy, which is nearly twice the lengthening noted for the Ni^{II} and Cu^{II} complexes. The 1-D chains pack in a pseudo-hexagonal arrangement, with the counterions occupying the interstices afforded by the packing of the chains (Figure 6).

Magnetic Properties

Magnetic susceptibility measurements were performed on $[Ni_2(abpy)(CH_3CN)_2(NO_3)_4]$ (**1**) and $[Cu_2(abpy)(CH_3CN)_8][BF_4]_4$ (**2**) at 1000 G. Compound **1** shows a $\chi_m T$ value at room temperature (2.17 emu·K·mol^{-1}) that is close to the expected spin-only value for two magnetically dilute Ni centers. The $\chi_m T$ value remains constant down to 200 K (Figure 8), and then shows a steady decrease which is indicative of the presence of antiferromagnetic interactions between the $S = 1$ Ni^{II} centers. The χ versus T graph depicted in Figure 9 shows a broad maximum at 18 K which is an obvious indication that the azo bridging ligand promotes antiferromagnetic interactions. This magnetic behavior was analyzed with an isotropic model for a Ni^{II} dimer. From the Hamiltonian: $H = -2J\,(S1 \cdot S2)$ where $S1 = S2 = S_{Ni} = 1$, a simple expression of χ_m was derived, to which an additional paramagnetic contribution was added [Equation (1)].

The best fit to the experimental data was obtained for $g = 2.03$ and $J = -7.5$ cm^{-1}. The paramagnetic term ($C = 0.075$) accounts for about 4% of monomer impurity in the sample.

$$\chi_m = \frac{3g^2\,(2e^{2J/T}+10e^{6J/T})}{8T(1+3e^{2J/T}+5e^{6J/T})} + \frac{C}{T} \quad (1)$$

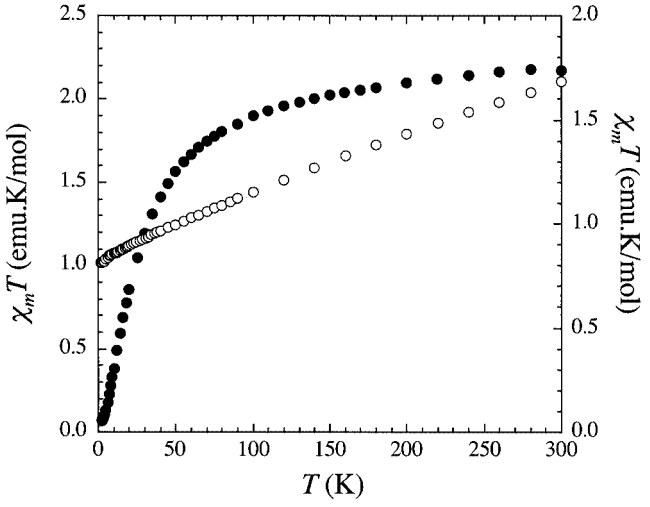

Figure 8. Plot of the $\chi_m T$ product vs. T for $[Ni_2(abpy)(CH_3CN)_2(NO_3)_4]\cdot 2CH_3CN$ (**1**, full circles) and $[Cu_2(abpy)(CH_3CN)_8][BF_4]_4$ (**2**, empty circles)

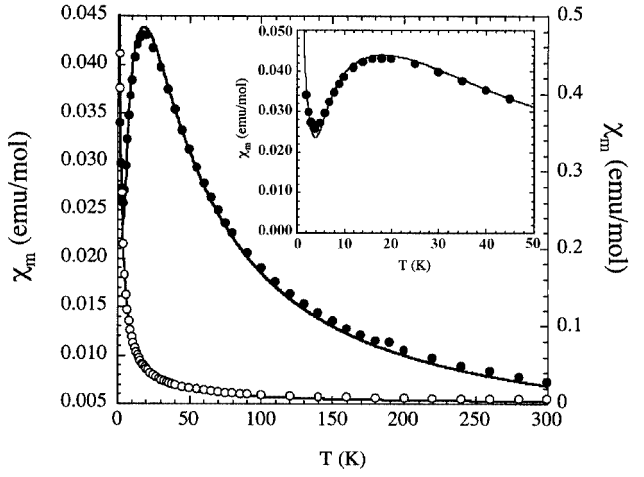

Figure 9. Plot of χ_m vs. T for $[Ni_2(abpy)(CH_3CN)_2(NO_3)_4]\cdot 2CH_3CN$ (**1**, full circles) and $[Cu_2(abpy)(CH_3CN)_8][BF_4]_4$ (**2**, empty circles); the corresponding lines represent the best fit obtained in each case

Compound **2** exhibits a $\chi_m T$ value (Figure 8) of 1.6 emu·K·mol^{-1} at room temperature, as compared to the expected spin-only value of 0.75 emu·K·mol^{-1} (for $g = 2$). The $\chi_m T$ plot gradually decreases with temperature and reaches a minimum value of 0.81 emu·K·mol^{-1} at 1.8 K. This behavior suggests the presence of a TIP (temperature-independent paramagnetism). The absence of a maximum in χ_m indicates that the magnetic interaction through the abpy ligand is small in this case. Indeed, the χ_m versus T graph (Figure 9) shows a typical exponential paramagnetic behavior. The data were fitted to a model for a Cu^{II} dimer, analogous to the one used for the Ni case, including a TIP contribution instead of a paramagnetic impurity contribution. From the expression derived for the susceptibility [Equation (2)], the fitting led to values of $g = 2.09$ and $J = -0.05$ cm^{-1}, and a TIP of 4×10^{-3} emu·mol^{-1}. These results support the conclusion that the interaction is essentially negligible in the Cu^{II} compound.

$$\chi_m = \frac{3g^2(2e^{2J/T})}{8T(1+3e^{2J/T})} + \chi_{TIP} \quad (2)$$

The fact that the magnetic interaction between Cu^{II} centers through the abpy ligand is much weaker than the corresponding interaction between Ni^{II} centers can be rationalized on the basis of geometrical considerations of the magnetic orbitals involved in the interaction, in addition to the longer distance between metal centers, when compared to the one observed for the Ni dimer. The X-ray studies reveal that the Cu^{II} centers exhibit a Jahn−Teller distortion of the axial elongation type along the N atoms of the azo group. The magnetic orbital therefore is $d_{x^2-y^2}$ which is orthogonal to the azo interaction. One would expect that superexchange through the pyridine ring and across the azo group to the adjacent pyridine ring would be very poor. Conversely, in the case of the Ni_2 compound both e_g orbitals are singly-occupied and there is no Jahn−Teller distortion. The improved overlap of the magnetic orbitals on the Ni^{II} ions with the N atoms of the bridging abpy ligand would be expected to lead to improved magnetic superexchange; this is corroborated by the magnetic measurements.

Conclusion

Two new paramagnetic dinuclear molecules were prepared by the reaction of Ni^{II} and Cu^{II} ions with the azo-2,2′-bypyridine (abpy) ligand. The compounds $[Ni_2(abpy)(CH_3CN)_2(NO_3)_4]$ and $[Cu_2(abpy)(CH_3CN)_8][BF_4]_4$ were fully characterized by X-ray crystallography, electrochemistry, electronic spectroscopy and magnetic susceptibility. The abpy ligand acts as a bridge between paramagnetic Ni^{II} and Cu^{II} centers in both cases and promotes antiferromagnetic interactions between the $S = 1$ Ni^{II} centers but does not provide a good pathway for superexchange in the $S = 1/2$ Cu^{II} dinuclear molecule. The different magnetic behavior can be explained by the fact that the Cu^{II} compound exhibits a Jahn−Teller distortion that leads to poor overlap of the magnetic orbitals through the bridging ligand.

The magnetic results allow for consideration of whether superexchange will be efficient through the abpy ligand. The antiferromagnetic exchange observed in the Ni^{II} compound is of the same order of magnitude found for ligands such as oxalate[28,29] and 2,2′-bipyrimidine.[30,31] On the ba-

Table 1. Crystallographic data and refinement parameters

	1·2CH_3CN	**2**	**3**
Formula	$C_{18}H_{20}N_{12}Ni_2O_{12}$	$C_{26}H_{32}B_4Cu_2F_{16}N_{12}$	$C_{10}H_8BCuF_4N_4$
Molecular weight	713.88	986.96	334.56
Space group	$P\bar{1}$	$P\bar{1}$	$P2_1/n$
Temperature (K)	110(2)	110(2)	110(2)
a (Å)	8.290(5)	10.240(2)	9.295(2)
b (Å)	8.343(5)	10.597(2)	9.541(2)
c (Å)	11.180(5)	10.712(2)	13.486(3)
α (deg)	105.357(5)	64.23(3)	90
β (deg)	94.387(5)	78.21(3)	91.58(3)
γ (deg)	107.564(5)	78.57(3)	90
V (Å^3)	700.5(7)	1026.7(3)	1195.5(4)
Z	1	1	4
ρ_{calc} (g/cm^3)	1.692	1.596	1.859
μ (Mo-K_α) (cm^{-1})	14.25	11.46	18.71
Reflections total/unique	8160/3252	7358/3484	11151/2040
$I > n\sigma$	2	4	4
Reflections/parameters	2815/199	2887/309	1096/133
R_1	0.0416	0.0662	0.0833
wR_2	0.1054	0.1688	0.2028
Goodness-of-fit	1.087	1.021	0.973

sis of this study, we conclude that the abpy ligand will be useful for the design of a range of magnetically interesting molecules and materials.

Experimental Section

General Remarks: All operations were performed under a nitrogen atmosphere using standard Schlenk-line techniques, unless otherwise indicated. Solvents were distilled prior to use from the appropriate drying agents. Acetonitrile was distilled from over 3 Å molecular sieves, whereas toluene and diethyl ether were distilled from over a Na/K amalgam. The reagent $Ni(NO_3)_2{\cdot}6H_2O$ was purchased from Aldrich and used without further purification. The compound $[Cu(CH_3CN)_4][BF_4]_2$ was synthesized according to published methods.[32] IR spectra were measured as Nujol mulls between KBr plates on a Nicolet 740 FT-IR spectrometer. Magnetic susceptibility measurements were performed in the range of 2−300 K with a Quantum Design SQUID magnetometer MPMS-XL. All measurements were performed on polycrystalline samples. Data were corrected for diamagnetic contributions calculated from Pascal constants.[33] The cyclic voltammetric studies were performed on a CH Instruments Electrochemical Analyzer in acetonitrile containing 0.1 M tetra-*n*-butylammonium hexafluorophosphate ([TBA][PF_6]) as the supporting electrolyte. The working electrode was a BAS Pt disk electrode, the reference electrode was Ag/AgCl and the counter electrode was a Pt wire. The Cp_2Fe/Cp_2Fe^+ couple occurs at +0.52 V vs. Ag/AgCl under the same experimental conditions.

$[Ni_2(abpy)(CH_3CN)_2(NO_3)_4]$ (1): A sample of $Ni(NO_3)_2{\cdot}6H_2O$ (100 mg, 0.34 mmol) was dissolved in 30 mL of acetonitrile to give a pale green solution which was stirred until the entire solid had dissolved, after which time abpy (32 mg, 0.17 mmol) was added. The resulting intensely green solution was stirred for 4 additional hours and then concentrated to 10 mL. Slow vapor diffusion of diethyl ether into the reaction solution afforded dark green crystals within 6 days. Yield = 80 mg (75%). IR (KBr): $\tilde{\nu}$ = 2724 cm^{-1} (w), 1620 (w), 1147 (w), 1039 (w), 1022 (w), 801 (w), 722 (w). UV/Vis (acetonitrile, $c = 9.8 \times 10^{-6}$ M): λ = 344 nm [$\varepsilon = 1.8 \times 10^4$ L(mol·cm)$^{-1}$].

$[Cu_2(abpy)(CH_3CN)_8][BF_4]_4$ (2): A sample of $[Cu(CH_3CN)_4][BF_4]_2$ (100 mg, 0.249 mmol) was dissolved in 20 mL of acetonitrile and treated with abpy (22 mg, 0.124 mmol). A color change from blue to pale green quickly ensued. The reaction mixture was stirred overnight, concentrated and treated with diethyl ether to the point of saturation. Light green platelet crystals of **2** were obtained by placing the solution in the freezer at −4 °C for a week. Yield = 82 mg (80%). IR (KBr): $\tilde{\nu}$ = 2724 cm^{-1} (w), 2296 (w), 2323 (w), 1589 (w), 1261 (w), 1229 (w), 1027 (br,s), 805 (w), 722 (w). UV/Vis (acetonitrile, $c = 8.0 \times 10^{-6}$ M): λ = 351 nm [$\varepsilon = 2.7 \times 10^4$ L(mol·cm)$^{-1}$], 230 [$\varepsilon = 1.98 \times 10^4$ L(mol·cm)$^{-1}$].

$\{[Cu(abpy)][BF_4]\}_\infty$ (3): A solution of **2** in acetonitrile layered with toluene produced dark green needle-like crystals of **3** after a period of one month.

X-ray Crystallographic Study: The X-ray data sets were collected on a SMART 1 K area detector diffractometer equipped with graphite monochromated Mo-K_α radiation (λ = 0.71073 Å). The frames were integrated with the Siemens SAINT[34] software package and the data were corrected for absorption using the SADABS program.[35] The structures were solved using the direct-methods programs SHELXS-97 (**1** and **3**),[36] and SIR97 (**2**). Crystal parameters and basic information pertaining to data collection and refinement are summarized in Table 1.

A dark green prismatic crystal of **1** was secured on the tip of a glass fiber with Dow Corning silicone grease and placed in a cold N_2(g) stream at 110 (2) K. A total of 8160 reflections were collected of which 3252 were unique. The final refinement cycle was based on 2815 reflections with $F_0 > 2\sigma(F_0)$ ($R1$ = 0.0416 and $wR2$ = 0.1054).

A light green platelet of **2** was secured on the tip of a glass fiber with Dow Corning silicone grease and placed in a N_2(g) stream at 110 (2)K. The data collection involved a total of 7358 reflections of which 3484 were unique. The final refinement cycle was based

on 2887 reflections with $F_0 > 4\sigma(F_0)$ that were used to fit 309 parameters which led to $R1 = 0.0662$ and $wR2 = 0.1688$. The goodness-of-fit index is 1.021, and the highest peak in the final difference map is 1.195 $e^-\cdot Å^3$.

A green needle-like crystal of **3** was covered with Paratone oil, secured on the tip of a glass fiber with Dow Corning silicone grease, and placed under a N_2(g) stream at 110 (2)K. A total of 11151 reflections were collected of which 2040 were unique. The final refinement cycle was based on 1096 reflections with $F_0 > 4\sigma(F_0)$ that were used to fit 181 parameters which led to $R1 = 0.0833$ and $wR2 = 0.2028$. The goodness-of-fit index is 0.973, and the highest peak in the final difference map is 1.765 $e^-\cdot Å^3$.

CCDC 183947 (**1**), -183948 (**2**) and -183949 (**3**) contain the supplementary crystallographic data for this paper. These data can be obtained free of charge at www.ccdc.cam.ac.uk/conts/retrieving.html [or from the Cambridge Crystallographic Data Centre, 12, Union Road, Cambridge CB2 1EZ, UK; fax: (internat.) +44-1223/336-033; E-mail: deposit@ccdc.cam.ac.uk].

Acknowledgments

We thank the National Science Foundation for a PI grant (CHE-9906583) and for equipment grants for the CCD X-ray equipment (CHE-9807975) and the SQUID magnetometer (NSF-9974899). Support from the Welch Foundation is also gratefully acknowledged. JRGM thanks the Spanish Ministerio de Ciencia y Tecnología for a research contract (Programa Ramón y Cajal).

[1] O. Kahn, C. J. Martinez, *Science* **1998**, *279*, 44−48.
[2] C. Joachim, J. K. Gimzewski, A. Aviram, *Nature* **2000**, *408*, 541−548.
[3] J. M. Tour, *Acc. Chem. Res.* **2000**, *33*, 791−804.
[4] C. S. Campos-Fernandez, R. Clérac, K. R. Dunbar, *Angew. Chem. Int. Ed.* **1999**, *38*, 3477−3479.
[5] C. S. Campos-Fernandez, R. Clérac, J. M. Koomen, D. H. Russell, K. R. Dunbar, *J. Am. Chem. Soc.* **2001**, *123*, 773−774.
[6] J. R. Galán-Mascarós, K. R. Dunbar, *Chem. Commun.* **2001**, 217−218.
[7] A. Aumüller, P. Erk, G. Klebe, S. Hünig, J. Schütz, H. Werner, *Angew. Chem. Int. Ed. Engl.* **1986**, *25*, 740−741.
[8] P. Erk, H. J. Gross, U. L. Hünig, H. Meixner, J. U. Von Schütz, H. C. Wolf, *Angew. Chem. Int. Ed. Engl.* **1989**, *28*, 1245−1246.
[9] M. L. Naklicki, R. J. Crutchley, *J. Am. Chem. Soc.* **1994**, *116*, 6045−6046.
[10] R. Kato, H. Kobayashi, A. Kobayashi, *J. Am. Chem. Soc.* **1989**, *111*, 5224−5232.
[11] W. Kaim, S. Kohlmann, *Inorg. Chem.* **1987**, *26*, 68−77.
[12] W. Kaim, S. Kohlmann, *Inorg. Chem.* **1986**, *25*, 3442−3448.
[13] H. Hartmann, T. Scheiring, J. Fiedler, W. Kaim, *J. Organomet. Chem.* **2000**, *604*, 267−272.
[14] S. Ernst, V. Kasack, W. Kaim, *Inorg. Chem.* **1988**, *27*, 1146−1148.
[15] S. Ernst, W. Kaim, *Inorg. Chem.* **1989**, *28*, 1520−1528.
[16] W. Kaim, S. Ernst, V. Kasack, *J. Am. Chem. Soc.* **1990**, *112*, 173−178.
[17] L. S. Kelso, D. A. Reitsma, R. Keene, *Inorg. Chem.* **1996**, *35*, 5144−5153.
[18] S. I. Gorelsky, E. S. Dodsworth, A. B. P. Lever, A. A. Vlcek, *Coord. Chem. Rev.* **1998**, *174*, 469−494.
[19] S. Kohlman, S. Ernst, W. Kaim, *Angew. Chem. Int. Ed. Engl.* **1985**, *24*, 684−685.
[20] W. Kaim, *Coord. Chem. Rev.* **2001**, *219−221*, 463−488.
[21] D. A. Baldwin, A. B. P. Lever, R. V. Parish, *Inorg. Chem.* **1969**, *8*, 107−115.
[22] W. Kaim, S. Kohlmann, J. Jordanov, D. Fenske, *Z. Anorg. Allg. Chem.* **1991**, *598−599*, 217−234.
[23] P. Kausikisankar, M. Shivakumar, P. Ghosh, A. Chakravorty, *Inorg. Chem.* **2000**, *39*, 195−199.
[24] E. Waldhör, J. Poppe, W. Kaim, E. Cutin, M. García, N. Katz, *Inorg. Chem.* **1995**, *34*, 3093−3096.
[25] A. J. Bellamy, I. S. MacKirdy, C. E. Niven, *J. Chem. Soc., Perkin. Trans. 2* **1983**, 183−185.
[26] M. B. Robin, P. Day, *Adv. Inorg. Chem. Radiochem.* **1967**, *10*, 247−422.
[27] R. Schäfer, W. Kaim, J. Fiedler, *Inorg. Chem.* **1993**, *32*, 3199−3200.
[28] E. Coronado, J. R. Galán-Mascarós, C. J. Gómez-García, *J. Chem. Soc., Dalton Trans.* **2000**, 205−210.
[29] E. Coronado, J. R. Galán-Mascarós, C. Giménez-Saiz, C. J. Gómez-García, C. Ruiz-Pérez, S. Triki, *Adv. Mater.* **1996**, *8*, 737−740.
[30] S. Triki, F. Thetiot, J. R. Galán-Mascarós, J. Sala-Pala, K. R. Dunbar, *New J. Chem.* **2001**, *25*, 954−958.
[31] G. De Munno, G. Viau, M. Julve, F. Lloret, J. Faus, *Inorg. Chim. Acta* **1997**, *257*, 121−129.
[32] B. J. Hathaway, D. G. Holah, A. E. Underhill, *J. Chem. Soc.* **1962**, 2444−2448.
[33] *Theory and Applications of Molecular Paramagnetism* (Eds.: E. A. Boudreaux, L. N. Mulay), John Wiley & Sons: New York, 1976.
[34] SAINT, Program for area detector absorption correction, Siemens Analytical X-ray Instruments Inc., Madison WI 53719, USA 1994−1996.
[35] Program in the SHELXTL software.
[36] SHELXL-97; G. M. Sheldrick, SHELXL-97, Program for refining crystal structures, University of Göttingen,1997.

Received May 13, 2002
[I02253]

Synthesis of (η^3-Allyl)bromodicarbonylbis(pyrazole)molybdenum(II) and Reactivity towards [Au(acac)PPh_3]: Structure and Dynamic Behavior of the Monometallic Pyrazole and Heterometallic Pyrazolate Complexes

Paloma Paredes,[a] Daniel Miguel,[a] and Fernando Villafañe*[a]

Keywords: Molybdenum / Gold / Heterometallic complexes / N ligands / Fluxionality

The reactions of [Mo(η^3-allyl)Br$(CO)_2(NCMe)_2$] and two equivalents of Hpz (pyrazole) or Hdmpz (3,5-dimethylpyrazole) lead to [Mo(η^3-allyl)Br$(CO)_2(Hpz)_2$] or [Mo(η^3-allyl)Br$(CO)_2(Hdmpz)_2$]. The Hpz and Hdmpz ligands are coordinated *cis* and *trans* with respect to the allyl group in the solid state, whereas in their solutions a slow trigonal twist process is detected. These complexes react with Tl(acac) giving [Mo(acac)(η^3-allyl)$(CO)_2$(Hpz)] and [Mo(acac)(η^3-allyl)$(CO)_2$(Hdmpz)], which also undergo a slow trigonal twist process in solution. The latter complex may also be obtained by the reaction of equimolar amounts of [Mo(η^3-allyl)Br$(CO)_2(Hdmpz)_2$] and [Au(acac)PPh_3], giving [Au$BrPPh_3$] as a by product. The reaction of these molybdenum acac complexes with [Au(acac)PPh_3] give rise to the heterobimetallic bridging pyrazolate complexes [Mo(acac)(η^3-allyl)$(CO)_2$(μ-pz)AuPPh_3] and [Mo(acac)(η^3-allyl)$(CO)_2$(μ-dmpz)AuPPh_3]. The solid state structure of the latter, which is also obtained from [Mo(η^3-allyl)Br$(CO)_2(Hdmpz)_2$] and two equivalents of [Au(acac)PPh_3], with [Au$BrPPh_3$] as a by product, reveals the coordination of the bridging dimethylpyrazolate ligand *trans* to the allyl group. Two different dynamic processes which are slowed down at low temperatures are detected in solution for each heterobimetallic complex: trigonal twist for the pyrazolate bridging complex, and hindered rotation of the Mo–N bond for the more hindered dimethylpyrazolate complex.
(© Wiley-VCH Verlag GmbH & Co. KGaA, 69451 Weinheim, Germany, 2003)

Introduction

Pyrazolate ligands are commonly used as bridging ligands since they allow for the study of the bimetallic moiety, holding both metals in close proximity but at the same time being flexible enough to adopt different geometries with a wide variety of metals.[1] The interest of these studies embraces different fields, such as the physical properties and the biological activity of new complexes, or their unusual chemical behavior and catalytic activity.[2]

The bridging pyrazolate heterobimetallic complexes are of special interest, and may be obtained by deprotonation of a terminal pyrazole complex when a second metallic substrate is present. This strategy allows the systematic synthesis of heterobimetallic systems, as has been successively used by different groups, mainly with middle and late transition elements.[3] Herein we report on the synthesis of molybdenum(II) complexes containing two terminal pyrazoles coordinated in a *cis* manner. We also present the first results of the use of these compounds as precursors for heterobimetallic systems: deprotonation of the pyrazole ligands, and further coordination to a late transition metal would lead to the synthesis of early-late bimetallic complexes. These are particularly interesting in the field of heterobimetallic systems, as the clear differences between both metals enhance the synergism responsible for their improved activity.[4]

Results and Discussion

Synthesis and Characterization of [MoBr(η^3-allyl)$(CO)_2(Hpz)_2$] and [MoBr(η^3-allyl)$(CO)_2(Hdmpz)_2$]

The reactions of [MoBr(η^3-allyl)$(CO)_2(NCMe)_2$] with a two-fold excess of pyrazole (Hpz) or dimethylpyrazole (Hdmpz) in dichloromethane are instantaneous at room temperature affording [MoBr(η^3-allyl)$(CO)_2(Hpz)_2$] (**1a**) and [MoBr(η^3-allyl)$(CO)_2(Hdmpz)_2$] (**1b**), respectively, isolated as yellow crystalline solids.

There are two possible geometries for these complexes, as depicted in Figure 1. They are pseudo-octahedral if the η^3-allyl ligand is considered as occupying one coordination po-

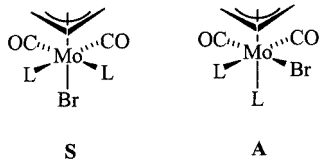

Figure 1. Two possible structures for complexes [MoBr(η^3-allyl)$(CO)_2L_2$]

[a] Departamento de Química Inorgánica, Facultad de Ciencias, Universidad de Valladolid, 47005 Valladolid, Spain

sition, having its terminal atoms oriented over the carbonyl groups, as has been demonstrated to be the most energetically favorable arrangement.[5] The two possible geometries are: **S** or symmetric, where the pyrazoles are coordinated in the *equatorial* positions, *trans* to the carbonyls; and **A** or asymmetric, where one of the pyrazoles is coordinated *trans* to the allyl group, in the *axial* position (Figure 1).

The NMR spectra provide very useful information for identifying the geometry of the complex, since both pyrazoles and both methylenes of the allyl group are equivalent in the symmetric isomer **S**, but inequivalent in the asymmetric isomer **A**. The latter is the only isomer detected in the ^1H and $^{13}C\{^1H\}$ NMR spectra of **1a** and **1b** at room temperature. However, some of the signals in the ^1H NMR spectra are broad, which might be a consequence of a slow exchange process before the coalescence.

These complexes $[MoX(\eta^3\text{-allyl})(CO)_2L_2]$ (X = halide or pseudo halide, L_2 = two monodentate ligands or a bidentate ligand) usually display a nondissociative trigonal twist process in which there is an intramolecular rotation of the XL_2 triangular face,[6] which would lead to the equilibrium depicted in Scheme 1. The isomers involved in this equilibrium are the symmetric **S** and both enantiomers of the asymmetric **A**. Therefore, if this exchange process is fast enough, a symmetric average spectrum should be observed.

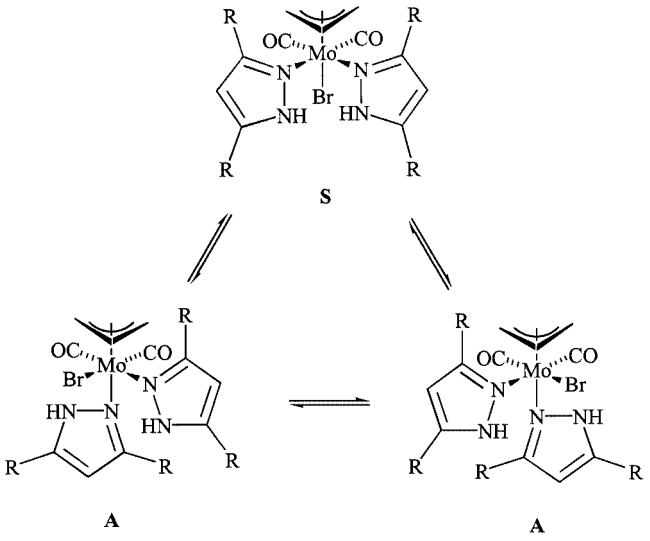

Scheme 1. Trigonal twist process observed for **1a** (R = H) and **1b** (R = CH_3)

Other dynamic processes in solution have been detected for these types of complexes, such as the $\eta^3-\eta^1-\eta^3$ rearrangement of the allyl,[7] or the recently described "pivoted double switch" process, where the *axial* ligand remains in the same position, while the bromo and the other ligand *trans* to the carbonyls switch between both *equatorial* positions.[8] The $\eta^3-\eta^1-\eta^3$ rearrangement of the allyl would render the H^{anti} and H^{syn} equivalent, giving an A_4X pattern for the allyl group in the ^1H NMR spectra. On the other hand, the "pivoted double switch" mechanism would never render both pyrazole ligands equivalent, since the pyrazole in the *axial* position would not exchange with the other pyrazole.

A variable temperature ^1H NMR spectroscopic study was carried out in order to understand the exact nature of the process in solution that leads to the broadening of the signals observed in the ^1H NMR spectra at room temperature for **1a** and **1b**.

The ^1H NMR spectrum of **1a** at 333 K shows signals due to a symmetric dynamic situation where both pyrazoles are equivalent, thus confirming the trigonal twist exchange process which is very slow at room temperature. On the other hand, a symmetric situation appears when the ^1H NMR spectrum of **1b** is recorded at 353 K in C_6D_6, as some of the signals of the different Hdmpz groups coincide, as well as those of different halves of the allyl group (see Exp. Sect.). Hence, the same trigonal twist exchange process is proposed for **1b**, but is slower than that of **1a**. This is in accordance with the higher steric requirements of Hdmpz compared with Hpz.

The allyl protons H^{anti} and H^{syn} always remain inequivalent, and the pyrazole ligands are equivalent when the processes are fast, which leads to both the $\eta^3-\eta^1-\eta^3$ rearrangement of the allyl and the "pivoted double switch" process being discarded.

Only the asymmetric isomer is detected in the ^1H NMR spectra of both complexes at low temperatures, indicating that the equilibrium occurs between the two asymmetric enantiomers **A** depicted in Scheme 1. The symmetric isomers **S** are not observed for any of the two complexes, which suggests that they are energetically very unfavorable.

The ^1H NMR spectra recorded at low temperatures display sharp signals. The H^4 signals in **1a** are pseudo quadruplets, due to coupling with the rest of pyrazolic protons including the pyrrolic proton, as was confirmed from selective homodecoupling experiments. Therefore, the broadness observed at room temperature might then also be due to a rapid prototropic exchange involving the pyrrolic proton, which is common in pyrazole complexes.[9] The homodecoupling experiments carried out on **1a** at low temperature allowed us to unequivocally assign the signals of the pyrazolic hydrogens. However, this assignment cannot be extended to the rest of the complexes described here, since the chemical shifts of the hydrogens or methyl groups in positions 3 and 5 seem to be affected by different factors, which are difficult to evaluate: whether the hydrogen (or methyl) group at position 3 resonates at a higher field than at position 5 or vice versa may vary in the same family of complexes,[3g] or even depend on the solvent used.[10] Therefore, the assignment proposed for the rest of the complexes in the Experim. Section may be considered as tentative.

The IR spectra of both complexes show two bands in the C−O stretching region in solution, although more bands are detected in the solid state. This is a common feature in carbonyl complexes and is attributed to the lower symmetry of the molecule in the crystal compared to the isolated molecule in solution. The C−O frequencies are slightly higher for **1a** than for **1b** when the IR is recorded in solution. This is to be expected considering that Hdmpz is a better donor

than Hpz, and is also observed for the rest of the complexes described in this work. However, the C−O frequencies of **1a** in the solid state are appreciably lower than those of **1b** (see Exp. Sect.). This has no immediate explanation, as the rest of the analytical and spectroscopic data are in accordance with the proposed geometries. Thus, we decided to carry out an X-ray study of both complexes in order to also obtain crystallographic data, and thus to determine whether this could shed some light on these anomalous frequencies.

The structures are shown in Figure 2 and relevant distances and angles are collected in Table 1. As indicated above, the molybdenum atoms are pseudo-octahedrally coordinated, assuming that the allyl groups occupy one site. The two carbonyls and the allyl group show the expected orientation, already described.[5,11] As evidenced by Table 1, the distances and angles are very similar in both complexes, and similar to those found in the previously reported structure of a bromodicarbonylmolybdenum(II) complex with pyrazole and phenylallyl.[12] It should be noted that one of the pyrazole ligands is coordinated *trans* to the allyl group in all three structures (asymmetric isomer **A** in Scheme 1), opposite to what is usually found in complexes of the type [MoX(η^3-allyl)$(CO)_2L_2$] (X = halide or pseudo halide, L_2 = nitrogen donor ligand), where the nitrogen donor ligands are always *trans* to the carbonyl groups (**S** isomer).[11]

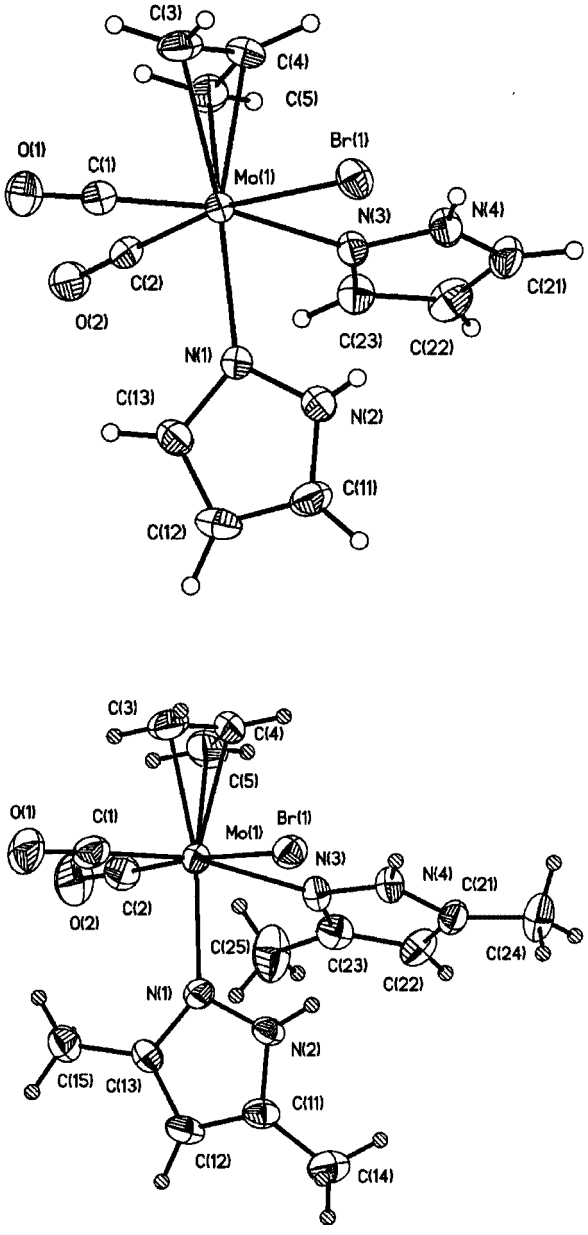

Figure 2. Perspective views of [Mo(η^3-allyl)$Br(CO)_2(Hpz)_2$], **1a** (above), and [Mo(η^3-allyl)$Br(CO)_2(Hdmpz)_2$], **1b** (below), showing the atom numbering

Table 1. Selected distances [Å] and angles [deg.] for [Mo(η^3-allyl)-$Br(CO)_2(Hpz)_2$] (**1a**) and [Mo(η^3-allyl)$Br(CO)_2(Hdmpz)_2$] (**1b**)

	1a	**1b**
Mo(1)−C(2)	1.940(3)	1.932(5)
Mo(1)−C(1)	1.957(3)	1.948(5)
Mo(1)−C(4)	2.215(3)	2.206(4)
Mo(1)−N(1)	2.222(2)	2.241(3)
Mo(1)−N(3)	2.268(2)	2.304(3)
Mo(1)−C(3)	2.325(3)	2.345(4)
Mo(1)−C(5)	2.338(3)	2.346(4)
Mo(1)−Br(1)	2.738(1)	2.771(1)
C(1)−O(1)	1.151(4)	1.160(4)
C(2)−O(2)	1.132(3)	1.160(5)
C(3)−C(4)	1.397(4)	1.396(6)
C(4)−C(5)	1.400(4)	1.381(6)
C(2)−Mo(1)−C(1)	80.06(12)	79.89(17)
C(2)−Mo(1)−N(1)	87.53(10)	91.27(15)
C(1)−Mo(1)−N(1)	90.33(10)	89.29(15)
C(2)−Mo(1)−N(3)	94.49(10)	99.27(14)
C(1)−Mo(1)−N(3)	169.26(10)	168.20(15)
N(1)−Mo(1)−N(3)	80.13(8)	78.95(11)
C(2)−Mo(1)−C(3)	107.15(13)	103.59(17)
C(1)−Mo(1)−C(3)	67.87(12)	68.76(19)
N(1)−Mo(1)−C(3)	150.34(10)	150.34(16)
N(3)−Mo(1)−C(3)	122.79(10)	122.54(16)
C(2)−Mo(1)−Br(1)	169.63(8)	172.85(12)
C(1)−Mo(1)−Br(1)	100.16(9)	95.11(12)
N(1)−Mo(1)−Br(1)	82.10(6)	83.52(8)
N(3)−Mo(1)−Br(1)	83.53(6)	84.58(8)

The Mo−C and C−O distances in the structures of **1a** and **1b** follow the expected sequence: those *trans* to the bromo ligand [C(1)−O(1)] are similar in both structures, whereas those *trans* to the pyrazoles are slightly different: C(2)−O(2) distance in **1a** is 1.132(3) Å vs. 1.160(5) Å in **1b**. This indicates that the C−O bond is stronger in **1a**, inferring that Hdmpz is a better donor than Hpz, as predicted. However, this result is difficult to rationalize with the frequencies observed from the solid-state IR spectra, which point to the opposite, since they are lower for **1a**. This feature might be explained considering lattice effects, since different space groups are detected for each molecular packing, and this should affect the C−O frequencies. This frequency anomaly might also be explained considering the short intermolecular distances where the oxygen atoms of the carbonyl groups are involved, as is discussed below.

The pyrrolic hydrogens in the structures of these two complexes are involved both in both intramolecular and in-

termolecular hydrogen bonds. The intramolecular hydrogen bonds affect the bromine atoms: 2.51 and 2.62 Å are found in **1a**, and 2.51 and 2.74 Å in **1b**, for Br(1)···H(4) and Br(1)···H(2), respectively. These distances are typical of weak hydrogen bonds,[13] and are always shorter those between the bromine atom and the pyrrolic hydrogen in the *equatorial* position. Similar hydrogen bond lengths have been found for other bromo complexes containing pyrazoles.[14]

The intermolecular hydrogen bonds involving the pyrrolic atoms clearly differ in both complexes: in **1a**, the acceptor atoms are the oxygens of the carbonyls giving distances expected for weak hydrogen bonds [H(2)···O(1) 2.75 Å, H(4)···O(2) 2.39 Å],[13] whereas no intermolecular interaction is observed for the pyrrolic hydrogens of **1b**. As indicated above, either the lattice effects or this feature (or both) might be responsible for the observed decrease in the C−O stretching frequencies in the solid IR for **1a**, since this interaction is only detected in this complex.

Acac Complexes

Once the two precursors needed to obtain heterobimetallic complexes had been synthesized, we decided to explore their reactivity towards different bases in order to deprotonate the pyrazoles and then react this pyrazolate complex with a second metal fragment. However, the treatment of either **1a** or **1b** with K_2CO_3, NEt_3, NaH, or KOH gave unchanged starting material or mixtures of unidentifiable products after forcing the conditions. This can be easily be explained in terms of the fact that these bases may act as nucleophiles, and the attack of nucleophiles on coordinated η^3-allyl groups is well-known. For [MoX(η^3-allyl)$(CO)_2L_2$] complexes, these reactions do not always afford the expected olefin,[15] but may lead to the substitution of the coordinated halogen by the nucleophile,[16] or even to decomposition.[17]

An alternative way of obtaining heterobimetallic complexes was the use of a base already coordinated to the metal fragment that was to be introduced. This fragment could immediately trap the pyrazolate formed by coordination to the second metal fragment. Thus, [Au(acac)PPh_3] was used, since the acetylacetonate could act as a base. Other acac complexes have previously been used for this purpose.[3a−3c]

The reaction of **1b** with a two-fold excess of [Au(acac)PPh_3] occurs at room temperature for 1 h in THF, and allows for the isolation of [Mo(acac)(η^3-allyl)$(CO)_2$(μ-dmpz)$AuPPh_3$] (**3b**) after separating [$AuBrPPh_3$] as a white solid by crystallization [Equation (1)]:

[MoBr(η^3-allyl)$(CO)_2$(Hdmpz)$_2$] (**1b**) + 2 [Au(acac)PPh_3] → [Mo(acac)(η^3-allyl)$(CO)_2$(μ-dmpz)$AuPPh_3$] (**3b**) + [$AuBrPPh_3$] + Hdmpz + Hacac (1)

As inferred from Equation (1), one equivalent of acac acts as a ligand, substituting one dimethylpyrazole and the bromo ligands, whereas the second acts as a base, removing the pyrrolic hydrogen and coordinating the pyrazolate ligand to the liberated "$AuPPh_3$" fragment. This sequence should coincide with the path followed by the reaction, since the products detected when the reaction was repeated using equimolar amounts of the reactants were [Mo(acac)(η^3-allyl)$(CO)_2$(Hdmpz)] (**2b**) and [$AuBrPPh_3$] [Equation (2)].

[MoBr(η^3-allyl)$(CO)_2$(Hdmpz)$_2$] (**1b**) + [Au(acac)PPh_3] → [Mo(acac)(η^3-allyl)$(CO)_2$(Hdmpz)] (**2b**) + [$AuBrPPh_3$] + Hdmpz (2)

This result led us to propose a more logical synthetic path in order to obtain these two new complexes: (a) the substitution of the bromo and pyrazole ligands by acetylacetonate was carried out with Tl(acac) instead of [Au(acac)PPh_3], and (b) this gold complex was used for the deprotonation of the remaining pyrazole and formation of the heterobimetallic complexes.

The reaction of Tl(acac) with equimolar amounts of **1a** or **1b** in dichloromethane at room temperature yielded, after separating TlBr as a precipitate, [Mo(acac)(η^3-allyl)$(CO)_2$(Hpz)] (**2a**) or [Mo(acac)(η^3-allyl)$(CO)_2$(Hdmpz)] (**2b**). The second equivalent of Hpz or Hdmpz liberated in the reaction remained in the mother liquor.

The allyl and acac signals in the ^{1}H NMR spectra of **2a** and **2b** at room temperature are indicative of a symmetric situation with respect to the plane that bisects the allyl and contains the metal atom. However some signals are broad, as occurred for complexes **1**, what is indicative of a dynamic process in solution. The ^{1}H NMR spectra at lower temperatures show signals of two isomers: one symmetric and one asymmetric, the ratio of the latter increasing as the temperature decreases. This is again in accordance with a trigonal twist process between the possible stereoisomers shown in Scheme 2. Contrarily to complexes **1**, the symmetric isomers **S** are detected in the solutions of complexes **2** (their ratio being higher as the temperature rises) which is indicative of their higher stability in this case.[18] The signals for both isomers are clearly differentiated in the $^{13}C\{^1H\}$ NMR spectra at 233 K of **2a** and **2b**.

The IR spectra of complexes **2a** and **2b** show two absorptions in the C−O stretching region, those of **2a** being slightly higher, as should be expected given the lower neat donor character of Hpz compared with Hdmpz. Another interesting feature is the N−H stretching bands, which show an important decrease for **2a**: 3159 cm^{-1}, vs. ca. 3300 cm^{-1} for **1a** and **1b**, or 3396 cm^{-1} for **2b**. In addition to this low frequency, the N−H stretching absorption observed for **2a** is very broad, which suggests that this hydrogen bond is stronger than those in complexes **1** and **2a**, which show sharp absorptions. These two factors point to a moderate hydrogen bond in **2a**, whereas those detected in the other complexes herein may be considered to be weak, as indicated above.[12,19]

Once acac has been incorporated to the molecules, they may be deprotonated to obtain the pyrazolate bridging het-

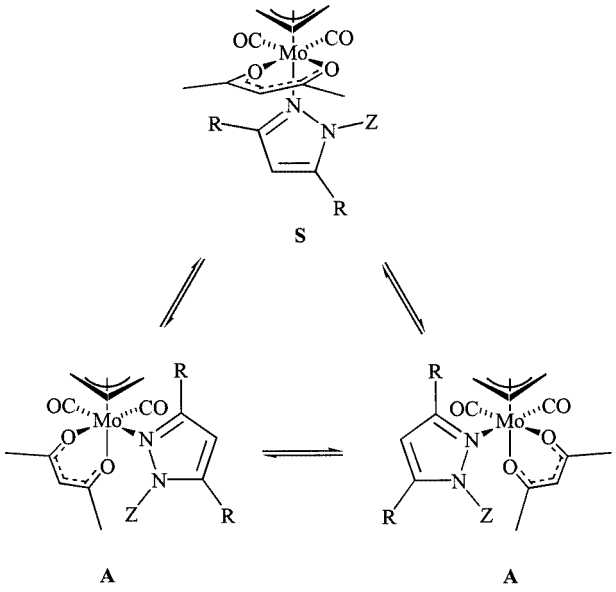

Scheme 2. Trigonal twist process observed for **2a** (R = H, Z = H), **2b** (R = CH_3, Z = H), and **3a** (R = H, Z = $AuPPh_3$).

erobimetallic complexes. The reactions of **2a** or **2b** with the equimolar amounts of [Au(acac)PPh_3] occur in 5 minutes at room temperature and in THF as the solvent, to give [Mo(acac)(η^3-allyl)$(CO)_2$(μ-pz)$AuPPh_3$] (**3a**) and [Mo(acac)(η^3-allyl)$(CO)_2$(μ-dmpz)$AuPPh_3$] (**3b**) as orange crystalline solids.

The IR spectra of **3a** and **3b** show two C−O absorptions, their frequencies being once again slightly higher for the Hpz complex, and no N−H bands are detected. Their ^{1}H NMR spectra at room temperature show allyl and acac signals indicative of a symmetric situation respect to the plane which bisects the allyl and contains the metal atom. The $^{31}P\{^1H\}$ NMR spectra show only one singlet at room temperature, whereas no $^{13}C\{^1H\}$ NMR spectra could be recorded due to the low solubility of the complexes. In this case, **3a** and **3b** showed different behavior when the variable temperature NMR spectroscopic study was carried out.

The behavior of **3a** at lower temperatures is similar to that described above for **2a**, since two isomers are detected, symmetric and asymmetric, although this time the ratio of the latter increases as the temperature decreases. This is observed both in the ^{1}H and $^{31}P\{^1H\}$ NMR spectra at low temperatures, and supports again a trigonal twist process between isomer **S** and the two enantiomers of isomer **A**, as shown in Scheme 2.

On the other hand, the $^{31}P\{^1H\}$ NMR spectra of **3b** at 213 K displays six singlets, one of them clearly more intense than the others. The ^{1}H NMR spectra at low temperature also show a major isomer with inequivalent halves for the acac and allyl ligands, and a mixture of minor isomers, although not all their signals could be completely interpreted due to their low ratio.

An X-ray diffractometric study was carried out in order to identify which isomer crystallizes. The result of this determination is shown in Figure 3, whereas Table 2 contains the more relevant distances and angles. The usual pseudo-octahedral geometry of (η^3-allyl)molybdenum complexes is found, with the open face of the allyl moiety oriented over the carbonyls. The acac ligands occupy the *equatorial* positions, whereas the *axial* position is occupied by the dimethylpyrazolate, which bridges the molybdenum and the gold atoms. The plane defined by the bridging pyrazole and the gold atom lies nearly perpendicular [91.4(1)°] to the plane defined by Mo, N(2), and the central atoms of the allyl and acac ligands [C(9) and C(5), respectively], which bisects the molybdenum complex.

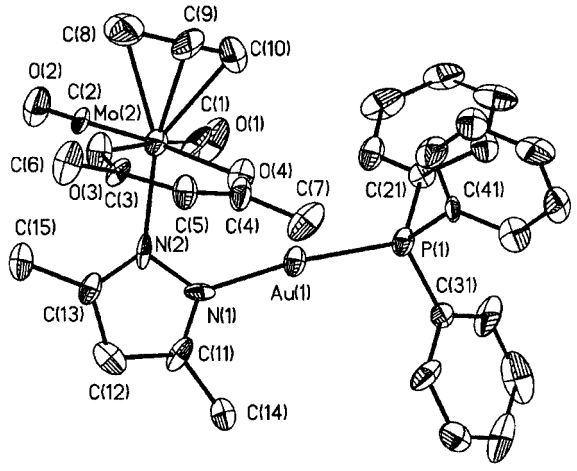

Figure 3. Perspective view of [Mo(acac)(η^3-allyl)$(CO)_2$(μ-dmpz)$AuPPh_3$] (**3b**) showing the atom numbering (the hydrogen atoms have been omitted for clarity)

The distances and angles of the "Mo(acac)(η^3-allyl)$(CO)_2$" moiety are very similar to those found in the structure of the complex [Mo(acac)(η^3-allyl)$(CO)_2$(py)],[20] where the acac also occupies the *equatorial* positions. The Au−N and Au−P distances [1.976(18) and 2.20(5) Å] are in the lower range of those previously reported for phosphanepyrazolylgold complexes [2.06(2) and 2.231(5)−2.334(5) Å, respectively].[21] The P−Au−N angle [171.9(6)°] is also in the lower limit with respect to those previously described [174.3(4)−178.0(5)°].[21]

Once the isomer in the solid state had been identified, the next step was to assign its signals in the NMR spectra. Therefore, the crystals were mixed with frozen $CDCl_3$ at 195 K, and the NMR spectra were recorded immediately after the solvent melted at 213 K. The ^{1}H and $^{31}P\{^1H\}$ NMR spectra show signals that correspond to the above mentioned major isomer. Small signals due to the minor isomers appear and increase as the solution is maintained at low temperature, until finally the same spectra as that described above, obtained when the solution was prepared at room temperature, is observed.

Hence, the isomer detected in the solid state is that labeled **S** in Scheme 2, but the $AuPPh_3$ moiety makes the plane bisecting the acac and the allyl ligands no longer a symmetry plane. This explains why its ^{1}H NMR spectrum shows inequivalent halves for the acac and allyl ligands, and suggests that the rotation of the Mo−N bond has been

Table 2. Selected distances [Å] and angles [deg.] for [Mo(acac)(η^3-allyl)$(CO)_2$(μ-dmpz)$AuPPh_3$] (**3b**)

Mo(2)−C(2)	1.89(2)
Mo(2)−C(1)	1.97(2)
Mo(2)−C(9)	2.10(3)
Mo(2)−N(2)	2.13(2)
Mo(2)−O(3)	2.148(14)
Mo(2)−O(4)	2.158(14)
Mo(2)−C(10)	2.32(2)
Mo(2)−C(8)	2.34(2)
Au(1)−N(1)	1.976(18)
Au(1)−P(1)	2.209(5)
C(1)−O(1)	1.14(2)
C(2)−O(2)	1.18(2)
O(3)−C(3)	1.22(2)
O(4)−C(4)	1.22(3)
C(8)−C(9)	1.31(3)
C(9)−C(10)	1.24(3)
C(2)−Mo(2)−C(1)	77.7(8)
C(2)−Mo(2)−C(9)	101.3(10)
C(1)−Mo(2)−C(9)	98.2(12)
C(2)−Mo(2)−N(2)	95.0(8)
C(1)−Mo(2)−N(2)	87.9(8)
C(9)−Mo(2)−N(2)	163.5(9)
C(2)−Mo(2)−O(3)	96.1(7)
C(1)−Mo(2)−O(3)	171.3(8)
C(9)−Mo(2)−O(3)	89.0(11)
N(2)−Mo(2)−O(3)	86.5(6)
C(2)−Mo(2)−O(4)	176.1(8)
C(1)−Mo(2)−O(4)	101.4(7)
C(9)−Mo(2)−O(4)	82.6(8)
N(2)−Mo(2)−O(4)	81.2(6)
O(3)−Mo(2)−O(4)	84.3(5)
N(1)−Au(1)−P(1)	171.9(6)
N(2)−N(1)−Au(1)	127.0(14)
N(1)−N(2)−Mo(2)	120.2(13)

stopped at low temperature. In complexes **2a**, **2b**, and **3a**, (Scheme 2) the Mo−N bonds rotate freely even at 213 K, as both halves of allyl and acac ligands are equivalent in the symmetric isomer **S**, opposite to what is observed for **3b**. Although the presence of isomers such as **A** in Scheme 2 cannot be completely ruled out, the isomers detected in the NMR spectra of **3b** should be different rotamers, the Mo−N bond rotation being slow at low temperature but fast at room temperature (Scheme 3).

Therefore, rotation of the Mo−N bond, which is only detected for **3b**, is fast for the rest of the complexes described herein. As **3b** contains bulkier substituents, this leads to the conclusion that the trigonal twist rearrangement is more energetically demanding. This is easily foreseeable considering that the scrambling of coordination sites should be more difficult to achieve than a bond rotation. In **3b**, both the presence of the methyl groups in the dimethylpyrazolate and its coordination to the $AuPPh_3$ fragment cooperate to brake the rotation of the Mo−N bond, which is too fast to be detected when only one of these factors (either in **2b** or **3a**) is absent. Thus the addition of these two factors allow the "molecular brake" to be obtained.

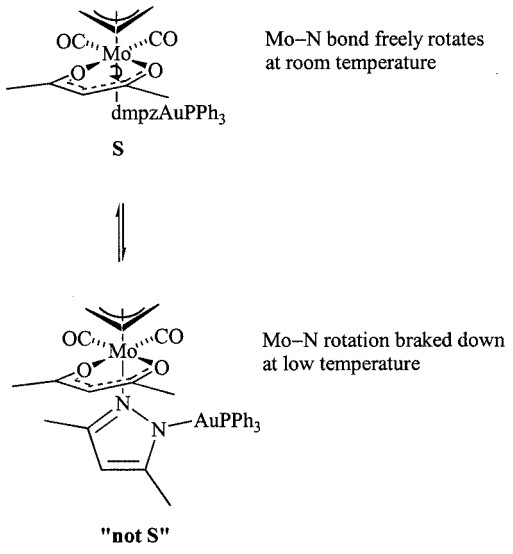

Scheme 3. Hindered rotation of the Mo−N bond observed for **3b**

Experimental Section

General Remarks: All manipulations were performed under a N_2 atmosphere following conventional Schlenk techniques. Filtrations were carried out on dry Celite under N_2. Solvents were purified according to standard procedures.[22] [Mo(η^3-allyl)Br$(CO)_2$-$(NCMe)_2$],[23] Tl(acac),[24] and [Au(acac)PPh_3][24] were obtained as described previously. All other reagents were obtained from the usual commercial suppliers, and used as received. Infrared spectra were recorded on Perkin−Elmer 1720X or RX I FT-IR apparatus on KBr pellets from 4000 to 400 cm^{-1}. NMR spectra were recorded on Bruker AC-300 or ARX-300 instruments in $CDCl_3$, at room temperature unless otherwise stated. NMR spectra are referred to the internal residual solvent peak for ^1H and $^{13}C\{^1H\}$ NMR or to external 85% aqueous H_3PO_4 for $^{31}P\{^1H\}$ NMR spectra. Assignment of the $^{13}C\{^1H\}$ NMR spectroscopic data was supported by DEPT experiments and relative intensities of the resonance signals. Elemental analyses were performed on a Perkin−Elmer 2400B microanalyzer.

[Mo(η^3-allyl)Br$(CO)_2(Hpz)_2$] (1a): [Mo(η^3-allyl)Br$(CO)_2(NCMe)_2$] (0.550 g, 1.5 mmol) was added to a solution of Hpz (0.205 g, 3 mmol) in CH_2Cl_2 (30 mL). The solution was stirred at room temperature for 5 min and hexane was added (ca. 30 mL). Concentration of the solution in vacuo and cooling to −20 °C gave a yellow microcrystalline solid, which was decanted, washed with hexane (3 × 3 mL approximately), and dried in vacuo, yielding 0.589 g (96%). IR (THF): $\tilde{\nu}$ = 1945 cm^{-1} vs, 1846 vs. IR (KBr): $\tilde{\nu}$ = 3304 cm^{-1} m, 3146 w, 3130 w, 1926 s, 1911 s, 1815 vs, 1654 vw, 1637 vw, 1466 w, 1404 vw, 1352 w, 1257 vw, 1158 vw, 1127 w, 1047 m, 911 vw, 792 w, 778 m, 719 vw, 675 vw, 602 vw, 590 vw, 502 vw. ^1H NMR (333 K, 300 MHz): 1.47 ppm (br., 2 H, H^{anti}), 3.50 (br., 2 H, H^{syn}), 4.04 (m, 1 H, H^c allyl), 6.33 (br., 2 H, H^4 Hpz), 7.39 (s, 2 H, H^3 Hpz), 7.70 (br., 1 H, H^5 Hpz), 8.10 (br., 1 H, H^5 Hpz), 11.75 (br., 2 H, *H*N). ^1H NMR (room temp., 300 MHz): 1.29 ppm (d, J = 9.2 Hz, 1 H, H^{anti}), 1.63 (d, J = 10.0 Hz, 1 H, H^{anti}), 3.19 (br., 1 H, H^{syn}), 3.84 (br., 1 H, H^{syn}), 4.03 (m, 1 H, H^c allyl), 6.25 (s, 1 H, H^4 Hpz), 6.43 (s, 1 H, H^4 Hpz), 7.40 (s, 2 H, H^3 Hpz), 7.57 (s, 1 H, H^5 Hpz), 8.37 (s, 1 H, H^5 Hpz), 11.61 (br., 1 H, *H*N), 11.78 (br., 1 H, *H*N) ppm. ^1H NMR (253 K, 300 MHz): 1.28 ppm (d, J = 9.4 Hz, 1 H, H^{anti}), 1.62 (d, J = 9.9 Hz, 1 H, H^{anti}), 3.19 (dd,

J = 6.4, 3.5 Hz, 1 H, H^{syn}), 3.82 (dd, J = 5.9, 3.5 Hz, 1 H, H^{syn}), 4.02 (m, 1 H, H^{c} allyl), 6.25 (q, J = 2.2 Hz, 1 H, H^{4} Hpz), 6.43 (q, J = 2.2 Hz, 1 H, H^{4} Hpz), 7.41 (s, 2 H, H^{3} Hpz), 7.54 (t, J = 1.8 Hz, 1 H, H^{5} Hpz), 8.39 (t, J = 1.8 Hz, 1 H, H^{5} Hpz), 11.52 (br., 1 H, HN), 11.74 (br., 1 H, HN). $^{13}C\{^{1}H\}$ NMR (room temp., 75.78 MHz): 57.5 ppm (s, CH$_2$), 63.6 (s, CH$_2$), 73.2 (s, CH allyl), 107.1 (s, C^{4}H Hpz), 107.5 (s, C^{4}H Hpz), 129.1 (s, $C^{3,5}$H Hpz), 129.2 (s, $C^{3,5}$H Hpz), 142.7 (s, $C^{5,3}$H Hpz), 144.8 (s, $C^{5,3}$H Hpz), 224.2 (s, CO), 225.1 (s, CO). $C_{11}H_{13}BrMoN_4O_2$: calcd. C 32.30, H 3.20, N 13.70; found C 32.65, H 3.08, N 13.70.

[Mo(η^3-allyl)Br(CO)$_2$(Hdmpz)$_2$] (1b): [Mo(η^3-allyl)Br(CO)$_2$(NCMe)$_2$] (0.147 g, 0.4 mmol) was added to a solution of Hdmpz (0.077 g, 0.8 mmol) in CH_2Cl_2 (15 mL). The solution was stirred at room temperature for 5 min, the volatiles were removed in vacuo, and the yellow residue was extracted with Et_2O (ca. 20 mL) and filtered. Hexane was added (ca. 20 mL) and the solution was concentrated and cooled to −20 °C, giving a yellow-orange microcrystalline solid, which was decanted, washed with hexane (3 × 3 mL approximately), and dried in vacuo, yielding 0.146 g (78%). IR (THF): $\tilde{\nu}$ = 1942 cm^{-1} vs, 1843 vs. IR (KBr): $\tilde{\nu}$ = 3294 cm^{-1}s, 3069 vw, 2994 vw, 2927 vw, 1948 s, 1930 s, 1854 vs, 1654 vw, 1636 vw, 1570 m, 1467 w, 1419 w, 1373 w, 1283 w, 1155 w, 1024 w, 799 w, 654 w, 572 vw, 512 vw, 474 vw. ^{1}H NMR (353 K, C_6D_6, 300 MHz): 1.44 ppm (br., 6 H, CH_3 Hdmpz + 2 H, H^{anti}), 2.12 (br., 3 H, CH_3 Hdmpz), 2.87 (br., 3 H, CH_3 Hdmpz), 4.20 (br., 2 H, H^{syn}), 4.32 (m, 1 H, H^{c} allyl), 5.35 (s, 2 H, H^{4} Hdmpz), 11.4 (br., 2 H, HN). ^{1}H NMR (room temp., 300 MHz): 1.25 ppm (d, J = 9.4 Hz, 1 H, H^{anti}), 1.51 (d, J = 9.9 Hz, 1 H, H^{anti}), 2.04 (s, 3 H, CH_3 Hdmpz), 2.05 (s, 3 H, CH_3 Hdmpz), 2.25 (s, 3 H, CH_3 Hdmpz), 2.95 (m partially hidden by the following signal, 1 H, H^{syn}), 2.97 (s, 3 H, CH_3 Hdmpz), 3.96 (m, 1 H, H^{syn}), 4.12 (m, 1 H, H^{c} allyl), 5.78 (s, 1 H, H^{4} Hdmpz), 5.93 (s, 1 H, H^{4} Hdmpz), 10.25 (br., 1 H, HN), 11.25 (br., 1 H, HN). ^{1}H NMR (243 K, 300 MHz): 1.26 ppm (d, J = 9.5 Hz, 1 H, H^{anti}), 1.47 (d, J = 9.8 Hz, 1 H, H^{anti}), 2.00 (s, 3 H, CH_3 Hdmpz), 2.03 (s, 3 H, CH_3 Hdmpz), 2.25 (s, 3 H, CH_3 Hdmpz), 2.91 (dd, J = 6.2, 3.3 Hz, 1 H, H^{syn}), 2.98 (s, 3 H, CH_3 Hdmpz), 3.95 (dd, J = 6.3, 3.3 Hz, 1 H, H^{syn}), 4.08 (m, 1 H, H^{c} allyl), 5.78 (s, 1 H, H^{4} Hdmpz), 5.94 (s, 1 H, H^{4} Hdmpz), 10.06 (br., 1 H, HN), 11.12 (br., 1 H, HN). $^{13}C\{^{1}H\}$ NMR (room temp., 75.78 MHz): 10.7 ppm (s, CH$_3$ Hdmpz), 10.9 (s, CH$_3$ Hdmpz), 14.1 (s, CH$_3$ Hdmpz), 15.7 (s, CH$_3$ Hdmpz), 58.8 (s, CH$_2$), 64.2 (s, CH$_2$), 75.4 (s, CH allyl), 106.5 (s, C^{4}H Hdmpz), 106.7 (s, C^{4}H Hdmpz), 139.9 (s, $C^{3,5}$ Hdmpz), 140.6 (s, $C^{3,5}$ Hdmpz), 152.2 (s, $C^{5,3}$ Hdmpz), 155.9 (s, $C^{5,3}$ Hdmpz), 224.5 (s, CO), 226.3 (s, CO). $C_{15}H_{21}BrMoN_4O_2$: calcd. C 38.73, H 4.55, N 12.04; found C 39.08, H 4.41, N 12.05.

[Mo(acac)(η^3-allyl)(CO)$_2$(Hpz)] (2a): Complex **1a** (0.245 g, 0.6 mmol) was added to a mixture of Tl(acac) (0.182 g, 0.6 mmol) in CH_2Cl_2 (30 mL) and the mixture was stirred at room temp. for 5 min. The solution was then filtered and the filtrate was evaporated to dryness. The yellowish residue was extracted with Et_2O (ca. 20 mL) and filtered. Hexane was added (ca. 30 mL) and the solution was concentrated and cooled to −20 °C, giving a yellow-orange microcrystalline solid, which was decanted, washed with hexane (3 × 3 mL approximately), and dried in vacuo, yielding 0.172 g (80%). IR (THF): $\tilde{\nu}$ = 1938 cm^{-1} vs, 1846 vs. IR (KBr): $\tilde{\nu}$ = 3159 cm^{-1} w, 1936 vs, 1842 vs, 1581 m, 1524 s, 1390 m, 1380 m, 1354 w, 1270 w, 1263 w, 1136 m, 1062 w, 1044 w, 1025 w, 932 w, 798 w, 753 w, 609 w, 571 w, 512 w. ^{1}H NMR (room temp., 300 MHz): 1.42 ppm (br., 2 H, H^{anti}), 1.90 (s, 6 H, CH_3 acac), 3.35 (br., 3 H, H^{c} allyl + H^{syn}), 5.26 (s, 1 H, CH acac), 6.40 (br., 1 H, H^{4} Hpz), 7.54 (br., 2 H, $H^{3,5}$ Hpz), 10.14 (br., 1 H, HN). ^{1}H NMR (253 K, 300 MHz): 1.18 ppm (d, J = 7.0 Hz, 1 H, H^{anti} isomer A), 1.38 (d, J = 7.6 Hz, 1 H, H^{anti} isomer A), 1.52 (d, J = 9.4 Hz, 2 H, H^{anti} isomer S), 1.89 (s, 6 H, CH_3 acac isomer S), 1.94 (s, 3 H, CH_3 acac isomer A), 1.99 (s, 3 H, CH_3 acac isomer A), 3.00 (br., 1 H, H^{syn} isomer S), 3.31 (m, 1 H, H^{syn} isomer A + 1 H, H^{c} isomer A + 1 H, H^{c} isomer S), 3.48 (br., 2 H, H^{syn} isomer S), 5.23 (s, 1 H, CH acac isomer A), 5.34 (s, 1 H, CH acac isomer S), 6.28 (s, 1 H, H^{4} Hpz isomer A), 6.52 (s, 1 H, H^{4} Hpz isomer S), 7.21 (s, 1 H, H^{3} Hpz isomer A), 7.62 (s, 1 H, H^{3} Hpz isomer S), 7.66 (s, 1 H, H^{5} Hpz isomer A), 8.20 (s, 1 H, H^{5} Hpz isomer S), 10.15 (s, 1 H, HN isomer S), 11.70 (s, 1 H, HN isomer A). Ratio isomer **A**/isomer **S** (253 K) = 1:0.7; ratio isomer **A**/isomer **S** (233 K) = 1:0.6; ratio isomer **A**/isomer **S** (213 K) = 1:0.5. $^{13}C\{^{1}H\}$ NMR (233 K, 75.78 MHz): 27.2 ppm (s, CH$_3$ acac, isomer A), 28.3 (s, CH$_3$ acac, isomer S), 28.5 (s, CH$_3$ acac, isomer A), 58.6 (s, CH$_2$, isomer A), 60.8 (s, CH$_2$, isomer A), 61.3 (s, CH$_2$, isomer S), 72.8 (s, CH allyl, isomer S), 73.0 (s, CH allyl, isomer A), 100.4 (s, CH acac, isomer S), 100.6 (s, CH acac, isomer A), 105.4 (s, C^{4}H Hpz, isomer A), 106.9 (s, C^{4}H Hpz, isomer S), 130.3 (s, $C^{3,5}$H Hpz, isomer S), 130.7 (s, $C^{3,5}$H Hpz, isomer A), 138.6 (s, $C^{5,3}$H Hpz, isomer A), 143.6 (s, $C^{5,3}$H Hpz, isomer S), 184.4 (s, CO acac, isomer A), 189.5 (s, CO acac, isomer S), 190.9 (s, CO acac, isomer A), 226.4 (s, CO, isomer A), 227.1 (s, CO, isomer A), 228.6 (s, CO, isomer S). $C_{13}H_{16}MoN_2O_4$: calcd. C 43.35, H 4.48, N 7.78; found C 43.22, H 4.36, N 8.14.

[Mo(acac)(η^3-allyl)(CO)$_2$(Hdmpz)] (2b): *Method A:* Complex **1b** (0.093 g, 0.2 mmol) was added to a mixture of Tl(acac) (0.061 g, 0.2 mmol) in CH_2Cl_2 (10 mL) and the mixture was stirred at room temp. for 45 min. The solution was then filtered and the filtrate was evaporated to dryness. The yellowish residue was extracted with Et_2O (ca. 10 mL) and filtered. Hexane was added (ca. 15 mL) and the solution was concentrated and cooled to −20 °C, giving a yellow microcrystalline solid, which was decanted, washed with hexane (3 × 3 mL approximately), and dried in vacuo, yielding 0.052 g (67%). *Method B:* Complex **1b** (0.093 g, 0.2 mmol) was added to a solution of [Au(acac)PPh$_3$] (0.112 g, 0.2 mmol) in THF (10 mL) and the mixture was stirred at room temperature for 45 min. The volatiles were removed in vacuo, and the yellow residue was extracted with hexane (15 mL) and filtered. The insoluble residue was spectroscopically identified as [AuBrPPh$_3$].[25] Concentration of the solution in vacuo and cooling to −20 °C gave a yellow microcrystalline solid, which was decanted, washed with hexane (3 × 3 mL approximately), and dried in vacuo, yielding 0.033 g (42%). IR (THF): $\tilde{\nu}$ = 1937 cm^{-1} vs, 1846 vs. IR (KBr): $\tilde{\nu}$ = 3396 cm^{-1} m, 3377 m, 2926 vw, 1927 vs, 1822 vs, 1582 s, 1526 s, 1424 w, 1391 w, 1373 m, 1272 w, 1154 w, 1026 w, 952 w, 804 w. ^{1}H NMR (room temp., 300 MHz): 1.41 ppm (br., 2 H, H^{anti}), 1.89 (s, 6 H, CH_3 acac), 2.14 (s, 3 H, CH_3 Hdmpz), 2.35 (br., 3 H, CH_3 Hdmpz), 3.31 (br., 3 H, H^{c} allyl + H^{syn}), 5.25 (br., 1 H, CH acac), 5.87 (br., 1 H, H^{4} Hdmpz), 9.12 (br., 1 H, HN). ^{1}H NMR (253 K, 300 MHz): 1.16 (d, J = 8.9 Hz, 1 H, H^{anti} isomer A), 1.36 (d, J = 9.2 Hz, 1 H, H^{anti} isomer A), 1.49 (d, J = 9.6 Hz, 2 H, H^{anti} isomer S), 1.90 (s, 6 H, CH_3 acac isomer A + 6 H, CH_3 acac isomer S), 2.14 (s, 3 H, CH_3 Hdmpz isomer A + 3 H, CH_3 Hdmpz isomer S), 2.38 (s, 3 H, CH_3 Hdmpz isomer A), 2.89 (m, 1 H, H^{c} allyl isomer A), 2.95 (s, 3 H, CH_3 Hdmpz isomer S), 3.31 (m, 2 H, H^{syn} isomer S + H^{c} allyl isomer S + 2 H, H^{syn} isomer A), 5.18 (s, 1 H, CH acac isomer S), 5.37 (s, 1 H, CH acac isomer A), 5.76 (s, 1 H, H^{4} Hdmpz isomer S), 6.01 (s, 1 H, H^{4} Hdmpz isomer A), 8.93 (s, 1 H, HN isomer A), 9.18 (s, 1 H, HN isomer S). Ratio isomer A/isomer S (253 K) = 1:0.6; ratio isomer A/isomer S (233 K) = 1:0.4; ratio isomer A/isomer S (213 K) = 1:0.2. $^{13}C\{^{1}H\}$ NMR (233 K, 75.78 MHz): 11.0 ppm (s, CH$_3$ Hdmpz, isomer A), 11.1 (s, CH$_3$ Hdmpz, isomer S),

14.0 (s, CH_3 Hdmpz, isomer A), 15.3 (s, CH_3 Hdmpz, isomer S), 27.6 (s, CH_3 acac, isomer A), 28.1 (s, CH_3 acac, isomer A), 28.3 (s, CH_3 acac, isomer S), 57.4 (s, CH_2, isomer A), 59.1 (s, CH_2, isomer A), 62.1 (s, CH_2, isomer S), 71.3 (s, CH allyl, isomer A), 72.8 (s, CH allyl, isomer S), 100.0 (s, CH acac, isomer S), 100.4 (s, CH acac, isomer A), 105.5 (s, C^4H Hdmpz, isomer A), 106.6 (s, C^4H Hdmpz, isomer S), 139.6 (s, $C^{3,5}$ Hdmpz, isomer A), 140.3 (s, $C^{3,5}$ Hdmpz, isomer S), 150.4 (s, $C^{5,3}$ Hdmpz, isomer A), 155.3 (s, $C^{5,3}$ Hdmpz, isomer S), 187.6 (s, CO acac, isomer A), 188.4 (s, CO acac, isomer A), 189.8 (s, CO acac, isomer S), 227.4 (s, CO, isomer A), 228.5 (s, CO, isomer S), 229.3 (s, CO, isomer A). $C_{15}H_{20}MoN_2O_4$: calcd. C 46.40, H 5.19, N 7.21; found C 46.09, H 4.93, N 7.09.

[Mo(acac)(η³-allyl)(CO)₂(μ-pz)AuPPh₃] (3a): Complex **2a** (0.090 g, 0.25 mmol) was added to a solution of [Au(acac)PPh_3] (0.140 g, 0.25 mmol) in THF (20 mL) and the solution, which rapidly turned orange, was stirred at room temperature for 5 min. The volatiles were removed in vacuo and the yellow residue was extracted in CH_2Cl_2/hexane (20:20 mL) and filtered. Concentration in vacuo and cooling to −20 °C gave a orange microcrystalline solid, which was decanted, washed with hexane (3 × 3 mL approximately), and dried in vacuo, yielding 0.154 g (72%) of **3a**·0.5CH_2Cl_2. IR (THF): $\tilde{\nu}$ = 1928 cm^{-1} vs, 1830 vs. IR (KBr): $\tilde{\nu}$ = 3059 cm^{-1} vw, 2991 vw, 1924 vs, 1824 vs, 1586 m, 1568 m, 1529 m, 1492 vw, 1481 vw, 1437 m, 1985 m, 1378 m, 1269 w, 1174 vw, 1162 vw, 1102 m, 1076 vw, 1055 w, 1026 w, 998 vw, 750 w, 748 w, 712 w, 696 m, 546 m, 513 w, 500 w. ^1H NMR (room temp., 300 MHz): 1.35 ppm (m, 2 H, H^{anti}), 1.72 (br., 6 H, CH_3 acac), 2.8−3.7 (br., 3 H, H^c allyl + H^{syn}), 4.97 (s, 1 H, CH acac), 6.17 (br., 1 H, H^4 pz), 7.20 (br., 1 H, H^3 pz), 7.3−7.9 (br., 16 H, C_6H_5 + H^5 pz). ^1H NMR (253 K, 300 MHz): 1.13 ppm (d, J = 8.8 Hz, 1 H, H^{anti} isomer A), 1.38 (d, J = 8.8 Hz, 1 H, H^{anti} isomer A), 1.43 (d, J = 8.3 Hz, 2 H, H^{anti} isomer S), 1.65 (s, 3 H, CH_3 acac isomer A), 1.75 (s, 6 H, CH_3 acac isomer S), 1.80 (s, 3 H, CH_3 acac isomer A), 2.94 (br., 2 H, H^{syn} isomer S), 3.38 (br., 1 H, H^c allyl isomer S + 1 H, H^{syn} isomer A), 3.55 (m, 1 H, H^c allyl isomer A + 1 H, H^{syn} isomer A), 4.96 (s, 1 H, CH acac isomer A), 5.12 (s, 1 H, CH acac isomer S), 6.14 (s, 1 H, H^4 pz isomer A), 6.28 (s, 1 H, H^4 pz isomer S), 7.15 (s, 1 H, H^3 pz isomer A), 7.22 (s, 1 H, H^3 pz isomer S), 7.37 (s, 1 H, H^5 pz isomer A), 7.4−7.9 (m, 15 H, C_6H_5 both isomers + 1 H, H^5 pz isomer S). Ratio isomer A/isomer S (253 K) = 1:0.5; ratio isomer A/isomer S (233 K) = 1:0.6; ratio isomer A/isomer S (213 K) = 1:0.7. $^{31}P\{^1H\}$ NMR (room temp., 121.49 MHz): 31.1 ppm (s, PPh_3). $^{31}P\{^1H\}$ NMR (213 K, 121.49 MHz): 33.6 ppm (s, PPh_3 isomer S), 39.3 (s, PPh_3 isomer A). $C_{63}H_{62}Au_2Cl_2Mo_2N_4O_8P_2$ (**3a**·0.5CH_2Cl_2): calcd. C 43.95, H 3.63, N 3.25; found C 43.62, H 3.52, N 3.20.

[Mo(acac)(η³-allyl)(CO)₂(μ-dmpz)AuPPh₃] (3b): *Method A:* Complex **2b** (0.039 g, 0.1 mmol) was added to a solution of [Au(acac)PPh_3] (0.056 g, 0.1 mmol) in THF (10 mL) and the solution, which rapidly turned orange, was stirred at room temperature for 5 min. The volatiles were removed in vacuo and the yellow residue was extracted in CH_2Cl_2/hexane (15:15 mL) and filtered. Concentration in vacuo and cooling to −20 °C gave a deep orange microcrystalline solid, which was decanted, washed with hexane (3 × 3 mL approximately), and dried in vacuo, yielding 0.055 g (65%). *Method B:* Complex **1b** (0.093 g, 0.2 mmol) was added to a solution of [Au(acac)PPh_3] (0.224 g, 0.4 mmol) in THF (10 mL) and the solution was stirred at room temp. for 1 h. The volatiles were removed in vacuo and the yellow residue was extracted in hexane/toluene (20:10 mL) and filtered. The insoluble residue was spectroscopically identified as [$AuBrPPh_3$].[25] The filtrate was evaporated to dryness and extracted in CH_2Cl_2/hexane (10:10 mL). Concentration in vacuo and cooling to −20 °C gave a deep orange microcrystalline solid, which was decanted, washed with hexane (3 × 3 mL

Table 3. Crystal data and refinement details for **1a**, **1b**, and **3b**

	Compound **1a**	Compound **1b**	Compound **3b**
Empirical formula	$C_{11}H_{13}BrMoN_4O_2$	$C_{15}H_{21}BrMoN_4O_2$	$C_{33}H_{34}AuMoN_2O_4P$
Formula mass	409.10	465.21	846.50
Crystal system	monoclinic	orthorhombic	triclinic
Space group	$P2_1/n$ (No. 14)	$P2_12_12_1$ (No. 19)	$P\bar{1}$ (No. 2)
a [Å]	8.368(1)	14.017(6)	8.142(4)
b [Å]	12.448(2)	14.739(6)	12.328(6)
c [A]	13.810(2)	18.347(7)	16.491(8)
α [deg]	90	90	77.122(8)
β [deg]	90.317(2)	90	84.196(9)
γ [deg]	90	90	81.489(7)
V [Å^3]	1.438.5(3)	3790.6(3)	1591.9(13)
Z	4	8	2
T [K]	293	293	293
d_{calc} [g cm^{-3}]	1.889	1.630	1.766
F(000)	800	1856	828
λ [Mo-$K_α$) [Å]	0.71073	0.71073	0.71073
Crystal size [mm]; color	0.15 × 0.15 × 0.10, yellow	0.25 × 0.17 × 0.15, yellow	0.16 × 0.06 × 0.02, orange
μ [mm^{-1}]	3.692	2.813	5.086
Scan range [deg]	2.2 ≤ θ ≤ 23.3	1.8 ≤ θ ≤ 23.3	1.3 ≤ θ ≤ 23.3
Absorption correction	SADABS	SADABS	SADABS
Corr. factors (min, max)	1.000, 0.725	1.000, 0.800	1.000, 0.646
Number of measured refelections	6182	17322	10236
Number of independent reflections [R(int)]	2063 (0.0235)	5470 (0.0316)	4570 (0.0983)
Number of observed reflections, $I \geq 2\sigma(I)$	1833	4880	2237
GOF on F^2	1.008	1.031	1.065
Number of parameters	180	424	371
Residuals R, $wR2$	0.0195, 0.0480	0.0225, 0.0403	0.0641, 0.1325

approximately), and dried in vacuo, yielding 0.073 g (43%). IR (THF): $\tilde{\nu}$ = 1924 cm^{-1} vs, 1825 vs. IR (KBr): $\tilde{\nu}$ = 3055 cm^{-1} w, 2990 w, 2914 w, 1913 vs, 1816 vs, 1585 s, 1521 s, 1482 w, 1437 m, 1393 m, 1374 m, 1264 w, 1184 vw, 1136 vw, 1102 m, 1020 w, 998 vw, 934 vw, 749 w, 712 w, 694 m, 545 m, 508 m. ^{1}H NMR (room temp., 300 MHz): 1.39 ppm (br., 2 H, H^{anti}), 1.60 (s, 6 H, CH_3 acac), 2.37 (s, 6 H, CH_3 dmpz), 3.27 (br., 1 H, H^c allyl), 3.38 (br., 2 H, H^{syn}), 4.80 (br., 1 H, CH acac), 5.88 (br., 1 H, H^4 dmpz), 7.52 (br., 10 H, C_6H_5,), 7.71 (br., 5 H, C_6H_5). ^{1}H NMR (213 K, 300 MHz, Major isomer): 1.37 ppm (d, J = 9.2 Hz, 1 H, H^{anti}), 1.44 (d, J = 8.9 Hz, 1 H, H^{anti}), 1.53 (s, 3 H, CH_3 acac), 1.69 (s, 3 H, CH_3 acac), 2.38 (s, 3 H, CH_3 dmpz), 2.40 (s, 3 H, CH_3 dmpz), 3.19 (m, 1 H, H^c allyl), 3.29 (br., 1 H, H^{syn}), 3.43 (br., 1 H, H^{syn}), 4.81 (s, 1 H, CH acac), 5.93 (s, 1 H, H^4 dmpz), 7.32 (m, 10 H, C_6H_5), 7.67 (m, 5 H, C_6H_5). Ratio major isomer/minor isomers = 1:0.3. ^{31}P{^{1}H} NMR (room temp., 121.49 MHz): 31.40 ppm (s, PPh$_3$). ^{31}P{^{1}H} NMR (213 K, 121.49 MHz): 30.4 (s, PPh$_3$, minor isomer), 30.6 (s, PPh$_3$, minor isomer), 31.0 (s, PPh$_3$, major isomer), 31.6 (s, PPh$_3$, minor isomer), 32.4 (s, PPh$_3$, minor isomer), 43.3 (s, PPh$_3$, minor isomer). The ^{1}H and ^{31}P{^{1}H} NMR spectra recorded at 213 K of a sample obtained immediately after mixing the solid complex and frozen $CDCl_3$ at −78 °C showed only signals of the major isomer. $C_{33}H_{34}AuMoN_2O_4P$: calcd. C 46.82, H 4.05, N 3.31; found C 46.45, H 3.85, N 3.05.

X-ray Crystallographic Study of 1a, 1b, and 3b: Crystals were grown by slow diffusion of hexane into concentrated solutions of the complexes in CH_2Cl_2 at −20 °C. Relevant crystallographic details are given in Table 3. A crystal was attached to a glass fiber and transferred to a Bruker AXS SMART 1000 diffractometer with graphite monochromatized Mo-K_α X-radiation and a CCD area detector. A hemisphere of the reciprocal space was collected up to 2θ = 48.6°. Raw frame data were integrated with the SAINT program.[26] The structure was solved by direct methods with SHELXTL.[27] A semi-empirical absorption correction was applied with the program SADABS.[28] All non-hydrogen atoms were refined anisotropically. Hydrogen atoms were set in calculated positions and refined as riding atoms, with a common thermal parameter. All calculations and graphics were made with SHELXTL. CCDC-189498 (**1a**), −189499 (**1b**), and −189500 (**3b**) contain the supplementary crystallographic data for this paper. These data can be obtained free of charge at www.ccdc.cam.ac.uk/conts/retrieving.html [or from the Cambridge Crystallographic Data Centre, 12, Union Road, Cambridge CB2 1EZ, UK; fax: (internat.) +44−1223/336-033; E-mail: deposit@ccdc.cam.ac.uk].

Acknowledgments

We thank the D.G.I.C.Y.T. (PB97 0470-C02-01) and the J.C.yL. (VA, 32/00B) for financial support.

[1] [1a] J. Reedijk, in: *Comprehensive Coordination Chemistry* (Eds.: G. Wilkinson, R. D. Gillard, J. A. McCleverty); Pergamon, Oxford, UK, **1987**; vol. 2., chapter 13.2.[1b]S. Trofimenko, *Prog. Inorg. Chem.* **1986**, *34*, 115−210. [1c] G. La Monica, G. A. Ardizzoia, *Prog. Inorg. Chem.* **1997**, *46*, 151−238.

[2] Some recent leading references: [2a] J. Barberá, A. Elduque, R. Giménez, L. A. Oro, J. L. Serrano, *Angew. Chem. Int. Ed. Engl.* **1996**, *35*, 2832−2835. [2b] C. Tejel, M. A. Ciriano, A. J. Edwards, F. J. Lahoz, L. A. Oro, *Organometallics* **1997**, *16*, 45−53. [2c] C. Tejel, M. A. Ciriano, J. A. López, F. J. Lahoz, L. A. Oro, *Organometallics* **1997**, *16*, 4718−4727. [2d] C. Tejel, M. A. Ciriano, J. A. López, F. J. Lahoz, L. A. Oro, *Angew. Chem. Int. Ed. Eng.* **1998**, *37*, 1542−1545. [2e] G. A. Ardizzoia, S. Cenini, G. La Monica, N. Masciocchi, A. Maspero, M. Moret, *Inorg. Chem.* **1998**, *37*, 4284−4292. [2f] C. Tejel, M. A. Ciriano, L. A. Oro, *Chem. Eur. J.* **1999**, *5*, 1131−1135. [2g] H. Matsushima, H. Hamada, K. Watanabe, M. Koikawa, T. Tokii, *J. Chem. Soc., Dalton Trans.* **1999**, 971−977. [2h] S. Komeda, M. Lutz, A. L. Spek, M. Chikuma, J. Reedijk, *Inorg. Chem.* **2000**, *39*, 4230−4236. [2i] E. Sola, F. Torres, M. V. Jiménez, J. A. López, S. E. Ruiz, F. J. Lahoz, A. Elduque, L. A. Oro, *J. Am. Chem. Soc.* **2001**, *123*, 11925−11932.

[3] See for example: [3a] L. A. Oro, D. Carmona, J. Reyes, C. Foces-Foces, F. H. Cano, *J. Chem. Soc., Dalton Trans.* **1986**, 31−37. [3b] D. Carmona, J. Ferrer, F. J. Lahoz, L. A. Oro, J. Reyes, M. Esteban, *J. Chem. Soc., Dalton Trans.* **1991**, 2811−2820. [3c] G. López, J. Ruiz, C. Vicente, J. M. Martí, G. García, P. A. Chaloner, P. B. Hitchcock, R. M. Harrison, *Organometallics* **1992**, *11*, 4090−4096. [3d] D. Carmona, J. Ferrer, R. Atencio, F. J. Lahoz, L. A. Oro, M. P. Lamata, *Organometallics* **1995**, *14*, 2057−2065. [3e] G. A. Ardizzoia, G. La Monica, A. Maspero, N. Masciocchi, M. Moret, *Eur. J. Inorg. Chem.* **1999**, 1301−1307. [3f] G. A. Ardizzoia, G. La Monica, A. Maspero, M. Moret, N. Masciocchi, *Eur. J. Inorg. Chem.* **2000**, 181−187. [3g] R. Contreras, M. Valderrama, E. M. Orellana, D. Boys, D. Carmona, L. A. Oro, M. P. Lamata, J. Ferrer, *J. Organomet. Chem.* **2000**, *606*, 197−202.

[4] [4a] P. Braunstein, J. Rose, in: *Comprehensive Organometallic Chemistry II* (Eds.: E. W. Abel, F. G. A. Stone, G. Wilkinson); Pergamon, Oxford, UK, **1995**; vol. 10, Ed. R. D. Adams, chapter 7. [4b]N. Wheatley, P. Kalck, *Chem. Rev.* **1999**, *99*, 3379−3419. [4c] R. D. Adams, *J. Organomet. Chem.* **2000**, *600*, 1−6.

[5] M. D. Curtis, O. Eisenstein, *Organometallics* **1984**, *3*, 887−895.

[6] J. W. Faller, D. A. Haitko, R. D. Adams, D. F. Chodosh, *J. Am. Chem. Soc.* **1979**, *101*, 865−876.

[7] [7a] S. K. Chowdhury, M. Nandi, V. S. Joshi, A. Sarker, *Organometallics* **1997**, *16*, 1806−1809. [7b] D. S. Frohnapfel, P. S. White, J. L. Templeton, H. Rüegger, P. S. Pregosin, *Organometallics* **1997**, *16*, 3737−3750. [7c] K.-B. Shiu, C.-J. Chang, Y. Wang, M.-C. Cheng, *J. Organomet. Chem.* **1991**, *406*, 363−369.

[8] P. Espinet, R. Hernando, G. Iturbe, F. Villafañe, G. A. Orpen, I. Pascual, *Eur. J. Inorg. Chem.* **2000**, 1031−1038.

[9] [9a] D. Carmona, L. A. Oro, M. P. Lamata, J. Elguero, M. C. Apreda, C. Foces-Foces, F. H. Cano, *Angew. Chem. Int. Ed. Engl.* **1986**, *25*, 1114−1115. [9b] D. Carmona, J. Ferrer, L. A. Oro, M. C. Apreda, C. Foces-Foces, F. H. Cano, J. Elguero, M. L. Jimeno, *J. Chem. Soc., Dalton Trans.* **1990**, 1463−1476. [9c] D. Röttger, G. Erker, M. Grehl, R. Fröhlich, *Organometallics* **1994**, *13*, 3897−3902. [9d] D. Carmona, J. Ferrer, J. M. Arilla, J. Reyes, F. J. Lahoz, S. Elipe, F. J. Modrego, L. A. Oro, *Organometallics* **2000**, *19*, 798−808.

[10] T. Beringhelli, G. D'Alonso, M. Panigati, F. Porta, P. Mercandelli, M. Moret, A. Sironi, *Organometallics* **1998**, *17*, 3282−3292.

[11] [11a] R. Davis, L. A. P. Kane-Maguire, in: *Comprehensive Organometallic Chemistry* (Eds.: G. Wilkinson, F. G. A. Stone, E. W. Abel); Pergamon, Oxford, UK, **1982**, vol. 8; 1156−1159. [11b] M. W. Whiteley, in: *Comprehensive Organometallic Chemistry II* (Eds.: E. W. Abel, F. G. A. Stone, G. Wilkinson); Pergamon, Oxford, UK, **1995**. vol. 12 (Eds.: J. A. Labinger, M. J. Winter); pp. 337−338.

[12] F. A. Cotton, R. L. Luck, *Acta Crystallogr., Sect. C* **1990**, *46*, 138−140.

[13] G. A. Jeffrey, *An Introduction to Hydrogen Bonding*; Oxford University Press, New York, **1997**, chapter 2.

[14] [14a] G. A. Ardizzoia, G. LaMonica, A. Maspero, M. Moret, N. Masciocchi, *Eur. J. Inorg. Chem.* **1998**, 1503−1511. [14b] J. Cámpora, J. A. López, C. M. Maya, P. Palma, E. Carmona, C. Ruiz, *Organometallics* **2000**, *19*, 2707−2715.

[15] [15a] B. M. Trost, M. Lautens, *J. Am. Chem. Soc.* **1982**, *104*, 5543−5545. [15b] B. M. Trost, M. Lautens, *J. Am. Chem. Soc.* **1987**, *109*, 1469−1478. [15c] B. M. Trost, C. A. Merlic, *J. Am.*

Chem. Soc. **1990**, *112*, 9590−9600. [15d] M. P. T. Sjögren, H. Frisell, B. Åkermark, P.-O. Norrby, L. Eriksson, A. Vitagliano, *Organometallics* **1997**, *16*, 942−950. [15e] B. M. Trost, I. Hachiya, *J. Am. Chem. Soc.* **1998**, *120*, 1104−1105.

[16] [16a] J. W. Faller, D. Linebarrier, *Organometallics* **1988**, *7*, 1670−1672. [16b] J. Pérez, L. Riera, V. Riera, S. García-Granda, E. García-Rodríguez, *J. Am. Chem. Soc.* **2001**, *123*, 7469−7470.

[17] A. T. T. Hsieh, B. O. West, *J. Organomet. Chem.* **1976**, *112*, 285−296.

[18] A referee has drawn our attention to the fact that the different populations of isomers **S** in complexes **1** and **2** could be related to the ligand *trans* to the allyl: pyrazole for **2**, but Br for **1**. In fact, there is a clear preference for the pyrazole against the bromo ligand in complexes **1**, whereas a more balanced competition between acac and the pyrazole seems to take place in complexes **2**.

[19] Ref.[13] paragraph 11.2.

[20] B. J. Brisdon, A. A. Woolf, *J. Chem. Soc., Dalton Trans.* **1978**, 291−295.

[21] F. Bachechi, A. Burini, R. Galassi, B. R. Pietroni, M. Severini, *J. Organomet. Chem.* **1999**, *575*, 269−277.

[22] D. D. Perrin, W. L. F. Armarego, *Purification of Laboratory Chemicals*; 3rd ed.; Pergamon Press: Oxford, **1988**.

[23] H. Tom Dieck, H. Friedel, *J. Organomet. Chem.* **1968**, *14*, 375−385.

[24] J. Vicente, M. T. Chicote, *Inorg. Synth.* **1998**, *32*, 172−177.

[25] P. F. Barron, L. M. Engelhardt, P. C. Healy, J. Oddy, A. H. White, *Aust. J. Chem.* **1987**, *40*, 1545−1555.

[26] *SAINT+.SAX* area detector integration program. Version 6.02. Bruker AXS, Inc., Madison, WI, **1999**.

[27] G. M. Sheldrick; *SHELXTL*, An integrated system for solving, refining, and displaying crystal structures from diffraction data. Version 5.1. Bruker AXS, Inc. Madison, WI, **1998**.

[28] G. M. Sheldrick; *SADABS*, Empirical Absorption Correction Program. University of Göttingen: Göttingen, Germany, **1997**.

Received July 15, 2002
[I02387]

Synthesis, Crystal Structure and Magneto-Structural Correlation of an Unusual Thiocyanato-Bridged Nickel(II) Compound, $[Ni(\mu\text{-}NCS)(dpt)(NCS)]_2$-$[Ni(\mu\text{-}NCS)(dpt)(NCS)]_4$ [dpt = bis(3-aminopropyl)amine]

Tapas Kumar Maji,[a] Golam Mostafa,[b] Juan M. Clemente-Juan,[c] Joan Ribas,*[d] Francesc Lloret,[c] Ken-ichi Okamoto,[e] and Nirmalendu Ray Chaudhuri*[a]

Keywords: Nickel / Bridging ligands / S ligands / Magnetic properties / N ligands

Reaction of $Ni(ClO_4)_2 \cdot 6H_2O$ with bis(3-aminopropyl)amine (dpt) and ammonium thiocyanate produces the novel thiocyanato-bridged nickel(II) compound $[Ni(\mu\text{-}NCS)(dpt)(NCS)]_2[Ni(\mu\text{-}NCS)(dpt)(NCS)]_4$, which has been structurally characterised. The structure determination reveals that there are two different molecules in the crystal lattice; one is dinuclear and other is tetranuclear. Low-temperature magnetic measurements show that there are ferro- as well as antiferromagnetic interactions. The ferromagnetic interaction arises from the dinuclear part and the doubly bridged part of the tetranuclear unit; the antiferromagnetic interaction occurs between singly bridged nickel centres in the tetranuclear unit.

(© Wiley-VCH Verlag GmbH & Co. KGaA, 69451 Weinheim, Germany, 2003)

Introduction

In the last few years there has been a considerable amount work dedicated to the design and elaboration of polymetallic molecular systems with extended structures and electronic properties, mainly molecular-based magnets and inorganic materials.[1−5] The precondition for synthesising these type of materials is that the metal ions should have an unpaired electron and should be assembled in a molecule containing a bridging moiety that can propagate this electron between the paramagnetic metal centres. The pseudohalogens are very versatile ligands for making such a bridge. Amongst them, the versatility of the azido ligand as a superexchange pathway in polynuclear complexes of Cu^{II}, Ni^{II} and Mn^{II} has been well explored.[6−11] In contrast, thiocyanato-bridged polynuclear systems are not common.[12−15] Curtis et al.[16] have reported the synthesis of $[NiL(NCS)_2]$ [L = bis(2-aminoethyl)amine (dien) or bis(2-aminopropyl)amine (dpt)] and have proposed structures with one bridging thiocyanate and one N-bonded terminal thiocyanate in the *cis* position on the basis of IR spectroscopy. Vicente et al.,[12,14] however, have reported the structures and magnetic properties of two polymeric complexes, $[Ni(\mu\text{-}NCS)(L)(NCS)]_n$ [L = bis(2-aminoethyl)methylamine (medien) or bis(3-aminopropyl)methylamine (medpt)] and have observed noticeable differences in the structures upon increasing the chain length of the triamine.

Recently, our group has also reported[17−19] some novel thiocyanato-bridged nickel(II) complexes and noticed some remarkable phenomena, such as that the chain length of the linear chain triamine, the alkyl group substitution on the donor atom of the triamine and the method of preparation play a very important role when synthesising complexes with different nuclearities. Starting with $Ni(NCS)_2$ in methanol, dien gives a dimeric structure whereas aepn [(2-aminoethyl)(3-aminopropyl)amine] yields a polymeric structure.[17] On the other hand, the reaction of medpt with $Ni(NCS)_2$ in methanol gives two dimeric fragments in the unit cell,[18] while the reaction between $Ni(ClO_4)_2 \cdot 6H_2O$ and NH_4NCS generates a 1D polymeric complex.[14]

The present paper reports the synthesis, X-ray structure analysis and magneto-structural correlation of a novel thiocyanato-bridged nickel(II) compound $[Ni(\mu\text{-}NCS)(dpt)(NCS)]_2[Ni(\mu\text{-}NCS)(dpt)(NCS)]_4$. The structure determination reveals that this is a rare type of thiocyanato-bridged

[a] Department of Inorganic Chemistry,
Indian Association for the Cultivation of Science,
Kolkata, 700 032, India
E-mail: icnrc@mahendra.iacs.res.in
Fax: (internat.) +91-33/2473-2805
[b] Department of Physics,
Krishnath College, Berhampur 742 109, India
[c] Departament and Instituto de Ciencia Molecular,
Universidad de Valencia, c/ Doctor Moliner, 50, 46100-Burjassot, Spain
[d] Departament de Química Inorgànica,
Universitat de Barcelona, c/ Diagonal, 647, 08028-Barcelona, Spain
E-mail: jribas@kripto.ub.es
[e] Department of Chemistry,
University of Tsukuba, Ibaraki 305, Japan

compound containing two different molecules in the crystal lattice: one is dinuclear and other is tetranuclear. Linear chain tetranuclear nickel(II) octahedral compounds are scarce in the literature.[20−21] Low-temperature magnetic measurements show that there are ferro- as well as antiferromagnetic interactions. The ferromagnetic interaction arises from the dinuclear part and the doubly bridged part of the tetranuclear unit; the antiferromagnetic interaction occurs between singly bridged nickel centres in the tetranuclear unit. To the best our knowledge this is the first report of a thiocyanato-bridged nickel(II) compound where ferro- as well as antiferromagnetic interactions are observed.

Results and Discussion

IR Spectroscopy

The compound shows two bands with medium intensity at $\tilde{\nu}$ = 3240, 3300 cm^{-1} corresponding to ν(N−H) and at $\tilde{\nu}$ = 2880, 2925 cm^{-1} assigned to the ν(C−H) stretching vibration of the triamine ligand. The occurrence of two strong peaks at 2080 and 2110 cm^{-1} in the IR spectrum, corresponding to ν(CN) stretching vibrations, suggests the presence of a bridging as well as a terminal linkage of the thiocyanate ligand. The higher frequency correlates to the bridging thiocyanate group whereas the lower frequency is assigned to a terminally bound thiocyanate ligand.[22]

Description of the Structure

The structure determination of the title complex reveals that there are two crystallographically independent molecules in the unit cell. One part of the complex is a dimer and other part is a tetramer (Figure 1). In the dimeric fragment two nickel atoms (Ni1 and its symmetry related counterpart) are bridged by two thiocyanate ligands in an end-to-end fashion; the other two thiocyanate groups exist as terminal ligands. The coordination polyhedron around the Ni1 atom in the dimeric fragment is best described as a distorted octahedron with an N_5S donor set. The three nitrogen atoms (N7, N8 and N9) from the triamine dpt ligand and one nitrogen atom (N1*; * =1 − *x*, 1 − *y*, 1 − *z*) from one of the bridging thiocyanate groups define the equatorial plane for Ni1 atom. The equatorial Ni1−N bond lengths are in the range 2.059(5)−2.114(4) Å (Table 1). The axial position is occupied by S1 [Ni1−S1, 2.577(2) Å] and N2 [Ni1−N2, 2.106(4) Å] from the bridging and terminal thiocyanate ligand, respectively. The Ni1 atom deviates from the mean plane by 0.008(2) Å and the maximum deviation of any equatorial atom (N1*) from the mean plane is 0.011(2) Å.

In the tetrameric part, the asymmetric unit comprises two nickel atoms (Ni2 and Ni3) with different coordination environments. The geometry around the Ni2 centre in the tetrameric part is distorted octahedral with an NiN_6 chromophore. The Ni2 atom is linked to Ni3 centre by only one bridging thiocyanate ligand. The other two terminal thiocy-

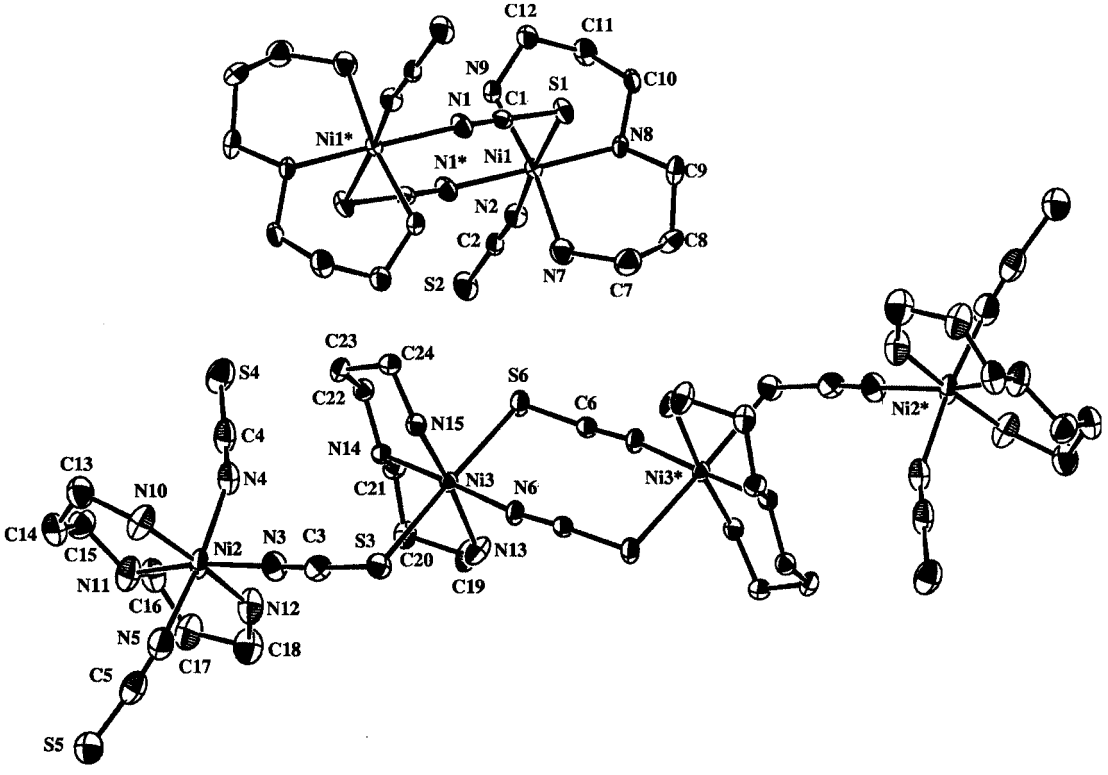

Figure 1. ZORTEP plot with atom labelling scheme of $[Ni(\mu_{N,S}\text{-NCS})(dpt)(NCS)]_2[Ni(\mu_{N,S}\text{-NCS})(dpt)(NCS)]_4$ (thermal ellipsoids are drawn at 50% probability for all non-hydrogen atoms)

Table 1. Selected bond lengths (Å) and angles (°) for [Ni(μ-NCS)(dpt)(NCS)]$_2$[Ni(μ-NCS)(dpt)(NCS)]$_4$

Ni1−S1	2.577(2)	Ni1−N2	2.106(4)
Ni1−N7	2.096(6)	Ni1−N8	2.114(4)
Ni1−N9	2.059(5)	Ni1−N1i[a]	2.105(4)
Ni2−N5	2.078(7)	Ni2−N10	2.075(7)
Ni2−N11	2.291(7)	Ni2−N12	2.022(7)
Ni2−N3	2.082(5)	Ni2−N4	2.133(6)
Ni3−N6	2.086(4)	Ni3−S3	2.667(2)
Ni3−S6	2.522(2)	Ni3−N15	2.062(4)
Ni3−N13	2.027(5)	Ni3−N14	2.117(4)
S1−Ni1−N2	175.66(11)	N3−Ni2−N4	89.9(2)
S1−Ni1−N7	90.49(15)	N3−Ni2−N11	168.3(2)
S1−Ni1−N8	87.45(12)	S3−Ni3−S6	175.62(5)
S1−Ni1−N9	90.94(13)	S3−Ni3−N6	83.70(11)
S1−Ni1−N1i[a]	92.46(13)	S6−Ni3−N13	96.12(15)
N2−Ni1−N7	88.85(19)	S6−Ni3−N14	88.83(11)
N2−Ni1−N8	88.32(15)	S6−Ni3−N15	92.90(11)
N2−Ni1−N9	90.35(18)	N6−Ni3−N13	85.97(19)
N1i−Ni1−N2[a]	91.79(16)	N6−Ni3−N14	178.26(18)
N7−Ni1−N8	94.45(19)	N6−Ni3−N15	88.66(17)
N7−Ni1−N9	171.31(18)	N13−Ni3−N14	92.55(19)
N1i−Ni1−N7[a]	86.52(19)	N13−Ni3−N15	169.67(18)
N8−Ni1−N9	94.18(16)	N14−Ni3−N15	92.66(17)
N1i−Ni1−N8[a]	179.02(19)	S3−Ni3−N14	95.28(11)
N1i−Ni1−N9[a]	84.85(16)	S3−Ni3−N15	85.43(11)
N3−Ni2−N12	88.8(2)	S3−Ni3−N13	85.21(15)
N4−Ni2−N5	173.7(3)	S6−Ni3−N6	92.22(11)
N4−Ni2−N10	92.1(2)	Ni1−S1−C1	102.54(18)
N4−Ni2−N11	91.9(2)	Ni3−S3−C3	104.5(2)
N4−Ni2−N12	89.6(3)	Ni3−S6−C6	102.24(19)
N5−Ni2−N10	83.7(3)	Ni1i−N1−C1[a]	163.7(4)
N5−Ni2−N11	84.0(3)	Ni1−N2−C2	165.2(3)
N5−Ni2−N12	94.4(3)	N10−Ni2−N11	96.5(2)
N10−Ni2−N12	175.9(3)	N11−Ni2−N12	79.7(3)
N3−Ni2−N5	95.1(2)	N3−Ni2−N10	95.0(2)
Ni2−N3−C3	176.5(5)	Ni2−N4−C4	155.8(6)
Ni2−N5−C5	161.9(7)	Ni3−N6−C6ii[a]	157.0(4)
S1−C1−N1	178.2(5)	S2−C2−N2	178.8(5)
S3−C3−N3	176.0(6)	S4−C4−N4	176.7(8)
S5−C5−N5	173.7(8)	S6−C6−N6	176.4(5)

[a] Symmetry code: i = 1 − x, 1 − y, 1 − z; ii = 3 − x, 2 − y, 1 − z.

anate groups are attached in a *cis* position to each other. The two nitrogen atoms (N4 and N5) [Ni2−N4, 2.133(6) Å; Ni2−N5, 2.078(7) Å] from the two pendent thiocyanate groups and other two nitrogen atoms (N10, N12) [Ni2−N10, 2.075(7) Å; Ni2−N12, 2.022(7) Å] (Table 1) form the equatorial plane around Ni2. One nitrogen atom (N3) [Ni2−N3, 2.082(5) Å] of the singly bridging thiocyanate ligand and a second nitrogen atom (N11) [Ni2−N11, 2.291(7) Å] of the triamine are in a *trans* axial position around Ni2. The maximum deviation of Ni2 from the mean plane formed by the four equatorial nitrogen atoms is 0.077(3) Å and the maximum deviation of any equatorial atom (N10) from the mean plane is 0.011(3) Å. In the case of Ni3 all the ligated thiocyanate groups are involved in bridging: two of them are attached to its symmetry related counterpart Ni3* and the other to Ni2. The coordination environment around Ni3 is pseudo-octahedral with an NiN_4S_2 chromophore. The two sulfur atoms (S6, S3) [Ni3−S6, 2.522(2) Å; Ni3−S3, 2.667(2) Å] from thiocyanate groups and N13 and N15 [Ni3−N13, 2.027(5) Å; Ni3−N15, 2.062(4) Å] (Table 1) from the triamine ligand define the equatorial plane around Ni3. The *trans* axial sites are occupied by N14 and N6 [Ni3−N14, 2.117(4) Å; Ni3−N6, 2.086(4) Å] of the triamine ligand and the bridging thiocyanate group, respectively. The maximum deviation of Ni3 from the mean plane formed by the four equatorial atoms is 0.088(2) Å and the maximum deviation of any equatorial atom (S3) from the mean plane is 0.005(2) Å.

The Ni−S−C, Ni−N−C and N−C−S angles in the bridge are 102.2(2)−104.5(3) Å, 157.0(4)−176.5(5) Å and 176.0(6)−178.2(5) Å, respectively. The Ni−N−C angle in the nonbridging thiocyanate group is 155.8(9)−166.9(5) Å. The Ni···Ni separation in the dimeric fragment is 5.736(9) Å and in the tetrameric fragment Ni2···Ni3 and Ni3···Ni3* are 5.998(2) and 5.682(3) Å, respectively. Weak intra- and intermolecular H-bonding (Table 2) results in a 1D supramolecular network lying on the *ab* plane (Figure 2). These H-bonding interactions are responsible for the overall conformation and stability of the crystal lattice.

Table 2. Hydrogen bonding interactions (Å,°) for [Ni(μ-NCS)(dpt)(NCS)]$_2$[Ni(μ-NCS)(dpt)(NCS)]$_4$

D−H···A[a]	D−H	H···A	D···A	D−H···A
N7−H7A···S6^{i}	0.90	2.865	3.696(6)	154.25
N15−H15A···S2^{ii}	0.90	2.711	3.500(6)	146.90

[a] Symmetry code: (i) =2 − x, 1 − y, 1 − z; (ii) = 3 − x, 1 − y, 1 − z.

Magnetic Measurements

Taking into account that there are two independent molecular entities — one dinuclear and the other tetranuclear — a plot of the magnetic data in the 200−2 K range is shown in Figure 3 as $\chi_M T$ vs. T for a molecular weight corresponding to six nickel(II) atoms. At 200 K, the $\chi_M T$ value is equal to 7.047 cm^3·mol^{-1}·K, a value that would be expected for six isolated nickel(II) ions with local S = 1 spins. $\chi_M T$ increases smoothly as T is lowered, reaching a maximum value of 7.35 cm^3·mol^{-1}·K at 22 K. From this temperature down to 2 K there is a clear and abrupt decrease of $\chi_M T$, reaching a minimum of 3.9147 cm^3·mol^{-1}·K at 2 K. These features are indicative of global weak ferromagnetic interactions between nickel(II) ions in the dinuclear and/or in the tetranuclear species present in the crystal, followed by a contribution of zero-field splitting, D, and antiferromagnetic coupling between the dinuclear and tetranuclear systems. Variable-temperature susceptibility data for a dinuclear moiety could be analysed using the isotropic Ginsberg [23] model from the Hamiltonian

$$H = -2JS_1S_2 - D(S_{1z}^2 + S_{2z}^2) - g\beta H(S_1 + S_2) - z'J'S\{S\}$$

where J is the intradimer exchange parameter, D the single-ion zero-field splitting and $z'J'$ the quantity for effective interdimer exchange; it is assumed that $g_x = g_y = g_z = g$. As previously indicated by Ginsberg, the parameters D and $z'J'$ are very strongly correlated with each other, but are

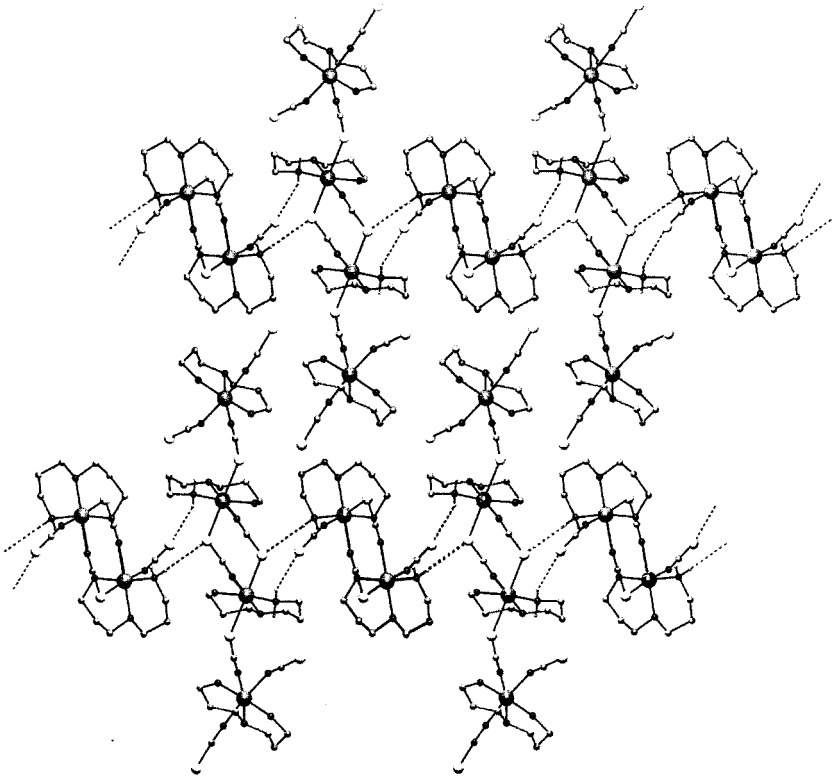

Figure 2. View of infinite one-dimensional H-bonded polymeric network of $[Ni(\mu_{N,S}\text{-}NCS)(dpt)(NCS)]_2[Ni(\mu_{N,S}\text{-}NCS)(dpt)(NCS)]_4$ (for clarity only relevant hydrogen atoms are shown)

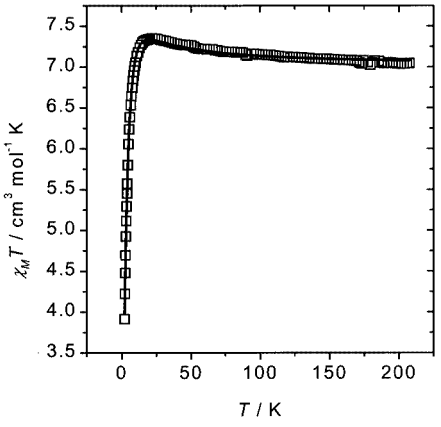

Figure 3. $\chi_M T$ vs. T plot for $[Ni(\mu_{N,S}\text{-}NCS)(dpt)(NCS)]_2[Ni(\mu_{N,S}\text{-}NCS)(dpt)(NCS)]_4$ [considering a molecular weight of 1836.58 corresponding to six nickel(II) centres]; the solid line corresponds to the best fit

The spin-Hamiltonian for all these tetranuclear nickel(II) complexes can easily be solved applying Kambe's method,[29] although for the linear systems a full diagonalization method is required and, seemingly, has never used for this kind of complex. The topological spin-scheme for this system is represented in Scheme 1.

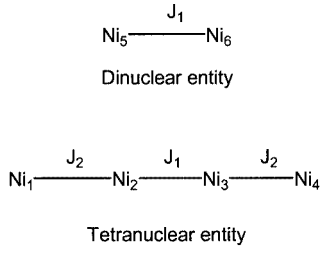

Scheme 1

only weakly correlated with g and J, therefore it is impossible to calculate D and $z'J'$ values accurately. Unfortunately, there is no mathematical expression which allows a fit of the tetranuclear part. The tetranuclear nickel(II) complexes reported in the literature are either planar, rhomboidal, cubanes or have square (cyclic) cores;[24−27] one zig-zag tetranuclear nickel(II) complex is known where two terminal nickel(II) atoms are in a square-planar geometry and thus show a diamagnetic behaviour.[28]

In this scheme, taking into account the structure, we assume that the coupling constants between the nickel(II) ions in the dinuclear entity (Ni1−Ni1*) and the central part (Ni3−Ni3*) of the tetranuclear entity (J_1) are the same. In both these cases, the two nickel(II) ions are linked by two thiocyanate bridges, although the terminal nickel(II) ions are linked to the central ones by only a thiocyanate bridge in the tetranuclear entity. Following this scheme, the ther-

mal variation of the $\chi_M T$ product was analysed using the following anisotropic Hamiltonian:

$$H = -2J_1(S_2S_3 + S_5S_6) - 2J_2(S_1S_2 + S_3S_4) + D(S_{1z}^2 + S_{2z}^2 + S_{3z}^2 + S_{4z}^2 + S_{5z}^2 + S_{6z}^2)$$

This Hamiltonian takes into account the interactions of one tetramer unit and one dimer unit at the same time. In order to remove the over-parametrization we have assumed some simplifications. Firstly, both exchange pathways through two end-to-end thiocyanate bridging ligands are associated to the same parameter, J_1, and secondly all single-ion parameters are identical (all single-ion anisotropies, D_i, are equal and collinear and all nickel(II) atoms have the same isotropic g value).

Evaluation of the susceptibility curve was performed with the MAGPACK programs package.[30−31] This efficient computing program allows the solution of the full spin-Hamiltonian by a numerical procedure and the calculation of the magnetic properties of spin clusters of arbitrary nuclearity, topology and anisotropy. Least-squares fitting of the magnetic data was accomplished with an adapted version of the function-minimization program MINUIT.[32] Using this conditions the best set of parameters is the following: $J_1 = +2.73$ cm^{-1}, $J_2 = -1.27$ cm^{-1}, $D = 3.12$ cm^{-1} and $g = 2.16$ ($R = 3.1 \times 10^{-3}$).

Magneto-Structural Correlations

The number of nickel(II) complexes with one or two bridging thiocyanate ligands is very limited. The magnetic data and the main structural parameters of these complexes, along with the title complex, are gathered in Tables 3 and 4. The J values found for the two systems with double end-to-end bridging thiocyanate ligand agree perfectly with those reported in the literature for the same kind of linkage. As can be seen from Table 3 the structural parameters are also very similar. However, the single thiocyanate bridging ligand in the tetrameric entity causes an antiferromagnetic coupling, while the other three complexes reported so far are ferromagnetically coupled. Comparing Tables 3 and 4 it is easy to realize that when there are two bridging thiocyanate ligands, J is always positive and greater than the values reported when there is only one thiocyanate ligand. On the other hand, the Ni−S−C and Ni−N−C angles are very different in the tetrameric entity from the other three complexes (Table 4). It has been postulated that these angles are the most important features for the character of the exchange coupling constant;[33] the Ni2−N3−S3−Ni3 torsion angle is −4.8°. It has been reported that, with the very similar OCN^- ligand, the effect of this torsion angle is similar to that reported for the azido bridging ligand: the maximum of the antiferromagnetic component corresponds to a torsion of 180° (or 0°), with a value close to zero for $J_{antiferro}$ (accidental orthogonality) for a torsion angle of 90°.[33] According to this idea, it is not surprising to find that other metal complexes with end-to-end bridging thiocyanate ligands show antiferromagnetic coupling. The $2J$ value for a dinuclear copper(II) complex is −148.2 cm^{-1},[34] and for some similar manganese(II) complexes the J values are −0.15 cm^{-1} and −2.5 cm^{-1}.[35−36]

New efforts are necessary for synthesising new complexes with this kind of structure in order to analyze their magnetic properties. This goal will not be easy, though, because there is a spontaneous tendency for four nickel(II) ions to give cubane-like or square-planar complexes.[24−27]

Table 3. Main structural and magnetic parameters for dinuclear nickel(II) complexes with double thiocyanate bridging bond

Compound[a]	Ni−S−C (°)	Ni−N−C (°)	Ni−N (Å)	Ni−S (Å)	J (cm^{-1})	Ref.
$[Ni_2(tren)_2(\mu\text{-}NCS)_2](BPh_4)_2$	100.0	167	2.04	2.61	2.4	[43]
$[Ni_2(terpy)(NCS)_2(\mu\text{-}NCS)_2]$	100.0(8)	159(2)	1.99	2.62	4.9	[44]
$[Ni_2(ibn)_3(NCS)_2(\mu\text{-}NCS)_2]$	100.7	165.2	2.06	2.55	4.3	[45]
	105.8	142.4	2.10	2.64		
$[Ni_2(ibn)_4(\mu\text{-}NCS)_2](PF_6)_2$	96.2	166.7	1.92	2.83	6.3	[45]
$[Ni_2(en)_4(\mu\text{-}NCS)_2]I_2$	100.0	167.0	2.04	2.61	4.5	[46,47]
dinuclear entity (*)	102.54	163.74	2.11	2.57	2.73	[b]
tetranuclear entity (*)	102.24	157.00	2.08	2.66	2.73	[b]

[a] (tren = 2,2′,2′′-triaminotriethylamine; terpy = 2,2′:6′,2′′-terpyridine; ibn = 1,2-diamino-2-methylpropane; en = 1,2-diaminoethane). [b] This work.

Table 4. Main structural and magnetic parameters for polymeric and polynuclear nickel(II) complexes with single thiocyanate bridging bond

Compound[a]	Ni−S−C(°)	Ni−N−C(°)	Ni−N (Å)	Ni−S(Å)	J (cm^{-1})	Ref.
$[Ni(medien)(NCS)(\mu\text{-}NCS)]_n$	100.24	167.5	2.04	2.66	0.96	[12]
$[Ni(en)_2(\mu\text{-}NCS)]_n(PF_6)_n$	100.8	171.5	2.10	2.62	0.2	[13]
$[Ni(medpt)(NCS)(\mu\text{-}NCS)]_n$	100.5	161.5	2.11	2.55	1.16	[14]
Tetranuclear entity	104.50	176.50	2.08	2.66	−1.27	[b]

[a] medien = bis(2-aminoethyl)methylamine; en = 1,2-diaminoethane; medpt = bis(3-aminopropyl)methylamine. [b] This work.

Experimental Section

Materials: High purity (98%) bis(3-aminopropyl)amine (dpt) was purchased from Aldrich Chemical Company Inc. and used as received. All other chemicals used were of AR grade.

Physical Measurements: Elemental analysis (C, H and N) was performed using a Perkin−Elmer 240C elemental analyser. IR spectra (4000−400 cm^{-1}) were taken using Nicolet Magna-IR 750 spectrometer series-II. Variable temperature (2−208 K) magnetic susceptibility measurements on polycrystalline sample was carried out with a Quantum Design SQUID magnetometer. Diamagnetic corrections of the constituent atoms were estimated from Pascal's constants.

Synthesis of [Ni(μ-NCS)(dpt)(NCS)]$_2$[Ni(μ-NCS)(dpt)(NCS)]$_4$: A methanolic solution (5 mL) of dpt (1 mmol) was added to an aqueous solution (15 mL) of $Ni(ClO_4)_2·6H_2O$ (1 mmol). Solid NH_4SCN (2 mmol) was then added slowly with constant stirring. The resulting solution was kept in a $CaCl_2$ desiccator and after a few days a blue crystalline complex separated out. This was dissolved in ethanol and filtered and the filtrate was kept in an open atmosphere. After some days blue single crystals suitable for X-ray diffraction were obtained. Yield ca. 80%. $C_8H_{17}N_5NiS_2$ (306.1): calcd. C 31.40, N 22.89, H 5.56, Ni 19.18; found C 31.40, N 22.88, H 5.54, Ni 19.20. IR: ν(NH_2), 3240, 3300 cm^{-1}; ν(CH_2), 2880, 2925 cm^{-1}; ν(CN), 2080, 2120 cm^{-1}.

Reaction Scheme:

$6Ni(ClO_4)_2·6H_2O + 12NH_4SCN + 6dpt = [Ni(μ\text{-}NCS)(dpt)(NCS)]_2[Ni(μ\text{-}NCS)(dpt)(NCS)]_4 + 12NH_4ClO_4 + 36H_2O$

Crystal-Data Collection and Refinement: A suitable single crystal of the title complex was mounted on a Rigaku AFC 7 diffractometer. The unit cell parameters and crystal orientation matrix were determined by least square refinement of 25 accurately centred reflections. Intensity data were collected in the ω-2θ scan mode using graphite-monochromated Mo-$K_α$ radiation. The crystal and instrument stabilities were monitored with a set of three standard reflections measured at a regular interval; in all cases no significant variations were found. The intensity data were corrected for Lorentz and polarisation effects[37] and an empirical absorption correction based on ψ-scans (T_{min}/T_{max} 0.678/0.968) was also employed. A total of 5865 reflections ($2.1 < θ < 27.5°$) were measured and all of them were assumed observed applying the condition $I > 2σ(I)$. The structure was solved by a Patterson synthesis and followed by successive Fourier and difference-Fourier syntheses. Full-matrix least-squares refinements on F^2 were carried out using SHELXL-97, with anisotropic displacement parameters for all non-hydrogen atoms. Hydrogen atoms were included in fixed calculated positions. At convergence the final residuals were $R = 0.045$; $wR = 0.122$. The final difference Fourier map showed a maximum and minimum peak height of 0.54 e·Å^{-3} and −0.39 e·Å^{-3} respectively, with no chemical significance. Complex neutral atom scattering factors[38] were used throughout. All calculations were carried out using the SHELXS-86,[39] SHELXL-97,[40] PLATON 99[41] and ZORTEP[42] programs. Crystal data are summarised in Table 5. Selected bond lengths and angles are listed in Table 1. Possible hydrogen bonds are displayed in Table 2.

Table 5. Crystal data and details of the structure determination for [Ni(μ-NCS)(dpt)(NCS)]$_2$[Ni(μ-NCS)(dpt)(NCS)]$_4$

Chemical formula	$C_{24}H_{51}N_{15}S_6Ni_3$
Molecular weight	918.29
T (K)	293(2)
λ (Å) (Mo-$K_α$)	0.71073
Crystal system	Triclinic
Space group	$P\bar{1}$ (No. 2)
a (Å)	7.680(10)
b (Å)	15.134(2)
c	18.719(4)
α (°)	70.550(10)
β (°)	81.540(10)
γ (°)	87.280(10)
V (Å^3)	2029.2(6)
Z	1
$ρ_{cal}$ (mg m^{-3})	1.503
μ (mm^{-1}) (Mo-$K_α$)	1.725
F(000)	960
Crystal size (mm)	0.50 × 0.40 × 0.20
θ range (°)	2.1−27.5
Reflections collected	5865
Reflections observed [$I > 2σ(I)$]	5865
$R(F)$[a]	0.0445
$wR(2)$	0.1221

[a] $R = ||F_o| - |F_c||/|F_o|$; $Rw = [\{w(F_o^2 - F_c^2)^2\}/\{w(F_o^2)^2\}]^{1/2}$.

CCDC-180314 contains the supplementary crystallographic data for this paper. These data can be obtained free of charge at www.ccdc.cam.ac.uk/conts/retrieving.html [or from the Cambridge Crystallographic Data Centre, 12, Union Road, Cambridge CB2 1EZ, UK; Fax: (internat.) +44-1223/336-033; E-mail: deposit@ccdc.cam.ac.uk].

Acknowledgments

The authors are grateful to the council of Scientific and Industrial Research (New Delhi) for financial support.

[1] *Magnetic Molecular Materials* (Eds.: D. Gatteschi, O. Kahn, J. S. Miller, F. Palacio), NATO ASI Series, No. E198; Kluwer Academic Publishers: Dordrecht, The Netherlands, **1991**.
[2] O. Kahn, *Adv. Inorg. Chem.* **1995**, *43*, 179−259.
[3] J. S. Miller, A. J. Epstein, W. M. Reiff, *Science* **1988**, *240*, 40−47.
[4] D. Gatteschi, *Adv. Mater.* **1994**, *6*, 635−645.
[5] *Magnetism: A Supramolecular Function* (Ed.: O. Kahn), NATO ASI Series, No. C484; Kluwer Academic Publishers: Dordrecht, The Netherlands, **1996**.
[6] J. Ribas, A. Escuer, M. Monfort, R. Vicente, R. Cortes, L. Lezema, T. Rojo, *Coord. Chem. Rev.* **1999**, *193−195*, 1027.
[7] L. K. Thompson, S. S. Tandon, *Comments Inorg. Chem.* **1996**, *18*, 125−144.
[8] P. S. Mukherjee, T. K. Maji, G. Mostafa, T. Mallah, N. Ray Chaudhuri, *Inorg. Chem.* **2000**, *39*, 5147−5150.
[9] T. K. Maji, P. S. Mukherjee, G. Mostafa, T. Mallah, J. Cano-Boquera, N. Ray Chaudhuri, *Chem. Commun.* **2001**, 1012.
[10] F. A. Mautner, R. Cortes, L. Lezema, T. Rojo, *Angew. Chem. Int. Ed. Engl.* **1996**, *35*, 96−98.
[11] J. Ribas, M. Monfort, R. Costa, X. Solans, *Inorg. Chem.* **1993**, *32*, 695−699.
[12] A. Escuer, S. B. Kumar, F. Mautner, R. Vicente, *Inorg. Chim. Acta* **1998**, *269*, 313−316.
[13] M. Monfort, C. Bastos, C. Diaz, J. Ribas, *Inorg. Chim. Acta* **1994**, *218*, 185−188.
[14] R. Vicente, A. Escuer, J. Ribas, X. Solans, *J. Chem. Soc., Dalton Trans.* **1994**, 259.
[15] R. Vicente, A. Escuer, E. Peñalba, X. Solans, M. Font-Bardía, *Inorg. Chim. Acta* **1997**, *255*, 7−12.
[16] N. F. Curtis, Y. M. Curtis, *Aust. J. Chem.* **1966**, *19*, 1423−1430.
[17] A. Mondal, C. Pariya, N. Ray Chaudhuri, N. P. Nayak, A. K. Mukherjee, A. Ghosh, *Polyhedron* **1997**, *16*, 39−45.

[18] A. K. Mukherjee, N. P. Nayak, A. Mondal, N. Ray Chaudhuri, *Acta Crystallogr., Sect. C* **1999**, *55*, 365−368.
[19] N. P. Nayak, A. K. Mukherjee, A. Mondal, N. Ray Chaudhuri, *Acta Crystallogr., Sect. C* **1998**, *54*, 208−210.
[20] S. Y Lai, T. W. Lin, Y. H. Chen, C. C. Wang, G. H. Lee, M.H. Yang, M. K. Leung, S. M. Peng, *J. Am. Chem. Soc.* **1999**, *121*, 250−251.
[21] S. Uozumi, H. Furutachi, M. Ohba, H. Okawa, D. E. Fenton, K. Shindo, S. Murata, D. J. Kitko, *Inorg. Chem.* **1998**, *37*, 6281−6287.
[22] K. Nakamoto, *Infrared and Raman Spectra of Inorganic and Coordination Compounds*, 3rd Edn, p 271−275, Wiley- Interscience, New York, **1978**.
[23] A. P. Ginsberg, R. L. Martin, R. W. Brookes, R. C. Sherwood, *Inorg. Chem.* **1972**, *11*, 2884−2891.
[24] K. S. Murray, *Adv. Inorg. Chem.* **1995**, *43*, 261−358 and references therein.
[25] M. A. Halcrow, J-S. Sun, J. C. Huffman, G. Christou, *Inorg. Chem.* **1995**, *34*, 4167−4177.
[26] C. S. Campos-Fernández, R. Clérac, K. R. Dunbar, *Angew. Chem. Int. Ed.* **1999**, *38*, 3477−3479.
[27] C. J. Matthews, K. Avery, Z. Xu, L. K. Thompson, L. Zhao, D. O. Miller, K. Biradha, K. Poirier, M. J. Zaworotko, C. Wilson, A. E. Goeta, J. A. K. Howard, *Inorg. Chem.* **1999**, *38*, 5266−5276.
[28] M. Mikuriya, K. Nakadera, T. Kotera, *Chem. Lett.* **1993**, 637.
[29] K. Kambe, *J. Phys. Soc. Jpn.* **1950**, *5*, 48−51.
[30] J. J. Borrás-Almenar, J. M. Clemente-Juan, E. Coronado, B. S. Tsukerblat, *Inorg. Chem.* **1999**, *38*, 6081−6088.
[31] J. J. Borrás-Almenar, J. M. Clemente-Juan, E. Coronado, S. Tsukerblat, *J. Comput. Chem.* **2001**, *22*, 985−991.
[32] F. James and M. Roos, *MINUIT Program, a System for Function-Minimization and Analysis of the Parameter Errors and Correlations Comput. Phys. Commun.* **1975**, *10*, 345.
[33] A. Escuer, R. Vicente, M. S. El Fallah, X. Solans, M. Font-Bardía, *J. Chem. Soc., Dalton Trans.* **1996**, 1013.
[34] J. A. R. Navarro, M. A. Romero, J. M. Salas, M. Quirós, E. R. T. Tiekink, *Inorg. Chem.* **1997**, *36*, 4988−4991.
[35] E. J. Laskowski, D. N. Hendrickson, *Inorg. Chem.* **1978**, *17*, 457−470.
[36] B. W. Dockum, G. A. Eisman, E. H. Witten, W. M. Reiff, *Inorg. Chem.* **1983**, *22*, 150−156.
[37] A. C. T. North, D. C. Philips, F. S. Mathews, *Acta Crystallogr., Sect. A* **1986**, *24*, 351.
[38] *International Tables for Crystallography*, Vol. C., Tables 4.2.6.8 and 6.1.1.4, **1992**.
[39] G. M. Sheldrick, SHELXS-86, *Program for the Solution of Crystal Structure*, University of Gottingen, Germany, **1986**.
[40] G. M. Sheldrick, SHELXL-97, *Program for the Solution of Crystal Structure*, University of Gottingen, Germany,**1997**.
[41] A. L. Spek, PLATON99, *Molecular Geometry Program*, **1999**, University of Utrecht, The Netherlands.
[42] L. Zsolani, ZORTEP. *A Program for the Presentation of Thermal Ellipsoids*, University Heidelberg, Germany, **1994**.
[43] D. M. Duggan, D. N. Hendrickson, *Inorg. Chem.* **1974**, *13*, 2929−2940.
[44] T. Rojo, R. Cortés, L. Lezama, M. I. Arriortua, K. Urtiaga, G. Villeneuve, *J. Chem. Soc., Dalton Trans.* **1991**, 1779.
[45] M. Monfort, J. Ribas, X. Solans, *Inorg. Chem.* **1994**, *33*, 4271.
[46] A. P. Ginsberg, R. C. Sherwood, R. W. Brookes, R. L Martin, *J. Am. Chem. Soc.* **1971**, *93*, 5927−5928.
[47] A. E. Shvelasvili, M. A. Porai-Koshity, A. S. Antsyshkins, *J. Struct. Chem. (Engl. Transl.)* **1969**, *10*, 552−557.

Received August 13, 2002
[I02459]

EurJIC
European Journal of Inorganic Chemistry

March 2003
Issue 6
Pages 1013–1254

Papers available ahead of print in Early View at www.interscience.wiley.com

Earliest available Table of Contents:
Automatically, free of charge by e-mail through
www.interscience.wiley.com/alerts

COVER PICTURE

The cover picture shows the arrangement of the 3-D $[Hg_7As_4]^{4+}$ host framework and the AgI_3^{2-} guest anions in a novel supramolecular architecture $[Hg_7As_4](AgI_3)_2$, self-assembled from a heterogeneous system at high temperature. Although the host–guest interaction is weak, it governs both the geometry of the host framework (mercury atoms, blue; arsenic atoms, pink) and guest anions (silver atoms, red; iodine atoms, violet) and the positioning of the guest in the framework cavities. A mutual adjustment of the host and guests results is the unusual off-plane geometry of the AgI_3^{2-} anion. Details are discussed in the article of A. V. Shevelkov et al. on p. 1053 ff.

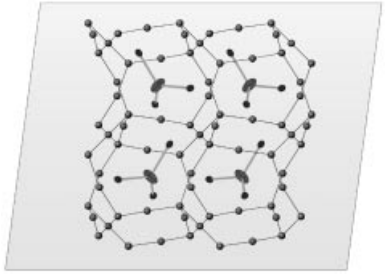

MICROREVIEW

Contents

1029 **M. Vallet-Regí,* C. V. Ragel, A. J. Salinas**

Glasses with Medical Applications

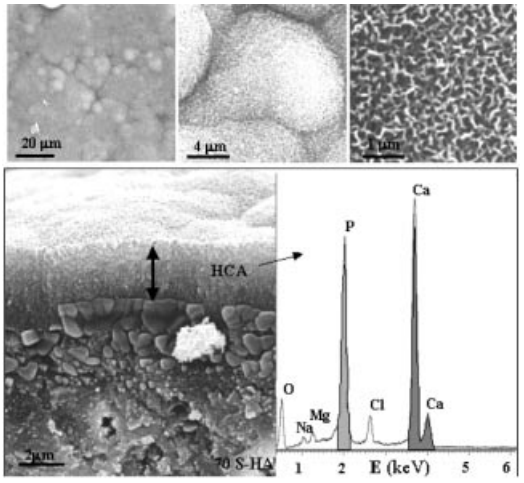

Keywords: Glasses / Materials science / Organic-inorganic hybrid composites / Metallic coatings / Textural properties

 © WILEY-VCH Verlag GmbH, 69451 Weinheim, Germany, 2003 1434–1948/03/0306–1017 $ 20.00+.50/0

SHORT COMMUNICATIONS

1043 **F. Chérioux,* B. Therrien, G. Süss-Fink**

First Star-Like Oligophenylene Molecules Containing a Dinuclear Organometallic Core

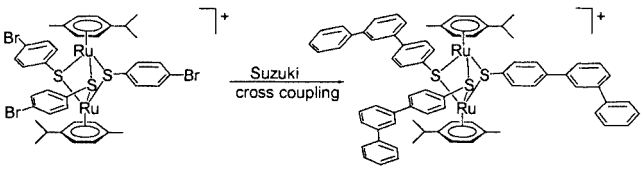

Keywords: Rhodium / Ruthenium / Oligomerization / Oligophenylene

1048 **R. Silaghi-Dumitrescu**

Nitric Oxide Reduction by Heme-Thiolate Enzymes (P450nor): A Reevaluation of the Mechanism

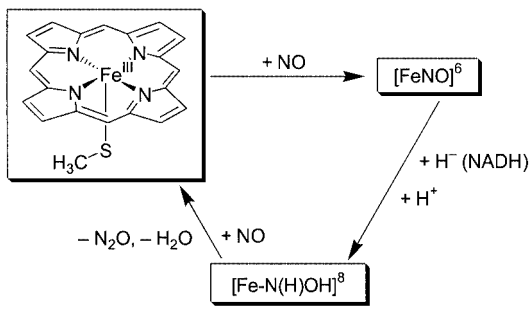

Keywords: Nitrogen oxides / Enzymes / Heme proteins / Density functional calculations / Bioinorganic chemistry

FULL PAPERS

1053 **A. V. Olenev, A. I. Baranov, O. S. Oleneva, I. I. Vorontsov, M. Y. Antipin, A. V. Shevelkov***

Synthesis, Crystal and Electronic Structure of $[Hg_7As_4](AgI_3)_2$, a Novel Supramolecular Complex with the Off-Plane AgI_3^{2-} Guest Anion

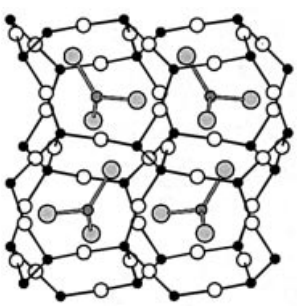

Keywords: Supramolecular chemistry / Inorganic chemistry / Mercury / Silver / Host-guest interactions

1058 **J. Wienold, R. E. Jentoft, T. Ressler***

Structural Investigation of the Thermal Decomposition of Ammonium Heptamolybdate by in situ XAFS and XRD

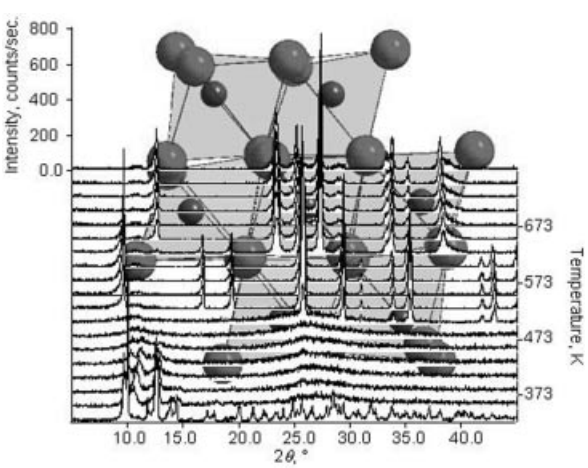

Keywords: X-ray absorption spectroscopy / X-ray diffraction / Molybdenum / Polyoxometalates

1072 **M. Krom, T. P. J. Peters, R. G. E. Coumans, T. J. J. Sciarone, J. Hoogboom, S. I. ter Beek, P. P. J. Schlebos, J. M. M. Smits, R. de Gelder, A. W. Gal***

3-Metalla-1,2-dioxolanes and Their Reactivity

Keywords: Formylmethyl complexes / Metallacycles / N ligands / Oxygenations / Rhodium

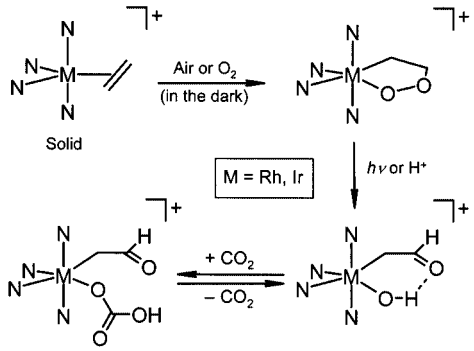

1088 **M. Tamm,* B. Dreßel, T. Lügger, R. Fröhlich, S. Grimme**

Chelate Complexes of Functionalized Cycloheptatrienyl Ligands: Molybdenum Complexes with Linked Cycloheptatrienyl-Phosphane Ligands and Their Use in Catalytic Carbon–Carbon Bond Formation

Keywords: Alkyne ligands / C–C coupling / Cycloheptatrienyl ligands / Density functional calculations / Hydride ligands

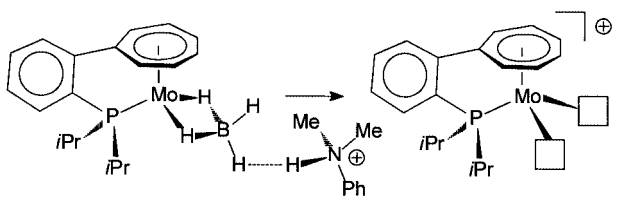

1099 **C. Benisch, D. B. Werz, R. Gleiter,* F. Rominger, T. Oeser**

Modes of Reactivity of Cyclic Diynes: Probing the *syn*/*anti* Selectivity of Tetrathiacycloalkadiynes and Mono(alkyne)cobalt Complexes

Keywords: Alkynes / Cobalt / Cyclobutadiene complexes / *syn-anti* selectivity

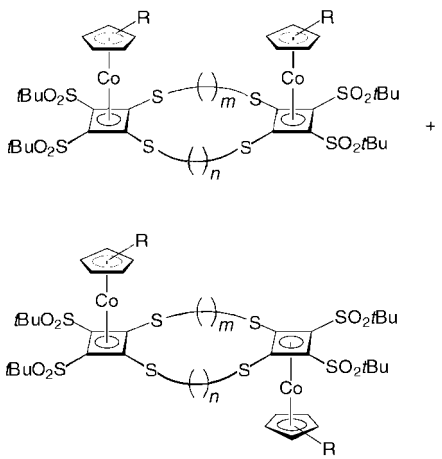

1113 **J. Pérez,* E. Hevia, L. Riera, V. Riera, S. García-Granda, E. García-Rodríguez, D. Miguel**

Mono- and Dimetallic Cyano Complexes with {Mo(η^3-allyl)$(CO)_2$(N–N)} Fragments

Keywords: Allylic compounds / Cyanides / Heterometallic compounds / Molybdenum / Manganese / Rhenium

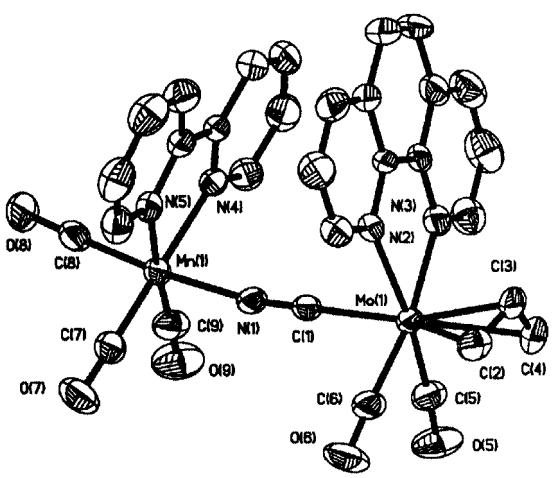

1121 **V. Torma, O. Vidoni, U. Simon, G. Schmid***

Charge-Transfer Mechanisms between Gold Clusters

Keywords: Gold / Cluster compounds / Charge transfer / Activation energy / Conductivity

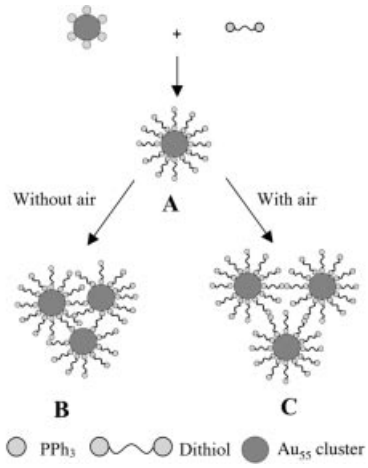

1128 **M. Vázquez, M. R. Bermejo,* M. Fondo, A. M. García-Deibe, J. Sanmartín, R. Pedrido, L. Sorace, D. Gatteschi**

Monohelical Complexes of a Novel Asymmetric N_4 Schiff Base: Unfamiliar Tetrahedral Environments of Manganese(II) and Iron(II) Helicates

Keywords: Electrochemistry / Helical structures / Schiff bases / Transition metals

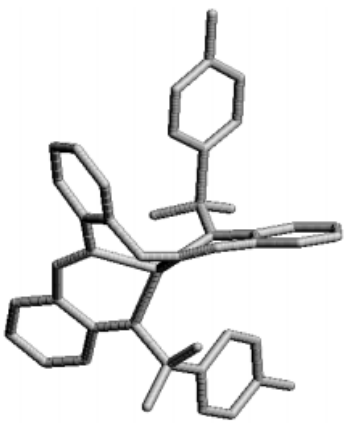

1136 **N. Margiotta, P. Papadia, F. P. Fanizzi, G. Natile***

Mono- and Bis-Guanosine Adducts of Platinum Complexes with Carrier Ligands Having In-Plane Steric Bulk: The Case of 1,10-Phenanthroline and 2,9-Dimethyl-1,10-phenanthroline

Keywords: Platinum / Nucleobases / Antitumour agents / Atropisomerism / NMR spectroscopy

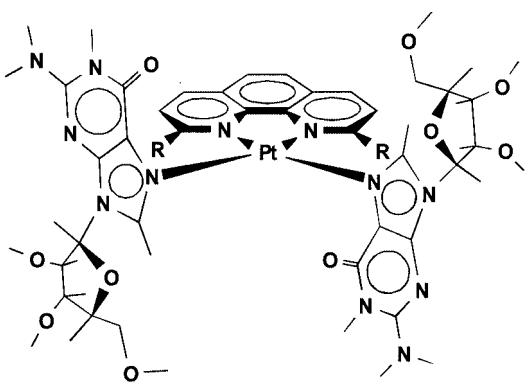

1145 **C. M. Armstrong, P. V. Bernhardt,* P. Chin, D. R. Richardson**

Structural Variations and Formation Constants of First-Row Transition Metal Complexes of Biologically Active Aroylhydrazones

Keywords: Hydrazones / Structure elucidation / Transition metals / N ligands

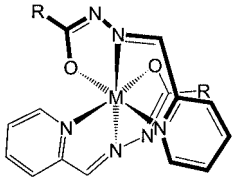

1157 **S. Sengupta, I. Chakraborty, A. Chakravorty***

New Rhenium(I) and Rhenium(II) Species Assembled by Stereospecific Azopyridine Chelation

Keywords: Rhenium / N ligands / Chelates / Back-bonding / Isomer specificity

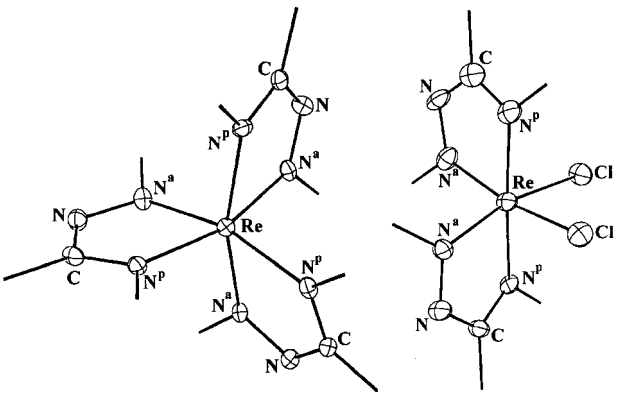

1161 **C. Mazet, L. H. Gade***

[Bis(oxazolinyl)pyrrole]palladium Complexes as Catalysts in Heck- and Suzuki-Type C−C Coupling Reactions

Keywords: Catalysis / Helical structures / N ligands / Palladium / Suzuki reaction / Heck reaction

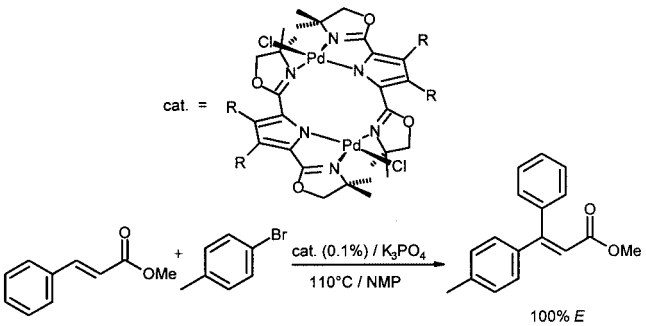

1169 **I. Shevchenko,* D. Shakhnin, H. Zhang, M. Lattman, G.-V. Röschenthaler**

The Synthesis and Structure of P−C−P Bridged Ferrocene

Keywords: Sandwich complexes / Phosphane ligands / Asymmetry / Bridging ligands

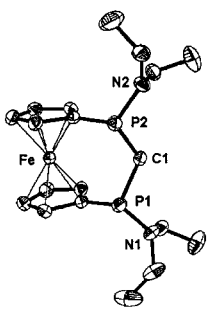

1175 **P. Brandão, A. Valente, A. Philippou, A. Fereira, M. W. Anderson, J. Rocha***

Hydrothermal Synthesis and Characterisation of Two Novel Large-Pore Framework Vanadium Silicates

Keywords: Microporous materials / Silicates / Vanadium / Catalysis / Hydrothermal synthesis

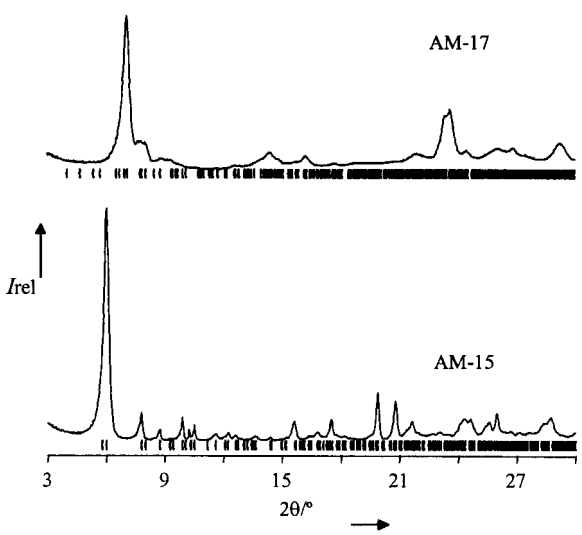

1181 **X. Zhang, C. Lu,* Q. Zhang, S. Lu, W. Yang, J. Liu, H. Zhuang**

Synthesis, Structure and Characterization of Two New Complexes $[Cu_2(C_3H_2O_4)_2(C_4H_4N_2)]\cdot 2H_2O$ and $[Zn_2(OH_2)_2(C_3H_2O_4)_2(C_4H_4N_2)]$

Keywords: Copper / N ligands / Supramolecular chemistry / Magnetic properties / Conducting materials

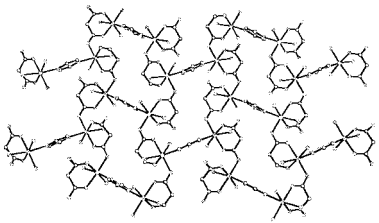

1186 **A. Arrais, E. Diana, R. Gobetto, M. Milanesio, D. Viterbo, P. L. Stanghellini***

Solid-State Adducts between C_{60} and Decamethylferrocene

Keywords: Donor-acceptor systems / Fullerenes / Infrared spectroscopy / Raman spectroscopy / Sandwich complexes

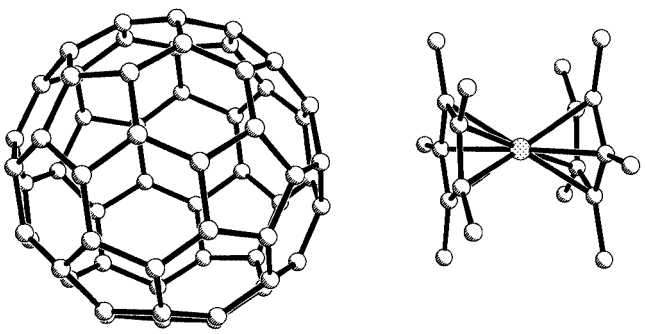

1193 **S. Kaskel,* C. W. Lehmann, G. Chaplais, K. Schlichte, M. Khanna**

Synthesis, Structure, and Characterization of $[RAl(\mu\text{-}NHEt)(\mu\text{-}NEt)_2Si(NHEt)]_2$ (R = Me, Et)

Keywords: Aluminium / Nitrogen / Precursor development / Silicon

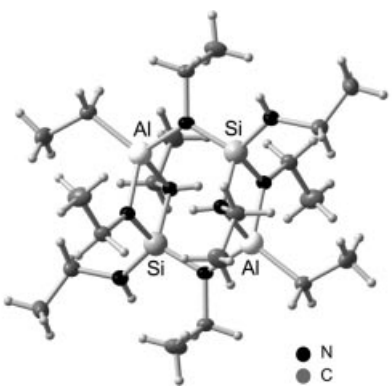

1197 **G. Battaini, L. Casella,* M. Gullotti, E. Monzani, G. Nardin, A. Perotti, L. Randaccio, L. Santagostini, F. W. Heinemann, S. Schindler**

Structure and Reactivity Studies on Dinuclear Copper Complexes of the Ligand α,α′-Bis{bis[1-(1′-methyl-2′-benzimidazolyl)methyl]amino}-*m*-xylene

Keywords: Bioinorganic chemistry / Copper / Dioxygen activation / Enzyme models

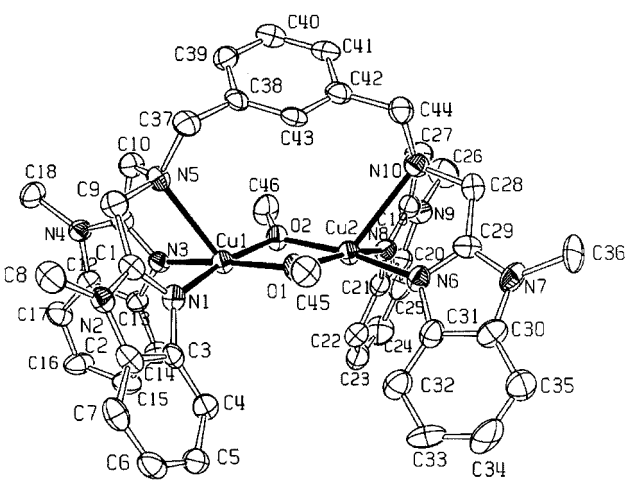

1206 **S. Fakih, V. P. Munk, M. A. Shipman, P. del S. Murdoch, J. A. Parkinson, P. J. Sadler***

Novel Adducts of the Anticancer Drug Oxaliplatin with Glutathione and Redox Reactions with Glutathione Disulfide

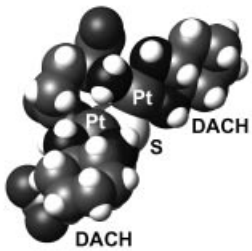

Keywords: Antitumour agents / Platinum / S ligands / Peptides / Redox chemistry

1215 **M. Poyatos, E. Mas-Marzá, J. A. Mata, M. Sanaú, E. Peris***

Synthesis, Reactivity, Crystal Structures and Catalytic Activity of New Chelating Bisimidazolium-Carbene Complexes of Rh

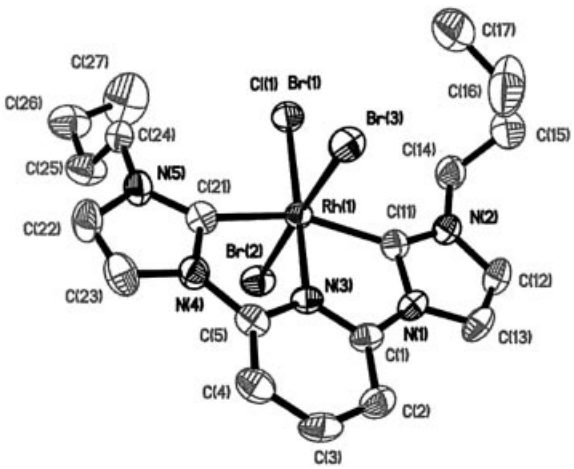

Keywords: Heterocycles / Carbenes / Rhodium / Homogeneous catalysis

1222 **Z. D. Tomic, V. M. Leovac, S. V. Pokorni, D. Zobel, S. D. Zarić***

Crystal Structure of Bis[acetone-1-naphthoylhydrazinato(−1)]copper(II) and Investigations of Intermolecular Interactions

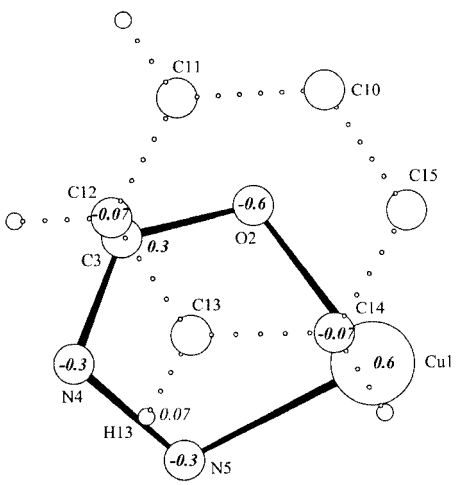

Keywords: Pi interactions / Stacking interactions / Copper / Chelates

1227 **C. Ma, C. Chen, Q. Liu,* D. Liao, L. Li**

The First Structurally Characterized Trinuclear Dipicolinato Manganese Complex and its Conversion into a Mononuclear Species by Ligand Substitution

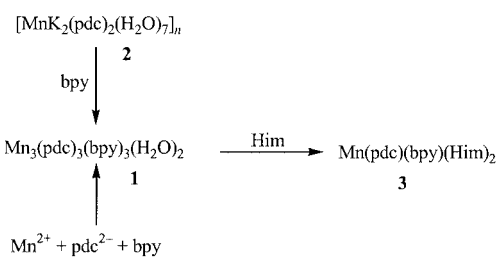

Keywords: Manganese / N ligands / Cluster compounds

1232 **M. Arca, A. J. Blake, V. Lippolis,* D. R. Montesu, J. McMaster, L. Tei, M. Schröder***

Coordination Chemistry of Nitrile and Amino Pendant Arm Derivatives of [9]aneN_2S and [9]aneNS_2 with Pd^{II} and Cu^{II}

Keywords: Macrocycles / Palladium / Copper / N ligands / S ligands

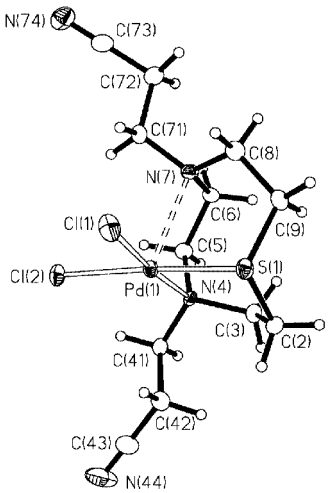

1242 **F. Leroux, P. Aranda,* J.-P. Besse, E. Ruiz-Hitzky**

Intercalation of Poly(Ethylene Oxide) Derivatives into Layered Double Hydroxides

Keywords: Layered compounds / Intercalations / Nanostructures

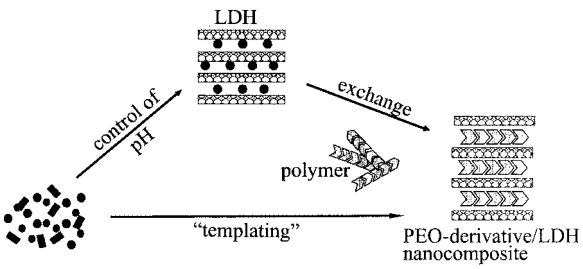

CORRECTION

1253 **R. W. Saalfrank,* B. Demleitner, H. Glaser, H. Maid, S. Reihs, W. Bauer, M. Maluenga, F. Hampel, M. Teichert, H. Krautscheid**

Synthesis of Tetrahemispheraplexes with Ammonium, Alkylammonium or Alkaline Metal Ions as Exohedral Guests via Self-Assembly or Guest Exchange

Keywords: Cage compounds / Supramolecular chemistry / Magnesium / Host-guest chemistry

Glasses with Medical Applications

María Vallet-Regí,*[a] C. Victoria Ragel,[a] and Antonio J. Salinas[a]

Keywords: Glasses / Materials science / Organic-inorganic hybrid composites / Metallic coatings / Textural properties

Bioactive glasses react chemically with the body fluids. The reaction product is an apatite, which, with the intervention of biological drivers, assists the generation of bone matrix and bone growth. The main application of these bioactive glasses in the clinical field is the filling of osseous cavities, manufacture of small parts for middle ear bone replacement and maxilofacial reconstruction and dental applications. Thanks to advances in related medical technologies, bioactive glasses are now undergoing a new stage of development, resulting in different mechanical properties, drug delivery capabilities, bioactive coating of metallic implants, protein and/or cell activation for tissue regeneration and tissue engineering, and are also finding use in biomimetics, nanotechnology, production of hybrid organic-inorganic materials and as bioactivity accelerators of mineral apatites or as bioactivity inductors of magnetic materials for hyperthermia treatment of osseous tumours.

(© Wiley-VCH Verlag GmbH & Co. KGaA, 69451 Weinheim, Germany, 2003)

1. Introduction

The discovery of the first *bioactive* ceramic took place 30 years ago, and since then has given rise to new strategies in the use of artificial materials in clinical bone repairs and replacement. The bioactive ceramics spontaneously bond to and integrate with living bone in the body without fibrous tissue forming around them. It was Hench et al.[1,2] who first introduced the idea of firmly bonding bone with synthetic materials through the chemical reactions that take place on a glass surface when it is implanted into a living body. Such an original line of thinking focussed attention on silica-based glasses, with the amorphous structure of silica glass, and on the chemical reactions that occurred on the surfaces of such materials. Bioglass® [1] and the subsequent family of bioactive glasses are now regarded, from the point of view of their application, as the earliest expression of all bioactive ceramics.

The characteristic amorphous quality of these glasses is generally a product of the structure of silicate glass, usually defined by [SiO_4] tetrahedra. These geometrical figures are linked together at all corners. While crystallised silica shows a uniform arrangement of these tetrahedra, as could be expected of any crystalline material (Figure 1, a), this is not

[a] Departamento de Química Inorgánica y Bioinorgánica, Facultad de Farmacia,
Universidad Complutense, 28040 Madrid, Spain
Fax: (internat.) + 34-91/394-1786
E-mail: vallet@farm.ucm.es

María Vallet-Regí (left, top) was born in Las Palmas, Spain, in 1946. She studied Chemistry at the Universidad Complutense de Madrid (UCM) and received her PhD at the same University in 1974. She is full professor of Inorganic Chemistry and Head of the Department of Inorganic Chemistry and Bioinorganic at the Faculty of Pharmacy (UCM). Her current research field is solid state chemistry, covering aspects of synthesis, characterisation and reactivity in oxides and bioceramics.

C. Victoria Ragel (right) was born in Madrid, Spain, in 1957. She studied Pharmacy at the Universidad Complutense de Madrid (UCM) and received her PhD at the same University in 1984. She was associate professor at the Department of Inorganic Chemistry and Bioinorganic at the Faculty of Pharmacy (UCM). In the last years, her research fields were the synthesis, characterisation and study of the properties of bioceramics, particularly bioactive sol-gel glasses to be included in drug release systems and biphasic materials. She passed away on June 1, 2002.

Antonio J. Salinas (left, bottom) was born in Madrid, Spain, in 1957. He studied Chemistry at the Universidad Complutense de Madrid (UCM) and received his PhD at the same University in 1992. He is associate professor at the Department of Inorganic Chemistry and Bioinorganic of the Faculty of Pharmacy (UCM). His current research field is the synthesis and characterisation of bioactive ceramics: gel glasses and glass ceramics, to be used in the osseous defects treatment.

MICROREVIEWS: This feature introduces the readers to the authors' research through a concise overview of the selected topic. Reference to important work from others in the field is included.

the case in silica glass. A common feature of both the crystalline − i.e., quartz − and the amorphous structures is that each oxygen ion links two tetrahedra, although forming a more open arrangement in the case of amorphous silica (Figure 1, b). Such a rather open structure facilitates the inclusion of cations referred to as network modifiers, and this feature allows a wide range of silica glasses to be obtained.

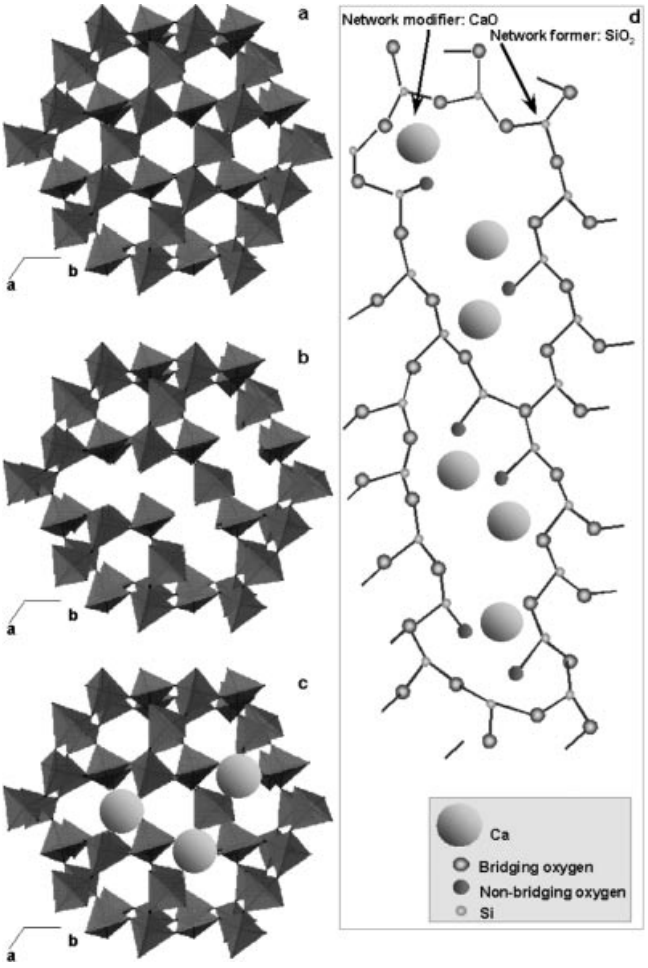

Figure 1. (a) Crystallised silica, (b) amorphous silica, (c) silica glass, (d) glassy network in two dimensions

The presence of cations such as Na^+, K^+ and Ca^{2+} (Figure 1, c) in the glass causes a discontinuity of the glassy network through the disruption of some Si−O−Si bonds. As a consequence, non-bridging oxygen is released. Figure 1, part d schematically depicts a glassy network in two dimensions. The network modifier in this case is an MO-type oxide, CaO, while the network former is SiO_2. Some Si atoms are bonded to other Si atoms through bridging oxygen, while others are coordinated through a non-bridging oxygen to the network of modifying ions. The purpose of the *network formers* is to build Si−O−Si bonds, while the *network modifiers* are there to break a proportion of those bonds, thus allowing the melt to solidify with a high degree of disorder. Its presence provides lower melting temperatures and viscosity values, reducing the economic costs of glass production, while ensuring a high degree of disorder.

This disordered structure, enhanced by the presence of network modifiers, gives rise to the high reactivity of these glasses in aqueous environments. This high reactivity is the main advantage of their application in periodontal repair and bone augmentation, as the reaction products obtained from these types of glasses and physiological fluids result in the crystallisation of the apatite-like phase, similar to the inorganic component of bones in vertebrate species.[3−9]

Bioactive glasses, from their beginnings in the 1970s, have reached a significant level of development, resulting since their discovery in the publication of several reviews on ceramics for medical applications, studying various aspects of their evolution.[11−18] This microreview reflects the more relevant results of our research in bioactive glasses.

2. Bioactive Glasses

Early bioactive glasses were prepared by the classic quenching of melts comprising SiO_2 and P_2O_5 as network formers and CaO and Na_2O as network modifiers.[1] This was the route followed for more than two decades in the synthesis of bioactive glasses.[3,19−24] In the early 1990s, sol-gel processing was introduced for the synthesis of bioactive glasses;[25] Figure 2 shows a scheme illustrating the main stages of the melting and sol-gel processes. The sol-gel route allows glasses of higher purity and homogeneity to be obtained, and the ranges of their compositions and textural properties to be expanded. In addition, all the steps in this route are carried out at temperatures notably lower than those required to obtain glasses by the melting method. It was therefore no longer necessary to include components intended to decrease the melting temperature (i.e., Na_2O), and the first bioactive gel glasses in the SiO_2·CaO·P_2O_5 system were obtained.

Our research group used the sol-gel route for preparation of bioactive glasses not only in the ternary SiO_2·CaO·P_2O_5 system,[26−43] but also in the quaternary SiO_2·CaO·P_2O_5·MgO[26,28,31,32,44] and the binary SiO_2·CaO[30,35,37,41−43,45−48] systems (see Table 1).

The addition of MgO to obtain quaternary gel glasses was performed in an attempt to improve the mechanical features of the glasses. The magnesium should be regarded as a network modifier, just as calcium, but it has different chemical behaviour and so substantial variations in the glass properties would be expected. Thus, Kokubo et al.[49] described the bioactive Apatite−Wollastonite glass-ceramic, based on an SiO_2·CaO·P_2O_5·MgO melt glass, with mechanical properties appreciably better than those of glasses.

The sol-gel method allows the ternary system to be simplified, P_2O_5 to be eliminated, and binary SiO_2·CaO bioglasses of a wide compositional range to be obtained. The objective of these studies was to determine the role of phosphorus in the gel glasses' bioactivity. This binary system can also help to understand the mechanism of bioactivity,

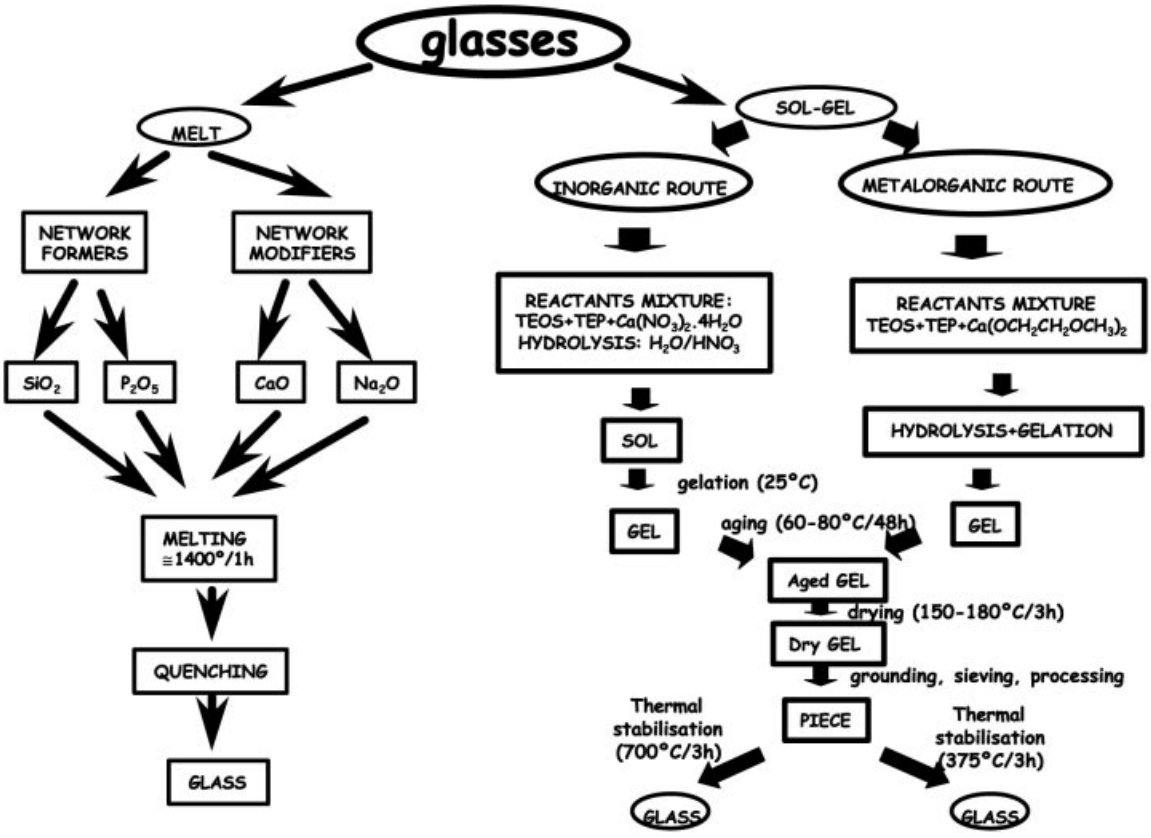

Figure 2. Diagram of the main stages in the melting and sol-gel processes (inorganic and metalorganic routes) to obtain bioactive glasses

since the phosphorus required for the apatite-like layer formation could now only originate from the assay solution.

In all cases, the syntheses of glasses were carried out by hydrolysis and polycondensation in the glass of stoichiometric amounts of the oxide precursors: tetraethyl orthosilicate (TEOS), triethyl phosphate (TEP), magnesium nitrate hexahydrate and calcium nitrate tetrahydrate (*inorganic route*) or calcium methoxyethoxide (*metalorganic route*),[39] by the scheme shown in Figure 2.

In the *inorganic route*, HNO_3 (2 N) was used to catalyse the TEOS and TEP hydrolyses, the (HNO_3 + H_2O/TEOS + TEP) molar ratio being constant and equal to 8. Reactants were added consecutively after 1-h intervals, with continuous stirring. The solution (*sol*) was poured into Teflon® containers, which were closed and kept at room temperature until gelation (*gel*) was reached (2−5 d depending on the *sol* composition). Ageing was achieved by a thermal treatment (70 °C/55 h) and the drying of the gel at 150 °C/72 h, after replacement of the container lid with another one with a small hole, allowing the gasses to leak. The dried gel was ground and sieved, and the 63−32 μm fractions were selected. Disks (13 mm diameter, 2 mm in height), were conformed by uniaxial (50 MPa) and isostatic (150 MPa) pressures on 0.5 g of dried gel powders. Nitrate elimination and material stabilisation was carried out at 700 °C/3 h, the temperature being determined by thermogravimetric analysis of the dried gels.

On the other hand, in view of the excellent bioactivity of the obtained gel glasses, we considered that their application field could be expanded through the preparation of new mixed materials, in which these glasses would be the bioactivity-inducing elements. We have thus obtained: (i) bioactive systems for controlled release of anti-inflammatory drugs and antibiotics, avoiding problems derived from implantation as bone substitutes, (ii) magnetic bioactive materials, for the treatment of osseous tumours by hyperthermia, and (iii) calcium phosphate based materials with improved kinetics for the formation of new apatite, thanks to the presence of the bioactive glass.

Finally, gel glasses have been used to prepare metallic substrate coatings (of Ti6Al4V) by dip-coating. These coatings allow the good mechanical properties of metals to be combined with the bioactivity of sol-gel glasses.

3. Ternary Compositions: SiO_2·CaO·P_2O_5 System

3.1 Characterisation of Glasses

Analyses of the compositions of gel glass by X-ray fluorescence (XRF) and energy dispersive X-ray spectroscopy (EDS) showed good agreement with the nominal compositions[26−43] (Table 1).

X-ray diffraction (XRD) characterisation confirmed the amorphous character of all the materials, but in some cases a diffuse maximum was observed at $2\theta \approx 32°$. This could

Table 1. Nominal compositions (mol %) of sol-gel glasses obtained by our research group

Glass	SiO_2	CaO	MgO	P_2O_5	Ref.
80S	80	16	–	4	[26,27,31,38]
80S17C	80	17	–	3	[30,35,37]
75S	75	21	–	4	[26,28,32,38]
76S	76	23	–	1	[39]
76SA	76	23	–	1	[39]
72.5S2.5P	72.5	25	–	2.5	[41,42]
70S	70	26	–	4	[29,26,40]
70S5P	70	25	–	5	[41,42]
77S	77	14	–	9	[43]
68S	68	23	–	9	[43]
65S	65	31	–	4	[26,28,32,38]
60S	60	36	–	4	[26,27,38,40]
58S	58	36	–	6	[34,38]
58S33	58	33	–	9	[43]
55S	55	41	–	4	[33,36]
80SM	80	12.8	3.2	4	[44]
80SM	80	13	3	4	[26,31]
80S7M	80	9	7	4	[31]
75SM	75	17	4	4	[26,28,32]
75SM	75	16.8	4.2	4	[44]
70SM	70	21	5	4	[26]
65SM	65	25	6	4	[26,28,32]
65SM	65	24.8	6.2	4	[44]
60SM	60	29	7	4	[26]
60SM	60	28.8	7.2	4	[44]
91S	91	–	–	9	[43]
90S10C	90	10	–	–	[48]
80S20C	80	20	–	–	[30,35,37,45–48]
75S25C	75	25	–	–	[41,42]
70S30C	70	30	–	–	[48]
60S40C	60	40	–	–	[48]
50S50C	50	50	–	–	[48]

be attributable to the more intense reflection of an apatite-like phase that could start to crystallise in the amorphous glass matrix.

The obtained Fourier-transform infrared (FTIR) spectra show bands attributable to the Si–O stretching vibrations (ν_a: ca. 1085 cm^{-1}; ν_s: ca. 802 cm^{-1}) and Si–O–Si bending vibrations (ca. 472 cm^{-1}). In addition, two low-intensity bands are registered at about 602 and 568 cm^{-1} and could be attributable to stretching vibrations of phosphate groups.

Characterisation by scanning electron microscopy (SEM) indicates that pieces of the glasses are made up of particle aggregates with a wide size distribution (ca. $1-25 \times 10^3$ nm) and with sharp edges, allowing numerous voids between them.

The textural properties (porosity and specific surface) were also determined,[32–34,38,42] by N_2 adsorption and intrusion mercury porosimetry. Figure 3 (see a) shows the nitrogen adsorption isotherms for the ternary, 60S, 65S, 75S and 80S gel glasses.[38] The inset shows the BET surface and mesoporous volume values obtained by this technique.

All the nitrogen adsorption isotherms can be identified as type IV isotherms with slight differences in the hysteresis loop.[50] Samples with SiO_2 contents under 70 mol % have an H1 type hysteresis loop in the mesoporous region (3–50 nm), characteristic of cylindrical pores with both sides open, with some narrow parts. In contrast, glasses with SiO_2 contents higher than 70 mol % present hysteresis loops of H2 type associated with inkbottle-like pores with variable size and narrow necks.

Figure 3, part b shows the pore volume as a function of the pore diameter in the macropore region (2×10^5 to 50 nm) obtained by mercury intrusion. The inset shows macropore diameter vs. SiO_2 content. As observed, the pore volume in this region increases when the SiO_2 content in the glasses decreases.

These results indicate that the textures of the sol-gel glasses in this system are determined by the relative amounts of the glass components. For the same contents in P_2O_5 (4 mol %), higher CaO percentages, and consequently lower SiO_2 contents, yield higher mesopore volumes. Simultaneously, pore diameter increases, whereas the surface area decreases. These results were explained by taking into account that increases in calcium content in the SiO_2 network increase the number of nonbonding oxygen atoms. A proportion of the micropores is therefore substituted by mesopores, producing a decrease in the specific surface.

It was observed that variations in the pore morphology parallel their modifications in volume and diameter. An increase in the pore size and volume joins the "inkbottle" pores together, producing cylindrical pores. A model presenting the transition in the pore morphology is depicted schematically in Figure 3, part c.

For constant CaO contents (25 mol %), however, the surface area increases and the pore diameter and volume decrease with increasing P_2O_5 content.[42] This was explained by considering that P_2O_5 bonds to calcium, decreasing the amount of this element that can interact with the silica network. An increase in the P_2O_5 content in the glass thus produces effects similar to those of a decrease in the CaO content (increasing the SiO_2 percentage).

Another point studied was the influence of the CaO precursor on the features of the sol-gel glasses obtained. With this as the objective, a glass composition was prepared from two different precursors (Figure 2): calcium nitrate tetrahydrate (*inorganic route*, 76S glass) and calcium methoxyethoxide (*metalorganic route*, 76SA glass).[39] 76SA has the following differences from 76S: it (i) was obtained in monolithic form, (ii) presented a lower pore volume (0.13 $cm^3 \times g^{-1}$ vs. 0.72 $cm^3 \times g^{-1}$ of 76S, obtained by Hg intrusion), and (iii) showed only one maximum (at 180 nm) in the pore size distribution, while 76S glass showed a bimodal distribution with maxima at 820 nm and 6 nm. Variations in texture can be explained by the porosity generated in the thermal treatment required for nitrate elimination in the synthesis of the 76S glass. This different textural properties give rise to different in vitro behaviour in the two glasses, as explained in the next section.

3.2 In Vitro Bioactivity Studies

There is a well-established relationship between the ability of a given material to form bonds with living tissues and its ability to grow an apatite-like layer when soaked in fluids mimicking human plasma, and so in vitro assays are pop-

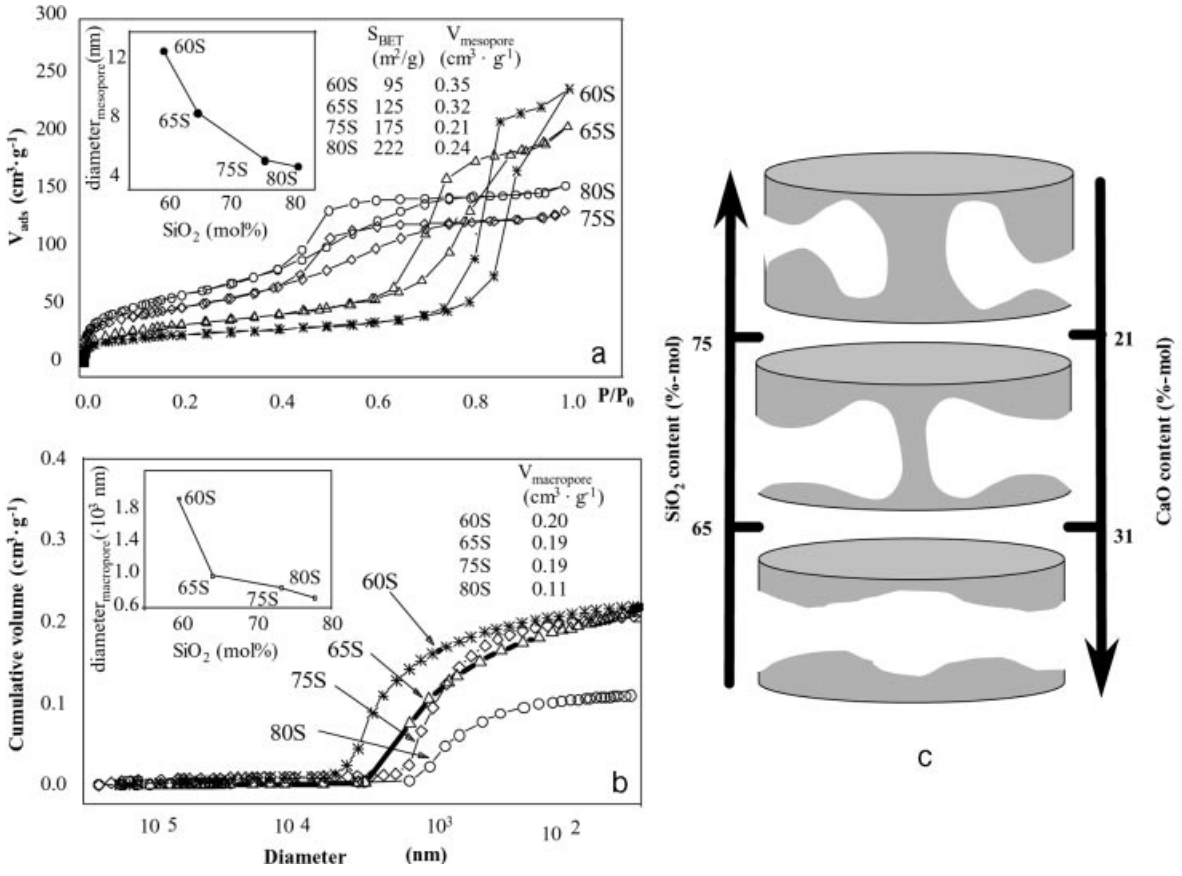

Figure 3. (a) N_2 adsorption isotherms of several $SiO_2 \cdot CaO \cdot P_2O_5$ sol-gel glasses; the inset shows the mesopore diameter versus SiO_2 content; BET surface and mesopore volume data are also included; (b) volume of intrusion Hg as a function of pore diameter; the inset shows the macropore diameter versus SiO_2 content; the macropore volume data are included; (c) model of the transition in the mesopore morphology as a function of the composition of the gel glasses

ular tools in the study of bioactivity of new candidate implant materials. In most of our research we have used the simulated body fluid (SBF) proposed by Kokubo et al.[7] SBF is an acellular, aqueous solution with an ionic composition that closely resembles that of human plasma, buffered to physiological pH (7.25−7.40) at 37 °C with a mixture of HCl/tris(hydroxymethyl)aminomethane. Figure 4 compares the ionic compositions of SBF and human blood plasma. Since this fluid contains Ca^{2+} and HPO_4^{2-} ions, it can be used to assess the in vitro bioactivity of a wide range of materials.

During the in vitro assays, the glass disks are soaked in SBF for time periods ranging from 1 h to 2 weeks. To homogenise our studies, to avoid effects due to volumetric differences, the relationship between the geometric areas of pieces and the volumes of solutions was 0.075 cm^{-1} in all cases. Disks are kept in a vertical position in a platinum scaffold (Figure 4). After the assays, pieces are washed with water and acetone and dried in air. Microorganism contamination of samples is avoided by performing all the manipulations inside a laminar flux cabinet and by filtering the SBF with a 0.22 μm Millipore® system.

In vitro bioactivity of glasses is evaluated by monitoring changes in pH and Ca^{II}, Si^{IV} and P^{V} concentrations in solution and by analysing the apatite layer formation on the surface of the pieces by XRD, FTIR, SEM-EDS, transmission electron microscopy (TEM) and electron diffraction (ED).

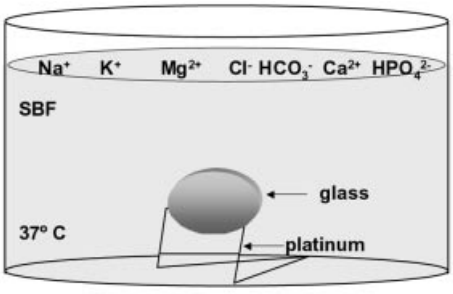

Ionic composition of SBF and Human Blood Plasma (mM)

	Na^+	K^+	Mg^{2+}	Ca^{2+}	Cl^-	HCO_3^-	HPO_4^{2-}	SO_4^{2-}
SBF	142.0	5.0	1.5	2.5	147.8	4.2	1.0	0.5
plasma	142.0	5.0	1.5	2.5	103.0	27.0	1.0	0.5

Figure 4. Schematic depiction of the in vitro bioactivity test; ion concentrations in SBF and in human blood plasma are also indicated

In general terms, as soaking time increases there is an increase in pH and in the Ca^{II} and Si^{IV} concentrations in SBF, whereas the P^{V} concentration in SBF decreases simultaneously. These effects are more pronounced in the first 12

h of assay and decrease after that. These variations agree with an exchange taking place between Ca^{2+} ions of the glass and H_3O^+ of the solution. This exchange favours the formation of Si−OH in the glass surface and increases the Ca^{2+} supersaturation in solution, inducing nucleation and crystallisation of apatite (Figure 5).

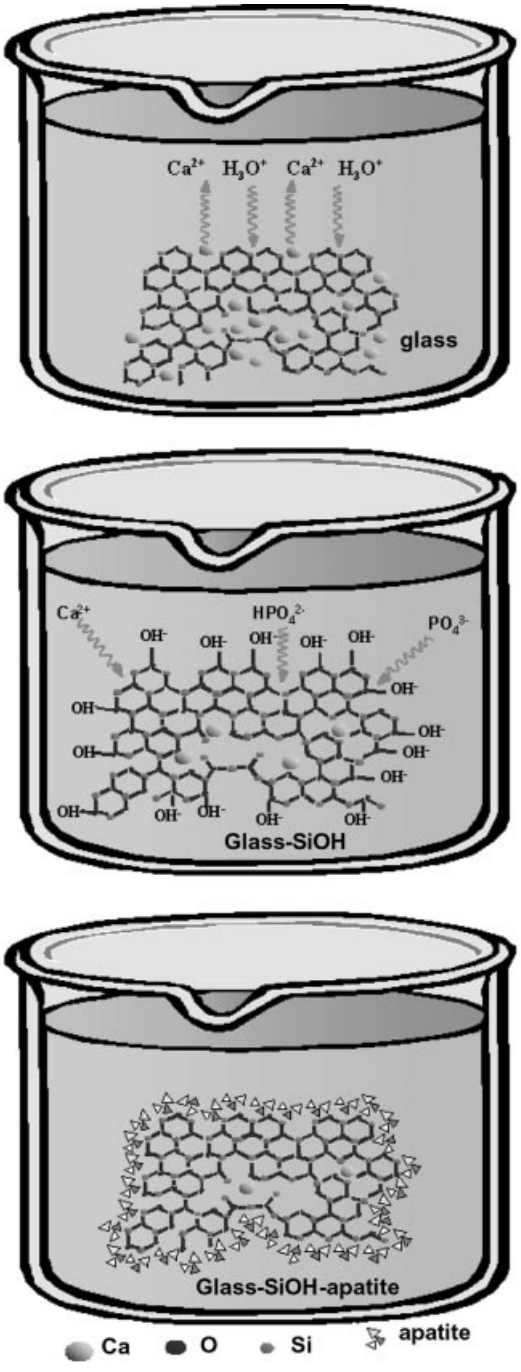

Figure 5. Depiction of the apatite formation mechanism as a function of the reactivity of bioactive glasses when in contact with physiological fluids, under in vitro conditions

Figure 6, part a shows the XRD diagrams of 60S glass before and after soaking for different periods in SBF. As the soaking time increases, diffraction maxima attributable to the more intense reflections of an apatite-like phase are registered. The intensities of these maxima increase with the immersion time as the apatite crystal size increases.

Figure 6, part b depicts FTIR spectra of 58S glass before and after soaking in SBF for different time periods. As the immersion time increases, the spectra develop bands attributable to the phosphate and carbonate groups, the intensities of these bands increasing with the soaking time. The presence of such bands shows that the material formed on the glass surface is hydroxycarbonate apatite (HCA), similar to biological apatites.[51,52]

SEM studies indicate that during the early soaking stages the glasses are totally coated by a layer of spheres of a diameter between 1 and 20×10^3 nm, identified by FTIR and EDS as amorphous calcium phosphate. For soaking times longer than 3−4 d, it was observed that the spheres were composed of numerous elongated particles (Figure 6, c). The times required for these processes varied with the gel glass composition but, in general, were lower for ternary gel glasses with high CaO contents.

The particles forming the spheres are made up of numerous crystalline aggregates, as confirmed by TEM (Figure 6, d). The correspondent ED diagram shows rings and diffraction maxima attributable to the more intense reflections of an apatite-like layer (Figure 6, e).[30] In addition, EDS analysis shows that the layer formed on 80S17C glass after 7 d in SBF is made up only of Ca, P and O (Figure 6, f).

The thickness of the newly formed layer can be studied by SEM, by cutting the pieces after the in vitro assays and applying the procedure shown in Figure 7. The EDS spectrum of the bulk glass (Figure 7, c) agrees with its nominal composition, whereas higher Ca and P concentrations and a lower Si content are detected in the layer, the thickness of which varies with glass composition and soaking time in SBF. For 55S glass, a thickness of 2×10^3 nm is measured after 15 h and increases up to a maximum value of 10×10^3 nm after 5 d of assay. In addition, the Ca/P molar ratio in the newly formed layer ranged between 1.4 and 1.7, within the common limit values for biological apatites.[53,54]

3.3 Texture − In Vitro Bioactivity Relationship in Sol-Gel Glasses

The formation of an Si-rich layer and a calcium phosphate layer on bioactive glasses is a well-established fact.[55−59] Figure 5 outlines the essential steps in the mechanism of formation of an apatite-like layer. The process takes place through the free surface of the glass, so those factors responsible for an increase in the specific surface of the initial glass also support an acceleration of the kinetics of this mechanism of chemical reactivity in bioactive glasses. This was in fact one of the main reasons to search for additional synthesis routes to these glasses, trying to enhance the specific surface and porosity of the final product.[60−64] The Si-rich layer is clearly seen on the bulk glass, and the calcium phosphate is seen as a light uppermost layer on the Si-rich gel.

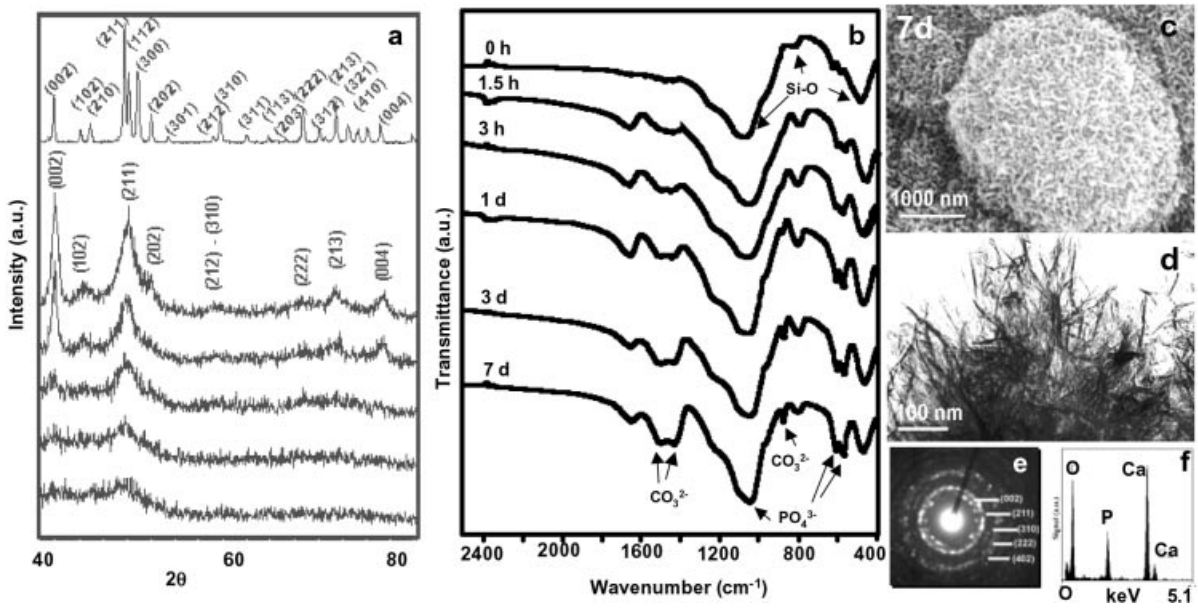

Figure 6. (a) XRD patterns of 70S before and after soaking different periods of time in SBF; an XRD pattern of hydroxyapatite is included as a reference; (b) FTIR spectra of 58S before and after soaking in SBF; (c) SEM micrographs; (d) TEM micrograph; (e) ED pattern, and (f) EDS spectra of 80S17C after a 7-d assay in SBF

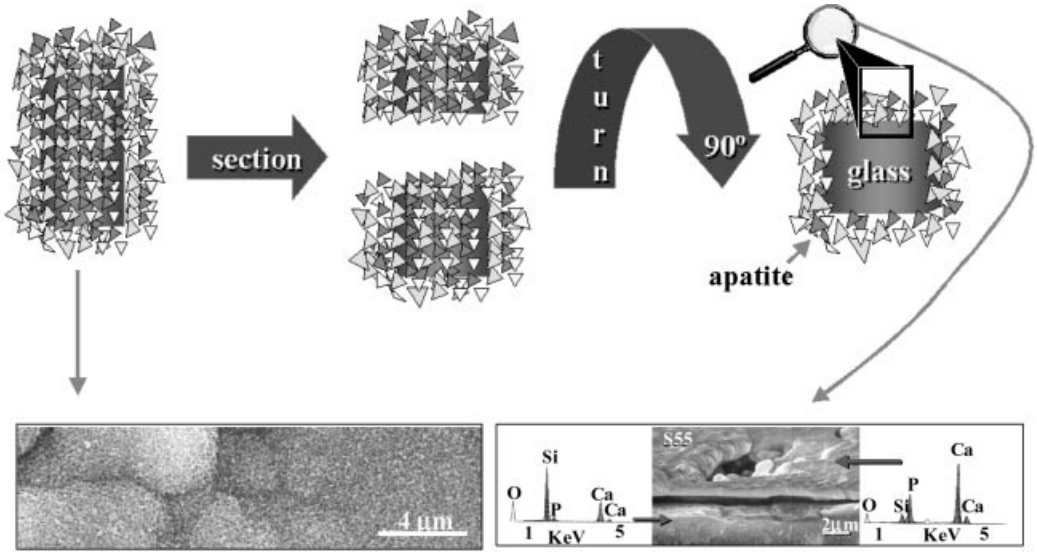

Figure 7. Schematic depiction of the sample treatment used to study the layer thickness by SEM-EDS; an SEM micrograph of 55S glass surface after 7 d soaking and SEM micrograph and EDS spectra of the inside of the glass and on the layer are also shown

High porosity in sol-gel glasses favours the formation of the apatite-like layer, since it facilitates rapid and massive release of Ca^{2+} ions from the glass into the solution. This release increases the Ca^{2+} saturation and pH in the medium, and induces silanol group (Si−OH) formation in the glass surface according to the following Equation:

$$2\ (Si{-}O)^{2-}\ Ca^{2+} + 2\ H_2O \rightarrow 2\ Si{-}OH + Ca^{2+} + 2\ OH^-$$

The formation of the silicon-rich layer is almost instantaneous, and it is covered within minutes by an amorphous phosphate layer, which in 2 or 3 d crystallises with an apatite structure. These processes also produce additional porosity, which facilitates the diffusion of more Ca^{2+} ions into the medium and the formation of new silanol groups. There are, however, other factors contributing to these reactions. CaO acts as network modifier, inducing instability in the system by provoking stress in the glassy network. Thus, generally speaking, a higher CaO content in the glass implies faster formation kinetics of the apatite phase.

The presence of CaO is also associated with a larger porosity of the glass, more so when introduced in the form of an inorganic salt such as $Ca(NO_3)_2$. In this context, a study on the differences between glasses in which CaO was included either as calcium alkoxide (76SA) or as calcium nitrate (76S) indicated that glasses obtained by the latter

method are more porous and less homogeneous.[39,65] In vitro studies of glasses indicate that both are bioactive. However, because of their better textural and structural properties, the layers formed on 76SA glass are thicker, more compact and more homogeneous.

3.4 Quantification of Bioactivity in SiO_2 Glasses

We have proposed a method to quantify and predict the bioactivity of silicate glasses;[40] it relates the SiO_2 network degradation with the factors that cause the formation of silanol groups on the glasses surface. As mentioned, these factors are mainly *composition* (amount of network modifiers: CaO, Na_2O, ...) and *textural* properties (surface area and porosity).

Preliminary studies show that the energy of activation (E_a) for the diffusion of $Si(OH)_4$, the soluble form of SiO_2, is closely related to the in vitro bioactivity of the studied glasses.[43] For melt and sol-gel silica glasses with in vitro bioactivity, it was observed that E_a for $Si(OH)_4$ diffusion after 6 h of assay is lower than 0.35 eV.

3.5 Sol-Gel Glasses Biocompatibility

The biocompatibility of these ternary sol-gel glasses was studied by means of osteoblast cell cultures.[41] It was observed that these materials allow and favour osseous cell growth.

In vivo studies involving the implantation of glass pieces in rabbit femur for time periods between 1 and 12 weeks were also performed;[66] the implants present excellent biocompatibility and osseous integration.

4. Quaternary Compositions: SiO_2·CaO·MgO·P_2O_5 System

As already indicated, the inclusion of certain quantities of MgO as a network modifier in the melt glass compositions can improve their mechanical properties. For that reason we performed the synthesis and an in vitro bioactivity study of sol-gel glasses of the SiO_2·MgO·P_2O_5 and SiO_2·CaO·MgO·P_2O_5 systems.

None of the compositions obtained in the SiO_2·MgO·P_2O_5 system show in vitro bioactivity. In the surface of SiO_2·CaO·MgO·P_2O_5 glasses, however, a phosphate-rich layer was formed after soaking in SBF at 37 °C.[26,28,31,32,44] In vitro studies show that the rate of formation of the new layer decreases with increasing magnesium content in glasses. Moreover, a whitlokite-like phase [β-$Ca_3(PO_4)_2$] was detected in the layer as well as the apatite, together with a noticeable increase in the layer thickness, reaching 20×10^3 nm for 80S7M glass.

In order to explain this decrease in the kinetics of layer formation in quaternary glasses, their textural properties were studied.[32,44] Increases in the MgO content were found to increase the surface area and pore volume, whereas the pore sizes remained almost constant. These differences are not sufficient to justify the strong inhibitory effect of MgO in the crystallisation and growth of apatite, since the opposite effect (that is, an increase in the apatite layer growth for larger surface areas) was observed in bioactive ternary SiO_2·CaO·P_2O_5 glasses.

Because of this, the surfaces of quaternary glasses were analysed by TEM-EDS. The study shows that the glasses are chemically heterogeneous at nanometric scales and that

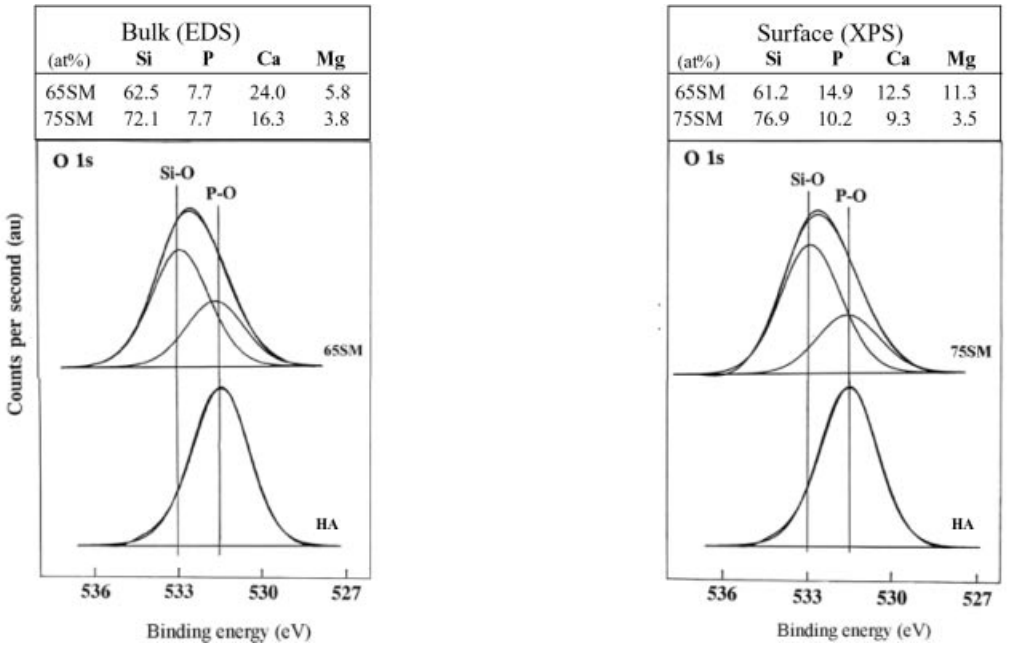

Figure 8. XPS spectra of oxygen 1s of the quaternary 65SM and 75SM glasses; hydroxyapatite spectra are included as reference; bulk (EDS) and surface (XPS) compositions of the glasses are also included

magnesium is always attached to Ca, P and Si, whereas pure calcium phosphate crystals were not detected. Therefore, Mg seems to inhibit the formation of calcium phosphate microdomains. These microdomains would eventually act as preferred centres for apatite crystallisation in Mg-free glasses, as they would offer a minimum interfacial energy for nucleation.[32]

To gain a deeper knowledge of the glass surface, a surface analysis technique, such as X-ray Photoelectron Spectroscopy (XPS), is needed. These studies show that the glasses' surfaces are richer in phosphorus and magnesium and poorer in calcium than the interiors (Figure 8).[32] Figure 8 shows the XPS spectra of O1s for 65SM and 75SM, together with that of hydroxyapatite (HA), included as a reference. The spectra of glasses can be deconvoluted into two components at 531.3 eV (P−O in HA) and 533.1 eV (Si−O).

Results from EDS-TEM and XPS studies suggest the existence of calcium-magnesium phosphate microdomains on the surface of quaternary glasses. Since the amount of calcium phosphate domains drastically decreased when MgO was included, this was regarded as the primary factor producing the bioactivity decrease in quaternary glasses containing magnesium.

5. Binary Compositions: SiO_2·CaO System

As already mentioned, addition of MgO to the SiO_2·CaO·P_2O_5 system modifies the textural properties and decreases the bioactivity of sol-gel glasses, while simultaneously increasing the complexity of the system. We therefore conjectured that the exclusion of a component of the ternary system, such as P_2O_5, might help understanding of the bioactivity mechanism in glasses, if the resultant glass was bioactive.

There are literature reports of bioactivity for SiO_2·CaO melt glasses with maximum SiO_2 contents of 65 mol %[67] (higher silica contents would produce phase separation by this synthesis method).

Our group has synthesised CaO·SiO_2 glasses with SiO_2 contents between 50 and 90 mol % by the sol-gel method.[42,45,48] In vitro bioactivity studies in all cases show the formation of an apatite-like layer. These results indicate that the presence of P_2O_5 in glasses of this system is not essential to ensure bioactivity, even at very high SiO_2 contents.

As with the ternary system, it was observed that the rate of formation of the new layer increases with the CaO content in the glasses.[30] In addition, in glasses with high CaO contents (40 and 50 mol %), calcite ($CaCO_3$) was also detected in the layer together with the apatite.

To understand the role of P_2O_5 in the glasses' bioactivity, the behaviour of an 80% SiO_2/20% CaO glass in SBF was compared with that of a ternary glass with identical silica content and 3% of P_2O_5.[30] Moreover, silicate glasses with identical CaO contents (25 mol %) and P_2O_5 contents of 0, 2.5 and 5 mol % were compared.[42]

The obtained results allow the conclusion that the presence of phosphorus retards the initial reactivity of glasses, defined as the time required for the initial formation of the amorphous calcium phosphate. Once some nuclei are formed, however, the growth of apatite crystals in the new layer is quicker and affords larger crystals when there is a small amount of P_2O_5 in the glass composition.

6. Procedures for the In Vitro Bioactivity Studies

During the in vitro studies described above, the assay solution was not renewed and so the ions released from the glass remain in the container. This method is termed *static* or *integral*. When materials with high reactivity in aqueous solutions are studied, however, ionic analysis of the solutions shows huge ionic concentration variations during the assay. As a result, some authors have proposed the so-called *differential* method,[5,6] in which the solution is renewed at predetermined intervals. For sol-gel glasses, our studies have shown that solution substitution should be at intervals so short that sample manipulations would affect the apatite formation process. For that reason, also to simulate the continuous flux of body fluids at the implant surface, we have proposed a new *dynamic* or *continuous* in vitro procedure, in which SBF is continuously renewed with the aid of a peristaltic pump. Figure 9 shows the scheme of the device used for *dynamic* in vitro assays.

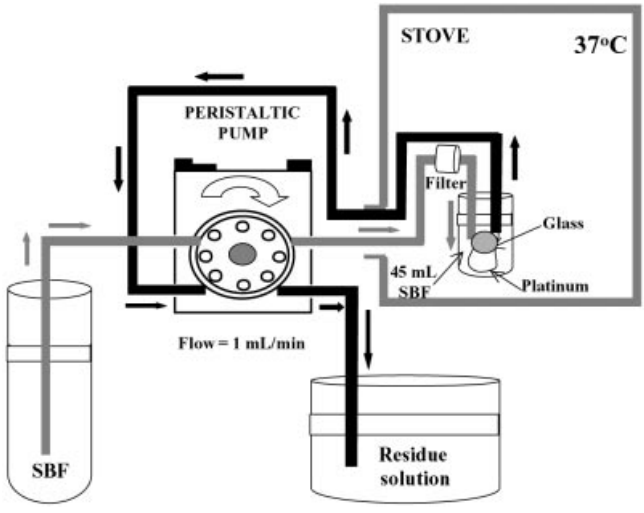

Figure 9. Representation of the dynamic procedure used for in vitro tests in SBF; a peristaltic pump continuously exchanges the assay solution to model the continuous flow of body fluids at the implant surface

This procedure was used for a bioactivity study of several glasses, results being compared with those obtained in *static* mode.[37,47] The use of a *dynamic* procedure allows complete bioactivity assays to be performed while keeping ionic concentration and pH almost equal to those of plasma. Fig-

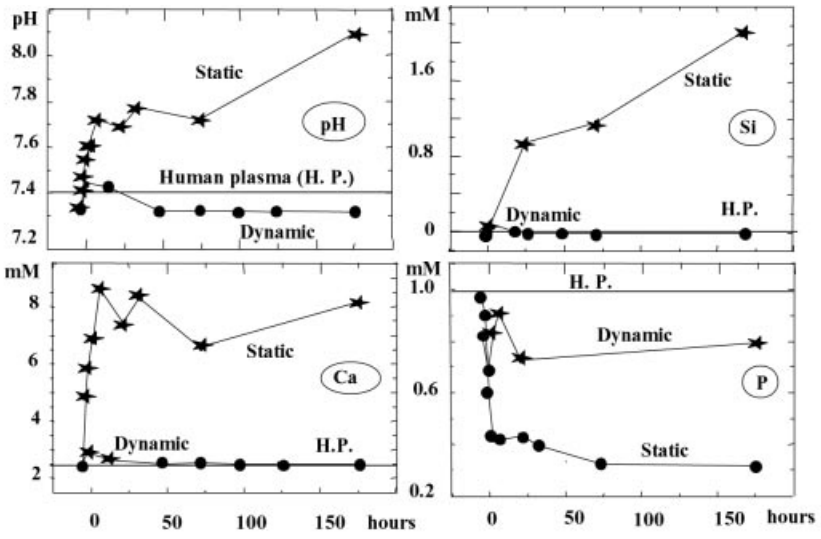

Figure 10. Variation of pH and Ca^{II}, P^{V} and Si^{IV} concentrations with soaking time in solution for 80S20C by use of static and dynamic in vitro procedures; the horizontal line in the figures indicates the values in human plasma

Table 2. Comparison between the two procedures used for in vitro studies of 80S20C and 80S17C sol-gel glasses

		Static	Dynamic
	SBF	Variations in solution after 7 d	
pH	7.30	8	7.30
Ca^{II} [mM]	2.5	8.5	2.5
P^{V} [mM]	1.0	0.3	0.8
Si^{IV} [mM]	0	2.1	0
		Variations in the layer	
Amorphous calcium phosphate		early formation	later formation
Apatite crystallisation		smaller crystals	bigger crystals
Layer composition		detected silicon	no silicon
Ca/P molar ratio		1.6	1.2

ure 10 shows variations with immersion time of Ca^{II}, P^{V}, Si^{IV} and pH in solution for 80S20C glass under *static* and *dynamic* conditions. Differences in solution composition, mainly pH, produced variations in the formation of calcium- and phosphorus-rich layers, shown schematically in Table 2. In *dynamic* mode, the amorphous phosphate layer was detected only after longer soaking times, but the size of the apatite crystals formed later is larger than in *static* mode. Regarding the layer composition, in contrast with static conditions, no traces of silicon were detected in *dynamic* mode and the Ca/P ratio was considerably lower (Figure 11, a). These differences were explained by the mechanism shown in Figure 11, b. The lower pH in *dynamic* mode (7.3) increases the HPO_4^{2-} ion concentration in solution compared with the static conditions under which the pH is close to 8. In this sense, use of the *dynamic* mode would favour the formation of calcium-deficient apatite, which might coexist with other calcium phosphates of lower Ca/P molar ratio.

7. Sol-Gel Glasses: Components of Mixed Materials

The excellent bioactivity of sol-gel glasses (SGGs) makes them potential candidates for osseous tissue regeneration. These glasses could be the optimal complement in systems for release of therapeutic action substances, such as antibiotics or anti-inflammatory agents, able to mitigate the problems originating from the material implantation.

The combination of these bioactive glasses with magnetic materials may also be an option for treatment of osseous tissues affected by tumours, since it should be possible to obtain bioactive and magnetic pieces capable of regenerating the bone, and to apply hyperthermia treatment. Moreover, the bioactive glass/hydroxyapatite (HA) combination can accelerate the bioactive response of HA. We have developed several SGG-polymer-drug, SGG-magnetic component and SGG-HA mixed materials, described below.

7.1 Sol-Gel Glass-Polymer-Drug

The study of systems for controlled release of drugs began with the synthesis of ceramic-polymer-drug materials including anti-inflammatory and antibiotic drugs.[68−73] In vitro studies showed that the release of the drug depends on its solubility and the piece matrix's porosity and capability to absorb liquid.

If a bioactive SSG is used as inorganic component in these systems,[74−77] a controlled release system, simultaneously bioactive, is produced. In this way, the osseous integration is improved and the drug release is favoured, due to the ionic interchange between the glass and medium.

On the other hand, the release of gentamicin from SSG implants was studied under in vivo conditions.[66] Gentamicin levels found in the organs analysed indicate that these

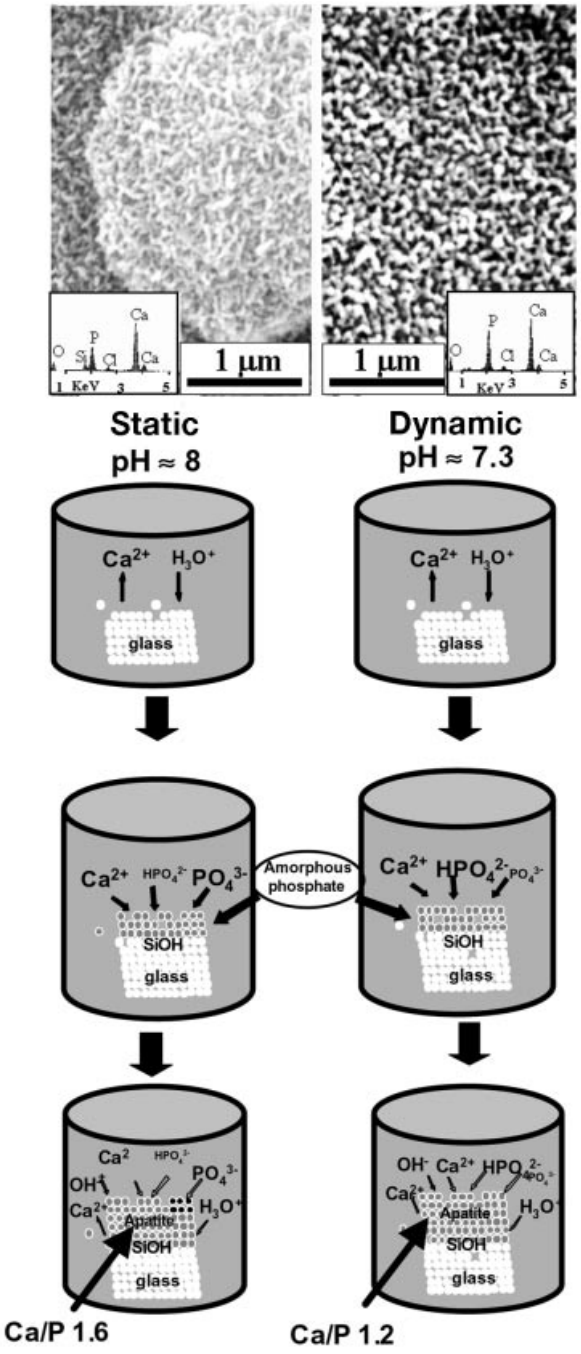

Figure 11. SEM micrographs and EDS patterns of 80S20C after 7 d soaking with use of static and dynamic in vitro bioactivity procedures and the proposed model to explain the different Ca/P molar ratio values obtained by EDS in the newly formed layer

implants are useful as drug release systems in bone during the 12 weeks of study.

7.2 Sol-Gel Glass-Magnetic Glass-Ceramic

The sensitivity of cancer cells to high temperatures was discovered 70 years ago, and the possibility of treating tumours by controlled heating has been studied since then. Nowadays, such therapy is termed *hyperthermia*. Among the techniques for application of this therapy, those of *interstitial hyperthermia* produce heat with the aid of devices directly implanted in the affected area. These devices can be magnetic materials, which will generate heat in an external alternating field, due to hysteresis losses or parasite currents. Heat is restricted to the desired volume without affecting the surrounding tissues.

Among those materials that have been proposed as *thermoseeds* in *interstitial hyperthermia*, magnetic glass-ceramics (MGCs) are interesting alternatives for the substitution and filling of osseous tissues exhibiting tumours.[78−82]

In our group we have studied the possibility of combining MGCs with bioactive glasses, synthesising biphasic materials presenting both properties. We have obtained several materials with varying proportions of the two components. Our studies showed that SGGs produce increases in the macro- and mesoporosity of the system, as well as higher reactivity in simulated body fluids, conferring high bioactivity on these biphasic materials.[83−84] However, the presence of SGGs seems partially to inhibit the incorporation of iron in the crystalline phases of the glass-ceramic, consequently decreasing the magnetic behaviour.[84]

7.3 Sol-Gel Glass-Hydroxyapatite

Hydroxyapatite (HA) is a highly suitable material for bone substitutions because it is not cytotoxic, presents excellent biocompatibility with living tissues, and is the material most similar to the mineral component of bone. However, the bioactivity of HA ceramics is lower than that of bioactive glasses.[85]

Our group has prepared and characterised SGG/HA biphasic materials offering more rapid kinetics of new apatite formation than pure HA.[86−88]

Figure 12 shows surface micrographs of 70S, HA and biphasic 70S/HA before and after soaking in SBF for different periods of time. As can be observed, the glass is coated by a layer of spheres after 7 d in SBF whereas the HA surface is not modified even after 45 d of immersion. Moreover, the biphasic 70S/HA is bioactive after only 12 h.

In addition, cross-sections of the biphasic materials before and after soaking for 3, 7 and 14 d in SBF were studied by SEM-EDS. The silicon content decreases from the inner part (ca. 30 μm) to the border, whereas Ca and P contents increase. The small amount of Si in the limit with the apatite-like layer obtained after 3 d of immersion is related to the lower thickness of this layer relative to those obtained after 7 or 14 d of treatment.

To visualise the newly formed layer better, Figure 13 shows the SEM micrographs, at different magnification, of the biphasic material surface after 7 d in SBF, as well as a cross section. The EDS spectrum of the new layer is also included. A layer thickness of approximately 3×10^3 nm and the absence of silicon in the new formed layer are observed.

8. Sol-Gel Glasses Coatings

Ceramic coatings of metallic pieces used as implants are of great interest because they combine the good mechanical

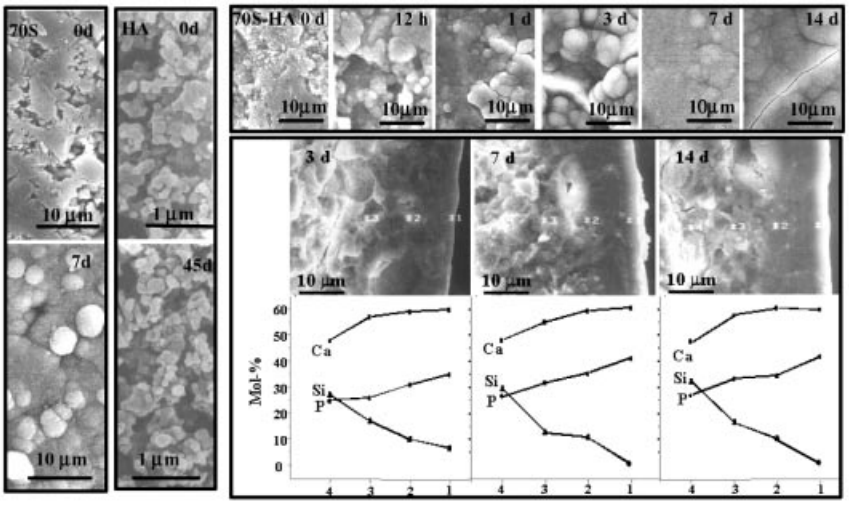

Figure 12. SEM micrographs of 70S glass, hydroxyapatite and 70S-HA biphasic material surfaces after SBF soaking several times; Ca, Si and P contents as a function of depth obtained by EDS in the transversal sections of biphasic material after SBF soaking for 3, 7 and 14 d are also included

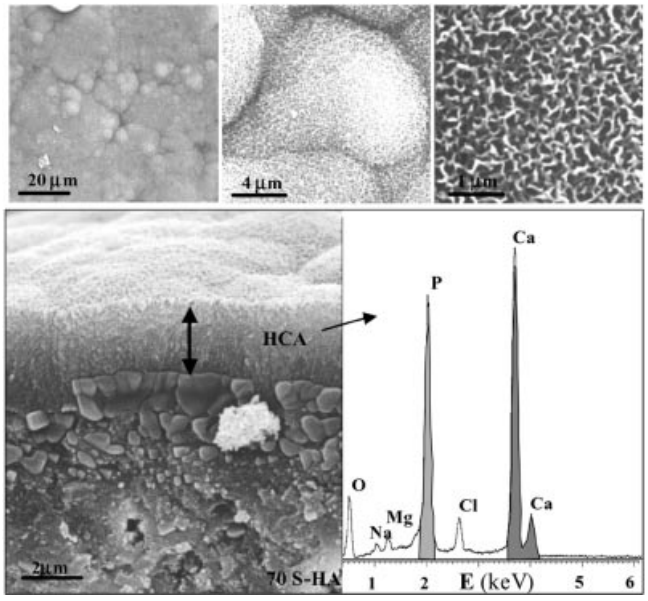

Figure 13. SEM micrographs of surface and a cross section of 70S-HA biphasic material after 7 d soaking; the EDS spectrum of the newly formed apatite layer is also included

properties of metals with the excellent biocompatibility and, in some cases, bioactivity of ceramics. At the same time, the metallic surface is protected from the biological medium, reducing corrosion and the release of ionic metals into the medium.

Sol-gel processing is ideal for the preparation of films by *dip-coating*. This method requires simple equipment and soft thermal treatments, and − its main advantage − allows a high degree of control over the microstructure and composition of the film, highly pure and homogeneous coatings being obtainable. *Dip-coating* technology is based on the capability of *sols* to form films on substrates introduced into them and extracted at a known rate. Many parameters affect the microstructure and thickness of the films, although the extraction velocity of substrate and the *sol* viscosity are strong limiting parameters. The extraction velocity must be lower than or equal to the gelling rate of the film in order to avoid flocculation processes and to maximise the adhesion to substrate.

Our group has prepared SiO_2·CaO system sol-gel coatings on metallic Ti6Al4V prostheses by *dip-coating*.[89] The characteristics of the method allow the porosity and thickness of coatings to be controlled by varying the properties of the starting solution. Figure 14 shows SEM and atomic force microscopy (AFM) micrographs of 80% SiO_2/20% CaO sol-gel coatings on a Ti6Al4V substrate.

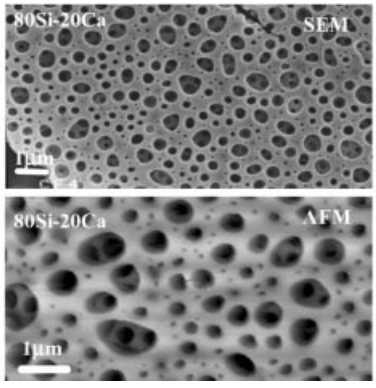

Figure 14. SEM and AFM micrographs of sol-gel glass coatings (80S20C glass) on metallic Ti6Al4V substrates

9. Future Expectations in Bioactive Glasses

From the advances in related medical technologies, bioactive materials appear to be entering a new stage of development in which they will have to be skilfully designed to exhibit a variety of new functions. These new functions include different mechanical properties, drug delivery capabil-

ity, the capability to activate proteins and/or cells for tissue regeneration and tissue engineering, biomimetics, nanotechnology, etc. Namely, there is significant increase in requirements for novel bioactive materials with different functions. To design a novel bioactive material successfully, the mechanism of bone-like apatite formation on the current bioactive materials should be specifically addressed and established.

Sol-gel glasses, as fibres or high-porosity monoliths, are good candidates with which to obtain biocompatible scaffolds for tissue engineering while maintaining mechanical properties during the resorption process. Growth factors (bone, platelet-derived, basic fibroblast) and polypeptides for their release can be included in the scaffolds.

On the other hand, the potential design of combinations of bioactive glasses and apatites could give very satisfactory results in terms of acceleration of the bioactivity of the apatites, which, due both to their composition and structure, are the ceramics most similar to the mineral component of the bone.

The new expectations on the field of hybrid organic/inorganic materials represent another route for future applications of bioactive glasses.

Acknowledgments

We would like to express our deepest gratitude to all our coworkers and friends who have contributed with their effort and thinking to these studies over the years. Financial support by the Spanish CICYT (MAT99-0466 and MAT01-1445-C02-01) is gratefully acknowledged.

[1] L. L. Hench, R. J. Splinter, W. C. Allen, T. K Greenlee, *J. Biomed. Mater. Res.* **1971**, *2*, 117−141.
[2] L. L. Hench, H. A. Paschall, *J. Biomed. Mater. Res.* **1973**, *7*, 25−42.
[3] L. L. Hench, *J. Am. Ceram. Soc.* **1991**, *74*, 1487−1510.
[4] C. G. Pantano, A. E. Clark, L. L. Hench, *J. Am. Ceram. Soc.* **1974**, *57*, 412−413.
[5] S. Radin, P. Ducheyne, B. Rothman, A. Conti, *J. Biomed. Mater. Res.* **1997**, *37*, 363−375.
[6] J. P. Zhong, D. C. Greenspan, in *Bioceramics 11* (Eds.: R. Z. LeGeros, J. P. LeGeros), World Scientific, Singapore, **1998**, p. 415−418.
[7] T. Kokubo, H. Kushitani, S. Sakka, T. Kitsugi, T. Yamamuro, *J. Biomed. Mater. Res.* **1990**, *24*, 721−734.
[8] P. Ducheyne, S. Brown, N. Blumenthal, L. L. Hench, A. Krajewski, G. Palavit, A. Ravaglioli, S. Steineman, S. Winderler, *Ann. N.Y. Acad. Sci.* **1988**, *523*, 257−263.
[9] T. Kokubo, H. Kushitani, C. Ohsuki, S. Sakka, T. Yamamura, *J. Mater. Sci.: Mater. Med.* **1992**, *3*, 79−83.
[10] K. Ohura, T. Nakamura, T. Yamamuro, T. Kokubo, Y. Ebisawa, Y. Kotoura, M. Oka, *J. Biomed. Mater. Res.* **1991**, *25*, 357−365.
[11] L. L. Hench, J. Wilson, *Science* **1984**, *226*, 630−636.
[12] G. Heimke, in *Handbook of Biomaterials Evaluation* (Ed.: A. F. Von Recum), Macmillan Publishing Company, New York, **1986**, p. 38−54.
[13] T. Kokubo, *J. Ceram. Soc. Jpn.* **1991**, *99*, 965−973.
[14] P. Ducheyne, *MRS Bulletin* **1998**, November 23, p. 43−49.
[15] L. L. Hench, T. Kokubo, in *Handbook of Biomaterials Properties* (Eds.: J. Black, G. Hastings), Chapman and Hall, London, **1998**, p. 355−363.
[16] M. Vallet-Regí, *J. Chem. Soc., Dalton Trans.* **2001**, 97−108.
[17] H. M. Kim, *J. Ceram. Soc. Jpn.* **2001**, *109*, S49−S57.
[18] L. L. Hench, J. M. Pollack, *Science* **2002**, *295*, 1014−1017.
[19] L. L. Hench, E. C. Ethridge, in *Biomaterials, An Interfacial Approach*, Academic Press, New York, **1982**, p. 139−148.
[20] Ö. H. Andersson, K. H. Karlsson, K. Kangasniemi, A. Yli-Urpo, *Glastech. Ber.* **1988**, *61*, 300−305.
[21] B. A. Blencke, H. Brömer, K. Deutcher, *J. Biomed. Mater. Res.* **1978**, *12*, 307−316.
[22] T. Kokubo, M. Shigematsu, Y. Nagashima, M. Tashiro, T. Nakamura, T. Yamamuro, S. Higashi, *Bull. Inst. Chem. Res. Kyoto Univ.* **1982**, *60*, 260−268.
[23] W. Vogel, W. Holland, *Angew. Chem. Int. Ed. Engl.* **1987**, *26*, 527−544.
[24] R. D. Rawlings, *J. Mater. Sci. Lett.* **1992**, *11*, 1340−1347.
[25] R. Li, A. E. Clark, L. L. Hench, *J. Appl. Biomat.* **1991**, *2*, 231−239.
[26] M. Vallet-Regí, F. Balas, M. Gil, E. Nogueroles, A. Romero, J. Román, A. J. Salinas, C. V. Ragel, in *Non-crystalline & nanoscale Materials* (Eds.: J. Rivas, M. A. Lopez Quintela), World Scientific, Singapore, **1998**, p. 55−60.
[27] A. J. Salinas, J. Román, M. Vallet-Regí, P. Fernández, J. Piqueras, in *Bioceramics* 11 (Eds.: R. Z. LeGeros, J. P. LeGeros), World Scientific, Singapore, **1998**, p. 707−710.
[28] F. Balas, J. Pérez-Pariente, M. Vallet-Regí, in *Bioceramics* 11 (Eds.: R. Z. LeGeros, J. P. LeGeros), World Scientific, Singapore, **1998**, p. 125−128.
[29] M. Vallet-Regí, A. M. Romero, C. V. Ragel, R. Z. LeGeros, *J. Biomed. Mater. Res.* **1999**, *44*, 416−421.
[30] M. Vallet-Regí, I. Izquierdo-Barba, A. J. Salinas, *J. Biomed. Mater. Res.* **1999**, *46*, 560−565.
[31] M. Vallet-Regí, A. J. Salinas, J. Román, M. Gil, *J. Mater. Chem.* **1999**, *9*, 515−518.
[32] J. Pérez-Pariente, F. Balas, M. Vallet-Regí, *Chem. Mater.* **2000**, *12*, 750−755.
[33] M. Vallet-Regí, A. Rámila, *Chem. Mater.* **2000**, *12*, 961−965.
[34] M. Vallet-Regí, D. Arcos, J. Pérez-Pariente, *J. Biomed. Mater. Res.* **2000**, *51*, 23−28.
[35] M. Vallet-Regí, J. Pérez-Pariente, I. Izquierdo-Barba, A. J. Salinas, *Chem. Mater.* **2000**, *12*, 3770−3775.
[36] A. Rámila, M. Vallet-Regí, *Biomaterials* **2001**, *22*, 2301−2306.
[37] A. J. Salinas, M. Vallet-Regí, I. Izquierdo-Barba, *J. Sol-Gel. Sci. Tech.* **2001**, *21*, 13−25.
[38] F. Balas, D. Arcos, J. Pérez-Pariente, M. Vallet-Regí, *J. Mater. Res.* **2001**, *16*, 1345−1348.
[39] A. Rámila, F. Balas, M. Vallet-Regí, *Chem. Mater.* **2002**, *14*, 542−548.
[40] D. Arcos, D. Greenspan, M. Vallet-Regí, *Chem. Mater.* **2002**, *14*, 1515−1522.
[41] M. Vallet-Regí, A. I. Martin, A. J. Salinas, N. Olmo, J. Turnay, M. A. Lizarbe, *Biol. Cell*, **2001**, *93*, 328−329.
[42] A. J. Salinas, A. I. Martín, M. Vallet-Regí, *J. Biomed. Mater. Res.* **2002**, *61*, 524−532.
[43] D. Arcos, D. Greenspan, M. Vallet-Regí, *J. Biomed. Mater. Res.*, in press.
[44] J. Pérez-Pariente, F. Balas, J. Román, A. J. Salinas, M. Vallet-Regí, *J. Biomed. Mater. Res.* **1999**, *47*, 170−175.
[45] I. Izquierdo-Barba, A. J. Salinas, M. Vallet-Regí, *J. Biomed. Mater. Res.* **1999**, *47*, 243−250.
[46] J. Pérez-Pariente, I. Izquierdo-Barba, J. L. García-Fierro, A. J. Salinas, M. Vallet-Regí, in *Bioceramics 12* (Eds.: H. Ohgushi, G. W. Hastings, T. Yoshikawa), World Scientific, Singapore, **1999**, p. 173−176.
[47] I. Izquierdo-Barba, A. J. Salinas, M. Vallet-Regí, *J. Biomed. Mater. Res.* **2000**, *51*, 191−199.
[48] A. Martínez, I. Izquierdo-Barba, M. Vallet-Regí, *Chem. Mater.* **2000**, *12*, 3080−3088.
[49] T. Kokubo, M. Shigematsu, Y. Nagashisma, M. Tashiro, T. Nakamura, T. Yamamuro, S. Higashi, *Bull. Inst. Chem. Res., Kyoto Univ.* **1982**, *60*, 260−268.
[50] S. J. Gregg, K. S. W. Sing, in *Adsorption, surface area and porosity*, Academic Press, New York, **1982**.

[51] R. Z. LeGeros, *Prog. Crystal Growth Charact.* **1981**, *4*, 1−45.
[52] R. Z. LeGeros, J. P. LeGeros, O. R. Trautz, E. Klein, *Dev. Appl. Spectrosc.* **1970**, *7B*, 13−22.
[53] A. Ravaglioli, A. Krajewski, G. C. Celoti, A. Piancastelli, B. Bacchini, L. Montanari, G. Zama, L. Piombi, *Biomaterials* **1996**, *17*, 617−622.
[54] C. Rey, A. Hina, A. Tofighi, M. J. Glimcher, *Cells Mater.* **1995**, *5*, 345−356.
[55] L. L. Hench, C. G. Pantano, P. J. Buscemi, D. C. Greenspan, *J. Biomed. Mater. Res.* **1977**, *11*, 267−281.
[56] Ö. H. Andersson, K. H. Karlsson, I. Kangasniemi, *J. Non-Cryst. Solids* **1990**, *119*, 290−296.
[57] E. Schepers, P. Ducheyne, De Clercq, *J. Biomed. Mater. Res.* **1989**, *23*, 735−742.
[58] Ö. H. Anderson, I. Kangasniemi, *J. Biomed. Mater. Res.* **1991**, *25*, 1019−1030.
[59] K. Ohura, T. Nakamura, T. Yamamuro, Y. Ebisawa, T. Kokubo, Y. Kotoura, M. Oka, *J. Mater. Sci. Mater. Med.* **1992**, *3*, 95−100.
[60] R. Li, A. E. Clark, L. L. Hench, in *Chemical Processing of Advanced Materials* (Eds.: L. L. Hench, J. K. West), John Wiley & Sons, Inc., New York, **1992**, p. 627−633.
[61] P. Li, K. Nakanish, T. Kokubo, K. De Groot, *Biomaterials* **1993**, *14*, 963−968.
[62] M. M. Pereira, A. E. Clark, L. L. Hench, *J. Am. Ceram. Soc.* **1995**, *78*, 2463−2468.
[63] M. M. Pereira, L. L. Hench, *J. Sol-Gel Sci. Tech.* **1996**, *7*, 59−68.
[64] M. M. Pereira, A. E. Clark, L. L. Hench, *J. Biomed. Mater. Res.* **1994**, *28*, 693−698.
[65] T. Peltola, M. Jokinen, H. Rahiala, E. Levänen, J. B. Rosenhold, I. Kangasniemi, A. Yli-Urpo, *J. Biomed. Mater. Res.* **1999**, *44*, 12−21.
[66] L. Meseguer-Olmo, M. J. Ros-Nicolas, M. Clavel-Sainz, V. Vicente-Ortega, M. Alcaraz-Baños, A. Lax-Pérez, D. Arcos, C. V. Ragel, M. Vallet-Regí, *J. Biomed. Mater. Res.* **2002**, *61*, 458−465.
[67] Y. Ebisawa, T. Kokubo, K. Ohura, T. Yamamuro, *J. Mater. Sci. Mater. Med.* **1990**, *1*, 239−244.
[68] D. Arcos, M. V. Cabañas, C. V. Ragel, M. Vallet-Regí, J. San Román, *Biomaterials* **1997**, *18*, 1235−1242.
[69] S. Granado, C. V. Ragel, V. Cabañas, J. San Román, M. Vallet-Regí, *J. Mater. Chem.* **1997**, *7*, 1581−1585.
[70] M. Vallet-Regí, S. Granado, D. Arcos, M. Gordo, M. V. Cabañas, C. V. Ragel, A. J. Salinas, A. L. Doadrio, J. San Román, *J. Biomed. Mat. Res.* **1998**, *39*, 423−428.
[71] M. Vallet-Regí, M. Gordo, C. V. Ragel, M. V. Cabañas, J. San Román, *Solid State Ionics* **1997**, *101−103*, 887−892.
[72] R. P. del Real, S. Padilla, M. Vallet-Regí, *J. Biomed. Mater. Res.* **2000**, *52*, 1−7.
[73] S. Padilla, R. P. del Real, M. Vallet-Regí, *J. Control Release* **2002**, *83*, 343−352.
[74] C. V. Ragel, M. Vallet-Regí, *J. Biomed. Mater. Res.* **2000**, *51*, 424−429.
[75] D. Arcos, C. V. Ragel, M. Vallet-Regi, *Biomaterials* **2001**, *22*, 701−708.
[76] S. Ladrón de Guevara, C. V. Ragel, M. Vallet-Regí, *Biomaterials*, submitted.
[77] A. Rámila, R. P. del Real, R. Marcos, P. Horcajada, M. Vallet-Regí, *J. Sol-Gel Sci. Tech.*, **2003**, *26*, 1195−1198.
[78] K. Ohura, M. Ikenaga, T. Nakamura, T. Yamamuro, Y. Ebisawa, T. Kokubo, Y. Kotoura, M. Oka, *J. Appl. Biomater.* **1991**, *2*, 153−159.
[79] Y. Ebisawa, Y. Sugimoto, T. Hayashi, T. Kokubo, K. Ohura, T. Yamamuro, *J. Ceram. Soc. Jpn.* **1991**, *99*, 7−13.
[80] M. Ikenaga, K. Ohura, T. Yamamuro, Y. Kotoura, M. Oka, T. Kokubo, *J. Orthop. Res.* **1993**, *11*, 849−855.
[81] Y. Ebisawa, F. Miyaji, T. Kokubo, K. Ohura, T. Nakamura, *J. Ceram. Soc. Jpn.* **1997**, *105*, 947−951.
[82] Y. Ebisawa, F. Miyaji, T. Kokubo, K. Ohura, T. Nakamura, *Biomaterials* **1997**, *18*, 1277−1284.
[83] D. Arcos, R. P. del Real, M. Vallet-Regí, *Biomaterials* **2002**, *23*, 2151−2158.
[84] D. Arcos, R. P. del Real, M. Vallet-Regí. *J. Biomed. Mater. Res.*, in press.
[85] H. Oonishi, L. L. Hench, J. Wilson, F. Sugihara, E. Tsuji, M. Matsuura, S. Kin, T. Yamamoto, S. Mizokawa, *J. Biomed. Mater. Res.* **2000**, *51*, 233−237.
[86] C. V. Ragel, M. Vallet-Regí, L. Rodríguez-Lorenzo, *Biomaterials* **2002**, *23*, 1865−1872.
[87] A. Ramila, S. Padilla, B. Muñoz, M. Vallet-Regí, *Chem. Mater.* **2002**, *14*, 24−39.
[88] M. Vallet-Regí, A. Ramila, S. Padilla, B. Muñoz. *J. Biomed. Mater. Res.*, in press
[89] I. Izquierdo-Barba, M. Vallet-Regí, J. M. Rojo, E. Blanco, L. Esquivias, *J. Sol-Gel Sci. Tech.*, **2003**, *26*, 1179−1182.

Received June 17, 2002
[I02312]

First Star-Like Oligophenylene Molecules Containing a Dinuclear Organometallic Core

Frédéric Chérioux,*[a] Bruno Therrien,[a] and Georg Süss-Fink[a]

Dedicated to Professeur Bernard Laude on the occasion of his 65th birthday

Keywords: Rhodium / Ruthenium / Oligomerization / Oligophenylene

The cationic complexes $Ru_2[(p\text{-}MeC_6H_4iPr)_2(p\text{-}SC_6H_4Br)_3]^+$ and $Rh_2[(C_5Me_5)_2(p\text{-}SC_6H_4Br)_3]^+$ are available in quantitative yields from the reaction of $p\text{-}HSC_6H_4Br$ with $[Ru(p\text{-}MeC_6H_4iPr)Cl_2]_2$ and $[Rh(C_5Me_5)Cl_2]_2$ respectively. These complexes are found to undergo triple Suzuki coupling with oligophenylene boronic acids to give $[Ru_2(p\text{-}MeC_6H_4iPr)_2\{p\text{-}S\text{-}(C_6H_4)_n\text{-}C_6H_5\}_3]^+$ and $[Rh_2(C_5Me_5)_2\{p\text{-}S\text{-}(C_6H_4)_n\text{-}C_6H_5\}_3]^+$ respectively. The star-like trisbromo complexes are potential precursors for the insertion of dinuclear organometallic entities into the main chain of conjugated molecules.
(© Wiley-VCH Verlag GmbH & Co. KGaA, 69451 Weinheim, Germany, 2003)

Introduction

During the two past decades there has been a growing interest in the field of conjugated molecules containing metal centers because of their electronic, nonlinear optical, magnetic and catalytic properties,[1−3] and more recently for the development of sensors.[4,5] It is quite impossible to be exhaustive because of the plethora of new compounds synthesized in all these fields of research, but, to the best of our knowledge, all relevant molecules are built around mononuclear building blocks coordinated by different types of organic ligand such as metallocenes, salens, dithiolenes or "nitrogen bridges" (terpyridines, bipyridines or porphyrins). These types of molecules are the most common in the literature because of their extraordinary ability to develop supramolecular structures.[1,6] However, the challenge remains to develop versatile and selective strategies with a view to creating new molecular designs and new bridging ligands.

Star-shaped molecules can lead to a strong enhancement of the physical properties — such as nonlinear optical susceptibilities[7,8] or electronic conductivities − in hyperbranched conjugated polymers.[9] Moreover, there is a large interest in conjugated oligomers for their intrinsic physical properties[10,11] as because they are model compounds for the study of the corresponding conductive polymers.[12] In this paper, we report the first example of dinuclear organometallic species in star-like conjugated molecules with sulfur connectivities of the type $[Ru_2(p\text{-}MeC_6H_4iPr)_2(p\text{-}SC_6H_4Br)_3]^+$ and $[Rh_2(C_5Me_5)_2(p\text{-}SC_6H_4Br)_3]^+$ and the increase of their conjugation length by Suzuki coupling reactions with oligophenylene boronic acids.

Results and Discussion

In accordance with our previous studies,[13] the dinuclear dichloro complexes $[Ru(p\text{-}MeC_6H_4iPr)Cl_2]_2$ and $[Rh(C_5Me_5)Cl_2]_2$ are found to react in ethanol with *p*-bromothiophenol to give the cationic complexes $[Ru_2(p\text{-}MeC_6H_4iPr)_2(p\text{-}SC_6H_4Br)_3]^+$ (**1**) and $[Rh_2(C_5Me_5)_2(p\text{-}SC_6H_4Br)_3]^+$ (**2**), respectively, which can be isolated in quantitative yield as the chloride salts (Scheme 1).

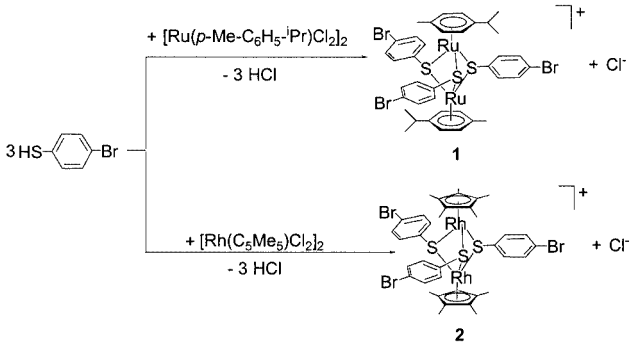

Scheme 1. Synthesis of star-like trisbromo complexes **1** and **2**

Both cations **1** and **2** are unambiguously characterized by their MS, IR, ^1H and ^{13}C NMR spectroscopic data as well as by satisfactory elemental analysis data of the chloride salts. These cationic complexes are readily soluble as their chloride salts in alcohols, acetone and chlorinated

[a] Institut de Chimie, Université de Neuchâtel,
Avenue de Bellevaux 51, 2007 Neuchâtel, Switzerland
Fax: (internat.) + 41-327/182-511
E-mail: frederic.cherioux@unine.ch

solvents. Their molecular structures were confirmed by a single-crystal X-ray structure analysis of [**1**]Cl and [**2**]Cl. The cations were found to consist of a closed trigonal bipyramid M_2S_3 framework (M = Ru or Rh), with each ruthenium or rhodium atom being coordinated to an η^6-Me-C_6H_4*i*Pr or an η^5-C_5Me_5 ligand, respectively, and each sulfur atom carrying a *p*-bromophenyl group. The molecular structures of **1** and **2** are shown in Figure 1.

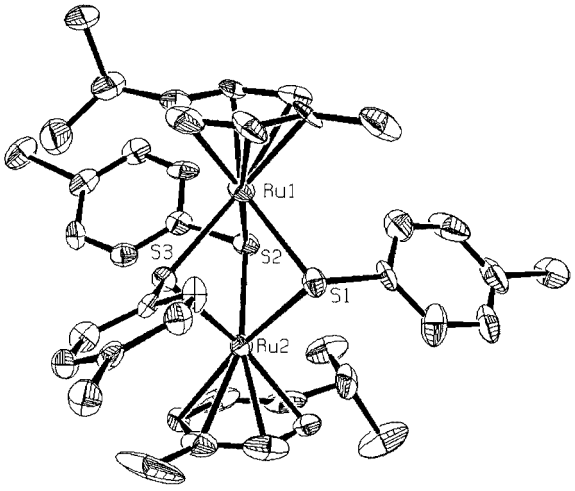

1

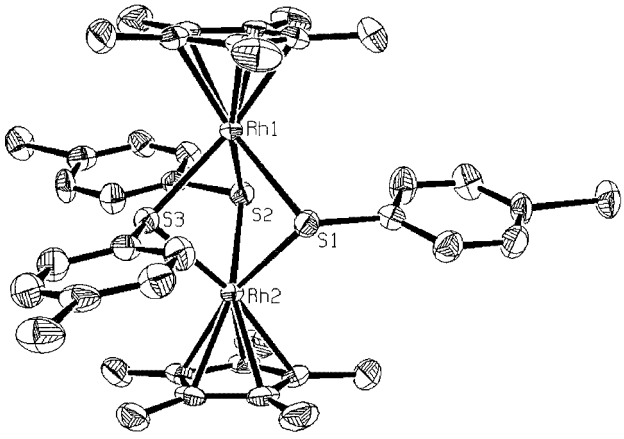

2

Figure 1. Molecular structure of [**1**]Cl and [**2**]Cl; the chloride ion, solvent molecules, and H atoms have been omitted for clarity; displacement ellipsoids are drawn at the 50% probability level; selected bond lengths (Å) and angles(°): [**1**]Cl Ru(1)−S(1) 2.392(2), Ru(1)−S(2) 2.4192(19), Ru(1)−S(3) 2.385(2), Ru(2)−S(1) 2.411(2), Ru(2)−S(2) 2.3989(19), Ru(2)−S(3) 2.402(2), Ru(1)−Ru(2) 3.3532(8); Ru(1)−S(1)−Ru(2) 88.56(7), Ru(1)−S(2)−Ru(2) 88.20(6), Ru(1)−S(3)−Ru(2) 88.92(8); [**2**]Cl Rh(1)−S(1) 2.3882(16), Rh(1)−S(2) 2.4145(17), Rh(1)−S(3) 2.3937(16), Rh(2)−S(1) 2.4112(17), Rh(2)−S(2) 2.3817(15), Rh(2)−S(3) 2.4059(16), Rh(1)−Rh(2) 3.2254(7); Rh(1)−S(1)−Rh(2) 84.45(5), Rh(1)−S(2)−Rh(2) 84.52(5), Rh(1)−S(3)−Rh(2) 84.44(5)

The bromo-ended star-shaped arrangement adopted by these complexes is very interesting as these compounds represent conductive organometallic nodes. The intramolecular charge transfer (ICT) between the organometallic moieties and the *p*-bromophenyl groups can be shown by the NMR spectroscopy. An important shielding of the arene (Cp* or *p*-MeC_6H_4*i*Pr) attached to the metal centers is observed in the NMR spectra, whereas a large deshielding of the signals of the *p*-bromophenyl groups is observed in the corresponding NMR spectra (see Exp. Sect.). This phenomenon is larger in the case of ruthenium-based complexes than in the rhodium derivatives. This is proof of the ICT between the *p*-bromophenyl group and the arene moieties through the sulfur bridges and the metal centers in cations **1** and **2**. The bromo sites at the periphery can lead to the insertion of original conductive nodes in the main chain of conjugated oligomers by organometallic cross-coupling Suzuki reactions[14] with appropriate boronic acid derivatives.

Cations **1** and **2** are found to react with boronic acids (a: phenylboronic acid; b: 3-biphenylboronic acid; c: 1-naphthylboronic acid) in ethanol with $Pd^0(PPh_3)_4$ as catalyst to give the star-shaped conjugated oligomers **3** and **4**, respectively, with yields ranging from 75 to 85% (See Scheme 2). We observed only the formation of the trisubstituted compounds.

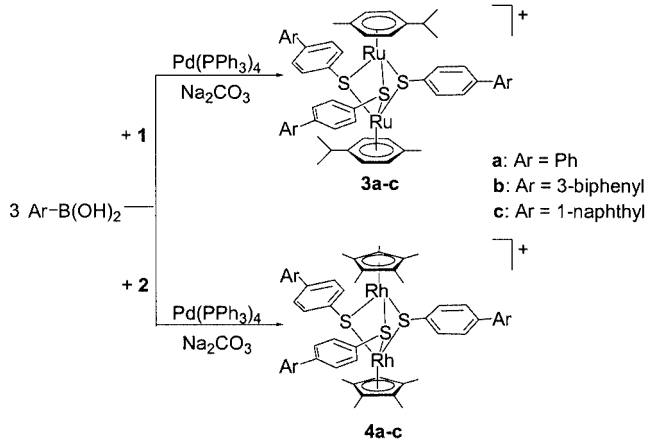

Scheme 2. Synthesis of star-shaped conjugated complexes **3** and **4**

Cations **3** and **4** were characterized by their MS and spectroscopic data (IR, ^1H and ^{13}C NMR) as well as by satisfactory elemental analysis data of the chloride salts. These cationic complexes are very soluble in alcohols, acetone and chlorinated solvents but not in water. The molecular structure of **4a** was confirmed by a single-crystal X-ray structure analysis of the PF_6 salt. The cation maintains the closed trigonal bipyramid M_2S_3 framework of its precursor **2**, as shown in Figure 2.

Consequently, the insertion of star-shaped dinuclear organometallic nodes into the main chain of a conjugated polymer during their growth is possible via Suzuki cross coupling reactions. These cations can be considered as star-shaped conductive reticulating agents for conjugated oligomers or polymers like 1,3,5-tribromobenzene and its derivatives[9,15]

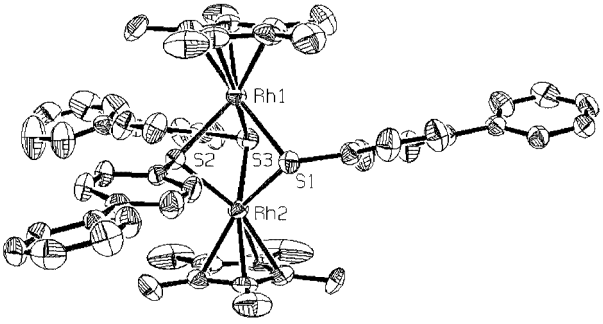

Figure 2. Molecular structure of [**4a**]PF_6; hexafluorophosphate, solvent molecules, and H atoms have been omitted for clarity; displacement ellipsoids are drawn at the 50% probability level; selected bond lengths (Å) and angles(°): Rh(1)−S(1) 2.4113(15), Rh(1)−S(2) 2.4006(15), Rh(1)−S(3) 2.4064(15), Rh(2)−S(1) 2.3835(14), Rh(2)−S(2) 2.3840(14), Rh(2)−S(3) 2.4121(17), Rh(1)−Rh(2) 3.2124(6); Rh(1)−S(1)−Rh(2) 84.13(5), Rh(1)−S(2)−Rh(2) 84.35(5), Rh(1)−S(3)−Rh(2) 83.63(5)

Conclusion

In conclusion, we report here the first synthesis of star-shaped dinuclear organometallic entities, based on a closed trigonal bipyramid M_2S_3 framework (M = Ru or Rh). We have demonstrated that these frameworks are conductive nodes that ensure the electronic connectivity of the *p*-bromophenyl group and the arene moieties through the three sulfur bridges and the two metal centers. Cations **1** and **2** react with oligophenylene boronic acid derivatives to give original star-shaped dinuclear organometallic complexes possessing three oligophenylene moieties. The electrochemical behavior, the electronic and optical properties of these conjugated star-shaped oligomers, as well as their insertion into the main chain of conductive polymers, are currently being investigated.

Experimental Section

General Remarks: All reactions were carried out under nitrogen, by using standard Schlenk techniques. Solvents were degassed prior to use. The dinuclear dichloro complexes $[Ru(p\text{-}MeC_6H_4iPr)Cl_2]_2$ and $[Rh(C_5Me_5)Cl_2]_2$ were synthesized by previously described methods.[16−18] All other reagents were purchased (Acros) and used as received. NMR spectra were recorded with a Varian Gemini 200 BB instrument and referenced to the signals of the residual protons in the deuterated solvents and TMS. The mass spectra were recorded at the University of Fribourg (Switzerland) by Prof. Titus Jenny. Microanalyses were carried out by the Laboratory of Pharmaceutical Chemistry, University of Geneva (Switzerland).

General Method for the Preparation of 1 and 2: The dinuclear dichloro complex $[Ru(p\text{-}MeC_6H_4iPr)Cl_2]_2$ (60 mg, 0.1 mmol) or $[Rh(C_5Me_5)Cl_2]_2$ (62 mg, 0.1 mmol) was refluxed in technical grade ethanol (25 mL). When the complex had completely dissolved, a solution of *p*-bromothiophenol (95 mg, 0.5 mmol) in 5 mL of ethanol was added dropwise to the hot solution. The resulting mixture was refluxed in ethanol for 3 hours. After cooling to 20 °C, the red solution was filtered through Celite, and the solvent was removed under reduced pressure. The oil obtained was purified by column chromatography (silica gel, dichloromethane/ethanol 5:1; r_f close to 0.8). Cations **1** and **2** were isolated in the form of their chloride salts, after evaporation of the solvent, as red-orange powders in quantitative yields.

$[Ru_2(p\text{-}Me\text{-}C_6H_4\text{-}iPr)_2(p\text{-}SC_6H_4Br)_3]^+$ (1): Yield: 107 mg; quantitative. ^{1}H NMR (200 MHz, $CDCl_3$, 21 °C): δ = 0.82 [d, $^3J_{H,H}$ = 7.0 Hz, 6 H, $(CH_3)_2CH$], 0.92 [d, $^3J_{H,H}$ = 7.0 Hz, 6 H, $(CH_3)_2CH$], 1.64 (s, 6 H, CH_3), 1.97 (sept, $^3J_{H,H}$ = 7.0 Hz, 2 H, $(CH_3)_2CH$), 5.23 (d, $^3J_{H,H}$ = 6.2 Hz, 2 H, C*H*-Ar), 5.26 (d, $^3J_{H,H}$ = 5.9 Hz, 2 H, C*H*-Ar), 5.32 (d, $^3J_{H,H}$ = 5.9 Hz, 2 H, C*H*-Ar), 5.60 (d, $^3J_{H,H}$= 6.2 Hz, 2 H, C*H*-Ar), 7.54 (d, $^3J_{H,H}$ = 8.8 Hz, 6 H, C*H*-Ar), 7.86 (d, $^3J_{H,H}$ = 8.8 Hz, 6 H, C*H*-Ar) ppm. ^{13}C NMR (50 MHz, $CDCl_3$, 21 °C): δ = 18.09 (*C*H_3), 22.12 [(*C*H_3)$_2$CH], 22.94 [(*C*H_3)$_2$CH], 30.00 [$(CH_3)_2CH$], 84.12 (Ru-*C*-Ar), 85.50 (Ru-*C*-Ar), 85.96 (Ru-*C*-Ar), 100.29 (Ru-*C*-Ar), 108.00 (Ru-*C*-Ar), 123.01 (*C*-Br), 132.60 (*C*-Ar), 134.61 (*C*-Ar), 137.16 (*C*-S) ppm. MS (ESI): *m*/*z* = 1036 [M^+]. $C_{38}H_{40}Br_3ClRu_2S_3$ (1070.23): calcd. C 42.65, H 3.77; found C 42.39, H 4.02.

$[Rh_2(C_5Me_5)_2(p\text{-}SC_6H_4Br)_3]^+$ (2): Yield: 107 mg; quantitative. ^{1}H NMR (200 MHz, $CDCl_3$, 21 °C): δ = 1.37 (s, 30 H, CH_3), 7.49 (d, $^3J_{H,H}$ = 8.4 Hz, 6 H, C*H*-Ar), 7.66 (d, $^3J_{H,H}$ = 8.4 Hz, 6 H, C*H*-Ar) ppm. ^{13}C NMR (50 MHz, $CDCl_3$, 21 °C): δ = 8.99 (*C*H_3), 98.51 (d, $^2J_{Rh,C}$ = 6.8 Hz; Rh-*C*-Ar), 123.74 (*C*-Br), 131.77 (*C*-Ar), 132.31 (*C*-Ar), 134.88 (*C*-S) ppm. MS (ESI): *m*/*z*: 1040 [M^+]. $C_{38}H_{42}Br_3ClRh_2S_3$ (1075.91): calcd. C 42.30, H 4.20; found C 42.18, H 4.33.

General Method for the Preparation of 3 and 4: The trisbromo dinuclear complex $[Ru_2(p\text{-}MeC_6H_4iPr)_2(p\text{-}SC_6H_4Br)_3]Cl$ (107 mg, 0.1 mmol) or $[Rh_2(C_5Me_5)_2(p\text{-}SC_6H_4Br)_3]Cl$ (108 mg, 0.1 mmol) and boronic acid derivatives C_6H_5-$B(OH)_2$ (**a**; 40 mg, 0.33 mmol), $C_{12}H_9$-$B(OH)_2$ (**b**; 65 mg, 0.33 mmol), and $C_{10}H_7$-$B(OH)_2$ (**c**; 57 mg, 0.33 mmol), were dissolved in technical grade ethanol. Then, an aqueous solution of Na_2CO_3 (1 mL, 2 N), and $Pd(PPh_3)_4$ catalyst (0.01 mmol, 11 mg) was added. The resulting mixture was refluxed in ethanol for 48 hours. After cooling to 20 °C, the red solution was filtered through Celite and the solvent was removed under reduced pressure. The oil obtained was purified by column chromatography (silica gel, dichloromethane/ethanol 10:1; r_f close to 0.8). Cations **3** and **4** were isolated in the form of their chloride salts, after evaporation of the solvent, as red-orange powders.

$[Ru_2(p\text{-}MeC_6H_4iPr)_2(p\text{-}SC_6H_4C_6H_5)_3]^+$ (3a): Yield: 90 mg; 85%. ^{1}H NMR (200 MHz, $CDCl_3$, 21 °C): δ = 0.81 [d, $^3J_{H,H}$ = 7.0 Hz, 6 H, $(CH_3)_2CH$], 0.92 [d, $^3J_{H,H}$ = 7.0 Hz, 6 H, $(CH_3)_2CH$], 1.70 (s, 6 H, CH_3), 2.03 (sept, $^3J_{H,H}$ = 7.0 Hz, 2 H, $(CH_3)_2CH$), 5.21 (d, $^3J_{H,H}$ = 5.9 Hz, 2 H, C*H*-Ar), 5.29 (d, $^3J_{H,H}$ = 5.9 Hz, 2 H, C*H*-Ar), 5.33 (d, $^3J_{H,H}$ = 5.9 Hz, 2 H, C*H*-Ar), 5.58 (d, $^3J_{H,H}$= 5.9 Hz, 2 H, C*H*-Ar), 7.40−7.54 (m, 9 H, C*H*-Ar), 7.68 (d, 12 H, $^3J_{H,H}$ = 8.4 Hz, C*H*-Ar), 8.05 (d, $^3J_{H,H}$ = 8.4 Hz, 6 H, C*H*-Ar) ppm. ^{13}C NMR (50 MHz, $CDCl_3$, 21 °C): δ = 18.14 (*C*H_3), 22.22 [(*C*H_3)$_2$CH], 22.90 [(*C*H_3)$_2$CH], 30.90 [$(CH_3)_2CH$], 84.14 (Ru-*C*-Ar), 85.08 (Ru-*C*-Ar), 85.58 (Ru-*C*-Ar), 85.66 (Ru-*C*-Ar), 100.31 (Ru-*C*-Ar), 107.55 (Ru-*C*-Ar), 127.19 (*C*-Ar), 127.91 (*C*-Ar), 129.28 (*C*-Ar), 133.43 (*C*-Ar), 137.24 (*C*-Ar), 140.04 (*C*-Ar), 141.31 (*C*-S) ppm. MS (ESI): *m*/*z* = 1027 [M^+]. $C_{56}H_{55}ClRu_2S_3$ (1061.83): calcd. C 63.34, H 5.22; found C 63.05, H 5.05.

$[Ru_2(p\text{-}MeC_6H_4iPr)_2\{p\text{-}SC_6H_4(m\text{-}C_6H_4C_6H_5)\}_3]^+$ (3b): Yield: 110 mg; 85%. ^{1}H NMR (200 MHz, $CDCl_3$, 21 °C): δ = 0.82 [d, $^3J_{H,H}$ = 7.0 Hz, 6 H, $(CH_3)_2CH$], 0.93 [d, $^3J_{H,H}$ = 7.0 Hz, 6 H, $(CH_3)_2CH$], 1.71 (s, 6 H, CH_3), 2.03 (sept, $^3J_{H,H}$ = 7.0 Hz, 2 H, $(CH_3)_2CH$], 5.24 (d, $^3J_{H,H}$ = 5.9 Hz, 2 H, C*H*-Ar), 5.31 (d, $^3J_{H,H}$ =

5.9 Hz, 2 H, C*H*-Ar), 5.36 (d, $^3J_{H,H}$ = 5.9 Hz, 2 H, C*H*-Ar), 5.60 (d, $^3J_{H,H}$= 5.9 Hz, 2 H, C*H*-Ar), 7.40−7.76 (m, 30 H, C*H*-Ar), 7.89 (s, 3 H, C*H*-Ar), 8.09 (d, $^3J_{H,H}$ = 8.1 Hz, 6 H, C*H*-Ar) ppm. ^{13}C NMR (50 MHz, $CDCl_3$, 21 °C): δ = 18.14 (*C*H$_3$), 22.19 [(*C*H$_3$)$_2$CH], 22.95 [(*C*H$_3$)$_2$CH], 30.90 [(CH$_3$)$_2$C*H*], 84.12 (Ru-*C*-Ar), 85.01 (Ru-*C*-Ar), 85.55 (Ru-*C*-Ar), 85.63 (Ru-*C*-Ar), 100.25 (Ru-*C*-Ar), 107.67 (Ru-*C*-Ar), 126.94 (*C*-Ar), 127.56 (*C*-Ar), 127.85 (*C*-Ar), 128.04 (*C*-Ar), 129.17 (*C*-Ar), 129.76 (*C*-Ar), 133.52 (*C*-Ar), 137.48 (*C*-Ar), 140.60 (*C*-Ar), 141.25 (*C*-Ar), 142.28 (*C*-S) ppm. MS (ESI): *m*/*z* = 1255 [M$^+$]. $C_{74}H_{67}ClRu_2S_3$ (1290.11): calcd. C 68.89, H 5.23, found C 68.65, H 5.35.

[Ru$_2$(*p*-Me-C$_6$H$_4$-*i*Pr)$_2$(*p*-SC$_6$H$_4$C$_{10}$H$_7$)$_3$]$^+$ (3c): Yield: 100 mg; 85%. ^{1}H NMR (200 MHz, $CDCl_3$, 21 °C): δ = 0.92 [d, $^3J_{H,H}$ = 7.0 Hz, 6 H, (C*H*$_3$)$_2$CH], 1.05 [d, $^3J_{H,H}$ = 7.0 Hz, 6 H, (C*H*$_3$)$_2$CH], 1.86 (s, 6 H, C*H*$_3$), 2.13 (sept, $^3J_{H,H}$ = 7.0 Hz, 2 H, (CH$_3$)$_2$C*H*], 5.32 (d, $^3J_{H,H}$ = 5.9 Hz, 2 H, C*H*-Ar), 5.40 (d, $^3J_{H,H}$ = 5.9 Hz, 2 H, C*H*-Ar), 5.44 (d, $^3J_{H,H}$ = 5.9 Hz, 2 H, C*H*-Ar), 5.71 (d, $^3J_{H,H}$= 5.9 Hz, 2 H, C*H*-Ar), 7.51−7.62 (m, 21 H, C*H*-Ar), 7.93 (d, $^3J_{H,H}$ = 8.1 Hz, 6 H, C*H*-Ar), 8.14 (d, $^3J_{H,H}$ = 8.1 Hz, 6 H, C*H*-Ar) ppm. ^{13}C NMR (50 MHz, $CDCl_3$, 21 °C): δ = 18.29 (*C*H$_3$), 22.54 [(*C*H$_3$)$_2$CH], 22.83 [(*C*H$_3$)$_2$CH], 30.95 [(CH$_3$)$_2$C*H*], 84.46 (Ru-*C*-Ar), 84.73 (Ru-*C*-Ar), 85.17 (Ru-*C*-Ar), 85.52 (Ru-*C*-Ar), 101.03 (Ru-*C*-Ar), 106.98 (Ru-*C*-Ar*)*, 125.75 (*C*-Ar), 126.26 (*C*-Ar), 126.62 (*C*-Ar), 127.35 (*C*-Ar), 128.43 (*C*-Ar), 128.81 (*C*-Ar), 131.10 (*C*-Ar), 131.51 (*C*-Ar), 132.95 (*C*-Ar), 134.15 (*C*-Ar), 137.20 (*C*-Ar), 139.22 (*C*-Ar), 141.24 (*C*-S) ppm. MS (ESI): *m*/*z* = 1177 [M$^+$]. $C_{68}H_{61}ClRu_2S_3$ (1212.00): calcd. C 67.39, H 5.07, found C 67.68, H 4.91.

[Rh$_2$(C$_5$Me$_5$)$_2$(*p*-SC$_6$H$_4$C$_6$H$_5$)$_3$]$^+$ (4a): Yield: 90 mg; 75%. ^{1}H NMR (200 MHz, $CDCl_3$, 21 °C): δ = 1.37 (s, 30 H, C*H*$_3$), 7.41−7.55 (m, 9 H, C*H*-Ar), 7.65 (d, $^3J_{H,H}$ = 8.4 Hz, 6 H, 6 H, C*H*-Ar), 7.71 (d, $^3J_{H,H}$ = 8.1 Hz, 6 H, 6 H, C*H*-Ar), 7.92 (d, $^3J_{H,H}$ = 8.1 Hz, 6 H, C*H*-Ar) ppm. ^{13}C NMR (50 MHz, $CDCl_3$, 21 °C): δ = 9.05 (*C*H$_3$), 98.20 (d, $^2J_{Rh,C}$ = 7.58 Hz, Rh-*C*-Ar), 127.08 (*C*-Ar), 127.40 (*C*-Ar), 128.23 (*C*-Ar), 129.30 (*C*-Ar), 131.97 (*C*-Ar), 134.01 (*C*-Ar), 139.75 (*C*-S) ppm. MS (ESI): *m*/*z* = 1031 [M$^+$]. $C_{56}H_{57}Cl_1Rh_2S_3$ (1067.51): calcd. C 63.01, H 5.38, found C 62.76, H 5.52.

[Rh$_2$(C$_5$Me$_5$)$_2${*p*-SC$_6$H$_4$(*m*-C$_6$H$_4$C$_6$H$_5$)}$_3$]$^+$ (4b): Yield: 97 mg; 75%. ^{1}H NMR (200 MHz, $CDCl_3$, 21 °C): δ = 1.44 (s, 30 H, C*H*$_3$), 7.41−7.77 (m, 30 H, C*H*-Ar), 7.89 (s, 3 H, C*H*-Ar), 7.95 (d, $^3J_{H,H}$ = 8.42 Hz, 6 H, C*H*-Ar) ppm. ^{13}C NMR (50 MHz, $CDCl_3$, 21 °C): δ = 9.05 (*C*H$_3$), 98.27 (d, $^2J_{Rh,C}$ = 5.3 Hz, Rh-*C*-Ar), 126.01 (*C*-Ar), 127.11 (*C*-Ar), 127.88 (*C*-Ar), 128.67 (*C*-Ar), 129.79 (*C*-Ar), 132.04 (*C*-Ar), 134.04 (*C*-Ar), 140.19 (*C*-Ar), 141.19 (*C*-Ar), 141.69 (*C*-Ar), 142.39 (*C*-S) ppm. MS (ESI): *m*/*z* = 1259 [M$^+$]. $C_{74}H_{69}Cl_1Rh_2S_3$ (1295.80): calcd. C 68.59, H 5.37, found C 68.75, H 5.09.

[Rh$_2$(C$_5$Me$_5$)$_2$(*p*-SC$_6$H$_4$C$_{10}$H$_7$)$_3$]$^+$ (4c): Yield: 91 mg; 75%. ^{1}H NMR (200 MHz, $CDCl_3$, 21 °C): δ = 1.47 (s, 30 H, C*H*$_3$), 7.51−7.65 (m, 21 H, C*H*-Ar), 7.81 (d, $^3J_{H,H}$ = 8.1 Hz, 6 H, C*H*-Ar), 8.01 (d, $^3J_{H,H}$ = 8.1 Hz, 6 H, C*H*-Ar) ppm. ^{13}C NMR (50 MHz, $CDCl_3$, 21 °C): δ = 9.05 (*C*H$_3$), 98.13 (d, $^2J_{Rh,C}$ = 5.5 Hz, Rh-*C*-Ar), 125.79 (*C*-Ar), 126.11 (*C*-Ar), 126.94 (*C*-Ar), 127.31 (*C*-Ar), 128.49 (*C*-Ar), 128.71 (*C*-Ar), 131.34 (*C*-Ar), 131.82 (*C*-Ar), 132.59 (*C*-Ar), 134.32 (*C*-Ar), 137.24 (*C*-Ar), 139.53 (*C*-Ar), 142.28 (*C*-S) ppm. MS (ESI): *m*/*z*: 1181 [M$^+$]. $C_{68}H_{63}Cl_1Rh_2S_3$ (1217.69): calcd. C 67.07, H 5.21, found C 67.39, H 4.97.

X-ray Crystallographic Study

[1]Cl·$CHCl_3$: $C_{39}H_{41}Br_3Cl_4Ru_2S_3$, *M* = 1189.57, orthorhombic, $P2_12_12_1$ (no. 19), *a* = 10.7690(6), *b* = 15.0037(8), *c* = 26.6643(16) Å, *U* = 4308.3(4) Å^3, *T* = 153 K, *Z* = 4, μ(Mo-K_α) = 3.905 mm^{-1}, 8018 reflections measured, 5392 unique (R_{int} = 0.0719) which were used in all calculations. The final *wR* (F^2) was 0.0827 (all data).

[2]Cl·3$CHCl_3$·0.5C_6H_6: $C_{44}H_{48}Br_3Cl_{10}Rh_2S_3$, *M* = 1473.05, monoclinic, $P2_1/n$ (no. 14), *a* = 14.0257(11), *b* = 24.8541(13), *c* = 15.9642(13) Å, β = 92.495(10)°, *U* = 5559.8(7) Å^3, *T* = 153 K, *Z* = 4, μ(Mo-K_α) = 3.374 mm^{-1}, 10607 reflections measured, 8186 unique (R_{int} = 0.0433) which were used in all calculations. The final *wR* (F^2) was 0.1567 (all data).

[4a]PF_6·2C_6H_6: $C_{68}H_{69}F_6PRh_2S_3$, *M* = 1333.20, monoclinic, $P2_1/c$ (no. 14), *a* = 19.5028(10), *b* = 15.0341(9), *c* = 22.5937(14) Å, β = 96.209(7)°, *U* = 6585.8(7) Å^3, *T* = 153 K, *Z* = 4, μ(Mo-K_α) = 0.675 mm^{-1}, 12536 reflections measured, 6576 unique (R_{int} = 0.0845) which were used in all calculations. The final *wR* (F^2) was 0.1191 (all data).

he data were measured using a Stoe Image Plate Diffraction system equipped with a φ circle, using Mo-K_α graphite monochromated radiation (λ = 0.71073 Å) with φ range 0−180°, increment 1°, 2θ range from 2.0−26°, D_{max}−D_{min} = 12.45−0.81 Å. The structures were solved by direct methods using the program SHELXS-97.[19] The refinement and all further calculations were carried out using SHELXL-97.[20] The H-atoms were included in calculated positions and treated as riding atoms using the SHELXL default parameters. The non-H atoms were refined anisotropically, using weighted full-matrix least-square on F^2.

CCDC-197151 ([**1**]Cl·$CHCl_3$), CCDC-197152 ([**2**]Cl·3$CHCl_3$·0.5C_6H_6) and CCDC-197153 ([**4a**]PF_6·2C_6H_6) contain the supplementary crystallographic data for this paper. These data can be obtained free of charge at www.ccdc.cam.ac.uk/conts/retrieving.html [or from the Cambridge Crystallographic Data Centre, 12, Union Road, Cambridge CB2 1EZ, UK; Fax: (internat.) +44-1223/336-033; E-mail: deposit@ccdc.cam.ac.uk].

Acknowledgments

Financial support of the Fond National Suisse de la Recherche Scientifique is gratefully acknowledged. The authors are also indebted to the Johnson Mathey Technology Centre for a loan of ruthenium trichloride hydrate.

[1] J.-M. Lehn, *Supramolecular Chemistry, Concepts and Perspectives*, VCH, Weinheim, **1995**.
[2] R. Ziessel, L. Charbonnière, M. Cesario, T. Prangé, H. Nierengarten, *Angew. Chem. Int. Ed.* **2002**, *41*, 975−979.
[3] K. Sénéchal, O. Maury, H. le Bozec, I. Ledoux, J. Zyss, *J. Am. Chem. Soc.* **2002**, *124*, 4560−4561.
[4] K. K.-W. Lo, W.-K. Hui, D. Chung-Ming Ng, *J. Am. Chem. Soc.* **2002**, *124*, 9344−9345.
[5] D. T. MacQuade, A. E. Pullen, T. M. Swager, *Chem. Rev.* **2000**, *100*, 2537−2574.
[6] U. S. Schubert, C. Eschbaumer, *Angew. Chem. Int. Ed.* **2002**, *41*, 2892−2926. and ref. therein.
[7] J. Zyss, I. Ledoux, *Chem. Rev.* **1994**, *94*, 77−105.
[8] C. Dhenault, I. Ledoux, I. D. W. Samuel, M. Bourgault, H. Le Bozec, *Nature* **1995**, *374*, 339−342.
[9] F. Chérioux, L. Guyard, *Adv. Func. Mater.* **2001**, *11*, 305−309.
[10] R. Anémian, J.-C. Mulatier, C. Andraud, O. Stephan, J.-C. Vial, *Chem. Commun.* **2002**, 1608−1609.
[11] *Electronic Materials: The Oligomer Approach* (Eds.: K. Müllen and G. Wegner), Wiley VCH, Weinheim, **1998**.
[12] L. L. Miller, Y. Yu, *J. Org. Chem.* **1995**, *60*, 6813−6819 and references cited therein.
[13] F. Chérioux, C. M. Thomas, B. Therrien, G. Süss-Fink, *Chem. Eur. J.* **2002**, *8*, 4377−4382.

[14] N. Miyaura, A. Suzuki, *Chem. Rev.* **1995**, *95*, 2457−2483.
[15] J. Pang, Y. Tao, S. Freiberg, X.-P. Yang, M. D'Iorio, S. Wang, *J. Mater. Chem.* **2002**, *12*, 206−212 and references cited therein.
[16] R. A. Zelonka, M. C. Baird, *Can. J. Chem.* **1972**, *50*, 3063−3068.
[17] J. W. Wang, K. Moseley, P. M. Maitlis, *J. Am. Chem. Soc.* **1969**, 5970−5977.
[18] M. A. Bennett, A. K. Smith, *J. Chem. Soc., Dalton Trans.* **1974**, 233−241.
[19] G. M. Sheldrick, *Acta Crystallogr., Sect. A* **1990**, *46*, 467.
[20] G. M. Sheldrick, SHELXL-97. University of Göttingen, Göttingen, Germany, **1999**.

Received November 28, 2002
[I02655]

Nitric Oxide Reduction by Heme-Thiolate Enzymes (P450nor): A Reevaluation of the Mechanism

Radu Silaghi-Dumitrescu[a]

Keywords: Nitrogen oxides / Enzymes / Heme proteins / Density functional calculations / Bioinorganic chemistry

The details of the heme-thiolate nitric oxide reductase (P450nor) catalytic mechanism are still controversial. One theory, supported by computational results [D. L. Harris, *Int. J. Quantum Chem.* **2002**, *88*, 183–200], assumes two sequential one-electron transfers from NAD(P)H to an initial $[FeNO]^6$ complex. The $[FeNO]^8$ species thus formed would react with NO, eventually liberating the unstable $ONNO^{2-}$ anion (most probably in its protonated form), which decomposes to N_2O and water. However, more recent experimental results [A. Daiber et al., *J. Inorg. Biochem.* **2002**, *88*, 343–352] suggest the first committed step of the mechanism to be direct hydride transfer from NAD(P)H to $[FeNO]^6$, presumably resulting in an iron-bound HNO unit, $[Fe\text{-}(H)NO]^8$, that would be readily protonated to $[Fe\text{-}(H)NOH]^8$. Subsequent NO addition would yield the unstable HO-N(H)-N=O, which would dissociate from the heme and decompose to H_2O and N_2O. Here, the DFT geometry optimization of all previously proposed reaction intermediates is reported. The first step of the mechanism is predicted to be hydride transfer to $[FeNO]^6$, to produce $[FeNOH]^8$ or $[Fe\text{-}N(H)O]^8$. Subsequent addition of NO to $[Fe\text{-}NOH]^8$ (but not to $[Fe\text{-}N(H)O]^8$ or $[Fe\text{-}N(H)OH]^8$) is predicted to lead to immediate liberation of $HN_2O_2^-$, without any stable intermediates. Contrary to what would be predicted according to the "thiolate push effect" dogma, the *thiolate ligand at the heme active site is shown to obstruct NO reduction*, rather than facilitate it. It is in fact shown that replacement of the thiolate by a neutral nitrogen ligand (i.e., lysine, as found in the active site of cytochrome c nitrite reductase, an enzyme that can reduce NO) clearly favors, from a thermodynamic point of view, NO reduction at the heme site.

(© Wiley-VCH Verlag GmbH & Co. KGaA, 69451 Weinheim, Germany, 2003)

Introduction

The active site of fungal nitric oxide reductases (enzymes that belong to the superfamily of cytochromes P450, and are commonly referred to as P450nor) consists of a solvent-exposed, cysteinate-ligated heme.[1,2] The widely accepted mechanism of P450nor[3–9] (Figure 1) involves binding of NO to the ferric form of the active site heme, followed by reduction of this $[FeNO]^6$ complex by NAD(P)H. Subsequent attack of a second molecule of NO leads to formation of a nitrogen-nitrogen bond and liberation of the very stable N_2O. Besides the starting $[FeNO]^6$ species, only one intermediate, absorbing at 444 nm, has been experimentally observed.[3]

The details of the P450nor mechanism, and in particular the identity of the 444 nm intermediate, are still controversial. One theory[5] (top half, Figure 1), supported by recent computational results,[9] assumes two sequential one-electron transfers from NAD(P)H to the initial $[FeNO]^6$ complex. The $[FeNO]^8$ species thus formed would constitute the 444-nm intermediate, and would react with NO, eventually liberating the unstable $ONNO^{2-}$ anion (most probably in its protonated form), which decomposes to N_2O and water. However, more recent experimental results[8] support a theory originally put forth by Averill,[11] suggesting the first committed step of the mechanism to be direct hydride transfer from NAD(P)H to the nitrogen atom of $[FeNO]^6$, resulting in an iron-bound HNO unit, $[Fe\text{-}(H)NO]^8$, that would undergo protonation to $[Fe\text{-}(H)NOH]^8$ (444-nm intermediate). Subsequent NO addition would yield the unstable HO-N(H)-N=O, which would dissociate from the heme and decompose to H_2O and N_2O. The present study reports DFT geometry optimization results on the putative reaction intermediates implied by the P450nor mechanisms proposed so far. These results not only provide a reasonable account of the P450nor mechanism, but also provide a basis for better understanding key notions in hemoproteins, such as "the thiolate push effect". Implications for other nitric oxide-reducing proteins (such as cytochrome c nitrite reductase) are also noted.

Results and Discussion

Geometry optimization results are shown in Table 1 and Table 2. Some of the models ($[FeNO]^{6,7,8}$) have already been

[a] Department of Chemistry and Center for Metalloenzyme Studies, University of Georgia,
Athens, GA 30602, USA
E-mail: silaghi@chem.uga.edu

Supporting information for this article is available on the WWW under http://www.eurjic.org or from the author.

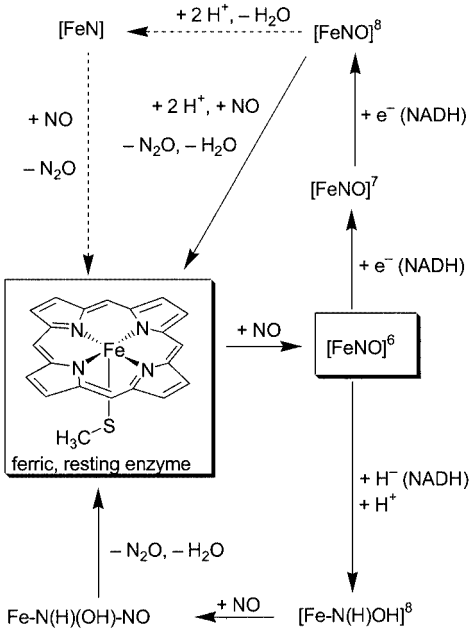

Figure 1. The two previously proposed mechanisms for P450nor (top half: supported by calculations,[9] bottom half: supported by experimental data[10]); species unambiguously known to be involved in the catalytic cycle are highlighted; species in the top and bottom right corners, respectively, have been proposed to constitute the experimentally-observed 444-nm intermediate;[9,10] an alternative pathway, based on partial DFT results, is marked with dashed arrows;[9] the Enemark−Feltham notation is used for iron-nitrosyl species $[FeNO]^n$, as well as for their protonated counterparts such as $[Fe\text{-}(H)NOH]^n$ (with the hydrogens counted as protons when summing up the electrons, "*n*", in the Enemark−Feltham formalism)

characterized elsewhere,[4,6,9,12] and are therefore not discussed in any detail here. It should be noted, however, that the predicted optimum geometries and spin states are in agreement with previously published data. Results on small molecules (i.e., NO, HNO, N_2O, H_2O, etc.), that would be useful as references when discussing overall energetics of the mechanism, are supplied as Supporting Information (see footnote on the first page of this article).

Regarding the first committed step of the P450nor mechanism, reduction of the $[FeNO]^6$ complex by NADH, two theories have been put forward to date.[9,11] Previous DFT results[9] have been used to support the idea that two electrons would be sequentially delivered to the active-site $[FeNO]^6$ complex by NADH in an outer-sphere mechanism, to generate $[FeNO]^8$ (which would be the experimentally observed 444-nm intermediate). According to this hypothesis, any one-electron reducing agent with a redox potential equal to or lower than that of NADH should yield the same $[FeNO]^8$ intermediate upon reaction with the $[FeNO]^6$ at the P450nor active site. Yet, this is known not to be the case: dithionite (redox potential lower than that of NADH by about 100 mV) can only reduce the active site $[FeNO]^6$ to $[FeNO]^7$.[3] Daiber et al.[8] have pointed out this shortcoming of the one-electron theory, and have instead shown kinetic isotope effects, using deuterium-substituted NADH, thereby concluding that hydride transfer from NADH to the nitrogen atom of $[FeNO]^6$ is the key step of the mechanism. The 444-nm intermediate would thus be $[Fe\text{-}N(H)OH]^8$, with the second proton provided by solvent and/or the protein matrix. These authors[8] were also able to generate the 444-nm intermediate by chemical reduction of $[FeNO]^6$ with borohydride, or by addition of pulse radiolysis-generated $NHOH^{\cdot}$ radicals to the ferric (resting) form of the active site heme. However, no evidence exists so far as to why a strong reducing agent like dithionite is not able to generate a $[FeNO]^8$ (protonated or not) species at the P450nor active site.

The energies listed in Table 1 suggest that a mechanism implying two sequential one-electron transfer steps for the reduction of $[FeNO]^6$ to $[FeNO]^7$ to $[FeNO]^8$ would be energetically unfeasible. That is, a $[FeNO]^7$ species would be generated as an intermediate, that is more than 200 kJ/mol more stable than the end-product $[FeNO]^8$, and some 150 kJ/mol more stable than $[FeNO]^6$. Thus, with one-electron reducing agents (such as dithionite) the P450nor site remains trapped in a $[FeNO]^7$ form that is too stable to be catalytically useful. By contrast, with a two-electron donor, such as NADH, reduction proceeds from $[FeNO]^6$ *directly*

Table 1. Results (energies in kJ/mol, distances in Å) for relevant P450nor models

Model	Energy	Fe−S	Fe−N	N−O	N−N	N−H/O−H	Fe−N−O
$[FeNO]^6$, $S = 0$	−7404902	2.30	1.67	1.18	–	–	163°[a]
$[FeNO]^7$, $S = 1/2$	−7405056	2.44	1.75	1.21	–	–	138°
$[FeNO]^8$, $S = 0$	−7404840	2.57	1.80	1.22	–	–	130°
$[FeNO]^8$, $S = 1$	−7404840	2.43	1.77	1.21	–	–	140°
$[Fe\text{-}N(H)O]^8$, $S = 0$	−7406619	2.37	1.81	1.26	–	1.06	135°
$[Fe\text{-}N(H)O]^8$, $S = 1$	−7406539	2.28	1.98	1.27	–	1.05	130°
$[Fe\text{-}NOH]^8$, $S = 0$	−7406522	2.42	1.74	1.40	–	0.98	116°
$[Fe\text{-}NOH]^8$, $S = 1$	−7406456	2.35	1.87	1.41	–	0.98	121°
$[Fe\text{-}N(H)OH]^8$, $S = 0$	−7407980	2.22	1.82	1.37	–	1.03/0.98	131°
$[Fe\text{-}N(H)OH]^8$, $S = 1$	−7407940	2.22	2.00	1.38		1.02/0.98	128°
Fe-N(O)-NOH, $S = 1/2$	−7747788	2.24	2.05	1.30/1.40[b]	1.29	1.03	123°
Fe-N(OH)-NO, $S = 1/2$	−7747788	2.24	2.01	1.39/1.31[b]	1.31	1.05	121°

[a] S−Fe−NO angle: 172°. This geometry accurately reproduces both previous DFT[9] results and the crystal structure of the P450nor $[FeNO]^6$ complex.[6] [b] Iron-bound nitrogen and non-iron-bound nitrogen, respectively, in this order.

Table 2. Charges and spin populations derived from NBO analyses (spin populations listed in parentheses) for relevant P450nor models

Model	Fe	S	N	O	L[a]	P[b]
$[FeNO]^6$, $S = 0$	1.27	−0.16	0.06	−0.16	−0.10	−0.91
$[FeNO]^7$, $S = 1/2$	1.28 (0.33)	−0.37 (0.13)	−0.07 (0.31)	−0.27 (0.20)	−0.34 (0.51)	−1.41 (0.04)
$[FeNO]^8$, $S = 0$	1.31	−0.49	−0.13	−0.33	−0.46	−2.03
$[FeNO]^8$, $S = 1$	1.30 (0.43)	−0.41 (0.11)	−0.09 (0.31)	−0.31 (0.19)	−0.40 (0.50)	−2.32 (0.96)
$[Fe\text{-}N(H)O]^8$, $S = 0$	1.29 (0.01)	−0.36	−0.27	−0.36	−0.29 (−0.01)	−1.39
$[Fe\text{-}N(H)O]^8$, $S = 0$	1.36 (0.96)	−0.25 (0.19)	−0.36 (0.39)	−0.37 (0.37)	−0.39 (0.76)	−1.63 (0.07)
$[Fe\text{-}NOH]^8$, $S = 0$	1.30 (0.01)	−0.38	−028 (−0.01)	−0.53	−0.33 (−0.01)	−1.43
$[Fe\text{-}NOH]^8$, $S = 1$	1.36 (0.81)	−0.31 (0.19)	−0.35	−0.56 (0.16)	−0.43 (0.16)	−1.48 (0.48)
$[Fe\text{-}N(H)OH]^8$, $S = 0$	1.32	−0.10	−0.42	−0.48	0.01	−1.12
$[Fe\text{-}N(H)OH]^8$, $S = 1$	1.35 (0.94)	−0.10 (0.26)	−0.41 (0.63)	−0.48 (0.21)	0.01 (0.84)	−1.17 (−0.04)
Fe-N(O)-NOH, $S = 1/2$	1.36 (0.87)	−0.20 (0.19)	−0.02/−0.04[c]	−0.54/−0.59[c]	−0.68 (0.04)	−1.36 (−0.10)
Fe-N(OH)-NO, $S = 1/2$	1.35 (0.87)	−0.20 (0.20)	−0.02/−0.04[c]	−0.59/−0.55[c]	−0.70 (0.04)	−1.35 (−0.10)

[a] Sum of partial atomic charges and spin populations over the NO ligand or its replacements. [b] Sum of partial atomic charges and spin populations over the porphyrin atoms. [c] Iron-bound nitrogen and non iron-bound nitrogen, respectively, in this order.

Table 3. Summary of geometry optimization results (energies in kJ/mol, distances in Å) for non-P450nor models; "X" is the axial ligand trans to NO

Model	X	Energy	Fe−N	N−O	Fe−N−O	Fe−X
X-$[FeNO]^6$, $S = 0$	−	−6253977	1.63	1.16	180°	−
X-$[FeNO]^7$, $S = 1/2$	−	−6254599	1.75	1.21	147°	−
X-$[FeNO]^8$, $S = 0$	−	−6254735	1.80	1.22	125°	−
X-$[FeNO]^6$, $S = 0$	CH_3NH_2	−6505813	1.65	1.15	177°	2.06
X-$[FeNO]^7$, $S = 1/2$	CH_3NH_2	−6506325	1.78	1.19	139°	2.21
X-$[FeNO]^8$, $S = 0$	CH_3NH_2	−6506425	2.33	1.81	125°	1.21

Table 4. Charges and spin populations derived from NBO analyses (spin populations listed in parentheses) for non-P450nor models; "X" is the axial ligand trans to NO

Model	X	Fe	X[a]	N	O	L[b]	P[c]
X-$[FeNO]^6$, $S = 0$	−	1.36	−	0.07	−0.10	−0.03	−0.33
X-$[FeNO]^7$, $S = 1/2$	−	1.33 (0.96)	−	−0.03 (0.04)	−0.20 (−0.01)	−0.23 (0.03)	−1.10 (0.01)
X-$[FeNO]^8$, $S = 0$	−	1.22	−	−0.08	−0.30	−0.38	−1.82
X-$[FeNO]^6$, $S = 0$	CH_3NH_2	1.35	−0.86	0.15	−0.07	0.08	−0.70
X-$[FeNO]^7$, $S = 1/2$	CH_3NH_2	1.33 (0.62)	−0.92 (0.03)	−0.01 (0.22)	−0.19 (0.14)	−0.20 (0.36)	−1.33 (−0.01)
X-$[FeNO]^8$, $S = 0$	CH_3NH_2	1.30	−0.93	−0.09	−0.31	−0.40	−1.95

[a] Sum of partial atomic charges and spin populations over atoms in "X". [b] Sum of partial atomic charges and spin populations over the NO ligand or its replacements. [c] Sum of partial atomic charges and spin populations over the porphyrin atoms.

to the (protonated or not) $[FeNO]^8$ stage. This observation also identifies the reason why the P450nor active site is solvent-exposed and allows NADH access to the heme,[2] unlike in any other member of the P450 protein[13] family. Thus, all other members of the P450 protein family have a heme active site buried inside the protein, and electrons are supplied to this heme by NADH in an indirect, outer-sphere, long-range manner, via flavin moieties, *in two sequential one-electron steps*.[13] Unlike P450nor, these other P450 proteins do not exhibit any nitric oxide reductase activity. Thus, the ability to perform the two-electron oxidation of NO at a heme-thiolate active site seems to depend on the possibility of performing the two-electron reduction *in a single step*.

Cytochrome c nitrite reductase (ccNirR) contains a heme at the active site, which can reduce NO to ammonia (with NO being, in fact, an intermediate product of nitrite reduction).[10] The electrons for this reduction are supplied by five neighboring heme units within the protein. Nitric oxide reduction by ccNiR may be deemed as unexpected, since no hydride donor appears to be required and the active site heme is actually not ligated by a thiolate, but by a lysine side-chain. Indeed, thiolate ligands are commonly believed to exert a certain "thiolate push effect" that would enable heme actives site to accomplish key reactions such as dioxygen activation or NO reduction. How can ccNiR perform the same chemistry as P450nor in the absence of a hydride donor *and* of a thiolate ligand? A simple answer is provided by calculations (cf. Table 3) on $[FeNO]^{6,7,8}$ models where the thiolate ligand was replaced by a methylamine unit to mimmick the ccNiR active-site heme. Unlike in P450nor, the ccNiR $[FeNO]^8$ complex is predicted to be more stable

than Fe[NO]^7. We propose this to be the reason why in ccNiR there is no need for a two-electron (hydride) donor. As shown in Table 3, the same situation as in the ccNiR models occurs if the axial ligand trans to NO is omitted altogether. A general observation may then be that nitrogenous heme axial ligands (such as lysine, and, most likely, histidine) favor easier reduction of NO (*thermodynamically speaking*) than anionic ligands such as thiolate. This raises an intriguing question: could the same type of argument ("thiolate obstruction") hold true for other heme enzymes, such as oxygen-activating (heme-thiolate) and oxygen-binding (heme-histidine) enzymes? The data in Table 1−4 clearly confirm that the "thiolate push effect" is a reality in the [FeNO]^{6,7,8} systems examined here. Indeed, in thiolate-ligated systems the electron density on the NO moiety is consistently higher (both charge-wise and spin-wise) than in their non-thiolate counterparts (Table 4). Nevertheless, the differences are not large enough (especially at the level of Fe−N and N−O distances) to warrant the assumption that this "push effect" significantly weakens the respective bonds to the extent that they would be easier to cleave.

With the one-electron theory now ruled out in P450nor by both DFT and experimental results, it follows that the first committed step in the P450nor mechanism can only be hydride transfer from NADH to [FeNO]^6, yielding [FeN(H)O]^8. Table 1 shows that the [Fe-N(H)O]^8 isomer is in fact more stable than its oxygen-protonated counterpart [FeNOH]^8. It is entirely conceivable that an [Fe-N(H)O]^8 species undergoes further protonation to [Fe-N(H)OH]^8 (presumably as a concerted process upon hydride addition), and Table 1 shows that such protonation would result in significant energetical stabilization. The active site has previously been shown to contain appropriate proton donors.[6] Thus, at this stage the Daiber mechanism has the full support of computational results, in that the [Fe-N(H)OH]^8 species appears the most likely candidate for the 444-nm intermediate.

The next step in the mechanism would then be addition of a second molecule of NO to the [Fe-N(H)OH]^8 intermediate, to form a nitrogen-nitrogen bond. Regardless of the exact mechanism of this step (see ref.[8]), this Fe-N(H)(OH)-NO complex would then decay to yield ferric heme, N_2O and H_2O, a process likely to occur by internal rearrangements of the $H_2N_2O_2$ moiety. Indeed, we found that geometry optimization of a putative $S = 5/2$ Fe-N(H)(OH)-NO model resulted in "cleavage" of the Fe−N bond, without an apparent energy barrier, leading to liberation of H_2N_2O. However, for $S = 1/2$ and $S = 3/2$ states of the same model, the Fe−N bond remained unperturbed and the N−N bond was "broken". Thus, Fe-N(H)(OH)-NO should not be conceived as a reaction intermediate, but rather as a transition state, with the observation that a spin crossover ($S = 1/2$ to $S = 5/2$) must occur in order for the interaction of the $S = 0$ [FeNHOH]^8 with $S = 1/2$ NO to be productive. However, for Fe-N(H)(OH)-NO models, $S = 1/2$ and $S = 3/2$ potential energy surfaces were more than 100 kJ/mol below $S = 5/2$, suggesting that, should the $S = 5/2$ pathway ever be active, it would have to be due to assistance from the protein matrix and/or solvent.[14] By contrast, if one assumes the 444-nm intermediate to be [FeNOH]^8 or even [FeNO]^8, addition of a second molecule of NO would result in formation of a strong nitrogen-nitrogen bond (cf. Table 1) and a significant weakening of the Fe−N bond, so that liberation of $HN_2O_2^-$ or (with further assistance from the protein) $H_2N_2O_2$, are entirely feasible reaction pathways. We note that in models where iron-nitrogen *and* nitrogen-nitrogen bonds exist, both electrons originating from NAD(P)H are located on the newly formed $N_2O_2H_x$ ($x = 1,2$) moiety, which is only loosely coordinated to Fe and is therefore likely to be readily displaced by solvent. Finally, it should be noted that attempts to dock an NADH molecule onto the P450nor active site using the Dock module of the Sybyl software package have consistently yielded conformations that would be appropriate for hydride transfer towards the oxygen — but not nitrogen — atom of the [FeNO]^6 unit. Thus, the above results suggest that [Fe-NOH]^8 and not its N-protonated versions is the productive intermediate that reacts with the second NO molecule. This conflict between theory and the Averill/Daiber mechanism may conceivably be solved by invoking active-site dynamics and solvation, which would then provide the extra energy required for the spin transition in the {[FeN(H)OH]^8-NO} system, to render the [FeN(H)OH]^8 + NO interaction productive.

Conclusion

A detailed account of the P450nor mechanism has been provided via geometry optimization of all possible reaction intermediates. The experimentally observed 444-nm intermediate is proposed to be a [FeNOH]^8 species, with [FeN(H)O]^8 or [FeN(H)OH]^8 not entirely ruled out as productive intermediates for reacting with the second NO molecule. Contrary to what would be predicted according to the "thiolate push" dogma, the *thiolate ligand in P450nor is shown to obstruct NO reduction*, rather than facilitate it. It is in fact shown that replacement of the thiolate with a neutral nitrogenous ligand (i.e., lysine, as found in the active site of cytochrome c nitrite reductase, an enzyme that can reduce NO) clearly facilitates (from a thermodynamic point of view) NO reduction at the heme site.

Experimental Section

Geometries of all models were optimized in the Spartan 02 (Windows)[15] package at the University of Georgia, on a Windows 2000-operated Pentium 4 PC (1.7 GHz, 1024 MB RAM). The UBP86 functional, which uses the gradient-corrected exchange functional proposed by Becke (1988) and the correlation functional by Perdew (1986), and the 6-31G** basis set were used as implemented in Spartan.[15] For the SCF calculations, a fine grid was used and the convergence criteria were set to 10^{-6} (for the root-mean square of electron density) and 10^{-8} (energy). For geometry optimization, convergence criteria were set to 0.001 au (maximum gradient criterion) and 0.0003 (maximum displacement criterion). Reported charges and spin densities were derived from NBO popu-

lation analyses. Energy differences between models of different sizes are fairly large, and therefore overall trends and relative energies are unlikely to be modified upon applying theoretically sophisticated and time-consuming corrections such as BSSE. Such corrections were therefore omitted from the present work.

All models were subjected to full geometry optimization, without any geometry or symmetry constraints. All models reported in Table 1 and 2 consisted of an unsubstituted heme coordinated axially by a methylthiolate unit (i.e., the species named "ferric, resting enzyme" in Figure 1), while the sixth coordination position was occupied by various ligands (see Table 1). All results reported in Table 1 for $[FeNO]^{6,7,8}$ models were obtained for end-on (monodentate) coordination, since $[FeNO]^6$ and $[FeNO]^7$ have already been characterized experimentally as being end-on complexes; a detailed theoretical treatment of $[FeNO]^{6,7,8}$ can be found elsewhere.[9] Attempts to model $[FeNO]^8$ as *bidentate* led to a *monodentate* geometry for the $S = 0$ state, and to a true bidentate geometry for $S = 1$ (details of this bidentate geometry are only listed as Supplementary Information; its energy was significantly higher than that of its monodentate isomer). Models reported in Table 3 and 4 consisted of an unsubstituted heme-coordinated NO, while the other axial coordination position was either empty, or occupied by a methylamine unit (see Table 2). Low-spin states ($S = 0$, 1/2) were chosen, for reasons detailed in ref.[10]

Acknowledgments

Dr. Donald M. Kurtz, Jr. is thanked for support and helpful discussions. Drs. Ioan Silaghi-Dumitrescu and Eric D. Coulter are thanked for helpful discussions. The Chemistry Department of the "Babeş-Bolyai University" in Cluj-Napoca, Romania, is thanked for a leave of absence to the author.

[1] K. Nakahata, T. Tanimoto, K. Hatano, K. Usuda, H. Shoun, *J. Biol. Chem.* **1993**, *268*, 8350−8355.
[2] S. Y. Park, *Nature Struct. Biol.* **1997**, *4*, 827−832.
[3] Y. Shiro, M. Fujii, T. Iizuka, S.-i. Adachi, K. Tsukamoto, K. Nakahara, H. Shoun, *J. Biol. Chem.* **1995**, *270*, 1617−1623.
[4] E. Obayashi, *J. Am. Chem. Soc.* **1997**, *119*, 7807−7816.
[5] E. Obayashi, S. Takahashi, Y. Shiro, *J. Am. Chem. Soc.* **1998**, *120*, 12964−12965.
[6] H. Shimizu, E. Obayashi, Y. Gomi, H. Arakawa, S.-Y. Park, H. Nakamura, S.-i. Adachi, H. Shoun, Y. Shiro, *J. Biol. Chem.* **2000**, *275*, 4816−4826.
[7] T. Kudo, N. Takaya, S.-Y. Park, Y. Shiro, H. Shoun, *J. Biol. Chem.* **2001**, *276*, 5020−5026.
[8] A. Daiber, T. Nauser, N. Takaya, T. Kudo, P. Weber, C. Hultschig, H. Shoun, V. Ullrich, *J. Inorg. Biochem.* **2002**, *88*, 343−352.
[9] D. L. Harris, *Int. J. Quantum Chem.* **2002**, *88*, 133−200.
[10] O. Einsle, A. Messerschmidt, R. Huber, P. M. H. Kroneck, F. Neese, *J. Am. Chem. Soc.* **2002**, *124*, 11737−11745.
[11] B. A. Averill, *Chem. Rev.* **1996**, *96*, 2951−2964.
[12] T. Wondimagegn, A. Ghosh, *J. Am. Chem. Soc.* **2001**, *123*, 5680−5683.
[13] M. Sono, M. P. Roach, E. D. Coulter, J. H. Dawson, *Chem. Rev.* **1996**, *96*, 2841−2888.
[14] The $S = 2$ state of the [Fe-N(H)-OH]^8 "complex" itself is, in fact, not a proper energetical minimum, as its geometry optimization leads to "dissociation" of the NH-OH moiety from iron, with the energy of the resulting "structure" more than 100 kJ/mol higher than that of the ground state, $S = 0$ [Fe-N(H)-OH]^8.
[15] SPARTAN '02 for Windows, *Wavefunction Inc.,* 18401 Von Karman Avenue, Suite 370 Irvine, CA 92612; *Q-Chem. Inc.* Four Triangle Drive, Suite 160 Export, PA 15632.

Received September 23, 2002
[I02537]

Synthesis, Crystal and Electronic Structure of $[Hg_7As_4](AgI_3)_2$, a Novel Supramolecular Complex with the Off-Plane AgI_3^{2-} Guest Anion

Andrei V. Olenev,[a] Alexei I. Baranov,[b] Olga S. Oleneva,[a] Ivan I. Vorontsov,[c] Mikhail Yu. Antipin,[c] and Andrei V. Shevelkov*[a]

Keywords: Supramolecular chemistry / Inorganic chemistry / Mercury / Silver / Host-guest interactions

A novel supramolecular inorganic complex $[Hg_7As_4](AgI_3)_2$ has been prepared and its crystal structure determined. It crystallizes in the cubic system (space group $Pa\bar{3}$) with the unit cell parameter a = 13.138(1) Å and Z = 4. The crystal structure comprises a three-dimensional positively charged host framework $[Hg_7As_4]^{4+}$ with AgI_3^{2-} guest anions trapped in each cavity of the framework. The guest anion shows an unusual off-plane geometry (C_{3v} symmetry), with a large, anisotropic thermal displacement parameter for the silver atom, which lowers significantly upon cooling from 293 down to 120 K. A study of the electronic structure shows that, although the host-guest interaction is weak and diffuse, it governs both the geometry of the guest anion and its positioning within the framework cavities.
(© Wiley-VCH Verlag GmbH & Co. KGaA, 69451 Weinheim, Germany, 2003)

Introduction

Supramolecular architectures with three-dimensional (3D) host frameworks possess a huge variety of crystal structures. A number of supramolecular complexes in which the positively charged 3D host substructures are built from linear mercury and tetrahedral pnicogen atoms have been reported over the past few years.[1−4] The combination of linear and tetrahedral units in the host substructure, together with the possibility of forming homonuclear bonds, provides a rich structural diversity of such complexes. Indeed, the crystal chemistry of the compounds under consideration ranges from phosphorus and arsenic analogues of the Millon phases[1] to a group of symmetric complexes with $[Hg_6Z_4]^{4+}$ host frameworks.[2] The positive charge of the host framework in these compounds is compensated by the halometallate anions of different shape and size that reside in the host framework cavities. Due to large separations between the host and guest moieties their interactions are limited to weak electrostatic forces.

It is well known that the guest moieties usually serve as templates during the formation of supramolecular complexes.[5] Host frameworks, in turn, may influence the geometry of the guests. Hence, the formation of a supramolecular architecture is often achieved by a mutual adjustment of the host and guest substructures. Examples of such an adjustment were shown in our previous work where we reported a family of new supramolecular complexes[4] in which the SnX_3^- (X = Cl, Br, I) guests are encapsulated in the cavities of the Hg−Z (Z = P, As, Sb) host framework. Evidently, the formation of a supramolecular complex is facilitated by a certain "crystallographic flexibility" of the guest, or, in general, by the possibility that the atoms of the guest moiety have different coordination (and oxidation) numbers. For silver, for example, the generic formula of the halometallate anions can be written as $AgX_n^{(n-1)-}$ ($2 \leq n \leq 4$; X = Cl, Br, I). Examining the possibility of the formation of supramolecular assemblies with $AgX_n^{(n-1)-}$ guest anions, we unexpectedly discovered a novel complex $[Hg_7As_4](AgI_3)_2$ in which an unusual off-plane AgI_3^{2-}anion resides in the cavities of a Hg−As cationic framework.

Here we report on the synthesis and crystal structure of $[Hg_7As_4](AgI_3)_2$. The host-guest interactions in the title compound, which lead to the observed off-plane geometry of the guest AgI_3^{2-} anion, are also discussed on the basis of the ab initio molecular structure and extended Hückel band-structure calculations.

Results

$[Hg_7As_4](AgI_3)_2$ was prepared from a stoichiometric mixture of mercury(II) iodide, arsenic, silver powder, and liquid mercury by a two-step ampoule synthesis (see Exp. Sect. for details). The sample formed as a dark-brown polycrystalline powder. The compound is air- and moisture-stable, and it melts incongruently at 675 K.

[a] Inorganic Synthesis Laboratory, Department of Chemistry, Moscow State University,
Leninskie Gory 1/3, Moscow 119992, Russia
[b] Department of Materials Sciences, Moscow State University, Leninskie Gory 1/3, Moscow 119992, Russia
[c] X-ray Structural Centre, Institute of Organoelement Compounds,
28 Vavilov St., B-334, Moscow 119991, Russia

For the structure investigation a suitable single crystal was selected from a sample prepared from a nonstoichiometric mixture of starting reagents as described in the Exp. Sect. The crystal structure of the new compound was determined by single-crystal X-ray diffraction methods at ambient temperature (Table 3). Analysis of the systematic absences in the data set revealed one possible space group $Pa\bar{3}$ (no. 205). The positions of the mercury, iodine, arsenic, and silver atoms were localized by direct methods (SHELXS 97[6]). It should be noted that the electron-density peak assigned to the silver atom position was the lowest one. Refinement of the crystal structure (SHELXL 97[6]) showed that the silver atom has a large thermal displacement parameter. Nevertheless, the refinement of the occupancy of the silver atom position confirmed this position to be fully occupied. Final anisotropic refinement led to quite acceptable R values ($R1 = 3.9\%$ $wR2 = 8.4\%$). However, it also revealed that the silver atom has a strongly prolate thermal ellipsoid, which could possibly indicate that the silver position is split. In order to check if this was the case, a low-temperature (120 K) X-ray structure investigation was carried out. The analysis of the diffraction frames showed the absence of superstructural reflections and confirmed the space group to be the same as that determined during the ambient-temperature diffraction experiment. The crystal structure was successfully refined ($R1 = 4.2\%$, $wR2 = 9.1\%$) with the atomic positions determined in the room-temperature experiment (Table 1). The thermal displacement parameters of all atoms, and especially of the silver atom (Table 1), lowered significantly. No electron-density peaks were observed near the position of the silver atom, which could be assigned to the split position of the silver.

Table 1. Atomic positions for $[Hg_7As_4](AgI_3)_2$ at 293 K and equivalent displacement parameters for the compound at 293 and 120 K

Atom	Wykoff	*x/a*	*y/b*	*z/c*	U_{eq} [Å^2][a] 293 K	120 K
Hg(1)	24d	0.2122(1)	0.4165(1)	0.4521(1)	0.0341(3)	0.0159(2)
Hg(2)	4b	1/2	1/2	1/2	0.0399(5)	0.0174(5)
I	24d	0.1659(1)	0.5524(1)	0.2453(1)	0.0270(3)	0.0121(3)
As(1)	8c	0.0528(1)	0.0528(1)	0.0528(1)	0.0132(6)	0.0054(7)
As(2)	8c	0.3903(1)	0.3903(1)	0.3903(1)	0.0143(7)	0.0079(8)
Ag	8c	0.2705(3)	0.2705(3)	0.2705(3)	0.101(1)	0.043(1)

[a] U_{eq} is defined as one third of the trace of the orthogonalized U_{ij} *tensor.*

Atomic parameters and selected interatomic distances and bond angles for $[Hg_7As_4](AgI_3)_2$ are listed in Tables 1 and 2, respectively. The crystal structure of the title compound (Figure 1) is composed of a positively charged $[Hg_7As_4]^{4+}$ host framework and AgI_3^{2-} guest anions encapsulated in the closed cavities of the host. The guest and host moieties are not connected by covalent bonds [d_{min}(Hg−I) = 3.31 Å], which is typical for supramolecular assemblies.

The host framework (Figure 1) is built from nearly linear-coordinated mercury and tetrahedrally coordinated arsenic

Table 2. Selected interatomic distances and bond angles for $[Hg_7As_4](AgI_3)_2$ at 293 K

Distances [Å]	
As(1)−As(1)	2.405(6)
As(1)−Hg(1)	2.510(1) ×3
As(2)−Hg(1)	2.500(1) ×3
As(2)−Hg(2)	2.497(3)
Ag−I	2.711(1) ×3
Hg(1)−I	3.307(1)
Hg(1)−I	3.446(1)
Hg(1)−I	3.573(1)
Hg(1)−I	3.575(1)
Angles [°]	
Hg(1)−As(1)−Hg(1)	113.00(6) ×3
As(1)−As(1)−Hg(1)	105.66(7) ×3
Hg(2)−As(2)−Hg(1)	105.84(7) ×3
Hg(1)−As(2)−Hg(1)	112.85(6) ×3
As(2)−Hg(1)−As(1)	166.94(9)
As(2)−Hg(2)−As(2)	180.00(6)
I−Ag−I	117.53(7) ×3

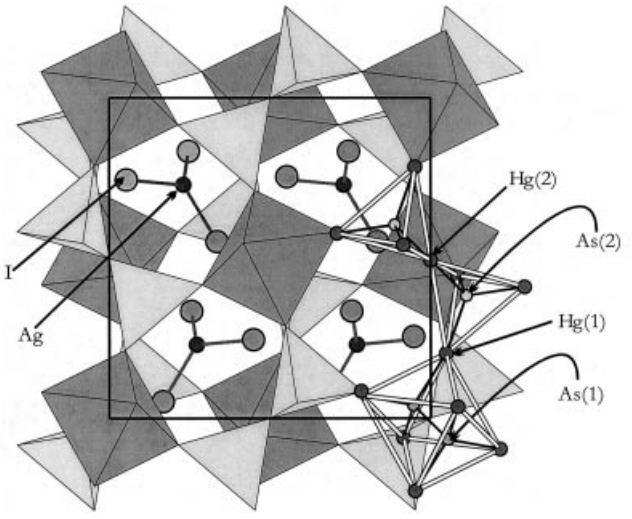

Figure 1. A view of the crystal structure of $[Hg_7As_4](AgI_3)_2$

atoms. There are two positions of the mercury atoms, Hg(1) and Hg(2), each of which is surrounded by two arsenic atoms. The additional neighbors of the Hg(2) atom lie 3.95 Å apart from it, and the As−Hg(2)−As angle appears to be 180°. In contrast with that, four iodine atoms of the guest anion serve as distant neighbors for the Hg(1) atom, the Hg−I separations being 3.31−3.56 Å. Thus, four iodine atoms of the guest complete the coordination sphere of the Hg(1) atom as a distorted octahedron, and, as a result, the As−Hg(1)−As angle (166.9°) departs from the ideal linear value.

The nearest neighbors of two crystallographically independent arsenic atoms are different (Figure 1). The As(1) atoms are joined into As_2^{4-} dumbbells and each As(1) atom is connected to one arsenic and three Hg(1) atoms. Six Hg(1) atoms surround the As(1)−As(1) dumbbell forming

an $Hg(1)_6As(1)_2$ octahedral building block. The As(2) atom has a tetrahedral arrangement of three Hg(1) and one Hg(2) atom. Two $As(2)Hg(1)_3Hg(2)$ tetrahedra share a common Hg(2) vertex forming an Hg_7As_2 bitetrahedral group. The Hg_7As_2 and Hg_6As_2 building blocks all share the Hg(1) vertices to form a 3D $[Hg_7As_4]^{4+}$ host framework. The As−As (2.41 Å) and As−Hg (2.50−2.51 Å) distances within the framework are in good agreement with the values found in the literature for numerous mercury pnictide halides.[1−4]

The $[Hg_7As_4]^{4+}$ host framework has eight cavities of equal size per unit cell. To compensate for the positive charge of the host, the AgI_3^{2-} guest anions occupy each cavity. The guest anion departs significantly from the expected configuration, which would be a regular triangle with an in-plane silver atom (D_{3h} symmetry). All the Ag−I separations in the anion are the same (2.71 Å), while the I−Ag−I angle (117.5°) indicates that the silver atom does not reside in the plane of three iodine atoms. It lies 0.41 Å apart from the ligand plane, therefore the actual symmetry of the guest anion is C_{3v}.

The equilibrium geometry of the AgI_3^{2-} anion was calculated at different levels of theory (RHF and DFT). All calculations exploiting different basis sets and correlation potentials resulted in the expected planar triangle geometry (D_{3h} symmetry), with the Ag−I distances ranging from 2.93 to 3.01 Å depending on the type of calculation. Then, the positions of the three iodine atoms were frozen according to their positions in the crystal structure, while the position of the silver atom was optimized. Such calculations at the RHF level with the MP2 correction resulted in the C_{3v} geometry of the anion with an off-plane shift of the silver atom of 0.36 Å and three equidistant Ag−I contacts of 2.69 Å.

The band-structure calculations (at the EH level, Figure 2) showed that the bands below the Fermi level are composed of p-orbitals of I and As, s-orbitals of Hg, and d-orbitals of Ag. Analysis of the overlap population revealed the existence of strong covalent Hg−As and As−As bonding within the host framework and Ag−I bonding in the guest anion, whereas the host-guest Hg−I interaction is weak. A detailed analysis of the molecular orbitals of the AgI_3^{2-} anion revealed two sets of MOs corresponding to the Ag−I interaction, d(Ag)−p(I) bonding (between −14.5 and −12.3 eV) and d(Ag)−p(I) antibonding (between −12.3 eV and E_F). Both sets contain σ- and π-orbitals whose energies are only slightly sensitive to the small deviation of the anion geometry from D_{3h} towards C_{3v} symmetry.

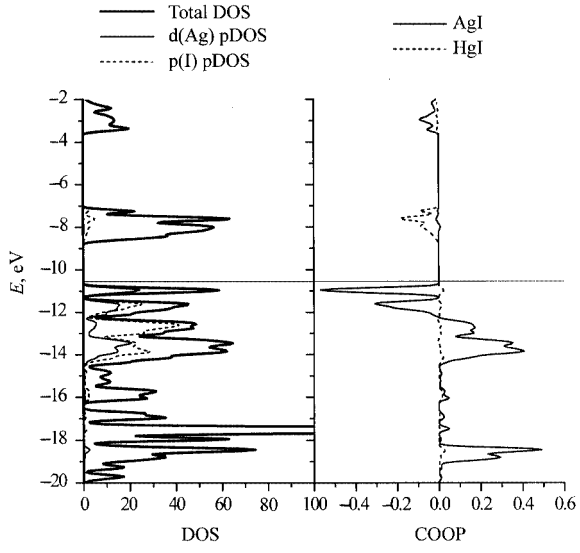

Figure 2. The Density of States (DOS) and Crystal Orbital Overlap Population (COOP) plots for $[Hg_7As_4](AgI_3)_2$

Discussion

The structure of the host framework of the title complex is similar to the structure of the hosts found in two earlier reported supramolecular architectures $[Hg_7As_4I_3]SnI_3$ and $[Hg_7P_4Br_3]SnBr_3$.[4] The main building blocks of the host frameworks of these two complexes are Hg_6Z_2 octahedra and Hg_7Z_2 bitetrahedal groups, their connection being the same as in the title compound. The main difference is that in the tin-containing complexes additional halogen atoms lie quite close to the mercury atoms thus modifying the host frameworks. The formulae of such frameworks can be written as $[Hg_7As_4I_3]^+$ and $[Hg_7P_4Br_3]^+$, respectively. They have two cavities of different size per formula unit and one guest anion − SnI_3^- or $SnBr_3^-$ − per formula unit is enough to compensate for the positive charge of the host framework These guest anions reside only in the larger cavities of the framework. In $[Hg_7As_4](AgI_3)_2$ the formal charge of the framework is +4, and all cavities in it have the same size. The electroneutrality of the complex is achieved by encapsulating the AgI_3^{2-} in each cavity of the host.

As was already mentioned, the geometry of the AgI_3^{2-} anion deviates considerably from the expected D_{3h} triangle. It is reasonable to compare the observed configuration of the guest anion with the geometry of AgX_3^{2-} (X = Cl, Br, I) anions in the literature. Analysis of the literature data surprisingly shows that there are only a small number of structurally characterized complexes that contain AgX_3^{2-}anions. The $AgCl_3^{2-}$ and $AgBr_3^{2-}$ anions have been isolated as their (dibenzo-18-crown-6)potassium and -rubidium salts.[7] In these two compounds the AgX_3^{2-} anions are regular (D_{3h} symmetry).

To the best of our knowledge there is only one known complex − $[PPh_3Me]_2[AgI_3]$[8] − that contains discrete AgI_3^{2-} anions. The triangular AgI_3^{2-} anion in it is reported to be only slightly distorted. The distance between the Ag atom and the ligand plane is only 0.04 Å. However, all three Ag−I distances in it are not equal and lie in the range 2.74−2.76 Å, thus lowering the symmetry of the anion from D_{3h} to effectively C_s.

The silver atom in the guest anion has a large thermal vibration amplitude in the direction perpendicular to the ligand plane. This indicate that the compound might undergo phase transformation (decomposition) at a relatively low temperature, or that the silver atom is distributed over two close crystallographic positions. However, neither the first nor the second supposition was proved to be the case.

The complex under investigation is stable up to 675 K, and the low-temperature X-ray diffraction experiment, as mentioned previously, unambiguously confirmed that the position of the silver atom is not split.

The off-plane construction of the AgI_3^{2-} guest anion, as well as the large thermal displacement parameter of the silver atom, deserve more discussion. It is clear from the results of the electronic structure calculations that the interaction of the host framework and guest anions is not strong and is predominantly of an electrostatic nature. Although the orbitals of As, Hg, Ag, and I apparently mix in the region below the Fermi level (from −10.8 to −14.5 eV), the overlap population analysis indicates that the Hg−I orbital interaction, which is responsible for the host-guest bonding, is weak and diffuse (Figure 2). On the contrary, bonding within the host and guest moieties is strongly covalent, and, consequently, the title compound can be formulated as pseudo-ionic: $[Hg_7As_4^{4+}](AgI_3^{2-})_2$. Each AgI_3^{2-} guest anion experiences the influence of 12 positively charged Hg(1) atoms of the host framework through distant Hg−I contacts (Figure 3). The Hg−I separations lying in the range of 3.31−3.58 Å are typical for a "secondary" Hg−I interaction. Analysis of the literature data[9] shows that the Hg−I separations in the 2+4 pseudo-octahedral array of mercury fall into two ranges: 2.62−2.64 Å for two collinear covalent Hg−I bonds, and 3.37−3.51 Å for four distant contacts. It is plausible to conclude that the positions of the iodine atoms in the title complex are governed by the arrangement of the positively charged mercury atoms of the rigid covalent framework. This leaves a limited space for the silver atom, forcing the latter to move from the ideal position at the center of the iodine triangle along its threefold axis. It should be noted that the observed 0.41 Å off-plane shift of Ag and the Ag−I distances of 2.72 Å are in very good agreement with the values calculated using a model with frozen iodine positions. Thus, the increase of the host anion energy due to the off-plane displacement of Ag is compensated for by the decrease of the energy of interaction between the host framework and the distorted AgI_3^{2-} guest anion. Furthermore, the off-plane shift of Ag is favored by an absence of neighbors along the threefold axis, the nearest, As(2), lying 3.66 Å apart. The absence of near neighbors in the direction of the threefold axis can also explain the large amplitude of the thermal vibrations along this axis, which lowers upon cooling (Figure 4).

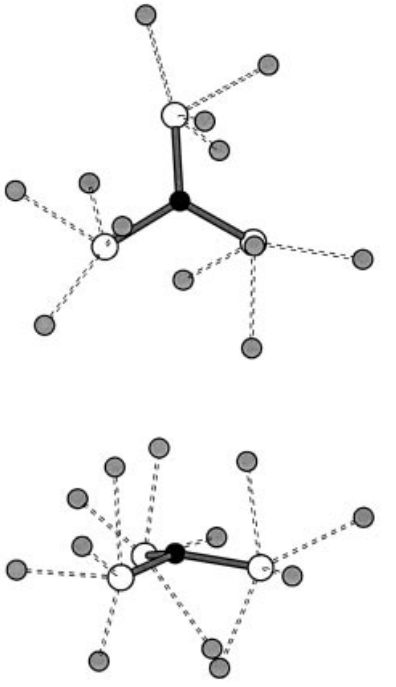

Figure 3. Coordination of the AgI_3^{2-} anion by the mercury atoms of the host framework; top: a view almost along the threefold axis; bottom: a side view; black circles, Ag; open circles, I; gray circles, Hg(1)

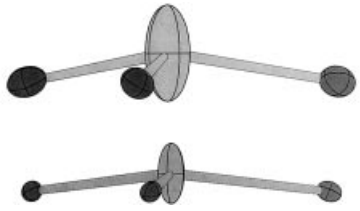

Figure 4. Thermal ellipsoids (50% probability) of the AgI_3^{2-} anion at 293 K (top) and 120 K (bottom); light gray, silver; dark gray, iodine

Experimental Section

Synthesis: A stoichiometric mixture of mercury(II) iodide, arsenic, silver powder, and liquid mercury (all > 99.99%; 0.5 g) was heated for 2 d at 775 K in a vacuum-sealed silica tube. Then, the ampoule was cooled down to 575 K and heated for further 2 d. A comparison of the diffraction pattern of the sample [STADI-P (STOE), Cu-$K_{\alpha 1}$ radiation] with the theoretical pattern calculated on the basis of the data obtained during the structure refinement revealed that the sample was almost phase-pure and had only a slight admixture of arsenic and Hg_2I_2.

Crystal Growth: Single crystals of the title compound were obtained by annealing a mixture of starting materials (3:4:2:3 molar ratio, total weight approx. 0.5 g) in a vacuum-sealed silica tube (60 mm length, 6 mm inner diameter) for 5 d at 675 K, and then cooling it down to ambient temperature at a rate of 30 K/h.

Crystal Structure Determination: For the ambient temperature experiment, a suitable single crystal of the reported compound was mounted on a CAD-4 (Nonius) goniometer head. The cubic unit-cell parameter was refined based on 24 well-centered reflections. The data collection parameters are listed in Table 3. A semiempirical absorption correction was introduced based on azimuthal scans of six reflections with χ angles close to 90°. The structure was solved by direct methods (SHELXS-97)[6] and refined anisotropically by a full-matrix least-squares method on F^2 (SHELXL-97)[6] to $R_1 = 0.0393$ and $wR_2 = 0.0839$. Final $\Delta\rho(xyz)$ synthesis revealed no chemically significant electron-density peaks. For the low-temperature structural investigations on the same single crystal, a data set was collected with a Bruker SMART 1000 CCD diffractometer at 120 K (Table 3). The absorption correction was applied by a standard routine (SADABS[10]). The crystal structure was refined (SHELXL-97,[6] anisotropic full-matrix least-squares

refinement on F^2, $R1 = 0.0419$, $wR2 = 0.0905$) using the starting atomic positions determined in the previous experiment. Further details of the crystal structure determination may be obtained from Fachinformationzentrum Karlsruhe, 76344 Eggenstein-Leopoldshafen, Germany, on quoting the depository numbers CSD-391131 and -391132.

Table 3. Data collection and structure refinement parameters for $[Hg_7As_4](AgI_3)_2$

Empirical formula	$Ag_2As_4Hg_7I_6$	
T [K]	293(2)	120(2)
Space group	$Pa\bar{3}$ (no. 205)	
Cell parameter a [Å]	13.138(1)	13.108(1)
V [Å^3]	2267.7(3)	2252.0(4)
Z	4	
Density (calcd.) [Mg/m^3]	7.853	7.907
μ [1/mm]	62.826	63.266
Crystal size [mm]	$0.13 \times 0.06 \times 0.05$	
Radiation, λ [Å]	Mo-K_α, 0.71069	
Data collection range [°]	$2.69 < \theta < 25.48$	$2.69 < \theta < 25.44$
Reflections collected	2123	6088
Independent reflections	707 [R(int) = 0.0944]	704 [R(int) = 0.0881]
Parameters refined	30	
R1,[a] $wR2$[b] [$F_o > 4\sigma(F_o)$]	0.0393, 0.0839	0.0419, 0.0905
R1, $wR2$ (all data)	0.0677, 0.0895	0.0595, 0.0952
Lagest diff. peak and hole [e/Å^3]	1.629 and −1.695	2.350 and −4.243
G.o.f. on F^2	1.047	0.947

[a] $R1 = \Sigma||F_o| - |F_c||/\Sigma|F_o||$. [b] $wR2 = [\Sigma w(F_o^2 - F_c^2)^2/\Sigma w(F_o^2)^2]^{1/2}$, $w = \{\sigma^2(F_o^2) + A[(F_o^2 + 2F_c^2)/3]^2\}^{-1}$; $A = 0.0195$ (293 K), 0.0472 (120 K).

Thermal Properties: A small quartz ampoule was completely filled with compound (approx. 0.2 g). The ampoule was evacuated and sealed. The differential thermal analysis curve was recorded with a modified PRT-1000m device at a 10 °C/min heating/cooling rate.

Calculational Details

Band Structure Calculations: Extended Hückel calculations of the band structure were performed with the YAeHMOP[11] program package utilizing the built-in atomic parameters. A mesh of 41 k-points taken within the irreducible wedge of the Brillouin zone was used.

Molecular Calculations: RHF (including MP2[12] correlation correction) and DFT (BLYP, VWN, and B3LYP[13] exchange-correlation potentials) calculations were performed using the GAMESS-US[14] program. The SBKJC effective core potentials were applied to all atoms and the SBKJC basis set[15] implemented in GAMESS was used. The starting geometry of the AgI_3^{2-} anion was taken from the crystal structure refinement. Geometry optimizations were performed by the quasi-Newton algorithm implemented in GAMESS.

[1] [1a] A. V. Shevelkov, E. V. Dikarev, M. Yu. Mustiakimov, B. A. Popovkin, *J. Chem. Soc., Dalton Trans.* **1995**, 147−148. [1b] A. V. Olenev, A. V. Shevelkov, B. A. Popovkin, *Zh. Neorg. Khim.* **1999**, *44*, 1911−1913; *Russ. J. Inorg. Chem.* **1999**, *44*, 1814−1816 (Engl. transl.).[1c] A. V. Olenev, A. V. Shevelkov, B. A. Popovkin, *Zh. Neorg. Khim.* **1999**, *44*, 1957−1965; *Russ. J. Inorg. Chem.* **1999**, *44*, 1853−1861 (Engl. transl.).

[2] [2a] A. V. Shevelkov, E. V. Dikarev, B. A. Popovkin, *J. Solid State Chem.* **1996**, *126*, 324−327. [2b] J. Beck, U. Neisel, *Z. Anorg. Allg. Chem.* **2000**, *626*, 1620−1626. [2c] J. Beck, S. Hedderich, U. Neisel, *J. Solid State Chem.* **2000**, *154*, 350−355. [2d] A. V. Olenev, M. M. Shatruk, A. V. Shevelkov, B. A. Popovkin, *Zh. Neorg. Khim.* **2001**, *46*, 1615−1618; *Russ. J. Inorg. Chem.* **2001**, *46*, 1462−1465 (Engl. transl.). [2e] A. V. Olenev, A. I. Baranov, M. M. Shatruk, A. S. Tyablikov, A. V. Shevelkov, *Russ. Chem. Bull.* **2002**, *3*, 414−418; *Russ. Chem. Bull.* **2002**, *3*, 444−448 (Engl. transl.).

[3] A. V. Olenev, A. V. Shevelkov, *Angew. Chem.* **2001**, *113*, 2415−2416; *Angew. Chem. Int. Ed.* **2001**, *40*, 2353−2354.

[4] [4a] A. V. Olenev, A. I. Baranov, A. V. Shevelkov, B. A. Popovkin, *Eur. J. Inorg. Chem.* **2000**, 265−270. [4b] A. V. Olenev, A. I. Baranov, A. V. Shevelkov, B. A. Popovkin, *Eur. J. Inorg. Chem.* **2002**, 547−553.

[5] A. Müller, H. Reuter, S. Dillinger, *Angew. Chem.* **1995**, *107*, 2505−2539; *Angew. Chem. Int. Ed. Engl.* **1995**, *34*, 2328−2361.

[6] [6a] G. M. Sheldrik, *SHELXS-97, Program for crystal structure solution*, University of Göttingen, Germany, **1997**.[6b] G. M. Sheldrik, *SHELXL-97, Program for crystal structure refinement*, University of Göttingen, Germany, **1997**.

[7] G. Helgesson, S. Jagner, *J. Chem. Soc., Dalton Trans.* **1993**, 1069−1072.

[8] G. A. Bowmaker, A. Camus, B. W. Skelton, A. H. White, *J. Chem. Soc., Dalton Trans.* **1990**, 727−731.

[9] [9a] H. J. Berthold, D. Haas, R. Tamme, K. Brodersen, K. P. Jensen, D. Messer, G. Thiele, *Z. Anorg. Allg. Chem.* **1979**, *456*, 29−40, and references therein.[9b] G. A. Jeffrey, M. Vlasse, *Inorg. Chem.* **1967**, *6*, 396−399. [9c] W. Rüdorf, K. Brodersen, *Z. Anorg. Allg. Chem.* **1953**, *274*, 323−340.

[10] G. M. Sheldrick, *SADABS, Bruker/Siemens Area Detector Absorption Correction Program*, Bruker AXS, Madison, Wisconsin, USA, **1998**, v.2.01.

[11] G. Landrum, W. Glassey, *Yet Another Extended Hückel Molecular Orbital Package* (YAeHMOP), www: http://overlap.-chem.cornell.edu:8080/yaehmop.html

[12] M. Dupuis, S. Chin, A. Marquez, in: *Relativistic and Electron Correlation Effects in Molecules* (Ed.: G. Malli), Plenum Press, NY, **1994**, pp. 315−338.

[13] [13a] R. G. Parr, M. Yang, *Density Functional Theory of Atoms and Molecules*, Oxford Scientific, Oxford, **1989**. [13b] W. Koch, M. C. Holthausen, *A Chemist's Guide to Density Functional Theory*, Wiley-VCH, **2001**.

[14] M. W. Schmidt, K. K. Baldridge, J. A. Boatz, S. T. Elbert, M. S. Gordon, J. J. Jensen, S. Koseki, N. Matsunaga, K. A. Nguyen, S. Su, T. L. Windus, M. Dupuis, J. A. Montgomery, *J. Comput. Chem.* **1993**, *14*, 1347−1363.

[15] [15a] W. J. Stevens, H. Basch, M. Krauss, *J. Chem. Phys.* **1984**, *81*, 6026−6033; [15b] W. J. Stevens, H. Basch, M. Krauss, P. Jasien, *Can. J. Chem.* **1992**, *70*, 612−630; [15c] T. R. Cundari, W. J. Stevens, *J. Chem. Phys.* **1993**, *98*, 5555−5565.

Received August 27, 2002
[I02482]

Structural Investigation of the Thermal Decomposition of Ammonium Heptamolybdate by in situ XAFS and XRD

Julia Wienold,[a] Rolf E. Jentoft,[a] and Thorsten Ressler*[a]

Keywords: X-ray absorption spectroscopy / X-ray diffraction / Molybdenum / Polyoxometalates

The decomposition of ammonium heptamolybdate (AHM, $(NH_4)_6Mo_7O_{24}\times4H_2O$) was studied in situ by X-ray diffraction and X-ray absorption spectroscopy, as well as by thermal analysis (TG/DTA). Decomposition conditions such as reactant atmospheres, (20% oxygen, 5% propene, 5% hydrogen, pure helium, and static air), heating rates, and gas flow rates were varied to investigate their influence on the decomposition process. The results obtained show that the reaction pathway is affected by the partial pressures of the gas-phase decomposition products. The partial pressures of the decomposition products, water and ammonia, at a given temperature, is influenced mainly by the reactant gas flow rate and the heating rate. Lowering the partial pressures of ammonia and water inhibits the crystallization of the intermediate ammonium tetramolybdate (ATM), and promotes the formation of the intermediate hexagonal MoO_3. The decomposition pathway under low gas phase product partial pressure is: (i) AHM; (ii) (ca. 335 K) X-ray amorphous phase; (iii) (ca. 520 K) hexagonal MoO_3; (iv) (ca. 650 K) the products, which depend on the reactant atmosphere, are mixtures of highly disordered Mo_4O_{11}, and/or α-MoO_3. Under different conditions the decomposition pathway is: (i) AHM; (ii) (ca. 350 K) X-ray amorphous phase; (iii) (ca. 470 K) ATM; (iv) (ca. 570 K) hexagonal MoO_3 + α-MoO_3; (ca. 650 K) α-MoO_3. Under a hydrogen containing atmosphere, a peculiar decomposition pathway is observed: an intermediate MoO_3 with an unusual texture is formed prior to the reduction to MoO_2 and the consecutive formation of orthorhombic Mo_4O_{11}.
(© Wiley-VCH Verlag GmbH & Co. KGaA, 69451 Weinheim, Germany, 2003)

Introduction

Numerous authors have investigated the thermal decomposition of ammonium heptamolybdate tetrahydrate [$(NH_4)_6Mo_7O_{24}\times4H_2O$, AHM] using several techniques.[1−24] The decomposition pathway of AHM has been the subject of most studies.[2−13,19,23,24] Thermogravimetric analysis [TGA] and/or differential thermal analysis [DTA],[2−12,19,24] infrared spectroscopy [IR],[6,9,12] and X-ray diffraction [XRD][3−7,9,10] have been used to identify the intermediates and final products. Other studies have compared the decomposition of AHM with that of compounds with similar composition.[8,18−21] The decomposition of AHM was also investigated with respect to the effect of varying decomposition conditions. The influence of dopants, such as vanadium,[14] cobalt,[15] and alkali metal ions,[16] the influence of supports,[17,19,22] and the influence of reactant atmosphere has also been investigated.[1,23] In most studies, flowing or static air was used, the exceptions being the studies by Yong (1990)[13], Thomazeau (2000),[22] and the thermo-Raman study by Murugan (2001),[23] which were carried out under H_2, Ar, and N_2 and O_2, respectively. The TG study by Hegedüs (1957),[1] was carried out under a variety of different atmospheres.

In Table 1, the results of several representative studies are summarized. For comparison, the total amounts of molybdenum and oxygen, reported in the formulas from the literature, were normalized to five molybdenum atoms for the first step (this phase is mostly reported as pentamolybdate), and eight molybdenum atoms for the second step (this phase is mostly reported as octamolybdate). Normalization was done without changing the stoichiometry and is valid since the reported stoichiometric formulae were all based on chemical analyses and not on structural analyses. Although four decomposition stages can be distinguished, as indicated in Table 1, not all the authors observed all stages, and the temperatures of the decomposition steps vary. The first step takes place at temperatures of about 370 K (335−400 K), affording $(NH_4)_4Mo_5O_{17}$ as an intermediate. At about 470 K (430−510 K), the second decomposition step takes place, and the intermediate formed is reported to be $(NH_4)_4Mo_8O_{26}$, with the exception of study 7. In studies 4, 5, and 6, the formation of hexagonal intermediates ($MoO_3 \times xH_2O \times yNH_3$) at about 520 K (510−545 K) is reported as the third step. The final step in all the studies is the formation of α-MoO_3 (orthorhombic), with the corresponding temperatures varying from 540 K to 630 K. In two studies, 4 and 6, this step is preceded by the formation of a hydrous MoO_3 species.

[a] Department of Inorganic Chemistry, Fritz-Haber-Institut der MPG
Faradayweg 4−6, 14195 Berlin, Germany
Fax: (internat.) + 49-30/8413-4405
E-mail: Ressler@FHI-Berlin.MPG.de

Table 1. Results of the study of AHM decomposition from selected publications

No.	Publication	Conditions; method			
		Decomposition scheme			
1	Ma et al., 1963	Static air; 7 K/min; TG/DTA, ex situ XRD characterization			
		400 K → $(NH_4)_4Mo_5O_{17;}$	510 K → $(NH_4)_4Mo_8O_{26}$		630 K → α-MoO_3
2	Schwing-Weill, 1967	No information on atmosphere and flow rate; 0.25 K/min; TG, ex situ XRD characterization and chemical analysis			
		370 K → $(NH_4)_4Mo_5O_{18;}$	460 K → $(NH_4)_4Mo_8O_{26}$		575 K → α-MoO_3
3	Louisy et al., 1970	static air; 0.25 K/min / TG/DTA, ex situ XRD characterization			
		350 K → $(NH_4)_4Mo_5O_{17}$	430 K → $(NH_4)_4Mo_8O_{26}$	525 K → dodecamolybdate	540 K → α-MoO_3
4	Kiss et al., 1970	Air; 277 ml/min; 5 and 10 K/ min; TG/DTA, in situ IR analysis of gaseous products, ex situ XRD and IR characterization			
		370 K → $(NH_4)_4$*$Mo_5O_{17;}$	(430 K → pseudo octamolybdate) 480 K → $(NH_4)_4Mo_8O_{26}$	530 K→$(NH_4)_2O$*$Mo_{14}O_{42}$(hex.) 545 K→$(NH_4)_2O$*$Mo_{22}O_{66}$(hex.)	550 K → MoO_3*× H_2O 570 K → α-MoO_3
5	Isa et al., 1981	static air 3 K/min; TG/DTA, in situ XRD analysis			
		335 K → decomposition starts	445 K → $(NH_4)_4Mo_8O_{26}$ + hex. MoO_3	525 K→ hex. MoO_3	630 K → α-MoO_3
6	Hanafi et al., 1980	No information on atmosphere and flow rate; 1.25 K/min; TG, ex situ XRD and IR characterization			
		370 K → $(NH_4)_4Mo_5O_{17;}$	480 K °C → $(NH_4)_4Mo_8O_{26}$	510 K→$(NH_4)_2O$*$Mo_{12}O_{36}$(hex.) 530 K→$(NH_4)_2O$*$Mo_{22}O_{66}$(hex.)	550 K → MoO_3*× H_2O 580 K → α-MoO_3
7	Said et al., 1994	Dry air; 40 ml/min; 10 K min; TG/DTA, ex situ XRD and IR characterization			
		395 K → $(NH_4)_{2.86}Mo_5O_{16,43}$*$1.43H_2O$	490 K → $(NH_4)_{2.28}Mo_8O_{25,14}$*$2.28H_2O$		575 K → α-MoO_3

In study 5, all the phases formed during the decomposition are identified in situ. This is the only study in which this is observed. In all the other studies, with the exception of study 6 where at least some intermediates are identified in situ, the characterization and identification of the intermediates and products were performed ex situ, and are based on chemical and XRD powder pattern analyses. The considerable variation in the reported decomposition step temperatures may be due to experimental conditions, i.e. different heating rates. The reasons for the differences in the observed phases and the wide temperature range for the formation of the final phase are not obvious. The results of study 5 are unique in that the first decomposition step is not observed at all, and after the second step at 445 K, two phases were reported, namely $(NH_4)_4Mo_8O_{26}$ and hexagonal MoO_3. In summary, although the decomposition process has already been studied to some extent, no description of the sequence of events that can explain the spread in materials and conditions of this key reaction in the production of molybdate heterogeneous catalysts exists.

An overview of the molybdenum-oxygen polyhedra found in the structures of the reported intermediates and products is presented in Figure 1. The structure of AHM is composed of monomers of seven distorted, edge-sharing, molybdenum-oxygen octahedra (Figure 1, A) [ICSD 4153]. The intermediate formed in the first step has been identified as $(NH_4)_4Mo_5O_{17}$, ammonium pentamolybdate, in several studies. Powder lines calculated from single crystal data of $(NH_4)_8Mo_{10}O_{34}$ [ICSD 67325] match the powder lines reported for this material [ICDD 21−971 and 26−77], and hence this intermediate can be identified as ammonium decamolybdate. This structure is composed of monomers of eight distorted, edge-sharing, molybdenum-oxygen octahedra and two distorted molybdenum-oxygen tetrahedra, which are linked to the cluster through bridging oxygen atoms. The resulting polyhedron is shown in Figure 1, B. The second intermediate, with the stoichiometry $(NH_4)_4Mo_8O_{26}$, can be identified as ammonium tetramolybdate, by comparing the literature powder lines [ICDD 18−117] with the powder diffraction data calculated from single crystal data of $(NH_4)_2Mo_4O_{13}$ [ICSD 68562]. In this structure, the distorted, edge-sharing, molybdenum-oxygen octahedra form one-dimensional oligomers, i.e. chains, as seen in Figure 1, C. The last intermediate is reported to be hexagonal. In studies 4 and 6, two phases with different stoichiometry, occurring successively and at nearly the same temperature (530/545 K), are reported. The powder patterns given for these phases are very similar and can be simulated with one single crystal data set with slightly varied lattice constants. The corresponding phase is $(NH_3)(MoO_3)_3$ [ICSD 62163], which can be understood as a hexagonal MoO_3 with NH_3 intercalated in the lattice. This phase is built from a three-dimensional network of distorted, edge and corner-sharing, molybdenum-oxygen octahedra that form six-fold channels in the structure, see Figure 1 (see D). The structure of the final product, α-MoO_3 (orthorhombic), is shown in Figure 1 (see E) [ICSD 35076], and is built from planes which are made from edge- and corner-sharing, distorted molybdenum-oxygen octahedra. A row of corner sharing, distorted molybdenum-oxygen octahedra, as indicated in Figure 1, constitute the structural unit in both hexagonal and α-MoO_3.

Our particular interest in the decomposition of AHM is because of its use as a precursor in the production of mol-

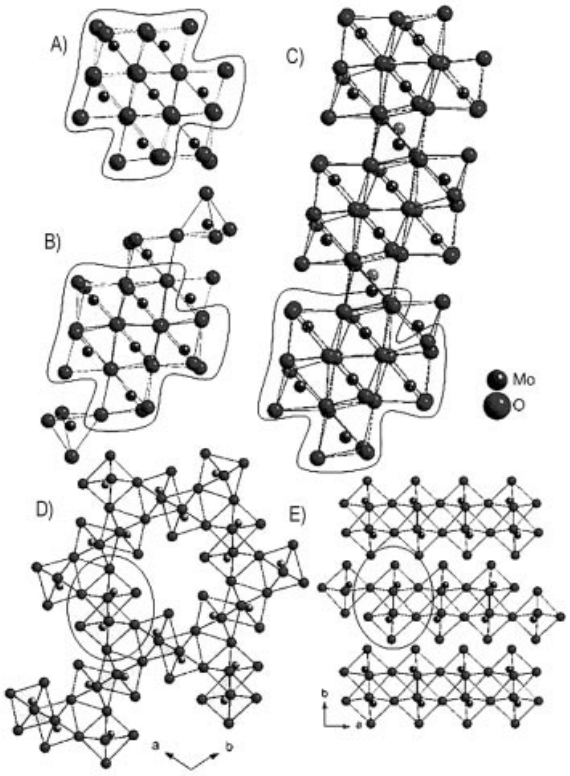

Figure 1. Schematic structural representation of potential intermediates in the decomposition of ammonium heptamolybdate: A, monomer of ammonium heptamolybdate; B, monomer of ammonium decamolybdate, C, sequence of the one-dimensional oligomer of ammonium tetramolybdate; D, hexagonal MoO_3 projected along the *c* axis; E, α-MoO_3 projected along the *c* axis. Only the molybdenum and oxygen atoms of the structures are shown. Ammonia and water are omitted. The structural units encircled in the monomers A and B and in the oligomer C are similar in all three phases. The structural units in hexagonal MoO_3 and α-MoO_3, encircled, indicate the rows of edge-shared octahedra, which are the same in the two structures

ybdenum trioxide (MoO_3) and partially reduced molybdenum oxide (MoO_{3-x}) catalysts. These oxides are suitable model systems[25] for the more complex mixed-oxide systems (molybdenum oxide with different additional components, for example Bi, W, V, Cu), which are used extensively as partial oxidation catalysts for light alkenes.[26] The catalytic activity of these materials depends on their properties,[27] i.e. their real structure (number and type of defects), their composition, and their particle sizes; which, in turn, will depend on the treatment of the precursor. Therefore, in order to learn how to control the textural and chemical properties of the resulting binary oxide, studies on the influence of different treatment parameters on the decomposition process, such as the composition of the gas phase or the heating rate, are required, together with a detailed analysis of the short- and long-range structure evolution.

In this work the decomposition of AHM is studied using in situ XRD and in situ X-ray absorption spectroscopy (XAS). The use of these two complementary methods allows us to follow the evolution of the short- and long-range structures of the phases formed. XRD is used to identify the phases and to reveal their crystallinity on a long-range order scale. The information gathered by XRD is used as a starting point for the analysis of the local structure by XAS. In addition, amorphous phases, which cannot be characterized by XRD, can be analyzed by XAS. The decomposition products in the gas phase are simultaneously analyzed by mass spectrometry. Additionally, the onset temperatures for the decomposition steps are obtained by TG/DTA coupled with evolved gas analysis (EGA) by mass spectrometry. Further, the influence of different atmospheres, such as pure helium, helium and oxygen, hydrogen, or propene, on the formation of intermediates and products is examined. In addition, the influence of the heating rate and the gas phase flow rate on the decomposition process is also investigated. The atmospheres are chosen to have oxidative, reductive, inert, and catalytically relevant reaction environments.

Results

Characterization of Ammonium Heptamolybdate

In Figure 2, the experimental diffraction pattern of ammonium heptamolybdate [$(NH_4)_6Mo_7O_{24}\times4H_2O$, AHM] in the range from 7 to 60° 2θ is shown, together with both the XRD powder pattern simulation employing single crystal data [ICSD 4153] (a = 8.393(1), b = 36.170(4), c = 10.472(1) Å, β = 116.0(0)°] and the difference between the experimental and simulated patterns. The refinement of the lattice parameters was performed with the software PowderCell 2.3. For the peak profile, the Pseudo-Voigt2 function was used and the full width at half maximum (FWHM) was taken as FWHM = $f(U,V,W)$, where only W was fitted and U = V = 0. The R_p value of the fit was 13.73. The resulting lattice constants are: a = 8.395(7), b = 36.204(3), c = 10.4765 Å, β = 115.884°. The good agreement between the experimental data and the single crystal data, the relatively small R_p value, and the fact that all the peaks in the experimental pattern of AHM were accounted for, indicate that the sample is pure and that the stoichiometry according to the structural formula is valid. The latter is also confirmed by the good agreement between the calculated and the measured weight loss for the decomposition of AHM in O_2/He with α-MoO_3 as the final product. In Figure 3, the IR absorption spectrum of AHM is shown. It is very similar to those previously reported for AHM and related compounds.[9,23,39,40] An assignment of the absorption bands is given in Table 2. For H_2O and NH_4^+, hydrogen bridging to the terminal oxygen of the Mo−O octahedra can be assumed from the structural data of AHM, whereas $O_{H2O}-O_{Molybdenum}$ = 2.72 Å and $N_{NH_4^+}-O_{Molybdenum}$ = 2.86 Å (stretching modes of H_2O at approximately 3400 cm^{-1} and of NH_4^+ at approximately 3100 cm^{-1}). The bending mode at 1640 cm^{-1} for H_2O refers to the free H_2O molecule. The bands below 1000 cm^{-1} are all assigned to the Mo−O modes, with the exception of the H_2O vibration mode at 636 cm^{-1}.

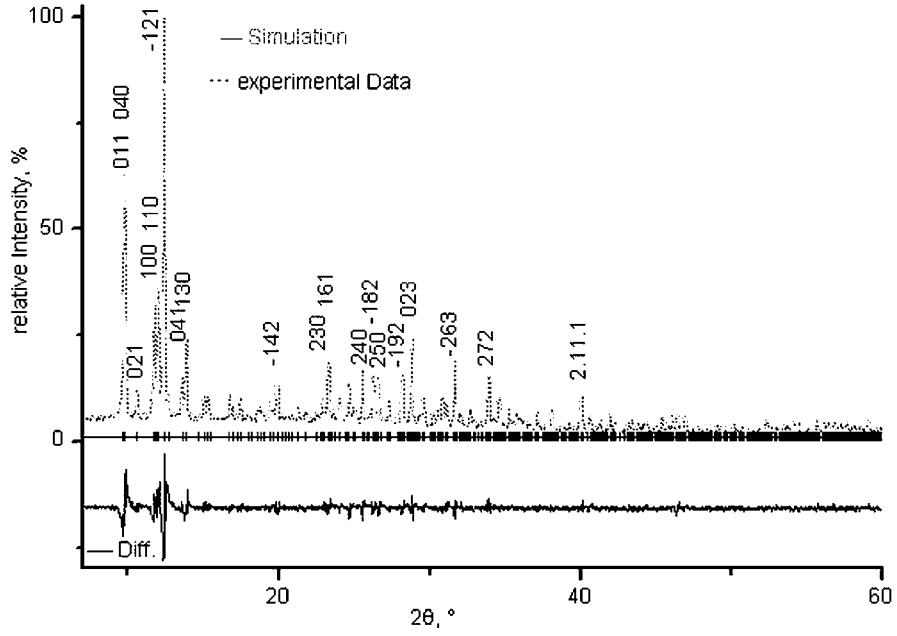

Figure 2. X-ray pattern of AHM (Aldrich), together with the fit of the theoretical data and the difference curve. Only the indices of peaks with $I_{rel.} > 5\%$ are given for clarity

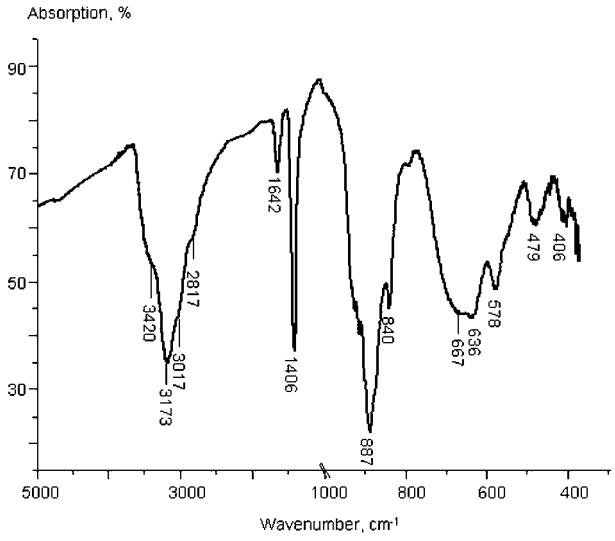

Figure 3. IR spectra of AHM (Aldrich). The *x*-axis is divided into two sections with different increments for clarity. Wavenumbers of distinct absorption bands are given. An assignment of the bands can be found in Table 2

Table 2. Vibrational spectrum for $(NH_4)_6Mo_7O_{24}\times4H_2O$ (in cm^{-1})

IR	Assignment
3420 (sh)[a]	$\nu(H_2O)$
3173 (vs)	$\nu(NH_4^+)$
3017 (sh)	$\nu(NH_4^+)$
2817 (sh)	
1642 (m)	$\delta(H_2O)$
1406 (vs)	$\delta(NH_4^+)$
925 (sh)	ν(Mo−O)
915 (sh)	
887 (vs)	ν(Mo−O)
875 (sh)	
840 (m)	
792 (vw)	
667 (m)	ν(Mo−O)
636 (m)	Lib. H_2O
578 (m)	ν(Mo−O)
479 (m)	
406 (m)	

[a] vs: very strong, s: strong, m: medium, w: weak, vw: very weak, sh: shoulder

TG/DTA

Figure 4 shows the progression of the TG curve, together with the DTA signal and the MS signals for $m/z = 18$ (assigned to H_2O) and $m/z = 15$ (assigned to NH), during the decomposition of AHM in 20% oxygen with a heating rate of 5 K/min. Four decomposition steps at 320, 460, 530, and 635 K, characterize the evolution of the weight loss, with a continuous weight loss between the first and the third decomposition steps. The change in the slope of the TG curve, corresponding to the second decomposition step at 460 K, is small and can only be observed in the first derivative of the curve. The weight loss after the third decomposition step at 530 K amounts to 17.22%, and after the fourth step at 635 K, to 18.61%. The latter value is in agreement with the calculated weight loss of 18.48%, if α-MoO_3 is assumed to be the decomposition product of the starting material $(NH_4)_6Mo_7O_{24}\times4H_2O$. During the first decomposition step, two endothermic DTA signals can be distinguished. The third decomposition step also shows endothermic character, while the second and fourth steps are exothermic. With the exception of the first step, which

begins with the evolution of water only, all steps are accompanied by the evolution of water and ammonia. The TG curve and the corresponding DTA signals for the decomposition of AHM in pure helium are almost identical to those obtained for the decomposition under a 20% O_2 atmosphere at the same heating rate of 5 K/min. The only difference is the slightly greater total weight loss of 18.95% after the last decomposition step at 635 K, instead of 18.61%.

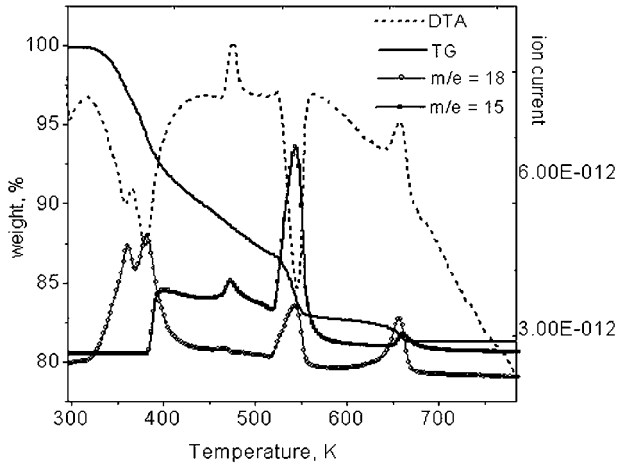

Figure 4. Evolution of the weight loss during decomposition of ground AHM in 20% oxygen in helium, together with MS signals for H_2O and NH_2^- and DTA signal (no axis inscription for the DTA signal). Heating rate: 5 K/min, flow rate: 100 mL/min

The influence of the different heating rates on the TG curve is shown in Figure 5. Lowering the heating rate from 5 K/min to 0.5 K/min does not affect the overall shape of the TG curve, however, the decomposition steps occur at lower temperatures and the weight loss prior to the third decomposition step increases. When the heating rate is increased from 5 K/min to 15 K/min, the overall shape of the TG curve changes. At this heating rate (15 K/min), the second decomposition step is accompanied by a visible change in the slope of the TG curve, resulting in a discernible stage. The total weight loss before the third decomposition step is less at the higher heating rate, and after the third decomposition step the weight loss increases from 17.22% to 18.03%. The total weight loss after the last step remains unchanged. All the decomposition steps take place at higher temperatures, except for the last step.

The influence of the heating rate and the gas flow on the TG curve is shown in Figure 6. A similar effect is observed on changing from a flowing to a static gas phase, as is seen on increasing the heating rate, i.e. lower weight loss at a given temperature and more distinct steps. A combination of accelerating the heating rate and a static gas phase results in a TG with four distinct decomposition steps, each resulting in a distinct stage. The corresponding weight loss for the steps is 6.63, 11.21, 18.03, and 18.6%. The weight

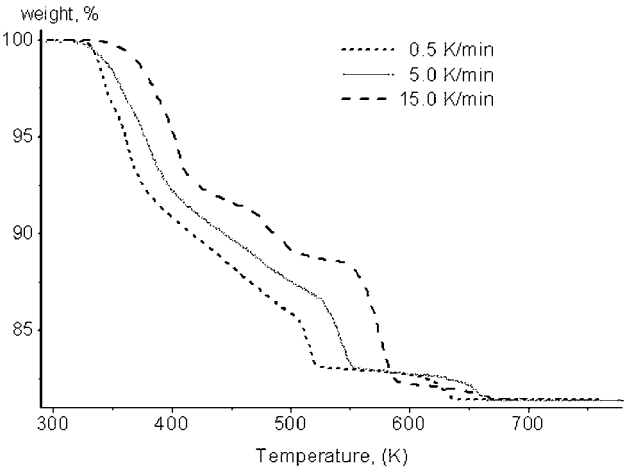

Figure 5. Comparison of the weight loss during decomposition of AHM in 20% oxygen in helium, flow rate 50 mL/min, with heating rates of 0.5, 5, and 15 K/min

loss for the first step is in excellent agreement with the calculated weight loss for the decomposition of AHM into ammonium decamolybdate (6.68%), and the second step corresponds to the formation of ammonium tetramolybdate with a weight loss of 11.09%.

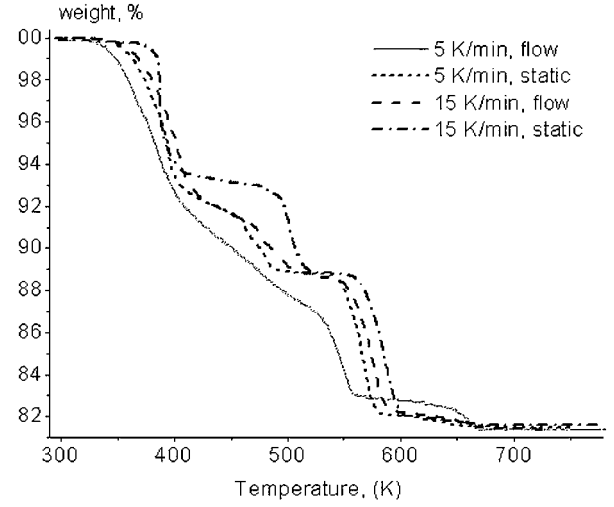

Figure 6. Comparison of the weight loss during decomposition of AHM in 20% oxygen in helium, flow rate 50 mL/min, with heating rates 5 and 15 K/min, and during decomposition of AHM in static air with heating rates of 5 and 15 K/min

The DTA signals in Figure 7 indicate that the exothermic character of the second decomposition step in Figure 4 is changed to an endothermic signal as the decomposition step becomes more pronounced due to the more rapid heating and static conditions as described above. Similarly, the exothermic signal of the last decomposition step becomes less distinct or is missing.

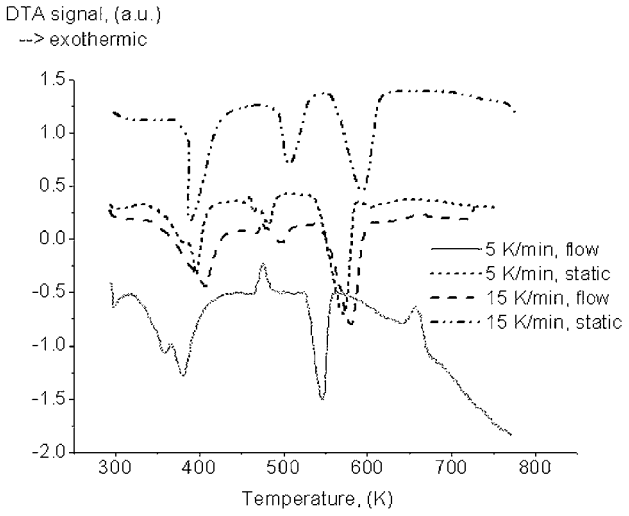

Figure 7. Comparison of the DTA signals, which belong to the TG curves shown in Figure 6. The DTA signals of the decomposition of AHM, 50 mL/min, 20% oxygen in helium, 0.5 K/min, are not shown, due to their weakness

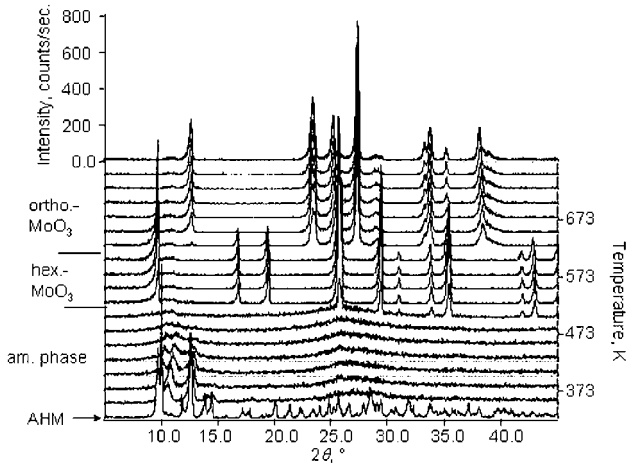

Figure 8. Evolution of the X-ray diffraction pattern during decomposition of AHM in 20% oxygen in helium. room temp. 770 K; effective heating rate: 0.1 K/min, Temperature held every 25 K for measurement; flow rate: 100 mL/min. The phases formed are indicated in the figure

In situ XRD and in situ XAS

Decomposition in 20% Oxygen

Figure 8 shows the evolution of the diffraction patterns during the decomposition of ground AHM in 20% oxygen with an effective heating rate of 0.1 K/min. Three distinct steps are visible in the diffraction patterns. In the first pattern at 320 K, changes from the expected pattern of AHM at room temperature are already observed, indicating that the decomposition has started. The patterns up to 420 K show a rapid decrease in crystallinity, and at 420 K show an X-ray amorphous phase. At 520 K, the formation of a new phase is observed which is identified as hexagonal $[H(_2O/NH_3)](MoO_3)_3$ [ICSD 62163], see Figure 1 (see D, denoted as hexagonal MoO_3 in the following). The splitting of the diffraction peak at approximately 25.7° 2θ with increasing temperature, can be explained by an expansion along the *a* and *b* axes. At 600 K, the hexagonal MoO_3 is transformed into α-MoO_3 [ICSD 35076]. Refinement of the lattice parameter of α-MoO_3 at 770 K affords a = 3.98(5) Å [3.96 Å], b = 14.222(3) Å [13.855 Å], c = 3.69(1) Å [3.69 Å] (the values in brackets are the initial values from the single crystal data [ICSD 35076] at room temperature). The variation of the lattice parameters indicates an anisotropic thermal expansion, which has also been reported by Kierkegard (1964).[33] The XRD investigations in 20% oxygen were performed with both, long and short ranges of 2θ in the XRD measurements, i.e. with effective heating rates of 0.1 K/min and 1 K/min. No differences are observed in the phases formed and the corresponding temperatures with the different effective heating rates.

Figure 9 (see A) shows the in situ XRD patterns obtained during the decomposition of AHM in 20% oxygen and with an effective heating rate of 1 K/min (short range of 2θ). The evolution of the radial-distribution-function {[FT(χ(*k*))],

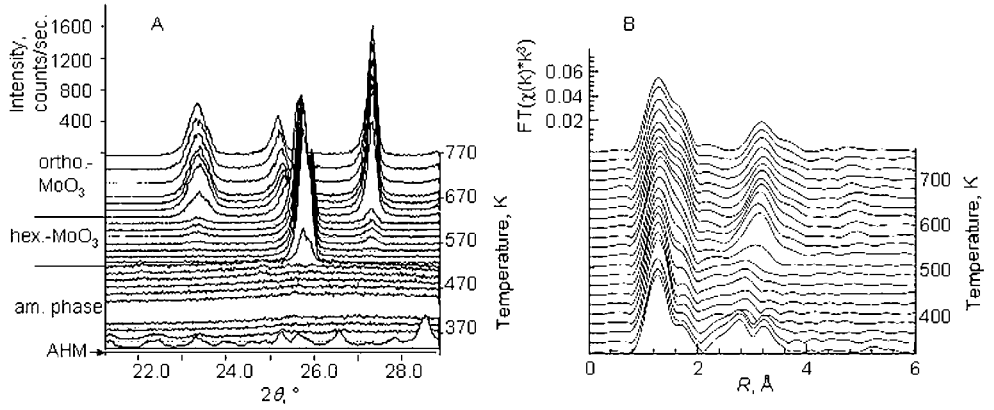

Figure 9. **A**: Evolution of the X-ray diffraction pattern during decomposition of AHM in 20% oxygen in helium. room temp. 770 K; effective heating rate: 1 K/min, Temperature held every 25 K for measurement; flow rate: 100 mL/min. **B**: Evolution of the radial distribution function (RDF) during decomposition of AHM in 20% oxygen in helium. Heating rate: 5 K/min, flow rate: 40 mL/min. The phases formed are indicated in the figure

RDF} from the corresponding in situ XAS experiment is presented in Figure 9 (see B). At the start of the decomposition process, the RDF corresponds to that of AHM. At about 345 K, the RDF exhibits a pronounced decrease in amplitude of the shells above 2 Å, indicating a loss of structural order. A comparison of the RDFs obtained between 450 K and 550 K and the RDF of crystalline ATM (the experimental RDF of ATM at 500 K is displayed in Figure 10) shows an agreement in the nodes and a comparable shape of the curve, and despite some small differences in the amplitudes, indicates a similar short-range order. At 520 K, a distinct change in the RDF occurs, corresponding to the phase change observed from the XRD data. However, in contrast to the XRD data, the RDF at about 600 K does not indicate the formation of a new phase. Despite the lack of changes in the RDF at 600 K, the simultaneously obtained MS data reveal the evolution of water and ammonia at 600 K, hence indicating a decomposition step. Although the hexagonal MoO_3 and the α-MoO_3 possess different long-range structures (see Figure 1, D and E), the pair distribution functions of the two phases within 6 Å are very similar, as is expected for phases which share the same structural features, as indicated in Figure 1. An overview of the bond lengths and coordination numbers of the two phases is given in Table 3. XAFS refinements on the RDFs between 520 K and 770 K, employing paths calculated with the FEFF7 code for either one of the two phases, result in similar distances (±0.05 Å). In Figure 11, the experimental RDF at 670 K is shown, together with a refinement using phases and amplitudes calculated for α-MoO_3.

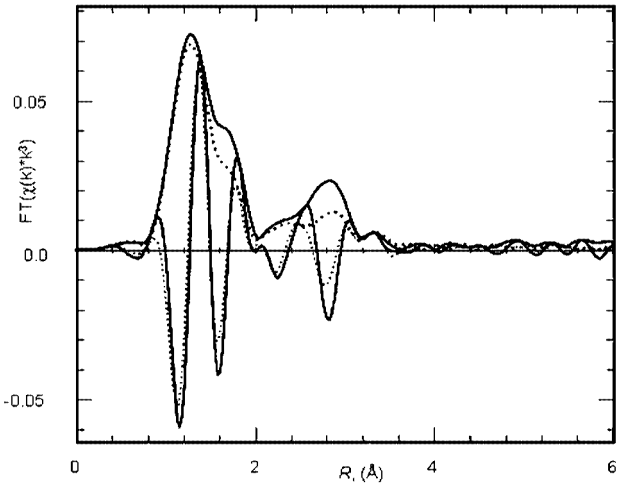

Figure 10. Comparison of the radial distribution function measured at 500 K during the decomposition in 20% oxygen (—) and the radial distribution function of ATM (· · · · ·)

Decomposition in Pure Helium

In Figure 12, A, diffraction patterns measured during the decomposition of AHM in pure helium with an effective heating rate of 1 K/min are presented. Figure 12, B shows the RDFs obtained from XAS measurements during the decomposition of AHM in pure helium. The evolution of the diffraction patterns for temperatures up to 600 K is similar to that observed for the decomposition of AHM in 20% oxygen. At temperatures above 600 K, the pattern of α-MoO_3 begins to show broad shoulders that can be identified as poorly crystallized Mo_4O_{11} (both monoclinic and orthorhombic). Mo_4O_{11} crystallizes with increasing temperature, without a decrease in the absolute intensity of α-MoO_3. The ratio between the monoclinic and orthorhombic Mo_4O_{11} phases changes from about 1:1 to 3:1 during crystallization. At 620 K, the evolution of the RDF during the decomposition of AHM in pure helium with a heating rate of 5 K/min exhibits a phase change, in contrast to the decomposition of AHM in 20% oxygen. The RDF of the phase formed at 620 K remains unchanged on further heating, i.e. there is no change in the short-range order with increasing temperature, in contrast to the changes in the long-range order observed with XRD. The evolution of the edge-shift with temperature, corresponding to the evolution

Table 3. Comparison of the distances between the central molybdenum atom and the surrounding atoms and coordination numbers of α-MoO_3 and hexagonal MoO_3

α-MoO_3			Hexagonal MoO_3		
Mo−O	1	1.671	Mo−O	1	1.645
Mo−O	1	1.734	Mo−O	1	1.687
Mo−O	2	1.948	Mo−O	2	1.941
Mo−O	1	2.251	Mo−O	1	2.210
Mo−O	1	2.332	Mo−O	1	2.378
Mo−Mo	2	3.438	Mo−Mo	2	3.299
Mo−O	2	3.552	Mo−O	2	3.563
Mo−O	2	3.554	Mo−O	2	3.694
Mo−Mo	2	3.696	Mo−Mo	2	3.726
Mo−O	1	3.764	Mo−O	1	3.755
			Mo−O	2	3.866
Mo−Mo	2	3.963	Mo−Mo	2	4.034
Mo−O	2	4.002			

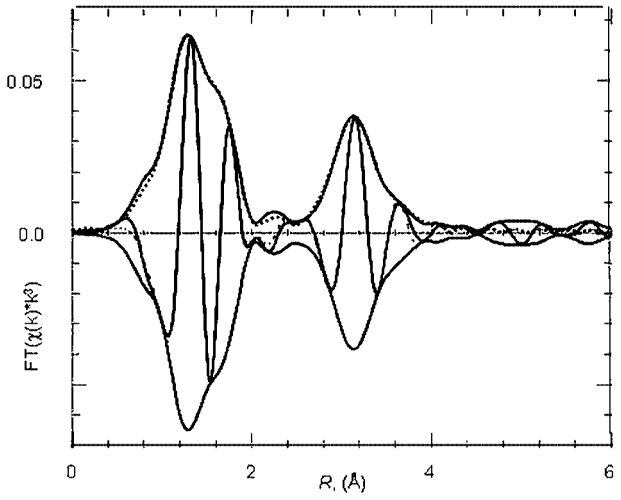

Figure 11. RDF of the decomposition in 20% oxygen in helium at 670 K (—) and the fit result of the simulation with single crystal data (· · · · ·). (*R*-value of the fit: 4.2)

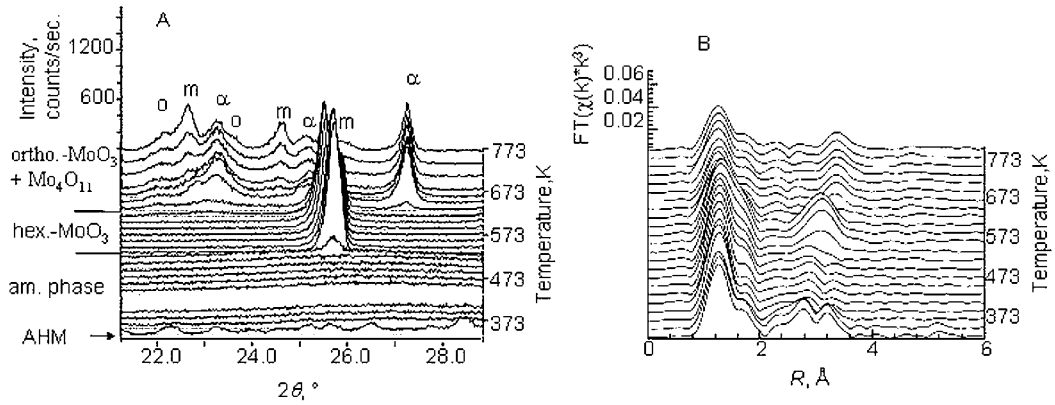

Figure 12. A: Evolution of the X-ray diffraction pattern during decomposition of AHM in helium. room temp. 770 K; temperature held every 25 K for measurement; effective heating rate: 1 K/min, flow rate: 100 mL/min. o: orthorhombic Mo_4O_{11}, m: monoclinic Mo_4O_{11}, α: orthorhombic MoO_3. B: Evolution of the RDF during decomposition of AHM in helium. Heating rate: 5 K/min, flow rate: 40 mL/min. The phases formed are indicated

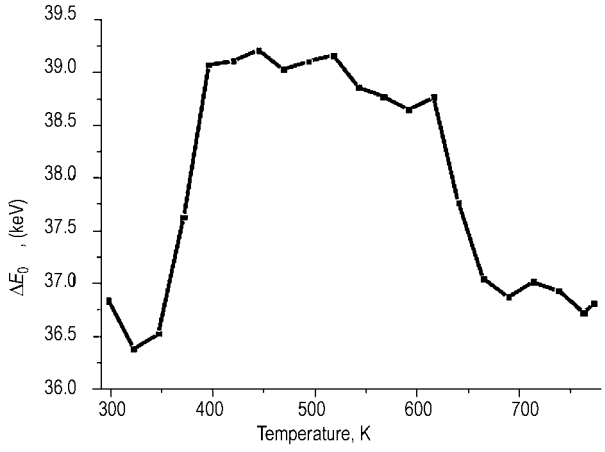

Figure 13. Evolution of the edge-shift with temperature from in situ XAS data of the decomposition of AHM in helium

of the radial distribution functions in Figure 12, B, is shown in Figure 13.

Decomposition in 5% Propene

The evolution of the diffraction patterns measured during the decomposition of AHM in 5% propene in helium with an effective heating rate of 1 K/min is shown in Figure 14, A. The corresponding RDFs are presented in Figure 14, B. For temperatures up to 600 K, the evolution of diffraction patterns is similar to that observed for the decomposition of AHM in pure helium or in 20% oxygen. At 620 K, poorly ordered orthorhombic and monoclinic Mo_4O_{11} is formed as intermediates. Subsequently, these phases are reduced to MoO_2, and at 700 K, the reduction to MoO_2 is complete. MoO_2 remains unchanged on further heating. In order to characterize the Mo_4O_{11} formed, this phase was isolated in situ, by stopping the flow of propene at the temperature of its formation, thus preventing further reduction to MoO_2. The evolution of the diffraction pat-

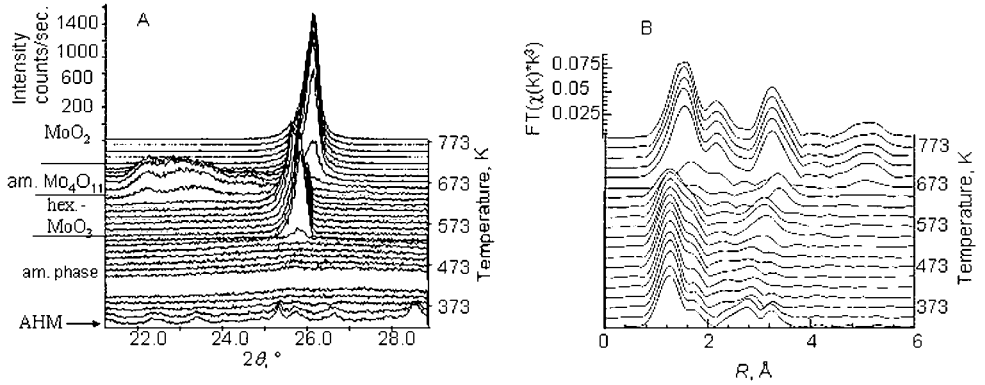

Figure 14. **A**: Evolution of the X-ray diffraction pattern during decomposition of AHM in 5% propene in helium. room temp. 770 K; temperature held every 25 K for measurement; effective heating rate: 1 K/min, flow rate: 100 mL/min. B. Evolution of the RDF during decomposition of AHM in 5% propene in helium. Heating rate: 5 K/min, flow rate: 40 mL/min. The phases formed are indicated

terns in the temperature range from 700 K to 770 K shows progressive crystallization of Mo_4O_{11}. A small amount of α-MoO_3 is also detected, and its absolute intensity remains constant with increasing temperature. The ratio between monoclinic and orthorhombic Mo_4O_{11} changes from about 1:2 to 1:1 during crystallization.

The evolution of the RDF during decomposition in 5% propene is similar to that during the decomposition in helium up to ca. 600 K. At 620 K, the RDF during the decomposition in 5% propene indicates a phase change. The phase formed is rapidly transformed into MoO_2, and can be identified at 645 K. The MoO_2 is identified by simulation of the RDF with an extended fine structure calculated from single crystal data.

Decomposition in Hydrogen

Figure 15, A shows the evolution of the diffraction patterns measured during the decomposition of AHM in 5% hydrogen with an effective heating rate of 1 K/min. Up to 520 K, the evolution of the diffraction patterns is similar to those described above. At 520 K, α-MoO_3 is obtained, in contrast to the decomposition processes in oxygen, helium, or propene where hexagonal MoO_3 is detected at 520 K. The α-MoO_3 formed possesses a strong preferred orientation which can be described as platelets with a (110) basal plane, according to the model of March.[34] This is different from the common (010) texture effects for α-MoO_3. The reduction of this phase to MoO_2 begins at 655 K, and at 745 K, the formation of Mo_4O_{11} is detected. Under these condition only the orthorhombic phase of Mo_4O_{11} is observed.

Evolution of the RDF of AHM during decomposition in 20% hydrogen is shown in Figure 15, B. The evolution of the RDF up to 620 K is similar to that in helium, and to that in 20% oxygen in helium. At about 600 K, the RDF of α-MoO_3 and/or hexagonal MoO_3 can be identified by comparison of the experimental RDF with a theoretical RDF of α-MoO_3. From 620 K to 770 K, the RDF changes continuously, corresponding to the formation of MoO_2.

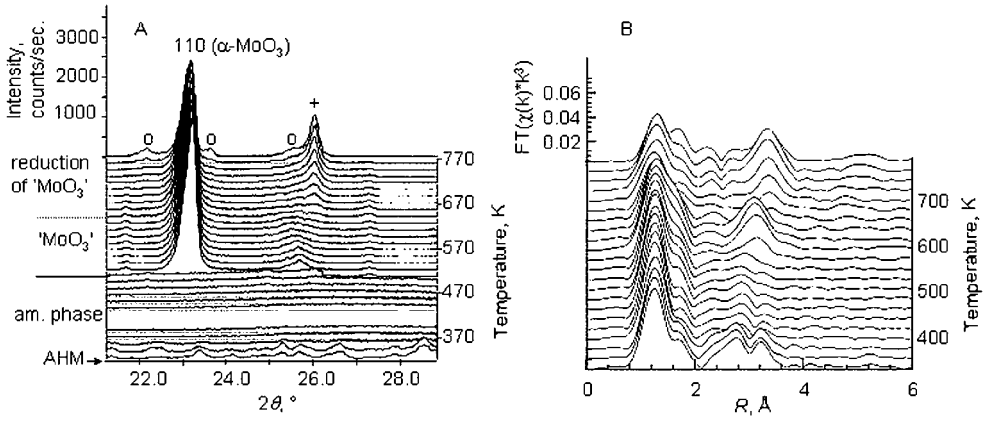

Figure 15. A: Evolution of the X-ray diffraction pattern during decomposition of AHM in 5% H_2 in helium. room temp. 770 K; temperature held every 25 K for measurement; effective heating rate: 1 K/min, flow rate: 100 mL/min. o: orthorhombic Mo_4O_{11}, +: MoO_2. B: Evolution of the RDF during decomposition of AHM in 20% H_2 in helium. Heating rate: 5 K/min, flow rate: 40 mL/min. The phases formed are indicated

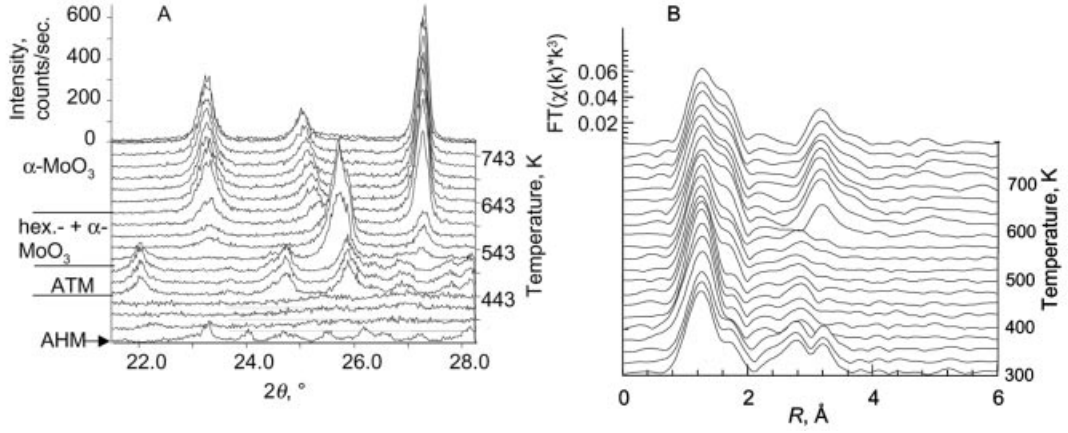

Figure 16. A: Evolution of the X-ray diffraction pattern during decomposition of AHM in static air. room temp. 770 K; temperature held every 25 K for measurement; effective heating rate: 1 K/min. B: Evolution of the RDF during decomposition of AHM in static air. Heating rate: 5 K/min, flow rate: 40 mL/min. The phases formed are indicated in the figure

Decomposition in Static Air

In Figure 16, the evolution of the diffraction patterns (1 K/min) and the RDFs measured during the decomposition of AHM in static air (5 K/min) are shown. Analysis of the XRD data shows that after the formation of an X-ray amorphous phase, ammonium tetramolybdate {ATM, $(NH_4)_2Mo_4O_{13}$, [ICSD 68562]} crystallizes at about 450 K. At 550 K, ATM decomposes into hexagonal MoO_3 and α-MoO_3. At 600 K, hexagonal MoO_3 transforms into α-MoO_3.

The evolution of the RDFs of AHM during decomposition in static air is similar to that during the decomposition in 20% O_2 (Figure 9, B). The formation of either hexagonal or α-MoO_3 can be seen at 640 K, instead of 620 K as in the decomposition in 20% O_2. During decomposition, the temperatures corresponding to the transformation of ATM to α-MoO_3/hexagonal MoO_3 in static air obtained from the XRD analysis are different from those obtained from the evolution of the RDFs (550 and 640 K, respectively). These differences may be attributed to a combination of the differences in the heating rates (1 or 5 K/min for XRD or XAS, respectively), and the differences in the reactor volume, which, under static conditions, may affect the gas phase composition.

Discussion

The experiments presented were performed to elucidate a reaction scheme for the decomposition of ammonium heptamolybdate, AHM, and to determine the effect of the gas phase composition, heating rate, and gas phase flow rate on the decomposition pathway. The emphasis herein was to obtain phase sequences from a phenomenological analysis of in situ experiments under controlled and comparable conditions. The results show that the decomposition scheme and the products formed are strongly influenced by the composition of the gas atmosphere in which the decomposition process takes place. Both the type of gas feed to the system, and the degree to which gas phase products are removed during the decomposition are important. These dependencies, hitherto not systematically recognized, and the knowledge of the sequence of phases formed during the various paths of decomposition explain the differences in the results which have been reported in the literature, and described in the introduction of this paper.

The TG/DTA experiments reveal that the pathway of the decomposition, i.e. the number of decomposition stages (Figures 4, 5, and 6) and the exothermicity or endothermicity of the step (DTA, Figure 7), depend on the heating rate and the gas flow rate. These observations suggest that all the reaction steps for the formation of α-MoO_3 from AHM are kinetically controlled. The extrinsic control variables, i.e. the processes at the gas-solid interface, including the transport of molecules and energy, are important for the reaction sequences. The intrinsic parameters, such as non-stoichiometry or morphology of the precursor, are not ruled out as additional control variables, however, these parameters were not investigated here.

The decomposition can be controlled, by the gas flow rate and the heating rate, to proceed through two phenomenologically different decomposition pathways: one with an extended region of continuous weight loss after the first decomposition step, denoted as Pathway 1; or alternatively through four distinct decomposition stages, denoted as Pathway 2 (Figures 4−6). Intermediate pathways in which the first and second decomposition stages are not pronounced can also be observed. Both pathways are characterized by DTA signals, and by the MS signals of water and ammonia, which indicate a decomposition process that occurs in four steps.

The heating rate and the gas flow rate affect the decomposition process in a similar manner, as indicated by the TG curves. The common parameter which influences the decomposition process is the partial pressure of the gas phase decomposition products, water and ammonia. The temperature at which decomposition occurs is dependent on the partial pressures of the gas phase products, which in turn is dependent on the heating rate and/or gas flow rate. The partial pressures of the gas phase products determine their availability for interaction with the solid. Decreasing the heating rate or increasing the gas flow rate reduces the partial pressure of ammonia and water and allows the decomposition to proceed at lower temperatures without the formation of distinct stages. Conversely, increasing the heating rate and/or decreasing the reactant gas flow rate increases the partial pressure of ammonia and water in the gas phase, stabilizes intermediate phases, and hence results in distinct stages. Under these conditions the decomposition progresses with distinct steps and stages. A similar correlation between the decomposition pathway and the interaction of the gas phase decomposition products with the base material has also been discussed by Maciejewski et al. (2000) for the decomposition of cobalt oxalate dihydrate.[35] They found that the primary gas- and solid-phase products reacted in secondary gas-solid and gas-gas reactions. Similarly, we suggest that the crystallization processes of the molecular structures of the intermediates after the first and second decomposition step, ammonium decamolybdate (possibly X-ray amorphous phase A), and ammonium tetramolybdate, may require water and/or ammonia as ligands. The crystallization of these intermediates results in the process of polycondensation (the formation of hexagonal MoO_3 and/or α-MoO_3) occurring at higher temperatures. The formation of hexagonal MoO_3 decreases with the formation of crystalline ATM, and thus appears to be induced by the low partial pressure of gaseous water and ammonia.

The kinetic reaction control discussed above would suggest that the effect of reactant gas composition on the decomposition pathway be studied at low heating rates, conditions under which product gases are purged and gas phase diffusion limitations are minimized. Such conditions allow analysis of the decomposition by structurally sensitive in situ XRD and in situ EXAFS experiments. Figure 5 indic-

ates that no qualitative changes are introduced into the sequence of events at low heating rates. Differences in the onset temperatures of the phase changes observed can be expected (≈ 20 K), because of the different heating rates.

From in situ XRD and XAS measurements, the sequence of phase transformations corresponding to the decomposition steps was elucidated. Decomposition in flowing reactants (20% oxygen, (Figure 9), pure helium, (Figure 10), and in 5% propene, (Figure 11), all proceed by a reaction scheme denoted as Pathway 1 (effective heating rate of 1 K/min for XRD and 5 K/min for XAS). The XAS data for the decomposition in oxygen suggest that the X-ray amorphous phase, present after the second decomposition step, is similar to ATM. On the basis of the XAS data, the X-ray amorphous phase has to be divided into two categories, X-ray amorphous phase A, formed after the first decomposition step at ca. 340 K, and X-ray amorphous phase B, formed after the second decomposition step at ca. 470 K. The relatively low barrier for the transition between the two amorphous phases explains the continuous weight loss observed in the TG curves (Figure 4). The sequence of phases formed is (i) AHM, as the starting phase, (ii) X-ray amorphous phase A, at ca. 340 K, (iii) X-ray amorphous phase B (ATM) at 470 K, (iv) amorphous phase B is transformed into hexagonal MoO_3 at 520 K, and (v) final products, which differ according to the reducing potential of the gas phase [α-MoO_3 (O_2), Mo_4O_{11} (He), or MoO_2 (propene)].

Pathway 1:

$$\text{AHM} \xrightarrow{340\ \text{K}} \text{X-ray amorphous phase A} \xrightarrow{470\ \text{K}} \text{B(ATM)} \xrightarrow{520\ \text{K}} \text{hex.}MoO_3 \xrightarrow{635\ \text{K}} \text{products}$$

The temperatures given for the decomposition steps should be considered only as reference points. They are a function of, not only the atmosphere, but also the heating rate and the gas flow rate.

The decomposition of AHM in 20% oxygen results in α-MoO_3, decomposition in helium results in α-MoO_3 and highly disordered Mo_4O_{11}, which recrystallizes with increasing temperature, and decomposition in 5% propene results in highly disordered Mo_4O_{11}, which is eventually reduced to MoO_2. The formation of highly dispersed Mo_4O_{11}, together with α-MoO_3 in the final step of the decomposition in helium is confirmed by the in situ XAS data (RDFs), which shows no change in the short-range structure with increasing temperature. The evolution of the corresponding edge-shift (Figure 13) reveals that the reduction takes place mainly during the decomposition of hexagonal MoO_3. A slight increase in the reduction with temperature is then observed, which is due to the mobility of lattice oxygen in this temperature region.[41] The changes observed by XRD after the decomposition of hexagonal MoO_3 are mainly due to recrystallization of Mo_4O_{11} with increasing temperature, and the formation of Mo_4O_{11} from MoO_3 and MoO_2.[29] The apparent oxidation during the decomposition of AHM at approximately 370 K (Figure 13) corresponds to the loss of NH_3 and H_2O during the formation of the amorphous phases (A+B), and thus oxidation of the remaining molybdenum oxide clusters. The Mo-*K* edge-shift observed during the decomposition in helium is representative for all decomposition conditions studied. However, under an oxidizing atmosphere (20% O_2 in helium), no reduction occurs during the decomposition of hexagonal MoO_3.

For the decomposition of AHM in a hydrogen containing atmosphere (Figure 15), Pathway 1 has to be modified. The XRD results indicate that the first decomposition step in hydrogen proceeds according to Pathway 1. The third decomposition step, however, yields MoO_3 with an unusual texture, instead of hexagonal MoO_3. With increasing temperature, α-MoO_3 is subsequently reduced to MoO_2.

The decomposition of AHM under static conditions follows a reaction scheme denoted as Pathway 2: (i) AHM, (ii) X-ray amorphous phase A, ca. 370 K, (iii) ATM is formed at ca. 500 K, followed by (iv) α-MoO_3 and hexagonal MoO_3, ca. 600 K, and (v) the decomposition of hexagonal MoO_3 to α-MoO_3 at 635 K. Since the influence of the heating rate may be more pronounced in a static atmosphere, larger differences were observed in the onset temperatures of the phase changes detected by in situ XRD and in situ XAS.

Pathway 2:

$$\text{AHM} \xrightarrow{370\ \text{K}} \text{X-ray amorphous phase A} \xrightarrow{500\ \text{K}} \text{ATM} \xrightarrow{635\ \text{K}} \alpha\text{-}MoO_3$$
$$\xrightarrow{600\ \text{K}} \text{hex.} + \alpha\text{-}MoO_3$$

Structural Relationships Between Intermediates and Products

Following the given sequence of phases, the transformation from the cluster structure of AHM to the three-dimensional MoO_3 structure can be described as a polycondensation. In the structural sequences of the two monomers, hepta- and decamolybdate, and the one-dimensional oligomer, tetramolybdate, the structural unit of 6 Mo-O octahedra is preserved, as indicated in Figure 1. In the tetramolybdate, however, the octahedra in this 6 membered unit are tilted (Figure 1, C). Nevertheless, for structural rearrangement between these 3 phases, considerable mass transport has to be assumed. For the transition from the heptamolybdate to the decamolybdate, a complete rearrangement of the clusters is required. In the decamolybdate and in the tetramolybdate, the clusters, and thus the Mo-O octahedra, are all uniquely oriented, neglecting the slight tilt in the tetramolybdate. This unique orientation of the octahedra is retained in hexagonal and α-MoO_3. The density of the phases hepta-, deca-, and tetramolybdate are 2.46, 2.84, and 3.32 g/cm^3, respectively (not including NH_3 and H_2O molecules).

The water and ammonia ligands in AHM play an important role in the transformation process. In the AHM structure, all the NH_4^+ and H_2O ligands differ in their coordination to the molybdenum-oxygen clusters (some bridging,

some singly coordinated). However, since the loss of NH_4^+ is not stoichiometric from one phase to another and since the structural relationships between the phases are not obvious, it is difficult to deduce which of the ligand molecules is being removed during the individual transformation steps.

The polymers, α-MoO_3 and hexagonal MoO_3, possess no readily visible structural relationships with the monomers and the oligomer, and thus a reconstructive phase transformation has to be assumed. Hexagonal and α-MoO_3 can be described as two different arrangements of the same structural subunits. These subunits are chains of edge-sharing distorted Mo-O octahedra, which are orientated along the *c* axis in both structures, as indicated in Figure 1. In α-MoO_3, these chains are connected along the *a* axis via edge-sharing of the octahedra, forming a layer structure. In hexagonal MoO_3, the chains are arranged around a three-fold axis via edge-sharing of the octahedra, forming a three-dimensional network. The resulting density of α-MoO_3, 4.7 g/cm^3, is higher than that of hexagonal MoO_3, 3.97 g/cm^3, calculated for the structures (not including NH_3 and H_2O molecules).

The X-ray amorphous phase A in Pathway 1 and 2 could not be identified with the data available. Isothermal decomposition of AHM over extended periods of time (up to eight days) produced only amorphous phases or phase mixtures unsuitable for the identification of the X-ray amorphous phase A. With respect to the observation of ammonium decamolybdate in the literature, besides the role of the ammonia and water ligands in the kinetic inhibition of the formation of sufficiently crystalline ammonium decamolybdate, two structural features may hinder the formation of crystalline decamolybdate. The first is the necessary rearrangement of the clusters in a way that all Mo−O octahedra exhibit the same orientation, as described above. Secondly, in ammonium decamolybdate, two out of ten molybdenum atoms are coordinated by oxygen in a four-fold manner, rather than in a six-fold manner. The rearrangement of the Mo-O octahedra is observed in the formation of crystalline ATM, hexagonal MoO_3 and α-MoO_3. However, molybdenum is not coordinated by oxygen in a four-fold manner in any of the crystalline phases detected.

A Unifying Decomposition Scheme

A schematic representation of decomposition Pathways 1 and 2 is shown in Figure 17. In comparison with the results reported in the literature (Table 1), Pathway 2 is in good agreement with the in situ study 6. A few differences should be noted. They are the formation of ATM, together with the formation of hexagonal MoO_3 at approximately 445 K, and only hexagonal MoO_3 is detected without α-MoO_3during the third decomposition stage. These differences may be due to the limited 2θ range used for the XRD analysis in study 5. No ammonium decamolybdate is observed in study 5, which is in agreement with the study presented here. If an intermediate pathway between Pathway 1 and Pathway 2 is achieved (depending on the experimental conditions), only a small amount of crystalline ammonium decamolybdate may be formed. The agreement of the results of study 6 with those of this work indicates significant differences between the phases identified from in situ and ex situ experiments.

Considerable differences can be seen between this work and the other studies included in Table 1, which were primarily performed ex situ. With the exception of study 8, the other studies also identified ammonium tetramolybdate in the second decomposition stage, albeit in this study it is also found in an amorphous form under conditions which favors Pathway 1. Hexagonal MoO_3 formed during step three of Pathway 2 has only been reported in studies 5, 6, and 7. However, in study 5, hexagonal MoO_3 was prepared ex situ , from aqueous solution, in order to verify the results of the phase analysis of the third decomposition stage. Hexagonal MoO_3 is reported in the literature[35−38] to be metastable, which may be a reason that it is not detected in some ex situ studies. So far we have not succeeded in preparing hexagonal MoO_3 by decomposition of AHM under controlled conditions. Only mixtures of hexagonal and α-MoO_3 were obtained. Furthermore, the temperatures given for the formation of α-MoO_3 in studies 2, 3, 4, and 8 actu-

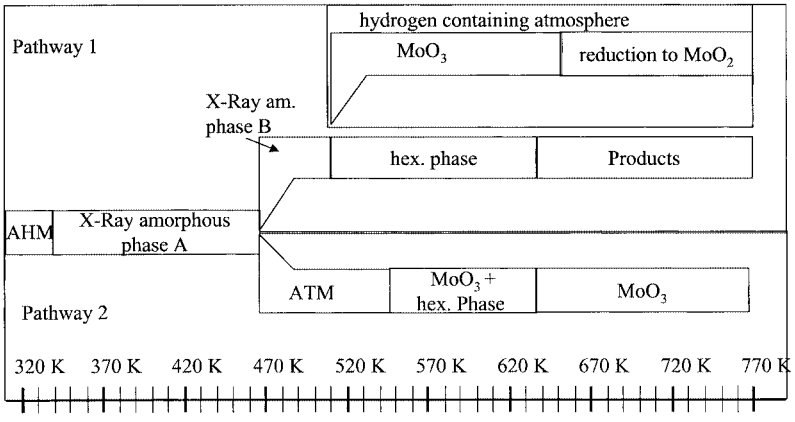

Figure 17. Schematic representation of the different pathways of the decomposition of AHM

ally correspond to step three in Pathway 2, where a mixture of hexagonal and α-MoO_3 is obtained.

With respect to the use of AHM as a catalyst precursor in the production of molybdenum oxide (MoO_{3-x}) based catalysts, the results show that it is possible, not only to control the reduction state but also the phase composition of the products. Apparently, this control can be most efficiently exerted at temperatures below ca. 520 K, where the molecular precursors persist with water as a spacer and ammonia as a counterion. In the temperature range from 610 K to 650 K, where molybdenum oxide catalysts exhibit the onset of catalytic activity, and hence are employed in the partial oxidation reactions of alkenes, the decomposition product obtained consists of partially reduced MoO_3 and mixtures of different oxides, rather than pure and defect-free MoO_3. In addition, this temperature range coincides with the onset of sufficient oxygen mobility in the molybdenum oxide lattice, a prerequisite for partial oxidation activity. This is in agreement with our previous results, that under partial oxidation reaction conditions, "MoO_3" corresponds to a partially reduced molybdenum oxide phase, probably with a considerable amount of shear-type defects in the regular structure. (For more detailed information see ref.[41] and references therein.)

This study demonstrates that control of the decomposition of AHM is possible. It is clear that the heating rate and reactant gas flow rate are coupled under the conditions investigated here. These parameters both function through their ability to affect the partial pressure of the gas phase decomposition products, which in turn control the decomposition path. This result indicates that it may be possible to direct the decomposition with a more complete control of the gas phase composition. Specifically, this control my be accomplished by purging with mixtures of product and/or reactant gases, with rates sufficient to minimize gas phase diffusion limitations and to allow only differential changes in the gas composition over the solid. This type of control could additionally be used to decouple the H_2O and NH_3 partial pressures, which are otherwise intrinsically coupled by the stoichiometry of the decomposition reactions.

Conclusion

The influence of the reactant atmosphere, and the heating rate and the gas flow rate on the decomposition of AHM has been shown. The results indicate that the decomposition scheme is sensitive to changes that affect the partial pressures of the gas phase decomposition products. In fact, differences in the gas phase product partial pressures, due perhaps to different flow rates, heating ramps, or experimental setups, are adequate to explain the differences in the results reported in the literature. The response of the system to changes in the gas phase decomposition product partial pressures is mainly important for the formation of hexagonal MoO_3, which depends on the preceding crystallization of ATM. Depending on the gas phase composition, two different Pathways can be distinguished:

Pathway 1 (low concentration of gaseous decomposition species at a given temperature)

(i) AHM; (ii) (≈ 335 K) X-ray amorphous phase A, (iii) (≈ 470 K) X-ray amorphous phase B (amorphous ATM), (iv) (≈ 520 K) hexagonal MoO_3; (v) (≈ 650 K) products (as a function of atmosphere, α-MoO_3, Mo_4O_{11}, or MoO_2).

Pathway 2 (high concentration of gaseous decomposition species at a given temperature)

(i) AHM, (ii) (≈ 350 K) X-ray amorphous phase A; (iii) (≈ 470 K) ATM.

(iv) (≈ 570 K) hexagonal MoO_3 + α-MoO_3; (v) (≈ 650 K) α-MoO_3.

Experimental Section

Ammonium Heptamolybdate Tetrahydrate: Ammonium heptamolybdate tetrahydrate, AHM, $(NH_4)_4Mo_7O_{24}\times 4\ H_2O$, was used as purchased (Aldrich, Analysis: total metallic impurities < 200 ppm). Phase purity and crystalline structure were verified by XRD and found to agree well with the simulated XRD powder patterns generated from single crystal data [ICSD 4153]. IR spectra of AHM were recorded with a FT-IR (Perkin−Elmer 2000), using the KBr disc technique. Chemical purity was confirmed by X-ray fluorescent analysis, which showed that there were no detectable impurities.

X-ray Diffraction: In situ XRD studies were performed with a Stoe STADI-P diffractometer (Ge secondary monochromator, Cu K_α radiation, Bragg−Brentano geometry), which is equipped with a Bühler HDK S1 high temperature cell (400 mL). Analysis of the gas phase was performed with a quadrupole mass spectrometer, QMS 200 (Pfeiffer), using a selective mass scan mode (≈ 12 s per scan). Measurements were performed in the temperature range from 300 K to 770 K, employing 2θ ranges of either 21.25−28.75° (short-range) or 5−45° (long-range). The shorter 2θ range was used to obtain more dynamic information, the longer 2θ range was sufficient for identification of the different phases. The short-range was selected in a 2θ region containing diffraction peaks of adequate intensities of all potential phases. With a heating rate of 5 K/min, diffractograms were recorded every 25 K for the long 2θ range, or every 15 K for the short 2θ range, resulting in effective heating rates of about 1 K/min or 0.1 K/min, respectively. The total gas flow rate was set to 100 mL/min. The concentrations of reactant gases in helium were 20% for oxygen, 5% for hydrogen, and 5% for propene. 30 mg of sample were suspended with acetone on the sample holder. A detailed description of the XRD set up can be found in Günter (2001).[28]

XRD studies of the ex situ samples were performed with a Stoe STADI-P diffractometer (Ge primary monochromator, Cu-K_α radiation, Debye−Scherrer geometry) equipped with a position sensitive detector.

Analysis of diffraction patterns was conducted using PowderCell for Windows, Version 2.3, and Stoe WinXPOW, Version 1.03. The ICDD (International center for diffraction data, former JC,PDS) database and the ICSD (Inorganic crystal structure database) were used for phase analysis.

X-ray Absorption Spectroscopy: In situ XAS measurements were performed in a flow reactor with a volume of ca. 4 mL, used in transmission geometry. Measurements were performed in a temperature range from 300 K to 770 K, with a heating rate of 5 K/·min.

The acquisition time was 4.5 minutes per spectrum, resulting in a temperature resolution of 22.5 K. Total flow rates of gases was set to 20 mL/min. Analysis of the gas phase was performed with a quadrupole mass spectrometer, QMS 200 (Pfeiffer), with a time resolution of ca. 12 s per scan using a selected mass scan mode. The AHM was mixed with boron-nitride (7 mg of AHM, 30 mg of BN) and pressed with a force of 1 ton into self-supporting pellets with a diameter of 5 mm. The resulting edge jump at the Mo-*K*-edge averages $\Delta\mu_x \approx 2$. For details of the experimental set up, see Ressler (2000).[29]

XAS measurements were performed at the Mo-*K* edge (19.999 keV) at the Hamburger Synchrotronstrahlungslabor, HASYLAB, beamline X1. The storage ring operated at 3.6 GeV with injection currents of 150 mA. A Si(311) double crystal monochromator was used.

Data analysis of the XAS spectra was performed using the software WinXAS 2.1.[30] The spectra were energy calibrated with respect to a molybdenum foil reference spectrum. Background subtraction and normalization were done using first order polynomials to fit the pre-edge and EXAFS region. Spectra were converted to k space using an E_0 defined as the second inflection point in the Mo-*K* edge. Atomic absorption, μ_0, fitting was performed using a cubic spline with 7 nodes and was optimized by minimization of peaks at low (< 1 Å) R value in the Fourier transformed $\chi(k)$.

Refinement of the local structure was performed in *R* space using the FEFF7 code[31] for calculation of amplitudes and phases for clusters with a radius of 6 Å around the absorber atom. The clusters were calculated from single crystal data of hexagonal and α-MoO_3 using the software Atoms.[32] All single scattering paths were considered, as well as multiple scattering paths with weights greater than 5% and a maximum of 4 legs. Fits were carried out in a range of ca. 0.4−3.9 Å, which resulted in 12 single scattering paths (SS) and 19 multiple-scattering paths (MS) for α-MoO_3 and hexagonal MoO_3. The number of free running parameters used during fitting was restricted to 19, well below the maximum of 28 allowed by the Nyquist theorem for the data range used. The free running parameters were (i) one Debye temperature for molybdenum and one for oxygen, (ii) one E_0 each for molybdenum and oxygen, (iii) - the distances of all SS paths, constrained to a maximum shift of ±0.1 Å, (iv) one third cumulant expansion factor for molybdenum and oxygen each and (v) the overall damping factor S_0.

TG/DTA: Weight loss measurements and differential thermal analysis (TG/DTA) were performed with a Seiko Instruments SSC/5200 (Pt-Rh 13% thermocouple). Measurements in 20% oxygen in helium and with a flow rate of 50 mL/min were carried out at heating rates of 0.5, 5, and 15 K/min. Three different flow rates 100 mL/min, 50 mL/min and no flow (static air), were examined with an atmosphere of 20% oxygen in helium and with a heating rate of 5 K/min. Additionally, a measurement in pure helium with a heating rate of 5 K/min and a flow rate of 50 mL/min was performed. Gas phase analyses were performed by using a Pfeiffer QMS 200 mass spectrometer.

Acknowledgments

We acknowledge the Hamburger Synchrotronstrahlungslabor HASYLAB for providing beam-time for this work. T. Ressler thanks the Deutsche Forschungsgemeinschaft "DFG" for financial support (Habilitationsstipendium). The authors are grateful to Prof. R. Schlögl for extended discussions and continuous support.

[1] A. J. Hegedüs, K. Sasvári, J. Neugebauer, *Z. Anorg. Allg. Chemie* **1957**, *293*, 56.
[2] M. Onchi, E. Ma, *J. Phys. Chem.* **1963**, *67*, 2240.
[3] E. Ma, *Bull. Chem. Soc. Jpn.* **1964**, *37(2)*, 171.
[4] E. Ma, *Bull. Chem. Soc. Jpn.* **1964**, *37(5)*, 648.
[5] M.-J. Schwing-Weill, *Bull. Soc. Chim. Fr.* **1967**, *10*, 3795.
[6] A. B. Kiss, P. Gadó, I. Asztalos, A. J. Hegedüs, *Acta Chim. Acad. Sci. Hung.* **1970**, *66(3)*, 235.
[7] A. Louisy, J. M. Dunoyer, *Bull. Soc. Chim. Fr.* **1970**, *67*, 1390.
[8] I. K. Bhatnagar, D. K. Chakrabarty, A. B. Biswas, *Indian J. Chem.* **1972**, *10*, 1025.
[9] Z. M. Hanafi, M. A. Khilla, M. H. Askar, *Thermochimica Acta* **1981**, *45*, 221.
[10] K. Isa, H. Ishimura, *Bull. Chem. Soc. Jpn.* **1981**, *54*, 3628.
[11] M. Topić, A. Moguš-Milanković, *Chroatica Chem. Acta* **1984**, *57(1)*, 75.
[12] I. B. Sharma, S. Batra, *J. Therm. Anal.* **1987**, *34*, 1273.
[13] W. J. Yong, *Thermochimica Acta* **1990**, *158*, 183.
[14] D. P. Shashkin, P. A. Shiryaev, M. Y. Kutyrev, O. V. Krylov, *Kin. Catal.* **1993**, *34(2)*, 302.
[15] S. A. Halawy, M. A. Mohamed, *J. Chem. Tech. Biotechnol.* **1993**, *58*, 237.
[16] A. A. Said, S. A. Halawy, *J. Therm. Anal.* **1994**, *41*, 1075.
[17] A. A. Said, *Thermochimica Acta* **1994**, *236*, 93.
[18] C. I. Cabello, I. L. Botto, H. J. Thomas, *Thermochimica Acta* **1994**, *232*, 183.
[19] M. Bi, H. Li, W.-P. Pan, W. G. Lloyd, B. H. Davis, *Thermochimica Acta* **1996**, *284*, 153.
[20] J.-C. Valmalette, R. Houriet, H. Hofmann, J.-R. Gavarri, *Eur. J. Solid State, Inorg. Chem.* **1997**, *34*, 317.
[21] Y. Zhoulan, L. Xinhai, C. Qiyuan, *Thermochimica Acta* **2000**, *352−353*, 107.
[22] C. Thomazeau, V. Martin, P. Afanasiev, *Appl. Cat. A* **2000**, *199*, 61.
[23] R. Murugan, H. Chang, *J. Chem. Soc., Dalton Trans.* **2001**, *20*, 3125.
[24] J.-L. Li, T. Inui, *Appl. Catal. A* **1996**, *137*, 105.
[25] J. Haber, E. Lalik, *Catalysis Today* **1997**, *30*, 119.
[26] R. K. Grasselli, *Catalysis Today* **1999**, *49*, 141.
[27] E. M. Gaigneaux, M. J. Genet, P. Ruiz, B. Delmon, *J. Phys. Chem. B* **2000**, *104*, 5724.
[28] M. M. Günter, T. Ressler, R. E. Jentoft, B. Bems, *J. Catal.* **2001**, *203*, 133.
[29] T. Ressler, R. E. Jentoft, J. Wienold, M. M. Günter, O. Timpe, *J. Phys. Chem. B* **2000**, *104*, 6360.
[30] T. Ressler, *J. Synchrotron Rad.* **1998**, *5*, 118.
[31] J. J. Rehr, C. H. Booth, F. Bridges, S. I. Zabinsky, *Phys. Rev. B* **1994**, *49*, 12347.
[32] B. Ravel, *J. Synchrotron Rad.* **2001**, *8*, 314.
[33] P. Kierkegaard, *Arkiv Kem.* **1964**, *23(21)*, 223.
[34] A. March, *Z. Kristallogr.* **1932**, *81*, 285.
[35] M. Maciejewski, E. Ingier-Stocka, W.-D. Emmerich, A. Baiker, *J. Thermal Anal.* **2000**, *60*, 735.
[36] J. L. Garin, J. M. Blanc, *J. Solid State Chem.* **1985**, *58*, 98.
[37] N. A. Caiger, S. Crouch-Baker, P. G. Dickens, G. S. James, *J. Solid State Chem.* **1987**, *67*, 369.
[38] J. Guo, P. Zavalij, M. S. Whittingham, *J. Solid State Chem.* **1995**, *117*, 323.
[39] I. L. Botto, C. I. Cabello, H. J. Thomas, *Mater. Chem. Phys.* **1997**, *47*, 37.
[40] I. L. Botto, A. C. Garcia, H. J. Thomas, *J. Phys. Chem. Solids* **1992**, *53(8)*, 1075.
[41] T. Ressler, J. Wienold, R. E. Jentoft, T. Neisius, *Journal of Catalysis*, **2002**, *210*, 67.

Received May 27, 2002
[I02275]

3-Metalla-1,2-dioxolanes and Their Reactivity

Monique Krom,[a] Theo P. J. Peters,[a] Ruud G. E. Coumans,[a] Timo J. J. Sciarone,[a] Johan Hoogboom,[a] Sandra I. ter Beek,[a] Paul P. J. Schlebos,[a] Jan M. M. Smits,[a] René de Gelder,[a] and Anton W. Gal*[a]

Keywords: Formylmethyl complexes / Metallacycles / N ligands / Oxygenations / Rhodium

The ethene complexes $[M^{I}(CH_2CH_2)]^+$ (M = Ir, Rh) can be oxygenated by molecular oxygen or air in the solid state, to form isolable unsubstituted 3-metalla-1,2-dioxolanes $[M^{III}(CH_2CH_2OO\text{-}\kappa^2C^1,O^2)]^+$. Such selectivity could not be achieved in solution. The stereoselectivity of the oxygenation process is highly dependent on the ligand, the metal and the counterion used. Oxygenation of $[(tpa)M(CH_2CH_2)]PF_6$ {tpa = tri(2-pyridylmethyl)amine; **4**PF_6, **7**PF_6} results in the formation of two isomeric 3-metalladioxolanes, whereas oxygenation of $[(tpa)M(CH_2CH_2)]BPh_4$ (**4**BPh_4, **7**BPh_4) only yields one isomer. Furthermore, oxygenation of [(Metpa)-$Rh(CH_2CH_2)]PF_6$ {**14**PF_6, Metpa = [(6-methyl-2-pyridyl)methyl]bis(2-pyridylmethyl)amine} proved to be much slower than that of $[(tpa)Rh(CH_2CH_2)]PF_6$ (**7**PF_6). The *solid* propene complex $[(tpa)Rh(CH_2CHCH_3)]BPh_4$ (**23**BPh_4) loses propene on reaction with molecular oxygen, and selectively forms the peroxo complex $[(tpa)Rh(\eta^2\text{-}O_2)]BPh_4$ (**24**BPh_4). The obtained 3-metalla-1,2-dioxolanes rearrange, both in the solid state and in solution, to formylmethyl hydroxy complexes on exposure to photons or protons. The isomeric 3-rhoda-1,2-dioxolanes $[(tpa)Rh(CH_2CH_2OO\text{-}\kappa^2C^1,O^2)]^+$ **8a**$^+$ and **8b**$^+$ differ in reactivity. On exposure of a solution of **8a**PF_6/**8b**PF_6 to glass-filtered daylight, isomer **8b**$^+$ rearranges to form the formylmethyl hydroxy complex **9b**$^+$. This rearrangement is three times faster than the rearrangement of **8a**$^+$ to **9a**$^+$. The iridadioxolanes are much more reactive than the corresponding rhodadioxolanes, whereas the iridium formylmethyl hydroxy complexes are less reactive than the corresponding rhodium formylmethyl hydroxy complexes. The tpa formylmethyl hydroxy complexes react reversibly with carbon dioxide to form formylmethyl hydrogen carbonate complexes.

(© Wiley-VCH Verlag GmbH & Co. KGaA, 69451 Weinheim, Germany, 2003)

Introduction

Transition metal catalyzed oxidation of olefins is one of the most important methods of converting these readily available and cheap starting materials into useful chemicals. For economical and environmental reasons, molecular oxygen or air are the most interesting oxidants. However, not much is known about the mechanisms involved in transition metal catalyzed olefin oxidations. In an attempt to investigate the validity of some of the earlier proposed mechanisms, we have investigated the oxygenation of rhodium and iridium ethene complexes by air.

3-Metalla-1,2-dioxolanes (κ^2-C^1,O^2-2-peroxyethyl metal complexes, see Structure) have been proposed as intermediates in the catalytic oxygenation of olefins by group VI and VIII metals.[1] These reactions include epoxidation[1d–1f] and oxidation to ketones.[1a–1c] Mimoun et al. have proposed that the rhodium-catalyzed olefin oxidation proceeds via a peroxo ethene complex. Insertion of ethene into the rhodium dioxygen bond then results in the formation of a 3-rhoda-1,2-dioxolane complex, which subsequently decomposes to acetaldehyde and a rhodium oxo complex (Scheme 1).[1a]

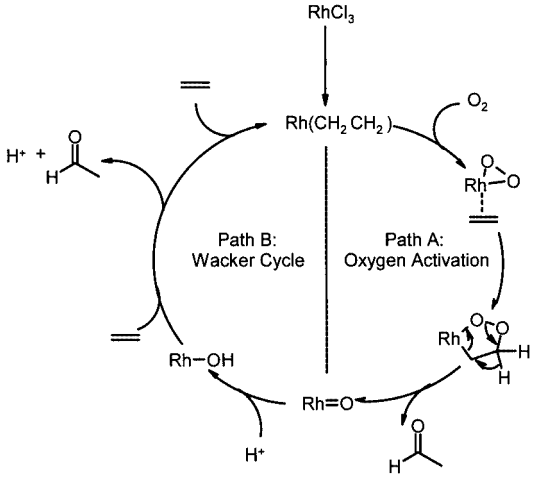

Scheme 1. Mechanism proposed by Mimoun for the rhodium catalyzed oxidation of ethene to acetaldehyde[1a]

[a] Department of Inorganic Chemistry, University of Nijmegen
Toernooiveld 1, 6525 ED Nijmegen, The Netherlands
Fax: (internat.) +31-24355-3450
E-mail: gal@sci.kun.nl

Supporting information for this article is available on the WWW under http://www.eurjic.org or from the author.

In the molybdenum catalyzed oxidation of olefins, Mimoun proposed that decomposition of 3-molybdena-1,2-dioxolanes results in the formation of a molybdenum oxo complex and ethylene oxide.[1e][1f] However, calculations by Frenking et al. have indicated that this would lead to the formation of acetaldehyde instead of ethylene oxide.[2]

3-Metalla-1,2-dioxolanes containing an *unsubstituted* 3-metalla-1,2-dioxolane fragment [M(κ^2C^1,O^2-CH_2CH_2OO-)] have not been reported before. However, tri- and tetra-substituted 3-platina-1,2-dioxolanes, with substituents that prevent β-hydrogen transfer, have been obtained from the reaction of [$(PPh_3)_2Pt(\eta^2$-$O_2)$] with electron-deficient olefins, and have been structurally characterized (**1** and **2**).[3] These *substituted* platinadioxolanes cannot be used as models for the further study of proposed metalladioxolane intermediates.

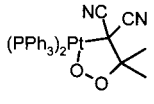

1

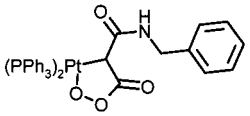

2

We now report on the synthesis of *unsubstituted* 3-metalla-1,2-dioxolanes, through the oxidation of rhodium and iridium ethene complexes by air or molecular oxygen. Oxidation by molecular oxygen was sometimes necessary due to the reactivity of the oxidation products towards water or carbon dioxide from the air. Rearrangement of the 3-metalla-1,2-dioxolanes to formylmethyl hydroxy complexes is also reported. Part of this work has been communicated previously.[4]

Results and Discussion

Synthesis of Ethene Complexes

Rhodium tpa Complexes

The complexes [(tpa)Rh(CH_2CH_2)]BPh_4 {**7**BPh_4, tpa = tris(2-pyridylmethyl)amine} and [(Metpa)Rh(CH_2CH_2)]-PF_6 {**14**PF_6, Metpa = [(6-methyl-2-pyridyl)methyl]bis(2-pyridylmethyl)amine} were synthesized according to a literature procedure. $NaBPh_4$ and KPF_6 were used to precipitate **7**BPh_4 and **14**PF_6, respectively.[5]

Iridium tpa Complexes

Bis(ethene) complexes **3**BPh_4 and **3**PF_6 were synthesized from in situ generated $IrCl(C_2H_4)_4$, tpa, and $NaBPh_4$ or KPF_6, respectively. Whereas a mono-ethene complex ($\mathbf{7}^+$) is formed for rhodium, a bis(ethene) complex is initially obtained for iridium, probably due to the better π-back-donating ability of iridium. However, an ethene molecule is easily lost from the bis(ethene) complex; when N_2 is bubbled through a solution containing $\mathbf{3}^+$, the mono-ethene complex $\mathbf{4}^+$ is obtained (Scheme 2). This reaction is reversible; when ethene is bubbled through a solution containing $\mathbf{4}^+$, the bis(ethene) complex $\mathbf{3}^+$ is obtained.

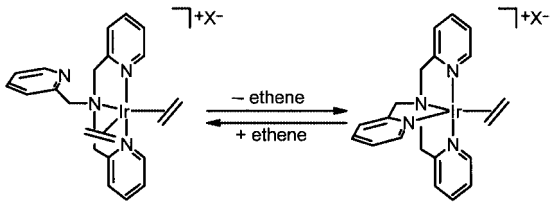

$\mathbf{3}^+$ $\mathbf{4}^+$

Scheme 2. Reactivity of bis(ethene) complex **3**PF_6 and mono-ethene complex **4**PF_6

The structure of complex $\mathbf{3}^+$, as determined by X-ray diffraction, is shown in Figure 1. The complex has a trigonal bipyramidal conformation and contains the tpa ligand in a meridional tridentate coordination mode. This coordination mode has not been observed before for bis(olefin) metal complexes stabilized by bpa-type ligands {bpa = bis(2-pyridylmethyl)amine}; in such complexes the bpa-type tridentate nitrogen donor ligand usually adopts a facial coordination mode.[6,7] The ^1H NMR spectrum of $\mathbf{3}^+$ at room temperature shows four triplets and its ^{13}C NMR spectrum shows four singlets for the ethene fragments, indicating that the fragments are not rotating, probably due to steric hindrance.

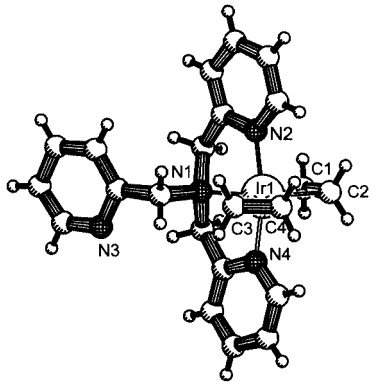

Figure 1. X-ray structure of bis(ethene) complex $\mathbf{3}^+$

Rhodium N_4Me_2 Complexes

To test the influence of the nitrogen donor ligand on the reactivity of the ethene complexes, bis(ethene) complex $\mathbf{5}^+$ (Scheme 3) was synthesized as the PF_6-salt from [{$(ethene)_2RhCl$}$_2$], N_4Me_2 and KPF_6. Complex $\mathbf{5}^+$ contains the rigid macrocyclic N_4 ligand, *N*,*N*′-dimethyl-2,11-diaza[3,3](2,6)pyridinophane[8] (N_4Me_2). As mentioned earlier, reaction of tpa with $IrCl(C_2H_4)_4$ initially gives a bis(ethene) complex, which easily and reversibly loses one ethene molecule. The same reaction with [{$(C_2H_4)_2RhCl$}$_2$] only produces the mono-ethene complex $\mathbf{7}^+$, even when carried out at low temperature. Rhodium apparently does not bind the second ethene molecule as strongly as iridium. Therefore, the initial formation of the bis(ethene) complex **5**PF_6 with N_4Me_2 was surprising. However, **5**PF_6 also loses an ethene molecule easily (see below). The synthesis of **5**PF_6 is discussed in more detail in the supporting information.

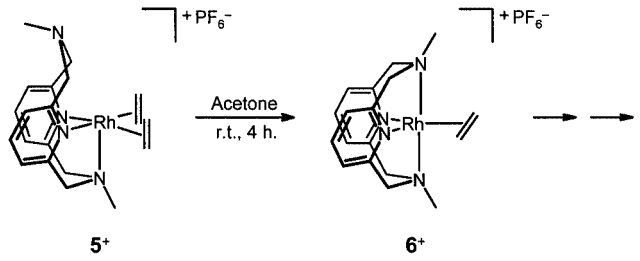

Scheme 3. Loss of ethene from bis(ethene) complex $\mathbf{5}PF_6$

The ^1H NMR and ^{13}C NMR resonances of the vinylic groups of $\mathbf{5}^+$ are broad at room temperature, which indicates the rotation of the ethene fragments. At −60 °C this rotation is frozen, resulting in an ABCD-pattern in the ^1H NMR spectrum. X-ray quality crystals of $\mathbf{5}PF_6$ were obtained by crystallization from acetone/diethyl ether (v/v = 1:3) over a period of nine days at −70 °C. The X-ray structure of the cation $\mathbf{5}^+$ is shown in Figure 2. This is the first reported X-ray structure of a bis(ethene) rhodium complex stabilized by three nitrogen donors.

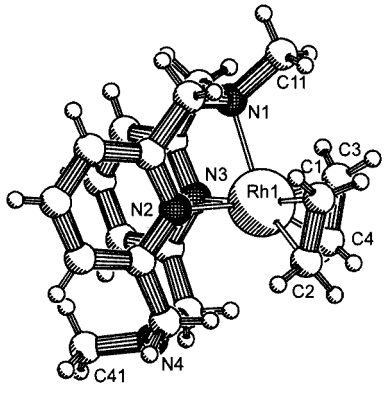

Figure 2. X-ray structure of bis(ethene) complex $\mathbf{5}^+$

Cation $\mathbf{5}^+$ has a pseudo square pyramidal geometry with the amine occupying the apical position, and the N_4Me_2 ligand in a tridentate coordination mode. Three complexes in which this coordination mode is found for N_4Me_2 (or an analogous ligand) have been reported earlier,[9] but usually this ligand adopts a tetradentate coordination mode.[10] In complex $\mathbf{5}^+$, as well as in the earlier reported κ^3-N_4Me_2 complexes,[9] the N_4Me_2 ligand adopts a *syn* (chair-boat) conformation. The X-ray structure of $\mathbf{5}^+$ is discussed in more detail in the supporting information.

Mono-ethene complex $\mathbf{6}PF_6$ is easily obtained by allowing $\mathbf{5}PF_6$ to stand in acetone solution under a nitrogen atmosphere at room temperature for approximately four hours (Scheme 3). This is not a reversible reaction; bubbling ethene through a solution of $\mathbf{6}PF_6$, or exposure of such a solution to an ethene atmosphere does not lead to the formation of $\mathbf{5}PF_6$. The rate and selectivity of the conversion of $\mathbf{5}^+$ to $\mathbf{6}^+$ are highly dependent on the counterion used. Formation of $\mathbf{6}^+$ is slower and more selective if PF_6^- is used as the counterion, instead of BPh_4^-. Furthermore, irrespective of the counterion, the selectivity is higher in acetone than in acetonitrile.

Since a square planar $[(\kappa^3\text{-}N_4Me_2)Rh(C_2H_4)]^+$ structure is not possible for complex $\mathbf{6}^+$ due to the rigidity of the N_4Me_2 ligand, we propose that the ligand has a κ^4-coordination mode, similar to tpa in $\mathbf{7}^+$.[5] Another indication for tetradentate coordination is the fact that the signals for the NMe groups in the ^1H NMR and ^{13}C NMR spectra are at approximately the same chemical shifts [$\delta(^1H)$ = 2.15 ppm, $\delta(^{13}C)$ = 49.8 ppm] as the signals for the coordinated NMe group in $\mathbf{5}^+$ [$\delta(^1H)$ = 2.25 ppm, $\delta(^{13}C)$ = 52.6 ppm].

Complex $\mathbf{6}PF_6$ is not stable in solution at room temperature, and decomposes within hours to a mixture of unidentified products. Thus, the formation of $\mathbf{6}PF_6$ is always accompanied by some decomposition, and analytically pure samples of it and its oxidation products (see below) could not be obtained.

Formation of 3-Metalla-1,2-dioxolanes from Ethene Complexes

Rhodium tpa Complexes

Oxidation of $\mathbf{7}BPh_4$ by air at room temperature *in solution* (acetone, acetonitrile, dichloromethane) results in the dissociation of ethene and the formation of a mixture of unidentified products. In marked contrast, exposure of *solid* $\mathbf{7}BPh_4$ to air for two days results in the formation of 3-rhoda-1,2-dioxolane $\mathbf{8a}BPh_4$ (Scheme 4).[11] A small amount of the hydroperoxy hydroxy complex $\mathbf{25}BPh_4$ is also formed (see below).

The ESI-MS spectrum of $\mathbf{8a}BPh_4$ shows a base peak at m/z = 453, corresponding to $[(tpa)Rh(CH_2CH_2) + O_2]^+$. The ^1H NMR spectrum shows the presence of a $Rh-CH_2-CH_2$ group. The $^3J(H_\alpha,H_\beta)$ coupling constant for this group (6.1 Hz, Table 1) suggests that it is part of a five-membered ring: the coupling constant is intermediate in magnitude between that observed in the four-membered 2-rhodaoxetane ring in $\mathbf{12b}^+$ and the six-membered ring in the rhodium 2-(acetimidoyloxy)ethyl complex $\mathbf{13b}^{2+}$ (Scheme 5).[5]

Crystals of $\mathbf{8a}BPh_4$ suitable for X-ray diffraction were obtained by slow diffusion of diethyl ether into a 1,2-dichloroethane/acetonitrile solution. The unit cell contains two crystallographically independent units, which are almost mirror images. The structure of one of the units is shown in Figure 3. The five-membered ring has an envelope conformation. The puckering of the 3-rhoda-1,2-dioxolane ring is virtually the same as in the 3-platina-1,2-dioxolane ring of **1**.[3a],[12] The average O1−O2 distance [1.500(17) Å] is normal compared with the O−O distances in **1** [1.482(15) Å][3a] and other M−O−O-C compounds (1.40−1.52 Å);[13] the average O2−C2 distance [1.443(10) Å] is also similar to that in **1** [1.407(19) Å] and other M−O−O-C compounds (1.40−1.47 Å).[14]

The nature of the counterion largely influences the selectivity of this solid-gas oxygenation reaction. On changing the counterion of $\mathbf{7}^+$ from BPh_4^- to PF_6^-, a 1:1 mixture of

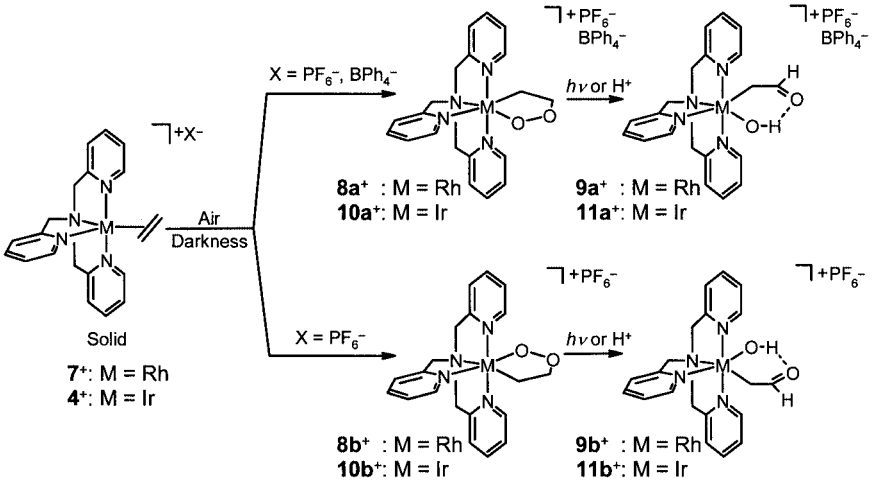

Scheme 4. Formation and rearrangement of 3-metalla-1,2-dioxolanes

Table 1. ^{1}H NMR chemical shifts (ppm) and coupling constants (Hz) of the $RhCH_2CH_nO$ fragments in CD_3CN

Compound	δ(MCH_2)	δ(CH_nO)[a]	$^3J_{H,H}$	$^2J_{H,Rh}$
8a$^+$	2.57(dt)	3.25(t)	6.1	2.4
8b$^+$	3.55 (dt)	3.41(t)	6.1	2.4
10a$^+$	2.03(t)	2.54(t)	6.2	–
10b$^+$	2.69(t)	2.63(t)	6.7	–
16$^+$	2.90(dt)	3.66(t)	6.5	2.5
12b$^+$	2.24(dt)	4.88(t)	7.5	2.5
9a$^+$	2.69(dd)	9.26(t)	5.1	2.9
9b$^+$	3.47(dd)	9.98(t)	4.9	2.9
11a$^+$	3.07(d)	9.21(t)	5.2	–
11b$^+$	3.66(d)	10.11(t)	4.9	–
17$^+$	3.14(dd)	9.57(t)	5.4	3.2
20a^{2+}	3.05(dd)	9.51(t)	4.9	2.7
21a$^+$	3.23(dd)	9.53(t)	4.7	2.5
22a$^+$	3.39(d)	9.46(t)	4.8	–
18$^+$	3.21(dd)	9.70(t)	5.5	2.8

[a] n = 1,2.

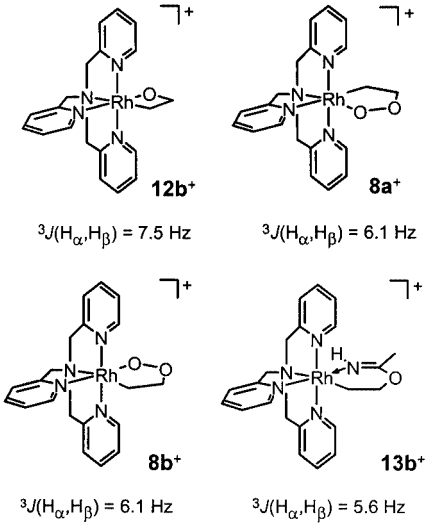

Scheme 5. Typical $^3J(H_\alpha,H_\beta)$ for $Rh-CH_2-CH_2$ fragments in four-membered (**12b**$^+$), five-membered (**8a**$^+$, **8b**$^+$), and six-membered (**13b**$^{2+}$) rings

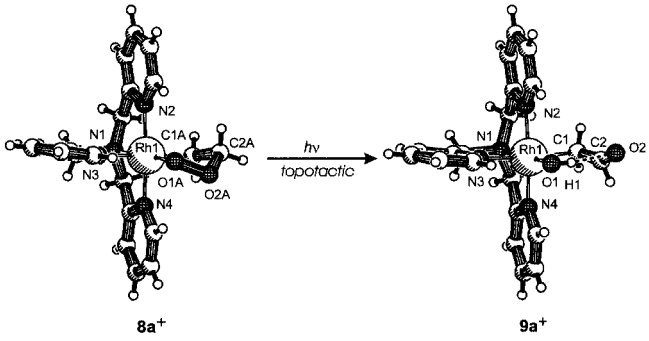

Figure 3. X-ray structures of 3-rhoda-1,2-dioxolane **8a**$^+$ and rhodium formylmethyl hydroxy complex **9a**$^+$

8aPF_6 and a new complex **8b**PF_6 is obtained after exposure to air for two days.[11] The ESI-MS and ^{1}H NMR spectra of the mixture of **8a**PF_6 and **8b**PF_6 in CD_3CN indicate that **8b**$^+$ is the isomeric 3-rhoda-1,2-dioxolane in Scheme 4. The C_α resonances in the ^{13}C NMR spectrum are at δ = 35.0 and δ = 44.8 ppm for **8a**$^+$ and **8b**$^+$, respectively, reflecting the stronger donor capacity of a pyridine versus an amine group (Table 2). The same trend is observed for **9a**$^+$/**9b**$^+$, **10a**$^+$/**10b**$^+$, and **11a**$^+$/**11b**$^+$, which are discussed below.

The NOE contacts in **8a**$^+$ and **8b**$^+$ are consistent with their proposed structures: isomer **8a**$^+$ shows NOE contacts between $Rh-CH_2-CH_2-$ and one proton each of the two equivalent $Rh-N_{amine}-CH_2-$ groups, and between $Rh-CH_2-CH_2-$ and the two equivalent py-H6 atoms; isomer **8b**$^+$ shows NOE contacts between $Rh-CH_2-CH_2-$ and all three py-H6 atoms, and between $Rh-CH_2-CH_2-$ and the two equivalent py-H6 atoms.

Possibly, the different packing in (microcrystalline) **7**BPh_4 and **7**PF_6 leads to the different accessibility of cation **7**$^+$ to O_2. Remarkably, oxidation of **7**$^+$ by hydrogen peroxide only leads to the formation of 2-rhodaoxetane **12b**$^+$ (N_{amine}, *C trans*) (Scheme 5).[5] Thus far, a 2-rhodaoxetane, **12a**$^+$ (N_{amine}, *O trans*), has not been observed.

Besides the influence of the counterion, small ligand changes also have a large effect on the reactivity of *solid* rhodium-ethene complexes towards air. Substitution of one

Table 2. ^{13}C NMR chemical shifts (ppm) and coupling constants (Hz) of the $RhCH_2CH_nO$ fragments in CD_3CN

Compound	δ(M*C*H$_2$)	δ(*C*H$_n$O)[a]	$^1J_{C,Rh}$
8a$^+$	35.0(d)	70.2(s)	25.0
8b$^+$	44.8(d)	72.8(s)	28.8
10a$^+$	15.8(s)	71.1 or 71.8(s)	–
10b$^+$	23.9(s)	71.6(s)	–
16$^+$	30.3(d)	71.7(s)	25
12b$^+$	1.3(d)[b]	78.7(d)	18.4[b]
9a$^+$	26.9(d)	209.0(s)	21.0
9b$^+$	34.5(d)	210.8(s)	25.0
11a$^+$	16.3(s)	209.4(s)	–
11b$^+$	20.7(s)	211.2(s)	–
17$^+$	33.4(d)	207.7(s)	21.2
20a^{2+}	27.8(d)	206.7(d)	20.4
21a$^+$	28.1(d)	210.1(s)	20.7
22a$^+$	14.8(s)	211.1(s)	–

[a] n = 1,2. [b] [D$_6$]Acetone.

Py-H6 of tpa for a methyl group, for example, leads to a large decrease in the reaction rate. According to the ^1H NMR spectrum (Scheme 6), exposure of *solid* **14**PF_6 to pure molecular oxygen for *7 months* results in approximately 45% conversion into a 2:1 mixture of **15a**$^+$ and **15b**$^+$ (the remainder being starting material). Exposure of *solid* **14**BPh_4 to pure molecular oxygen for a similar period of time also results in the formation of a mixture of **15a**$^+$ and **15b**$^+$. This was unexpected since exposure of the analogous complex **7**BPh_4 only results in the formation of isomer **8a**$^+$. Again, different packing in **7**BPh_4 and **14**BPh_4 might be responsible for this difference in selectivity.

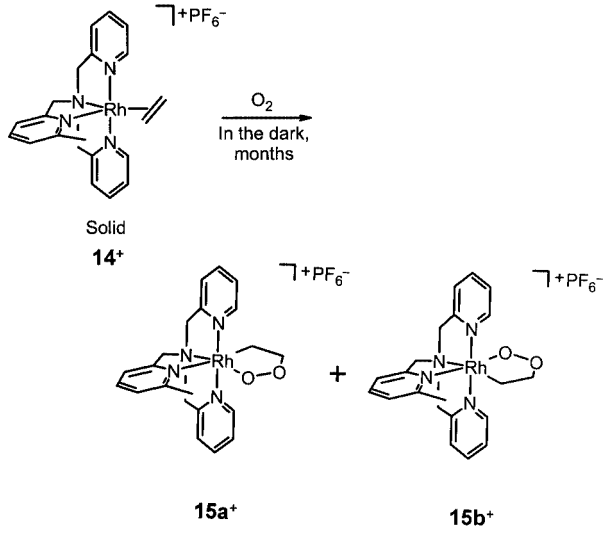

Scheme 6. Oxygenation of rhodium ethene complex **14**PF_6

Iridium tpa Complexes

Exposure of a *solution* of **4**BPh_4 to air leads to a mixture of unidentified products, whereas exposure of *solid* **4**BPh_4 to air leads to the formation of 3-irida-1,2-dioxolane **10a**BPh_4 (Scheme 4). Exposure of *solid* **4**PF_6 to air results in the formation of a mixture of the isomeric iridadioxolanes **10a**PF_6 and **10b**PF_6, in an approximate ratio of 2:5 (Scheme 4). Powder X-ray diffraction spectra of **4**PF_6 and **7**PF_6 show that these complexes are isomorphous, which indicates that the different ratios in which the isomeric 3-rhoda- and 3-iridadioxolanes are formed do not stem from the different packing of the starting materials.

ESI-MS spectra of **10a**BPh_4 and **10a**PF_6/**10b**PF_6 could not be obtained because of the instability of these complexes in solution at room temperature (see below). The ^1H NMR spectra show two triplets for the $Ir-CH_2-CH_2-$ fragment, with $^3J(H_\alpha,H_\beta)$ = 6.2 and 6.7 Hz for **10a**$^+$ and **10b**$^+$, respectively. This indicates that the fragments are part of five-membered rings (Table 1, Scheme 5). The ^1H NMR signals for Ir*C*H_2- and for $-CH_2O-$ were assigned by analogy with the 3-rhoda-1,2-dioxolanes (Table 1).

Rhodium N_4Me_2 Complexes

On reaction of *solid* **6**PF_6 with dioxygen (instead of air; see below), at room temperature in the dark, **16**PF_6 was formed within a few days.[11] The ^1H NMR spectrum of **16**PF_6 shows two double triplets at δ = 2.94 ppm and at δ = 3.70 ppm, indicating the presence of a $RhCH_2CH_2X$ fragment (Table 1). A coupling constant of $^3J_{H,H}$ = 6.5 Hz for these signals indicates that a five-membered ring is formed (Table 1). The ESI-MS spectrum shows a base peak at m/z = 431, which is in accordance with the formation of 3-rhodadioxolane **16**$^+$ (Scheme 7). All attempts to obtain X-ray quality crystals of **16**$^+$ failed, partly because of its instability in solution.

Rearrangement of 3-Metalla-1,2-dioxolanes to Formylmethyl Hydroxy Complexes

Rhodium tpa Complexes

Exposure of microcrystalline **8a**BPh_4 to glass-filtered daylight under N_2 results in the selective conversion into the corresponding rhodium formylmethyl hydroxy complex **9a**BPh_4, in several weeks (Scheme 4). Similarly, exposure of a solution of **8a**BPh_4 in CD_3CN to the glass-filtered light of a high-pressure mercury lamp at −30 °C results in the conversion into **9a**BPh_4. Monitoring of this reaction by ^1H NMR indicates that an optimum yield of 90% **9a**BPh_4 is obtained after 90 minutes of illumination (see Supporting Information).

The ESI-MS spectrum of **9a**$^+$ is similar to that of **8a**$^+$, with the exception of a peak at m/z = 435, which corresponds to the loss of water from the parent cation. Such loss of water in the gas-phase has been observed earlier for the transient formylmethyl hydroxy complex [(MeCN)(Bzbpa-κ^3)Rh(CH_2CHO-κ^1)(OH)]BPh_4 (**19**BPh_4), which is the only other formylmethyl hydroxy complex reported thus far,[15,16] although several other formylmethyl complexes have been reported.[17]

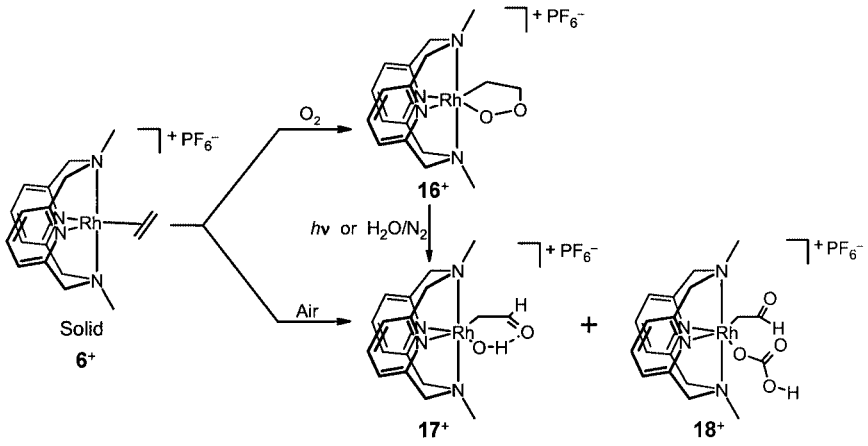

Scheme 7. Formation and rearrangement of rhodadioxolane **16**PF_6 and subsequent reaction with CO_2

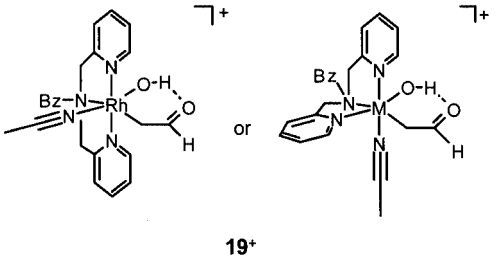

The ^1H NMR and ^{13}C NMR spectra of **9a**BPh_4 show signals typical of a metal-bound formylmethyl group, similar to those found in **19**BPh_4 (Tables 1 and 2).[16] Complex $\mathbf{9a}^+$ shows a strong IR absorption at 1655 cm^{-1}, in accordance with the presence of a carbonyl group.

After repeated attempts to obtain X-ray quality crystals of **9a**BPh_4 had failed, an attempt was made to photochemically convert a single crystal of **8a**BPh_4 to a single crystal of **9a**BPh_4. The crystal that had been used for the X-ray structure determination of **8a**BPh_4 was exposed to glass-filtered daylight for one week and its crystal structure was re-determined. It was found that $\mathbf{8a}^+$ had been fully converted into $\mathbf{9a}^+$ leaving the crystal packing virtually unchanged (a "topotactic" transformation).[18]

The crystal structure of $\mathbf{9a}^+$ shows that the hydroxy group forms a hydrogen-bond with the formyl fragment, thus forming a puckered six-membered ring (Figure 3). The bridging hydrogen (H1) was refined at an O1−H1 distance of 0.80(5) Å [Rh−O1−H1 = 99(4)°] and a H1−O2 distance of 1.92(5) Å [O1−H1−O2 = 168(5)°]. The puckering of the six-membered ring results from the rotation of the formyl fragment around the C1−C2 bond [torsion angle Rh−C1−C2−O2 = −72(3)°]. The crystal structure of $\mathbf{9a}^+$ is discussed in more detail in the supporting information.

We propose that the photochemical rearrangement of $\mathbf{8a}^+$ to $\mathbf{9a}^+$ involves photolysis of the O−O bond, followed by abstraction of a β-hydrogen atom from $-CH_2-CH_2-O^{\cdot}$ by $-O^{\cdot}$ (Scheme 8, a). In the solid state, the puckering of the 3-rhoda-1,2-dioxolane ring positions a β-hydrogen in close proximity of the O1 atom (Figure 3). Therefore, this reaction would not be hindered by the constraints of the lattice. The mechanism, shown in Scheme 8 (see a), is supported by preliminary DFT calculations.[19]

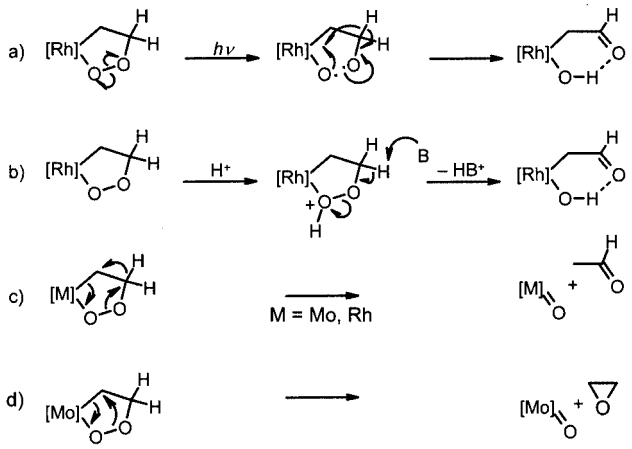

Scheme 8. Proposed mechanisms for rearrangement of 3-metalla-1,2-dioxolanes: a) photochemically, to a formylmethyl hydroxy complex b) proton assisted, to a formylmethyl hydroxy complex c) directly, to an oxo complex species and acetaldehyde[1a,2] and d) directly, to an oxo complex and ethylene oxide[1f]

Analogous to microcrystalline 3-rhoda-1,2-dioxolane **8a**BPh_4, the microcrystalline mixture of the isomeric 3-rhoda-1,2-dioxolanes **8a**PF_6 and **8b**PF_6 (**8a**PF_6/**8b**PF_6) rearranges photochemically to a mixture of the isomeric formylmethyl hydroxy complexes **9a**PF_6 and **9b**PF_6 (**9a**PF_6/**9b**PF_6; Scheme 4). However, **8a**BPh_4 and **8a**PF_6/**8b**PF_6 react differently when exposed to a N_2 atmosphere saturated with H_2O; complex **8a**BPh_4 proved to be stable, whereas **8a**PF_6/**8b**PF_6 rearranges to **9a**PF_6/**9b**PF_6. Since **8a**PF_6/**8b**PF_6 is stable under dry N_2, this reactivity must have been triggered by the presence of H_2O. Since there is no obvious mechanism by which H_2O would directly cause O−O bond breaking in the rhodadioxolane, we considered the possibility that a trace of acid (possibly generated from hydrolysis of a small amount of PF_6^- to $PF_2O_2^-$ and HF) catalyzes the conversion. To investigate proton-assisted ring opening in solution, 0.1 equivalent of the noncoordinating acid $[H(OEt_2)_2]B[C_6H_3(CF_3)_2]_4$ ($HBAr^F_4$) was added to a solu-

tion of **8a**BPh_4 in CD_3CN. In a typical experiment, the ^1H NMR spectrum shows that **8a**$^+$ is converted into the formylmethyl hydroxy complex **8a**$^+$ (87%) within 10 minutes, and a small amount (8%) of the formylmethyl aqua complex **20a**$^{2+}$ (i.e. protonated **9a**$^+$) is also formed.[20] Likewise, addition of 1.1 equivalent of $HBAr^F_4$ to a solution of **8a**BPh_4 results in the formation of **20a**$^{2+}$ in approximately 85% yield within 10 minutes.[20] In the latter case, any **9a**$^+$ formed is apparently directly protonated. This protonation results in a downfield shift of the Rh−CH_2−CHO and Rh−CH_2−C*H*O ^1H NMR signals from δ = 2.69 to δ = 3.05 ppm and from δ = 9.26 to δ = 9.51 ppm, respectively. The base-peak in the ESI-MS spectrum of the obtained solution has the correct isotope distribution pattern and *m*/*z* value (227) for **20a**$^{2+}$. As demonstrated by its formylmethyl ^1H NMR signals, a trace of **20a**$^{2+}$ is also formed in the conversion of *solid* **8a**PF_6/**8b**PF_6 to **9a**PF_6/**9b**PF_6 under N_2 saturated with H_2O. This supports our hypothesis of an acid-catalyzed ring opening.

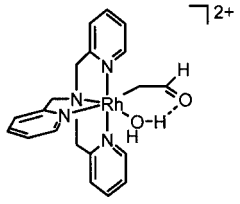

20a^{2+}

A possible mechanism for the acid-catalyzed ring opening is shown in Scheme 8, b. Protonation of **8a**$^+$ at O_α induces heterolytic splitting of the O−O bond, followed by the deprotonation at C_β by an external base and the formation of a carbonyl double bond. This mechanism was supported by preliminary DFT calculations.[19]

The isomeric 3-rhodadioxolanes **8a**$^+$ and **8b**$^+$ clearly differ in their photoreactivity: on exposure of a CD_3CN solution of **8a**$^+$ and **8b**$^+$ to glass-filtered daylight at room temperature, the relative intensities of the ^1H NMR 2-peroxyethyl signals show that the initial reaction rate of **8b**$^+$ is three times faster than that of **8a**$^+$ (Figure 4).

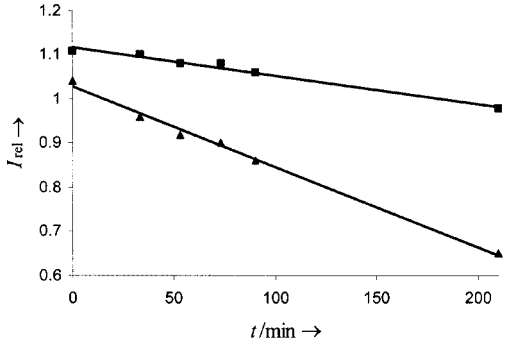

Figure 4. Relative intensities of the 2-peroxyethyl ^1H NMR signals of **8a**$^+$ (■) and **8b**$^+$ (▲) on exposure to glass-filtered daylight

Formylmethyl hydroxy complexes **9a**$^+$ and **9b**$^+$ decompose to a mixture of unidentified products in solution at room temperature on prolonged exposure to light.

Iridium tpa Complexes

Both **10a**$^+$ and **10b**$^+$ rearrange to iridium formylmethyl hydroxy complexes (**11a**$^+$ and **11b**$^+$) on exposure to light. The ESI-MS spectra of **11a**BPh_4 and **11a**PF_6/**11b**PF_6 show the expected base peak at *m*/*z* = 543. For **11a**BPh_4, the daughter ion spectrum from this base peak shows a peak at *m*/*z* = 525, corresponding to the loss of water.

There is a large difference in reactivity between the 3-rhodadioxolanes and the 3-iridadioxolanes: 3-iridadioxolanes rearrange to form formylmethyl hydroxy complexes in solution at room temperature, whereas 3-rhodadioxolanes need to be exposed to light or protons before rearrangement can take place. It is possible that the iridadioxolanes are more sensitive to traces of adventitious acid, e.g. on glass surfaces, than the rhodadioxolanes. Another possibility is that for iridium, water is already a strong enough acid to induce the conversion. Finally, an alternative conversion mechanism, not requiring any acid, may be possible for iridium.

The iridium formylmethyl hydroxy complexes **11a**$^+$ and **11b**$^+$ are stable in CH_3CN solution at room temperature when exposed to light, whereas the rhodium analogues decompose under these conditions.

Rhodium N_4Me_2 Complexes

Both in the presence and absence of visible light, the *solid* mono-ethene complex **6**PF_6 reacts with air, within a few days at room temperature, to form a mixture of two formylmethyl complexes in an approximate ratio of 5:1, according to the ^1H NMR spectrum in CD_3CN. The ESI-MS spectrum of the mixture in CH_3CN shows a base peak at *m*/*z* = 431, in accordance with the presence of the formylmethyl hydroxy complex **17**$^+$, and a peak at *m*/*z* = 475, corresponding to the formylmethyl hydrogen carbonate complex **18**$^+$. Water present in the air probably induces an acid-catalyzed rearrangement of the initially formed dioxolane to a formylmethyl hydroxy complex. Although rearrangement on exposure to a nitrogen atmosphere saturated with water had been observed earlier for the tpa complexes (see above), rearrangement on exposure to air was not observed. Furthermore, the resulting formylmethyl hydroxy complex reacts with carbon dioxide from the air, forming **18**$^+$. This has not been observed for the tpa complexes either. However, exposure of **9a**BPh_4 or **11a**BPh_4 to a CO_2 atmosphere leads to the full conversion into the formylmethyl hydrogen carbonate complexes **21a**BPh_4 and **22a**BPh_4, respectively (Scheme 9). On removal of the CO_2 atmosphere, CO_2 is released and the formylmethyl hydroxy complexes **9a**BPh_4 or **11a**BPh_4 are regenerated. Formation of rhodium and iridium hydrogen carbonate complexes from metal hydroxy complexes and CO_2, and vice versa have been reported before.[21]

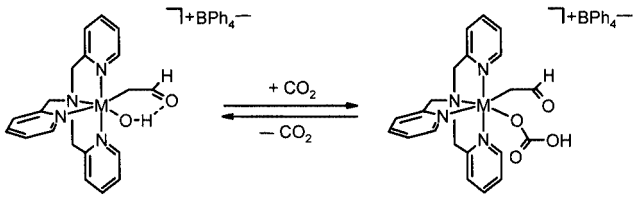

Scheme 9. Reversible reaction of formylmethyl hydroxy complexes $\mathbf{9a}^+$ and $\mathbf{11a}^+$ with CO_2

Exposure of *solid* $\mathbf{16}PF_6$ (obtained from $\mathbf{6}PF_6$ and dioxygen; see above) to visible light and N_2 leads to the conversion into $\mathbf{17}PF_6$, as shown by the ESI-MS, ^1H NMR and ^{13}C NMR spectra in CD_3CN (Tables 1 and 2). Exposure of $\mathbf{16}PF_6$ to water vapour/N_2 also leads to the formation of $\mathbf{17}PF_6$, probably due to the PF_6^- counterion (see above).

Oxidation of a Rhodium Propene Complex to a Peroxo Complex and Its Reactivity towards Water

As mentioned earlier, exposure of *solid* $\mathbf{7}BPh_4$ to air not only produces 3-rhoda-1,2-dioxolane $\mathbf{8a}BPh_4$, but also a small amount of the hydroperoxy hydroxy complex $\mathbf{25}BPh_4$. Exposure of *solid* $\mathbf{7}BPh_4$ to pure dioxygen, however, leads to the formation of $\mathbf{8a}BPh_4$ and a small amount of the peroxo complex $\mathbf{24}BPh_4$. This peroxo complex can be obtained more efficiently by the oxidation of *solid* $[(tpa)Rh(CH_2CHCH_3)]BPh_4$ ($\mathbf{23}BPh_4$) with molecular oxygen (Scheme 10).

Complex $\mathbf{23}BPh_4$ was synthesized from $[\{(ethene)_2RhCl\}_2]$, propene, tpa, and $NaBPh_4$. It is the first reported rhodium propene complex stabilized by a tetradentate nitrogen donor ligand. Propene coordinates less strongly to the rhodium center than ethene, resulting in an easier loss of olefin from the complex and the quantitative formation of $\mathbf{24}BPh_4$ on oxidation with molecular oxygen. Oxidation with air results in a mixture of unidentified products. The reason for this is still unclear. Possibly, further reactions of $\mathbf{24}BPh_4$ with water (see below), and subsequently with CO_2 occur. The ^1H NMR and ^{13}C NMR spectra of $\mathbf{24}BPh_4$ only show signals for the (coordinated) tpa ligand. The ESI-MS spectrum of $\mathbf{24}BPh_4$ shows a base peak at $m/z = 425$, corresponding to $[(tpa)Rh + O_2]^+$, and the loss of O_2 from the parent cation.[22]

Exposure of complex $\mathbf{24}BPh_4$ to a nitrogen atmosphere saturated with water leads to the complete conversion into $\mathbf{25}BPh_4$. The ^1H NMR and ^{13}C NMR spectra of $\mathbf{25}BPh_4$ again only show signals for the (coordinated) tpa ligand. The ESI-MS spectrum shows a base peak at $m/z = 443$, corresponding to $\mathbf{25}^+$, and the loss of H_2O, HO_2, and H_2O_3 from the parent cation. Complex $\mathbf{25}BPh_4$ is the first rhodium hydroperoxy hydroxy complex reported, but other metal hydroperoxy hydroxy complexes have been reported earlier.[23] Analytically pure samples of $\mathbf{24}BPh_4$ and $\mathbf{25}BPh_4$ were not obtained, due to their instability in solution at room temperature. Since the decomposition of $\mathbf{25}BPh_4$ is a problem in solution at −30 °C as well, no ^{13}C NMR spectroscopic data were obtained for this complex.

Conclusions

We have achieved selective oxidation of $[M]^I$(ethene) (M = Rh, Ir) complexes by air or dioxygen to form isolable 3-metalla-1,2-dioxolanes for the first time. Remarkably selective dioxygenation was only achieved for ethene complexes embedded in a crystalline matrix. The reasons for this difference between solid phase reactivity and solution phase reactivity have not yet been elucidated. However, our results clearly indicate that solid-gas reactions should be considered as a useful alternative to conventional solution phase chemistry, not only under heterogeneous conditions (high pressures and temperatures), but also at room temperature and atmospheric pressure.

Small changes have a large effect on the reactivity of the ethene complexes. The dioxygenation of $\mathbf{14}PF_6$ is much slower than of $\mathbf{7}PF_6$. Using a completely different N_4-ligand (N_4Me_2) results in a higher reactivity of not only the ethene

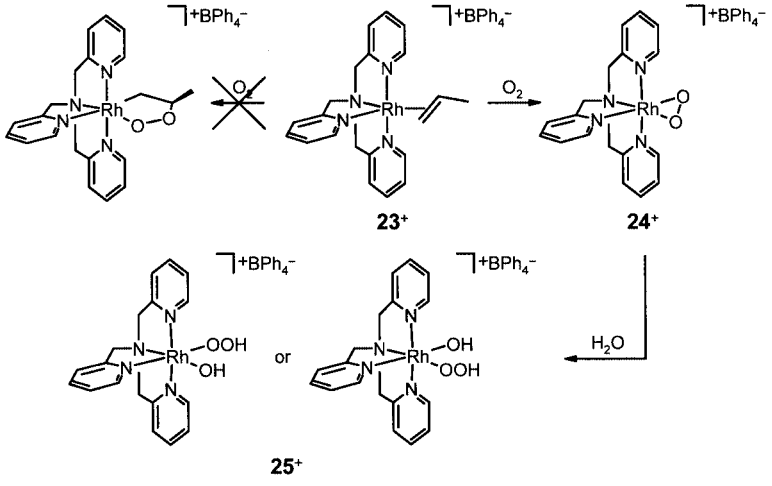

Scheme 10. Reaction of propene complex $\mathbf{23}BPh_4$ with dioxygen

complex, but also of the 3-rhodadioxolane and the formylmethyl hydroxy complex. More interestingly, even the counterion affects the oxidation chemistry; oxygenation of **7**PF_6 results in the formation of two isomeric 3-rhodadioxolanes, whereas oxygenation of **7**BPh_4 only yields one isomer. Thus, it appears that for these solid-gas reactions, new opportunities for reaction tuning exist.

The observed rearrangement of 3-metalla-1,2-dioxolanes to formylmethyl hydroxy complexes is in marked contrast with the rearrangements proposed earlier for 3-metalla-1,2-dioxolanes i.e. direct rearrangement to a metal oxo complex and acetaldehyde, or to a metal oxo complex and ethylene oxide.[1f] However, the formylmethyl complexes may still be intermediates in the formation of acetaldehyde and a rhodium oxo or hydroxy complex.

In the 1980's Read et al. proposed that 3-rhodadioxolanes are intermediates in the co-oxygenation of terminal or cyclic olefins and triphenylphosphane, to ketones and triphenylphosphane oxide (Scheme 11).[1b] The 3-rhodadioxolane is converted into a 2-rhodaoxetane via the transfer of an O atom to triphenylphosphane. The triphenylphosphane oxide stabilized 2-rhodaoxetane then successively loses triphenylphosphane oxide and a ketone. Our findings do not support such a mechanism. 3-Rhoda-1,2-dioxolane **8a**BPh_4 does not react with triphenylphosphane, and the formation of 2-rhodaoxetanes from 3-rhoda-1,2-dioxolanes have not been observed.

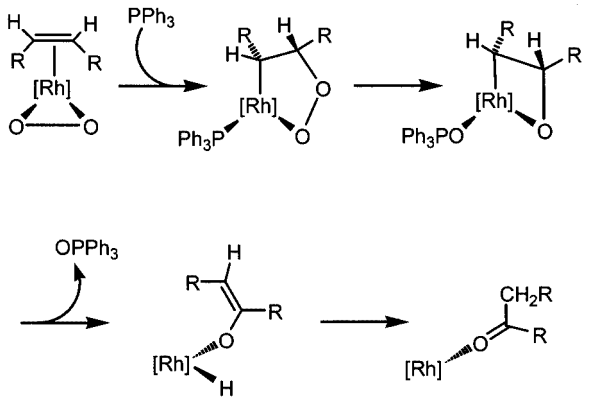

Scheme 11. Mechanism proposed by Read for rhodium catalyzed co-oxygenation of olefins and triphenylphosphane to ketones and triphenylphosphane oxide[1b]

Both Mimoun and Read proposed the formation of 3-rhoda-1,2-dioxolanes from rhodium peroxo ethene complexes.[1a,1b] We have not observed such peroxo ethene intermediates in the formation of 3-rhoda-1,2-dioxolanes. Our group has isolated iridium peroxo ethene complexes, generated through the reaction of iridium ethene complexes with dioxygen in solution, however, these complexes are quite stable and the formation of 3-irida-1,2-dioxolanes is not observed from these complexes.[6c]

Experimental Section

General Methods: All procedures were performed under a nitrogen atmosphere using standard Schlenk techniques, unless indicated otherwise. The solvents (p.a.) were deoxygenated by bubbling through a stream of nitrogen.

NMR experiments were carried out on Bruker DPX200, Bruker AC300, Bruker WM400, and Bruker AM-500. Solvent shift references for ^1H NMR are: CD_2Cl_2 $\delta(^1H)$ = 5.31 ppm, CD_3CN $\delta(^1H)$ = 1.94 ppm and [D_6]acetone $\delta(^1H)$ = 2.05 ppm. Solvent shift references for ^{13}C NMR are: CD_3CN $\delta(^{13}C)$ = 118.1 ppm and [D_6]acetone $\delta(^{13}C)$ = 206.18 ppm. Abbreviations used are: s = singlet, d = doublet, dd = double doublet, t = triplet, dt = double triplet, q = quadruplet, qq = quadruplet of quadruplets, m = multiplet, dm = double multiplet, br. = broad. Mass spectra (ESI) were recorded on a Finnigan MAT 900S and a Finnigan TSQ 7000 mass spectrometer. Elemental analyses (C, H N) were carried out on an Hanau Elementar-Analyzer CHN-O-Rapid. Infrared spectra were measured on a Perkin−Elmer 1720X spectrometer.

Compounds [{$(CH_2CH_2)_2RhCl$}$_2$],[24] tpa,[25] Metpa,[26] [(Metpa)$Rh(CH_2CH_2)$]BPh_4/PF_6,[5] [(tpa)$Rh(CH_2CH_2)$]BPh_4/PF_6,[5] N_4Me_2,[27] [{$(C_8H_{14})IrCl$}$_2$],[28] and $[H(OEt_2)_2]B[C_6H_3(CF_3)_2]_4$ ($HBAr^F_4$)[29] were prepared according to literature procedures. All other chemicals were obtained commercially and were used without further purification.

X-ray Diffraction: Crystals of **3**PF_6 suitable for X-ray diffraction were obtained by slow diffusion of diethyl ether into an acetonitrile solution. Crystals of **5**PF_6 were obtained by crystallization from acetone/diethyl ether (v/v = 1:3) over a period of nine days at −70 °C. Crystals of **8a**BPh_4 were obtained through slow diffusion of diethyl ether into a 1,2-dichloroethane/acetonitrile solution. A crystal of **9a**BPh_4 was obtained by exposure of a crystal of **8a**BPh_4 to glass-filtered daylight for one week.

X-ray diffraction data for **3**PF_6 and **5**PF_6 were collected at 208(2) K on an Enraf−Nonius CAD4 diffractometer, using graphite monochromatized Mo-K_α radiation (λ = 0.71073 Å) and Cu-$K\alpha$ radiation (λ = 1.54184 Å), respectively. X-ray diffraction data for **8a**BPh_4 and **9a**BPh_4 were collected at 150(2) K on a Nonius KappaCCD diffractometer with rotating anode, using graphite monochromatized Mo-K_α radiation (λ = 0.71073 Å). The structures were solved by the PATTY[30] option of the DIRDIF[31] program system. All non-hydrogen atoms were refined with anisotropic temperature factors. The bridging hydrogen atom of the formyl fragment in **9a**BPh_4 was taken from a difference Fourier map and was freely refined. All other hydrogen atoms were placed at calculated positions and were refined isotropically in riding mode. Subsequently, for **5**PF_6, the hydrogen atoms were freely refined. Selected bond lengths and angles are shown in Tables 3 and 4. Other relevant crystal data are summarized in Table 5. Drawings were generated with the program PLATON.[32]

3PF_6**:** Geometrical calculations (PLATON, Spek 1995)[33] revealed neither unusual geometric features, nor unusual short intermolecular contacts. The calculations revealed no higher symmetry and no solvent accessible areas.

5PF_6**:** There is a disordered solvent molecule present in the crystal structure. Calculations (PLATON, Spek,1995)[33] showed a void of 95 Å^3, containing 31 electrons, at 0.0032, 0.466, 0.842. Based on the synthetic route, the electron density most probably represents one acetone molecule (C_3H_6O, 32 electrons). The SQUEEZE pro-

Table 3. Selected bond lengths [Å] for $\mathbf{3}^+$, $\mathbf{5}^+$, $\mathbf{8a}A^+$, $\mathbf{8a}B^+$, and $\mathbf{9a}^+$ (M = Rh or Ir)

	$\mathbf{3}^+$	$\mathbf{5}^+$	$\mathbf{8a}A^+$	$\mathbf{8a}B^+$	$\mathbf{9a}^+$
N1−M	2.175(8)	2.311(5)	2.054(2)	2.054(2)	2.040(3)
N2−M	2.027(10)	2.145(5)	2.015(3)	2.015(3)	2.018(4)
N3−M	−	2.163(5)	2.133(3)	2.133(3)	2.102(3)
N4−M	2.056(8)	−	2.030(3)	2.030(3)	2.033(4)
C1−M	2.164(11)	2.113(7)	2.030(16)	2.076(16)	2.085(4)
C2−M	2.126(13)	2.143(7)	−	−	−
C3−M	2.157(11)	2.104(8)	−	−	−
C4−M	2.118(10)	2.125(8)	−	−	−
O1−M	−	−	2.01(2)	1.97(2)	2.014(3)
O1−O2	−	−	1.504(18)	1.496(16)	−
O1−H1	−	−	−	−	0.80(5)
H1−O2	−	−	−	−	1.92(5)
O2−C2	−	−	1.430(11)	1.455(9)	1.103(11)
C2−C1	1.419(16)	1.411(11)	1.563(11)	1.534(11)	1.245(12)
C3−C4	1.416(16)	1.341(11)	−	−	−

Table 4. Selected angles and torsion angles [°] for $\mathbf{3}^+$, $\mathbf{5}^+$, $\mathbf{8a}A^+$, $\mathbf{8a}B^+$, and $\mathbf{9a}^+$ (M = Rh or Ir)

	$\mathbf{3}^+$	$\mathbf{5}^+$	$\mathbf{8a}A^+$	$\mathbf{8a}B^+$	$\mathbf{9a}^+$
N1−M−N2	82.2(3)	78.41(19)	84.04(10)	84.04(10)	83.54(13)
N1−M−N3	−	78.2(2)	81.87(10)	81.87(10)	82.83(12)
N1−M−N4	82.1(3)	−	82.91(10)	82.91(10)	82.44(13)
N2−M−N3	−	77.72(19)	88.47(10)	88.47(10)	87.78(13)
N2−M−N4	164.1(4)	−	166.33(10)	166.33(10)	165.46(13)
N3−M−N4	−	−	93.70(10)	93.70(10)	94.27(13)
C1−M−O1	−	−	84.6(4)	84.7(4)	90.18(18)
C2−C1−M	69.2(6)	71.8(4)	106.0(9)	102.2(8)	111.4(5)
O2−C2−C1	−	−	106.2(18)	111.5(10)	146(2)
O1−O2−C2	−	−	106.1(15)	101.7(11)	−
M−O1−O2	−	−	106.3(10)	110.8(12)	−
C1−M−N1	95.7(4)	95.3(3)	99.3(3)	95.9(3)	96.18(15)
C1−M−N2	89.4(4)	96.7(3)	91.2(4)	87.5(4)	89.26(16)
C1−M−N3	−	172.1(3)	178.7(3)	175.6(4)	176.97(16)
C1−M−N4	90.1(4)	−	86.9(4)	89.8(4)	88.44(17)
O1−M−N1	−	−	175.9(4)	179.1(7)	173.63(15)
O1−M−N2	−	−	97.0(12)	95.3(11)	96.19(15)
O1−M−N3	−	−	94.2(3)	97.5(3)	90.80(15)
O1−M−N4	−	−	96.3(12)	97.7(11)	98.17(15)
M−O1−H1	−	−	−	−	99(4)
O1−H1−O2	−	−	−	−	168(5)
M−C1−C2−O2	−	−	−	−	−72(3)
C1−M−C3	−	89.9(4)	−	−	−
C2−M−C4	−	84.4(4)	−	−	−
C1−C2−M	72.1(7)	69.5(4)	−	−	−
C3−C4−M	72.1(6)	70.7(5)	−	−	−
C4−C3−M	69.2(6)	72.3(5)	−	−	−

cedure was applied to account for the electron density of the solvent molecule.

8aBPh$_4$: The five-membered dioxolane ring has the envelope form and occurs in two conformations. As expected there is considerable positional overlap for some of the atoms (C1A and C1B, C2A and C2B, O1A and O1B). Therefore, some geometrical constraints had to be applied: the two conformations were 'SAMEd' and the anisotropic thermal displacement parameters were tied. Calculations (PLATON, Spek 1995)[33] showed two distinct voids, one of 229 Å^3, containing 68 electrons, around a two-fold axis (position 4e, 0, *y*, 1/4; $y = -0.036$), and one of 152 Å^3, containing 44 electrons, around an inversion center (position 4b: 1/2, 0, 0). Based on the synthetic route and evidence from NMR spectroscopy, it is assumed that these electron densities represent one molecule of diethyl ether ($C_4H_{10}O$, 42 electrons) plus one molecule of acetonitrile (CH_3CN, 22 electrons) in the first void (64 electrons, 28.5 Å^3/atom), and one molecule of dichloroethane ($C_2H_4Cl_2$, 50 electrons) in the second void (30.2 Å^3/atom). It was not possible to assign any physically meaningful parameters to the electron densities found in the difference fourier map. Therefore the SQUEEZE procedure was applied to account for these electron densities.

9aBPh$_4$: Hydrogen atom H1 was clearly visually observed in a difference fourier map and its position was subsequently determined automatically. Its positional and thermal parameters were refined freely and this refinement proved to be stable. The position of H1 is well outside the regions influenced by the SQUEEZE procedure described later on.

From the anisotropic thermal displacement parameters for C2 and O2 it is clear that these atoms show a large positional disorder. Although it is possible to use several partially occupied positions for these atoms, no physically reasonable models result from these parameters, at least not any better than the model presented here. Splitting up these atoms serves no other purpose but to lower the *R*-value. The calculated hydrogen positions on C2 are therefore merely indications of possible positions.

Calculations (PLATON, Spek 1995)[33] showed two distinct voids, one of 239 Å^3, containing 58 electrons, around a two-fold axis (position 4e, 0, *y*, 1/4; $y = -0.041$), and one of 152 Å^3, containing 39 electrons, around an inversion center (position 4b: 1/2, 0, 0). Based on the synthetic route and evidence from NMR spectroscopy, it is assumed that these electron densities possibly represent one molecule of diethyl ether ($C_4H_{10}O$, 42 electrons) plus one molecule of acetonitrile (CH_3CN, 22 electrons) in the first void (64 electrons, 29.9 Å^3/non-hydrogen atom), and one molecule of dichloroethane ($C_2H_4Cl_2$, 50 electrons) in the second void (38.0 Å^3/non-hydrogen atom). These assumptions are in accordance with the earlier crystal structure determination of the original crystal of **8a**BPh$_4$ before its exposure to glass-filtered daylight, and account for the calculated physical molecular properties as reported in this paper.

It was not possible to assign any physically meaningful parameters to the electron densities found in the difference fourier map. Therefore, the SQUEEZE procedure was applied to account for these electron densities.

CCDC-187013 (**3**PF$_6$), CCDC-187012 (**5**PF$_6$), CCDC-157414 (**8a**BPh$_4$), and CCDC-170096 (**9a**BPh$_4$) contain the supplementary crystallographic data for this paper. These data can be obtained free of charge at www.ccdc.cam.ac.uk/conts/retrieving.html [or from the Cambridge Crystallographic Data Centre, 12, Union Road, Cambridge CB2 1EZ, UK; Fax: (internat.) +44−1223/336-033; E-mail: deposit@ccdc.cam.ac.uk].

Synthesis

Bis(ethene)[*N*-(2-pyridylmethyl)-*N*,*N*-bis(2-pyridylmethyl-κ*N*)amine-κ*N*]iridium(I) Hexafluorophosphate (3PF$_6$): Ethene was bubbled through a solution of $[(C_8H_{14})_2IrCl]_2$ (325 mg, 0.36 mmol) in MeOH (13 mL) until a clear solution was obtained. Under an ethene atmosphere, tpa (216 mg, 0.74 mmol) was added and the reaction mixture was stirred for 10 minutes. KPF_6 (167 mg, 0.91 mmol) was then added under an ethene atmosphere, and after stirring for 1 hour, the solution was cooled to −78 °C. The cold suspension was filtered under a nitrogen atmosphere and the white

Table 5. Crystallographic data

	3^+	5^+	$8a^+$	$9a^+$
Empirical formula	$C_{22}H_{26}F_6IrN_4P$	$C_{47}H_{54}BN_4ORh$	$C_{48}H_{50.50}BClN_{4.50}O_{2.50}Rh$	$C_{48}H_{50.50}BClN_{4.50}O_{2.50}Rh$
Crystal color	Light yellow transparent	Transparent yellow-brown	Transparent yellow	Transparent yellow
Crystal shape	Regular platelet	Irregular fragment	Irregular fragment	Irregular fragment
Crystal size [mm]	0.53 × 0.46 × 0.10	0.36 × 0.24 × 0.10	0.29 × 0.22 × 0.13	0.29 × 0.22 × 0.13
Molecular weight	683.64	804.66	879.60	879.60
T [K]	208(2)	208(2)	150(2)	150(2)
Crystal system	Monoclinic	Monoclinic	Monoclinic	Monoclinic
Space group	P 21/c	P 21/n	C 2/c	C 2/c
Unit cell dim. from N refl.	23	21	17718	14986
a [Å]	7.538(2)	11.555(2)	35.8688(5)	36.0362(2)
b [Å]	14.831(3)	17.523(5)	10.7328(2)	10.77600(10)
c [Å]	20.753(10)	19.686(5)	24.2609(4)	24.2975(2)
α [°]	90	90	90	90
β [°]	90.07(3)	97.38(2)	116.6660(10)	116.3883(4)
γ [°]	90	90	90	90
V [Å^3]	2320.2(13)	3952.9(17)	8346.4(2)	8452.21(11)
$\rho_{calcd.}$ [g·cm^{-3}]	1.957	1.352	1.400	1.382
Z	4	4	8	8
Diffractometer	Enraf−Nonius CAD4	Enraf−Nonius CAD4	Nonius Kappa CCD with rotating anode	Nonius Kappa CCD with rotating anode
Abs. Coefficient [mm^{-1}]	5.890	3.805	0.520	0.514
Scan	ω-2θ	ω-2θ	Area detector, and ω scan	Area detector, and ω scan
Radiation (graphite mon.)	Mo-K_α	Cu-Kα	Mo-K_α	Mo-K_α
Wavelength [Å]	0.71073	1.54184	0.71073	0.71073
F(000)	1328	1688	3656	3656
Θ range [°]	2.70−27.48	3.39−69.93	1.27−27.48	1.73−25.35
Index ranges	$-9 \le h \le 0$	$0 \le h \le 14$	$-46 \le h \le 46$	$-43 \le h \le 43$
	$-19 \le k \le 0$	$0 \le k \le 21$	$-13 \le k \le 13$	$-12 \le k \le 12$
	$-26 \le l \le 26$	$-23 \le l \le 23$	$-31 \le l \le 31$	$-29 \le l \le 29$
Abs. Corr.	Semi-empir. Ψ-scan[a]	Semi-empir. Ψ-scan[a]	None	None
Range of rel. transm. fac.	4.786, 0.696	1.083, 0.947	−	−
Measured reflections	5707	7865	17718	14986
Unique reflections	5314	7478	9548	7719
[R_{int}]	[0.0481]	[0.0633]	[0.0508]	[0.0294]
Observed reflections [$I_0 > 2\sigma(I_0)$]	4542	4765	5801	5510
Data/restraints/parameters	5314/0/308	7478/0/485	9548/184/506	7719/0/473
Goodness-of-fit on F^2	1.090	1.004	0.963	1.054
SHELXL-97 weight parameters	0.1169, 42.6696	0.0970, 0.0000	0.0586, 0.0000	0.0870, 6.0419
Final $R1$, $wR2$ [$I > 2\sigma(I)$]	0.0657, 0.1843	0.0702, 0.1617	0.0459, 0.1080	0.0494, 0.1402
$R1$, $wR2$ [all data]	0.0766, 0.1992	0.1140, 0.1815	0.0904, 0.1186	0.0721, 0.1492
Diff. Peak and hole [e·Å^{-3}]	6.907, −3.638	1.635, −1.208	0.770, −0.508	0.899, −0.643

[a] A. C. T. North, D. C. Philips, F. S. Mathews, *Acta Crystallogr.* **1968**, *A24*, 351−359.

residue was washed with MeOH (3 × 1 mL) and dried in vacuo. Complex **3**PF_6 was obtained as a white powder. Yield: 290 mg (58%). ^{1}H NMR (200 MHz, CD_2Cl_2, 300 K): δ = 8.69 (ddd, $^3J_{H,H}$ = 4.9, $^4J_{H,H}$ = 1.8, $^5J_{H,H}$ = 0.9 Hz, 1 H, Py_a-H6), 7.80 (dt, $^3J_{H,H}$ = 7.7, $^4J_{H,H}$ = 1.9 Hz, 1 H, Py_a-H4), 7.73 (dt, $^3J_{H,H}$ = 7.8, $^4J_{H,H}$ = 1.6 Hz, 2 H, Py_b-H4), 7.60 (d, $^3J_{H,H}$ = 4.9 Hz, 2 H, Py_b-H6), 7.37 (m, 3 H, Py-H3), 7.14 (t, $^3J_{H,H}$ = 7.0 Hz, 3 H, Py-H5), 5.50 (d[AB], $^2J_{H,H}$ = 15.4 Hz, 2 H, NCH_2Py_b), 4.65 (d[AB], $^2J_{H,H}$ = 15.6 Hz, 2 H, NCH_2Py_b), 4.39 (s, 2 H, NCH_2Py_a), 3.36 (br.t, $^3J_{H,H}$ = 9.4 Hz, 2 H, CH_2CH_2), 3.22 (t, $^3J_{H,H}$ = 9.7 Hz, 2 H, CH_2CH_2), 1.94 (t, $^3J_{H,H}$ = 9.8 Hz, 2 H, CH_2CH_2), 1.85 (br.t, $^3J_{H,H}$ = 9.7 Hz, 2 H, CH_2CH_2) ppm; $^{13}C\{^1H\}$ NMR (125 MHz, CD_3CN, 243 K): δ = 166.2 (Py_b-C2), 154.6 (Py_a-C2), 150.8 (Py_a-C6), 150.4 (Py_b-C6), 138.8(Py_b-C4), 138.2 (Py_a-C4), 127.2 (Py_a-C3/5), 126.6 (Py_b-C3/5), 124.8 (Py_b-C3/5), 124.5 (Py_a-C3/5), 65.4 (NCH_2Py_b), 65.3 (NCH_2Py_a), 39.8 (br., CH_2CH_2), 37.3 (br., CH_2CH_2), 34.8 (CH_2CH_2), 30.3 (CH_2CH_2) ppm; elemental analysis for **3**PF_6 ($C_{22}H_{26}F_6IrN_4P$; 683.66): calcd. C 38.65, H 3.83, N 8.20; found C 38.78, H 3.90, N 8.36 %.

Bis(ethene)[*N*-(2-pyridylmethyl)-*N*,*N*-bis(2-pyridylmethyl-κ*N*)amine-κ*N*]iridium(I) Tetraphenylborate (3BPh_4): Complex **3**BPh_4 was obtained by the same procedure as **3**PF_6, using $NaBPh_4$ instead of KPF_6.

(Ethene)[*N*,*N*,*N*-tris(2-pyridylmethyl-κ*N*)amine-κ*N*]-iridium(I) Hexafluorophosphate (4PF_6): Complex **4**PF_6 was synthesized according to the same procedure as bis(ethene) complex **3**PF_6, but nitrogen was bubbled through the MeOH solution before the addition of KPF_6. Complex **4**PF_6 was obtained as a yellow/orange powder. Yield: 83%. ^{1}H NMR (200 MHz, CD_3CN, 300 K): δ = 9.19 (d, $^3J_{H,H}$ = 5.2 Hz, 1 H, Py_a-H6), 8.28 (d, $^3J_{H,H}$ = 5.3 Hz, 2 H, Py_b-H6), 7.64 (t, $^3J_{H,H}$ = 7.8 Hz, 3 H, Py-H4), 7.21 (m, 4 H, Py-H3 and Py_a-H5), 7.05 (t, $^3J_{H,H}$ = 6.6 Hz, 2 H, Py_b-H5), 5.11 (d[AB], $^2J_{H,H}$ = 15.3 Hz, 2 H, NCH_2Py_b), 4.83 (d[AB], $^2J_{H,H}$ =

15.3 Hz, 2 H, NCH_2Py$_b$), 4.69 (s, 2 H, NCH_2Py$_a$), 1.28 (m, 4 H, CH_2CH_2) ppm; ^{13}C{^{1}H} NMR (75 MHz, CD_3CN, 300 K): δ = 165.5 (Py$_b$-C2), 161.1 (Py$_a$-C2), 152.4 (Py$_a$-C6), 151.4 (Py$_b$-C6), 137.8 (Py$_a$-C4), 136.3 (Py$_b$-C4), 125.8 (Py$_b$-C3/5), 124.6 (Py$_a$-C3/5), 123.4 (Py$_b$-C3/5), 122.3 (Py$_a$-C3/5), 71.6 (NCH$_2$Py$_b$), 65.9 (NCH$_2$Py$_a$), 4.3 (CH$_2$CH$_2$), 4.1 (CH$_2$$CH_2$) ppm. ESI-MS (THF): 511 [M − PF$_6$]$^+$, 483 [M − CH$_2$CH$_2$ − PF$_6$]$^+$; elemental analysis for **4**PF$_6$ ($C_{20}H_{22}F_6IrN_4P$; 655.61): calcd. C 36.64, H 3.38, N 8.55; found C 36.63, H 3.44, N 8.66 %.

(Ethene)[*N*,*N*,*N*-tris(2-pyridylmethyl-κ*N*)amine-κ*N*]-iridium(I) Tetraphenylborate (4BPh$_4$): Complex **4**BPh$_4$ was obtained by the same procedure as **4**PF$_6$, using NaBPh$_4$ instead of KPF$_6$.

Bis(ethene){3,11-dimethyl-3,11,17,18-tetraazatricyclo-[11.3.1.1^{5,9}]octadeca-1(17),5(18),6,8,13,15-hexaene-κ^4*N*^{1},*N*^{2},*N*^{3}} rhodium(I) Hexafluorophosphate (5PF$_6$): [Rh(μ-Cl)(C$_2$H$_4$)$_2$]$_2$ (100 mg, 0.26 mmol) was added to a suspension of NaHCO$_3$ (100 mg, 1.2 mmol) in methanol (5 mL) at −20 °C. The reaction mixture was stirred for 15 minutes, after which N_4Me_2 (138 mg, 0.51 mmol) was added. After stirring for 5 minutes at −20 °C, the reaction mixture was cooled to −78 °C and stirred for 30 minutes. Undissolved material was removed by filtration. A solution of KPF$_6$ (100 mg, 0.54 mmol) in methanol (1 mL) was then added to the filtrate at −78 °C, causing the precipitation of a light yellow solid. After stirring for 1 hour, the solid was collected by filtration. Additional KPF$_6$ (60 mg, 0.33 mmol) was added to the filtrate. The solution was warmed to room temperature for two minutes, after which it was cooled to −78 °C again. This produced a second batch of solid, which was collected by filtration after stirring for 15 minutes. The combined solids were washed with methanol and dried under vacuum. Yield: 245 mg (83%). ^{1}H NMR (500 MHz, [D$_6$]acetone, 203 K): δ = 7.73 (t, $^3J_{H,H}$ = 7.8 Hz, 2 H, Py-H4), 7.37 (d, $^3J_{H,H}$ = 7.5 Hz, 2 H, Py-H3/5), 7.28 (d, $^3J_{H,H}$ = 7.8 Hz, 2 H, Py-H3/5), 6.06 (d[AB], $^2J_{H,H}$ = 14.1 Hz, 2 H, NCH_2Py), 5.17 (d[AB], $^2J_{H,H}$ = 16.7 Hz, 2 H, NCH_2Py), 4.51 (d[AB], $^2J_{H,H}$ = 16.9 Hz, 2 H, NCH_2Py), 4.46 (d[AB], $^2J_{H,H}$ = 14.1 Hz, 2 H, NCH_2Py), 3.84 (s, 3 H, NCH_3), 3.22 (m, 2 H, CH_2CH_2), 2.92 (br.t, $^3J_{H,H}$ = 10.3 Hz, 2 H, CH_2CH_2), 2.53 (br.t, $^3J_{H,H}$ = 10.9 Hz, 2 H, CH_2CH_2), 2.25 (s, 3 H, NCH_3), 1.72 (m, 2 H, CH_2CH_2) ppm; ^{13}C{^{1}H} NMR (100 MHz, [D$_6$]acetone, 243 K): δ = 160.0 (Py-C2/6), 158.1 (Py-C2/6), 138.4 (Py-C4), 126.3 (Py-C3/5), 121.9 (Py-C3/5), 68.1 (NCH$_2$Py), 65.4 (NCH$_2$Py), 57.7 (br., CH$_2$$CH_2$), 52.6 (N$CH_3$), 46.6 (br., CH$_2$$CH_2$), 37.7 (N$CH_3$) ppm. ESI-MS ($CH_3CN$): 427 [M − PF$_6$]$^+$, 399 [M − (CH$_2CH_2$) − PF$_6$]$^+$.

(Ethene){3,11-dimethyl-3,11,17,18-tetraazatri-cyclo[11.3.1.1^{5,9}]octadeca-1(17),5(18),6,8,13,15-hexaene-κ^4*N*^{1},*N*^{2},*N*^{3},*N*^{4}}rhodium(I) Hexafluorophosphate (6PF$_6$): After stirring **5**PF$_6$ (245 mg, 0.43 mmol) in [D$_6$]acetone (10 mL) for 4 hours, diethyl ether (40 mL) was added. A red solid precipitated and was collected by filtration and washed with diethyl ether. The obtained brick-red solid was isolated by filtration, washed with diethyl ether and dried in vacuo. Yield 112 mg (48%). ^{1}H NMR (200 MHz, CD_3CN, 298 K): δ = 7.62 (t, $^3J_{H,H}$ = 7.9 Hz, 2 H, Py-H4), 7.11 (d, $^3J_{H,H}$ = 7.8 Hz, 4 H, Py-H3 and Py-H5), 4.01 (d[AB], $^2J_{H,H}$ = 15.1 Hz, 4 H, NCH_2Py), 3.82 (d[AB], $^2J_{H,H}$ = 15.0 Hz, 4 H, NCH_2Py), 2.54 (d, $^2J_{H,Rh}$ = 2.4 Hz, 4 H, CH_2CH_2), 2.15 (d, $^3J_{H,Rh}$ = 1.3 Hz, 6 H, NCH_3) ppm; ^{13}C{^{1}H} NMR (75 MHz, [D$_6$]acetone, 297 K): δ = 155.4 (Py-C2 and Py-C6), 136.6 (Py-C4), 121.3 (Py-C3 and Py-C5), 76.1 (NCH$_2$Py), 49.8 (NCH$_3$), 24.8 (d, $J_{C,Rh}$ = 18 Hz, CH$_2$$CH_2$) ppm. ESI-MS ($CH_3CN$): 399 [M − PF$_6$]$^+$, 371 [M − (CH$_2CH_2$) − PF$_6$]$^+$.

(2-Peroxyethyl-κ^2*C*^{1},*O*^{2})[*N*,*N*,*N*-tris(2-pyridylmethyl-κ*N*)-amine-κ*N*]rhodium(III) Tetraphenylborate (8aBPh$_4$): Compound **7**BPh$_4$ was ground with a mortar and exposed to air at room temperature and was left in the dark for 2 days at atmospheric pressure.[11] **8a**BPh$_4$ was obtained in > 90% yield, as determined by ^{1}H NMR spectroscopy. Crystals obtained from a 1,2-dichloroethane solution proved to be unsuitable for X-ray diffraction. However, the crystals obtained were used for elemental analysis. Both ^{1}H NMR spectroscopy and elemental analysis of these crystals showed that they contained 1.5 molecules of 1,2-dichloroethane per cation. ^{1}H NMR (300 MHz, CD_3CN, 297 K): δ = 8.75 (d, $^3J_{H,H}$ = 5.4 Hz, 1 H, Py$_a$-H6), 8.66 (d, $^3J_{H,H}$ = 5.5 Hz, 2 H, Py$_b$-H6), 7.81 (dt, $^3J_{H,H}$ = 7.8, $^4J_{H,H}$ = 1.7 Hz, 2 H, Py$_b$-H4), 7.69 (dt, $^3J_{H,H}$ = 7.8, $^4J_{H,H}$ = 1.7 Hz, 1 H, Py$_a$-H4), 7.40 (d, $^3J_{H,H}$ = 8.0 Hz, 2 H, Py$_b$-H3), 7.35 (m, 3 H, Py$_a$-H5 and Py$_b$-H5), 7.28 (m, 8 H, BAr-H2), 7.16 (dt, $^3J_{H,H}$ = 7.8, $^4J_{H,H}$ = 0.9 Hz, 1 H, Py$_a$-H3), 6.99 (t, $^3J_{H,H}$ = 7.4 Hz, 8 H, BAr-H3), 6.84 (t, $^3J_{H,H}$ = 7.3 Hz, 4 H, BAr-H4), 4.88 (d[AB], $^2J_{H,H}$ = 15.6 Hz, 2 H, NCH_2Py$_b$), 4.71 (d[AB], $^2J_{H,H}$ = 15.1 Hz, 2 H, NCH_2Py$_b$), 4.57 (s, 2 H, NCH_2Py$_a$), 3.25 (t, $^3J_{H,H}$ = 6.1 Hz, 2 H, RhCH$_2$CH_2OO), 2.57 (dt, $^3J_{H,H}$ = 6.1, $^2J_{H,Rh}$ = 2.4 Hz, 2 H, RhCH_2CH$_2$OO) ppm; ^{13}C{^{1}H} NMR (75 MHz, CD_3CN, 297 K): δ = 164.6 (q, $^1J_{C,B}$ = 49.5 Hz, BAr-C1), 162.7 (Py$_b$-C2), 158.6 (Py$_a$-C2), 150.1 (Py$_b$-C6), 149.5 (Py$_a$-C6), 139.4 (Py$_a$-C4), 139.3 (Py$_b$-C4), 136.5 (BAr-C2), 126.4 (q, $^3J_{C,B}$ = 2.8 Hz, BAr-C3), 125.5 (Py$_b$-C3), 125.4 (Py$_a$-C3), 124.2 (Py$_b$-C5), 122.6 (BAr-C4), 121.9 (Py$_a$-C5), 72.9 (NCH$_2$Py$_a$), 70.2 (N-CH$_2$-Py$_b$ and RhCH$_2$CH_2OO), 35.0 (d, $^1J_{C,Rh}$ = 25.0 Hz, RhCH$_2$CH$_2$OO) ppm. ESI-MS (CD_3CN): 453 [M − BPh$_4$]$^+$, 425 [M − CH$_2$CH$_2$ − BPh$_4$]$^+$, 409 [M − C$_2$H$_4$O − BPh$_4$]$^+$, 393 [M − C$_2$H$_4$O$_2$ − BPh$_4$]$^+$, 391 [M − C$_2$H$_4$O$_2$ − H$_2$ − BPh$_4$]$^+$; elemental analysis for **8a**BPh$_4$·1^1/$_2$C$_2$H$_4$Cl$_2$ ($C_{47}H_{48}BCl_3N_4O_2Rh$; 921.00): calcd. C 61.36, H 5.26, N 6.09; found C 61.36, H 5.44, N 6.17 %.

(2-Peroxyethyl-κ^2*C*^{1},*O*^{2})[*N*,*N*,*N*-tris(2-pyridylmethyl-κ*N*)-amine-κ*N*]rhodium(III) Hexafluorophosphate (8aPF$_6$/8bPF$_6$): Complex **7**PF$_6$ was ground with a mortar and exposed to air at room temperature and was left in the dark for 2 days at atmospheric pressure.[11] A mixture of **8a**PF$_6$ and **8b**PF$_6$ in an approximate ratio of 1:1 was obtained in > 90% yield, as determined by ^{1}H NMR spectroscopy. The data for **8b**PF$_6$ are given: ^{1}H NMR (500 MHz, CD_3CN, 298 K): δ = 8.86 (d, $^3J_{H,H}$ = 5.4 Hz, 1 H, Py$_a$-H6), 8.56 (d, $^3J_{H,H}$ = 5.4 Hz, 2 H, Py$_b$-H6), 7.83 (dt, $^3J_{H,H}$ = 7.8, $^4J_{H,H}$ = 1.4 Hz, 2 H, Py$_b$-H4),7.63 (t, $^3J_{H,H}$ = 7.3 Hz, 1 H, Py$_a$-H4), 7.48 (d, $^3J_{H,H}$ = 7.8 Hz, 2 H, Py$_b$-H3), 7.35 (t, $^3J_{H,H}$ = 6.6 Hz, 2 H, Py$_b$-H5), 7.25 (m, 1 H, Py$_a$-H5), 7.14 (d, $^3J_{H,H}$ = 7.8 Hz, 1 H, Py$_a$-H3), 5.12 (d[AB], $^2J_{H,H}$ = 15.6 Hz, 2 H, NCH_2Py$_b$), 5.00 (d[AB], $^2J_{H,H}$ = 15.6 Hz, 2 H, NCH_2Py$_b$), 4.80 (s, 2 H, NCH_2Py$_a$), 3.55 (dt, $^3J_{H,H}$ = 6.1, $^2J_{H,Rh}$ = 2.4 Hz, 2 H, RhCH_2CH$_2$OO), 3.41 (t, $^3J_{H,H}$ = 6.1 Hz, 2 H, RhCH$_2$CH_2OO) ppm; ^{13}C{^{1}H} NMR (50 MHz, CD_3CN, 300 K): δ = 164.6 (Py$_b$-C2), 162.7 (Py$_a$-C6), 152.5 (Py$_a$-C6), 150.5 (Py$_b$-C6), 139.7 (Py$_b$-C4), 138.7 (Py$_a$-C4), 125.9 (Py$_b$-C3), 125.5 (Py$_a$-C3), 124.6 (Py$_b$-C5), 122.6 (Py$_a$-C5), 72.8 (RhCH$_2$$CH_2$OO), 67.9 (N$CH_2Py_b$), 65.4 (N$CH_2Py_a$), 44.8 (d, $^1J_{C,Rh}$ = 28.8 Hz, RhCH$_2$CH$_2$OO) ppm. ESI-MS (CD_3CN): 453 [M − PF$_6$]$^+$, 425 [M − CH$_2$CH$_2$ − PF$_6$]$^+$, 409 [M − C$_2$H$_4$O − PF$_6$]$^+$, 393 [M − C$_2$H$_4$O$_2$ − PF$_6$]$^+$, 391 [M − C$_2$H$_4$O$_2$ −H$_2$ − PF$_6$]$^+$.

(2-Peroxyethyl-κ^2*C*^{1},*O*^{2})[*N*,*N*,*N*-tris(2-pyridylmethyl-κ*N*)-amine-κ*N*]iridium(III) Tetraphenylborate (10aBPh$_4$): Compound **4**BPh$_4$ was ground with a mortar and exposed to air for 5 days. **10a**BPh$_4$ was obtained in > 90% yield, as determined by ^{1}H NMR spectroscopy.[11] ^{1}H NMR (500 MHz, CD_3CN, 243 K): δ = 8.67 (m, 3 H, Py-H6), 7.77 (dt, $^3J_{H,H}$ = 7.8, $^4J_{H,H}$ = 1.6 Hz, 2 H, Py$_b$-H4), 7.68 (dt, $^3J_{H,H}$ = 7.8, $^4J_{H,H}$ = 1.6 Hz, 1 H, Py$_a$-H4), 7.38 (d, $^3J_{H,H}$ = 7.7 Hz, 2 H, Py$_b$-H3), 7.30 (m, 3 H, Py-H5), 7.26 (m, 8 H, BAr-H2), 7.16 (d, $^3J_{H,H}$ = 7.7 Hz, 1 H, Py$_a$-H3), 6.98 (t, $^3J_{H,H}$ =

7.5 Hz, 8 H, BAr-H3), 6.82 (t, $^3J_{H,H}$ = 7.3 Hz, 4 H, BAr-H4), 4.92 (d[AB], $^2J_{H,H}$ = 15.4 Hz, 2 H, NCH_2Py$_b$), 4.67 (d[AB], $^2J_{H,H}$ = 15.4 Hz, 2 H, NCH_2Py$_b$), 4.56 (s, 2 H, NCH_2Py$_a$), 2.54 (t, $^3J_{H,H}$ = 6.2 Hz, 2 H, RhCH$_2$CH_2OO), 2.03 (t, $^3J_{H,H}$ = 6.2 Hz, 2 H, RhCH_2CH$_2$OO) ppm; ^{13}C{^{1}H} NMR (125 MHz, CD$_3$CN, 243 K): δ = 164.8 (Py$_b$-C2), 163.9 (q, ^1J (C,B)= 49.2 Hz, BAr-C1), 159.3 (Py$_a$-C2), 149.0 (Py$_b$-C6), 148.1 (Py$_a$-C6), 138.5 (Py$_a$-C4), 138.0 (Py$_b$-C4), 135.8 (q, $^2J_{C,B}$ = 1.3 Hz, BAr-C2), 126.1 (q, $^3J_{C,B}$ = 2.9 Hz, BAr-C3), 124.9 (Py$_b$-C3/5 and Py$_a$-C3/5), 123.9 (Py$_b$-C3/5), 122.1 (BAr-C4), 121.3 (Py$_a$-C3/5), 72.1 (NCH$_2$Py$_b$), 71.8 (NCH$_2$Py$_\alpha$ or IrCH$_2$CH_2OO), 71.1 (NCH$_2$Py$_\alpha$ or IrCH$_2$CH_2OO), 15.8 (IrCH$_2$CH$_2$OO) ppm.

(2-Peroxyethyl-κ²*C*¹,*O*²)[*N*,*N*,*N*-tris(2-pyridylmethyl-κ*N*)-amine-κ*N*]iridium(III) Hexafluorophosphate (10aPF$_6$/10bPF$_6$): Compound **4**PF$_6$ was ground with a mortar and exposed to air for 5 days.[11] A mixture of the isomeric 3-irida-1,2-dioxolanes **10a**PF$_6$ and **10b**PF$_6$ in an approximate ratio of 2:5 was formed in > 90% yield, as determined by ^{1}H NMR spectroscopy. The data for **10b**PF$_6$ are given: ^{1}H NMR (500 MHz, CD$_3$CN, 243 K): δ = 8.93 (d, $^3J_{H,H}$ = 5.5 Hz, 1 H, Py$_a$-H6), 8.58 (d, $^3J_{H,H}$ = 5.13 Hz, 2 H, Py$_b$-H6), 7.75 (dt, $^3J_{H,H}$ = 7.8, $^4J_{H,H}$ = 1.3 Hz, 2 H, Py$_b$-H4), 7.56 (dt, $^3J_{H,H}$ = 7.8, $^4J_{H,H}$ = 1.3 Hz, 1 H, Py$_a$-H4), 7.42 (d, $^3J_{H,H}$ = 8.1 Hz, 2 H, Py$_b$-H3), 7.27 (t, $^3J_{H,H}$ = 6.2 Hz, 2 H, Py$_b$-H5), 7.15 (m, 2 H, Py$_a$-H5 and Py$_a$-H3), 5.04 (d[AB], $^2J_{H,H}$ = 15.4 Hz, 2 H, NCH_2Py$_b$), 4.94 (d[AB], $^2J_{H,H}$ = 15.8 Hz, 2 H, NCH_2Py$_b$), 4.76 (s, 2 H, NCH_2Py$_a$), 2.69 (t, $^3J_{H,H}$ = 6.7 Hz, 2 H, IrCH_2CH$_2$OO), 2.63 (t, $^3J_{H,H}$ = 6.7 Hz, 2 H, IrCH$_2$CH_2OO) ppm. ^{13}C NMR (125 MHz, CD$_3$CN, 243 K): δ = 165.9 (Py$_b$-C2), 162.6 (Py$_a$-C2), 152.4 (Py$_a$-C6), 149.5 (Py$_b$-C6), 138.7 (Py$_b$-C4), 137.3 (Py$_a$-C4), 125.3 (Py$_b$-C3/5), 125.1 (Py$_a$-C3/5), 124.2 (Py$_b$-C3/5), 121.8 (Py$_a$-C3/5), 71.6 (IrCH$_2$CH_2OO), 69.2 (NCH$_2$Py$_b$), 66.4 (NCH$_2$Py$_a$), 23.9 (IrCH$_2$-CH$_2$OO) ppm.

(2-Peroxyethyl-κ²*C*¹,*O*²){3,11-dimethyl-3,11,17,18-tetraazatricyclo[11.3.1.1^{5,9}]octadeca-1(17),5(18),6,8,13,15-hexaene-κ⁴*N*¹,*N*²,*N*³,*N*⁴}rhodium(III) Hexafluorophosphate (16PF$_6$): Complex **6**PF$_6$ was exposed to an oxygen atmosphere at room temperature for 5 days at atmospheric pressure.[11] The color changed from red to yellow ochre. ^{1}H NMR (200 MHz, CD$_3$CN, 298 K): δ = 7.75 (t, $^3J_{H,H}$ = 7.9 Hz, 1 H, Py-H4), 7.66 (t, $^3J_{H,H}$ = 7.9 Hz, 1 H, Py-H4), 7.28 (d, $^3J_{H,H}$ = 7.8 Hz, 2 H, Py-H3/5), 7.14 (d, $^3J_{H,H}$ = 7.8 Hz, 2 H, Py-H3/5), 4.57 (d[AB], $^2J_{H,H}$ = 15.3 Hz, 2 H, NCH_2Py), 4.36 (d[AB], $^2J_{H,H}$ = 16.6 Hz, 2 H, NCH_2Py), 4.16 (d[AB], $^2J_{H,H}$ = 15.2 Hz, 4 H, NCH_2Py), 3.66 (dt, $^3J_{H,H}$ = 6.4, $^3J_{H,Rh}$ = 0.7 Hz, 2 H, RhCH$_2$CH_2OO), 2.90 (dt, $^3J_{H,H}$ = 6.5, $^2J_{H,Rh}$ = 2.5 Hz, 2 H, RhCH_2CH$_2$OO), 2.71 (d, $^3J_{H,Rh}$ = 1.2 Hz, 6 H, NCH_3) ppm; ^{13}C{^{1}H} NMR (125 MHz, CD$_3$CN, 243 K): δ = 157.0 (Py-C2/6), 155.0 (Py-C2/6), 139.3 (Py-C4), 138.2 (Py-C4), 121.6 (Py-C3/5), 120.8 (Py-C3/5), 74.4 (NCH$_2$Py), 72.5 (NCH$_2$Py), 71.7 (RhCH$_2$CH_2OO), 50.1 (NCH$_3$), 30.3 (d, $J_{C,Rh}$ = 25 Hz, RhCH$_2$CH$_2$OO) ppm. ESI-MS (CH$_3$CN): 431 [M − PF$_6$]$^+$.

(Formylmethyl-κ*C*¹)(hydroxy)[*N*,*N*,*N*-tris(2-pyridylmethyl-κ*N*)amine-κ*N*]rhodium(III) Tetraphenylborate (9aBPh$_4$). Method A: A stirred solution of **8a**BPh$_4$ in CD$_3$CN under nitrogen was exposed to the glass-filtered light of a high pressure mercury vapor lamp[34] for 90 minutes at −30 °C. **9a**BPh$_4$ was obtained in > 90% yield, as determined by ^{1}H NMR spectroscopy.

Method B: HBAr$^F_4$ (5.5 mg, 5.4 μmol) was added to a solution of **8a**BPh$_4$ (41.8 mg, 54 μmol) in CD$_3$CN (1 mL) under N$_2$. **9a**BPh$_4$ was obtained in approximately 70% yield in approximately 1 hour, as determined by ^{1}H NMR spectroscopy. ^{1}H NMR (200 MHz, CD$_3$CN, 300 K): δ = 9.26 (t, $^3J_{H,H}$ = 5.0 Hz, 1 H, RhCH$_2$CHO), 9.21 (br.d, $^3J_{H,H}$ = 6.0 Hz, 1 H, Py$_a$-H6), 8.62 (br.d, $^3J_{H,H}$ = 5.6 Hz, 2 H, Py$_b$-H6), 7.84 (dt, $^3J_{H,H}$ = 7.8, $^4J_{H,H}$ = 1.6 Hz, 2 H, Py$_b$-H4), 7.73 (dt, $^3J_{H,H}$ = 7.8, $^4J_{H,H}$ = 1.6 Hz, 1 H, Py$_a$-H4), 7.32 (m, 6 H, Py-H3 and Py-H5), 7.27 (m, 8 H, BAr-H2), 6.99 (t, $^3J_{H,H}$ = 7.4 Hz, 8 H, BAr-H3), 6.83 (t, $^3J_{H,H}$ = 7.2 Hz, 4 H, BAr-H4), 5.01 (d[AB], $^2J_{H,H}$ = 15.9 Hz, 2 H, NCH_2Py$_b$), 4.71 (d[AB], $^2J_{H,H}$ = 14.9 Hz, NCH_2Py$_b$), 4.67 (s, 2 H, NCH_2Py$_a$), 2.69 (dd, $^3J_{H,H}$ = 5.1, $^2J_{H,Rh}$ = 2.9 Hz, 2 H, RhCH_2CHO) ppm; ^{13}C{^{1}H} NMR (125 MHz, CD$_3$CN, 243 K): δ = 209.0 (RhCH$_2$$C$HO), 163.9 (q, $^1J_{C,B}$ = 49.2 Hz, BAr-C1), 162.4 (Py$_b$-C2), 159.0 (Py$_a$-C2), 149.9 (Py$_b$-C6), 147.2 (Py$_a$-C6), 139.3 (Py$_b$-C4), 139.2 (Py$_a$-C4), 135.7 (BAr-C2), 126.1 (q, $^3J_{C,B}$ = 2.7 Hz, BAr-C3), 125.4 (Py$_b$-C5/C3), 124.9 (Py$_a$-C5/C3), 124.4 (Py$_b$-C5/C3), 122.1 (BAr-C4), 121.2 (Py$_a$-C5/C3), 70.7 (NCH$_2$Py$_a$), 68.3 (NCH$_2$Py$_b$), 26.9 (d, $^1J_{C,Rh}$ = 21.0 Hz, RhCH$_2$CHO) ppm. ESI-MS (CD$_3$CN): 453 [M − BPh$_4$]$^+$, 435 [M − H$_2$O − BPh$_4$]$^+$, 425 [M − C$_2$H$_4$ − BPh$_4$]$^+$, 409 [M − C$_2$H$_4$O − BPh$_4$]$^+$, 393 [M − C$_2$H$_4$O$_2$ − BPh$_4$]$^+$, 391 [M − C$_2$H$_4$O$_2$ − H$_2$ − BPh$_4$]$^+$. IR (KBr): $\tilde{\nu}$ = 1655 cm^{-1}.

(Formylmethyl-κ*C*¹)(hydroxy)-[*N*,*N*,*N*-tris(2-pyridylmethyl-κ*N*)amine-κ*N*]rhodium(III) Hexafluorophosphate (9aPF$_6$/9bPF$_6$): *Solid* **8a**PF$_6$/**8b**PF$_6$ was exposed to a N$_2$ atmosphere saturated with H$_2$O for three days at room temperature. A mixture of **9a**PF$_6$ and **9b**PF$_6$ in an approximate ratio of 1:1 was obtained in > 90% yield, according to ^{1}H NMR spectroscopy. The data for **9b**PF$_6$ are given: ^{1}H NMR (500 MHz, CD$_3$CN, 243 K): δ = 9.98 (t, $^3J_{H,H}$ = 4.9 Hz, 1 H, RhCH$_2$CHO), 8.68 (d, $^3J_{H,H}$ = 5.5 Hz, 2 H, Py$_b$-H6), 8.53 (d, $^3J_{H,H}$ = 5.5 Hz, 1 H, Py$_a$-H6), 7.84 (m, 2 H, Py$_b$-H4), 7.66 (dt, $^3J_{H,H}$ = 7.7, $^4J_{H,H}$ = 1.5 Hz, 1 H, Py$_a$-H4), 7.48 (d, $^3J_{H,H}$ = 8.2 Hz, 2 H, Py$_b$-H3), 7.36 (t, $^3J_{H,H}$ = 6.6 Hz, 2 H, Py$_b$-H5), 7.28 (t, $^3J_{H,H}$ = 6.6 Hz, 1 H, Py$_a$-H5), 7.17 (d, $^3J_{H,H}$ = 8.8 Hz, 1 H, Py$_a$-H3), 5.39 (d[AB], $^2J_{H,H}$ = 15.0 Hz, 2 H, NCH_2Py$_b$), 4.88 (s, 2 H, NCH_2Py$_a$), 4.76 (d[AB], $^2J_{H,H}$ = 15.0 Hz, 2 H, NCH_2Py$_b$), 3.47 (dd, $^3J_{H,H}$ = 4.8, $^2J_{H,Rh}$ = 2.9 Hz, 2 H, RhCH_2CHO) ppm; ^{13}C{^{1}H} NMR (125 MHz, CD$_3$CN, 243 K): δ = 210.8 (d, $^2J_{C,Rh}$ = 9.6 Hz, RhCH$_2$$C$HO), 165.0 (Py$_b$-C2), 163.5 (Py$_a$-C2), 151.5 (Py$_b$-C6), 150.2 (Py$_a$-C6), 139.6 (Py$_b$-C4), 138.8 (Py$_a$-C4), 125.4 (Py$_b$-C5/C3), 125.1 (Py$_a$-C5/C3), 124.4 (Py$_b$-C5/C3), 122.1 (Py$_a$-C5/C3), 66.4 (N$CH_2Py_b$), 66.2 (N$CH_2Py_a$), 34.5 (d, $^1J_{C,Rh}$ = 25.0 Hz, RhCH$_2$CHO) ppm. ESI-MS (CH$_3$CN): 453 [M − PF$_6$]$^+$.

(Formylmethyl-κ*C*¹)(aqua)[*N*,*N*,*N*-tris(2-pyridylmethyl-κ*N*)-amine-κ*N*]rhodium(III) Tetraphenylborate Tetra[3,5-bis(trifluoromethyl)phenyl]borate (20a[BPh$_4$][BAr$^F_4$]): HBAr$^F_4$ (57 mg, 0.11 mmol) was added to a solution of **8a**BPh$_4$ (40 mg, 0.1 mmol) in CD$_3$CN (1.0 mL) under N$_2$. **20a**(BPh$_4$)(BAr$^F_4$) was obtained in approximately 85% yield, as determined by ^{1}H NMR spectroscopy. ^{1}H NMR (200 MHz, CD$_3$CN, 300 K): δ = 9.51 (t, $^3J_{H,H}$ = 4.8 Hz, 1 H, RhCH$_2$CHO), 8.96 (d, $^3J_{H,H}$ = 5.5 Hz, 1 H, Py$_a$-H6), 8.52 (d, $^3J_{H,H}$ = 5.7 Hz, 2 H, Py$_b$-H6), 7.95 (dt, $^3J_{H,H}$ = 7.8, $^4J_{H,H}$ = 1.6 Hz, Py$_b$-H4), 7.81 (dt, $^3J_{H,H}$ = 7.8, $^4J_{H,H}$ = 1.6 Hz, Py$_a$-H4),7.73 (m, 8 H, BAr$^F_4$-H2), 7.68 (s, 4 H, BAr$^F_4$-H4), 7.6−7.4 (m, 5 H, Py$_b$-H3, Py$_b$-H5 and Py$_a$-H3/5), 7.33 (m, 8 H, BAr-H2), 7.21 (m, 1 H, Py$_a$-H3/5), 7.01 (t, $^3J_{H,H}$ = 7.4 Hz, 8 H, BAr-H3), 6.85 (t, $^3J_{H,H}$ = 6.9 Hz, 4 H, BAr-H4), 5.15 (d[AB], $^2J_{H,H}$ = 16.4 Hz, 2 H, NCH_2Py$_b$), 4.82 (s, 2 H, NCH_2Py$_a$), 4.69 (d[AB], $^2J_{H,H}$ = 16.6 Hz, 2 H, NCH_2Py$_b$), 3.05 (dd, $^3J_{H,H}$ = 4.9, $^2J_{H,Rh}$ = 2.7 Hz, 2 H, RhCH_2CHO) ppm; ^{13}C{^{1}H} NMR (125 MHz, CD$_3$CN, 243 K): δ = 206.7 (d, $^2J_{C,Rh}$ = 1.9 Hz, RhCH$_2$$C$HO), 164.0 (q, $^1J_{C,B}$ = 49.2 Hz, BAr-C1), 161.9 (q, $^1J_{C,B}$ = 49.8 Hz, BAr^F-C1), 161.6 (Py$_b$-C2), 158.0 (Py$_a$-C2), 151.5 (Py$_b$-C6), 148.7 (Py$_a$-C6), 140.9 (Py$_b$-C4), 140.4 (Py$_a$-C4), 135.8 (BAr-C2), 134.9 (BAr^F-C2), 129.0 (qq, $^2J_{C,F}$ = 31.4, $^3J_{C,B}$ = 2.9 Hz, BAr^F-C3), 126.4 (Py$_b$-C5/C3), 126.2 (q, $^3J_{C,B}$ = 2.6 Hz, BAr-C3), 125.8 (Py$_a$-C5/C3), 125.4 (Py$_b$-C5/C3), 124.6 (q, $^1J_{C,F}$ = 271.9 Hz, BAr^F-CF$_3$), 122.3 (BAr-C4), 122.1 (Py$_a$-C5/C3), 73.5 (NCH$_2$Py$_a$), 69.6 (NCH$_2$Py$_b$), 27.8 (d, $^1J_{C,Rh}$ =

20.4 Hz, Rh*C*H$_2$CHO) ppm. (The signal for BAr^F-C4 is obscured by one of the solvent signals). ESI-MS (CH_3CN): 227 [M − BPh_4 − BAr^F_4]$^{2+}$, 218 [M − H_2O − BPh_4 − BAr^F_4]$^{2+}$.

(Formylmethyl-κ*C*^{1})(hydroxy)[*N*,*N*,*N*-tris(2-pyridylmethyl-κ*N*)amine-κ*N*]iridium(III) Tetraphenylborate (11aBPh_4): A solution of **10a**BPh_4 (85.2 mg, 99 μmol) in CH_3CN (1 mL) was stirred at room temperature. After 4 hours, diethyl ether was added and a yellow solid precipitated. After filtration, the solid was washed with diethyl ether and dried in vacuo. Yield: 49.1 mg (58%). ^{1}H NMR (500 MHz, CD_3CN, 298 K): δ = 9.25 (br.d, $^3J_{H,H}$ = 5.7 Hz, 1 H, Py$_a$-H6), 9.21 (t, $^3J_{H,H}$ = 5.1 Hz, 1 H, IrCH$_2$C*H*O), 8.71 (d, $^3J_{H,H}$ = 5.7 Hz, 2 H, Py$_b$-H6), 7.78 (dt, $^3J_{H,H}$ = 7.8, $^4J_{H,H}$ = 1.5 Hz, 2 H, Py$_b$-H4), 7.68 (dt, $^3J_{H,H}$ = 7.8, $^4J_{H,H}$ = 1.6 Hz, 1 H, Py$_a$-H4), 7.4−7.1 (m, 6 H, Py-H3 and Py-H5), 7.29 (m, 8 H, BAr-H2), 7.00 (t, $^3J_{H,H}$ = 7.4 Hz, 8 H, BAr-H3), 6.84 (t, $^3J_{H,H}$ = 7.2 Hz, 4 H, BAr-H4), 4.86 (s, 2 H, NC*H*$_2$Py$_b$), 4.85 (s, 2 H, NC*H*$_2$Py$_b$), 4.56 (s, 2 H, NC*H*$_2$Py$_a$), 3.07 (d, $^3J_{H,H}$ = 5.3 Hz, 2 H, IrC*H*$_2$CHO) ppm; ^{13}C{^{1}H} NMR (125 MHz, CD_3CN, 298 K): δ = 209.4 (IrCH$_2$*C*HO), 165.8 (Py$_b$ -C2), 164.6 (q, ^1J (C,B)= 49.3 Hz, BAr-C1), 160.8 (Py$_a$-C2), 149.7 (Py$_b$-C6), 146.3 (Py$_a$-C6), 139.2 (Py$_a$-C4), 139.0 (Py$_b$-C4), 136.5 (BAr-C2), 126.4 (q, $^3J_{C,B}$ = 2.8 Hz, BAr-C3), 125.7 (Py$_b$-C3/5), 125.1 (Py$_a$-C3/5), 124.7 (Py$_b$-C3/5), 122.6 (BAr-C4), 121.5 (Py$_a$-C3/5), 72.9 (N*C*H$_2$Py$_a$), 71.4 (N*C*H$_2$Py$_b$), 16.3 (Ir*C*H$_2$CHO) ppm. ESI-MS (CH_3CN): 543 [M − BPh_4]$^+$, 525 [M − H_2O − BPh_4]$^+$, 499 [M − C_2H_4O − BPh_4]$^+$, 483 [M − $C_2H_4O_2$ − BPh_4]$^+$, 391 [M − $CH_2C_5H_4N$ − H_4O_2 − BPh_4]$^+$. IR (KBr): $\tilde{\nu}$ = 1654 cm^{-1}.

(Formylmethyl-κ*C*^{1})(hydroxy)[*N*,*N*,*N*-tris(2-pyridylmethyl-κ*N*)amine-κ*N*]iridium(III) Hexafluorophosphate (11aPF_6/11bPF_6): 11aPF_6/11bPF_6 was prepared by a procedure similar to that of **11a**BPh_4, using **10a**PF_6/**10b**PF_6 instead of **10a**BPh_4. Yield: 93%. ^{1}H NMR (500 MHz, CD_3CN, 298 K): δ = 10.11 (t, $^3J_{H,H}$ = 5.0 Hz, 1 H, IrCH$_2$C*H*O), 8.73 (d, $^3J_{H,H}$ = 5.9 Hz, 3 H, Py-H6), 7.81 (dt, $^3J_{H,H}$ = 7.7, $^4J_{H,H}$ = 1.5 Hz, 2 H, Py$_b$-H4), 7.61 (dt, $^3J_{H,H}$ = 7.7, $^4J_{H,H}$ = 1.5 Hz, 1 H, Py$_a$-H4), 7.48 (d, $^3J_{H,H}$ = 8.1 Hz, 2 H, Py$_b$-H3), 7.30 (t, $^3J_{H,H}$ = 6.4 Hz, 2 H, Py$_b$-H5), 7.23 (t, $^3J_{H,H}$ = 6.8 Hz, 1 H, Py$_a$-H5), 7.17 (d, $^3J_{H,H}$ = 7.7 Hz, 1 H, Py$_a$-H3), 5.40 (d, $^2J_{H,H}$ = 15.0 Hz, 2 H, NC*H*$_2$Py$_b$), 4.82 (s, 2 H, NC*H*$_2$Py$_a$), 4.77 (d, $^2J_{H,H}$ = 14.7 Hz, 2 H, NC*H*$_2$Py$_b$), 3.66 (d, $^3J_{H,H}$ = 4.8 Hz, 2 H, IrC*H*$_2$CHO) ppm; ^{13}C{^{1}H} NMR (125 MHz, CD_3CN, 300 K): δ = 211.2 (IrCH$_2$*C*HO), 167.1 (Py$_b$-C2), 164.9 (Py$_a$-C2), 152.0 (Py$_b$-C6), 151.1 (Py$_a$-C6), 139.5 (Py$_b$-C4), 138.4 (Py$_a$-C4), 125.9 (Py$_b$-C3/5), 125.7 (Py$_a$-C3/5), 124.5 (Py$_b$-C3/5), 122.2 (Py$_a$-C3/5), 69.3 (N*C*H$_2$Py$_a$), 68.6 (N*C*H$_2$Py$_b$), 20.7 (Ir*C*H$_2$CHO) ppm. ESI-MS (CH_3CN): 543 [M − PF_6]$^+$, 541 [M − H_2 − PF_6]$^+$.

(Formylmethyl-κ*C*^{1})(hydroxy){3,11-dimethyl-3,11,17,18-tetraazatricyclo[11.3.1.1^{5,9}]octadeca-1(17),5(18),6,8,13,15-hexaene-κ^4*N*^{1},*N*^{2},*N*^{3},*N*^{4}}rhodium(III) Hexafluorophosphate (17PF_6): *Solid* **16**PF_6 was put under a nitrogen atmosphere saturated with H_2O vapor for 4 days. The product was dried in vacuo. ^{1}H NMR (400 MHz, CD_3CN, 297 K): δ = 9.57 (t, $^3J_{H,H}$ = 5.4 Hz, 1 H, C*H*O), 7.77 (t, $^3J_{H,H}$ = 7.8 Hz, 1 H, Py-H4), 7.66 (t, $^3J_{H,H}$ = 8.0 Hz, 1 H, Py-H4), 7.29 (d, $^3J_{H,H}$ = 8.0 Hz, 2 H, Py-H3/5), 7.18 (d, $^3J_{H,H}$ = 8.0 Hz, 2 H, Py-H3/5), 4.76 (d[AB], $^2J_{H,H}$ = 16.5 Hz, 2 H, NC*H*$_2$Py), 4.51 (d[AB], $^2J_{H,H}$ = 16.5 Hz, 2 H, NC*H*$_2$Py), 4.30 (d[AB], $^2J_{H,H}$ = 16.5 Hz, 2 H, NC*H*$_2$Py), 4.29 (d[AB], $^2J_{H,H}$ = 15.9 Hz, 2 H, NC*H*$_2$Py), 3.14 (dd, $^3J_{H,H}$ = 5.3, $^3J_{H,Rh}$ = 3.2 Hz, 1 H, RhC*H*$_2$CHO), 2.95 (s, 6 H, NC*H*$_3$) ppm; ^{13}C{^{1}H} NMR (125 MHz, CD_3CN, 243 K): δ = 207.7 (RhCH$_2$*C*HO), 157.4 (Py-C2/6), 155.7 Py-C2/6), 139.9 (Py-C4), 138.7 (Py-C4), 121.4 (Py-C3/5), 74.7 (N*C*H$_2$Py), 72.6 (N*C*H$_2$Py), 50.8 (N*C*H$_3$), 33.4 (d, $^1J_{C,Rh}$ = 21.2 Hz, Rh*C*H$_2$CHO) ppm. FAB-MS (NPOE, CH_3CN): 431 [M − PF_6]$^+$. ESI-MS (CH_3CN): 431 [M − PF_6]$^+$, 413 [M − H_2O − PF_6]$^+$, 287 [M − C_2H_4O − PF_6]$^+$, 371 [M − $C_2H_4O_2$ − PF_6]$^+$, 369 [M − $C_2H_4O_2$ − H_2 − PF_6]$^+$. IR (CD_3CN): $\tilde{\nu}$ = 1651 cm^{-1}.

(Formylmethyl-κ*C*^{1})(hydrogen carbonate)[*N*,*N*,*N*-tris(2-pyridylmethyl-κ*N*)amine-κ*N*]rhodium(III) Tetraphenylborate (21aBPh_4): A solution of **9a**BPh_4 was left standing under a CO_2 atmosphere. **21a**BPh_4 was formed within 5 minutes in a quantitative yield, according to ^{1}H NMR spectroscopy. Isolation of **21a**BPh_4 was not possible, since the insertion of CO_2 is a reversible reaction. Precipitation and filtration led to the isolation of **9a**BPh_4. ^{1}H NMR (200 MHz, CD_3CN, 298 K): δ = 9.53 (t, $^3J_{H,H}$ = 4.6 Hz, 1 H, RhCH$_2$C*H*O), 8.99 (d, $^3J_{H,H}$ = 4.8 Hz, 1 H, Py$_a$-H6), 8.86 (d, $^3J_{H,H}$ = 5.8 Hz, 2 H, Py$_b$-H6), 7.85 (dt, $^3J_{H,H}$ = 7.8, $^4J_{H,H}$ = 1.6 Hz, 2 H, Py$_b$-H4), 7.73 (dt, $^3J_{H,H}$ = 7.7, $^4J_{H,H}$ = 1.6 Hz, 1 H, Py$_a$-H4), 7.5−7.2 (m, 5 H, Py-H5 and Py$_b$-H3), 7.29 (m, 8 H, BAr-H2), 7.15 (d, $^3J_{H,H}$ = 7.9 Hz, 1 H, Py$_a$-H3), 6.99 (t, $^3J_{H,H}$ = 7.4 Hz, 8 H, BAr-H3), 6.84 (t, $^3J_{H,H}$ = 7.2 Hz, 4 H, BAr-H4), 4.99 (d[AB], $^2J_{H,H}$ = 16.2 Hz, 2 H, NC*H*$_2$Py$_b$), 4.58 (s, 2 H, NC*H*$_2$Py$_a$), 4.50 (d[AB], $^2J_{H,H}$ = 15.8 Hz, 2 H, NC*H*$_2$Py$_b$), 3.23 (dd, $^3J_{H,H}$ = 4.8, $^2J_{H,Rh}$ = 2.5 Hz, 2 H, RhC*H*$_2$CHO) ppm; ^{13}C{^{1}H} NMR (50 MHz, CD_3CN): δ = 210.1 (RhCH$_2$*C*HO), 164.6 (q, $^1J_{C,B}$ = 49.3 Hz, BAr-C1), 162.3 (Py$_b$-C2), 158.4 (Py$_a$-C2), 152.2 (Py$_b$-C6), 148.4 (Py$_a$-C6), 140.4 (Py$_b$-C4), 140.1 (Py$_a$-C4), 136.5 (BAr-C2), 126.40 (q, $^3J_{C,B}$ = 2.6 Hz, BAr-C3), 125.9 (Py$_b$-C3/5), 125.5 (CO_2), 124.9 (Py$_b$-C3/5), 122.6 (BAr-C4), 121.9 (Py$_a$-C3/5), 73.2 (N*C*H$_2$Py$_a$), 70.0 (N*C*H$_2$Py$_b$), 28.1 (d, $^1J_{C,Rh}$ = 20.7 Hz, Rh*C*H$_2$CHO) ppm. (The signal for Py$_a$-C3/5 is obscured by one of the other signals). IR (CD_3CN): $\tilde{\nu}$ = 1694, 1664 cm^{-1}.

(Formylmethyl-κ*C*^{1})(hydrogen carbonate)[*N*,*N*,*N*-tris(2-pyridylmethyl-κ*N*)amine-κ*N*]iridium(III) Tetraphenylborate (22aBPh_4): **22a**BPh_4 was prepared by a procedure similar to that of **21a**BPh_4, using **11a**BPh_4 instead of **9a**BPh_4. Complex **22a**BPh_4 was also obtained in a quantitative yield, according to ^{1}H NMR spectroscopy, but could not be isolated. ^{1}H NMR (500 MHz, CD_3CN, 298 K): δ = 9.46 (t, $^3J_{H,H}$ = 4.8 Hz, 1 H, IrCH$_2$C*H*O), 9.02 (d, $^3J_{H,H}$ = 5.5 Hz, 1 H, Py$_a$-H6), 8.95 (d, $^3J_{H,H}$ = 5.5 Hz, 2 H, Py$_b$-H6), 7.82 (dt, $^3J_{H,H}$ = 7.9, $^4J_{H,H}$ = 1.5 Hz, 2 H, Py$_b$-H4), 7.71 (dt, $^3J_{H,H}$ = 7.7, $^4J_{H,H}$ = 1.5 Hz, 1 H, Py$_a$-H4), 7.44 (d, $^3J_{H,H}$ = 7.7 Hz, 2 H, Py$_b$-H3), 7.40 (t, $^3J_{H,H}$ = 6.6 Hz, 1 H, Py$_a$-H5), 7.33 (t, $^3J_{H,H}$ = 6.6 Hz, 2 H, Py$_b$-H5), 7.29 (m, 8 H, BAr-H2), 7.18 (d, $^3J_{H,H}$ = 8.0 Hz, 1 H, Py$_a$-H3), 6.99 (t, $^3J_{H,H}$ = 7.3 Hz, 8 H, BAr-H3), 6.84 (t, $^3J_{H,H}$ = 7.1 Hz, 4 H, BAr-H4), 4.93 (d[AB], $^2J_{H,H}$ = 15.3 Hz, 2 H, NC*H*$_2$Py$_b$), 4.75 (d[AB], $^2J_{H,H}$ = 15.7 Hz, 2 H, NC*H*$_2$Py$_b$), 4.55 (s, 2 H, NC*H*$_2$Py$_a$), 3.39 (d, $^3J_{H,H}$ = 4.8 Hz, 2 H, IrC*H*$_2$CHO) ppm; ^{13}C{^{1}H} NMR (125 MHz, CD_3CN, 298 K): δ = 211.1 (IrCH$_2$-*C*HO), 164.6 (q, ^1J (C,B)= 49.4 Hz, BAr-C1), 164.5 (Py$_b$ -C2), 159.9 (Py$_a$-C2), 152.4 (Py$_b$-C6), 147.9 (Py$_a$-C6), 139.8 (Py$_a$-C4), 139.7 (Py$_b$-C4), 136.5 (BAr-C2), 126.4 (q, $^3J_{C,B}$ = 2.8 Hz, BAr-C3), 125.9 (Py$_b$-C3/5), 125.6 (Py$_b$-C3/5), 124.7 (Py$_a$-C3/5), 122.6 (BAr-C4), 121.8 (Py$_a$-C3/5), 74.9 (N*C*H$_2$Py$_a$), 72.1 (N*C*H$_2$Py$_b$), 14.8 (Ir*C*H$_2$CHO) ppm. ESI-MS (CO_2 saturated CH_3CN): 587 [M − BPh_4]$^+$, 543 [M − CO_2 − BPh_4]$^+$. IR (CH_3CN): $\tilde{\nu}$ = 1663, 1635 cm^{-1}.

(Propene)[*N*,*N*,*N*-tris(2-pyridylmethyl-κ*N*)amine-κ*N*]-rhodium(I) Tetraphenylborate (23bBPh_4): Propene was bubbled through a solution of [(ethene)$_2$RhCl]$_2$ (54 mg, 0.14 mmol) and $NaHCO_3$ (50 mg) in MeOH (3 mL) at room temperature for 30 minutes. Tpa (81 mg, 0.28 mmol) was then added, and the reaction mixture was stirred for 1 hour. After filtration the residue was washed with methanol (2 × 0.25 mL) and $NaBPh_4$ (85.5 mg, 0.25 mmol) was added to the filtrate. The reaction mixture was stirred for 1 hour, filtered, washed with MeOH (3 × 1 mL) and

dried in vacuo. Yield: 130 mg (69%). ^{1}H NMR (200 MHz, [D$_6$]acetone, 300 K): δ = 9.39 (d, $^3J_{H,H}$ = 4.7 Hz, 1 H, Py-H6), 8.33 (d, $^3J_{H,H}$ = 5.5 Hz, 1 H, Py-H6), 8.03 (d, $^3J_{H,H}$ = 5.3 Hz, 1 H, Py-H6), 7.67 (m, 3 H, Py-H4), 7.35 (m, 11 H, BAr-H2 and Py-H3/5), 7.17 (m, 3 H, Py-H3/5), 6.92 (t, $^3J_{H,H}$ = 7.2 Hz, 8 H, BAr-H3), 6.77 (t, $^3J_{H,H}$ = 6.9 Hz, 4 H, BAr-H4), 5.68 (d[AB], $^2J_{H,H}$ = 15.1 Hz, 1 H, NC*H*$_2$Py), 5.57 (d[AB], $^2J_{H,H}$ = 15.1 Hz, 1 H, NC*H*$_2$Py), 4.93 (d[AB], $^2J_{H,H}$ = 15.3 Hz, 1 H, NC*H*$_2$Py), 4.92 (d[AB], $^2J_{H,H}$ = 15.5 Hz, 1 H, NC*H*$_2$Py), 4.63 (s, 2 H, NC*H*$_2$Py), 2.47 (m, 1 H, CH$_2$C*H*CH$_3$), 2.28 (dm, $^3J_{H,H}$ = 7.8 Hz, 1 H, C*H*$_2$CHCH$_3$), 1.93 (dm, $^3J_{H,H}$ = 9.8 Hz, 1 H, C*H*$_2$CHCH$_3$), 0.87 (dd, $^3J_{H,H}$ = 6.2, $^2J_{H,Rh}$ = 1.3 Hz, 3 H, CH$_2$CHC*H*$_3$) ppm; ^{13}C{^{1}H} NMR (100 MHz, [D$_6$]acetone, 297 K): δ = 165.0 (q, $^1J_{C,B}$ = 49.7 Hz, BAr-C1), 164.1 (Py-C2), 163.5 (Py-C2), 159.3 (Py-C2), 152.4 (Py-C6), 151.9 (Py-C6), 151.2 (Py-C6), 138.3 (Py-C4), 137.5 (Py-C4), 137.4 (Py-C4), 137.1 (BAr-C2), 126.1 (m, BAr-C3), 125.5 (Py-C3/5), 125.2 (Py-C3/5), 124.7 (Py-C3/5), 123.7 (Py-C3/5), 123.4 (Py-C3/5), 122.4 (Py-C3/5), 122.4 (BAr-C4), 70.1 (N*C*H$_2$Py), 69.9 (N*C*H$_2$Py), 64.6 (N*C*H$_2$Py), 40.3 (d, $^1J_{C,Rh}$ = 19.7 Hz, *C*H$_2$CHCH$_3$/CH$_2$*C*HCH$_3$), 33.8 (d, $^1J_{C,Rh}$ = 19.8 Hz, *C*H$_2$CHCH$_3$/CH$_2$*C*HCH$_3$), 20.6 (CH$_2$CH*C*H$_3$) ppm. ESI-MS (acetone): 435 [M − BPh$_4$], 393 [M − C$_3$H$_6$ − BPh$_4$], 301 [M − C$_3$H$_6$ − CH$_2$C$_5$H$_4$N − BPh$_4$].

(Peroxo-κ^2*O*^{1},*O*^{2})[*N*,*N*,*N*-tris(2-pyridylmethyl-κ*N*)amine-κ*N*]-rhodium(III) Tetraphenylborate (24BPh$_4$): Complex **23**BPh$_4$ was exposed to air for 3 days. **24**BPh$_4$ was obtained in > 90% yield, as determined by ^{1}H NMR spectroscopy. ^{1}H NMR (500 MHz, CD$_3$CN, 233 K): δ = 9.23 (d, $^3J_{H,H}$ = 5.5 Hz, 1 H, Py$_a$-H6), 8.37 (d, $^3J_{H,H}$ = 5.1 Hz, 2 H, Py$_b$-H6), 7.77 (dt, $^3J_{H,H}$ = 7.8, $^4J_{H,H}$ = 1.6 Hz, 2 H, Py$_b$-H4), 7.65 (dt, $^3J_{H,H}$ = 7.8, $^4J_{H,H}$ = 1.6 Hz, 1 H, Py$_a$-H4), 7.34 (d, $^3J_{H,H}$ = 7.7 Hz, 2 H, Py$_b$-H3), 7.28 (m, 11 H, BAr-H2, Py-H5), 7.12 (d, $^3J_{H,H}$ = 7.7 Hz, 1 H, Py$_a$-H3), 6.98 (t, $^3J_{H,H}$ = 7.3 Hz, 8 H, BAr-H3), 6.81 (t, $^3J_{H,H}$ = 7.2 Hz, 4 H, BAr-H4), 5.21 (d[AB], $^2J_{H,H}$ = 16.1 Hz, 2 H, NC*H*$_2$Py$_b$), 4.82 (d[AB], $^2J_{H,H}$ = 16.1 Hz, 2 H, NC*H*$_2$Py$_b$), 4.53 (s, 2 H, NC*H*$_2$Py$_a$) ppm; ^{13}C{^{1}H} NMR (125 MHz, CD$_3$CN, 233 K): δ = 163.8 (q, $^1J_{C,B}$ = 49.2 Hz, BAr-C1), 162.8 (Py$_b$-C2), 159.8 (Py$_a$-C2), 152.5 (Py$_a$-C6), 150.1 (Py$_b$-C6), 139.4 (Py$_b$-C4), 139.1 (Py$_a$-C4), 135.6 (BAr-C2), 126.0 (q, $^3J_{C,B}$ = 2.7 Hz, BAr-C3), 125.4 (Py$_b$-C3/5), 123.4 (Py$_b$-C3/5), 122.1 (BAr-C4), 121.8 (Py$_a$-C3/5), 70.4 (N*C*H$_2$Py$_b$), 67.6 (N*C*H$_2$Py$_a$) ppm. (The signal for Py$_a$-C3/5 is obscured by one of the other signals). ESI-MS (CH$_3$CN): 425 [M − BPh$_4$]$^+$, 393 [M − O$_2$ − BPh$_4$]$^+$, (467 [?]$^+$ [22]).

(Hydroperoxy)(hydroxy)[*N*,*N*,*N*-tris(2-pyridylmethyl-κ*N*)-amine-κ*N*]rhodium(III) Tetraphenylborate (25BPh$_4$): Complex **24**BPh$_4$ was exposed to a N$_2$ atmosphere saturated with water for 3 days. **25**BPh$_4$ was obtained in > 90% yield, as determined by ^{1}H NMR spectroscopy. ^{1}H NMR (200 MHz, CD$_3$CN, 300 K): δ = 8.76 (d, $^3J_{H,H}$ = 5.9 Hz, 1 H, Py$_a$-H6), 8.70 (d, $^3J_{H,H}$ = 5.7 Hz, 2 H, Py$_b$-H6), 7.86 (dt, $^3J_{H,H}$ = 7.8, $^4J_{H,H}$ = 1.6 Hz, 2 H, Py$_b$-H4), 7.69 (dt, $^3J_{H,H}$ = 7.8, $^4J_{H,H}$ = 1.7 Hz, 1 H, Py$_a$-H4), 7.5−7.3 (m, 5 H, Py$_b$-H3 and Py-H5), 7.28 (m, 8 H, BAr-H2), 7.11 (d, $^3J_{H,H}$ = 7.8 Hz, 1 H, Py$_a$-H3), 6.99 (t, $^3J_{H,H}$ = 7.3 Hz, 8 H, BAr-H3), 6.83 (t, $^3J_{H,H}$ = 7.0 Hz, 4 H, BAr-H4), 5.35 (d[AB], $^2J_{H,H}$ = 15.5 Hz, 2 H, NC*H*$_2$Py$_b$), 4.75 (m, 4 H, NC*H*$_2$Py$_b$ and NC*H*$_2$Py$_a$) ppm. ESI-MS (CH$_3$CN): 443 [M − BPh$_4$]$^+$, 425 [M − H$_2$O − BPh$_4$]$^+$, 410 [M − HO$_2$ − BPh$_4$]$^+$, 393 [M − OH − O$_2$H − BPh$_4$]$^+$, 300 [M − CH$_2$C$_5$H$_4$N − O$_2$H − H$_2$O − BPh$_4$]$^+$.

Acknowledgments

This work was supported by the Netherlands Organization for Scientific Research (NWO-CW). We thank Johnson Matthey Ltd. for a generous loan of RhCl$_3$·3H$_2$O. S. Thewissen, P. M. van Galen, and H. I. V. Amatdjais-Groenen are gratefully acknowledged for the ESI-MS measurements. Prof. Dr. P. Chen from the ETH Zürich is kindly acknowledged for allowing us to use the Finnigan TSQ 7000 mass spectrometer. Prof. Dr. Hans-Jörg Krüger (Universität Kaiserslautern, Germany) is kindly acknowledged for providing us with details on the synthesis of N$_4$Me$_2$.

[1] [1a] H. Mimoun, M. M. P. Machirant, I. Seree de Roch, *J. Am. Chem. Soc.* **1978**, *100(17)*, 5437−5444. [1b] G. Read, *J. Mol. Catal.* **1988**, *44*, 15−33. [1c] M. Bressan, F. Morandini, A. Morvillo, P. Rigo, *J. Organomet. Chem.* **1985**, *280*, 139−146. [1d] R. A. Sheldon, J. A. van Doorn, *J. Organomet. Chem.* **1975**, *94*, 115−129. [1e] H. Mimoun, *Angew. Chem.* **1982**, *21*, 734; *Angew. Chem. Int. Ed. Engl.* **1982**, *94*, 750−766. [1f] H. Mimoun, I. Seree de Roch, L. Sajus, *Tetrahedron* **1970**, *26*, 37−50.

[2] D. V. Deubel, J. Sundermeyer, G. Frenking, *J. Am. Chem. Soc.* **2000**, *122*, 10101−10108.

[3] [3a] G. Read, M. Urgelles, A. M. R. Galas, M. B. Hursthouse, *J. Chem. Soc., Dalton Trans.* **1983**, 911−913. [3b] L. Pandolfo, G. Paiaro, G. Valle, P. Ganis, *Gazz. Chim. Ital.* **1985**, *115*, 59−63.

[4] [4a] M. Krom, R. G. E. Coumans, J. M. M. Smits, A. W. Gal, *Angew. Chem.* **2001**, *113*, 2164−2166; *Angew. Chem. Int. Ed.* **2001**, *40(11)*, 2106−2108. [4b] M. Krom, R. G. E. Coumans, J. M. M. Smits, A. W. Gal, *Angew. Chem.* **2002**, *114*, 595−599; *Angew. Chem. Int. Ed.* **2002**, *41(4)*, 575−579.

[5] B. de Bruin, M. J. Boerakker, J. A. W. Verhagen, R. de Gelder, J. M. M. Smits, A. W. Gal, *Chem. Eur. J.* **2000**, *6*, 298−312.

[6] [6a] B. de Bruin, J. A. Brands, J. J. J. M. Donners, M. P. J. Donners, R. de Gelder, J. M. M. Smits, A. W. Gal, A. L. Spek, *Chem. Eur. J.* **1999**, *5*, 2921−2936. [6b] B. de Bruin, R. J. N. A. M. Kicken, N. F. A. Suos, M. P. J. Donners, C. J. den Reijer, A. J. Sandee, R. de Gelder, J. M. M. Smits, A. W. Gal, A. L. Spek, *Eur. J. Inorg. Chem.* **1999**, 1581−1592. [6c] B. de Bruin, Th. P. J. Peters, J. B. M. Wilting, S. Thewissen, J. M. M. Smits, A. W. Gal, *Eur. J. Inorg. Chem.* **2002**, 2671.

[7] The X-ray structures of three other iridium bis(ethene) complexes stabilized by tridentate nitrogen donor ligands have been reported: [7a] Y. Alvarado, O. Boutry, E. Gutiérrez, A. Monge, M. C. Nicasio, M. L. Poveda, P. J. Pérez, C. Ruíz, C. Bianchini, E. Carmona, *Chem. Eur. J.* **1997**, *3*, 860−873. [7b] J. S. Wiley, W. J. Oldham, Jr., D. M. Heinekey, *Organometallics* **2000**, *19*, 1670−1676. The third complex is stabilized by a tpa-type ligand.[6c]

[8] *N*,*N*′-Dimethyl-2,11-diaza[3,3](2,6)pyridinophane = 3,11-dimethyl-3,11,17,18-tetraazatricyclo[11.3.1.1^{5,9}]octadeca-1(17),5(18),6,8,13,15-hexaene.

[9] [9a] H. Kelm, H. J. Kruger, *Eur. J. Inorg. Chem.* **1998**, 1381−1385. [9b] T. Sciarone, J. Hoogboom, P. P. J. Schlebos, P. H. M. Budzelaar, R. de Gelder, J. M. M. Smits, A. W. Gal, *Eur. J. Inorg. Chem.* **2002**, 457−464. [9c] S. Plentz Meneghetti, P. J. Lutz, J. Kress, *Organometallics* **2001**, *20*, 5050−5055.

[10] [10a] H. Sakaba, C. Kabuto, H. Horino, M. Arai, *Bull. Chem. Soc. Jpn.* **1990**, *63*, 1822−1824. [10b] H. Kelm, H. J. Kruger, *Inorg. Chem.* **1996**, *35*, 3533−3540. [10c] W. O. Koch, V. Schunemann, M. Gerdan, A. X. Trautwein, H. J. Kruger, *Chem. Eur. J.* **1998**, *4(7)*, 1255−1265. [10d] W. O. Koch, V. Schunemann, M. Gerdan, A. X. Trautwein, H. J. Kruger, *Chem. Eur. J.* **1998**, *4(4)*, 686−691. [10e] H. J. Krüger, *Chem. Ber.* **1995**, *128*, 531−539. [10f] W. O. Koch, H. J. Kruger, *Angew. Chem. Int. Ed. Engl.* **1995**, *34 (23/24)*, 2671−2674.

[11] Samples as prepared required the reported reaction time for full conversion. The different reaction times found for different complexes could reflect differences in reactivity and/or differences in particle size distribution.

[12] O$_\beta$ and C$_\beta$ (O2 and C2) are positioned above and below the O1−M−C1 plane: the displacement of O2 from this plane is +0.51 Å in **8a**A$^+$ and −0.47 Å in **8a**B$^+$, versus +0.49 Å in the

3-platina-1,2-dioxolane **1**. The displacement of C2 is −0.26 Å in **8a**A^+ and +0.29 Å in **8a**B^+, versus −0.29 in the 3-platina-dioxolane.

[13] This range is based on O−O distances in 48 crystal structures containing a M−O−O−C fragment (M = any metal); 4 outliers were not taken into account.

[14] This range is based on O−C distances in 48 crystal structures containing a M−O−O−C fragment (M = any metal); 9 outliers were not taken into account.

[15] Bzbpa = *N*-benzyl-*N*,*N*-bis(2-pyridylmethyl)amine.

[16] B. de Bruin, J. A. W. Verhagen, C. H. J. Schouten, A. W. Gal, D. Feichtinger, D. A. Plattner, *Chem. Eur. J.* **2001**, *7(2)*, 416−422.

[17] For some examples see: [17a] J. C. M. Ritter, R. G. Bergman, *J. Am. Chem. Soc.* **1997**, *119*, 2580−2581. [17b] K. J. Del Rossi, X. X. Zhang, B. B. Wayland, *J. Organomet. Chem.* **1995**, *504*, 47−56.

[18] Space group before and after transformation: *C*2/*c*. Cell dimensions before transformation: a = 35.8688(5), b = 10.7328(2), c = 24.2609(4) Å, β = 116.666(1)°, V = 8346.4(2) Å^3. Cell dimensions after transformation: a = 36.0362(2), b = 10.7760(1), c = 24.2975(2) Å, β = 116.3883(4)°, V = 8452.2(2) Å^3 (see Table 5).

[19] A. N. J. Blok, P. H. M. Budzelaar, M. Krom, A. W. Gal, paper to be published.

[20] Yields and reaction times highly depend on the presence of (small amounts of) water and protonation of the counterion, which both influence the acidity of the solution.

[21] [21a] B. R. Flynn, L. Vaska, *J. Am. Chem. Soc.* **1973**, *95(15)*, 5081−5083. [21b] T. Yoshida, D. L. Thorn, T. Okano, J. A. Ibers, S. Otsuka, *J. Am. Chem. Soc.* **1979**, *101(15)*, 4212−4221. [21c] S. F. Hossain, K. M. Nicholas, C. L. Teas, R. E. Davis, *J. Chem. Soc., Chem. Commun.* **1981**, 268−269.

[22] The ESI-MS spectrum also shows a peak at m/z = 467, but since both the ^{1}H NMR and ^{13}C NMR spectra (measured at 233 K) do not show any peaks that could stem from a second product, we have no explanation for the origin of this peak.

[23] See e.g.: [23a] H. Büning, J. Altman, H. Zorbas, W. Beck, *J. Inorg. Biochem.* **1999**, *75(4)*, 269−279. [23b] K. Tajima, S. Oka, T. Edo, S. Miyake, H. Mano, K. Mukai, H. Sakurai, K. Ishizu, *J. Chem. Soc., Chem. Commun.* **1995**, (*15*), 1507−1508. [23c] P. N. Balasubramanian, E. S. Schmidt, T. C. Bruice, *J. Am. Chem. Soc.* **1987**, *109(25)*, 7865−7873.

[24] R. Cramer, *Inorg. Synth.* **1990**, *28*, 86−88.

[25] G. Anderegg, F. Wenk, *Helv. Chim. Acta* **1967**, *50(243)*, 2330−2332.

[26] H. Nagao, N. Komeda, M. Mukaida, M. Suzuki, K. Tanaka, *Inorg. Chem.* **1996**, *35*, 6809−6815.

[27] [27a] F. Bottino, M. De Grazia, P. Finocchario, F. R. Fronczek, A. Mamo, S. Pappalardo, *J. Org. Chem.* **1988**, *53*, 3521−3529. [27b] H. J. Krüger, personal communication.

[28] J. L. Herdé, J. C. Lambert, C. V. Senoff, *Inorg. Synth.* **1974**, *15*, 18−20.

[29] M. Brookhart, B. Grant, A. F. Volpe Jr., *Organometallics* **1992**, *11*, 3920−3922.

[30] P. T. Beurskens, G. Beurskens, M. Strumpel, C. E. Nordman, in: *Patterson and Pattersons* (Eds.: J. P. Glusker, B. K. Patterson, M. Rossi) Clarendon Press, Oxford, **1987**, 356−367.

[31] *DIRDIF-96.* A computer program system for crystal structure determination by Patterson methods and direct methods applied to difference structure factors: P. T. Beurskens, G. Beurskens, W. P. Bosman, R. de Gelder, S. García-Granda, R. O. Gould, R. Israël, J. M. M. Smits, Crystallography Laboratory, University of Nijmegen, The Netherlands, **1996**.

[32] A. L. Spek, *Acta Crystallogr., Sect. A* **1990**, *46*, C-34.

[33] *PLATON-93.* Program for display and analysis of crystal and molecular structures: A. L. Spek, University of Utrecht, The Netherlands, **1995**.

[34] Immersion Lamp TQ 150 of Heraeus Noblelight GmbH; power consumption: 150 W. The experimental setup is available as Supporting Information.

Received July 23, 2002
[I02410]

Chelate Complexes of Functionalized Cycloheptatrienyl Ligands: Molybdenum Complexes with Linked Cycloheptatrienyl-Phosphane Ligands and Their Use in Catalytic Carbon−Carbon Bond Formation

Matthias Tamm,*[a][‡] Bernd Dreßel,[a][‡] Thomas Lügger,[a] Roland Fröhlich,[b] and Stefan Grimme[b]

Keywords: Alkyne ligands / C−C coupling / Cycloheptatrienyl ligands / Density functional calculations / Hydride ligands

The synthesis of *P*-functionalized molybdenum chelate complexes incorporating the linked cycloheptatrienyl-phosphane ligand [2-(diisopropylphosphanyl)phenyl]cycloheptatrienyl (*o*-*i*Pr_2P–C_6H_4–C_7H_6) is described. From the ligand precursor [2-(cyclohepta-2,4,6-trienyl)phenyl]diisopropylphosphane (**1**) the paramagnetic 17-electron dibromide [(*o*-*i*$Pr_2PC_6H_4$-η^7-C_7H_6)$MoBr_2$(*P–Mo*)] (**2**) can readily be obtained. This is a versatile starting material for the preparation of cycloheptatrienyl molybdenum hydrides [(*o*-*i*$Pr_2PC_6H_4$-η^7-C_7H_6)Mo(η^2-BH_4)(*P–Mo*)] (**3**) and [(*o*-*i*$Pr_2PC_6H_4$-η^7-C_7H_6)Mo(PPh_3)-H(*P–Mo*)] (**4**). Treatment of **3** with dimethylanilinium tetraphenylborate ([$PhNMe_2H$][BPh_4]) allows the production of the cationic 14-electron complex fragment [(*o*-*i*$Pr_2PC_6H_4$-η^7-C_7H_6)Mo(*P–Mo*)]$^+$ (**13**), which can be stabilized in the presence of suitable ligands L. The complexes [(*o*-*i*$Pr_2PC_6H_4$-η^7-C_7H_6)MoL_2(*P–Mo*)]BPh_4 [L = dimethylphenyl isocyanide, (**5**)BPh_4; L_2 = η^4-2,5-norbornadiene, (**6**)BPh_4; L_2 = η^2-phenylacetylene, (**7**)BPh_4; L_2 = η^2-*tert*-butylacetylene, (**8**)BPh_4] can thus be isolated in good yields. The alkyne complex (**7**)BPh_4 can be used as a single-source catalyst for the oligomerization of phenylacetylene, affording a mixture of triphenylbenzenes and linear oligomers. Quantum chemical calculations reveal an intimate relationship between the catalytically active 14-electron complex fragment [(*o*-*i*$Pr_2PC_6H_4$-η^7-C_7H_6)Mo(*P–Mo*)]$^+$ (**13**) and *hypothetical* isoelectronic and isolobal complexes of the type [(*o*-*i*$Pr_2PC_6H_4$-η^5-C_5H_4)M(*P–M*)]$^+$ (M = Ru, **14**; M = Os, **15**), indicating that cycloheptatrienyl molybdenum systems might in general be a suitable replacement for cyclopentadienyl ruthenium and osmium catalysts.
(© Wiley-VCH Verlag GmbH & Co. KGaA, 69451 Weinheim, Germany, 2003)

Introduction

Ruthenium half-sandwich complexes of the type [(η-C_5R_5)Ru(PR'_3)$_2$Cl] (R = H, Me; R′ = alkyl, aryl) are among the most important starting materials in organotransition metal chemistry and have played key roles in the stabilization of highly reactive species such as vinylidenes and allenylidenes by metal coordination.[1] In addition, extensive studies have shown that these complexes are particularly useful for effective ruthenium-catalyzed C−C bond formation.[2] The actual active catalyst system in this process is generated by splitting off of the halide and one phosphane ligand, resulting in the formation of the doubly coordinatively unsaturated complex fragment [(η-C_5R_5)Ru(PR'_3)]$^+$ (**I**), which allows various organic substrates to be brought together and coupled in its coordination sphere.[2,3] The similarity between the isoelectronic and isolobal fragments [(η-C_5R_5)Ru] and [(η-C_7H_7)Mo] prompted us to pursue a general study on the possibility of replacing the frequently used ruthenium catalysts by the analogous but much cheaper molybdenum systems. Consequently, similar chemical and physical properties may be expected in complexes possessing an identical set of co-ligands upon substitution of the [(η-C_5R_5)Ru] unit by [(η-C_7H_7)Mo] unit.[4,5]

Our goal of introducing cycloheptatrienyl molybdenum complexes into homogeneous catalysis is based on the concept of donor functionalization, extremely successful in cyclopentadienyl chemistry in particular,[6−9] and we have already been able to synthesize complexes with novel cycloheptatrienyl ligands bearing pendant O-, N-, S- and P-donor groups capable of coordinating to a transition metal center in a chelating η^7:η^1-fashion.[10,11] Complexes with linked cycloheptatrienyl-phosphane ligands seemed to be particularly well suited for applications in catalytic C−C coupling reactions, and so we have started to prepare precursor complexes that should allow us to obtain coordin-

[a] Institut für Anorganische und Analytische Chemie, Westfälische Wilhelms-Universität,
Wilhelm-Klemm-Str. 8, 48149 Münster, Germany
E-mail: matthias.tamm@ch.tum.de
[b] Organisch-Chemisches Institut, Westfälische Wilhelms-Universität,
Corrensstr. 40, 48149 Münster, Germany
[‡] Current Address: Anorganisch-chemisches Institut, Lehrstuhl für Anorganische Chemie, Technische Universität München,
Lichtenbergstr. 4, 85747 Garching
Fax: (internat.) + 49−(0)89/289−13473

atively unsaturated molybdenum complex fragments of type **II** (Scheme 1).[12] In this contribution we present the syntheses of tetrahydroborate complexes of type [(*o*-$R_2PC_6H_4$-η^7-C_7H_6)Mo(η^2-BH_4)(*P*-*Mo*)] (R = *i*Pr, Ph), from which the cationic 14-electron complex fragments [(*o*-$R_2PC_6H_4$-η^7-C_7H_6)Mo(*P*-*Mo*)]$^+$ can be generated and stabilized in the presence of suitable co-ligands.

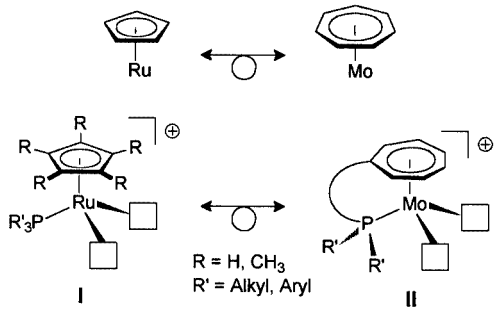

Scheme 1. Isolobal relationship between cyclopentadienyl ruthenium and cycloheptatrienyl molybdenum complex fragments

Results and Discussion

Preparation and Reactions of Molybdenum Hydride Complexes

We have recently reported on the preparation of a cycloheptatriene with a diphenylphosphanyl donor group, and were able to demonstrate that the resulting paramagnetic 17-electron complexes of the type [(*o*-$Ph_2PC_6H_4$-η^7-C_7H_6)MoX_2(*P*-*Mo*)] (X = Br, CH_2SiMe_3) can be used in the ring-opening metathesis polymerization of norbornene.[11] In order to render the donor moiety more sterically demanding and electron-rich, we aimed at replacement of the phenyl substituents with isopropyl groups, and the corresponding ligand precursor [2-(cyclohepta-2,4,6-trienyl)-phenyl]diisopropylphosphane (**1**) used in this contribution was prepared by addition of 2-(diisopropylphosphanyl)-phenyllithium to the tropylium cation $C_7H_7^+$. A three-step synthesis starting from the air-sensitive **1** and $Mo(CO)_6$ affords the 17-electron dibromo complex **2** (Scheme 2). Full details of the preparation of **1** and **2**, together with the spectroscopic and structural properties of all reaction intermediates, will be presented elsewhere.[13]

Reduction of paramagnetic **2** can be achieved by use of $NaBH_4$ in ethanol solution, resulting in the formation of the tetrahydroborate complex **3** (Scheme 2). In contrast, Suzuki and co-workers have shown that the corresponding treatment of isoelectronic ruthenium(III) complexes of the type [(η-C_5Me_5)Ru(PR_3)Cl_2] (R = Ph, *i*Pr, *cyclo*-C_6H_{11}) does indeed also give tetrahydroborate complexes [(η-C_5Me_5)Ru(PR_3)(η^2-BH_4)], but that these undergo immediate ethanolysis under these conditions to yield the trihydrides [(η-C_5Me_5)Ru(PR_3)H_3].[14] In our hands, **2** could not be converted into a trihydride complex and remained perfectly stable toward hydrolysis even in wet ethanol solution. The molecular structure of **3** is shown in Figure 1 (top), and selected bond lengths and angles are listed in Table 1.

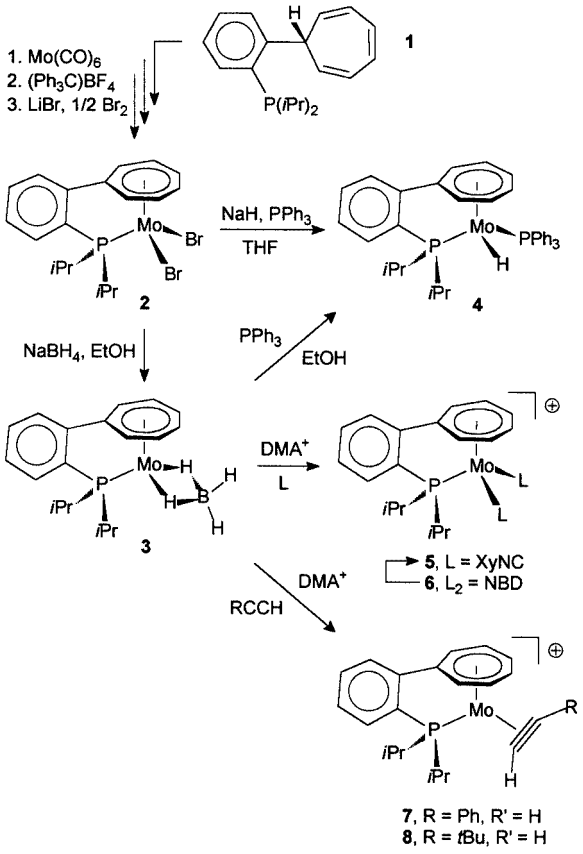

Scheme 2. XyNC = 2,6-dimethylphenyl isocyanide; NBD = 2,5-norbornadiene; DMA^+ = dimethylanilinium $(PhNMe_2\ H)^+$

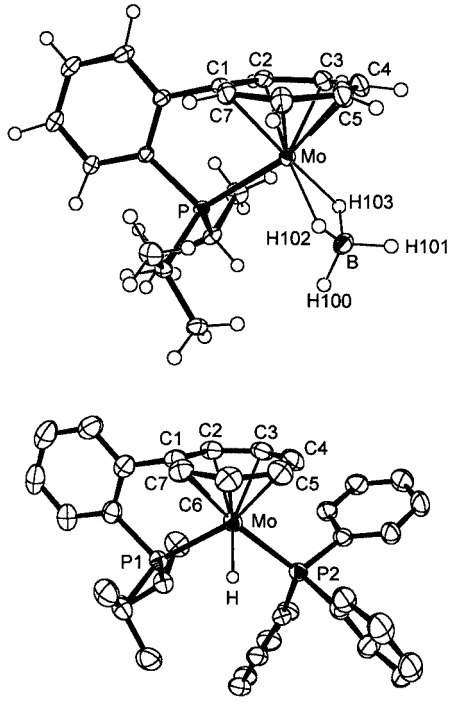

Figure 1. ORTEP drawings of **3** (top) and **4** (bottom) with thermal ellipsoids drawn at 50% probability

Table 1. Selected bond lengths (Å) and angles (°) for **3**, **4**, (**5**)$BPh_4 \cdot C_5H_{12}$, (**6**)$BPh_4 \cdot CH_2Cl_2$, (**7**)BPh_4, and (**10**)$BPh_4 \cdot 3C_4H_8O$

	3	**4**	(**5**)$BPh_4 \cdot C_5H_{12}$	(**6**)$BPh_4 \cdot CH_2Cl_2$	(**7**)BPh_4	(**10**)$BPh_4 \cdot 3C_4H_8O$
C1−C2	1.4218(19)	1.425(3)	1.417(6)	1.420(5)	1.408(4)	1.403(5)
C2−C3	1.413(2)	1.401(3)	1.376(7)	1.391(5)	1.402(4)	1.435(5)
C3−C4	1.418(2)	1.407(3)	1.404(7)	1.410(6)	1.422(5)	1.411(5)
C4−C5	1.402(2)	1.406(3)	1.401(7)	1.392(6)	1.380(5)	1.403(6)
C5−C6	1.427(2)	1.419(3)	1.401(7)	1.422(6)	1.415(5)	1.404(6)
C6−C7	1.414(2)	1.409(3)	1.403(6)	1.392(6)	1.405(4)	1.413(5)
C1−C7	1.419(2)	1.409(3)	1.416(6)	1.406(5)	1.410(4)	1.421(5)
C1−C8	1.5042(18)	1.497(3)	1.509(6)	1.502(5)	1.496(4)	1.500(5)
C14−C15/C26−C27					1.292(4)	1.279(5)
C15−C16/C27−C28					1.457(4)	1.465(5)
C20−C21				1.371(6)		
C23−C24				1.368(5)		
C20−N1			1.164(5)			
C29−N2			1.165(6)			
Mo−C1	2.2527(12)	2.286(2)	2.264(5)	2.324(3)	2.373(3)	2.366(3)
Mo−C2	2.2744(14)	2.316(2)	2.321(5)	2.294(4)	2.292(3)	2.325(3)
Mo−C3	2.2557(14)	2.319(2)	2.298(5)	2.272(4)	2.221(3)	2.226(3)
Mo−C4	2.3191(13)	2.323(2)	2.313(5)	2.343(4)	2.324(3)	2.311(3)
Mo−C5	2.3168(14)	2.310(2)	2.301(5)	2.343(4)	2.343(3)	2.351(4)
Mo−C6	2.2550(13)	2.261(2)	2.286(5)	2.270(4)	2.241(3)	2.246(3)
Mo−C7	2.2736(11)	2.294(2)	2.301(4)	2.311(4)	2.280(3)	2.268(3)
Mo−C14/C26					2.023(3)	2.035(3)
Mo−C15/C27					2.090(3)	2.090(3)
Mo−C20			2.076(5)	2.381(4)		
Mo−C21				2.401(4)		
Mo−C23				2.400(4)		
Mo−C24				2.388(4)		
Mo−C29			2.078(5)			
Mo−P/P1	2.4824(3)	2.4912(5)	2.4958(13)	2.5863(10)	2.5283(8)	2.5073(9)
Mo−P2		2.4886(6)				
C14−C15−C16/ C26−C27−C28					136.6(3)	138.4(3)

The positions of all hydrogen atoms were refinable, indicating that the BH_4 anion is coordinated to the molybdenum atom through two three-center, two-electron bonds, thereby simultaneously blocking two coordination sites. This bidentate M(μ^2-H_2BH_2) ligation represents the most common mode of bonding in tetrahydroborate transition metal complexes.[15] In addition, it is possible to establish the angles between the centroid of the cycloheptatrienyl ring, the C_7 carbon atoms, and the adjacent hydrogen atoms, to reveal a significant out-of-plane displacement for the C_7 ring hydrogen atoms. The average bending is about 9° toward the molybdenum center, such deviation having previously been attributed to a reorientation of the large seven-membered ring for a better metal overlap.[4,16]

As described above, **3** remained perfectly stable in ethanol solution. In the presence of Lewis bases such as PPh_3, however, rapid ethanolysis and cleavage of the BH_4 ligand can be achieved, and formation of the monohydride complex **4** is observed together with evolution of dihydrogen. The reaction can be followed by ^{31}P NMR spectroscopy, which reveals two doublets at 74.5 and 53.7 ppm for the two different phosphorus nuclei in **4** ($^2J_{P,P}$ = 31 Hz) together with the singlet at δ = 67.9 ppm for complex **3**. Pure hydrides such as **4** can also be efficiently prepared directly from the dibromide **2** by use of various hydride sources in the presence of Lewis bases. Consequently, treatment of **2** with sodium hydride in the presence of PPh_3 affords **4** in good yield. In **4**, the pseudotetrahedrally coordinated molybdenum center has four different ligands, and so the complex is obtained as a racemic mixture of two enantiomers. As this representative of so-called "chiral-at-metal" half-sandwich compounds[17−19] is configurationally stable, the diastereotopic cycloheptatrienyl hydrogen atoms give rise to six different ^1H NMR resonances between 3.8 and 5.5 ppm. This portion of the 600 MHz spectrum is shown in Figure 2. Correspondingly, seven ^{13}C NMR resonances are observed for the C_7H_6 carbon atoms, together with six resonances for the phenylene bridge and six resonances for the diastereotopic isopropyl groups. The hydride resonance in **4** is observed as a doublet of doublets at −2.88 ppm with 62 and 41 Hz couplings to the two different phosphorus nuclei (Figure 2). Recrystallization of **4** from hexane afforded single crystals suitable for structure determination by X-ray diffraction; the molecular structure is shown in Figure 1 (bottom). The position of the Mo−H hydrogen atom could be refined to reveal a molybdenum hydrogen

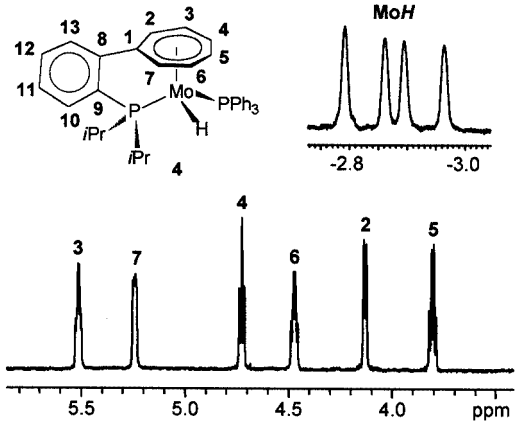

Figure 2. Selected parts of the ^{1}H NMR spectrum (600 MHz, [D_8]toluene) of **4**

bond length of 1.69(2) Å. As would be expected, this distance is slightly shorter than the Mo−H distances of 1.88(2) and 1.96(2) Å in **3**.

Compound **4** is a rare example of a cycloheptatrienyl transition metal hydride, and to the best of our knowledge, [(η^7-C_7H_7)Mo(dppe)H] represents the only previously reported closely related example,[20] apart from a series of tungsten complexes of the type [(η^7-C_7H_7)W(PR_3)(CO)H] (R = OMe, O*i*Pr, Ph).[21] Furthermore, chiral hydrides such as **4** might − in view of the extensive chemistry of related cyclopentadienyl iron, ruthenium, and osmium hydrides − be interesting starting materials for hydrometalation or hydrogenation reactions.[22] For instance, protonation of the hydride ligand in **4** might result in the formation of a cationic dihydrogen complex [(*o*-*i*$Pr_2PC_6H_4$-η^7-C_7H_6)Mo(PPh_3)(H_2)(*P*-*Mo*)]$^+$, from which the 14-electron complex fragment [(*o*-*i*$Pr_2PC_6H_4$-η^7-C_7H_6)Mo(*P*-*Mo*)]$^+$ could be generated by splitting of the phosphane and the dihydrogen ligands. To our disappointment, however, decomposition was mainly observed upon treatment of **4** with HBF_4·Et_2O.

More conveniently, the tetrahydroborate **3** proved to be an ideal starting material for the generation of our target 14-electron complex by cleavage of the boranate ligand. In fact, this unit can be made available by treatment of **3** with dimethylanilinium (DMA^+) salts, widely used as mild acids in metallocene chemistry.[23] Treatment of **3** with [$HNMe_2Ph$][BPh_4] proceeds with evolution of dihydrogen, and the formation of stable cationic adducts is observed in THF and acetonitrile solutions. The bis(acetonitrile) complex can even be isolated in crystalline form. The two available coordination sites can be blocked irreversibly by addition of more strongly coordinating ligands. If the protonolysis is carried out in the presence of 2,6-dimethylphenyl isocyanide (XyNC), for instance, the stable diisocyanide complex (**5**)BPh_4 is obtained. The CN stretching frequencies of 2099 and 2066 cm^{-1} show that the cationic [(*o*-*i*$Pr_2PC_6H_4$-η^7-C_7H_6)Mo(*P*-*Mo*)]$^+$ unit has a relatively strong electron-releasing capability, although significantly stronger metal-to-ligand backbonding is observed in, for instance, *trans*-diisocyanide molybdenum(0) complexes containing only additional phosphane ligands.[24,25] Accordingly, the molecular structure of the cation in (**5**)BPh_4·C_5H_{12} (Figure 3, top) has longer Mo-C bond lengths [2.076(5) and 2.078(5) Å] to the isocyanide carbon atoms, together with slightly shorter C≡N bond lengths [1.164(5) and 1.165(6) Å], in comparison with the values found for the centrosymmetric structure of *trans*-[$Mo(dppe)_2(CNPh)_2$] [2.031(6) and 1.171(6) Å].[25] Only slight deviation from linearity is observed for the Mo-C−N and C−N−C bond angles in **5** (168.7(5) − 174.6(5)°).

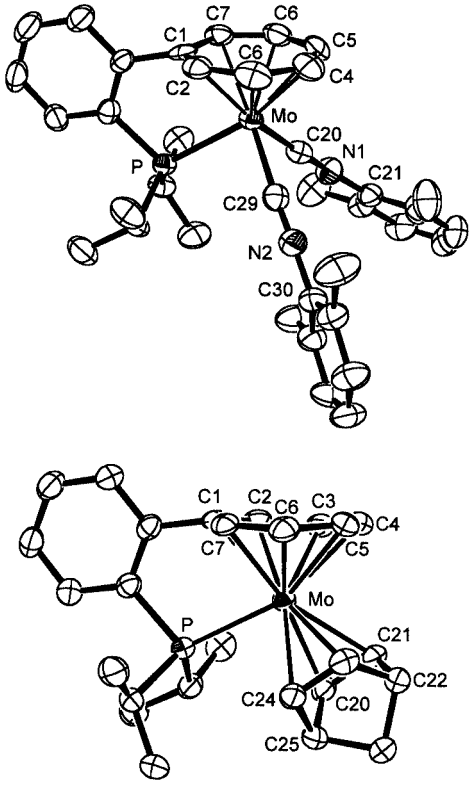

Figure 3. ORTEP drawings of the cations in (**5**)BPh_4·C_5H_{12} (top) and (**6**)BPh_4·CH_2Cl_2 (bottom) with thermal ellipsoids drawn at 50% probability

In a similar fashion, treatment of **3** with [$HNMe_2Ph$][BPh_4] in the presence of norbornadiene gives the diolefin complex (**6**)BPh_4, which is also a versatile starting material for further ligand substitution reactions. Treatment of (**6**)BPh_4 with XyNC thus results in the quantitative formation of (**5**)BPh_4. The norbornadiene complex was also characterizable by X-ray diffraction analysis, and the molecular structure of the cation in (**6**)BPh_4·CH_2Cl_2 is shown in Figure 3 (bottom). Although the structural parameters about the molybdenum centers again fall in the expected ranges (Table 1),[11] the norbornadiene ligand seems to cause some steric congestion at the metal center, and so an elongated Mo−P bond length of 2.5863(10) Å together with a slight puckering of the seven-membered ring can be observed with the longest molybdenum-carbon bonds to C4 and C5, which are adjacent to the diolefin ligand. A similar observation has been made in the related ruthenium complex [(η-C_5Me_5)Ru(PPh_3)(η^4-NBD)]ClO_4.[26]

Preparation of Molybdenum Alkyne Complexes

Cyclopentadienyl ruthenium complexes are extensively used for C−C bond formation through the employment of terminal alkynes, which can either be oligomerized or coupled with various other substrates such as allyl alcohols or alkenes.[2,3] We have consequently studied the cleavage of the tetrahydroborate ligand in the presence of phenyl- and *tert*-butylacetylene, resulting in the formation of crystalline (**7**)BPh_4 and (**8**)BPh_4. Both complexes contain η^2-coordinated alkyne ligands, which stabilize both available coordination sites with their π-electrons and must therefore act as four-electron donors. This fact is easily deduced from their ^{1}H NMR spectra, which exhibit characteristic resonances at low field for the acetylenic *H*C-hydrogen atoms.[27] These resonances appear as doublets at δ = 10.41 ppm ($^3J_{H,P}$ = 29.4 Hz) for **7** and at δ = 10.03 ppm, ($^3J_{H,P}$ = 33.0 Hz) for **8**. A similar downfield shift is observed in the ^{13}C NMR spectra for the acetylenic carbon atoms. For the phenylacetylene complex **7**, these resonances are found as doublets at δ = 178.5 ppm ($^2J_{C,P}$ = 28.4 Hz, ≡CH) and at δ = 173.2 ppm ($^2J_{C,P}$ = 4.5 Hz, ≡CPh). Surprisingly, the order of these resonances is reversed for the *tert*-butylacetylene complex **8**, its ^{13}C NMR spectrum exhibiting a broad singlet at δ = 191.2 ppm (≡C*t*Bu) and a doublet at 177.8 ppm ($^2J_{C,P}$ = 30.1 Hz, ≡CH).

In addition, the molecular structure of the cation **7** (Figure 4, top) shows the structural parameters for the alkyne ligand, with an elongated C≡C (C14−C15) bond length of 1.291(4) Å, together with a small C≡C−C(Ph) (C14−C15−C16) angle of 136.5(3)°, which are clearly indicative of a four-electron donor alkyne ligand.[27] The geometry around the molybdenum atom can be interpreted as a two-legged piano stool with the acetylenic C14−C15 carbon bond and the Mo−P axis in the same plane, and the P-Mo-C14−C15 torsion angle is 173.7°. The acetylenic phenyl and the *ortho*-phenylene rings are also almost coplanar (interplanar angle of 16.7°), so the complex can be regarded as being essentially C_s-symmetric if the two isopropyl groups are neglected. The molybdenum distances to the ring carbon atoms range from 2.221(3) Å (Mo-C3) to 2.373(3) Å (Mo-C1), indicating a fairly significant deviation from planarity (Table 1), and the mean and maximum deviations from the least-squares plane (C1−C7) are 0.075 and −0.108 Å (for C3), respectively. Nevertheless, these structural parameters are still strongly indicative of an η^7-coordinated cycloheptatrienyl ligand. We are not aware of any related ruthenium complex containing an η^2-bonded alkyne ligand. Very recently, however, the molecular structure of a related osmium complex [(η-C_5H_5)Os(η^2-HC≡CCPh_2OH)(P*i*Pr_3)]PF_6 containing a coordinated propargyl alcohol has been reported.[28] Comparison of the bond lengths and angles with those in **7** demonstrates that cycloheptatrienyl molybdenum complexes are also strongly related to cyclopentadienyl osmium systems, with which they exist in a diagonal relationship.

For purposes of comparison, we also studied the possibility of synthesizing the corresponding tetrahydroborate complex **9** containing the linked cycloheptatrienyl-phosphane ligand with a diphenylphosphanyl donor group, the synthesis and coordination chemistry of which have been reported before.[11] Treatment of [(*o*-$Ph_2PC_6H_4$-η^7-C_7H_6)$MoBr_2$-(*P*−*Mo*)] with $NaBH_4$ in EtOH does indeed result in the formation of **9**, which could be isolated in relatively low yield as a green, air-sensitive solid. The crude product was only characterized by ^{1}H and ^{31}P NMR spectroscopy and was used without further purification for the preparation of the alkyne complex (**10**)BPh_4. Thus, treatment of **9** with [$HNMe_2$Ph][BPh_4] in the presence of phenylacetylene afforded (**10**)BPh_4 as a stable, crystalline compound (Scheme 3). Single crystals of (**10**)BPh_4·3THF could be obtained by recrystallization from THF/hexane solution, and Figure 4 (bottom) shows an ORTEP presentation of the cation **10**. The alkyne ligand in **10** seems to be somewhat more weakly coordinated than in **7**, as it has a slightly shorter C≡C bond length [1.279(5) vs. 1.292(4) Å], together with a slightly larger C≡C−C(Ph) angle [138.4(3) vs. 136.5(3)°]. The overall geometry, though, is similar to that observed for **7** (Table 1), although the phenylacetylene ligand deviates more strongly from a perfectly C_s-symmetric conformation, as indicated by the torsion angle of 169.8° between the P-Mo-C26−C27 atoms and by the interplanar angle of 26.6° between the least-squares planes containing the acetylenic phenyl and phenylene carbon atoms. From the difficulties encountered in particular with the synthesis of the tetrahydroborate derivative **9**, we were able to ascertain that in our hands the more sterically demanding diisopropylphosphane donor seems to be superior to its diphenylphosphane analogue. We have generally observed increased stability upon replacement of the phenyl groups with isopropyl groups, and so both our experimental work and our catalytic studies have mainly focused on, and

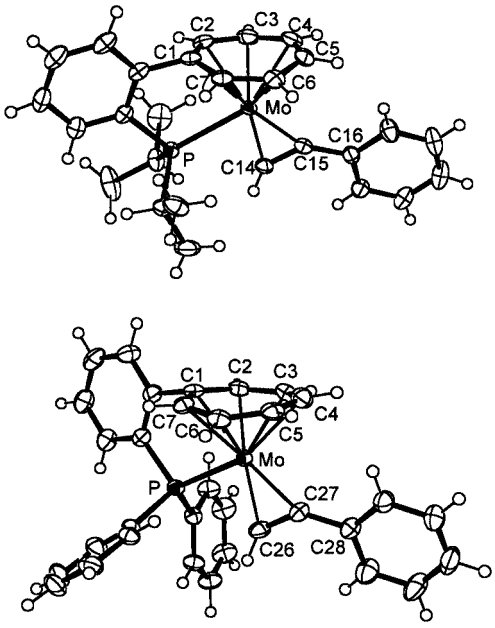

Figure 4. ORTEP drawings of the cations in (**7**)BPh_4 (top) and (**10**)BPh_4·C_6H_{14} (bottom) with thermal ellipsoids drawn at 50% probability

mainly will continue to focus on, the use of complexes containing the [2-(diisopropylphosphanyl)phenyl]cycloheptatrienyl ligand.

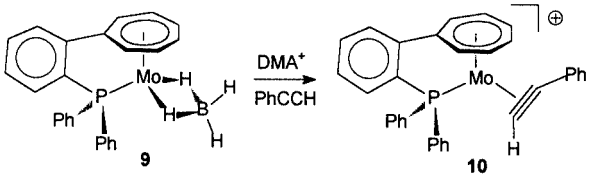

Scheme 3. DMA^+ = dimethylanilinium $(PhNMe_2\ H)^+$

Catalytic Study

Alkyne complexes such as **7**, **8**, and **10** could be intermediates in the catalytic coupling of acetylenes at cationic molybdenum complex fragments of type II (Scheme 1).[2,3] We have therefore studied the use of (**7**)BPh_4 (5 mol %) as a catalyst for the oligomerization of phenylacetylene[29] in THF solution at 80 °C. Our preliminary results indicate that this system is indeed efficient at catalyzing the above reaction, affording a product mixture of cyclotrimers (80%) and linear oligomers (20%). Surprisingly, cyclotrimerization to give 1,3,5-triphenylbenzene (52%, unambiguously characterized by X-ray diffraction analysis)[30] and 1,2,4-triphenylbenzene (28%) is predominantly observed, in addition to the formation of a linear dimer (12%) and a linear trimer (8%) (Scheme 4). This result contrasts with the reaction involving ruthenium catalysts, in which linear dimers and trimers are formed almost exclusively.[3b,3e,3f] Further work will be directed toward the elucidation of the oligomerization mechanism[31] effective with our novel molybdenum catalyst system. Thus, (**7**)BPh_4 and our related alkyne complexes represent ideal starting materials for further controlled stoichiometric transformations, which will hopefully allow additional possible intermediates in the catalytic cycle to be identified.

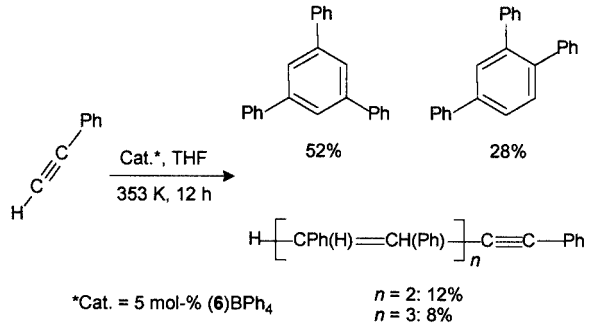

Scheme 4. Catalytic oligomerization of phenylacetylene

Theoretical Study

To study the (C_7H_7)Mo-(C_5R_5)M-relationship (M = Ru, Os) by theoretical methods, we chose the molybdenum phenylacetylene complex **7** for comparison with the *hypothetical* cyclopentadienyl ruthenium and osmium complexes **11** and **12**, each containing an identical diisopropylphosphanylphenyl substituent (Scheme 5). The structures of all three cationic complexes were optimized by DFT methods employing the BP86 functional (Figure 5). The alkyne conformations in all three complexes are very similar and are in agreement with the expected nearly C_s-symmetric geometry about the metal centers. The phenylacetylene ligand in each complex exhibits the expected lengthening of the C≡C

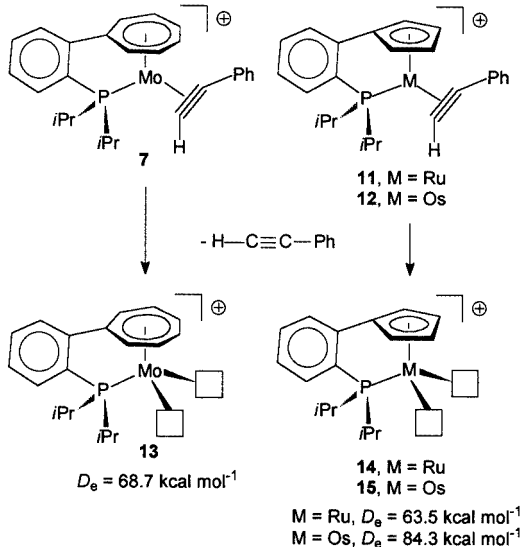

Scheme 5. Alkyne bond dissociation energies (D_e) of phenylacetylene complexes

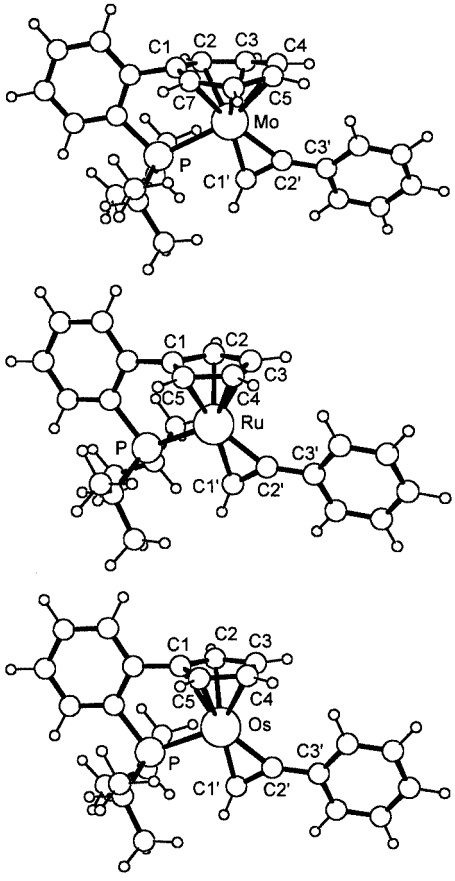

Figure 5. Calculated structures of the cations **7**, **11**, and **12**

Table 2. Experimentally measured and calculated bond lengths (Å) and angles (°) for **7**, **11**, and **12**

	(**7**)BPh_4	**7**	**11**	**12**
C1−C2	1.408(4)	1.423	1.439	1.429
C2−C3	1.402(4)	1.426	1.442	1.435
C3−C4	1.422(5)	1.426	1.427	1.420
C4−C5	1.380(5)	1.405	1.440	1.432
C5−C1			1.440	1.432
C5−C6	1.415(5)	1.428		
C6−C7	1.405(4)	1.424		
C1−C7	1.410(4)	1.421		
C1′−C2′	1.292(4)	1.318	1.309	1.306
C2′−C3′	1.457(4)	1.450	1.445	1.446
M−C1	2.373(3)	2.403	2.220	2.275
M−C2	2.292(3)	2.300	2.193	2.246
M−C3	2.221(3)	2.246	2.210	2.258
M−C4	2.324(3)	2.356	2.215	2.262
M−C5	2.343(3)	2.343	2.205	2.253
M−C6	2.241(3)	2.259		
M−C7	2.280(3)	2.338		
M−C1′	2.023(3)	2.033	2.004	2.004
M−C2′	2.090(3)	2.113	2.029	2.031
M−P	2.5283(8)	2.580	2.388	2.416
P−M−C1′	76.52(9)	76.8	81.2	82.3
P−M−C2′	112.86(8)	113.7	119.1	120.0
C1′−C2′−C3′	136.6(3)	138.8	143.8	142.7

bond length, together with a small C≡C−C(Ph) angle (Table 2). For the molybdenum complex **7**, the computed optimized geometry is in excellent agreement with the structure determined by X-ray diffraction analysis (Table 2, Figure 3), and the puckering of the seven-membered ring is also accurately reproduced. This deviation from planarity is significantly less pronounced in **11** and **12**, the structural data of which are very similar and in excellent agreement with the experimentally measured and calculated geometric parameters of unbridged cyclopentadienyl osmium alkyne complexes.[28]

Scheme 5 shows the theoretically predicted alkyne bond dissociation energies (D_e) of **7**, **11**, and **12**, calculated as the energy difference between the alkyne complex on one hand, and the *unoptimized* complex fragments **13** −**15** and the phenylacetylene ligand at its optimized geometry on the other (vertical D_e). The predicted D_e for the molybdenum complex **7** (68.7 kcal·mol^{-1}) takes an intermediate position between the values calculated for the Ru (D_e = 63.5 kcal·mol^{-1}) and Os systems (D_e = 84.3 kcal·mol^{-1}). Comparative calculations employing the popular B3LYP hybrid functional result in D_e values approximately 10 kcal·mol^{-1} lower, but the differences between the three complexes are very similar. Figure 6 shows a representation of the frontier orbitals in the unoptimized 14-electron complexes **13** −**15** formed by splitting of the phenylacetylene ligand.

In each complex, the symmetry properties of the two lowest unoccupied molecular orbitals (LUMOs), which are essentially vacant d-orbitals, match those of the occupied $\pi_{\|}$ and $\pi_{\perp}$ orbitals of an alkyne ligand. Consequently, this can act as a four-electron donor, providing 18-electron complexes.[27,28,32] Comparison of the energies and shapes of the relevant frontier orbitals reveals the close resemblance between **13**, **14**, and **15** and confirms the intimate relationship between the isoelectronic and isolobal [(η-C_7H_7)Mo] and [(η-C_5R_5)M] fragments (M = Ru, Os).

Conclusion

In summary, we present a new method for the generation and stabilization of coordinatively unsaturated cycloheptatrienyl molybdenum complexes, which can be used for catalytic alkyne-alkyne coupling reactions. These results indicate that cycloheptatrienyl complexes can indeed be potentially useful for applications in homogeneous transition metal catalysis, the goal of these studies being the develop-

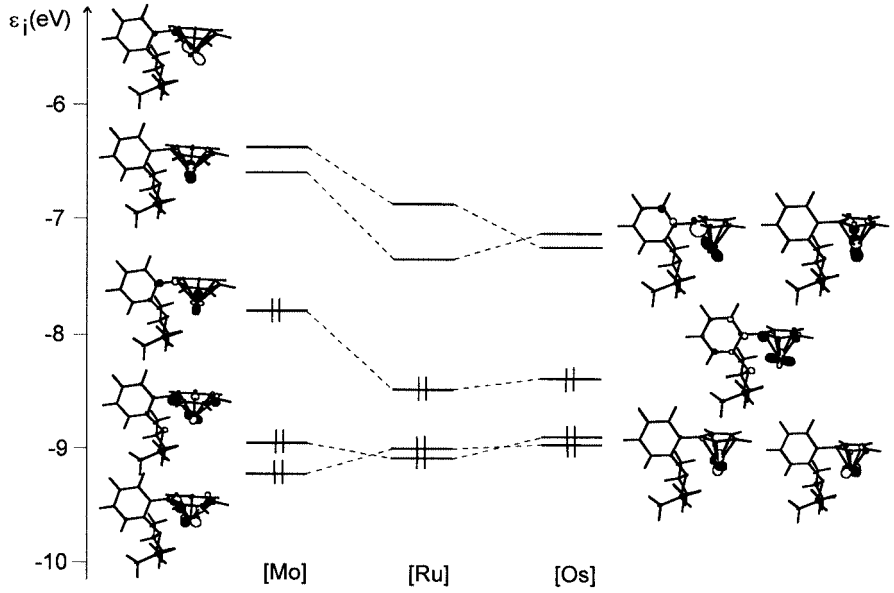

Figure 6. Frontier orbitals of the 14-electron complexes **13** [M = Mo], **14** [M = Ru], and **15** [M = Os]

ment of novel effective catalyst systems that should allow the precious metal ruthenium (and also osmium) to be substituted with the much cheaper molybdenum. This work is part of our general goal to extend the chemistry of cycloheptatrienyl complexes and to raise their level of significance in comparison with those of cyclopentadienyl and benzene complexes.

Experimental Section

General: All operations were performed under an atmosphere of dry argon by Schlenk and vacuum techniques. Solvents were dried by standard methods and distilled prior to use.

Dimethylanilinium tetrafluoroborate was prepared by published procedures.[33] Full details of the preparation of **1** and **2**, together with the spectroscopic and structural properties of all reaction intermediates, will be presented elsewhere.[13] Elemental analyses (C, H N) were performed on a Heraeus CHNS-Rapid elemental analyzer. EI and ESI mass spectra were recorded on a Varian MAT 212 or on a Micromass Quattro LCZ mass spectrometer, respectively. ^{1}H and ^{13}C NMR spectra were measured on Bruker AC 200, Bruker AMX 400, or Varian U 600 spectrometers with the solvent as internal standard, whereas ^{31}P NMR measurements were run on a Bruker AC 200 spectrometer with aqueous H_3PO_4 (85%) as an external reference. IR spectra were recorded on a Bruker Vector 22 instrument. The assignment of all ^{1}H and ^{13}C NMR resonances was supported by two-dimensional NMR spectroscopy (COSY and NOE experiments). For the atomic numbering schemes used in the Exp. Sect., see Figure 2.

[(*o*-*i*Pr$_2$PC$_6$H$_4$-η^7-C$_7$H$_6$)Mo(η^2-BH$_4$)(*Mo*−*P*)] (3): A solution of **2** (500 mg, 0.93 mmol) in ethanol was treated at 0 °C with $NaBH_4$ (250 mg, 6.52 mmol) and stirred for 3 h at ambient temperature. The solvent was removed in vacuo, and the residue was extracted with diethyl ether/hexane (1:1). After evaporation of the solvent, **3** could be isolated as a light green compound. Purification by recrystallization from diethyl ether/hexane was possible, affording green crystals of **3**. Yield: 342 mg (91%). ^{1}H NMR ([D$_8$]toluene, 600 MHz): δ = 7.56 (dm, 1 H, C_6H_4), 7.31 (tm, 1 H, C_6H_4), 7.19 (m, 2 H, C_6H_4), 5.48 (m, 2 H, C_7H_6), 4.49 (m, 4 H, C_7H_6), 1.86 (sept, 1 H, *i*Pr: CH), 1.84 (sept, 1 H, *i*Pr: CH), 0.72 (dd, 6 H, *i*Pr: CH_3), 0.64 (dd, 6 H, *i*Pr: CH_3), −5.72 (br. s, 4 H, BH_4) ppm. ^{13}C NMR ([D$_8$]toluene, 150.9 MHz): δ = 155.2 (d, $^2J_{C,P}$ = 24.8 Hz, C-8), 138.7 (d, $^1J_{C,P}$ = 33.8 Hz, C-9), 130.2 (br. s, C_6H_4), 129.6 (br. s, C_6H_4), 114.2 (d, $^3J_{C,P}$ = 2.6 Hz, C-1), 90.3 (d, $^2J_{C,P}$ = 5.4 Hz, C_7H_6), 85.8 (d, $^2J_{C,P}$ = 2.0 Hz, C_7H_6), 76.6 (s, C_7H_6), 25.0 (d, $^1J_{C,P}$ = 17.2 Hz, *i*Pr: CH), 19.1 (d, $^2J_{C,P}$ = 7.0 Hz, *i*Pr: CH_3), 19.0 (d, $^2J_{C,P}$ = 1.5 Hz, *i*Pr: CH_3) ppm. ^{31}P NMR ([D$_8$]toluene, 81 MHz): δ = 68.0 ppm. MS (EI): *m*/*z* (%) = 394 (100) [M]$^+$, 379 (80) [M$^+$ − BH_4]. $C_{19}H_{28}BMoP$ (394.1): calcd. C 57.90, H 7.16; found C 57.65, H 6.77.

[(*o*-*i*Pr$_2$PC$_6$H$_4$-η^7-C$_7$H$_6$)Mo(PPh$_3$)H(*Mo*−*P*)] (4): A solution of **2** (1.184 g, 2.20 mmol) and PPh_3 (576 mg, 2.20 mmol) in THF was treated with NaH (421 mg, 17.54 mmol) and stirred for 12 h. The reaction mixture was filtered, and the solvent was removed by evaporation. The crude product was recrystallized from hexane to afford **4** as a brown crystalline solid. Yield: 848 mg (60%). ^{1}H NMR ([D$_8$]toluene, 600 MHz): δ = 7.74 (t, 3 H, PPh_3), 7.52 (dm, 1 H, C_6H_4), 7.32 (m, 6 H, PPh_3), 7.16 (m, 1 H, C_6H_4), 7.05 (m, 1 H, C_6H_4), 7.04 (m, 6 H, PPh_3), 6.98 (t, 1 H, C_6H_4), 5.57 (m, 1 H, C_7H_6), 5.29 (m, 1 H, C_7H_6), 4.78 (t, 1 H, C_7H_6), 4.52 (q, 1 H, C_7H_6), 4.18 (d, 1 H, C_7H_6), 3.86 (q, 1 H, C_7H_6), 2.10 (m, 1 H, *i*Pr: CH), 1.09 (d sept, 1 H, *i*Pr: CH), 0.86 (m, 6 H, *i*Pr: CH_3), 0.81 (dd, 3 H, *i*Pr: CH_3), 0.68 (dd, 3 H, *i*Pr: CH_3), −2.82 (dd, 1 H, MoH) ppm. ^{13}C NMR ([D$_8$]toluene, 150.9 MHz): δ = 154.0 (d, $^2J_{C,P}$ = 25.8 Hz, C-8), 141.4 (d, $^1J_{C,P}$ = 28.7 Hz, *ipso*-C_6H_5), 140.5 (d, $^1J_{C,P}$ = 28.3 Hz, C-9), 134.2 (d, $^3J_{C,P}$ = 11.0 Hz, *o*-PPh_3), 134.0 (d, $^2J_{C,P}$ = 19.9 Hz, *m*-PPh_3), 129.1 (m, C-10), 128.3 (d, $^3J_{C,P}$ = 1.9 Hz, C-11), 127.2 (d, $J_{C,P}$ = 8.5 Hz, *p*-PPh_3), 126.9 (d, $^3J_{C,P}$ = 7.7 Hz, C-13), 126.7 (d, $J_{C,P}$ = 4.1 Hz, C-12), 105.4 (t, $^2J_{C,P}$ = 2.0 Hz, C-1), 88.3 (d, $^2J_{C,P}$ = 1.5 Hz, C-7), 87.9 (d, $^2J_{C,P}$ = 3.1 Hz, C-5), 87.9 (s, C-6), 85.9 (d, $^2J_{C,P}$ = 5.1 Hz, C-4), 84.6 (dd, $^2J_{C,P}$ = 8.3 Hz, C-2), 80.6 (s, C-3), 26.5 (d, $^1J_{C,P}$ = 21.4 Hz, *i*Pr: CH), 25.7 (dd, $^1J_{C,P}$ = 14.4 Hz, *i*Pr: CH), 19.9 (d, $^2J_{C,P}$ = 27.2 Hz, *i*Pr: CH_3), 18.9 (d, $^2J_{C,P}$ = 3.7 Hz, *i*Pr: CH_3), 18.7 (d, $^2J_{C,P}$ = 6.3 Hz, *i*Pr: CH_3), 17.4 (d, $^2J_{C,P}$ = 3.7 Hz, *i*Pr: CH_3) ppm. ^{31}P NMR ([D$_8$]toluene, 81 MHz): δ = 74.5 (d, $^2J_{P,P}$ = 31.0 Hz, P*i*Pr$_2$), 53.7 (d, $^2J_{P,P}$ = 31.0 Hz, PPh_3) ppm. MS (EI): *m*/*z* (%) = 642 (100) [M]$^+$. $C_{19}H_{28}BMoP$ (642.7): calcd. C 69.14, H 6.27; found C 70.45, H 6.51.

[(*o*-*i*Pr$_2$PC$_6$H$_4$-η^7-C$_7$H$_6$)Mo(XyNC)$_2$(*Mo*−*P*)]BPh$_4$ (5)BPh$_4$: A solution of **3** (250 mg, 0.63 mmol) in THF (50 mL) was treated at room temperature with [HNMe$_2$Ph][BPh_4] (355 mg, 0.76 mmol). After addition of an excess of 2,6-dimethylphenyl isocyanide, the reaction mixture was subsequently stirred at ambient temperature for 12 h. After evaporation of the solvent, the residue was extracted with a small amount of dichloromethane and added dropwise to rapidly stirred diethyl ether. Purification by recrystallization from dichloromethane/diethyl ether at 0 °C was possible, affording air-stable, brown crystals. Yield: 472 mg (78%). ^{1}H NMR (CD_2Cl_2, 600 MHz): δ = 7.81 (dm, 1 H, C_6H_4), 7.68 (tm, 1 H, C_6H_4), 7.64 (m, 2 H, C_6H_4), 7.41 (br. m, 8 H, *o*-BPh_4), 7.28 (t, 2 H, *p*-$C_6H_3Me_2$), 7.22 (d, 4 H, *m*-$C_6H_3Me_2$), 7.08 (t, 8 H, *m*-BPh_4), 6.93 (t, 4 H, *p*-BPh_4), 5.50 (m, 4 H, C_7H_6), 5.04 (dd, 2 H, C_7H_6), 2.55 (m, 2 H, *i*Pr: CH), 2.44 (s, 12 H, *o*-CH_3), 1.21 (dd, 6 H, *i*Pr: CH_3), 1.11 (dd, 6 H, *i*Pr: CH_3) ppm. ^{13}C NMR (CD_2Cl_2, 150.9 MHz): δ = 177.8 (d, $^2J_{C,P}$ = 16.6 Hz, CNR), 164.4 (q, $^1J_{C,B}$ = 49.4 Hz, *ipso*-BPh_4), 150.2 (d, $^2J_{C,P}$ = 25.9 Hz, C-8), 137.8 (d, $^1J_{C,P}$ = 35.9 Hz, C-9), 136.3 (s, *o*-BPh_4), 134.8 (s, *o*-$C_6H_3Me_2$), 131.6 (d, $J_{C,P}$ = 2.6 Hz, C_6H_4), 130.7 (s, C_6H_4), 129.5 (s, *p*-$C_6H_3Me_2$), 129.4 (d, $J_{C,P}$ = 5.1 Hz, C_6H_4), 128.7 (s, *m*-$C_6H_3Me_2$), 127.5 (d, $J_{C,P}$ = 9.3 Hz, C_6H_4), 127.3 (s, *ipso*-$C_6H_3Me_2$), 125.9 (q, $^3J_{C,B}$ = 2.6 Hz, *m*-BPh_4), 122.0 (s, *p*-BPh_4), 118.0 (d, $^3J_{C,P}$ = 2.5 Hz, C-1), 92.9 (s, C_7H_6), 91.1 (d, $^2J_{C,P}$ = 3.9 Hz, C_7H_6), 91.0 (s, C_7H_6), 26.2 (d, $^1J_{C,P}$ = 21.1 Hz, *i*Pr: CH), 19.2 (s, $C_6H_3\mathit{Me}_2$), 18.6 (d, $^2J_{C,P}$ = 5.1 Hz, *i*Pr: CH_3), 18.1 (s, *i*Pr: CH_3) ppm. ^{31}P NMR (CD_2Cl_2, 81 MHz): δ = 75.7 ppm. MS (ESI): *m*/*z* (%) = 641 (100) [M − BPh_4]$^+$. IR (CH_2Cl_2): ṽ = 2099 ν(CN), 2067 ν(CN) cm^{-1}. $C_{61}H_{62}BMoN_2P$ (960.9): calcd. C 76.25, H 6.50, N 2.92; found C 75.59, H 6.02, N 2.37.

[(*o*-*i*Pr$_2$PC$_6$H$_4$-η^7-C$_7$H$_6$)Mo(η^4-NBD)(*Mo*−*P*)]BPh$_4$ (6)BPh$_4$: Compound (**6**)BPh_4 could be prepared in a manner similar to that described for (**5**)BPh_4, by treatment of a solution of **3** (157 mg, 0.40 mmol) in THF with [HNMe$_2$Ph][BPh_4] (175 mg, 0.40 mmol), followed by addition of norbornadiene (44 mg, 0.48 mmol). Yield: 258 mg (82%). ^{1}H NMR (CD_2Cl_2, 600 MHz): δ = 7.80 (d, 1 H, C_6H_4), 7.74 (dd, 1 H, C_6H_4), 7.45 (t, 1 H, C_6H_4), 7.40 (dm, 1 H, C_6H_4), 7.34 (br. m, 8 H, *o*-BPh_4), 7.03 (t, 8 H, *m*-BPh_4), 6.88 (t, 4 H, *p*-BPh_4), 5.66 (m, 2 H, C_7H_6), 5.22 (m, 2 H, C=CH), 4.93 (m, 2 H, C_7H_6), 4.85 (dd, 2 H, C_7H_6), 3.52 (m, 2 H, C=CH), 3.43 (br. s, 1 H, CH), 3.27 (br. s, 1 H; CH), 2.92 (m, 2 H, *i*Pr: CH), 1.29 (dd, 6 H, *i*Pr: CH_3), 1.23 (dd, 6 H, *i*Pr: CH_3), 1.02 (s, 2 H, CH_2) ppm. ^{13}C NMR (CD_2Cl_2, 150.9 MHz): δ = 164.9 (br. s, *ipso*-BPh_4),

136.3 (q, $^2J_{C,B}$ = 1.3 Hz, *o*-BPh_4), 135.0 (s, C_6H_4), 131.6 (d, $^2J_{C,P}$ = 2.0 Hz, C-8), 131.3 (s, C-1), 129.9 (s, C_6H_4), 129.4 (d, $^1J_{C,P}$ = 4.6 Hz, C-9), 128.2 (s, C_6H_4), 126.9 (d, $J_{C,P}$ = 9.1 Hz, C_6H_4), 126.0 (q, $^3J_{C,B}$ = 3.2 Hz, *m*-BPh_4), 122.1 (s, *p*-BPh_4), 93.4 (d, $^2J_{C,P}$ = 2.0 Hz, C_7H_6), 90.6 (d, $^2J_{C,P}$ = 1.3 Hz, C_7H_6), 88.3 (s, C_7H_6), 75.6 (s, NBD), 71.3 (s, NBD), 61.1 (s, NBD), 50.5 (d, $J_{C,P}$ = 2.5 Hz, NBD), 47.9 (s, NBD), 28.1 (d, $^1J_{C,P}$ = 18.2 Hz, *i*Pr: CH), 19.0 (d, $^2J_{C,P}$ = 4.2 Hz, *i*Pr: CH_3), 18.2 (s, *i*Pr: CH_3) ppm. ^{31}P NMR (CD_2Cl_2, 81 MHz): δ = 66.5 ppm. MS (ESI): *m*/*z* (%) = 471 (100) $[M - BPh_4]^+$. $C_{50}H_{52}BMoP$ (790.7): calcd. C 75.95, H 6.63; found C 76.30, H 6.24.

[(*o*-*i*Pr$_2$PC$_6$H$_4$-η^7-C$_7$H$_6$)Mo(η^2-HCCPh)(*Mo*−*P*)]BPh$_4$ (7)BPh$_4$: Compound (**7**)BPh_4 could be prepared in a manner similar to that described for (**5**)BPh_4, by treatment of a solution of **3** (397 mg, 1.01 mmol) in THF with $[HNMe_2Ph][BPh_4]$ (532 mg, 1.21 mmol), followed by the addition of phenylacetylene. Yield: 576 mg (72%). ^{1}H NMR (CD_2Cl_2, 600 MHz): δ = 10.41 (d, $^3J_{H,P}$ = 29.4 Hz, 1 H, C≡C), 7.77−7.45 (m, 9 H, C_6H_4 + BPh_4), 7.34 (br. m, 8 H, *o*-BPh_4), 7.01 (t, 8 H, *m*-BPh_4), 6.87 (t, 4 H, *p*-BPh_4), 5.74 (dd, 2 H, C_7H_6), 5.54 (dd, 2 H, C_7H_6), 5.30 (m, 2 H, C_7H_6, 2.83 (m, 2 H, *i*Pr: CH), 1.22 (dd, 6 H, *i*Pr: CH_3), 1.01 (dd, 6 H, *i*Pr: CH_3) ppm. ^{13}C NMR (CD_2Cl_2, 150.9 MHz): δ = 178.5 (d, $^2J_{C,P}$ = 28.4 Hz, ≡CH), 173.2 (d, $^2J_{C,P}$ = 4.5 Hz, ≡CPh), 164.4 (q, $^1J_{C,B}$ = 49.9 Hz, *ipso*-BPh_4), 149.8 (d, $^2J_{C,P}$ = 21.7 Hz, C-8), 136.3 (s, *o*-BPh_4), 132.4 (d, $^4J_{C,P}$ = 2.0 Hz, C-12), 131.7 (d, $^1J_{C,P}$ = 38.2 Hz, C-9), 131.2 (s, C-10), 130.6 (s, *p*-C_6H_5), 130.0 (d, $^3J_{C,P}$ = 5.1 Hz, C-11), 129.6 (s, *m*-C_6H_5), 129.5 (s, *o*-C_6H_5), 127.4 (d, $^3J_{C,P}$ = 8.1 Hz, C-13), 126.0 (q, $^3J_{C,B}$ = 2.6 Hz, *m*-BPh_4), 122.1 (s, *p*-BPh_4), 118.4 (d, $^2J_{C,P}$ = 2.6 Hz, C-1), 95.7 (d, $^2J_{C,P}$ = 2.6 Hz, C-4,5), 94.7 (d, $^2J_{C,P}$ = 2.4 Hz, C-2,7), 82.9 (s, C-3,6), 27.6 (d, 23.0 Hz, *i*Pr: CH), 19.8 (d, $^2J_{C,P}$ = 4.0 Hz, *i*Pr: CH_3), 19.0 (s, *i*Pr: CH_3) ppm. ^{31}P NMR (CD_2Cl_2, 81 MHz): δ = 72.4 ppm. MS (ESI): *m*/*z* (%) = 481 (100) $[M - BPh_4]^+$. $C_{51}H_{50}BMoP$ (800.7): calcd. C 76.50, H 6.29; found C 75.50, H 5.93.

[(*o*-*i*Pr$_2$PC$_6$H$_4$-η^7-C$_7$H$_6$)Mo(η^2-HCC-*t*Bu)(*Mo*−*P*)]BPh$_4$ (8)BPh$_4$: Compound (**8**)BPh_4 could be prepared in a manner similar to that described for (**5**)BPh_4, by treatment of a solution of **3** (235 mg, 0.60 mmol) in THF with $[HNMe_2Ph][BPh_4]$ (315 mg, 0.72 mmol), followed by the addition of *tert*-butylacetylene. Yield: 400 mg (86%). ^{1}H NMR (CD_2Cl_2, 600 MHz): δ = 10.03 (d, $^3J_{H,P}$ = 33.0 Hz, 1 H, C≡CH), 7.70 (m, 1 H, C_6H_4), 7.65 (m, 2 H, C_6H_4), 7.59 (m, 1 H, C_6H_4), 7.33 (br. m, 8 H, *o*-BPh_4), 7.01 (t, 8 H, *m*-BPh_4), 6.88 (t, 4 H, *p*-BPh_4), 6.08 (dd, 2 H, C_7H_6), 5.49 (dd, 2 H, C_7H_6), 5.32 (m, 2 H, C_7H_6), 2.75 (m, 2 H, *i*Pr: CH), 1.44 (s, 9 H, *t*Bu), 1.16 (dd, 6 H, *i*Pr: CH_3), 0.94 (dd, 6 H, *i*Pr: CH_3) ppm. ^{13}C NMR (CD_2Cl_2, 150.9 MHz): δ = 191.2 (s, ≡C*t*Bu), 177.8 (d, $^2J_{C,P}$ = 30.1 Hz, ≡CH), 164.3 (q, $^1J_{C,B}$ = 50.5 Hz, *ipso*-BPh_4), 149.7 (d, $^2J_{C,P}$ = 22.4 Hz, C-8), 136.3 (s, *o*-BPh_4), 132.2 (d, $^4J_{C,P}$ = 1.9 Hz, C-12), 131.8 (d, $^1J_{C,P}$ = 39.0 Hz, C-9), 131.1 (s, C-10), 129.9 (d, $^3J_{C,P}$ = 5.3 Hz, C-11), 127.3 (d, $^3J_{C,P}$ = 7.9 Hz, C-13), 125.9 (q, $^3J_{C,B}$ = 2.6 Hz, *m*-BPh_4), 122.1 (s, *p*-BPh_4), 118.4 (d, $^2J_{C,P}$ = 2.5 Hz, C-1), 94.6 (d, $^2J_{C,P}$ = 2.5 Hz, C-4,5), 94.2 (d, $^2J_{C,P}$ = 1.9 Hz, C-2,7), 81.6 (s, C-3,6), 31.6 (s, *t*Bu), 27.4 (d, 23.6 Hz, *i*Pr: CH), 19.7 (d, $^2J_{C,P}$ = 3.9 Hz, *i*Pr: CH_3), 18.9 (s, *i*Pr: CH_3) ppm. ^{31}P NMR (CD_2Cl_2, 81 MHz): δ = 72.9 ppm. $C_{49}H_{54}BMoP$ (780.7): calcd. C 75.38, H 6.97; found C 75.63, H 6.48.

[(*o*-Ph$_2$PC$_6$H$_4$-η^7-C$_7$H$_6$)Mo(η^2-BH$_4$)(*Mo*−*P*)] (9): A solution of [(*o*-$Ph_2PC_6H_4$-η^7-C_7H_6)$MoBr_2$(*Mo*−*P*)] (500 mg, 0.72 mmol) in ethanol was treated at 0 °C with $NaBH_4$ (250 mg, 6.52 mmol) and stirred for 1 h at ambient temperature. The solvent was removed by evaporation, and the residue was extracted with diethyl ether/hexane (1:1). After evaporation of the solvent, **9** was isolated as a light green compound. Purification by recrystallization from diethyl ether/hexane was possible, affording green crystals of **9**. Yield: 165 mg (36%). ^{1}H NMR ([D$_6$]benzene, 200 MHz): δ = 7.34 (m, 1 H, C_6H_4), 7.12−7.00 (m, 2 H, C_6H_4), 6.86−6.72 (m, 6 H, C_6H_4 + C_6H_5), 6.65 (m, 5 H, C_6H_4+C_6H_5), 5.12 (dd, 2 H, C_7H_6), 4.40 (dd, 2 H, C_7H_6), 4.18 (tm, 2 H, C_7H_6), −5.56 (br. s, 4 H, BH_4) ppm. ^{31}P NMR ([D$_6$]benzene, 81 MHz): δ = 52.6 ppm.

[(*o*-Ph$_2$PC$_6$H$_4$-η^7-C$_7$H$_6$)Mo(η^2-HCCPh)(*Mo*−*P*)]BPh$_4$ (10)BPh$_4$: Compound (**10**)BPh_4 could be prepared in a manner similar to that described for (**5**)BPh_4, by treatment of a solution of **9** (165 mg, 0.36 mmol) in THF with $[HNMe_2Ph][BPh_4]$ (188 mg, 0.43 mmol), followed by the addition of large excess of phenylacetylene. Yield: 186 mg (60%). ^{1}H NMR (CD_2Cl_2, 200 MHz): δ = 10.08 (d, $^3J_{H,P}$ = 34.2 Hz, 1 H, C≡CH), 7.86−7.41 (br. m, 14 H, C_6H_4 + PC_6H_5), 7.31 (br. m, 8 H, *o*-BPh_4), 6.98 (br. t, 8 H, *m*-BPh_4), 6.83 (br. t, 4 H, *p*-BPh_4), 5.86 (m, 2 H, C_7H_6), 5.60 (m, 2 H, C_7H_6), 5.25 (m, 2 H, C_7H_6) ppm.^{31}P NMR ([D$_6$]benzene, 81 MHz): δ = 95.1 ppm.

Catalytic Study: A solution of phenylacetylene (0.2 mL, 3.03 mmol) in THF (10 mL) was treated with (**7**)BPh_4 (128 mg, 0.16 mmol, 5 mol %), and the reaction mixture was stirred at 80 °C for 12 h. The solvent was evaporated, and the residue was transferred to a chromatography column (SiO_2, 4% H_2O). Elution with hexane afforded a yellow oil (245 mg, 65%). GC/MS studies revealed that the mixture contained a linear dimer (12%, *m*/*z* = 204, presumably one regioisomer of diphenyl-1,3-butenyne), 1,3,5-triphenylbenzene (52%, *m*/*z* = 306), a linear trimer (8%, *m*/*z* = 306, presumably one regioisomer of triphenylhex-1-yne-3,5-diene) and 1,2,4-triphenylbenzene (28%, *m*/*z* = 306). Crystals of 1,3,5-triphenylbenzene were isolated from the mixture and characterized by X-ray diffraction analysis.[30] Subjection of these crystals to a GC/MS study confirmed the formation of 1,3,5-triphenylbenzene as the main product.

X-ray Crystallography:[34] Data sets were collected at −75 °C [for **4** and (**5**)BPh_4] with an Enraf−Nonius KappaCCD or at −120 °C [for **3**, (**6**)BPh_4, (**7**)BPh_4, and (**10**)BPh_4] with a Bruker AXS APEX diffractometer, both equipped with a rotating anode and both using Mo-K_α radiation (λ = 0.71073 Å). Empirical absorption correction with SORTAV[35] [for **4** and (**5**)BPh_4] or SADABS[36] [for **3**, (**6**)BPh_4, (**7**)BPh_4, and (**10**)BPh_4] was applied to the raw data. Structure solution in all cases with SHELXS[37] and refinement with SHELXL[38] with anisotropic thermal parameters for all atoms. Hydrogen atoms were added to the structure models on calculated positions and were refined as riding atoms [**4**, (**5**)BPh_4] or are unrefined (for (**10**)BPh_4). Hydrogen atoms for **3**, (**6**)BPh_4, and (**7**)BPh_4 were located in the difference Fourier map and were refined with isotropic thermal parameters. ORTEP[39] was used for all drawings. Additional crystallographic data are listed in Table 3.

Computational Details: All quantum chemical calculations were performed with the TURBOMOLE suite of programs.[40] The phenylacetylene complexes have been fully optimized at the density functional (DFT) level employing the BP86 functional[41] and Gaussian AO basis sets of valence-triple-ξ quality including polarization functions (TZVP, C:[5s3p1d], H:[3s1p], P:[5s4p1d]).[42] For the metals the quasi-relativistic pseudo potentials of the Stuttgart group with a 28 (Mo, Ru) and 60 (Os) electron core, respectively, are used.[43] The corresponding optimized AO basis sets (Mo, Ru: [5s3p3d1f], Os: [6s3p3d1f]) have been taken from the TURBOMOLE library.[44] The calculated dissociation energies have been obtained by freezing the metal fragment without the phenylacetylene ligand in the optimized geometry of the complex (vertical D_e). Comparative calculations have also been performed with the popular B3LYP hybrid functional.[45]

Table 3. Crystallographic data for **3**, **4**, (**5**)$BPh_4 \cdot C_5H_{12}$, (**6**)$BPh_4 \cdot CH_2Cl_2$, (**7**)BPh_4, and (**10**)$BPh_4 \cdot C_6H_{14}$

	3	**4**	(**5**)$BPh_4 \cdot C_5H_{12}$	(**6**)$BPh_4 \cdot CH_2Cl_2$	(**7**)BPh_4	(**10**)$BPh_4 \cdot 3C_4H_8O$
Empirical formula	$C_{19}H_{28}BMoP$	$C_{37}H_{40}MoP_2$	$C_{66}H_{74}BMoN_2P$	$C_{51}H_{54}BCl_2MoP$	$C_{51}H_{50}BMoP$	$C_{69}H_{70}BMoO_3P$
Formula mass, amu	394.13	642.57	1032.99	875.56	800.63	1084.97
a, Å	22.2257(11)	17.635(1)	21.534(1)	10.0047(8)	19.1772(10)	11.1097(5)
b, Å	22.2257(11)	8.681(1)	13.622(1)	14.6763(12)	19.0903(10)	21.2852(10)
c, Å	7.4034(5)	21.649(1)	21.592(1)	14.8010(12)	22.2170(12)	23.4095(11)
α, deg	90.0	90.00	90.0	82.037(2)	90.0	90.00
β, deg	90.0	107.65(1)	118.55(1)	84.542(2)	90.0	96.1750(10)
γ, deg	90.0	90.00	90.0	82.248(2)	90.0	90.00
V, Å^3	3657.1(4)	3158.2(4)	5563.5(5)	2126.2(3)	8133.6(7)	5503.6(4)
$d_{calcd.}$, g cm^{-1}	1.432	1.351	1.233	1.368	1.308	1.309
Crystal system	orthorhombic	monoclinic	monoclinic	triclinic	orthorhombic	monoclinic
Space group	I_{4bar}	$P21/c$	$P2_1/n$	$P\bar{1}$	Pbca	Cc
Z	8	4	4	2	8	4
μ, mm^{-1}	0.799	0.541	0.306	0.507	0.397	0.316
Unique data	11271	7965	9754	5549	5308	12468
observed data $\{I > 2\sigma(I)\}$	10309	6685	5162	4631	4130	11347
*R*1 (obsd. data),%	2.57, *wR*1 = 5.48	3.23, w*R*1 = 7.61	5.98, w*R*1 = 10.42	3.78, w*R*1 = 8.86	2.89, w*R*1 = 6.35	4.43, w*R*1 = 10.97
*R*2 (all data),%	2.88, *wR*2 = 5.53	4.35, *wR*2 = 8.11	14.48, *wR*2 = 12.86	5.00, *wR*2 = 9.48	4.61, *wR*2 = 7.09	4.96, *wR*2 = 11.24
GoF	0.949	1.037	0.990	1.033	1.013	1.045
No. of variables	311	369	650	713	687	650
Res. electron density, e/ Å^3	0.667 /−0.873	0.410 /−0.509	0.560 /−0.430	0.473 /−0.435	0.470/−0.204	1.462/−1.529

Acknowledgments

This work was financially supported by the Deutsche Forschungsgemeinschaft, the Fonds der Chemischen Industrie, and the government of North Rhine-Westphalia (Bennigsen-Foerder-Preis 2000 to M. T.). We are indebted to Dr. Klaus Bergander for carrying out valuable NMR experiments.

[1] M. I. Bruce, *Chem. Rev.* **1998**, *98*, 2797−2858.
[2] B. M. Trost, F. D. Toste, A. B. Pinkerton, *Chem. Rev.* **2001**, *101*, 2067−2096.
[3] For selected publications, see: [3a] B. M. Trost, A. B. Pinkerton, F. D. Toste, M. Sperrle, *J. Am. Chem. Soc.* **2001**, *123*, 12504−12509. [3b] M. I. Bruce, B. C. Hall, B. W. Skelton, A. H. White, N. N. Zaitseva, *J. Chem. Soc., Dalton Trans.* **2000**, 2279−2286. [3c] E. Rüba, W. Simanko, K. Mauthner, K. M. Soldouzi, C. Slugovc, K. Mereiter, R. Schmid, K. Kirchner, *Organometallics* **1999**, *18*, 3843−3850. [3d] B. M. Tost, B. Vidal, M. Thommen, *Chem. Eur. J.* **1999**, 1055−1069. [3e] C. S. Yi, N. Liu, *Organometallics* **1998**, *17*, 3158−3160. [3f] C. S. Yi, N. Liu, *Organometallics* **1996**, *15*, 3968−3971. [3g] T. Braun, O. Gevert, H. Werner, *J. Am. Chem. Soc.* **1995**, *117*, 7291−7292.
[4] M. L. H. Green, D. K. P. Ng, *Chem. Rev.* **1995**, *95*, 439−473.
[5] [5a] C. E. Davies, I. M. Gardiner, J. C. Green, M. L. H. Green, N. J. Hazel, P. D. Grebenik, V. S. B. Mtetwa, K. Prout, *J. Chem. Soc., Dalton Trans.* **1985**, 669−683. [5b] J. S. Adams, C. Bitcon, J. R. Brown, D. Collison, M. Cunningham, M. W. Whiteley, *J. Chem. Soc., Dalton Trans.* **1987**, 3049−3053. [5c] C. Bitcon, R. Breeze, P. F. Miller, M. W. Whiteley, *J. Organomet. Chem.* **1989**, *364*, 181−193. [5d] R. L. Beddoes, R. W. Grime, Z. I. Hussain, M. W. Whiteley, *J. Chem. Soc., Dalton Trans.* **1996**, 3893−3895.
[6] [6a] J. Okuda, T. Eberle in *Metallocenes* (Eds.: A. Togni, R. L. Halterman), Wiley-VCH, Weinheim, **1998**, Vol. 1, p. 415. [6b] J. Okuda, *Comment, Inorg. Chem.* **1994**, *16*, 185.
[7] P. Jutzi, T. Redeker, *Eur. J. Inorg. Chem.* **1998**, 663−674.
[8] U. Siemeling, *Chem. Rev.* **2000**, *100*, 1495−1526.
[9] H. Butenschön, *Chem. Rev.* **2000**, *100*, 1527−1564.
[10] M. Tamm, T. Bannenberg, B. Dreßel, R. Fröhlich, C. Holst, *Inorg. Chem.* **2002**, *41*, 47−59.
[11] M. Tamm, K. Baum, T. Lügger, R. Fröhlich, K. Bergander, *Eur. J. Inorg. Chem.* **2002**, 918−928.
[12] M. Tamm, B. Dreßel, V. Urban, T. Lügger, *Inorg. Chem. Commun.* **2002**, *5*, 837−840.
[13] M. Tamm, B. Dreßel, K. Baum, T. Lügger, T. Pape, *J. Organomet. Chem.*, submitted.
[14] H. Suzuki, D. H. Lee, N. Oshima, Y. Moro-oka, *Organometallics* **1987**, *6*, 1569−1575.
[15] S. L. J. Conway, L. H. Doerrer, M. L. H. Green, M. A. Leech, *Organometallics* **2000**, *19*, 630−637, and references cited therein.
[16] M. Elian, M. M. L: Chen, D. M. P. Mingos, R. Hoffmann, *Inorg. Chem.* **1976**, *15*, 1148−1155.
[17] [17a] H. Brunner, *Eur. J. Inorg. Chem.* **2001**, 905−912. [17b] H. Brunner, *Angew. Chem.* **1999**, *111*, 1248−1263; *Angew. Chem. Int. Ed.* **1999**, *38*, 1194−1209.
[18] H. Brunner, M. Muschiol, I. Bernal, G. M. Reisner, *J. Organomet. Chem.* **1980**, *198*, 169−178.
[19] For a related chiral ruthenium complex of the type [(η-C_5Me_5)Ru(PPh_3)(PR_3)H] (R = OMe), see: T. Arliguie, B. chaudret, F. A. Jalon, A. Otero, J. A. Lopez, F. J. Lahoz, *Organometallics* **1991**, *10*, 1888−1896.
[20] M. L. H. Green, R. B. A. Pardy, *Polyhedron* **1985**, *4*, 1035−1041.
[21] E. Schwed, H.-U. Hund, H. W. Bosch, H. Berke, *Helv. Chim. Acta* **1991**, *74*, 189−196.
[22] *Comprehensive Organometallic Chemistry II* (Eds.: E. W. Abel, F. G. A. Stone, G. Wilkinson), vol. 7 (Vol. Eds. D. F. Shriver, M. I. Bruce), Chapman and Hall, Oxford, **1995**.
[23] G. J. P. Britovsek, V. C. Gibson, D. F. Wass, *Angew. Chem.* **1999**, *111*, 448−468; *Angew. Chem. Int. Ed.* **1999**, *38*, 428−447.
[24] J. Chatt, C. M. Elson, A. J. L. Pombeiro, R. L. Richards, G. H. D. Royston, *J. Chem. Soc., Dalton Trans.* **1978**, 165−169.
[25] H. Seino, C. Arita, D. Nonokawa, G. Nakamura, Y. Harada, Y. Mizobe, M. Hidai, *Organometallics* **1999**, *18*, 4165−4173.
[26] R. Usón, L. A. Oro, M. A. Ciriano, M. M. Naval, M. C. Apreda, C. Foces-Foces, F. H. Cano, S. Garcia-Blanco, *J. Organomet. Chem.* **1983**, *256*, 331−347.
[27] J. L. Templeton, *Adv. Organomet. Chem.* **1989**, *29*, 1−100.
[28] J. J. Carbó, P. Crochet, M. A. Esteruelas, Y. Jean, Agustí

Lledós, A. M. López, E. Oñate, *Organometallics* **2002**, *21*, 305−314.
[29] [29a] W. E. Douglas, *J. Chem. Soc., Dalton Trans.* **2000**, 57−62. [29b] M. G. L. Petrucci, A. K. Kakkar, *J. Chem. Soc., Chem. Commun.* **1995**, 1577−1578. [29c] H.-F. Klein, M. Mager, S. Isringhausen-Bley, U. Flörke, H.-J. Haupt, *Organometallics* **1992**, *11*, 3174−3175.
[30] Crystal data for 1,3,5-triphenylbenzene: a = 7.4779(3), b = 19.7314(9), c = 11.2217(5) Å, Z = 4, orthorhombic, space group $Pna2_1$, final R = 3.79% based on 2137 observed structure factors [$I \geq 2\ \sigma(I)$].
[31] L. S. Meriwether, M. F. Leto, E. C. Colthup, G. W. Kennerly, *J. Org. Chem.* **1962**, *27*, 3930−3941.
[32] G. Frenking, N. Fröhlich, *Chem. Rev.* **2000**, *100*, 717−774.
[33] M. Haufe, R. D. Köhn, R. Weimann, G. Seifert, D. Zeigan, *J. Org. Chem.* **1996**, *520*, 121−129.
[34] CCDC-CCDC-183826, -183827, -183828, -183829, -192130, and -192131 contain the supplementary crystallographic data for this paper. These data can be obtained free of charge at www.ccdc.cam.ac.uk/conts/retrieving.html [or from the Cambridge Crystallographic Data Centre, 12, Union Road, Cambridge CB2 1EZ, UK; fax: (internat.) +44-1223/336-033; E-mail: deposit@ccdc.cam.ac.uk].
[35] SORTAV, R. H. Blessing, *J. Appl. Crystallogr.* **1997**, *30*, 421−426.
[36] SMART, Bruker AXS, **2000**.
[37] SHELXS-97, G. M. Sheldrick, *Acta Crystallogr., Sect. A* **1990**, *46*, 467−473.
[38] SHELXL-97, G. M. Sheldrick, Universität Göttingen, **1997**.
[39] ORTEP-3, L. J. Farrugia, University of Glasgow, **1999**.
[40] R. Ahlrichs, M. Bär, H.-P. Baron, R. Bauernschmitt, S. Böcker, M. Ehrig, K. Eichkorn, S. Elliott, F. Furche, F. Haase, M. Häser, H. Horn, C. Huber, U. Huniar, M. Kattannek, C. Kölmel, M. Kollwitz, K. May, C. Ochsenfeld, H. Öhm, A. Schäfer, U. Schneider, O. Treutler, M. von Arnim, F. Weigend, P. Weis, H. Weiss, TURBOMOLE (vers. 5.3), Universität Karlsruhe, **2000**.
[41] [41a] A. D. Becke, *Phys. Rev. A* **1988**, *38*, 3098−3100. [41b] J. P. Perdew, *Phys. Rev. B* **1986**, *33*, 8822−8824.
[42] A. Schäfer, C. Huber, R. Ahlrichs, *J. Chem. Phys.* **1994**, *100*, 5829−5835.
[43] D. Andrae, U. Häussermann, M. Dolg, H. Stoll, H. Preuss, *Theor. Chim. Acta* **1990**, *77*, 123−130.
[44] The AO basis sets used are available at (anonymous) ftp://ftp.chemie.uni-karlsruhe.de/pub/basen
[45] [45a] A. D. Becke, *J. Chem. Phys.* **1993**, *98*, 5648−5652. [45b] P. J. Stephens, F. J. Devlin, C. F. Chabalowski, M. J. Frisch, *J. Phys. Chem.* **1994**, *98*, 11623−11627.

Received August 26, 2002
[I02478]

Modes of Reactivity of Cyclic Diynes: Probing the *syn*/*anti* Selectivity of Tetrathiacycloalkadiynes and Mono(alkyne)cobalt Complexes

Christoph Benisch,[a] Daniel B. Werz,[a] Rolf Gleiter,*[a] Frank Rominger,[a] and Thomas Oeser[a]

Keywords: Alkynes / Cobalt / Cyclobutadiene complexes / *syn-anti* selectivity

Cyclic tetrathiaalkadiynes in which two 1,4-dithiaalkyne units are connected with alkane bridges of length *n* and *m* [**A(*m*.*n*)**] were treated with [η^2-bis(*tert*-butylsulfonyl)acetylene]carbonyl(η^5-cyclopentadienyl)cobalt(I) (**8a**) and several substituted analogues (**8b**–**8e**) in order to probe the reactivity of electron-rich cyclic diynes. Both mono- [**B(*m*.*n*)**] and bis(cyclobutadiene) [**C(*m*.*n*)**] complexes were isolated as products of these reactions and the *anti*/*syn* ratio of **C(*m*.*n*)** was determined. For *m*, *n* < 4 the *syn* isomers dominate and this is attributed to the configuration of the intermediate metallacycle which is correlated with the conformations of the rings in the mono(cyclobutadiene) products **B(*m*.*n*)**. This analysis was corroborated by X-ray structural investigations of the products.
(© Wiley-VCH Verlag GmbH & Co. KGaA, 69451 Weinheim, Germany, 2003)

Introduction

Dicarbonyl(η^5-cyclopentadienyl)cobalt [$CpCo(CO)_2$] (**1**) is a very convenient and efficient reagent for the di- and trimerisation of alkynes.[1] Two different mechanisms have been proposed for this reaction. One involves (alkyne)dicobalt complexes[2] whereas the other assumes that the reaction occurs on one CpCo fragment only.[3–5] The latter seems to be preferred at low temperatures whereas polynuclear complexes may play a role at higher temperatures.[2] The mechanism involving only one $CpCoL_2$ unit, in which the ligands are replaced successively by the alkyne to yield a 16-electron metallacycle which is converted to an 18-electron species **4** by an additional ligand L, is outlined briefly in Scheme 1.

The fact that derivatives of **2** and **4** have been isolated at room temperature[6–9] and that the alkynes react either to cyclobutadiene (**6**)[10] or to aromatic species (**5**)[4] support this mechanism.

Recently, we found a mild and efficient procedure to isolate congeners of **2** by treating **1** with bis(*tert*-butylsulfonyl)-acetylene (BTSA, **7**).[7] The resulting complex **8** reacts under very mild conditions with electron-rich alkynes to yield the cyclobutadiene complexes **9**. The reactions with dithiaalkynes (R = SR′ in Scheme 2) were especially efficient.[11]

In view of the complex mechanism of cyclobutadiene formation (Scheme 1) it is of general interest to test the reactivity of electron-rich cyclic diynes with the electrophile **8**, and to see if there is any preference for one of the two possible products (*syn* or *anti*). For cyclic tetrathiadiynes **A(*m*.*n*)** the anticipated products **B(*m*.*n*)R**, and *syn*- and *anti*-**C(*m*.*n*)R** are shown in Scheme 3.

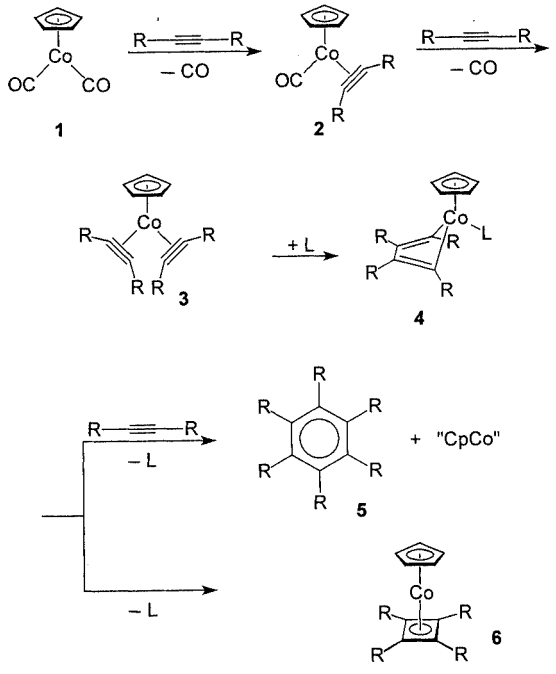

Scheme 1

Results

We used the recently prepared cyclic tetrathiadiynes **A(2.2)** to **A(5.5)**[12] and [η^2-bis(*tert*-butylsulfonyl)acetylene]-

[a] Organisch-Chemisches Institut der Universität Heidelberg, Im Neuenheimer Feld 270, 69120 Heidelberg, Germany
E-mail: rolf.gleiter@urz.uni-heidelberg.de

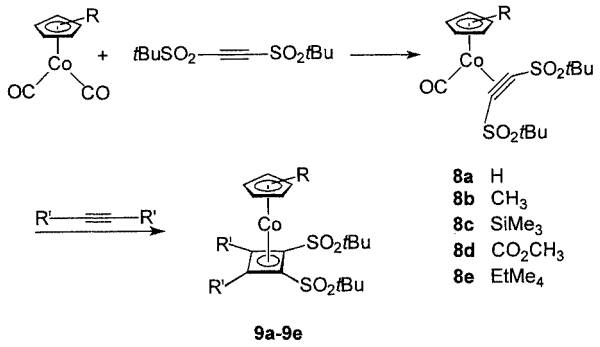

Scheme 2

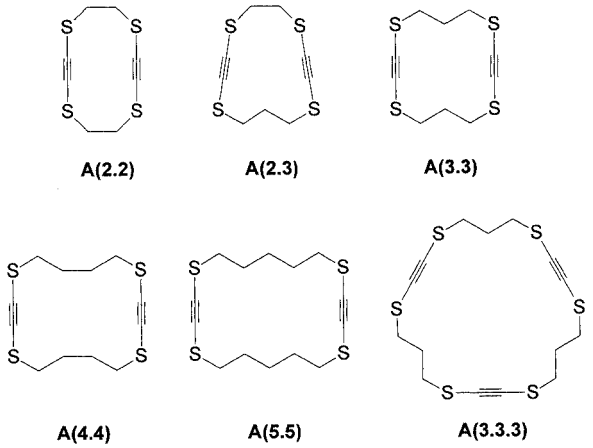

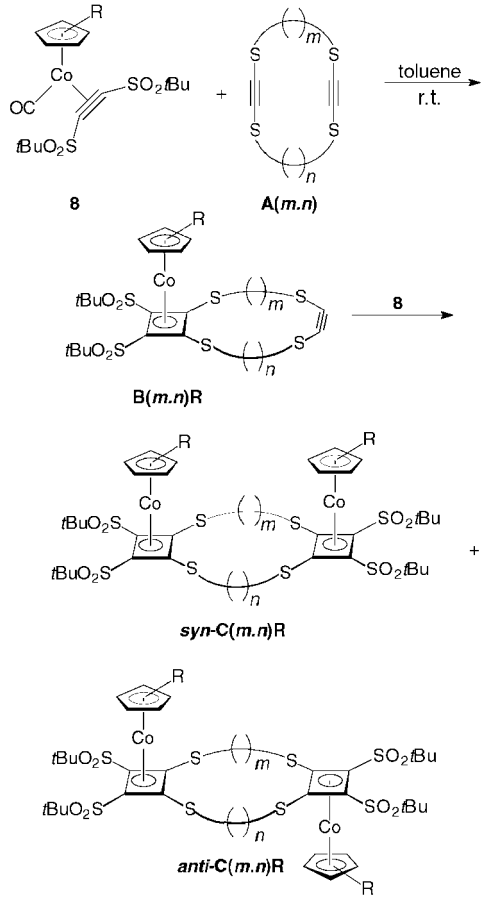

Scheme 3

carbonyl(η^5-cyclopentadienyl)cobalt(I) (**8a**) and several analogues **8b**−**8e** substituted at the Cp ring[7] as starting materials.

The cyclic tetrathiadiynes **A(*m.n*)** were treated with **8a**−**8e** in 1:1 and 2:1 ratios at room temperature in toluene as solvent to give the 1:1 and 2:1 cyclobutadienes. The yields of the products **B(*m.n*)R** and **C(*m.n*)R** are reported in Table 1.

Because the solubility of the cyclobutadiene complexes decreases with reduced ring size we treated cycles **A(2.2)** and **A(2.3)** with **8c** only. The $SiMe_3$ substituent in the products ensured reasonable solubilities. The yields listed in Table 1 were obtained as follows: The reaction was monitored by thin layer chromatography, and as soon as no monoalkyne complex was present or no further reaction could be detected, we removed the solvent in vacuo and separated the products by column chromatography. In the case of **A(5.5)** the *syn*/*anti* ratio was determined by NMR spectroscopy since the stereoisomers could not be separated.

When the reaction was carried out such that **8**/**A** = 1:1, good yields of **B(*m.n*)R** were obtained (30−60%), whereas the yields of the 2:1 products were low. A closer look (Table 2) at the distributions of the *anti*/*syn*-**C(*m.n*)** product ratios shows a considerable variation.

In the case of the twelve-membered ring system **A(2.2)**, the *syn* isomer of **C(2.2)SiMe$_3$** was formed predominantly in about 13% yield. For **A(2.3)** and **A(3.3)** the *syn* isomers dominated, whereas for **A(4.4)** the *anti* isomer of **C(4.4)R** was preferred. Only when both triple bonds were separated by pentamethylene chains [**A(5.5)**] was the *anti*/*syn* ratio of the product [**C(5.5)**] found to be 1. These results reveal that thermodynamic factors are not important for the *anti*/*syn* selectivity observed, because the *anti*-**C(*m.n*)R** isomers should be more stable than the *syn* isomers due to steric reasons. We believe that it is the conformation of the large ring of the monosubstituted product **B(*m.n*)R** which primarily influences the *anti*/*syn* ratio of **C(*m.n*)R**. The *anti*/*syn* selectivity in the reactions of **A(3.3)** and **A(4.4)** with **8a**−**8c** (Table 3) allows estimation of the influence of the substituents on the Cp ring. The *anti*/*syn* ratio of the products **C(3.3)** and **C(4.4)** remains essentially constant for **C(3.3)R** and increases in the case of **C(4.4)R** with increasing size of R.

Reaction of triyne **A(3.3.3)** with a large excess of **8c** gave the trinuclear cobalt complexes *anti*-**C(3.3.3)SiMe$_3$** and all-*syn*-**C(3.3.3)SiMe$_3$** in 56 and 13% yield, respectively. In the former, two of the three cobalt centres are above the plane of the ring, whereas in the latter, all three cobalt atoms are on the same side.

Table 1. Yields of the products **B(*m.n*)R** and **C(*m.n*)R** as a function of the ratio of starting materials [**8**: **A(*m.n*)**]

	Ratio **8**/**A**	Isomer	R = H	R = Me	R = $SiMe_3$	R = CO_2Me	R = $EtMe_4$
A(2.2)	1:1	mono			41		
		anti			<1		
		syn			5		
	2:1	mono			60		
		anti			<1		
		syn			13		
A(2.3)	1:1	mono			41		
		anti			<1		
		syn			<1		
	2:1	mono			8		
		anti			23		
		syn			32		
A(3.3)	1:1	mono	27	18	57	12	19
		anti	8	13	14	28	<1
		syn	14	32	11	12	<1
	2:1	mono	11	<1	10	1	13
		anti	14	16	16	15	5
		syn	26	58	25	33	<1
A(4.4)	1:1	mono	34	43	57	41	
		anti	<1	<1	<1	<1	
		syn	<1	<1	<1	8	
	2:1	mono	20	<1	10	3	9
		anti	26	53	31	29	<1
		syn	16	19	11	29	<1
A(5.5)	1:1	mono	22	30		48	
		anti	3	9		<1	
		syn	3	9		<1	
	2:1	mono	13	<1		<1	
		anti	16	28		32	
		syn	16	28		32	

Table 2. Averaged *anti*/*syn* ratios of the isomers obtained in the reaction of bis(cyclopentadienylcobalt) complexes with the tetrathiadiynes **A(2.2)** to **A(5.5)**

Diyne	**A(2.2)**	**A(2.3)**	**A(3.3)**	**A(4.4)**	**A(5.5)**
anti/*syn*	< 1:13	1:1.4	1:2	2 :1	1:1

Table 3. Yield of *syn* and *anti* **C(3.3)R** and **C(4.4)R** as a function of the substituents R

		8a (H)	**8b** (CH_3)	**8c** ($SiMe_3$)
C(3.3)	anti	14	16	16
	syn	26	58	25
C(4.4)	anti	26	53	31
	syn	16	19	11

X-ray Investigations

Isolation of single crystals of mono- and disubstitution products of the 12-, 13-, 14- and 16-membered rings **A(2.2)**, **A(2.3)**, **A(3.3)** and **A(4.4)** allowed a detailed study of their molecular structures using X-ray techniques. The molecular structures of **B(2.2)SiMe$_3$** and *syn*-**C(2.2)SiMe$_3$** are shown in Figure 1.

As can be seen from the conformation of the 12-membered ring of the monoadduct, the triple bond is situated relatively close (472 pm) to the cyclobutadiene (Cb) ring. The distances between the metal atom and the centres of the Cp ring and the Cb ring are 167 and 168 pm, respectively. Owing to the sizeable $SiMe_3$ substituent, the Cp and Cb rings are not parallel but are tilted by 8.3°. It is interesting to note that the torsion angle between the CH_2-S bonds at the triple bond of **B(2.2)SiMe$_3$** is 93.0°. In *syn*-**C(2.2)SiMe$_3$** (Figure 1) the two Cb rings are separated by 538 pm and 645 pm, corresponding to an angle between the two Cb planes of 42.7°.

The structure of **B(2.3)SiMe$_3$** in the crystal (Figure 2) shows that the 13-membered ring is more remote from the Cb ring (556 pm) and also from the $CpSiMe_3$ group. The interplanar angle between the Cp and Cb rings (4.1°) is smaller than in **B(2.2)SiMe$_3$**.

The X-ray structure of the *anti*-**C(2.3)SiMe$_3$** isomer is also shown in Figure 2. In this structure, both Cb rings are tilted towards each other by 62.0°.

The X-ray analysis of single crystals of **B(3.3)SiMe$_3$** revealed two molecules as asymmetric unit. The quality of the data was somewhat marginal and, while the distances and angles must therefore be viewed with caution, only the conformation of the 14-membered ring could be elucidated (Figure 3).

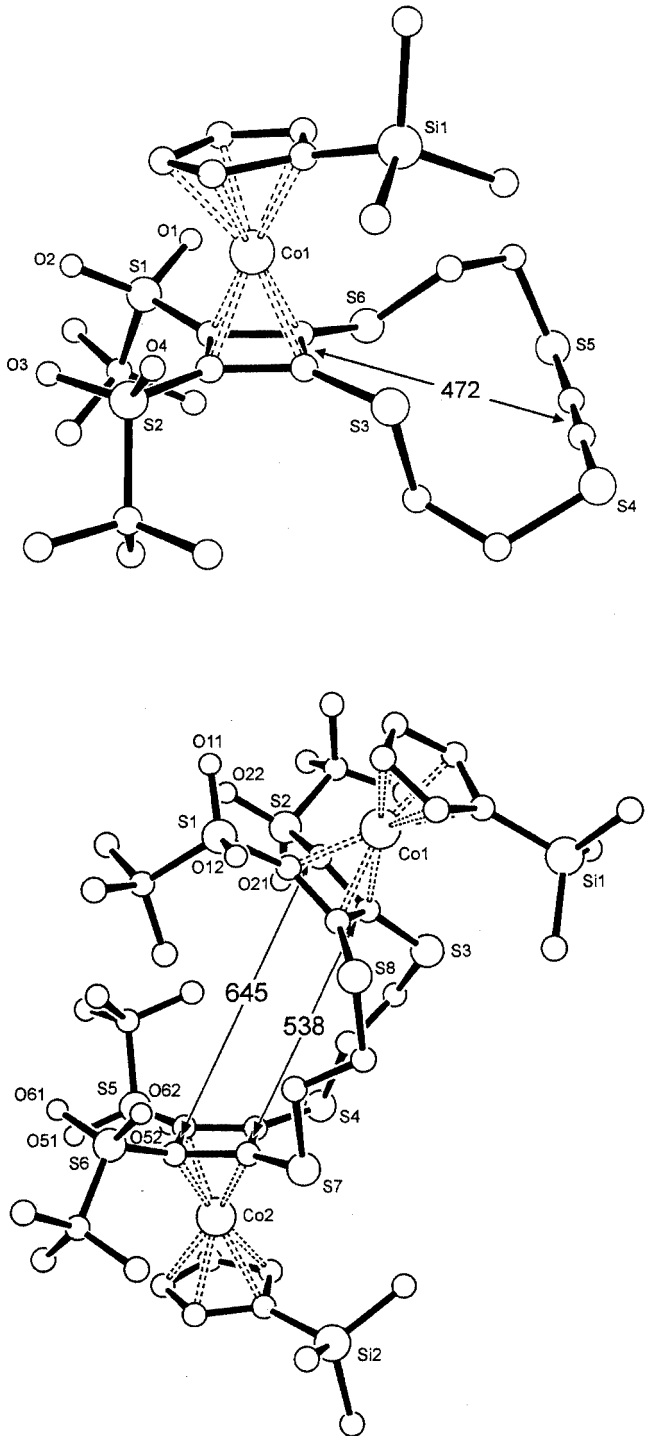

Figure 1. Molecular structures of **B(2.2)SiMe$_3$** and *syn*-**C(2.2)SiMe$_3$**; distances between the π-units defined by the arrows are given

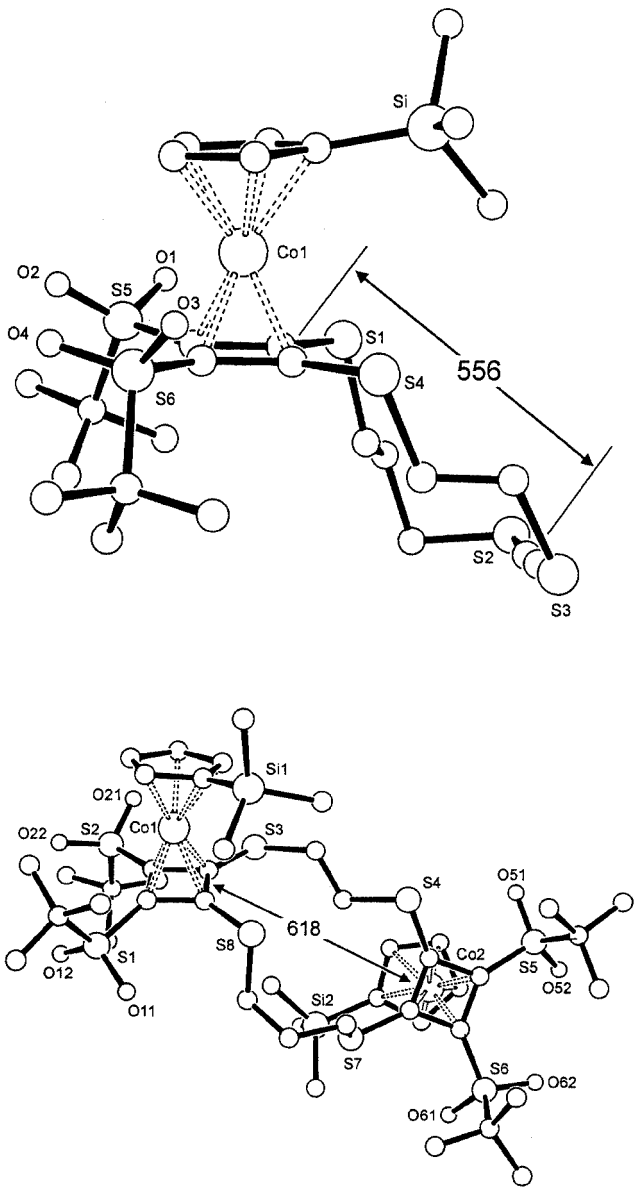

Figure 2. Molecular structures of **B(2.3)SiMe$_3$** and *anti*-**C(2.3)SiMe$_3$**; distances between the π-units defined by the arrows are given

The quality of the structure of *syn*-**C(3.3)SiMe$_3$** (R_w = 0.147) is similar to that of **B(3.3)SiMe$_3$**, and therefore a structural diagram has not been included. However, it can be deduced that the conformation of *syn*-**C(3.3)SiMe$_3$** is similar to that of *anti*-**C(2.3)SiMe$_3$** insofar as the planes of the two cyclobutadiene rings are twisted by about 72°. All *tert*-butylsulfonyl groups are bent away from the $SiMe_3CpCo$ moieties. Figure 3 also shows the structure of *anti*-**C(3.3)SiMe$_3$** in the crystal. As in the *syn* isomer the two Cb rings are twisted, but the twist angle is 54° (calculated as "torsion angle" between the two nearest Cb bonds of both rings), less than in the *syn* isomer. The distance between the cyclobutadiene rings in the *anti* isomer (685 pm) is larger than that found in *syn*-**C(3.3)SiMe$_3$** (661 pm). Both *tert*-butylsulfonyl moieties are bent away from the $SiMe_3CpCo$ fragment.

The triple bond in **B(4.4)CH$_3$** (Figure 4) is relatively far remote from the cyclobutadiene ring (705 pm) and is nearly in plane with the cyclobutadiene ring. The large ring adopts an armchair conformation. In both *syn*- and *anti*-**C(4.4)CH$_3$** (Figure 4) a chair-like conformation of the central ring is maintained. A comparison of the structures of

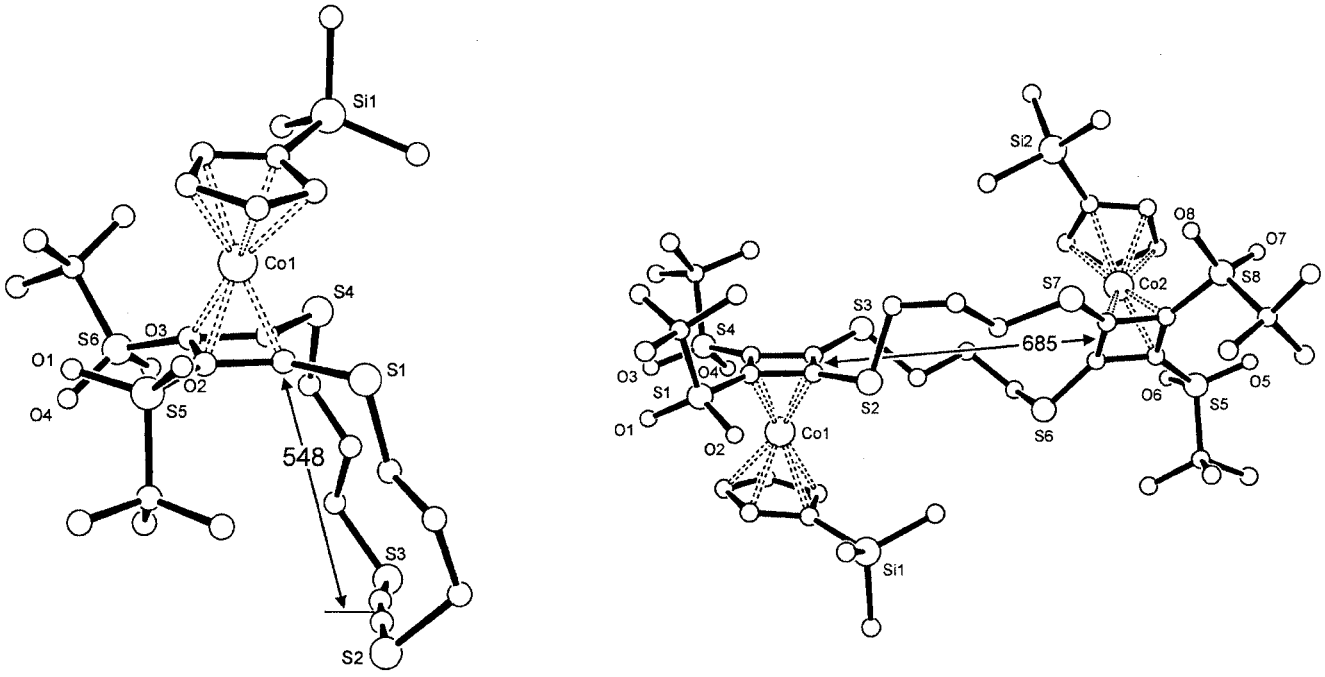

Figure 3. Molecular structures of **B(3.3)SiMe$_3$** (only one of both independent molecules is shown) and *anti*-**C(3.3)SiMe$_3$**; distances between the π-units defined by the arrows are given

B(4.4)CH$_3$ and **C(4.4)CH$_3$** shows an increase in the distance between the former triple bonds [779 pm in *syn*-**C(4.4)CH$_3$**]. The "torsion angle" between the two nearest bonds of both cyclobutadiene units is 3.8°. All four *tert*-butylsulfonyl groups point away from the MeCpCo moieties. In *anti*-**C(4.4)CH$_3$** the central ring adopts a chair-like conformation. A crystallographic inversion center is found and consequently both cyclobutadiene rings are parallel to each other. As anticipated, the distance between both cyclobutadiene units (776 pm) is larger than in **B(4.4)CH$_3$**. The distance between the cobalt atoms is larger in the *anti* isomer (1080 pm) than in the *syn* isomer (1024 pm). The CpMe unit adopts a conformation which places the CH_3 group mostly between the SO_2 groups. Such a conformation has previously never been encountered for bulky $SiMe_3$ substituents.

Table 4 gives a comparison of the transannular distances *d* between the π units of **A(*m.n*)**, **B(*m.n*)R** and **C(*m.n*)R**, as well as the torsional angles α between the unsaturated bonds as defined in Figure 5. This shows that the transannular distance *d* between the triple bonds in **A(*m.n*)** is increased in the complexes. This increase is anticipated because it is due to the rehybridisation of the sp centres into sp^2 centres. Thus, the former C(sp)−C(sp)−S angles are reduced from 180 to about 120°. There are small torsion angles α between the triple bonds and the cyclobutadiene rings in the **B(*m.n*)R** complexes. It is interesting to note that the chair conformation of the 14-membered ring of **A(3.3)** is changed to a twisted conformation in both *syn*- and *anti*-**C(3.3)SiMe$_3$**, with α = 66.4 and 54.2°, respectively. The opposite is found in the case of the 16-membered ring of **A(4.4)**. Here the twisted conformation (α = 58.7°) is transformed into an armchair and a chair conformation, respectively, with small torsion angles. Figure 6 shows the molecular structure of the trinuclear cobalt complex all-*syn*-**C(3.3.3)SiMe$_3$**.

Discussion

The rationalisation of our results is difficult since the system contains a number of unknowns. As outlined in Scheme 1 the metal-supported cyclobutadiene formation follows a sequence of several steps. A further complication arises from the unknown minimum energy conformation of the medium-sized ring in **B(*m.n*)** in solution. In order to rationalise the outcome of our experiments we assume that the transition state which determines the stereochemistry of the products is close in energy and structure to the intermediate metallacycle (e.g. **4** in Scheme 1) and rather different to the cyclobutadiene product. We furthermore assume that the barrier to ring inversion in the metallacycles is in the order of 5 kcal/mol.[8] Steric effects should therefore be important in determining the *syn*/*anti* ratios.

In order to discuss the reaction mechanism, two conformations of **B(*m.n*)**, **D1** and **D2** (Figure 7) must be considered. In **D1** the triple bond is situated on the same level with the cyclobutadiene system, whereas in **D2** it is placed below the cyclobutadiene ring. Which of the two geometries is favoured depends mainly on the conformations of the methylene chains and, to a minor extent, on the substituents at the Cp ring. The methylene chains favour a zig-zag arrangement, as demonstrated for several cyclic diynes[13] and especially for cyclic tetrathiadiynes[11] and tetrathiaenynes.[14] In these ring systems a staggered conformation is achieved.

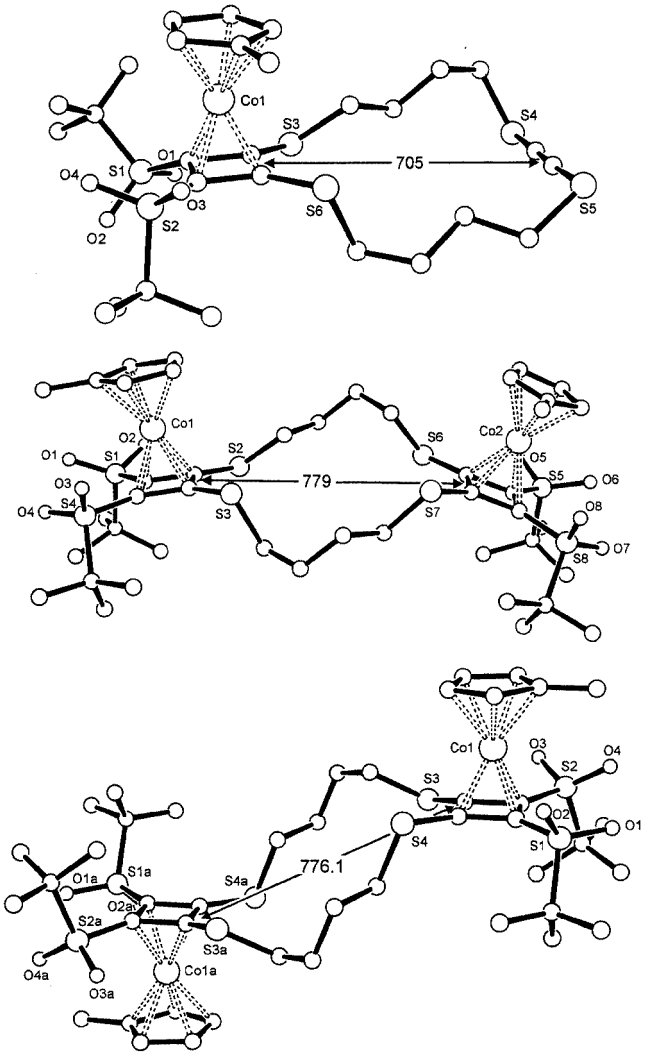

Figure 4. Molecular structures of **B(4.4)Me** (top), *syn*-**C(4.4)Me** (centre) and *anti*-**C(4.4)Me** (bottom); distances between the π-units defined by the arrows are given

Table 4. Transannular distances *d* [pm] and torsional angles α [°] for **A(*m*.*n*)**, **B(*m*.*n*)R** and **C(*m*.*n*)R** ($m = 2-4$, $n = 2-4$) as defined in Figure 5

m	*n*	R		**A(*m*.*n*)**	**B(*m*.*n*)R**	**C(*m*.*n*)R** *syn*	*anti*
2	2	$SiMe_3$	*d*	356	472	539	–
			α	0.0	5.8	20.9	–
2	3	$SiMe_3$	*d*	405	556	–	61.8
			α	13.9	3.3	–	59.1
3	3	$SiMe_3$	*d*	545	548/561	661/652	685
			α	0.0	9.6/10.6	66.4/89.7	54.2
4	4	Me	*d*	535	705	779	776
			α	58.7	1.6	3.8	0.0

The two conformations **D1** and **D2** yield two intermediates **E1** and **E2** (Figure 7). In **E1** the repulsion between the two Cp rings is minimised. Reaction via **E1** should lead to the *anti* isomer, whereas **E2** will give the *syn* isomer. The close distance between the triple bond and the cyclobutadiene ring (472 pm) and the bulky $SiMe_3$ substituent in **B(2.2)SiMe$_3$** should clearly favour **E1** even when the triple bond and cyclobutadiene ring are situated at the same level (Figure 1). The strong preference for *syn*-**C(2.2)SiMe$_3$** (Tables 1 and 2) can be rationalised by assuming that the energy difference between the conformation shown in Figure 1 and one close to that found for **B(2.3)SiMe$_3$** (Figure 2) should be small. This assumption is supported by X-ray studies of (*Z*)-1,4,7,10-tetrathiacyclododeca-2-en-8-yne (**9**).[14] The conformation of **9** is given in Figure 8 and resembles that of the enyne fragment of **B(2.3)SiMe$_3$**. In this conformation the triple bond is rather close to the *tert*-butyl groups, and therefore the metallacycle with the CpCo fragment on the *syn* side should be favoured. The same holds for **B(2.3)SiMe$_3$** and **B(3.3)SiMe$_3$**. Owing to the stair-like arrangement of double and triple bonds, and the close proximity of the *tert*-butyl groups and the triple bond, a *syn* product should be favoured as indicated in Table 2. The results summarised in Table 3 suggest that, for the reaction of **B(3.3)R** with **8a**–**8c**, a transition state similar to **E2** should be preferred, whereas in the reaction of **B(4.4)R** with **8a**–**8c**, a geometry closely related to **E1** should be favoured. These conclusions are in agreement with the structures of **B(3.3)SiMe$_3$** and **B(4.4)SiMe$_3$** in the crystal.

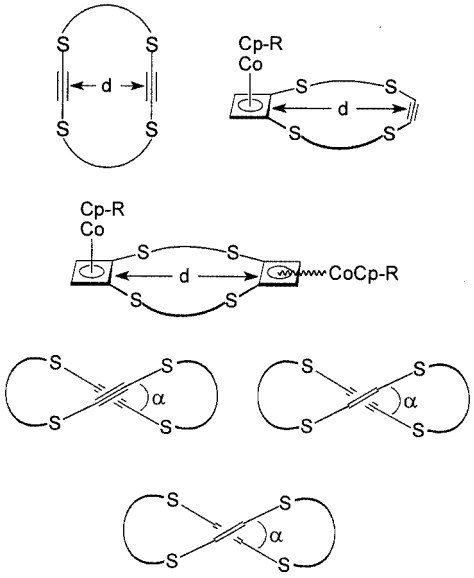

Figure 5. Definition of *d* and α for the values listed in Table 4

Conclusions

In the beginning of our investigations we raised the question of the *syn*/*anti* selectivity in the twofold cyclobutadiene formation in nonconjugated cyclic diynes. We have been able to determine the *syn*/*anti* ratio in the reaction of the medium-sized rings **A(*m*.*n*)** ($n = 2-4$ and $m = 2-4$) by using highly reactive nucleophilic tetrathiaalkadiynes and strongly electrophilic mono(alkyne)cobalt complexes. No selectivity was observed for larger rings ($m, n > 4$). For smaller rings, *syn* selectivity was preferred for **A(2.2)**, **A(2.3)**

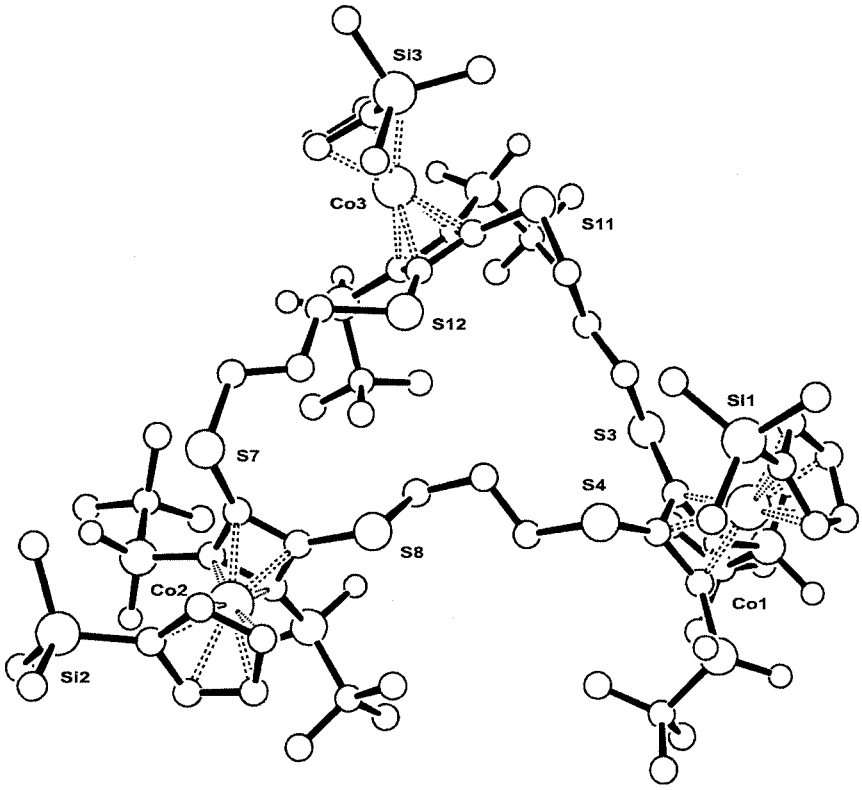

Figure 6. Molecular structure of all-*syn*-**C(3.3.3)SiMe$_3$**

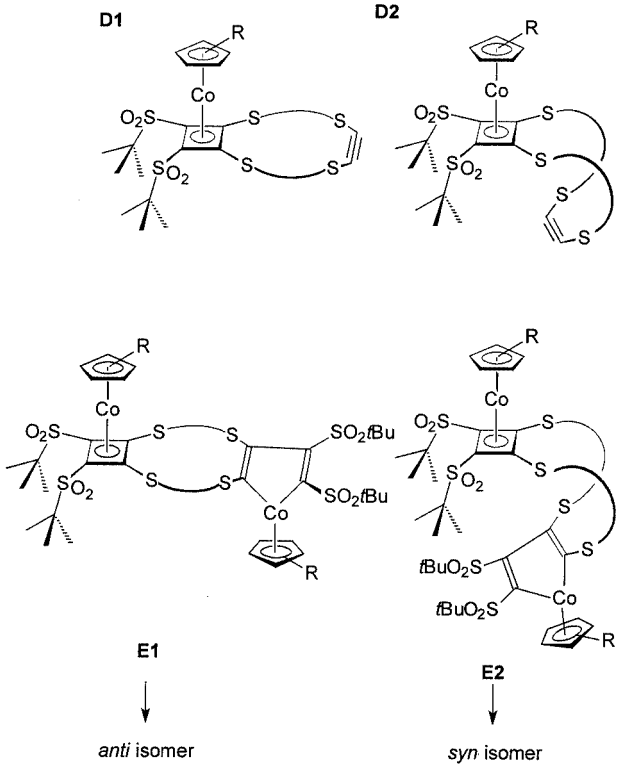

Figure 7. Possible conformations, **D1** and **D2**, of the 1:1 products **B(*m.n*)R** (top); resulting intermediates, **E1** and **E2**, from the reactions of **D1** and **D2** with **8a**−**8e**

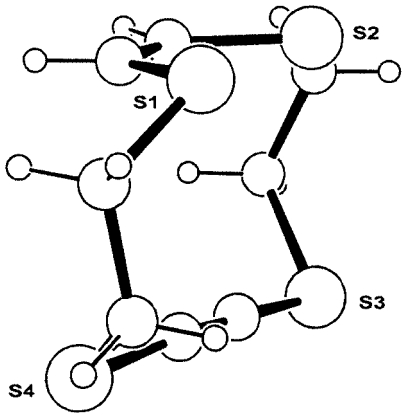

Figure 8. The conformation of (*Z*)-1,4,7,10-tetrathiacyclododeca-2-en-8-yne (**9**) in the crystal that resembles that of the enyne fragment of **B(2.3)SiMe$_3$**

and **A(3.3)**, whereas for **A(4.4)** *anti* selectivity prevails. Our X-ray investigations on the mono- and disubstituted complexes revealed that the selectivity is mainly determined by the conformation of the medium-sized chain. For short chains (m, $n < 4$) we found that the ring with the dithiaalkyne unit in **B(*m.n*)** is bent away from the CpCo moiety. This conformation favours the formation of the second metallacycle *syn* to the CpCo-stabilised cyclobutadiene complex. These studies suggest that a stepwise synthesis of cyclic oligomers[15] should be possible if the chain length between the triple bonds is small. For pure hydrocarbons the chain length should be below six CH_2 groups.

Experimental Section

General Methods: Moisture- and oxygen-sensitive reactions were conducted in oven-dried glassware under argon. Toluene was dried with sodium/benzophenone and distilled under argon before use. Petroleum ether and diethyl ether were distilled before use. Melting points are uncorrected. Materials used for column chromatography: Silica gel 60 (Machery−Nagel). ^{1}H and ^{13}C NMR: Bruker AS 200 (^{1}H at 200 MHz and ^{13}C at 50.33 MHz), Bruker Avance 300 (^{1}H at 300 MHz and ^{13}C at 75.47 MHz), Bruker Avance 500 (^{1}H at 500 MHz and ^{13}C at 125.77 MHz) using the solvent as internal standard. The signals were assigned by NMR correlation techniques. IR: Bruker Vector 22 FT-IR. MS: Low resolution: ZAB-2F; high resolution: JEOL JMS-700. Elemental analyses were carried out by the Mikroanalytisches Laboratorium der Universität Heidelberg. Complexes **8a**−**8e**[7] and the tetrathiacyclodiynes **A(2.2)** to **A(5.5)**[12] were prepared according to literature methods.

General Procedure for the Preparation of the Cyclobutadiene Complexes: The mono(alkyne)cobalt complex was dissolved in toluene (150 mL) and the tetrathiacycloalkadiyne was added in one portion. The reaction mixture was stirred at room temperature. After completion of the reaction, the solvent was removed by rotary evaporation and the products were isolated by column chromatography (SiO_2; diethyl ether/petroleum ether, 1:1 → 2:1 → 5:1 → dichloromethane/methanol, 30:1).

Reaction of A(2.2) with [CpSiMe$_3$Co(CO)(BTSA)] (8c). Reaction A: 8c (134 mg, 0.27 mmol) and **A(2.2)** (70 mg, 0.30 mmol). Yield: 77 mg (41%) of **B(2.2)SiMe$_3$** and 15 mg (5%) of *syn*-**C(2.2)SiMe$_3$**. **Reaction B: 8c** (324 mg, 0.66 mmol) and **A(2.2)** (70 mg, 0.30 mmol). Yield: 126 mg (60%) of **B(2.2)SiMe$_3$** and 46 mg (13%) of *syn*-**C(2.2)SiMe$_3$**.

B(2.2)SiMe$_3$: Yellow solid, m.p. 186 °C. ^{1}H NMR (300 MHz, $CDCl_3$): δ = 0.36 [s, 9 H, $Si(CH_3)_3$], 1.45 [s, 18 H, $C(CH_3)_3$], 2.97/3.60 (m, 8 H, SCH_2), 5.32/5.68 (pt, 4 H, CpH) ppm. ^{13}C NMR (75 MHz, $CDCl_3$): δ = −0.4 [$Si(CH_3)_3$], 24.7 [$C(CH_3)_3$], 33.1/34.1 (SCH_2), 61.6 [$C(CH_3)_3$], 78.3 [*C*(Cb)SO_2tBu], 81.6 [*C*(Cb)S], 87.3 (≡C), 88.5/90.1 [*C*(Cp)H], 93.7 [*C*(Cp)$SiMe_3$] ppm. IR (KBr): $\tilde{\nu}$ = 2966 cm^{-1}, 2929, 1631, 1358, 1309, 1250, 1121. UV/Vis (CH_2Cl_2): λ_{max} (log ε) = 316 nm (4.35). MS (FAB+): 694 [M$^+$]. HRMS (FAB+): [M$^+$] $C_{26}H_{39}CoO_4S_6Si$: calcd. 694.0274; found 694.0244. $C_{26}H_{39}CoO_4S_6Si$ (695.0): calcd. C 44.93, H 5.66, S 27.68; found C 45.22, H 5.74, S 27.39.

***syn*-C(2.2)SiMe$_3$:** Yellow solid, m.p. 230 °C. ^{1}H NMR (300 MHz, $CDCl_3$): δ = 0.32 [s, 18 H, $Si(CH_3)_3$], 1.41 [s, 36 H, $C(CH_3)_3$], 2.79/3.51 (m, 8 H, SCH_2), 4.95/5.61 (pt, 8 H, CpH) ppm. ^{13}C NMR (75 MHz, $CDCl_3$): δ = −0.3 [$Si(CH_3)_3$], 24.6 [$C(CH_3)_3$], 36.7 (SCH_2), 61.9 [$C(CH_3)_3$], 77.5 [*C*(Cb)SO_2tBu], 81.2 [*C*(Cb)S], 88.8/91.5 [*C*(Cp)H], 94.7 [*C*(Cp)$SiMe_3$] ppm. IR (KBr): $\tilde{\nu}$ = 2955 cm^{-1}, 1633, 1307, 1123. UV/Vis (CH_2Cl_2): λ_{max} (log ε) = 258 (4.77), 316 nm (4.70). MS (FAB+): 1156 [M$^+$], 1083 [M$^+$ − *t*BuO]. HRMS (FAB+): [M$^+$] $C_{44}H_{70}Co_2O_8S_8Si_2$: calcd. 1156.1039; found 1156.1047. $C_{44}H_{70}Co_2O_8S_8Si_2{\cdot}0.25C_4H_{10}O$ (1176.1): calcd. C 45.96, H 6.21, S 21.81; found C 46.10, H 6.15, S 22.08.

Reaction of A(2.3) with [CpSiMe$_3$Co(CO)(BTSA)] (8c). Reaction A: 8c (127 mg, 0.26 mmol) and **A(2.3)** (70 mg, 0.30 mmol). Yield: 76 mg (41%) of **B(2.3)SiMe$_3$**. **Reaction B: 8c** (307 mg, 0.62 mmol) and **A(2.3)** (70 mg, 0.30 mmol). Yield: 15 mg (8%) of **B(2.3)SiMe$_3$**, 74 mg (23%) of *anti*-**C(2.3)SiMe$_3$** and 106 mg (32%) of *syn*-**C(2.3)SiMe$_3$**.

B(2.3)SiMe$_3$: Yellow solid, m.p. 200 °C (dec.). ^{1}H NMR (300 MHz, $CDCl_3$): δ = 0.35 [s, 9 H, $Si(CH_3)_3$], 1.49 [s, 18 H, $C(CH_3)_3$], 2.15 (m, 2 H, $CH_2CH_2CH_2$), 2.60/2.98 (m, 2 H, $CH_2CH_2CH_2SC$≡), 2.74/2.98 (m, 2 H, SCH_2CH_2SC≡), 3.19 (m, 2 H, SCH_2CH_2SC≡), 3.31/3.47 (m, 2 H, $CH_2CH_2CH_2SC$≡), 5.06/5.70 (pt, 4 H, CpH) ppm. ^{13}C NMR (125 MHz, CD_2Cl_2): δ = −0.3 [$Si(CH_3)_3$], 25.38/25.42 [$C(CH_3)_3$], 30.9 ($CH_2CH_2CH_2$), 35.3 (SCH_2CH_2SC≡), 36.2 ($CH_2CH_2CH_2SC$≡), 36.5 ($CH_2CH_2CH_2SC$≡), 37.0 (SCH_2CH_2SC≡), 62.4 [$C(CH_3)_3$], 77.9/78.9 [*C*(Cb)SO_2tBu], 82.9 [*C*(Cb)SCH_2CH_2S], 83.8 [*C*(CBD)$SCH_2CH_2CH_2$], 86.0 (SCH_2CH_2SC≡), 89.1 ($CH_2CH_2CH_2SC$≡), 89.3/89.4/91.4 [*C*(Cp)H], 95.3 [*C*(Cp)$SiMe_3$] ppm. IR (KBr): $\tilde{\nu}$ = 2970 cm^{-1}, 2930, 1632, 1356, 1307, 1248, 1192, 1163, 1121. UV/Vis (CH_2Cl_2): λ_{max} (log ε) = 258 (4.19), 314 nm (4.08). MS (FAB+): 708 [M$^+$], 635 [M$^+$ − *t*BuO]. HRMS (FAB+): [M$^+$] $C_{27}H_{41}CoO_4S_6Si$: calcd. 708.0430; found 708.0470. $C_{27}H_{41}CoO_4S_6Si$ (709.0): calcd. C 45.74, H 5.83, S 27.13; found C 45.86, H 5.82, S 27.08.

***anti*-C(2.3)SiMe$_3$:** Yellow solid, m.p. 235 °C (dec.). ^{1}H NMR (500 MHz, CD_2Cl_2): δ = 0.30 [s, 18 H, $Si(CH_3)_3$], 1.41/1.45 [s, 36 H, $C(CH_3)_3$], 1.94 (m, 2 H, $CH_2CH_2CH_2$), 3.08 (m, 4 H, $CH_2CH_2CH_2$), 3.18/3.45 (m, 4 H, SCH_2CH_2S), 5.08/5.16 (pt, 4 H, CpH), 5.63 (m, 4 H, CpH) ppm. ^{13}C NMR (125 MHz, CD_2Cl_2): δ = −0.4 [$Si(CH_3)_3$], 24.68/24.74 [$C(CH_3)_3$], 28.2 ($CH_2CH_2CH_2$), 35.9 ($CH_2CH_2CH_2$), 36.2 (SCH_2CH_2S), 61.8/61.9 [$C(CH_3)_3$], 77.2/79.0 [*C*(Cb)SO_2tBu], 78.5 [*C*(Cb)$SCH_2CH_2CH_2$], 84.6 [*C*(CBD)SCH_2CH_2S], 88.3/89.2/90.2/90.7 [*C*(Cp)H], 94.2 [*C*(Cp)$SiMe_3$] ppm. IR (KBr): $\tilde{\nu}$ = 2956 cm^{-1}, 2932, 1632, 1474, 1357, 1309, 1250, 1122. UV/Vis (CH_2Cl_2): λ_{max} (log ε) = 258 (4.47), 314 nm (4.38). MS (FAB+): 1170 [M$^+$], 1097 [M$^+$ − $SiMe_3$], 1024 [M$^+$ − 2 $SiMe_3$]. HRMS (FAB+): [M$^+$] $C_{45}H_{72}Co_2O_8S_8Si_2$: calcd. 1170.1195; found 1170.1246. $C_{45}H_{72}Co_2O_8S_8Si_2$ (1171.6): calcd. C 46.13, H 6.19, S 21.90; found C 46.29, H 6.26, S 21.87.

***syn*-C(2.3)SiMe$_3$:** Yellow solid, m.p. 244 °C (dec.). ^{1}H NMR (500 MHz, CD_2Cl_2): δ = 0.35 [s, 18 H, $Si(CH_3)_3$], 1.45/1.46 [s, 36 H, $C(CH_3)_3$], 2.04 (m, 2 H, $CH_2CH_2CH_2$), 3.00/3.42 (m, 4 H, $CH_2CH_2CH_2$), 3.19/3.42 (m, 4 H, SCH_2CH_2S), 5.16/5.73 (pt, 8 H, CpH) ppm. ^{13}C NMR (125 MHz, CD_2Cl_2): δ = −0.4 [$Si(CH_3)_3$], 25.21/25.29 [$C(CH_3)_3$], 29.1 ($CH_2CH_2CH_2$), 36.0 ($CH_2CH_2CH_2$), 36.1 (SCH_2CH_2S), 62.3/62.5 [$C(CH_3)_3$], 77.4/78.6 [*C*(Cb)SO_2tBu], 80.8 [*C*(Cb)SCH_2CH_2S], 81.9 [*C*(Cb)$SCH_2CH_2CH_2$], 89.5/90.2/91.5 [*C*(Cp)H], 94.5 [*C*(Cp)$SiMe_3$] ppm. IR (KBr): $\tilde{\nu}$ = 2967 cm^{-1}, 1632, 1474, 1357, 1309, 1250, 1122. UV/Vis (CH_2Cl_2): λ_{max} (log ε) = 258 (4.18), 316 nm (4.07). MS (FAB+): 1170 [M$^+$], 1097 [M$^+$ − $SiMe_3$]. HRMS (FAB+): [M$^+$] $C_{45}H_{72}Co_2O_8S_8Si_2$: calcd. 1170.1195; found 1170.1218. $C_{45}H_{72}Co_2O_8S_8Si_2{\cdot}0.5\ C_4H_{10}O$ (1208.7): calcd. C 46.71, H 6.42, S 21.22; found C 46.83, H 6.32, S 21.59.

Reaction of A(3.3) with [CpCo(CO)(BTSA)] (8a). Reaction A: 8a (117 mg, 0.28 mmol) and **A(3.3)** (80 mg, 0.31 mmol). Yield: 49 mg (27%) of **B(3.3)H**, 11 mg (8%) of *anti*-**C(3.3)H** and 20 mg (14%) of *syn*-**C(3.3)H**. **Reaction B: 8a** (296 mg, 0.71 mmol) and **A(3.3)** (80 mg, 0.31 mmol). Yield: 21 mg (11%) of **B(3.3)H**, 44 mg (14%) of *anti*-**C(3.3)H** and 84 mg (26%) of *syn*-**C(3.3)H**.

B(3.3)H: Yellow solid, m.p. 157 °C. ^{1}H NMR (500 MHz, $CDCl_3$): δ = 1.47 [s, 18 H, $C(CH_3)_3$], 2.21 (m, 4 H, $CH_2CH_2CH_2$), 2.76 (m, 4 H, CH_2SC≡), 3.20 (m, 4 H, $SCH_2CH_2CH_2SC$≡), 5.40 (s, 5 H, CpH) ppm. ^{13}C NMR (125 MHz, $CDCl_3$): δ = 25.2 [$C(CH_3)_3$], 30.5 ($CH_2CH_2CH_2$), 35.3/36.9 (SCH_2), 62.1 [$C(CH_3)_3$], 78.7 [*C*(Cb)SO_2tBu], 84.6 [*C*(Cb)SCH_2], 86.3 [*C*(Cp)], 87.0 (C≡) ppm. IR (KBr): $\tilde{\nu}$ = 2929 cm^{-1}, 1632, 1309, 1121. UV/Vis (CH_2Cl_2): λ_{max} (log ε) = 250 (4.14), 314 nm (3.93). MS (FAB+): 650 [M$^+$], 577 [M$^+$ − *t*BuO]. HRMS (FAB+): [M$^+$] $C_{25}H_{35}CoO_4S_6$: calcd. 650.0192; found 650.0197. $C_{25}H_{35}CoO_4S_6$ (650.9): calcd. C 46.13, H 5.42; found C 46.08, H 5.71.

***anti*-C(3.3)H:** Yellow solid, m.p. 286 °C (dec.). ^{1}H NMR (500 MHz, $CDCl_3$): δ = 1.46 [s, 36 H, $C(CH_3)_3$], 2.10 (m, 4 H, $CH_2CH_2CH_2$),

3.18 (m, 8 H, SCH_2), 5.42 (s, 10 H, CpH) ppm. ^{13}C NMR (125 MHz, $CDCl_3$): δ = 25.2 [C(CH_3)$_3$], 29.0 ($CH_2CH_2CH_2$), 37.0 (SCH_2), 62.2 [$C(CH_3)_3$], 78.7 [C(Cb)SO_2tBu], 83.6 [C(Cb)SCH_2], 86.3 [C(Cp)] ppm. IR (KBr): $\tilde{\nu}$ = 2961 cm^{-1}, 2929, 1727, 1632, 1307, 1122. UV/Vis (CH_2Cl_2): λ_{max} (log ε) = 248 (4.35), 310 (4.10), 358 nm (3.38). MS (FAB+): 1140 [M$^+$], 967 [M$^+$ − *t*BuO]. HRMS (FAB+): [M$^+$] $C_{40}H_{58}Co_2O_8S_8$: calcd. 1040.0561; found 1040.0560. $C_{40}H_{58}Co_2O_8S_8$ (1041.3): calcd. C 46.14, H 5.61, S 24.64; found C 46.07, H 5.64, S 24.44.

***syn*-C(3.3)H:** Yellow solid, m.p. 290 °C (dec.). ^{1}H NMR (500 MHz, $CDCl_3$): δ = 1.47 [s, 36 H, $C(CH_3)_3$], 2.12 (m, 4 H, $CH_2CH_2CH_2$), 3.26 (m, 8 H, SCH_2), 5.41 (s, 10 H, CpH) ppm. IR (KBr): $\tilde{\nu}$ = 2925 cm^{-1}, 2854, 1307, 1121. UV/Vis (CH_2Cl_2): λ_{max} (log ε) = 252 (4.27), 310 (3.99), 356 nm (3.23). MS (FAB+): 1140 [M$^+$], 967 [M$^+$ − *t*BuO]. HRMS (FAB+): [M$^+$] $C_{40}H_{58}Co_2O_8S_8$: calcd. 1040.0561; found 1140.0580. $C_{40}H_{58}Co_2O_8S_8$ (1041.3): calcd. C 46.14, H 5.61, S 24.64; found C 46.04, H 5.89, S 24.45.

Reaction of A(3.3) with [CpMeCo(CO)(BTSA)] (8b). Reaction A: 8b (122 mg, 0.28 mmol) and **A(3.3)** (80 mg, 0.31 mmol). Yield: 34 mg (18%) of **B(3.3)Me**, 20 mg (13%) of *anti*-**C(3.3)Me** and 47 mg (32%) of *syn*-**C(3.3)Me**. **Reaction B: 8b** (305 mg, 0.71 mmol) and **A(3.3)** (80 mg, 0.31 mmol). Yield: 54 mg (16%) of *anti*-**C(3.3)Me** and 191 mg (58%) of *syn*-**C(3.3)Me**.

B(3.3)Me: Yellow solid, m.p. 172 °C. ^{1}H NMR (500 MHz, $CDCl_3$): δ = 1.47 [s, 18 H, $C(CH_3)_3$], 2.10 (s, 3 H, CpCH_3), 2.19 (m, 4 H, $CH_2CH_2CH_2$), 2.73 (m, 4 H, $CH_2SC{\equiv}$), 3.17 (m, 4 H, $SCH_2CH_2CH_2SC{\equiv}$), 5.14/5.31 (pt, 4 H, CpH) ppm. ^{13}C NMR (125 MHz, $CDCl_3$): δ = 12.9 (CpCH_3), 25.2 [C(CH_3)$_3$], 30.5 ($CH_2CH_2CH_2$), 35.4/36.1 (SCH_2), 62.1 [$C(CH_3)_3$], 78.3 [C(Cb)SO_2tBu], 82.7 [C(Cb)SCH_2], 85.5/86.8 [C(Cp)H], 87.0 (C≡), 101.2 [C(Cp)CH_3] ppm. IR (KBr): $\tilde{\nu}$ = 2928 cm^{-1}, 1634, 1476, 1356, 1305, 1121. UV/Vis (CH_2Cl_2): λ_{max} [nm] (log ε) = 254 (4.23), 314 (4.06), 366 (3.38). MS (FAB+): 664 [M$^+$], 591 [M$^+$ − *t*BuO]. HRMS (FAB+): [M$^+$] $C_{26}H_{37}CoO_4S_6$: calcd. 664.0348; found 664.0359.

***anti*-C(3.3)Me:** Yellow solid, m.p. 277 °C (dec.). ^{1}H NMR (300 MHz, $CDCl_3$): δ = 1.46 [s, 36 H, $C(CH_3)_3$], 2.09 (m, 4 H, $CH_2CH_2CH_2$), 2.12 (s, 6 H, CpCH_3), 3.18 (m, 8 H, SCH_2), 5.22/5.34 (pt, 8 H, CpH) ppm. ^{13}C NMR (75 MHz, $CDCl_3$): δ = 12.9 (CpCH_3), 25.2 [C(CH_3)$_3$], 29.1 ($CH_2CH_2CH_2$), 36.6 (SCH_2), 62.2 [$C(CH_3)_3$], 77.9 [C(Cb)SO_2tBu], 82.4 [C(Cb)SCH_2], 85.3/86.7 [C(Cp)H], 101.1 [C(Cp)CH_3] ppm. IR (KBr): $\tilde{\nu}$ = 2971 cm^{-1}, 2929, 1633, 1476, 1349, 1308, 1194, 1121. UV/Vis (CH_2Cl_2): λ_{max} (log ε) = 252 (4.52), 312 (4.34), 356 nm (3.74). MS (FAB+): 1068 [M$^+$], 995 [M$^+$ − *t*BuO]. HRMS (FAB+): [M$^+$] $C_{42}H_{62}Co_2O_8S_8$: calcd. 1068.0874; found 1068.0881. $C_{42}H_{62}Co_2O_8S_8$ (1069.3): calcd. C 47.18, H 5.84, S 23.99; found C 47.08, H 5.87, S 23.71.

***syn*-C(3.3)Me:** Yellow solid, m.p. 290 °C (dec.). ^{1}H NMR (300 MHz, $CDCl_3$): δ = 1.47 [s, 36 H, $C(CH_3)_3$], 2.10 (m, 4 H, $CH_2CH_2CH_2$), 2.12 (s, 6 H, CpCH_3), 3.19 (m, 8 H, SCH_2), 5.23/5.35 (pt, 8 H, CpH) ppm. ^{13}C NMR (75 MHz, $CDCl_3$): δ = 12.9 (CpCH_3), 25.2 [C(CH_3)$_3$], 29.1 ($CH_2CH_2CH_2$), 36.6 (SCH_2), 62.2 [$C(CH_3)_3$], 77.9 [C(Cb)SO_2tBu], 82.4 [C(Cb)SCH_2], 85.3/86.7 [C(Cp)H], 101.0 [C(Cp)CH_3] ppm. IR (KBr): $\tilde{\nu}$ = 2973 cm^{-1}, 2929, 1634, 1476, 1353, 1307, 1193, 1121. UV/Vis (CH_2Cl_2): λ_{max} (log ε) = 242 (4.57), 318 (4.26), 372 nm (3.65). MS (FAB+): 1168 [M$^+$], 995 [M$^+$ − *t*BuO]. HRMS (FAB+): [M$^+$] $C_{42}H_{62}Co_2O_8S_8$: calcd. 1068.0874; found 1068.0867. $C_{42}H_{62}Co_2O_8S_8$ (1069.3): calcd. C 47.18, H 5.84, S 23.99; found C 46.90, H 5.88, S 23.85.

Reaction of A(3.3) with [CpSiMe$_3$Co(CO)(BTSA)] (8c). Reaction A: 8c (138 mg, 0.28 mmol) and **A(3.3)** (80 mg, 0.31 mmol). Yield: 115 mg (57%) of **B(3.3)SiMe$_3$**, 23 mg (14%) of *anti*-**C(3.3)SiMe$_3$** and 18 mg (11%) of *syn*-**C(3.3)SiMe$_3$**. **Reaction B: 8c** (348 mg, 0.71 mmol) and **A(3.3)** (80 mg, 0.31 mmol). Yield: 22 mg (10%) of **B(3.3)SiMe$_3$**, 57 mg (16%) of *anti*-**C(3.3)SiMe$_3$** and 93 mg (25%) of *syn*-**C(3.3)SiMe$_3$**.

B(3.3)SiMe$_3$: Yellow solid, m.p. 159 °C. ^{1}H NMR (300 MHz, $CDCl_3$): δ = 0.31 [s, 9 H, $Si(CH_3)_3$], 1.47 [s, 18 H, $C(CH_3)_3$], 2.21 (m, 4 H, $CH_2CH_2CH_2$), 2.71 (m, 4 H, $CH_2SC{\equiv}$), 3.13 (m, 4 H, $SCH_2CH_2CH_2SC{\equiv}$), 5.10/5.75 (pt, 4 H, CpH) ppm. ^{13}C NMR (125 MHz, $CDCl_3$): δ = 0.4 [$Si(CH_3)_3$], 25.3 [C(CH_3)$_3$], 30.6 ($CH_2CH_2CH_2$), 35.4/36.3 (SCH_2), 62.3 [$C(CH_3)_3$], 78.2 [C(Cb)SO_2tBu], 82.9 [C(Cb)SCH_2], 87.2 (C≡), 89.4/90.9 [C(Cp)H], 94.6 [C(Cp)$SiMe_3$] ppm. IR (KBr): $\tilde{\nu}$ = 2929 cm^{-1}, 1650, 1358, 1304, 1250, 1122. UV/Vis (CH_2Cl_2): λ_{max} (log ε) = 258 (4.18), 314 nm (4.04). MS (FAB+): 722 [M$^+$], 649 [M$^+$ − *t*BuO]. HRMS (FAB+): [M$^+$] $C_{28}H_{43}CoO_4S_6Si$: calcd. 722.0587; found 722.0587.

***anti*-C(3.3)SiMe$_3$:** Yellow solid, m.p. 204 °C. ^{1}H NMR (300 MHz, $CDCl_3$): δ = 0.31 [s, 18 H, $Si(CH_3)_3$], 1.47 [s, 36 H, $C(CH_3)_3$], 2.03 (m, 4 H, $CH_2CH_2CH_2$), 3.13 (m, 8 H, SCH_2), 5.20/5.74 (pt, 8 H, CpH) ppm. ^{13}C NMR (75 MHz, $CDCl_3$): δ = 0.3 [$Si(CH_3)_3$], 25.3 [C(CH_3)$_3$], 29.5 ($CH_2CH_2CH_2$), 36.8 (SCH_2), 62.4 [$C(CH_3)_3$], 78.3 [C(Cb)SO_2tBu], 82.4 [C(Cb)SCH_2], 89.2/90.7 [C(Cp)H], 94.2 [C(Cp)$SiMe_3$] ppm. IR (KBr): $\tilde{\nu}$ = 2963 cm^{-1}, 1632, 1309, 1250, 1122. UV/Vis (CH_2Cl_2): λ_{max} (log ε) = 258 (4.45), 316 nm (4.32). MS (FAB+): 1184 [M$^+$], 1111 [M$^+$ − *t*BuO]. HRMS (FAB+): [M$^+$] $C_{46}H_{74}Co_2O_8S_8Si_2$: calcd. 1184.1352; found 1184.1340. $C_{46}H_{74}Co_2O_8S_8Si_2$ (1185.7): calcd. C 46.60, H 6.29, S 21.64; found C 46.79, H 6.25, S 21.51.

***syn*-C(3.3)SiMe$_3$:** Yellow solid, m.p. 230 °C (dec.). ^{1}H NMR (300 MHz, $CDCl_3$): δ = 0.35 [s, 18 H, $Si(CH_3)_3$], 1.48 [s, 36 H, $C(CH_3)_3$], 2.01 (m, 4 H, $CH_2CH_2CH_2$), 3.19 (m, 8 H, SCH_2), 5.22/5.75 (pt, 8 H, CpH) ppm. ^{13}C NMR (75 MHz, $CDCl_3$): δ = 0.4 [$Si(CH_3)_3$], 25.3 [C(CH_3)$_3$], 28.8 ($CH_2CH_2CH_2$), 36.5 (SCH_2), 62.5 [$C(CH_3)_3$], 77.9 [C(Cb)SO_2tBu], 82.1 [C(Cb)SCH_2], 89.2/90.5 [C(Cp)H], 94.2 [C(Cp)$SiMe_3$] ppm. IR (KBr): $\tilde{\nu}$ = 2954 cm^{-1}, 1632, 1308, 1249, 1122. UV/Vis (CH_2Cl_2): λ_{max} (log ε) = 258 (4.45), 314 nm (4.32). MS (FAB+): 1184 [M$^+$], 1111 [M$^+$ − *t*BuO]. HRMS (FAB+): [M$^+$] $C_{46}H_{74}Co_2O_8S_8Si_2$: calcd. 1184.1352; found 1184.1382. $C_{46}H_{74}Co_2O_8S_8Si_2$ (1185.7): calcd. C 46.60, H 6.29, S 21.64; found C 46.47, H 6.32, S 21.51.

Reaction of A(3.3) with [CpCOOMeCo(CO)(BTSA)] (8d). Reaction A: 8d (133 mg, 0.28 mmol) and **A(3.3)** (80 mg, 0.31 mmol). Yield: 24 mg (12%) of **B(3.3)COOMe**, 45 mg (28%) of *anti*-**C(3.3)COOMe** and 19 mg (12%) of *syn*-**C(3.3)COOMe**. **Reaction B: 8d** (294 mg, 0.62 mmol) and **A(3.3)** (70 mg, 0.27 mmol). Yield: 47 mg (15%) of *anti*-**C(3.3)COOMe** and 103 mg (33%) of *syn*-**C(3.3)COOMe**.

B(3.3)COOMe: Yellow solid, m.p. 146 °C. ^{1}H NMR (300 MHz, $CDCl_3$): δ = 1.48 [s, 18 H, $C(CH_3)_3$], 2.20 (m, 4 H, $CH_2CH_2CH_2$), 2.74 (m, 4 H, $CH_2SC{\equiv}$), 3.26 (m, 4 H, $SCH_2CH_2CH_2SC{\equiv}$), 3.90 (s, 3 H, $COOCH_3$), 5.63/5.73 (pt, 4 H, CpH) ppm. ^{13}C NMR (75 MHz, $CDCl_3$): δ = 25.4 [C(CH_3)$_3$], 30.4 ($CH_2CH_2CH_2$), 34.8/35.1 (SCH_2), 52.9 ($COOCH_3$), 62.5 [$C(CH_3)_3$], 78.9 [C(Cb)SO_2tBu], 84.9 [C(Cb)SCH_2], 87.1 (C≡), 87.6/89.0 [C(Cp)H], 90.4 [C(Cp)COOMe], 166.0 (C=O) ppm. IR (KBr): $\tilde{\nu}$ = 2966 cm^{-1}, 1724, 1472, 1366, 1308, 1193, 1148, 1121. UV/Vis (CH_2Cl_2): λ_{max} (log ε) = 318 (4.02), 366 nm (3.42). MS (FAB+): 709 [M + H$^+$], 635 [M$^+$ − *t*BuO]. HRMS (FAB+): [M + H$^+$] $C_{27}H_{38}CoO_6S_6$: calcd. 709.0325; found 709.0326.

***anti*-C(3.3)COOMe:** Yellow solid, m.p. 226 °C. ^{1}H NMR (300 MHz, $CDCl_3$): δ = 1.47 [s, 36 H, $C(CH_3)_3$], 2.03 (m, 4 H, $CH_2CH_2CH_2$), 3.29 (m, 8 H, SCH_2), 3.91 (s, 6 H, $COOCH_3$), 5.65/5.84 (pt, 8 H, CpH) ppm. ^{13}C NMR (75 MHz, $CDCl_3$): δ = 25.1 [C(CH_3)$_3$], 28.8 ($CH_2CH_2CH_2$), 35.4 (SCH_2), 53.0 ($COOCH_3$), 62.6

[$C(CH_3)_3$], 79.2 [C(Cb)SO_2tBu], 84.3 [C(Cb)SCH_2], 87.2/89.0 [C(Cp)H], 90.4 [C(Cp)COOMe], 166.0 (C=O) ppm. IR (KBr): $\tilde{\nu}$ = 2933 cm^{-1}, 1722, 1632, 1473, 1367, 1309, 1194, 1148. UV/Vis (CH_2Cl_2): λ_{max} (log ε) = 254 (4.43), 314 (4.26), 356 nm (3.55). MS (FAB+): 1157 [M + H^+], 1083 [M^+ − tBuO]. HRMS (FAB+): [M^+] $C_{44}H_{62}Co_2O_{12}S_8$: calcd. 1156.0671; found 1156.0709. $C_{44}H_{62}Co_2O_{12}S_8$ (1157.4): calcd. C 45.66, H 5.40, S 22.16; found C 45.80, H 5.39, S 22.07.

***syn*-C(3.3)COOMe:** Yellow solid, m.p. 254 °C (dec.). ^{1}H NMR (300 MHz, $CDCl_3$): δ = 1.47 [s, 36 H, $C(CH_3)_3$], 2.06 (m, 4 H, $CH_2CH_2CH_2$), 3.24 (m, 8 H, SCH_2), 3.85 (s, 6 H, $COOCH_3$), 5.64/5.83 (pt, 8 H, CpH) ppm. ^{13}C NMR (75 MHz, $CDCl_3$): δ = 25.2 [$C(CH_3)_3$], 29.4 ($CH_2CH_2CH_2$), 35.6 (SCH_2), 52.9 ($COOCH_3$), 62.5 [$C(CH_3)_3$], 79.3 [C(Cb)SO_2tBu], 84.7 [C(Cb)SCH_2], 87.2/89.0 [C(Cp)H], 90.4 [C(Cp)COOMe], 166.1 (C=O) ppm. IR (KBr): $\tilde{\nu}$ = 2934 cm^{-1}, 1722, 1634, 1473, 1367, 1308, 1194, 1148, 1122. UV/Vis (CH_2Cl_2): λ_{max} (log ε) = 242 (4.60), 320 (4.28), 366 nm (3.65). MS (FAB+): 1157 [M + H^+], 1083 [M^+ − tBuO]. HRMS (FAB+): [M^+] $C_{44}H_{62}Co_2O_{12}S_8$: calcd. 1156.0671; found 1156.0702. $C_{44}H_{62}Co_2O_{12}S_8$ (1157.4): calcd. C 45.66, H 5.40, S 22.16; found C 45.51, H 5.41, S 22.26.

Reaction of E(3.3) with [$EtMe_4$CpCo(CO)(BTSA)] (5). Reaction A: 8e (140 mg, 0.28 mmol) and **A(3.3)** (80 mg, 0.31 mmol). Yield: 40 mg (19%) of **B(3.3)EtMe_4**. **Reaction B: 8e** (360 mg, 0.71 mmol) and **A(3.3)** (80 mg, 0.31 mmol). Yield: 29 mg (13%) of **B(3.3)EtMe_4** and 20 mg (5%) of *anti*-**C(3.3)EtMe_4**.

B(3.3)EtMe_4: Yellow solid, m.p. 169 °C. ^{1}H NMR (500 MHz, $CDCl_3$): δ = 0.98 (t, ^3J = 7.6 Hz, 3 H, CH_2CH_3), 1.42 (s, 18 H, $C(CH_3)_3$], 1.92/1.93 (s, 12 H, CpCH_3), 2.13 (m, 4 H, $CH_2CH_2CH_2$), 2.51 (q, ^3J = 7.6 Hz, 2 H, CH_2CH_3), 2.57/2.84 (m, 4 H, CH_2SC≡), 2.73/3.22 (m, 4 H, $SCH_2CH_2CH_2SC$≡) ppm. ^{13}C NMR (125 MHz, $CDCl_3$): δ = 10.0/10.3 (CpCH_3), 14.4 (CH_2CH_3), 18.4 (CH_2CH_3), 25.7 [$C(CH_3)_3$], 30.8 ($CH_2CH_2CH_2$), 35.9/36.2 (SCH_2), 62.3 [$C(CH_3)_3$], 77.2 [C(Cb)SO_2tBu], 78.4 [C(Cb)SCH_2], 87.2 (C≡), 95.7/96.7 [C(Cp)CH_3], 101.0 [C(Cp)CH_2CH_3] ppm. IR (KBr): $\tilde{\nu}$ = 2967 cm^{-1}, 2926, 1630, 1303, 1117. UV/Vis (CH_2Cl_2): λ_{max} (log ε) = 268 (4.22), 320 (4.21), 370 (3.31). MS (FAB+): 734 [M^+]. HRMS (FAB+): [M + H^+] $C_{31}H_{48}CoO_4S_6$: calcd. 735.1209; found 735.1209.

***anti*-C(3.3)EtMe_4:** Yellow solid, m.p. 263 °C (dec.). ^{1}H NMR (500 MHz, $CDCl_3$): δ = 0.97 (t, ^3J = 7.6 Hz, 6 H, CH_2CH_3), 1.42 [s, 36 H, $C(CH_3)_3$], 1.90/1.91 (s, 24 H, CpCH_3), 2.48 (q, ^3J = 7.6 Hz, 2 H, CH_2CH_3), 2.73 (m, 4 H, $CH_2CH_2CH_2$), 2.59/3.20 (m, 8 H, SCH_2) ppm. ^{13}C NMR (75 MHz, $CDCl_3$): δ = 10.0/10.2 (CpCH_3), 14.3 (CH_2CH_3), 18.3 (CH_2CH_3), 25.8 [$C(CH_3)_3$], 35.2 ($CH_2CH_2CH_2$), 36.7 (SCH_2), 62.3 [$C(CH_3)_3$], 77.2 [C(Cb)], 77.6 [C(Cb)], 95.8/96.7 [C(Cp)CH_3], 101.2 [C(Cp)CH_2CH_3] ppm. IR (KBr): $\tilde{\nu}$ = 2968 cm^{-1}, 2929, 1632, 1457, 1349, 1306, 1193, 1118. UV/Vis (CH_2Cl_2): λ_{max} (log ε) = 268 (4.54), 320 (4.56), 370 nm (3.69). MS (FAB+): 1208 [M^+]. HRMS (FAB+): [M + H^+] $C_{52}H_{83}Co_2O_8S_8$: calcd. 1209.2518; found 1209.2535.

Reaction of A(4.4) with [CpCo(CO)(BTSA)] (8a). Reaction A: 8a (105 mg, 0.25 mmol) and **A(4.4)** (80 mg, 0.28 mmol). Yield: 57 mg (34%) of **B(4.4)H**. **Reaction B: 8a** (267 mg, 0.64 mmol) and **A(4.4)** (80 mg, 0.28 mmol). Yield: 38 mg (20%) of **B(4.4)H**, 81 mg (26%) of *anti*-**C(4.4)H** and 48 mg (16%) of *syn*-**C(4.4)H**.

B(4.4)H: Yellow solid, m.p. 206 °C. ^{1}H NMR (500 MHz, $CDCl_3$): δ = 1.47 [s, 18 H, $C(CH_3)_3$], 1.84 (m, 4 H, $CH_2CH_2CH_2SC$≡), 2.00 (m, 4 H, $CH_2CH_2CH_2SC$≡), 2.68 (m, 4 H, CH_2SC≡), 3.17 (m, 4 H, $CH_2CH_2CH_2CH_2SC$≡), 5.41 (s, 5 H, CpH) ppm. ^{13}C NMR (125 MHz, $CDCl_3$): δ = 25.2 [$C(CH_3)_3$], 27.8 (CH_2CH_2SC≡), 28.7 ($CH_2CH_2CH_2SC$≡), 35.8 (CH_2SC≡), 37.3 ($CH_2CH_2CH_2CH_2SC$≡), 62.0 [$C(CH_3)_3$], 77.9 [C(Cb)SO_2tBu], 84.3 [C(Cb)SCH_2], 85.9 [C(Cp)], 86.6 (C≡) ppm. IR (KBr): $\tilde{\nu}$ = 2929 cm^{-1}, 1633, 1306, 1122. UV/Vis (CH_2Cl_2): λ_{max} (log ε) = 250 (4.20), 316 (4.00), 356 nm (3.31). MS (FAB+): 678 [M^+], 605 [M^+ − tBuO]. HRMS (FAB+): [M + H^+] $C_{27}H_{40}CoO_4S_6$: calcd. 679.0583; found 679.0616. $C_{27}H_{39}CoO_4S_6.CH_3OH$ (711.0): calcd. C 47.31, H 6.09, S 27.08; found C 47.27, H 5.92, S 26.95.

***anti*-C(4.4)H:** Yellow solid, m.p. 293 °C (dec.). ^{1}H NMR (500 MHz, $CDCl_3$): δ = 1.46 [s, 36 H, $C(CH_3)_3$], 1.88 (m, 8 H, $CH_2CH_2CH_2CH_2$), 3.08 (m, 8 H, CH_2S), 5.37 (s, 10 H, CpH) ppm. ^{13}C NMR (125 MHz, $CDCl_3$): δ = 25.2 [$C(CH_3)_3$], 29.0 ($CH_2CH_2CH_2CH_2$), 37.3 (CH_2S), 62.1 [$C(CH_3)_3$], 78.3 [C(Cb)SO_2tBu], 84.4 [C(Cb)SCH_2], 86.1 [C(Cp)] ppm. IR (KBr): $\tilde{\nu}$ = 2971 cm^{-1}, 2931, 1633, 1308, 1122. UV/Vis (CH_2Cl_2): λ_{max} (log ε) = 250 (4.44), 314 (4.24), 356 nm (3.66). MS (FAB+): 1068 [M^+], 995 [M^+ − tBuO]. HRMS (FAB+): [M^+] $C_{42}H_{62}Co_2O_8S_8$: calcd. 1068.0874; found 1068.0872. $C_{42}H_{62}Co_2O_8S_8$ (1069.34): calcd. C 47.17, H 5.84, S 23.99; found C 47.01, H 5.86, S 23.77.

***syn*-C(4.4)H:** Yellow solid, m.p. 273 °C (dec.). ^{1}H NMR (500 MHz, $CDCl_3$): δ = 1.46 [s, 36 H, $C(CH_3)_3$], 1.87 (m, 8 H, $CH_2CH_2CH_2CH_2$), 3.06 (m, 8 H, CH_2S), 5.37 (s, 10 H, CpH) ppm. ^{13}C NMR (125 MHz, $CDCl_3$): δ = 25.1 [$C(CH_3)_3$], 29.0 ($CH_2CH_2CH_2CH_2$), 37.1 (CH_2S), 62.1 [$C(CH_3)_3$], 78.3 [C(Cb)SO_2tBu], 84.0 [C(Cb)SCH_2], 86.3 [C(Cp)] ppm. IR (KBr): $\tilde{\nu}$ = 2931 cm^{-1}, 1632, 1308, 1122. UV/Vis (CH_2Cl_2): λ_{max} (log ε) = 248 (4.49), 312 (4.28), 354 nm (3.59). MS (FAB+): 1068 [M^+], 995 [M^+ − tBuO]. HRMS (FAB+): [M^+] $C_{42}H_{62}Co_2O_8S_8$: calcd. 1068.0874; found 1068.0900.

Reaction of A(4.4) with [CpMeCo(CO)(BTSA)] (8b). Reaction A: 8b (109 mg, 0.25 mmol) and **A(4.4)** (80 mg, 0.28 mmol). Yield: 74 mg (43%) of **B(4.4)Me**. **Reaction B: 8b** (276 mg, 0.64 mmol) and **A(4.4)** (80 mg, 0.28 mmol). Yield: 164 mg (53%) of *anti*-**C(4.4)Me** and 59 mg (19%) of *syn*-**C(4.4)Me**.

B(4.4)Me: Yellow solid, m.p. 174 °C. ^{1}H NMR (500 MHz, $CDCl_3$): δ = 1.45 [s, 18 H, $C(CH_3)_3$], 1.81 (m, 4 H, $CH_2CH_2CH_2SC$≡), 1.98 (m, 4 H, CH_2CH_2SC≡), 2.10 (s, 3 H, CpCH_3), 2.65 (m, 4 H, CH_2SC≡), 3.10 (m, 4 H, $CH_2CH_2CH_2CH_2SC$≡), 5.19/5.30 (pt, 4 H, CpH) ppm. ^{13}C NMR (125 MHz, $CDCl_3$): δ = 12.9 (CpCH_3), 25.2 [$C(CH_3)_3$], 27.8/28.7 ($CH_2CH_2CH_2CH_2$), 35.8/36.8 (SCH_2), 62.0 [$C(CH_3)_3$], 77.2 [C(Cb)SO_2tBu], 83.1 [C(Cb)SCH_2], 85.9/86.5 [C(Cp)H], 86.6 (C≡), 100.8 [C(Cp)CH_3] ppm. IR (KBr): $\tilde{\nu}$ = 2964 cm^{-1}, 2927, 1632, 1475, 1455, 1305, 1236, 1193, 1121. UV/Vis (CH_2Cl_2): λ_{max} (log ε) = 254 (4.19), 316 (4.07), 358 nm (3.46). MS (FAB+): 692 [M^+], 619 [M^+ − tBuO]. HRMS (FAB+): [M^+] $C_{28}H_{41}CoO_4S_6$: calcd. 693.0739; found 693.0750. $C_{28}H_{41}CoO_4S_6$. 0.25 $C_4H_{10}O$ (711.5): calcd. C 48.96, H 6.16, S 27.04; found C 48.78, H 6.01, S 26.93.

***anti*-C(4.4)Me:** Yellow solid, m.p. 266 °C (dec.). ^{1}H NMR (500 MHz, $CDCl_3$): δ = 1.46 [s, 36 H, $C(CH_3)_3$], 1.85 (m, 8 H, $CH_2CH_2CH_2CH_2$), 2.10 (s, 6 H, CpCH_3), 3.04 (m, 8 H, SCH_2), 5.14/5.29 (pt, 8 H, CpH) ppm. ^{13}C NMR (125 MHz, $CDCl_3$): δ = 12.8 (CpCH_3), 25.2 [$C(CH_3)_3$], 29.0 ($CH_2CH_2CH_2CH_2$), 36.6 (SCH_2), 62.1 [$C(CH_3)_3$], 77.3 [C(Cb)SO_2tBu], 82.5 [C(Cb)SCH_2], 85.4/86.7 [C(Cp)H], 101.0 [C(Cp)CH_3] ppm. IR (KBr): $\tilde{\nu}$ = 2970 cm^{-1}, 2930, 1633, 1475, 1456, 1355, 1307, 1121. UV/Vis (CH_2Cl_2): λ_{max} (log ε) = 252 (4.59), 314 (4.27), 354 nm (3.73). MS (FAB+): 1096 [M^+], 1023 [M^+ − tBuO]. HRMS (FAB+): [M^+] $C_{44}H_{66}Co_2O_8S_8$: calcd. 1096.1188; found 1096.1172.

***syn*-C(4.4)Me:** Yellow solid, m.p. 266 °C. ^{1}H NMR (500 MHz, $CDCl_3$): δ = 1.46 [s, 36 H, $C(CH_3)_3$], 1.85 (m, 8 H, $CH_2CH_2CH_2CH_2$), 2.10 (s, 6 H, CpCH_3), 3.04 (m, 8 H, SCH_2), 5.14/5.29 (pt, 8 H, CpH) ppm. ^{13}C NMR (125 MHz, $CDCl_3$): δ = 12.8 (CpCH_3), 25.2 [$C(CH_3)_3$], 29.1 ($CH_2CH_2CH_2CH_2$), 36.6

(S*C*H$_2$), 62.1 [*C*(CH$_3$)$_3$], 77.8 [*C*(Cb)SO$_2$*t*Bu], 82.5 [*C*(Cb)SCH$_2$], 85.4/86.8 [*C*(Cp)H], 101.0 [*C*(Cp)CH$_3$] ppm. IR (KBr): $\tilde{\nu}$ = 2970 cm^{-1}, 2929, 1633, 1476, 1456, 1355, 1308, 1122. UV/Vis (CH$_2$Cl$_2$): λ_{max} (log ε) = 252 (4.53), 314 (4.38), 354 nm (3.70). MS (FAB+): 1096 [M$^+$], 1023 [M$^+$ − *t*BuO]. HRMS (FAB+): [M$^+$] C$_{44}$H$_{66}$Co$_2$O$_8$S$_8$: calcd. 1096.1188; found 1096.1188. C$_{44}$H$_{66}$Co$_2$O$_8$S$_8$ (1097.4): calcd. C 48.16, H 6.06, S 23.38; found C 48.22, H 6.07, S 23.26.

Reaction of A(4.4) with CpSiMe$_3$Co(CO)(BTSA) (8c). Reaction A: 8c (123 mg, 0.25 mmol) and **A(4.4)** (80 mg, 0.28 mmol). Yield: 107 mg (57%) of **B(3.3)SiMe$_3$**. **Reaction B: 8c** (314 mg, 0.64 mmol) and **A(4.4)** (80 mg, 0.28 mmol). Yield: 22 mg (10%) of **B(4.4)SiMe$_3$**, 104 mg (31%) of *anti*-**C(4.4)SiMe$_3$** and 38 mg (11%) of *syn*-**C(4.4)SiMe$_3$**.

B(4.4)SiMe$_3$: Yellow solid, m.p. 193 °C. ^{1}H NMR (500 MHz, CDCl$_3$): δ = 0.34 [s, 9 H, Si(CH$_3$)$_3$], 1.46 [s, 18 H, C(CH$_3$)$_3$], 1.79 (m, 4 H, C*H*$_2$CH$_2$CH$_2$SC≡), 1.95 (m, 4 H, C*H*$_2$CH$_2$SC≡), 2.65 (m, 4 H, CH$_2$SC≡), 2.98/3.15 (m, 4 H, C*H*$_2$CH$_2$CH$_2$CH$_2$SC≡), 5.26/5.73 (pt, 4 H, CpH) ppm. ^{13}C NMR (125 MHz, CDCl$_3$): δ = 0.3 [Si(CH$_3$)$_3$], 25.3 [C(*C*H$_3$)$_3$], 27.7 (*C*H$_2$CH$_2$CH$_2$SC≡), 28, 6 (*C*H$_2$CH$_2$SC≡), 35.7 (CH$_2$SC≡), 37.2 (*C*H$_2$CH$_2$CH$_2$CH$_2$SC≡), 62.2 [*C*(CH$_3$)$_3$], 76.8 [*C*(Cb)SO$_2$*t*Bu], 84.0 [*C*(Cb)SCH$_2$], 86.6 (C≡), 88.9/90.2 [*C*(Cp)H], 94.3 [*C*(Cp)SiMe$_3$] ppm. IR (KBr): $\tilde{\nu}$ = 2929 cm^{-1}, 1633, 1456, 1307, 1248, 1192, 1121. UV/Vis (CH$_2$Cl$_2$): λ_{max} (log ε) = 258 (4.16), 318 (4.05), 362 nm (3.41). MS (FAB+): 750 [M$^+$], 677 [M$^+$ − SiMe$_3$]. HRMS (FAB+): [M$^+$] C$_{30}$H$_{47}$CoO$_4$S$_6$Si: calcd. 750.0900; found 750.0909. C$_{30}$H$_{47}$CoO$_4$S$_6$Si.0.25 C$_4$H$_{10}$O (769.6): calcd. C 48.38, H 6.48, S 25.00; found C 48.56, H 6.41, S 25.21.

***anti*-C(4.4)SiMe$_3$:** Yellow solid, m.p. 202 °C. ^{1}H NMR (500 MHz, CDCl$_3$): δ = 0.35 [s, 18 H, Si(CH$_3$)$_3$], 1.47 [s, 36 H, C(CH$_3$)$_3$], 1.88 (m, 8 H, CH$_2$C*H*$_2$C*H*$_2$CH$_2$), 2.99 (m, 8 H, C*H*$_2$S), 5.15/5.73 (pt, 8 H, CpH) ppm. ^{13}C NMR (125 MHz, CDCl$_3$): δ = −0.4 [Si(CH$_3$)$_3$], 25.3 [C(*C*H$_3$)$_3$], 28.2 (CH$_2$*C*H$_2$*C*H$_2$CH$_2$), 36.4 (S*C*H$_2$), 61.6 [*C*(CH$_3$)$_3$], 77.3 [*C*(Cb)SO$_2$*t*Bu], 82.8 [*C*(Cb)SCH$_2$], 88.5/89.8 [*C*(Cp)H], 93.8 [*C*(Cp)SiMe$_3$] ppm. IR (KBr): $\tilde{\nu}$ = 2931 cm^{-1}, 1457, 1355, 1310, 1249, 1122. UV/Vis (CH$_2$Cl$_2$): λ_{max} (log ε) = 328 (4.34), 360 (3.69), 370 nm (3.77). MS (FAB+): 1212 [M$^+$], 1139 [M$^+$ − SiMe$_3$]. HRMS (FAB+): [M + H$^+$] C$_{48}$H$_{79}$Co$_2$O$_8$S$_8$Si$_2$: calcd. 1213.1743; found 1213.1743. C$_{48}$H$_{78}$Co$_2$O$_8$S$_8$Si$_2$.0.5 C$_4$H$_{10}$O (1250.8): calcd. C 48.02, H 6.69, S 20.51; found C 48.29, H 6.65, S 20.26.

***syn*-C(4.4)SiMe$_3$:** Yellow solid, m.p. 274 °C (dec.). ^{1}H NMR (300 MHz, CDCl$_3$): δ = 0.32 [s, 18 H, Si(CH$_3$)$_3$], 1.48 [s, 36 H, C(CH$_3$)$_3$], 1.85 (m, 8 H, CH$_2$C*H*$_2$C*H*$_2$CH$_2$), 3.00 (m, 8 H, C*H*$_2$S), 5.12/5.72 (pt, 8 H, CpH) ppm. ^{13}C NMR (75 MHz, CDCl$_3$): δ = 0.3 [Si(CH$_3$)$_3$], 25.3 [C(*C*H$_3$)$_3$], 28.8 (CH$_2$*C*H$_2$*C*H$_2$CH$_2$), 37.3 (S*C*H$_2$), 62.3 [*C*(CH$_3$)$_3$], 77.9 [*C*(Cb)SO$_2$*t*Bu], 84.0 [*C*(Cb)SCH$_2$], 89.2/90.4 [*C*(Cp)H], 99.8 [*C*(Cp)SiMe$_3$] ppm. IR (KBr): $\tilde{\nu}$ = 2931 cm^{-1}, 1633, 1457, 1356, 1309, 1249, 1121. UV/Vis (CH$_2$Cl$_2$): λ_{max} (log ε) = 260 (4.48), 316 (4.37), 360 nm (3.69). MS (FAB+): 1212 [M$^+$], 1139 [M$^+$ − SiMe$_3$]. HRMS (FAB+): [M + H$^+$] C$_{48}$H$_{79}$Co$_2$O$_8$S$_8$Si$_2$: calcd. 1213.1743; found 1213.1741. C$_{48}$H$_{78}$Co$_2$O$_8$S$_8$Si$_2$.0.5 C$_4$H$_{10}$O (1250.8): calcd. C 48.02, H 6.69, S 20.51; found C 47.78, H 6.64, S 20.32.

Reaction of A(4.4) with CpCOOMeCo(CO)(BTSA) (8d). Reaction A: 8d (120 mg, 0.25 mmol) and **A(4.4)** (80 mg, 0.28 mmol). Yield: 75 mg (41%) of **B(4.4)COOMe**, and 12 mg (8%) of *syn*-**C(4.4)COOMe**. **Reaction B: 8d** (304 mg, 0.64 mmol) and **A(4.4)** (80 mg, 0.28 mmol). Yield: 6 mg (3%) of **B(4.4)COOMe**, 97 mg (29%) of *anti*-**C(4.4)COOMe** and 97 mg (29%) of *syn*-**C(4.4)COOMe**.

B(4.4)COOMe: Yellow solid, m.p. 155 °C. ^{1}H NMR (500 MHz, CDCl$_3$): δ = 1.45 [s, 18 H, C(CH$_3$)$_3$], 1.81 (m, 4 H, C*H*$_2$CH$_2$CH$_2$SC≡), 1.97 (m, 4 H, C*H*$_2$CH$_2$SC≡), 2.65 (m, 4 H, CH$_2$SC≡), 3.17 (m, 4 H, C*H*$_2$CH$_2$CH$_2$CH$_2$SC≡), 3.89 (s, 3 H, COOCH$_3$), 5.65/5.82 (pt, 4 H, CpH) ppm. ^{13}C NMR (125 MHz, CDCl$_3$): δ = 25.1 [C(*C*H$_3$)$_3$], 28.0/28.6 (CH$_2$*C*H$_2$*C*H$_2$CH$_2$), 35.70/35.73 (SCH$_2$), 52.9 (COO*C*H$_3$), 62.4 [*C*(CH$_3$)$_3$], 78.1 [*C*(Cb)SO$_2$*t*Bu], 85.7 [*C*(Cb)SCH$_2$], 86.5 (C≡), 86.9/88.8 [*C*(Cp)H], 90.4 [*C*(Cp)COOMe], 166.2 (C=O) ppm. IR (KBr): $\tilde{\nu}$ = 2931 cm^{-1}, 1724, 1632, 1472, 1308, 1146. UV/Vis (CH$_2$Cl$_2$): λ_{max} (log ε) = 240 (4.35), 324 (4.05), 364 nm (3.41). MS (FAB+): 736 [M$^+$], 633 (M$^+$ − *t*BuO). HRMS (FAB+): [M + H$^+$] C$_{29}$H$_{42}$CoO$_6$S$_6$: calcd. 737.0638; found 737.0639. C$_{29}$H$_{41}$CoO$_6$S$_6$·CH$_3$OH (769.0): calcd. C 46.86, H 5.90, S 25.02; found C 46.51, H 5.78, S 25.29.

***anti*-C(4.4)COOMe:** Yellow solid, m.p. 246 °C. ^{1}H NMR (500 MHz, CDCl$_3$): δ = 1.47 (s, 36 H, C(CH$_3$)$_3$], 1.86 (m, 8 H, CH$_2$C*H*$_2$C*H*$_2$CH$_2$), 3.13 (m, 8 H, C*H*$_2$S), 3.86 (s, 6 H, COOCH$_3$), 5.63/5.79 (pt, 8 H, CpH) ppm. ^{13}C NMR (125 MHz, CDCl$_3$): δ = 24.4 (C(*C*H$_3$)$_3$], 28.1 (CH$_2$*C*H$_2$*C*H$_2$CH$_2$), 35.0 (S*C*H$_2$), 52.7 (COO*C*H$_3$), 61.7 [*C*(CH$_3$)$_3$], 77.9 [*C*(Cb)SO$_2$*t*Bu], 85.0 [*C*(Cb)SCH$_2$], 86.4/88.2 [*C*(Cp)H], 90.7 [*C*(Cp)COOMe], 166.1 (C=O) ppm. IR (KBr): $\tilde{\nu}$ = 2934 cm^{-1}, 1721, 1633, 1473, 1367, 1308, 1122. UV/Vis (CH$_2$Cl$_2$): λ_{max} [nm] (log ε) = 240 (4.64), 322 (4.35), 366 nm (3.76). MS (FAB+): 1184 [M$^+$], 1111 (M$^+$ − *t*BuO). HRMS (FAB+): [M + H$^+$] C$_{46}$H$_{67}$Co$_2$O$_{12}$S$_8$: calcd. 1185.1062; found 1185.1056. C$_{46}$H$_{66}$Co$_2$O$_{12}$S$_8$ (1185.4): calcd. C 46.61, H 5.61, S 21.64; found C 46.66, H 5.66, S 21.56.

***syn*-C(4.4)COOMe:** Yellow solid, m.p. 193 °C. ^{1}H NMR (500 MHz, CDCl$_3$): δ = 1.45 [s, 36 H, C(CH$_3$)$_3$], 1.85 (m, 8 H, CH$_2$C*H*$_2$C*H*$_2$CH$_2$), 3.12 (m, 8 H, C*H*$_2$S), 3.89 (s, 6 H, COOCH$_3$), 5.61/5.77 (pt, 8 H, CpH) ppm. ^{13}C NMR (125 MHz, CDCl$_3$): δ = 25.1 (C(*C*H$_3$)$_3$], 28.8 (CH$_2$*C*H$_2$*C*H$_2$CH$_2$), 35.5 (S*C*H$_2$), 52.9 (COO*C*H$_3$), 62.5 [*C*(CH$_3$)$_3$], 78.4 [*C*(Cb)SO$_2$*t*Bu], 85.1 [*C*(Cb)SCH$_2$], 87.4/88.9 [*C*(Cp)H], 90.5 [*C*(Cp)COOMe], 166.0 (C=O) ppm. IR (KBr): $\tilde{\nu}$ = 2934 cm^{-1}, 1721, 1633, 1473, 1367, 1308, 1122. UV/Vis (CH$_2$Cl$_2$): λ_{max} (log ε) = 242 (4.66), 320 (4.35), 366 nm (3.68). MS (FAB+): 1184 [M$^+$], 1111 [M$^+$ − *t*BuO]. HRMS (FAB+): [M$^+$] C$_{46}$H$_{66}$Co$_2$O$_{12}$S$_8$: calcd. 1184.0984; found 1184.0986. C$_{46}$H$_{66}$Co$_2$O$_{12}$S$_8$ (1185.4): calcd. C 46.61, H 5.61, S 21.64; found C 46.59, H 5.62, S 21.49.

Reaction of A(4.4) with EtMe$_4$CpCo(CO)(BTSA) (8e). Reaction A: 8e (126 mg, 0.25 mmol) and **A(4.4)** (80 mg, 0.28 mmol). Yield: 17 mg (9%) of **B(4.4)EtMe$_4$**. **Reaction B: 8e** (322 mg, 0.64 mmol) and **A(4.4)** (80 mg, 0.28 mmol). Yield: 30 mg (14%) of **B(4.4)EtMe$_4$**.

B(4.4)EtMe$_4$: Yellow solid, m.p. 184 °C. ^{1}H NMR (500 MHz, CDCl$_3$): δ = 0.98 (t, ^3J = 7.5 Hz, 3 H, CH$_2$C*H*$_3$), 1.41 [s, 18 H, C(CH$_3$)$_3$], 1.75 (m, 4 H, C*H*$_2$CH$_2$CH$_2$SC≡), 1.93 (m, 4 H, C*H*$_2$CH$_2$SC≡), 1.92/1.94 (s, 12 H, CpC*H*$_3$), 2.51 (q, ^3J = 7.5 Hz, 2 H, C*H*$_2$CH$_3$), 2.62/2.70 (m, 4 H, CH$_2$SC≡), 2.70/3.03 (m, 4 H, C*H*$_2$CH$_2$CH$_2$CH$_2$SC≡) ppm. ^{13}C NMR (125 MHz, CDCl$_3$): δ = 10.0/10.3 (Cp*C*H$_3$), 14.4 (CH$_2$*C*H$_3$), 18.4 (C*H*$_2$CH$_3$), 25.7 [C(*C*H$_3$)$_3$], 28.0 (*C*H$_2$CH$_2$CH$_2$SC≡), 28.8 (*C*H$_2$CH$_2$SC≡), 35.8 (*C*H$_2$SC≡), 37.1 (*C*H$_2$CH$_2$CH$_2$CH$_2$SC≡), 62.3 [*C*(CH$_3$)$_3$], 76.4 [*C*(Cb)SO$_2$*t*Bu], 78.6 [*C*(Cb)SCH$_2$], 86.7 (C≡), 95.5/96.5 [*C*(Cp)CH$_3$], 100.9 [*C*(Cp)CH$_2$CH$_3$] ppm. IR (KBr): $\tilde{\nu}$ = 2964 cm^{-1}, 2928, 2867, 1456, 1357, 1307, 1237, 1193, 1117, 1024. UV/Vis (CH$_2$Cl$_2$): λ_{max} (log ε) = 266 (4.26), 322 (4.29), 364 nm (3.40). MS (FAB+): 762 [M$^+$], 689 [M$^+$ − *t*BuO]. HRMS (FAB+): [M$^+$] C$_{33}$H$_{51}$CoO$_4$S$_6$: calcd. 762.1444; found 762.1474. C$_{33}$H$_{51}$CoO$_4$S$_6$·0.5CH$_3$OH (795.1): calcd. C 51.65, H 6.86, S 24.69; found C 51.80, H 6.64, S 24.59.

Reaction of A(5.5) with CpCo(CO)(BTSA) (8a). Reaction A: 8a (84 mg, 0.20 mmol) and **A(5.5)** (70 mg, 0.22 mmol). Yield: 31 mg (22%) of **B(5.5)H** and 12 mg (5%) of a mixture of *anti*-**C(5.5)H** and *syn*-**C(5.5)H**. **Reaction B: 8a** (213 mg, 0.51 mmol) and **A(5.5)** (80 mg, 0.22 mmol). Yield: 20 mg (13%) of **B(5.5)H** and 75 mg (31%) of a mixture of *anti*-**C(5.5)H** and *syn*-**C(5.5)H**.

B(5.5)H: Yellow solid, m.p. 132 °C. ^{1}H NMR (500 MHz, $CDCl_3$): δ = 1.47 [s, 18 H, $C(CH_3)_3$], 1.59 (m, 4 H, $CH_2CH_2CH_2SC\equiv$), 1.76 (m, 4 H, $CH_2CH_2CH_2CH_2SC\equiv$), 1.83 (m, 4 H, $CH_2CH_2SC\equiv$), 2.63 (m, 4 H, $CH_2SC\equiv$), 3.02 (m, 4 H, $CH_2CH_2CH_2CH_2CH_2SC\equiv$), 5.35 (s, 5 H, CpH) ppm. ^{13}C NMR (125 MHz, $CDCl_3$): δ = 25.2 [$C(CH_3)_3$], 28.1 ($CH_2CH_2CH_2SC\equiv$), 29.6 ($CH_2CH_2SC\equiv$), 30.4 ($CH_2CH_2CH_2CH_2SC\equiv$), 36.2 ($CH_2SC\equiv$), 37.6 ($CH_2CH_2CH_2CH_2CH_2SC\equiv$), 62.0 [$C(CH_3)_3$], 78.3 [$C(Cb)SO_2t$Bu], 84.3 [$C(Cb)SCH_2$], 86.2 [$C$(Cp)], 86.6 (C≡) ppm. IR (KBr): $\tilde{\nu}$ = 2964 cm^{-1}, 2928, 2855, 1456, 1349, 1310, 1193, 1122. UV/Vis (CH_2Cl_2): λ_{max} (log ε) = 248 (3.48), 312 (4.01), 356 nm (3.35). MS (FAB+): 706 [M^+], 633 [$M^+ - t$BuO]. HRMS (FAB+): [M^+] $C_{29}H_{43}CoO_4S_6$: calcd. 706.0818; found 706.0825.

Data for the Mixture of *anti*-C(5.5)H and *syn*-C(5.5)H: Yellow solid. ^{1}H NMR (500 MHz, $CDCl_3$): δ = 1.45 [s, 72 H, $C(CH_3)_3$], 1.63 (m, 8 H, $CH_2CH_2CH_2CH_2CH_2$), 1.72 (m, 16 H, $CH_2CH_2CH_2CH_2CH_2$), 3.05 (m, 16 H, $CH_2CH_2CH_2CH_2CH_2$), 5.36 (s, 10 H, CpH), 5.37 (s, 10 H, CpH) ppm. ^{13}C NMR (125 MHz, $CDCl_3$): δ = 25.1 [$C(CH_3)_3$], 28.8 ($CH_2CH_2CH_2CH_2CH_2$), 29.5 ($CH_2CH_2CH_2CH_2CH_2$), 37.7/37.8 ($CH_2CH_2CH_2CH_2CH_2$), 62.03/62.05 [$C(CH_3)_3$], 78.1/78.2 [C(Cb)SO_2tBu], 84.38/84.43 [C(Cb)SCH_2], 85.98/86.00 [C(Cp)] ppm. IR (KBr): $\tilde{\nu}$ = 2971 cm^{-1}, 2931, 2858, 1458, 1351, 1309, 1194, 1122. UV/Vis (CH_2Cl_2): λ_{max} (log ε) = 250 (4.45), 314 (4.25), 362 nm (3.54). MS (FAB+): 1096 [M^+], 1023 [$M^+ - t$BuO]. HRMS (FAB+): [M^+] $C_{44}H_{66}Co_2O_8S_8$: calcd. 1096.1187; found 1096.1215. $C_{44}H_{66}Co_2O_8S_8$ (1097.4): calcd. C 48.16, H 6.06, S 23.38; found C 48.28, H 6.03, S 23.27.

Reaction of A(5.5) with CpMeCo(CO)(BTSA) (8b). Reaction A: 8b (87 mg, 0.20 mmol) and **A(5.5)** (70 mg, 0.22 mmol). Yield: 44 mg (30%) of **B(5.5)Me** and 39 mg (17%) of a mixture of *anti*-**C(5.5)Me** and *syn*-**C(5.5)Me**. **Reaction B: 8b** (220 mg, 0.51 mmol) and **A(5.5)** (70 mg, 0.22 mmol). Yield: 137 mg (55%) of a mixture of *anti*-**C(5.5)Me** and *syn*-**C(5.5)Me**.

B(5.5)Me: Yellow solid, m.p. 122 °C. ^{1}H NMR (500 MHz, $CDCl_3$): δ = 1.47 [s, 18 H, $C(CH_3)_3$], 1.59 (m, 4 H, $CH_2CH_2CH_2SC\equiv$), 1.75 (m, 4 H, $CH_2CH_2CH_2CH_2SC\equiv$), 1.82 (m, 4 H, $CH_2CH_2SC\equiv$), 2.09 (s, 3 H, $CpCH_3$), 2.63 (m, 4 H, $CH_2SC\equiv$), 2.99 (m, 4 H, $CH_2CH_2CH_2CH_2CH_2SC\equiv$), 5.12/5.28 (pt, 4 H, CpH) ppm. ^{13}C NMR (125 MHz, $CDCl_3$): δ = 12.8 ($CpCH_3$), 25.2 [$C(CH_3)_3$], 28.1 ($CH_2CH_2CH_2SC\equiv$), 29.6 ($CH_2CH_2SC\equiv$), 30.4 ($CH_2CH_2CH_2$-$CH_2SC\equiv$), 36.2 ($CH_2SC\equiv$), 37.1 ($CH_2CH_2CH_2CH_2CH_2SC\equiv$), 62.0 [$C(CH_3)_3$], 77.8 [$C(Cb)SO_2t$Bu], 83.0 [$C(Cb)SCH_2$], 85.3/86.7 [$C$(Cp)H], 86.6 (C≡), 100.9 [C(Cp)CH_3] ppm. IR (KBr): $\tilde{\nu}$ = 2959 cm^{-1}, 2929, 2857, 1475, 1456, 1354, 1309, 1222, 1194, 1122. UV/Vis (CH_2Cl_2): λ_{max} (log ε) = 254 (4.25), 314 (4.08), 360 nm (3.32). MS (FAB+): 720 [M^+], 647 [$M^+ - t$BuO]. HRMS (FAB+): [M^+] $C_{30}H_{45}CoO_4S_6$: calcd. 720.0974; found 720.0984.

Data for the Mixture of *anti*-C(5.5)Me and *syn*-C(5.5)Me: Yellow solid. ^{1}H NMR (300 MHz, $CDCl_3$): δ = 1.44 (s, 72 H, $C(CH_3)_3$], 1.69 (m, 24 H, $CH_2CH_2CH_2CH_2CH_2$), 2.08 (s, 6 H, $CpCH_3$), 2.09 (s, 6 H, $CpCH_3$), 3.05 (m, 16 H, $CH_2CH_2CH_2CH_2CH_2$), 5.15/5.28 (pt, 16 H, CpH) ppm. ^{13}C NMR (125 MHz, $CDCl_3$): δ = 12.82/12.83 ($CpCH_3$), 25.2 [$C(CH_3)_3$], 28.9 ($CH_2CH_2CH_2CH_2CH_2$), 29.5 ($CH_2CH_2CH_2CH_2CH_2$), 37.7 ($CH_2CH_2CH_2CH_2CH_2$), 62.03/62.04 [$C(CH_3)_3$], 77.43/77.54 [C(Cb)SO_2tBu], 83.2 [C(Cb)SCH_2], 85.0/86.5 [C(Cp)H], 100.8 [C(Cp)CH_3] ppm. IR (KBr): $\tilde{\nu}$ = 2969 cm^{-1}, 2929, 2858, 1476, 1457, 1353, 1311, 1194, 1123. UV/Vis (CH_2Cl_2): λ_{max} (log ε) = 254 (4.59), 314 (4.43), 360 nm (3.65). MS (FAB+): 1124 [M^+], 1051 [$M^+ - t$BuO]. HRMS (FAB+): [M + H^+] $C_{46}H_{71}Co_2O_8S_8$: calcd. 1125.1579; found 1125.1584. $C_{46}H_{70}Co_2O_8S_8$ (1125.5): calcd. C 49.09, H 6.27, S 22.79; found C 49.25, H 6.23, S 22.70.

Reaction of A(5.5) with CpCOOMeCo(CO)(BTSA) (8d). Reaction A: 8d (96 mg, 0.20 mmol) and **A(5.5)** (70 mg, 0.22 mmol). Yield: 48 mg (31%) of **B(5.5)COOMe**. **Reaction B: 8d** (242 mg, 0.51 mmol) and **A(5.5)** (70 mg, 0.22 mmol). Yield: 165 mg (61%) of a mixture of *anti*-**C(5.5)COOMe** and *syn*-**C(5.5)COOMe**.

B(5.5)COOMe: Orange oil. ^{1}H NMR (300 MHz, $CDCl_3$): δ = 1.47 [s, 18 H, $C(CH_3)_3$], 1.60 (m, 4 H, $CH_2CH_2CH_2SC\equiv$), 1.78 (m, 8 H, $CH_2CH_2CH_2CH_2SC\equiv$), 2.63 (m, 4 H, $CH_2SC\equiv$), 3.07 (m, 4 H, $CH_2CH_2CH_2CH_2CH_2SC\equiv$), 3.88 (s, 3 H, $COOCH_3$), 5.62/5.74 (pt, 4 H, CpH) ppm. ^{13}C NMR (75 MHz, $CDCl_3$): δ = 25.1 [$C(CH_3)_3$], 28.0 ($CH_2CH_2CH_2SC\equiv$), 29.5/30.3 ($CH_2CH_2CH_2CH_2SC\equiv$), 36.0/36.2 (CH_2S), 52.8 ($COOCH_3$), 62.4 [$C(CH_3)_3$], 78.6 [C(Cb)SO_2tBu], 85.4 [C(Cb)SCH_2], 86.6 (C≡), 87.3/88.9 [C(Cp)H], 90.4 [C(Cp)CH_3], 166.1 ($COOCH_3$) ppm. IR (KBr): $\tilde{\nu}$ = 2929 cm^{-1}, 1720, 1472, 1308, 1283, 1192, 1147. UV/Vis (CH_2Cl_2): λ_{max} (log ε) = 240 (4.99), 320 (4.66), 364 nm (3.47). MS (FAB+): 764 [M^+], 691 [$M^+ - t$BuO]. HRMS (FAB+): [M^+] $C_{31}H_{45}CoO_6S_6$: calcd. 764.0872; found 764.0891.

Data for the Mixture of *anti*-C(5.5)COOMe and *syn*-C(5.5)COOMe: Yellow solid. ^{1}H NMR (300 MHz, $CDCl_3$): δ = 1.46 [s, 72 H, $C(CH_3)_3$], 1.68 (m, 24 H, $CH_2CH_2CH_2CH_2CH_2$), 3.11 (m, 16 H, $CH_2CH_2CH_2CH_2CH_2$), 3.85 (s, 6 H, $COOCH_3$), 3.90 (s, 6 H, $COOCH_3$), 5.63/5.79 (pt, 16 H, CpH) ppm. ^{13}C NMR (75 MHz, $CDCl_3$): δ = 24.4 [$C(CH_3)_3$], 28.84/28.87 ($CH_2CH_2CH_2CH_2CH_2$), 29.4 ($CH_2CH_2CH_2CH_2CH_2$), 36.14/36.26 ($CH_2CH_2CH_2CH_2CH_2$), 52.76/52.88 ($COOCH_3$), 62.44/62.47 [$C(CH_3)_3$], 78.32/78.45 [C(Cb)SO_2tBu], 85.65/85.88 [C(Cb)SCH_2], 87.03/87.10/88.78/ 88.81 [C(Cp)H], 90.31/90.34 [C(Cp)$COOCH_3$], 166.13 ($COOCH_3$) ppm. IR (KBr): $\tilde{\nu}$ = 2932 cm^{-1}, 1720, 1650, 1472, 1367, 1309, 1193, 1147, 1122. UV/Vis (CH_2Cl_2): λ_{max} (log ε) = 242 (4.56), 322 (4.25), 364 nm (3.58). MS (FAB+): 1212 [M^+], 1139 [$M^+ - t$BuO]. HRMS (FAB+): [M + H^+] $C_{48}H_{71}Co_2O_{12}S_8$: calcd. 1213.1375; found 1213.1399. $C_{48}H_{70}Co_2O_{12}S_8$ (1213.5): calcd. C 47.51, H 5.81; found C 47.19, H 5.83.

Reaction of A(3.3.3) with [CpSiMe$_3$Co(CO)(BTSA)] (8c). Synthesis of A(3.3.3): A suspension of lithium acetylide in THF and a solution of 1,3-dithiocyanatopropane in THF were added simultaneously at −40 °C to THF (1 L) over a period of 4 h. After complete addition, the reaction mixture was allowed to warm to room temperature overnight. The solvent was removed by rotary evaporation and polymers and salts were removed by flash filtration [SiO_2; 3% NEt_3(v/v), toluene]. After removal of the solvent, the product was isolated by column chromatography [SiO_2; 3% NEt_3 (v/v), *n*-hexane/toluene, 3:1]. Starting material: Dilithium acetylide, prepared from *n*BuLi (60 mmol) in THF (250 mL) and 1,3-dithiocyanatopropane (4.51 g, 28.5 mmol) in THF (250 mL). Yield: 107 mg (3%) of **A(3.3.3)**.

A(3.3.3): Colourless solid, m.p. 100 °C. ^{1}H NMR (300 MHz, $CDCl_3$): δ = 2.24 (quint, 6 H, SCH_2CH_2), 2.81 (t, ^3J = 7.1 Hz, 12 H, SCH_2) ppm. ^{13}C NMR (75 MHz, $CDCl_3$): δ = 28.5 (SCH_2CH_2), 34.4 (SCH_2), 86.2 (C≡) ppm. IR (KBr): $\tilde{\nu}$ = 2929 cm^{-1}, 2058, 1437. MS (EI+): 390 [M^+], 204, 88. HRMS (EI+): [M^+] $C_{15}H_{18}S_6$: calcd. 389.9733; found 389.9725. $C_{15}H_{18}S_6$ (390.7): calcd. C 46.11, H 4.64, S 49.25; found C 46.22, H 4.70, S 48.99.

Starting material: **A(3.3.3)** (60 mg, 0.15 mmol) and **8c** (453 mg, 0.92 mmol). Yield: 154 mg (56%) of *anti*-**C(3.3.3)SiMe$_3$**, 36 mg (13%) of *all-syn*-**C(3.3.3)SiMe$_3$**.

***anti*-C(3.3.3)SiMe$_3$:** Yellow solid, m.p. 103 °C (dec.). ^{1}H NMR (500 MHz, $CDCl_3$): δ = 0.29 [s, 9 H, $Si(CH_3)_3$], 0.32 [s, 18 H, $Si(CH_3)_3$], 1.47 [s, 48 H, $C(CH_3)_3$], 1.99 (m, 6 H, $CH_2CH_2CH_2$), 3.03 (m, 12 H, SCH_2), 5.19/5.73 (pt, 12 H, CpH) ppm. ^{13}C NMR (75 MHz, $CDCl_3$): δ = −0.2 [$Si(CH_3)_3$], 24.7 [$C(CH_3)_3$], 29.5 ($CH_2CH_2CH_2$), 29.6 ($CH_2CH_2CH_2$), 36.1 (SCH_2), 36.1 (SCH_2), 36.3 (SCH_2), 61.8 [$C(CH_3)_3$], 61.8 [$C(CH_3)_3$], 61.9 [$C(CH_3)_3$], 76.4 [C(Cb)SO_2tBu], 76.5 [C(Cb)SO_2tBu], 76.6 [C(Cb)SO_2tBu], 82.9 [C(Cb)SCH_2], 83.6 [C(Cb)SCH_2], 83.6 [C(Cb)SCH_2], 88.5/88.6/88.6/89.6/89.8/90.3 [C(Cp)H], 93.7/93.9 [C(Cp)$SiMe_3$] ppm. IR (KBr): $\tilde{\nu}$ = 2958 cm^{-1}, 1631, 1351, 1122. UV/Vis (CH_2Cl_2): λ_{max} [nm] (log ε) = 258 (4.34), 316 (4.22). MS (FAB+): 1778 [M$^+$]. HRMS (FAB+): [M + Na$^+$] $C_{69}H_{111}Co_3O_{12}S_{12}Si_3Na$: calcd. 1799.1926; found 1799.1908. $C_{69}H_{111}Co_3O_{12}S_{12}Si_3$ (1778.5): calcd. C 46.60, H 6.29, S 21.64; found C 46.96, H 6.41, S 21.49.

***all-syn*-C(3.3.3)SiMe$_3$:** Yellow solid, m.p. 105 °C (dec.). ^{1}H NMR (500 MHz, $CDCl_3$): δ = 0.35 [s, 27 H, $Si(CH_3)_3$], 1.46 [s, 48 H, $C(CH_3)_3$], 1.98 (m, 6 H, $CH_2CH_2CH_2$), 3.04 (m, 6 H, SCH*H*), 3.07 (m, 6 H, SCH*H*), 5.21/5.72 (pt, 12 H, CpH) ppm. ^{13}C NMR (125 MHz, $CDCl_3$): δ = −0.2 [$Si(CH_3)_3$], 24.7 [$C(CH_3)_3$], 29.5 ($CH_2CH_2CH_2$), 36.1 (SCH_2), 61.8 [$C(CH_3)_3$], 76.4 [C(Cb)SO_2tBu], 83.4 [C(Cb)SCH_2], 88.5/90.0 [C(Cp)H], 94.0 [C(Cp)$SiMe_3$] ppm. IR (KBr): $\tilde{\nu}$ = 2956 cm^{-1}, 1631, 1309, 1250, 1121. UV/Vis (CH_2Cl_2): λ_{max} (log ε) = 258 (4.60), 316 (4.47), 364 (3.69), 408 nm (3.40). MS (FAB+): 1778 [M$^+$]. HRMS (FAB+): [M$^+$] $C_{69}H_{112}Co_3O_{12}S_{12}Si_3$: calcd. 1777.2106; found 1777.2108. $C_{69}H_{111}Co_3O_{12}S_{12}Si_3$.0.25 $C_4H_{10}O$ (1797.0): calcd. C 47.15, H 6.51, S 20.98; found C 46.97, H 6.56, S 20.76.

X-ray Diffraction Analyses: Reflections were collected using Nonius CAD4, Bruker Smart CCD and Bruker APEX diffractometers (Mo-K_α radiation, graphite monochromator). Intensities were corrected for Lorentz and polarisation effects. Numerical (face indexing) or empirical absorption corrections were applied using SADABS.[16] The structures were solved by direct methods. The structural parameters of the non-hydrogen atoms were refined anisotropically according to a full-matrix least-squares technique (F^2). Hydrogen atom positions were calculated according to stereochemical aspects. In **B(2.3)SiMe$_3$** the *tert*-butyl groups (6:4) and the thiaalkyne side chain (7:3) were disordered. In *syn*-**C(2.2)SiMe$_3$** one ethano moiety was disordered (1:1:1). In *syn*-**C(3.3)SiMe$_3$** two methylene units were disordered (3:1). The minor positions were refined isotropically. Structure solution and refinement were carried out using the SHELXTL software package.[16] Tables 5 and 6 contain the crystallographic data, details of the data collection and the refinement procedure. ORTEP drawings were obtained using ORTEP-3 for Windows.[17] CCDC-193187 to -193198 contain the supplementary crystallographic data for this paper. These data can be obtained free of charge at www.ccdc.cam.ac.uk/conts/retrieving.html [or from the Cambridge Crystallographic Data Centre, 12 Union Road, Cambridge CB2 1EZ, UK; Fax: (internat.) + 44-1223/336-033; E-mail: deposit@ccdc.cam.ac.uk].

Acknowledgments

We are grateful to the Deutsche Forschungsgemeinschaft (SFB, 623), the Fonds der Chemischen Industrie and the BASF Aktienge-

Table 5. Crystallographic data for **B(2.2)SiMe$_3$**, **B(2.3)SiMe$_3$**, **B(3.3)SiMe$_3$**, **B(4.4)Me**, *syn*-**C(2.2)SiMe$_3$** and *anti*-**C(2.3)SiMe$_3$**

	B(2.2)SiMe$_3$	**B(2.3)SiMe$_3$**	**B(3.3)SiMe$_3$**	**B(4.4)Me**	*syn*-**C(2.2)SiMe$_3$**	*anti*-**C(2.3)SiMe$_3$**
Empirical formula	$C_{26}H_{39}CoO_4S_6Si$	$C_{27}H_{41}CoO_4S_6Si$	$C_{28}H_{43}CoO_4S_6Si$	$C_{28}H_{41}CoO_4S_6$	$C_{44}H_{70}Co_2O_8S_8Si_2$	$C_{45}H_{72}Co_2O_8S_8Si_2$
Formula mass [g/mol]	695.01	708.98	723.06	692.96	1157.60	1171.63
Crystal colour	orange	orange	yellow	dark yellow	orange	orange
Crystal size [mm]	0.24 × 0.20 × 0.17	0.40 × 0.20 × 0.15	0.48 × 0.14 × 0.12	0.42 × 0.38 × 0.15	0.42 × 0.18 × 0.13	0.30 × 0.17 × 0.16
Crystal shape	polyhedron	polyhedron	polyhedron	polyhedron	polyhedron	polyhedron
Temperature [K]	200(2)	293(2)	200(2)	200(2)	200(2)	200(2)
Crystal system	triclinic	orthorhombic	orthorhombic	triclinic	monoclinic	monoclinic
Space group	$P\bar{1}$	Pbca	$Pca2_1$	$P\bar{1}$	$P2_1/c$	$P2_1/n$
Z	2	8	8	2	4	4
a [Å]	11.3932(2)	32.031(8)	20.8028(3)	10.7867(3)	14.3890(3)	15.9129(1)
b [Å]	11.4211(1)	16.732(5)	9.8930(2)	11.9069(4)	27.0985(5)	20.7595(2)
c [Å]	13.6488(1)	12.517(3)	33.4337(2)	13.5096(4)	15.5620(3)	17.3414(2)
α [°]	68.160(1)	90	90	108.122(1)	90	90
β [°]	79.717(1)	90	90	94.780(1)	115.870(1)	102.561(2)
γ [°]	81.728(1)	90	90	99.355(1)	90	90
V [Å^3]	1616.23(3)	6708(3)	6880.73(18)	1610.45(8)	5459.85(18)	5591.49(9)
$D_{calcd.}$ [g/cm^3]	1.428	1.404	1.396	1.429	1.408	1.392
μ [mm^{-1}]	0.986	0.951	0.929	0.954	1.004	0.981
h_{min}/h_{max}	−13/13	0/42	−24/24,	−12/12	−18/18	−18/18
k_{min}/k_{max}	−13/13	0/22	−11/11,	−13/14	−35/35	−24/24
l_{min}/l_{max}	−15/14	0/16	−40/40	−15/16	−20/20	−19/20
Refl. collected	12061	8064	48399	12022	56008	41137
Refl. unique	5384	8064	11929	5349	12514	9678
Refl. observed	4756	3877	9825	4866	9065	7489
Parameter	352	407	722	359	604	604
S (Gof) on F^2	1.04	1.01	1.14	1.03	1.02	1.07
$R(F)$	0.025	0.054	0.066	0.023	0.045	0.033
$R_w(F^2)$	0.063	0.142	0.163	0.058	0.093	0.065
$(\Delta\rho)_{max}$ [eA^{-3}]	0.30	0.94	1.94	0.30	0.89	0.31
$(\Delta\rho)_{min}$ [eA^{-3}]	−0.28	−0.47	−0.50	−0.25	−0.98	−0.34

Table 6. Crystallographic data for *syn*- and *anti*-**C(3.3)SiMe$_3$**, *syn*- and *anti*-**C(4.4)Me**, **A(3.3.3)** and all-*syn*-**C(3.3.3)SiMe$_3$**

	syn-**C(3.3)SiMe$_3$**	*anti*-**C(3.3)SiMe$_3$**	*syn*-**C(4.4)Me**	*anti*-**C(4.4)Me**	**A(3.3.3)**	all-*syn*-**C(3.3.3)SiMe$_3$**
Empirical formula	$C_{46}H_{74}Co_2O_8S_8Si_2$[a]	$C_{46}H_{74}Co_2O_9S_8Si_2$[b]	$C_{44}H_{66}Co_2O_8S_8$	$C_{58}H_{82}Co_2O_8S_8$[c]	$C_{15}H_{18}S_6$	$C_{69}H_{111}Co_3O_{12}S_{12}Si_3$
Formula mass [g/mol]	1185.65	1185.65	1097.40	1097.40	390.65	1778.40
Crystal colour	orange	orange	yellow	yellow	colorless	yellow
Crystal size [mm]	0.22 × 0.17 × 0.16	0.23 × 0.21 × 0.13	0.48 × 0.20 × 0.11	0.48 × 0.10 × 0.09	0.15 × 0.08 × 0.06	0.23 × 0.15 × 0.05
Crystal shape	polyhedron	polyhedron	polyhedron	needle	polyhedron	plate
Temperature [K]	200(2)	200(2)	200(2)	200(2)	200(2)	203(2)
Crystal system	Triclinic	orthorhombic	tetragonal	monoclinic	monoclinic	monoclinic
Space group	$P\bar{1}$	$Pna2_1$	$P4_2/n$	$P2_1/c$	$P\bar{1}$	$C2/c$
Z	4	4	8	2	2	8
a [Å]	17.3542(1)	11.0539(1)	31.6670(3)	9.8439(1)	5.1841(2)	42.073(4)
b [Å]	17.7849(3)	49.9314(1)	31.6670(3)	25.6281(4)	11.0558(2)	15.933(1)
c [Å]	22.0769(3)	10.5457(1)	9.9244(1)	12.2894(1)	16.4672(5)	30.183(3)
α [°]	112.615(1)	90	90	90	80.108(2)	90
β [°]	108.785(1)	90	90	94.812(1)	83.827(2)	113.086(2)
γ [°]	91.480(1)	90	90	90	87.066(2)	90
V [Å^3]	5866.94(13)	5820.56(8)	9952.18(17)	3089.45(6)	923.87(5)	18612(3)
$D_{calcd.}$ [g/cm^3]	1.371	1.389	1.465	1.378	1.404	1.269
μ [mm^{-1}]	0.939	0.947	1.052	0.858	0.731	0.885
h_{min}/h_{max}	−20/20	−13/13	−37/37	−11/11	−6/6	−56/56
k_{min}/k_{max}	−20/21	−57/60	−36/36	−29/31	−14/14	−21/20
l_{min}/l_{max}	−25/26	−12/12	−12/11	−14/14	−21/21	−40/35
Refl. collected	44201	42573	75080	22631	9565	68596
Refl. unique	19571	9823	8896	5339	4202	23118
Refl. observed	12704	8924	6897	4316	2495	11339
Parameter	1256	633	574	404	190	919
S (Gof) on F^2	1.03	1.03	1.03	1.06	0.99	0.93
$R(F)$	0.061	0.032	0.045	0.045	0.045	0.073
$R_w(F^2)$	0.147	0.070	0.097	0.106	0.083	0.168
$(\Delta\rho)_{max}$ [eA^{-3}]	0.77	0.54	0.63	1.22	0.30	1.54
$(\Delta\rho)_{min}$ [eA^{-3}]	−0.78	−0.39	−0.63	−0.31	−0.37	−0.46

[a] The single crystal contained 2 independent molecules and 1.75 molecules of methanol in the asymmetric unit (not completely occupied). [b] The single crystal contained 1 molecule of methanol in the asymmetric unit. [c] The single crystal contained 1 molecule of disordered toluene in the unit cell.

sellschaft, Ludwigshafen, for financial support. D. B. W. thanks the Studienstiftung des deutschen Volkes for a graduate fellowship. We thank Mrs. U. Wiesinger for her help in crystal preparation and Mrs. A. Reule for typing the manuscript.

[1] [1a] J. P. Collman, L. S. Hegedus, J. R. Norton, R. G. Finke, *Principles and Applications of Organotransition Metal Chemistry*, University Science Books, Mill Valley, California, **1987**. [1b] R. D. W. Kemmit, D. R. Russell in: *Comprehensive Organometallic Chemistry* (Eds.: F. G. A. Stone, E. W. Abel), Pergamon Press, Oxford, **1982**, vol. 5, p. 248.

[2] W.-S. Lee, H. H. Brintzinger, *J. Organomet. Chem.* **1977**, *127*, 93−103.

[3] M. D. Rausch, G. F. Westover, E. Mintz, G. M. Reisner, I. Bernal, A. Clearfield, J. M. Troup, *Inorg. Chem.* **1979**, *18*, 2605−2615.

[4] [4a] K. P. C. Vollhardt, *Angew. Chem.* **1984**, *96*, 525−541; *Angew. Chem. Int. Ed. Engl.* **1984**, *23*, 539−555. [4b] H. Bönnemann, *Angew. Chem.* **1985**, *97*, 264−279; *Angew. Chem. Int. Ed. Engl.* **1985**, *24*, 248−263.

[5] J. H. Hardesty, J. B. Koerner, T. A. Albright, G.-Y. Lee, *J. Am. Chem. Soc.* **1999**, *121*, 6055−6067.

[6] [6a] A. Krebs, J. Wilke, *Top. Curr. Chem.* **1983**, *109*, 189−233. [6b] B. Jessel, Dissertation, Universität Hamburg, **1984**.

[7] C. Benisch, J. Chávez, R. Gleiter, B. Nuber, H. Irngartinger, T. Oeser, H. Pritzkow, F. Rominger, *Eur. J. Inorg. Chem.* **1998**, 629−632.

[8] Y. Wakatsuki, O. Nomura, K. Kitaura, K. Morokuma, H. Yamazaki, *J. Am. Chem. Soc.* **1983**, *105*, 1907−1912.

[9] R. Diercks, B. E. Eaton, S. Gürtzgen, S. Jalisatgi, A. J. Matzger, R. H. Radde, K. P. C. Vollhardt, *J. Am. Chem. Soc.* **1998**, *120*, 8247−8248.

[10] [10a] A. Efraty, *Chem. Rev.* **1977**, *77*, 691−744. [10b] R. Gleiter, *Angew. Chem.* **1992**, *104*, 29−46; *Angew. Chem. Int. Ed. Engl.* **1992**, *31*, 27−44.

[11] C. Benisch, R. Gleiter, T. H. Staeb, B. Nuber, T. Oeser, H. Pritzkow, F. Rominger, *J. Organomet. Chem.* **2002**, *641*, 102−112.

[12] C. Benisch, S. Bethke, R. Gleiter, T. Oeser, H. Pritzkow, F. Rominger, *Eur. J. Org. Chem.* **2000**, 2479−2488.

[13] [13a] J. Dale, *Angew. Chem.* **1966**, *78*, 1070−1093; *Angew. Chem. Int. Ed. Engl.* **1966**, *3*, 1000−1221. [13b] R. Gleiter, M. Ramming, H. Weigl, V. Wolfart, H. Irngartinger, T. Oeser, *Liebigs Ann./Recueil* **1997**, 1545−1550.

[14] T. H. Staeb, R. Gleiter, F. Rominger, *Eur. J. Org. Chem.* **2002**, 2815−2822.

[15] R. J. Schaller, R. Gleiter, J. Hofmann, F. Rominger, *Angew. Chem.* **2002**, *114*, 1231−1234; *Angew. Chem. Int. Ed.* **2002**, *41*, 1181−1183.

[16] G. M. Sheldrick, Bruker Analytical X-ray-Division, Madison, WI, **2000**.

[17] ORTEP-3 for Windows: A Version of ORTEP-III with a Graphical User Interface (GUI): L. J. Farrugia, *J. Appl. Crystallogr.* **1997**, *72*, 565.

Received September 26, 2002
[I02510]

Mono- and Dimetallic Cyano Complexes with {Mo(η^3-allyl)$(CO)_2$(N−N)} Fragments

Julio Pérez,*[a] Eva Hevia,[a] Lucía Riera,[a] Víctor Riera,[a] Santiago García-Granda,[a] Esther García-Rodríguez,[b] and Daniel Miguel[c]

Keywords: Allylic compounds / Cyanides / Heterometallic compounds / Molybdenum / Manganese / Rhenium

Treatment of [MoCl(η^3-allyl)$(CO)_2$(phen)] with NaCN in CH_2Cl_2/MeOH afforded [Mo(CN)(η^3-allyl)$(CO)_2$(phen)] [allyl = C_3H_5 (**1a**); 2-MeC_3H_4 (**1b**)] as the sole products (no products of cyanide attack on the allyl group were detected). Treatment of **1a**,**b** with [Mo(OTf)(η^3-C_3H_5)$(CO)_2$(phen)] and $NaBAr'_4$ in CH_2Cl_2 yielded the compounds [{Mo(η^3-allyl)$(CO)_2$(phen)}(μ-CN){Mo(η^3-C_3H_5)$(CO)_2$(phen)}]BAr'_4 (**2a**,**b**). Analogous treatment of **1a** with *fac*-[M(OTf)$(CO)_3$(bipy)] (M = Mn, Re) and $NaBAr'_4$ resulted in the synthesis of [{Mo(η^3-C_3H_5)$(CO)_2$(phen)}(μ-CN){M$(CO)_3$(bipy)}]BAr'_4 (**3**, **4**), in which the C and N atoms of the cyano bridge are bonded to Mo and M (M = Mn, Re), respectively. The linkage isomer of **4** (C and N atoms of the cyano group bonded to Re and Mo, respectively) (**6**) was prepared by treatment of [Re(CN)$(CO)_3$(bipy)] (**5**) with [Mo(OTf)(η^3-C_3H_5)$(CO)_2$(phen)] and $NaBAr'_4$. Compounds **1a**, **2b**, **3**, and **6** were characterized by X-ray diffraction.

(© Wiley-VCH Verlag GmbH & Co. KGaA, 69451 Weinheim, Germany, 2003)

Introduction

Monometallic complexes with terminal cyano ligands can act as metalloligands toward a second metal fragment through the uncoordinated nitrogen atom of the cyano group, affording dimetallic complexes with CN bridges,[1−6] simpler models of the supramolecular and solid-state entities in which cyano groups act as links between metal atoms.

We have recently found that pseudooctahedral [MoX(η^3-allyl)$(CO)_2$(N−N)] (N−N = 2,2′- bipyridine, bipy; 1,10-phenanthroline, phen) complexes react with organolithium or organomagnesium reagents and with sodium alkoxides to afford new alkyl,[7] alkynyl,[8] and alkoxo[9] complexes by selective halide substitution. A similar reactivity pattern would provide access to the previously unknown [Mo(CN)(η^3-allyl)$(CO)_2$(N−N)] complexes. Attractive features of the known [MoX(η^3-allyl)$(CO)_2$(N−N)] compounds are their ease of preparation[10] and the robustness of the {Mo(η^3-allyl)$(CO)_2$(N−N)} fragment[11] that directs the reactivity towards the remaining coordination position.[7−9] This paper summarizes the results of our study on the reactivity of [MoX(η^3-allyl)$(CO)_2$(N−N)] complexes towards cyanide, as well as the behavior of the resulting cyano complexes as ligands.

[a] Departamento de Química Orgánica e Inorgánica/ I.U.Q.O.E.M., Facultad de Química, Universidad de Oviedo − C.S.I.C.,
Julián Clavería s/n, 33071 Oviedo, Spain
Fax: (internat.) + 34-985/103446
E-mail: japm@sauron.quimica.uniovi.es
[b] Departamento de Química Física y Analítica, Facultad de Química, Universidad de Oviedo − C.S.I.C.,
Julián Clavería s/n, 33071 Oviedo, Spain
[c] Departamento de Química Inorgánica, Facultad de Ciencias, Universidad de Valladolid,
47071 Valladolid, Spain

Results and Discussion

Treatment of [MoCl(η^3-C_3H_5)$(CO)_2$(phen)][12] with excess sodium cyanide in CH_2Cl_2/MeOH resulted in the formation of [Mo(CN)(η^3-C_3H_5)$(CO)_2$(phen)] (**1a**) as the only product, as depicted in Scheme 1. Employment of methanol as co-solvent was needed to provide sufficient solubility for the sodium cyanide. The product **1a** was easily separated from the excess sodium cyanide and the sodium chloride by-product by extraction into pure CH_2Cl_2, followed by filtration and crystallization.

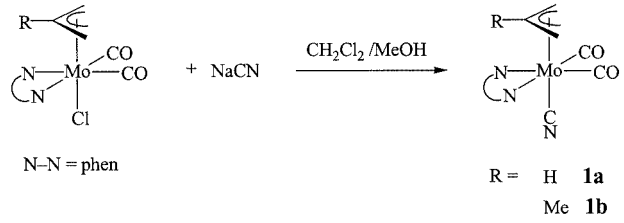

Scheme 1

The IR spectrum of **1a** shows, in addition to the two strong bands corresponding to the *cis*-Mo$(CO)_2$ fragment, a weak band indicative of the presence of a cyano group.[1,2] Its ν_{CN} value (2113 cm^{-1}) is higher than that of the free cyanide anion (2080 cm^{-1}), as is typically found for C-

bound cyano ligands in transition metal complexes.[13] The ^{1}H NMR spectrum of **1a** reveals the presence of a molecular mirror plane (four signals for the phen ligand), and a symmetric, static η^3-allyl group. The methallyl complex [Mo(CN)(η^3-2-MeC_3H_4)(CO)$_2$(phen)] (**1b**) was prepared in a similar manner. Its spectroscopic features are also indicative of a geometry like that of **1a**, and so the structures shown in Scheme 1 are assumed. The low solubility of **1a**,**b** in organic solvents precluded the observation of significant ^{13}C NMR spectroscopic data, but the structure of **1a** was determined by single-crystal X-ray diffraction. A view of the molecule is displayed in Figure 1, and selected distances and angles are given in Table 1.

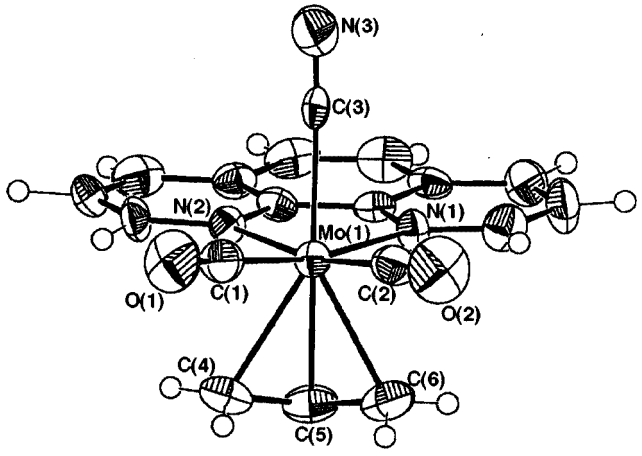

Figure 1. Molecular structure and numbering scheme of [Mo(CN)(η^3-C_3H_5)(CO)$_2$(phen)] (**1a**); thermal ellipsoids are drawn at the 30% probability level

Table 1. Selected bond lengths [Å] and angles [°] for [Mo(CN)(η^3-C_3H_5)(CO)$_2$(phen)] (**1a**)

Mo(1)−C(1)	1.966(7)	Mo(1)−N(1)	2.243(5)
Mo(1)−C(2)	1.959(9)	Mo(1)−N(2)	2.255(5)
Mo(1)−C(4)	2.329(7)	C(1)−O(1)	1.140(7)
Mo(1)−C(5)	2.229(7)	C(2)−O(2)	1.155(8)
Mo(1)−C(6)	2.325(7)	C(3)−N(3)	1.103(8)
Mo(1)−C(3)	2.188(8)		
C(1)−Mo(1)−C(2)	79.0(3)	C(2)−Mo(1)−C(3)	89.0(2)
N(1)−Mo(1)−N(2)	73.65(17)	C(3)−Mo(1)−N(1)	81.5(2)
C(1)−Mo(1)−N(1)	169.8(2)	C(3)−Mo(1)−N(2)	81.09(19)
C(2)−Mo(1)−N(2)	169.6(2)	N(3)−C(3)−Mo(1)	178.3(6)
C(1)−Mo(1)−C(3)	88.4(2)		

The molecule is isostructural with previously known [MoX(η^3-allyl)(CO)$_2$(N−N)] compounds.[14] It can thus be described, if the η^3-allyl group is regarded as occupying one coordination position, as pseudooctahedral: the molybdenum atom is surrounded by the two carbonyl groups, the cyano group, the η^3-allyl group, and the two nitrogen atoms of the phenanthroline ligand. The two CO groups are mutually *cis*, and each is *trans* to a phen nitrogen atom. The cyano and allyl groups are therefore mutually *trans*. The C(3)−N(3) [1.103(8) Å] and N(3)−C(3)−Mo(1) [178.3(6) °] values are typical for M−C−N groupings,[1,2] and the Mo(1)−C(3) distance [2.188(8) Å] is similar to Mo-C(alkynyl) distances recently found in isostructural complexes.[8,15]

This structure concurs with the static structure in solution as deduced from the spectroscopic data (see above). In fact, X-ray diffraction does not allow clear differentiation between carbonyl and cyano groups, and so the spectroscopic data constitute the stronger evidence of their relative positions (two *cis*-carbonyl ligands related by a mirror plane). The cyano complexes **1a**,**b** are obtained in good yield, and no products resulting from cyanide anion attack on the allyl group could be detected. It is worth noting that, in general, attack on the allyl moiety is preferred for stabilized, soft nucleophiles, whereas hard ones preferentially attack the metal atom.[16,17] For [MoX(η^3-allyl)(CO)$_2$(L−L)] complexes in particular, stabilized carbanions − such as those resulting from deprotonation of dialkyl malonates − attack the allyl ligand.[18] In contrast, we have found here that the soft cyanide anion attacks the metal atom.

We aimed to explore the potential of the cyano complexes **1a**,**b** as ligands. We recently found that triflate abstraction from [Mo(OTf)(η^3-allyl)(CO)$_2$(phen)] can be smoothly effected by use of NaBAr′$_4$[19] [Ar′ = 3,5-bis(trifluoromethyl)phenyl] in CH_2Cl_2.[20] We thus treated equimolar amounts of this triflato complex, **1a**,**b**, and NaBAr′$_4$, in each case obtaining a single product, the IR ν_{CN} band of which showed the shift to higher wavenumber values expected for a change in the coordination mode of the cyano group from terminal to bridge (ν_{CN}: 2129 cm^{-1} for **2a** and 2132 cm^{-1} for **2b**) (Scheme 2).[1,2]

These compounds, partly due to the presence of the BAr′$_4$ anion, displayed high solubility in dichloromethane, allowing the acquisition of their ^{13}C NMR spectra. The most characteristic features are the weak signals at δ = 169.8 ppm (**2a**) and δ = 169.9 ppm (**2b**), attributable to the CN groups. Red crystals of **2a** could be obtained from CH_2Cl_2/hexane mixtures, but an attempt to determine its structure by X-ray diffraction was complicated by the severe disorder affecting one of the allyl groups. The analogous dimetallic compound **2b** did not suffer from this problem, and its structure could be determined with acceptable accuracy (see Figure 2 for a view of the cation, Tables 2 and 5 for selected geometrical data). The cation of **2b** consists of two {Mo(η^3-allyl)(CO)$_2$(N−N)} fragments, isostructural with that of **1a**, bridged by a CN group in linear fashion [Mo(1)−C(1)−N(1) = 176.2(8)°, C(1)−N(1)−Mo(2) = 179.4(8)°].

The bond between the cyano group and a second metal fragment is therefore formed without disruption of the Mo−CN bond. In contrast, the alkynyl group (for which similarities with CN as a ligand have been noted)[21] is transferred from {Mo(η^3-allyl)(CO)$_2$(N−N)} to other metal fragments.[15] Since the two metal fragments of **2b** are distinguishable, and only one species is present both in solution and in the crystal, the complex is stable with respect to CN $\rightleftarrows$ NC isomerization of the bridge.

We wanted to evaluate the ability of the new monometallic cyanomolybdenum complexes to act as ligands towards

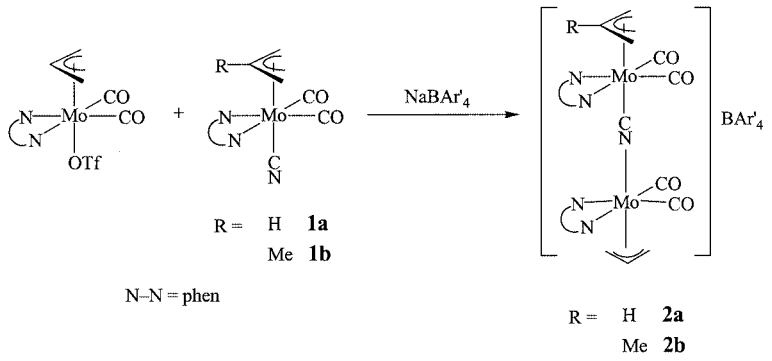

Scheme 2

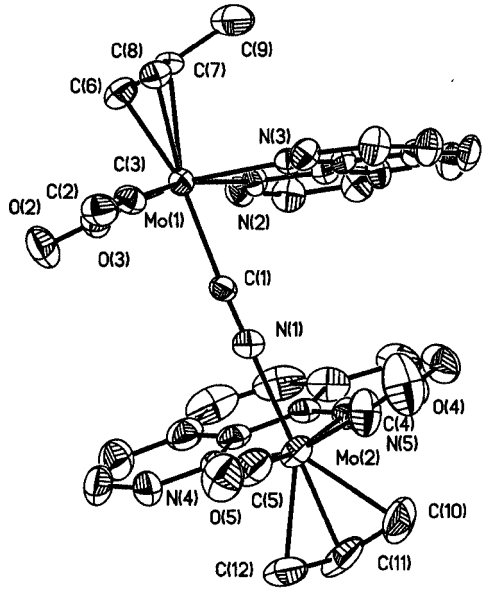

Figure 2. Thermal ellipsoid (30% probability) plot of the [{Mo(η³-C_3H_4-Me-2)$(CO)_2$(phen)}(μ-CN){Mo(η³-C_3H_5)$(CO)_2$(phen)}]⁺ cation of **2b**, with hydrogen atoms omitted for clarity

Table 2. Selected bond lengths [Å] and angles [°] for the [{Mo(η³-C_3H_4-Me-2)$(CO)_2$(phen)}(μ-CN){Mo(η³-C_3H_5)$(CO)_2$(phen)}]⁺ cation of **2b**

Mo(1)−C(2)	1.930(11)	Mo(2)−C(4)	1.966(12)
Mo(1)−C(3)	1.935(11)	Mo(2)−C(5)	1.904(13)
Mo(1)−C(6)	2.330(8)	Mo(2)−C(10)	2.325(11)
Mo(1)−C(7)	2.250(9)	Mo(2)−C(11)	2.226(12)
Mo(1)−C(8)	2.317(8)	Mo(2)−C(12)	2.258(11)
Mo(1)−C(1)	2.135(9)	Mo(2)−N(1)	2.195(8)
Mo(1)−N(2)	2.229(7)	Mo(2)−N(4)	2.250(8)
Mo(1)−N(3)	2.219(7)	Mo(2)−N(5)	2.249(8)
C(2)−O(2)	1.172(10)	C(4)−O(4)	1.173(11)
C(3)−O(3)	1.168(10)	C(5)−O(5)	1.193(12)
C(1)−N(1)	1.142(9)		
C(2)−Mo(1)−C(3)	82.0(4)	C(4)−Mo(2)−C(5)	76.3(5)
C(2)−Mo(1)−N(3)	167.1(3)	C(4)−Mo(2)−N(4)	164.3(4)
C(3)−Mo(1)−N(2)	167.7(3)	C(5)−Mo(2)−N(5)	170.1(4)
N(2)−Mo(1)−N(3)	74.3(3)	N(4)−Mo(2)−N(5)	73.4(3)
C(1)−Mo(1)−C(2)	87.7(4)	N(1)−Mo(2)−C(4)	86.2(4)
C(1)−Mo(1)−C(3)	89.7(4)	N(1)−Mo(2)−C(5)	87.9(4))
C(1)−Mo(1)−N(2)	78.8(3)	N(1)−Mo(2)−N(4)	79.0(3)
C(1)−Mo(1)−N(3)	79.5(3)	N(1)−Mo(2)−N(5)	82.8(3)
Mo(1)−C(1)−N(1)	176.2(8)	C(1)−N(1)−Mo(2)	179.4(8)

different metal centers. Treatment of the triflato complex [Re(OTf)$(CO)_3$(bipy)] with the salt NaBAr′$_4$ in the presence of neutral, two-electron ligands has recently been used to synthesize [Re(L)$(CO)_3$(bipy)]BAr′$_4$ compounds.[22] Similarly, [Mo(CN)(η³-C_3H_5)$(CO)_2$(phen)] (**1a**) reacted with [M(OTf)$(CO)_3$(bipy)] (M = Mn, Re)[23] and NaBAr′$_4$ to afford the dimetallic compounds **3** and **4**, respectively, as presented in Scheme 3.

The new compounds **3** and **4** could be isolated as solids by filtration, followed by crystallization (see Exp. Sect.). The simultaneous presence of the molybdenum and the manganese or rhenium fragments was indicated by the appearance of both the bipy and phen signals in a 1:1 ratio in the ^{1}H NMR spectra. Accordingly, the IR spectra of **3** and **4**, in their ν(CO) regions, show two bands of similar intensity, attributed to the *cis*-Mo$(CO)_2$ moiety, and bands similar to those of cationic *fac*-[M$(CO)_3$(bipy)(L)]⁺ (M = Mn, Re) complexes. For the rhenium compound **4** the latter bands are some 10 cm^{-1} lower than those of [Re$(CO)_3$(bipy)(NCR)]BAr′$_4$ (R = Me, Ph),[22] indicating that the cyano complex is a stronger donor than nitriles. On the other hand, the frequencies corresponding to the *cis*-Mo$(CO)_2$ fragment are little shifted with respect to those of the monometallic precursor. Thus, coordination of the cyano nitrogen atom to the rhenium atom modifies the electron density at the molybdenum center only a little. The presence of the bridging cyano group is shown by the weak C−N stretches in the IR spectra (2145 cm^{-1} for **3**, 2140 cm^{-1} for **4**), and by the low-intensity signals in the ^{13}C NMR spectra (δ = 166.6 and 163.8 ppm for **3** and **4**, respectively). The close similarity between these ^{13}C NMR chemical shifts and those of the homodimetallic compounds **2a**,**b** is consistent with coordination of the cyano bridge to the molybdenum atom through the carbon atom in compounds **3** and **4** (see below for carbon coordination to a rhenium atom). Crystals of **3** suitable for structural determination by X-ray diffraction were obtained, and the results are presented in Figure 3, Tables 3 and 5. These results confirm the [{Mo(η³-C_3H_5)$(CO)_2$(phen)}(μ-CN){Mn$(CO)_3$(bipy)}]BAr′$_4$ formulation for **3**.

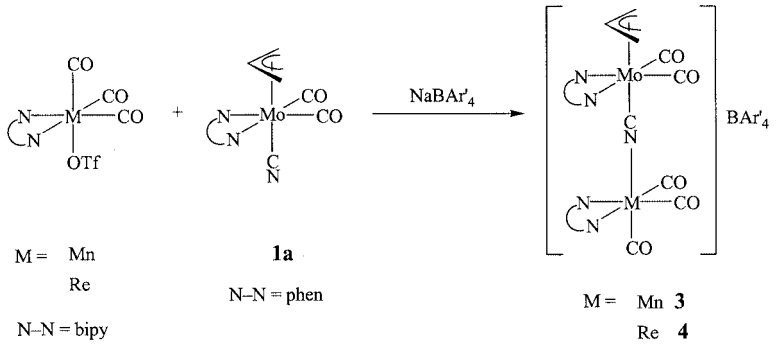

Scheme 3

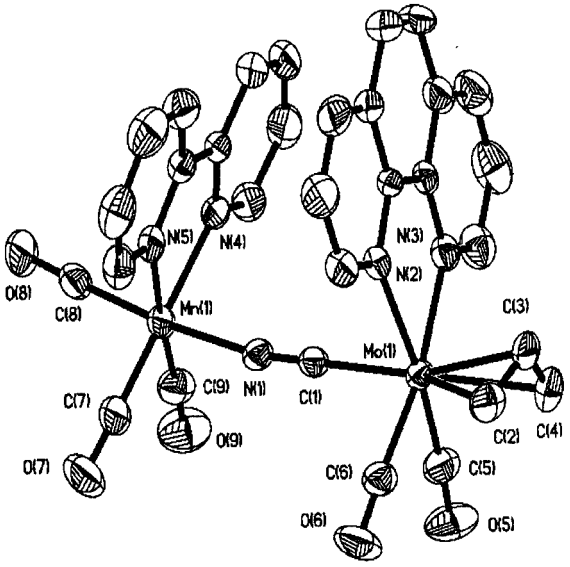

Figure 3. Thermal ellipsoid (30% probability) plot of the [{Mo(η^3-C_3H_5)$(CO)_2$(phen)}(μ-CN){Mn$(CO)_3$(bipy)}]$^+$ cation of **3**, with hydrogen atoms omitted for clarity

Table 3. Selected bond lengths [Å] and angles [°] for the [{Mo(η^3-C_3H_5)$(CO)_2$(phen)}(μ-CN){Mn$(CO)_3$(bipy)}]$^+$ cation of **3**

Mn(1)−N(1)	2.008(4)	Mo(1)−C(6)	1.956(7)
Mo(1)−C(1)	2.161(5)	Mo(1)−C(5)	1.943(7)
C(1)−N(1)	1.148(6)	Mo(1)−N(2)	2.255(4)
Mn(1)−C(8)	1.812(6)	Mo(1)−N(3)	2.246(4)
Mn(1)−C(7)	1.809(7)	Mo(1)−C(2)	2.347(6)
Mn(1)−C(9)	1.797(8)	Mo(1)−C(3)	2.230(5)
Mn(1)−N(5)	2.051(5)	Mo(1)−C(4)	2.336(6)
Mn(1)−N(4)	2.051(4)		
N(1)−C(1)−Mo(1)	179.9(7)	C(6)−Mo(1)−C(1)	86.8(2)
C(1)−N(1)−Mn(1)	170.5(4)	C(5)−Mo(1)−C(1)	86.8(2)
C(8)−Mn(1)−N(1)	174.2(2)	C(1)−Mo(1)−N(3)	83.31(16)
C(7)−Mn(1)−N(1)	93.2(2)	C(1)−Mo(1)−N(2)	82.72(16)
C(9)−Mn(1)−N(1)	93.4(2)	N(3)−Mo(1)−N(2)	73.20(16)
N(5)−Mn(1)−N(4)	78.65(18)		

Given the asymmetric nature of the cyano bridge (i.e., one metal atom is bound to a carbon and the other to a nitrogen atom), heterodimetallic cyano-bridged complexes such as **3** and **4** have linkage isomers. For complexes **3** and **4**, those isomers would feature Mo−N and M−C (M = Mn or Re) bonds. As recently pointed out, linkage isomers of cyano-bridged dimetallic complexes have been isolated in only a few instances.[24] This prompted us to attempt the synthesis of the linkage isomers of **3** and **4**. The Mo/Mn complex proved to be labile in solution, and attempts to isolate it by crystallization afforded crystals of the dimolybdenum compound **2a**. Therefore, only the Mo/Re complex is discussed.

The first step, just as in the synthesis of **3** and **4**, was to prepare the mononuclear cyano complexes. [Re(CN)$(CO)_3$(bipy)] had previously been synthesized by heating [ReCl$(CO)_3$(bipy)] at reflux with a 100-fold molar excess of sodium cyanide in water or an ethanol/water mixture and subsequent extraction with dichloromethane.[25,26]

We have found that [Re(CN)$(CO)_3$(bipy)] (**5**) can be conveniently prepared by treatment of the labile triflato complex [Re(OTf)$(CO)_3$(bipy)] with tetraethylammonium cyanide. The reaction takes place in dichloromethane within 2 h at room temperature when 1.2 equiv. of [Et_4N]CN is used, and the IR spectrum of the resulting solution shows only the bands of [Re(CN)$(CO)_3$(bipy)] (**5**). The coordinated cyano group appears as a weak signal at δ = 156.1 ppm in the ^{13}C NMR spectrum. However, the isolated material (see Exp. Sect.) was contaminated with [Et_4N]CN, as indicated by the ^{1}H NMR spectrum. Since purification of this mononuclear complex proved difficult, the crude material was employed for the synthesis of the targeted dimetallic compound. Thus, by the methodology used for the synthesis of **2**, [Re(CN)$(CO)_3$(bipy)] (**5**) was added to the filtered solution obtained from the reaction between [Mo(η^3-allyl)(OTf)$(CO)_2$(phen)] and NaBAr′$_4$ in CH_2Cl_2.

The formation of the dimetallic compound [{Mo(η^3-allyl)$(CO)_2$(phen)}(μ-NC){Re$(CO)_3$(bipy)}]BAr′$_4$ (**6**), depicted in Scheme 4, was instantaneous, as indicated by IR monitoring, and the product could be purified and isolated by crystallization and characterized by spectroscopy and single-crystal X-ray diffraction. The cyano ligand of **6** gives rise to a signal at δ = 155.1 ppm in the ^{13}C NMR spectrum. This value, very close to that found for the mononuclear complex **5**, strongly supports C-coordination to Re in **6** (see above for the chemical shifts values found for the C−Mo isomer). The results of the structural determination of the

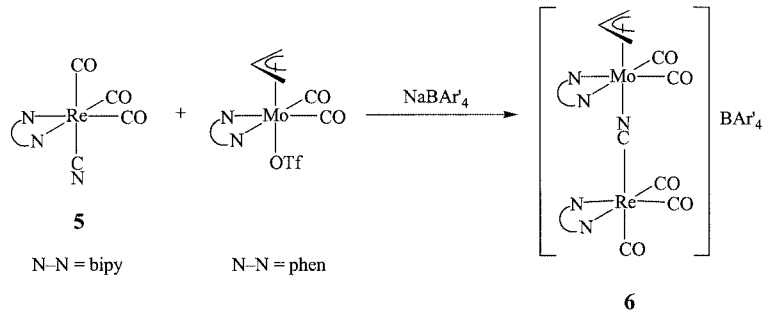

Scheme 4

cation are displayed in Figure 4, Tables 4 and 5. The cationic complex consists of a cyano bridge N-bonded to the molybdenum of an {Mo(η³-allyl)(CO)₂(phen)} fragment, and C-bonded to the rhenium atom of a {Re(CO)₃(bipy)} fragment.

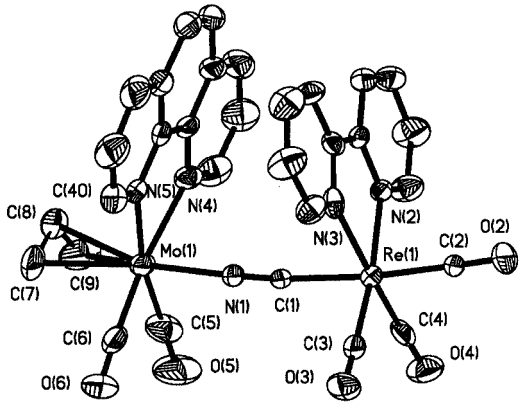

Figure 4. Thermal ellipsoid (30% probability) plot of the [{Mo(η³-C_3H_5)(CO)₂(phen)}(μ-NC){Re(CO)₃(bipy)}]⁺ cation of **6**, with hydrogen atoms omitted for clarity

Table 4. Selected bond lengths [Å] and angles [°] for the [{Mo(η³-C_3H_5)(CO)₂(phen)}(μ-NC){Re(CO)₃(bipy)}]⁺ cation of **6**

Mo(1)−N(1)	2.151(7)	Mo(1)−C(5)	1.916(13)
Re(1)−C(1)	2.123(8)	Mo(1)−C(6)	1.961(13)
C(1)−N(1)	1.143(9)	Mo(1)−N(4)	2.257(7)
Re(1)−C(2)	1.928(8)	Mo(1)−N(5)	2.228(8)
Re(1)−C(3)	1.948(9)	Mo(1)−C(7)	2.350(11)
Re(1)−C(4)	1.889(10)	Mo(1)−C(8)	2.227(9)
Re(1)−N(2)	2.162(6)	Mo(1)−C(9)	2.329(12)
Re(1)−N(3)	2.155(7)		
N(1)−C(1)−Re(1)	174.8(6)	C(5)−Mo(1)−N(1)	89.4(4)
C(1)−N(1)−Mo(1)	176.9(6)	C(6)−Mo(1)−N(1)	88.5(3)
C(2)−Re(1)−C(1)	174.5(3)	N(4)−Mo(1)−N(1)	82.0(2)
C(3)−Re(1)−C(1)	94.0(3)	N(5)−Mo(1)−N(1)	80.0(2)
C(4)−Re(1)−C(1)	91.1(3)	N(4)−Mo(1)−N(5)	73.9(3)
N(2)−Re(1)−N(3)	74.9(2)		

As in the isomer **4**, the IR spectrum of **6** shows sets of bands attributable to *cis*-{Mo(CO)₂} and *fac*-{Re(CO)₃}, together with a weak ν_{CN} absorption at a higher frequency (2143 cm^{-1}) than that of the starting monometallic cyano complex (2122 cm^{-1}).

Conclusion

In summary, [Mo(CN)(η³-allyl)(CO)₂(phen)] complexes were easily synthesized and employed as building blocks for the preparation of cationic homo- and heterodimetallic cyano-bridged complexes by treatment with neutral triflato complexes in the presence of the salt NaBAr′₄ as triflate abstractor. This strategy was extended to prepare the two linkage isomers of [{Mo(η³-allyl)(CO)₂(phen)}(μ-NC){Re(CO)₃(bipy)}]BAr′₄.

Experimental Section

General Remarks: All manipulations were carried out under nitrogen by standard Schlenk techniques. Solvents were distilled from freshly wired Na (hexanes) or CaH_2 (CH_2Cl_2 and MeOH) prior to use. CD_2Cl_2 was degassed by three freeze-pump-thaw cycles, dried with molecular sieves (4 Å), and stored in the dark in a Young tube. Elemental analyses were obtained with a Perkin−Elmer 240-B microanalyzer. The IR and NMR spectra were recorded with Perkin−Elmer FT 1720-X and Bruker AC 200 or AC 300 spectrometers, respectively. [MoCl(η³-C_3H_5)(CO)₂(phen)],[12] [MoCl(η³-C_3H_4-2-Me)(CO)₂(phen)],[27] [Mo(OTf)(η³-C_3H_5)(CO)₂(phen)],[20] [M(OTf)(CO)₃(bipy)] (M = Mn, Re),[23] and NaBAr′₄ [19] were prepared according to literature procedures. All other chemicals were used as received from commercial sources. H_s and H_a designate the *syn*- and *anti*-H atoms, respectively, of the allyl and methallyl ligands; H_c is the central H atom of the allyl ligand. The atom-labeling scheme for the allyl, 1,10- phenanthroline, and BAr′₄ groups is shown below.

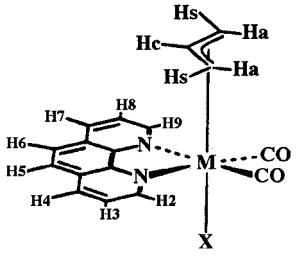

[Mo(CN)(η³-C_3H_5)(CO)₂(phen)] (1a): NaCN (0.013 g, 0.294 mmol) was added to a solution of [MoCl(η³-C_3H_5)(CO)₂(phen)] (0.100 g, 0.245 mmol) in a mixture of CH_2Cl_2 (20 mL) and MeOH (3 mL), and the mixture was stirred for 2 h at room temperature. The red solution obtained was concentrated in vacuo, and the residue was

Table 5. Crystal data and refinement details for complexes **1a**, **2b**, **3**, and **6**

	1a	**2b**	**3**	**6**
Empirical formula	$C_{18}H_{13}MoN_3O_2 \cdot CH_2Cl_2$	$C_{68}H_{40}BF_{24}Mo_2N_5O_4 \cdot 0.25CH_2Cl_2$	$C_{64}H_{35}BF_{24}MnMoN_5O_5 \cdot CH_2Cl_2$	$C_{64}H_{35}BCl_2F_{24}MoN_5O_5Re \cdot CH_2Cl_2$
Molecular mass	484.18	1670.47	1642.56	1773.82
Crystal system	orthorhombic	monoclinic	monoclinic	monoclinic
Space group	Pbca	$P2_1/c$	$P2_1/c$	$P2_1/c$
a [Å]	14.5230(10)	12.6202(19)	17.9066(12)	18.3397(18)
b [Å]	12.5750(10)	18241(3)	20.2195(14)	20.457(2)
c [Å]	21.0800(10)	31.537(5)	19.5450(13)	18.6142(18)
β [°]	90	100.241(3)	105.8300(10)	97.957(2)
V [Å^3]	3849.8(4)	7144.2(19)	6808.1(8)	6916.4(12)
Z	8	4	4	4
T [K]	293(2)	295(2)	297(2)	299(2)
D_c [g cm^{-3}]	1.671	1.553	1.603	1.703
F(000)	1936	3320	3264	3464
λ(Mo-K_α) [Å]	1.54184	0.71073	0.71073	0.71073
Crystal size [mm]		0.19 × 0.13 × 0.06	0.14 × 0.20 × 0.34	0.09 × 0.14 × 0.24
μ [mm^{-1}]	8.297	0.483	0.566	2.123
Scan range [°]	5.10 to 68.17	1.29 to 23.33	1.18 to 23.29	1.12 to 23.33
No. of reflections measured	4259	31565	43929	30961
No. of ind. reflections	2782	10321	9791	9984
No. of data/ restraints/parameters	2782/0/298	10321/0/960	9791/ 0/925	9984/ 0/298
Goodness-of-fit on F^2	1.002	1.013	1.028	1.019
R_1/R_{w2} [$I > 2\sigma(I)$]	0.0533/0.1258	0.0686/0.1571	0.0602/0.1646	0.0489/0.1184
R_1/R_{w2} (all data)	0.0697/0.1312	0.1436/0.1780	0.0759/0.1840	0.0822/0.1353

redissolved in CH_2Cl_2 and filtered through Celite. The volatiles were removed in vacuo, and the residue was washed with hexane (3 × 10 mL). Slow diffusion of hexane into a solution of [Mo(CN)(η^3-C_3H_5)(CO)$_2$(phen)] (**1a**) in CH_2Cl_2 (15 mL) at room temperature produced red crystals of **1a**. A single crystal obtained in this way was used for the X-ray analysis. Yield: 0.088 g, 90%. $C_{18}H_{13}MoN_3O_2$ (399.26): calcd. C 54.15, H 3.28, N 10.52; found C 54.11, H 3.07, N 10.15. IR (CH_2Cl_2): $\tilde{\nu}$ = 2113 ($\nu_{C\equiv N}$), 1952, 1868 (ν_{CO}) cm^{-1}. ^{1}H NMR (CD_2Cl_2): δ = 9.06 (dd, $J_{2,3\text{-H}} = J_{9,8\text{-H}}$ = 5.0, $J_{2,4\text{-H}} = J_{7,9\text{-H}}$ = 1.5 Hz, 2 H, 2,9-H), 8.52 (dd, $J_{H4,3} = J_{H7,8}$ = 8.3 Hz, 2 H, 4,7-H), 7.98 (s, 2 H, 5,6-H), 7.81 (dd, 2 H, 3,8-H), 3.35 (d, $J_{Hs,c}$ = 6.5, 2 H, H_s), 3.01 (m, 1 H, H_c), 1.83 (d, $J_{Ha,c}$ = 9.8 Hz, 2 H, H_a) ppm.

[Mo(CN)(η^3-2-MeC_3H_4)(CO)$_2$(phen)] (1b): The procedure was similar to that described above for the preparation of **1a**, starting from [MoCl(η^3-2-MeC_3H_4)(CO)$_2$(phen)] (0.100 g, 0.237 mmol) and NaCN (0.014 g, 0.284 mmol). Yield: 0.090 g, 92%. $C_{19}H_{15}MoN_3O_2$ (413.28): calcd. C 55.22, H 3.66, N 10.17; found C 55.01, H 3.34, N 10.38. IR (CH_2Cl_2): $\tilde{\nu}$ = 2112 ($\nu_{C\equiv N}$), 1950, 1870 (ν_{CO}) cm^{-1}. ^{1}H NMR (CD_2Cl_2): δ = 9.02 (dd, $J_{2,3\text{-H}} = J_{9,8\text{-H}}$ = 5.0, $J_{2,4\text{-H}} = J_{7,9\text{-H}}$ = 1.3, 2 H, 2,9-H), 8.53 (dd, $J_{4,3\text{-H}} = J_{7,8\text{-H}}$ = 8.2 Hz, 2 H, 4,7-H), 8.00 (s, 2 H, 5,6-H), 7.83 (dd, 2 H, 3,8-H), 3.10 (s, 2 H, H_s), 1.81 (s, 2 H, H_a), 0.59 [s, 3 H, η^3-C_3H_4(CH_3)] ppm.

[{Mo(η^3-C_3H_5)(CO)$_2$(phen)}$_2$(μ-CN)]BAr′$_4$ (2a): NaBAr′$_4$ (0.093 g, 0.105 mmol) was added to a solution of [Mo(OTf)(η^3-C_3H_5)(CO)$_2$(phen)] (0.055 g, 0.105 mmol) in CH_2Cl_2 (20 mL), and the resulting slurry was stirred for 15 min. The solution was filtered by cannula into a solution of [Mo(CN)(η^3-C_3H_5)(CO)$_2$(phen)] (**1a**, 0.038 g, 0.105 mmol) in CH_2Cl_2 (15 mL) and the deep red solution obtained was stirred for 2 h. The solution was then concentrated in vacuo to a volume of 5 mL, and slow diffusion of hexane at room temperature gave red crystals of **2a**. Yield: 0.110 g, 71%. $C_{67}H_{38}BF_{24}Mo_2N_5O_4$ (1635.73): calcd. C 49.20, H 2.34, N 4.28; found C 48.93, H 2.38, N 4.34. IR (CH_2Cl_2): $\tilde{\nu}$ = 2129 ($\nu_{C\equiv N}$), 1958, 1878 (ν_{CO}) cm^{-1}. ^{1}H NMR (CD_2Cl_2): δ = 8.75, 8.59, 8.46, 7.96, 7.95 and 7.68 (m, 16 H, 2 × phen), 7.78 (m, 8 H, C_o-H), 7.58 (m, 4 H, C_p-H), 3.27 (d, $J_{Hs,c}$ = 6.4 Hz, 2 H, H_s), 3.19 (d, $J_{Hs,c}$ = 6.4 Hz, 2 H, H_s), 2.87 (m, 2 H, H_c), 1.75 (d, $J_{Ha,c}$ = 9.5 Hz, 2 H, H_a), 1.45 (d, $J_{Ha,c}$ = 9.4 Hz, 2 H, H_a) ppm. ^{13}C{^{1}H} NMR (CD_2Cl_2): δ = 223.7 and 223.2 (CO), 169.8 (CN), 152.3, 152.1, 144.7, 138.6, 138.3 and 130.3 (phen), 162.1 (q, J = 49.8 Hz, C_i), 135.2 (C_o), 129.3 (q, J = 31.4 Hz, C_m), 124.9 (q, J = 272.4 Hz, CF_3), 117.9 (C_p), 79.0 (C-2 of η^3-C_3H_5), 60.2 (C-1 and C-3 of η^3-C_3H_5), 57.8 (C-1 and C-3 of η^3-C_3H_5) ppm.

[{Mo(η^3-C_3H_4-Me-2)(CO)$_2$(phen)}(μ-CN){Mo(η^3-C_3H_5)(CO)$_2$-(phen)}]BAr′$_4$ (2b): The procedure was similar to that described above for the preparation of **2a**, starting from [Mo(CN)(η^3-2-MeC_3H_4)(CO)$_2$(phen)] (**1b**, 0.047 g, 0.115 mmol), [Mo(OTf)(η^3-C_3H_5)(CO)$_2$(phen)] (0.060 g, 0.115 mmol) and NaBAr′$_4$ (0.102 g, 0.115 mmol) to give complex **2b**. Yield: 0.143 g, 79%. $C_{68}H_{40}BF_{24}Mo_2N_5O_4$ (1649.75): calcd. C 49.51, H 2.44, N 4.24; found C 49.17, H 2.38, N 4.01. IR (CH_2Cl_2): $\tilde{\nu}$ = 2132 ($\nu_{C\equiv N}$), 1959, 1878 (ν_{CO}) cm^{-1}. ^{1}H NMR (CD_2Cl_2): δ = 8.73, 8.54, 8.47, 7.98 and 7.68 (m, 16 H, 2 × phen), 7.74 (m, 8 H, C_o-H), 7.56 (m, 4 H, C_p-H), 3.17 (d, $J_{Hs,c}$ = 6.5 Hz, 2 H, H_s), 3.01 (s, 2 H, H_s), 2.99 (d, $J_{Hs,c}$ = 6.7 Hz, 2 H, H_s),1.70 (s, 2 H, H_a), 1.68 (d, $J_{Ha,c}$ = 9.2 Hz, 2 H, H_a), 1.42 (d, $J_{Ha,c}$ = 9.3 Hz, 2 H, H_a), 0.42 [s, 3 H, C_3H_4(CH_3)] ppm. ^{13}C{^{1}H} NMR (CD_2Cl_2): δ = 223.7 and 223.6 (CO), 169.9 (CN), 152.1, 151.9, 144.8, 138.7, 138.1, 130.5, 127.8, 127.7, 125.4, 125.3, 125.2 and 119.5 (2 × phen), 162.1 (q, J = 49.4 Hz, C_i), 135.1 (C_o), 129.2 (q, J = 34.2 Hz, C_m), 124.9 (q, J = 272.4 Hz, CF_3), 117.8 (C_p), 88.9, 73.6, 71.4, 58.3, 58.1 and 57.7 [C-1, C-2 and C-3 of η^3-C_3H_5 and η^3-C_3H_4(CH_3)], 17.6 [η^3- C_3H_4(CH_3)] ppm.

[{Mo(η^3-C_3H_5)(CO)$_2$(phen)}(μ-CN){Mn(CO)$_3$(bipy)}]BAr′$_4$ (3): NaBAr′$_4$ (0.099 g, 0.112 mmol) was added to a solution of [Mn(OTf)(CO)$_3$(bipy)] (0.050 g, 0.112 mmol) in CH_2Cl_2 (15 mL)

and the resulting solution was stirred for 15 min at room temperature. The color of the solution turned from yellow to orange. The solution was filtered by cannula into a solution of [Mo(CN)(η³-C_3H_5)(CO)$_2$(phen)] (**1a**, 0.045 g, 0.112 mmol) in CH_2Cl_2 (15 mL) and the color of the solution turned bright red. The resulting solution was concentrated in vacuo to a volume of 5 mL, and slow diffusion of hexane at −20 °C gave dark orange crystals of **3**. A single crystal obtained in this way was used for the X-ray analysis. Yield: 0.105 g, 62%. $C_{63}H_{33}BF_{24}MnMoN_5O_5$ (1557.64): calcd. C 48.58, H 2.13, N 4.50; found C 48.78, H 1.98, N 4.85. IR (CH_2Cl_2): $\tilde{\nu}$ = 2145 ($\nu_{C\equiv N}$), 2042, 1957, 1877 (ν_{CO}) cm^{-1}. ^{1}H NMR (CD_2Cl_2): δ = 8.77, 8.64, 8.45 and 7.94 (m, 2 H each bipy and phen), 7.76 (m, 10 H, C_o-H and 4 H, bipy), 7.57 (m, 4 H C_p-H), 7.39 (m, 2 H, phen), 3.33 (m, 2 H, H_s), 2.96 (m, 1 H, H_c), 1.81 (m, 2 H, H_a) ppm. ^{13}C{^{1}H} NMR (CD_2Cl_2): δ = 223.9 (2 CO, Mo−CO), 219.4 (2 CO, Mn−CO) 217.1 (1 CO, Mn−CO), 166.6 (CN), 155.4, 153.3, 152.5, 144.9, 139.4, 138.94, 130.4, 127.8, 127.0, 125.3 and 122.6 (bipy and phen), 78.5 (C-1 and C-3 of η³-C_3H_5), 59.9 (C-2 of η³-C_3H_5) ppm.

[{Mo(η³-C_3H_5)(CO)$_2$(phen)}(μ-CN){Re(CO)$_3$(bipy)}]BAr′$_4$ (4): The procedure was similar to that described above for the preparation of **3**, starting from [Re(OTf)(CO)$_3$(bipy)] (0.050 g, 0.087 mmol), [Mo(CN)(η³-C_3H_5)(CO)$_2$(phen)] (**1a**, 0.034 g, 0.087 mmol), and NaBAr′$_4$ (0.077 g, 0.087 mmol), to give complex **4** as a microcrystalline red powder. Yield: 0.040 g, 69%. $C_{60}H_{28}BF_{24}MoN_5O_5Re$ (1647.84): calcd. C 43.73, H 1.71, N 4.25; found C 43.44, H 1.89, N 4.57. IR (CH_2Cl_2): $\tilde{\nu}$ = 2140 ($\nu_{C\equiv N}$), 2033, 1958, 1930, 1877 (ν_{CO}) cm^{-1}. ^{1}H NMR (CD_2Cl_2): δ = 8.76, 8.63 and 8.50 (m, 2 H each bipy and phen), 8.12 (m, 4 H, bipy), 7.99 (m, 2 H, phen), 7.76 (m, 8 H, C_o-H, 2 H, phen and 2 H, bipy), 7.57 (m, 4 H C_p-H), 7.45 (m, 2 H, phen), 3.36 (d, $J_{Hs,c}$ = 6.5 Hz, 2 H, H_s), 2.98 (m, 1 H, H_c), 1.83 (d, $J_{Ha,c}$ = 9.2 Hz, 2 H, H_a) ppm. ^{13}C{^{1}H} NMR (CD_2Cl_2): δ = 225.3 (2 CO, Mo−CO), 196.1 (2 CO, Re−CO), 189.8 (1 CO, Re−CO), 163.8 (CN), 157.7, 155.2, 154.5, 146.9, 142.3, 140.6, 132.6, 129.9, 128.7, 127.4 and 119.9 (bipy and phen), 81.0 (C-1 and C-3 of η³-C_3H_5), 62.5 (C-2 of η³-C_3H_5) ppm.

[Re(CN)(CO)$_3$(bipy)] (5): NEt_4CN (0.016 g, 0.104 mmol) was added to a solution of [Re(OTf)(CO)$_3$(bipy)] (0.050 g, 0.087 mmol) in CH_2Cl_2 (20 mL), the mixture was stirred for 2 h at room temperature, and the color of the solution turned from yellow to orange. The volatiles were removed in vacuo and the residue was washed with Et_2O (3 × 15 mL). IR (CH_2Cl_2): $\tilde{\nu}$ = 2122 ($\nu_{C\equiv N}$), 2023, 1920 (ν_{CO}) cm^{-1}. ^{1}H NMR (CD_2Cl_2): δ = 9.02, 8.36, 8.14 and 7.56 (2 H each, bipy), 3.24 (q, J = 7.1 Hz, CH_2, Et_4N), 1.31 (t, J = 7.1 Hz, CH_3, Et_4N) ppm. ^{13}C{^{1}H} NMR (CD_2Cl_2): δ = 196.1 and 191.2 (CO), 156.1 (CN), 153.6, 143.1, 139.7, 127.7 and 124.1 (bipy), 53.86 (CH_2, Et_4N), 7.11 (CH_3, Et_4N) ppm.

[{Mo(η³-C_3H_5)(CO)$_2$(phen)}(μ-NC){Re(CO)$_3$(bipy)}]BAr′$_4$ (6): NaBAr′$_4$ (0.093 g, 0.105 mmol) was added to a solution of [Mo(OTf)(η³-C_3H_5)(CO)$_2$(phen)] (0.055 g, 0.105 mmol) in CH_2Cl_2 (20 mL), and the resulting slurry was stirred for 15 min. The solution was filtered by cannula into a solution of [Re(CN)(CO)$_3$(bipy)] (**5**, 0.047 g, 0.105 mmol) in CH_2Cl_2 (15 mL), and the deep red solution obtained was stirred for 2 h. The solution was then concentrated in vacuo to a volume of 5 mL, and slow diffusion of hexane at room temperature gave red crystals of **6**. Yield: 0.151 g, 87%. $C_{60}H_{28}BF_{24}MoN_5O_5Re$ (1647.84): calcd. C 43.73, H 1.71, N 4.25; found C 43.61, H 2.03, N 4.17. IR (CH_2Cl_2): $\tilde{\nu}$ = 2143 ($\nu_{C\equiv N}$), 2030, 1947, 1926, 1875 (ν_{CO}) cm^{-1}. ^{1}H NMR (CD_2Cl_2): δ = 8.89, 8.49, 8.15, 8.06 and 7.37 (m, 32 H, bipy, phen and BAr′$_4$), 3.26 (d, $J_{Hs,c}$ = 6.0 Hz, 2 H, H_s), 2.70 (m, 1 H, H_c), 1.51 (d, $J_{Ha,c}$ = 9.3 Hz, 2 H, H_a) ppm. ^{13}C{^{1}H} NMR (CD_2Cl_2): δ = 225.75 and 224.15 (2 CO, Mo−CO), 193.61 (2 CO, Re−CO) 191.78 (1 CO, Re−CO), 162.49 (q, J = 49.9 Hz, C_i), 155.67 (CN), 155.66, 153.35, 152.35, 139.95, 138.98 (bipy and phen), 135.20 (C_o), 130.48, 130.40 (bipy and phen), 129.27 (q, J = 31.9 Hz, C_m), 127.92, 127.86, 126.79 (bipy and phen), 124.38 (q, J = 272.3 Hz, CF_3), 119.57 (phen), 117.91 (C_p), 73.87 (C-1 and C-3 of η³-C_3H_5), 59.9 (C-2 of η³-C_3H_5) ppm.

X−ray Crystallographic Study:[28] The crystal of **1a** was measured with a Nonius CAD4 diffractometer. Profile analysis was performed on all reflections.[29,30] Symmetry-equivalent and other redundant reflections were averaged, and drift, Lorentz, and polarization corrections were applied. The structure was solved by Patterson methods with DIRDIF-96.[31] Isotropic least-squares refinement was carried out on F^2 by use of SHELXL-97.[32] An empirical absorption correction was applied at this stage, by use of XABS2.[33] All atoms were located by Fourier synthesis. During the final stages of the refinement, all positional parameters and the anisotropic temperature factors of all the non-H atoms were refined with SHELXL-97.[31] The atoms were isotropically refined. Plots were made with the EUCLID package.[34] Geometrical calculations were performed with PARST.[35] Data in common for compounds **2b**, **3**, and **6**: Bruker AXS SMART 1000 CCD diffractometer, φ and ω scans, Mo-K_α radiation (λ = 0.71073 Å), graphite monochromator, T = 295 K. Raw frame data integrated by use of the SAINT[36] program. Structures were solved by direct methods with SHELXTL,[37] semiempirical absorption correction with SADABS.[38] All non-hydrogen atoms were refined anisotropically. Hydrogen atoms were set in calculated positions and refined as riding atoms, with a common thermal parameter. All calculations were performed with SHELXTL.

Acknowledgments

We thank the Ministerio de Ciencia y Tecnología (Projects MCT-00-BQU-0220 and BQU2002-03414) and FICYT (PR-01-GE-7) for support, and predoctoral scholarships (to E. H. and L. R.).

[1] W. P. Fehlhammer, M. Fritz, *Chem. Rev.* **1993**, *93*, 1243−1280.
[2] K. R. Dunbar, R. A. Heintz, *Prog. Inorg. Chem.* **1997**, *45*, 283−391.
[3] D. Bellamy, N. G. Connelly, O. M. Hicks, A. G. Orpen, *J. Chem. Soc., Dalton Trans.* **1999**, 3185−3190.
[4] D. Bellamy, N. C. Brown, N. G. Connelly, A. G. Orpen, *J. Chem. Soc., Dalton Trans.* **1999**, 3191−3195.
[5] N. G. Connelly, O. M. Hicks, G. R. Lewis, A. G. Orpen, A. J. Wood, *J. Chem. Soc., Dalton Trans.* **2000**, 1637−1643.
[6] K. M. Anderson, N. G. Connelly, N. J. Goodwin, G. R. Lewis, M. T. Moreno, A. G. Orpen, A. J. Wood, *J. Chem. Soc., Dalton Trans.* **2001**, 1421−1427.
[7] J. Pérez, L. Riera, V. Riera, S. García-Granda, E. García-Rodríguez, *J. Am. Chem. Soc.* **2001**, *123*, 7469−7470.
[8] J. Pérez, L. Riera, V. Riera, S. García-Granda, E. García-Rodríguez, D. Miguel, *Organometallics* **2002**, *21*, 1622−1626.
[9] E. Hevia, J. Pérez, L. Riera, V. Riera, D. Miguel, *Organometallics* **2002**, *21*, 1750−1752.
[10] H. tom Dieck, H. Friedel, *J. Organomet. Chem.* **1968**, *14*, 375−385.
[11] B. J. Brisdon, M. Cartwright, A. G. Hodson, *J. Organomet. Chem.* **1984**, *277*, 85−90.
[12] B. J. Brisdon, G. F. Griffin, *J. Chem. Soc., Dalton Trans.* **1975**, 1999−2002.
[13] K. Nakamoto, *Infrared and Raman Spectra of Inorganic and Coordination Compounds. Part B: Applications in Coordination, Organometallic and Bioinorganic Chemistry*, 5th ed., John Wiley & Sons, **1997**, p. 105−113.

[14] P. K. Baker, *Adv. Organomet. Chem.* **1995**, *40*, 45−115.
[15] J. Pérez, L. Riera, V. Riera, S. García-Granda, E. García-Rodríguez, D. Miguel, *Chem. Commun.* **2002**, 384−385.
[16] G. Consiglio, R. M. Waymouth, *Chem. Rev.* **1989**, *89*, 257−276. See also ref.[14]
[17] B. M. Trost, D. L. Van Vranken, *Chem. Rev.* **1996**, *96*, 395−422. The terms "hard" and "soft" are used here as defined in these reviews.
[18] B. M. Trost, M. Lautens, *J. Am. Chem. Soc.* **1982**, *104*, 5543−5545.
[19] M. Brookhart, B. Grant, A. F. Volpe, *Organometallics* **1992**, *11*, 3920−3922.
[20] D. Morales, J. Pérez, L. Riera, V. Riera, R. Corzo-Suárez, S. García-Granda, D. Miguel, *Organometallics* **2002**, *21*, 1540−1545.
[21] J. Manna, K. D. John, M. D. Hopkins, *Adv. Organomet. Chem.* **1995**, *38*, 79−154.
[22] E. Hevia, J. Pérez, V. Riera, D. Miguel, A. Rheingold, S. Kassel, *Inorg. Chem.* **2002**, *41*, 4673−4679.
[23] Triflato complexes of this kind have been previously prepared. See for instance: J. Guerrero, O. E. Pino, E. Wolcan, M. R. Feliz, G. Ferraudi, S. A. Moya, *Organometallics* **2001**, *20*, 2842−2853. See also ref.[9]
[24] G. A. Stark, A. M. Arif, J. A. Gladysz, *Organometallics* **1997**, *16*, 2909−2918.
[25] R. M. Leasure, L. Sacksteder, D. Nesselrodt, G. A. Reitz, J. N. Demas, B. A. DeGraff, *Inorg. Chem.* **1991**, *30*, 3722−3728.
[26] The related $[Mn(CN)(CO)_3(dppe)]$ complex was prepared by reaction of aqueous NaCN with $[Mn(CO)_3(dppe)(OH_2)]BF_4$ [dppe = 1,2-bis(diphenyphosphanyl)ethane]: S. K. Mandal, D. M. Ho, M. Orchin, *Inorg. Chem.* **1991**, *30*, 2244−2248.
[27] P. Powell, *J. Organomet. Chem.* **1977**, *129*, 175−179.
[28] CCDC-193528 (**1a**), -193529 (**2b**), -193530 (**3**) and -193531 (**6**) contain the supplementary crystallographic data for this paper. These data can be obtained free of charge at www.ccdc.cam.ac.uk/conts/retrieving.html [or from the Cambridge Crystallographic Data Centre, 12 Union Road, Cambridge CB2 1EZ, UK; Fax: (internat.) + 44-1223/336-033; E-mail: deposit@ccdc.cam.ac.uk].
[29] M. S. Lehman, F. K. Larsen, *Acta Crystallogr., Sect. A* **1974**, *30*, 580.
[30] D. F. Grant, E. J. Gabe, *J. Appl. Crystallogr.* **1978**, *11*, 114.
[31] P. T. Beurskens, G. Admiraal, G. Beurskens, W. P. Bosman, S. García-Granda, R. O. Gould, J. M. M. Smits, C. Smykalla, *The DIRDIF96 program system*, Technical Report of the Crystallography Laboratory, University of Nijmegen, The Netherlands, **1996**.
[32] G. M. Sheldrick, *SHELXL-97, Program for the Refinement of Crystal Structures*, University of Göttingen, Germany, **1989**.
[33] S. Parkin, B. Moezzi, H. Hope, *J. Appl. Crystallogr.* **1995**, *28*, 53.
[34] A. L. Spek, "The EUCLID package", in: *Computational Crystallography* (Ed.: D. Sayre), Clerendon Press, Oxford, **1982**, p. 528.
[35] M. Nardelli, *Comput. Chem.* **1983**, *7*, 95.
[36] *SAINT+ SAX area detector integration program*, version 6.02, Bruker AXS, Inc., Madison, WI, **1999**.
[37] G. M. Sheldrick, *SHELXTL, An integrated system for solving, refining, and displaying crystal structures from diffraction data*, version 5.1, Bruker AXS, Inc., Madison, WI, **1998**.
[38] G. M. Sheldrick, *SADABS, Empirical Absorption Correction Program*, University of Göttingen, Göttingen, Germany, **1997**.

Received September 17, 2002
[I02524]

Charge-Transfer Mechanisms between Gold Clusters

Viktoria Torma,[a] Olivia Vidoni,[a] Ulrich Simon,[b] and Günter Schmid*[a]

Keywords: Gold / Cluster compounds / Charge transfer / Activation energy / Conductivity

Electron-transfer processes in complex chemistry are usually described by Taube's "outer sphere" and "inner sphere" mechanisms. A behaviour related to these electron-transfer mechanisms in complex chemistry can be observed for charge-transfer transport between ligand protected Au_{55} nanoclusters. A linear dependence between cluster-cluster distance and activation energy for electron transfer is observed if a noncovalent linkage exists; this interaction is independent of the distance in covalently linked clusters. Instead, the activation energy depends on the electronic nature of the linking molecules. The dithiols 1,5-dithionaphthaline (**1**), 4,4′-thiobis(benzenethiol) (**2**), and 2,8-dithio-6-hydroxypurine (**3**) have been used as bifunctional covalent linkers either in their monomeric form (**2**) or, in the presence of air, dimerized via S–S bonds (**1**, **2**, **3**), causing an increase in the distance between the clusters and leading to the cluster networks **4**–**7**. Noncovalent cluster networks are formed either by pellets of clusters with monodentate ligands in **8** and **11**, linked only by van der Waals forces, or by using bifunctional spacers that interact with the clusters by ion attractions (**9**, **10**).

A study of the activation energies clearly indicates that in the case of noncovalently organized nanoparticles only the cluster spacing is of relevance, even if conjugated π-systems like in **10** are used. This behaviour corresponds to an outer-sphere mechanism. On the contrary, for covalently linked clusters the distances between them does not play a visible role. The activation energies all lie below those of the noncovalent examples, and a relation between cluster-cluster distance and activation energy is not obvious. In those cases the relationship suggests an inner-sphere mechanism where the transport properties of the spacer play a decisive role.

These findings possibly help to explain contradictory reports on the conductivity behaviour of organic molecules.

(© Wiley-VCH Verlag GmbH & Co. KGaA, 69451 Weinheim, Germany, 2003)

Introduction

The study of the electric properties of nanosized materials is a rapidly emerging field of great fundamental and practical interest owing to their potential as building blocks in future nanoelectronic devices. Much of the recent work is therefore driven by prospective applications in nanoelectronics, nonlinear optics, sensors etc. The charge-transfer properties of individual particles,[1−3] monolayers,[4−6] multilayers,[7,8] as well as of three-dimensional structures[9−11] have been investigated. Generally, it was found that the electrical conductivity depends on the size of the particles[12] and on the distance between them.[13] Whereas particles with diameters larger than about 2 nm were suggested to be used for the fabrication of nanowires to connect electrical circuit elements,[14] particles smaller than 2 nm are promising candidates for room-temperature single electron transistors[15] since the rate-limiting step of the electron-transfer process is the charging of the particles. Therefore, charge transport is connected with a relatively high activation energy.

In order to vary the activation energy for electron transfer between nanoparticles many different ligand molecules or interconnecting spacers have been applied. Among these are thiols and dithiols,[7,16−18] dicyanides,[5] phosphanes,[9,10,15] and other molecules with or without conjugated π-systems.[5,19] There is, however, no agreement among different authors whether and/or in which way the chemical nature of the spacers influences the conduction properties of the nanoparticle arrangement[4,5] or not.[13,15,20] It has been shown that the resistance of an adsorbed monolayer on a surface, measured by STM, depends on the nature of the end groups of the adsorbed molecules.[21] This effect was interpreted by the conduction through the highest occupied molecular orbitals (HOMOs) or the lowest unoccupied states (LUMOs).

On the other hand we found that the activation energy for charge transport in three-dimensional cluster arrangements depends simply on the cluster spacing rather than on the chemical nature of the molecules between them.[22] This is reflected by an almost linear dependence of the activation energy on the cluster spacing that is observed provided that

[a] Universität Essen, Institut für Anorganische Chemie, 45117 Essen, Germany
Fax: (internat.) +49−201/183-4195
E-mail: guenter.schmid@uni-essen.de
[b] RWTH Aachen, Institut für Anorganische Chemie, 52056 Aachen, Germany
Fax: (internat.) +49−241/8099003
E-mail: ulrich.simon@ac.rwth-aachen.de

the cluster linkage results from ionic coupling instead of a covalent linkage. A simple approach based on the Landauer formula, which allows a first-order estimate of the resistance of the linking molecules, leads to the conclusion that the charge transport between clusters via organic molecules (ligands/spacers) involves tunnelling rather than propagation.[20]

Results and Discussion

In this paper we report on the synthesis and electrical characterisation of different types of covalently crosslinked Au_{55} clusters in order to compare the charge-transfer properties with those of previously described noncovalently organized systems. For that purpose we used three different dithiols, since sulfur−gold bonds are of a strongly covalent character and dithiol-protected clusters can be three-dimensionally linked through direct Au-dithiol-Au bonds or S−S bonds formed by smooth oxidation of the second SH groups.

As dithiols we used

1,5-dithionaphthaline (DNP)

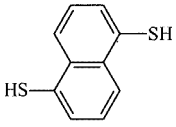

1

4,4'-thiobis(benzenethiol (TBBT)

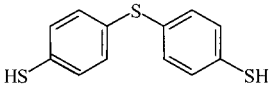

2

and 2,8-thio-6-hydroxypurine (purine)

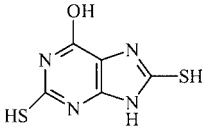

3

The process aimed is illustrated schematically in Figure 1.

The formation of the dithiol-stabilized gold clusters results from ligand-transfer reactions and has been performed previously with various other thiol ligands.[7,23,24] As shown in Figure 1, the first step should represent the formation of individual thiol-stabilized clusters (A) which have not been isolated. Afterwards, two further reactions can take place: in the absence of air, the terminal thiols can interact directly with other clusters (B) (due to the high steric hindrance, this exchange can need several weeks), whereas in the presence of air, fast oxidation of the free SH groups to S−S disulfide bridges occurs, crosslinking the clusters (C). This process can be followed by the formation of brown precipitates, consisting of three-dimensionally linked cluster-dithiol hybrid materials, and residual colourless solutions.

Under a nitrogen atmosphere, well-ordered arrangements of Au_{55} clusters, directly linked by the spacer molecule **2**

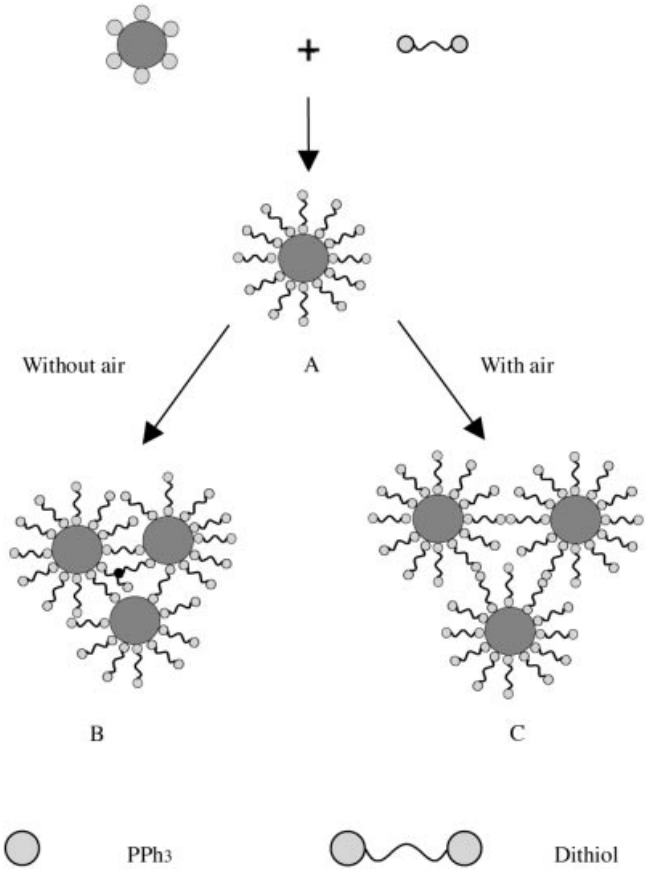

Figure 1. Schematic representation of the cross-linkage of Au_{55} clusters with dithiols (A); without air, aggregates of type B are formed, whereas in the presence of air aggregates C, with S−S bridges, result

through formation of Au−S bonds, were observed (**4**, Figure 2, top). In air, various assemblies of clusters were formed (**6**, Figure 2, middle). These clusters do not adopt a specific ordering, but a regular average distance of 2.3 nm between two adjacent particles attests to the presence of a disulfide bridge. In contrast to **4**, which took about two weeks to form and precipitate, the formation of **6** was finished after two hours so no higher organization is possible. This lack of organisation can be explained by the fact that the spacer molecules used are long and flexible enough to fold during the experiments modifying the inter-particle distance. The number of spacer molecules present around one Au_{55} cluster depends on the ligands used. Because of the nature of the product (insoluble polymer), the elemental analysis does not allow the determination of the exact stoichiometry of the compounds, but only an estimation concerning the number of linkers present around each cluster. The results are the following:

entity 4: $Au_{55}[TBBT]_{22/2}$; entity 5: $Au_{55}[purine]_{16}$; entity 6: $Au_{55}[TBBT]_{14}$; entity 7: $Au_{55}[DNP]_{18}$.

As a blank, one drop of a solution of gold clusters was deposited onto a TEM grid (Figure 2, bottom). In this case, no special kind of organisation of the gold particles was observed. For the electrical measurements the washed and

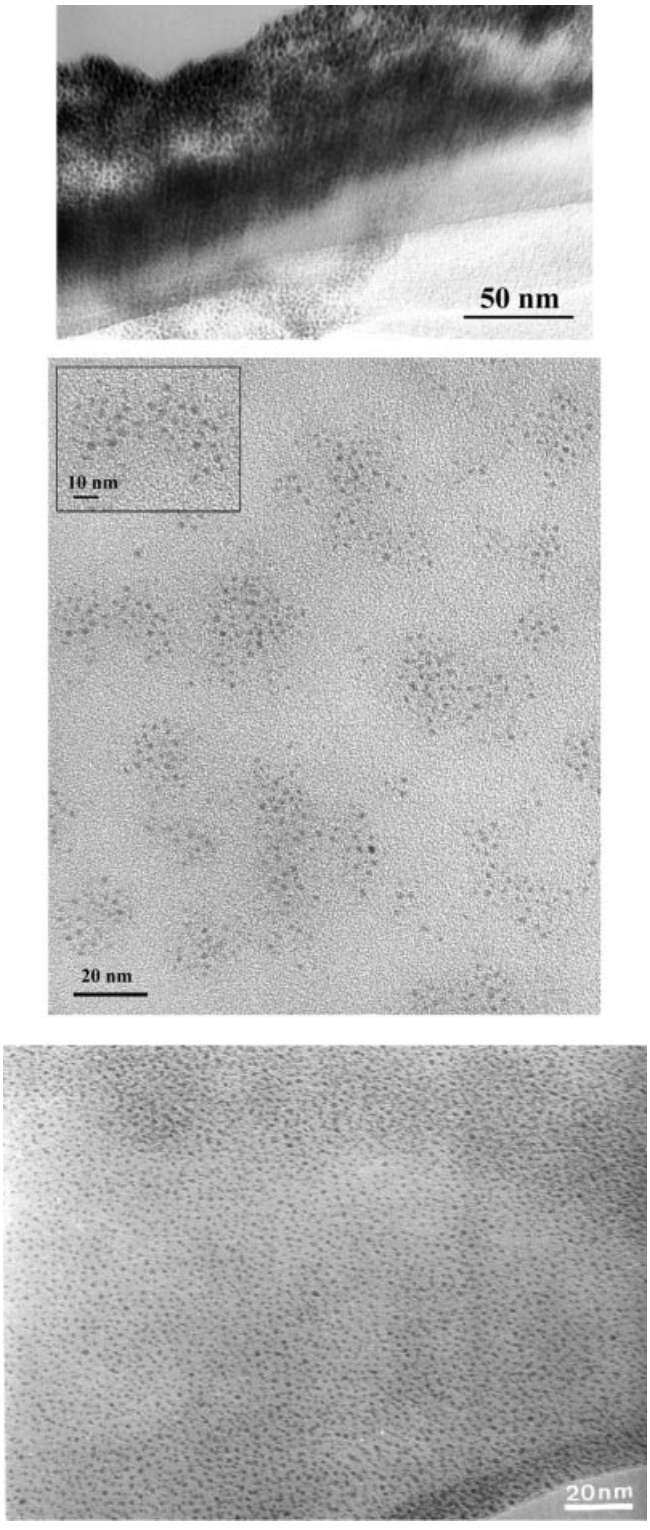

Figure 2. (top): TEM image of an ordered arrangement of $[Au_{55}Cl_6(PPh_3)_{12}]$ clusters linked by the spacer molecule **2** without oxygen (sample **4**); (middle): TEM image of $[Au_{55}Cl_6(PPh_3)_{12}]$ clusters linked by the spacer molecules **2** in the presence of air (sample **6**); the insert shows the magnified aggregate below; (bottom): TEM image of nonlinked $[Au_{55}Cl_6(PPh_3)_{12}]$ clusters

carefully dried precipitates were pressed into pellets and contacted on the top and bottom with silver paint. The activation energies were determined by temperature-dependent conductivity measurements. The temperature dependence shows simply activated behaviour for a temperature range between 200 K and 300 K. In this temperature range the charge transport is due to thermally activated electron exchange between neighbouring clusters. The corresponding activation energy E_a i.e. the charging energy of the particles in the three-dimensional arrangement, is determined by the respective particle size and spacing. Thus, E_a represents the charge disproportionation energy, which needs to be overcome to create mobile charge carriers.[25] Below 200 K a transition from nearest neighbour exchange to variable range exchange is observed, leading to a temperature dependent activation energy. In these experiments E_a was determined between 200 K and 300 K by a regression line fit. Figure 3 contains the experimental curves of the investigated samples and Table 1 summarises these data together with the calculated cluster distances. In addition, the corresponding data for the non-covalently crosslinked clusters of our previous investigations[15,25,26] are included for comparison.

Figure 4 illustrates the data of Table 1. As already mentioned, in the case of noncovalently crosslinked Au_{55} clusters there is a linear relation (correlation coefficient: 0.992) between cluster-cluster distances and activation energies, indicating that only the distance between the nanoparticles determines the energy of the hopping processes. The chemical nature of the linking molecules obviously plays a minor role. This can be understood due to the fact that there is no direct electronic interaction between the clusters via either the stabilizing ligand molecules in a close packing in samples **8** and **11** (van der Waals attraction), or the crosslinking spacer molecules in **9** and **10** (ionic attraction between spacer and functional groups and outer ligand sphere). This is most visible in the case of the spacer in sample **10**, which comprises a conjugated π-system along its backbone and from which a molecular conducting behaviour might be expected. Instead, E_a also depends on its length, implying that propagation along the π-system is blocked by the ionic interconnection between spacer and ligand.

On the contrary, the dithiol spacers link the clusters directly by covalent bonds. The activation energies are characteristically lower and do not depend linearly on the cluster spacing. Although a direct relation between the molecule length, electron density, symmetry etc. and E_a could not be established, it is obvious that the chemical nature of these molecules, which differ considerably among each other, essentially affect the transition probability for electrons between the clusters. This suggests an electron-transport mechanism, where bonding and/or antibonding molecular orbitals of the linking molecules are involved in the conductivity process.

In a first-order approximation the difference between directly (covalent) and nondirectly (van der Waals, ionic) linked clusters can be compared with the mechanisms of classical redox processes, which have been divided into "outer sphere" and "inner sphere" mechanisms.[27–31] The inner-sphere mechanism of electron transfer is characterised

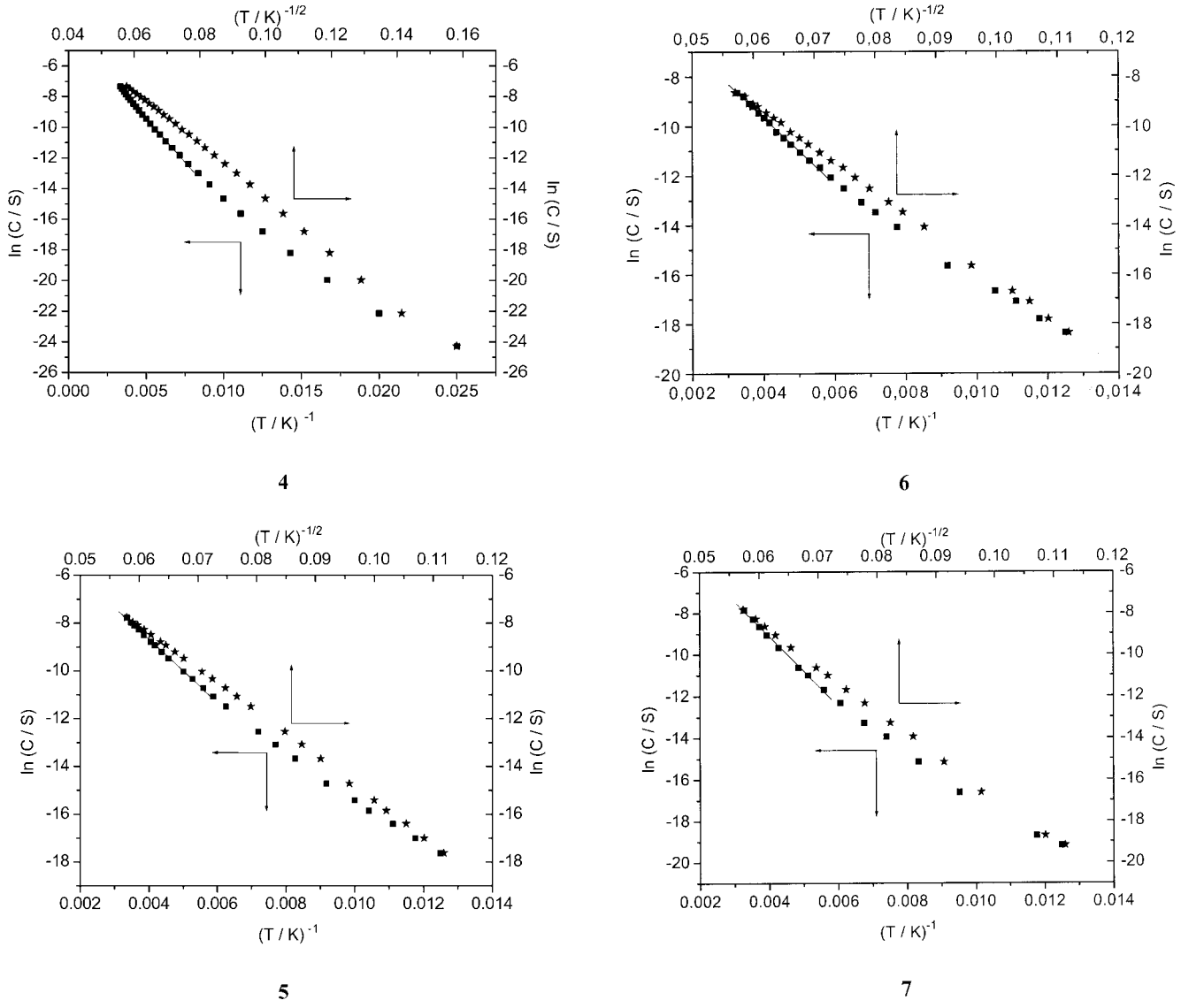

Figure 3. Experimental curves (temperature versus conductance) of **4**, **5**, **6**, and **7**

by the participation of a bridging ligand between the oxidizing and the reducing metal ion. In the outer-sphere process the coordinated metal ions simply touch each other via their coordination spheres, and the electron transfer has to occur through the ligand shell and probably involves a deformation of the coordination spheres. Electron transfer between clusters can indeed be compared with those redox processes. The initial step for the creation of free charge carriers is the charge disproportionation of two initially neutral clusters in the immediate vicinity. Thus, charged cluster pairs represent both reduced and oxidized species, and E_a corresponds to the inverse of the electron-transfer rate, which is essentially higher in redox pairs with direct coupling (inner-sphere mechanism).

Conclusion

We have shown that electron-transfer processes between Au_{55} clusters can occur in two different ways: compared with classical inner-sphere redox processes, noncovalently linking molecules simply act as spacers, independent of their chemical nature, and require activation energies that correspond only to their length. Covalently cluster-linking

Table 1. Activation energies and cluster-cluster distances of the covalently and the non-covalently organized systems

Linking System		Distance [nm][a]	E_a [eV]
Covalently Linked			
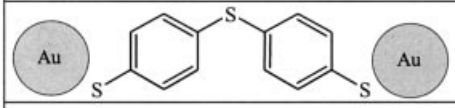	**4**	1.1	0.095
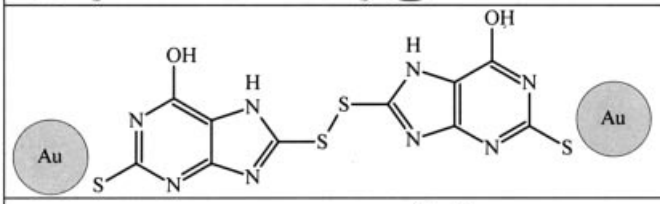	**5**	1.6	0.11
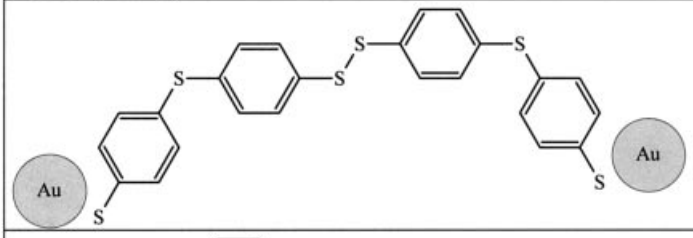	**6**	2.3	0.12
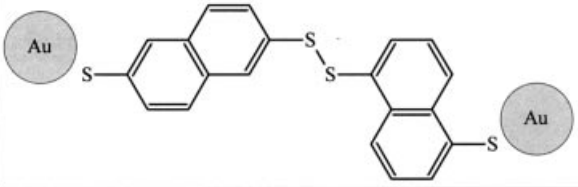	**7**	1.5	0.14
Noncovalently Linked			
Linking System		Distance [nm][a]	E_a [eV]
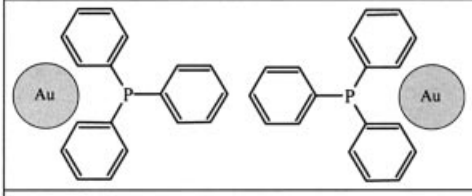	**8**	0.7	0.16
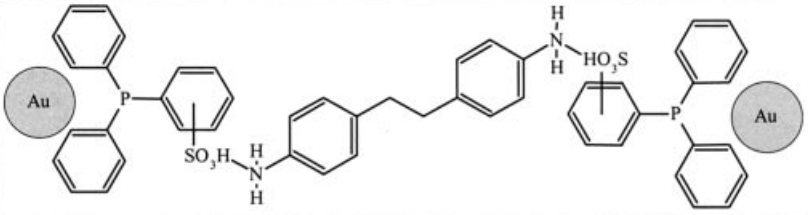	**9**	1.9	0.2
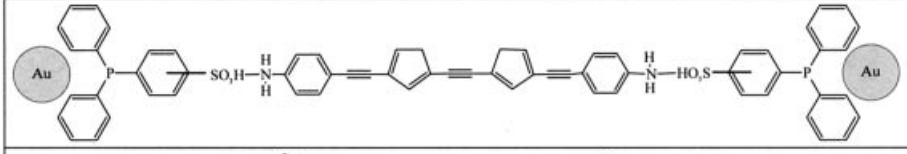	**10**	2.8	0.23
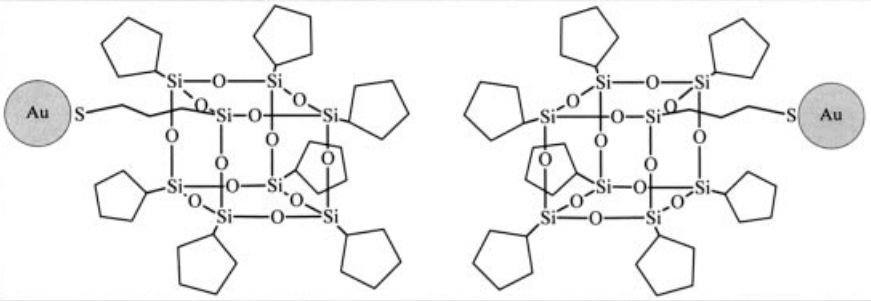	**11**	3.1	0.26

[a] The length of the molecules was determined using the program ACD-ChemSketch.

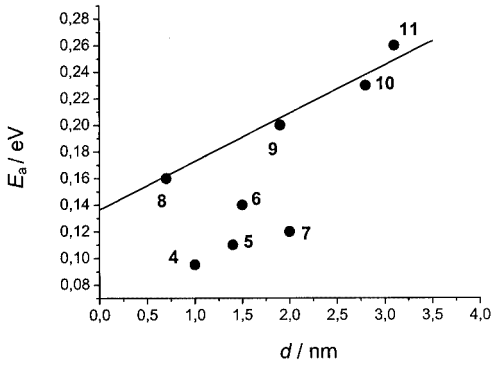

Figure 4. Activation energies versus cluster-cluster distances of the covalently (**4**−**7**) and the noncovalently (**8**−**11**) organized systems

species, possessing delocalised π-electrons, enable inter-cluster electron transfers by lower activation energies, depending on the electronic situation in the molecule, not only on their lateral extension. These results give a new insight into the charge-transport mechanism between nanoparticles, and long and controversial questions concerning the nature of this transport − whether it involves propagation via the organic molecules or whether it predominantly involves tunnelling − can now be considered as at least partially to be answered.

Experimental Section

General: 4,4′-Thiobis(benzenethiol) (**2**) and 2,8-dimercapto-6-hydroxypurine (**3**) were purchased from Aldrich (98% purity) and from Avocado (98% purity), respectively. 1,5-Dithionaphthalene (**1**) was synthesised from 1,5-naphthalenedisulfonic acid sodium salt hydrate (Aldrich, 95% purity) following described synthetic procedures.[32,33] $[Au_{55}Cl_6(PPh_3)_{12}]$ was synthesised as described previously.[34] Transmission electron microscopy was performed with a Philips CM 2000 FEG at 200 kV, the electrical measurements were done with a Keithley 6517 ElectroMeter and a Keitheley 2400 SourceMeter in a CryVac cooling system under N_2.

4: A solution of **2** (53 mg, $2.1\cdot10^{-4}$ mol) was added dropwise under a nitrogen atmosphere to a stirred solution of $[Au_{55}(PPh_3)_{12}Cl_6]$ (100 mg, $7\cdot10^{-6}$ mol) in dichloromethane (300 mL). After three weeks, the black precipitate isolated from a colourless solution by filtration was washed carefully several times with CH_2Cl_2 and dried under reduced pressure. Yield 52 mg; Au 58.7, S 11.2.

5, 6, 7: All experiments were performed using the same procedure. Only the solvents were modified, depending on the solubility of the linker: Et_2O for **1**, CH_2Cl_2 for **2**, and DMF for **3**. In a typical experiment, 100 mL of a solution of **1**, **2**, **3** ($2\cdot10^{-4}$ mol) was added dropwise to a stirred dichloromethane solution (300 mL) of $[Au_{55}Cl_6(PPh_3)_{12}]$ (100 mg, $7\cdot10^{-6}$ Mole) under an atmosphere of nitrogen. After addition the reaction was continued for ca. 12 h under an atmosphere of air, leading to a brown precipitate, which was isolated by filtration from the colourless solution. After careful washing with CH_2Cl_2 and the corresponding linker solvent the products (**5**, **6**, **7**) were dried under reduced pressure and used for the electrical measurements.

Product 5: Yield 66 mg; Au 63.6, S 6.17.

Product 6: Yield 78 mg; Au 65.7, S 8.18.

Product 7: Yield 53 mg; Au 65.0, S 6.76.

Acknowledgments

We thank J. Jockel and W. Oßwald for assisting in the conductivity measurements. We also acknowledge support by the Deutsche Forschungsgemeinschaft (Graduiertenkolleg 689/1, SFB 452), and the Fonds der Chemischen Industrie, Frankfurt am Main.

[1] R. P. Andres, T. Bein, M. Dorogi, S. Feng, J. I. Henderson, C. P. Kubiak, W. Mahoney, R. Osifchin, R. Reifenberger, *Science* **1996**, *272*, 1323−1325.
[2] D. L. Klein, P. L. McEuen, J. E. Bowen Katari, R. Roth, A. P. Alivisatos, *Appl. Phys. Lett.* **1996**, *68*, 2574−2576.
[3] C. P. Vinod, G. U. Kulkarni, C. N. R. Rao, *Chem. Phys. Lett.* **1998**, *289*, 329−333.
[4] R. P. Andres, J. D. Bielefeld, J. I. Henderson, D. B. Janes, V. R. Kolagunta, C. P. Kubiak, W. J. Mahoney, R. Osifchin, *Science* **1996**, *273*, 1690−1963.
[5] R. P. Andres, S. Datta, M. Dorogi, J. Gomez, J. I. Henderson, D. B. Janes, V. R. Kolagunta, C. P. Kubiak, W. Mahoney, R. Osifchin, R. Reifenberger, M. P. Samanta, W. Tian, *J. Vac. Sci. Technol.* **1996**, *A14*, 1178−1183.
[6] G. Schmid, Y.-P. Liu, M. Schumann, T. Raschke, C. Radehaus, *Nano Lett.* **2001**, *1*, 405−407.
[7] R. H. Terril, T. A. Postlethwaite, C. Chen, C. Poon, A. Tersis, A. Chen, J. E. Hutchison, M. R. Clark, G. Wignall, J. D. Londono, R. Superfine, M. Falvo, C. S. Johnson, E. T. Samulski, R. W. Murray, *J. Am. Chem. Soc.* **1995**, *117*, 12537−12548.
[8] V. Torma, G. Schmid, U. Simon, *ChemPhysChem.* **2001**, 321−325.
[9] G. Schön, U. Simon, *Colloid Polym. Sci.* **1995**, *273*, 101−117.
[10] G. Schön, U. Simon, *Colloid Polym. Sci.* **1995**, *273*, 202−218.
[11] U. Simon, *Adv. Mater.* **1998**, *10*, 1487−1492.
[12] A. W. Snow, H. Wohltjen, *Chem. Mater.* **1998**, *10*, 947−949.
[13] U. Simon, R. Flesch, H. Wiggers, G. Schön, G. Schmid, *J. Mater. Chem.* **1998**, *8*, 517−518.
[14] S. Datta, D. B. Janes, R. P. Andres, C. P. Kubiak, R. Reifenberger, *Semiconductor Sci. Techn.* **1998**, *13*, 1347−1353.
[15] G. Schmid, L. F. Chi, *Adv. Mater.* **1998**, *10*, 515−526.
[16] S. Chen, *Adv. Mat.* **2000**, *12*, 186−189.
[17] F. L. Leibowitz, W. X. Zheng, M. M. Maye, C. J. Zhong, *Anal. Chem.* **1999**, *71*, 5076−5083.
[18] J. F. Hicks, F. P. Zamborini, A. J. Osisek, R. W. Murray, *J. Am. Chem. Soc.* **2001**, *123*, 7048−7053.
[19] R. P. Andres, S. Datta, D. B. Janes, C. P. Kubiak, R. Reifenberger, in: *Handbook of Nanostructured Materials and Nanotechnology* (Ed.: H. S. Nalwa), Academic Press **2000**, vol. 3, p. 179.
[20] U. Simon, *Mat. Res. Soc. Symp. Proc.* **2000**, *581*, 77−82.
[21] S. Hong, R. Reifenberger, *Superlattices Microstruct.* **2000**, *28*, 289−303.
[22] U. Simon, G. Schön, in: *Handbook of Nanostructured Materials and Nanotechnology* (Ed.: H. S. Nalwa), Academic Press **2000**, vol. 3, p. 131.
[23] G. Schmid, R. Pugin, J.-O. Malm, J.-O. Bovin, *Eur. J. Inorg. Chem.* **1998**, *6*, 813−817.
[24] G. Schmid, R. Pugin, W. Meyer-Zaika, U. Simon, *Eur. J. Inorg. Chem.* **1999**, *11*, 2051−2055.
[25] M. P. I. van Staveren, H. B. Brom, L. J. de Jongh, *Phys. Rev.* **1991**, *208*, 1−96.

[26] U. Simon, Habilitationsschrift, University of Essen, **1998**.
[27] H. Taube, H. Myers, R. L. Rich, *J. Am. Chem. Soc.* **1953**, *75*, 4118−4119.
[28] H. Taube, *Electron Transfer Reactions of Complex Ions in Solution*, Academic Press, New York **1970**.
[29] A. Haim, *Acc. Chem. Res.* **1975**, *8*, 264−272.
[30] D. E. Pennington, in: *Coordination Chemistry* (Ed.: A. E. Martell), vol. 3, ACS Monograph 174, American Chemical Society, Washington DC **1978**, p. 476.
[31] H. Taube, *Science* **1984**, *226*, 1028−1036.
[32] S. Fujita, *Synthesis* **1982**, 423−424.
[33] P. D. Caesar, *Org. Synth.* **1953**, 693−695.
[34] G. Schmid, *Inorg. Synth.* **1990**, *7*, 214−217.

Received September 25, 2002
[I02538]

Monohelical Complexes of a Novel Asymmetric N_4 Schiff Base: Unfamiliar Tetrahedral Environments of Manganese(II) and Iron(II) Helicates

Miguel Vázquez,[a] Manuel R. Bermejo,*[a] Matilde Fondo,[a] Ana M. García-Deibe,[a] Jesús Sanmartín,[a] Rosa Pedrido,[a] Lorenzo Sorace,[b] and Dante Gatteschi[b]

Keywords: Electrochemistry / Helical structures / Schiff bases / Transition metals

The electrochemical reaction of the bis-bidentate H_2ABATs Schiff base [H_2ABATs = *N*,*N*′-bis(2-tosylaminobenzylidene)-2-aminobenzylamine] with manganese, iron, cobalt, nickel, copper, zinc and cadmium was investigated. The reaction cell yields products of empirical formula M(ABATs). X-ray diffraction studies show that [Mn(ABATs)]·0.75H_2O (**1**), [Fe(ABATs)]·0.75H_2O (**2**), [Ni(ABATs)]·0.75H_2O (**3**), [Cu(ABATs)]·0.5H_2O (**4**) and [Zn(ABATs)]·0.75H_2O (**5**) are mononuclear distorted tetrahedral helical complexes in the solid state. Complexes **1** and **2** confirm the ability of this type of ligand to dictate the geometry around the metal centre, as is shown by the unfamiliar tetrahedral environments of manganese(II) and iron(II) ions in complexation with the Schiff bases.
(© Wiley-VCH Verlag GmbH & Co. KGaA, 69451 Weinheim, Germany, 2003)

Introduction

Molecular architectures featuring helical arrangements of multidentate ligands around one or more metal centres are one of the goals of supramolecular chemistry.[1−4] In this search, many studies have been performed in order to develop synthetic procedures for new multidentate ligands exhibiting the potential to give bridged polynuclear species.[5−11] Among the various ligand systems capable of promoting self-assembly of mononuclear and/or polynuclear helical coordination complexes, careful design of imine-based ligands[12−20] demonstrates that this can be an inexpensive approach to supramolecular chemistry. These ligands have the advantage of being easily modified, allowing changes in the features (length, flexibility, donor ability) of the spacer, the position of the donor atoms and the presence of different groups that can give rise to intermolecular interactions and/or induce torsion of the ligand. A systematic study of the factors affecting the isolation of helical complexes can therefore be done by changing just one of the variables.

We have recently prepared some bis-bidentate Schiff bases containing bulky tosyl groups and different spacers.[21−22] These ligands yield mononuclear and/or dinuclear helicates, depending on the flexibility and/or the length of the spacer, as well as on the nature of the metal atom. In fact, a Schiff base with a flexible propylene spacer separating the *N*-imine donors can give rise to complexes of different nuclearity, depending on the metal ion.

Regardless of the mono- or dinuclear nature of the helix, all complexes prepared with this kind of Schiff base show coordination numbers of four for the metal centres. It therefore seems that the stereochemical preferences of the metal do not play a fundamental role in the nuclearity of the complex in this case study. Until now, however, neither manganese(II) nor iron(II) complexes of this type had been crystallographically characterised, these metals having special preference for an octahedral coordination. To the best of our knowledge, in fact, no tetrahedral Schiff-base complexes with these metal atoms have been structurally characterised.

In an attempt to determine whether the presence of the tosyl groups can always dictate the geometry around the metal centre, and to examine the influence of the flexibility of the spacer on the nuclearity of the helix, the new H_2ABTs ligand (Scheme 1), with a semi-rigid benzylidene group (three carbon atoms) between the two imine moieties, was prepared. The interaction of H_2ABATs with manganese, iron, cobalt, nickel, copper, zinc and cadmium in an electrochemical cell was investigated and the results achieved are described.

Results and Discussion

Synthesis of the Ligand

The Schiff base H_2ABATs was prepared by conventional condensation between 2-tosylaminobenzaldehyde and 2-aminobenzylamine. The yellow solid showed a satisfactory

[a] Departamento de Química Inorgánica, Facultade de Química, Universidade de Santiago de Compostela, 15706 Santiago de Compostela, Spain
E-mail: qimb45@usc.es
[b] Dipartimento di Chimica, Universita degli Studi di Firenze, Polo Scientifico Universitario, 50099 Sesto Fiorentino (Fi), Italy

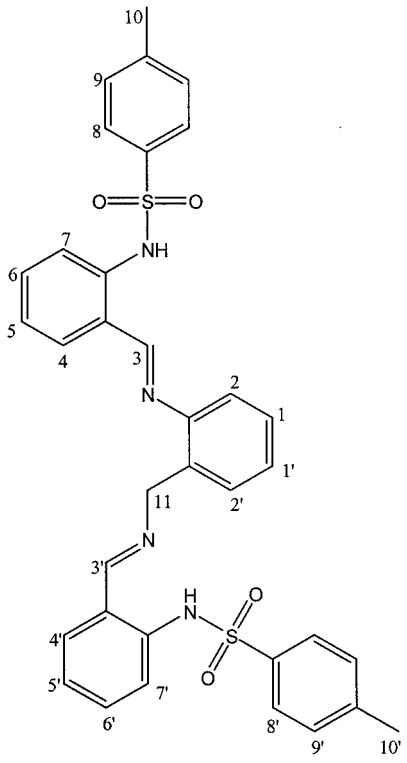

Scheme 1. H_2ABATs

elemental analysis and was further characterised by IR and ^{1}H NMR spectroscopy and FAB mass spectrometry.

Electrochemical Synthesis of the Complexes

All the complexes were prepared by a previously described electrochemical method.[21]

Elemental analyses show that all metals employed here react with the ligand in a 1:1 molar ratio to afford complexes of the bis-deprotonated $[ABATs]^{2-}$ with high purity. All these neutral metal complexes are obtained in good yields and appear to be stable both in the solid state and in solution. It therefore seems that although an inert atmosphere is necessary for the isolation of pure manganese(II) and iron(II) complexes, these compounds are air-stable once formed.

X-ray Studies

The crystal structures of $[Mn(ABATs)]\cdot 0.75H_2O$ (**1**), $[Fe(ABATs)]\cdot 0.75H_2O$ (**2**), $[Ni(ABATs)]\cdot 0.75H_2O$ (**3**), $[Cu(ABATs)]\cdot 0.5H_2O$ (**4**) and $[Zn(ABATs)]\cdot 0.75H_2O$ (**5**) were solved as detailed below.

The five complexes are isomorphous and isostructural, and so only the ORTEP diagram of **1** is shown in Figure 1. Experimental details are recorded in Table 1 and the main bond distances and angles in Table 2.

Metal-Ion Geometry

All the complexes consist of mononuclear compounds with water as solvate. In each case the ligand uses its four nitrogen atoms (two imine and two amide) to link to the metal atom. In addition, one oxygen atom of each tosyl group interacts weakly with the metal centre (Table 2). These distances are too long to be regarded as true coordinated bonds, and are better described as secondary intramolecular interactions. The metal centre is therefore in a tetracoordinated environment, with the tosyl groups playing an important role in the adopted coordination number. However, it is noteworthy that the higher preference for an octa-

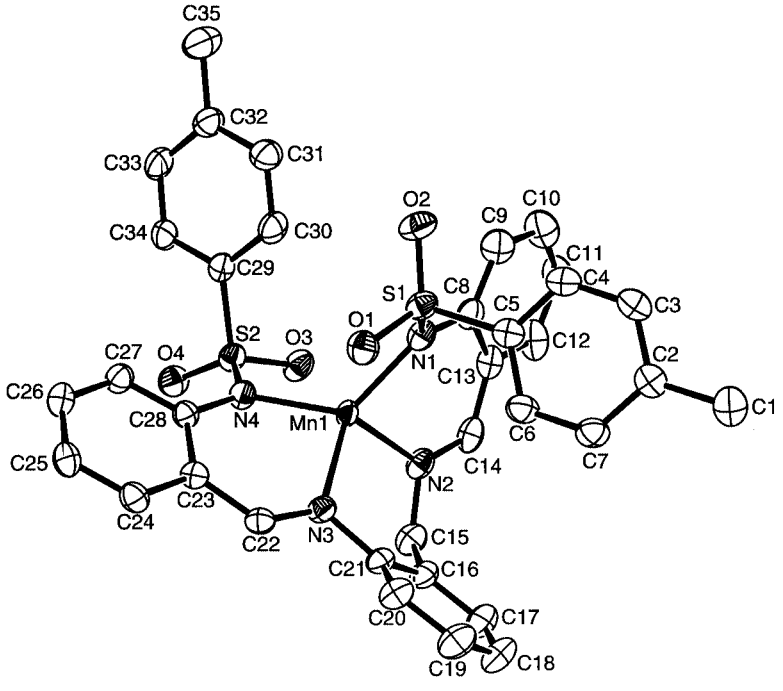

Figure 1. An ORTEP view of complex **1**, showing the *P* enantiomer (thermal ellipsoids are drawn at the 30% probability level; hydrogen atoms and solvent molecules have been omitted for clarity)

Table 1. Crystal data and structure refinement for **1**−**5**

	1	**2**	**3**	**4**	**5**
Empirical formula	$C_{35}H_{31.50}MnN_4O_{4.75}S_2$	$C_{35}H_{31.50}FeN_4O_{4.75}S_2$	$C_{35}H_{31.50}NiN_4O_{4.75}S_2$	$C_{35}H_{31}CuN_4O_{4.5}S_2$	$C_{35}H_{31.50}ZnN_4O_{4.75}S_2$
Molecular weight	703.20	704.11	706.97	707.30	713.63
Crystal system	Monoclinic	Monoclinic	Monoclinic	Monoclinic	Monoclinic
Space group	*P*2/*c* (No.13)	*P*2/*c* (No.13)	*P*2/*c* (No.13)	*P*2/*c* (No.13)	*P*2/*c* (No.13)
a (Å)	19.486(3)	19.51830(10)	19.3080(5)	19.207(5)	19.296(3)
b (Å)	10.696(2)	10.6748(2)	10.7143(3)	10.636(4)	10.736(2)
c (Å)	17.636(3)	17.6367(10)	17.7497(4)	17.760(5)	17.755(4)
α (°)	90	90	90	90	90
β (°)	114.74(2)	114.8230(10)	115.1580(10)	114.98(2)	114.823(13)
γ (°)	90	90	90	90	90
V (Å^3)	3338.4(10)	3335.2(2)	3323.59(15)	3288.7(18)	3338.3(11)
Z	4	4	4	4	4
Absorption coefficient (mm^{-1})	0.568	0.625	0.757	0.838	0.908
Crystal size (mm^3)	0.25 × 0.15 × 0.10	0.20 × 0.10 × 0.05	0.40 × 0.25 × 0.15	0.40 × 0.25 × 0.15	0.40 × 0.25 × 0.10
Reflections collected	20493	17037	16931	16721	16789
Independent reflections	7647 [*R*(int) = 0.0367]	7652 [*R*(int) = 0.0638]	7625 [*R*(int) = 0.0585]	7554 [*R*(int) = 0.0888]	7607 [*R*(int) = 0.0371]
θ range (°)	1.90−27.54	1.91−27.52	1.17−27.58	2.24−27.53	1.16−27.55
Data/restraints/parameters	7647/0/423	7652/0/429	7625/0/423	7554/0/419	7607/0/429
Final *R* indices [$I > 2\sigma(I)$]	*R*1 = 0.0538	*R*1 = 0.0698	*R*1 = 0.0590	*R*1 = 0.0774	*R*1 = 0.0488
	*wR*2 = 0.1153	*wR*2 = 0.1456	*wR*2 = 0.1570	*wR*2 = 0.1539	*wR*2 = 0.1100
R indices (all data)	*R*1 = 0.0924	*R*1 = 0.1422	*R*1 = 0.1084	*R*1 = 0.1705	*R*1 = 0.0866
	*wR*2 = 0.1329	*wR*2 = 0.1765	*wR*2 = 0.1863	*wR*2 = 0.1944	*wR*2 = 0.1325

Table 2. Selected bond lengths [Å] and angles (°) for 1−5

	1	**2**	**3**	**4**	**5**
M(1)−N(1)	2.047(3)	2.029(4)	1.989(3)	1.978(4)	1.990(3)
M(1)−N(2)	2.053(2)	2.056(3)	1.961(3)	1.940(4)	2.015(3)
M(1)−N(3)	2.091(3)	2.096(3)	2.000(3)	1.977(4)	2.045(2)
M(1)−N(4)	2.017(2)	2.008(3)	1.937(3)	1.956(4)	1.962(2)
M(1)···O(1)	2.680(2)	2.634(3)	2.828(3)	2.765(4)	2.763(2)
M(1)···O(3)	2.595(2)	2.519(3)	2.552(2)	2.647(4)	2.681(2)
N(1)−M(1)−N(2)	87.07(11)	86.23(14)	89.55(13)	90.79(19)	90.82(11)
N(1)−M(1)−N(3)	132.97(10)	132.22(14)	126.27(12)	136.85(19)	130.14(11)
N(1)−M(1)−N(4)	123.65(10)	126.44(14)	117.93(13)	108.20(18)	120.20(10)
N(2)−M(1)−N(3)	92.18(10)	91.80(14)	94.50(13)	94.53(19)	92.36(10)
N(2)−M(1)−N(4)	135.32(11)	135.16(15)	140.19(13)	143.2(2)	133.52(11)
N(3)−M(1)−N(4)	88.15(10)	86.41(13)	91.26(12)	92.43(18)	91.83(10)

hedral geometry is displayed in the shorter M···O_{tosyl} distance.

The dihedral angle θ between the two MNN terminal planes (ca. 62.3° for **1**, 62.6° for **2**, 65.3° for **3**, 55.9 for **4** and 64.9° for **5**) shows that the metal ion displays a tetrahedral geometry with a square-planar distortion (θ = 0° for square-planar geometry and θ = 90° for tetrahedral geometry). The value of θ for **4** indicates that the geometry around the copper atom could in fact be viewed as intermediate between tetrahedral and square-planar. This geometry is quite unfamiliar for manganese(II) and iron(II) Schiff-base complexes, which display clear stereochemical preferences for octahedral environments, and even for Ni^{II}, which also prefers octahedral or square-planar rather than tetrahedral geometries. To the best of our knowledge, no manganese Schiff-base complexes with this geometry have been described previously, and just one iron(II) tetrahedral complex of a bidentate Schiff base (FeL_2) has recently been characterised.[23] Nevertheless, it should be noted that this complex was prepared in non-polar, non-coordinating solvents under an inert atmosphere. In our case the iron centre maintains its tetrahedral environment despite the presence of water in the solvent and trapped in the unit cell, which demonstrates the ability of this type of ligand to predetermine the coordination polyhedron. It therefore seems that the steric hindrance induced by the tosyl groups, in conjunction with the second order interactions of the metal with the tosyl oxygen atoms, prevent any other donor from coordinating to the metal ion.

In addition, it must be pointed out that Zn and Ni form dinuclear complexes with H_2PTs [*N*,*N*′-bis(2-tosylaminobenzylidene)-1,3-diaminopropane],[21] while they afford mononuclear compounds with H_2ABATs. The related H_2PTs ligand, like H_2ABATs, contains three carbon atoms

between the imine moieties. However, the spacer in H_2PTs is an aliphatic chain and this emphasises the role of the spacer flexibility in the nuclearity of the helix.

The M−N (M = Ni, Cu, Zn) distances are typical of tetracoordinate tetrahedral complexes,[21−22] but are shorter than those found for octahedral complexes with similar ligands,[24] reflecting the lower coordination number. The $M-N_{imine}$ (M−N2 and M−N3) distances decrease monotonically from **1** to **4** and increase for **5**, following the trend (**1** ≈ **2** > **5** > **3** > **4**) of the ionic radii. The $M-N_{amide}$ (M−N1 and M−N4) distances show the same pattern.

The wide range of angles observed around the metal centres, varying between ca. 87° and 143.2°, compares fairly well with those previously reported for this kind of complex and reflects the severe distortion from the ideal tetrahedral geometry.

Chelate Rings and Helical Coiling

The ligand forms three chelate rings around the central metal atom. The two terminal six-membered rings are reasonably planar while the central six-membered ring is less so, as would be expected, due to the presence of one sp^3 carbon atom. The loss of planarity between the N_{imine} atoms is also shown by the N(2)C(15)C(16)C(21) torsion angles, which range from −58.7(5)° for **3** to 63.0(4)° for **2**, showing the strain of the ligand. The central N(2)C(15)C(16)C(21)N(3) chelate ring forms angles of ca. 46° and 27° for **1**−**3** and **5** and of ca. 41° and 23° for **4** with N(1)C(8)C(13)C(14)N(2) and N(3)C(22)C(23)C(28)N(4), respectively. These angles show the screwing of this thread, which affords monohelical single-stranded molecules. The twisting of the ligand can be attributed to an attempt by the additional peripheral tosyl groups to minimise the steric hindrance, being orientated in different directions, as shown in Figure 2.

The extent of helical coiling in these chiral complexes can be described in terms of the ligand wrapping angle. However, the value of this angle, and of the helical pitch of the thread, can change significantly depending on different considerations, such as the actual helix top-ends or the helical axis declination, so only qualitative aspects are considered.

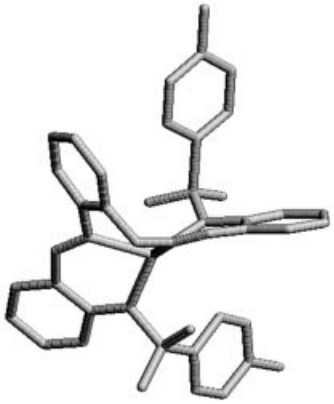

Figure 2. Stick view of **1**, showing the wrapping of the ligand

It can clearly be observed (Figure 2) that, if only the donor atoms are taken into account, the wrapping angle is always shorter than 360°. Nevertheless, if the tosyl groups are included, the ligand wraps slightly more than once. In that sense, the S···S distances could be taken as a close value for the pitch, being ca. 5.0 Å for **1**, 4.98 Å for **2**, 4.88 Å for **3**, 4.74 Å for **4** and 4.99 Å for **5**. These distances show that the shortest pitch corresponds to **4**, which is in agreement with its more distorted (tetrahedral towards square-planar) geometry.

Finally, the space group and the analysis of the crystal data indicate the formation of a racemic mixture, with both *P* and *M* enantiomers present in the unit cell with 50% yield for all the complexes.

IR Spectra

The IR spectra of the free ligand and complexes show two bands at ca. 1605 and 1630 cm^{-1}, in agreement with the presence of two inequivalent imine groups. Both ν(C=N) bands are shifted to higher wavenumber values (1−15 cm^{-1}) with respect to the free ligand for most of the complexes. In addition, all complexes show a negative shift of ν(C−N) relative to free H_2ABATs. This suggests the coordination of the ligand to the metal centre through the imine and amide nitrogen atoms. In addition, two bands in the ranges 1250−1261 cm^{-1} and 1127−1138 cm^{-1} are attributable to the asymmetric and symmetric vibration modes of the SO_2 group, respectively.[25−26] Finally, no bands above 2500 cm^{-1} were detected for any of the complexes, indicating the deprotonation of the NH groups and, therefore, the dianionic character of the ligand.

Magnetic Studies

The magnetic moments of all the paramagnetic complexes were recorded in the solid state between 2 and 280 K. In agreement with the observed long distances between magnetic centres (ca. 9.5 Å), and with the absence of any efficient exchange pathway, the temperature dependence of the magnetic susceptibilities between 2 and 280 K for all the complexes shows deviation from Curie behaviour only at low temperature, with the exception of the Ni^{II} complex for which, due to the expected partially unquenched orbital contribution, a deviation is observed below 50 K (Figure 3). The values of the magnetic moment, obtained by the Curie−Weiss fit of $1/\chi$ vs. *T* plots (Table 3), are very close to those expected for magnetically diluted tetrahedral M^{II} ions, with *g* values that, except for Mn^{II}, differ greatly from that of the free electron.[27] This provides confirmation of the oxidation state +II for the metal centre, indicating the deprotonation of the Schiff-base ligand, and the achieved high-spin configuration for [Mn(ABATs)] and [Fe(ABATs)], as would be expected. The EPR spectra essentially confirm this picture; indeed, a typical tetrahedral Cu^{II} spectrum is observed for the complex [Cu(ABATs)], which yielded *g* values $g_{\|}$ = 2.185 $g_{\perp}$ = 2.095 with an average *g* value of 2.125, in good agreement with the magnetic moment observed at room temperature. On the other hand, the EPR

spectrum of the Mn^{II} derivative, recorded at low temperature, clearly shows a fine structure deriving from a non-negligible zero field splitting (ZFS) of the $S = 5/2$ multiplet (Figure 4). Finally, no EPR spectra are observed for the Fe^{II} and Co^{II} derivatives: the absence of a spectrum for the former is in agreement with the expected large ZFS and integer spin state that usually make tetrahedral high-spin Fe^{II} complexes silent at EPR X-band frequencies.[28] The non-observation of an EPR spectrum for the Co^{II} derivative, a Kramers ion, could be attributable to fast relaxation.[29]

Thus, in view of the formulations of the complexes and their magnetic moments, it seems quite reasonable to propose a tetrahedral environment around the metal atoms for all the paramagnetic complexes, as the crystal structures of **1** to **5** confirm.

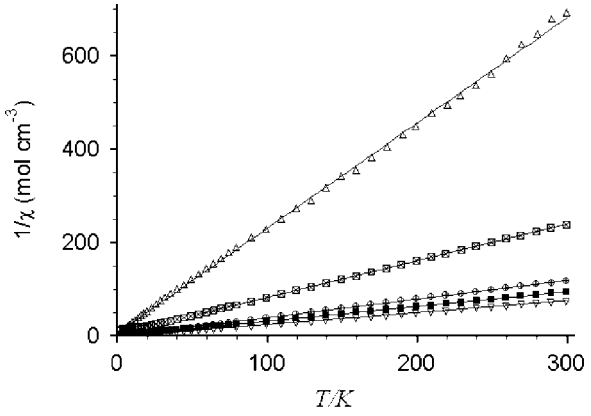

Figure 3. Curie−Weiss plots for paramagnetic complexes; Δ Cu derivative, □ Ni derivative, ○ Co derivative, ■ Fe derivative and ▽ Mn derivative

Table 3. Value of the Curie constant for the complexes

Complex	C ($cm^3 \cdot K \cdot mol^{-1}$)
Mn(ABATs)	3.88
Fe(ABATs)	3.17
Co(ABATs)	2.5
Ni(ABATs)	1.28
Cu(ABATs)	0.44

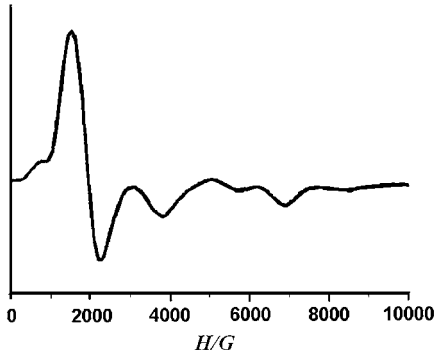

Figure 4. EPR band spectrum (at 9.225 GHz) of Mn(ABATs) recorded at 4.2 K

FAB Mass Spectra

FAB mass spectra of all the complexes show peaks due to $[M(ABATs)]^+$ fragments (M = Mn, Fe, Co, Ni, Cu, Zn or Cd), corroborating the coordination of the ligand to the metal. However, no peaks attributable to $[ML]_2^+$ fragments could be detected for any of the complexes, suggesting mononuclear natures in solution for all of them.

NMR Studies

The ^1H NMR spectra of H_2ABATs, [Zn(ABATs)] and [Cd(ABATs)] were recorded in [D_6]DMSO as solvent. The spectra show two sets of aromatic signals in a 1:1 ratio, indicating that the two arms are not magnetically equivalent. The assignments of the signals were based on COSY and NOESY experiments, as well as on previous results.[21−22]

The comparison of the free ligand spectrum with those of the complexes allows some conclusions to be drawn:

1. The NH protons present in the free ligand disappear in the spectra of the complexes, in agreement with bis-deprotonation of the Schiff base.
2. The imine hydrogen atoms (3-H and 3′-H) show a shift to lower field for the zinc complex, while 3-H is shifted to higher field in the cadmium complex, indicating that the coordination of the imine groups to the metal centre induces opposite shielding effects on these hydrogen atoms. This situation was also found for zinc and cadmium complexes with ligands containing an aliphatic spacer.[21b]

The imine protons of the cadmium complex are flanked by satellites arising from spin-spin coupling to $^{111/113}$Cd, suggesting that the complex is kinetically inert on the NMR timescale.

3. The methylene protons (11-H) are magnetically equivalent in the free ligand and appear as a singlet at δ = 5.08 ppm. However, the room-temperature spectrum of the zinc complex contains a well resolved AB doublet of doublets for the 11-H protons. The AB pattern for the methylene hydrogen atoms implies that the strong coordination of the hard imine nitrogen to the zinc atom abolishes the erstwhile enantiotopic nature of these protons to make them diastereotopic. This observation can be interpreted in terms of a helical conformation of the new complex, making it chiral. It therefore seems that the zinc complex in solution maintains the structure found in solid state.

The spectrum of the cadmium complex at room temperature shows just one broad signal at $\delta = 4.97$ ppm for the 11-H protons. This could indicate that the complex is not chiral or that a fast interconversion of enantiomers of the chiral single helicate takes place in solution.

Finally, it should be noted that just one diastereoisomer exists in solution for both complexes, as no additional peaks indicative of a second species could be detected.

Conclusions

The electrochemical interaction of manganese, iron, cobalt, nickel, copper, zinc and cadmium with the bis-bidentate H_2ABATs Schiff base yields mononuclear [M^{II}(ABATs)] complexes. The bulky tosyl groups induce torsion in the ligand, giving rise to monohelical, single-stranded, tetrahedral compounds. This geometry is quite unusual for manganese(II) and iron(II) with Schiff bases. In fact, to the best of our knowledge, there are no previous crystallographically characterised examples of this type of complex obtained from non-anhydrous solvents. This demonstrates the ability of this type of ligand to dictate the coordination number in spite of the geometrical preferences of the metal.

Finally, this work further contributes to make the role of the flexibility of the spacer in the nuclearity of the helix evident: nickel and zinc double-helical compounds have previously been reported for a related ligand (H_2PTs) with a flexible propylene spacer (three aliphatic carbon atoms between imine-N atoms), while the semi-rigid benzylidene spacer in H_2ABATs (three carbon atoms, two aromatic and one aliphatic, between imine-N atoms) only allows the isolation of monohelical complexes.

Experimental Section

General: Elemental analyses were performed on a Carlo Erba EA 1108 analyser. Infrared spectra were recorded as KBr pellets on a Bio-Rad FTS 175 spectrophotometer in the 4000−600 cm^{-1} range. NMR spectra were recorded on a Bruker AMX 500 spectrometer in [D_6]DMSO as solvent. Fast atom bombardment (FAB) mass spectra were performed on a Kratos MS-50 mass spectrometer, employing Xe atoms at 70 keV in *m*-nitrobenzyl alcohol as matrix. EPR spectra were recorded on a Varian ESR9 spectrometer working at the X-band frequency (9.225 GHz) equipped with a ^{4}He continuous flow cryostat for low temperature measurements. Magnetic measurements were performed between 2 and 280 K with a Cryogenics Squid S600 magnetometer with applied field of 1 T. The data were corrected for sample holder contribution and diamagnetism of the sample by the use of Pascal constants.

Synthesis: All the starting materials were purchased from Aldrich and used without further purification. 2-Tosylaminobenzaldehyde was prepared and characterised according to the literature.[30−31]

Ligand Preparation: 2-Aminobenzylamine (1.13 g, 9.1 mmol) was added to a solution of 2-tosylaminobenzaldehyde (5.0 g, 18.2 mmol) in chloroform (150 mL), and the mixture was heated to reflux. The volume of the solution was reduced to ca. 50 mL over a 4 h period with the aid of a Dean−Stark trap, and the mixture was then allowed to cool. The resultant yellow solution was concentrated to ca. 10 mL. The solid that precipitated was collected by filtration, washed with diethyl ether (4 mL) and dried in vacuo. Yield: 5.20 g (90%); m.p. 187 °C. $C_{35}H_{32}N_4O_4S_2$ (636): calcd. C 66.0, H 5.1, N 8.8, S 10.1; found C 66.1, H 5.1, N 8.7, S 10.2. IR (KBr): $\tilde{\nu}$ = 1628, 1605 [s, ν(C=N)], 1339 [s, ν(C−N)], 1285, 1165 [s, ν(SO_2)] cm^{-1}. FAB-MS: *m*/*z* = 637.3 [H_3L^+]. ^{1}H NMR (500 MHz, [D_6]DMSO): δ = 2.09 (s, 3 H, 10′-H), 2.22 (s, 3 H, 10-H), 5.09 (s, 2 H, 11-H), 6.95−7.0 (m, 4 $H_{arom.}$), 7.10−7.13 (m, 4 $H_{arom.}$), 7.38−7.53 (m, 9 $H_{arom.}$), 7.67 (d, 2 H, 8-H), 7.76 (d, 1 H, 4-H), 8.65 (s, 1 H, 3′-H), 8.88 (s, 1 H, 3-H), 12.82 (s, 1 H, NH), 12.94 (s, 1 H, NH) ppm.

Synthesis of the Complexes: All the complexes were obtained by an electrochemical procedure. The cell can be summarised as: Pt(−)|H_2ABATs + MeCN|M(+), where M stands for the metal. The synthesis can be typified by the preparation of Cu(ABATs). A suspension of the ligand (0.2 g, 0.32 mmol) in acetonitrile (80 mL), containing tetramethylammonium perchlorate (10 mg), was electrolysed with a current of 10 mA for 3.4 h. Concentration of the resultant solution to a third of its initial volume yielded a yellow-brown solid that was washed with diethyl ether and dried under vacuum. Recrystallisation of the bulk sample by diffusion of diethyl ether into an acetonitrile solution, produced dark-green crystals of [Cu(ABATs)]·0.5H_2O (**4**).

CAUTION: Perchlorate salts are potentially explosive and should therefore be handled with the appropriate care.

The synthetic procedure is the same for all the metals except for manganese and iron. These two compounds were prepared in a closed cell under an argon atmosphere. Prismatic crystals of [Mn(ABATs)]·0.75H_2O (**1**, orange brown), [Fe(ABATs)]·0.75H_2O (**2**, brown), [Ni(ABATs)]·0.75H_2O (**3**, brown), [Cu(ABATs)]·0.5H_2O (**4**, dark green) and [Zn(ABATs)]·0.75H_2O (**5**, yellow) were obtained by slow evaporation of a saturated acetonitrile solution in air. No crystals suitable for X-ray studies could be obtained for [Co(ABATs)] or [Cd(ABATs)].

[Mn(ABATs)]: Dark red solid. Yield 0.17 g (78%). $C_{35}H_{30}MnN_4O_4S_2$ (688.9): calcd. C 60.9, H 4.3, N 8.1, S 9.3; found C 60.9, H 4.4, N 8.2, S 9.3. IR (KBr): $\tilde{\nu}$ = 1632, 1605 [s, ν(C=N)], 1281 [s, ν(C−N)], 1250, 1127 [s, ν(SO_2)] cm^{-1}. FAB-MS: *m*/*z* = 690.2 [MnL]$^+$. μ (280 K) = 5.6 BM.

[Fe(ABATs)]: Red solid. Yield 0.15 g (70%). $C_{35}H_{30}FeN_4O_4S_2$ (689.5): calcd. C 60.9, H 4.3, N 8.1, S 9.3; found C 60.8, H 4.5, N 8.1, S 9.2. IR (KBr): $\tilde{\nu}$ = 1636, 1606 [s, ν(C=N)], 1290 [s, ν(C−N)], 1255, 1136 [s, ν(SO_2)] cm^{-1}. FAB-MS: *m*/*z* = 691.1 [FeL]$^+$. μ (280 K) = 5.0 BM.

[Co(ABATs)]: Dark red solid. Yield 0.17 g (81%). $C_{35}H_{30}CoN_4O_4S_2$ (692.9): calcd. C 60.6, H 4.3, N 8.1, S 9.2; found C 60.7, H 4.4, N 8.0, S 9.2. IR (KBr): $\tilde{\nu}$ = 1632, 1605 [s, ν(C=N)], 1285 [s, ν(C−N)], 1258, 1134 [s, ν(SO_2)], cm^{-1}. FAB-MS: *m*/*z* = 694.1 [CoL]$^+$. μ (280 K) = 4.3 BM.

[Ni(ABATs)]: Dark green solid. Yield 0.15 g (72%). $C_{35}H_{30}N_4NiO_4S_2$ (692.7): calcd. C 60.6, H 4.3, N 8.1, S 9.2; found C 60.6, H 4.4, N 8.2, S 9.0. IR (KBr): $\tilde{\nu}$ = 1640, 1605 [s, ν(C=N)], 1285 [s, ν(C−N)], 1254, 1138 [s, ν(SO_2)] cm^{-1}. FAB-MS: *m*/*z* = 693.1 [NiL]$^+$. μ (280 K) = 2.7 BM.

[Cu(ABATs)]: Dark green solid. Yield 0.15 g (69%). $C_{35}H_{30}CuN_4O_4S_2$ (697.5): calcd. C 60.2, H 4.3, N 8.0, S 9.2; found C 60.1, H 4.3, N 8.0, S 9.0. IR (KBr): $\tilde{\nu}$ = 1636, 1605 [s, ν(C=N)],

1285 [s, ν(C−N)], 1258, 1138 [s, ν(SO_2)], cm^{-1}. FAB-MS: *m*/*z* = 698.2 $[CuL]^+$. μ (280 K) = 2.1 BM.

[Zn(ABATs)]: Yellow solid. Yield 0.17 g (80%). $C_{35}H_{30}N_4O_4S_2Zn$ (699.4): calcd. C 60.0, H 4.3, N 8.0, S 9.1; found C 60.1, H 4.3, N 8.1, S 9.2. IR (KBr): $\tilde{\nu}$ = 1643, 1615 [s, ν(C=N)], 1296 [s, ν(C−N)], 1261, 1138 [s, ν(SO_2)], cm^{-1}. FAB-MS: *m*/*z* = 699.1 $[ZnL]^+$. ^1H NMR (500 MHz, [D_6]DMSO): δ = 2.22 (s, 3 H, 10′-H), 2.35 (s, 3 H, 10-H), 4.72 (d, 1 H, 11-H), 5.44 (d, 1 H, 11-H), 6.95−7.03 (m, 3 H, 2 × 9′-H + 6′-H), 7.26−7.38 (m, 7 H, 2 × 9-H + 7-H + 7′-H + 6-H + 5-H + 4′-H + 2′-H), 7.44−7.73 (m, 6 H, 2 × 8′-H + 7-H + 2-H + 1-H + 1′-H), 7.81(d, 1 H, 4-H), 7.90 (d, 2 H, 8-H), 8.75 (s, 1 H, 3′-H), 8.92 (s, 1 H, 3-H) ppm.

[Cd(ABATs)]: Pale yellow solid. Yield 0.19 g (83%). $C_{35}H_{30}CdN_4O_4S_2$ (746.4): calcd. C 56.2, H 4.0, N 7.5, S 8.6; found C 56.2, H 3.9, N 7.5, S 8.7. IR (KBr): $\tilde{\nu}$ = 1636, 1613 [s, ν(C=N)], 1289 [s, ν(C=N)], 1258, 1127 [s, ν(SO_2)] cm^{-1}. FAB-MS: *m*/*z* = 749.1 $[CdL]^+$. ^1H NMR (500 MHz, [D_6]DMSO): δ = 2.26 (s, 3 H, 10′-H), 2.28 (s, 3 H, 10-H), 4.97 (br., 2 H, 2 × 11-H), 6.75 (t, 1 H, 5′-H), 6.97 (t, 1 H, 5-H), 7.08−7.16 (m, 6 H, 2 × 9-H + 2 × 9′-H + 6′-H + 7′-H), 7.25 (t, 1 H, 6-H), 7.33−7.36 (m, 2 H, 4′-H + 2′-H), 7.41−7.50 (m, 4 H, 7-H + 2-H + 1-H + 1′H), 7.67 (d, 1 H, 4-H), 7.74 (d, 2 H, 8′H), 7.82 (d, 2 H, 8-H), 8.68 (s, 1 H, 3′-H), 8.70 (s, 1 H, 3-H) ppm.

Crystallographic Measurements: Crystals of **1** to **5** suitable for X-ray diffraction studies were obtained as described previously. Data were collected on a Siemens SMART CCD diffractometer for **1**, **2**, **4** and **5** and on a Siemens P4 diffractometer for **3**, with graphite monochromatised Mo-K_α radiation (λ = 0.71073 Å), at room temperature. The structures were solved by direct methods and refined by full-matrix, least-squares based on F^2 with the SHELX-97 program package.[32] Absorption corrections were carried out semiempirically from equivalents by use of the Sadabs program.[33] All non-hydrogen atoms were refined anisotropically, except for some of those corresponding to solvated water molecules (**2−4**), which are disordered over two different positions (0.5 and 0.25 occupancies sites) for **1−3** and **5**. Hydrogens bonded to carbon atoms were included in the model at geometrically calculated positions and refined with a riding model. Only some H atoms corresponding to solvated water molecules could be located, fixed and given isotropic displacement parameters of 0.1 $Å^2$.

CCDC-190797−190801 (**1−5**, respectively) contain the supplementary crystallographic data for this paper. These data can be obtained free of charge at www.ccdc.cam.ac.uk/conts/retrieving.html [or from the Cambridge Crystallographic Data Centre, 12, Union Road, Cambridge CB2 1EZ, UK; Fax: (internat.) +44-1223/336-033; E-mail: deposit@ccdc.cam.ac.uk].

[1] *Transition Metals in Supramolecular Chemistry* (Eds.: L. Fabrizzi and A. Poggi), Kluwer Academic, Dordecht, **1994**.

[2] J. M. Lehn, *Supramolecular Chemistry-Concepts and Perspectives*, VCH, Weinheim, **1995**.

[3] [3a] E. C. Constable, in *Comprehensive Supramolecular Chemistry, Vol. 9* (Eds.: J. P. Sauvage, M. W. Hosseini), Pergamon, Oxford, **1996**, 213−252. [3b]E. C. Constable, C. E. Housecroft, M. Neuburger, D. Phillips, P. R. Raithby, E. Schofield, E. Sparr, D. A. Tocher, M. Zehnder, Y. Zimmermann, *J. Chem. Soc., Dalton Trans.* **2000**, 2219−2228.

[4] C. Piguet, G. Bernarddinelli, G. Hopfgartner, *Chem. Rev.* **1997**, *97*, 2005−2062.

[5] Y. Zhang, A. Thompson, S. J. Rettig, D. Dolphin, *J. Am. Chem. Soc.* **1998**, *120*, 13537−13538.

[6] [6a] P. N. W. Baxter, J. M. Lehn, K. Rissanen, *Chem. Commun.* **1997**, 1323−1324. [6b] K. M. Gardinier, R. G. Khoury, J. M. Lehn, *Chem. Eur. J.* **2000**, *6*, 4124−4131.

[7] [7a] J. S. Fleming, K. L. V. Mann, S. M. Couchman, J. C. Jeffery, J. A. McCleverty, M. D. Ward, *J. Chem. Soc., Dalton Trans.* **1998**, 2047−2052. [7b] C. R. Rice, S. Wörl, J. C. Jeffery, R. L. Paul, M. D. Ward, *J. Chem. Soc., Dalton Trans.* **2001**, 550−559.

[8] G. Baum, E. C. Constable, D. Fenske, C. E. Housecroft, T. Kulke, M. Neuburger, M. Zehnder, *Chem. Eur. J.* **2000**, *6*, 4510−4517.

[9] [9a] C. Piguet, *J. Incl. Phenom. Macrocycl. Chem.* **1999**, *34*, 361−391. [9b] G. Muller, J. C. G Bunzli, K. J. Schenk, C. Piguet, G. Hopfgartner, *Inorg. Chem.* **2001**, *40*, 2642−2651.

[10] [10a] M. Albrecht, *Chem. Soc. Rev.* **1998**, *27*, 281−288. [10b] M. Albrecht, O. Blau, H. Röttele, *New J. Chem.* **2000**, *24*, 619−622.

[11] O. Mamula, A. von Zelewsky, T. Bark, G. Bernardinelli, *Angew. Chem. Int. Ed. Eng.* **1999**, *38*, 2945−2948.

[12] [12a] L. Zhu, Y-X. Tong, X-M. Cheng, *J. Chem. Soc., Dalton Trans.* **2000**, 4182−4186. [12b] G. Yang, S. L. Zheng, X-M. Chen, H. K. Lee, Z-Y. Zhou, T. C. W. Mak, *Inorg. Chim. Acta* **2000**, *303*, 86−93.

[13] G. C. van Stein, G. van Koten, K. Vrieze, C. Brevard, A. L. Spek, *J. Am. Chem. Soc.* **1984**, *106*, 4486−4492.

[14] P. K. Boyer, K. A. Porter, A. D. Rae, A. C. Willis, B. Wild, *Chem. Commun.* **1998**, 1153−1154.

[15] [15a] M. J. Hannon, C. L. Painting, A. Jackson, J. Hamblin, W. Errington, *Chem. Commun.* **1997**, 1807−1808. [15b] M. J. Hannon, S. Bunce, A. J. Clarke, N. W. Alcock, *Angew. Chem. Int. Ed.* **1999**, *38*, 1277−1278. [15c] L. J. Chields, N. W. Alcock, M. J. Hannon, *Angew. Chem. Int. Ed.* **2001**, *40*, 1079−1081.

[16] V. Amendola, L. Fabbrizzi, L. Linati, C. Mangano, P. Pallavicini, V. Pedrazzini, M. Zema, *Chem. Eur. J.* **1999**, *5*, 3679−3688.

[17] H. Cheng, D. Chun-Ying, F. Chen-Jie, M. Qing-Jin, *J. Chem. Soc., Dalton Trans.* **2000**, 2419−2424.

[18] [18a] N. Yoshida, K. Ichikawa, *Chem. Commun.* **1997**, 1091−1092. [18b] N. Yoshida, H. Oshio, T. Ito, *Chem. Commun.* **1998**, 63−64. [18c] N. Yoshida, K. Ichikawa, M. Shiro, *J. Chem. Soc., Perkin Trans.* **2000**, 17−26.

[19] L. Carbonaro, M. Isola, V. Liuzzo, F. Marchetti, F. Balzano, C. S. Pomelli, A. Raffaelli, *Eur. J. Inorg. Chem.* **2001**, 353−357.

[20] [20a] J. Sanmartín, M. R. Bermejo, A. M. García-Deibe, O. Piro, E. E. Castellano, *Chem. Commun.* **1999**, 1953−1954. [20b] J. Sanmartín, M. R. Bermejo, A. M. García-Deibe, A. L. Llamas-Saiz, *Chem. Commun.* **2000**, 795−796.

[21] [21a] M. Vázquez, M. R. Bermejo, M. Fondo, A. M. González, J. Mahía, L. Sorace, D. Gatteschi, *Eur. J. Inorg. Chem.* **2001**, 1863−1868. [21b] M. Vázquez, M. R. Bermejo, M. Fondo, A. García- Deibe, A. M. González, R. Pedrido, *Eur. J. Inorg. Chem.* **2002**, 465−472.

[22] [22a] M. Vázquez, M. R. Bermejo, M. Fondo, A. M. García-Deibe, A. M. González, R. Pedrido, J. Sanmartín, *Z. Anorg. Allg. Chem.* **2002**, *628*, 1068−1074. [22b] M. Vázquez, M. R. Bermejo, J. Sanmartin, A. M. Garcia-Deibe, C. Lodeiro, J. Mahia, *J. Chem. Soc., Dalton Trans.* **2002**, 870−877.

[23] M. A. Torzilli, S. Colquhoun, J. Kim, R. H. Beer, *Polyhedron* **2002**, *21*, 705−713.

[24] [24a] M. R. Bermejo, A. Sousa, M. Fondo, M. Helliwell, *New. J. Chem.* **2000**, *24*, 33−41. [24b] A. Sousa, M. R. Bermejo, M. Fondo, A. García-Deibe, A. Sousa-Pedrares, O. Piro, *New J. Chem.* **2001**, *25*, 647−654.

[25] M. Morioka, M. Kato, H. Yoshida, T. Ogata, *Heterocycles* **1997**, *45*, 1173−1181.

[26] K. Nakamoto, in *Infrared and Raman Spectra of Inorganic and Coordination Compounds*, John Wiley & Sons, New York, **1997**.

[27] J. S. Griffith, "*The Theory of Transition Metal Ions*", Cambridge University Press, Cambridge, **1961**.

[28] M. J. Knapp, J. Krzystek, L. C. Brunel, D. N Hendrickson, *Inorg. Chem.* **2000**, *39*, 281−288.

[29] A. Bencini, D. Gatteschi, in *Transition Metal Chemistry* (Eds.:

B. N. Figgis, G. Melson) vol. 8, p. 1, Marcel Dekker, New York, **1982**.
[30] N. I. Chernova, Y. S. Ryabokobylky, V. G. Brudz, B. M. Bolotin, *Zh. Neorg. Khim.* **1971**, 1680−1684.
[31] J. Mahia, M. Maestro, M. Vázquez, M. R. Bermejo, A. M. Gonzalez, M. Maneiro, *Acta Crystallogr., Sect. C* **1999**, *C55*, 2158−2160.
[32] G. M. Sheldrick, SHELX-97 (SHELXS 97 and SHELXL 97), Programs for Crystal Structure Analyses, University of Göttingen, Germany, **1998**.
[33] SADABS, Area-Detector Absorption Correction. Siemens Industrial Automation Inc., Madison, WI, **1996**.

Received October 8, 2002
[I02557]

Mono- and Bis-Guanosine Adducts of Platinum Complexes with Carrier Ligands Having In-Plane Steric Bulk: The Case of 1,10-Phenanthroline and 2,9-Dimethyl-1,10-phenanthroline

Nicola Margiotta,[a] Paride Papadia,[a] Francesco P. Fanizzi,[b,c] and Giovanni Natile*[a]

Keywords: Platinum / Nucleobases / Antitumour agents / Atropisomerism / NMR spectroscopy

The steric hindrance generated by carrier ligands, in particular in *cis*-Pt$\mathbf{A}_2\mathbf{G}_2$ adducts ($\mathbf{A}_2$ = diamine, **G** = guanine derivative), has often been used to slow down rotation about the platinum-guanine bonds, thus allowing the characterisation of different conformers and the analysis of the interactions that are involved in the stabilisation of cisplatin adducts with DNA. In a previous study concerning 1,10-phenanthroline and 2,9-dimethyl-1,10-phenanthroline (phen and Me_2phen, respectively), the Me_2phen ligand was reported to form an unusual bis-guanosine derivative with a *trans* disposition of the nucleobases and monodentate Me_2phen. The present investigation has demonstrated that phen and Me_2phen, like other bidentate ligands, allow formation of both mono- and bis-guanosine derivatives, the latter having the usual *cis* configuration. In both the phen and Me_2phen carrier ligands the rigidity of the phenanthroline skeleton is able to hinder rotation of the guanosine base(s) about the Pt–N(7) bond(s) and render the interconversion between rotamers slow on the NMR timescale even at 350 K (the highest temperature explored). However there are noticeable differences between the two ligands. As a consequence of the increased in-plane steric bulk of Me_2phen: (i) the H(8) chemical shifts within the *HH* (*Head-to-Head*) conformer and between the *HT* (*Head-to-Tail*) conformers become closer, (ii) the average H(8) chemical shift of the *HT* conformers is at higher field and that of the *HH* form at lower field, and (iii) the *HT* rotamers become even more favoured than the *HH* rotamer. Observation (ii) is in agreement with the *HT* rotamers preferring the "6-in" conformation, which brings the six-membered rings of the guanines closer to one another and is also in agreement with the phen ligand allowing a greater canting of the guanine bases than Me_2phen. Moreover, free chloride ion readily displaces the coordinated guanosines, particularly in solvents of lower dielectric constants than water.
(© Wiley-VCH Verlag GmbH & Co. KGaA, 69451 Weinheim, Germany, 2003)

Introduction

Despite undesirable side effects, cisplatin {*cis*-$[PtCl_2(NH_3)_2]$} remains one of the most widely used drugs in the treatment of several tumours.[1,2] There is general consensus that nuclear DNA is the main target of cisplatin and that 1,2-intrastrand cross-links between adjacent purines are responsible for the anticancer activity of the drug.[3]

A huge number of models of the 1,2-intrastrand cross-link have been investigated.[4,5] In particular, carrier ligands able to introduce steric hindrance in the coordination sphere of platinum and to slow down dynamic motions about the platinum-ligand bonds have proven to be very informative.[6−12] By slowing down the rotation of the nucleobases about the Pt−N(7) bonds different rotamers, with *HT* (*Head-to-Tail*) and *HH* (*Head-to-Head*) conformations, have been identified.[13,14]

In principle 1,10-phenanthroline (phen) and, even better, 2,9-Me_2-1,10-phenanthroline (Me_2phen, neocuproine) could be used to introduce steric bulk in the coordination plane (Figure 1). 1,10-Phenanthrolines, differently from

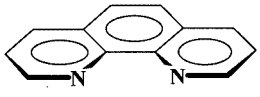

phen

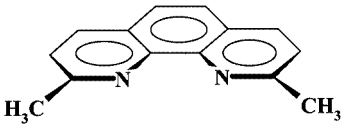

Me2phen

Figure 1. Schematic representation of 1,10-phenanthroline (phen) and 2,9-dimethyl-1,10-phenanthroline (Me_2phen) ligands

[a] Dipartimento Farmaco-Chimico, Università di Bari,
Via E. Orabona 4, 70125 Bari, Italy
E-mail: natile@farmchim.uniba.it
[b] Dipartimento di Scienze e Tecnologie Biologiche ed Ambientali, Università di Lecce,
Via Monteroni, 73100 Lecce, Italy
[c] Consortium CARSO Cancer Research Centre,
70100 Valenzano, Bari, Italy
Supporting information for this article is available on the WWW under http://www.eurjic.org or from the author.

other chelating diamines, have a very rigid structure and the lone pairs on the nitrogen atoms are convergent and hence ideally oriented for complexation to a metal centre.[15] Because of these distinctive properties, 1,10-phenanthrolines have found biological application as complexing agents of metal ions (removal of essential metal can lead to inactivation of cellular proteins and enzymes) and as bacteriostatic, fungistatic, antihelmintic, tuberculostatic, antispermatozoal, and antifibrilatory agents.[16,17] Moreover, some phenanthrolines are endowed with antitumour activity against sarcomas in mice and inhibit formation of carcinomas in rats.[18,19]

In a recent study the reaction of guanosine with phen-Pt^{II} and Me_2phen-Pt^{II} substrates was investigated.[20] The results were interpreted as being due to formation of bis-guanosine adducts of formula *cis*-[Pt(*N*,*N*-phen)$(Guo)_2]^{2+}$ and *trans*-[PtCl(*N*-Me_2phen)$(Guo)_2]^{+}$. The presence of two H(8) resonances in *cis*-[Pt(*N*,*N*-phen)$(Guo)_2]^{2+}$ was interpreted as formation of two rotamers: one *HH* and one *HT*. However the *HH* rotamer should have inequivalent G moieties and therefore should give two H(8) signals of equal intensities. Moreover, two *HT* rotamers are possible (Λ*HT* and Δ*HT*), each of which should have equivalent G's, but the H(8) chemical shifts should be different for the two *HT* rotamers. In the second case examined (Me_2phen complex) the structure was essentially deduced from the observation of two signals in the methyl region with an intensity ratio of ca. 1:1. This was interpreted as being due to the presence of a *trans*-[PtCl(*N*-Me_2phen$)(Guo)_2]^{+}$ complex, with monocoordinated Me_2phen undergoing slow exchange of the donor atoms. The latter result was rather unusual since, in all complexes previously investigated by us and containing monocoordinated Me_2phen, the diamine undergoes fast exchange between the two nitrogens at room temperature.[21−23] The discrepancy between the newly reported data and those reported in the literature for analogous systems prompted us to reinvestigate the reaction of guanosine with platinum substrates containing phen and Me_2phen as carrier ligands.

Results and Discussion

Stereochemistry of *cis*-PtA_2G_2 Adducts

Previous reports have demonstrated that the 1,2-intrastrand cross-links formed by cisplatin with double-strand oligonucleotides have the guanines in a *Head-to-Head* (*HH*) conformation with both H(8)'s on the same side of the platinum coordination plane (Figure 2).[24−26] The phosphodiester linkage and the GC Watson−Crick base pairing of the vicinal guanosines are supposed to constrain such adducts in the *HH* conformation. In the case of cisplatin adducts with two guanine bases untethered by a phosphodiester linkage, the *Head-to-Tail* (*HT*) conformation is by far the most favoured at equilibrium, although the *HH* conformer should account for 50% on a statistical basis.[27]

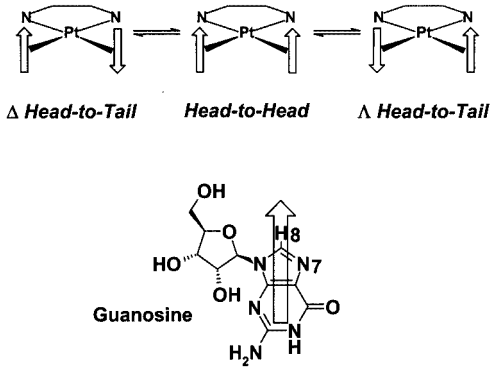

Figure 2. Schematic representation of *HH* and *HT* rotamers; arrows represent guanosines having H(8) coincident with the pointed end

Rotation about the Pt−**G**(N7) bonds in *cis*-PtA_2G_2 adducts [$\mathbf{A_2}$ = two monodentate or one bidentate amine ligand, **G** = N(7)-bound guanine base], interconverts *HH* and *HT* rotamers (Figure 2). When A_2 is a nonbulky ligand, the rotation about the Pt−**G**(N7) bonds is fast on the NMR timescale and only one set of NMR signals, which is an average of several conformations, is observed. In contrast, when A_2 is bulky, the rotation is restricted by steric interactions between the rotating guanines and the A_2 ligand(s) and different sets of signals are observed in the NMR spectra. In this respect the signals of the **G**(H8) protons are particularly informative. The number of H(8) signals detectable in solution for each *cis*-PtA_2G_2 conformer depends upon the symmetry of the A_2 carrier ligand and of the substituents at N(9) of the **G** residues. For carrier ligands of C_2, or higher, symmetry and asymmetric N(9) substituents the two **G**'s are equivalent within each *HT* conformer (Δ-*HT* and Λ-*HT*), and inequivalent within the *HH* conformer.

Complexes with Me_2phen (1 and 2)

[Pt(Me₂phen)(Guo)₂]Cl₂ (1)

The procedure used for the preparation of [Pt(Me_2phen)-$(Guo)_2]Cl_2$ (**1** in Figure 3) was different from that reported by Clement et al.[20] Instead of performing the reaction in water at high temperature (80 °C, 24 h) we carried out the reaction at room temperature (so reducing the risk of decomposition) in chloroform/methanol since the starting substrate [$PtCl_2$(Me_2phen)] is soluble in chloroform and guanosine is soluble in methanol. The desired product was formed in a shorter time (2 h) and with higher yield (90%) than reported in reference 20 (60% yield).

The ^{1}H NMR spectrum of complex **1**, in D_2O and pH* = 2.90 (the asterisk denotes pH values uncorrected for the effect of deuterium on the glass electrode), is reported in Figure 4 (a small amount of free guanosine was added to the sample for comparison). Two strong signals of unequal intensity (at δ = 8.51 and 8.52 ppm, intensity ratio 1:1.25) and two much weaker signals of equal intensities (at δ = 9.00 and 9.01 ppm) are observed in the region of H(8). The

downfield shift of the H(8) resonances relative to that for free guanosine (δ = 7.87 ppm at pH* = 2.90) is a clear indication that the nucleobases are coordinated to platinum through N(7).[28] This was further confirmed by pH titration experiments (Figure S1 in the Supporting Information, see also the footnote on the first page of this article). The two strong and more-shielded signals of unequal intensities are assigned to the *HT* rotamers (Δ-*HT* and Λ-*HT*), while the two weak and less-shielded signals of equal intensities

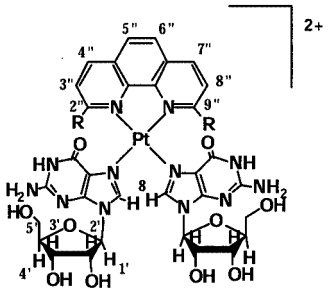

Figure 3. Schematic drawing and numbering schemes for compounds **1**–**4**

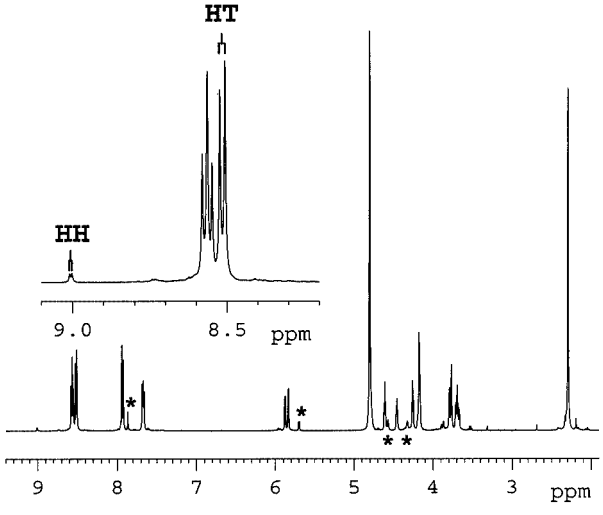

Figure 4. ^{1}H NMR spectrum of complex **1** in D_2O (pH* = 2.90, T = 298 K); the asterisks mark the signals of free guanosine added to the sample for comparison; the H(8) signals of the *HH* and *HT* rotamers are also labelled

are assigned to the *HH* conformer. Literature data indicate that the *HT* orientation can be stabilised with respect to the *HH* orientation in *cis*-Pt$\mathbf{A}_2\mathbf{G}_2$ adducts because of a better dipole-dipole interaction between the two guanine residues.

Three singlets at δ = 2.29, 2.32, and 2.33 ppm (intensity ratios 36:1:1) are observed for the methyl protons. Therefore, a large upfield shift (ca. 1 ppm) is experienced by these methyls upon substitution of the two chlorides by two guanosine molecules (for [$PtCl_2$(Me_2phen)] the Me chemical shift is at δ = 3.12 ppm in CD_3OD). The most intense signal, at δ = 2.29 ppm, is assigned to the two *HT* conformers, which therefore give coincident signals for the methyls in positions 2′′ and 9′′ of the phenanthroline moiety (see Figure 3 for the numbering scheme). The less-intense signals at δ = 2.32 and 2.33 ppm of 1:1 intensities are assigned to the *HH* conformer (for which the two methyls of Me_2phen are expected to be inequivalent). The chemical shifts of the phenanthroline Me's are influenced mostly by the shielding effect of the *cis*-coordinated nucleobase, while the effect of the chiral ribose, which should be responsible for the difference in chemical shift between *HT* rotamers and within the *HH* rotamer, is practically negligible.

The pattern of the methyl protons (1 ppm upfield shift) clearly indicates that Me_2phen is biscoordinated to platinum and the other two coordination positions are occupied by guanosine molecules. This complex composition is also supported by the absence of the typical Pt−Cl stretching frequency,[29] which is found in the IR spectrum of the precursor complex [$PtCl_2$(Me_2phen)] at 341 cm^{-1}.

The complete ^{1}H NMR analysis of the [Pt(Me_2phen)($Guo)_2$]$^{2+}$ complex with the assignments of all proton signals pertinent to the various rotamers is given in Table 1. The aliphatic region of a gradient-enhanced COSY spectrum showing the sequential assignment of the resonance peaks of the ribose protons is reported in Figure S2 (Supporting Information).

An interesting observation from the NOESY experiment is the presence of strong cross-peaks between H(8) and the sugar proton H(1′) for both *HT* rotamers (Figure S3). The presence of a cross-peak between H(8) of the guanine and the anomeric proton H(1′) is an indication that there is a *syn* contribution to the conformation of the nucleoside (the conformation is *anti* in natural B-DNA).[30−33] This result was also confirmed by a ROESY experiment (Figure S4) showing cross-peaks between the H(8) proton of the guanine and the sugar protons H(1′), H(2′) and H(3′). The ratio between the volumes of cross-peaks H(8)/H(1′) and H(8)/H(2′) is 2.1 and 1.8 for the two *HT* conformers, thus confirming the partial *syn* character of the nucleosides in these adducts. The 4.8 Hz value of the $^3J_{H1',H2'}$ coupling constant observed for the *HT* rotamers suggests a higher percentage of *S* puckering of the ribose rings (S/N sugar pucker ratio of ca. 54:46). None of the above NOE's was observed for the *HH* rotamer because of its low concentration in solution.

^{1}H NMR spectra were also recorded at higher temperatures in order to detect possible interconversion between the *HH* and the *HT* conformers. Under the experimental

Table 1. ^{1}H NMR chemical shifts (ppm) of the complexes (numbering of the protons as indicated in Figure 3); $^3J_{H,H}$ values (in Hz) are given in parentheses; s = singlet, d = doublet, dd = doublet of doublets, t = triplet, m = multiplet

			Phenanthroline							Guanosine					
Comp.	Conform.	Solv.	Me/H(2")	H(3")	H(4")	H(5"/6")	H(7")	H(8")	Me/H(9")	H(8)	H(1′)	H(2′)	H(3′)	H(4′)	H(5′)
1	*HT*$_M$	D_2O[a]	2.29 s	7.68d (8.3)	8.57 d (8.3)	7.94 s	8.57 d (8.3)	7.68 d (8.3)	2.29 s	8.51 s	5.84 d (4.9)	4.60 t	4.26 t	4.17 m	3.80−3.67 m
	HT$_m$	D_2O	2.29 s	7.66 d (8.3)	8.55 d (8.3)	7.92 s	8.55 d (8.3)	7.66 d (8.3)	2.29 s	8.52 s	5.88 d (4.9)	4.46 t	4.17 t	4.17 m	3.80−3.67 m
	HH	D_2O	2.32 s	7.60 dd (8.7)	[b]	7.95 s	[b]	7.60 dd (8.7)	2.33 s	9.01 s, 9.00 s	5.96 d, 5.94 d (5.0)	4.59 t, 4.68 t	4.19 t	4.34	4.00−3.92 m
2	M	CD_3OD	3.27 s	7.79 d (8.2)	8.65 d (8.2)	8.05 s	8.64 d (8.2)	7.67 d (8.2)	2.27 s	8.79 s	5.99 d (4.2)	4.50 t	4.32 t	4.14 m	3.94−3.74 m
	m		3.27 s	7.79 d (8.2)	8.66 d (8.2)	8.05 s	8.64 d (8.2)	7.67 d (8.2)	2.26 s	8.73 s	5.92 d (4.4)	4.58 t	4.30 t	4.14 m	3.94−3.74 m
3	*HT*$_M$	D_2O[c]	8.27	7.90 dd (8.3)	8.94	8.21 s	8.94	7.90 dd (8.3)	8.27	8.80 s	6.05 d (4.9)	4.65 t	4.31 t	4.25	3.95−3.60 m
	HT$_m$	D_2O	8.27	7.90 dd (8.3)	8.94	8.20 s	8.94	7.90 dd (8.3)	8.27	8.75 s	6.03	4.85 t	4.42	4.25	3.95−3.60 m
	HH	D_2O	8.36	7.90 d (8.3)	8.94	8.22 s	8.94	7.90	8.36	8.91 s, 8.86 s	6.05 d, 6.03 d (4.9)	4.67 t	4.43 t	4.25	3.90−3.70 m
4	M	CD_3OD	9.72	8.09	8.93	8.20 s	8.50	7.88	8.93	8.86 s	6.06 d (4.3)	4.68 t	4.37 m	4.14 m	3.94−3.72 m
	m		9.72	8.09	8.93	8.20 s	8.50	7.88	8.93	8.81 s	6.00 d (4.3)	4.57 t	4.37 m	4.14 m	3.94−3.72 m

[a] pH* = 2.90. [b] Obscured by overlapping signal of the *HT* conformers. [c] pH* = 3.00.

conditions used (solvent D_2O, pH* = 3.5), only a slight broadening of the resonance peaks was observed upon raising the temperature to 353 K (Figure S5). Complex **1** proved to be stable at high temperature for quite a long time as indicated by the similarity between the initial spectrum and that recorded at 298 K after a long stay at 353 K. The slow interconversion between rotamers, on the NMR timescale, was also confirmed by the absence of EXSY cross-peaks between the H(8) signals of the three rotamers in the NOESY-EXSY experiment (Figure S3).

Effect of Chloride Ions on the Ligand Exchange in Complex 1: Formation of [PtCl(Me$_2$phen)(Guo)]Cl (2)

It is well documented that in *cis*-Pt**A$_2$G$_2$** species the nucleobases are strongly bound to the platinum centre[34] and their displacement requires the use of strong nucleophiles such as CN^- or sulfur donor ligands. For example, the displacement of guanine from *cis*-$[Pt(NH_3)_2(Guanine)_2]^{2+}$ by thiourea has been calculated from ^{13}C NMR spectroscopic data to have a rate constant of 1.5×10^{-5} M^{-1} s^{-1} at 316 K.[35,36] Only in the case of strong *trans*-labilizing ligands, such as phosphanes, has the ready displacement of a coordinated guanosine by chloride been observed.[37]

The situation appears to be different when a solvent with a lower dielectric constant than water is used.[38] For instance $[Pt(Me_2phen)(Guo)_2]Cl_2$ dissolved in CD_3OD gave rise to a dissociation equilibrium in which two new species were formed, one of which was easily recognised as free guanosine. The second species shows two signals in the region of H(8) (δ = 8.79 and 8.73 ppm) and three singlets (δ = 3.27, 2.27, and 2.26 ppm, relative intensities 2:1:1) in the region of the methyl protons. Moreover, integration of the aromatic protons shows that only one molecule of guanosine is present per molecule of neocuproine. Therefore the new complex can be formulated as [PtCl(Me$_2$phen)(Guo)]Cl with a bidentate Me$_2$phen, one chloride, and one guanosine in the coordination sphere of platinum. Such a complex is expected to have inequivalent Me's with one Me (the one *cis* to the guanosine) more shielded than the other. The presence of two signals for H(8) and two signals at high field for the Me's (δ = 2.27 and 2.26 ppm) is indicative of the presence of two conformers stemming from restricted rotation of the guanosine about the Pt−N(7) bond (as observed for compound **1**). The two conformers are made diastereomeric by the presence of the asymmetric ribose. A noteworthy observation is that the average H(8) chemical shifts of the mono-guanosine derivative (δ = 8.76 ppm), which is not influenced by the magnetic anisotropy of a *cis*-**G**, falls right in between the average H(8) chemical shifts of the *HT* and *HH* rotamers of the bis-guanosine derivative. (δ = 8.51 and 9.01 ppm, respectively). Although some caution is needed since the overall charge of the complex (+1 and +2 for compounds **2** and **1**, respectively) and the set of donor atoms are different in the two cases, it nevertheless appears that, with respect to the monoadduct, in the bis-guanosine derivative the H(8)'s are shielded by the *cis* **G** in the *HT* rotamer and are deshielded by the *cis* **G** in the *HH* rotamer.

The same complex, [PtCl(Me$_2$phen)(Guo)]Cl (**2**), was prepared independently and fully characterised by ele-

mental analysis and ^{1}H NMR spectroscopy (the ^{1}H NMR spectrum in CD_3OD is reported in Figure S6). The complete assignment of the ^{1}H NMR chemical shifts for the two conformers of compound **2** is reported in Table 1. NOESY cross-peaks were observed (Figure S7) between the guanosine H(8)'s and the sugar protons H(1′) and H(2′). The H(8)−H(1′) cross-peaks indicate that the nucleoside conformation has a partial *syn* character, while the value of 4.4 Hz for the $^3J_{H1',H2'}$ coupling indicates a higher percentage of N-pucker for the ribose (S/N of ca. 49:51).

^{1}H NMR spectra were recorded at different temperatures in order to investigate the effect of the temperature upon the rate of interconversion between conformers in compound **2**. Unfortunately the monosubstituted guanosine derivative started to decompose at temperatures slightly above 50 °C. This shows that the attempt by Clement and co-workers[20] to prepare the bis-guanosine derivative of Me_2phen from a reaction in H_2O at 80 °C is probably not the most appropriate.

The dependence of the dissociation equilibrium of **1** in methanol [Equation (1)] upon the Cl^- concentration was confirmed by addition of KCl (three times the stoichiometric amount) to a solution of **1** in CD_3OD (NMR tube).

$$[Pt(Me_2phen)(Guo)_2]^{2+} + Cl^- \rightleftharpoons [PtCl(Me_2Phen)(Guo)_2]^+ + Guo \quad (1)$$

The molar ratio **1**:**2** changed from 3:1 to 2:1, supporting the involvement of the chloride ion in the equilibrium of displacement of one guanosine from complex **1**.

The observation of the displacement of a guanosine derivative by a chloride ion in a different solution environment (the phenomenon was not observed in water) could be relevant to the biochemistry of this type of substrates in lipophilic environments.

Complexes with phen (3 and 4)

[Pt(phen)(Guo)$_2$](NO$_3$)$_2$ (3)

Because of the low solubility of the starting dichloro complex [$PtCl_2$(phen)], this substrate was first converted into the solvato species $[Pt(phen)(DMF)_2]^{2+}$ by reaction with a stoichiometric amount of $AgNO_3$ in DMF and then allowed to react, at room temperature, with a stoichiometric amount of guanosine (ratio 1:2) to give [Pt(phen)-$(Guo)_2](NO_3)_2$. Once more our experimental conditions were different from those used by Clement and co-workers (starting material [$PtCl_2$(phen)] and reaction performed in water at 65 °C for three days).

The ^{1}H NMR spectrum of complex **3** in D_2O at pH* 3.0 is reported in Figure 5 (a small amount of free guanosine was added to the sample for comparison) and the complete assignment of the NMR spectroscopic data is reported in Table 1. Four peaks are observed in the H(8) region: two signals are much more intense and rather shielded (δ = 8.80 and 8.75 ppm, relative intensities 1.1:1) and two signals are very weak, rather deshielded, and of equal intensities (δ = 8.91 and 8.86 ppm). The two strong signals with different intensities were assigned to the two *HT* rotamers, each one having equivalent H(8) protons, while the two weaker signals were assigned to the *HH* conformer with inequivalent H(8)'s.

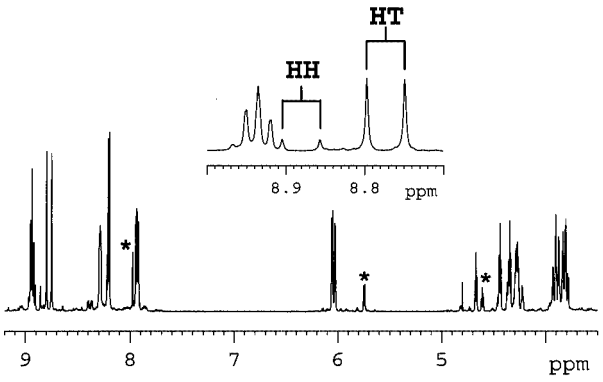

Figure 5. ^{1}H NMR spectrum of complex **3** in D_2O (pH* = 3.00, 298 K); the asterisks mark the peaks of free guanosine added to the sample for comparison; the H(8) peaks of the *HH* and *HT* rotamers are also labelled

The chemical shifts of the H(8) protons are indicative of N(7) coordination of the guanosine ligands. This type of coordination was also confirmed by a pH titration experiment.

A COSY experiment (Figure S8) allowed the assignment of all resonances (Table 1). A comparison of the 2D maps obtained in the ^{1}H-^{13}C HSQC experiments performed on complexes **3** and **1** (Figure 6) indicates that, differently from Clement's assignment,[20] the less-shielded signal (δ = 8.94 ppm) belongs to protons 4"/7′′ and the more-shielded signal (δ = 8.27 ppm) to protons 2"/9′′. It is likely that the aromatic ring current of the *cis*-coordinated guanosines is responsible for the shielding of protons 2"/9′′ (a similar effect has already been observed for methyls 2"/9′′ in the analogous complex **1**). Further support for our assignment of the aromatic protons comes from the presence of a ROESY cross-peak (C in Figure 7) between protons 5"/6′′ (δ = 8.21 ppm) and the less-shielded signal here assigned to protons 4"/7′′ (δ = 8.94 ppm). Significant ROESY cross-peaks are also observed between H(8) and H(2"/9") and between H(8) and H(1′) for the two *HT* rotamers (cross-peaks **B** and E, respectively). Similarly to the case of complexes **1** and **2**, the latter cross-peak gives an indication that the base/sugar conformation has some *syn* character. The ratios between the integrals of the ROESY cross-peaks H(8)−H(1′) and H(8)−H(2′) are equal to 2.17 and 1.63 for the two *HT* rotamers, respectively, suggesting a high percentage of S-pucker for the ribose. Such a pucker was also confirmed by the value of the $^3J_{H1'-H2'}$ coupling constant (4.9 Hz, which corresponds to an S/N ratio of ca. 55:45).

The effect of temperature on the rate of interconversion between *HT* and *HH* conformers was also investigated. The ^{1}H NMR spectrum of a sample of **3** in D_2O at pH* 3.50 and 355 K shows only a slight broadening of the peaks of the aromatic protons (Figure S9) with respect to the spectrum at 295 K, indicating that, even at the highest temperature explored, the rate of interconversion between rota-

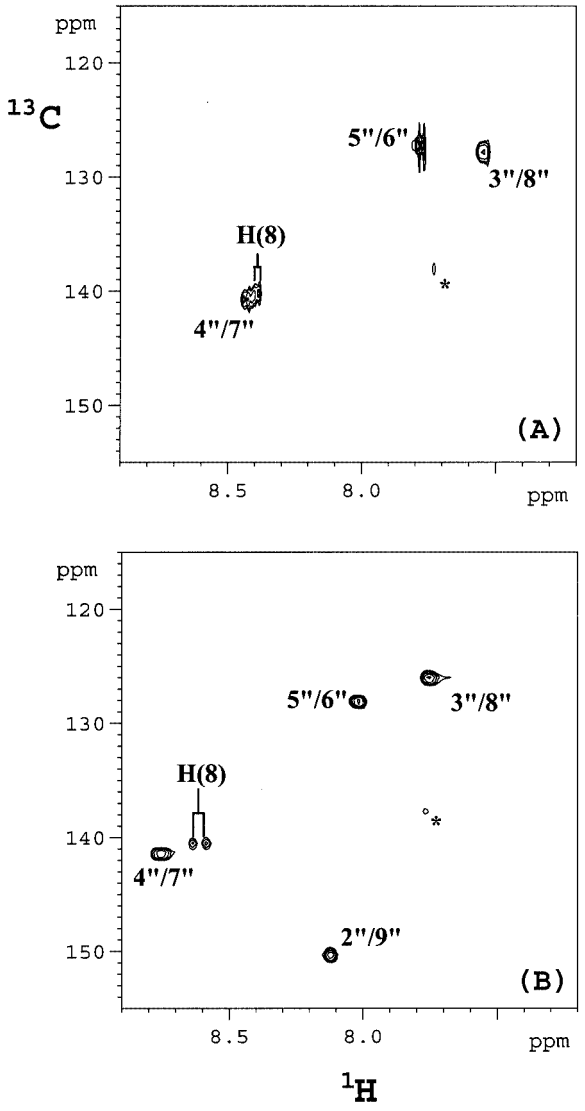

Figure 6. ^{1}H-^{13}C HSQC contour map of complex **1** (A) and complex **3** (B) in D_2O (pH* 2.90 and 3.00 for **1** and **3**, respectively; T = 298 K for both experiments); the asterisks mark the peaks of free guanosine added to the samples for comparison

mers is slow on the NMR timescale. Therefore the steric hindrance of the protons in positions 2′′ and 9′′ of phen is sufficient to prevent the free rotation of the guanosines about the Pt−N(7) bonds.

The analogy between the behaviour of **3** and that of **1** was quite unexpected since protons 2"/9′′ were not believed to inhibit the rotation around the Pt−N(7) bond to the same extent as the methyls 2"/9′′ of Me_2phen.

[PtCl(phen)(Guo)](NO$_3$) (4)

For the preparation of [PtCl(phen)(Guo)](NO_3) (**4**) the starting [$PtCl_2$(phen)] was first treated with one equivalent of $AgNO_3$ in DMF and then with one equivalent of guanosine. A small amount of complex **3** was always formed as a by-product in this reaction.

Similarly to the case of complex **2**, two sharp H(8) signals (at δ = 8.86 and 8.81 ppm, ratio 1.2:1) indicate the presence

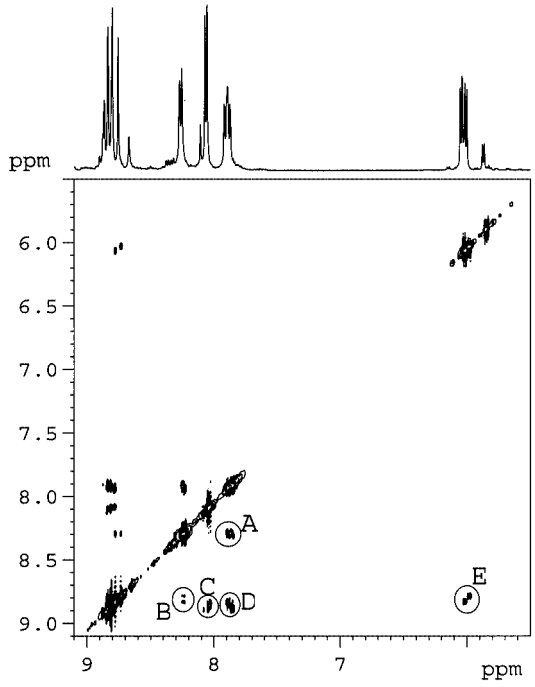

Figure 7. 2D-ROESY contour map of complex **3** in D_2O; the labelled cross-peaks are in antiphase with respect to the diagonal and represent intraresidual spatial couplings between protons of the *HT* rotamers: H(3"/8")−H(2"/9"), A; H(2"/9")−H(8), B; H(5"/6")−H(4"/7"), C; H(3"/8")−H(4"/7"), D; H(8)−H(1′), E

of two conformers in slow interconversion on the NMR timescale (Figure S10). The assignment of the ^{1}H NMR signals was facilitated by a COSY experiment (Figure 8) and is reported in Table 1. One *ortho* proton of phen is less shielded (δ = 9.72 ppm) and is assigned to the proton *cis* to the chlorine ligand (2′′ in Figure 3), since a similar chemical shift was observed for the *ortho* protons in the starting [$PtCl_2$(phen)] complex (δ = 9.80 ppm in [D_7]DMF). In con-

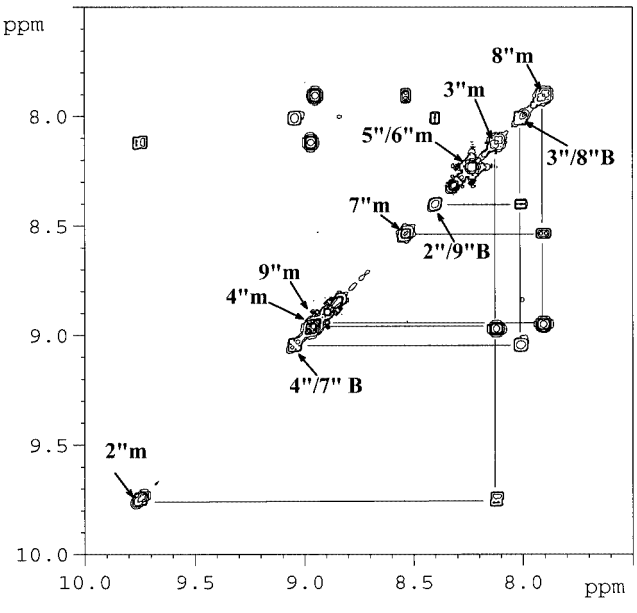

Figure 8. 2D-COSY contour map of complex **4** (resonances labelled m); resonances labelled B belong to complex **3**

trast, the *ortho* proton 9′′ undergoes an upfield shift of ca. 1 ppm which appears to be typical for an *ortho* proton *cis* to a guanine base. A similar upfield shift was observed for the *ortho* methyl(s) of Me_2phen *cis* to a guanine base.

The presence of two conformers indicates that there is also restricted rotation about the Pt−N(7) bond in the case of the monoadduct, and that the in-plane steric hindrance of the *ortho* protons of phen is sufficient to inhibit the free rotation of a *cis* guanosine.

The partial *syn* character of the guanosine conformation was also revealed by a ROESY experiment for compound **4**. The value of the $^3J_{H1',H2'}$ coupling (4.3 Hz) corresponds to an S/N pucker ratio of ca. 48:52.

As for Me_2phen and for phen the monoadduct has a slightly higher percentage of N pucker than the bis adduct and the average chemical shift of the H(8) protons falls in between the average H(8) chemical shifts of the *HH* and *HT* rotamers of the bis adduct.

Comparison between Me_2phen and Phen Derivatives

The differences in chemical shift between the H(8) signals of the two *HT* rotamers and between the two H(8) signals of the single *HH* rotamer observed in compounds **1** and **3** are very small ($\leq$ 0.05 ppm) when compared to those observed in similar compounds with C_2-symmetrical ligands having a strong asymmetry with respect to the coordination plane. These latter ligands were named Chirality Controlling Chelates, **CCC**, since they are able to favour one *HT* rotamer over the other and to induce a difference in the H(8) chemical shift between *HT* rotamers of the order of 0.2−0.4 ppm and a difference in chemical shift between the two guanines of the *HH* rotamer of the order of 0.8−1.1 ppm.[39−41]

The large dispersion of the H(8) signals within the *HH* conformer and between the two *HT* conformers observed in the platinum compounds with **CCC** ligands is mostly determined by the ability of these ligands to induce a preferential canting (either right- or left-handed) to the nucleobases. For a given direction of canting one *HT* rotamer will have the H(8) protons leaning towards the *cis* amine and deshielded while the second *HT* rotamer will have the H(8) protons leaning towards the *cis*-**G** and shielded. The two forms have been termed "6-in" and "6-out" since the former has the six-membered rings of the guanines closer to one another and the latter further apart. The *HH* rotamer will have one "6-in" and one "6-out" guanine, the former guanine will have a deshielded signal and the latter a shielded H(8) signal. Differently from **CCC** ligands, the phenanthroline ligands are perfectly symmetrical with respect to the coordination plane and cannot induce preferential canting of the nucleobases. Therefore the average canting could either be zero for all rotamers or, in the case of *HT* rotamers, be driven by the rotamer chirality. We will see (following section) that the latter is the case here. However there is no question that in **1** and **3** the differences between *HT* rotamers and between the two guanines of the *HH* conformer are determined entirely by the chiral ribose substituent, and are small.

There are some significant differences in chemical shifts between **3** and **1**. First, the chemical shift difference between the H(8) signals of the two *HT* rotamers and between the two H(8) signals of the single *HH* form is ca. 0.05 ppm in **3** and ca. 0.01 ppm in **1**. Second, the average H(8) chemical shift of the *HT* rotamers is at lower field in compound **3** than in compound **1** (δ = 0.26 ppm). Finally, the average H(8) chemical shift of the *HH* rotamer is at higher field in compound **3** than in **1** (δ = 0.12 ppm). All these features can be explained by assuming that, because of the smaller steric hindrance of the *ortho* substituents, the two guanosines have significantly greater wagging freedom in the case of phen than in the case of Me_2phen.

Therefore, with reference to the first point, the effect of the ribose in rendering the guanine bases within the *HH* rotamer and between the two *HT* rotamers magnetically inequivalent will be greater in **3** than in **1**.

With reference to the second point, the smaller shielding of the H(8) protons in the HT rotamers of **3** than in **1** is in agreement with the *HT* rotamers preferring the "6-in" conformation and the phen ligand allowing a greater canting of the guanine bases. The "6-in" conformation moves the six-membered ring of each guanine towards the *cis* **G** while the H(8) proton is moved towards the *cis* amine; it follows, therefore, that the more canted the bases are, the more deshielded the H(8) protons. The latter observation can be taken as proof that in the absence of other factors, such as the preferential canting imposed by **CCC** ligands, the canting of the bases is driven by the chirality of the *HT* conformer. The Δ-*HT* conformer induces an R canting and the Λ-*HT* conformer an L canting so that in both cases the six-membered rings move closer to each other and give a better internucleoside interaction. The canting direction [right-handed (R) or left-handed (L)] is defined by the chirality of two screw lines, one passing through the N(7) atoms of the two coordinated guanines and the other passing through H(8) and bisecting the given guanine.

With reference to the third point, we have to consider that in the *HH* rotamer the guanine with the "6-out" orientation is generally more canted and has a more-shielded H(8) signal than the guanine with the "6-in" orientation. Moreover, in the case of canting neutral phen ligands each guanine oscillates between the "6-in" and "6-out" conformations leading to an average H(8) signal which is similar for the two guanines. However, since the phen ligand allows for a more canted "6-out" conformation, the average H(8) chemical shift of the *HH* rotamer will be at higher field in compound **3** (δ = 0.12 ppm) than in compound **1**, in which the guanosines are more constrained to an orthogonal position.

Conclusions

This investigation has shown that phen and Me_2phen behave like other bidentate ligands, allowing the formation of platinum complexes in which one or both of the remaining two coordination positions can host guanosine ligands.

The features of the mono- and bis-guanosine adducts are strongly influenced by the special stereochemistry of the phen and Me_2phen ligands. First, both the Me_2phen and the phen carrier ligands are able to hinder rotation of the guanosine bases about the Pt−N(7) bonds so that the interconversion between rotamers becomes slow on the NMR timescale. Such a result was rather unexpected for phen. It is likely that the rigidity of the phenanthroline skeleton amplifies the steric impediment created by the small *ortho*-hydrogen atoms and restricts the free rotation of the *cis* guanosine ligand.

An interesting result of this investigation is that, by increasing the in-plane steric bulk of the carrier ligand (Me's instead of H's in positions 2/9 of the phenanthroline), the degree of wagging of the guanosine ligands is reduced and, in the case of Me_2phen, these ligands are forced to be more strictly orthogonal to the coordination plane. As a consequence: (i) the H(8) chemical shifts within the *HH* conformer and between *HT* conformers become more similar ($\Delta\delta$ of 0.01 ppm in the Me_2phen system as compared to 0.05 ppm in the case of phen), (ii) the H(8) protons of the *HT* conformers are more shielded ($\Delta\delta$ of 0.26 ppm), (iii) the H(8) protons of the *HH* rotamer are less shielded ($\Delta\delta$ of 0.12 ppm), and (iv) the *HT*/*HH* ratio is greater (ca. 18 and 8 in Me_2phen and phen, respectively).

Another result of this investigation is that in all the reported compounds the guanosine conformation appears to have some *syn* character.

Finally, the different behaviour of compound **1** in water and methanol solutions indicates that the solvent can play an important role in the stabilisation of cationic platinum adducts with purine bases when coordinating anions, such as Cl^-, are also present in solution.

Experimental Section

Physical Measurements: Elemental analyses were performed using a Carlo Erba Elemental Analyzer mod. 1106 instrument. IR Spectra were recorded on a Perkin−Elmer Spectrum One spectrometer using KBr as solid support for pellets. ^{1}H NMR spectra were recorded on a DPX 300 MHz WB Avance Bruker instrument. Chemical shifts are referenced to TMS using the residual protic peak of the solvent as internal reference (δ = 4.80 ppm for D_2O and δ = 3.30 ppm for CD_3OD). ^{1}H NMR experiments at different temperatures were performed using the heating control unit of the spectrometer. 2D ^{1}H NMR experiments were performed on a DRX 500 MHz WB Avance Bruker Instrument.

A Crison Micro-pH meter Model 2002 equipped with a Crison micro-combination electrode (9 mm diameter) and calibrated with Crison standard buffer solutions at pH 4.00 and 7.02 was used for all pH measurements. The pH readings for D_2O solutions are indicated as pH* values and are uncorrected for the effect of deuterium on glass electrodes.

Calculations of pK_a Values: The pH titration curves were fitted to the Henderson−Hasselbach equation using the program Kaleidagraph 3.0 for Macintosh.[42]

Starting Materials: Commercial reagent-grade chemicals, 2,9-Me_2-1,10-phenanthroline (Me_2phen, neocuproine), 1,10-phenanthroline (phen), guanosine (Guo), dimethyl sulfoxide (DMSO) and dimethylformamide (DMF) were used without further purification. $[PtCl_2(DMSO)_2]$ was prepared from an aqueous solution of K_2PtCl_4 and DMSO.[43] $[PtCl_2(Me_2phen)]$ was prepared by previously reported procedures.[21]

Preparation of Complexes

$[PtCl_2(phen)]$: A suspension of $[PtCl_2(DMSO)_2]$ (359 mg, 0.85 mmol) in methanol (100 mL) was treated with 1,10-phenanthroline (170 mg, 0.85 mmol). After stirring for one day, the newly formed precipitate was collected by filtration of the reaction mixture. The filtrate was concentrated to half its volume by evaporation of the solvent under reduced pressure and kept at room temperature for a few more days while another crop of yellow precipitate was formed. The combined solid fractions were washed with methanol and dried under vacuum to give 367 mg of product (97% yield based on starting platinum complex). $C_{12}H_8Cl_2N_2Pt$ (446.2): calcd. C 22.9, H 1.3, N 4.5; found C 22.6, H 1.3, N 4.4.

$[Pt(Me_2phen)(Guo)_2]Cl_2$ (1): $[PtCl_2(Me_2phen)]$ (250 mg, 0.53 mmol) was dissolved in methanol/chloroform (150 mL; 2:1, v/v) and a solution of guanosine in methanol (299 mg, 1.06 mmol, in 100 mL of solvent) was added dropwise to the resulting solution. The reaction mixture was stirred for two hours at room temperature and then taken to dryness by evaporation of the solvents under vacuum. The solid residue was treated with water (10 mL) and the mixture stirred overnight. The water solution was then filtered and taken to dryness by evaporation of the solvent under vacuum. The yellow residue proved to be pure $[Pt(Me_2phen)(Guo)_2]Cl_2$ (496 mg, 90% yield). $C_{34}H_{38}Cl_2N_{12}O_{10}Pt$ (1040.7): calcd. C 39.2, H 3.7, N 16.2; found C 39.8, H 3.5, N 16.8.

$[PtCl(Me_2phen)(Guo)]Cl$ (2): $[PtCl_2(Me_2phen)]$ (100 mg, 0.21 mmol) was dissolved in methanol/chloroform (80 mL; 2:1, v/v) and a stoichiometric amount (1:1 molar ratio) of guanosine dissolved in methanol (119 mg, 0.1 mmol, in 50 mL of solvent) was added dropwise to the resulting solution. The reaction mixture was stirred for two hours at room temperature and then concentrated under vacuum to 50 mL. Addition of diethyl ether induced the precipitation of a yellow product which was separated by filtration of the reaction mixture, washed with diethyl ether, and dried under vacuum to give 135 mg of product (85% yield). $C_{24}H_{25}Cl_2N_7O_5Pt$ (757.5): calcd. C 38.1, H 3.3, N 12.9; found C 37.8, H 3.1, N 12.7.

$[Pt(phen)(Guo)_2](NO_3)_2$ (3): $[PtCl_2(phen)]$ (200 mg, 0.56 mmol) was dissolved in DMF (70 mL) and treated with $AgNO_3$ (190 mg, 1.12 mmol) previously dissolved in the minimum amount of water. The solution was left stirring in the dark for 12 hours and a white precipitate of AgCl formed. The reaction mixture containing the solvato species $[Pt(DMF)_2(phen)]^{2+}$ was filtered through celite and treated with guanosine (317 mg, 1.12 mmol) previously dissolved in the minimum amount of DMF. This mixture was stirred for 5 hours at room temperature and then treated with diethyl ether to induce the formation of a yellow precipitate. The solid product was separated by filtration of the mother liquor, washed with several aliquots of diethyl ether and dried under vacuum to give 477 mg of product (80% yield). $C_{32}H_{34}N_{14}O_{16}Pt$ (1065.8): calcd. C 36.1, H 3.2, N 18.4; found C 36.6, H 3.3, N 18.2.

$[PtCl(phen)(Guo)](NO_3)$ (4): The procedure used for the preparation of $[PtCl(phen)(Guo)](NO_3)$ was similar to that used for compound **3** with the only difference being that only one equivalent of $AgNO_3$ and guanosine were added per mol of platinum substrate. In addition to compound **4** some compound **3** was also formed as

side-product, this prevented the characterisation of **4** by elemental analysis.

Acknowledgments

The authors thank the University of Bari, the "Ministero dell'Istruzione Università e Ricerca (MIUR)" (Cofin. N. 2001053898 and 2000 N. MMO3027791), and the EC (COST Chemistry projects D20/0001/2000 and D20/0003/01) for financial support. The authors are also grateful to Vincenzo Alicino for the help in the synthesis of the complexes.

[1] J. Reedijk, *Chem. Commun.* **1996**, 801−806.
[2] *Cisplatin. Chemistry and Biochemistry of a Leading Anticancer Drug* (Ed.: B. Lippert), Wiley VCH, Zurich, **1999**.
[3] S. E. Sherman, S. J. Lippard, *Chem. Rev.* **1987**, *87*, 1153−1181.
[4] A. Eastman, *Pharmacol. Ther.* **1987**, *34*, 155−166.
[5] A. M. J. Fichtinger-Schepman, J. L. van der Veer, J. H. J. Den Hartog, P. H. M. Lohman, J. Reedijk, *Biochemistry.* **1985**, *24*, 707−713.
[6] L. G. Marzilli, S. O. Ano, F. P. Intini, G. Natile, *J. Am. Chem. Soc.* **1999**, *42*, 9133−9142.
[7] K. M. Williams, L. Cerasino, F. P. Intini, G. Natile, L. G. Marzilli, *Inorg. Chem.* **1998**, *37*, 5260−5268.
[8] M. Carlone, F. P. Fanizzi, F. P. Intini, N. Margiotta, L. G. Marzilli, G. Natile, *Inorg. Chem.* **2000**, *39*, 634−641.
[9] S. T. Sullivan, A. Ciccarese, F. P. Fanizzi, L. G. Marzilli, *Inorg. Chem.* **2000**, *39*, 836−842.
[10] S. T. Sullivan, A. Ciccarese, F. P. Fanizzi, L. G. Marzilli, *Inorg. Chem.* **2001**, *40*, 455−462.
[11] H. C. Wong, R. Coogan, F. P. Intini, G. Natile, L. G. Marzilli, *Inorg. Chem.* **1999**, *38*, 777−787.
[12] D. Kiser, F. P. Intini, Y. Xu, G. Natile, L. G. Marzilli, *Inorg. Chem.* **1994**, *33*, 4149−4158.
[13] R. E. Cramer, P. L. Dahlstrom, *J. Am. Chem. Soc.* **1979**, *101*, 3679−3681.
[14] R. E. Cramer, P. L. Dahlstrom, *Inorg. Chem.* **1985**, *24*, 3420−3424.
[15] P. G. Sammes, G. Yahioglu, *Chem. Soc. Rev.* **1994**, *23*, 327−334.
[16] M. Nozaki, K. Ono, T. Nakazawa, S. Kotani, O. Hayaishi, *J. Biol. Chem.* **1968**, *243*, 2682−2690.
[17] A. R. Katritzky, A. J. Boulton, *Adv. Heteroc. Chem.* **1978**, *22*, 1−69 and references therein.
[18] J. Leiter, J. L. Hartwell, J. S. Kahler, I. Kline. M. J. Shear, *J. Natl. Cancer Inst.* **1953**, *14*, 365−374.
[19] Z. Broda, S. Bulba, *Res. Commun. Chem. Pathol. Pharmacol.* **1972**, *3*, 383−391.
[20] O. Clement, D. Macartney, E. Buncel, *Inorg. Chim. Acta* **1997**, *264*, 117−124.
[21] F. P. Fanizzi, F. P. Intini, L. Maresca, G. Natile, M. Lanfranchi, A. Tiripicchio, *J. Chem. Soc., Dalton Trans.* **1991**, 1007−1015.
[22] F. P. Fanizzi, M. Lanfranchi, G. Natile, A. Tiripicchio, *J. Chem. Soc., Dalton Trans.* **1994**, *33*, 3331−3339.
[23] R. J. H. Clark, F. P. Fanizzi, G. Natile, C. Pacifico, C. G: van Rooyen, D. A. Tocher, *Inorg. Chim. Acta* **1995**, *235*, 205−213.
[24] S. O. Ano, Z. Kuklenyik, L. G. Marzilli, in *Cisplatin. Chemistry and Biochemistry of a Leading Anticancer Drug* (Ed.: B. Lippert), Wiley VCH, Zurich, **1999**.
[25] G. Admiraal, J. H. van der Veer, R. A. G. de Graaff, J. H. J. den Hartog, J. Reedijk, *J. Am. Chem. Soc.* **1987**, *109*, 592−594.
[26] S. O. Ano, F. P. Intini, G. Natile, L. G. Marzilli, *J. Am. Chem. Soc.* **1998**, *120*, 12017−12022.
[27] S. O. Ano, F. P. Intini, G. Natile, L. G. Marzilli, *J. Am. Chem. Soc.* **1997**, *119*, 8570−8571.
[28] S. J. Berners-Price, U. Frey, J. D. Ranford, P. J. Sadler, *J. Am. Chem. Soc.* **1993**, *115*, 8649−8659.
[29] K. Nakamoto, *Infrared and Raman Spectra of Inorganic and Coordination Compounds*, John Wiley & Sons, inc., New York, **1997**.
[30] K. Wuthrich, *NMR of Proteins and Nucleic Acids*, John Wiley & Sons, New York, **1986**.
[31] J. S. Saad, T. Scarcia, K. Shinozuka, G. Natile, L. G. Marzilli, *Inorg. Chem.* **2002**, *41*, 546−557.
[32] L. G. Marzilli, S. O. Ano, F. P. Intini, G. Natile, *J. Am. Chem. Soc.* **1999**, *121*, 9133−9142.
[33] M. Polak, J. Plavec, A. Trifonova, A. Földesi, J. Chattopadhyaya, *J. Chem. Soc., Perkin Trans.* **1999**, *1*, 2835−2843.
[34] F. Basolo, R. G. Pearson, in *Mechanism of Inorganic Reactions*, John Wiley & Sons, New York, **1967**, Chapt. 5.
[35] J. A. Beaty, M. M. Jones, *Inorg. Chem.* **1992**, *31*, 2547−2551.
[36] M. Mikola, K. D. Kilka, A. Hakala, J. Arpalahti, *Inorg. Chem.* **1999**, *38*, 571−578.
[37] A. Habtemariam, J. A. Parkinson, N. Margiotta, T. W. Hambley, S. Parsons, P. J. Sadler, *J. Chem. Soc., Dalton Trans.* **2001**, 362−372.
[38] N. Margiotta, F. P. Fanizzi, J. Kobe, G. Natile, *Eur. J. Inorg. Chem.* **2001**, *5*, 1303−1310.
[39] L. G. Marzilli, F. P. Intini, D. Kiser, H. C. Wong, S. O. Ano, P. A. Marzilli, G. Natile, *Inorg. Chem.* **1998**, *37*, 6898−6905.
[40] S. O. Ano, F. P. Intini, G. Natile, L. G. Marzilli, *Inorg. Chem.* **1999**, *38*, 2989−2999.
[41] Y. Xu, G. Natile, F. P. Intini, L. G. Marzilli, *J. Am. Chem. Soc.* **1990**, *112*, 8172−8179.
[42] Kaleidagraph, Version 3.0 for Macintosh Computers, Abelbeck Software, **1993**.
[43] Yu. N. Kukushkin, Yu. E. Vyaz′menskii, L. I. Zorina, Yu. L. Pazukhina, *Zh. Neorg. Khim.* **1968**, *13*, 1595−1599.

Received May 21, 2002
[I02262]

Structural Variations and Formation Constants of First-Row Transition Metal Complexes of Biologically Active Aroylhydrazones

Claire M. Armstrong,[a] Paul V. Bernhardt,*[a] Piao Chin,[a] and Des R. Richardson[b]

Keywords: Hydrazones / Structure elucidation / Transition metals / N ligands

Iron chelators of the 2-pyridinecarbaldehyde isonicotinoylhydrazone (HPCIH) class show high potential for the treatment of iron overload diseases. In the present study, selected first-row transition metal (from Mn to Zn) complexes with HPCIH and 2-pyridinecarbaldehyde (4′-aminobenzoyl)hydrazone (HPCAH) were synthesised and characterised. Crystallography reveals that HPCAH exclusively forms bis complexes with divalent transition metals, with each ligand coordinating meridionally through its pyridine-N, imine-N and carbonyl-O atoms, forming distorted octahedral *cis*-MN_4O_2 complexes. Complexes of HPCIH were more varied and unpredictable, with metal/ligand ratios of 1:1, 1:2, 2:2 and 3:2 obtained with different metal ions. The isonicotinoyl ring N-atom in HPCIH was found to be an effective ligand, and this resulted in the varied metal/ligand ratios observed. The formation constants of divalent metal complexes with HPCIH were determined by potentiometric titrations and the values obtained were consistent with similar tridentate ligands and with the Irving–Williams order.

(© Wiley-VCH Verlag GmbH & Co. KGaA, 69451 Weinheim, Germany, 2003)

Introduction

In recent years the search for an orally effective drug for iron (Fe) overload diseases has gained increasing attention.[1−3] The motivating factors behind this interest are that the chelator in current clinical use, desferrioxamine B (DFO, see Scheme 1),[4] is expensive, is found to cause serious side effects in some patients, and is orally ineffective. In fact, DFO requires frequent and long periods of subcutaneous infusion leading to poor patient compliance.[5,6]

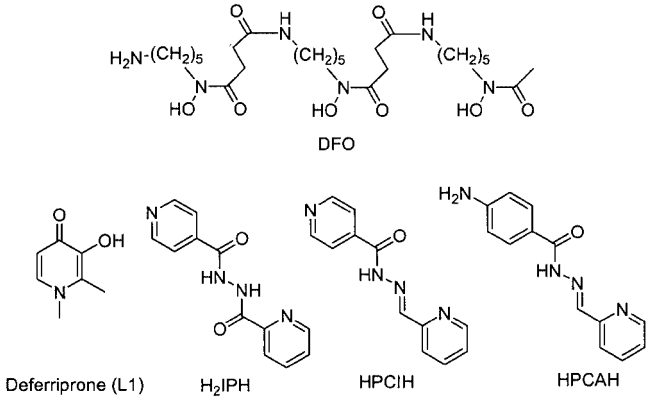

Scheme 1

An orally active alternative drug, deferiprone (also known as L1, see Scheme 1), was developed and extensively tested in the 1980s and 1990s,[7,8] but was found to result in myelotoxicity, liver fibrosis and have limited ability to reduce hepatic Fe levels.[9−11] Indeed, the use of this chelator remains controversial.[12] However, recent studies have shown more promise,[13−15] particularly when DFO is combined with Deferiprone.[16,17] Lipophilic Fe chelators have also been proposed for the treatment of other Fe-loading diseases such as the severe neurological disease Friedreich's ataxia.[18] If successful, this strategy will provide a new therapeutic application for these compounds.[18,19]

Our research program revolves around the design and synthesis of ligands that exhibit high Fe chelation efficacy and are potentially orally effective. We have designed and patented a novel class of ligands based on 2-pyridinecarbaldehyde isonicotinoylhydrazone (HPCIH, see Scheme 1), that have shown great promise in vitro, demonstrating a high Fe chelation efficacy.[20−22] Moreover, these chelators show very low toxicity in vitro in cultured cells and the compounds are simple and economical to prepare by a Schiff-base condensation reaction.[19−23]

Interestingly, and unexpectedly, the parent chelator of this class, HPCIH, has been shown to be oxidized by Fe^{III} to the diacylhydrazine, *N*-(isonicotinoyl)-*N*′-(picolinoyl)hydrazine (H_2IPH; see Scheme 1).[23] In contrast, in the absence of Fe^{III}, the parent hydrazone is not oxidized in aerobic aqueous solution.[23] To examine whether the diacylhydrazine H_2IPH could be responsible for the biological ef-

[a] Department of Chemistry, University of Queensland, Brisbane, Queensland 4072, Australia
Fax: (internat.) + 61-7/3365-4299
E-mail: P.Bernhardt@mailbox.uq.edu.au
[b] Children's Cancer Institute Australia for Medical Research, P. O. Box 81, High St, Randwick, Sydney, New South Wales 2031, Australia

fects of PCIH, their Fe chelation efficacy was compared. Unlike its parent hydrazone, the diacylhydrazine showed little Fe chelation activity, probably because the latter ligand was charged at physiological pH (pH = 7.4), hindering its access across membranes to cellular Fe pools.[23] In contrast, the IPH-Fe complex was charge-neutral, which would permit passage through cell membranes. These data allow a model of Fe chelation for this compound to be proposed: the parent aroylhydrazone (HPCIH) diffuses through cell membranes to bind Fe and is subsequently oxidized to the IPH-Fe complex, which then diffuses from the cell.[23] However, other diacylhydrazine ligands showed much higher activity, probably because they had a neutral charge.[23]

As part of our continuing research into the properties of this class of ligand we have investigated their coordination chemistry with divalent metal ions of the first transition series (Mn to Zn). This was relevant to our work as many of these metal ions are biologically important. From this class of chelators, HPCIH itself was examined as it represented the parent compound of these potential drugs and our earlier studies demonstrated that it possessed interesting properties.[23] For comparison, another member of this group has been assessed in parallel, namely, 2-pyridinecarbaldehyde (4-aminobenzoyl)hydrazone (HPCAH, Scheme 1), which does not bear a potentially bridging N-donor atom. The role of this latter ligating atom in HPCIH was important to assess as it could play a role in the chelation of some transition metal ions and result in different complexes to those found for HPCAH.

We were also interested to assess whether the unprecedented Fe-catalysed oxidation of HPCIH to its diacylhydrazine analogue H_2IPH discovered in our previous investigation[23] could be observed in HPCAH, or in the presence of other metal ions. The results obtained in this study are important for understanding the biological activity of HPCIH and its analogues, especially in terms of their affinity towards other biologically important divalent metal ions that can act as competitors against Fe in vivo.

Results and Discussion

Synthesis and Spectroscopic Properties

Upon reaction of 1 equiv. of the divalent metal ion (chloride salt), 2.5 equiv. of the ligand, and 2 equiv. of Et_3N in methanol, divalent complexes of the general formula ML_2 (M = Mn, Ni, Cu and Zn; L = $PCIH^-$ and $PCAH^-$) were obtained. The 2 equiv. of Et_3N accept protons released from the amide functional group upon complexation. The use of a suitable base was found to be important to afford good yields of the bis(complex), as the same experiments conducted without base gave poor yields or no product at all.

If the same synthesis is applied to the Fe^{II} and Co^{II} analogues, mixtures of products were obtained comprising varying ratios of metal and ligand. The synthesis in MeCN was straightforward by comparison. The Fe^{II} and Co^{II} complexes yield solid-state spin-only magnetic moments of 4.87 and 4.59 B.M., respectively, which are both indicative of high-spin d^6 and d^7 electronic ground states in pseudo-octahedral coordination environments.

In addition to the formation of ML_2 complexes, HPCIH exhibited a variety of other metal/ligand stoichiometries. Complexes of (H)PCIH with metal/ligand ratios of 1:1, 2:2 and 3:2 were obtained, although not with the HPCAH analogue, despite the application of similar conditions. This behaviour may be attributed to the presence of the unhindered N-donor on the isonicotinoyl ring of HPCIH. As seen from crystal structures of the three unusual complexes to be discussed later, the participation of the isonicotinoyl nitrogen atom in coordination evidently changes the way the complexes are formed. By contrast, the free amino group on HPCAH is an ineffective ligand as a result of conjugation of the N-atom lone pair with the aromatic ring.

The free ligand amide N−H (ca. 3450 cm^{-1}) and C=O (ca. 1650 cm^{-1}) stretching vibrations[24,25] are not observed in the IR spectra of the divalent $[M(PCAH)_2]$ and $[M(PCIH)_2]$ complexes. However, the complexes exhibit a strong absorption band at ca. 1600 cm^{-1} not observed in the free ligands, which is due to the conjugated C=N−N=C−O^- moiety.[26] Thus, in each ML_2 complex, the deprotonated ligands are predominantly in the enolate resonance form (Figure 1). The trivalent complex $[Co(PCAH)_2]Cl$ exhibits an IR spectrum essentially the same as the divalent bis complexes. By contrast, the IR spectrum of $[Zn(HPCIH)]SO_4$, where the amide N-atom is not deprotonated, exhibits both the amide N−H and C=O vibration bands (3422, 1684 and 1653 cm^{-1}) and the 1600 cm^{-1} peak characteristic of the deprotonated ligand is absent.

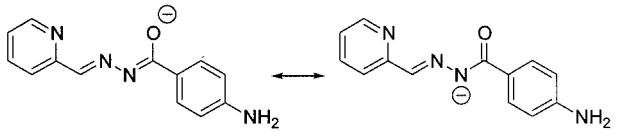

Figure 1. Line drawing of enol and keto resonance forms of $PCAH^-$

The ^{1}H NMR spectrum of $[Co(PCAH)_2]Cl$ shows that both ligands are deprotonated, with the amide-H being absent from the spectrum. In the ^{13}C NMR spectrum, the signals of the carbonyl and imine carbon atoms are shifted downfield by ca. 20 ppm, as expected when this ligand is coordinated through the imine-N and amide-O. Similar results were obtained with the $[Co(PCIH)_2]^+$ analogue.

The electronic spectra of the ML_2 complexes of $PCIH^-$ and $PCAH^-$ in methanol are very similar, and are dominated by intense ligand-based transitions in the near UV region (Table 1). However, the Ni^{II} complexes display weak maxima at ca. 840 nm while complexes of Cu^{II} exhibit maxima at ca. 690 nm, which are both due to d-d transitions. All bis(complexes) show one intense band at ca. 360 nm and one or two less-intense absorptions in the range 240−300 nm. In general, the ligand-based transitions for the (H)PCAH complexes are at lower energy than those for (H)PCIH complexes. Similar red-shifted maxima have been

Table 1. Electronic spectroscopic data (methanol, 298 K)

	λ_{max} [nm] (ε [dm^3 mol^{-1} cm^{-1}])
[Mn(PCAH)$_2$]	389 (24700), 328 (36100)
[Fe(PCAH)$_2$]	633 (2180), 381 (33500), 332 (32800)
[Co(PCAH)$_2$]	392 (25500), 291 (12400)
[Co(PCAH)$_2$]Cl	427 (43900), 284 (26500)
[Ni(PCAH)$_2$]	851 (49), 395 (55000), 295 (19000)
[Cu(PCAH)$_2$]	690 (250), 396 (100000), 300 (47600), 270 (47900)
[Zn(PCAH)$_2$]	391 (35800), 299 (14700), 268 (11600)
[Mn(PCIH)$_2$]	363 (56900), 280 (32400)
[Fe(PCIH)$_2$]	649 (4010), 349 (39000), 268 (19500), 229 (35200)
[Co(PCIH)$_2$]	490 sh (ca. 1000), 356 (30200), 275 (15100)
[Co(PCIH)$_2$]NO$_3$	430 sh (ca. 7700), 381 (17600), 273 (30700)
[Ni(PCIH)$_2$]	857 (21), 373 (17200), 278 (10000)
[Cu(PCIH)$_2$]	699 (53), 367 (25500), 241 (21700)
[Zn(PCIH)$_2$]	363 (25100), 277 (12000)

observed for similar Mn, Fe and Cu complexes when the substituent on the ligand becomes more strongly electron-donating.[27−33] In the electronic spectrum of [Co(PCAH)$_2$]Cl, the intense absorption at ca. 360 nm observed in the other bis(complexes) is shifted significantly to a lower energy at 427 nm (Table 1). This suggests that this electronic transition is of ligand-to-metal charge-transfer origin, with the lower energy reflecting the greater ease of reduction of the trivalent metal ion than the other divalent analogues.

Description of Crystal Structures

HPCAH

The crystal structure of HPCAH·H$_2$O (Table 2) has been determined and a view of the molecule is shown in Figure 2. The bond lengths and angles (Table 3) are as expected for a compound of this type and agree with the other ligands belonging to the HPCIH series.[21] Of note is the C7−O1 bond length, which is typical of a double bond, and the N2−N3 bond, which has a bond order intermediate between a single and a double bond.

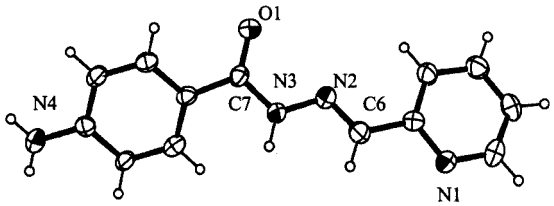

Figure 2. View of HPCAH structure (30% probability ellipsoids)

[M(PCAH)$_2$]·H$_2$O (M = Mn, Ni, Cu and Zn)

The molecular structure of Mn(PCAH)$_2$ is shown in Figure 3. Structures of the Ni^{II}, Cu^{II} and Zn^{II} analogues are very similar and are not shown. Selected bond lengths and angles are listed in Table 3. Each metal ion has a *cis*-N$_4$O$_2$ coordination sphere, where the two deprotonated ligands bind meridionally through their pyridine-N, imine-N and carbonyl-O atoms. The coordinated ligands from two five-membered chelate rings, imposing large distortions on the ideally octahedral coordination angles. The *trans*-N2A−M−N2B angles are close to 180°, whereas the *trans*-N1A(B)−M−O1A(B) angles defined by each meridionally coordinated ligand deviate markedly from linearity; this distortion is greatest for the largest metal ions in the series (Mn^{II} and Zn^{II}). Distortion of the *cis* coordination angles defined by the five-membered chelate rings also increases with metal ion size. The M−N(pyridine), M−N(imine) and M−O bond lengths observed here are within the range reported for other similar complexes of divalent metal ions.[32−36] The variations in C−C, C−N, C−O and N−N bond lengths and angles across the [M(PCAH)$_2$] series are very small, as expected. In general, the average M−N2A(B) distances are significantly shorter than the M−N1A(B) distances, which can be attributed to greater π-back-bonding in the M−N(imine) bond than in the M−N(pyridine)

Table 2. Crystal data for HPCAH and its complexes

	HPCAH·H$_2$O	[Mn(PCAH)$_2$]·H$_2$O	[Ni(PCAH)$_2$]·H$_2$O	[Cu(PCAH)$_2$]·H$_2$O	[Zn(PCAH)$_2$]·H$_2$O
Empirical formula	$C_{13}H_{14}N_4O_2$	$C_{26}H_{24}MnN_8O_3$	$C_{26}H_{24}N_8NiO_3$	$C_{26}H_{24}CuN_8O_3$	$C_{26}H_{24}N_8O_3Zn$
Formula mass	258.28	551.47	555.24	560.07	561.90
Crystal system	orthorhombic	monoclinic	monoclinic	monoclinic	monoclinic
a [Å]	6.38280(5)	9.339(1)	9.379(3)	9.375(2)	9.366(2)
b [Å])	18.2310(2)	13.534(2)	13.616(2)	13.739(1)	13.643(2)
c [Å]	22.071(1)	20.846(3)	20.180(2)	20.147(2)	20.417(3)
β [°]		102.880(3)	103.255(9)	103.330(10)	103.190(10)
V [Å^3]	2568.3(1)	2568.5(6)	2508.4	2525.1	2540.1(8)
T [K]	296	296	296	296	296
Z	8	4	4	4	4
Space group	*Pbca*	*P*2$_1$/*n*	*P*2$_1$/*c*	*P*2$_1$/*n*	*P*2$_1$/*c*
μ (Mo-K_α [mm^{-1}])	0.094	0.559	0.819	0.911	1.012
Indep. reflections (R_{int})	2253 (0.000)	4510 (0.0347)	4400 (0.0732)	4431 (0.0724)	4464 (0.0767)
R_1 (obsd. data)	0.0490	0.0657	0.0695	0.0524	0.0703
wR_2	0.1139	0.1650	0.1274	0.1163	0.1445

Table 3. Selected bond lengths [Å] and angles [°] of free ligand and metal complexes of HPCAH

	$HPCAH·H_2O$	$[Mn(PCAH)_2]·H_2O$	$[Ni(PCAH)_2]·H_2O$	$[Cu(PCAH)_2]·H_2O$	$[Zn(PCAH)_2]·H_2O$
M−N1A	−	2.321(5)	2.095(7)	2.180(6)	2.259(7)
M−N1B	−	2.282(5)	2.125(7)	2.234(7)	2.207(7)
M−N2A	−	2.170(4)	1.976(7)	1.949(6)	2.048(7)
M−N2B	−	2.169(4)	1.976(7)	1.956(6)	2.051(7)
M−O1A	−	2.137(4)	2.100(6)	2.124(5)	2.113(6)
M−O1B	−	2.152(4)	2.100(6)	2.173(5)	2.139(5)
N1A−M−O1A	−	143.76(15)	154.8(3)	154.6(2)	150.4(2)
N1B−M−O1B	−	142.95(16)	155.2(3)	152.6(2)	149.9(2)
N2A−M−N2B	−	173.72(17)	178.7(4)	178.0(3)	175.2(3)
N1A−M−N1B	−	90.45(17)	93.9(3)	93.0(2)	91.7(2)
N1A−M−N2B	−	102.05(16)	102.3(3)	101.5(2)	100.0(3)
N2A−M−N1B	−	106.32(17)	100.2(3)	104.7(2)	105.1(2)
N1A−M−N2A	−	71.82(17)	78.5(3)	77.8(2)	75.3(3)
N2A−M−O1A	−	72.20(15)	76.4(3)	76.8(2)	75.2(3)
C6A−N2A	1.265(7)	1.290(7)	1.260(11)	1.282(9)	1.261(10)
C6B−N2B	−	1.256(7)	1.274(11)	1.281(9)	1.259(10)
C7A−N3A	1.374(8)	1.362(7)	1.350(11)	1.344(9)	1.347(10)
C7B−N3B	−	1.324(7)	1.349(10)	1.344(10)	1.338(10)
C7A−O1A	1.228(7)	1.276(6)	1.268(9)	1.274(8)	1.267(8)
C7B−O1B	−	1.280(6)	1.257(9)	1.256(8)	1.272(9)
N2A−N3A	1.365(6)	1.365(6)	1.367(9)	1.360(7)	1.367(9)
N2B−N3B	−	1.372(6)	1.361(9)	1.380(7)	1.369(8)

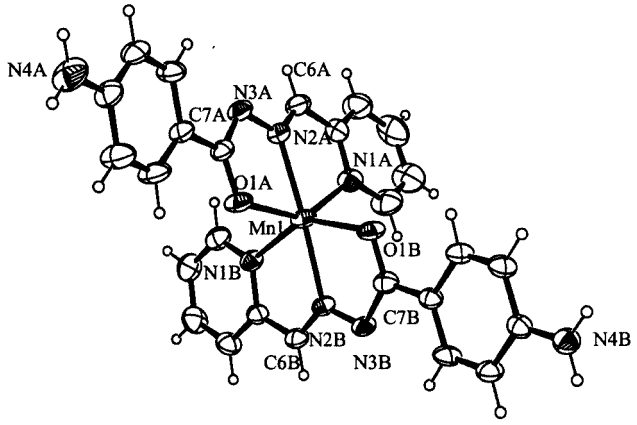

Figure 3. View of the $[Mn(PCAH)_2]$ molecule (30% probability ellipsoids)

bond[36,37] and also to the steric requirements of the meridionally coordinated ligand.

Although the C6A(B)−N2A(B) and N2A(B)−N3A(B) bond lengths are unaffected by complexation [ca. 1.27 and 1.37 Å in the complexes compared with 1.265(7) and 1.365(6) Å in the free ligand, respectively], the C7A(B)−O1A(B) bond lengthens significantly (by ca. 0.04 Å); variations in the C7A(B)−N3A(B) bond upon complexation are less pronounced. Overall, these observations are consistent with the enolate resonance form of the ligand (Figure 1) being dominant in the deprotonated coordinated ligand, and this is supported by the IR spectroscopic data.[36,38−45]

HPCIH Complexes

Crystal data and selected bond lengths and angles of the various HPCIH complexes are given in Tables 4 and 5 respectively. The molecular structure of $[Cu(PCIH)_2]$ is shown in Figure 4. The four (Cu, Ni and both Co) bis(complexes) of HPCIH share common structural characteristics with the ML_2 complexes of $PCAH^-$ described above. All metal ions have *cis*-N_4O_2 coordination spheres, where each of the two ligands binds the metal ion meridionally via the pyridine-N, imine-N and carbonyl-O atoms. In most cases the bond lengths in the $[M(PCIH)_2]$ complexes (Table 5) are similar to those found in $PCAH^-$ analogues (Table 3). This implies that the coordinated HPCIH ligand also exists predominantly in the enolate resonance form with the conjugated C=N−N=C−O^- moiety, agreeing with the IR spectra.

Two Co^{III} complexes of HPCIH were isolated, shown in Figures 5 and 6. $[Co(HPCIH)(PCIH)](NO_3)_2$ exhibits a structure (Figure 5) similar to the Cu^{II} and Ni^{II} bis(complexes), except that one of the ligands is protonated at its isonicotinoyl N-atom; i.e., the protonated ligand is present in a zwitterionic (pyridinium/amidate) form. The other cobalt complex of HPCIH consists of two cobalt ions: an octahedral Co^{III} coordinated within the expected N_4O_2 donor set and a tetrahedral Co^{II} ion coordinated to three chloride ions and the nitrogen atom of the isonicotinoyl ring (Figure 6, Table 6). Since a 1:2 ratio of Co/HPCIH was used in the synthesis, the formation of this complex may be attributed to the strong tendency for the free isonicotinoyl nitrogen atom to coordinate.

The fact that DMSO is an effective ligand, together with the presence of residual chloride ions and the strongly coordinating isonicotinoyl nitrogen atom, are compounding reasons that lead to the isolation of $[\{MnCl_2(DMSO)(HPCIH)\}_2Mn(DMSO)_2Cl_2]$, as an unusual M_3L_2 complex (Figure 7, Table 6). The bridging Mn (Mn1), at a centre of symmetry, bears no chelate rings, so all *cis* coordination angles are close to 90°. The coordination

Table 4. Crystal data of metal complexes of HPCIH

	[{$MnCl_2$(DMSO)-(HPCIH)}$_2$Mn(DMSO)$_2Cl_2$]	[Co(PCIH)$_2CoCl_3$]·$2H_2O$	[Co(HPCIH)(PCIH)]-$(NO_3)_2$·H_2O·$^1/_2CH_3OH$	[Ni(PCIH)$_2$]·$2H_2O$	[Cu(PCIH)$_2$]	[Zn(HPCIH)]SO_4·$3^1/_2H_2O$
Empirical formula	$C_{32}H_{44}Cl_6Mn_3N_8O_6S_4$	$C_{24}H_{22}Cl_3Co_2N_8O_4$	$C_{24.5}H_{23}CoN_{10}O_{9.5}$	$C_{24}H_{22}N_8NiO_4$	$C_{24}H_{18}CuN_8O_2$	$C_{12}H_{17}N_4O_{8.5}SZn$
Formula mass	1142.52	710.71	688.46	545.21	514.00	450.73
Crystal system	monoclinic	triclinic	triclinic	triclinic	monoclinic	monoclinic
a [Å]	17.169(4)	12.101(1)	9.947(1)	8.2500(9)	8.2361(5)	6.654(2)
b [Å]	7.1321(5)	12.3805(9)	12.741(2)	8.656(2)	20.290(3)	15.034(2)
c [Å]	20.389(3)	13.542(2)	13.744(2)	17.305(3)	13.695(1)	16.878(4)
α [°]		97.726(8)	62.27(1)	91.17(2)		
β [°]	105.82(2)	116.009(9)	72.472(9)	94.86(1)	102.518(7)	97.90(3)
γ [°]		107.599(7)	84.753(9)	93.03(1)		
V [Å^3]	2402.1(7)	1651.4(3)	1467.8(3)	1229.2(4)	2234.2(4)	1672.4(7)
T [K]	296	296	296	296	296	296
Z	4	2	2	2	4	4
Space group	$P2_1/a$	$P\bar{1}$	$P\bar{1}$	$P\bar{1}$	$P2_1/a$	$P2_1/n$
μ [mm^{-1}]	1.332	1.287	0.656	0.837	1.019	1.649
Indep. reflections (R_{int})	4232 (0.0286)	5785 (0.0878)	5144 (0.0243)	4323 (0.0496)	3908 (0.0367)	2930 (0.0392)
R_1 (obsd. data)	0.0841	0.1018	0.0715	0.0554	0.0408	0.0459
wR_2	0.2110	0.2788	0.2242	0.1204	0.0942	0.1019

Table 5. Selected bond lengths [Å] and angles [°] for mononuclear metal complexes of HPCIH

	[Co(HPCIH)(PCIH)]$(NO_3)_2$·H_2O·$^1/_2CH_3OH$	[Ni(PCIH)$_2$]·$2H_2O$	[Cu(PCIH)$_2$]	[Zn(HPCIH)]SO_4·$3^1/_2H_2O$
M−N1A	1.920(5)	2.109(5)	2.118(3)	2.120(5)
M−N1B	1.915(4)	2.128(4)	2.301(4)	–
M−N2A	1.848(5)	1.975(4)	1.946(3)	2.091(5)
M−N2B	1.858(5)	1.976(4)	1.992(3)	–
M−O1A	1.915(4)	2.121(4)	2.096(3)	2.219(4)
M−O1B	1.918(4)	2.093(4)	2.328(3)	–
N1A−M−O1A	165.11(18)	154.48(15)	153.36(12)	149.25(17)
N1B−M−O1B	165.02(18)	153.63(16)	148.58(11)	–
N2A−M−N2B	176.6(2)	176.7(2)	172.00(15)	–
N1A−M−N1B	92.0(2)	87.17(18)	97.20(13)	–
N1A−M−N2B	99.7(2)	103.67(18)	104.45(13)	–
N2A−M−N1B	99.3(3)	99.40(18)	96.03(13)	–
N1A−M−N2A	83.0(2)	78.62(19)	78.12(13)	76.62(18)
N2A−M−O1A	82.12(19)	75.87(17)	77.04(12)	72.71(15)
C6A−N2A	1.278(8)	1.288(7)	1.284(5)	1.254(7)
C6B−N2B	1.286(7)	1.282(7)	1.277(5)	–
C7A−N3A	1.309(8)	1.334(7)	1.333(5)	1.345(7)
C7B−N3B	1.322(7)	1.339(7)	1.332(5)	–
C7A−O1A	1.299(7)	1.255(6)	1.269(4)	1.230(7)
C7B−O1B	1.289(7)	1.267(6)	1.250(5)	–
N2A−N3A	1.381(7)	1.382(6)	1.360(4)	1.359(6)
N2B−N3B	1.375(6)	1.358(6)	1.367(5)	–

sphere comprises two DMSO ligands, two chloride ions and two isonicotinoyl residues. The symmetry-related Mn ions (Mn2 and Mn2′) are each coordinated in a tridentate fashion to an HPCIH ligand. It is interesting to note that the two chloride ions on the central Mn1 are *trans* oriented, whereas on Mn2 the chloride ions are *cis*. A large distortion from octahedral geometry is imposed by the tridentate coordinated HPCIH ligand on the ideally linear N1−Mn−O1 bond angle, which is contracted to 138.1(2)°. No substantial C7−O1 bond lengthening or C7−N3 bond shortening is observed in the complex relative to free ligand. The amide N3 atom is not deprotonated, thus preventing the formation of enolate ion and the conjugated C=N−N=C−O$^-$ moiety.

In the case of [Zn(HPCIH)SO_4], the participation of the isonicotinoyl nitrogen atom and sulfate anions in coordination led to a surprising result (Figure 8). The N_2O-tridentate HPCIH is again bonded to Zn^{II} meridionally in addition to an isonicotinoyl nitrogen atom *trans* to the imine nitrogen atom. These ZnN_3O moieties are arranged in parallel planes, with bridging sulfate anions occupying the sites perpendicular to this plane. The result is a three-dimensional coordination polymer. This mode of coordination is in contrast to the other complexes reported herein, which

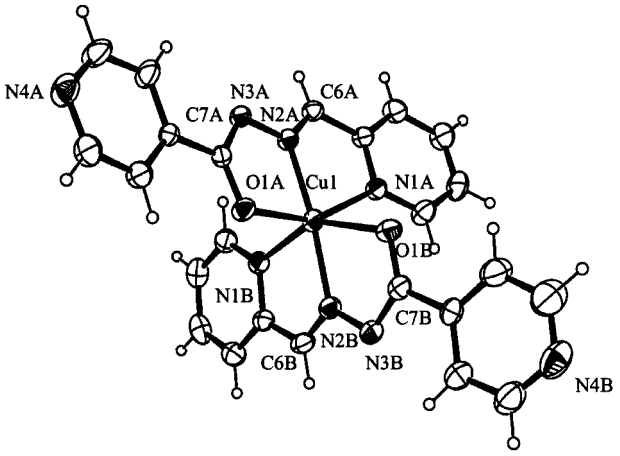

Figure 4. View of the $[Cu(PCIH)_2]$ molecule (30% probability ellipsoids)

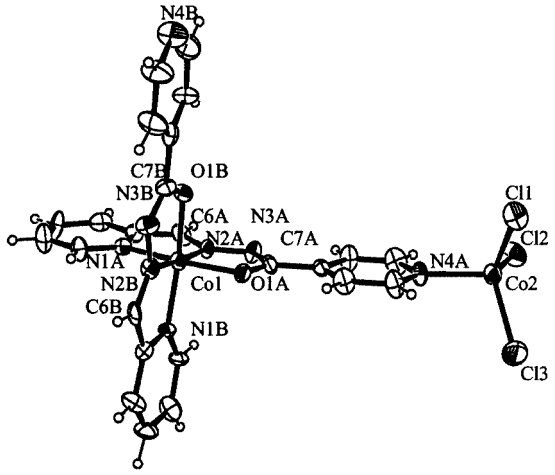

Figure 6. View of the $[Co(PCIH)_2CoCl_3]$ molecule (30% probability ellipsoids)

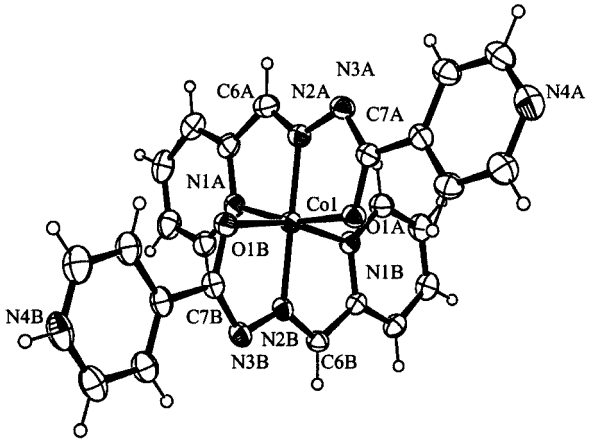

Figure 5. View of the $[Co(HPCIH)(PCIH)]^{2+}$ cation (30% probability ellipsoids)

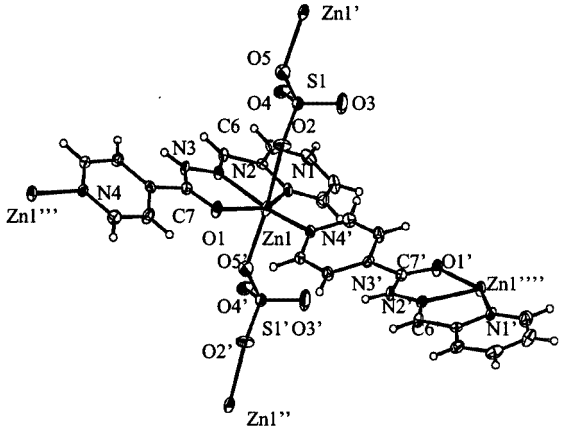

Figure 8. Partial view of the polymeric $[Zn(HPCIH)]SO_4$ structure (30% probability ellipsoids)

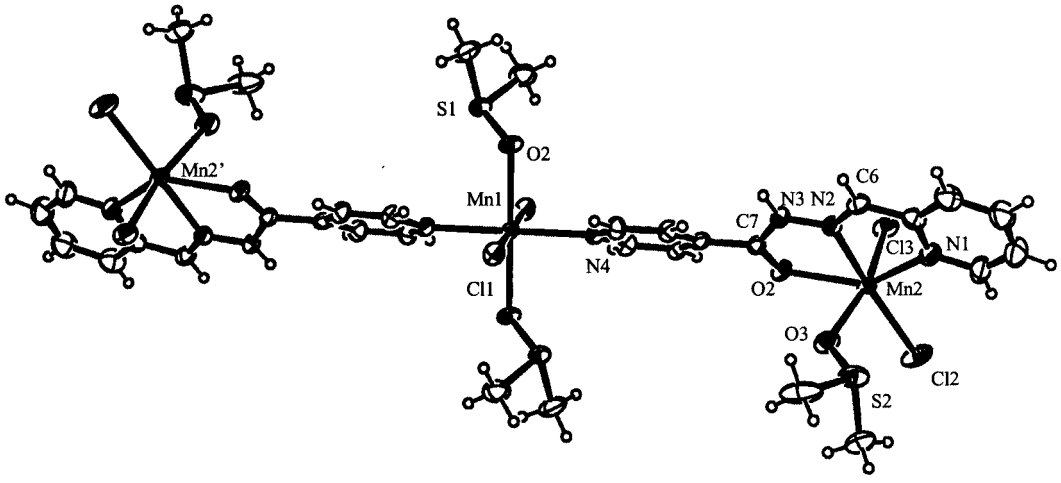

Figure 7. View of $[\{MnCl_2(DMSO)(HPCIH)\}_2Mn(DMSO)_2Cl_2]$ structure (30% probability ellipsoids)

are discrete molecules. While the *trans*-O2−Zn−O3′ and -N2−Zn−N4′ bonds are almost linear, the *trans*-N1−Zn−O1 bond is bent to 149.3(2)°. The C7−O1 and C7−N3 bond lengths in this complex are similar to those in the free ligand. The fact that the hydrazone remains protonated in this complex results in these bonds retaining their double bond character in the absence of the electron delocalisation seen in the complexed deprotonated ligands.

Table 6. Selected bond lengths [Å] and angles [°] of oligonuclear HPCIH complexes

	[{$MnCl_2$(DMSO)-(HPCIH)}$_2$Mn(DMSO)$_2Cl_2$]	[Co(PCIH)$_2$-$CoCl_3$]·$2H_2O$
M1−N1A	2.312(6)	1.925(13)
M1−N1B	−	1.896(13)
M1−N2A	2.258(6)	1.850(12)
M1−N2B	−	1.847(13)
M1−O1A	2.311(4)	1.907(11)
M1−O1B	−	1.915(11)
M2−N4A	2.292(5)	2.034(13)
M2−Cl3	2.499(2)	2.242(7)
N1A−M1−O1A	138.14(19)	165.1(5)
N1B−M1−O1B	−	165.4(5)
N2A−M1−N2B	−	174.4(7)
N1A−M1−N1B	−	91.7(6)
N1A−M1−N2B	−	99.2(6)
N2A−M1−N1B	−	101.4(6)
N1A−M1−N2A	69.2(2)	82.7(6)
N2A−M1−O1A	68.96(17)	82.4(5)
N4A−M2−Cl3	88.14(14)	105.6(5)
C6A−N2A	1.266(8)	1.27(2)
C6B−N2B	−	1.29(2)
C7A−N3A	1.344(8)	1.32(2)
C7B−N3B	−	1.31(2)
C7A−O1A	1.233(8)	1.326(19)
C7B−O1B	−	1.309(19)
N2A−N3A	1.356(7)	1.348(17)
N2B−N3B	−	1.375(19)

Overall, it can be concluded that the active participation of the isonicotinoyl nitrogen of HPCIH in bonding has led to a much more varied and unpredictable coordination chemistry.

EPR Spectroscopy of Copper(II) Complexes

The Jahn−Teller distortions observed in most six-coordinate Cu^{II} complexes[46] are revealed in the crystal structure of [Cu(PCIH)$_2$], where the *trans*-Cu−N1B and -Cu−O1B bonds are exceptionally long [2.301(4) and 2.328(3) Å, respectively] compared to the other four coordination bonds (Table 5). However, this distortion is not apparent in the structure of [Cu(PCAH)$_2$]·H_2O (Table 3). EPR spectroscopy was employed to resolve this issue. [Cu(PCIH)$_2$] and [Cu(PCAH)$_2$] exhibit identical EPR spectra (Figure 9) and these could be simulated with identical, axially symmetric spin Hamiltonian parameters ($g_{\|}$ = 2.262, $g_{\perp}$ = 2.09, $A_{\|}$ = 122 *G* and $A_{\perp}$ = 25 G). These parameters are consistent with a tetragonally elongated d^9 complex in a $d_{x^2-y^2}$ ground state ($g_{\|} > g_{\perp}$ and $A_{\|} > A_{\perp}$) with significant distortion of the in-plane *cis* coordinate angles away from 90° ($A_{\|} <<$ 200 G). Note that the broad feature around 3300 G ($g \approx$ 2) is due to an impurity in the EPR spectrometer cavity, and so the experimental and simulated spectra are obviously different in this region. The EPR results indicate that the copper ions are in the same electronic environment in both [Cu(PCIH)$_2$] and [Cu(PCAH)$_2$] despite their apparent structural differences. That is, the bond lengths found in [Cu(PCIH)$_2$] are representative of the true tetragonally elongated structures of both [Cu(PCIH)$_2$] and [Cu(PCAH)$_2$], whereas the geometry defined by the crystal structure of [Cu(PCAH)$_2$] is a weighted average of two tetragonally elongated forms, and thus apparently (but not really) tetragonally compressed.

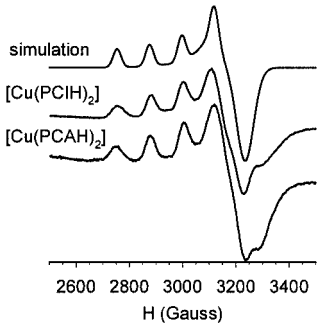

Figure 9. Experimental X-band (9.303 GHz) EPR spectra of [Cu(PCAH)$_2$] (bottom) and [Cu(PCIH)$_2$] (centre): conditions: 1 mM complex in DMF/H_2O (1:2), 77 K; the simulated spectrum is shown at the top (see text for simulation parameters); broad, high-field resonances ($g \approx 2$) in experimental spectra are due to cavity impurities

Ligand Oxidation

One interesting observation while preparing the Co-HPCIH complexes was that the HPCIH ligand is not oxidised when the redox-active Co^{II} is oxidised to Co^{III} by dissolved atmospheric oxygen in the solution during complex formation. This is in contrast to our earlier report of the oxidation of HPCIH to the diacylhydrazine *N*-(isonicotinoyl)-*N*′-(picolinoyl)hydrazone (H_2IPH) while trying to prepare the Fe^{III} complex of HPCIH.[23] We successfully duplicated the preparation of the trivalent complex [Fe(HIPH)(IPH)] from Fe^{II} salts and HPCIH as starting materials, but as yet have been unable to isolate the trivalent [Fe(PCIH)$_2$]$^+$ complex. We believe that the ligand oxidation is not a straightforward process. Indeed, it probably involves Fe^{III}, water and O_2 in the mechanism, since a similar oxidation is not observed with Co^{II} and Co^{III}, or any other transition metals investigated in this report. Nevertheless, the divalent [FeL_2] (L = PCIH and PCAH) complexes have been synthesised and the [Fe(PCIH)$_2$] complex formation constants have been demonstrated by potentiometric titration (see below). So far our work on HPCAH has not shown any evidence of ligand oxidation in the presence of either Fe^{II} or Fe^{III}. This adds another dimension to the ligand oxidation phenomenon such that oxidation seems to be peculiar to HPCIH. We are currently working toward an understanding of this oxidation mechanism.

Formation Constants

The formation constants of the bis(complexes) of HPCIH with divalent first-row transition metals from manganese to zinc have been determined. The results are shown in Table 7. The values obtained are similar to those obtained with similar tridentate ligands and consistent with the Irving−Williams order.[47] The exceptionally low log K_2 value ($ML + L \rightleftarrows ML_2$) of Cu^{II} at 7.42 is expected, since

the addition of a second ligand forces the Cu^{II} centre into a strained tetragonally elongated six-coordinate configuration evident from the crystal structure (Table 5) and EPR spectrum (Figure 9) of $[Cu(PCIH)_2]$, where the rigid meridionally coordinated second ligand must span the elongated axis of the coordination sphere.

Table 7. Formation constants of complexes of (H)PCIH with divalent first row transition metals

	Mn^{II}	Fe^{II}	Co^{II}	Ni^{II}	Cu^{II}	Zn^{II}
$\log K_1$ (ML)	4.71(3)	7.02(3)	7.67(5)	9.27(4)	10.83(8)	7.41(7)
$\log\beta_2$ (ML_2)	9.20(3)	13.37(2)	14.42(5)	16.97(4)	18.25(9)	13.85(7)

A typical speciation plot, such as that for the Ni^{II} complex shown in Figure 10, illustrates the transition from free metal ions to bis(complexes) as pH increases. At lower pH, the monoligand complex is the prevailing species, with $[Ni(PCIH)]^+$ beginning to form at pH = 2.5 (while $[Cu(PCIH)]^+$ begins to form at pH = 1.5). As the pH increases, bis(complexes) begin to form, eventually becoming the only species at pH = 7 and beyond. The Mn^{II} complex is the exception due to the closeness of log K_1 ($M + L \rightleftarrows ML$) and log K_2 ($ML + L \rightleftarrows ML_2$) values (4.71 and 4.49, respectively). $[Mn(PCIH)]^+$ only begins to form at pH = 5 while $[Mn(PCIH)_2]$ begins to form at pH = 7. Both species coexist in equilibrium through to pH = 12. Thus, the isolation of $[\{MnCl_2(DMSO)(HPCIH)\}_2Mn(DMSO)_2Cl_2]$ can be further rationalised by considering the formation constants, which illustrate that the formation of $[Mn(PCIH)_2]$ is least favourable of all ML_2 metal complexes in this series.

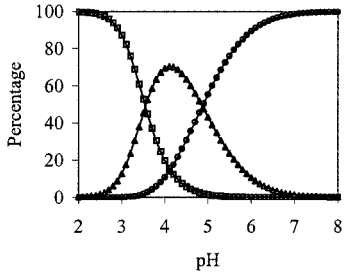

Figure 10. pH speciation plot for Ni^{II} complexes of HPCIH; key: squares: free Ni^{2+} ions; triangles: $[Ni(PCIH)]^+$; circles: $[Ni(PCIH)_2]$

Biological Activity

The Fe chelation efficacy of the HPCIH analogues is now established.[19−21] An important question concerns the physiologically relevant form of these chelators and their complexes upon encountering intracellular Fe and other competing metal ions. The HPCIH analogues form divalent Fe complexes even in the presence of oxygen. This is in contrast with other biologically active Fe chelators such as DFO, which spontaneously oxidises Fe^{II} to its trivalent state under aerobic conditions.

Given the reactivity of the Fe^{III} complex of $PCIH^-$ and the ready formation of the divalent complex in our synthetic studies,[23] it appears that the trivalent complexes of the HPCIH analogues will not be the major species in vivo, and the biological activity of the chelators may be attributed to their ability to act as intracellular Fe^{II} chelators rather than Fe^{III} chelators. The formation constants of HPCIH with Fe^{II} are not particularly high (Table 7) and there is nothing to suggest that the ligands are selective for divalent Fe over any of the other metal ions. In fact, at face value, the ligands should form more stable divalent complexes with Cu and Zn which are also present in biological fluids. However, intracellular Fe is present in much higher concentrations than other transition metals, and this will naturally influence the outcome under physiological conditions.

It is well known that charge neutrality and lipophilicity are desirable features in facilitating passage across cell membranes and thus enhancing Fe mobilisation activity. It is pertinent that the divalent complexes of HPCIH are charge-neutral, so the metal-free chelators may enter the cell in a charge-neutral form and the Fe complexes also may leave the cell in a charge-neutral form. A similar charge neutrality has been sought in tribasic ligands such as DFO and tris-L1 in complexes with trivalent Fe. Although the FeL_2 (L = PCIH, PCAH) complexes may be oxidised to their trivalent forms with mild oxidants, they are highly reactive and would be unlikely to survive in vivo. Furthermore, they would necessarily carry a positive charge, which may inhibit their exit from the cell.

An alternative, but less likely, hypothesis to explain the pronounced Fe mobilisation activity of these chelators is that ligand dehydrogenation of the unstable trivalent Fe complexes of the HPCIH (hydrazone) analogues occurs generating the corresponding hydrazine (H_2IPH) complex within the cell, by analogy with observations of the chemistry of these complexes on a preparative scale.[23] At this point, we prefer the former argument, as the hydrazine analogue of HPCIH (H_2IPH) exhibits very poor Fe mobilisation activity,[23] and its biological role in the activity of the HPCIH analogues is doubtful. Even though the formation constants of bis(complexes) of HPCAH with divalent first-row transition metals have not been determined, we would expect their values to exhibit the same trend and order of magnitude as those of HPCIH due to the similarities of the two ligands. In fact, the crystallographic and spectroscopic data reported herein show that the local coordination environments of the $[M(PCIH)_2]$ and $[M(PCAH)_2]$ complexes are indistinguishable. The main feature that distinguishes the HPCIH analogues in terms of their biological activity appears to be their lipophilicity, which affects their ability to cross the cell membrane and gain access to intracellular Fe pools.

Conclusion

Divalent first-row transition metals (Mn, Fe, Co, Ni, Cu and Zn) readily form similar bis(complexes) with HPCAH as shown by spectroscopy and X-ray crystallography. How-

ever, complexes of HPCIH are less predictable, forming complexes of various metal/ligand ratios. Such behaviour is attributed to the active participation of the unhindered isonicotinoyl nitrogen atom in bonding. In the case of the trinuclear complex $[\{MnCl_2(DMSO)(HPCIH)\}_2Mn(DMSO)_2Cl_2]$, the low formation constant of $[Mn(PCIH)_2]$ coupled with competition from ligands like DMSO and chloride, as well as participation of the isonicotinoyl nitrogen atom in coordinate bonding, led to the formation of this unique compound. From the IR spectra and crystal data, it is evident that the deprotonated hydrazone ligands exist predominantly in the enolate resonance form. Oxidation of HPCIH and HPCAH in the presence of divalent metal ions was not observed in this study, which further strengthens our belief that the unique participation of Fe^{III} and oxygen is the key to this unprecedented oxidation of HPCIH to H_2IPH. On the other hand, formation constants of the divalent metal complexes of HPCIH show that the affinity of this ligand for Fe^{II} is not particularly great, although the chelator is successful in mobilising iron as shown by our cell culture experiments.[23] Other factors such as the greater bioavailability of Fe or, less likely, the intracellular oxidation of HPCIH to H_2IPH could be the answer and further studies are being undertaken to ascertain these unresolved questions.

Experimental Section

Materials: The chemicals and solvents used in this work were of analytical grade, available commercially, and were used without further purification.

Physical Measurements: Solution UV/Vis spectra were measured with a Perkin−Elmer Lambda 40 spectrophotometer. Infrared spectra were measured with a Perkin−Elmer 1600 series instrument, with compounds being dispersed as KBr discs. ^1H NMR spectra were obtained with a Bruker AC200F spectrometer using TMS as the internal standard. Electron paramagnetic resonance (EPR) spectra were recorded at 77 K with a Bruker ER200D spectrometer at X-band frequency (9.303 GHz). Samples were made up as 1 mM solutions in a DMF/water (1:2) mixture. Spectra were simulated with the program EPR50F.[48] Potentiometric titrations were performed under nitrogen at 298 K with a Metrohm E665 Dosimat autotitrator equipped with a 5-mL burette. The titrant was 0.1 M Et_4NOH standardised with HCl. Solutions of pure ligands (1 mM) were used in the titrations for the determination of protonation constants. The chelators were prepared in $HClO_4$ (6 mM) and Et_4NClO_4 (0.1 M) as supporting electrolyte to maintain a constant ionic strength throughout the titration. Solutions of transition metal ions plus ligands used in the titration for the determination of metal complex formation constants contained transition metal ions as the perchlorate salt (0.5 mM), ligand (1.25 mM) (calculated at a 1:2 metal ion/ligand ratio, with 25% excess ligand added), $HClO_4$ (6−12 mM) and Et_4NClO_4 (0.1 M). Care was taken to pre-purge all solutions with nitrogen so as to prevent complications from redox reactions. Milli-Q water was used to make up the transition metal salt solutions, which were also pre-purged with nitrogen before dissolution. The solution potential was measured using an Orion 720A pH meter and an Ionode IJ44 intermediate junction pH electrode. The electrode was calibrated by strong acid-strong base titration prior to every potentiometric titration of the ligands or complexes. Data obtained were fitted to the Nernst equation and the pK_a values or formation constants were determined using the program SuperQuad.[49] In each case, a minimum of four titrations was performed in the range $2 < pH < 12$.

Ligand Syntheses: HPCIH and HPCAH were synthesised by a Schiff-base condensation between 2-pyridinecarbaldehyde and the respective acid hydrazides as described previously.[20,21,50] Slow concentration of an aqueous methanol (1:1) solution of HPCAH afforded crystals suitable for X-ray work.

HPCIH·2H$_2$O: $C_{12}H_{14}N_4O_3$ (262.2): calcd. C 54.96, H 5.38, N 21.36; found C 55.10, H 5.34, N 21.55. IR: $\tilde{\nu}_{max}$ = 3448 s, 3050 w, 3007 w, 1681 vs, 1660 vs, 1552 vs, 1473 s, 1437 s, 1411 s, 1370 s, 1293 vs, 1147 s, 1071 s, 1002 w, 929 w, 845 w, 783 s, 742 s, 692 vs, 625 w and 521 w cm^{-1}. ^1H NMR ([D$_4$]methanol):δ = 7.47 (m, 1 H), 7.92 (m, 3 H), 8.28 (d, 1 H), 8.45 (s, 1 H), 8.60 (m, 1 H) and 8.78 (dd, 2 H) ppm. ^{13}C NMR ([D$_4$]methanol):δ = 122.4, 123.2, 126.3, 138.7, 142.1, 150.3, 150.7, 151.1, 154.1 and 164.9 ppm.

HPCAH·H$_2$O: $C_{13}H_{14}N_4O_2$ (258.3): calcd. C 60.46, H 5.46, N 21.69; found C 60.43, H 5.42, N 21.65. IR: $\tilde{\nu}_{max}$ = 3528 s, 3466 s, 3434 vs, 3316 s, 3208 s, 3034 w, 2987 w, 1646 vs, 1629 vs, 1603 vs, 1551 s, 1514 s, 1472 s, 1434 s, 1348 s, 1283 vs, 1183 vs, 1150 s, 1076 w, 1000 w, 938 w, 843 s, 770 w, 744 w, 694 s, 666 w and 620 s cm^{-1}. ^1H NMR ([D$_6$]DMSO): δ = 5.87 (s, 1 H), 6.63 (d, 2 H), 7.36 (m, 1 H), 7.72 (d, 2 H), 7.86 (m, 2 H), 8.44 (s, 1 H), 8.58 (d, 1 H) and 11.73 (s, 1 H). ^{13}C NMR ([D$_6$]DMSO): δ = 112.9, 119.4, 119.9, 124.3, 129.9, 137.0, 146.4, 149.7, 152.8, 153.9 and 163.7 ppm.

Complex Syntheses

Bulk Syntheses of [M(PCIH)$_2$] and [M(PCAH)$_2$] Complexes (M = Mn, Ni, Cu and Zn): The ligand (HPCIH or HPCAH; 2.5 mmol) was dissolved in 30 mL of methanol. The chloride salt of the respective metal (1 mmol) was added to the solution, followed by triethylamine (Et_3N; 2 mmol). The mixture was gently refluxed for 3 h and then concentrated to approximately one third of the original volume. The resulting precipitate was collected by vacuum filtration and washed with distilled water. Complexes ML_2 of Mn^{II}, Ni^{II} and Cu^{II} were all brown in colour, while the Zn^{II} complexes were bright yellow. Yields of the first crops of compound were 20−40%. Further crops were obtained from concentration of the filtrates.

Bulk Syntheses of [M(PCIH)$_2$] and [M(PCAH)$_2$] Complexes (M = Fe and Co): The ligand (HPCIH or HPCAH; 4 mmol) was dissolved in 50 mL of MeCN. Triethylamine (30 mmol) was added, followed by the perchlorate salt of the respective metal (1.6 mmol). The mixture was gently refluxed for 3 h and then concentrated to approximately one third of the original volume. The resulting precipitate was collected by vacuum filtration and washed with MeOH and then with distilled water. The Fe^{II} complexes were green and the Co^{II} complexes were deep purple. Yields of the first crops of compound were 75−80%.

[Mn(PCIH)$_2$]·H$_2$O: $C_{24}H_{20}MnN_8O_3$ (524.4): calcd. C 55.07, H 3.85, N 21.41; found C 54.97, H 3.42, N 21.38. IR: $\tilde{\nu}_{max}$ = 3070 w, 3023 w, 1607 s, 1591 s, 1568 s, 1497 vs, 1487 vs, 1460 vs, 1358 vs, 1308 s, 1150 s, 1068 vs, 782 w, 755 s and 699 s cm^{-1}.

[Fe(PCIH)$_2$]·0.5H$_2$O: $C_{24}H_{10}FeN_8O_{2.5}$ (515.3): calcd. C 55.94, H 3.72, N 21.74; found C 55.42, H 3.44, N 21.79. IR: $\tilde{\nu}_{max}$ = 3072 w, 3021 w, 1601 s, 1566 s, 1498 vs, 1482 vs, 1456 vs, 1362 vs, 1344 vs, 1308 s, 1151 s, 1063 vs, 784 w, 754 s and 700 s cm^{-1}.

[Co(PCIH)$_2$]: $C_{24}H_{18}CoN_8O_2$ (509.4): calcd. C 56.59, H 3.56, N 22.00; found C 56.67, H 3.53, N 22.03. IR: $\tilde{\nu}_{max}$ = 3014 w, 1604 s, 1567 s, 1484 vs, 1457 vs, 1359 vs, 1308 s, 1149 s, 1072 vs, 785 w, 755 s and 700 s cm^{-1}.

[Ni(PCIH)$_2$]·3H$_2$O: $C_{24}H_{24}N_8NiO_5$ (563.2): calcd. C 51.18, H 4.30, N 19.90; found C 51.57, H 3.82, N 19.78. IR: $\tilde{\nu}_{max}$ = 1609 vs, 1567 s, 1488 vs, 1460 vs, 1357 vs, 1153 s, 1312 s, 1153 s, 1078 vs, 784 w, 758 s and 701 s cm^{-1}.

[Cu(PCIH)$_2$]: $C_{24}H_{18}CuN_8O_2$ (514.0): calcd. C 56.08, H 3.53, N 21.80; found C 55.84, H 3.51, N 21.61. IR: $\tilde{\nu}_{max}$ = 3068 w, 3020 w, 1603 s, 1586 s, 1570 vs, 1519 vs, 1486 vs, 1458 vs, 1364 vs, 1351 vs, 1339 vs, 1306 vs, 1151 s, 1064 vs, 784 s, 754 s and 700 s cm^{-1}.

[Zn(PCIH)$_2$]·0.5H$_2$O: $C_{24}H_{19}N_8O_{2.5}Zn$ (524.9): calcd. C 54.92, H 3.65, N 21.35; found C 55.22, H 3.45, N 21.63. IR: $\tilde{\nu}_{max}$ = 3072 w, 3020 w, 1609 w, 1591 s, 1569 s, 1500 vs, 1486 vs, 1462 vs, 1355 vs, 1307 s, 1149 s, 1073 s, 784 s, 756 s and 700 s cm^{-1}.

[Mn(PCAH)$_2$]·H$_2$O: $C_{26}H_{24}MnN_8O_3$ (551.4): calcd. C 56.63, H 4.39, N 20.32; found C 56.42, H 4.41, N 19.99. IR $\tilde{\nu}_{max}$ = 3354 s, 3210 s, 2677 w, 1624 s, 1599 vs, 1551 w, 1484 s, 1456 s, 1421 s, 1354 vs, 1291 vs, 1174 vs, 1146 vs, 1102 s, 1070 vs, 914 w, 851 w, 767 s, 678 w, 637 s and 503 w cm^{-1}.

[Fe(PCAH)$_2$]·2.5H$_2$O: $C_{26}H_{27}N_8O_{4.5}Fe$ (579.4): calcd. C 53.90, H 4.70, N 19.34; found C 54.08, H 4.26, N 19.34. IR: $\tilde{\nu}_{max}$ = 3332 s, 3214 s, 1632 s, 1604 vs, 1560 w, 1472 s, 1448 s, 1411 s, 1363 vs, 1289 vs, 1175 vs, 1150 vs, 1110 s, 1068 vs, 846 w, 761 s, 681 w and 506 w cm^{-1}.

[Co(PCAH)$_2$]·H$_2$O: $C_{26}H_{24}$ Co N_8O_3 (555.5): calcd. C 56.22, H 4.35, N 20.17; found C 55.90, H 4.46, N 19.97. IR: $\tilde{\nu}_{max}$ = 3344 s, 3214 s, 1628 s, 1598 vs, 1548 w, 1482 s, 1456 s, 1420 s, 1354 vs, 1289 vs, 1175 vs, 1147 vs, 1105 s, 1079 vs, 847 w, 765 s, 679 w and 504 w cm^{-1}.

[Ni(PCAH)$_2$]·H$_2$O: $C_{26}H_{24}N_8NiO_3$ (555.3): calcd. C 56.24, H 4.36, N 20.18; found C 56.23, H 4.45, N 19.76. IR: $\tilde{\nu}_{max}$ = 3336 s, 3218 s, 1628 s, 1599 vs, 1552 w, 1485 vs, 1458 s, 1424 s, 1353 vs, 1339 vs, 1288 vs, 1174 vs, 1147 vs, 1107 s, 1083 vs, 847 w, 767 s, 679 w, 642 w and 504 w cm^{-1}.

[Cu(PCAH)$_2$]·H$_2$O: $C_{26}H_{24}CuN_8O_3$ (560.1): calcd. C 55.76, H 4.32, N 20.01; found C 55.61, H 4.40, N 19.63. IR: $\tilde{\nu}_{max}$ = 3329 s, 3212 s, 1628 w, 1598 vs, 1551 w, 1522 w, 1483 s, 1459 s, 1424 w, 1354 vs, 1337 vs, 1289 vs, 1174 vs, 1148 vs, 1104 s, 1075 s, 846 w, 766 s, 681 w, 622 w, and 505 w cm^{-1}.

[Zn(PCAH)$_2$]·H$_2$O: $C_{26}H_{24}N_8O_3Zn$ (561.9): calcd. C 55.58, H 4.30, N 19.94; found C 55.39, H 4.36, N 19.67. IR: $\tilde{\nu}_{max}$ = 3347 s, 3216 w, 1628 w, 1600 vs, 1553 w, 1521 w, 1487 s, 1460 s, 1426 w, 1354 vs, 1338 vs, 1289 vs, 1174 vs, 1147 vs, 1104 s, 1081 s, 851 w, 768 s, 680 w, 640 w and 504 w cm^{-1}. ^{1}H NMR ([D$_6$]DMSO): δ = 5.60 (s, 2 H), 6.50 (d, 2 H), 7.28 (m, 1 H), 7.64 (d, 1 H), 7.80 (d, 2 H), 7.91 (m, 2 H) and 8.55 (s, 1 H) ppm.

Crystals of [M(PCAH)$_2$]·H$_2$O (M = Mn, Ni, Cu, Zn) and [Cu(PCIH)$_2$]: The perchlorate salt of the respective metal (14 μmol) and the ligand (35 μmol; 1:2.5 ratio) were dissolved in 6 mL of MeCN/toluene (3:2) and 40 μL of Et_3N was added to the solution. The solutions were allowed to concentrate slowly and crystals suitable for X-ray work were formed. IR spectra of the crystals were found to be identical to the spectra of their respective counterparts in the bulk syntheses. Crystals of [Ni(PCIH)$_2$]·2H$_2$O were obtained from vapour diffusion of 2-propanol into a concentrated DMSO solution of the complex.

Trivalent and Oligomeric Complexes

[Co(PCIH)$_2$][CoCl$_3$]·2H$_2$O: HPCIH (0.5 g, 2 mmol) was dissolved in methanol (50 mL). $CoCl_2$·6H$_2$O (0.26 g, 1 mmol) was added to the solution and the mixture was refluxed for 16 h. Dichloromethane vapour diffusion into the concentrated reaction mixture afforded red-brown crystals suitable for X-ray work. Further crops were obtained from diethyl ether vapour diffusion into a concentrated methanolic solution of the solid. Total yield was 21%. $C_{24}H_{22}Cl_3Co_2N_8O_4$ (710.1): calcd. C 40.56, H 3.12, N 15.73; found C 40.45, H 3.02, N 15.87. IR: $\tilde{\nu}_{max}$ = 1618 s, 1484 vs, 1446 vs, 1380 vs, 1341 s, 1209 s, 1151 s, 1077 s, 848 w, 727 s and 606 s cm^{-1}.

[Co(HPCIH)(PCIH)](NO$_3$)$_2$·H$_2$O·0.5CH$_3$OH: HPCIH (0.5 g, 2 mmol) was dissolved in 50 mL of methanol. Co(NO$_3$)$_2$·6H$_2$O (0.32 g, 1.1 mmol) was added to the solution and the mixture gently refluxed for 16 h. A precipitate of the product formed on cooling and was collected and washed with diethyl ether. Diethyl ether vapour diffusion into a concentrated methanolic solution of the mother liquor afforded crystals suitable for X-ray work. More crystals were obtained from slow concentration of the mother liquor. Total yield was 16%. $C_{24.5}H_{23}CoN_{10}O_{9.5}$ (668.5): calcd. C 44.02, H 3.47, N 20.95; found C 44.10, H 3.40, N 21.07. IR: $\tilde{\nu}_{max}$ = 1636 s, 1540 s, 1483 s, 1448 vs, 1383 vs, 1208 s, 1148 s, 1078 s, 1000 w, 928 w, 844 w, 750 s, 716 s, 682 w and 607 w cm^{-1}.

[Co(HPCIH)$_2$](NO$_3$)$_3$·2H$_2$O: HPCIH (1.0 g, 4 mmol) was dissolved in 50 mL of methanol. Co(NO$_3$)$_2$·6H$_2$O (0.55 g, 2 mmol) was added to the solution and the mixture gently refluxed for 48 h. A precipitate of the product formed on cooling and was collected and washed with diethyl ether. Total yield was 81%. $C_{24}H_{26}CoN_{11}O_{13}$ (733.5): calcd. C 39.30, H 3.30, N 21.01; found C 39.36, H 2.94, N 21.02. IR: $\tilde{\nu}_{max}$ = 3063 s, 2526br, 1636 s, 1527 s, 1482 s, 1448 vs, 1384 vs, 1300 s, 1213 s, 1151 s, 1077 s, 1006 w, 930 w, 826 w, 749 s, 716 s, 682 w and 600 w cm^{-1}.

[Co(PCIH)$_2$]NO$_3$·2H$_2$O: Addition of 2 equiv. of Et_3N to an aqueous solution of [Co(HPCIH)$_2$](NO$_3$)$_3$·2H$_2$O resulted in immediate precipitation of the product, which was collected and washed with diethyl ether. Total yield was 75%. $C_{24}H_{22}CoN_9O_7$ (607.4): calcd. C 47.46, H 3.65, N 20.75; found C 47.52, H 3.42, N 20.73. IR: $\tilde{\nu}_{max}$ =1610 s, 1567 w, 1483 s, 1443 vs, 1384 vs, 1340 s, 1209 s, 1150 s, 1079 s, 927 w, 840 w, 780 w, 750 w, 713 s, and 607 w cm^{-1}.

[Co(PCAH)$_2$]Cl·4H$_2$O: HPCAH (0.5 g, 2 mmol) was dissolved in 50 mL of methanol. $CoCl_2$·6H$_2$O (0.23 g, 1 mmol) was added to the solution and the mixture was gently refluxed for 16 h. A red precipitate of the product formed on cooling. The solution was concentrated to approximately one third of the original volume and the precipitate collected and washed with cold methanol and then with distilled water. Total yield was 48%. $C_{26}H_{30}ClCoN_8O_6$ (645.0): calcd. C 48.42, H 4.69, N 17.37; found C 48.04, H 4.34, N 17.05. IR: $\tilde{\nu}_{max}$ = 3328 s, 3207 w, 1624 w, 1601 vs, 1559 w, 1522 w, 1479 s, 1451 s, 1374 vs, 1287 s, 1215 w, 1174 vs, 1148 s, 1079 s, 843 w, 758 w, 682 w, 636 w and 511 w cm^{-1}. ^{1}H NMR ([D$_6$]DMSO): δ = 6.14 (s, 2 H), 6.47 (d, 2 H), 7.39 (t, 1 H), 7.64 (d, 2 H), 7.85 (d, 1 H), 8.07 (m, 2 H) and 9.39 (s, 1 H). ^{13}C NMR ([D$_6$]DMSO): δ = 112.8, 116.2, 126.4, 127.7, 131.4, 141.8, 148.6, 151.6, 153.8, 160.7 and 184.0 ppm.

[{MnCl$_2$(DMSO)(HPCIH)}$_2$Mn(DMSO)$_2$Cl$_2$]: The preparation of [Mn(PCIH)$_2$] (described above) occasionally resulted in a product contaminated with small amounts of $MnCl_2$ as a co-precipitate. Dissolution of this crude compound in DMSO followed by vapour diffusion of 2-propanol into the mixture afforded yellow crystals suitable for X-ray work. [{MnCl$_2$(DMSO)(HPCIH)}$_2$Mn-

$(DMSO)_2Cl_2$]. $C_{32}H_{44}Cl_6Mn_3N_8O_6S_4$ (1142.5): calcd. C 33.64, H 3.88, N 9.81; found C 33.59, H 3.80, N 9.76.

[Zn(HPCIH)SO_4]·3.5H_2O: HPCIH (0.5 g, 2 mmol) was dissolved in 15 mL of methanol. Then $ZnSO_4·7H_2O$ (0.28 g, 1 mmol) was added to the solution and the mixture gently refluxed for 18 h. The mixture was cooled and a yellow precipitate of the product was collected and washed with diethyl ether. A small amount of the product was dissolved in minimum amount of acetonitrile/toluene (1:1) mixture. Slow concentration of the solution yielded crystals suitable for X-ray work. Total yield was 20%. $C_{12}H_{17}N_4O_{8.5}SZn$ (450.7): calcd. C 31.98, H 3.80, N 12.43; found C 32.10, H 3.60, N 12.37. IR: $\tilde{\nu}_{max}$ = 1684 vs, 1653 vs, 1575 vs, 1551 vs, 1472 s, 1433 s, 1406 s, 1361 s, 1298 vs, 1147 s, 1071 s, 926 s, 846 s, 781 s, 750 s and 686 vs cm^{-1}.

Crystallography: Cell constants were determined by a least-squares fit to the setting parameters of 25 independent reflections measured with an Enraf−Nonius CAD4 four-circle diffractometer employing graphite-monochromated Mo-K_α radiation. Data reduction, absorption correction (ψ-scans) and all calculations were performed with the WINGX suite of programs.[51] Structures were solved by direct methods for HPCAH, [Mn(PCAH)$_2$], [Ni(PCAH)$_2$], [Cu(PCAH)$_2$], [Zn(PCAH)$_2$] and [Cu(PCIH)$_2$] and Patterson methods for [Ni(PCIH)$_2$], [Co^{III}(PCIH)$_2$$Co^{II}Cl_3$] and [$Co^{III}$(HPCIH)(PCIH)]$NO_3$ with SHELXS,[52−54] and with SIR92 for [{$MnCl_2$(DMSO)(HPCIH)}$_2$Mn(DMSO)$_2$$Cl_2$] and [Zn(HPCIH)]$SO_4$.[55] Structures were refined by full-matrix least-squares analysis with SHELXL-97.[56] All non-H atoms were refined with anisotropic thermal parameters. Aryl and amino H-atoms were included at estimated positions whereas amide H-atoms (if any) were first located from difference maps then restrained in a similar manner to that employed for the remaining H-atoms. Crystal data appear in Tables 2 and 4 and selected bond lengths and angles are presented in Tables 3, Table 5 and 6. The atomic nomenclature is defined in Figures 2−8 and drawn with programs PLATON[57] and ORTEP-3.[58] CCDC-182551 to -182561 contain the supplementary crystallographic data for this paper. These data can be obtained free of charge at www.ccdc.cam.ac.uk/conts/retrieving.html [or from the Cambridge Crystallographic Data Centre, 12 Union Road, Cambridge CB2 1EZ, UK; Fax: (internat.) + 44-1223/336-033; E-mail: deposit@ccdc.cam.ac.uk].

Acknowledgments

P. C. thanks the Department of Chemistry, University of Queensland for a departmental scholarship. P. V. B. acknowledges financial support from the University of Queensland. D. R. thanks the National Health and Medical Research Council for grant and fellowship support. We also thank Mr. K. Thurecht for assistance with the EPR spectral measurements.

[1] J. B. Porter, E. R. Huehns, R. C. Hider, *Baillière's Clin. Haematol.* **1989**, *2*, 257.
[2] C. Hershko, *Baillière's Clin. Haematol.* **1994**, *7*, 965.
[3] Z. D. Liu, R. C. Hider, in *Molecular and Cellular Iron Transport* (Ed.: D. M. Templeton), Marcel Dekker, Inc., New York, **2001**, p. 321.
[4] D. R. Richardson, P. Ponka, *Am. J. Hematol.* **1998**, *58*, 299.
[5] N. F. Olivieri, G. M. Brittenham, *Blood* **1997**, *90*, 1161.
[6] N. F. Olivieri, G. M. Brittenham, *Blood* **1999**, *94*, 3302.
[7] G. J. Kontoghiorghes, Ph. D thesis, University of Essex, Colchester, **1982**.
[8] N. F. Olivieri, G. M. Brittenham, D. Matsui, M. Berkovitch, L. M. Blendis, R. G. Cameron, R. A. McClelland, P. P. Liu, D. M. Templeton, G. Koren, *N. Engl. J. Med.* **1995**, *332*, 918.
[9] F. N. al-Refaie, B. Wonke, A. V. Hoffbrand, *Eur. J. Hematol.* **1994**, *53*, 298.
[10] A. V. Hoffbrand, F. Al-Refaie, B. Davis, N. Siritanakatkul, B. F. A. Jackson, J. Cochrane, E. Prescott, B. Wonke, *Blood* **1998**, *91*, 295.
[11] N. F. Olivieri, G. M. Brittenham, C. E. McLaren, D. M. Templeton, R. G. Cameron, R. A. McClelland, A. D. Burt, K. A. Fleming, *N. Engl. J. Med.* **1998**, *339*, 417.
[12] D. R. Richardson, *J. Lab. Clin. Med.* **2001**, *137*, 324.
[13] L. J. Anderson, B. Wonke, E. Prescott, S. Holden, J. M. Walker, D. J. Pennell, *Lancet* **2002**, *360*, 516.
[14] D. R. Richardson, *Lancet* **2002**, *360*, 501.
[15] I. R. Wanless, G. Sweeney, A. P. Dhillon, M. Guido, A. Piga, R. Galanello, M. R. Gamberini, E. Schwartz, A. R. Cohen, *Blood* **2002**, *100*, 1566.
[16] Y. Aydinok, G. Nisli, K. Kavakli, C. Coker, M. Kantar, N. Centingul, *Acta Haematol.* **1999**, *102*, 17.
[17] G. Link, A. M. Konijn, W. Breuer, Z. I. Cabantchik, C. Hershko, *J. Lab. Clin. Med.* **2001**, *138*, 130.
[18] E. Becker, D. R. Richardson, *Int. J. Biochem. Cell Biol.* **2001**, *33*, 1.
[19] D. R. Richardson, C. Mouralian, P. Ponka, E. Becker, *Biochim. Biophys. Acta-Mol. Basis Dis.* **2001**, *1536*, 133.
[20] E. Becker, D. R. Richardson, *J. Lab. Clin. Med.* **1999**, *134*, 510.
[21] D. R. Richardson, E. Becker, P. V. Bernhardt, *Acta Crystallogr., Sect. C* **1999**, *55*, 2102.
[22] D. Richardson, P. V. Bernhardt, E. M. Becker, in *PCT Int. Appl.*, University of Queensland, Australia, Heart Research Institute Ltd., 0117530, **2001**, p. 50.
[23] P. V. Bernhardt, P. Chin, D. R. Richardson, *J. Biol. Inorg. Chem.* **2001**, *6*, 801.
[24] W. Kemp, in *Organic Spectroscopy*, 2nd ed., Macmillan Education Ltd, Hampshire, **1987**, p. 65.
[25] R. M. Silverstein, G. C. Bassler, T. C. Morrill, in *Spectrometric Identification of Organic Compounds*, 4th ed., John Wiley & Sons, Inc., **1981**, p. 124.
[26] L. El-Sayed, M. F. Iskander, *J. Inorg. Nucl. Chem.* **1971**, *33*, 435.
[27] A. V. Lakshmi, N. R. Sangeetha, S. Pal, *Indian J. Chem. Sect A* **1997**, *36*, 844.
[28] N. R. Sangeetha, S. Pal, *J. Coord. Chem.* **1997**, *42*, 157.
[29] J. W. Pyrz, A. L. Roe, L. J. Stern, L. Que, *J. Am. Chem. Soc.* **1985**, *107*, 614.
[30] R. N. Mukherjee, O. A. Rajan, A. Chakravorty, *Inorg. Chem.* **1982**, *21*, 785.
[31] R. J. P. Williams, *J. Chem. Soc.* **1955**, 137.
[32] S. Pal, G. V. Karunakar, N. R. Sangeetha, V. Susila, *J. Coord. Chem.* **2000**, *50*, 51.
[33] S. Pal, A. Choudhury, B. Geetha, N. R. Sangeetha, V. Kavita, V. Susila, *J. Coord. Chem.* **1999**, *48*, 87.
[34] H. Oshio, E. Ino, I. Mogi, T. Ito, *Inorg. Chem.* **1993**, *32*, 5697.
[35] M. H. Moore, L. R. Nassimbeni, M. L. Niven, *J. Chem. Soc., Dalton Trans.* **1987**, 2125.
[36] S. Seth, S. Chakraborty, *Acta Crystallogr., Sect. C* **1984**, *C40*, 1530.
[37] A. Seal, S. Ray, *Acta Crystallogr., Sect. C* **1984**, *C40*, 929.
[38] N. R. Sangeetha, C. K. Pal, P. Ghosh, S. Pal, *J. Chem. Soc., Dalton Trans.* **1996**, 3293.
[39] A. Mangia, M. Nardelli, C. Pelizzi, G. Pelizzi, *J. Chem. Soc., Dalton Trans.* **1973**, 1141.
[40] S. Dutta, V. Manivannan, L. G. Babu, S. Pal, *Acta Crystallogr., Sect. C* **1995**, *51*, 813.
[41] M. R. Maurya, D. C. Antony, S. Gopinathan, V. G. Puranik, S. S. Tavale, C. Gopinathan, *Bull. Chem. Soc. Jpn.* **1995**, *68*, 2847.
[42] X. M. Zhang, X. Z. You, X. Wang, *Polyhedron* **1996**, *15*, 1793.
[43] W. Wang, F. L. Zeng, X. Wang, M. Y. Tan, *Polyhedron* **1996**, *15*, 1699.
[44] S. P. Rath, S. Mondal, A. Chakravorty, *Inorg. Chim. Acta* **1997**, *263*, 247.
[45] N. R. Sangeetha, K. Baradi, R. Gupta, C. K. Pal, V. Manivannan, S. Pal, *Polyhedron* **1999**, *18*, 1425.

[46] F. A. Cotton, G. Wilkinson, C. A. Murillo, M. Bochmann, in *Advanced Inorganic Chemistry*, 6th ed., John Wiley & Sons, Inc., **1999**, p. 865.
[47] A. E. Martell, R. M. Smith, R. J. Motekaitis, *Critically selected stability constants of metal complexes database*, 4th ed., Texas A & M University, **1997**.
[48] R. A. Martinelli, G. R. Hanson, J. S. Thompson, B. Holmquist, J. R. Pilbrow, D. S. Auld, B. L. Vallee, *Biochemistry* **1989**, *28*, 2251.
[49] P. Gans, A. Sabatini, A. Vacca, *J. Chem. Soc., Dalton Trans.* **1985**, 1195.
[50] S. G. Komurcu, S. Rollas, M. Ulgen, J. W. Gorrod, A. Cevikbas, *Boll. Chim. Farmac.* **1995**, *134*, 375.
[51] L. J. Farrugia, *J. Appl. Crystallogr.* **1999**, *32*, 837.
[52] G. M. Sheldrick, University of Göttingen, Germany, **1997**.
[53] G. M. Sheldrick, *Acta Crystallogr., Sect. A* **1990**, *46*, 467.
[54] G. M. Sheldrick, Z. Dauter, K. S. Wilson, H. Hope, L. C. Sieker, *Acta Crystallogr. Sect D* **1993**, *49*, 18.
[55] A. Altomare, G. Cascarano, C. Giacovazzo, A. Gualardi, *J. Appl. Crystallogr.* **1993**, *26*, 343.
[56] G. M. Sheldrick, University of Göttingen, Germany, **1997**.
[57] A. L. Spek, *Acta Crystallogr., Sect. A* **1990**, *46*, C34.
[58] L. J. Farrugia, *J. Appl. Crystallogr.* **1997**, *30*, 565.

Received July 10, 2002
[I02376]

New Rhenium(I) and Rhenium(II) Species Assembled by Stereospecific Azopyridine Chelation

Suman Sengupta,[a] Indranil Chakraborty,[a] and Animesh Chakravorty*[a,b]

Keywords: Rhenium / N ligands / Chelates / Back-bonding / Isomer specificity

The spontaneous reaction of $[ReO(OEt)I_2(PPh_3)_2]$ with 2,2′-azobipyridine (L) in acetonitrile, and of $[ReOCl_3(PPh_3)_2]$ with L in toluene, proceeds stereospecifically furnishing the green tris-chelate $[Re^{I}L_3]I$ (**1**) and the red bis-chelate $[Re^{II}Cl_2L_2]$ (**2**), respectively. A structure determination reveals that the coordination geometry of **1** is facial and that of **2** is *cis*(Cl,Cl)-*trans*(N^p,N^p)-*cis*(N^a,N^a) (N^p is a pyridine nitrogen and N^a is an azo nitrogen). The isomer preference is exclusive in both cases and no other isomer has been observed. The average N–N distance in both compounds is about 1.35 Å, signifying the presence of strong d(Re)-π*(azo) back-bonding which plays a crucial role in controlling isomer specificity. The bis-chelate **2** is a one-electron paramagnet and displays a six-line EPR spectrum in fluid solution with g = 2.080 and A = 320 G. The ^{1}H NMR spectrum of diamagnetic **1** is consistent with the facial geometry. In acetonitrile solution **1** displays an Re^{II}/Re^{I} couple and **2** an Re^{III}/Re^{II} couple, the reduction potentials being 0.60 and 0.50V vs. SCE respectively. The violet-coloured imide complex $[Re^{V}Cl_3(NC_6H_4Cl\text{-}p)L]$ (**3**) is also reported; it displays an Re^{VI}/Re^{V} redox wave at 1.33 V vs. SCE. The stabilization of the lower rhenium oxidation states in **1** and **2** is consistent with the decrease of metal reduction potential with progressive L chelation.

(© Wiley-VCH Verlag GmbH & Co. KGaA, 69451 Weinheim, Germany, 2003)

Introduction

In the design of potential radiopharmaceuticals based on rhenium the higher oxidation states of the metal (especially +5) have commonly been employed, although lower states like +1 and +2 are now receiving increasing attention.[1,2] This has prompted us to investigate the synthesis and characterization of new rhenium(I) and rhenium(II) species. Herein we report the unprecedented rhenium coordination types $Re^{I}N_6$ and $Re^{II}Cl_2N_4$ in the form of **1** and **2**, respectively, assembled by 2,2′-azobipyridine (L) chelation. The compounds occur exclusively in a single geometrical form: facial in the case of **1** and *cis*(Cl,Cl)-*trans*(N^p,N^p)-*cis*-(N^a,N^a) in the case of **2**.

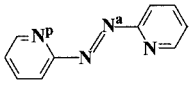

L

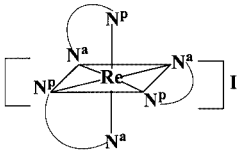

1

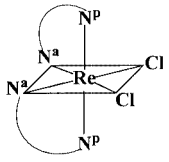

2

Results and Discussion

The reaction of $[ReO(OEt)I_2(PPh_3)_2]$ with excess L in boiling acetonitrile afforded the green tris-complex $[ReL_3]I$ (**1**). On the other hand a 1:2.5 mixture of $[ReOCl_3(PPh_3)_2]$ and L reacted in boiling toluene furnishing red coloured $[ReCl_2L_2]$ (**2**). The latter displays two Re−Cl stretches ($\tilde{\nu}$ = 320, 330 cm^{-1}) in the IR spectrum corresponding to the *cis*-$ReCl_2$ moiety and is paramagnetic (1.95 μB; t_{2g}^5, S = 1/2) displaying a six-line EPR spectrum (^{185}Re and ^{187}Re: I = 5/2)[3] in dichloromethane solution (300 K) with g = 2.080 and A = 320 G. The ^{1}H NMR spectrum of diamagnetic (t_{2g}^6) **1** is consistent with a facial geometry in which the three chelate rings are equivalent in solution.

The geometries of **1** and **2** have been authenticated by an X-ray structure determination. Molecular views are shown in Figure 1 and 2.

Careful chromatographic workup during the syntheses did not reveal the presence of the meridional isomer of **1** or of any of the other theoretically possible isomers (*cis-cis-cis, trans-cis-cis, cis-cis-trans*, and *trans-trans-trans*) of **2**. Bond length data provide a clue to this geometrical specifi-

[a] Department of Inorganic Chemistry, Indian Association for the Cultivation of Science,
Kolkata 700 032, India
Fax: (internat.) + 91-33/2473-2805
E-mail: icac@mahendra.iacs.res.in
[b] Jawaharlal Nehru Centre for Advanced Scientific Research,
Bangalore 560 064, India

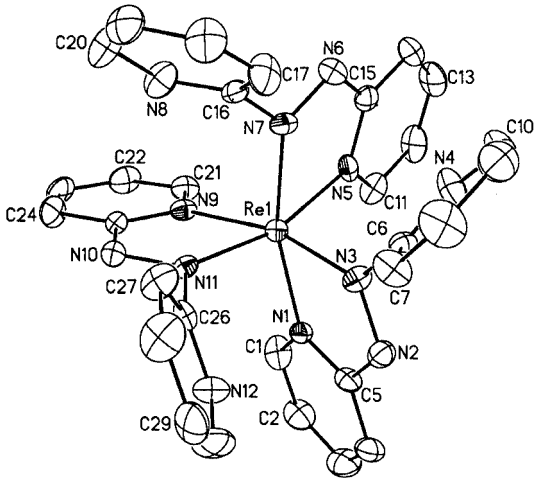

Figure 1. Perspective view and atom labeling scheme of $[ReL_3]^+$; all non-hydrogen atoms are represented by 30% thermal probability ellipsoids (hydrogen atoms are omitted for clarity); selected bond lengths [Å]: Re1−N3 1.965(9), Re1−N7 1.999(9), Re1−N5 2.111(8), Re1−N11 1.982(7), Re1−N1 2.110(8), Re1−N9 2.115(8), N2−N3 1.360(12), N10−N11 1.333(10), N6−N7 1.312(11); selected bond angles [°]: N3−Re1−N11 96.1(3), N11−Re1−N7 96.0(3), N11−Re1−N1 97.0(3), N3−Re1−N5 96.7(3), N7−Re1−N5 73.4(4), N3−Re1−N9 164.9(3), N7−Re1−N9 97.1(3), N5−Re1−N9 95.3(3), N3−Re1−N7 95.1(4), N3−Re1−N1 74.5(3), N7−Re1−N1 164.1(3), N11−Re1−N5 164.0(3), N1−Re1−N5 95.5(3), N11−Re1−N9 73.8(3), N1−Re1−N9 95.2(3)

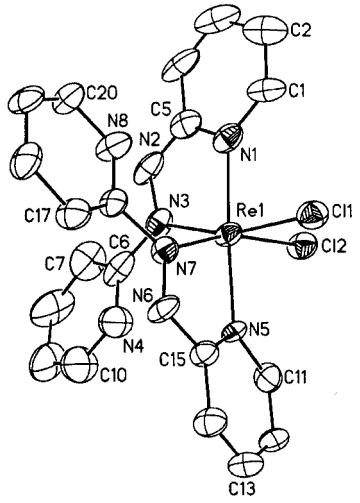

Figure 2. Perspective view and atom labeling scheme of $[ReL_2Cl_2]$; all non-hydrogen atoms are represented by 30% thermal probability ellipsoids (hydrogen atoms are omitted for clarity); selected bond lengths [Å]: Re1−N3 2.001(13), Re1−N5 2.043(10), Re1−N7 2.005(11), Re1−N1 2.080(13), Re1−Cl2 2.374(4), Re1−Cl1 2.384(4), N2−N3 1.37(2), N6−N7 1.32(2); selected bond angles [°]: N3−Re1−N7 91.8(5), N7−Re1−N5 74.4(4), N7−Re1−N1 108.3(5), N3−Re1−Cl2 93.4(4), N5−Re1−Cl2 90.3(3), N3−Re1−Cl1 163.4(4), N5−Re1−Cl1 88.6(3), Cl2−Re1−Cl1 92.25(14), N3−Re1−N5 106.9(5), N3−Re1−N1 75.0(6), N5−Re1−N1 176.8(4), N7−Re1−Cl2 164.7(3), N1−Re1−Cl2 87.0(3), N7−Re1−Cl1 86.8(4), N1−Re1−Cl1 89.7(4)

city. The average Re−N^a and Re−N^p lengths are 1.98 and 2.11 Å in **1** and 2.00 and 2.06 Å in **2**. The average N−N length in both compounds is about 0.1 Å longer than the uncoordinated azo length (1.25 Å).[4] These data clearly underline the presence of strong d(Re)-π*(azo) back-bonding in **1** and **2**. In osmium(II) bis-chelates[5,6] of azoheterocyclic ligands related to L, the N−N length is shorter by about 0.04 Å than that in **2**, signifying the π-basicity order $Re^{II} > Os^{II}$.

The *cis* (as opposed to *trans*) disposition of the two N^a donor sites ensures lack of competition between them for the same metal d-orbitals, thus maximizing back-bonding. In facial $[ReL_3]^+$ three *cis* ReN^a pairs are present, representing a model situation for back-bonding. This geometry is, however, more crowded (aryl groups pendant from the same face) than the unobserved meridional form which has only two *cis* ReN^a pairs. It is proposed that the stronger back-bonding more than offsets the steric disadvantage of the facial geometry which alone becomes observable. As a π-base rhenium(I) is superior to isoelectronic osmium(II) and this has a dramatic geometrical consequence. Osmium(II) tris-chelates of 2-arylazopyridines (pendant pyridine ring of L replaced by, for example, phenyl) occur primarily in the meridional form.[5]

In the case of $[ReCl_2L_2]$ the *cis-trans-cis* form is sterically more favourable than the other two possible but unobserved isomers — *cis-cis-cis* and *trans-cis-cis* — with a *cis* ReN^a pair. In the case of azoheterocyclic bis-chelates of $M^{II}X_2$ (M = Ru,[7] Os;[5,6] X = Cl, Br) isomers have been isolated and these undergo spontaneous thermal conversion into the stable *cis-trans-cis* form.[8] The stability is more critically poised for $[ReCl_2L_2]$, which occurs only in the *cis-trans-cis* form **2**.

A comment on the redox stabilization of rhenium oxidation states by L is in order here. In acetonitrile solution the nearly reversible (peak-to-peak separation 70−80 mV)

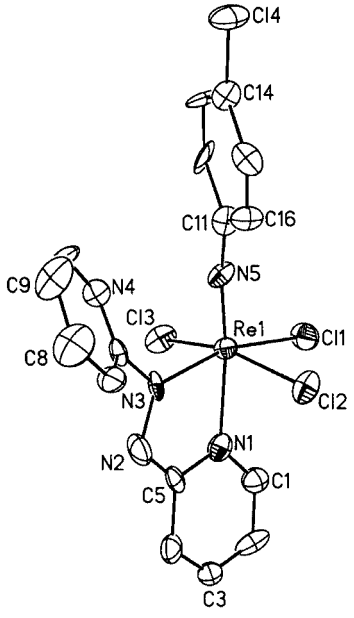

Figure 3. Perspective view and atom labeling scheme of $[ReCl_3(NC_6H_4Cl\text{-}p)L]$; all non-hydrogen atoms are represented by 30% thermal probability ellipsoids (hydrogen atoms are omitted for clarity) selected bond lengths [Å]: Re1−N5 1.72(2), Re1−N1 2.18(3), Re1−N3 2.00(2), Re1−Cl1 2.354(9), Re1−Cl2 2.386(9), Re1−Cl3 2.335(9), N2−N3 1.30(4)

cyclic voltammetric metal redox couples Re^{II}/Re^{I} in **1** and Re^{III}/Re^{II} in **2** have $E_{1/2}$ values of 0.60 and 0.50 V versus SCE respectively. No other metal redox couples are observed in the accessible potential window. On the other hand the rhenium(V) state has been realized in the violet-coloured imide complex $[ReCl_3(NC_6H_4Cl\text{-}p)L]$ (**3**; Figure 3) synthesized by reacting $[ReOCl_3(PPh_3)_2]$ with L in 1:1.5 ratio in the presence of excess $p\text{-}ClC_6H_4NH_2$.

It displays a single metal redox couple Re^{VI}/Re^{V} having an $E_{1/2}$ of 1.33V. Evidently the $E_{1/2}$ of a given Re^{n+1}/Re^{n} couple increases dramatically as the number of L chelate rings increase. The variation of this number along with coligand control provides an excellent handle for stabilizing various oxidation states of rhenium under ambient conditions. Monochelation stabilizes rhenium(V) as has also been documented for related azoheterocyclic ligands.[9,10] Tris- and bis-chelation are now shown to make the mono- and divalent states accessible in the form of **1** and **2**, respectively.

Conclusion

So far rhenium(I) compounds have been primarily known to involve[11,12] carbon monoxide, isocyanide and tertiary phosphane coordination. On the other hand, authentic mononuclear rhenium(II) compounds generally incorporate[11,13] nitrosyl/thionitrosyl and phosphane binding, with a few exceptions.[1,14] The $[ReL_3]I$ and $[ReCl_2L_2]$ chelates add a new dimension to compound types that can span the +1 and +2 oxidation states of rhenium.

Experimental Section

General: $[ReOCl_3(PPh_3)_2]$,[15] $[ReO(OEt)I_2(PPh_3)_2]$,[16] and 2,2′-azobipyridine[4] were prepared by reported methods. For electrochemical work HPLC-grade acetonitrile was used. All other chemical and solvents were of reagent grade and were used as received. Spectral measurements were made with the following equipment: IR (KBr disk), Perkin−Elmer 783 IR spectrometer; X-band EPR, Varian E-109C spectrometer. ^1H NMR, Bruker 300 MHz FT spectrometer (the proton numbering scheme used is the same as in crystallography and the assignments are based on chemical shifts, coupling constants and previous work[5]). The magnetic susceptibility was measured on a PAR 155 vibrating-sample magnetometer. Electrochemical measurements were performed under a nitrogen atmosphere using a PAR 370−4 electrochemistry system with platinum working electrode.[17] The supporting electrolyte was tetraethylammonium perchlorate (TEAP), and the potentials are referenced to the saturated calomel electrode (SCE) without junction correction.

Complex 1: L (107 mg, 0.582 mmol) was added to a solution of $[ReO(OEt)I_2(PPh_3)_2]$ (100 mg, 0.097 mmol) in acetonitrile (15 mL). The resulting mixture was heated to reflux for 3 h, affording a brownish green solution. The solvent was then removed under reduced pressure. The mass thus obtained was dissolved in a minimum amount of dichloromethane and subjected to chromatography on a silica gel column (20 × 1 cm, 60−120 mesh). A deep-green band was eluted out with a toluene/acetonitrile (1:1) mixture. Removal of solvent from the eluate gave $[ReL_3]I$ (**1**) in pure form. It was finally dried under vacuo over fused calcium chloride {**1:** 51 mg, 60% yield based on $[ReO(OEt)I_2(PPh_3)_2]$}. ^1H NMR (300 MHz, $CDCl_3$, 298 K): δ = 8.12 (d, J = 3.7 Hz, H1), 7.85 (complex multiplet, H2), 7.85 (complex multiplet, H3), 8.00 (d, J = 6.0, H4), 6.99 (d, J = 6.0, H7), 7.47 (t, J = 6.0, H8), 7.59 (t, J = 8.7, H9), 7.20 (d, J = 5.6, H10)

Complex 2: L (55.3 mg, 0.300 mmol) was added to a suspension of $[ReOCl_3(PPh_3)_2]$ (100 mg, 0.120 mmol) in toluene (25 mL). The resulting mixture was refluxed for 20 min affording a reddish solution. The solvent was then quickly removed under reduced pressure and the solid mass thus obtained was dissolved in a small amount of dichloromethane and subjected to chromatography in the same manner as mentioned above. A reddish orange band was eluted out with a toluene/acetonitrile (25:2) mixture. Solvent removal under reduced pressure afforded $[ReCl_2L_2]$ (**2**) in pure form which was dried under vacuo over fused calcium chloride {**2:** 49 mg, 65% yield based on $[ReOCl_3(PPh_3)_2]$}.

Complex 3: L (33 mg, 0.180 mmol) and *p*-chloroaniline (76 mg, 0.600 mmol) were added to a suspension of $[ReOCl_3(PPh_3)_2]$ (100 mg, 0.120 mmol) in toluene (25 mL). The mixture was heated to reflux for 2.5 h, affording a violet solution. The solvent was then removed under reduced pressure, and the mass thus obtained was subjected to chromatographic workup as before. Excess amine ($p\text{-}ClC_6H_4NH_2$) was eluted with toluene. A violet band was eluted with a toluene/acetonitrile (25:1) mixture. Solvent removal from the eluate under reduced pressure afforded $[ReCl_3(NC_6H_4Cl\text{-}p)L]$ (**3**) as a dark solid {**3:** 43 mg, 60% yield based on $[ReOCl_3(PPh_3)_2]$}.

Crystal Structure Determination: Single crystals of complexes **1**, **2** and **3** were grown by slow diffusion of hexane into dichloromethane solutions of the respective compounds. Data were collected on a Nicolet R3m/V four-circle diffractometer with graphite-monochromated Mo-K_α radiation (λ = 0.71073 Å) by the ω-scan technique in the range $3° \le 2\theta \le 47°$ for complexes **1** and **3** and $3° \le 2\theta \le 50°$ for **2**. All data were corrected for Lorentz-polarization and absorption.[18] The metal atoms were located from Patterson maps and the rest of the non-hydrogen atoms emerged from successive Fourier syntheses. The structures were then refined by a full-matrix least-squares procedure on F^2. All non-hydrogen atoms were refined anisotropically. All hydrogen atoms were included in calculated positions. Calculations were performed using the SHELXTL™ V 5.03 Program package.[19] In the structure of **3** there are two very similar but crystallographically independent molecules in the asymmetric unit. Figure 3 refers to molecule 1.

Crystal Data for 1: $C_{30}H_{24}IN_{12}Re$, monoclinic, *C*2/*c* (no. 15) a = 22.914(5), b = 13.236(3), c = 21.722(4) Å, β = 110.61(3)°, V = 6166(2) Å^3, Z = 8, Mo-K_α (λ = 0.71073 Å), 4589 unique reflections (R_{int} = 0.0360). Final residuals R_1 = 0.0391 and wR_2 = 0.0826 [$I > 2\sigma(I)$], 403 parameters.

Crystal Data for 2: $C_{20}H_{16}Cl_2N_8Re$, orthorhombic, *Pbcn* (no. 60), a = 19.190(9), b = 15.431(9), c = 15.062(14) Å, V = 4460(5) Å^3, Z = 8, Mo-K_α (λ = 0.71073 Å), 3937 unique reflections (R_{int} = 0.0338). Final residuals R_1 = 0.0603 and wR_2 = 0.1356 [$I > 2\sigma(I)$], 280 parameters.

Crystal Data for 3: $C_{16}H_{13}Cl_3N_5Re$, triclinic, $P\bar{1}$ (no. 2), a = 13.379(5), b = 13.652(5), c = 13.992(6) Å, α = 61.90(3), β = 65.44(3), γ = 66.12(3)°, V = 1980(1) Å^3, Z = 4, Mo-K_α (λ = 0.71073 Å), 5815 unique reflections (R_{int} = 0.0368). Final residuals R_1 = 0.0981 and wR_2 = 0.2232 [$I > 2\sigma(I)$], 464 parameters.

CCDC-192908 (**1**), -192909 (**2**) and -192910 (**3**) contain the supplementary crystallographic data for this paper. These data can be obtained free of charge at www.ccdc.cam.ac.uk/conts/retrieving.html [or from the Cambridge Crystallographic Data Centre, 12,

Union Road, Cambridge CB2 1EZ, UK; Fax: (internat.) +44−1223/336−033; E-mail: deposit@ccdc.cam.ac.uk].

Acknowledgments

We thank the Department of Science and Technology and Council of Scientific and Industrial Research, New Delhi for financial support.

[1] G. E. D. Mullen, P. J. Blower, D. J. Price, A. K. Powell, M. J. Howard, M. J. Went, *Inorg. Chem.* **2000**, *39*, 4093−4098.
[2] J. R. Dilworth, S. J. Parrott, *Chem. Soc. Rev.* **1998**, *27*, 43−55; S. Top, H. E. Hafa, A. Vessieres, J. Quivy, J. Vaissermann, D. W. Hughes, M. J. McGlinchey, J. P. Mornon, E. Thoreau, G. Jaouen, *J. Am. Chem. Soc.* **1995**, *117*, 8372−8380.
[3] B. K. Dirghangi, M. Menon, S. Banerjee, A. Chakravorty, *Inorg. Chem.* **1997**, *36*, 3595−3601.
[4] M. Shivakumar, K. Pramanik, I. Bhattacharyya, A. Chakravorty, *Inorg. Chem.* **2000**, *39*, 4332−4338; K. Pramanik, M. Shivakumar, P. Ghosh, A. Chakravorty, *Inorg. Chem.* **2000**, *39*, 195−199.
[5] B. K. Ghosh, A. Mukhopadhyay, S. Goswami, S. Ray, A. Chakravorty, *Inorg. Chem.* **1984**, *23*, 4633−4639.
[6] P. Byabartta, S. Pal, T. Misra, C. Sinha, F.-L. Liao, K. Panneerselvam, T.-H. Lu, *J. Coord. Chem.* **2002**, *55*, 479−496.
[7] R. A. Krause, K. Krause, *Inorg. Chem.* **1980**, *19*, 2600−2603; S. Goswami, A. R. Chakravarty, A. Chakravorty, *Inorg Chem.* **1981**, *20*, 2246−2250; A. H. Velders, H. Kooijman, A. L. Spek, J. G. Haasnoot, D. deVos, J. Reedijk, *Inorg. Chem.* **2000**, *39*, 2966−2967.
[8] T. Bao, K. Krause, R. A. Krause, *Inorg. Chem.* **1988**, *27*, 759−761; A. K. Deb, M. Kakoti, S. Goswami, *J. Chem. Soc., Dalton Trans.* **1991**, 3249−3251; T. K. Misra, D. Das, C. Sinha, P. Ghosh, C. K. Pal, *Inorg. Chem.* **1998**, *37*, 1672−1678.
[9] I. Chakraborty, S. Bhattacharyya, S. Banerjee, B. K. Dirghangi, A. Chakravorty, *J. Chem. Soc., Dalton Trans.* **1999**, 3747−3753.
[10] S. Banerjee, S. Bhattacharyya, B. K. Dirghangi, M. Menon, A. Chakravorty, *Inorg. Chem.* **2000**, *39*, 6−13.
[11] F. A. Cotton, G. Wilkinson, C. A. Murillo, M. Bochmann, *Advanced Inorganic Chemistry*, John Wiley and Sons, Inc., 5th Edn., **1999**.
[12] M. L. Kuznetsov, A. J. L. Pombeiro, A. I. Dementlev, *J. Chem. Soc., Dalton Trans.* **2000**, 4413−4421; K. Wang, L. Huang, L. Gao, L. Jin, C. Hoang, *Inorg. Chem.* **2002**, *41*, 3353−3358.
[13] A. Voigt, U. Abram, R. Kirmse, *Z. Anorg. Allg. Chem.* **1999**, *625*, 1658−1663; M. Goeldner, A. Kienast, H. Homborg, *Z. Anorg. Allg. Chem.* **1998**, *624*, 141−146.
[14] M. Stebler, A. Gutierrez, A. Ludi, B. Hans-Beat, *Inorg. Chem.* **1987**, *26*, 1449−1451.
[15] J. Chatt, G. A. Rowe, *J. Chem. Soc.* **1962**, 4019−4033.
[16] G. Francociani, G. D'Alfonso, P. Romiti, A. Sironi, M. Freni, *Inorg. Chim. Acta* **1983**, *72*, 29−37.
[17] A. Pramanik, N. Bag, D. Ray, G. K. Lahiri, A. Chakravorty, *Inorg. Chem.* **1991**, *30*, 410−417.
[18] A. C. T. North, D. C. Philips, F. S. Mathews, *Acta Crystallogr., Sect. A* **1968**, *24*, 351−359.
[19] G. M. Sheldrick, SHELXTL™ V 5.03, Bruker analytical X-ray systems, Madison, WI, 1994.

Received September 17, 2002
[I02515]

[Bis(oxazolinyl)pyrrole]palladium Complexes as Catalysts in Heck- and Suzuki-Type C−C Coupling Reactions

Clément Mazet[a] and Lutz H. Gade*[a]

Keywords: Catalysis / Helical structures / N ligands / Palladium / Suzuki reaction / Heck reaction

The two bis(oxazoline)pyrrole ligand precursors 2,5-bis(4,4′-dimethyl-4,5-dihydrooxazol-2-yl)pyrrole ("dmoxpH", **2**) and 2,5-bis(4,4′-dimethyl-4,5-dihydrooxazol-2-yl)-3,4-diethylpyrrole ("Et_2dmoxpH", **5**) have been synthesised and metallated by treatment with *n*-butyllithium at −78 °C in diethyl ether. Treatment of the lithium pyrrolide with 1.1 mol-equiv. of [$PdCl_2$(COD)] gave the corresponding helical dinuclear palladium complexes [Pd_2Cl_2(dmoxp)$_2$] (**6**) and [Pd_2Cl_2(Et_2dmoxp)$_2$] (**7**). In both complexes the tridentate bis(oxazolinyl)pyrrolide ligands bridge the two metal centres, with one of the oxazoline rings and the charged pyrrolide being coordinated to the one Pd centre while the second oxazoline ring is twisted relative to the pyrrolide unit and coordinates to the second palladium atom. Complexes **6** and **7** were found to be precursors for active catalysts for Heck coupling reactions of styrene and ethyl acrylate, with turnover numbers of over 9000 for the former, as well as for disubstituted alkenes such as methyl crotonate and methyl cinnamate. Complex **6** was found to be a very active catalyst for Suzuki coupling reactions of activated and deactivated bromoarenes.

(© Wiley-VCH Verlag GmbH & Co. KGaA, 69451 Weinheim, Germany, 2003)

Introduction

In recent years, nitrogen donor ligands have increasingly been employed as ancillary ligands in molecular catalysis.[1] This is due to the great variety of synthetic strategies available. Nitrogen-based catalysts may generate catalytically active complexes complementary to the known phosphane-based systems. Oxazolines and their derivatives have been intensely studied in a wide range of applications, particularly in asymmetric catalysis.[2,3]

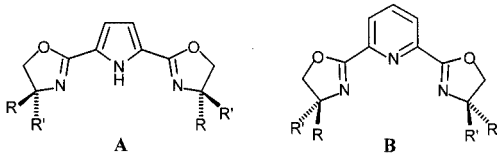

A

B

We recently began to develop the coordination chemistry of a new class of potentially tridentate, monoanionic N-donor ligands based on the combination of two oxazoline rings and a central pyrrole unit (**A**).[4] This class of compounds may be viewed as precursors to monoanionic analogues of the well-established family of pybox ligands (**B**), which have found widespread application in asymmetric catalysis in recent years.[5] The monoanionic charge of the deprotonated molecule and the more open structure of this derivative of the five-membered pyrrole ring in comparison with the ligands containing a central pyridine unit would be expected to result in somewhat different complex structures in comparison to pybox complexes. In a preliminary study of their coordination chemistry we discovered that the arrangement of its three N-donor atoms does not permit meridional tris(coordination) to a single metal centre.[4] This gives rise to dinuclear complexes that dissociate in solution only at higher temperatures.[6]

In this paper we report the synthesis of two achiral type **A** bis(oxazolinyl)pyrroles, one of which is alkyl-substituted in the 3- and 4-positions of the pyrrole ring, and the synthesis of two helical dinuclear palladium complexes. The principle focus was to assess their suitability as precursors for efficient catalytic C−C coupling reactions. To this end, a series of Heck and Suzuki coupling reactions were carried out as benchmark reactions in order to test these novel molecular systems.

Results and Discussion

Synthesis of the Two Ligand Precursors 2,5-Bis[2-(4,4′-dimethyl-4,5-dihydrooxazolyl)]pyrrole ("dmoxpH", 2) and 2,5-Bis[2-(4,4′-dimethyl-4,5-dihydrooxazolyl)]-3,4-diethylpyrrole ("Et_2dmoxpH", 5)

As a starting material in the synthesis of 2,5-bis(4,4′-dimethyl-4,5-dihydrooxazol-2-yl)pyrrole ("dmoxpH", **2**) we chose pyrrole-2,5-dicarbonitrile (**1**), for which we had previously developed an efficient synthetic route.[6] Its cyclisation with two mol-equiv. of 2-amino-2-methyl-1-propanol was

[a] Laboratoire de Chimie Organométallique et de Catalyse, CNRS UMR 7513, Institut Le Bel, Université Louis Pasteur, 4, rue Blaise Pascal, 67070 Strasbourg, France

carried out by the method reported by Witte and Bolm.[7] Heating at reflux in chlorobenzene in the presence of 0.5 mol-equiv. of activated $ZnCl_2$ for 12 h gave crude **2**, which was purified by flash chromatography to give a cream-coloured solid. The formulation of compound **2** was confirmed by elemental analysis and mass spectrometry, while its ^1H, ^{13}C NMR and infrared spectra were consistent with the structure depicted in Scheme 1.

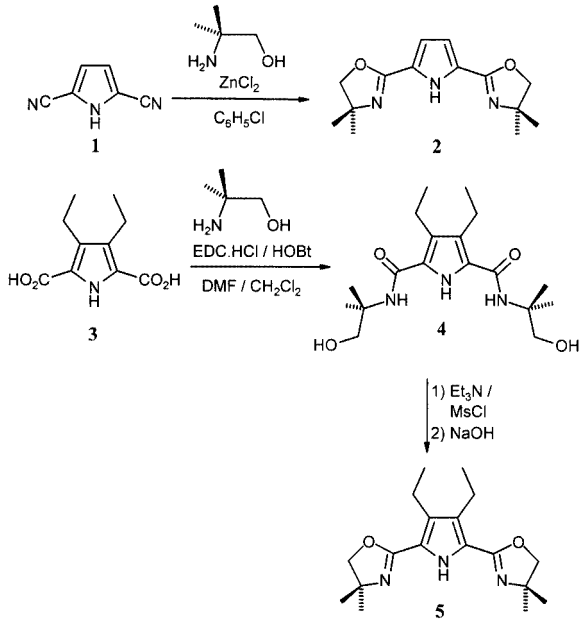

Scheme 1. Synthesis of the two bis(oxazolinyl)pyrroles **2** and **5**

The 3,4-diethylpyrrole analogue of **2**, 2,5-bis(4,4′-dimethyl-4,5-dihydrooxazol-2-yl)-3,4-diethylpyrrole ("Et_2dmoxpH", **5**) was synthesised in two steps, starting from the known 3,4-diethylpyrrole-2,5-dicarboxylic acid (**3**).[8] This has frequently been used as a starting material in porphyrin synthesis, and several efficient preparative procedures have been published in recent years.[9] The purpose behind the replacement of the central pyrrole ring by a diethylpyrrole unit was the variation of the donor capacity of the pyrrolide ligand, an approach previously pursued in oligopyrrole (notably porphyrin) chemistry.[9] In the first reaction step the dicarboxylic acid **3** was treated with 2.5 mol-equiv. of the amino alcohol in the presence of the well-established amide coupling reagent *N*′-[3-(dimethylamino)propyl]-*N*-ethylcarbodiimide (EDC·HCl) and 1-hydroxybenzotriazole (HOBt) (Scheme 1).[10] The diamide **4** was dimesylated and then cyclized in the presence of an excess of NaOH in methanol. After workup, the target compound **5** was obtained as a pale yellow oil, which was characterised by elemental analysis, mass spectrometry and infrared and ^1H and ^{13}C NMR spectroscopy.

Synthesis and Structural Characterisation of the Helical Dinuclear Palladium Complexes $[Pd_2Cl_2(dmoxp)_2]$ (6) and $[Pd_2Cl_2(Et_2dmoxp)_2]$ (7)

Deprotonation of the pyrrole rings in dmoxpH (**2**) and Et_2dmoxpH (**5**) with *n*-butyllithium at −78 °C in diethyl ether and subsequent stirring of the lithium pyrrolide with 1.1 mol-equiv. of $[PdCl_2(COD)]$ gave the corresponding palladium complexes $[Pd_2Cl_2(dmoxp)_2]$ (**6**) and $[Pd_2Cl_2(Et_2dmoxp)_2]$ (**7**) after chromatographic workup (Scheme 2).

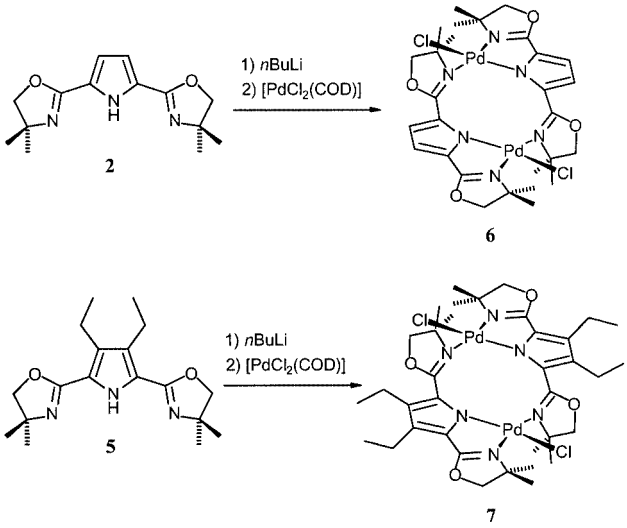

Scheme 2. Synthesis of the helical dinuclear palladium complexes $[Pd_2Cl_2(dmoxp)_2]$ (**6**) and $[Pd_2Cl_2(Et_2dmoxp)_2]$ (**7**)

In order to establish their molecular structures, X-ray diffraction studies of both complexes **6** and **7** were carried out. Two views of their very similar molecular structures are depicted in Figures 1 and 2, together with the principal bond lengths and interbond angles.

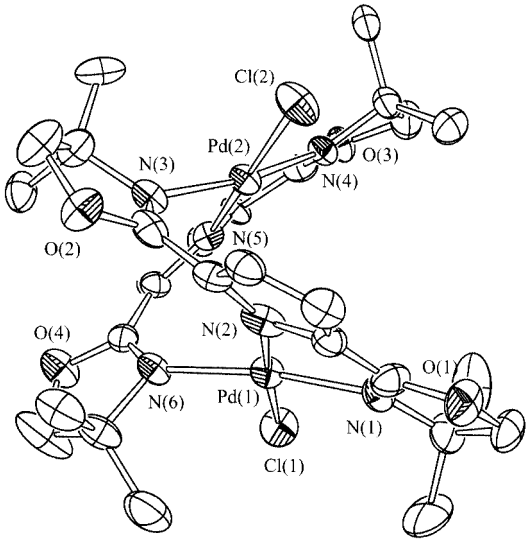

Figure 1. Molecular structure of the palladium complex $[Pd_2Cl_2(dmoxp)_2]$ (**6**); selected bond lengths [Å] and angles [°]: Pd(1)−N(1) 2.052(8), Pd(1)−N(2) 2.039(8), Pd(1)−N(6) 2.036(8), Pd(1)−Cl(1) 2.296(3), Pd(2)−Cl(2) 2.287(3), Pd(2)−N(3) 2.043(8), Pd(2)−N(4) 2.025(7), Pd(2)−N(5) 2.039(8); N(2)−Pd(1)−N(6) 97.7(3), N(1)−Pd(1)−N(2) 79.8(3), Cl(1)−Pd(1)−N(1) 96.5(2), N(3)−Pd(2)−N(5) 97.7(3), N(4)−Pd(2)−N(5) 79.9(3), N(2)−C(28)−C(8)−N(3) 29.3(5), N(5)−C(19)−C(22)−N(6) 26.4(5)

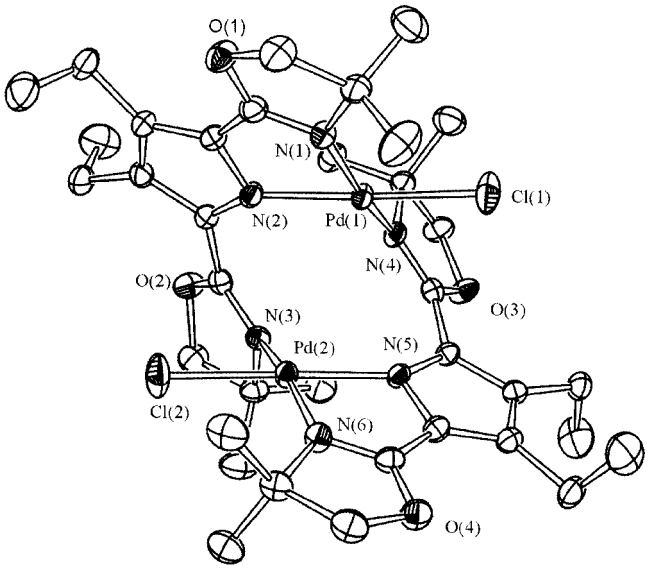

Figure 2. Molecular structure of the palladium complex $[Pd_2Cl_2(Et_2dmoxp)_2]$ (**7**); selected bond lengths [Å] and angles [°]: Pd(1)−N(1) 2.031(2), Pd(2)−N(3) 2.043(2), Pd(1)−Cl(1) 2.2922(7), Pd(1)−N(2) 2.036(2), Pd(2)−N(5) 2.031(2), Pd(2)−Cl(2) 2.0311(7), Pd(1)−N(4) 2.035(2), Pd(2)−N(6) 2.036(2); N(1)−Pd(1)−Cl(1) 94.94(6), N(6)−Pd(2)−Cl(2) 95.75(6), N(1)−Pd(1)−N(2) 80.01(8), N(3)−Pd(2)−N(5) 94.48(8), N(2)−Pd(1)−N(4) 96.80(8), N(5)−Pd(2)−N(6) 79.86(8), N(2)−C(7)−C(14)−N(3) 21.4(5), N(4)−C(21)−C(24)−N(5) 28.3(5)

Both compounds **6** and **7** are dinuclear complexes in which the tridentate bis(oxazolinyl)pyrolide ligands bridge the two metal centres. Whereas one of the oxazoline rings and the charged pyrrolide are coordinated to the one Pd centre, adopting an almost coplanar arrangement, the second oxazoline ring is twisted relative to the pyrrolide unit [**6**: 26.4 and 29.3°; **7**: 21.4 and 28.3°] and coordinates to the second palladium atom. The coordination geometry at each metal centre is distorted square-planar, with the chloro ligand disposed *trans* to the pyrrolide. Although neither of the complexes **6** and **7** possesses exact crystallographic symmetry, both have an approximate twofold molecular symmetry axis relating the {Pd(ligand)Cl} fragments. Overall, the two bis(oxazolinyl)pyrrolide ligands are wrapped around the two metal centres to give helical arrangements,[11] with Pd−Pd distances of 3.389 and 3.426 Å for **6** and **7**, respectively. It is interesting to note that complex **6** crystallised in the polar space group *C*2 as a conglomerate of (*P*)- and (*M*)-helical enantiomers, although we were unable to separate them mechanically. For the solution of the crystal structure of **6** we selected by chance a crystal containing the (*M*) enantiomer, which is depicted in Figure 1.

The dimerisation of both **6** and **7** to give the helical dinuclear complexes implies the loss of all local symmetry elements at the metal centres. Only the two tridentate ligands as a whole are related by a twofold rotational axis. This loss in local symmetry is reflected in the signal patterns of the ^1H and ^{13}C NMR spectra of both compounds, in which all the ^1H and ^{13}C nuclei in the individual ligands are chemically inequivalent. Consistent with this reduced symmetry with respect to the ligand precursors **2** and **5** is the observation of two vibrational C=N bands for the two inequivalent oxazoline rings at 1632 and 1608 cm^{-1} for **6** and at 1622 and 1600 cm^{-1} for **7**.

Heck Coupling Reactions with Mono- and 1,2-Disubstituted Alkenes, Catalysed by $[Pd_2Cl_2(dmoxp)_2]$ (6) and $[Pd_2Cl_2(Et_2dmoxp)_2]$ (7)

Originally, Pd-catalysed Heck and Suzuki coupling reactions were based almost entirely on phosphane or phosphane-derived systems.[12] In recent years, however, a whole range of alternative ligand systems for this reaction has been successfully tested. These include *N*-heterocyclic carbenes,[13,14] N-, O- and S-containing palladacycles,[15,16] cyclometallated imines[17] and diazabutadienes[18] which act as mono- or polydentate ancillary ligands.

We tested the activities of compounds **6** and **7** in Heck coupling reactions. In an initial study, the reaction conditions (solvent, base, reaction temperature) were optimised for the reference reaction between bromobenzene and styrene, in the presence of 0.1 mol % of the catalyst precursor (Scheme 3). The best results were obtained at 110 °C in *N*-methylpyrrolidone with K_3PO_4 as a base, and these reaction conditions were chosen for all subsequent catalytic runs. It should be pointed out that the palladium catalysts were stable under these conditions throughout the conversions. Precipitation of "Pd-black", potentially due to the degradation of the molecular catalysts, was not observed in any case. The results of a comparative study with $[Pd_2Cl_2(dmoxp)_2]$ (**6**) and $[Pd_2Cl_2(Et_2dmoxp)_2]$ (**7**) are depicted in Table 1.

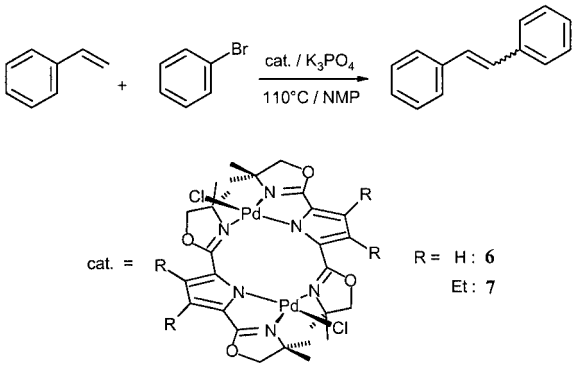

Scheme 3. Application of the palladium complexes $[Pd_2Cl_2(dmoxp)_2]$ (**6**) and $[Pd_2Cl_2(Et_2dmoxp)_2]$ (**7**) in the Heck reaction between bromobenzene and styrene

Table 1. Comparative study of the catalytic activities of catalysts **6** and **7** in the Heck reaction between bromobenzene and styrene

Entry	Catalyst	Cat./Sub.	Time	Conv. [(*Z*) + (*E*)]	T.O.N.
1	6	10^{-3}	3 d	97.1%	971
2	7	10^{-3}	3 d	96.6%	966
3	6	10^{-4}	3 d	87.3%	8730
4	7	10^{-4}	3 d	85.4%	8540
5	6	$5{\cdot}10^{-5}$	4 d	47.4%	9480
6	7	$5{\cdot}10^{-5}$	4 d	43.2%	8640

In general, there does not seem to be a significant difference in the catalytic performances of complexes **6** and **7**. A minimum catalyst/substrate ratio of $5 \cdot 10^{-5}$ was employed, and this, after 4 d reaction time at 110 °C, gave degrees of conversion to the product stilbene of 47 and 43%, respectively. The electronic effect expected from the introduction of the ethyl substituent on the pyrrolide ring[9] is not reflected in a modulation of the catalytic activity. It should be noted, though, that the turnover numbers of 9480 and 8640 place these catalysts among the most efficient systems containing exclusively nitrogen donor ligands.[19,20]

The results of the coupling of methyl acrylate with several substituted bromobenzene derivatives catalysed by compound **6** (Scheme 4) is shown in Table 2. The degree of conversion after a reaction time of 3 d was high and the stereoselectivity in favour of the (*E*) isomers essentially quantitative. In none of the cases did we observe traces of the geminally disubstituted coupling product.[21] No activity was observed for derivatives of chlorobenzene for the coupling either of styrene or of methyl acrylate.

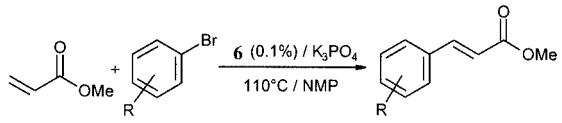

Scheme 4. Coupling of methyl acrylate with substituted bromobenzene derivatives

Table 2. Results of the Heck reactions between methyl methacrylate and substituted bromobenzene derivatives, catalysed by **6**

Entry	R	Time	Conversion	(*E*)/(*Z*)
1	2-Me	3 d	77%	100:0
2	4-Me	3 d	97%	100:0
3	4-OMe	3 d	85%	99:1

The use of the Heck coupling reaction for the synthesis of trisubstituted alkenes has received much less attention than the standard conversions affording disubstituted C=C double bonds.[20,22,23] We therefore carried out several tests to investigate the activity of **6** towards (*E*)-1,2-disubstituted alkenes. With a catalyst loading of 0.1 mol %, the reactions of methyl crotonate and methyl cinnamate with 4-bromotoluene gave the corresponding trisubstituted olefins after a reaction time of 7 d (Scheme 5).

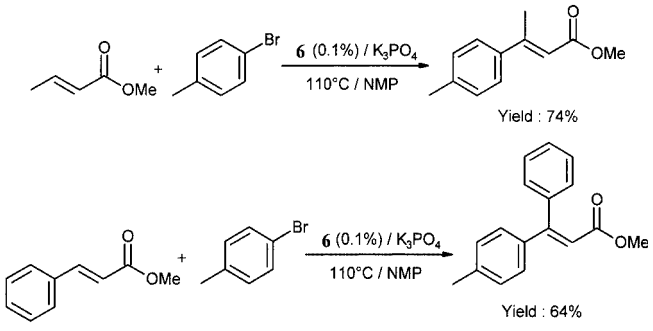

Scheme 5. Heck reactions giving trisubstituted alkenes

The most remarkable aspect of these conversions is the complete stereoselectivity in the positioning of the entering aryl group in the reaction products. The configuration was established by NOESY experiments, NOEs between the α-olefin proton and the *ortho*-protons of the tolyl group providing the key assignment. It was not possible to detect any other stereoisomer even in trace quantities by GC, GCMS or by NMR spectroscopy. The exclusive formation of the (*E*) stereoisomers may be explained by the stereospecificity of the migratory insertion step resulting in the coupling of the olefin and the Pd-bonded aryl group and of the subsequent β-elimination step (Scheme 6).

We have shown in a previous study that these dissociate in solution at temperatures above 70 °C,[6] and it is within this thermodynamic regime that their catalytic activities in Heck and Suzuki C−C coupling reactions have been observed. We therefore only consider monomeric species in the following mechanistic discussion. The *endo* approach of the aryl group in the intermediates **Ia** and **IIa** stereospecifically generates the alkyl complexes **Ib** and **IIb**, in which rotation around a C−C bond gives access to a conformation (**Ic** and **IIc**, respectively) in which the β-H is oriented towards the metal centre and from which β-elimination occurs. This gives the intermediates **Id** and **IId**, both of which liberate exclusively the (*E*) isomer.

Buchwald et al. have previously found a high degree of stereoselectivity in non-phosphane/palladium-catalysed Heck reactions of 1,2-substituted α,β-unsaturated carboxyl esters.[20] They also pointed out that the generally accepted mechanism of the catalytic Heck coupling implied a stereospecific reaction sequence as detailed above. The deviations from ideal stereoselection were interpreted as being due to an isomerisation of the configuration at the C=C double bond after the Heck coupling step. For the two cases described above we were unable to establish such an post-Heck equilibration, which may be due to the short lifetime of the hydridopalladium intermediate after decoordination of the product olefin. In fact, such a hydrido species may play a role either before or after the Heck reaction:

a) It may in principle coordinate the disubstituted alkene starting material (**IIIa** in Scheme 6), which is isomerised to the (*Z*)-1,2-disubstituted alkene in a sequence of migratory insertion and β-elimination (liberated from **IIId** in Scheme 6).

b) Alternatively, given a sufficient lifetime of the hydridopalladium complex, the reaction products liberated from **Id** and **IId** may recoordinate to the metal centre, and the migratory insertion into the Pd−H bond may then take place in part with a reversed regioselectivity (migration of the H atom to the C atom adjacent to the carboxyl function). A subsequent β-elimination from such an intermediate may indeed give the other isomer and, since all steps are reversible, the product distribution may be under thermodynamic control.

The fact that no isomerisation is observed in the case at hand even after the considerable reaction time of 7 d, necessary because of the low catalyst loadings of 0.1 mol %, indicates the short lifetime of the hydridopalladium species.

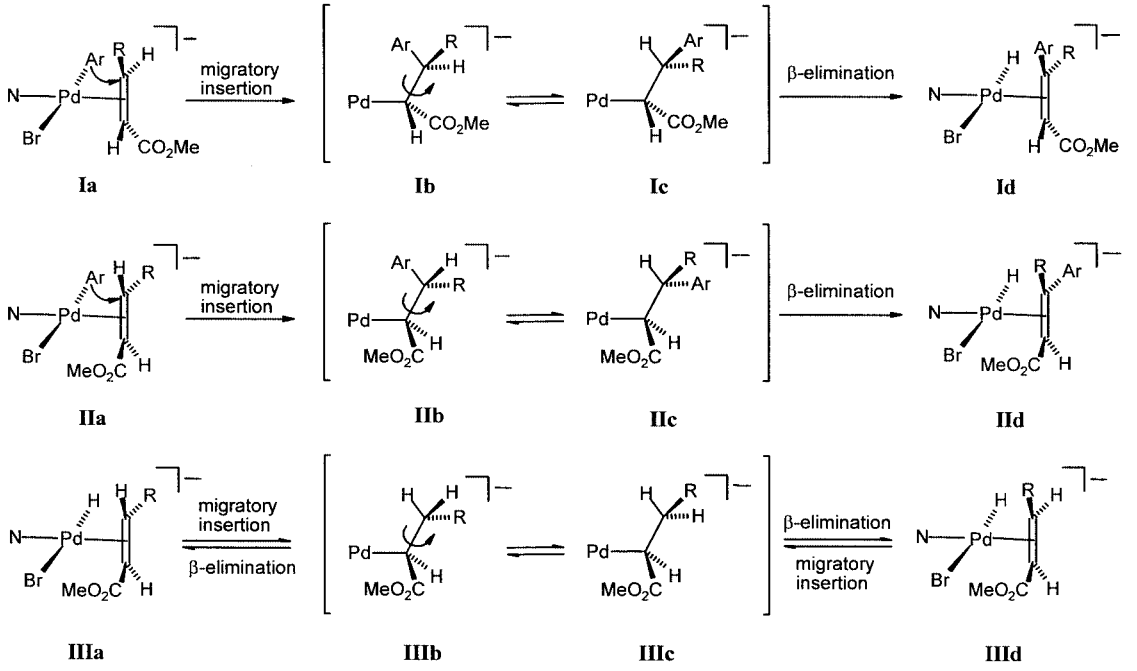

Scheme 6. Mechanistic scheme representing the stereospecific migratory insertion-β-elimination sequence in the Heck reaction involving 1,2-disubstituted alkenes

This may in part be due to the proximity of the relatively basic oxazoline functions attached to the pivotal pyrrolide ligand.

Suzuki Coupling Reactions Catalysed by $[Pd_2Cl_2(dmoxp)_2]$ (6)

Compound **6** was found to be a highly active catalyst for the Suzuki-type coupling of phenylboronic acid with aryl bromides at relatively moderate temperatures (Table 3). In the general procedure a catalyst/substrate ratio of 10^{-4} was used and the aryl bromide and phenylboronic acid were stirred at 70 °C in toluene in the presence of K_2CO_3 as auxiliary base.

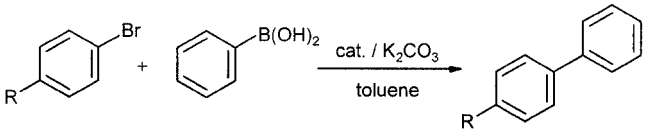

Scheme 7. Suzuki coupling between bromobenzene derivatives and phenylboronic acid

As observed for the Heck-type coupling reactions discussed above, catalyst **6** was found to be highly stable under Suzuki coupling conditions, and no palladium-black was formed during the reaction. The catalytic reaction was monitored by GC MS, and 100% conversion was obtained with both activated and deactivated bromides after 1−6 h. A decrease in the catalyst/substrate ratio to 10^{-5} still gave an 82% isolated yield of 4-bromoacetophenone and 54% of 4-methoxyacetophenone after 4 h, corresponding to turnover numbers of 82000 and 54000, respectively. In contrast to the reactivity towards aryl bromides, the catalyst proved to possess only very low activity towards the aryl chlorides, the reaction effectively stopping after a few cycles at 110 °C. As in the case of the Heck coupling reactions discussed in the previous section, the use of the diethyl-substituted derivative $[Pd_2Cl_2(Et_2dmoxp)_2]$ (**7**) gave essentially identical results in the catalytic conversions.

Table 3. Results of the Suzuki reactions between phenylboronic acid and substituted bromobenzene derivatives, catalysed by **6**

Entry	R	Product	Time	Cat./Sub.	Temp.	Yield	T.O.N.
1	H	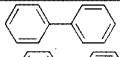	2 h	10^{-4}	70 °C	97 %	9700
2	CH_3	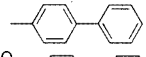	2 h	10^{-4}	70 °C	89 %	8900
3	$C(O)CH_3$	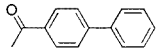	1 h	10^{-4}	70 °C	92 %	9200
4	$C(O)OCH_3$	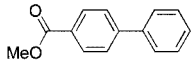	4 h	10^{-4}	70° C	95 %	9500
5	OCH_3	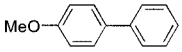	6 h	10^{-4}	70 °C	88 %	8800
6	$C(O)OCH_3$	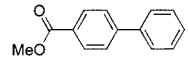	4 h	10^{-5}	110 °C	82 %	**82000**
7	OCH_3	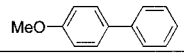	4 h	10^{-5}	110 °C	54 %	**54000**

Conclusions

Through the charging and deformation of the well-established pybox ligand **B** systems by replacement of the central pyridine unit by a formally charged pyrrolide ring, the more open "pyrrbox" ligands **A** have been obtained. The specific arrangement of the three nitrogen donor functions in these has given rise to helical dinuclear complexes if coordinated

to palladium(II). Whereas their activity is lower than those found for some Pd complexes bearing phosphane or N-heterocyclic arene ligands, they are nevertheless among the most active catalysts containing exclusively nitrogen-donor ligands. The observation of the high stereoselectivity in the Heck reactions with 1,2-disubstituted alkenes described in this work is remarkable and has initiated a more systematic investigation into this aspect, currently underway in our laboratory.

Experimental Section

General: Solvents were dried by standard procedures and saturated with nitrogen. Solids were separated from suspensions by centrifugation, thus avoiding filtration procedures, with a Hettich Rotina 48 centrifuge equipped with a specifically designed Schlenk tube rotor (Hettich Zentrifugen, Tuttlingen, Germany).[24] Optical rotations were recorded with a thermostated Perkin−Elmer Otopol III instrument in a 1.0-dm cell. The ^1H and ^{13}C NMR spectra were recorded with Bruker AC 300 (^1H 300 MHz; $^{13}C\{^1H\}$ 75 MHz), Bruker AM 400 (^1H 400 MHz; $^{13}C\{^1H\}$ 100 MHz), and Bruker ARX 500 (^1H 500 MHz; $^{13}C\{^1H\}$ 125 MHz) spectrometers. Infrared spectra were recorded with a Perkin−Elmer 1600 FT-IR spectrometer. EI mass spectra were recorded with a Shimadzu QP5050-GC/MS system. The elemental analyses were carried out by the Service Commun de Microanalyse de l'Université Louis Pasteur at Strasbourg. Pyrrole-2,5-dicarbonitrile,[6] 3,4-diethylpyrrole-2,5-dicarboxylic acid[8] and $[PdCl_2(1,5\text{-}COD)]$[25] were prepared by published procedures. All other chemicals used as starting materials were obtained commercially and used as received without further purification.

Preparation of 2,5-Bis(4,4′-dimethyl-4,5-dihydrooxazol-2-yl)pyrrole ("dmoxpH", 2): $ZnCl_2$ (1.164 g, 8.54 mmol, 0.5 equiv.) was melted under vacuum and then cooled under nitrogen for 15 min. A slurry of pyrrole-2,5-dicarbonitrile (2 g, 17.6 mmol) and 2-amino-2-methyl-1-propanol (4.263 g, 47.82 mmol, 2.8 equiv.) in chlorobenzene (25 mL) was added, and the mixture was heated at reflux for 24 h. The solvent was removed in vacuo and the orange-brown residue was chromatographed on silica gel (hexanes/EtOAc, 1:1); R_f = 0.43, yielding 4.263 g of an off-white solid (yield 72%). ^1H NMR (300 MHz. $CDCl_3$): δ = 11.40 (br. s, 1 H, NH_{pyrr}), 6.71 (s, 2 H, $H_{3/4,pyrr}$), 4.05 (s, 4 H, $CH_{2,oxa}$), 1.34 (s, 12 H, $CH_{3,oxa}$) ppm. $^{13}C\{^1H\}$ NMR (75 MHz. $CDCl_3$): δ = 155.6 ($C{=}N_{oxa}$), 123.0 (C-2/5$_{pyrr}$), 112.9 (C-3/4$_{pyrr}$), 79.0 ($CH_{2,oxa}$), 67.4 ($C_{quat,oxa}$), 28.2 ($CH_{3,oxa}$) ppm. IR (KBr): $\tilde{\nu}$ = 3436 (s), 2969 (m), 1660 (s), 1612 (m), 1499 (s), 1404 (m), 702 (m) cm^{-1}. MS (EI, 70 eV): *m*/*z* = 261 $[M]^+$, 246 $[M - CH_3]^+$, 174 $[M - CH_3 - (CH_3)_2CCH_2O]^+$. $C_{14}H_{19}N_3O_2$ (261.15): calcd. C 64.35, H 7.33, N 16.08; found C 63.89, H 7.25 N 15.99.

Preparation of Compound 4: A mixture of 3,4-diethylpyrrole-2,5-dicarboxylic acid (4.1 g, 19.4 mmol), amino alcohol (5.191 g, 58.2 mmol), EDC·HCl (11.164 g, 58.2 mmol), and HOBt (7.870 g, 58.2 mmol) in 75 mL of CH_2Cl_2 and 75 mL of DMF was stirred under nitrogen at room temperature for 48 h. The reaction mixture was poured into a saturated NH_4Cl/CH_2Cl_2 solution, and the aqueous layer was extracted with CH_2Cl_2. The combined organic layers were washed with 1 N HCl, water, saturated $NaHCO_3$ and brine, and then dried with anhydrous Na_2SO_4. After removal of the solvent, the product was isolated as a pale yellow oil (5.2 g, 14.7 mol, 77% yield). ^1H NMR (300 MHz, $CDCl_3$): δ = 10.4 (br. s, 1 H, NH_{pyrr}), 6.39 (s, 2 H, NH), 3.61 (s, 4 H, CH_2), 2.64 (q, 4 H, $CH_{2,pyrr}$), 1.38 (s, 12 H, CH_3), 1.20 (t, 6 H, $CH_{3,oxa}$) ppm. $^{13}C\{^1H\}$ NMR (75 MHz, $CDCl_3$): δ = 162.1 (C-3/4$_{pyrr}$), 128.1 (C=O or C-2/5$_{pyrr}$), 123.9 (C-2/5$_{pyrr}$ or C=O), 69.9 (CH_2), 56.2 [*C*$(CH_3)_2$], 24.8 (CH_3), 17.9 ($CH_{2,pyrr}$), 15.8 ($CH_{3,pyrr}$) ppm. IR ($CHCl_3$): $\tilde{\nu}$ = 3423 (m), 2971 (s), 2253 (s), 1634 (s), 1516 (s), 1469 (s), 1301 (s), 1062 (m), 651 (s) cm^{-1}. $C_{18}H_{31}N_3O_4$ (353.23): calcd. C 61.17, H 8.84, N 11.89; found C 61.24, H 8.67 N 11.74.

Preparation of 2,5-Bis(4,4′-dimethyl-4,5-dihydrooxazol-2-yl)-3,4-diethylpyrrole ("Et$_2$dmoxpH", 5): MsCl (1.18 mL, 15.2 mmol) was slowly added to an ice-cold solution of **3** (2.440 g, 6.9 mmol) and Et_3N (3.30 mL, 30.4 mmol) in 20 mL of dichloromethane. The mixture was allowed to warm to room temperature and was then stirred for 1 h. After washing with water (5 mL), the organic phase was dried with Na_2SO_4, and the volatiles were removed in vacuo to give a yellow oil, which was used in the next step without purification. The bis(mesylated) compound was treated with KOH (0.4 g, 7.1 mmol) in 25 mL of an MeOH/H_2O mixture (5:1). The reaction mixture was stirred at room temperature for 3 d, then washed with water and dried with Na_2SO_4. The solvents were removed to give the ligand precursor as a pale yellow oil in 73% yield (1.6 g). ^1H NMR (300 MHz, $CDCl_3$): δ = 9.6 (br. s, 1 H, NH_{pyrr}), 4.24 (s, 4 H, $CH_{2,oxa}$), 2.70 (q, 4 H, $CH_{2,pyrr}$), 1.32 (s, 12 H, CH_3), 1.15 (t, 6 H, $CH_{3,oxa}$) ppm. $^{13}C\{^1H\}$ NMR (75 MHz, $CDCl_3$): δ = 156.6 ($C{=}N_{oxa}$), 130.1 (C-2/5$_{pyrr}$), 118.6 (C-3/4$_{pyrr}$), 79.0 ($CH_{2,oxa}$), 66.9 [*C*$(CH_3)_2$], 28.2 (CH_3), 17.7 ($CH_{2,pyrr}$), 15.8 ($CH_{3,pyrr}$) ppm. IR ($CHCl_3$): $\tilde{\nu}$ = 3437 (m), 2969 (s), 1640 (s), 1461 (m), 1353 (m), 1305 (m), 1197 (m), 651 (s) cm^{-1}. MS (EI, 70 eV): *m*/*z* = 317 $[M]^+$, 302 $[M - CH_3]^+$, 160 $[M - 2\,CH_2CH_3]^+$. $C_{18}H_{27}N_3O_2$ (317.21): calcd. C 68.11, H 8.57, N 13.24; found C 68.02, H 8.52 N 13.15.

General Procedure for the Preparation of the Palladium Complexes [Pd$_2$Cl$_2$(dmoxp)$_2$] (6) and [Pd$_2$Cl$_2$(Et$_2$dmoxp)$_2$] (7): A solution of *n*BuLi (1.6 M) in hexanes (3.59 mL) was added to a diethyl ether (50 mL) solution of the bis(oxazolinyl)pyrrole (5.74 mmol), which was cooled to −78 °C. The reaction mixture was stirred for 15 min and then allowed to warm to room temperature. After an additional hour, a suspension of dichlorobis(1,5-cyclooctadiene)palladium (1.639 g; 5.74 mmol) in diethyl ether (20 mL) was added and the resulting mixture was stirred for 12 h at room temperature. The reaction mixture was then filtered and the resulting orange oil was purified by flash chromatography (silica gel, hexanes/EtOAc, 1:1) to give **6** (and **7**) as orange, air-stable solids.

[Pd$_2$Cl$_2$(dmoxp)$_2$] (6): Yield: 42%. R_f = 0.56. ^1H NMR (300 MHz, $CDCl_3$): δ = 6.64 (br. d, 2 H, 3/4-H_{pyrr}), 4.38 (d, 1 H, $CH_{2,oxa}$), 4.24 (t, 2 H, $CH_{2,oxa}$), 4.17 (d, 1 H, $CH_{2,oxa}$), 1.92 (s, 3 H, $CH_{3,oxa}$), 1.57 (s, 3 H, $CH_{3,oxa}$), 1.43 (s, 3 H, $CH_{3,oxa}$), 1.15 (s, 3 H, $CH_{3,oxa}$) ppm. $^{13}C\{^1H\}$ NMR (125 MHz, $CDCl_3$): δ = 167.8 ($C{=}N_{oxa}$), 164.9 ($C{=}N_{oxa}$), 133.1 (C-2/5$_{pyrr}$), 131.9 (C-5/2$_{pyrr}$), 117.1 (C-3/4$_{pyrr}$), 112.2 (C-3/4$_{pyrr}$), 83.2 ($CH_{2,oxa}$), 80.0 ($CH_{2,oxa}$), 67.9 [*C*$(CH_3)_2$], 65.9 [*C*$(CH_3)_2$], 30.4 ($CH_{3,oxa}$), 27.8 ($CH_{3,oxa}$), 27.5 ($CH_{3,oxa}$), 26.7 ($CH_{3,oxa}$) ppm. IR (KBr): $\tilde{\nu}$ = 2964, 1632, 1608, 1521, 1376, 721, 362 cm^{-1}. $C_{28}H_{38}Cl_2N_6O_5Pd_2$ (822.36): calcd. C 41.81, H 4.51; found C 41.95, H 4.73.

[Pd$_2$Cl$_2$(Et$_2$dmoxp)$_2$] (7): Yield 30%. R_f = 0.47. ^1H NMR (500 MHz, C_6D_6): δ = 3.72 (m, 3 H, $CH_{2,oxa}$), 3.52 (d, $^3J_{H,H}$ = 8.3 Hz, 1 H, $CH_{2,oxa}$), 2.92 (m, 1 H, $CH_{2,pyrr}$), 2.79 (m, 2 H, $CH_{2,pyrr}$), 2.68 (m, 1 H, $CH_{2,pyrr}$), 1.77 (s, 3 H, $CH_{3,oxa}$), 1.53 (s, 3 H, $CH_{3,oxa}$), 1.41(m, 6 H, $CH_{3,oxa}$ and $CH_{3,pyrr}$), 1.32 (t, $^3J_{H,H}$ = 8 Hz, 3 H, $CH_{3,pyrr}$), 1.04 (s, 3 H, $CH_{3,oxa}$) ppm. $^{13}C\{^1H\}$ NMR (125 MHz, C_6D_6): δ = 168.3 ($C{=}N_{oxa}$), 165.5 ($C{=}N_{oxa}$), 133.0 (C-2/5$_{pyrr}$), 131.1 (C-3/4$_{pyrr}$), 130.0 (C-3/4$_{pyrr}$), 128.4 (C-3/4$_{pyrr}$), 83.2

($CH_{2,oxa}$), 80.0 ($CH_{2,oxa}$), 67.4 [$C(CH_3)_2$], 65.2 [$C(CH_3)_2$], 31.0 ($CH_{3,oxa}$), 27.6 ($CH_{3,oxa}$), 27.4 ($CH_{3,oxa}$), 26.6 ($CH_{3,oxa}$), 18.8 ($CH_{2,pyrr}$), 17.9 ($CH_{2,pyrr}$), 17.3 ($CH_{3,pyrr}$), 17.2 ($CH_{3,pyrr}$) ppm. IR (KBr): $\tilde{\nu}$ = 2965 (m), 1622 (s), 1600 (s), 1519 (m), 1406 (s), 1189 (s), 1151 (s), 965 (m), 742 (m), 349 (w) cm^{-1}. $C_{36}H_{52}Cl_2N_6O_5Pd_2$ (914.15): calcd. C 47.17, H 5.72; found C 47.21, H 5.56.

General Procedure for the Heck Coupling Reactions: The aryl bromide (1.1 mmol), the olefinic substrate (1.0 mmol, 6.0 mmol in the case of methyl acrylate) and K_3PO_4 (1.1 mmol) were dissolved in 3 mL of dry NMP. The catalyst (or a solution of the catalyst) was then added the reaction mixture was purged three times with nitrogen and heated to 110 °C. The reaction was monitored by GCMS analysis until the generation of the product olefin had ceased. The (*Z*)/(*E*) ratio and the degree of conversion were determined by GC analysis.

General Procedure for the Heck Coupling Reactions with 1,2-Disubstituted Alkenes: The aryl bromide (1.1 mmol), the olefin (1.0 mmol) and K_3PO_4 (1.1 mmol) were dissolved in 3 mL of dry NMP. The catalyst (0.1%) was then added and the reaction mixture was purged three times with nitrogen and heated to 110 °C. When the reaction was complete, as determined by GCMS analysis, the reaction mixture was allowed to cool to room temperature, diluted with diethyl ether and washed three times with water. The organic layer was dried with $MgSO_4$ and concentrated in vacuo to give the crude product. Purification by flash chromatography (hexane 100%, then hexanes/EtOAc, 1:1) afforded the analytically pure alkene product.

General Procedure for the Suzuki Cross-Coupling Reactions: The arylboronic acid and K_2CO_3 (2 equiv.) were placed in a Schlenk tube equipped with a stirring bar. Three nitrogen/vacuum cycles were performed before addition of dry toluene (5 mL), the aryl bromide (1.1 equiv.) and the palladium catalyst (or a solution of the palladium catalyst). The reaction was performed at the temperature indicated in Table 3. On completion of the reaction, the mixture was diluted with Et_2O, filtered through a pad of Celite, washed three times with water, concentrated and purified by column chromatography or recrystallisation. All the products were characterised by standard spectroscopic and analytical methods. Their spectroscopic data are in agreement with those found in the literature.[26]

X-ray Crystallographic Study of 6 and 7: Suitable crystals of the complexes **6** and **7** were obtained by layering concentrated solutions of the compounds in dichloromethane with *n*-hexane and allowing slow diffusion at room temperature. The crystal data were collected at −100 °C with a Nonius Kappa CCD diffractometer and transferred to a DEC Alpha workstation; for all subsequent calculations the Nonius OpenMoleN package was used.[27] The structures were solved by direct methods with absorption corrections being part of the scaling procedure of the data reductions. After refinement of the heavy atoms, difference Fourier maps revealed the maxima of residual electron density close to the positions expected for the hydrogen atoms; they were introduced as fixed contributors in the structure factor calculations with fixed coordinates (C−H: 0.95 Å) and isotropic temperature factors [B(H) = 1.3 B_{equiv}(C) Å^2] but not refined. Full least-squares refinements on F^2. A final difference map revealed no significant maxima of electron density. The scattering factor coefficients and the anomalous dispersion coefficients were taken from ref.[28] Crystal data and experimental details for the crystals of compounds **6** and **7** are given in Table 4. CCDC-173019 (**6**) and -194957 (**7**) contain the supplementary crystallographic data for this paper. These data can be obtained free of charge at www.ccdc.cam.ac.uk/conts/retrieving.html [or from the Cambridge Crystallographic Data Centre, 12 Union Road, Cambridge CB2 1EZ, UK; Fax: (internat.) + 44-1223/336-033; E-mail: deposit@ccdc.cam.ac.uk].

Table 4. X-ray experimental data of compounds **6** and **7**

	6	**7**
Empirical formula	$C_{28}H_{36}Cl_2N_6O_4Pd_2{\cdot}H_2O$	$C_{36}H_{52}Cl_2N_6O_4Pd_2$
Formula mass	822.36	916.56
Crystal system	monoclinic	monoclinic
Space group	*C*2	$P2_1/c$
a [Å]	19.733(1)	11.4766(1)
b [Å]	9.9775(5)	18.3485(3)
c [Å]	16.8832(9)	19.8285(3)
β [°]	95.021(5)	103.820(5)
V [Å^3]	3311.3(3)	4054.58(9)
Z	4	4
$D_{calcd.}$ [g cm^{-3}]	1.65	1.50
F(000)	1656	1872
μ [mm^{-1}]	1.293	1.063
T [K]	173	173
λ [Å]	0.71073	0.71073
Radiation	Mo-K_α	Mo-K_α
θ limits [°]	2.5/27.09	2.5/30.03
Number of data measured	5478	20064
Number of data with $I > 3\sigma(I)$	4263	7971
Number of variables	387	451
R	0.048	0.029
Rw	0.066	0.036
GOF	1.179	1.159
Largest peak in final difference [e·Å^{-3}]	1.758	1.267

Acknowledgments

We thank the CNRS (France), the Institut Universitaire de France, and the Ministère de l'Education Nationale, de la Recherche et de la Technologie (PhD grant for C. M.) for funding. We are grateful to Dr. André De Cian and N. Gruber for X-ray diffraction studies

[1] A. Togni, L. M. Venanzi, *Angew. Chem.* **1994**, *106*, 517−546; *Angew. Chem. Int. Ed. Engl.* **1994**, *33*, 497−526.

[2] [2a] R. E. Lowenthal, A. Abiko, S. Masamune, *Tetrahedron Lett.* **1990**, *31*, 6005−6008. [2b] D. A. Evans, K. A. Woerpel, M. M. Hinman, M. M. Faul, *J. Am. Chem. Soc.* **1991**, *113*, 726−728. [2c] D. Müller, G. Umbricht, B. Weber, A. Pfaltz, *Helv. Chim. Acta* **1991**, *74*, 232−240. [2d] E. J. Corey, N. Imai, H. Y. Zhang, *J. Am. Chem. Soc.* **1991**, *113*, 728−729. For reviews of chiral oxazoline ligands in asymmetric catalysis, see: [2e] F. Fache, E. Schulz, M. Lorraine Tommasino, M. Lemaire, *Chem. Rev.* **2000**, *100*, 2159−2231. [2f] M. Gomez, G. Muller, M. Rocamora, *Coord. Chem. Rev.* **1999**, *193*, 769−835. [2g] A. K. Ghosh, P. Mathivanan, J. Cappiello, *Tetrahedron: Asymmetry* **1998**, *9*, 1−45.

[3] Selected recent references: [3a] Mukaiyama−Michael reactions: D. A. Evans, K. A. Scheidt, J. N. Johnston, M. C. Willis, *J. Am. Chem. Soc.* **2001**, *123*, 4480−4491. [3b] Cycloadditions of silyl ketenes: D. A. Evans, J. M. Janey, *Org. Lett.* **2001**, *3*, 2125−2128. [3c] Henry reactions: C. Christensen, K. Juhl, K. A. Jørgensen, *Chem. Commun.* **2001**, 2222−2223. [3d] Friedel−Crafts reactions: W. Zhuang, N. Gathergood, R. G. Hazell, K. A. Jørgensen, *J. Org. Chem.* **2001**, *66*, 1009−1013. [3e] Hetero Diels−Alder reactions: D. A. Evans, J. S. Johnson,

E. J. Olhava, *J. Am. Chem. Soc.* **2000**, *122*, 1635−1649. [3f] Molybdenum-catalysed allylic alkylation: F. Glorius, A. Pfaltz, *Org. Lett.* **1999**, *1*, 141−144.
[4] C. Mazet, L. H. Gade, *Organometallics* **2001**, *20*, 4144−4146.
[5] [5a] H. Nishiyama, H. Sakagushi, T. Nakamura, M. Horihata, M. Kondo, K. Itoh, *Organometallics* **1989**, *8*, 846−848. [5b] H. Nishiyama, M. Kondo, T. Nakamura, K. Itoh, *Organometallics* **1991**, *10*, 500−508. [5c] D. A. Evans, M. C. Kozlowski, J. A. Murry, C. S. Burgey, K. R. Campos, B. T. Connell, R. J. Staples, *J. Am. Chem. Soc.* **1999**, *121*, 669−685. [5d] D. A. Evans, C. S. Burgey, M. C. Kozlowski, S. W. Tregay, *J. Am. Chem. Soc.* **1999**, *121*, 686−699. [5e] D. A. Evans, D. M. Barnes, J. S. Johnson, T. Lectka, P. von Matt, S. J. Miller, J. A. Murry, R. D. Norcross, E. A. Shaughnessy, K. R. Campos, *J. Am. Chem. Soc.* **1999**, *121*, 7582−7594. [5f] D. A. Evans, Z. K. Sweeney, T. Rovis, J. S. Tedrow, *J. Am. Chem. Soc.* **2001**, *123*, 12095−12096. [5g] H. Nishiyama, Y. Itoh, H. Matsumoto, K. Itoh, *J. Am. Chem. Soc.* **1994**, *116*, 2223−2224. [5h] H. Nishiyama, Y. Itoh, Y. Sugawara, H. Matsumoto, K. Aoti, K. Itoh, *Bull. Chem. Soc. Jpn.* **1995**, *68*, 1247−1262. [5i] Y. Motoyama, K. Murata, O. Kurihara, T. Naitoh, K. Aoki, H. Nishiyama, *Organometallics* **1998**, *17*, 1251−1253. [5j] H. Nishiyama, T. Naitoh, Y. Motoyama, K. Aoki, *Chem. Eur. J.* **1998**, *5*, 3509−3513.
[6] C. Mazet, L. H. Gade, *Chem. Eur. J.* **2002**, *8*, 4308−4318.
[7] [7a] C. Bolm, K. Weickhardt, M. Zehnder, D. Glasmacher, *Helv. Chim. Acta* **1991**, *74*, 717−726. [7b] C. Bolm, K. Weickhardt, M. Zehnder, T. Ranff, *Chem. Ber.* **1991**, *124*, 1173−1180.
[8] [8a] L. Knorr, *Ber. Dtsch. Chem. Ges.* **1884**, *17*, 1635−1642. [8b] L. Knorr, *Justus Liebigs Ann. Chem.* **1886**, *236*, 290−332. [8c] U. Eisner, A. Lichtarowicz, R. P. Linstead, *J. Chem. Soc.* **1957**, 733−738. [8d] J. B. Paine, III, R. B. Woodward, D. Dolphin, *J. Org. Chem.* **1976**, *41*, 2826−2835. [8e] H. W. Whitelock, R. Hanauer, *J. Org. Chem.* **1968**, *33*, 2169−2171.
[9] *The Porphyrins Handbook* (Eds.: K. M. Kadish, K. M. Smith, R. Guilard), Academic, San Diego, CA, **2000**.
[10] [10a] Y. S. Klausner, M. Bodansky, *Synthesis* **1972**, 453−463. [10b] S. R. Gilbertson, C. W. T. Chang, *J. Org. Chem.* **1998**, *63*, 8424−8431.
[11] For reviews of helical complexes, see: [11a] E. C. Constable, *Tetrahedron* **1992**, *48*, 10013−10059. [11b] C. Piguet, G. Bernardinelli, G. Hopfgartner, *Chem. Rev.* **1997**, *97*, 2005−2062. [11c] M. Albrecht, *Chem. Rev.* **2001**, *101*, 3457−3498. [11d] U. Knof, A. von Zelewsky, *Angew. Chem. Int. Ed.* **1999**, *38*, 302−322.
[12] For recent reviews of the cross-coupling of organoboron compounds, see: [12a] A. Suzuki, *Pure Appl. Chem.* **1991**, *63*, 419−422. [12b] N. Miaura, A. Suzuki, *Chem. Rev.* **1995**, *95*, 2457−2483. [12c] A. Suzuki, *J. Organomet. Chem.* **1999**, *576*, 147−168. Selected references: [12d] M. Beller, H. Fischer, W. A. Herrmann, K. Öfele, C. Brossmer, *Angew. Chem. Int. Ed. Engl.* **1995**, *34*, 1848−1849. [12e] M. Gomez Andreu, A. Zapf, M. Beller, *Chem. Commun.* **2000**, 2475−2476. [12f] A. F. Littke, G. C. Fu, *Angew. Chem. Int. Ed.* **1998**, *37*, 3387−3388. [12g] J. P. Wolfe, S. L. Buchwald, *Angew. Chem. Int. Ed.* **1999**, *38*, 2413−2416. [12h] J. P. Wolfe, R. A. Singer, B. H. Yang, S. L. Buchwald, *J. Am. Chem. Soc.* **1999**, *121*, 9550−9561.
[13] [13a] W. A. Herrmann, C. P. Reisinger, M. Spiegler, *J. Organomet. Chem.* **1998**, *557*, 93−96. [13b] T. W. Weskamp, V. P. Böhm, W. A. Herrmann, *J. Organomet. Chem.* **1999**, *585*, 348−352. [13c] C. Zhang, J. Huang, M. L. Trudell, S. P. Nolan, *J. Org. Chem.* **1999**, *64*, 3804−3805. [13d] C. Zhang, M. L. Trudell, *Tetrahedron Lett.* **2000**, *41*, 595−598. [13e] M. V. Baker, B. W. Skelton, A. H. White, C. C. Williams, *J. Chem. Soc., Dalton Trans.* **2001**, 111−120. [13f] D. A. Albisson, R. B. Bedford, S. E. Lawrence, P. N. Scully, *Chem. Commun.* **1998**, 2095−2096. [13g] R. B. Bedford, S. M. Draper, P. N. Scully, S. L. Welch, *New J. Chem.* **2000**, *24*, 745−747. [13h] R. B. Bedford, S. L. Welch, *Chem. Commun.* **2001**, 129−130.
[14] [14a] S. Gründemann, M. Albrecht, J. A. Loch, J. W. Faller, R. H. Crabtree, *Organometallics* **2001**, *20*, 5485−5488. [14b] E. Peris, J. A. Loch, J. Mata, R. H. Crabtree, *Chem. Commun.* **2001**, 201−202. [14c] J. A. Loch, M. Albrecht, E. Peris, J. Mata, J. W. Faller, R. H. Crabtree, *Organometallics* **2002**, *21*, 700−706.
[15] [15a] I. P. Beletskaya, A. V. Chuchurjukin, H. P. Dijkstra, G. P. M. van Klink, G. van Koten, *Tetrahedron Lett.* **2000**, *41*, 1075−1079. [15b] I. P. Beletskaya, A. N. Kashin, N. B. Karlstedt, A. V. Mitin, A. V. Cheprakov, G. M. Kazankov, *J. Organomet. Chem.* **2001**, *622*, 89−96.
[16] D. Zim, A. S. Gruber, G. Ebeling, J. Dupont, A. L. Monteiro, *Org. Lett.* **2000**, *18*, 2881−2884.
[17] H. Weissman, D. Milstein, *Chem. Commun.* **1999**, 1901−1902.
[18] G. A. Grasa, A. C. Hillier, S. P. Nolan, *Org. Lett.* **2001**, *3*, 1077−1080.
[19] W. Cabri, I. Candiani, A. Bedeschi, R. Santi, *Synlett* **1992**, 871−872.
[20] C. Gürtler, S. L. Buchwald, *Chem. Eur. J.* **1999**, *5*, 3107−3112.
[21] V. César, S. Bellemin-Laponnaz, L. H. Gade, *Organometallics* **2002**, *21*, 5204.
[22] A. F. Littke, G. C. Fu, *J. Am. Chem. Soc.* **2001**, *123*, 6989−7000.
[23] [23a] S. Cacchi, P. G. Ciattini, E. Morera, G. Ortar, *Tetrahedron Lett.* **1987**, *28*, 3039−3042. [23b] A. Amorese, A. Arcadi, E. Bernocchi, S. Cacchi, S. Cerrini, W. Fedeli, G. Ortar, *Tetrahedron* **1989**, *45*, 813−829. [23c] M. Moreno-Manas, M. Pérez, R. Pleixats, *Tetrahedron Lett.* **1996**, *37*, 7449−7452. [23d] M. Moreno-Manas, R. Pleixats, A. Roglans, *Synlett* **1997**, 1157−1158. [23e] M. Beller, T. H. Riermeier, *Tetrahedron Lett.* **1996**, *37*, 6535−6538. [23f] M. Beller, T. H. Riermeier, *Eur. J. Inorg. Chem.* **1998**, 29−35.
[24] K. W. Hellmann, L. H. Gade, *Verfahrenstechnik (Berlin)* **1997**, *31*(5), 70−71.
[25] D. Drew, J. R. Doyle, *Inorg. Synth.* **1972**, *13*, 47−65.
[26] [26a] A. F. Littke, G. C. Fu, *J. Org. Chem.* **1999**, *64*, 10−11. [26b] A. F. Littke, C. Dai, G. C. Fu, *J. Am. Chem. Soc.* **2000**, *122*, 4020−4028.
[27] Nonius *OpenMoleN, Interactive Structure Solution*, Delft, **1997**.
[28] D. T. Cromer, J. T. Waber, *International Tables for X-ray Crystallography*, The Kynoch Press, Birmingham, **1974**.

Received October 7, 2002
[I02552]

The Synthesis and Structure of P−C−P Bridged Ferrocene

Igor Shevchenko,*[a] Dmitrii Shakhnin,[a] Hongming Zhang,[b] Michael Lattman,[b] and Gerd-Volker Röschenthaler[c]

Keywords: Sandwich complexes / Phosphane ligands / Asymmetry / Bridging ligands

The reaction of dilithioferrocene **12** with methylene-bis(dialkylaminochlorophosphanes) **13a,b** (**a** = CH_3, **b** = C_2H_5) leads to the formation of compounds **14a,b** in which the two cyclopentadiene rings are bridged by a P–C–P chain. Because of the cyclic structure, *cis*- and *trans*-isomerism is expected. The *cis*- and *trans*-isomers of the sulfur derivative **16b** have been separated by column chromatography.

(© Wiley-VCH Verlag GmbH & Co. KGaA, 69451 Weinheim, Germany, 2003)

Introduction

Phosphane-substituted ferrocene derivatives have been intensively investigated in the last two decades. Particular attention was paid to the study of non-racemic ferrocene derivatives, as they have found wide application as ligands for catalysts of numerous asymmetric reactions. The chemistry of chiral ferrocene derivatives has been extensively reviewed up to 1997.[1−3]

The main method of synthesis of non-racemic ferrocene derivatives is based on the lithiation of *N*,*N*-dimethyl-1-ferrocenylethylamine (**1**; Scheme 1) followed by the addition of chlorophosphane **2**. This reaction can result in the formation of either the monophosphane **4** or the diphosphane derivative **5**.

The presence of the asymmetric substituent R* (*N*,*N*-dimethyl-1-ethylamine) at one of the rings brings about selective lithiation of the ring.

The bridging of dilithioferrocene **3** with methylene-bis(dichlorophosphane) **6** should give rise to isomerism caused by different positions of the substituents R at the phosphorus atom. Taking into account that one of the ferrocene rings bears the substituent R*, four isomers **7**−**10** are possible. These ligands may be useful in the design of asymmetric catalysts.

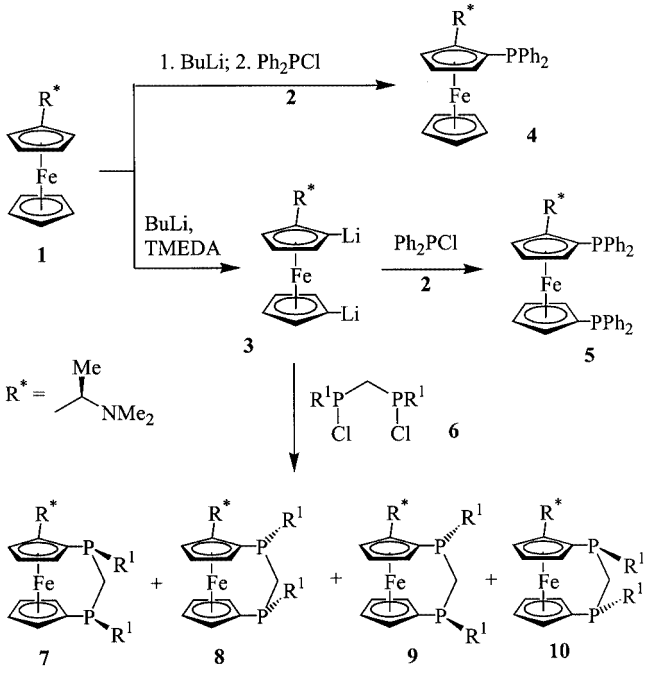

Scheme 1

[a] Institute of Bioorganic Chemistry,
Murmanskaya Street 1, 02094 Kiev, Ukraine
Fax:(internat.) +38-044/573-2552
E-mail: ishev@bpci.kiev.ua
[b] Department of Chemistry, Southern Methodist University,
Dallas, Texas 75275, USA
Fax: (internat.) +1-214/768-4089
E-mail: mlattman@mail.smu.edu
[c] Institute of Inorganic and Physical Chemistry, Universität Bremen, NW2, C2350,
Leobener Str, 28334 Bremen, Germany
Fax: (internat.) +49-(0)421/218-4267
E-mail: gvr@chemie.uni-bremen.de

Results and Discussion

To the best of our knowledge, there are no examples in which two cyclopentadiene rings are bridged by a diphosphane unit. P-B bridged species are known[4] and a P-bridged derivative has also been reported.[5] In addition, there have been several P−N−P-bridged ferrocenes reported where the bridge is part of a cyclic triphosphazene.[6−9] For the first step of the proposed ap-

proach we have chosen a simple model, namely bridging of the unsubstituted ferrocene **11** with methylene-bis(dialkylaminochlorophosphanes) **13a,b** (**a** = CH_3, **b** = C_2H_5; Scheme 2). The dialkylamino-substituted chlorophosphanes **13a,b** are easier to synthesise than other methylene-bis(chlorophosphanes).

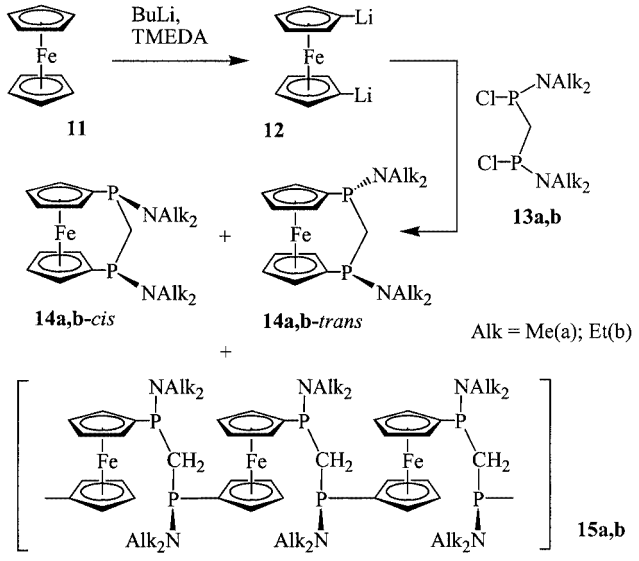

Scheme 2

The lithiation of both rings of the ferrocene **11** proceeds easily with *n*BuLi at room temperature, in the presence of TMEDA.[10] The dilithium derivative **12** crystallizes from the reaction mixture as a complex with TMEDA and can be isolated as dark-red crystals. This compound was immediately used for the reaction with **13a,b** in a solution of THF. The *cis*- and *trans*-isomers of the reaction products **14a,b** possess different spectral characteristics and show separate singlets in their ^{31}P NMR spectra. The presence of the two reaction centers in each starting compound led to the formation of oligomeric/polymeric by products. In their ^{31}P NMR spectra these compounds display broad signals with chemical shifts close to that of the respective monomers. Dilution of the reaction mixture and lowering of the temperature reduced the formation of these by products.

Both isomers were formed in approximately equal proportions (*cis*:*trans* = 45:55), and do not interconvert at room temperature. The differences in physical characteristics allowed the isomers to be separated. Unlike **14a,b-*trans***, the **14a,b-*cis*** isomers possess a more compact structure and crystallize more readily from the reaction mixture. The isolation of the pure *trans*-isomers in this manner was not possible as they crystallized together with the remaining *cis*-isomer. Unfortunately the purification of the **14a,b-*trans*** isomers by column chromatography was not possible either, as the P−N bond in trivalent phosphorus compounds is rather sensitive to moisture.

Compounds in which a plane of symmetry divides the P−P or P−C−P system into two equal parts display signals of substituents at the phosphorus atoms in the NMR spectra as an $AX_nA'X'_n$ spin system. Thus, PH- or PC-coupling may appear, not as doublets, but as pseudo-triplets. Recently, for example, we have noted this to be the case for carbodiphosphoranes.[11] ^{13}C NMR spectroscopic studies of **14a,b-*cis*** isomers revealed that the carbon atoms of the ferrocene cyclopentadienyl rings also appear as pseudo-triplets.

Compounds **14a**,**b** easily react with sulfur to give the sulfur derivatives **16a**,**b** quantitatively (Scheme 3). They are not sensitive to moisture and oxygen and can be used for the separation of *cis*- and *trans*-isomers by column chromatography. For separation purposes, the diethylamino derivative **16b** was chosen, as it is more soluble than **16a**.

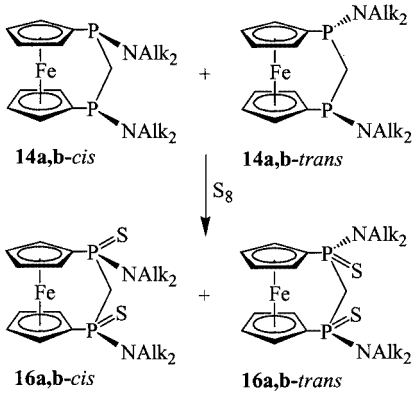

Scheme 3

The detailed structure of compounds **14b-*cis*** (Figure 1), **16b-*cis*** (Figure 2) and **16b-*trans*** (Figure 3) have been determined by X-ray analysis. Selected bond lengths and angles are collected in Table 1. Both *cis* molecules have very similar Fe−Cp carbon distances with a spread of only 3 pm. The *trans* molecule shows a slightly greater spread of distances (5 pm). In all three derivatives, the Cp rings are planar with no carbon atom more than 0.5(5) pm from its mean plane. The Cp rings in each molecule are almost coplanar with "tilt" angles of 5.07(3)°, 2.9(3)°, and 3.1(5)° for **14b-*cis***, **16b-*cis*** and **16b-*trans***, respectively. In addition, one of the phosphorus atoms in each molecule lies somewhat more out of the Cp plane than does the other, with deviations from the mean Cp planes being P(1): 13(1), 3(1), 3(1) pm, and P(2): 6(1), 11(1), 17(1) pm for **14b-*cis***, **16b-*cis*** and **16b-*trans***, respectively. One important structural feature is the degree to which the Cp rings are staggered or eclipsed, since there is a variation in these molecules despite the fact that the rings are bridged by a P−C−P unit in each case. The C(11)-ring centroid-ring centroid-C(16) torsion angles are 3.0°, −7.6°, and −17.3°, for **14b-*cis***, **16b-*cis*** and **16b-*trans***, respectively. Thus, these molecules adopt more of an eclipsed, rather than a staggered, conformation; however, **16b-*trans*** is essentially halfway between the eclipsed and staggered geometries. These structures can be compared with the known Si−O−Si bridged ferrocenes $O(R_2SiCp)_2Fe$ (R = Me, Ph),[12] as well as the P−N−P phosphazene-bridged ferrocenes mentioned above.[6−9] All are similar in

structure with a slight trend towards increasing torsion angles (i.e., eclipsed to staggered) in the order P−N−P, P−C−P, Si−O−Si. This tendency may simply be due to crystal packing forces.[13]

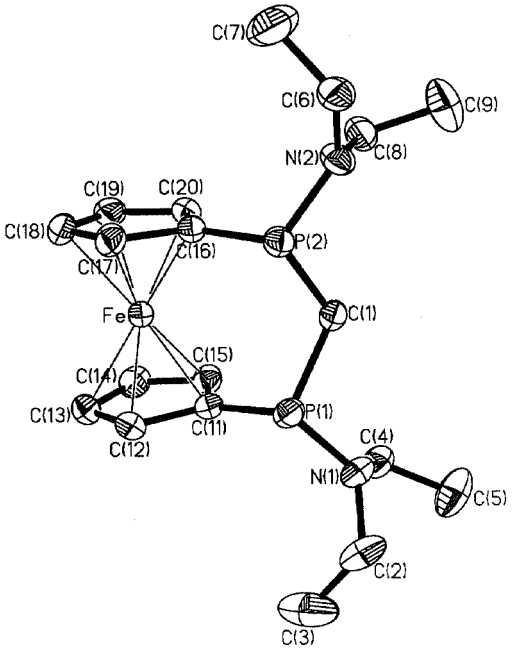

Figure 1. Perspective view and labeling scheme for the molecule **14b-*cis***

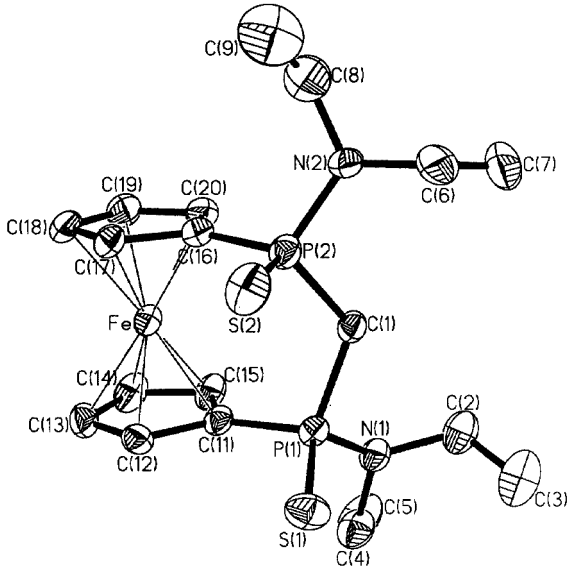

Figure 2. Perspective view and labeling scheme for the molecule **16b-*cis***

Finally, the P−C−P angle in these derivatives shows a large variation from the ideal tetrahedral angle of 107.9(1)° in **14b-*cis*** to 122.7(4)° in **16b-*trans***. Large variations in P−C−P-containing molecules have been observed before[14] and illustrate the ability of this unit to accommodate various geometrical constraints.

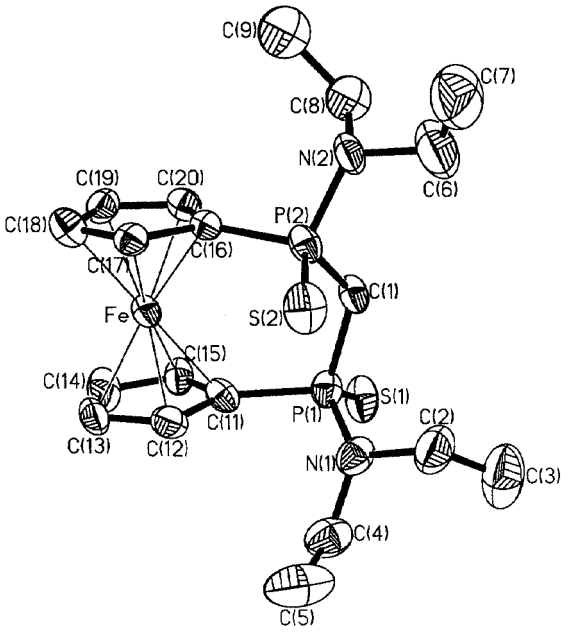

Figure 3. Perspective view and labeling scheme for the molecule **16b-*trans***

Experimental Section

General Remarks: All operations were performed under nitrogen in a dry box. The solvents were dried by the usual procedures. The NMR spectra were recorded with JEOL FX-90Q, Bruker DPX 200 and Bruker AMX 360 spectrometers. The ^{1}H and ^{13}C chemical shifts were referenced to tetramethylsilane (TMS). The ^{31}P chemical shifts were referenced to 85% aqueous orthophosphoric acid as an external standard. As usual, high frequency shifts are given positive signs. The digital resolutions were 0.25 Hz, 0.5 Hz and 1.25 Hz for the ^{1}H, ^{13}C and ^{31}P NMR spectra, respectively. Compounds **13a,b** were obtained from methylenebis(dichlorophosphane)[15] and *N*,*N*-dimethyl- or *N*,*N*-diethyltrimethylsilylamine in petroleum ether at 0 °C and isolated in 60% yield by distillation [b.p. 77−78 °C (**13a**), 108−110 °C (**13b**); 0.04 Torr].

Compound 12: Ferrocene (710 mg, 3.81 mmol) was dissolved in diethyl ether (12 mL) in a closed flask at 40 °C and, after cooling to room temperature, the solution obtained was added to a mixture of TMEDA (1.155 g; 9.96 mmol) and *n*BuLi (9.5 mmol of 1.6 M solution in hexane) in diethyl ether (6 mL). After 16 h the reaction mixture was decanted from the precipitated red crystals of **12** which were quickly dried under a stream of dry nitrogen (yield 1.180 g, 2.74 mmol, 72%) and immediately dissolved in THF (20 mL).

Compound 14a-*cis*: A freshly obtained solution of **12** (1.180 g, 2.74 mmol) in THF (20 mL) (see above) was cooled to −80 °C and a solution of **13a** (644 mg, 2.74 mmol) in THF (10 mL) was added to it in portions while stirring, keeping the temperature constant. The mixture was stirred at −80 °C for 20 min, then slowly warmed to −15 °C and left at this temperature overnight. The solvents were then evaporated in vacuo and the dry residue was extracted with petroleum ether (70−100 °C, 3 × 10 mL, boiling each portion for 1 min). The solvents were evaporated from the combined extracts in vacuo, the residue was re-extracted with boiling petroleum ether (70−100 °C, 5 mL) and the solution obtained was left at −15 °C. After 16 h, 130 mg of **14a-*cis*** contaminated with **14a-*trans*** was isol-

Table 1. Selected bond lengths (pm) and bond angles (deg)

14b-*cis*		**16b-*cis***		**16b-*trans***	
Fe−C(11)	203.7(2)	Fe−C(11)	203.2(4)	Fe−C(11)	201.2(7)
Fe−C(12)	204.7(2)	Fe−C(12)	203.8(4)	Fe−C(12)	202.0(7)
Fe−C(13)	205.7(2)	Fe−C(13)	205.2(4)	Fe−C(13)	201.8(7)
Fe−C(14)	204.1(2)	Fe−C(14)	204.2(5)	Fe−C(14)	205.6(7)
Fe−C(15)	202.7(2)	Fe−C(15)	203.3(4)	Fe−C(15)	203.1(7)
Fe−C(16)	203.9(2)	Fe−C(16)	202.1(4)	Fe−C(16)	200.9(6)
Fe−C(17)	204.6(2)	Fe−C(17)	204.1(4)	Fe−C(17)	203.3(6)
Fe−C(18)	205.5(2)	Fe−C(18)	205.9(4)	Fe−C(18)	204.5(8)
Fe−C(19)	204.4(2)	Fe−C(19)	203.8(4)	Fe−C(19)	204.6(7)
Fe−C(20)	202.7(2)	Fe−C(20)	202.5(4)	Fe−C(20)	201.0(6)
P(1)−N(1)	169.8(2)	P(1)−S(1)	194.2(2)	P(1)−S(1)	195.6(3)
P(1)−C(1)	184.8(2)	P(1)−N(1)	167.2(3)	P(1)−N(1)	165.2(6)
P(1)−C(11)	183.0(2)	P(1)−C(1)	181.9(4)	P(1)−C(1)	181.4(7)
P(2)−N(2)	169.4(2)	P(1)−C(11)	179.2(4)	P(1)−C(11)	180.9(7)
P(2)−C(1)	184.4(2)	P(2)−S(2)	194.1(2)	P(2)−S(2)	194.8(3)
P(2)−C(16)	183.4(2)	P(2)−N(2)	167.5(4)	P(2)−N(2)	165.2(6)
N(1)−C(2)	146.3(2)	P(2)−C(1)	182.6(4)	P(2)−C(1)	182.1(7)
N(1)−C(4)	146.7(3)	P(2)−C(16)	179.4(4)	P(2)−C(16)	178.9(6)
N(2)−C(8)	145.6(3)	N(1)−C(4)	146.7(6)	N(1)−C(4)	146.9(9)
N(2)−C(6)	146.6(3)	N(1)−C(2)	147.2(6)	N(1)−C(2)	147.8(10)
		N(2)−C(8)	145.4(8)	N(2)−C(8)	146.4(11)
		N(2)−C(6)	149.3(6)	N(2)−C(6)	149.7(12)
N(1)−P(1)−C(1)	102.81(10)	N(1)−P(1)−C(1)	101.2(2)	N(1)−P(1)−C(11)	103.4(3)
N(1)−P(1)−C(11)	107.26(10)	N(1)−P(1)−C(11)	101.8(2)	N(1)−P(1)−C(1)	107.8(3)
C(11)−P(1)−C(1)	99.74(11)	C(11)−P(1)−C(1)	108.2(2)	C(11)−P(1)−C(1)	107.4(3)
N(2)−P(2)−C(1)	102.11(11)	N(1)−P(1)−S(1)	118.16(14)	N(1)−P(1)−S(1)	118.5(2)
N(2)−P(2)−C(16)	107.20(11)	C(11)−P(1)−S(1)	112.0(2)	C(11)−P(1)−S(1)	110.0(2)
C(16)−P(2)−C(1)	100.17(11)	C(1)−P(1)−S(1)	114.2(2)	C(1)−P(1)−S(1)	109.1(2)
C(2)−N(1)−C(4)	116.1(2)	N(2)−P(2)−C(1)	100.5(2)	N(2)−P(2)−C(16)	105.3(3)
C(2)−N(1)−P(1)	115.2(2)	N(2)−P(2)−C(16)	103.9(2)	N(2)−P(2)−C(1)	105.8(3)
C(4)−N(1)−P(1)	121.9(2)	C(16)−P(2)−C(1)	105.7(2)	C(16)−P(2)−C(1)	103.9(3)
C(8)−N(2)−C(6)	116.0(2)	N(2)−P(2)−S(2)	117.2(2)	N(2)−P(2)−S(2)	114.3(3)
C(8)−N(2)−P(2)	123.7(2)	C(16)−P(2)−S(2)	112.8(2)	C(16)−P(2)−S(2)	112.7(2)
C(6)−N(2)−P(2)	115.8(2)	C(1)−P(2)−S(2)	115.1(2)	C(1)−P(2)−S(2)	113.9(3)
P(2)−C(1)−P(1)	107.89(12)	C(4)−N(1)−C(2)	114.6(4)	C(4)−N(1)−C(2)	114.6(6)
C(15)−C(11)−C(12)	106.2(2)	C(4)−N(1)−P(1)	115.5(3)	C(4)−N(1)−P(1)	117.6(5)
C(15)−C(11)−P(1)	132.1(2)	C(2)−N(1)−P(1)	122.6(3)	C(2)−N(1)−P(1)	121.3(5)
C(12)−C(11)−P(1)	121.5(2)	C(8)−N(2)−C(6)	117.0(4)	C(8)−N(2)−C(6)	104.6(10)
C(20)−C(16)−C(17)	106.2(2)	C(8)−N(2)−P(2)	122.2(3)	C(8)−N(2)−P(2)	124.2(9)
C(20)−C(16)−P(2)	132.1(2)	C(6)−N(2)−P(2)	116.2(3)	C(6)−N(2)−P(2)	116.7(6)
C(17)−C(16)−P(2)	121.6(2)	P(1)−C(1)−P(2)	119.7(2)	P(1)−C(1)−P(2)	122.7(4)
		C(12)−C(11)−C(15)	107.1(4)	C(12)−C(11)−C(15)	107.1(6)
		C(12)−C(11)−P(1)	126.6(3)	C(12)−C(11)−P(1)	128.7(6)
		C(15)−C(11)−P(1)	126.3(3)	C(15)−C(11)−P(1)	124.1(5)
		C(20)−C(16)−C(17)	107.7(4)	C(20)−C(16)−C(17)	106.2(6)
		C(20)−C(16)−P(2)	128.4(3)	C(20)−C(16)−P(2)	130.5(5)
		C(17)−C(16)−P(2)	123.8(3)	C(17)−C(16)−P(2)	122.9(5)

ated. The pure *cis*-isomer was obtained after recrystallization from dichloromethane/hexane at −15 °C. Yield 80 mg, (8.4%). M.p. 217−218 °C. ^{1}H NMR (200 MHz, $CDCl_3$): δ = 3.27 (dt, $^2J_{H,H}$ = 11.4, $^2J_{P,H}$ = 2.6 Hz, 1 H, P-CH_2-P), 4.18 (pseudo t, $^3J_{P,H}$ = 5.6 Hz, 12 H, NCH_3), 5.22 (dt, $^2J_{H,H}$ = 11.4, $^2J_{P,H}$ = 4.4 Hz, 1 H, P-CH_2-P), 5.67−5.81 [m, 2 H, Fe(Cpd$_2$)], 5.87−6.04 [m, 4 H, Fe(Cpd$_2$)], 6.09−6.24 [m, 2 H, Fe(Cpd$_2$)] ppm. ^{13}C NMR (22.5 MHz, $CDCl_3$): δ = 32.4 (t, $^1J_{P,C}$ = 17.56 Hz, 1 C, P-*C*-P), 41.6 (pseudo t, $^2J_{P,C}$ = 6.7 Hz, 4 C, NCH_3), 69.9 [pseudo t, $^2J_{P,C}$ = 5.8 Hz, 2 C, Fe(Cpd$_2$)], 70.1 [pseudo t, $^2J_{P,C}$ = 2.9 Hz, 2 C, Fe(Cpd$_2$)], 71.9 [s, 4 C, Fe(Cpd$_2$)], 77.1 [pseudo t, $^1J_{P,C}$ = 24.4 Hz, 2 C, Fe(Cpd$_2$)] ppm. ^{31}P NMR (36.2 MHz, $CDCl_3$): δ = 42.3 (s, 2 P, *P*-C-*P*) ppm. $C_{15}H_{22}FeN_2P_2$ (348.15): calcd. C 51.75, H 6.37; found C 50.78, H 6.27.

Compound 14b-*cis*: A freshly obtained solution of **12** (1.180 g, 2.74 mmol) in THF (20 mL) (see above) was cooled to −80 °C and a solution of **13b** (798 mg, 2.74 mmol) in THF (10 mL) was added to it in portions while stirring, keeping the temperature constant. The mixture was stirred at −80 °C for 20 min, then slowly warmed to −15 °C and left at this temperature overnight. The solvents were then evaporated in vacuo and the dry residue was extracted with hexane (5 × 15 mL, boiling each portion for 1 min). The combined extracts were evaporated in vacuo and the residue was dissolved in hexane (3 mL) at boiling and left at −15 °C for 48 h. Recrystallization was not needed as the *cis*:*trans* ratio was 98:2. Yield 234 mg, (21%). M.p. 113−116 °C. ^{1}H NMR (200 MHz, $CDCl_3$): δ = 0.98 (t, $^3J_{H,H}$ = 7.0 Hz, 12 H, NCH_2CH_3), 1.62 (dt, $^2J_{H,H}$ = 11.4, $^2J_{P,H}$ = 2.6 Hz, 1 H, P-CH_2-P), 2.8−3.3 (m, 8 H, NCH_2CH_3), 3.83

(dt, $^2J_{H,H}$ = 11.4, $^2J_{P,H}$ = 4.1 Hz, 1 H, P-CH_2-P), 4.1−4.2 [m, 2 H, Fe(Cpd_2)], 4.3−4.4 [m, 4 H, Fe(Cpd_2)], 4.5−4.7 [m, 2 H, Fe(Cpd_2)] ppm. ^{13}C NMR (22.5 MHz, $CDCl_3$): δ = 14.5 (pseudo t, $^3J_{P,C}$ = 2.0 Hz, 4 C, NCH_2CH_3), 35.5 (t, $^1J_{P,C}$ = 17.6 Hz, 1 C, P-*C*-P), 43.9 (pseudo t, $^2J_{P,C}$ = 6.8 Hz, 4 C, NCH_2CH_3), 69.3 [pseudo t, $^2J_{P,C}$ = 5.9 Hz, 2 C, Fe(Cpd_2)], 69.5 [pseudo t, $^2J_{P,C}$ = 3.0 Hz, 2 C, Fe(Cpd_2)], 71.4 [s, 2 C, Fe(Cpd_2)], 76.2 [pseudo t, $^1J_{P,C}$ = 25.4 Hz, 2 C, Fe(Cpd_2)], 81.0 [pseudo t, $^3J_{P,C}$ = 12.6 Hz, 2 C, Fe(Cpd_2)] ppm. ^{31}P NMR (36.2 MHz, $CDCl_3$): δ = 37.0 (s, 2 P, *P*-C-*P*) ppm. $C_{19}H_{30}FeN_2P_2$ (404.26): calcd. C 56.45, H 7.48, N 6.93; found C 55.86, H 7.48, N 6.74.

Compounds 16a,b-*cis*: Sulfur (20 mg, 0.63 mmol) was added to a solution of **14a-*cis*** or **14b-*cis*** (0.12 mmol) in dichloromethane (0.5 mL) and the reaction mixture was stirred at room temperature for 2 h. According to NMR spectroscopic data the reaction proceeds quantitatively. The reaction solution was diluted with hexane until it became turbid and left at −15 °C overnight. The crystalline product that formed was separated and dried in vacuo. Yield after crystallization 46−50%.

16a-*cis*: M.p. 230 °C (dec.). ^{1}H NMR (90 MHz, $CDCl_3$): δ = 2.47 (d, $^3J_{PH}$ = 15.5 Hz, 12 H, NCH_3), 3.36 (t, $^2J_{P,H}$ = 15.5 Hz, 1 H, P-CH_2-P), 3.38 (t, $^2J_{P,H}$ = 17.0 Hz, 1 H, P-CH_2-P), 4.38−4.54 [m, 4 H, Fe(Cpd_2)], 4.50−4.64 [m, 2 H, Fe(Cpd_2)], 5.01−5.17 [m, 2 H, Fe(Cpd_2)] ppm. ^{13}C NMR (22.5 MHz, $CDCl_3$): δ = 37.2 (s, 4 C, NCH_3), 44.2 (t, $^1J_{P,C}$ = 73.1 Hz, 1 C, P-*C*-P), 69.9−70.6 [m, 4 C, Fe(Cpd_2)], 71.8−72.7 [m, 2 C, Fe(Cpd_2)], 73.2−74.0 [m, 2 C, Fe(Cpd_2)], 77.3−78.3 [m, $^2J_{P,C}$ = 17.6 Hz, 2 C, Fe(Cpd_2)] ppm. ^{31}P NMR (36.2 MHz, $CDCl_3$): δ = 66.6 (s, 2 P, *P*-C-*P*) ppm. $C_{15}H_{22}FeN_2P_2S_2$ (412.27): calcd. C 43.70, H 5.38, N 6.80; found C 43.61, H 5.23, N 7.24.

16b-*cis*: M.p. 175−180 °C (dec.). ^{1}H NMR (300 MHz, $CDCl_3$): δ = 1.06 (t, $^3J_{H,H}$ = 7.0 Hz, 12 H, NCH_2CH_3), 2.87−3.10 (m, 8 H, NCH_2CH_3), 3.20 (dt, $^2J_{H,H}$ = 13.8, $^2J_{P,H}$ = 17.1 Hz, 1 H, P-CH_2-P), 3.40 (q, $^2J_{H,H}$ = 13.8, $^2J_{P,H}$ = 13.8 Hz, 1 H, P-CH_2-P), 4.37−4.46 [m, 4 H, Fe(Cpd_2)], 4.47−4.55 [m, 2 H, Fe(Cpd_2)], 5.04−5.12 [m, 2 H, Fe(Cpd_2)] ppm. ^{13}C NMR (22.5 MHz, $CDCl_3$): δ = 14.5 (m, 4 C, NCH_2CH_3), 40.90 (m, 4 C, NCH_2CH_3), 44.32 (t, $^1J_{P,C}$ = 71.2 Hz, 1 C, P-*C*-P), 69.45−70.15 [m, 4 C, Fe(Cpd_2)], 71.65−72.38 [m, 2 C, Fe(Cpd_2)], 72.80−73.45 [m, 2 C, Fe(Cpd_2)], 77.65−78.55 [m, $^2J_{P,C}$ = 17.6 Hz, 2 C, Fe(Cpd_2)] ppm. ^{31}P NMR (36.2 MHz, $CDCl_3$): δ = 60.0 [s, 2 P, *P*-C-*P*) ppm. $C_{19}H_{30}FeN_2P_2S_2$ (468.38): calcd. C 48.72, H 6.46; found C 47.86, H 6.48.

Compound 16b-*trans*: An excess of sulfur (300 mg) was added to the mother liquor left after crystallization of **14b-*cis***, which contained about 970 mg of dissolved compounds (*cis*:*trans* = 15:85) (see above) and the mixture was stirred vigorously at room temperature for 12 h. The reaction mixture was dried in vacuo, dissolved in a minimum amount of dichloromethane and passed through a column with silica gel (45 g) using dichloromethane (about 1200 mL) as solvent. Fractions with R_f = 0.65 yielded 200 mg of **16b-*trans***. (R_f **16b-*cis*** = 0.45). M.p. 128−129 °C (dec.). ^{1}H NMR (90 MHz, $CDCl_3$): δ = 1.06 (t, $^3J_{H,H}$ = 7.1 Hz, 12 H, NCH_2CH_3), 2.91−3.40 (m, 8 H, NCH_2CH_3), 3.61 (t, $^2J_{P,H}$ = 14.6 Hz, 2 H, P-CH_2-P), 4.27−4.44 [m, 2 H, Fe(Cpd_2)], 4.44−4.60 [m, 2 H, Fe(Cpd_2)], 4.78−4.92 [m, 2 H, Fe(Cpd_2)], 4.92−5.07 [m, 2 H, Fe(Cpd_2)] ppm. ^{13}C NMR (22.5 MHz, $CDCl_3$): δ = 13.8 (pseudo t, $^3J_{P,C}$ = 2.4 Hz, 4 C, NCH_2CH_3), 40.3 (pseudo t, $^2J_{P,C}$ = 1.5 Hz, 4 C, NCH_2CH_3), 47.3 (t, $^1J_{P,C}$ = 61.4 Hz, 1 C, P-*C*-P), 71.9 [t, $^3J_{P,C}$ = 6.0 Hz, 4 C, Fe(Cpd_2)], 73.9 [t, $^2J_{P,C}$ = 4.8 Hz, 2 C, Fe(Cpd_2)], 74.8 [t, $^2J_{P,C}$ = 4.8 Hz, 2 C, Fe(Cpd_2)], 78.2 [m, $^2J_{P,C}$ = 8.3 Hz, 2 C, Fe(Cpd_2)] ppm. ^{31}P NMR (36.2 MHz, $CDCl_3$): δ = 62.2 (s, 2 P, *P*-C-*P*) ppm. $C_{19}H_{30}FeN_2P_2S_2$ (468.38): calcd. C 48.72, H 6.46; found C 48.16, H 6.41.

X-ray Crystallographic Study: Crystals of complexes **14b-*cis*, 16b-*cis*,** and **16b-*trans*** are all orange in color. The diffraction data of the three structures were collected on a Bruker P4 diffractometer. Diffraction data for **14b-*cis*** were collected at room temperature, while data for **16b-*cis*** and **16b-*trans*** were collected at −45 °C. The pertinent crystallographic data and conditions for data collection are summarized in Table 2. The data were corrected for Lorentz and polarization effects. ψ-Scan absorption studies were carried out

Table 2. Crystal data for compounds **14b-*cis*, 16b-*cis*,** and **16b-*trans***

	14b-*cis*	**16b-*cis***	**16b-*trans***
Formula	$C_{19}H_{30}N_2P_2Fe$	$C_{19}H_{30}N_2P_2S_2Fe$	$C_{19}H_{30}N_2P_2S_2Fe$
Mol. wt.	404.2	468.4	468.4
Crystal system	monoclinic	monoclinic	monoclinic
Space group	$P2_1/n$	$P2_1/c$	$P2_1/n$
a, Å	6.291(1)	14.036(1)	10.590(1)
b, Å	20.152(1)	12.883(1)	7.837(1)
c, Å	15.802(1)	12.544(1)	27.029(2)
β, °	92.242(5)	98.093(6)	98.615(7)
V, Å^3	2003.1(4)	2245.7(3)	2217.9(4)
Z	4	4	4
$D_{calcd.}$, g cm^{-3}	1.34	1.38	1.40
Abs coeff, mm^{-1}	0.916	1.01	1.02
Crystal dmns, mm	0.30 × 0.25 × 0.15	0.35 × 0.35 × 0.20	0.35 × 0.35 × 0.15
Scan type	w/2θ	w/2θ	w/2θ
2θ range, °	3.5−50.0	3.5−44.0	3.5−44.0
Scan speed, min, max, °	3.5, 35.0	3.5, 35.0	3.5, 35.0
Decay of data,%	3.85	2.70	6.20
Data collected	3867	2898	2878
Obsd reflctns, $F > 4\sigma(F)$	2897	2424	2220
Parameters refined	218	241	236
Goodness-of-fit	1.03	1.05	1.08
R_1	0.033	0.042	0.058
wR_2	0.085	0.116	0.150

on the three structures with T_{min} and T_{max} 0.713 and 0.784 for **14b-*cis***, 0.806 and 0.987 for **16b-*cis***, 0.764 and 1.000 for **16b-*trans***. The crystal structures were solved by direct methods and subsequent difference Fourier syntheses using the *SHELXTL-Plus* package.[16] Full-matrix least-squares refinement was performed. Scattering factors, as well as anomalous-dispersion correction for heavy atoms, were taken from ref.[17] All structures were refined on F^2 (SHELXL-93).[18] One methyl [C(9)] of **16b-*cis*** is disordered, with site occupancy factors of C(9) 0.840, C(9′) 0.160. As for **16b-*trans***, one ethyl group [C(8) and C(9)] is disordered, C(8) and C(9) 0.479, C(8′) and C(9′) 0.521. The above-mentioned disordered moieties were all elastically constrained during the final stages of refinement. H atoms of the three structures were located on a riding model. The final values of R_1 and weighted wR_2 are listed in Table 2. A full list of atomic coordinates, all bond lengths and angles, anisotropic thermal parameters, the positions of H atoms, and tables of structural factors were supplied in the supplementary materials.[19]

Acknowledgments

We thank the Deutsche Forschungsgemeinschaft and Robert A. Welch Foundation for financial support.

[1] M. Sawamura, Y. Ito, *Chem. Rev.* **1992**, *92*, 857−871.
[2] Ferrocenes. *Homogeneous Catalysis, Organic Synthesis, Materials Science* (Eds.: A. Togni, T. Hayashi); VCH: Weinheim, Germany, 1995.
[3] Ch. J. Richards, A. J. Locke, *Tetrahedron: Asymmetry* **1998**, *9*, 2377−2407.
[4] K. A. O. Starzewski, W. M. Kelly, A. Stumph, D. Freitag, *Angew. Chem. Int. Ed.* **1999**, *38*, 2439−2443.
[5] J. H. Shin, T. Hascall, G. Parkin, *Organometallics* **1999**, *18*, 6−9.
[6] H. R. Allcock, K. D. Lavin, G. H. Riding, R. R. Whittle, M. M. Parvez, *Organometallics* **1986**, *5*, 1626−1635.
[7] I. Manners, W. D. Coggio, M. N. Mang, M. Parvez, H. R. Allcock, *J. Am. Chem. Soc.* **1989**, *111*, 3481−3482.
[8] H. R. Allcock, W. D. Coggio, I. Manners, M. Parvez, *Organometallics* **1991**, *10*, 3090−3098.
[9] H. R. Allcock, J. A. Dodge, I. Manners, M. Parvez, G. H. Riding, K. B. Visscher, *Organometallics* **1991**, *10*, 3098−3104.
[10] M. A. Carroll, D. A. Widdowson, D. J. Williams, *Synlett* **1994**, *12*, 1025−1026.
[11] I. Shevchenko, R. Mikolenko, S. Loss, H. Grützmacher, *Eur. J. Inorg. Chem.* **1999**, 1665−1671.
[12] C. Angelakos, D. B. Zamble, D. A. Foucher, A. J. Lough, I. Manners, *Inorg. Chem.* **1994**, *33*, 1709−1718.
[13] We thank a referee for making this suggestion.
[14] I. Shevchenko, H. Zhang, M. Lattman, *Inorg. Chem.* **1995**, *34*, 5405−5409.
[15] S. Hietkamp, H. Sommer, O. Stelzer, *Inorg. Synth.* **1989**, *25*, 120−123.
[16] G. M. Scheldrick, *SHELXTL-Plus* (1990), Bruker Analytical X-ray Systems, Inc., USA.
[17] *International Tables for X-ray Crystallography* (1974), *Vol. IV*, Birmingham: Kynoch Press.
[18] G. M. Sheldrick, *SHELXL-93, Program for the refinement of Crystal Structures* (1993). University of Göttingen, Germany.
[19] CCDC-178178 (**14b-*cis***), -178179 (**16b-*cis***) and -178180 (**16b-*trans***) contain the supplementary crystallographic data for this paper. These data can be obtained free of charge at www.ccdc.cam.ac.uk/conts/retrieving.html [or from the Cambridge Crystallographic Data Centre, 12, Union Road, Cambridge CB2 1EZ, UK; Fax: (internat.) +44-1223/336-033; E-mail: deposit@ccdc.cam.ac.uk].

Received May 29, 2002
[I02282]

Hydrothermal Synthesis and Characterisation of Two Novel Large-Pore Framework Vanadium Silicates

Paula Brandão,[a] Anabela Valente,[a] Andreas Philippou,[b] Artur Ferreira,[c] Michael W. Anderson,[b] and João Rocha*[a]

Keywords: Microporous materials / Silicates / Vanadium / Catalysis / Hydrothermal synthesis

Two new large-pore sodium vanadium silicates, denoted AM-15 and AM-17 (Aveiro-Manchester, structures number 15 and 17) with framework composition $Na_6Si_{14}V_4O_{39}$ and $Na_4CaSi_{10}V_2O_{27}$, respectively, are reported. Electron paramagnetic resonance (EPR), Fourier transform infrared (FTIR) and diffuse reflectance ultraviolet-visible (DR UV/Vis) spectroscopy reveal that as-prepared AM-15 contains both V^{IV} and V^{V} in a square pyramidal and tetrahedral coordination, respectively, while AM-17 contains predominantly octahedral V^{IV}. The thermal stability of AM-15 in air is modest (ca. 380 °C), while AM-17 is stable up to 450 °C. The acid-base and redox properties of AM-17 have been assessed by the conversion of isopropanol and ethanol oxidation, respectively.
(© Wiley-VCH Verlag GmbH & Co. KGaA, 69451 Weinheim, Germany, 2003)

Introduction

Microporous vanadium silicates are a new class of materials with potential for applications as selective heterogeneous catalysts for acid-catalysed and oxidation reactions.[1−3] In such systems, catalyst deactivation is a major issue, associated with reduced thermal stability and leaching phenomena.[4] As a result, much research has been carried out in order to prepare vanadium silicates with improved catalytic behaviour.[5−14]

In 1997 we reported the first example of a large-pore vanadium silicate containing stoichiometric amounts of hexacoordinate vanadium (Si/V = 5).[15] This material, dubbed AM-6, is a structural analogue of titanium silicate ETS-10, where titanium has been fully replaced by vanadium. ETS-10 has a framework consisting of "TiO_2" rods, which run in two orthogonal directions and are surrounded by tetrahedral silicate units. The pore structure consists of twelve-, seven-, five- and three-membered rings and has a three-dimensional channel system whose minimum diameter is defined by twelve-membered ring apertures.[16] Jacobson and co-workers reported two novel small-pore vanadium silicates $K_2(VO)(Si_4O_{10})\cdot H_2O$ (VSH-1) and $Cs_2(VO)(Si_6O_{14})\cdot 3H_2O$ (VSH-2), whose structures are closely related to the structures of cavansite and pentagonite.[17] Cavansite and pentagonite, dimorphs of the mineral $Ca(VO)(Si_4O_{10})\cdot 4H_2O$, are small-pore materials containing V^{IV} in a square-pyramidal coordination.[18,19] The framework of cavansite is formed by silicate layers of four- and eight-membered rings of tetrahedra connected vertically by V^{IV} cations. Calcium cations and water molecules reside in the channels formed by the eight-membered rings and between the SiO_2 layers. Cavansite has channels running parallel to the *c* direction with a free diameter of only 3.3 Å in the hydrated state. Recently, the same authors reported on a series of novel vanadium silicates with open-framework and microporous structures with general formula $A_r[(VO)_s(Si_2O_5)_p(SiO_2)_q]\cdot tH_2O$, where A is Na, K, Rb, Cs, or a combination of these metals.[20] Two other large-pore vanadium silicates, AM-13 and AM-14 with Si/V molar ratios of 4 and 10, respectively, have also been reported.[21] In the as-prepared samples, both V^{IV} and V^{V} occur simultaneously in different coordination environments. Like AM-6, AM-14 contains essentially hexacoordinate V^{IV}, while in AM-13 V^{IV} may be in a square-pyramidal coordination. The preparation of these two materials depends strongly on variables such as gel pH, cations present, time and temperature.[22] AM-13 requires a pH between 10.6 and 11.0 whereas AM-14 is obtained in the pH range 10.3−10.5. The AM-13 gel contains 60% Na and 40% Ca, whereas AM-14 crystallises in the presence of Na cations. Here we wish to report the synthesis and characterisation of two novel large-pore vanadium silicates, AM-15 and AM-17.

[a] Department of Chemistry, University of Aveiro, CICECO, 3810-193 Aveiro, Portugal
Fax: (internat.) + 351-34/370-084
E-mail: ROCHA@DQ.UA.PT
[b] Department of Chemistry, UMIST, P. O. Box 88, Manchester M60 1QD, UK
[c] ESTGA, University of Aveiro, CICECO, 3810-193 Aveiro, Portugal

Results and Discussion

Powder XRD

The powder XRD patterns of AM-15 and AM-17 are shown in Figure 1 with the corresponding d-spacings and intensities listed in Table 1 and 2, respectively. The AM-15 cell is monoclinic with $a = 29.612$, $b = 17.892$, $c = 11.400$ Å, $\beta = 97.39°$ (volume 5990 Å^3). The most probable space group is $P2_1/n$ (no.14). The AM-17 cell is orthorhombic with $a = 37.712$, $b = 26.973$, $c = 16.456$ Å, (volume 16740 Å^3). The most probable space group is *Pba*2 (no. 32).

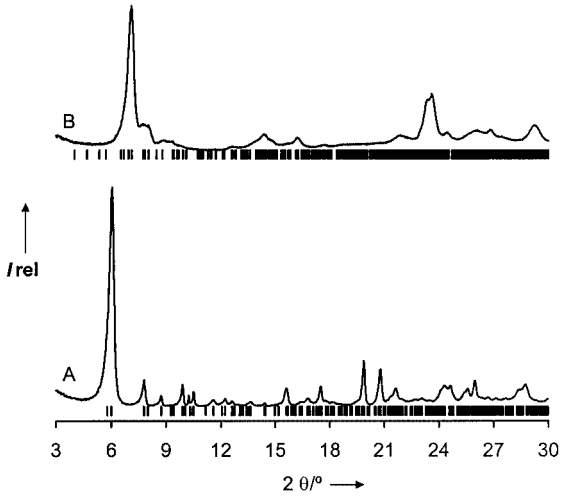

Figure 1. Powder XRD patterns of: A) AM-15 and B) AM-17; the tick marks depict Bragg reflections

Table 1. Powder XRD data of AM-15

d (Å)	I/I_0	d (Å)	I/I_0
14.568	100	4.273	17
11.332	12	4.106	7
10.110	5	3.917	1
8.923	10	3.855	2
8.410	7	3.663	7
7.643	3	3.612	7
7.224	3	3.478	5
7.011	2	3.429	10
6.503	2	3.340	1
6.144	1	3.283	1
5.672	8	3.226	1
5.399	1	3.143	5
5.286	3	3.108	8
5.064	9	2.972	2
4.890	1	2.929	4
4.465	22	2.899	5

SEM and EDAX

SEM images of the AM-15 samples (Figure 2) reveal that the crystals consist of thin plates with a particle size of ca. 5 μm. EDAX analysis of different AM-15 crystals shows a similar molar composition: Si/V = 3.7, Na/V = 1.5. No other phases rich in silicon or vanadium were detected. Assuming that all vanadium is present as V^{IV} (which is probably not entirely correct, see below) the ideal formula of dehydrated AM-15 is $Na_6Si_{14}V_4O_{39}$. AM-17 crystals consist of plates with a size of ca. 1−2 μm, with the following molar ratios: Si/V = 4.4, Na/Ca = 2.9, Na/V = 1.0. The ideal formula of AM-17 is $Na_6Ca_2Si_{24}V_6O_{65}$, where all vanadium is assumed to be present as V^{IV}.

Table 2. Powder XRD data of AM-17

d (Å)	I/I_0	d (Å)	I/I_0
21.674	<1	5.006	2
16.325	<1	4.729	2
12.394	100	4.079	8
11.397	17	4.052	8
10.974	16	3.800	34
9.987	5	3.765	38
9.448	5	3.637	9
9.123	3	3.521	5
7.037	2	3.503	7
6.864	2	3.433	10
6.499	3	3.405	11
6.343	6	3.321	11
6.165	11	3.134	4
5.991	6	3.066	13
5.638	4	3.049	14
5.459	7	3.031	10

Thermal Analysis

The thermal stability of AM-15 and AM-17 was investigated using TGA/DSC in air, and variable temperature (25−650 °C) in-situ powder XRD in air and in vacuo. The AM-15 and AM-17 total mass loss between 30 and 600 °C is ca. 12.0% and 9.8%, respectively. DSC exhibits exothermic peaks centred at 380 °C (AM-15) and 450 °C (AM-17) probably due to the collapse of the crystalline structure (Figure 3). When calcined in vacuo, both materials retain their structural integrity up to about 600 °C (not shown). Upon calcination in air at temperatures of ca. 400 °C the structure of AM-15 collapses, while AM-17 is stable until ca. 450 °C (Figure 4).

Adsorption Measurements

Nitrogen adsorption isotherms are of type I, with a slight upward distortion (Figure 5), suggesting that microporosity (pore width < 2 nm, according to IUPAC) is associated with significant external surface area. These vanadium silicates have similar specific surface areas (330−380 m^2/g) and micropore volumes (0.1−0.13 cm^3/g; Table 3). A narrow pore-size distribution with median pore width of 8 and 7.3 Å is obtained for AM-15 and AM-17, respectively. Both materials adsorb benzene, *m*-xylene and mesitylene and the sorption capacities (taken at $p/p_0 \approx 0.4$) decrease with increasing size of the diffusing molecule (molecular dimension in brackets): benzene (6.8 Å) > *m*-xylene (7.4 Å) > mesitylene (8.4 Å; Table 4). The above results suggest that AM-15 and AM-17 have large accessible pores with a width of 7−8 Å.

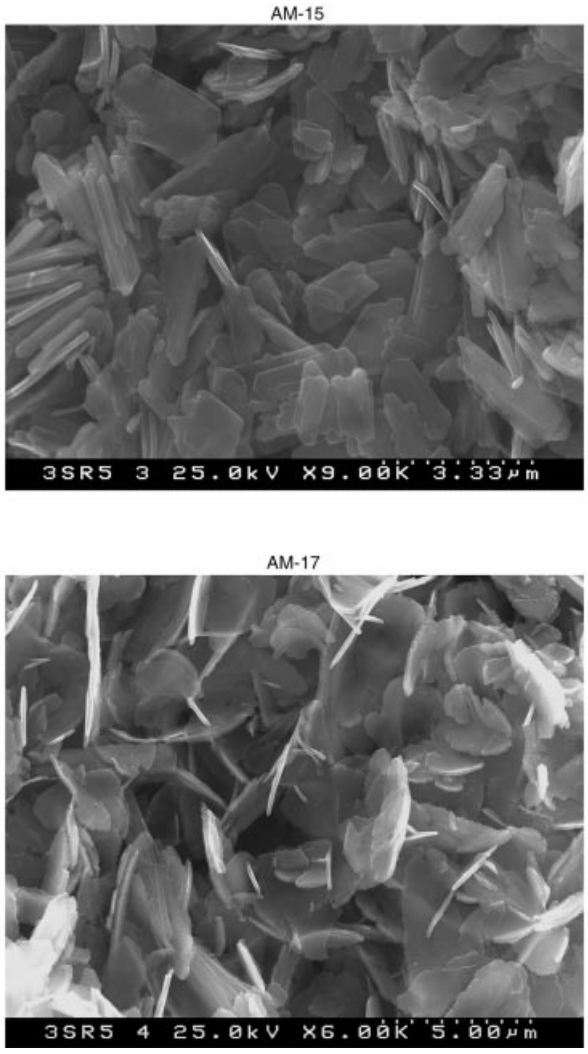

Figure 2. SEM images of AM-15 and AM-17

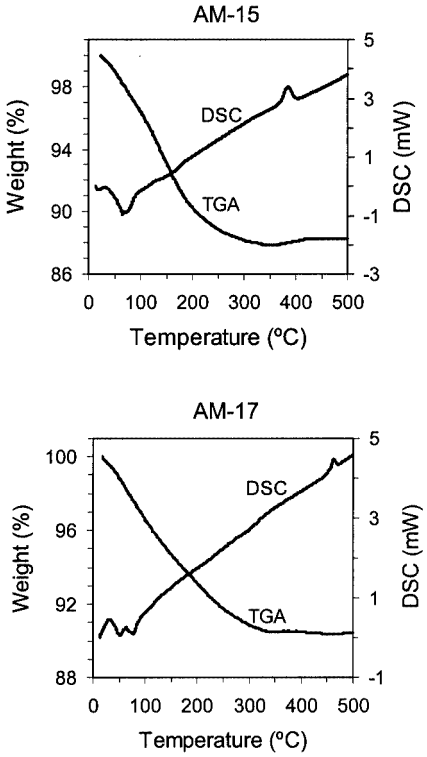

Figure 3. TGA and DSC curves of AM-15 and AM-17, recorded in air

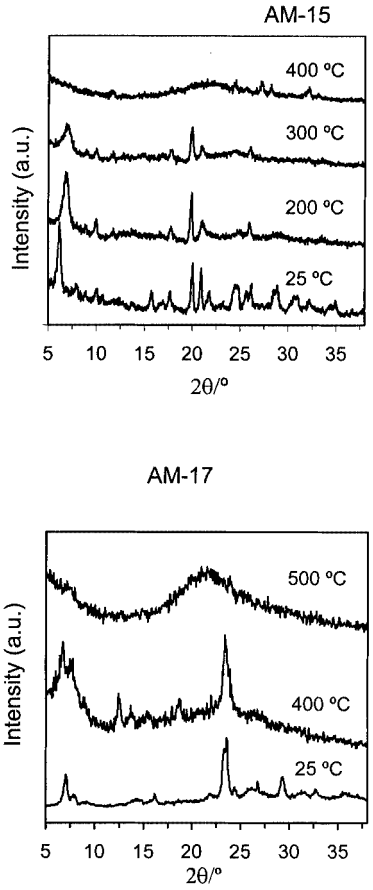

Figure 4. Powder XRD patterns of AM-15 and AM-17, recorded in situ at different temperatures in air

Electron Paramagnetic Resonance

The oxidation state of vanadium atoms in as-synthesised AM-15 and AM-17 was studied by EPR spectroscopy at room temperature. The spectra of AM-15 and AM-17 display a broad signal centred at $g = 2.357$ and 2.415, respectively (Figure 6). No hyperfine structure is observed, indicating the presence of (nonisolated) V^{IV} dipolar-coupled to other V^{IV} ions.

Fourier Transform Infrared Spectroscopy

FTIR spectra of AM-15, AM-17 and, for comparison, AM-6 and crystalline V_2O_5 (Aldrich) are shown in Figure 7. Since the characteristic FTIR bands at $\tilde{\nu} = 838$ and 605 cm^{-1} are not observed, the presence of crystalline V_2O_5 in AM-15 and AM-17 is ruled out. The band at $\tilde{\nu} = 872$ cm^{-1} in the spectrum of AM-6 is ascribed to V^{IV} in an octahedral coordination. The IR absorption spectrum of AM-17 shows a small band at $\tilde{\nu} = 887$ cm^{-1} which, by comparison with

Table 3. Texture parameters of AM-15 and AM-17

Sample	S_{Lang}[a] (m^2/g)	TPV [b] (cm^3/g)	$V_{micropore}$ [c] (cm^3/g)	Pore size [d] (Å)
AM-15	375	0.17	0.13	8.0
AM-17	337	0.16	0.11	7.3

[a] Langmuir specific surface area. [b] Total pore volume. [c] Micropore volume derived from t-plot. [d] Median pore diameter derived from DFT calculations.

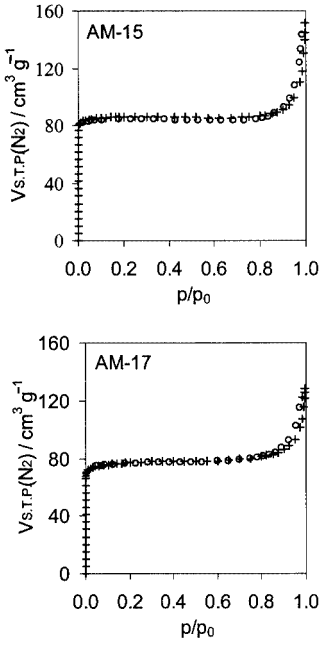

Figure 5. Nitrogen adsorption (+) and desorption (O) isotherms of AM-15 and AM-17

Table 4. Adsorption of hydrocarbons on AM-15 and AM-17 at 298 K

Sample	Benzene	*m*-Xylene ($\mu mol \cdot g_{solid}^{-1}$) [a]	Mesitylene
AM-15	740	430	248
AM-17	910	526	304

[a] Uptake at $p/p_0 \approx 0.4$.

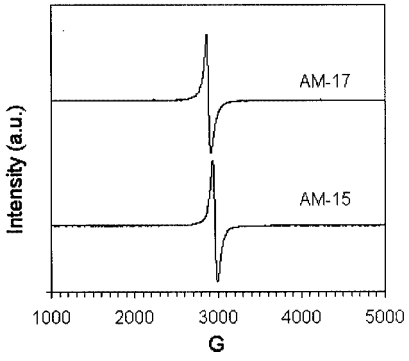

Figure 6. Room temperature EPR spectra of AM-15 and AM-17

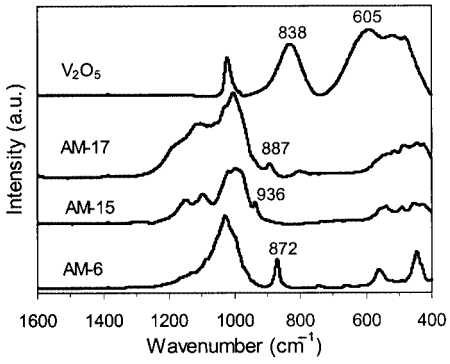

Figure 7. FTIR absorption spectra of AM-15, AM-17, AM-6 and V_2O_5

AM-6, is assigned to hexacoordinate V^{IV}. The AM-15 band at $\tilde{\nu} = 936\ cm^{-1}$ indicates the presence of V=O bonds, which usually give bands in the region $\tilde{\nu} = 900-1000\ cm^{-1}$.[23] No band is observed in the range of octahedral V^{IV}.

Diffuse-Reflectance UV/Visible Spectroscopy

Additional structural information on vanadium coordination may be obtained by DR UV/Vis spectroscopy. AM-6 is used as a DR UV/Vis reference compound, since it contains hexacoordinate V^{IV}. All samples exhibit broad bands at about 600, 435, and 220−270 nm (Figure 8). Charge transfer (CT) associated with O to V^{IV} electron transfer occurs in the range 220−270 nm.[10,24] The bands at 600 and 435 nm are assigned to V^{IV} d-d transitions and are responsible for the green colour of the solids. These observations suggest that both vanadium silicates contain V^{IV}. However, AM-15 gives a band at 340 nm, which is absent from the AM-6 and AM-17 spectra. In general, the spectra of materials containing V^{V} ions exhibit CT absorption bands in the region 280−340 nm.[9,25] Therefore, the AM-15 UV band observed in this region may be ascribed to the presence of tetrahedral V^{V}. Combining the DR UV/Vis and FTIR evidence, we propose that in AM-15 V^{IV} and V^{V} may be in a square pyramidal and tetrahedral coordination, respectively, while AM-17 contains essentially hexacoordinate V^{IV}.

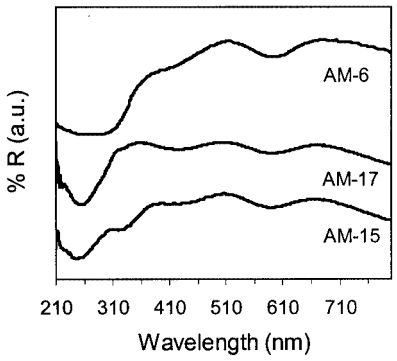

Figure 8. Diffuse reflectance UV/Vis spectra of AM-6, AM-15 and AM-17

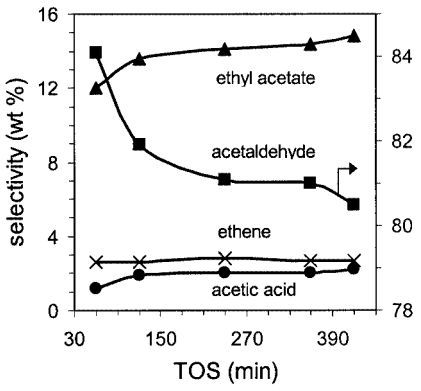

Figure 9. Effect of TOS on the products distribution of ethanol oxidation (T = 300 °C; WHSV = 0.4 h^{-1}), over AM-17

Catalytic Tests

Given the modest thermal stability of AM-15 the catalytic reactions in the gas phase were carried out over AM-17.

Isopropanol Conversion

A preliminary characterisation of the acid-base properties of AM-17 was performed by means of 2-propanol conversion, a probe reaction which is tailored for both acidity and basicity.[26] AM-17 yields mainly acetone, resulting from base-catalysed dehydrogenation of 2-propanol, whereas propene, formed by acid-catalysed dehydration, was produced in smaller amounts (Table 5). These results point to the basic character of AM-17.

Ethanol Oxidation

The oxidation activity of AM-17 was studied using the oxidation of ethanol with air as a model reaction.[27] The catalytic results obtained at 300 °C are shown in Table 5. AM-17 yields mainly acetaldehyde (84.1% selectivity at 23.7% conversion) and ethyl acetate (12% selectivity), along with minor amounts of ethene and acetic acid. Acetaldehyde is formed in the dehydrogenation process. As seen in Figure 9, long times on stream (TOS) favour the formation of ethyl acetate at the expense of acetaldehyde. The consecutive reaction of acetaldehyde with ethanol and oxygen produces ethyl acetate.[28,29] AM-17 possesses little dehydration activity in this process, evidenced by the formation of minor amounts of ethene (2.3% selectivity). After the catalytic tests, AM-17 was characterised by powder XRD, and the results show 21% crystallinity loss. The above results indicate that AM-17 is a basic solid with potential in redox catalysis.

Table 5. Conversion and product selectivity (wt %) of 2-propanol.[a] and ethanol oxidation[b] over AM-17

	Isopropanol	Ethanol
Conversion	31.2	23.7
Acetone	73.8	–
Propene	26.2	–
Acetaldehyde	–	84.1
Ethyl acetate	–	12.1
Ethene	–	2.6
Acetic acid	–	1.2

[a] $T_{reaction}$ = 350 °C; TOS = 60 min; WHSV = 2 h^{-1}; carrier gas: argon. [b] $T_{reaction}$ = 300 °C; TOS = 60 min; WHSV = 0.4 h^{-1}; carrier gas: air.

Conclusions

Two novel large-pore sodium vanadium silicates, AM-15 and AM-17, with approximate framework compositions $Na_6Si_{14}V_4O_{39}$ and $Na_6Ca_2Si_{24}V_6O_{65}$, respectively, have been prepared hydrothermally. Spectroscopic techniques suggest that as-synthesised AM-15 contains both square pyramidal V^{IV} and tetrahedral V^{V}, whereas V^{IV} in AM-17 assumes octahedral coordination. The latter is an interesting catalyst for dehydrogenation reactions.

Experimental Section

Synthesis: The synthesis of AM-15 and AM-17 was carried out in Teflon-lined autoclaves under static hydrothermal conditions.

Synthesis of AM-15. An alkaline solution was made by mixing 5.08 g of sodium silicate solution (Na_2O 8 wt%, SiO_2 27 wt%, Merck), 8.27 g of H_2O and 0.55 g of NaOH (Merck). A second solution was made by mixing 7.61 g of H_2O with 1.02 g of $VOSO_4 \cdot 5H_2O$ (Merck). These two solutions were combined and stirred thoroughly.

Synthesis of AM-17. An alkaline solution was made by mixing 5.01 g of sodium silicate solution (Merck), 10.35 g of H_2O, and 0.10 g of $Ca(OH)_2$ (Aldrich). A second solution was made by mixing 5.53 g of H_2O with 1.00 g of $VOSO_4 \cdot 5H_2O$ (Merck). The AM-15 gel with a composition $6.7Na_2O{:}11.4SiO_2{:}V_2O_5{:}441H_2O$, and the AM-17 gel with a composition $3.3Na_2O{:}0.7CaO{:}11.3SiO_2{:}V_2O_5{:}441H_2O$, were autoclaved for three days at 230 °C. The crystalline powders were filtered off, washed and dried at room temperature.

Catalytic Tests: The catalytic reactions were carried out at atmospheric pressure in a fixed-bed stainless-steel reactor (height = 16 cm, internal diameter = 0.5 cm), which was charged with 50 mg

of catalyst. Prior to reaction, the catalyst was activated at 350 °C in a flow of argon (10 mL/min) for 2-propanol conversion or in a flow of air (2 mL/min) for ethanol oxidation. The reactant was fed using a syringe pump and mixed with the flowing gas before entering the reactor tube. The products were analysed by gas chromatography with a 30-metre long capillary column (DP1 fused silica phase) and an FID (flame ionisation detector).

Techniques: Powder XRD data were collected on an X'Pert MPD Philips diffractometer (CuK_α X-radiation) with a curved graphite monochromator, a fixed divergence slit (0.5°, irradiated length 10.00 mm), a progressive receiving slit (slit's height 0.2 mm) and a flat-plate sample holder, in a Bragg−Brentano para-focusing optics configuration. Intensity data were collected by the step counting method, step 0.02°, time 120 (AM-17) and 64 s (AM-15) in the 2θ range 3−40°. X-ray diffraction pattern auto-indexing was performed with DICVOL[30] from the resolved first 22 lines and checked with the Chekcell package.[31]

SEM images were recorded on a Hitachi S-4100 Field Emission Gun tungsten filament working with a voltage of 25000 V. Chemical composition was determined by energy dispersive analysis of X-rays (EDAX). TGA and DSC curves were measured with TGA-50 and DSC Shimadzu analysers. Samples were heated under air with a rate of 2 °C/min. Variable temperature in situ powder XRD was carried out using an Anton Parr high-temperature chamber with a 10 °C/min heating rate. Nitrogen adsorption measurements were performed using a Micromeritics ASAP 2010 V1.01 B automatic instrument at 77 K. Pore-size distributions were determined using the density functional theory (DFT) Plus Software for data files generated from the ASAP instrument. Adsorption of benzene, *m*-xylene and mesitylene was measured at 298 K using a gravimetric adsorption apparatus equipped with a CI electronic MK2−M5 microbalance and an Edwards Barocel pressure sensor. Before measurements, the samples were outgassed overnight at 573 K. EPR spectra were obtained at room temperature on a Bruker ESP 300E spectrometer, operating at 9.53 GHz. The g-values were obtained by reference to standard diphenylpicrylhydrazine (DPPH, $g = 2.0037$). FTIR spectra were recorded in absorbance mode on a Mattson Mod 7000 spectrophotometer, as KBr pellets, in the range 400−4000 cm^{-1}. The pellets were prepared by sample dispersion (0.2 mg) in a KBr matrix (150 mg) and pressed. The spectra were typically an average of 64 scans with 4 cm^{-1} resolution. DR UV/Vis was performed on a Jasco V-560 PC spectrometer using $BaSO_4$ as the reference material.

Acknowledgments

The authors thank, FCT, PRAXIS XXI, POCTI and FEDER (Portugal) for financial support.

[1] J. I. W. C. E. Arends, R. A. Sheldon, M. W. Wallau, V. Schuchardt, *Angew. Chem. Int. Ed. Engl.* **1997**, *36*, 1144.
[2] M. Zahedi-Niaki, S. J. M. Zaidi, S. Kaliaguine, *Appl. Catal. A: Gen.* **2000**, *196*, 9.
[3] P. R. H. Rao, A. A. Belhekar, S. G. Hedge, A. V. Ramaswamy, P. Ratnasamy, *J. Catal.* **1993**, *141*, 595.
[4] Y. Deng, C. Lettmann, W. F. Maier, *Appl. Catal. A: Gen.* **2001**, *214*, 31.
[5] P. R. H. Rao, R. Kumar, A. V. Ramaswamy, P. Ratnasamy, *Zeolites* **1993**, *13*, 663.
[6] T. Sen, V. Ramaswamy, S. Ganapathy, P. R. Rajamohanan, S. Sivasanker, *J. Phys. Chem.* **1996**, *100*, 3809.
[7] S. H. Chien, J. C. Ho, S. S. Mon, *Zeolites* **1997**, *18*, 182.
[8] Z. Luan, J. Xu, H. He, J. Klinowski, L. Kevan, *J. Phys. Chem.* **1996**, *100*, 19595.
[9] Z. Luan, D. Zhao, L. Kevan, *Microporous Mesoporous Mater.* **1998**, *20*, 93.
[10] G. Catana, R. R. Rao, B. M. Weckhuysen, P. Van Der Voort, E. F. Vansant, R. A. Schoonheydt, *J. Phys. Chem. B* **1998**, *102*, 8005.
[11] D. Wei, H. Wang, X. Feng, W. Chuch, P. Ravikovitch, M. Lyubovsky, C. Li, T. Takeguchi, G. L. Haller, *J. Phys. Chem. B* **1999**, *103*, 2113.
[12] Z. Luan, J. Y. Bae, L. Kevan, *Chem. Mater.* **2000**, *12*, 3202.
[13] L. X. Dai, K. Tabata, E. Suzuki, T. Tatsumi, *Chem. Mater.* **2001**, *13*, 208.
[14] M. Mathieu, P. Van Der Voort, B. M. Weckhuysen, R. R. Rao, G. Catana, R. A. Schoonheydt, E. F. Vansant, *J. Phys. Chem. B* **2001**, *105*, 3393.
[15] J. Rocha, P. Brandão, Z. Lin, M. W. Anderson, V. Alfredsson, O. Terasaki, *Angew. Chem. Int. Ed. Engl.* **1997**, *36*, 100.
[16] M. W. Anderson, O. Terasaki, T. Ohsuna, A. Philippou, S. P. Mackay, A. Ferreira, J. Rocha, S. Lidin, *Nature* **1994**, *367*, 347.
[17] X. Wang, L. Liu, A. J. Jacobson, *Angew. Chem. Int. Ed.* **2001**, *40*, 2174.
[18] H. T. Evans, *J. Am. Mineral. Sect. B* **1973**, *58*, 412.
[19] R. Rinaldi, J. J. Pluth, J. V. Smith, *Acta Crystallogr., Sect. B* **1975**, *31*, 1598.
[20] X. Wang, L. Liu, A. J. Jacobson, *J. Am. Chem. Soc.* **2002**, *124*, 7812.
[21] P. Brandão, H. Hanif, A. Philippou, A. Ferreira, P. Ribeiro-Claro, J. Rocha, M. W. Anderson, *Chem. Mater.* **2002**, *14*, 1053.
[22] P. Brandão, N. Hanif, A. Philippou, J. Rocha, M. W. Anderson,. *Proceedings of the 13th International Zeolite conference*, Montpellier, **2001**, 176.
[23] D. C. M. Dutoit, M. Schneider, P. Fabrizioli, A. Baiker, *Chem. Mater.* **1996**, *8*, 734.
[24] L. Frunza, P. Van Der Voort, E. F. Vansant, A. Schoonheydt, B. M. Weckhuysen, *Microporous Mesoporous Mater.* **2000**, *39*, 493.
[25] S. Higashimoto, M. Matsuoka, H. Yamashita, M. Anpo, O. Kitao, H. Hidaka, M. Che, E. Giamello, *J. Phys. Chem. B* **2000**, *104*, 10288.
[26] P. E. Hathaway, M. E. Davies, *J. Catal.* **1989**, *116*, 263.
[27] J. M. Miller, L. J. Lakshmi, *J. Catal.* **1999**, *184*, 68.
[28] L. Wang, R. Eguchi, H. Arai, T. Seiyama, *Chem. Lett.* **1986**, 1173.
[29] N. Iwasa, O. Yamamoto, R. Tamura, M. Nishikubo, N. Takezawa, *Catal. Lett.* **1999**, *62*, 179.
[30] A. Boultif, D. Louër, *J. Appl. Crystallogr.* **1991**, *21*, 987.
[31] J. Laugier, B. Bochu, *Programme D'affinement des Paramètres de Maille à Partir d'un Diagramme de Poudre*; Laboratoire des Matériaux et du Génie Physisque, École Nationale Supérieure de Physisque de Grenoble (INGP), Saint Martin d'Hères, France.

Received July 1, 2002
[I02357]

Synthesis, Structure and Characterization of Two New Complexes $[Cu_2(C_3H_2O_4)_2(C_4H_4N_2)]\cdot 2H_2O$ and $[Zn_2(OH_2)_2(C_3H_2O_4)_2(C_4H_4N_2)]$

Xiutang Zhang,[a] Canzhong Lu,*[a] Quanzheng Zhang,[a] Shaofang Lu,[a] Wenbin Yang,[a] Jiacheng Liu,[a] and Honghui Zhuang[a]

Keywords: Copper / N ligands / Supramolecular chemistry / Magnetic properties / Conducting materials

Two new complexes with three-dimensional extended frameworks linked by pyrazine and malonate ligands, namely $[Cu_2(C_3H_2O_4)_2(C_4H_4N_2)]\cdot 2H_2O$ and $[Zn_2(OH_2)_2(C_3H_2O_4)_2(C_4H_4N_2)]$, have been prepared and characterized by X-ray crystallography, IR, EPR and UV/Vis spectroscopy, their magnetic properties and electrical conductivity.
(© Wiley-VCH Verlag GmbH & Co. KGaA, 69451 Weinheim, Germany, 2003)

Introduction

In the past decade, transition metal complex polymers in which a ligand bridges two or more metal centers have received increasing attention due to the potential applications of their physical and/or chemical properties.[1] It is well-known that pyrazine and RCO_2^- can act as excellent bridging ligands for the syntheses of such compounds.[2] Most compounds, however, have either chain-like structures or two-dimensional layer-like structures.[3] For three-dimensional coordination frameworks, it is often difficult to predict the structures and obtain single crystals for X-ray structural analysis. Recently, we have chosen pyrazine and malonate as ligands and attempted to explore the synthetic strategies and structural features. In this paper, the syntheses and structural characterization of two new complexes with 3-D coordination frameworks, $[Cu_2(C_3H_2O_4)_2(C_4H_4N_2)]\cdot 2H_2O$ (**1**) and $[Zn_2(OH_2)_2(C_3H_2O_4)_2(C_4H_4N_2)]$ (**2**), are reported. The magnetic behavior and temperature dependence of the electric conductivity of complex **1** are also described.

Results and Discussion

Blue crystalline blocks of **1** were obtained from the reaction of $Cu(C_3H_2O_4)\cdot 2H_2O$, malonic acid and pyrazine, and its structure determined by a single crystal X-ray diffraction study. An ORTEP diagram of **1** is shown in Figure 1 with selected bond distances and angles listed in Table 1. The crystal structure reveals that the copper(II) ion is pentacoordinate with four oxygen atoms from three malonate ligands and a nitrogen atom from the pyrazine ligand. The coordination geometry of the Cu^{II} ion can be described as square-based pyramidal, the square plane being defined by O(1), O(3), O(4), and N(1) with an average Cu−O bond length of 1.950 Å. The Cu−N distance is 2.045(3) Å, while the Cu−O(2) distance is slightly longer at 2.252 Å. The Cu^{II} center and the four atoms forming the base are displaced from the least-squares plane by −0.0338, +0.0346, −0.0343, +0.0334, and +0.1151 Å respectively, while the capping atom O(2) is 2.3553 Å away from the corresponding least-squares plane. As described in previous reports,[4] each malonate ligand has two different coordination modes both of which are seen in compound **1**. In the first mode, each malonate acts as a bridge for three Cu^{II} ions, whilst in the second mode each malonate forms a six-membered chelate ring with one Cu^{II} ion in a boat-type configuration. As shown in Figure 2, four Cu^{II} ions are bridged by malonate ligands forming a square 4.848×4.848 Å in size which is slightly bigger than that previously reported.[4] Such square arrangements are then linked by four pyrazines forming a two-dimensional network, leaving a much bigger square (11.685×11.685 Å) in the same plane. Finally, the two-dimensional network is further linked into a three-dimensional structure via malonate ligands (Figure 3). Interestingly, the interstices of the structure are filled with water molecules.

Colorless rhombohedral crystals of **2** were obtained by a similar method to those of **1**. The molecular structure has been determined by a single crystal X-ray diffraction study and an ORTEP diagram of the structure is shown in Figure 4. Selected distances and angles are listed in Table 2. The crystal structure reveals that each Zn^{II} ion is six-coordinate and the coordination geometry of the Zn^{II} centers is octahedral. Each Zn^{II} ion is chelated by two oxygen atoms from one malonate, two oxygen atoms from two neighbor-

[a] The State Key Laboratory of Structural Chemistry, Fujian Institute of Research on the Structure of Matter, The Chinese Academy of Sciences,
Fuzhou, Fujian, 350002, China
E-mail: czlu@ms.fjirsm.ac.cn
Supporting information for this article is available on the WWW under http://www.eurjic.org or from the author.

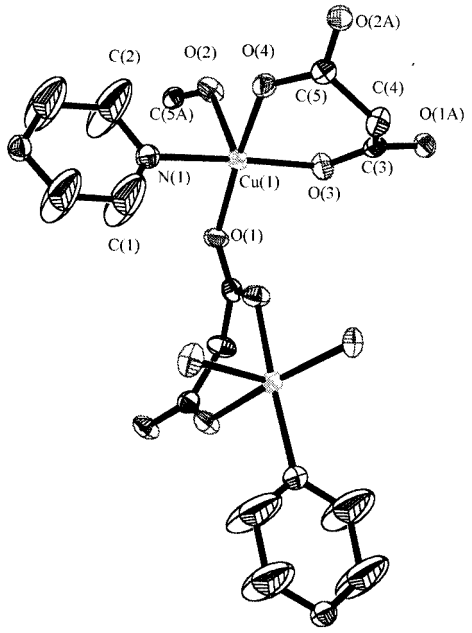

Figure 1. ORTEP diagram of $[Cu_2(C_3H_2O_4)_2(C_4H_4N_2)]\cdot 2H_2O$ **1**

Table 1. Selected bond lengths [Å] and angles [°] in complex **1**

Cu(1)−O(1)	1.956(3)	Cu(1)−O(4)	1.927(3)
Cu(1)−O(2)	2.252(3)	Cu(1)−N(1)	2.045(3)
Cu(1)−O(3)	1.968(3)		
O(4)−Cu(1)−O(1)	171.19(12)	O(3)−Cu(1)−N(1)	175.37(13)
O(4)−Cu(1)−O(3)	92.03(12)	O(4)−Cu(1)−O(2)	89.14(12)
O(1)−Cu(1)−O(3)	87.76(12)	O(1)−Cu(1)−O(2)	99.67(11)
O(4)−Cu(1)−N(1)	87.66(13)	O(3)−Cu(1)−O(2)	90.10(11)
O(1)−Cu(1)−N(1)	91.84(13)	N(1)−Cu(1)−O(2)	94.52(12)

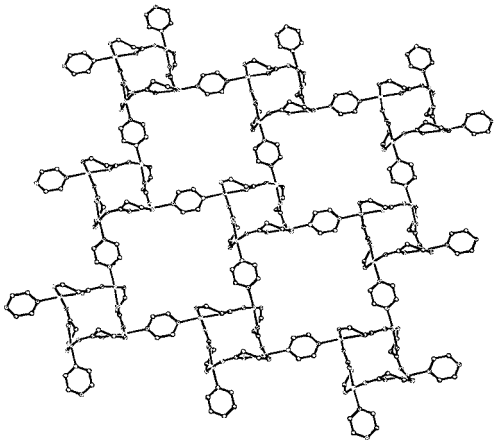

Figure 2. View of the two-dimensional network of **1**

ing malonates, one water molecule, and one nitrogen atom from the pyrazine ligand. The Zn−O bond lengths are in the range 2.065(2)−2.181(3) Å and the Zn−N distance is 2.251(3) Å. The equatorial plane is defined by O(2), O(3),

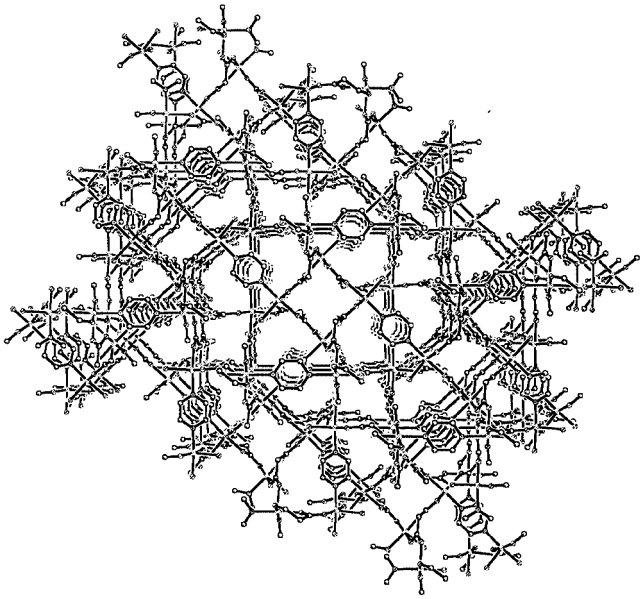

Figure 3. Packing diagram of **1** along the *z*-axis

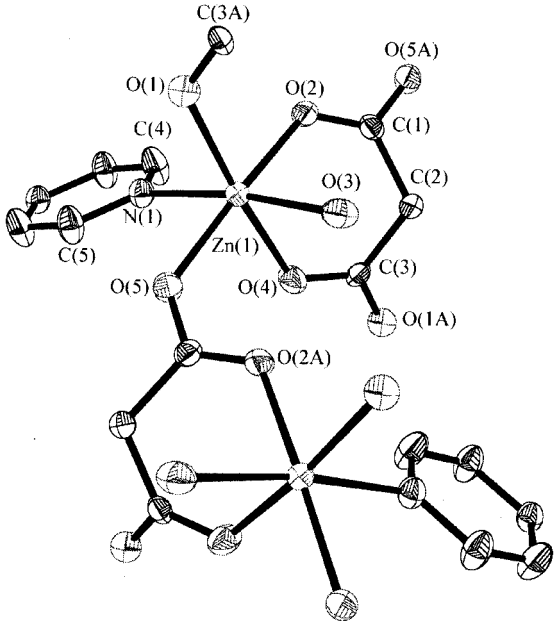

Figure 4. ORTEP diagram of $[Zn_2(OH_2)_2(C_3H_2O_4)_2(C_4H_4N_2)]$ (**2**)

O(5), and N(1) and the deviations of those atoms and the Zn^{II} center from this plane are −0.0045, +0.0046, −0.0049, +0.0047, and −0.1077 Å, respectively, while the axial atoms O(1) and O(4) are −2.1704 and +1.9738 Å away from the corresponding least-squares plane. As in compound **1**, the malonate in complex **2** displays similar coordination modes. As shown in Figure 5, the two-dimensional layer that can be seen is formed in the following way: Zn^{II} ions are first coordinated by malonate ligands to form a chain along the *x*-axis, such chains are then linked by pyrazine units along the *y*-axis to form a wall-like layer. Finally, these layers are

Table 2. Selected bond lengths [Å] and angles [°] in complex of **2**

Zn(1)−O(5)	2.065(2)	Zn(1)−O(2)	2.085(2)
Zn(1)−O(1)	2.075(3)	Zn(1)−O(3)	2.181(3)
Zn(1)−O(4)	2.082(3)	Zn(1)−N(1)	2.251(3)
O(5)−Zn(1)−O(1)	98.68(10)	O(4)−Zn(1)−O(3)	87.33(11)
O(5)−Zn(1)−O(4)	88.80(11)	O(2)−Zn(1)−O(3)	92.20(10)
O(1)−Zn(1)−O(4)	172.06(10)	O(5)−Zn(1)−N(1)	84.91(10)
O(5)−Zn(1)−O(2)	173.69(10)	O(1)−Zn(1)−N(1)	91.00(10)
O(1)−Zn(1)−O(2)	86.90(10)	O(4)−Zn(1)−N(1)	86.99(11)
O(4)−Zn(1)−O(2)	85.50(10)	O(2)−Zn(1)−N(1)	92.08(10)
O(5)−Zn(1)−O(3)	90.23(10)	O(3)−Zn(1)−N(1)	172.60(10)
O(1)−Zn(1)−O(3)	95.26(10)		

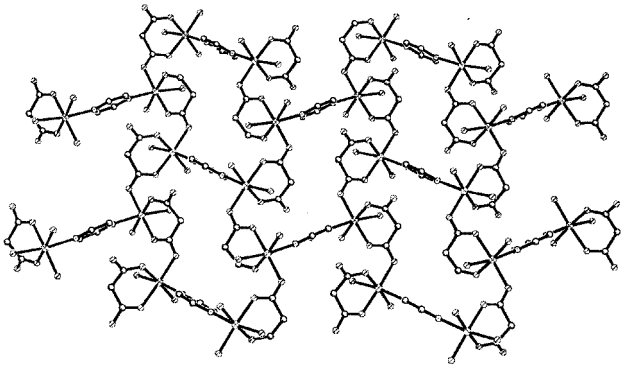

Figure 5. View of the two-dimensional network of **2** in the *ab* plane

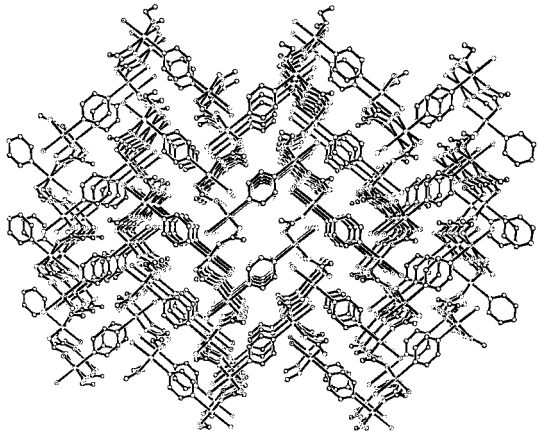

Figure 6. Network structure for complex **2** viewed along the *z*-axis

linked by malonate ligands to form a three-dimensional network possessing polygonal channels (Figure 6).

The magnetic susceptibility of a powder sample of compound **1** was measured using a Quantum Design SQUID magnetometer on the MPMS-7 system with a 10000Qe magnetic field in the temperature range of 5.0−300 K. Its magnetic behavior is highlighted by plots of $\chi_M T$ vs. T and

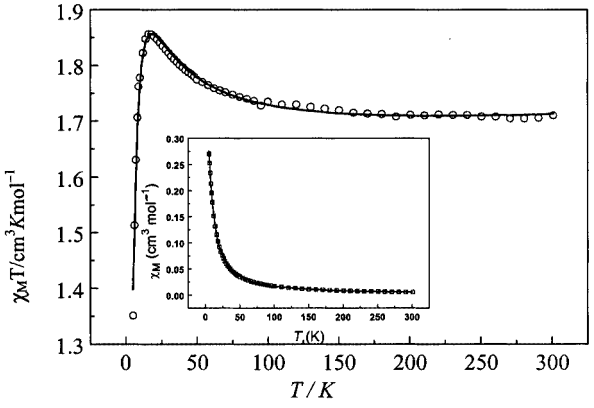

Figure 7. Plots of the experimental temperature dependence of $\chi_M T$ and χ_M for **1**

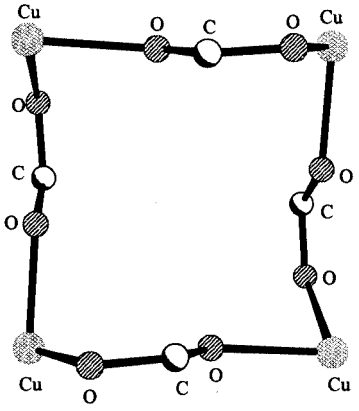

Figure 8. The magnetic exchange path of Cu−O−C(R)−O′−Cu′ in the tetranuclear "Cu_4" mini-square

χ_M vs. T as shown in Figure 7. The temperature dependence of χ^{-1} is in good agreement with the Curie−Weiss law with C = 0.42(1) cm^3·K·mol^{-1} and Θ = 1.51(1) K, indicating that overall, complex **1** displays ferromagnetic behavior. As the temperature decreases, the $\chi_M T$ values increase gradually from 1.71 cm^3·K·mol^{-1} at 300 K, reaching 1.856 cm^3·K·mol^{-1} at 16 K, and then drop rapidly to 1.351 cm^3·K·mol^{-1} at 5 K. On the basis of the geometrical structure, the magnetic exchange involves a Cu−O−C(R)−O′−Cu′ superexchange path through *syn-anti* bridging binary carboxylate groups in the tetranuclear "Cu_4" mini-square (Figure 8) and a Cu−L−Cu (L = pyrazine) interaction between the "Cu_4" clusters. Using the Van Vleck equation results in Equations (1) and (2) for χ_M' and χ_M.

$$\chi_M' = \frac{2Ng^2\beta^2}{kT} \times \frac{e^{2x} + 2e^{4x} + 5e^{6x}}{1 + 3e^{2x} + 7e^{4x} + 5e^{6x}}, \text{ where } x = J/k \quad (1)$$

$$\chi_M = \frac{\chi_M'}{1 - \frac{2zj\chi_M'}{Ng^2\beta^2}} + \text{TIP} \quad (2)$$

J is the exchange constant for Cu−O−C(R)−O′−Cu′. j and z are the exchange constant for Cu−L−Cu and the number of nearest neighbors respectively. TIP is temperature-independent paramagnetism. A good agreement of $R = 8.55\cdot10^{-5}$ [$R = [(\chi_M T)_{obs} - (\chi_M T)_{cal}]^2/(\chi_M T)^2_{obs}$] is obtained with $J = 5.62(3)$ cm^{-1}, $j = -0.284$ cm^{-1} [for $zj = -1.138(8)$cm^{-1}, $z = 4$, $g = 2.092(4)$, $TIP = 0.00015(3)$]. These results indicate that there is ferromagnetic exchange between Cu^{II} through the *syn-anti* [Cu−O−C(R)−O′−Cu′] bridge, and the whole [Cu−O−C(R)−O′−Cu′]$_n$ chain skeleton is non-planar. This is consistent with the results of the magnetic properties of the compounds [Cu$_4$(DZB)$_3$(DZBH)(NO$_3$)-(H$_2$O)]·2H$_2$O[5] and [CuL(H$_2$O)]$_n$[6] reported previously. The exchange interaction between the Cu^{II} centers through pyrazine is more complicated. When the dihedral angle between the pyrazine plane and the coordination plane of Cu^{II} in the reported complex [Cu(NO$_3$)(pyz)]$_x$,[7] is around 50°, the antiferromagnetic exchange interaction parameter j is about -7.4 cm^{-1}. The corresponding dihedral angle in compound **1** is about 65.3°, and the exchange constant $j = -0.2845$, indicating the antiferromagnetic exchange between Cu^{II} through pyrazine is very weak.

It is worthwhile noting that the g value of 2.092(4) mentioned above corresponds well with the results from the EPR measurements at room temperature and at liquid nitrogen temperature ($g = 2.152$ and 2.155, respectively).

In recent years, polymeric unconventional semiconductors have been of much interest.[8] Consequently, we were prompted to investigate the temperature dependence of the electrical conductivity of **1**. Measurements were been carried out using a small pressed disc of the powdered sample on a ZL5-LCR conductometer, giving conductivity values from $2.500\cdot10^{-5}$ S·cm^{-1} to $7.095\cdot10^{-5}$ S·cm^{-1} as the temperature was increased from 298 K to 353 K (Figure 9). These results indicate that complex **1** belongs to the class of semiconductors[9] and this might be mainly due to the interesting structural feature of the copper(II) being linked by aromatic pyrazine and RCOO$^-$ (possessing delocalized π bonding[10]) units.

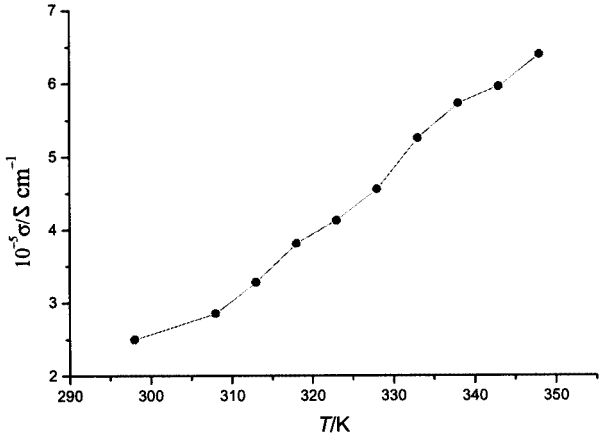

Figure 9. Temperature-dependent electrical conductivity of **1**

Crystalline samples of **1** and **2** were heated from 30 °C to 830 °C. For **1,** TGA showed that the first weight loss, estimated at about 8.15%, occurred between 80 °C and 110 °C which is consistent with the loss of two H$_2$O molecules (calcd. 8.05% for **1)**. The other ligands in **1** (pyrazine and malonate) were lost gradually from 215 °C. In **2**, the loss of two coordinated water molecules and other ligands occurred from 195 °C.

Experimental Section

Syntheses

Preparation of Complex 1: 1) A solution of basic cupric carbonate [CuCO$_3$·Cu(OH)$_2$·xH$_2$O, ca. 0.05 mol] and malonic acid (0.1 mol) in H$_2$O (200 mL) was heated to reflux for 10 minutes and then filtered. The filtrate was concentrated to approximately 10 mL and filtered again. The resultant precipitates from the filtrations were then dried. 2) To a solution of the dry precipitates (0.2 g) in H$_2$O (30 mL), was added, dropwise, a solution of pyrazine (0.08 g, 2 mmol) in EtOH (15 mL). The solution was filtered and then evaporated slowly in air. Blue crystalline blocks were obtained after several hours. Yield 0.29 g. Analysis: found C 26.88, H 2.57, N 6.30, Cu 28.34; calcd. C, 26.85, H 2.70, N 6.26, Cu 28.41%. IR (KBr, cm^{-1}): ν(OH) 3431−3587, ν(−C−H, =C−H) 3053−3132, δ(OH) 1647, ν(COO) 1558~1429, ν(Cu−O, Cu−N) 228−482.

Preparation of Complex 2: 1) A solution of zinc carbonate (0.1 mol) and malonic acid (0.1 mol) in H$_2$O (200 mL) was heated to reflux for 10 minutes and then filtered. The filtrate was concentrated to ca. 10 mL and filtered again. The resultant precipitates were then dried. 2) To a solution of the above dry precipitates (0.2 g) in H$_2$O (30 mL) was added, dropwise, a solution of pyrazine (0.08 g, 2 mmol) in EtOH (15 mL). The solution was filtered and the filtrate was sealed in flask. Colorless rhombohedral crystals were obtained after several days. Yield 0.26 g. Analysis: found C 26.68, H 2.18, N 6.10; Zn, 29.10; calcd. C, 26.63, H 2.23, N 6.21; Zn, 29.00%. IR (KBr, cm^{-1}): ν(OH) 3248, ν(−C−H, =C−H) 3053−3122, δ(OH) 1626, ν(COO) 1574~1417, ν(Zn−O, Zn−N) 239−463.

X-ray Crystallography

Crystal Data for 1: Crystal dimensions 0.26 × 0.10 × 0.06 mm, Cu$_2$C$_{10}$H$_{12}$N$_2$O$_{10}$, $M = 447.30$, tetragonal, space group P-42(1)c, $a = 12.6075(4)$, $c = 9.1944(4)$ Å, $V = 1461.44(9)$ Å^3, $Z = 4$, $D_{calcd.} = 2.033$ g·cm^{-3},μ(Mo-K_α) = 2.969 mm^{-1}, $T = 293(2)$ K. The data were collected on a Siemens SMART CCD diffractometer over the range $2.28 < \theta < 25.04°$. 4349 Reflections were collected of which 1291 were considered to be observed [$I > 2\sigma(I)$]. The structure solution by Patterson methods and full-matrix least-squares refinement were carried out using the SHELXL-97 software package[11] with anisotropic thermal parameters for all skeleton non-hydrogen atoms. All non-hydrogen atoms were refined anisotropically, whilst hydrogen atoms of dissociated water were placed in calculated positions and not refined. It should be pointed out that the U(eq) values for C(1) and C(2) are relatively large and could not be improved with an alternative data set from another crystal. The final agreement factors are R [$I > 2\sigma(I)$] = 0.0279, $R_w = 0.0719$ and GOF = 1.059.

Crystal Data for 2: Crystal dimensions 0.46 × 0.24 × 0.06 mm, Zn$_2$C$_{10}$H$_{12}$N$_2$O$_{10}$. $M = 450.99$, monoclinic, space group $P2_1/n$, $a = 6.9659(5)$, $b = 14.3405(9)$, $c = 7.4477(5)$ Å, β = 92.179(2)°, $V = 743.45(9)$ Å^3, $Z = 2$, $D_{calcd.} = 2.014$ g·cm^{-3}, μ(Mo-K_α) = 3.284

mm^{-1}, $T = 293(2)$ K. Data were collected on a Siemens SMART CCD diffractometer over the range $2.84 < \theta < 25.01°$. 2428 reflections were collected of which 1117 were considered observed [$I > 2\sigma(I)$]. The structure solution by direct methods and the full-matrix least-squares refinement were carried out using the SHELXL-97 software package[11] with anisotropic thermal parameters for all skeleton non-hydrogen atoms. All non-hydrogen atoms were refined anisotropically, whilst hydrogen atoms of coordinated water molecules were placed in calculated positions and not refined. The final agreement factors are R [$I > 2\sigma(I)$] = 0.0350, R_w = 0.0943 and GOF = 1.053.

CCDC-184200 and CCDC-184201 contain the supplementary crystallographic data for this paper. These data can be obtained free of charge at www.ccdc.cam.ac.uk/conts/retrieving.html [or from the Cambridge Crystallographic Data Centre, 12, Union Road, Cambridge CB2 1EZ, UK; Fax: (internat.) + 44-1223/336-033; E-mail: deposit@ccdc.cam.ac.uk].

Acknowledgments

We gratefully acknowledge financial support from the Chinese Academy of Sciences, the National Science Foundation of China (20073048) and the NSF of Fujian (2002F015).

[1] [1a] V. Tangoulis, G. Psomas, C. Dendrinou-Samara, C. P. Raptopoulou, A. Terzis, D. P. Kessissoglou, *Inorg. Chem.* **1996**, *35*, 7655−7660. [1b] J. Y. Lu, M. A. Lawandy, J. Li, T. Yuen, C. L. Lin, *Inorg. Chem.* **1999**, *28*, 2695−2704. [1c] X. Hao, Y. Wei, S. Zhang, *Chem. Commun.* **2000**, 2271−2272. [1d] R.-K. Chiang, C.-C. Huang, C.-S. Wur, *Inorg. Chem.* **2001**, *40*, 3237−3239. [1e] S. Hayami, Z. Gu, Y. Einaga, Y. Kobayasi, Y. Ishikawa, Y. Yamada, A. Fujishima, O. Sato, *Inorg. Chem.* **2001**, *40*, 3240−3242.

[2] [2a] C. Creutz, H. Taube, *J. Am. Chem. Soc.* **1969**, *91*, 3988−3989. [2b] J. Beattie, N. S. Hush, P. R. Taylor, *Inorg. Chem.* **1976**, *15*, 992−993. [2c] T. J. Meyer, M. J. Powers, D. J. Salmon, *J. Am. Chem. Soc.* **1977**, *99*, 1064−1073. [2d] T. J. Meyer, *Acc. Chem. Res.* **1978**, *11*, 94−100. [2e] J. A. Baumann, D. J. Salmon, S. T. Wilson, T. J. Meter, *Inorg. Chem.* **1979**, *18*, 2472−2479. [2f] P. W. Charreck, M. Goldstein, E. M. McPartlin, W. E. Unsworth, *J. Chem. Soc., Dalton Trans.* **1971**, 1632−1637. [2g] M. Inoue, M. Kubo, *Coord. Chem. Rev.* **1976**, *21*, 1−21. [2h] H. W. Richardson, J. R. Wasson, W. E. Hatfield, *Inorg. Chem.* **1977**, *16*, 484−486. [2i] A. B. Blake, W. E. Hatfield, *J. Chem. Soc., Dalton Trans.* **1978**, 861−868. [2j] M. S. Haddad, D. N. Hendrickson, J. P. Cannady, R. S. Drago, D. S. Bieckza, *J. Am. Chem. Soc.* **1979**, *101*, 898−899. [2k] J. Darriet, M. S. Haddad, E. N. Duesler, D. N. Hendrickson, *Inorg. Chem.* **1979**, *18*, 2679−2682.

[3] [3a] J. F. Villa, W. E. Hatfield, *J. Am. Chem. Soc.* **1971**, *93*, 4081−4082. [3b] E. B. Fleischer, D. Jeter, R. Florian, *Inorg. Chem.* **1974**, *13*, 1042−1047. [3c] H. W. Richardson, W. E. Hatfield, *J. Am. Chem. Soc.* **1976**, *98*, 835−839. [3d] M. S. Haddad, D. N. Hendrickson, J. P. Cannady, R. S. Drago, D. S. Bieksza, *J. Am. Chem. Soc.* **1979**, *101*, 899−906. [3e] C. J. O'Connor, C. L. Klein, R. J. Majeste, L. M. Trefonas, *Inorg. Chem.* **1982**, *21*, 64−67. [3f] H. Oschio, U. Nagashima, *Inorg. Chem.* **1990**, *29*, 3321−3325.

[4] J. Li, H. Zeng, J. Chen, Q. Wang, X. Wu, *Chem. Commun.* **1997**, 1213.

[5] E. Colacio, J.-P. Costes, R. Kivekäs, J.-P. Laurent, J. Ruiz, *Inorg. Chem.* **1990**, *29*, 4240−4246.

[6] E. Colacio, J.-M. Dominguez-Vera, J.-P. Costes, R. Kivekäs, J.-P. Laurent, J. Ruiz, M. Sandbery, *Inorg. Chem.* **1992**, *31*, 774−778.

[7] C. Creutz, H. Taube, *J. Am. Chem. Soc.* **1969**, *91*, 3988−3991.

[8] G. C. Papavassiliou, *Prog. Solid State Chem.* **1997**, *25*, 125−270.

[9] R. E. Newnham, in: *Structure-Property Relations*, Springer-Verlag, Berlin/Heidelberg/New York, **1975**.

[10] [10a] C. M. Che, M.-C. Tse, M. C. W. Chan, K.-K. Cheung, D. L. Philips, K.-H. Leung, *J. Am. Chem. Soc.* **2000**, *122*, 2464−2468. [10b] M. Munakata, L. P. Wu, T. Kuroda-Sowa, *Adv. Inorg. Chem.* **1998**, *46*, 172−173. [10c] V. W. W. Yam, K. K. W. Lo, N. K.-M. Fung, C. R. Wang, *Coord. Chem. Rev.* **1998**, *171*, 3−16.

[11] G. M. Sheldrick, Universität Göttingen, Germany, **1997**.

Received July 23, 2002
[I02411]

Solid-State Adducts between C_{60} and Decamethylferrocene

Aldo Arrais,[a] Eliano Diana,[a] Roberto Gobetto,[a] Marco Milanesio,[b] Davide Viterbo,[b] and Pier Luigi Stanghellini*[b]

Keywords: Donor-acceptor systems / Fullerenes / Infrared spectroscopy / Raman spectroscopy / Sandwich complexes

Co-deposition from concentrated solutions of C_{60} and $Fe[C_5(CH_3)_5]_2$ affords two solid products in different yields. The major product **1**, in the form of regular shaped crystals, has been investigated by X-ray diffraction, ^{13}C CPMAS NMR and vibrational spectroscopy, which showed it to be a co-crystalline adduct of C_{60} and $Fe[C_5(CH_3)_5]_2$ with no significant electron charge transfer between the two building blocks. The minor product **2**, in the form of an amorphous powder, has been investigated by vibrational techniques. Both IR and Raman spectra are consistent with a solid structure in which electron transfer between the two units appears to be possible.
((© Wiley-VCH Verlag GmbH & Co. KGaA, 69451 Weinheim, Germany, 2003)

Introduction

Interesting chemical and physical properties indicate fullerene C_{60} to be a useful building block for the preparation of new materials with particular electronic and magnetic properties.[1−4] C_{60} behaves as a mild electron acceptor, capable of incorporating up to six electrons in the cage[5−8] and of forming salts with several inorganic and organic cations.[9] The most fascinating example of these species are the alkali metal salts M_nC_{60}, which show superconductivity properties at quite high temperatures.[10−11]

On the other hand, C_{60} can form molecular adducts with several organic and organometallic electron donors D,[12−22] giving rise to molecular charge-transfer (CT) complexes $D_n(C_{60})$. Presumably, there is no neat distinction between ionic complexes and CT molecular complexes, in that the formally neutral systems probably imply some electron transfer from the donors to C_{60} through π-stacking interactions, particularly favourable when the donor exhibits a largely delocalised π-structure. It might be expected that even a fractional electron transfer should change the spectroscopic (vibrational and magnetic) properties of both the donor and the C_{60} acceptor. Spectroscopic data on C_{60} and its anions are available in the literature, and while they usually indicate that the effect of the charge on the cage is not very evident, careful study can allow their extents to be estimated.[23−27] A clear example is given by the ionic salt $[TDAE]^+[C_{60}]^-$ [TDAE = tetrakis(dimethylamino)ethylene]: the transfer of one electron from TDAE to C_{60} has been associated with subtle modification of the Raman spectrum of C_{60} itself.[28] A parallel opportunity is offered by changes in the spectroscopic properties of the donor molecule as a consequence of electron transfer.[29]

On the basis of our knowledge of the metallocene complexes and their cations, primarily ferrocene (Fc) and decamethylferrocene (*Fc),[30,31] we performed the reaction between C_{60} and *Fc, and the products have been characterised by vibrational and NMR spectroscopy and, when possible, by X-ray diffraction methods. The results, also in comparison with the spectroscopic data concerning the well-known $C_{60}(Fc)_2$,[14] form the object of this paper.

Results and Discussion

Adduct 1

Description of the Structure

The main features of the crystal structure of the adduct **1** are illustrated in Figures 1 and 2. The C_{60} molecule sits with the centre of the "ball" on a crystallographic inversion centre. There are two different types of *Fc molecules: one (molecule A with Fe1 atom) in a general position and one (molecule B with Fe2 atom) with the iron atom sitting on a crystallographic inversion centre. Both rings of molecule A (Figure 1) face two pentagons of the fullerene, in an almost staggered way, and without relevant side shift. On the other hand, molecules B form unconnected layers between the layers of $C_{60}[*Fc_2(A)]$ complexes (Figure 2). In these last layers, each fullerene molecule is surrounded by four

[a] Dipartimento di Chimica I.F.M., Università di Torino, via P. Giuria 7, 10125 Torino, Italy
[b] Dipartimento di Scienze e Tecnologie avanzate, Università del Piemonte Orientale "A. Avogadro", corso T. Borsalino 54, 15100 Alessandria, Italy
Fax: (internat.) + 39-0131/287416
E-mail: pierluigi.stanghellini@mfn.unipmn.it
Supporting information for this article is available on the WWW under http://www.eurjic.org or from the author.

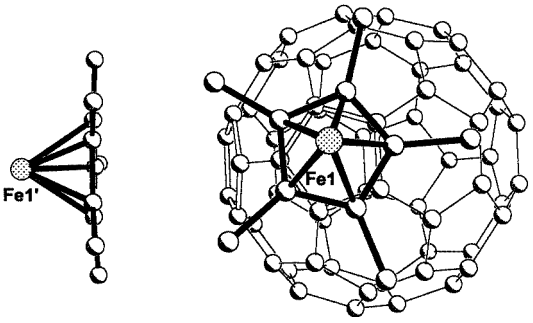

Figure 1. The two different staggered facings of the two *Cp moieties linked to Fe1 and Fe1′ (molecule A) with the five-membered rings of fullerene

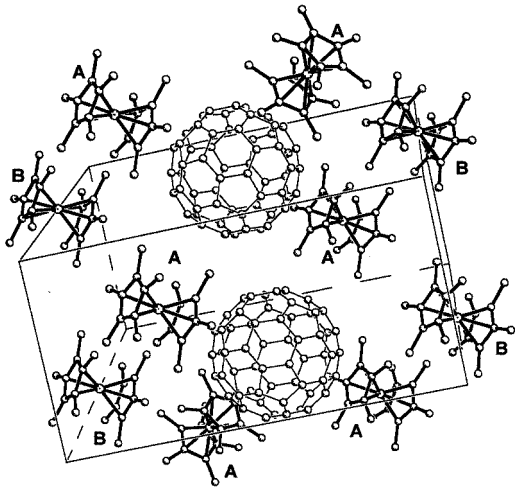

Figure 2. Crystal packing of adduct **1**, showing both the interacting (A) and the non-interacting (B) *Fc molecules in the unit cell

*Fc(A) molecules. The facing of the two rings of molecule A is rather different: one is almost parallel to the pentagon of the C_{60} ring [dihedral angle 4.7(8)°], with a centre-to-centre distance of 3.26(1) Å, while the other is tilted by 14.0(8)°, with a centre-to-centre distance of 3.35(1) Å. The values of the centre-to-centre distances are typical of π interactions between aromatic molecules and are in keeping with the interplane distance of 3.35 Å in graphite. The facing is stabilised by a number of weak C−H···π interactions between methyl hydrogen atoms and fullerene six-membered rings. The shortest distances are found for hydrogen atoms linked to C17 [distance from H to the centre of the ring: 2.94(3) Å] and to C18 [distance from H to the centre of the ring: 2.80(3) Å], belonging to the cyclopentadienyl ring most tilted with respect to the fullerene pentagon. This may suggest that the tilting allows better anchoring of the ring to C_{60}, hindering its free rotation as a sort of a wedge. All other "H-to-ring" distances are greater than 3.0 Å.

The geometry of the fullerene molecule shows the usual bimodal distribution of the C−C distances: the average hexagon−hexagon bond is 1.39(1) Å, while the average hexagon−pentagon bond is 1.45(1) Å. The distances between the centre of the ball and the 30 independent carbon atoms vary from 3.53(1) to 3.56(1) Å. An analysis of the distances between the centre of the ball and the 30 independent carbon atoms does not indicate any systematic deformation, such as is found in the ionic structure of decamethylnickelocenium fulleride.[22]

The crystal structure of **1** is quite different from that of the $C_{60}Fc_2$ adduct,[14] in which only one ring of the single ferrocene molecule faces (with a sideways slipping of 0.8 Å) a fullerene pentagon in an almost eclipsed way.

In order to carry out a more accurate comparison of the *Fc molecules in **1** with the same molecule alone, we also redetermined the crystal structure of *Fc, at 150 K. However, the resulting resolved structure did not substantially differ from that reported by Freyberg et al.,[32] which was carried out at room temperature. The molecule has a C_{2h} crystallographic site symmetry with the iron atom sitting on an inversion centre, and so the two cyclopentadienyl rings must be exactly staggered. The three independent Fe−C, C−C, and C−CH_3 distances and the C−C−C angles differ by less than 3σ and their average values are reported in Table 1. With respect to the plane through the five-membered rings, the methyl carbon atoms are slightly (about 0.06 Å) displaced in the direction away from the central Fe atom. In all the methyl groups, two hydrogen atoms point towards the Fe and are relatively close to the cyclopentadienyl plane, while the third H sticks out of the plane away from the Fe. This pattern was also found in a series of $Fe(Me_4RCp)_2$ derivatives.[33,34]

The two different *Fc molecules in compound **1** are somewhat less regular than in *Fc alone; nevertheless, average values of selected distances and angles are very similar in the two structures. Table 1 summarises the most significant distance and angle values for A and B in **1**, in comparison with those in *Fc. The disposition of the methyl groups

Table 1. Main geometrical parameters of the *Fc moiety from the crystal structure of adduct **1**, in comparison with *Fc alone

	Adduct **1** − molecule A			Adduct **1** − molecule B			*Fc
Distance [Å]	Minimum	Maximum	Average	Minimum	Maximum	Average	Average
Fe−C	2.038(6)	2.068(6)	2.053(6)	2.035(7)	2.063(7)	2.047(7)	2.053(2)
C−C	1.417(9)	1.437(9)	1.428(9)	1.397(10)	1.440(10)	1.416(10)	1.430(3)
C−CH_3	1.489(9)	1.519(9)	1.508(9)	1.477(10)	1.529(10)	1.509(11)	1.500(3)
Angle [°]							
C−C−C	107.3(6)	109.0(6)	108.0(6)	105.5(7)	109.2(7)	108.0(7)	108.0(2)

is similar to that found in *Fc alone, and their deviations from the cyclopentadienyl plane are also of the same order of magnitude and in the same direction.

Solid-State ^{13}C NMR

The ^{13}C CPMAS spectrum of **1** shows the presence of five resonances, at δ = 142.1, 79.9, 79.3, 78.8, and 10.8 ppm. The low-field resonance falls in the range typical of the C_{60} peak. The fact that all 60 carbon atoms are equivalent indicates that rapid isotropic motion of C_{60} on the NMR timescale is occurring in the solid at room temperature.[35−36] This result is apparently in conflict with the X-ray data, which allow complete refinement of the fullerene structure, but one should consider the different measurement temperatures and the different timescales involved in X-ray and NMR analyses.[37] Unfortunately, further attempts to observe the static ^{13}C CPMAS spectrum at low temperature were precluded by the low signal/noise ratio, probably due to the increasing of relaxation times with decreasing temperature.

The three resonances in the range δ = 70−80 ppm can readily be assigned to the cyclopentadienyl carbon atoms. Bearing in mind that inequivalences in the solid state can arise from the crystal packing, these data are in full agreement with the solid-state structure, which shows the presence of three different environments for the *Cp rings. The single resonance found for each *Cp ligand in the ^{13}C CPMAS spectrum is an indication that the rings are in a fast rearrangement process in the solid state. As previously shown in the case of *Fc,[38] the dynamic process corresponds to a rotation of the *Cp rings in the planes perpendicular to their C_5 coordination axes. Finally, the resonance at higher field appears as a broad signal due to partial overlapping of the slightly different methyl ligands.

Vibrational Spectra

The infrared and Raman features of adduct **1** are nearly coincident with those of the two separated components, as Figures 3 and 4 clearly show. Table 2 reports the frequency values and the assignments. In particular, neither the different crystallographic position of the *Fc molecules, nor the different orientations of the *Cp rings strongly affect the vibrational behaviour.

Adduct 2

The adduct **2** was always obtained only in trace amounts, as a faint light brown powder accompanying the crystals of adduct **1**. Any attempt to recrystallise the powder failed: the result was the recovery of the starting components. The only reliable experimental data that we were able to obtain are the infrared and Raman spectra in the solid state. Although the vibrational patterns of *Fc and C_{60} would not be expected to change greatly as a consequence of electron transfer,[39] a careful examination finds significant differences. First of all, the ν(CH) pattern is significantly shifted towards higher frequency by ca. 6−8 cm^{-1} and it is surprisingly similar to that of the adduct [*Fc][TCNE] (TCNE = tetracyanoethylene), for which an ionic structure is proposed.[40] In a recent study on the spectra of permethylated metallocene complexes we proposed the shift of the ν(CH) modes as a measure of the positive charge on the metallocene unit.[31] In order to allow a quantitative estimate of this effect, we compared the frequency of the most intense Raman band in this region, which ranges from 2894 and 2895 cm^{-1} for *Fc and adduct **1** to 2904 cm^{-1} for adduct **2**, to 2919 cm^{-1} for the TCNE adduct, and up to 2926 cm^{-1} for the PF_6^- salt. The same trend is shown by the $\delta(CH_3)$ symmetric mode, the frequency of which (1384 cm^{-1}) is close to those in $[*Fc]^+[TCNE]^-$ (1386 cm^{-1}) and $[*Fc]^+[PF_6]^-$ (av. 1385 cm^{-1}) and significantly different from those of *Fc (av. 1375 cm^{-1}) and adduct **1** (av. 1372 cm^{-1}).

Even more interesting is the Raman pattern between 1600 and 1350 cm^{-1}. This includes some $\delta(CH_3)$ and ν(CC)

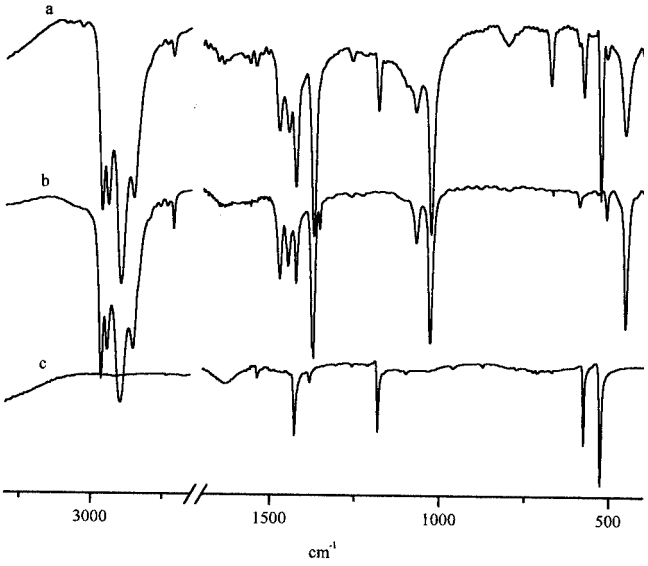

Figure 3. Infrared spectra (KBr disk) of (a) adduct **1**, (b) *Fc, (c) C_{60}

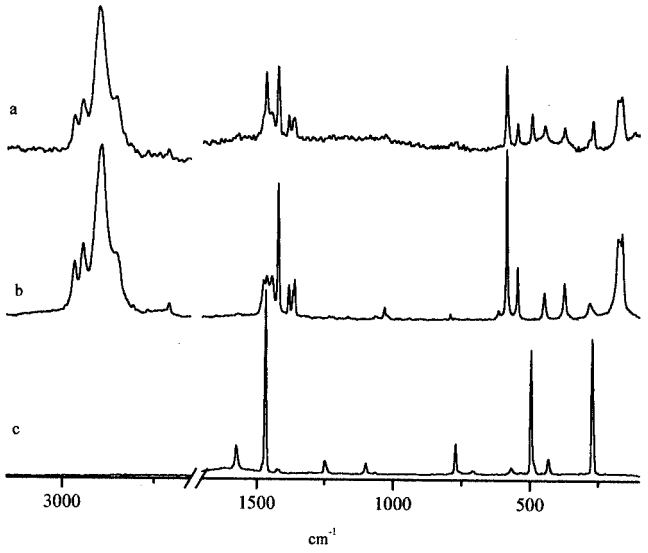

Figure 4. Raman spectra (crystals) of (a) adduct **1**, (b) *Fc, (c) C_{60}

Table 2. Infrared and Raman frequencies [cm^{-1}] and assignment of the vibrational modes of adduct **1**

Infrared	Raman	Assignments
2963 m	2967 w	$\nu_{as}(C-H)$
2942 m	2944 m	$\nu_{as}(C-H)$
2895 s, br	2898 s	$\nu_{s}(C-H)$
2852 m	2852 m, sh	$2\delta(CH_3)$
2713 w	2710 vw	$2\delta(CH_3)$
	1573 m	C_{60} (H_g)
1477 w	ca. 1476 w, br.	$\delta_{as}(CH_3)$
	1466 m	C_{60} (A_{1g})
1449 w	ca. 1445 w	$\delta_{as}(CH_3)$
1427 m		C_{60} (T_{1u})
	1423 m	$\delta_{as}(CH_3)/\nu(C=C)$
	1385 m	$\delta_{s}(CH_3)/\nu(C=C)$
ca. 1375 m, sh		$\delta_{s}(CH_3)$
1371 s	ca. 1370 w, sh	$\delta_{s}(CH_3)$
	1364 m	δ_{s} (CH_3)
1182 m		C_{60} (T_{1u})
1072 w		$\nu(C-CH_3)$
1027 s	1032 w	$\rho(CH_3)$
	772 w	C_{60} (T_{1g})
674 w		
	587 s	Cp ring breathing
577 m		C_{60} (T_{1u})
	547 m	asym. tilt(Cp−Fe−Cp)
528 s		C_{60} (T_{1u})
	495 m	C_{60} (A_{1g})
453 m, br	450 w	ν_{as}(Cp−Fe)
	431 w	C_{60} (H_g)
381 vw	375 w	sym. tilt(Cp−Fe−Cp)
	ca. 284 w	
	272 m	C_{60} (H_g)
	179 s	ν_{s}(Cp−Fe)
	165 s	ν_{s}(Cp−Fe)

modes of *Fc and the highest frequency modes − $H_g(8)$, $H_g(7)$, and $A_g(2)$ − of C_{60}. In Figure 5 the Raman spectrum of adduct **2** is compared with those of *Fc and C_{60}: the difference in the frequency and in the shape of the bands is clearly evident. More informative data can be obtained by a deconvolution of the spectral pattern between 1550 and 1350 cm^{-1}. Figure 6 shows the experimentally measured spectrum and the fitted curve obtained as a sum of five mixed Lorentzian/Gaussian curves centred at 1475, 1451, 1423, 1384, and 1367 cm^{-1}. The good quality of the matching between the experimentally measured and the fitted curve is shown by the value of the correlation coefficient (0.99857). The band at 1451 cm^{-1} is attributable to the $A_g(2)$ mode of C_{60} (the others are *Fc modes). The $H_g(8)$ mode appears at 1562 cm^{-1}.[41] These modes show significant low-energy shifts of 12 and 16 cm^{-1} for H_g and A_g, respectively. Other C_{60} modes show similar shifts: such as A_g, from 495 to 486 cm^{-1}, and H_g, from 271 to 249 cm^{-1}. In addition, the bands of adduct **2** are clearly broadened with respect to those of C_{60} [e.g., the full width at half maximum (fwhm) of the $A_g(2)$ mode is ca. 22 cm^{-1} for adduct **2** and ca. 6 cm^{-1} for C_{60} alone]. Both effects have been already reported for the compound C_{60}/TDAE and ascribed to electron-transfer from TDAE to C_{60}.[28] All the vibrational data and assignments are listed in Table 3.

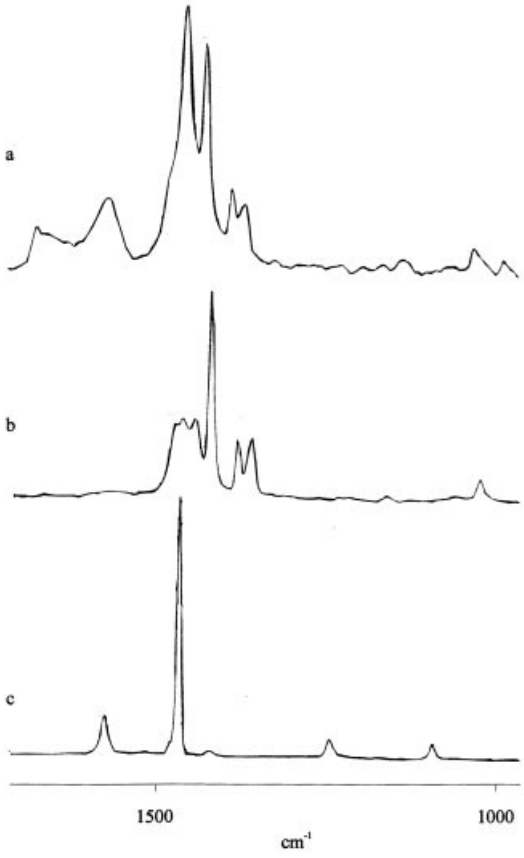

Figure 5. Raman spectra (crystals) in the 1600−1000 cm^{-1} range for (a) adduct **2**, (b) *Fc, (c) C_{60}

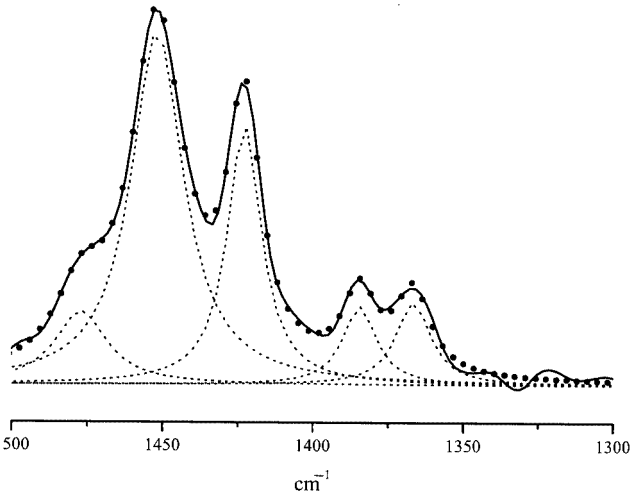

Figure 6. Deconvolution of the Raman band pattern in the 1500−1300 cm^{-1} range for the adduct **2**; the solid line is the experimentally measured spectrum; the small dashed lines are the individual fitted curves and the dots indicate the resultant fitted curve

A Comparison with Fc_2C_{60} Adduct

The molecular structure of this adduct was described almost ten years ago.[14] The crystal packing of the Fc molecules is simpler than that shown in adduct **1**. Only one Fc molecule in a general crystallographic position is present

Table 3. Infrared and Raman frequencies [cm^{-1}] and assignment of the vibrational modes of adduct **2**

Infrared	Raman	Assignments
2960 m	2966 m	$\nu_{as}(C-H)$
	2945 w, sh	$\nu_{as}(C-H)$
2902 m, br.	2904 vs	$\nu_{s}(C-H)$
2854 w	2851 w, sh	$2\delta(CH_3)$
	1562 m, br.	C_{60} (H_g)
	ca. 1475 m, sh	$\nu(C=C)$
	1451 s	C_{60} (A_{1g})
1428 s		C_{60} (T_{1u})
	1423 m	$\delta_{as}(CH_3)/\nu(C=C)$
1383 s	1384 w	$\delta_{as}(CH_3)/\nu(C=C)$
	1367 w	$\delta_{s}(CH_3)/\nu(C=C)$
1182 m		C_{60} (T_{1u})
1027 m	1034 w, br.	$\rho(CH_3)$
	991 w	
	858 w, br.	C_{60} (T_{1g})
	708 w	
674 w		
	586 s	Cp ring breathing
576 m		C_{60} (T_{1u})
	546 m	asym. tilt(Cp−Fe−Cp)
526 vs		C_{60} (T_{1u})
	486 m, br.	C_{60} (A_{1g})
454 m, br.	447 w	$\nu_{as}(Cp-Fe)$
	374 m	symm. tilt(Cp−Fe−Cp)
	ca. 282 w, br.	
	229 w	
	177 s, sh	$\nu_{s}(Cp-Fe)$
	164 s	$\nu_{s}(Cp-Fe)$

and only one Cp ring faces one of the C_{60} pentagons. We explored its spectroscopic features further.

The ^{13}C CPMAS spectrum is consistent with the crystal structure. Two peaks of equal intensity at $\delta = 71.09$ and 72.20 ppm are attributable to the cyclopentadienyl carbon atoms. The splitting of the expected unique peak is consistent with the different environments of the two rings, due to the proximity of one ring to the C_{60} cage. A resonance at $\delta = 144.43$ ppm is attributable to the C_{60} carbon atoms. The narrowness of the peak and the absence of spinning side bands confirm the high mobility of the fullerene molecule at room temperature.

At very first sight, the infrared and Raman spectra appear as a simple superpositions of the spectra of the single components, but careful inspection reveals that some spectral features differ significantly, in that the bands show small frequency shifts or changes in their relative intensities. This is particularly evident in the 3200−3000 cm^{-1}, 900−800 cm^{-1}, and 500−300 cm^{-1} regions, which are typical of the ν(CH), γ(CH), and Fe−ring stretching modes. Not surprisingly, they belong to the vibrations that, more than the others, are involved in possible interactions between the Cp rings and fullerene. See, for instance, Figure 7, which shows the spectra of Fc and Fc_2C_{60} in the low-wavenumber region. The intensity and the frequency of the infrared and Raman features corresponding to the skeletal motion of the Fc unit in the Fc_2C_{60} adduct are significantly different from those of Fc alone, presumably reflecting the

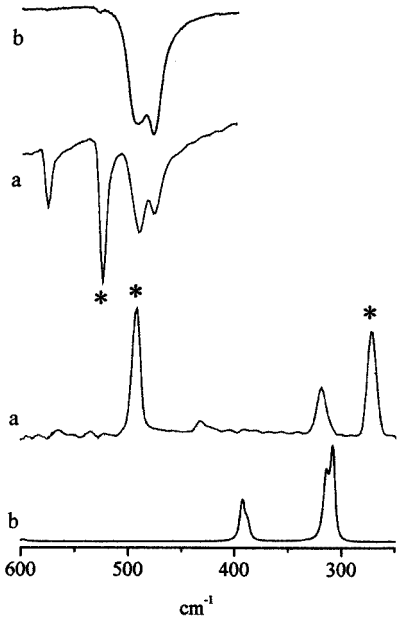

Figure 7. Infrared (top curves, KBr disk) and Raman (bottom curves, crystals) spectra of Fc_2C_{60} adduct (a) and Fc (b); the bands marked with * correspond to C_{60} modes

interaction of one Cp ring with C_{60}. On the other hand, the bands of the C_{60} component also show small but significant changes with respect to those of the free C_{60}. Thus, the Raman feature at 493 cm^{-1}, the totally symmetric A_g breathing mode of the cage,[42,43] which can be expected to interact with the sym. Cp−Fe−Cp stretching, is clearly shifted (2.5 cm^{-1}). In addition, the band at 1464 cm^{-1}, regarded as a measure of electron transfer from the donor metallocene to C_{60}, shows a small (4 cm^{-1}) low-energy shift. Other figures (Figures S1 and S2), illustrating selected regions of the spectra, and a table (Table S1), listing the frequency data and assignment, are included as Supporting Information (see also footnote on the first page of this article).

Conclusion

The formation of co-crystals of organic and organometallic species with fullerene molecules is governed both by structural and by electronic aspects: a curved surface of co-blocks[44] allows a better fit in the formation of a solid-state complex structure, and the interaction of the electron acceptor C_{60} with good electron-donating systems is thermodynamically favoured. Nevertheless, the fullerene species exhibit behaviour determined by the aromatic character of its bonds and, like planar aromatic molecules, are able to enter into intermolecular interactions through the π electron density, without net electron transfer between the C_{60} and a donor molecule. For example, the C_{60} benzene solvate[45] can be viewed as a co-crystal between C_{60} and C_6H_6. The benzene rings are parallel to the surface of the C_{60} and lie over the (6,6) bond, where the electron density is most localized. Similarly, the facing of the pentagonal ring of C_{60} with the five-carbon ring of the permethylated

ferrocene may suggest an interaction between the HOMO of the *Fc and the LUMO of C_{60}.

While **1** is undoubtedly a molecular adduct, the vibrational data suggest that the minor product **2** has an ionic structure, similar to those of Cp^*_2Mn/C_{60}, Cp^*_2Ni/C_{60}, and bis(toluene)$_2$Cr/C_{60}.[46] In the absence of any other experimental support, we are confident that the vibrational behaviour is a strong indicator of the charge transfer between the donor and the acceptor molecules, as it has been demonstrated for C_{60}[28] and *Fc[31], separately linked to other species. In this light, the spectra also suggest a small degree of electron transfer from Fc to C_{60} in the Fc_2C_{60} molecular adduct.

Experimental Section

Reactants and Solvents: All manipulations were performed by standard Schlenk techniques under an inert gas. C_{60} was purchased from Hoechst and used without further purification. *Fc (Aldrich) was purified by sublimation. The solvents were distilled from sodium (benzene and toluene) or P_4O_{10} (1,2-dichlorobenzene) and then stored under argon.

Synthesis of Adducts of *Fc and C_{60}: The preparation of intermolecular adducts of C_{60} is influenced by the starting material's low solubility. Solvents able to dissolve both *Fc and C_{60} significantly are benzene, toluene, and 1,2-dichlorobenzene. Any attempted co-crystallisation in these solvents by changing the stoichiometric ratio between *Fc and C_{60} always gave the same results: well-shaped, black crystals of adduct **1**, mixed with a small amount of light brown powder identified as the adduct **2**. In a typical preparation, C_{60} (50 mg, 0.069 mmol) was dissolved in benzene (35 mL) in a Schlenk tube and mixed with *Fc (45 mg, 0.14 mmol), previously dissolved in a few drops of benzene. The solution was slowly concentrated under an inert gas in a dry-box. After concentration, a thin layer of light brown dust mixed with black, lustrous crystals had deposited on the wall of the tube. The excess of deposited *Fc was removed by sublimation. The two compounds were mechanically separated from the solid mixture. Shiny black crystals of adduct **1** suitable for X-ray analysis were obtained by recrystallization of a 1,2-dichlorobenzene solution of the crude product at −30 °C.

X-ray Crystal Structure Analyses: Crystallographic data and details of data collection and refinement for adduct **1** and *Fc[47] are given in Table 4. Both sets of data collection were carried out with a four-circle automatic diffractometer at 150 K. Structure solutions were obtained by direct methods and refinements by full-matrix, least squares on F^2 (non-H atoms with anisotropic displacement parameters, H atoms geometrically positioned and treated as riding atoms). The computer programs used were: XSCANS[48] for data collection, SIR92[49] for structure solution, SHELXL-97[50] for structure refinement and MOLDRAW[51] and XP[52] for graphic analysis.

NMR Spectra: The ^{13}C CPMAS spectrum was acquired with a Jeol GSE-270 spectrometer operating at 67.8 MHz. The MAS rotor was spun with air at ca. 5.2 kHz, the contact time was 3.5 ms and the recycle delay 10 s. The Hartmann−Hann condition was optimised with hexamethylbenzene. ^{13}C chemical shifts are given in ppm from external tetramethylsilane reference.

Infrared Spectra: The infrared spectra were collected with a Bruker Equinox 55 FT-IR spectrophotometer, with a resolution of 2 cm^{-1} and an average 64 scans.

Table 4. Crystal data and structure refinement parameters for adduct **1** and *Fc

Compound	Adduct **1**	*Fc
Empirical formula	$(C_{120}H_{90}Fe_3)/2$	$C_{20}H_{30}Fe$
Formula mass	849.74	326.29
Crystal system	monoclinic	orthorhombic
Space group	$P2_1/c$	$Cmca$
a [Å]	10.287(11)	15.113(4)
b [Å]	20.199(14)	11.592(3)
c [Å]	19.932(17)	9.958(3)
β [°]	100.29(4)	90
V [Å^3]	4075(6)	1744.5(8)
Z	4	4
F(000)	1776	704
Density (calcd.) [g cm^{-3}]	1.385	1.242
Temperature [K]	150(2)	
Diffractometer	Siemens P4	
Radiation (graph-monochr.) [Å]	0.71073	
Absorption coefficient [mm^{-1}]	0.584	0.857
Crystal size [mm]	0.20×0.23×0.48	0.22×0.44×0.46
Colour	black	orange
Shape	prism	prism
Scan method	ω	
Scan speed [°/min]	variable: 3.0−20.0	
Scan range [°]	0.90	1.40
θ range [°]	1.5−25.0	1.5−35.0
Index ranges	$-6 \le h \le 12$, $-6 \le k \le 24$, $-4 \le l \le 23$	$0 \le h \le 24$, $0 \le k \le 18$, $-16 \le l \le 0$
Reflections collected	5869	1995
Independent reflections	5750	1981
Absorption correction	n/a	n/a
Refinement method	Full-matrix, least-squares on $\|F_o\|^2$	
Observed reflections	3086 [$I > 2\sigma(I)$]	1354 [$I > 2\sigma(I)$]
Data/restraints/parameters	5750/0/556	1981/0/62
Goodness of fit on $\|F_o\|^2$	1.088	1.040
R indices [$I > 2\sigma(I)$]	$R1 = 0.0621$, $wR2 = 0.1194$	$R1 = 0.0470$, $wR2 = 0.1006$
R indices (all data)	$R1 = 0.1543$, $wR2 = 0.1647$	$R1 = 0.0841$, $wR2 = 0.1159$
Largest diff. peak and hole [e·Å^{-3}]	0.439, −0.436	0.590, −0.715
Weight (calculated)	$w = 1/[\sigma^2(\|F_0\|^2) + (gP)^2 + qP]$, $P = (\|F_0\|^2 + 2\|F_c\|^2)/3$	
	$g = 0.054$, $q = 3.352$	$g = 0.049$, $q = 1.030$

Raman Spectra: The Raman spectra were collected with a Bruker RFS 100 FT Raman spectrophotometer, by use of NIR laser radiation at 1064 nm and a Ge diode (laser power 100 mW, res. 4 cm^{-1}). To minimize decomposition of the sample, the complexes were sealed in capillary glass tubes under nitrogen. Adduct **2**, which shows a significant fluorescence background, required low laser power (30 mW) and an average of 2000 scans, obtained by a sequence of several scan-packets (50−100 scans each) to give a good spectrum.

Acknowledgments

Financial support from the MIUR (COFIN 2000 to E. D., R. G. and P. L. S.) is gratefully acknowledged.

[1] P. W. Stephens, D. Cox, J. W. Lauher, L. Mihaly, J. B. Wiley, P. M. Allemand, A. Hirsch, K. Holczer, Q. Li, J. D. Thompson, F. Wudl, *Nature* **1992**, *355*, 331.
[2] W. J. Blau, J. H. Byrne, D. J. Cardin, T. J. Dennis, J. P. Hare, H. W. Kroto, R. Taylor, D. R. M. Walton, *Phys. Rev. Lett.* **1991**, *67*, 1423.
[3] R. Taylor, D. R. M. Walton, *Nature* **1993**, *363*, 685.
[4] D. M. Guldi, *Chem. Commun.* **2000**, 321.
[5] Q. Xie, E. Pérez-Cordero, L. Echegoyen, *J. Am. Chem. Soc.* **1992**, *114*, 3978.
[6] Y. Ohsawa, T. Saji, *J. Chem. Soc., Chem. Commun.* **1992**, 781.
[7] I. Noviandri, R. D. Bolskar, P. A. Lay, C. A. Reed, *J. Phys. Chem. B* **1997**, *101*, 6350.
[8] L. Echegoyen, L. E. Echegoyen, *Acc. Chem. Res.* **1998**, *31*, 593.
[9] C. A. Reed, R. D. Bolskar, *Chem. Rev.* **2000**, *100*, 1075.
[10] A. F. Hebard, M. J. Rosseinsky, R. C. Haddon, D. W. Murphy, S. H. Glarum, T. T. M. Palstra, A. P. Ramirez, A. R. Kortan, *Nature* **1991**, *350*, 600.
[11] D. W. Murphy, M. J. Rosseinsky, R. M. Fleming, R. Tycko, A. P. Ramirez, R. C. Haddon, T. Siegrist, G. Dabbagh, J. C. Tully, R. E. Walstedt,, *J. Phis. Chem. Solids* **1992**, *53*, 1321.
[12] *Anthracene:* J. A. Schlueter, J. M. Seaman, S. Taha, H. Cohen, K. R. Lykke, H. H. Wang, J. M. Williams, *J. Chem. Soc., Chem. Commun.* **1993**, 972.
[13] *$Fe_4(CO)_4(\eta^5\text{-}C_5H_5)_4$:* J. D. Crane, P. B. Hitchcock, *J. Chem. Soc., Dalton Trans.* **1993**, 2537.
[14] *Ferrocene:* J. D. Crane, P. B. Hitchcock, H. W. Kroto, R. Taylor, D. R. M. Walton, *J. Chem. Soc., Chem. Commun.* **1992**, 1764.
[15] *N,N-Diethylaniline:* Y. Wang, *J. Phys. Chem.* **1992**, *96*, 764.
[16] *1,4-Diazabicyclooctane:* K. I. Priyadarsini, H. Mohan, A. K. Tyagi, J. P. Mittal, *Chem. Phys. Lett.* **1994**, *230*, 317.
[17] *Hexamethylenetetratellurafulvalene:* T. Pradeep, K. K. Singh, A. P. B. Sinha, D. E. Morris, *J. Chem. Soc., Chem. Commun.* **1992**, 1747.
[18] *Bis(ethylenedithio)tetrathiafulvalene:* A. Izuoka, T. Tachikawa, T. Sugawara, Y. Suzuki, M. Konno, Y. Saito, H. Shinohara, *Chem. Commun.* **1992**, 1472.
[19] *Triethylamine:* Y. A. Sun, B. Ma, G. E. Lawson, *Chem. Phys. Lett.* **1995**, *233*, 57.
[20] *P_4:* R. E. Douthwaite, M. L. H. Green, S. J. Heyes, M. J. Rosseinsky, J. F. C. Turner, *J. Chem. Soc., Chem. Commun.* **1994**, 1367.
[21] *Hydroquinone:* O. Ermer, *Helv. Chim. Acta* **1991**, *74*, 1339.
[22] *-$C_5(CH_3)_5]_2Ni$:* W. C. Wan, (X. Liu, G. M. Sweeney, W. E. Broderick, *J. Am. Chem. Soc.* **1995**, *117*, 9580.
[23] G. A. Heath, J. E. Mc Grady, R. L. Martin, *J. Chem. Soc., Chem. Commun.* **1992**, 1272.
[24] J. Stinchcombe, A. Pénicaud, P. Bhyrappa, P. W. D. Boyd, C. A. Reed, *J. Am. Chem. Soc.* **1993**, *115*, 5212.
[25] M. L. Mc Glashen, M. E. Blackwood Jr., T. G. Spiro, *J. Am. Chem. Soc.* **1993**, *115*, 2074.
[26] Y. Zhang, Y. Du, J. R. Shapeley, M. J. Weaver, *Chem. Phys. Lett.* **1993**, *205*, 6; Y. Zhang, Y. Du, J. R. Shapeley, M. J. Weaver, *Chem. Phys. Lett.* **1993**, *205*, 6, 508.
[27] J. Fulana, M. Jakobi, J. P. Maier, *Chem. Phys. Lett.* **1993**, *21*, 43; J. Fulana, M. Jakobi, J. P. Maier, *Chem. Phys. Lett.* **1993**, *21*, 43, 227.
[28] D. V. S. Muthu, M. N. Shashikala, A. K. Sood, R. Seshadri, C. N. R. Rao, *Chem. Phys. Lett.* **1994**, *217*, 146.
[29] K. Tanaka, T. Sato, T. Yamabe, *J. Phys. Chem.* **1996**, *100*, 3980.
[30] E. Diana, R. Rossetti, P. L. Stanghellini, S. F. A. Kettle, *Inorg. Chem.* **1997**, *36*, 382.
[31] P. L. Stanghellini, E. Diana, E. Boccaleri, R. Rossetti, *J. Organomet. Chem.* **2000**, *593−594*, 36.
[32] D. P. Freyberg, J. L. Robbins, K. N. Raymond, J. C. Smart, *J. Am. Chem. Soc.* **1979**, *101*, 892.
[33] U. Siemeling, U. Vorfeld, B. Neumann, H. G. Stammler, *Chem. Ber.* **1995**, *128*, 481.
[34] M. Hobi, O. Ruppert, V. Gramlich, A. Togni, *Organometallics* **1997**, *16*, 1384.
[35] C. S. Yannony, R. D. Jonson, G. Meijer, D. S. Bethune, J. R. Salem, *J. Phys. Chem.* **1991**, *95*, 9.
[36] H. He, J. Barras, J. Foulkes, J. Klinowski, *J. Phys. Chem. B* **1996**, *101*, 117.
[37] P. Day, in: *The Time Domain in Surface and Structural Dynamics* (Eds.: G. J. Long, F. Grandjean), Kluwer Academic Publishers, The Netherlands, **1987**, p. 1.
[38] D. E. Wemmer, D. J. Ruben, A. Pines, *J. Am. Chem. Soc.* **1981**, *103*, 28.
[39] T. Pradeep, K. K. Swigh, A. P. B. Sinha, D. E. Harris, *J. Chem. Soc., Chem. Commun.* **1992**, 1747.
[40] E. Adman, M. Rosenblum, S. Sullivan, T. N. Margulis, *J. Am. Chem. Soc.* **1967**, *89*, 4540.
[41] The remaining mode, $H_g(7)$, gives rise to a weak band at 1423 cm^{-1} in the Raman spectrum of C_{60} and cannot be detected by the deconvolution procedure.
[42] R. E. Stanton, M. D. Newton, *J. Phys. Chem.* **1988**, *92*, 2141.
[43] C. H. Choi, M. Kertesz, L. Mihaly, *J. Phys. Chem. A* **2000**, *104*, 102.
[44] T. Ishii, N. Aizawa, M. Yamashita, H. Matsuzaka, T. Kodama, K. Kikuchi, I. Ikemoto, Y. Iwasa, *J. Chem. Soc., Dalton Trans.* **2000**, 4407.
[45] M. F. Meidine, P. B. Hitchcock, H. W. Kroto, R. Taylor, D. R. M. Walton, *J. Chem. Soc., Chem. Commun.* **1992**, 1534.
[46] A. Hönnerscheid, L. van Wüllen, M. Jansen, *J. Chem. Phys.* **2001**, *115*, 7161.
[47] Supplementary material (coordinates of H atoms, anisotropic thermal parameters, bond lengths and angles) has been deposited at the Cambridge Crystallographic Data Centre, with deposition numbers CCDC-190842 (**1**) and -190841 (*Fc) at 150 K.
[48] Bruker, *P3/PC Diffractometer Program*, Version 3.13, Bruker Analytical X-ray Systems, Inc., Madison, Wisconsin, USA, **1989**.
[49] A. Altomare, G. Cascarano, C. Giacovazzo, A. Guagliardi, M. C. Burla, G. Polidori, M. Camalli, *J. Appl. Crystallogr.* **1994**, *27*, 435.
[50] G. M. Sheldrick, *SHELXL-97*, University of Göttingen, Germany, **1997** (website: http://shelx.uni-ac.gwdg.de/SHELX/).
[51] P. Ugliengo, D. Viterbo, G. Chiari, *Z. Kristallogr.* **1993**, *207*, 9 (website: http://www.ch.unito.it/ifm/fisica/moldraw/moldraw.html).
[52] G. M. Sheldrick, *SHELXTL/IRIS*, Bruker Analytical X-ray Systems, Inc., Madison, Wisconsin, USA, **1990**.

Received August 7, 2002
[I02447]

Synthesis, Structure, and Characterization of $[RAl(\mu\text{-}NHEt)(\mu\text{-}NEt)_2Si(NHEt)]_2$ (R = Me, Et)

Stefan Kaskel,*[a] Christian W. Lehmann,[a] Gerald Chaplais,[a] Klaus Schlichte,[a] and Meik Khanna[a]

Keywords: Aluminium / Nitrogen / Precursor development / Silicon

The reaction between tetrakis(ethylamino)silane, $Si(NHEt)_4$ (**1**) and trialkylaluminium compounds AlR_3 [R = Me (**2**), R = Et (**3**)] results in partial deprotonation of **1** and subsequent formation of a new dimeric alumosilazane in high yield. Single-crystal X-ray analyses reveal the structure of two new four-membered ring compounds $[RAl(\mu\text{-}NHEt)(\mu\text{-}NEt)_2Si(NHEt)]_2$ [R = Me (**4**), R = Et (**5**)]. They are isostructural and crystallize in the triclinic space group $P\bar{1}$ (No. 2) with a = 8.3052(8) Å, b = 9.8323(9) Å, c = 10.324(1) Å, α = 115.498(4)°, β = 97.684(4)°, γ = 94.382(4)° (**4**) and a = 8.2319(3) Å, b = 9.3748(5) Å, c = 10.8221(6) Å, α = 107.035(2)°, β = 104.435(2)°, γ = 94.375(2)° (**5**). The alternating edge- and corner-sharing SiN_4- and $AlCN_3$-tetrahedra represent a new structural motif with μ-NHEt and μ-NEt groups in one double bridge. The compounds were further characterized by elemental analysis, mass spectrometry, and NMR and IR spectroscopy.
(© Wiley-VCH Verlag GmbH & Co. KGaA, 69451 Weinheim, Germany, 2003)

Introduction

The design of new oxygen-free molecular precursors is crucial for the development of new nitride ceramics, porous non-oxide materials, and nanocomposites. Our interest is in the development of such precursors for the manufacture of porous non-oxide materials and gels, especially for catalytic applications in solid base catalysis.[1–4] For the synthesis of three-dimensional zeolitic frameworks such as nitridosilicates, molecular alumosilazanes may be suitable.[5,6] However, the known and well characterized triaminosilanes that form cage-type compounds in the reaction with $AlMe_3$ or $LiAlMe_4$ are expensive and require several synthesis steps.[7] We have therefore explored the reactions between AlR_3 and silanes such as $Si(NHEt)_4$, which on one hand is accessible in high yield from a one-step reaction between aminoethane and tetrachlorosilane,[8] and on the other hand is known to be transformable into $Si(NH)_2$ under mild conditions.[9] An important feature in comparison with other silane precursors is the absence of Si–C bonds. Si–C bonds are extremely stable, and so their cleavage and conversion into imides or nitrides under ammonothermal conditions requires high temperatures.

AlH_3 is known to form polymers of a wide compositional range in its reaction with $Si(NHMe)_4$. These are suitable precursors for the design of Si_3N_4/AlN nanocomposites.[10] Surprisingly, we found that AlR_3 (R = Me, Et) and $Si(NHEt)_4$ do not form polymers. Instead, molecular, crystalline compounds of the type $[RAl(\mu\text{-}NHEt)(\mu\text{-}NEt)_2Si(NHEt)]_2$ (R = Me, Et) with a fixed Al:Si ratio of 1:1 are obtained. They each have a cyclic four-membered ring structure, with bridging and terminal ethylamino ligands, and form through deprotonation of two ethylamino groups per $Si(NHEt)_4$. We report below on the preparation of the two isostructural compounds $[RAl(\mu\text{-}NHEt)(\mu\text{-}NEt)_2Si(NHEt)]_2$ (R = Me, Et) and on their structural and spectroscopic characterization by single-crystal X-ray analysis and spectroscopic methods.

Results and Discussion

Synthesis and Spectra

The compounds $[RAl(\mu\text{-}NHEt)(\mu\text{-}NEt)_2Si(NHEt)]_2$ [R = Me (**4**), R = Et (**5**)] are directly prepared by dropwise addition of trimethylaluminium ($AlMe_3$) or triethylaluminium ($AlEt_3$) to tetrakis(ethylamino)silane, $Si(NHEt)_4$ (**1**) (Scheme 1). The synthesis may be carried out either with or without solvent. If $AlEt_3$ is added slowly to the pure silane without solvent dilution the generation of gas bubbles is rather vigorous and the reaction vessel should be cooled.

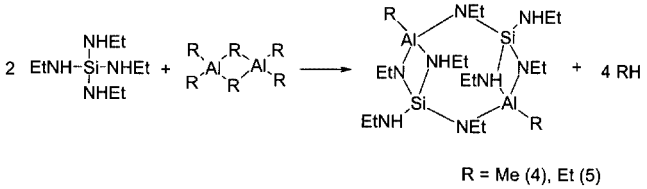

Scheme 1

[a] Max-Planck-Institut für Kohlenforschung
Kaiser-Wilhelm-Platz 1, 45470 Mülheim a.d. Ruhr, Germany
Fax: (internat.) + 49-(0)208/3062995
E-mail: kaskel@mpi-muelheim.mpg.de

After several minutes, ethane formation begins to slow down. The product is obtained after twelve hours, in the form of transparent crystals. Without the use of solvent dilution, in fact, the vessel is completely filled with white, crystalline product.

The reaction may also be carried out in pentane solution. In that case the solvent is removed in vacuo after twelve hours reaction time and the product is obtained as a white, crystalline solid.

Both compounds were characterized by mass spectrometry, IR and NMR spectroscopic studies, elemental analysis, and single-crystal X-ray diffraction.

The EI mass spectrum of **4** shows the molecular ion peak [M^+] at m/z = 488 (19%) and a signal due to the [$M^+ - CH_3$] fragment at m/z = 473 (100%). The EI mass spectrum of **5** does not show the molecular ion peak, but a signal due to the [$M^+ - C_2H_5$] fragment is seen at m/z = 487 (100%). The molecular ion peak [$M^+ + H$] of **5** at m/z = 517 (35%) is only recorded if chemical ionization (isobutane) is used.

The ^{1}H NMR spectrum of **4** shows broad signals at δ = 2.88−3.14 and 1.06−1.40, due to the methylene and methyl protons in the amino ethane groups. The protons of the methyl groups bound to the aluminium center appear as a singlet (δ = −0.20 ppm). At 300 K the signals due to the methylene protons appear as two broad, overlapping peaks, whereas the methyl protons appear as three broad peaks. At lower temperatures (243 K, [D_8]toluene), on the other hand, the methyl protons are resolved as four triplets, two of which are separated (δ = 1.30 and 1.18 ppm) while two overlap with each other (δ = 1.09 and 1.04 ppm). The signals at δ = 2.88−3.14 appear at 243 K as a complicated structure of overlapping multiplets.

The ^{1}H NMR spectrum of **5** is very similar to that of **4**, but the broadening of the signals at 300 K is less pronounced. The methylene protons in the vicinity of the aluminium atom appear at δ = 0.37 ppm.

The temperature-dependent linewidth in the proton NMR spectra indicates inter- or intramolecular exchange of terminal and bridging groups on the NMR timescale in solution (benzene, toluene).

The molecular compounds each show two distinct absorptions in the IR spectrum, at 3413 (**4**) [3410 (**5**)] and 3262 (**4**) [3254 (**5**)] cm^{-1}. These are attributable to the N−H stretching frequency of the terminal ethylamino group, similar to that in Si(NHEt)$_4$ (3414 cm^{-1}), and the N−H stretching frequency of the μ-NHEt groups in the double bridge (Scheme 1).

The simultaneous presence of alkyl groups bound to aluminium and residual acidic protons in the aminoethane ligands is similar to the situation seen in an incomplete condensation reaction between a primary amine and an alkylaluminium compound and is not uncommon,[6] subsequent formation of alane-amine adducts, aminoalanes, and poly(*N*-alkylimino)alanes typically being observed in such reactions.[11] For **4** and **5**, further intramolecular condensation is difficult to achieve without complete rearrangement of the molecular structure, so further condensation of the terminal ethylamino and alkyl groups would probably result in polymerization. Obviously, this polymerization does not take place at room temperature because several alkyl groups are pointing outwards, acting as a protective shell for the cluster and hindering further polymerization.

X-ray Structures of [MeAl(μ-NHEt)(μ-NEt)$_2$Si(NHEt)]$_2$ (4) and [EtAl(μ-NHEt)(μ-NEt)$_2$Si(NHEt)]$_2$ (5)

Single-crystal X-ray structure determinations carried out at 100 K show that compounds **4** and **5** both crystallize in the $P\bar{1}$ space group, with one cagelike molecule per unit cell, situated on an inversion center. The basic structural motif in **4** and **5** is a heterocyclic eight-membered ring composed of alternating Al and Si atoms with interspersed N(Et) groups (Figure 1). Two additional NHEt groups, each bridging one pair of Si-Al atoms, produce a formally tricyclic ring system. The tetrahedral coordination of the Si and Al atoms is completed with an additional EtNH group for silicon and alkyl groups for aluminium, to give an overall neutral molecule. The cage is therefore made up of two pairs of edge-sharing $AlCN_3$ and SiN_4 tetrahedra linked through the corners to form a four-membered cycle (Figure 2). Two crystallographically and chemically different EtN groups can be distinguished. Both are μ_2-bridging ligands between Al and Si centers, but one has a common corner (top and bottom in Figure 2) of two tetrahedral units whereas the other is part of a common edge of two tetrahedra. The two μ_2-ligands forming a common edge of two tetrahedra are termed a "double-bridge" below.

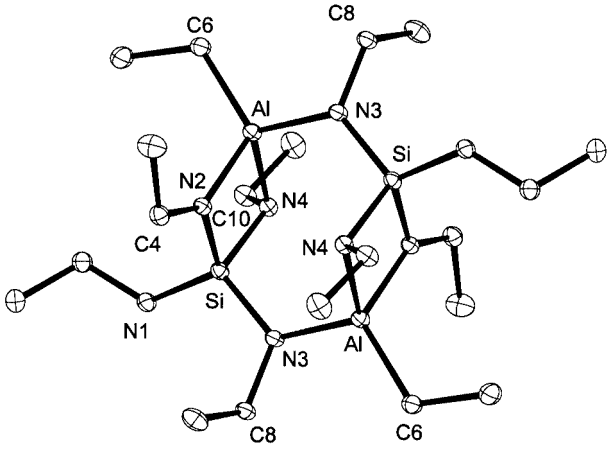

Figure 1. Crystal structure of **5** (hydrogen atoms are omitted for clarity); selected bond length [Å] and angles [°] are given in Table 1

The deviation of the coordination from an ideal tetrahedron (Figures 1 and 3, Table 1) is noticeable for the aluminium center, since the double bridges give rise to compression of one of the tetrahedron angles (N2−Al−N4) to only 80.4(1)°, whereas all other angles except for one (N3−Al−N4: 107.6(1)°] are expanded (113.5−119.4°). The Al−C6 bond length is 1.971(2) Å in **5** and 1.967(4) Å in **4,** close to Al−C distances typically observed in organoaluminium compounds (LiAlEt$_4$: d(Al−C) = 2.023 Å[12]). The Al−N bond lengths to the bridging EtN nitrogens [Al−N2: 1.849(2), Al−N3: 1.851(2) Å in **5**; 1.858(3) and 1.856(3) Å

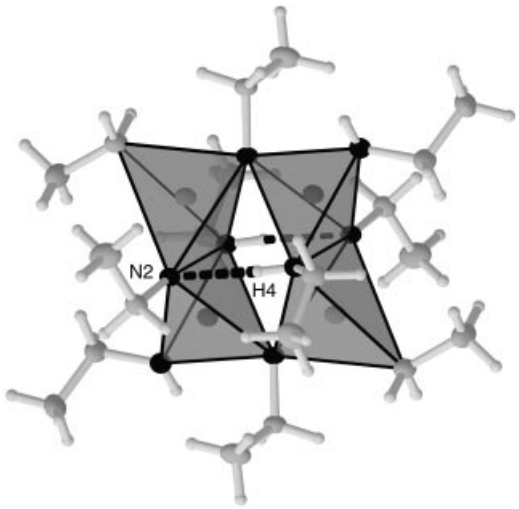

Figure 2. Polyhedral representation of **5**; the proton in position H4 was located in the Fourier map and refined without constraints; the dashed line indicates a secondary interaction between EtNH and EtN groups in neighboring double bridges

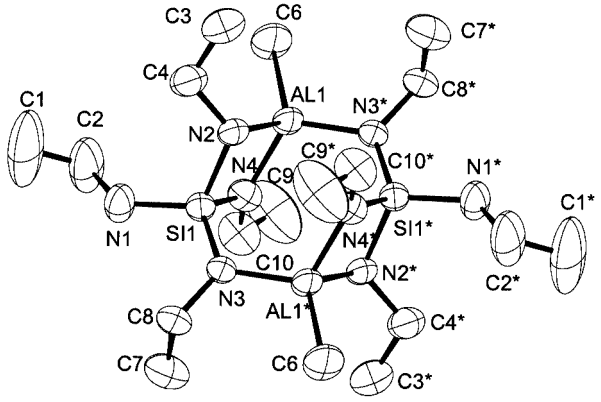

Figure 3. Molecular structure of **4**

Table 1. Selected bond lengths [Å] and angles [°] in compound **5**

Al−N2	1.849(2)	Al−N3	1.851(2)
Al−N4	2.006(2)	Al−C6	1.971(2)
Si−N1	1.700(2)	Si−N2	1.699(2)
Si−N3	1.704(2)	Si−N4	1.833(2)
N4−H4	0.80(2)	N1−H1	0.80(3)
N2−Al−N3	115.2(1)	N2−Al−C6	119.4(1)
N3−Al−C6	113.5(1)	N2−Al−N4	80.4(1)
N3−Al−N4	107.6(1)	C6−Al−N4	116.1(1)
N2−Si−N1	114.1(1)	N2−Si−N3	118.3(1)
N1−Si−N3	110.8(1)	N2−Si−N4	89.6(1)
N1−Si−N4	112.2(1)	N3−Si−N4	110.1(1)
C4−N2−Si	125.3(1)	C8−N3−Si	119.7(1)
C4−N2−Al	134.9(1)	C8−N3−Al	118.2(1)
Si−N2−Al	99.9(1)	Si−N3−Al	119.8(1)
C10−N4−Si	118.3(1)		
Si−N4−Al	90.0(1)		
C10−N4−Al	121.1(1)		

in **4**] are significantly shorter than the bond to the EtNH ligand [Al−N4: 2.006(2) Å in **5**, 1.992(3) Å in **4**].

For silicon, compression of the tetrahedral environment along the double bridge is less severe [N2−Si−N4: 89.6(1)°] and the other N−Si−N angles are between 110 and 114°, with one exception [N2−Si−N3: 118.3(1)°]. As in the $AlCN_3$ tetrahedron, the Si−N bond length to the μ_2-bridging EtNH group is longer [Si−N4: 1.833(2) Å (**5**); 1.826(3) Å (**4**)] than the other Si−N bonds [1.699(2)−1.704(2) Å].

An interesting feature is that only 50% of the original EtNH groups are deprotonated. Bridging EtN groups are clearly different from the bridging EtNH ligands in geometry. In the former, the nitrogen atoms (N2 and N3) show a distorted trigonal planar coordination [C4−N2−Si: 125.3(1)°, C4−N2−Al: 134.9(1)°, Si−N2−Al: 99.9(1)°, sum: 360.1°; C8−N3−Si: 119.7(1)°, C8−N3−Al: 118.2(1)°, Si−N3−Al: 119.8(1)° sum: 357.7° (359.7° for **4**)] whereas in the latter N4 has a pseudotetrahedral arrangement of non-hydrogen atoms [C10−N4−Si: 118.3(1)°, Si−N4−Al: 90.0(1)°, C10−N4−Al: 121.1(1)°, sum: 329.4° (332.2° for **4**)].

The simultaneous presence of bridging EtNH and EtN groups is a unique structural feature of the new cluster. The proton H4, attached to N4, was located in the difference Fourier map and refined without constraints to give an N4−H4 distance of 0.80(2) Å. Interestingly, the distance between H4 and the non-covalently bonded N2 in the neighboring double bridge is only 2.49(2) Å (Figure 2, dashed line), so a secondary interaction between the EtNH and the EtN ligand in the neighboring double bridge is probably the reason for the unusual structural motif. The H4 location is also ideal for an intramolecular exchange of the proton from the EtNH to the EtN ligand, which is unprecedented and would explain some of the broadening in the NMR spectra.

The position of the proton in the terminal EtNH group attached to silicon was also located in the course of the structural refinement.

Although differentiation between aluminium and silicon and location of the hydrogen position are not trivial, the assignment of positions is evident from the synthesis and the geometrical considerations outlined above. The good solubilities of **4** and **5** in non-polar solvents such as pentane are also in agreement with the overall zero charge on the molecule deduced from the structural analysis, especially since the ethyl groups point outwards from the cluster to provide an overall hydrophobic shell. Hydrophobic interactions between those groups therefore also largely determine the lattice energy and packing of the clusters in the crystal structure.

Overall, the structures of the new compounds are a remarkable new element in alane chemistry. Tetrameric iminoalanes commonly possess cubane-type skeletons.[11] However, for an Al_2Si_2 skeleton the cubane structure, for reasons of charge-matching, would not only require one unusual terminal EtN ligand ($[RAl(\mu_3\text{-}NEt)_2Si(NEt)]_2$) but would also produce neighboring aluminium tetrahedra, obviously less favorable than alternating silicon and aluminium tetrahedra. Interestingly, the latter can be seen as a molecular analogy of Löwenstein's rule, which states that the Al:Si

ratio in zeolites can never exceed 1.0 because Al−O−Al linkages are avoided.[13]

Conclusion

We have shown that heterocyclic precursors containing aluminium and silicon in a fixed ratio of 1:1 are accessible as crystalline compounds in high yield. They represent pre-organized structural building units for the assembly of tetrahedral framework materials such as nitrido zeolites. Preliminary investigations in our group show that they are suitable precursors for the generation of porous aluminium silicon imide materials with high accessible surface area by use of ammonothermal transamination in supercritical ammonia.

Experimental Section

Synthesis of 4 and 5: All operations were performed either in a glove box (Argon, $O_2 < 1$ ppm, $H_2O < 1$ ppm) or with use of a vacuum line and dry solvents. Tetrakis(ethylamino)silane was obtained from aminoethane and silicon chloride (9:1) and purified by distillation in vacuo (99.7%, GC).[8]

Typically, AlR_3 (5 mmol) was added dropwise at room temperature either to a stirred solution of $Si(NHEt)_4$ (5 mmol, 1 g) in pentane or to pure $Si(NHEt)_4$. The liquid mixture was stirred at room temperature for 12 hours. For reactions carried out in the absence of solvent the vessel was completely filled with white, crystalline product after 12 h. For reactions carried out in pentane, the solvent was removed in vacuo and a solid product was obtained [yield: 98%, 1.198 g (**4**), 100%, 1.292 g (**5**)].

Compound 4: $C_{18}H_{50}Al_2N_8Si_2$ (488.80) Calcd. C 44.23, H: 10.31, N 22.93, Al 11.04, Si 11.49; found C 44.15, H 10.19, N 23.11, Al 11.15, Si 11.81. MS(EI): *m/z* (%) = 488 (19) [M^+], 473 (100) [$M^+ - CH_3$]. ^{1}H NMR (300 MHz, 300 K, [D_6]benzene, ppm): δ = −0.20 (s, 6 H, $AlCH_3$), 1.06−1.40 (m, 24 H, N-CH_2−CH_3), 2.88−3.14 (m, 16 H, N-CH_2−CH_3). IR (KBr): $\tilde{\nu}$ = 3413cm^{-1}(m), 3262 (m)(N−H), 2960(s), 2927(s), 2862(s)(C−H), 2683(w), 2589(w), 1475(m), 1449(m), 1395(s), 1371(s), 1298(m), 1265(m), 1192(s), 1125(s), 1065(s), 929(s), 887(s), 864(s), 779(s), 699(m), 657(m).

Compound 5: $C_{20}H_{54}Al_2N_8Si_2$ (516.86) Calcd. C 46.48, H 10.53, N 21.68, Al 10.44, Si 10.87; found C 46.11, H 10.26, N 21.39, Al 10.59, Si 11.31. MS(CI, *i*-butane): *m/z* (%) = 517 (35) [M^+ + H], 487 (100) [$M^+ - C_2H_5$]. ^{1}H NMR (300 MHz, 300 K, [D_6]benzene, ppm): δ = 0.37 (m, 4 H, $AlCH_2CH_3$), 1.01−1.49 (m, 30 H, CH_2−CH_3), 2.70−3.03 (m, 16 H, N-CH_2−CH_3). IR (KBr): $\tilde{\nu}$ = 3410(m) cm^{-1}, 3254(m) (N−H), 2958(s), 2895(s), 2861(s) (C−H), 2680(w), 2589(w), 1449(s), 1393(s), 1371(s), 1350(s), 1296(w), 1265(s), 1188(s), 1125(s), 1065(s), 991(m), 926(s), 861(s), 780(s), 692(m), 628(m), 542(m).

Crystal Data Collection and Refinement of the Structure of 4: $C_{18}H_{50}Al_2N_8Si_2$, M_r = 488.80 g·mol^{-1}, triclinic, space group $P\bar{1}$ (No.2), a = 8.3052(8) Å, b = 9.8323(9) Å, c = 10.3240(10) Å, α = 115.498(4)°, β = 97.684(4)°, γ = 94.382(4)°, V = 745.60(12) Å^3, Z = 1, $D_{calcd.}$ = 1.089 g·cm^{-3}, μ = 0.198 mm^{-1}, $F(000)$ = 536 e, T = 100 K. Convergence of the 141 variable parameters by full-matrix, least-squares refinement on F^2 reaches R_1 = 0.0766 [$I > 2\sigma(I)$] and wR_2= 0.2515 with a goodness-of-fit of 0.870.The data were collected on a Siemens SMART-CCD diffractometer by use of graphite monochromatized Mo-K_α radiation (λ = 0.71073 Å).

Crystal Data Collection and Refinement of the Structure of 5: $C_{20}H_{54}Al_2N_8Si_2$, M_r = 516.86 g·mol^{-1}, triclinic, space group $P\bar{1}$ (No.2), a = 8.2319(3) Å, b = 9.3748(5) Å, c = 10.8221(6) Å, α = 107.035(2)°, β = 104.435(2)°, γ = 94.375(2)°, V = 763.20(6) Å^3, Z = 1, $D_{calcd.}$ = 1.125 g·cm^{-3}, μ = 0.196 mm^{-1}, $F(000)$ = 568 e, T = 100 K. Convergence of the 158 variable parameters by full-matrix, least-squares refinement on F^2 reaches R_1 = 0.0671 [$I > 2\sigma(I)$] and wR_2= 0.1471 with a goodness-of-fit of 1.007. The data were collected on a Nonius Kappa-CCD diffractometer by use of graphite monochromatized Mo-K_α radiation (λ = 0.71073 Å).

CCDC-190148 (**5**) and CCDC-190147 (**4**) contain the supplementary crystallographic data for this paper. These data can be obtained free of charge at www.ccdc.cam.ac.uk/conts/retrieving.html [or from the Cambridge Crystallographic Data Centre, 12, Union Road, Cambridge CB2 1EZ, UK; Fax: (internat.) + 44-1223/336-033; E-mail: deposit@ccdc.cam.ac.uk].

Acknowledgments

We thank F. Schüth for helpful discussions and financial support.

[1] D. Farrusseng, K. Schlichte, B. Spliethoff, A. Wingen, S. Kaskel, J. S. Bradley, F. Schüth, *Angew. Chem.* **2001**, *113*, 4336−4339; *Angew. Chem. Int. Ed.* **2001**, *40*, 4204−4207.
[2] S. Kaskel, D. Farrusseng, K. Schlichte, *Chem. Commun.* **2000**, 2481−2482.
[3] S. Kaskel, K. Schlichte, *J. Catal.* **2001**, *201*, 270−274.
[4] S. Kaskel, K. Schlichte, B. Zibrowius, *Phys. Chem. Chem. Phys.* **2002**, *4*, 1675−1681.
[5] P. Böttcher, H. W. Roesky, M. G. Walawalkar, H. G. Schmidt, *Organometallics* **2001**, *20*, 790−793.
[6] C. Rennekamp, P. Müller, J. Prust, H. Wessel, H. W. Roesky, I. Uson, *Eur. J. Inorg. Chem.* **2000**, 1861−1868.
[7] K. Wraage, A. Künzel, M. Noltemeyer, H. G. Schmidt, H. W. Roesky, *Angew. Chem.* **1995**, *107*, 2954−2956; *Angew. Chem. Int. Ed. Engl.* **1996**, *34*, 2645−2647.
[8] D. M. Narsavage, L. V. Interrante, P. S. Marchetti, G. E. Maciel, *Chem. Mater.* **1991**, *3*, 721−730.
[9] U. Wannagat, A. Schervan, M. Jansen, H.-P. Baldus, A. Eiling, **1991**, EP 0479050A1.
[10] J. Löffelholz, M. Jansen, *Adv. Mater.* **1995**, *7*, 289−292.
[11] M. F. Lappert, P. P. Power, A. R. Sanger, R. C. Srivastava, *Metal and Metalloid Amides*, 1st Ed. John Wiley & Sons, Chichester, **1980**.
[12] R. L. Gerteis, R. E. Dickerson, T. L. Brown, *Inorg. Chem.* **1964**, *3*, 872−875.
[13] W. Loewenstein, *Am. Mineral.* **1954**, *39*, 92−96.

Received August 16, 2002
[I02464]

Structure and Reactivity Studies on Dinuclear Copper Complexes of the Ligand α,α′-Bis{bis[1-(1′-methyl-2′-benzimidazolyl)methyl]amino}-*m*-xylene

Giuseppe Battaini,[a] Luigi Casella,*[a] Michele Gullotti,[b] Enrico Monzani,[a] Giorgio Nardin,[c] Angelo Perotti,[a] Lucio Randaccio,[c] Laura Santagostini,[b] Frank W. Heinemann,[d] and Siegfried Schindler[d]

Keywords: Bioinorganic chemistry / Copper / Dioxygen activation / Enzyme models

The ligand α,α′-bis{bis[1-(1′-methyl-2′-benzimidazolyl)-methyl]amino}-*m*-xylene (L-55) forms the complexes $[Cu^{I}_2$(L-55)$(MeCN)_2](PF_6)_2$ (**1**) and $[Cu^{II}_2$(L-55)$(OMe)_2][ClO_4]_2$ (**2**), in which an extremely weak axial amine interaction is imposed by the small five-membered benzimidazole chelating ring units. This structural feature has been characterized by X-ray crystal structure determination. In **1**, the Cu^{I} centers are three-coordinate with ligation from two benzimidazolyl and one acetonitrile N-donors, in a slightly distorted trigonal arrangement. In **2**, each Cu^{II} center has a distorted square-planar geometry and coordinates to the benzimidazolyl N atoms and the bridging methoxy groups in the basal positions, with a much weaker interaction with the tertiary amine N in an apical position. These structural features affect the reactivities of the copper(I)– and copper(II)–L-55 complexes toward dioxygen and hydrogen peroxide, respectively. $[Cu^{I}_2$(L-55)$(MeCN)_2]^{2+}$ does not produce a stable peroxo complex, but undergoes an irreversible oxidation to copper(II) species, while $[Cu^{II}_2$(L-55)$(H_2O)_2]^{4+}$ reacts slowly with hydrogen peroxide to undergo regiospecific hydroxylation of the ligand at one benzylic carbon atom, which causes decomposition of the complex. $[Cu_2$(L-55)$(H_2O)_2]^{4+}$ is easily converted into its bis(μ-hydroxo) adduct $[Cu_2$(L-55)$(OH)_2]^{2+}$. This pH-driven equilibrium was monitored by paramagnetic ^1H NMR spectroscopy, and the solution magnetic properties of the complexes were determined by the Evans susceptibility method.

(© Wiley-VCH Verlag GmbH & Co. KGaA, 69451 Weinheim, Germany, 2003)

Introduction

The interactions between synthetic copper complexes and dioxygen have become increasingly important in the last decade,[1−4] in connection with the enzymatic reactions catalyzed by copper enzymes,[5−9] particularly tyrosinase, and potential applications in catalytic transformations of organic substrates.[10,11] In the best characterized systems, the μ-η^2:η^2-peroxodicopper(II) or bis(μ-oxo)dicopper(III) complexes have been found to be able to effect C−H bond cleavage of the ligand[12−18] or an exogenous substrate[19,20] with insertion of an oxygen atom. In other dinuclear copper systems the putative copper−dioxygen intermediate could not be characterized, due to high reactivity even at low temperature.[21−26] The first and most intensely studied example of a tyrosinase model, $[Cu_2$(*m*-XYLpy$_2$)$]^{2+}$,[12,13,27−29] performs ligand arene hydroxylation, to produce a μ-hydroxo-μ-phenoxodicopper(II) species, through the peroxo complex derived from the reaction with dioxygen. In the same system, xylyl ligand hydroxylation can also be achieved by treatment of the dinuclear Cu^{II} complex $[Cu_2$(*m*-XYLpy$_2$)$]^{4+}$ with hydrogen peroxide.[30] The monooxygenase reaction by Cu^{I} and dioxygen is not observed when the pyridine rings in the chelating arms of the *m*-xylyl-containing ligand are replaced by other nitrogen heterocycles such as imidazoles or benzimidazoles.[23,31−34] However, the dicopper(I) complex $[Cu_2$(L-66)$]^{2+}$, in which the ligand L-66 contains *N*-methylbenzimidazole rather than pyridine rings,[32] forms a peroxodicopper(II) complex capable of hydroxylating an exogenous phenol.[19] In addition, when $[Cu_2$(L-66)$]^{4+}$ is treated with hydrogen peroxide, the resulting hydroperoxodicopper(II) complexes effect double hydroxylation of the xylyl aromatic ring, to produce a hydroquinone complex.[34] In this paper we report structure and reactivity studies on the dicopper(I) and dicopper(II) complexes of the ligand L-55 (L-55 = α,α′-bis{bis[1-(1′-methyl-2′-benzimidazolyl)-

[a] Dipartimento di Chimica Generale, Università di Pavia, Via Taramelli 12, 27100 Pavia, Italy
Fax: (internat.) + 39-0382/528544
E-mail: bioinorg@unipv.it
[b] Dipartimento C.I.M.A., Università di Milano, Centro CNR, Via Venezian 21, 20133 Milano, Italy
[c] Dipartimento di Scienze Chimiche, Università di Trieste, Via L. Giorgieri 1, 34127 Trieste, Italy
[d] Institute of Inorganic Chemistry, University of Erlangen-Nürnberg, Egerlandstraße 1, 91058 Erlangen, Germany

methyl]amino}-*m*-xylene, Scheme 1),[35] which is related both to L-66, containing longer chains on the benzimidazolyl arms connected to the diamino-*m*-xylene unit, and to EBA, where a more flexible carbon chain replacing the *m*-xylyl unit[26] (Scheme 1). The synthesis and spectroscopic characterization of the copper(I) and copper(II) complexes of L-55 in solution have been reported before.[33,35] The X-ray crystal structure investigation of the $[Cu^{I}_2(L\text{-}55)(MeCN)_2](PF_6)_2$ (**1**) and $[Cu^{II}_2(L\text{-}55)(OMe)_2][ClO_4]_2$ (**2**) complexes reported here shows an extremely weak Cu−amine axial interaction, constrained by the small five-membered chelating ring units. This structural feature strongly affects the properties of the resulting copper complexes, particularly the reactivity patterns of the reduced and oxidized forms of the L-55 complexes towards dioxygen and hydrogen peroxide, respectively.

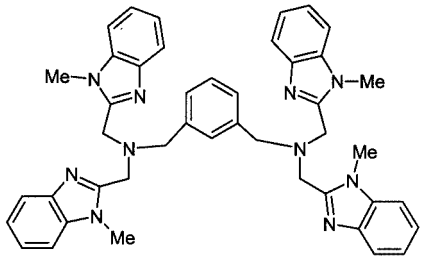

L - 55

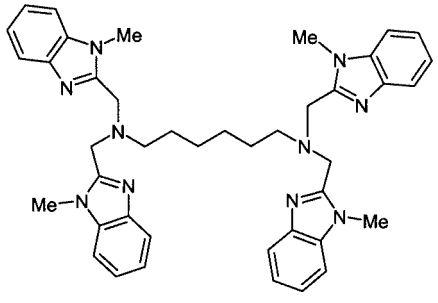

EBA

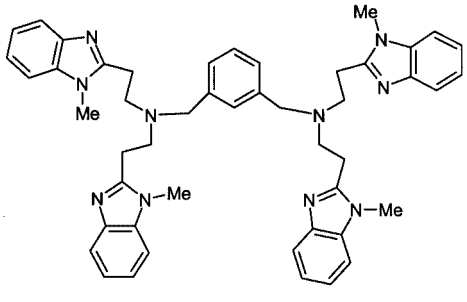

L- 66

Scheme 1

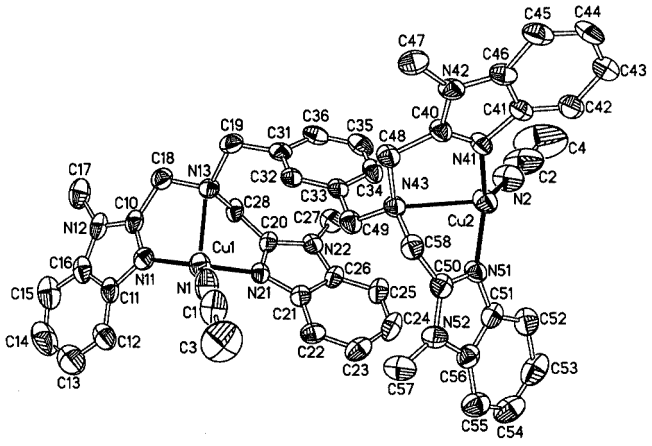

Figure 1. ORTEP[37] diagram of the cation **1** with the atom numbering labels

Results and Discussion

X-ray Structure of $[Cu^{I}_2(L\text{-}55)(MeCN)_2](PF_6)_2$ (1)

The structure of **1** consists of discrete $[Cu^{I}_2(L\text{-}55)(MeCN)_2]^{2+}$ cations and PF_6^- anions. An ORTEP view of the cation, including the labelling scheme, is shown in Figure 1. The two crystallographically independent Cu^{I} centers are three-coordinate with ligation from two benzimidazolyl N-donors and one acetonitrile N-donor, in a slightly distorted trigonal arrangement. The Cu−NCMe distances are slightly shorter than the other two. A long contact to the tertiary amino nitrogen donor [Cu1−N13, 2.602(5) Å, and Cu2−N43, 2.707(5) Å] is observed, the $N(sp^3)$ lone pair pointing approximately towards the copper ion; this may be indicative of a weak bonding interaction. The geometry around Cu is similar to the coordination around one copper(I) ion in a dinuclear complex derived from the ligand 1,3-bis[bis(2-pyridylmethy1)amino]benzene, although the Cu−N distance here is shorter [2.39(2) Å].[36] The geometry of **1** differs significantly from that found in the $[Cu^{I}_2(m\text{-}XYLpy_2)]^{2+}$ cation,[27] in which *m*-$XYLpy_2$ = $[(2\text{-}pyCH_2CH_2)_2N{-}CH_2C_6H_4CH_2{-}N(2\text{-}pyCH_2CH_2)_2]$. In the latter, in fact, each Cu^{I} achieves tricoordination through ligation of two pyridyl donors at short distances, slightly more than 1.90 Å, and the $N(sp^3)$ amino donor at a long distance, around 2.2 Å. Furthermore, the planar arrangement of the N donors around the copper ions is dramatically distorted from ideal trigonal geometry towards a T-shaped geometry with an angle of about 150° between the two Cu−benzimidazolyl distances.

The differences observed in the Cu^{I} coordination in the two cations may mainly be ascribed to the presence in $[Cu^{I}_2(L\text{-}55)(MeCN)_2]^{2+}$ of a methylene group bridging the $N(sp^3)$ atom to the benzimidazole residues. This does not allow ring-closure at a suitable Cu−$N(sp^3)$ coordination distance, as occurs in $[Cu^{I}_2(m\text{-}XYLpy_2)]^{2+}$, in which $N(sp^3)$ and the pyridyl moieties are joined by ethylene bridges. Consequently, the coordinatively unsaturated Cu^{I} center binds an acetonitrile molecule, so the two Cu^{I} ions in the two kinds of cations have dramatically different coor-

Table 1. Crystal data and structure refinement for $[Cu^{I}_2(L\text{-}55)(MeCN)_2](PF_6)_2\cdot 3MeCN$ [(**1**)·3MeCN] and $[Cu^{II}_2(L\text{-}55)(OMe)_2][ClO_4]_2\cdot 1.25MeOH$ (**2**)

Empirical formula	$C_{54}H_{59}Cu_2F_{12}N_{15}P_2$	$C_{47.25}H_{50}Cl_2Cu_2N_{10}O_{11.25}$
Formula mass	1335.18	1135.95
Temperature	200(2) K	293(2) K
Wavelength	0.71073 Å	0.71069 Å
Crystal system, space group	triclinic, $P\bar{1}$	triclinic, $P\bar{1}$
Unit cell dimensions	a = 13.022(3) Å, α = 81.85(3)°	a = 10.462(4) Å, α = 78.08(3)°
	b = 13.944(3) Å, β = 74.18(3)°	b = 13.226(4) Å, β = 89.18(3)°
	c = 18.433(6) Å, γ = 69.02(1)°	c = 20.149(7) Å, γ = 80.07(2)°
Volume	3003(2) $Å^3$	2686.4(16) $Å^3$
Z, calculated density	2, 1.477 Mg/m^3	2, 1.404 Mg/m^3
Absorption coefficient	0.849 mm^{-1}	0.957 mm^{-1}
F(000)	1368	1171
Crystal size	0.50 × 0.40 × 0.30 mm	0.6 × 0.4 × 0.4 mm
Reflections collected/unique	12110/10581 [R(int) = 0.1246]	9476/9449 [R(int) = 0.0230]
Refinement method	full-matrix, least-squares on F^2	full-matrix, least-squares on F^2
Data/restraints/parameters	10578/17/797	9476/0/653
Goodness-of-fit on F^2	0.936	1.057
Final R indices [$I > 2\sigma(I)$]	$R1$ = 0.0756, $wR2$ = 0.1850	$R1$ = 0.0856, $wR2$ = 0.1958
R indices (all data)	$R1$ = 0.1414, $wR2$ = 0.2067	$R1$ = 0.1950, $wR2$ = 0.2564
Largest diff. peak and hole	0.864 and −0.709 e·$Å^{-3}$	0.697 and −0.504 e·$Å^{-3}$

dinations and possibly different electronic configurations. Crystal data and structure refinement are given in Table 1. Complete tables of atomic parameters and bond lengths and angles are deposited with the CCDC.

X-ray Structure of $[Cu^{II}_2(L\text{-}55)(OMe)_2][ClO_4]_2\cdot 1.25MeOH$ (2)

The crystals consist of dinuclear $[Cu^{II}_2(L\text{-}55)(OMe)_2]^{2+}$ cations and two ClO_4^- anions. These crystals spontaneously formed from a methanolic solution of the bis(μ-hydroxo)-bridged complex $[Cu_2(L\text{-}55)(OH)_2][ClO_4]_2$. Crystal data and structure refinement are shown in Table 1, and an ORTEP drawing, together with the atom numbering scheme of the cation, is shown in Figure 2.[37] The cation has an approximate mirror symmetry, the mirror plane containing the two bridging OMe, C40, and C43 atoms. The structure of the cation is similar to that of $[Cu_2(EBA)(OH)_2]^{2+}$, in which the ligand has a flexible spacer of six methylene carbon atoms instead of the five carbon atoms of the L-55 ligand. Each Cu has a highly distorted square-pyramidal geometry and coordinates to the tertiary amine in the apical position and the two sp^2-N atoms of the tridentate arm in two *cis* basal positions. The other two equatorial positions are occupied by the bridging methoxy groups. (Figure 2). In spite of the different spacer, the overall geometries of the $N_5Cu_2O_2N_5$ moieties are very similar in L-55 and EBA derivatives, as are the coordination geometries about the metal ions. These are compared in Table 2, together with the length of the spacer (N5···N10) and the intermetallic distances.

The basal donors of Cu1 and Cu2 are coplanar within 0.013 and 0.005 Å, respectively, and the displacements of Cu1 and Cu2 out of their respective mean planes toward the apical N donor are 0.114(4) and 0.149(4) Å, respectively. The two N_2O_2 basal planes make a dihedral angle (β) of 19.1(2)°, very similar to that observed in the EBA derivative

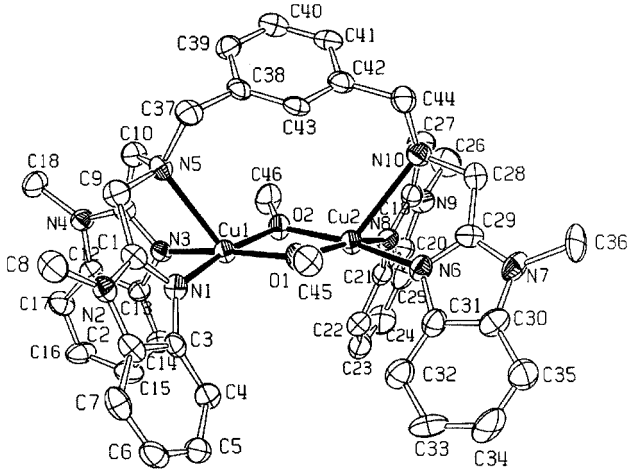

Figure 2. ORTEP[37] representation of the crystal structure of the cation **2**

[β = 20.0(2)°]. The geometry of the cation of **2** differs significantly from that reported for $[Cu_2L_3(OMe)_2]^{2+}$ [L_3 = (2-py$(CH_2CH_2)_2$N$(CH_2)_3$N(2-pyCH_2CH_2py)$_2$],[38] which has a crystallographic mirror symmetry, the L_3 ligand having aminobis(2-CH_2CH_2-pyridyl) arms [instead of aminobis(2-CH_2-benzimidazolyl)ones] and a trimethylene spacer. The Cu coordination in the latter cation is less distorted than that in the cation of **2**, with a small shortening of the apical Cu−N distance of about 0.2 Å, and a small, but significant, lengthening of the basal distances of about 0.03 Å (Table 2). Correspondingly, the N(sp^3)−N(sp^3) distance is more than 1 Å shorter than that in the L-55 and EBA analogues. This is due to the large difference in the spacer length (Table 2) and to N(sp^3)$(CH_2)_n$N(sp^3) arms, as previously suggested.[26] Notwithstanding, the geometries of the CuO_2Cu moieties are similar in the three dinuclear cations (Table 2). However, the *m*-xylyl plane in the cation of **2** is not parallel

Table 2. Comparison of coordination bond lengths and angles in $[Cu_2(L\text{-}55)(OMe)_2][ClO_4]_2$, $[Cu_2(EBA)(OH)_2][PF_6]_2$, and $[Cu_2L_3(OMe)_2][ClO_4]_2$

	$[Cu_2(L\text{-}55)(OMe)_2][ClO_4]_2$	$[Cu_2(EBA)(OH)_2][PF_6]_2$	$[Cu_2L_3(OMe)_2][ClO_4]_2$
Bond lengths [Å]:			
Cu1−O1	1.911(6)	1.892(11)	1.934(9)
Cu1−O2	1.913(6)	1.941(10)	1.934(8)
Cu1−N1	1.970(7)	1.930(12)	1.992(12)
Cu1−N3	1.957(7)	1.918(13)	2.004(14)
Cu1−N5	2.503(7)	2.487(11)	2.363(13)
Cu2−O1	1.926(6)	1.882(10)	−
Cu2−O2	1.921(6)	1.887(12)	−
Cu2−N6	1.947(7)	1.942(11)	−
Cu2−N8	1.958(7)	1.983(12)	−
Cu2−N10	2.586(8)	2.548(11)	−
Cu1···Cu2	3.003(2)	2.988(2)	3.070(3)
N5···N10	6.096(10)	6.050(15)	4.75(1)
Bond angles [°]:			
O1−Cu1−O2	76.8(2)	75.2(4)	74.8(5)
O1−Cu1−N1	95.0(3)	98.4(5)	74.8(5)
O1−Cu1−N3	169.4(3)	165.9(5)	152.2(6)
O1−Cu1−N5	114.0(2)	116.2(4)	115.3(5)
O2−Cu1−N1	170.1(3)	170.4(5)	168.4(6)
O2−Cu1−N3	95.4(3)	92.5(5)	94.1(5)
O2−Cu1−N5	111.8(2)	113.0(4)	101.7(6)
N1−Cu1−N3	92.0(3)	92.9(3)	91.7(6)
N1−Cu1−N5	76.4(3)	76.1(4)	89.0(5)
N3−Cu1−N5	75.3(3)	74.7(4)	91.7(6)
Cu1−O1−Cu2	103.0(2)	104.7(5)	105.0(7)
Cu1−O2−Cu2	103.1(2)	102.6(5)	105.0(6)
O1−Cu2−O2	76.2(2)	76.8(5)	−
O1−Cu2−N6	95.6(3)	94.8(5)	−
O1−Cu2−N8	164.3(3)	168.8(5)	−
O1−Cu2−N10	121.5(3)	116.1(4)	−
O2−Cu2−N6	170.3(3)	166.6(4)	−
O2−Cu2−N8	92.7(3)	94.5(5)	−
O2−Cu2−N10	113.8(2)	118.0(4)	−
N6−Cu2−N8	94.3(3)	92.4(5)	−
N6−Cu2−N10	74.8(3)	75.0(4)	−
N8−Cu2−N10	73.0(3)	74.0(4)	−

to the CuO_2Cu mean plane {as it is to the propylene spacer carbon atom in $[Cu_2L_3(OMe)_2]^{2+}$}, making an interplanar angle of 31.7(3)°.

Reactivity of L-55 Complexes: Cu^I_2 vs. O_2 and Cu^{II}_2 vs. H_2O_2

The reactivity of the Cu^I complex $[Cu_2(L\text{-}55)(CH_3CN)_2]^{2+}$ toward dioxygen has been tested in different solvents and at various temperatures. When solutions of the complex are oxygenated at −85 °C in acetone, −90 °C in CH_2Cl_2, or −95 °C in THF, a moderately intense band near 350 nm (CT, $\varepsilon \approx 6000\ M^{-1}\cdot cm^{-1}$) and a weaker band at 500 nm (d-d envelope, $\varepsilon \approx 200\ M^{-1}\cdot cm^{-1}$) rapidly develop. In neither case can the reaction be reversed by application of vacuum/argon purge cycles, even upon mildly warming the solution. The UV band is bleached by the addition of a small excess of acid at low temperature, and no trace of hydrogen peroxide could be detected by peroxidase assay[19] after quenching of the reactions. Therefore, on reaction with dioxygen, $[Cu_2(L\text{-}55)(CH_3CN)_2]^{2+}$ does not produce a stable peroxo complex, but undergoes an irreversible oxidation to copper(II) species. Furthermore, application of the low-temperature stopped-flow method, a technique that has proved extremely useful for the spectroscopic detection of "copper−dioxygen adducts",[28,39] did not allow the observation of a peroxo intermediate complex. The spectral characteristics of the formed species are different from those of L-55 (hydroxo)dicopper(II) complexes that we have reported previously.[35] However, these oxygenated solutions are highly sensitive to moisture, and their UV/Vis spectra change quickly upon exposure to air, producing LMCT bands at 300 nm ($\varepsilon \approx 4300\ M^{-1}\cdot cm^{-1}$) and 335 nm ($\varepsilon \approx 3500\ M^{-1}\cdot cm^{-1}$), which testify to the formation of the previously characterized bis(hydroxo)dicopper(II) adduct.[35] The spectroscopic data and the sensitivity to water suggest that the low-temperature oxygenation of **1** affords a μ-oxodicopper(II) complex, which may be formed in a fast reaction as the Cu_2O_2 intermediate reacts with excess Cu^I [Equation (1)].

$$Cu^I\cdots Cu^I + O_2 \rightarrow [Cu_2O_2] + Cu^I\cdots Cu^I \rightarrow 2\,Cu^{II}-O-Cu^{II} + H_2O \rightarrow 2\,Cu^{II}-(OH)_2-Cu^{II} \quad (1)$$

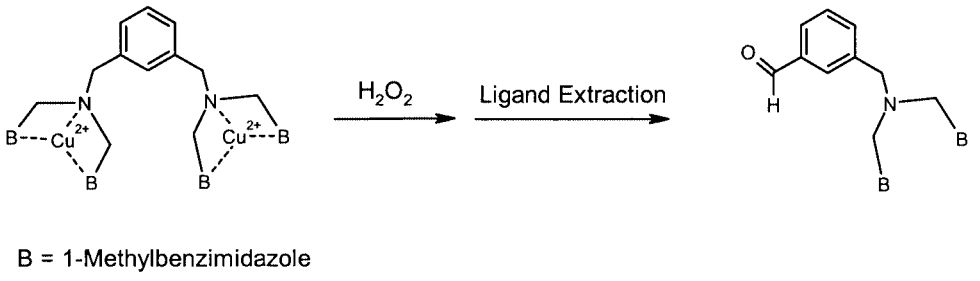

Scheme 2

The positions of the LMCT bands developing during the low-temperature experiments do, in fact, agree with those reported for other μ-oxodicopper(II) complexes.[40,41] The oxygenation behavior of $[Cu_2(EBA)]^{2+}$, in which the copper coordination set is identical to that of $[Cu_2(L\text{-}55)(CH_3CN)_2]^{2+}$, is also similar.[26] The extreme electrophilicity of the putative oxygen intermediate $[Cu_2O_2]$ is not unexpected in view of the structural features of **1** and **2**, in which essentially only two poorly basic benzimidazole nitrogen donors of the ligand are coordinated to the copper ions (Figures 1 and 2). With $[Cu_2(L\text{-}66)]^{2+}$, in contrast, a stable and reversible dioxygen complex is formed at low temperature.[19] In this case, the larger size and flexibility of the chelate rings allows the ligand to bind each Cu^I with three nitrogen donors and the copper(I) centers to attain a more regular tetrahedral geometry. This is confirmed by the electrochemical data, which show that the ligand L-66 stabilizes the copper(I) state more than L-55 or EBA.[26,35] Furthermore, the ligand flexibility more easily supports the structural reorganization involved in the Cu^{II}/Cu^I redox exchange.[35]

The reactivity of $[Cu_2(L\text{-}55)(H_2O)_2]^{4+}$ toward hydrogen peroxide was also investigated. A tenfold excess of H_2O_2, after 12 h reaction time at room temperature, produced a regiospecific hydroxylation of the ligand at one benzylic carbon atom, followed by decomposition of the complex, in 50% yield (Scheme 2). Isolation of the oxidized ligand showed the presence of an aldehyde group, with a characteristic ^1H NMR peak at $\delta \approx 10$ ppm. The loss of a chelating arm of the ligand was confirmed by ESI-MS analysis (see Exp. Sect.). It is interesting to note that in the related complex $[Cu_2(L\text{-}66)]^{4+}$,[34] and also in $[Cu_2(m\text{-}Xylpy_2)]^{4+}$,[30] hydrogen peroxide effects ligand hydroxylation at the central xylyl residue. Therefore, the coordination environment of Cu^{II} centers, and in particular the five- or six-membered chelate ring size, plays a major role in effecting the hydroxylation reaction and in controlling the regiochemistry of C−H attack. Oxidative cleavage at the benzylic carbon atom, with production of an aromatic aldehyde, has previously been observed in the oxygenation of the Cu^I complexes $[Cu(PhCH_2Py)_2]^+$ [41] and $[Cu_2(m\text{-}Xyl^{i\text{Pr}4})]^{2+}$.[42]

Ligand Protonation and Stability Constants of Copper(II)−L-55 Complexes

The protonation and Cu^{2+} complex-forming equilibria of the ligand L-55 were investigated potentiometrically in a mixture of acetonitrile/water (4:1, v/v). We were able to monitor five protonation steps for L-55 and to determine their cumulative logβ values as 8.04 (0.2), 14.94 (0.2), 19.85 (0.3), 23.98 (0.1), 25.85 (0.3). The ligand easily and simultaneously incorporates two copper(II) ions according to the equilibrium in Equation (2).

$$2\,Cu^{2+} + \text{L-55} \rightleftarrows [Cu_2(\text{L-55})]^{4+} \quad \log\beta_{120} = 20.62\,(0.1) \tag{2}$$

The stability constant of this complex is similar to that of the corresponding dinuclear Cu^{II} complex derived from L-66 ($\log\beta_{120} = 19.89$[34]), while that of the $[Cu_2(EBA)]^{4+}$ complex is much larger ($\log\beta_{120} = 37.68$[26]), indicating that the longer and flexible carbon chain of EBA enables the repulsion between the positively charged cationic centers to be reduced.

With increasing pH, the two copper ions, each containing coordinated water molecules, undergo stepwise deprotonation of coordinated water molecules, as shown in the species distribution diagram in Figure 3, according to the equilibria in Equation (3) and (4) which occur with pK_a values of 6.93 and 6.25, respectively.

$$[Cu_2(\text{L-55})(H_2O)_2]^{4+} \rightleftarrows [Cu_2(\text{L-55})(H_2O)(OH)]^{3+} + H^+ \tag{3}$$

$$[Cu_2(\text{L-55})(H_2O)(OH)]^{3+} \rightleftarrows [Cu_2(\text{L-55})(OH)_2]^{2+} + H^+ \tag{4}$$

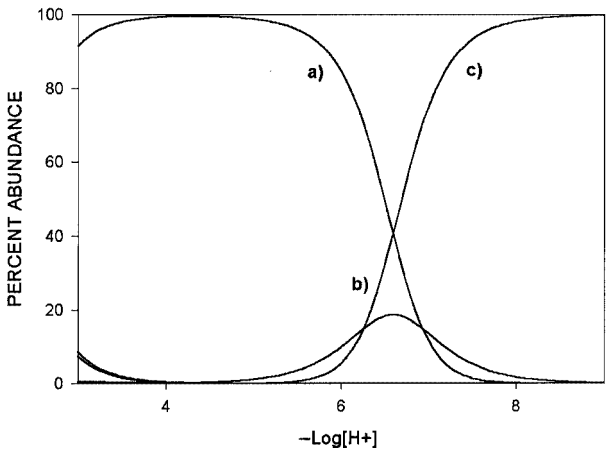

Figure 3. Species distribution in the 2Cu/L-55 system as a function of pH in acetonitrile/water solution: a) $[Cu_2(L\text{-}55)(H_2O)_2]^{4+}$; b) $[Cu_2(L\text{-}55)(H_2O)(OH)]^{3+}$; c) $[Cu_2(L\text{-}55)(OH)_2]^{2+}$

Both pK_a values are rather low and consistent with the formation of a bis(μ-hydroxo)dicopper(II) species. It may be noted that the second deprotonation occurs with lower pK_a values, even though the charge decreases after the first step. This behavior is not surprising. As is suggested by the X-ray crystal structure of $[Cu_2(L\text{-}55)(OMe)_2][ClO_4]_2$ (**2**), formation of the bis(μ-hydroxo) bridge probably drives proton dissociation, accounting for pK_{a2} < pK_{a1}. Therefore, as we have previously noted,[26] the monohydroxo species that forms after the first deprotonation step preorganizes the complex and facilitates the formation of the dibridged complex containing the ring-closed $Cu_2(OH)_2$ core. Deprotonation of coordinated water in the related complex $[Cu_2(EBA)(OH)_2]^{4+}$ follows the same trend (pK_{a2} < pKa1), but both pK_a values are larger.[26] This indicates that the *m*-xylyl residue of L-55 more readily favors the adoption of the folded conformation, stabilizing the bis(μ-hydroxo) bridge with respect to the long aliphatic chain of EBA.

NMR Studies on Copper(II)−L55 Complexes

The pH-driven equilibrium between $[Cu_2(L\text{-}55)(H_2O)_2]^{4+}$ (**3**) and its bis(μ-hydroxo) adduct **4** reported above can conveniently be monitored by ^{1}H NMR spectroscopy. The ^{1}H NMR spectrum of **3** in DMSO solution shows typical paramagnetic behavior, with broad signals (Figure 4a) resulting from the presence of only weakly coupled metal centers. The unresolved and broad peaks are spread between δ = 30 and −3 ppm, and increasing temperature shifts the downfield resonances towards the diamagnetic region, obeying Curie behavior, as shown in Figure 5a. In agreement with the above interpretation, the μ_{eff}/Cu was 1.27 μ_B, confirming the existence of a moderate interaction between the copper centers. This interaction is probably mediated by bridging water molecule(s) between the dicopper(II) centers. The addition of 2 equiv. of OH^- to the DMSO solution of **3** completely changes the NMR spectral shape. Formation of the bis(μ-hydroxo) bridge in **4** strongly increases the ex-

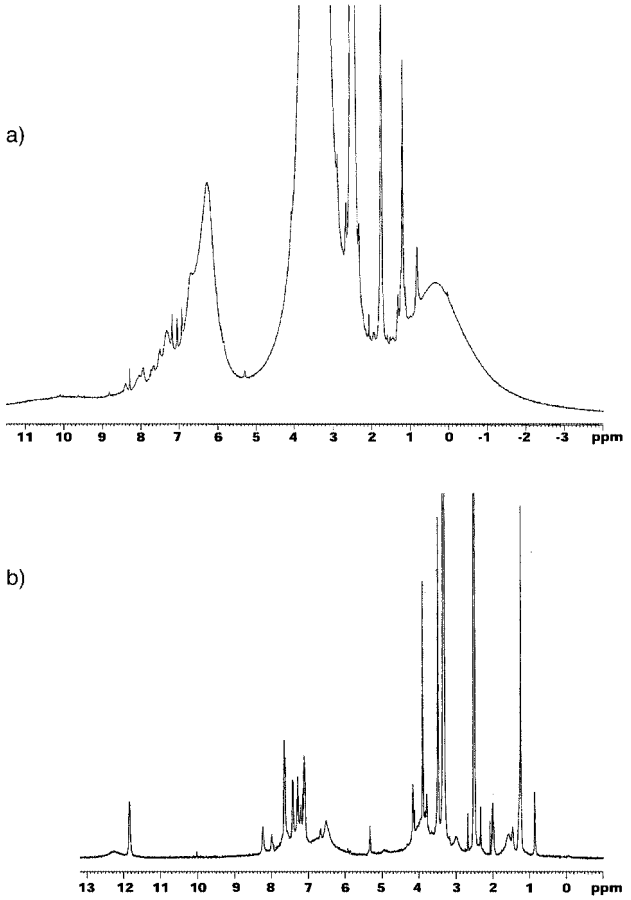

Figure 4. Diamagnetic regions of the ^{1}H NMR (δ values, ppm) spectra of $[Cu_2(L\text{-}55)(H_2O)_2]^{4+}$ and $[Cu_2(L\text{-}55)(OH)_2]^{2+}$ in DMSO solutions (1.5 mM) at 25 °C

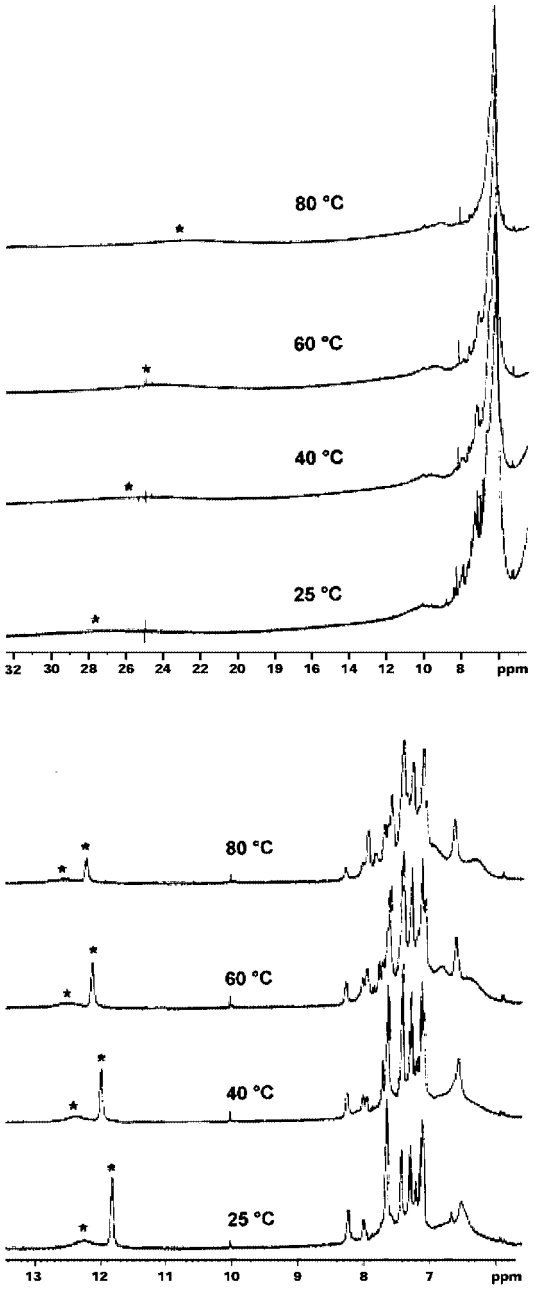

Figure 5. Upfield shifted resonances of a) $[Cu_2(L\text{-}55)(H_2O)_2]^{4+}$ and b) $[Cu_2(L\text{-}55)(OH)_2]^{2+}$; ^{1}H NMR spectra were recorded in DMSO at different temperatures

change interaction between the metal centers. The compound gives a diamagnetic-type NMR spectrum in which broadening of the peaks is reduced dramatically (Figure 4b), and the signals are detected only between $\delta = 0$ and 14 ppm. The temperature dependence of these signals was studied over the temperature range between 25 and 80 °C. As shown in Figure 5b, the downfield resonances clearly shift away from the diamagnetic region as the temperature increases, obeying anti-Curie law behavior. The magnetic properties of **4** in solution were confirmed by the Evans susceptibility method. At 25 °C, μ_{eff}/Cu was reduced to 0.47 μ_B, indicating a strong exchange coupling between the copper(II) centers. In the bridged bis(μ-hydroxo)dicopper(II) complexes the exchange interaction between the electron spins of the metal ions affects both the relaxation and the paramagnetic shift properties.[43,44] Hence, ^{1}H NMR spectroscopy strongly confirms the double-bridged structure of $[Cu_2(L\text{-}55)(OH)_2]^{2+}$ in solution, which should be clearly similar to those reported for **2** and $[Cu_2(EBA)(OH)_2]^{2+}$.[26] It can be noted that this coordination arrangement for $[Cu_2(L\text{-}55)(OH)_2]^{2+}$ was previously postulated on the basis of UV/Vis titration data.[35]

Conclusion

The reaction between $[Cu^I_2(L\text{-}55)(MeCN)_2]^{2+}$ and dioxygen produces $[Cu^{II}_2(L\text{-}55)(OH)_2]^{2+}$ through the formation of a species that we formulate as the μ-oxo-bridged complex $[Cu^{II}_2(L\text{-}55)O]^{2+}$, on the basis of its spectral properties and reaction with water. With $[Cu^I_2(L\text{-}66)]^{2+}$, in contrast, the isolation and characterization of the $[Cu_2(L\text{-}66)O_2]^{2+}$ peroxo complex at low temperatures was possible.[19] On raising the temperature, this peroxo complex also undergoes a similar irreversible oxidation (Scheme 3, a). However, when $[Cu^I_2(m\text{-}Xylpy_2)]^{2+}$ reacts with O_2, the resulting Cu_2O_2 complex effects a hydroxylation of the aromatic ring (Scheme 3b), giving a five-coordinate μ-phenoxo,μ-hydroxo-bridged dicopper(II) complex.[27] Structural results for compounds **1** and **2**, in comparison with those for the corresponding *m*-Xylpy$_2$ complexes, suggest that the different behavior of the Cu^I species toward dioxygen should be principally related to the different structural environments of the Cu^I ions, in spite of the apparently favorable orientation of the xylyl ring. Although the structure of the starting Cu^I compound is not known, the Cu^I−EBA complex should behave like the L-55 derivative, as suggested by the long Cu···N(amine) distance found in Cu^{II}−EBA,[26] close to that found for **2**. The reactivity of the putative dioxygen intermediates involved in the reaction pathways of L-55 and EBA complexes (Scheme 3a) are strictly related to their structural features. The absent or weak axial interaction offered by the amine group of the ligands increases the electrophilic reactivity of the $[Cu_2O_2]^{2+}$ moiety. Even at low temperature, as soon as the $[Cu_2(L\text{-}55)O_2]^{2+}$ or $[Cu_2(EBA)O_2]^{2+}$ complexes form, they probably react rapidly with excess Cu^I species present in solution (Scheme 3a), producing their corresponding μ-oxodicopper(II) complexes.

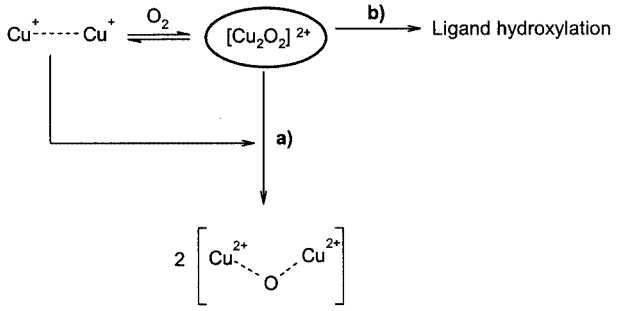

Scheme 3

The reactivity of the Cu^{II} complexes with hydrogen peroxide also elicits important differences in the behavior of L-55 vs. L-66 or *m*-Xylpy$_2$ complexes. In the last two cases, in fact, formation of a hydroperoxo intermediate results in hydroxylation of the central *m*-xylyl ring.[30,34] With $[Cu_2(L\text{-}55)(H_2O)_2]^{4+}$ a similar reaction through a putative μ-hydroperoxodicopper(II) complex seems possible, judging from the crystal structure of **2**, but the observed hydroxylation is much slower and occurs at the benzylic position. To clarify these differences, our current efforts are directed to the characterization of the so far elusive hydroperoxo intermediate formed by $[Cu_2(L\text{-}55)(H_2O)_2]^{4+}$.

Experimental Section

General: All reagents were purchased from commercial sources and were used as received unless otherwise noted. The ligand L-55 and the corresponding dinuclear copper(I) and copper(II) complexes studied here were prepared by published procedures.[33,35] NMR spectra were recorded with a Bruker Avance 400 spectrometer. Optical spectra were measured with HP 8452A and 8453 diode array spectrophotometers. Electrospray ionization MS spectra were acquired with a Finnigan MAT system equipped with an ion trap detector. Solutions were introduced into the electrospray source by syringe pump at 10 μL·min^{-1}. The ESI source was operated at 3.5 kV, the capillary temperature was set at 180 °C, and its voltage at 10 V; the experiments were performed in positive ion mode.

Single-Crystal X-ray Structure Determination of 1: Crystals of **1** were obtained by diffusion of diethyl ether into a solution of **1** in acetonitrile under an inert gas. Single crystals were coated with polyfluoropolyalkyl ether oil and mounted on a glass fiber. Data were collected with a Siemens P4 diffractometer. Lorentz and polarization corrections were applied. The structures were solved by direct methods and refined on F^2 by full-matrix, least-squares techniques.[45] Non-hydrogen atoms were refined with anisotropic thermal parameters. The PF_6^- anions are partly situated on inversion centers and disordered; they were refined by use of SIMU restraints. All hydrogen atoms are positioned geometrically. No hydrogen atoms were included in the description of three not very well defined acetonitrile solvate molecules.

Single-Crystal X-ray Structure Determination of 2: The crystals used in the X-ray analysis were grown by slow concentration of a methanol solution of $[Cu_2(L\text{-}55)(OH)_2][ClO_4]_2$. For data collection, a crystal of 0.6 × 0.4 × 0.4 mm, sealed in a glass capillary tube, in the presence of mother liquor, was used. The diffraction data were

collected at room temperature with an Enraf−Nonius CAD4 four-circle automated diffractometer with graphite-monochromated Mo-K_α radiation. Accurate unit cell parameters and orientation matrix were determined by least-squares refinement of the setting angles of 25 well-centered reflections in the range $22° < 2\theta < 30°$. Reflections were collected in the ω/2θ-scan mode. No decay was observed throughout the data collection. Correction for Lorentz polarization and scan absorption was applied. A total of 9476 (9449 independent) reflections were collected, 4424 of which having $I > 2\sigma(I)$. Unit cell parameters are a = 10.462(4), b = 13.226(4), c = 20.149(7) Å, α= 78.08(3), β= 89.18(3), and γ = 80.07(2)° for the triclinic $P\bar{1}$ space group, V = 2686.4(16) Å^3, Z = 2, M_w = 1135.9 and $D_{calcd.}$ = 1.404 Mg/m^3. The structure was solved by conventional Patterson and Fourier methods and refined by least-squares methods.[46,47] All the non-H atoms were treated anisotropically, except those of the solvent methanol, and the H atom contribution was held constant in the final refinement of 653 parameters. The final R index was 0.086 (Rw = 0.196) for reflections with $I > 2\sigma(I)$. Crystal collection and refinement data are given in Table 1. Complete tables of atomic parameters and bond lengths and angles are deposited with the CCDC. CCDC-198231 (**2**) and -198232 (**1**) contain the supplementary crystallographic data for this paper. These data can be obtained free of charge at www.ccdc.cam.ac.uk/conts/retrieving.html [or from the Cambridge Crystallographic Data Centre, 12 Union Road, Cambridge CB2 1EZ, UK; Fax: (internat.) + 44-1223/336-033; E-mail: deposit@ccdc.cam.ac.uk].

Low-Temperature Spectroscopy: Low-temperature spectra (−80 °C and below) recorded during the reaction between $[Cu_2(L\text{-}55)(CH_3CN)_2]^{2+}$ and dioxygen were obtained with a custom-designed immersible fiber-optic quartz probe (Hellma) fitted to a Schlenk vessel and connected with an HP 8452A diode array spectrophotometer. Experiments were performed by bubbling chilled dioxygen into ca. 1.5 mM solutions of the complexes, formed in situ by mixing stoichiometric amounts of ligand and copper(I) BArF salt {BArF = $[\{3,5\text{-}(CF_3)_2C_6H_3\}_4B]^-$} in the appropriate solvent.[40,48]

Potentiometric Determinations: Potentiometric determination of L-55 in the absence and in the presence of copper(II) ions were performed with an apparatus and by methods described elsewhere[49] in 50 mL of an acetonitrile/water mixture (80:20, v/v) made up to 0.1 M in ionic strength with $NaClO_4$ at 298 K. The electrodes were dipped in the above solvent mixture for more than 1 h before standardization of the system, which was also made as described previously.[49] The HYPER-QUAD program was used to process the data to calculate both the protonation and stability constant.[50]

Solution Susceptibility Measurements: The susceptibility of the sample was measured by the modified Evans method.[51,52] A coaxial NMR tube was used with *tert*-butyl alcohol as an internal reference. The solution of the paramagnetic species (5 mM, DMSO) of which the susceptibility was to be determined was introduced into the inner narrow-bore tube, while the solvent containing the reference compound (4%, v/v) was placed into the outer tube. The paramagnetic solution also contained the reference compound, in an identical amount. The methyl proton signals of *tert*-butyl alcohol were recorded and the separation of the two signals ($\Delta\nu$) was monitored and regarded as the paramagnetic shift. Mass susceptibility (χ_p) is correlated to the above measured $\Delta\nu$ as given in Equation (5) where c is the concentration of the solution (mol/L), M the molecular weight of the complex, ν_0 the operating rf of the spectrometer, and χ_0 the susceptibility of pure solvent.

$$\chi_p = \chi_0 + \frac{3000 \cdot \Delta\nu}{4\pi\nu_0 cM} \quad (5)$$

Molar susceptibility (χ_M) can then be calculated after the usual correction.[53] The magnetic moment in solution (μ_{eff}) was obtained from the same shift data as reported in the literature.[54] The reliability of our measurement method was tested with $CuSO_4 \cdot 5H_2O$ as paramagnetic standard. The χ_p, χ_M, μ_{eff} values for this compound agreed perfectly with those previously calculated and available in the literature.[51,52]

Isolation of the Hydroxylated Ligand: The complex $[Cu_2(L\text{-}55)(H_2O)_2]^{4+}$ (100 mg, 0.07 mmol) was dissolved in a mixture of MeOH/phosphate buffer (50 mM, pH = 7, 8:2, v/v), and a concd. aqueous solution of hydrogen peroxide (0.7 mmol) was added. The solution was allowed to react for 12 h whilst stirring at room temperature. It was then concentrated under reduced pressure and chromatographed on a Sephadex LH-20 column (1.5 × 40 cm). The resulting fraction was collected, and the solvent volume was reduced by rotary evaporation and added to 100 mL of a mixture of concentrated ammonia/CH_2Cl_2 (1:1, v/v). The aqueous layer was separated and further extracted with cold CH_2Cl_2 (50 mL, 3 times). The organic extracts were combined, washed with water, and dried with $MgSO_4$. The final organic mixture was purified by silica gel column, by eluting with a mixture of CH_2Cl_2/MeOH (9:1, v/v) to which an increasing amount of concentrated NEt_3, from 1 to 15%, was added. The fraction containing the product was collected by spectrophotometric monitoring of the UV absorptions of the benzimidazole ring (284, 276, 254 nm) in the eluate, and after evaporation of the solvent afforded a light yellow, unstable oil (overall yield 50%). ^{1}H NMR ($CDCl_3$): δ = 9.8 (s, 1 H, HCO), δ = 7.6 (m, 8 H, Bz + Xy), 4.1 (t, 4 H, CH_2), 3.9 (s, 2 H, CH_2-Xy), 3.6 (s, 6 H, CH_3-Bz) ppm. ESI-MS: m/z = 424.4 $[L + H]^+$.

Acknowledgments

The authors thank the Italian CNR, the University of Pavia (FAR), and COST for support. S. S. gratefully acknowledges financial support from the DFG and Prof. Rudi van Eldik (University of Erlangen-Nürnberg).

[1] A. G. Blackman, W. B. Tolman, *Struct. Bonding* **2000**, *97*, 179−211.
[2] K. D. Karlin, A. D. Zuberbühler, in: *Bioinorganic Catalysis*, 2nd ed., revised and expanded (Eds.: J. Reedijk, E. Bouwman), Dekker, New Jork, **1999**, pp. 469−534.
[3] S. Schindler, *Eur. J. Inorg. Chem.* **2000**, 2311−2326.
[4] H.-C. Liang, M. Dahan, K. D. Karlin, *Curr. Opin. Chem. Biol.* **1999**, *3*, 168−175.
[5] E. I. Solomon, P. Chen, M. Metz, S.-K. Lee, A. E. Palmer, *Angew. Chem. Int. Ed.* **2001**, *40*, 4570−4590.
[6] E. I. Solomon, U. M. Sundaram, T. E. Machonkin, *Chem. Rev.* **1996**, *96*, 2563−2605.
[7] M. A. McGuirl, D. M. Dooley, *Curr. Opin. Chem. Biol.* **1999**, *3*, 138−144.
[8] H. Decker, R. Dillinger, F. Tuczek, *Angew. Chem. Int. Ed.* **2000**, *39*, 1591−1595.
[9] P. L. Holland, W. B. Tolman, *Coord. Chem. Rev.* **1999**, *190−192*, 855−869.
[10] P. Gamez, P. G. Aubel, W. L. Driessen, J. Reedijk, *Chem. Soc. Rev.* **2001**, *30*, 376−385.
[11] C. S. Foote, J. S. Valentine, A. Greenberg, J. F. Liebman, *Active Oxygen in Chemistry*, Chapman & Hall, London, **1995**.
[12] K. D. Karlin, M. S. Nasir, B. I. Cohen, R. W. Cruse, S. Kaderli,

A. D. Zuberbühler, *J. Am. Chem. Soc.* **1994**, *116*, 1324−1336.
[13] E. Pidcock, H. V. Obias, C. X. Zhang, K. D. Karlin, E. I. Solomon, *J. Am. Chem. Soc.* **1998**, *120*, 7841−7847.
[14] P. L. Holland, K. R. Rodgers, W. B. Tolman, *Angew. Chem. Int. Ed.* **1999**, *38*, 1139−1142.
[15] J. A. Halfen, V. G. Young, Jr., W. B. Tolman, *Inorg. Chem.* **1998**, *37*, 2102−2103.
[16] S. Itoh, M. Taki, H. Nakao, P. L. Holland, W. B. Tolman, L. Que, Jr., S. Fukuzumi, *Angew. Chem. Int. Ed.* **2000**, *39*, 398−400.
[17] V. Mahadevan, J. L. DuBois, B. Hedman, K. O. Hodgson, T. D. P. Stack, *J. Am. Chem. Soc.* **1999**, *121*, 5583−5584.
[18] V. Mahadevan, M. J. Henson, E. I. Solomon, T. D. P. Stack, *J. Am. Chem. Soc.* **2000**, *122*, 10249−10250.
[19] L. Santagostini, M. Gullotti, E. Monzani, L. Casella, R. Dillinger, F. Tuczek, *Chem. Eur. J.* **2000**, *6*, 519−522.
[20] S. Itoh, H. Kumei, M. Taki, S. Nagatomo, T. Kitagawa, S. Fukuzumi, *J. Am. Chem. Soc.* **2001**, *123*, 6708−6709.
[21] L. Casella, M. Gullotti, G. Pallanza, R. Rigoni, *J. Am. Chem. Soc.* **1988**, *110*, 4221−4227.
[22] O. J. Gelling, F. van Bolhuis, A. Meetsma, B. L. Feringa, *J. Chem. Soc., Chem. Commun.* **1988**, 552−554.
[23] T. N. Sorrell, V. A. Vankai, M. L. Garrity, *Inorg. Chem.* **1991**, *30*, 207−210.
[24] G. Alzuet, L. Casella, M. Villa, O. Carugo, M. Gullotti, *J. Chem. Soc., Dalton Trans.* **1997**, 4789−4794.
[25] D. Ghosh, P. Mukherjee, *Inorg. Chem.* **1998**, *37*, 6597−6605.
[26] E. Monzani, G. Battaini, A. Perotti, L. Casella, M. Gullotti, L. Santagostini, G. Nardin, L. Randaccio, S. Geremia, P. Zanello, G. Opromolla, *Inorg. Chem.* **1999**, *38*, 5359−5369.
[27] K. D. Karlin, J. C. Hayes, Y. Gultneh, R. W. Cruse, T. W. McKown, J. P. Hutchinson, J. Zubieta, *J. Am. Chem. Soc.* **1984**, *106*, 2121−2128.
[28] K. D. Karlin, S. Kaderli, A. D. Zuberbühler, *Acc. Chem. Res.* **1997**, *30*, 139−147.
[29] M. Becker, S. Schindler, K. D. Karlin, T. A. Kaden, S. Kaderli, T. Palanche, A. D. Zuberbühler, *Inorg. Chem.* **1999**, *38*, 1989−1995.
[30] R. W. Cruse, S. Kaderli, C. J. Meyer, A. D. Zuberbühler, K. D. Karlin, *J. Am. Chem. Soc.* **1988**, *110*, 5020−5024.
[31] T. N. Sorrell, M. L. Garrity, *Inorg. Chem.* **1991**, *30*, 210−215.
[32] L. Casella, M. Gullotti, R. Radaelli, P. Di Gennaro, *J. Chem. Soc., Chem. Commun.* **1991**, 1611−1612.
[33] L. Casella, E. Monzani, M. Gullotti, D. Cavagnino, G. Cerina, L. Santagostini, R. Ugo, *Inorg. Chem.* **1996**, *35*, 7516−7525.
[34] G. Battaini, E. Monzani, A. Perotti, C. Para, L. Casella, L. Santagostini, M. Gullotti, R. Dillinger, C. Näther, F. Tuczek, *J. Am. Chem. Soc.*, submitted for publication.
[35] L. Casella, O. Carugo, M. Gullotti, S. Garofani, P. Zanello, *Inorg. Chem.* **1993**, *32*, 2056−2057.
[36] S. Schindler, D. J. Szalda, C. Creutz, *Inorg. Chem.* **1992**, *31*, 2255−2264.
[37] C. K. Johnson, *Report ORNL-5138, ORTEP*, Oak Ridge National Laboratory, Oak Ridge, TN, **1976**.
[38] K. D. Karlin, J. Shi, J. C. Hayes, J. W. McKown, J. P. Hutchinson, J. Zubieta, *Inorg. Chim. Acta* **1984**, *91*, L3−L7.
[39] M. Weitzer, M. Schatz, F. Hampel, F. W. Heinemann, S. Schindler, *J. Chem. Soc., Dalton Trans.* **2002**, 686−694.
[40] H. V. Obias, Y. Lin, N. N. Murthy, E. Pidcock, E. I. Solomon, M. Ralle, N. J. Blackburn, Y.-M. Neuhold, A. D. Zuberbühler, K. D. Karlin, *J. Am. Chem. Soc.* **1998**, *120*, 12960−12961.
[41] I. Sanyal, M. Mahroof-Tahir, M. S. Nasir, P. Ghosh, B. I. Cohen, Y. Gultneh, R. W. Cruse, A. Farooq, K. D. Karlin, S. Liu, J. Zubieta, *Inorg. Chem.* **1992**, *31*, 4322−4332.
[42] S. Mahapatra, S. Kaderli, A. Llobet, Y.-M. Neuhold, T. Palanche, J. A. Halfen, V. G. Young, Jr., T. A. Kaden, L. Que, A. D. Zuberbühler, W. B. Tolman, *Inorg. Chem.* **1997**, *36*, 6343−6356.
[43] V. Clementi, C. Luchinat, *Acc. Chem. Res.* **1998**, *31*, 351−361.
[44] N. N. Murthy, K. D. Karlin, I. Bertini, C. Luchinat, *J. Am. Chem. Soc.* **1997**, *119*, 2156−2162.
[45] G. M. Sheldrick, Siemens Analytical X-ray Inst., Inc., WI, USA, **1994**.
[46] G. M. Sheldrick, Universität Göttingen, Göttingen, Germany, **1993**.
[47] G. M. Sheldrick, *Acta Crystallogr., Sect. A* **1990**, *A46*, 467−473.
[48] M. Brookhart, B. Brant, A. F. Volpe Jr., *Organometallics* **1992**, *11*, 3920−3922.
[49] E. Monzani, L. Quinti, A. Perotti, L. Casella, M. Gullotti, L. Randaccio, S. Geremia, G. Nardin, P. Faleschini, G. Tabbi, *Inorg. Chem.* **1998**, *37*, 553−562.
[50] A. Sabatini, A. Vacca, P. Gans, *Coord. Chem. Rev.* **1992**, *120*, 389−405.
[51] D. F. Evans, *J. Chem. Soc.* **1959**, 2003−2005.
[52] S. K. Sur, *J. Magn. Reson.* **1989**, *82*, 169−173.
[53] R. L. Carlin, *Magnetochemistry*, Springer, New York, **1986**.
[54] I. Bertini, C. Luchinat, *NMR of Paramagnetic Substances*, Elsevier, Amsterdam, **1996**.

Received September 2, 2002
[I02493]

Novel Adducts of the Anticancer Drug Oxaliplatin with Glutathione and Redox Reactions with Glutathione Disulfide

Sarah Fakih,[a] Vivienne P. Munk,[a] Michelle A. Shipman,[a] Piedad del Socorro Murdoch,[a] John A. Parkinson,[a] and Peter J. Sadler*[a]

Keywords: Antitumour agents / Platinum / S ligands / Peptides / Redox chemistry

Reactions of [Pt(*rac*-1,2-DACH)Cl_2], [Pt(1*R*,2*R*-DACH)Cl_2] and the anticancer drug oxaliplatin with the tripeptide glutathione and glutathione disulfide have been studied by HPLC, ESI-MS and NMR methods. The same two major products are formed in each reaction: a thiolate-bridged dimer and a novel thiolate-bridged dinuclear macrochelate containing a nine-membered chelate ring. Redox reactions of Pt^{II} anticancer drugs with biological disulfides are of potential importance to their mechanism of action.

(© Wiley-VCH Verlag GmbH & Co. KGaA, 69451 Weinheim, Germany, 2003)

Introduction

cis-Diamminedichloroplatinum(II) or cisplatin (**1**) has been used as an anticancer drug since it entered clinical trials in the 1970s.[1] Its effectiveness against ovarian and testicular cancers is well established, and it has also been used to improve the response rate of head, neck and lung tumours.[2] Although one of the most effective anticancer drugs known to date, cisplatin possesses inherent disadvantages, namely limited solubility and extreme side-effects, including nausea, vomiting and nephrotoxicity.[3] Furthermore, many tumours have displayed a natural resistance to cisplatin while others develop resistance during treatment.[4] Thus, the use of the drug is limited to a narrow class of tumours. The occurrence of such adverse side-effects has been addressed by the introduction of hyperhydration therapies and serotonin antagonists.[5] Concurrently, there has been a major effort in the production of alternative drugs, which display all of the activity of cisplatin but with fewer side-effects.[6] A large library of platinum complexes has been synthesised and their antitumour activity examined, resulting in the determination of structure-activity relationships.

The nature of the amine has a pronounced effect on the activity observed. Preclinical studies of platinum complexes containing diaminocyclohexane (DACH) have demonstrated activity against cisplatin-resistant cell lines.[7] The drug (1*R*,2*R*)-diaminocyclohexaneoxalatoplatinum(II), oxaliplatin (**2**), has recently been approved for use in the treatment of colorectal and ovarian cancers in Europe, Asia and South America.[8,9] In the clinical trials of oxaliplatin, the drug was highly active in solid tumour types, and particularly effective against advanced colorectal cancer when administered with 5′-fluorouracil.[5,10] Oxaliplatin shows no nephrotoxicity or myeloid toxicity. However, the dose-limiting toxicity is governed by peripheral sensory neuropathy.[11] Evidence also exists that cisplatin analogues containing the bulky, nonpolar ligand DACH, such as oxaliplatin, do not elicit resistance in mismatch repair-deficient cells.[12] Thus, oxaliplatin may be able to overcome tumour resistance caused by loss of mismatch repair. Studies have shown that [Pt(1,2-DACH)Cl_2] is nearly twice as cytotoxic to HT-29 cells as oxaliplatin, although cellular uptake of oxaliplatin is considerably higher.[11]

Although cellular DNA is the ultimate target for platinum anticancer drugs,[13−15] many other biomolecules can also interact with platinum drugs, especially thiols and thioethers. Such biomolecules could either aid the transport of the drug or, equally, hinder transport by effectively capturing it, thereby preventing it from ever reaching its intended target site.

The thiol-containing tripeptide glutathione (γ-L-Glu-L-Cys-Gly, GSH, **3**) is present in most cells in millimolar concentrations (0.5−10 mM).[16,17] Intracellular interactions between glutathione and cisplatin have previously been found to be deactivating, and cisplatin-resistant tumour cells often contain elevated levels of glutathione.[18,19] There is strong evidence that GS-X pumps can facilitate the active transport of Pt drugs from the cell.[20] Interestingly, however, the strong affinity of sulfur for platinum complexes has led to the coadministration of platinum drugs with glutathione as a chemoprotectant.[21,22] The toxic side-effects are reduced due to reversal or prevention of Pt-S adducts in proteins, while the antitumour activity of cisplatin remains un-

[a] School of Chemistry, University of Edinburgh, West Mains Road, Edinburgh, EH9 3JJ, UK
Fax: (internat.) + 44−131 650 6452
E-mail: P.J.Sadler@ed.ac.uk
Supporting information for this article is available on the WWW under http://www.eurjic.org or from the author.

affected.[23] Platinum-sulfur adducts might constitute drug reservoirs from which the platinum could later be transferred onto the target DNA.[17] Could this provide an alternative pathway to the direct attack of the drug (or its aqua adducts) on DNA? Such a question has provided the stimulus for a number of studies into reactions between platinum drugs and potential sulfur nucleophiles.[24−28]

The major product from the reaction of cysteine derivatives with *cis*-diam(m)ineplatinum(II) complexes is thought to be the bridged dimer $[(am)_2Pt(\mu_2\text{-}SR)_2Pt(am)_2]$, where "am" is am(m)ine or one half of a diamine. However, these bridged complexes are unlikely to be reactive towards DNA bases, although the ammine complexes can slowly release ammonia.[29,30] Reactions carried out with [PtCl(dien)]Cl and methionine (Met) or methylated glutathione (GSMe)[26,27] and 5′ GMP have indicated that the platinum−sulfur adducts $[Pt(dien)(Met\text{-}S)]^{2+}$ and $[Pt(dien)(GSMe\text{-}S)]^{2+}$ are formed initially with subsequent intermolecular displacement of the thioether in the Pt−S adducts by 5′ GMP-N7. Interestingly, this displacement of guanine-N7 has been observed only with thioether adducts and not for reactions with thiolate complexes.[30] The biotransformation products of oxaliplatin have been investigated in patients with gastrointestinal cancers and there is evidence of nucleophilic substitution of the oxalate leaving group, with mono- and dichlorinated DACH-platin and glutathione-DACH-platin adducts being present as metabolites in the blood plasma and urine.[31]

In work reported here, we have isolated and characterised new products formed from reactions of either GSH or GSSG (GSH disulfide, **4**) with oxaliplatin, and (1*R*,2*R*)-diaminocyclohexanedichloroplatinum(II), [Pt(1*R*,2*R*-DACH)-Cl_2], **5**. These reactions have been carried out under physiological conditions, and for each complex a glutathione-bridged dinuclear platinum(II) macrochelate has been isolated. This is a potentially reactive species and could play a role in the mechanism of action of platinum anticancer drugs.

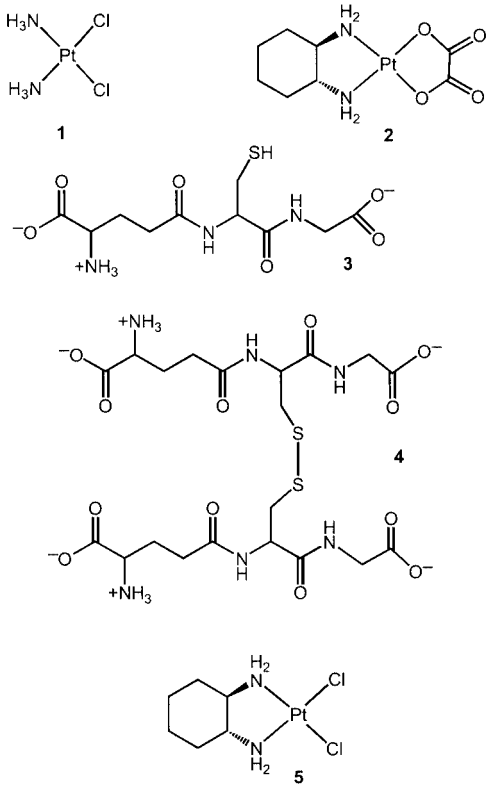

Results

Reactions of [Pt(1,2-DACH)Cl_2] with GSH and GSSG

UV/Vis Measurements

The time-courses of reactions between [Pt(*rac*-1,2-DACH)Cl_2] with GSH or GSSG at 310 K were studied using UV/Vis spectroscopy. Two molar equivalents of GSH or GSSG (10 μL, 20 mM, pH 7) were added to a solution of [Pt(*rac*-1,2-DACH)Cl_2] (1 mL, 100 μM). Typical spectra are shown in Figure 1. In both experiments a major new absorption band was observed at 220 nm which increased in intensity with time over a period of ca. 24 h. Interestingly, the reaction with GSH was only slightly faster than that with GSSG [see also Figure 8(b)].

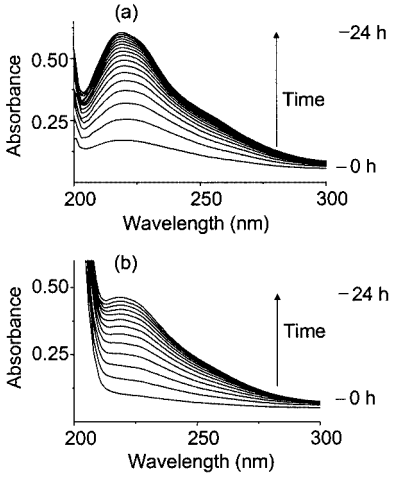

Figure 1. The change in absorbance with time for reactions of [Pt(*rac*-1,2-DACH)Cl_2] with two molar equivalents of (a) GSH, or (b) GSSG in aqueous solution (pH 7); measurements were taken at 310 K at regular hourly intervals for the first 24 hours of the reaction

HPLC Measurements

HPLC techniques were used to isolate two major products (labelled **A** and **B** in Figure 2) which formed during six-day incubations at 310 K of [Pt(*rac*-1,2-DACH)Cl_2] (2 mL, 100 μM) with two molar equivalents of GSH or GSSG (20 μL, 20 mM) initially at pH 7. Small amounts of unchanged GSH and GSSG were still present in the reaction mixture after six days. The major product peaks eluted at 20.6 min (peak **A**) and 21.6 min (peak **B**) using a gradient of acetonitrile (0−30% over 25 min) in water, with 0.1% trifluoroacetic acid as an ion pairing agent. Other minor peaks were also observed in the chromatogram, but these peaks were not isolated or identified.

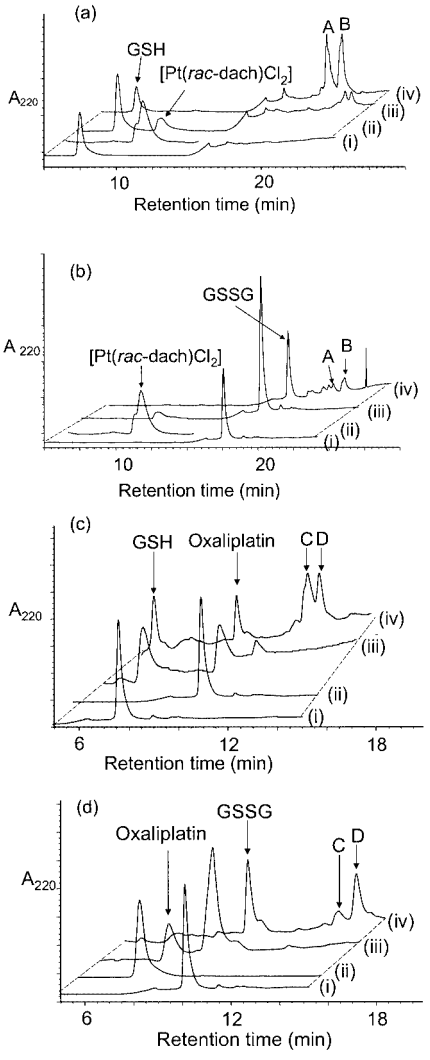

Figure 2. HPLC chromatograms (C_{18} reverse phase column eluted with a CH_3CN/H_2O gradient containing 0.1% of the ion pairing agent, monitored at 220 nm) for reactions of [Pt(*rac*-1,2-DACH)Cl_2] with two molar equivalents of either (a) GSH, or (b) GSSG (310 K, initially at pH 7), and oxaliplatin with two molar equivalents of either (c) GSH, or (d) GSSG (310 K, initially at pH 7); labels for chromatograms: (i) GSH or GSSG alone, (ii) [Pt(*rac*-1,2-DACH)Cl_2] or oxaliplatin alone (iii) after 5 min of reaction and (iv) after six days of reaction; baseline drifts in the chromatograms are observed due to a change in the refraction index of the solvent

Using the same acetonitrile gradient, the reaction of [Pt(*rac*-1,2-DACH)Cl_2] (2 mL, 100 μM) with two molar equivalents of GSH (20 μL, 20 mM, pH 7) at 310 K was monitored at hourly intervals for 24 h. The resulting chromatograms are shown in Figure S1 in the Supporting Information. The chromatograms show that the peaks for the starting materials decrease and the intensities of the product peaks **A** and **B** increase with time. No intermediates were observed during the course of the reaction. The reaction was complete after ca. 24 h, at which point the peaks due to the starting materials, 8.1 min (GSH) and 8.9 min ([Pt(*rac*-1,2-DACH)Cl_2]), have almost disappeared and the peaks for the products, 19.1 min (**A**) and 22.1 min (**B**), reach maximum intensity.

Reactions of [Pt(*rac*-1,2-DACH)Cl_2] with increasing GSH concentrations (1, 2, 4, 8 and 10 molar equivalents) were investigated by HPLC using a different acetonitrile gradient (4−20% over 30 min). The resulting chromatograms are shown in Figure 3. With this acetonitrile gradient the peaks that represent the major products, peaks **A** and **B**, do not appear as the single peaks previously seen in Figure 2, but as a series of split peaks. This difference can be attributed to changes in the HPLC elution conditions and the possible presence of isomers. The chromatograms clearly indicate a steady increase in the area of the peaks for product **A** (ca. 14 min) with increasing concentrations of GSH, while the intensities of the peaks for product **B** (ca. 18 min) decrease with increasing GSH concentrations. The areas of the peaks for products **A** and **B** are approximately equal at a 2:1 molar ratio of GSH to [Pt(*rac*-1,2-DACH)Cl_2].

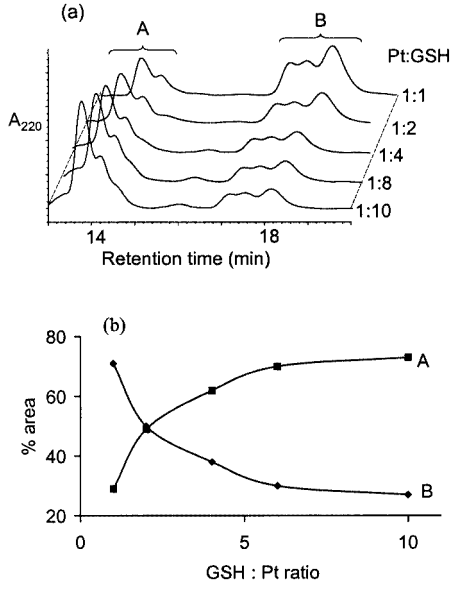

Figure 3. (a) Effect of variation of the molar ratio of [Pt(*rac*-1,2-DACH)Cl_2]:GSH on the intensities of the groups of peaks **A** and **B** in the HPLC chromatogram from reactions incubated at 310 K for 6 days; (b) variation of the intensities of peaks **A** and **B** with Pt:GSH molar ratio

To investigate the possibility that the split peaks observed in the HPLC chromatograms shown in Figure 3 are due to the presence of isomers, an analogous reaction of GSH (20 μL, 20 mM, pH 7) with enantiomerically pure [Pt(1*R*,2*R*-DACH)Cl_2] (2 mL, 100 μM) was carried out at 310 K. The resulting HPLC chromatogram, obtained using a 4−20% acetonitrile gradient over 30 min, is shown in Figure 4, together with the HPLC trace of products from the reaction of [Pt(*rac*-1,2-DACH)Cl_2] and GSH for comparison. The chromatogram for the reaction products of the enantiomerically pure platinum complex contains two single peaks in a ratio of ca. 1:2. The overall ratio of peak areas **A**:**B** is similar for reactions of the racemic and enantiomerically pure DACH complexes. The small change in HPLC retention times can be attributed to slight differences in the HPLC elution conditions.

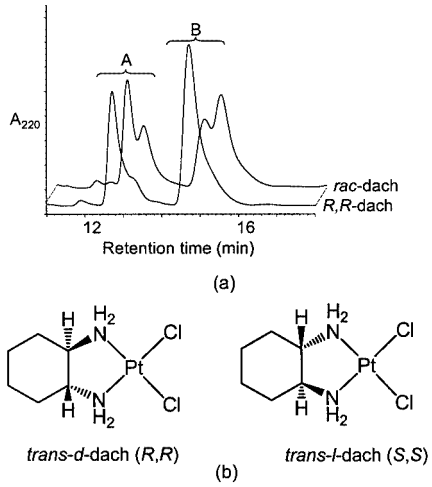

Figure 4. (a) HPLC chromatograms for products formed at 310 K from the reaction of [Pt(*rac*-1,2-DACH)Cl_2] or [Pt(1*R*,2*R*-1,2-DACH)Cl_2] with two molar equivalents of GSH in aqueous solution (initially at pH 7); HPLC elution conditions are slightly different from those in Figures 2 and 3, accounting for slight variations in the retention times; (b) structures of the two optical isomers of [Pt(1,2-DACH)Cl_2], [Pt(1*R*,2*R*-DACH)Cl_2] and [Pt(1*S*,2*S*-DACH)Cl_2]

The absorption coefficients of the separated products **A** (ε = 32,000 $M^{-1}cm^{-1}$) and **B** (ε = 34,000 $M^{-1}cm^{-1}$) at 220 nm were determined by freeze-drying the collected peaks, redissolution in water, measurement of their absorption spectra and determination of the platinum concentration in the same solution by ICP-AES.

Since GSH in cells is likely to be present in high molar excess over the platinum complex, an analogous reaction of [Pt(1*R*,2*R*-DACH)Cl_2] and a 100-fold molar excess of GSH was also monitored by HPLC. Two product peaks were formed in this reaction, and their identities (peaks **A** and **B**) were confirmed by ESI-MS (see below).

ESI-MS Measurements

The positive ion ESI-MS data of the reaction mixtures of [Pt(*rac*-1,2-DACH)Cl_2] with GSSG or GSH revealed the presence of peaks for two major products at *m*/*z* = 462 and *m*/*z* = 615 for both of the reactions (Figure S2 in the Supporting Information). The only other observed peaks are attributable to small amounts of the starting materials. Peaks **A** and **B** were separated by HPLC, and ESI-MS measurements of the collected fractions indicated that each peak consists of a single product. The observed ESI-MS spectrum for each of these products is shown in Figure 5. Both peaks show a cluster of ions characteristic of the isotopic distributions of Pt and N. The most abundant molecular ion obtained from collected peak **A** has a molecular ion [M^{2+}] at *m*/*z* = 615. Isotope modelling suggested that peak **A** corresponds to the molecular formula of $[Pt_2C_{32}H_{58}N_{10}O_{12}S_2]^{2+}$, assignable to an *S*-bridged dimer [Figure 6(a)]. The fraction associated with peak **B** [Figure 5(b)] has a molecular ion [M^{2+}] at *m*/*z* = 462, and isotope modelling suggested a molecular formula

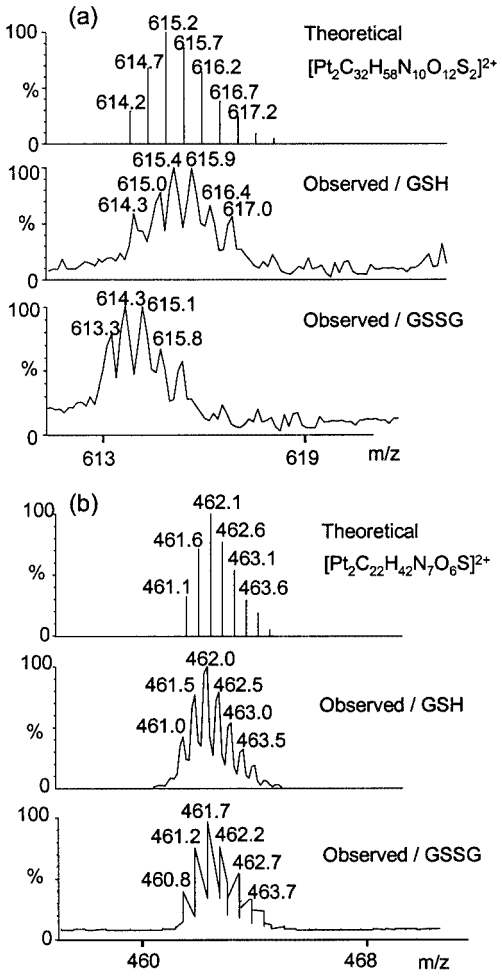

Figure 5. Positive ion ESI-MS spectra for HPLC peaks (a) **A** and (b) **B** separated from the reaction of [Pt(*rac*-1,2-DACH)Cl_2] with two molar equivalents of GSH or GSSG (310 K, initially at pH 7, six days); the HPLC conditions for the separation of these species are the same as in Figure 2; the HPLC peaks were collected, concentrated by lyophilisation and redissolved in acetonitrile/water, 1:1, for ESI-MS measurements; the observed and theoretical isotope patterns of the proposed structures for each peak are shown; the full ESI-MS spectrum is shown in Figure S2 in the Supporting Information

$[Pt_2C_{22}H_{42}N_7O_6S]^{2+}$, assignable to a glutathione-bridged macrochelate [Figure 6(b)].

NMR Analysis

1D ^1H and 2D ^1H DQFCOSY, NOESY, TOCSY and ROESY NMR experiments were carried out on a ca. 1.3 mM solution of product **B** in 90% H_2O/10% D_2O, pH 4. Specific assignments were determined for most of the ^1H NMR resonances based on the 2D TOCSY NMR spectroscopic data (Figure 7): Gly-N*H* (δ = 7.90 ppm) couples to two doublets of doublets at δ = 4.10 ppm (Gly−Hα^a) and δ = 3.61 ppm (Gly−Hα^b). Cys−Hα (δ = 5.02 ppm) couples to Cys−Hβ^b (δ = 2.79 ppm) but not to its geminal partner Cys−Hβ^a (δ = 2.66 ppm). Both of these signals are clearly visible in the 1D ^1H NMR spectrum (Figure S3 in the Supporting Information, which also shows the atom labelling scheme). A spin system consisting of six resonances was

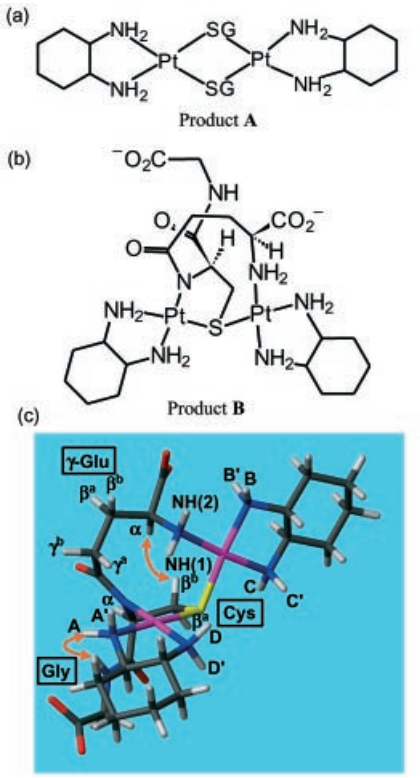

Figure 6. Proposed structures for the products of the reactions of [Pt(*rac*-DACH)Cl_2] with GSH or GSSG, which give rise to HPLC peaks (a) **A**, and (b) **B**; (c) capped-stick representation of the structure of the product corresponding to HPLC peak **B** formed between GSH with [Pt(1*R*,2*R*-DACH)Cl_2], as determined by ^{1}H NMR spectroscopy; two key structural ^{1}H-^{1}H rOes are shown by double-headed arrows; of the N*H* signals, the highest frequency resonance is that of NH(1) of γ-Glu; the space-filled representation explains how this shift may arise since the proton sits above one of the platinum centres (see contents entry); this proton therefore experiences a larger deshielding effect compared to all other N*H* protons in the molecule

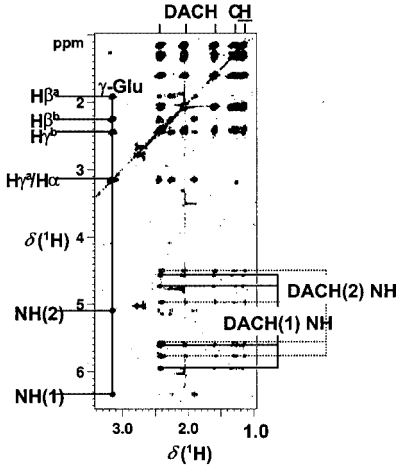

Figure 7. Section of the 600 MHz ^{1}H 2D TOCSY NMR spectroscopic data for peak **B** formed between GSH with [Pt(1*R*,2*R*-DACH)Cl_2], showing assignments for γ-Glu and DACH ligand resonances; despite several overlaps between DACH C*H* protons, it is still possible to distinguish two independent spin systems from the DACH N*H* resonances; resonance assignments are summarised in Table 1

assigned to γ-Glu: $\delta_{NH(1)}$ = 6.33 ppm; $\delta_{NH(2)}$ = 5.10 ppm; $\delta_{H\alpha}$ = 3.15 ppm; $\delta_{H\beta}{}^{b}$ = 2.25 ppm; $\delta_{H\beta}{}^{a}$ = 1.91 ppm; $\delta_{H\gamma}{}^{a}$ = 3.25 ppm; $\delta_{H\gamma}{}^{b}$ = 2.40 ppm. In addition, two complete spin systems are visible for two independent DACH units (Figure 7). Stereospecific assignments for the ring protons were not made due to resonance overlap. The NMR signal assignments are given in Table 1.

Table 1. ^{1}H NMR resonance assignments for the 2:1 macrochelate (peak **B**) formed between [Pt(1*R*,2*R*-DACH)Cl_2] and GSH; for proton labelling see Figures 6(c) and Figure S3 in the Supporting Information

		δ (NH)				
{Pt-DACH}		5.95 (A), 4.56 (A′) 5.62 (D), 4.75 (D′)			5.78 (C), 4.96 (C′) 5.57 (B), 4.50 (B′)	
H_2-SG	δ (NH)	δ (Hα)	δ (Hβ^a)	δ (Hβ^b)	δ (Hβγ^a)	δ (Hβγ^b)
Gly	7.90	4.10[a], 3.61[b]				
Cys	– [a]	5.02	2.66[b]	2.79[c]		
γ-Glu	6.33 (NH1), 5.10 (NH2)	3.15	1.91	2.25	3.16	2.40

[a] The NH signal is absent, consistent with the N of Cys being bound directly to one of the two platinum metal centres. [b] $^3J_{H,H}$ = 0, $^2J_{H,H}$ = 14 Hz. [c] $^3J_{H,H}$ = 6.4, $^2J_{H,H}$ = 14 Hz.

A molecular model of product **B** was constructed as a glutathione-bridged macrochelate molecule, $[Pt_2C_{22}H_{42}N_7O_6S]^{2+}$, which accounts for three specific observed rOes: Gly-N*H* shows an rOe to the NH proton A of DACH(1); Cys-Hβ^b shows an rOe to γ-Glu−Hα; γ-Glu−Hγ^a shows an rOe to the NH proton A′ of DACH(1). The energy-minimised model incorporating these constraints is shown in Figure 6(c).

pH Considerations

No buffers were used in these investigations, since buffer ions (e.g. phosphate) are potential ligands for Pt^{II}. The pH of each solution was regularly monitored during the course of each reaction. The pH of the glutathione and glutathione disulfide solutions was adjusted to 7 prior to addition of the platinum complex solution. Following addition of the platinum complex, the pH of the reaction mixture dropped within ca. 4 h to a value of between 4.5 and 5. The ^{1}H NMR spectra of products **A** and **B** show little change over the pH range 2.8−8.7, and therefore these species appear to be stable over a wide pH range.

Reactions of Oxaliplatin with GSH and GSSG

UV/Vis Measurements

The reaction between oxaliplatin (1 mL, 100 μM) and GSH (10 μL, 20 mM, pH 7) at 310 K gives rise to a new absorption band at 220 nm, which increases in intensity over a period of 48 h (Figure 8). The reaction between oxaliplatin and GSSG, which was monitored over 96 hours, is also slow and gives rise to a similar new absorption band. In comparison with the similar reactions of [Pt(*rac*-1,2-

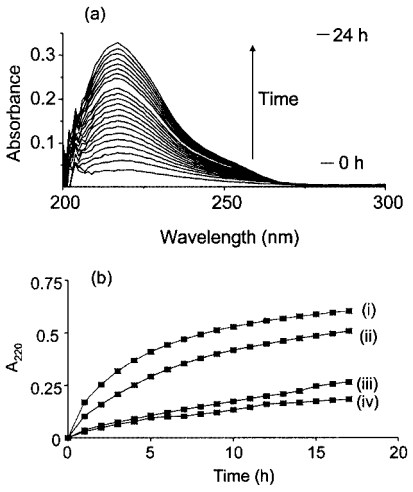

Figure 8. (a) The change in absorbance with time for reactions of oxaliplatin with two molar equivalents of GSH (initially at pH 7) in aqueous solution; measurements were taken at 310 K at regular hourly intervals for the first 24 hours of the reaction; (b) comparison of the changes in absorbance at 220 nm with time for reactions of [Pt(*rac*-1,2-DACH)Cl_2] or oxaliplatin with two molar equivalents of GSH or GSSG; labels for graphs: (i) [Pt(*rac*-1,2-DACH)Cl_2]/GSH, (ii) [Pt(*rac*-1,2-DACH)Cl_2]/GSSG, (iii) oxaliplatin/GSH and (iv) oxaliplatin/GSSG

DACH)Cl_2], those of oxaliplatin are approximately three times slower [Figure 8(b)].

HPLC Measurements

The HPLC chromatograms for reaction mixtures of oxaliplatin (2 mL, 100 μM) with two molar equivalents of GSH or GSSG (20 μL, 20 mM, pH 7, 310 K) using a 4−20% acetonitrile gradient over 30 min are shown in Figure 2(c) and (d). Peaks for two major products which elute at 14.8 min (**C**) and 15.5 min (**D**) appear in both chromatograms and increase in intensity over a period of 48 h, whilst the peaks corresponding to the reactants decrease in intensity. Small amounts of the starting materials were still present in the reaction mixtures after five days. Some minor peaks for unidentified products were also observed. For the GSH reactions, the relative areas of peaks **C** and **D** are similar, whereas for GSSG, peak **D** is more intense than peak **C**. A timecourse study (Figure S1 in the Supporting Information) showed that this preference for formation of product **D** was similar throughout the 0−24 h period that the reaction was studied.

ESI-MS Measurements

HPLC peaks **C** and **D** were collected for reactions between oxaliplatin and GSH or GSSG, and analysed by ESI-MS (Figure 9). Each peak corresponds to only one major product, with molecular ions at m/z = 615 (**C**) and m/z = 462 (**D**). Isotope modelling of the data showed that peak **C** was assignable to the molecular formula $[Pt_2C_{32}H_{58}N_{10}O_{12}S_2]^{2+}$ [the S-bridged dimer shown in Figure 6(a)] and peak **D** assignable to the formula $[Pt_2C_{22}H_{42}N_7O_6S]^{2+}$ [the glutathione-bridged macrochelate shown in Figure 6(b)]. These data are consistent with the

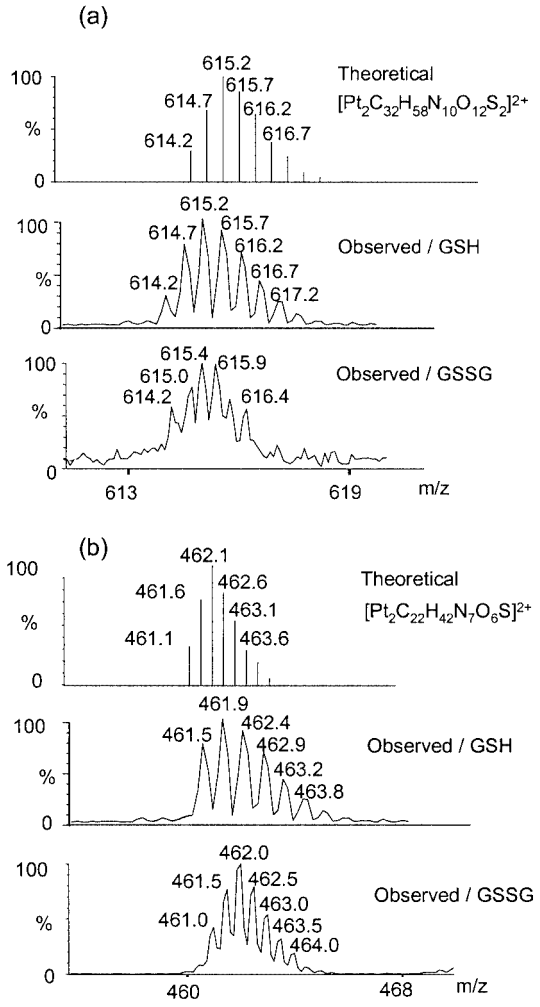

Figure 9. Positive ion ESI-MS spectra obtained from HPLC peaks (a) **C**, and (b) **D**, products from the reaction of oxaliplatin with two molar equivalents of GSH (310 K, initially at pH 7, six days), separated and collected using the elution conditions shown in Figure 2, and concentrated by lyophilisation; the observed and theoretical isotope patterns for the proposed structures are shown

products giving rise to peaks **C** and **D** from the oxaliplatin reactions being identical to those of peaks **A** and **B**, respectively, from the reactions of [Pt(1,2-DACH)Cl_2].

Discussion

Although cisplatin is an effective anticancer drug, a major clinical problem is the development of resistance.[4] Early on it was discovered that diaminocyclohexane (DACH) platinum(II) complexes are non-cross resistant with cisplatin and this has led to the clinical approval of one such DACH derivative, [Pt(1*R*,2*R*-DACH)(oxalate)] (oxaliplatin), for the treatment of metastatic colorectal cancer.[8,32] For [Pt(DACH)Cl_2] complexes containing the *trans*-DACH geometrical isomer, the *R*,*R* diastereomer is more active than *S*,*S*, and both are more active than the meso (*R*,*S*) adduct.[33] Since thiols such as the tripeptide glutathione (GSH), present in cells at concentrations of

0.5−10 mM,[16] can play a major role in cellular resistance mechanisms, there is a need to elucidate reactions between Pt-DACH anticancer complexes and glutathione.

In the only previous study (as far as we are aware) of such reactions, two products from the reaction of [Pt(1,2-DACH)Cl_2] and GSH were separated by HPLC.[34] They were found to be 1:1 (Pt:GSH) adducts, but were not further characterised. In this work we have studied reactions of both GSH and its oxidised form GSSG with both racemic (1*R*,2*R*/1*S*,2*S*) and enantiomerically pure [Pt(1*R*,2*R*-DACH)Cl_2], as well as the drug oxaliplatin. The time dependence of the reactions was followed by both UV/Vis spectroscopy and by HPLC. Remarkably, reactions of both GSH and GSSG gave rise to a similar broad band at ca. 220 nm (Figures 1 and 8), assignable to a thiolate-to-platinum charge-transfer band ($\varepsilon > 30{,}000\ M^{-1}cm^{-1}$). Reactions with GSSG were more than three times slower than with GSH. HPLC studies showed that reactions of [Pt(*rac*-1,2-DACH)Cl_2] with both GSH and GSSG gave rise to the same two major products [**A** and **B**, Figure 2(a) and (b)], which were identified by ESI-MS as 2(Pt):2(GSH) (**A**) and 2(Pt):1(GSH) (**B**) adducts.

Displacement of oxalate from oxaliplatin by GSH (or GSSG) leads to products **C** and **D**, which are identical to products **A** and **B** from reactions of the dichloro complex, from which the chloro ligands are displaced. Reactions of oxaliplatin with GSH and GSSG were much slower than those of [Pt(1,2-DACH)Cl_2]. This is not surprising in view of the presence of chelated oxalate in oxaliplatin.

Remarkably, therefore, GSSG undergoes redox reactions with platinum(II) complexes, leading to cleavage of the disulfide bond and formation of Pt^{II}-GSH adducts. Such redox chemistry of platinum(II) anticancer drugs has received relatively little previous attention. Lempers et al. have suggested that cleavage of GSSG by $[Pt(dien)Cl]^+$ involves H_2O as the reducing agent[16] and Fazlur-Rahman and Verkade have detected initial binding of GSSG to $[Pt(dien)]^{2+}$.[35] Ohta et al. have reported that *trans*-$[PtCl_2(NH_3)_2]$ can cleave disulfide bonds in human serum albumin,[36] and they also found that GSH reacts with cisplatin 17 times faster than with GSSG, and six times faster with the monoaqua adducts.[37] Further work is needed to elucidate the mechanism of such redox reactions.

The resolution of the reverse-phase HPLC chromatograms is very sensitive to the elution conditions (solvent gradient and temperature), but under certain conditions diastereomeric products were separable for reactions of the racemic complex. On the basis of ESI-MS and NMR spectroscopic data, product **A** can be identified as a thiolate-bridged dimer [Figure 6(a)] and product **B** as a novel dinuclear glutathione-bridged macrochelate [Figure 6(b)]. Evidence for the latter structure was provided by comparing 1D ^1H NMR, 2D [^1H, ^1H] TOCSY and NOESY data with those for products from similar reactions of the ethylenediamine complex [Pt(en)Cl_2], for which a comprehensive NMR study was possible with the use of ^{15}N-labelled en.[38] ^{15}N-DACH was not available for the present study.

In particular, similarities in the chemical shifts of the peptide ^1H NMR resonances and between the chemical shifts of the N*H* resonances of the diamine ligand are notable (Figures S3−S5 in the Supporting Information). A large doublet with a broadened base at $\delta = 6.33$ ppm, assignable to γ-Glu NH(1), is evidence for the presence of an unsymmetrical *bis* adduct. Differential couplings are consistent with torsion angles Cys−(Hβ^a−Cβ−Cα−Hα) = 90° and Cys−(Hβ^b−Cβ−Cα−Hα) = 30°; no signal was detected for Cys−N*H*, consistent with formation of a Cys−N(S) chelate ring. The macrochelate **B** contains a five-membered N,S chelate ring formed by the deprotonated amide N and S of the cysteine residue of GSH, and a nine-membered macrochelate ring formed by coordination of the γ-Glu α-amino group to the second Pt(DACH) unit.

Although the S-bridged dimer **A** is likely to be a stable end product, the macrochelate **B** is expected to be more reactive. Since we found that **B** is still formed even in the presence of a large excess of GSH (as would be the case inside cells), further studies of this species may well have physiological significance. Protonation of the Cys−N would produce a reactive coordination site, and the pH on the surface of DNA may be as low as 5;[39] however, complex **B** appeared to be stable down to pH 2.8.

Conclusions

Previous studies of the mechanism of action of platinum anticancer drugs have mostly been centred on the nature of hydrolysis reactions that activate chloro complexes, and reactions with DNA bases that lead to structural changes such as DNA bending. Whilst it is well recognised that platinum(IV) anticancer drugs are readily reduced in physiological media giving active platinum(II) products,[40] and that Pt^{II} can react with amides and imides to form mixed-valence "platinum blues",[41] little attention has been given to redox reactions of platinum(II) drugs with disulfides. We have shown here that reactions of the drug oxaliplatin with glutathione disulfide are only slightly slower than analogous reactions with the reduced form of glutathione. Remarkably, reactions of oxaliplatin with glutathione and glutathione disulfide lead to the same major products, both platinum(II) adducts of glutathione. Clearly, oxaliplatin can induce reductive cleavage of the disulfide bond of glutathione disulfide. Since platinum is still in oxidation state +2 in the products, the electrons must be supplied by another component of the reaction, probably water. The formation of the unusual macrochelate **B**, even in the presence of excess glutathione, could potentially be of biological importance.

Experimental Section

Materials: Potassium oxalate, *rac*-1,2-DACH and (1*R*,2*R*)-DACH were purchased from Aldrich. Potassium tetrachloroplatinate(II) was provided by Johnson Matthey. Enantomerically pure [Pt(1*R*,2*R*-DACH)Cl_2], [Pt(*rac*-1,2-DACH)Cl_2] and oxaliplatin

were prepared using previously described procedures.[42−45] Glutathione (GSH) was purchased from Acros and glutathione disulfide (GSSG) from Sigma.

Instrumental Methods: High pressure liquid chromatography (HPLC) was carried out on a Hewlett Packard 1100 system with UV detection. For all analytical separations, a RP C18 column (250 × 4.6 mm, 100 Å, 5 μM, Hichrom) with UV detection at 220 nm, eluting with 0−50% acetonitrile gradients over varying time intervals with 0.1% trifluoroacetic acid as an ion-pairing agent. ESI-MS positive ion electrospray mass spectrometry (ESI-MS) was performed using a Platform-II mass spectrometer (Micromass, Manchester, UK). A Corning 240 pH meter equipped with an Aldrich microcombination electrode standardised with Aldrich buffers at pH 4, 7 and 10 was used to make pH measurements. Electronic absorption spectra were recorded over a range of 800 to 200 nm at 310 K on a Perkin−Elmer Lambda-16 spectrometer using a cell with a path length of 1 cm. ICP-AES determination of platinum concentrations was carried out using a Thermo Jarrell Ash *IRIS* ICP-AES, calibrated with 0−100 ppm standards purchased from BDH.

NMR spectroscopic data were acquired using a Varian ^{UNITY}*INOVA* 600 NMR spectrometer equipped with a z-field gradient triple resonance NMR probe and operating at a ^{1}H resonance frequency of 599.841 MHz. A sample of the 2:1 adduct between [Pt(1*R*,2*R*-DACH)Cl$_2$] and GSH (1.3 mM, 90% H_2O/10% D_2O, pH = 4, separated by HPLC) was used for the acquisition of all NMR spectroscopic data. 1D ^{1}H NMR spectroscopic data sets were typically acquired under the following conditions: frequency width 7 kHz, acquisition time 2.34 s, number of data points 32 *k*, relaxation delay 2 s, number of transients 128, pulse angle 90°. Homonuclear ^{1}H 2D NOESY (τ_m = 150 and 500 ms), TOCSY (τ_m = 70 ms), DQFCOSY and ROESY (τ_m = 120 ms) NMR spectroscopic data sets were typically acquired over a 5 kHz frequency width in both ω2 and ω1 for which 32 transients were acquired into 2 k complex data points (acquisition time 205 ms) for each of 2 × 400 hypercomplex t_1 increments. For all data accumulation, solvent suppression was achieved using either WET[46] or excitation sculpting.[47] The sample temperature was maintained at 298 K throughout data acquisition. Data were converted (Xwin-NMR version 2.0, Bruker, U.K. Ltd.) and processed using suitable apodization functions. Referencing of all data was made internally to the methyl singlet of TSP at δ = 0 ppm. A model for [{Pt(1*R*,2*R*-DACH)}$_2$(μ$_2$-*S*G)] was constructed on the basis of the structure calculated for [Pt(en)$_2$(μ$_2$-*S*G)][38] using Sybyl (version 6.3, Tripos Inc.). The presence of an rOe in the NMR spectroscopic data was used to define upper (3.5 Å) and lower (2.5 Å) distance bounds between associated protons in the molecule. Distance range force constants, k_{NOE}, were set to 20 kcal·mol^{-1} Å^{-2} for each distance restraint. A single torsion angle restraint was also incorporated (γ-Glu−(Hα−Cα−Cβ−Hβ^a); θ_{tor} = 90°, k_{tor} = 0.01 kcal·mol^{-1} deg^{-2}). Energy minimization of the model was carried out with repeated conjugate gradient steps until the structure was stable.

Reactions of [Pt(1,2-DACH)Cl$_2$] and Oxaliplatin with Glutathione (GSH) or Glutathione Disulfide (GSSG): The pH of GSH or GSSG solutions (20 mM) was adjusted to 7 with NaOH. [Pt(1,2-DACH)Cl$_2$] or oxaliplatin (100 μM, 2 mL) was added to an aliquot of GSH or GSSG (20 μL, 2 mol equiv.), and the reaction mixture was incubated at 310 K for 24 h ([Pt(1,2-DACH)Cl$_2$]) or 48 h (oxaliplatin). The pH of the reaction was monitored at regular intervals. Analytical separation of the products was carried out by HPLC methods as described above.

Acknowledgments

We thank the BBSRC, EPSRC and Wellcome Trust (Edinburgh Protein Interaction Centre) for their support for this work. We also thank members of EC COST D8/D20 for stimulating discussions.

[1] B. Rosenberg, in "*Cisplatin − Chemistry and Biochemistry of a leading anticancer drug*" (Ed.: B. Lippert), Wiley-VCH, Zürich, **1999**, pp. 3−27.
[2] P. J. Loehrer, L. H. Einhorn, *Ann. Intern. Med.* **1984**, *100*, 704−713.
[3] C. J. Ziegler, A. P. Silverman, S. J. Lippard, *J. Biol. Inorg. Chem.* **2000**, *5*, 774−783.
[4] L. Chen, P. F. Lee, J. D. Ranford, J. J. Vittal, S. Y. Wong, *J. Chem. Soc., Dalton Trans.* **1999**, 1209−1212.
[5] I. R. Judson, L. R. Kelland, *Drugs* **2000**, *59*, 29−36.
[6] A. Zenker, M. Galanski, T. L. Bereuter, B. K. Keppler, W. Lindner, *J. Biol. Inorg. Chem.* **2000**, *5*, 498−504.
[7] O. Rixe, W. Ortuzar, M. Alvarez, R. Parker, E. Reed, K. Paull, T. Fojo, *Biochem. Pharm.* **1996**, *52*, 1855−1865.
[8] M. A. Graham, G. F. Lockwood, D. Greenslade, S. Brienza, M. Bayssas, E. Gamelin, *Clin. Cancer Res.* **2000**, *6*, 1205−1218.
[9] B. Springler, D. A. Whittington, S. J. Lippard, *Inorg. Chem.* **2001**, *40*, 5596−5602.
[10] D. Machova, E. Diaz-Rubio, A. de Gramont, A. Schilf, J. J. Gastiaburu, S. Brienza, M. Itzhaki, G. Metzger, D. N′Daw, J. Vignoud, A. Abad, E. Farancois, E. Gamelin, M. Marty, J. Sastre, J. F. Seitz, M. Ychou, *Ann. Oncol.* **1996**, *7*, 95−98.
[11] F. R. Luo, S. D. Wyrick, S. G. Chaney, *Oncol. Res.* **1998**, *10*, 595−603.
[12] Z. Z. Zdraveski, J. A. Mello, C. K. Farinelli, J. M. Essigmann, M. G. Marinus, *J. Biol. Inorg. Chem.* **2002**, *277*, 1255−1260.
[13] S. E. Sherman, S. J. Lippard, *Chem. Rev.* **1987**, *87*, 1153−1181.
[14] J. Reedijk, *Inorg. Chim. Acta* **1992**, *198−200*, 873−881.
[15] E. R. Jamieson, S. J. Lippard, *Chem. Rev.* **1999**, *99*, 2467−2498.
[16] E. L. M. Lempers, K. Inagaki, J. Reedijk, *Inorg. Chim. Acta* **1988**, *152*, 201−207.
[17] J. Reedijk, *Chem. Rev.* **1999**, *99*, 2499−2510.
[18] A. Eastman, *Pharmac. Ther.* **1987**, *34*, 155−166.
[19] S. J. Berners-Price, P. W. Kuchel, *J. Inorg. Biochem.* **1990**, *38*, 305−326.
[20] T. Ishikawa, C. D. Wright, H. Ishizuka, *J. Biol. Chem.* **1994**, *269*, 29085−29093.
[21] E. F. Bernstein, H. A. Pass, J. R. Glass, A. M. Deluca, S. Cook, J. Fisher, J. A. Cook, *Int. J. Oncol.* **1995**, *7*, 353−358.
[22] J. Sastre, E. Diaz-Rubio, J. Blanco, L. Cifuentes, *Oncol. Rep.* **1996**, *3*, 1149−1152.
[23] R. T. Dorr, in "*Platinum and Other Metal Coordination Compounds in Cancer Chemotherapy 2*" (Eds.: H. M. Pinedo, J. H. Schornagel), Plenum Press, New York, **1996**, pp. 131−154.
[24] E. L. M. Lempers, J. Reedijk, *Inorg. Chem.* **1990**, *29*, 217−222.
[25] K. A. Mitchell, K. C. Streveler, C. M. Jensen, *Inorg. Chem.* **1993**, *32*, 2608−2609.
[26] K. J. Barnham, M. I. Djuran, P. d. S. Murdoch, P. J. Sadler, *J. Chem. Soc., Chem. Commun.* **1994**, 721−722.
[27] K. J. Barnham, M. I. Djuran, P. d. S. Murdoch, J. D. Ranford, P. J. Sadler, *J. Chem. Soc., Dalton Trans.* **1995**, 3721−3726.
[28] T. G. Appleton, *Coord. Chem. Rev.* **1997**, *166*, 313−359.
[29] T. G. Appleton, J. W. Connir, J. R. Hall, P. D. Prenzler, *Inorg. Chem.* **1989**, *28*, 2030−2037.
[30] E. L. M. Lempers, M. J. Bloemink, J. Brouwer, Y. Kidani, J. Reedijk, *J. Inorg. Biochem.* **1990**, *40*, 23−35.
[31] J. M. Allen, M. A. Graham, J. W. Firth, S. Woolfrey, D. Greenslade, J. G. Morrison, S. McDougall, P. Ross, D. Cunningham, in "*8th International symposium on platinum and other metal coordination compounds in cancer chemotherapy*" (Ed.: L. R. Kelland), Oxford, UK, **1999**.
[32] P. J. O′Dwyer, J. P. Stevenson, S. W. Johnson, in "*Platinum-*

Based Drugs in Cancer Therapy'' (Eds.: L. R. Kelland, N. Farrell), Humana Press, Totawa, NJ, **2000**, pp. 231−249.
[33] M. Noji, K. Okamoto, Y. Kidani, *J. Med. Chem.* **1981**, *24*, 508−515.
[34] S. K. Mauldin, F. A. Richard, M. Plescia, S. D. Wy, A. Sancar, S. G. Chaney, *Anal. Biochem.* **1986**, *157*, 129−143.
[35] A. K. Fazlur-Rahman, J. G. Verkade, *Inorg. Chem.* **1992**, *31*, 2064−2069.
[36] N. Ohta, D. Chen, S. Ito, T. Futo, T. Yotsuyanagi, K. Ikeda, *Int. J. Pharm.* **1995**, *118*, 85−93.
[37] N. Ohta, K. Inagaki, H. Muta, T. Yotsuyaagi, T. Matsuo, *Int. J. Pharm.* **1998**, *161*, 15−21.
[38] P. d. S. Murdoch, N. A. Kratchowil, J. A. Parkinson, M. Patriarca, P. J. Sadler, *Angew. Chem. Int. Ed.* **1999**, *38*, 2949−2951.
[39] G. Lamm, G. R. Pack, *Proc. Natl. Acad. Sci. USA* **1990**, *87*, 9033−9036.
[40] M. D. Hall, T. W. Hambley, *Coord. Chem. Rev.* **2002**, *232*, 49−67.
[41] B. Lippert, in "*Cisplatin − Chemistry and Biochemistry of a leading anticancer drug''* (Ed.: B. Lippert), Wiley-VCH, Zürich, **1999**, pp. 379−403.
[42] B. A. Howell, R. Rashidianfar, J. R. Glass, B. J. Hutchinson, D. A. Johnson, *Inorg. Chim. Acta* **1988**, *142*, 181−183.
[43] A. H. Talebian, D. Bensley, A. Ghiorghis, C. F. Hammer, P. S. Schein, *Inorg. Chim. Acta* **1991**, *179*, 281−287.
[44] J. A. Zuleta, J. M. Bevilacqua, D. M. Proserpio, P. D. Harvey, R. Eisenberg, *Inorg. Chem.* **1992**, *31*, 2396−2404.
[45] Y. Kidani, K. Inagaki, M. Iogo, A. Hoshi, K. Kuretani, *J. Med. Chem.* **1978**, *21*, 1315−1318.
[46] S. H. Smallcombe, S. L. Patt, P. A. Keifer, *J. Magn. Res., Series A* **1995**, *117*, 295−303.
[47] T.-L. Hwang, A. J. Shaka, *J. Magn. Res. Series A* **1995**, *112*, 275−279.

Received September 2, 2002
[I02494]

Synthesis, Reactivity, Crystal Structures and Catalytic Activity of New Chelating Bisimidazolium-Carbene Complexes of Rh

Macarena Poyatos,[a] Elena Mas-Marzá,[a] José A. Mata,[a] Mercedes Sanaú,[b] and Eduardo Peris*[a]

Keywords: Heterocycles / Carbenes / Rhodium / Homogeneous catalysis

A series of new bridging, chelating and pincer *N*-heterocyclic carbenes of Rh^{I} and Rh^{III} have been obtained under mild conditions. The compounds have been fully characterised and their crystal structures determined. The chelate-pincer coordination of the ligands means that the stability of these compounds is significantly greater than other carbene complexes of Rh. The compounds have been tested in catalytic reactions such as hydrogen transfer from alcohols to ketones, and hydrosilylation of terminal olefins and alkynes; they show a high activity for both processes.
(© Wiley-VCH Verlag GmbH & Co. KGaA, 69451 Weinheim, Germany, 2003)

Introduction

The number of synthetic applications of homogeneous catalysts has increased enormously during the last three decades. Highly active and selective catalysts have been prepared to activate a large variety of bonds, thus providing efficient methods to obtain new products with important industrial and pharmaceutical applications. However, homogeneous catalysts are far from being widely used in industrial processes, mainly due to their low chemical and thermal stability and to their low potential to provide recyclable systems. With this in mind, recent research in this area has focused mainly on the search for new methods for the synthesis of stable, effective and recyclable catalysts, since this would combine both economic and environmental benefits.

Homogeneous organometallic catalysis has long depended on phosphane ligands.[1,2] Despite their effectiveness in controlling reactivity and selectivity, phosphane catalysts require air-free handling to prevent the oxidation of the ligand and are subject to P−C activation at elevated temperatures.[3] As an alternative to the use of phosphanes, *N*-heterocyclic carbenes are currently being used in the design of new homogeneous catalysts.[4] The chemical versatility of these compounds and their easy access provide methods to obtain ligands with tunable steric and electronic properties. The precursor imidazolium salts are often easier to obtain than phosphanes, but their coordination to the metal often requires harsh preactivation conditions, in most cases needing the addition of strong bases such as *n*BuLi.[5,6] Once bound to the metal, however, monodentate carbenes are often reactive and undergo decomposition processes that can reduce the catalytic efficiency at high temperatures.

In order to improve the stability of the carbene-imidazolium compounds we[7−10] and others,[6,11−17] have reported a series of compounds whose stability is entropically improved by the chelate effect. In this sense, a series of bis-chelate and pincer-bis-carbene compounds have been reported, providing catalysts which resist higher temperatures than other classical homogeneous catalysts.

Most of the tridentate pincer CNC bis-carbene ligands reported so far are Pd-based and have been used in catalytic C-C bond formation reactions (Heck, Suzuki, Sonogashira).[9,10,15] Due to the high thermal stability of these catalysts, traditionally inert bonds such as C−Cl are readily activated providing the highest turnover numbers reported to date in the Heck C−C coupling.[9] Pincer CNC ligands have also allowed the preparation of recyclable heterogeneous catalysts which have also been effectively used in the Heck C−C coupling reaction.[18]

Despite their obvious potential applications, the use of bis-carbene chelate or pincer ligands with other metals is limited to a few papers reporting Rh[7] and Ru[13] complexes whose catalytic applications were envisaged.

Based on our previous findings, we now report the synthesis and reactivity of a series of CNC-bis-carbene complexes of Rh^{I} and Rh^{III}. The crystal structures of several of the reported compounds are described. We also report the

[a] Departamento de Química Inorgánica y Orgánica. Universitat Jaume I,
12080 Castellón. Spain
Fax: (internat.) +34-(0)96/472-8214
E-mail: eperis@qio.uji.es
[b] Departamento de Química Inorgánica, Universitat de València, c/Dr. Moliner 50, 46100 Valencia, Spain

catalytic applications of our compounds toward the hydrosilylation of terminal olefins and alkynes, and hydrogen transfer between alcohols and ketones.

Results and Discussion

Synthesis and Reactivity of the Compounds

In order to obtain the new Rh compounds, we used the ligand precursors **1**-R_2 [9] (R = Me, Bu) and **2**-Me_2. The preactivation of the ligand (deprotonation) was performed with NEt_3, since we have previously found that this base affords good results under mild reaction conditions. As metal complex we used $[RhCl(COD)]_2$.

Scheme 1 shows the general method for the synthesis of complexes **3**, **4** and **5**. The reaction of $[RhCl(COD)]_2$ with **1**-R_2 allowed the synthesis, in high yield, of two different compounds, depending on the reaction conditions used. Under inert conditions, using a Rh/**1**-R_2 molar ratio of 1:1, compound **3** was obtained (65−80% yield). The complex **3**-Bu_2 was recently obtained and fully characterized in our group,[19] and **3**-Me_2 has very similar spectroscopic features[19] allowing for the obvious differences derived from changing the two Bu wingtips by two methyl groups. The more relevant NMR spectroscopic features arise from the fact that the twofold symmetry of the ligand is maintained upon coordination, and that the ^{13}C NMR spectrum of the complex shows Rh−C coupling ($^1J_{Rh,C}$ = 49.2 Hz, δ = 184.8 ppm), which confirms that metallation of the ligand has occurred.

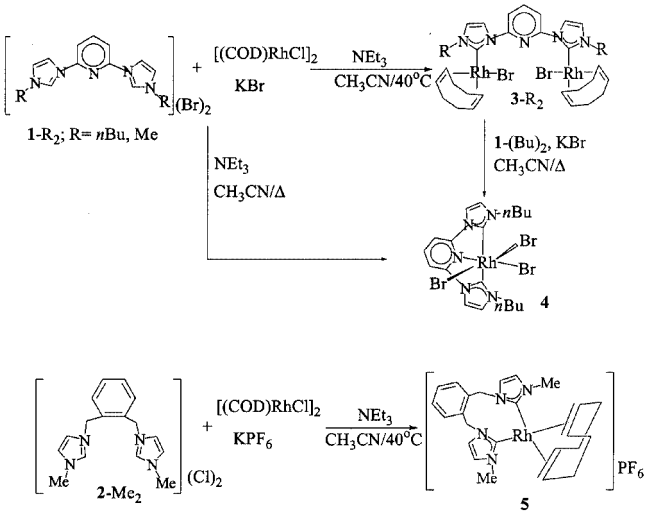

Scheme 1

The synthesis of **4** can proceed both from $[RhCl(COD)]_2$ and from **3** (Scheme 1). The mechanism of this reaction is not well understood, but it looks as if the oxidation of the starting Rh^I complex is the first step in the reaction, which is why aerating the initial CH_3CN solution increases the reaction yields. In fact, when the reaction is carried out under a completely inert atmosphere, much lower yields are obtained, and most of the starting $[RhCl(COD)]_2$ complex is recovered, together with the Rh^I complex **3**, which can be considered as a reaction intermediate in the synthesis of **4**. KBr is added to the reaction medium in order to favour the formation of the perbrominated complex, although in most occasions mixtures of the Cl and Br complexes were still obtained. In the absence of KBr, mixtures of [Rh(CNC-Bu_2)Br_3] and *trans*-[Rh(CNC-Bu_2)Br_2Cl] were obtained, which we could not separate by conventional methods (i.e. column chromatography, crystallization, etc.).

The ^1H NMR spectrum of **4** shows the typical pattern of the bis-carbene ligand coordinated in the pincer form, very similar to that of related Pd complexes.[9,10] In the ^{13}C NMR spectrum, the carbene signal is observed as a doublet at δ = 177.5 ppm with a coupling constant that is diagnostic for Rh binding ($^1J_{Rh,C}$ = 33.7 Hz).

In order to confirm that **3** is in fact a reaction intermediate in the synthesis of **4**, we reacted **3**-Bu_2 with an equimolar amount of **1**-Bu_2 in refluxing CH_3CN, with the formation of **4** in almost quantitative yield (Scheme 1). We still do not have a satisfactory explanation for the oxidation step from **3**-Bu_2 to **4**, although we have observed that aerated solvents provide better yields. A possible explanation for this process may be the oxidation of traces of Br^- to Br_2 by dioxygen, with the subsequent oxidative addition of Br_2 to **3**. Further studies on this matter are being carried out in more detail.

All attempts to coordinate **1**-Bu_2 and **1**-Me_2 to Rh^I in the pincer form were unsuccessful. Although all these attempts were with $[RhCl(COD)]_2$, we believe that any other Rh^I starting compound would have given us similar results. Reduction of the corresponding Rh^{III} species was unsuccessful, with decomposition of the compound and the formation of unknown species.

We also wanted to see whether a chelating bis-carbene coordination to Rh^I was possible, since all attempts made so far have resulted in the oxidation to Rh^{III}, both in the results that we now present and in our previous work.[7] With this aim in mind, we tried to coordinate the ligand precursor **2**-Me_2, made from direct reaction of dichloro-*o*-xylene and methylimidazole. The reaction of **2**-Me_2 with $[RhCl(COD)]_2$ in CH_3CN in the presence of NEt_3 yielded compound **5** in high yield (85%). The synthesis of **5** occurs without the formation of any Rh^{III} species, which could support the idea that prior oxidation of the halide (in this case Cl^- to Cl_2 obviously would be not possible) by air is needed for the oxidation of Rh^I to Rh^{III}. Evidence for the chelate coordination of the bis-carbene ligand comes again from NMR spectroscopy, which shows that the imidazole rings are symmetry related. The metallation of the ligand is confirmed by the presence of a doublet (δ = 180.8 ppm; $^2J_{Rh,C}$ = 52.6 Hz) in the ^{13}C NMR spectrum. The coordination sphere of the rhodium atom is completed by the presence of a molecule of 1,5-COD.

The molecular structures of **3**-Me_2, **4** and **5** were unambiguously confirmed by single crystal X-ray diffraction.

The molecular structure of **3**-Me_2 (Figure 1) is virtually identical to that of complex **3**-Bu_2 which we have published previously.[19] The compound consists of a dirhodium struc-

ture bridged by 2,6-bis(1-methyl imidazolylidene-3-yl)pyridine, with the nitrogen atom of the pyridine unbound. The geometry about each rhodium atom is pseudo-square-planar, with Rh−C_{imid} distances of 1.948(11) and 2.029(11) Å suggesting that these bonds have a major σ contribution with very little back-donation.

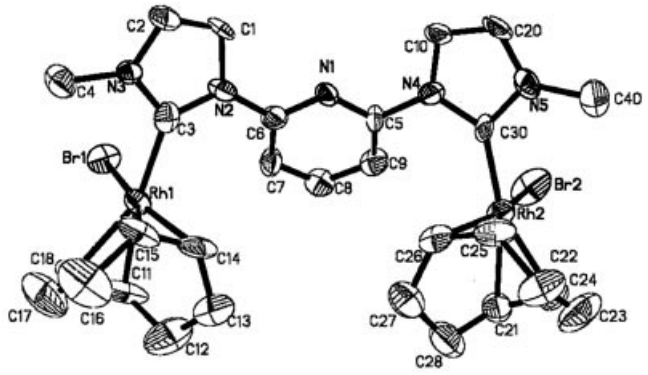

Figure 1. ORTEP diagram of **3**-Me_2 with 50% probability ellipsoids; hydrogen atoms omitted for clarity; selected bond lengths (Å) and angles (°): Rh(1)−C(3) 2.029(11), Rh(1)−C(15) 2.095(12), Rh(1)−C(14) 2.105(12), Rh(1)−C(11) 2.200(12), Rh(1)−C(18) 2.220 (11), Rh(1)−Br(1) 2.5172(17), Rh(2)−C(30) 1.948(11), Rh(2)−C(26) 2.101(11), Rh(2)−C(25) 2.157(12), Rh(2)−C(22) 2.189(11), Rh(2)−C(21) 2.216(11), Rh(2)−Br(2) 2.5169(18); C(3)−Rh(1)−Br(1) 87.7(3), C(30)−Rh(2)−Br(2) 90.2(3)

Figure 2 shows the molecular structure of complex **4**. The crystal contains a mixture of [Rh(CNC-Bu_2)Br_3] and *trans*-[Rh(CNC-Bu_2)Br_2Cl], and was refined with a 50% occupancy for each. The molecular structure shows the Rh atom in a distorted octahedral coordination, with a pincer-ligand bite angle of 79.9°. The imidazole and pyridine rings are virtually coplanar, and the two butyl groups point out of these planes. The Rh−C bond length (2.05 Å) is slightly longer than that obtained for a similar *cis*-chelate rhodium(III) bis-carbene reported in our group (1.99 Å),[7] due to the mutual trans influence.

The molecular diagram of **5** is shown in Figure 3. The structure shows the Rh atom in a distorted square-planar coordination with a chelate bite angle of 90.55°. The Rh−C bond lengths of 2.03 and 2.05 Å are similar to those of compound **3**, implying that the Rh−C bond has a major σ contribution. To the best of our knowledge, this is the first Rh^I chelate-bis-carbene complex reported so far.

Catalytic Hydrosilylation

Hydrosilylation of multiple bonds represents a useful class of catalytic processes for the functionalization of organic molecules. Vinylsilanes, which are widely used intermediates for organic synthesis, can be efficiently prepared by transition-metal-catalyzed addition of silanes to alkynes. Most of the recent efforts in the study of catalytic hydrosilylation concern the design of new and efficient catalysts that enable the preparation of both (*Z*)- and (*E*)-alkenylsilanes independently.[20−25] For this reason, the number of reports regarding mechanistic studies in order to rationalize the factors affecting the selectivity of this reaction have increased over the last few years.[20,22,25−27] In view of the compounds that we report in this paper, we thought that catalytic hydrosilylation could be a good test of the catalytic potential of these new complexes. Our Rh^I complexes (**3**-Me_2, **3**-Bu_2 and **5**) display all the structural and chemical requirements for this catalytical system, and could throw some light onto the reaction process.

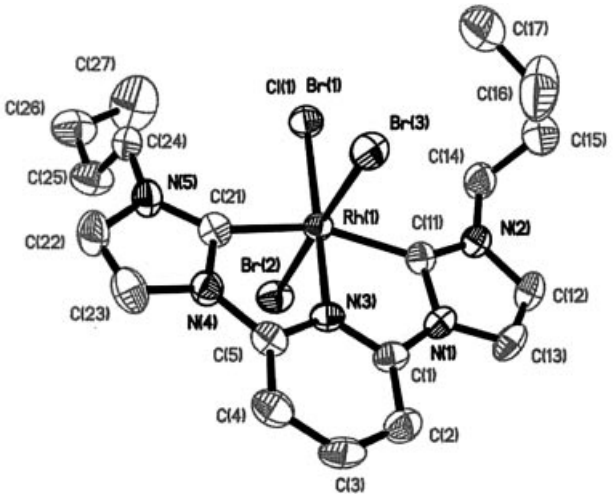

Figure 2. ORTEP diagram of **4** with 50% probability ellipsoids; hydrogen atoms omitted for clarity; selected bond lengths (Å) and angles (°): Rh(1)−N(3) 1.969(4), Rh(1)−C(21) 2.045(5), Rh(1)−C(11) 2.055(5), Rh(1)−Br(1) 2.4382(12), Rh(1)−Br(3) 2.4922(12); N(3)−Rh(1)−C(27) 78.7(2), N(3)−Rh(1)−C(11) 78.9(2)

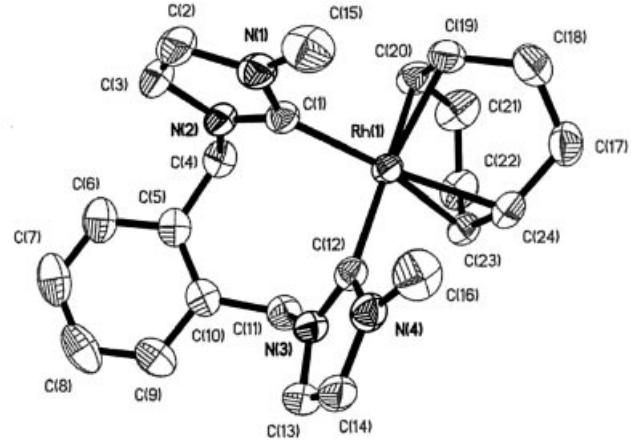

Figure 3. ORTEP diagram of **5** with 50% probability ellipsoids; hydrogen atoms omitted for clarity; selected bond lengths (Å) and angles (°): Rh(1)−C(12) 2.027(3), Rh(1)−C(1) 2.050(3), Rh(1)−C(23) 2.193(3), Rh(1)−C(19) 2.199(3), Rh(1)−C(24) 2.222(3), Rh(1)−C(20) 2.225(3); C(12)−Rh(1)−C(1) 90.55(11), C(19)−Rh(1)−C(24) 80.57(12), C(23)−Rh(1)−C(20) 80.95(12)

Table 1 shows the catalytic results for the hydrosilylation of several terminal alkynes with $HSi(OEt)_3$ and $HSiMe_2Ph$. All the reactions were carried out without any special need for inert conditions, since the catalysts used proved to be fairly stable under oxygen-containing atmospheres, even at high temperatures. The reactions were carried out in $CDCl_3$ at 60 °C, with 1 mol % catalyst. For all the reactions studied, all the catalysts used give a mixture of the β-(*E*),

Table 1. Hydrosilylation of alkynes

Entry[a]	RC≡CH	$HSiR_3$	Catalyst	Time (h)	*E*/*Z*/α	Yield (%)
1	PhC≡CH	$HSiMe_2Ph$	**3**-Me_2	72	83/0/17	95
2	PhC≡CH	$HSiMe_2Ph$	**3**-Bu_2	24	33/50/17	95
3	PhC≡CH	$HSiMe_2Ph$	**5**	72	80/11/9	100
4	PhC≡CH	$HSi(OEt)_3$	**3**-Me_2	72	57/30/13	92
5	PhC≡CH	$HSi(OEt)_3$	**3**-Bu_2	72	50/33/17	90
6	PhC≡CH	$HSi(OEt)_3$	**5**	72	66/26/8	85
7	*n*BuC≡CH	$HSiMe_2Ph$	**3**-Me_2	24	61/39/0	95
8	*n*BuC≡CH	$HSiMe_2Ph$	**3**-Bu_2	72	64/35	100
9	*n*BuC≡CH	$HSiMe_2Ph$	**5**	72	68/32/0	100
10	*n*BuC≡CH	$HSi(OEt)_3$	**3**-Me_2	24	50/50/0	70
11	*n*BuC≡CH	$HSi(OEt)_3$	**3**-Bu_2	72	50/50	50
12	*n*BuC≡CH	$HSi(OEt)_3$	**5**	72	61/39	100

[a] 0.077 mmol of alkyne, 0.085 mmol of silane. and 1% mol catalyst used in $CDCl_3$. T = 60 °C. Yields determined by ^1H NMR spectroscopy.

β-(*Z*) and α-isomers, although the β-(*E*) isomer is preferred in all cases where the process is carried out for long reaction times (72 h). In most metal-catalyzed hydrosilylations, the regioselectivity is affected by factors such as types of alkynes and silanes, catalyst, solvent or temperature. However, it has been reported that cationic Rh complexes catalyze the hydrosilylation of alkynes to give the β-(*E*)-vinylsilanes as the major products, while neutral Rh complexes show a higher preference to yield the β-(*Z*) ones.[20,28−30] Since initially we did not see this tendency for the neutral complexes, we decided to follow the reaction more carefully, and study how the isomer ratio evolves with time (Figure 4).

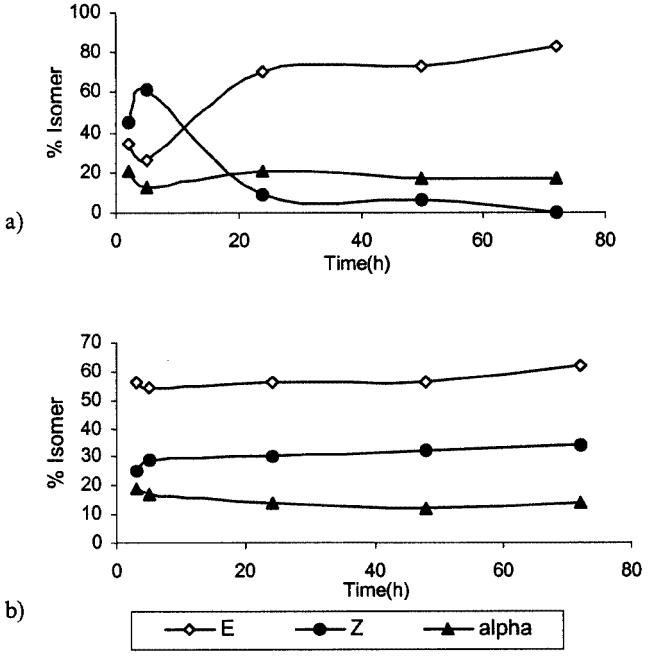

Figure 4. Reaction profiles for the hydrosilylation reactions of phenylacetylene by using **3**-Me_2 (1 mol % ratio) with: (a) $HSiMe_2Ph$, and (b) $HSi(OEt)_3$; percentage of isomer relative to molar fraction ($E + Z + \alpha = 100$)

As seen from Figure 4a, the reaction of phenylacetylene with $HSiMe_2Ph$ using **3**-Me_2 as catalyst starts by showing a higher preference for the β-(*Z*) isomer. As the reaction proceeds, there is a conversion from the (*Z*)- to the (*E*)-isomer, until total conversion into the (*E*)-isomer is achieved. A similar behavior is observed for the *n*BuC≡CH/$HSiMe_2Ph$ system with both neutral catalysts. These results confirm that the rate of isomerization of the initially preferred (*Z*)-isomer to the thermodynamically more stable (*E*)-isomer competes with the hydrosilylation process. The fact that no (*Z*)-vinylsilane is observed at the end of the reaction probably implies that the isomerization occurs via a reversible addition of the (*Z*) product in the last step of the reaction mechanism rather than a change in the selectivity of the catalyst due to a modification of its nature during the reaction.[20,27] When $HSi(OEt)_3$ is used, there is a clear preference for the (*E*)-isomer from the start of the reaction, and no (*Z*)-(*E*) conversion is observed with time (Figure 4b).

For the cationic catalyst **5**, the tendency to produce the (*E*)-vinylsilane isomer is observed from the beginning of the reaction. A higher selectivity for the (*E*)-isomer is obtained when $HSiMe_2Ph$ is used instead of $HSi(OEt)_3$.

These results are in agreement with other reports on rhodium-catalyzed alkyne-hydrosilylation reactions, in which a mixture of isomers is always obtained.[31] $[Rh(nbd)(dppe)_2]PF_6$ gives no β-(*Z*) isomer, although some α-isomer is formed.[22]

The relative efficiencies of these Rh complexes as olefin hydrosilylation catalysts were compared by means of a standard reaction of styrene with $HSi(OEt)_3$ and $HSiMe_2Ph$ (Table 2). No induction periods were observed, and the formation of the silylated compounds proceeded without detectable by-products by NMR spectroscopy. As seen from the results shown in Table 2, there is a predominant tendency to yield the linear (terminal) phenethyl isomer. The cationic complex **5** has a better ability to yield the mentioned isomer, displaying higher selectivities.

It is difficult to determine whether the neutral dimetallic precatalysts **3**-Me_2 and **3**-Bu_2 remain dimetallic under the reaction conditions of the hydrosilylation process. In fact, we cannot exclude that the compounds evolve to a stable Rh^{III} species with the chelate carbene bound and a Rh^{I} compound without carbene, which could be the true cata-

Table 2. Hydrosilylation of styrene

Entry[a]	$HSiR_3$	Catalyst	Time (h)	Linear/ branched	Yield (%)
1	$HSiMe_2Ph$	**3**-Me_2	48	82/18	88
2	$HSiMe_2Ph$	**3**-Bu_2	24	65/35	78
3	$HSiMe_2Ph$	**5**	72	90/10	100
4	$HSi(OEt)_3$	**3**-Me_2	72	55/45	20
5	$HSi(OEt)_3$	**3**-Bu_2	24	56/44	70
6	$HSi(OEt)_3$	**5**	72	85/25	80

[a] 0.077 mmol of olefin, 0.085 mmol of silane and 1% mol catalyst used in $CDCl_3$. T = 60 °C. Yields determined by ^1H NMR spectroscopy.

lytic species. However, according to our previous results on the hydroformylation of olefins,[19] we have observed that **3**-Me_2 and **3**-Bu_2 do not decompose to mononuclear species under the harsh conditions required for hydroformylation, thus suggesting that the complexes may maintain their dinuclear nature under the much milder conditions used in hydrosilylation.

Catalytic Hydrogen Transfer

The pseudo-octahedral Rh^{III} complex fulfills the electronic and structural requirements to catalyze the hydrogenation of the C=O groups of ketones via hydrogen transfer from *i*PrOH/KOH. The reactions are slow at room temperature, but proceed at very good rates at 80 °C. Again, the high stability of **4** allowed us to run all the reactions under non-inert conditions, with solvents used as purchased and in the absence of any precautions concerning the presence of air or moisture. As seen from the data shown in Table 3, the hydrogenation rates of the aromatic ketones are significantly higher than those shown for the aliphatic ones. The catalytic activity of this compound is similar to that reported by us for another Rh^{III} bis-carbene complex,[7] although in that case aliphatic ketones were hydrogenated faster than the aromatic ones.

In order to check whether incubation of the catalyst is important for this system we studied the reaction profiles of the hydrogen transfer to the three ketones used. As seen in Figure 5, the reaction profile is a sigmoid curve for the acetophenone case, indicating that a preactivation period of 3−4 h is necessary only for this substrate. This result is also observable for the reaction performed with 6×10^{-3} mol % catalyst (not shown in Figure 5). We still do not have a satisfactory explanation for this observation, although further studies are being carried out.

Transfer hydrogenation to alkenes failed with our catalyst, which in fact allows chemoselective reduction of C=O bonds in conjugated enones.

Table 3. Selected results for catalytic hydrogenation transfer of ketones with **4** as catalyst

Entry[a]	Substrate	Time (h)	Catalyst (mol %)	TON	TOF
1	Cyclohexanone	7	0.06	1322	189
2	Cyclohexanone	24	0.06	1322	55
3	Acetophenone	7	0.06	500	71
4	Acetophenone	24	0.06	1107	46
5	Acetophenone	6	0.006	3500	583
6	Benzophenone	7	0.06	1357	194
7	Benzophenone	24	0.06	1357	57
8	Benzophenone	3	0.006	3636	1212
9	Benzophenone	7	0.006	6450	921
10	Benzophenone	24	0.006	10580	441

[a] 2 mmol of substrate, 10 mL 0.1 M KOH in *i*PrOH T = 80 °C. Yields determined by ^{1}H NMR spectroscopy. TON = mol product/mol catalyst. TOF = mol product/(mol catalyst × hour).

Conclusion

We have obtained new bis-carbene complexes of Rh^{I} and Rh^{III}, and complex **4** is the first CNC-pincer complex of Rh described to date. The synthetic methods that we have described provide high yields under mild conditions, and establish a new method of activating bis-imidazolium salts in order to perform their coordination to metal complexes. The complexes obtained have been tested in the catalytic hydrosilylation of alkynes and olefins, and in the hydrogen transfer from alcohols to ketones; they show high catalytic activity. All in all, we have shown that a new family of Rh bis-carbene complexes can be easily obtained, providing a new and versatile class of catalysts whose properties deserve to be exploited.

Experimental Section

General Remarks: NMR spectra were recorded on Varian Innova 300 MHz and 500 MHz spectrometers, with $CDCl_3$ or [D_6]DMSO as solvents. The ligand precursors **1**-R_2 [7] (R = Me, *n*Bu) and the complex **3**-Bu_2 [19] were prepared according to literature methods. All other reagents are commercially available and were used as received.

Synthesis of [*o*-(CH_3-imid-CH_2)$_2$Ph](Cl)$_2$ (2): A mixture of α,α′-dichloro-*o*-xylene (2 g, 11.2 mmol) and *N*-methylimidazole (1.93 mL, 22.4 mmol) was heated at 150 °C for 12 h. The resulting solid was then washed with CH_2Cl_2 and filtered, yielding pure **2** (95%). ^{1}H NMR ($CDCl_3$, 500 MHz): δ = 9.61 (s, 2 H, NC*H*N), 7.92 (s, 2 H, imid), 7.84 (s, 2 H imid), 7.48 (2 H, Ph), 7.38 (2 H, Ph), 5.82 (s, 4 H, CH_2), 3.92 (s, 6 H, CH_3) ppm. $C_{16}H_{20}Cl_2N_4$

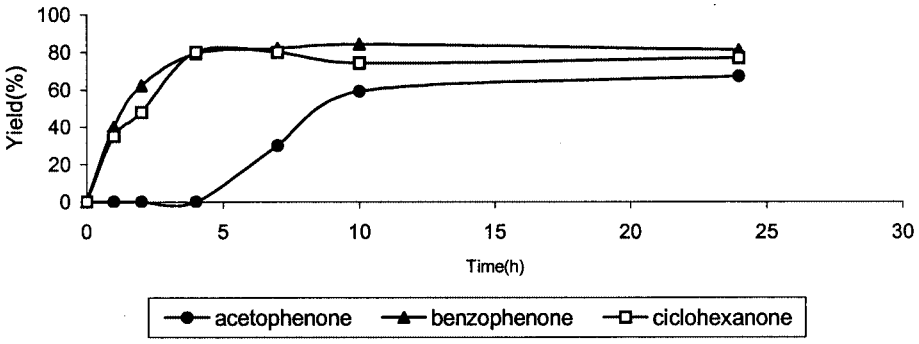

Figure 5. Reaction profile for the hydrogen-transfer reaction; 80 °C and 0.06 mol % catalyst (**4**)

(339.0): calcd. C 56.6, H 5.89, N 16.52; found C 56.2, H 5.67, N 16.87.

Synthesis of [(COD)RhBr]$_2$(μ-CNC-Me$_2$) (3-Me$_2$) and [(COD)RhBr]$_2$(μ-CNC-Bu$_2$) (3-Bu$_2$): A mixture of [RhCl(COD)]$_2$ (200 mg, 0.41 mmol), **1**-Me$_2$ (327 mg, 0.82 mmol), KBr (300 mg) and NEt$_3$ (0.5 mL, 3.5 mmol) was heated at 45 °C for 12 h in CH_3CN. The reaction mixture was filtered and the solvent was eliminated under vacuum. The resulting solid was redissolved in CH_2Cl_2 and the solution was transferred to a chromatography column. Elution with CH_2Cl_2 separated a minor yellow band that contained [RhCl(COD)]$_2$. Further elution with a gradient of CH_2Cl_2/acetone (10:1) allowed the separation of a major yellow band that contained **3**-Me$_2$ (yield 80%). $C_{29}H_{37}Br_2N_5Rh_2$ (820.9): calcd. C 42.42, H 4.51, N 8.53; found C 42.1, H 4.49, N 8.59.

[(COD)RhBr]$_2$(CNC-Me$_2$), (3-Me$_2$): ^{1}H NMR ($CDCl_3$, 300 MHz): δ = 10.05 (d, $^2J_{H,H}$ = 8.1 Hz, pyridine-*H*), 8.28 (t, $^2J_{H,H}$ = 8.0 Hz, pyridine-*H*), 7.80 (imidazole-H), 6.99 (imidazole-*H*), 4.21 (s, 6 H, NCH_3) ppm. ^{13}C NMR ([D$_6$]DMSO, 300 MHz): δ = 184.8 (d, $^2J_{Rh-C}$ = 49.2 Hz, N*C*N), 149.8 (C_{ipso}), 139.7 (C_{ortho}), 123.1 (im-C), 123 (C_{meta}), 116.2 (im-C), 98.8, 97.5, 70.2 (COD), 39.6 (CH_3), 29.8, 29.3 (COD) ppm.

Synthesis of Rh(CNC-Bu$_2$)Br$_3$ (4): A mixture of [RhCl(COD)]$_2$ (200 mg, 0.41 mmol), **1**-Bu$_2$ (400 mg, 0.82 mmol), KBr (300 mg) and NEt$_3$ (0.5 mL, 3.6 mmol) was refluxed in 10 mL of CH_3CN for 12 h. During this time the solvent was aerated several times by bubbling a steam of air through the reaction medium. The reaction mixture was filtered and the solvent of the filtrate was removed under vacuum. The crude solid was redissolved in CH_2Cl_2 and the solution was transferred to a column chromatography. Elution with CH_2Cl_2 separated a minor yellow band that contained [RhCl(COD)]$_2$. Further elution with a gradient of CH_2Cl_2/acetone (10:1) afforded the separation of an orange band containing **4** (yield 53%). Complex **4** can also be obtained from **3** as follows: a mixture of **3**-Bu$_2$ (100 mg, 0.12 mmol), **1**-Bu$_2$ (59 mg, 0.12 mmol), KBr (100 mg) and NEt$_3$ (150 μL) was refluxed in CH_3CN for 5 h. After this time the workup was similar to that described above (yield 62%).

Rh(CNC-Bu$_2$)Br$_3$ (4): ^{1}H NMR ([D$_6$]DMSO, 300 MHz): δ = 8.54 (d, $^3J_{H,H}$ = 1.5 Hz, 2 H, imidazole−*H*), 8.39 (t, $^3J_{H,H}$ = 7.8 Hz, 1 H, pyridine−*H*), 8.04 (d, $^3J_{H,H}$ = 8.1 Hz, 2 H, pyridine−*H*), 7.77 (d, $^3J_{H,H}$ = 1.5 Hz, 2 H, imidazole−*H*), 4.77 (t, 4 H, N*C*H_2CH$_2$CH$_2$CH$_3$), 2.48 (quintet, 4 H, NCH$_2$*C*H_2CH$_2$CH$_3$), 1.89 (sextet, 4 H, NCH$_2$CH$_2$*C*H_2CH$_3$), 0.88 (t, 6 H, NCH$_2$CH$_2$CH$_2$*C*H_3) ppm. ^{13}C NMR ([D$_6$]DMSO, 300 MHz): δ = 177.5 (d, $^1J_{Rh,C}$ = 33.7 Hz, N*C*N), 152.5 (C_{ipso}), 144.51 (C_{ortho}), 124.97 (im-C), 118.54 (C_{meta}), 108.44 (im-C), 50.39 (*C*H$_2$CH$_2$CH$_2$CH$_3$), 33.70 (CH$_2$*C*H$_2$CH$_2$CH$_3$), 20.02 (CH$_2$CH$_2$*C*H$_2$CH$_3$), 14.68 (CH$_2$CH$_2$CH$_2$*C*H$_3$) ppm. $C_{19}H_{25}Br_{2.5}Cl_{0.5}N_5Rh$ (643.85): calcd. C 35.42, H 3.88, N 10.87; found C 35.42, H 4.11, N 10.07.

Synthesis of [Rh(COD)(C∧C)]PF$_6$ (5): A mixture of [RhCl(COD)]$_2$ (200 mg, 0.41 mmol), **2**-Me$_2$ (275 mg, 0.82 mmol), KCl (400 mg) and NEt$_3$ (0.5 mL, 3.5 mmol) was heated at 45 °C for 12 h in CH_3CN. The reaction mixture was filtered and washed with CH_2Cl_2, and the solvent was then eliminated under vacuum. The crude solid was redissolved in CH_2Cl_2 and the solution was transferred to a chromatography column. Elution with CH_2Cl_2 separated a minor yellow band that contained [RhCl(COD)]$_2$. The solution was eluted with a gradient of CH_2Cl_2/acetone/KPF_6 allowing the separation of a major yellow band that contained **5** (yield 85%).

[Rh(COD)(C∧C)]PF$_6$ (5): ^{1}H NMR ($CDCl_3$, 300 MHz): δ = 7.84 (m, 2 H, phenylene-*H*), 7.55 (d, 2 H, imidazole-*H*), 7.40 (m, 2 H, phenylene-H), 7.19 (d, imidazole-*H*), 6.48 (d, 2 H, NCH_2), 5.12 (d, 2 H, NCH$_2$) ppm. ^{13}C NMR ([D$_6$]DMSO, 300 MHz): δ = 180.8 (d, $^2J_{Rh,C}$ = 52.6 Hz, N*C*N), 136.4 (C_{ortho}, phenylene), 132.4 (C, phenylene), 129.7 (C, phenylene), 124.3 (im-C), 121.9 (im-C), 90.2, 88.9 (COD), 51.3 (CH_2), 39.2 (CH_3), 31.0 (COD) ppm. $C_{24}H_{30}F_6N_4PRh$ (621.9): calcd. C 46.32, H 4.82, N 9.02; found C 46.7, H 4.73, N 8.82.

Hydrosilylation of 1-Alkynes and Olefins with Silanes. General Procedure: In a 5 mm NMR tube, *n*BuC≡CH or PhC≡CH (0.077 mmol), silane [HSi(OEt)$_3$ or HSiMe$_2$Ph, 0.085 mmol] and a catalytic amount of **3**-Me$_2$, **3**-Bu$_2$ or **5** (1 mol %, 7.7×10^{-5} mmol) were dissolved in $CDCl_3$ (0.5 mL). The mixture was kept at 60 °C by immersion in a hot oil bath. The progress of the reaction was monitored by ^{1}H NMR spectroscopy, according to the data of the products obtained from the literature.[28,30]

Hydrogen-Transfer Catalysis: A mixture of the ketone (2 mmol), KOH (10 mL, 0.2 M in *i*PrOH) and a suspension of **4** (0.06% or 0.006% mol vs. substrate) in CH_2Cl_2 was heated to reflux. After the desired reaction times, aliquots were extracted from the reaction vessel and added to an NMR tube containing 0.5 mL of $CDCl_3$. Yields were determined by ^{1}H NMR spectroscopy.

X-ray Diffraction Studies: Single crystals of **3**-Me$_2$, **4** and **5** were mounted on a glass fiber in a random orientation. Crystal data are summarized in Table 4. Data collection was performed at room temperature on a Siemens Smart CCD diffractometer using graphite monochromated Mo-K_α radiation (λ = 0.71073 Å) with a nominal crystal-to-detector distance of 4.0 cm. A hemisphere of data was collected based on three ω-scan runs (starting with ω = −28°) at φ values of 0°, 90° and 180° with the detector at 2θ = 28°. After each of these runs, frames (606, 435 and 230) were collected at 0.3° intervals and 30 s per frame. Space group assignment was based on systematic absences, E statistics and successful refinement of the structures. The structures were solved by direct methods with the aid of successive difference Fourier maps and were refined using the SHELXTL 5.1 software package.[32] All non-hydrogen were refined anisotropically. Hydrogen atoms were assigned to ideal positions and refined using a riding model. Details of the data collection, cell dimensions and structure refinement are given in Table 4. The diffraction frames were integrated using the SAINT[33] package and corrected for absorption with SADABS.[34]

CCDC-194088 (**3**), -194089 (**4**) and -194090 (**5**) contain the supplementary crystallographic data for this paper. These data can be obtained free of charge at www.ccdc.cam.ac.uk/conts/retrieving.html [or from the Cambridge Crystallographic Data Centre, 12, Union Road, Cambridge CB2 1EZ, UK; fax: (internat.) +44-1223/336-033; E-mail: deposit@ccdc.cam.ac.uk].

Acknowledgments

We gratefully acknowledge financial support from the MCYT (MAT2002−04421−002−02) and Bancaixa (P1.1B2001−03) for financial support. We also thank the Generalitat Valenciana for a fellowship (J.A.M.). We would also like to thank Prof. Robert H. Crabtree for his helpful comments.

[1] G. W. Parshall, S. D. Ittel, *Homogeneous Catalysis*, second ed., John Wiley & Sons, Inc., New York, **1992**.
[2] B. Cornils, W. A. Herrmann, *Applied Homogenous Catalysis with Organometallic Compounds*, VCH, New York, **1996**.
[3] P. Garrou, *Chem. Rev.* **1981**, *81*, 229.

Table 4. Crystallographic data

	3-Me_2	**4**	**5**
Empirical formula	$C_{29}H_{37}Br_2N_5Rh_2$	$C_{19}H_{25}Br_{2.50}Cl_{0.50}N_5Rh$	$C_{24}H_{30}F_6N_4PRh$
Molecular mass	821.28	643.85	622.40
Wavelength	0.71073 Å	0.71073 Å	0.71073 Å
Crystal system	Monoclinic	Monoclinic	Monoclinic
Space group	$P2_1/c$	$P2_1/c$	$P2_1/c$
a (Å)	14.635(5)	12.777(4)	12.717
b (Å)	10.547(4)	10.882(4)	13.849
b (Å)	19.842(7)	16.432(5)	14.887
α	90°	90°	90°
β	99.015(9)°	103.653(7)°	100.097(5)°
γ	90°	90°	90°
V (Å)^3	3024.8(19)	2220.2(12)	2581.4(12)
Z	4	4	4
Density (calculated)	1.803 Mg/m^3	1.926 Mg/m^3	1.602 Mg/m^3
Absorption coefficient	3.760 mm^{-1}	5.344 mm^{-1}	0.788 mm^{-1}
Reflections collected	24380	10540	20616
Goodness-of-fit on F^2	0.855	1.039	1.058
Final R indices [$I > 2\sigma(I)$]	$R1 = 0.0677$ $wR2 = 0.1863$	$R1 = 0.0323$, $wR2 = 0.0753$	$R1 = 0.0414$, $wR2 = 0.1026$

[4] W. A. Herrmann, *Angew. Chem. Int. Ed.* **2002**, *41*, 1291.
[5] V. P. W. Bohm, C. W. K. Gstottmayr, T. Weskamp, W. A. Herrmann, *J. Organomet. Chem.* **2000**, *595*, 186.
[6] J. Schwarz, V. P. W. Bohm, M. G. Gardiner, M. Grosche, W. A. Herrmann, W. Hieringer, G. Raudaschl-Sieber, *Chem. Eur. J.* **2000**, *6*, 1773.
[7] M. Albrecht, R. H. Crabtree, J. Mata, E. Peris, *Chem. Commun.* **2002**, 32.
[8] S. Grundemann, M. Albrecht, J. A. Loch, J. W. Faller, R. H. Crabtree, *Organometallics* **2001**, *20*, 5485.
[9] J. A. Loch, M. Albrecht, E. Peris, J. Mata, J. W. Faller, R. H. Crabtree, *Organometallics* **2002**, *21*, 700.
[10] E. Peris, J. A. Loch, J. Mata, R. H. Crabtree, *Chem. Commun.* **2001**, 201.
[11] A. M. Magill, D. S. McGuinness, K. J. Cavell, G. J. P. Britovsek, V. C. Gibson, A. J. P. White, D. J. Williams, A. H. White, B. W. Skelton, *J. Organomet. Chem.* **2001**, *617*, 546.
[12] D. S. McGuinness, K. J. Cavell, *Organometallics* **2000**, *19*, 741.
[13] A. A. Danopoulos, S. Winston, W. B. Motherwell, *Chem. Commun.* **2002**, 1376.
[14] A. A. D. Tulloch, A. A. Danopoulos, R. P. Tooze, S. M. Cafferkey, S. Kleinhenz, M. B. Hursthouse, *Chem. Commun.* **2000**, 1247.
[15] A. A. D. Tulloch, A. A. Danopoulos, G. J. Tizzard, S. J. Coles, M. B. Hursthouse, R. S. Hay-Motherwell, W. B. Motherwell, *Chem. Commun.* **2001**, 1270.
[16] W. A. Herrmann, J. Schwarz, M. G. Gardiner, *Organometallics* **1999**, *18*, 4082.
[17] M. G. Gardiner, W. A. Herrmann, C. P. Reisinger, J. Schwarz, M. Spiegler, *J. Organomet. Chem.* **1999**, *572*, 239.
[18] M. Poyatos, F. Márquez, E. Peris, C. Claver, E. Fernandez, *New J. Chem.* **2002**, *27*, 425.
[19] M. Poyatos, P. Uriz, J. A. Mata, C. Claver, E. Fernandez, E. Peris, *Organometallics* **2003**, *22*, 440.
[20] J. W. Faller, D. G. D′Alliessi, *Organometallics* **2002**, *21*, 1743.
[21] M. Isobe, R. Nishizawa, T. Nishikawa, K. Yoza, *Tetrahedron Lett.* **1999**, *40*, 6927.
[22] J. Cervantes, G. Gonzalez-AlaTorre, D. Rohack, K. H. Pannell, *App. Organomet. Chem.* **2000**, *14*, 146.
[23] A. K. Dash, I. Gourevich, J. Q. Wang, J. X. Wang, M. Kapon, M. S. Eisen, *Organometallics* **2001**, *20*, 5084.
[24] K. Itami, K. Mitsudo, A. Nishino, J. Yoshida, *J. Org. Chem.* **2002**, *67*, 2645.
[25] H. Katayama, K. Taniguchi, M. Kobayashi, T. Sagawa, T. Minami, F. Ozawa, *J. Organomet. Chem.* **2002**, *645*, 192.
[26] Y. Maruyama, K. Yamamura, T. Sagawa, H. Katayama, F. Ozawa, *Organometallics* **2000**, *19*, 1308.
[27] C. H. Jun, R. H. Crabtree, *J. Organomet. Chem.* **1993**, *447*, 177.
[28] R. Takeuchi, S. Nitta, D. Watanabe, *J. Chem. Soc., Chem. Commun.* **1994**, 1777.
[29] A. Mori, E. Takahisa, H. Kajiro, K. Hirabayashi, Y. Nishihara, T. Hiyama, *Chem. Lett.* **1998**, 443.
[30] R. Takeuchi, S. Nitta, D. Watanabe, *J. Org. Chem.* **1995**, *60*, 3045.
[31] A. Onopchenko, E. T. Sabourin, D. L. Beach, *J. Org. Chem.* **1983**, *48*, 5101.
[32] G. M. Sheldrick, *SHELXTL, version 5.1, Bruker AXS, Inc*, Madison, WI, **1997**.
[33] *SAINT, Bruker Analytical X-ray System, version 5.0*, Madison, WI, **1998**.
[34] G. M. Sheldrick, *SADABS empirical absorption program*, University of Göttingen, Göttingen, **1996**.

Received September 23, 2002
[I02533]

Crystal Structure of Bis[acetone-1-naphthoylhydrazinato(−1)]copper(II) and Investigations of Intermolecular Interactions

Zoran D. Tomić,[a] Vukadin M. Leovac,[b] Srdjan V. Pokorni,[c] Dieter Zobel,[d] and Snežana D. Zarić*[c]

Keywords: Pi interactions / Stacking interactions / Copper / Chelates

In the crystal structure of the bis(acetone-1-naphthoylhydrazinato)copper(II) complex there are interactions of neighbouring molecules via naphthyl groups; the naphthyl group of one molecule interacts with the copper centre and CH_3 group of another molecule. The geometry of the crystal structure and dispositions of charges in the naphthyl and chelate rings indicate that there are stacking interactions between the aromatic ring and, not only the copper atom, but also the whole chelate ring.

(© Wiley-VCH Verlag GmbH & Co. KGaA, 69451 Weinheim, Germany, 2003)

Introduction

In the past decades, investigations of non-covalent forces involving aromatic rings, such as weak hydrogen bonds, π-π interactions, and cation-π interactions, have attracted considerable interest.[1−12] Extended ab initio calculations on the orientation of two benzene molecules have shown that T-shaped and slipped-parallel orientations are more stable than a parallel orientation. It has also been shown that long range interactions such as electrostatic and dispersion interactions are a major source of attraction and that they are responsible for the directionality of the interactions.[13,14]

Noncovalent interactions of aromatic rings in transition metal complexes have been investigated by searching databases of crystal structures,[15−19] by quantum chemical calculations[18−22] and by spectroscopic methods.[23] These interactions play a role in crystal engineering,[11,12,16] and in the stability of metal complexes[10,18,23] and metalloproteins,[17] and it was proposed that these interactions can play a role in the mechanism of enzymatic reactions.[17]

Here we report on a crystal structure of the bis(acetone-1-naphthoylhydrazinato)copper(II) complex (complex I) and the study of a special type of noncovalent interaction between an aromatic ring and a transition metal complex.

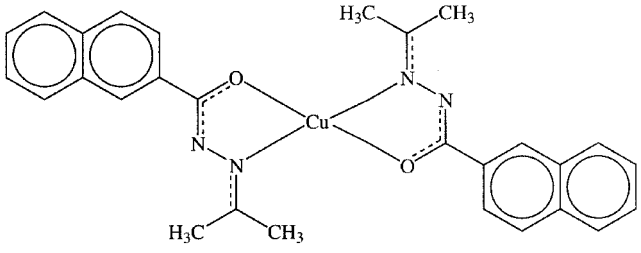

Complex I

In transition metal complexes with square planar and square pyramidal geometries, there are possibilities for noncovalent interactions that involve a metal atom. Noncovalent interactions of carbon atoms with the Cu^{II} metal ion have been noticed in our previously published crystal structure of aqua(4-methyl-1-naphth-1-yl-2,3-diaza-1,3,5-heptatriene-1,6-diolato-*N*,*O*,*O*,′)copper(II),[24] (complex II) and in other crystal structures of copper(II) complexes.[25−27] Small magnetic interactions transmitted through the interaction between the metal ion and the aromatic ring were recently identified and evaluated by EPR measurements in the crystal structure of the L-(tryptophylglycinato)copper(II) complex.[28]

[a] Institute of Nuclear Sciences "Vinča", P. O. Box 522, 11001 Belgrade, Yugoslavia
E-mail: zorant@vin.bg.ac.yu
[b] Institute of Chemistry, Faculty of Sciences, University of Novi Sad,
Trg Dositeja Obradovica 3, 21000, Novi Sad, Yugoslavia
[c] Department of Chemistry, University of Belgrade,
Studentski trg 16, P. O. Box 158, 11001 Belgrade, Yugoslavia
Fax:(internat.) + 381-11/638-785
E-mail: szaric@chem.bg.ac.yu
[d] Department of Biology, Chemistry and Pharmacy, Institute of Chemistry, Free University of Berlin,
Takustrasse 6, 14195 Berlin, Germany

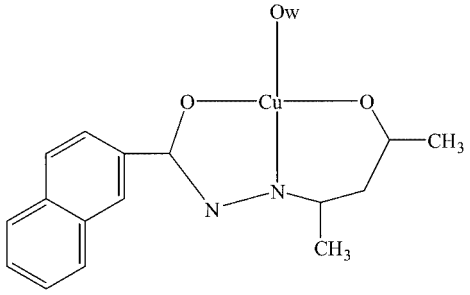

Complex II

For the newly synthesised complex I, a square-planar geometry was anticipated since there is a tendency for bis(chelate) Cu^{II} complexes to adopt such geometries.[29] Due to the absence of hydrogens on the nitrogen and oxygen atoms, the hydrogen bonding potential of this complex is diminished. Thus, it was anticipated that intermolecular contacts of the complex molecules would primarily be determined by the interactions involving aromatic rings. Indeed, in the crystal structure a naphthyl ring is involved in some kind of stacking interaction with a coordination plane of the other molecule.

Results and Discussion

Crystal Structure

The structure is built up of isolated units with a copper ion located at the centre of symmetry. Two molecules of the acetone-1-naphthoylhydrazinato ligand are coordinated through the O and terminal N atoms arranged in a distorted square-planar geometry resulting in a *trans* disposition of these ligands (Figure 1). The Cu−N and Cu−O bond lengths are 2.032(3) and 1.904(2) Å, respectively, while the bite angle of the chelate ring, N5−Cu1−O2 is 80.31°.

The bond lengths in the chelate ring indicate a delocalisation of electrons in the O2−C3−N4 fragment [C3−O2 1.299(3), C3−N4 1.299(3) Å] and the presence of a localised double bond N5−C16 [1.298(4) Å]. These naphthalene fragments are nearly planar and are twisted with respect to the chelate ring about the C3−C6 bond, the dihedral angle between the mean planes of the naphthalene and chelate rings being 16.20(7)°.

Intermolecular interactions between the outer six-membered ring and the Cu atom link the molecules into an infinite one-dimensional chain along the A axis (Figure 2). The Cu···centroid distance is 3.89 Å, while the distance of the Cu atom to the nearest C atom of the naphthyl ring is 3.185(3) Å. The dihedral angle between the mean planes of the chelate and the aromatic ring involved in the Cu···ring interaction is 16.35°. The second nearest C atom is at a distance of 3.529(4) Å. These arrangements are also associated with C−H···π interactions between the methyl hydrogen atom H(17C) and the inner six-membered ring of the neighbouring molecule (H···centroid 2.80 Å, C−H···centroid angle 132.20°). The corresponding distance from the ring centroid to the projection of the H atom position on the plane of the ring is 0.33 Å. This is in accordance with the preference of the hydrogen bond involved in the X−H··· π interaction to be directed towards the centre of the phenyl ring.[30] Adjacent chains are linked by van der Waals forces and weak C−H···π interactions of the methyl hydrogen atom H18C with the outer six-membered ring (H···centroid 3.01 Å, C−H···centroid angle 160.25°) to form sheets across the *ab* plane. The H···centroid distance

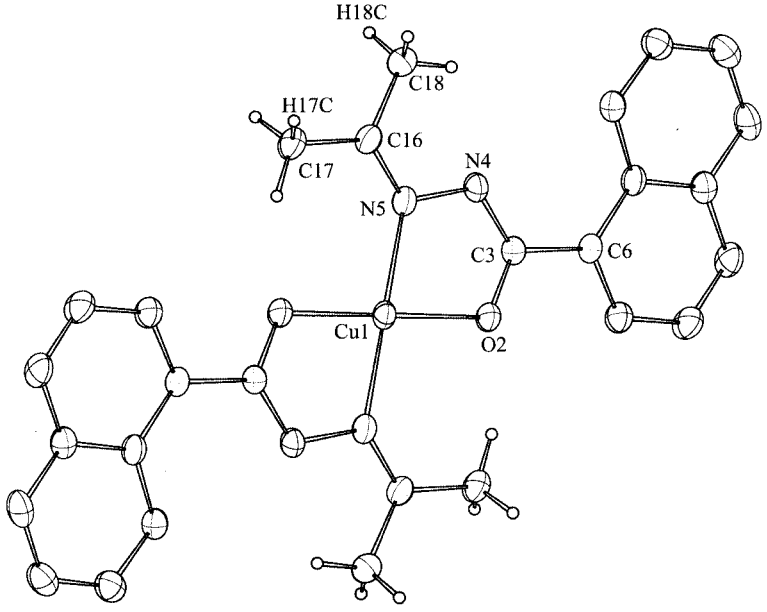

Figure 1. ORTEP[38] view (50% probability ellipsoids) of complex I showing the atom labelling

is slightly larger than the sum of the van der Waals radii of 3.05 Å.[31] However it was shown[32] that, besides the H···acceptor distance, the directional properties of the corresponding fragment must be considered, bearing in mind the tendency of the X−H···acceptor fragment to form a linear angle. The nearest intra- and inter-chain Cu···Cu separation is 6.261(5) and 8.474(7) Å, respectively.

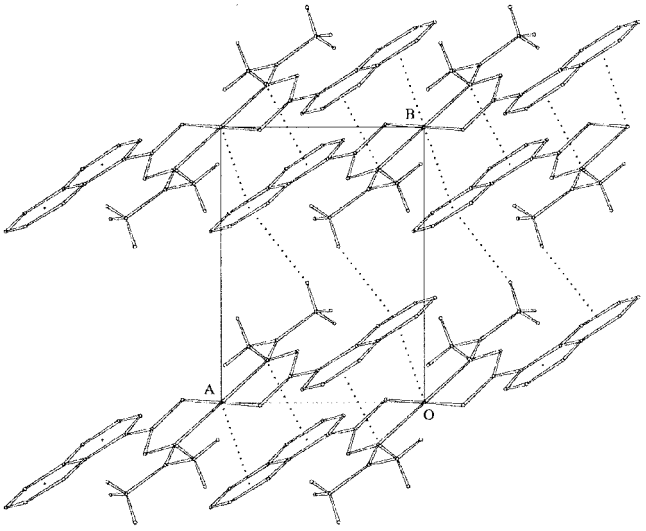

Figure 2. Arrangement of molecules into chains along the a axis and interchain contacts (dotted lines: C−H···π, and Cu···centroid)

We noticed that intermolecular forces in this crystal structure are similar to the forces reported in the previously published crystal structure of compound II.[24] In that structure, the molecules in the unit cell form chains with alternating O−H···π and Cu-naphthalene interactions. This arrangement is associated with a distance of 3.52/3.68 Å for the Cu···centroid of the six-membered ring, and a Cu···C distance of 3.116/3.061 Å.

A comparison of the two crystal structures shows that in both crystals a chain formation is achieved via X−H···π and Cu···phenyl contacts, associated with the distance of the Cu-centroid of the six-membered ring, in the range of 3.5−3.9 Å. The six-membered ring in both crystal structures is in a slipped-parallel position with respect to the chelate ring.

It is also interesting to compare the structure of complex I with the crystal structure of bis(*N*-isopropylidene-*N*′-salicyloylhydrazinato)copper(II) (complex III).[33] Although the ligands are very similar, the OH group on the aromatic ring in complex III has a large influence on the intermolecular interactions. Oxygen atoms have a large affinity to interact with Cu^{II} ions, hence in this crystal structure there is a Cu−O interaction (Cu···O distance of 2.764 Å), and no interaction of the Cu^{II} atom with the aromatic ring.

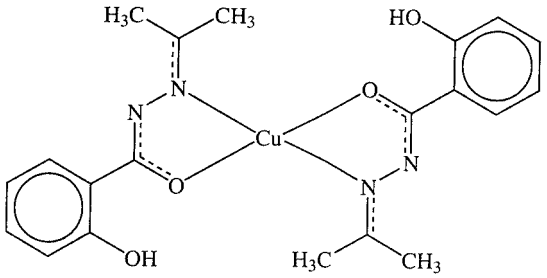

Complex III

Chelate Ring−Aromatic Ring Contacts

Chelate rings with delocalised bonds are considered to be similar to aromatic rings.[19,34] We assume that the slipped-parallel orientation in the structures of complexes I and II is a result of the balance of interacting forces, similar to that for two benzene molecules, for which the slipped-parallel orientation is very stable.[13] The slipped-parallel orientation can also been found in crystal structures of metal complexes, as can the usual π-interaction for aromatic nitrogen-containing ligands.[15] Since it is known that electrostatic interactions are important for interactions between aromatic rings,[13] we calculated the charges for complex I. Some atoms of the chelate ring are partially positively charged [Cu (0.6), C3 (0.3)], while some atoms are partially negatively charged [O2 (−0.6), N4 (−0.3), N5 (−0.3)]. The geometry of the crystal structure shows that the partially positively charged atoms of the chelate ring (Cu and C) have the shortest distance to the partially negatively (−0.07) charged carbons of the aromatic ring (C1···C14 3.185 Å, C12···C3 3.393 Å), whereas the nitrogen atoms from the chelate ring have the shortest distance to the partially positively (0.07) charged hydrogen atom (N4···H13 2.942, N5···H13 2.975 Å) (Figure 3).

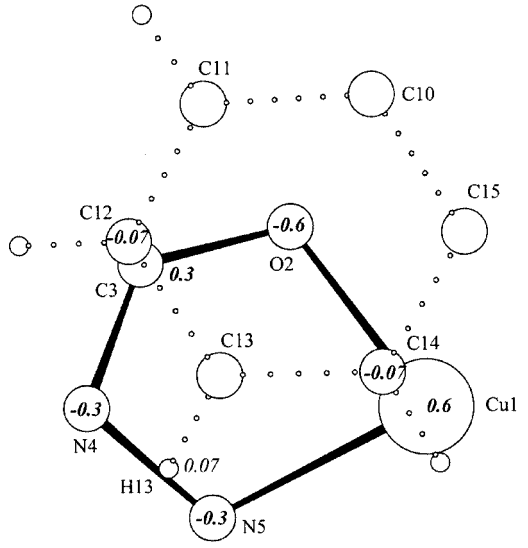

Figure 3. Interaction of the chelate ring and aromatic ring in complex I showing partial atomic charges; orientation is in the direction normal to the chelate mean plane; the aromatic ring is represented by dots

It should be mentioned that in the crystal structure of complex III[33] there is no slipped-parallel orientation of the chelate and phenyl ring; however, inspection of the crystal packing showed that the shortest distances between atoms from two molecules are the distances between partially positively charged atoms and partially negatively charged atoms (Cu···O 2.764 Å, N1···C7 3.354 Å).

Conclusion

In the crystal structure of bis(acetone-1-naphthoylhydrazinato)copper(II) the intermolecular distances between the copper and aromatic carbons indicates that interactions may occur. A mutual slipped-parallel orientation of the chelate and the aromatic ring, similar to the stable orientation of two benzene molecules, suggests that these interactions involve not only the copper atom but also the whole chelate ring. This assumption is supported by analysis of the distances in the crystal structure connected with the partial atomic charges on the aromatic ring and the chelate ring. This indicates that a modification of the chelate ring could modify the interaction of the aromatic ring with the Cu^{II} atom, in square-planar copper(II) complexes.

Experimental Section

Preparation

A synthesis of the title compound has been reported[35] although crystals of the product were not suitable for X-ray diffraction analysis. In the modified procedure the compound was unexpectedly obtained from a reaction of an acetone/ethyl alcohol (1:1) solution of acetone-1-naphthoylhydrazone and a methyl alcohol solution of $Cu(NO_3)_2{\cdot}3H_2O$ and NH_4NCS (molar ratio 1:1:2, respectively). After precipitation of CuNCS, the solution was filtered, allowed to stand and after a few days, crystals of the title complex suitable for X-ray diffraction were obtained.

X-ray Crystallography

Crystal data for $C_{28}H_{26}CuN_4O_2$: M = 514.07, monoclinic space group $P2_1/c$, a = 6.261(5) Å, b = 8.474(5) Å, c = 21.830(5) Å, β = 90.110(5)°, V = 1158.2(12) Å^3, D_c = 1.474 mg/m^3, λ (Mo-K_α radiation) = 0.71073 Å, F_{000} = 534. Diffraction data were measured on a Stoe 4-circle diffractometer with graphite monochromator, using ω/2θ scans. Lattice parameters were determined from 43 reflections in the range $15 < 2\theta < 30$. 5866 reflections were measured ($\theta < 28$), of which 2786 were independent. The data were corrected for Lorentz and polarisation factors, but not for absorption. The structure was solved by direct methods using SIR92 [36] and refined by applying a full-matrix least-squares method based on F^2, including all reflections. All non-hydrogen atoms were refined anisotropically using SHELXL-97.[37] Hydrogen atoms were included at calculated positions and allowed to ride on their parent atoms. The refinement converged at R = 0.051, and wR = 0.1453 for 2068 reflections satisfying the condition $I > 2\sigma(I)$, (wR = 0.1565 for all reflections). The maximum and minimum residual electron densities in the final ΔF map were 0.797 and −0.521 e/Å^3, respectively. The structure diagram was generated using ORTEP 3[38] and geometrical analysis was performed using PLATON-99.[39] All calculations were done using WinGX as an integrated system for all the crystallographic programs.[40]

CCDC-183111contains the supplementary crystallographic data for this paper. These data can be obtained free of charge at www.ccdc.cam.ac.uk/conts/retrieving.html [or from the Cambridge Crystallographic Data Centre, 12, Union Road, Cambridge CB2 1EZ, UK; Fax: (internat.) +44-1223/336-033; E-mail: deposit@ccdc.cam.ac.uk].

Computational Details

Quantum chemical calculations of partial charges were performed on a model system built from the crystal structure, using the B3LYP[41,42] method and LACVP** basis set. Calculations were done with the Jaguar 4.1 program.[43]

Acknowledgments

The authors would like to thank Prof. E. W. Knapp for useful discussions. S. D. Z. was supported by a Alexander von Humboldt fellowship, S. P. was supported by a DAAD fellowship. The calculations were carried out at the computer centre of the Free University of Berlin.

[1] G. R. Desiraju, T. Steiner, *The Weak Hydrogen Bonds in Structural Chemistry and Biology*, Oxford University Press, **1999**.
[2] M. J. Calhorda, *Chem. Commun.* **2001**, 801−809.
[3] D. A. Dougherty, *Science* **1996**, *271*, 163−168.
[4] J. C. Ma, D. A. Dougherty, *Chem. Rev.* **1997**, *97*, 1303−1324.
[5] J. P. Gallivan, D. A. Dougherty, *J. Am. Chem. Soc.* **2000**, *122*, 870−874.
[6] J. P. Gallivan, D. A. Dougherty, *Proc. Natl. Acad. Sci. USA* **1999**, *96*, 9459−9464.
[7] Z. Shi, A. Olson, N. R. Kallenbach, *J. Am. Chem. Soc.* **2002**, *124*, 3284−3291.
[8] E. V. Pletneva, A. T. Laederach, D. B. Fulton, N. M. Kostić, *J. Am. Chem. Soc.* **2001**, *123*, 6232−6245.
[9] T. P. Burghardt, N. Juranić, S. Macura, K. Ajtai, *Biopolymers* **2002**, *63*, 261−272.
[10] O. Sénèquè, M. Giorgi, O. Reinaud, *Chem. Commun.* **2001**, 984−985.
[11] D. Braga, F. Grepioni, *Acc. Chem. Res.* **2000**, *33*, 601−608.
[12] D. Braga, F. Grepioni, *Coord. Chem. Rev.* **1999**, *183*, 19−41.
[13] S. Tsuzuki, K. Honda, T. Uchimaru, M. Mikami, K. Tanabe, *J. Am. Chem. Soc.* **2002**, *124*, 106−114.
[14] P. Hobza, H. L. Selzle, E. W. Schlag, *J. Phys. Chem.* **1996**, *100*, 18790−18794.
[15] C. Janiak, *J. Chem. Soc., Dalton Trans.* **2000**, 3885−3896.
[16] D. Braga, F. Grepioni, E. Tedesco, *Organometallics* **1998**, *17*, 2669−2672.
[17] S. D. Zarić, D. Popović, E. W. Knapp, *Chem. Eur. J.* **2000**, *6*, 3935−3942.
[18] M. Milčić, S. D. Zarić, *Eur. J. Inorg. Chem.* **2001**, 2143−2150.
[19] G. A. Bogdanović, A. Spasojević-de Biré, S. D. Zarić, *Eur. J. Inorg. Chem.* **2002**, 1599−1602.
[20] S. D. Zarić, *Chem. Phys. Lett.* **1999**, *311*, 77−80.
[21] A. Zmirić, M. Milčić, S. D. Zarić, *Inter. J. Quant. Chem.* **2002**, 354−359.
[22] J. Šponer, J. E. Šponer, J. Leszczynski, *J. Biomol. Struct. Dyn.* **2000**, *17*, 1087−1096.
[23] H. Kumita, T. Kato, K. Jitsukawa, H. Einaga, H. Masuda, *Inorg. Chem.* **2001**, *40*, 3936−3942.
[24] R. Fazlic, V. Divjakovic, V. M. Leovac, S. Y. Chundak, *Acta Crystallogr., Sect. C* **1991**, *47*, 714−715.
[25] W. A. Franks, D. van der Helm, *Acta Crystallogr., Sect. B* **1971**, *27*, 1299−1310.
[26] H. Masuda, A. Odani, O. Yamauchi, *Inorg. Chem.* **1989**, *28*, 624−625.

[27] O. R. Nascimento, A. J. Costa-Filho, D. I. De Morais, J. Ellena, L. F. Delboni, *Inorg. Chim. Acta* **2001**, *312*, 133−138.
[28] A. J. Costa-Filho, O. R. Nascimento, L. Ghivelder, R. Calvo, *J. Phys. Chem. B* **2001**, *105*, 5039−5047.
[29] P. R. Raithby, G. P. Shields, F. H. Allen, W. D. S. Motherwell, *Acta Crystallogr., Sect. B* **2000**, *56*, 444−454.
[30] Z. Ciunik, G. R. Desiraju, *Chem. Commun.* **2001**, 703−704.
[31] F. A. Cotton and G. Wilkinson, *Inorganic Chemistry*, Wiley, New York, 1st ed., 1967, p. 115.
[32] T. Steiner, G. R. Desiraju, *Chem. Commun.* **1998**, 891−892.
[33] P. Domiano, A. Musatti, G. Predieri, *Cryst. Struct. Commun.* **1974**, *3*, 717−720.
[34] H. Masui, *Coord. Chem. Rev.* **2001**, *957−992*, 219−221.
[35] V. M. Leovac, D. Ž. Obadović, S. Yu. Chundak, F. Skuban, *Thermochim. Acta* **1992**, *210* 193−203.
[36] A. Altomare, G. Cascarano, G. Giacovazzo, A. Guagliardi, M. C. Burla, G. Polidori, M. Camalli, *J. Appl. Crystallogr.* **1994**.
[37] G. M. Sheldrick, SHELXL-97, *Program for the Refinement of Crystal Structures*, University of Goettingen, Germany **1997**.
[38] L. J. Farrugia, ORTEP 3, *J. Appl. Crystallogr.* **1997**, *30*, 565−565.
[39] A. L. Spek, PLATON-99, *Molecular Geometry Program*, University of Utrecht, The Netherlands **1999**.
[40] L. J. Farrugia, *J. Appl. Cryst.* **1999**, *32*, 837−838.
[41] A. D. Becke, *J. Chem. Phys.* **1993**, *98* 5648−5652.
[42] C. Lee, W. Yang, R. G. Parr, *Phys. Rev. B* **1988**, *37*, 785−789.
[43] Jaguar 4.1, Schrodinger, Inc., Portland, Oregon, **2000**.

Received April 8, 2002
[I02182]

The First Structurally Characterized Trinuclear Dipicolinato Manganese Complex and its Conversion into a Mononuclear Species by Ligand Substitution

Chengbing Ma,[a] Changneng Chen,[a] Qiutian Liu,*[a] Daizheng Liao,[b] and Licun Li[b]

Keywords: Manganese / N ligands / Cluster compounds

The novel complex $[Mn_3(pdc)_3(bpy)_3(H_2O)_2]$ (**1**) (H_2pdc = 2,6-pyridinedicarboxylic acid, also known as 2,6-dipicolinic acid; bpy = 2,2′-bipyridine), has been obtained from the reaction of polymeric $[MnK_2(pdc)_2(H_2O)_7]_n$ (**2**) with bpy, and is the first example of a structurally characterized, trinuclear Mn complex incorporating dipicolinato ligands. All the Mn^{II} centers are seven-coordinate in severely distorted pentagonal-bipyramidal geometries. The conversion of **1** to mononuclear $[Mn(pdc)(bpy)(Him)_2]$ (**3**) (Him = imidazole), which is the first seven-coordinate Mn complex with a Him ligand, has also been achieved by substitution of the labile ligand in **1** by Him.
(© Wiley-VCH Verlag GmbH & Co. KGaA, 69451 Weinheim, Germany, 2003)

Introduction

Much attention has been paid to the design and synthesis of transition metal complexes incorporating 2,6-dipicolinic acid due to the versatile bidentate, tridentate, or bridging coordination modes of the ligand,[1] its diverse biological activity and its capacity to stabilize unusual oxidation states,[2] as well as its application to diverse areas of technology.[3] Up to now, the control of product architecture has been elusive and remains a major challenge of modern chemistry.[4] Only one example of a trinuclear 2,6-dipicolinate complex is known in the literature,[5] although many examples of mononuclear and dinuclear dipicolinates, as well as complexes with chain structures, have been reported.[6] Manganese complexes of 2,6-dipicolinates are nevertheless rare.[7] Recently, we obtained a Mn/K polymer, $[MnK_2(pdc)_2(H_2O)_7]_n$, from a reaction system containing Mn^{2+}, H_2pdc, and alkali metal hydrate as a member of the family $[MnK_2(pdc)_2(H_2O)_7]_n$ (M = Mn, Co, Zn etc.).[8] Here we report the reaction of the Mn/K polymer with bpy, from which the first example of a dipicolinato, trinuclear Mn complex, $[Mn_3(pdc)_3(bpy)_3(H_2O)_2]$ (**1**), was obtained. Further study of the reaction leads to the mononuclear complex $[Mn(pdc)(bpy)(Him)_2]$ (**3**) with three different ligands within the coordination sphere.

[a] State Key Laboratory of Structural Chemistry, Fujian Institute of Research on the Structure of Matter, Chinese Academy of Sciences,
Fuzhou 350002, China
Fax: (internat.) +86-(0)591/371-4946
E-mail: lqt@ms.fjirsm.ac.cn
[b] Department of Chemistry, Nankai University,
Tianjing 300071, China

Results and Discussion

Dipicolinates commonly ligate to transition metals by either carboxylate bridges between metal centers, to form polymeric complexes, or tridentate (O,N,O′) chelation to one metal ion.[9] With the intention of preparing pdc-coordinated oligomers as model compounds for Mn-containing enzymes,[10] the bpy ligand, which strongly favours bidentate coordination, was used to cleave the carboxylate bridges of **2**, and a trinuclear cluster (**1**·9H_2O) was successfully isolated as single crystals. Complex **1** can also be obtained directly from a reaction mixture containing Mn^{2+}, pdc^{2-}, and bpy. However, the excess pdc^{2-} used in this direct synthesis gives rise to the formation of impurities and does not allow the formation of good quality single crystals. Upon reaction of **1** with an excess of imidazole (Him) in DMF/H_2O, substitution of H_2O by Him occurs and the trinuclear **1** decomposes, resulting in mononuclear **3**. Related reactions are compiled in Scheme 1.

Single-crystal X-ray analysis revealed **1** to be a discrete trimanganese cluster. As shown in Figure 1, all Mn atoms

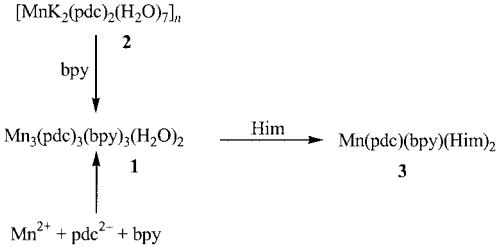

Scheme 1. Preparation of **1** and its decomposition to produce **3**

are seven-coordinate, although two types of inequivalent Mn atoms are observed. Both bpy and pdc^{2-} ligands chelate to each Mn center in bi- and tridentate mode (N,N′ and O,N,O′) respectively, while one additional terminal water molecule binds to Mn1 and Mn2, giving the same coordination sphere for the Mn1 and Mn2 sites. In addition to bpy and pdc^{2-} chelation, Mn3 is bidentately coordinated by a carboxylate group of the pdc^{2-} ligand bound to the central Mn2 atom. Interestingly, the three pdc^{2-} ligands exhibit diverse coordination modes. The pdc^{2-} bridges between the Mn ions are also different from each other: double μ-O bridges occur between Mn1 and Mn2 and both carboxylate (μ-OCO) and μ-O bridges exist between Mn2 and Mn3. Consequently, each of the three metals possesses a highly asymmetrical coordination environment, forming a pentagonal bipyramidal geometry around each Mn^{II} center. The intracluster Mn···Mn separations were found to be 3.739(2) Å for Mn1···Mn2, and 4.607(2) Å for Mn2···Mn3; the difference of 0.86 Å in Mn···Mn separation in a single structure is rather rare.[11] Complex **1** is the first dipicolinato trimanganese complex, although a similar triiron dipicolinate [{Fe(pdc)(Hpdc)}$_2$Fe(H$_2$O)$_4$] has been reported.[5] High spin d^5 compounds can be expected to adopt geometries dictated by electrostatic effects, and many seven-coordinate Fe^{III} compounds are known.[12] Seven-coordinate Mn^{II} complexes are often observed with a quinquedentate ligand such as 15-crown-5,[13] which serves to define a pentagonal plane on the equator and leaves two axial positions open for further coordination to give a regular pentagonal bipyramid. However, the coordination sphere in **1** is severely distorted (Table 1) because the two planar ligands (bpy and pdc^{2-}) do not coexist in the equatorial plane and, therefore, large steric strain results between the ligands. On the other hand, linear connection between the metal centers and ligand distortion offer the possibility of further reaction with certain reagents, such as imidazole, to give mononuclear,

Table 1. Selected bond lengths [Å] and angles [°] with estimated standard deviations for **1**

Mn1−O13	2.168(5)	Mn2−O6	2.315(4)
Mn1−N1	2.260(5)	Mn2−N7	2.330(6)
Mn1−N5	2.293(6)	Mn2−O7	2.422(5)
Mn1−O2	2.310(5)	Mn3−N3	2.226(5)
Mn1−O6	2.315(4)	Mn3−N9	2.267(6)
Mn1−N4	2.323(6)	Mn3−O11	2.271(5)
Mn1−O4	2.401(4)	Mn3−N8	2.289(6)
Mn2−O14	2.183(5)	Mn3−O8	2.317(5)
Mn2−O4	2.236(4)	Mn3−O10	2.351(5)
Mn2−N6	2.276(5)	Mn3−O7	2.368(4)
Mn2−N2	2.288(5)		
O13−Mn1−N5	166.3(2)	N9−Mn3−O8	165.0(2)
O13−Mn1−O2	83.2(2)	N9−Mn3−O11	98.8(2)
O13−Mn1−O6	80.23(18)	N9−Mn3−N8	71.7(2)
O13−Mn1−N1	94.72(19)	N9−Mn3−N3	96.0(2)
O13−Mn1−N4	96.0(2)	N9−Mn3−O10	88.39(19)
O13−Mn1−O4	109.36(18)	N9−Mn3−O7	111.32(19)
N5−Mn1−N1	95.03(19)	O8−Mn3−N3	98.78(19)
N5−Mn1−O6	100.91(18)	O8−Mn3−O11	88.54(19)
N5−Mn1−O2	91.1(2)	O8−Mn3−N8	96.8(2)
N5−Mn1−N4	70.9(2)	O8−Mn3−O7	55.78(16)
N5−Mn1−O4	83.29(18)	O8−Mn3−O10	94.30(18)
O4−Mn2−O7	153.40(16)	O14−Mn2−O7	76.24(17)
O4−Mn2−N6	109.70(18)	N6−Mn2−O7	84.34(18)
O4−Mn2−N2	131.59(17)	N2−Mn2−O7	67.88(17)
O4−Mn2−O6	69.08(16)	O6−Mn2−O7	135.86(16)
O4−Mn2−O14	83.96(17)	N7−Mn2−O7	79.77(18)
O4−Mn2−N7	83.82(19)		

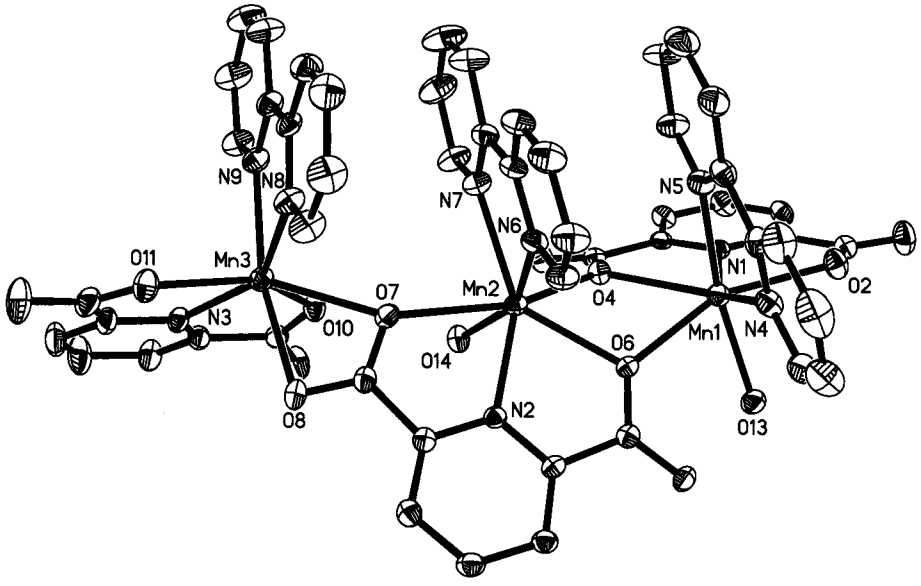

Figure 1. ORTEP drawing of **1** with independent atom-labeling showing thermal ellipsoids at 30% probability

seven-coordinate **3** containing three different ligands (pdc, bpy and Him). To the best of our knowledge, **3** is the first seven-coordinate Mn complex containing imidazole. A single-crystal X-ray analysis confirmed that the sphere around the seven-coordinate Mn^{II} center in **3** has a slightly

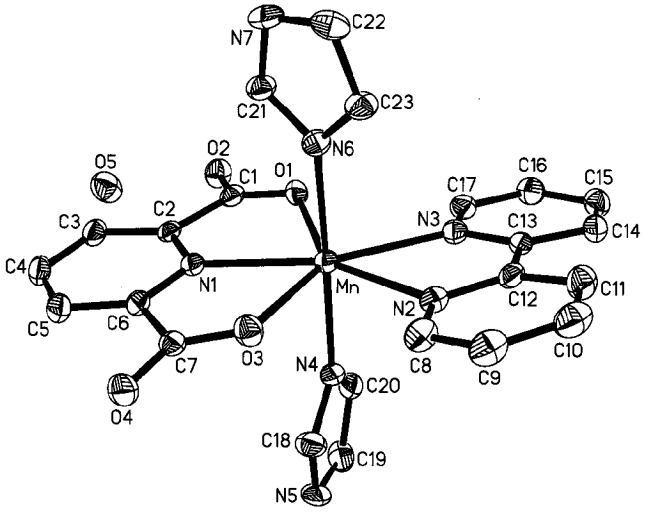

Figure 2. ORTEP drawing of $3{\cdot}H_2O$ with independent atom-labeling showing thermal ellipsoids at 30% probability

distorted pentagonal bipyramidal geometry (Figure 2). Three arene N atoms and two carboxylate O atoms from tridentate pdc^{2-} and bidentate bpy chelate to the Mn^{II} center and form the equatorial plane [a maximum deviation of 0.1494(2) Å from the plane occurs for N3], and two Him N atoms occupy the axial sites. The axial bond angle of 177.45(2)° for N4−Mn−N6 gives a more or less regular pentagonal bipyramid (Table 2). This arrangement of the

Table 2. Selected bond lengths [Å] and angles [°] with estimated standard deviations for **3**

Mn−N6	2.248(5)	Mn−O1	2.372(4)
Mn−N4	2.250(5)	Mn−N2	2.393(5)
Mn−N1	2.324(5)	Mn−N3	2.423(5)
Mn−O3	2.349(4)		
N6−Mn−N4	177.43(18)	N4−Mn−N2	93.30(17)
N6−Mn−N1	93.59(17)	N1−Mn−N2	146.13(18)
N4−Mn−N1	85.51(17)	O3−Mn−N2	78.11(17)
N6−Mn−O3	90.12(17)	O1−Mn−N2	145.91(17)
N4−Mn−O3	87.31(17)	N6−Mn−N3	93.38(17)
N1−Mn−O3	68.02(16)	N4−Mn−N3	88.72(17)
N6−Mn−O1	88.21(17)	N1−Mn−N3	145.32(18)
N4−Mn−O1	93.67(17)	O3−Mn−N3	145.85(17)
N1−Mn−O1	67.75(16)	O1−Mn−N3	78.57(16)
O3−Mn−O1	135.53(16)	N2−Mn−N3	68.27(18)
N6−Mn−N2	86.09(17)		

three ligands is evidently favorable to stabilize the structure and promotes the conversion of trinuclear **1** into mononuclear **3**.

The room-temperature magnetic moment measured for **3** (μ_{eff} = 10.3 B.M.) is close to that expected for the spin-only value of 10.24 B.M. for three uncoupled S = 5/2 sites. The effective magnetic moment remains essentially constant with decreasing temperature, but μ_{eff} decreases rapidly below 40 K, exhibiting a characteristic antiferromagnetic interaction between the neighboring Mn^{II} ions. A model containing a linear Mn_3 system was used for fitting the experimental magnetic data by invoking an exchange pathway through the carboxylate bridges, in which the magnetic exchange constant (J) between Mn2 and Mn1 (or Mn3) is assumed to be equal, for simplification, and the interaction between Mn1 and Mn3 is omitted. The spin-spin coupling

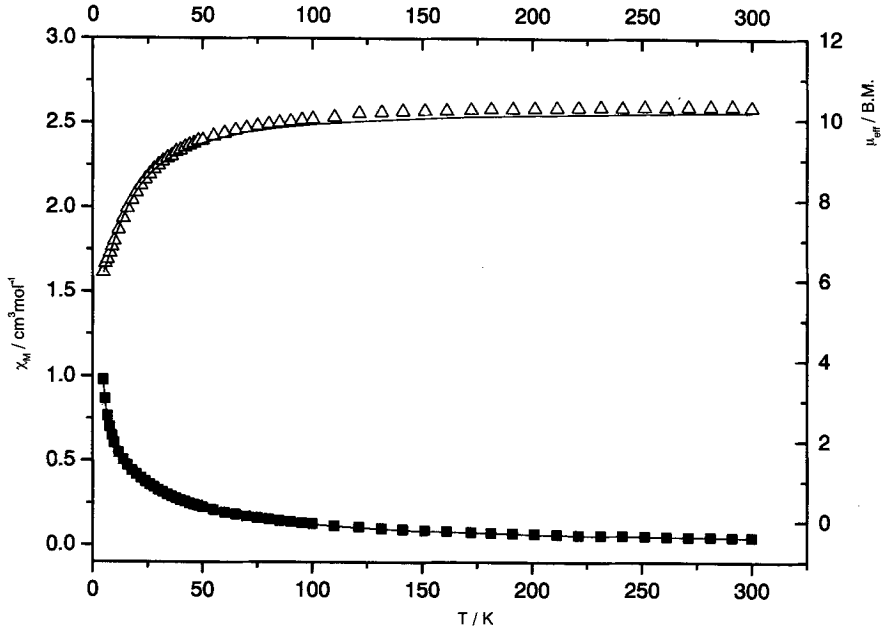

Figure 3. Experimental susceptibilities (χ_M, marked as square) and effective magnetic moment (μ_{eff}, marked as triangle) as functions of temperature for **1**; the solid lines represent the calculated values

Hamiltonian appropriate for describing the magnetic exchange interaction of the model is presented in Equation (1).

$$\hat{H} = -2J(\hat{S}_1\hat{S}_2 + \hat{S}_2\hat{S}_3)$$

$$\chi_M = \frac{Ng^2\beta^2}{3kT}\left[\frac{A}{B}\right]$$

$$A = 2040e^{-32x} + 1860e^{-17x} + 858e^{-4x} + 495e^{7x} + 252e^{16x} + 105e^{23x} + 1365e^{-27x} + 858e^{-14x} + 495e^{-3x} + 252e^{6x} + 105e^{13x} + 30e^{18x} + 858e^{-22x} + 492e^{-11x} + 252e^{-2x} + 105e^{5x} + 30e^{10x} + 3e^{13x} + 252e^{-8x} + 105e^{-x} + 30e^{4x} + 252e^{-12x} + 105e^{-5x} + 30 + 105e^{-7x}$$

$$B = 32e^{-32x} + 48e^{-17x} + 24e^{-4x} + 24e^{7x} + 16e^{16x} + 12e^{23x} + 28e^{-27x} + 24e^{-14x} + 20e^{-3x} + 16e^{6x} + 12e^{13x} + 8e^{18x} + 24e^{-22x} + 20e^{-11x} + 16e^{-2x} + 12e^{5x} + 8e^{10x} + 4e^{13x} + 16e^{-8x} + 12e^{-x} + 8e^{4x} + 16e^{-12x} + 12e^{-5x} + 8 + 12e^{-7x}$$

$$x = \frac{-J}{kT} \qquad (1)$$

The best fitting curves are depicted in Figure 3 for **1**. The best fitting parameters are $J = -0.81$ cm^{-1}, $g = 2.02$, and $R = [(\chi_M)_{obsd.} - (\chi_M)_{calcd.}]^2/(\chi_M)^2_{obsd.}] = 1.84 \times 10^{-4}$, showing weak antiferromagnetic exchange interactions between the metal atoms.

Conclusion

This work has described the synthesis and structure of a novel trinuclear Mn complex **1** derived from a polymeric Mn/K precursor **2**, as well as the conversion of **1** into a mononuclear species, **3**, which represents a preliminary result in the control of product nuclearity by ligand exchange or substitution. The control of product architecture is yet to be explored.

Experimental Section

General: All manipulations were performed under aerobic conditions with materials as received. Polymeric $[MnK_2(pdc)_2(H_2O)_7]_n$ was prepared from the reaction of dipicolinic acid and KOH with $Mn(OAc)_2{\cdot}4H_2O$.[8] The IR spectra were recorded on a Bio-Rad FTS-40 Model spectrophotometer. The variable-temperature susceptibilities were measured on a Model CF-1 superconducting extraction sample magnetometer with a crystalline sample kept in a capsule between 5 and 300 K. Diamagnetic corrections were made with Pascal's constants. Elemental analyses were performed by a Vario EL Elemental Analyzer.

$[Mn_3(pdc)_3(bpy)_3(H_2O)_2]{\cdot}9H_2O$ ($1{\cdot}9H_2O$): 2,2′-Bipyridine (0.32 g, 2 mmol) in 10 mL of EtOH was added to a solution of $[MnK_2(pdc)_2(H_2O)_7]_n$ (1.18 g, 2 mmol) in 5 mL of H_2O with continuous stirring. The mixture was refluxed for six days, producing large plate-like crystals of $1{\cdot}9H_2O$. Yield: 0.39 g (44%). $C_{51}H_{55}Mn_3N_9O_{23}$ (1326.86): calcd. C 46.17, H 4.18, N 9.50, Mn 12.42; found C 46.11, H 4.15, N 9.54, Mn 12.47. IR (KBr pellet): $\tilde{\nu}$ = 3396 (br. s), 1645 (m), 1616 (s), 1603 (s), 1579 (s), 1566 (s), 1493 (w), 1475 (m), 1439 (s), 1375 (s), 1363 (s), 1317 (w), 1277 (m), 1246 (w), 1186 (m), 1161 (w), 1119 (w), 1076 (m), 1063 (w), 1043 (w), 1016 (s), 962 (w), 916 (m), 862 (w), 837 (w), 773 (s), 762 (s), 737 (m), 698 (m), 661 (m), 625 (w), 530 (w), 432 (m), 413 cm^{-1} (w).

$[Mn(pdc)(bpy)(Him)_2]{\cdot}H_2O$ ($3{\cdot}H_2O$): Imidazole (0.68 g, 10 mmol) was added to a solution of $1{\cdot}9H_2O$ (1.33 g, 1 mmol) dissolved in 20 mL of H_2O/DMF (1:4, v/v). The mixture was refluxed for two hours and was then filtered. The filtrate was left in a desiccator with $CaCl_2$ for six days to produce yellow crystals of $3{\cdot}H_2O$. Yield: 0.86 g (54%). $C_{23}H_{21}MnN_7O_5$ (530.41): calcd. C 52.08, H 3.99, N 18.49, Mn 10.36; found C 52.02, H 3.97, N 18.44, Mn 10.42. IR (KBr pellet): $\tilde{\nu}$ = 3492 (s), 3379 (br. s), 3107 (m), 3045 (w), 2846 (m), 2611 (w), 1622 (s), 1587 (m), 1531 (m), 1437 (s), 1377 (s), 1327 (w), 1279 (m), 1244 (w), 1184 (m), 1159 (w), 1136 (m), 1101 (m), 1065 (s), 1011 (m), 935 (m), 904 (w), 843 (m), 804 (w), 768 (s), 725 (s), 698 (m), 661 (s), 642 (w), 623 (m), 521 (w), 415 cm^{-1} (w).

X-ray Crystallography: Data were collected at 293 K on a Siemens SMART CCD diffractometer for $1{\cdot}9H_2O$ and $3{\cdot}H_2O$ with graphite monochromated Mo-K_α radiation (λ = 0.71073 Å) using the ω-scan mode, and were corrected with the SADABS program. Structure solutions were made with the SHELXTL program.[14] The structures were solved by direct methods. All non-hydrogen atoms were refined anisotropically with three exceptions: O20, O21 and O22 of the solvate water molecules in $1{\cdot}9H_2O$ are disordered over two positions with occupancies of 0.5 each.

Crystal Data for $1{\cdot}9H_2O$: $C_{51}H_{55}Mn_3N_9O_{23}$, M_r = 1326.86, monoclinic, space group $P2_1/n$, a = 21.2089(3), b = 10.0559(2), c = 28.1400(1) Å, β = 108.017(1)°, V = 5707.26(1) Å^3, Z = 4, $D_{calcd.}$ = 1.544 g/cm^3, $F(000)$ = 2732, μ = 0.743 mm^{-1}. R = 0.0754 and Rw = 0.1683 for 5979 observed reflections with $I > 2\sigma(I)$.

Crystal Data for $3{\cdot}H_2O$: $C_{23}H_{21}MnN_7O_5$, M_r = 530.41, monoclinic, space group $P2_1/n$, a = 8.1309(1), b = 16.9103(5), c = 17.3252(5) Å, β = 102.017(2)°, V = 2329.94(1) Å^3, Z = 4, D_c = 1.512 g/cm^3, $F(000)$ = 1092, μ = 0.618 mm^{-1}. R = 0.0698 and Rw = 0.1956 for 2766 observed reflections with $I > 2\sigma(I)$.

CCDC-188829 (**$1{\cdot}9H_2O$**) and -188830 (**$3{\cdot}H_2O$**) contain the supplementary crystallographic data for $1{\cdot}9H_2O$ and $3{\cdot}H_2O$. These data can be obtained free of charge at www.ccdc.cam.ac.uk/conts/retrieving.html [or from the Cambridge Crystallographic Data Centre, 12 Union Road, Cambridge CB2 1EZ, UK; Fax: (internat. +44-1223/336-033; E-mail: deposit@ccdc.cam.ac.uk].

Acknowledgments

This work was supported by State Key Basic Research and Development Plan of China (G1998010100), the NNSFC (29973047, 30170229 and 39970177) and Expert Project of Key Basic Research from Ministry of Science & Technology.

[1] [1a] G. Chessa, G. Marangoni, B. Pitteri, V. Bertoasi, V. Ferreti, *Inorg. Chim. Acta* **1991**, *185*, 201−210. [1b] P. P. Quaglieri, H. Loiseleur, G. Thomas, *Acta Crystallogr., Sect. B* **1972**, *28*, 2583−2590. [1c] S. K. Sengupta, S. K. Shani, R. N. Kapoor, *Polyhedron* **1983**, *2*, 317−322.

[2] [2a] B. S. Church, H. Halvorson, *Nature* **1959**, *183*, 124−125. [2b] G. Scapin, S. G. Reddy, R. Zheng, J. S. Blanchard, *Biochemistry* **1997**, *36*, 15081−15087. [2c] D. L Hoof, D. G. Tisley, R. A. Walton, *J. Chem. Soc., Dalton Trans.* **1973**, 200−204.

[3] [3a] Y. Pocker, C. T. O. Fong, *Biochemistry* **1980**, *19*, 2045−2050. [3b] C. G. Pope, E. Matijevic, R. C. Patel, *J. Colloid Interface Sci.* **1981**, *80*, 874−879.

[4] [4a] S. O. H. Gutschke, A. K. Powell, P. T. Wood, *Angew. Chem. Int. Ed.* **1999**, *38*, 1088−1090. [4b] S. S. Y. Chui, S. M. F. Lo, A. G. Orpen, I. D. Williams, *Science* **1999**, *283*, 1148−1150.

[5] P. Lainé, A. Gourdon, J.-P. Launay, *Inorg. Chem.* **1995**, *34*, 5138−5149.

[6] [6a] J. G. H. du Preez, H. E. Rohwer, B. J. van Brecht, M. R. Caira, *J. Chem. Soc., Dalton Trans.* **1984**, 975−980. [6b] G. R.

Willery, T. J. Woodman, M. Fisher, M. G. B. Drew, *Transition Met. Chem.* **1998**, *23*, 467−471. [6c] K. A. Abbound, C. Xu, R. S. Drago, *Acta Crystallogr., Sect. C* **1998**, *54*, 1270−1272. [6d] A. J. Edwards, D. R. Slim, J. E. Guerchais, R. Kergoat, *J. Chem. Soc., Dalton Trans.* **1980**, 289−291. [6e] C. C Ou, W. J. Borowski, J. A. Potenza, H. J. Schugar, *Acta Crystallogr., Sect. B* **1977**, *33*, 3246−3248. [6f] J. A. Thich, C. C Ou, D. Powers, B. Vasiliou, D. Mastropaolo, J. A. Potenza, H. J. Schugar, *J. Am. Chem. Soc.* **1976**, *98*, 1425−1432. [6g] P. Guerriero, U. Casellato, S. Sitran, P. A. Vigato, R. Graziani, *Inorg. Chim. Acta* **1987**, *133*, 337−345. [6h] P. M. L. Goodgame, T. E. Müller, D. J. Williams, *Polyhedron* **1992**, *11*, 1513−1516. [6i] A. Yu. Leontiev, M. D. Arion, I. M. Razdobreev, G. A. Kiosse, V. Yu. Yablokov, T. I. Malinovskii, G. A. Popovich, *Dokl. Akad. Nauk SSSR* **1988**, *300*, 1129−1140.

[7] [7a] J. Limburg, G. W. Brudvig, R. H. Crabtree, *J. Am. Chem. Soc.* **1997**, *119*, 2761−2762. [7b] S. K. Chandra, P. Chakraborty, A. Chakravorty, *Proc. Indian Acad. Sci., Chem. Sci.* **1992**, *104*, 351−360. [7c] N. Okabe, N. Oya, *Acta Crystallogr., Sect. C* **2000**, *56*, 1416−1417.

[8] C. Ma, C. Chen, F. Chen, X. Zhang, H. Zhu, Q. Liu, D. Liao, L. Li, *Bull. Chem. Soc. Jpn.*, in press.

[9] [9a] P. Starynowicz, *Acta Crystallogr., Sect. C* **1992**, *48*, 1428−1430. [9b] M. G. B. Drew, R. W. Matthews, R. A. Walton, *J. Chem. Soc. A* **1970**, 1405−1410. [9c] N. Okabe, N. Oya, *Acta Crystallogr., Sect. C* **2000**, *56*, 305−308.

[10] N. A. Law, M. T. Caudle, V. L. Pecoraro, *Adv. Inorg. Chem.* **1999**, *46*, 305−440.

[11] R. L. Rardin, A. Bino, P. Poganiuch, W. B. Tolman, S. Liu, S. J. Lippard, *Angew. Chem. Int. Ed. Engl.* **1990**, *29*, 812−813.

[12] [12a] G. J. Palenik, D. W. Wester, U. Rychlewska, R. C. Palenik, *Inorg. Chem.* **1976**, *15*, 1814−1819. [12b] D. C. Finnen, A. A. Pinkerton, W. R. Dunham, R. H. Sands, M. O. Funk, Jr., *Inorg. Chem.* **1991**, *30*, 3960−3964. [12c] C. A. Chang, L. C. Francesconi, M. F. Malley, K. Kumar, J. Z. Gougoutas, M. F. Tweedle, D. W. Lee, L. J. Wilson, *Inorg. Chem.* **1993**, *32*, 3501−3508. [12d] E. J. Seddon, J. Yoo, K. Folting, J. C. Huffman, D. N. Hendrickson, G. Christou, *J. Chem. Soc., Dalton Trans.* **2000**, 3640−3648. [12e] J. Sanchiz, S. Dominguez, A. Mederos, F. Brito, J. M. Arrieta, *Inorg. Chem.* **1997**, *36*, 4108−4114. [12f] Z. Xu, L. K. Thomson, D. O. Miller, H. J. Clase, J. A. K. Howard, A. E. Goeta, *Inorg. Chem.* **1998**, *37*, 3620−3627. [12g] L. Karki, K. V. Lakshmi, V. A. Szalai, G. W. Brudvig, *J. Am. Chem. Soc.* **2000**, *122*, 5180−5188. [12h] M. Mizuno, S. Funahashi, N. Nakasuka, M. Tanaka, *Inorg. Chem.* **1991**, *30*, 1550−1553.

[13] [13a] H. O. N. Reid, I. A. Kahwa, A. J. P. White, D. J. Williams, *Chem. Commun.* **1999**, 1565−1566. [13b] C. Pelizzi, G. Pelizzi, G. Predieri, S. Resola, *J. Chem. Soc., Dalton Trans.* **1982**, 1349−1354. [13c] A. H. Othman, K.-L. Lee, H.-K. Fun, B.-C. Yip, *Acta Crystallogr., Sect. C* **1996**, *52*, 602−605. [13d] N. W. Alcock, D. C. Liles, M. McPartlin, P. A. Tasker, *J. Chem. Soc., Chem. Commun.* **1974**, 727−728. [13e] M. V. Capparelli, P. De Meester, D. M. L. Goodgame, S. J. Gunn, A. C. Skapski, *Inorg. Chim. Acta* **1985**, *97*, L37−L39. [13f] G. J. Palenik, D. W. Wester, *Inorg. Chem.* **1978**, *17*, 864−870. [13g] S. Brooker, V. McKee, W. B. Shepard, L. K. Pannell, *J. Chem. Soc., Dalton Trans.* **1987**, 2555−2562. [13h] S. McCann, M. McCann, M. T. Casey, M. Devereux, V. McMichael, J. G. McCrea, *Polyhedron* **1997**, *16*, 4247−4252.

[14] SHELXTL: Siemens, *SAINT and SHELXTL* (*Version 5.0*), Siemens Analytical X-ray Instruments Inc., Madison, Wisconsin, USA, **1994**.

Received August 5, 2002
[I02445]

Coordination Chemistry of Nitrile and Amino Pendant Arm Derivatives of [9]aneN$_2$S and [9]aneNS$_2$ with Pd^{II} and Cu^{II}

Massimiliano Arca,[a] Alexander J. Blake,[b] Vito Lippolis,*[a] Daniela R. Montesu,[a] Jonathan McMaster,[b] Lorenzo Tei,[a,b] and Martin Schröder*[b]

Keywords: Macrocycles / Palladium / Copper / N ligands / S ligands

Palladium(II) and copper(II) complexes [Pd(**L^1**)Cl$_2$], [Pd(**L^3**)Cl$_2$], [Cu(**L^1**)Cl$_2$], [Cu(**L^3**)Cl$_2$], [Pd(**L^2**)][BF$_4$]$_2$, [Pd(**L^4**)Cl]BF$_4$, [Cu(**L^2**)][NO$_3$]$_2$ and [Cu(**L^4**)Cl]PF$_6$ of the nitrile (**L^1** and **L^3**) and amino (**L^2** and **L^4**) pendant arm derivatives of 1-thia-4,7-diazacyclononane ([9]aneN$_2$S) and 7-aza-1,4-dithiacyclononane ([9]aneNS$_2$) have been prepared and fully characterised. In each case, a square-pyramidal coordination sphere is observed at both metal ions with either one or two Cl$^-$ anions completing the donor set. The tridentate nine-membered macrocyclic moiety adopts a [333] conformation in all the complexes obtained. The five-membered chelate rings involving the donor atoms of the basal plane adopt a *gauche* configuration with very similar degrees of puckering. The "innocent" nitrile pendant arms in **L^1** and **L^3** do not bind to the metal ions, but still appear to influence the binding of the tridentate macrocyclic frameworks via the tertiary amine sites.

(© Wiley-VCH Verlag GmbH & Co. KGaA, 69451 Weinheim, Germany, 2003)

Introduction

1,4,7-Triazacyclononane ([9]aneN$_3$) and 1,4,7-trithiacyclononane ([9]aneS$_3$; Scheme 1) have been extensively studied, and afford bis(sandwich) octahedral complexes in which the ligands bind to the metal centre in a facial manner; [9]aneN$_3$ has been used mainly to complex 3d transition metal ions[1,2] whereas the trithia analogue, [9]aneS$_3$, because of the soft nature of its donor atoms, has also been considered for complexation with 4d and 5d transition metal ions.[3] Thus, a range of complexes of noble metal ions having uncommon oxidation states have been synthesised.[3] The two related nine-membered ring macrocycles [9]aneN$_2$S (1,4-diaza-7-thiacyclononane) and [9]aneNS$_2$ (1-aza-4,7-dithiacyclononane) are of particular interest since the loss of threefold symmetry and the presence of both hard N- and soft S-donors can potentially have interesting stereochemical consequences and thereby offer specific coordination selectivity. However, their coordination chemistry has not been studied extensively,[4] perhaps in part due to the greater difficulty in preparing these mixed donor macrocycles. In comparison to [9]aneN$_3$,[5] even less attention has been directed to the *N*-functionalisation of [9]aneN$_2$S and [9]aneNS$_2$ by incorporation of pendant arms bearing coordinating donor groups to give potentially tetra- and pentadentate ligands, respectively.[4,6–13] In particular, the coordination chemistry of nitrile and amino pendant arm derivatives of [9]aneN$_2$S and [9]aneNS$_2$ such as **L^1**–**L^4** is unknown, although **L^1** and **L^2** have been described previously as free ligands.[14,15] The ethyl-bridged bis([9]aneNS$_2$), which can also be formally considered as an amino pendant arm derivative of [9]aneNS$_2$, is also known.[13] Interestingly, **L^1** and **L^4** can impose stereorestrictive modes of coordination at metal centres such as Pd^{II} and Cu^{II} by forming potentially four- or five-coordinate complexes possessing unusual and interesting coordination and/or redox properties. Due to their electronic requirements, Pd^{II} and Cu^{II} typically form square-planar and Jahn–Teller distorted octahedral complexes, respectively, and as a result, five-coordinate complexes of these metal ions would represent potential models for intermediates in associative substitution reactions at square-planar d^8 complexes, and in dissociative reactions of hexacoordinate compounds, respectively. Furthermore, five-coordinate metal complexes of coordinatively unsaturated metal centres such as Cu^{II} lead to the possibility of binding and activation of small molecules and therefore represent useful models of enzymatic systems. As a continuation of our studies[4,6–11] of the coordination chemistry of *N*-functionalised pendant arms derivatives of tridentate mixed thia/aza nine-membered macrocycles, we report herein our studies of the complexation of Pd^{II} and Cu^{II} centres with **L^1**, **L^2**, **L^3** and **L^4**.

[a] Dipartimento di Chimica Inorganica ed Analitica, Università degli Studi di Cagliari SS
554 Bivio per Sestu, 09042 Monserrato (CA), Italy
[b] School of Chemistry, The University of Nottingham, University Park, Nottingham NG7 2RD, UK

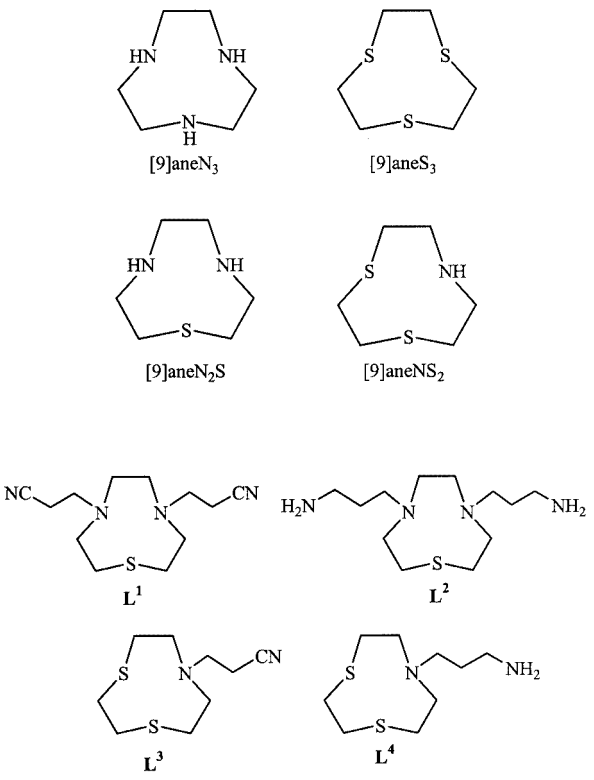

Scheme 1

Results and Discussion

Coordination to Pd^{II}

Reaction of $PdCl_2$ with 1 mol-equiv. of **L^1** in refluxing MeCN for 12 h gave an orange solution. After partial removal of the solvent and filtration through a pad of Celite, dark-red crystals of [Pd(**L^1**)Cl$_2$] were formed upon diffusion of Et_2O vapour into the remaining solution. The X-ray crystal structure of [Pd(**L^1**)Cl$_2$] (Figure 1, top; Table 1) shows a square-planar $NSCl_2$ coordination sphere at Pd^{II} with two mutually *cis*-Cl$^-$ ligands *trans* to N- and S-donors of the [9]aneN$_2$S macrocyclic framework. The remaining N-donor of the [9]aneN$_2$S ring is oriented towards the Pd^{II} centre and lies above the $NSPdCl_2$ coordination plane with a Pd···N(7) distance of 2.638(4) Å. Thus, an overall [NS+N] coordination for the [9]aneN$_2$S framework is observed. The Pd(1)−N(7) vector shows a slight deviation from perpendicularity to the Pd^{II} coordination plane with N(7)−Pd(1)−X angles [X = S(1), N(4), Cl(1) or Cl(2)] ranging from 77.23(12) to 101.23(8)°. The Pd^{II} centre lies only 0.006 Å above the mean $NSCl_2$ coordination plane and the two nitrile-functionalised pendant arms do not bind to the metal centre.

Examples of long-range Pd···N apical interactions in square-based pyramidal complexes of tridentate nine-membered macrocycles are very rare. The complex cations $[Pd([9]aneN_3)_2]^{2+}$ and $[Pd([9]aneN_3)(H[9]aneN_3)]^{3+}$ have square-planar coordination geometries at Pd^{II},[16,17] but with the remaining apical N-centres oriented away from the axial site of the PdN_4 plane at a distance of 3.499(5) Å for centrosymmetric $[Pd([9]aneN_3)_2]^{2+}$,[16] and 2.982(11)−3.079(11) Å for $[Pd([9]aneN_3)(H[9]aneN_3)]^{3+}$.[17]

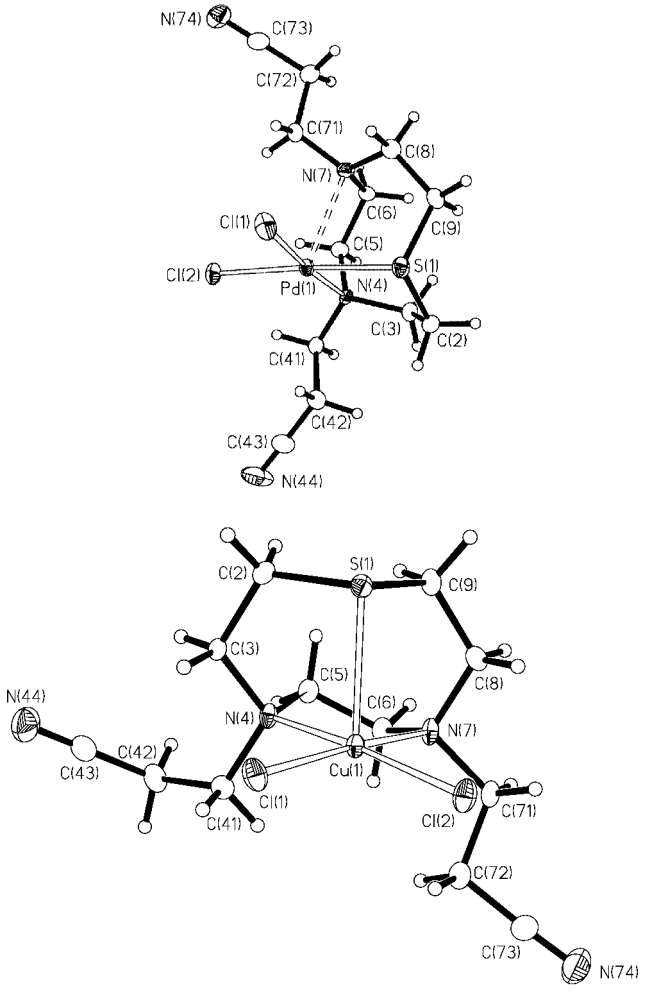

Figure 1. Structures of [Pd(**L^1**)Cl$_2$] (top) and [Cu(**L^1**)Cl$_2$] (bottom) with the numbering scheme adopted; displacement ellipsoids are drawn at 50% probability

Table 1. Selected bond lengths [Å] and angles [°] for [Pd(**L^1**)Cl$_2$] and [Cu(**L^1**)Cl$_2$]

	M = Pd	M = Cu
M(1)−S(1)	2.2492(13)	2.577(4)
M(1)−N(4)	2.124(4)	2.132(6)
M(1)−N(7)	2.638(4)	2.095(5)
M(1)−Cl(1)	2.3093(12)	2.272(2)
M(1)−Cl(2)	2.3388(12)	2.268(4)
S(1)−M(1)−N(4)	87.42(10)	82.6(2)
S(1)−M(1)−N(7)	82.02(9)	87.5(2)
S(1)−M(1)−Cl(1)	88.89(4)	97.33(11)
S(1)−M(1)−Cl(2)	176.54(4)	103.42(13)
N(4)−M(1)−N(7)	77.23(12)	83.4(2)
N(4)−M(1)−Cl(1)	175.20(10)	92.6(2)
N(4)−M(1)−Cl(2)	92.09(10)	172.4(2)
N(7)−M(1)−Cl(1)	99.23(9)	173.3(2)
N(7)−M(1)−Cl(2)	101.23(8)	92.1(2)
Cl(1)−M(1)−Cl(2)	91.79(4)	91.28(11)

Interesting exceptions are represented by the complex cation $[Pd(py_3[9]aneN_3)]^{2+}$ {$py_3[9]aneN_3$ = 1,4,7-tris(2-pyridylmethyl)-1,4,7-triazacyclononane}[2] in which one of the N-donors of the [9]aneN$_3$ framework occupies the apical site [Pd−N$_{ap}$ 2.580 Å] of a square-based pyramidal geometry. A similar geometry is observed in $[Pd(NCMe)_2(Me_3[9]aneN_3)]^{2+}$ in which the apical N-donor of the macrocycle is sited 2.523(8) from the Pd^{II} centre.[18] It is also interesting to compare the coordination modes of [9]aneN$_2$S and **L^1** to Pd^{II}. In the sandwich complexes $[Pd([9]aneN_2S)_2][PF_6]_2$ and $[Pd([9]aneN_2S)_2]Cl_2\cdot H_2O$ each metal centre is bound by four N-donors of the two macrocycles in a square-planar arrangement, with the thioether S-donors showing either long-range apical interactions with the Pd^{II} centre {as in $[Pd([9]aneN_2S)_2][PF_6]_2$} or no interaction at all {as in $[Pd([9]aneN_2S)_2]Cl_2\cdot H_2O$}.[19] A [2N+S] coordination is also observed for the [9]aneN$_2$S units in the trinuclear complex $[Pd_3([9]aneN_2S)_4Cl_2]Cl_4\cdot 2H_2O$,[19] and similar structural features have been observed for Pt^{II} complexes with both [9]aneN$_3$ and [9]aneN$_2$S[1,4,6−11] and for the complex $[Au([9]aneN_2S)Cl_2]^+$.[20] Therefore, the [NS+N] coordination of the [9]aneN$_2$S macrocyclic framework in [Pd(**L^1**)Cl$_2$] is unusual: it may have its origins in either electronic or steric effects which arise from the combination of the two nitrile functionalised pendant arms and the two bound Cl$^-$ ligands. [Pd(**L^1**)Cl$_2$] units interact with each other in the crystal lattice through long-range Cl···S contacts [3.527(2) Å] (Figure 2) to form polymeric chains of [Pd(**L^1**)Cl$_2$] which run along the (010) direction.

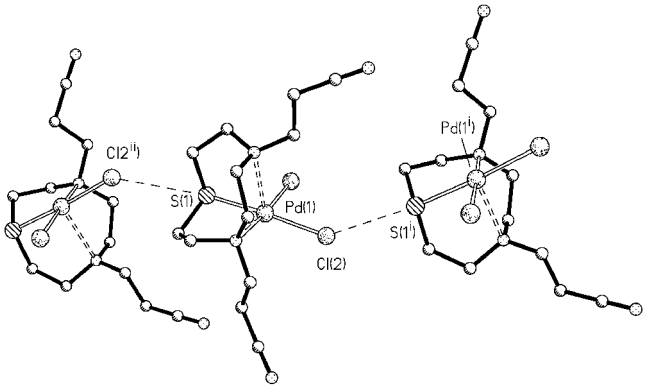

Figure 2. Partial view of the crystal packing in [Pd(**L^1**)Cl$_2$]: Cl(2)···S(1^i) 3.527(2) Å; Pd(1)−Cl(2)−S(1^i) 141.56(5), Pd(1)−S(1)−Cl(2^{ii}) 171.25(5)°; i = 1 − *x*, 1/2 + *y*, 1/2−z; ii = 1 − *x*, −1/2 + *y*, 1/2 − *z*

In order to study the effect that nitrile-functionalised pendant arms can have upon the coordination mode of mixed thia/aza nine-membered macrocyclic derivatives towards Pd^{II}, we treated **L^3** with PdCl$_2$ under the same conditions used for the synthesis of [Pd(**L^1**)Cl$_2$]. The red-orange crystals of [Pd(**L^3**)Cl$_2$] obtained after recrystallisation from DMF/Et$_2$O were analysed by X-ray diffraction. The Pd^{II} centre is bound by the two S-donors of the macrocyclic ring and two Cl$^-$ ligands to form an approximate S$_2$PdCl$_2$ plane (Figure 3, top; Table 2). The remaining tertiary N-atom of the [9]aneNS$_2$ moiety is disposed apically relative to this coordination plane with N(7)−Pd(1)−X angles [X = S(1), S(4), Cl(1) or Cl(2)] ranging from 79.24(5) to 100.94(6)°. The Pd^{II} centre is displaced 0.007 Å out of the S$_2$PdCl$_2$ mean plane in the direction of the apical N-centre. Therefore, as for [Pd(**L^1**)Cl$_2$], the addition of a nitrile pendant arm to the N-centre in [9]aneNS$_2$ leads to the macrocyclic framework adopting an unusual [2S+N] coordination in [Pd(**L^3**)Cl$_2$], with the N-centre occupying the apical position of a "flat" square-pyramidal coordination geometry. In contrast an [NS+S] coordination mode has been observed for [9]aneNS$_2$ in the complex cation $[Pd([9]aneNS_2)_2]^{2+}$ where the Pd^{II} centre is bound to two N- and two S-donors in a square-planar configuration with the remaining two S-atoms interacting apically.[21] Significantly, in the related half-sandwich complex [Pd([9]aneS$_2$O)Cl$_2$], the macrocyclic ligand assumes a facial [2S+O] coordination mode at the metal centre with the oxygen atom lying above the basal S$_2$PdCl$_2$ plane and pointing toward the Pd centre.[22] At this stage it is difficult to conclude whether the observed [NS+N] and [2S+N] coordination modes of **L^1** and **L^3** in [Pd(**L^1**)Cl$_2$] and [Pd(**L^3**)Cl$_2$], respectively, are determined by the steric requirements of the nitrile pendant arms, by electronic effects or by the binding of soft S-donors to soft Pd^{II}. It might be argued that the pendant arms in [Pd(**L^1**)Cl$_2$] and [Pd(**L^3**)Cl$_2$] tend to dispose themselves as far as possible from the Cl$^-$ ligands because of steric requirements. Alternatively, the tertiary nitrogen centres in **L^1** and **L^3** may have a weaker σ-donor character than the analogous secondary N-donors in [9]aneN$_2$S and [9]aneNS$_2$. According to molecular orbital calculations performed by Rossi and Hoffmann for d^8 low-spin metal centres,[23] this would lead to a tendency for the N-donor to lie in the apical position of a square-based pyramidal coordination geometry. However, thioether donors in macrocyclic systems have a limited π-donor/acceptor capacity,[3] and according to calculations performed by Rossi and Hoffmann for a five-coordinate, square-based pyramidal geometry, the disposition and the relative bond strengths of the substituents in the apical and basal positions, as well as the degree of pyramidality, are the result of a delicate balance between σ- and π-substituent effects.[23]

In both [Pd(**L^1**)Cl$_2$] and [Pd(**L^3**)Cl$_2$] the nitrile groups of the pendant arms are directed away from the metal centre. We argued that conversion of nitriles to amine functions would switch the coordination mode at Pd^{II} and restore the more usual [2N+S] and [NS+S] binding of the [9]aneN$_2$S and [9]aneNS$_2$ moieties in **L^2** and **L^4**, respectively. This would be driven by the formation of six-membered chelate rings on coordination of the strongly donating amine pendant arms to Pd^{II}. The reaction of **L^2** with 1 mol-equiv. of $[Pd(CH_3CN)_4](BF_4)_2$ in MeCN/MeOH at room temperature yielded a yellow solid after removal of the solvent. Recrystallisation by diffusion of Et$_2$O into a solution of the complex in MeNO$_2$ afforded pale-yellow crystals which, according to analytical and mass spectrometric data, had the formulation [Pd(**L^2**)][BF$_4$]$_2$. A crystal structure determination confirmed the formation of the cation [Pd(**L^2**)]$^{2+}$ (Figure 4, top; Table 3), with the pentadentate ligand **L^2** impos-

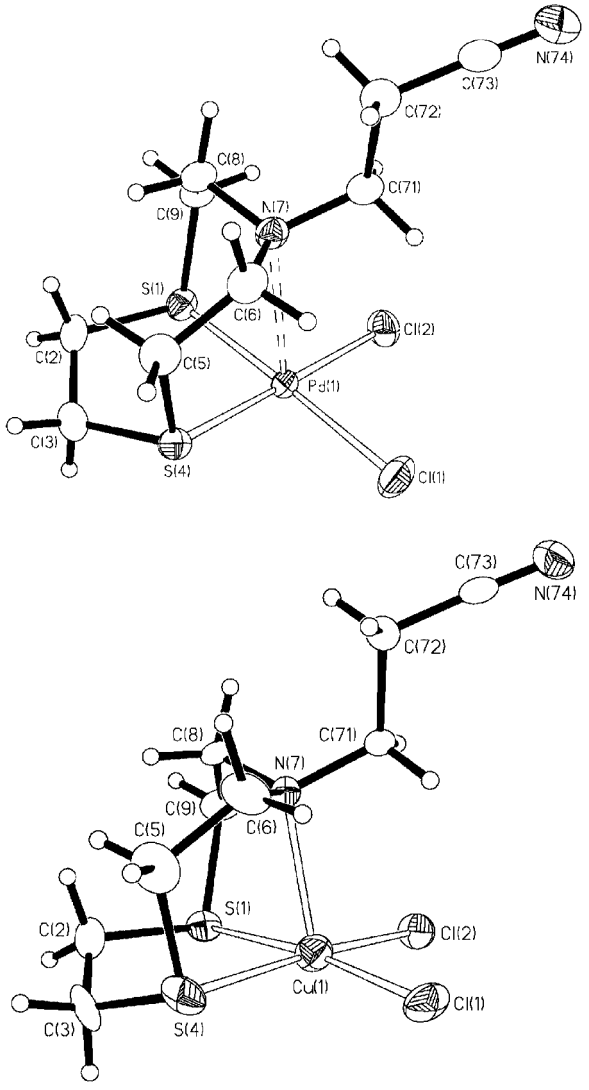

Figure 3. Structures of [Pd(**L^3**)Cl$_2$] (top) and [Cu(**L^3**)Cl$_2$] (bottom) with the numbering scheme adopted; displacement ellipsoids are drawn at 50% probability

Table 2. Selected bond lengths [Å] and angles [°] for [Pd(**L^3**)Cl$_2$] and [Cu(**L^3**)Cl$_2$]

	M = Pd	M = Cu
M(1)−S(1)	2.2685(8)	2.313(2)
M(1)−S(4)	2.2532(9)	2.340(2)
M(1)−N(7)	2.722(2)	2.333(4)
M(1)−Cl(1)	2.3282(9)	2.256(2)
M(1)−Cl(2)	2.3258(9)	2.277(2)
S(1)−M(1)−S(4)	89.76(3)	87.40(6)
S(1)−M(1)−N(7)	79.24(5)	85.34(10)
S(1)−M(1)−Cl(1)	177.90(3)	172.70(6)
S(1)−M(1)−Cl(2)	89.29(3)	86.90(6)
S(4)−M(1)−N(7)	81.31(6)	85.38(10)
S(4)−M(1)−Cl(1)	88.20(3)	88.37(6)
S(4)−M(1)−Cl(2)	179.03(3)	171.18(7)
N(7)−M(1)−Cl(1)	100.94(6)	100.25(10)
N(7)−M(1)−Cl(2)	98.70(6)	100.85(10)
Cl(1)−M(1)−Cl(2)	92.74(3)	

ing a formal [4+1] coordination sphere at the Pd^{II} centre, which is bound by the two tertiary N-donors of the [9]aneN$_2$S ring and the nitrogen atoms of both amino pendant arms forming an approximate PdN$_4$ plane. The S-donor of the macrocyclic ring occupies an apical site of a distorted square-pyramidal geometry with a long-range Pd···S(1) interaction of 3.0865(11) Å. The Pd^{II} centre is displaced 0.07 Å out of the mean plane defined by the atoms N(4), N(7), N(44) and N(74) towards S(1), with the angles S(1)−Pd(1)−N$_{eq}$ ranging from 75.60(9) to 106.72(9)°. Therefore, the introduction of coordinating functionalised pendant arms does indeed switch the [9]aneN$_2$S moiety of **L^2** to adopt a facial [2N+S] donation to Pd^{II} rather than the [NS+N] mode observed for **L^1** in [Pd(**L^1**)Cl$_2$] (see above). The Pd···S(1) distance in [Pd(**L^2**)]$^{2+}$ is consistent with those for long-range Pd···S apical interactions found in other sandwich and half-sandwich Pd^{II} complexes with thia- and mixed thia/aza macrocycles.[3,19−21,24−32] In [Pd(**L^2**)]$^{2+}$ (Figure 4, top) there are one five- and two six-membered chelate rings involving the metal centre. The former adopts a *gauche* conformation with a torsion angle at the C(5)−C(6) bond of 45.7(5)°, while the latter adopt chair forms. The chelate angles range from 86.47(13) [N(4)−Pd(1)−N(7)] to 93.02(14)° [N(4)−Pd(1)−N(44)] and do not suggest any particular structural or steric constraints imposed by the five- and six-membered chelate rings.

Reaction of [Pd(CH$_3$CN)$_4$](BF$_4$)$_2$ with **L^4** affords a brown oil which was treated with 1 mol-equiv. of aqueous NaCl at room temperature to give, after removal of the solvent, a brown solid which could be recrystallised from MeCN/Et$_2$O. The fast-atom bombardment (FAB) mass spectrum of the product exhibited peaks with the correct isotopic distribution for [^{106}PdCl(**L^4**)]$^+$ (*m*/*z* = 362) and for [^{106}Pd(**L^4**)]$^+$ (*m*/*z* = 327). These, together with elemental analytical data, suggest a formulation [Pd(**L^4**)Cl]BF$_4$. An X-ray diffraction study confirmed the formation of the complex cation [Pd(**L^4**)Cl]$^+$ in which a formal [4+1] square-based pyramidal geometry is achieved at the metal centre (Figure 5, top; Table 4). One N- and one S-donor of the macrocyclic framework, the amino group of the pendant arm and one Cl$^-$ ligand are coordinated to the Pd^{II} centre in a square-planar arrangement. The remaining S-donor of [9]aneNS$_2$ shows a long-range apical Pd···S(4) interaction of 2.9278(9) Å, with the metal atom displaced only 0.004 Å out of the N$_2$SCl mean plane towards S(4). Symmetry-related [Pd(**L^4**)Cl]$^+$ complex cations interact with each other to form dimeric units through Pd···Cl contacts of 3.6091(11) Å, while the S-donors in the PdN$_2$SCl coordination plane interact with F$^-$ centres in BF$_4^-$ counter-anions (Figure 6, top).

Significantly, the Pd···S$_{ap}$ interaction in [Pd(**L^4**)Cl]$^+$ is shorter than that observed in the sandwich complex cation [Pd([9]aneNS$_2$)$_2$]$^{2+}$ [3.011(3) Å],[21] even though the overall cationic charge of the former is lower. This demonstrates once again that apical interactions in square-pyramidal Pd^{II} and Pt^{II} complexes are influenced significantly by the electronic nature of the equatorial ligands. As predicted, the binding of **L^2** and **L^4** to Pd^{II} drives the [9]aneN$_2$S and

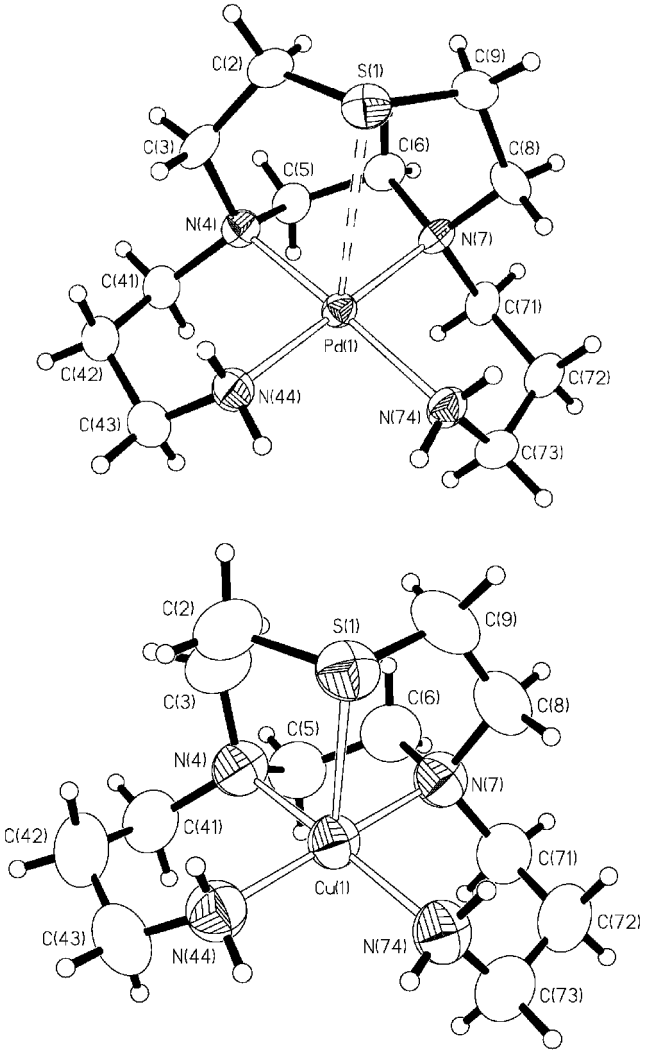

Figure 4. Structures of the complex cations $[Pd(\mathbf{L^2})]^{2+}$ (top) and $[Cu(\mathbf{L^2})]^{2+}$ (bottom) with the numbering scheme adopted; displacement ellipsoids are drawn at 50% probability

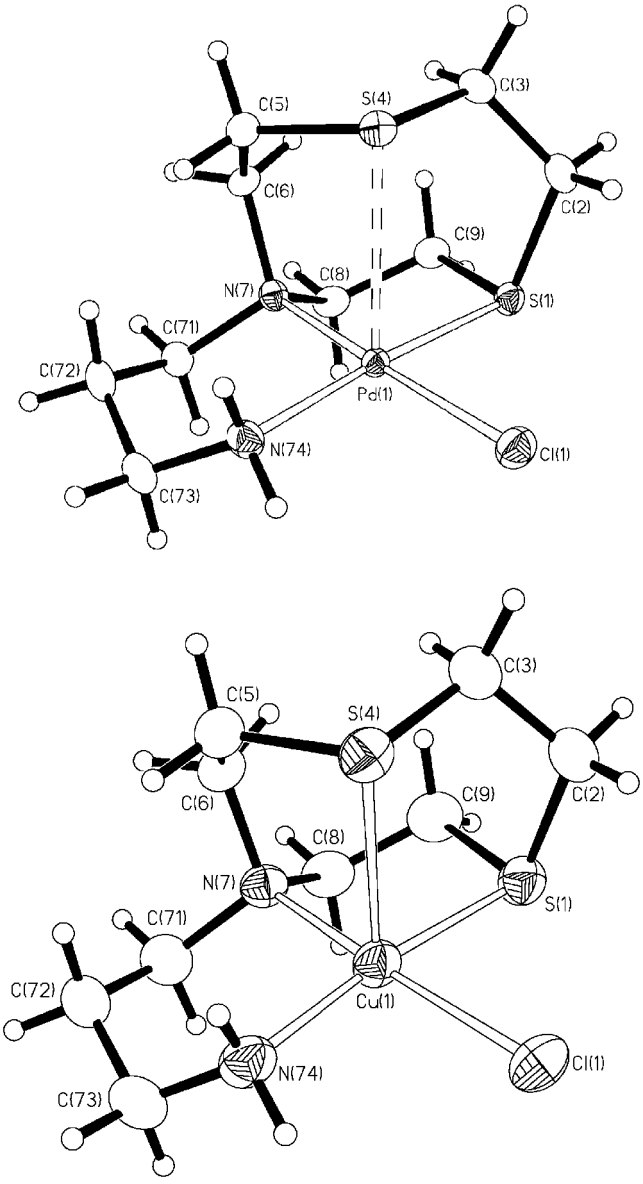

Figure 5. Structures of the complex cations $[Pd(\mathbf{L^4})Cl]^{+}$ (top) and $[Cu(\mathbf{L^4})Cl]^{+}$ (bottom) with the numbering scheme adopted; displacement ellipsoids are drawn at 50% probability

Table 3. Selected bond lengths [Å] and angles [°] for $[Pd(\mathbf{L^2})][BF_4]_2$ and $[Cu(\mathbf{L^2})][NO_3]_2$

	M = Pd	M = Cu
M(1)−S(1)	3.0865(11)	2.5608(13)
M(1)−N(4)	2.075(4)	2.070(4)
M(1)−N(7)	2.077(3)	2.093(4)
M(1)−N(44)	2.052(3)	2.025(4)
M(1)−N(74)	2.064(3)	2.013(4)
S(1)−M(1)−N(4)	80.19(10)	88.07(11)
S(1)−M(1)−N(7)	75.60(9)	85.80(11)
S(1)−M(1)−N(44)	104.80(10)	96.61(13)
S(1)−M(1)−N(74)	106.72(9)	99.71(12)
N(4)−M(1)−N(7)	86.47(13)	84.5(2)
N(4)−M(1)−N(44)	93.02(14)	93.6(2)
N(4)−M(1)−N(74)	172.14(14)	170.6(2)
N(7)−M(1)−N(44)	179.29(13)	176.8(2)
N(7)−M(1)−N(74)	91.60(12)	90.8(2)
N(44)−M(1)−N(74)	88.84(14)	90.8(2)

[9]aneNS$_2$ moieties to bind facially with long-range S-donor apical interactions as opposed to long-range N-donor interactions in the case of $\mathbf{L^1}$ and $\mathbf{L^2}$.

While the macrocyclic ligands in $[Pd([9]aneN_3)_2]^{2+}$,[16] half-sandwich Pd^{II} complexes with [9]aneS$_3$[25] and $[Pt([9]aneS_3)phen]^{2+}$[32] have been shown to be fluxional in solution, no evidence of similar behaviour has yet been reported for mixed thia/aza macrocycles [9]aneN$_2$S and [9]aneNS$_2$ or their derivatives. For $[Pd(py_2[9]aneN_2S)]^{2+}$ it has been shown by NMR spectroscopy that the ligand is nonfluxional in solution, with the axial S-donor believed to maintain a constant position by weak interaction with the Pd^{II} centre.[26] The structures of $[Pd(\mathbf{L^1})Cl_2]$ and $[Pd(\mathbf{L^3})Cl_2]$ clearly demonstrate the possibility for [9]aneN$_2$S, [9]aneNS$_2$ and their derivatives to adopt different facial coordination

Table 4. Selected bond lengths [Å] and angles [°] for [Pd(**L**^{4})Cl]BF$_4$ and [Cu(**L**^{4})Cl]PF$_6$

	M = Pd	M = Cu
M(1)−S(1)	2.2633(8)	2.2938(11)
M(1)−S(4)	2.9278(9)	2.5962(11)
M(1)−N(7)	2.087(2)	2.103(3)
M(1)−N(74)	2.077(2)	1.996(3)
M(1)−Cl(1)	2.3381(9)	2.3567(11)
S(1)−M(1)−S(4)	84.00(3)	87.91(4)
S(1)−M(1)−N(7)	87.04(6)	87.01(9)
S(1)−M(1)−N(74)	175.91(7)	173.49(11)
S(1)−M(1)−Cl(1)	89.37(3)	86.76(4)
S(4)−M(1)−N(7)	84.56(6)	87.52(9)
S(4)−M(1)−N(74)	99.19(7)	97.87(11)
S(4)−M(1)−Cl(1)	96.26(3)	95.89(4)
N(7)−M(1)−N(74)	95.79(9)	96.20(13)
N(7)−M(1)−Cl(1)	176.21(6)	172.78(9)
N(74)−M(1)−Cl(1)	87.74(7)	89.65(10)

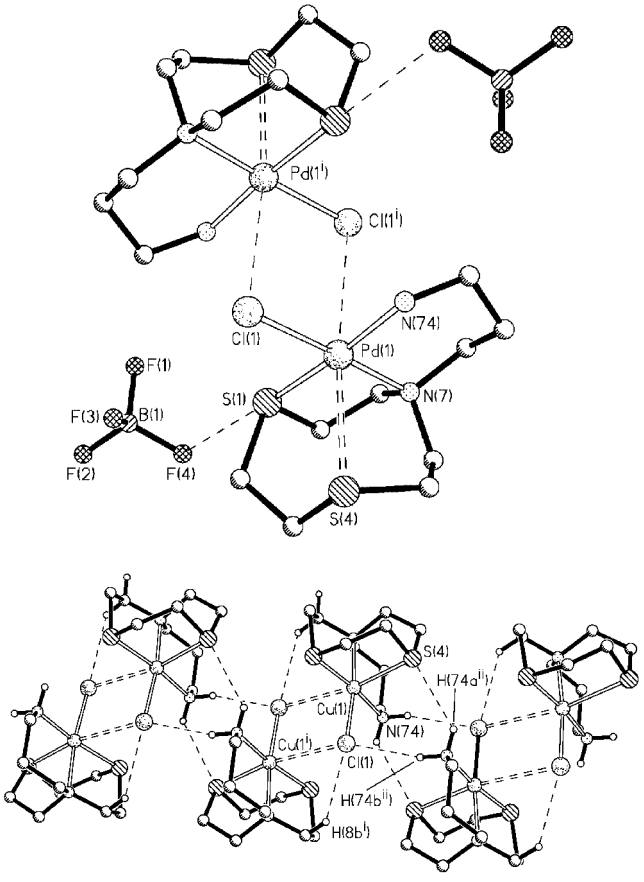

Figure 6. Top: dimeric units of [Pd(**L**^{4})Cl]$^+$ complex cations interacting with BF_4^- anions [Pd···Cl(1^i) 3.6091(11) Å; Cl(1^i)···Pd(1)−S(4) 167.13(2), Pd(1)−Cl(1)···Pd(1^i) 84.55(2)°; S(1)···F(4) 3.179(2) Å; F(4)···S(1)−Pd(1) 173.51(5)°; i = 1 − *x*, 2 − *y*, 1 − *z*]; bottom: view of part of an infinite ribbon of [Cu(**L**^{4})Cl]$^+$ cations running along the (100) direction; only those H atoms which are involved in hydrogen bonding are shown [Cu(1^i)···Cl(1) 3.1514(12), Cl(1)···H(8b^i) 2.801, Cl(1)···H(74b^{ii}) 2.656, S(4)···H(74a^{ii}) 2.903 Å; Cu(1)−Cl(1)···H(8b^i) 141.8°; i = − *x*, 2 − *y*, 1 − *z*; ii = 1 − *x*, 2 − *y*, 1 − *z*]

modes at low-spin d^8 metal centres. Furthermore, the structure of [Pd([9]aneN$_2$S)$_2$]Cl$_2$·H$_2$O shows that the S-centres do not interact apically with the metal centre[19] and this situation could represent the first step towards a dynamic structure in solution in which the metal atom undergoes a series of inner-sphere substitution reactions with the ligand rotating between [2N+S] and [NS+N] configurations. Although the results herein apply only to situations in the solid state, they confirm the low energy differences between these different possible coordination modes and suggest that fluxional behaviour in solution may be possible for [9]aneN$_2$S and [9]aneNS$_2$ within sandwich and half-sandwich complexes with Pd^{II} and Pt^{II}. Unfortunately, due to the very low solubilities of [Pd(**L**^{1})Cl$_2$] and [Pd(**L**^{3})Cl$_2$] we have not been able to demonstrate this in solution.

Coordination to Cu^{II}

Reaction of **L**^{1} with 1 mol-equiv. of CuCl$_2$·2H$_2$O in MeCN afforded a green solution after 1 h of reflux under N$_2$. Slow concentration of this solution yielded green crystals having the formulation [Cu(**L**^{1})Cl$_2$] according to analytical and mass spectrometric data. A crystal structure determination (Figure 1, bottom; Table 1) shows the metal centre in a distorted square-pyramidal environment, with the basal positions occupied by the two tertiary N-donors of the [9]aneN$_2$S moiety of **L**^{1} and by two Cl$^-$ ligands. The S-donor S(1) of the macrocyclic ring occupies the apical position whereas the nitrile functionalised pendant arms are directed away from the metal centre. The Cu^{II} centre is displaced 0.1145 Å out of the mean plane defined by the atoms N(4), N(7), Cl(1) and Cl(2), in the direction of S(1). The structure of [Cu(**L**^{1})Cl$_2$] is very similar to that reported for the half-sandwich complex [Cu([9]aneN$_2$S)Br$_2$],[33] where the macrocyclic ligand also adopts a facial [2N+S] coordination at the metal centre [Cu−N$_{eq}$ 2.03(1), 2.02(1) Å; Cu−S$_{ap}$ 2.567(3) Å] but with two Br$^-$ ligands at basal positions completing the square-pyramidal geometry. However, the Cu−N$_{eq}$ distances appear significantly longer in the case of [Cu(**L**^{1})Cl$_2$] (Table 1) and this could be due to an increased steric repulsion at the tertiary N-centres in **L**^{1} compared to the secondary N-centres in [9]aneN$_2$S. Cu−S$_{ap}$ bonds longer than those reported for [Cu([9]aneN$_2$S)Br$_2$][33] and [Cu(**L**^{1})Cl$_2$] have been observed for the sandwich complex [Cu([9]aneN$_2$S)$_2$]$^{2+}$ [Cu−N$_{eq}$ 2.027(3), 2.067(3); Cu−S$_{ap}$ 2.707(1) Å] in which the macrocyclic ligand also adopts a facial [2N+S] coordination mode.[34,35] [Cu(**L**^{1})Cl$_2$] provides an interesting contrast to [Pd(**L**^{1})Cl$_2$] in that changing the metal centre from low-spin d^8 to d^9 causes the [9]aneN$_2$S framework of **L**^{1} to pass from the [NS+S] to the [2N+S] facial coordination mode. This is clearly consistent with the preference of Cu^{II} for binding N-donor centres, as also demonstrated by the structure of the sandwich complex [Cu([9]aneN$_2$S)$_2$]$^{2+}$ in which the four N-donors occupy the equatorial sites of a distorted octahedral geometry and the two S-donors occupy the axial positions.[33,34]

In order to investigate the coordinative behaviour of the [9]aneNS$_2$ moiety in **L**^{3} towards Cu^{II}, **L**^{3} was treated with

1 mol-equiv. of $CuCl_2 \cdot 2H_2O$ in MeCN under the same experimental conditions used for the synthesis of $[Cu(\mathbf{L^1})Cl_2]$. Well-shaped crystals of $[Cu(\mathbf{L^3})Cl_2]$ suitable for X-ray diffraction studies were obtained after recrystallisation from DMF/Et_2O. The [2S+N] ligand arrangement in $[Cu(\mathbf{L^3})Cl_2]$ (Figure 3, bottom; Table 2) is very similar to that observed in $[Pd(\mathbf{L^3})Cl_2]$ but contrasts with that observed for $[Cu(\mathbf{L^1})Cl_2]$. In $[Cu(\mathbf{L^3})Cl_2]$ it appears that the preference of Cu^{II} for N-donors is offset by steric effects of the bulky tertiary N-donors which induces the [9]aneNS$_2$ framework to adopt the observed [2S + N] coordination mode. A similar coordination mode is observed in $[Cu([9]aneNS_2)_2]^{2+}$ with the S-donors occupying the equatorial sites of an octahedral geometry [Cu−S_{eq} 2.547(1)−2.539(1) Å] and the N-donors at the axial positions average [Cu−N_{eq} 2.016(4) Å].[36] In this case the average Cu−N_{eq} distance is much shorter and the Cu−S_{eq} are much longer than the corresponding bond lengths observed in $[Cu(\mathbf{L^3})Cl_2]$ suggesting a possible opposite direction of the Jahn−Teller effect in the two complexes. It appears, therefore, that a delicate balance between electronic and steric factors might be responsible for the type of donation of the macrocyclic framework in the square-pyramidal complexes $[M(\mathbf{L^1})Cl_2]$ and $[M(\mathbf{L^3})Cl_2]$ (M = Pd, Cu).

$[Cu(\mathbf{L^3})Cl_2]$ units in the crystal lattice interact with each other via long Cl···Cu contacts to give infinite zigzag chains which run along the *c* axis, with the nitrile-functionalised pendant arms dangling away from the metal centres (Figure 7).

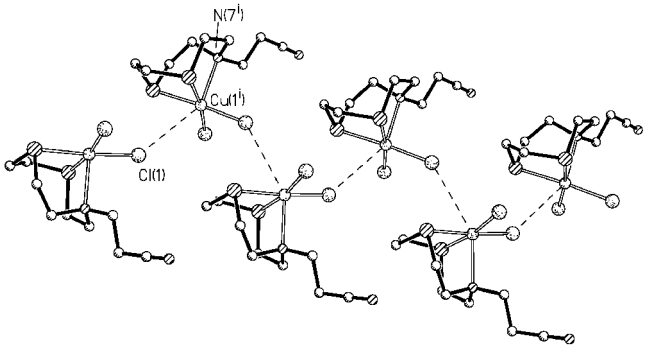

Figure 7. Partial view along the (110) direction of zigzag chains of $[Cu(\mathbf{L^3})Cl_2]$ molecules running along the (001) direction: Cl(1)···Cu(1^{i}) 3.5886(11) Å; Cl(1)···Cu(1^{i})−N(7^{i}) 150.52(10)°; i = 1 − *x*, − *y*, *z* − 1/2

Given that structural data on CuN_4S systems are relatively rare in the literature, we treated $\mathbf{L^2}$ with 1 mol-equiv. of $Cu(NO_3)_2 \cdot 3H_2O$ in MeCN/EtOH at room temperature. A blue colour was immediately formed and the residue obtained after removal of the solvent was repeatedly crystallised from EtOH/Et_2O to give blue blocky crystals having the formulation $[Cu(\mathbf{L^2})][NO_3]_2$.

As observed for $[Pd(\mathbf{L^2})]^{2+}$, the structure of the cation $[Cu(\mathbf{L^2})]^{2+}$ (Figure 4, bottom; Table 3) shows the ligand encapsulating the metal ion in a distorted square-based pyramidal geometry. The basal coordination sites are occupied by the N-atoms of the [9]aneN$_2$S moiety and by the primary amino groups of the pendant arms, with the remaining S-donor of the pentadentate ligand $\mathbf{L^2}$ occupying the apical position. The metal ion is displaced out of the N_4 plane by 0.0965 Å in the direction of the S donor. The Cu−N_{eq} bond lengths [average 2.05(2) Å] are typical for an N_4-donor set arranged in a plane around the Cu^{II} centre, and similar average Cu−N_{eq} bond lengths have been observed for Cu^{II} complexes of amino-functionalised pendant arm derivatives of [9]aneN$_3$ and ethyl-bridged bis([9]aneN$_3$).[37] The Cu−S_{ap} bond length [2.5608(13) Å] is towards the lower end of the range [2.56−2.82 Å] expected for axial Cu−S contacts.[34] The structure of $[Cu(\mathbf{L^2})]^{2+}$ can be compared to those of $[Cu(py_2[9]aneN_2S)]^{2+}$ [Cu−S_{ap} = 2.496(8), Cu−N_{eq} = 2.02(1) Å][38] and [Cu(*b*[10.5.2][19]aneN$_4$S)]$^{2+}$ bicyclo [Cu−S_{ap} = 2.549(2), Cu−N_{eq} = 2.04(1) Å][14] {py$_2$[9]aneN$_2$S = 4,7-bis(2-pyridylmethyl)-1-thia-4,7-diazacyclononane; *b*[10.5.2][19]aneN$_4$S = 15-thia-1,5,8,12-tetraazabicyclo[10.5.2]nonadecane}. These represent the only examples of structurally characterised CuN_4S systems with a square-pyramidal coordination sphere at the metal centre. Py$_2$[9]aneN$_2$S differs from $\mathbf{L^2}$ in that it has pyridyl-functionalised pendant arms, whereas *b*[10.5.2][19]aneN$_4$S can be considered as derived from $\mathbf{L^2}$ by formally joining the primary amino groups of the pendant arms with a $-CH_2CH_2-$ bridge to form a tetraazamacrocycle fused with a [9]aneN$_2$S moiety. In the case of $[Cu(py_2[9]aneN_2S)]^{2+}$, the structural data seem to indicate the presence of significant geometric constraints imposed by the pentadentate ligand py$_2$[9]aneN$_2$S. Indeed, the Cu−S_{ap} bond is particularly short and, although the mean Cu−N_{eq} bond length is similar for all three complexes, the Cu−N_{eq} bonds involving the pyridine donors in $[Cu(py_2[9]aneN_2S)]^{2+}$ are significantly shorter.[14,38] A similar trend in M−S_{ap} and M−N_{eq} distances is observed when comparing $[Pd(\mathbf{L^2})]^{2+}$ with $[Pd(py_2[9]aneN_2S)]^{2+}$.[26] Finally, the rather strained square-pyramidal coordination imposed on Cu^{II} by py$_2$[9]aneN$_2$S is also seen in the strong distortion of the basal plane in $[Cu(py_2[9]aneN_2S)]^{2+}$ where the metal centre suffers by far the greatest displacement (0.22 Å) from the N_4 plane towards the apical S-donor in the three complexes considered.

The ligand $\mathbf{L^4}$ was treated with 1 mol-equiv. of $CuCl_2 \cdot 2H_2O$ in MeOH at room temperature to give a deep blue solution. Addition of excess NH_4PF_6 followed by removal of the solvent gave a blue product, which was recrystallised from MeCN/Et_2O. The fast-atom bombardment (FAB) mass spectrum of this product exhibits peaks with the correct isotopic distribution for $[^{63}Cu(\mathbf{L^4})Cl]^+$ (*m*/*z* = 319) and for $[^{63}Cu(\mathbf{L^4})]^+$ (*m*/*z* = 284), and elemental analytical data suggested a formulation $[Cu(\mathbf{L^4})Cl]PF_6$. A structure determination confirmed the formation of a $[Cu(\mathbf{L^4})Cl]^+$ cation (Figure 5, bottom; Table 4) having structural features very similar to those observed in the analogous Pd^{II} complex $[Pd(\mathbf{L^4}Cl)]^+$. The square-pyramidal coordination geometry in $[Cu(\mathbf{L^4})Cl)]^+$ involves an N_2SCl donor set defining the basal plane and an S-donor at the apical site. The Cu−S_{ap} bond length is 2.5962(11) Å and, as expected, the Cu−N_{eq} distance involving the amino pen-

dant arm group [1.996(3) Å] is shorter than that involving the tertiary N-donor of the macrocyclic ring [2.103(3) Å]. The metal centre is displaced 0.1307 Å out of the mean plane defined by the atoms N(74), N(7), S(1) and Cl(1) in the direction of the apical S-donor S(4). In [Cu(**L^4**)Cl]$^+$, as in [Pd(**L^4**)Cl]$^+$, the coordination of the amino pendant arm to the metal centre with the formation of a six-membered chelate ring has driven the [9]aneNS$_2$ framework to adopt a facial [NS+S] coordination mode in contrast to the [2N+S] binding observed in [Cu(**L^2**)Cl$_2$] and [Pd(**L^2**)Cl$_2$]. [Cu(**L^4**)Cl]$^+$ units are associated in pairs via long-range Cu···Cl contacts and Cl···H hydrogen bonds, giving a Cu···Cu distance of 4.001(1) Å (Figure 6, bottom). Also, pairs of [Cu(**L^4**)Cl]$^+$ cations interact with each other through hydrogen bonds involving the amino pendant arm of the ligand to give ribbons which run along the *a* axis.

Conclusions

The binding of **L^1**−**L^4** to Pd^{II} and Cu^{II} is the same for each pair of complexes (Table 5) except for [M(**L^1**)Cl$_2$] for which both [NS+N] (M = Pd) and [2N + S] (M = Cu) coordination modes are observed. Generally, the amine ligands **L^2** and **L^4** show strong basal coordination of the N-donors of the macrocycle and of the primary amine. This is driven by the excellent binding properties of the primary amine donors and by the inherent stability of the chelate rings thus formed. The apparently "innocent" nitrile pendant arms are found to modulate the binding of the macrocyclic units within complexes of **L^1** and **L^3** and afford rare examples of long-range apical Pd···N$_{ap}$ interactions.

Experimental Section

General: Melting points are uncorrected. Microanalyses were performed by the University of Nottingham School of Chemistry Microanalytical Service. IR spectra were recorded as KBr discs using a Perkin−Elmer 598 spectrometer over the range 400−4000 cm^{-1}. NMR spectra (^{1}H and ^{13}C) were recorded at 298 K with a Bruker DPX300 instrument. UV/Vis spectra were measured in quartz cells using a Perkin−Elmer Lambda 9 spectrophotometer. Reagents and analytical-grade materials were obtained from commercial suppliers and used without further purification. All solvents were dried by conventional methods, freshly distilled and degassed. All reactions of air- and water-sensitive materials were performed in oven-dried glassware under dinitrogen. **L^1**,[14,39,40] **L^2** [14] and **L^3** [39,40] were synthesised according to literature procedures.

Table 5. Summary of coordination modes in Pd^{II} and Cu^{II} complexes of **L^1**−**L^4**

	M = Pd	M = Cu
[M(**L^1**)Cl$_2$]	[NS + N]	[2N + S]
[M(**L^2**)]$^{2+}$	[2N + S]	[2N + S]
[M(**L^3**)Cl$_2$]	[2S + N]	[2S + N]
[M(**L^4**)Cl]$^+$	[NS + S]	[NS + S]

Synthesis of L^4: A mixture of **L^3** (0.879 g, 3.99 × 10^{-3} mol) and BH$_3$·THF (1 M THF solution, 25 mL) was refluxed under N$_2$ for 48 h. The mixture was cooled and water (40 mL) was slowly added to destroy excess BH$_3$. The solvent was removed in vacuo and the solid residue was treated with 2 M HCl (50 mL) under reflux for 2 h. The solvent was removed under reduced pressure and the residue dried in vacuo. The white solid obtained was dissolved in water and the solution passed through an ion-exchange resin (Dowex 1X8-200) to give, after removal of the solvent, a colourless oil (0.585 g, 65% yield). EI$^+$ MS: *m*/*z* = 161 [M$^+$ − CH$_2$CH$_2$S], 147 [M$^+$ − CH$_2$ − CH$_2$CH$_2$S]. ^{1}H NMR (CDCl$_3$, 300 MHz): δ = 1.52 (quint, *J* = 7.23 Hz, 2 H, NCH$_2$*C*H$_2$CH$_2$NH$_2$), 2.43−2.81 (m, 12 H, NC*H*$_2$CH$_2$C*H*$_2$NH$_2$, NC*H*$_2$C*H*$_2$S), 3.06 (s, 4 H, SC*H*$_2$C*H*$_2$S) ppm. ^{13}C NMR (CDCl$_3$, 75.47 MHz): δ = 31.2, 32.6 (*C*H$_2$S*C*H$_2$), 34.2 (NCH$_2$*C*H$_2$CH$_2$NH$_2$), 39.8 (NCH$_2$CH$_2$*C*H$_2$NH$_2$), 54.7 (N*C*H$_2$CH$_2$CH$_2$NH$_2$), 57.7 (N*C*H$_2$CH$_2$S) ppm. IR spectrum (film between KCl discs): ṽ = 3277 br. m, 2911 s, 2800 s, 1627 m, 1572 m, 1461 m, 1405 m, 1305 m, 1144 w, 1111 w, 1022 w, 905 w, 811 w cm^{-1}.

[Pd(L^1)Cl$_2$]: A mixture of **L^1** (30 mg, 0.12 mmol) and PdCl$_2$ (21.08 mg, 0.12 mmol) in MeCN (10 mL) was refluxed overnight under N$_2$. The solvent was partially removed under reduced pressure and the resulting orange solution was filtered. Et$_2$O vapour was allowed to diffuse into the filtrate solution giving 37 mg (72% yield) of dark red microcrystals. Diffraction-quality crystals were obtained by recrystallisation from MeCN/Et$_2$O. M.p. 200−204 °C (dec.).C$_{12}$H$_{20}$Cl$_2$N$_4$PdS (429.68): calcd. C 33.54, H 4.69, N 13.04; found C 33.32, H 4.13, N 12.88. ES$^+$ MS: *m*/*z* = 427; calcd. for [^{106}Pd(**L^1**)Cl$_2$]$^+$ [M$^+$] 428. UV/Vis (MeCN): λ$_{max}$ (ε$_{max}$) = 400 nm (606 dm^3 mol^{-1} cm^{-1}). IR (KBr disc): ṽ = 2926 m, 2875 w, 2823 w, 2242 s, 1478 m, 1456 s, 1412 m, 1356 m, 1286 m, 1236 w, 1207 m, 1187 w, 1126 m, 1094 m, 1008 m, 931 m, 940 w, 908 w, 860 w, 760 m, 586 w cm^{-1}.

[Pd(L^3)Cl$_2$]: A mixture of **L^3** (20 mg, 0.092 mmol) and PdCl$_2$ (16.31 mg, 0.092 mmol) in MeCN (10 mL) was refluxed overnight under N$_2$. The resulting solution was filtered through a pad of Celite and the solvent removed under reduced pressure to give a red-brown residue. Recrystallisation by diffusion of Et$_2$O vapour into a DMF solution of the obtained solid gave red-orange crystals (20 mg, 55% yield). M.p. 260−262 °C (dec.). C$_9$H$_{16}$Cl$_2$N$_2$PdS$_2$ (393.66): calcd. C 27.46, H 4.10, N 7.12; found C 26.98 , H 3.88, N 6.90. FAB MS [3-nitrobenzyl alcohol(3-noba)]: *m*/*z* = 359; calcd. for [^{106}PdCl(**L^3**)]$^+$ [M$^+$] 358. UV/Vis (DMF): λ$_{max}$ (ε$_{max}$) = 410 nm (945 dm^3 mol^{-1} cm^{-1}). IR spectrum (KBr disc): ṽ = 2978 m, 2950 m, 2827 m, 2246 m, 1453 m, 1440 m, 1400 s, 1371 m, 1346 s, 1298 m, 1132 m, 1113 m, 1045 w, 1011 m, 959 m, 926 m, 896 w, 808 w, 736 w, 654 w, 580 w cm^{-1}.

[Pd(L^2)][BF$_4$]$_2$: A mixture of **L^2** (50 mg, 0.1920 mmol) and Pd(CH$_3$CN)$_4$(BF$_4$)$_2$ (85.3 mg, 0.1920 mmol) in MeCN/MeOH (1:1, v/v; 10 mL) was stirred at room temperature for 4 h. The solvent was removed in vacuo to give a yellow solid. Diffusion of Et$_2$O vapour into a solution of the complex in MeNO$_2$ afforded pale yellow crystals (77.5 mg, 75% yield). M.p. 214−216 °C. C$_{12}$H$_{28}$B$_2$F$_8$N$_4$PdS (540.46): calcd. C 26.67, H 5.22, N 10.37; found C 27.09, H 5.53, N 10.77. FAB MS (3-noba): *m*/*z* = 453, 366; calcd. for [^{106}Pd(**L^2**)(BF$_4$)]$^+$ [M$^+$] 454 and [^{106}Pd(**L^2**)]$^+$ [M$^+$] 367. UV/Vis (MeCN): λ$_{max}$ (ε$_{max}$) = 300 (459), 396 nm (60 dm^3 mol^{-1} cm^{-1}). IR (KBr disc): ṽ = 3310 s, 3276 s, 3171 m, 3096 m, 2944 m, 1612 s, 1469 m, 1328 m, 1175 s, 1087 s, 992 s, 771 m, 540 m, 420 w cm^{-1}.

[Pd(L^4)Cl]BF$_4$: A mixture of **L^4** (21 mg, 0.0953 mmol) and Pd(CH$_3$CN)$_4$(BF$_4$)$_2$ (42.33 mg, 0.0953 mmol) in MeCN (5 mL) was

stirred at room temperature for 48 h. The solvent was removed in vacuo to give a brown-orange oil. This oil was dissolved in H_2O (4 mL), NaCl (5.57 mg, 0.095 mmol) was added and the resulting mixture was stirred at room temperature for 24 h. The solvent was removed under reduced pressure to give a brown solid, which was taken up in MeCN. The suspension was filtered off, and Et_2O was allowed to diffuse into the filtrate to give dark red crystals (8.2 mg, 19% yield). M.p. 214−220 °C with decomposition. $C_9H_{20}BClF_4N_2PdS_2$ (449.05): calcd. C 24.07, H 4.49, N 6.24; found C 23.85, H 4.24, N 6.10. FAB MS (3-noba): *m*/*z* = 363, 325; calcd. for $[^{106}PdCl(\mathbf{L^4})]^+$ $[M^+]$ 362 and $[^{106}Pd(\mathbf{L^4})]^+$: $[M^+]$ 327. UV/Vis (MeCN): λ_{max} (ε_{max}) = 350 (464), 452 nm (51 dm^3 mol^{-1} cm^{-1}). IR (KBr disc): $\tilde{\nu}$ = 3422 s, 3289 m, 3189 m, 3133 m, 3089 m, 2955 w, 1589 m, 1444 m, 1400 m, 1289 m, 1200 w, 1072 s, 917 w, 805 w, 733 w, 533 m, 522m cm^{-1}.

[Cu(L^1)Cl$_2$]: A mixture of **L^1** (46.9 mg, 0.18 mmol) and $CuCl_2{\cdot}2H_2O$ (30.12 mg, 0.18 mmol) was refluxed in MeCN (15 mL) for 1 h under N_2. The solvent of the resulting green solution was allowed to evaporate and after 2 d green crystals of the complex were formed (46.4 mg, 65.5% yield). M.p. 128−130 °C. $C_{12}H_{20}Cl_2CuN_4S$ (386.82): calcd. C 37.26, H 5.21, N 14.48; found C 37.50, H 5.29, N 14.46. FAB MS (3-noba): *m*/*z* = 350, 315; calcd. for $[^{63}Cu(\mathbf{L^1})Cl]^+$ $[M^+]$ 351 and $[^{63}Cu(\mathbf{L^1})]^+$ $[M^+]$ 316. UV/Vis (MeCN): λ_{max} (ε_{max}) = 250 (1670), 335 (4912), 419 (1093), 716 nm (39 dm^3 mol^{-1} cm^{-1}). IR (KBr disc): 2940 w, 2905 w, 2880 w, 2840 w, 2220 m, 1480 m, 1440 s, 1410 s, 1400 s, 1350 s, 1300 s, 1270 m, 1230 w, 1210 w, 1120 w, 1080 s, 1060 m, 1045 m, 1030 m, 1010 w, 1000 w, 985 s, 970 m, 960 w, 940 m, 880 w, 730 m, 710 w, 525 w, 475 w, 380 w, 365w cm^{-1}.

[Cu(L^3)Cl$_2$]: A solution of $CuCl_2{\cdot}2H_2O$ (48.4 mg, 0.28 mmol) in MeCN (4 mL) was added to a solution of **L^3** (61.5 mg, 0.28 mmol) in MeCN (4 mL). A green solid was immediately formed and the mixture was stirred at room temperature for 2 h. The solid was filtered off, washed with Et_2O and dried under reduced pressure (67.4 mg, 68% yield). Single crystals suitable for X-ray diffraction studies were grown by diffusion of Et_2O vapour into a DMF solution of the green solid. M.p. 158−160 °C with decomposition. $C_9H_{16}Cl_2CuN_2S_2$ (350.80): calcd. C 30.81, H 4.60, N 7.98; found C 30.84, H 4.73, N 8.26. FAB MS (3-noba): *m*/*z* = 314, 279; calcd. for $[^{63}Cu(\mathbf{L^3})Cl]^+$ $[M^+]$ 315 and $[^{63}Cu(\mathbf{L^3})]^+$ $[M^+]$ 280. UV/Vis (MeCN): λ_{max} (ε_{max}) = 251 (530), 281 (327), 347 (1090), 428 (348), 762 nm (34 dm^3 mol^{-1} cm^{-1}). IR (KBr disc): $\tilde{\nu}$ = 2978 w, 2929 m, 2243 s, 1472 s, 1444 s, 1409 m, 1366 m, 1344 m, 1305 m, 1119 m, 1097 m, 1037 m, 961 m, 906 m, 834 w, 819 w, 756 w, 734 w, 671 w, 634 w, 595 w, 527 w, 445w cm^{-1}.

[Cu(L^2)][NO$_3$]$_2$: A solution of $Cu(NO_3)_2{\cdot}3H_2O$ (49.5 mg, 0.21 mmol) in MeCN (2 mL) was added to a solution of **L^2** (53.3 mg, 0.21 mmol) in MeCN/EtOH (1:1, v/v; 10 mL). A blue colour immediately developed and the mixture was stirred at room temperature for 1 h. The solvent was removed in vacuo and the residue repeatedly crystallised from EtOH/Et_2O to give blue block-like crystals (48.3 mg, 55% yield). M.p. 190−192 °C. $C_{12}H_{28}CuN_6O_6S$ (448.00): calcd. C 32.17, H 6.30, N 18.76; found C 31.95, H 6.10, N 18.45. FAB MS (3-noba): *m*/*z* = 385, 323; calcd. for $[^{63}Cu(\mathbf{L^2})(NO_3)]^+$ $[M^+]$ 386 and $[^{63}Cu(\mathbf{L^2})]^+$ $[M^+]$ 324. UV/Vis (MeOH): λ_{max} (ε_{max}) = 281 (3013), 556 nm (102 dm^3 mol^{-1} cm^{-1}). IR (KBr disc): $\tilde{\nu}$ = 3378 s, 3200 s, 3100 s, 2922 m, 2855 m, 1611 w, 1372 s, 1205 w, 1161 w, 1083 m, 1069 m, 1041 m, 1020 m, 923 w, 864 w, 826 w, 729 w, 688 w, 542w cm^{-1}.

[Cu(L^4)Cl]PF$_6$: A solution of $CuCl_2{\cdot}2H_2O$ (23.18 mg, 0.14 mmol) in MeOH (4 mL) was added to a solution of **L^4** (30 mg, 0.14 mmol) in MeOH (4 mL); an intense blue colour developed immediately and the mixture was stirred at room temperature for 2 h. The solvent was partially removed under reduced pressure and a large excess of NH_4PF_6 in MeOH solution was added. The solvent was completely removed and the residue washed with water to give a blue solid that was dried under reduced pressure (22.3 mg, 35% yield). Single crystals suitable for X-ray diffraction studies were obtained by recrystallisation from MeCN/Et_2O. M.p. 168 °C. $C_9H_{20}ClCuF_6N_2PS_2$ (464.35): calcd. C 23.28, H 4.34, N 6.03; found C 23.15, H 4.25, N 5.88. FAB MS (3-noba): *m*/*z* = 318, 283; calcd. for $[^{63}Cu(\mathbf{L^4})Cl]^+$ $[M^+]$ 319 and $[^{63}Cu(\mathbf{L^4})]^+$ $[M^+]$ 284. UV/Vis (MeCN): λ_{max} (ε_{max}) = 240 (1671), 312 (3996), 624 nm (126 dm^3 mol^{-1} cm^{-1}). IR (KBr disc): $\tilde{\nu}$ = 3291 s, 3214 s, 3140 w, 2959 w,

Table 6. Summary of crystal data and refinement results

	[Pd(**L^1**)Cl$_2$]	[Pd(**L^2**)][BF$_4$]$_2$	[Pd(**L^3**)Cl$_2$]	[Pd(**L^4**)Cl]BF$_4$	[Cu(**L^1**)Cl$_2$]	[Cu(**L^2**)][NO$_3$]$_2$	[Cu(**L^3**)Cl$_2$]	[Cu(**L^4**)Cl]PF$_6$
Empirical formula	$C_{12}H_{20}Cl_2N_4PdS$	$C_{12}H_{28}B_2F_8N_4PdS$	$C_9H_{16}Cl_2N_2PdS_2$	$C_9H_{20}BClF_4N_2PdS_2$	$C_{12}H_{20}Cl_2CuN_4S$	$C_{12}H_{28}CuN_6O_6S$	$C_9H_{16}Cl_2CuN_2S_2$	$C_9H_{20}ClCuF_6N_2PS_2$
M	429.68	540.46	393.66	449.05	386.82	448.00	350.80	464.35
Crystal size [mm]	0.26×0.21×0.12	0.58×0.37×0.23	0.43×0.39×0.19	0.67×0.31×0.10	0.29×0.12×0.11	0.27×0.27×0.27	0.29×0.19×0.13	0.47×0.24×0.16
Crystal system	monoclinic	orthorhombic	monoclinic	monoclinic	monoclinic	monoclinic	orthorhombic	triclinic
Space group	$P2_1/c$ (no. 14)	$P2_12_12_1$ (no. 19)	$C2/c$ (no. 15)	$P2_1/c$ (no. 14)	$P2_1/n$ (no. 14)	$P2_1/c$ (no. 14)	$Pna2_1$ (no. 33)	$P\bar{1}$ (no. 2)
a [Å]	7.796(3)	9.3480(11)	12.766(2)	12.473(3)	10.758(10)	9.5927(9)	13.9378(7)	7.2762(6)
b [Å]	15.313(4)	13.8508(16)	7.9708(10)	7.389(2)	6.850(9)	13.602(2)	11.9995(8)	9.8513(9)
c [Å]	13.522(2)	15.3511(17)	26.698(3)	17.786(3)	21.56(4)	14.6767(13)	8.2728(6)	12.3494(11)
α [°]	90	90	90	90	90	90	90	72.515(6)
β [°]	90.16	90	92.183(15)	107.18(2)	101.38(12)	106.177(8)	90	79.886(5)
γ [°]	90	90	90	90	90	90	90	89.105(6)
V [Å^3]	1614.3(8)	1987.6(4)	2714.8(6)	1566.1(6)	1558(4)	1839.2(3)	1383.6(2)	830.53(13)
Z	4	4	8	4	4	4	4	2
$D_{calcd.}$ [g·cm^{-3}]	1.768	1.806	1.926	1.905	1.650	1.618	1.684	1.857
T [K]	150(2)	220(2)	220(2)	150(2)	150(2)	220(2)	220(2)	220(2)
μ (Mo-K_α) [mm^{-1}]	1.605	1.117	2.043	1.652	1.874	3.132	2.241	7.149
Reflect. collected	2844	3446	4135	2765	2714	4042	3328	2376
Unique. reflect. R_{int}	2844,--	2349, 0.011	2387, 0.021	2765, --	2528, 0.064	2703, 0.031	2023, 0.017	2376, --
*R*1	0.0349	0.0215	0.0253	0.0218	0.0553	0.0542	0.0349	0.0377
*wR*2	0.0765	0.0541	0.0596	0.0528	0.211	0.159	0.0943	0.0982

2921 w, 1586 s, 1474 s, 1409 m, 1206 w, 1152 m, 1080 m, 995 m, 846vs, 730 w, 642 w, 559s cm^{-1}.

Crystallography: A summary of the crystal data and refinement details for the compounds is given in Table 6. The crystals were cooled using an Oxford Cryosystems open-flow dinitrogen cryostat.[41] For all the compounds diffraction data were collected with a Stoë Stadi-4 four-circle diffractometer using ω-θ scans. Data were corrected for Lorentz and polarisation effects and absorption corrections were applied using numerical or ψ-scan methods. For [Pd(**L^1**)Cl$_2$], and [Pd(**L^4**)Cl]BF$_4$ and [Cu(**L^2**)][NO$_3$]$_2$ a Patterson synthesis using *SHELXS-97*[42] provided a satisfactory set of starting parameters for the heavier atoms. The other structures were solved by direct methods using either *SIR92*[43] or *SHELXS*[42] and developed through subsequent difference Fourier synthesis.[44] All non-H atoms were refined anisotropically and H atoms were located from difference Fourier synthesis (solvent methyl H atoms) or introduced at calculated positions and thereafter incorporated into a riding model with $U_{iso}(H) = xU_{eq}(C)$ (x = 1.2 for CH_2, 1.5 for CH_3). For [Cu(**L^2**)][NO$_3$]$_2$ the NO_3^- anions were restrained to planarity and to have equal N−O bond lengths. In the case of [Cu(**L^4**)Cl]PF$_6$ the PF_6^- ion was found to be disordered during refinement. The disorder was modelled by a partial occupancy model over two sites for each of the four F atoms in the equatorial plane with occupancy factors of 0.59 and 0.41. The two F atoms in the axial positions could be treated as ordered. All the P−F bond lengths were restrained to have the same value during refinement. CCDC-181045 to -181052 contain the supplementary crystallographic data for this paper. These data can be obtained free of charge at www.ccdc.cam.ac.uk/conts/retrieving.html [or from the Cambridge Crystallographic Data Centre, 12 Union Road, Cambridge CB2 1EZ, UK; Fax: (internat.) + 44-1223/336-033; E-mail: deposit@ccdc.cam.ac.uk].

Acknowledgments

We thank the EPSRC and the University of Nottingham for financial support and the EPSRC Mass Spectrometry Service at the University of Swansea for mass spectra.

[1] P. Chaudhuri, K. Wieghardt, *Prog. Inorg. Chem.* **1987**, *35*, 329−436.
[2] P. V. Bernhardt, G. A. Lawrance, *Coord. Chem. Rev.* **1990**, *104*, 297−343.
[3] A. J. Blake, M. Schröder, *Adv. Inorg. Chem.* **1990**, *35*, 1−80.
[4] J. P. Danks, N. R. Champness, M. Schröder, *Coord. Chem. Rev.* **1998**, *174*, 417−468.
[5] K. P. Wainwright, *Coord. Chem. Rev.* **1997**, *166*, 35−90.
[6] A. J. Blake, I. A. Fallis, R. O. Gould, S. Parsons, S. A. Ross, M. Schröder, *J. Chem. Soc., Chem. Commun.* **1994**, 2467−2469.
[7] A. J. Blake, J. P. Danks, V. Lippolis, S. Parsons, M. Schröder, *New J. Chem.* **1998**, *22*, 1301−1303.
[8] A. J. Blake, J. P. Danks, A. Harrison, S. Parsons, P. Schooler, G. Whittaker, M. Schröder, *J. Chem. Soc., Dalton Trans.* **1998**, 2335−2340.
[9] A. D. Pidwell, S. R. Collinson, S. J. Coles, M. B. Hursthouse, M. Schröder, D. W. Bruce, *Chem. Commun.* **2000**, 955−956.
[10] L. Tei, G. Baum, A. J. Blake, D. Fenske, M. Schröder, *J. Chem. Soc., Dalton Trans.* **2000**, 2793−2799.
[11] A. J. Blake, D. W. Bruce, J. P. Danks, I. A. Fallis, D. Guillon, S. A. Ross, H. Richtzenhain, M. Schröder, *J. Mat. Chem.* **2001**, *11*, 1011−1018 and references therein.
[12] W. S. Striejewske, R. R. Conry, *Chem. Commun.* **1998**, 555−556.
[13] D. Parker, A. S. Craig, G. Ferguson, A. J. Lough, *Polyhedron* **1989**, *8*, 2951−2952.
[14] D. G. Fortier, A. McAuley, *Inorg. Chem.* **1989**, *28*, 655−662.
[15] L. R. Gaham, G. A. Lawrance, A. M. Sargeson, *Aust. J. Chem.* **1982**, *35*, 1119−1131.
[16] G. Hunter, A. McAuley, T. W. Whitcombe, *Inorg. Chem.* **1988**, *27*, 2634−2639.
[17] A. J. Blake, L. M. Gordon, A. J. Holder, T. I. Hyde, G. Reid, M. Schröder, *J. Chem. Soc., Chem. Commun.* **1988**, 1452−1454.
[18] A. J. Blake, A. J. Holder, Y. V. Roberts, M. Schröder, *J. Chem. Soc., Chem. Commun.* **1993**, 260−262.
[19] U. Heinzel, R. Mattes, *Inorg. Chim. Acta* **1992**, *194*, 157−161.
[20] U. Heinzel, R. Mattes, *Polyhedron* **1991**, *10*, 19−25.
[21] A. J. Blake, R. D. Crofts, B. DeGroot, M. Schröder, *J. Chem. Soc., Dalton Trans.* **1993**, 485−486.
[22] C. R. Lucas, W. Liang, D. O. Miller, J. N. Bridson, *Inorg. Chem.* **1997**, *36*, 4508−4513.
[23] A. R. Rossi, R. Hoffmann, *Inorg. Chem.* **1975**, *14*, 365−374.
[24] A. J. Blake, A. J. Holder, T. I. Hyde, Y. V. Roberts, A. J. Lavery, M. Schröder, *J. Organomet. Chem.* **1987**, *323*, 261−270.
[25] A. J. Blake, Y. V. Roberts, M. Schröder, *J. Chem. Soc., Dalton Trans.* **1996**, 1885−1895.
[26] B. Chak, A. McAuley, T. W. Whitcombe, *Can. J. Chem.* **1994**, *72*, 1525−1532.
[27] K. Wieghardt, H.-J. Küppers, E. Raabe, C. Krüger, *Angew. Chem. Int. Ed. Engl.* **1986**, *25*, 1101−1103.
[28] S. Chandrasekhar, A. McAuley, *Inorg. Chem.* **1992**, *31*, 2663−2665.
[29] G. J. Grant, K. A. Sanders, W. N. Setzer, D. G. VanDerveer, *Inorg. Chem.* **1991**, *30*, 4053−4056.
[30] A. J. Blake, R. O. Gould, A. J. Lavery, M. Schröder, *Angew. Chem. Int. Ed. Engl.* **1986**, *25*, 274−276.
[31] G. Reid, A. J. Blake, T. I. Hyde, M. Schröder, *J. Chem. Soc., Chem. Commun.* **1988**, 1397−1399.
[32] H. Nikol, H.-B. Bürgi, K. I. Hardcastle, H. B. Gray, *Inorg. Chem.* **1995**, *34*, 6319−6322.
[33] R. D. Hancock, S. M. Dobson, J. C. A. Boeyens, *Inorg. Chim. Acta* **1987**, *133*, 221−231.
[34] J. C. A. Boeyens, S. M. Dobson, R. D. Hancock, *Inorg. Chem.* **1985**, *24*, 3073−3076.
[35] L. R. Gahan, C. H. L. Kennard, G. Smith, T. C. W. Mak, *Transition Met. Chem.* **1986**, *11*, 465−466.
[36] A. J. Blake, J. P. Danks, I. A. Fallis, A. Harrison, W.-S. Li, S. Parsons, S. A. Ross, G. Whittaker, M. Schröder, *J. Chem. Soc., Dalton Trans.* **1998**, 3969−3976.
[37] A. J. Blake, J. P. Danks, W.-S. Li, V. Lippolis, M. Schröder, *J. Chem. Soc., Dalton Trans.* **2000**, 3034−3040.
[38] K. Wasielewski, R. Mattes, *Acta Crystallogr., Sect. C* **1990**, *46*, 1826−1828.
[39] L. Tei, A. J. Blake, P. A. Cooke, C. Caltagirone, F. Demartin, V. Lippolis, F. Morale, C. Wilson, M. Schröder, *J. Chem. Soc., Dalton Trans.* **2002**, 1662−1670.
[40] V. Lippolis, A. J. Blake, P. A. Cooke, F. Isaia, W.-S. Li, M. Schröder, *Chem. Eur. J.* **1999**, *5*, 1987−1991.
[41] J. Cosier, A. M. Glazer, *J. Appl. Crystallogr.* **1986**, *19*, 105−107.
[42] *SHELXS*-86 and *SHELXS*-97: G. M. Sheldrick, *Acta Crystallogr., Sect. A* **1990**, *46*, 467−473.
[43] A. Altomare, M. C. Burla, M. Camelli, G. Giacovazzo, A. Guagliardi, G. Polidori, *J. Appl. Crystallogr.* **1994**, *27*, 435−436.
[44] G. M. Sheldrick, *SHELXL*-93 and *SHELXL*-97, *Programs for Crystal Structure Refinement*, University of Göttingen, Germany, **1993** and **1997**.

Received September 10, 2002
[I02506]

Intercalation of Poly(Ethylene Oxide) Derivatives into Layered Double Hydroxides

Fabrice Leroux,[a] Pilar Aranda,*[b] Jean-Pierre Besse,[a] and Eduardo Ruiz-Hitzky[b]

Keywords: Layered compounds / Intercalations / Nanostructures

Mono- and bi-functional guest molecules, poly(ethylene glycol)-*n*-alkyl-3-sulfopropyl diether (PEG-AS) and poly(ethylene glycol)dicarboxylic acid (PEG-DC), containing hydrophilic polyoxyethylene (PEO) chains of different ethylene oxide units (EOUs) are incorporated between the layers of $Cu_2Cr(OH)_6Cl{\cdot}nH_2O$ hydrotalcite-type materials. The intercalation compounds are characterized by chemical analysis, adsorption measurements, XRD, SEM, FTIR and ^{13}C CP-MAS spectroscopy. It is found that the polyoxyethylene chain of PEG-DC distorts its helical symmetry when it is intercalated in the LDH galleries. The basal spacing of PEG-AS nanocomposites is independent of the number, *n*, of EOUs in the polymer chain. In addition to changes in the IR bands, ^{13}C CP-MAS spectra are modified with new resonance peaks at more deshielded values. These facts suggest a strong interaction of polyether chains with the LDH inner-surface, with the hydrophobic alkyl tail dangling into the interlamellar space. It is shown that the terminal functionalities dictate the arrangement of the PEO chains.

(© Wiley-VCH Verlag GmbH & Co. KGaA, 69451 Weinheim, Germany, 2003)

Introduction

The preparation of hybrid organic-inorganic nanocomposites has generated a lot of interest.[1] Layered materials are well-known to be highly suitable as host matrices for the incorporation of a large variety of organic species, readily accommodating the guest molecules via topotactic reactions. The development of tunable systems synergically enhanced by their two components is topical, the main interest being to obtain desirable properties that are unattainable from only one of the two components. This notion has also been extended to reinforced composites in which the inorganic part is usually finely dispersed or exfoliated within a polymer that supplies the mechanical strength.[2]

Due to their applications in heterogeneous catalysis, a lot of interest has been devoted to layered double hydroxides (LDH), also known as hydrotalcite-like solids, as host materials.[3] $Mg(OH)_2$ brucite material has been used, in which the M^{2+} cations are partially substituted by M^{3+} cations. The substitution creates a positive net charge counterbalanced by the presence of anions located in the interlamellar region. The exchange capacity of LDH materials, defined by the trivalent to divalent cation ratio, is usually two to three times greater than that of cations in smectite clay minerals. This may be considered as a drawback for incorporating a large organic guest, when considering the packing between the layers. Nevertheless, large molecules with variable functionalities lying parallel to the LDH plan have been incorporated, such as DNA[4] or polymers.[5] It was found that the match between the charge density and the monomeric repetition of the LDH layer, viz. the projected area of the anionic function, is of great importance in obtaining complete exchange with large molecules and the ordered nanocomposites of the stiff polymer.[5d]

With regard to the nanocomposites, a lot of attention has been paid to the intercalation of poly(ethylene oxide) (PEO) into different lamellar inorganic frameworks, such as smectites,[6] V_2O_5,[7] MoO_3,[8] and other host lattices,[9] giving hybrid materials with improved properties such as ion-conductivity or mechanical strength. PEO is known to present a flexible helical arrangement[10] that can be distorted to obtain zigzag conformations, depending on its environment and in particular on the presence of alkali-metals or other complexing ions. Besides this application, we were also interested to know how the PEO chain could be accommodated in the LDH gallery. As intercalation in LDH hosts is limited to anionic species, we focussed our attention on two charged polymers (Table 1), one an acid monofunctional, poly(ethylene glycol)alkenylsulfonic acid (PEG-AS) and the other a bifunctional, poly(ethylene glycol)dicarboxylic acid (PEG-DC), presenting an average of 11 or 7 and 12 (OCH_2CH_2) units (EOUs), respectively.

The morphology and flexibility of layered structures are important factors for topotactic reactions. For this reason, the $Cu_2Cr(OH)_6Cl{\cdot}nH_2O$ (noted as [CuCr] host structure) LDH sample, which is presented as corrugated sheets,[11] is

[a] Laboratoire des Matériaux Inorganiques, CNRS-UMR n°6002, Université Bla Pascal,
63177 Aubière cédex, France
E-mail: fleroux@chimtp-univ.bpclermont.fr
[b] Instituto de Ciencia de Materiales de Madrid, Cantoblanco, 28049 Madrid, Spain
E-mail: aranda@icmm.csic.es

Table 1. Polyethylene oxide compounds used in this work

Polymer	Formula	Characteristics
PEG-DC	$HO_2C(CH_2OCH_2)_nCO_2H$	n ≈ 12; Mw average 600 Dalton
PEG-AS 11	$R(OCH_2CH_2)_nO(CH_2)_3SO_3K$	R = $CH_3(CH_2)_y$, y = 12-14; $n \approx 11$
PEG-AS 7	$R(OCH_2CH_2)_nO(CH_2)_3SO_3K$	R = $CH_3(CH_2)_y$, y = 12-14; $n \approx 7$

taken as the host material. In addition, its acid character will prevent contamination by carbonate anion uptake, thus avoiding competition with polymer incorporation.

In this work we have tried several synthetic procedures to incorporate the two PEO-based polymers indicated above for the preparation of new polymer/LDH nanocomposites. The study of the adsorption and intercalation processes of both polymers between the sheets of the [CuCr] host structure and characterization of the resulting nanocomposites by a combination of technique, such as X-ray diffraction, FTIR and ^{13}C solid state NMR spectroscopy, employed to postulate models for the polymer arrangements. Some results concerning another LDH host solid, ($Zn_2Cr(OH)_6Cl{\cdot}nH_2O$) noted as [ZnCr], will also be discussed.

Results

Polymer Incorporation

A powder X-ray diffraction pattern of [CuCr], typical of hydrotalcite-type material, was refined using an $R\bar{3}m$ space group in rhombohedral symmetry (Figure 1a). The cell parameters **a** and **c** (equal to three times the interlamellar distance) are equal to 0.31 nm and 2.31 nm, respectively, in agreement with previous results.[11]

The uptake of PEG-DC between the LDH layers is confirmed by an expansion of the d-spacing. The intercalation of PEG-DC performed in an aqueous medium for four hours induces an increase of the basal spacing from 0.77 to 3.03 nm (Figure 1b). Longer reaction times (up to three days) give rise to a lower d-spacing of 2.60 nm (Figure 1c). To explain this result it is necessary to suppose that the sample is altered by the progressive action of the solution containing PEG-DC or invoking a reorganization of the polymer chain inside the interlayer space of the LDH. This could be due to a reorganization of the polymer in the LDH galleries. An XRD pattern of the sample synthesized in butanol (BuOH) solution is very similar to the one prepared by direct exchange in an aqueous medium, although a d-spacing of 2.95 nm is obtained (Figure 1d). It is noteworthy that other alternatives such as the guest displacement or templating methods, appear to be unsuccessful in completing the exchange, giving rise to a mixture of an intercalated phase with a d-spacing of about 2.6 nm and to the pristine host material.

In comparison with the pristine host material, the broadness of the diffraction peaks is affected by the polymer incorporation. This broadening indicates the presence of either some turbostatic effects or of a large decrease in the stacking sequence, as usually observed after topotactic reactions. This is even more pronounced after a longer exchange reaction time (Figure 1c). The incorporation of PEG-AS 11, by an exchange reaction, is also visible from the variation of the 2D-periodicity from 0.77 to 3.79 nm (Figure 2a). Since the diffusion of PEG-AS into the LDH gallery may be thermodynamically and/or sterically hindered, the templating method was carried out. During the co-precipitation, the polymer is entrapped between LDH sheets.

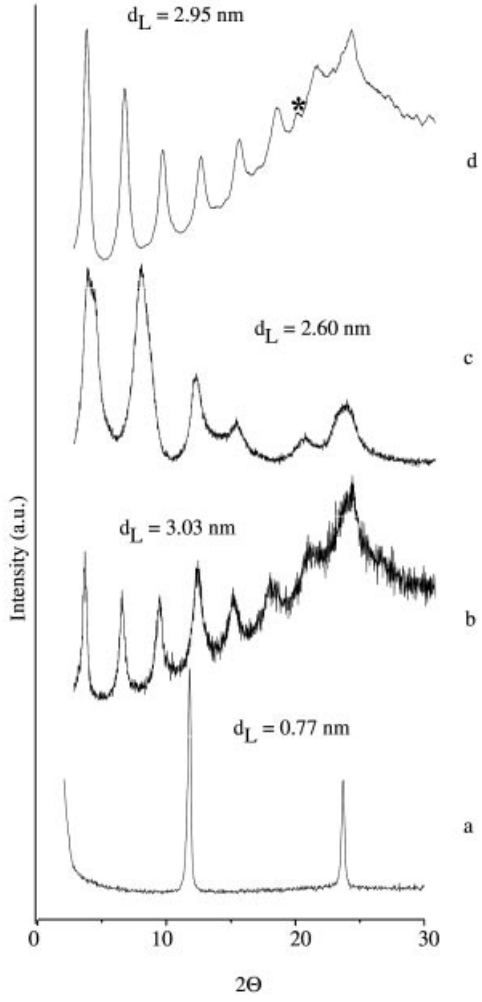

Figure 1. XRD patterns of: a) [CuCr] LDH pristine material, and PEG-DC/LDH nanocomposites obtained after b) 4 hours and c) 3 days of exchange reaction in water, and d) 4 hours of exchange reaction in butanol (* indicates a non-harmonic peak observed at 19.3°, i.e. 0.46 nm)

This is associated with a greater expansion of the d-spacing of up to 4.30 nm (Figure 2b). In Figure 2, the set of the first three harmonics is of different intensity. This is related to the arrangement of the organic molecule within the interlayer space. The polymer organization is then sensitive to the synthetic pathway. Additionally, a broad scattering hump is observed between 20−30° in 2θ, suggesting that a part of the polymer remains associated with the surface of the material. This occurs because the polymer is used in excess and can be adsorbed on the surface during the co-precipitation; the use of less polymer during the formation of $Cu_2Cr(OH)_6Cl{\cdot}nH_2O$ has not been explored.

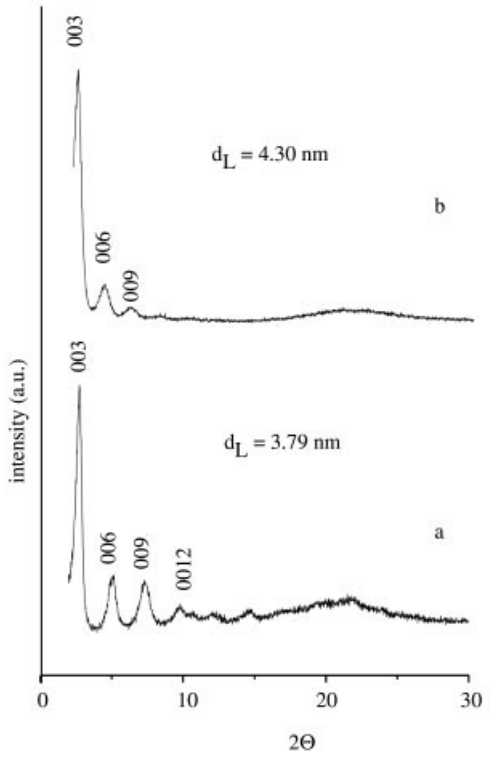

Figure 2. XRD patterns of PEG-AS (11 EOUs)/[CuCr] nanocomposites obtained via: a) exchange reaction in water, and b) co-precipitation

Our findings may be compared with the incorporation of $C_{12}H_{25}(OCH_2CH_2)_mSO_4^-$ surfactant molecules (m = 1, 2, 4) between LDH materials as reported by Kopka et al.[12] The authors noticed that the degree of exchange decreased with the increase of EOUs (90 and 71% of exchange for m = 1 and 4, respectively) reaching a d-spacing of 3.31 nm for m = 4. In our case, this implies a highly constrained environment of PEG-AS 11 between LDH sheets because the d-spacing changes from 3.60 to 3.79 nm for the polymer with 7 and 11 EOUs, respectively.

It is noteworthy that for the exchange reaction, and after repeated centrifugations, the solution still remains a pale green color. This shows the presence of finely dispersed particles. Such behavior must be related to the colloidal properties of PEG-AS that induces the formation of micelles, thus giving rise to the disassembly of the LDH microcrystals. This approach could be an alternative to other exfoliation processes.[13]

The carbon content of the nanocomposites is lower than what was theoretically expected from the complete exchange reaction. The polymer content per formula [$Cu_2Cr(OH)_6$] is found to be in the range of 0.24−0.76 for PEG-AS and 0.53−0.84 for PEG-DC (Table 2). These differences depend strongly on the synthetic approach and may be explained by the limited diffusion of the polymer between the LDH sheets, as reported for the intercalation of cumbersome molecules.[14] The presence of chlorine anions was detected in the material, showing that the host structure encounters a co-intercalation phenomenon. A peculiar arrangement of the EOU units may also induce strong effects (see below).

Polymer Adsorption Measurements

Adsorption isotherms (Figure 3) exhibit features characteristic of the H(2) Langmuir type according to the classification of Giles et al.;[15] this usually occurs when the solute consists of large units such as ionic micelles or polymeric molecules. It shows that both polymers possess a strong affinity for the LDH surface, and are completely adsorbed at a low concentration range. The Langmuir-type process is modeled according to Equation (1),[16] where C_e is the concentration of adsorbate at equilibrium (mmol/L), q_e the amount adsorbed at equilibrium (mmol/g), X_m (mmol/g) the maximum amount of adsorbate that can be adsorbed in a monolayer, and K_e the Langmuir constant related to the energy of adsorption.

$$C_e/q_e = 1/X_mK_e + C_e/X_m \quad (1)$$

The q_e versus C_e curve was fitted according to Equation (1) (inset Figure 3, a and b). The fitting and the correlation parameters for both polymers are indicated in the figure caption. X_m and K_e are equal to 0.48 and 0.37, respectively, for the adsorption process of PEG-DC, and 1.18 and 5.76, respectively, for the PEG-AS with 11 EOUs. The energy of adsorption is much higher for PEG-AS than it is for PEG-DC. This agrees with the stronger acid character of sulfonic versus carboxylic species.

It is interesting to note that the adsorption mechanism could be different for each polymer. In fact, the analysis of the shape of the plateau and the maximum adsorbed amount is quite different for each one. In both cases, the polymer must be strongly reorganized in the interlayer space, as shown by the variations in the adsorbed amount of polymer and d-spacing values.

For PEG-DC the maximum of the adsorbed amount is lower than 0.50 mmol per gram, which corresponds to 0.16 mol per formula. There is no complete ion-exchange even for the most concentrated equilibrium solutions. There is a progressive intercalation as the amount of polymer increases, and the basal spacing of the organic intercalated phase is modified. The maximum adsorption has not been reached and so even for the 0.46 mmol/g material there are

Table 2. Characteristics of PEG-DC/ and PEG-AS/ nanocomposites prepared in this work

Nanocomposites	Method of synthesis	Δd_L (nm)	%C in the solid	Tentative formula[a]
PEG-DC/CuCr	ion-exchange in H_2O	2.55	17.3	$Cu_2Cr(OH)_6 \cdot PEG\text{-}DC_{0.32}Cl_{0.36} \cdot nH_2O$
	ion-exchange in BuOH	2.47	29.5	$Cu_2Cr(OH)_6$ $PEG\text{-}DC_{0.76} \cdot nH_2O$[c]
	co-precipitation	2.12[b]	14.6	$Cu_2Cr(OH)_6$ $PEG\text{-}DC_{0.24}Cl_{0.52} \cdot nH_2O$
PEG-AS/CuCr	ion-exchange of PEG-AS 11 EOUs in H_2O	3.31	30.1	$Cu_2Cr(OH)_6$ $PEG\text{-}AS_{0.53}Cl_{0.47} \cdot nH_2O$
	ion-exchange of PEG-AS 7 EOUs in H_2O	3.12	33.5	$Cu_2Cr(OH)_6$ $PEG\text{-}AS_{0.70}Cl_{0.30} \cdot nH_2O$
	co-precipitation in presence of PEG-AS 11 EOUs	3.82	36.2	$Cu_2Cr(OH)_6$ $PEG\text{-}AS_{0.84}Cl_{0.16} \cdot nH_2O$
PEG-AS/ZnCr	ion-exchange of PEG-AS 11 EOUs in H_2O	3.22	33.1	$Zn_2Cr(OH)_6$ $PEG\text{-}AS_{0.66}Cl_{0.34} \cdot nH_2O$
	ion-exchange of PEG-AS 7 EOUs in H_2O	3.07	32.3	$Zn_2Cr(OH)_6$ $PEG\text{-}AS_{0.65}Cl_{0.35} \cdot nH_2O$

[a] Tentative formula calculated assuming that the anionic polymers are intercalated by replacing Cl^- ions of the pristine $Cu_2Cr(OH)_6Cl \cdot nH_2O$ or $Zn_2Cr(OH)_6Cl \cdot nH_2O$ LDH matrices. [b] Also a phase of pristine LDH is observed. [c] Incorporated amount of PEG-DC exceeds the ion-exchange capacity.

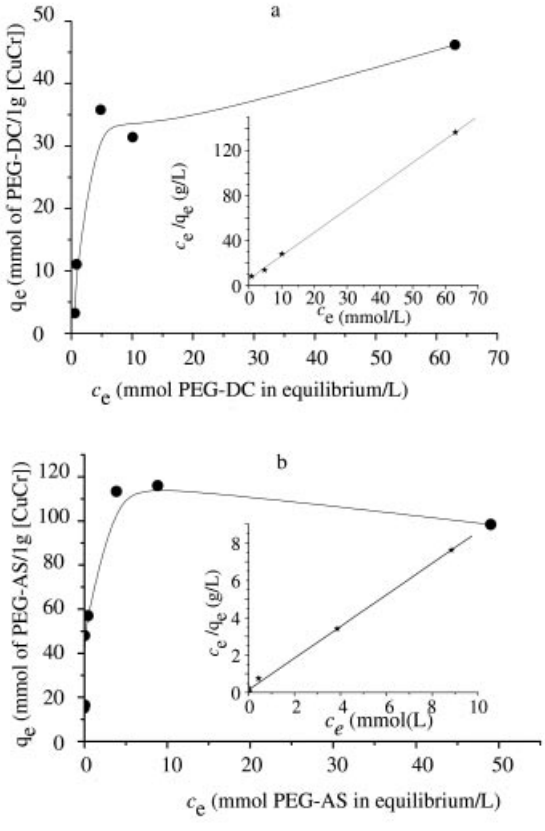

Figure 3. Adsorption isotherm from water solutions of: a) PEG-DC and b) PEG-AS containing 11 EOUs on [CuCr]; the fit is displayed in the inset [according to Equation (1)]: a) $C_e/q_e = 5.55 + 0.0033292\ C_e$ ($R = 0.99968$), b) $C_e/q_e = 0.1468 + 0.00109\ C_e$ ($R = 0.9989$)

still peaks associated with the pristine solid [CuCr]. An incorporation of PEG-DC as high as 0.76 mol per [CuCr] formula unit is reached using BuOH as the solvent (Table 2). Such high polymer content may be explained by the preparation method. The use of BuOH under reflux conditions is known to break up the LDH structure, thus creating an increase in the interface. A part of the polymer must coat the surface of the crystallites.

For the PEG-AS (11 EOUs) there is a maximum in the adsorption close to 120 mmol/g (0.40 mmol per formula unit) for equilibrium concentrations below 20 mmol/L. At higher C_e values, a slight decrease is observed for the adsorbed amount of about 0.35 mol per formula unit. The XRD patterns still exhibit the diffraction peak of pristine [CuCr] LDH material. The formation of an intercalated phase progresses along with an increase in the amount of polymer to the point where the LDH structure starts to dissolve, as illustrated by the large scatter between 20 and 30° in 2θ. A green color indicates that a disassembly of the 2D-host matrix occurs, probably entangled by the polymer. The monofunctional polymer may play the role of a spacer acting at the edge of the crystallites like dodecylsulfate molecules for the LDH delamination.[13a][13b]

FTIR Spectroscopy

IR spectroscopy of the resulting PEO/LDH nanocomposites affords significant information on how the polymer is associated into the 2D host solid. The lattice vibration bands arising from M−O and O−M−O (M= Cu, Cr) bonds are observed in the 400−800 cm^{-1} region and there are no important differences between LDH and the nanocomposites (Figure 4 and 5). In the 1300−1350 cm^{-1} region several vibration bands appear that are related to the wagging vibration of the $-CH_2-O-$ groups, which give crucial information about characteristics of the polyoxyethylene skeleton and its deformation. This is exemplified by the vibration band at 1346 cm^{-1} for PEG-DC (Figure 4), characteristic of $-CH_2-O-$ groups of polyether chains in a helical conformation. The presence of a weak band at 1325

cm^{-1} in the non-intercalated pristine polymer suggests a very slight distortion of the helix. However, for the PEG-DC/LDH nanocomposites the band at higher wavenumber can be shifted towards 1330 cm^{-1} and a new and intense band develops at 1314 cm^{-1}. These facts indicate that the polyoxyethylene chain presents EOUs in a *trans* conformation[10] and therefore the helix is distorted. The degree of distortion depends on the nature of the host-guest matrix interactions. Some of the nanocomposites show planar zigzag conformations of the polymer as is observed for other poly(ethylene oxide) intercalation compounds.[6]

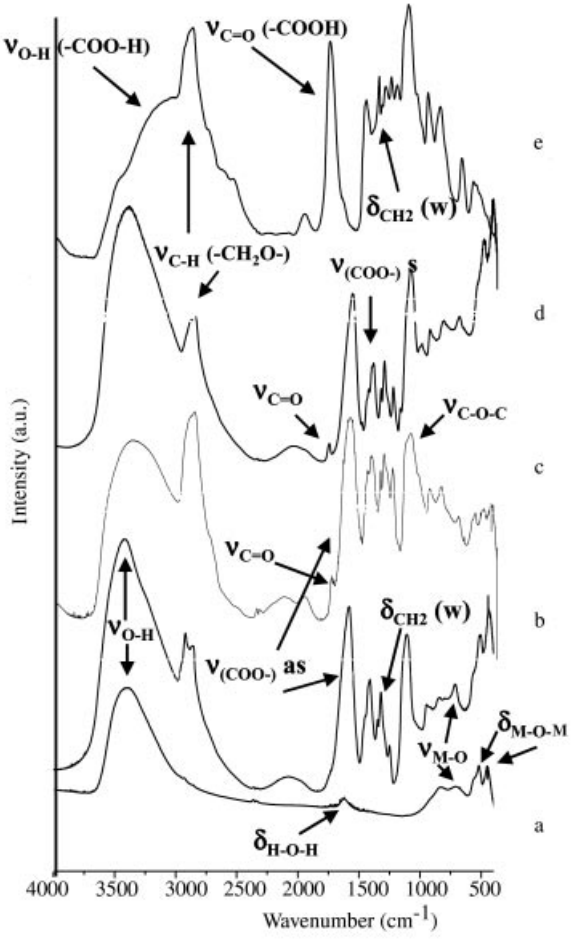

Figure 4. FTIR spectra of: (a) LDH pristine material, and PEG-DC/LDH nanocomposites obtained via b) ion-exchange in water, c) ion-exchange in butanol, d) co-precipitation, and e) pure PEG-DC

The assignment of the different vibration bands is displayed in Table 3. In the case of PEG-DC based nanocomposites, the bands associated with the $\nu_{C=O}$ stretch of the carboxylic groups are split into two at around 1578 cm^{-1} and 1407 cm^{-1}, corresponding to the antisymmetric and symmetric $\nu_{C=O}$ mode of the COO^- groups, respectively, as the acid is intercalated in the anionic form. In spite of this, the spectra of the nanocomposites, prepared by co-precipitation and BuOH under reflux, still show weak bands at around 1770 cm^{-1} and 1240 cm^{-1}, indicating the presence of free acid groups in the polymer associated with the solid.

The $\nu_{O=S=O}$ vibration bands of the SO_3^- group are observed at around the same wavenumber, 1190 and 1040 cm^{-1} for the antisymmetric and symmetric contribution, respectively, for pure PEG-AS and PEG-AS/LDH nanocomposites (Figure 5). The inversion in their relative intensity suggests that the SO_3^- group is in a more symmetric environment for the nanocomposites; this is probably a consequence of the interaction with the hydroxide sheet. For PEG-AS (11 EOUs)/LDH nanocomposites prepared by different synthetic approaches, either in [CuCr] or [ZnCr] LDHs, the striking difference when compared with the pristine polymer or even with the nanocomposites based on PEG-AS of 7 EOUs, is the appearance of two new bands around 1720 and 1570 cm^{-1} (Figure 5). The assignment of these bands is still unclear as there are no appreciable alterations, either in the organic backbone vibration bands or in those corresponding to the inorganic host (Figure 4). The vibration band at around 1720 cm^{-1} is indicative of a carbonyl group, suggesting that the polymer chain can be partially altered by heterolytic oxidation reactions.

^{13}C Solid-State NMR Spectroscopic Study

In order to get more information on the guest/host interaction in the PEG-AS/[CuCr] nanocomposite, ^{13}C solid-state CP MAS spectroscopy experiments were performed (Figure 6). The spectrum of PEG-AS of 11 EOUs exhibits several resonance peaks, with chemical shifts attributed as follows: δ = 72.2 ppm to carbon nuclei in the (-OCH_2CH_2-) ethylene oxide chain, δ = 48.4 ppm for C attached to an SO_3^- group, and several peaks lumped together (shoulder Figure 6a) from δ = 30.2 to δ = 14.4 ppm associated with the different methylene groups, and the terminal CH_3, respectively. The latter contribution is also observed for the LDH derivatives (Figure 6b and c), only the response is broader. For the C linked to the S, an up-field shift is observed up to δ = 42.5 ppm; this shielding may correspond to an electrostatic attraction between the molecule and the sheets of [CuCr] as observed in other systems.[17] The same effect, but much less pronounced, is observed for carbon nuclei in the ethylene chain with a shielding from δ = 72.2 to 71.1 ppm. However, it is interesting to note that the relative carbon nuclei population of the polymer is very different from that of the organic-inorganic phase. Even if the CP experiment does not strictly supply quantitative information, it is obvious that the population relative to carbon in the polyoxyethylene chain has decreased.

Surprisingly, some new peaks at δ = 127.0, 121.9 and 149.8 ppm appear for the nanocomposite that are absent for PEG-AS. These are not spinning side-bands since they are present in the spectra recorded at the two different fields. Such chemical shift values are typical of aromatic or highly deshielded carbons such as carbonyl carbons. It is noteworthy that these down-field contributions are not observed for PEG-DC hybrid materials.

Table 3. IR vibration bands (cm^{-1}) and their assignment for the PEG-DC and PEG-AS polymers and some of their LDH nanocomposites derivatives

PEG-DC	PEG-DC/CuCr ion-exchange	PEG-DC/CuCr co-precipitation	PEG-AS (11 EOUs)	PEG-AS (11 EOUs)/CuCr ion-exchange	PEG-AS (11 EOUs)/CuCr co-precipitation	PEG-AS (11 EOUs)/ZnCr ion-exchange	PEG-AS (7 EOUs)/CuCr ion-exchange	Assignment [a]
≈ 3200[b]	3414	3406		3436	3422	3464	3442	ν_{O-H} ν_{O-H} (-COO-H)
			2914	2920	2914	2918	2918	ν_{C-H} ($-CH_2-$)
2878	2864	2870	2858	2848	2850	2848	2846	ν_{C-H} ($-CH_2-O-$)
1742		1771		1724	1760[c], 1718[c]	1724[c]		$\nu_{C=O}$ (COOH)
				1618	1620	1618	1621	δ_{HOH} (H_2O)
	1578	1578		1570 [c]	1570[c]	1574[c]		$\nu_{C=O}$ (COO^-) asym
			1462	1456	1450	1456	1457	δ_{CH2} w ($-CH_2-$)
	1407	1407						$\nu_{C=O}$ (COO^-) sym
1346 m	1332 w	1350 w	1342	1344	1344	1344	1346	δ_{CH2} w ($-CH_2-O-CH_2-$)[d]
1325 w	1314 m	1314 m						
1242	1243	1242	1276		1288	1294		δ_{CH2} t
			1188	1182	1192	1182	1186	$\nu_{O=S=O}$ asym ($-SO_3^-$)
				1146[c]	1150[c]	1140[c]	1150[c]	ν_{C-O}[c]
1104	1102	1100	1100	1100	1112	1112	1110	ν_{C-O-C} asym
			1058, 1038	1038	1041	1038	1038	$\nu_{O=S=O}$ sym ($-SO_3^-$)
942	936	940	948	945	948	942	942	ν_{CH2} r
			840	850	851		865	$\nu_{S=O}$ ($-SO_3^-$)
				790[c]		788[c]	790[c]	$\nu_{(COO-)}$ formate
	707	707		735		731	728	ν_{M-O}
					570	574		ν_{C-S}
	504, 432	500, 436		508, 434	506, 428	506, 380	510, 436	δ_{O-M-O}

[a] Asym: antisymmetric; sym: symmetric; w: wagging; t: twisting; r: rocking. [b] Very broad and strong band centred around 3200 cm^{-1}. [c] Tentative assignation of the bands to vibration modes of C=O functions related to oxidation products of the oxyethylene polymer chain. [d] When two bands are observed the relative intensity of both of them is signalled (m = medium; w = weak).

SEM Observations

SEM pictures of the pristine material and derivative phases are displayed in Figure 7. The starting chloride-exchanged [CuCr] material gives rise to a platelet-like shape, this morphology being characteristic of the applied method of synthesis.[5b] This is found to be different for the PEG-DC nanocomposites, which show a leaf aspect.

For PEG-AS/LDH nanocomposites with either 7 or 11 EOUs, the crystallite surface presents a crumpled shape. The part of the polymer coating the material (see above) must be the origin of the irregularities. Moreover, the polymer chains must be linked to close chunks, giving rise to a large ill-defined piece. In the inset of Figure 7 (see f), the 2D-character is evidenced for these hybrid organic-inorganic phases.

Discussion

To shed some light on the present results, different hypotheses must be considered in order to postulate a model for the intercalated materials. The conformation of the PEO chain is an important factor for the polymer geometry between the layers. PEO presents a repetition of ($-OCH_2CH_2-$) units adopting a helical structure in its crystalline state.[10] Instead of taking the EOU linear size as three methylene groups in a zigzag conformation,[12] a flexible polyoxyethylene chain adopting a helix with either a $9_{1/2}$ or $7_{1/2}$ symmetry must be considered for long PEO chains.[10] The first gives rise to a dimension of 1.95 nm for 9 EOUs, and the second 1.90 nm for 7 EOUs.

By subtracting the LDH layer width of 0.48 nm from the d-spacing, we access the space available to accommodate the polymer between the sheets. For the PEG-DC nanocomposite prepared by ion-exchange, this gives a space of around 2.60 nm (Table 2), which is in agreement with a polyoxyethylene chain in a $9_{1/2}$ helical symmetry (expected value of 2.72 nm considering 12 EOUs instead of 9 in the helical conformation with the size of the two carboxylic groups being 0.12 nm[14]). After a longer reaction time, the gallery size is shortened to 2.17 nm (Figure 1, c), showing that the polyoxyethylene chains are strongly confined and the helix is distorted by chain-chain interactions and/or with OH from the LDH layer or H_2O molecules. This interpretation is supported by the high intensity of the δ_{CH2} (w) vibration band at 1314 cm^{-1} (Table 3).

For the PEG-DC/[CuCr] nanocomposite prepared by an exchange reaction in BuOH, eight well-defined harmonics are observed suggesting that the stacking is good. An additional peak at 19.3° (d = 0.46 nm) is also observed. In the absence of other possible explanations, this was related to a superlattice ($\sqrt{3}$ times the perpendicular distance between [100] planes).[18] Since this material presents an excess of polymer over the ion-exchange capacity determined from the chemical analysis (Table 2), a portion of the organics should be intercalated either in their acid form and/or adsorbed on the surface through interaction with OH groups. The first interpretation is supported by the presence of a

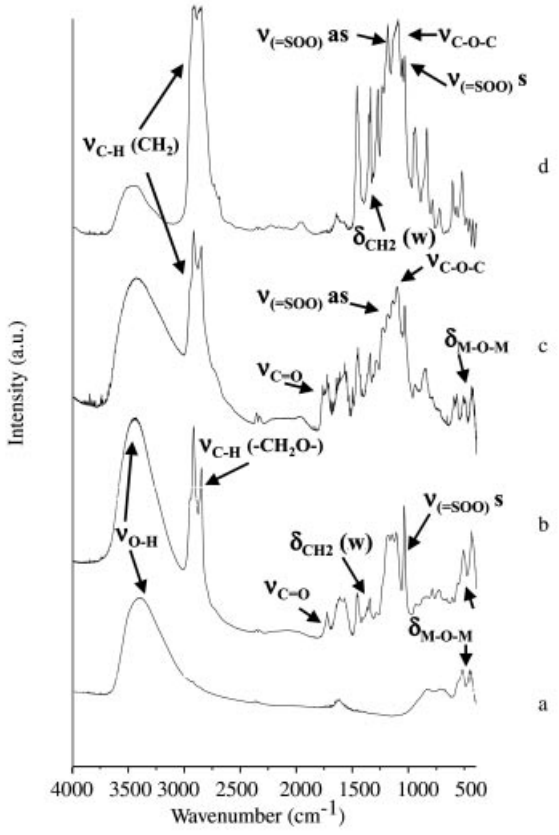

Figure 5. FTIR spectra of: (a) [CuCr] LDH pristine material, and PEG-AS/LDH nanocomposites obtained via b) ion-exchange in water, c) co-precipitation, and d) potassium salt of PEG-AS of 11 EOUs

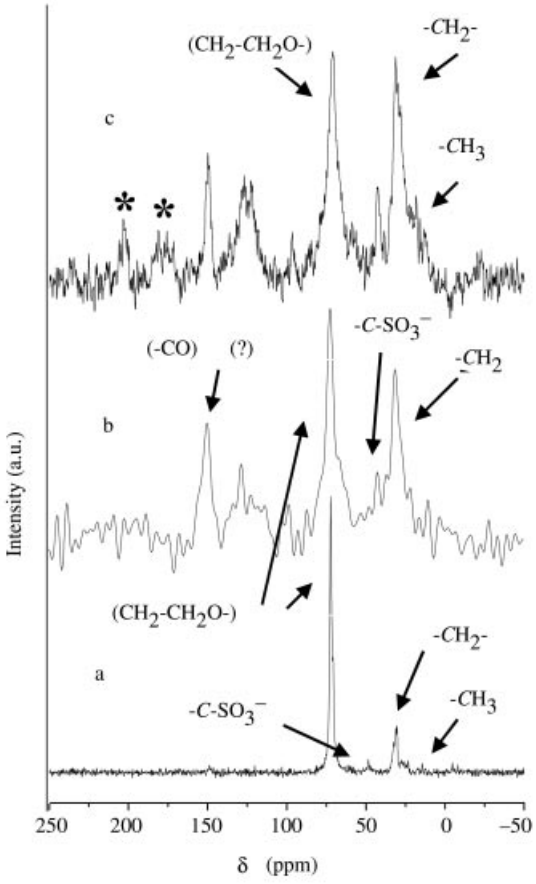

Figure 6. ^{13}C NMR spectra of: (a) the potassium salt of PEG-AS of 11 EOUs, and the PEG-AS/ [CuCr] nanocomposites recorded at (b) 7.04 T (300 MHz), and c) 9.39 T (400 MHz); spinning sidebands are indicated with an asterisk

band at 1742 cm^{-1} (Figure 4, c) assignable to the $\nu_{C=O}$ vibration mode of a free carboxylic group.

Bearing all of the above considerations in mind, we propose a model in which the molecule is intercalated with each of its functional groups interacting with one of the hydroxide surfaces in the interlayer space and with the polyoxyethylene chain being more or less twisted (Figure 8a). This model takes into account the possibility of obtaining nanocomposites with different arrangements of PEG-DC in which the amount of intercalated polymer and its interaction with OH groups of the layer and with H_2O molecules induce distortions in the polyether chain. The vibration bands and switching in intensity of the δ_{CH2} wagging vibration bands for $(-CH_2O-CH_2-)$ groups are affected (Table 2). As for PEO/montmorillonite nanocomposites,[6] the nature of the interlayer space may affect the distortion of the polyoxyethylene chains.

The same approach was taken to unravel the arrangement, between the LDH sheets, of the PEG-AS with 11 EOUs. Using similar calculations for the organic moieties, the size of the polymeric molecule is 4.73 and 5.39 nm, depending on the $9_{1/2}$ or $7_{1/2}$ helical symmetry, respectively. This calculation was made considering the following dimensions from Kopka and co-workers:[12] 0.127 nm per CH_2 group, and 0.30 nm for the $-CH_3$ and 0.18 nm for the $-CH_2SO_3^-$ groups. This appears to be much larger than that of the available space of 3.31 to 3.82 nm, depending on the synthesis (Table 2) of the [CuCr] LDH sheets. It underlines a different arrangement between the two guest molecules. At this point, two hypotheses may be considered: i) the PEG chain is strongly confined, but presents no significant interaction with the LDH layers. In this case, the molecule adopts an angle to the LDH surface, and ii) the PEG chains are close to the LDH layers, and may interact through their hydroxy groups.

The FTIR spectra of PEG-AS/LDH nanocomposites show only a band at around 1345 cm^{-1}, which is assigned to the δ_{CH2} (w) vibration mode of the EOUs in the helical conformation; this is different from that of the PEG-DC/LDH derivatives. However, from ^{13}C CP MAS and FTIR spectroscopy, highly deshielded carbon atoms were observed in these latter nanocomposites compared to the polymer alone. This was also associated with the appearance of a new vibration at 1720 cm^{-1}, and may be interpreted as a strong interaction of some of the EOUs with the LDH sheets. This situation was also observed for other organic surfactants, where ethoxy groups were found to be folded in a "hairpin" conformation and remained in contact with

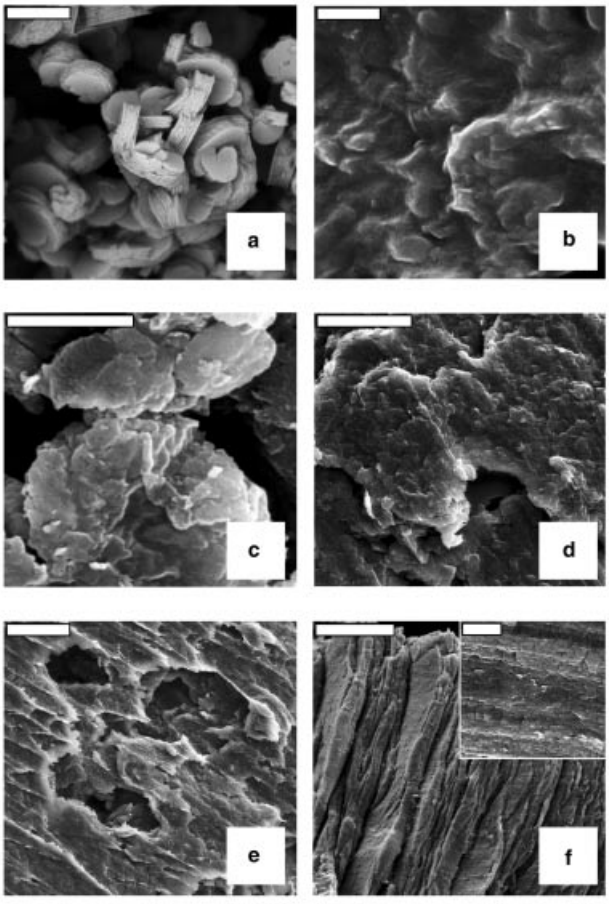

Figure 7. SEM pictures of (a) [CuCr] LDH pristine material; PEG-DC/[CuCr] nanocomposites obtained via (b) ion-exchange in water, (c) co-precipiation, and PEG-AS/[CuCr] nanocomposites of the polymer of 11 EOUs prepared via (d) ion-exchange in water, (e) co-precipitation, and the polymer of 7 EOUs prepared via (f) ion-exchange in water (in inset, the view is perpendicular to the stacking direction). The bar represents 2, 2, 2, 10, 20, 50, 5 (inset) μm, respectively

the LDH surface.[12] However, as PEO and PEO-salt complexes in certain circumstances can easily be oxidized following different mechanisms,[19] giving a complex mixture of primary products including ester, aldehyde, carboxylic acid and formate-end groups, the IR absorption bands observed in the 1500−1900 cm^{-1} region could be attributed to the oxidative degradation of the polymer catalyzed by the host LDH. Thus, for instance, the band at around 1720 cm^{-1} developed from the intercalates of PEG-AS of 11 EOUs (Table 3) could be ascribed to the formation of formate end-functions (-CH_2-O-CHO).

To corroborate this interpretation, PEG-AS of 7 EOUs was intercalated into [CuCr] and [ZnCr] LDH frameworks. These are materials that present the same layer charge density. From the XRD patterns (Figure 9) of nanocomposites derived from the polymer with 11 EOUs intercalated by ion-exchange in the two hosts, the space available for the guest molecule, calculated from the third harmonic position, varies from 3.31 to 3.22 nm for [CuCr] and [ZnCr] derivatives, respectively (Table 2). Thus, PEG-AS may also

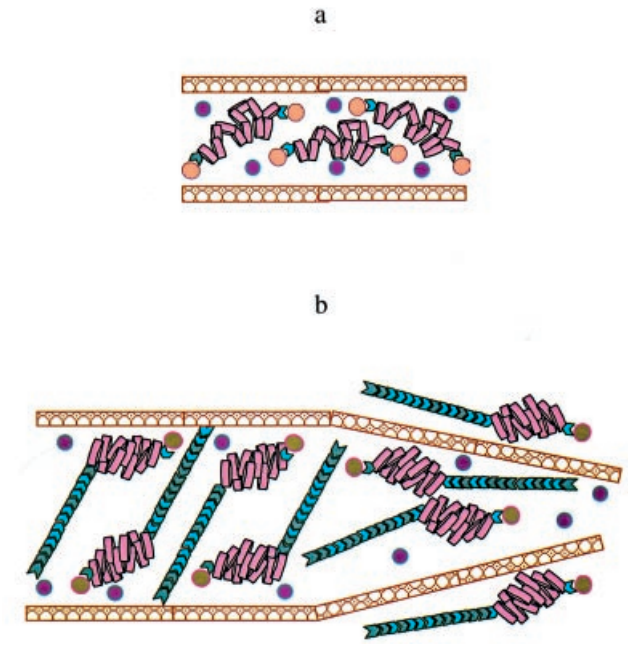

Figure 8. Proposed models for the [CuCr] LDH nanocomposites incorporating (a) PEG-DC and (b) PEG-AS

adopt a highly confined arrangement within the layers of the [ZnCr] LDH structure. For the polymer with 7 EOUs, the situation is slightly modified to 3.12 and 3.07 nm, respectively (Table 2).

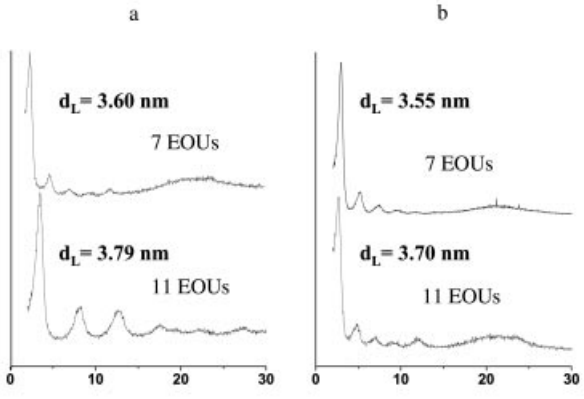

Figure 9. XRD patterns of nanocomposites prepared by ion-exchange reaction of PEG-AS of different EOUs (*n*) with (a) [CuCr] and (b) [ZnCr]; the values of *n* are displayed

The small difference between the variation of basal spacing from 7 to 11 EOUs for the PEG-AS/LDH nanocomposites cannot be explained by the increase in size of the polyoxyethylene chain. This fact proves that the polyoxyethylene chains are not directly contributing to the expansion of the interlayer space available for the molecule. These results are supported by a model in which the polyether chain interacts with the corrugated [CuCr] LDH inner-surface, with the alkyl tails dangling in the interlayer space

(Figure 8b). Qualitatively, this is the same as a polymer literally gluing the inner and outer surface of the matrix, as illustrated by SEM micrographs (Figure 7) and as pointed out by the adsorption measurements, which indirectly give rise to a large surface covered by the mono-functional guest molecule. The existence of such an interaction might also be the cause of a break in the polyether chain that originates, in certain cases, in the presence of carbonyl functions, as deduced from IR and NMR spectroscopic studies and consistent with the observations of other authors.[19]

Conclusion

This paper provides clear evidence of the intercalation of the mono- and bifunctional molecules, PEG-DC and PEG-AS polymers, containing flexible oxyethylene groups between the sheets of LDH [CuCr]. For the macromolecule PEG-DC, the basal spacing of the hybrid phase is small, and has to be explained by assuming a highly distorted helical situation for the polyoxyethylene chain. For PEG-AS, the polymer chain must be in a helical symmetry, although complementary results gathered by FTIR and NMR spectroscopy seem to indicate the presence of additional intricate effects. From these results, we assume that the polyether chain must interact strongly with the LDH layers, giving rise to a distribution of chemical shifts depending on the orientation of the helix with the positively charged layers.

Experimental Section

All the reagents are of analytical grade: $CuCl_2{\cdot}2H_2O$, CuO, $CrCl_3{\cdot}6H_2O$, $ZnCl_2$, NaOH and BuOH are commercial products from Aldrich. Water soluble polymers (Table 1), potassium poly(ethylene glycol) (ca. 7 and 11 ethylene oxide units, EOUs) −[*n*-alkyl(C_{13}−C_{15})− (3-sulfopropyl diether] salt [$R(OCH_2CH_2)_nO(CH_2)_3SO_3$]K, noted as PEG-AS-*n* of 7 or 11 EOUs, respectively], poly(ethylene glycol)dicarboxylic acid [$HO_2C(CH_2OCH_2)_nCO_2$ H, average M_n 600, $n \approx 12$ EOUs − noted as PEG-DC] are available from Aldrich. Deionized water was used for the synthesis and washing procedures.

LDH starting material, [CuCr] of general composition $Cu_2Cr(OH)_6Cl{\cdot}nH_2O$ was prepared by either co-precipitation or salt-oxide methods.[20] For the former, the solutions of transition metal chlorides were slowly added at a controlled pH of 4.9 ($CuCl_2$: 10^{-2} M, $CrCl_3$: 5×10^{-3} M).[20a] For the second preparation, $CrCl_3$ was added to a solution containing CuO that was finely dispersed in water by sonication.[20b] The resulting precipitates were kept overnight in the mother liquor for aging, then separated by three repeated washing/centrifugation cycles and, finally, dried in air at room temperature. In the present study, the second method was preferred, giving rise to more crystalline materials. Co-precipitation was used for the templating reaction (see below). $Zn_2Cr(OH)_6Cl{\cdot}nH_2O$ LDH material, noted as [ZnCr], was prepared by the co-precipitation method at a constant pH of 5.5.

Intercalation of the Polymers

1) Direct exchange was performed as follows: the LDH material (30 mg) was ultrasonicated (5 minutes) in decarbonated water (25 mL) and added to a solution containing the polymer neutralized at pH 7. The amount of dissolved polymer corresponded to two to five times the anionic exchange capacity (AEC) of the LDH material (270 mequiv. per 100 g for [CuCr]). The exchange reaction was performed under nitrogen gas for 3 to 12 h. The resulting powder was centrifuged, washed several times and finally dried at room temperature. In some cases, a mixture of solvents [such as H_2O/MeOH,H_2O/EtOH (1:1)] was used instead of pure water.
2) The method defined as "solvent-assisted preparation", consists of dispersing the LDH sample into butanol. The exchange was then carried out under reflux conditions at 90 °C with vigorous stirring.
3) Co-precipitation is an approach similar to the "templating" method used by Oriaki et al.[5b] for the incorporation of polysulfonated polymers. The hybrid LDH phase was synthesized in the presence of the polymer previously dissolved in aqueous solution (the amount of polymer corresponds to twice the AEC of the solid which, hypothetically, results in the complete formation from the initial salts concentration) on adjusting the pH to 7.0.

The adsorption isotherms were measured by the batch equilibration technique. Thus, a known amount of hydrotalcite-like material (ca. 50 mg) was sonically dispersed in 25 mL of deionized water and then kept in contact with the polymer solution at 25 °C for 24 h. The polymer concentration ranged from 10^{-4} to 5×10^{-2} M. The amount of organic matter adsorbed by the solid, expressed in mmol per gram of LDH (q_e), was determined from HCN elemental microanalyses. The final concentration (C_e, adsorbate concentration at equilibrium after a contact time of 24 hours) was determined by subtracting the quantity of polymer (m) retained by the solid from the total content in the original solution: $C_e = (C_i \times V - q_e \times m)/V$. The adsorption isotherms were obtained by plotting q_e versus C_e (relative error $< 1\%$).

Elemental chemical analysis of the LDH materials was performed using the inductive conduction plasma coupled to atomic emission spectroscopy (ICP/AES) at Center d'Analyse de Vernaison, France. The organic content was determined by conventional HCN chemical analysis (Perkin−Elmer 240C). Materials were characterized by the XRD technique with a D500 Siemens or a Philips 1710 spectrometer, both operating with Cu-K_α radiation. FTIR was performed with a Nicolett 20SXC apparatus employing the KBr dilution technique for solid samples. SEM observations were performed on a SEM-EDX microscope (Zeiss DSM 960) operating at 15.0 kV. ^{13}C solid-state NMR spectroscopy experiments were performed with a 300 Bruker spectrometer at 75.47 MHz, using a 4-mm diameter zirconia rotor and working under magic angle spinning (MAS) condition of 10 kHz. A second spectrometer 400 Bruker (^{13}C Larmor frequency of 100.63 MHz) was also employed. ^{13}C spectra obtained by the proton-enhanced cross-polarization method (CP) were referenced to the carbonyl of the glycine calibrated at $\delta = 176.03$ ppm or tetramethylsilane (TMS).

Acknowledgments

The authors would like to thank Pr. C. Forano for fruitful discussions and Dr. I. Sobrados and Mr. F. Pinto for helpful assistance in the NMR spectroscopic study and SEM characterization, respectively. F. L and P. A. thank the CNRS and CSIC for a French−Spanish cooperation grant (France n°7945, Spain 2000FR0024) and to the CICYT (Spain, MAT2000-1585-C03-01 and MAT2000-1451 projects) for financial support.

[1] [1a] S. Komarni, *J. Mater. Chem.* **1992**, *2*, 1219−1230. [1b] E. Ruiz-Hitzky, *Adv. Mater.* **1993**, *5*, 334−340. [1c] E. Giannelis,

Adv. Mater. **1996**, *8*, 29−35. [1d] B. M. Novak, *Adv. Mater.* **1993**, *5*, 422−433. [1e] G. Lagaly, *Appl. Clay Sci.* **1999**, *15*, 1−9. [1f] *Polymer-Clay Nanocomposites* (Eds.: T. J. Pinnavaia & G. W. Beall), John Wiley & Sons, West Sussex, **2000**.

[2] [2a] E. Ruiz-Hitzky, *Mol. Cryst. Liq. Cryst.* **1988**, *161*, 433−452. [2b] Z. Wang, T. Lan, T.J. Pinnavaia, *Chem. Mater.* **1996**, *8*, 2200−2204. [2c] J. Bujdak, E. Hackett, E. P. Giannelis, *Chem. Mater.* **2000**, *12*, 2168−2174.

[3] A. Vaccari, *Applied Clay Science* **1999**, *14*, 161−198.

[4] J.-H. Choy, S.-Y. Kwak, J.-S. Park, Y.-J. Jeong, J. Portier, *J. Am. Chem. Soc.* **1999**, *121*, 1399−1400.

[5] [5a] P. B. Messersmith, S. I. Stupp, *Chem. Mater.* **1995**, *7*, 454−460. [5b] C. O. Oriakhi, I. V. Farr, M. M. Lerner, *J. Mater. Chem.* **1996**, *6*, 103−107. [5c] S. Rey, J. Mérida-Robles, K.-S. Han, L. Guerlou-Demourgues, C. Delmas, E. Duguet, *Polym. Int.* **1999**, *48*, 277−282. [5d] F. Leroux, J.-P. Besse, *Chem. Mater.* **2001**, *13*, 3507−3515.

[6] [6a] P. Aranda, E. Ruiz-Hitzky, *Adv. Mater.* **1990**, *2* 545−547. [6b] P. Aranda, E. Ruiz-Hitzky, *Chem. Mater.* **1992**, *4*, 1395−1403. [6c] P. Aranda, E. Ruiz-Hitzky, *Appl. Clay Sci.* **1999**, *15*, 119−135.

[7] [7a] Y.-J. Liu, D. C. DeGroot, J. L. Schindler, C. R. Kannewurf, M. G. Kanatzidis, *Chem. Mater.* **1991**, *3*, 992−994. [7b] E. Ruiz-Hitzky, P. Aranda, B. Casal, *J. Mater. Chem.* **1992**, *2*, 581−582. [7c] Y.-J. Liu, J. L. Schindler, D. C. DeGroot, C. R. Kannewurf, W. Hirpo, M. G. Kanatzidis, *Chem. Mater.* **1996**, *8*, 525−534.

[8] [8a] L. F. Nazar, H. Wu, W. P. Power, *J. Mater. Chem.* **1995**, *5*, 1985−1993. [8b] L. Wang, J. Schindler, C. R. Kannewurf, M. G. Kanatzidis, *J. Mater. Chem.* **1997**, *7*, 1277−1283.

[9] [9a] E. Ruiz-Hitzky, P. Aranda, *Anales Química Int. Ed.* **1997**, *93*, 197−212. [9b] E. Ruiz-Hitzky, P. Aranda, in *Polymer-Clay Nanocomposites* (Eds.: T. J. Pinnavaia & G.W.Beall), John Wiley & Sons, West Sussex **2000**, pp. 19−46.

[10] [10a] W. H. T. Davison, *J. Chem. Soc.* **1955**, 3270−3275. [10b] H. Tadokoro, Y. Chatani, T. Yoshihara, S. Tahara, S. Murahashi, *Makromol. Chem.* **1964**, *73*, 109−127. [10c] B. L. Papke, M. A. Ratner, D. F. Shriver, *J. Phys. Chem. Solids* **1981**, *42*, 493−500.

[11] H. Roussel, V. Briois, E. Elkaïm, A. de Roy, J.-P. Besse, *J. Phys. Chem. B* **2000**, *104*, 5915−5923.

[12] H. Kopka, K. Beneke, G. Lagaly, *J. Colloid Interface Sci.* **1988**, *123*, 427−436.

[13] [13a] M. Adachi-Pagano, C. Forano, J.-P. Besse, *Chem. Com.* **2000**, 91−92. [13b] F. Leroux, M. Adachi-Pagano, M. Intissar, S. Chauvière, C. Forano, J.-P. Besse, *J. Mater. Chem.* **2001**, *11*, 105−112. [13c] T. Hibino, W. Jones, *J. Mater. Chem.* **2001**, *11*, 1321−1323.

[14] M. Meyn, K. Beneke, G. Lagaly, *Inorg. Chem.* **1990**, *29*, 5201−5207.

[15] C. H. Giles, T. H. MacEwan, S. N. Nakhwa, D. Smith, *J. Chem. Soc.* **1960**, 3973−3993.

[16] [16a] R. Calvet, *Environmental Health Perpectives* **1989**, *83*, 145−177. [16b] Y. Yu, Y.-Y. Zhuang, Z.-H. Wang, *J. Colloid Inter. Sci.* **2001**, *242*, 288−293. [16c] F. A. Banat, B. Al-Bashir, S. Al-Ashed, O. Hayajneh, *Environ. Pollution* **2000**, *107*, 391−398.

[17] [17a] Y. Komori, K. Sugahara, K. Kuroda, *Chem. Mater.* **1999**, *11*, 3081−3085. [17b] E. M. Moujahid, J. Inacio, J.-P. Besse, F. Leroux, *J. Mater. Chem.* **2002**, *12*, 3324−3330.

[18] [18a] M. Vucelic, G. D. Moggridge, W. Jones, *J. Phys. Chem.* **1995**, *99*, 8328−8337. [18b] A. S. Bookin, V. I. Cherkashin, V.A. Drits, *Clays Clay Miner.* **1993**, *41*, 558−564.

[19] [19a] L. Costa, A.M. Gad, G. Camino, *Macromolecules* **1992**, *25*, 5512−5518. [19b] C. Wilheilm, J.-L. Gardette, *Polymer* **1998**, *39*, 5973−5980. [19c] S. Morlat, J.-L. Gardette, *Polymer* **2001**, *42*, 6071−6079.

[20] [20a] S. Miyata, *Clays Clay Miner.* **1983**, *31*, 305−311. [20b] A. De Roy, C. Forano, K. El Malki, J.-P. Besse, in *Synthesis of Microporous Materials Vol. II. Expanded Clays and Other Microporous Solids* (Eds.: L. Occelli, H. Robson), Van Nostrand Reinhold, New York, **1992**, pp. 108−169.

Received June 19, 2002
[I02325]

Synthesis of Tetrahemispheraplexes with Ammonium, Alkylammonium or Alkaline Metal Ions as Exohedral Guests via Self-Assembly or Guest Exchange

Rolf W. Saalfrank,* Bernhard Demleitner, Horst Glaser, Harald Maid, Stefan Reihs, Walter Bauer, Monica Maluenga, Frank Hampel, Markus Teichert, Harald Krautscheid

Keywords: Cage compounds / Supramolecular chemistry / Magnesium / Host-guest chemistry

In the printed article,[1] *the stereo views of Figure 1 on page 824 and Figures 2 and 3 on page 826 have erroneously been expanded horizontally, thus causing difficulties in obtaining the intended 3D impression. Therefore, Figures 1−3 are reproduced here with the correct separation. The electronic version is not affected by this error.*

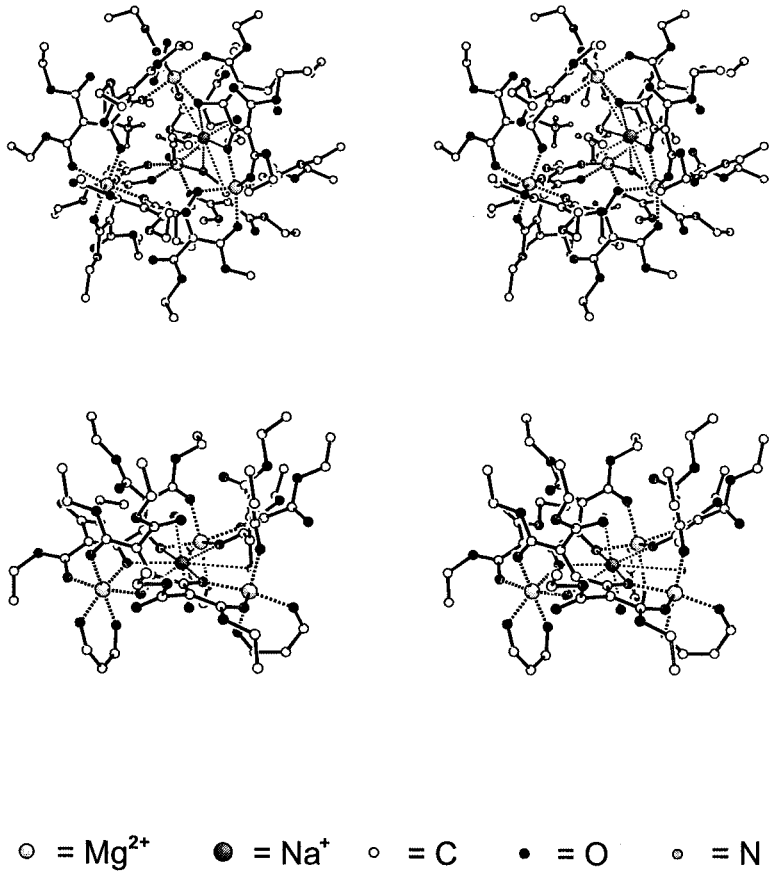

Figure 1. (Stereo view): Top: Structure of {$Na(Et\text{-}NH_3)_3 \cap [Mg_4(L^2)_6]$} **4** ($L^2$: R = Et) in the crystal. Bottom: Selected tetrahedral face highlighting its metalla-coronate character. Solvent molecules and hydrogen atoms except ammonium hydrogens are not depicted for clarity

 © 2003 WILEY-VCH Verlag GmbH & Co. KGaA, 69451 Weinheim 1434−1948/03/0306−1253 $ 20.00+.50/0

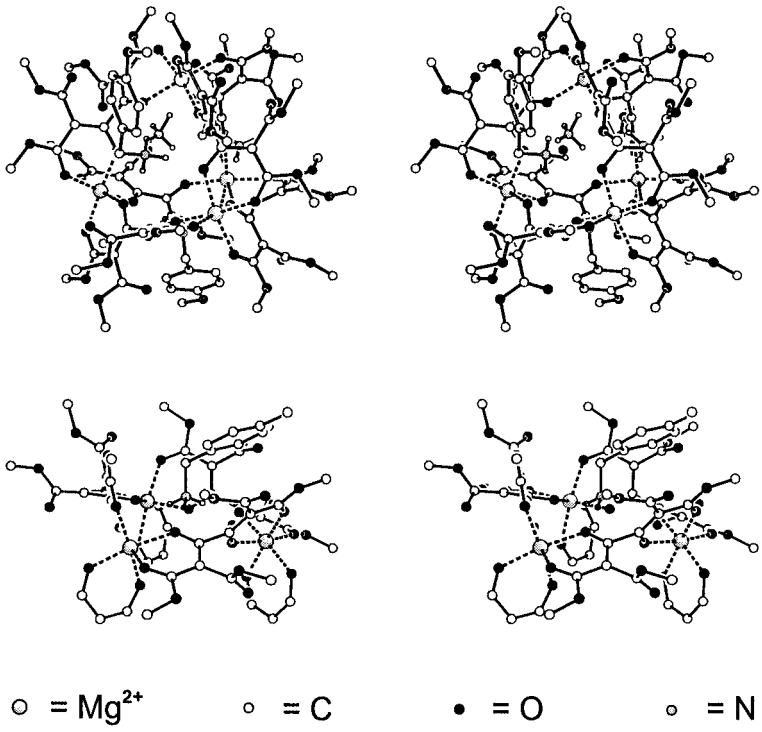

Figure 2. (Stereo view): Top: Structure of $\{(NH_4)_2(R^2-NH_3)_2\cap[Mg_4(L^1)_6]\}$ **6** (L^1: R = Me; R^2 = *p*-$MeOC_6H_4CH_2$) in the crystal. Bottom: Selected tetrahedral face hosting *p*-methoxybenzylammonium. Solvent molecules and hydrogen atoms except ammonium hydrogens are not depicted for clarity

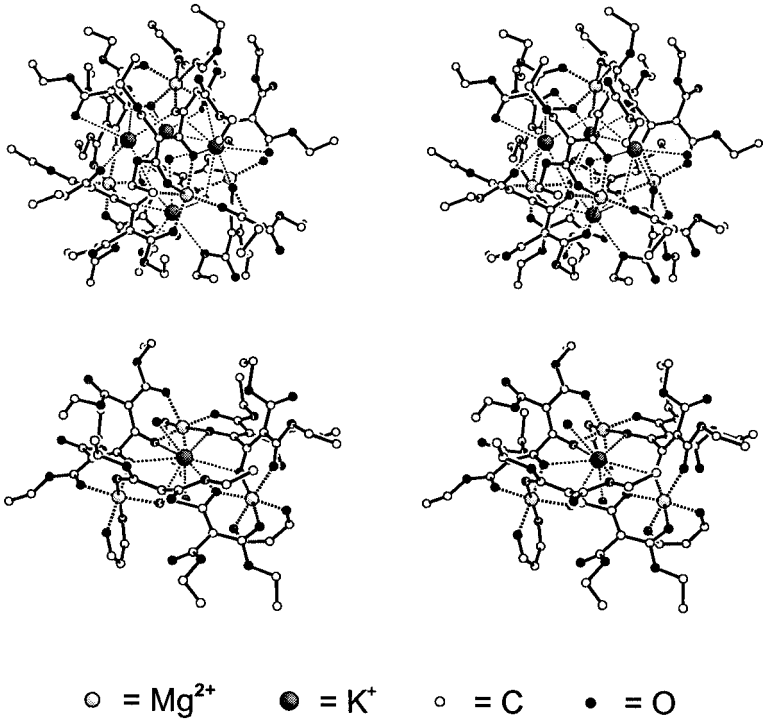

Figure 3. (Stereo view): Top: Structure of $\{K_4\cap[Mg_4(L^2)_6]\}$ **7a** (L^2: R = Et) in the crystal. Bottom: Selected tetrahedral face highlighting its metalla-coronate character. Solvent molecules and hydrogen atoms are not depicted for clarity

[1] R. W. Saalfrank, B. Demleitner, H. Glaser, H. Maid, S. Reihs, W. Bauer, M. Maluenga, F. Hampel, M. Teichert, H. Krautscheid, *Eur. J. Inorg. Chem.* **2003**, 822−829.

The Editors
[I02474C]

EurJIC
European Journal of Inorganic Chemistry

April 2003
Issue 7
Pages 1255–1468

Papers available ahead of print in Early View at www.interscience.wiley.com

Earliest available Table of Contents:
Automatically, free of charge by e-mail through
www.interscience.wiley.com/alerts

COVER PICTURE

The cover picture shows the X-ray structure of [Pd(Et_2timdt)-Br_2] (left; Et_2timdt = diethylimidazolidine-2,4,5-trithione), obtained by treating the symmetrically substituted dithiolene [Pd(Et_2timdt)$_2$] with Br_2 or IBr. This complex has been exploited as a starting material for the synthesis of the new mixed-ligand, push-pull dithiolene [Pd(Et_2timdt)(mnt)] (mnt = maleonitriledithiolate), whose X-ray molecular structure is depicted on the right. Details are discussed in the Short Communication by M. Arca et al. on p. 1291 ff.

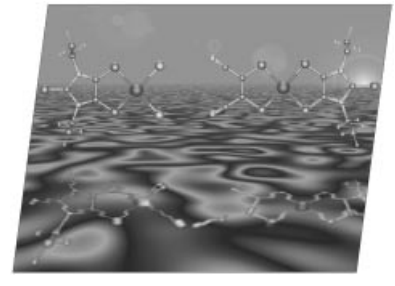

MICROREVIEW

Contents

1271 **R. Llusar,* S. Uriel**

Heterodimetallic Chalcogen-Bridged Cubane-Type Clusters of Molybdenum and Tungsten Containing First-Row Transition Metals

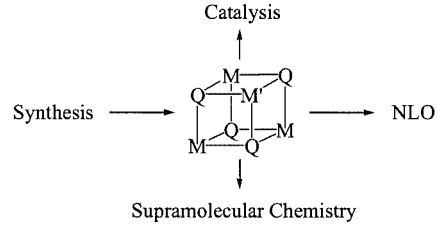

Keywords: Molybdenum / Tungsten / Cluster compounds / Sulfur / Selenium / Heterometallic complexes

 © 2003 WILEY-VCH Verlag GmbH & Co. KGaA, 69451 Weinheim 1434–1948/03/0407–1259 $ 20.00+.50/0

SHORT COMMUNICATIONS

1291 **M. C. Aragoni, M. Arca,* C. Denotti, F. A. Devillanova, E. Grigiotti, F. Isaia, F. Laschi, V. Lippolis, L. Pala, A. M. Z. Slawin, P. Zanello, J. D. Woollins**

A Facile Synthesis of a Push-Pull Mixed-Ligand Pd-Dithiolene Complex Containing the Et_2timdt Ligand (Et_2timdt = Monoreduced Diethyl-imidazolidine-2,4,5-trithione)

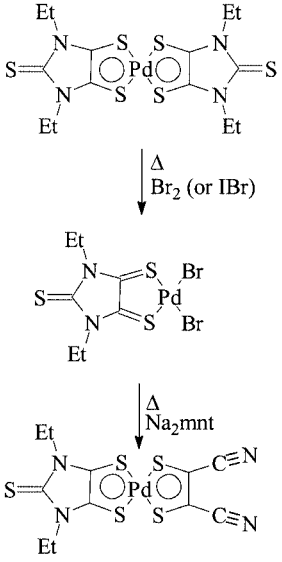

Keywords: Palladium / Halogenation / S ligands / Density functional calculations / Non-linear optics

1296 **E. Theunissen, C. E. A. Kirschhock, S. P. B. Kremer, D. D. Habermacher, J. A. Martens***

Preferential Siting of Iron Atoms in an MFI-type Ferrisilicate Zeolite Framework: An Attempt to Explain Experimental Data with TPA-Silicate Solution Chemistry

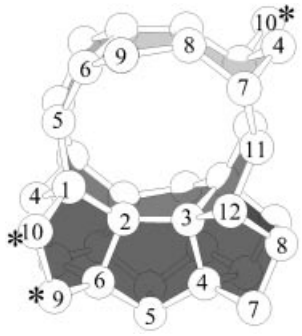

Keywords: Zeolites / Transition metals / Iron / X-ray diffraction

1299 **C. Klein, E. Graf, M. W. Hosseini,* A. De Cian, N. Kyritsakas**

Design and Structural Analysis of Metalla-macrocycles Based on Zinc Halides and a V-Shaped Bismonodentate Ligand of the Cyclophane Type

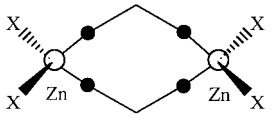

Keywords: Cyclophanes / Pyridine / Zinc / Metallacycles

1303 **D. Sun, R. Cao,* Y. Sun, W. Bi, M. Hong**

A Novel Open-Framework Gallium Phosphate Containing Two Different Building Units

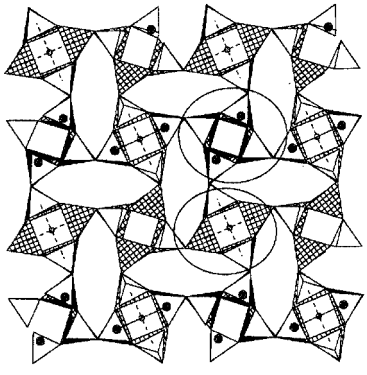

Keywords: Zeolite analogues / Gallium / Phosphates / Alkali metals / Fluorides

FULL PAPERS

1307 **A. Eichhöfer,* O. Hampe, M. Blom**

Synthesis, Structures, and Properties of a Series of $[Cd_8Se(SePh)_{12}Cl_4]^{2-}$ Cluster Compounds with Different Counterions

Keywords: Cluster compounds / Cadmium / Selenium / X-ray diffraction / UV/Vis spectroscopy / Mass spectrometry

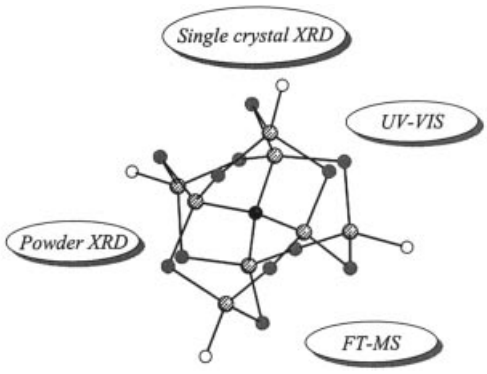

1315 **R. Vivas-Reyes, F. De Proft, M. Biesemans, R. Willem, P. Geerlings***

A DFT Study of Tin- and Crown-Ether-Based Host Molecules Capable of Binding Anions and Cations Simultaneously

Keywords: Acidity / Basicity / Crown compounds / Density functional calculations / Host-guest systems / Tin

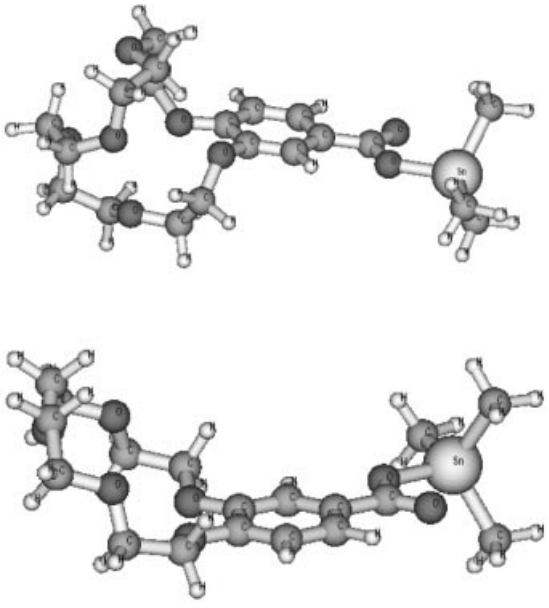

1325 **B. F. G. Johnson,* S. Hermans, T. Khimyak**

Synthesis and Structure of Two New High Nuclearity Ru/Pt Mixed-Metal Clusters

Keywords: Cluster compounds / Ruthenium / Platinum / Heterometallic complexes / Bridging ligands

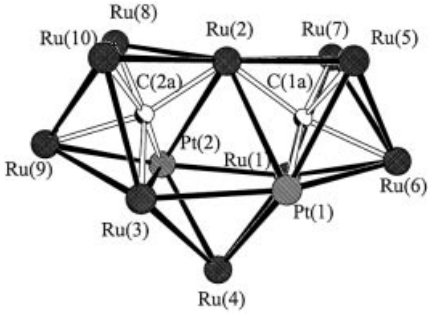

1332 **D. Imbert, N. Fatin-Rouge, J.-C. G. Bünzli***

Lanthanide Chelates Based on Diethylenetriamine Fitted with *O*-Benzoic Acid Pendant Arms

Keywords: Carboxylate ligands / Lanthanides / Luminescence / Podand / Stability constant

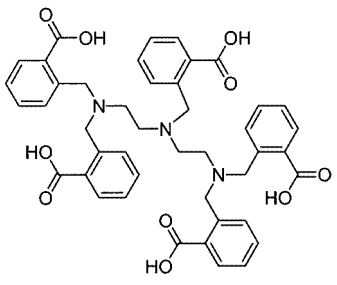

1340 **K. Hegetschweiler,* O. Maas, A. Zimmer, R. J. Geue, A. M. Sargeson, J. Harmer, A. Schweiger, I. Buder, G. Schwitzgebel, V. Reiland, W. Frank**

The Coordination Chemistry of the Pentadentate 2,2,6,6-Tetrakis(aminomethyl)-4-azaheptane (ditame)

Keywords: Amine ligands / Chelates / Ligand design / Stability constants

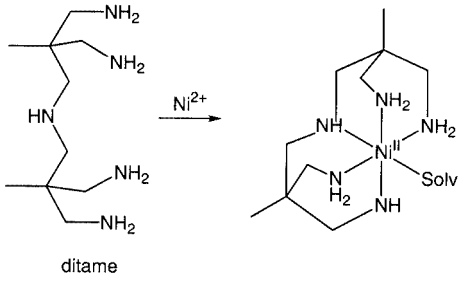

1355 **Y.-B. Wang, X.-J. Zheng, W.-J. Zhuang, L.-P. Jin***

Hydrothermal Synthesis and Characterization of Novel Lanthanide 2,2′-Diphenyldicarboxylate Complexes

Keywords: Hydrothermal synthesis / Lanthanides / Coordination polymer / X-ray diffraction

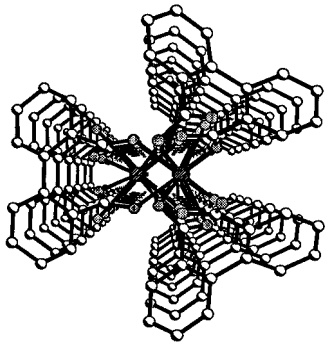

1361 **L. Balazs, H. J. Breunig,* E. Lork, C. Silvestru**

Low-Valent Organobismuth Compounds with Intramolecular Coordination: *cyclo*-R_3Bi_3, *cyclo*-R_4Bi_4, $RBi[W(CO)_5]_2$, and R_4Bi_2 [R = 2-$(Me_2NCH_2)C_6H_4$]

Keywords: Bismuth / Metallacycles / Tungsten

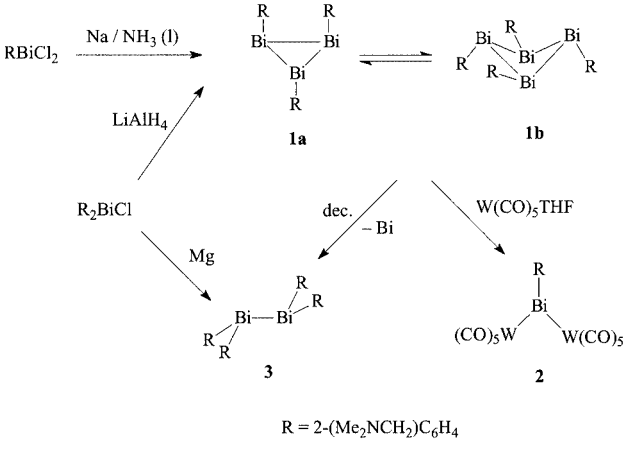

1366 **R. D. Gougeon,* M. Soulard, M. Reinholdt, J. Miehé-Brendlé, J.-M. Chézeau, R. Le Dred, R. Marchal, P. Jeandet***

Polypeptide Adsorption on a Synthetic Montmorillonite: A Combined Solid-State NMR Spectroscopy, X-ray Diffraction, Thermal Analysis and N_2 Adsorption Study

Keywords: Peptides / Adsorption / Clays / NMR spectroscopy / X-ray diffraction

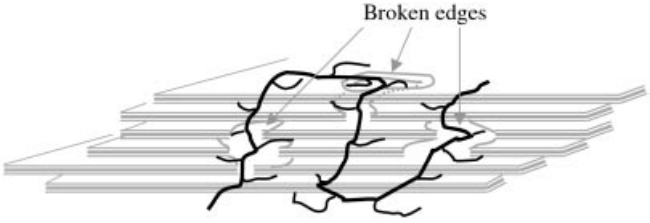

1373 **M. P. Suh,* K. S. Min, J. W. Ko, H. J. Choi**

Assembly of Hydrogen-Bonded Organic Layers with Macrocyclic Complexes Acting as Pillars

Keywords: Hydrogen bonds / Layered compounds / Macrocyclic ligands / Nickel / Self-assembly

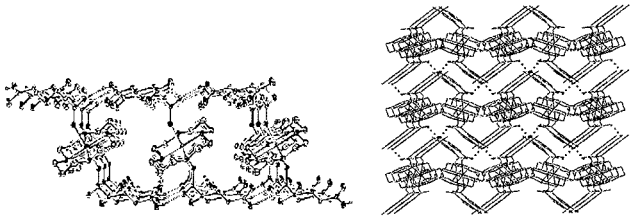

1 **2**

1380 **H.-F. Klein,* R. Beck, U. Flörke, H.-J. Haupt**

Five- and Six-Membered Cobaltocycles with C,P-Chelating Ligands through Regiospecific Cyclometalation of Mono(2-Substituted) Triphenylphosphane

Keywords: Chelates / Cobalt / Metalation / Metallacycles / Structure elucidation

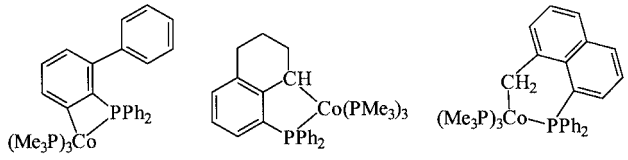

1388 **S. M. Cendrowski-Guillaume,* G. Le Gland, M. Nierlich, M. Ephritikhine***

A Comparison of Analogous 4f- and 5f-Element Compounds: Syntheses and X-ray Crystal Structures of the Mixed Sandwich Complexes $[M(\eta\text{-}C_8H_8)(L)\{OP(NMe_2)_3\}]$ (M = Nd or U; L = $\eta\text{-}C_5Me_5$ or $\eta\text{-}C_4Me_4P$)

Keywords: Cyclopentadienyl ligands / P ligands / Lanthanides / Actinides / Sandwich complexes

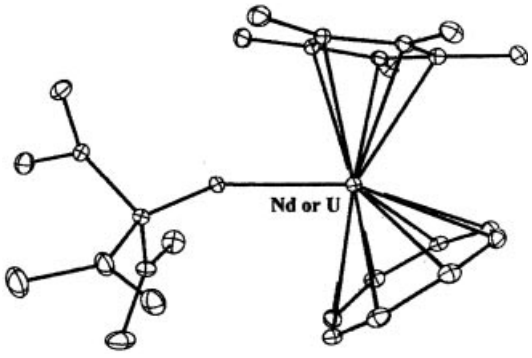

1394 **G. Aromí, P. Gamez, H. Kooijman, A. L. Spek, W. L. Driessen, J. Reedijk***

Two New Dinuclear Sterically Crowded Cu^{II} Complexes as Catalyst Precursors for the Oxidative Coupling of 2,6-Dimethylphenol

Keywords: Copper / N ligands / Homogeneous catalysis / Oxidations

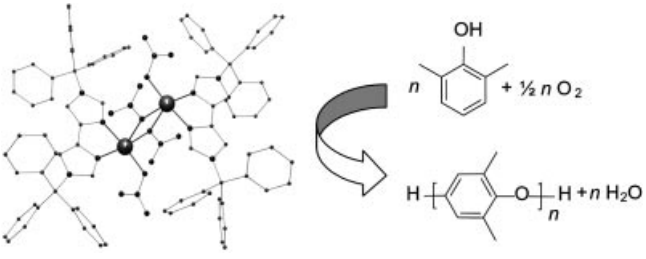

1401 **S. Autzen, H.-G. Korth, R. Boese, H. de Groot,* R. Sustmann***

Studies of Pyridinyl-Containing 14-Membered Macrocyclic Copper(II) Complexes

Keywords: Macrocyclic ligands / Copper / Enzyme models / Superoxide dismutase

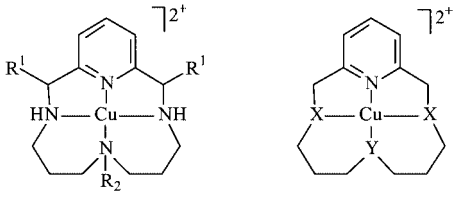

R^1 = H, Me
R^2 = H, 2-MeO-C_6H_4-CH_2

X = O, NH
Y = O, NH

1411 **S. Schlecht,* K. Friese**

Direct Synthesis of $(PhSe)_4Ge$ and $(PhTe)_4Ge$ from Activated Hydrogenated Germanium – Crystal Structure and Twinning of $(PhTe)_4Ge$

Keywords: Germanium / Tellurium / Van der Waals interactions / Active metals

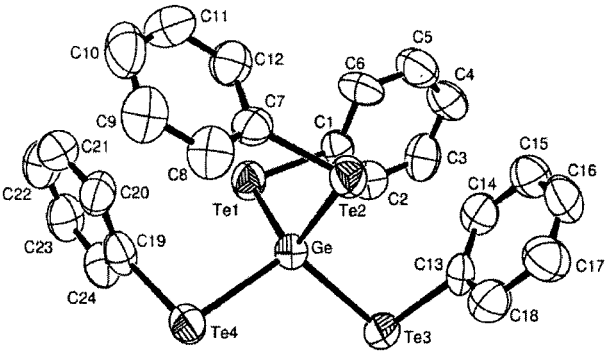

1416 **J. P. Dunne, M. Tacke,* C. Selinka, D. Stalke**

Arylcalcium Hydrides as Precursors to Alkoxides and Aryloxides of Calcium

Keywords: Calcium / C–H activation / Cocondensation / Hydrides

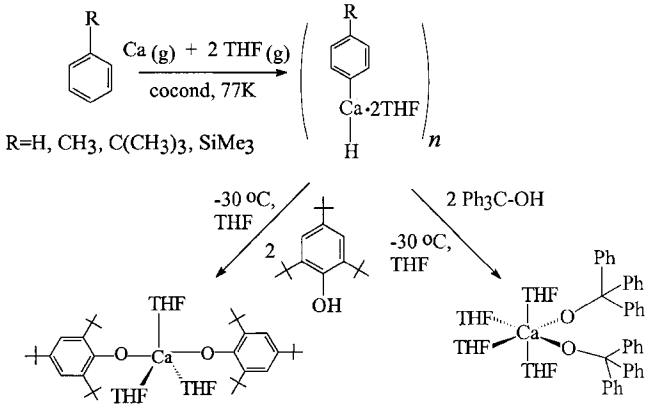

1426 **O. V. Pryma, S. R. Petrusenko,* V. N. Kokozay, B. W. Skelton, O. V. Shishkin, T. S. Teplytska**

A Facile Direct Synthesis of Bimetallic $Cu^{II}Zn^{II}$ Complexes with Ethylenediamine Revealing Different Types of Chain Crystal Structures

Keywords: Heterometallic complexes / Copper / Zinc / N ligands

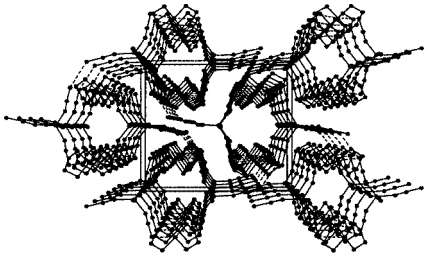

1433 **A. D. Burrows,* R. W. Harrington, M. F. Mahon, S. J. Teat**

Structural Manipulation of Hydrogen Bond Networks Using Sulfonated Phosphane Ligands and Their Complexes: Competition and Interplay Between Strong and Weak Hydrogen Bonds

Keywords: Crystal engineering / Phosphane ligands / Hydrogen bonds / X-ray crystal structures

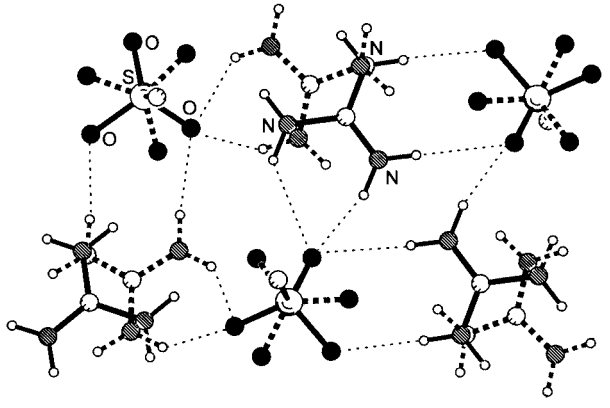

1440 **P.-C. Kuo, J.-H. Huang,* C.-H. Hung, G.-H. Lee, S.-M. Peng**

Synthesis and Characterization of Five-Coordinate Gallium and Indium Complexes Stabilized by Tridentate, Substituted Pyrrole Ligands

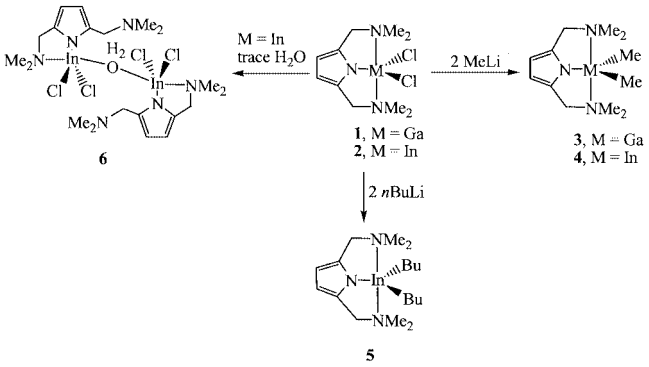

Keywords: Gallium / Indium / N ligands / Bridging ligands

1445 **I. Mayer,* O. Jacobsohn, T. Niazov, J. Werckmann, M. Iliescu, M. Richard-Plouet, O. Burghaus, D. Reinen**

Manganese in Precipitated Hydroxyapatites

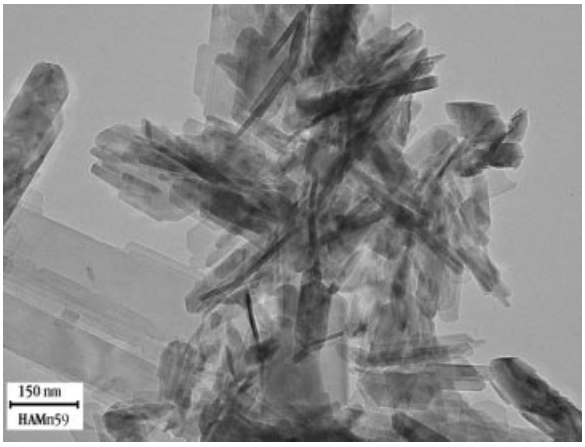

Keywords: Manganese / Hydroxyapatite / EPR spectroscopy / Thermal properties

1452 **A. Penoni, R. Wanke, S. Tollari, E. Gallo, D. Musella, F. Ragaini, F. Demartin, S. Cenini***

Cyclopropanation of Olefins with Diazoalkanes, Catalyzed by Co^{II}(porphyrin) Complexes − A Synthetic and Mechanistic Investigation and the Molecular Structure of $Co^{III}(TPP)(CH_2CO_2Et)$ (TPP = Dianion of *meso*-Tetraphenylporphyrin)

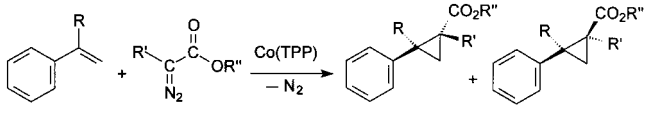

Keywords: Cobalt / Cyclopropanation / Olefins / Porphyrinoids

1461 **P. Kilian, P. Bhattacharyya, A. M. Z. Slawin, J. D. Woollins***

Phosphorus-Selenium Heterocycles from the Tetraphospholane $(PhP)_4CH_2$

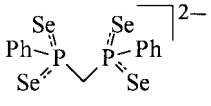

Keywords: Phosphanes / Heterocycles / Isomers / Phosphorus / Selenium

Heterodimetallic Chalcogen-Bridged Cubane-Type Clusters of Molybdenum and Tungsten Containing First-Row Transition Metals

Rosa Llusar*[a] and Santiago Uriel[b]

Keywords: Molybdenum / Tungsten / Cluster compounds / Sulfur / Selenium / Heterometallic complexes

Transition metal cluster chalcogenides with cubane-type structures are relevant to our understanding of several industrial and biological catalytic processes. Recent advances in cluster chemistry owe much to the development of rational synthetic approaches, an aspect that is emphasised in this review which focuses on cuboidal clusters of molybdenum and tungsten (M) with $M_2M'_2S_4$ and $M_3M'Q_4$ (Q = S, Se) central units that incorporate a first-row transition metal atom (M′). Special attention has been paid to the non-aqueous chemistry of these compounds. The structural features of these complexes are discussed in relation to their electronic structures within the framework of molecular orbital theory, spectroscopic, magnetic and electrochemical experimental data. Finally, the importance of these clusters in catalysis, nonlinear optics and in the formation of supramolecular adducts is discussed.
(© Wiley-VCH Verlag GmbH & Co. KGaA, 69451 Weinheim, Germany, 2003)

Introduction

Transition metal chalcogenide clusters with a cubane-type structure, where the metal and chalcogen atoms occupy adjacent vertices in a cube, are a unique area within cluster chemistry. These compounds are of interest not only because of their contribution to the development of modern chemistry, but also for their potential use as models for various industrial and biological catalytic processes.[1−3] In addition, these complexes have recently been utilised as optical limiters and contrast agents.[4−7]

The first cuboidal cluster to be identified contained the Fe_4S_4 core, a redox-active unit present in the electron-transfer protein ferredoxin. In addition to this homonuclear system, several important metalloenzymes contain heteronuclear transition metal sites. For example, nitrogenase contains the unique Fe-Mo cofactor, which is a major part of the dinitrogen activation system. The characterisation of the Fe-Mo cofactor by X-ray diffraction techniques has

[a] Departament de Ciències Experimentals, Universitat Jaume I, Campus de Riu Sec, P. O. Box 224, 12080 Castelló, Spain
Fax: (internat.) + 34-964/728066
E-mail: llusar@exp.uji.es
[b] Departamento de Química Orgánica − Química Física, Centro Politécnico Superior, Universidad de Zaragoza, María de Luna 3, 50015 Zaragoza, Spain
Fax: (internat.) + 34-976/761879
E-mail: suriel@posta.unizar.es

Rosa Llusar was born in Almenara (Spain). She studied chemistry at the University of Valencia (Spain) and received Ph.D. degrees from Valencia University in 1987 and from Texas A&M University (USA) in 1988 under the guidance of Prof. F. Albert Cotton. After working for industry for three years, she spent one year (1992) with Prof. John D. Corbett at the Ames Laboratory (Iowa State University, USA). Since 1993, she has held a position at the University Jaume I of Castelló (Spain) and became Associate Professor of Physical Chemistry in 1995. Her research has focussed on the chemistry of transition metal clusters, especially the relationship between their molecular and electronic structures and their properties.

Santiago Uriel was born in Madrid (Spain). He received his PhD degree in 1992 from Zaragoza University. His doctoral work, under the supervision of Dr. J. Garín, dealt with the synthesis of new (aminomethyl)tetrathiafulvalene derivatives. He then spent three years with Dr. Patrick Batail, first at Laboratoire de Physique the Solides of the University of Paris XI (Orsay) supported by an E. U. Human Capital and Mobility fellowship, and subsequently at the Institut de Matériaux de Nantes as Research Associate at the Centre National de la Recherche Scientifique. He worked on the molecular chemistry of octahedral rhenium clusters and their association within organic-inorganic materials. He joined the research group of Dr. R. Llusar in 1997 at the Jaume I University of Castellón (Spain) supported by Ministerio de Educación y Ciencia and he is currently Profesor Asociado at the Organic Chemistry Department of the University of Zaragoza. His research interests include synthesis, structural chemistry and physical properties of transition metal molecular ions.

MICROREVIEWS: This feature introduces the readers to the authors′ research through a concise overview of the selected topic. Reference to important work from others in the field is included.

shown the presence of a $MoFe_7S_8$ core structure with two partial thiocubane substructures, each of which contains an open Fe_3 face.[8,9] Synthetic efforts to prepare chemical analogues of the cofactor have been extensively reviewed and will not be covered here.[10,11]

This review is limited to heterodimetallic cuboidal $M_2M'_2$ and M_3M' cluster chalcogenides of molybdenum and tungsten (M) that incorporate a first-row transition metal (M′). Heterodimetallic clusters with $M_2M'_2S_4$ and $M_3M'S_4$ cores (M′ = Ni, Co) are considered as discrete molecular models for substrate binding in the hydrodesulfurisation process (HDS), due to the fact that cobalt and nickel are known to act as promoters of the catalytic activity of the molybdenum sulfide industrial heterogeneous catalysts.[12] Sulfur- or selenium-containing transition metal clusters with MM'_3S_3Br or $M_3M'Se_4$ (M = Mo and W; M′ = Cu and Ag) cubane-like structures are also known to possess strong optical limiting effects.[4,5,13,14] In the past ten years, several review articles have appeared covering the most important aspects of the chemistry of molybdenum and tungsten transition metal chalcogenides.[1,15−19] Special attention has been given to the aqueous chemistry of heterodimetallic molybdenum and tungsten $M_3M'Q_4$ clusters that incorporate a second transition metal atom.[1,15,17,18]

In this work we place our emphasis on the non-aqueous chemistry of these complexes, a field of particular interest to us. In addition, we have included results reported on the $M_2M'_2S_4$ systems for comparative purposes. We have restricted M′ to the first-row transition elements, again motivated by our own research interests. The review is organised as follows. The first section provides a general overview of the synthesis, structure and electron counts of clusters with $M_2M'_2S_4$ and $M_3M'Q_4$ central units. Each subsection is defined based on the nature of the surrounding ligands around the group-6 metal atom. The next section discusses the electronic structure, electrochemistry and magnetism of these $M_2M'_2S_4$ and $M_3M'Q_4$ clusters. The final section deals with some selected properties that we have decided to emphasise, based on their potential applications such as catalysis, nonlinear optics and the capability of these cluster compounds to form supramolecular adducts.

Synthesis, Structure and Electron Counts

The development of the chemistry of transition metal clusters is closely related to the discovery of rational synthetic routes for the preparation of these compounds. In recent years, different strategies have evolved for the synthesis of molecular transition metal sulfide systems. These strategies can be roughly classified into six different categories: (i) spontaneous self-assembly where the structure of the reactant is not preserved in the final product; (ii) fragmentation of clusters of higher nuclearity; (iii) cluster excision from solid-state polymers; (iv) building-block synthesis from lower nuclearity species; (v) transmetallation or replacement of one metal atom by another, and (vi) substitution of peripheral ligands. The first two procedures suffer from the disadvantage that the structures of the products cannot be easily predicted.

The building-block approach has been the most widely used method for the construction of cuboidal heterodimetallic $M_2M'_2S_4$ and $M_3M'Q_4$ (Q = S, Se) cluster complexes. Using this approach, $M_2M'_2S_4$ complexes can be prepared from a dinuclear precursor and two mononuclear complexes according to the so-called [2 + 1 + 1] route, or from two dinuclear compounds according to a strategy designated as [2 + 2]. $M_3M'Q_4$ clusters can be prepared in an analogous fashion by adding a monomeric compound to a triangular metal complex, this method being termed a [3 + 1] synthesis. Scheme 1 gives a graphical representation of these three methods.

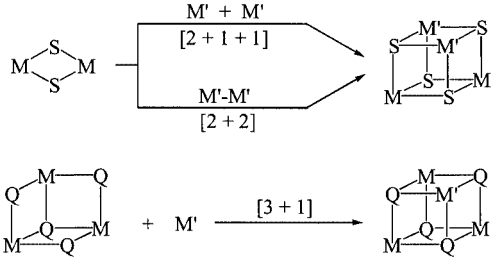

Scheme 1. Building-block synthetic methods for heterometallic cubane clusters

Once the heterodimetallic tetrameric unit has been formed, it can undergo different chemical transformations without changing its nuclearity. For example, one of the metal atoms can be substituted for a different metal atom (transmetallation) or the outer ligands can be replaced by other ligands (ligand substitution). In addition, the structure of the cluster core can rearrange in the presence of certain reagents.

The trinuclear and dinuclear precursors have been prepared by a variety of methods such as self-assembly, cluster fragmentation and cluster excision. This last method has represented a major advance in the field because it both allows the synthesis of previously inaccessible compounds and gives significant improvements in the yields of the cluster formation reactions. In this section we will first present details of the synthesis of the dinuclear or trinuclear precursors for each particular group of compounds, and then continue with a general description of the synthesis employed to obtain $M_2M'_2S_4$ and $M_3M'Q_4$ cluster complexes.

Clusters with $M_2M'_2S_4$ Central Units

A simplified representation of the structures of representative compounds with $Mo_2M'_2S_4$ and $W_2M'_2S_4$ cluster units is given in Figure 1. All structures have been drawn to emphasise the familiar thiocubane core and the coordination environments of the metal atoms. No analogous compounds of selenium have yet been reported to our knowledge. A summary of intermetallic distances for some representative cluster compounds within this series is given in Table 1.

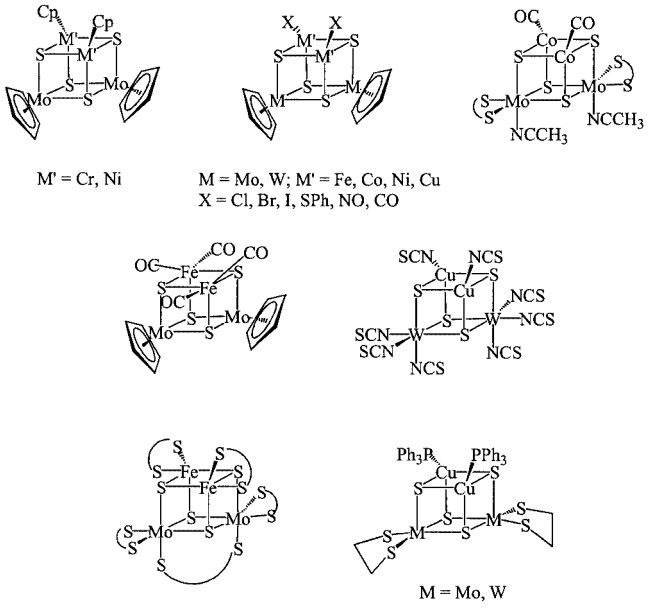

Figure 1. Schematic representations of the different coordination environments in $M_2M'_2S_4$ cubane-type clusters

Dimeric molybdenum and tungsten sulfur-rich complexes with cyclopentadienyl (Cp) and sulfur-containing ligands (dithiocarbamates, 1,2-dimercaptoethane or polysulfides) have been used as precursors for the synthesis of heterometallic $M_2M'_2S_4$ clusters through [2 + 1 + 1] or [2 + 2] building block strategies. These complexes behave as metalloligands towards heterometal atoms by using the lone-pair electrons of the sulfur atoms. The most widely used building block is the M_2S_4 unit, particularly the molybdenum- and tungsten(V) $[M_2S_2(\mu_2\text{-}S)_2]$ isomeric forms. Note however, that the tetrabridged molybdenum(IV) complex $[Mo_2(\mu_2\text{-}S)_2(\mu_2\text{-}SH)_2Cp_2]$ is often used for the synthesis of (cyclopentadienyl)molybdenum derivatives. The heterometal M′ is usually incorporated as a mononuclear or a dinuclear carbonyl complex except in the case of copper, where incorporation has always been accomplished by reaction with copper halides. The coordination environment of the heteroatom depends on the composition of the carbonylmetal compound.

$M_2M'_2S_4$ Clusters with Cyclopentadienyl Ligands

The dinuclear cyclopentadienyl building blocks $[M_2S_4Cp_2]$ are prepared by reaction of the molybdenum(I) or the tungsten(I) dinuclear complex $[MCp^*(CO)_2]_2$ with elemental sulfur in refluxing toluene to produce a mixture of isomers with metal atoms in oxidation states ranging from III to V.[34] The product distribution depends on the reaction conditions. Typical reaction yields for the $[M_2S_4Cp_2]$ dimer are 40% for Mo and 60% for W. In the case of tungsten, the *syn*-$[W_2S_2(\mu_2\text{-}S)_2]$ isomer is obtained in 54% yield, while the molybdenum analogue is produced in only 10% yield. Alternatively, the *trans*-$[Mo_2S_2(\mu_2\text{-}S)_2Cp^*_2]$ isomer can be prepared in 65% yield by treating the hydridomolybdenum complex $[MoCp^*H(CO)_3]$ with elemental sulfur in refluxing THF.[35] The preparation of the widely used $[Mo_2(\mu_2\text{-}S)_2(\mu_2\text{-}SH)_2Cp^{\#}_2]$ precursor is car-

Table 1. Selected bond lengths [Å] and infrared CO or NO stretching frequencies [cm^{-1}] for some representative $Mo_2M'_2S_4$ and $W_2M'_2S_4$ cubane-type clusters (standard deviations for averaged values are given in brackets)

Cluster	No. of metal electrons	M−M	M−M′	M′−M′	ν(CO) or ν(NO)[a] [b]	Ref.
Mo octahedral and M′ tetrahedral coordination:						
$[Mo_2Fe_2S_4Cp^*_2Cl_2]$	16	2.8219(7)	2.757[4]	2.791(1)	–	[20]
$[Mo_2Co_2S_4Cp^{Et}_2Cl_2]$	18	2.804(1)	2.756[5]	2.955(2)	–	[21]
$[Mo_2Co_2S_4Cp^{Et}_2I_2]$	18	2.803(1)	2.738[4]	2.936(1)	–	[21]
$[Mo_2Co_2S_4Cp^{Et}_2(PhS)_2]$	18	2.8156(3)	2.733[1]	2.7414(6)	–	[21]
$[Mo_2Fe_2S_4Cp^{Et}_2(NO)_2]$	20	2.8419(7)	2.7654[7]	2.704(1)	1736/1715	[22]
$[Mo_2Co_2S_4(S_2CNEt_2)_2(CH_3CN)_2(CO)_2]$	20	2.788(1)	2.676[6]	2.533(1)	1983/1960	[23]
$[Mo_2Co_2S_4Cp'_2(CO)_2]$	20	2.8313(5)	2.701[5]	2.5816(9)	1984/1965	[24]
$[Mo_2Co_2S_4Cp'_2(CO)_2]^-$	21	2.838(1)	2.739[9]	2.746(1)	1898/1865[b]	[25]
$[Mo_2Co_2S_4Cp^{Et}_2(CO)_2]^-$	21	2.846(1)	2.731[6]	2.735(1)	1902/1873[b]	[26]
$[Mo_2Co_2S_4Cp^{Et}_2(NO)_2]$	22	2.8135(6)	2.766[4]	3.116(1)	1747/1717	[22]
$[Mo_2Ni_2S_4Cp'_2(CO)_2]$	22	2.829(1)	2.722[2]	2.960(1)	1990/1970	[27]
$[Mo_2Cu_2S_4Cp^*_2Cl_2]$	22	2.865(1)	2.788[9]	3.058(3)	–	[28]
Mo octahedral coordination and M′ pentacoordinate:						
$[Mo_2Fe_2S_4(\mu\text{-}dtc)(dtc)_4]$	15	2.734(2)	2.75[2]	2.784(3)	–	[29]
$[Mo_2Fe_2S_4Cp^*_2(CO)_4]$	18	2.761(1)	2.81[2]	3.334	1995/1962/1934	[30]
Mo pentacoordinate and M′ tetrahedral coordination:						
$[Mo_2Cu_2S_4(edt)_2(PPh_3)_2]$	22	2.8576(7)	2.81[2]	3.095(2)	–	[31]
W octahedral and M′ tetrahedral coordination:						
$[W_2Fe_2S_4Cp^*_2(NO)_2]$	20	2.8198(9)	2.766[4]	2.735(3)	1736/1715	[22]
$[W_2Co_2S_4Cp^*_2(NO)_2]$	22	2.7984(5)	2.780[4]	3.131(1)	1732/1709	[22]
$[W_2Cu_2S_4(SCN)_8]^{4-}$	22	2.845(2)	2.76[3]	2.999	–	[32]
W pentacoordinate and M′ tetrahedral coordination:						
$[W_2Cu_2S_4(edt)_2(PPh_3)_2]$	22	2.851(1)	2.82[2]	3.090	–	[33]

[a] All IR data are referred to the CO or NO stretching frequency in KBr unless otherwise indicated. [b] IR data in CH_3CN solutions.

ried out through reduction of the polymeric phase $\{Mo_2S_xCp^{\#}\}_n$ ($Cp^{\#}$ = Cp, Cp′, Cp*; with Cp′ = methylcyclopentadienyl and Cp* = pentamethylcyclopentadienyl) with an excess of lithium ethylborohydride.[36] This phase is obtained by treating $[MoCp^{\#}(CO)_3]_2$ with elemental sulfur.[35,37] The intermetallic distance in $[Mo_2(\mu_2\text{-}S)_2(\mu_2\text{-}SH)_2Cp^{\#}_2]$ as well as in $[M_2S_2(\mu_2\text{-}S_2)Cp^*_2]$ is consistent with the presence of a metal−metal single bond.

The Mo_2Cr_2 core is formed by photolysis of the carbonylchromium(I) complex $[CrCp(CO)_2]_2$ in the presence of $[Mo_2S_4Cp^*_2]$, which affords the cubane-like diamagnetic cluster $[Mo_2Cr_2S_4Cp^*_2Cp_2]$ in 41% yield according to Equation (1).[38]

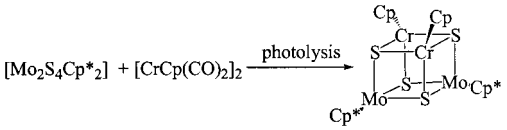

(1)

The equivalent $[Mo_2Cr_2S_4Cp_2Cp^*_2]$ complex has also been prepared by treating a chromium sulfide dimer $[Cr_2(\mu_2,\eta^2\text{-}S_2)(\mu_2,\eta^1\text{-}S_2)(\mu_2\text{-}S)Cp^*_2]$ with the corresponding carbonylmolybdenum compound $[MoCp(CO)_2]_2$. The final oxidation state of both Mo and Cr in the cluster is III and consequently there are 12 metal cluster electrons available for metal−metal bonding. The analogous nickel cluster $[Mo_2Ni_2S_4Cp'_2Cp_2]$ has been synthesised in 15% yield from $[Mo_2(\mu_2\text{-}S)_2(\mu\text{-}SH)_2Cp'_2]$ and $[NiCp(CO)]_2$ in refluxing THF to produce a 22 metal electron cluster, for which the oxidation state assignment $Mo^{III}_2Ni^{II}_2$ has been proposed.[27] Consequently, the reaction implies reduction of the dimolybdenum sulfide (Mo^{IV} to Mo^{III}), with concomitant oxidation of the carbonylnickel compound from Ni^I to Ni^{II}. Although these tetrametallic $Mo_2Cr_2S_4$ and $Mo_2Ni_2S_4$ clusters have not been characterised by X-ray structural analysis, a cubane-type structure has been proposed based on spectroscopic evidence. The complex $[Mo_2(\mu_2\text{-}S)_2(\mu_2\text{-}SH)_2Cp'_2]$ does not react with $[Fe_2Cp_2(CO)_4]$ or $[CoCp(CO)_2]$ under the conditions used for the synthesis of the Mo_2Ni_2 complex.[27]

The hydridosulfides $[Mo_2(\mu_2\text{-}S)_2(\mu_2\text{-}SH)_2Cp^{\#}_2]$ ($Cp^{\#}$ = Cp, Cp′) react rapidly (< 2 h) with $[Ni(CO)_4]$, $[Fe_2(CO)_9]$ and $[Co_2(CO)_8]$ in organic solvents, but only in the case of nickel can $M_2M'_2S_4$ thiocubane clusters be isolated. These have the formula $[Mo_2Ni_2S_4Cp^{\#}_2(CO)_2]$ and are obtained in 25 and 50% yields for Cp and Cp′, respectively, as represented in Scheme 2.[27,36]

These nickel compounds, also with 22 metal cluster electrons, adopt a cubane-butterfly structure with the Ni atoms placed at the wing tips (Ni···Ni = 2.962 Å) In the case of iron, the complexes $[Mo_2Fe_2(\mu_3\text{-}S)_2(\mu_2\text{-}S)_2Cp^{\#}_2(CO)_6]$ ($Cp^{\#}$ = Cp, Cp′) are obtained. These contain a planar Mo_2Fe_2 core and have the μ_3-S ligands lying on opposite sites of the Mo_2Fe_2 plane. Reaction with the carbonylcobalt compound affords the tetranuclear clusters $[Mo_2Co_2(\mu_3\text{-}S)_2(\mu_4\text{-}S)Cp^{\#}_2(CO)_4]$ in 50% yield. These have an $Mo_2Co_2S_3$ core containing a μ_4-S sulfido ligand. The Cp′ derivative

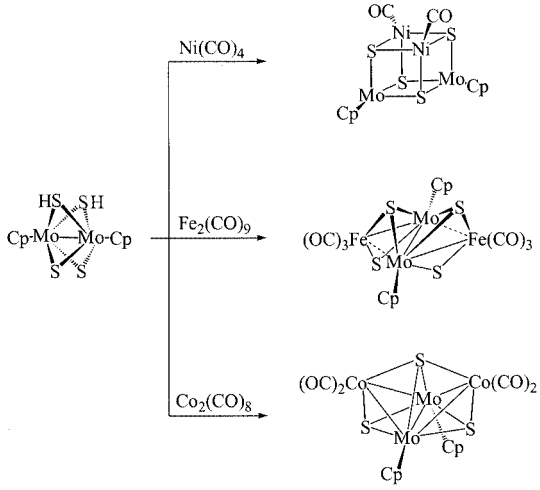

Scheme 2. Reactions of $[Mo_2(\mu_2\text{-}S)_2(\mu_2\text{-}SH)_2Cp_2]$ with carbonylmetal compounds

undergoes thermal decomposition by heating with pyridine at 150 °C to give a trimolybdenum cuboidal cluster $[Mo_3CoS_4Cp'_3(CO)]$ in 15% yield.[24]

The $[Mo_2Co_2(\mu_3\text{-}S)_2(\mu_4\text{-}S)Cp'_2(CO)_4]$ complex deserves special attention due to its relevance as a molecular model for hydrodesulfurisation catalysis.[25,39] This $Mo_2Co_2S_3$ cluster compound reacts with a variety of organic thiols RSH (R = *tert*-butyl, isopentyl, phenyl) in near quantitative yield to give the corresponding hydrocarbon and the $[Mo_2Co_2(\mu_3\text{-}S)_4Cp'_2(CO)_2]$ cubane having 20 metal electrons. Treatment of the $Mo_2Co_2S_4$ cluster with a CO/H_2 mixture (1:4) at 150 °C and 13.4×10^5 Pa affords the $[Mo_3CoS_4Cp'_3(CO)]$ complex in 15−30% yield, according to Scheme 3.[24]

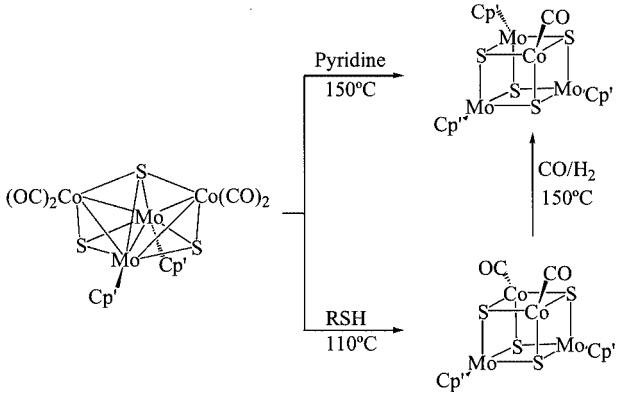

Scheme 3. Rearrangement reactions of the $Mo_2Co_2S_3$ core

An analogue of $[Mo_2Co_2(\mu_3\text{-}S)_4Cp'_2(CO)_2]$ can be obtained in better yields (72%) from the sulfur-rich dinuclear complex $[Mo_2S_4Cp^*_2]$ and $[Co_2(CO)_8]$ in toluene.[40] This procedure can be extended to tungsten to afford the $[W_2Co_2S_4Cp^*_2(CO)_2]$ cubane compound in 51% yield.[22] The $M_2Co_2S_4$ cluster unit in these compounds having 20 metal electrons shows a complete metal tetrahedron with six intermetallic bonds (see Table 1), in contrast to the Ni

complex analogue where only five metal−metal bonds are present. If one neglects the intermetallic bonds, the coordination environment around the heterometal in both the Ni and the Co clusters is nearly tetrahedral.

Reduction of the carbonylcobalt cubane $[Mo_2Co_2S_4Cp^{Et}_2(CO)_2]$ (Cp^{Et} = ethyltetramethylcyclopentadienyl) with sodium amalgam in THF affords the extremely air-sensitive one-electron reduction product which was crystallised as the $[Na(15\text{-crown-}5)_{1.5}]^+$ salt in 44% yield. Alternatively, the analogous Cp′ complex has been prepared by the thermal decomposition of the thiolate adduct $[Mo_2Co_2S_3Cp'_2(CO)_2(SAr)]^-$ (Ar= *p*-tolyl) formed from $[Mo_2Co_2S_3Cp'_2(CO)_4]$ and *p*-toluene thiolate in acetonitrile. The addition of an electron causes an increase of ca. 0.4 Å in the Co−Co bond length with respect to the neutral 20 metal electron cluster, while the Mo−Mo and Mo−Co distances remain practically unchanged.[26] Thus, in a formal sense, changes in the number of metal electrons mainly involve the Co atoms; these are reduced from Co^{2+} to $Co^{1.5+}$.

Oxidation of the heterodimetallic sulfidocobalt cluster $[Mo_2Co_2S_4Cp^{Et}_2(CO)_2]$ with X_2 (X = Cl, Br, I, SPh) causes oxidative substitution of the carbonyl groups by halogens or PhS to give the 18 metal electron clusters $[Mo_2Co_2S_4Cp^{Et}_2X_2]$ in 48−83% yields, as shown in Equation (2).[21,41]

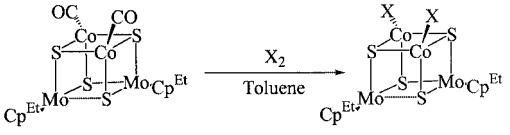

(2)

The $Mo_2Co_2S_4$ core in these 18 electron metal clusters shows a cubane butterfly structure with five metal−metal bonds. The Co···Co distances in these complexes are 2.934(3) and 2.953(3) Å for the iodine and the chlorine derivatives, respectively, and 2.741(1) Å for the thiolato cluster. This last value is very similar to that found for the radical anion $[Na(15\text{-crown-}5)_{1.5}][Mo_2Co_2S_4Cp^{Et}_2(CO)_2]$ [2.735(1) Å] that was associated with a formal Co···Co bond order of 1/2.

A (carbonyl)$Mo_2Fe_2S_4$ cubane-type cluster of formula $[Mo_2Fe_2S_4Cp^*_2(CO)_4]$ has been synthesised from the molybdenum(IV) complex $[Mo_2(\mu_2,\eta^2\text{-}S_2)(\mu_2\text{-}S)_2Cp^*_2]$, by reaction with $[Fe_2(CO)_9]$ in THF at room temperature (33% yield) or by photochemical reaction with $[Fe(CO)_5]$ (10% yield).[30] Two heterodimetallic Mo_2FeS_2 trimers with a trigonal-bipyramidal core are also obtained from this reaction. The $[Mo_2Fe_2S_4Cp^*_2(CO)_4]$ complex possesses 18 metal cluster electrons which agrees with a formal oxidation state assignment of $Mo^{III}_2Fe^{II}_2$. The cubane cluster with 18 metal cluster electrons adopts a butterfly structure and consequently five metal−metal bonds. The coordination sphere around the iron atom consists of three μ_3-S sulfur atoms and two carbonyl groups in a square-pyramidal geometry.

In the case of iron, the cyclopentadienyl halide derivative $[Mo_2Fe_2S_4Cp^*_2Cl_2]$ has been prepared through a self-assembly reaction between the molybdenum(IV) monomer $[MoCp^*(S(tBu)_3)]$ and $FeCl_3$ in THF that unexpectedly gives the cubane cluster $[Mo_2Fe_2S_4Cp^*_2Cl_2]$ in 39% yield.[20] The resulting $[Mo_2Fe_2S_4]$ complex has 16 metal cluster electrons, and in spite of the uncertainty related to the oxidation state definition in cluster compounds, a possible assignment is $Mo^{IV}_3Fe^{II}_2$. The reduction of iron from Fe^{III} to Fe^{II} is considered to occur during the cluster formation reaction, with simultaneous cleavage of the C−S bond. The electron deficiency in this cluster mainly affects the Fe−Fe distance which is ca. 0.09 Å longer than in similar iron complexes having 20 metal electrons, as can be observed in Table 1. Reaction of $[Mo_2Fe_2S_4Cp^*_2Cl_2]$ with Li_2S_2 gives rise to a tricubane cluster where the three $Mo_2Fe_2S_4$ cluster units are linked by three Fe−Fe bonds (2.610 Å) and three $\mu_2,\eta^2\text{-}S^{2-}_4$ ligands, as represented in Equation (3).

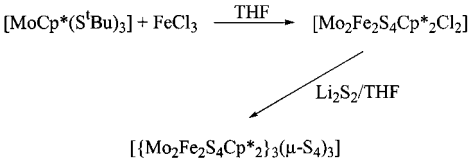

(3)

The only example of a heterodimetallic Mo_2Cu_2 cluster with cyclopentadienyl ligands is the $[Mo_2Cu_2S_4Cp^*_2Cl_2]$ complex, prepared by reaction of $[Mo_2S_4Cp^*_2]$ with 2 equiv. of CuCl in acetonitrile. Three different isomeric forms of the dinuclear sulfido starting material have been used, namely $[Mo_2(\mu_2,\eta^2\text{-}S_2)S_2Cp^*_2]$, $[Mo_2(\mu_2,\eta^2\text{-}S_2)(\mu_2\text{-}S)_2Cp^*_2]$, and $[Mo_2(\mu_2\text{-}S)_2S_2Cp^*_2]$, and the best yields (81%) are obtained for the first of these. In all three cases, other trimetallic Mo_2Cu and noncuboidal tetrametallic Mo_2Cu_2 complexes are also obtained as coproducts. The resulting $[Mo_2Cu_2S_4Cp^*_2Cl_2]$ complex having 22 metal electrons has a similar cubane-butterfly structure to the one observed for the 22 electron Mo_2Ni_2 systems.[28]

Finally, several nitrosyl derivatives of the $M_2M'_2S_4$ unit derived from (cyclopentadienyl)group-6 complexes have been prepared with Fe and Co as heterometals. These complexes have the chemical formula $[M_2M'_2S_4Cp^{\#}_2(NO)_2]$ (M = Mo and W and M′ = Fe and Co).[22,42] The clusters $[Mo_2Fe_2S_4Cp^{\#}_2(NO)_2]$ ($Cp^{\#}$ = Cp, Cp^{Et}, Cp*) were synthesised using different Mo/S synthons and two (nitrosyl)Fe complexes as the source of the FeNO vertex, as summarised in Scheme 4. Typical yields for these reaction are ca. 40%. In contrast to the carbonylcobalt findings, the reaction between the (sulfhydryl)molybdenum complex $[Mo_2S_2(SH)_2Cp_2]$ and $[Fe(CO)_2(NO)_2]$ does not lead to the "$Mo_2Fe_2S_3$" cluster, isoelectronic with $[Mo_2Co_2S_3Cp^{Et}_2(CO)_2]$.[22] It is interesting to point out that when the 22 electron cluster $[Mo_2Cu_2S_4Cp^*_2Cl_2]$ is irradiated in the presence of $[Fe(NO)(CO)_3]^+$, the CuCl fragments are replaced by Fe(NO) to afford the 20 metal electron cluster $[Mo_2Fe_2S_4Cp^*_2(NO)_2]$.[28]

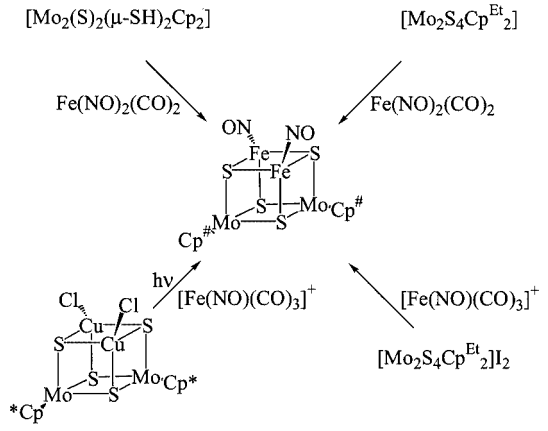

Scheme 4. Synthetic routes to the $[Mo_2Fe_2S_4Cp^{\#}(NO)_2]$ cubane.

The analogous (nitrosyl)W_2Fe_2 complex is obtained by reaction of $[W_2S_4Cp^*_2]$ with $[Fe(NO)_2(CO)_2]$ in refluxing toluene to afford $[W_2Fe_2S_4Cp^*_2(NO)_2]$ in 36% yield. These $[M_2Fe_2S_4Cp^{\#}_2(NO)_2]$ compounds have 20 metal cluster electrons and their structures show six metal−metal bonds and an NO ligand attached to the tetrahedral Fe atom. Similar cluster complexes are obtained for cobalt by treating $[Mo_2S_4Cp^{Et}_2]$, $[W_2S_4Cp^*_2]$ or $[Mo_2(\mu_2\text{-}S)_2(\mu\text{-}SH)_2Cp_2]$ with $[Co(CO)_3(NO)]$ in toluene to afford complexes with formula $[M_2Co_2S_4Cp^{\#}_2(NO)_2]$ in low to moderate (30−50%) yields.[22] The change of iron for cobalt increases the number of metal cluster electrons from 20 to 22. The formal oxidation states of the metal atoms in these clusters are M^{III} and Co^{I} (the nitrosyl ligand is assumed to be NO^+) and consequently, replacement of Fe by Co has the same effect as substitution of a carbonyl by a nitrosyl group. The Co−Co distances of ca. 3.12 Å in the $[M_2Co_2S_4Cp^{\#}_2(NO)_2]$ clusters (see Table 1) are well beyond the typical Co−Co single bond lengths and the metal atoms adopt the butterfly disposition already observed for other 22 metal electron clusters.

$M_2M'_2S_4$ Clusters with Sulfur-Containing Ligands

The number of $M_2M'_2$ clusters with sulfur-containing ligands is more limited than their cyclopentadienyl counterparts. All known examples contain dithiolate or dithiocarbamate as ancillary ligands and metal electron counts between 15 and 20. The main building block fragment used for this chemistry is the *syn*-$[M_2(\mu_2\text{-}S)_2S_2]$ unit, in particular the molybdenum and tungsten dimers $[M_2S_4(dtc)_2]$ (dtc = diethyldithiocarbamate) and $[Et_4N]_2[M_2S_4(edt)_2]$ (edt = 1,2-ethanedithiolate). The *syn* isomers of the molybdenum complexes $[Mo_2(\mu_2\text{-}S)_2S_2(dtc)_2]$ and $[Mo_2(\mu_2\text{-}S)_2S_2(edt)_2]^{2-}$ are prepared in 82 and 75% yield, respectively, by reaction of $[NH_4]_2[Mo_2(S-S)_6]$ with an excess (20−25 equiv.) of Na[dtc] or Na_2[edt] in refluxing methanol.[43] The excess thiolate serves both as the reductant of the disulfide ligand and as a peripheral ligand in the final product. The neccessity for excess thiolate may be obviated by using triphenylphosphane as the reducing agent. A more general route for the synthesis of $[Et_4N]_2[Mo_2(\mu_2\text{-}S)_2S_2(edt)_2]$ has been developed, and this can also be used to prepare the analogous tungsten complex. $[NH_4]_2[MS_4]$ is treated with 1,3-ethanedithiol in DMF, and addition of tetraethylammonium bromide precipitates the $[Et_4N]_2[M_2(\mu_2\text{-}S)_2S_2(edt)_2]$ salt in 63 and 55% yields for Mo and W respectively.[44,45] The tungsten complex $[W_2(\mu_2\text{-}S)_2S_2(dtc)_2]$ can be obtained in 75% yield by treatment of $(Et_4N)_2[W_2(\mu_2\text{-}S)_2S_2(S_4)]$ with sodium diethyldithiocarbamate, triphenylphosphane and NH_4PF_6 in acetonitrile.[45] The sulfur-rich $[W_2(\mu_2\text{-}S)_2S_2(S_4)_2]^{2-}$ anion has also been employed as a building block. This tungsten(V) dimer is obtained in 83% yield by heating $[NH_4]_2[WS_4]$ and elemental sulfur in DMF.[45] It can also be obtained at room temperature by using a reducing agent such as $NH_2NH_2{\cdot}HCl$.[32]

The synthesis of the cubane cluster $[Mo_2Fe_2S_4(S_2CNEt_2)_5]$ in 18% yield has been reported, using a one-pot reaction between $[NH_4]_2[MoS_4]$, $FeCl_3$, Na[dtc], PhSH and $NaOCH_3$ in methanol/DMF solutions, as shown in Equation (4).[29]

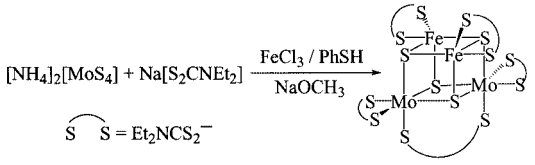

(4)

It is very likely that the reducing conditions used in this reaction (PhS^- and $Et_2NCS_2^-$) cause the formation of an intermediate molybdenum(V) dimer with an $M_2(\mu_2\text{-}S)_2S_2$ central core, as found for tungsten. The $Mo_2Fe_2S_4$ cluster skeleton has a cubane-type structure where each metal atom is coordinated by three μ_3-S atoms and two sulfur atoms of the dithiocarbamate chelating terminal ligand. In addition, the fifth $Et_2NCS_2^-$ group acts as a bridging ligand between two Mo atoms, resulting in an octahedral environment for that metal atom. The coordination geometry around the iron atom is an irregular triangular bipyramid. The intermetallic distances within this cluster are listed in Table 1. The Mo−Mo and Mo−Fe bond lengths are consistent with metal−metal single bonds, while the Fe−Fe bond length of 2.784 Å lies outside the single bond range. In consequence there are in total five metal−metal bonds, with the metal atoms defining a butterfly arrangement in which the Mo atoms occupy the hinge positions. The dithiocarbamate bridging ligand causes a shorthening of the Mo−Mo bond length (2.734 Å) in the $[Mo_2Fe_2S_4(S_2CNEt_2)_5]$ cluster, while the other intermetallic Mo−Fe and Fe−Fe bond lengths are similar to those observed in the 16 metal electron cluster $[Mo_2Fe_2S_4Cp^*_2Cl_2]$.

The $Mo_2Co_2S_4$ cluster $[Mo_2Co_2S_4(S_2CNEt_2)_2(CH_3CN)_2(CO)_2]$ having 20 metal cluster electrons has been prepared by reaction of $[Mo_2(\mu_2\text{-}S)_2S_2(dtc)_2]$ with an equimolar amount of $[Co_2(CO)_8]$ in THF or acetonitrile, as represented in Equation (5).[23]

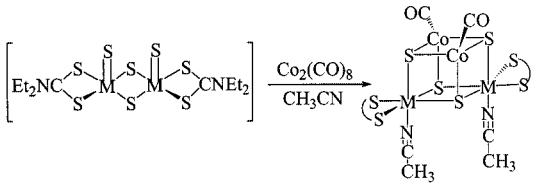

(5)

The analogous tungsten complex is prepared from $[W_2(\mu_2\text{-}S)_2S_2(dtc)_2]$ in acetonitrile.[45] The structure of the parent $[M_2S_4(dtc)_2]$ fragment remains essentially unchanged in the final cluster, where the M_2Co_2 atoms define a tetrahedron. The dinuclear precursor shows no tendency to bind acetonitrile, in contrast to the final cubane product, and thus it appears that the presence of cobalt enhances the affinity for ligands at the molybdenum or tungsten site *trans* to the μ_3-S atom. There are no known examples of $M_2Ni_2S_4$ derivatives with sulfur-containing ligands and examples with copper are restricted to the molybdenum and tungsten $[M_2Cu_2S_4(SCH_2CH_2S)_2(PPh_3)_2]$ complexes. When $[Et_4N]_2[MoS_4(edt)_2]$ reacts with 2 equiv. of $[Cu(PPh_3)_3Cl]$ under an inert gas, the cubane cluster compound $[Mo_2Cu_2S_4(edt)_2(PPh_3)_2]$ is obtained. The isomorphous tungsten compound $[W_2Cu_2S_4(edt)_2(PPh_3)_2]$ was synthesised from $[Et_4N]_2[WS_4(edt)_2]$, $CuCl_2{\cdot}H_2O$ and PPh_3 in CH_2Cl_2/EtOH solution.[31] The coordination sphere around the Mo or W atoms in these complexes consists of three μ_3-S sulfido ligands and two sulfur atoms from the bidentate ligand, arranged in a tetragonal-pyramidal geometry. The four metal atoms adopt a cubane-butterfly structure, as found in the (cyclopentadienyl)M_2Cu_2 derivatives which also have 22 metal cluster electrons.[33] Alternatively, the reaction of $[Et_4N]_2[M_2S_4(edt)_2]$ (M = Mo, W) with $[Cu(PPh_3)_2(dtp)]$ (dtp = $^-S_2P(OCH_2{-}CH_3)_2$, dithiophosphate] in CH_2Cl_2/CH_3CN solution at room temperature gives the incomplete cubane cluster $[Et_4N][M_2CuS_4(edt)_2(PPh_3)]$ (M = Mo, W), as summarised in Scheme 5.[46]

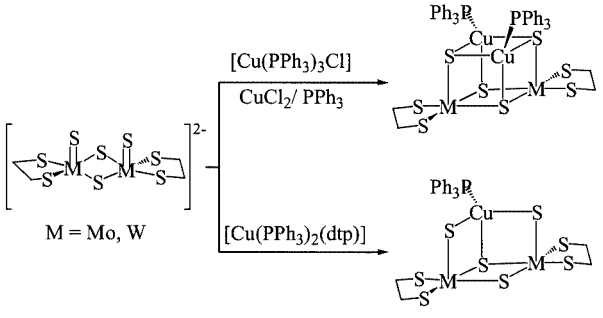

Scheme 5. Incorporation of one or two copper atoms to $(Et_4N)_2[M_2S_2(\mu_2\text{-}S)_2(edt)_2]$

No interconversion between the trinuclear and the tetranuclear species, as has been found in similar systems with noble metals instead of copper, has been reported.[47]

Finally, the air-stable complex $[Et_4N]_4[W_2Cu_2S_4(SCN)_8]$ having 22 metal cluster electrons has been prepared in 45% yield by reacting $[Et_4N]_2[W_2S_4(S_4)_2]$ with CuCl in the presence of KSCN.[32] In contrast to the other complexes described in this section, the tungsten atom is coordinated to the nitrogen atoms of the thiocyanate ligands in a octahedral coordination environment. The thiocyanate ligands attached to the Cu atoms define a tetrahedron. All the reported $M_2Cu_2S_4$ clusters are electron-precise, having 22 metal cluster electrons (see Table 1) and a cuboidal−butterfly arrangement of the metal atoms, where the nonbonding distance corresponds to the Cu···Cu interaction.

Clusters with $M_3M'Q_4$ Central Units

In contrast to the above-reported cuboidal complexes where, with the exception of the $[\{Mo_2Fe_2S_4Cp^*_2\}_3(\mu\text{-}S_4)_3]$ tricubane cluster, only isolated single-cube structures have been found, compounds with $M_3M'Q_4$ central cores exhibit single, edge linked double-cube and corner-shared double-cube structures, as represented in Figure 2. In the case of first-row transition heterometals, only the first two structural types have been encountered to date.

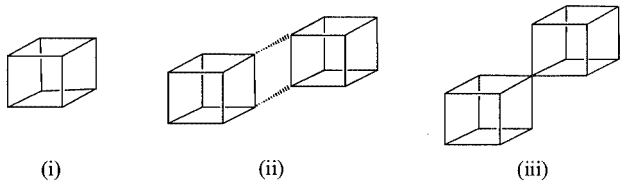

Figure 2. Structural types of $M_3M'Q_4$ aquo cuboidal clusters: (i) single cubane (ii) edge-linked double cubane (iii) corner-shared double cubane

The chemistry of heterodimetallic clusters with $M_3M'Q_4$ cores has been developed predominantly in aqueous media, and major advances have been made in the field of molybdenum clusters, where the heterometals incorporated into the incomplete cuboidal $[Mo_3S_4(H_2O)_9]^{4+}$ aquo ion according to a [3 + 1] synthetic strategy range from group-6 to -15 elements.[18] For tungsten, the number of heterometals incorporated is more restricted, a fact that has been attributed to the greater difficulty in reducing tungsten as compared to molybdenum. Reactivity studies of $[M_3Se_4(H_2O)_9]^{4+}$ complexes towards a second metal are limited to some preliminary results regarding the incorporation of Ni and Pd into the molybdenum selenide aquo ion[48] and Mo insertion into the W_3Se_4 aquo ion.[49] This chemistry has been extensively reviewed in the past year, and for this reason we will only comment on the most relevant aspects regarding the insertion of first-row transition metals into the M_3Q_4 aquo ion. However, we will give a detailed description of the non-aqueous chemistry of these $M_3M'Q_4$ heterodimetallic clusters.[17−19] Figure 3 presents a number of representative $M_3M'Q_4$ clusters that have been

reported, where again the familiar cubane core has been emphasised.

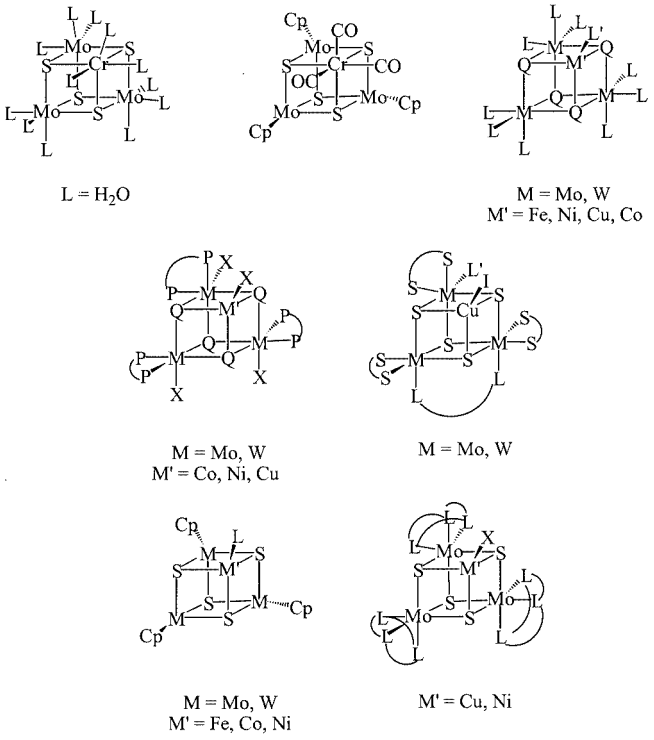

Figure 3. Schematic representations of cubane structures and metal environments of $M_3M'Q_4$ clusters

$M_3M'Q_4$ Clusters as Derivatives of the M_3Q_4 Aquo Ion

Since Shibahara's report in 1986 of the reaction of the molybdenum aquo cluster $[Mo_3S_4(H_2O)_9]^{4+}$ with iron metal to give the molybdenum−iron mixed-metal cluster $[Mo_3FeS_4(H_2O)_{10}]^{4+}$, much work has been carried out in the field.[50] The insertion of other metal atoms has been successfully achieved as previously mentioned, and the analogous tungsten and selenium building blocks M_3Q_4 have been prepared.

The synthesis of the green aquo cluster $[Mo_3S_4(H_2O)_9]^{4+}$ has been recently reviewed.[17] This aquo ion was first prepared in low yields (ca. 20%) by two different routes; the self-assembly reaction of $[Mo(CO)_6]$ with anhydrous Na_2S in acetic anhydride[51] and oxidative fragmentation of the tetrametallic $[Mo_4S_4(H_2O)_{12}]^{5+}$ aquo ion in acidic solutions.[52,53] An almost quantitative synthesis of this aquo ion has been developed that involves abstraction of sulfur from the $[Mo_3(\mu_3\text{-}S)(\mu_2\text{-}S_2)_3X_6]^{2-}$ (X = Cl, Br) trimer with PPh_3.[54] The analogous selenium cluster $[Mo_3Se_4(H_2O)_9]^{4+}$ has been prepared in a similar manner from the selenium-rich trimer $[PPh_4]_2[Mo_3(\mu_3\text{-}Se)(\mu_2\text{-}Se_2)_3Cl_6]$, which was aquated in acid prior to the diselenide reduction to selenide with PPh_3.[55] The most efficient method for the synthesis of the $[W_3Q_4(H_2O)_9]^{4+}$aquo ions (yields ca. 60−70%) involves treatment of the corresponding $\{W_3Q_7Br_4\}_x$ polymeric phases with hypophosphorous acid in hot HCl.[56,57] Purification of the aquo ions is achieved by cation exchange chromatography. The sulfur-bridged trimers are stable in acidic solution, but the selenium analogues are less stable, giving a deposit of red selenium after a week.[57,58]

First-row transition metal incorporation into the $[Mo_3S_4]^{4+}$ aquo ion has been achieved by treating $[Mo_3S_4(H_2O)_9]^{4+}$ with iron,[50] cobalt,[59] nickel[60] and copper metal[61] (M′) in acidic solution, HCl or *p*-toluenesulfonic acid (Hpts), to afford the corresponding heterodimetallic $[Mo_3M'S_4(H_2O)_{10}]^{4+}$ complexes with 14, 15, 16 and 17 metal cluster electrons for M′ = Fe, Co, Ni and Cu, respectively, as shown in Equation (6).

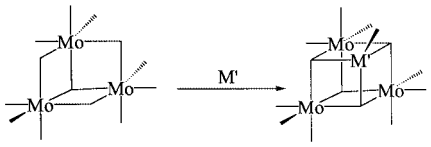

(6)

This synthetic strategy has also been applied to obtain the selenido derivative $[Mo_3NiSe_4(H_2O)_{10}]^{4+}$ [48] or the tungsten-containing cluster sufides $[Mo_{3-x}W_xNiS_4(H_2O)_{10}]^{4+}$ (x = 0−3).[62] Alternatively, the $[Mo_3NiS_4(H_2O)_{10}]^{4+}$ aquo ion has been synthesised by a self-assembly reaction between $[NH_4]_2[MoS_4]$ and nickel metal in HCl solution or by reduction of an Ni^{2+} salt in the presence of $[Mo_3S_4(H_2O)_9]^{4+}$.[63,64] With the exception of the $[Mo_3NiS_4(H_2O)_{10}]^{4+}$ complex, the remaining heterodimetallic aquo ions, especially the cobalt derivative, are very air-sensitive.

The Mo_3Fe and Mo_3Ni aquo ions, having an even number of cluster metal electrons, crystallised from *p*-toluensulfonic acid solutions as isolated single cubes of formula $[Mo_3M'S_4(H_2O)_{10}](pts)_4\cdot 7H_2O$ (pts = *p*-toluenesulfonate), while the analogous Co and Cu heterodimetallic clusters, having an odd number of metal electrons, crystallise under the same conditions as an edge-linked double cuboidal structure formulated as $[\{Mo_3M'S_4(H_2O)_9\}_2](pts)_8\cdot nH_2O$ (M′ = Co, n = 18; M′ = Cu, n = 20). The Co−Co and Cu−Cu bond lengths in these double cubes are 2.498 and 2.426 Å, respectively, corresponding to an M′−M′ single bond. A summary of intermetallic distances for $M_3M'S_4$ cubanes is presented in Table 2.

In contrast to the $[M_2M'_2S_4]$ heterodimetallic complexes, changes in the heterometal within the $[Mo_3M'S_4]^{4+}$ aquo ion series does not produce significant differences in the intermetallic distances that can be correlated with the number of metal cluster electrons. The single-to-double cube dimerisation reaction is reversible in the case of Cu, as shown in Equation (7).[76,77]

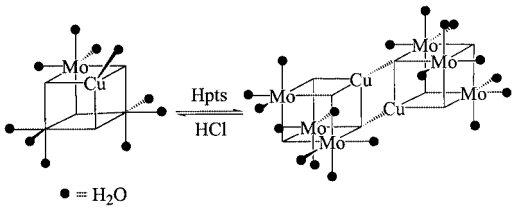

(7)

Table 2. Selected bond lengths [Å] for some representative $M_3M'S_4$ cubane-type clusters (standard deviations for averaged values are given in brackets)

Cluster	No. of metal electrons	M−M	M−M′	Ref.
Single cubes:				
$[Mo_3FeS_4(H_2O)_{10}]^{4+}$	14	2.767[7]	2.671[11]	[65]
$[Mo_3FeS_4Cp'_3(SH)]$	14	2.86[2]	2.79[2]	[24]
$[Mo_3CoS_4Cp'_3CO]$	16	2.838[11]	2.745[11]	[24]
$[Mo_3NiS_4(H_2O)_{10}]^{4+}$	16	2.755[10]	2.640[9]	[60]
$[Mo_3NiS_4(H_2O)_9CO]^{4+}$	16	2.744[8]	2.677[7]	[66]
$[\{Mo_3NiS_4Cp'_3\}_2(\mu\text{-}C_4H_8S_2)]^{2+}$	16	2.819[13]	2.71[1]	[67]
$[W_3NiS_4(H_2O)_9(C_2H_4)]^{4+}$	16	2.7137(9)	2.701(2)	[62]
$[W_3NiS_4Cp'_3(PPh_3)]^{+}$	16	2.809[1]	2.733[9]	[68]
$[Mo_3CuS_4(Hnta)_3Cl]^{2-}$	16	2.778(1)	2.838(2)	[69]
$[Mo_3CuS_4(dmpe)_3Cl_4]^{+}$	16	2.782[1]	2.823[8]	[5]
$[W_3CuS_4(dmpe)_3Br_4]^{+}$	16	2.780[2]	2.884[7]	[5]
$[Mo_3CuS_4(dtp)_3(\mu\text{-}OAc)(DMF)I]$	16	2.73[5]	2.85[4]	[70]
$[Mo_3CuS_4(n\text{Pr}_2PS_2)_3(\mu\text{-}n\text{Pr}_2PS_2)(py)I]$	16	2.769[9]	2.857[14]	[71]
$[W_3CuS_4(dtp)_3(\mu\text{-}O_2CCl_3)(CH_3CN)I]$	16	2.73[3]	2.87[5]	[72]
$[Mo_3CuS_4(Et_2NCS_2)_3(\mu\text{-}Et_2NCS_2)(py)I]$	16	2.76[3]	2.849[13]	[73]
$[Mo_3CuS_4(tdci)_3Br]^{3+}$	17	2.832[9]	2.916[12]	[74]
$[Mo_3CuSe_4(dmpe)_3Cl_4]^{+}$	16	2.839[4]	2.839[4]	[75]
Edge-linked double cubes:				
$[\{Mo_3CoS_4(H_2O)_9\}_2]^{8+}$	15	2.744[11]	2.64[2]	[59]
$[\{W_3NiS_4(H_2O)_9\}_2]^{8+}$	16	2.747[7]	2.66[4]	[62]
$[\{Mo_3CuS_4(H_2O)_9\}_2]^{8+}$	17	2.730[7]	2.89[8]	[61]

The $[Mo_2WNi]^{4+}$ aquo ions crystallise as single cuboidal clusters in the same way as the analogous Mo_3Ni complexes. However, further substitution of Mo for W results in the formation of $[\{Mo_nW_{3-n}NiS_4(H_2O)_9\}_2](pts)_8\cdot 20H_2O$ (n = 0, 1) edge-linked double cuboidal structures, with Ni−Ni bond lengths of 2.549 Å for MoW_2Ni and 2.56 Å for the W_3Ni cluster.[62]

In contrast to the reactivity just reported for the incomplete cuboidal molybdenum sulfide versus a first-row transition metal, the $[Mo_3S_4]^{4+}$ aquo ion does not react with chromium metal. Instead, the $[Mo_3CrS_4(H_2O)_{12}]^{4+}$ cluster is prepared by treating $[Mo_3S_4(H_2O)_9]^{4+}$ with $[Cr(H_2O)_6]^{2+}$. This Mo_3Cr cube has only been characterised spectroscopically in solution.[78] The reaction of the $[Mo_3S_4]^{4+}$ aquo ion with Cu^+, or with a Cu^{2+} salt in the presence of sodium borohydride, gives the 16 electron metal cluster $[Mo_3CuS_4(H_2O)_{10}]^{5+}$ in contrast to the 17 electron species obtained by direct reaction between the trimer and the metal.[76] The 16 electron Mo_3Cu clusters are air-stable in HCl due to coordination of Cl^- to the heterometal, but they tend to disproportionate to Cu^{2+}(aq.) and $[Mo_3CuS_4]^{4+}$in noncoordinating acids.[69] The existence of the 16 metal electron $[Mo_3CuS_4]^{5+}$ complex is also detected as the first step of the oxidation reaction of the corresponding 17 metal electron cluster.[76] The transmetallation reaction of $[Mo_3M'S_4(H_2O)_{10}]^{4+}$ (M′ = Fe, Ni) in the presence of a 10 molar excess of a Cu^{2+} salt in 2 M HCl also produces the 16 electron $[Mo_3CuS_4(H_2O)_9Cl]^{3+}$ aquo complex as the major reaction product.[79] When the cluster concentration is increased to ca. 0.1 M, the reaction of $[Mo_3FeS_4(H_2O)_{10}]^{4+}$ with a Cu^{2+} salt under similar conditions instead affords the 17 electron cluster $[Mo_3CuS_4(H_2O)_9Cl]^{4+}$ as the major product (yield = 37%), while the 16 electron cluster is only obtained in 5% yield.[69] Further investigations are required to understand these replacement reactions.

In the same way that chlorine coordination to the heteroatom stabilises the $[Mo_3CuS_4]^{4+}$ cluster core, substitution of the water molecule coordinated to the extremely air-sensitive $[Mo_3CoS_4]^{4+}$ aquo ion affords the more stable $[Mo_3CoS_4(H_2O)_9(CO)]^{4+}$ cluster.[48] The nickel aquo cluster also coordinates CO and ethylene (L) in aqueous or organic solutions to give $[M_3NiS_4(H_2O)_9L]^{4+}$ and $[Mo_3NiSe_4(H_2O)_9L]^{4+}$.[62] Coordination of ethylene is favoured by an increase in the number of tungsten atoms in the cluster core.

The heterodimetallic $[M_3M'S_4]^{4+}$ cluster aquo ions can also be derivatised by substitution of the water molecules coordinated to the group-6 metal by mono-,[65] bi-[80] or tridentate ligands.[60] In some cases, this substitution results in complexes having an enhanced stability, a fact that has allowed the crystallisation and further X-ray characterisation of certain cluster cores. For example, addition of nitrilotriacetate (H_3nta + base) to the $[Mo_3CuS_4(H_2O)_9Cl]^{4+}$ aquo complex allows crystallisation of the single cube $[Mo_3CuS_4(Hnta)_3Cl]^{2-}$ as the K^+ or $[NH_4]^+$ salt.[69] The Mo−Mo and Mo−Cu distances in this 16 metal electron cluster are similar to those observed for the $[\{Mo_3CuS_4(H_2O)_9\}_2](pts)_8\cdot 20H_2O$ double cube with 17 metal electrons per cubane unit. In other cases, derivatisation of the heterodimetallic $[M_3M'S_4]^{4+}$ cluster aquo ions produces unexpected results. For example, reaction of $[Mo_3CuS_4(H_2O)_{10}]^{4+}$ with concentrated ammonia yields the $[\{(NH_3)_6(H_2O)(OH)Mo_3CuS_4(\mu_2\text{-}O)\}_2]Cl_4\cdot 8H_2O$ com-

plex in which two cuboidal $[Mo_3CuS_4]^{5+}$ cores are bridged by two oxygen atoms. The oxidant of the cluster core in this reaction remains unidentified.[81]

$M_3M'S_4$ Clusters with Cyclopentadienyl Ligands

$[Mo_3M'S_4Cp_3]^{n+}$ (n = 0, 1) cluster compounds with M′ = Cr, Fe, Co and Ni have been prepared through [3 + 1] building-block synthetic strategies using the $[Mo_3S_4Cp_3]^+$ incomplete cuboidal cluster as the precursor in the case of Cr and Ni, or by rearrangement of tetrametallic cluster species with Mo_2Fe_2 and Mo_2Co_2 units. Of the analogous tungsten complexes, only the nickel derivative $[W_3NiS_4Cp'_3]^+$ has been prepared.

The synthesis of the trinuclear complex $[Mo_3S_4Cp_3][Sn(CH_3)_3Cl_2]$ was first reported in 1971 from the reaction of $[MoCp(CO)_3Cl]$ with $[Sn(CH_3)_3]_2S$ in 1,2-dimethoxyethane in 50% yield.[82] An improved synthetic procedure for this trimer that uses the $[Mo_3S_4]^{4+}$ aquo ion as the starting material has recently been reported. This synthesis can also be used to prepare the analogous tungsten complex. Reaction of the $[M_3S_4(H_2O)_9]^{4+}$ ion (M = Mo or W) with triethyl orthoformate in the presence of a catalytic amount of *p*-toluenesulfonic acid converts the aquo ligands into ethanol ligands which can be further replaced by acetonitrile and tetrahydrofuran. Finally, addition of TlCp or TlCp′ results in formation of the desired $[M_3S_4Cp^{\#}_3](pts)$ ($Cp^{\#}$ = Cp or Cp′) species. Treatment with CH_3CN prior to THF is carried out to ensure removal of traces of $(CH_3CH_2O)_3CH$ and results in an improvement of the final yield. Typical yields for these reactions are 85% for molybdenum and 22% for tungsten.[68,83,84] The reduced $[Mo_3S_4Cp^{\#}_3]$ ($Cp^{\#}$ = Cp, Cp*) species have been synthesised by reaction of $[MoH(CO)_3Cp]$ or $[MoH(CO)_2Cp[P(OC_6H_5)_3]$ with propylene sulfide in THF or by reduction of $[Mo\{S(tBu_3)_3\}Cp^*]$ with sodium amalgam in 88% yield.[85,86]

$[Mo_3S_4Cp_3](pts)$ reacts with $[Cr(CO)_3(CH_3CN)_3]$ in CH_2Cl_2 to produce $[Mo_3CrS_4Cp_3(CO)_3][pts]$ in 64% yield, as represented in Equation (8).[83]

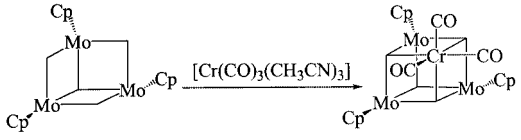

(8)

This Mo_3CrS_4 cluster is stable in air for at least a few days and soluble in common polar organic solvents. This reaction also works for the analogous molybdenum and tungsten carbonylmetal compounds, showing that the [3 + 1] insertion reactions are not restricted to aqueous media. A nickel atom can also be incorporated into the $[Mo_3S_4Cp'_3][pts]$ and $[W_3S_4Cp'_3][pts]$ complexes by treating these trimeric precursors with $[Ni(cod)_2]$ (cod = 1,5-cyclooctadiene) to yield the coordinatively unsaturated cubane-like cluster $[M_3NiS_4Cp'_3][pts]$ in high yields.[68,87] The reaction produces an instant colour change from green to dark brown in the case of molybdenum while, for the tungsten complex, the colour change from violet to brown takes approximately 3 h, probably due to solubility problems. Addition of various ligands to the reaction mixture [triphenylphosphane, M = W; dimethyl sulfide, diethyl sulfide, di(*tert*-butyl) sulfide, tetrahydrothiophene, 1,4-dithiane, thiochroman-4-ol, pyridine, quinoline, 4,4′-bipyridine, M = Mo] saturates the vacant Ni coordination site, as represented in Scheme 6.[67]

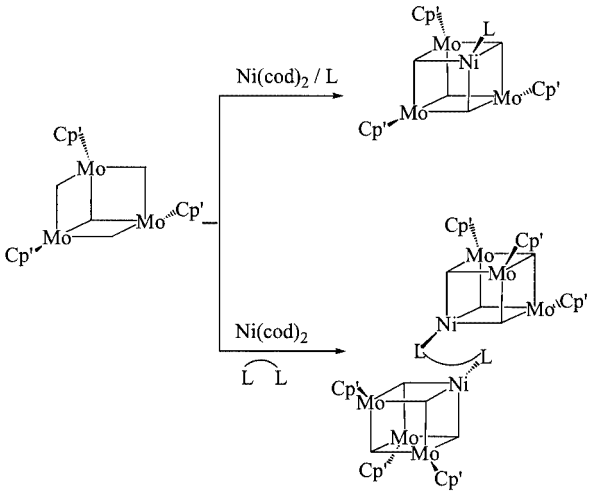

Scheme 6. Coordination of mono- and bidentate ligands to the $[Mo_3NiS_4Cp'_3]^+$ cluster

The crystal structures of the tungsten derivative $[W_3NiS_4Cp'_3(PPh_3)][pts]$ and the molybdenum derivatives $[\{Mo_3NiS_4Cp'_3\}_2(\mu_2\text{-}C_4H_8S_2)][pts]_2$ and $[\{Mo_3NiS_4Cp'_3\}_2(\mu_2\text{-}(4,4'\text{-bipy})][pts]_2$ have been determined. In the last two examples, the 1,4-dithiane and the 4,4′-bipyridine ligands act as bridges between two cubane units. The intermetallic distances for these M_3Ni complexes having 16 metal electrons are similar to those found for the analogous aquo derivatives (see Table 2). Structural data for the molybdenum complexes, where the Ni atom coordinates a sulfur or a nitrogen atom, do not indicate any activation of the C−S or C−N bond.

The trimolybdenum cluster $[Mo_3CoS_4Cp'_3(CO)]$ is formed in ca. 15% yield by heating $[Mo_2Co_2(\mu_3\text{-}S)_2(\mu_4\text{-}S)Cp'_2(CO)_4]$ in pyridine at 150 °C for 3 h, or by treatment of $[Mo_2Co_2(\mu_3\text{-}S)_4Cp'_2(CO)_2]$ with a CO/H_2 mixture in toluene at 250 °C (15−30% yield), as represented in Scheme 3.[24] The resulting Mo_3Co cluster appears to be a thermodynamic sink for the decomposition of the two Mo_2Co_2 complexes. The intermetallic Mo−Mo and Mo−Co distances in this 16 electron Mo_3Co complex are ca. 0.09 and 0.027 Å longer than the corresponding distances in the 16 electron Mo_3Ni cluster. Finally, the cuboidal $[Mo_3FeS_4Cp'_3(SH)]$ compound is obtained in low yields from the reaction between the butterfly-type cluster $[Mo_2Fe_2(\mu_3\text{-}S)_2Cp'_2(CO)_8]$ and thiophene at 150 °C in a pressure reactor.[24] The Mo−Mo and Mo−Fe distances in this cluster are 0.09 and 0.12 Å longer than the equivalent

distances in the $[Mo_3FeS_4]^{4+}$ aquo cluster which also possesses 14 metal cluster electrons.

$M_3M'S_4$ Clusters with Sulfur-Containing Ligands

In parallel to the development of the aqueous chemistry of the $M_3M'Q_4$ complexes, a non-aqueous chemistry arises from inserting Cu into M_3S_4 units derivatised with dithiophosphates [dtp = $(EtO)_2PS_2^-$]. This was subsequently extended to other sulfur-containing ligands such as dithiocarbamates (dtc = $Et_2NCS_2^-$) and dithiophosphinates ($R_2PS_2^-$). These complexes are always prepared through [3 + 1] synthetic routes. The trimeric molybdenum and tungsten dithiophosphate precursors $[M_3S_4\{(EtO)_2PS_2)_3(\mu_2\text{-}(EtO)_2PS_2\}(H_2O)]$ have been synthesised by reaction of $MoCl_3{\cdot}H_2O$ in ethanol or EtOH/HCl solutions.[88] The water molecule is easily replaced by other ligands such as dimethylformamide and pyridine. The dithiocarbamate and dithiophosphinate derivatives have been prepared by reduction of the disulfido μ_2-S_2 bridging ligand in $[Mo_3(\mu_2\text{-}S_2)_3(\mu_3\text{-}S)(Et_2NCS_2)_3]^+$ and $[Mo_3(\mu_2\text{-}S_2)_3(\mu_3\text{-}S)(R_2PS_2)_3](R_2PS_2)$ (R = Et, *n*Pr) with triphenylphosphane to yield $[Mo_3(\mu_2\text{-}S)_3(\mu_3\text{-}S)(Et_2NCS_2)_3(\mu_2\text{-}Et_2NCS_2)(H_2O)]$ and $[Mo_3(\mu_2\text{-}S)_3(\mu_3\text{-}S)(R_2PS_2)_3(\mu_2\text{-}R_2PS_2)(py)]$, respectively.[89–92] The structures of these trinuclear clusters are similar to other M_3Q_4 trimers, with octahedral metal environments and with the bidentate chelating ligand occupying positions *trans* to the capping and one bridging sulfur atoms. The remaining coordination site is occupied by the sulfur atom of the bridging bidentate ligand for two of the metal atoms, and by a water or pyridine molecule for the remaining metal atom. This ligand arrangement gives rise to chirality.[93]

A series of heterodimetallic complexes with $[M_3CuS_4]^{5+}$ cores and consequently 16 metal cluster electrons has been synthesised by treating $[M_3S_4((EtO)_2PS_2)_3(\mu_2\text{-}(EtO)_2PS_2)(L)]$ (L = H_2O, CH_3CN) with CuI in organic solvents in the presence of various acetates, producing tetranuclear clusters of the general formula $[M_3CuS_4((EtO)_2PS_2)_3(\mu_2\text{-}O_2CR)L]$ (R = CH_3, CF_3, CCl_3; L = DMF, DMSO, py, CH_3CN), as shown in Equation (9).[70,94,95]

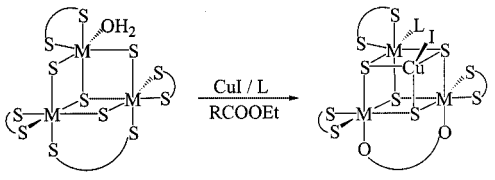

(9)

The Mo_3CuS_4 dithiocarbamate and dithiophosphinate complexes $[Mo_3CuS_4(Et_2NCS_2)_3(\mu_2\text{-}Et_2NCS_2)(py)I]$ and $[Mo_3CuS_4(R_2PS_2)_3(\mu_2\text{-}R_2PS_2)(py)I]$ (R = Et, *n*Pr) have also been prepared by reaction of the corresponding trimeric precursors with CuI in pyridine.[71,96,97] The presence of acetate ligands in the reaction media does not cause substitution of the bridging dithiocarbamate or dithiophosphinate, as is observed for the analogous dithiophosphate compound. This ligand environment provides these M_3CuS_4 complexes with great stability towards air oxidation, in contrast to the equivalent aquo complexes.

The structures of several of these derivatives have been determined by single-crystal X-ray diffraction experiments. Intermetallic distances for some representative complexes are listed in Table 2. The coordination environment around the M atoms is pseudooctahedral, as observed for the trinuclear starting materials, although in the case of the dithiophosphate derivatives the bridging μ_2-$(EtO)_2PS_2^-$ ligand has been substituted for a bridging acetate ligand. The pseudotetrahedral Cu atom is coordinated to the iodine atom. The average M−M and M−Cu bond lengths are similar to those reported for the 16 metal electron aquo derivative $[Mo_3CuS_4Cl(Hnta)_3]^{2+}$. However, the presence of a ligand bridging two molybdenum or tungsten atoms causes a shortening of this M−M bond length by ca. 0.08 Å, with concomitant lengthening of the M−Cu bonds by ca. 0.05−0.08 Å. The M−Cu distances are between 0.1 and 0.2 Å longer than the M−M′ (M′ = Co or Ni) bond lengths observed for other 16 metal electron clusters.

$M_3M'S_4$ Clusters with Phosphanes

A series of heterodimetallic clusters of molybdenum and tungsten with $M_3M'Q_4$ (Q = S, Se) units have been reported for M′ = Cu, where the group-6 metal atom is coordinated to different bidentate phosphanes such as dmpe or dppe. Recent work in our group has shown that the procedures employed can also be extended to Co and Ni.[98] The preparation of these tetrametallic species has also been achieved through a [3 + 1] synthetic strategy, using the molecular clusters $[M_3Q_4(diphosphane)_3X_3]^+$ [M = Mo, W; Q = S, Se; X = Cl, Br; diphosphane = 1,2-bis(dimethylphosphanyl)ethane (dmpe), 1,2-bis(diphenylphosphanyl)ethane (dppe)] as starting materials. The excision of polymeric $\{M_3Q_7X_4\}_x$ phases with chalcogen-abstracting ligands such as phosphanes has proved to be a general method for the preparation of M_3Q_4 incomplete cuboidal clusters having phosphanes as ancillary ligands.[54,99–101] The cationic $[M_3S_4(dmpe)_3X_3]^+$ trimers are obtained in high yields (> 90%) by excision of the corresponding $\{M_3S_7X_4\}_x$ polymers with dmpe in refluxing acetonitrile.[102] The analogous dppe derivatives $[M_3S_4(dppe)_3X_3]^+$ are obtained in ca. 75% under similar reaction conditions. This synthetic method can also be extended to selenium, with typical yields of 50−65% for the $[M_3Se_4(dmpe)_3X_3]^+$ complexes and 67−85% for the $[M_3Se_4(dppe)_3X_3]^+$ compounds.[75,98,103,104] Alternatively, the $[M_3S_4(diphosphane)_3X_3]^+$ [diphosphane = dmpe, 1,2-bis(diethylphosphanyl)ethane (depe)] complexes can be obtained in 15−55% yields by treating the metal halides with NaHS in THF/methanol in the presence of an excess of dmpe or depe.[105–107] The synthesis of the (dppe)molybdenum derivatives in approximately 50% yield has been reported from the reaction of the molecular cluster $[Mo_3S_7X_6]^{2-}$ (X = Cl, Br) with dppe in methanol.[54] In addition, the $[M_3Se_4(dppe)_3X_3]^+$ cationic cluster can be obtained by excision of the polymeric precursor in molten

dppe, with an overall reaction yield of 40 and 62% for the Mo and W derivatives, respectively.[108] These $[M_3Q_4(diphosphane)_3X_3]^+$ complexes have one phosphorus atom *trans* to the capping sulfur atom and another *trans* to the bridging sulfur atom, as shown in Figure 4. This arrangement results in chiral complexes with an effective C_3 symmetry. However, the nonstereospecificity of the reaction leads to racemic mixtures.

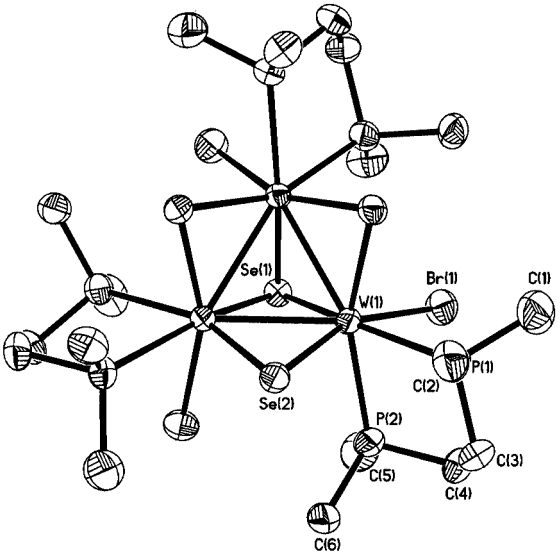

Figure 4. ORTEP representation of the $[W_3Se_4(dmpe)_3Br_3]^+$ cation; only the atoms in the asymmetric unit are labeled

The first attempt to introduce a first-row transition metal atom into an incomplete cuboidal M_3S_4 unit was the reaction between the molybdenum(IV) trimer $[Mo_3S_4Cl_4(PEt_3)_3(MeOH)_2]$ and $[Ni(cod)_2]$ in THF which afforded a pentanuclear $Mo_3Ni_2S_4$ cluster instead of the expected Mo_3Ni cubane. X-ray structural analysis of this pentanuclear sulfido cluster revealed a square-pyramidal core with an Mo_2Ni_2 base, an Mo atom at the vertex, and short intermetallic distances: d(Mo−Mo) = 2.65−2.67 Å, d(Mo−Ni) = 2.50−2.67 Å and d(Ni−Ni) = 2.71 Å. An oxidation state assignment of $Mo_3^{IV}Ni_2^0$ has been proposed based on the XPS spectra, suggesting that Ni incorporation into the Mo trimer occurs without changes in the metal oxidation states.[101]

Cubane-type Mo_3CuQ_4 and W_3CuS_4 clusters have been obtained by reaction of the trimers $[Mo_3Q_4(dmpe)_3X_3][PF_6]$ and $[W_3S_4X_3(dmpe)_3][PF_6]$ in THF with CuX, or with $[Cu(CH_3CN)_4][PF_6]$ in the presence of a tetrabutylammonium halide salt, to give the corresponding $[M_3CuQ_4(dmpe)_3X_4][PF_6]$ heterodimetallic tetramers, according to Equation (10).[5,75]

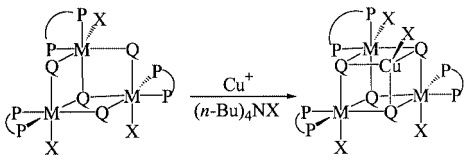

(10)

The products are air-stable and soluble in common organic solvents such as CH_2Cl_2 and CH_3CN. Typical yields for the reaction range from 40 to 73%. The reaction takes place without overall changes in the oxidation states of the metal atoms, and these M_3CuQ_4 clusters possess 16 electrons for metal−metal bonding. X-ray structural analysis reveals that there is no significant structural rearrangement on going from M_3Q_4 to M_3CuQ_4, and in consequence the resulting heterodimetallic clusters are also chiral, although the product is again obtained as a racemic mixture. Metal−metal distances for some representative complexes are listed in Table 2. The M−M distances do not change significantly between molybdenum and tungsten, while the M−M bonds in the selenido derivatives are ca. 0.06 Å longer than the corresponding distances in the sulfido complexes. The Mo−Cu bonds in the sulfido clusters are 0.04 Å longer than the Mo−Mo distance, while the W−Cu bond is 0.1 Å longer than the W−W distance. This distortion of the tetrametallic unit can be regarded as an elongation along the C_3 axis through Cu, and is less pronounced for the selenido clusters in comparison to the analogous sulfido complexes. The average M−M and M−Cu bond lengths are similar to those reported for other M_3CuQ_4 clusters having an identical metal electron population of 16 e^-.

As previously mentioned, trinuclear $[M_3Q_4(diphosphane)_3X_3]^+$ (diphosphane = dmpe, dppe; X = Cl, Br) complexes can also incorporate atoms of other metals such as nickel or cobalt through reaction of the trimeric cations with $[Ni(cod)_2]$ or $[Co_2(CO)_8]$.[98] Alternatively, an entry to these complexes through the $[Mo_3NiS_4(H_2O)_9Cl]Cl_3$ aquo ion has been proposed. Water substitution takes place by treating the solid aquo ion with dppe in methanol to afford $[Mo_3NiS_4(dppe)_3Cl_4]$ in 43% yield.[80] In contrast to the reactivity observed at the Ni site in the analogous cyclopentadienyl complexes, the Cl ligand attached to the Ni atom cannot be replaced by CO, PMe_3 or PMe_2Ph. On the other hand, electrospray mass spectrometry of the Ni derivatives prepared by direct Ni insertion into the trimer $[M_3S_4(diphosphane)_3X_3]^+$ shows coordination of a solvent molecule to the heteroatom. This solvent molecule can then be substituted for a various N- and S-donor ligands.

$M_3M'S_4$ Clusters with N−O Donor Tripodal Ligands

There is only one example of this type of clusters but it deserves special mention because it is the only case of an Mo_3CuS_4 complex with a simple cubane structure and an odd number of metal cluster electrons (17 e^-). The compound $[Mo_3CuS_4(tdci)_3Br]^{3+}$ [tdci = 1,3,5-trideoxy-1,3,5-tris(dimethylamino)-*cis*-inositol] was prepared in 55% yield by treating the trinuclear precursor $[Mo_3S_4(tdci)_3]^{4+}$ with copper metal in ethanol.[74] This synthetic route contrasts with the other procedure reported in non-aqueous solvents, in that Cu metal is used as starting material instead of a Cu^I halide, and this difference results in a change in the number of cluster metal electrons from 16 to 17. This complex has been structurally characterised and the intermetallic distances are listed in Table 2. The observed Mo−Mo and Mo−Cu distances in $[Mo_3CuS_4(tdci)_3Br]^{3+}$ are longer

than those found in all reported Mo_3CuS_4 complexes having single cube structures and 16 metal electrons.

Electronic Structure, Electrochemistry and Magnetism

$M_2M'_2S_4$ Clusters

The most common ligand arrangement for the $M_2M'_2$ cubane-type clusters results in a pseudooctahedral geometry around the 4d or 5d metal, M, and a pseudotetrahedral coordination environment for the first-row transition metal, M′. Harris et al. have developed a qualitative molecular orbital (MO) scheme for this system.[109] In this model, the metal M "t_{2g}" and the M′ "t_2" orbitals combine to form a set of six bonding and six antibonding orbitals, while the M "e_g" and the M′ "e" orbitals remain nonbonding. This results in a total of ten metal-based MOs; four nonbonding low-lying MOs which are predominately M′ in character and six bonding "t" symmetry MOs of higher energy. Based on this model, a cluster metal electron count of 20 is expected to be necessary for a completely bonding metal $M_2M'_2$ tetrahedron and any metal electrons in excess of this number are expected to occupy antibonding orbitals.

Table 1 lists intermetallic distances together with carbonyl and nitrosyl frequencies for some representative complexes with $Mo_2M'_2S_4$ and $W_2M'_2S_4$ central units. The strongest metal−metal interactions occur between the 4d or 5d metals in these complexes, and the weakest interactions are between the two 3d metals. These clusters can exist with metal electron counts between 16 and 22, although in the case of Cu and Ni only 22 electron systems have been reported to date. In the 20 electron clusters there are nominally six metal−metal bonds, and a bond order of one is assigned to the M′−M′ bond. Differences in bond lengths between the Fe and Co complexes can be ascribed to the slightly larger covalent radius of Fe as compared to Co. All 20 electron clusters are diamagnetic.

The clusters with 16 or 18 metal electrons show a marked increase in the M′−M′ distance. In the 18 e^- systems, eight electrons will occupy the low-lying nonbonding orbitals leaving ten electrons to fill five metal−metal bonding orbitals. Different situations arise depending on the nature of these MOs, which may be highly delocalised over the tetrametallic core or localised between metal pairs. In the $[Mo_2Co_2S_4Cp^{Et}_2X_2]$ (X = halogen) clusters, it appears that the electron density has been removed from the Co−Co bond, resulting in a long nonbonding Co···Co distance. In the thiolato cluster $[Mo_2Co_2S_4Cp^{Et}_2(SPh)_2]$, much less electron density appears to be removed from the Co−Co bond and an apparent bond order near 0.5 results.[21] These differences can be attributed to the differences in electronegativities and π-donor characteristics of the ligands on the Co atoms. These differences evidently affect the degree of localisation/delocalisation of the metal-based MOs involved in Co−Co bonding. In the 16 electron $[Mo_2Fe_2S_4Cp^*_2X_2]$ cluster, the electron density is also preferentially removed from the Fe−Fe bond.[20] The ^{1}H NMR spectrum of this complex in $CDCl_3$ showed a broad singlet at δ = 1.81 ppm, indicating the weak paramagnetic nature of this compound. On the other hand, the ^{1}H NMR spectrum of the 18 e^- $[Mo_2Co_2S_4Cp^{Et}_2X_2]$ (X = I, Br, Cl) complexes showed clear NMR peaks corresponding to those expected for Cp^{Et} ligands on diamagnetic clusters even though these complexes are paramagnetic both in solution and in the solid state. These $[Mo_2Co_2]^{12+}$ halo compounds exhibit complex spin equilibria with thermally accessible S = 1, 2 and 3 spin states and consequently there is no simple explanation for their apparently diamagnetic ^{1}H NMR spectra. In contrast, the analogous thiolate cluster shows simple paramagnetism consistent with an S = 1 spin state, which may simply mean that the S = 2 state is not thermally accessible at the temperature studied since the thiolate ligands are better π-donors than halide ligands. No ^{1}H NMR signal is observed for the $[Mo_2Co_2S_4Cp^{Et}_2(SPh)_2]$ thiolate cluster, as expected for a paramagnetic system. The differences in magnetic behaviour between the halide and thiolate $[Mo_2Co_2]^{12+}$ complexes are not well understood and require further investigation.

The butterfly arrangement observed in the 16 and 18 metal electron clusters is also seen in the 21 and 22 e^- complexes, and the M−M and M−M′ distances correspond to single bonds (see Table 1). The M′−M′ distance in the 22 metal electron complex is nonbonding, suggesting that the HOMO is an M′−M′ σ* antibonding orbital. The Co−Co bond lengths of 2.75 Å found in the 21 e^- clusters are halfway between the fully bonded distance of 2.57 Å found in the 20 electron clusters and the nonbonding distance observed for the 22 electron systems, supporting the M′−M′ antibonding character of the HOMO. This interpretation is also supported by the ESR spectrum of the $[Mo_2Co_2S_4Cp^{Et}_2(CO)_2]^-$ complex which is consistent with the odd electron being delocalised over two Co atoms, each with spin I = 7/2; 13 of the expected 15 lines were observed, with the outer two being too weak.[26] Addition of another electron reduces the M′−M′ bond order to zero, producing diamagnetic complexes.

Qualitative bonding schemes have also been developed for other M_2M_2' cubane sulfido clusters with different metal coordination environments to the ones previously discussed. Changes in the symmetry of the system result in different electron counts for the formation of intermetallic cluster bonds. For example, the Dahl group has developed an MO energy diagram for homometallic $[M_4S_4Cp_4]$ clusters based on the cubic T_d symmetry of the metallic tetrahedron that makes it possible to predict and understand the changes in metal−metal bonding which accompany changes in the number of electrons.[110] The number of metal electrons required for a completely filled set of six M−M bonding orbitals (a_1 + e + t_2) is 12. This bonding scheme is also assumed to be applicable to the relatively rare heterometallic $[M_2M'_2S_4Cp_4]$ clusters. Although there are no structural data on these clusters, spectroscopic evidence suggests that the $[Mo_2Cr_2S_4Cp^*_2Cp_2]$ complex with 12

cluster electrons has a cubane-type structure with presumably a fully bonded metal tetrahedron.[38]

Another combination of metal coordination geometries is found in the $[Mo_2Fe_2Cp_2(CO)_4]$ cluster with a square-pyramidal "$FeS_3(CO)_3$" fragment. Fenske−Hall calculations on this complex predict that a cluster electron count anywhere between 12 and 16 e^- should lead to a completely bonding metal tetrahedron.[111] In the 18 electron $[Mo_2Fe_2Cp_2(CO)_4]$ compound, two electrons will occupy an Fe−Fe antibonding orbital and the long Fe−Fe distances observed in this complex agree with this prediction. On the other hand, the $[Mo_2Fe_2S_4(\mu_2\text{-}S_2CNEt_2)(S_2CNEt_2)_4]$ complex, also with a pentacoordinate iron fragment (albeit trigonal-bipyramidal instead of square-pyramidal) and 15 metal cluster electrons, has a full set of six metal−metal bonds.

Finally, the $[M_2Cu_2S_4(S_2C_2H_4)_2(PPh_3)_2]$ complexes with a pentacoordinate environment for the molybdenum and tungsten atoms that differs from the octahedral coordination found in the remaining $M_2M'_2$ clusters have the same butterfly-cubane geometry found in the octahedrally coordinated Mo and W complexes. Although no qualitative MO energy diagram of this system has been developed, the structural findings also agree with the existence of an antibonding HOMO localised between the two copper atoms, as theoretically predicted for the $M_2M'_2S_4$ cyclopentadienyl derivatives.

A comparison of the IR spectra of the Mo clusters and their W analogues shows that the ν_{CO} or ν_{NO} values are lower for the tungsten clusters in all cases, indicating a higher back-donation for the heavier metal which is effectively more electron-rich. This is consistent with the electrochemical results. Cyclic voltammetry studies show that these systems undergo reversible or quasireversible conversions between the 20, 21 and 22 metal electron species. The reported redox potentials for representative $M_2M'_2$ compounds are listed in Table 3. The tungsten clusters are more difficult to reduce and easier to oxidise than their molybdenum analogues, which is also consistent with the tungsten complexes being more electron-rich.

$M_3M'Q_4$ Clusters

Fenske−Hall MO calculations on $M_3M'S_4$ complexes show the presence of a group of three strongly bonding cluster MOs (1e and $1a_1$), a doubly degenerate M′-based bonding orbital (2e), a group of three weakly antibonding cluster MOs ($2a_1$ and 3e) and three strongly antibonding cluster MOs (4e and $3a_1$).[112] In the clusters having electron counts of 14 and 16 e^-, 12 metal electrons will occupy the cluster bonding orbitals and the weakly antibonding $2a_1$ orbital, and two or four electrons will partially or fully occupy the 3e HOMO. Metal electrons in excess of 16 will occupy strongly antibonding 4e and $3a_1$ cluster MOs.

This MO scheme is supported by magnetic susceptibility measurements on powdered samples of single crystals of $[Mo_3M'S_4(H_2O)_{10}][pts]_4\cdot 7H_2O$ (M′ = Fe, Ni) which give effective moments of 2.78 B.M. at 2.16 K and 3.26 B.M. at 269.95 K for M′ = Fe and 0.11 B.M. at 2.00 K and 1.26 B.M. at 260.7 K for M′ = Ni.[65,113,114] These results are consistent with the presence of two unpaired electrons in the Mo_3Fe 14 metal electron cluster and no unpaired electrons in the Mo_3Ni 16 metal electron cluster. No ESR spectra could be observed for frozen solutions of $[Mo_3FeS_4(H_2O)_{10}]^{4+}$ in 2 M HCl or $HClO_4$ at temperatures down to 4.2 K, in agreement with an S = 1 ground state for this system. The magnetic susceptibility data for $[Mo_3M'S_4(H_2O)_{10}](pts)_4\cdot 7H_2O$ (M′ = Fe, Ni) were analysed using the vector model formalism of Kambe and the

Table 3. Redox potentials [V vs. Fc] of some representative $Mo_2M'_2S_4$ cubane-type clusters

Cluster[a]	No. of metal electrons	E_{red}	E_{ox}	Conditions	Correction	Ref.
$[Mo_2Fe_2S_4Cp^*_2Cl_2]$	16	−1.44 (rev.)		glassy carbon electrode THF/$[Bu_4N][ClO_4]$	[b]	[20]
$[Mo_2Fe_2S_4\ Cp^{Et}_2(NO)_2]$	20	−1.12 (rev.) −1.52 (rev.) −1.86 (rev.)	0.22 (irr.) 0.60 (irr.) 0.90 (irr.)	platinum electrode $CH_3CN/[Bu_4N][PF_6]$	[c]	[22]
$[W_2Fe_2S_4Cp^*_2(NO)_2]$	20	−1.72 (rev.) −1.90 (rev.) −2.33 (qrev.)	0.08 (irr.) 0.40 (irr.) 1.14 (qrev.)	platinum electrode $CH_3CN/[Bu_4N][PF_6]$	[c]	[22]
$[Mo_2Co_2S_4Cp^{Et}_2(CO)_2]$	20	−1.44 (rev.)	−0.20 (irr.) 0.22 (irr.)	platinum electrode $CH_3CN/[Bu_4N][PF_6]$	[c]	[22]
$[Mo_2Ni_2S_4Cp^*_2Cp_2]$	20	−1.47 (rev.) −2.30 (irr.)	−0.22 (rev.) 0.24 (rev.)	platinum electrode $CH_3CN/[Bu_4N][BF_4]$	[d]	[27]
$[Mo_2Co_2S_4Cp^{Et}_2(NO)_2]$	22	−1.93 (rev.)	−0.60 (rev.)	platinum electrode $CH_3CN/[Bu_4N][PF_6]$	[c]	[22]
$[W_2Co_2S_4Cp^*_2(NO)_2]$	22	−2.15 (rev.)	−0.47 (rev.)	platinum electrode $CH_3CN/[Bu_4N][PF_6]$	[c]	[22]
$[Mo_2Ni_2S_4Cp'_2(CO)_2]$	22	−1.65 (rev.) −2.18 (rev.)	0.15 (irr.) 0.35 (irr.)	platinum electrode $CH_3CN/[Bu_4N][BF_4]$	[d]	[27]
$[Mo_2Cu_2S_4(C_2H_4S_2)_2(PPh_3)_2]$	22	−1.22 (irr.)	−	platinum electrode $CH_2Cl_2/[Bu_4N][ClO_4]$	[e]	[31]
$[W_2Cu_2S_4(C_2H_4S_2)_2(PPh_3)_2]$	22	−1.66 (irr.)	−	platinum electrode $CH_2Cl_2/[Bu_4N][ClO_4]$	[e]	[31]

[a] Half-wave potential ($E_{1/2}$) is given unless the wave is irreversible (irr.), in which case the peak potential (E_p) is given. [b] Fc 0.56 V vs. SCE (THF/$[NBu_4][PF_6]$); conversion into Fc approximate. [c] Fc 0.40 V vs. NHE.[22] [d] Fc 0.07 V vs. $Ag[NO_3]/Ag$.[27] [e] Fc 0.46 V vs. SCE ($CH_2Cl_2/[NBu_4][PF_6]$); conversion into Fc approximate.

experimental data were fitted to a model with an $Mo^{IV}Mo_2^{III}M'^{II}$ core. The ground state assignment agrees with the experimental results of ^{57}Fe-Mössbauer spectroscopy, where the oxidation state of the iron atom in the Mo_3Fe cluster has been determined to be +2.39. The order of the binding energies of Mo $3d_{3/2}$ and Mo $3d_{5/2}$ for these tetranuclear clusters and their trinuclear Mo_3 precursor have been obtained from X-ray photoelectronic spectra to give the following values: $E(Mo_3)$ = 233.7, 230.7 eV; $E(Mo_3Fe)$ = 233.1, 230.0 eV and $E(Mo_3Ni)$ = 233.3, 230.3 eV. The fact that $E(Mo_3) > E(Mo_3M')$ indicates a real charge transfer from the incorporated metal atom to the Mo_3 trimer, in good agreement with the previous $Mo^{IV}Mo_2^{III}M'^{II}$ metal oxidation state assignment.

A comparison of the bond lengths between the 14 and 16 metal electron M_3M' clusters with single-cube structures (see Table 2) does not show any clear relationship between the intermetallic distances and the number of metal electrons, in contrast to the general findings for $M_2M'_2$ complexes. This fact can be attributed to the highly delocalised nature of the bond in the M_3M' system. On the other hand, significant differences are observed in the metal−metal bond lengths between clusters with identical $Mo_3M'S_4$ cores and the same number of metal electrons, indicating that changes in the donor ability of the outer ligands have important effects on the electronic structure of the cluster.

Fenske−Hall calculations also show that the bonding/antibonding character of the middle group of cluster orbitals ($2a_1$ and 3e) is affected by the relative energies of the M′ and M_3 fragment orbitals.[112] As the M′ fragment orbitals increase in energy relative to the Mo_3 fragment orbitals, they mix more strongly with the unoccupied Mo_3S_4 fragment orbitals and as a result, the middle group of cluster orbitals becomes more bonding (or in this case, less antibonding). The energies of the M′ fragment increase in the order Cu < Ni < Co < Fe and thus the antibonding character of the ($2a_1$ and 3e) orbitals decrease according to the sequence Cu > Ni > Co > Fe. Consequently, the strength of the M−M′ interaction increases in the order Cu < Ni < Co < Fe. This effect is seen in the calculated M−M′ bond orders of 0.561 and 0.432 for $[Mo_3CoS_4Cp'_3(CO)]$ and $[Mo_3NiS_4(H_2O)_9(CO)]^{4+}$, respectively.

Discrete variational (DV) Xα calculations carried out on $[Mo_3M'S_4(H_2O)_{10}]^{4+}$ (M′= Fe, Ni) complexes agree with the general picture of the bond provided by the Fenske−Hall scheme, except that the Xα method gives a HOMO with "a" symmetry for both the Mo_3Fe and the Mo_3Ni complexes.[65] In the case of nickel the HOMO symmetry matches the LUMO of small molecules such as carbon monoxide or ethylene, thus explaining the reactivity of the Mo_3Ni cluster towards these molecules. The absence of reactivity found for the iron complex has been attributed to the lack of symmetry matching between the Mo_3Fe cluster HOMO and the LUMO of these small molecules.

The only compounds with $[M_3M'Q_4]$ cores and 17 metal cluster electrons to have been structurally characterised are those with M = Mo, M′ = Cu and Q = S, and two different structural types, isolated cube and double cubane, have been identified. In all cases, the Mo−Cu distances are longer than those observed for the analogous 16 electron clusters. Extended Hückel MO calculations on isolated Mo_3CuS_4 complexes suggest that the extra electron in the 17 e^- cluster occupies a strongly antibonding Mo−Mo and Mo−Cu orbital, thus explaining the longer Mo−Mo and Mo−Cu distances observed for $[Mo_3CuS_4(tdci)_3Br]^{3+}$ [tdci = *cis*-1,3,5-tris(dimethylamino)inositol].[74,77]

EPR studies on the 17 electron mixed-metal single-cubane cluster $[Mo_3CuS_4(H_2O)_{10}]^{4+}$, generated by decomposition of the double cubane cluster complex $[\{Mo_3CuS_4(H_2O)_9\}_2]^{8+}$, indicate that the complex is paramagnetic with S = 1/2 and the hyperfine splitting is consistent with a metal oxidation state formulation of $Mo_2^{IV}Mo^{III}Cu^{I}$ in which the paramagnetic centre is mainly located on one of the molybdenum atoms. The Mo^{III} site is not fixed at a specific position but moves over the three molybdenum sites at a rate of the order of 10^7 s^{-1}.[77] Extended Hückel MO calculations on the $[Mo_3CuS_4(H_2O)_{10}]^{4+}$ aquo ion agree with a large spin distribution on Mo, as observed experimentally.

The redox properties of these $M_3M'Q_4$ complexes have been investigated by cyclic voltammetry and a list of selected potentials is presented in Table 4.

In general, the M_3M' clusters are easier to reduce than their $M_2M'_2$ counterparts and, with the exception of the $[Mo_3NiS_4(dppe)_3Cl_4]$ complex which has a reversible oxidation wave at 0.2 V (vs. Fc), no oxidation processes have been reported for the M_3M' compounds, in contrast to the rich electrochemical activity found for the $M_2M'_2$ clusters upon oxidation.[80] As found for the $M_2M'_2$ system, the tungsten derivatives are more difficult to reduce than those of molybdenum. An interesting point arises when comparing the electrochemical behaviours of the tetrametallic $M_3M'Q_4$ clusters with those of their trimeric M_3Q_4 precursors. In the case of the Fe or Ni incorporation into the $[Mo_3S_4]^{4+}$ aquo ion, the resulting $[Mo_3M'S_4(H_2O)_{10}]^{4+}$ (M′ = Fe, Ni) complexes are ca. 0.45 V more difficult to reduce than their precursor aquo trimers.[65] These observations suggest a formal oxidation state for the metals of $Mo^{IV}Mo_2^{III}M'^{II}$, in agreement with the Mössbauer and XPS experimental results. The three reduction waves can then be attributed to three monoelectronic processes, namely $Mo^{IV}Mo_2^{III}M'^{II} \rightleftarrows Mo^{IV}Mo_2^{III}M'^{I} \rightleftarrows Mo^{IV}Mo_2^{III}M'^{0} \rightleftarrows Mo_3^{III}M'^{0}$, taking into account that the peak potential for the third reduction of these Mo_3Fe and Mo_3Ni complexes is very close to that for the third reduction of the $[Mo_3S_4]^{4+}$ aquo precursor in which $Mo^{IV}Mo_2^{III}$ is reduced to Mo_3^{III}.

In contrast to the Fe and Ni findings, Cu insertion into the $[M_3Q_4(dmpe)_3X_3]^+$ trimers results in an anodic shift of the redox potential in the sulfides and selenides of both molybdenum and tungsten.[5,75] This fact, together with the $Mo_2^{IV}Mo^{III}Cu^{I}$ oxidation state assignment of the 17 electron $[Mo_3CuS_4]^{4+}$ aquo ion (based on EPR results) and close inspection of the redox potential values for the Mo_3Cu complexes and their Mo_3 precursors (see Table 4), has led us to propose the following reduction mechanism: $Mo_3^{IV}Cu^{I} \rightleftarrows Mo_2^{IV}Mo^{III}Cu^{I} \rightleftarrows Mo^{IV}Mo_2^{III}Cu^{I}$. Note that the potential

Table 4. Redox potentials [V vs. Fc] of some representative $M_3M'Q_4$ cubane-type clusters and their trinuclear M_3S_4 precursors

Cluster[a]	No. of metal electrons	E_{red}	Conditions	Correction	Ref.
$[Mo_3S_4(H_2O)_9]^{4+}$	6	−0.54 (qrev.) −1.10 (qrev.) −1.83 (irr.)	glassy carbon electrode $CH_3CN/[Bu_4N][PF_6]$	[b]	[65]
$[Mo_3FeS_4(H_2O)_{10}]^{4+}$	14	−1.00 (irr.) −1.56 (irr.) −1.90 (irr.)	glassy carbon electrode $CH_3CN/[Bu_4N][PF_6]$	[b]	[65]
$[Mo_3NiS_4(H_2O)_{10}]^{4+}$	16	−1.00 (irr.) −1.57 (irr.) −1.81 (irr.)	glassy carbon electrode $CH_3CN/[Bu_4N][PF_6]$	[b]	[65]
$[Mo_3S_4(dmpe)_3Cl_3]^{+}$	6	−1.13 (qrev.) −1.82 (irr.)	platinum electrode $CH_3CN/[Bu_4N][PF_6]$	[c]	[102]
$[Mo_3CuS_4(dmpe)_3Cl_4]^{+}$	16	−0.81 (qrev.) −1.19 (irr.)	platinum electrode $CH_3CN/[NBu_4][PF_6]$	[d]	[5]
$[Mo_3S_4(dmpe)_3Br_3]^{+}$	6	−1.00 (qrev.) −1.64 (irr.)	platinum electrode $CH_3CN/[Bu_4N][PF_6]$	[c]	[102]
$[Mo_3CuS_4(dmpe)_3Br_4]^{+}$	16	−0.73 (qrev.) −1.08 (irr.)	platinum electrode $CH_3CN/[Bu_4N][PF_6]$	[d]	[5]
$[Mo_3Se_4(dmpe)_3Br_3]^{+}$	6	−0.98 (irr.) −1.31 (irr.) −1.64 (irr.)	platinum electrode $CH_3CN/[Bu_4N][PF_6]$	[c]	[75]
$[Mo_3CuSe_4(dmpe)_3Br_4]^{+}$	16	−0.73 (qrev.) −1.31 (irr.) −1.56 (irr.)	platinum electrode $CH_3CN/[Bu_4N][PF_6]$	[c]	[75]

[a] Half-wave potential ($E_{1/2}$) is given unless the wave is irreversible (irr.), in which case the peak potential (E_p) is given. [b] Fc 0.094 V vs. Ag^+/Ag.[65] [c] Fc 0.44 V vs. Ag^+/Ag.[102] [d] Fc 0.5 V vs. Ag^+/Ag.[5]

values for the second reduction process of the Mo_3Cu complexes are similar to the peak potential of the first bielectronic wave found for the sulfide trimers, where Mo_3^{IV} is reduced to $Mo^{IV}Mo_2^{III}$. They are also similar to the peak potential of the second monoelectronic wave observed in the trinuclear selenides, where $Mo_2^{IV}Mo^{III}$ is reduced to $Mo^{IV}Mo_2^{III}$. A similar mechanism could be tentatively extended to the W_3CuS_4 complexes. In general the selenido clusters are more easily reduced than the analogous sulfides.

Properties and Applications

In this last section we highlight some properties of these $M_2M'_2S_4$ and $M_3M'Q_4$ transition metal chalcogenido clusters that make these complexes useful as materials with potential technological applications. We have chosen these properties based on our own interests in catalysis, nonlinear optics and the capability of these complexes to form supramolecular adducts.

Catalysis

The only molecular clusters of the type discussed in this microreview that have proved to resemble the industrial HDS heterogeneous catalyst are the $Mo_2Co_2S_x$ ($x = 3, 4$) complexes. As described in a previous section, $[Mo_2Co_2(\mu_3\text{-}S)_2(\mu_4\text{-}S)Cp'_2(CO)_4]$ reacts with thiols at temperatures of several hundred degrees below that used in the HDS of petroleum feed stocks to give the cubane cluster $[Mo_2Co_2S_4Cp'_2(CO)_2]$ in almost quantitative yields together with the corresponding hydrocarbon. No molecular rearrangement or alkene formation is observed in the course of the reaction. This fact, together with the stereospecificity of the reaction, indicates homolytic cleavage of the C−S bond.[25,115] The reaction of $[Mo_2Co_2S_3Cp'_2(CO)_4]$ with the thiolate $MeC_6H_4S^-$ was studied at −60 °C by NMR spectroscopy and it provides the first insight into the mechanism of desulfurisation. Initially, the thiolate ion binds a cobalt atom to form a red adduct. An increase of the temperature to −24 °C causes a transformation of this red adduct to a green compound in which the thiolate bridges the Co−Mo bond. Desulfurisation occurs upon heating this bridged adduct under reflux conditions in deuterated MeCN to produce $[D_1]$toluene (MeC_6H_4D) plus the radical anion $[Mo_2Co_2(\mu_3\text{-}S)_4Cp'_2(CO)_2]^-$, again supporting the idea of homolytic cleavage of the C−S bond.[25]

This $Mo_2Co_2S_3$ cluster also cleaves the C−S bond in thiols by an apparent free radical mechanism. The kinetics of thiol desulfurisation are first-order in both cluster and thiol concentration. When the reaction product $[Mo_2Co_2(\mu_3\text{-}S)_4Cp'_2(CO)_2]$ is heated at 150 °C with CO at 69 atm, a 20% conversion into $[Mo_2Co_2(\mu_3\text{-}S)_2(\mu_4\text{-}S)Cp'_2(CO)_4]$ and OCS is obtained. The combination of the sulfur abstraction reaction and the regeneration of $[Mo_2Co_2S_3Cp'_2(CO)_4]$ constitutes a cycle for catalytic carbonyl desulfurisation of organic sulfides, as represented in Scheme 7.[21,25,41,115]

The cluster $[Mo_2Co_2(\mu_3\text{-}S)_4Cp^{Et}_2(CO)_2]$ reacts with good sulfur donors such as thiiranes and thietanes to give the organic hydrocarbons that result from their hydrodesulfurisation, together with an insoluble black solid for which a polymeric structure of $[Mo_2Co_2(\mu_3\text{-}S)_4Cp^{Et}_2]$ cubes linked together by sulfur bridges has been proposed.[116]

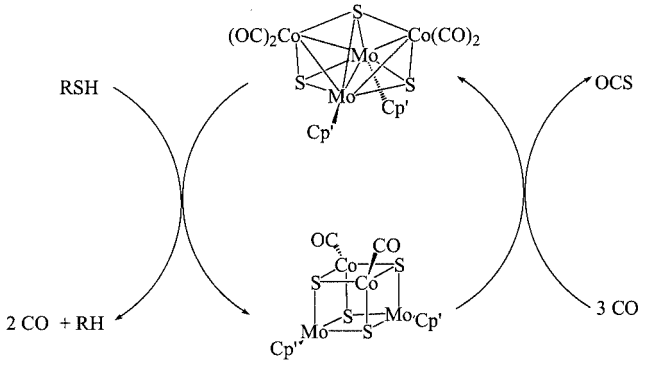

Scheme 7. Catalytic desulfurisation cycle of organic sulfides

$[Mo_2Co_2(\mu_3\text{-}S)_4Cp^{Et}_2(SPh)_2]$, obtained by oxidation of the carbonyl starting material cluster, was used to model the sulfur-bridged polymer. When $[Mo_2Co_2(\mu_3\text{-}S)_4Cp^{Et}_2(SPh)_2]$ is treated with H_2 (13.4×10^5 Pa)/CO (13.4×10^5 Pa) at 130 °C, the carbonyl cluster $[Mo_2Co_2(\mu_3\text{-}S)_4Cp^{Et}_2(CO)_2]$ is regenerated and gives PhSSPh as the sole organic product. Furthermore, a catalytic cycle for the conversion of PhSH to PhSSPh with the $Mo_2Co_2S_4$ cluster as catalyst is feasible.[21] It is interesting to point out that these $Mo_2Co_2S_x$ ($x = 3, 4$) clusters are capable of cleaving C−S bonds at temperatures several hundred degrees below that used in the industrial heterogeneous hydrodesulfurisation process, suggesting that C−S bond activation is not the rate-determining step in the industrial process, but rather the removal of sulfur from the surface of the catalyst.

The cluster $[Mo_2Co_2(\mu_3\text{-}S)_2(\mu_4\text{-}S)Cp'_2(CO)_4]$ has been supported on alumina and subjected to temperature-programmed decomposition under hydrogen. The activity and selectivity of this $MoCoS/Al_2O_3$ system for thiophene hydrodesulfurisation are similar to those of conventionally prepared catalysts under similar reaction conditions. Spectroscopic characterisation of the cluster-derived catalyst suggests that the clusters undergo oxidation by the surface upon loss of the organic ligands.[117]

The uptake of CO is often used as a measure of the HDS activity of a heterogeneous catalyst. The fact that several $M_3M'Q_4$ complexes react with CO supports the idea that these clusters may be functional models in homogeneous HDS catalysis.[63] The ability of the heterometal atoms in the $[M_3M'Q_4]^{n+}$ (M′= Fe, Co, Ni, Cu) aquo ions to bind CO has been correlated with the number of metal cluster electrons. The Mo_3CoS_4 and M_3NiQ_4 cubes with 15 and 16 metal electrons react with CO to afford the $[Mo_3CoS_4(H_2O)_9(CO)]^{4+}$, $[Mo_3NiQ_4(H_2O)_9(CO)]^{4+}$ and $[W_3NiS_4(H_2O)_9(CO)]^{4+}$ cationic clusters, which are more stable than their starting aquo ions. In the case of nickel, the presence of chloride ions in the reaction media precludes formation of the carbonyl adduct, and CO is replaced by Cl^- on addition of concentrated HCl to $[M_3NiQ_4(H_2O)_9(CO)]^{4+}$. Coordination of CO to $[Mo_3CoS_4(H_2O)_{10}]^{4+}$ is reversible, and bubbling nitrogen through $[Mo_3CoS_4(H_2O)_9(CO)]^{4+}$ regenerates the starting aquo ion. The $[Mo_3CuS_4(H_2O)_{10}]^{5+}$ cluster, which has the same 16 metal electron count as the Ni complexes, reacts with CO in a different manner to produce the trinuclear $[Mo_3S_4]^{4+}$aquo ion plus $[Cu(CO)]^+$. As observed for the cobalt system, bubbling of nitrogen regenerates the starting aquo cluster. On the other hand, the $[Mo_3FeS_4(H_2O)_{10}]^{4+}$ and $[Mo_3CuS_4(H_2O)_{10}]^{4+}$ clusters, with 14 and 17 metal cluster electrons, respectively, do not react with CO.[48]

The IR spectra of $[M_3NiS_4(H_2O)_9(CO)]^{4+}$ show CO stretching bands at 2077 cm^{-1} for M = Mo and 2045 cm^{-1} for M = W. IR spectra of heterogeneous NiWS catalysts after CO uptake display a CO band at 2090 cm^{-1}, suggesting that there are differences in the chemical environment between the nickel atoms in the NiMS heterogeneous catalyst and in the $[M_3NiS_4(H_2O)_9(CO)]^{4+}$ aquo ions. The structural characterisation of $[Mo_3NiS_4Cp'_3L]^+$ compounds in which the nickel atom is coordinated to organic sulfur- or nitrogen-containing ligands (L), do not indicate any activation of the C−S or C−N bonds, as reported in a previous section. In addition, the reaction between $[Mo_3NiS_4Cp'_3L]^+$ and benzothiophene/quinoline at 30 bar of H_2 and 130 °C does not reveal the formation of any of the expected hydrodesulfurisation or hydrodenitrogenation products.[67] This lack of HDS activity has been attributed to the low electron density on Ni, based on quantum mechanical calculations.[112] However, the limited backbonding to CO, a consequence of the low electron density on the heterometal, is also observed in the industrial MNiS catalysts. Further investigations are needed to understand these observations.

One of the key problems in the hydrodesulfurisation of light oil is the low reactivity of 4-methyldibenzothiophene and 4,6-dimethyldibenzothiophene, since the methyl groups hinder the approach of sulfur to the active sites of the catalyst. In order to overcome this limitation, $[Mo_3S_4(H_2O)_9]^{4+}$ and $[Mo_3NiS_4(H_2O)_9Cl]^{3+}$ have been loaded into zeolites in the hope that the acidic properties of zeolites might be capable of activating the alkyl group(s) in the thiophenic derivatives as the cluster core promotes the desulfurisation reaction. The Mo_3S_4 and Mo_3NiS_4 complexes have been incorporated into zeolites (NaY, HUSY, NaHβ, Na mordenite and KL) by aqueous ion-exchange without destruction of the zeolite structure.[118−120] The trinuclear cluster remains virtually intact after ion exchange. On the other hand, partial decomposition of the NiMo cluster to Ni^{2+} and the Mo_3S_4 trimer has been observed after ion exchange. The HDS activity of benzothiophenone is significantly affected by the zeolite structure and the best results are found for NaY or KL. The catalysts prepared by incorporation of the nickel heterodimetallic cluster were more active in the HDS reaction than those prepared by ion exchange of the Mo_3S_4 cluster with nickel nitrate solutions in the zeolites. The effectiveness of employing the MoNi mixed cluster suggests some similarities between the structure of the active sites and that of the Mo_3Ni heterodimetallic cluster.

Recent work in our group shows that the $[Mo_3CuS_4(dmpe)_3Cl_4]^+$ cationic cluster is a useful catalyst for the cyclopropanation of diazo compounds. The reaction of 1-diazo-5-penten-2-one in dichloromethane solutions un-

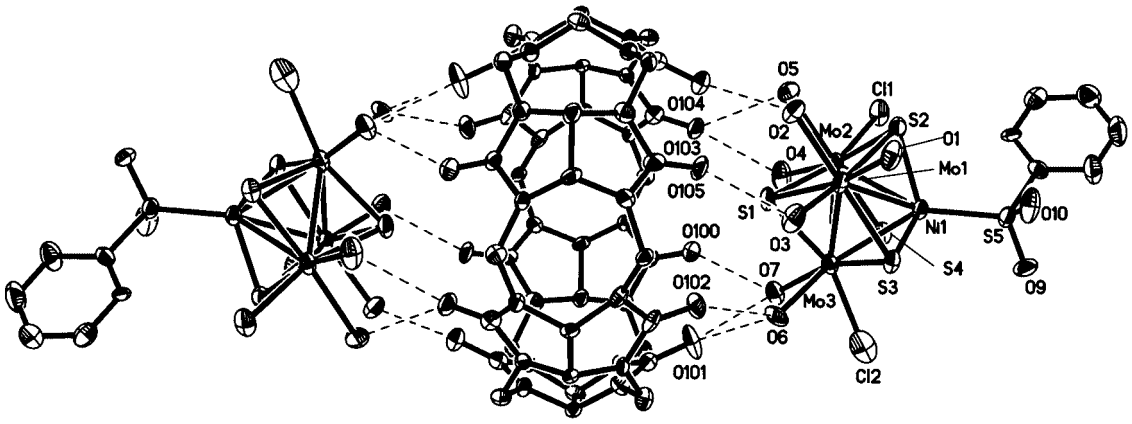

Figure 5. Drawing of the $[\{Mo_3[Ni(PhSO_2)]S_4(H_2O)_{7.83}Cl_{1.17}\}_2(C_{36}H_{36}N_{24}O_{12})]^{3.66+}$ supramolecular adduct with partial atom-numbering scheme

der reflux conditions for 3 d affords the cyclopropanation product bicyclo[3.1.0]pentan-2-one in yields greater than 95%.[121]

Nonlinear Optics

The optical-limiting merit of transition metal clusters has attracted much interest recently because these compounds combine the advantages of the presence of heavy atoms with structural versatility of the coordination environment. The clusters $[M_3CuS_4(dmpe)_3X_4]^+$ (X = Cl, Br) as well as their trinuclear precursors $[M_3Q_4(diphosphane)_3X_3]^+$ (diphosphane = dmpe, dppe) are all efficient optical limiters.[5,108] A large ratio of the effective excited-state cross section (σ_{eff}) to ground-state absorption cross section (σ_0) is one criterion for assessing potential as optical limiters. Values of σ_{eff}/σ_0 for these trinuclear and tetranuclear clusters lie within an order of magnitude (from 1.1 to 12), suggesting a common power-limiting mechanism, possibly purely thermal in origin. The threshold-limiting fluence in these optical limiters decreases on proceeding from the tetranuclear cluster to its trinuclear precursor and from the tungsten-containing to its molybdenum-containing analogue.

Formation of Supramolecular Adducts

The $M_3M'S_4$ aquo ions yield supramolecular compounds on reaction with macrocyclic ligands such as cucurbituril (cuc).[122,123] In cases where M′ is a first-row transition metal, this ligand forms stable compounds with cations such as $[Mo_3NiS_4(H_2O)_7Cl_3]^+$, $[Mo_3NiS_4(H_2O)_8Cl_2]^{2+}$ and $[Mo_3NiS_4(H_2O)_9(PhSO_2)]^{3+}$.[124,125] The typical arrangement (cluster)(cucurbituril)(cluster) is shown in Figure 5 for the latter derivative. The driving force for the crystallisation process is the formation of several complementary hydrogen bonds between the C=O groups and the water molecules coordinated to the cluster, and as a result, addition of cucurbituril is often used as a method to facilitate crystallisation of cuboidal aquo ions.

This entry to supramolecular chemistry also allows the development of host−guest chemistry. This is illustrated by the crystallisation of the supramolecular adduct $\{[Mo_3NiS_4(H_2O)_8Cl_2](pyH^+\subset cuc)\}Cl_3\cdot 14\cdot 5H_2O$ with a pyridinium cation inside the cucurbituril cavity.

Acknowledgments

This work was supported by the Spanish Dirección General de Enseñanza Superior e Investigación Científica (DGESIC, research project PB98-1044), Generalitat Valenciana (CTIDIB/2002/330) and Fundació Caixa Castelló-UJI (research project P1·1B2001-07).

[1] E. I. Stiefel, K. Matsumoto, *Transition Metal Sulfur Chemistry, ACS Symposium Series*, Honolulu (Hawai), **1995**.
[2] V. P. Fedin, J. Czyzniewska, R. Prins, T. Weber, *Appl. Catal. A* **2001**, *213*, 123−132.
[3] T. Weber, R. Prins, R. A. van Santen, *Transition Metal Sulfides − Chemistry and Catalysis*, Eds. Kluwer, Dordrecht, **1998**.
[4] Q.-F. Zhang, Y.-N. Xiong, T.-S. Lai, W. Ji, X.-Q. Xin, *J. Phys. Chem. B* **2000**, *104*, 3446−3449.
[5] M. Feliz, J. M. Garriga, R. Llusar, S. Uriel, M. G. Humphrey, N. T. Lucas, M. Samoc, B. Luther-Davies, *Inorg. Chem.* **2001**, *40*, 6132−6138.
[6] S.-B. Yu, A. B. Watson, *Chem. Rev.* **1999**, *99*, 2353−2377.
[7] S. B. Yu, M. Droege, B. Segal, S. H. Kim, T. Sanderson, A. D. Watson, *Inorg. Chem.* **2000**, *39*, 1325−1328.
[8] R. H. Holm, P. Kennepohl, E. I. Solomon, *Chem. Rev.* **1996**, *96*, 2239−2314.
[9] J. B. Howard, D. C. Rees, *Chem. Rev.* **1996**, *96*, 2965−2982.
[10] S. M. Malinak, D. Coucouvanis, *Prog. Inorg. Chem.* **2001**, *49*, 599−662.
[11] B. E. Schimth, *Adv. Inorg. Chem.* **1999**, *47*, 160−218.
[12] P. Braunstein, R. Jacky, *Metal Clusters in Chemistry* (Eds.: P. Braunstein, L. A. Oro, P. R. Raithby), Wiley-VCH Verlag GmbH, Weinheim, Germany, **1999**, vol. 2, p. 616−677.
[13] S. Shi, W. Ji, J. P. Lang, X. Q. Xin, *J. Phys. Chem.* **1994**, *98*, 3570−3572.
[14] S. Shi, W. Ji, S. H. Tang, J. P. Lang, X. Q. Xin, *J. Am. Chem. Soc.* **1994**, *116*, 3615−3616.
[15] T. Shibahara, *Coord. Chem. Rev.* **1992**, *123*, 73−147.
[16] T. Saito, *Adv. Inorg. Chem.* **1996**, *44*, 45.
[17] R. Hernandez-Molina, A. G. Sykes, *J. Chem. Soc., Dalton Trans.* **1999**, 3137−3148.
[18] R. Hernandez-Molina, M. N. Sokolov, A. G. Sykes, *Acc. Chem. Res.* **2001**, *34*, 223−230.
[19] M. Hidai, S. Kuwata, Y. Mizobe, *Acc. Chem. Res.* **2000**, *33*, 46−52.

[20] H. Kawaguchi, K. Yamada, S. Ohnishi, K. Tatsumi, *J. Am. Chem. Soc.* **1997**, *119*, 10871−10872.
[21] M. A. Mansour, M. D. Curtis, J. W. Kampf, *Organometallics* **1997**, *16*, 3363−3370.
[22] M. A. Mansour, M. D. Curtis, J. W. Kampf, *Organometallics* **1997**, *16*, 275−284.
[23] T. R. Halbert, S. A. Cohen, E. I. Stiefel, *Organometallics* **1985**, *4*, 1689−1690.
[24] M. D. Curtis, U. Riaz, O. J. Curnow, J. W. Kampf, A. L. Rheingold, B. S. Haggerty, *Organometallics* **1995**, *14*, 5337−5343.
[25] S. H. Druker, M. D. Curtis, *J. Am. Chem. Soc.* **1995**, *117*, 6366−6367.
[26] M. D. Curtis, S. H. Druker, L. Goossen, J. W. Kampf, *Organometallics* **1997**, *16*, 231−235.
[27] M. D. Curtis, P. D. Williams, W. M. Butler, *Inorg. Chem.* **1988**, *27*, 2853−2862.
[28] H. Brunner, R. Grabl, J. Wachter, B. Nuber, M. L. Ziegler, *J. Organomet. Chem.* **1990**, *393*, 119−129.
[29] J. Xu, J. Qian, Q. Wei, *Inorg. Chim. Acta* **1989**, *164*, 55−58.
[30] H. Brunner, N. Janietz, J. Wachter, T. Zahn, M. L. Ziegler, *Angew. Chem. Int. Ed. Engl.* **1985**, *24*, 133−135.
[31] N. Y. Zhu, Y. Zheng, X. Wu, *J. Chem. Soc., Chem. Commun.* **1990**, 780−781.
[32] J. Wu, N. Zhu, S. Du, X. Wu, J. Lu, *Inorg. Chim. Acta* **1991**, *185*, 181−185.
[33] N. Zhu, R. Wu, X. Wu, *Acta Crystallogr., Sect. C* **1991**, *47*, 1537−1539.
[34] H. Brunner, W. Meier, J. Wachter, E. Guggolz, T. Zahn, M. L. Ziegler, *Organometallics* **1982**, *1*, 1107−1113.
[35] M. R. Dubois, D. L. Dubois, M. C. VanDerveer, R. C. Haltiwanger, *Inorg. Chem.* **1981**, *20*, 3064−3071.
[36] M. D. Curtis, P. D. Williams, *Inorg. Chem.* **1983**, 2661−2662.
[37] R. A. Schunn, C. J. Fritchie, C. T. Prewitt, *Inorg. Chem.* **1966**, *5*, 892−899.
[38] H. Brunner, H. Kauermann, J. Wachter, *J. Organomet. Chem.* **1984**, *265*, 189−198.
[39] U. Riaz, O. J. Curnow, M. D. Curtis, *J. Am. Chem. Soc.* **1994**, *116*, 4357−4363.
[40] H. Brunner, J. Wachter, *J. Organomet. Chem.* **1982**, *240*, C41−C44.
[41] M. A. Mansour, M. D. Curtis, J. W. Kampf, *Organometallics* **1995**, *14*, 5460−5462.
[42] H. Brunner, H. Kauermann, J. Wachter, *Angew. Chem. Int. Ed. Engl.* **1983**, *22*, 549−550.
[43] K. F. Miller, A. E. Bruce, J. L. Corbin, S. Wherland, E. I. Stiefel, *J. Am. Chem. Soc.* **1980**, *102*, 5102−5104.
[44] W.-H. Pan, T. Chandler, J. H. Enemark, E. I. Stiefel, *Inorg. Chem.* **1984**, *23*, 4265−4269.
[45] S. A. Cohen, E. I. Stiefel, *Inorg. Chem.* **1985**, *24*, 4657−4662.
[46] N. Y. Zhu, Y. Zheng, X. Wu, *Inorg. Chem.* **1990**, *29*, 2705−2707.
[47] T. Ikada, S. Kuwata, Y. Mizobe, M. Hidai, *Inorg. Chem.* **1998**, *37*, 5793−5797.
[48] R. Hernandez-Molina, A. G. Sykes, *Coord. Chem. Rev.* **1999**, *187*, 291−302.
[49] I. J. McLean, R. Hernandez-Molina, M. N. Sokolov, M. S. Seo, A. V. Virovets, M. R. J. Elsegood, W. Clegg, A. G. Sykes, *J. Chem. Soc., Dalton Trans.* **1998**, 2557−2562.
[50] T. Shibahara, H. Akashi, H. Kuroya, *J. Am. Chem. Soc.* **1986**, *108*, 1342−1343.
[51] F. A. Cotton, Z. Dori, R. Llusar, W. Schwotzer, *J. Am. Chem. Soc.* **1985**, *107*, 6734−6735.
[52] T. Shibahara, H. Kuroya, *Polyhedron* **1986**, *5*, 357−361.
[53] P. Kathirgamanathan, M. Martinez, A. G. Sykes, *J. Chem. Soc., Chem. Commun.* **1985**, 953−954.
[54] V. P. Fedin, M. N. Sokolov, Y. V. Mironov, B. A. Kolesov, S. V. Tkachev, V. Y. Fedorov, *Inorg. Chim. Acta* **1990**, *167*, 39−45.
[55] R. Hernandez-Molina, D. N. Dybtsev, V. P. Fedin, M. R. J. Elsegood, W. Clegg, A. G. Sykes, *Inorg. Chem.* **1998**, *37*, 2995−3001.
[56] V. P. Fedin, M. N. Sokolov, A. G. Sykes, *J. Chem. Soc., Dalton Trans.* **1996**, 4089−4092.
[57] V. P. Fedin, M. N. Sokolov, A. V. Virovets, N. V. Podberezskaya, V. Y. Fedorov, *Inorg. Chim. Acta* **1998**, *269*, 292−296.
[58] R. Hernandez-Molina, M. R. J. Elsegood, W. Clegg, A. G. Sykes, *J. Chem. Soc., Dalton Trans.* **2001**, 2173−2178.
[59] T. Shibahara, H. Akashi, M. Yamasaki, K. Hashimoto, *Chem. Lett.* **1991**, 689−692.
[60] T. Shibahara, M. Yamasaki, H. Akashi, T. Katayama, *Inorg. Chem.* **1991**, *30*, 2693−2699.
[61] T. Shibahara, H. Akashi, H. Kuroya, *J. Am. Chem. Soc.* **1988**, *110*, 3313−3314.
[62] T. Shibahara, G. Sakane, M. Maeyama, H. Kobashi, T. Yamamoto, T. Watase, *Inorg. Chim. Acta* **1996**, *251*, 207−225.
[63] I. Schmidt, J. Hyldoft, J. Hjortkjaer, C. J. Jacobsen, *Acta Chem. Scan.* **1996**, *50*, 871−874.
[64] P. W. Dimmock, G. J. Lamprecht, A. G. Sykes, *J. Chem. Soc., Dalton Trans.* **1991**, 955−959.
[65] T. Shibahara, G. Sakane, Y. Naruse, K. Taya, H. Akashi, A. Ichimura, H. Adachi, *Bull. Chem. Soc. Jpn.* **1995**, *68*, 2769−2782.
[66] T. Shibahara, S. Mochida, G. Sakane, *Chem. Lett.* **1993**, 89−92.
[67] K. Herbst, M. Monari, M. Brorson, *Inorg. Chem.* **2002**, *41*, 1336−1338.
[68] K. Herbst, L. Dahlenburg, M. Brorson, *Inorg. Chem.* **2001**, *40*, 1989−1992.
[69] H. Akashi, T. Shibahara, *Inorg. Chim. Acta* **2000**, *300−302*, 572−580.
[70] X. Wu, S. Lu, L. Zu, Q. Wu, J. Lu, *Inorg. Chim. Acta* **1987**, *133*, 39−42.
[71] H. Diller, H. Keck, W. Kuchen, D. Mootz, R. Wiskemann, *Z. Naturforsch., Teil B* **1993**, *48*, 291−296.
[72] Y. Zheng, H. Zhan, X. Wu, *Acta Crystallogr., Sect. C* **1989**, *45*, 1990−1992.
[73] S. Lu, H. Chen, J. Huang, Q. Wu, Q. Sun, J. Li, J. Lu, *Inorg. Chim. Acta* **1995**, *232*, 43−50.
[74] K. Hegetschweiler, M. Wörh, M. D. Meienberger, R. Nesper, H. W. Schmalle, R. D. Hancock, *Inorg. Chim. Acta* **1996**, *250*, 35−47.
[75] R. Llusar, S. Uriel, C. Vicent, *J. Chem. Soc., Dalton Trans.* **2001**, 2813−2818.
[76] M. Nasreldin, Y.-J. Li, E. M. Frank, A. G. Sykes, *Inorg. Chem.* **1994**, *33*, 4283−4289.
[77] R. Miyamoto, S. Kawata, M. Iwaizumi, H. Akashi, T. Shibahara, *Inorg. Chem.* **1997**, *36*, 542−546.
[78] C. A. Routledge, M. Humanes, Y.-J. Li, G. Sykes, *J. Chem. Soc., Dalton Trans.* **1994**, 1275−1282.
[79] T. Shibahara, T. Asano, G. Sakane, *Polyhedron* **1991**, *10*, 2351−2352.
[80] D. Masui, Y. Ishii, M. Hidai, *Bull. Chem. Soc. Jpn.* **2000**, *73*, 931−938.
[81] H. Akashi, T. Shibahara, *Inorg. Chim. Acta* **1998**, *282*, 50−54.
[82] P. Vergamini, H. Vahrenkamp, L. Dahl, *J. Am. Chem. Soc.* **1971**, *93*, 6327−6329.
[83] B. Rink, M. Brorson, *Organometallics* **1999**, *18*, 2309−2313.
[84] K. Herbst, M. Monari, M. Brorson, *Inorg. Chem.* **2001**, *40*, 2979−2985.
[85] W. Beck, W. Danzer, G. Thiel, *Angew. Chem. Int. Ed. Engl.* **1973**, *12*, 582−583.
[86] R. E. Cramer, K. Yamada, H. Kawaguchi, K. Tatsumi, *Inorg. Chem.* **1996**, *35*, 1743−1746.
[87] K. Herbst, B. Rink, L. Dahlenburg, M. Brorson, *Organometallics* **2001**, *20*, 3655−3660.
[88] J. Q. Huang, J. L. Huang, M. Y. Shang, S. F. Lu, X. T. Lin, Y. H. Lin, M. D. Huang, H. H. Zhuang, J. X. Lu, *Pure Appl. Chem.* **1988**, *60*, 1185−1192.
[89] H. Zimmermann, K. Hegetschweiler, T. Keller, V. Gramlich, H. Schmalle, W. Petter, W. Schneider, *Inorg. Chem.* **1991**, *30*, 4336−4341.

[90] M. J. Mayor-López, J. Weber, K. Hegetschweiler, M. D. Meienberger, F. Joho, S. Leoni, R. Nesper, G. J. Reiss, W. Frank, B. A. Kolesov, V. P. Fedin, V. E. Fedorov, *Inorg. Chem.* **1998**, *37*, 2633−2644.
[91] H. Keck, W. Kuchen, J. Mathow, B. Meyer, D. Mootz, H. Wunderlich, *Angew. Chem. Int. Ed. Engl.* **1981**, *20*, 975−976.
[92] H. Keck, W. Kuchen, J. Mathow, B. Meyer, D. Mootz, H. Wunderlich, *Angew. Chem. Int. Ed. Engl.* **1982**, *21*, 929−930.
[93] R. Hernandez-Molina, M. Sokolov, W. Clegg, P. Esparza, A. Mederos, *Inorg. Chim. Acta* **2002**, *331*, 52−58.
[94] H. Zhan, Y. Zheng, X. Wu, J. Lu, *Inorg. Chim. Acta* **1989**, *156*, 277−280.
[95] Y. Zheng, H. Zhan, X. Wu, J. Lu, *Transition Met. Chem.* **1989**, *14*, 161−164.
[96] S. F. Lu, H. B. Chen, J. Q. Huang, Q. J. Wu, Q. L. Sun, J. Li, J. X. Lu, *Inorg. Chim. Acta* **1995**, *232*, 43−50.
[97] [97a] H. Diller, H. Keck, H. Wunderlich, W. Kuchen, *J. Organomet. Chem.* **1995**, *489*, 123−127. [97b] H. Diller, H. Keck, A. Kruse, W. Kuchen, D. Mootz, R. Wiskemann, *Z. Naturforsch., Teil B* **1993**, *48*, 548−554.
[98] M. Feliz, R. Llusar, S. Uriel, C. Vicent, unpublished results.
[99] T. Saito, N. Yamamoto, T. Yamagata, H. Imoto, *Chem. Lett.* **1987**, 2025−2028.
[100] F. A. Cotton, P. A. Kibala, M. Matusz, C. S. McCaleb, R. B. W. Sandor, *Inorg. Chem.* **1989**, *28*, 2623−2630.
[101] T. Saito, Y. Kajitani, T. Yamagata, H. Imoto, *Inorg. Chem.* **1990**, *29*, 2951−2955.
[102] F. Estevan, M. Feliz, R. Llusar, J. A. Mata, S. Uriel, *Polyhedron* **2001**, *20*, 527−535.
[103] V. P. Fedin, M. N. Sokolov, A. O. Gerasko, A. V. Virovets, N. V. Podberezskaya, V. Y. Fedorov, *Inorg. Chim. Acta* **1991**, *187*, 81−90.
[104] V. P. Fedin, M. N. Sokolov, K. G. Myakishev, O. A. Gerasko, V. Y. Fedorov, *Polyhedron* **1991**, *10*, 1311−1317.
[105] F. A. Cotton, R. Llusar, *Polyhedron* **1987**, *6*, 1741−1745.
[106] F. A. Cotton, R. Llusar, C. T. Eagle, *J. Am. Chem. Soc.* **1989**, *111*, 4332−4338.
[107] F. A. Cotton, S. K. Mandal, *Inorg. Chim. Acta* **1992**, *192*, 71−79.
[108] M. Feliz, R. Llusar, S. Uriel, C. Vicent, M. G. Humphrey, N. T. Lucas, M. Samoc, B. Luther-Davies, *Inorg. Chim. Acta*, accepted for publication.
[109] S. Harris, *Polyhedron* **1989**, *8*, 2843−2882.
[110] Trinh-Toan, B. K. Teo, J. A. Ferguson, T. J. Meyer, L. F. Dahl, *J. Am. Chem. Soc.* **1977**, *99*, 408−416.
[111] S. Harris, *Inorg. Chem.* **1987**, *26*, 4278−4285.
[112] C. S. Bahn, A. Tan, S. Harris, *Inorg. Chem.* **1998**, *37*, 2770−2778.
[113] H. Akashi, T. Shibahara, N. Uryu, *Inorg. Chim. Acta* **1997**, *261*, 53−57.
[114] P. W. Dimmock, P. E. Dickson, A. G. Sykes, *Inorg. Chem.* **1990**, *29*, 5120−5125.
[115] U. Riaz, O. J. Curnow, M. D. Curtis, *J. Am. Chem. Soc.* **1994**, *116*, 4357−4363.
[116] M. D. Curtis, S. H. Druker, *J. Am. Chem. Soc.* **1997**, *119*, 1027−1036.
[117] M. D. Curtis, J. E. Penner-Hahn, J. Schwank, O. Barait, D. J. McCabe, L. Thompson, G. Waldo, *Polyhedron* **1988**, *7*, 2411−2420.
[118] T. Tastumi, M. Tanaguchi, H. Ishige, Y. Ishii, T. Murata, M. Hidai, *Appl. Surf. Sci.* **1997**, *121/122*, 500−504.
[119] M. Taniguchi, D. Imamura, H. Ishige, Y. Ishii, T. Murata, M. Hidai, T. Tatsumi, *J. Catal.* **1999**, *187*, 139−150.
[120] M. Taniguchi, Y. Ishii, T. Murata, T. Tatsumi, M. Hidai, *J. Chem. Soc., Chem. Commun.* **1995**, 2533−2534.
[121] R. Llusar, J. Pérez-Prieto, M. Barberis, M. Feliz, C. Vicent, S. Uriel, unpublished results.
[122] M. N. Sokolov, A. V. Virovets, D. N. Dybtsev, A. Gerasko, V. P. Fedin, R. Hernandez-Molina, W. Clegg, A. G. Sykes, *Angew. Chem. Int. Ed.* **2000**, *39*, 1659−1661.
[123] V. P. Fedin, A. V. Virovets, M. N. Sokolov, D. N. Dybtsev, O. A. Gerasko, W. Clegg, *Inorg. Chem.* **2000**, *39*, 2227−2230.
[124] V. Fedin, V. Gramlich, M. Worle, T. Weber, *Inorg. Chem.* **2001**, *40*, 1074−1077.
[125] M. N. Sokolov, R. Henández-Molina, D. N. Dybtsev, E. V. Chubarova, S. F. Solodovnikov, N. V. Pervukhina, C. Vicent, R. Llusar, V. Fedin, *Z. Anorg. Allg. Chem.* **2002**, *628*, 2335−2339.

Received October 15, 2002
[I02569]

A Facile Synthesis of a Push-Pull Mixed-Ligand Pd-Dithiolene Complex Containing the Et_2timdt Ligand (Et_2timdt = Monoreduced Diethylimidazolidine-2,4,5-trithione)

M. Carla Aragoni,[a] Massimiliano Arca,*[a] Carla Denotti,[a] Francesco A. Devillanova,[a] Emanuela Grigiotti,[b] Francesco Isaia,[a] Franco Laschi,[b] Vito Lippolis,[a] Luca Pala,[a] Alexandra M. Z. Slawin,[c] Piero Zanello,[b] and J. Derek Woollins[c]

Keywords: Palladium / Halogenation / S ligands / Density functional calculations / Nonlinear optics

The reaction of the dithiolene [Pd(Et_2timdt)$_2$] (Et_2timdt = formally monoreduced diethylimidazolidine-2,4,5-trithione) with Br_2 or IBr yields the complex [Pd(Et_2timdt)Br_2], a good starting material for the synthesis of novel push-pull mixed-ligand Pd-dithiolenes. The synthesis and characterisation of the unsymmetrical dithiolene [Pd(Et_2timdt)(mnt)] (mnt = maleonitriledithiolato dianion) is also reported.

(© Wiley-VCH Verlag GmbH & Co. KGaA, 69451 Weinheim, Germany, 2003)

In recent years, non-linear optical (NLO) materials have attracted great interest because of their wide range of possible applications in several fields, such as laser technology, telecommunications, data storage, and optical switches.[1] So far, most reports have dealt with inorganic and organometallic compounds with extended delocalized π-systems.[2] Among these, "non-innocent"[3] metal-dithiolenes represent a very promising class of compounds in view of their peculiar electronic structure accompanied by high thermal and photochemical stabilities.[4]

Recently, we have reported a new class of neutral dithiolenes [M(R,R′timdt)$_2$] (M = Ni, Pd, Pt),[5] which shows remarkable stability and an unusually intense NIR absorption at about 1000 nm, whose energy is tunable by changing the metal ion and/or substituents R and R′.[6−9] The intense NIR absorption makes these dithiolenes good candidates as Q-switching and/or mode-locking dyes in the technology of Nd-lasers (such as Nd:YLF and Nd:YAG, emitting at 1053 and 1064 nm, respectively), and for applications in solid-state NIR-photodetectors.[10] These compounds are structurally analogous to the metal dithiolenes that derive from the ligand dmit (dmit = 2-thioxo-1,3-dithiol-4,5-dithiolate), while differing in that NR groups are present instead of endocyclic S atoms in the heterocyclic organic framework of the ligand.[11] However, while [M(R,R′timdt)$_2$] dithiolenes are isolated in the neutral state, [M(dmit)$_2$] complexes have been reported as anions with integer or fractional charges, and have been used as building blocks to prepare materials with interesting conducting properties.[12,13]

DFT calculations have confirmed that the terminal sulfur atoms in the two classes of dithiolenes are differently charged: those in the neutral [M(dmit)$_2$] dithiolenes carry a small positive charge, while those in the neutral [M(R,R′timdt)$_2$] dithiolenes carry a non-negligible negative charge.[8] The donor properties of the latter complexes have been exploited in the reactions with iodine: the interaction of I_2 at the terminal sulfur atoms gives CT adducts bearing linear S−I−I groups.[6,7] The reactions of [Ni(R,R′timdt)$_2$] with Br_2 and IBr generally occur with elimination of the central Ni ion. For example, in the case of the reaction of [Ni(*i*Pr_2timdt)$_2$] with IBr, together with other unidentified by-products, the corresponding 1,3,6,8-tetrasubstituted 4,5,9,10-tetrathiocino-[1,2-*b*:5,6:*b*′]diimidazolyl-2,7-dithione was identified by X-ray diffraction.[14]

Unexpectedly, the reaction between [Pd(Et_2timdt)$_2$] (**1**)[7] and either IBr or Br_2 in molar ratios ranging from 1:1 to 1:20 gave very tiny bronze crystals, with an elemental analysis that corresponds to the formula of [Pd(Et_2timdt)Br_2] (**2**). Although the quality of these crystals was not good enough to obtain reliable structural data (see Exp. Sect.), it is possible to note that on passing from **1** to **2**, the Pd ion maintains a square-planar coordination geometry, which is achieved for **2** by coordination to one Et_2timdt ligand and two bromide ions.

[a] Dipartimento di Chimica Inorganica ed Analitica, Università degli Studi di Cagliari,
S.S. 554 bivio per Sestu, 09042 Monserrato-Cagliari, Italy
Fax: (internat.) +39-070/675-4456
E-mail: marca@unica.it
[b] Dipartimento di Chimica, Università degli Studi di Siena,
Via A. Moro, 53100 Siena, Italy
[c] School of Chemistry, University of St. Andrews,
St. Andrews, Fife, UK KY16 9ST

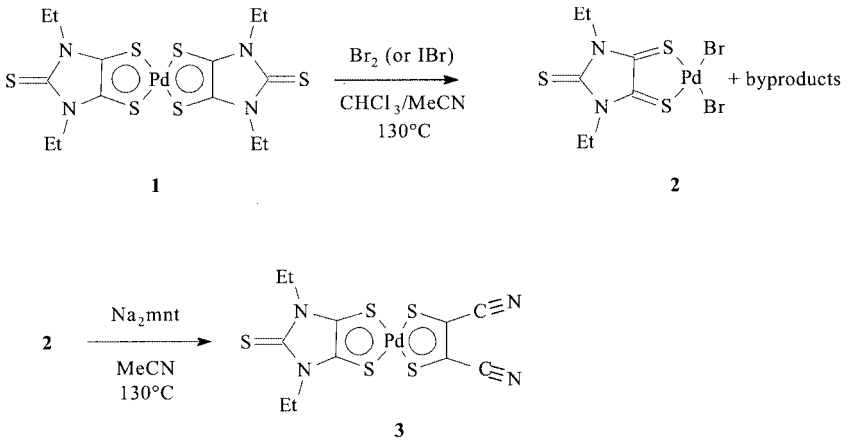

Scheme 1

The reaction of **2** with [Na_2mnt] (mnt = maleonitriledithiolate) in MeCN (Scheme 1) yielded dark crystals, whose X-ray crystal structure determination showed that they consist of the mixed-ligand dithiolene [Pd(Et_2timdt)(mnt)] (**3**; Figure 1).[15] In **3**, the C(1)−C(2) bond length within the Et_2timdt ligand is longer than that found in **1** [1.453(4) and 1.397(9) Å, respectively], while the C(1)−S(1) and C(2)−S(2) distances [corresponding averaged value in **1** 1.689(8) Å][7] are shorter [1.661(3) and 1.655(3) Å, respectively]. On comparing the two C_2S_2Pd metallacycles in **3**, the C−C length in the mnt unit [1.354(4) Å] is shorter than that in the Et_2timdt one, while the C−S distances are longer in the mnt ligand [C(3)−S(3) 1.731(3); C(4)−S(4) 1.734(3) Å]. The structural features in **1**,[7] **3**, and [Pd$(mnt)_2$], [characterised as (perylene)$_2$Pd$(mnt)_2$][16] clearly indicate that the Et_2timdt ligand in **3** shows a remarkable trithione character, while mnt occurs in the dithiolato form.[17]

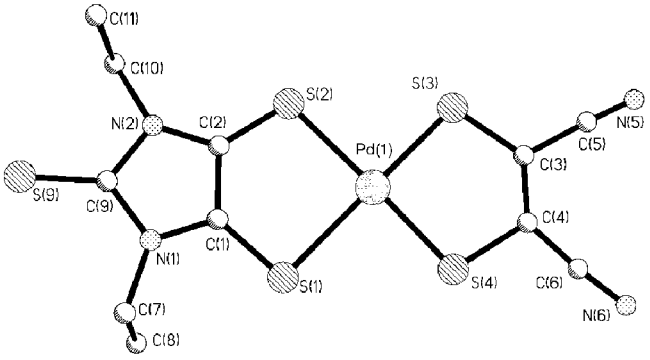

Figure 1. Molecular structure and atom labelling scheme for [Pd(Et_2timdt)(mnt)] (**3**); selected bond lengths (Å) and angles (°): Pd(1)−S(1) 2.3293(8), Pd(1)−S(2) 2.3300(8), Pd(1)−S(3) 2.2633(8), Pd(1)−S(4) 2.2526(8), C(1)−S(1) 1.660(3), C(2)−S(2) 1.655(3), C(3)−S(3) 1.731(3), C(4)−S(4) 1.734(3), C(1)−C(2) 1.453(4), C(3)−C(4) 1.354(4); S(1)−Pd(1)−S(2) 91.02(3), S(3)−Pd(1)−S(4) 90.59(3), S(1)−C(1)−C(2) 124.4(2), S(2)−C(2)−C(1) 124.3(2), S(3)−C(3)−C(4) 122.6(2), S(4)−C(4)−C(3) 122.1(2)

The dithiolato nature of mnt in **3** is also confirmed by its FT-Raman spectrum in the solid state: the C=C stretching vibration of the mnt unit is found at 1485 cm^{-1}, in very good agreement with the value of 1482 cm^{-1} reported for $[Pd(mnt)_2]^{2-}$.[18]

These experimental results are in agreement with a push-pull nature for **3**, also supported by DFT calculations carried out on the corresponding model complex [Pd(H_2timdt)(mnt)] (**4**). In this dithiolene, the HOMO and LUMO are π-type molecular orbitals (Figure 2): while the HOMO is mainly centred on the mnt dithiolato ligand and the terminal sulfur atom of the H_2timdt trithione ligand, the LUMO has a remarkable contribution from the H_2timdt ligand.

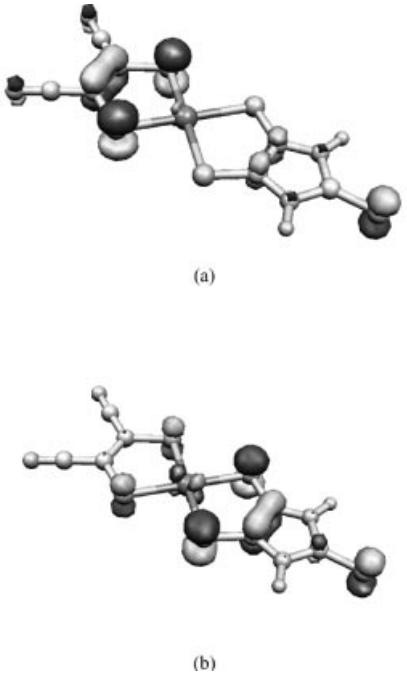

Figure 2. Kohn−Shan HOMO (a) and LUMO (b) calculated for [Pd(H_2timdt)(mnt)] (**4**)

Due to the different nature of the two ligands, a strong intramolecular polarisation can be expected for **3**, as confirmed by its remarkable solvatochromism (the position of the maximum in the NIR spectrum ranges between 920 nm in MeCN and 1060 nm in $CHCl_3$, Figure 3). On the other hand, the NBO[19] charge distribution calculated for **4** [Pd(1) 0.348, S(1,2) 0.055, S(3,4) 0.052, C(1,2) 0.016, C(3,4)

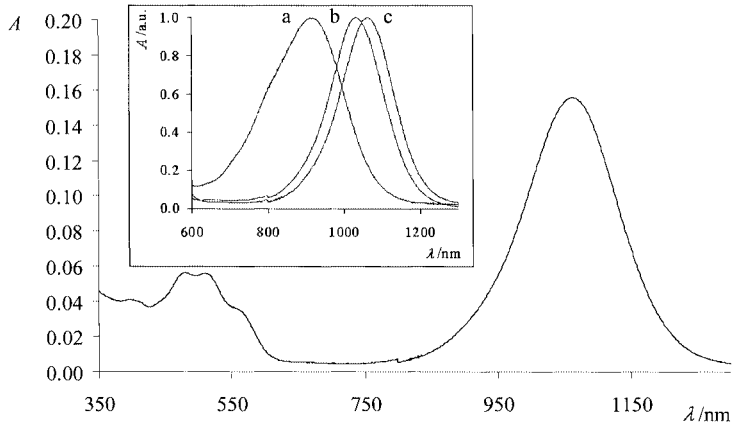

Figure 3. UV/Vis-NIR spectrum of **3** in $CHCl_3$ solution ($1.2 \cdot 10^{-5}$ M); the inset shows the superimposed normalised NIR spectra in MeCN (a), CH_2Cl_2 (b) and $CHCl_3$ (c)

−0.027, N(1,2) −0.583, C(5,6) 0.280, N(5,6) −0.271 e] agrees with a strong intramolecular polarisation. The cyclic voltammetry (Figure 4a) of complex **3** in CH_2Cl_2 shows two consecutive, (coulometrically tested) one-electron reversible reductions [$E^{\circ\prime}_{0/-1} = +0.41$; $E^{\circ\prime}_{-1/-2} = -0.27$ V, vs. SCE]. A one-electron irreversible oxidation (not shown in Figure 3a) is also present close to the solvent discharge ($E_{pa,\ 0/+} = +1.43$ V). On the basis of the nature of the calculated Kohn−Shan HOMO and LUMO, the reduction process should be considered as being centred mainly on the Et_2timdt ligand, while oxidation occurs mostly on the mnt unit.

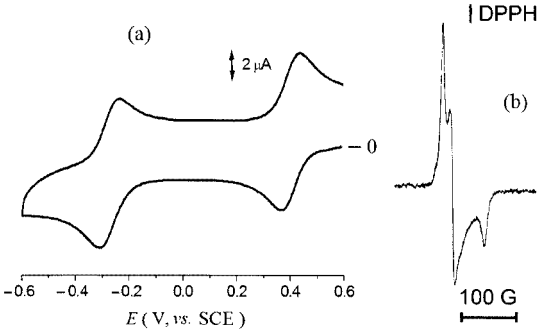

Figure 4. (a) Cyclic voltammogram recorded at a platinum electrode on a CH_2Cl_2 solution of **3** ($0.7 \cdot 10^{-3}$ M); scan rate 0.5 $V \cdot s^{-1}$; (b) X-band EPR spectrum recorded at 100 K on the electrogenerated $[\mathbf{3}]^-$ monoanion

Both the monoanion and the dianion also proved to be stable over the longer time-span of macroelectrolysis. Figure 4b shows the low-temperature EPR spectrum recorded on a CH_2Cl_2 solution of the electrogenerated $[Pd(Et_2timdt)(mnt)]^{\cdot -}$ radical monoanion. The $<g>$ value of the rhombic absorption [$<g> = 1/3(g_l + g_m + g_h) = 2.013$] proved to be appreciably higher than $g_{electron}$ (2.002), confirming that the central palladium atom partly contributes to the LUMO of **3**, even though the low Δg value ($\Delta g = g_l - g_h = 0.048$) agrees with a predominantly ligand-centred reduction process.

In conclusion, by exploring the reactivity of $[M(R,R'timdt)_2]$ towards Br_2 and IBr we have found an alternative method to easily prepare non-centrosymmetric push-pull [M(R,R′timdt)L] dithiolenes (L is a dithiolate ligand) with potential NLO applications.

Experimental Section

Materials and Methods: All solvents and reagents were purchased from Aldrich and used as received. The degree of purity of each compound was checked by elemental and TLC analyses. Elemental analysis, and FT-Raman, and UV/Vis-NIR spectroscopy were carried out as previously reported.[8] Cyclic voltammetry was performed in an anhydrous dichloromethane solution using electrochemical grade $[NBu_4][PF_6]$ as supporting electrolyte in a three-electrode cell containing a platinum working electrode surrounded by a platinum-spiral counter electrode and an aqueous saturated calomel reference electrode (SCE) mounted with a Luggin capillary. A BAS 100 W electrochemical analyser was used as polarising unit. Controlled potential coulometry was performed in an H-shaped cell with anodic and cathodic compartments separated by a sintered-glass disk. The working macroelectrode was a platinum gauze; a mercury pool was used as the counter electrode. All potential values are referred to the SCE (under the present experimental conditions, the one-electron oxidation of ferrocene occurs at $E^{\circ\prime} = +0.39$ V). X-band electron spin resonance (ESR) spectra were recorded with an ER 200 D-SRC Bruker spectrometer operating at a frequency of 9.62 GHz using a HS Bruker rectangular cavity. The operational frequency was controlled with a Hewlett−Packard x 5−32 B wavemeter and the magnetic field was calibrated with a DPPH (diphenylpicrylhydrazyl) free radical as a suitable field marker. The temperature was controlled with a Bruker ER 4111 VT device (±1 K). The g values are referred to DPPH ($g = 2.0036$) used as the external standard reference. The starting dithiolene **1** was synthesised according to the previously described method.[7]

Synthesis of $[Pd(Et_2timdt)Br_2]$ (2): Compound **1** (50 mg, $9.2 \cdot 10^{-5}$ mol) was reacted with an excess of bromine (100 mg, $6.8 \cdot 10^{-4}$ mol) in 30 mL of a mixture of $CHCl_3$ and MeCN (1:2 v/v) for 10 minutes in an Aldrich pressure tube at 130 °C. After cooling, the precipitate was filtered off, washed with light petroleum ether, and dried under vacuum. Yield 27 mg, 60%. M.p. > 250 °C. $C_7H_{10}Br_2N_2PdS_3$ (484.6): calcd. C 17.35, H 2.08, N 5.78, S 19.85; found C 17.48, H

2.03, N 5.76, S 19.91. FT-Raman (1500−50 cm^{-1}; solid state): $\tilde{\nu}$ = 1433 (1.0), 1350 (3.5), 1300 (10.0), 1257 (3.0), 1166 (0.9), 446 (7.5), 425 (2.1) cm^{-1} (relative intensities in parentheses).

Synthesis of [Pd(Et_2timdt)(mnt)] (3): Compound **2** (31 mg, $6.3\cdot10^{-5}$ mol) was reacted with [Na_2mnt] (21 mg, $1.12\cdot10^{-4}$ mol) in 30 mL of MeCN for 30 minutes in an Aldrich pressure tube at 130 °C. After cooling, the precipitate was filtered off, washed with water, and dried under vacuum. Yield 12 mg, 40%. M.p. > 250 °C. $C_{11}H_{10}N_4PdS_5$ (464.9): calcd. C 28.42, H 2.17, N 12.05, S 34.48; found C 28.82, H 2.15, N 11.98, S 33.89. FT-Raman (1500−50 cm^{-1}; solid state): $\tilde{\nu}$ = 1485 (4.7), 1348 (5.2), 1292 (10.0), 1165 (2.7), 1059 (3.3), 530 (4.7), 449 (6.8), 362(8.7), 332 (6.7) cm^{-1} (relative intensities in parentheses).

X-ray Crystal Structure Determination: Data collections were performed on a SMART CCD area detector diffractometer with graphite-monochromated Mo-K_α radiation (λ = 0.71073 Å). Data collection was performed at 125 K for **2** and at room temperature for **3**. A full hemisphere of data with 0.3° steps was collected. SADABS corrections were applied. The non-hydrogen atoms were refined anisotropically except for the carbon atoms in **2** (the crystals available for **2** were very thin needles, numerous samples were examined and several types of absorption corrections performed with no improvement in the quality of the collected data or of this refinement); the calculations employed the SHELXTL program system.[20]

X-ray Structure Determination of 2: $C_7H_{10}Br_2N_2PdS_3$, monoclinic, space group $P2_1/n$, a = 13.7244(15) Å, b = 23.829(3) Å, c = 16.4013(17) Å, β = 91.404(2)°, V = 5362.3(10) $Å^3$, Z = 16, D_c = 2.401 Mg/m^3, T = 125 K. R = 0.0525, wR = 1.004 for 7627 observed independent data.

X-ray Structure Determination of 3: $C_{11}H_{10}N_4PdS_5$, monoclinic, space group $P2_1/n$, a = 7.8685(3) Å, b = 14.0557(5) Å, c = 14.9088(6) Å, β = 90.985(1)°, V = 1648.63(11) $Å^3$, Z = 4, D_c = 1.873 Mg/m^3, T = 293 K. R = 0.0210, wR = 0.0459 for 2364 observed independent data.

CCDC-188021 (**2**) and CCDC-188022 (**3**) contain the supplementary crystallographic data for this paper. These data can be obtained free of charge at www.ccdc.cam.ac.uk/conts/retrieving.html [or from the Cambridge Crystallographic Data Centre, 12, Union Road, Cambridge CB2 1EZ, UK; Fax: (internat.) +44-1223/336-033; E-mail: deposit@ccdc.cam.ac.uk].

Theoretical Calculations: Hybrid-DFT calculations were performed with the Gaussian 98 package[21] on compounds [Pd(H_2timdt)$_2$], [Pd(H_2timdt)Br_2], and **4**. In all cases both the Becke3LYP[22] and MPW1PW[23] hybrid functionals were used, along with the Schafer et al. basis set[24] for all atoms except Pd, for which the Hay−Wadt LANL2DZ basis set[25] with Effective Core Potentials was preferred. For each molecule, after the geometry optimisation, a normal mode frequency calculation was performed. The experimental structures are in better agreement with those calculated using the MPW1PW functional.

Supporting information: (See Footnote on the first page of this article). Optimized geometries in Cartesian coordinate form and frontier Kohn−Shan orbital energies for complexes [Pd(H_2timdt)$_2$], [Pd(H_2timdt)Br_2] and **4** are available from the authors on request.

Acknowledgments

The "Ministero dell'Istruzione dell'Università della Ricerca" is thankfully acknowledged for financial support. CINECA (Centro Interuniversitario Nord Est Calcolo Automatico) is also acknowledged for computational facilities.

[1] *Molecular Nonlinear Optics: Materials, Physical and Devices* (Ed.: J. Zyss), Academic Press, Boston, MA, **1993**; C.-T. Chen, S.-Y. Liao, K.-J. Lin, L.-L. Lai, *Adv. Mater.* **1998**, *10*, 334−338; D.-L. Long, W.-T- Wong, S. Shi, X.-Q. Xin, J.-S Huang, *J. Chem. Soc., Dalton Trans.* **1997**, 4361−4365; Z. Sun, M. Tong, H. Zeng, L. Ding, Z. Wang, Z. Xu, J. Dai, G. Bian, *Chem. Phys. Lett.* **2001**, *342*, 323−327.

[2] P. A. Franken, A. E. Hill, C. W. Peters, *Phys. Rev. Lett.* **1961**, *7*, 118−119; X.-M. Zhang, B.-Z. Shan, C.-Y. Duan, X.-Z. You, *Chem. Commun.* **1997**, 1131−1132; S. N. Oliver, S. V. Kershaw, A. E. Underhill, C. A. S. Hill, A. Charlton, *Nonlinear Optics* **1995**, *10*, 87−99.

[3] M. D. Ward, J. A. McCleverty, *J. Chem. Soc., Dalton Trans.* **2002**, 275−288; *Proc. Indian Acad. Sci. (Chem. Sci.)* **2002**, *114*, 291−309.

[4] U. T. Mueller-Westerhoff, B. Vance, D. I. Yoon, *Tetrahedron* **1991**, *47*, 909−932; J. A. McCleverty, *Prog. Inorg. Chem.* **1968**, *10*, 49−221.

[5] R,R′timdt = formally monoreduced disubstituted imidazolidine-2,4,5-trithione. Attention should be paid to the fact that through the paper R,R′timdt is used for both the neutral and the negatively charged ligand, since the assignment of the net charges on the central metal and on the ligands is not straightforward due to the non-innocent nature of the ligands in dithiolenes.[3] Nevertheless, on passing from the neutral trithione ligand to its mono- or dianionic dithiolato species, the C−C and C−S bonds are shortened and lengthened, respectively. Therefore, the experimental structural values of these bond lengths give information on the nature of the ligand in each compound.

[6] F. Bigoli, P. Deplano, F. A. Devillanova, V. Lippolis, P. J. Lukes, M. L. Mercuri, M. A. Pellinghelli, E. F. Trogu, *J. Chem. Soc., Chem. Commun.* **1995**, 371−372; F. Bigoli, P. Deplano, F. A. Devillanova, J. R. Ferraro, V. Lippolis, P. J. Lukes, M. L. Mercuri, M. A. Pellinghelli, E. F. Trogu, *Inorg. Chem.* **1997**, *36*, 1218−1226.

[7] M. Arca, F. Demartin, F. A. Devillanova, A. Garau, F. Isaia, F. Lelj, V. Lippolis, S. Pedraglio, G. Verani, *J. Chem. Soc., Dalton Trans.* **1998**, 3731−3736.

[8] M. C. Aragoni, M. Arca, F. Demartin, F. A. Devillanova, A. Garau, F. Isaia, F. Lelj, V. Lippolis, G. Verani, *J. Am. Chem. Soc.* **1999**, *121*, 7098−7107.

[9] M. C. Aragoni, M. Arca, T. Cassano, C. Denotti, F. A. Devillanova, R. Frau, F. Isaia, F. Lelj, V. Lippolis, L. Nitti, P. Romaniello, R. Tommasi, G. Verani, *Eur. J. Inorg. Chem.*, in press.

[10] M. C. Aragoni, M. Arca, T. Cassano, C. Denotti, F. A. Devillanova, F. Isaia, V. Lippolis, D. Natali, L. Nitti, M. Sampietro, R. Tommasi, *Inorg. Chem. Commun.* **2002**, *5*, 869−872.

[11] A. E. Pullen, R.-M. Olk, *Coord. Chem. Rev.* **1999**, *188*, 211−262.

[12] P. Cassoux, L. Valade, H. Kobayashi, A. Kobayashi, R. A. Clark, A. E. Underhill, *Coord. Chem. Rev.* **1991**, *110*, 115−160.

[13] P. Cassoux, *Coord. Chem. Rev.* **1999**, *185−186*, 213−232; E. Canadell, *Coord. Chem. Rev.* **1999**, *185−186*, 629−651.

[14] F. Bigoli, P. Deplano, M. L. Mercuri, M. A. Pellinghelli, G. Pintus, E. F. Trogu, G. Zonnedda, H. H. Wang, J. M. Williams, *Inorg. Chim. Acta* **1998**, *273*, 175−183.

[15] [Ni(*i*Pr_2timdt)(mnt)] — a neutral dithiolene similar to **3** — has been synthesised by the metathesis reaction between [Ni(*i*Pr_2timdt)$_2$] and [Ni(mnt)$_2$]$^{2-}$ followed by oxidation of the resulting [Ni(*i*Pr_2timdt)(mnt)]$^-$ with I_2, but it has not been structurally characterised: F. Bigoli, C.-T. Chen, W.-C. Wu, P. Deplano, M. L. Mercuri, M. A. Pellinghelli, L. Pilia, G. Pintus, A. Serpe, E. F. Trogu, *Chem. Commun.* **2001**, 2246−2247 and references therein.

[16] A. Domingos, R. T. Henriques, V. Gama, M. Almeda, *Synth. Metals* **1988**, *27*, B411−B416.

[17] The structural features of **2**, supported by DFT calculations carried out on the [Pd(H_2timdt)Br_2] model compound, indicate a trithione character for the organic ligand [average structural values (corresponding optimised distances in parentheses) C(1)−C(2) 1.474 (1.458), C(1,2)−S(1,2) 1.655 (1.658) Å].
[18] R. J. H. Clark, P. C. Turtle, *J. Chem. Soc., Dalton Trans.* **1977**, 2142−2148.
[19] E. D. Geldening, J. K. Badenshoop, A. E. Reed, J. E. Carpenter, F. Weinhold, Theoretical Chemistry Institute, University of Wisconsin, Madison, **1992**; A. E. Reed, R. B. Weinstock, F. Weinhold, *Chem. Rev.* **1988**, *88*, 899−926.
[20] SHELXTL, Bruker AXS, Madison, New York, **1998**.
[21] Gaussian 98, Revision A.7, M. J. Frisch, G. W. Trucks, H. B. Schlegel, G. E. Scuseria, M. A. Robb, J. R. Cheeseman, V. G. Zakrzewski, J. A. Montgomery, Jr., R. E. Stratmann, J. C. Burant, S. Dapprich, J. M. Millam, A. D. Daniels, K. N. Kudin, M. C. Strain, O. Farkas, J. Tomasi, V. Barone, M. Cossi, R. Cammi, B. Mennucci, C. Pomelli, C. Adamo, S. Clifford, J. Ochterski, G. A. Petersson, P. Y. Ayala, Q. Cui, K. Morokuma, D. K. Malick, A. D. Rabuck, K. Raghavachari, J. B. Foresman, J. Cioslowski, J. V. Ortiz, A. G. Baboul, B. B. Stefanov, G. Liu, A. Liashenko, P. Piskorz, I. Komaromi, R. Gomperts, R. L. Martin, D. J. Fox, T. Keith, M. A. Al-Laham, C. Y. Peng, A. Nanayakkara, C. Gonzalez, M. Challacombe, P. M. W. Gill, B. Johnson, W. Chen, M. W. Wong, J. L. Andres, C. Gonzalez, M. Head-Gordon, E. S. Replogle, J. A. Pople, Gaussian, Inc., Pittsburgh PA, **1998**.
[22] A. D. Becke, *J. Chem. Phys.* **1993**, *98*, 1372−1377; A. D. Becke, *J. Chem. Phys.* **1993**, *98*, 5648−5652; C. Lee, W. Yang, R. G. Parr, *Phys. Rev. B* **1988**, *37*, 785−789.
[23] C. Adamo, V. Barone, *J. Chem. Phys.* **1998**, *108*, 664−675.
[24] A. Schafer, H. Horn, R. Ahlrichs, *J. Chem. Phys.* **1992**, *97*, 2571−2577.
[25] P. J. Hay, W. R. Wadt, *J. Chem. Phys.* **1985**, *82*, 270−298.

Received November 25, 2002
[I02641]

Preferential Siting of Iron Atoms in an MFI-type Ferrisilicate Zeolite Framework: An Attempt to Explain Experimental Data with TPA-Silicate Solution Chemistry

Elisabeth Theunissen,[a] Christine E. A. Kirschhock,[a] Sebastien P. B. Kremer,[a] David D. Habermacher,[a] and Johan A. Martens*[a]

Keywords: Zeolites / Transition metals / Iron / X-ray diffraction

In this paper an attempt is made to explain the experimentally observed iron siting in ferrisilicate MFI-type zeolites based on TPA-silicate solution chemistry. A critical molecular step in the formation of Silicalite-1 zeolite is the formation of the precursor, counting 36 T-atoms, by condensation of three pentacyclic dodecamers around a TPA molecule. Incorporation of a tetracyclic undecamer instead of a pentacyclic dodecamer results in a precursor with a missing Si atom at a position that becomes a T_9 or T_{10} site of the orthorhombic unit cell of the MFI-type zeolite. The incorporation of iron at these empty positions of the precursor explains the experimentally observed preferred iron positions. Close examination of the precursor formation mechanism reveals that the iron is incorporated at the same T-atom positions, viz. T_9 and T_{10}, when the precursor is formed from an iron-containing pentacyclic dodecamer.
(© Wiley-VCH Verlag GmbH & Co. KGaA, 69451 Weinheim, Germany, 2003)

Introduction

In the field of heterogeneous catalysis, zeolites with the MFI framework topology are important materials.[1] Incorporation of heteroatoms, and particularly of aluminum, iron or titanium in the MFI-type silicate framework, leads to unique acid-base and redox catalytic properties. MFI-type zeolites have been given particular names according to their chemical composition or assignment of the inventors, such as Silicalite-1 for the purely siliceous version,[2] ZSM-5 for the aluminosilicate,[3] TS-1 for the titanosilicalite composition,[4] and Fe-ZSM-5, or Fe-MFI for the iron-containing analogue.[5,6] The ferrisilicate composition has received much attention in the recent literature as it is an effective catalyst for a variety of reactions.[7−11]

MFI zeolites have orthorhombic or monoclinic symmetry, and possess 12 or 24 crystallographically different T-atom sites, respectively. The distribution of the heteroatoms over the framework positions has already been the subject of numerous experimental[12−15] and computational studies.[16−18] The evidence for the occurrence of isomorphous substitution is convincing, and although there is general agreement that the distribution of the heteroatoms over the different T-sites is non-random, the precise location remains uncertain. The kinetic rather than thermodynamic control over the formation of siliceous zeolite phases and over the incorporation of heteroatoms[19,20] complicates the theoretical studies.[16−18]

Recently, structural evidence for preferential iron siting at the T_9 and T_{10} sites of Fe-MFI could be obtained using synchrotron radiation single-crystal X-ray diffraction.[21] Identification of the iron positions was done based on the localization of the sodium counterions in the channels of the MFI structure and comparison of T−O distances in Silicalite-1 and Fe-MFI. In parallel with this development, the initial molecular steps involved in the formation of Silicalite-1 were recently revealed.[22,23] In this paper, we explain how the oligomerization chemistry responsible for the formation of the Silicalite-1 framework can offer an explanation for the experimentally determined iron atom siting.

Discussion

The tetrapropylammonium hydroxide (TPA) directed silica oligomerization sequence, identified by ^{29}Si NMR spectroscopy, involves a bicyclic pentamer (**1**), a pentacyclic octamer (**2**), a tetracyclic undecamer (**3**), and a pentacyclic dodecamer (**4**; Figure 1).[22,23] These polyanions have curved surfaces and are hydrophobic on the inside and hydrophilic on the outside. The propyl arms of the TPA molecule interact favorably with the hydrophobic internal surface. The assembly of three dodecamers around the TPA molecule leads to the formation of the precursor (**5**; Figure 1). The precursor has the same connectivity as in the MFI framework. The T-sites of the MFI framework are

[a] Centrum voor Oppervlaktechemie en Katalyse, K.U. Leuven
Kasteelpark Arenberg 23, 3001 Leuven, Belgium
Fax: (internat.) +32-16/321-998
E-mail: johan.martens@agr.kuleuven.ac.be

mapped onto a model of the precursor in Figure 2. Aggregation of the precursor in the three directions leads to an MFI framework without missing T-atoms. The pentacyclic dodecamer (**4**) was detected as an intermediate in a polymerization experiment at 0 °C. At room temperature, it is a short-lived species and is quickly transformed into the precursor. The assembly of three pentacyclic dodecamers leads to precursors (**5**) containing 36 T-atoms. When a tetracyclic undecamer (**3**) is incorporated into precursor (**5**) instead of pentacyclic dodecamers (**4**), a T-atom is missing.

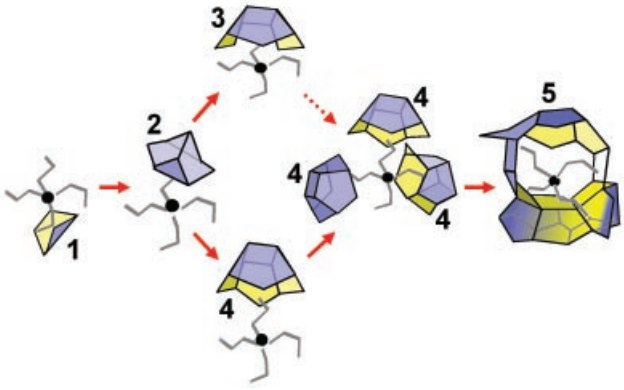

Figure 1. TPA-directed molecular steps involved in the formation of the 36-mer precursor:[22,23] (**1**) pentamer, (**2**) pentacyclic octamer, (**3**) tetracyclic undecamer, (**4**) pentacyclic dodecamer, and (**5**) precursor

In order to determine which T-atoms are missing, a close examination of the tetracyclic undecamer (**3**), pentacyclic dodecamer (**4**) and precursor (**5**) formation mechanism is needed. Incorporation of a tetracyclic undecamer (**3**) into the precursor (**5**) requires opening of the four-ring, which results in an intermediate with a three five-ring sequence, corresponding to the ones occurring in the precursor (**5**). Incorporation of the pentacyclic dodecamers (**4**) needs the opening of two rings, one five-ring and one four-ring. Comparison of the two opened intermediates shows that in the intermediate obtained from the tetracyclic undecamer (**3**), the Q^1-atom is missing. The latter atoms are always positioned in the precursor at positions that become T_9 or T_{10} sites of the orthorhombic MFI framework. They are marked with an asterisk in Figure 2. The T_9 and T_{10} sites represent extremities of the precursor (Figure 2). Incorporation of trivalent iron at these missing T-positions does not interfere with the hydrophobic interactions of the inner surface of the precursor with the TPA molecule. Near the T_9 and T_{10} sites of the precursor, there is ample space for the cation necessary for balancing the framework charge generated by incorporation of a trivalent iron atom as well as for possible non-framework ligands of iron when adopting a higher than fourfold coordination (Figure 2).

The T_9 and T_{10} positions constitute the four-rings in the MFI framework (Figure 2 bottom). Preferential substitution of aluminum in four-membered rings was earlier proposed based on upper substitution limits.[24] For iron incorporation into ferrisilicate MFI, the upper limit according to Szostak et al.[6] corresponds to an Si/Fe atomic ratio of 36, or 2.5 iron atoms per unit cell. When higher iron loadings are attempted, part of the iron is located at non-framework sites.[25] The experimentally observed maximum iron loading of one iron atom per 36 T-atoms suggests the incorporation of one iron atom per precursor. The achievement of higher iron loadings of the MFI zeolite would require the formation of precursors with two irons incorporated. Formation of these precursors is difficult, and coupling with other doubly substituted precursors will be impossible due to the Löwenstein's rule and/or formation of four-rings with double iron substitution. These doubly substituted four-rings are unlikely to form considering the preferred octahedral coordination of iron. This explains the maximum iron loading of one iron per 36 T-atoms.

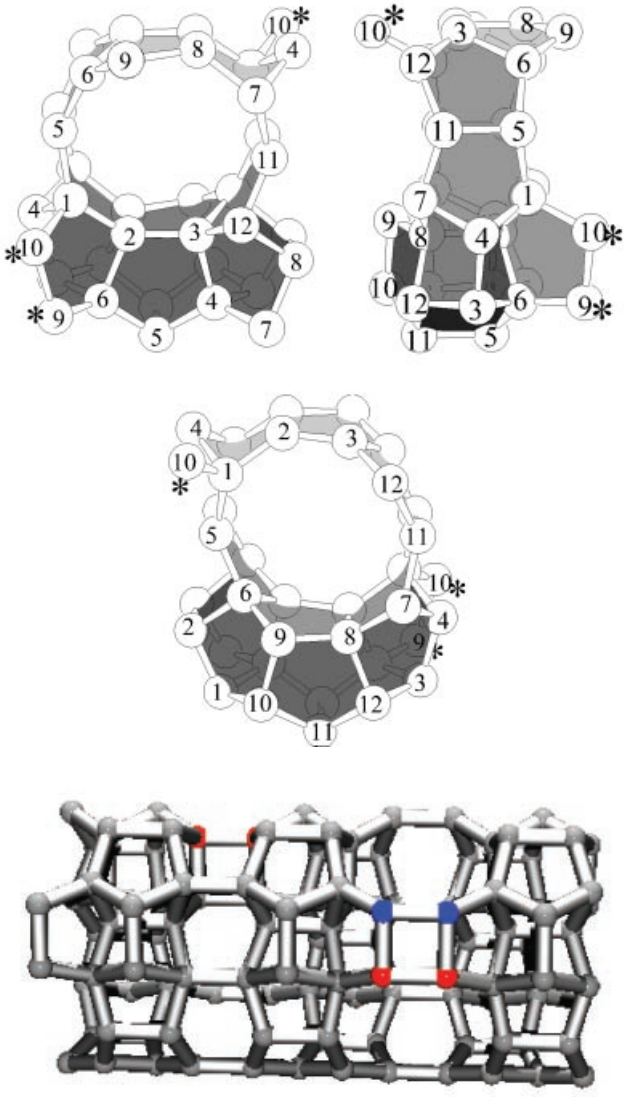

Figure 2. (top) Three views of the precursor model and T-atom numbering; at the T-atoms marked with an asterisk, the Si atom is missing when tetracyclic undecamer (**3**) is incorporated instead of pentacyclic dodecamer (**4**) and Fe^{3+} incorporated; (bottom) coupling of the precursor (**5**) into the MFI framework showing T_9 (blue) and T_{10} (red) sites forming four-rings

If the exclusive pathway for iron incorporation were through occupation of missing T-sites in the precursor (**5**), to obtain this maximum ratio each precursor would have to be defective. It is therefore likely that iron atoms can already be part of pentacyclic dodecamers (**4**). In view of the large atomic radius of iron, these heteroatoms will preferably be at the Q^2-positions of the pentacyclic dodecamers (**4**). Fe^{3+}-containing rings are the least stable, and ring opening preceding the precursor formation will occur in this ring, inevitably resulting in Fe^{3+}-atoms at the T_9 or T_{10} positions of the precursor.

Conclusion

In conclusion, the early molecular steps involved in the TPA-directed formation of Silicalite-1 offer an explanation for the experimentally observed iron location at T_9 and T_{10} [21] sites in the niche of the sinusoidal channel of the MFI-type framework. Examination of the synthesis model reveals that trivalent iron can be incorporated into the pentacyclic undecamer and at T-site vacancies created by the incorporation of tetracyclic undecamers in the precursor. Both incorporation mechanisms result in the same iron siting, viz. T_9 and T_{10}.

Acknowledgments

This work was sponsored by the Flemish government through a Concerted Research Action (GOA). C.E.A.K. acknowledges the Flemish FWO for a postdoctoral fellowship. The Belgian government is acknowledged for supporting the work through the IAP-PAI cooperative network.

[1] I. E. Maxwell, W. H. J. Stork, *Stud. Surf. Sci. Catal.* **2001**, *137*, 747−813.
[2] E. M. Flanigen, J. M. Bennett, R. W. Grose, J. P. Cohen, R. L. Patton, R. M. Kirchner, J. V. Smith, *Nature* **1978**, *271*, 512−516.
[3] G. T. Kokotailo, S. L. Lawton, D. H. Olson, W. M. Meier, *Nature* **1978**, *272*, 437−438.
[4] G. Perego, G. Bellussi, C. Corno, M. Taramasso, F. Buonomo, A. Esposit,o in *Proc. Seventh Int. Conf. on Zeolites* (Eds: Y. Murakami, A. Tijima, J. W. Ward), Elsevier, 1986, Tokyo Tonk Kodansha Amsterdam, p129.
[5] P. Ratnasamy, R. Kumar, *Catal. Today* **1991**, *9*, 329−416.
[6] R. Szostak, T. L. Thomas, *J. Catal.* **1986**, *100*, 555−557.
[7] G. Vorbeck, M. Richter, R. Fricke, B. Parlitz, E. Schreier, K. Szulzewsky, B. Zibrowius, *Stud. Surf. Sci. Catal.* **1991**, *65*, 631−644.
[8] T. Inui, H. Matsuda, O. Yamase, H. Nagata, K. Fukuda, T. Ukawa, A. Miyamoto, *J. Catal.* **1986**, *98*, 491−501.
[9] G. P. Handreck, T. D. Smith, *J. Chem. Soc., Faraday Trans. 1* **1989**, *85*, 3215−3220.
[10] A. S. Kharitonov, V. B. Fenelonov, T. P. Voskresenskaya, N. A. Rudina, V. V. Molchanov, L. M. Plyasova, G. I. Panov, *Zeolites* **1995**, *15*, 253−258.
[11] X. B. Feng, W. K. Hall, *Catal. Lett.* **1996**, *41*, 47−53.
[12] J. Patarin, H. Kessler, J. L. Guth, *Zeolites* **1990**, *10*, 674−679.
[13] P. Ratnasamy, R. Kumar, *Catal. Today* **1991**, *9*, 329−416.
[14] N. Matsubayashi, H. Shimada, M. Imamura, T. Sato, K. Okabe, Y. Yoshimura, A. Nishijima, *Catal. Today* **1996**, *29*, 273−277.
[15] C. A. Hijar, R. M. Jacubinas, J. Eckert, N. J. Henson, P. J. Hay, K. C. Ott, *J. Phys. Chem. B* **2000**, *104*, 12157−12164.
[16] R. Vetrivel, S. Pal, S. Krishnan, *J. Mol. Catal.* **1991**, *66*, 385−397.
[17] D. W. Lewis, C. R. A. Catlow, G. Sankar, S. W. Carr, *J. Phys. Chem.* **1995**, *99*, 2377−2383.
[18] A. Chatterjee, A. K. Chandra, *J. Mol. Catal. A-Chem.* **1997**, *119*, 51−56.
[19] P. M. Piconne, S. Yang, A. Navrotsky, M. E. Davis, *J. Phys. Chem. B* **2002**, *106*, 3629−3638.
[20] N. J. Henson, A. K. Cheetman, J. D. Gale, *Chem. Mater.* **1994**, *6*, 1647−1650.
[21] M. Milanesio, C. Lamberti, R. Aiello, F. Testa, M. Piana, D. Viterbo, *J. Phys. Chem. B* **2000**, *104*, 9951−9951.
[22] C. E. A. Kirschhock, R. Ravishankar, L. Van Looveren, P. A. Jacobs, J. A. Martens, *J. Phys. Chem. B* **1999**, *103*, 4972−4978.
[23] C. E. A. Kirschhock, S. P. B. Kremer, P. J. Grobet, P. A. Jacobs, J. A. Martens, *J. Phys. Chem. B* **2002**, *106*, 4897−4900.
[24] P. A. Jacobs, J. A. Martens, *Stud. Surf. Sci. Catal.* **1987**, *33*, 280.
[25] R. Szostak, V. Nair, T. L. Thomas, *J. Chem. Soc., Faraday Trans. 1* **1987**, *83*, 487−494.

Received November 4, 2002
[I02606]

Design and Structural Analysis of Metallamacrocycles Based on Zinc Halides and a V-Shaped Bismonodentate Ligand of the Cyclophane Type

Cédric Klein,[a] Ernest Graf,[a] Mir Wais Hosseini,*[a] André De Cian,[a] and Nathalie Kyritsakas[b]

Keywords: Cyclophanes / Pyridine / Zinc / Metallacycles

The ligand **1**, based on the [1,1,1,1]cyclophane skeleton and bearing two pyridine units as monodentate coordination sites on the same face of the backbone, leads, in the presence of ZnX_2 (X = Cl, Br or I) complexes, to three isostructural neutral metallamacrocycles with an M/L ratio of 2:2. All three binuclear complexes have been characterised in the solid state by single-crystal X-ray diffraction. All three metallamacrocycles possess a roof-shaped geometry affording a pocket with a single opening. The latter is occupied by solvent molecules in the solid state. A correlation between the size of the halide and dimensions of the pocket is described.

(© Wiley-VCH Verlag GmbH & Co. KGaA, 69451 Weinheim, Germany, 2003)

Introduction

Over the last decade considerable efforts have been invested in the design and synthesis of macro(poly)cyclic structures of the metallamacrocycle type.[1−9] These molecules are based on the interconnection of organic fragments (L) bearing coordination sites and metal centres (M). The topology (macrocyclic, macrobicyclic etc.) and the nuclearity (M/L ratio) of such complexes have been shown to be dependent on both the structural and coordination features of the organic ligand (number of coordination sites, denticity of the coordination units and their spatial arrangement) and on the stereochemical demands of the metal centre (coordination geometry, number of available coordination sites and their disposition within the coordination sphere of the metal).

In a continuation of our investigations on the design and formation of metallamacrocycles,[10−15] we designed the V-shaped ligand **1** and explored its ability to form metallamacrocycles with an imposed 2:2 nuclearity.

We report here the formation of a homologous series of metallamacrocycles based on ZnX_2 (X = Cl, Br, I) and the V-shaped ligand **1**, and their solid state structures.

Results and Discussion

The design of the ligand **1** is based on the [1.1.1.1]metacyclophane skeleton (Scheme 1), which adopts the thermally stable 1,3-alternate conformation.[16] The functionalisation of the two distal aromatic moieties by two pyridine derivatives leads to ligand **1**, for which the two monodentate coordination sites are located on the same face of the backbone. The connection between the cyclophane skeleton and pyridines was achieved through C−C bonds at the *para* position of the pyridine ring.

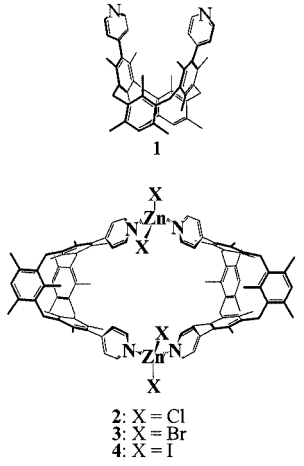

Scheme 1

Due to the rather rigid nature of the ligand **1** and its V-shaped geometry (angle of 30−40° between the pyridine rings), it appeared interesting to explore the possibility of preparing metallamacrocycles using this ligand. The majority of metallamacrocycles reported to date are based on square-planar protected Pd^{II} and Pt^{II} complexes,[2−4] however, based on the geometry of **1** and the orientation of the two pyridines, metal centres adopting a tetrahedral coordination geometry appeared to be the most interesting ones

[a] Université Louis Pasteur, Laboratoire de Chimie de Coordination Organique
4, rue Blaise Pascal, 67000 Strasbourg, France
Fax: (internat.) + 33-3/90241325
E-mail: hosseini@chimie.u-strasbg.fr
[b] Service Commun des Rayons X, Institut Le Bel,
4, rue Blaise Pascal, 67000 Strasbourg, France

for the formation of metallamacrocycles. Thus, three zinc halides (ZnX_2, X = Cl, Br, I) were used. The rationale behind the choice of this type of complex was based on the fact that, taking into account the neutral nature of the ligand **1** and the rather strong biding ability of halides towards Zn^{2+} dication, the combination of **1** and ZnX_2 would lead to neutral metallamacrocycles **2**−**4**. In other words, for a neutral ZnX_2 complex adopting a tetrahedral coordination geometry, two vertices would be occupied by two halides and thus the remaining two coordination positions would be available for coordination to two molecules of **1** through their pyridines. It is perhaps interesting to note that the majority of metallamacrocycles are obtained using *cis*-protected square-planar metal complexes such as diphosphane or ethylenediamine complexes of Pd^{II} and Pt^{II}, whereas in the present case, the connecting metal cation adopts a tetrahedral coordination geometry. This aspect has been recently demonstrated by Braga et al.[7] Furthermore, it was believed that by changing the steric demand of the halogen, one could tailor the geometric features of the metallamacrocycles. Indeed, the increase in the size of the halogen from chloride to bromide and finally to iodide must induce a strong deformation of the tetrahedral Zn complex by increasing the X−Zn−X angle and, consequently, would lead to a decrease in the N−Zn−N angle.

Dealing with the synthesis of metallamacrocycles, an important issue is the control of the nuclearity (Figure 1), i.e. the M/L ratio. Indeed, using rigid and linear organic bismonodentate ligands, depending on the metal cation used, a variety of cyclic compounds such as [2.2]- (Figure 1a), [3.3]- (Figure 1b), [4.4]- (Figure 1c), [5.5]- (Figure 1d) and [6.6]metallamacrocycles (Figure 1e) may be obtained. Based on the angular characteristics of the ligand **1**, we believed that use of ZnX_2 complexes as connecting centres would favour the formation of the [2,2]metallamacrocycle (Figure 1a).

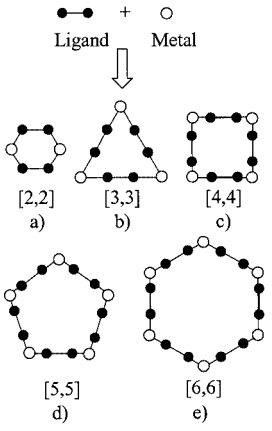

Figure 1. Schematic representation of the formation of metallamacrocycles with different M/L ratio

Metallamacrocycles **2** and **3** were obtained in quantitative yield by mixing the ligand **1** and ZnX_2 (X = Cl or Br) in CH_2Cl_2 at room temperature and then evaporating the solvent. Both binuclear complexes are soluble in $CHCl_3$. They were characterised in solution by ^1H and ^{13}C NMR spectroscopy, and by X-diffraction studies on single crystals in the solid state.

In solution, the ^1H NMR investigations in $CDCl_3$ at 25 °C revealed that the signals corresponding to H atoms belonging to the pyridine units are significantly downfield shifted for both complexes **2** and **3** with respect to the free ligand **1** (Figure 2). Interestingly, addition of an excess of $ZnCl_2$ or $ZnBr_2$ to a solution containing **2** and **3**, respectively, has no effect on the line-widths and chemical shifts of the signals, indicating that the species present in solution are the metallamacrocycles **2** and **3** with a well-defined 2M/2 L ratio.

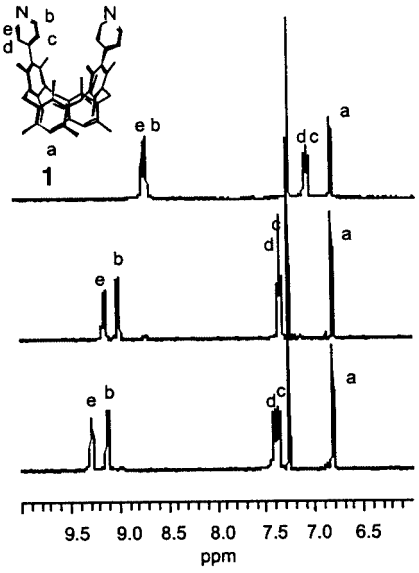

Figure 2. ^1H NMR (300 MHz, $CDCl_3$) studies at room temperature of the free ligand **1** (top) and metallamacrocycles **2** (middle) and **3** (bottom); only signals corresponding to protons belonging to pyridine units are presented

Compound **4**, due to its insolubility in $CHCl_3$, was not characterised in solution under the same conditions but only in the solid state by single-crystal X-ray diffraction.

In the solid state, the X-ray diffraction investigations revealed that, for all three compounds, neutral metallamacrocycles of the [2,2]-type are formed.

In the case of **2** (Figure 3a), the crystal is composed of $(\mathbf{1}\cdot ZnCl_2)_2$, and one ethanol and eight chlorobenzene molecules. The coordination sphere around the metal centre is composed of two Cl^- anions and two N atoms belonging to two pyridine units of two ligands **1**, with Zn−N and Zn−Cl bond lengths in the range 2.03−2.07 Å and 2.19−2.23 Å, respectively. The metal centre adopts a distorted tetrahedral coordination geometry with N−Zn−N and Cl−Zn−Cl angles of 101.3−101.7°, and 122.0−126.0°, respectively. Due to the rigidity of **1** and the tetrahedral geometry around the zinc(II) cation, the metallamacrocycle adopts a roof-type conformation with an average angle between the two main cyclophane axes of 110° and a Zn−Zn separation of 11.37 Å. Due to the peculiar arrangement of the two cyclophane units **1**, a pocket-type cavity possessing a single opening is formed; this is occupied by one chlorobenzene molecule.

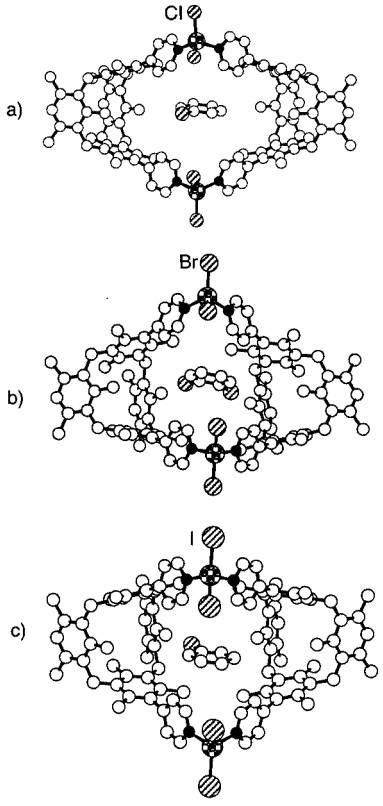

Figure 3. The solid-state structures of the metallamacrocycles **2** (a), **3** (b) and **4** (c); non-included solvent molecules and H atoms are omitted for clarity; see text for bond lengths and angles

In the case of **3** (Figure 3b), the crystal is composed of a $(\mathbf{1}\cdot ZnBr_2)_2$ metallamacrocycle and nine 1,2-dichlorobenzene molecules. Again, the coordination sphere around the metal centre is composed of a set of two Br^- anions and two N atoms with average Zn−N and Zn−Br bond lengths of 2.07 Å and 2.34 Å, respectively. The Zn^{2+} cation adopts a more distorted tetrahedral coordination geometry, with N−Zn−N and Br−Zn−Br angles of 93.7°, and 123.4°, respectively. Once again, the metallamacrocycle **3** adopts a roof-type conformation, as expected, with an average angle between the two main cyclophane axes of 82° and a Zn−Zn separation of 10.92 Å. The pocket-type cavity is occupied by a 1,2-dichlorobenzene molecule.

In the case of **4** (Figure 3c), the crystal is composed of a $(\mathbf{1}\cdot ZnI_2)_2$ metallamacrocycle and three chlorobenzene molecules. The latter were found to be disordered over two positions. Again, the coordination sphere around the metal centre is composed of a set of two I^- anions and two N atoms with average Zn−N and Zn−I bond lengths of 2.07 Å and 2.54 Å, respectively. The Zn^{2+} cation adopts an even more distorted tetrahedral coordination geometry with N−Zn−N and I−Zn−I angles of 92.6° and 121.6°, respectively. Once again, the metallamacrocycle **4** adopts a roof-type conformation, as expected, with an average angle between the two main cyclophane axes of 77.0° and a Zn−Zn separation of 11.21 Å. The pocket-type cavity is occupied by a disordered chlorobenzene molecule.

For all metallamacrocycles **2**−**4**, except for a few van der Waals contacts, no particular host-guest type interactions can be identified.

In $CDCl_3$ solution, no trace of the inclusion complexes of **2** and **3** could be observed by H-H NOESY investigations.

In summary, owing to the rigidity of the V-shaped bismonodentate ligand **1** and the orientation of the pyridine units, three isostructural neutral metallamacrocycles **2**−**4** of the 2M/2 L-type have been obtained in the presence of ZnX_2 (X = Cl, Br or I). All three metallamacrocycles have been characterised in the solid state by single-crystal X-ray diffraction. Due to the geometry of the ligand, the binuclear metallamacrocycles contain a pocket-type cavity possessing a single opening. The dimension of the cavity is determined by the size of the halide. In all three cases, the cavity is occupied by solvent molecules. Using the ligand **1**, the formation of other types of finite metallamacrocycles using other metal centres and the generation of infinite coordination networks are currently under investigations.

Experimental Section

Synthesis of Metallamacrocycles 2−4

General: All commercially available reagents were purchased and used without further purification. ^1H and ^{13}C NMR spectra were recorded on Bruker spectrometers at 400 and 300 MHz and at 50 MHz, respectively. Microanalyses were performed by the Service de Microanalyses de la Fédération de Recherche Chimie, Université Louis Pasteur, Strasbourg.

$(\mathbf{1}\cdot ZnCl_2)_2$ 2: A mixture of ligand **1**[16] (20 mg, 0.029 mmol) and $ZnCl_2$ (3.9 mg, 0.029 mmol) in CH_2Cl_2 (7 mL) was stirred at room temp. for 2 hours. Subsequent evaporation of the solvent gave the pure complex **2** as a white powder in quantitative yield (23 mg). $C_{100}H_{108}Cl_4N_4Zn_2\cdot 0.5CH_2Cl_2$ (1681.1): calcd. C 71.80, H 6.53, N 3.33; found C 71.78, H 6.55, N 3.27.^1H NMR ($CDCl_3$, 300 MHz, 25 °C): δ = 1.19 (s, 12 H, *p*-CH_3), 1.28 (s, 12 H, *p*-CH_3), 1.99 (s, 24 H, *o*-CH_3), 2.34 (s, 24 H, *o*-CH_3), 3.90 et 3.98 (AB, 2d, 16 H, *J* = 17 Hz, Ar-CH_2-Ar), 6.81 (s, 4 H, H-Ar), 7.34 (d, *J* = 5 Hz, 4 H, H-Py), 7.36 (d, *J* = 5 Hz, 4 H, H-Py), 9.00 (d, *J* = 5 Hz, 4 H, H-Py), 9.15 (d, *J* = 5 Hz, 4 H, H-Py) ppm. ^{13}C NMR ($CDCl_3$, 50 MHz, 25 °C): δ = 17.5, 18.1, 19.5, 21.4, 32.2, 126.4, 127.6, 130.1, 130.6, 144.4, 135.4, 136.8, 137.4, 138.2, 148.9, 149.1 ppm.

$(\mathbf{1}\cdot ZnBr_2)_2$ 3: A mixture of ligand **1**[16] (20 mg, 0.029 mmol) and $ZnCl_2$ (6.5 mg, 0.029 mmol) in CH_2Cl_2 (7 mL) was stirred at room temp. for 2 hours. Subsequent evaporation of the solvent gave the pure complex **3** as a white powder in quantitative yield (26 mg). $C_{100}H_{108}Br_4N_4Zn_2\cdot 2CH_2Cl_2$ (1986.3): calcd. C 61.68, H 5.68, N 2.82; found C 61.84, H 5.62, N 2.80. ^1H NMR ($CDCl_3$, 300 MHz, 25 °C): δ = 1.19 (s, 12 H, *p*-CH_3), 1.28 (s, 12 H, *p*-CH_3), 1.98 (s, 24 H, *o*-CH_3), 2.34 (s, 24 H, *o*-CH_3), 3.89 et 3.98 (AB, 2d, 16 H, *J* = 17 Hz, Ar-CH_2-Ar), 6.81 (s, 4 H, H-Ar), 7.37 (d, *J* = 5.5 Hz, 4 H, H-Py), 7.41 (d, *J* = 5.5 Hz, 4 H, H-Py), 9.12 (d, *J* = 5.5 Hz, 4 H, H-Py), 9.29 (d, *J* = 5.5 Hz, 4 H, H-Py) ppm. ^{13}C NMR ($CDCl_3$, 50 MHz, 25°C): δ = 17.5, 18.1, 19.5, 21.3, 32.1, 126.5, 127.8, 130.1, 130.5, 133.4, 135.3, 136.6, 136.9, 137.3, 138.2, 148.9, 149.0, 153.4, 157.1 ppm.

$(\mathbf{1}\cdot ZnI_2)_2$ 4: Due to the insolubility of complex **4** in CH_2Cl_2, this metallamacrocycle was generated directly as crystals in a crystallis-

ing tube upon slow diffusion of an ethanol solution (0.75 mL) of ZnI_2 (5.7 mg, 0.018 mmol) into a chlorobenzene (0.5 mL) solution of ligand **1**[16] (5 mg, 0.0073 mmol).

Crystallisation Conditions

Metallamacrocycles 2 and 3: An EtOH solution (1 mL) of ZnX_2 (4.4 mg for X = Cl, 7.2 mg for X = Br) was added dropwise to a stirred solution (5 mL) of **1** (20 mg, 0.029 mmol) in chlorobenzene (X = Cl) or 1,2-dichlorobenzene (X = Br). After stirring at room temperature for two hours, EtOH (3 mL) was diffused into the solution. Complexes **2** and **3** were obtained as colourless crystals after about a week.

Single crystals of the binuclear metallamacrocycle **4** were obtained as described above.

Crystal Structure Characterisation: X-ray diffraction data collection was carried out on a Kappa CCD diffractometer equipped with an Oxford Cryosystem liquid N_2 device, using graphite-monochromated Mo-K_α radiation. For all structures, diffraction data were corrected for absorption and analysed with the OpenMolen package.[17] All non-H atoms were refined anisotropically.

Crystal Data for 2 ($1{\cdot}ZnCl_2)_2$: Colourless crystals, 173 K, $C_{200}H_{216}Cl_8N_8Zn_4{\cdot}8C_6H_5Cl{\cdot}C_2H_5OH$, M = 4223.66, triclinic, space group $P\bar{1}$, a = 12.4464(2), b = 21.8475(2), c = 22.8606(3) Å, α = 112.173(5)°, β = 90.786(5)°, γ = 92.262(5)°, V = 5749.4(1) Å^3, Z = 1, D_c = 1.22 g cm^{-3}, μ = 0.653 mm^{-1}, 14989 data with $I > 3\sigma(I)$, R = 0.117, Rw = 0.142.

Crystal Data for 3 ($1{\cdot}ZnBr_2)_2$: Colourless crystals, 173 K, $C_{50}H_{52}Br_2N_2Zn{\cdot}4.5C_6H_4Cl_2$, M = 1567.69, monoclinic, space group $C2/c$, a = 36.3141(4), b = 11.4622(1), c = 36.2867(4) Å, β = 107.446(5)°, V = 14409.2(3) Å^3, Z = 8, D_c = 1.45 g cm^{-3}, μ = 1.828 mm^{-1}, 8040 data with $I > 3\sigma(I)$, R = 0.053, Rw = 0.080.

Crystal data for 4 ($1{\cdot}ZnI_2)_2$: Colourless crystals, 173 K, $C_{50}H_{54}I_2N_2Zn{\cdot}3C_6H_5Cl$, M = 1337.84, monoclinic, space group $C2/c$, a = 34.2298(5), b = 11.7252(2), c = 34.6599(7) Å, β = 117.237(5)°, V = 12368.4(6) Å^3, Z = 8, D_c = 1.44 g cm^{-3}, μ = 1.566 mm^{-1}, 8235 data with $I > 3\sigma(I)$, R = 0.078, Rw = 0.091.

CCDC 199799−199801 (**2**−**4**) contain the supplementary crystallographic data for this paper. These data can be obtained free of charge at www.ccdc.cam.ac.uk/conts/retrieving.html or from the Cambridge Crystallographic data Centre, 12 Union Road, Cambridge CB2 1EZ, UK; fax: (internat.) +44-1223/336-033; E-mail: deposit@ccdc.cam.ac.uk.

Acknowledgments

We would like to thank the Université Louis Pasteur and the Ministry of Research and Technology for financial support and a scholarship to C. K.

[1] R. W. Saalfrank, A. Stark, K. Peters, H.-G. von Schnering, *Angew. Chem. Int. Ed. Engl.* **1988**, *27*, 851−853.
[2] M. Fujita, in *Comprehensive Supramolecular Chemistry* (Eds.: J. L. Atwood, J. E. D. Davies, D. D. MacNicol, F. Vögtle), *Vol. 9* (Eds.: J. P. Sauvage, M. W. Hosseini), Elsevier, Oxford, **1996**, pp. 253−282.
[3] P. J. Stang, B. Olenyuk, *Acc. Chem. Res.* **1997**, *30*, 502−518.
[4] G. F. Swiegers, T. J. Malefetse, *Chem. Rev.* **2000**, *100*, 3483−3537.
[5] J. K. M. Sanders, in *Comprehensive Supramolecular Chemistry* (Eds.: J. L. Atwood, J. E. D. Davies, D. D. MacNicol, F. Vögtle, *Vol. 9* (Eds.: J. P. Sauvage, M. W. Hosseini), Elsevier, **1996**, pp. 131−164.
[6] C. M. Drain, J.-M. Lehn, *J. Chem. Soc., Chem. Commun.* **1994**, 2313−2314.
[7] D. Braga, M. Polito, M. Bracaccini, D. D'Addario, E. Tagliavini, D. M. Proserpio, F. Grepioni, *Chem. Commun.* **2002**, 1080−1081.
[8] F. M. Romero, R. Ziessel, A. Dupont-Gervais, A. van Dorsselaer, *Chem. Commun.* **1996**, 551−552.
[9] T. Habicher, J. F. Nierengarten, V. Gramlich, F. Diederich, *Angew. Chem. Int. Ed.* **1998**, *37*, 1916−1919.
[10] R. Schneider, M. W. Hosseini, J.-M. Planeix, A. De Cian, J. Fischer, *Chem. Commun.* **1998**, 1625−1626.
[11] M. Lo, M. W. Hosseini, A. Jouaiti, A. De Cian, J. Fischer, *Eur. J. Inorg. Chem.* **1999**, 1981−1985.
[12] A. Jouaiti, M. Lo, M. W. Hosseini, A. De Cian, *Chem. Commun.* **2000**, 2085−2086.
[13] V. Jullien, J.-M. Planeix, M. W. Hosseini, A. De Cian, *J. Organomet. Chem.* **2002**, *643*−*644*, 376−380.
[14] A. Jouaiti, M. W. Hosseini, N. Kyritsakas, *Eur. J. Inorg. Chem.* **2002**, 57−61.
[15] P. Grosshans, A. Jouaiti, M. W. Hosseini, A. De Cian, N. Kyritsakas, *Tetrahedron Lett.* **2002**, *43*, in press.
[16] C. Klein, E. Graf, M. W. Hosseini, A. De Cian, N. Kyritsakas-Gruber, *Eur. J. Org. Chem.* **2002**, 395−399.
[17] OpenMolenN, Interactive Structure Solution, Nonius B. V., Delft, The Netherlands, 1997.

Received December 17, 2002
[I02682]

A Novel Open-Framework Gallium Phosphate Containing Two Different Building Units

Daofeng Sun,[a] Rong Cao,*[a] Yanqiong Sun,[a] Wenhua Bi,[a] and Maochun Hong[a]

Keywords: Zeolite analogues / Gallium / Phosphates / Alkali metals / Fluorides

A novel open-framework fluorinated gallium phosphate has been prepared hydrothermally. X-ray diffraction shows each double four-ring (D4R) links four 1D gallium phosphate chains made up of single four-rings (S4R) to form a 3D framework with eight-ring channels where potassium ions reside.

(© Wiley-VCH Verlag GmbH & Co. KGaA, 69451 Weinheim, Germany, 2003)

Since the discovery of the family of crystalline aluminophosphates (ALPOs) in 1982,[1] microporous zeolite-like materials have attracted much interest due to their potential applications in, for example, ion-exchangers, catalysts and adsorbents.[2,3] In the past decade, the replacement of Al in ALPOs by Ga has resulted in a large number of gallium phosphates with a wide range of structure types[4,5] because of the ability of gallium to adopt a more variable and expanded coordination environment compared to aluminum. Recently, fluoride ion has been discovered to play a major role in the gallium phosphate system and many fluoride gallium phosphates have been synthesized.[6] Férey and others have prepared a series of fluoride gallium phosphates that show interesting templating effects and structure types. Some of these gallium phosphate materials, such as cloverite,[7] ULM-5,[8] ULM-18[9] and Mu-15,[10] contain a double four-ring unit (D4R), with a fluoride ion occluded at its center. This has resulted in the postulation that the fluoride ion acts as a template for the formation of the D4R species and makes the cuboidal D4R an attractive target because of its rigid 3D shape.[11] In the synthesis of materials containing D4R units, the use of organic amines as structure-directing and charge-compensation agents is very common, but that of alkali metal ions is rare. In this communication, we report a novel gallium phosphate containing fluoride-templating D4R units and potassium ion charge-compensation agents.

In an attempt to prepare new a gallium phosphate material with 1-(2-aminoethyl)piperazine as the structure-directing agent, an open framework fluoride gallium phosphate, $K[(GaPO_4)\{F_{1/4}(GaPO_4)\}_4]$ (**1**), was obtained. This novel material was prepared by a hydrothermal synthesis with KF as a source of fluoride ions. Single-crystal X-ray diffraction indicates that **1** possesses a three-dimensional open framework containing one-dimensional channels along the *c* axis, in which potassium ions reside.

Two crystallographically independent gallium and phosphate centers, Ga(1), P(1) and Ga(2), P(2), which form different second building units (SBUs), are present in the structure. The first SBU is a $Ga_2(PO_4)_2$ single four-ring (S4R; Figure 1, Part I, left) made up of Ga(1) and P(1). The gallium atom is four-coordinate and is linked by corner-sharing PO_4 tetrahedra with an average Ga−O distance of 1.875(4) Å. This distance is slightly longer than that found in complex ULM-16,[5d] in which the $Ga_2(PO_4)_2$ unit links layers to form a 3D open framework. As is well known, the linkage of S4Rs often results in 2D layers containing eight-ring windows, and this phenomenon has been observed for a number of zeolites and zeolite analogues.[12,13] Interestingly, in **1**, a one-dimensional infinite gallium phosphate chain is formed by the linkage of S4Rs, in which the gallium atom and the phosphate tetrahedron alternate (Figure 1, Part I, right).

The second SBU is a double four-ring unit (D4R; Figure 1, Part II) formed by Ga(2) and P(2), similar to that observed in many gallium phosphate molecular sieves.[7−10] A fluoride ion resides in the D4R unit as observed in cloverite[7] and other ULM complexes.[8−10] In this case, the fluoride atoms lie a long distance from the four gallium atoms, with a relatively long contact of 2.459 Å, which is longer than that found in CYCLAM-GaPO (2.286 Å)[14] and illustrates that the fluoride ion less strongly bound in the D4R center. The average Ga−O distance in the D4R unit is 1.865(4) Å, shorter than that in the S4R unit. In previous reports, D4R is usually linked through its corners to other D4R units to give rise to a 2D or 3D ACP topology first reported by Stucky.[15] Surprisingly, in **1**, the D4Rs themselves have no linkage, each D4R links four above mentioned 1D gallium phosphate chains by its four corners with a Ga−O distance of 1.920(4) Å, and a 3D open framework with eight-ring channels (9.657 × 3.763 Å) is formed along the *c* axis, in which the potassium ions reside. As

[a] State Key Laboratory of Structural Chemistry, Fujian Institute of Research on the Structure of Matter
Chinese Academy of Sciences,
Fujian, Fuzhou 350002, China

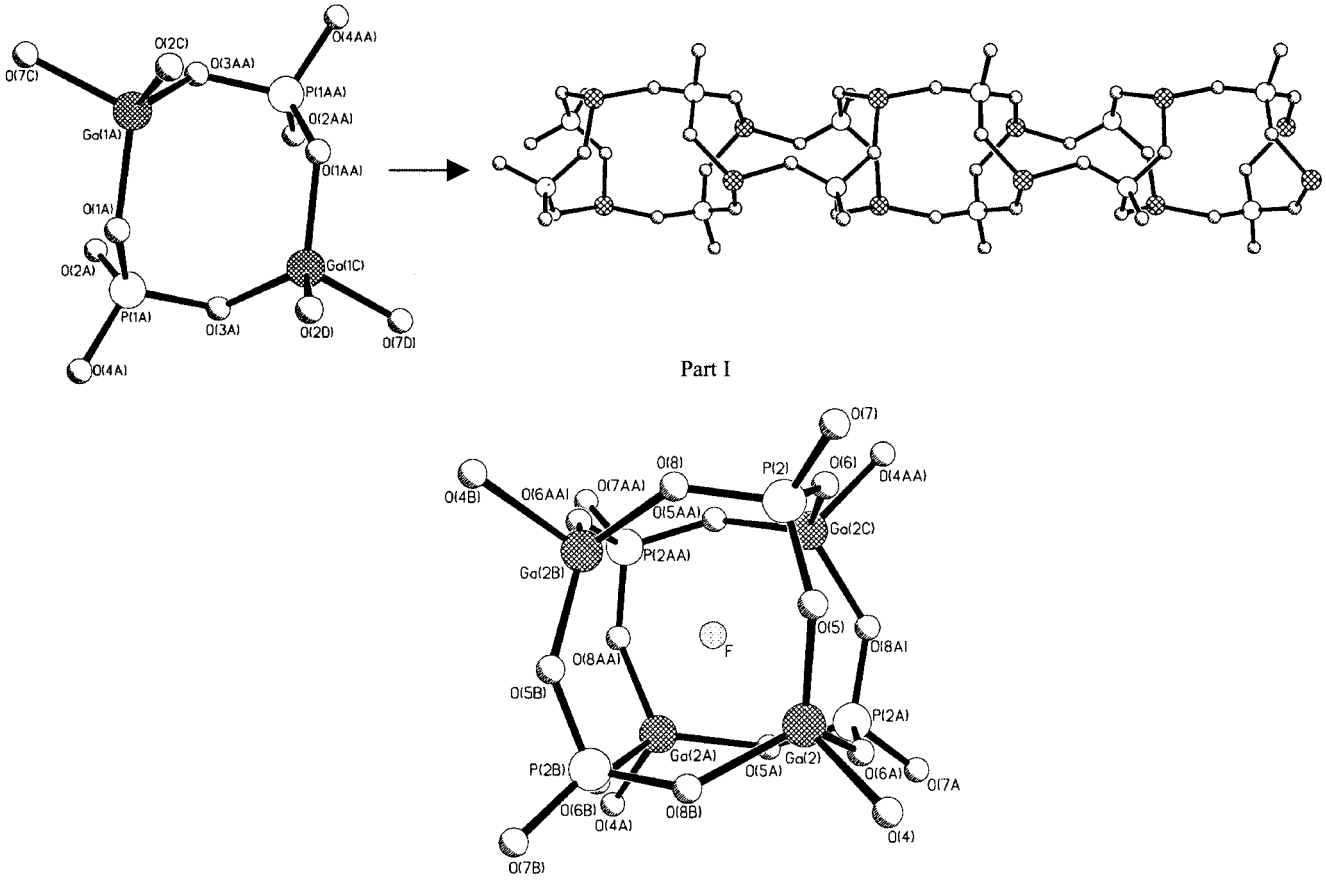

Figure 1. The one-dimensional chain and D4R unit in **1**; selected bond lengths (Å) and angles (°): Ga(1)−O(1) 1.880(3), Ga(1)−O(3) 1.884(4), Ga(2)−O(7) 1.834(4), Ga(2)−O(8) 1.850(4), Ga(2)−O(9) 1.856(3), Ga(2)−O(6) 1.920(4), P(1)−O(4) 1.526(4), P(1)−O(6) 1.533(4), P(1)−O(1) 1.534(3), P(1)−O(2) 1.537(3), P(2)−O(7) 1.535(3)

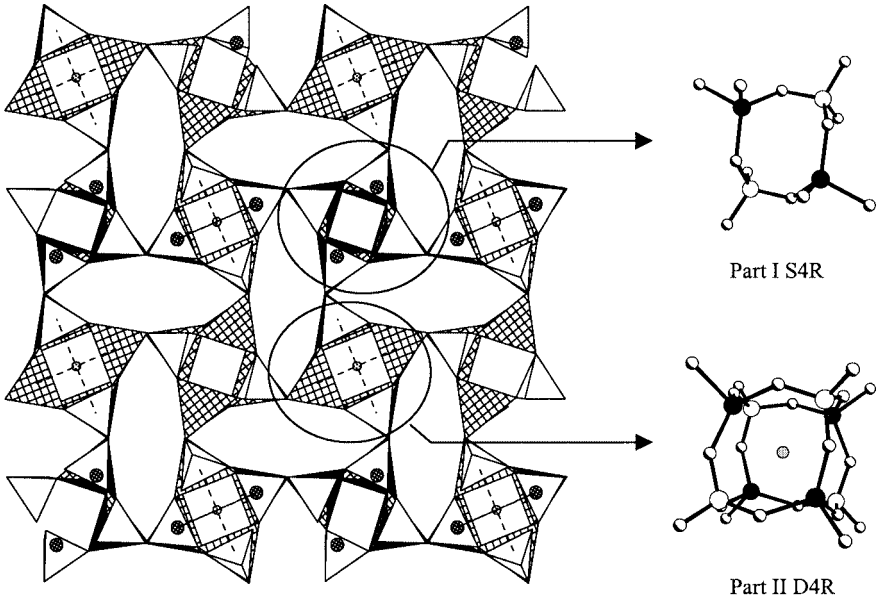

Figure 2. The 3D open framework showing the arrangement of single four-ring and double four-ring units to form eight-ring channels along *c* axis; potassium ions are omitted for clarity

shown in Figure 2, every two adjacent eight-membered rings are almost perpendicular to each other.

TGA determination shows that complex **1** possesses a high degree of thermal stability and there is no weight loss even upon heating to more than 800 °C, indicating that **1** is thermally more stable than potassium templating gallium phosphatooxalate.[16] After heating a sample of **1** to 800 °C the XRPD pattern remains essentially the same, although slight changes in the strength of some peaks were observed. This result validates the stability of **1** and is in agreement with the structural data.

Experimental Section

Synthesis of 1: Ga_2O_3 (0.023 g, 0.0625 mmol) was dispersed in 16 mL of distilled water by vigorous stirring, and then phosphoric acid (0.5 g, 85% weight aqueous solution) was added. After stirring for 15 minutes, 1-(2-aminoethyl)piperazine (0.1 mL) and KF (0.03 g, 0.5 mmol) were added and stirred to homogeneity. The mixture was sealed in a Teflon-lined stainless autoclave and heated at 160 °C for three days under autogenous pressure, then cooled to room temperature over 8 hours. The resulting product, consisting of colorless prism-like crystals was collected by filtration. Yield: 35%.

X-ray Crystallography: $F_{0.25}Ga_2KO_8P_2$, (**1**), M = 373.23, *tetragonal*, space group $P4_2/n$, a = 13.2322(19), b = 13.2322(19), c = 8.6535(17) Å, U = 1515.2(4) Å^3, T = 293 K, Z = 4, D_c = 1.636 g/cm^3, λ = 0.71073 Å, 1730 unique reflections were used in the calculations. $R1$ = 0.0350 and $wR2$ = 0.1308. The intensity data were collected on a Smart CCD diffractometer with graphite-monochromated Mo-K_α (λ = 0.71073 Å) radiation at room temperature in the ω-2θ scan mode. An empirical absorption correction was applied to the data using the SADABS program. The structures were solved by direct methods. All calculations were performed using the SHELXTL program. Crystallographic data for the complex **1** are given in Table 1.

Table 1. Crystallographic data for complex **1**

	1
Empirical formula	$F_{0.25}Ga_2KO_8P_2$
F_w	373.23
Crystal system	tetragonal
Space group	$P4_2/n$
a, Å	13.2322(19)
b, Å	13.2322(19)
c, Å	8.6535(17)
α, deg	90
β, deg	90
γ, deg	90
V, Å^3	1515.2(4)
Z	4
D_c, g·cm^{-3}	1.636
μ, mm^{-1}	4.051
R_1 [$I > 2\sigma(I)$][a]	0.0350
wR_2 (all data)[b]	0.1454

[a] $R_1 = ||F_o| - |F_c||/|F_o|$. [b] $wR_2 = [w(F_o^2 - F_c^2)^2/w(F_o^2)^2]^{1/2}$.

Further details of the crystal-structure investigation(s) may be obtained from the Fachinformationszentrum Karlsruhe, 76344 Eggenstein-Leopoldshafen, Germany, on quoting the depository number CSD-412582

Acknowledgments

We are grateful for financial support from NNSF of China (90206040, 29901005), NSF of Fujian Province and the key and the "One Hundred Talent" projects from CAS. We also thank Prof. Guoyu Yang for the thermogravimetric analysis.

[1] S. T. Wilson, B. M. Lok, C. A. Messina, T. R. Cannan, E. M. Flanigen, *J. Am. Chem. Soc.* **1982**, *104*, 1146−1147.
[2] [2a] J. M. Thomas, *Angew. Chem. Int. Ed. Engl.* **1994**, *33*, 913−916. [2b] M. E. Davis, *Microporous Mesoporous Mater.* **1998**, *21*, 173−182. [2c] F. S. Xiao, S. Qiu, Q. W. Pang, R. Xu, *Adv. Mater.* **1999**, *11*, 1091−1099. [2d] C. N. R. Rao, S. Natarajan, A. Choudhury, S. Neeraj, A. A. Ayi, *Acc. Chem. Res.* **2001**, *34*, 80−87.
[3] [3a] B. Zhang, A. Clearfield, *J. Am. Chem. Soc.* **1997**, *119*, 2751−2752. [3b] A. K. Cheetham, G. Férey, T. Loiseau, *Angew. Chem. Int. Ed.* **1999**, *38*, 3268−3292. [3c] J. Y. Ying, M. S. Wong, *Angew. Chem. Int. Ed.* **1999**, *38*, 56−77.
[4] [4a] X. T. Yin, L. F. Nazar, *J. Chem. Soc., Chem. Commun.* **1994**, 2349−2350. [4b] A. R. Cowley, A. M. Chippindale, *Chem. Commun.* **1996**, 673−674. [4c] X. H. Bu, P. Y. Feng, G. D. Stucky, *Science* **1997**, *278*, 2080−2085.
[5] [5a] S. H. Feng, X. T. Xu, G. D. Yang, R. R. Xu, F. P. Glasser, *J. Chem. Soc., Dalton. Trans.* **1995**, 2147−2153. [5b] S. J. Weigel, S. C. Weston, A. K. Cheetham, G. D. Stucky, *Chem. Mater.* **1997**, *9*, 1293−1295. [5c] K. H. Lii, C. Y. Chen, *Inorg. Chem.* **2000**, *39*, 3374−3378. [5d] C. Sassoye, J. Marrot, T. Loiseau, G. Férey, *Chem. Mater.* **2002**, *14*, 1340−1347.
[6] [6a] R. I. Walton, F. Millange, A. Le Bail, T. Loiseau, C. Serre, D. O'Hare, G. Ferey, *Chem. Commun.* **2000**, 203−204. [6b] F. Bonhomme, S. G. Thoma, T. M. Nenoff, *J. Mater. Chem.* **2001**, *11*, 2559−2563. [6c] P. Caullet, J. L. Guth, J. Hazm, J. M. Lamblin, H. Gies, *Eur. J. Solid State Inorg. Chem.* **1991**, *28*, 345−351.
[7] M. Estermann, L. B. McCusker, C. Baerlocher, A. Merrouche, H. Kessler, *Nature* **1991**, *352*, 320−325.
[8] G. Férey, *J. Fluor. Chem.* **1995**, *72*, 187−193.
[9] F. Taulelle, A. Samoson, T. Loiseau, G. Férey, *J. Phys. Chem. B* **1998**, *102*, 8588−8598.
[10] A. Matijasic, J. L. Paillaud, J. Patarin, *J. Mater. Chem.* **2000**, *10*, 1345−1351.
[11] D. S. Wragg, R. E. Morris, *J. Am. Chem. Soc.* **2000**, *122*, 11246−11247.
[12] [12a] D. S. Wragg, I. Bull, B. G. Hix, R. E. Morris, *Chem. Commun.* **1999**, 2037−2038. [12b] W. M. Meier, D. H. Olson and Ch. Baerlocher, *Atlas of Zeolite Structural Types*, Elsevier, New York, 4th edn., 1996.
[13] [13a] T. Loiseau, F. Serpaggi, G. Férey, *Chem. Commun.* **1997**, 1093−1094. [13b] G. Férey, *C. R. Acad. Sci. Ser. C* **1998**, *1*, 1−9.
[14] D. S. Wragg, G. B. Hix, R. E. Morris, *J. Am. Chem. Soc.* **1998**, *120*, 6822−6823.
[15] P. Feng, X. Xu, G. D. Stucky, *Nature* **1997**, *388*, 735−741.
[16] L. C. Hung, H. M. Kao, K. H. Lii, *Chem. Mater.* **2000**, *12*, 2411−2417.

Received December 15, 2002
[I02687]

Synthesis, Structures, and Properties of a Series of $[Cd_8Se(SePh)_{12}Cl_4]^{2-}$ Cluster Compounds with Different Counterions

Andreas Eichhöfer,*[a] Oliver Hampe,[a] and Martine Blom[a]

Keywords: Cluster compounds / Cadmium / Selenium / X-ray diffraction / UV/Vis spectroscopy / Mass spectrometry

A series of seven single-crystalline ionic CdSe cluster compounds, all possessing the cluster anion $[Cd_8Se(SePh)_{12}Cl_4]^{2-}$, but with different counterions, has been synthesized. The compounds were characterized in the solid state, solution, and gas phases using single-crystal XRD, powder XRD, UV/Vis spectroscopy, and FT mass spectrometry. The results of the crystal structure determination show that the increasing size of the different counterions does not simply lead to an increase in the shortest inter-cluster distance, but rather to changes in the crystal structure. Room-temperature UV/Vis absorption and reflectance spectra of the crystalline powders are virtually identical, proving that the electronic transitions in the energy range probed can be attributed to the cluster anion $[Cd_8Se(SePh)_{12}Cl_4]^{2-}$. The band of the first transition in the solid-state UV/Vis spectra are broadened relative to that in the solution spectra, as it is possibly affected by the collective interactions between the nanoclusters in the three-dimensional crystal lattice. Interestingly, in solution, the position and feature of the lowest-energy transition band changes as the solvent is varied. As FT mass spectrometry gives clear evidence for the existence of the intact $[Cd_8Se(SePh)_{12}Cl_4]^{2-}$ cluster anion in all these solutions, these shifts can be interpreted in terms of solvatochromic effects.
(© Wiley-VCH Verlag GmbH & Co. KGaA, 69451 Weinheim, Germany, 2003)

Introduction

Recent progress in the syntheses of CdSe cluster molecules has led to the development of a series of homologous compounds, namely $[NPr_4^+]_2[Cd_4(SePh)_6Cl_4]^{2-}$ $[Cd_{10}Se_4(SePh)_{12}(PPr_3)_4]$, $[Cd_{17}Se_4(SePh)_{24}(PPh_2Pr)_4]^{2+}[Cd_8Se(SePh)_{12}Cl_4]^{2-}$, and $[Cd_{32}Se_{14}(SePh)_{36}(PPh_3)_4]$ (Ph = phenyl, Pr = *n*-propyl).[1] As the largest clusters already overlap in size with the smallest nanocrystals, these clusters of semiconductor materials, composed of tens of atoms with bonding resembling that present in the solid state, are interesting molecular models for the investigation of the evolution of properties with size.[2−4] Systematic studies of the size-dependent optical and electronic properties of the CdSe cluster molecules mentioned above show that the onset of the absorption and low-temperature photoluminescence excitation of the clusters systematically shift to the blue in smaller clusters, manifesting the quantum confinement effect well known for larger CdSe nanocrystals. Photo-darkening experiments on the ionic cluster $[Cd_{17}Se_4(SePh)_{24}(PPh_2Pr)_4]^{2+}[Cd_8Se(SePh)_{12}Cl_4]^{2-}$ provide the first evidence for collective interactions between the cluster molecules within the crystalline solids. The results from a recent report by Döllefeld et al. on the absorption and reflectance spectra of $[Cd_{17}S_4(SCH_2CH_2OH)_{26}]$ cluster molecules show that collective interactions in the crystalline state also influence the lowest energy transition bands relative to the those in solution.[5,6]

In the work presented herein, we study the influence of the subsequent change in the type of counterion used in the synthesis of the cluster anion $[Cd_8Se(SePh)_{12}Cl_4]^{2-}$ on the properties of the compounds formed in solution and in the solid state. The compounds were characterised using X-ray diffraction on single crystals and crystalline powders, as well as by using different spectroscopic methods such as UV/Vis spectroscopy and electrospray Fourier transform mass spectrometry. The latter has proven to be a powerful tool in identifying charged, large cluster species present in solution.[7]

Results and Discussion

Cluster compounds **1**−**7** have been synthesised according to Scheme 1. Different conditions were optimised for the crystallisation of the different clusters, depending on the type of counterion present.

Structure Determination by Single-Crystal X-ray Diffraction

For all the compounds, crystal structures have been determined by single-crystal X-ray analysis. The molecular structure of the cluster anion $[Cd_8Se(SePh)_{12}Cl_4]^{2-}$ is similar for all the compounds studied (Figure 1).[8,9] A central selenium atom Se1 is tetrahedrally surrounded by four "in-

[a] Institut für Nanotechnologie, Forschungszentrum Karlsruhe, Postfach 3640, 76021 Karlsruhe, Germany
Fax: (internat.) + 49-7247/82-6368
E-mail: eichhoefer@int.fzk.de

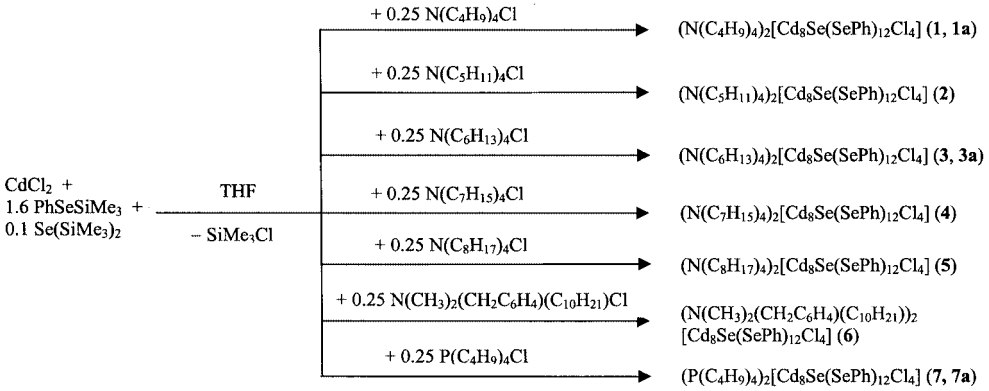

Scheme 1

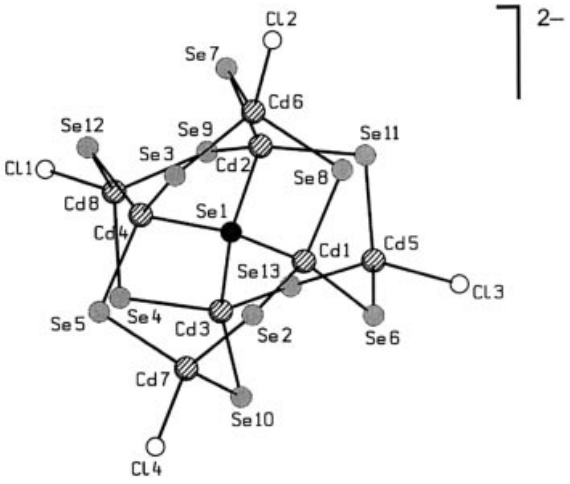

Figure 1. Molecular structure of the cluster anion $[Cd_8Se(SePh)_{12}Cl_4]^{2-}$ in **1**–**7**; C and H atoms are omitted for clarity; Se^{2-}: black, μ_2-$SePh^-$: grey, Cd^{2+}: hatched, and Cl^-: open circles

ner" cadmium atoms Cd1 to Cd4. Each of these four inner cadmium atoms is bound, through three μ_2-$SePh^-$ ligands (Se2 to Se13), to one of the four "outer" cadmium atoms Cd5 to Cd8, which also form a tetrahedron. In addition, each of the four outer cadmium atoms is bound to a terminal chloro ligand (Cl1 to Cl4). Each of the eight cadmium atoms has a distorted tetrahedral coordination sphere. The selenium atoms form a distorted icosahedron with the eight cadmium atoms bridging the triangular faces, whereby four of the cadmium atoms lie within, and four outside the icosahedron. The ranges of selected bond lengths are listed in Table 1 and display similar values for **1**–**7**, with the exception of the Cd–Se1 bond length range in **6**. In this compound a THF molecule is located close to Cd1 (Cd1–O2 2.813 Å), which possibly elongates the Cd1–Se1 bond length to a value of 2.672 Å.

The main difference in the structures of **1**–**7** arises as a result of the different crystal packing of the cluster anions and the ammonium or phosphonium cations. An interesting feature is the variation in the cluster–cluster distance in the crystal lattice. In Table 1, the variation of the shortest inter-cluster distances, measured as the distance between the central selenium atoms of the molecules, is shown (**1**: 15.076 Å, **1a**: 14.741 Å, **2**: 15.160 Å, **3**: 14.238 Å, **3a**: 14.995, **4**: 15.320 Å, **5**: 14.086 Å, **6**: 13.947 Å, **7**: 14.020 Å, **7a**: 14.145 Å). For all cluster molecules, the shortest inter-cluster distance varies from 13.95 Å in **6** to 15.32 Å in **4**. The trend in the variation of these distances is also followed by the shortest inter-cluster interactions between the selenium atoms. Interestingly, these values do not show a systematic increase with increasing length of the alkyl chain of the ammonium counterion. Even in **2**, **3a**, and **4**, which crystallise in the same space group with similar packing of the cluster molecules, inter-cluster distances do not systematically increase. In addition, different values for the pairs of similar compounds **1**, **1a** and **3**, **3a** and **7**, **7a** show that the size of the counterion is not the only parameter influencing the inter-cluster distance. The flexibility of the alkyl chains

Table 1. Selected ranges of bond lengths for **1**–**7a** including inter-cluster distances

	1	**1a**	**2**	**3**	**3a**	**4**	**5**	**6**	**7**	**7a**
Se1–Cd [Å]	2.616–2.630(2)	2.604–2.627(2)	2.613–2.622(1)	2.603–2.621(1)	2.612–2.625(2)	2.610–2.620(1)	2.608–2.628(2)	2.619–2.672(1)	2.612–2.627(1)	2.610–2.619(1)
μ_2-PhSe–Cd [Å]	2.627–2.691(2)	2.621–2.681(2)	2.629–2.696(2)	2.621–2.682(1)	2.617–2.678(2)	2.617–2.691(1)	2.617–2.681(1)	2.622–2.677(1)	2.629–2.701(2)	2.630–2.683(1)
Cl–Cd [Å]	2.432–2.448(5)	2.443–2.451(3)	2.425–2.445(3)	2.421–2.460(3)	2.416–2.447(3)	2.422–2.447(2)	2.426–2.458(4)	2.444–2.460(2)	2.434–2.445(3)	2.443–2.444(2)
Shortest inter-cluster distances [Å][a]	15.076	14.741	15.160	14.238	14.995	15.320	14.086	13.947	14.020	14.145

[a] Inter-cluster distances were measured as the distances between the central selenium atoms of the cluster molecules.

allows for the variable arrangements of the cations in the space between the $[Cd_8Se(SePh)_{12}Cl_4]^{2-}$ cluster anions, which, in addition to the incorporation of a varying number of solvent molecules, leads to the formation of different crystal packings. We found that the crystals incorporate more solvent molecules with increasing length of the alkyl chain of the ammonium cations, and as a result the crystal decomposes faster when separated from the mother liquor. Cations with more rigid and more bulky organic ligands than the "structurally weak" alkyl groups used here could lead to a better spacing of the cluster ions.

Powder X-ray Diffraction

In order to check the purity of the samples with respect to the possibility of the crystallisation of mixtures of different crystalline cluster compounds, as observed for **3**, **3a** and **7**, **7a**, powder X-ray diffraction patterns were measured for all compounds and compared with the calculated peak patterns from the data of the corresponding single-crystal X-ray analysis. The diffraction pattern of **4** (Figure 2, top) displays a good agreement between theory and experiment, however, those for **1**, **1a**, **2**, **3**, **3a**, **5**, **6**, **7**, and **7a** do not match the calculated patterns. Although the powder patterns show intense peaks in the low-angle region, the position of the peaks does not fit and the patterns could not be indexed. However, elemental analyses, UV/Vis spectra, and FT mass spectra (see below) all indicate the existence of the clusters determined by single-crystal X-ray diffraction. The powder patterns display no phase change on cooling from room temperature to 200 K. Determinations of the cell parameters of the single crystals at different temperatures also do not support the occurrence of phase changes, although difficulties do arise from the easy decomposition of the crystals at higher temperatures as a result of the loss of solvent molecules. Therefore, we suggest that the diffraction patterns of the dried crystalline powders show that the cluster molecules still present an order, but with a slight change in the lattice due to the loss of solvent molecules during the drying of the powder samples. In good agreement with this suggestion is the fact that the diffraction patterns of the crystalline powders in the mother liquor perfectly fit those calculated. The change in the curves by subsequent drying of the crystalline powder of **6** is shown in Figure 2 (bottom). The powder patterns of **3**, **3a** and **7**, **7a** measured in this way display peaks of both crystallographic species.

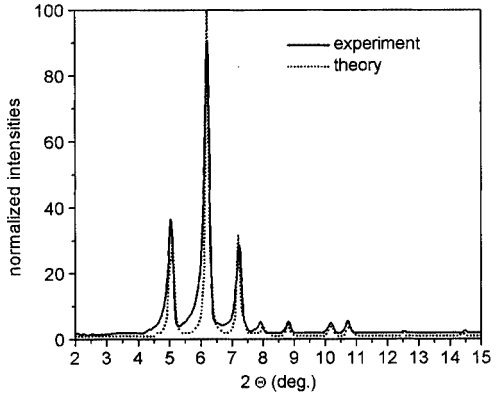

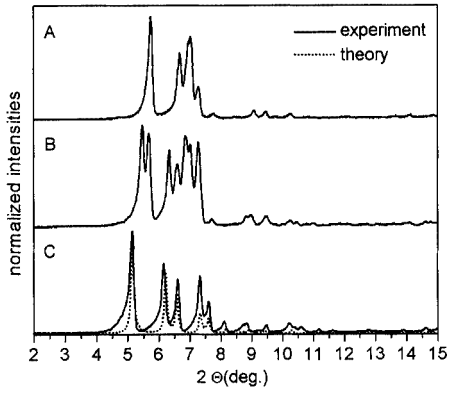

Figure 2. Top: room-temperature powder diffraction patterns of the dried crystalline powders of $[N(C_7H_{15})_4]_2[Cd_8Se(SePh)_{12}Cl_4]$ (**4**); bottom: change in room-temperature powder diffraction pattern of $[N(CH_3)_2(CH_2C_6H_4)(C_{10}H_{21})]_2[Cd_8Se(SePh)_{12}Cl_4]$ (**6**) by subsequent drying; A: dried under vacuum (10^{-3} bar); B: dried under nitrogen flow; C: as a suspension in THF (theoretical curve shown as dotted line)

FT Mass Spectrometry

Figure 3 shows a negative ion mass spectrum obtained by spraying a solution of crystalline **1** in 1,2-dichloroethane at a cone voltage of 25 V. It shows four peaks A−D that we identify as double negatively charged species: $[Cd_8Se(SePh)_{11}Cl_5]^{2-}$, $[Cd_8Se(SePh)_{12}Cl_4]^{2-}$, $[Cd_8Se(SePh)_{13}Cl_3]^{2-}$, $[Cd_8Se(SePh)_{14}Cl_2]^{2-}$, respectively. The inset compares the high-resolution mass spectrum of peak B with the simulated isotope distribution pattern of $[Cd_8Se(SePh)_{12}Cl_4]^{2-}$.

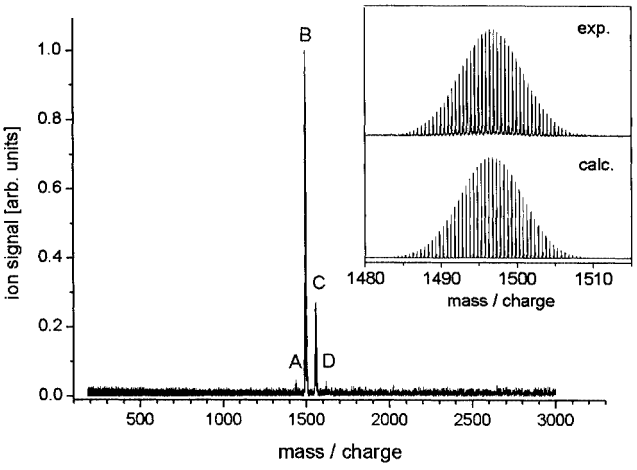

Figure 3. Electrospray FT mass spectrum of $[N(C_4H_9)_4^+]_2[Cd_8Se(SePh)_{12}Cl_4]^{2-}$ (**1**) in negative ion mode; the inset shows the high-resolution peak B ($[Cd_8Se(SePh)_{12}Cl_4]^{2-}$), experiment and simulation

Table 2. Assignment of the observed negative ions in the ESI mass spectra (as shown in Figure 3)

Peak	Ion	*m/z* (exp.)	*m/z* (calcd.)	Rel. intensity
A	$[Cd_8Se(SePh)_{11}Cl_5]^{2-}$	1436.41	1436.24	0.04
B	$[Cd_8Se(SePh)_{12}Cl_4]^{2-}$	1496.41	1496.55	1.00
C	$[Cd_8Se(SePh)_{13}Cl_3]^{2-}$	1556.92	1556.87	0.25
D	$[Cd_8Se(SePh)_{14}Cl_2]^{2-}$	1616.93	1617.18	0.03

The results are summarised in Table 2. It is worth noting that no fragmentation of the cluster ion occurred as long as cone voltages were kept below 30 V. This proves the high stability of these cluster complexes and also strongly suggests that these species are present intact in solution. Mass spectra taken from all seven compounds **1**−**7**, under virtually identical conditions, reveal very similar results, with slight variations in the relative intensities of peaks A−D. The observation of peaks A, C, and D next to the parent ion B is indicative of a ligand exchange process. Ligand exchange reactions were recently observed in electrospray mass spectrometric studies on thiophenolate-capped clusters of CdS, CdSe, and ZnS,[10−12] under conditions where partial fragmentation also takes place. Contrary to these studies, the mass spectra of our selenophenolate-bridged clusters do not show any ion signal due to Cl^- or $SePh^-$.

Given the relative ion intensities observed, the cluster has a tendency to lose Cl^- in favour of $SePh^-$, while keeping the total number of ligands constant. This could indicate that the cluster keeps its original structure as shown in Figure 1. This exchange can be attributed to the fact that $SePh^-$ is a better bridging ligand than Cl^-. However, the observation of $[Cd_8Se(SePh)_{11}Cl_5]^{2-}$ proves that a bridging $SePh^-$ ligand which is replaced by Cl^- potentially leads to a species with halide bridging. As the FT mass spectra show the same peaks when using different solvents, namely THF, acetonitrile, dichloromethane, and 1,2-dichloroethane, we deduce that this ligand exchange is a direct result of intercluster reactions.

Warming and cooling of the solutions of the cluster molecules do not lead to a change in the observed mass spectra or UV/Vis spectra (see next chapter). Mass spectra taken from solutions after one week also do not differ from the original spectra, showing their intrinsic stability.

UV/Vis Spectroscopy

UV/Vis absorption spectra of solutions of **1**−**7** in 1,2-dichloroethane were measured. All compounds display a very similar spectrum, with a maximum at 301 nm and a minimum at 284 nm. Figure 4 shows the absorption spectra of **2** with $\varepsilon = 6.12 \cdot 10^4\ M^{-1}cm^{-1}$ at 301 nm (dashed line). According to these results, it is obvious that the different counterions have virtually no effect on the absorption behaviour of the cluster anions in solution. Solid state reflectance spectra of **1**−**7** were measured directly on the milled crystalline powders or as a mull in oil between two quartz plates inside an integrating sphere (Figure 4). For all compounds, the onset of the absorption shifts slightly to

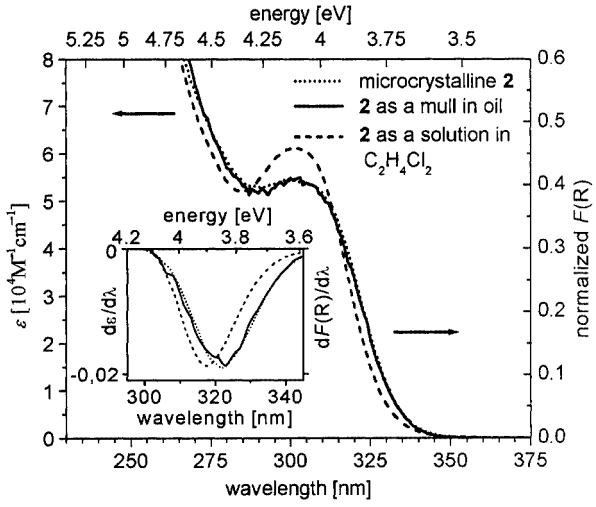

Figure 4. UV/Vis absorption spectrum of $[N(C_5H_{11})_4]_2[Cd_8Se(SePh)_{12}Cl_4]$ (**2**) in $C_2H_4Cl_2$ (dashed line) and UV/Vis reflectance spectra of **2** as a mull in mineral oil (straight line) and as a microcrystalline powder (dotted line); the inset shows part of the first derivative spectra

lower energies relative to that in the solution spectra. This is accompanied by a loss of structure, as can be seen from the spectra of **2** in Figure 4. Slight differences in the solid state spectra of **1**−**7** are thought to arise mostly from the quality of the mull, since the concentration and grain sizes cannot be kept constant for all the samples. Therefore, these differences cannot be related to the different spacing of the $[Cd_8Se(SePh)_{12}Cl_4]^{2-}$ cluster anions in the crystal lattice. Further, the powder X-ray diffraction patterns reveal that the crystals lose solvent molecules on drying, which is accompanied by a change in the packing in the crystal lattice. This leads to the deduction that the different counterions have no distinct influence on the UV/Vis absorption spectra of the $[Cd_8Se(SePh)_{12}Cl_4]^{2-}$ cluster anion in the solid state as well.

The broadening of the solid state spectra, indicated by a shift of the maximum of the first derivative by about 55 meV to lower energies with respect to the spectra in solution, could result from the effect of the crystal packing and/or of the counterion on the electronic properties in the solid state, as was recently suggested by Döllefeld et al. for crystals of $[Cd_{17}S_4(SCH_2CH_2OH)_{26}]$.[5] They found a shift of the first electronic transition to lower energies by about 150 meV in the reflectance spectra of micron-sized crystals, relative to that in their solution spectra in DMF. They suggest that both the electronic and the dipole−dipole interactions play a role in the complete description of the interactions between semiconductor nanoclusters in crystalline superstructures. Besides the difference in charges, the main difference between the compound $[Cd_{17}S_4(SCH_2CH_2OH)_{26}]$ investigated by Döllefeld et al. and the $[Cd_8Se(SePh)_{12}Cl_4]^{2-}$ cluster anions in this work is the fact that the former are directly bonded in the crystal lattice to one another by bridging thiolato ligands. The remarkable change in the solid state and solution spectra in this case may arise from

the breaking of the covalent bonds of the bridging thiolato groups by the strongly coordinating solvent DMF. This suggestion is also supported by the fact that the authors can find for thin layers of this cluster deposited from DMF solutions only a broadening of the lowest energy transition in comparison to the spectra of the DMF solutions.[6]

Regarding the $[Cd_8Se(SePh)_{12}Cl_4]^{2-}$ cluster anions, the use of various solvents, with a range of dielectric constants (ε_r), has a clear effect on the absorption properties of the cluster molecules, as can be seen for **7**, **7a** (Figure 5). The absorption spectra in dichloromethane (ε_r = 8.9) and 1,2-dichloroethane (ε_r = 10.2) are very similar, whereas the first absorption maximum in acetonitrile (ε_r = 37.5) is shifted by about 41 meV to a higher energy. The shape of the first absorption peak in the spectra of **7**, **7a** in THF (ε_r = 7.6) is more featureless and broader than those in the other solution spectra. While the value for the first absorption maximum is similar to that found in acetonitrile, the inflection point (maximum of the first derivative) is similar to that in the two chlorinated solvents. Therefore, the shift of the lowest energy absorption band does not simply follow the change in the permittivity of the medium, but is probably more affected by the different coordination properties of the various solvents. In this context, it can be seen that a THF molecule coordinates one cadmium atom of the $[Cd_8Se(SePh)_{12}Cl_4]^{2-}$ cluster anion in **6**, leading to a coordination number of five for this metal atom.

FT mass spectrometry clearly shows the existence of the intact $[Cd_8Se(SePh)_{12}Cl_4]^{2-}$ cluster anion in all solutions. However, the observed ligand exchange reaction of chlorine atoms for phenylselenolato ligands could also have an effect on the UV/Vis absorption spectra, although we cannot rule out that these reactions take place in the electrospraying step. Interestingly, the use of the different solvents, THF, acetonitrile, dichloromethane, and 1,2-dichloroethane, leads to virtually identical products of ligand exchange, with slightly varying intensities in the FT mass spectra.

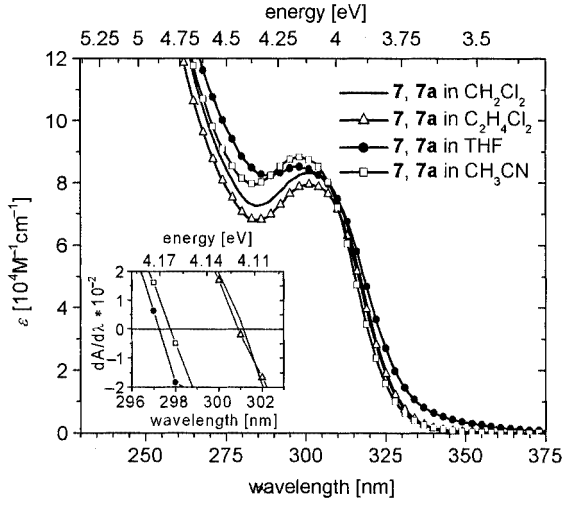

Figure 5. UV/Vis absorption spectra of $[P(C_4H_9)_4]_2[Cd_8Se(SePh)_{12}Cl_4]$ (**7**, **7a**) dissolved in different solvents; the inset shows part of the first derivative spectra; values for the relative dielectric constants, ε_r, of the solvents are: 8.9 (CH_2Cl_2), 10.2 ($C_2H_4Cl_2$), 7.6 (THF), 37.5 (CH_3CN)

Conclusions

A series of seven single-crystalline CdSe cluster molecules with the same $[Cd_8Se(SePh)_{12}Cl_4]^{2-}$ cluster anion has been synthesised by altering the counterion. The cluster molecules were characterised by a detailed analytical investigation, which included single-crystal XRD, powder XRD, UV/Vis spectroscopy, as well as FT mass spectrometry. The results of the crystal structure determination show that the increasing size of the different counterions does not simply lead to an increase in the shortest inter-cluster distances, but rather to changes in the crystal structure. Room-temperature UV/Vis absorption and reflectance spectra of the crystalline powders are virtually identical, proving that the electronic transitions in the energy range probed can be attributed to the cluster anion $[Cd_8Se(SePh)_{12}Cl_4]^{2-}$. The band of the lowest energy transition in the solid-state UV/Vis spectra are broadened relative to that in the solution spectra, as it is possibly affected by the collective interactions between the nanoclusters in the three-dimensional crystal lattice. Interestingly, in solution, the position and feature of the lowest energy transition band changes as the solvent is varied. As FT mass spectrometry gives clear evidence for the existence of the intact $[Cd_8Se(SePh)_{12}Cl_4]^{2-}$ cluster anion in all these solutions, these shifts can be interpreted in terms of solvatochromic effects.

Further studies will focus on the use of other counterions, including higher charged species and more rigid organic ligands, and on the crystallisation of larger ionic cluster molecules that are shown to be stable from simple theoretical calculations.[13] Additional synthetic interest arises from the possibility to form covalently linked two- or three-dimensional networks of these cluster molecules, through reaction of the four reactive Cd−Cl bonds with bifunctional silylated chalcogen compounds, such as $(Me_3Si)Se-R-Se(SiMe_3)$, where R = C_2H_4, C_3H_6, C_4H_8. Interesting collective phenomena based on direct cluster−cluster interactions are to be expected in these compounds.

Experimental Section

Syntheses: Standard Schlenk techniques were employed throughout the syntheses using a double manifold vacuum line with high-purity dry nitrogen. The solvents tetrahydrofuran and diethyl ether were dried with sodium/benzophenone and distilled under nitrogen. Anhydrous $CdCl_2$, as well as ammonium and phosphonium salts, were purchased from Aldrich. $PhSeSiMe_3$ [14] and $Se(SiMe_3)_2$ [15] were prepared according to standard literature procedures.

$[N(n\text{-}C_4H_9)_4]_2[Cd_8Se(SePh)_{12}Cl_4]$ (1, 1a): $CdCl_2$ (0.20 g, 1.09 mmol) and $N(n\text{-}C_4H_9)_4Cl$ (0.08 g, 0.27 mmol) were suspended in 130 mL of THF. $PhSeSiMe_3$ (0.33 mL, 1.74 mmol) was then added, and the resulting clear solution stirred overnight. Addition of $Se(SiMe_3)_2$ (0.025 mL, 0.11 mmol) at −40 °C, and warming to room temper-

ature led to the formation of colourless hexagonal plates of **1**, **1a**, with a total yield of 60% after further concentration of the solution. $C_{104}H_{132}Cd_8Cl_4N_2Se_{13}$ (3477.48): calcd. C 35.92, H 3.83, N 0.83; found C 35.93, H 3.98, N 0.88. Suitable crystals for single-crystal XRD were obtained either by layering the concentrated filtered solution with diethyl ether to yield **1**, or by recrystallising the white crystalline powder from THF at −20 °C to give **1a**.

$[N(n\text{-}C_5H_{11})_4]_2[Cd_8Se(SePh)_{12}Cl_4]$ (2): $CdCl_2$ (0.24 g, 1.31 mmol) and $N(n\text{-}C_5H_{11})_4Cl$ (0.11 g, 0.33 mmol) were suspended in 70 mL of THF. $PhSeSiMe_3$ (0.40 mL, 2.10 mmol) was then added, and the resulting clear solution was stirred overnight. Addition of $Se(SiMe_3)_2$ (0.029 mL, 0.13 mmol) at −30 °C, and warming to room temperature led to the formation of colourless crystals of **2** with a yield of 74%. **2** can be recrystallised from THF on careful addition of small aliquots of diethyl ether. $C_{112}H_{148}Cd_8Cl_4N_2Se_{13}$ (3589.99): calcd. C 37.47, H 4.16, N 0.78; found C 37.89, H 4.39, N 0.82.

$[N(n\text{-}C_6H_{13})_4]_2[Cd_8Se(SePh)_{12}Cl_4]$ (3, 3a): $CdCl_2$ (0.24 g, 1.31 mmol) and $N(n\text{-}C_6H_{13})_4Cl$ (0.13 g, 0.33 mmol) were suspended in 70 mL of THF. $PhSeSiMe_3$ (0.40 mL, 2.10 mmol) was then added, and the resulting clear solution stirred overnight. Addition of $Se(SiMe_3)_2$ (0.029 mL, 0.13 mmol) at −30 °C, and warming to room temperature led to the formation of colourless crystals of **3**, **3a**, with a yield of 62%. Suitable crystals of **3** were obtained directly from the reaction solution at room temperature, while crystals of **3a** were grown at 0 °C. $C_{120}H_{164}Cd_8Cl_4N_2Se_{13}$ (3702.21): calcd. C 38.93, H 4.46, N 0.76; found C 38.72, H 4.48; N 0.85.

$[N(n\text{-}C_7H_{15})_4]_2[Cd_8Se(SePh)_{12}Cl_4]$ (4): $CdCl_2$ (0.18 g, 0.98 mmol) and $N(n\text{-}C_7H_{15})_4Cl$ (0.11 g, 0.25 mmol) were suspended in 75 mL of THF. $PhSeSiMe_3$ (0.30 mL, 1.57 mmol) was then added, and the resulting clear solution stirred overnight. Addition of $Se(SiMe_3)_2$ (0.022 mL, 0.098 mmol) at −30 °C, and warming to room temperature led to the formation of a small amount of a precipitate of unknown composition. This was filtered, and on addition of 5 mL of diethyl ether, colourless crystals of **4** were formed with a 68% yield. **4** can be recrystallised from THF on addition of aliquots of diethyl ether. $C_{128}H_{180}Cd_8Cl_4N_2Se_{13}$ (3814.42): calcd. C 40.30, H 4.76, N 0.73; found C 38.98, H 4.76, N 0.63.

$[N(n\text{-}C_8H_{17})_4]_2[Cd_8Se(SePh)_{12}Cl_4]$ (5): $CdCl_2$ (0.21 g, 1.15 mmol) and $N(n\text{-}C_8H_{17})_4Cl$ (0.14 g, 0.25 mmol) were suspended in 50 mL of THF. $PhSeSiMe_3$ (0.35 mL, 1.84 mol) was then added, and the resulting clear solution stirred overnight. Addition of $Se(SiMe_3)_2$ (0.026 mL, 0.12 mmol) at −30 °C, and warming to room temperature led to the formation of a clear colourless solution. Concentration to 3 mL led to the formation of thin needles in a white precipitate of unknown composition. This was filtered, and on addition of 8 mL of diethyl ether, colourless crystals of **5** were formed with a 65% yield. **5** can be recrystallised from THF on addition of aliquots of diethyl ether. $C_{136}H_{196}Cd_8Cl_4N_2Se_{13}$ (3926.64): calcd. C 41.60, H 5.03, N 0.71; found C 41.08, H 4.99, N 0.75.

$[N(CH_3)_2(CH_2C_6H_4)(n\text{-}C_{10}H_{21})]_2[Cd_8Se(SePh)_{12}Cl_4]$ (6): $CdCl_2$ (0.17 g, 0.093 mmol) and $N(CH_3)_2(CH_2C_6H_4)(n\text{-}C_{10}H_{21})Cl$ (0.07 g, 0.23 mmol) were suspended in 60 mL of THF. $PhSeSiMe_3$ (0.28 mL, 1.49 mmol) was then added, and the resulting clear solution stirred overnight. Addition of $Se(SiMe_3)_2$ (0.021 mL, 0.093 mmol) at −30 °C, and warming to room temperature led to the formation of colourless crystals of **6**; concentration led to the further precipitation of crystals, yielding 71% of **6**. $C_{110}H_{128}Cd_8Cl_4N_2Se_{13}$ (3545.81): calcd. C 37.26, H 3.64, N 0.79; found C 38.61, H 4.02, N 0.94.

$[P(n\text{-}C_4H_9)_4]_2[Cd_8Se(SePh)_{12}Cl_4]$ (7, 7a): $CdCl_2$ (0.25 g, 1.36 mmol) and $P(n\text{-}C_4H_9)_4Cl$ (0.10 g, 0.34 mmol) were suspended in 150 mL of THF. $PhSeSiMe_3$ (0.42 mL, 2.18 mmol) was then added, and the resulting clear solution stirred overnight. Addition of $Se(SiMe_3)_2$ (0.031 mL, 0.14 mmol) at −30 °C, and warming to room temperature led to the formation of a colourless solution. Colourless crystals of **7**, **7a** were formed after concentration, with a 76% yield. Recrystallisation from THF/diethyl ether also yielded a mixture of crystals of **7** and **7a**. $C_{104}H_{132}Cd_8Cl_4P_2Se_{13}$ (3511.71): calcd. C 35.57, H 3.79 found C 35.58, H 3.94.

Structure Determinations: Crystals suitable for single-crystal X-ray diffraction were obtained directly from the reaction solutions of compounds **2**, **3**, **3a**, **4**, **6**, **7**, and **7a**. In the case of **1a** and **5**, crystals were grown by recrystallisation of the obtained microcrystalline powders. **1** was crystallised by layering of the concentrated reaction solution. Single-crystal X-ray diffraction data were collected using graphite-monochromatised Mo-K_α radiation (λ = 0.71073 Å) with a STOE IPDS (Imaging Plate Diffraction System), equipped with a SCHNEIDER rotating anode. All the structures were solved with the direct methods program SHELXS[16] of the SHELXTL PC suite programs, and they were refined with the use of the full-matrix least-squares program SHELXL.[16] Molecular diagrams were prepared using the program SCHAKAL 97.[17] All Cd, Se, and Cl atoms were refined with anisotropic displacement parameters. In **1a**, **3a**, **5**, **6**, **7**, and **7a**, the N, P, and the C atoms of the SePh rings were also refined anisotropically. The C atoms of the phenyl groups in **1** were refined isotropically as a rigid group. In **6**, the atoms C1 to C6, and in **3**, the atoms C55 to C60 are disordered. The C atoms of the ammonium and phosphonium counterions were all refined isotropically and show some disorder in the case of **3**, **6**, and **7**. In **5**, some of the C atoms of the $N(C_8H_{17})_4^+$ counterions show high thermal parameters due to the flexibility of the long alkyl chain and could only be refined with reduced occupancy. For one octyl chain in **5**, only four carbon atoms could be located in the difference fourier map. These problems probably arise from the fact that the crystals decompose, even at 110 K after 1 d of measurement. THF and Et_2O solvent molecules were mostly refined with half occupancy because of a high degree of disorder and large thermal parameters. The H atoms of the SePh groups were included in the calculated positions for **2**, **3a**, **4**, **7**, and **7a**. X-ray powder diffraction data (XRD) were collected with a STOE STADI P diffractometer (Cu-K_α radiation, germanium monochromator, Debye−Scherrer geometry). The measurements were performed on crystalline powders, dried or in mother liquor, in 0.5 mm sealed glass capillaries. Theoretical powder diffraction patterns for **1**−**7** were calculated on the basis of the atom coordinates obtained from single-crystal X-ray analysis using the program package STOE WinXPOW.[18] Crystal data for each compound are listed in Tables 3 and 4.[19]

UV/Vis Measurements: Absorption spectra of cluster molecules in solution were measured with a Perkin−Elmer Lambda 900 spectrophotometer in quartz cuvettes. Solid state reflectance spectra were measured with a Varian Cary 500 as micron-sized crystalline powders or as nujol mulls between quartz plates inside a Labsphere integrating sphere.

FT-Mass Spectrometry: Mass spectra were measured with a 7-Tesla-APEX II Fourier transform mass spectrometer (Bruker Daltonics) equipped with an electrospray ionisation source (Analytica of Branford). Freshly prepared solutions of compounds **1**−**7** in $C_2H_4Cl_2$ (ca. 0.1 mmol/L) were sprayed employing a syringe infusion pump (Cole-Parmer), at typical rates of 300 μL/h. Neat nitro-

Table 3. Crystallographic data for $[N(n\text{-}C_4H_9)_4]_2[Cd_8Se(SePh)_{12}Cl_4]$ (**1**, **1a**), $[N(n\text{-}C_5H_{11})_4]_2[Cd_8Se(SePh)_{12}Cl_4]$ (**2**), and $[N(n\text{-}C_6H_{13})_4]_2[Cd_8Se(SePh)_{12}Cl_4]$ (**3**, **3a**)

	1·0.5C_4H_8O	**1a**·5C_4H_8O	**2**·0.5C_4H_8O	**3**·0.5C_4H_8O	**3a**·2C_4H_8O
Formula mass [g/mol]	3513.65	3838.12	3622.83	3738.06	3846.22
Crystal system	triclinic	monoclinic	orthorhombic	monoclinic	orthorhombic
Space group	$P\bar{1}$	$P2_1/c$	$Pna2_1$	$P2_1/n$	$Pna2_1$
a [Å]	21.471(2)	19.543(4)	27.818(6)	21.510(4)	28.077(6)
b [Å]	26.694(5)	29.694(6)	22.156(4)	29.364(6)	21.500(4)
c [Å]	28.815(5)	32.266(7)	24.009(5)	24.494(5)	25.113(5)
α [°]	114.08(2)	90	90	90	90
β [°]	90.99(2)	103.09(3)	90	91.79(3)	90
γ [°]	90.04(2)	90	90	90	90
V [Å^3]	15076(4)	18238(6)	14798(5)	15463(5)	15160(5)
Z	4	4	4	4	4
T [K]	200	110	200	200	200
d_c [g·cm^{-3}]	1.548	1.398	1.626	1.606	1.685
μ(Mo-K_α) [mm^{-1}]	4.35	3.604	4.434	4.25	4.334
F[000]	6736	7456	6980	7248	7488
$2\theta_{max}$ [°]	50	52	50	50	50
Meas. reflns.	67932	96163	62906	73397	58768
Unique reflns.	45880	35341	23880	26235	24285
R_{int}	0.0863	0.1106	0.0627	0.0931	0.1095
Reflns. with $I > 2\sigma(I)$	25771	25515	19147	19591	20914
Refined params.	812	1220	703	776	1125
$R1$ [$I > 2\sigma(I)$][a]	0.0791	0.0883	0.0470	0.0705	0.0668
$wR2$ (all data)[b]	0.2976	0.2580	0.1368	0.2156	0.1920
Abs. structure parameter	–	–	0.201(8)	–	0.160(10)

[a] $R1 = \Sigma||F_o| - |F_c||/\Sigma|F_o|$. [b] $wR2 = \{\Sigma[w(F_o^2 - F_c^2)^2]/\Sigma[w(F_o^2)^2]\}^{1/2}$.

Table 4. Crystallographic data for $[N(n\text{-}C_7H_{15})_4]_2[Cd_8Se(SePh)_{12}Cl_4]$ (**4**), $[N(n\text{-}C_8H_{17})_4]_2[Cd_8Se(SePh)_{12}Cl_4]$ (**5**), $[N(CH_3)_2(CH_2C_6H_4)(n\text{-}C_{10}H_{21})]_2[Cd_8Se(SePh)_{12}Cl_4]$ (**6**), and $[P(n\text{-}C_4H_9)_4]_2[Cd_8Se(SePh)_{12}Cl_4]$ (**7**, **7a**)

	4·0.5C_4H_8O	**5**·2.25C_4H_8O·1.25$C_4H_{10}O$	**6**·1C_4H_8O	**7**·2C_4H_8O	**7a**·1.5C_4H_8O
Formula mass [g/mol]	3832.26	4217.36	3617.73	3655.72	3675.78
Crystal system	orthorhombic	triclinic	monoclinic	triclinic	monoclinic
Space group	$Pna2_1$	$P\bar{1}$	$P2_1/n$	$P\bar{1}$	$C2/c$
a [Å]	28.359(6)	26.221(5)	21.690(4)	16.984(3)	23.741(5)
b [Å]	22.153(4)	29.220(6)	28.180(6)	19.390(2)	25.649(5)
c [Å]	24.495(5)	31.148(6)	23.327(5)	26.151(5)	27.885(6)
α [°]	90	112.82(3)	90	100.417(18)	90
β [°]	90	97.12(3)	94.26(3)	93.81(2)	101.53(3)
γ [°]	90	113.43(3)	90	107.572(17)	90
V [Å^3]	15388(5)	19061(7)	14218(5)	8007(2)	16637(6)
Z	4	4	4	2	4
T [K]	200	110	200	200	200
d_c [g·cm^{-3}]	1.654	1.470	1.69	1.516	1.468
μ(Mo-K_α) [mm^{-1}]	4.269	3.455	4.615	4.117	3.964
F[000]	7468	8330	6944	3520	7088
$2\theta_{max}$ [°]	48	50	50	50	50
Meas reflns.	68066	63913	87029	83284	52866
Unique reflns.	23831	48059	24660	28015	13722
R_{int}	0.0459	0.0374	0.0581	0.1091	0.0751
Reflns. with $I > 2\sigma(I)$	19804	36989	18584	28015	11223
Refined params.	762	2531	760	1084	611
$R1$ [$I > 2\sigma(I)$][a]	0.0429	0.0570	0.0555	0.0726	0.0422
$wR2$ (all data)[b]	0.1246	0.1787	0.1949	0.2245	0.1662
Abs. structure parameter	0.027(8)	–	–	–	–

[a] $R1 = \Sigma||F_o| - |F_c||/\Sigma|F_o|$. [b] $wR2 = \{\Sigma[w(F_o^2 - F_c^2)^2]/\Sigma[w(F_o^2)^2]\}^{1/2}$.

gen was used as the spraying and drying gas, both kept at room temperature. Cone voltages were kept low enough to minimise fragmentation.

Acknowledgments

This work was supported by the German-Israel Fund, the Deutsch-Israelisches Programm (DIP) and the Forschungszentrum

Karlsruhe. A. E. wants to thank Dr. A. Eychmüller, Dr. M. Haase, and Dr. H. Döllefeld for helpful discussions concerning the measurement of the UV/Vis spectra of the solid samples, and Prof. Dr. H. Krautscheid for careful revision of the document. The authors are also grateful to E. Tröster for her invaluable assistance in the practical work.

[1] V. Soloviev, A. Eichhöfer, D. Fenske, U. Banin, *J. Am. Chem. Soc.* **2001**, *123*, 2354−2364.
[2] I. G. Dance, A. Choy, M. L. Scudder, *J. Am. Chem. Soc.* **1984**, *106*, 6285−6295.
[3] N. Herron, J. C. Calabrese, W. E. Farneth, Y. Wang, *Science* **1993**, *259*, 1426−1428.
[4] T. Vossmeyer, G. Reck, L. Katsikas, E. Haupt, B. Schulz, H. Weller, *Science* **1995**, *267*, 1476−1479.
[5] H. Döllefeld, H. Weller, A. Eychmüller, *Nanoletters* **2001**, *1*, 267−269.
[6] H. Döllefeld, H. Weller, A. Eychmüller, *J. Phys. Chem. B* **2002**, *106*, 5604−5608.
[7] D. Fenske, T. Langetepe, M. Kappes, O. Hampe, P. Weis, *Angew. Chem.* **2000**, *112*, 1925−1928; *Angew. Chem. Int. Ed.* **2000**, *39*, 1857−1860.
[8] G. S. H. Lee, K. J. Fisher, D. C. Craig, M. L. Scudder, I. G. Dance, *J. Am. Chem. Soc.* **1990**, *112*, 6435−6437.
[9] S. Behrens, D. Fenske, *Ber. Bunsenges. Phys. Chem.* **1997**, *101*, 1588−1592.
[10] J-J. Gaumet, G. F. Strouse, *J. Am. Soc. Mass Spectrom.* **2000**, *11*, 338−344.
[11] T. Løver, W. Henderson, G. A. Bowmaker, J. M. Seakins, R. P. Cooney, *Inorg. Chem.* **1997**, *36*, 3711−3723.
[12] T. Løver, G. A. Bowmaker, W. Henderson, R. P. Cooney, *Chem. Commun.* **1996**, *36*, 683−685.
[13] I. Dance, G. S. H. Lee, in: *The Chemistry of the Copper and Zinc Triads* (Eds.: A. J. Welch, S. K. Chapman), Royal Society of Chemistry, Cambridge, **1993**, p. 87.
[14] N. Miyoshi, H. Ishii, K. Kondo, S. Mui, N. Sonoda, *Synthesis* **1979**, 301−304.
[15] H. Schmidt, H. Ruf, *Z. Anorg. Allg. Chem.* **1963**, *321*, 270−273.
[16] G. M. Sheldrick, *SHELXTL, PC version 5.1, An Integrated System for Solving, Refining, and Displaying Crystal Structures from Diffraction Data*, Bruker Analytical X-ray Systems, Karlsruhe, **2000**.
[17] E. Keller, *SCHAKAL 97, A Computer Program for the Graphic Representation of Molecular and Crystallographic Models*, Universität Freiburg, **1997**.
[18] STOE, *WinXPOW*, STOE & Cie GmbH, Darmstadt, **2000**.
[19] CCDC-192112 to -192121 contain the supplementary crystallographic data for this paper. These data can be obtained free of charge at www.ccdc.cam.ac.uk/conts/retrieving.html [or from the Cambridge Crystallographic Data Centre, 12 Union Road, Cambridge CB2 1EZ, UK; Fax: (internat.) + 44-1223/336-033; E-mail: deposit@ccdc.cam.ac.uk].

Received August 22, 2002
[I02476]

A DFT Study of Tin- and Crown-Ether-Based Host Molecules Capable of Binding Anions and Cations Simultaneously

Ricardo Vivas-Reyes,[a,b] Frank De Proft,[b] Monique Biesemans,[c] Rudolph Willem,[c] and Paul Geerlings*[b]

Keywords: Acidity / Basicity / Crown compounds / Density functional calculations / Host-guest systems / Tin

DFT calculations are reported for a series of tin- and crown-ether-based host compounds {i.e., the trimethyl derivatives [18]-crown-6-$C_6H_3COOSn(CH_3)_3$ and [15]-crown-5-$C_6H_3COOSn(CH_3)_3$} capable of binding cations and anions simultaneously. The B3LYP functional together with the 6-31G* basis set was used for the atoms C, H, N, O, S, Na and K and the 3-21G* basis set for Sn in order to obtain insights into the factors determining the nature of the interactions of these compounds with the neutral molecules acetone and H_2O, the SCN^- anion, and the Na^+ and K^+ cations. The interaction strength pattern with these molecules was explained by the use of a series of reactivity descriptors such as the Fukui function, hardness, local softness, and the MEP (molecular electrostatic potential). In all cases studied in this paper, the complexes with Na^+ were more stable than those with K^+, correlating with the size of the cation and the volume available in the crown ether. Moreover, this finding is also in accordance with the greater hardness of Na^+ relative to K^+, in combination with the hard environment of the crown ether moiety. This region was also analysed by computation of electrostatic potentials, which showed that highly negative values are associated with the inside region of the cavity of the crown, this region thus being amenable to electrophilic attack. The HSAB principle, characterising the reactive sites on the basis of local softness and the Fukui function, provided a firm explanation of the reactivity of the tin atom of the crown ether benzocarboxylate towards SCN^-, acetone and water. The HSAB concept was also successfully used to explain the preference of the tin atoms in both crown ethers to bind with the nitrogen atom rather than the sulfur atom of SCN^-. This result is a confirmation that the tin atoms in the compounds under consideration behave as hard atoms. Overall, these results fit remarkably well with previous experimentally measured NMR spectroscopy data and demonstrate that the interactions of this kind of molecules can be predicted and interpreted by the use of DFT calculations and DFT-based reactivity descriptors, as well as MEP calculations.

(© Wiley-VCH Verlag GmbH & Co. KGaA, 69451 Weinheim, Germany, 2003)

1. Introduction

The complexation of host molecules capable of binding an anion and a cation simultaneously is still a relatively unexplored topic in chemistry.[1] Numerous studies, however, have been devoted either to the interactions between cations and preorganised host molecules,[2] or to fixation of anions by neutral molecules containing Lewis acidic metal centres.[3] Studies on interactions between crown ethers and various inorganic and organic cations have spawned wide applications in chemistry, biology, medicine and technology,[4] while the Lewis acidity of the tin atom in, for instance, organotin halides is well documented.[5] Fewer studies have been reported on interactions of Lewis bases with organotin carboxylates,[6] despite widespread interest in their in vitro antitumour activity[7] and their rich structural diversity in the solid state.[8]

We recently reported a novel type of salt complexation by a new class of host molecules, containing both a crown ether susceptible to interaction with the cation and a Lewis acidic tin centre potentially acting as an anion carrier.[9] It was demonstrated that tri-*n*-butyl and triphenyltin derivatives of 4-carboxybenzo-[18]crown-6 or [15]crown-5 are receptors capable of binding M^+SCN^- ion pairs heterotopically. The Lewis acidic complexation of Sn by the thiocyanate anion cooperates with the crown ether complexation by the alkali metal cation and gives rise to a large charge separation, as evidenced by X-ray data in the crystalline state for the triphenyltin derivatives and by NMR spectroscopic data in solution for the tri-*n*-butyltin analogues.

This paper presents a theoretical investigation of the trimethyltin analogues of these compounds {i.e., [18]crown-6-$C_6H_3COOSn(CH_3)_3$ and [15]crown-5-$C_6H_3COOSn(CH_3)_3$,

[a] Grupo de Quimica Cuantica y Teorica, Universidad de Cartagena, Chemistry Department,
A.A 1661 Cartagena, Colombia
[b] Eenheid Algemene Chemie, Faculteit Wetenschappen, Vrije Universiteit Brussel,
Pleinlaan 2, 1050 Brussels, Belgium
Fax: (internat.) + 32-2/6293317
E-mail pgeerlin@vub.ac.be
[c] High Resolution NMR Centre, Vrije Universiteit Brussel,
Pleinlaan 2, 1050 Brussels, Belgium

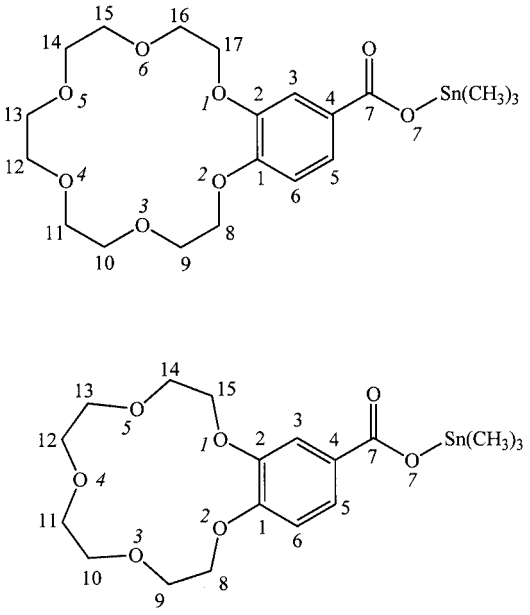

Figure 1. Molecular structures of [18]crown-6-$C_6H_3COOSn(CH_3)_3$ and [15]crown-5-$C_6H_3COOSn(CH_3)_3$

see Figure 1, the triphenyltin and tributyltin analogues being computationally too time-consuming}, in order to gain more insight into the factors determining the nature of the interactions of these molecules with the SCN^- anion and the Na^+ and K^+ cations. Moreover, as far as the inductive effects of the functional groups attached to the tin atom are concerned, the methyl group lies in between the +I *n*-butyl group and the −I phenyl group, and so also constitutes an optimal choice from that point of view. The studies were performed at a nonempirical ab initio level, still relatively rare for tin-containing compounds,[10] and interpreted by the use of DFT-based descriptors and principles.

Of particular interest in the understanding of chemical reactivity are the so-called response functions of the system to perturbations in the number of electrons or external potential, commonly referred to as atomic or molecular reactivity descriptors.[11−17] These descriptors have a sound basis in density functional theory (DFT).[18] Electronic chemical potential (μ), electronegativity (χ), hardness (η) and softness (*S*) are examples of such reactivity descriptors (for detailed accounts see refs.[18b−18d]). In this work, the basic quantities to be addressed are hardness and softness both at the global (i.e., molecular) and at the local (i.e., atomic sites in molecules) levels. A detailed discussion of these quantities can be found elsewhere.[18−24]

The local properties[18] developed are the Fukui function (FF) and the local softness typically describing the local role of a specific atom within a molecule in the reactivity of the latter.[18]

Fukui function and local softness, which are related to changes in the electron density function $\rho(r)$ with the total number of electrons at constant external potential $[\partial\rho(r)/\partial N]_v$, have been used to determine the site of reactivity of a system.[25] The FF was originally used essentially as an indicator of intramolecular reactivity sequences[26] (regioselectivity), the local softness being involved in intermolecular reactivity sequences. When the HSAB principle is used at a local level, the consideration of local softness turns out to be essential for estimating relative interaction energies of different sites in a molecule towards electrophilic or nucleophilic reagents.

In this study, and also in the context of a series of papers aiming at the description of properties of tin compounds with the aid of DFT reactivity indicators,[27−28] we investigate the use of the FF and the local softness to describe the interactions between the tin atom and the SCN^- anion, as well as neutral molecules such as acetone for which experimental NMR spectroscopic data are available,[9] Pearson's hard and soft acids and bases (HSAB) principle[19−21] being expected to act as the guiding principle.[29,30] When the HSAB principle is applied in a local sense,[31] regioselectivity problems can be addressed on the basis of the idea that soft (or hard) regions of one reaction partner will preferentially interact with soft (or hard) regions of the other partners.[32−34] We are also interested in knowing whether (i) only the cation or the anion is involved in a monotopic interaction, or (ii) both ions are involved in a heterotopic interaction.[1k] If the latter holds, an additional question is whether anions and cations remain electrostatically paired or undergo a charge separation from their initial ion pair.

The molecular electrostatic potential (MEP) is also used to predict the behaviour of the crown ether moiety, because its cavity is expected to be hard, as it is found to interact with hard cations such as Na^+ and K^+.

The MEP[35−37] has indeed been found suitable for the description of electrostatic (i.e., nonorbital-based) interactions, and has been used in recent years to study the structures and reactivities of polyoxometallate cages and, in our group, the $(CH_3Sn)_{12}O_{14}(OH)_6^{2+}$ cationic cluster.[28] The spatial distribution and the values of the MEP can be taken, at least in the case of a fairly hard reagent, as an indicator of where a nucleophilic or electrophilic attack is likely to take place. We used MEP calculations to describe the interactions between the oxygen atoms of the crown ether and Na^+ and K^+ cations.

2. Theory and Computational Details

As a detailed presentation and discussion of the reactivity parameters used in this paper can be found elsewhere,[18,38] only the relevant expressions used for the evaluation of different quantities for the crown ethers [15]crown-5-$C_6H_3COOSn(CH_3)_3$ and [18]crown-6-$C_6H_3COOSn(CH_3)_3$ are given here.

The global hardness (η) and the global softness (*S*) are calculated from Equations (1) and (2), by use of the finite-difference approximation, where *IE* and *EA* are the vertical ionisation energy and electron affinity, respectively.

$$\eta = \frac{IE - EA}{2} \quad (1)$$

$$S = \frac{1}{2\eta} \tag{2}$$

The Fukui function $f(r)$ is defined as the partial derivative of the total electron density at a given point r, $\rho(r)$, with respect to the number of electrons N, at constant external potential $v(r)$ (the potential exerted by the nuclei) determined for the N values considered. Parr and Yang[18,19,25] have proposed an association of different reactivity indices through Equation (3).

$$f(\underline{r}) = \left(\frac{\partial \rho(\underline{r})}{\partial N}\right)_{v(\underline{r})} \tag{3}$$

The expressions used to investigate nucleophilic or electrophilic attack on the system are given by Equation (4) for a nucleophilic attack and Equation (5) in the case of an electrophilic attack.

$$f^{+}(\underline{r}) = \left(\frac{\partial \rho(\underline{r})}{\partial N}\right)^{+}_{v(\underline{r})} \tag{4}$$

$$f^{-}(\underline{r}) = \left(\frac{\partial \rho(\underline{r})}{\partial N}\right)^{-}_{v(\underline{r})} \tag{5}$$

The superscripts + and − refer to right and left derivatives, respectively. In a finite difference approach, $f^{+}(r)$ and $f^{-}(r)$ can be approximated by Equations (6) and (7),[18,25,39] where ρ_N, ρ_{N+1} and ρ_{N-1} are the electron densities of the systems with N, $N + 1$ and $N - 1$ electrons, respectively.

$$f^{+}(\underline{r}) \approx \rho_{N+1}(\underline{r}) - \rho_{N}(\underline{r}) \tag{6}$$

$$f^{-}(\underline{r}) \approx \rho_{N}(\underline{r}) - \rho_{N-1}(\underline{r}) \tag{7}$$

Because of the constraint of a constant external potential, the quantities ρ_{N+1} and ρ_{N-1} are calculated with the same geometry as the N electron system.

The f^{o} function, which governs radical attack, is considered to be the average of $f^{+}(r)$ and $f^{-}(r)$, and can therefore be approximated by Equation (8).

$$f^{o}(\underline{r}) \approx \frac{1}{2}[\rho_{N+1}(\underline{r}) - \rho_{N-1}(\underline{r})] \tag{8}$$

Yang and Mortier[26] have also proposed a condensed version of Equations (6) to (8). The information contained in $f(r)$ in the neighbourhood of a given atom A can be approximated by use of the atomic population N_A, obtained by population analysis on the considered atom.[40] Accordingly, the condensed Fukui function on the atom A, f_A, is obtained as Equations (9) to (11), where $N_A(N)$ stands for the atomic population on atom A in the N electron system.

$$f_A^{+} \approx N_A(N+1) - N_A(N) \tag{9}$$

$$f_A^{-} \approx N_A(N) - N_A(N-1) \tag{10}$$

$$f_A^{o} \approx \frac{1}{2}[N_A(N+1) - q_A(N-1)] \tag{11}$$

According to the relation given in Equation (12) the corresponding condensed local softness parameters can easily be calculated from the condensed Fukui function and the global softness, as in Equation (13).

$$s(\underline{r}) = Sf(\underline{r}) \tag{12}$$

$$s_A^{+} = Sf_A^{+} \tag{13}$$

The MEP,[36,37] $V(r)$, was calculated in the usual way, neglecting polarisation and nuclear rearrangement effects, as described in Equation (14), where the summation runs over all nuclei A with charge Z_A and coordinate R_A.

$$V(\underline{r}) = \sum_A \frac{Z_A}{|\underline{R}_A - \underline{r}|} - \int \frac{\rho(\underline{r}')}{|\underline{r}' - \underline{r}|} d\underline{r}' \tag{14}$$

The first term on the right-hand side of Equation (14) gives the contribution of the nuclei, the second term reflects the effect of the electrons.

In this contribution, the MEP has been computed in a plane containing three oxygen atoms (oxygen O1, O2 and O3; see Figure 1) of the crown ether moiety, for both the [18]crown-6 and the [15]crown-5 systems (see Figures 3 and 4, respectively). The MEP was also calculated on a straight line perpendicular to the plane containing the oxygen atoms used to calculate the MEP contours, starting at 5 Å above and ending 5 Å below the mean crown ether plane, with steps of 0.01 Å.

Structures and energies were calculated with the aid of the Gaussian98[41] program. All geometries were completely optimised at the DFT level with the B3LYP[42−44] functional, with a 6-31G*[45] basis set for H, C, O, Na and K and 3-21G*[45] for Sn.

The geometries of all the complexes between the tin atoms of the crown ether derivatives and the nucleophiles (SCN^{-}, acetone and water) interacting with the tin atom, and the cations (Na^{+} and K^{+}) interacting with the crown ether moiety itself were fully optimised.

3. Results and Discussion

The stabilisation energies resulting from the interactions between [15]crown-5-$C_6H_3COOSn(CH_3)_3$ and [18]crown-6-

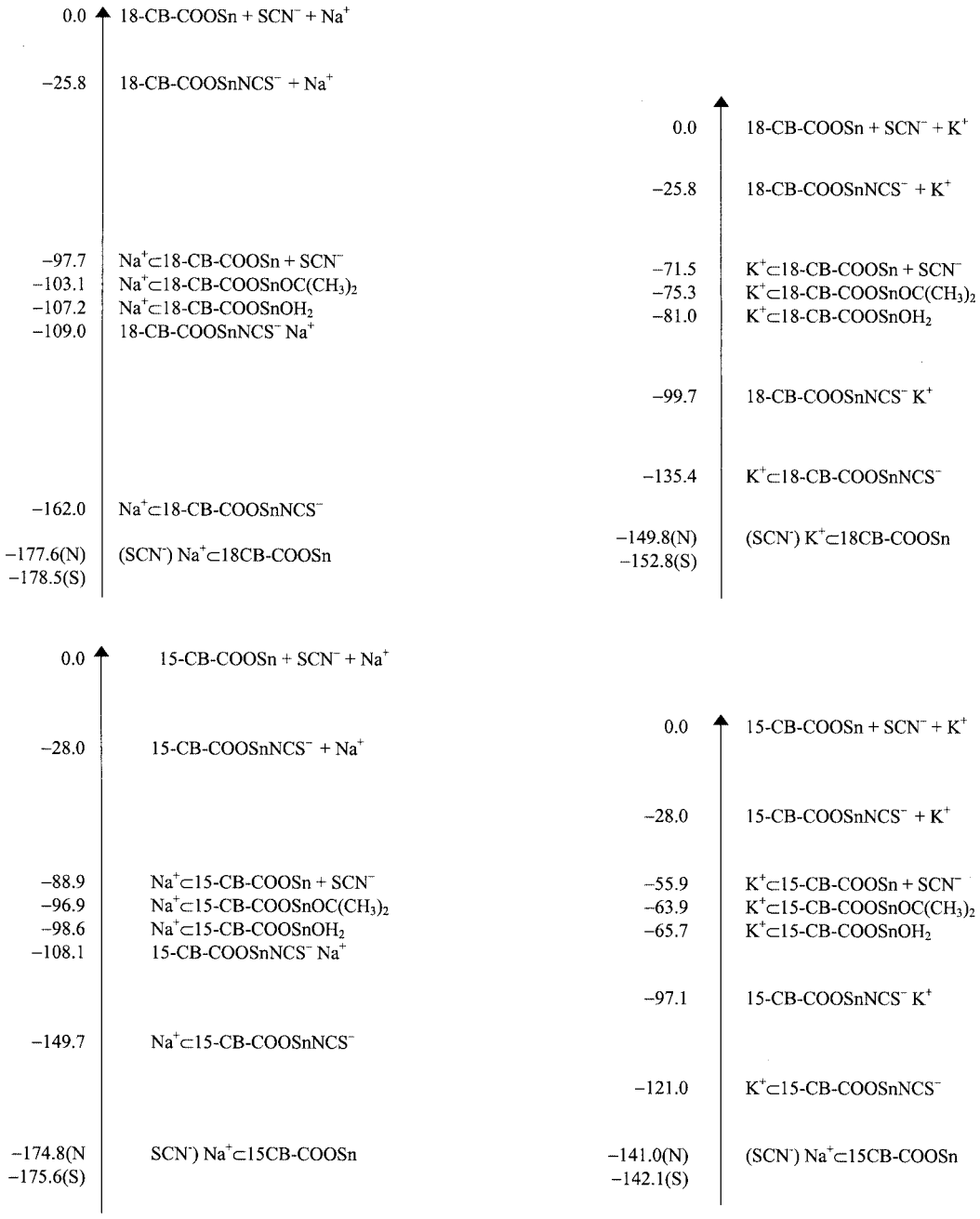

Figure 2. Diagram of stabilisation energies (B3LYP level) for (top left) the [18]crown ether complexes with different nucleophiles and Na^+, (top right) the [18]crown ether complexes with different nucleophiles and K^+, (bottom left) the [15]crown ether complexes with different nucleophiles and Na^+, and (bottom right) the [15]crown ether complexes with different nucleophiles and K^+; the methyl groups on tin are omitted for clarity

$C_6H_3COOSn(CH_3)_3$, nucleophiles either charged or uncharged and of variable softness (SCN^-, acetone and H_2O), and cations (Na^+ and K^+) are shown in Figures 2a−d. The hardness sequence of the above nucleophiles was calculated at the level outlined in the previous section to yield: H_2O (8.42 eV) > acetone (5.91 eV) > SCN^- (4.36 eV). The investigated complexes displayed interactions between a nucleophile and the tin atom on one hand, and on the other hand between the alkali cations and either the crown ether cavity or the nucleophilic sulfur atom of the SCN^- anion.

The stabilisation energies for the complexation of the crown ether tin derivative with SCN^-, H_2O and acetone were calculated both with Na^+ and with K^+ in the crown ether moiety of the molecule. Initially the nucleophiles were positioned at a distance of 2.20 Å from the tin atom and forming an angle of 180° between the attacking atom of the nucleophile (the oxygen atom for water or acetone and the N atom for SCN^-), the tin atom and the oxygen atom of the carboxylate group bound to tin. The final geometry of the complex of acetone and water with Sn was almost ident-

ical for both crown ether tin derivatives, the final distance between the Sn atom and the attacking nucleophilic atom in all cases being between 2.55 and 2.56 Å. The deviations with respect to the original NSnO(7) angle in the X-ray data were only 3.2° and 3.5° for both crown ethers. For the complex with SCN^-, the final distance between the Sn atom and the attacking N atom was 2.10 Å and the deviation in the angle was 3.0°.

This orientation (attacking N and not S) was considered first in view of the crystallographic data,[9] this regioselectivity being further discussed below.

The much smaller Sn−N distances of 2.10 Å − in comparison with the Sn−O distance of 2.55 Å − in the water and acetone complexes suggest a stronger complex (vide infra).

The results of the calculations of the stabilisation energies obtained as a result of the interaction of the SCN^-, H_2O and acetone nucleophiles with the tin atom and the Na^+ or K^+ cations with the crown ether moiety are shown in Figure 2a−d.

The influence of the nature of the cation and the crown ether size is discussed first on the basis of MEP calculations. The MEP contours of the crown ethers (see Figures 3 and 4) show that the crown cavity is associated with negative values of the electrostatic potential while the regions outside the crown ether ring are associated with positive values of the electrostatic potential. This behaviour of the MEP thus straightforwardly explains the positions of the Na^+ and K^+ cations in the crown ether cavity.

In order to find where the minimum (expected to appear in a region with a substantial accumulation of electronic density) was located, we calculated the potential on a straight line over a distance of 10 Å from 5 Å above to 5 Å below the averaged crown ether plane. The results of this calculation can be seen in Figure 5; the minimum was found exactly at the point where the cation should be located and, moreover, a more negative value is associated with the [18]crown-6 ether (−0.1452 a.u.) than for the [15]crown-5 ether (−0.1062 a.u.).

Na^+ complexes are systematically more stable than K^+ complexes, which can be correlated with the larger ionic radius of K^+ (133 pm versus 68 pm for Na^+) taking into account the space available in the crown ether.[46] It is also in accordance with the greater hardness of Na^+ than of K^+, thus interacting more favourably with the hard environment constituted by the ring oxygen atoms of the crown ether moieties. These observations are confirmed by the stabilisation energies calculated for the [18]crown-6 with Na^+ (97.7 kcal·mol^{-1}) and with K^+ (71.5 kcal·mol^{-1}) and for the [15]crown-5 ether, for which the stabilisation energy with Na^+ is 88.9 kcal·mol^{-1} and with K^+ 55.9 kcal·mol^{-1} (see Figure 2). As can be observed, higher stabilisation energies are observed for both cations with the [18]crown ether than with the [15]crown.

The interaction with the cation turns out to be more stabilizing than the interaction with the nucleophile. Note, however, that the interaction energies of SCN^--containing complexes are not additive, with deviations of 38.5 and 38.9

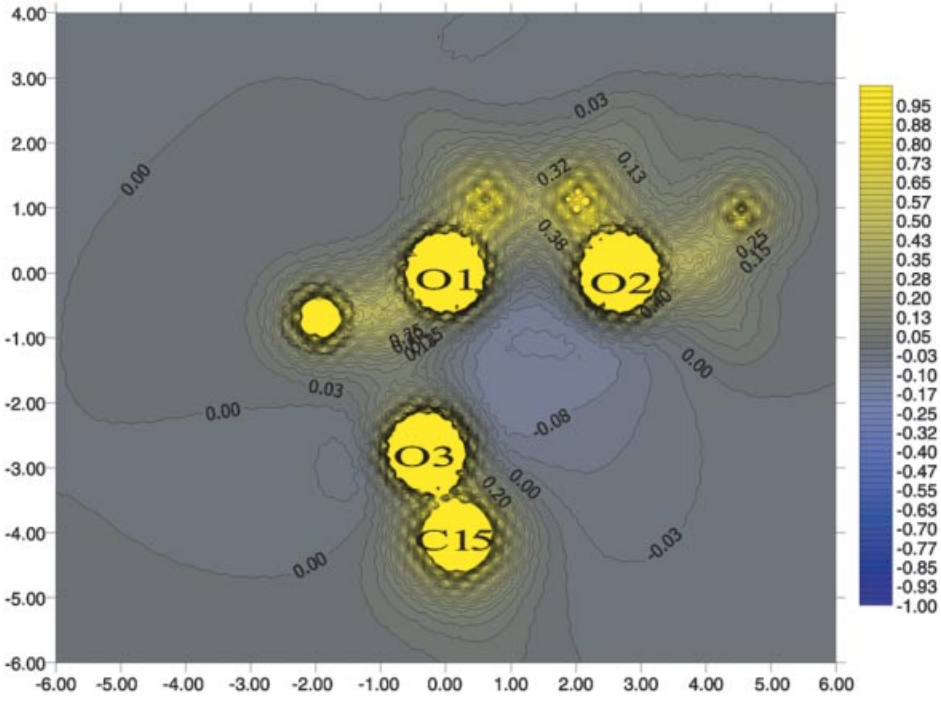

Figure 3. The MEP for the plane containing three of the six oxygen atoms (O1, O2, O3) in the crown ether moiety in [18]crown-6-$C_6H_3COOSn(CH_3)_3$

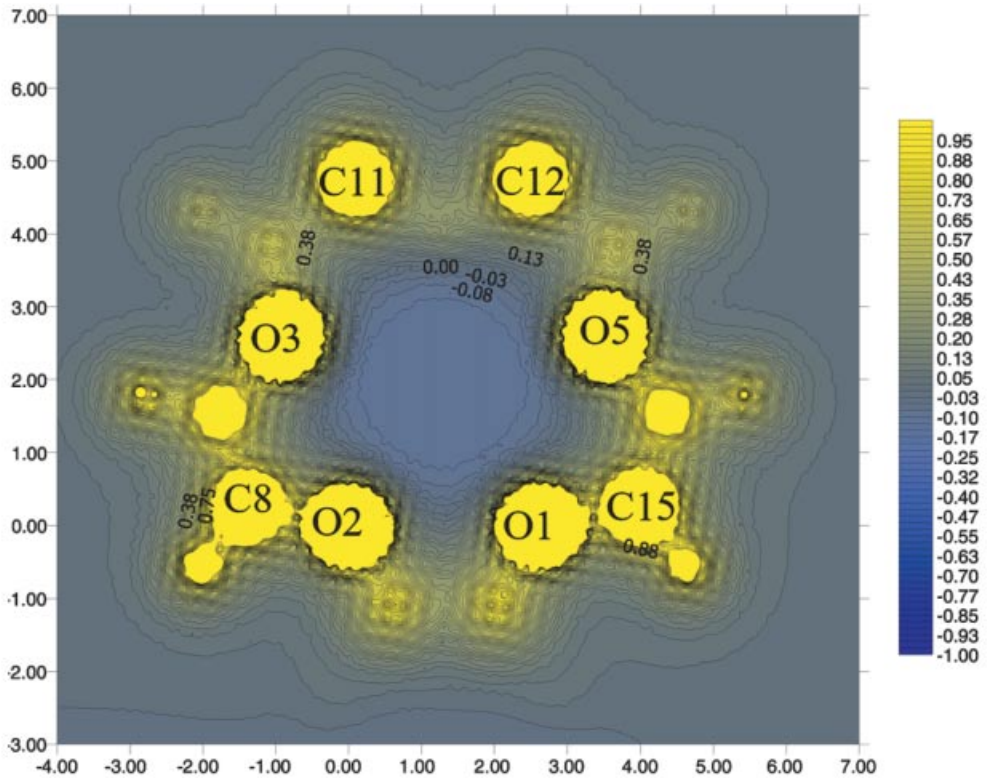

Figure 4. The MEP for the plane containing three of the five oxygen atoms (O1, O2, O3) in the crown ether moiety [15]crown-5-$C_6H_3COOSn(CH_3)_3$

kcal·mol^{-1} for the [18]crown ether with Na^+ and K^+, respectively, and 32.4 and 37.2 for the [15]crown ether with Na^+ and K^+, respectively.

One may note that the complexes formed between the tin atom of the crown benzocarboxylate moiety and SCN^- are always more stable (i.e., display more negative values) than for water and acetone both for the Na^+ and for the K^+ cations, and also both for the [15]crown and for the [18]crown ethers. At first glance, this sequence is in line with the softness sequence $SCN^- >$ acetone $> H_2O$, suggesting that the Sn acts as a soft centre (soft Lewis acid).

In the case of the interaction with SCN^-, however, a problem is posed by the regioselectivity. It is known from previous detailed studies on the Fukui function,[47−49] by the present authors among others, that the S atom is the soft centre. It was indeed shown that the sulfur atom in SCN^- was softer than the nitrogen atom, the values being 0.667 a.u. for the condensed Fukui function f^-_S as compared to 0.342 a.u. for the f^-_N (obtained at the QCISD/aug-cc-pVDZ level by use of Bader's population analysis[50]). These values show the same trend as the values calculated in this work (see Table 1).

Table 1 shows that this result is in fair agreement with our calculations, the sequence of local softness values being $s^-_S(SCN^-) > s^-_O(H_2O) \approx s^-_O(\text{acetone}) > s^-_N(SCN^-)$.

This result is a first indication that the Sn atom in the compounds under consideration behaves as a hard atom, since it preferentially interacts with the harder part of SCN^-. Note that the charge on the tin atom in both compounds is of the order of +1 a.u. (1.001 a.u. for the [18]crown ether and 1.002 a.u. for the [15]crown ether). This relatively high charge may be due to the structure of the crown ether, where the pentacoordination of Sn, resulting in an almost ideal trigonal-bipyramidal structure[9] in which the two electronegative ligands (the carboxylate group and the nitrogen atom of SCN^-) occupy the two apical positions, gives rise to longer bonds with little s character and hence a higher ionic contribution.

The reason that SCN^- as a whole interacts more strongly than acetone or water can then again be traced back to interaction between the Sn moiety and nucleophiles in which charge control (i.e., hard−hard interactions; SCN^- carries a negative charge) dominate. It is found that, in the absence of a net negative charge on the molecule, the oxygen atoms in H_2O and acetone have net charges of 0.72 and 0.40, respectively, making these atoms hard, the sequence being in line with the interaction strength $H_2O >$ acetone. Here we took the net atomic charge as a first indicator of local hardness (see ref.[51] for an in-depth discussion of the problem of finding a well-suited counterpart to local softness).

The hardness of the tin atom has been a point of controversy. From the position of the atom in the Periodic Table, one could conclude that Sn should be relatively soft; indeed, a low value of 3.05 eV is found for the absolute hardness for the isolated atom.[18] In our previous study[36] on the nanocluster $[(RSn)_{12}O_{14}(OH)_6]^{2+}$ (R = CH_3), however, we found a local softness value of 0.0074, of the same order as

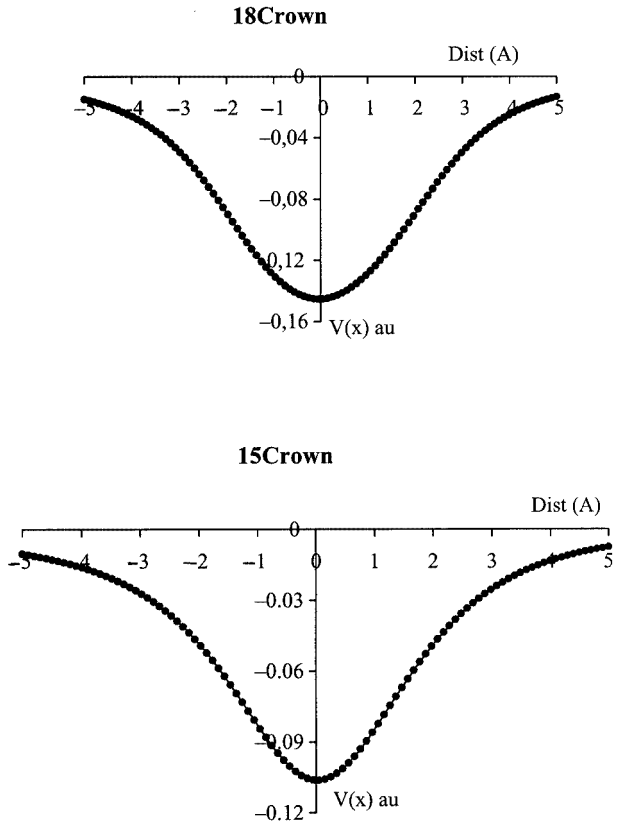

Figure 5. The MEP $V(x)$ (a.u.) for [18]crown-6-$C_6H_3COOSn(CH_3)_3$ and [15]crown-5-$C_6H_3COOSn(CH_3)_3$ along a straight line starting at 5 Å perpendicular to the plane containing the oxygen atoms used in the calculation of the MEP contours (Figures 3 and 4), the intersection point being the Na^+ or K^+ cation position, in steps of 0.01 Å

the value found here (0.0076), indicating in both cases that the oxophilicity of the tin atom makes it a hard centre, preferring to interact with hard molecules. In addition, the well-known tendency of the tin atom to involve intra- and intermolecularly bridging fluorine atoms is in line with the hardness of Sn in tin fluorides.[52]

Confirmation of a preference for N−Sn interaction over S−Sn interaction was found when the possibility of complexation through the S atom of SCN^- was explicitly studied. In these cases the sulfur atom was placed at the same position as the N atom in the other complexes. Geometry optimisation starting from this alternative complexation mode, however, never provided stable complexes. Moreover, complexes of Sn with SCN^- through the N atom have also been reported elsewhere.[53]

We also calculated complexes in which the nucleophile interacted with the tin atom and the Na^+ or K^+ were infinitely remote. For the [18]crown-6 we found that the stabilisation energy is 25.8 kcal·mol^{-1} and for the [15]crown-5 28.0 kcal·mol^{-1}. By comparison with the data above, it appears that the cation alone in the crown ether hole stabilises the molecule more than when only the nucleophiles are interacting with the tin atom. This can be explained by considering that the crown ether moiety is harder than the Sn atom region. A numerical confirmation (e.g., through the MEP) is quite difficult though, as one region is nucleophilic whereas the other part is electrophilic in nature.

We also studied cases in which SCN^- is bound to the tin atom through the N atom, and the sodium and potassium ions are bound to the S atom of SCN^- (the initial distance between the S atom of SCN^- and the sodium and potassium cations being 2.35 and 2.71 Å, respectively). The energies show the same trends as already obtained in the previous calculations, according to which the [18]crown-6 complex was more stable than the [15]crown-5. They are all less stable than when the cation is trapped in the crown ether cavity. As may be expected in view of the very soft nature of the S centre of SCN^-, hard cations interact preferentially with the hard, oxygen-rich crown ether hole.

A final set of complexes for the two kinds of trimethyltin crown ether benzocarboxylates was also assessed. In these new cases, SCN^- is directly interacting with the Na^+ or K^+ ions located in the crown ether hole. For these calculations, both possibilities − that the ions could interact with the N or with the S atom of SCN^- − were considered. The SCN^- was placed at a distance of 2.2 Å from the cation, forming an angle of 90° with the cation and oxygen atoms 1 and 2 (see Figure 1). This geometry was used for both tin ether moieties. For each of the two crown ethers and the two cations, the geometry optimisation was started with a binding situation in which the cation was exclusively interacting either with the nitrogen atom or with the sulfur atom. The optimised end geometries appeared to be roughly identical, since, when starting from the N^-Na^+ interaction in the [18]crown ether, optimised $N^-−Na^+$ and $S^-−Na^+$ distances of 2.30 and 4.64 Å were obtained, while when starting from the S^-Na^+ interaction fairly similar optimised distances of 2.33 and 4.21 Å, with very close interaction energies of −177.6 and −178.5 kcal·mol^{-1} respectively, were

Table 1. Calculated hardnesses η [eV], softnesses S [eV^{-1}], condensed Fukui functions f^+ and f^- (atomic units, a.u.) and local softness values s^+ and s^- (a.u. eV^{-1}); atoms to which condensed functions refer are given in parentheses

Molecule	η	S	f^+	f^-	s^+	s^-
[18]Crown-6	4.07	0.246	0.0316 (Sn)		0.00776 (Sn)	
[15]Crown-5	4.04	0.248	0.0309 (Sn)		0.00765 (Sn)	
SCN^-	4.36	0.229		0.264 (N)		0.0299 (N)
				0.620 (S)		0.1420 (S)
Acetone	5.91	0.169		0.365 (O)		0.0619 (O)
H_2O	8.42	0.119		0.662 (O)		0.0786 (O)

calculated. Similar calculations for the [18]crown K^+ complex give 2.71 and 4.56 Å when starting from N^-K^+ and 2.96 and 3.34 Å when starting from S^-K^+, with interaction energies of −149.8 and −152.2 kcal·mol^{-1}, respectively. For the [15]crown ether, optimised N^-Na^+ and S^-Na^+ distances of 2.28 and 4.14 Å were obtained, while when starting from the S^-Na^+ interaction, optimised distances of 2.75 and 3.54 Å, with very close interaction energies of −174.8 and −175.6 kcal·mol^{-1}, respectively, were calculated. Similar calculations for the [15]crown K^+ complex give 2.75 and 3.54 Å when starting from N^-K^+, and 2.95 and 3.28 Å when starting from S^-K^+, with interaction energies of −141.0 and −142.1 kcal·mol^{-1}, respectively. These final geometries show very clearly that wherever the N atom of SCN^- is initially located, the final structure always has the nitrogen atom closer to the cation, although with the nitrogen and sulfur atoms arranged in such a way that a bidentate chelation mode with the cation results.

The final geometries of these complexes always yield a pentacoordinate tin atom, since the carboxylate ligands also bind to Sn in a bidentate mode, the oxygen atom of the carbonyl group expanding its coordination (see Scheme 1).

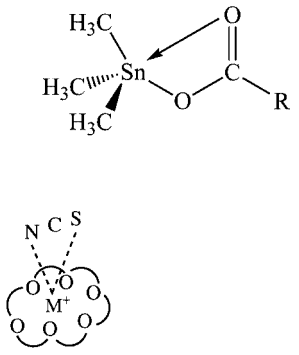

Scheme 1. Bidentate chelating mode of the carboxylate ligand in triorganotin carboxylates, and of SCN^- with the cation positioned in the crown ether

These complexes are more stable (see values above) than the complexes reported in Figure 2. This stability can be attributed to the simultaneous presence of a chelating bidentate mode of the nucleophiles at the levels of both the tin atom and the alkali cation.

Overall, these results fit remarkably well with previous experimental findings from multinuclear NMR studies[9] from which a mixture of several species was proposed to exist in dynamic equilibrium in acetone solution (Figure 6). No direct evidence for species b and c could be given in the NMR study. In the current ab initio study, the species actually merge into a single one with a bidentate mode for NCS^- with the alkali cation. The reason for the lack of NMR evidence lies in the poor sensitivity of ^{23}Na chemical shifts to coordination changes, the chemical shift difference between completely free Na^+ and Na^+ interacting with six oxygen atoms amounting to only ca. 10 ppm. A supplementary interaction with external SCN^- is therefore hardly able also to influence the ^{23}Na chemical shifts. In the crystalline state, the only species observed is the one with the cation trapped in the crown ether cavity and the anion bound to Sn (i.e., of the species calculated here, the most stable one; after $M^+\subset CBCOOSnNCS^-$, species a). In solution, this coexists with the third most stable species, the one where the cation interacts with the sulfur atom of the anion, itself bound to Sn through the nitrogen atom ($CBCOOSnNCS^-M^+$). In addition, ^{117}Sn NMR chemical shift data reveal that the tin−nitrogen interaction is broken up with increasing temperature, favouring a species in which acetone from the solvent is complexing Sn [$M^+\subset CBCOOSnOC(CH_3)_2$].

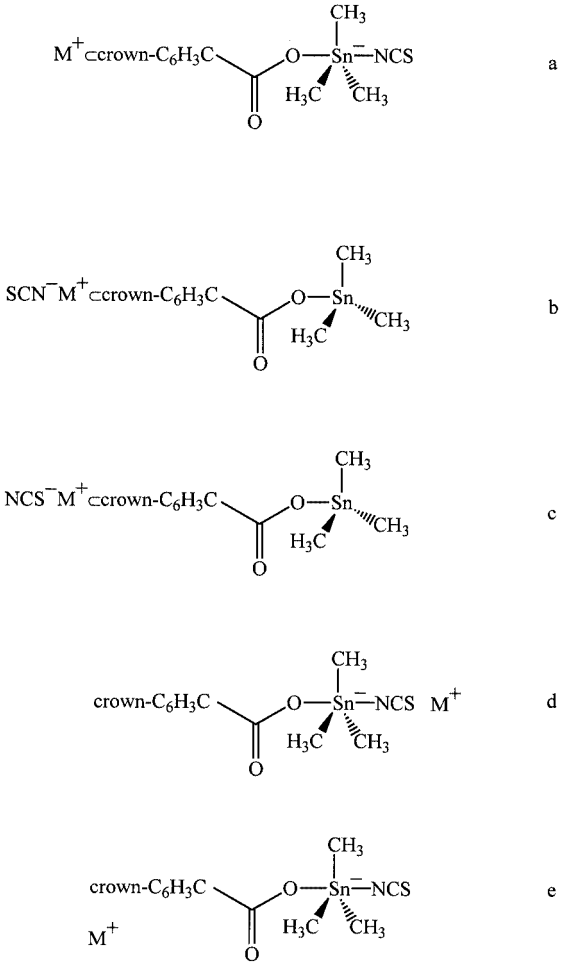

Figure 6. Possible zwitterionic ion pairings

Finally, ^{23}Na NMR spectroscopic data show the existence of an equilibrium between free Na^+ and Na^+ trapped in the crown ether hole, this equilibrium favouring Na^+ trapping much more for the [18]crown ether than for the [15]crown ether, in line with the results of our calculations indicating more stable alkali cation complexation with the former crown ether than with the latter. Interestingly, when the cation interacts with the sulfur atom of the thiocyanate anion complexing Sn through the nitrogen atom or does not interact at all, the stabilisation energy of the complexes are essentially independent of the crown ether sizes, as they actually should be.

These experiments are also in line with the electrostatic attraction between the positive charge of the cation and the negative values of the MEP being more pronounced for the [18]- than for the [15]crown ether ring (see Figure 5).

4. Conclusion

In conclusion, this paper clearly demonstrates that the sites of interactions of the trimethyltin derivatives of [18]crown-6 and [15]crown-5 benzo-4-carboxylates can be predicted by use of DFT-based reactivity descriptors such as the hardness, softness and Fukui function, as well as MEP calculations. The agreement with experimental results is good to excellent, so such calculations both help in interpreting experimental data as well as providing a firm theoretical basis for the different cases of complexation observed.

The HSAB principle, characterising the reactive sites on the basis of local softness, and the Fukui function provide a firm explanation for the reactivity of the tin atom of the crown ether benzocarboxylate towards SCN^-, acetone and water. The HSAB concept was also successfully used to explain the preferences of the tin atoms in both crown ethers for binding with the nitrogen atom of SCN^- rather than with the sulfur atom.

Acknowledgments

R. V. R. wishes to thank the Colombian Institute for Science and Development, Colciencias, and the Universidad de Cartagena (Cartagena, Colombia) for a PhD fellowship. P. G. and F. D. P. acknowledge the Research Council of Free University of Brussels (VUB) and the Fund for Scientific Research − Flanders (Belgium) (F.W.O.) for continuous support to their group. R. W. and M. B. acknowledge financial support from the Fund for Scientific Research − Flanders (Belgium) (F.W.O.) (Grants G.0192.98 and G.0016.02) and from the Research Council of the VUB.

[1] [1a] I. Haiduc, F. T. Edelmann, in *Supramolecular Organometallic Chemistry*, Wiley-VCH, Weinheim, **1999**, pp. 42−43. [1b] N. Pelizzi, A. Casnati, A. Friggeri, R. Ungaro, *J. Chem. Soc., Perkin Trans. 2* **1998**, 1307−1311. [1c] P. D. Beer, J. B. Cooper, *Chem. Commun.* **1998**, 129−130. [1d] P. D. Beer, S. W. Dent, *Chem. Commun.* **1998**, 825−826. [1e] M. T. Blanda, M. A. Herren, *Chem. Commun.* **2000**, 343−344. [1f] J. E. Redman, P. D. Beer, S. W. Dent, M. G. B. Drew, *Chem. Commun.* **1998**, 231−232. [1g] M. T. Reetz, C. M. Niemeyer, K. Harms, *Angew. Chem. Int. Ed. Engl.* **1991**, *30*, 1472−1474. [1h] M. T. Reetz, C. M. Niemeyer, K. Harms, *Angew. Chem. Int. Ed. Engl.* **1991**, *30*, 1474−1476. [1i] J. Scheerder, J. P. M. van Duynhoven, J. F. J. Engbersen, D. N. Reinhoudt, *Angew. Chem. Int. Ed. Engl.* **1996**, *35*, 1090−1093. [1j] D. M. Rudkevich, Z. Brzozka, M. Palys, H. C. Visser, W. Verboom, D. N. Reinhoudt, *Angew. Chem. Int. Ed. Engl.* **1994**, *33*, 467−468. [1k] J. M. Lehn, in *La chimie supramoléculaire*, Deboeck Université, Paris, **1997**, p. 37.

[2] [2a] D. J. Cram, *Science* **1988**, *240*, 760−767. [2b] J. J. Christensen, D. J. Eatough, R. M. Izatt, *Chem. Rev.* **1974**, *74*, 351−384. [2c] R. M. Izatt, K. Pawlak, J. S. Bradshaw, R. L. Bruening, *Chem. Rev.* **1991**, *91*, 1721−2085.

[3] [3a] M. F. Hawthorne, X. Yang, Z. Zheng, *Pure Appl. Chem.* **1994**, *66*, 245−254. [3b] B. Dietrich, *Pure Appl. Chem.* **1993**, *65*, 1457−1464. [3c] F. D. Schmidtchen, M. Berger, *Chem. Rev.* **1997**, *97*, 1609−1646.

[4] [4a] *Crown ethers and analogs* (Ed.: S. Pataï), John Wiley & Sons, Chichester, **1989**. [4b] F. Vögtle, in *Supramolecular Chemistry*, John Wiley & Sons, Chichester, **1991**. [4c] *Comprehensive Supramolecular Chemistry*, vol. I−XI (Eds.: J. M. Lehn, J. L. Atwood, J. E. D. Davies, D. D. MacNicol, F. Vögtle), Pergamon, Oxford, **1996**.

[5] [5a] T. J. Karol, J. P. Hutchinson, J. R. Hyde, H. G. Kuivila, J. A. Zubieta, *Organometallics* **1983**, *2*, 106−114. [5b] M. Gielen, K. Jurkschat, *J. Organomet. Chem.* **1984**, *273*, 303−312. [5c] M. Austin, K. Gebreyes, H. G. Kuivila, K. Swami, J. A. Zubieta, *Organometallics* **1987**, *6*, 834−842. [5d] K. Jurkschat, H. G. Kuivila, S. Liu, J. A. Zubieta, *Organometallics* **1989**, *8*, 2755−2759. [5e] J. H. Horner, P. J. Squatritto, N. McGuire, J. P. Riebenspies, M. Newcomb, *Organometallics* **1991**, *10*, 1741−1750. [5f] D. Dakternieks, K. Jurkschat, H. Zhu, E. R. T. Tiekink, *Organometallics* **1995**, *14*, 2512−2521. [5g] R. Altmann, K. Jurkschat, M. Schürmann, D. Dakternieks, A. Duthie, *Organometallics* **1997**, *16*, 5716−5723. [5h] R. Altmann, O. Gausset, D. Horn, K. Jurkschat, M. Schürmann, M. Fontani, P. Zanello, *Organometallics* **2000**, *19*, 430−443.

[6] [6a] C. H. Yoder, R. A. Morreall, C. I. Butoi, W. J. Kowalski, J. N. Spencer, *J. Organomet. Chem.* **1993**, *448*, 59−61. [6b] S. W. Ng, J. M. Hook, M. Gielen, *Main Group Met. Chem.* **1999**, *22*, 649−654. [6c] S. W. Ng, *Z. Kristallogr.* **1999**, *214*, 424−426. [6d] J. K. Tsagatakis, N. A. Chaniotakis, K. Jurkschat, S. Damoun, P. Geerlings, A. Bouhdid, M. Gielen, I. Verbruggen, M. Biesemans, J. C. Martins, R. Willem, *Helv. Chim. Acta* **1999**, *82*, 531−542.

[7] [7a] M. Gielen, *Coord. Chem. Rev.* **1996**, *151*, 41−51. [7b] M. Gielen, P. Lelieveld, D. de Vos, R. Willem, in *Metal Complexes in Cancer Chemotherapy* (Ed.: B. K. Keppler), VCH, Weinheim, **1993**, pp. 383−390. [7c] D. de Vos, R. Willem, M. Gielen, K. E. van Wingerden, K. Nooter, *Met. Based Drugs* **1998**, *5*, 179−188.

[8] [8a] E. R. T. Tiekink, *Appl. Organomet. Chem.* **1991**, *5*, 1−23. [8b] E. R. T. Tiekink, *Trends Organomet. Chem.* **1994**, *1*, 71−116.

[9] M. Kemmer, M. Biesemans, M. Gielen, J. C. Martins, V. Gramlich, R. Willem, *Chem. Eur. J.* **2001**, *17*, 4686−4695.

[10] [10a] A. Marquez, G. G. Gonzalez, J. Fernandez-Sanz, *Chem. Phys.* **1989**, *138*, 99−104. [10b] G. Stewart, E. R. T. Tiekink, M. A. Buntine, *J. Phys. Chem.* **1997**, *101*, 5638−5373. [10c] M. A. Buntine, V. J. Hall, F. J. Kosovel, E. R. T. Tiekink, *J. Phys. Chem. A* **1998**, *102*, 2472−2482. [10d] J. Leszczynki, I. J. Yanov, *J. Phys. Chem. A.* **1999**, *103*, 396−401. [10e] G. Barone, M. C. Ramusino, R. Barbieri, G. Lamanna, *J. Mol. Struct. (Theochem).* **1999**, *469*, 143−149. [10f] M. Yasuda, K. Chiba, A. Baba, *J. Am. Chem. Soc.* **2000**, *122*, 7549−7555. [10g] D. Duca, G. Barone, G. La Manna, T. Fiore, C. Pellerito, R. Di Stefano, M. Scopello, L. Pellerito, *Appl. Organomet. Chem.* **2001**, *15*, 581.

[11] S. Krishnamurty, R. K. Roy, R. Vetrivel, S. Iwata, S. Pal, *J. Phys. Chem.* **1997**, *101*, 7253−7257.

[12] R. Ch. Deka, R. Vetrivel, S. Pal, *J. Phys. Chem.* **1999**, *103*, 5978−5982.

[13] S. Pal, K. R. S. Chandrakumar, *J. Am. Chem. Soc.* **2000**, *122*, 4145−4153.

[14] R. K. Roy, S. Krishnnamurty, P. Geerlings, S. Pal, *J. Phys. Chem.* **1998**, *102*, 3746−3755.

[15] S. Damoun, W. Langenaeker, P. Geerlings, *J. Phys. Chem.* **1997**, *101*, 6951−6954.

[16] S. Damoun, G. Van de Woude, F. Mendez, P. Geerlings, *J. Phys. Chem.* **1997**, *101*, 886−893.

[17] S. Damoun, G. Van de Woude, K. Choho, P. Geerlings, *J. Phys. Chem.* **1999**, *103*, 7861−7866.

[18] [18a] R. G. Parr, W. Yang, *Density Functional Theory of Atoms and Molecules*, Oxford University Press, New York, **1989**. [18b] H. Chermette, *J. Comp. Chem.* **1999**, *20*, 129. [18c] P. Geerlings, F. De Proft, W. Langenaeker, *Chem. Rev.*, in press. [18d] F. De Proft, P. Geerlings, *Chem. Rev.* **2001**, *101*, 1451−1464. [18e] P. Geerlings, F. De Proft, *Int. J. Mol. Sci.* **2002**, *3*, 276−309.

[19] R. G. Parr, R. G. Pearson, *J. Am. Chem. Soc.* **1983**, *105*, 7512−7516.
[20] R. G. Pearson, *J. Am. Chem. Soc.* **1963**, *85*, 3533−3539.
[21] R. G. Pearson, *Coord. Chem. Rev.* **1990**, *100*, 403−425.
[22] R. G. Parr, P. K. Chattaraj, *J. Am. Chem. Soc.* **1991**, *113*, 1855−1856.
[23] R. G. Parr, P. K. Chattaraj, *J. Am. Chem. Soc.* **1991**, *113*, 1854−1855.
[24] P. K. Chattaraj, G. H. Liu, R. G. Parr, *Chem. Phys. Lett.* **1995**, *237*, 171−176.
[25] [25a] R. G. Parr, W. Yang, *J. Am. Chem. Soc.* **1984**, *106*, 4049−4050. [25b] W. Yang, R. G. Parr, *Proc. Natl. Acad. Sci. USA* **1985**, *82*, 6723−6726.
[26] W. Yang, W. J. Mortier, *J. Am. Chem. Soc.* **1986**, *108*, 5708−5711.
[27] R. Vivas-Reyes, F. De Proft, M. Biesemans, R. Willem, P. Geerlings, *J. Phys. Chem. A* **2002**, *106*, 2753−2759.
[28] R. Vivas-Reyes, F. De Proft, P. Geerlings, M. Biesemans, R. Willem, F. Ribot, C. Sanchez, *New. J. Chem.* **2002**, *9*, 1108−1117.
[29] P. Geerlings, F. De Proft, W. Langenaeker, in *Density Functional Methods: Applications in Chemistry and Material Science* (Ed.: M. Springborg), chapter 2, John Wiley, New York, **1997**.
[30] P. Geerlings, F. De Proft, W. Langenaeker, *Adv. Quant. Chem.* **1999**, *33*, 303−328.
[31] J. L. Gazquez, F. Mendez, *J. Chem. Phys.* **1994**, *98*, 4591−4593.
[32] F. Mendez, J. Tamariz, P. Geerlings, *J. Phys. Chem. A* **1998**, *102*, 6292−6296.
[33] F. Mendez, M. L. de Romero, F. De Proft, P. Geerlings, *J. Org. Chem.* **1998**, *63*, 5774−5778.
[34] T. N. Le, L. T. Nguyen, F. De Proft, A. K. Chandra, P. Geerlings, M. T. Nguyen, *J. Chem. Soc., Perkin Trans. 2* **1999**, 1249−1255.
[35] R. Bonaccorsi, E. Scrocco, J. Tomasi, *J. Chem. Phys.* **1970**, *51*, 5270−5284.
[36] M. M. Rohmer, M. Bénard, J. P. Blaudeau, J. P. Maestre, J. M. Poblet, *Coord. Chem. Rev.* **1998**, *178−180*, 1015−1045, and refs. cited therein.
[37] J. Tomasi, B. Menuci, R. Cammi, in *Molecular Electrostatic Potentials: Concepts and Applications, Theoretical and Computational Chemistry*, (Eds.: J. S. Murray, K. D. Sen), Elsevier, Amsterdam, **1996**, vol. 3.
[38] P. Geerlings, F. De Proft, *Int. J. Quant. Chem.* **2000**, *80*, 227−235.
[39] C. Lee, W. Yang, R. G. Parr, *J. Mol. Struct.* **1988**, *163*, 305−313.
[40] R. S. Mulliken, *J. Chem. Phys.* **1955**, *23*, 1833−1840.
[41] M. J. Frisch, G. W. Trucks, H. B. Schlegel, G. E. Scuseria, M. A. Robb, J. R. Cheeseman, V. G. Zakrzewski, J. A. Montgomery, R. E. Stratmann, J. C. Burant, S. Dapprich, J. M. Millam, A. D. Daniels, K. N. Kudin, M. C. Strain, O. Farkas, J. Tomasi, V. Barone, M. Cossi, R. Cammi, B. Mennucci, C. Pomelli, C. Adamo, S. Clifford, J. Ochterski, G. A. Petersson, P. Y. Ayala, Q. Cui, K. Morokuma, D. K. Malick, A. D. Rabuck, K. Raghavachari, J. B. Foresman, J. Cioslowski, J. V. Ortiz, B. B. Stefanov, G. Liu, A. Liashenko, P. Piskorz, I. Komaromi, R. Gomperts, R. L. Martin, D. J. Fox, T. Keith, M. A. Al-Laham, C. Y. Peng, A. Nanayakkara, C. Gonzalez, M. Challacombe, P.M. W. Gill, B. G. Johnson, W. Chen, M. W. Wong, J. L. Andres, M. Head Gordon, E. S. Replogle, J. A. Pople, *Gaussian 98* (Revision A.7), Gaussian, Inc., Pittsburgh, PA, **1998**.
[42] A. D. Becke, *J. Chem. Phys.* **1993**, *98*, 5648−5652.
[43] C. Lee, W. Yang, R. G. Parr, *Phys. Rev. B.* **1998**, *37*, 785−789.
[44] P. J. Stephens, F. J. Delvin, C. F. Chablowski, M. J. Frisch, *J. Phys. Chem.* **1994**, *98*, 11623−11627.
[45] W. J. Hehre, L. Radom, P. V. R. Schleyer, J. A. Pople, *Ab Initio Molecular Orbital Theory*, Wiley, New York, **1986**.
[46] F. Vögtle, *Supramolecular Chemistry*, John Wiley & Sons, New York, **1993**.
[47] P. Geerlings, F. De Proft, J. M. L. Martin, in *Theoretical and Computational Chemistry*, vol.4 (“Recent Developments and Applications of Modern Density Functional Theory”) (Ed.: J. M. Seminario), Elsevier, Amsterdam, **1996**, p. 773.
[48] D. Gonnissen, W. Langenaeker, A. Hubin, P. Geerlings, *J. Raman Spectrosc.* **1998**, *29*, 1031−1039.
[49] F. Tielens, M. Saeys, E. Tourwé, G. B. Marin, A. Hubin, P. Geerlings, *J. Phys. Chem. A* **2002**, *106*, 1450−1457.
[50] R. F. W. Bader, *Atoms in Molecules, A Quantum Theory*, Clarendon Press, Oxford, **1990**, p. 192.
[51] G. Klopman, *J. Am. Chem. Soc.* **1968**, *90*, 223−234.
[52] [52a] N. Pieper, C. Klaus-Mrestani, M. Schürmann, K. Jurkschat, M. Biesemans, I. Verbruggen, J. C. Martins, R. Willem, *Organometallics* **1997**, *16*, 1043−1052. [52b] A. Meddour, F. Mercier, J. C. Martins, M. Gielen, M. Biesemans, R. Willem, *Inorg. Chem.* **1997**, *36*, 5712−5715. [52c] J. Beckmann, M. Biesemans, K. Hassler, K. Jurkschat, J. C. Martins, M. Schürmann, R. Willem, *Inorg. Chem.* **1998**, *37*, 4891−4897. [52d] F. A. G. Mercier, A. Meddour, M. Gielen, M. Biesemans, R. Willem, E. R. T. Tiekink, *Organometallics* **1998**, *17*, 5933−5936.
[53] E. J. Gabe, F. L. Lee, L. E. Khoo, F. E. Smith, *Inorg. Chim. Acta* **1986**, *112*, 41−46.

Received June 3, 2002
[I02290]

Synthesis and Structure of Two New High Nuclearity Ru/Pt Mixed-Metal Clusters

Brian F. G. Johnson,*[a] Sophie Hermans,[a] and Tetyana Khimyak[a]

Keywords: Cluster compounds / Ruthenium / Platinum / Heterometallic complexes / Bridging ligands

The reaction of the dianion $[Ru_5C(CO)_{14}]^{2-}$ with $[PtCl_2(MeCN)_2]$ in the presence of silica yields $[Ru_5PtC(CO)_{16}]$ (**1**) and the new compound $[PPN]_2[Ru_{10}Pt_2C_2(CO)_{28}]$ (**2**), while, in a related reaction, $[Ru_6C(CO)_{16}]^{2-}$ undergoes addition of $[PtCl_2(MeCN)_2]$ to yield the cluster $[Ru_{12}PtC_2(CO)_{32}(MeCN)_2]$ (**3**). The high nuclearity compounds **2** and **3** have been fully characterized and their structures determined by single crystal X-ray analysis.
(© Wiley-VCH Verlag GmbH & Co. KGaA, 69451 Weinheim, Germany, 2003)

Introduction

Our recent success in the preparation of ruthenium-palladium mixed-metal nanoparticles which have been shown to possess high catalytic activity for a number of processes,[1] has led us to consider the possibility of extending our studies to embrace similar systems containing ruthenium and platinum. To this end, we have investigated the possibility of preparing appropriate high nuclearity derivatives based on both the Ru_5C and Ru_6C sub-cores, and which fall in the nanometer scale. In this paper we wish to report the synthesis and complete characterization of two such new high nuclearity clusters based on $[Ru_{10}Pt_2C_2]$ and $[Ru_{12}PtC_2]$ central units, one of which having already been used successfully as a nano-catalyst precursor.[2] These two compounds are reminiscent of the "sandwich" Ru-Pd clusters reported previously, which were obtained by reacting $[Ru_6C(CO)_{16}]^{2-}$ with $[Pd(MeCN)_4]^{2+}$.[3] Our investigations have also led us to a potentially highly valuable method involving the use of silica as a "synthetic" reagent for the stabilization of highly active cationic metal fragments, a process that has already been reported elsewhere,[4] but is extended further here.

Results and Discussion

When the salt $[PPN]_2[Ru_5C(CO)_{14}]$ {$[PPN]^+$ = bis-(triphenylphosphane)iminium cation} was reacted with $[PtCl_2(MeCN)_2]$ in dichloromethane in the presence of silica, the solution darkened immediately. After separation by thin layer chromatography, two compounds were obtained. The first red compound was identified as the known $[Ru_5PtC(CO)_{16}]$ (**1**) on the basis of its mass and IR spectra.[5] The second, brown, compound, isolated in 21% yield, was identified as $[PPN]_2[Ru_{10}Pt_2C_2(CO)_{28}]$ (**2**) on the basis of its mass spectrum, which shows a high intensity peak at m/z = 1104.7 corresponding to half the mass of the anionic $[Ru_{10}Pt_2C_2(CO)_{28}]^{2-}$. A weaker peak at m/z = 2209.4 could be attributed to the same formulation, but only singly charged. The IR spectrum of **2** contains one broad peak at 2026 cm^{-1} corresponding to terminal CO ligands and two weak peaks at 1823 and 1789 cm^{-1} attributable to bridging carbonyls. Compound **2** could also be isolated as its Ph_4P^+ salt, whose crystal structure is reported here. Crystals suitable for X-ray structure determination were obtained by slow diffusion of diethyl ether into a solution of **2** in dichloromethane. Compound **2** crystallises in the monoclinic space group $P2_1/n$ and the molecular structure of the dianion $[Ru_{10}Pt_2C_2(CO)_{28}]^{2-}$ is presented in Figure 1, together with selected bond lengths and angles in Table 1.

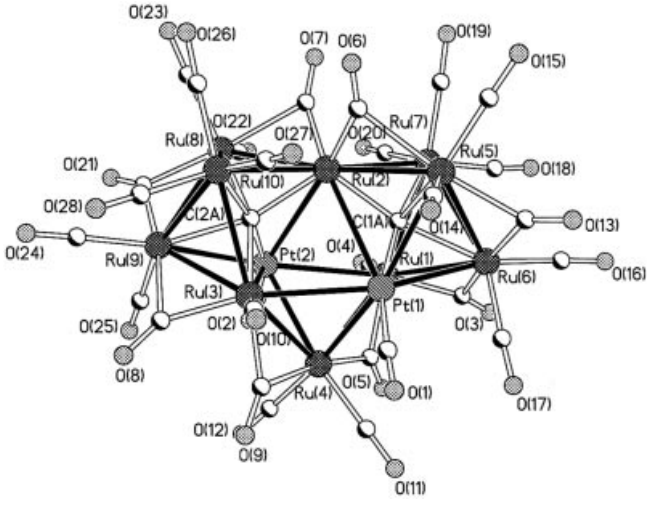

Figure 1. Molecular structure of the dianion $[Ru_{10}Pt_2C_2(CO)_{28}]^{2-}$ of **2** (labels on C atoms of carbonyl ligands correspond to those on O atoms and are omitted for clarity)

[a] University Chemical Laboratory,
Lensfield Road, Cambridge CB2 1EW, UK

Table 1. Selected bond lengths (Å) and angles (°) for $[Ph_4P]_2[Ru_{10}Pt_2C_2(CO)_{28}]$ (**2**)

Ru(2)−Pt(1)	3.0800(9)	Ru(5)−Ru(6)	2.8057(13)
Ru(4)−Pt(1)	2.7872(8)	Ru(6)−Ru(7)	2.9333(12)
Ru(2)−Pt(2)	3.1029(9)	Ru(8)−Ru(9)	2.7984(12)
Ru(4)−Pt(2)	2.7905(9)	Ru(9)−Ru(10)	2.9164(11)
Ru(2)−Ru(5)	2.8127(12)	Ru(2)−C(1a)	2.069(10)
Ru(2)−Ru(7)	2.8652(13)	Ru(2)−C(2a)	2.055(10)
Ru(2)−Ru(8)	2.7988(12)	Ru(6)−C(1a)	2.210(10)
Ru(2)−Ru(10)	2.8854(13)	Ru(9)−C(2a)	2.218(10)
Pt(1)−C(1a)−Ru(2)	96.7(5)	Pt(2)−C(2a)−Ru(2)	100.2(4)
Ru(1)−C(1a)−Ru(2)	114.7(4)	Ru(3)−C(2a)−Ru(2)	115.8(5)
Ru(1)−C(1a)−Ru(5)	161.9(6)	Ru(3)−C(2a)−Ru(8)	160.6(5)
Ru(2)−C(1a)−Ru(6)	162.9(5)	Ru(2)−C(2a)−Ru(9)	162.0(5)
Pt(1)−C(1a)−Ru(7)	169.6(5)	Pt(2)−C(2a)−Ru(10)	169.4(6)

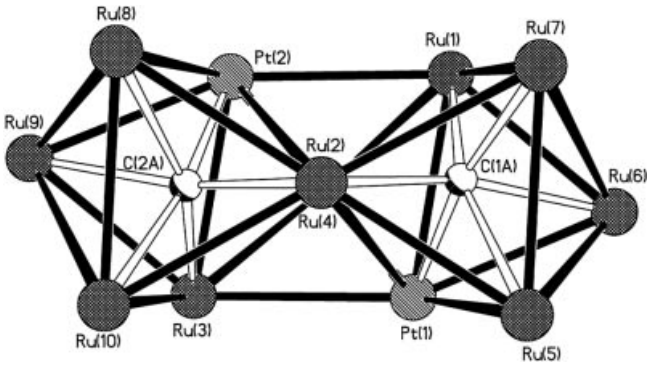

Figure 2. View down the C_2 axis passing through Ru(2) (top) and Ru(4) (bottom) atoms of the metal core of the dianion **2**

The structure of the dianion of **2** may be viewed in two different ways. The first considers the cluster core as three square-based pyramidal units [Pt(1)Ru(1)Ru(5)Ru(6)Ru(7), Pt(1)Pt(2)Ru(1)Ru(3)Ru(4), and Pt(2)Ru(3)Ru(8)-Ru(9)Ru(10)] sharing two edges [Pt(1)−Ru(1) and Pt(2)−Ru(3)] and bound together through the Ru(2) atom. The two outer pyramids correspond to Ru_4Pt units whereas the central pyramid accounts for Ru_3Pt_2. Alternatively, the structure may be viewed as three face-sharing octahedra with the two common edges — Ru(1)−Ru(2) and Ru(3)−Ru(2) — missing. The Ru(1)−Ru(2) (3.475 Å) and Ru(2)−Ru(3) (3.511 Å) distances indicate little or no direct metal-metal bonding. All Pt−Ru distances are within the expected range[5,6] with the shortest being Pt(1)−Ru(4) and Pt(2)−Ru(4) [2.7872(8) and 2.7905(9) Å, respectively] and the longest Pt(1)−Ru(2) and Pt(2)−Ru(2) [3.0800(9) and 3.1029(9) Å, respectively]. The Ru−Ru distances are similar to those reported previously for hexanuclear ruthenium clusters,[7−9] and lie between 2.7984(12) Å and 2.9333(12) Å, with the shortest being Ru(8)−Ru(9) [2.7984(12) Å] and Ru(5)−Ru(6) [2.8057(13) Å] and the longest Ru(9)−Ru(10) [2.9164(11) Å] and Ru(6)−Ru(7) [2.9333(12) Å], all these belonging to the outer pyramids. The bases of the two outer pyramids are inclined at an angle of 40° with respect to each other. The interstitial carbon atoms in each of these pyramids are shifted towards the Ru(2) atom and deviate from the plane of the base [by −0.244 Å and 0.269 Å for C(1a) and C(2a), respectively]. In agreement with the infrared data, eight carbonyl ligands are in bridging mode while the remaining twenty are terminally bonded. The Ru(2) atom bears only two bridging carbonyl ligands — the Ru(7) and Ru(10) atoms have each three terminal carbonyls — but all the other Ru atoms bear two terminal CO ligands and share two bridging CO ligands with neighboring Ru atoms. The platinum atoms are connected only to terminal carbonyls. The overall symmetry of the anion is C_2 with a twofold axis passing through Ru(2) and Ru(4) (Figure 2).

The cluster $[Ru_{10}Pt_2C_2(CO)_{28}]^{2-}$ (**2**) has a total of 166 valence electrons, which is four more than the 162 electrons predicted for three face-sharing octahedra, according to the condensed polyhedra approach proposed by Mingos. The four additional electrons might account for the two non-existing Ru−Ru bonds. This has also been noted in other Ru-Pt mixed-metal clusters, such as $[PtRu_5C(CO)_{13}(\mu\text{-}RC_2R)(\mu_3\text{-}RC_2R)]$ (R = Et,[6] Ph[10]) with a capped square-based-pyramidal metal core. These compounds have a total electron count of 88, which is two more than predicted by the PSEPT rules and is accounted for by the presence of two unusually long, and consequently weakened, Ru−Ru bonds.

The formation mechanism of compound **2** is unclear. The silica present in the reaction mixture is presumed to assist the formation of the active fragment $[Pt(MeCN)_2]^{2+}$, which undergoes addition to $[Ru_5C(CO)_{14}]^{2-}$ (by analogy with the reactions involving $[PtCl_2(COD)]$, see ref.[4]). The hypothetical monomer $[Ru_5PtC(CO)_{14}(MeCN)_2]$ is probably unstable and readily undergoes rearrangement to form compounds **1** and **2**. The fact that the ratio of the two metals in **2** is 10:2 is consistent with this view involving as it does prior formation of a Ru_5Pt adduct. The same product, $[Ru_{10}Pt_2C_2(CO)_{28}]^{2-}$, was obtained when $[PPN]_2[Ru_5C(CO)_{14}]$ was reacted with $[PtCl_2(PhCN)_2]$ in dichloromethane in the presence of silica. Its identity was proven by infrared spectroscopy and mass spectrometry. This result further supports our view on the mechanism of formation of **2**.

If the reaction leading to the formation of **2** does follow the proposed mechanism, then the formation of $[Ru_5PtC(CO)_{16}]$ (**1**) would be dependent upon the availability of CO that could substitute the acetonitrile in the intermediate (the simple adduct formed initially). Therefore, a reaction of $[Ru_5C(CO)_{14}]^{2-}$ with $[PtCl_2(MeCN)_2]$ was carried out under an atmosphere of carbon monoxide. Indeed, compound **1** was isolated in 11% yield, to compare with 1.7% obtained from the reaction carried out under N_2. The second product isolated was identified as $[PPN]_2[Ru_{10}Pt_3C_2(CO)_{32}]$. The detailed synthesis and structure of this compound will be reported elsewhere.[11]

Similarly, in an alternative set of experiments, we find that when the salt $[PPN]_2[Ru_6C(CO)_{16}]$ is treated with the same platinum compound, $[PtCl_2(MeCN)_2]$, in dichloromethane, in the presence of silica, a high nuclearity cluster is

also obtained. In this case the product was found to be $[\{Ru_6C(CO)_{16}\}_2Pt(MeCN)_2]$ (**3**) on the basis of a single crystal X-ray structure determination. In its infrared spectrum, bands attributable to both terminal (2076 and 2002 cm^{-1}) and bridging CO ligands (1869 and 1844 cm^{-1}) were observed. In the ^1H NMR spectrum, recorded in CD_2Cl_2, two peaks, at δ = 1.32 (3 H) and 0.89 (3 H) ppm, may be assigned to the two MeCN ligands. In the mass spectrum, a molecular peak was not observed, but instead a peak at m/z = 1096 corresponding to $[Ru_6C(CO)_{17}]$ was found. Crystals suitable for X-ray diffraction structure determination were grown by slow diffusion of hexane into a solution of **3** in dichloromethane. The structure obtained is shown in Figure 3 and relevant bond lengths and angles are listed in Table 2.

The asymmetric unit of the crystal structure contains two independent but structurally similar molecules. The overall molecular structure of **3** consists of two $[Ru_6C(CO)_{16}]$ octahedra linked by a single Pt atom and one bridging acetonitrile ligand (Figure 4). This MeCN ligand forms an unusual triple bridge, linked through its nitrogen atom to the platinum and one ruthenium atom [Ru(10)], and through the carbon to a second ruthenium atom [Ru(1)]. A second acetonitrile ligand is terminally bound to the platinum atom through its nitrogen lone pair. The Ru(2)−Ru(3) distance in one of the Ru_6 octahedra is beyond the range usually considered as a Ru−Ru bond. A compound in which two Ru_3 cluster subunits are linked by a single platinum atom has been previously reported but is of lower nuclearity (Ru_3-Pt-Ru_3).[12] The geometry of the two $[Ru_6C(CO)_{16}]$ moieties in **3** is not unusual, except for the "missing" Ru-Ru edge. The two carbide atoms lie at the centre of the octahedra. The Ru−Ru bond lengths range from 2.806(2) to 3.114(2) Å in molecule 1 and from 2.803(2) to 3.085(2) Å in molecule 2. These span a wider range than those found in $[Ru_6C(CO)_{17}]$ [2.827(5)−3.034(5) Å], but average to the same value (ca. 2.90 Å).[5] Three carbonyl ligands bridge Ru-Ru edges in the first Ru_6 unit [containing the long Ru(2)−Ru(3) bond], while only two occupy a bridging position in the second Ru_6 unit. All the other carbonyl ligands are terminal and almost linear. The Ru-Ru edges spanned by bridging CO ligands are amongst the shortest. The longest Ru-Ru edges are associated with the Ru atoms bonded to the bridging acetonitrile ligand [Ru(1) and Ru(10)], which is presumably due to the increased electron density on these atoms. The Ru-Pt distances vary from 2.7412(14) to 2.8734(12) Å in molecule 1 and from 2.7562(12) to 2.8897(13) Å in molecule 2. As such there are two short and one longer Ru−Pt bonds. These distances are very similar to the mean value (2.789 Å) that can be calculated over all the compounds containing a Ru−Pt bond that have been characterised crystallographically. The MeC-N bond length in the acetonitrile ligand bound in a terminal fashion is 1.16(2) Å in molecule 1 and 1.17(2) Å in molecule 2. These values are typical of a C≡N triple bond (theoretical value: 1.16 Å) and fall within the range [1.03(7)−1.22(8) Å] reported for a number of "end-on" nitrile complexes characterised by X-ray crystallography.[13] The second acetonitrile ligand is not linear: the Pt−N−C angle is 133.9(10)° in molecule 1 and 131.6(10)° in molecule 2, while the N−C−CH_3 angle is 120.1(13)° in molecule 1 and 120.5(12)° in molecule 2. The MeC-N distance of 1.28(2) Å in both molecules is

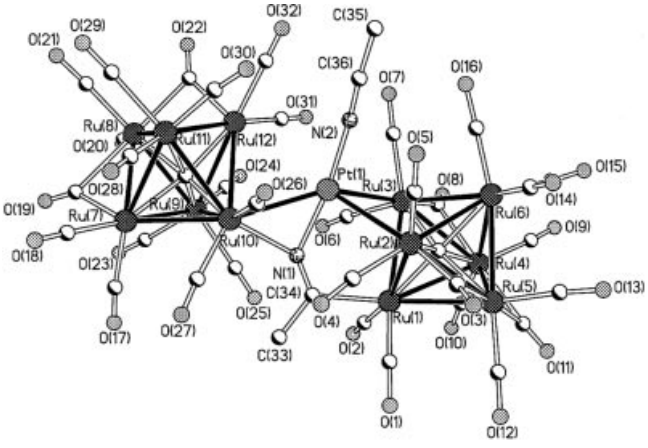

Figure 3. Molecular structure of $[\{Ru_6C(CO)_{16}\}_2Pt(MeCN)_2]$ (**3**) (labels on C atoms of carbonyl ligands correspond to those on O atoms and are omitted for clarity)

Table 2. Selected bond lengths (Å) and angles (°) for $[\{Ru_6C(CO)_{16}\}_2Pt(MeCN)_2]$ (**3**)

	Molecule 1	Molecule 2		Molecule 1	Molecule 2
Ru(3)−Pt(1)	2.7769(13)	2.7882(12)	Ru(2)−Pt(1)−N(2)	94.1(3)	97.3(3)
Ru(2)−Pt(1)	2.8734(12)	2.8897(13)	Ru(3)−Pt(1)−N(2)	97.6(3)	93.4(3)
Ru(10)−Pt(1)	2.7412(14)	2.7562(12)	Ru(2)−Pt(1)−Ru(3)	71.36(3)	71.17(4)
Pt(1)−N(1)	1.963(12)	1.949(11)	Ru(2)−Pt(1)−N(1)	87.4(3)	87.2(3)
Pt(1)−N(2)	1.990(13)	1.990(13)	Ru(3)−Pt(1)−N(1)	95.1(3)	97.2(3)
N(2)−C(36)	1.16(2)	1.17(2)	Ru(10)−Pt(1)−N(1)	50.5(3)	49.0(3)
C(36)−C(35)	1.53(2)	1.43(2)	Ru(10)−Pt(1)−N(2)	119.1(3)	120.7(3)
N(1)−C(34)	1.28(2)	1.28(2)	Ru(10)−Pt(1)−Ru(2)	122.14(4)	117.74(4)
N(1)−Ru(10)	2.127(10)	2.086(11)	Ru(10)−Pt(1)−Ru(3)	137.53(4)	141.05(4)
C(34)−C(33)	1.49(2)	1.53(2)	N(1)−Pt(1)−N(2)	167.0(5)	169.3(4)
C(34)−Ru(1)	2.081(13)	2.116(14)	Pt(1)−N(2)−C(36)	175.4(13)	177.8(12)
C−O (mean)	1.154(4)	1.146(3)	N(2)−C(36)−C(35)	176.8(17)	176.8(16)
			Pt(1)−N(1)−C(34)	133.9(10)	131.6(10)
			N(1)−C(34)−C(33)	120.1(13)	120.5(12)

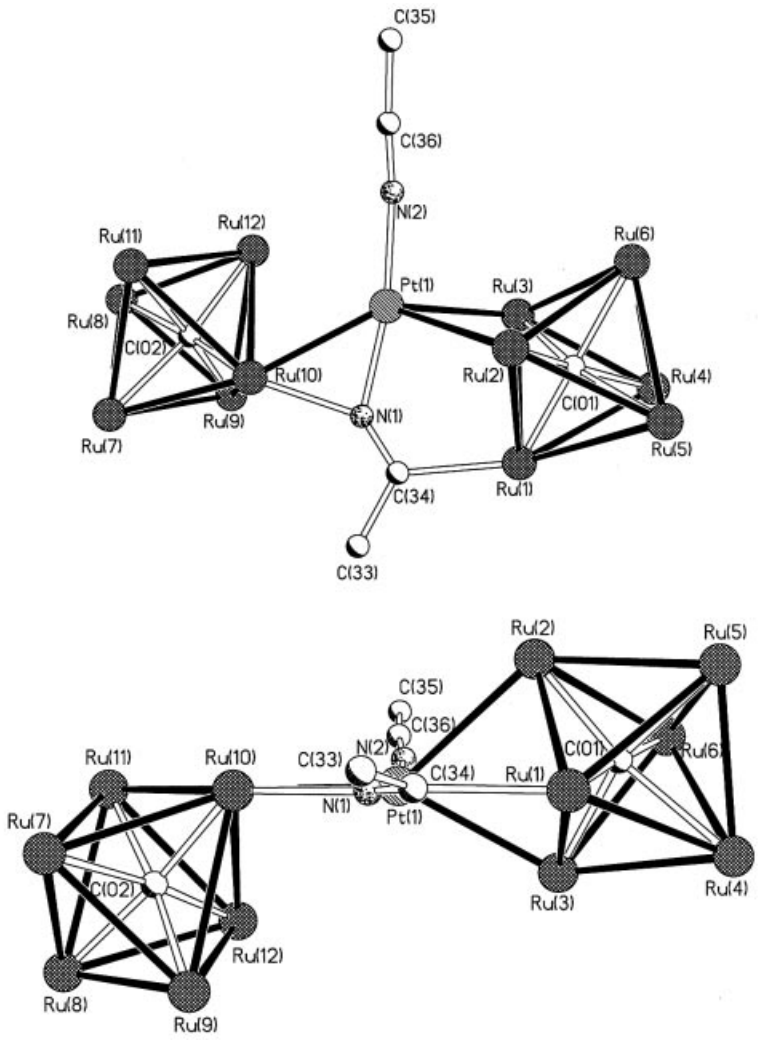

Figure 4. Side views of the structure of $[\{Ru_6C(CO)_{16}\}_2Pt(MeCN)_2]$ (**3**), emphasising the coordination of both MeCN ligands (top) and the planarity of the bridging acetonitrile ligand (bottom); carbonyl ligands are omitted for clarity

typical of a C=N double bond (theoretical value: 1.28 Å). These angles (close to the ideal 120° value) and bond length indicate that the C(34) and N(1) atoms are sp^2 rehybridised in the bridging MeCN. Indeed, the N-C atoms of the ligand are coplanar with the bridged platinum and two ruthenium atoms. The view shown in Figure 4 (bottom) emphasises the planarity of the bridging acetonitrile.

This type of triply bridging nitrile ligand has been reported only in one previous instance, in the compound $[Os_6Pt(CO)_{17}(NCMe)(COD)]$.[14] The C−N bond length in that case was intermediate between a triple and a double bond [1.22(3) Å], and the distribution of metal-metal bonds between the atoms bridged by the MeCN unit was different. The bridging nitrile was considered to be a four-electron donor. The shift of the second MeCN ligand in $[\{Ru_6C(CO)_{16}\}_2Pt(MeCN)_2]$ (**3**) from a terminal to a triply bridging bonding mode is thus accompanied by a change from a two-electron donor to a four-electron donor capacity. This additional pair of available electrons might explain the observed lengthening of one Ru−Ru distance in one of the octahedra. The Ru_6 unit displaying this elongated Ru−Ru distance is associated with the greatest number of interactions with the platinum fragment (two Ru−Pt bonds and one Ru−N bond, as opposed to one Ru−Pt and one Ru−N bond for the other Ru_6 unit). The coordination geometry at the platinum atom can be described either as a distorted trigonal bipyramid [N(1) and N(2) axials] or a distorted square pyramid [Ru(2) axial]. A five-coordinate Pt atom is indicative of the metal centre being in the +2 oxidation state,[15] and non-planar Pt^{II} usually respects the 18-electron rule. Indeed, in **3**, eight electrons are provided by the platinum, and each of the three Pt−Ru bonds accounts for two electrons, as do each of the two Pt−N bonds, reaching a total of 18 around the Pt atom. The oxidation state of the platinum is thus unchanged during the course of the reaction. If the reaction is considered as the addition of two $[Ru_6C(CO)_{16}]^{2-}$ "ligands" to the $[Pt(MeCN)_2]^{2+}$ fragment, the resulting adduct should be doubly negatively charged. An oxidation of one $[Ru_6C(CO)_{16}]^{2-}$ unit to $[Ru_6C(CO)_{16}]$ must have occurred, probably at the expense of some $[PtCl_2(MeCN)_2]$ undergoing reduction to platinum(0). This would explain the low

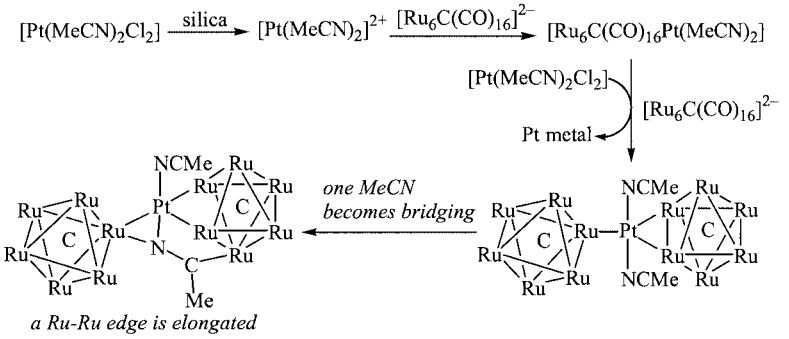

Scheme 1. Suggested mechanism for the reaction leading to $[\{Ru_6C(CO)_{16}\}_2Pt(MeCN)_2]$ (**3**); carbonyl ligands are omitted for clarity

yield of the reaction. Scheme 1 summarises our view on the mechanism of the reaction leading to the formation of $[\{Ru_6C(CO)_{16}\}_2Pt(MeCN)_2]$ (**3**).

Conclusions

In this paper we have reported the synthesis of two high nuclearity Ru-Pt clusters, obtained by reacting $[Ru_5C(CO)_{14}]^{2-}$ or $[Ru_6C(CO)_{16}]^{2-}$ with $[PtCl_2(MeCN)_2]$ in the presence of silica. The idea that $[Ru_5C(CO)_{14}]^{2-}$ and $[Ru_6C(CO)_{16}]^{2-}$ may serve as simple bidentate ligands (for the platinum) in a conventional sense is attractive and has certainly been of benefit previously in our interpretation of the chemistry of certain Ru-Sn systems.[16] Here this view is complicated by further reaction, leading to rearrangement of the cluster core in **2** and the formation of a triply bridging MeCN ligand in **3**. Additionally, in these reactions, the role of the silica is crucial and its net action is to remove Cl^-. High yields of other Ru-Pt clusters of predictable nuclearity were obtained following this method,[4] while the use of more conventional chloride scavengers (such as $AgBF_4$) did not prove as efficient. No reaction is observed in the absence of silica, leading to the conclusion that an initial reaction of $[PtCl_2(MeCN)_2]$ with surface Si−OH occurs, resulting in surface-bonded and stabilised $[Pt(MeCN)_2]^{2+}$ units, that can then react with the ruthenium clusters in a controlled way. This aspect is under further exploration.

Experimental Section

All the reactions were carried out using standard Schlenk techniques, under water- and oxygen-free nitrogen. All solvents were dried and distilled immediately before use. Reactants and chemicals were purchased from Aldrich Chemicals and used without further purification. The silica used in reaction media was Silica gel 60 (0.040−0.063 mm) for column chromatography purchased from Merck. The clusters $[PPN]_2[Ru_5C(CO)_{14}]$[17] and $[PPN]_2[Ru_6C(CO)_{16}]$[8] were synthesised following literature procedures.

All chromatographic separations were performed on the open bench without any precaution to exclude air. Thin-layer chromatography (TLC) was carried out using glass plates (20 × 20 cm) coated with a layer of silica gel 60 F_{254}, supplied by Merck. The eluents used were standard grade laboratory solvents.

Infrared spectra were collected in dichloromethane solution using a NaCl liquid cell (0.5 mm path length) supplied by Specac Ltd., on a Perkin−Elmer Paragon 1000 FT-IR spectrometer. The mass spectra were obtained on a Kratos Concept spectrometer (*) using electron impact ionisation (EI) in positive mode or on a Micromass Quattro-LC spectrometer using the electrospray ionisation technique (ESI) in negative mode (‡). The ^1H NMR spectrum was recorded on a Bruker DPX-400 instrument. The elemental analyses were performed by the microanalysis service of the department.

Preparation of $[Ru_5PtC(CO)_{16}]$ (1) and $[PPN]_2[Ru_{10}Pt_2C_2(CO)_{28}]$ (2): $[PPN]_2[Ru_5C(CO)_{14}]$ (100 mg, 0.050 mmol) was dissolved in dichloromethane (20 mL). A slight excess of $[PtCl_2(MeCN)_2]$ (20 mg, 0.057 mmol) and two spoons of silica (ca. 1 g) were added, inducing an immediate darkening of the solution. After five hours stirring at room temperature, the mixture was filtered, and the solvent evaporated. The residue was separated into its component compounds by thin layer chromatography, using hexane/acetone/dichloromethane (50:5:45, v/v) as eluent. The top orange band was identified as $[Ru_5PtC(CO)_{16}]$ (**1**), obtained in very low yield (1 mg, 1.7%), and $[PPN]_2[Ru_{10}C_2Pt_2(CO)_{28}]$ (**2**) (17 mg, 21%) was isolated from the bottom. Compound **2** can also be isolated as its $[Ph_4P]^+$ salt.

$[Ru_5PtC(CO)_{16}]$ (1): IR (CH_2Cl_2): ν_{CO} 2065.0(s), 2049.7(vs), 2003.0(w, sh), 1873.1(vw, br) cm^{-1}. EI-MS (*): m/z = 1163 (calcd. for $Ru_5PtC(CO)_{16}$: 1162, M^+), followed by loss of 16 CO ligands.

$[Ph_4P]_2[Ru_{10}Pt_2C(CO)_{28}]$ (2): IR (CH_2Cl_2): ν_{CO} 2026vs (br), 2002m (sh), 1964w (sh), 1823m (br), 1789m (br) cm^{-1}. ESI-MS (‡): m/z = 1104.7 (calcd. for $[Ru_{10}Pt_2C_2(CO)_{28}]^{2-}$: 1104.6, $M^{2-}/2$), 2209.4 (calcd. for $[Ru_{10}Pt_2C_2(CO)_{28}]^-$: 2209.2, M^-). $C_{78}H_{40}O_{28}P_2Pt_2Ru_{10}$ (2888.0): calcd. C 32.44, H 1.40; found C 32.26, H 1.56.

Reaction of $[PPN]_2[Ru_5C(CO)_{14}]$ with $[Pt(PhCN)_2Cl_2]$: $[PPN]_2[Ru_5C(CO)_{14}]$ (100 mg, 0.050 mmol) was dissolved in dichloromethane (20 mL). An equivalent of $[PtCl_2(PhCN)_2]$ (24 mg, 0.050 mmol) and two spoons of silica (ca. 1 g) were added, inducing an immediate darkening of the solution. After five hours stirring at room temperature, the mixture was filtered, and the solvent evaporated. The residue was separated into its component compounds by thin layer chromatography, using hexane/acetone/dichloromethane (40:20:40, v/v) as eluent. The top orange band was identified as $[Ru_5PtC(CO)_{16}]$ (**1**), obtained in very low yield (less than 1 mg), and $[PPN]_2[Ru_{10}C_2Pt_2(CO)_{28}]$ (**2**) (21 mg, 26%) was isolated from the bottom.

Reaction of $[PPN]_2[Ru_5C(CO)_{14}]$ with $[PtCl_2(MeCN)_2]$ under CO: One equivalent of $[PtCl_2(MeCN)_2]$ (18 mg, 0.05 mmol) and silica

Table 3. Crystal data for $[Ph_4P]_2[Ru_{10}Pt_2C_2(CO)_{28}]$ (**2**) and $[\{Ru_6C(CO)_{16}\}_2Pt(MeCN)_2]$ (**3**)

	2	**3**
Chemical formula	$C_{78}H_{40}O_{28}P_2Pt_2Ru_{10}$	$C_{38.75}H_{7.50}Cl_{1.50}N_2O_{32}PtRu_{12}$
Mol. wt.	2887.92	2474.07
Wavelength (Å)	0.71073	0.71069
T (K)	180(2)	180(2)
Crystal size (mm)	0.32 × 0.12 × 0.02	0.18 × 0.07 × 0.01
Crystal system	monoclinic	monoclinic
Space group	$P2_1/n$	$P2_1/c$
a (Å)	21.8793(5)	10.392(2)
b (Å)	14.2035(3)	44.191(3)
c (Å)	28.6527(7)	24.911(2)
β (°)	111.3430(10)	98.9(3)
V (Å^3)	8293.5(3)	11299.4(3)
Z	4	8
D_{calc} (mg m^{-3})	2.313	2.909
μ (mm^{-1})	5.204	5.737
F(000)	5432	9132
2θ range (deg)	7.12 − 54.96	2.48−50.02
No of reflections collected	41483	30770
No. of indep reflections	18548	18539
R_{int}	0.0798	0.0716
Refinement method	full-matrix least-square on F^2	full-matrix least-square on F^2
Refined parameters	1005	845
Goodness of fit on F^2	1.027	0.997
Final R indices [$I > 2\sigma(I)$]		
$R1$,[a] $wR2$[b]	0.0607, 0.1249	0.0553, 0.1029
(all data)	0.1253, 0.1472	0.1255, 0.2073
Largest diff peak/hole (e·Å^{-3})	2.813/−1.338	2.214/−1.915

[a] $R1 = \Sigma F_0 - F_c/\Sigma F_0$. [b] $wR2 = [\Sigma w(F_0^2 - F_c^2)^2/\Sigma w(F_0^2)^2]^{1/2}$.

(approx. 1 g) were added to a solution of $[PPN]_2[Ru_5C(CO)_{14}]$ (100 mg, 0.05 mmol) in CH_2Cl_2 (20 mL). The mixture was stirred for 3 hours under carbon monoxide and then left to stir overnight under nitrogen. Subsequently, the silica was filtered off and the solvent evaporated to dryness in vacuo. The crude product was dissolved in a minimum amount of CH_2Cl_2 and purified by TLC using a mixture of CH_2Cl_2/acetone/hexane (45:5:50, v/v) as eluent. The top red band was identified as $[PtRu_5C(CO)_{16}]$ (**1**) (11 mg, 0.009 mmol, 19% yield) and the bottom violet band was identified as $[PPN]_2[Pt_3Ru_{10}C_2(CO)_{32}]$ (4 mg, 0.001 mmol, 2.5% yield).

$[Ru_5PtC(CO)_{16}]$ (1): IR (CH_2Cl_2): ν_{CO} 2064.5(s), 2049.9(vs), 2004(w, sh), 1869(vw, br) cm^{-1}. EI-MS (*): m/z = 1162 (calcd. for $Ru_5PtC(CO)_{16}$: 1162, M^+), followed by loss of 16 CO ligands.

Preparation of $[\{Ru_6C(CO)_{16}\}_2Pt(MeCN)_2]$ (3): The reaction was performed in a similar fashion, starting from $[PPN]_2[Ru_6C(CO)_{16}]$ (100 mg, 0.0466 mmol) and $[PtCl_2(MeCN)_2]$ (16 mg, 0.0466 mmol) and purification by thin-layer chromatography, using hexane/dichloromethane (3:2, v/v) as eluent. The eluting brown fraction is $[\{Ru_6C(CO)_{16}\}_2Pt(MeCN)_2]$ (**3**), obtained in very low yield (3.4 mg, 3.03%).

$[\{Ru_6C(CO)_{16}\}_2Pt(MeCN)_2]$ (3): IR (CH_2Cl_2): ν_{CO} 2076(m), 2063(s), 2048(vs), 2018 (w, sh), 2002(w, sh), 1869(w, br), 1844(w, br) cm^{-1}. ^{1}H NMR (400 MHz, CD_2Cl_2, 25 °C): δ = 0.89 (s, 3 H, MeCN), 1.32 (s, 3 H, MeCN) ppm. EI-MS (*): m/z = 1096 (calcd. for $Ru_6C(CO)_{17}$: 1095), with CO losses. $C_{38}H_6N_2O_{32}Pt_1Ru_{12}$ (2410.4): calcd. C 18.94, H 0.25, N 1.16; found C 21.40, H 3.17, N 0.33. Crystals suitable for X-ray diffraction structure determination were grown by slow diffusion of hexane into a solution of **3** in dichloromethane.

Crystallography: Single crystal X-ray diffraction analyses were performed on a Nonius Kappa CCD system with a sealed-tube Mo-K_α source equipped with an Oxford Cryostream apparatus for low-temperature data collection. The structures were solved by direct methods using teXsan,[18] and refined by full-matrix least-squares on F^2 with the SHELXL-97[19] (**2**) and SHELXL-93[20] (**3**) software packages. In the case of **2**, all non-hydrogen atoms, apart from the solvent molecules and disordered groups (one of the Ph_4P cations is disordered over two positions), were refined with anisotropic atomic displacement parameters. In the case of **3**, only the Ru and Pt metal atoms were refined with anisotropic atomic displacement parameters. All hydrogen atoms were placed in idealised positions, assigned isotropic displacement parameters and allowed to ride on the parent carbons. The crystal data for **2** and **3** are summarised in Table 3.

CCDC-191419 (**2**) and 191420 (**3**) contain the supplementary crystallographic data for this paper. These data can be obtained free of charge at www.ccdc.cam.ac.uk/conts/retrieving.html [or from the Cambridge Crystallographic Data Centre, 12 Union Road, Cambridge CB2 1EZ, UK; fax: (internat.) +44-1223/336-033; E-mail: deposit@ccdc.cam.ac.uk].

Acknowledgments

We are very grateful to John E. Davies and Andrew D. Bond for data collection for compounds **2** and **3** and structure refinement for compound **3**, and to the European Commission and Newnham College, Cambridge, for funding to SH, to the Cambridge Overseas Trust (Schlumberger Research) and ICI for funding to TK, and to the EPSRC for a grant to BFGJ.

[1] R. Raja, G. Sankar, S. Hermans, D. S. Shephard, S. Bromley, J. M. Thomas, B. F. G. Johnson, T. Maschmeyer, *Chem. Commun.* **1999**, 1571−1572.
[2] R. Raja, T. Khimyak, J. M. Thomas, S. Hermans, B. F. G. Johnson, *Angew. Chem. Int. Ed.* **2001**, *40*, 4638−4642.
[3] T. Nakajima, A. Ishiguro, Y. Wakatsuki, *Angew. Chem. Int. Ed.* **2000**, *39*, 1131−1134.
[4] S. Hermans, T. Khimyak, B. F. G. Johnson, *J. Chem. Soc., Dalton Trans.* **2001**, 3295−3302.
[5] R. D. Adams, W. Wu, *J. Cluster Sci.* **1991**, *2*, 271−290.
[6] R. D. Adams, W. Wu, *J. Cluster Sci.* **1993**, *4*, 245−258.
[7] D. Braga, F. Grepioni, P. J. Dyson, B. F. G. Johnson, P. Frediani, M. Bianchi, F. Piacenti, *J. Chem. Soc., Dalton Trans.* **1992**, 2565−2571.
[8] B. F. G. Johnson, J. Lewis, S. W. Sankey, K. Wong, M. McPartlin, W. J. H. Nelson, *J. Organomet. Chem.* **1980**, *191*, C3−C7.
[9] B. F. G. Johnson, J. Lewis, J. N. Nicholls, J. Puga, P. R. Raithby, M. J. Rosales, M. McPartlin, W. Clegg, *J. Chem. Soc., Dalton Trans.* **1983**, 277−290.
[10] R. D. Adams, W. G. Wu, *Organometallics* **1993**, *12*, 1238−1242.
[11] B. F. G. Johnson, T. Khimyak, *manuscript in preparation*.
[12] L. J. Farrugia, *Organometallics* **1990**, *9*, 105−110.
[13] B. N. Storhoff, H. C. Lewis, *Coord. Chem. Rev.* **1977**, *23*, 1−29.
[14] C. Couture, D. H. Farrar, *J. Chem. Soc., Dalton Trans.* **1987**, 2245−2252.
[15] F. A. Cotton, G. Wilkinson, *Advanced Inorganic Chemistry*, Wiley, New York, 5th ed., **1988**, ch. 19, p. 918.
[16] S. Hermans, B. F. G. Johnson, *Chem. Commun.* **2000**, 1955−1956.
[17] B. F. G. Johnson, J. Lewis, W. J. H. Nelson, J. N. Nicholls, J. Puga, P. R. Raithby, M. J. Rosales, M. Schröder, M. D. Vargas, *J. Chem. Soc., Dalton Trans.* **1983**, 2447−2457.
[18] teXsan, Version 1.7. Molecular Structure Corporation, **1995**.
[19] G. Sheldrick, *SHELX-97*, University of Göttingen, **1997**.
[20] G. Sheldrick, *SHELXL-93*, University of Göttingen, **1993**.

Received August 19, 2002
[I02467]

Lanthanide Chelates Based on Diethylenetriamine Fitted with *O*-Benzoic Acid Pendant Arms

Daniel Imbert,[a] Nicolas Fatin-Rouge,[a] and Jean-Claude G. Bünzli*[a]

Keywords: Carboxylate ligands / Lanthanides / Luminescence / Podand / Stability constant

A new polycarboxylate ligand H_5L has been synthesized by the attachment of five benzoate subunits onto a diethylenetriamine framework. Seven pK_a values have been determined by potentiometry, spectrophotometry and NMR spectroscopy as 1.9(2), 2.8(2), 3.87(5), 4.58(6), 4.87(6), 9.19(6) and 11.68(5), the first four corresponding to the carboxylic functions and the last three to amine sites. The interaction between H_5L and Ln^{III} ions in dilute aqueous solution has been examined by UV/Vis absorption and emission spectrometries, and has been found to result in monometallic complexes that are moderately stable in the pH range 3.7–7.5. Conditional stability constants at pH 5.3 are logK_{11} = 5.3(2), 6.6(1), 6.5(1) and 7.2(3) for La, Eu, Tb and Lu, respectively. In the case of Tb^{III}, the stability constants for $[Tb(HL)]^-$ and $[Tb(H_2L)]$ are logβ_{111} = 22.0(2) and logβ_{121} = 29.8(1), giving a pTb of 10.0. In the pH range 4–7, more than 90% of the Tb^{III} ions are in the form of the neutral species $[Tb(H_2L)]$. Lifetime determinations of the Eu($^5D_0$) and Tb($^5D_4$) excited levels in both H_2O and D_2O at pH 5.3 indicate 4.8 ± 0.5 (Eu) and 4.5 ± 0.5 (Tb) water molecules being bound in the inner coordination sphere of the Ln^{III}. The triplet state of the ligand in water lies at around 26000 cm^{-1}, resulting in a sizeable sensitisation of the Tb-centred luminescence (absolute quantum yield: φ_{abs} = 10.3%), while the luminescence of Eu^{III} is only poorly sensitised (φ_{abs} = 1.5%).

(© Wiley-VCH Verlag GmbH & Co. KGaA, 69451 Weinheim, Germany, 2003)

Introduction

Stable chelates of trivalent lanthanide ions are of interest as contrast enhancement agents in magnetic resonance imaging,[1] as catalysts for the cleavage of phosphodiester bonds in DNA and RNA,[2] as precursors for various functional materials,[3] including doped polymers for optical amplifiers,[4] or as luminescent probes for biomedical analysis,[5–7] for responsive analytical sensors[8] or for imaging of cancerous cells.[9] The main difficulty associated with the design of luminescent probes and sensors lies in overcoming the very low molar absorption coefficients of the Ln^{III} ions, due to the forbidden nature of the f-f transitions. To sensitise the metal ion efficiently, there are specific requirements for ligand molecules i.e. that they should be strong complexation agents, have large absorption coefficients and offer a series of photophysical properties allowing efficient energy transfer from the ligand onto the metal ion and minimization of quenching processes.[5]

Several synthetic strategies intended to meet all these requirements have been examined,[3] including the use of preorganised (macrocyclic)[10] or predisposed receptors,[11,12] leading to induced cavities; these receptors can also be obtained by self-assembly processes[13] or by the use of flexible podands.[14] These latter are readily available, cheap and are easy to derivatize. In this paper we attempt to combine the stability of Ln^{III} complexes with ligands derived from polyaminocarboxylates, such as dtpa,[15] with the large

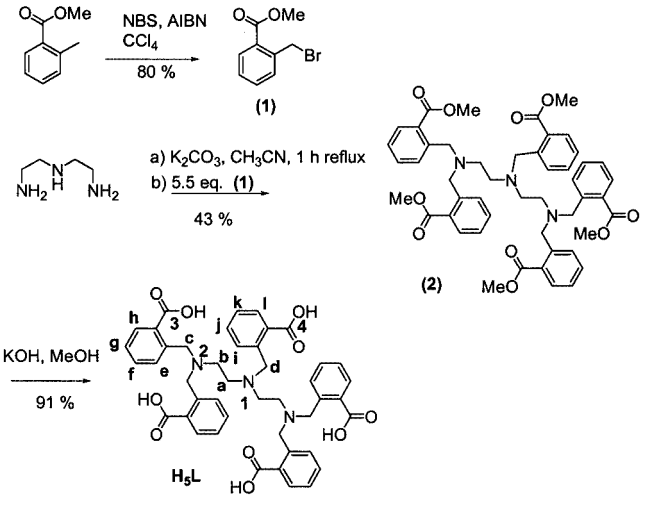

Scheme 1

[a] Swiss Federal Institute of Technology Lausanne, Institute of Molecular and Biological Chemistry
1015 Lausanne, Switzerland
Fax: (internat.) +41-21/693-9825
E-mail: jean-claude.bunzli@epfl.ch

Supporting information for this article is available on the WWW under http://www.eurjic.org or from the author.

sensitisation of Tb^{III} ion luminescence (and also other Ln^{III} ions) achieved by incorporation of the benzoate chromophore,[5,16] absolute quantum yields of 100 and 20% having been reported for Tb^{III} and Eu^{III}, respectively, in the solid state.[17] We have therefore synthesized the polydentate ligand H_5L [1,4,7-heptanetriamine-*N,N,N′,N′,N″*-pentakis-(2-methylbenzoic acid), Scheme 1] and investigated its complexation and sensitisation properties towards trivalent lanthanide ions.

Results and Discussion

Acidity Constants of the Ligand

The ligand H_5L was prepared in three steps (Scheme 1) in an overall yield of 31%. Its acidity constants were determined separately by potentiometry (Figure 1) and spectrophotometry (Figure 2) and further confirmed by ^1H NMR spectroscopy. The extracted pK_a values, defined by the following equations and obtained by titration in the 2−12 pH range, are summarized in Table 1.

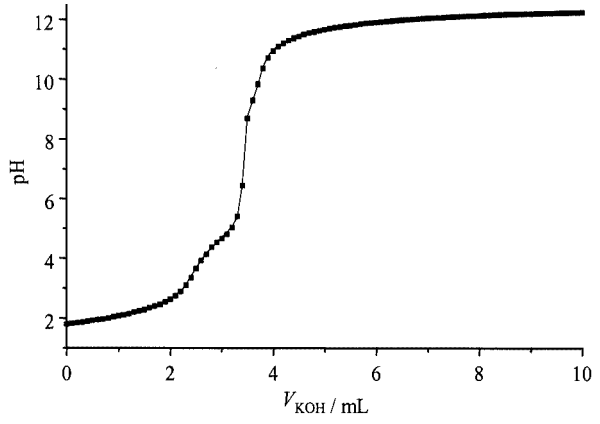

Figure 1. Potentiometric titration of H_7L^{2+} with OH^- in H_2O/CH_3OH (98:2 v/v); T = 20.0 ± 0.2 °C; μ = 0.1 M (KCl)

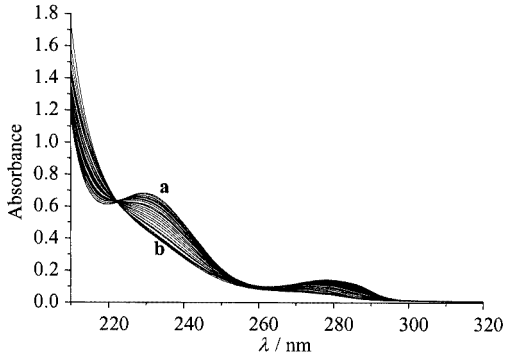

Figure 2. UV/Visible absorption spectra of H_7L^{2+} as a function of pH in H_2O/CH_3OH (98:2 v/v); T = 20.0 ± 0.2 °C; μ = 1 M (KCl): curve a (pH = 1.37), curve b (pH = 12.04)

Table 1. Acidity constants of H_7L^{2+} (± σ) and dtpa (see text for the definition of K_{ai})

	L[a]	L[b]	L[c]	dtpa[d]
pK_{a1}	–	1.9(2)	1.7(4)	1.45
pK_{a2}	–	2.8(2)	2.9(3)	1.75
$pK_{a1} + pK_{a2}$	4.20(8)	4.7(4)	4.6(7)	3.20
pK_{a3}	3.87(5)	–	–	2.06
pK_{a4}	4.58(6)	4.5(2)	4.7(1)	2.73
pK_{a5}	4.87(6)	–	–	4.28
pK_{a6}	9.19(6)	9.4(3)	9.0(4)	8.65
pK_{a7}	11.68(5)	11.6(3)	11.6(4)	10.59

[a] Potentiometric data. $[L]_0 = 1.0\cdot10^{-3}$ M; I = 0.1 M (KCl); T = 20.0 °C. [b] Spectrophotometric data. $[L]_0 = 2.0\cdot10^{-5}$ M; I = 1 M (KCl); T = 20.0 °C. [c] ^1H NMR spectroscopic data. $[L]_0 = 1.0\cdot10^{-3}$ M; T = 20 °C. [d] ^1H NMR spectroscopic data. I = 0.1 M (KNO_3); T = 25.0 °C.[34]

$$(H_{8-i}L)^{(3-i)+} \rightleftarrows (H_{7-i}L)^{(2-i)+} + H^+ \qquad (1)$$
$$pK_{ai}\ (i = 0-4, \text{carboxylic functions})$$

$$(H_{8-i}L)^{(3-i)+} \rightleftarrows (H_{7-i}L)^{(2-i)+} + H^+ \qquad (2)$$
$$pK_{ai}\ (i = 5-7, \text{amine functions})$$

The agreement between the values from various experimental techniques is quite good, and the dissociation constants display behaviour similar to that reported for dtpa: five pK_a values are in the 2 to 5 range while the last two are between 9 and 12. A fit of the data with eight pK_a values did not converge, indicating that pK_{a0}, corresponding to the deprotonation of a carboxylic group (see below, NMR spectra), probably lies below pH 2. However, the protolytic groups of H_5L are less acidic than those of dtpa. The first is only slightly less acidic ($\Delta\log K_a$ = 0.35), but the difference increases up to $\Delta\log K_a$ = 1.9 for pK_{a4}. The electron-donor ability of the benzene moieties and the larger number of bonds separating the nitrogen atoms from the carboxylate groups explain this trend.

^1H NMR spectra were measured from pH 12.2 to 1.1 in D_2O/CD_3OD (95:5) solutions (Figure 3), and the resonances were attributed on the basis of their chemical shifts, signal intensities and ^1H-^1H COSY experiments. In the aromatic region, because of superimposed signals, only the protons labelled (i) and (h) could be unambiguously assigned. The eight protons labelled (c) and the two protons labelled (d) appear to be equivalent, pointing to an averaged structure of the molecule on the NMR timescale. The (a) and (b) protons are nonequivalent and appear as two broad peaks because of spin coupling and conformational motions.

The variation of the chemical shifts with pH is shown at the bottom of Figure 3. At pH 12.2, corresponding to a solution containing mainly the totally deprotonated ligand L^{5-}, the resonances for the (c) and (d) protons have very similar chemical shifts, and this is also true for protons (a) and (b). A decrease in the pH to 10.4 by the addition of one equivalent of acid causes only slight variations in the

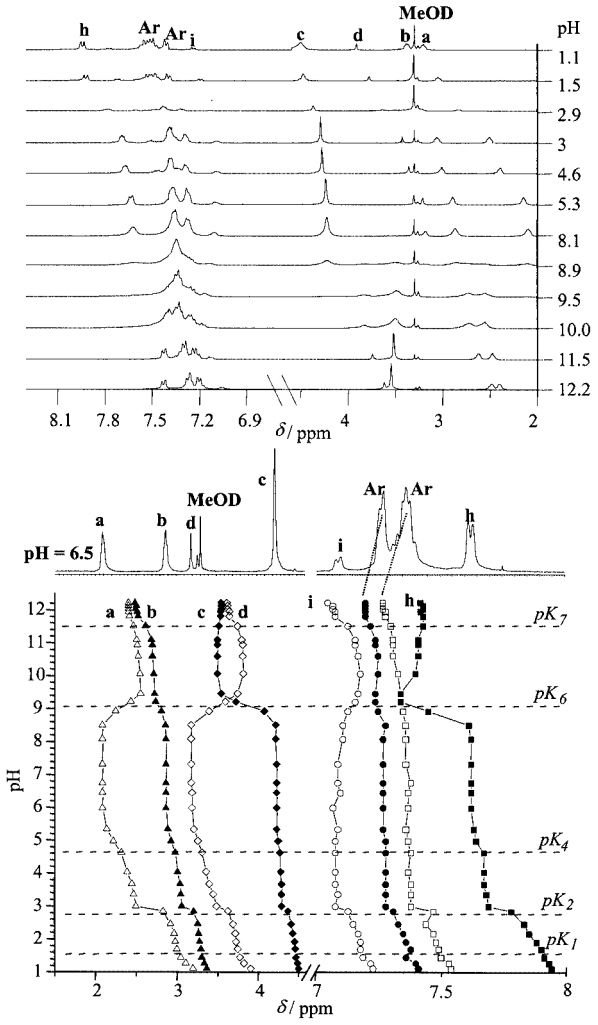

Figure 3. (Top) ^{1}H NMR spectra of $H_nL^{(5-n)-}$ vs. pH in D_2O/CD_3OD (95:5 v/v) at T = 20 °C, and (bottom) variation of the ^{1}H NMR chemical shifts vs. pH

shifts of the methylene protons, which become more shielded, except for protons (d), which become deshielded. Similarly, the aromatic protons undergo small positive shifts, except for protons (h), which become deshielded. Further addition of acid again results in relatively small changes until around pH 9, except that the shift tendency inverts for protons (d) and (i), which become more shielded. In the pH range 9 to 3, dramatic changes occur for the methylene protons and for protons (h); in particular, the resonances of protons (a) and (b) on one hand and (c) and (d) on the other become clearly separated. After a discontinuity at pH 3, all the protons, particularly protons (h), become more shielded upon further addition of acid.

The observed shift of the methylene protons is in fact an average value reflecting the mean time that each proton spends in a given chemical environment.[18] Quantitative analysis of the pH dependence of these chemical shifts can therefore be performed by assuming that the contributions to the shift of a given proton i (δ_i) are additive and linearly related to the fraction of time spent in each environment. As a result, the preferred protonation sites and the extent of protonation can be estimated from a simple model taking into account only the two closest protonation sites, where f is the fractional population of a given protonation site, C is the chemical shift increment caused by the presence of the proton in this site, and the indices α and β refer to the position of the protonated nitrogen atom relative to the resonant proton.

$$\delta_a = \delta_a^0 + f_1 \times C_{N\alpha} + f_2 \times C_{N\beta} \quad (3)$$

$$\delta_b = \delta_b^0 + f_2 \times C_{N\alpha} + f_1 \times C_{N\beta} \quad (4)$$

$$\delta_c = \delta_c^0 + f_2 \times C_{N\alpha} + f_3 \times C_{O3} \quad (5)$$

$$\delta_d = \delta_d^0 + f_1 \times C_{N\alpha} + f_4 \times C_{O4} \quad (6)$$

We have set C_{O3}, C_{O4}, C_O to be equal. The δ_i^0 values were taken as equal to the chemical shifts measured at pH 12.2. Finally, the f_i values were normalised by the following relationship, where n is the number of equivalents of acid added to the fully deprotonated ligand L^{5-}.

$$f_1 + 2f_2 + 4f_3 + f_4 = n \quad (7)$$

Values of f_1, f_2 and $C_{N\alpha}$, $C_{N\beta}$ were obtained only for n = 1 and 2, because the data become too imprecise beyond this amount of acid. For n = 0−2, f_3 and f_4 were set as equal to zero, which is a reasonable assumption. The best results for n = 1 were obtained at pH 1/2(pK_{a6} + pK_{a7}), and Equations (3), (4), (6) and (7) give f_1 = 0.22, f_2 = 0.39, $C_{N\alpha}$ = 0.59 ppm and $C_{N\beta}$ = 0.05 ppm. Generally speaking, the C values have large error margins because of the fairly small chemical shift changes. The calculated $C_{N\alpha}$ value is in good agreement with literature data for dtpa (0.75), but the value found for $C_{N\beta}$ is much lower than the reported value of about 0.35 ppm.[18] At pH 1/2(pK_{a4} + pK_{a3}), different values of n were again tested and n = 2 gave the best result, with Equations (3)−(5) and Equation (7) yielding f_1 = 0.38, f_2 = 0.81, $C_{N\alpha}$ = 0.82 ppm, and $C_{N\beta}$ = 0.77 ppm. These calculations offer evidence of the drastic change in the charge repartition on the three nitrogen atoms on going from n = 1 to n = 2, consistent with the data for dtpa.[18] At n = 2, for instance, the protons are mainly bound to the end nitrogen atoms N2, as a result of electrostatic repulsion. Further attempts to determine quantitatively the extent of protonation of the benzoate groups with pH failed. Nevertheless, the similar values of the three largest pK_a values for dtpa and for H_5L point to the protonation of L^{5-} occurring first on the three nitrogen atoms. However, distribution diagrams show that protonation of the benzoate sites starts while full protonation of the central nitrogen atom is not yet complete.

Interaction with Trivalent Lanthanide Ions

The interaction between Ln^{III} ions (Ln = La, Eu, Tb, Lu) and H_5L was first monitored in dilute aqueous solu-

tions by UV/Vis spectrophotometry at pH 5.3. The variation of the absorbance versus $R = [Ln^{III}]_{tot}/[H_5L]_{tot}$ (Figure 3) points to the presence of a single 1:1 complex species in the stoichiometry range investigated ($0 < R < 5$). This is in agreement with the ESI-MS spectra. The conditional stability constants extracted from these data amount to $\log K_{11} = 5.3(2)$, 6.6(1), 6.5(1) and 7.2(3), respectively (Figure S1, Supporting Information, see also the footnote on the first page of this article). The linear relationship between the magnitude of the binding constants and the charge density of the cation is a clear indication that there is no steric effect in the coordination of the metal ions. To determine the influence of the pH on the speciation, we titrated the ligand in the presence of one equivalent of Tb^{III} and monitored the experiment both by spectrophotometry (Figure 4) and by luminescence spectroscopy (Figure 5). Potentiometry could not be used because of precipitation of the metal complexes at concentrations greater than 10^{-3} M. The best model used to fit the titration data was fairly complex, with ten different $[Ln_i(OH)_jH_kL_l]^{(3i-j+k-5l)+}$ species: one hydroxide moiety ($i = 1$; $j = 3$; $k = l = 0$), six protonated forms of the ligand ($i = j = 0$) determined independently from the potentiometric titration described above, and two protonated 1:1 complexes ($i = 1$, $j = 0$, $k = 1$ and 2, $l = 1$). The absorption maxima of the different species are given in Table 2. The two proton-dependent stability constants refined amount to $\log\beta_{111} = 22.0(2)$ [Equation (8)] and $\log\beta_{121} = 29.8(1)$ [Equation (9)].

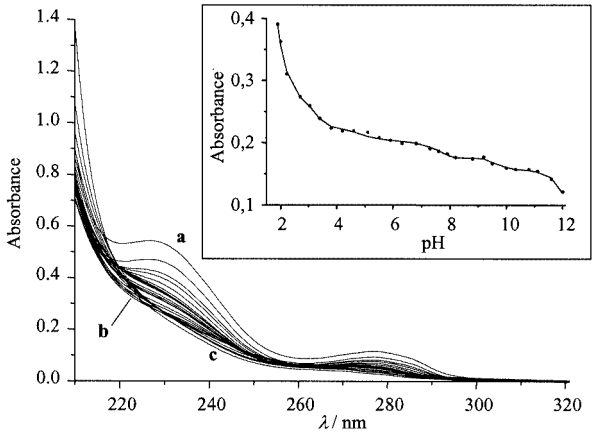

Figure 4. UV/Visible absorption spectra of H_7L^{2+} $2\cdot10^{-5}$ M in H_2O/CH_3OH (98:2 v/v), $\mu = 0.1$ M (KCl) in the presence of one equivalent of Tb^{III}, at $T = 20.0 \pm 0.2$ °C at various pH; curve a, b, and c: pH = 1.92, 9.22, and 12.0; the inset shows the absorbance variation at 240 nm

$$Tb^{3+} + H^+ + L^{5-} \overset{\beta_{111}}{\rightleftharpoons} [TbHL]^- \quad (8) \qquad (8)$$

$$Tb^{3+} + 2H^+ + L^{5-} \overset{\beta_{121}}{\rightleftharpoons} [TbH_2L] \quad (9) \qquad (9)$$

The calculated distribution curves from these stability constants are presented in Figure 6. In the pH range 3.5−7.5, the neutral species $[Tb(H_2L)]$ is clearly dominant,

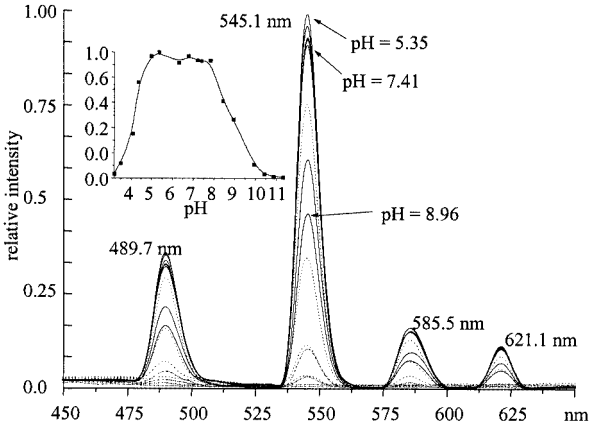

Figure 5. Emission spectra of H_7L^{2+} $2\cdot10^{-5}$ M in H_2O/CH_3OH (98:2 v/v), $\mu = 0.1$ M (KCl) in the presence of one equivalent of Tb^{III}, at $T = 20.0 \pm 0.2$ °C as a function of pH; inset: phosphorescence intensity at 545 nm vs. pH

Table 2. Absorption maxima of the ligand species at $T = 20$ °C

Species	λ_{max} (nm)[a]	ε_{max} ($M^{-1}\cdot cm^{-1}$)[b]	Species	λ_{max} (nm)[a]	ε_{max} ($M^{-1}\cdot cm^{-1}$)[b]
$[L]^{5-}$	268 sh	3300	$[H_5L]$	230	33800
				278	7200
$[HL]^{4-}$	268 sh	3600	$[H_7L]^{2+}$	277	6700
$[H_2L]^{3-}$	272	4300	$[TbHL]^-$	272 sh	3600
$[H_3L]^{2-}$	228sh	30000	$[TbH_2L]$	272	3700
	275	5600			
$[H_4L]^-$	229	33900			
	278	6600			

[a] ± 2 nm. [b] ± 10%.

which explains the difficulty in solubilising the metal complexes after their isolation as solid-state samples. At lower pH, competition with protons dissociates the complex, while very stable hydroxides are the major species at pH values higher than 8.5. Altogether, the metal complexes are moderately stable, as shown by the pTb value of 10.0,[19] calculated with $[Tb]_{tot} = 10^{-6}$ M, $[H_5L]_{tot} = 10^{-5}$ M and pH 7.4, in comparison with 19.2 for $[Tb(dtpa)]^-$ [20] and with 6.7 for terbium benzoate. This result is a clear indication that the nitrogen atoms of the H_5L ligand are most probably nonbonding and remain protonated in the metal complexes, as indicated by the unchanged values of the two highest apparent pK_a values upon addition of Ln^{III} ions.

Photophysical Properties of the Ligand and the $[LnH_2L]$ Complexes

In water, the ligand displays two main adsorption bands around 46080 (shoulder at 42370 cm^{-1}) and 39370 cm^{-1}. The high-energy band is slightly blue-shifted (ca. 400−500 cm^{-1}) in the Ln^{III} complexes. The photophysical properties of the ligand and of its 1:1 complexes with La, Lu, Eu and Tb in water (pH 5.3) and in frozen glycerol/water mixtures are summarized in Table 3. UV excitation in the $\pi \rightarrow \pi^*$ and $n \rightarrow \pi^*$ absorption bands of the ligand results in a

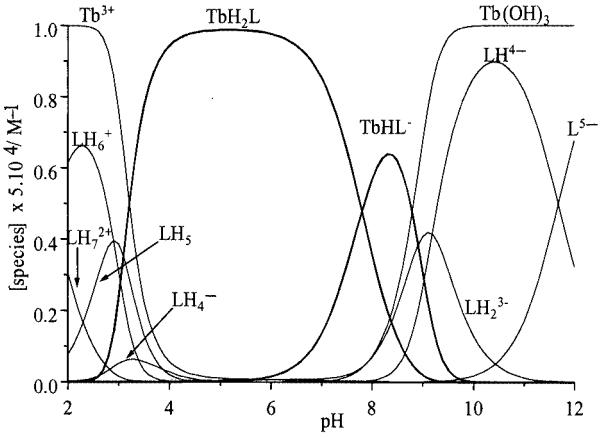

Figure 6. Corresponding formation curves of proton and terbium complexes, computed from the stability constants given in the text; $[L]_{tot} = [Tb^{III}]_{tot} = 2.0 \cdot 10^{-5}$ M; $\lambda_{exc} = 274$ nm; $T = 20$ °C

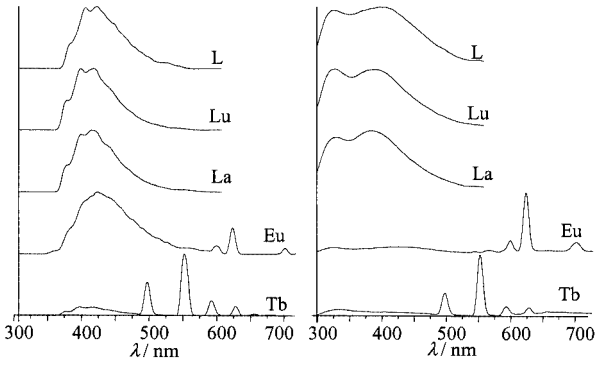

Figure 7. Emission spectra of the $[LnH_2L]$ complexes (Ln = La, Eu, Tb, Lu), pH = 5.3; (left) phosphorescence spectra in solutions of glycerol/water, 10:90% at 77 K; (right) fluorescence spectra at 295 K in water

ligand-centred emission displaying two overlapping bands assigned to emission from the $^1\pi\pi^*$ (33110 cm^{-1}) and $^3\pi\pi^*$ states (Figure 7). The absolute fluorescence quantum yield of the fully deprotonated ligand (L^{5-}) is small at 0.3%, a value that increases slightly for the $[Ln(H_2L)]$ complexes: 0.4 and 0.5% for La and Lu, respectively, at pH 5.3. At 77 K, the $^3\pi\pi^*$ state emission is structured with a vibrational progression of 1350 ± 30 cm^{-1}, corresponding to a ring breathing mode and its 0-phonon transition is located at 26520 cm^{-1}. The gap between the $^3\pi\pi^*$ and $^1\pi\pi^*$ states (ca. 6320 cm^{-1}) is favourable for a relatively efficient intersystem crossing process.[5] The emission spectra of the ligand and its complexes at room temperature are consistent with this finding, since they display emission from both the singlet and triplet states, although very weakly for Eu and Tb. The $^3\pi\pi^*$ lifetime amounts to 1.88 s, a value close to that obtained for benzoic acid ($\tau = 2$ s).[21] As would be expected from the relatively high energy of the $^3\pi\pi^*$ 0-phonon component, both the Eu^{III} ions, with $\Delta E(^3\pi\pi^* - {}^5D_0) \approx 9700$ cm^{-1}, and the Tb^{III} ions, with $\Delta E(^3\pi\pi^* - {}^5D_4) \approx 6500$ cm^{-1}, are reasonably well sensitised (Figure 7). This is in agreement with what has been observed for Tb^{III} poly(aminocarboxylates), for which the best antenna effect was observed for $^3\pi\pi^*$ states around 26000 cm^{-1}.[22]

The high-resolution excitation spectrum of a solid-state sample of $[EuH_2L]$ in the $^5D_0 \leftarrow {}^7F_0$ spectral range, obtained by analysis of the maximum on the $^5D_0 \rightarrow {}^7F_2$ transition at 10 K, displays a single broad and symmetrical peak at 17246 cm^{-1} with a full width at half height (fwhh) of 26.9 cm^{-1}, which is consistent with the presence of a single site for the Eu^{III} ion.

The metal-centred luminescence of diluted aqueous solutions is pH dependent, due to the distribution of the various species present in solution. The Tb complex displays emission over a large pH range, from pH 3.5 to 10.5 (Figure 4), with maximum intensity occurring in the pH range 5−8, in which $[TbH_2L]$ is the major species in solution. The average numbers of water molecules bound to the metal ions were determined from the experimental lifetimes at room temperature for solutions of $[LnH_2L]$ (Ln = Eu, Tb) in H_2O (pH 5.3) and D_2O (pD 5.7).[23,24] For the Eu complex, the measured lifetimes ($\tau = 1.41 \pm 0.04$ ms in D_2O and 0.20 ± 0.01 ms in H_2O) give $q = 4.8 \pm 0.5$, while $q = 4.5 \pm 0.5$ is obtained for the Tb podate ($\tau = 1.47 \pm 0.01$ ms in D_2O and 0.61 ± 0.01 ms in H_2O). The presence of at least eight OH oscillators in the inner coordination sphere is consistent with the reasoning, based on the stability constants, that at least four benzoate units are coordinated to the metal ions (in a monodentate fashion), but the nitrogen atoms are not. The large number of water molecules in the first coordination sphere explains the inability of the ligand to sensitise the luminescence of the Dy^{III}, Er^{III} and Tm^{III} ions. Despite this, the quantum yields of metal-centred luminescence in

Table 3. Ligand-centred absorption and emission properties of the ligand (pH 12) and $[LnH_2L]$ podates at pH 5.3

Compound	E (cm^{-1})[a]	E (cm^{-1})[a] $^1\pi\pi^*$[c]	$^3\pi\pi^*$[c]	$^3\pi\pi^*$[b]	$\tau(^3\pi\pi^*)$ (ms)[b]
$[L]^{5-}$	46080, 42370 sh, 39370	33110	25706	26790, *25360*, 23980	1879 ± 26
$[LuH_2L]$	46510, 42370 sh, 39275	33005	26140	26920, *25540*, 24240, 22910, 21530	789 ± 12
$[LaH_2L]$	46590, 42370 sh, 39525	33445	26040	26880, *25510*, 24210, 22940, 21600	809 ± 6
$[EuH_2L]$	46619, 42370 sh, 36490	33655	25445	26920, *25610*, 24230	1363 ± 14
$[TbH_2L]$	46619, 42370 sh, 36490	33700	25640	26920, *25610*, 24270	456 ± 12

[a] The most intense component is italicised. [b] Luminescence data and lifetimes for frozen solutions in glycerol/water 10:90% (77 K). [c] Electronic spectroscopic data at 295 K in water; energies are given for the maximum of the band envelope (sh: shoulder).

water at pH 5.3 remain sizeable, at 1.5 and 10.3% for the Eu and Tb podates, respectively (Table 4). This points to fairly efficient energy transfer from the ligand to the Tb($^5D_4$) level. It is noteworthy that the quantum yield of [Tb(H_2L)] increases significantly upon addition of HMPA, which is know to be a good complexation agent for Ln^{III} ions and which removes the water from the inner coordination sphere (2 eqs: +45%, 4, 10, 100 and 500 eqs: +105%). Moreover, a graph of the quantum yield of [Tb(H_2L)] vs. pH (Figure S2, Supporting Information) reflects the distribution curve of this species reasonably well.

Conclusion

The solution studies described in this paper show that podand H_5L gives stable Ln^{III} complexes in water that are resistant toward hydrolysis and show interesting photophysical properties. Thermodynamically stable 1:1 neutral podates [Ln(H_2L)] form in the pH range 3.7−8. No nitrogen atom is involved in the binding, as a result of the protonation of the amine functions, preventing the wrapping of the ligand around the metal ion. The emission lifetimes of the Eu^{III} and Tb^{III} complexes recorded in D_2O and H_2O point to four water molecules completing the coordination sphere of the metal ions. The luminescence study shows that the ligand exhibits a good antenna effect with respect to the Tb^{III} ion, due to efficient intersystem crossing ($^1\pi\pi^*$- to-$^3\pi\pi^*$) and ligand-to-metal energy transfer. Despite the large number of coordinated water molecules, the quantum yields of the metal-centred luminescence in the Tb^{III} (and Eu^{III}) complexes are encouraging and demonstrate that benzoate is a potentially interesting moiety for attachment onto a flexible receptor for Ln^{III} ions.

Experimental Section

Starting Materials and General Procedures: Analytical grade solvents and chemicals (Fluka AG) were used without further purification, except for acetonitrile, which was distilled from CaH_2. Solutions were prepared just before use with freshly boiled, doubly distilled water saturated with N_2. Stock solutions of $LnX_3{\cdot}nH_2O$ (X = ClO_4, CF_3SO_3) were prepared from lanthanide oxides (99.99%, Rhône Poulenc) and the corresponding acid. They were systematically acidified with HCl to a pH of about 4 before titration to avoid hydroxide precipitation. The concentrations were determined by complexometric titrations with a standardized Na_2H_2EDTA solution in urotropine-buffered medium and with xylenol orange as indicator.[25] Elemental analyses were performed by Dr. Eder, Microchemical Laboratory, University of Geneva.

1-D and 2-D NMR spectroscopic data were collected on Bruker DPX 400 or AM 360 spectrometers. ^1H NMR and ^{13}C NMR spectra were recorded in $CDCl_3$, D_2O or CH_3OD and their assignment was based on ^1H coupling and 2-D ^1H-^{13}C correlation spectra. The mass spectra were recorded in electrospray ionisation mode on a Finnigan quadrupole mass spectrometer (T_{matrix} = 240 °C). The instrument was calibrated with a horse myoglobin standard. The analyses were conducted in positive mode. The ion spray voltage was 4.6 kV. Assignment of the species was based on the isotopic distribution of the peaks. Electronic UV/Vis spectra were recorded on a Perkin−Elmer Lambda 900 spectrometer. Infra-red spectra were measured on a FT-IR Mattson Alpha Centauri spectrometer (4000−400 cm^{-1}, KBr pellets).

Syntheses (see Scheme 1). Methyl 2-(Bromomethyl)benzoate (1): This compound was synthesized by a known procedure.[26]

1,4,7-Heptanetriamine-*N,N,N′,N′,N″*-pentakis(methyl 2-methylbenzoate) (2): Potassium carbonate (10.04 g, 72.7 mmol) was added under nitrogen atmosphere to a solution of diethylenetriamine (500 mg, 4.9 mmol) in freshly distilled acetonitrile (100 mL). The resulting mixture was heated at reflux for 30 min, and a solution of **1** (6.08 g, 26.7 mmol) in dry acetonitrile (50 mL) was added over 2 h. The mixture was stirred and heated at reflux for an additional 12 h and filtered while hot. The solvents were then evaporated to give a black oil, which was dissolved in dichloromethane, washed with brine and dried with Mg_2SO_4, and the solvents were evaporated to dryness. The residue was purified by column chromatography (silica gel; 2% MeOH in CH_2Cl_2). Yield: 1.76 g (43%), orange foam. IR (KBr): $\tilde{\nu}$ = 1711 (C=O), 1452, 1384 cm^{-1}. ^1H NMR (300 MHz, $CDCl_3$, 25 °C): δ = 2.46 (m, 8 H, CH_2), 3.72 (s, 8 H, CH_2), 3.76 (s, 2 H, CH_2), 3.82 (s, 12 H, CH_3), 3.86 (s, 3 H, CH_3), 7.21 (m, 5 H, ArH), 7.27 (dt, ^1J = 7.5, ^2J = 1.3 Hz, 1 H, ArH), 7.34 (dt, ^1J = 7.8, ^2J = 1.3 Hz, 4 H, ArH), 7.41 (d, J = 7.5 Hz, 1 H, ArH), 7.58 (d, J = 7.8 Hz, 4 H, ArH), 7.68 (dd, ^1J = 7.5, ^2J = 1.3 Hz, 1 H, ArH), 7.74 (dd, ^1J = 7.8, ^2J = 1.3 Hz, 4 H, ArH) ppm. ^{13}C NMR ($CDCl_3$): δ = 51.7, 51.8 (CH_3), 52.5, 52.6, 57.0, 57.6 (CH_2), 126.3, 129.3, 129.7, 129.9 (CH), 130.1, 130.4 (Cq), 131.3, 131.6 (CH), 141.4 (Cq), 168.2, 168.4 (C=O) ppm. ESI-MS (CH_3CN, H_2O, CH_3CO_2H): m/z = 844.3 (calcd. 844.3) $[M + H]^+$, 422.8 (calcd. 422.7) $[M + 2H]^{2+}$. $C_{49}H_{53}N_3O_{10}$ (843.97): calcd. C 69.73, H 6.33, N 4.98; found C 69.72, H 6.31, N 4.96.

1,4,7-Heptanetriamine-*N,N,N′,N′,N″*-pentakis(2-methylbenzoic acid) (H_5L): Compound **2** (500 mg, 0.59 mmol) was dissolved in a solution of methanol (200 mL) and KOH in water (1 M, 15 mL). The resulting mixture was heated at reflux for 4 h, and the solvents were evaporated. The residue was dissolved in water (400 mL), cooled to 0 °C and acidified to pH 2 with aqueous HCl. The yellow precipitate was collected, washed with water and then diethyl ether, and dried. Yield: 417 mg (91%), yellow solid. IR (KBr): $\tilde{\nu}$ = 3426 br (OH), 2606 br (OH), 1700 (C=O), 1590, 1552, 1451, 1381, 1295, 1145, 1085, 752 cm^{-1}. ^1H NMR (300 MHz, D_2O, 20 °C): δ = 2.8 (m, 4 H, CH_2), 3.3 (m, 4 H, CH_2), 3.63 (s, 2 H, CH_2), 4.44 (s, 8 H, CH_2), 7.2 (m, 1 H, ArH), 7.3−7.4 (m, 14 H, ArH), 7.74 (m, 1 H, ArH), 7.93 (m, 4 H, ArH) ppm. ^{13}C NMR (D_2O, 20 °C): δ = 51.1, 55.4, 56.7, 57.9, 58.1 (CH_2), 127.2, 129.6, 130.6, 130.8 (CH), 131.4, 131.6 (quat. C), 133.1, 134.4 (CH), 137.5 (quat. C), 170.7 (C=O) ppm. ESI-MS (CH_3CN, H_2O, CH_3CO_2H): m/z = 774.4 (calcd. 774.3) $[M + H]^+$, 387.8 (calcd. 387.7) $[M + 2H]^{2+}$. $H_5L{\cdot}H_2O$ $C_{44}H_{45}N_3O_{11}$ (791.85): calcd. C 66.74, H 5.73, N 5.31; found C 66.72, H 5.60, N 5.20.

Preparation of [Ln(H_2L)]·nH_2O Complexes (Ln = La, Eu, Tb, Lu): Freshly titrated $LnClO_4.nH_2O$ solutions (10^{-3} M, 0.039 mmol) were added over 4 h, at room temperature, to an aqueous solution of H_5L (40 mL, 0.039 mmol, 10^{-3} M, pH = 5.3, adjusted with HCl). The mixture was stirred for an additional 2 h and the resulting white precipitate was filtered, washed successively with water (several times) and diethyl ether, and further dried for 3 days at 65 °C and 0.01 Torr. These complexes being very hygroscopic, variable numbers of water molecules were found when performing microanalyses.

[La(H_2L)]·$5H_2O$ (75%): IR (KBr): $\tilde{\nu}$ = 3422 br (OH), 1554 and 1399 (ν_{as}, ν_s COO), 1606, 1498, 1449, 1294, 1203, 1151, 1120, 1089,

753 cm^{-1}. $C_{44}H_{50}LaN_3O_{15}$ (999.80): calcd. C 52.86, H 5.04, N 4.20; found C 52.27, H 4.50, N 4.27.
$[Eu(H_2L)]\cdot 3H_2O$ (89%): IR (KBr): $\tilde{\nu}$ = 3413 br (OH), 1556 and 1403 (ν_{as}, ν_s COO), 1607, 1490, 1449, 1294, 1202, 1150, 1120, 1094, 752 cm^{-1}. ESI-MS: a stoichiometric mixture of $Eu(ClO_4)_3\cdot xH_2O$ (x = 4.2) and H_5L 10^{-4} M in pure methanol gave $[EuH_3L]^+$ m/z = 923.4 (calcd. 923.4). $C_{44}H_{46}EuN_3O_{13}$ (976.81): calcd. C 54.10, H 4.75, N 4.30; found C 53.65, H 4.59, N 4.30.
$[Tb(H_2L)]\cdot 7H_2O$ (84%): IR (KBr): $\tilde{\nu}$ = 3416 br (OH), 1556 and 1407 (ν_a, ν_s COO), 1608, 1491, 1450, 1295, 1203, 1151, 1120, 1087, 752 cm^{-1}. $C_{44}H_{54}N_3O_{17}Tb$ (1055.83): calcd. C 50.05, H 5.15, N 3.98; found C 49.16, H 4.78, N 3.72. Complexometry: calcd. Tb 15.05; found Tb 15.28 ± 0.28.
$[Lu(H_2L)]\cdot 4H_2O$ (92%): IR (KBr): $\tilde{\nu}$ = 3417 br (OH), 1561 and 1410 (ν_{as}, ν_s COO), 1608, 1491, 1450, 1294, 1203, 1152, 1120, 1088, 752 cm^{-1}. $C_{44}H_{48}N_3O_{14}Lu$ (1017.84): calcd. C 51.92, H 4.75, N 4.13; found C 51.98, H 4.41, N 4.14.

Physical Measurements. Potentiometric Titrations: H_7L^{2+} was titrated with a 5.1 mL sample ($[H_7L^{2+}]_{tot}$ = $3.7\cdot10^{-3}$ M, solvent: H_2O/CH_3OH 98:2 v/v) in a thermostatted (20.0 ± 0.1 °C) glass-jacketed vessel under an Ar atmosphere. The ionic strength was fixed with KCl (μ = 0.1 M). The solution was acidified to a pH of about 1.8 (HCl) 30 min before titration. Titrations were carried out with an automatic Metrohm Titrino 736 GP potentiometer linked to an IBM PS/2 computer (resolution 0.1 mV, accuracy 0.2 mV) and by use of constant volume addition (0.05 mL). An automatic burette (Metrohm 6.3013.210, 10 mL, accuracy 0.03 mL) was used, together with a Metrohm 6.0238.000 glass electrode. The standard base solution (KOH = 0.050 M, μ = 0.1 M, KCl) was added inside the solution through a capillary tip attached to the automatic burette. The data (200 points, drift < 1 mV/min) were mathematically treated by use of the program SUPERQUAD[27] with a Marquardt algorithm while the distribution of species was calculated with the program Haltafall.[28] Calibration of the pH meter and the electrode system was performed prior to each measurement with a standardized HCl solution (μ = 0.1 M, KCl) at 20.0 °C: 10 mL of the latter were titrated with a standardized 0.1 M KOH solution at a ionic strength of 0.1, and the electrode potential readings were converted to pH. The ion product of solvent (pK_w = 13.91) and electrode potential were refined by use of the program Scientist® by Micromath® (Version 2.0).

Spectrophotometric Titrations: Electronic spectra were recorded with a Perkin–Elmer Lamdba 900 spectrophotometer at 20 °C (210–350 nm, 60 nm min^{-1} scan speed, spectral width 2 nm) in 1 cm Suprasil® quartz cells. Titrations of 10 mL samples were performed in a thermostatted (20.0 ± 0.1 °C), glass-jacketed vessel filled with Ar, at μ = 1 M (KCl); H_7L^{2+} (pH, 2) was titrated with KOH (0.1 M), H_5L (pH, 5.3, HCl) with $Ln(ClO_4)_3$ (≈ $4.0\cdot10^{-3}$ M, Ln = La, Eu, Tb, Lu) at pH = 5.3, and $[Tb(H_2L)]$ $2.0\cdot10^{-5}$ M at pH_0 ≈ 2 by KOH (0.050 M). Aliquots of the titrant were added through a Socorex® micropipette. The pH values of the titrated solutions were monitored continuously. After a 15 min delay, 3 mL of solution was transferred into the quartz cell with a Teflon® syringe. The stability constants were computed by use of the Specfit program.[29] Differences between the measured and the computed absorbances were less than 7×10^{-3} absorbance unit at any wavelength and exhibited statistical behaviour.

NMR Titration: A solution of H_5L (11.6 mg, $7.3\cdot10^{-3}$ M) was prepared in 2 mL of a D_2O/CD_3OD (95:5, v/v) mixture, by addition of a concentrated KOD/D_2O aliquot (pD_0 ≈ 12). Samples with different pD values were prepared by addition of dilute D_2SO_4/D_2O (Fluka, puriss). Precipitation of ligand occurred at pD values lower than 3.2. The pH values of the solutions were determined with a Metrohm Titrino 736 GP potentiometer equipped with a calibrated Metrohm 6.0234.100 glass electrode in H_2O. Ionic strength was not adjusted. The pD values were obtained from the equation $pD = pH_{measd.} + 0.4$.[30]

Luminescence Titrations: The solutions {$[H_5L]_0$ = $2.0\cdot10^{-5}$ M, $[Tb(ClO_4)_3]_0$ = $2.0\cdot10^{-5}$ M, 10 mL, pH_0 ≈ 2; $[KOH]_{tit}$ = 0.050 M; μ = 0.1 M (KCl)} were identical to those used for the spectrophotometric pH-dependent titration described previously. After a 15 min delay, 3 mL of solution were transferred into a quartz cell and degassed with Ar for 5 min. Absorbance at the excitation wavelength was measured (A < 0.05) and emission (λ_{exc} = 285 nm) and excitation spectra were collected.

Luminescence Measurements: Low-resolution luminescence measurements (spectra and lifetimes) were recorded on a Perkin–Elmer LS-50B spectrofluorimeter. Phosphorescence lifetimes (τ) were measured with the instrument in time-resolved mode, on frozen glycerol/water (10:90%) solutions in a quartz capillary or a 1-cm Suprasil® cell. They are the average of at least three independent measurements, made by monitoring the decay at the maxima of the emission spectra, enforcing a 0.03–0.04 ms delay. The decays were mono-exponential and were analysed by use of the FLDM program (Perkin–Elmer). Solutions of $[Ln(H_jL)]^{(3+j-5)+}$ were prepared in water at pH = 5.3, with stock solutions of H_5L ($2.0\cdot10^{-3}$ M) and $Ln(ClO_4)_3\cdot xH_2O$ (x ≈ 4.5, Ln = La, Eu, Tb, Lu; ≈ $4\cdot10^{-3}$ M). Quantum yields of L^{5-} (10^{-5} M, pH = 12) and $[Ln(H_2L)]$ (Ln = La, Eu, Tb, Lu, 10^{-5} M in H_2O) were determined in degassed water relative to quinine sulfate in 0.05 M aqueous H_2SO_4 (absolute quantum yield: 0.546)[31] and cresol violet (absolute quantum yield: 0.52);[32] estimated error ±10%. The number of coordinated water molecules (q) for the Eu and Tb complexes were calculated from $q = A(\tau_H^{-1} - \tau_D^{-1} - k_{corr})$, where τ_H and τ_D are the lifetimes in H_2O and D_2O respectively, A = 1.2 (Eu) and 5.0 (Tb), and k_{corr} = 0.25 (Eu) and 0.06 (Tb) ms^{-1}.[24] High-resolution spectra were recorded on a previously described setup.[33]

Table 4. Absolute quantum yield of the ligand-centred fluorescence in $[L]^{5-}$ (pH = 12) and $[LnH_2L]$ (Ln = La, Lu) and of the metal-centred phosphorescence in $[LnH_2L]$ (Ln = Eu, Tb) measured in water at 295 K and pH = 5.3 (values in D_2O are italicised)

Compound	λ_{exc} (nm)	φ_{abs} (%)
$[L]^{5-}$	268	0.3
$[LuH_2L]$	273	0.4
$[LaH_2L]$	273	0.5
$[EuH_2L]$	270	1.5, *3.3*
$[TbH_2L]$	270	10.3, *18.9*

Acknowledgments

This work is supported through grants from the Swiss National Science Foundation and the Swiss Federal Office for Science and Education (COST Action D18). We thank Frédéric Gumy for his help in recording the high-resolution luminescence data.

[1] The chemistry of contrast agents in medical magnetic resonance imaging, eds A. E. Merbach and E. Tóth, Wiley, London, **2001**.
[2] Z. P. Zheng, *Chem. Commun.* **2001**, 2521–2529.
[3] J.-C. G. Bünzli, C. Piguet, *Chem. Rev.* **2002**, *102*, 1897–1928.

[4] L. H. Slooff, A. van Blaaderen, A. Polman, G. A. Hebbink, S. I. Klink, F. C. J. M. Van Veggel, D. N. Reinhoudt, J. W. Hofstraat, *J. Appl. Phys.* **2002**, *91*, 3955−3980.
[5] J.-C. G. Bünzli, C. Piguet, in *Encylopedia of Materials: Science and Technology* (Eds.: K. H. J. Buschow, R. W. Cahn, M. C. Flemings, B. Ilschner, E. J. Kramer, S. Mahajan), Elsevier Science Ltd, Oxford, **2001**, *10*, Ch. 1. 10. 4, 4465−76.
[6] V. W. W. Yam, K. K. W. Lo, *Coord. Chem. Rev.* **1999**, *184*, 157−240.
[7] G. Mathis, in *Rare Earths* (Eds.: R. Saez Puche, P. Caro), Editorial Complutense, Madrid, **1998**, 285−97.
[8] D. Parker, *Coord. Chem. Rev.* **2000**, *205*, 109−130.
[9] D. J. Bornhop, D. S. Hubbard, M. P. Houlne, C. Adair, G. E. Kiefer, B. C. Pence, D. L. Morgan, *Anal. Chem.* **1999**, *71*, 2607−2615.
[10] G. Zucchi, A.-C. Ferrand, R. Scopelliti, J.-C. G. Bünzli, *Inorg. Chem.* **2002**, *41*, 2459−2465.
[11] F. M. Ramirez, L. J. Charbonnière, G. Muller, R. Scopelliti, J.-C. G. Bünzli, *J. Chem. Soc., Dalton Trans.* **2001**, 3205−3213.
[12] C. Piguet, J.-C. G. Bünzli, *Chem. Soc. Rev.* **1999**, *28*, 347−358.
[13] M. Elhabiri, R. Scopelliti, J.-C. G. Bünzli, C. Piguet, *J. Am. Chem. Soc.* **1999**, *121*, 10747−10762.
[14] N. Fatin-Rouge, E. Tóth, D. Perret, R. H. Backer, A. E. Merbach, J.-C. G. Bünzli, *J. Am. Chem. Soc.* **2000**, *122*, 10810−10820.
[15] J.-C. G. Bünzli, in *Rare Earths* (Eds.: R. Saez Puche, P. Caro), Editorial Complutense, Madrid, **1998**, 223−259.
[16] W. Shrott, H. Büchner, U. E. Steiner, *J. Inf. Recording* **1996**, *23*, 79−84.
[17] M. Bredol, U. Kynast, C. Ronda, *Adv. Mat.* **1991**, *3*, 361−367.
[18] J. L. Sudmeier, C. N. Reilley, *Anal. Chem.* **1964**, *36*, 1698−1706.
[19] K. N. Raymond, G. Muller, F. Matzanke, *Top. Curr. Chem.* **1984**, *123*, 49−102.
[20] J. R. Duffield, F. Marsicano, D. R. Williams, *Polyhedron.* **1991**, *10*, 1105−1111.
[21] H. J. Maria, S. P. McGlynn, *J. Chem. Phys.* **1970**, *52*, 3399−3402.
[22] M. Latva, H. Takalo, V. M. Mukkala, C. Matachescu, J.-C. Rodriguez-Ubis, J. Kankare, *J. Lumin.* **1997**, *75*, 149−169.
[23] J.-C. G. Bünzli, in *Lanthanide Probes in Life, Chemical and Earth Sciences. Theory and Practice* (Eds.: J.-C. G. Bünzli, G. R. Choppin), Elsevier Science Publ. B. V., Amsterdam, **1989**, chapter 7, 219−93.
[24] A. Beeby, I. M. Clarkson, R. S. Dickins, S. Faulkner, D. Parker, L. Royle, A. S. de Sousa, J. A. G. Williams, M. Woods, *J. Chem. Soc., Perkin Trans. 2* **1999**, 493−504.
[25] G. Schwarzenbach, *Complexometric Titrations*, Chapman & Hall, London, **1957**.
[26] D. A. Quagliato, P. M. Andrae, E. M. Matelan, *J. Org. Chem.* **2000**, *65*, 5037−5042.
[27] P. Gans, A. Sabatini, A. Vacca, *J. Chem. Soc., Dalton Trans.* **1985**, 1195−1200.
[28] N. Ingri, W. Kakolowicz, L. G. Sillen, B. Warnqvist, *Talanta* **1967**, *14*, 1261−1286.
[29] H. Gampp, M. Maeder, C. J. Meyer, A. D. Zuberbühler, *Talanta* **1986**, *33*, 943−951.
[30] K. Mikkelsen, S. O. Nielsen, *J. Phys. Chem.* **1960**, *64*, 632−637.
[31] S. R. Meech, D. C. Phillips, *J. Photochem.* **1983**, *23*, 193−217.
[32] D. Magde, J. H. Brannon, T. L. Cremers, J. Olmsted, III, *J. Phys. Chem.* **1979**, *83*, 696−699.
[33] R. Rodriguez-Cortinas, F. Avecilla, C. Platas-Iglesias, D. Imbert, J.-C. G. Bünzli, A. de Blas, T. Rodriguez-Blas, *Inorg. Chem.* **2002**, *41*, 5336−5349.
[34] P. Letkeman, A. E. Martell, *Inorg. Chem.* **1979**, *18*, 1284−1289.

Received October 4, 2002
[I02550]

The Coordination Chemistry of the Pentadentate 2,2,6,6-Tetrakis(aminomethyl)-4-azaheptane (ditame)

Kaspar Hegetschweiler,*[a] Oliver Maas,[a] Anja Zimmer,[a] Rodney J. Geue,[b] Alan M. Sargeson,[b] Jeffrey Harmer,[c] Arthur Schweiger,[c] Irmgard Buder,[d] Günter Schwitzgebel,[d] Vera Reiland,[e] and Walter Frank[e]

Dedicated to Professor Walter Schneider on the occasion of his 75th birthday

Keywords: Amine ligands / Chelates / Ligand design / Stability constants

The protonation and metal complex formation of the branched pentaamine ligand 2,2,6,6-tetrakis(aminomethyl)-4-azaheptane (ditame, L) with Co^{II}, Co^{III}, Ni^{II}, Cu^{II}, Zn^{II}, and Cd^{II} have been studied. The crystal structures of $[Ni(ditame)(EtOH)]Br_2$, $[Co_2(ditame)_2(O_2)]Cl_4{\cdot}4H_2O$, and $[Co_2(ditame)_2(O_2)]Cl_2[ZnCl_4][ZnCl_3(H_2O)]{\cdot}H_2O$ were determined by X-ray diffraction analyses. The metal complexes showed octahedral coordination geometries with exclusive formation of six-membered chelate rings, the four primary amino groups being in equatorial positions and the secondary amino group (N^{sec}) apical. This geometry enforces a relatively short M–N^{sec} bond. Complex formation in aqueous solution was evaluated by potentiometric titration. The ditame ligand forms a surprisingly stable Ni^{II} complex with $\log K_{NiL} = 17.8$ (25 °C, 0.1 M KNO_3), and formation of protonated species $[Ni(H_n ditame)]^{(n+2)+}$ (n = 1, 2) is not significant. Different behavior is evident for Zn^{II} and Cd^{II}, with which protonated species are extensively formed, while the stability of $[ML]^{2+}$ is relatively low. Complex formation between ditame and Cu^{II} in the range $3 < pH < 7$ resulted in the formation of $[Cu(H_2ditame)]^{4+}$. In slightly alkaline solution, the dinuclear $[Cu_2(ditame)_2]^{4+}$ appears to be formed. The structural assignment of this dimer is based on its UV/Vis and EPR characteristics, with the EPR data indicating a $Cu^{II}\cdots Cu^{II}$ separation of about 5.9 Å. The redox behavior of the Ni and Co complexes was investigated by cyclic voltammetry. The mononuclear species showed quasi-reversible electron transfer for the $Ni^{II/III}$ and $Co^{II/III}$ couples. For the dinuclear peroxo/superoxo-bridged Co^{III} complexes, quasi-reversible electron transfer corresponding to oxidation/reduction of the O_2^{2-}/O_2^- bridge was observed.

(© Wiley-VCH Verlag GmbH & Co. KGaA, 69451 Weinheim, Germany, 2003)

Introduction

Ligand design is a well-established field in modern coordination chemistry.[1] Tailored complexing agents are of importance for the construction of catalysts,[2] and as building blocks for coordination polymers,[3,4] since they allow specific modulation of the electronic and steric properties of a metal complex.[5] Pentadentate chelators are of particular interest, since the high denticity often gives rise to high stability, while the binding of an additional ligand (e.g. a substrate) to the metal cation within an octahedral environment is still possible.[6–16] As regards complex formation with late transition metal cations, aliphatic polyamines are of particular relevance.[17,18] Various aliphatic and alicyclic pentaamines have been prepared and their coordination chemistry explored. They comprise a series of pentaaza macrocycles[19] as well as tetraaza and triaza macrocycles with pendant amine groups.[20] Macrobicyclic pentaaza ligands are also known,[19] and a number of open-chain, linear, and branched aliphatic pentaamines have been described.[6,7,21–25] The synthesis of the doubly branched 2,2,6,6-tetrakis(aminomethyl)-4-azaheptane, or ditame (Scheme 1), has recently been reported by some of us, and the structure and reactivity of its Co^{III} complex have been discussed in detail.[21] Metal complex formation by a related pyridine analogue has been published by Grohmann and

[a] Anorganische Chemie, Universität des Saarlandes
Postfach 15 11 50, 66041 Saarbrücken, Germany
Fax: (internat.) + 49-681/302-2663
E-mail: hegetschweiler@mx.uni-saarland.de
[b] Research School of Chemistry, Australian National University, Canberra, ACT 0200, Australia
[c] Laboratorium für Physikalische Chemie, ETH Hönggerberg, 8093 Zürich, Switzerland
[d] Physikalische Chemie, Universität des Saarlandes
Postfach 15 11 50, 66041 Saarbrücken, Germany
[e] Institut für Anorganische Chemie und Strukturchemie, Heinrich-Heine-Universität Düsseldorf,
Universitätsstr. 1, 40225 Düsseldorf, Germany
Supporting information for this article is available on the WWW under http://www.eurjic.org or from the author.

co-workers.[10−16] This investigation explores the stability of labile coordination complexes of ditame in comparison with the coordination chemistry of two related hexadentate ligands (Scheme 1), 1,1,1-tris(5-amino-2-azapentyl)ethane (stn) and 1,1,1-tris(4-amino-2-azabutyl)ethane (sen).[26]

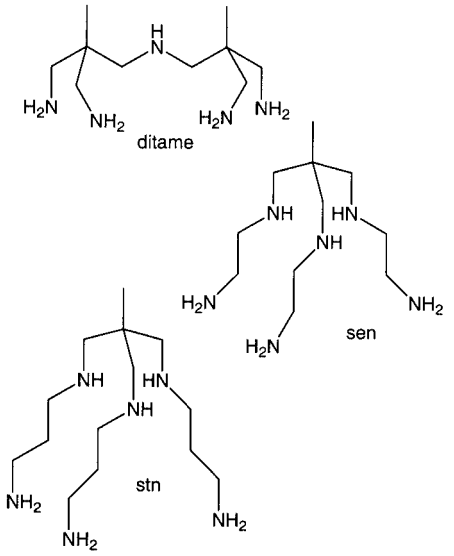

Scheme 1

Results and Discussion

Protonation of ditame

Because of the fairly high charges of multiply protonated amines, increased electrostatic effects have to be taken into account. It is known that some cyclic, multiply protonated polyamines selectively bind suitable anions such as chloride or nitrate through hydrogen bonding.[19] Such interactions could influence the acidity constants of the ligand. Since precise pK_a values of the ligand are a prerequisite for conclusive analysis of metal complex formation in aqueous solution, a series of pK_a determinations was performed, with the nature and concentration of the inert electrolyte (KCl and KNO_3, 0.1 and 1.0 M) as well as the total concentration of ditame (1−10 mM) being varied. Inspection of the corresponding values (Table 1) reveals a significant dependence of the pK_a values on the ionic strength. The acidities of multiply protonated species decrease at higher salt concentrations, and this effect increases with increasing degree of protonation.[27] The effect of the anion (Cl^- versus NO_3^-) was negligible, so specific binding of these anions by the open-chained H_xL^{x+} appears not to be significant in aqueous solution. However, a weak but significant dependence of the pK_a values on total ligand concentration is evident, indicating some deviation from ideal behavior for solutions in which the ratio of total ditame to the ionic strength exceeds a value of 1:500.

Table 1. pK_a values of ditame (25 °C) for different inert electrolytes

Ionic strength [M]	0.1	0.1	1.0	1.0	1.0
Inert electrolyte	KCl	KNO_3	KCl	KCl	KNO_3
Total L [M]	0.001	0.001	0.002	0.010	0.010
p$K_{a,1}$[a]	–[b]	–[b]	1.7(1)	1.8(1)	1.8(1)
p$K_{a,2}$	6.77	6.83	7.32	7.36	7.40
p$K_{a,3}$	7.90	7.90	8.26	8.32	8.33
p$K_{a,4}$	9.47	9.44	9.61	9.72	9.76
p$K_{a,5}$	11.10	11.09	11.06	11.25	11.28

[a] $pK_{a,i} = -\log K_{a,i}$, $K_{a,i} = [H_{5-i}L] \times [H] \times [H_{6-i}L]^{-1}$, estimated standard deviations are 0.01 or less unless otherwise noted. [b] Value too low for determination by pH-metric methods.

A series of pD-dependent ^1H NMR spectra were measured in D_2O (Figure 1). These exhibit four signals for the H(−C) protons of the C_{2v}-symmetric[21] H_xL^{x+} entity, a singlet for the two homotopic methyl groups (X), an additional singlet (Y) for the enantiotopic methylene protons [$H^{(Y1)}$ and $H^{(Y2)}$], and an AB system for the diastereotopic protons $H^{(Za)}$ and $H^{(Zb)}$ of the four methylene groups (Z). Since the chemical shifts of $H^{(Za)}$ and $H^{(Zb)}$ differ only slightly over the entire pD range, a mean value corresponding to the center of the AB system (Z) is presented in Figure 1. The pD-dependence of these signals was modeled by minimization of $\Sigma(\delta_{obs} - \delta_{calc})^2$, assuming a rapid equilibrium with weighted averaged shifts (δ_{obs}) for the six macrospecies H_xL^{x+} ($0 \le x \le 5$, see Table S1).[28,29] The resulting pK_a values of 0.9, 7.2, 8.0, 9.3, and 11.0 agree well with the values obtained from potentiometric titrations. In the fully protonated and the fully deprotonated forms, the two types of methylene groups (Y and Z) have rather similar environments, with similar chemical shifts. For some of the intermediate forms H_xL^{x+} ($2 \le x \le 4$), however, the chemical shifts of Y and Z differ significantly. This observation is attributed to different tautomeric forms that have to be taken into account for the partially protonated species, with the secondary nitrogen atom either protonated or not protonated. Additionally, the four primary amino groups of H_2L^{2+} and H_3L^{3+} can be protonated in different ways, which results in the generation of further tautomers. However, since the four primary amino groups appear to be symmetry-equivalent on the NMR timescale, the latter type of tautomerism can be taken account of by means of an averaged, partial protonation of the NH_2 groups. A total of two microspecies for each of the partially protonated forms is thus sufficient for a suitable description of the NMR characteristics. A set of empirically derived deshielding parameters was used to elucidate the equilibrium between the different microspecies.[28,29] These parameters were determined by use of the well-established observation that protonation of an amino group generally results in a deshielding of nearby H(−C) protons, and that this effect decreases with increasing distance.[30,31] In the range $10 < pD < 12$, the related pD dependence of Y and Z is indicative of fairly unspecific binding of the first proton. The quantit-

ative analysis suggests 25% protonation at the secondary amino group in HL^+, approximately corresponding to a statistical distribution of the proton over the five basic sites. Obviously, there is no significant difference in basicity between the secondary and primary nitrogen donors. For H_2L^{2+}, protonation at the secondary nitrogen atom is < 10%, and in H_3L^{3+} and H_4L^{4+} the protons are exclusively bonded to the primary amino groups. Therefore, consecutive protonation of L up to H_4L^{4+} resulted in increasing protonation at the primary amino groups and decreasing protonation at the secondary amino group. Consequently, the chemical shifts of X and Z increase steadily with increasing protonation (Figure 1), whereas the methylene protons Y are less deshielded in H_2L^{2+} than in HL^+. A dramatic deshielding of Y is observed on final protonation of H_4L^{4+}. However, since H_4L^{4+} is a rather weak base, the exclusive presence of the fully protonated H_5L^{5+} is only observed in strongly acidic solutions (pD = 0).

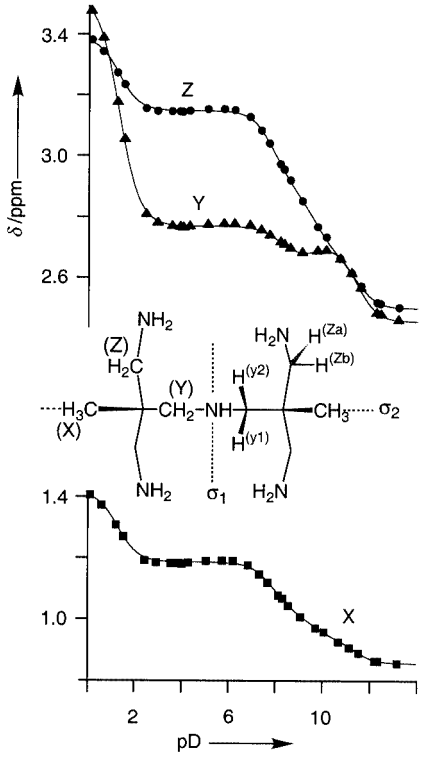

Figure 1. pD dependence of the ^1H NMR resonances of $H_x$ditame^{x+}; the points correspond to experimental values, the lines are calculated (least-squares), by assuming a rapid equilibrium; the values of Z correspond to the center of the AB system of Z^a and Z^b; the schematic formula indicates the observed C_{2v} symmetry with the mirror plane σ_1 and the pseudo mirror plane σ_2[21]

Crystal Structures

[Ni(ditame)(EtOH)]Br$_2$ (1Br$_2$)

The complex cations $\mathbf{1}^{2+}$ and the Br^- anions are arranged in linear chains along the crystallographic *b* axis through $Ni^{II}-N-H\cdots Br^-$ and $Ni^{II}-O-H\cdots Br^-$ hydrogen bonding. Two such chains, related through a crystallographic screw axis, form a double-chain structure. The $\mathbf{1}^{2+}$ cation (Figure 2) is situated on a crystallographic mirror plain, approximately corresponding to the molecular pseudo-plane σ_2 (Figure 1). However, the symmetry operation σ_2 requires either a planar geometry or rapid inversion of the pyramidal configuration for the secondary nitrogen atom. Obviously, neither requirement can be met in the metal complex, and the inherent violation of this symmetry has resulted in a characteristic disorder. The cation was thus refined by two superimposed, but completely independent models (mirror images) with occupancies of 50% each (Figure S1). A similar type of disorder has previously been reported for [Co(ditame)Cl][$ZnCl_4$].[21]

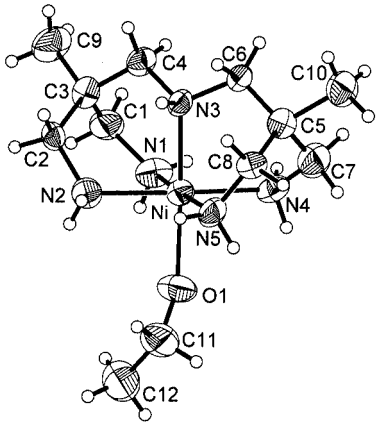

Figure 2. Molecular structure of $[Ni(ditame)(EtOH)]^{2+}$ ($\mathbf{1}^{2+}$); the atomic displacement ellipsoids are drawn at the 50% probability level; hydrogen atoms are shown as spheres of arbitrary size; selected bond lengths [A] and angles [°]: Ni−N1 2.111(7), Ni−N2 2.107(7), Ni−N3 2.050(5), Ni−N4 2.115(7), Ni−N5 2.113(7), Ni−O1 2.172(6); N1−Ni−N2 85.0(3), N1−Ni−N3 93.2(3), N1−Ni−N4 92.4(4), N1−Ni−N5 176.9(4), N1−Ni−O1 86.8(3), N2−Ni−N3 86.8(3), N2−Ni−N4 177.1(3), N2−Ni−N5 98.1(4), N2−Ni−O1 90.2(3), N3−Ni−N4 92.2(3), N3−Ni−N5 87.2(2), N3−Ni−O1 177.0(3), N4−Ni−N5 84.6(3), N4−Ni−O1 90.8(3), N5−Ni−O1 92.9(3)

[Co$_2$(ditame)$_2$(O$_2$)]Cl$_4$·4H$_2$O (2Cl$_4$·4H$_2$O)

The Co−O−O−Co group of the peroxo complex $\mathbf{2}^{4+}$ was located on a twofold rotational axis. It could be refined without problems, although considerable anisotropy for the atomic displacement of the primary nitrogen atoms indicated some conformational disorder within the ditame moieties (Figure 3). The dimeric cation $\mathbf{2}^{4+}$ and the counterions again form a chain structure. The chains are oriented parallel to *b* and coincide with the twofold rotational axes, forming a type of distorted hexagonal rod packing.

[Co$_2$(ditame)$_2$(O$_2$)]Cl$_2$[ZnCl$_4$][ZnCl$_3$(H$_2$O)]·H$_2$O {3Cl$_2$[ZnCl$_4$][ZnCl$_3$(H$_2$O)]·H$_2$O}

The centrosymmetric superoxo complex $\mathbf{3}^{5+}$ (Figure 4) was located and refined without problems, although the counter-ion and the water of crystallization showed some disorder. The positive charge of +2.5 in the asymmetric

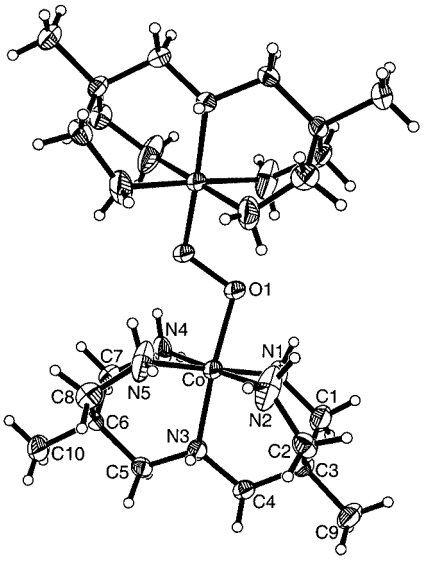

Figure 3. Molecular structure of $[Co_2(ditame)_2O_2]^{4+}$ ($\mathbf{2}^{4+}$); the atomic displacement ellipsoids are drawn at the 50% probability level; hydrogen atoms are shown as spheres of arbitrary size; selected bond lengths [Å] and angles [°]: Co−N1 1.987(8), Co−N2 1.950(8), Co−N3 1.920(7), Co−N4 1.973(8), Co−N5 1.978(8), Co−O1 1.951(7), O1−O1′ 1.495(11); N1−Co−N2 86.7(4), N1−Co−N3 92.7(4), N1−Co−N4 92.8(5), N1−Co−N5 177.6(6), N1−Co−O1 79.8(4), N2−Co−N3 88.1(5), N2−Co−N4 177.9(6), N2−Co−N5 95.4(5), N2−Co−O1 93.8(5), N3−Co−N4 93.9(4), N3−Co−N5 88.5(5), N3−Co−O1 172.1(5), N4−Co−N5 85.1(4), N4−Co−O1 84.1(4), N5−Co−O1 98.9(4), O1′−O1−Co: 110.4(5)

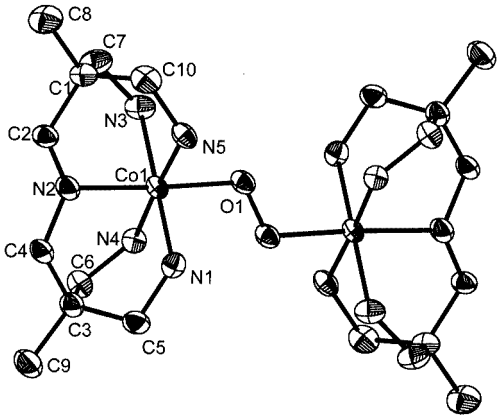

Figure 4. Molecular structure of $[Co_2(ditame)_2O_2]^{5+}$ ($\mathbf{3}^{5+}$); the atomic displacement ellipsoids are drawn at the 50% probability level; hydrogen atoms are omitted for clarity; selected bond lengths [Å] and angles [°] Co−N1 1.956(6), Co−N2 1.949(6), Co−N3 1.963(6), Co−N4 1.966(6), Co−N5 1.970(6), Co−O1 1.917(5), O1−O1′ 1.341(10); N1−Co−N2 91.6(3), N1−Co−N3 176.9(3), N1−Co−N4 88.6(3), N1−Co−N5 90.3(3), N1−Co−O1 92.8(2), N2−Co−N3 87.5(3), N2−Co−N4 88.1(3), N2−Co−N5 94.5(3), N2−Co−O1 175.4(2), N3−Co−N4 94.3(3), N3−Co−N5 86.8(3), N3−Co−O1 88.1(2), N4−Co−N5 177.2(3), N4−Co−O1 90.8(2), N5−Co−O1 86.7(2), O1′−O1−Co 116.0(5)

unit is balanced by a Cl^- anion and an additional tetrahedral ZnX_4 moiety. Three of these X positions could be unambiguously refined as Cl atoms; the fourth position exhibited two maxima in an electron density map with a separation of 0.69(2) Å. These two positions were refined as a Cl and an O atom, each with 50% occupancy. The corresponding distances to the Zn center, of 2.28(1) and 2.08(3) Å, are in agreement with a Zn−Cl and a Zn−OH_2 bond, respectively.[32,33] Obviously, the ZnX_4 positions are equally and randomly shared by $[ZnCl_4]^{2-}$ and $[ZnCl_3(OH_2)]^-$ anions; the simultaneous presence of these two anions has frequently been observed in solid-state structures.[33] An additional water molecule, located in proximity to two ZnX_4 moieties, was distributed over three positions with site occupancies of 28−36%. The zincate anions and the water molecule form chains of composition $[ZnCl_4]\cdots H_2O\cdots[ZnCl_3(H_2O)]\cdots$ along the crystallographic *c* axis. Additional chains along *c* were formed by $\mathbf{3}^{5+}$ and the Cl^- counter-ions. They are stabilized by Co−N−H···Cl^- hydrogen bonds.

Molecular Structures of the ditame Complexes

The crystal structures of two mononuclear Co^{III}(ditame) complexes have been reported previously.[21] The structures of $\mathbf{1}^{2+}$ and of the dinuclear $\mathbf{2}^{4+}$ and $\mathbf{3}^{5+}$ (Figures 2−4) each display a closely related coordination mode for the ditame ligand, with exclusive formation of six-membered chelate rings. The four primary nitrogen donors form an almost regular square, with a slight distortion towards an isosceles trapezium: The $N^{prim}\cdots N^{prim}$ distances in one tripodal tris(aminomethyl)ethane (= tame) cap are slightly shorter than corresponding distances between the nitrogen atoms belonging to different caps. Moreover, the inter-tame N···N distances are inequivalent, the N···N distance with a *cisoid* orientation towards the (N^{sec})−H hydrogen is longer than that with a *transoid* orientation. In all three complexes, the M(ditame) moiety exhibits approximate local C_s symmetry, although the corresponding mirror plain (σ_1 in Figure 1) never corresponds to a crystallographic symmetry element. The M−N^{sec} bond is always somewhat shorter than the corresponding bonds to the primary amino groups. This is also the case if a ligand with a significant *trans* influence[34−36] such as O_2^{2-} is bonded *trans* to N^{sec}, and it appears that the short M−N^{sec} bond is a consequence of the steric requirements of this particular ligand.[15]

The Co−O−O−Co structures of $\mathbf{2}^{4+}$ and $\mathbf{3}^{5+}$ exhibited characteristic differences. The O−O lengths of 1.495 and 1.341 Å are indicative of an O_2^{2-} and an O_2^- bridge, respectively. Corresponding distances for related monobridged (pentaamine)Co^{III} complexes are 1.42−1.53 Å for O_2^{2-} and 1.27−1.34 Å for O_2^-.[6−9,15,23,34−43] The presence of a peroxo bridge in $\mathbf{2}^{4+}$ is also indicated by the Raman data, with an O−O stretch vibration at 810 cm^{-1}.[7,15,35,44] The $Co^{III}-O_2^-$ bond of 1.917(5) Å in the superoxo complex $\mathbf{3}^{5+}$ is in good agreement with literature values, but the $Co^{III}-O_2^{2-}$ bond [1.951(7) Å] in $\mathbf{2}^{4+}$ is unusually long (reported range: 1.83−1.92 Å).[6,8,9,15,23,34−39] The Co^{III}−O−O angles and the average Co^{III}−N distances in both complexes are all normal. The superoxo complex $\mathbf{3}^{5+}$ has a planar, *transoid* Co−O−O−Co grouping with a torsional angle τ of 180°, whereas the Co−O−O−Co grouping in the peroxo complex $\mathbf{2}^{4+}$ is twisted with τ = 138.1°. In agreement with our findings, dinuclear, monobridged

Co^{III}(pentaamine)(superoxo) complexes reported to date are centrosymmetric[7,15,40−42] or nearly centrosymmetric[43] ($\tau = 175°$). For (pentaamine)Co^{III}(peroxo) complexes, both planar *transoid*[6,23,34,35,37,38] and bent[8,9,15,36,39] structures have been described, examples with $\tau = 180°$ predominating. The known non-centrosymmetric, bent structures have torsional angles τ of 146−177.5°.[45] Obviously, $\mathbf{2}^{4+}$ exhibits a particularly high degree of such torsional twist. It has been argued that the value of τ is strongly influenced by inter- and intramolecular hydrogen bonding. In particular, hydrogen bonds between the coordinated amino groups and the remote oxygen atom of the peroxo bridge have been proposed to be a major structure-determining factor.[15,23] However, the corresponding $N\cdots O^{remote}$ distances depend on the rotation around the Co−O bond rather than about O−O. A conclusive discussion of the different types of rotamers requires consideration of three torsional angles τ, φ^a, and φ^b (Scheme 2, φ^a and φ^b are defined as the torsional angles $O-O\cdots N^{sec}-H$). The symmetry types of the various conformers can be mapped as functions of these three parameters; *transoid* conformations ($\tau = 180°$) with $\varphi^a = \varphi^b = 180°$ or $\varphi^a = \varphi^b = 0°$ have the highest possible symmetry (C_{2h}).[42] Further *transoid* conformations have C_s ($\varphi^a = 0$, $\varphi^b = 180°$), C_i ($\varphi^a = -\varphi^b$), or C_2 ($\varphi^a = \varphi^b$) symmetry. For $\tau < 180°$ and $\varphi^a = \varphi^b$ the symmetry remains C_2. Evidently, all conformations with $0° < |\varphi^a| \neq |\varphi^b| < 180°$ are completely asymmetric (C_1). The prerequisite for the formation of four equal intramolecular $N-H\cdots O^{remote}$ hydrogen bonds is $|\varphi^a|, |\varphi^b| = 0$, 90, or 180°. Several of the symmetry types described above match these requirements (even C_1). Neither a centrosymmetric structure nor the *transoid* conformation is required.[23]

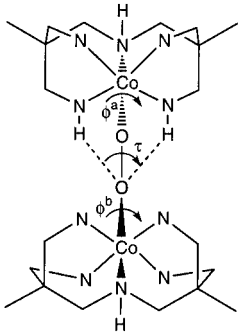

Scheme 2

In the crystal structures reported here, the superoxo and the peroxo complexes have a C_i ($\tau = 180°$, $\varphi^a = 86.2°$, $\varphi^b = -86.2°$) and a C_2 ($\tau = 138.1°$, $\varphi^a = -82.7°$, $\varphi^b = -82.7°$) structure, respectively. Only one strong $N-H\cdots O^{remote}$ hydrogen bond per Co(ditame) moiety is formed in each complex. Since the two Co(ditame) moieties are twisted against each other by an angle of almost 90°, the four methyl groups are not equivalent. In solution (D_2O, pD = 7), however, we observed only one single signal for these methyl groups in the ^1H and the ^{13}C NMR spectra of the peroxo complex $\mathbf{2}^{4+}$. The methylene groups exhibited three AB systems (six unique H atoms) in the ^1H NMR, and the ^{13}C NMR showed a total of five lines. These characteristics are only compatible with a C_{2h} structure. Variation in temperature did not produce any unusual line-broadening effect, and it appears that the barriers of rotation for the Co−O and the O−O bonds are − as would be expected − fairly small. The different values of τ reported in the literature are thus most probably based on the crystal packing and not on any electronic effect.

Evidence of the different conformations of $\mathbf{2}^{4+}$ in solution and in the solid state is also provided by UV/Vis spectroscopy. In solution the typical spectrum of a monobridged, centrosymmetric complex[46−48] with $\lambda_{max} = 296$ nm, $\log \varepsilon = 4.1$ (π_σ* CT), and shoulders around 420 and 520 nm has been observed. In the solid state, an intense CT band remained at about 300 nm, but an additional shoulder appeared at about 380 nm while the 420 and 520 nm bands gained in intensity. This behavior is clearly indicative of the diminished symmetry in the solid state, in which some transitions, symmetry-forbidden in the C_{2h} forms, become allowed. A more detailed discussion on the electronic properties of this complex will be given elsewhere.[49] The spectrum of the superoxo complex $\mathbf{3}^{5+}$ has maxima at 471 nm ($\log \varepsilon = 2.3$) and 695 nm ($\log \varepsilon = 2.9$). These values agree well with the characteristics reported for monobridged Co^{III}(pentaamine)(superoxo) complexes.[7,15,41,42,50]

Complex Formation of ditame (= L) with Co^{II}, Ni^{II}, Zn^{II}, and Cd^{II} in Aqueous Solution

Potentiometric measurements were performed to evaluate complex formation as a function of pH (Figure 5), and to determine the corresponding formation constants (Table 2). For Co^{II}, Ni^{II}, Zn^{II}, and Cd^{II} the predominant species at $8 < pH < 11$ is the 1:1 complex $[ML]^{2+}$. The observed order of stability $Co^{II} < Ni^{II} > Zn^{II}$ is in agreement with the well-established Irving−Williams series.[51] Differences between 0.1 M KNO_3 and 0.1 M KCl are generally small, with the exception of Cd, for which formation of chloro complexes must be taken into account.[28] The difference between Cd^{II} and Zn^{II} ($\Delta\log \beta_{110} = 2.8$ in 0.1 M KNO_3) is fairly large. Such an effect can be attributed to the formation solely of six-membered chelate rings, which is more favorable for the smaller cation.[52] Additional species of composition $[M(HL)]^{3+}$ and $[M(H_2L)]^{4+}$ appeared at lower pH values. Formation of such protonated components is almost negligible for Co^{II} and Ni^{II} but more significant for Zn^{II} and Cd^{II}. In these latter species, the donor set is necessarily only partially bonded to the metal cation, one or two nitrogen atoms of the primary amino groups remaining protonated. In the alkaline range, hydroxo complexes of composition $[ML(OH)]^+$ formed, thus indicating additional coordination of a solvent molecule which can be deprotonated. A corresponding octahedral NiN_5O structure has been established by X-ray analysis (Figure 2) and was confirmed in solution by the Vis spectrum of $[Ni(ditame)(H_2O)]^{2+}$, with bands at 338, 533, and 884 nm.[4] The pK_a values of the $[ML(H_2O)]^{2+}/[ML(OH)]^+$ couples can be calculated as $pK_a = \log \beta_{110} - \log \beta_{11-1}$. For the divalent cations, they

showed only minor differences: 11.7 (Co^{II}), 12.0 (Ni^{II}), 11.8 (Zn^{II}), and 11.7 (Cd^{II}). For the inert Co^{III}, the corresponding value was determined directly by acid-base titration. As was to be expected,[15,17,24] the water molecule bonded to this trivalent cation was considerably more acidic (pK_a = 6.38).

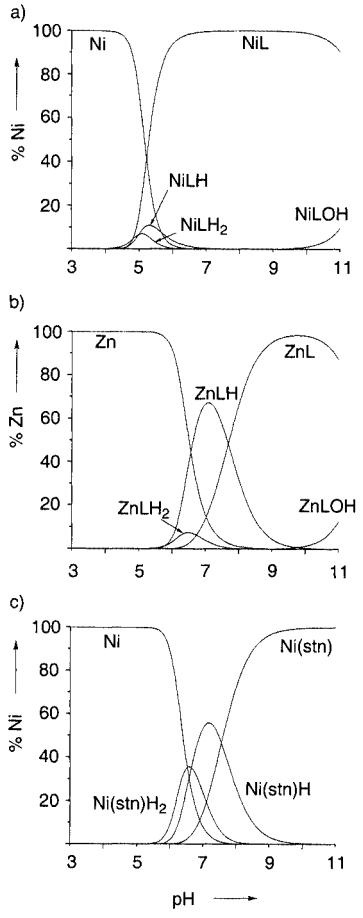

Figure 5. Species distribution plots for equilibrated aqueous solutions; a) Ni^{II} and ditame, b) Zn^{II} and ditame, c) Ni^{II} and stn; total metal and total ligand (L = ditame) concentrations are 1 mM; only metal-containing species are shown; the equilibrium constants listed in Tables 1 and 2 were used for the calculations

Stability constants for metal complexes with representative pentaamine ligands are given in Table 3. These values clearly show that ditame forms a surprisingly stable complex with Ni^{II}. The formation constant of the 1:1 complex has the same order of magnitude as those observed for corresponding complexes with the linear, open-chained tetren or the macrocyclic [16]aneN5. For Zn^{II} and Cd^{II} the situation is different; here the linear and the macrocyclic representatives form 1:1 complexes of higher stability. Obviously, the ditame geometry appears to be particularly suited for the accommodation of relatively small metal ions with a pronounced preference for an octahedral coordination. The particular metal-binding properties of ditame can be elucidated further by comparison with ligands representing different types of substructures with the ditame geometry (Table 4). It is particularly interesting that the addition of two aminomethyl branches to the linear 1,5,9-triazanonane (3,3-tri) ligand at the 3- and the 7-positions increases the stability of the Ni^{II} complex by almost nine orders of magnitude. Again, this effect is much less pronounced for Zn^{II} and Cd^{II}. Similarly, the fusion of two "tame" fragments to the ditame structure is particularly effective for Ni^{II}. Some examples listed in Tables 3 and 4 also support the notion that an increasing number of six-membered chelate rings usually results in a reduction in complex stability. Such destabilization is not observed for ditame, however, although this ligand forms six-membered chelate rings exclusively. The *penta*dentate ditame forms more stable complexes with Co^{II} and Ni^{II}, than the *hexa*dentate stn. This behavior is consistent with the observation that protonated Ni(ditame) complexes are minor species whereas $[Ni(Hstn)]^{3+}$ and $[Ni(H_2stn)]^{4+}$ are substantial components in neutral solution (Figure 5). Even the sen ligand, with three five-membered and three six-membered chelate rings, has a higher

Table 3. Comparison of formation constants (log β_{110}) for selected pentaamine ligands

Polyamine[a]	Co^{II}	Ni^{II}	Zn^{II}	Cd^{II}
ditame	12.8	17.8	11.4	8.7
tetren	13.4	17.4	15.1	13.8
[15]aneN5	16.8[b]		17.9	18.0
[16]aneN5	16.0[b]	17.7	17.9	18.1
pydien	14.8	19.2	13.7	
pydpt	11.5	15.4	11.2	

[a] $\beta_{110} = [ML] \times [M]^{-1} \times [L]^{-1}$; the data are from ref.[53] and are given for 25 °C and an ionic strength of 0.1 M unless otherwise noted; abbreviation of ligands (see also Scheme 1): tetren: 1,4,7,10,13-pentaazatridecane, [15]aneN5: 1,4,7,10,13-pentaazacyclopentadecane, [16]aneN5: 1,4,7,10,13-pentaazacyclohexadecane, pydien: 1,9-bis(2-pyridyl)-2,5,8-triazanonane, pydpt: 1,11-bis(2-pyridyl)-2,6,10-triazaundecane. [b] 35 °C.

Table 2. Formation constants (log β_{xyz}) of ditame complexes (25 °C) with estimated standard deviations in parenthesis (0.1 M KNO_3 or 0.1 M KCl as indicated)

x y z[a]	Co^{II}		Ni^{II}		Zn^{II}		Cd^{II}	
	KNO_3	KCl	KNO_3	KCl	KNO_3	KCl	KNO_3	KCl
1 1 0	12.79(2)	12.93(1)	17.77(2)	17.77(2)	11.43(2)	11.35(1)	8.67(2)	8.19(2)
1 1 1	18.6(2)	18.80(6)	22.42(8)	22.58(8)	19.12(1)	19.03(1)	16.79(2)	16.63(2)
1 1 2	24.8(2)	24.8(2)	27.4(2)	27.7(2)	24.90(6)	25.32(3)	24.02(4)	24.25(2)
1 1 −1	1.04(8)	1.01(6)	5.8(1)	6.6(1)	−0.41(4)	0.96(2)	−2.98(5)	−3.05(3)

[a] $\beta_{xyz} = [M_xL_yH_z] \times [M]^{-x} \times [L]^{-y} \times [H]^{-z}$.

Table 4. Comparison of formation constants (log β_{110}) for some relevant polyamine ligands

Ligand[a]	Denticity	No. of chelate rings five-/six-membered	Co^{II}	Ni^{II}	Zn^{II}	Cd^{II}
ditame[b]	5	0/6	12.8	17.8	11.4	8.7
3,3-tri	3	0/2	6.9	9.2	7.9	6.6
2,2-tri	3	2/0	8.0	10.6	8.8	8.2
tamm[c]	3	0/3	6.3	9.9		5.4
tame[d]	3	0/3		10.1	6.6	
stn[b,e]	6	0/6	10.9	15.6	10.6	9.8
sen	6	3/3	18.0[f]	23.4[b,e]	16.9[b,e,g]	13.4[f]

[a] $\beta_{110} = [ML] \times [M]^{-1} \times [L]^{-1}$; the values given are for $T = 25$ °C, $\mu = 0.1$ M, and are from ref.[53] unless otherwise noted; abbreviation of ligands: 3,3-tri: 1,5,9-triazanonane, 2,2-tri: 1,4,7-triazaheptane, tamm: tris(aminomethyl)methane, tame: 1,1,1-tris(aminomethyl)ethane, stn: 1,1,1-tris(5-amino-2-azapentyl)ethane, sen: 1,1,1-tris(4-amino-2-azabutyl)ethane. For ditame, stn, and sen: see also Scheme 2. [b] This work. [c] 20 °C. [d] 0.5 M KCl. [e] The following pK_a values were used for H_6L^{6+} (25 °C, 0.1 M KCl): 10.92, 10.15, 9.56. 8.52, 6.49, 3.71 for L = stn; and 10.53, 9.61, 9.03, 6.74, 4.70, ca. 2.1 for L = sen. See Tables S4 and S5 in the Supporting Information for further details. [f] 0.5 M KCl.[54] [g] A value $\log\beta_{110} = 17.0(1)$ is reported for 0.5 M KCl.[54]

proportion of such protonation products (Figure S2). The detachment of an amino group in $[Ni(ditame)(H_2O)]^{2+}$ is obviously a particularly unfavorable process, and ditame appears to be unique within the family of ligands forming exclusively six-membered chelate rings.

Formation of Cu^{II} Complexes in Aqueous Solution

Comparison of Ni^{II} and Cu^{II} complex formation with ditame in aqueous solution reveals significant differences. When a 1:1 mixture of $H_5ditame^{5+}$ and Ni^{II} is titrated with 5 equiv. of base, a single, continuous buffer region is observed, according to the reaction $H_5ditame^{5+} + Ni^{2+} + 5\ OH^- \rightarrow [Ni(ditame)]^{2+} + 5\ H_2O$. For Cu^{II}, two individual buffer regions are observed (Figure S3), corresponding to the abstraction of three and of two protons from $H_5ditame^{5+}$ in two sequential and separated steps. It is noteworthy that for the second buffer region, the curve of Cu^{II} lies above that of Ni^{II}, indicating that binding of subsequent amino groups to Ni^{II} is favored at this stage.

For further characterization of the Cu complexes formed, the titration was monitored photometrically. This method allowed the assignment of a spectrum to each individual colored species (Figure S4). The first buffer region could unambiguously be evaluated in terms of $[Cu(H_2L)]^{4+}$ formation (Figure 6). This protonated species predominated in the range $4 < pH < 6$. A meridional coordination mode with two detached $-CH_2-NH_3^+$ branches is proposed for this complex. This assignment is supported by the characteristics of the d-d band with $\lambda_{max} = 619$ nm in comparison to $\lambda_{max} = 616$ nm reported for $[Cu(3,3\text{-tri})]^{2+}$.[55] E. Prenesti et al. reported an empirically derived equation for the estimation of λ_{max} in equatorially coordinated Cu^{II}(amine) complexes,[56] yielding a value of 608 ± 10 nm for such a meridional triamine configuration.

A conclusive assignment for the species appearing in the second buffer region was more difficult. According to the potentiometric measurements, a species of composition Cu^{II}/ditame/H^+ = 1:1:0 was finally formed. The titrations could be interpreted by the assumption of the formation of the simple $[Cu(ditame)]^{2+}$ complex. The corresponding

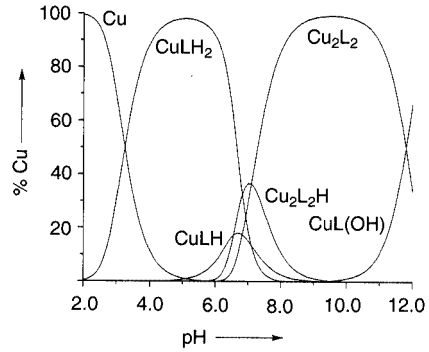

Figure 6. Species distribution plots for equilibrated aqueous solutions with total Cu and total ditame concentration of 10 mM; only metal-containing species are shown; the abundance is given in % of total Cu rather than the amount of species formed; the equilibrium constants listed in Tables 1 and 5 were used for the calculations

λ_{max} of 567 nm, however, is indicative of a tetraammine configuration with the four nitrogen atoms all equatorial.[57] For CuN_5 coordination with an additional nitrogen at the apex, a shift of about 50 nm to *longer* wavelengths would be expected ("pentaamine effect").[4,58] Interestingly, the spectral properties of this species strongly depend on the solvent. Addition of glycerol to a complex solution at pH = 9 resulted in a significant shift of λ_{max} to longer wavelengths (Figure S5). For a glycerol content of 20%, λ_{max} was found at 606 nm. Upon further addition of glycerol this value remained constant. This change can be interpreted as an equilibrium between two different complexes with a Cu^{II}/ditame/H^+ = 1:1:0 composition. An obvious choice for such an equilibrium is the dimerization $2\ [CuL]^{2+} \rightleftarrows [Cu_2L_2]^{4+}$, with the monomer having the square-pyramidal CuN_5 ($\lambda_{max} = 606$ nm) and the dimer a square-planar CuN_4 ($\lambda_{max} = 567$ nm) chromophore. Obviously, $\Delta G°$ for the dimerization is close to 0 under the experimental conditions and this equilibrium is sensitive to subtle changes in the solvent. A conceivable structure for such a dimer would consist of two Cu^{II} centers bonded to the primary amino groups of two ditame ligands. Various conformers of this type, with Cu···Cu separations of 4.0−7.5 Å, were analyzed

by Molecular Mechanics calculations.[59] The structure shown in Figure 7 was found to be of particularly low strain and so can be regarded as a possible model for such a dimer. A series of potentiometric titrations with variable total Cu concentration and variable total Cu/total ditame ratios was now performed, and these measurements could be interpreted well by assuming $[Cu_2L_2]^{4+}$, $[Cu_2L(HL)]^{5+}$, and $[Cu(HL)]^{3+}$ as relevant species (Table 5, Figure 6). The formation of some other Cu^{II} dimers with branched polyamine ligands has recently been described.[60] The spectra of the two dinuclear species $[Cu_2L_2]^{4+}$ and $[Cu_2L(HL)]^{5+}$ did not differ significantly. This is in keeping with the structure shown in Figure 7, in which one of the noncoordinating, secondary nitrogen atoms may be protonated, possibly through intramolecular N−H···N hydrogen bond formation.

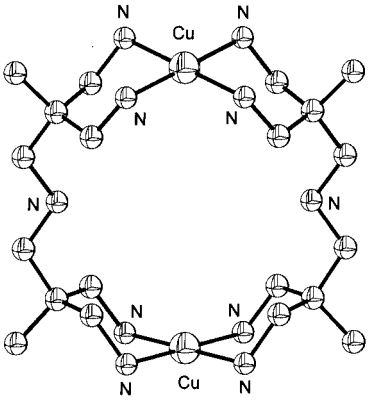

Figure 7. Minimum-energy structure (hydrogen atoms omitted for clarity), calculated by Molecular Mechanics,[59] for the $[Cu_2(ditame)_2]^{4+}$ complex with a square-planar arrangement of the tetraamine donor set; the possible binding of an additional solvent (= H_2O) molecule in the apical positions is omitted in this graphical representation

Table 5. Final model (log $\beta_{x\,y\,z}$) of the Cu(ditame) system (25 °C, 1.0 M KNO_3)

$x\ y\ z$	log $\beta_{x\,y\,z}$[a]
1 1 1	25.5
1 1 2	32.6
1 1 −1	7.1
2 2 0	39.8
2 2 1	46.9

[a] Estimated standard deviations are 0.1 or less.

Further addition of base to an aqueous $[Cu_2L_2]^{4+}$ solution resulted in formation of the hydroxo complex $[CuL(OH)]^+$. This species has a λ_{max} of 606 nm, which is in agreement with an elongated octahedral structure, with N^{sec} and the OH^- ligand in the apices.[58] A pK_a of about 11 was estimated for the $[CuL(OH_2)]^{2+} \rightleftarrows [CuL(OH)]^+ + H^+$ equilibrium. Obviously, $[CuL(OH_2)]^{2+}$ is a slightly stronger acid than the corresponding Co^{II}, Ni^{II}, Zn^{II}, and Cd^{II} complexes.

EPR Characteristics of $[Cu_2(ditame)_2]^{4+}$

For unambiguous identification of the dimer, a comprehensive EPR investigation was performed. The addition of DMSO to a Cu(ditame) complex solution at pH = 9, unlike that of glycerol, did not result in any spectral changes (λ_{max} remained at 567 nm). Most of the low-temperature experiments were therefore performed in frozen DMSO/water solutions. CW EPR measurements were performed primarily to verify the existence of dimers. Figure 8 shows the CW EPR spectra of frozen solutions (2.5 mM Cu) in H_2O with 10% DMSO at pH = 9 (**4**), 10% DMSO at pH = 12 (**5**), and 50% glycerol at pH = 9 (**6**) in the field ranges 260−360 mT (a) and 120−200 mT (b). Simulation parameters for the three samples are given in Table 6. The low-field signal of **4** belongs to the $\Delta M_s = \pm 2$ transitions and arises from magnetic dipole couplings between two Cu^{II} ions. The observation of this low-field spectrum unambiguously shows that sample **4** contains dimers. However, the lack of such a signal in the spectra of **5** and **6** does not necessarily mean that these copper complexes are monomers, since the $\Delta M_s = \pm 2$ transitions can be very low in intensity and difficult to detect. The ratio of the intensity of the forbidden $\Delta M_s = \pm 2$ to the allowed $\Delta M_s = \pm 1$ transitions can be used to estimate the Cu−Cu distance r by the expression[61] $r = [k/I_r(9.1/\nu)^2]^{1/6}$, where k is a constant of approximately 20, I_r is the relative intensity, and ν the microwave frequency. For the dimer of sample **4**, $I_r = 4.4 \cdot 10^{-4}$ yields a distance $r = 5.9$ Å. This estimate is consistent with the proposed structure of the dimer (Figure 7).

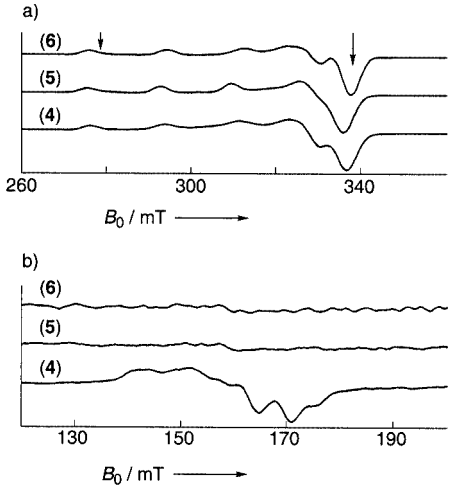

Figure 8. CW EPR spectra of Cu^{II}(ditame); (a) allowed transitions $\Delta M_s = \pm 1$ recorded at 120 K; (b) low-field forbidden transitions $\Delta M_s = \pm 2$ recorded at 10 K; samples: 2.5 mM Cu(ditame) in H_2O with 10% DMSO at pH = 9 (**4**), 10% DMSO at pH = 12 (**5**) and 50% glycerol at pH = 9 (**6**); the two arrows in (a) indicate the observer positions used in ENDOR and HYSCORE experiments

Further information on the coordination of ^{14}N and ^1H nuclei was achieved through ENDOR and HYSCORE experiments.[62] ENDOR spectra on all three samples showed signals from strongly coupled ^{14}N nuclei with hyperfine couplings A between 28 and 34 MHz overlapping with the

Table 6. Principal values of g and A^{Cu} of Cu(ditame) complexes derived from CW EPR

Sample	$g_{\parallel}$	$g_{\perp}$	$\lvert A_{\parallel}^{Cu}\rvert$ [MHz]	$\lvert A_{\perp}^{Cu}\rvert$ [MHz]
^{63}Cu(ditame) in H_2O with				
10% DMSO at pH = 9 (**4**)	2.227	2.051	550	45
10% DMSO at pH = 12 (**5**)	2.238	2.050	530	35
50% Glycerol at pH = 9 (**6**)	2.222	2.048	560	45

signals from weakly coupled ^{1}H nuclei. Spectra from the Cu/ditame dimer sample (Figure 8, sample **4**) taken at the two observer positions indicated in Figure 8a are shown in Figure 9. With weak and long microwave pulses the proton signals dominate, whereas with strong and short microwave pulses the signals of the weakly coupled ^{1}H nuclei are attenuated and the nitrogen signals centered at $A/2$ become clearly visible. The hyperfine couplings of the ^{14}N nuclei are typical for equatorially coordinated nitrogen nuclei with the unpaired electron in the $d_{x^2-y^2}$ orbital of the copper(II) ion.[63]

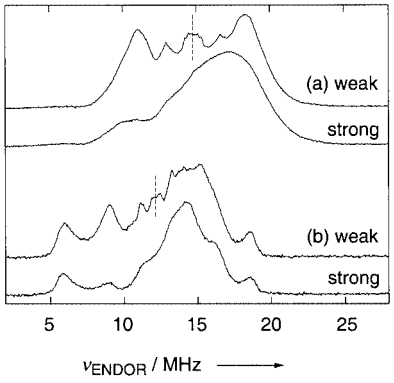

Figure 9. Davies-ENDOR spectra of 2.5 mM Cu(ditame) in H_2O with 10% DMSO at pH = 9 (**4**); spectra were recorded at $g_{\perp}$ (a) and $g_{\parallel}$ (b) by use of weak and strong microwave pulses, respectively (see arrows in Figure 8a); the dashed lines indicate the ^{1}H Larmor frequency

Figure 10 shows two HYSCORE spectra recorded at the high-field position indicated by the arrow in Figure 8a. The spectrum in Figure 10a was measured on the dimer sample **4** and shows large couplings from equatorial ^{1}H nuclei. The spectrum in Figure 10b was measured on sample **5**. In addition to the equatorial ^{1}H nuclei, signals from a ^{14}N nucleus are observed, as indicated in the Figure. Simulations of the ^{14}N HYSCORE spectra, measured at several field positions (Figure S6), resulted in the hyperfine couplings $A_{iso} = -5.6$ MHz, $A_{\parallel} - A_{iso} = 1.8$ MHz, $A_{\perp} - A_{iso} = -0.9$ MHz, and in the nuclear quadrupole coupling $|e^2qQ/h| = 1.3$ MHz with the asymmetry parameter $\eta = 0.4$. They allowed assignment to an axially coordinated ^{14}N nucleus, in agreement with the proposed structure for the monomeric complex. By use of the point-dipole model,[62] the hyperfine anisotropy is given by $T = (\mu_o/2\pi)(gg_n\beta_e\beta_n/hr^3)$. For $T = 0.9$ MHz, a distance of $r = 1.9$ Å between the nitrogen atom and the electron is calculated, a value consistent with expectations. The proton HYSCORE spectra for both complexes show hyperfine couplings of up to 13 MHz, consistent with the ENDOR data.

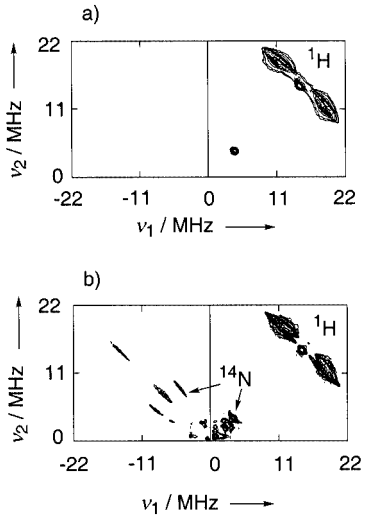

Figure 10. HYSCORE spectra recorded at the high-field position (arrow in Figure 8a) for: 2.5 mM Cu(ditame) in H_2O with 10% DMSO at pH = 9 (Figure 8, sample **4**) (a), 10% DMSO at pH = 12 (Figure 8, sample **5**) (b)

Electrochemistry

Cyclic voltammograms of $[Co(ditame)(H_2O)]^{3+/2+}$ were recorded by use of a hanging Hg drop electrode. Attempts to measure CVs with Au, Pt, or glassy carbon electrodes were not successful. CV scans in neutral and alkaline aqueous solutions showed one single redox step with a strongly pH-dependent potential $E_{obs}^{1/2}$, which decreased with increasing pH in the range $6 < pH < 13$. In aqueous 0.1 M KNO_3, the peak separation ΔE_P was 0.086 V at a scan rate v of 10 mV/s, increasing to $\Delta E_P = 0.162$ V at $v = 200$ mV/s (pH = 9). The ratio of the anodic and cathodic peak current I_{pa}/I_{pc} was 1.0, and I_{pc} depended linearly on $v^{0.5}$. All these observations are in agreement with quasi-reversible electron transfers. The pH dependence was interpreted in terms of a deprotonation of the coordinated water ligand. The species $[Co^{II}L(H_2O)]^{2+}/[Co^{II}L(OH)]^{+}$ ($pK_a^{II} = 11.75$) and $[Co^{III}L(OH_2)]^{3+}/[Co^{III}L(OH)]^{2+}$ ($pK_a^{III} = 6.38$) were taken into consideration. For $pK_a^{III} < pH < pK_a^{II}$, $E_{obs}^{1/2}$ corresponded to an intermediate between the values of the aqua and the hydroxo couples (Figure 11),[24] giving $E^{1/2} = -0.15(1)$ V for $[Co(ditame)(H_2O)]^{3+/2+}$ and $E^{1/2} = -0.47(1)$ V for $[Co(ditame)(OH)]^{2+/+}$ (vs. NHE). For comparison, the corresponding ammine and chloro complexes $[Co(ditame)(NH_3)]^{3+}$ and $[Co(ditame)Cl]^{2+}$ were also studied; they exhibited quasireversible redox behavior with $Co^{3+/2+}$ potentials of -0.41 and -0.20 V (Au electrode), respectively.

CV measurements were performed on the dinuclear Co^{III} complex by use either of the peroxo or of the superoxo forms as starting materials (1 M KCl, Au electrode). Quasireversible redox behavior was found with $E^{1/2} = 0.72$ V vs.

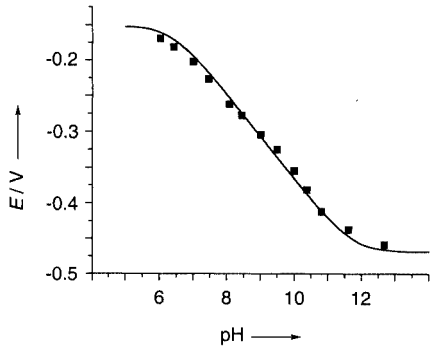

Figure 11. Observed redox potentials $E^{1/2}_{obs}$ for the $[Co(ditame)(OH_2)]^{3+/2+}$ – $[Co(ditame)(OH)]^{2+/+}$ system; squares represent the measured values; the line was calculated by use of the equation $E^{1/2}_{obs} = E^{1/2}{}_{Co^{III/II}L(H_2O)} - RT/F \times \ln\{(1 + K^{III}_a/[H^+])/(1 + K^{II}_a/[H^+])\}$ with $pK^{III}_a = 6.36$, $pK^{II}_a = 11.75$, and $E^{1/2}{}_{Co^{III/II}L(H_2O)} = -0.15$ V; $E^{1/2}{}_{Co^{III/II}L(OH)}$ can be calculated as $E^{1/2}{}_{Co^{III/II}L(H_2O)} - 2.303\ RT/F \times (pK^{II}_a - pK^{III}_a) = -0.47$ V

NHE. This value showed no significant pH dependence in the range $3 < pH < 8$. ΔE_P increased steadily with increasing v ($\Delta E_P = 70$ mV at $v = 10$ mV/s, $\Delta E_P = 120$ mV at $v = 200$ mV/s). I_{pc} was again found to depend linearly on $v^{0.5}$. I_{pa}/I_{pc} varied between 0.8 and 1.2. Similar behavior has been reported for other dinuclear, peroxo-bridged (pentaamine)Co^{III} complexes, with $E^{1/2}_{obs}$ being assigned to reversible oxidation of the O_2^{2-} bridge.[7,15,35,48,64]

In aqueous solutions of $[Ni(ditame)]^{2+}$ (0.1 M KNO_3), cyclic voltammetry indicated formation of an Ni^{III} species. A quasi-reversible one-electron transfer was observed, with $E^{1/2}_{obs} = 0.95$ V vs. NHE ($\Delta E_P = 79$ mV, $v = 5$ mV/s, Au electrode). ΔE_P again increased with increasing v. Unlike in the case of the Co complexes, I_{pa}/I_{pc} depended significantly on v, with $I_{pa}/I_{pc} < 1$ for $v < 100$ mV/s. At $v > 100$ mV/s the ratio was close to unity. $E^{1/2}_{obs}$ did not depend on H^+ concentration in the range $7 < pH < 11$. At higher pH values a significant drop in the potential was noted. Under these conditions, however, the reaction was no longer reversible, and deposition of solid materials on the surface of the electrode was observed. The electrochemical oxidation of Ni^{II}(polyamine) complexes to corresponding Ni^{III} species is well established.[65,66] For $[Ni(sen)]^{3+/2+}$, $E^{1/2}_{obs} = 0.92$ V has been reported.[66] The absence of any pH dependence for the $[Ni(ditame)]^{3+/2+}$ couple at $pH < 11$ is a clear indication that deprotonation of an acidic aqua ligand in the Ni^{III} species does not occur.[67,68] This could be attributable to the Jahn–Teller distortion caused by the low-spin d^7-electron configuration. The drastic drop in the potential at higher pH is coupled with decomposition. A possible explanation of this reactivity would be N–H deprotonation of a coordinated amino group, followed by an intramolecular oxidation of the ligand by Ni^{III}.[68,69]

Conclusions

The pentadentate ditame ligand (= L) forms $[NiLX]^{2+}$ complexes (X = solvent molecule) of surprisingly high stability and selectivity. We attribute the high selectivity to the peculiar ligand geometry, which appears to be particularly well suited for accommodation of late transition metal ions of fairly small size and a distinct preference for octahedral coordination. This conclusion is based on the following observations:

(i) ditame and stn (Scheme 1) can both be regarded as extensions of the tripodal tris(aminomethyl)ethane (tame), with exclusive formation of six-membered chelate rings. However, with respect to $[NiL]^{2+}$ formation, the complex with the *penta*dentate ditame is significantly more stable than the complex with the *hexa*dentate stn. The situation is different for Cd^{II}, for which the complex with stn is of slightly higher stability.

(ii) The favorable geometry of ditame for Ni^{II} binding is further demonstrated by the low capacity of $[Ni(ditame)]^{2+}$ to dissociate partially and to protonate an amino group. This type of reactivity is usually a feature of polyamine complexes with multiple six-membered chelate rings. For $[Zn(ditame)]^{2+}$, partial dissociation and partial protonation of the ligand is indeed extensively observed.

(iii) The geometry of ditame appears to induce a rather short $M-N^{sec}$ bond. This feature is most readily attained in complexes with an approximately octahedral structure. As a consequence, $[Cu(ditame)]^{2+}$ has a rather low stability, which does not fit normal Irving–Williams behavior. Two primary amino groups are readily detached and protonated, forming a meridional $[Cu(H_2ditame)]^{4+}$ complex, which appears to predominate in slightly acidic solutions. Furthermore, the EPR measurements provided unambiguous evidence that in slightly alkaline solution, in which the noncoordinating ammonium groups of $[Cu(H_2ditame)]^{4+}$ become deprotonated, the mononuclear species is in equilibrium with a dimer, $[Cu_2(ditame)_2]^{4+}$. In this dimer, Cu^{II} is probably bonded to the four primary amino groups with a square-planar arrangement.

From the high stability and the possibility for additional binding of a monodentate entity X (a "substrate"), octahedral complexes such as $[NiLX]^{2+}$ or $[CoLX]^{3+}$ would have ideal prerequisites for synthetic or even catalytic applications. The dimeric Co^{III}(peroxo)/(superoxo) complexes $\mathbf{2}^{4+}$ and $\mathbf{3}^{5+}$, in which reversible one-electron transfer was observed for the dioxygen bridge over a wide pH range (2–9), may be regarded as models for this type of reactivity.

Experimental Section

Materials and Instrumentation: ditame·5HCl,[21] [Co(ditame)Cl][$ZnCl_4$],[21] [Co(ditame)(NH_3)]Cl[$ZnCl_4$],[21] sen·6HCl,[26] and stn·6HCl[26] were prepared as described. Unless otherwise stated, all chemicals used for the synthetic work were commercially available products of reagent-grade quality. H_2O was distilled twice (quartz apparatus). Organic solvents were purified by distillation prior to use. For the potentiometric and spectrophotometric titrations, metal salts of the highest available quality (> 99.95%) were used. $^{63}CuCl_2$ (for EPR) was purchased (98.6% isotopically enriched) from CAMPRO Scientific (Berlin, Germany). Dowex 50 W-X2 (100–200 mesh, H^+ form) and Dowex 2-X8 (50–100 mesh,

Cl^- form) were purchased from Fluka. The anion resin was converted into the OH^- form or the NO_3^- form by use of 0.3 M aqueous NaOH or concd. KNO_3, respectively. UV/Vis spectra of the Ni^{II} complexes were measured with a Uvikon 941 spectrophotometer (H_2O, 25±3 °C), while a solid-state UV/Vis spectrum of **2**Cl_4·$4H_2O$ was recorded with sapphire plates and a Cary 5 spectrometer. IR spectra were recorded with a Bruker Vector 22 FT IR spectrometer equipped with a Golden Gate ATR unit. Raman spectra were measured with a Dilor-XY spectrometer, with an Ar^+/Kr^+-mixed gas laser used for excitation (λ = 647.1 nm). C,H,N analyses were performed by H. Feuerhake (Universität des Saarlandes).

Measurement and Interpretation of NMR Spectra: ^1H and $^{13}C\{^1H\}$ NMR spectra were measured in D_2O (28 °C) with a Bruker DRX 500 spectrometer (resonance frequencies: 500.13 MHz for ^1H and 125.9 MHz for ^{13}C). Chemical shifts (in ppm) are given relative to sodium [D_4](trimethylsilyl)propionate as an internal standard (δ = 0 ppm). A Hamilton SPINTRODE glass electrode, fitted with an internal Ag/AgCl reference (H_2O), was used within the NMR tube for a direct measurement of pD (corrected).[29] Least-squares calculations [$\Sigma(\delta_{obs} - \delta_{calc})^2$ = min] were performed with the computer program NMR-Tit,[70] the resulting parameters (pK_a and δ_{calc}) of the macro species are listed in Table S1. The constants P^α, S^α, P^χ, and S^χ were used to model the deshielding of the CH_2 and CH_3 protons in the individual microspecies caused by protonation of a primary (*P*) or the secondary (*S*) amine site, respectively. The distances between the protonated site and the hydrogen atom under consideration are indicated as α (N−C−H) and χ (N−C−C−C−H). Effects over longer distances were not considered. From symmetry arguments, the protonation of a primary amino group was always treated in a statistical manner by distributing the protons equally over all four sites. Because of the low number of observations (i.e., the resonances X, Y, Z in Figure 1), the same distance dependence was assumed for the primary and the secondary amine sites: $P^\chi/P^\alpha = S^\chi/S^\alpha = x$. From the data for the fully protonated and the fully deprotonated form one obtains: (i) $P^\alpha + xP^\alpha + xS^\alpha = 0.89$; (ii) $S^\alpha + 2x\,P^\alpha = 1.066$; (iii) $2xP^\alpha + x\,S^\alpha = 0.558$; and subsequently $P^\alpha = 0.495$, $S^\alpha = 0.748$, and $x = 0.32$. It is noteworthy that the value of 0.32 for *x* is significantly larger than corresponding ratios previously reported for methylene groups of macrocyclic polyamines.[31] The observed shifts of the macrospecies HL^+, H_2L^{2+}, H_3L^{3+}, and H_4L^{4+} were then interpreted as weighted averages of the two micro species (Table S2).

EPR: CW EPR measurements were performed with a Bruker ESP300 spectrometer (microwave frequency 9.43 GHz) equipped with a liquid nitrogen cryostat and a liquid helium cryostat from Oxford Inc. HYSCORE and ENDOR experiments[62] were carried out at X-band frequencies with a Bruker Elexsys spectrometer (microwave frequency 9.68 GHz) at 20 K. The HYSCORE experiments with the pulse sequence $\pi/2-\tau-\pi/2-t_1-\pi-t_2-\pi/2-\tau-$echo used 40-ns $\pi/2$ pulses, a 16-ns transfer π pulse, and an eight-step phase cycle. Two Davies-ENDOR experiments were measured by using the pulse sequence $\pi-T-\pi/2-\tau-\pi-$echo. One sequence employed a 120-ns π pulse and the second sequence employed a 32-ns π pulse to suppress weakly coupled proton nuclei. A radio frequency pulse with a length of 8 μs and a flip angle of π for the matrix protons was used. All measurements were carried out in frozen aqueous solutions with addition of DMSO or glycerol, using ^{63}Cu. Oxygen-free samples were obtained by degassing (freeze-pump-thaw method under vacuum). CW EPR and HYSCORE simulations were calculated with the EasySpin package[71] and the TRYSCORE program,[72] respectively.

Electrochemistry: Cyclic voltammograms of $[CoL(NH_3)]^{3+/2+}$, $[CoLCl]^{2+/+}$, $[NiL(H_2O)]^{3+/2+}$, and $[Co_2L_2(O_2)]^{5+/4+}$ (L = ditame) were recorded with a BAS C2 cell and a BAS 100B/W 2 potentiostat at ambient temperature (23±3 °C) with an Au working electrode, a Pt counter-electrode, and an Ag/AgCl reference. The $[CoL(H_2O)]^{3+/2+}$ couple was investigated by using an Hg (hanging drop) working electrode and $Na_2B_4O_7$·$10H_2O$ or 4-(2-hydroxyethyl)piperazin-1-propanesulfonic acid (HEPPS) as buffers. Potentials quoted were calculated relative to the normal hydrogen electrode (NHE), with a value of 0.46 V used for the $[Fe(CN)_6]^{3-/4-}$ couple (0.01 M NaOH).

Potentiometric Measurements: Potentiometric titrations (50 mL sample solution) were carried out under nitrogen at 25.0±0.1 °C as described previously.[4,29] Solid, analytically pure samples of ditame·5HCl, ditame·$5HNO_3$·$0.5H_2O$, stn·6HCl·$2H_2O$, or sen·6HCl were applied to determine the pK_a values of the ligands. Metal-containing samples (Co, Ni, Cu, Zn, Cd) were prepared from standardized aqueous stock solutions (w/w) of the metal chlorides or metal nitrates. Details of the various titrations are summarized in Tables S3−S5. Formation of Ni^{II} complexes with sen and stn proved to be too slow for continuous titration, and a batch method with individually sealed sample solutions was applied.

Spectrophotometric Titrations: The titration cell used for the potentiometric titrations was equipped with an immersion probe (HELLMA) connected to a diode array spectrophotometer (J&M, TIDAS-UV/NIR/100-1). An in-house computer program was used to control the addition of the titrant (1 M KOH) and to trigger a spectrum of the sample solution (0.01−0.02 M total Cu, 1 M KNO_3, 25.0±0.1 °C) prior to the addition of each aliquot of titrant.

Calculations of Equilibrium Constants: All equilibrium constants were calculated as concentration constants and the pH was defined as $-\log [H^+]$. The potentiometric data were evaluated by use of the computer program HYPERQUAD.[73] The pK_w (13.78 for μ = 0.1 M, 13.71 for μ = 1.0 M)[53] and the total concentrations of the reactants were treated as fixed values. Additionally, the protonation constants of the ligands were also fixed (Table 1) when refining formation constants of metal-containing species. The model for Cu(ditame) complexes was established by collective evaluation of several titration experiments with total Cu and total ditame concentrations ranging from 0.25 to 10.0 mM. The spectrophotometric data were evaluated by use of the computer program SPECFIT.[74] The spectrum of the free Cu^{2+} was measured separately and was not refined; ditame and its protonation products were regarded as colorless.

Crystal Structure Determination:[75] X-ray diffraction data of **1**Br_2, **2**Cl_4·$4H_2O$, and **3**$Cl_2[ZnCl_4][ZnCl_3(H_2O)]$·$H_2O$ were collected with a STOE imaging Plate Diffraction System by use of graphite-monochromatized Mo-K_α radiation (λ = 0.71073 Å) at 25(2) °C. Further details are summarized in Table 7. No indication of crystal decay was noted for any of the crystals during data collection. All data sets were corrected for Lorentz and polarization effects. *Specific comments for* **1***Br*$_2$ *and* **2***Cl*$_4$·$4H_2O$*:* The symmetries of diffraction patterns and systematic extinctions were consistent with space group types *Pnma* and $Pna2_1$ for **1**Br_2, and *I*2/*m*, *Im*, and *I*2 for **2**Cl_4·$4H_2O$. The structures were solved by direct methods.[76] Approximate positions of all the hydrogen atoms were found in different stages of refinements by full-matrix, least-squares calculations on F^2.[77] Refinements suffered from the high pseudosymmetry of the cations $\mathbf{1}^{2+}$ and $\mathbf{2}^{4+}$ and the possibility of disorder on sites of higher symmetry had to be taken into account with respect to their

shape and the symmetry of their solid-state environments. In both cases, none of the possible space groups allowed a complete set of physically reasonable atomic and anisotropic displacement parameters to be refined without use of appropriate weak restraints to overcome correlation problems. Consistent with E-statistics, significantly better results were observed for a model with 1:1 orientationally disordered cations on a site of symmetry *m* in centrosymmetric space group *Pnma* in the case of $\mathbf{1}Br_2$ ($S = 1.06$), and for a C_2-symmetric model on a site of corresponding symmetry in the chiral space group *I*2 in the case of $\mathbf{2}Cl_4{\cdot}4H_2O$ ($S = 1.07$).[77] The absolute structure of $\mathbf{2}Cl_4{\cdot}4H_2O$ could be determined reliably.[78] Anisotropic displacement parameters were refined for all non-hydrogen atoms with the exception of O4 and O5, representing disordered water molecules of $\mathbf{2}Cl_4{\cdot}4H_2O$ in partially occupied general positions (occupation 0.25 and 0.25). All H atoms were treated with fixed idealized O−H, N−H, or C−H distances. With idealized geometries assumed for the CH_3, CH_2, NH_2, and NH groups, the riding model was applied for the H atoms. In addition, the H atoms of methyl groups were allowed to move collectively around the neighboring C−C axis. The water molecules of $\mathbf{2}Cl_4{\cdot}4H_2O$ were treated as rigid groups with idealized bond lengths and angles. The orientation of the OH group of the ethanol ligand of $\mathbf{1}^{2+}$ was refined. Isotropic displacement parameters of H atoms were kept equal to 120% of the equivalent isotropic displacement parameters of the parent oxygen, nitrogen, and carbon atoms for the OH, NH, NH_2, and CH_2 groups and equal to 150% for the CH_3 groups and water molecules. *Specific comments for* $\mathbf{3}Cl_2[ZnCl_4]{\cdot}[ZnCl_3(H_2O)]{\cdot}H_2O$: The structure was solved by direct methods (SHELXS-97) and refined by full-matrix, least-squares calculations on F^2 by use of SHELXL-97.[76,77] One water molecule of crystallization (O2) was found to be distributed over three sites (O2A, O2B, O2B′, with O2B−O2B′ being related by $= -x, y, -z + 1/2$) with site occupancies of 0.28, 0.36, and 0.36. The O(4A)−Cl(4A) part of the two counter-ions $[ZnCl_4]^{2-}$and $[ZnCl_3(H_2O)]^-$ (which were related through a center of inversion), was also found to be disordered. Some preliminary isotropic refinement found an occupancy of 50±2% for O(4A) and Cl(4A). In the final refinement, the occupancy of these atoms was fixed at 50%, and anisotropic displacement parameters were used for all non-hydrogen atoms. The positions of the H atoms were calculated (riding model with $U_{iso} = 1.2 \times U_{eq}$ of the pivot atom).

Molecular Modeling Calculations: These were carried out with the commercially available program MOMEC97.[59]

[Ni(ditame)(EtOH)]Br_2: ditame·5HCl[21] (2.20 g, 5.50 mmol) was dissolved in H_2O (100 mL) and deprotonated with Dowex 2 (OH^- form). The solution was concentrated to dryness under reduced pressure. The oily residue was redissolved in H_2O (20 mL), and a solution of $NiBr_2{\cdot}3H_2O$ (1.47 g, 5.39 mmol) in H_2O (20 mL) was added dropwise. A color change to violet was noted. The solution was concentrated to dryness, and the residue was recrystallized from EtOH (40 mL)/H_2O (6 mL) at 5 °C. The resulting violet precipitate was washed with EtOH and Et_2O and dried in vacuo over P_2O_5 (1.07 g, 41%). $C_{12}H_{33}Br_2N_5NiO$ (482.0): calcd. C 29.91, H 6.90, N 14.53; found C 30.06, H 6.93, N 14.70. UV/Vis: λ_{max} (ε) = 338 (10.1), 533 (7.6), 884 (9.9) nm. Single crystals suitable for X-ray crystallography were grown by layering a concentrated aqueous complex solution with EtOH.

ditame·5HCl: A high-purity sample required for the potentiometric titrations was obtained from the Ni complex. [Ni(ditame)(EtOH)]Br_2 was recrystallized twice from EtOH/H_2O. The resulting, analytically pure, violet compound was dissolved in H_2O and heated to 50 °C. Concd. HCl was added to the solution in small portions until a color change to green was noted. The clear green solution was diluted with water to pH = 1 and sorbed on Dowex 50. The column was eluted with water and with 0.5 M HCl until all the Ni had been removed (checked with dimethylglyoxime). Elution with 6 M HCl yielded a colorless solution of ditame·5HCl, which was concentrated to dryness. The resulting white solid was recrystallized from concd. HCl/MeOH/EtOH (yield 72%). $C_{10}H_{32}Cl_5N_5$ (399.7): calcd. C 30.05, H 8.07, N 17.52; found C 30.06, H 8.19, N 17.30. ^{1}H NMR (D_2O, pD < 2): δ = 1.27 (s, 6 H), 3.06 (s, 4 H), 3.23 (AB system, 8 H) ppm. ^{13}C NMR (D_2O, pD < 2): δ = 20.1, 38.7, 46.4, 57.0 ppm.

ditame·5HNO$_3$·0.5H$_2$O: ditame·5HCl (1.40 g, 3.50 mmol) was dissolved in H_2O (1400 mL) and sorbed on Dowex 2 (NO_3^- form). The column was eluted *slowly* (over 24 h) with water and the resulting solution was concentrated to dryness. The oily residue was carefully dried in vacuo over P_2O_5, and recrystallized from MeOH/H_2O (yield 72%). $C_{10}H_{33}N_{10}O_{15.5}$ (541.4): calcd. C 22.18, H 6.14, N 25.87; found C 22.32, H 6.14, N 25.59. ^{1}H NMR (D_2O, pD < 2) identical with that of ditame·5HCl.

[Zn(ditame)(EtOH)]Br$_2$: The Zn complex was prepared by the same procedure as reported for the Ni complex and was obtained as a colorless, crystalline solid (38%). $C_{12}H_{33}Br_2N_5OZn$ (488.6): calcd. C 29.50, H 6.81, N 14.33; found C 29.31, H 6.73, N 14.52.

[Co$_2$O$_2$(ditame)$_2$]Cl$_4$·4H$_2$O: ditame·5HCl (800 mg, 2 mmol) was dissolved in H_2O (5 mL) and deprotonated on Dowex 2 (OH^- form). The alkaline eluent was concentrated to dryness under reduced pressure, and the oily residue was redissolved in H_2O (10 mL). $CoCl_2{\cdot}6H_2O$ (476 mg, 2 mmol), dissolved in H_2O (10 mL), was then added dropwise, and a stream of O_2 was passed through the solution over a period of 3 h. The color changed from yellow to deep brown. The solution was allowed to stand for 3 d at 5 °C, and the resulting brown solid was collected by filtration. The remaining clear, brown solution was concentrated to a volume of 20 mL, cooled, and allowed to stand for 3 d at 5 °C. After collection of a second fraction of the product, the two fractions were combined, washed with Et_2O, and dried in vacuo (367 mg, 47%). $C_{20}H_{62}Cl_4Co_2N_{10}O_6$ (798.5): calcd. C 30.09, H 7.83, N 17.54; found C 30.04, H 7.89, N 17.74. UV/Vis: λ_{max} (log ε) = 296 (4.1) nm. IR: $\tilde{\nu}$ = 3358, 3177, 3079, 2954, 2907, 2873, 1603, 1461, 1409, 1202, 1155, 1117, 1083, 1020, 969, 910, 735, 629, 562, 505 cm^{-1}. ^{1}H NMR (D_2O): δ = 0.86 (s, 12 H), 2.36 (4 H), 2.47 (8 H), 2.56 (8 H), 2.73 (4 H) ppm. ^{13}C NMR (D_2O): δ = 23.5, 42.3, 47.8, 49.2, 59.2 ppm. Single crystals suitable for X-ray crystallography were grown from a saturated aqueous solution by slow concentration at room temperature.

[Co$_2$O$_2$(ditame)$_2$]Cl$_5$·2H$_2$O: $[Co_2O_2(ditame)_2]Cl_4{\cdot}4H_2O$ (270 mg, 0.338 mmol) was suspended in H_2O (50 mL). $Ce(SO_4)_2{\cdot}4H_2O$ (140 mg, 0.346 mmol) was separately dissolved in H_2O (10 mL). Both solutions were acidified to pH = 1 with a few drops of 8 M HCl. The Ce^{IV} solution was added rapidly (within 1 min) to the suspension of the μ-peroxo complex, and the resulting deep green solution was stirred for 10 min. EtOH (200 mL) was added, and the mixture was allowed to stand for 72 h at 5 °C. The green precipitate was collected, washed carefully with EtOH and Et_2O, and air-dried (200 mg, 74%). $C_{20}H_{58}Cl_5Co_2N_{10}O_4$ (797.9): calcd. C 30.11, H 7.33, N 17.55; found C 30.25, H 7.30, N 17.16. UV/Vis: λ_{max} (log ε) = 312 (3.9), 471 (2.3), 695 (2.85) nm. Single crystals of composition $\mathbf{5}Cl_2[ZnCl_4][ZnCl_3(H_2O)]{\cdot}H_2O$ suitable for X-ray crystallography were grown at 5 °C from a saturated aqueous solution (10 mL) of the pentachloride salt after addition of a solution (10 mL) of HCl (8 M) and $ZnCl_2$ (1 g).

Table 7. Crystallographic data of $[Ni(ditame)(EtOH)]Br_2$ (**1**Br_2), $[Co_2(ditame)_2O_2]Cl_4{\cdot}4H_2O$ (**2**$Cl_4{\cdot}4H_2O$), and $[Co_2(ditame)_2O_2]Cl_2[ZnCl_4][ZnCl_3(H_2O)]{\cdot}H_2O$ (**3**$Cl_2[ZnCl_4][ZnCl_3(H_2O)]{\cdot}H_2O$)

Complex	$\mathbf{1}^{2+}$	$\mathbf{2}^{4+}$	$\mathbf{3}^{5+}$
Empirical formula	$C_{12}H_{33}Br_2N_5NiO$	$C_{20}H_{62}Cl_4Co_2N_{10}O_6$	$C_{20}H_{58}Cl_9Co_2N_{10}O_4Zn_2$
Formula mass	481.96	798.46	1070.41
Crystal system	orthorhombic	monoclinic	monoclinic
Space group	*Pnma* (no. 62)	*I*2 (no. 5)	*C*2/*c* (no. 15)
a [Å]	20.509(4)	14.291(3)	23.190(5)
b [Å]	7.7354(15)	7.2447(14)	14.244(3)
c [Å]	12.436(3)	18.488(4)	16.165(3)
β [°]	90	108.80(3)	127.97(3)
V [Å^3]	1972.9(7)	1812.0(6)	4209(2)
Z	4	2	4
$D_{calcd.}$ [g cm^{-3}]	1.623	1.463	1.689
μ [mm^{-1}]	5.040	1.257	2.512
Crystal size [mm]	0.4 × 0.1 × 0.1	0.50 × 0.32 × 0.28	0.3 × 0.2 × 0.1
θ_{min}, θ_{max} [°]	1.92, 24.12	3.01, 25.79	1.81, 22.50
Data set	−23/23; −8/8; −14/13	−17/17; −8/8; −22/22	−24/19; 0/15; 0/17
Total/unique data	12136, 1670	12816, 3240	2753, 2753
Parameter/restraints	194/38	198/9	231/0
R_1, wR_2 [$I > 2\sigma(I)$]	0.0462, 0.1075	0.0639, 0.1286	0.0567, 0.1342
R_1, wR_2 (all data)	0.0579, 0.1122	0.0712, 0.1322	0.0579, 0.1348
Abs. struct. param.		0.06(3)	
Max. peak/hole [e/Å^3]	0.907/−0.884	0.541/−0.312	0.593/−0.565

[Co(ditame)(H_2O)](CF_3SO_3)$_3$: [Co(ditame)Cl][$ZnCl_4$][21] (100 mg, 193 μmol) was dissolved in H_2O (10 mL) and sorbed on Dowex 50. The column was washed with H_2O, 0.1 M HCl, 0.5 M HCl, and 1 M HCl (200 mL each). Further elution with 3 M HCl gave a dark red fraction, which was concentrated to dryness. The resulting solid was redissolved in H_2O (20 mL) and heated to 80 °C. A solution of $AgCF_3SO_3$ was added dropwise until the precipitation of solid AgCl was completed. The solid was removed by filtration (Celite) and the reddish-orange, clear solution was concentrated to dryness. (142 mg, 100%). $C_{13}H_{29}CoF_9N_5O_{10}S_3$ (741.5): calcd. C 21.06, H 3.94, N 9.44; found C 21.42, H 4.09, N 9.42. UV/Vis: λ_{max} = 345, 487 nm. ^{1}H NMR (D_2O): δ = 0.93 (s, 6 H), 2.06 (2 H), 2.33 (2 H), 2.45 (2 H), 2.62 (2 H) 2.74 (2 H), 2.77 (2 H) ppm. ^{13}C NMR (D_2O): δ = 22.8, 42.8, 47.1, 48.4, 57.7, 122.3 (q, *J* = 316 Hz) ppm.

[Ni(stn)]$Br_2{\cdot}2.5H_2O$: The procedure reported above for the ditame complex was applied, with $NiBr_2{\cdot}3H_2O$ (534 mg, 1.96 mmol) and crude[26] stn·6HCl·$2H_2O$ (1.09 g, 2 mmol). The resulting violet solid was recrystallized from H_2O (10 mL) and EtOH (20 mL) at 5 °C (70%). $C_{14}H_{41}Br_2N_6NiO_{2.5}$ (552.0): calcd. C 30.46, H 7.49, N 15.22; found C 30.52, H 7.48, N 15.19. UV/Vis: λ_{max} (ε) = 341 (13.9), 539 (10.6), 858 (8.3) nm.

stn·6HCl·$2H_2O$: A high-purity sample required for the titration experiments was prepared from crystalline, analytically pure [Ni(stn)]$Br_2{\cdot}2.5H_2O$ (570 mg, 1.03 mmol). The complex was decomposed by HCl and sorbed on Dowex 50 as described above for ditame·5HCl. The protonated polyamine was eluted with 8 M HCl, and the solution was concentrated to a total volume of 10 mL. MeOH (20 mL) was added slowly, and the mixture was allowed to stand at 5 °C for 72 h. The colorless, crystalline solid was removed by filtration, washed with EtOH and EtOEt, and dried in vacuo (81%). $C_{14}H_{46}Cl_6N_6O_2$ (543.3): calcd. C 30.95, H 8.53, N 15.47; found C 30.90, H 8.57, N 15.28. ^{1}H NMR (D_2O, pD < 3): δ = 1.39 (s, 3 H), 2.18 (m, 6 H), 3.12 (t, *J* = 8 Hz, 6 H), 3.26 (t, *J* = 8 Hz, 6 H), 3.38 (s, 6 H) ppm. ^{13}C NMR (D_2O, pD < 3): δ = 21.0, 26.7, 38.8, 39.6, 49.4, 55.4 ppm.

[Ni(sen)]Br_2:[66] The procedure reported above for the ditame complex was applied, with $NiBr_2{\cdot}3H_2O$ (545 mg, 2 mmol) and crude[26] sen·6HCl (930 mg, 2 mmol). The resulting violet solution was concentrated to a total volume of 10 mL. EtOH (50 mL) was added, and the solution was allowed to stand at 5 °C for 72 h. Violet needles (572 mg, 62%). $C_{11}H_{30}Br_2N_6Ni$ (464.9): calcd. C 28.42, H 6.50, N 18.08; found C 28.72, H 6.56, N 17.77. UV/Vis: λ_{max} (ε) = 337 (10.0), 522 (8.2), 803 (10.0) nm.

sen·6HCl: A high-purity sample required for the titration experiments was prepared from crystalline, analytically pure [Ni(sen)]Br_2 (1664 mg, 3.58 mmol). The complex was decomposed with HCl and sorbed on Dowex 50 as described above for ditame·5HCl. The protonated polyamine was eluted with 8 M HCl and the solution was concentrated to a total volume of 20 mL. MeOH (100 mL) and EtOH (50 mL) were added slowly, and the mixture was allowed to stand at 5 °C for 72 h. The colorless, crystalline solid was removed by filtration, washed with EtOH and EtOEt, and dried in vacuo (1.20 g, 72%). $C_{11}H_{36}Cl_6N_6$ (465.2): calcd. C 28.40, H 7.8, N 18.07; found C 28.30, H 7.86, N 17.69. ^{1}H NMR (D_2O, pD < 3): δ = 1.44 (s, 3 H), 3.47 (s, 6 H), 3.53 (m, 12 H) ppm. ^{13}C NMR (D_2O, pD < 3): δ = 21.1, 38.4, 39.3, 48.9, 55.1 ppm.

Supporting Information: Supporting information for this article is available (see footnote on the first page of this article). Tables S1−S5 list NMR parameters and potentiometric data. Figures S1−S6 show the disorder of [Ni(ditame)(EtOH)]Br_2, pH-dependent species distribution plots of the Co^{II}/ditame, Cd^{II}/ditame, and Ni^{II}/sen systems, titration curves of Cu^{2+}/Ni^{2+}/ditame·$5HNO_3$ solutions, and Vis and EPR data for the Cu(ditame) complexes.

Acknowledgments

The Raman and solid-state UV/Vis spectra were measured by Prof. Dr. Felix Tuczek (Kiel). MM calculations were carried out by Dr. Dirk Kuppert (Saarbrücken). Part of the synthetic work was performed by Anton Zaschka (Saarbrücken). X-ray diffraction data

for $\mathbf{5}Cl_2[ZnCl_4][ZnCl_3(H_2O)]\cdot H_2O$ were recorded by Dr. Volker Huch (Saarbrücken). We thank Stefan Steinhauser and Bernd Morgenstern (Saarbrücken) for valuable help and suggestions. Financial support from the Saarland (O. M.) and the Fonds der Chemischen Industrie (K. H.) is gratefully acknowledged.

[1] [1a] D. S. C. Black, A. J. Hartshorn, *Coord. Chem. Rev.* **1973**, *9*, 219−274. [1b] K. Hegetschweiler, *Chem. Soc. Rev.* **1999**, *28*, 239−249.
[2] [2a] P. Braunstein, F. Naud, *Angew. Chem. Int. Ed.* **2001**, *40*, 680−699. [2b] C. Gambs, S. Chaloupka, G. Consiglio, A. Togni, *Angew. Chem. Int. Ed.* **2000**, *39*, 2486−2488.
[3] T. Bark, M. Düggeli, H. Stoeckli-Evans, A. von Zelewsky, *Angew. Chem. Int. Ed.* **2001**, *40*, 2848−2851.
[4] A. Zimmer, D. Kuppert, T. Weyhermüller, I. Müller, K. Hegetschweiler, *Chem. Eur. J.* **2001**, *7*, 917− 931.
[5] [5a] R. J. Geue, J. V. Hanna, A. Höhn, C. J. Qin, S. F. Ralph, A. M. Sargeson, A. C. Willis, *Adv. Chem. Ser.* **1997**, *253*, 137−150. [5b] A. M. Allgeier, C. A. Mirkin, *Angew. Chem. Int. Ed.* **1998**, *37*, 894−908.
[6] B. M. Gatehouse, G. McLachlan, L. L. Martin, R. L. Martin, L. Spiccia, *Aust. J. Chem.* **1991**, *44*, 351−359.
[7] P. V. Bernhardt, G. A. Lawrance, T. W. Hambley, *J. Chem. Soc., Dalton Trans.* **1990**, 235−241.
[8] J. H. Timmons, A. Clearfield, A. E. Martell, R. H. Niswander, *Inorg. Chem.* **1979**, *18*, 1042−1047.
[9] J. H. Timmons, R. H. Niswander, A. Clearfield, A. E. Martell, *Inorg. Chem.* **1979**, *18*, 2977−2982.
[10] A. Grohmann, F. Knoch, *Inorg. Chem.* **1996**, *35*, 7932−7934.
[11] C. Dietz, F. W. Heinemann, J. Kuhnigk, C. Krüger, M. Gerdan, A. X. Trautwein, A. Grohmann, *Eur. J. Inorg. Chem.* **1998**, 1041−1049.
[12] A. Grohmann, F. W. Heinemann, P. Kofod, *Inorg. Chim. Acta* **1999**, *286*, 98−102.
[13] T. Poth, H. Paulus, H. Elias, R. van Eldik, A. Grohmann, *Eur. J. Inorg. Chem.* **1999**, 643−650.
[14] C. Dietz, F. W. Heinemann, A. Grohmann, *Eur. J. Inorg. Chem.* **1999**, 2147−2156.
[15] S. Schmidt, F. W. Heinemann, A. Grohmann, *Eur. J. Inorg. Chem.* **2000**, 1657−1667.
[16] C. Zimmermann, F. W. Heinemann, A. Grohmann, *Eur. J. Inorg. Chem.* **2001**, 547−555.
[17] D. A. House, *Coord. Chem. Rev.* **1977**, *23*, 223−322.
[18] D. A. House, *Compr. Coord. Chem.* **1987**, *2*, 23−72.
[19] A. Bianchi, M. Micheloni, P. Paoletti, *Coord. Chem. Rev.* **1991**, *110*, 17−113.
[20] [20a] E. Kimura, M. Haruta, T. Koike, M. Shionoya, K. Takenouchi, Y. Iitaka, *Inorg. Chem.* **1993**, *32*, 2779−2784. [20b] T. W. Hambley, G. A. Lawrance, M. Maeder, E. N. Wilkes, *Inorg. Chim. Acta* **1996**, *246*, 65−71. [20c] L. R. Gahan, G. A. Lawrance, A. M. Sargeson, *Aust. J. Chem.* **1982**, *35*, 1119−1131.
[21] B. Fabius, R. J. Geue, R. G. Hazell, W. G. Jackson, F. K. Larsen, C. J. Qin, A. M. Sargeson, *J. Chem. Soc., Dalton Trans.* **1999**, 3961−3972.
[22] D. A. Buckingham, W. G. Jackson, P. A. Marzilli, A. M. Sargeson, *Aust. J. Chem.* **1999**, *52*, 185−204.
[23] M. Zehnder, U. Thewalt, *Z. Anorg. Allg. Chem.* **1980**, *461*, 53−60.
[24] M. Maeder, H. R. Mäcke, *Inorg. Chem.* **1994**, *33*, 3135−3140.
[25] [25a] A. Zimmer, I. Müller, G. J. Reiß, A. Caneschi, D. Gatteschi, K. Hegetschweiler, *Eur. J. Inorg. Chem.* **1998**, 2079−2086. [25b] G. J. Reiss, A. Zimmer, K. Hegetschweiler, *Acta Crystallogr., Sect. C* **2000**, *56*, 284−288.
[26] R. J. Geue, G. H. Searle, *Aust. J. Chem.* **1983**, *36*, 927−935.
[27] [27a] F. J. Millero, D. R. Schreiber, *Am. J. Science* **1982**, *282*, 1508−1540. [27b] F. J. Millero, *Geochim. Cosmochim. Acta* **1992**, *56*, 3123−3132.
[28] J. W. Pauly, J. Sander, D. Kuppert, M. Winter, G. J. Reiss, F. Zürcher, R. Hoffmann, T. F. Fässler, K. Hegetschweiler, *Chem. Eur. J.* **2000**, *6*, 2830−2846.
[29] D. Kuppert, J. Sander, C. Roth, M. Wörle, T. Weyhermüller, G. J. Reiss, U. Schilde, I. Müller, K. Hegetschweiler, *Eur. J. Inorg. Chem.* **2001**, 2525−2542.
[30] A. Blaskó, C. A. Bunton, S. Bunel, C. Ibarra, E. Moraga, *Carbohydr. Res.* **1997**, *298*, 163−172.
[31] J. L. Sudmeier, C. N. Reilley, *Anal. Chem.* **1964**, *36*, 1698−1706.
[32] [32a] J. Springborg, C. E. Olsen, I. Søtofte, *Acta Chem. Scand.* **1995**, *49*, 555−563. [32b] M. Kubiak, T. Glowiak, *Acta Crystallogr., Sect. C* **1986**, *42*, 419−421. [32c] K. M. Doxsee, J. R. Hagadorn, T. J. R. Weakley, *Inorg. Chem.* **1994**, *33*, 2600−2606, and references therein.
[33] [33a] P. D. W. Boyd, M. Gerloch, G. M. Sheldrick, *J. Chem. Soc., Dalton Trans.* **1974**, 1097−1102. [33b] F. A. Cotton, Z. Dori, R. Llusar, W. Schwotzer, *Inorg. Chem.* **1986**, *25*, 3654−3658.
[34] [34a] J. R. Fritch, G. G. Christoph, W. P. Schaefer, *Inorg. Chem.* **1973**, *12*, 2170−2175. [34b] R. M. Hartshorn, S. G. Telfer, *J. Chem. Soc., Dalton Trans.* **2000**, 2801−2808. [34c] F. R. Fronczek, W. P. Schaefer, R. E. Marsh, *Acta Crystallogr., Sect. B* **1974**, *30*, 117−121.
[35] D. Ramprasad, A. G. Gilicinski, T. J. Markley, G. P. Pez, *Inorg. Chem.* **1994**, *33*, 2841−2847.
[36] [36a] W. P. Schaefer, *Inorg. Chem.* **1968**, *7*, 725−731. [36b] N. F. Curtis, W. T. Robinson, D. C. Weatherburn, *Aust. J. Chem.* **1992**, *45*, 1663−1680.
[37] [37a] U. Thewalt, M. Zehnder, S. Fallab, *Helv. Chim. Acta* **1977**, *60*, 867−873. [37b] T. Shibahara, S. Koda, M. Mori, *Bull. Chem. Soc. Jpn.* **1973**, *46*, 2070−2074.
[38] G. J. Gainsford, W. G. Jackson, A. M. Sargeson, *Aust. J. Chem.* **1986**, *39*, 1331−1336.
[39] M. Zehnder, U. Thewalt, S. Fallab, *Helv. Chim. Acta* **1979**, *62*, 2099−2108.
[40] [40a] R. E. Marsh, W. P. Schaefer, *Acta Crystallogr., Sect. B* **1968**, *24*, 246−251. [40b] W. P. Schaefer, S. E. Ealick, D. Finley, R. E. Marsh, *Acta Crystallogr., Sect. B* **1982**, *38*, 2232−2235.
[41] D. D. Dexter, C. N. Sutherby, M. W. Grieb, R. C. Beaumont, *Inorg. Chim. Acta* **1984**, *86*, 19−31.
[42] V. M. Miskowski, B. D. Santarsiero, W. P. Schaefer, G. E. Ansok, H. B. Gray, *Inorg. Chem.* **1984**, *23*, 172−176.
[43] W. P. Schaefer, S. E. Ealick, R. E. Marsh, *Acta Crystallogr., Sect. B* **1981**, *37*, 34−38.
[44] [44a] K. Nakamoto, *Coord. Chem. Rev.* **1990**, *100*, 363−402. [44b] H. A. O. Hill, D. G. Tew, *Compr. Coord. Chem.* **1987**, *2*, 315−333.
[45] A rather small twist angle $\tau = 100.4°$ has been reported for a dinuclear Co^{III}(*tetra*amine)(peroxo) complex with an additional ligating sugar oxygen atom: T. Tanase, T. Onaka, M. Nakagoshi, I. Kinoshita, K. Shibata, M. Doe, J. Fujii, S. Yano, *Inorg. Chem.* **1999**, *38*, 3150−3159.
[46] E. I. Solomon, F. Tuczek, D. E. Root, C. A. Brown, *Chem. Rev.* **1994**, *94*, 827−856.
[47] S. Fallab, M. Zehnder, *Helv. Chim. Acta* **1984**, *67*, 392−398.
[48] S. Fallab, P. R. Mitchell, *Adv. Inorg. Bioinorg. Mech.* **1984**, *3*, 311−377.
[49] F. Tuczek, K. Hegetschweiler, unpublished.
[50] G. A. Lawrance, P. A. Lay, *J. Inorg. Nucl. Chem.* **1979**, *41*, 301−304.
[51] H. Irving, R. J. P. Williams, *Nature* **1948**, *162*, 746−747.
[52] R. D. Hancock, *Acc. Chem. Res.* **1990**, *23*, 253−257.
[53] R. M. Smith, A. E. Martell, R. J. Motekaitis, *Critically Selected Stability Constants of Metal Complexes*, NIST Standard Reference Database 46, version 6.0, Gaithersburg, MD, USA, **2001**.
[54] G. K. Hollingshed, G. A. Lawrance, M. Maeder, M. Rossignoli, *Polyhedron* **1991**, *10*, 409−413.
[55] A. Wojciechowska, L. Bolewski, L. Lomozik, *Monatsh. Chem.* **1991**, *122*, 131−138.

[56] E. Prenesti, P. G. Daniele, M. Prencipe, G. Ostacoli, *Polyhedron* **1999**, *18*, 3233−3241.
[57] In ref.[55] λ_{max} = 575 nm is reported for $[Cu(1,3\text{-diaminopropane})_2]^{2+}$; the estimation according to ref.[56] yields a value of 556±10 nm).
[58] J. Bjerrum, B. V. Agarwala, *Acta Chem. Scand., Ser. A* **1980**, *34*, 475−481.
[59] [59a] P. Comba, T. W. Hambley, G. Lauer, N. Okon, *MOMEC97*, Version 2.1.3. a Molecular Modeling Package for Inorganic Compounds, Heidelberg, **1996**. [59b] P. Comba, T. W. Hambley, *Molecular Modeling of Inorganic Compounds*, 2nd ed., VCH, Weinheim, **2001**.
[60] P. V. Bernhardt, *Inorg. Chem.* **2001**, *40*, 1086−1092.
[61] S. S. Eaton, K. M. More, B. M. Sawant, G. R. Eaton, *J. Am. Chem. Soc.* **1983**, *105*, 6560−6567.
[62] A. Schweiger, G. Jeschke, *Principles of Pulse Electron Paramagnetic Resonance*, Oxford University Press, Oxford, **2001**.
[63] e.g. CuTPP, see: T. G. Brown, B. M. Hoffman, *Mol. Phys.* **1980**, *39*, 1073−1109.
[64] D. T. Richens, A. G. Sykes, *J. Chem. Soc., Dalton Trans.* **1982**, 1621−1624.
[65] L. Fabbrizzi, A. Perotti, A. Profumo, T. Soldi, *Inorg. Chem.* **1986**, *25*, 4256−4259.
[66] A. McAuley, S. Subramanian, T. W. Whitcombe, *J. Chem. Soc., Dalton Trans.* **1993**, 2209−2214.
[67] C. K. Murray, D. W. Margerum, *Inorg. Chem.* **1982**, *21*, 3501−3506.
[68] G. De Santis, L. Fabbrizzi, A. Poggi, A. Taglietti, *Inorg. Chem.* **1994**, *33*, 134−139.
[69] B. de Castro, J. Gomes, M. P. M. Marques, C. F. G. C. Geraldes, *J. Chem. Soc. Dalton Trans.* **1995**, 2041−2044.
[70] A. Ries, K. Hegetschweiler, *NMR-Tit*, Program for the Simulation of pH-Dependent Shifts in NMR Spectra, version 2.0, Saarbrücken, **1999**.
[71] See website http://www.esr.ethz.ch
[72] R. Szosenfogel, D. Goldfarb, *Mol. Phys.* **1998**, *95*, 1295−1308.
[73] P. Gans, A. Sabatini, A. Vacca, *Talanta* **1996**, *43*, 1739−1753.
[74] [74a] R. A. Binstead, B. Jung, A. D. Zuberbühler, *SPECFIT/32*, version 3.0, Spectrum Software Associates, Marlborough, MA 01752, USA, **2000**. [74b] H. Gampp, M. Maeder, C. J. Meyer, A. D. Zuberbühler, *Talanta* **1985**, *32*, 95−101.
[75] CCDC-106171, -106173, and -106611 (excluding structure factors) for **1**Br_2, **2**$Cl_4{\cdot}4H_2O$, and **3**$Cl_2[ZnCl_4][ZnCl_3(H_2O)]{\cdot}H_2O$ contain the supplementary crystallographic data for this paper. These data can be obtained free of charge at www.ccdc.cam.ac.uk/conts/retrieving.html [or from the Cambridge Crystallographic Data Centre, 12 Union Road, Cambridge CB2 1EZ, UK; Fax: (internat.) + 44-1223/336-033; E-mail: deposit@ccdc.cam.ac.uk].
[76] G. M. Sheldrick, *SHELXS-97, Program for Crystal Structure Solution*, Göttingen, **1990**.
[77] G. M. Sheldrick, *SHELXL-97, Program for Crystal Structure Refinement*, Göttingen, **1997**.
[78] H. D. Flack, *Acta Crystallogr., Sect. A* **1983**, *39*, 876−881.

Received October 4, 2002
[I02553]

Hydrothermal Synthesis and Characterization of Novel Lanthanide 2,2′-Diphenyldicarboxylate Complexes

Yi-Bo Wang,[a] Xiang-Jun Zheng,[a] Wen-Juan Zhuang,[a] and Lin-Pei Jin*[a]

Keywords: Hydrothermal synthesis / Lanthanides / Coordination polymer / X-ray diffraction

Lanthanide complexes with a one-dimensional chain, $[Ln_2(dpdc)_3(H_2O)_2]_n$ [Ln = La (**1**), Pr (**2**), Eu (**3**), Tb (**4**); dpdc = 2,2′-diphenyldicarboxylate] were obtained by hydrothermal reaction of lanthanide(III) chlorides and 2,2′-diphenyldicarboxylic acid, and characterized by X-ray diffraction. The crystal structure data reveal that they are isostructural. In the asymmetric unit, the two Ln^{3+} ions are both eight-coordinate but they have different coordination environments. Lanthanide ions arranged in a zigzag manner are bridged by the dpdc ligands into a 1-D chain, while the structure appears like a pinwheel viewed along the *c* axis. In these complexes, 2,2′-diphenyldicarboxylate anions exhibit tetradentate and pentadentate coordination modes. A laser-induced high-resolution spectrum (resolution: 0.2 cm^{-1}) of **3** was obtained, which shows two Eu^{3+} sites in **3**. This is in agreement with the results of single-crystal X-ray diffraction studies of **3**.
(© Wiley-VCH Verlag GmbH & Co. KGaA, 69451 Weinheim, Germany, 2003)

Introduction

The crystal engineering and synthesis of one-, two-, and three-dimensional coordination polymers have been areas of renewed interest and have undergone explosive growth in recent years.[1−11] In principle, the physical and chemical properties of polymer networks are decisively dependent on the properties of the individual molecular components and their distribution within the crystal lattice. In terms of molecular composition, the inorganic-organic coordination polymers have many advantages over simple inorganic and organic materials. This is because varieties of organic ligands coordinating to metal atoms construct coordination polymers with many fascinating structures, in which the metal atoms display many kinds of coordination geometries,[12−17] and these polymers may possess distinctive and attractive properties. Therefore, the choice of appropriate bridging ligands is a key step in forming interesting structures.

The coordination chemistry of aromatic polycarboxylic acids coordinated to metal atoms has been extensively investigated for their potential applications such as magnetic,[18−20] luminescent,[21,22] and microporous materials.[23,24] In constructing coordination polymers with networks or channels, 2,2′-diphenyldicarboxylic acid (H_2dpdc) is a useful starting material and possesses several interesting structural features. Two carboxyl groups may be partially or completely deprotonated, resulting in novel structures of coordination polymers by various coordination modes. Dpdc is a flexible ligand in which the carboxyl groups may not be coplanar with the phenyl ring due to steric hindrance in the coordination process. It can form an infinite variety of architectures in different directions. In the crystal structures of many reported transition metal complexes with 2,2′-diphenyldicarboxylate, the dpdc ligand exhibits diverse types of coordination modes[25−29] with multiple coordination sites. Owing to the higher coordination number and attractive luminescent properties, applied in fluorescent probes, the reactions of dpdc and lanthanide ions may generate polymers with different coordination modes and properties distinct from transition metal complexes of dpdc. To the best of our knowledge, lanthanide 2,2′-diphenyldicarboxylate complexes have never been reported.

To obtain the coordination polymers, reaction of the lanthanide chloride and sodium 2,2′-diphenyldicarboxylate was carried out by the conventional solution method. The uncharacterized precipitate is insoluble in water and common organic solvents. This led us to adopt hydrothermal synthesis to obtain single crystals suitable for X-ray structure analysis. It is well known that hydrothermal reactions are useful in the synthesis of zeolites, phosphates, phosphonates, and polyoxalkoxometalates.[30,31] Hydrothermal methods are also an effective approach to produce metastable compounds and promote the growth of crystals.[32] More recently, we have used this method in the synthesis of lanthanide coordination polymers. Herein, we report the synthesis and structural characterization of lanthanide 2,2′-diphenyldicarboxylate complexes.

Results and Discussion

Structural Description

The crystallographic data of **1**−**4** are shown in Table 1. The structural data show that the four coordination poly-

[a] Department of Chemistry, Beijing Normal University, Beijing, 100875, People's Republic of China
Fax: (internat.) + 86-010/6220-0567
E-mail: lpjin@bnu.edu.cn

Table 1. Crystal data for **1**−**4**

Compound	**1**	**2**	**3**	**4**
Empirical formula	$La_2C_{42}H_{28}O_{14}$	$Pr_2C_{42}H_{28}O_{14}$	$Eu_2C_{42}H_{28}O_{14}$	$Tb_2C_{42}H_{28}O_{14}$
FW	1034.46	1038.46	1060.56	1074.48
Crystal system	Monoclinic	Monoclinic	Monoclinic	Monoclinic
Space group	*C*2/*c*	*C*2/*c*	*C*2/*c*	*C*2/*c*
a, Å	20.970(7)	21.004(6)	20.914(6)	20.938(7)
b, Å	21.613(8)	21.587(7)	21.409(6)	21.363(7)
c, Å	8.377(3)	8.345(3)	8.234(2)	8.207(3)
α, deg	90	90	90	90
β, deg	103.773(7)	103.888(5)	104.028(5)	104.052(5)
γ, deg	90	90	90	90
Z	4	4	4	4
V, Å^3	3688(2)	3673(2)	3576.8(17)	3561(2)
ρ_{calcd}, g·cm^{-3}	1.863	1.878	1.969	2.004
Temp, K	293(2)	293(2)	293(2)	293(2)
μ, mm^{-1}	2.360	2.696	3.551	4.016
Reflections collected	6320, 2657	7509, 3233	6187, 2573	7181, 3103
Total, independent, R_{int}	0.0504	0.0242	0.0558	0.0202
λ (Mo-K_α), Å	0.71073	0.71073	0.71073	0.71073
R_1, wR_2 [$I > 2\sigma(I)$]	0.0314, 0.0682	0.0214, 0.0488	0.0340, 0.0810	0.0182, 0.0406

mers are isostructural. Each polymer can be regarded as a one-dimensional infinite chain composed of $[Ln_2(dpdc)_3(H_2O)_2]$ units. Herein, only complex **3** will be described in detail. Complex **3** is composed of one-dimensional chains of $[Eu_2(dpdc)_3(H_2O)_2]_n$. Two carboxylate groups of each dpdc ligand are deprotonated, and the dpdc ligands adopt two types of coordination modes, as shown in Scheme 1. $[Eu_2(dpdc)_3(H_2O)_2]$ consists of two crystallographically independent europium(III) ions as shown in Figure 1. Eu(1) is coordinated to eight oxygen atoms, two oxygen atoms [(O6A), (O6B)] from two bridging bidentate carboxylate groups of two tetradentate dpdc ligands, two oxygen atoms [O(3), O(3A)] from two bridging bidentate carboxylate groups of two pentadentate dpdc ligands, two oxygen atoms [O(1), O(1A)] from the two chelating-bridging tridentate carboxylate groups of the two pentadentate dpdc ligands, and two oxygen atoms [O(7), O(7A)] from two coordinated water molecules. The Eu(1)−O(carboxylate) bond lengths vary from 2.307 Å to 2.465 Å, and the Eu(1)−O(w) distances are both 2.521 Å. The O−Eu(1)−O bond angles range from 66.2° to 147.4°. Eu(2) is also ligated to eight oxygen atoms, two oxygen atoms [O(5), O(5A)] from two bridging bidentate carboxylate groups of a tetradentate dpdc ligand, four oxygen atoms [O(1), O(2), O(1B), O(2A)] from two chelating-bridging tridentate carboxylate groups of two pentadentate dpdc ligands, and two oxygen atoms [O(4A), O(4B)] from two bridging bidentate carboxylate groups of other two pentadentate dpdc ligands. The Eu(2)−O(carboxylate) distances fall in the range 2.318−2.594 Å, and the O−Eu(2)−O bond angles are in the range 35.8−150.7°. The results show that Eu(1) is surrounded by two tetradentate dpdc ligands, two pentadentate dpdc ligands, and two water molecules, while around Eu(2) there are one tetradentate dpdc ligand and four pentadentate dpdc ligands; the coordination environments of the two Eu^{III} ions are therefore different. However, the coordination geometries of the two Eu^{III} ions can both be described as slightly distorted triangular dodecahedra.

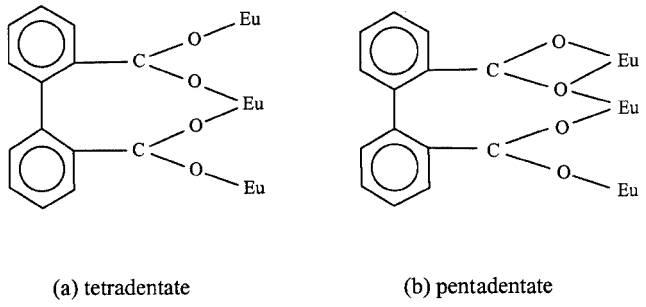

Scheme 1. Two coordination modes of dpdc ligand in **3**

Each carboxylate moiety of the dpdc ligands bridges two adjacent Eu^{III} ions, and each ligand bridges three adjacent Eu^{III} ions through carboxylate oxygen atoms of these bridging dpdc groups, resulting in one-dimensional infinite polymeric chains along the *c* axis (Figure 2). The Eu^{III} ions are arranged in a zigzag manner, and the distance between two adjacent Eu^{III} ions is 4.459 Å. The tetradentate dpdc ligands and pentadentate dpdc ligands are located around the $Eu^{III}\cdots Eu^{III}$ chain and the number of pentadentate dpdc ligands is double the number of tetradentate ones. From Figure 2, we can see that the coordination environments of Eu(1A), Eu(1B), and Eu(1C) are the same as Eu(1) in Figure 1, and those of Eu(2A), Eu(2B), and Eu(2C) are the same as Eu(2) in Figure 1. In a tetradentate dpdc ligand, the two phenyl rings are not coplanar, and the dihedral angle is 56.2°. In addition, each of the two carboxylic groups of a tetradentate dpdc ligand is not coplanar with the connected phenyl ring, and the dihedral angles are both 122.5°; the two carboxylic groups of the tetradentate dpdc ligand are, however, coplanar. In the pentadentate dpdc ligand, one of the two carboxylate groups adopts a chelating-bridg-

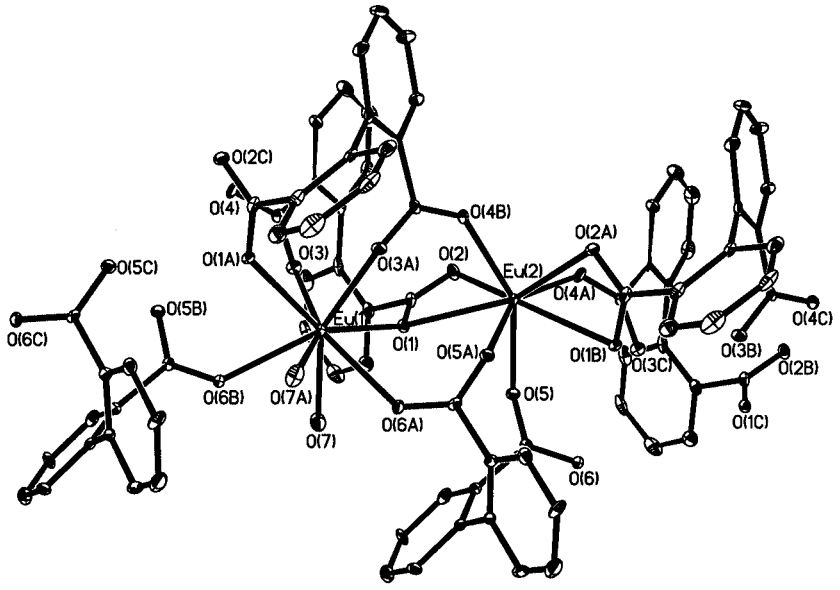

Figure 1. Coordination environment of the two Eu^{III} ions in **3** with thermal ellipsoids at 15% probability; all hydrogen atoms have been omitted for clarity

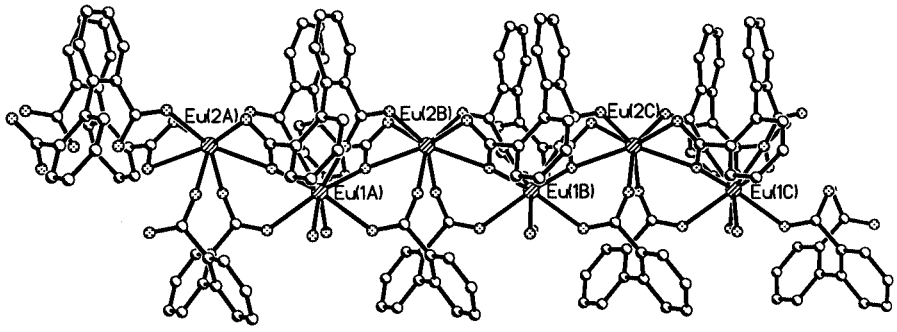

Figure 2. 1-D chain of **3** viewed along the *a* axis; all hydrogen atoms and uncoordinated water molecules have been omitted for clarity

ing tridentate mode, the other group adopts a bridging bidentate mode. Two oxygen atoms of the bridging bidentate carboxylate group coordinate to two Eu^{III} ions [Eu(1A), Eu(2B)], while two oxygen atoms of the other carboxylate group chelate to the third Eu^{III} ion [Eu(2A)] (see Figure 2) and, moreover, one oxygen atom of the chelating carboxylic group acts as a μ_2-O atom. In the pentadentate ligand, the bridging bidentate carboxylate group and the connected phenyl ring are not coplanar and the dihedral angle is 34.9°. The chelating-bridging tridentate carboxylate group and the connected phenyl ring are not coplanar either, and the dihedral angle is 67.4°. The two phenyl rings in a pentadentate dpdc ligand are not coplanar and the dihedral angle is 70.1°. This may result from the steric effect of the coordination. In the tetradentate ligand, the two bridging bidentate O−C−O bond angles are 124.6°, whereas the chelating-bridging tridentate O−C−O bond angles (122.6°) are all smaller than the bridging bidentate ones (123.9°) in the pentadentate ligand, as expected.

Every chain looks like a pinwheel viewed along the *c* axis (Figure 3). Eu^{III} ions reside at the centers of the pinwheel and are grouped into two parts, arranged in two rows. The ligands fall into three groups and are well distributed

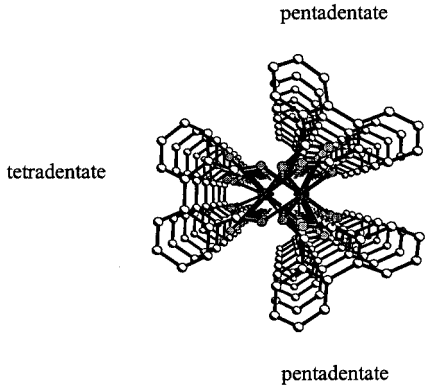

Figure 3. Pinwheel structure of **3**

around the centers of the Eu^{III} ions. The phenyl rings of the dpdc ligands belonging to the same group of a chain are all parallel to each other and the distances between the parallel phenyl rings are in the range of 6.4490 Å to 7.0314 Å.

The phenyl rings of dpdc ligands in adjacent 1-D chains of complex **3** are interdigitated, forming channels with a cavity of size 9.676 × 4.520 Å in the *c* direction (see Figure 4).

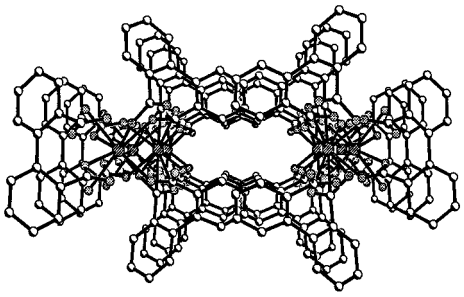

Figure 4. Packing of **3** viewed along the *c* axis

In the four lanthanide coordination polymers, the mean La−O(carboxylate), Pr−O(carboxylate), Eu−O(carboxylate), and Tb−O(carboxylate) distances are 2.501 Å, 2.470 Å, 2.413 Å, and 2.386 Å, respectively; the La−O(w), Pr−O(w), Eu−O(w), and Tb−O(w) distances are 2.633 Å, 2.579 Å, 2.521 Å, and 2.470 Å, respectively. The separations of La···La, Pr···Pr, Eu···Eu, and Tb···Tb are 4.555 Å, 4.529 Å, 4.459 Å, and 4.440 Å, respectively. We can thus conclude that the Ln^{III}−O and Ln···Ln distances decrease with the contraction of the ionic radii from La^{III} to Tb^{III} ions.

In the two reported isostructural complexes with 2,2′-diphenyldicarboxylic acid, $[M_2(O_2CC_{12}H_8CO_2)_2(H_2O)_8]$, [M = cobalt(II), nickel(II)],[25] the M−O distances of the two transition metal complexes are both shorter than those of complexes **1**−**4**. The coordination environments of the two transition metal ions are both slightly distorted octahedra, and the M^{II} ions are all six-coordinate, with two oxygen atoms from two carboxylate groups of a dpdc ligand and four oxygen atoms from four coordinated water molecules. Obviously, there are two more atoms coordinated to the Ln^{III} ion in **1**−**4**, producing an eight-coordinate metal center. The dihedral angles of the aromatic rings of the dpdc ligand in the two transition metal complexes are 85.96° and 87.2° for Co^{II} and Ni^{II}, respectively, which are larger than those in the tetradentate dpdc ligand and pentadentate dpdc ligand of **3** (56.2° and 70.1°, respectively). This may be a result of the higher coordination number of the lanthanide ions and thus the steric hindrance effect results in the formation of coordination polymers. Similarly, compounds **1**−**4** exhibit more complicated coordination modes than the transition metal dpdc complexes. This is due to the larger radii of Ln^{III} ions, and corresponding large coordination number, as well as the different coordination modes that are required by lanthanide ions.

Thermogravimetric Analyses

Thermogravimetric analyses of **1**−**4** were performed to observe their thermal behaviors. The thermogravimetric analysis data for **1**, **2**, **3**, and **4** are listed in Table 2. Loss of two coordinated water molecules of the four complexes was observed as the first weight loss. Their dehydration temperatures are in the range of 178.6 °C to 225.1 °C, and further decomposition processes begin at temperatures above 459 °C, giving the final products Ln_2O_3 (Ln = La, Eu), Pr_6O_{11}, and Tb_4O_7. Taking **1** as an example, the TGA curve shows that the process of first weight loss is between 178.6 and 221.5 °C with 3.5% total weight, which is in accordance with the removal of two water molecules per formula unit (calculated: 3.6%). Then, further decomposition of **1** begins at temperatures above 461.2 °C, giving rise to La_2O_3.

Photophysical Properties of 3

Complex **3** emits intense red fluorescence when it is irradiated by UV light. Figure 5 shows its high-resolution emission spectrum excited at a wavelength of 355 nm at 77 K, corresponding to $^5D_0 \rightarrow {}^7F_J$ (J = 0−4) transitions in

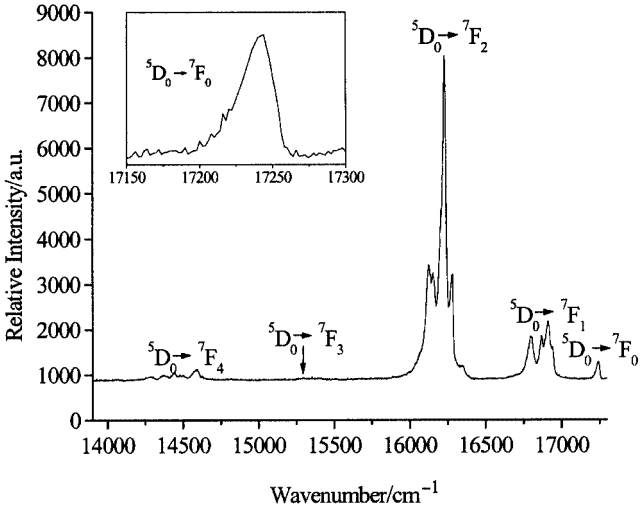

Figure 5. Emission spectrum of **3** corresponding to $^5D_0 \rightarrow {}^7F_J$ (J = 0−4) transitions at 77 K, λ_{exc} = 355 nm

Table 2. Thermogravimetric analysis data of **1**−**4**

	1	**2**	**3**	**4**
Dehydration temperature [°C]	178.6−221.5	197.6−208.3	209.1−225.1	199.3−215.3
Loss of water calcd. (found) [%]	3.6 (3.5)	3.5 (3.6)	3.4 (3.3)	3.3 (3.5)
Further decomposition temperature [°C]	461.2	460.9	459.5	463.8

the range 13900−17300 cm^{-1}. The $^5D_0 \rightarrow {}^7F_2$ transition is the induced electric dipole transition, which is greatly affected by the coordination environment, while the $^5D_0 \rightarrow {}^7F_1$ transition is the magnetic dipole transition, which is much less sensitive to the environment. The intensity ratio of $^5D_0 \rightarrow {}^7F_2/{}^5D_0 \rightarrow {}^7F_1$ is 3.73, which shows that the Eu^{3+} ions are not at an inversion center. For the $^5D_0 \rightarrow {}^7F_J$ transition, the peak number should obey the $(2J + 1)$ rule. However, the broad and asymmetric spectrum of the $^5D_0 \rightarrow {}^7F_0$ transition (see inset in Figure 5), as well as the shoulder of the three peaks in the $^5D_0 \rightarrow {}^7F_1$ transition indicate that $2\times(2J + 1)$ partly overlapping signals are expected in the low-temperature luminescence spectrum of **3**, and thus the europium ions in **3** are not located in the same chemical environment. To further study the local structural characteristics, a selective excitation technique has been applied. Setting 16213 cm^{-1} and 16143 cm^{-1} as the analyzing wave number, respectively, the excitation spectra *a* and *b* arising from the $^5D_0 \leftarrow {}^7F_0$ transition were obtained, as shown in Figure 6. Obviously, there are two peaks located at 579.57 nm and 579.83 nm in both excitation spectra *a* and *b*, which confirms two Eu^{3+} ion sites in the complex **3**.[33] This is in good agreement with the results of the single-crystal X-ray diffraction. It can be concluded that there are two different La^{3+}, Pr^{3+}, and Tb^{3+} ion sites in the complexes **1**, **2**, and **4**, respectively.

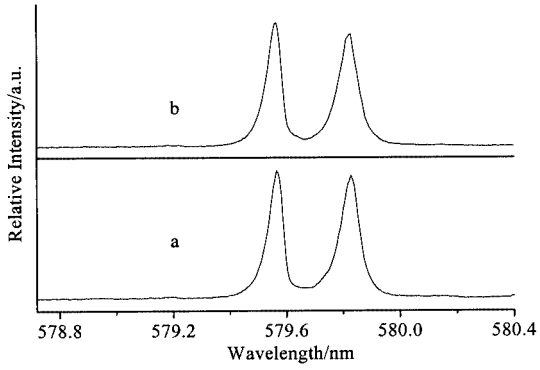

Figure 6. Excitation spectra of **3** at 77 K; analyzing wave number: (a) 16 213 cm^{-1}; (b) 16 143 cm^{-1}

Conclusion

The first examples of structural characterization of lanthanide coordination polymers with 2,2′-biphenyldicarboxylic acid were obtained. The dpdc ligands in **1**, **2**, **3**, and **4** have two coordination modes, tetradentate and pentadentate. Coordination polymers **1**−**4** are isostructural, and 1-D chains of **1**−**4** are composed of $Ln_2(dpdc)_3(H_2O)_2$ building blocks, in which the lanthanide(III) ions have two chemical environments. The Ln−O bond lengths and Ln···Ln separations show a lanthanide contraction over the series.

Experimental Section

Materials: $LaCl_3{\cdot}7H_2O$, $PrCl_3{\cdot}6H_2O$, $EuCl_3{\cdot}6H_2O$, and $TbCl_3{\cdot}6H_2O$ were prepared by dissolving their oxides in hydrochloric acid, and then drying. 2,2′-Diphenyldicarboxylic acid was purchased from Aldrich and used without further purification,while all the other reagents are commercially available and were used as received.

Instrumentation: Elemental analyses were performed on an Elementar Vario EL analyzer. The IR spectra were recorded with a Nicolet Avatar 360 FT-IR spectrometer using the KBr pellet technique. Thermogravimetric analyses were performed on a ZRY-2P Thermal Analyzer. The excitation light source was a YAG-Nd laser that emits at 1.064 μm, and the excitation wavelength was 355 nm. The sample was placed in a Dewar and cooled with liquid nitrogen. The fluorescence was collected at right angles through a Spex 1403 monochromator with a photomultiplier tube, then averaged by a Boxcar integrator, and finally data were transferred to a computer.

X-ray Crystallographic Study: The single-crystal X-ray data collections for complexes **1**, **2**, **3**, and **4** were performed on a Bruker Smart 1000 CCD diffractometer, using graphite-monochromated MoK_α radiation (λ = 0.71073 Å). Semiempirical absorption corrections were applied using the SADABS program. The structures were solved by direct methods and refined by full-matrix least-squares on $|F|^2$ using the SHELXTL-97 program.[34] All non-hydrogen atoms were refined anisotropically. The hydrogen atoms were generated geometrically and treated by a mixture of independent and constrained refinements.

CCDC 195399−195402 (**1**−**4**) contain the supplementary crystallographic data for this paper. These data can be obtained free of charge at ww.ccdc.cam.ac.uk/conts/retrieving.html [or from the Cambridge Crystallographic Data Centre, 12, Union Road, Cambridge CB2 1EZ, UK; fax: (internat.) +44-1223/336-033; E-mail: deposit@ccdc.cam.ac.uk].

$[La_2(dpdc)_3(H_2O)_2]_n$ (1): A mixture of $LaCl_3{\cdot}7H_2O$ (0.111 g, 0.3 mmol), 2,2′-diphenyldicarboxylic acid (0.109 g, 0.45 mmol), H_2O (10 mL), and an aqueous solution of NaOH (0.4 mL, 0.26 mmol) was sealed in a 25-mL stainless-steel reactor with a Teflon liner, heated to 170 °C for 72 h, and then slowly cooled to room temperature. The products were filtered, washed with ethanol, and then dried in air. Colorless transparent crystals of **1** were obtained in 70.4% yield (0.109 g). $C_{42}H_{28}La_2O_{14}$ (1034.44): calcd. C 48.77, H 2.73; found C 48.66, H 2.52. IR data (KBr pellet): $\tilde{\nu}$ = 3549(m) cm^{-1}, 1615(s), 1548(s), 1523(s), 1442(s), 1406 (s), 771(m), 760(m).

$[Pr_2(dpdc)_3(H_2O)_2]_n$ (2): A mixture of $PrCl_3{\cdot}6H_2O$ (0.107 g, 0.3 mmol), 2,2′-diphenyldicarboxylic acid (0.109 g, 0.45 mmol), H_2O (10 mL), and an aqueous solution of NaOH (0.3 mL, 0.20 mmol) was sealed in a 25-mL stainless-steel reactor with a Teflon liner, heated to 200 °C for 72 h, and then slowly cooled to room temperature. The products were filtered, washed with ethanol, and then dried in air. Light green crystals of **2** were obtained in 71.5% yield (0.111 g). $C_{42}H_{28}O_{14}Pr_2$ (1038.44): calcd. C 48.58, H 2.91; found C 48.67, H 2.43. IR data (KBr pellet): $\tilde{\nu}$ = 3550(m) cm^{-1}, 1617(s), 1548(s), 1522(s), 1442(s), 1406 (s), 771(m), 761(m).

$[Eu_2(dpdc)_3(H_2O)_2]_n$ (3): The synthesis of **3** was similar to that of **1**. The products were filtered, washed with ethanol, and then dried in air. Reddish brown transparent crystals of **3** were obtained in 67.4% yield (0.107 g). $C_{42}H_{28}Eu_2O_{14}$ (1060.64): calcd. C 47.54, H 2.66; found C 47.59, H 2.30. IR data (KBr pellet): $\tilde{\nu}$ = 3551(m) cm^{-1}, 1622(s), 1553(s), 1525(s), 1443(s), 1408(s), 772(m), 762(m).

$[Tb_2(dpdc)_3(H_2O)_2]_n$ (4): The synthesis of **4** was similar to that of **2**. The products were filtered, washed with ethanol, and then dried in air. Colorless transparent crystals of **4** were obtained in 68.9%

yield (0.111 g). Calcd. for $C_{42}H_{28}Tb_2O_{14}$ (1074.44): calcd. C 46.95, H 2.81; found C 46.97, H 2.38. IR data (KBr pellet): $\tilde{\nu}$ = 3552(m) cm^{-1}, 1624(s), 1555(s), 1527(s), 1443(s), 1409(s), 763(m).

Acknowledgments

This work is supported by the National Natural Science Foundation of China (29971005 and 20071004) and the State Key Project of Fundamental Research (G1998061308).

[1] B. F. Hoskins, R. Robson, *J. Am. Chem. Soc.* **1990**, *112*, 1546−1554.
[2] H. J. Choi, M. P. Suh, *J. Am. Chem. Soc.* **1998**, *120*, 10622−10628.
[3] O. M. Yaghi, H. Li, T. L. Groy, *J. Am. Chem. Soc.* **1996**, *118*, 9096−9101.
[4] L. Pan, E. B. Woodlock, X. Wang, *Inorg. Chem.* **2000**, *39*, 4174−4178.
[5] A. K. Cheetham, G. Férey, T. Loiseau, *Angew. Chem. Int. Ed.* **1999**, *38*, 3268−3292.
[6] P. J. Hagrman, D. Hagrman, J. Zubieta, *Angew. Chem. Int. Ed.* **1999**, *38*, 2638−2684.
[7] D.-L. Long, A. J. Blake, N. R. Champness, M. Schröder, *Chem. Commun.* **2000**, 1369−1370.
[8] T. J. Prior, M. J. Rosseinsky, *Chem. Commun.* **2001**, 495−496.
[9] G. Guilera, J. W. Steed, *Chem. Commun.* **1999**, 1563−1564.
[10] B. Gomea-Lor, E. Gutierrez-Puebla, M. Iglesias, M. A. Monge, C. Ruiz-Valero, N. Snejko, *Inorg. Chem.* **2002**, *41*, 2429−2432.
[11] C. L. Bowes, G. A. Ozin, *Adv. Mater.* **1996**, *8*, 13−28.
[12] R. Cao, D. Sun, Y. Liang, M. Hong, K. Tatsumi, Q. Shi, *Inorg. Chem.* **2002**, *41*, 2087−2094.
[13] C.-D. Wu, C.-Z. Lu, W.-B. Yang, S.-F. Lu, H.-H. Zhuang, J.-S. Huang, *Eur. J. Inorg. Chem.* **2002**, 797−800.
[14] T. M. Reineke, M. Eddaoudi, M. O'Keeffe, O. M. Yaghi, *Angew. Chem. Int. Ed.* **1999**, *38*, 2590−2594.
[15] G. B. Gardner, D. Venkataraman, J. S. Moore, S. Lee, *Nature* **1995**, *374*, 792−795.
[16] S. B. Copp, S. Subramanian, M. J. Zaworotko, *J. Am. Chem. Soc.* **1992**, *114*, 8719−8720.
[17] G.-F. Liu, Z.-P. Qiao, H.-Z. Wang, X.-M. Chen, G. Yang, *New J. Chem.* **2002**, *26*, 791−795.
[18] D. M. J. Doble, C. H. Benison, A. J. Blake, D. Fenske, M. S. Jackson, R. D. Kay, W.-S. Li, M. Schröder, *Angew. Chem. Int. Ed.* **1999**, *38*, 1915−1918.
[19] J. Lisowski, P. Starynowicz, *Inorg. Chem.* **1999**, *38*, 1351−1355.
[20] X.-M. Chen, S. M. J. Aubin, Y.-L. Wu, Y.-S. Yang, T. C. W. Mak, D. N. Hendrickson, *J. Am. Chem. Soc.* **1995**, *117*, 9600−9601.
[21] T. M. Reineke, M. Eddaoudi, M. Fehr, D. Kelley, O. M. Yaghi, *J. Am. Chem. Soc.* **1999**, *121*, 1651−1657.
[22] C. Reinhard, H. U. Gudel, *Inorg. Chem.* **2002**, *41*, 1048−1055.
[23] A. Kamiyama, T. Noguchi, T. Kajiwara, T. Ito, *Angew. Chem. Int. Ed.* **2000**, *39*, 3130−3132.
[24] H. Li, M. Eddaoudi, M. O'Keeffe, O. M. Yaghi, *Nature* **1999**, *402*, 276−279.
[25] J.-M. Rueff, S. Pillet, N. Claiser, G. Bonaventure, M. Souhassou, P. Rabu, *Eur. J. Inorg. Chem.* **2002**, 895−900.
[26] M. S. Islam, M. M. Uddin, *Polyhedron* **1992**, 2913−2916.
[27] J. Gao, S.-L. Ma, C.-Y. Jin, D.-Z. Liao, *Polyhedron* **1996**, 2633−2639.
[28] J. Gao, S.-H. Zhong, *J. Mol. Catal. A: Chemical* **2000**, *164*, 1−7.
[29] M. S. Islam, M. M. Uddin, *Synth. React. Inorg. Met.-Org. Chem.* **1991**, *21*, 1093−1105.
[30] M. I. Khan, L. M. Meyer, R. C. Haushalter, A. L. Schweitzer, J. Zubieta, J. L. Dye, *Chem. Mater.* **1996**, *8*, 43−53.
[31] G. Bonavia, R. C. Haushalter, C. J. O'Connor, J. Zubieta, *Inorg. Chem.* **1996**, *35*, 5603−5612.
[32] J. Gopalakrishnan, *Chem. Mater.* **1995**, *7*, 1265−1275.
[33] J.-C. G. Bünzli, in *Lanthanide Probes in Life, Chemical and Earth Sciences. Theory and Practice* (Eds.: J.-C. G. Bünzli, G. R. Choppin), Elsevier Scientific Publishers; Amsterdam, 1989; Chapter 7.
[34] G. M. Sheldrick, SHELX-97, PC-version, University of Göttingen, Germany, 1997.

Received October 18, 2002
[I02577]

Low-Valent Organobismuth Compounds with Intramolecular Coordination: *cyclo*-R_3Bi_3, *cyclo*-R_4Bi_4, $RBi[W(CO)_5]_2$, and R_4Bi_2 [R = 2-$(Me_2NCH_2)C_6H_4$]

Lucia Balazs,[a] Hans J. Breunig,*[a] Enno Lork,[a] and Cristian Silvestru[b]

Keywords: Bismuth / Metallacycles / Tungsten

The cyclobismuthanes R_nBi_n, [R = 2-$(Me_2NCH_2)C_6H_4$; n = 3 (**1a**), 4 (**1b**)] have been synthesised by reduction of $RBiCl_2$ with Na in liquid NH_3 or by reaction of R_2BiCl with $LiAlH_4$ in Et_2O. The reaction of **1a/b** with $W(CO)_5$·THF afforded the bismuthinidene complex $RBi[W(CO)_5]_2$ (**2**). R_2BiCl reacts with Mg in THF to give the dibismuthane R_4Bi_2 (**3**). Single-crystal X-ray structure analyses of **1b**, **2**, and **3** reveal intramolecular coordination of the pendant CH_2NMe_2 groups to the bismuth atom.

(© Wiley-VCH Verlag GmbH & Co. KGaA, 69451 Weinheim, Germany, 2003)

Introduction

Relativistic effects[1] are expected to favour the lower oxidation states of bismuth and to stabilize singlet bismuthinidenes RBi. Known examples of Bi^I derivatives[2] are the dibismuthenes RBi=BiR [R = 2,4,6-$[(Me_3Si)_2CH]_3C_6H_2$,[3,4] 2,6-$(Me_3C_6H_2)_2C_6H_3$[5]], *cyclo*-R_nBi_n oligomers [n = 3, 4; R = $(Me_3Si)_2CH$,[6] $(Me_3Si)_3Si$[7] and n = 5; R = Me_3SiCH_2[8]], and a complex of R_2Bi_2 (R = Me_3SiCH_2), i.e. $[(RBi=BiR)\{W(CO)_5\}_2]$.[8] Monomeric bismuthinidenes have not been isolated, but RBi groups have been incorporated into *cyclo*-$[RBiFe(CO)_4]_2$ (R = Me,[9] Ph,[10] *i*Bu[11]). The oxidation state of bismuth in these complexes is, however, ambiguous. Bismuth(II) compounds are known as dibismuthanes R_4Bi_2.[12–16] All low-valent organobismuth compounds tend to decompose with formation of elemental Bi and R_3Bi, unless protected by bulky groups or stabilized by complexation. Usually, monodentate alkyl or aryl ligands are used for steric protection. We expected additional stabilization with substituents containing a pendant donor group available for internal coordination at Bi. Examples of compounds with internal coordination at Bi^{III} are the 2-(dimethylaminomethyl)phenyl derivatives R_2BiCl,[17] $RBiI_2$,[17] or R_3Bi[18] [R = 2-$(Me_2NCH_2)C_6H_4$]. We report here on arylbismuth(I) and -bismuth(II) compounds with internal nitrogen coordination of the 2-$(Me_2NCH_2)C_6H_4$ ligand.

[a] Institut für Anorganische und Physikalische Chemie, Universität Bremen,
28334 Bremen, Germany
Fax: (internat.) + 49-421/2184042
E-mail: breunig@chemie.uni-bremen.de
[b] Facultatea de Chimie si Inginerie Chimica, Universitatea Babes-Bolyai,
3400 Cluj-Napoca, Romania
Fax: (internat.) + 40-64/190818
E-mail: cristi@chem.ubbcluj.ro

Results and Discussion

Both the reduction of $RBiCl_2$ with Na in liquid ammonia at −70 °C and the reaction of R_2BiCl with $LiAlH_4$ in Et_2O resulted in isolation of a black-green product (49 and 65% yield, respectively), which was identified as *cyclo*-R_nBi_n (**1**) by elemental analysis. A possible intermediate for the latter reaction is R_2BiH, which gives **1** by elimination of RH (Scheme 1). Three- (**1a**) and four-membered (**1b**) R_nBi_n rings were identified by NMR spectroscopy in solution, whereas the crystals of **1** consist of the four-membered ring **1b**, the structure of which was established by a single-crystal X-ray diffraction study.

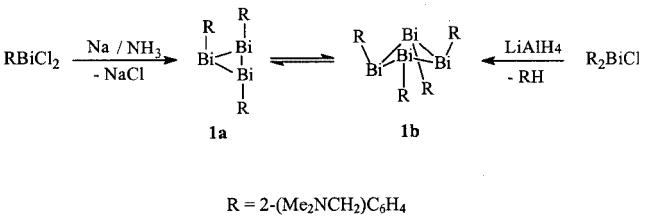

Scheme 1

Crystals of **1b** are stable for a long time at room temperature under argon. Solutions of **1** in hydrocarbon solvents are more sensitive, however, and in sealed tubes at 25 °C the R_nBi_n rings decompose after several hours to R_4Bi_2 (**2**) and metallic bismuth. At −28 °C, however, they are stable for weeks. The colour of the crystals is dark green, while solutions in hydrocarbon solvents are dark red. Variable-temperature and concentration-dependent ^1H NMR spectra in $C_6D_5CD_3$ enable the rings **1a** and **1b** to be easily distinguished. Two sets of signals (1:2 intensity ratio) for the 2-(dimethylaminomethyl)phenyl group could be assigned to the *cyclo*-trimer **1a** in the *cis-trans* configuration. For the tetramer **1b** only one set of signals was observed, corre-

sponding to the *all-trans* configuration with equivalent substituents. Each set consists of two singlets, for the CH_3 and the CH_2 protons respectively, and a group of signals for the spin system of the aromatic protons. The ^{1}H NMR spectroscopic data suggest rapid reversible dissociation of the pendant CH_2NMe_2 arm in solution.

The relative concentration of **1a** and **1b** in solution depends on the temperature and the absolute concentration of the ring systems. Lower temperatures and higher concentrations favour the four-membered ring **1b** at the expense of the three-membered ring **1a**. Similar solution equilibria following the principle of Le Chatelier were also reported for *cyclo*-$[(Me_3Si)_2CH]_nBi_n$ (n = 3, 4)[6] and *cyclo*-$(Me_3SiCH_2)_nBi_n$ (n = 3, 5).[8] In contrast to the *cyclo*-$(Me_3SiCH_2)_nBi_n$ system, where the equilibrium between the trimer and the pentamer is frozen at −15 °C, the equilibrium between **1a** and **1b** occurs even at −45 °C. The equilibrium constant $K = [\mathbf{1a}]^4/[\mathbf{1b}]^3$ is 36±5 mol/L at 0 °C.

Additional signals for species containing equivalent R groups were observed at high dilution and high temperature. These signals can be assigned to [2-(Me_2NCH_2)-C_6H_4]Bi or [2-$(Me_2NCH_2)C_6H_4]_2Bi_2$.

Single crystals of **1b** suitable for X-ray diffraction studies were obtained by cooling a petroleum ether solution of a mixture of the rings to −28 °C. The molecular structure is depicted in Figure 1. The structure consists of a folded four-membered bismuth ring with the 2-$(Me_2NCH_2)C_6H_4$ substituents in the *all-trans* configuration, consistent with the NMR spectroscopic data in solution. The Bi_3-Bi_3 dihedral angles are 107.9 and 109.4°, respectively. The Bi−Bi bond lengths [3.0095(16)−3.0221(16) Å] compare well with the analogous values found in $[(Me_3Si)_2CH]_4Bi_4$ [2.970(5)−3.044(2) Å][6] and $[(Me_3Si)_3Si]_4Bi_4$ [3.013(1)−3.028(1) Å].[7] The Bi−C bonds [2.24(3)−2.30(3) Å] are shorter than the corresponding bonds in $[(Me_3Si)_2CH]_4Bi_4$ [2.33(2)−2.39(2) Å].[6] The 2-$(Me_2NCH_2)C_6H_4$ groups act as bidentate chelating ligands with weak N→Bi intramolecular interactions [2.97(3)−3.05(2) Å] *trans* to a Bi−Bi bond. The N−Bi distances lie between the sum of the covalent (2.2 Å) and van der Waals radii (3.7 Å) of N and Bi. Comparable interactions were observed in [2-$(Me_2NCH_2)C_6H_4]_3Bi$ [Bi−N 3.04(2)−3.11(3) Å][17] and [2-$(Me_2NCH_2)C_6H_4]_2BiCl$ [Bi−N 2.570(5), 3.047(5) Å].[18] The orientation of the aryl groups leads to a propeller-like arrangement. The geometry about the bismuth atoms is distorted pseudo-trigonal-bipyramidal with one of the neighbouring bismuth atoms and the nitrogen atom in axial positions [Bi−Bi−N 158.7(6)−163.5(5)°]. The second bismuth atom, the *ipso*-carbon atom and the lone pair of electrons are in equatorial positions. The Bi−Bi−Bi angles [76.79(4)−79.51(4)°] are similar to those found in *cyclo*-$[(Me_3Si)_2CH]_4Bi_4$ [78.97(8)−79.93(6)°].[6] The transanular Bi···Bi distances in **1b** [3.753(1), 3.857(1) Å] and *cyclo*-$[(Me_3Si)_2CH]_4Bi_4$[6] [3.834, 3.859 Å] are also similar.

Coordination of the bismuthinidene [2-(Me_2NCH_2)-C_6H_4]Bi was achieved by treatment of the **1a/1b** mixture with $W(CO)_5$·THF in at 0 °C affording the complex $RBi[W(CO)_5]_2$ (**2**) [Equation (1)].

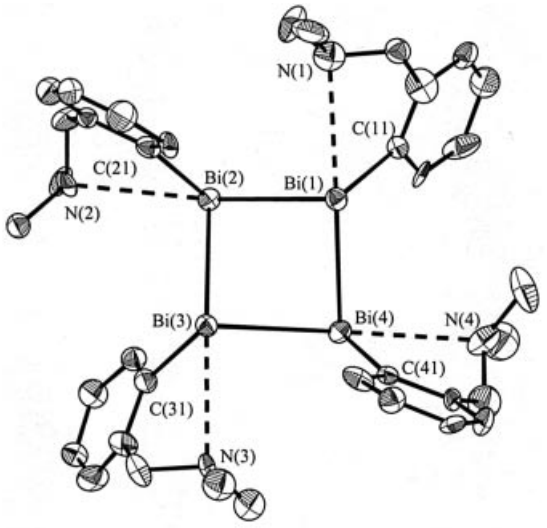

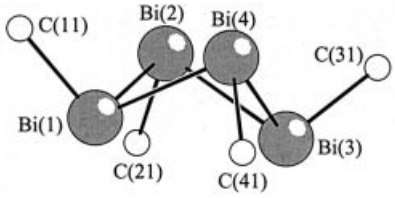

Figure 1. Structure of **1b** in the crystal; the ellipsoids represent 40% probability; selected bond lengths [Å] and angles [°]: Bi(1)−Bi(2) 3.0095(16), Bi(1)−Bi(4) 3.0206(16), Bi(2)−Bi(3) 3.0187(15), Bi(3)−Bi(4) 3.0221(16), Bi(1)−C(11) 2.24(3), Bi(2)−C(21) 2.30(3), Bi(3)−C(31) 2.28(3), Bi(4)−C(41) 2.28(3); Bi(2)−Bi(1)−Bi(4) 79.51(4), Bi(1)−Bi(2)−Bi(3) 77.01(4), Bi(2)−Bi(3)−Bi(4) 79.34(4), Bi(1)−Bi(4)−Bi(3) 76.79(4), Bi(2)−Bi(1)−C(11) 99.4(7), Bi(4)−Bi(1)−C(11) 98.6(7), Bi(1)−Bi(2)−C(21) 97.7(7), Bi(3)−Bi(2)−C(21) 93.2(7), Bi(2)−Bi(3)−C(31) 96.7(8), Bi(4)−Bi(3)−C(31) 101.7(7), Bi(1)−Bi(4)−C(41) 92.3(6), Bi(3)−Bi(4)−C(41) 94.4(7)

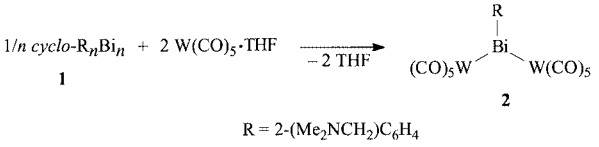

(1)

Red-orange crystals of **2** were obtained from a red toluene solution at −28 °C. The ^{1}H NMR spectrum of **2** shows the expected two singlets for the CH_3 and CH_2 groups, respectively, and the signals for the aryl protons. In the CI mass spectrum, the molecular ion peak of **2** was observed as the one with highest mass. The molecular structure of this bismuthinidene complex with intramolecular base coordination is depicted in Figure 2.

The [2-$(Me_2NCH_2)C_6H_4$]Bi group bridges two pentacarbonyltungsten fragments. The bismuth atom is tetra-coordinate in an irregular trigonal-pyramidal environment. The Bi−W bond lengths [2.8248(8) and 2.8362(8) Å] are similar to the values observed in $[Ph_3BiW(CO)_5]$ [2.8294(5) Å],[19] $[(Ph_3P)_2N][Ph_2Bi\{W(CO)_5\}_2]$ [2.891(2), 2.997(3) Å][20] and $[(Bi_2)W_2(CO)_8\{MeBiW(CO)_5\}]$ [2.851(2)−3.001(3) Å].[21]

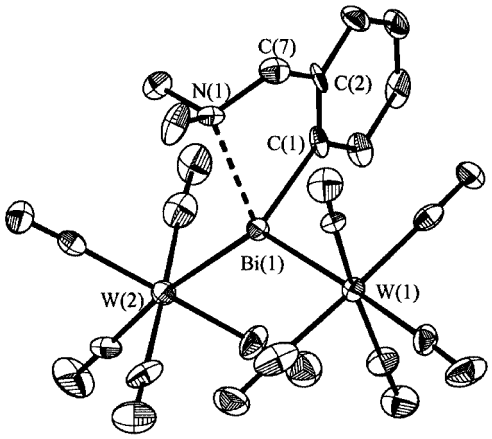

Figure 2. Structure of **2** in the crystal; the ellipsoids represent 40% probability; selected distances [Å] and angles [°]: Bi(1)−C(1) 222.3(16), Bi(1)−N(1) 2.435(12), Bi(1)−W(2) 2.8248(8), Bi(1)−W(1) 2.8362(8); C(1)−Bi(1)−N(1) 73.7(5), C(1)−Bi(1)−W(2) 108.8(3), N(1)−Bi(1)−W(2) 111.7(3), C(1)−Bi(1)−W(1) 105.7(3), N(1)−Bi(1)−W(1) 109.2(3), W(2)−Bi(1)−W(1) 132.13(3)

The intramolecular N−Bi distance [2.435(12) Å] in **2** is shorter than in R_2BiCl [2.570(5) Å][18] or $RBiI_2$ [2.503(6) Å],[18] [R = 2-$(Me_2NCH_2)C_6H_4$]. The W_2BiC framework of the Bi(*C,N*)W_2 core is almost planar (the sum of angles around Bi is 346.53°), with the Bi atom situated only 0.5 Å above the W_2C plane. Compound **2** can be described as a complex of an RBi ligand with two sp^2-orbitals containing lone pairs of electrons and an empty p-orbital at the bismuth atom. The filled orbitals are involved in the dative bonds to the tungsten atoms and the empty p-orbital accepts electron density from the amine group and the tungsten atoms. The structure is certainly also influenced by the constraints imposed by the five-membered chelate ring.

Analogous base-stabilized bismuthinidene complexes with donation of two lone pairs of electrons to two 16-electron complex fragments are unknown. Closely related compounds are the dinuclear complexes with phosphinidene, arsinidene, or stibinidene ligands, which have been studied by Huttner et al. They found that the tendency to form adducts with Lewis bases is considerably stronger for the heavier group-15 element ligands.[22] The formation of **2** does not prove unambiguously the presence of a monomeric bismuthinidene in the reaction solution. Alternatively, the reaction of the rings **1a** or **1b** with $W(CO)_5$·THF followed by splitting of the Bi−Bi bond might lead to **2**. It is remarkable that the analogous reaction of *cyclo*-$(Me_3SiCH_2)_nBi_n$ with $W(CO)_5$·THF, carried out under very similar conditions, gave the dibismuthene complex $[(RBi{=}BiR)\{W(CO)_5\}_2]$ (R = Me_3SiCH_2) instead of a bismuthinidene complex.[8]

The dibismuthane R_4Bi_2 (**3**) was synthesised by reduction of $[2\text{-}(Me_2NCH_2)C_6H_4]_2BiCl$ with Mg in THF at −40 °C [Equation (2)] and was isolated in 78% yield as a dark red hydrocarbon-soluble solid. Solutions of **3** are air-sensitive, but under an inert gas they are stable at room temperature for a long time ($\tau_{1/2}$ = 14 d). Crystals of **3** are stable in air for several hours.

$$2\ R_2BiCl + Mg \xrightarrow[-40\ ^\circ C]{THF} \underset{\mathbf{3}}{R_2Bi{-}BiR_2} + MgCl_2 \quad (2)$$

R = 2-$(Me_2NCH_2)C_6H_4$

The ^1H NMR spectrum of **3** shows one singlet for the methyl groups and an AB spin system for the CH_2 groups, indicating that all substituents are equivalent in solution. Variation of the temperature between +20 and −60 °C does not result in significant changes in the ^1H NMR spectrum. The EI mass spectrum of **3** displays a peak for the R_2Bi^+ fragment at highest mass. Single crystals of **3** were obtained from diethyl ether at −28 °C and the structure was determined by a single-crystal X-ray diffraction study. The molecular structure is depicted in Figure 3. Compound **3** is a dibismuthane exhibiting an antiperiplanar (*trans*) conformation [φ = lp−Bi−Bi−lp 132.18(1)°; lp = assumed position of the lone pair of electrons], which brings two organic groups on different metal atoms in an almost ecliptic position relative to each other [C(31)−Bi(2)−Bi(1)−C(11) 35.2(2)°]. This behaviour contrasts with the ideal *trans* conformation found in other dibismuthanes, $R_2Bi{-}BiR_2$ [R = Ph: φ = 180.00(5);[14] R = Me_3Si: φ = 180.00(3)[15]]. Intramolecular N−Bi coordination occurs through three of the four nitrogen atoms, the pendant arm carrying the N(1) atom being twisted far from the Bi(1) atom.

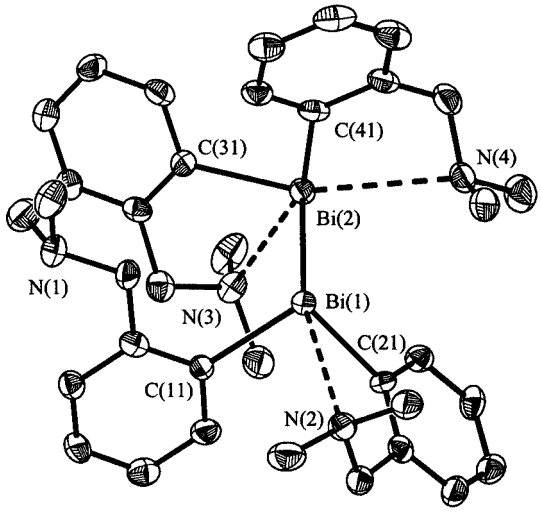

Figure 3. Structure of **3** in the crystal; the ellipsoids represent 40% probability; selected distances [Å] and angles [°]: Bi(1)−Bi(2) 3.0657(5), Bi(1)−C(11) 2.272(5), Bi(1)−C(21) 2.295(6), Bi(1)−N(2) 2.952(5), Bi(2)−C(31) 2.287(5), Bi(2)−C(41) 2.317(5), Bi(2)−N(3) 3.027(4), Bi(2)−N(4) 3.170(4); C(11)−Bi(1)−C(21) 96.29(19), C(11)−Bi(1)−N(2) 85.15(16), C(21)−Bi(1)−N(2) 67.39(18), C(11)−Bi(1)−Bi(2) 101.20(13), C(21)−Bi(1)−Bi(2) 96.04(15), N(2)−Bi(1)−Bi(2) 162.97(10), C(31)−Bi(2)−C(41) 94.3(2), C(31)−Bi(2)−N(3) 66.54(17), C(41)−Bi(2)−N(3) 159.83(18), C(31)−Bi(2)−Bi(1) 106.33(15), C(41)−Bi(2)−Bi(1) 81.77(14), N(3)−Bi(2)−Bi(1) 97.24(10), C(31)−Bi(2)−N(4) 159.31(17), C(41)−Bi(2)−N(4) 65.72(17), N(3)−Bi(2)−N(4) 133.92(13), Bi(1)−Bi(2)−N(4) 77.10(9)

This results in a wide range of Bi−Bi−C angles [81.77(14)−106.33(14)°] and different overall coordination geometries at the metal atoms. Bi(1) is in a distorted pseudo-trigonal-bipyramidal environment similar to that of the bismuth atoms in **1b**, with N(2) and Bi(2) in axial positions [N(2)−Bi(1)−Bi(2) 162.97(10)°].

The coordination geometry around Bi(2) is distorted tetragonal-pyramidal, with Bi(1) in the apical position and a C_2N_2 basal plane. The Bi−N distances [2.952(5), 3.027(4), and 3.170(4) Å] in the molecule of **3** are similar to the corresponding Bi−N bond lengths in **1b** [2.97(3)−3.05(2) Å], while the Bi−Bi distance in **3** [3.0657(5) Å] corresponds to a normal single bond as found in **1b** [3.0095(16)−3.0221(16) Å] or Ph_4Bi_2 [2.990(2) Å].[14] The Bi−Bi−C angles in **3** lie in the range between 81.77(14) and 106.33(15)°.

Conclusions

The present results show that the use of the 2-(dimethylaminomethyl)phenyl group stabilizes di- and *cyclo*-bismuthanes through intramolecular coordination of the pendant CH_2NMe_2 arm. The stabilizing effect is, however, not sufficient to allow the isolation of the monomeric 8-electron bismuthinidene species, RBi. This moiety was trapped by formation of a complex with pentacarbonyltungsten.

Experimental Section

General Comments: Syntheses were carried out under argon using dried solvents freshly distilled under argon. NMR spectra were recorded with a Bruker DPX 200 instrument. Mass spectra were recorded with a Finnigan MAT 8222 instrument and IR spectra with an FT-IR SPEKTRUM 1000. Compounds with the formulae $[2\text{-}(Me_2NCH_2)C_6H_4]_nBiCl_{3-n}$ were prepared according to the literature method.[17] The crystal structure measurement and refinement data for **1b**, **2**, and **3** are given in Table 1. Data for **1b** and **2** were collected with a Siemens P4 four-circle diffractometer. Data for **3** were collected with a STOE IPDS diffractometer. In both cases a graphite monochromator was used to produce a wavelength (Mo-K_α) of 0.71073 Å. The crystals were attached with Kel-F oil to a glass fibre and cooled under a nitrogen stream at 173 K. The structures were solved by direct methods (full-matrix least squares on F^2). All non-hydrogen atoms were refined with anisotropic thermal parameters. Structure solutions and refinements were carried out using the SHELX-97 software package.[23] Diagrams were created using the Diamond program by Crystal Impact GbR.[24] CCDC-195483 (**1b**), -195484 (**2**), and -195482 (**3**) contain the supplementary crystallographic data for this paper. These data can be obtained free of charge at www.ccdc.cam.ac.uk/conts/retrieving.html

Table 1. Data for the X-ray structure determinations of **1b**, **2**, and **3**

	1b	**2**	**3**
Empirical formula	$C_{36}H_{48}Bi_4N_4$	$C_{19}H_{12}BiNO_{10}W_2$	$C_{36}H_{48}Bi_2N_4$
Formula mass	1372.70	990.98	954.74
Colour	dark green	orange	red
Temp. [K]	173(2)	173(2)	173(2)
Crystal size [mm]	0.40 × 0.30 × 0.30	0.25 × 0.10 × 0.05	0.5 × 0.4 × 0.3
Wavelength [Å]	0.71073	0.71073	0.71073
Crystal system	orthorhombic	triclinic	monoclinic
Space group	$P2_12_12_1$	$P\bar{1}$	$P2_1/c$
a [Å]	11.589(3)	9.8730(10)	19.759(4)
b [Å]	14.460(4)	10.2640(10)	11.045(2)
c [Å]	23.807(4)	12.1440(10)	16.315(3)
α [°]	90	81.25	90
β [°]	90	82.83	90.12(3)
γ [°]	90	84.72	90
Z	4	2	4
$d_{calcd.}$ [g cm^{-3}]	2.285	2.735	1.781
μ [mm^{-1}]	17.618	16.880	9.900
F(000)	2496	888	1832
θ range [°]	2.22−27.51°	2.54−27.49	2.11−25.89
Index ranges	$-15 \le h \le 9$, $-18 \le k \le 18$, $-10 \le l \le 30$	$-12 \le h \le 1$, $-13 \le k \le 13$, $-15 \le l \le 15$	$-24 \le h \le 24$, $-13 \le k \le 13$, $-19 \le l \le 19$
No. of measured data	6237	6579	48837
No. of unique data [R(int)]	5889 [R(int) = 0.0270]	5521 [R(int) = 0.0399]	6873 [R(int) = 0.1091]
Data/restraints/parameters	5889/108/408	5521/0/303	6873/0/390
Absorption correction	empirical (SHELXA)	empirical (SHELXA)	empirical (SHELXA)
$R1$ [$I > 2\sigma(I)$]	0.0657	0.0571	0.0277
$wR2$ [$I > 2\sigma(I)$]	0.1161	0.1107	0.0440
$R1$ (all data)	0.1238	0.1023	0.0553
$wR2$ (all data)	0.1374	0.1279	0.0474
Goodness-of-fit on F^2	1.018	1.006	0.824
Residual density [e·Å^{-3}]	1.854, −1.818	2.320, −2.006	0.548, −0.766

[or from the Cambridge Crystallographic Data Centre, 12 Union Road, Cambridge CB2 1EZ, UK; Fax: (internat.) + 44-1223/336-033; E-mail: deposit@ccdc.cam.ac.uk].

Synthesis of [2-(Me_2NCH_2)C_6H_4]$_n$$Bi_n$ [*n* = 3 (1a), 4 (1b)]. Procedure 1: Na (1.0 g, 44.4 mmol) was dissolved in liquid ammonia (ca. 150 mL) and [2-(Me_2NCH_2)C_6H_4]$BiCl_2$ (9.0 g, 21.7 mmol) was added. The reaction mixture was stirred for 9 h and the liquid ammonia evaporated. The remaining black residue was extracted with petroleum ether (250 mL). After filtration, the petroleum ether was evaporated leaving a black-green solid (3.7 g, 49.5%). Compound **1b** [m.p. 53 °C (dec.)] separated as dark-green crystals from petroleum ether at −28 °C after a few weeks. ^{1}H NMR (200 MHz, 25 °C, $C_6D_5CD_3$, TMS): R_3Bi_3 (**1a**): δ = 2.29 (s, 12 H, *cis*-CH_3), 2.34 (s, 6 H, *trans*-CH_3), 3.38 (s, 4 H, *cis*-CH_2), 3.34 (s, 2 H, *trans*-CH_2), 6.42−6.99 (m, 9 H, 3−5-H), 7.57 (dd, $^3J_{H,H}$ = 7.4, $^4J_{H,H}$ = 1.3, 2 H, *cis*-6-H), 7.87 (dd, $^3J_{H,H}$ = 7.4, $^4J_{H,H}$ = 1.3, 1 H, *trans*-6-H); R_4Bi_4 (**1b**): δ = 1.91 (s, 24 H, CH_3), 3.43 (s, 8 H, CH_2), 6.68−6.99 (m, 12 H, 3−5-H), 8.93 (d, $^3J_{H,H}$ = 6.2, 4 H, 6-H). $C_{36}H_{48}Bi_4N_4$ (1372.70): calcd. C 31.50, H 3.52; found C 31.39, H 3.42. **Procedure 2:** $LiAlH_4$ (0.4 g, 10.7 mmol) was added with stirring to a solution of [2-(Me_2NCH_2)C_6H_4]$_2$BiCl (5.0 g, 9.7 mmol) in Et_2O (90 mL) at −78 °C. The reaction mixture was then warmed slowly to −30 °C. At −30 °C the solution was filtered through a precooled glass frit. The dark red filtrate was concentrated in vacuo at −30 °C leaving dark green crystals of **1b** (2.2 g, 65.9%). The identity of the product was established by ^{1}H NMR and X-ray diffraction (determination of the unit cell parameters).

Synthesis of [{2-(Me_2NCH_2)C_6H_4}Bi{$W(CO)_5$}$_2$] (2): A solution of [$W(CO)_5$THF] (2.3 g, 5.8 mmol) in THF (100 mL) was added to **1** (1.0 g, 0.7 mmol) in THF (40 mL) at 0 °C and the mixture was stirred for 3 h at 0 °C. After removal of the solvent in vacuo, the residue was extracted with toluene (100 mL) and then filtered through a glass frit covered with kieselguhr. The clear filtrate was concentrated and cooled to −28 °C to give orange-red crystals of **2** (1.6 g, 57.6%) (m.p. 82−85 °C). ^{1}H NMR (200 MHz, 25 °C, C_6D_6, TMS): δ = 1.99 (s, 6 H, CH_3), 3.07 (s, 2 H, CH_2), 6.88−7.21 (m, 3 H, 3−5-H), 7.58 (dd, $^3J_{H,H}$ = 7.2, 1 H, 6-H) ppm. ^{13}C NMR (50 MHz, 25 °C, C_6D_6, TMS): δ = 49.85 (s, CH_3), 72.73 (s, CH_2), 131.59 (s, C-4), 134.96 (s, C-3), 143.48 (s, C-5), 163.74 (s, C-6), 198.07 (s, CO_{eq}), 200.89 (s, CO_{ax}) ppm. IR (nujol): $\tilde{\nu}$ = 2072, 2054, 1940, 1908 cm^{-1} (C=O). MS (EI, 70 eV): *m*/*z* (%) = 990 (5) [M^+], 822 (2) [M^+ − 6 CO], 794 (3) [M^+ − 7 CO], 766 (2) [M^+ − 8 CO], 583 (10) [$RW(CO)_2^+$], 343 (60) [RBi^+], 134 (76) [R^+], 58 (100) [$Me_2NCH_2^+$]. $C_{19}H_{12}BiO_{10}W_2$ (990.98): calcd. C 23.03, H 1.22; found C 22.79, H 1.23.

Synthesis of [2-(Me_2NCH_2)C_6H_4]$_4$$Bi_2$ (3): A solution of [2-(Me_2NCH_2)C_6H_4]$_2$BiCl (7.0 g, 13.8 mmol) in THF (70 mL) was added dropwise at −40 °C to Mg (0.5 g, 21.4 mmol) activated with 1,2-dibromoethane (0.5 mL). The reaction mixture was stirred for 3 h and then the temperature was raised to 0 °C. The solvent was removed in vacuo leaving a dark red solid. After extraction with petroleum ether (150 mL) and filtration, the solvent was evaporated to dryness and the residue dissolved in Et_2O (20 mL). Cooling to −28 °C gave **3** (4.9 g, 78.3%) as red crystals (m.p. 69−79 °C). ^{1}H NMR (200 MHz, 25 °C, C_6D_6, TMS): δ = 1.93 (s, 6 H, CH_3), AB spin system with δ_A = 3.14 and δ_B = 3.32 ($^2J_{H,H}$ = 12.8, 2 H, CH_2), 6.99 (ddd, $^3J_{H,H}$ = 7.1, $^4J_{H,H}$ = 1.5, 1 H, 4-H), 7.13 (ddd, $^3J_{H,H}$ = 7.4, $^4J_{H,H}$ = 1.5, 5-H), 7.24 (dd, $^3J_{H,H}$ = 7.4, $^4J_{H,H}$ = 1.2, 1 H, 3-H), 8.67 (dd, $^3J_{H,H}$ = 7.1, $^4J_{H,H}$ = 1.5, 1 H, 6-H) ppm. ^{13}C NMR (50 MHz, 25 °C, C_6D_6, TMS): δ = 45.12 (s, CH_3), 69.13 (s, CH_2), 126.75 (s, C-4), 129.75 (s, C-3), 129.99 (s, C-5), 145.46 (s, C-6), 146.31 (s, C-1), 151.73 (s, C-2) ppm. MS (EI, 70 eV): *m*/*z* (%) = 477 (100) [R_2Bi^+], 342 (8) [RBi^+], 134 (50) [R^+]. $C_{36}H_{48}Bi_2N_4$ (954.74): calcd. C 45.29, H 5.07; found C 45.10, H 5.05.

Acknowledgments

We thank the Deutsche Forschungsgemeinschaft and the University Bremen for financial support.

[1] P. Pyykkö, *Chem. Rev.* **1988**, *88*, 563.
[2] C. Silvestru, H. J. Breunig, H. Althaus, *Chem. Rev.* **1999**, *99*, 3277.
[3] N. Tokitoh, Y. Arai, R. Okazaki, S. Nagase, *Science* **1997**, *277*, 78.
[4] N. Tokitoh, *J. Organomet. Chem.* **2000**, *611*, 217.
[5] B. Twamley, C. D. Sofield, M. M. Olmstead, P. P. Power, *J. Am. Chem. Soc.* **1999**, *121*, 3357.
[6] H. J. Breunig, R. Rösler, E. Lork, *Angew. Chem.* **1998**, *110*, 3361; *Angew. Chem. Int. Ed.* **1998**, *37*, 3175.
[7] G. Linti, W. Köstler, *Z. Anorg. Allg. Chem.* **2002**, *628*, 63.
[8] L. Balazs, H. J. Breunig, E. Lork, *Angew. Chem.* **2002**, *13*, 2411−2414, *Angew. Chem. Int. Ed.* **2002**, *41*, 2309−2312.
[9] K. H. Whitmire, M. Shieh, J. M. Cassidy, *Inorg. Chem.* **1989**, *28*, 3164.
[10] J. M. Cassidy, K. H. Whitmire, *Inorg. Chem.* **1991**, *30*, 2788.
[11] M. Shieh, Y. Liou, S.-M. Peng, G.-H. Lee, *Inorg. Chem.* **1993**, *32*, 2212.
[12] F. A. Paneth, H. Loleit, *J. Chem. Soc.* **1935**, 366.
[13] H. J. Breunig, D. Müller, *Angew. Chem.* **1982**, *94*, 448; *Angew. Chem. Int. Ed. Engl.* **1982**, *21*, 439.
[14] F. Calderazzo, R. Poli, G. Pelizzi, *J. Chem. Soc., Dalton Trans.* **1984**, 2365.
[15] O. Mundt, G. Becker, M. Rössler, C. Witthauer, *Z. Anorg. Allg. Chem.* **1983**, *506*, 42.
[16] A. J. Ashe, J. W. Kampf, D. B. Puranik, S. M. Al-Taweel, *Organometallics* **1992**, *11*, 2743.
[17] S. Kamepalli, C. J. Carmalt, R. D. Culp, A. H. Cowley, R. A. Jones, *Inorg. Chem.* **1996**, *35*, 6179.
[18] C. J. Carmalt, A. H. Cowley, R. D. Culp, R. A. Jones, S. Kamepalli, N. C. Norman, *Inorg. Chem.* **1997**, *36*, 2770.
[19] N. J. Holmes, W. Levason, M. Webster, *J. Organomet. Chem.* **1997**, *545−546*, 111.
[20] R. E. Bachman, K. H. Whitmire, *Inorg. Chem.* **1995**, *34*, 1542.
[21] A. M. Arif, A. H. Cowley, N. C. Norman, M. Pakulski, *J. Am. Chem. Soc.* **1985**, *107*, 1062.
[22] G. Huttner, in: *Multiple Bonds and Low Coordination in Phosphorus Chemistry* (Eds.: M. Regitz, O. J. Scherer), Thieme Stuttgart, **1990**.
[23] G. M. Sheldrick, *SHELX-97*, Universität Göttingen, Göttingen, Germany, **1997**.
[24] K. Brandenburg, *DIAMOND*, Version 2.1c, Crystal Impact GbR, **1999**.

Received October 24, 2002
[I02588]

Polypeptide Adsorption on a Synthetic Montmorillonite: A Combined Solid-State NMR Spectroscopy, X-ray Diffraction, Thermal Analysis and N_2 Adsorption Study

Régis D. Gougeon,*[a] Michel Soulard,[b] Marc Reinholdt,[b] Jocelyne Miehé-Brendlé,[b] Jean-Michel Chézeau,[b] Ronan Le Dred,[b] Richard Marchal,[a] and Philippe Jeandet*[a]

Keywords: Peptides / Adsorption / Clays / NMR spectroscopy / X-ray diffraction

Two homopolypeptides, polylysine and polyglutamic acid, were adsorbed on a synthetic montmorillonite clay, in acidic medium. These organic-inorganic complexes can be heated up to 110 °C without any degradation of the polypeptide. ^{1}H-^{13}C CP-MAS NMR spectra show that these polypeptides, which exhibit a mixture of α-helical and random coil conformations in the bulk, tend to unfold and adopt a more extended random coil structure on adsorption on the phyllosilicate. The values of the basal spacing measured by X-ray diffraction on dehydrated samples clearly indicate that in the presence of adsorbed polypeptide, the silicate layers do not collapse. The incorporation of polypeptide fragments within the interlayer space is also revealed by the decrease in the specific surface areas measured by N_2-adsorption BET experiments.

(© Wiley-VCH Verlag GmbH & Co. KGaA, 69451 Weinheim, Germany, 2003)

Introduction

Specific interactions between polymers or proteins and clay mineral solid surfaces are at the basis of both natural processes and technological applications. In soil chemistry for instance, such organic-inorganic interactions are considered to be of prime importance in the regulation of the microbially mediated decomposition processes of soil organic matter.[1] Alternatively, membrane filtration[2] or advanced hybrid materials[3,4] are examples of the efficient use of the macromolecule-clay mineral interactions for new industrially relevant techniques. On the other hand, bentonites have been used for more than 60 years as adsorbents in winemaking, to remove proteins from musts and wines.[5] This particular affinity of proteins for phyllosilicates is based on the commonly high specific-surface areas associated with swelling and cation-exchange properties of the latter. Due to intralayer octahedral and/or tetrahedral substitutions, montmorillonites exhibit an overall negative surface charge that is balanced by hydrated cations such as sodium or calcium which are located within the interlayer spaces.[6] At pH values below their isoelectric points (i.e.p.), proteins are positively charged and their adsorption is basically seen as a cation-exchange process based on electrostatic, hydrophobic and/or hydrophilic interactions.[7]

To characterize the way in which proteins interact with solid surfaces, several studies have pointed out the important features arising from the modification of the conformation of interacting macromolecules. In particular, FTIR and enzymatic activity studies have emphasized the pH-dependent modification[8] and/or pH-dependent orientation[9] effects on the adsorbed enzymes, characterized by structural unfolding due to electrostatic interactions with montmorillonite. However, the mechanisms by which proteins are adsorbed on clay minerals are still subject to many questions.[10] A detailed description of the part of the protein that interacts with the mineral surface and the distance of interaction is required to understand the proteins/solid surface interactions.[11]

The aim of this study is to investigate model samples that can be considered as representative of protein−clay mineral complexes. This is accomplished through the analysis of the adsorption of two homopolypeptides, polylysine and polyglutamic acid (Scheme 1), on a synthetic montmorillonite,[12] using complementary approaches.

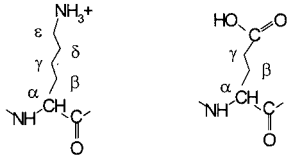

Scheme 1. Lysine (left) and glutamic acid (right) units

[a] Laboratoire d'œnologie URVVC, Université de Reims, UPRES EA 2069, Faculté des Sciences,
Moulin de la Housse, B. P. 1039, 51687 Reims Cedex 2, France
[b] Laboratoire de Matériaux Minéraux, Ecole Nationale Supérieure de Chimie, UMR-CNRS 7016,
3, Rue A. Werner, 68093 Mulhouse cedex, France

Thermal analyses (TG-DTA) can provide a rather accurate determination of the amount of adsorbed polypeptides on the solid surfaces,[13] and can also afford useful indirect information about the strength of the organic-inorganic interaction, from the decomposition temperature of the organic matter.[14]

Despite its low sensitivity, solid-state NMR spectroscopy has been successfully applied to the study of interfaces. In particular, this technique does not require any mechanical treatment and can provide, under certain circumstances, a direct three-dimensional picture of polypeptides in the bulk or in the adsorbed state.[13,15] Solid-state NMR spectroscopy has already been applied to the qualitative and/or quantitative characterization of soil organic matter,[16] but rarely to the characterization of adsorbed proteins on clay minerals.[17]

Several features can be obtained from powder X-ray diffraction patterns of smectites, e.g. the basal spacing, which is equal to the sum of the interlayer spacing and the thickness of the silicate layer, and which is given by the measurement of the (001) peak position.[18] Numerous studies have reported the d_{001} values of clay minerals onto which organic molecules such as amino acids[19] or alkylammonium ions[20] were adsorbed. These results provide a good basis for the comparison of values measured for polypeptide-adsorbed montmorillonite, either under controlled humidity or after dehydration.

Finally, one of the most interesting properties to explore when dealing with porous solids is the specific surface area and its variation resulting from the adsorption of organic molecules. However, measuring the actual specific surface area of montmorillonites corresponds to the determination of the surface area between the silicate layers which, in the absence of any adsorbed molecule, is theoretically equal to 760 m^2/g.[21] Such a result is classically obtained by the adsorption of a probe molecule such as methylene blue,[22] which can displace some interlayer species, and therefore cannot be used in the presence of previously adsorbed polypeptides. Consequently, nitrogen was used to determine the BET surface areas. It must be noted that the whole interlayer microporous surface of montmorillonites is theoretically not accessible to nitrogen molecules owing to the reversible collapse of the silicate layers on outgassing.

Results and Discussion

Thermal Analyses

The DTA curve (Figure 1, a) of the synthetic montmorillonite (**M**) is characterized by a major endothermic peak at 100 °C, which corresponds to interlayer dehydration, followed by a second weaker and broader endothermic peak, with a minimum at 650 °C, for the dehydroxylation of the layer.[12] On adsorption of polypeptides, the DTA curves (Figure 1, a) show additional exothermic signals in the range 260−700 °C, which correspond to the oxidative degradation of the adsorbed organic molecules. For **M/PL**, a strong exothermic peak occurs at 320 °C, and is followed by a second weaker exothermic peak at 600 °C. Two broader peaks are also observed for **M/PG**, but with weaker intensities and with the first peak occurring at a higher temperature than that for **M/PL**.

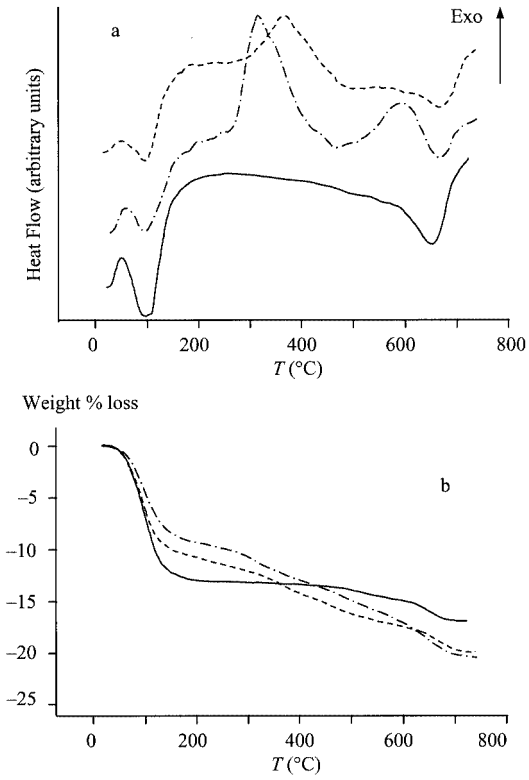

Figure 1. (a) DTA and (b) TG curves of **M** (plain line), **M/PL** (dashed dotted line) and **M/PG** (dotted line)

The amounts of adsorbed polypeptide were determined from the analysis of the TG curves (Figure 1, b), since the distinct exothermic peaks are solely due to the combustion of the organic matter. However, weight losses recorded at higher temperatures include the dehydroxylation process. The latter can be quantified from the experiment on **M** alone, and then subtracted from the weight losses determined for the organic-inorganic complexes. Table 1 gathers the calculated amounts of **PL**, **PG** and **PL/PG** adsorbed on **M**. For each separate adsorption (**M/PL** and **M/PG**), nearly all the polypeptide introduced is adsorbed. When both polypeptides are simultaneously introduced, and in higher quantities (**M/PL/PG**), they are also almost completely adsorbed (Table 1). In the case of **M/PL/PG**, the amount of **PL** introduced was set to present approximately 100 mequiv. of side chain NH_3^+ charges per 100 g of calcined

Table 1. Weight-percent amount, relative to dehydrated montmorillonite, of polypeptide introduced and adsorbed, from TG analyses; errors are ± 0.2

	M/PL	M/PG	M/PL/PG
Introduced	7.0	5.0	12.0 + 12.0
Adsorbed	7.0	4.7	21.0
After outgassing	4.6	3.3	20.3

montmorillonite, i.e. the initial cation exchange capacity of **M**.[12] Therefore, if **PL** is adsorbed via an electrostatic mechanism, in order to replace the Na^+ cations and balance the negative charge of **M**, **PG**, which does not bear positively charged side chains, is adsorbed via a different mechanism.

In order to assess the thermal stability of these organic-inorganic complexes, similar TG-DTA measurements were performed on the samples which had previously been outgassed under vacuum to a temperature of 110 or 150 °C, as required for nitrogen adsorption experiments. The corresponding weight losses are also given in Table 1. On outgassing at 150 °C under vacuum, both **M/PL** and **M/PG** have lost part of the initial amount of adsorbed organic matter. This loss of matter is higher for **M/PL** than for **M/PG**. In contrast, the total amount of adsorbed **PL** and **PG** is kept unchanged after having heated **M/PL/PG** to 110 °C, under vacuum. Furthermore, as shown below by ^{13}C NMR spectroscopy, the structure of the remaining adsorbed polypeptides is kept unchanged, which indicates that outgassing has basically lowered the amount of adsorbed matter, and that any decomposition products, volatile or not, have been outgassed.

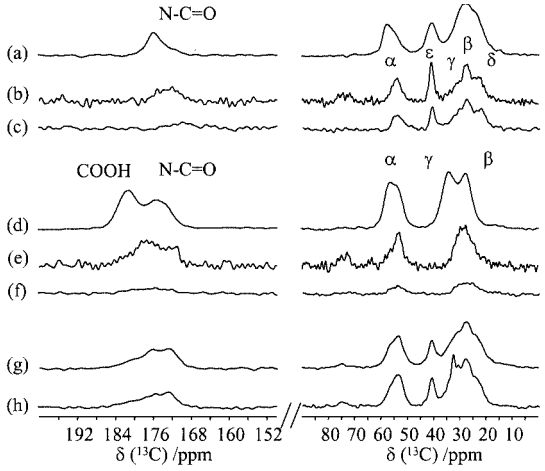

Figure 2. ^1H-^{13}C CP-MAS spectra of: (a) **PL**, (b) **M/PL**, (c) **M/PL** outgassed, (d) **PG**, (e) **M/PG**, (f) **M/PG** outgassed, (g) **M/PL/PG** and (h) **M/PL/PG** outgassed; contact time of 1 ms; only the peak regions are displayed

^{13}C NMR Chemical Shifts and Line Widths

^1H-^{13}C CP-MAS spectra of the bulk **PL** and **PG** samples, and the three polypeptide-adsorbed samples (**M/PL**, **M/PG** and **M/PL/PG**) are presented in Figure 2, with peak assignments taken from the literature.[23] The chemical shifts for the different resolved peaks along with their corresponding line widths are given in Table 2, and an example of deconvolution, for **PL** is given in Figure 3.

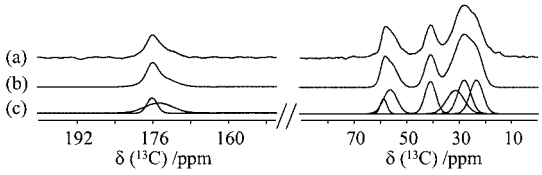

Figure 3. Deconvolution of the ^1H-^{13}C CP-MAS spectrum of **PL**: (a) experimental spectrum, (b) simulated spectrum and (c) individual components

The ^1H-^{13}C CP-MAS spectra of bulk **PL** (Figure 2, a) shows four distinct signals, which are composed of eight components (Figure 3 and Table 2): the backbone carbonyl (δ = 176.1 and 174.7 ppm), the backbone α-CH (δ = 58.3 and 55.8 ppm), the side chain ε-CH_2 (δ = 40.8 ppm), and the three remaining side chain methylene carbon atoms (δ = 31.3, 28.0 and 23.4 ppm) corresponding to the γ, β and δ-CH_2 carbon atoms, respectively. The distribution of the chemical shifts for both the carbonyl and the α-CH carbon atom clearly indicates the heterogeneous secondary structure of bulk **PL**. This is based on the well-established rule that the α-helix to β-sheet transformation in polypeptides is accompanied by a shift towards lower frequencies of the backbone α- and carbonyl carbon atoms, and a shift towards higher frequencies of the side chain β-carbon atom.[23] Intermediate shifts between these two extremes reflect the presence of random coils. For the α-CH group of **PL**, literature values of δ = 57.6 and 57.4 ppm are given for a helical conformation, and values of δ = 51.4 and 52.3 ppm for the β-sheet conformation.[23a,23c] Likewise, for the carbonyl group, literature values of δ = 175.7 and 171.5 ppm or δ = 170.4 ppm are given for the α-helix and the β-sheet, respectively.[23a] This indicates that **PL** displays a mixture of α-helical and random coil secondary structures

Table 2. ^{13}C chemical shifts (δ) and line widths (Δ) in ppm, of the different resolved peaks in the ^1H-^{13}C CP-MAS spectra; where possible, proportions of populations are indicated

	COO^-			NC=O			α-CH		ε-CH_2		γ-CH_2		β-CH_2		δ-CH_2	
	δ	Δ	%	δ	Δ	%	δ	Δ	δ	Δ	δ	Δ	δ	Δ	δ	Δ
PL			28	176.1	2.6	22	58.3	2.9	40.8	4.9	31.3	7.7	28.0	5.8	23.4	5.7
			72	174.7	6.8	78	55.8	6.1								
M/PL				173.0	5.9		54.1	4.3	40.8	2.2	30.5	6.3	27.5	2.7	23.3	5.6
PG	181.3	5.0	50	176.1	3.7	50	57.3	4.2			34.3	6.1	27.7	5.4		
			50	173.3	4.1	50	53.5	4.5								
M/PG	176.9	4.6		172.3	4.0	20	57.4	3.4			29.6	6.7	26.5	7.4		
	181.1	5.4				80	53.3	4.1								
M/PL/PG	181.0	5.8		176.5	3.2		57.4	3.4	40.7	3.0						
				173	5.9		53.3	4.1								

with proportions of about 25 and 75%, respectively (Table 2).

Similar observations can be made with regard to the **PG** ^{13}C chemical shifts (Figure 2, d). The backbone α-carbon resonance is clearly composed of two peaks at δ = 57.3 and 53.5 ppm, indicating the simultaneous α-helical and random coil secondary structures.[23a,23b] Likewise, two components are observed for the carbonyl resonance. From the deconvolutions of both the α-CH and the carbonyl resonances of **PG**, the α-helical and random coil conformations are in equal proportions (Table 2). As for **PL**, the heterogeneous nature of the **PG** secondary structure is in good agreement with the fact that the molecular weights of **PL** and **PG** are intermediate in value between low values, which favor β-sheet conformations and high values, which favor α-helices. The resonance of the carboxylic group at δ = 181.3 ppm is in the expected region for the Na salt form of the **PG** side chains.[24]

On adsorption of polylysine (sample **M/PL**, Figure 2, b), both the backbone carbonyl and α-CH peaks give rise to more symmetrical signals, shifted to lower frequencies at δ = 173.0 and 54.1 ppm, respectively. This directly reflects an overall loss of helicity of polylysine, and the adoption of a single more extended conformation. The α-helices are no longer detected. Besides, three different resolved signals are now observed for the γ, β and δ side chain methylene carbon atoms, which are shifted to lower frequencies (Table 2). This discrepancy is characterized by an apparent shielding of the three side chain −CH− carbon atoms, whereas the β-carbon peak, which should have shifted towards higher frequencies with the loss of helicity,[23a] can be directly correlated to the simultaneous approach of these carbon atoms near the negatively charged clay layer surface.[25] Furthermore, for **M/PL**, the three signals are narrower than for **PL**. The more significant narrowing occurs for the side chain ε-CH_2 peak, whose line width at half height (Δ) halves on adsorption (Table 2). This general line narrowing suggests an increase in the conformational order of these adsorbed polylysine side chain carbons within the clay interlayer space.

For **M/PG** (Figure 2, e), both the carbonyl and the α-CH peaks are shifted to lower frequencies (Table 2), indicating a similar loss of helicity. However, for the latter, a shoulder representing 20% of the signal is still observed at δ = 57.4 ppm, which indicates that the change in conformation is not complete, in contrast with **M/PL**. The side chain carboxylic peak shifts to lower frequencies, but a shoulder also remains at δ = 181.1 ppm, as in bulk **PG**. A shift to lower frequencies of the carboxylic isotropic chemical shift is in good agreement with the protonation of the side chain group.[24] Hence, on adsorption of **PG** onto **M**, most of the polyglutamic acid side chains are protonated, though a minor part remains unprotonated. Taken together with the conclusion drawn from the α-CH chemical shifts, these results confirm that **PG** side chains are directly involved in the adsorption process. However, unlike **PL** side chains, they do not have any positive charges at pH = 3.4. Therefore, to overcome the repulsion from the negative charges of the clay, carboxylic groups have to be protonated, as already shown for BSA adsorbed onto clays.[9b] Furthermore, the broadening of the $-CH_2-$ peaks (Figure 2, e) indicates that unlike for polylysine, adsorption of polyglutamic acid is not accompanied by an apparent increased ordering of the side chains.

The ^{1}H-^{13}C CP-MAS spectrum of **M/PL/PG** (Figure 2, g) displays both the characteristic ε-CH_2 signal (δ = 40.7 ppm) of **M/PL** and the characteristic carboxylic signal (δ = 181 ppm) of **M/PG**, indicating that the two polypeptides have been adsorbed. From the deconvolution of the carboxylic and carbonyl peaks and on the basis of the results of the deconvolutions on the spectra of **M/PL** and **M/PG**, an estimated ratio of 50:50 for the proportions of adsorbed **PL** and **PG** is found, which is consistent with the TG results. As for **M/PL** and **M/PG**, the carboxylic, the carbonyl and the α-CH peaks of **M/PL/PG** shift towards lower frequencies (Table 2). A part of the **PG** molecules retain the bulk secondary structure, as revealed by the carboxylic signal at δ = 181 ppm, and the α-CH signal is narrower than in bulk **PL**. Therefore, it seems that in terms of conformation, each polypeptide has been adsorbed as if the other one was not present.

When the samples were outgassed under vacuum, the ^{1}H-^{13}C CP-MAS spectra still exhibit comparable chemical shifts with those of the unheated samples (Figure 2 c, f, h), thus confirming that this high temperature treatment has not significantly modified the secondary structure of the adsorbed **PL** and **PG** molecules. This is more clearly seen for the **M/PL/PG** sample, which exhibits the highest amount of adsorbed organic matter. Only a weak modification of the conformation of some of the side chain $-CH_2-$ carbon atoms is observed, as suggested by the narrow peak at δ = 32 ppm (Figure 2, h). It must be noted that owing to the small quantities of samples left, spectra in Figure 2 c, f, h were recorded with a Bruker 2.5-mm probe, thus explaining the poor signal-to-noise ratio, particularly for **M/PG**.

X-ray Diffraction

The d_{001} peak region of each sample was recorded under controlled humidity (P/P_0 = 0.79) and after dehydration at 110 °C under vacuum (Figure 4). Unfortunately, we did not succeed in recording the diffractogram of **M/PG** after dehydration due to the lack of sample. The corresponding d_{001} values, which directly reflect the basal spacing of the samples, are presented in Table 3. This spacing is equal to the sum of the interlayer distance and the thickness of the layer, which is about 9.6 Å for a 2:1 phyllosilicate. As already reported, under a relative humidity of P/P_0 = 0.79, **M** exhibits a d_{001} value of 16.1 Å (Table 3).[12] On dehydration, the value falls to 10.5 Å, indicating the almost complete collapse of the layers, with interlayer cations partially inserted into hexagonal openings formed by the silicon tetrahedra.

Under a relative humidity of P/P_0 = 0.79, the d_{001} value of the two **PL**-containing samples (**M/PL** and **M/PL/PG**) is slightly higher (16.4 and 16.5 Å, respectively) than that

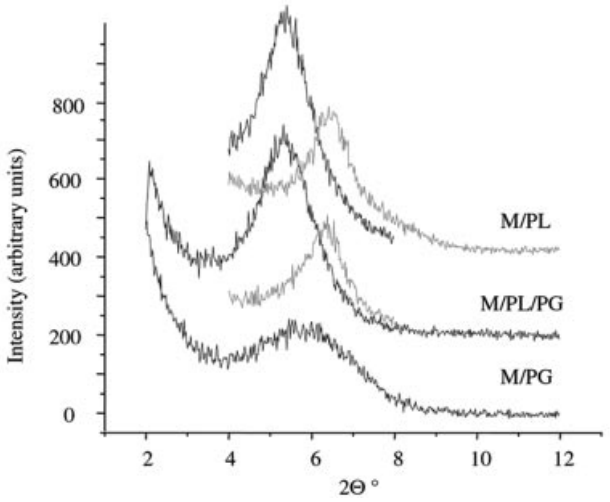

Figure 4. XRD patterns showing the d_{001} region for **M/PL** (top), **M/PL/PG** (center) and **M/PG** (bottom), under a relative humidity of 79% (black) and after dehydration (gray)

Table 3. XRD d_{001} values [Å]

	M	M/PL	M/PG	M/PL/PG
P/P_0 = 79%	16.1	16.4	15.4	16.5
Dehydrated	10.5	13.7		13.9

of **M**, whereas the d_{001} value of **M/PG** is slightly lower (15.4 Å), suggesting that the cumulative volume of adsorbed water molecules and polypeptide moieties is higher for **PL** than for **PG**. However, the highest value of 16.5 Å indicates that, in any case, only one layer of polypeptide moieties is intercalated within the interlayer space, which is consistent with the short length of the side chains of both **PL** and **PG**.[26] On dehydration, the d_{001} values for **M/PL** and **M/PL/PG** (13.7 and 13.9 Å, respectively) remain significantly higher than the thickness of the layers, and are conversely, in very good agreement with those reported for the monolayer adsorption of short chain length alkylammonium cations.[26] Therefore, only the polypeptide side chains appear to be adsorbed within the interlayer space of **M**.[11]

Nitrogen Adsorption

Nitrogen adsorption-desorption isotherms are given for samples **M** and **M/PL/PG** in Figure 5, a and are representative of the other samples. They both exhibit an important hysterisis loop, which is a mixing of type H3 and H4, characteristic of adsorbents containing slit-shaped pores.[27] The first part of these isotherms (P/P_0 between 0 and 0.2) clearly indicates a higher microporous character for **M** (type I isotherm) relative to **M/PL/PG** (type IIb isotherm), whereas the last part (P/P_0 above 0.7) reflects a higher swelling ability of **M** relative to **M/PL/PG**.

The specific surface areas calculated from the BET method are presented in Table 4, along with the corresponding proportions of microporous and external surfaces, as determined from the analyses of the *t*-plot (Figure 5, b).

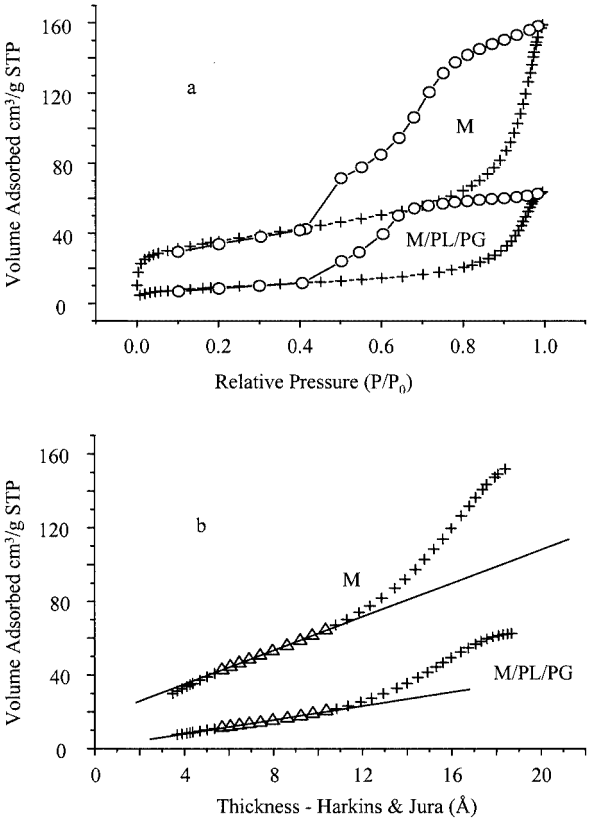

Figure 5. (a) Adsorption (+)-desorption (o) isotherms of nitrogen at 77 K on **M** and **M/PL/PG**; (b) *t*-plot representations for the same samples; triangles represent the experimental points considered for the analysis and the straight line represents the corresponding linear fit

Table 4. Specific surface areas determined from the BET measurements and proportions of external and microporous surface obtained from the *t*-plot analyses; values are expressed in m^2 per gram of dry montmorillonite and corrected for the mass of polypeptide adsorbed

	M	M/PL	M/PG	M/PL/PG
BET	128	110	92	41
External	72	63	63	37
Microporous	56	47	29	4

In the *t*-plots, the volume of nitrogen adsorbed is represented vs. the mean thickness of the adsorbed layer of nitrogen molecules,[28] and a positive intercept of the fitted linear region between ca. 5 and 10 Å directly reflects and quantifies the presence of micropores. Cumulative histogram plots (Figure 6) represent, for each sample, the sum of the microporous and external specific surface areas, which equals to the BET surface area. The above-mentioned microporosity has been attributed to the broken edge face of the particles due to the irregular stacking of the layers, which gives rise to slit-shaped pores.[29] Hence, this microporosity has been shown to be more accessible to hydration, for instance, than interlamellar porosity.[29] Therefore, although being external, this microporosity can be seen basically as interme-

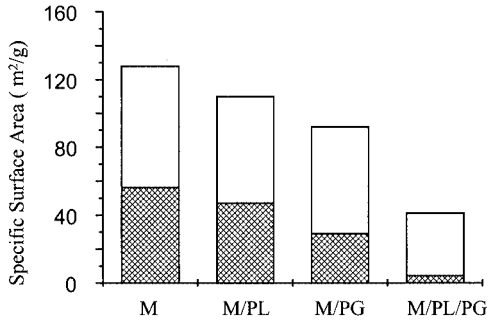

Figure 6. Cumulative histogram representing the microporous (bottom) and external (top) specific surface areas of the different samples; their sum corresponds to the BET surface for each sample

diate between the external surface of particles and the interlayer porosity.

Adsorption of polypeptides clearly leads to a decrease in the BET specific surface area of **M**, with the microporous component being the major contributor to this decrease (Figure 5, b and Figure 6). The higher BET value of **M/PL** compared with that of **M/PG** is in agreement with the thermal analyses, which have shown that on dehydration, **M/PL** has lost a more important proportion of the polypeptide than **M/PG**. In the case of **M/PL/PG**, where more polypeptides were initially adsorbed, nearly all the microporosity is lost. The external specific surface area also decreases on adsorption of the polypeptides, which indicates that the interparticle surface decreases.

Therefore, adsorption of these polypeptides can be described as a plugging process, more specifically, at the broken edges of the **M** particles, with side chains incorporated within the interlayer spaces (Scheme 2). This description agrees with all our results and explains the decrease in both the microporous character and the swelling ability of **M** on adsorption of polypeptides (Figure 5, a).

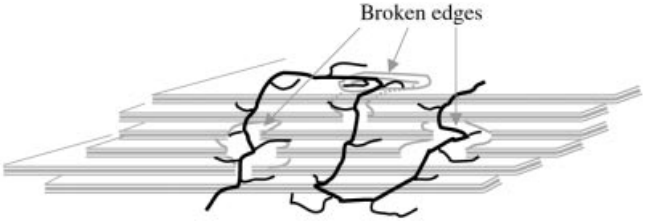

Scheme 2. Proposed description for the plugging of an unfolded polypeptide fragment at the broken edges of the **M** particles, with side chains pointing into the interlayer spaces

Conclusion

Understanding the mechanisms by which polypeptides and proteins adsorb on clay minerals is of major importance for several scientific areas, particularly in areas where this organic-inorganic interaction is at the basis of advanced composite materials. In this study, the use of complementary approaches has led to a more detailed description of the interaction between polylysine and polyglutamic acid with a synthetic montmorillonite. ^{13}C NMR chemical shifts of the backbone α- and carbonyl carbon atoms have shown that both polypeptides, which exhibit a mixture of α-helical and random coil conformations in the bulk, tend to unfold and adopt a more extended random coil structure on adsorption. Furthermore, analysis of the ^{13}C NMR line widths has shown that adsorption of the basic polylysine is accompanied by an increased ordering of the side chains, which is not the case for polyglutamic acid. However, in agreement with thermal analyses, the secondary structure of the adsorbed polypeptides is not significantly modified by heating at temperatures of up to 150 °C under vacuum. Based on this observation, we were able to compare the basal spacing of the polypeptide-adsorbed samples kept under controlled humidity ($P/P_0 = 0.79$) with that measured after dehydration under vacuum. The montmorillonite sheets collapse in the absence of adsorbed polypeptides, whereas they remain about 3.5 Å apart in their presence. Finally, nitrogen adsorption experiments, which are also based on dehydration under vacuum of the samples, were run to compare the accessible specific surface areas of the different samples. We observed that the higher the amount of polypeptide adsorbed, the lower the BET surface. The major contribution to this decrease in measured specific surface area is attributed to the microporous component of the external surface, as deduced from the analyses of the *t*-plots. All together, our results lead to the hypothesis that polypeptides are adsorbed at the periphery of the montmorillonite particles through specific interaction between the polypeptide side chains and the silicate sheets, whereas the polypeptide backbones do not enter the interlayer space.

Experimental Section

Samples: Poly-D-lysine (HBr salt) of average molecular weight 20900 and polydispersity 1.15, and poly-D-glutamic acid (sodium salt) of average molecular weight 19900 and polydispersity 1.3, were purchased from Sigma−Aldrich Chimie and used as received. Montmorillonite (**M**), whose synthesis and characterization is detailed elsewhere,[12] is a Mg-containing 2:1 dioctahedral clay with Na^+ cations in its interlayer space to balance the layer negative charge. Separate adsorption of each polypeptide was realized by mixing a solution of poly-D-lysine (**PL**) (ca. 30 mg), or poly-D-glutamic acid (**PG**) (ca. 30 mg), dissolved in a 15-mL acidic solution (pH = 3.4) with a solution of montmorillonite (**M**) (500 mg), initially suspended for 5 d in 25 mL of the same acidic buffer, at 10 °C for 6 h. Co-adsorption of the two polypeptides was realized under similar conditions by adding a solution of **PL** (50 mg) and **PG** (50 mg) dissolved in 50 mL of the acidic buffer to a solution of **M** (240 mg), initially suspended in 25 mL of the acidic buffer. After filtration through 0.45 μm filters and repeated washes with the buffer and deionized water, the three polypeptide-adsorbed samples **M/PL**, **M/PG** and **M/PL/PG** were dried overnight at room temperature in air and stored at 4 °C.

Thermal Analysis: TG-DTA measurements were carried out with a Setaram Labsys apparatus under air-flow condition, with a heating rate of 5 °C/min, from 18 to 750 or 800 °C.

X-ray Powder Diffraction: X-ray diffractograms were recorded with a STOE STADI-P powder X-ray diffractometer, equipped with a linear position-sensitive detector ($2\theta = 6°$) in Debye−Scherrer geometry and employing Ge-monochromated Cu-$K_{\alpha 1}$ radiation (λ = 1.5406 Å). Records, in the range $2\theta = 2-12°$, were performed on samples under controlled humidity ($P/P_0 = 0.79$) and on samples dehydrated at 110 °C under vacuum for 10 h. For the former, capillaries were filled with powder kept under controlled humidity, just before starting the experiment, whereas for the latter, capillaries were filled in a glove box under argon. In both cases, the capillaries were sealed immediately after filling up.

N_2 Adsorption: Complete nitrogen gas adsorption-desorption cycles were obtained with a Micromeritics ASAP 2001 apparatus. BET specific surface areas were determined from the initial part of the adsorption branches (typically in the range $P/P_0 = 0.04-0.2$), and the *t*-plot analysis of the adsorption permitted the determination of the microporous and external surface proportions. Prior to experiments, about 100 mg of each sample was outgassed to a residual pressure of less than 0.8 Pa at 110 or 150 °C for about 15 h.

Solid-State NMR Spectroscopy: ^{13}C NMR spectroscopic experiments were run with a Bruker DSX 400 spectrometer operating at frequencies of 100.6 MHz, and a Bruker MSL 300 spectrometer operating at a frequency of 75.4 MHz. ^1H-^{13}C Cross-Polarization-MAS (CP-MAS) experiments were performed using a Bruker double-channel 4-mm probe or a Bruker double-channel 2.5-mm probe. Hartmann−Hahn matching for the ^1H-^{13}C CP-MAS experiments was set on adamantane for ^1H and ^{13}C radio-frequency fields of ca. 60 kHz. Proton T_1 spin-lattice relaxation times ranged between 100 and 500 ms for the different proton species observed in the ^1H MAS spectra of mineral/polypeptide products. In the case of bulk polypeptides, rotors were packed in a glove box under argon in order to prevent interaction with ambient moisture. This resulted in higher ^1H T_1 values (ca. 1 s), mainly attributed to the absence of the paramagnetic O_2 relaxing agent. Chemical shifts for ^{13}C spectra were referenced to adamantane (δ_C = 29.47 ppm for the low-frequency peak). Deconvolution of the ^1H-^{13}C CP-MAS spectra was performed with the WINFIT software.[30]

Acknowledgments

We are grateful to the Region Champagne − Ardennes for financial support through the grant of R. D. G. Drs. L. Delmotte and X. Bourdon are acknowledged for helpful discussions.

[1] H. Quiquampoix, *Mechanisms of protein adsorption on surfaces and consequences for extracellular enzyme activity in soil*, in Soil Biochemistry (Eds: J. M. Bollag, G. Stotzky), Marcel Dekker, Inc., New York, **2000**, vol. 10, p. 171−206.
[2] C. Causserand, K. Jover, P. Aimar, M. Meireles, *J. Membr. Sci.* **1997**, *137*, 31−44.
[3] E. P. Giannelis, *Adv. Mater.* **1996**, *8*, 29−35.
[4] [4a] A. Clearfield, *Chem. Mater.* **1998**, *10*, 2801−2810. [4b] C. Breen, R. Watson, *J. Colloid Interface Sci.* **1998**, *208*, 422−429.
[5] M. R. Sarmento, J. G. Oliveira, R. B. Boulton, *Int. J. Food. Sci. Tech.* **2000**, *35*, 41−47.
[6] J. T. Kloprogge, S. Komarneni, J. E. Amonette, *Clays Clay Miner.* **1999**, *47*, 529−554.
[7] [7a] W. Norde, *Adv. Colloid Interface Sci.* **1986**, *25*, 267−328. [7b] C. A. Haines, W. Norde, *Colloids Surf. B* **1994**, *2*, 517−525. [7c] S. Staunton, H. Quiquampoix, *J. Colloid Interface Sci.* **1994**, *166*, 89−94. [7d] A. Pantazaki, M. H. Baron, M. Revault, C. Vidal-Madjar, *J. Colloid Interface Sci.* **1998**, *207*, 324.
[8] [8a] R. K. Sandwick, K. J. Schray, *J. Colloid Interface Sci.* **1987**, *115*, 130. [8b] H. Quiquampoix, S. Staunton, M. H. Baron, R. G. Ratcliffe, *Colloids Surf. A* **1993**, *75*, 85−93.
[9] [9a] M. H. Baron, M. Revault, S. Servagent-Noinville, J. Abadie, H. Quiquampoix, *J. Colloid Interface Sci.* **1999**, *214*, 319−332. [9b] S. Servagent-Noinville, M. Revault, H. Quiquampoix, M. H. Baron, *J. Colloid Interface Sci.* **2000**, *221*, 273−283.
[10] C. H. Yu, M. A. Norman, S. Q. Newton, D. M. Miller, B. J. Teppen, L. Schäfer, *J. Mol. Struct.* **2000**, *556*, 95−103.
[11] [11a] R. D. Gougeon, M. Reinholdt, L. Delmotte, J. Miehé-Brendlé, J-M. Chézeau, R. Le Dred, R. Marchal, P. Jeandet, *Langmuir* **2002**, *18*, 3396−3398. [11b] T. Coradin, O. Durupthy, J. Livage, *Langmuir* **2002**, *18*, 2331−2336. [11c] J. N. Cha, G. D. Stucky, D. E. Morse, T. J. Deming, *Nature* **2000**, *403*, 289−292.
[12] M. Reinholdt, J. Miehé-Brendlé, L. Delmotte, M-H. Tuilier, R. Le Dred, R. Cortès, A-M. Flank, *Eur. J. Inorg. Chem.* **2001**, 2831−2841.
[13] V. L. Fernandez, J. A. Reimer, M. M. Denn, *J. Am. Chem. Soc.* **1992**, *114*, 9634−9642.
[14] W. Xie, Z. Gao, K. Liu, W-P. Pang, R. Vaia, D. Hunter, A. Singh, *Thermochim. Acta* **2001**, *339*, 367−368.
[15] W. J. Shaw, J. R. Long, J. L. Dindot, A. A. Campbell, P. S. Stayton, G. P. Drobny, *J. Am. Chem. Soc.* **2000**, *122*, 1709−1716.
[16] [16a] A. Golchin, P. Clarke, J. M. Oades, *Biogeochemistry* **1996**, *34*, 71−97. [16b] D. W. Hopkins, J. A. Chudek, S. F. I. Haslam, E. A. Webster, *NMR Microbiol.* **2000**, 431−451. [16c] N. J. Mathers, X. A. Mao, Z. H. Xu, P. G. Saffigna, S. J. Berners-Price, M. C. S. Perera, *Aust. J. Soil Res.* **2000**, *38*, 769−787.
[17] H. Quiquampoix, R. G. Ratcliffe, *J. Colloid Interface Sci.* **1992**, *148*, 343−352.
[18] E. S. Boeck, P. V. Coveney, N. T. Skipper, *J. Am. Chem. Soc.* **1995**, *117*, 12608−12617.
[19] O. Sieskind, *C. R. Acad. Sci. Fr.* **1960**, *250*, 2392−2393.
[20] G. Lagaly, *Clay Minerals* **1981**, *16*, 1−21.
[21] R. Greene-Kelly, *Clay Min. Bull.* **1964**, *5*, 392−400.
[22] P. T. Hang, G. W. Brindley, *Clays Clay Miner.* **1970**, *18*, 203−212.
[23] [23a] H. R. Kricheldorf, D. Müller, *Macromolecules* **1983**, *16*, 615−623. [23b] A. Shoji, O. Takuo, H. Saitô, R. Tabeta, I. Ando, *Macromolecules* **1984**, *17*, 1472−1479. [23c] H. Saitô, *Magn. Reson. Chem.* **1986**, *24*, 835−852.
[24] Z. Gu, A. McDermott, *J. Am. Chem. Soc.* **1993**, *115*, 4282−4285.
[25] C. H. Chiang, N. I. Liu, J. L. Koenig, *J. Colloid Interface Sci.* **1982**, *86*, 26−34.
[26] A. R. Mermut, G. Lagaly, *Clays Clay Miner.* **2001**, *49*, 393−397.
[27] F. Rouquerol, J. Rouquerol, K. Sing, *Adsorption by Powders & Porous Solids*, Academic Press, San Diego, **1999**.
[28] J. H. de Boer, B. C. Lippens, B. G. Linsen, J. C. P. Broekhollf, A. Van der Heuvel, Th. J. Osinga, *J. Colloid Interface Sci.* **1966**, *21*, 405.
[29] J. M. Cases, I. Bérend, G. Besson, M. François, J. P. Uriot, F. Thomas, J. E. Poirier, *Langmuir* **1992**, *8*, 2730−2739.
[30] D. Massiot, Web site: http://crmht.cnrs-orleans.fr/Pole1/ThemeDM/

Received July 24, 2002
[I02416]

Assembly of Hydrogen-Bonded Organic Layers with Macrocyclic Complexes Acting as Pillars

Myunghyun Paik Suh,*[a] Kil Sik Min,[a] Jung Woo Ko,[a] and Hye Jin Choi[a]

Keywords: Hydrogen bonds / Layered compounds / Macrocyclic ligands / Nickel / Self-assembly

Novel supramolecular networks of 2D $\{[Ni(cyclam)][C_6H_9(COOH)_2(COO)]_2\}_n$ (**1**) and 3D $\{[Ni(cyclam)][C_6H_3(OH)_2(COO)]_2\}_n$ (**2**) have been constructed by the self-assembly of $[Ni(cyclam)](ClO_4)_2$ with *cis,cis*-1,3,5-cyclohexanetricarboxylic acid (H_3CTC) and 3,5-dihydroxybenzoic acid (HDHB), respectively, in py/MeCN/H_2O. In the crystal structure of **1**, each nickel(II) macrocyclic complex binds two H_2CTC^- ions at the axial sites. The coordinated H_2CTC^- ions form hydrogen bonds with one another, which results in organic bilayers having macrocyclic complexes as pillars. In the crystal structure of **2**, each nickel(II) macrocyclic complex binds two DHB^- ions in the *trans* position. Two free hydroxyl groups and one carbonyl oxygen atom of the coordinated DHB^- ion are extensively hydrogen-bonded with the DHB^- ligand of the neighboring complexes, which results in a 3D network where 2D organic layers are linked by the macrocyclic complexes acting as pillars.

(© Wiley-VCH Verlag GmbH & Co. KGaA, 69451 Weinheim, Germany, 2003)

Introduction

Supramolecular solids with various network topologies and with interesting properties have been prepared by the self-assembly of transition metal ions and organic building blocks.[1,2] In the self-assembly of supramolecules, hydrogen bonding,[3] metal-ligand coordination,[4] and π-π interactions[5] are involved in multidimensional intermolecular interactions. In particular, directional hydrogen-bonding interactions are important for materials design[6] and molecular recognition.[7,8] It has been demonstrated that extensive hydrogen-bonding interactions in organic compounds result in remarkably robust three-dimensional networks.[9] In addition, frameworks with different topologies can be constructed by changing the hydrogen-bonding mode.[10,11] Macrocyclic complexes have been rarely employed as metal building blocks in the self-assembly of supramolecular networks.[12,13] Recently, a molecular floral lace with 1D channels, $[Ni(cyclam)(H_2O)_2]_3[C_6H_3(COO)_3]_2\cdot 24H_2O$ (**A**), was assembled by the extensive hydrogen-bonding interactions between the coordinated water molecules of $[Ni(cyclam)(H_2O)_2]^{2+}$ and 1,3,5-benzenetricarboxylate.[12]

Here we report 2D $\{[Ni(cyclam)][C_6H_9(COOH)_2(COO)]_2\}_n$ (**1**) and 3D $\{[Ni(cyclam)][C_6H_3(OH)_2(COO)]_2\}_n$ (**2**) supramolecular networks, which are assembled from $[Ni(cyclam)](ClO_4)_2$ with *cis,cis*-1,3,5-cyclohexanetricarboxylic acid (H_3CTC) and 3,5-dihydroxybenzoic acid (HDHB), respectively, in the presence of pyridine. Multidimensional networks **1** and **2** are generated by the extensive hydrogen-bonding interactions between the organic building blocks, giving rise to 2D layers with the macrocyclic complexes acting as pillars connecting the organic layers. To the best of our knowledge, this is the first example where macrocyclic complexes are involved as pillars linking the organic layers in the supramolecular networks. This synthetic strategy can be applied to construct hybrid materials that consist of alternately packed organic-inorganic layers.

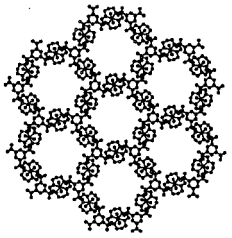

A

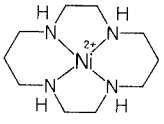

$[Ni(cyclam)]^{2+}$

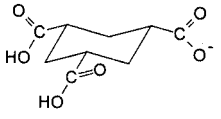

cis,cis-H_2CTC^-

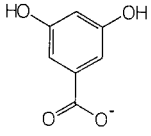

DHB^-

Results and Discussion

Self-Assembly and Properties of 2D and 3D Networks

Our synthetic strategy to build multidimensional networks was based on the hydrogen-bonding interactions be-

[a] School of Chemistry and Molecular Engineering, and Center for Molecular Catalysis, Seoul National University, Seoul 151-747, Republic of Korea
Fax: (internat.) +82-2/886-8516
E-mail: mpsuh@snu.ac.kr

Supporting information for this article is available on the WWW under http://www.eurjic.org or from the author.

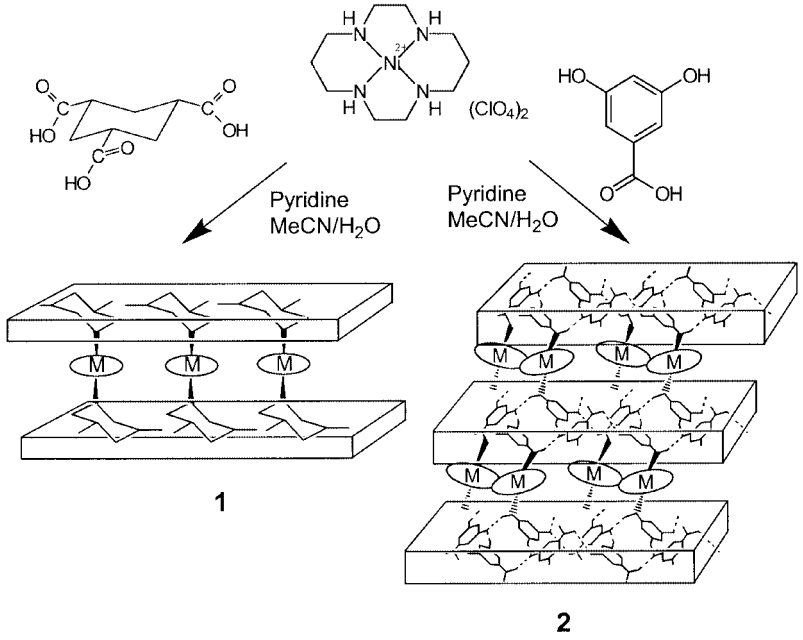

Scheme 1. Synthetic strategy for **1** and **2**

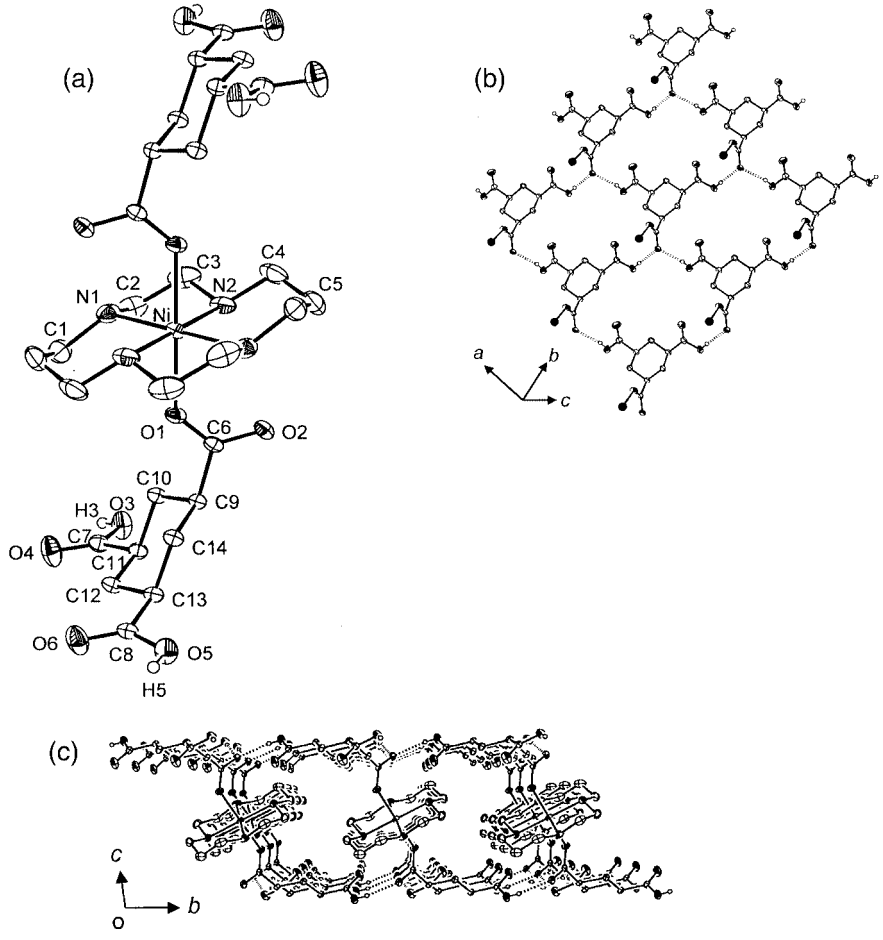

Figure 1. (a) An ORTEP view of **1** with atomic numbering scheme; the atoms are represented by 40% probability thermal ellipsoids; (b) the 2D organic layer, showing 26-membered supramolecular synthons constructed by the hydrogen bonding interactions between the coordinated H_2CTC^- ions; metal ions are indicated as filled black circles and intermolecular hydrogen bonds are indicated as dotted lines; (c) a view from the *bc* plane, showing the bilayer network where macrocyclic complexes act as pillars

tween organic ligands, which led to 2D organic layers with the macrocyclic complexes linking the organic layers as pillars. For this, $[Ni(cyclam)](ClO_4)_2$[14] and the carboxylate anions derived from *cis*,*cis*-1,3,5-cyclohexanetricarboxylic acid (H_3CTC) and 3,5-dihydroxybenzoic acid (HDHB) were used as the building blocks (Scheme 1).

When $[Ni(cyclam)](ClO_4)_2$ was reacted in MeCN/H_2O (1:1 v/v) with *cis*,*cis*-1,3,5-cyclohexanetricarboxylic acid (H_3CTC) in the presence of pyridine, only one proton of H_3CTC was removed and $[Ni(cyclam)]^{2+}$ was coordinated by two H_2CTC^- anions to form $\{[Ni(cyclam)][C_6H_9(COOH)_2(COO)]_2\}_n$ (**1**). When $[Ni(cyclam)](ClO_4)_2$ was reacted in MeCN/H_2O (1:1 v/v) with 3,5-dihydroxybenzoic acid (HDHB) in the presence of pyridine, the carboxylic acid group of HDHB was deprotonated and $[Ni(cyclam)]^{2+}$ was coordinated with two DHB^- anions to form $\{[Ni(cyclam)][C_6H_3(OH)_2(COO)]_2\}_n$ (**2**).

The supramolecular compounds **1** and **2** are pink and air-stable. They are insoluble in all solvents except water. In water, they are dissociated into the building blocks, as evidenced by the UV/Vis spectra, which exhibit the characteristic chromophore (λ_{max} = 445 nm) of the starting material $[Ni(cyclam)]^{2+}$. The diffuse reflectance spectrum measured for a powdered sample of **1** shows maximum absorptions at 332, 505, and 648 nm and that of **2** at 300, 511, and 661 nm, which correspond to the chromophores of nickel(II) ions coordinated by N_4O_2 donors.[15] The TGA and DSC traces of **1** and **2** (Figures S1 and S2) show that decomposition starts at 240 and 220 °C, respectively.

X-ray Crystal Structure of 1

An ORTEP[16] drawing of **1** is shown in Figure 1a. Table 1 shows selected bond lengths and angles. In the crystal structure of **1**, the nickel(II) ion of the macrocyclic complex $[Ni(cyclam)]^{2+}$ is coordinated to two carboxylate oxygen atoms of H_2CTC^- ions at the axial sites (Figure 1a). The complex has an inversion center at the nickel(II) ion. The average Ni−N bond length is 2.042(1) Å and the average Ni−O bond length is 2.171(1) Å, similar to those of open-framework **A**.[12] The coordinated H_2CTC^- ligands are linked to one another by the extensive hydrogen-bonding interactions. Each carbonyl oxygen atom of the coordinated carboxylate group of H_2CTC^- behaves as a hydrogen acceptor to form bifurcated hydrogen bonds with two carboxylic acid groups belonging to two different H_2CTC^- ions of the adjacent macrocyclic complexes [O2···O3′(x − 1, y, z): 2.701(2) Å; O2···H3′−O3′: 172.73°; O2···O5′′(x, y − 1, z): 2.700(2) Å; O2···H5′′−O5′′: 172.74°), and two free carboxylic acid groups of the H_2CTC^- ligand behave as hydrogen donors and form hydrogen bonds with the carbonyl oxygen atoms of the H_2CTC^- ligands belonging to two different adjacent complexes. The extensive hydrogen-bonding interactions between H_2CTC^- ligands construct 26-membered supramolecular synthons that propagate infinitely parallel to the crystallographic *ab* plane to give rise to a 2D organic network (Figure 1b). Due to the hydrogen-bonding interactions, the free C=O bond length of H_2CTC^- [C6−O2, 1.266(2) Å] is longer than that of the coordinated C−O bond length [C6−O1, 1.241(2) Å]. Since both of the H_2CTC^- ions coordinating a nickel(II) macrocyclic complex are involved in the formation of two different 2D organic layers, the structure becomes a bilayer containing nickel(II) macrocycles acting as pillars (Figure 1c). The interlayer distance within the bilayer is 5.692(4) Å and the shortest distance between two adjacent bilayers (C···O) is 3.399(3) Å.

Table 1. Selected bond lengths (Å) and angles (°) for **1**[a]

Ni1−N1	2.042(2)	C1−C5′	1.501(5)
Ni1−N2	2.042(2)	C2−C3	1.498(4)
Ni1−O1	2.171(1)	C4−C5	1.498(5)
O1−C6	1.241(2)	C6−C9	1.526(2)
O2−C6	1.266(2)	C7−C11	1.507(3)
O3−C7	1.314(3)	C8−C13	1.504(3)
O4−C7	1.200(3)	C9−C10	1.527(2)
O5−C8	1.317(3)	C9−C14	1.528(2)
O6−C8	1.199(3)	C10−C11	1.530(2)
N1−C2	1.458(3)	C11−C12	1.520(3)
N1−C1	1.471(3)	C12−C13	1.518(3)
N2−C3	1.458(3)	C13−C14	1.530(2)
N2−C4	1.475(3)		
N1−Ni1−N2	85.82(9)	O4−C7−O3	122.43(19)
N1−Ni1−O1	89.44(7)	O4−C7−C11	124.64(18)
N2−Ni1−O1	90.72(7)	O3−C7−C11	112.86(17)
O1′−Ni1−O1	180.00(7)	O6−C8−O5	122.27(19)
C6−O1−Ni1	132.12(12)	O6−C8−C13	124.74(18)
C2−N1−C1	114.1(2)	O5−C8−C13	112.92(17)
C2−N1−Ni1	105.27(15)	C6−C9−C10	110.17(14)
C1−N1−Ni1	116.57(16)	C6−C9−C14	110.29(14)
C3−N2−C4	114.1(2)	C10−C9−C14	111.21(15)
C3−N2−Ni1	105.33(15)	C9−C10−C11	111.28(14)
C4−N2−Ni1	116.56(16)	C7−C11−C12	110.50(15)
N1−C1−C5′	113.1(2)	C7−C11−C101	10.13(15)
N1−C2−C3	108.9(2)	C12−C11−C10	110.15(15)
N2−C3−C2	108.8(2)	C13−C12−C11	110.59(15)
N2−C4−C5	113.0(2)	C8−C13−C12	110.61(15)
C4−C5−C1′	115.4(2)	C8−C13−C14	110.46(15)
O1−C6−O2	124.30(17)	C12−C13−C14	109.89(15)
O1−C6−C9	117.66(16)	C9−C14−C13	111.58(15)
O2−C6−C9	118.04(16)		

[a] Symmetry transformations used to generate equivalent atoms: ′: $-x$, $-y$, $-z$.

X-ray Crystal Structure of 2

An ORTEP[16] drawing of **2** is shown in Figure 2a. Table 2 shows selected bond lengths and angles. In the crystal structure of **2**, the nickel(II) ion of the macrocyclic complex binds two carboxylate oxygen atoms of DHB^- ions at the axial sites (Figure 2a). The complex has an inversion center at the nickel(II) ion. The average Ni−N and Ni−O bond lengths are 2.065(1) and 2.130(1) Å, respectively, which are similar to those of **1**. The aromatic ring of the DHB^- ion is tilted with respect to the square coordination plane of the macrocycle [dihedral angle = 51.3(1)°]. The DHB^- ligand is not planar since the dihedral angle between the carboxylate group and the aromatic ring of DHB^- ion is 29.9(3)°. Within the molecule, there are hydrogen-bonding interactions between the carbonyl oxygen atoms of the carboxylate ions and the secondary amines of the macrocy-

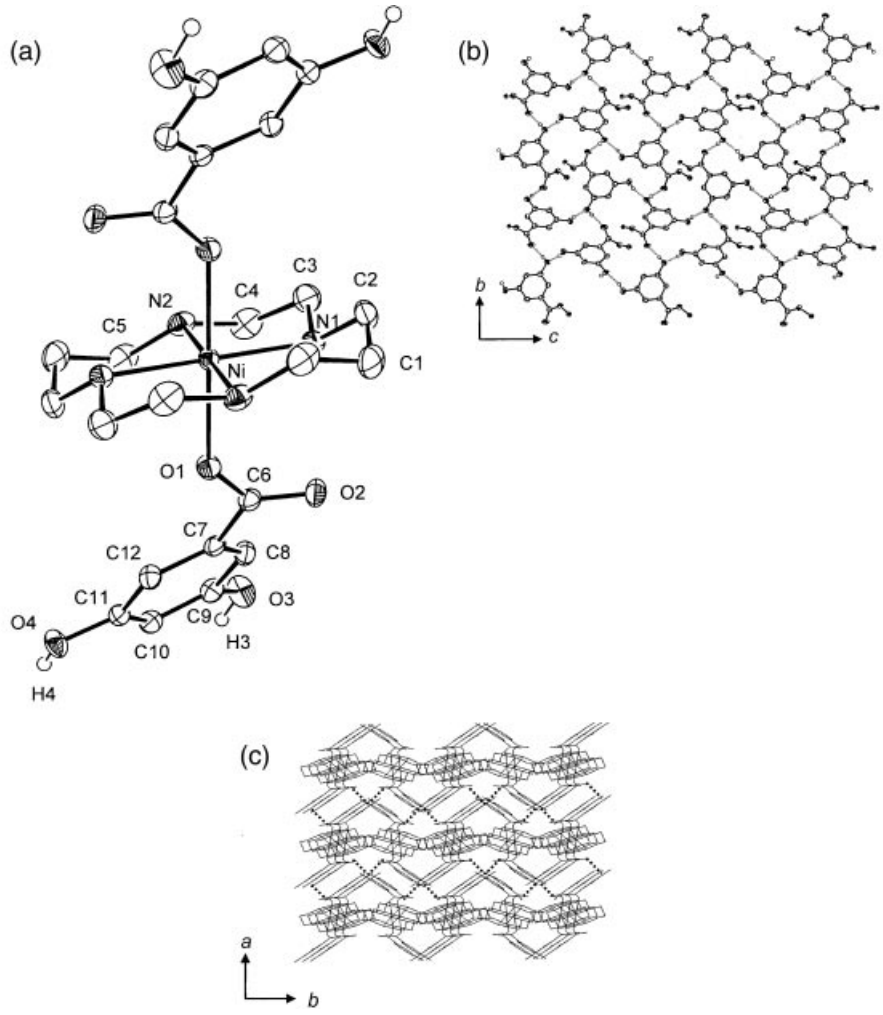

Figure 2. (a) An ORTEP view of **2** with atomic numbering scheme; the atoms are represented by 40% probability thermal ellipsoids; intramolecular hydrogen bonds are indicated as dotted lines; (b) a 2D organic layer constructed by the hydrogen-bonding interactions between the coordinated DHB^- ligands; (c) a view of the 3D network on the *ab* plane, showing how the thick 2D organic layers are linked by the macrocyclic complexes acting as pillars, interlayer hydrogen bonds are indicated as ·····

cle to form six-membered rings (O2···N1: 2.980(3) Å; O2···H1−N1: 162°). The six-coordinate nickel(II) macrocyclic complexes are linked together by extensive hydrogen-bonding interactions between the DHB^- ligands. Each DHB^- ion coordinating the metal above the plane forms hydrogen bonds with two neighboring DHB^- ligands, via hydroxyl groups [O3···O4(#1) (#1: x, $-y - 0.5$, $z + 0.5$): 2.763(2) Å; O3−H3(#1)···O4(#1): 164°], to build a 1D chain that extends along the crystallographic *c* axis, undulating in the *b* and *a* directions (Figure 2b; A in Scheme 2). Similarly, each DHB^- ligand coordinating a metal below the macrocyclic coordination plane also forms hydrogen bonds with two adjacent DHB^- ligands to construct another undulating 1D chain that also extends along the *c* direction (B in Scheme 2). These two kinds of chains are alternately aligned toward the *b* direction, and they are connected to one another by the hydrogen-bonding interactions via the free carbonyl oxygen atom of the coordinated carboxylate group of DHB^- belonging to one chain and the hydroxyl group of DHB^- belong to the other chain [O2···O4(#2) (#2 = $-x - 1$, $y + 0.5$, $-z + 0.5$): 2.610(2) Å; O2···H4(#2)−O4(#2): 175°]. There are π-π interactions between the phenyl rings of DHB^- belonging to the adjacent chains [centroid···centroid distance: 6.032 Å; closest C···C distance: 3.917(4) Å]. Since the interchain hydrogen-bonding interactions extend along the *b* direction and undulate in the *a* direction, the DHB^- ligands construct a

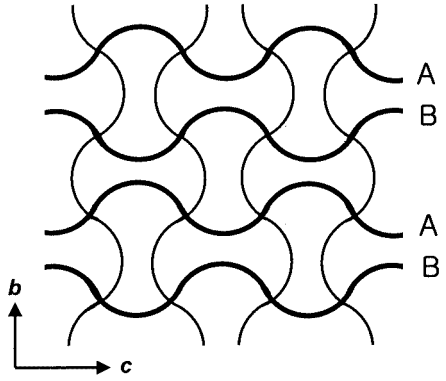

Scheme 2. Schematic drawing of formation of 2D organic layer in **2**

Table 2. Selected bond lengths (Å) and angles (°) for **2**[a]

Ni−N1	2.065(2)	C1−C5′	1.515(4)
Ni−N2	2.065(2)	C1−C2	1.517(4)
Ni−O1	2.130(2)	C3−C4	1.513(4)
N1−C3	1.465(3)	C6−C7	1.498(3)
N1−C2	1.478(3)	C7−C12	1.389(3)
N2−C5	1.469(3)	C7−C8	1.393(3)
N2−C4	1.482(3)	C8−C9	1.386(3)
O1−C6	1.258(3)	C9−C10	1.388(3)
O2−C6	1.258(3)	C10−C11	1.387(3)
O3−C9	1.360(3)	C11−C12	1.392(3)
O4−C11	1.368(3)		
N2−Ni−N1	85.23(8)	O1−C6−O2	124.4(2)
N2−Ni−O1	92.00(7)	O1−C6−C7	116.47(17)
N1−Ni−O1	92.92(7)	O2−C6−C7	119.05(19)
C3−N1−C2	113.62(19)	C12−C7−C8	120.12(19)
C3−N1−Ni	106.20(14)	C12−C7−C6	119.92(18)
C2−N1−Ni	116.08(14)	C8−C7−C6	119.83(19)
C5−N2−C4	114.4(2)	C9−C8−C7	119.8(2)
C5−N2−Ni	115.88(16)	O3−C9−C8	116.7(2)
C4−N2−Ni	106.24(15)	O3−C9−C10	122.55(19)
C6−O1−Ni	132.68(14)	C8−C9−C10	120.73(19)
C5′−C1−C2	115.8(2)	C11−C10−C9	119.02(19)
N1−C2−C1	112.45(19)	O4−C11−C10	122.09(19)
N1−C3−C4	109.08(19)	O4−C11−C12	116.91(19)
N2−C4−C3	108.9(2)	C10−C11−C12	120.99(19)
N2−C5−C1′	111.77(19)	C7−C12−C11	119.33(19)

[a] Symmetry transformations used to generate equivalent atoms: ′: $-x$, $-y$, $-z$.

thick 2D organic layer (Figure 2b and 2c). The thickness of the organic layer is 4.872(3) Å. These thick 2D organic layers are linked by the macrocyclic complexes located on a plane parallel to the *bc* plane, and thus the whole structure can be viewed as a 3D network where macrocyclic complexes act as pillars (Figure 2c).

Conclusion

A 2D bilayered framework (**1**) and a 3D supramolecular network (**2**), where macrocyclic complexes behave as pillars linking 2D organic layers, have been prepared by the self-assembly of the nickel(II) macrocyclic complex $[Ni(cyclam)]^{2+}$ with *cis*,*cis*-1,3,5-cyclohexanetricarboxylate (H_2CTC^-) and 3,5-dihydroxybenzoate (DHB^-), respectively. The multi-dimensional networks are constructed by the extensive hydrogen-bonding interactions between the organic ligands coordinating the nickel(II) ions. The synthetic strategy can be applied to construct hybrid materials that consist of organic layers and layers of transition metal complexes packed alternately.

Experimental Section

General Remarks: All chemicals and solvents used in the synthesis were of reagent grade and used without further purification. $[Ni(cyclam)](ClO_4)_2$ was prepared according to the literature procedures previously reported.[14] Infrared spectra were recorded with a Perkin−Elmer 2000 FT-IR spectrophotometer. Elemental analyses were performed by the analytical laboratory of Seoul National University. UV/Vis diffuse reflectance spectra were recorded with a Cary 300 Bio UV/Vis spectrophotometer. Thermogravimetric analysis (TGA) and differential scanning calorimetry (DSC) were performed at a scan rate of 5 °C/min using a DuPont TGA 2050 and a DuPont DSC 2100 TA instrument, respectively.

Safety Note: *Perchlorate salts of metal complexes with organic ligands are often explosive and should be handled with great caution, although we have experienced no problem with the compounds reported in this work.*

$\{[Ni(cyclam)][C_6H_9(COOH)_2(COO)]_2\}_n$ (1): An MeCN solution (6 mL) of *cis*,*cis*-1,3,5-cyclohexanetricarboxylic acid (H_3CTC; 0.14 g, 0.76 mmol) mixed with pyridine (1 mL) was added dropwise to an MeCN/H_2O (1:1 v/v, 12 mL) solution of $[Ni(cyclam)](ClO_4)_2$ (0.17 g, 0.38 mmol). The yellow color of the nickel(II) solution turned to pale pink. The solution was allowed to stand at room temperature until pale pink crystals of $\{[Ni(cyclam)][C_6H_9(COOH)_2(COO)]_2\}_n$ formed, which were filtered, washed with MeCN/H_2O (1:1 v/v), and dried in air. There is no other form of aggregation present in the solution. Yield: 0.20 g (77%). $C_{28}H_{46}N_4NiO_{12}$: calcd. C 48.78, H 6.73, N 8.13; found C 48.60, H 6.55, N 8.50. FT-IR (Nujol mull): $\tilde{\nu}$ = 3300 (s), 3123 (s), 3084 (s), 1721 (s), 1548 (s), 1251 (s), 1177 (s), 954 (s), 870 (s), 730 (s), 649 (s) cm^{-1}. UV/Vis (diffuse reflectance spectrum): λ_{max} = 332, 505, 648 nm.

$\{[Ni(cyclam)][C_6H_3(OH)_2(COO)]_2\}_n$ (2): An MeCN solution (6 mL) of 3,5-dihydroxybenzoic acid (0.14 g, 0.88 mmol) and pyridine (1 mL) was added dropwise to an MeCN/H_2O (1:1 v/v, 12 mL) solution of $[Ni(cyclam)](ClO_4)_2$ (0.20 g, 0.44 mmol). The yellow color of the nickel(II) solution turned to pale pink. The solution was allowed to stand at room temperature until pale pink crystals of $\{[Ni(cyclam)][C_6H_3(OH)_2(COO)]_2\}_n$ formed, which were filtered off, washed with MeCN/H_2O (1:1 v/v), and dried in air. There is no other form of aggregation present in the solution. Yield: 0.19 g (75%). $C_{24}H_{34}N_4NiO_8$: calcd. C 51.00, H 6.06, N 9.91; found C 50.27, H 6.17, N 9.98. FT-IR (Nujol mull): $\tilde{\nu}$ = 3306 (s), 3200 (s), 3062 (s), 2554 (s, br), 1558 (s), 1393 (s), 1284 (s), 1156 (s), 1025 (s), 958 (s), 792 (s), 689 (s) cm^{-1}. UV/Vis (diffuse reflectance spectrum): λ_{max} = 248, 300, 511, 661 nm.

X-ray Crystallographic Study: Single crystals of **1** and **2** were mounted on an Enraf−Nonius CAD4 diffractometer. The unit-cell parameters were determined from 25 machine-centered reflections with $22° < 2\theta < 28°$ for **1** and $22° < 2\theta < 27°$ for **2**. Intensities were collected with graphite-monochromated Mo-K_α radiation (λ = 0.71069 Å), using the ω-2θ scan. Three standard reflections were measured every 2 h for the orientation and intensity control; no significant intensity decay was observed. The data were corrected for Lorentz and polarization effects. No absorption correction was made. For **1**, among 2618 reflections measured in the range $3.78 < 2\theta < 49.88$, 2552 were assumed to be observed [$F > 4\sigma(F)$]. For **2**, among 2193 reflections measured in the range $4.80 < 2\theta < 49.94$, 1842 were assumed to be observed [$F > 4\sigma(F)$]. The crystal structures were solved by direct methods[17] and refined by full-matrix least-squares methods using the SHELXL-97 computer program.[18] For **1** and **2**, the positions of all non-hydrogen atoms were refined with anisotropic displacement factors. The carboxylic acid protons and hydroxyl protons were located from the difference Fourier maps and refined with isotropic thermal parameters. The remaining hydrogen atoms were allowed to ride on their bonded atoms with the isotropic displacement factors fixed with values of 1.2-times those of the bonded atoms. ORTEP drawings were made

Table 3. Crystallographic data for **1** and **2**

	1	**2**
Formula	$C_{28}H_{46}N_4NiO_{12}$	$C_{24}H_{34}N_4NiO_8$
M	689.40	565.26
Crystal system	Triclinic	Monoclinic
Space group	$P\bar{1}$	$P2_1/c$
a (Å)	8.349(2)	8.563(1)
b (Å)	8.361(3)	13.079(2)
c (Å)	10.803(4)	11.283(3)
α (°)	85.75(3)	90
β (°)	85.82(2)	98.74(1)
γ (°)	88.23(2)	90
V (Å^3)	749.8(4)	1249.0(4)
Z	1	2
μ (mm^{-1})	0.719	0.834
T (K)	293(2)	293(2)
Total measured reflections	2857	2372
Total unique reflections	2618 (R_{int} = 0.0069)	2193 (R_{int} = 0.0127)
Observed reflections [$I > 2\sigma(I)$]	2552	1842
$R1$ (all data)[a]	0.0348	0.0412
$wR2$ (all data)[b]	0.0931	0.0860

[a] $R1 = \Sigma||F_0| - |F_c||/\Sigma|F_0|$. [b] $wR2 = [\Sigma[w(|F_0|^2 - |F_c|^2)^2]/\Sigma[w(|F_0|)^4]]^{1/2}$.

with ORTEP-3 for Windows.[16] The crystallographic data of **1** and **2** are summarized in Table 3.

CCDC-193023 (**1**) and -193024 (**2**) contain the supplementary crystallographic data for this paper. These data can be obtained free of charge at www.ccdc.cam.ac.uk/conts/retrieving.html [or from the Cambridge Crystallographic Data Centre, 12, Union Road, Cambridge CB2 1EZ, UK; fax: (internat.) +44-1223/336-033; E-mail: deposit@ccdc.cam.ac.uk].

Acknowledgments

This work was supported by the Korea Science and Engineering Foundation (R01-1999-000-00041-0) and the Center for Molecular Catalysis.

[1] [1a] K. S. Min, M. P. Suh, *J. Am. Chem. Soc.* **2000**, *122*, 6834. [1b] M. Eddaoudi, D. B. Li, H. Moler, B. Chen, T. M. Reineke, M. O'Keeffe, O. M. Yaghi, *Acc. Chem. Res.* **2001**, *34*, 319. [1c] M. Eddaoudi, J. Kim, M. O'Keeffe, O. M. Yaghi, *J. Am. Chem. Soc.* **2002**, *124*, 376. [1d] T. L. Hennigart, D. C. Macquarrie, P. Losier, R. D. Rogers, M. J. Zaworotko, *Angew. Chem. Int. Ed. Engl.* **1997**, *36*, 972.

[2] [2a] P. J. Hagrman, D. Hagrman, J. Zubieta, *Angew. Chem. Int. Ed.* **1999**, *38*, 2639. [2b] Y.-H. Kiang, G. B. Gardner, S. Lee, Z. Xu, *J. Am. Chem. Soc.* **2000**, *122*, 6871. [2c] E. Corradi, S. V. Meille, M. T. Messina, P. Metrangolo, G. Resnati, *Angew. Chem. Int. Ed.* **2000**, *39*, 1782. [2d] H. Gudbjartson, K. Biradha, K. M. Poirier, M. J. Zaworotko, *J. Am. Chem. Soc.* **1999**, *121*, 2599.

[3] [3a] C. B. Aakeröy, K. R. Seddon, *Chem. Soc. Rev.* **1993**, *22*, 397. [3b] S. Subramanian, M. J. Zaworotko, *Coord. Chem. Rev.* **1994**, *137*, 357. [3c] S. Scheiner, *Hydrogen Bonding, A Theoretical Perspective*, Oxford University Press, Oxford, **1997**.

[4] [4a] S. R. Batten, R. Robson, *Angew. Chem. Int. Ed.* **1998**, *37*, 1461. [4b] O. M. Yaghi, H. Li, C. Davis, D. Richardson, T. L. Groy, *Acc. Chem. Res.* **1998**, *31*, 474. [4c] S. R. Seidel, P. J. Stang, *Acc. Chem. Res.* **2002**, *35*, 972−983.

[5] [5a] G. R. Desiraju, *Crystal Engineering: The Design of Organic Solids*, Elsevier, New York, **1989**, ch. 4. [5b] C. A. Hunter, J. Singh, J. M. Thornton, *J. Mol. Biol.* **1991**, *218*, 837. [5c] A. S. Shetty, J. Zhang, J. S. Moore, *J. Am. Chem. Soc.* **1996**, *118*, 1019.

[6] [6a] C. B. Aakeröy, *Acta Crystallogr., Sect. B* **1997**, *53*, 569. [6b] P. Bhyrappa, S. R. Wilson, K. S. Suslick, *J. Am. Chem. Soc.* **1997**, *119*, 8492. [6c] K. Kobayashi, M. Koyanagi, K. Endo, H. Masuda, Y. Aoyama, *Chem. Eur. J.* **1998**, *4*, 417.

[7] [7a] G. A. Jeffrey, W. Saenger, *Hydrogen Bonding in Biological Structures*, Springer, New York, **1991**. [7b] A. D. Hamilton, *J. Chem. Educ.* **1990**, *67*, 821. [7c] M. M. Chowdhry, D. M. P. Mingos, A. J. P. White, D. J. Williams, *Chem. Commun.* **1996**, 899. [7d] J. Bernstein, R. J. Davey, J. O. Henck, *Angew. Chem. Int. Ed.* **1999**, *38*, 3441−3461. [7e] J. Bernstein, *Polymorphism in Molecular Crystals* **2002**, Oxford University Press.

[8] [8a] B. J. B. Folmer, R. P. Sijbesma, H. Kooijman, A. L. Spek, E. W. Meijer, *J. Am. Chem. Soc.* **1999**, *121*, 9001. [8b] B. Gong, Y. Yan, H. Zeng, E. Skrzypczak-Jankunn, Y. W. Kim, J. Zhu, H. Ickes, *J. Am. Chem. Soc.* **1999**, *121*, 5607. [8c] H. Zeng, R. S. Miller, R. A. Flowers, B. Gong, *J. Am. Chem. Soc.* **2000**, *122*, 2635.

[9] [9a] X. Wang, M. Simard, J. D. Wuest, *J. Am. Chem. Soc.* **1994**, *116*, 12119. [9b] P. Brunet, M. Simard, J. D. Wuest, *J. Am. Chem. Soc.* **1997**, *119*, 2737.

[10] M. Munakata, L. P. Wu, M. Yamamoto, T. Kuroda-Sowa, M. Maekawa, *J. Am. Chem. Soc.* **1996**, *118*, 3117.

[11] [11a] C. B. Aakeröy, A. M. Beatty, D. S. Leinen, *J. Am. Chem. Soc.* **1998**, *120*, 7383. [11b] I. L. Karle, D. Ranganathan, S. Kurur, *J. Am. Chem. Soc.* **1999**, *121*, 7156. [11c] C. B. Aakeröy, A. M. Beatty, D. S. Leinen, *Angew. Chem. Int. Ed.* **1999**, *38*, 1815. [11d] N. C. Gianneschi, E. R. T. Tiekink, L. M. Rendina, *J. Am. Chem. Soc.* **2000**, *122*, 8474.

[12] H. J. Choi, T. S. Lee, M. P. Suh, *Angew. Chem. Int. Ed.* **1999**, *38*, 1405.

[13] [13a] H. J. Choi, M. P. Suh, *J. Am. Chem. Soc.* **1998**, *120*, 10622. [13b] H. J. Choi, M. P. Suh, *Inorg. Chem.* **1999**, *38*, 6309. [13c] K. S. Min, M. P. Suh, *Chem. Eur. J.* **2001**, *7*, 303. [13d] K. S. Min, M. P. Suh, *Eur. J. Inorg. Chem.* **2001**, 449. [13e] M. P. Suh, J. W. Ko, H. J. Choi, *J. Am. Chem. Soc.* **2002**, *124*, 10976. [13f] J. W. Ko, K. S. Min, M. P. Suh, *Inorg. Chem.* **2002**, *41*, 2151.

[14] E. K. Barefield, F. Wagner, A. W. Herlinger, A. R. Dahl, *Inorg. Synth.* **1976**, *16*, 220.
[15] F. L. Urbach, in *Coordination Chemistry of Macrocyclic Compounds* (Ed.: G. A. Melson), Plenum Press, New York, **1979**, pp. 350−355.
[16] L. J. Farrugia, ORTEP-3 for Windows, Version 1.03, University of Glasgow, Scotland, **1997**.
[17] G. M. Sheldrick, *Acta Crystallogr., Sect. A* **1990**, *46*, 467.
[18] G. M. Sheldrick, SHELXL-97, *Program for the Refinement of Crystal Structures*, University of Göttingen, Göttingen, Germany, **1997**.

Received September 10, 2002
[I02508]

Five- and Six-Membered Cobaltocycles with C,P-Chelating Ligands through Regiospecific Cyclometalation of Mono(2-Substituted) Triphenylphosphane

Hans-Friedrich Klein,*[a] Robert Beck,[a] Ulrich Flörke,[b] and Hans-Jürgen Haupt[b]

Keywords: Chelates / Cobalt / Metalation / Metallacycles / Structure elucidation

Cyclometalation in the aliphatic ring occurs in the reaction between $[CoCH_3(PMe_3)_4]$ and 5-(diphenylphosphanyl)-1,2,3,4-tetrahydronaphthalene to give [{8-(diphenylphosphanyl)-1,2,3,4-tetrahydronaphthyl-(C^1,P)}tris(trimethylphosphane)cobalt] (**1**), containing a five-membered metallacycle as shown in the molecular structure. While 1-(diphenylphosphanyl)naphthalene reacts accordingly, affording [{8-(diphenylphosphanyl)naphthyl-(C^1,P)}tris(trimethylphosphane)cobalt] (**2**), 2-(diphenylphosphanyl)biphenyl yields *ortho*-metalated [{2-(diphenylphosphanyl)-3-phenylphenyl-(C^1,P)}tris(trimethylphosphane)cobalt] (**3**), containing a four-membered metallacycle**.** 1-**(**Diphenylphosphanyl)-8-methylnaphthalene is metalated in the aliphatic substituent to form [{[8-(diphenylphosphanyl)naphth-1-yl]methyl-(*C*,*P*)}tris(trimethylphosphane)cobalt] (**4**). The molecular structure shows a trigonal-bipyramidal configuration of the cobalt atom accommodating a six-membered metallacycle. 2-(Diphenylphosphanyl)styrene replaces two trimethylphosphane ligands to give [{2-(diphenylphosphanyl)styrene-(*C*,*C*-η^2,*P*)}methylbis(trimethylphosphane)cobalt] (**5**), avoiding metalation. Replacement of equatorial trimethylphosphane in compounds **1**–**3** by ethene gives π-ethene complexes **6**–**8**. In the molecular structure of **7** the C–C vector of the π-ethene ligand is arranged in the equatorial plane of a trigonal bipyramid. Under 1 bar of CO, compound **2** forms a monocarbonyl complex **9**, in which an equatorial carbonyl ligand is found in the molecular structure. Iodomethane transforms **2** into pentacoordinate [{2-(diphenylphosphanyl)naphthyl-(C^1,P)}iodobis(trimethylphosphane)cobalt] (**10**) with retention of the metallacycle.

(© Wiley-VCH Verlag GmbH & Co. KGaA, 69451 Weinheim, Germany, 2003

Introduction

Cyclometalation reactions with mono(2-substituted) triphenylphosphanes and $[CoCH_3(PMe_3)_4]$ proceed with elimination of methane, whereby the selective product formation is rendered irreversible.[1] The observed regiospecificity, based on the orientation of C−H bonds situated in the vicinity of the metal atom, is sterically controlled by the preferred substrate conformation. Four-membered cobaltocycles have been found to originate from an *ortho*-metalation process, while in exceptional cases five-membered rings arise from attack in the side chain, although on the basis of C−H and C−Co bond energies the balance is believed to be less favorable for C(sp^3)−H bonds.[2] With the aim of selectively generating larger metallacycles we have metalated some pre-chelate phosphane ligands capable of forming five- and six-membered cobaltocycles (Scheme 1). An optional *ortho*-metalation route, disregarding the *ortho*-CH groups in the phenyl substituents, is also indicated for all four pre-chelate systems under investigation.

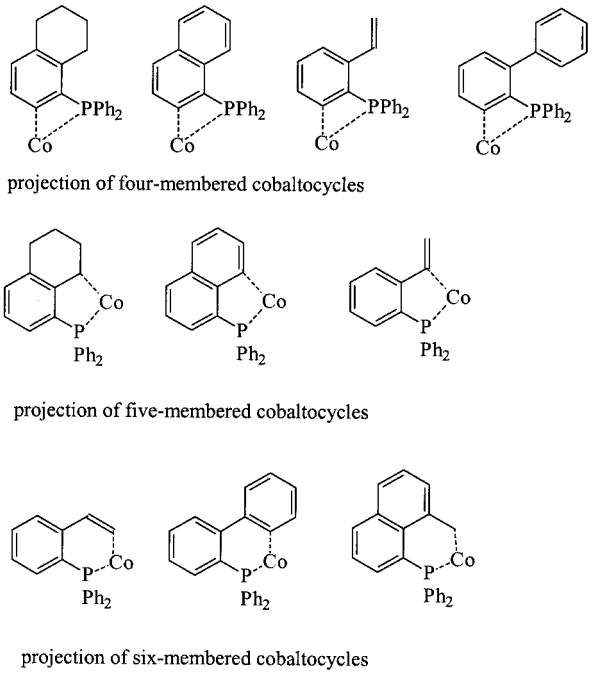

Scheme 1. Projection of cyclometalation reactions

[a] Eduard-Zintl-Institut für Anorganische und Physikalische Chemie der Technischen Universität Darmstadt,
Petersenstrasse 18, 64285 Darmstadt, Germany
[b] Anorganische und Analytische Chemie der Universität Paderborn,
Warburger Straße, 33098 Paderborn, Germany

Results and Discussion

The $ArCH_3 \rightarrow ArCH_2 \rightarrow ArCH$ Line

Proximity of a C−H bond to the metal atom and a perpendicular orientation are believed to be necessary prerequisites for a cyclometalation reaction to occur. The unusual switching of selectivities from side-chain attack (2-methyl substituent) to *ortho*-metalation (2-ethyl substituent), which is steric in origin, prompted us to clarify the cyclometalation process further by restricting the proximity conformations. Rotational orientations of C−H bonds will be restricted in an aliphatic ring when 5-(diphenylphosphanyl)-1,2,3,4-tetrahydronaphthalene is chosen as a prechelate reactant. Reaction with $[CoCH_3(PMe_3)_4]$ proceeds below 20 °C [Equation (1)].

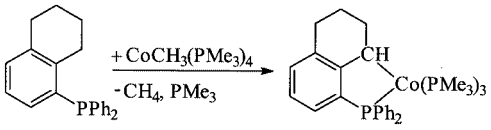

(1)

1

Red-brown crystals of **1**, melting with decomposition above 121 °C, were obtained from pentane. In the ^{31}P NMR spectrum, the observed coordination chemical shift of $\delta \approx 80$ ppm is only compatible with the PPh_2 group ($\delta = 64$ ppm) as part of a five-membered cobaltocycle. This configuration was confirmed in the molecular structure of **1** (Figure 1).

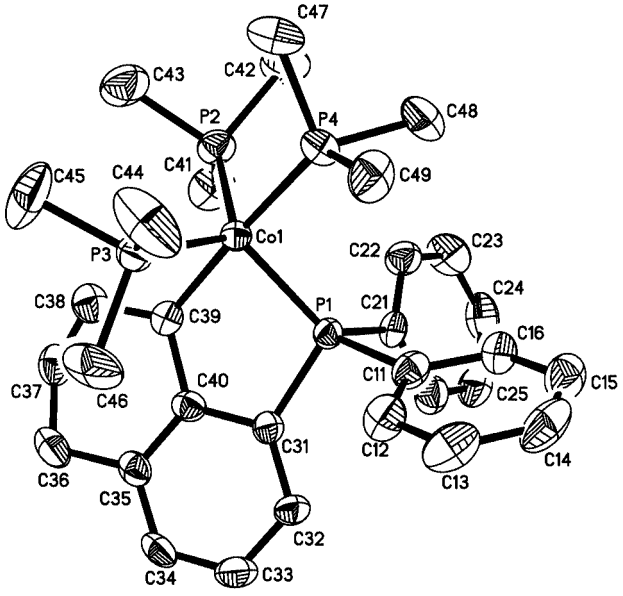

Figure 1. Molecular structure of **1** (ORTEP plot with hydrogen atoms omitted); selected bond lengths [Å] and angles [°]: Co−C39 2.082(6), Co−P1 2.1612(17), Co−P2 2.2189(17), Co−P3 2.1911(18), Co−P4 2.223(2), P1−C31 1.837(6), C31−C40 1.401(8), C39−C40 1.487(8); C39−Co−P1 81.18(17), C39−Co−P2 88.12(18), C39−Co−P3 85.34(19), C39−Co−P4 176.58(18), P1−Co−P2 120.50(7), P1−Co−P3 117.05(7), P1−Co−P4 95.56(6), P2−Co−P3 120.11(7), P2−Co−P4 94.45(7), P3−Co−P4 95.29(7), Co−P1−C31 105.26(19), P1−C31−C40 110.3(4), C31−C40−C39 117.8(5), Co−C39−C40 116.5(4)

The cobalt atom is centered in a trigonal bipyramid with axial CH and PMe_3 groups and a five-membered metallacycle spanning C-axial and P-equatorial positions with a C39−Co−P1 bite angle of 81.18(17)°. The Co−C bond is unusually long [Co−C39 = 2.082(6) Å], and while the adjacent distance $C(sp^3)-C(sp^3)$ is shortened [C39−C38 = 1.422(8) Å] the $C(sp^3)-C(sp^2)$ distance is normal [C39−C40 = 1.487(8) Å]. A multiplet arising from multiple phosphorus coupling at $\delta = 1.08$ ppm (1 H) in the ^1H NMR spectrum at 296 K is attributable to the CoCH group, and there is nothing remarkable in the remaining cycloaliphatic proton signals ($\delta = 2.20-2.63$ ppm, 6 H). As there are no unusual anisotropic properties of the carbon atoms, and as split models for the atomic positions of C39 and C38 were found insufficient, the structural irregularity in the cycloaliphatic ring is attributed to packing forces.

Incorporation of the CH_2 group in a cyclohexenyl ring switches the cyclometalation reaction from *ortho*-metalation of a $C(sp^2)-H$ bond to side-chain attack at a $C(sp^3)-H$ bond.

1-(Diphenylphosphanyl)naphthalene, providing two in-plane *ortho*-$C(sp^2)-H$ bonds, reacts with $[CoCH_3(PMe_3)_4]$ at −70 °C [Equation (2)] to afford **2** exclusively, isolated in 85% yield. The ^{31}P NMR chemical shifts and coupling constants at 193 K are found in positions and of an order expected for a five-membered cobaltocycle. The configuration of **2** was confirmed by monosubstitution with carbon monoxide to afford **9** (see below). Formation of a similar metallacycle starting from iridium(III) chloride was reported to require reflux conditions in 2-methoxyethanol.[3]

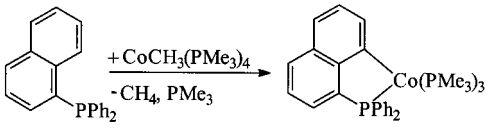

(2)

2

In order to address the matter of preference of six- or four-membered cobaltocycles, 2-(diphenylphosphanyl)biphenyl was treated with $[CoCH_3(PMe_3)_4]$ [Equation (3)].

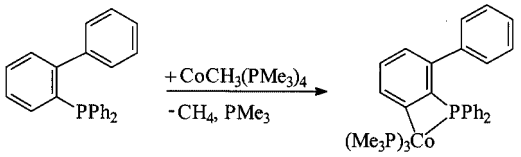

(3)

3

After evolution of gas, the mixture became red-brown in color and afforded **3** as a waxy solid, which was characterized by spectroscopy but gave no satisfactory elemental analysis. Evidence for the presence of a four-membered cobaltocycle was substantiated by its π-ethene derivative **8** (see below).

Metalation of the congested methyl group in 1-(diphenylphosphanyl)-8-methylnaphthalene should provide a six-

membered cobaltocycle, if not dominated by *ortho*-metalation (Scheme 1). The relative proximity effects at the cobalt center upon coordination of the anchoring PPh_2 group allow reaction with $[CoCH_3(PMe_3)_4]$ at −70 °C and evolution of methane to proceed within 5 min.

Metalation occurs specifically at the naphthylmethyl group, forming the six-membered metallacycle [Equation (4)]. Compound **4** was crystallized from pentane as short, dark brown rods. The ^{31}P NMR spectrum shows two doublets of triplets and a doublet of doublets, as in the five-membered cobaltocycles of **1** or **2**. The observed pattern is in agreement with axial CH_2 and PMe_3 groups and three P donor functions in equatorial positions. A six-membered chelate ring spanning axial C and equatorial P sites of a trigonal bipyramid is shown in the molecular structure of **4** (Figure 2).

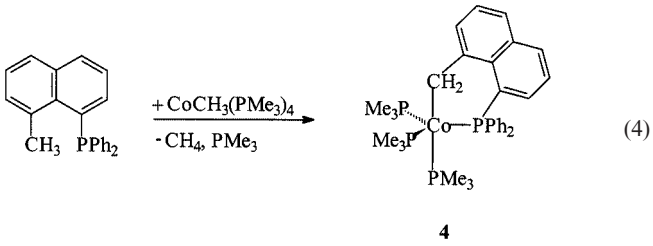

(4)

4

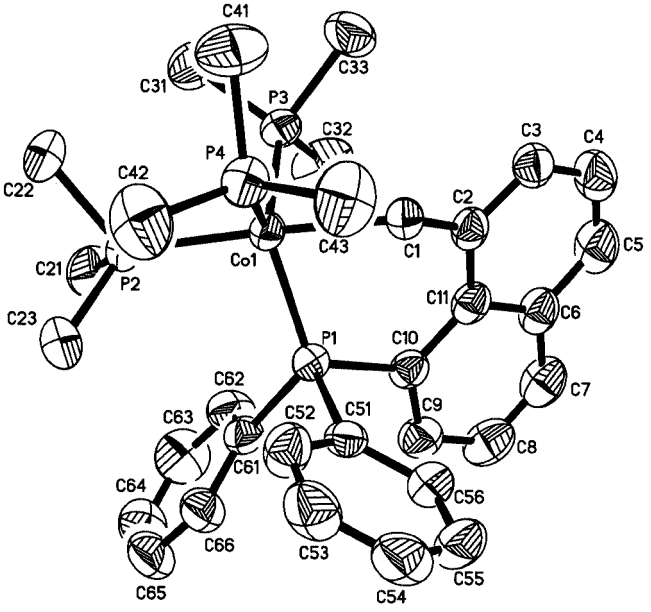

Figure 2. Molecular structure of **4** (ORTEP plot with hydrogen atoms omitted); selected bond lengths [Å] and angles [°]: Co−C1 2.090 (3), Co−P1 2.1438(9), Co−P2 2.1904(12), Co−P3 2.1932(10), Co−P4 2.2180(11), P1−C10 1.859(3), C10−C11 1.421(4), C2−C11 1.420(4), C1−C2 1.484(4); C1−Co−P1 79.72(9), C1−Co−P2 176.61(10), C1−Co−P3 88.32(10), C1−Co−P4 85.25(9), P1−Co−P2 98.60(4), P1−Co−P3 120.87(4), P1−Co−P4 121.21(4), P2−Co−P3 95.06(4), P2−Co−P4 93.18(4), P3−Co−P4 115.02(4), Co−P1−C10 117.05(10), P1−C10−C11 120.4(2), C2−C11−C10 123.5(2), C11−C2−C1 121.7(3), Co−C1−C2 123.4(2)

The cobalt atom is situated 109.5(1) pm above the best plane in the chelate ring. Bond lengths and angles show only minor deviations from the molecular structure of **1** (Figure 1).

Formation of all three ring sizes can be envisaged in 2-(diphenylphosphanyl)styrene (Scheme 1). However, treatment with $[CoCH_3(PMe_3)_4]$ failed to show evolution of gas, proceeding instead by substitution of two trimethylphosphane ligands [Equation (5)].

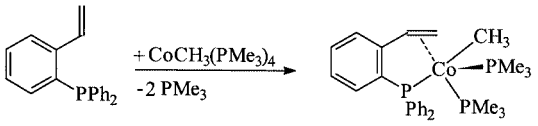

(5)

5

Compound **5** was obtained as an orange solid, decomposing above 152 °C under argon and stable in air under ambient conditions for at least 2 h. In the ^1H NMR spectrum at 296 K, a doublet of triplets at $\delta = -0.85$ ppm (3 H) represents the $CoCH_3$ group, while in the ^{31}P NMR spectrum at 233 K, two doublets of doublets for an axial and two anisochronic equatorial P-donor atoms indicate a tbp-coordinated cobalt atom with local C_s symmetry caused by an equatorial π-vinyl ligand. 2-(Diphenylphosphanyl)styrene appears to be trapped as a neutral chelating ligand[4] that does not undergo a metalation reaction.

Reactions with Ethene

π-Olefin coordination in aryl(trimethylphosphane)cobalt(I) complexes is usually achieved through a smooth substitution reaction.[1a,5] Complex **6** was observed to crystallize much better under 1 bar of ethene than under argon.

The underlying replacement of dissociated trimethylphosphane by ethene [Equations (6) and (7)] converts **1** and **2** into π-ethene compounds that form orange plates (**6**) and short orange rods (**7**) from pentane solutions.

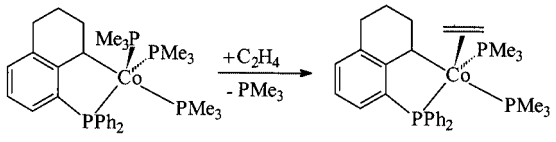

(6)

1 **6**

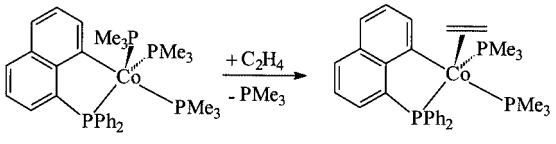

(7)

2 **7**

When the complexes are heated under argon, decomposition (**6**: > 101 °C; **7**: > 105 °C) proceeds with release of ethene, and no alteration in the five-membered metallacycle was indicated (IR) prior to deposition of cobalt. The expected tbp configuration was confirmed in the molecular structure of **7** (Figure 3).

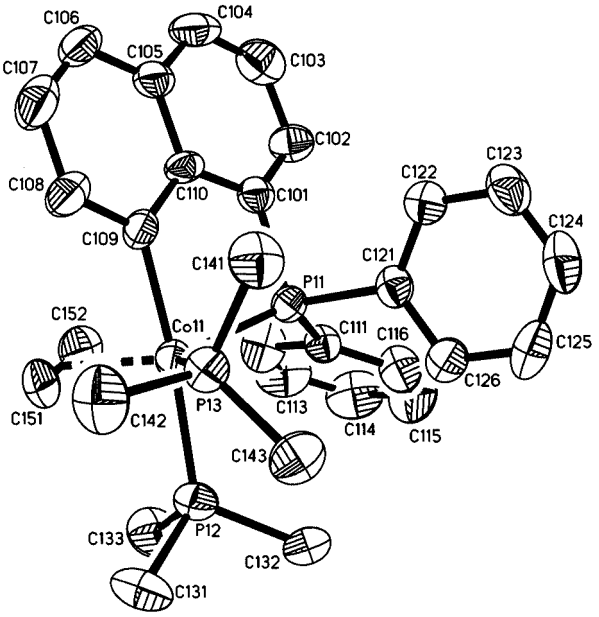

Figure 3. Molecular structure of **7** (molecule A) (QRTEP plot with hydrogen atoms omitted); selected bond lengths [Å] and angles [°]: Co−C109 2.001(5), Co−C151 2.026(6), Co−C152 2.045(7), Co−P11 2.1830(16), Co−P12 2.2413(18), Co−P13 2.2097(17), P11−C101 1.821(6), C101−C110 1.409(7), C109−C110 1.432(7); C109−Co−P11 83.82(16), C109−Co−P12 174.07(16), C109−Co−P13 88.06(17), P11−Co−P12 99.20(6), P11−Co−P13 105.74(6), P12−Co−P13 95.98(7), Co−P11−C101 102.55(18), P11−C101−C110 111.0(4), C101−C110−C109 119.0(5), Co−C109−C110 118.5(4)

A cobalt atom is found in the central position of a trigonal bipyramid with axial C and PMe_3 donor groups and a side-on coordinated ethene ligand with its C−C vector arranged in the equatorial plane, although crowded by PPh_2 and PMe_3 groups. The chelate bite angle [C109−Co−P = 83.82(16)°] is only 2° larger than in **1**, and the axial P−Co distance [Co−P12 = 2.2413(18) Å] is again the longest in the molecule, due to the *trans* influence of the naphthyl ligand.

Irrespective of the ring size or the heteroatom in P,C-, P,N-, and P,O-cobaltocycles, coordination of ethene in tbp complex molecules is regioselective, due to a better overlap with the strongest π-acceptor ligand in an equatorial position.[6]

A smooth replacement of trimethylphosphane by ethene also proceeds [Equation (8)] with complex **3**, which contains a four-membered cobaltocycle.

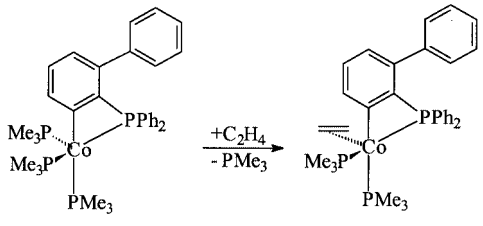

3 **8** (8)

Three doublets of doublets in the ^{31}P NMR spectrum of **8**, at δ = −11, 9, and 21 ppm, fall in the positions corresponding to a four-membered cobaltocycle expected from data for *ortho*-metalated compounds[1] and indicate an equatorial position of the π-ethene ligand.

Reaction with Carbon Monoxide

In solution under 1 bar of CO at 20 °C, **2** forms a monocarbonyl complexe **9** [Equation (9)].

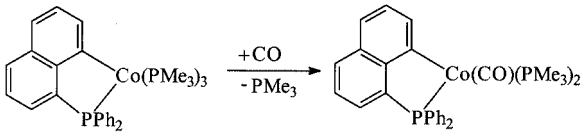

2 **9** (9)

The dark red crystals of **9** are thermally about 30 K more stable than their parent trimethylphosphane compound and are less air-sensitive. ^{31}P NMR spectra obtained from THF solutions show a mixture of isomers with $J_{P,P}$ coupling constants consistent with tbp configurations in which a terminal carbonyl ligand resides either in an axial or in an equatorial position. In toluene solution, only the isomer with axial CO is observed.

The molecular structure of **9** (Figure 4) shows the tbp configuration of the isomer containing an equatorial carbonyl ligand and, in view of the otherwise similar infrared spectra, confirms the presence of a five-membered cobaltocycle in **2**. The chelate bite angle in **9** [C38−Co−P1 = 83.97(12)°] is as in **7**, and the sum of internal angles (534.7°) indicates little deviation from planarity. The Co−CO dis-

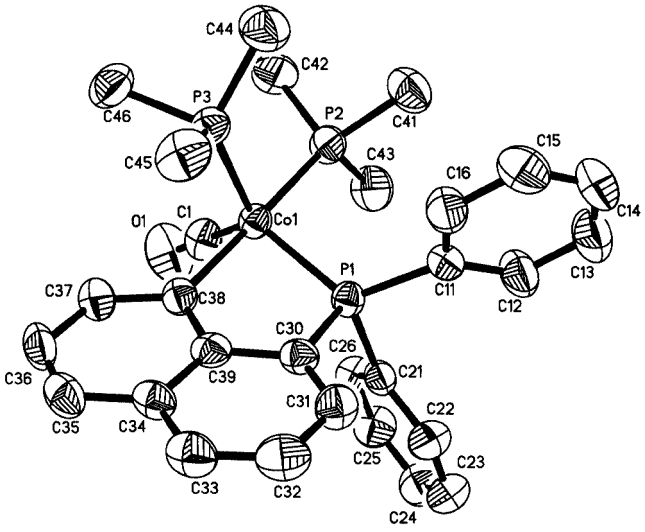

Figure 4. Molecular structure of **9** (ORTEP plot with hydrogen atoms omitted); selected bond lengths [Å] and angles [°]: Co−C38 1.996(4), Co−C1 1.720(5), Co−P1 2.1753(12), Co−P2 2.1935(13), Co−P3 2.2213(13), P1−C30 1.824(4), C30−C39 1.410(6), C38−C39 1.445(5); C38−Co−P1 83.97(12), C38−Co−P2 176.71(13), C38−Co−P3 85.07(12), P1−Co−P2 98.10(5), P1−Co−P3 113.16(5), P2−Co−P3 96.41(5), Co−P1−C30 103.09(14), P1−C30−C39 110.1(3), C30−C39−C38 119.6(4), Co−C38−C39 118.0(3)

tance [Co−C1 = 1.720(5) Å] is at the short end of the range for monocarbonylcobalt(I) complexes although in most cases the CO ligand occupies an axial position.[7]

Reactions with Iodomethane

Iodomethane oxidizes **2** [Equation (10)] to form a cobalt(II) complex **10** without there being evidence of a cobalt(III) intermediate.[1a] Although the molecular geometry of **10** has not been clarified, the magnetic moment of 1.91 is as would be expected for a tbp configuration at the cobalt atom (d^7).[1a,8]

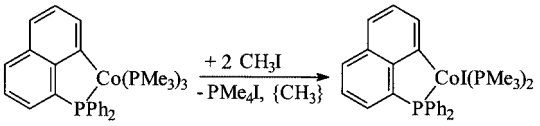

2 **10** (10)

Conclusion

The irreversible cyclometalation processes with $[CoCH_3(PMe_3)_4]$ appear to depend on the conformation of the 2-substituent when accommodated within the first coordination sphere of the metal atom. As soon as proximity to the electron-rich metal center is optimized, the product is formed by a sequence of fast steps involving oxidative addition of an aliphatic or an aromatic CH group, followed by elimination of methane. The ring size of the C,P-cobaltocycles in the product complex may be four, five, or six and does not dictate the regiospecificity of the cyclometalation reaction. Neither cobaltocycle inserts a π-coordinated ethene ligand into the Co−C bond and neither is expanded by CO uptake as with four-membered cobaltocycles.[1]

Experimental Section

General Procedures and Materials: All air-sensitive and volatile materials were handled by use of standard vacuum techniques and were kept under argon. Microanalyses: Kolbe Microanalytical Laboratory, Mülheim/Ruhr, FRG. Melting points/decomposition temperatures: sealed capillaries, uncorrected values. Chemicals (Merck/Schuchardt) were used as purchased. Literature methods were applied in the preparation of 1-iodo-8-methylnaphthalene,[9] 5-(diphenylphosphanyl)-1,2,3,4-tetrahydronaphthalene,[10] 2-(diphenylphosphanyl)biphenyl,[11] 2-(diphenylphosphanyl)stryrene,[12] and $[CoCH_3(PMe_3)_4]$.[13] IR: Nujol mulls between KBr discs, Bruker spectrophotometer type FRA 106. ^1H and ^{13}C NMR spectra (300 MHz and 75 MHz, respectively) were recorded with a Bruker ARX 300 spectrometer, ^{31}P NMR spectra (81 MHz) with a Bruker AM 200 instrument. ^{13}C and ^{31}P resonances were obtained with broad-band proton decoupling. Magnetic susceptibility data were obtained by the Faraday method with a Cahn D 200 torsion balance (Bruker) at 1.5 Tesla.

1-(Diphenylphosphanyl)-8-methylnaphthalene: *n*BuLi (9.7 mL 1.6 N in hexane, 15.7 mmol) was added slowly at −70 °C to 1-iodo-8-methylnaphthalene (4.20 g, 15.7 mmol) in 50 mL of diethyl ether, and the mixture was allowed to warm to −30 °C. After 2 h, chlorodiphenylphosphane (3.45 g, 15.7 mmol) was added, and the resulting suspension was stirred at 20 °C for 4 h. The volatiles were then removed in vacuo and the residue was extracted with two portions of methylcyclohexane (each 50 mL). On cooling of the combined extracts to 4 °C, white cubic crystals (1.89 g, 37%) were formed; m.p. 131−132 °C. ^1H NMR (300 MHz, CD_2Cl_2, 296 K): δ = 3.08 (d, $J_{P,H}$ = 4.2 Hz, 3 H, CH_3), 7.12 (ddd, ^3J = 6.5, $^4J_{P,H}$ = 5.0, ^4J = 1.5 Hz, 1 H, CH), 7.21−7.28 (m, 6 H, CH), 7.31−7.32 (m, 1 H, CH), 7.34 −7.38 (m, 6 H, CH), 7.73 (d, ^3J = 7.9 Hz, 1 H, CH), 7.85 (dd, ^3J = 8.1, ^4J = 1.4 Hz, 1 H, CH) ppm. ^{13}C NMR (75.4 MHz, CD_2Cl_2, 296 K): δ = 27.5 (d, $^1J_{P,C}$ = 32.0 Hz, CH_3), 125.2 (s, CH), 125.9 (s, CH), 126.6 (d, $^2J_{P,C}$ = 16.3 Hz, C), 128.5 (s, CH), 129.2 (d, $^2J_{P,C}$ = 16.5 Hz, CH), 131.3 (s, CH), 131.9 (s, CH), 132.2 (m, CH), 134.6 (d, $^3J_{P,C}$ = 20.4 Hz, CH), 135.5 (d, $^3J_{P,C}$ = 29.3 Hz, C), 135.9 (s, CH), 136.0 (s, C), 136.7 (s, C), 139.1 (d, $^2J_{P,C}$ = 14.0 Hz, C) ppm. ^{31}P NMR (81 MHz, CD_2Cl_2, 296 K): δ = −0.5 ppm. $C_{23}H_{19}P$ (326.2): calcd. C 84.64, H 5.87; found C 84.17, H 5.98.

[{8-(Diphenylphosphanyl)-1,2,3,4-tetrahydronaphthyl-(*C*^{1},*P*)}tris-(trimethylphosphane)cobalt(I)] (1): 5-(Diphenylphosphanyl)-1,2,3,4-tetrahydronaphthalene (685 mg, 2.16 mmol) in THF (50 mL) was mixed at −70 °C with $[CoCH_3(PMe_3)_4]$ (820 mg, 2.16 mmol) in THF (50 mL). On warming, the mixture turned red-brown and was stirred at 20 °C for 16 h. The volatiles were then removed in vacuo, and the waxy residue was extracted with pentane (two 50-mL portions). At 4 °C, the solution afforded deep-red octahedral crystals of **1**, suitable for X-ray diffraction. Yield 535 mg (41%); m.p. 121−123 °C. ^1H NMR (300 MHz, [D$_8$]THF, 296 K): δ = 0.98 (d, $^2J_{P,H}$ = 6.3 Hz, 9 H, PCH_3), 1.08 (m, 1 H, CoCH), 1.25 (m, 18 H, PCH_3), 2.20 (m, 2 H, CH_2), 2.48 (m, 2 H, CH_2), 2.63 (dd, $^2J_{P,H}$ = 8.2, 7.6 Hz, 2 H, CH_2), 5.89 (m, 1 H, CH), 6.75−6.79 (m, 2 H, CH), 7.09−7.12 (m, 6 H, CH), 7.52−7.55 (m, 4 H, CH) ppm. ^{13}C NMR (75.4 MHz, [D$_8$]THF, 296 K): δ = 21.7 (m, PCH_3), 23.1 (m, CoCH), 23.9 (m, CH_2), 25.6 (m, CH_2), 27.4 (m, CH_2), 123.1(d, $^3J_{P,C}$ = 4.3 Hz, CH), 125.4 (s, CH), 126.1 (d, $^3J_{P,C}$ = 7.6 Hz, CH), 126.2 (s, CH), 126.5 (s, CH), 131.9 (d, $^2J_{P,C}$ = 13.0 Hz, CH), 133.6 (s, C) ppm. ^{31}P NMR (81 MHz, [D$_8$]THF, 233 K): δ = −3 (dd, $^2J_{Peq,Peq}$ = 97, $^2J_{Peq,Pax}$ = 53 Hz, 2 P, PCH_3), 24 (dt, $^2J_{Pax,Peq}$ = 53, $^2J_{Pax,Peq}$ = 53 Hz, 1 P, PCH_3), 64 (dt, $^2J_{Peq,Peq}$ = 97, $^2J_{Peq,Pax}$ = 53 Hz, 1 P, PPh_2) ppm. $C_{31}H_{47}CoP_4$ (602.5): calcd. C 61.79, H 7.86, P 20.56; found C 61.47, H 7.47, P 21.05.

[{8-(Diphenylphosphanyl)naphthyl-(*C*^{1},*P*)}tris(trimethylphosphane)-cobalt(I)] (2): 1-(Diphenylphosphanyl)naphthalene (710 mg, 2.27 mmol) in THF (50 mL) was mixed at −70 °C with $[CoCH_3(PMe_3)_4]$ (860 mg, 2.27 mmol) in THF (50 mL). On warming, the mixture turned red-brown and was stirred at 20 °C for 16 h. The volatiles were then removed in vacuo, and the waxy residue was extracted with diethyl ether (three 80-mL portions). At −27 °C, the solution afforded black rhombuses of **2**. Yield 1150 mg (85%); m.p. 107−109 °C (dec.). ^1H NMR (300 MHz, [D$_8$]THF, 296 K): δ = 1.01 (d, $^2J_{P,H}$ = 6.4 Hz, 9 H, PCH_3), 1.09 (m, 18 H, PCH_3), 6.88 (t, ^3J = 7.6 Hz, 1 H, CH), 7.12 (m, 2 H, CH), 7.19−7.21 (m, 2 H, CH), 7.39−7.47 (m, 7 H, CH), 7.61−7.69 (m, 4 H, CH) ppm. ^{13}C NMR (75.4 MHz, [D$_8$]THF, 296 K): δ = 21.9 (dd, $^1J_{P,C}$ = 14.2, $^3J_{P,C}$ = 7.6 Hz, PCH_3), 22.5 (m, PCH_3), 117.6 (s, CH), 122.6 (s, CH), 122.8 (d, $^3J_{P,C}$ = 6.1 Hz, CH), 124.6 (s, CH), 126.2 (d, $^3J_{P,C}$ = 7.6 Hz, CH), 126.4 (s, CH), 127.2 (s, CH), 131.6 (d, $^1J_{P,C}$ = 15.2 Hz, C), 132.2 (d, $^2J_{P,C}$ = 12.2 Hz, CH), 139.8 (d, $^2J_{P,C}$ = 12.2 Hz, C), 142.3 (m, C) ppm. ^{31}P NMR (81 MHz, [D$_8$]THF, 233 K): δ = −3 (dd, $^2J_{Peq,Peq}$ = 100, $^2J_{Peq,Pax}$ = 54 Hz, 2 P, PCH_3),

24 (dt, $^2J_{Pax,Peq}$ = 54, $^2J_{Pax,Peq}$ = 54 Hz, 1 P, PCH_3), 64 (dt, $^2J_{Peq,Peq}$ = 100, $^2J_{Peq,Pax}$ = 54 Hz, 1 P, PPh_2) ppm. $C_{31}H_{43}CoP_4$ (598.5): calcd. C 62.21, H 7.24, P 20.70; found C 61.43, H 7.36, P 21.11.

[{2-(Diphenylphosphanyl)-3-phenylphenyl-(C^1,P)}tris(trimethylphosphane)cobalt(I)] (3): 2-(Diphenylphosphanyl)biphenyl (608 mg, 1.79 mmol) in THF (50 mL) was mixed at −70 °C with $[CoCH_3(PMe_3)_4]$ (680 mg, 1.79 mmol) in THF (30 mL). After warming, the dark red mixture was stirred at 20 °C for 5 h, and the volatiles were then removed in vacuo. The solid residue was extracted with pentane (80 mL). No crystallization was achieved either at 4 or at −27 °C from pentane, diethyl ether, THF, or mixtures of these solvents. Evaporation of solvent afforded **3** as a dark-red, waxy solid. Crude yield 940 mg. ^{1}H NMR (300 MHz, [D$_8$]THF, 296 K): δ = 1.05 (d, $^2J_{P,H}$ = 6.4 Hz, 9 H, PCH_3), 1.30 (t′, $|^2J_{P,H} + {}^4J_{P,H}|$ = 4.6 Hz, 18 H, PCH_3), 5.40−7.70 (m, 18 H, CH) ppm. ^{31}P NMR (81 MHz, [D$_8$]THF, 233 K): δ = −21 (dt, $^2J_{Peq,Peq}$ = 90, $^2J_{Peq,Pax}$ = 71 Hz, 1 P, PPh_2), −4 (dd, $^2J_{Peq,Peq}$ = 90, $^2J_{Peq,Pax}$ = 48 Hz, 2 P, PCH_3), 21 (dt, $^2J_{Pax,Peq}$ = 71, $^2J_{Pax,Peq}$ = 48 Hz, 1 P, PCH_3) ppm.

[{[8-(Diphenylphosphanyl)naphth-1-yl]methyl-(C,P)}tris(trimethylphosphane)cobalt(I)] (4): 1-(Diphenylphosphanyl)-8-methylnaphthalene (740 mg, 2.26 mmol) in THF (50 mL) was added at −78 °C to a solution of $[CoCH_3(PMe_3)_4]$ (857 mg, 2.26 mmol) in THF (50 mL). A rapid change of color from dark red to brown was observed as the solution warmed up. After 5 h, the solvent was removed in vacuo and the residue was extracted with pentane (two portions of 50 mL). Crystallization at 4 °C afforded dark brown cubes of **4**, suitable for X-ray diffraction. Yield 625 mg (45%); m.p. 146−148 °C (dec.). ^{1}H NMR (300 MHz, [D$_8$]THF, 296 K): δ = 1.02 (s, 27 H, PCH_3), 1.92 (q, $^3J_{P,H}$ = 11.7 Hz, 2 H, $CoCH_2$), 6.72 (dt, ^3J = 7.5, ^4J = 0.8 Hz, 1 H, CH), 7.03 (dt, ^3J = 7.8, ^4J = 2.5 Hz, 2 H, CH), 7.16−7.21 (m, 6 H, CH), 7.31−7.33 (m, 2 H, CH), 7.42−7.47 (m, 4 H, CH), 7.67 (d, ^3J = 8.0 Hz, 1 H, CH) ppm. ^{13}C NMR (75.4 MHz, [D$_8$]THF, 296 K): δ = 11.6 (m, $CoCH_2$), 19.8 (m, PCH_3), 122.0 (d, $^3J_{P,C}$ = 4.3 Hz, CH), 125.4 (s, CH), 126.1 (d, $^3J_{P,C}$ = 7.6 Hz, CH), 126.2 (s, CH), 126.5 (s, CH), 131.9 (d, $^2J_{P,C}$ = 13.0 Hz, CH), 133.6 (s, C) ppm. ^{31}P NMR (81 MHz, [D$_8$]THF, 203 K): δ = −3 (dd, $^2J_{Peq,Peq}$ = 102, $^2J_{Peq,Pax}$ = 40 Hz, 2 P, PCH_3), 20 (dt, $^2J_{Pax,Peq}$ = 46, $^2J_{Pax,Peq}$ = 40 Hz, 1 P, PCH_3), 48 (dt, $^2J_{Peq,Peq}$ = 102, $^2J_{Peq,Pax}$ = 46 Hz, 1 P, PPh_2) ppm. $C_{32}H_{45}CoP_4$ (612.5): calcd. C 62.75, H 7.40, P 20.23; found C 62.72, H 7.38, P 20.39.

[{2-(Diphenylphosphanyl)styrene-(C,C-η^2,P)}methylbis(trimethylphosphane)cobalt(I)] (5): 2-(Diphenylphosphanyl)stryrene (571 mg, 1.98 mmol) in diethyl ether (40 mL) was mixed at −70 °C with $[CoCH_3(PMe_3)_4]$ (750 mg, 1.98 mmol) in diethyl ether (40 mL). After warming, the orange mixture was stirred at 20 °C for 3 h, and the volume was then reduced to 40 mL. Pentane (50 mL) was added with vigorous stirring to precipitate **5** as a light brown solid. This was isolated by filtration and washing with pentane. Yield 652 mg (64%); m.p. 152−154 °C (dec.). ^{1}H NMR (300 MHz, [D$_8$]THF, 296 K): δ = −0.85 (dt, $^3J_{P,H}$ = 8.1, 1.8 Hz, $CoCH_3$), 0.78 (d, $^2J_{P,H}$ = 5.6 Hz, 9 H, PCH_3), 1.30 (d, $^2J_{P,H}$ = 5.5 Hz, 9 H, PCH_3), 1.80 (m, 2 H, $=CH_2$), 2.64 (m, 1 H, =CH), 6.86 (t, ^3J = 7.3 Hz, CH), 7.01 (dt, ^3J = 6.3, ^4J = 1.3 Hz, 1 H, CH), 7.18 (t, ^3J = 6.7 Hz, 1 H, CH), 7.26−7.31 (m, 6 H, CH), 7.31−7.33 (m, 1 H, CH), 7.38−7.41 (m, 2 H, CH), 7.77−7.83 (m, 2 H, CH) ppm. ^{13}C NMR (75.4 MHz, [D$_8$]THF, 296 K): δ = 17.6 (d, $^1J_{P,C}$ = 14.7 Hz, PCH_3), 18.9 (d, $^1J_{P,C}$ = 16.7 Hz, PCH_3), 50.8 (s, $=CH_2$), 62.1 (d, $^2J_{P,C}$ = 18.2 Hz, =CH), 121.7 (d, $^4J_{P,C}$ = 4.1 Hz, CH), 123.4 (d, $^2J_{P,C}$ = 112.6 Hz, CH), 126.4 (d, $^3J_{P,C}$ = 7.9 Hz, CH), 126.7 (d, $^3J_{P,C}$ = 7.7 Hz, CH), 127.3 (s, CH), 127.8 (s, CH), 130 (s, CH), 132.8 (d, $^2J_{P,C}$ = 10.5 Hz, C), 133.2 (d, $^2J_{P,C}$ = 9.8 Hz, CH), 137.8 (s, C), 138.4 (s, C) ppm. ^{31}P NMR (81 MHz, [D$_8$]THF, 233 K): δ = 9 (dd, $^2J_{Peq,Pax}$ = 44, $^2J_{Peq,Pax}$ = 26 Hz, 2 P, PCH_3), 71 (dd, $^2J_{Pax,Peq}$ = 26, $^2J_{Pax,Peq}$ = 44 Hz, 1 P, PPh_2) ppm. $C_{27}H_{38}CoP_3$ (514.2): calcd. C 63.04, H 7.45, P 18.06; found C 63.44, H 6.79, P 18.18.

[{8-(Diphenylphosphanyl)-1,2,3,4-tetrahydronaphthyl-(C^1,P)}-(ethene)bis(trimethylphosphane)cobalt(I)] (6): A sample of **3** (620 mg, 1.03 mmol) in diethyl ether (30 mL) was stirred under 1 bar of ethene for 1 h to provide an orange-red solution. The volatiles were removed in vacuo and the solid residue was extracted with pentane (40 mL). Crystallization at 4 °C afforded orange, hexagonal plates of **6**. Yield 490 mg (86%); m.p. 101−103 °C (dec.). ^{1}H NMR (300 MHz, [D$_8$]THF, 296 K): δ = 0.98 (d, $^2J_{P,H}$ = 6.3 Hz, 9 H, PCH_3), 1.08 (m, 1 H, CoCH), 1.25 (br. s, 9 H, PCH_3), 2.19−2.21 (m, 2 H, CH_2), 2.48 (m, 2 H, CH_2), 2.63 (dd, ^3J = 8.2, ^3J = 7.6 Hz, 2 H, CH_2), 5.89 (m, 1 H, CH), 6.75−6.79 (m, 2 H, CH), 7.09−7.12 (m, 2 H, CH), 7.52−7.55 (m, 4 H, CH) ppm. ^{1}H NMR (300 MHz, [D$_8$]toluene, 296 K): δ = 0.53 (d, $^2J_{P,H}$ = 6.4 Hz, 9 H, PCH_3), 0.86 (m, 1 H, CoCH), 1.05 (d, $^2J_{P,H}$ = 5.0 Hz, 9 H, PCH_3), 1.88−2.54 (m, 6 H, CH_2), 1.90 (m, 2 H, $=CH_2$), 2.29 (m, 2 H, $=CH_2$), 5.35 (m, 1 H, CH), 6.42−6.59 (m, 2 H, CH), 6.92−7.03 (m, 2 H, CH), 7.61−7.84 (m, 4 H, CH) ppm. ^{13}C NMR (75.4 MHz, [D$_8$]THF, 296 K): δ = 16.3 (d, $^1J_{P,C}$ = 19.5 Hz, PCH_3), 19.1 (d, $^1J_{P,C}$ = 19.5 Hz, PCH_3), 23.4 (m, CoCH), 25.4 (m, CH_2), 27.6 (s, CH_2), 29.1 (s, CH_2), 39.2 (m, $=CH_2$), 40.9 (m, $=CH_2$), 121.1 (s, CH), 123.2 (d, $^3J_{P,C}$ = 5.2 Hz, CH), 124.7 (s, CH), 126.1 (d, $^2J_{P,C}$ = 12.3 Hz, C), 126.2 (d, $^1J_{P,C}$ = 15.1 Hz, C), 126.9 (d, $^2J_{P,C}$ = 12.7 Hz, CH), 127.2 (d, $^1J_{P,C}$ = 20.5 Hz, CH), 131.8 (d, $^1J_{P,C}$ = 16.3 Hz, C), 132. 4 (d, $^2J_{P,C}$ = 11.8 Hz, CH), 140.2 (s, C) ppm. ^{13}C NMR (75.4 MHz, [D$_8$]toluene, 296 K): δ = 18.1 (d, $^1J_{P,C}$ = 18.4 Hz, PCH_3), 21.8 (d, $^1J_{P,C}$ = 19.3 Hz, PCH_3), 23.3 (m, CoCH), 26.8 (m, CH_2), 29.0 (s, CH_2), 30.5 (s, CH_2), 41.1 (d, $^2J_{P,C}$ = 18.2 Hz, $=CH_2$), 42.4 (d, $^2J_{P,C}$ = 16.4 Hz, $=CH_2$), 122.8 (s, CH), 124.7 (d, $^2J_{P,C}$ = 14.2 Hz, CH), 124.8 (s, CH), 127.6 (d, $^2J_{P,C}$ = 11.2 Hz, CH), 128.4 (s, C), 133.2 (d, $^3J_{P,C}$ = 10.5 Hz, CH), 133.5 (d, $^3J_{P,C}$ = 9.5 Hz, CH), 134.4 (d, $^2J_{P,C}$ = 16.1 Hz, C), 141.7 (d, $^2J_{P,C}$ = 22.6 Hz, CH), 155.0 (d, $^1J_{P,C}$ = 43.7 Hz, C) ppm. ^{31}P NMR (81 MHz, [D$_8$]THF, 213 K): δ = 5 (dd, $^2J_{Peq,Pax}$ = 46, $^2J_{Peq,Peq}$ = 38 Hz, 1 P, PCH_3), 17 (dd, $^2J_{Pax,Peq}$ = 32, $^2J_{Pax,Peq}$ = 46 Hz, 1 P, PCH_3), 75 (dd, $^2J_{Peq,Pax}$ = 32, $^2J_{Peq,Peq}$ = 38 Hz, 1 P, PPh_2) ppm. $C_{30}H_{42}CoP_3$ (554.5): calcd. C 64.98, H 7.63, P 16.76; found C 65.36, H 7.82, P 16.39.

[{2-(Diphenylphosphanyl)naphthyl-(C^1,P)}(ethene)bis(trimethylphosphane)cobalt(I)] (7): A sample of **2** (680 mg, 1.13 mmol) in diethyl ether (50 mL) was stirred under 1 bar of ethene for 1 h to provide a light red solution. The volatiles were removed in vacuo, and the solid residue was extracted with pentane (three 50-mL portions). Crystallization at 4 °C afforded short orange rods of **7**, suitable for X-ray diffraction. Yield 506 mg (81%); m.p. 105−107 °C (dec.). ^{1}H NMR (300 MHz, [D$_8$]THF, 296 K): δ = 0.90 (d, $^2J_{P,H}$ = 6.5 Hz, 9 H, PCH_3), 1.05 (d, $^2J_{P,H}$ = 6.0 Hz, 9 H, PCH_3), 1.49 (m, 2 H, $=CH_2$), 2.47 (m, 2 H, $=CH_2$), 6.95 (t, ^3J = 7.5 Hz, 2 H, CH), 7.15 (dd, ^3J = 6.8, ^4J = 1.6 Hz, 1 H, CH), 7.17 (dd, ^3J = 8.3, ^4J = 1.3 Hz, 1 H, CH), 7.21 (dd, ^3J = 4.4, ^4J = 1.8 Hz, 1 H, CH), 7.26−7.33 (m, 7 H, CH), 7.46 (m, 2 H, CH), 7.54 (dd, ^3J = 7.6, ^4J = 1.8 Hz, 1 H, CH), 7.67−7.71 (m, 2 H, CH) ppm. ^{13}C NMR (75.4 MHz, [D$_8$]THF, 296 K): δ = 17.6 (d, $^1J_{P,C}$ = 11.3 Hz, PCH_3), 20.3 (d, $^1J_{P,C}$ = 18.8 Hz, PCH_3), 25.4 (m, CH_2), 40.1 (d, $^2J_{P,C}$ = 16.9 Hz, $=CH_2$), 42.1 (d, $^2J_{P,C}$ = 15.9 Hz, $=CH_2$), 119.8 (s, CH), 124.4 (d, $^3J_{P,C}$ = 5.4 Hz, CH), 125.9 (s, CH), 127.4 (s, CH), 127.6

(d, $^1J_{P,C}$ = 14.0 Hz, C), 127.9 (s, CH), 128.9 (d, $^1J_{P,C}$ = 23.9 Hz, CH), 132.6 (d, $^2J_{P,C}$ = 10.7 Hz, CH), 133.1 (d, $^3J_{P,C}$ = 7.3 Hz, CH), 133.7 (d, $^3J_{P,C}$ = 12.3 Hz, C), 141.2 (d, $^3J_{P,C}$ = 6.4 Hz, CH), 145.8 (m, C), 149.4 (s, C), 150.1 (s, C) ppm. ^{31}P NMR (81 MHz, [D$_8$]THF, 213 K): δ = 4 (dd, $^2J_{Peq,Pax}$ = 45, $^2J_{Peq,Peq}$ = 36 Hz, 1 P, PCH_3), 17 (dd, $^2J_{Pax,Peq}$ = 33, $^2J_{Pax,Peq}$ = 45 Hz, 1 P, PCH_3), 75 (dd, $^2J_{Peq,Pax}$ = 33, $^2J_{Peq,Peq}$ = 36 Hz, 1 P, PPh_2) ppm. $C_{30}H_{38}CoP_3$ (550.4): calcd. C 65.46, H 6.96, P 16.88; found C 64.81, H 6.71, P 17.27.

[{2-(Diphenylphosphanyl)-3-phenylphenyl-(*C*^{1},*P*)}(ethene)bis(trimethylphosphane)cobalt(I)] (8): A sample of **3** (940 mg, ca. 1.5 mmol) in THF (40 mL) was stirred under 1 bar of ethene for 3 h. The volatiles were removed in vacuo, and the oily residue was extracted with pentane (50 mL). Crystallization at 4 °C afforded short, orange rods of **8.** Yield 503 mg (58%); m.p. 95−97 °C (dec.). ^{1}H NMR (300 MHz, [D$_8$]THF, 296 K): δ = 0.82 (d, $^2J_{P,H}$ = 6.3 Hz, 9 H, PCH_3), 1.10 (d, $^2J_{P,H}$ = 5.9 Hz, 9 H, PCH_3), 1.66 (m, 1 H, =CH), 1.91 (m, 2 H, $=CH_2$), 2.31 (m, 1 H, =CH), 6.51 (m, 1 H, CH), 6.72 (dd, ^3J = 5.0, ^4J = 1.5 Hz, 2 H, CH), 7.15 (dd, ^3J = 6.8, ^4J = 1.6 Hz, 1 H, CH), 7.17 (dd, ^3J = 8.3, ^4J = 1.3 Hz, 1 H, CH), 6.85 (m, 3 H, CH), 6.95 (dd, ^3J = 7.3, ^4J = 1.4 Hz, 1 H, CH), 7.16 (dd, ^3J = 7.2, ^4J = 1.5 Hz, 1 H, CH), 7.21 (m, 6 H, CH), 7.41(dd, ^3J = 9.4, ^4J = 1.5 Hz, 1 H, CH), 7.42 (m, 2 H, CH), 7.68 (dd, ^3J = 9.4, ^4J = 1.9 Hz, 1 H, CH), 7.70 (dd, ^3J = 5.8, ^4J = 2.6 Hz, 1 H, CH) ppm. ^{13}C NMR (75.4 MHz, [D$_8$]THF, 296 K): δ = 16.5 (d, $^1J_{P,C}$ = 18.1 Hz, PCH_3), 20.3 (d, $^1J_{P,C}$ = 18.4 Hz, PCH_3), 32.5 (d, $^2J_{P,C}$ = 10.4 Hz, $=CH_2$), 38.8 (d, $^2J_{P,C}$ = 18.1 Hz, $=CH_2$), 121.5 (s, CH), 124.7 (s, CH), 125.9 (s, CH), 126.6 (d, $^2J_{P,C}$ = 8.8 Hz, CH), 127.1 (s, CH), 127.8 (s, CH), 128.2 (s, CH), 128.6 (d, $^1J_{P,C}$ = 15.2 Hz, C), 131.9 (d, $^2J_{P,C}$ = 12.1 Hz, CH), 132.2 (d, $^2J_{P,C}$ = 12.2 Hz, CH), 135.6 (d, $^1J_{P,C}$ = 16.4 Hz, CH), 136.9 (s, C), 139.1 (d, $^1J_{P,C}$ = 17.5 Hz, C), 140.7 (d, $^3J_{P,C}$ = 4.3 Hz, C), 146.4 (s, C), 153.0 (m, CoC) ppm. ^{31}P NMR (81 MHz, [D$_8$]THF, 233 K): δ = −11 (dd, $^2J_{Peq,Pax}$ = 47, $^2J_{Peq,Peq}$ = 51 Hz, 1 P, PPh_2), 9 (dd, $^2J_{Pax,Peq}$ = 31, $^2J_{Pax,Peq}$ = 47 Hz, 1 P, PCH_3), 21 (dd, $^2J_{Peq,Pax}$ = 31, $^2J_{Peq,Peq}$ = 51 Hz, 1 P, PCH_3) ppm. $C_{32}H_{40}CoP_3$ (576.2): calcd. C 66.67, H 6.99, P 16.22; found C 66.45, H 7.41, P 16.14.

[(Carbonyl){2-(diphenylphosphanyl)naphthyl-(*C*^{1},*P*)}bis(trimethylphosphane)cobalt(I)] (9): A sample of **2** (770 mg, 1.28 mmol) in THF (40 mL) was stirred under 1 bar of CO for 1 h to provide a light red solution. The volatiles were removed in vacuo, and the solid residue was extracted with pentane (three 70-mL portions). Crystallization at −27 °C afforded short, orange rods of **9** suitable for X-ray diffraction. Yield 616 mg (87%); m.p. 112−114 °C (dec.). IR (Nujol): $\tilde{\nu}$ = 1905 cm^{-1} (C≡O). ^{1}H NMR (300 MHz, [D$_8$]THF, 296 K): CO-eq isomer (12%): δ = 0.68 (d, $^2J_{P,H}$ = 6.3 Hz, 18 H, PCH_3), 1.12 (d, $^2J_{P,H}$ = 7.9 Hz, 18 H, PCH_3), 7.01−8.02 (m, 16 H, CH) ppm; CO-ax isomer (88%): δ = 0.69 (d, $^2J_{P,H}$ = 6.3 Hz, 9 H, PCH_3), 1.00 (t′, $|^2J_{P,H} + {}^4J_{P,H}|$ = 6.8 Hz, 18 H, PCH_3), 1.19 (d, $^2J_{P,H}$ = 7.9 Hz, 9 H, PCH_3), 7.08 (d, ^3J = 6.6 Hz, 1 H, CH), 7.10 (t, ^3J = 7.4 Hz, 1 H, CH), 7.26−7.29 (m, 8 H, CH), 7.43−7.49 (m, 4 H, CH), 7.61 (d, ^3J = 6.9 Hz, 1 H, CH), 7.70 (d, ^3J = 6.9 Hz, 1 H, CH), 7.84 (d, ^3J = 7.0 Hz, 1 H, CH), 7.97 (d, ^3J = 8.2 Hz, 1 H, CH) ppm. ^{13}C NMR (75.4 MHz, [D$_8$]THF, 296 K) CO-ax isomer (88%): δ = 19.8 (m, PCH_3), 120.5 (s, C), 125.5 (d, $^3J_{P,C}$ = 5.4 Hz, CH), 125.8 (s, CH), 126.5 (s, C), 128.6 (d, $^1J_{P,C}$ = 15.5 Hz, C), 128.8 (d, $^2J_{P,C}$ = 8.4 Hz, CH), 129.4 (s, CH), 130.4 (s, CH), 132.6 (d, $^2J_{P,C}$ = 12.7 Hz, CH), 133.3 (s, C), 134.7 (d, $^1J_{P,C}$ = 14.3 Hz, C), 138.9 (m, CH), 141.6 (s, C), 142.0 (s, C), 203.2 (s, CO) ppm. ^{31}P NMR (81 MHz, [D$_8$]THF, 233 K) CO_{ax} isomer (12%): δ = 5 (d, $^2J_{Peq,Peq}$ = 96 Hz, 2 P, PCH_3), 63 (t, $^2J_{Peq,Peq}$ = 96 Hz, 1 P, PPh_2) ppm; CO_{eq} isomer (88%): δ = −1 (dd, $^2J_{Peq,Peq}$ = 81, $^2J_{Peq,Pax}$ = 48 Hz, 1 P, PCH_3), 23 (dd, $^2J_{Pax,Peq}$ = 48, $^2J_{Pax,Peq}$ = 48 Hz, 1 P, PCH_3), 70 (dd, $^2J_{Peq,Peq}$ = 81, $^2J_{Peq,Pax}$ = 48 Hz, PPh_2) ppm. $C_{29}H_{34}CoOP_3$ (550.4): calcd. C 63.28, H 6.23, P 16.88; found C 62.67, H 5.78, P 17.30.

[{2-(Diphenylphosphanyl)naphthyl-(*C*^{1},*P*)}iodobis(trimethylphosphane)cobalt(II)] (10): A sample of **2** (670 mg, 1.12 mmol) in diethyl ether (50 mL) was mixed at −70 °C with iodomethane (365 mg, 2.57 mmol, slight excess). After 1 h at 20 °C, the mixture was filtered and the solution was kept at 4 °C to afford dark-brown crystals of **10**. The solid was extracted with diethyl ether (two 80-mL portions) to give a second fraction of **10**, which was combined with the first. Yield 421 mg (58%); m.p. 158−160 °C (dec.). Magnetic moment: μ_{eff} = 1.91 μ_B. $C_{28}H_{34}CoIP_3$ (649.3): calcd. C 51.79, H 5.28, P 14.31; found C 51.78, H 5.41, P 14.26.

Crystal Structure Analyses: Crystal data are presented in Tables 1 and 2. Complex **1**: A crystal was sealed under argon in a glass capillary and mounted on a Bruker AXS P4 diffractometer. Reflections were collected (ω-scans) by use of graphite-monochromated Mo-K_α radiation; a Lorentz polarization correction and an absorption correction based on ψ-scans were applied. The structure was solved by direct and conventional Fourier methods. All non-hydrogen atoms were treated anisotropically, hydrogen atoms were treated with a riding model in idealized positions. Complex **4**: Crystal mounting, data collection, structure solution, and refinement as for **1**. Complex **7**: Crystal mounting, data collection, structure solution, and refinement as for **1**. Two independent molecules per asymmetric unit. Complex **9**: Crystal mounting, data collection, structure solution, and refinement as for **1**. CCDC-184425 (**1**), -184426 (**4**), -184427 (**7**), and -184428 (**9**) contain the supplementary crystallographic data for this paper. These data can be obtained free of charge at www.ccdc.cam.ac.uk/conts/retrieving.html [or from the Cambridge Crystallographic Data Center, 12 Union Road, Cambridge CB2 1EZ, UK; Fax: (internat.) + 44-1223/336-033; E-mail: deposit@ccdc.cam.ac.uk].

Table 1. Crystal data for compounds **1** and **4**

	1	**4**
Empirical formula	$C_{31}H_{47}CoP_4$	$C_{32}H_{45}CoP_4$
Molecular mass	602.5	612.5
Crystal size [mm]	0.50 × 0.45 × 0.45	0.44 × 0.40 × 0.40
Crystal system	orthorhombic	monoclinic
Space group	$P2_12_12_1$	$P2_1/c$
a [Å]	10.929(3)	9.096(3)
b[Å]	16.544(3)	35.594(3)
c [Å]	17.501(9)	9.913(2)
β [°]	90	98.79(2)
V [Å^3]	3164.3(19)	3171.8(13)
Z	4	4
$D_{calcd.}$ [g/cm^3]	1.265	1.283
μ (Mo-K_α) [mm^{-1}]	0.763	0.762
Temperature [K]	203(2)	293(2)
Data coll. range [°]	$4.7 \le 2\theta \le 55$	$4.6 \le 2\theta \le 55$
h	$-1 \le h \le 14$	$-1 \le h \le 11$
k	$-1 \le k \le 21$	$-1 \le k \le 46$
l	$-1 \le l \le 22$	$-12 \le l \le 12$
No. reflect. measured	4975	8877
No. unique data	4759 (R_{int} = 0.0323)	7266 (R_{int} = 0.0310)
Parameters	335	334
GoF on F^2	1.010	0.968
$R1$ [$I \ge 2\sigma(I)$]	0.0578	0.0484
$wR2$ (all data)	0.1243	0.1051

Table 2. Crystal data for compounds **7** and **9**

	7	**9**
Empirical formula	$C_{30}H_{38}CoP_3$	$C_{29}H_{34}CoOP_3$
Molecular mass	550.4	550.4
Crystal size [mm]	0.40 × 0.35 × 0.30	0.38 × 0.15 × 0.06
Crystal system	monoclinic	monoclinic
Space group	$P2_1/c$	$P2_1/c$
a [Å]	9.697(2)	18.242(2)
b [Å]	16.411(2)	9.016(1)
c [Å]	35.970(6)	18.301(2)
β [°]	97.36(2)	111.94(1)
V [Å^3]	5677.0(17)	2792.0(5)
Z	8	4
$D_{calcd.}$ [g/cm^3]	1.288	1.309
μ (Mo-K_α) [mm^{-1}]	0.790	0.806
Temperature [K]	293(2)	293(2)
Data coll. range [°]	$4.2 \le 2\theta \le 54$	$4.5 \le 2\theta \le 50$
h	$-12 \le h \le 1$	$-1 \le h \le 21$
k	$-1 \le k \le 20$	$-1 \le k \le 10$
l	$-45 \le l \le 45$	$-21 \le l \le 20$
No. reflect. measured	15436	6135
No. unique data	12400 (R_{int} = 0.0584)	4910 (R_{int} = 0.0378)
Parameters	638	313
GoF on F^2	0.977	0.984
$R1$ [$I \ge 2\sigma(I)$]	0.0665	0.0469
$wR2$ (all data)	0.1677	0.1304

Acknowledgments

Financial support of this work by Fonds der Chemischen Industrie is gratefully acknowledged.

[1] [1a] H.-F. Klein, R. Beck, U. Flörke, H.-J. Haupt, *Eur. J. Inorg. Chem.*, **2003**, 853−862. [1b] H.-F. Klein, S. Schneider, M. He, U. Flörke, H.-J. Haupt, *Eur. J. Inorg. Chem.* **2000**, 2295−2301.
[2] [2a] W. D. Jones, F. J. Feher, *Acc. Chem. Res.* **1989**, *22*, 91−100. [2b] A. E. Shilov, G. B. Shul'pin, *Chem. Rev.* **1997**, *97*, 2879−2932.
[3] J. M. Duff, B. L. Shaw, *J. Chem. Soc., Dalton Trans.* **1972**, 2219−2225.
[4] [4a] M. A. Bennett, J. Chatt, E. Erskine, J. Lewis, R. F. Long, R. S. Nyholm, *J. Chem. Soc. A* **1967**, 501−509. [4b] M. A. Bennett, E. J. Hann, R. N. Johnson, *J. Organomet. Chem.* **1977**, *124*, 189−211. [4c] M. A. Bennett, R. N. Johnson, I. B. Tomkins, *J. Am. Chem. Soc.* **1974**, *96*, 61−69.
[5] H.-F. Klein, R. Beck, U. Flörke, H.-J. Haupt, *Eur. J. Inorg. Chem.* **2002**, 3305−3312.
[6] T. A. Albright, J. K. Burdett, M. H. Whangbo, *Orbital Interactions in Chemistry*, John Wiley & Sons, New York, **1985**, p. 361.
[7] [7a] A. G. Orpen, L. Brammer, F. H. Allen, O. Kennard, D. G. Watson, R. Taylor, *J. Chem. Soc., Dalton Trans.* **1989**, S1−S83. [7b] H.-F. Klein, X. Li, U. Flörke, H.-J. Haupt, *Z. Naturforsch., Teil B* **2000**, *55*, 707−717.
[8] [8a] H.-F. Klein, H. H. Karsch, *Chem. Ber.* **1976**, *109*, 1453−1464. [8b] M. Bressan, P. Rigo, *Inorg. Chem.* **1975**, *14*, 38−42. [8c] W. P. Leung, H. K. Lee, L. H. Weng, Z. Y. Zhou, T. C. W. Mak, *J. Chem. Soc., Dalton Trans.* **1997**, 779−783.
[9] J. Blum, D. Gelinan, W. Baldossi, E. Shakh, A. Rosenfeld, Z. Aizenshtat, *J. Org. Chem.* **1997**, *62*, 8681−8686.
[10] F. H. Carré, C. Chuit, R. J. P. Corriu, W. E. Douglas, D. M. H. Guy, C. Reye, *Eur. J. Inorg. Chem.* **2000**, 647−653.
[11] T. Bartik, T. Himmler, H.-G. Schulte, K. Seevogel, *J. Organomet. Chem.* **1984**, *272*, 29−41.
[12] [12a] M. A. Bennett, R. S. Nyholm, J. D. Saxby, *J. Organomet. Chem.* **1967**, *10*, 301−306. [12b] M. A. Bennett, W. R. Kneen, R. S. Nyholm, *J. Organomet. Chem.* **1971**, *26*, 293−303.
[13] H.-F. Klein, H. H. Karsch, *Chem. Ber.* **1975**, *108*, 944−954.

Received September 20, 2002
[I02520]

A Comparison of Analogous 4f- and 5f-Element Compounds: Syntheses and X-ray Crystal Structures of the Mixed Sandwich Complexes $[M(\eta\text{-}C_8H_8)(L)\{OP(NMe_2)_3\}]$ (M = Nd or U; L = $\eta\text{-}C_5Me_5$ or $\eta\text{-}C_4Me_4P$)

Sophie M. Cendrowski-Guillaume,*[a][‡] Gildas Le Gland,[a] Martine Nierlich,[a] and Michel Ephritikhine*[a]

Keywords: Cyclopentadienyl ligands / P ligands / Lanthanides / Actinides / Sandwich complexes

The series of complexes [M(COT)(L)(HMPA)] {M = Nd or U; COT = $\eta\text{-}C_8H_8$; L = $\eta\text{-}C_5Me_5$ (Cp^*) or $\eta\text{-}C_4Me_4P$ (tmp), HMPA = $OP(NMe_2)_3$} have been synthesized. [Nd(COT)(Cp^*)(HMPA)] (**1b**) was prepared by substitution of the THF ligand of [Nd(COT)(Cp^*)(THF)]; [Nd(COT)(tmp)(HMPA)] (**3**) was prepared by reaction of the neodymium cation $[Nd(COT)(THF)_4][BPh_4]$ with Ktmp followed by the addition of HMPA to the dimeric compound $[Nd(COT)(tmp)]_2$ (**2**); [U(COT)(Cp^*)(HMPA)] (**4**) was isolated from the reaction of the uranium cation $[U(COT)(HMPA)_3][BPh_4]$ with KCp^*, and $[U(COT)(tmp)(HMPA)_2]$ (**5**) was obtained upon reduction of the uranium(IV) cation of $[U(COT)(tmp)(HMPA)_2][BPh_4]$ with sodium amalgam. The X-ray crystal structures of **1b**, **3**, and **4** have been determined. In the isostructural compounds **1b** and **4**, the differences between the U–C and Nd–C bond lengths are smaller than those predicted from the ionic radii of the trivalent ions; in particular, the average M–C(Cp^*) distances are equal to 2.77 Å for both M = Nd and U.
(© Wiley-VCH Verlag GmbH & Co. KGaA, 69451 Weinheim, Germany, 2003)

Introduction

The differentiation of trivalent lanthanide (Ln) and actinide (An) ions should be facilitated by the precise knowledge of the metal−ligand bond and the respective role of the 4f- and 5f-electrons. Such a discrimination between Ln^{III} and An^{III} complexes represents an important problem for both its fundamental aspects and its applications, especially in the management of nuclear wastes.[1] In this context, much attention is currently focused on highlighting the possible significant variations in the structural parameters of analogous Ln^{III} and U^{III} coordination complexes.[2−5]

Recently, we reported the synthesis and structural characterization of the unique cyclooctatetraenyllanthanide cation $[Nd(COT)(L)_x][BPh_4]$ {COT = $\eta\text{-}C_8H_8$; L = THF and x = 4; L = $OP(NMe_2)_3$ (HMPA) and x = 3},[6,7] of the first cationic monocyclooctatetraenyluranium(III) complex, the analog $[U(COT)(HMPA)_3][BPh_4]$,[7] and of the first organometallic dication of an f-element, $[U(COT)(HMPA)_3][BPh_4]_2$.[8] These cationic compounds form the $[M(COT)(HMPA)_3]^{n+}$ series (M = Nd and n = 1; M = U and n = 1 or 2), which allowed a direct structural comparison of the Nd^{III}/U^{III} and U^{III}/U^{IV} analogous derivatives.[7] These investigations revealed that the variations in the metal−ligand bond lengths were proportional to the differences in the ionic radii of the metals.

In contrast to the numerous mixed cyclooctatetraenyl-/cyclopentadienyllanthanide complexes characterized by X-ray crystallography,[9] the only such compound of actinide(III) is [U(COT)(Cp*)(Me_2bpy)] (Cp* = $\eta\text{-}C_5Me_5$; Me_2bpy = 4,4′-dimethyl-2,2′-bipyridine).[10] While phospholyl derivatives of the f-elements are well known,[11−13] a few mixed cyclooctatetraenyl/phospholyl complexes of Nd^{III}, Sm^{III},[14] and U^{III} [15] have been recently isolated; the crystal structures of [Nd(COT)(Dsp)(THF)] {Dsp = 3,4-dimethyl-2,5-bis(trimethylsilyl)phospholyl}[14] and [U(COT)(tmp)(BH_4)(THF)] (tmp = $\eta\text{-}C_4Me_4P$)[15] have been determined.

Here we present the syntheses and X-ray crystal structures of the analogous neutral complexes in the mixed COT/Cp* or tmp series, [M(COT)(L)(HMPA)] with M = Nd or U and L = Cp* or tmp.

Results and Discussion

Synthesis and Characterization

The borohydride and cationic compounds $[Nd(COT)(BH_4)(THF)]_2$,[6a] and $[Nd(COT)(THF)_4][BPh_4]$,[6,7] proved to be valuable precursors for the synthesis of monocyclooctatetraenyllanthanide derivatives;[6,7,16] they are also at the origin of the neodymium

[a] Service de Chimie Moléculaire, DSM − DRECAM, Laboratoire Claude Fréjacques, CNRS URA 331, CEA Saclay, 91191 Gif-sur-Yvette Cedex, France
Fax: (internat.) + 33-1/69086640
E-mail: ephri@drecam.cea.fr
[‡] Present address: Laboratoire de Chimie des Polymères Organiques, CNRS UMR 5629, ENSCP; Université Bordeaux 1; 16 Avenue Pey-Berland; 33607 Pessac cedex, France; Fax: (internat.) + 33-5/56848487; E-mail: guillaume@enscpb.fr

complexes studied in the present work. The mixed COT/Cp* sandwich derivative [Nd(COT)(Cp*)(THF)] was prepared in high yield from either the neutral or cationic parent complex, the procedure using the cation being more efficient and more selective.[6] Exchanging the THF solvent molecule for HMPA gave the green derivative [Nd(COT)(Cp*)(HMPA)$_2$] (**1a**) in 93% yield; green crystals of [Nd(COT)(Cp*)(HMPA)] (**1b**) were obtained by crystallization from THF/pentane. These complexes are the only examples among the [Ln(COT)(Cp*)] series (Ln = Sc, Y, La, Pr, Sm, Gd, Tb, Dy, Er, Lu) that have not been prepared by a metathesis reaction from a lanthanide chloride precursor.[9] Addition of Ktmp to a THF solution of [Nd(COT)(THF)$_4$][BPh$_4$] afforded the mixed COT/tmp compound [Nd(COT)(tmp)]$_2$ (**2**), which was obtained as a green powder in 75% yield. Considering that the Nd(COT)(Cp*) species was isolated as the THF adduct [Nd(COT)(Cp*)(THF)], it is very likely that the isosteric moiety Nd(COT)(tmp), which is less electron-rich because the tmp group is less electron-donating than the Cp* ligand,[12] adopts in the solid state a dimeric structure ensured by a μ-η^5,η^1-bridging tmp ligand. The ability of the phospholyl ligand to bridge two metal centers through the available lone pair on the P atom is well documented, and can be illustrated with the structures of the U^{III} complexes [U(tmp)$_2$(BH$_4$)]$_2$ and [U(tmp)(Cp*)(BH$_4$)]$_2$.[13] Complex **2** certainly forms monomeric adducts in coordinating solvents and with Lewis bases; in the presence of HMPA, it was readily transformed into the dark green derivative [Nd(COT)(tmp)(HMPA)] (**3**), which crystallized from THF/pentane.

Treatment of [U(COT)(HMPA)$_3$][BPh$_4$] with KCp* led to the formation of [U(COT)(Cp*)(HMPA)] (**4**), which was isolated as dark brown crystals in 70% yield. The adducts U(COT)(Cp*)(L) (L = THF, Me$_2$bpy) have been synthesized in THF from the reaction of [U(Cp*)I$_2$(THF)$_2$] and K$_2$COT, in the presence of Me$_2$bpy for the latter.[10] The dark brown powder of [U(COT)(tmp)(HMPA)$_2$] (**5**) was obtained in 57% yield after reduction of the uranium(IV) cation [U(COT)(tmp)(HMPA)$_2$][BPh$_4$] with sodium amalgam. A similar reduction of a cationic tetravalent cyclooctatetraenyluranium compound was already performed to make [U(COT)(HMPA)$_3$][BPh$_4$] from [U(COT)(HMPA)$_3$][BPh$_4$]$_2$.[7] Complex **5** is the first mixed cyclooctatetraenyl/phospholyl complex of uranium(III). Unfortunately, no crystals suitable for X-ray diffraction analysis could be obtained. The synthesis of **4** and **5** provide further examples of the usefulness of cationic uranium compounds as precursors of derivatives in the +3 oxidation state.

As previously observed with [U(COT)(tmp)(BH$_4$)(THF)] and [U(COT)(tmp)(HMPA)$_2$][BPh$_4$],[15] protonation of the tmp ligand of **2** and **5** with NEt$_3$HBPh$_4$ afforded the parent cationic complexes. Thus, **2** was transformed in THF into [Nd(COT)(THF)$_4$][BPh$_4$], while **5** also underwent oxidation to give [U(COT)(HMPA)$_3$][BPh$_4$]$_2$ (NMR spectroscopic experiments). Protonolysis of the U−P bond was also observed with the phosphido complex [U(NEt$_2$)$_3$(PPh$_2$)], which was transformed into [U(NEt$_2$)$_3$][BPh$_4$] by reaction with (NEt$_3$H)BPh$_4$.[17]

Complexes **1**−**5** were characterized by elemental analyses (except **4**) and ^{1}H NMR spectra. The crystal structures of **1b**, **3** and **4** have been determined.

Crystal Structures of [Nd(COT)(Cp*)(HMPA)], [Nd(COT)(tmp)(HMPA)], and [U(COT)(Cp*)(HMPA)]

The two analogous neodymium and uranium COT/Cp* complexes **1b** and **4** are isostructural; the crystal structure of **4** is shown in Figure 1. The crystal structure of **3**, the tmp analog of **1b**, is shown in Figure 2. Selected bond lengths and angles of the three complexes are listed in Table 1.

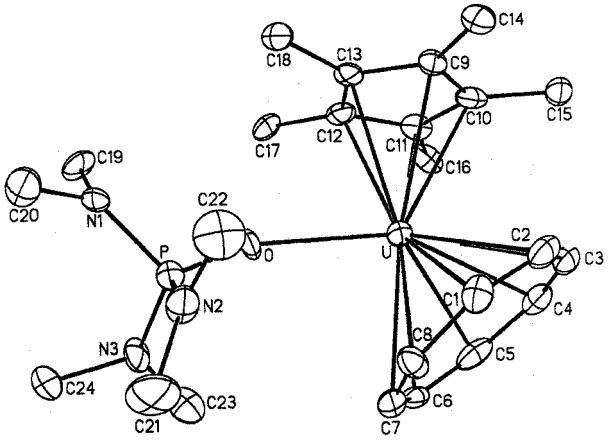

Figure 1. View of the crystal structure of [U(COT)(Cp*)(HMPA)] with thermal ellipsoids drawn at the 30% probability level

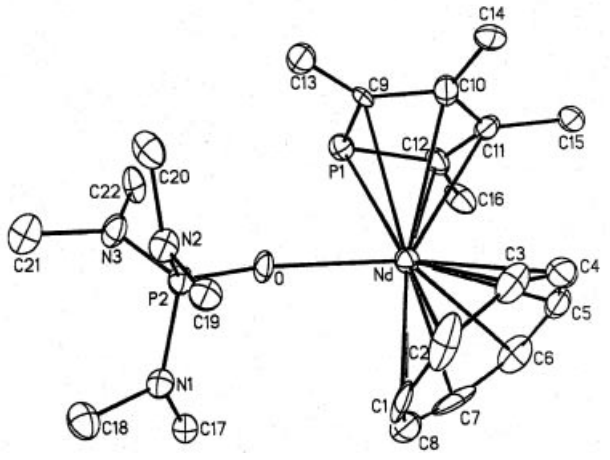

Figure 2. View of the crystal structure of [Nd(COT)(tmp)(HMPA)] with thermal ellipsoids drawn at the 30% probability level

These complexes adopt the same trigonal configuration as that encountered in [Nd(COT)(Dsp)(THF)][14] and [Gd(COT)(η-C$_5$H$_9$C$_5$H$_4$)(THF)],[18] considering the COT, Cp*, and tmp ligands as monodentate. Coordination of the COT ligand in **1b** and **3** is similar to that found in other monocyclooctatetraenylneodymium complexes; the Nd−COT(centroid) distances of 1.99(2) Å in **1b** and 1.97(1)

Table 1. Selected bond lengths [Å] and angles [°] for the complexes

	[Nd(COT)(Cp*)(HMPA)] (**1b**)	[Nd(COT)(tmp)(HMPA)] (**3**)	[U(COT)(Cp*)(HMPA)] (**4**)
M−C(1)	2.749(4)	2.698(17)	2.711(15)
M−C(2)	2.773(4)	2.67(2)	2.676(14)
M−C(3)	2.732(5)	2.635(19)	2.721(14)
M−C(4)	2.685(5)	2.665(19)	2.712(14)
M−C(5)	2.699(4)	2.636(15)	2.706(16)
M−C(6)	2.697(5)	2.657(14)	2.726(13)
M−C(7)	2.662(4)	2.625(17)	2.778(13)
M−C(8)	2.675(5)	2.72(2)	2.781(14)
M−C(9)	2.780(4)	2.840(9)	2.794(10)
M−C(10)	2.809(4)	2.884(14)	2.805(11)
M−C(11)	2.766(4)	2.943(11)	2.776(14)
M−C(12)	2.750(4)	2.887(13)	2.739(15)
M−C(13) or Nd−P	2.745(4)	2.968(8)	2.748(13)
M−O	2.441(3)	2.434(8)	2.461(8)
<M−C(COT)>	2.71(4)	2.66(3)	2.73(4)
<M−C(Cp*)>	2.77(2)	2.88(4)	2.77(2)
M−COT(centroid)	1.99(2)	1.97(2)	2.01(1)
M−Cp* or −tmp(centroid)	2.49(2)	2.59(1)	2.50(1)
COT−M−Cp* or −tmp(centroid)	141(1)	139(1)	141(1)
O−M−COT(centroid)	120(1)	120(1)	120(1)
O−M−Cp* or −tmp(centroid)	98(1)	101(1)	99(1)

Å in **3** can be compared with those measured in $[Nd(COT)(\eta\text{-}C_5H_9C_5H_4)(THF)_2]$ (2.011 Å),[18] [Nd(COT)(Dsp)(THF)] (1.94 Å),[14] and $[Nd(COT)(HMPA)_3][BPh_4]$ [1.984(5) Å].[7] The Cp* ligation in **1b** is also unexceptional; the Nd−Cp*(centroid) distance of 2.49(2) Å is similar to that of 2.48 Å in $[Nd(Cp^*)I_2(pyridine)_3]\cdot C_7H_8$.[19] In the crystal structure of **3**, the Nd−tmp(centroid) distance of 2.59(1) Å compares well with the corresponding value of 2.57 Å in [Nd(COT)(Dsp)(THF)];[14] the Nd−P bond length is equal to 3.0195(4) Å in the latter and to 2.968(8) Å in **3**. As previously observed in other analogous tmp and Cp* compounds,[12] the Nd−tmp(centroid) distance in **3** is longer, by 0.1 Å, than the Nd−Cp*(centroid) distance in **1b**. The Nd−O distances in **1b** and **3**, 2.441(3) and 2.434(8) Å, are longer than the average Nd−O bond length of 2.36(3) Å in $[Nd(COT)(HMPA)_3][BPh_4]$[7] while the Nd−C(COT) distances are practically the same. This feature likely results from the more positive charge on the cationic Nd^{III} center, which induces a stronger interaction with the Lewis base.

The structural parameters of the U(COT)(Cp*) unit in **4** are quite similar to those determined in $[U(COT)(Cp^*)(Me_2bipy)]$.[10] The U−COT(centroid) distance is equal to 2.01(1) Å in both compounds while the U−Cp*(centroid) distances are 2.50(1) and 2.49 Å, respectively. The U−O bond length of 2.46(1) Å in **4** is, here again, longer than the average U−O distance of 2.40(6) Å in the cation $[U(COT)(HMPA)_3][BPh_4]$[7] while the U−C(COT) distances are identical, reflecting the weaker interaction between the metal center and the oxygen donor ligand.

More interesting is the comparison of the crystal structures of the Nd^{III} and U^{III} analogs **1b** and **4**. In contrast to what was observed in the cations $[M(COT)(HMPA)_3]^+$ (M = Nd, U),[7] where the differences <U−O> − <Nd−O> and <U−C> − <Nd−C> perfectly reflect the +0.04 Å difference between the ionic radii of the trivalent uranium and neodymium ions,[20] it seems that the average U−O, U−C(COT), and U−C(Cp*) distances in **4** are shorter than those expected from a purely ionic model, the <U−X> − <Nd−X> differences (X = C or O) being lower than 0.04 Å. Most notably, there is no difference between the mean U−C(Cp*) and Nd−C(Cp*) bond lengths which are both equal to 2.77(3) Å. Similar small deviations (0.02−0.05 Å) between the differences in metal−ligand bond lengths and the differences in metal ionic radii, which must be considered with caution in view of the experimental errors, have previously been detected in the crystal structures of analogous uranium and lanthanide complexes with polydentate nitrogen ligands: $[M(Mentb)_2]X_3$ {M = La and X = ClO_4, M = U and X = I; Mentb = tris(*N*-methylbenzimidazol-2-ylmethyl)amine},[2] $[MI_3(tpa)(C_5H_5N)]$ {M = La or U; tpa = tris[(2-pyridyl)methyl]amine},[2] $[MI_3(bipy)(C_5H_5N)]$ (M = Ce or U; bipy = 2,2′-bipyridine),[3] and $[M(terpy)_3]I_3\cdot 2MeCN$ (M = La, Ce, Nd, U; terpy = 2,2′:6′,2″-terpyridine).[4] A difference of +0.047 Å was also measured between the average La−S and U−S distances in the complexes $[M(1,4,7\text{-trithiacyclononane})I_3(MeCN)_2]$ (M = La, U),[5] while the ionic radius of the U^{III} ion is only 0.01 Å shorter than that of the La^{III} ion.[20] It is solely in the phosphorous complexes $[M(\eta\text{-}C_5H_4Me)_3L]$ {M = Ce or U; L = PMe_3 or $P(OCH_2)_3CEt$}[21] and in the tris(btp) compounds $[M(btp)_3]I_3\cdot n C_5H_5N$ {M = Ce or U; btp = 2,6-bis(5,6-dialkyl-1,2,4-triazin-3-yl)pyridine}[4] that the U−P and U−N bond lengths were found to be significantly shorter, by 0.1 Å, than the Ce−P and Ce−N distances, while the ionic radius of the U^{III} ion is 0.01 Å longer than that of the Ce^{III} ion.[20] In all these pairs of analogous Ln^{III} and U^{III} complexes, the deviations of the U−X distances

(X = N, P, S) from the ionic bonding model have been explained by a stronger π back-bonding interaction between the metal atom and the ligand that is much less likely in the lanthanide analogs. If significant, the variations observed in the crystal structures of **1b** and **4**, especially the apparent shortening of the U−C(Cp*) bonds, could also be accounted for by a metal to ligand π back-donation which, as expected,[22] is more important and detectable than in the cationic parent compounds $[M(COT)(HMPA)_3][BPh_4]$ (M = Nd, U).

Conclusion

The synthesis of the mixed cyclooctatetraenyl/cyclopentadienyl or phospholyl compounds **1**−**5** further demonstrate the utility of cationic complexes as precursors in organo-f-element chemistry.[6−8,23] The crystal structures of the isostructural neodymium and uranium complexes **1b** and **4** revealed that the differences between the U−C and Nd−C bond lengths are smaller than those predicted from the ionic radii of the trivalent ions; in particular, the mean M−C(Cp*) distances are equal in both compounds. These structures would provide a unique example in which the more covalent character of the uranium−ligand bond is observed primarily with an anionic hydrocarbon ligand, and not a neutral Lewis base. Further studies on analogous Ln^{III} and U^{III} organometallic compounds are necessary to confirm these observations.

Experimental Section

General: All manipulations and reactions were carried out under argon (less than 3 ppm of oxygen and water) using standard Schlenk and vacuum-line techniques or in a glove box. Solvents were thoroughly dried and deoxygenated by standard methods and distilled immediately prior to use. Deuterated solvents were dried with Na/K alloys. The ^{1}H NMR spectra were recorded with a Bruker DPX 200 instrument and were referenced internally using the residual protio solvent resonances relative to tetramethylsilane (δ = 0). Elemental analyses were performed by the Analytische Laboratorien at Lindlar (Germany). $[Nd(COT)(THF)_4][BPh_4]$,[6] [Nd(COT)(Cp*)(THF)],[6] $[U(COT)(HMPA)_3][BPh_4]$,[7] and [U(COT)-(tmp)$(HMPA)_2$]$[BPh_4]$[15] were synthesized as previously reported.

Synthesis of [Nd(COT)(Cp*)$(HMPA)_2$] (1a): HMPA (10 μL, 10.3 mg, 57.48 μmol) was added to a solution of [Nd(COT)(Cp*)-(THF)] (13.03 mg, 28.60 μmol) in THF (5 mL). After 45 min, the green solution was concentrated to dryness. After washing with toluene (5 mL), the green powder of **1a** was dried under vacuum (19.7 mg, 93%). ^{1}H NMR ([D$_8$]THF): δ = 6.12 (br. s, $w_{1/2}$ = 27 Hz, 15 H, Cp*), 3.56 (br. s, $w_{1/2}$ = 21 Hz, 36 H, HMPA), −13.52 (br. s, $w_{1/2}$ = 67 Hz, 8 H, COT) ppm. $C_{30}H_{59}N_6O_2P_2Nd$ (741): calcd. C 48.56, H 8.01, N 11.32, P 8.35; found C 48.30, H 7.94, N 11.07. Green single crystals of **1b** were obtained at 20 °C within a week from a THF solution of [Nd(COT)(Cp*)(THF)] (24.1 mg, 52.88 μmol) and HMPA (28 μL, 28.8 mg, 160.94 μmol, 3.04 equiv.), layered with pentane.

Synthesis of [Nd(COT)(tmp)]$_2$ (2): A flask was charged with $[Nd(COT)(THF)_4][BPh_4]$ (160.1 mg, 187.02 μmol), Ktmp (33.2 mg, 186.40 μmol) and THF (25 mL). After stirring for 3 h at 20 °C, the green solution was filtered and the solvents evaporated to dryness.

Table 2. Crystal data and structure refinement for the complexes

	[Nd(COT)(Cp*)(HMPA)] (**1b**)	[Nd(COT)(tmp)(HMPA)] (**3**)	[U(COT)(Cp*)(HMPA)] (**4**)
Empirical formula	$C_{24}H_{41}N_3NdOP$	$C_{22}H_{38}N_3NdOP_2$	$C_{24}H_{41}N_3OPU$
M [g mol^{-1}]	562.81	566.73	656.60
Crystal system	orthorhombic	orthorhombic	orthorhombic
Space group	Pbca	$Pna2_1$	Pbca
a [Å]	18.324(4)	27.919(6)	18.396(4)
b [Å]	14.538(3)	7.481(1)	14.523(3)
c [Å]	19.201(4)	11.669(2)	19.288(4)
V [Å^3]	5115.0(18)	2437.2(8)	5153.1(18)
Z	8	4	8
$\rho_{calcd.}$ [g cm^{-3}]	1.462	1.545	1.693
μ (Mo-K_α) [mm^{-1}]	2.112	2.279	6.381
Crystal size [mm]	0.20 × 0.10 × 0.10	0.15 × 0.10 × 0.10	0.12 × 0.10 × 0.05
T_{min}/T_{max}	0.772/0.801	0.728/0.785	0.401/0.752
F(000)	2312	1156	2568
T [K]	123(2)	123(2)	123(2)
2θ range [°]	2.77−24.72	2.82−24.79	2.62−24.70
No. of data collected	32170	12796	31863
No. of unique data	4311	3904	4321
Observed data [$I > 2\sigma(I)$]	3168	2840	2262
R_{int}	0.0532	0.1232	0.1240
No. of parameters	271	262	271
R_1 [a]	0.0317	0.0581	0.0609
wR_2 [b]	0.0697	0.1199	0.1062
S	1.012	1.035	0.947
$\Delta\rho_{min}$ [e·Å^{-3}]	−0.644	−0.723	−1.595
$\Delta\rho_{max}$ [e·Å^{-3}]	0.538	0.993	1.023

[a] $R_1 = \Sigma(||F_o| - |F_c||)/\Sigma|F_o|$ (observed reflections). [b] $wR_2 = [\Sigma w(||F_o| - |F_c||)^2/\Sigma w(|F_o|)^2]^{1/2}$ (observed reflections).

The resulting product was further extracted with THF (15 mL) and after evaporation of the solvent, the green powder of **2** was washed with toluene (5 mL) and dried under vacuum (54.0 mg, 75%). ^{1}H NMR ([D$_8$]toluene): δ = 11.01 (br. s, $w_{1/2}$ = 42 Hz, 6 H, Me), 1.20 (br. s, $w_{1/2}$ = 40 Hz, 6 H, Me), −15.62 (br. s, $w_{1/2}$ = 95 Hz, 8 H, COT) ppm. ^{1}H NMR ([D$_8$]THF): δ = 10.64 (br. s, $w_{1/2}$ = 20 Hz, 6 H, Me), 2.70 (br. s, $w_{1/2}$ = 22 Hz, 6 H, Me), −15.0 (br. s, $w_{1/2}$ = 50 Hz, 8 H, COT) ppm. $C_{16}H_{20}PNd$ (387): calcd. C 49.59, H 5.20, P 7.99; found C 49.32, H 5.33, P 8.13.

Synthesis of [Nd(COT)(tmp)(HMPA)] (3): HMPA (64.0 μL, 65.9 mg, 0.37 mmol), was added to a solution of **2** (118.4 mg, 0.153 mmol) in THF (30 mL); the initial green solution became darker. After stirring at 20 °C for 2 h, the solution was concentrated to dryness, leaving a dark green powder of **3** (159.4 mg, 92%). ^{1}H NMR ([D$_8$]THF): δ = 12.30 (br. s, $w_{1/2}$ = 20 Hz, 6 H, Me), 5.68 (br. s, $w_{1/2}$ = 62 Hz, 18 H, HMPA), −2.32 (br. s, $w_{1/2}$ = 27 Hz, 6 H, Me), −12.20 (br. s, $w_{1/2}$ = 53 Hz, 8 H, COT) ppm. $C_{22}H_{38}N_3OP_2Nd$ (660): calcd. C 46.62, H 6.76 N 7.41, P, 10.93; found C 46.41, H 6.86, N 7.55, P 10.67. Green crystals of **3** were grown from a saturated THF solution layered with pentane.

Synthesis of [U(COT)(Cp*)(HMPA)] (4): Addition of KCp* (22.5 mg, 129.1 μmol) to [U(COT)(HMPA)$_3$][BPh$_4$] (153.6 mg, 128.1 μmol) in THF (40 mL) induced a color change of the solution from dark green to dark brown within 30 min. After stirring at 20 °C for 2 h, the solution was filtered and the solvents were evaporated to dryness to give a brownish solid that was then extracted with toluene (10 mL). After concentration to dryness, the dark brown solid was crystallized from THF/pentane, affording brown crystals of **4** (60.1 mg, 70%). ^{1}H NMR ([D$_8$]toluene): δ = 1.67 (d, 7 Hz, 18 H, HMPA), −10.07 (s, 15 H, Cp*), −50.18 (s, 8 H, COT) ppm. ^{1}H NMR ([D$_8$]THF): δ = 1.97 (d, 9 Hz, 18 H, HMPA), −8.45 (s, 15 H, Cp*), −48.94 (s, 8 H, COT) ppm.

Synthesis of [U(COT)(tmp)(HMPA)$_2$] (5): Reduction of [U(COT)(tmp)(HMPA)$_2$][BPh$_4$] (303.3 mg, 261.7 μmol) with 2% Na(Hg) (596.5 mg, 518.7 μmol of Na) in THF (40 mL) over 24 h afforded a dark brown suspension. After filtration and concentration to dryness, the crude product was extracted with toluene (3 × 15 mL) and then precipitated upon addition of pentane, affording a dark brown powder of **5** (125.5 mg, 57%). ^{1}H NMR ([D$_8$]toluene): δ = 1.87 (s, 36 H, HMPA), −3.91 (s, 6 H, Me), −25.57 (s, 6 H, Me), −43.16 (s, 8 H, COT) ppm. ^{1}H NMR ([D$_8$]THF): δ = 3.07 (s, 36 H, HMPA), −1.15 (br. s, $w_{1/2}$ = 60 Hz, 6 H, Me), −22.39 (br. s, $w_{1/2}$ = 90 Hz, 6 H, Me), −41.44 (br. s, $w_{1/2}$ = 55 Hz, 8 H, COT) ppm. $C_{28}H_{56}N_6O_2P_3U$ (839): C 40.05, H 6.72, N 10.01, P 11.07; found C 39.94, H 6.63, N 9.79, P 10.80.

Reactions of 2 and 5 with (NEt$_3$H)BPh$_4$. a) An NMR tube was charged with **2** (8.1 mg, 10.45 μmol) and (NEt$_3$H)BPh$_4$ (9.0 mg, 21.35 μmol) in [D$_8$]THF (0.3 mL). After 45 min at 20 °C, the spectrum of the green solution showed the formation of [Nd(COT)(THF)$_4$][BPh$_4$] as the sole organometallic product. **b)** An NMR tube was charged with **5** (7.3 mg, 8.64 μmol) and (NEt$_3$H)BPh$_4$ (5.0 mg, 11.8 μmol) in [D$_8$]THF (0.3 mL). Precipitation of an orange solid was immediate. The precipitate was identified as [U(COT)(HMPA)$_3$][BPh$_4$]$_2$ by its ^{1}H NMR spectrum in pyridine.

X-ray Crystallography of 1b, 3, and 4: Diffraction collections were carried out with a Nonius Kappa-CCD diffractometer. The lattice parameters were determined from 10 images recorded with 2° Φ-scans and later refined on all data. A 180° Φ range was scanned with 2° steps and 10 s of exposure time per frame with a crystal-to-detector distance fixed at 30 mm. Data were corrected for Lorentz polarization and absorption effects.[24] The structures were solved by the heavy-atom method and refined by full-matrix least squares on F^2 with anisotropic thermal parameters for all non-hydrogen atoms. H atoms were introduced at calculated positions as riding atoms with an isotropic displacement parameter equal to 1.2 (CH, CH$_2$) or 1.5 (CH$_2$, CH$_3$) times that of the parent atom. All calculations were performed with an O2 Silicon Graphics Station using the SHELXTL package.[25] Crystal data and details of data collection and refinement are given in Table 2. CCDC-195294 (**1b**), -195292 (**3**), and -195293 (**4**) contain the supplementary crystallographic data for this paper. These data can be obtained free of charge at www.ccdc.cam.ac.uk/conts/retrieving.html [or from the Cambridge Crystallographic Data Centre, 12 Union Road, Cambridge CB2 1EZ, UK; Fax: (internat.) + 44-1223/336-033; E-mail: deposit@ccdc.cam.ac.uk].

[1] [1a] K. L. Nash, *Solv. Extr. Ion Exch.* **1993**, *11*, 729−768. [1b] K. L. Nash, in: *Handbook on the Physics and Chemistry of the Rare Earths. Lanthanides/Actinides: Chemistry* (Eds.: K. A. Gschneidner, L. Eyring, G. R. Choppin, G. H. Lander), North-Holland, Amsterdam, **1994**, vol. 18, p. 197.

[2] R. Wietzke, M. Mazzanti, J. M. Latour, J. Pécaut, *J. Chem. Soc., Dalton Trans.* **2000**, 4167−4173.

[3] C. Rivière, M. Nierlich, M. Ephritikhine, C. Madic, *Inorg. Chem.* **2001**, *40*, 4428−4435.

[4] [4a] J. C. Berthet, Y. Miquel, P. B. Iveson, M. Nierlich, P. Thuéry, C. Madic, M. Ephritikhine, *J. Chem. Soc., Dalton Trans.* **2002**, 4167−4173. [4b] P. B. Iveson, C. Rivière, D. Guillaneux, M. Nierlich, P. Thuéry, M. Ephritikhine, C. Madic, *Chem. Commun.* **2001**, 1512−1513.

[5] L. Karmazin, M. Mazzanti, J. Pécaut, *Chem. Commun.* **2002**, 654−655.

[6] [6a] S. M. Cendrowski-Guillaume, M. Nierlich, M. Lance, M. Ephritikhine, *Organometallics* **1998**, *17*, 786−788. [6b] S. M. Cendrowski-Guillaume, G. Le Gland, M. Nierlich, M. Ephritikhine, *Organometallics* **2000**, *19*, 5654−5660.

[7] S. M. Cendrowski-Guillaume, M. Nierlich, M. Ephritikhine, *Eur. J. Inorg. Chem.* **2001**, *6*, 1495−1498.

[8] S. M. Cendrowski-Guillaume, M. Lance, M. Nierlich, M. Ephritikhine, *Organometallics* **2000**, *19*, 3257−3259.

[9] [9a] H. Schumann, J. A. Meese-Marktscheffel, L. Esser, *Chem. Rev.* **1995**, *95*, 865−986. [9b] F. T. Edelmann, *New. J. Chem.* **1995**, *19*, 535−550. [9c] M. Visseaux, D. Barbier-Baudry, O. Blacque, A. Hafid, P. Richard, F. Weber, *New. J. Chem.* **2000**, *24*, 939−942. [9d] Q. Liu, X. Shen, J. Huang, Y. Qian, A. S. C. Chan, W. T. Wong, *Polyhedron* **2000**, *19*, 453−456.

[10] A. R. Schake, L. R. Avens, C. J. Burns, D. L. Clark, A. P. Sattelberger, W. H. Smith, *Organometallics* **1993**, *12*, 1497−1498.

[11] [11a] F. Nief, *Coord. Chem. Rev.* **1998**, *178−180*, 13−81. [11b] P. Gradoz, D. Baudry, M. Ephritikhine, F. Nief, F. Mathey, *J. Chem. Soc., Dalton Trans.* **1992**, 3047−3051. [11c] D. Baudry, M. Ephritikhine, F. Nief, L. Ricard, F. Mathey, *Angew. Chem. Int. Ed. Engl.* **1990**, *29*, 1485−1486.

[12] P. Gradoz, D. Baudry, M. Ephritikhine, M. Lance, M. Nierlich, J. Vigner, *J. Organomet. Chem.* **1994**, *466*, 107−118.

[13] P. Gradoz, M. Ephritikhine, M. Lance, J. Vigner, M. Nierlich, *J. Organomet. Chem.* **1994**, *481*, 69−73.

[14] M. Visseaux, F. Nief, L. Ricard, *J. Organomet. Chem.* **2002**, *647*, 139−144.

[15] S. M. Cendrowski-Guillaume, M. Nierlich, M. Ephritikhine, *J. Organomet. Chem.* **2002**, *643−644*, 209−213.

[16] S. M. Cendrowski-Guillaume, G. Le Gland, M. Lance, M. Nierlich, M. Ephritikhine, *C. R. Acad. Sci., Chimie, IIc* **2002**, *5*, 73−80.

[17] S. M. Cendrowski-Guillaume, M. Ephritikhine, *J. Organomet. Chem.* **1990**, *577*, 161−166.

[18] J. Jin, X. Zhuang, Z. Jin, W. Chen, *J. Organomet. Chem.* **1995**, *490*, C8−C13.
[19] D. L. Clark, J. C. Gordon, B. L. Scott, J. G. Watkin, *Polyhedron* **1999**, *18*, 1389−1396.
[20] R. D. Shannon, *Acta Crystallogr., Sect. A* **1976**, *32*, 751−767.
[21] J. G. Brennan, S. D. Stults, R. A. Andersen, A. Zalkin, *Organometallics* **1988**, *7*, 1329−1334.
[22] M. del Mar Conejo, J. S. Parry, E. Carmona, M. Schultz, J. G. Brennann, S. M. Beshouri, R. A. Andersen, R. D. Rogers, S. Coles, M. Hursthouse, *Chem. Eur. J.* **1999**, *5*, 3000−3009.
[23] [23a] S. M. Cendrowski-Guillaume, M. Ephritikhine, *J. Chem. Soc., Dalton Trans.* **1996**, 1487−1491. [23b] J. -C. Berthet, M. Ephritikhine, *Coord. Chem. Rev.* **1998**, *178−180*, 83−116.
[24] A. L. Spek, *MULABS, PLATON*, University of Utrecht, The Netherlands, **1998**.
[25] G. M. Sheldrick, *SHELXTL*, University of Göttingen, Germany, distributed by Bruker-AXS, Madison, WI, **1999**.

Received October 17, 2002
[I02574]

Two New Dinuclear Sterically Crowded Cu^{II} Complexes as Catalyst Precursors for the Oxidative Coupling of 2,6-Dimethylphenol

Guillem Aromí,[a] Patrick Gamez,[a] Huub Kooijman,[b] Anthony L. Spek,[b] Willem L. Driessen,[a] and Jan Reedijk*[a]

Keywords: Copper / N ligands / Homogeneous catalysis / Oxidations

The molecular structure and spectroscopic properties of the first two bis(μ-η^1-nitrato)-bridged, dinuclear Cu complexes containing 4,4′-biimidazole ligands are presented. ^{1}H NMR, EPR, and UV/Vis spectroscopy indicate that their solid-state structure is not retained in solution. Dioxygen uptake measurements show that the presence of a methyl group at the 2-position of the imidazole rings leads to a dramatic increase of the rate of the catalytic polymerization of 2,6-dimethylphenol. Detailed examination of the molecular structures of both catalyst precursors in the crystalline state suggests that this may either be caused by the difference in basicity of the biimidazole ligands or by a small but important steric effect of the 2-Me groups affecting the coplanarity of equatorial Cu^{II} ligands and the orientation of the axial nitrate ligands.
(© Wiley-VCH Verlag GmbH & Co. KGaA, 69451 Weinheim, Germany, 2003)

Introduction

Our longstanding interest in the preparation and spectroscopic study of copper coordination compounds with azole-based ligands[1−6] originates from two main driving forces. First, it is well established that many important enzymes hold a copper-active site mainly by means of the imidazole moieties from protein histidine amino acids.[7] Second, the unique characteristics of the Cu^{II}/Cu^{I} redox couple render many of their complexes especially suited for the catalysis of organic oxidation reactions, in some cases with industrial relevance.[8]

Since its discovery in 1959,[9] the oxidative polymerization of 2,6-dimethylphenol (DMP) catalyzed by Cu complexes of N-based ligands has been used on an industrial scale. The product, poly(1,4-phenylene ether) (PPE), is a valuable thermoplastic with vast worldwide applications thanks to its excellent mechanical properties and chemical resistance.[10,11] An unwanted side product of this reaction is diphenoquinone (DPQ), which results from the C−C coupling and subsequent oxidation of two DMP units. Considerable research effort has been dedicated to improve the performance and selectivity of the reaction and to elucidate its mechanism. For example, we have recently found conditions that have led to a dramatic increase of the reaction rates compared with those still encountered in large-scale production.[12] Although the exact mechanism of the reaction remains a matter of discussion, several hypotheses have been put forward. Early proposals favored a pathway involving phenoxy radicals as key intermediates.[13,14] More recently, the presence of a dinuclear phenolate-bridged Cu^{II} complex has been suggested.[15−17] Quite diverse approaches have been adopted to obtain mechanistic details of the reaction. These include kinetic studies using various kinds of ligands,[18−24] the use of different substrates such as oligomers,[16] ab initio calculations,[25] or changing the proportions between the various components (Cu, ligand, base, water, substrate) and studying the influence on the catalytic activity.[12,19,26] Another strategy has been to examine the molecular structure of various catalyst precursors or potential reaction intermediates to establish possible correlations between geometric parameters and activity. In this context, we decided to explore the coordination properties of the two chelating 4,4′-biimidazole (bi) ligands shown in Scheme 1.[27]

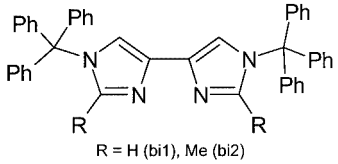

Scheme 1

In sharp contrast to their isomeric 2,2′-analogues, 4,4′-biimidazole chelates have not been found as part of any structurally characterized coordination compound, most likely owing to the difficulty in preparing these ligands. In

[a] Leiden Institute of Chemistry, Gorlaeus Laboratories, Leiden University,
P. O. Box 9502, 2300 RA Leiden, The Netherlands
Fax: (internat.) + 31-71/527-4671
E-mail: reedijk@chem.leidenuniv.nl
[b] Bijvoet Center for Biomolecular Research, Crystal and Structural Chemistry, Utrecht University,
Padualaan 8, 3584 CH, Utrecht, The Netherlands

this paper we report synthetic procedures to prepare the complexes $[Cu(\mu\text{-}\eta^1\text{-}NO_3)(NO_3)(bi)]_2$ [bi = bi1 (**1**), bi2 (**2**)], the first examples containing 4,4′-biimidazole ligands. Their catalytic activity during the oxidation of DMP into PPE is examined and discussed in the light of their single-crystal X-ray structure and their solution properties.

Results and Discussion

Complexes **1** and **2** both crystallize from acetonitrile directly from reaction mixtures containing the stoichiometric amount of the appropriate components. In both cases, well-formed crystals collapse immediately upon exposure to air, probably reflecting loss of lattice solvent, which is detected crystallographically, but not from microanalysis (see below). The fact that the complexes are hygroscopic is reflected in repeated experiments of elemental analysis.

Description of the Structures

Crystallographic data for $[Cu(\mu\text{-}\eta^1\text{-}NO_3)(NO_3)(bi1)]_2$ (**1**) and $[Cu(\mu\text{-}\eta^1\text{-}NO_3)(NO_3)(bi2)]_2$ (**2**) are collected in Table 4. Selected interatomic distances and angles for complexes **1** and **2** are listed in Table 1 and the respective molecular structures are represented in Figures 1 and 2.

Table 1. Selected interatomic distances [Å] and angles [°] for $[Cu(\mu\text{-}\eta^1\text{-}NO_3)(NO_3)(bi1)]_2$ (**1**) and $[Cu(\mu\text{-}\eta^1\text{-}NO_3)(NO_3)(bi2)]_2$ (**2**)

1		**2**	
Cu(1)−O(91)	2.403(3)	Cu(1)−O(91)	1.9754(15)
Cu(1)−N(21)	2.002(3)	Cu(1)−N(21)	1.9781(19)
Cu(1)−O(96)	1.970(3)	Cu(1)−O(96)	1.9626(17)
Cu(1)−O(91)a	1.996(3)	Cu(1)−O(91)a	2.3598(17)
Cu(1)−O(97)	2.643(5)	Cu(1)−O(97)	2.6972(23)
Cu(1)−N(11)	1.996(3)	Cu(1)−N(11)	1.9728(17)
Cu(1)···Cu(1)a	3.4106(8)	Cu(1)···Cu(1)a	3.530(1)
O(91)−Cu(1)−O(96)	93.37(7)	O(91)−Cu(1)−O(96)	94.43(12)
O(91)−Cu(1)−N(21)	91.54(7)	O(91)−Cu(1)−N(21)	97.76(12)
O(96)−Cu(1)−N(11)	93.66(7)	O(96)−Cu(1)−N(11)	96.06(12)
N(11)−Cu(1)−N(21)	81.60(8)	N(11)−Cu(1)−N(21)	83.24(12)
O(91)−Cu(1)−O(91)a	76.60(6)	O(91)−Cu(1)−O(91)a	73.64(10)
O(96)−Cu(1)−N(21)	174.29(7)	O(96)−Cu(1)−N(21)	167.80(15)
N(11)−Cu(1)−O(91)a	100.22(7)	N(11)−Cu(1)−O(91)a	169.28(13)
O(91)−Cu(1)−N(11)	172.34(8)	O(91)−Cu(1)−N(11)	95.95(12)
O(96)−Cu(1)−O(91)a	91.17(6)	O(96)−Cu(1)−O(91)a	87.46(11)
N(21)−Cu(1)−O(91)a	92.80(7)	N(21)−Cu(1)−O(91)a	95.44(11)
Cu(1)−O(91)−Cu(1)a	103.40(6)	Cu(1)−O(91)−Cu(1)a	106.36(11)

$[Cu(\mu\text{-}\eta^1\text{-}NO_3)(NO_3)(bi1)]_2$ (1)

The structure of **1** shows a dinuclear centrosymmetric complex consisting of two Cu^{II} ions bridged by two monodentate $\mu\text{-}\eta^1\text{-}NO_3^-$ ligands. This bridging mode is relatively uncommon for nitrate,[28] which usually bridges Cu ions in a didentate fashion. The bridging nitrate ligand is bound to the Cu centers through a short [1.975(2) Å] and a long bond [2.360(2) Å], which occupy an equatorial and an axial position, respectively, of the nearly square-pyramidal coordination environment observed around the Cu centers ($\tau = 0.03$, where τ is 0 and 1 for the perfect square-pyramidal and trigonal-bipyramidal geometries, respectively).[29] The remaining equatorial positions of each metal ion are completed by the N donors of one chelating bi1 ligand [at distances of 1.973(2) and 1.978(2) Å, respectively] and by one O atom of a terminal NO_3^- ligand [1.963(2) Å]. A second O atom of the latter lays 2.697(2) Å apart from the Cu^{II} ion. The intermetallic Cu···Cu distance is 3.4106(8) Å. The crystal packing shows no unusual features. Complexes **1** and **2** (vide infra) are the first crystallographically characterized complexes of a 4,4′-biimidazole ligand.

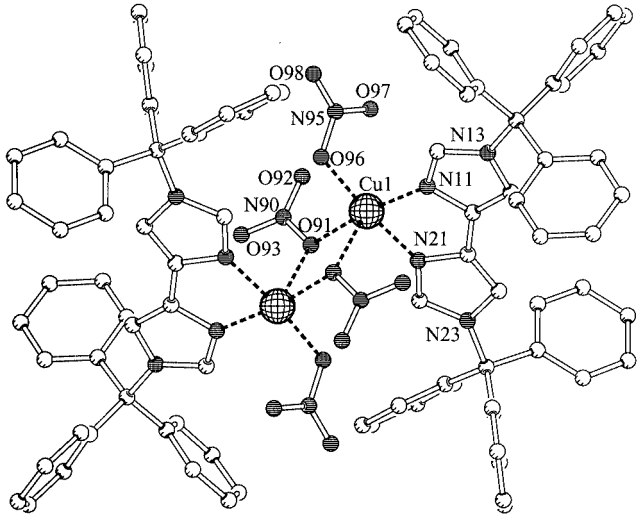

Figure 1. PLATON[38] representation of $[Cu(\mu\text{-}\eta^1\text{-}NO_3)(NO_3)(bi1)]_2$ (**1**)

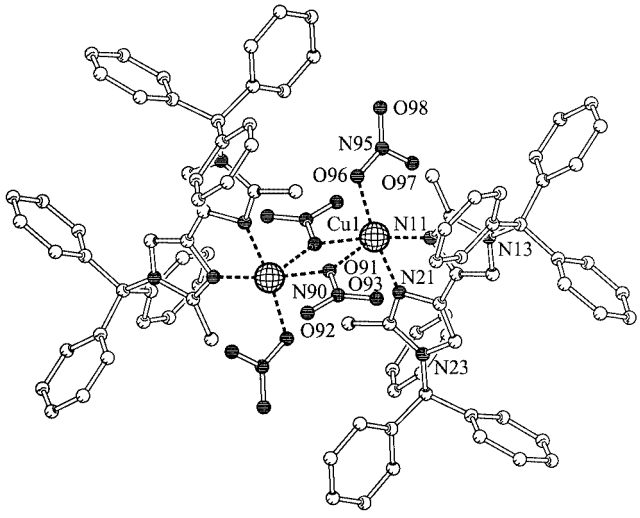

Figure 2. PLATON[38] representation of $[Cu(\mu\text{-}\eta^1\text{-}NO_3)(NO_3)(bi2)]_2$ (**2**)

$[Cu(\mu\text{-}\eta^1\text{-}NO_3)(NO_3)(bi2)]_2$ (2)

Complex **2** is isostructural with complex **1**. The presence of a methyl substituent at the 2- and 2′-positions of the imidazole rings does not appear to affect significantly the

overall structure of the complex. The metal centers maintain the square-pyramidal coordination geometry (with $\tau = 0.02$), and are slightly more separated [Cu···Cu = 3.530(1) Å] than in **1**. The bridging nitrate ligand is bound to the Cu centres at 1.996(3) and 2.403(3) Å, and the oxygen donor of the terminal nitrate group is separated from the metal ion by 1.970(3) Å. The long O···Cu contact featured by this ligand is 2.643(5) Å. The orientations of the nonbridging nitrato groups do differ from complex **1**, which is ascribed to the steric effect of the 2-Me group. The chelating ligands display Cu−N distances of 1.996(3) and 2.002(3) Å.[30,31] The packing in this structure is also uneventful and involves mainly van der Waals forces.

Spectroscopic Studies

The infrared (IR) spectra of complexes **1** and **2** were measured in the solid state. Both compounds exhibit a strong absorption (1279 and 1282 cm^{-1}, respectively) in the region characteristic for ν(NO) of monodentate-coordinated nitrates.[32]

The electronic spectra of **1** and **2** were collected from polycrystalline samples, using the diffuse reflectance technique. Both spectra have the same qualitative appearance, with the bands of complex **1** being slightly red-shifted with respect to those of **2**. One broad absorption band is observed (Table 2) in the 712−770-nm range (14000−12900 cm^{-1}) that can be assigned to d−d transitions involving the Cu^{II} ion in a square-pyramidal environment.[33,34] Near-ultraviolet absorption bands at ca. 400 nm (25000 cm^{-1}, shoulder; **1**) and 452 nm (22000 cm^{-1}; **2**) were also detected, and are assigned as charge-transfer transitions from a nitrate nonbonding orbital to the copper ion. In addition, both spectra display LMCT transitions from the chelating ligands at ca. 320 and 261 nm (31100 and 38100 cm^{-1}; **1**) and at ca. 320 and 274 nm (31100 and 36300 cm^{-1}; **2**). The electronic spectra of both compounds where also measured in CH_2Cl_2 solution. The above-mentioned various bands were found at very similar positions, but a dramatic decrease of intensity of the visible absorptions with respect to the ultraviolet bands was evident. This could be due to a change of the dipolar integral for some transitions, caused by an alteration of the symmetry within the complex upon dissolution or by dissociation. Furthermore, a new band could be seen at very high energy (227 nm, i.e. 43800 cm^{-1} for both complexes), most probably corresponding to an intra-ligand transition.

Complexes **1** and **2** were studied by paramagnetic ^1H NMR in $CDCl_3$ solution (Figure 3). A list of the chemical shifts of the different observed resonances is included in Table 2. Both complexes show a unique set of three paramagnetically broadened signals in the range δ = 6−8 ppm, corresponding to the phenyl rings of the biimidazole ligands. Complex **2** also displays a very broadened and shifted resonance at δ ≈ −9 ppm attributed to the methyl substituents on the imidazole rings of the ligand bi2. The signals corresponding to the protons directly on the imidazole rings were broadened beyond detection. Thus, the spectra of **1** and **2** show that both complexes exhibit higher symmetry in solution than in the solid state. This could be due to a rapid fluxional process rendering both halves of the ligand equivalent, or to the dissociation of the dimers in solution, leading to more symmetric mononuclear species. The second hypothesis was supported by a variable temperature ^1H NMR study, conducted down to ca. 110 K, in which no sign of any de-coalescence process could be observed (data not shown).

The solid-state and solution X-band EPR spectra of **1** and **2**, respectively, were compared at room temperature and ca. 77 K. The solution (CH_2Cl_2/toluene, 2:1) spectrum

Table 2. Spectroscopic data for complexes **1** and **2**

	Complex **1**	Complex **2**
Ligand field (solid)[a]	38100, 31100, ca. 25500, 13900	36300, ca. 31100, 22000, 13300
Ligand field (solution)[b]	43800, 39300, 25500, 14000	43800, 38100, 22000, 12900
EPR (solution)[c]	$g_{iso} = 2.15$	$g_{iso} = 2.16$
EPR (frozen solution)[d]	$g_{\|} = 2.30$ ($A_{\|} = 166$ G), $g_{\perp} = 2.07$	$g_{\|} = 2.31$ ($A_{\|} = 150$ G), $g_{\perp} = 2.07$
EPR (solid)[e]	$g = 2.05$	$g = 2.11$
300 MHz ^1H NMR[f]	7.41 (*m*-Ph), 7.05 (*p*-Ph), 6.44 (*m*-Ph)	7.47 (*m*-Ph), 7.04 (*p*-Ph), 6.51 (*m*-Ph), ca. −9 (CH_3)

[a] In cm^{-1}, registered in solid state at 298 K, diffuse reflectance. [b] In cm^{-1}, registered in CH_2Cl_2 solutions at 298 K. [c] At 77 K, frozen solution in CH_2Cl_2/toluene (2:1). At 298 K, solution in CH_2Cl_2/toluene (2:1). [d] At 77 K, frozen solution in CH_2Cl_2/toluene (2:1). [e] At 77 K, polycrystalline sample. [f] In ppm, in $CDCl_3$.

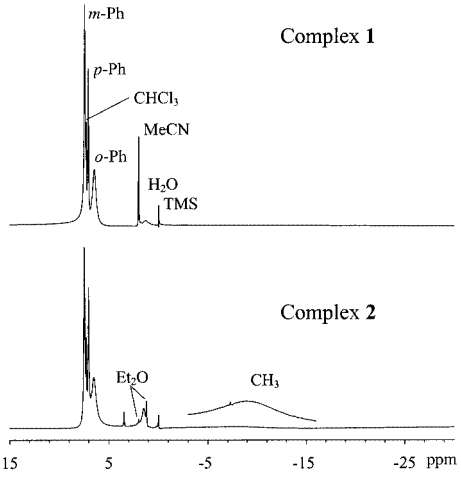

Figure 3. 300 MHz ^1H NMR spectra of complexes **1** and **2** in $CDCl_3$; the labels used for the top spectrum apply also to the bottom spectrum

at room temperature (not shown) displays for both species a band typical for mononuclear Cu^{II}, with g_{iso} = 2.15/2.16 (**1**/**2**). Both bands are split into four signals (A_{iso} = 68/62 G) due to hyperfine coupling of the spin with the Cu nuclei ($I = {}^3/_2$). In frozen solution, both compounds feature typical axial spectra (Figure 4) where $g_{\|}$ = 2.30/2.31 and $g_{\perp}$ = 2.07/2.07. From these values, the isotropic g constants reported above can be calculated from $g_{iso} = 1/3(2\times g_{\perp} + g_{\|})$. The parallel resonance in both compounds display hyperfine splitting due to the coupling with Cu ($A_{\|}$ = 166/150 G). Also, both spectra show superhyperfine splitting of the perpendicular signal due to interaction with the ^{14}N nuclei of the biimidazole ligands. These spectra are consistent with the presence of mononuclear species in solution. A possible distribution of species could be tetragonally elongated [Cu-$(NO_3)_2(bi)_2$] along with solvated $Cu(NO_3)_2$. Because $A_{\|}$ in **1** is slightly higher than in **2** the first type of species may well be EPR-active in both systems, the complex of **2** experiencing a larger distortion from planarity at the equatorial plane caused by the methyl substituents of bi2. A much broader signal underlying the spectra (especially visible in the frozen solution spectrum of **2**) could be attributed to the second type of species. The solid-state EPR spectra of **1** and **2** are also very similar to each other and distinct from the corresponding solution spectra. In both cases, a broad, isotropic signal is observed at g = 2.05/2.11. These bands could be ascribed to a triplet state, and the dramatic difference with the frozen solution spectra clearly indicates that the dinuclear structure of **1** and **2** observed in the solid state is not maintained in solution. No attempts were made to analyze the triplet signals in detail.

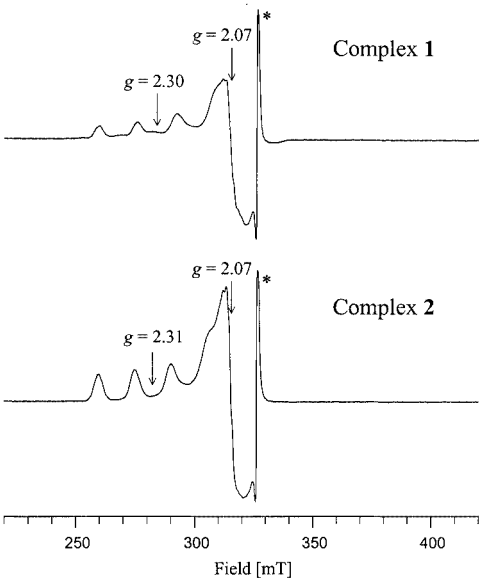

Figure 4. X-band EPR spectra of complexes **1** and **2** at 77 K in CH_2Cl_2/toluene (2:1) frozen solution; the signal labeled "*" corresponds to the reference radical used for calibration (see Exp. Sect.)

Catalytic Properties

$[Cu(\mu\text{-}\eta^1\text{-}NO_3)(NO_3)(bi1)]_2$ (**1**) and $[Cu(\mu\text{-}\eta^1\text{-}NO_3)(NO_3)(bi2)]_2$ (**2**) were tested as catalysts for the polymerization of 2,6-dimethylphenol (DMP) to ascertain the influence of the ligand derivatives on the catalytic activity of these precursors, in relation to their structural properties. Interestingly, the catalytic activity of complex **2** (which contains the 2,2′-dimethylbiimidazole ligand) is more than ten times faster than that of **1** (Table 3). This confirms the results achieved with ligands Meim and Dmeim (1-methylimidazole and 1,2-dimethylimidazole, respectively), where a methyl group on the 2-position of the imidazole ring led to a dramatic enhancement of activity[18] (see Table 3). The crystal structures of complexes **1** and **2** (see above) have revealed that the presence of methyl groups at the 2,2′-positions of the imidazole rings has almost no influence on the metric parameters of the rest of the complex. This suggests that the main reason for the difference in activity is the differential basicity of the ligands. It has been proposed that the N-based ligands of the catalyst might act as a Brønsted base during the catalytic cycle. In such a case the pK_b of the ligand could affect the rate of conversion. In this particular system the structural factors influencing the catalytic activity might be dominated by the much larger triphenylmethyl substituents common to both compounds. It would be interesting to expand the present study using the corresponding ligands 4,4′-biimidazole and 2,2′-dimethyl-4,4′-biimidazole. Here, however, an influence of the steric properties on the catalytic activity cannot be completely excluded, since no structural details of intermediates containing the reaction substrate, DMP, are known.

Conclusion

Single-crystal X-ray diffraction has revealed the solid-state molecular structure of the two copper dimeric com-

Table 3. Catalytic activity of Cu^{II} with didentate ligands bi1 and bi2 during the polymerization of DMP in acetonitrile, compared with that with Meim and Dmeim[18]

Ligand L	L/Cu	Conversion [%]	Reaction time [h]	R_0 [10^{-5} molL^{-1}s^{-1}]	PPE [%]
bi1	1	68	1.50	3	95.1
bi2	1	43	0.30	31	95.0
Meim[a]	4	68	0.08	142	> 95
Dmeim[b]	4	76	0.08	200	> 95

[a] Meim = 1-methylimidazole. [b] Dmeim = 1,2-dimethylimidazole.

plexes $[Cu(\mu\text{-}\eta^1\text{-}NO_3)(NO_3)(bi1)]_2$ (**1**) and $[Cu(\mu\text{-}\eta^1\text{-}NO_3)(NO_3)(bi2)]_2$ (**2**) are similar, despite the fact that the 2-Me group of the latter is close to the coordination sphere of Cu^{II}. These are the first crystallographically characterized coordination compounds featuring 4,4′-biimidazole ligands. Spectroscopic studies indicate that the solid-state structure of compounds **1** and **2** is not preserved in solution. The various data suggest that dissociation into mononuclear species takes place. Complexes **1** and **2** have been used as catalyst precursors for the oxidative coupling of DMP into PPE. In view of the solid-state molecular structure of both precursors, their dramatic difference in activity is interpreted in terms of the difference in ligand basicity. The EPR solution spectra, however, indicate that the presence of an Me group might distort the mononuclear complexes present in solution, thereby affecting their catalytic activity. The preparation and crystallographic characterization of additional catalyst precursors for this reaction will establish any correlations between structural parameters and the catalytic activity of these species.

Experimental Section

General Remarks: The biimidazole ligands 1,1′-bis(triphenylmethyl)-4,4′-biimidazole (bi1) and 2,2′-dimethyl-1,1′-bis(triphenylmethyl)-4,4′-biimidazole (bi2) were prepared according to the method reported by Pyne et al.[27] Solvents and chemicals were commercially available and were used as received unless otherwise indicated. The syntheses of all organic compounds were performed under argon and their purification was commonly performed in air. Infrared spectra were collected with a Perkin−Elmer Paragon 1000 spectrophotometer equipped with a Golden Gate Diamond ATR as a sample support. ^1H NMR spectra were recorded with a 200 MHz Jeol JNM FX-200 instrument and a 300 MHz Bruker DPX 300 spectrometer. Vis/NIR spectra where measured with a Perkin−Elmer Lambda 900 spectrophotometer in CH_2Cl_2 solution or using the diffuse reflectance technique, with MgO as a reference. X-band EPR spectra were recorded with a JEOL ESR spectrometer equipped with an Esprit 330 data system at room temperature and at 77 K, with dpph as an internal reference ($g = 2.0036$). Elemental analyses were performed at the Microanalytical Laboratory of the University College, Dublin, Ireland or at the Mikroanalytisches Labor Pascher, Remagen-Bandorf, Germany.

Dioxygen Uptake Measurements: In a typical quantitative, time-resolved dioxygen-uptake experiment, one compartment of a special in-house made two-compartment reaction vessel was filled with 5 mL of a 0.01 M Cu^{II}/ligand solution, and the other with 10 mL of the substrate (3 mmol) solution. Intense shaking in under dioxygen combined these solutions and started the reaction. The resulting reaction mixture was 3.33 mM in Cu and 0.2 M in DMP (**3**). The polymerization reactions were performed at 25 °C under pure dioxygen at atmospheric pressure. In this particular case, a ligand/Cu ratio of 1 and an NaOMe/Cu ratio of 2 were used. The catalytic activity was determined from the initial dioxygen-uptake rate R_0. A detailed description of the dioxygen-uptake experiments and the processing of the experimental data have been previously published.[35]

$[Cu(\mu\text{-}\eta^1\text{-}NO_3)(NO_3)(bi1)]_2$ (1): A slurry of bi1 (62 mg, 0.1 mmol) in MeCN (5 mL) was added to a stirred blue solution of $Cu(NO_3)_2{\cdot}3H_2O$ (26 mg, 0.1 mmol) in MeCN (5 mL). The ligand dissolved completely upon reaction. After a few minutes, the blue solution was left unperturbed and the solvent was allowed to slowly evaporate for a few days. After this time, blue block-shaped crystals suitable for X-ray crystallography had deposited. The crystals were collected by filtration and dried in vacuo. The yield was 44%. IR (neat): $\tilde{\nu}$ [cm^{-1}] = 1511.8 m, 1490.0 m, 1471.6 s, 1445.7 m, 1278.9 vs, 1214.0 m, 1085.8 m, 1002.1 m, 947.3 w, 845.8 w, 744.6 vs, 697.7 vs, 659.4 vs, 638.8 m, 374.0 w, 345.3 m, 316.6 w. $C_{88}H_{68}Cu_2N_{12}O_{12}(H_2O)_2$ (1648.72): calcd. C 64.11, H 4.40, N 10.19; found C 63.86, H 4.12, N 9.96.

$[Cu(\mu\text{-}\eta^1\text{-}NO_3)(NO_3)(bi2)]_2$ (2): A slurry of bi2 (259 mg, 0.4 mmol) in MeCN (10 mL) was added to a stirred blue solution of $Cu(NO_3)_2{\cdot}3H_2O$ (96 mg, 0.4 mmol) in MeCN (20 mL). After a few minutes, the resulting green solution was filtered with paper and the filtrate was left unperturbed for the slow evaporation of the solvent. After a few days, green needles suitable for X-ray crystallography were obtained. The solid was collected by filtration and turned gray upon contact with air. The sample was dried in vacuo (yield 31%). IR (neat): $\tilde{\nu}$ [cm^{-1}] = 1489.7 s, 1446.0 m, 1394.1 w, 1281.8 vs, 1232.9 m, 1149.5 w, 1010.1 m, 747.9 vs, 700.1 vs, 668.2 m, 655.7 w, 637.9 m, 586.0 w, 499.4 w, 398.2 w, 336.4 w. $C_{92}H_{76}Cu_2N_{12}O_{12}(H_2O)$ (1686.81): calcd. C 65.51, H 4.66, N 9.96; found C 65.67, H 4.78, N 9.48.

X-ray Crystallography: Crystals of complexes **1** and **2** were mounted on Lindemann glass capillaries and transferred into the cold nitrogen stream of a Nonius KappaCCD diffractometer on a rotating anode, (Mo-K_α radiation, graphite monochromator, λ = 0.71073 Å, T = 150 K). Pertinent data for the structure determinations are collected in Table 4. Structures were solved with direct methods using SHELXS86.[36] Refinement on F^2 was performed with SHELXL-97-2.[37] The hydrogen atoms were included in the refinement on calculated positions riding on their carrier atoms. The non-hydrogen atoms were refined with anisotropic thermal parameters. The hydrogen atoms were refined with a fixed isotropic displacement parameter related to the value of the equivalent isotropic displacement parameter of their carrier atoms. The structures of both **1** and **2** contain an area filled with acetonitrile. In **1** the solvent could be described with an ordered model, albeit with relatively high displacement parameters. In **2** the volume of the solvent area was significantly larger, and no satisfactory model could be constructed. Therefore, for this complex, the contribution to the structure factors associated with the solvent was taken into account using the SQUEEZE procedure as incorporated in PLATON.[38] A total of 126 electrons were found in a system of channels running parallel to a and c of 600 Å^3 per unit cell, corresponding to approximately six molecules of acetonitrile. The nitrate ions and one of the phenyl rings of **2** displayed high anisotropy in their displacement factors. Mild rigid bond restraints were applied to ensure realistic values for the displacement parameters. Neutral atom scattering factors and anomalous dispersion corrections were taken from the International Tables for Crystallography.[39] Geometrical calculations and illustrations were performed with PLATON.[38] CCDC-194207 (**1**) and -194208 (**2**) contain the supplementary crystallographic data for this paper. These data can be obtained free of charge at www.ccdc.cam.ac.uk/conts/retrieving.html [or from the Cambridge Crystallographic Data Centre, 12 Union Road, Cambridge CB2 1EZ, UK; Fax: (internat.) + 44-1223/336-033; E-mail: deposit@ccdc.cam.ac.uk].

Table 4. Crystallographic data for $[Cu(\mu\text{-}\eta^1\text{-}NO_3)(NO_3)(bi1)]_2$ (**1**) and $[Cu(\mu\text{-}\eta^1\text{-}NO_3)(NO_3)(bi2)]_2$ (**2**)

	1	**2**
Crystal data:		
Empirical formula	$C_{88}H_{68}Cu_2N_{12}O_{12}\cdot 4C_2H_3N$	$C_{92}H_{76}Cu_2N_{12}O_{12}\cdot 6C_2H_3N$[a]
Formula mass [g·mol^{-1}]	1776.86	1915.09[a]
Crystal system	triclinic	triclinic
Space group	$P\bar{1}$ (no. 2)	$P\bar{1}$ (no. 2)
a [Å]	13.4436(15)	11.286(2)
b [Å]	13.5376(10)	15.320(2)
c [Å]	13.944(3)	15.520(3)
α [°]	90.437(17)	105.442(12)
β [°]	118.674(11)	99.655(10)
γ [°]	94.982(10)	106.171(10)
V [Å^3]	2214.6(5)	2397.9(7)
$\rho_{calcd.}$ [g·cm^{-3}]	1.332	1.326[a]
Z	1	1
F(000)	922	998[a]
T [K]	150	150
μ [mm^{-1}] (Mo-K_α)	0.552	0.538[a]
Crystal colour	blue	blue−green
Crystal size [mm]	0.1 × 0.3 × 0.3	0.2 × 0.3 × 0.3
Data collection:		
θ_{min}, θ_{max} [°]	1.6, 27.46	1.6, 25.25
X-ray exposure [h]	1.8	2.4
Data set	−17:17, −17:17, −18:18	−13:12, −18:17, −18:18
Total data	29969	22466
Total unique data	10077	8443
R_{int}	0.0699	0.0529
R_σ	0.0548	0.0452
Absorption correction range	0.864−0.977 [MULABS][38]	[4]
Refinement:		
No. of refined parameters	570	534
Final $R1$[b]	0.0458 [8188 I > 2σ(I)]	0.0618 [7237 I > 2σ(I)]
Final $wR2$[c]	0.1243	0.1622
Goodness of fit	1.030	1.045
w^{-1}[d]	$\sigma^2(F_{obs}^2) + (0.0597P)^2 + 1.34P$	$\sigma^2(F_{obs}^2) + (0.0582P)^2 + 5.48P$
$(\Delta/\sigma)_{av}$, $(\Delta/\sigma)_{max}$	< 0.001, 0.001	< 0.001, 0.001
Min., max. residual density [e·Å^{-3}]	−0.76, 0.63	−0.54, 0.66

[a] Including the estimated contribution of the disordered solvent. [b] $R1 = \Sigma||F_o| - |F_c||/\Sigma|F_o|$. [c] $wR2 = \{\Sigma[w(F_o^2 - F_c^2)^2]/\Sigma[w(F_o^2)^2]\}^{1/2}$. [d] $P = [\mathrm{Max}(F_o^2,0) + 2F_c^2)/3$.

Acknowledgments

Financial support by the European Union, under contract HPMF-CT-1999-00113 (Marie Curie Fellowship) to G. A. and COST Action D21/003/2001 (P. G.), the Dutch National Research School Combination Catalysis (HRSMC and NIOK) the WFMO (J. R.) and the CW-NWO (A. L. S.) are thankfully acknowledged.

[1] M. Zoeteman, E. Bouwman, R. A. G. De Graaff, W. L. Driessen, J. Reedijk, P. Zanello, *Inorg. Chem.* **1990**, *29*, 3487.
[2] G. J. A. A. Koolhaas, W. L. Driessen, J. Reedijk, J. L. Van der Plas, R. A. G. De Graaff, D. Gatteschi, H. Kooijman, A. L. Spek, *Inorg. Chem.* **1996**, *35*, 1509.
[3] G. J. A. A. Koolhaas, P. M. Van Berkel, S. C. Van der Slot, G. MendozaDiaz, W. L. Driessen, J. Reedijk, H. Kooijman, N. Veldman, A. L. Spek, *Inorg. Chem.* **1996**, *35*, 3525.
[4] G. Tabbi, W. L. Driessen, J. Reedijk, R. P. Bonomo, N. Veldman, A. L. Spek, *Inorg. Chem.* **1997**, *36*, 1168.
[5] C. J. Campbell, W. L. Driessen, J. Reedijk, W. J. J. Smeets, A. L. Spek, *J. Chem. Soc., Dalton Trans.* **1998**, 2703.
[6] M. Beretta, E. Bouwman, L. Casella, B. Douziech, W. L. Driessen, L. Gutierrez-Soto, E. Monzani, J. Reedijk, *Inorg. Chim. Acta* **2000**, *310*, 41.
[7] S. J. Lippard, J. M. Berg, *Principles of Bioinorganic Chemistry*, University Science Books, Mill Valley, **1994**.
[8] N. Kitajima, Y. Morooka, *Chem. Rev.* **1994**, *94*, 737.
[9] A. S. Hay, H. S. Stafford, G. F. Endres, J. W. Eustance, *J. Am. Chem. Soc.* **1959**, *81*, 6335.
[10] J. Heijboer, *J. Polym. Sci. C* **1968**, *16*, 3755.
[11] F. E. Karasz, J. M. O'Reilly, *J. Polym. Sci., Pol. Lett.* **1965**, *3*, 561.
[12] P. Gamez, C. Simons, R. Steensma, W. L. Driessen, G. Challa, J. Reedijk, *Eur. Polym. J.* **2001**, *37*, 1293.
[13] A. S. Hay, *J. Polym. Sci.* **1962**, *58*, 581.
[14] H. L. Finkbeiner, A. S. Hay, D. M. White, in: *Polymerization Processes*, vol. XXIV (Ed.: C. E. Schildnecht), Wiley, New York, **1977**, p. 537.
[15] P. J. Baesjou, W. L. Driessen, G. Challa, J. Reedijk, *J. Mol. Catal. A* **1998**, *135*, 273.
[16] P. J. Baesjou, W. L. Driessen, G. Challa, J. Reedijk, *J. Mol. Catal. A* **1999**, *140*, 241.
[17] F. J. Viersen, G. Challa, J. Reedijk, *Polymer* **1990**, *31*, 1368.
[18] P. Gamez, C. Simons, G. Aromí, W. L. Driessen, G. Challa, J. Reedijk, *Appl. Catal. A* **2001**, *214*, 187.
[19] F. J. Viersen, G. Challa, J. Reedijk, *Polymer* **1990**, *31*, 1361.
[20] W. Chen, G. Challa, *Eur. Polym. J.* **1990**, *26*, 1211.

[21] E. Tsuchida, M. Kaneko, H. Nishide, *Makromol. Chem.* **1972**, *151*, 221.
[22] C. E. Koning, G. Challa, F. B. Hulsbergen, J. Reedijk, *J. Mol. Cat.* **1986**, *34*, 355.
[23] K.-T. Li, *Polym. Bull.* **1995**, *34*, 419.
[24] A. Camus, M. S. Garozzo, N. Marsich, M. Mari, *J. Mol. Catal. A* **1996**, *112*, 353.
[25] P. J. Baesjou, W. L. Driessen, G. Challa, J. Reedijk, *J. Am. Chem. Soc.* **1997**, *119*, 12590.
[26] P. J. Baesjou, PhD Thesis thesis, Leiden University, Leiden, **1997**.
[27] M. D. Cliff, S. G. Pyne, *Synthesis* **1994**, 681.
[28] T. Otieno, S. J. Rettig, R. C. Thompson, J. Trotter, *Inorg. Chem.* **1995**, *34*, 1718.
[29] A. W. Addison, T. N. Rao, J. Reedijk, J. van Rijn, G. C. Verschoor, *J. Chem. Soc., Dalton Trans.* **1984**, 1349.
[30] M. Handa, T. Idehara, K. Nakano, K. Kasuga, M. Mikuriya, N. Matsumoto, M. Kodera, S. Kida, *Bull. Chem. Soc. Jpn.* **1992**, *65*, 3241.
[31] A. R. Oki, J. Sanchez, R. J. Morgan, *J. Coord. Chem.* **1995**, *36*, 167.
[32] K. Nakamoto, in: *Infrared and Raman Spectra of Inorganic and Coordination Compounds*, 4th ed., John Wiley, New York, **1986**, pp. 254.
[33] B. J. Hathaway, *J. Chem. Soc., Dalton Trans.* **1972**, 1196.
[34] G. Murphy, P. Nagle, B. Murphy, B. Hathaway, *J. Chem. Soc., Dalton Trans.* **1997**, 2645.
[35] P. J. Baesjou, W. L. Driessen, G. Challa, J. Reedijk, *J. Mol. Catal. A* **1996**, *110*, 195.
[36] G. M. Sheldrick, *SHELX86, Program for crystal structure determination*, University of Götingen, Germany, **1986**.
[37] G. M. Sheldrick, *SHELXL-97-2, Program for crystal structure refinement*, University of Götingen, Germany, **1996**.
[38] A. L. Spek, *PLATON, A multi-purpose crystallographic tool*, Utrecht University, The Netherlands, **2002**; internet: http://www.cryst.chem.uu.nl/platon
[39] A. J. C. Wilson (Ed.), *International Tables for Crystallography*, Kluwer Academic Publishers, Dordrecht, The Netherlands, **1992**, vol. C.

Received November 6, 2002
[I02610]

Studies of Pyridinyl-Containing 14-Membered Macrocyclic Copper(II) Complexes

Sabrina Autzen,[a] Hans-Gert Korth,[a] Roland Boese,[b] Herbert de Groot,*[c] and Reiner Sustmann*[a]

Keywords: Macrocyclic ligands / Copper / Enzyme models / Superoxide dismutase

Six copper(II) complexes of tetracoordinating, pyridinyl-containing 14-membered macrocycles with varying ratios of nitrogen and oxygen donor atoms were prepared and characterized by IR, UV/Vis, and EPR spectroscopy and cyclic voltammetry. A distorted tetragonal coordination of the copper center in the solid-state was established by X-ray crystallography for the tetraazamacrocyclic complex **Cu-3** carrying a methoxybenzyl pendent arm and the trioxaaza complex **Cu-6**. The superoxide dismutase-like activity of the Cu^{II} complexes was investigated by inhibition of NADH oxidation. Although the UV/Vis and EPR spectra of the complexes were strongly affected when the coordinating nitrogen atoms were successively replaced by oxygen atoms, no significant change in their reactivity towards superoxide was observed. In all cases a 1:1 or 1:2 stoichiometry for the reaction with superoxide was found, with the exception of the methoxybenzyl-substituted tetraaza complex, which showed a low catalytic activity with a turnover number of about 10.
(© Wiley-VCH Verlag GmbH & Co. KGaA, 69451 Weinheim, Germany, 2003)

Introduction

Our present studies are concerned with the preparation of transition metal complexes of 14-membered, pyridine-containing macrocycles and the examination of their spectroscopic properties to elucidate their potential enzyme-mimetic qualities. We have recently reported the catalase-mimetic activity of some non-heme iron(III) complexes.[1] Copper is another biologically significant metal, being found in various enzymes, such as the important Cu-Zn superoxide dismutase (Cu_2Zn_2-SOD), which is used in living organisms to detoxify the superoxide radical anion, $O_2^{\cdot -}$, [Equation (1)].[2]

$$2\,O_2^{\cdot -} + 2\,H^+ \xrightarrow{SOD} H_2O_2 + O_2 \qquad (1)$$

[a] Institut für Organische Chemie, Universität Essen, Universitätsstr. 5, 45117 Essen, Germany
Fax: (internat.) + 49-201/183-4259
E-mail: reiner.sustmann@uni-essen.de
[b] Institut für Anorganische Chemie, Universität Essen, Universitätsstr. 5, 45117 Essen, Germany
[c] Institut für Physiologische Chemie, Universitätsklinikum Essen, Hufelandstr. 55, 45122 Essen, Germany
Fax: (internat.) + 49-201/723-5943
E-mail: h.de.groot@uni-essen.de

Numerous transition metal (preferably Cu, Fe, Mn) complexes of various kinds have been investigated with regard to their reactivity toward superoxide. The use of copper complexes as SOD mimics has been reviewed.[3,4] Although several investigated compounds exhibit good SOD-like activities, systematic studies concerning the factors which govern the enzyme-mimicking reactivities are scarce.[5] We report here on the copper(II) complexes **Cu-1**−**Cu-6** of ligands **1**−**6** in which the sp^3-nitrogen atoms of the parent macrocycle **1** are successively replaced by oxygen atoms. Spectroscopic properties were compared to determine the influence of the coordinating atoms on the SOD-like activities of the complexes. Complexes **Cu-1** and **Cu-2** have previously been described,[6−9] but their SOD activity was not investigated. Complex **Cu-3**, carrying a methoxybenzyl pendent arm, was included in this study to determine whether a possible coordination by the phenolic oxygen atom to the fifth coordination site at the copper atom might influence the catalytic activity. Coordination of phenolate groups to the fifth position in square-planar Cu^{II} complexes has been reported before;[10] however, to the best of our knowledge, coordination of phenyl ether substituents to the axial position has not been reported. There is, however, a recent report[11] in which phenyl ether moieties within the chain of a 20-membered macrocyclic ligand bind to the axial position of a tetra-*N*-coordinated copper(II) complex. X-ray crystal structures of the copper(II) complexes **Cu-3** and **Cu-6** are presented. X-ray structures of eight 14-membered *endo*-pyridine Cu^{II} complexes, including the PF_6^- salt of

Cu-1,[9] can be found in the Cambridge Structural Database.[12]

Results and Discussion

Synthesis

Macrocycle **2** was prepared from its nickel complex as described by Karn and Busch.[13] Compound **5** was prepared from ditosylated pyridine-2,6-diyldimethanol and the alkanediol, compound **6**[14] from pyridine-2,6-diyldimethanol and the appropriate alkanediyl ditosylate. Macrocycles **1**[6] and **3**[1] were prepared according to literature procedures in a copper-template reaction. The preparation of ligands **1**, **3** and **4** was devised starting from pyridine-2,6-dicarbaldehyde, which was treated with the appropriate diamine in a copper-template reaction to give the macrocycle. Diimine reduction by sodium borohydride and removal of copper(II) as sulfide provided the free ligands. Unfortunately, attempts to prepare the macrocycles **7** and **8**, in which the position of the nitrogen and oxygen atoms was exchanged with respect to compounds **4** and **5**, respectively, were not successful (Scheme 1).

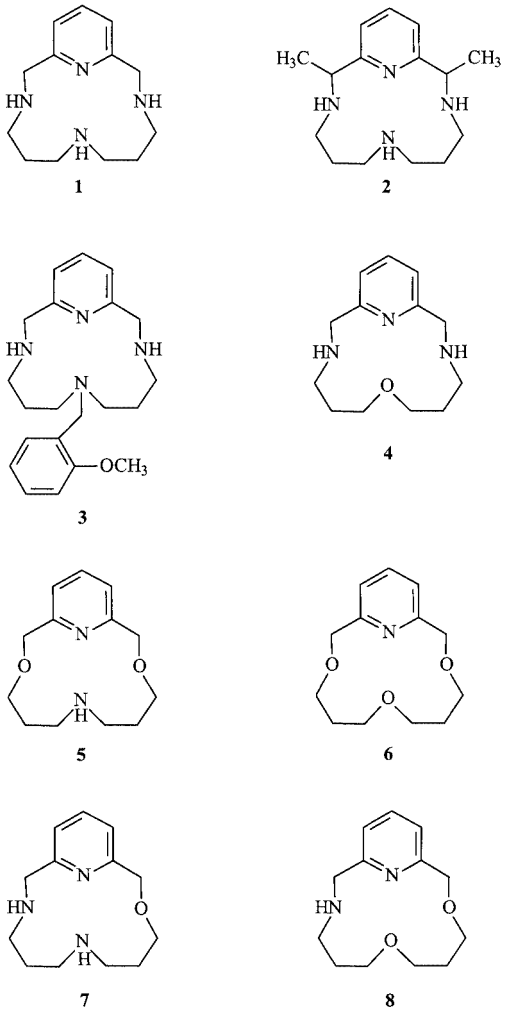

Scheme 1

Facile formation of the copper(II) complexes was achieved by addition of an equimolar ethanolic solution of copper(II) perchlorate to an ethanolic solution of the ligands at room temperature and subsequent crystallization. As expected, for the ligands **1**, **2**, and **4**−**6** the corresponding copper complexes **Cu-1**, **Cu-2**, and **Cu-4**−**Cu-6** (Scheme 2) with two perchlorate counterions were obtained.

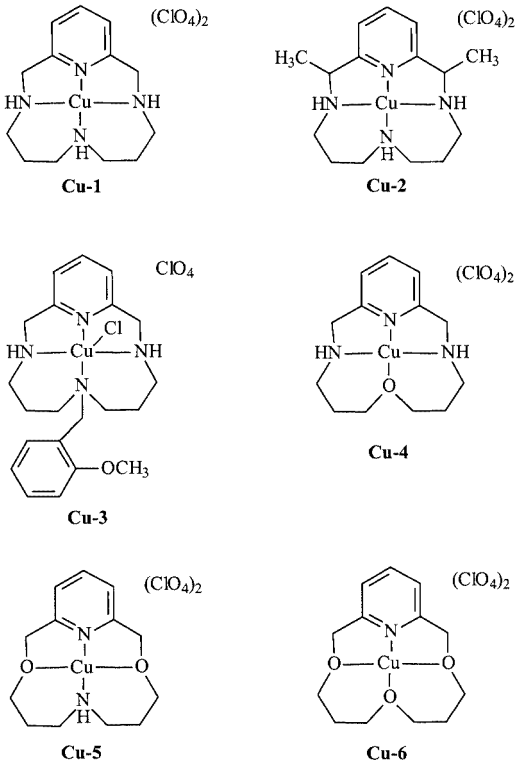

Scheme 2

Unexpectedly, X-ray structural and elemental analysis revealed that the copper complex **Cu-3** of ligand **3** contained one chloride ion as a counterion, although no chloride was involved in any steps of the synthesis. Thus, perchlorate must have been reduced during complex formation. Although perchlorate (which is a weakly chelating, relatively large anion) is a strong oxidant it is generally kinetically stable to reductants and is therefore frequently used to regulate the ion strength in kinetic and thermodynamic studies.[15] Because perchlorate reduction was not observed in the preparation of the related complexes **Cu-1** and **Cu-2**, it is very likely that the methoxybenzyl side chain of **3** facilitated this reduction. This conclusion is supported by the rapid formation of a Cu^{II}+**3** complex of 1:2 stoichiometry, $[Cu^{II}(\mathbf{3})_2](ClO_4)_2$, after mixing of copper(II) perchlorate and **3** (see Exp. Sect.). When kept in the reaction mixture, this complex slowly (within 12 h) converted into complex **Cu-3**. We propose that the initial 1:2 complex may have been formed by a kinetically controlled, exocyclic complexation, probably involving the oxygen atom of the methoxybenzyl

substituent. In solution, this exocyclic complex then rearranges to the thermodynamically more stable complex **Cu-3**, thereby re-releasing one ligand molecule. Concomitantly, partial reduction of perchlorate to chloride takes place. Given the rather mild reaction conditions used here it is not clear how the perchlorate might have been reduced, i.e. which chemical entity would have been the reductant. The copper(II) ion is unlikely to be oxidized under the applied conditions (compare the inertness of **Cu-1**, **Cu-2**), whereas the electron-rich phenyl group of the side arm might be a chemically reasonable target. A reduction of perchlorate to chloride during the preparation of a macrocyclic iron complex has been described by Goedken et al.[16] who discussed the formation of an unspecified, yet very reactive, intermediate. Elucidation of the mechanism of this interesting reaction is beyond the scope of this paper and will be the subject of a separate study.

Crystal Structure

The crystal structure of **Cu-1** with two PF_6^- counterions instead of perchlorate has been reported.[9] The crystal structures and the unit-cell diagrams of **Cu-3** and **Cu-6** are displayed in Figures 1 and 2. Selected bond lengths and angles are listed in the captions. It can be seen that in **Cu-3** copper(II) has a fivefold coordination environment. The four in-plane distances are of lengths commonly found in square-based pyramidal structures, with the $Cu-N_{pyr}$ distance (1.94 Å) being somewhat shorter than the other C−N distances (2.02−2.05 Å). This bond-length pattern seems to be characteristic of complexes of tetraazamacrocyclic ligands containing a pyridine moiety (see refs.[1,9] and references cited therein). The copper(II) ion in **Cu-3** is lifted out of the plane of the four coordinating ligand atoms by ρ(**Cu-3**) = 0.311 Å with a $Cu^{II}-Cl$ distance of 2.564 Å. The tetrahedral distortion of 0.311 Å is significantly increased compared with that in **Cu-1**·$(PF_6)_2$ (ρ = 0.133 Å),[9] which may be related to the coordination of Cl^-. The methoxybenzyl group, C(15)−C(21) and O(1), with the riding hydrogen atoms and the methylene hydrogen atoms H(14A/14B) is disordered over two sites with occupancies of 0.6 and 0.4 together; O(31) and C(32) of the methoxy group are disordered over two sites with occupancies of 0.5. In the crystal, the oxygen atom of the 2-methoxybenzyl group is not coordinated to the central ion. The second counterion is essentially noncoordinating perchlorate. Unlike **Cu-3**, in **Cu-6** the copper atom is essentially located in-plane [ρ(**Cu-6**) = 0.003 Å], with a Cu−N distance of 1.89 Å and Cu−O lengths of 1.93−1.96 Å. One of the perchlorate anions is

Table 1. Crystallographic data of **Cu-3** and **Cu-6**

Compound	**Cu-3**	**Cu-6**
Empirical formula	$C_{21}H_{30}ClCuN_4O\cdot ClO_4\cdot 0.5[CH_4O]$	$C_{13}H_{19}CuNO_3\cdot 2[ClO_4]$
Formula mass	568.95	499.73
Temperature [K]	203(2)	203(2)
Wavelength [Å]	0.71073	0.71073
Crystal system	triclinic	monoclinic
Space group	$P\bar{1}$	$P2_1$
a [Å]	6.8494(12)	9.739(2)
b [Å]	10.764(2)	7.1341(17)
c [Å]	17.819(3)	13.785(3)
α [°]	87.336(4)	90
β [°]	79.461(4)	105.772(4)
γ [°]	73.991(4)	90
Volume [Å^3]	1241.4 (4)	921.7(4)
Z	2	2
Density (calculated) [g cm^{-3}]	1.522	1.801
Absorption coefficient [mm^{-1}]	1.137	1.535
F(000)	592	510
Crystal size [mm]	0.28 × 0.14 × 0.12	0.28 × 0.24 × 0.05
Crystal color	blue	blue
Crystal description	rod	plate
θ range of data collection [°]	1.97−28.33	2.17−28.40
Index range	$-9 \le h \le 6$ $-6 \le k \le 14$ $-14 \le l \le 23$	$-12 \le h \le 13$ $-9 \le k \le 9$ $-18 \le l \le 18$
Reflections collected	10779	11593
Independent reflections	4805 [R_{int} = 0.0627]	4565 [R_{int} = 0.0338]
Absorption correction	Siemens SADABS program multi-scan	Bruker AXS Saint program Vers. 6.0
Max./min. transmission	1.00/0.69	−/−
Refinement method	full-matrix least-squares on F^2	full-matrix least-squares on F^2
Data/restraints/parameters	2970/0/364	3533/1/263
Goodness-of-fit on F^2	0.933	0.985
Final *R* indices [$I > 2\sigma(I)$]	*R*1 = 0.0571, *wR*2 = 0.1332	*R*1 = 0.0606, *wR*2 = 0.1574
R indices (all data)	*R*1 = 0.0928, *wR*2 = 0.1515	*R*1 = 0.0774, *wR*2 = 0.1770
Largest diff. peak/hole [e·Å^{-3}]	0.811/−0.440	0.993/−0.577

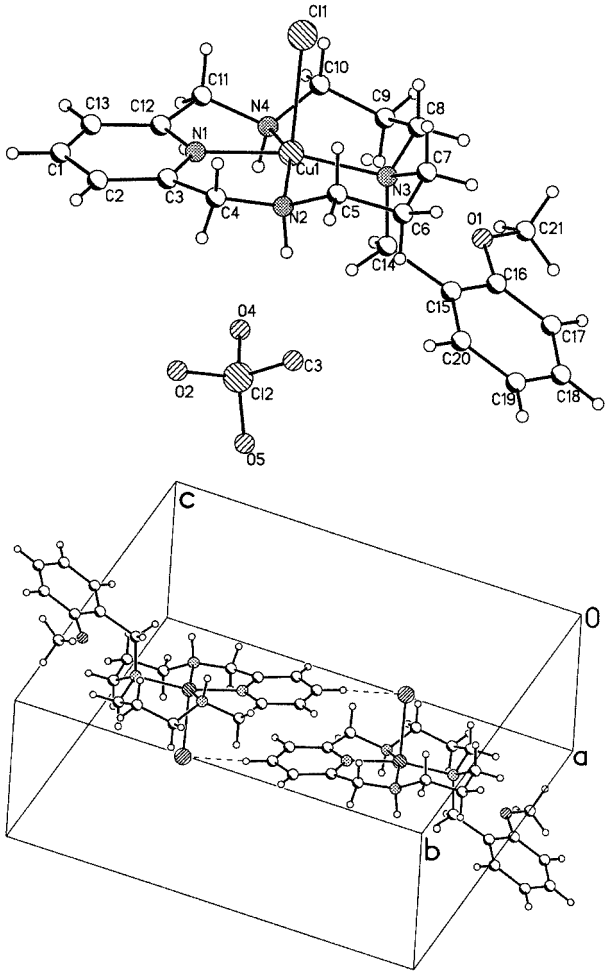

Figure 1. Molecular structure of **Cu-3** in the crystal; selected bond lengths [Å] and angles [°]: Cu1−Cl1 2.564, Cu1−N1 1.938, Cu1−N2 2.023, Cu1−N3 2.026, Cu1−N4 2.054; N1−Cu1−Cl1 92.8, N2−Cu1−Cl1 100.8, N3−Cu1−Cl1 101.1, N4−Cu1−Cl1 97.4, N2−Cu1−N1 81.9, N3−Cu1−N1 166.1, N4−Cu1−N1 81.0, N3−Cu1−N2 95.6, N4−Cu1−N2 155.6, N4−Cu1−N3 96.7

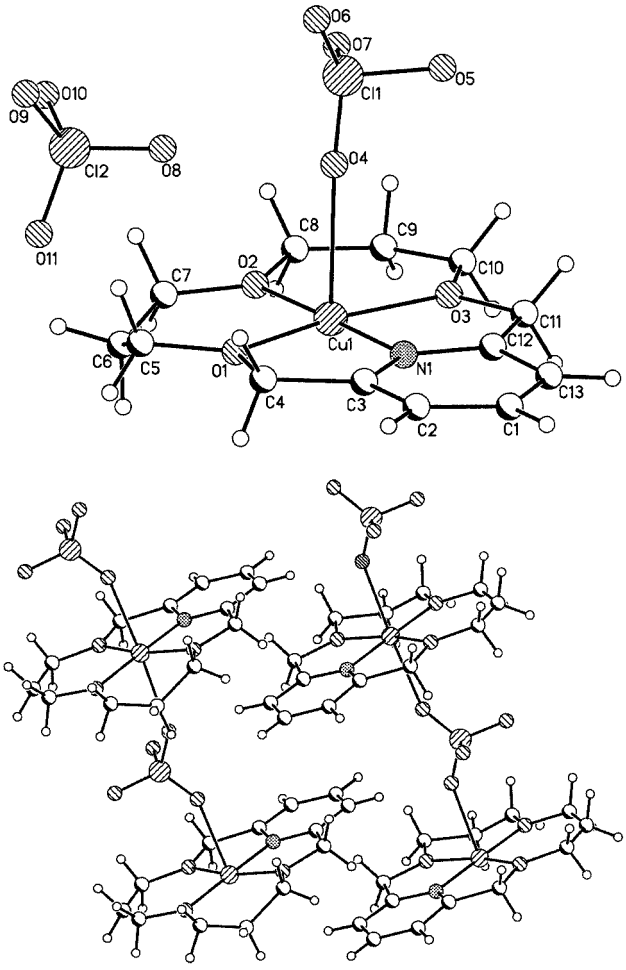

Figure 2. Molecular structure of **Cu-6** in the crystal; selected bond lengths [Å] and angles [°]: Cu1−N1 1.885, Cu1−O1 1.955, Cu1−O2 1.931, Cu1−O3 1.964, Cu1−O4 2.425; O1−Cu1−N1 81.5, O2−Cu1−N1 178.7, O3−Cu1−N1 81.6, O4−Cu1−N1 89.6, O2−Cu1−O1 98.1, O3−Cu1−O1 163.0, O4−Cu1−O1 91.9, O3−Cu1−O2 98.8, O4−Cu1−O2 91.6, O4−Cu1−O3 86.9

coordinated to two Cu^{II} centers as a bridging ligand with Cu^{II}−O distances of 2.425 and 2.433 Å, respectively, in a range (2.2−2.9 Å) commonly observed for axial Cu−O bond lengths.[17] Thus, the coordination geometry of **Cu-6** is essentially tetragonal-octahedral. Oxygen atom O(5) is disordered over two sites with occupancies of 0.68−0.32. In both complexes, the pyridine ring adopts an offset face-to-face orientation.

Infrared Spectra

The spectra of the free ligands **1**−**5** show sharp, medium-intensity bands at 3250−3300 cm^{-1} for the N−H valence vibrations. All ligands showed two bands around 1590 cm^{-1} for the C=N valence vibration of the pyridine ring (Table 2). On Cu^{II} complexation, the N−H valence bands are shifted by about 15−150 cm^{-1} to lower frequencies. For **Cu-1** and **Cu-2** two N−H valence vibrations are observed,

Table 2. Characteristic infrared frequencies [cm^{-1}] of complexes **Cu-1**−**Cu-6**; frequencies of the free ligands **1**−**6** are given in parentheses; the most intense lines are in italics

Complex	$\tilde{\nu}$(N−H)	$\tilde{\nu}$(C=N)	$\tilde{\nu}$(ClO_4^-)
Cu-1	3250, 3221 (3242, 3220)	1609, 1583 (1588, 1576)	1098, 1068, 624
Cu-2	3240, 3223 (3247, 3218)	1605, 1582 (1589, 1571)	1122, 1064, 624
Cu-3	3225, 3163 (3378)	1600, 1583 (1598, 1560)	*1107*, 1054, 623
Cu-4	3243 (3310)	1608, 1585 (1593, 1576)	*1108*, 1066,[a] 624
Cu-5	3354 (3369, 3288)	1607, 1585 (1594, 1578)	1147, 1111, *1091*,[a] 627
Cu-6	– –	1608, 1585 (1590, 1574)	*1085*, 1061, 1038,[a] 621

[a] Assignment ambiguous due to superposition with $\tilde{\nu}$(C−O).

in line with the different chemical environment of the NH groups located in *cis* and *trans* positions with respect to the pyridine nitrogen atom. As the higher wavenumber vibration is missing in the spectra of **Cu-3** and **Cu-4** but found in **Cu-5** (for which the lower wavenumber is absent), we assign this band to the *trans*-oriented NH group. In the complexes, the pyridine ν(C=N) bands are uniformly shifted to higher frequencies by 10−20 cm^{-1}, but virtually unaffected by the variation of the coordinating ring atoms.

The typical ν_3 (antisymmetric stretch) and ν_4 (antisymmetric bent) modes of noncoordinated perchlorate give rise to single, strong absorptions. In complexes **Cu-1**−**Cu-6** the perchlorate absorption at about 1100 cm^{-1} (ν_3) is split into two or three components, whereas the sharp strong band at 620 cm^{-1} (ν_4) remained a singlet. Thus, in the solid state, the symmetry of the perchlorate ions in these complexes is lowered.[7] However, it is not certain whether this is the result of coordination or of crystal packing effects. The latter appears to be more likely because the X-ray structure of **Cu-3** revealed that here the perchlorate is not coordinated to Cu^{II}.

Electronic Absorption

Complexes **Cu-1**−**Cu-6** show broad electronic absorptions in the 550−800-nm region (Table 3), typical for d−d transitions of Cu^{II} in a weak tetragonal field.[24] The absorption maxima show a red-shift (i.e. decreasing ligand-field strength) with increasing number of coordinating oxygen atoms, ranging from λ_{max} = 560 nm for the tetra-*N*-substituted complexes **Cu-1**−**Cu-3** to 793 nm for the tris-O complex **Cu-6**. This red-shift is accompanied by a similar decrease of the molar extinction coefficient ε. With respect to the parent complex **Cu-1**, the methyl and methoxybenzyl substituents in **Cu-2** and **Cu-3**, respectively, have virtually no effect on the absorption maxima but appear to decrease slightly the molar extinction. However, the red-shift of the absorption maxima is markedly different for the various positions with respect to the pyridine ring. Replacement of the nitrogen atom *trans* to the pyridine ring by an oxygen atom, viz. **Cu-1**−**Cu-3** → **Cu-4** and **Cu-5** → **Cu-6**, shifts the absorption maximum by $\Delta\lambda \approx 40$ nm^{-1} toward longer wavelengths, whereas replacement of the *cis* nitrogen atoms, viz. **Cu-1**−**Cu-3** → **Cu-5** and **Cu-4** → **Cu-6**, induces an approximate fivefold stronger shift of $\Delta\lambda \approx 190-200$ nm^{-1}. This discontinuity in the λ_{max} values on *cis*-N→O replacement is paralleled by a decrease of the extinction coefficient ε and a "jump" in the *g* values of the EPR spectra (see below), both indicating a significant change of the coordination geometry from a distorted tetragonal (square-based pyramidal) to a more octahedral tetragonal structure. In line with the stronger effect exerted by a *cis*-oxygen atom, the Cu^{II}-EDTA complex, having a *cis*-2N-2O coordination arrangement, shows a λ_{max} value of ca. 730 nm.[19] For the observed dependencies of the d−d transitions on the ligand substitution pattern, possible Cu^{II} complexes of the hitherto unknown ligands **7** and **8** should have absorption maxima around 700 and 740 nm, respectively.

Table 3. Visible electronic absorptions of Cu^{II} complexes in aqueous solution (298 K)

Complex	λ_{max} [nm]	lgε [$M^{-1}cm^{-1}$]
Cu-1	565[a]	2.56
Cu-2	560[b]	2.29
Cu-3	563	2.13
Cu-4	603	2.18
Cu-5	757	1.42
Cu-6	793	1.36
Cu-EDTA[19]	730	
$Cu(ClO_4)_2$	820	1.04
Cu_2Zn_2SOD[20]	680	2.1

[a] Ref.[21] 544 (2.24) nm, in nitromethane. [b] Ref.[7] 560 (2.25) nm, in methanol; ref.[8] 560 (1.87) nm, in 0.1 M $NaNO_3$.

Electron Paramagnetic Resonance

To check whether the characteristics of the X-ray structures, the UV/Vis spectra, and/or the SOD-like activities (see below) of our Cu complexes are reflected by their EPR spectral features, the EPR spectra of **Cu-1**−**Cu-6** were examined in liquid (Figure 3, Table 4) and frozen (77 K) aque-

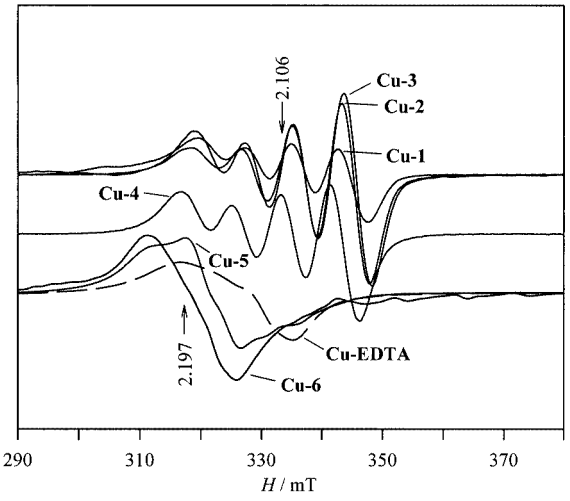

Figure 3. EPR spectra of the copper complexes **Cu-1**−**Cu-6** in aqueous solution (298 K)

Table 4. EPR parameters of Cu^{II} complexes in aqueous solution (298 K)

Complex[a]	g_{app}	A_{iso} [mT]
Cu-1	2.101	7.80
Cu-2	2.099	8.05
Cu-3	2.102	8.32
Cu-4	2.112	8.18
Cu-5	2.176	ca. 4.9
Cu-6	2.197	n.r.[b]
Cu-EDTA	2.134	n.r.

[a] Instrument settings: scan range 150 mT, modulation amplitude 0.5 mT, modulation frequency 100 kHz, microwave power 20 mW, microwave frequency 9.77−9.79 GHz. [b] Not resolved.

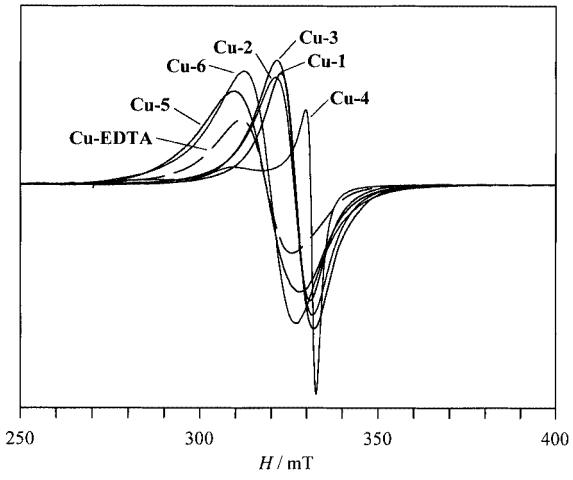

Figure 4. EPR spectra of the copper complexes **Cu-1**−**Cu-6** in frozen aqueous solution (77 K)

Table 5. EPR parameters of Cu complexes in frozen aqueous solution (77 K)

Complex[a]	g_{app}	$g_\perp$	$g_\parallel$	$A_\parallel$ [mT]
Cu-1	2.090	2.086[b]	2.107	≤ 5.5
Cu-2	2.085	2.084[c]	2.105	≤ 5.5
Cu-3	2.082	2.082	2.200	17.4
Cu-4	–	2.056	2.209	≤ 1.5
Cu-5	2.139	–	–	–
Cu-6	2.134	2.128	2.180	8.4
Cu-EDTA	2.136	–	–	–
Cu_2Zn_2SOD[24]	–	2.073	2.267	13.3

[a] Instrument settings: scan range 150 mT, modulation amplitude 0.5 mT, modulation frequency 100 kHz, microwave power 20 mW, microwave frequency 9.52−9.55 GHz. [b] Ref.[8] $g_1 = 2.040$, $g_2 = 2.110$, $g_3 = 2.178$, $A_1 = 4.8$, $A_2 = 9.8$, $A_3 = 199.3$ cm^{-1}; in 1 M $NaClO_4$. [c] Ref. [7] $g_\perp = 2.052$, $g_\parallel = 2.19$; polycrystalline sample, 298 K.

ous solutions (Figure 4, Table 5). The spectra show the expected characteristics of distorted (axially elongated) tetragonal coordination of Cu^{II} ($S = 1/2$) with $g_\parallel > g_\perp$,[18,22] thus indicating a $d_{x^2-y^2}$ ground state. EPR data for Cu^{II}-EDTA and Cu_2Zn_2-SOD are given for comparison. In liquid solution, **Cu-1**−**Cu-3** show virtually identical, nearly isotropic EPR spectra with a well-resolved $^{63/65}$Cu hyperfine splitting in the range of 8 mT (Figure 3), confirming that the additional ring substituents in **Cu-2** and **Cu-3** have only a marginal effect on the spectral properties, in agreement with the absorption spectral properties.

Replacement of the *trans*-nitrogen atom by an oxygen atom in **Cu-4** yields a similarly resolved spectrum with only the apparent *g* factor slightly shifted to higher values. Replacement of the *cis*-nitrogen atoms by oxygen atoms (**Cu-5**), however, results in both a stronger *g* shift to higher values and an increased anisotropy of the spectra, as well as a reduced copper splitting [$a(^{63/65}Cu) \approx 4.9$ mT]. These effects are further pronounced for **Cu-6**. Thus, a replacement of a *cis*-N by O has a stronger effect on the *g* factor than replacement of the *trans*-N by O. These observations strikingly parallel the above-mentioned shifts of the UV/Vis absorption maxima. In addition, the apparent *g* factor of Cu^{II}-EDTA,[23] which has a 2N-2O coordination pattern similar to the arrangement in the macrocycle **8**, lies in between the *g* factors of **Cu-1**−**Cu-4** and **Cu-5** and **Cu-6**. The small spectral features between 330 and 370 mT in the EPR spectrum of **Cu-6** are probably due to a Cu^{II}-containing impurity. Because these signals could not be diminished by repeated recrystallization, they might belong to a copper complex formed from, and in equilibrium with, **Cu-6** in the aqueous phase. The uncommonly low *g* value of about 1.951 [$a(^{63/65}Cu) \approx 8.9$ mT] of this feature would indicate a d_z^2 ground state ($g_\perp > g_\parallel \approx 2$)[18,22] for this species.

In frozen (77 K) aqueous solution (Figure 4) a $^{63/65}$Cu hyperfine splitting can no longer be resolved in any of the spectra. The spectra of **Cu-1**−**Cu-3**, **Cu-5**, and **Cu-6** all consist of a single, broad line with apparent *g* values as given in Table 5. The spectral resolution could not be improved by tenfold dilution and lower microwave power and modulation settings, in agreement with observations by Costa and Delgado[8] who noted for **Cu-1** and related complexes the loss of resolution in solutions of low ionic strength (Table 5, footnote[b]). The anisotropic parameters (Table 5) were evaluated by spectral simulation and are approximate values because of the low resolution. Nevertheless, they are typical for Cu^{II} in a distorted tetragonal environment. As was observed for liquid aqueous solution, the apparent *g* factors are shifted to higher values, from 2.085 to about 2.140, with increasing number of oxygen atoms in the macrocyclic ring. However, two distinct differences compared with the liquid-phase spectra are apparent. First, the spectra of **Cu-5** and **Cu-6** now show approximately the same apparent *g* factor (ca. 2.134−9), similar to that of Cu-EDTA; second, the spectrum of **Cu-4** displays a clear separation of the parallel and perpendicular components of the *g* tensor and also has a smaller linewidth than the other spectra. We have no straightforward explanation for this unique feature of **Cu-4**. As the spectrum of **Cu-4** is strikingly similar to those observed for polycrystalline samples of **Cu-2** and related complexes at ambient temperature,[4] it might indicate that the coordination sphere in frozen water is very similar to that in the solid state.

Electrochemical Properties

Cyclic voltammograms of complexes **Cu-1**−**Cu-4** and **Cu-6** were examined in oxygen-free aqueous solution at room temperature. Potassium chloride was employed as supporting electrolyte to achieve a better correspondence with the conditions of the SOD activity measurements (see below). All complexes showed a quasi-reversible redox wave (E^1) in the range +0.37 to +0.42 V vs. NHE and an apparent irreversible cathodic peak (E^2_{pc}) between −0.13 and −0.36 V (Table 6). The latter potential might be quasi-reversible but the corresponding anodic peak was overlayed by a strong adsorption peak which appeared between 0 and +0.15 V on the subsequent oxidation cycle. Very similar voltammograms were obtained for hydrated Cu^{II} ions from solutions of copper(II) perchlorate and copper(II) sulfate un-

der the same conditions. The data of Table 6 display no dramatic variation of the potentials with the nature of the ligands. The quasi-reversible potentials $E^1_{1/2}$ of **Cu-1**−**Cu-3** differ only by 10 mV, the cathodic peak potentials E^2_{pc} by ca. 50 mV. Replacement of N by O in the macrocyclic ligand (**Cu-4**, **Cu-6**) shifted the E^1 potentials toward slightly (20−40 mV) more positive values, approaching the values for $CuSO_4$ and $Cu(ClO_4)_2$. The same is true for E^2_{pc} with the exception of **Cu-4** for which a cathodic shift of ca. 200 mV was observed. However, inspection of Table 6 clearly reveals that neither the E^1 nor the E^2_{pc} potential would account for the unique, though low SOD activity of **Cu-3** (see below, Table 7), as its anodic redox potential does not differ from those of **Cu-1** and **Cu-2**, and, also, the SOD activities of all copper compounds (see below) do not parallel the variation of the E^2_{pc} values. Thus, the redox potentials of the Cu^{II} complexes are not essentially associated with their SOD activities.

Table 6. Cyclic voltammetric data [V vs. NHE] of the copper(II) complexes

Compound[a]	E^1_{pa}	E^1_{pc}	$E^1_{1/2}$[b]	E^2_{pc}[c]
Cu-1	0.439	0.322	0.381	−0.164
Cu-2	0.438	0.317	0.378	−0.138
Cu-3	0.465	0.287	0.376	−0.214
Cu-4	0.491	0.318	0.405	−0.358
Cu-6	0.466	0.366	0.416	−0.056
$Cu(ClO_4)_2$	0.463	0.335	0.400	−0.068
$CuSO_4$	0.446	0.314	0.414	−0.005

[a] At 1 mM and a scan rate of 0.1 V s^{-1}. [b] Quasi-reversible, $E_{1/2} = (E_{pa} + E_{pc})/2$. [c] Irreversible or quasi-reversible.

Superoxide Dismutase Activity

Copper(II) complexes **Cu-2**−**Cu-4**, and **Cu-6** were examined with regard to their Superoxide Dismutase (SOD) mimetic activity by the method of Paoletti et al.[25] For comparison purposes, hydrated Cu^{II} [employed as $Cu(ClO_4)_2$] was also investigated. The applied method is based on the oxidation of β-nicotinamide adenine dinucleotide (β-NADH) by mercaptoethanol/EDTA/Mn^{2+} at pH = 7.4. In the presence of molecular oxygen, this system generates superoxide ($O_2^{\cdot -}$), which, in turn, oxidizes NADH to NAD^+. Based on the kinetics of the oxidation of NADH in the presence and absence (control) of copper(II) complexes, the SOD-mimetic potential was determined. Addition of SOD or a SOD-active compound inhibits the oxidation of NADH, which is monitored UV-spectroscopically by the retarded decay of the absorption of NADH at 340 nm. After an initially progressive course, the decline of the absorption follows apparent zero-order kinetics (Figure 5, inset). These parts of the decay traces were used for the subsequent evaluation of the rates. To determine the SOD activity, the percentage of the rate of inhibition of NADH oxidation (control: absence of SOD-mimic = 100%) was plotted against the initial concentration of the copper complexes (Figure 5). For all complexes the inhibition of the oxidation rate is not proportional to the concentrations of copper complexes but rather follows an exponential dependence. The IC_{50} value, that is the amount of complex reducing the rate of the NADH oxidation by 50%, was extracted from the graphs (Table 7). Since catalase does not interfere in the above reaction, this enzyme was used to remove the produced hydrogen peroxide so as to determine whether the peroxide and/or its possible reaction products affect the assay. As the catalytic activity in the presence of catalase[26] did not change, inhibition by hydrogen peroxide and its possible products can be excluded.

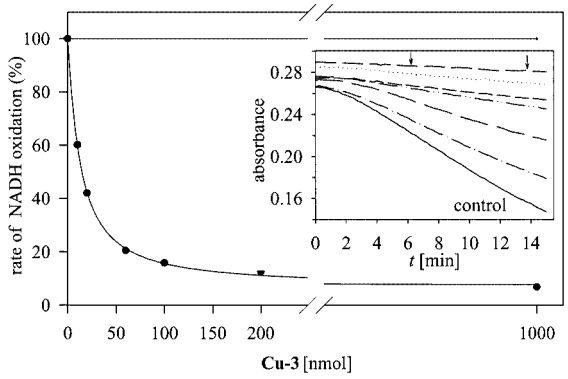

Figure 5. Inhibition of NADH oxidation as a function of **Cu-3** concentration; inset: kinetic traces of NADH oxidation monitored at 340 nm at different concentrations of **Cu-3**

Table 7. Comparison of superoxide dismutase activity at 296 K

Compound	IC_{50} [μM]	Cu/NADH ratio
Cu-2	247	1:1.07
Cu-3	28	1:9.46
Cu-4	206	1:1.29
Cu-6	126	1:2.10
$Cu(ClO_4)_2$	247	1:1.07

The IC_{50} values and the Cu/NADH ratios listed in Table 7 reveal that complexes **Cu-2** and **Cu-4** do not show any true catalytic activity, rather, they convert $O_2^{\cdot -}$ in a roughly 1:1 stoichiometric ratio, similar to copper(II) perchlorate. Likewise, **Cu-6** does not appear to be a catalyst, reacting with $O_2^{\cdot -}$ in a 1:2 stoichiometry. Hence, simple exchange of the coordinating atoms, i.e. N vs. O, in the macrocyclic ring does not effect the SOD-like activity of this type of Cu^{II} complexes. However, for complex **Cu-3**, which carries a methoxybenzyl pendent arm, a low but unequivocal catalytic activity is found. The data indicate a turnover of about 10, i.e. one molecule of the complex decomposes about ten molecules of superoxide before being deactivated.

Investigation of the SOD-mimetic activity of complexes by employing indirect methods like the one chosen here are frequently hampered because "free" (hydrated) Cu^{II} ions also react with $O_2^{\cdot -}$, as is demonstrated here by $Cu(ClO_4)_2$. Thus, the question arises as to whether the present copper complexes or low amounts of free Cu^{II} ions, deriving from dissociation of the complexes or impurities, are responsible for the observed reaction. The latter possibility can be ex-

cluded on the basis of the control experiments with copper(II) perchlorate. Further, the stability of our complexes was confirmed by EPR experiments in which a tenfold excess of EDTA added to aqueous solutions of the complexes produced no detectable changes in the EPR spectra of **Cu-1**−**Cu-6**.

The catalytic activity of **Cu-3** is rather surprising as the above spectroscopic and electrochemical data do not indicate any unique physicochemical properties in solution compared with the analogues **Cu-1** and **Cu-2**. Indeed, the oxygen-substituted systems **Cu-4**−**Cu-6** which indeed show marked variations in their UV/Vis and EPR spectra, behave very similarly to **Cu-1** and **Cu-2**. Exploratory experiments were performed with regard to the mechanistic background for the enhanced activity of **Cu-3**. In complex **Cu-3**, the fifth coordination site in the solid state is occupied by a chloride ion, whereas in the nonactive complexes **Cu-2**, **Cu-4**, and **Cu-6** this site is occupied by a second perchlorate ion. Thus, the chloride coordination might be responsible for the catalytic activity of **Cu-3**. Experiments were, therefore, performed in which large amounts (50 mM) of potassium chloride were added to the reaction mixture. However, no changes in the catalytic activities of all complexes were detected. As neither contamination by "free" Cu^{II} nor different coordinating counterions account for the different activity of **Cu-3**, it appears that the methoxybenzyl side chain in **Cu-3** is responsible. The X-ray structure of **Cu-3** showed that the methoxybenzyl substituent is not coordinated via the oxygen atom to the copper center but rather directed outward (Figure 3). Such an arrangement would make a significant influence of the pendent arm on the SOD activity very unlikely. However, in solution the situation might change due to free rotational movement of the methoxybenzyl group. Trial PM3(tm) calculations indeed favor (at least in the gas phase) an arrangement of the substituent where the methoxy oxygen atom is coordinated to the central Cu^{II} ion (Figure 6).

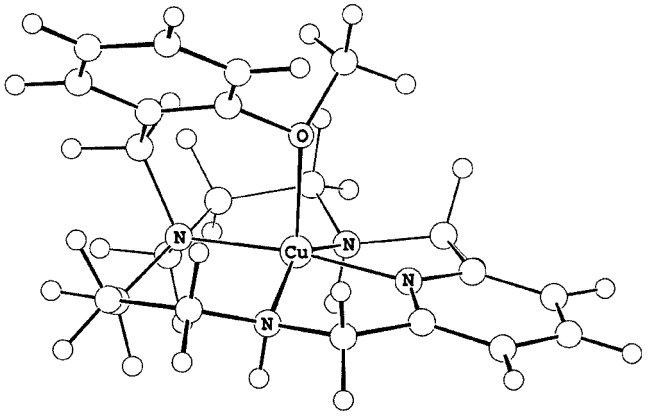

Figure 6. Optimized PM3 structure for **Cu-3**

Therefore, in aqueous solution the methoxybenzyl substituent might "protect" one of the axial positions against further, deactivating reactions (e.g. from attack of a second superoxide molecule) when the substrate superoxide has associated to the opposite side. Such a blocking function might be a crucial feature for the catalytic activity of the complex. However, from the currently available data, no further conclusions concerning the reaction mechanism can be made. Further work is necessary for a deeper insight into the mechanism of superoxide dismutation.

Experimental Section

Instrumentation: ^1H and ^{13}C NMR spectra: Bruker DRX 500 and Varian Gemini 200. Melting points (uncorrected): Elektrothermal 9100. IR: Bio-Rad Series FTS 135 FT-IR. UV/Vis: J&M TIDAS Detector NMC 301. EPR: Bruker ESP 300E. Elemental analysis: Carlo Erba 1010 CHNSO. Cyclic voltammetry: ECO-Chemie Autolab GPES.

Materials: The following compounds were prepared according to published procedures: pyridine-2,6-dicarbaldehyde,[27] 3,7,11,17-teraazabicyclo[11.3.1]heptadeca-1(17),13,15-triene (**1**),[6] {2,12-dimethyl-3,7,11,17-tetraazabicyclo[11.3.1]heptadeca-1(17),2,11,13,15-pentaene}nickel(II) perchlorate,[13] {2,12-dimethyl-3,7,11,17-tetraazabicyclo[11.3.1]heptadeca-1(17),13,15-triene}nickel(II) perchlorate,[13] (2*R*,12*S*)-2,12-dimethyl-3,7,11,17-tetraazabicyclo[11.3.1]-heptadeca-1(17),13,15-triene monohydrate (**2**),[28,29] *N*,*N*-bis(2-cyanoethyl)-2-methoxybenzylamine, *N*,*N*-bis(3-aminopropyl)-2-methoxybenzylamine,[1] 7-(2-methoxybenzyl)-3,7,11,17-tetraazabicyclo[11.3.1]heptadeca-1(17),13,15-triene (**3**),[1] 2,6-bis[(tosyloxy)methyl]pyridine,[30] dipropanolamine,[31] 4-oxa-1,7-heptanediol,[14] 4-oxaheptane-1,7-diyl ditosylate,[14] 3,7,11-trioxa-17-azabicyclo[11.3.1]heptadeca-1(17),13,15-triene (**6**).[14] Reduced adenine dinucleotide (β-NADH, disodium salt) and diethyleneaminotetraacetic acid (EDTA) were obtained from Sigma, while manganese(II) chloride dihydrate and 2-mercaptoethanol were supplied by Merck and 3,3′-oxydipropionitrile by Fluka. Reagents and solutions: triethanolamine/diethanolamine (Tea-Dea) buffer (100 mM each, pH = 7.4); NADH (7.5 mM); EDTA/$MnCl_2$ (100 mM/50 mM); mercaptoethanol (10 mM).

3,3′-Oxydipropaneamine: The literature synthesis[32] was improved as follows: Raney nickel (3 g) was added to a solution of 3,3′-oxydipropionitrile (2.06 g, 16.6 mmol), dissolved in methanol (40 mL), containing anhydrous ammonia (5.2 g, 0.31 mol). The nitrile was hydrogenated under pressure (8 bar) at room temperature, until no drop in pressure was observed (10 h). The residue was filtered off and the product obtained by distillation under reduced pressure (2.0 g, 15.1 mmol, 91%). ^1H NMR (500 MHz, CD_3OD): δ = 1.66 (m, 4 H, 2 × CH_2), 2.66 (t, ^3J = 6.5 Hz, 4 H, 2 × CH_2), 3.44 (t, ^3J = 6.2 Hz, 4 H, 2 × CH_2) ppm. ^{13}C NMR (75 MHz, CD_3OD): δ = 33.77 (2 × CH_2), 40.11 (2 × CH_2), 70.13 (2 × CH_2) ppm.

7-Oxa-3,11,17-triazabicyclo[11.3.1]heptadeca-1(17),13,15-triene (4): A solution of pyridine-2,6-dicarbaldehyde (3.25 g, 24.0 mmol) in ethanol was added to a stirred solution of copper nitrate trihydrate (5.80 g, 24.0 mmol) in water (65 mL), resulting in a pale green mixture. A solution of 3,3′-oxydipropioamine (3.24 g, 24.5 mmol) in ethanol (10.0 mL) was then added dropwise with rapid stirring over 30 min and the resulting dark blue solution was refluxed for 2 h, then cooled to 5 °C in an ice/brine bath and sodium borohydride (2.30 g, 60.4 mmol) added. After 30 min, the solution was stirred at room temperature for 2 h, heated at 60 °C for 1 h, and stirred further at room temperature for several hours. The copper(II) was removed by treating the mixture with sodium sulfide nonahydrate (14.41 g, 60 mmol) followed by stirring at 60 °C for 1 h, and the solution was then cooled and the copper(II) sulfide removed by

filtration through Celite. Ethanol was evaporated, the residue extracted three times with dichloromethane, and the combined extracts dried with $MgSO_4$. After removal of the dichloromethane by evaporation, the resultant light brown residue was purified by chromatography (chloroform, neutral aluminium oxide). The product was obtained as a colourless solid (3.16 g, 13.4 mmol, 56%). ^{1}H NMR (500 MHz, $CDCl_3$): δ = 1.82 (m, 4 H, CH_2), 2.59 (t, ^3J = 5.5 Hz, 4 H, CH_2), 3.54 (t, ^3J = 5.5 Hz, 4 H, CH_2), 3.70 (s, 2 H, N*H*), 3.89 (s, 4 H, CH_2), 6.99 (d, ^3J = 7.6 Hz, 2 H, C*H*), 7.52 (dd, 1 H, ^3J = 7.6 Hz, C*H*) ppm. ^{13}C NMR (75 MHz, $CDCl_3$): δ = 29.28 (*C*H$_2$), 45.39 (*C*H$_2$), 53.91 (*C*H$_2$), 68.34 (*C*H$_2$), 120.81 (*C*H), 136.72 (*C*H), 158.53 (*C*) ppm. $C_{13}H_{21}N_3O$ (235.33): calcd. C 66.35, H 8.99, N 17.86; found C 66.05, H 9.17, N 17.61.

3,11-Dioxa-7,17-diazabicyclo[11.3.1]heptadeca-1(17),13,15-triene (5): Macrocycle **5** was prepared from (1.81 g, 4.0 mmol) 2,6-bis[(tosyloxy)methyl]pyridine and dipropanolamine (0.54 mg, 4.0 mmol) in a similar fashion to the procedure of Bradshaw et al.[14] The product thus obtained was a colourless solid (0.51 g, 2.16 mmol, 54%). ^{1}H NMR (200 MHz, $CDCl_3$): δ = 1.91 (m, 4 H, CH_2), 3.05 (br. m, 8 H, CH_2), 4.67 (s, 4 H, CH_2), 7.20 (d, 2 H, C*H*), 7.68 (dd, 1 H, C*H*) ppm. ^{13}C NMR (50 MHz, $CDCl_3$): δ = 30.12 (*C*H$_2$), 49.15 (*C*H$_2$), 65.83 (*C*H$_2$), 72.72 (*C*H$_2$), 117.12 (*C*H), 123.52 (*C*H), 158.88 (*C*) ppm. $C_{13}H_{20}N_2O_2$ (236.31): calcd. C 66.07, H 8.53, N 11.86; found C 66.33, H 8.55, N 11.92.

Copper Complexes Cu-1−Cu-6: The preparation of **Cu-1**[6] and **Cu-2**[7] has been reported before. All solid complexes were obtained in good yields (> 65%) by mixing ethanolic solutions of the appropriate ligands with equimolar solutions of cupric perchlorate hexahydrate in ethanol at room temperature. The precipitated complexes were isolated by filtration and purified by washing several times with cold ethanol. Whereas complexes **Cu-1**, **Cu-2**, and **Cu-4−Cu-6** were instantaneously formed on mixing of the reactants, addition of an equimolar amount of copper(II) perchlorate in ethanol to an ethanolic solution of ligand **3** initially led to rapid formation of a yellow precipitate which according to elemental analysis and EPR spectroscopy represented a Cu^{II}−ligand complex of 1:2 stoichiometry, $[Cu^{II}(\mathbf{3})_2](ClO_4)_2$ (60% yield relative to **3**). When the reaction mixture without prior separation of this complex was allowed to stand for 12 h at ambient temperature, violet crystals of complex **Cu-3** were obtained in 68% yield.

CAUTION: Metal perchlorate salts containing organic ligands are potentially explosive, and should be handled with care!

Characterization of Complexes Cu-1−Cu-6

Cu-1: Blue-purple powder (0.39 g, 68%). IR (KBr): $\tilde{\nu}$ = 3242 (NH), 3084 (CH_{Ph}), 2936 (CH_{aliph}), 624 (ClO_4) cm^{-1}. $C_{13}H_{22}Cl_2CuN_4O_8$ (496.80): calcd. C 31.43, H 4.46, Cu 12.79, N 11.28; found C 31.14, H 4.41, Cu 12.58, N 10.99. UV (water): λ_{max} (lg ε) = 565 (2.56) nm.

Cu-2: Violet-blue powder (0.76 g, 76%), decomp. 254 °C. IR (KBr): $\tilde{\nu}$ = 3223 (NH), 3094 (CH_{Ph}), 2943 (CH_{aliph}), 624 (ClO_4) cm^{-1}. $C_{15}H_{26}Cl_2CuN_4O_8$ (524.86): calcd. C 34.33, H 4.99, Cu 12.11, N 10.68; found C 34.29, H 4.97, Cu 11.84, N 10.39. UV (water): λ_{max} (lg ε) = 254 (3.90), 560 (2.29) nm.

Cu-3: Violet-blue crystals (0.39 g, 68%), decomp. 231 °C. IR (KBr): $\tilde{\nu}$ = 3226 (NH), 3068 (CH_{Ph}), 2934 (CH_{aliph}), 2893 ($CH_{methyl\ ether}$), 1600 (NH), 1248 ($CO_{aryl\ alkyl\ ether}$), 622 (ClO_4) cm^{-1}. $C_{21}H_{30}Cl_2CuN_4O_5$ (553.73): calcd. C 45.61, H 5.47, Cu 11.49, N 10.13; found C 45.31, H 5.55, Cu 11.41, N 9.84. FAB (glycerol): *m/z* (%) = 516 (3), 417 (15), 355 (34). UV (water): λ_{max} (lg ε) = 256 (3.89), 563 (2.13) nm.

Cu-4: Blue crystals (0.83 g, 73%), decomp. 290 °C. IR (KBr): $\tilde{\nu}$ = 3242 (NH), 3092 (CH_{Ph}), 2951 (CH_{aliph}), 1608 (NH), 1108 (COC), 624 (ClO_4) cm^{-1}. $C_{13}H_{21}Cl_2CuN_3O_9$ (497.78): calcd. C 31.37, H 4.25, Cu 12.77, N 8.44; found C 31.72, H 4.26, Cu 12.66, N 8.52. FAB (glycerol): *m/z* (%) = 397 (22), 298 (30). UV (water): λ_{max} (lg ε) = 255 (3.82), 603 (2.15) nm.

Cu-5: Light blue crystals (0.24 g, 65%), decomp. 291 °C. IR (KBr): $\tilde{\nu}$ = 3078 (CH_{Ph}), 2957 (CH_{aliph}), 1605 (NH), 627 (ClO_4) cm^{-1}. $C_{13}H_{20}Cl_2CuN_2O_{10}$ (498.76): calcd. C 31.31, H 4.04, Cu 12.74, N 5.62; found C 30.98, H 3.94, Cu 12.89, N 5.47. UV (water): λ_{max} (lg ε) = 757 (1.42) nm.

Cu-6: Turquoise crystals (0.36 g, 72%), decomp. 292 °C. IR (KBr): $\tilde{\nu}$ = 3084 (CH_{Ph}), 2957 (CH_{aliph}), 621 (ClO_4) cm^{-1}. $C_{13}H_{19}Cl_2CuNO_{11}$ (499.73): calcd. C 31.24, H 3.83, Cu 12.72, N 2.80; found C 31.52, H 3.82, Cu 12.43, N 2.99. FAB (glycerol): *m/z* (%) = 300 (100), 238 (83). UV (water): λ_{max} (lg ε) = 264 (3.59), 793 (1.36) nm.

Aqueous solutions of the complexes all had pH values between 7 and 8.

Kinetic Measurements: The principle of the method is based on the oxidation of NADH, mediated by superoxide radical, in a purely chemical system developed by Paoletti et al.[25] To monitor the assay we added the following solutions (see materials) into a cuvette (1-mm cell): 400 μL Tea-Dea buffer (100 mM each), 20 μL NADH solution (7.5 mM), 12.5 μL EDTA/$MnCl_2$ solution (100 mM/50 mM) and 50 μL of sample or buffer were mixed thoroughly. In a second series of experiments the reaction mixture was supplemented with 50 mM KCl. The reaction was started by rapid mixing with 50 μL of mercaptoethanol (10 mM). Rates of NADH oxidation, observed at 340 nm, were initially low, then increased progressively to yield good linear kinetics and an 8-min window was used for our calculations. The maximal rates obtained are expressed as a percentage of the control and plotted against the complex concentracion. One unit of the SOD-mimic is the amount of copper complex capable of inhibiting by 50% the rate of NADH oxidation observed in the control.

EPR Spectroscopy: X-band (9.5 GHz) EPR spectra were recorded from 1−3 mM solutions of the complexes in oxygen-free, deionized water in a TM_{110} wide-bore cavity (Bruker). For liquid solutions, a 0.4 mm inner diameter quartz flat cell (Wilmad) was used; measurements at 77 K were performed in 4 mm Suprasil quartz tubes immersed in a liquid nitrogen dewar insert. Spectral simulations were carried out with the Simfonia program (Bruker). The concentration of the copper complexes in liquid and frozen solution was checked by numerical double integration (WinEPR software, Bruker) of the EPR spectra and comparison with the integrated EPR signal of a 1 mM Cu^{II}-EDTA solution. In all cases the integration accounted for > 90% purity of the complexes.

Cyclic Voltammetry: Cyclic voltammetric measurements were performed at 20 °C in aqueous solution under nitrogen. Complex concentrations of 1 mM were employed, and 100 mM KCl was used as supporting electrolyte. A 3 mm diameter glassy-carbon working electrode, an Ag/AgCl reference electrode, and a Pt-wire counter electrode were used. Scan rates were varied from 0.01 to 1.0 V s^{-1}. Electrochemical potentials were converted into the normal hydrogen electrode (NHE) scale by addition of 0.222 V.

X-ray Crystallographic Study: CCDC-188550 (**Cu-3**) and -188551 (**Cu-6**) contain the supplementary crystallographic data for this paper. These data can be obtained free of charge at

www.ccdc.cam.ac.uk/conts/retrieving.html [or from the Cambridge Crystallographic Data Centre, 12 Union Road, Cambridge CB2 1EZ, UK; Fax: (internat.) + 44-1223/336-033; E-mail: deposit@ccdc.cam.ac.uk].

Acknowledgments

This work was supported by the Deutsche Forschungsgemeinschaft (SFB, 452).

[1] S. Autzen, H.-G. Korth, H. de Groot, R. Sustmann, *Eur. J. Org. Chem.* **2001**, 3119−3125.
[2] B. Halliwell, *New Phytol.* **1974**, *73*, 1075−1086.
[3] T. Nagano, *Yuki Gosei Kagaku* **1989**, *47*, 843−854. K. Jitsukawa, M. Harata, H. Arii, H. Sakurai, H. Masuda, *Inorg. Chim. Acta* **2001**, *324*, 108−116.
[4] J. R. Sorenson, *Prog. Med. Chem.* **1989**, *26*, 437−568.
[5] D. P. Riley, *Chem. Rev.* **1999**, *99*, 2573−2587.
[6] K. P. Balakrishnan, H. A. A. Omar, P. Moore, N. W. Alcock, G. A. Pike, *J. Chem. Soc., Dalton Trans.* **1990**, 2965−2969.
[7] L. F. Lindoy, N. E. Tokel, L. B. Anderson, D. H. Busch, *J. Coord. Chem.* **1971**, *1*, 7−16.
[8] J. Costa, R. Delgado, *Inorg. Chem.* **1993**, *32*, 5257−5265.
[9] V. Felix, M. J. Calhorda, J. Costa, R. Delgado, C. Brito, M. T. Duarte, T. Arcos, M. G. B. Drew, *J. Chem. Soc., Dalton Trans.* **1996**, 4543−4553.
[10] P. Chaudhuri, K. Wieghardt, *Progr. Inorg. Chem.* **2001**, *50*, 151−216.
[11] R. R. Fenton, R. Gauci, P. C. Junk, L. F. Lindoy, R. C. Luckay, G. V. Meehan, J. R. Price, P. Turner, G. Wei, *J. Chem. Soc., Dalton Trans.* **2002**, 2185−2193.
[12] E. V. Rybak- Akimova, A. Y. Nazarenko, S. S. Silchenko, *Inorg. Chem.* **1999**, *38*, 2974−2980. M. Mikuriya, K. Hamada, S. Kida, I. Murase, *Bull. Chem. Soc. Jpn*, **1985**, *58*, 1839−1840. J. Costa, R. Delgado, M. G. B. Drew, V. Felix, *J. Chem. Soc., Dalton Trans.* **1999**, 4331−4339. M. Di Casa, L. Fabbrizzi, M. Licchelli, A. Poggi, D. Sacchi, M. Zema, *J. Chem. Soc., Dalton Trans.* **2001**, 1671−1675. K. Panneerselvam, T.-H. Lu, T.-Y. Chi, F.-L. Liao, C.-S. Chung, *Anal. Sci.,* **2000**, *16*, 441−442. K. Mochizuki, S. Miyashita, *Chem. Lett.* **1996**, 899−900. H. Keypour, S. Salehzadeh, R. G. Pritchard, R. V. Parish, *Inorg. Chem.* **2000**, *39*, 5787−5790.
[13] J. L. Karn, D. H. Busch, *Inorg. Chem.* **1969**, *8*, 1149−1153.
[14] J. S. Bradshaw, J. M. Guynn, S. G. Wood, B. E. Wilson, N. K. Dalley, R. M. Izatt, *J. Heterocycl. Chem.* **1987**, *24*, 415−419.
[15] M. M. Abu-Omar, L. D. McPherson, J. Arias, V. M. Béreau, *Angew. Chem.* **2000**, *112*, 4480−4483; *Angew. Chem. Int. Edit.* **2000**, *39*, 4310−4313.
[16] V. L. Goedken, Y.-A. Park, *J. Chem. Soc., Chem. Commun.* **1975**, 214−215.
[17] T. Murakami, S. Hatakeyama, S. Igarashi, Y. Yukawa, *Inorg. Chim. Acta* **2000**, *310*, 96− 102.
[18] B. J. Hathaway in *Comprehensive Coordination Chemistry*, vol. 5, chapter 53 (Ed.: G. Wilkinson), Pergamon Press, Oxford, **1987**, p. 594−744.
[19] C. K. Jørgensen, *Acta Chem. Scand.* **1955**, *9*, 1362−1377.
[20] M. Linss, U. Weser, *Inorg. Chim. Acta* **1986**, *125*, 117−121.
[21] N. W. Alcock, K. P. Balakrishnan, P. Moore, G. A. Pike, *J. Chem. Soc., Dalton Trans.* **1987**, 889−894.
[22] J. R. Pilbrow *Transition Metal Ion Electron Paramagnetic Resonance*, Clarendon Press, Oxford, **1990**, pp. 9, 30, 154, 484.
[23] F. S. Stephens, *J. Chem. Soc. A* **1969**, 1723−1734.
[24] R. A. Lieberman, R. H. Sands, J. A. Fee, *J. Biol. Chem.* **1982**, *257*, 336−344.
[25] F. Paoletti, D. Aldinucci, A. Mocali, A. Caparrini, *Anal. Biochem.* **1986**, *154*, 536−541.
[26] F. Paoletti, A. Mocali, *Methods Enzymol.* **1990**, *186*, 209−220.
[27] N. W. Alcock, R. G. Kingston, P. Moore, C. Pierpoint, *J. Chem. Soc., Dalton Trans.* **1984**, 1937−1943.
[28] A. C. Melnyk, N. K. Kildahl, A. R. Rendina, D. H. Busch, *J. Am. Chem. Soc.* **1979**, *101*, 3232−3240.
[29] C. J. Cairns, R. A. Heckman, A. C. Melnyk, W. M. Davis, D. H. Busch, *J. Chem. Soc., Dalton Trans.* **1987**, 2505−2510.
[30] J. S. Bradshaw, P. Huszthy, C. W. McDaniel, C. Y. Zhu, N. K. Dalley, R. M. Izatt, *J. Org. Chem.* **1990**, *55*, 3129−3137.
[31] C. Granier, R. Guilard, *Tetrahedron* **1995**, *51*, 1197−1208.
[32] P. F. Wiley, *J. Am. Chem. Soc.* **1946**, *68*, 1867−1868.

Received July 12, 2002
[I02379]

Direct Synthesis of $(PhSe)_4Ge$ and $(PhTe)_4Ge$ from Activated Hydrogenated Germanium − Crystal Structure and Twinning of $(PhTe)_4Ge$

Sabine Schlecht*[a] and Karen Friese[b]

Keywords: Germanium / Tellurium / Van der Waals interactions / Active metals

The germanium chalcogenolates $(PhSe)_4Ge$ and $(PhTe)_4Ge$ were synthesized from activated hydrogenated germanium (Ge*) and diphenyldiselenide or diphenylditelluride, respectively. $(PhTe)_4Ge$ is the first homoleptic organotellurolate of germanium. It was characterized spectroscopically and by X-ray crystal structure analysis. $(PhTe)_4Ge$ crystallizes in the monoclinic space group $P2_1/c$ with a = 12.8018(14), b = 9.1842(9), c = 23.690(3) Å and β = 105.458(8)°. The molecules show a tetrahedral $GeTe_4$ core. Weak Te-Te interactions connect neighbouring tetrahedra to infinite helices along [010].
(© Wiley-VCH Verlag GmbH & Co. KGaA, 69451 Weinheim, Germany, 2003)

Introduction

In the last two decades, organochalcogenolates of group 14 elements have gained increasing importance as molecular precursors for IV/VI semiconductors.[1−3] In the case of the homoleptic series $(RCh)_4E$ with Ch = Se, S and E = Ge, Sn only rather elaborate and low-to-medium yield synthetic routes are known in the literature.[4−6] Analogous tellurolates $(RTe)_4E$ with E = Ge or Sn have not been described so far.

Hence, a direct synthesis of this class of compounds from R_2Ch_2 (R = alkyl, aryl; Ch = Se, Te) and the group 14 element is highly desirable, especially in the case of the tellurium compounds.

Results and Discussion

Commercially available elemental germanium or tin powder does not react with diorganodichalcogenides at temperatures below the decomposition temperature of these organoelement compounds. Thus, a chemical activation of germanium is necessary in order to make such a direct reaction feasible.

We used solvochemically produced hydrogenated germanium, which is highly reactive and a good reductand and can be obtained from $GeCl_2$·dioxane and $Li[Et_3BH]$ in THF according to Equation (1).[7]

$$GeCl_2\cdot\text{dioxane} + 2\,Li[Et_3BH] \rightarrow \underset{\mathbf{1}}{Ge^*} + 2\,Et_3B + 2\,LiCl + H_2 + \text{dioxane} \quad (1)$$

The activated germanium thus obtained indeed inserted into the Se−Se bond and Te−Te bond of Ph_2Se_2 and Ph_2Te_2 at surprisingly low temperatures to give homoleptic $(PhSe)_4Ge$ (**2**) at 65 °C and $(PhTe)_4Ge$ (**3**) at room temperature [Equation (2) and (3)].

$$\underset{\mathbf{1}}{Ge^*} + 2\,Ph_2Se_2 \rightarrow \underset{\mathbf{2}}{Ge(SePh)_4} \quad (2)$$

$$\underset{\mathbf{1}}{Ge^*} + 2\,Ph_2Te_2 \rightarrow \underset{\mathbf{3}}{Ge(TePh)_4} \quad (3)$$

The same type of direct reaction with Ph_2Se_2 has also been observed for activated nanocrystalline tin and also yielded the homoleptic product $(PhSe)_4Sn$.[8]

In the reaction of Ge* (**1**) with diphenyldiselenide at 65 °C in THF solvent, the selenolate **2** is obtained in 92% yield. This yield is significantly higher than the 60−65% yield that could be obtained in reactions of LiSePh with $GeCl_4$.[4,5] In addition, our direct synthesis from activated germanium and Ph_2Se_2 does not produce any by-products in significant amounts and therefore no separation procedure is required.[5]

The reaction of **1** with Ph_2Te_2 is less straightforward, but tellurolate **3** was obtained in 26% yield as a deep red solid. Although all suspended Ge* was consumed after two hours of stirring at room temperature and a clear red solution had formed, we were not able to isolate pure **3** from that solution. Instead, a mixture of Ph_2Te_2, amorphous brownish

[a] Philipps-Universität Marburg, Fachbereich Chemie
Hans-Meerwein-Strasse, 35032 Marburg, Germany
Fax: (internat.) + 49-(0)6421/28-28917
E-mail: schlecht@chemie.uni-marburg.de
[b] Max-Planck-Institut für Festkörperforschung
Heisenbergstrasse 1, 70569 Stuttgart, Germany

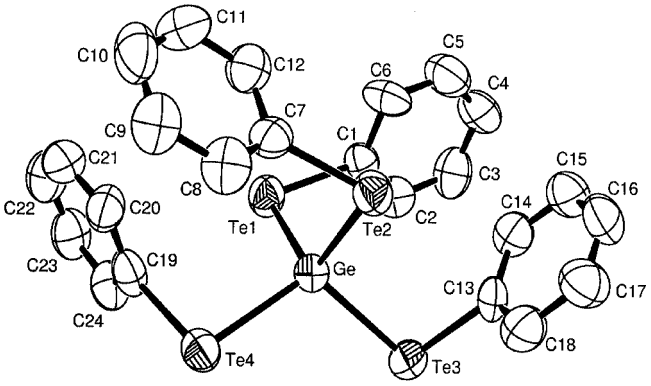

Figure 1. Molecular structure of $(PhTe)_4Ge$ (**3**) (ORTEP representation[19]); thermal ellipsoids are represented at a 50% probability level

germanium and product **3** was obtained after removal of the tetrahydrofuran. This mixture was re-dissolved in diethyl ether and the amorphous germanium was separated by filtration. The filtrate was evaporated to dryness and Ph_2Te_2 and **3** were separated by an extraction with ice-cold diethyl ether in which only Ph_2Te_2 is soluble. The deep-red product that remained was pure **3** and was recrystallized at room temperature by slow evaporation of a concentrated solution in diethyl ether.

Table 1. Experimental parameters for the X-ray diffraction measurement and details concerning the structure determination for $GeTe_4C_{24}H_{20}$ (**3**)

Crystal system	monoclinic
Space group	$P2_1/c$
a [Å]	12.8018(14)
b [Å]	9.1842(9)
c [Å]	23.690(3)
β [°]	105.458(8)
V [Å^3]	2684.6(5)
Calculated density [g/cm^3]	2.22
Crystal shape	Prismatic
Crystal colour	Dark red
Crystal size [mm]	0.02 × 0.04 × 0.03
Diffractometer	Stoe IPDS II
1st run; 2nd run	φ = 0; ω = 0−180; φ = 90; ω = 0−180
Δω [°]	1
Exposure time [min]	10
Detector distance [mm]	100
Wavelength [Å]	0.71073
2Θ-range for data collection [°]	2.3−59.5
hkl_{min}, hkl_{max}	−17, −17, −19; −17, 17, 19
Absorption coefficient [mm^{-1}]	5.41
Absorption correction	Gaussian
T_{min}, T_{max}	0.2766, 0.8018
Total number of reflections	22297
Unique reflections	5949 (3149 >3σ)
Structure solution	Sir97 [17]
Structure refinement	Jana2000[18]
Parameters refined	325
R(obs) (>3σ)	0.0418
R_w(obs) (>3σ)	0.0273
R(all)	0.0764
R_w(all)	0.0276
Twin matrix	(−1 0 0 | 0 1 0 | −2/7 0 1)
Volume fraction individual I	0.867(1)
Volume fraction individual II	0.133(1)
Extinction coefficient	0.408(9)

Table 2. Atomic coordinates and isotropic displacement parameters of **3**

Atom	x	y	z	U_{iso}
Ge	0.14730(8)	0.01670(9)	0.82455(4)	0.0504(4)
Te1	0.25306(6)	0.23134(6)	0.88289(3)	0.0634(3)
Te2	0.27185(5)	−0.18240(6)	0.80162(3)	0.0620(3)
Te3	0.02920(5)	0.09922(7)	0.72343(3)	0.0615(2)
Te4	0.02559(5)	−0.07486(7)	0.88825(3)	0.0637(3)
C1	0.3212(7)	0.2951(8)	0.8146(4)	0.052(3)
C2	0.2708(9)	0.3988(9)	0.7752(4)	0.067(4)
C3	0.3187(11)	0.4432(10)	0.7315(5)	0.082(5)
C4	0.4195(10)	0.3873(12)	0.7285(5)	0.077(5)
C5	0.4664(9)	0.2864(13)	0.7683(6)	0.087(5)
C6	0.4212(8)	0.2351(10)	0.8123(5)	0.074(5)
C7	0.3340(7)	−0.2477(10)	0.8899(4)	0.059(4)
C8	0.2895(9)	−0.3591(9)	0.9127(5)	0.072(5)
C9	0.3345(12)	−0.4047(12)	0.9700(5)	0.081(6)
C10	0.4256(13)	−0.3392(15)	0.0040(6)	0.094(6)
C11	0.4716(10)	−0.2248(17)	0.9815(6)	0.109(7)
C12	0.4270(9)	−0.1779(11)	0.9254(5)	0.074(5)
C13	0.1342(8)	0.0011(10)	0.6777(3)	0.059(4)
C14	0.2310(8)	0.0652(10)	0.6766(4)	0.064(4)
C15	0.2967(9)	−0.0048(11)	0.6480(4)	0.071(5)
C16	−0.2656(11)	0.3603(14)	0.8777(5)	0.087(6)
C17	−0.1748(10)	0.2952(11)	0.8765(5)	0.082(5)
C18	−0.1022(9)	0.3620(11)	0.8472(5)	0.081(5)
C19	0.1225(8)	0.0246(9)	0.9661(4)	0.063(4)
C20	0.2144(9)	−0.0489(11)	0.9993(4)	0.070(4)
C21	0.2761(9)	0.0221(13)	0.0480(5)	0.078(5)
C22	0.2526(11)	0.1571(12)	0.0647(5)	0.081(5)
C23	0.1664(11)	0.2256(11)	0.0317(5)	0.076(5)
C24	0.0954(9)	0.1649(10)	0.9826(4)	0.070(5)

The X-ray crystal structure of germanium tellurolate **3** is depicted in Figure 1. Details of the crystal structure determination are given in Table 1, and atomic coordinates can be found in Table 2.

The structure of the molecule is similar to that of $(PhSe)_4Ge$ and $(PhSe)_4Sn$, of which an orthorhombic and a monoclinic polymorph are known.[5] The germanium centre is surrounded by an almost regular tetrahedron of tellurium atoms. The Ge−Te bond lengths span from 257.5 pm to 258.2 pm (Table 3) and are similar to the distances

Table 3. Selected bond lengths [pm] and bond angles [°] of **3**

Ge−Te1	257.51(10)	Te1−C1	211.6(10)
Ge−Te2	257.75(11)	Te2−C7	211.7(8)
Ge−Te3	258.24(10)	Te3−C13	213.8(10)
Ge−Te4	258.17(13)	Te4−C19	213.4 (9)
Te3−Te4′	393.23(8)		
Te1−Ge−Te2	112.95(4)	Ge−Te1−C1	93.8(2)
Te1−Ge−Te3	111.54(3)	Ge−Te2−C7	94.8(3)
Te1−Ge−Te4	104.39(4)	Ge−Te3−C13	93.1(2)
Te2−Ge−Te3	104.76(4)	Ge−Te4−C19	93.7(3)
Te2−Ge−Te4	113.32(4)		
Te3−Ge−Te4	110.03(4)		

found in the literature for other $GeTe_4$ tetrahedra (e.g. K_2GeTe_4: 250.8−264.0 pm;[9] Ag_8GeTe_6: 254.4 pm;[10] Cs_4GeTe: 253.7−262.3 pm[11]).

The angles around the four symmetrically independent tellurium atoms range from 93.1° to 94.8° and are generally more oblique than in the related selenium compounds [$(PhSe)_4Ge$ (**2**): 96.2−96.7°; orthorhombic $(PhSe)_4Sn$: 95.9−96.4°]. Only in monoclinic $(PhSe)_4Sn$ are similar angles (93.5−95.6°) observed.

The main difference between $(PhTe)_4Ge$ (**3**) and the other related compounds becomes evident when looking at the spatial arrangement of the molecules. In the orthorhombic compounds the molecules are arranged in such a way that the tetrahedral cores are relatively isolated from each other and, consequently, the intertetrahedral Se−Se distances are significantly longer than the intratetrahedral distances [$(PhSe)_4Ge$: intratetrahedral distances: 374.7−397.4; shortest intertetrahedral distance: 468.5 pm; orthorhombic $(PhSe)_4Sn$: intratetrahedral distances: 403.2−424.6 pm; shortest intertetrahedral distance: 434.9 pm]. In the monoclinic polymorph of $(PhSe)_4Sn$ some of the intertetrahedral distances (the shortest is 382.3 pm) are shorter than the intratetrahedral distances (404.1−414.4 pm), yet still too long to assume Se−Se interactions. In $(PhTe)_4Ge$ (**3**) the shortest intertetrahedral Te−Te distance is 393.2 pm, which is significantly shorter than all intratetrahedral distances (407.44−431.0 pm). Furthermore, this distance is well below the sum of the van der Waals radii (440 pm)[12] and in this case it is indeed reasonable to assume weak, attractive Te−Te interactions. These interactions connect Te atoms of neighbouring tetrahedra and lead to the formation of helical chains consisting of germanium and tellurium atoms along the crystallographic *b* direction (see Figure 2 and 3). The type of helix that is formed by the tellurium and germanium atoms in the backbone of the chain resembles the anionic chain of tetrahedra in K_2GeTe_4[9] and the chain of tellurium atoms found in the tellurium subchloride Te_3Cl_2,[13] except for the differences in the bond angles. The observed Te−Te distance in **3** is similar to that observed in other compounds, for example in $Te[N(SiMe_3)_2]_2$ (377 pm),[14] with van der Waals interactions between the tellurium atoms. These distances are longer than the interchain distance in elemental tellurium (350 pm),[15] but they are again similar to the Te−Te distances at the van der Waals gap of extended layered tellurides such as Ta_2Te_3,[16] where a value of 373 pm was found.

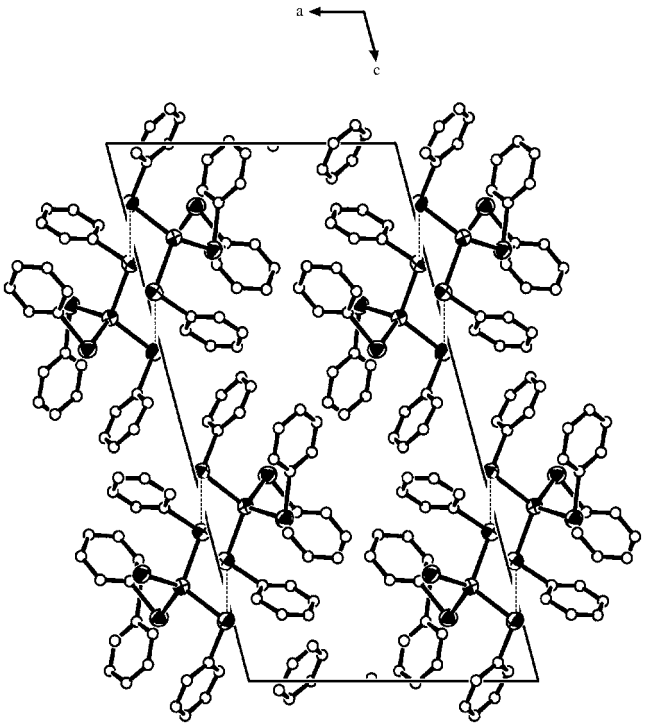

Figure 2. Projection of the crystal structure of **3** along [010]; Te−Te interactions are indicated as dashed lines (ORTEP representation[19]); thermal ellipsoids are represented at a 50% probability level

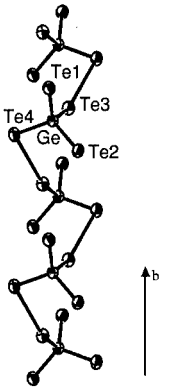

Figure 3. Helical chain of interconnected tetrahedra of $GeTe_4$ units (ORTEP representation[19]); thermal ellipsoids are represented at a 50% probability level

Conclusion

Activated hydrogenated germanium **1** allows the direct one-step synthesis of $(PhSe)_4Ge$ (**2**) and $(PhTe)_4Ge$ (**3**) from Ph_2Se_2 or Ph_2Te_2 and **1** in an oxidative addition leading directly to the tetravalent germanium species. The homoleptic tellurolate **3** shows short intertetrahedral Te−Te contacts that lead to the formation of helical chains consisting of germanium and tellurium atoms in this compound. The easy accessibility of $(PhSe)_4Ge$ (**2**) and $(PhTe)_4Ge$ (**3**) makes these compounds ideal candidates for molecular precursors leading to IV/VI semiconductors. Investigations on the low-temperature synthesis of germanium(II) chalcogenides from $(PhSe)_4Ge$ and $(PhTe)_4Ge$ are currently under way.

Experimental Section

All manipulations were carried out under dry, oxygen-free argon, except where stated otherwise. $Li[Et_3BH]$ (1 M in THF), diphenylditelluride, diphenyldiselenide and tetrahydrofuran were purchased from Aldrich. $GeCl_2$·dioxane was purchased from ABCR. THF

was dried over CaH_2 under argon atmosphere and freshly distilled prior to use. The reactions were carried out in standard Schlenk glassware. Activated hydrogenated germanium (**1**) was prepared as described in the literature.[7]

$(PhSe)_4Ge$ (2): $GeCl_2$·dioxane (232 mg, 1.0 mmol) was reduced to Ge* (**1**) by 2.0 mL of a 1.0 M solution of $Li[Et_3BH]$ in THF as described previously.[7] The resulting **1** was suspended in 60 mL of THF and Ph_2Se_2 (624 mg, 2.0 mmol) was added. The reaction mixture was heated to gentle reflux for 4 h and a clear yellow solution was obtained. This was allowed to cool to room temperature and then the THF was removed under vacuum. The yellow solid obtained was washed with 10 mL of hexane and dried again. The product was identified as $(PhSe)_4Ge$ (**2**)[5] by ^1H, ^{13}C and ^{77}Se NMR spectroscopy, elemental analysis and powder diffraction data. Yield: 641 mg (92%).

$(PhTe)_4Ge$ (3): $GeCl_2$·dioxane (232 mg, 1.0 mmol) was reduced with 2.0 mL of a 1 M solution of $Li[Et_3BH]$ in THF as described above. The resulting **1** was suspended in 60 mL of THF and Ph_2Te_2 (818 mg, 2.0 mmol) was added. The reaction mixture was stirred at room temperature for 2 h and a clear red solution formed. The THF was quickly evaporated under vacuum and an orange-red powder remained. Diethyl ether (40 mL) was added and the solution was filtered. The filtrate was evaporated to dryness under vacuum and the remaining mixture of Ph_2Te_2 and **3** was extracted with 3 × 5 mL of ice-cold diethyl ether. A dark red solid remained. Yield: 232 mg (26%). ^1H NMR (300 MHz, CD_2Cl_2, 25 °C): δ = 7.19 (t, 8 H), 7.38 (t, 4 H), 7.61 (t, 8 H) ppm. ^{13}C NMR (75 MHz, CD_2Cl_2, 25 °C): δ = 129.1, 130.0, 141.5 ppm. IR (nujol mull): $\tilde{\nu}$ 1573 cm^{-1} (w), 1153 (w), 1014 (w), 996 (w), 688 (m), 450 (m, νTe-C), 252 (m, νGe-Te), 238 (m, νGe-Te), 178 (w). MS (EI, 70 eV): *m/z* (%) = 766 (2) $[(PhTe)_2Ge(Te)(TeC_2H_3)]^+$, 561 (10) $[(PhTe)Ge(Te)(TeC_2H_3)]^+$, 410 (20) $[Ph_2Te_2]^+$, 305 (50) $[(PhTe)Ge(C_2H_3)]^+$, 206 (30) $[PhTeH]^+$, 154 (42) $[TeC_2H_3]^+$, 77 (100) $[Ph]^+$. $C_{24}H_{20}GeTe_4$ (891.01): calcd. C 32.32, H 2.24; found C 32.03, H 2.51.

X-ray Crystallographic Study: The overall distribution of intensities in the diffraction pattern of $Ge(TePh)_4$ (**3**) can be explained assuming a monoclinic lattice with a = 12.8018(14), b = 9.1842(9), c = 23.690(3) Å and β = 105.458(8) and an additional twinning operation (Figure 4). Two twin individuals of different volume fractions have to be taken into account. The twinning can be classified as twinning by reticular merohedry. The two individual lattices have the *hk*0 plane in common and generally all reflections $l = 7n$ overlap completely, while reflections $l \neq 7n$ correspond to reflections of a single individual. This implies that it is inevitable to consider the twinning operation in the refinement process. If the two twin individuals were of equal volume, orthorhombic Laue symmetry 2/*m*2/*m*2/*m* would be simulated for the overall diffraction pattern. The reduction of the symmetry of one individual to Laue class 2/*m* leaves the remaining four symmetry operations $2'/m'-2'/m'$ as possible choices for the twinning operation. We chose the mirror plane perpendicular to a^* as twin law corresponding to the matrix (−1 0 0 | 0 1 0 | −2/7 0 1).

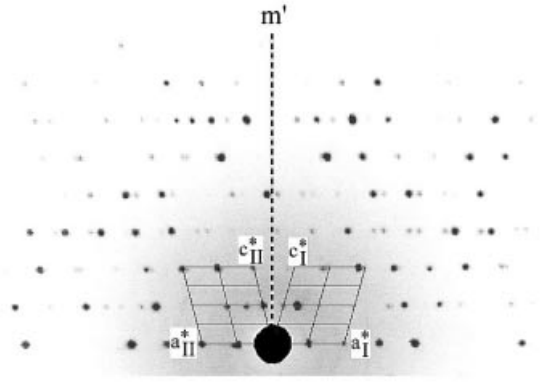

Figure 4. h0l plane of the reciprocal space of $(PhTe)_4Ge$; unit cells of the two different twin individuals and the twinning operation are indicated

Although in the structure solution process (with the program SIR97[17]) all reflections were taken into account (i.e. also the overlapping ones) no problems were encountered and the positions of all heavy atoms were easily identified. Structure refinement employing the above -described twin law was carried out with the program Jana2000.[18] Hydrogen atoms were taken from the difference Fourier synthesis map.

CCDC-190899 contains the supplementary crystallographic data for this paper. These data can be obtained free of charge at www.ccdc.ac.uk/conts/retrieving.html [or from the Cambridge Crystallographic Data Centre, 12, Union Road, Cambridge CB2 1EZ, UK; fax: (internat.) +44-1223/336-033; E-mail: deposit@ccdc.cam.ac.uk].

Acknowledgments

S.S. thanks the Fonds der Chemischen Industrie and the BMBF for a Liebig-Fellowship. Financial support by the BMBF is gratefully acknowledged. We are grateful to Prof. Dr. Martin Jansen for his continuous support.

[1] P. Boudjouk, D. J. Seidler, D. G. Grier, G. J. McCarthy, *Chem. Mater.* **1996**, *8*, 1189−1196.
[2] P. Boudjouk, M. P. Remington, D. G. Grier, W. Triebold, B. R. Jarabek, *Organometallics* **1999**, *18*, 4534−4537.
[3] J. Arnold, *Progr. Inorg. Chem.* **1995**, *43*, 353−417.
[4] H. J. Backer, J. B. G. Hurenkamp, *Recl. Trav. Chim. Pays-Bas* **1942**, *61*, 802−808.
[5] H. J. Gysling, H. R. Luss, *Organometallics* **1989**, *8*, 363−368.
[6] D. H. R. Barton, H. Dadoun, A. Gourdon, *Nouveau J. Chim.* **1982**, *6*, 53−57.
[7] S. Schlecht, *Angew. Chem.* **2002**, *114*, 1237−1239; *Angew. Chem. Int. Ed.* **2002**, *41*, 1178−1180.
[8] S. Schlecht, M. Budde, L. Kienle, *Inorg. Chem.* **2002**, *42*, 6001−6005.
[9] B. Eisenmann, H. Schrod, H. Schaefer, *Mater. Res. Bull.* **1984**, *19*, 293−298.
[10] N. Rysanek, P. Laruelle, A. Katty, *Acta Crystallogr., Sect. B* **1976**, *32*, 692−696.
[11] C. Brinkmann, B. Eisenmann, H. Schaefer, *Mater. Res. Bull.* **1985**, *20*, 1207−1211.
[12] L. Pauling, *The Nature of the Chemical Bond*, 3rd ed., Cornell University Press: Ithaka, New York, **1960**, Ch. 7.
[13] R. Kniep, D. Mootz, A. Rabenau, *Angew. Chem.* **1973**, *85*, 504−505; *Angew. Chem. Int. Ed. Engl.* **1973**, *12*, 499−500.
[14] M. Björgvinsson, H. W. Roesky, F. Pauer, D. Stalke, G. M. Sheldrick, *Inorg. Chem.* **1990**, *29*, 5140−5143.
[15] N. N. Greenwood, A. Earnshaw, *Chemistry of the Elements*; Pergamon Press, Oxford, 1984, p. 887.
[16] M. Conrad, B. Harbrecht, *J. Alloys Comp.* **1992**, *187*, 181−192.

[17] A. Altomare, G. Cascarano, C. Giacovazzo, A. Guagliardi, A. G. G. Moliterni, M. C. Burla, G. Polidori, M. Camilli, R. Spagna, *SIR97 − a package for crystal structure solution by direct methods and refinement*, Computer programme. Dip. Geomineralogico, University of Bari, Italy, **1997**.
[18] V. Petříček, M. Dušek, *JANA2000 − crystallographic computing system*, Institute of Physics, Academy of the Czech Republic, Praha.
[19] L. J. Farrugia, *J. Appl. Crystallogr.* **1997**, 565.

Received August 6, 2002
[I02446]

Arylcalcium Hydrides as Precursors to Alkoxides and Aryloxides of Calcium

John P. Dunne,[a] Matthias Tacke,*[a] Carola Selinka,[b] and Dietmar Stalke[b]

Keywords: Calcium / C−H activation / Cocondensation / Hydrides

Calcium atoms react with +I-substituted benzene derivatives under cocondensation conditions to yield arylcalcium hydrides. With toluene, *tert*-butylbenzene, and trimethyl(phenyl)silane the reaction showed no selectivity for C–H activation, resulting in the formation of each of the three possible isomers, while with *m*-xylene the reaction resulted in selective activation of the bond *meta* to the CH_3 groups. Treatment of (*tert*-butylphenyl)calcium hydride with di- and trisubstituted phenols such as 2,6-di-*tert*-butylphenol, 2,6-di-*tert*-butyl-4-methylphenol, and 2,4,6-tri-*tert*-butylphenol resulted in the formation of calcium aryloxides in yields > 95%. $[Ca(2,4,6\text{-}tBu_3C_6H_2O)_2(THF)_3]$ crystallises from a THF solution as a distorted trigonal bipyramid, with two THF ligands in the *trans*-axial positions and the third THF ligand and both aryloxide groups in equatorial positions. The $Ca–O_{Aryl}$ bond length was found to average at 2.181(3) Å. The $Ca–O–C_{Aryl}$ angles are almost linear, with Ca1–O1–C1 and Ca1–O2–C19 being 173.9(3)° and 178.8(3)°, respectively, while the O1–Ca1–O2 angle was determined as 152.04(12)°. A reaction between (*tert*-butylphenyl)calcium hydride and triphenylmethanol resulted in the formation of the corresponding monomeric calcium bis(alkoxide) $Ca(OCPh_3)_2(THF)_4$ in 95% yield. The structure was determined as a distorted octahedron with the alkoxide ligands in a *cis*-equatorial arrangement. The Ca–O bond length was determined at 2.1609(17) Å. The $Ca–O–C_{Aryl}$ angle of 177.46(16)° is almost linear, while the O1–Ca1–O1A angle was determined at 110.12(19)°.

(© Wiley-VCH Verlag GmbH & Co. KGaA, 69451 Weinheim, Germany, 2003)

Introduction

Until the mid 1980s, complexes of calcium were among the longest known, yet least understood class of compounds. Since the early 1990s, however, there has been renewed interest in this field.[1] The reasons for this slow development have been due to numerous factors. Firstly, calcium complexes have rather poor solubility in hydrocarbon solvents and many are thermally unstable.[1] Secondly, there are only a limited number of starting reagents and preparative techniques for the formation of calcium compounds.[1]

The most popular preparative technique is to use non-elemental forms of calcium (as shown in Figure 1), utilising a salt such as CaI_2 or calcium bis(trimethylsilyl)amide as the source of calcium. Another method is by deprotonation with an activated hydrocarbon, as shown in Equation (C) in Figure 1.

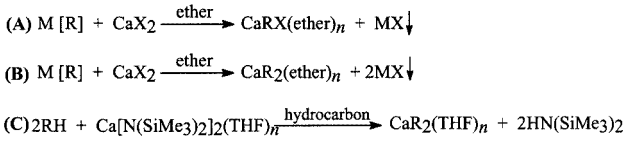

Figure 1. Reactions using non-elemental forms of calcium

Another synthetic method is to use bulk calcium metal for reaction, but a major difficulty encountered with this technique is its relative inertness to reaction. There are a number of different methods to activate the bulk metal, including the formation of an activated powder by displacement of calcium by potassium from a calcium dihalide (Rieke calcium),[2] or by decomposition of alkaline earth metal/anthracene complexes (Bogdanovic method).[3] Alternatively, the metal can be dissolved in liquid ammonia[4] or dispersed in THF.[5]

Metal vapour synthesis (MVS) takes a different approach to the above methods to overcome the inertness of bulk calcium metal. The above procedures are in reality a cleaning of the metal surface. Metal atom techniques are different, in that they utilise the vaporisation enthalpy of calcium as the reaction enthalpy. This technique has received only sporadic attention to date. In the late 1980s, MVS was used to prepare $[Ca(cot)(THF)_n]$[6] and the bis(cyclopentadienyl)-calcium complex $[Ca\{\eta\text{-}C_5H_3\text{-}1,3\text{-}(SiMe_3)_2\}_2(THF)]$,[7] and more recently $[Ca\{CH(SiMe_3)_2\}_2(THF)_3]$,[8] while in the mid 1980s Mochida et al.[9] reported the C−H bond activation of benzene by calcium atoms to form PhCaH, which was not isolated but characterised by its organic products as outlined in Figure 2. In these systems the high reactivity of calcium atoms is stored in the products' highly reactive bonds.

Recently performed theoretical work showed that the molecule "PhCaH" should be able to exist in donor solv-

[a] Department of Chemistry, University College Dublin, Belfield, Dublin 4, Ireland
[b] Institut für Anorganische Chemie, Universität Würzburg, Am Hubland, 97074 Würzburg, Germany

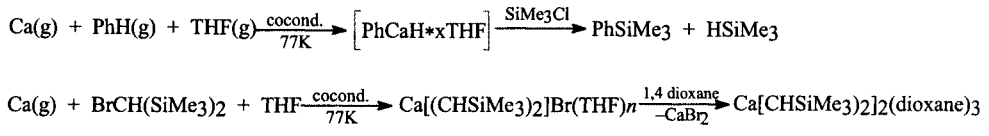

Figure 2. Cocondensation reactions with calcium atoms

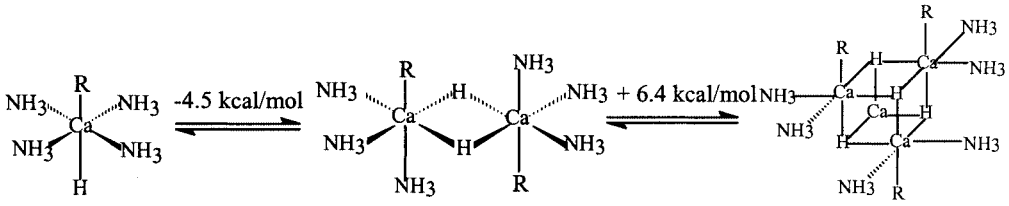

Figure 3. Calculated structures for PhCaH in donor solvents

ents such as THF in different aggregation states.[10] As a means of developing a convenient theoretical model for arylcalcium hydride in donor solvents, ammonia was used to simulate an amine and the elimination of H_2 was suppressed. These calculations show that a concentration-dependent equilibrium exists in donor solvents (as outlined in Figure 3). At low concentrations of "PhCaH", a monomeric species is energetically favoured, while at higher concentrations a tetrameric species with triply bridging hydride ligands exists. However, at average concentrations of "PhCaH" the energetically favoured structure is a dimer.

Calcium alkoxides are used as CVD precursors and for sol-gel synthesis.[1,11] As well as this, alkaline earth metal alkoxides are noted for their rich variety of structures and reactions.[1] This is due to the conformational and bonding flexibility of the alkoxide ligand (e.g., μ^1-, μ^2-, and μ^3-bonding modes are known). Crystallographically identified structural types range from discrete monomeric species such as $[Ca(BHT)_2(THF)_3]$ (BHT = 2,6-*tert*-butyl-4-methylphenolate)[12] to large polynuclear aggregates such as $[Ca_9(OCH_2CH_2OMe)_{18}(HOCH_2CH_2OMe)_2]$.[13]

The aim of this work was firstly to use calcium atoms to activate the aromatic C−H bonds of +I-substituted benzene derivatives, thus forming arylcalcium hydrides, and secondly to use these arylcalcium hydrides as starting reagents for the formation of calcium alkoxides and aryloxides. To date, relatively few examples of monomeric alkoxides and aryloxides have been structurally characterised [examples include $[Ca(BHT)_2(THF)_3]$ and $[Ca(cox)_2(THF)_3]$·THF {cox = $C(Ph)_2(CH_2C_6H_4Cl\text{-}4)$}.[12] The reasons for this arise from difficulties in preventing oligomerisation or polymerisation of the calcium alkoxides and their low solubilities in most solvents. For this purpose a series of sterically bulky alcohols and phenols were chosen, in order to prevent oligomerisation and increase solubility in hydrocarbons.

Results

Experimental Study

Under cocondensation conditions, calcium atoms react with +I-substituted benzene derivatives to form extremely air- and moisture-sensitive, dark red solids in yields ranging from 78 to 97%. When calcium atoms were cocondensed with benzene in the presence of THF (as outlined in Scheme 1), a dark red, pyrophoric solid of composition PhCaH·2THF was obtained in a yield of 78%. An IR spectrum in Nujol mull showed a strong vibration at 1094 cm^{-1} and a weaker signal at 1031 cm^{-1}. We assign these as the Ca−H vibration at 1094 cm^{-1} and C−H bond deformations of the phenyl ring at 1031cm^{-1}, based on similar trends seen in our DFT-modelled vibrations. Because of the low solubility of the product in organic solvents and its extremely high sensitivity to air and moisture, however, NMR spectroscopic data were not obtained for this or any other arylcalcium hydride species. Instead, **1a** was treated at −30 °C with $SiMe_3Cl$ (as shown in Scheme 1) and the organic derivative trimethyl(phenyl)silane was identified by GC MS and NMR techniques. Further characterisation to show the presence of the hydride moiety was performed by treatment of **1a** with the hydride-abstracting agent $Ph_3C^+BF_4^-$. The product isolated from this reaction was triphenylmethane, as shown in Scheme 2.

A change of the aromatic compound from benzene to toluene resulted in a higher yield of 97%. The elemental analysis of the solid compound showed that it was composed of a C_7H_7CaH·2THF moiety. As with the benzene cocondensation product, a Ca−H vibration was found at 1092 cm^{-1}. In order to ascertain which C−H bond was activated, **1b** was converted into an organic compound by treating it with chlorotrimethylsilane. In this case, GC MS detected the presence of three different isomers in similar abundances. In conjunction with NMR spectroscopic data,

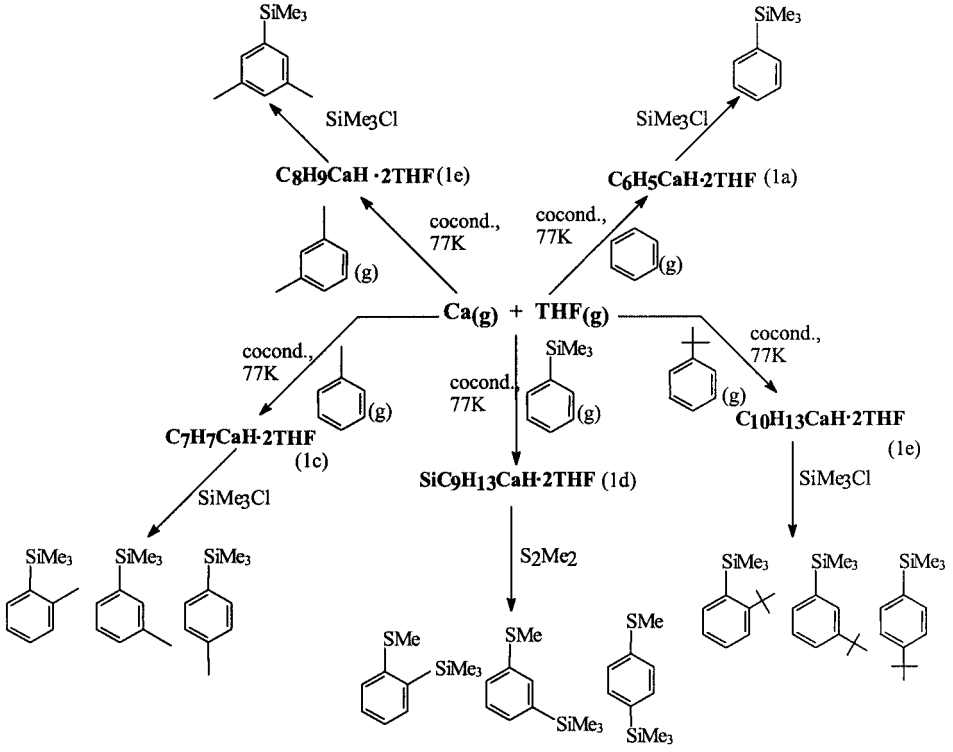

Scheme 1. Cocondensation of calcium atoms with +I-substituted benzene derivatives in the presence of THF

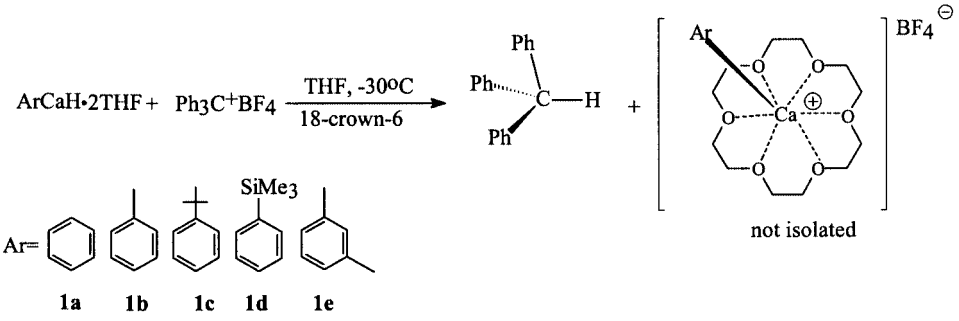

Scheme 2. Reaction of arylcalcium hydrides with $Ph_3C^+BF_4^-$

these were identified as the *ortho*, *meta*, and *para* isomers of trimethyl(methylphenyl)silane, as outlined in Scheme 1.[14–16] As before, **1b** was treated with $Ph_3C^+BF_4^-$, resulting in the isolation of triphenylmethane as outlined in Scheme 2. No attack at the thermodynamically favoured benzyl position was detected.

When *tert*-butylbenzene was used instead of toluene (as outlined in Scheme 1), a slightly lower yield of 93% was obtained. Like the previous cocondensation products, elemental analysis showed it to be composed of a $C_{10}H_{13}CaH{\cdot}2THF$ moiety, and a Ca–H vibration was found at 1094 cm^{-1}. As in the toluene cocondensation, **1c** was treated with chlorotrimethylsilane to identify which C–H bonds were activated. As in the case of the toluene reaction product, GC MS and NMR showed the presence of *ortho*, *meta*, and *para* isomers of (*tert*-butylphenyl)trimethylsilane in similar abundances, as outlined in Scheme 1.[17–19] As in the previous cocondensations, **1c** was treated with $Ph_3C^+BF_4^-$ to form triphenylmethane, thus indicating the presence of a hydride ligand, as outlined in Scheme 2.

A change of the +I benzene derivative to *m*-xylene resulted in a lower yield of 85%. As in the previous cocondensation products, elemental analysis shows the product to be of the composition $C_8H_9CaH{\cdot}2THF$, and the Ca–H vibration was detected at 1095 cm^{-1}. To confirm the regiochemistry of this reaction, **1d** was again treated with chlorotrimethylsilane. Unlike in the toluene and *tert*-butylbenzene cocondensations, though, GC MS and NMR showed that a single species had been formed, and this was identified as (3,5-dimethylphenyl)trimethylsilane, as outlined in Scheme 1.[20] Treatment of **1d** with $Ph_3C^+BF_4^-$ as outlined in Scheme 2 confirmed the presence of the hydride ligand.

When trimethyl(phenyl)silane was cocondensed with calcium atoms in the presence of THF, a similar lack of selectivity was observed. The isolated dark red solid (86% yield) had the composition $C_9H_{13}SiCaH{\cdot}2THF$. As in the previous cocondensation products, a Ca–H vibration was found

at 1094 cm^{-1}. For ease of characterisation, **1c** was treated with dimethyl disulfide rather than chlorotrimethylsilane in order to elucidate the selectivity of this reaction. GC MS measurements showed the presence of three different isomers in similar abundances. In conjunction with NMR spectroscopic data, these were identified as the *ortho*, *meta*, and *para* isomers of trimethyl[4-(methylthio)phenyl]silane, as outlined in Scheme 1.[17,19] As in all the previous cocondensations, **1c** was treated with $Ph_3C^+BF_4^-$ (as outlined in Scheme 2) to confirm the presence of a hydride ligand.

These arylcalcium hydrides can be redissolved in THF and utilised as reagents for the formation of new calcium compounds. When arylcalcium hydrides were treated at room temperature with bulky phenols (**3a**−**3c**), the corresponding bis(aryloxides) were formed in excellent yields (all > 95%), as outlined in Scheme 3. IR and NMR techniques identified all species as bis(aryloxides) of calcium. A characteristic ^{13}C NMR signal for the *ipso*-carbon atom (C−O^-) can be seen at δ ≈ 164.4 (for **3a**), 163.9 (for **3b**) and 163.4 ppm (for **3c**). The calcium aryloxides **3b** and **3c** have been reported previously and the NMR and IR data agree with the literature.[12,21] However, no crystal structure for **3c** had been reported in the literature. Integration of the THF signals in the ^1H NMR shows that **3a** has a coordination number of six, while **3b** has the lower coordination number of five.

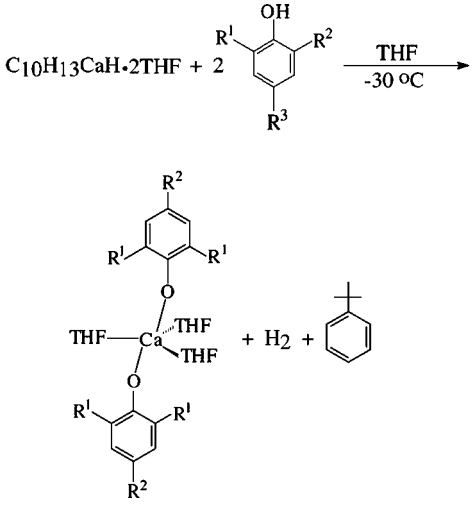

3a: $R^1 = t$Bu, R^2 = H
3b: $R^1 = t$Bu, $R^2 = CH_3$
3c: $R^1 = t$Bu, $R^2 = t$Bu

Scheme 3. Synthesis of calcium aryloxides using **1c**

A single crystal of **3c** suitable for X-ray diffraction was grown over 5 d at +5 °C in THF. The result of the structure determination is depicted in Figure 4. The coordination number for the calcium is five, with two aryloxide and three THF ligands arranged in a distorted trigonal-bipyramidal coordination polyhedron around the calcium centre. Two and a half further uncoordinated THF molecules could be detected as lattice solvent. Bond lengths and angles are listed in Table 1.

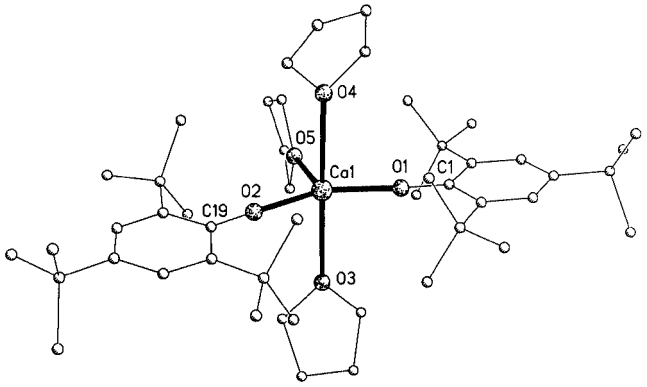

Figure 4. Crystal structure of Ca[2,4,6-tBu$_3$C$_6$H$_2$O]$_2$(THF)$_3$ (**3c**)

Table 1. Selected bond lengths [Å] and angles [°] for **3c**

Bond	Bond length [Å]	Angle	[°]
Ca1−O1	2.180(3)	O3−Ca1−O4	177.78(12)
Ca1−O2	2.183(3)	O1−Ca1−O2	152.08(12)
Ca1−O3	2.399(3)	O1−Ca1−O5	103.39(10)
Ca1−O4	2.395(3)	O2−Ca1−O5	104.45(11)
Ca1−O5	2.393(3)	C1−O1−Ca1	173.8(3)
O1−C1	1.325(5)	C19−O2−Ca1	178.7(3)
O2−C19	1.336(5)		

The calcium aryloxide **3c** crystallises as a monomer with two aryloxide ligands and a single THF donor molecule in the equatorial plane and two THF donors in axial positions. The Ca atom and three equatorial oxygen atoms are located in a plane with a mean deviation of 0.03 Å. The axial (THF)O−Ca−O(THF) angle of 177.78(12)° is almost linear, but the equatorial ArO−Ca−OAr angle of 152.08(12)° is markedly widened from the expected 120° for an ideal trigonal bipyramid. As a consequence, the angles for the other equatorial ligands are smaller [103.93(10)° for O1−Ca1−O5 and 104.45(11)° for O2−Ca1−O5]. The C_6 planes of the aryl ligands intersect at an angle of 8.2°. The two calcium−oxygen ($^-$OAr) bond lengths of 2.183(3) Å (av.) are almost identical. The Ca−O(THF) bonds are almost invariant at 2.395(3) Å. The carbon−oxygen bonds in the alkoxide ligands are identical within estimated standard deviations [1.324(5) Å for O1−C1 and 1.336(5) Å for O2−C19], and hence considerably shorter than standard C−O single bonds (1.43 Å).[22] In addition, the Ca−O−C angles of 173.8(3)° for Ca1−O1−C1 and 178.7(3)° for Ca1−O2−C19 are almost linear. Similar bond shortening and linearity was found in the analogous complex {[Ca(BHT)$_2$(THF)$_3$]·THF[12] and in the thiolate complex [Ca(SMes)$_2$(THF)$_4$] (Smes = 2,4,6-tBu$_3$C$_6$H$_2$S)}.[23]

The arylcalcium hydride **1c** also reacts with alcohols to form the corresponding bis(alkoxides) of calcium. When triphenylmethanol was allowed to react with **1c**, it produced the previously unrecorded calcium alkoxide **4** in 94% yield, as shown in Scheme 4. A single crystal of **4** was grown for X-ray diffraction over 10 d at +5 °C in THF. The coordina-

tion polyhedron around the central calcium atom is made up of six oxygen atoms, two of the Ph_3CO^- anions in adjacent equatorial positions and four of THF molecules in the remaining equatorial and axial positions (Figure 5). An additional THF molecule is found uncoordinated in the crystal lattice. Bond lengths and angles are described in full in Table 2.

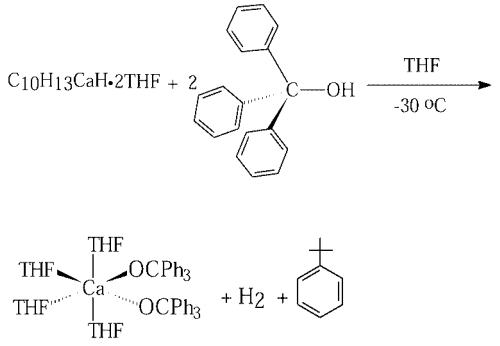

4

Scheme 4. Synthesis of **4** using **1c**

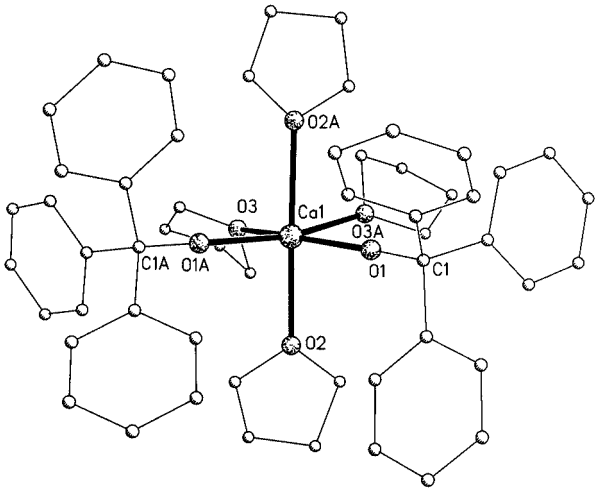

Figure 5. Crystal structure of $Ca[OCPh_3]_2(THF)_4$

Table 2. Selected bond lengths [Å] and angles [°] for **4**

Bond	Bond length [Å]	Angle	[°]
Ca1−O1	2.1609(16)	O1−Ca1−O1A	110.16(9)
Ca1−O2	2.440(2)	O1−Ca1−C3A	87.9(2)
Ca1−O3	2.482(7)	O3−Ca1−O3A	76.3(4)
O1−C1	1.375(2)	O2−Ca1−O2A	166.67(8)
C1−C2	1.565(3)	C1−O1−Ca1	177.47(13)
C1−C8	1.550(3)		
C1−C14	1.565(3)		

The distorted octahedral arrangement is evident from the deviation from linearity of the angle O2−Ca1−O2A, at 166.67(8)°. The calcium atom and four equatorial oxygen atoms are located in a plane with a mean standard deviation of 0.22 Å. The angle O1−Ca1−O1A between the two triphenylmethoxy ligands and the calcium atom is 110.16(9)°, while the angle between the two equatorial THF ligands at the calcium atom is considerably smaller at 76.3(4)°. This deformation in the octahedral geometry can clearly be attributed to the greater steric demand of the alkoxide ligands than of the THF ligands. Both axial THF ligands are bent away from the alkoxide ligands. Again, the angle $Ca-O-C_{Aryl}$, at 177.47(13)°, indicates near linearity. The Ca−O bond length in the alkoxide ligand is 2.1609(16) Å, and hence almost as long as in **3c**. The $O-C_{Aryl}$ single bonds in **4** − at 1.375(2) Å − are slightly longer than in **3c**.

Theoretical Study

In order to gain further insight into the proposed compositions of the arylcalcium hydrides a series of theoretical calculations were performed. As in previous reported theoretical work,[10] the AKR4/6-31g** basis set combination was used. This has proved to give reasonable geometries without greatly increasing the calculation time. As before, ammonia was chosen as a model Lewis base to decrease calculation time.

The aim of this theoretical study was to examine a possible mechanism for this reaction. The first step examined was the direct insertion of calcium atoms into the C−H bond. This is unlikely, since the calculated reaction enthalpy of +10.8 kcal/mol for the formation of PhCaH (**8**) is too large to occur at 77 K (outlined in Figure 6). This would indicate that a highly endothermic reaction is occurring at such a low temperature. The calculated Ca−H bond length for **8** was 2.037 Å and the Ca−C bond length was found to be 2.324 Å. The optimised structure **8** (as shown in detail in Table 3) showed an agostic interaction between the calcium atom and the *ortho* C−H bond of the phenyl ligand. This agostic bond length was calculated as 2.534 Å and the angle between the phenyl ligand, the calcium atom and the hydride ligand (C−Ca−H angle) was found to be 144.8°. This bending of the C−Ca−H angle in conjunction with an agostic C−H bond indicates coordinative unsaturation of the calcium centre in **8**. This is to be expected, since a coordination number of two for calcium is extremely low, particularly in view of the lack of steric bulk in the phenyl and hydride ligands. It would be reasonable to expect that, in the presence of donor solvents such as THF, a higher coordination number would be achieved through the coordination of donor solvent molecules.

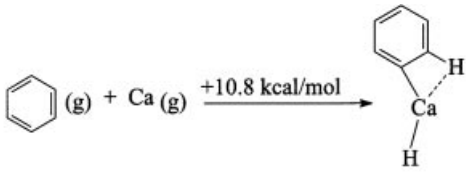

8

Figure 6. Reaction of calcium atoms with benzene

In a previous theoretical study,[10] it was reported that phenylcalcium hydride exists in donor solvents as a hydride-bridged dimer with a coordination number of six. Here it is extended to show that the *trans* "$PhCaH\cdot3NH_3$" dimer

Table 3. Comparison of bond lengths and IR frequencies in calculated arylcalcium hydride species

	PhCaH	*trans*-PhCaH·3NH$_3$	*cis*-PhCaH·3NH$_3$
Ca−H [Å]	2.037	2.305	2.318
Ca−C [Å]	2.324	2.552	2.528
Ca−N [Å]	N/A	2.569	2.575
Ca−Ca [Å]	N/A	3.461	3.532
ν_s(Ca−H) [cm^{-1}]	N/A	991 (sym)	849 (sym)
ν_{as}(Ca−H) [cm^{-1}]	N/A	1048 (antisym)	930 (antisym)

species **9** has a reaction enthalpy −13.9 kcal/mol lower than that of the *cis* dimer species **10**, as described in Figure 7. For the *trans* species **9**, the calculated Ca−H bond length is 2.305 Å, the Ca−C bond length is 2.552 Å and the Ca−N bond length is 2.569 Å; these values are outlined in Table 3. The Ca−H antisymmetric vibration, which is IR-active, is calculated as 1078 cm^{-1}. Slightly different values (as shown in Table 3) are seen for **10**. The calculated Ca−H bond (2.318 Å) is slightly longer than in **9**, while the Ca−C bond length was found to be 2.528 Å, shorter than in **9**. The Ca−H antisymmetric vibration in **10** is 930 cm^{-1}. This value is lower than that of **9** (1078 cm^{-1}). It should be possible to distinguish whether "solvated PhCaH" exists in either *cis* or *trans* form in solution by IR methods.

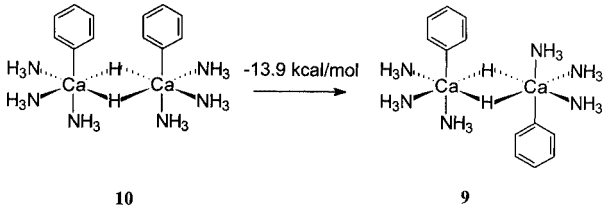

10 **9**

Figure 7. Energy difference between *cis* and *trans* isomers of PhCaH·3NH$_3$

Discussion

Composition of Arylcalcium Hydrides

Mochida originally proposed that the product from the reaction between benzene and calcium atoms was "PhCaH",[9] but he failed to isolate this compound. Instead, it was allowed to react with D_2O and $SiMe_3Cl$. On repeating this experiment in THF, we isolated a dark red, air- and moisture-sensitive solid in 78% yield, as shown in Scheme 1. This is an extremely high yield for an MVS experiment, and it appears moreover that the loss in yield stems from a relatively high-melting matrix in the vessel, which hinders collection of the entire sample. In the benzene cocondensation, for example the matrix is a benzene/THF mixture. The melting point of benzene is 5.5 °C and the melting point of THF is −103 °C. However, the toluene cocondensation has a lower melting matrix of toluene/THF (melting point of toluene −95 °C) and hence a higher yield. This reaction type was expanded to include other +I-substituted benzene derivatives, as in the similar lithium atom reaction.[20] Calcium atoms were able to activate the C−H bonds of toluene, *tert*-butylbenzene, trimethyl(phenyl)silane, and *m*-xylene, as outlined in Scheme 1. It is clear from the derivatisation reactions with chlorotrimethylsilane (as shown in Scheme 1) and $Ph_3C^+BF_4^-$ (shown in Scheme 2) that the backbone of **1a** is composed of the anionic ligands Ph^- and H^-. However, the elemental analysis indicates that the composition is (PhCaH·2THF)$_x$: The existence of coordinated Lewis base molecules such as THF is a well-known facet of calcium chemistry.[1]

Theoretical calculations show the tendency towards oligomerisation through hydride bridging and the uptake of THF to fill the coordination sphere of the calcium atom. These calculations showed that the formation of PhCaH is energetically unfavourable by +10.8 kcal/mol and that an aggregated state through hydride bridging is favoured over a monomeric species.[6] These calculations also showed that the favoured coordination number is six and that a solvent-dependent equilibrium exists in donor solvents. The calculations show that the aggregation state can be elucidated from the IR data on the Ca−H vibration. The calculated IR frequency for a terminal hydride ligand (e.g., monomeric PhCaH·4NH$_3$) is 897 cm^{-1}. When the hydride ligand is bridging, as in a dimeric species, the calculated Ca−H vibration is higher, at 1048 cm^{-1}. The calculated data for this dimeric species are in good agreement with the experimentally measured value of 1094 cm^{-1}. However, the possibility of higher aggregates such as tetramers (in which the hydride ligand would be triply bridging) or an oligomeric species through mixed bridging of the phenyl and hydride ligands cannot be gauged from these data.

Selectivity of C−H Activation with Calcium Atoms

Lithium atoms have been reported to activate aromatic C−H bonds of +I-substituted benzene derivatives selectively in the *para* position.[24] By use of an approach similar to Mochida's and by treatment of the "ArCaH" with chlorotrimethylsilane at −30 °C, easy identification of the activated positions on the aromatic ring by NMR and GC MS is possible. On expanding this reaction type to other aromatic compounds [e.g., toluene, *tert*-butylbenzene, trimethyl(phenyl)silane, and *m*-xylene], it was expected that selective C−H bond activation in the *para* position would be observed, in a reaction series analogous to that of lithium atoms.[20] However, this was not observed; instead, a lack of selectively was noted. All benzene derivatives except xylene experienced the activation of the *ortho*, *meta*, and *para* C−H bonds. This lack of selectivity is different to the case of the lithium atom reaction, in which the *para* position was selectively attacked.[24] Another difference was that xylene, which had failed to react with lithium atoms, reacted with calcium atoms. [Calcium atoms react with mesitylene, which does not react with lithium atoms, to yield an extremely pyrophoric, insoluble, red solid.]

One similarity to the lithium atom reaction is that the reaction between calcium atoms and toluene does not result in the activation of the thermodynamically favoured benzyl position. In the case of lithium atoms, it was shown the a key intermediate was the formation of a π complex between

the benzene ring and an Li_2 cluster, which favours the activation of the aromatic C−H bonds.[24]

Reactions of Arylcalcium Hydrides

These arylcalcium hydrides can be redissolved in THF and allowed to react with sterically bulky phenols and alcohols to form bis(aryloxides)/-(alkoxides) of calcium in improved yields (all > 95%).[12]

The structure of **3c** is similar to those of **5** and **7**, which are shown in Figure 8 and have been reported previously.[12,23] It is monomeric, in a distorted trigonal-bipyramidal arrangement, with the Ca−O(phenolate) bond length of 2.182(3) Å av. for **3c** being shorter than that for **5** at 2.197 Å. Like those in **5** and **7**, the aryloxide ligands in **3c** are in the equatorial positions. Another similarity between **3c** and **5** is the almost linear Ca−O−C angle. It is not clear what causes this linearity (and shortened Ca−O bond) in calcium aryloxides.[12] One possible explanation is the steric load on the ligands in both **3c** and **5**; another might lie in π-bonding.[25,26] This is not as unreasonable as it appears, since aryloxides are good π-donor ligands and it has been shown that calcium possesses low-lying d orbitals that influence the structure of molecules.[27−29] It can be very difficult to separate steric and electronic effects.[30] It has been demonstrated that the M−O−C angle has no simple correlation with the degree of π-bonding.[25] A similar comparison can be made between the calcium alkoxide **4** and the previously reported species **6** and **8**.[12,31] There is a pronounced difference between the structures. In **4**, the crystal was grown from THF and crystallised as a monomer of coordination number six, while compounds **6** and **8** were grown from toluene and crystallised as dimers with lower coordination numbers of four and three, respectively. The Ca−O bond length for the terminal alkoxide in **6** is 2.105 Å, shorter than the same Ca−O bond length, of 2.1609(17) Å, in **4** and more akin to the Ca−O bond lengths found in the aryloxide species **3d** [2.182(3) Å] and **8** (2.121 Å). Unlike those in the above species **3c**, **4**, and **5**, the Ca−O−C angle in **6** is bent at 167.4°, while in **4** the Ca−O−C angle is 177.46(14)°. This is almost linear and similar in value to those in the aryloxide species **3c** and **5**.

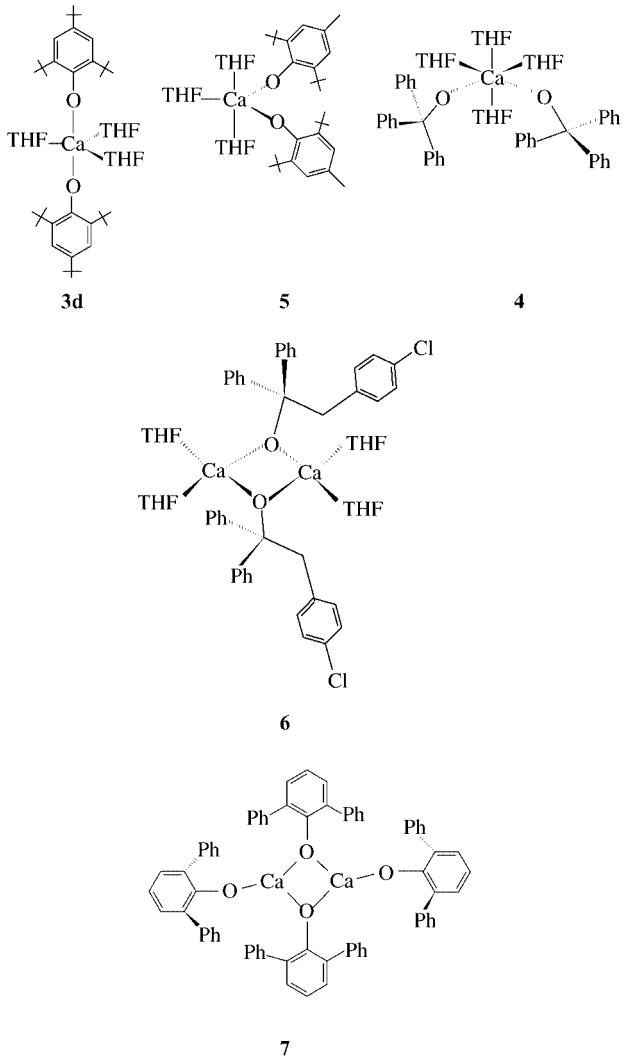

Figure 8. A comparison of some selected group-II bis(alkoxides)

Conclusion

Calcium atoms react unselectively with toluene, *tert*-butylbenzene and trimethyl(phenyl)silane to form the *ortho*, *meta*, and *para* isomers of each arylcalcium hydride. However, when *m*-xylene was cocondensed with calcium atoms in the presence of THF, selective C−H bond activation in the position *meta* to the methyl groups was observed. These arylcalcium hydrides are useful reagents for the formation of calcium bis(alkoxides). The reactions between (*tert*-butylphenyl)calcium hydride and different *tert*-butyl-substituted phenols resulted in the formation of the corresponding aryloxides in high yields. In $Ca(2,4,6\text{-}tBu_3C_6H_2O)_2(THF)_3$ the five oxygen atoms furnish a distorted trigonal-bipyramidal coordination polyhedron with the sterically bulky aryloxide ligands in the equatorial positions. In a similar reaction, triphenylmethanol yielded the alkoxide $[Ca\{OC(C_6H_5)_3\}_2(THF)_4]$ in a similar high yield. This compound shows a distorted octahedron of six oxygen atoms around the central metal atom and the two alkoxide ligands in a *cis* equatorial geometry.

Experimental Section

General: All experimental procedures were performed by use of standard Schlenk techniques under dry argon. Solvents such as THF, benzene, toluene, *m*-xylene, and *tert*-butylbenzene were dried and distilled prior to use from sodium benzophenone ketyl under argon. Trimethyl(phenyl)silane was dried and distilled from calcium dihydride under argon. Pentane was dried and distilled prior to use from sodium/potassium amalgam under argon. The solvents were then degassed by three freeze-pump-thaw cycles. Triphenylcarbenium tetrafluoroborate and 18-crown-6 were purchased from Aldrich and dried under high vacuum for 2 d. Celite was stored in an oven at 120 °C overnight and was dried under vacuum for 3 h before use. Approximately 6 cm of Celite was used for each filtra-

tion. ^{1}H and ^{13}C NMR spectra were obtained with either a Varian 300 MHz or a Varian 500 MHz NMR machine. All chemical shifts are reported in ppm and are referenced to TMS. All the GC MS samples were run as ethyl acetate solutions with a Finnigan Trace GC MS, on a room temp. X-5MS 15-m column. Warwick Analytical Service, Warwick, UK, performed the elemental analysis.

Typical Cocondensation Experiment: Calcium (1.5 g, 0.0375 mol) was vaporised from an alumina crucible over 90 min (5.6 V and 56 A) and cocondensed with a mixture of the aromatic compound (20 mL) and THF (80 mL). The pressure measured at the bottom of the cocondensation vessel was kept below 10^{-5} mbar to avoid gas-phase reactions between the metal atoms and reactants. The apparatus used has been described previously.[24] At the end of the experiment, the frozen matrix was allowed to warm up under argon. The molten mixture flowed through an internal drain into a Schlenk tube. The solution was filtered through 6 cm of Celite and the solvent was evaporated under reduced pressure to yield a dark red, pyrophoric solid $\{(ArCaH{\cdot}2THF)_x\}$ in yields ranging from 78 to 97%.

Cocondensation of Benzene with Calcium Atoms in THF: This cocondensation yielded a dark red, pyrophoric solid $\{(PhCaH{\cdot}2THF)_x\}$(**1a**) in 78% yield. $C_6H_5CaH{\cdot}2THF$ (262.4): calcd. C 64.1, H 8.4, Ca 15.3; found C 63.5, H 7.9, Ca 15.2. IR (Nujol mull; major peaks): $\tilde{\nu}$ = 3369 (s), 1285 (m), 1224 (s), 1094 (vs), 1031 (w), 981 (m), 905 (s), 837 (s), 751 (m), 726 (m), 696 (m) cm^{-1}.

Cocondensation of Toluene with Calcium Atoms in THF: This cocondensation yielded a brown, pyrophoric solid $\{(C_7H_7CaH{\cdot}2THF)_x\}$ (**1b**) in 97% yield. $C_7H_7CaH{\cdot}2THF$ (276.4): calcd. C 65.2, H 8.8, Ca 14.5; found C 64.4, H 8.8, Ca 14.3. IR (Nujol mull; major peaks): $\tilde{\nu}$ = 3368 (s), 1285 (m), 1223 (s), 1093 (vs), 1032 (w), 986 (m), 908 (s), 837.9 (s), 752 (m), 728 (m), 691 (m) cm^{-1}.

Cocondensation of *tert*-Butylbenzene with Calcium Atoms in THF: This cocondensation yielded a dark red, pyrophoric solid $\{(C_{10}H_{13}CaH{\cdot}2THF)_x\}$ (1c) in 93% yield. $C_{10}H_{13}CaH{\cdot}2THF$ (318.5): calcd. C 67.9, H 9.5, Ca 12.6; found C 67.0, H 9.2, Ca 12.3. IR (Nujol mull; major peaks): $\tilde{\nu}$ = 3370 (s), 1264 (s), 1112 (s), 1094 (vs), 1033 (w), 982 (m), 835 (s), 761.6 (m), 723 (m), 697 (m) cm^{-1}.

Cocondensation of *m*-Xylene with Calcium Atoms in THF: This cocondensation yielded a dark red, pyrophoric solid $\{(C_8H_9CaH{\cdot}2THF)_x\}$ (**1d**) in 85% yield. $C_8H_9CaH{\cdot}2THF$ (290.5): calcd. C 66.2, H 9.0, Ca 13.8; found C 65.9, H 8.7, Ca 13.6. IR (Nujol mull; Major peaks): $\tilde{\nu}$ = 3372 (s), 1288 (m), 1220 (s), 1096 (vs), 10323 (w), 989 (m), 912 (s), 838.4 (s), 757 (m), 732 (m), 686 (m)cm^{-1}.

Cocondensation of Trimethyl(phenyl)silane with Calcium Atoms in THF: This cocondensation yielded a dark red, pyrophoric solid $\{(C_9H_{13}CaH{\cdot}2THF)_x\}$ in 86% yield. $C_9H_{13}SiCaH{\cdot}2THF$ (334.6): calcd. C 61.0, H 9.0, Ca 12.0, Si 8.4; found C 59.8 H 8.8, Ca 12.3, Si 8.0. IR (Nujol mull; major peaks): $\tilde{\nu}$ = 3372 (s), 1591 (w), 1306 (w), 1260 (s), 1206 (m), 1114 (m), 1094 (vs), 1034 (m), 1019 (s), 837 (m), 801 (br), 751 (m), 725 (s), 698 (m), 618 (m) cm^{-1}.

Typical Derivatisation of the Arylcalcium Hydride with Chlorotrimethylsilane: Chlorotrimethylsilane (0.06 mL, 0.73 mmol) in THF (5 mL) was added dropwise at −30 °C to a stirred solution of arylcalcium hydride (1.0 g, dissolved in 50 mL of THF). The dark red colour turned yellow over a period of 5 min. After this time, the stirring was continued, while the solution was allowed to warm to room temperature. Water (15 mL) was added to this solution. The organic layer was separated and dried with magnesium sulfate, and the solvent was removed under reduced pressure to yield the corresponding substituted silane as a dark red oil.

Derivatisation of 1b with Chlorotrimethylsilane: All three possible trimethyl(methylphenyl)silane isomers were detected by GC MS ([M$^+$]: *m*/*z* = 164.1). Trimethyl(2-methylphenyl)silane: ^{1}H and ^{13}C NMR spectroscopic data agree with literature values.[14] Trimethyl(3-methylphenyl)silane: ^{1}H and ^{13}C NMR spectroscopic data agree with literature values.[15] Trimethyl(4-methylphenyl)silane: ^{1}H and ^{13}C NMR spectroscopic data agree with literature values.[16]

Treatment of 1c with Chlorotrimethylsilane. All three possible (*tert*-butylphenyl)trimethylsilane isomers were detected by GC MS ([M$^+$]: *m*/*z* = 206.4). (2-*tert*-Butylphenyl)trimethylsilane: ^{1}H and ^{13}C NMR spectroscopic data agree with literature values.[17] (3-*tert*-Butylphenyl)trimethylsilane: ^{1}H and ^{13}C NMR spectroscopic data agree with literature values.[18] (4-*tert*-Butylphenyl)trimethylsilane: ^{1}H and ^{13}C NMR spectroscopic data agree with literature values.[19]

Treatment of 1e with Chlorotrimethylsilane: Only one compound was detected by GC MS ([M$^+$]: *m*/*z* = 178.4), corresponding to (3,5-dimethylphenyl)trimethylsilane as identified by ^{1}H and ^{13}C NMR data.[20]

Treatment of 1d with Dimethyl Disulfide: Dimethyl disulfide (0.07 mL, 0.73 mmol) in THF (5 ml) was added dropwise at −30 °C to a stirred solution of **1d** (1.0 g, 0.091 mmol, dissolved in 50 mL of THF). The workup was performed as for the derivatisation above. All three isomers of trimethyl[(methylthio)phenyl]-silane were detected by GC MS ([M$^+$]: *m*/*z* = 196.4). Trimethyl[2-(methylthio)phenyl]silane: ^{1}H NMR ($CDCl_3$): δ = 0.33 (s, 9 H, $SiMe_3$), 2.52 (s, 3 H, SCH_3), 7.31 (2 H, Ar-H), 7.5 (2 H, ArH) ppm.^{13}C NMR ($CDCl_3$): δ = −1.1 ($SiMe_3$), 15.6 (SCH_3), 124.4 ($C_{meta'}$), 125.9 (C_{meta}), 129.0 (C_{para}), 132.5 ($C_{ortho'}$), 138.1 (C_{ipso} $CSiMe_3$), 144.1 (C_{ortho} CSMe). Trimethyl[3-(methylthio)phenyl]silane: ^{1}H and ^{13}C NMR spectroscopic data agree with literature values.[17] Trimethyl[4-(methylthio)phenyl]silane: ^{1}H and ^{13}C NMR spectroscopic data agree with literature values.[19]

Typical Hydride Abstraction Reaction of the Arylcalcium Hydride with Ph_3CBF_4: The appropriate arylcalcium hydride (0.52 g, 1.9 mmol) was dissolved in toluene (30 mL) and 18-crown-6 (0.5 g, 1.9 mmol) and placed in a pressure-equalising dropping funnel. This solution was added slowly at −30 °C and with vigorous stirring to a suspension of triphenylcarbenium tetrafluoroborate (0.65 g, 1.9 mmol) in toluene (20 mL). After completion of the addition, the dark red solution was stirred at −30 °C for 1 h. Any unchanged solid was removed by filtration and the toluene solvent was removed in vacuo to yield triphenylmethane.

Typical Synthesis of Calcium Bis(alkoxides) by Use of 1c: Compound **1c** (1.27 g, 0.001 mol) was dissolved in THF (150 mL). The substituted alcohol or phenol (0.008 mol), dissolved in THF (50 mL), was added dropwise to this solution over 15 min at −30 °C. The solution was kept at −30 °C with vigorous stirring until the evolution of H_2 had ceased. The solution was then allowed to warm up slowly to room temperature. The solvent was removed under vacuum to yield a beige, moisture-sensitive solid. This was washed twice with pentane and the remaining solid was dried under vacuum to yield the corresponding bis(alkoxide) of calcium in high yields ranging from 95 to 98%.

Synthesis of $[Ca(2,6\text{-}tBu_2C_6H_2O)_2(THF)_3]$ (3a): This reaction yielded 0.53 g (96% yield) of **3a** as an off-white solid. ^{1}H NMR

(500 MHz, C_6H_6) δ = 7.3 (d, 4 H), 6.7 (t, 2 H), 3.4 (s, 12H THF), 1.9 (s, 12 H, THF), 1.4 (s, 36 H, CH_3) ppm. ^{13}C NMR (500 MHz, C_6H_6) 164.4 (C_{ipso}), 137.4 C_{ortho}), 125.0 (C_{meta}), 112.8 (C_{para}), 69.1 (THF), 35.4 $(CCH_3)_3$, 31.4 (CH_3), 25.1 (THF) ppm. IR (Nujol mull; major vibrations): $\tilde{\nu}$ = 2887 (m), 1416 (m) 1382 (s), 1228 (m), 1037 (s), 898 (m), 809 (m), 519 (m) cm^{-1}.

Synthesis of [Ca(2,6-*t*Bu$_2$-4-MeC$_6$H$_2$O)$_2$(THF)$_3$] (3b): This reaction yielded 0.55 g (98% yield) of **3b** as an off-white solid. ^1H and ^{13}C NMR spectroscopic data (500 MHz C_6H_6) agree with literature values.[12]

Synthesis of [Ca(2,4,6-*t*Bu$_3$C$_6$H$_2$O)$_2$]·3THF (3c): This reaction yielded 0.59 g (97%) of **3c** as an off-white solid. ^1H and ^{13}C NMR (500 MHz C_6H_6) agree with literature values.[32] X-ray quality crystals were grown from a concentrated THF solution at +5 °C over a period of one week.

Synthesis of [Ca{OC(C$_6$H$_5$)$_3$}$_2$(THF)$_3$] (4): This reaction yielded 0.77 g (95%) of **4** as a pale white solid. A colourless single crystal of **4** for X-ray diffraction studies was grown from a concentrated THF solution at +5 °C over 10 d. ^1H NMR (500 MHz, C_6H_6) δ = 7.30 (d, 12 H, CH C_6H_5), 7.10−7.01 (m, 18 H, C_6H_5), 3.41 (m, 16 H, THF), 1.36 (m, 16 H, THF) ppm. IR (Nujol mull; major bands): $\tilde{\nu}$ = 3056 (s), 2919 (m), 1490 (m), 1444 (m), 1230 (s), 1031 (vs), 1015 (s), 823 (m), 776 (m), 754 (m), 727 (m), 700 (s), 671 (m), 617 (m), 512 (m) cm^{-1}.

X-ray Crystallographic Study of 3c and 4: The data for **3c** and **4** were collected at 173(2) K from shock-cooled crystals with a BRUKER SMART-APEX diffractometer (graphite-monochromated Mo-K_α radiation, λ = 71.073 pm), equipped with a low-temperature device.[32] The crystal data are summarized in Table 4. The structure was solved by direct methods (SHELXS-NT97)[33] and refined by full-matrix, least-squares methods against F^2 (SHELXL-NT97).[34] R values defined as $R1 = \Sigma||F_o| - |F_c||/\Sigma|F_o|$, $wR2 = [\Sigma w(F_o^2 - F_c^2)^2/\Sigma w(F_o^2)^2]^{0.5}$, $w = [\sigma^2(F_o^2) + (g_1P)^2 + g_2P]^{-1}$, $P = 1/3[\max(F_o^2,0) + 2F_c^2]$. SADABS 2.0 was employed as a program for empirical absorption correction.[35] In addition to the calcium complex **3c**, the unit cell also contained 2.5 noncoordinating THF molecules. The THF molecule (O7−C57) is disordered and was refined to split occupancies of 0.68/0.32. The disordered *tert*-butyl moiety (C12−C14) was refined to a split occupancy of 0.65/0.35. All non-hydrogen atoms were refined anisotropically. All hydrogen atoms were geometrically idealised and refined with a riding model. In addition to the calcium complex **4**, the unit cell also contains one noncoordinating THF molecule. The coordinated THF molecule (O3−C27) was disordered and could be refined to split occupancies of 0.73/0.27. Bond length and similarity restraints were used in the refinement of the disorder. All non-hydrogen atoms were refined anisotropically. The hydrogen atoms were geometrically idealised and refined with a riding model. CCDC-190905 (**3c**) and -190906 (**4**) contain the supplementary crystallographic data for this paper. These data can be obtained free of charge at www.ccdc.cam.ac.uk/conts/retrieving.html [or from the Cambridge Crystallographic Data Centre, 12 Union Road, Cambridge CB2 1EZ, UK; Fax: (internat.) + 44-1223/336-033; E-mail: deposit@ccdc.cam.ac.uk].

Theoretical Methods: For determination of the structures, spectroscopic data, and reaction enthalpies of intermediates in the reaction mechanisms, the application of theoretical methods has proven advantageous. For this purpose the program package GAUSSIAN98[36] implemented on a DEC Alpha workstation (500 MHz CPU/256 MB RAM) or an Origin 200 eight-processor cluster (SGI, 180 MHz CPU/2 GB RAM) was used. Ab initio calculations were performed at the DFT level of theory (B3LYP) with the 6-31G** basis set for C, H, and N. The chosen general basis set for calcium was AKR4, which was used by us in another study on organocalcium complexes.[6] Harmonic vibrational frequencies, calculated at the same level, characterised stationary points and gave the zero-point energies. The difference in the sum of the electronic and the zero-point energies were interpreted as reaction enthalpies at 0 K.

Table 4. Crystallographic data for [Ca{2,4,6-*t*Bu$_3$C$_6$H$_2$O}$_2$(THF)$_3$] (**3c**) and [Ca(OPh$_3$)$_2$(THF)$_4$] (**4**) at T = 173 K

	3c	**4**
Empirical formula	$C_{48}H_{82}CaO_5$+2.5C_4H_8O	$C_{58}H_{70}CaO_7$
Formula mass	959.48	919.22
Crystal system	monoclinic	orthorhombic
Space group	$P2_1/c$	*Pccn*
a [Å]	9.942(2)	14.564(8)
b [Å]	35.933(8)	16.580(9)
c [Å]	16.138(3)	21.182(13)
β [°]	94.206(4)	90
V [Å^3]	5750(2)	5115(5)
Z	4	4
Calcd. density [Mg/m^3]	1.108	1.194
Absorption coeff. [mm^{-1}]	0.158	0.174
F(000)	2120	1976
Crystal size [mm]	0.3 × 0.3 × 0.2	0.6 × 0.5 × 0.3
θ range [°]	1.39−22.46	1.86−25.03
Reflections collected	62291	48730
Independent reflections	11975 [R(int) = 0.0612]	5776 [R(int) = 0.0274]
Completeness at $\theta_{max.}$ [%]	99.9	100.0
Data/restraints/param.	7481/636/761	4528/110/367
Goodness-of-fit on F^2	1.192	1.156
Final R indices [$I > 2\sigma(I)$]	$R1$ = 0.0890, $wR2$ = 0.1979	$R1$ = 0.0550, $wR2$ = 0.1313
R indices (all data)	$R1$ = 0.0949, $wR2$ = 0.2015	$R1$ = 0.0575, $wR2$ = 0.1331
Largest diff. peak/hole [e·A^{-3}]	0.601/−0.417	0.336/−0.266

Acknowledgments

This work was supported by the Centre for High-Performance Computing Applications at University College Dublin, Ireland. C. S. and D. S. thank the Deutsche Forschungsgemeinschaft and the Fonds der Chemischen Industrie for financial support.

[1] For some recent reviews see: [1a] T. P. Hanusa, *Polyhedron* **1990**, *9*, 1345−1362. [1b] T. P. Hanusa, *Chem. Rev.* **1993**, *93*, 1023−1036. [1c] D. Stalke, *Angew. Chem. Int. Ed. Engl.* **1994**, *33*, 2168−2171. [1d] M. Westerhausen, *Coord. Chem. Rev.* **1998**, *176*, 157−210. [1e] M. Westerhausen, *Angew. Chem. Int. Ed.* **2001**, *40*, 2975−2977. [1f] T. P. Hanusa, *Coord. Chem. Rev.* **2000**, *210*, 329−367. [1g] T. P. Hanusa, *Organometallics* **2002**, *21*, 2559−2571.

[2] T. C. Wu, R. Xiong, R. D. Rieke, *J. Org. Chem.* **1990**, *55*, 5045−5051.

[3] [3a] B. Bogdanovic, *Acc. Chem. Res.* **1988**, *21*, 261−267. [3b] B. Bogdanovic, *Main Group Met. Chem.* **1990**, *13*, 341.

[4] S. R. Drake, D. J. Otway, S. P. Perlepes, *Main Group Met. Chem.* **1991**, *14*, 243.

[5] K. Mochida, T. Yamanishi, *J. Organomet. Chem.* **1987**, *332*, 247−252.

[6] D. S. Hutchings, P. C. Junk, W. C. Patalinghug, C. L. Raston, A. H. White, *J. Chem. Soc., Chem. Commun.* **1989**, 973−974.

[7] L. M. Engelhardt, P. C. Junk, C. L. Raston, A. H. White, *Chem. Commun.* **1988**, 1500−1501.

[8] P. B. Hitchcock, M. F. Lappert, G. A. Lawless, B. Royo, *Chem. Commun.* **1990**, *17*, 1141−1143.

[9] K. Mochida, H. Takeuchi, Y. Hiraga, H. Ogawa, *Organometallics* **1987**, *6*, 2293−2297.

[10] J. P. Dunne, M. Tacke, S. Fox, *J. Mol. Struct. THEOCHEM* **2001**, *543*, 157−166.

[11] [11a] D. C. Bradley, *Chem. Rev.* **1989**, *89*, 1317−1322. [11b] W. A. Wojtczak, P. F. Fleig, M. J. Hampden-Smith, *Adv. Organomet. Chem.* **1996**, *40*, 215−329. [11c] J. S. Matthews, W. S. Rees, *Adv. Inorg. Chem.* **2000**, *50*, 173−192.

[12] K. F. Tesh, T. P. Hanusa, J. C. Huffman, C. J. Huffman, *Inorg. Chem.* **1992**, *31*, 5572−5579.

[13] S. C. Geol, M. A. Matchett, M. Y. Chiang, W. E. Buhro, *J. Am. Chem. Soc.* **1991**, *113*, 1844−1845.

[14] J. A. Albanese, D. E. Gingrich, C. D. Schaeffer Jr, S. M. Coley, J. C. Otter, *J. Organomet. Chem.* **1989**, *365*, 23−35.

[15] H. J. Reich, J. E. Holladay, J. D. Mason, W. H. Sikorski, *J. Am. Chem. Soc.* **1995**, *117*, 12137−12150.

[16] L. Hevesi, M. Dehon, R. Crutzen, A. Lazarescu-Grigore, *J. Org. Chem.* **1997**, *62*, 2006−2012.

[17] F. Effenberger, D. Hablich, *Liebigs Ann. Chem.* **1979**, *6*, 842−857.

[18] C. D. Schaeffer, J. J. Zuckerman, C. H. Yoder, *J. Organomet. Chem.* **1974**, *80*, 29−35.

[19] C. A. van Walree, X. Y. Lauteslager, A. M. A. van Waginingen, J. W. Zwickler, L. W. Jeneskens, *J. Organomet. Chem.* **1995**, *496*, 117−125.

[20] P. A. Deck, C. L. Beswick, T. J. Marks, *J. Am. Chem. Soc.* **1998**, *120*, 1772−1784.

[21] S. R. Drake, D. J. Ottway, M. B. Hursthouse, K. M. Abdul Malik, *Polyhedron* **1992**, *11*, 1995−2007.

[22] P. Rademacher, *Strukturen organischer Moleküle*, VCH, Weinheim, **1987**, p. 56.

[23] U. Englich, K. Ruhlandt-Senge, *Z. Anorg. Allg. Chem.* **2001**, *627*, 851−856.

[24] [24a] M. Tacke, *Chem. Ber.* **1995**, *128*, 91−92. [24b] M. Tacke, *Chem. Ber.* **1996**, *129*, 1369−1371. [24c] M. Tacke, *Eur. J. Inorg. Chem.* **1998**, 537−541. [24d] J. P. Dunne, M. Bockmeyer, M. Tacke, *Eur. J. Inorg. Chem.*, in press.

[25] G. D. Smith, P. E. Fanwick, I. P. Rothwell, *Inorg. Chem.* **1990**, *29*, 3221−3226.

[26] T. W. Coffindaffer, B. D. Steffy, I. P. Rothwell, K. Folting, K. Huffman, J. C. Streib, *J. Am. Chem. Soc.* **1989**, *111*, 4742−4749.

[27] M. Kaupp, P. v. R. Schleyer, *J. Am. Chem. Soc.* **1992**, *114*, 491−497.

[28] M. Kaupp, P. v. R. Schleyer, H. Stoll, H. Preuss, *J. Am. Chem. Soc.* **1991**, *113*, 6012−6020.

[29] M. Kaupp, P. v. R. Schleyer, H. Stoll, H. Preuss, *J. Chem. Phys.* **1991**, *94*, 1360−1366.

[30] R. Fleischer, D. Stalke, *Inorg. Chem.* **1997**, *36*, 2413−2419.

[31] G. B. Deacon, C. M. Forsyth, P. C. Junk, *J. Organomet. Chem.* **2000**, *607*, 112−119.

[32] [32a] D. Stalke, *Chem. Soc. Rev.* **1998**, *27*, 171. [32b] T. Kottke, R. J. Lagow, D. Stalke, *J. Appl. Crystallogr.* **1996**, *29*, 465. [32c] T. Kottke, D. Stalke, *J. Appl. Crystallogr.* **1993**, *26*, 615.

[33] G. M. Sheldrick, *Acta Crystallogr., Sect. A* **1990**, *46*, 467.

[34] G. M. Sheldrick, *SHELXL-NT97, Program for Crystal Structure Refinement*, Universität Göttingen, **1997**.

[35] G. M. Sheldrick, *Program for empirical absorption correction*, Universität Göttingen, **2000**.

[36] M. J. Frisch, G. W. Trucks, H. B. Schlegel, G. E. Scuseria, M. A. Robb, J. R. Cheeseman, V. G. Zakrzewski, J. A. Montgomery, Jr., R. E. Stratmann, J. C. Burant, S. Dapprich, J. M. Millam, A. D. Daniels, K. N. Kudin, M. C. Strain, O. Farkas, J. Tomasi, V. Barone, M. Cossi, R. Cammi, B. Mennucci, C. Pomelli, C. Adamo, S. Clifford, J. Ochterski, G. A. Petersson, P. Y. Ayala, Q. Cui, K. Morokuma, D. K. Malick, A. D. Rabuck, K. Raghavachari, J. B. Foresman, J. Cioslowski, J. V. Ortiz, A. G. Baboul, B. B. Stefanov, G. Liu, A. Liashenko, P. Piskorz, I. Komaromi, R. Gomperts, R. L. Martin, D. J. Fox, T. Keith, M. A. Al-Laham, C. Y. Peng, A. Nanayakkara, C. Gonzalez, M. Challacombe, P. M. W. Gill, B. Johnson, W. Chen, M. W. Wong, J. L. Andres, C. Gonzalez, M. Head-Gordon, E. S. Replogle, J. A. Pople, *Gaussian98, Revision A.7*, Gaussian, Inc., Pittsburgh, PA, **1998**.

Received August 12, 2002
[I02456]

A Facile Direct Synthesis of Bimetallic $Cu^{II}Zn^{II}$ Complexes with Ethylenediamine Revealing Different Types of Chain Crystal Structures

Oksana V. Pryma,[a] Svitlana R. Petrusenko,*[a] Volodymyr N. Kokozay,[a] Brian W. Skelton,[b] Oleg V. Shishkin,[c] and Tetyana S. Teplytska[c]

Keywords: Heterometallic complexes / Copper / Zinc / N ligands

Unactivated copper metal powder and zinc oxide readily react with ethylenediamine (en) in nonaqueous [methanol, dimethylformamide (dmf), dimethyl sulfoxide (dmso), acetonitrile] solutions of ammonium salts under ambient conditions producing, in high yields, a series of heterobimetallic complexes of general formula $[Cu(en)_2ZnX_4]\cdot(Solv)$, where X = Cl, Br, NCS, CH_3COO (OAc); Solv = dmf, dmso, CH_3CN, H_2O. The single-crystal X-ray analysis of the complexes reveals chain structures, which are based on the completion of the octahedral coordination of Cu^{II} by two bridging X atoms from ZnX_4^{2-}. The ZnX_4^{2-} is shown to be a distorted tetrahedron (Cl, Br, NCS) or a very distorted octahedron (OAc) and to behave as a one- or two-linking centre bridging ligand. The chains are found to be zigzag $[Cu(en)_2ZnCl_4]\cdot$dmso (**1**), $[Cu(en)_2ZnCl_4]\cdot$dmf (**2**), $[Cu(en)_2Zn(NCS)_4]\cdot CH_3CN$ (**3**), quasi linear $[Cu(en)_2Zn(OAc)_4]$ (**4**), or helical, $[Cu(en)_2Zn(NCS)_4]\cdot 0.5H_2O$ (**5**), depending on the nature of the anion and solvent. Complex **4** represents the first compound containing $Zn(OAc)_4^{2-}$ to be crystallographically authenticated.

(© Wiley-VCH Verlag GmbH & Co. KGaA, 69451 Weinheim, Germany, 2003)

Introduction

The one-pot synthesis of metal complexes using elemental metals as starting materials, the so called "direct synthesis of coordination compounds" (DS),[1] has become an active research field and is undergoing rapid progress. Among the various methods of DS — cryosynthesis, electrochemical synthesis, mechanosynthesis — the oxidative dissolution of unactivated coarse-grain metal powders in solutions of ligands is one of the most important because of its simplicity and versatility. This method has provided a route to the synthesis of almost all the main types of monometal coordination compounds.[1,2]

Recently we have expanded this approach to the preparation of mixed-metal complexes that are of current interest due to their promising physical and biological properties. The synthetic procedure shown in Scheme 1 has been used to produce a series of new heterobimetallic Cu^{II}/M^{II} (M = Co, Ni, Zn, Pb) complexes with amino alcohols (HL).[2–8]

[a] Department of Inorganic Chemistry, National Taras Shevchenko University,
Volodimirska st. 64, Kyiv 01033, Ukraine
Fax: (internat.) + 380-44/296-2467
E-mail: kokozay@chem.univ.kiev.ua
[b] Department of Chemistry, University of Western Australia, Crawley, Western Australia 6009, Australia
[c] Scientific Research Department of Alkali Halide Crystals, STC "Institute for Single Crystals", National Academy of Sciences of Ukraine,
Lenina Ave 60, Khar'kov 61001, Ukraine

$$Cu^0 - M^0/MX_2 \text{ - HL - Solv (in air)}$$

Scheme 1

The synthetic route (Scheme 1) is effective when using proton-donating ligands. In this paper we suggest developing DS for the use of aprotic ligands (L). The essence of the proposed approach is to use ammonium salts as both proton- and anion-donating reagents (Scheme 2).

$$Cu^0 \text{ - } M^0/MO \text{ - L - } NH_4X \text{ - Solv (in air)}$$

Scheme 2

Ethylenediamine was employed in our synthesis as an aprotic ligand. It has been shown that ethylenediamine can take part in the activation of the metal surface and also in electron transfer in the reacting system.[9] Moreover, it is a strong coordinating agent that is efficiently applied in supramolecular design.[10–13]

Exploiting this approach (Scheme 2), we have synthesized a number of $Cu^{II}Zn^{II}$ complexes with ethylenediamine, which have the general formula $[Cu(en)_2ZnX_4]\cdot n$ Solv (X = Cl, Br, SCN, OAc; Solv = dmf, dmso, CH_3CN, and H_2O which is produced in the reaction; n = 0, 0.5, 1). The reactions proceed in the following way:

$$Cu^0 + ZnO + 2\,en + 4\,NH_4X + 1/2\,O_2 + n\,Solv \rightarrow [Cu(en)_2ZnX_4]\cdot n\,Solv + 4\,NH_3 + 2\,H_2O$$

In each case the reactions were conducted in air, at 50–60 °C and with stirring for 1–2 h. The yields of the products were up to 90%.

Details of the syntheses, crystal structures and IR spectroscopic investigations of the complexes are reported.

Results and Discussion

Zigzag CuZn Chain Structures of $[Cu(en)_2ZnCl_4]\cdot$dmso (1), $[Cu(en)_2ZnCl_4]\cdot$dmf (2), and $[Cu(en)_2Zn(NCS)_4]\cdot CH_3CN$ (3)

All the titled complexes possess the same type of crystal structure. The tetrahedral ZnX_4^{2-} anions behave as one-linking centre bridging ligands, spanning the square planar $Cu(en)_2^{2+}$ cations in the *trans* positions with the Cl (in **1**, **2**) or S (in **3**) atoms, building up one-dimensional networks (Figure 1). The unusual coordination mode of ZnX_4^{2-} in these complexes is most probably due to the set of hydrogen bonds (ca. 3.0−3.2 Å) between the amino groups of ethylenediamine and the donor atoms of the nonbridged X ligands. Usually, the coordination is two-linking for similar complexes, as in $[ZnL_2][ZnCl_4]$ (L = diacetone alcohol).[14] Additionally the structure is supported by the guest dimethyl sulfoxide, dimethylformamide or acetonitrile molecules accommodated in the interchain space and hydrogen bonded through the O (dmso, dmf) or N (CH_3CN) atoms to the NH_2 groups (Figure 1). The lengths of the en-solvate hydrogen bonds show the strongest connection in case of dmso molecule [$d(N\cdots O_{dmso})$ are 2.95(1) and 2.94(1) Å (**1**), $d(N\cdots O_{dmf})$ are 3.171(7) and 2.973(8) Å (**2**), $d(N\cdots N)$ are 3.13(2) and 3.07(2) Å (**3**)].

The chains of Cu−Zn atoms have a zigzag shape with the Cu−Zn−Cu angle [89.06(2)° (**1**), 82.88(2)° (**2**), 66.05(3)° (**3**)] being dependant on both the nature of the X ligands in the ZnX_4^{2-} anion and the nature of the solvate molecule. The Cu···Cu distances within the chains are 5.910(1), 5.5130(5) and 6.308(3) Å for **1**, **2** and **3**, respectively.

Bond lengths in the en ligands and Cu−N distances (Table 2) are in accordance with those found in the literature for similar copper(II) complexes.[15,16] The axial Cu−X distances are 3.117(3) and 3.085(4) Å (Cu−Cl, **1**), 2.9285(8) Å (Cu−Cl, **2**), 3.202(4) Å and 3.232(4) Å (Cu−S, **3**). These are quite long but do occur in complexes that have an elongated tetragonal or rhombic octahedral stereochemistry of the copper(II) ion, e.g. the $Cu-Cl_{ax}$ distances of ca. 3.0−3.2 Å are found in $Cs_3[Cu_2Cl_7(H_2O)_2]$,[17] $(Me_3NH)_2[Cu_4Cl_{10}]$,[18] $[Pt(NH_3)_4CuCl_4]$,[19] and the $Cu-S_{ax}$ of 3.00 and 3.27 Å in $[Cu(NH_3)_4(SCN)_2]$[20] and $[Cu(en)_2(SCN)_2]$,[21] respectively. The geometrical parameters of ZnX_4^{2-}, namely nonequivalence of the Zn−Cl and Zn−N bond lengths (Table 2), lend additional support to the conclusion that the complex anions are weakly or *semi*-coordinated[22] to the copper(II) ion and not just positioned by van der Waals forces.

Quasi Linear CuZn Chain Structure of $[Cu(en)_2Zn(OAc)_4]$ (4)

Although the main building blocks of the acetate complex $Cu(en)_2^{2+}$ and $Zn(OAc)_4^{2-}$ show a formal resemblance

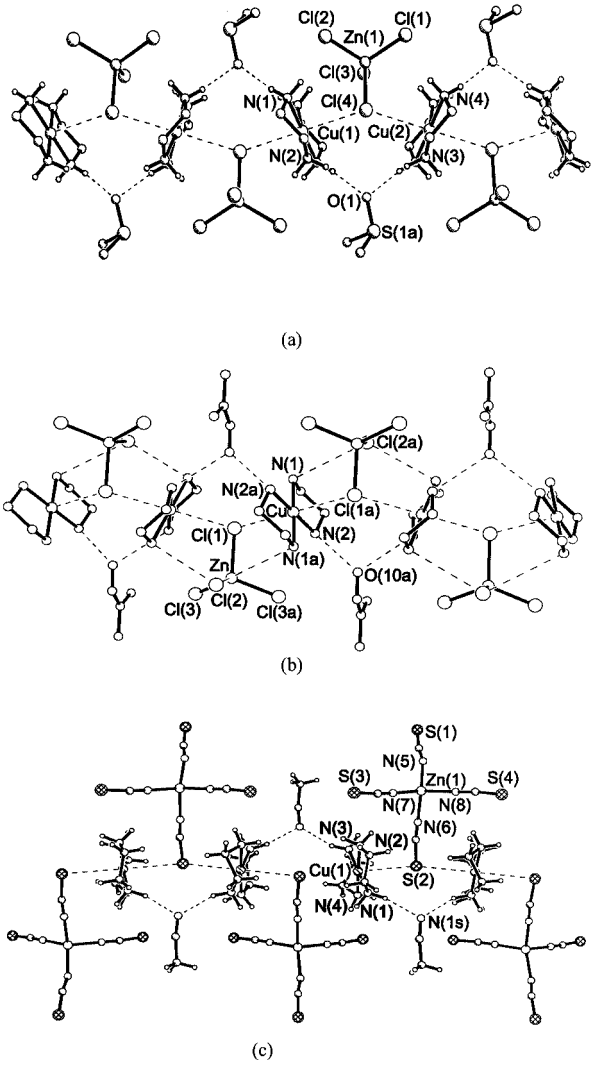

Figure 1. Structures of zigzag CuZn chains in (a) $[Cu(en)_2ZnCl_4]\cdot$dmso (**1**), (b) $[Cu(en)_2ZnCl_4]\cdot$dmf (**2**), (c) $[Cu(en)_2Zn(NCS)_4]\cdot CH_3CN$ (**3**), with atomic numbering

to **1**−**3**, the differences in their crystal structures are quite significant. Most importantly, the Zn atom in the tetraacetatozincate ion is not four- but now six-coordinate through two asymmetrically chelating and two monatomic bridging bidentate acetate groups (Figure 2). The octahedron ZnO_6 is very distorted: the Zn−O distances and O−Zn−O angles vary from 2.00−2.41 Å and 57.0−154.4°, respectively (Table 2). Because no crystallographic data was found for $Zn(OAc)_4^{2-}$ a structural comparison was made with $M(OAc)_4^{2-}$ (M = Cu, Cd)[23] and $Zn(NO_3)_4^{2-}$.[24] In these complexes the symmetry of the resulting coordination polyhedron is approximately D_{2d} and depicted as a distorted dodecahedron. The differences in the bond lengths M−O within a chelate carboxylate group or nitrate ring are very significant [Cu−O(OAc) = 1.97−2.79 Å and Zn−O(NO_3) = 2.03−2.52 Å]. In the case of the tetranitratozincate complex the distortions observed were explained by the tendency of the Zn^{II} ion to undergo tetrahedral coor-

dination; this explanation may also be applicable in our case.

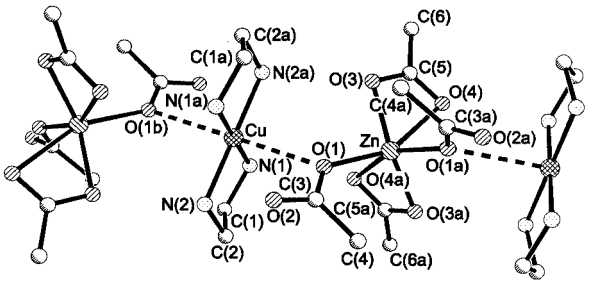

Figure 2. Structure of quasi linear CuZn chain in $[Cu(en)_2Zn(OAc)_4]$ (**4**) with atomic numbering.

It is worth noting that the absence of data on the crystal structure of $Zn(OAc)_4^{2-}$ may not be accidental but due to its low thermodynamic stability. A search for isomorphous crystals of $CaCu(OAc)_4{\cdot}6H_2O$ was undertaken by Langs and Hare,[23] but all attempts to substitute the Zn atoms for Cu atoms were met with failure. The existence of the $Zn(OAc)_4^{2-}$ in **4** is presumably stabilized by the $Cu(en)_2^{2+}$ cation, which is apt to the formation of numerous hydrogen bonds. Indeed, all the acetate oxygen atoms [except O(1), which is bridging the Cu and Zn atoms] take part in hydrogen bonding (Table 3).

The arrangement of the Cu and Zn atoms is almost linear, with the angle at the Cu atom (on an inversion centre) being 180° and that at the Zn atom, 170.25(2)°. The Cu···Zn distances are 4.1064(7) Å.

Helical CuZn Chain Structure of $[Cu(en)_2Zn(NCS)_4]{\cdot}0.5H_2O$ (5)

One of the more interesting structures is given in Figure 3 where a helical type of chain crystal structure is presented. A comparison of the structures of **3** and **5** demonstrates seemingly insignificant changes in composition, such as the replacement of an included acetonitrile molecule for a water molecule, associated with dramatic changes in the supramolecular structure. In contrast to **3**, in the hydrate complex a $Zn(NCS)_4^{2-}$ ion acts as a two-linking centre bridging ligand connecting the $Cu(en)_2^{2+}$ moieties in an infinite bimetallic spiral. The spirals, running along the *a* axis, form channels filled with uncoordinated water molecules (Figure 3, see b).

The Zn^{II} coordination environment closely approximates tetrahedral symmetry, the N−Zn−N bond angle being 107−112°. The thiocyanato groups are almost linear with a mean value of the N−C−S angles of 177(2)°. The Zn−N−C linkages are bent with angles varying from 159(1)° to 177(2)°; those with maximal deviations from linearity have the NCS^- groups bridging Zn and Cu atoms with the minimal values being those of the N(6)C(6)S(2) group, which bridges the Zn atoms such that the Zn-NCS···Zn′ atoms are essentially linear [the S(2)···Zn distance and C(6)S(2)Zn angle are ca. 3.64 Å and 171° respectively] (Figure 3, see a). The S−C average distance of 1.62(2) Å, and C−N average distances of 1.14(2) Å are in accordance with the values observed in other thiocyanato-containing metal complexes.[25,26]

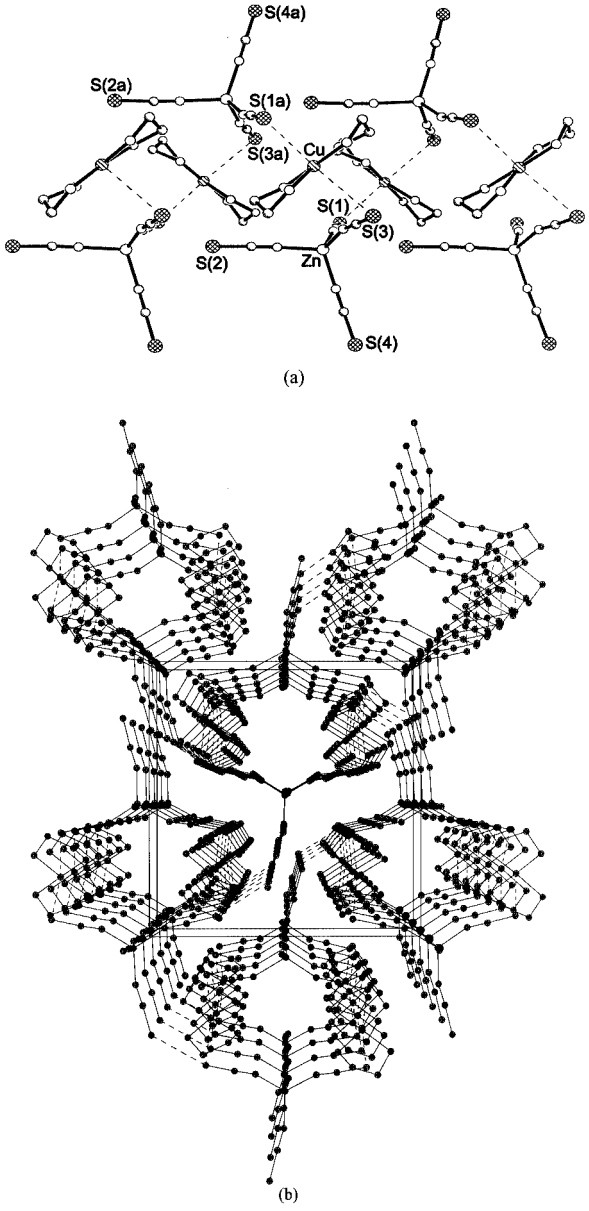

Figure 3. (a) Structure of helical CuZn chain in $[Cu(en)_2Zn(NCS)_4]{\cdot}0.5H_2O$ (**5**) with atomic numbering; (b) packing diagram of **5** revealing the channels down the a axis; hydrogen atoms and water molecules are omitted for clarity.

The Cu^{II} ion has asymmetric (4+1+1) surroundings; the axial positions are occupied by the S(1) and S(3) atoms from the thiocyanate groups: Cu−S(1) = 2.921(6) and Cu−S(3) = 3.218(5) Å; the S(1)−Cu−S(3) angle is 170.7(1)°. The CuN_4 fragment is largely planar and its geometrical parameters are consistent with those normally observed.[16]

IR Spectroscopic Measurements

The infrared spectra for complexes **1**−**5** contain characteristic ν(N−H), ν(C−H), δ(HNH), ν(C−N) and ν(C−C)

frequencies for ethylenediamine in the ranges 3325−3130, 2990−2890, 1605−1580 (in **4** the corresponding mode of en is obscured by stretching vibrations of the carboxylate group), 1105−1053 and 990−980 cm^{-1}, respectively. Evidence for the coordination of en is provided by the shift of asymmetrical and symmetrical NH stretching frequencies of ca. 30−100 cm^{-1} to lower values and CH stretching frequencies of ca. 50−80 cm^{-1} to higher values compared with corresponding ones for en itself [3355, 3270 cm^{-1} − ν(NH); 2925, 2855 cm^{-1} − ν(CH)].[27,28] Two strong and broad absorption bands found for the acetate groups in complex **4** (1630− 580 and 1430−1390 cm^{-1}) lead to the Δ value [$\Delta = \nu_{as}(COO) - \nu_s(COO)$] in the range 150−240 cm^{-1}. This value is consistent with bridging unidentate or asymmetrical chelate (''pseudo-unidentate'') carboxylate coordination.[29] The coordinated thiocyanate groups in **3** and **5** are confirmed by the presence of the intense absorption at 2090 cm^{-1} attributed to $\nu_{as}(C\equiv N)$ and the weak ν(CS) absorption at 835 cm^{-1}.[26] The presence of the solvate molecules in **1**−**3** can be identified by the peaks at 1020 and 950 cm^{-1} (for dmso, **1**), 1650 cm^{-1} (for dmf, **2**), and 2250 cm^{-1} (for CH_3CN, **3**). It should be noted that the peaks of ν(SO) and ν(CO) found in **1** and **2** are typical for coordinated dmso and dmf[26] but in our case the shift of the frequencies to lower values can be explained by the participation of the solvates in hydrogen bonding.

Conclusion

This paper describes a novel synthetic method for the preparation of bimetallic Cu/Zn complexes with ethylenediamine using zerovalent copper in powdered form. We consider that such an approach can also be used for the synthesis of other mixed-metal compounds, e.g. Cu/Cd, Cu/Ni and Cu/Co, with ethylenediamine or related ligands (diethylenetriamine, triethylenetetramine). Further work in this direction is in progress and will be presented in subsequent papers.

Experimental Section

General: All chemicals were of reagent grade and used as received, all experiments were carried out in air. Elemental analyses for

Table 1. Crystal data and structure refinement for **1**−**5**

	1	**2**	**3**	**4**	**5**
Crystal parameters:					
Empirical formula	$C_6H_{22}Cl_4CuN_4OSZn$	$C_7H_{23}Cl_4CuN_5OZn$	$C_{10}H_{19}CuN_9S_4Zn$	$C_{12}H_{28}CuN_4O_8Zn$	$C_8H_{17}CuN_8O_{0.5}S_4Zn$
Formula mass	469.05	464.04	522.49	485.29	490.47
Crystal system	Monoclinic	Monoclinic	Monoclinic	Monoclinic	Orthorombic
Space group	$P2_1/c$	$P2_1/m$	$P2_1$	$C2/c$	$P2_12_12_1$
a/Å	11.820(2)	8.407(1)	9.496(3)	14.213(3)	8.293(3)
b/Å	8.247(2)	11.026(1)	12.615(3)	14.840(3)	15.267(6)
c/Å	18.169(4)	9.429(1)	9.859(3)	9.334(2)	15.573(3)
α/°	90	90	90	90	90
β/°	94.33(3)	96.856(2)	115.45(3)	94.60(3)	90
γ/°	90	90	90	90	90
V/Å^3	1766.1(7)	867.8(2)	1066.4(5)	1962.4(7)	1971.7(11)
Z	4	2	2	4	4
$D_{calcd.}$/g·cm^{-3}	1.764	1.776	1.627	1.643	1.649
μ/mm^{-1}	3.28	3.22	2.526	3.257	2.727
F(*000*)	948	470	530	1004	988
Data collection:					
Diffractometer	CAD-4	Siemens SMART	Siemens P3/PC	CAD-4	Siemens P3/PC
Monochromator	Graphite	Graphite	Graphite	Graphite	Graphite
Radiation	Mo-K_α (λ = 0.71073 Å)	Mo-K_α (λ = 0.71073 Å)	Mo-K_α (λ = 0.71073 Å)	Cu-K_α (λ = 1.54178 Å)	Mo-K_α (λ = 0.71073 Å)
T/K	293(2)	150	293(2)	293(2)	293(2)
2θ scan range /°	2.25−24.97	2−26.4	2.29−30.07	4.31−59.94	2.78−25.07
h, k, l ranges	+12, +9, ±21	±10, +13, +11	+13, +17, ±13	±15, +16, +10	+9, +18, +18
Reflections collected	3218	8636	2831	1559	1905
Independent reflections [R_{int}]	2977 [0.013]	1873[0.089]	2526[0.0634]	1456 [0.0239]	1905
Refinement:					
Final *R* indices [$I > 2\sigma(I)$]	$R1 = 0.053$ $wR2 = 0.073(F)$	$R1 = 0.061$ $wR2 = 0.068(F)$	$R1 = 0.0734$ $wR2 = 0.1723$	$R1 = 0.0480$ $wR2 = 0.1233$	$R1 = 0.0623$ $wR2 = 0.1473$
R indices (all data)	$R1 = 0.088$ $wR2 = 0.085$	$R1 = 0.071$ $wR2 = 0.076$	$R1 = 0.0958$ $wR2 = 0.1838$	$R1 = 0.0562$ $wR2 = 0.1352$	$R1 = 0.1141$ $wR2 = 0.1721$
G.O.F. (F^2)	1.042(*F*)	1.649(*F*)	1.036	1.027	1.006
Δ(ρ)/e· Å^{-3}	+1.07, −0.95	+1.973, −1.206	+0.923, −0.730	+0.658, −0.990	+0.998, −0.580

Table 2. Selected bond lengths (Å) and angles (°) around metal atoms for **1**−**5** (symmetry transformations used to generate equivalent atoms: **1** *a* < −*x*, −*y*, −*z* >, *b* < 1 −*x*, −*y*, −*z* >; **2** *a* < *x*, 1/2 − *y*, *z* >; **4** *a* < −*x* + 1, *y*, −*z* + 1/2>, *b* < −*x* + 1/2, −*y* + 1/2, −*z* >)

1					
Cu(1)−N(1)	1.981(8)	N(1)−Cu(1)−N(2)	84.7(3)	Cl(1)−Zn(1)−Cl(2)	113.01(9)
Cu(1)−N(2)	2.013(8)	N(1)−Cu(1)−N(1a)	180.0	Cl(1)−Zn(1)−Cl(3)	109.9(1)
Cu(2)−N(3)	1.993(8)	N(1)−Cu(1)−N(2a)	95.3(3)	Cl(1)−Zn(1)−Cl(4)	109.2(1)
Cu(2)−N(4)	1.985(7)	N(2)−Cu(1)−N(2a)	180.0	Cl(2)−Zn(1)−Cl(3)	109.8(1)
Zn(1)−Cl(1)	2.246(3)	N(3)−Cu(2)−N(4)	85.0(3)	Cl(2)−Zn(1)−Cl(4)	108.3(1)
Zn(1)−Cl(2)	2.242(3)	N(3)−Cu(2)−N(3b)	180.0	Cl(3)−Zn(1)−Cl(4)	106.40(9)
Zn(1)−Cl(3)	2.271(3)	N(4)−Cu(2)−N(3b)	95.0(3)		
Zn(1)−Cl(4)	2.302(3)	N(4)−Cu(2)−N(4b)	180.0		
2					
Cu−N(1)	2.021(6)	N(1)−Cu−N(2)	85.2(2)	Cl(1)−Zn−Cl(2)	101.7(1)
Cu−N(2)	2.008(6)	Cl(1)−Cu−N(1)	85.5(2)	Cl(1)−Zn−Cl(3)	109.13(6)
Zn−Cl(1)	2.318(3)	Cl(1)−Cu−N(2)	89.6(2)	Cl(2)−Zn−Cl(3)	110.69(6)
Zn−Cl(2)	2.278(3)			Cl(3)−Zn−Cl(3a)	114.74(8)
Zn−Cl(3)	2.250(2)				
3					
Cu(1)−N(1)	1.918(10)	N(1)−Cu(1)−N(2)	84.8(5)	N(5)−Zn(1)−N(6)	122.9(3)
Cu(1)−N(2)	2.085(9)	N(1)−Cu(1)−N(3)	177.6(5)	N(5)−Zn(1)−N(7)	114.2(5)
Cu(1)−N(3)	2.085(8)	N(1)−Cu(1)−N(4)	94.3(4)	N(5)−Zn(1)−N(8)	103.6(5)
Cu(1)−N(4)	1.990(8)	N(2)−Cu(1)−N(3)	96.9(4)	N(6)−Zn(1)−N(7)	99.8(5)
Zn(1)−N(5)	1.949(8)	N(2)−Cu(1)−N(4)	178.1(5)	N(6)−Zn(1)−N(8)	105.7(5)
Zn(1)−N(6)	2.000(7)	N(3)−Cu(1)−N(4)	84.0(3)	N(7)−Zn(1)−N(8)	110.3(4)
Zn(1)−N(7)	1.886(12)				
Zn(1)−N(8)	2.043(11)				
4					
Cu−N(1)	1.995(4)	N(1)−Cu−N(2)	84.7(2)	O(1)−Zn−O(4a)	90.89(13)
Cu−N(2)	2.010(4)	N(1)−Cu−N(1a)	180.0	O(3)−Zn−O(4)	57.02(12)
Zn−O(1)	2.003(3)	N(1)−Cu−N(2a)	95.3(2)	O(3)−Zn−O(1a)	108.58(11)
Zn−O(3)	2.054(3)	N(2)−Cu−N(2a)	180.0	O(3)−Zn−O(3a)	136.9(2)
Zn−O(4)	2.410(4)	O(1)−Zn−O(3)	97.90(11)	O(3)−Zn−O(4a)	90.10(13)
		O(1)−Zn−O(4)	154.42(11)	O(4)−Zn−O(4a)	84.7(2)
		O(1)−Zn−O(1a)	103.2(2)	O(1)−Cu−O(1b)	180.0
5					
Cu(1)−N(1)	2.04(1)	N(1)−Cu(1)−N(2)	96.8(5)	N(5)−Zn(1)−N(6)	107.0(7)
Cu(1)−N(2)	2.02(1)	N(1)−Cu(1)−N(3)	178.7(5)	N(5)−Zn(1)−N(7)	109.4(5)
Cu(1)−N(3)	1.99(1)	N(1)−Cu(1)−N(4)	84.4(5)	N(5)−Zn(1)−N(8)	112.3(6)
Cu(1)−N(4)	1.99(1)	N(2)−Cu(1)−N(3)	84.5(5)	N(6)−Zn(1)−N(7)	108.1(7)
Zn(1)−N(5)	2.01(1)	N(2)−Cu(1)−N(4)	175.3(5)	N(6)−Zn(1)−N(8)	109.5(6)
Zn(1)−N(6)	1.96(1)	N(3)−Cu(1)−N(4)	94.3(6)	N(7)−Zn(1)−N(8)	110.3(6)
Zn(1)−N(7)	1.95(1)				
Zn(1)−N(8)	1.93(1)				

Table 3. Hydrogen bond parameters for **4** (symmetry operations: *a* <1 − *x*,*y*, 1/2 − *z*>, *b* <1/2 − *x*, 1/2 − *y*, − *z*>)

	Distances (Å)			Angles (°)
D−H···A	D···A	D−H	H···A	D−H···A
N(1)−H(1N)···O(4a)	2.891(6)	1.07(5)	1.93(5)	148(4)
N(2)−H(3N)···O(3b)	2.931(5)	0.80(5)	2.14(5)	173(5)
N(2)−H(4N)···O(2)	2.995(5)	0.82(6)	2.26(5)	149(5)
N(1)−H(2N)···O(2b)	2.999(5)	0.74(4)	2.32(5)	154(4)

metals were performed by atomic absorption spectroscopy, by standard titrimetric methods for anions and with a Carlo Erba Strumentazion Analyser (for C, H and N). Thermogravimetric analyses (TGA) were performed on polycrystalline samples *ca.* 150 mg in air at a scan speed of 10 °C/min on a derivatograph "Q−1500". Infrared spectra were recorded with KBr discs and in Nujol mulls on a UR−10 spectrophotometer in the 4000−400 cm^{-1} region using conventional techniques.

$[Cu(en)_2ZnCl_4]$·dmso (1): Copper powder (0.32 g, 0.005 mol), zinc oxide (0.41 g, 0.005 mol), ammonium chloride (1.54 g, 0.02 mol), dmso (20 cm^3) and ethylenediamine (0.7 cm^3, 0.01 mol) were placed in a flask in the above order, heated to 60 °C and magnetically stirred until total dissolution of Cu^0 and ZnO was observed (110 minutes). The dark-violet crystals suitable for X-ray crystallography formed immediately after cooling the resulting solution. The crystals were filtered out and dried in vacuo at room temperature. Mass collected 2.1 g, yield 89%. $C_6H_{22}Cl_4CuN_4OSZn$ (469.05): calcd. C 15.36, H 4.74, N 11.95, Cu 13.55, Zn, 13.94, Cl 30.23; found C 15.2, H 4.63, N 11.9, Cu 13.9, Zn, 14.3, Cl 29.9. TGA results indicated that **1** exhibited a weight loss of 41.71% in the temperature range 170−340 °C (calcd. 42.28% for the loss of one dmso and two ethylenediamine molecules per formula unit). IR (cm^{-1}): $\tilde{\nu}$ = 3315 s, 3260 s, 3145 s, 2990 w, 2950 sh, 1605 s, 1580 m, 1450 w, 1285 w, 1185 m, 1090 s, 1045 vs, 1020 vs, 975 w, 950 s, 710 s, 540 m. The compound is soluble in water, dmso and dmf.

$[Cu(en)_2ZnCl_4]\cdot$dmf (2): This complex was obtained in a similar manner to **1**, except for the use of dmf (20 cm^3) instead of dmso. Mass collected 1.9 g, yield 82%. $C_7H_{23}Cl_4CuN_5OZn$ (464.04): calcd. C 18.12, H 5.01, N 15.12, Cu 13.71, Zn, 14.11, Cl 30.60; found C 18.3, H 4.9, N 16.0, Cu 14.0, Zn, 13.5, Cl 29.2. TGA results showed an initial weight loss of 15.03% in the temperature range 110−190 °C (calcd. 15.75% for the loss of one dmf molecule per formula unit). IR (cm^{-1}): $\tilde{\nu}$ = 3310 s, 3260 s, 3160 w, 2980 w, 2895 w, 1650 vs, 1600 s, 1585 sh, 1455 w, 1410 w, 1385 m, 1325 w, 1285 w, 1250 w, 1095 m, 1045 vs, 975 w, 705 m, 660 w, 535w, 475w, 420w. The compound is soluble in water, dmso and dmf.

$[Cu(en)_2Zn(NCS)_4]\cdot CH_3CN$ (3): This complex was obtained in a similar manner to **1**, except for the use of NH_4NCS instead of NH_4Cl in CH_3CN (25 cm^3). Mass collected 1.62 g, yield 62%. $C_{10}H_{19}CuN_9S_4Zn$ (522.49): calcd. C 22.99, H 3.67, N 15.12, Cu 13.71, Zn14.11; NCS 50.14; found C 22.7, H 3.5, N 15.3, Cu 13.7, Zn, 13.7; NCS 49.9. TGA results showed a weight loss of 8.00% in the temperature range 50−130 °C (7.86% for the loss of one CH_3CN molecule per formula unit). IR (cm^{-1}): $\tilde{\nu}$ = 3325 m, 3270 m, 3235 m, 3155 w, 2955 w, 2890 w, 2250 w, 2090 vs, 1585 m, 1460 w, 1385 w, 1370 w, 1360 w, 1325 w, 1280 w, 1180−1150 br, 1095 m, 1045 s, 1010 w, 980 w, 880 w, 690 w, 535 w, 520 w, 480 w. The compound is insoluble in water but soluble in dmso and dmf.

$[Cu(en)_2Zn(CH_3COO)_4]$ (4): This complex was obtained in a similar manner to **1**, except for the use of CH_3COONH_4 instead of NH_4Cl. Mass collected 0.95 g, yield 39%. $C_{12}H_{28}CuN_4O_8Zn$ (485.29): calcd. C 29.69, H 5.83, N 11.55, Cu 13.09, Zn 13.47; found C 29.3, H 6.1, N 11.6, Cu 13.3; Zn, 13.5. TGA results showed an initial decomposition of **4** at 40 °C but no well-separated weight loss steps were observed. IR (cm^{-1}): $\tilde{\nu}$ = 3340−3305 br, 3275 sh, 3140 s, 2985−2955 br, 2900 w, 1625 sh, 1575 vs, 1425 vs, 1405 sh, 1340 m, 1280 w, 1185−1165 br, 1105 w, 1050 vs, 1020 m, 985 w, 915 m, 735 w, 660 s, 615 w, 550 w, 525 w, 480 w, 415 w. The compound is soluble in water, dmso and dmf.

$[Cu(en)_2Zn(NCS)_4]\cdot 0.5\ H_2O$ (5): This complex was obtained in a similar manner to **1**, except for the use of NH_4NCS instead of NH_4Cl in CH_3OH (25 cm^3). Mass collected 0.47 g, yield 19%. $C_8H_{17}CuN_8O_{0.5}S_4Zn$ (490.47): calcd. C 19.59, H 3.50, N 20.54, Cu 11.65, Zn 11.98; NCS 42.59; found C 20.1, H 3.4, N 21.5, Cu 11.5, Zn 12.2; NCS 39.5. The presence of water molecules in **5** is clearly indicated in the TGA results, which exhibited an initial weight loss of 1.99% in the temperature range 180−205 °C [calcd. 1.84% for the loss of half a water molecule per formula unit]. IR (cm^{-1}): $\tilde{\nu}$ = 3320 m, 3290 sh, 3230 m, 3130 w, 2980−2950 br, 2930 sh, 2885 w, 2090 vs, 1580 s, 1455 w, 1320 w, 1275 w, 1165 w, 1090 m, 1040 s, 1010 w, 980 w, 830 w, 690 m, 520 w, 475 w. The compound is insoluble in water and soluble in dmso and dmf.

X-ray Data Collection and Processing: Well-shaped crystals of **1**−**5** were suitable for X-ray analysis. Crystal data and details of structure solutions are summarized in Table 1 and selected bond lengths and angles in Table 2.

The data were corrected for Lorentz-polarisation effects and for the effects of absorption by the gausian for **1** and multiscan methods for **2**. The non-hydrogen atoms were refined with anisotropic displacement parameters. All hydrogen atoms (except those of the water molecule in **5**) were located in Fourier difference syntheses or assigned at geometrically calculated positions and refined using a riding model (**1**, **4**) or fixed (**2**, **3**, **5**). The structures were solved by direct methods and refined by full-matrix least-squares methods using the SHELXL−93, SHELXL-97[30−32] and XTAL3.4 programs.[33] For **1**, the dmso S atom and Me groups were modelled as being disordered over two sites.

CCDC-174059−174063 contains the supplementary crystallographic data for this paper. These data can be obtained free of charge at www.ccdc.cam.ac.uk/conts/ retrieving.html [or from the Cambridge Crystallographic Data Centre, 12, Union Road, Cambridge CB2 1EZ, UK; Fax: (internat.) +44-1223/336-033; E-mail: deposit@ccdc.cam.ac.uk].

Acknowledgments

The work was in part supported by the Science and Technology Center in Ukraine (Project Gr-32j).

[1] *Direct Synthesis of Coordination and Organometallic Compounds*, Eds. A. D. Garnovskii, B. I. Kharissov, Elsevier Science, Amsterdam, **1999**.
[2] V. N. Kokozay, O. Yu. Vassilyeva, P. Weinberg, M. Wasinger, W. Linert, *Rev. Inorg. Chem.* **2000**, *20*, 255−282.
[3] O. Yu. Vassilyeva, V. N. Kokozay, N. I. Zhukova, L. A. Kovbasyuk, *Polyhedron* **1997**, *16*, 263−266.
[4] O. Yu. Vassilyeva, L. A. Kovbasyuk, V. N. Kokozay, B. W. Skelton, W. Linert, *Polyhedron* **1998**, *17*, 85−91.
[5] L. A. Kovbasyuk, O. Yu. Vassilyeva, V. N. Kokozay, W. Linert, J. Reedijk, B. W. Skelton, A. G. Oliver, *J. Chem. Soc., Dalton Trans.* **1998**, *16*, 2735−2738.
[6] L. A. Kovbasyuk, O. Yu. Vassilyeva, V. N. Kokozay, W. Linert, B. W. Skelton, A. G. Oliver, *New J. Chem.* **1998**, *22*, 931−932.
[7] V. G. Makhankova, O. Yu. Vassilyeva, V. N. Kokozay, B. W. Skelton, J. Reedijk, G. A. Van Albada, L. Sorace, D. Gatteschi, *New J. Chem.* **2001**, *25*, 685−689.
[8] V. G. Makhankova, O. Yu. Vassilyeva, V. N. Kokozay, B. W. Skelton, G. A. Van Albada, J. Reedijk, *Z. Naturforsch., Teil B* **2001**, *56*, 931−936.
[9] Y. Li, Z. Wang, Y. Ding, *Inorg. Chem.* **1999**, *38*, 4737−4740.
[10] T. Iwamoto, *Supramolecular Chemistry in Cyanometallate Systems*, in *Comprehensive Supramolecular Chemistry* (Eds. D. D. MacNicol, F. Toda, R. Bishop), Pergamon Press, Oxford, **1996**.
[11] A. Yuan, J. Zou, B. Li, Z. Zha, C. Duan, Y. Liu, Z. Xu, S. Keizer, *Chem. Commun.* **2000**, 1297−1298.
[12] N. Fukita, M. Ohba, H. Okawa, K. Matsuda, H. Iwamura, *Inorg. Chem.* **1998**, *37*, 842−848.
[13] D. B. Leznoff, B. Y. Xue, R. J. Batchelor, F. W. B. Einstein, B. O. Patrick, *Inorg. Chem.* **2001**, *40*, 6026−6034.
[14] O. Schneider, E. Gerstner, F. Weller, K. Dehnicke, *Z. Anorg. Allg. Chem.* **1999**, *625*, 1101−1106.
[15] Brian J. Hathaway, in *Comprehensive Coordination Chemistry: Copper* (Eds. G. Wilkinson, R. D. Gillard, J. A. McCleverty), Pergamon Press, Oxford, **1987**.
[16] A. F. Wells, *Structural Inorganic Chemistry*, 5th ed., Clarendon Press, Oxford, **1986**.
[17] Von W. Vogt, H. Haas, *Acta Crystallogr., Sect. B* **1971**, *27*, 1528−1532.
[18] R. E. Caputo, M. J. Vukosavovich, R. D. Willet, *Acta Crystallogr., Sect. B* **1976**, *32*, 2516−2518.
[19] B. Morosin, P. Fallon, J. S. Vallentine, *Acta Crystallogr., Sect. B* **1975**, *31*, 2220−2223.
[20] M. A. Porai-Koshits, *Zh. Struct. Khim.* **1963**, *4*, 584−593.
[21] B. W. Brown, E. C. Lingafetter, *Acta Crystallogr., Sect. B* **1964**, *17*, 254−259.
[22] I. M. Procter, B. J. Hathaway, P. Nicholls, *J. Chem. Soc. A* **1968**, *7*−*8*, 1678−1684.
[23] D. A. Langs, C. R. Hare, *J. Chem. Soc., Chem. Commun.* **1967**, *17*, 890−891.
[24] C. Bellito, L. Gastaldi, A. A. G. Tomlinson, *J. Chem. Soc., Dalton Trans.* **1976**, *11*, 989−992.

[25] M. Kabešová, R. Boca, M. Melník, D. Valigura, M. Dunaj-Jurco, *Coord. Chem. Rev.* **1995**, *140*, 115−135.
[26] *Chemistry of Pseudohalides* (Eds. A. Golub, H. Kohler, V. Skopenko), Elsevier Science, Amsterdam, **1986**.
[27] C. J. Pouchert, *The Aldrich Library of FT-IR Spectra*, 1st ed., **1985**.
[28] Yu. Ya. Kharitonov, I. K. Kireeva, A. N. Goryachev, *Koord. Khim.* **1975**, *1*, 1118−1133.
[29] G. B. Deacon, R. J. Phillips, *Coord. Chem. Rev.* **1980**, *33*, 227−250.
[30] G. M. Sheldrick, *SHELXL-97*, *Program for the Refinement of Crystal Structures*, University of Gottingen, Germany, **1997**.
[31] G. M. Sheldrick, *SHELXL-93*, *Program for the Refinement of Crystal Structures*, University of Gottingen, Germany, **1993**.
[32] G. M. Sheldrick, *Acta Crystallogr., Sect. A* **1990**, *46*, 467−473.
[33] S. R. Hall, G. S. D. King, J. M. Stewart, *XTAL3.4*, *User's Manual*, University of Western Australia, Lamb, Perth, **1995**.

Received September 25, 2002
[I02539]

Structural Manipulation of Hydrogen Bond Networks Using Sulfonated Phosphane Ligands and Their Complexes: Competition and Interplay Between Strong and Weak Hydrogen Bonds

Andrew D. Burrows,*[a] Ross W. Harrington,[a] Mary F. Mahon,[a] and Simon J. Teat[b]

Keywords: Crystal engineering / Phosphane ligands / Hydrogen bonds / X-ray crystal structures

Using the sulfonated phosphane $[PPh_2(C_6H_4\text{-}m\text{-}SO_3)]^-$, $\mathbf{L}^-$, we have demonstrated that metal centres can readily be incorporated into guanidinium sulfonate (GS) hydrogen-bonded networks, and that the increase in steric bulk on going from $[C(NH_2)_3][\mathbf{L}]$ (**1**) to $[C(NH_2)_3][AuCl(\mathbf{L})]$ (**2**) leads to a flattening of the GS sheets. The crystal structures of $[C(NH_2)_3][\mathbf{LS}]$ **3** and $[C(NH_2)_3][\mathbf{LSe}]$ **4** ($\mathbf{LS}^- = [SPPh_2(C_6H_4\text{-}m\text{-}SO_3)]^-$, $\mathbf{LSe}^- = [SePPh_2(C_6H_4\text{-}m\text{-}SO_3)]^-$) reveal disorder in both the sulfonate groups and the guanidinium cations, which is a consequence of *pseudo*-sixfold phenyl embraces between the anions. These interactions, identical to those observed in Ph_3PS and Ph_3PSe, position the sulfonate groups too close together for regular quasihexagonal hydrogen bonding motifs to be formed. The regular GS hydrogen bonding patterns can also be disrupted by using an anion containing two sulfonate groups such as that in $[C(NH_2)_3]_2\{cis\text{-}[PdCl_2(\mathbf{L})_2]\}$ (**5**). In this case the incorporation of two sulfonate groups from each anion into the same hydrogen-bonded sheet also serves to constrain the distance between the sulfur atoms to a value incommensurate with that enabling a guanidinium cation to hydrogen bond to both groups. In this case irregular GS sheets are formed involving fewer N–H···O hydrogen bonds than in **1** and **2**.

(© Wiley-VCH Verlag GmbH & Co. KGaA, 69451 Weinheim, Germany, 2003)

Introduction

The use of intermolecular interactions in the design and synthesis of solid-state structures — a process often referred to as crystal engineering — has attracted enormous interest over the past few years.[1] Previously, we have reported the use of multiple hydrogen bonds to control the aggregation of metal complex cations and anions containing complementary hydrogen bonding groups.[2] The incorporation of two hydrogen bond donors (D) on each cation face and two hydrogen bond acceptors (A) on each anion face, giving an overall DD:AA interaction, ensures that secondary interactions are all favourable, thus enhancing the total energy of the interaction.

The guanidinium sulfonate (GS) system is another case in which the cations and anions are linked together by pairs of hydrogen bonds in the DD:AA arrangement, though, since both cations and anions contain three hydrogen bonding faces, the hydrogen bond interactions in this system lead to quasihexagonal arrays and the formation of infinite two-dimensional sheets.[3,4] These GS sheets are particularly robust to changes in the steric and electronic properties of the sulfonate substituents, and bilayer or pillared-brick structures incorporating disulfonates can be used to include many guest molecules.[5] In this paper we show how monosulfonated triphenylphosphane $[PPh_2(C_6H_4\text{-}m\text{-}SO_3)]^-$, $\mathbf{L}^-$, a ligand initially prepared for biphasic catalysis,[6] can be incorporated into GS arrays, therefore providing a means of introducing metal centres into hydrogen-bonded networks in which two dimensions are controlled by the hydrogen bonds. A recent communication from Kathó and coworkers[7] using guanidinium to crystallise sulfonated phosphanes has prompted us to report our findings.[8] To this end, the syntheses and crystal structures of $[C(NH_2)_3][\mathbf{L}]$ (**1**), $[C(NH_2)_3][AuCl(\mathbf{L})]$ (**2**), $[C(NH_2)_3][\mathbf{LS}]$ (**3**), $[C(NH_2)_3][\mathbf{LSe}]$ (**4**) and $[C(NH_2)_3]_2\{cis\text{-}[PdCl_2(\mathbf{L})_2]\}$ (**5**) are reported ($\mathbf{LS}^- = [SPPh_2(C_6H_4\text{-}m\text{-}SO_3)]^-$, $\mathbf{LSe}^- = [SePPh_2(C_6H_4\text{-}m\text{-}SO_3)]^-$). Analysis of the structures reveals that predetermination of the relative positions of the sulfonate groups, either through interactions between the triphenylphosphane groups or through coordination of two phosphane ligands to a metal centre, can lead either to disruption of the quasihexagonal hydrogen bonding motif or to disorder in the GS sheets.

Results and Discussion

Metathesis of Na[**L**] with guanidinium chloride in methanol gave colourless crystals of $[C(NH_2)_3][\mathbf{L}]$ (**1**) suitable for analysis by X-ray crystallography. The asymmetric unit of

[a] Department of Chemistry, University of Bath, Claverton Down, Bath BA2 7AY, UK
E-mail: a.d.burrows@bath.ac.uk
[b] CLRC Daresbury Laboratory, Daresbury, Warrington WA4 4AD, UK

1 showed the presence of two independent guanidinium cations and two independent triphenylphosphane sulfonate anions. Hydrogen bond interactions between the cations and anions lead to the formation of the anticipated quasihexagonal GS arrays [Figure 1 (top)], despite the steric bulk of the triphenylphosphane group. A single-layer sheet structure is adopted, with PPh_3 groups located on both sides of the GS sheets. The sheets are corrugated, with a "hinge" between hydrogen-bonded ribbons [Figure 1 (bottom)], and this is reflected in an inter-ribbon angle of 103°, based on the angle between guanidinium planes in neighbouring ribbons. Similar distortions to GS sheets have been observed previously,[3] and occur as a means of minimising void space within the structure.

The single-layer sheet structure ensures that triphenylphosphane groups from neighbouring sheets project into the inter-sheet space. The major interaction between these groups involves pairs of $[\mathbf{L}]^-$ anions, based on P(1) and P(2) in neighbouring sheets, which adopt sixfold phenyl embraces (6PEs).[9] Two C−H···O interactions are also evident [C(8)···O(1) 3.548(10), H(8)···O(1) 2.66(1) Å, C(8)−H(8)···O(1) 160.8(5)°; and C(36)···O(6) 3.639(10), H(36)···O(6) 2.75(1) Å, C(36)−H(36)···O(6) 161.0(5)°].

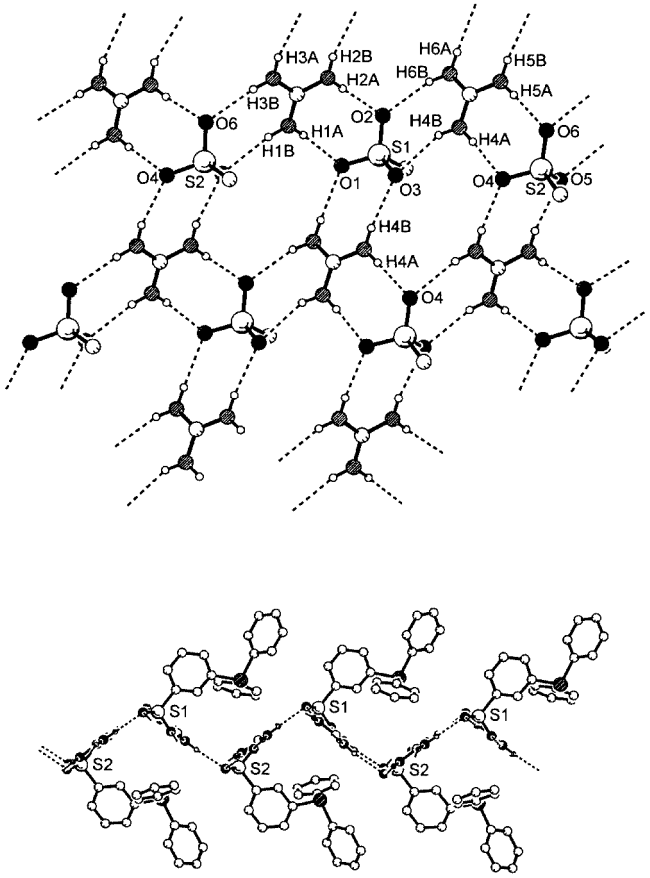

Figure 1. (top) Quasihexagonal hydrogen-bonded GS sheets in the crystal structure of $[C(NH_2)_3][\mathbf{L}]$ (**1**); hydrogen bond lengths (Å) and angles (°): N(1)···O(1) 2.974, H(1A)···O(1) 2.12, N(1)−H(1A)···O(1) 176; N(1)···O(5) 3.056, H(1B)···O(5) 2.24, N(1)−H(1B)···O(5) 158; N(2)···O(5) 3.010, H(2A)···O(5) 2.16, N(2)−H(2A)···O(5) 170; N(2)···O(2) 3.008, H(2B)···O(2) 2.15, N(2)−H(2B)···O(2) 176; N(3)···O(4) 3.061, H(3A)···O(4) 2.20, N(3)−H(3A)···O(4) 177; N(3)···O(6) 3.038, H(3B)···O(6) 2.20, N(3)−H(3B)···O(6) 165; N(4)···O(3) 3.050, H(4A)···O(3) 2.21, N(4)−H(4A)···O(3) 167; N(4)···O(4) 3.053, H(4B)···O(4) 2.20, N(4)−H(4B)···O(4) 175; N(5)···O(6) 2.981, H(5A)···O(6) 2.12, N(5)−H(5A)···O(6) 174; N(5)···O(3) 3.046, H(5B)···O(3) 2.20, N(5)−H(5B)···O(3) 166; N(6)···O(2) 3.021, H(6A)···O(2) 2.18, N(6)−H(6A)···O(2) 166; N(6)···O(1) 2.981, H(6B)···O(1) 2.13, N(6)−H(6B)···O(1) 171; (bottom) side-on view of one of the GS sheets in the structure of **1**

The gold complex $Na[AuCl(\mathbf{L})]$ was formed from the reaction of $[AuCl(SC_4H_8)]$ and $Na[\mathbf{L}]$ in acetone, and recrystallised from methanol. Metathesis of $Na[AuCl(\mathbf{L})]$ with guanidinium chloride in methanol gave colourless crystals of $[C(NH_2)_3][AuCl(\mathbf{L})]$ (**2**) which were suitable for X-ray crystallography. The structural analysis of **2** showed the presence of one guanidinium cation and one $[AuCl(\mathbf{L})]^-$ anion in the asymmetric unit. As in **1**, the sulfonate groups form quasihexagonal hydrogen-bonded arrays through N−H···O interactions with guanidinium cations, and these lead to the formation of GS sheets [Figure 2 (top)]. Although the interactions within the sheets are similar to those in **1**, there are two main differences. Firstly, the presence of the AuCl group coordinated to each phosphane serves to flatten the sheets, and the inter-ribbon angle in **2** is increased to 161° [Figure 2 (bottom)]. In other GS sheet structures, increase in steric bulk or inclusion of guest molecules can have the effect of reducing the degree of distortion from planarity, hence the AuCl group can be regarded as a "guest" within the $[C(NH_2)_3][\mathbf{L}]$ lattice, albeit one with a directional coordination binding site. Secondly, the quasihexagonal sheets are distorted such that the intra-ribbon S···S distance is increased to 8.105 Å, equal to the unit cell parameter *a*. In simple guanidinium sulfonate structures[3,4] closest S···S distances within the GS sheets range from 6.57 to 7.77 Å. The distortion of the GS sheets in **2** is also apparent in the values of the N−H···O angles.

These distortions are related to the interactions between the (triphenylphosphane)gold chloride units. Dance and Scudder have shown[10] the importance of interactions between multiple phenyl groups in the crystal structures of PPh_3 complexes. In **2**, *pseudo*-sixfold phenyl embraces serve to link the $AuCl(PPh_3)$ units into chains running perpendicular to the direction of the hydrogen-bonded ribbons (Figure 3). In these *pseudo*-sixfold phenyl embraces, the AuCl unit acts in a similar manner to a phenyl group, so that each embrace involves three phenyl rings on one anion and two phenyl rings and the AuCl group on the other. These interactions bring the phosphorus atoms on closest phosphane groups to within 6.49 Å of each other, and position sulfur atoms from the same sheet at 11.29 Å, equal to the unit cell parameter *b*, from each other. *Pseudo*-sixfold phenyl embraces in which gold-containing groups are involved have been shown to be recurrent structural motifs in the crystal structures of gold-PPh_3 complexes.[11] Au···Au interactions have previously been exploited as crystal engineering tools in conjunction with hydrogen bond networks.[12] However, in the crystal structure of **2** there are no aurophilic interactions, the shortest Au···Au distance being 7.35 Å.

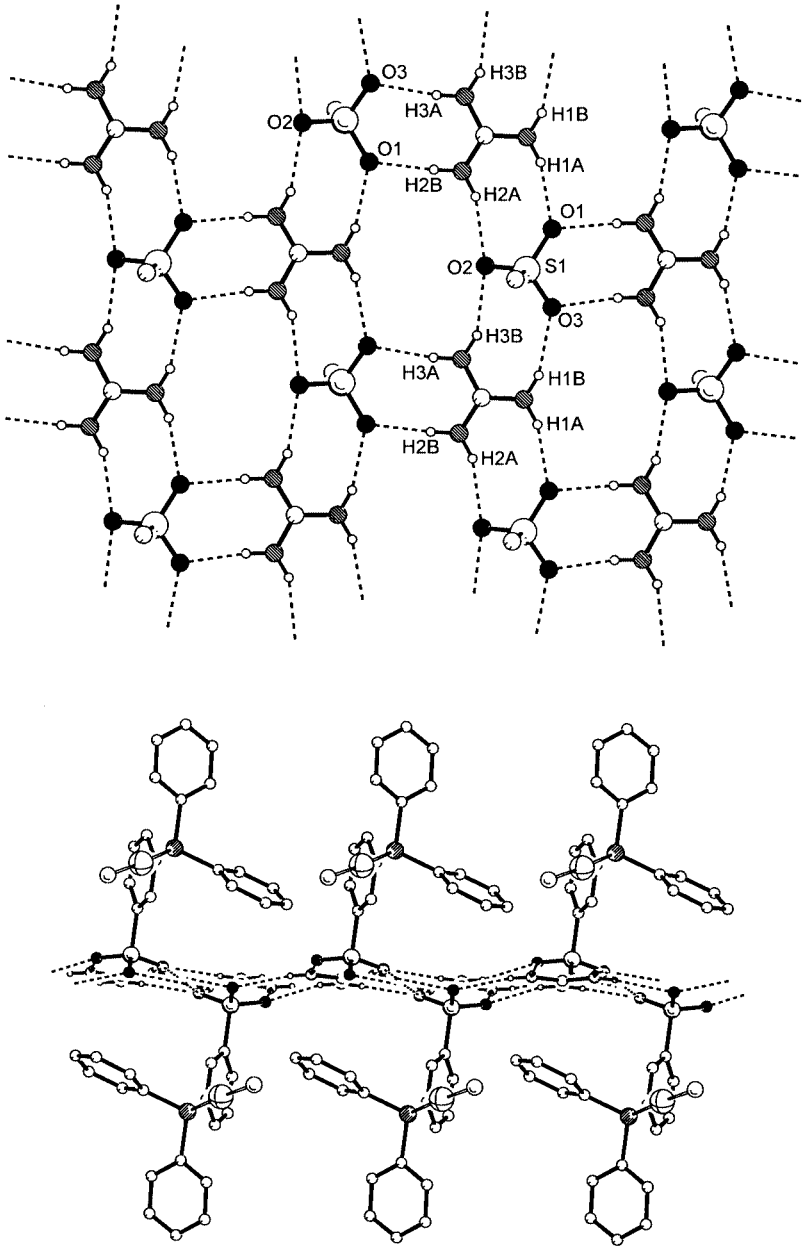

Figure 2. (top) Quasihexagonal hydrogen-bonded GS sheets in the crystal structure of $[C(NH_2)_3][AuCl(\mathbf{L})]$ (**2**); hydrogen bond lengths (Å) and angles (°): N(1)···O(1) 2.988, H(1A)···O(1) 2.16, N(1)−H(1A)···O(1) 157; N(1)···O(3) 3.030, H(1B)···O(3) 2.19, N(1)−H(1B)···O(3) 160; N(2)···O(2) 3.024, H(2A)···O(2) 2.19, N(2)−H(2A)···O(2) 159; N(2)···O(1) 2.907, H(2B)···O(1) 2.03, N(2)−H(2B)···O(1) 175; N(3)···O(3) 2.913, H(3A)···O(3) 2.05, N(3)−H(3A)···O(3) 169; N(3)···O(2) 3.049, H(3B)···O(2) 2.23, N(3)−H(3B)···O(2) 155; (bottom) side-on view of one of the GS sheets in the structure of **2**

The compounds Na[**L**S] and Na[**L**Se] were prepared from the oxidation of Na[**L**] with elemental sulfur or selenium in methanol. Metathesis with $[C(NH_2)_3]Cl$ in methanol gave colourless crystals of $[C(NH_2)_3][\mathbf{L}S]$ (**3**) and $[C(NH_2)_3][\mathbf{L}Se]$ (**4**) respectively. X-ray structural analyses of **3** and **4** showed that both compounds possess one cation and one anion in their asymmetric units, and that they are essentially isostructural. Both **3** and **4** are disordered with regard to the sulfonate oxygen atom positions (1:1 ratio between two sets of positions) and the guanidinium cations (2:1:1 ratio between three positions in **3**, 50:37:13 between similar positions in **4**). Although GS sheets are formed [Figure 4 (top)], the presence of this disorder makes an unambiguous evaluation of the inter-ribbon angle impossible, though estimated values of 150° for **3** and 153° for **4** suggest that, as anticipated, the Group 16 atom is less sterically demanding than the AuCl fragment [Figure 4 (bottom)]. The disorder in these structures can be rationalised by consideration of the interactions between the triphenylphosphane sulfide (or selenide) units.

In a similar manner to the (triphenylphosphane)gold chloride units in **2**, the triphenylphosphane sulfides and selenides form *pseudo*-sixfold phenyl embraces involving three phenyl rings on one anion and two phenyl rings and the

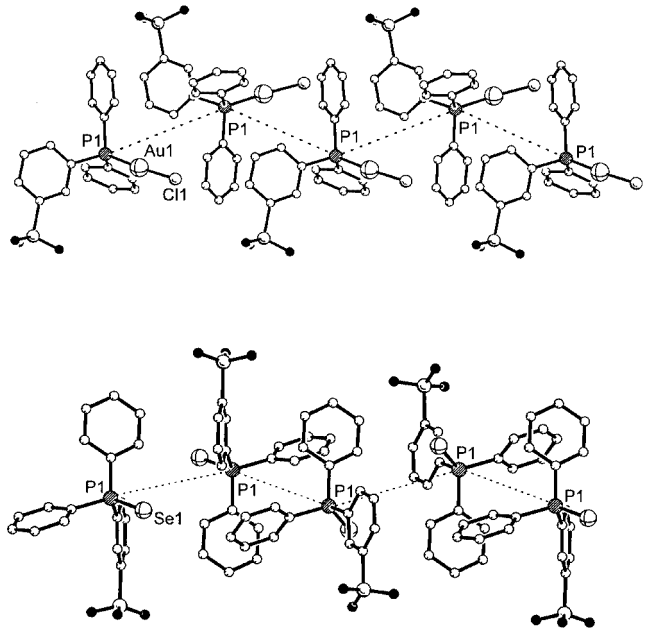

Figure 3. *Pseudo*-sixfold phenyl embraces linking the anions into chains in the crystal structures of $[C(NH_2)_3][AuCl(\mathbf{L})]$ (**2**) and $[C(NH_2)_3][\mathbf{L}Se]$ (**4**)

Group 16 atom on the other. These embraces lead to the formation of chains running in the same direction as the hydrogen-bonded ribbons, which possess closest P···P distances of 6.17 Å for **3** and 6.27 Å for **4** (Figure 3). This chain formation ensures that sulfonate groups within the same sheet are positioned with S···S distances of 9.27 Å for **3** and 9.49 Å for **4**, in both cases equal to the respective unit cell parameter *b*. In addition to these interactions, each triphenylphosphane sulfide or selenide unit forms a second *pseudo*-sixfold phenyl embrace, approximately perpendicular to the first, in this case arising from neighbouring centrosymmetrically related pairs of anions, and involving two phenyl rings and the Group 16 atom. This interaction leads to P···P distances of 5.75 Å and 5.90 Å for **3** and **4**, respectively. Both types of *pseudo*-sixfold phenyl embrace are also observed in the crystal structures of Ph_3PS[13] and Ph_3PSe,[14] and together they serve to dictate the relative positions of the sulfonate groups in **3** and **4**. These groups are too close together for the guanidinium cations to form regular hydrogen bonding patterns, and as a consequence the cations are disordered. In one of the three orientations, N−H groups are directed out of the plane of the GS sheets, and form N−H···S or N−H···Se hydrogen bonds to the sulfide or selenide together with $R_2^1(6)$ rings [N(1B)···S(1) 3.35(1), H(1B2)···S(1) 2.52(1) Å, N(1B)−H(1B2)···S(1) 157(1)° and N(3B)···S(1) 3.41(1), H(3B1)···S(1) 2.61(1) Å, N(3B)−H(3B1)···S(1) 151(1)° for **3**; N(1B)···Se(1) 3.29(2), H(1B1)···Se(1) 2.46(2) Å, N(1B)−H(1B1)···Se(1) 158(1)° and N(3B)···Se(1) 3.44(3), H(3B2)···Se(1) 2.67(2) Å, N(3B)−H(3B2)···Se(1) 148(2)° for **4**].

The complex $Na_2\{cis\text{-}[PdCl_2(\mathbf{L})_2]\}$ was formed from the reaction of $[PdCl_2(cod)]$ with Na[**L**] in acetonitrile/methanol. Metathesis of this sodium salt with guanidinium nitrate in the same solvent mix gave several products including small, yellow crystals of $[C(NH_2)_3]_2\{cis\text{-}[PdCl_2(\mathbf{L})_2]\}$ (**5**) suitable for analysis at the SRS facility. The structural analysis of **5** showed the presence of GS sheets [Figure 5 (top)], with both of the sulfonate groups from each complex anion incorporated into the same sheet. The hydrogen bonding patterns in **5** are less regular than those observed in **1** and **2**. Only two of the six independent guanidinium faces are involved in DD:AA interactions. Of the remaining faces, two form $R_2^1(6)$ rings with sulfonate oxygen atoms whereas another forms bifurcated N−H···O hydrogen bonds. The final guanidinium face is not involved in any N−H···O hydrogen bonding, instead forming N−H···Cl interactions to the metal-bound chlorides.[15] The distortions from the regular pattern observed for **1** and **2** are a consequence of the distance constraint imposed by virtue of the two sulfonate groups arising from the same anion (S···S 9.21 Å) coupled with the triangular shape of the guanidinium cation. It is not possible to orientate the cation to enable it to form two N−H···O hydrogen bonds with both sulfonates as the groups are too far apart.

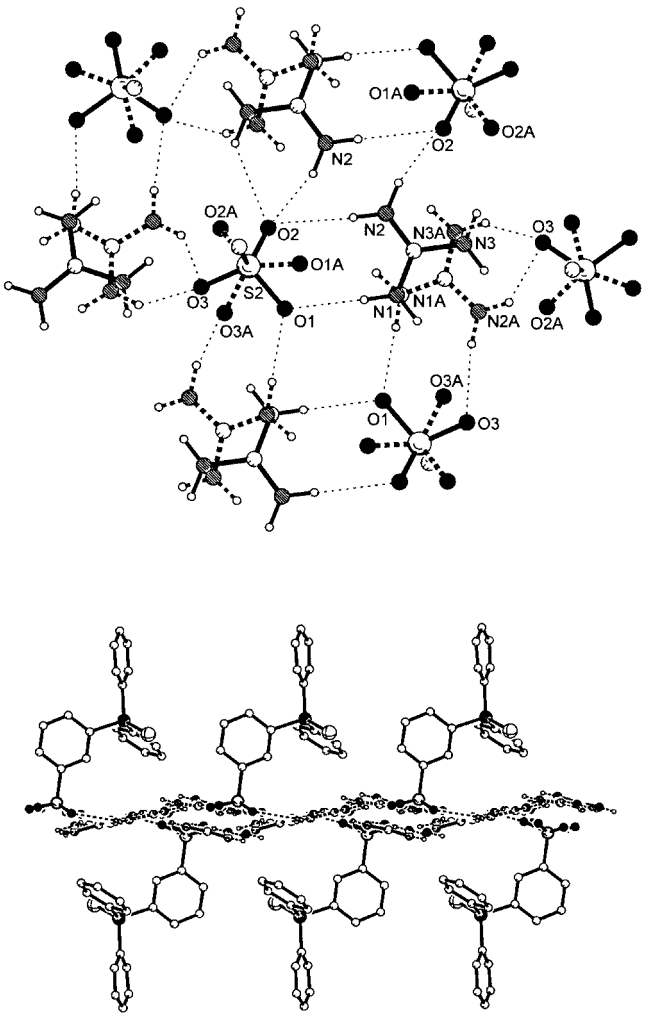

Figure 4. (top) GS sheet formation in $[C(NH_2)_3][\mathbf{L}S]$ (**3**); for the guanidinium cations only two of the three positions are shown for clarity; (bottom) side-on view of one of the GS sheets in the structure of **3**

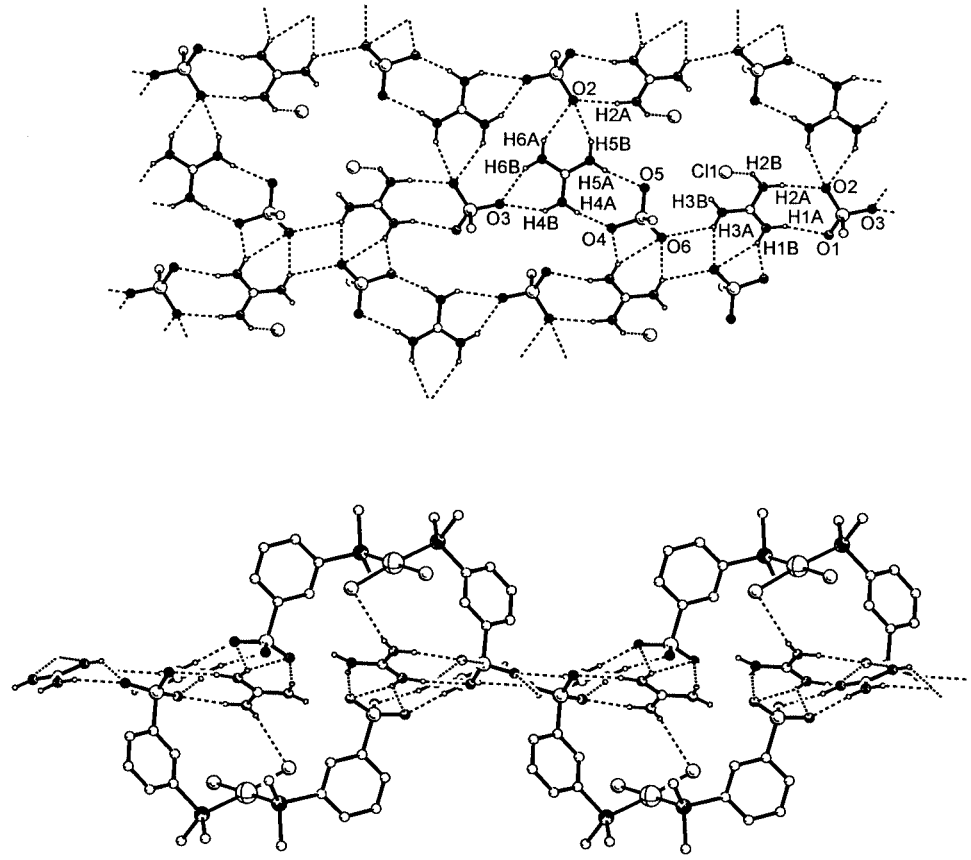

Figure 5. (top) GS sheet formation in $[C(NH_2)_3]_2\{cis\text{-}[PdCl_2(\mathbf{L})_2]$ (**5**); hydrogen bond lengths (Å) and angles (°): N(1)···O(1) 2.911, H(1A)···O(1) 2.06, N(1)−H(1A)···O(1) 162; N(1)···O(4) 2.893, H(1B)···O(4) 2.12, N(1)−H(1B)···O(4) 146; N(1)···O(6) 3.219, H(1B)···O(6) 2.43, N(1)−H(1B)···O(6) 150; N(2)···O(2) 2.902, H(2A)···O(2) 2.04, N(2)−H(2A)···O(2) 168; N(2)···Cl(1) 3.253, H(2B)···Cl(1) 2.56, N(2)−H(2B)···Cl(1) 136; N(3)···O(6) 3.140, H(3A)···O(6) 2.32, N(3)−H(3A)···O(6) 154; N(3)···O(6) 3.003, H(3A)···O(6) 2.50, N(3)−H(3A)···O(6) 117; N(4)···O(4) 2.810, H(4A)···O(4) 1.94, N(4)−H(4A)···O(4) 168; N(4)···O(3) 2.855, H(4B)···O(3) 2.11, N(4)−H(4B)···O(3) 142; N(5)···O(5) 2.923, H(5A)···O(5) 2.05, N(5)−H(5A)···O(5) 171; N(5)···O(2) 2.994, H(5B)···O(2) 2.19, N(5)−H(5B)···O(2) 153; N(6)···O(2) 3.079, H(6A)···O(2) 2.30, N(6)−H(6A)···O(2) 147; N(6)···O(3) 2.927, H(6B)···O(3) 2.21, N(6)−H(6B)···O(3) 139; (bottom) side-on view of one of the GS sheets in the structure of **5**; for clarity only the *ipso* carbon atoms on the unfunctionalised phenyl rings are shown

As with compounds **1**−**4**, the phosphanes are located on either side of the GS sheets [Figure 5 (bottom)]. Parallel fourfold phenyl embraces (P4PEs) link centrosymmetrically related pairs of phosphanes based on P(1), and pairs of phosphanes based on P(2), and, as in the structures of **2**−**4**, these interactions serve to constrain the distances between sulfonate groups.

The structures reported in this paper clearly demonstrate that sulfonated phosphane ligands and their metal complexes can be incorporated into hydrogen-bonded networks based on guanidinium sulfonate sheets. This system is sufficiently robust to cope with the increased steric bulk that accompanies inclusion of a coordination centre. The interactions between phosphane groups − involving C−H···π interactions and *pseudo*-sixfold phenyl embraces − observed in the crystal structures of molecules such as Ph_3PS and Ph_3PSe can be preserved in their guanidinium sulfonate adducts, and these are important in determining the relative positions of the sulfonate groups. Although the GS motif is flexible to a range of S···S distances, if the sulfonates are positioned too closely to each other, guanidinium cations are unable to form regular hydrogen bonding patterns, and disorder in both the cation and the anion sulfonate groups is observed. In contrast, when the S···S distance is constrained by having two sulfonate groups from the same complex incorporated into the same sheet, significant distortions from the quasihexagonal array may result.

Taken together, these structural analyses demonstrate that supramolecular interactions that are generally considered weak can compete effectively with strong hydrogen bonds in determining gross structures. Clearly, the disorder and the distortions observed in the GS networks in **3**, **4** and **5** occur with loss of some, but not all, of the stabilisation energy. Non-disordered structures in the cases of **3** and **4** would involve either steric clashes or voids within the structure, both of which are energetically unfavourable. Similarly, non-distorted GS sheets in **5** would result in unfavourable bond lengths and/or angles within the anions, which would also be energetically less favourable than the loss of hydrogen bonding in the distorted GS network.

We are currently exploring the use of bis(phosphane) complexes containing unsaturated metal centres to bridge between GS sheets with a view to exploring the reversible coordination of small molecules.

Experimental Section

Synthesis of metal complexes of [**L**]$^-$ were routinely carried out using Schlenk-line techniques under pure dry dinitrogen using dioxygen-free solvents. Metathesis reactions were carried out with no special precautions to exclude air. Microanalyses (C, H and N) were carried out by Mr. Alan Carver (University of Bath Microanalytical Service). Infrared spectra were recorded on a Nicolet Nexus FT-IR spectrometer as KBr pellets. The compounds Na[**L**][16] and [AuCl(SC_4H_8)][17] was prepared according to the literature methods.

Synthesis of Na[AuCl(L)]: Na[**L**] (0.182 g, 0.50 mmol), dissolved in acetone (10 cm^3) was added to a solution of [AuCl(SC_4H_8)] (0.158 g, 0.50 mmol) in acetone (10 cm^3). The resultant solution was stirred for 2 h, filtered, and the solvent removed in vacuo. Recrystallisation from methanol gave a colourless crystalline material. Yield 0.188 g (64%). ^{31}P NMR (CD_3OD): δ = 46.0 (s) ppm. IR: ν(SO_3) 1670s cm^{-1} (br).

Synthesis of Na[AuCl(LS)]: An excess of elemental sulfur was added to a solution of Na[**L**] (0.200 g, 0.55 mmol) in wet methanol (30 cm^3) and the mixture stirred vigorously for 3 h. Unreacted sulfur was removed by filtration, then the solvent was removed in vacuo and the crude solid recrystallised from methanol. Yield 0.191 g (88%). ^{31}P NMR (CD_3OD): δ = 46.3 (s) ppm.

Na[AuCl(**L**Se)] was prepared in an analogous manner using elemental selenium.

Synthesis of Na$_2$\{*cis*-[PdCl$_2$(L)$_2$]\}: A solution of Na[**L**] (0.276 g, 0.70 mmol) in methanol (25 cm^3) was added dropwise with stirring to a solution of [$PdCl_2$(cod)] (0.100 g, 0.35 mmol) in acetonitrile (30 cm^3) giving a slight darkening of colour. Stirring was continued for 45 min, and then the solvent was removed in vacuo and the crude yellow-orange solid recrystallised from methanol. Yield 0.235 g (74%). ^{31}P NMR (CD_3OD): δ = 25.6 (s) ppm. IR: ν(SO_3) 1641s cm^{-1} (br), 1536s.

Synthesis of [C(NH$_2$)$_3$][L] (1): Na[**L**] (0.100 g, 0.27 mmol) and [$C(NH_2)_3$]Cl (0.026 g, 0.27 mmol) were dissolved in methanol (10 cm^3), and the solvent allowed to slowly evaporate. After two weeks colourless crystals were harvested. Yield 0.077 g (70%). $C_{19}H_{20}N_3O_3PS$ (401.4): calcd. C 56.9, H 5.02, N 10.5; found C 57.2, H 4.99, N 10.0. IR: ν(NH) 3380s cm^{-1} (br), 3195s (br); ν(SO_3)/δ(NH_2) 1684s, 1571s, 1431m.

Synthesis of [C(NH$_2$)$_3$][AuCl(L)] (2): Na[AuCl(**L**)] (0.100 g, 0.17 mmol) and [$C(NH_2)_3$]Cl (0.016 g, 0.17 mmol) were dissolved in methanol (10 cm^3), and the solvent allowed to slowly evaporate. After one week colourless crystals were harvested. Yield 0.085 g (80%). $C_{19}H_{20}AuClN_3O_3PS$ (633.8): calcd. C 36.0, H 3.18, N 6.63; found C 36.0, H 3.16, N 6.44. IR: ν(NH) 3400s cm^{-1} (br), 3273s, 3202s; ν(SO_3)/δ(NH_2) 1684s, 1569m, 1479m.

Synthesis of [C(NH$_2$)$_3$][LS] (3): Na[**L**S] (0.100 g, 0.25 mmol) and [$C(NH_2)_3$]Cl (0.024 g, 0.23 mmol) were dissolved in methanol (10 cm^3), and the solvent allowed to slowly evaporate. After two weeks colourless crystals were harvested. Yield 0.085 g (80%). $C_{19}H_{20}N_3O_3PS_2$ (433.5): calcd. C 52.2, H 4.65, N 9.70; found C 52.6, H 4.51, N 9.60. IR: ν(NH) 3388s cm^{-1} (br), 3208s (br); ν(SO_3)/δ(NH_2) 1664s, 1577s, 1431s.

Crystals of [$C(NH_2)_3$][**L**Se] **4** were prepared in a similar manner from Na[**L**Se] and [$C(NH_2)_3$]Cl.

Synthesis of [C(NH$_2$)$_3$]$_2$\{*cis*-[PdCl$_2$(L)$_2$]\} (5): Na$_2$\{*cis*-[$PdCl_2$(**L**)$_2$]\} (0.050 g, 0.045 mmol) in methanol (5 cm^3) was added to [$C(NH_2)_3$]NO_3 (0.013 g, 0.10 mmol) in acetonitrile (5 cm^3). The solvent was allowed to slowly evaporate, and after two weeks small yellow crystals were obtained.

Crystallography

Single crystals of compounds **1**−**5** were prepared by the methods above. Data were collected using a Enraf−Nonius CAD4 automatic four-circle diffractometer for **1** and a Nonius Kappa CCD diffractometer for **2**, **3** and **4**. Crystals of **5** were too small to ana-

Table 1. Crystal data for compounds **1**−**5**

Complex	**1**	**2**	**3**	**4**	**5**
Empirical formula	$C_{19}H_{20}N_3O_3PS$	$C_{19}H_{20}AuClN_3O_3PS$	$C_{19}H_{20}N_3O_3PS_2$	$C_{19}H_{20}N_3O_3PSSe$	$C_{38}H_{40}Cl_2N_6O_6P_2PdS_2$
M	401.41	633.83	433.47	480.37	980.12
Temperature/K	296(2)	170(2)	150(2)	150(2)	150(2)
Crystal system	Orthorhombic	Monoclinic	Monoclinic	Monoclinic	Triclinic
Space group	$Pca2_1$	$P2_1$	$P2_1/n$	$P2_1/n$	$P\bar{1}$
a (Å)	19.4240(10)	8.1050(4)	14.3160(4)	14.4130(2)	10.145(2)
b (Å)	7.969(5)	11.2910(5)	9.2710(3)	9.49200(10)	12.763(3)
c (Å)	25.621(4)	12.1120(6)	16.1200(7)	16.0910(2)	17.019(4)
α (°)					85.125(9)
β (°)		98.475(3)	108.1670(10)	107.9850(10)	84.163(9)
γ (°)					79.192(9)
V (Å^3)	3966(3)	1096.31(9)	2032.85(12)	2093.81(4)	2148.4(9)
Z	8	2	4	4	2
μ(Mo-K_α) (mm^{-1})	0.268	7.025	0.366	1.994	0.780
Reflections collected	3733	13383	29789	19837	11184
Independent reflections	3571	4567	3543	3698	7062
R(int)	0.0089	0.0495	0.0931	0.0782	0.0322
*R*1, *wR*2 [$I > 2\sigma(I)$]	0.0541, 0.1357	0.0345, 0.0762	0.0482, 0.1071	0.0410, 0.0898	0.0578, 0.1294
R indices (all data)	0.0788, 0.1486	0.0374, 0.0773	0.0809, 0.1230	0.0787, 0.1056	0.0706, 0.1352

lyse at Bath so data were collected at Station 9.8 of the SRS, Daresbury. Corrections for Lorentz and polarisation were implemented in all cases, with extinction corrections being merited for **2** and **3**. All atoms were refined anisotropically. Absorption corrections were also applied to data for **2** and **4**. In **2**, the largest residual peak and hole are proximate to C(11) (1.54 Å) and Au(1) (0.84 Å) respectively. These are artifacts of the data and are not chemically significant. Details of the data collections and structure solutions are given in Table 1.

As mentioned above, the structures of **3** and **4** were subject to considerable disorder. In **3**, there was 1:1 disorder of sulfonate oxygens between O(1)−O(3) and O(1A)−O(3A). Threefold disorder was also observed in the guanidinium moiety (ratio 2:1:1) between atoms labelled therein without suffix, atoms with suffix "A" and atoms with suffix "B" respectively. These fragments were refined subject to being flat, and atomic displacement parameters therein were also constrained. Compound **4**, which is isostructural with **3**, was treated similarly during refinement, with the exception of the occupancies assigned to the disordered guanidinium fragments. All structures were solved using SHELXS-97 and refined using SHELXL-97.[18] Hydrogen atoms were readily located in the penultimate difference Fourier maps for the non-disordered structures **1**, **2** and **5** but in the final least-squares cycles they were included at calculated positions throughout.

CCDC-191297 (**1**), -191298 (**2**), -191299 (**3**), -191300 (**4**) and -191301 (**5**) contain the supplementary crystallographic data for this paper. These data can be obtained free of charge at www.ccdc.cam.ac.uk/conts/retrieving.html [or from the Cambridge Crystallographic Data Centre, 12 Union Road, Cambridge CB2 1EZ, UK; fax: (internat.) +44-1223/336-033; E-mail: deposit@ccdc.cam.ac.uk].

Acknowledgments

The EPSRC is thanked for financial support.

[1] D. Braga, *J. Chem. Soc., Dalton Trans.* **2000**, 3705−3713; C. B. Aakeröy, A. M. Beatty, *Aust. J. Chem.* **2001**, *54*, 409−421; R. E. Meléndez, A. D. Hamilton, *Topics Curr. Chem.* **1998**, *198*, 97−129 − B. Moulton, M. J. Zaworotko, *Chem. Rev.* **2001**, *101*, 1629−1658; A. D. Burrows, C.-W. Chan, M. M. Chowdhry, J. E. McGrady, D. M. P. Mingos, *Chem. Soc. Rev.* **1995**, *24*, 329−339.

[2] A. D. Burrows, D. M. P. Mingos, A. J. P. White, D. J. Williams, *Chem. Commun.* **1996**, 97−99; A. D. Burrows, S. Menzer, D. M. P. Mingos, A. J. P. White, D. J. Williams, *J. Chem. Soc., Dalton Trans.* **1997**, 4237−4240; M. T. Allen, A. D. Burrows, M. F. Mahon, *J. Chem. Soc., Dalton Trans.* **1999**, 215−221.

[3] V. A. Russell, M. C. Etter, M. D. Ward, *J. Am. Chem. Soc.* **1994**, *116*, 1941−1952; V. A. Russell, M. C. Etter, M. D. Ward, *Chem. Mater.* **1994**, *6*, 1206−1217.

[4] M. J. Horner, K. T. Holman, M. D. Ward, *Angew. Chem. Int. Ed.* **2001**, *40*, 4045−4048.

[5] V. A. Russell, C. C. Evans, W. Li, M. D. Ward, *Science* **1997**, *276*, 575−579; J. A. Swift, A. M. Reynolds, M. D. Ward, *Chem. Mater.* **1998**, *10*, 4159−4168; J. A. Swift, A. M. Pivovar, A. M. Reynolds, M. D. Ward, *J. Am. Chem. Soc.* **1998**, *120*, 5887−5894; C. C. Evans, L. Sukarto, M. D. Ward, *J. Am. Chem. Soc.* **1999**, *121*, 320−325.

[6] F. Joó, A. Kathó, *J. Mol. Catal. A* **1997**, *116*, 3−26; A. F. Borowski, D. J. Cole-Hamilton, G. Wilkinson, *Nouv. J. Chim.* **1978**, *2*, 137−144.

[7] A. Kathó, A. C. Bényei, F. Joó, M. Sági, *Adv. Synth. Catal.* **2002**, *344*, 278−282.

[8] A. D. Burrows, R. W. Harrington, M. F. Mahon, in *Dalton Discussion Meeting 3: Inorganic Crystal Engineering*, Bologna, Italy, 2000.

[9] I. Dance, M. Scudder, *Chem. Eur. J.* **1996**, *2*, 481−486; M. Scudder, I. Dance, *J. Chem. Soc., Dalton Trans.* **1998**, 3155−3165.

[10] I. Dance, M. Scudder, *J. Chem. Soc., Dalton Trans.* **2000**, 1579−1585.

[11] I. Dance, M. Scudder, *J. Chem. Soc., Dalton Trans.* **2000**, 1587−1594.

[12] B. C. Tzeng, A. Schier, H. Schmidbaur, *Inorg. Chem.* **1999**, *38*, 3978−3984; W. J. Hunks, M. C. Jennings, R. J. Puddephatt, *Inorg. Chem.* **2002**, *41*, 4590−4598.

[13] B. Ziemer, A. Rabis, H.-U. Steinberger, *Acta Crystallogr., Sect. C* **2000**, *56*, E58−E59.

[14] P. G. Jones, C. Kienitz, C. Thone, *Z. Kristall.* **1994**, *209*, 80−81.

[15] G. Aullón, D. Bellamy, L. Brammer, E. A. Bruton, A. G. Orpen, *Chem. Commun.* **1998**, 653−654.

[16] S. Ahrland, J. Chatt, N. R. Davies, A. A. Williams, *J. Chem. Soc.* **1958**, 276−288.

[17] R. Usón, A. Laguna, M. Laguna, *Inorg. Synth.* **1989**, *26*, 85−91.

[18] G. M. Sheldrick, *Acta Crystallogr., Sect. A* **1990**, *46*, 467−473; G. M. Sheldrick, *SHELXL-97, Computer Program for Crystal Structure Refinement*, University of Göttingen, **1997**.

Received November 14, 2002
[I02625]

Synthesis and Characterization of Five-Coordinate Gallium and Indium Complexes Stabilized by Tridentate, Substituted Pyrrole Ligands

Pei-Cheng Kuo,[a] Jui-Hsien Huang,*[a] Chen-Hsiung Hung,[a] Gene-Hsiang Lee,[b] and Shie-Ming Peng[b]

Keywords: Gallium / Indium / N ligands / Bridging ligands

Five-coordinate gallium and indium complexes stabilized by tridentate, substituted pyrrole ligands have been synthesized and characterized. The reaction of MCl_3 with 1 equiv. of $Li[NC_4H_2(CH_2NMe_2)_2\text{-}2,5]$ in diethyl ether affords $[\{NC_4H_2(CH_2NMe_2)_2\text{-}2,5\}MCl_2]$ [M = Ga (**1**), In (**2**)] in high yield. Reaction of **1** with 2 equiv. of MeLi in diethyl ether at −78 °C followed by heating to reflux for 30 min affords the alkylated product $[\{NC_4H_2(CH_2NMe_2)_2\text{-}2,5\}GaMe_2]$ (**3**). Similarly, the reaction of **2** with 2 equiv. of MeLi or *n*BuLi affords the dialkylated complexes **4** and **5**, respectively. Complex **2** is a strong Lewis acid which readily absorbs H_2O forming $[\{[C_4H_2N(CH_2NMe_2)_2\text{-}2,5]InCl_2\}_2(\mu\text{-}OH_2)]$ (**6**). Complexes **3**, **4**, and **6** have been characterized by X-ray crystallography.

(© Wiley-VCH Verlag GmbH & Co. KGaA, 69451 Weinheim, Germany, 2003)

Introduction

Lewis acids catalyze a wide range of reactions. The reactivity and selectivity of these reactions are often related to the Lewis acid's electronic and steric properties.[1] Among the Lewis acid catalysts derived from group-13 metals, those of aluminum are well known for serving as catalysts in organic synthesis, and more recently for polymerization reactions.[2−4] The number of metal complexes reported, however, declines upon descending the group from aluminum to indium. Indium-mediated organometallic reactions have received considerable attention recently, due to their tolerance of polar solvents, including water.[5−11] Lewis acidic indium complexes are dominated by a low coordination number at the metal center (three or four)[12−14] but a few complexes of higher coordination number (five and six) have been reported.[15−21]

We have been interested in the chemistry of group-13[22−23] and early transition metal complexes[24−25] stabilized by bi- or tridentate substituted pyrrole ligands.[26−27] These complexes are Lewis acids with the potential to serve as catalysts in organic synthesis or for the polymerization of olefins. We report here the syntheses, intramolecular rearrangement, and X-ray crystal structures of Ga and In complexes.

[a] Department of Chemistry, National Changhua University of Education,
Changhua 50058, Taiwan
E-mail: juihuang@cc.ncue.edu.tw
[b] Department of Chemistry and Instrumentation Center, National Taiwan University,
Taipei 10764, Taiwan

Results and Discussion

Synthesis and Characterization

Reaction of $Li[NC_4H_2(CH_2NMe_2)_2\text{-}2,5]$ with MCl_3 (M = Ga, In) in diethyl ether affords $[\{NC_4H_2(CH_2NMe_2)_2\text{-}2,5\}MCl_2]$ [M = Ga (**1**), In (**2**)] in yields of 98 and 81%, respectively (Scheme 1). However, suitable crystals of complexes **1** and **2** could not be obtained. The ^1H and ^{13}C NMR spectra of both **1** and **2** show the signals of one type of CH_2 and NMe_2 units at $\delta \approx 3.6$ and 2.5 ppm, respectively, which are consistent with symmetrical structures.

Reaction of complex **1** with 2 equiv. of 1.6 M methyllithium in diethyl ether solution at −78 °C followed by heating to reflux for 30 min afforded the dimethylgallium complex $[\{NC_4H_2(CH_2NMe_2)_2\text{-}2,5\}GaMe_2]$ (**3**) in 75% yield. The ^1H NMR spectrum of **3** shows signals of one set of CH_2, NMe_2, and GaMe units at $\delta = 3.47$, 2.29, and −0.37 ppm, respectively.

Similarly, treatment of **2** with 2 equiv. of MeLi or *n*BuLi in a diethyl ether solution at −78 °C, allowing to warm to room temperature, and then heating to reflux for 30 min generated the pure dimethyl complex **4** and the dibutyl complex **5** in yields of 61 and 65%, respectively. Complexes **3**, **4**, and **5** are thermally robust and show no decomposition upon heating in toluene at 100 °C for over 12 h.

Complex **2** is very Lewis acidic and reacts readily with moisture upon exposure to air. During recrystallization of **2** from a toluene solution at −20 °C, the Schlenk flask was occasionally opened to air resulting in the deposition of the water-bridged complex $[\{[C_4H_2N(CH_2NMe_2)_2\text{-}2,5]InCl_2\}_2(\mu\text{-}OH_2)]$ (**6**). The procedure was carried out several times in both toluene and diethyl ether, and the same result was obtained. Attempts to let **2** react with 0.5 equiv. of H_2O

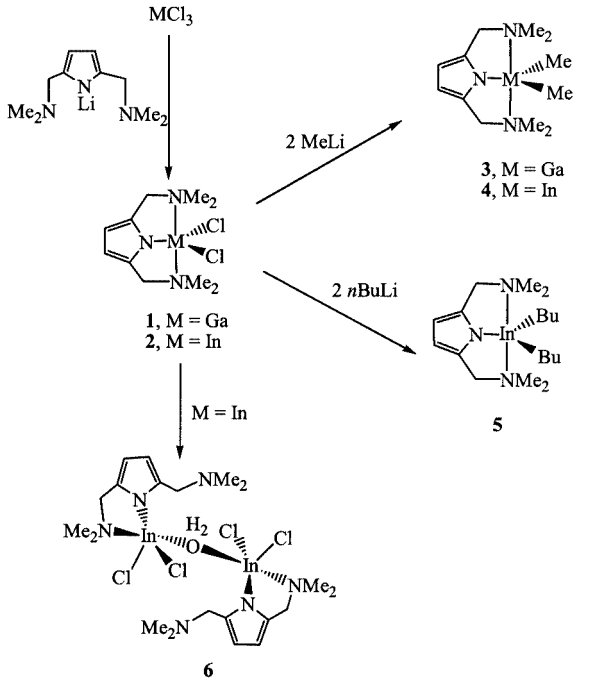

Scheme 1

in either toluene or diethyl ether afforded a mixture, from which only a small amount of **6** was isolated. Similarly, diffusion of H_2O vapor into a toluene solution of **2** yielded the same results. The ^1H NMR spectrum of **6** in CD_2Cl_2 at room temperature indicates an asymmetric arrangement, which is consistent with the X-ray crystal structure (vide infra). Complex **6** gives rise to three methyl resonances for the two NMe_2 units at $\delta = 2.50$, 2.59, and 2.84 ppm in the ratio of 1:1:2. Four doublets for the two AB systems of the CH_2N units were observed at $\delta = 3.16$, 3.70, 4.56, and 4.72 ppm in the ratio of 1:1:1:1. Selective homonuclear decoupling of the ^1H NMR spectrum of **6** revealed that one AB pattern of a CH_2N unit gives rise to the resonances at $\delta = 3.16$ and 4.56 ppm while the other unit can be attributed to the resonances at $\delta = 3.70$ and 4.72 ppm.

Solid-State Structures of Complexes 3, 4, and 6

Crystals of **3** suitable for X-ray structure determination were obtained from a saturated diethyl ether solution stored at −20 °C. Crystals of **4** were obtained by sublimation from a flask in the glove box under nitrogen. Details of the data collections for **3** and **4** are summarized in Table 2 with selected bond lengths and angles listed in Table 1. The ORTEP diagram of complex **3** is depicted in Figure 1. The gallium atom is surrounded by two methyl groups and three nitrogen atoms of the tridentate pyrrolyl ligand, $[NC_4H_2(CH_2NMe_2)_2\text{-}2,5]$, forming a distorted trigonal-bipyramidal structure. The tridentate pyrrolyl ligand is arranged at the meridional positions, with the pyrrolyl nitrogen atom occupying the equatorial position and the two NMe_2 units occupying the axial positions. The axial N(1)−Ga−N(3) angle of 146.68(6)° deviates from linearity

Table 1. Selected bond lengths [Å] and angles [°] for compounds **3**, **4**, and **6**

3

Ga−N(2)	1.920(2)	Ga−C(2)	1.953(2)	Ga−C(1)	1.969(2)	Ga−N(1)	2.307(2)
Ga−N(3)	2.736(2)						
N(2)−Ga−C(2)	121.38(10)	N(2)−Ga−C(1)	114.36(9)	C(2)−Ga−C(1)	123.10(11)	N(2)−Ga−N(1)	77.13(7)
C(2)−Ga−N(1)	102.57(9)	C(1)−Ga−N(1)	99.66(9)	N(2)−Ga−N(3)	69.92(6)	C(2)−Ga−N(3)	90.63(8)
C(1)−Ga−N(3)	98.27(9)	N(1)−Ga−N(3)	146.68(6)				

4

In(1)−N(2)	2.108(5)	In(1)−C(2)	2.173(6)	In(1)−C(1)	2.187 (6)	In(1)−N(1)	2.519(5)
In(1)−N(3)	2.681(6)	In(2)−N(5)	2.117(5)	In(2)−C(14)	2.087(7)	In(2)−C(13)	2.161(6)
In(2)−N(4)	2.516(6)	In(2)−N(6)	2.670(6)				
N(2)−In(1)−C(2)	113.1(2)	N(2)−In(1)−C(1)	121.2(2)	C(2)−In(1)−C(1)	124.6(3)	N(2)−In(1)−N(1)	71.9(2)
C(2)−In(1)−N(1)	105.4(2)	C(1)−In(1)−N(1)	101.3(2)	N(2)−In(1)−N(3)	69.5(2)	C(2)−In(1)−N(3)	94.5(3)
C(1)−In(1)−N(3)	94.0(2)	N(1)−In(1)−N(3)	140.96(19)	N(5)−In(2)−C(14)	112.7(3)	N(5)−In(2)−C(13)	119.5(2)
C(14)−In(2)−C(13)	127.0(3)	N(5)−In(2)−N(4)	71.5(2)	C(14)−In(2)−N(4)	106.1(3)	C(13)−In(2)−N(4)	98.4(2)
N(5)−In(2)−N(6)	68.5(2)	C(14)−In(2)−N(6)	95.2(3)	C(13)−In(2)−N(6)	95.6(2)	N(4)−In(2)−N(6)	139.5(2)

6·C_7H_8

In(1)−O(1)	2.136(4)	In(1)−N(2)	2.167(5)	In(1)−N(1)	2.334(5)	In(1)−Cl(1)	2.434(2)
In(1)−Cl(1)	2.519(2)	In(2)−N(5)	2.146(5)	In(2)−O(1)	2.175(4)	In(2)−N(4)	2.366(5)
In(2)−Cl(3)	2.462(2)	In(2)−Cl(4)	2.4750(14)				
O(1)−In(1)−N(2)	97.5(2)	O(1)−In(1)−N(1)	156.9(2)	N(2)−In(1)−N(1)	78.7(2)	O(1)−In(1)−Cl(1)	106.64(10)
N(2)−In(1)−Cl(1)	102.8(1)	N(1)−In(1)−Cl(1)	96.4(1)	O(1)−In(1)−Cl(2)	84.7(1)	N(2)−In(1)−Cl(2)	154.2(1)
N(1)−In(1)−Cl(2)	89.2(1)	Cl(1)−In(1)−Cl(2)	101.14(6)	N(5)−In(2)−O(1)	96.9(2)	N(5)−In(2)−N(4)	77.6(2)
O(1)−In(2)−N(4)	161.3(2)	N(5)−In(2)−Cl(3)	98.7(1)	O(1)−In(2)−Cl(3)	98.2(1)	N(4)−In(2)−Cl(3)	100.4(1)
N(5)−In(2)−Cl(4)	163.8(1)	O(1)−In(2)−Cl(4)	84.7(1)	N(4)−In(2)−Cl(4)	95.8(1)	Cl(3)−In(2)−Cl(4)	97.03(6)
In(1)−O(1)−In(2)	108.6(2)						

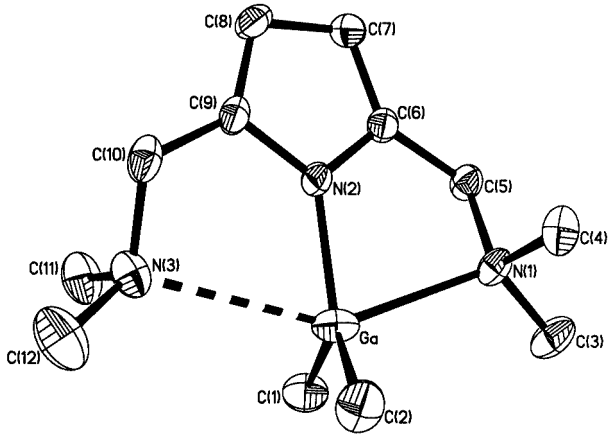

Figure 1. ORTEP diagram of complex **3**; thermal ellipsoids at the 50% probability level and hydrogen atoms are omitted for clarity

by 33.32° due to the geometrical constraints of the two fused five-membered rings. It is noteworthy that the N(1)−Ga and N(3)−Ga bond distances of 2.307(2) and 2.736(2) Å, respectively, are significantly different. The unit cell of **4** contains two independent molecules and the structure of one of these is shown in Figure 2. The structure of **4** is very similar to that of complex **3**. However, the difference of 0.14 Å in the metal-to-axial-nitrogen bond lengths In(1)−N(1) [2.519(5) Å] and In(1)−N(3) [2.661(6) Å] is smaller in **4** than in the corresponding gallium species. This is consistent with the larger atomic radius of indium. The axial angle, N(1)−In−N(3) [140.96(19)°], deviates from linearity by 39.04° due to the steric constraints imposed by the two fused five-membered rings.

Crystals of complex **6** were obtained by dissolving **2** in toluene and cooling to −20 °C. The reaction of **2** with moisture was effected by slowly exposing the solution to air occasionally. This caused crystals of **6** to appear in the flask. The crystals were collected and characterized by ^{1}H NMR spectroscopy and a single-crystal X-ray diffraction study. Details of the data collection for complex **6** are summarized in Table 2 with selected bond lengths and angles listed in Table 1. The ORTEP diagram of **6** is shown in Figure 3. The structure of **6** can be described as corner-sharing bis(square-pyramidal), in which the oxygen atom acts as the corner atom with Cl(1) and Cl(3) occupying the apical positions. A view of the coordination spheres of the two indium centers is shown in Figure 4, where the two square planes are joined by the oxygen atom. The In(1) and In(2) atoms are displaced from the planes defined by N(1)−N(2)−O(1)−Cl(2) and N(4)−N(5)−O(1)−Cl(4) by 0.4717 and 0.3389 Å, respectively. The question has been raised as to whether the oxygen-containing bridging groups should be viewed as water molecules or dianionic oxo groups. Although the hydrogen atoms of the bridging group were not found either in the ^{1}H NMR spectrum or in the X-ray crystal structure, three points support the water-bridged formulation for the dinuclear indium complex: (1) In both **4** and **6**, both pyrrolyl groups exist as σ-coordinated ligands with similar In−N distances [2.108(5) vs. 2.17 Å]. Furthermore, accommodation of the two methyl groups results in an oxidation state of +3 for the In center. These data suggest that the oxygen atom is coordinated to the indium

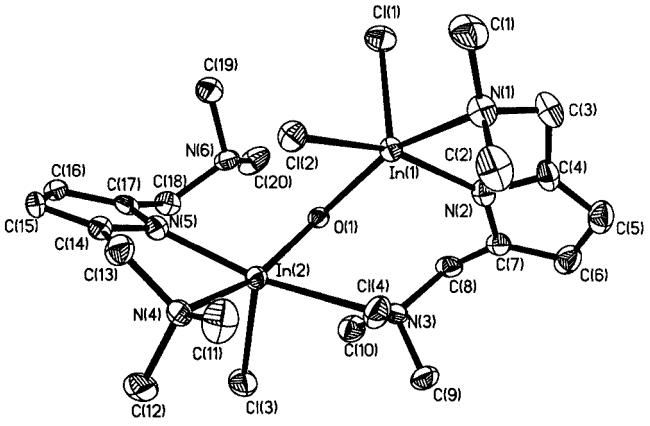

Figure 3. ORTEP diagram of complex **6**; thermal ellipsoids are at the 50% probability level and hydrogen atoms are omitted for clarity

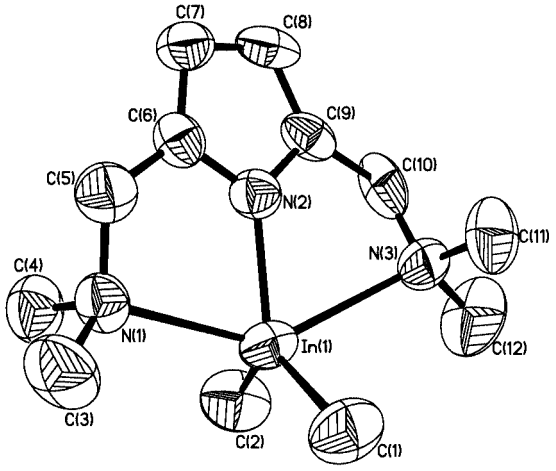

Figure 2. ORTEP diagram of complex **4**; thermal ellipsoids are at the 50% probability level and hydrogen atoms are omitted for clarity

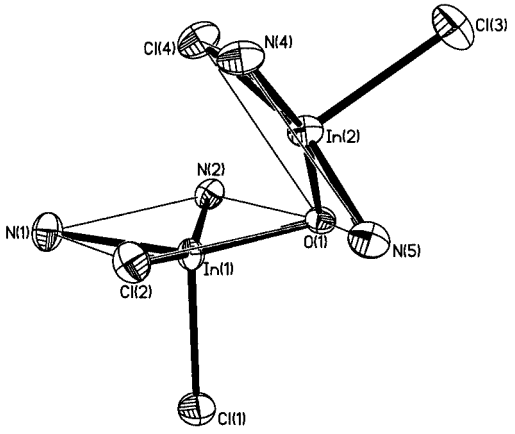

Figure 4. View of the coordination spheres of complex **6** showing only atoms coordinated to the indium atom; thermal ellipsoids are at the 50% probability level

atom via a lone pair of electrons. (2) The bond angle subtended by In(2)−O(1)−In(1) in complex **6** is 108.6(2)°, which is very close to the sp^3 bonding angle of 109.28. (3) Finally, an IR spectrum of **6** supports the existence of the bridged H_2O molecule, since a broad characteristic OH stretching peak was observed at 3460 cm^{-1}. Oxygen-atom-bridged dinuclear indium complexes have been observed often,[28−30] however, water-bridged diindium complexes have not been reported.

Experimental Section

General Procedures: All reactions were performed under dry nitrogen using standard Schlenk techniques or a glove box. Toluene, diethyl ether, and tetrahydrofuran were dried by heating to reflux in the presence of sodium benzophenone ketyl. CH_2Cl_2 was dried with P_2O_5. All solvents were distilled and stored under nitrogen in solvent reservoirs containing 4-Å molecular sieves. ^1H and ^{13}C NMR spectra were recorded with a Bruker AC 200 spectrometer. Chemical shifts for ^1H and ^{13}C spectra were recorded in ppm relative to the residual protons of the solvent or the ^{13}C resonances of the deuterated solvent: $CDCl_3$ (δ = 7.24, 77.0 ppm), C_6D_6 (δ = 7.15, 128.0 ppm), or CD_2Cl_2 (δ = 5.24, 54.0 ppm). Elemental analyses were performed with a Heraeus CHN-OS Rapid Elemental Analyzer at the Instrument Center, NCHU. $[C_4H_3N(CH_2NMe_2)_2$-2,5] and Li$[C_4H_2N(CH_2NMe_2)_2$-2,5] were prepared according to previously reported procedures.[23−25] $InCl_3$ (Strem) and MeLi (Aldrich) were used as received.

[{$C_4H_2N(CH_2NMe_2)_2$-2,5}$GaCl_2$] (1): A 100-mL Schlenk flask was charged with a solution of $GaCl_3$ (5.0 g, 28.57 mmol) in diethyl ether (30 mL). This solution was added dropwise to a suspension of Li$[C_4H_2N(CH_2NMe_2)$-2,5] (5.34 g, 28.57 mmol) in diethyl ether (20 mL) with stirring at −78 °C. The mixture was allowed to warm to room temperature and stirred for 5 h. The resultant suspension was filtered through Celite. The filtrate was concentrated to dryness and the resultant solid was recrystallized from diethyl ether to afford **1** (9.0 g, 98%). ^1H NMR ($CDCl_3$): δ = 2.52 (s, 12 H, N*Me*$_2$), 3.63(s, 4 H, CH_2N), 5.95 (s, 2 H) ppm. ^{13}C NMR ($CDCl_3$): δ = 47.0 (q, $J_{C,H}$ = 136 Hz, N*Me*$_2$), 58.8 (t, $J_{C,H}$ = 139 Hz, *C*H_2N), 105.2 (d, $J_{C,H}$ = 167 Hz), 128.0 (s) ppm. $C_{10}H_{18}Cl_2GaN_3$ (320.90): calcd. C 37.43, H 5.65, N 13.09; found C 36.93, H 5.68, N 12.55.

[{$C_4H_2N(CH_2NMe_2)_2$-2,5}$InCl_2$] (2): This complex was prepared in a similar way to that described for **1**, starting from $InCl_3$ (3.0 g, 13.6 mmol) and Li$[C_4H_2N(CH_2NMe_2)$-2,5] (2.53 g, 13.6 mmol). Yield: 4.03 g (81%). ^1H NMR ($CDCl_3$): δ = 2.54 (s, 12 H, N*Me*$_2$), 3.65 (s, 4 H, CH_2N), 5.99 (s, 2 H) ppm. ^{13}C NMR ($CDCl_3$): δ = 46.5 (q, $J_{C,H}$ = 137 Hz, N*Me*$_2$), 59.3 (t, $J_{C,H}$ = 138 Hz, *C*H_2N), 106.4 (d, $J_{C,H}$ = 167 Hz), 129.5 (s) ppm. $C_{10}H_{18}Cl_2InN_3$ (365.99): calcd. C 32.82, H 4.96, N 11.48; found C 32.26, H 4.54, N 10.92.

[{$C_4H_2N(CH_2NMe_2)_2$-2,5}$GaMe_2$] (3): A 50-mL Schlenk flask was charged with diethyl ether (20 mL) and **1** (2.0 g, 6.23 mmol) and the resultant solution was cooled to −78 °C. To this solution was added MeLi (1.4 M in diethyl ether, 4.45 mL, 12.5 mmol) via syringe. The mixture was stirred at room temperature for 5 h, and the resultant suspension was heated to reflux for 30 min and filtered through Celite. The filtrate was concentrated to dryness affording **3** in 75% yield (1.30 g). ^1H NMR ($CDCl_3$): δ = −0.37 (s, 6 H, Ga*Me*), 2.29 (s, 12 H, N*Me*$_2$), 3.48 (s, 4 H, CH_2N), 5.89 (s, 2 H) ppm. ^{13}C NMR ($CDCl_3$): δ = −9.32 (q, $J_{C,H}$ = 121 Hz), 45.9 (q, $J_{C,H}$ = 137 Hz, N*Me*$_2$), 58.9 (t, $J_{C,H}$ = 136 Hz, *C*H_2N), 103.0 (d, $J_{C,H}$ = 163 Hz), 131.9 (s) ppm. $C_{12}H_{24}GaN_3$ (280.06): calcd. C 51.46, H 8.64, N 15.00; found C 49.802, H 8.036, N 14.51. The error in the elemental analysis may be due to traces of LiBr in the final product.

[{$C_4H_2N(CH_2NMe_2)_2$-2,5}$InMe_2$] (4) and [{$C_4H_2N(CH_2NMe_2)_2$-2,5}$InBu_2$] (5): A similar procedure described for the preparation of complexe **3** was applied for the preparation of **4** and **5**. The yield of **4** was 61% (0.54 g, based on 1.0 g of **2**). ^1H NMR ($CDCl_3$): δ = −0.31 (s, 6 H, In*Me*), 2.31 (s, 12 H, N*Me*$_2$), 3.47 (s, 4 H, CH_2N), 5.91 (s, 2 H) ppm. ^{13}C NMR ($CDCl_3$): δ = −10.6 (q, $J_{C,H}$ = 126 Hz), 46.1 (q, $J_{C,H}$ = 135 Hz, N*Me*$_2$), 59.4 (t, $J_{C,H}$ = 135 Hz, *C*H_2N), 103.0 (d, $J_{C,H}$ = 164 Hz), 131.9 (s) ppm. $C_{12}H_{24}InN_3$ (325.16): calcd. C 44.33, H 7.44, N 12.92; found C 44.92, H 6.96, N 12.65. For **5** the yield was 65% (0.73 g, based on 1.0 g of **2**) of a brown viscous liquid after removing all volatiles. Due to the viscosity of complex **5**, it could not be purified by recrystallization or distillation. ^1H NMR ($CDCl_3$): δ = 0.66 (t, 4 H, In*CH*$_2$CH$_2$CH$_2$CH$_3$), 0.89 (t, 6 H, InCH$_2$CH$_2$CH$_2$*CH*$_3$), 1.31 (m, 4 H, InCH$_2$*CH*$_2$CH$_2$CH$_3$), 1.57 (m, 4 H, InCH$_2$CH$_2$*CH*$_2$CH$_3$), 2.34 (s, 12 H, N*Me*$_2$), 3.45 (s, 4 H, CH_2N), 5.91 (s, 2 H) ppm. ^{13}C NMR ($CDCl_3$): δ = 13.2 (t, $J_{C,H}$ = 140 Hz), 13.7 (q, $J_{C,H}$ = 123 Hz), 28.8 (t, $J_{C,H}$ = 125 Hz), 30.3 (t, $J_{C,H}$ = 128 Hz), 46.8 (q, $J_{C,H}$ = 137 Hz, N*Me*$_2$), 60.0 (t, $J_{C,H}$ = 135 Hz, *C*H_2N), 103.0 (d, $J_{C,H}$ = 164 Hz), 132.7 (s). No elemental analysis was performed due to a small amount of impurity present in the product.

[{[$C_4H_2N(CH_2NMe_2)_2$-2,5]$InCl_2$}$_2$(μ-OH_2)] (6): The same procedure was applied for the preparation of **6** as that used to synthesize **2**, with the exception that during recrystallization of complex **2** from a toluene solution at −20 °C the Schlenk flask was periodically opened to air. This resulted in the deposition of **6** on the bottom of the flask (1.03 g,13%, based on 5 g of $InCl_3$). ^1H NMR (CD_2Cl_2): δ = 2.50 (br. s, 6 H, N*Me*$_2$), 2.59 (br. s, 6 H, N*Me*$_2$), 2.84 (br. s, 12 H, N*Me*$_2$), 3.16 (d, 4 H, CH_2N), 3.70 (d, 4 H, CH_2N), 4.56 (d, 4 H, CH_2N), 4.72 (d, 4 H, CH_2N), 6.01 (d, 2 H), 6.26 (d, 2 H) ppm. ^{13}C NMR (CD_2Cl_2): 47.8 (q, $J_{C,H}$ = 136 Hz, N*Me*$_2$), 49.6 (q, $J_{C,H}$ = 135 Hz, N*Me*$_2$), 50.2 (q, $J_{C,H}$ = 135 Hz, N*Me*$_2$), 60.6 (t, $J_{C,H}$ = 139 Hz, *C*H_2N), 61.3 (t, $J_{C,H}$ = 145 Hz, *C*H_2N), 106.3 (d, $J_{C,H}$ = 167 Hz), 114.9 (d, $J_{C,H}$ = 164 Hz), 122.5 (s), 136.0 (s). A small amount of complex **2** was present in **6** (less than 3% by ^1H NMR spectroscopy), which prevented a reasonable elemental analysis from being obtained.

X-ray Structure Determination of Complexes 3, 4, and 6: Crystals were mounted on a glass fiber using epoxy resin and transferred to the goniostat. Data collections were preformed at 150 K under liquid nitrogen vapor for complexes **3** and **6** and at 293 K for complex **4**. Data were collected with a Bruker SMART CCD diffractometer with graphite-monochromated Mo-K_α radiation. Structural determinations were carried out using the SHELXTL package of programs. All refinements were carried out by the full-matrix least-squares method using anisotropic displacement parameters for all non-hydrogen atoms. All the hydrogen atoms were placed in calculated positions. The crystal data are summarized in Table 2. CCDC-185057 and -185059 contain the supplementary crystallographic data for this paper. These data can be obtained free of charge at www.ccdc.cam.ac.uk/conts/retrieving.html [or from the Cambridge Crystallographic Data Centre, 12 Union Road, Cambridge CB2 1EZ, UK; Fax: (internat.) + 44-1223/336-033; E-mail: deposit@ccdc.cam.ac.uk].

Acknowledgments

We thank the National Science Council of Taiwan for financial support and the National Center for High Performance Computing

Table 2. Summary of crystallographic data for compounds **3**, **4**, and **6**

	3	**4**	**6**
Empirical formula	$C_{12}H_{24}GaN_3$	$C_{24}H_{48}In2N_6$	$C_{27}H_{46}Cl_4In_2N_6O$
Formula mass	280.06	650.32	842.14
Temperature [K]	150(1)	293(2)	150(1)
Crystal system	orthorhombic	monoclinic	monoclinic
Space group	Pbca	*C*2/*c*	$P2_1/c$
a [Å]	12.1751(6)	27.4334(17)	9.3723(1)
b [Å]	15.2278(7)	9.1830(6)	17.6586(3)
c [Å]	15.6050(7)	27.5320(17)	21.9571(2)
β [°]	90	117.23(1)	92.704(1)
Volume [Å^3]/*Z*	2893.2(2)/8	6173.1(7)/8	3629.89(8)/4
Density (calcd.) [Mg/m^3]	1.286	1.399	1.541
Absorption coefficient [mm^{-1}]	1.884	1.514	1.594
F(000)	1184	2656	1696
Crystal size [mm]	0.50 × 0.40 × 0.10	0.36 × 0.31 × 0.07	0.20 × 0.10 × 0.10
θ range [°]	2.51 to 27.50	1.66 to 27.51	1.48 to 27.50
No. of reflns. collected	16753	19182	20140
No. of indep. reflns.	3318 (R_{int} = 0.0375)	7066 (R_{int} = 0.0339)	8096 (R_{int} = 0.08533)
Max./min. trans.	0.6471/0.4120	0.9486/0.8740	0.8621/0.5674
No. of data/restraints/params.	3318/0/146	7066/0/297	8095/0/362
Goodness of fit on F^2	1.094	1.014	1.017
Final *R* indices [$I > 2\sigma(I)$], R_1[a]	0.0363	0.0409	0.0581
wR_2[b]	0.0754	0.0830	0.1007
R indices (all data), R_1[a]	0.0463	0.1177	0.1045
wR_2[b]	0.0793	0.1137	0.1169
Largest diff. peak/hole [e·Å^{-3}]	0.674/−0.615	0.765/−0.739	1.812/−1.210

[a] $R_1 = \Sigma||F_o| - |F_c||/\Sigma|F_o|$. [b] $wR_2 = \{\Sigma[w(F_o^2 - F_c^2)^2]/\Sigma[w(F_o^2)^2]^{1/2}\}$.

for databank searches. We also thank Dr. Darin Tiedtke for helpful discussions and for proofreading this manuscript.

[1] H. Yamamoto (Ed.), *Lewis Acids in Organic Synthesis*, Wiley-VCH, Weiheim, **2000**.
[2] M. Bochmann, D. M. Dawson, *Angew. Chem. Int. Ed. Engl.* **1996**, *35*, 2226−2228.
[3] D. A. Atwood, J. A. Jegier, D. Rutherford, *J. Am. Chem. Soc.* **1995**, *117*, 6779−6780.
[4] M. P. Coles, R. F. Jordan, *J. Am. Chem. Soc.* **1997**, *119*, 8125−8126.
[5] S. Araki, T. Kamei, T. Hirashita, H. Yamamura, M. Kawai, *Org. Lett.* **2000**, *2*, 847−849.
[6] N. Fujiwara, Y. Yamamoto, *J. Org. Chem.* **1997**, *62*, 2318−2319.
[7] B. C. Ranu, A. Majee, *Chem. Commun.* **1997**, 1225−1226.
[8] P. Cintas, *Synlett* **1995**, 1087−1096.
[9] L. A. Paquette, R. R. Rothhaar, M. Issac, L. M. Rogers, R. D. Rogers, *J. Org. Chem.* **1998**, *63*, 5463−5472.
[10] T. H. Chan, Y. Yang, *J. Am. Chem. Soc.* **1999**, *121*, 3228−3229.
[11] C. J. Li, T. H. Chan, *Organic Reactions in Aqueous Media*, John Wiley & Sons, New York, **1997**.
[12] C. D. Abernethy, M. L. Cole, C. Jones, *Organometallics* **2000**, *19*, 4852−4857.
[13] L. A. Mîinea, S. Suh, D. M. Hoffman, *Inorg. Chem.* **1999**, *38*, 4447−4454.
[14] A. M. Arif, A. H. Cowley, T. M. Elkins, R. A. Jones, *J. Chem. Soc., Chem. Commun.* **1986**, 1776−1777.
[15] Y. Zhou, D. S. Richeson, *Organometallics* **1995**, *14*, 3558−3561.
[16] J. T. Leman, H. A. Roman, A. R. Barron, *Organometallics* **1993**, *12*, 2986−2990.
[17] Y. Zhou, D. S. Richeson, *Inorg. Chem.* **1996**, *35*, 1423−1424.
[18] J.-H. Park, P. O'Brien, A. J. P. White, D. J. Williams, *Inorg. Chem.* **2001**, *40*, 3629−3631.
[19] S. Suh, D. M. Hoffman, *J. Am. Chem. Soc.* **2000**, *122*, 9396−9404.
[20] C. J. Olazabal, F. P. Gabbai, A. H. Cowley, *Organometallics* **1994**, *13*, 421−423.
[21] M. Stender, U. Segerer, J. Sieler, E. Hey-Hawkins, *Z. Anorg. Allg. Chem.* **1998**, *624*, 85−90.
[22] J.-H. Huang, H.-J. Chen, J.-C. Chang, C.-C. Zhou, G.-H. Lee, S.-M. Peng, *Organometallics* **2001**, *20*, 2647−2650.
[23] J.-C. Chang, C.-H. Hung, J.-H. Huang, *Organometallics* **2001**, *20*, 4445−4447.
[24] J.-H. Huang, P.-C. Kao, G.-H. Lee, S.-M. Peng, *J. Chin. Chem. Soc.* **2000**, *47*, 1191−1195.
[25] J.-H. Huang, L.-S. Chi, F.-M. Huang, P.-C. Kao, G.-H. Lee, S.-M. Peng, *J. Chin. Chem. Soc.* **2000**, *47*, 895−900.
[26] W. Herz, K. Dittmer, *J. Am. Chem. Soc.* **1947**, *69*, 1698−1700.
[27] H. Kim, R. L. Elsenbaumer, *Tetrahedron Lett.* **1998**, *39*, 1087−1090.
[28] D. C. Bradley, H. Chudzynska, D. M. Frigo, M. B. Hursthouse, M. A. Mazid, *J. Chem. Soc., Chem. Commun.* **1988**, 1258−1259.
[29] D. C. Bradley, H. Chudzynska, D. M. Frigo, M. E. Hammond, M. B. Hursthouse, M. A. Mazid, *Polyhedron* **1990**, *9*, 719−726.
[30] For examples of dianionic O-bridged diindium complexes, see: S. Abram, C. Maichle-Mössmer, U. Abram, *Polyhedron* **1998**, *17*, 131−143.

Received July 17, 2002
[I02392]

Manganese in Precipitated Hydroxyapatites

Isaac Mayer,*[a] Orit Jacobsohn,[a] Tamara Niazov,[a] Jacques Werckmann,[b] Monica Iliescu,[b] Mireille Richard-Plouet,[b] Olaf Burghaus,[c] and Dirk Reinen[c]

Keywords: Manganese / Hydroxyapatite / EPR spectroscopy / Thermal properties

The synthesis of Mn-containing hydroxyapatite (HA) samples was carried out by precipitation from an aqueous solution with and without carbonate at pH 5.8–6.0. Chemical analyses have shown that Mn uptake (about 70%) is proportional to the amount of initially added Mn. The molar Ca/P ratios of the samples (1.53–1.63) indicate the formation of nonstoichiometric HA, with the higher values being obtained for the carbonated samples. Powder X-ray diffraction (XRD) and IR spectroscopy have shown well-defined patterns with structural data characteristic of HA. The calculated lattice constants were found to be similar to those known for HA, without any effect of the varying Mn content. High temperature treatment of selected samples was studied by XRD and IR and showed that the apatite structure is stable up to 400 °C for all samples. At 600 °C samples with low carbonate content transform partially, and at 800 °C completely, to β-$Ca_3(PO_4)_2$, while for samples with higher carbonate content (3.5–6.0%) the apatite structure is stable up to 800 °C, and a colour change to blue occurs. EPR spectroscopy reveals that manganese is divalent in all precipitated samples and present in a cubic impurity phase. After heating above 600 °C it is partially oxidized to Mn^V in the samples with high carbonate content and enters the HA lattice as the blue MnO_4^{3-} ion. In the carbonate-poor solids Mn^{2+} seems to partly occupy the Ca^{2+} sites in β-$Ca_3(PO_4)_2$ when sintered at temperatures above 400 °C.
(© Wiley-VCH Verlag GmbH & Co. KGaA, 69451 Weinheim, Germany, 2003)

Introduction

Various calcium hydroxyapatites (HA) containing Mn^{2+} ions were prepared in the course of a project dealing with the surface improvement of metal implants. HA is frequently used in implant materials for orthopaedic applications because of its biocompatibility. The addition of Mn^{2+} ions to HA in the present work was due to the fact that divalent Mn^{2+} has been linked to the activation of integrins,[1] a family of receptors which mediate cellular interactions with extracellular matrix and cell-surface ligands. In the presence of Mn^{2+} ions the ligand affinity of integrin increases and cell adhesion is promoted.

It is well-known that Mn^{2+} may enter the divalent M^{II} metal positions of apatites at the doping level, preferentially the M(I) site on a C_3 axis and with the coordination number 9 with respect to oxygen. The EPR spectra of Mn^{2+} in the Ca(I) position of the fluoride apatite $Ca_5(PO_4)_3F$ have been reported, indicating an axial lower-symmetry ligand field according to a zero-field splitting, D, of 428 G (about four times larger than the hyperfine splitting A).[2] Single crystal spectra of Mn^{2+}-doped $Cd_5(PO_4)_3Cl$ yield rather similar values ($D \approx 457$ G; $A \approx 92$ G).[3] Manganese may also enter the tetrahedral positions in the (+V) oxidation state, however, and a series of detailed single-crystal and powder studies centred on the optical and EPR properties have been published.[4]

Results

Chemical Analyses

Table 1 is a partial list of the analytical results of the synthesised samples (for preparation see Exp. Sect.). The molar Ca/P ratios found were in the range of 1.51−1.62, lower than the ratio for stoichiometric HA (1.67), thus indicating that under the experimental conditions used nonstoichiometric HA is obtained. Higher values of Ca/P are usually obtained for carbonate-containing samples. The Mn contents found in the samples were proportional to the initial amounts of Mn ions added and were about 70% of the original percentages.

Crystal Phase Analyses

Powder XRD patterns of the samples consisted of well defined reflections with the characteristic $P6_3/m$ hexagonal structure of apatites and with no additional crystal phases. The calculated lattice constants are listed in Table 1, and

[a] Department of Inorganic & Analytical Chemistry, Hebrew University, 91904 Jerusalem, Israel
[b] IPCMS, Universite Louis Pasteur, Strasbourg, France
[c] Fachbereich Chemie and Zentrum für Materialwissenschaften, Philipps Universität, 35032 Marburg, Germany

Table 1. Hydroxyapatite samples with different amounts of carbonate and Mn Lattice constants and Ca/P values

Sample	Mn^{2+} added (mg)	Mn^{2+} found (%)	CO_3^{2-} added (mL)	CO_3^{2-} found (%)	Lattice constants a (Å)	c (Å)	Ca/P
HAMn20	12.1	0.28	–	2.4	9.397	6.862	1.61
HAMn21	24.2	0.54	–	–	9.397	6.862	1.65
HAMn19	36.2	0.74	–	1.3	9.391	6.846	1.62
HAMn18	48.3	1.08	–		9.397	6.862	1.62
HAMn25	12.1	0.27	10	0.9	9.423	6.871	1.57
HAMn22	24.2	0.55	10	0.9	9.402	6.846	1.53
HAMn24	36.2	0.80	10	–	9.439	6.871	1.51
HAMn23	12.1	0.25	5	2.3	9.407	6.871	1.58
HAMn28	24.2	0.55	5	2.8	9.423	6.862	1.54
HAMn53	8.8	0.17	–	1.8	9.410	6.868	1.61
HAMn52	17.5	0.33	–	3.2	9.394	6.852	1.59
HAMn51	26.2	0.52	–		9.376	6.854	1.59
HAMn50	35.0	0.68	–	1.9	9.391	6.862	1.55
HAMn57	8.8	0.15	10	5.0	9.421	6.882	1.60
HAMn56	17.5	0.33	10	4.0	9.414	6.873	1.63
HAMn55	26.2	0.47	10	3.6	9.412	6.868	1.63
HAMn54	35.0	0.66	10	3.3	9.407	6.862	1.60
HAMn58	–	–	–	1.6	9.410	6.862	1.59
HAMn59	–	–	10	4.0	9.412	6.879	1.61
HAMn60	26.2	0.52	–	1.2	9.381	6.854	1.61
HAMn65	26.2	0.45	–	1.1	9.407	6.865	1.58
HAMn61	26.2	0.44	10	2.6	9.428	6.884	1.61
HAMn63	17.5	0.29	–	1.2	9.409	6.869	1.59
HAMn69	8.8	0.14	15	5.9	9.391	6.829	1.63
HAMn66	17.5	0.30	15	3.0	9.414	6.877	1.62
HAMn62	26.2	0.45	15	2.8	9.410	6.873	1.62
HAMn68	35.0	0.72	15	4.4	9.422	6.886	1.62

are close to those of pure HA. The amount of Mn added during precipitation has no apparent effect on the lattice constant values.

The IR spectra of the samples display the characteristic phosphate, hydroxide and water bands of HA. The carbonate bands appear around 1420 and 1470 cm^{-1}, indicating the replacement of phosphate by carbonate (B-type). In samples without carbonate HPO_4^{2-} could be detected by a band at around 866 cm^{-1}.

Thermal Properties

The thermal properties of selected samples were studied by heating them during four hours in the temperature range of 400−800 °C in 200 °C intervals. The samples were then analysed by XRD. The results of this thermal treatment are summarised in Table 2. The XRD patterns of the samples heated up to 800 °C display very sharp and well-defined peaks, an indication of improved crystallinity. The samples show no change in their crystal structure after heating up to 400 °C, and only one crystal phase − the apatite structure − is present. At 600 °C the apatite structure is still the only crystal phase found for the samples containing more than 4% carbonate. The XRD powder patterns of all the other samples have, in addition to the apatite phase, the diffraction peaks of β-$Ca_3(PO_4)_2$ (β-TCP),[5] indicating the partial transformation of HA to β-TCP. At 800 °C samples without, or with up to 2%, carbonate transform almost completely to β-TCP. The samples with a carbonate content equal to or higher than 4% do not decompose at all during thermal treatment but their colour turns to blue above 600 °C. This colour change is most pronounced in samples with low Mn content (around 0.1%); above 1.0% Mn, part of the crystallites are brownish. No such colour changes were observed for the samples which transform to β-TCP.

EPR Spectroscopy

Figure 1 shows the Q-band spectrum and the second derivative of a sample after precipitation and drying. The spectrum is characteristic of Mn^{2+} in a cubic environment, with a well-resolved sextet due to the hyperfine interaction with the manganese nucleus. A significant zero- field splitting, indicating lower-symmetry crystal field components − which should be observable if Mn^{2+} substitutes into the Ca^{2+} position of the apatite lattice[3] − cannot be detected. Apparently, Mn^{2+} is present as an impurity phase (oxidic or hydroxy), sometimes with manganese clustering, which shows up in an only partly resolved hyperfine structure of many samples.

Annealing at 400 °C leads already to distinct changes in the environment of part of the Mn^{2+} ions, obviously induced by the onset of migration of manganese into the apatite lattice. This is deduced from the Q-band spectrum in Figure 2 (top), for example, where new lines beside the original sextet appear, but even more distinctly in the X-band region, where more or less pronounced additional absorptions, in particular at lower magnetic fields, supplement the original broad signal around 3300 G (Figure 2; bottom). However, more precise information is obtained by looking

Table 2. Mn-containing HA samples heated at temperatures above 400 °C; structure stability and colour changes are indicated

Sample	600 °C	800 °C	Mn (%)	CO_3 (%)	600 °C	800 °C
HAMn20		Transf.	0.56	–		white
HAMn28		Transf.	0.52	2.8		white
HAMn56	Minor Transf.	No Transf.	0.33	4.0	light grey	blue grey
HAMn52	Partial Transf.	Partial Transf.	0.33	3.2	white	light grey
HAMn64	Minor Transf.	Partial Transf.	–	1.2	white	white
HAMn54		Partial Transf.	0.66	3.3		light grey
HAMn57	No Transf.	No Transf.	0.15	5.0	light blue	blue grey
HAMn68	Minor Transf.	No Transf.	0.72	4.4	grey	grey
HAMn69	No Transf.	No Transf.	0.19	5.9	blue	blue
HAMn50	Partial Transf.	Transf.	0.68	1.9	white	light grey
HAMn55		Minor Transf.	0.47	3.6		light grey
HAMn61		Minor Transf.	0.41	2.6		light grey
HAMn65		Partial Transf.	0.45	1.1		light grey
HAMn75	Minor Transf.	Minor Transf.	0.70	3.6	blue	blue grey
HAMn73	Minor Transf.	Minor Transf.	0.30	3.6	white	blue
HAMn77	Partial Transf.	Partial Transf.	0.59	2.6	light blue	grey
HAMn83	No Transf.	No Transf.	0.30	4.2	light blue	blue grey
HAMn86	No Transf.	Partial Transf.	0.17	1.0	white	white

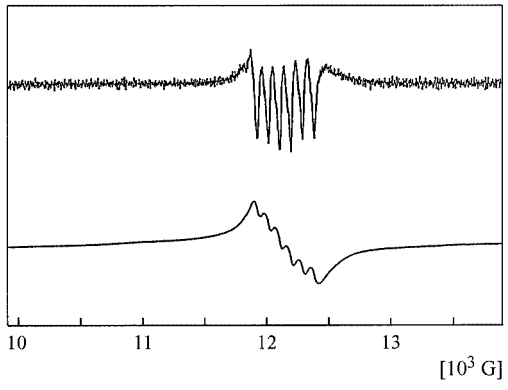

Figure 1. Q-band spectrum of the non heated sample HAMn61 (33.99 GHz, 298 K); the second derivative spectrum is also shown (above)

at the EPR spectra samples after heat treatment at 600 °C and 800 °C. The Q-band spectrum in Figure 3 depicts the typical situation for compounds with vanishingly small or very low CO_3^{2-} contents, which transform to β-TCP when heated to higher temperatures. This spectrum is typical for zero-field effects, displaying a centrosymmetric intensity distribution; the fine structure transitions are broad and not resolved into hyperfine sextets, except in the central part. The optical spectra give no evidence for oxidation states of manganese beyond +II, in agreement with the white colour. A moderate zero-field splitting *D* of about 500 G is estimated, which is near to the value for Mn^{2+} doped into the Cd^{2+} position of the $Cd_5(PO_4)_3Cl$ apatite.[3] One can easily follow this argument by direct comparison. The group of lines five (I–V) due to the zero-field splitting, which is induced by the non-cubic ligand-field component, are each nicely resolved into the six hyperfine components in the case of Mn^{2+}-doped $Cd_5(PO_4)_3Cl$ (powdered single crystals); they are also present in the β-TCP sample, however, as broad absorptions — presumably because of Mn^{2+} clustering in the host. We therefore conclude that Mn^{2+} has partly entered one of the five Ca^{2+} positions in β-TCP – presumably Ca(5) with a pseudo-octahedral coordination.[6]

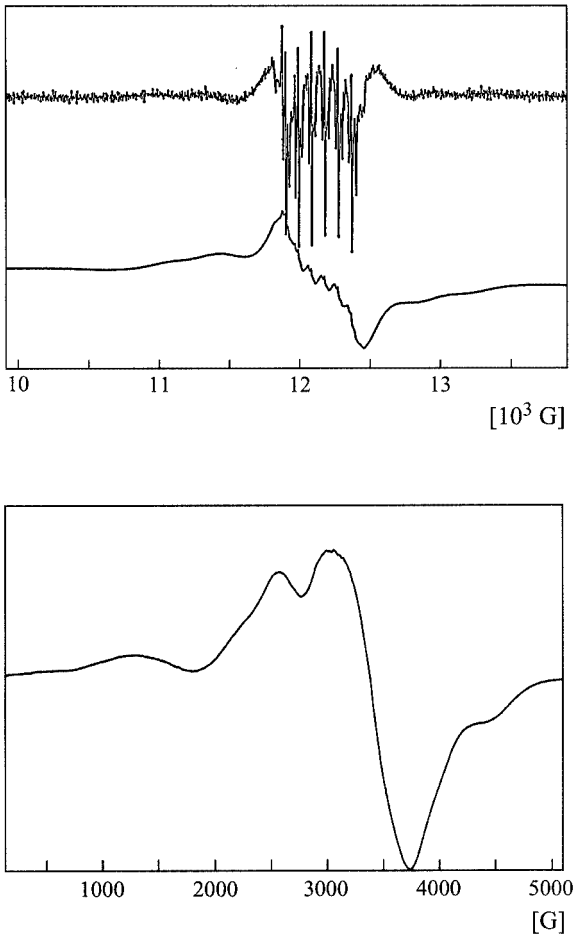

Figure 2. Q-band spectrum and second derivative of sample HAMn21, annealed at 400 °C (33.98 GHz, 298 K; top) and X-band spectrum of the same sample (9.23 GHz, 120 K; bottom)

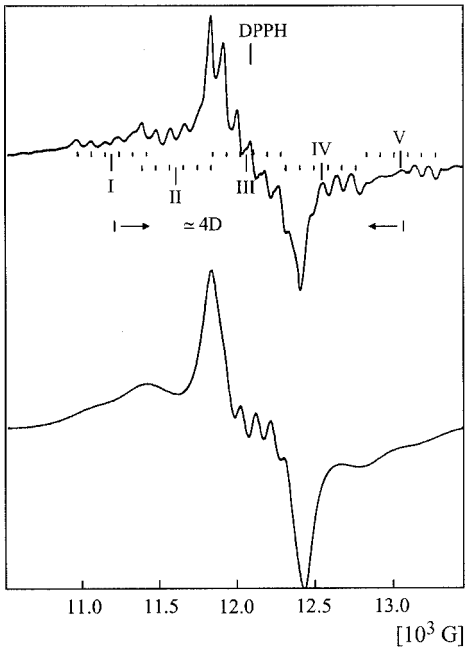

Figure 3. Q-band spectrum of sample HAMn28 with low carbonate content and annealed at 800 °C (33.98 GHz, 298 K; bottom) in comparison with the Q-band spectrum of Mn^{2+}-doped $Cd_5(PO_4)_3Cl$ (adapted from ref.;[3] top)

A different situation arises when looking at the samples with higher carbonate content, heated to temperatures above 400 °C. They turn bluish and the optical spectra indicate $Mn^{V}O_4$ tetrahedra; the split and intensity-dominating $^3A_2(e^2) \rightarrow {}^3T_1(\approx e^1t_2^1)$ transition shows the same structure and appears at the same energy (Figure 4) as the colour-determining band of Mn^{V}-doped apatites synthesised by high-temperature solid-state reactions.[7a,7b] Correspondingly, a diverse spectral intensity distribution becomes apparent in the EPR spectra, with a considerably larger fine

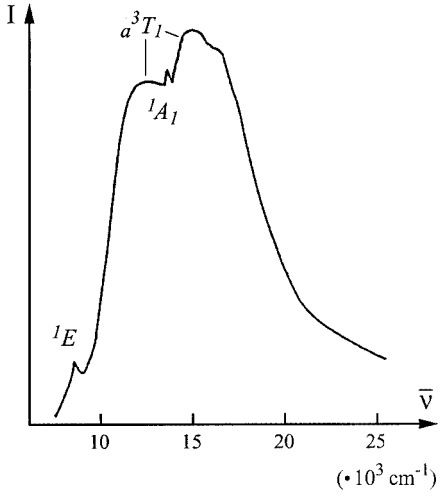

Figure 4. The optical powder reflection spectrum of sample HAMn69, heated at 800 °C, between 8000 and 28000 cm^{-1}; besides the allowed $^3A_2 \rightarrow {}^3_aT_1$ band around 12000 to 15000 cm^{-1} the characteristic narrow spin-forbidden transitions $^3A_2 \rightarrow {}^1E$, $^1A_1$ within the e^2 ground-state configuration are seen at 8700 and 13500 cm^{-1}, respectively

structure splitting. This is particularly observable in the X-band spectra, where signal groups extend down to 700 G, in contrast to the former case with low carbonate content (Figure 5). The described features roughly correspond to those typical for tetrahedral Mn^{V} in apatites.[7a] Apparently part of the manganese present has been oxidized and has entered the apatite lattice. A reaction where CO_3^{2-} is positioned on a PO_4^{3-} lattice position and OH^- is a constituent of the apatite host [depicted in Equation (1)] would offer an explanation for these spectral findings.

$$Mn^{II}(OH)_2 + CO_3^{2-} + OH^- + 3/4O_2 \rightarrow Mn^{V}O_4^{3-} + CO_2 + 3/2H_2O \quad (1)$$

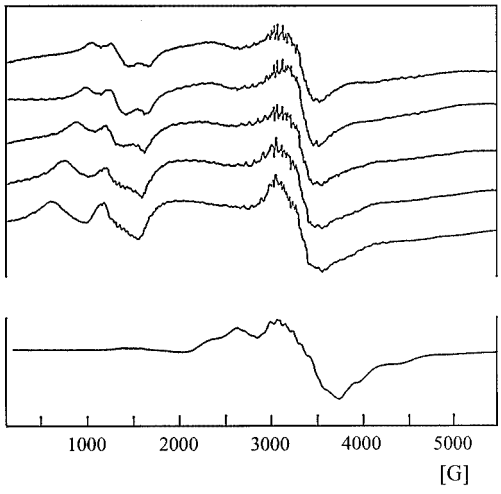

Figure 5. X-band spectra (9.21 GHz) of sample HAMn69, after heating to 800 °C, at temperatures 340, 293, 280, 170 and 117 K (above) and of sample HAMn86 (below), after heating to 800 °C, at 298 K

EDX Analysis and TEM Electron Microscopy

The results of the EDX analysis of two representative samples, HAMn23 and HAMn61, are shown in Figure 6 and 7. The Ca/P ratios and the Mn content obtained at different locations within the samples show that the Ca/P ratio is relatively constant, while Mn is not homogeneously dispersed in the samples.

The results of the TEM analysis of selected samples have shown that in the samples with and without carbonate and with Mn, crystals appear in the form of sticks and platelets. Figure 8 and 9 are TEM pictures of samples HAMn2 (no CO_3, 0.56% Mn) and HAMn61 (2.6% CO_3, 0.44% Mn). Sticks and plates appear in both and in the case of HaMn61 fibres can also be seen. In Figure 9 (sample HAMn59) wider sticks and plates appear, but no fibres are present, which indicates that Mn may play a role in the formation of fibres. The main morphological observations obtained are summarised in Table 3.

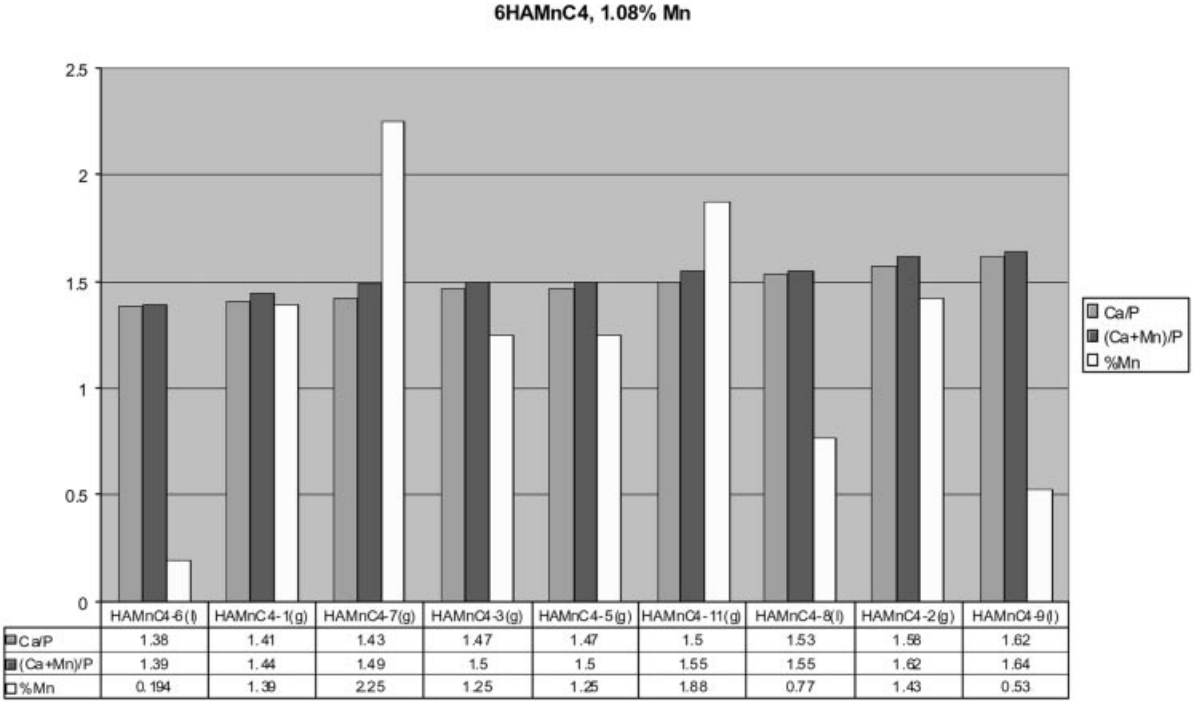

	HAMnC4-6(l)	HAMnC4-1(g)	HAMnC4-7(g)	HAMnC4-3(g)	HAMnC4-5(g)	HAMnC4-11(g)	HAMnC4-8(l)	HAMnC4-2(g)	HAMnC4-9(l)
Ca/P	1.38	1.41	1.43	1.47	1.47	1.5	1.53	1.58	1.62
(Ca+Mn)/P	1.39	1.44	1.49	1.5	1.5	1.55	1.55	1.62	1.64
%Mn	0.194	1.39	2.25	1.25	1.25	1.88	0.77	1.43	0.53

Figure 6. EDX analysis results of sample HAMn23

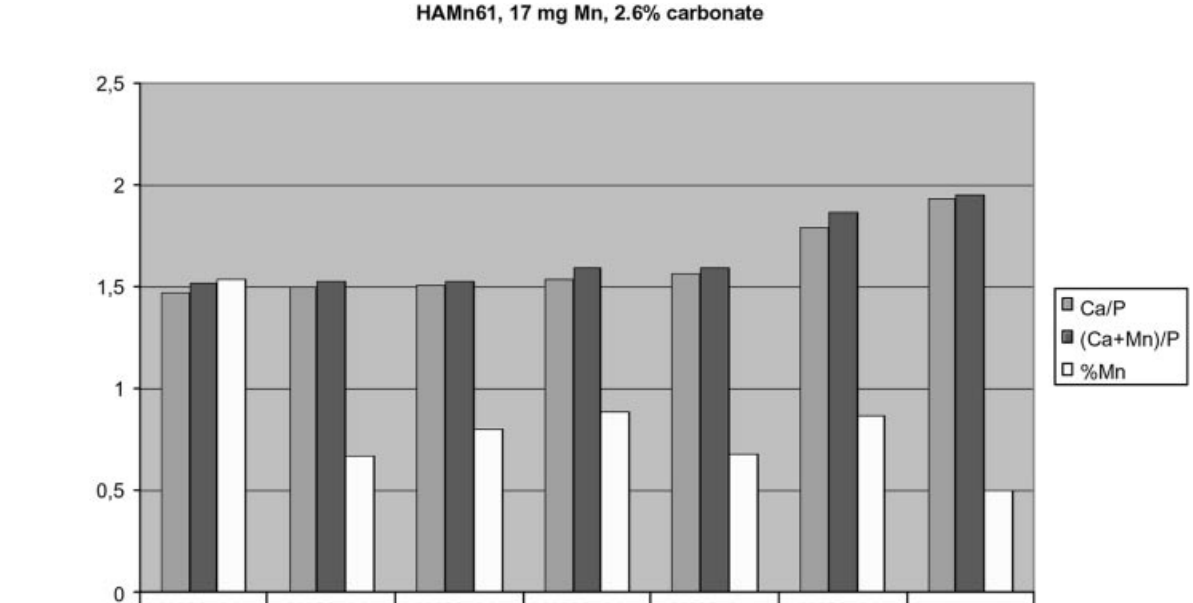

	HAMn61-4(g)	HAMn61-1(g)	HAMn61-5(g)	HAMn61-3(g)	HAMn61-2(g)	HAMn61-6(p)	HAMn61-7(f)
Ca/P	1,47	1,5	1,51	1,54	1,57	1,79	1,93
(Ca+Mn)/P	1,52	1,53	1,53	1,6	1,6	1,87	1,95
%Mn	1,54	0,67	0,8	0,89	0,68	0,87	0,5

Figure 7. EDX analysis results of sample HAMn 61

Discussion

The main aim of this work was to prepare precipitated HA samples in the presence of Mn^{2+} and to investigate their properties. The analytical data concerning the chemical composition of the samples, as well as their XRD and FTIR data, prove that apatite-type HA samples were obtained with their typical structural characteristics. The non-stochiometry of the samples, with molar Ca/P ratios of less than 1.67, is most probably due to the presence of HPO_4^{2-}

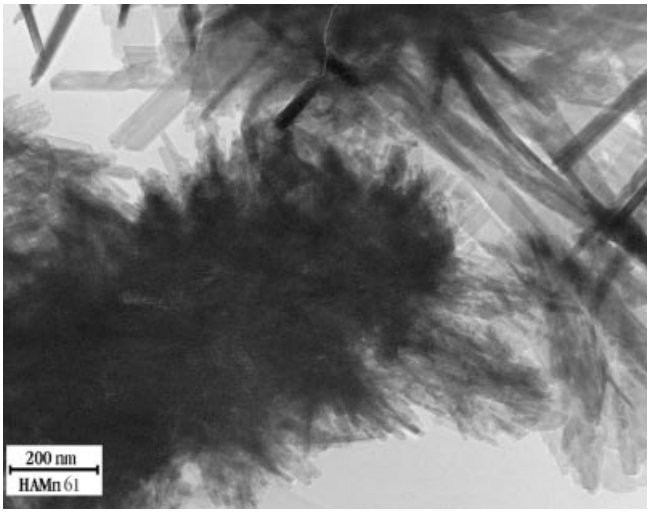

Figure 8. TEM picture of sample HAMn61

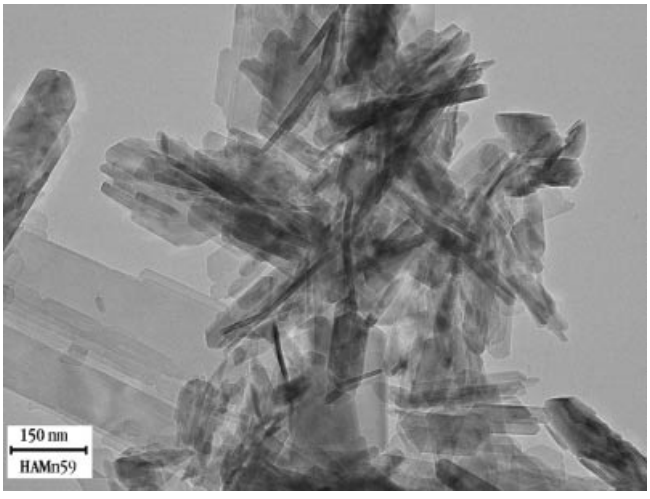

Figure 9. TEM picture of sample HAMn59

Table 3. Morphological data of various Mn-containing HA samples; l: length; w: width; e: thickness

Sample	CO_3 (%)	Mn (%)	Platelets (nm)	Fibers (nm)	Sticks (nm)
HAMn2	–	0.56	$w < 200$	–	$l < 500$; $e < 6$
HAMn4	–	1.08	$w < 200$	–	$l < 500$; $e \approx 10$
HAMnC2	0.9	0.55	$w < 120$	$l > 2\mu$; $e < 10$	
HAMnC4	–	1.08	$w < 150$	$l > 1\mu$; $e < 10$	
HAMnC6	2.6	0.54	$w < 100$	–	$l < 1\mu$; $e < 10$
HAMn65	1.1	0.45	$w < 250$	–	$l < 300$; $e < 10$
HAMn58	1.6	–	$l < 600$	–	
HAMn59	4.6	–	$l < 600$, $w < 150$	–	$l < 500$; $e < 10$

ions which occupy a small part of the anion sites of the compounds together with the PO_4^{3-} ions. Such an assumption is in good agreement with the structural and spectroscopic findings discussed below. The Ca/P ratios found by EDX analysis locally, and by global analyses as well, are close to the chemical analysis results. EPR spectroscopy shows that Mn is in the divalent state in all the samples. Mn^{2+} is present as a cubic (oxidic or hydroxy) impurity phase, which is not homogeneously distributed over the samples, as is clearly indicated by EDX analysis and also suggested by EPR spectroscopy.

TEM observations have shown that the morphology of the crystals is that of platelets, sticks and fibres. Platelets and sticks have also been found in HA samples precipitated in the presence of Zn[8] and Al.[9] In the present work fibre-like crystals were also observed. Apparently, further studies are needed to determine the role of Mn in the formation of fibre-type crystals.

Two types of high temperature behaviour have been observed: HA samples without or with carbonate contents up to about 3.5% transform partially or completely above 600 °C to β-TCP; samples with carbonate contents higher than 4% retain the apatite structure and their colour changes to blue above 600 °C. There is definite spectroscopic evidence that $Mn^{V}O_4^{3-}$ ions – generated by oxidation of Mn^{2+} and presumably substituting CO_3^{2-} ($+OH^-$) [cf. Equation (1)] in the HA structure – are responsible for this colour. In contrast manganese in the samples with low carbonate content remain in the (+II) oxidation state and partly migrate into Ca^{2+} positions of β-TCP and of HA as well, when heated to temperatures from 400 °C to 800 °C.

The simultaneous effect of $HPO_4^{2-}$and CO_3^{2-} ions on the thermal transformation of HA to β-TCP was discussed in a previous work[10] and it was shown that HPO_4^{2-} ions support this transformation; the CO_3^{2-} ions in carbonate-containing apatites prevent the incorporation of HPO_4^{2-} ions. The assumption of HPO_4^{2-} substituting PO_4^{3-} in the apatite lattice as the cause of the lower molar Ca/P ratios is well in agreement with the high temperature properties of precipitated HA samples. As Equation (2) indicates for an extreme case the presence of vacancies in the Ca^{2+} sublattice and the release of water on heating – which leaves the OH^- positions unoccupied – destabilizes the apatite structure and favours the structural transformation to β-TCP. Indeed, such a transformation is often observed for HA samples with small molar Ca/P ratios. On the other hand, the presence of larger amounts of carbonate, which is known to replace phosphate in HA to a certain extent, prevents the formation of β-TCP on annealing,[10] as Equation (3) – again for an extreme case – illustrates nicely.

$$\square_{0.5}Ca_{4.5}(PO_4)_2(HPO_4)OH \rightarrow 1.5\,Ca_3(PO_4)_2 + H_2O \quad (2)$$

$$\square_{0.5}Ca_{4.5}(PO_4)_2(HPO_4)_{0.7}(CO_3)_{0.3}OH \rightarrow 0.9Ca_5(PO_4)_3OH + 0.3CO_2 + 0{\cdot}4H_2O \quad (3)$$

It is clearly the basic character of CO_3^{2-} that stabilizes the apatite lattice, as well as the fact that the substitution of PO_4^{3-} by CO_3^{2-} in the lattice raises the Ca/P ratio towards that characteristic for stoichiometric apatite (Table 1). The basic (O^{2-} donor) properties of CO_3^{2-} are

also needed for the oxidation from Mn^{II} to Mn^{V} [Equation (1)]. If the manganese concentration becomes too high, such an oxidation process is only partly possible; most of the manganese is oxidized to Mn^{IV} in that case − where O^{2-} donors are not needed − as indicated by the brownish colour (MnO_2 impurities).

In a very recent EPR study[11] it was suggested that in precipitated HA (carbonate-free, manganese presence), heated to 400 °C, Mn^{2+} has partly migrated into the Ca^{2+} position − in perfect agreement with the results presented here.

Experimental Section

Sample Preparation and Characterisation

Samples of HA with Mn (0.1−2.0%), and with (1.0−6.0%) and without carbonate, were prepared by a precipitation method described in more detail elsewhere.[12] A phosphate solution [3.7 g of $(NH_4)_2HPO_4$ in 200 mL of triply distilled water (TDW)] was added dropwise to a calcium solution [9.47 g $Ca(NO_3)_2{\cdot}4H_2O$ in 200 mL TDW]. Carbonate was added [5.0, 10.0, 15.0 and 20.0 mL] from a 1 M $NaHCO_3$ stock solution. These additions were designed to give 2.5−3.5 and 3.5−6.0% carbonate in the final sample. The amount of Mn added was 0, 2.5, 5.0, 10, 15.0, 20.0 and 25.0 mL per sample from a 0.025 M $MnCl_2$ solution.

For the preparation of HA samples with Mn^{2+} the pH of 5.8−6.0 was chosen because it was found that at this pH Mn^{2+} is not oxidized to a higher valence state. The pH was maintained constant during precipitation by adding NaOH solution using a Mettler pH-stat automatic titrator. The precipitation was carried out during 2 h, and following this the temperature was raised to boiling point and the system was refluxed for 2 h. The sample was then washed with TDW and dried overnight in air at 120 °C.

The Ca, P and Mn contents of the samples were determined by ICP-atomic emission spectroscopy with a precision of ±0.1, ±0.5, and ±0.3% for Ca, P and Mn respectively.

Powder X-ray Diffraction (XRD) was used for crystal phase and lattice constant determination. The X-ray diffraction analyses were made by a Philips Automatic Diffractometer using Cu-K_α radiation. The samples were scanned in the 2θ range of 20−55°. The lattice parameters were calculated by a least-square computer program. The maximum deviation of the lattice constants was ±0.003 Å.

The characterisation of the samples by infrared spectroscopy (IR) was performed by a Nicolet FTIR spectrometer. Samples of approx. 1 mg were pressed into pellets with approx. 150 mg KBr. The carbonate content of the samples was estimated by IR analysis using the extinction ratio of the carbonate (1420 cm^{-1}) and phosphate (575 cm^{-1}) bands. Carbonate is determined by this method with an accuracy of ±5%.[13]

Thermal analyses of selected samples were carried out by heating in porcelain crucibles up to 800 °C in an electric furnace.

EPR measurements were performed at X- and Q-band frequencies between 300 and 80 K with a Bruker ESP-300 spectrometer. UV/Vis spectra were recorded using the powder diffuse-reflection technique with a Zeiss PMQII spectrometer.

Samples were also examined by EDX analysis and by TEM electron microscopy. For this purpose they were ground and sonicated in ethanol. The thus-obtained suspension was deposited onto a carbon-coated grid. In local analysis of the samples the beam diameter was 18 nm, in global analysis 15 μ and 56 and 700 nm.

Acknowledgments

This work was supported by a grant from the European Union SIMI Contract G5RD-CT.

[1] A. Armulik, G. Svineng, K. Wennerberg, R. Faessler, S. Johansson, *Experimental Cell Res.* **2000**, *254*, 55−63.
[2] P. H. Kasai, *J. Phys. Chem.* **1962**, *66*, 674.
[3] I. Mayer, H. Diab, D. Reinen, Ch. Albrecht, *J. Mater. Sci.* **1993**, *28*, 2428−2432.
[4] D. Reinen, W. Rauw, U. Kesper, M. Atanasov, H. U. Gûdel, M. Hazenkamp, U. Oetliker, *J. Alloys Comp.* **1997**, *246*, 193−208, and references cited therein.
[5] *International Centre for Diffraction Data*. Powder Diffraction File, 09-0169, **2001**.
[6] B. Dickens, L. W. Schroeder, W. E. Brown, *J. Solid State Chem.* **1974**, *10*, 232−248.
[7] [7a] D. Reinen, H. Lachwa, R. Allmann, *Z. Anorg. Allg. Chem.* **1986**, *542*, 71−88. [7b] H. Lachwa, D. Reinen, *Inorg. Chem.* **1989**, *28*, 1044−1053.
[8] F. J. G. Cuisinier, P. Steuer, J. C. Voegel, F. Apfelbaum, I. Mayer, *J. Mater. Sci. Mater. Med.* **1995**, *6*, 85−89.
[9] J. D. Layani, F. J. G. Cuisinier, P. Steuer, H. Cohen, J. C. Voegel, I. Mayer, *J. Biomed. Mater. Res.* **2000**, *50*, 199−207.
[10] F. Apfelbaum, I. Mayer, J. D. B. Featherstone, *J. Inorg. Biochem.* **1990**, *38*, 1−8.
[11] B. Sutter, T. Wasowicz, T. Howard, L. R. Hossner, D. W. Ming, *Soil Science Society of America Journal* **2002**, *66*, 1359−1366.
[12] J. D. B. Featherstone, I. Mayer, F. C. M. Driessens, R. M. H. Verbeeck, M. Heijligers, *Calcif. Tissue Int.* **1983**, *35*, 169−171.
[13] J. D. B. Featherstone, S. Pearson, R. Z. LeGeros, *Caries Res.* **1984**, *18*, 63−66.

Received August 19, 2002
[I02466]

Cyclopropanation of Olefins with Diazoalkanes, Catalyzed by Co^{II}(porphyrin) Complexes − A Synthetic and Mechanistic Investigation and the Molecular Structure of $Co^{III}(TPP)(CH_2CO_2Et)$ (TPP = Dianion of *meso*-Tetraphenylporphyrin)

Andrea Penoni,[a] Riccardo Wanke,[a] Stefano Tollari,[b] Emma Gallo,[a] Danilo Musella,[a] Fabio Ragaini,[a] Francesco Demartin,[c] and Sergio Cenini*[a]

Dedicated to Prof. Mauro Graziani on the occasion of his 65th birthday

Keywords: Cobalt / Cyclopropanation / Olefins / Porphyrinoids

Cobalt(II) porphyrin complexes catalyze reactions between ethyl diazoacetate (EDA) and styrenes to give the corresponding cyclopropanes with *trans* selectivity. The reactions of other diazoalkanes and other olefins have also been carried out, and the mechanism of the reaction has been investigated. Kinetic data and stoichiometric reactions support the formation of a diazoalkane cobalt-porphyrin complex that reacts with the olefins to generate the cyclopropane. Diethyl maleate and fumarate are not formed in the presence of an excess of olefin. On treatment of EDA with Co^{II}(TPP) (TPP = dianion of *meso*-tetraphenylporphyrin) in the absence of the olefin, an alkyl cobalt(III) complex $Co^{III}(TPP)(CH_2CO_2Et)$ was isolated, and its structure has been solved by X-ray diffraction.
(© Wiley-VCH Verlag GmbH & Co. KGaA, 69451 Weinheim, Germany, 2003)

Introduction

A vast number of investigations into metal complex-catalyzed cyclopropanations of alkenes with diazo compounds have recently been reported.[1] A variety of transition metal compounds have been employed as catalysts for diazo decomposition, and the most efficient compounds have been found to be based on copper[2] and rhodium.[3]

In the last few years, transition metal-porphyrin complexes of iron,[4] rhodium,[5] osmium,[6] and ruthenium[7−9] have been extensively employed as catalysts in the cyclopropanation of olefins and, in the case of ruthenium, excellent enantioselectivity was obtained in this reaction.

The mechanism of the metal−porphyrin-catalyzed reactions has also been investigated. Carbene complexes have always been implicated, and the molecular structures of these carbene complexes have in several cases been determined by X-ray diffraction. Carbene complexes of ruthenium-,[7,9b,10] iron-,[4a,11] and osmium-porphyrins[10b,12] are known. In the case of rhodium, while no stable carbene complex has been isolated from reactions involving diazo compounds, one has been spectroscopically characterized and its reactivity investigated.[13] A stable rhodium-porphyrin carbene complex has been obtained by a different route and crystallographically characterized, but its reactivity with olefins was not investigated.[14]

Recently we have reported on the catalytic activity of cobalt(II) porphyrin complexes in the amination reactions of olefins[15] and benzylic C−H bonds,[16] with aromatic azides as aminating agents. Since diazo compounds are isoelectronic with aryl azides, we considered that cobalt(II) porphyrin complexes may also act as catalysts for the cyclopropanation reaction, and the results of our studies are reported here.

To the best of our knowledge, this is the first time that cobalt(II) porphyrin complexes have been used as catalysts for cyclopropanation reactions, though cobalt(II) Schiff bases[17,18] and dioximato complexes[19] are excellent catalysts for the cyclopropanation of olefins. Several reports concerning stoichiometric reactions between cobalt porphyrins and diazo compounds have been published.[20−22] Both cobalt(III) and cobalt(II) porphyrin complexes have been used as substrates, but in the latter case the reactions were always performed in $CHCl_3$ and in air, so chloride-containing cobalt(III) complexes were obtained as products in any case. The chloride anion clearly derives from a radical activation of the solvent, and in the only reaction employing

[a] Dipartimento di Chimica Inorganica Metallorganica e Analitica and ISTM-CNR,
Via Venezian 21, 20133 Milano, Italy
Fax: (internat.) + 39-02/5031-4405
E-mail: sergio.cenini@unimi.it
[b] Dipartimento di Scienze Chimiche, Fisiche e Matematiche,
Via Valleggio 11, 22100, Como, Italy
[c] Dipartimento di Chimica Strutturale e Stereochimica Inorganica,
Via Venezian 21, 20133 Milano, Italy

Co^{II}(OEP) and ethyl diazoacetate with exclusion of air, the same cobalt(III) chloride complex was obtained as in the presence of air, although after a longer time and in a lower yield.[20a] The identity of the major product depends on the amounts of the reagents and the identity of the diazo compound, but with ethyl diazoacetate the primary product from Co(OEP)[20a] or Co(TPP)[20b] was Co^{III}(porphyrin)-(Cl)(CHCOOEt), with a carbene group bridging cobalt and one of the pyrrole nitrogen atoms. Relevantly to this work, all attempts to trap the carbene group by treatment with an olefin failed, indicating that the cobalt(III) carbene complex is not an active species in cyclopropanation reactions. No cyclopropanation activity has been reported even for the other complexes obtained under different experimental conditions or with other diazo compounds or porphyrins.

Results and Discussion

Catalytic Reactions

Ethyl diazoacetate reacts with an excess of olefin, in the presence of catalytic amounts of Co(porphyrin) complexes (1%), to give the corresponding cyclopropanes in good yields [Equation (1)]. The results are listed in Table 1. Fumaric and maleic acid esters were never detected in these reactions, consistently with literature data, which show that these by-products are not generally formed when catalytic systems based on cobalt complexes are employed.[17–19] It is also important to note that no polystyrene was formed either, as evidenced by the lack of any signal in the $-CH_2-$ region in the ^1H NMR spectra of reactions run in deuterated solvents (see also later).

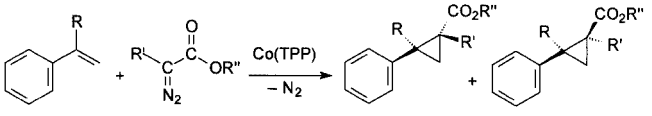

(1)

The reaction between styrene (R = H) and EDA (R′ = H, R′′ = Et) in refluxing CH_2Cl_2, catalyzed by Co(TPP) (TPP = dianion of *meso*-tetraphenylporphyrin), gave a mixture of *trans*- and *cis*-cyclopropanes (**1**) in 85:15 ratio (Table 1, entry 1).

The most active catalyst for the synthesis of cyclopropanes, although slightly less diastereoselective as far as the *trans*/*cis* ratio is concerned, is Co(*p*-ClTPP) (*p*-ClTPP = dianion of *meso*-tetra-*p*-chlorophenylporphyrin) (entry 2). Co(*p*-OMeTPP) (*p*-OMeTPP = dianion of *meso*-tetra-*p*-methoxyphenylporphyrin) and Co(OEP) (OEP = dianion of *beta*-octaethylporphyrin) are also effective catalysts (entries 3 and 4).

With methyl phenyldiazoacetate (MPhDA, R′ = Ph, R′′ = CH_3) as the diazoalkane and again with styrene as the olefin and Co(*p*-ClTPP) as catalyst, a slower reaction was observed, as would be expected in view both of the greater stability of the starting diazo compound and of the steric hindrance of the derived carbene. The cyclopropane (**2**) was obtained in a 40% yield. Surprisingly, the most abundant cyclopropane isomer is the one with two phenyl groups in a *cis* arrangement (39:61 *trans*/*cis* ratio). The use of MPhDA will be investigated further, because many metal catalysts afford excellent *trans* selectivities,[2b,3,23] but only a few examples showing *cis* selectivity have been reported.[24]

With other diazoalkanes such as ethyl diazoacetacetate (EDAA, R′ = $COCH_3$, R′′ = Et) and with the diethyl ester of diazomalonic acid (EDM, R′ = COEt, R′′ = Et) we did not observe any reaction.

Other olefins were also tested. The reaction between 1,1-diphenylethylene (R = Ph) and EDA (R′ = H, R′′ = Et), catalyzed by Co(TPP), was fast and gave high yields of the cyclopropane (**3**, entry 5). With this olefin the most efficient catalyst appears to be Co(TPP), while Co(*p*-XTPP) (X = Cl, OMe) and Co(OEP) were less active and less selective. However the differences are not marked enough to allow any speculation about the electronic effects of the porphyrin ring. Again, with a hindered and more stable diazoalkane such as EDAA, a slower reaction was observed (**4**, 42% yield).

Table 1. Reactions of EDA with olefins catalyzed by Co^{II}(porphyrin)

Entry[a]	Substrate	Catalyst	*t*/h[b]	Cyclopropane yield%[c]	*trans*/*cis* ratio[d]
1	styrene	Co(TPP)	21	62 (**1**)	85:15
2	styrene	Co(*p*-ClTPP)	22	99 (**1**)	75:25
3	styrene	Co(*p*-OMeTPP)	22	80 (**1**)	76:24
4	styrene	Co(OEP)	24	71 (**1**)	83:17
5	1,1-diphenylethylene	Co(TPP)	7	99 (**3**)	–
6	1,1-diphenylethylene	Co(*p*-ClTPP)	10	88 (**3**)	–
7	1,1-diphenylethylene	Co(*p*-OMeTPP)	19	85 (**3**)	–
8	1,1-diphenylethylene	Co(OEP)	20	65 (**3**)	–
9	α-methylstyrene	Co(TPP)	19	95 (**5**)	70:30
10	α-methylstyrene	Co(*p*-ClTPP)	17	91 (**5**)	75:25
11	α-methylstyrene	Co(*p*-OMeTPP)	20	72 (**5**)	77:23
12	α-methylstyrene	Co(OEP)	21	65 (**5**)	85:15

[a] Reaction carried out in refluxing dichloromethane (10 mL), with $1.2 \cdot 10^{-3}$ mmol of catalyst and a catalyst/diazoalkane/styrene ratio of 1:100:500. [b] Time required to reach complete conversion of EDA. [c] Isolated yields, calculated with respect to the initial amount of the diazoalkane. [d] Determined by ^1H NMR spectroscopy.

The reaction between α-methyl styrene (R = CH_3) and EDA, catalyzed by Co(TPP), gave good yields of the cyclopropanes (**5**, entry 9). The dominant isomer is the cyclopropane with the phenyl and the $-CO_2Et$ groups *trans* to each other. Small variations were observed on using the other porphyrin complexes as catalysts, while the use of the more hindered and stable EDAA gave slower reactions both when using Co(TPP) (**6**, 29% yield, 62:38 = *trans*/*cis* ratio) and when using Co(*p*-ClTPP) (**6**, 40% yield, 60:40 = *trans*/*cis* ratio).

The reactions between other olefins, such as norbornene and indene, and EDA with Co(*p*-ClTPP) as catalyst gave the corresponding cyclopropanes in low yields in mixtures with other compounds.

With 1-octene and cyclohexene, Co(*p*-ClTPP) as catalyst and EDA as the diazoalkane, we observed no derivatives originating from the attack of the carbene moiety on the alkene. On the other hand, we observed the products of coupling of two carbene units − that is, diethyl maleate and fumarate − for the first time. The formation of these coupling products when unreactive olefins are employed is in line with the results of the mechanistic study described below.

Preliminary studies were carried out with 2,3-dimethyl-1,3-butadiene as a representative diene. The efficiency of the catalytic system was checked under the same reaction conditions, and we observed the complete consumption of the EDA. Analysis of the ^1H NMR of the crude product verified the formation only of the monocyclopropanation derivative, and no coupling products were detected

Finally, when a 4:1 ratio between EDA and Co(TPP) was used, the products of the attack of the carbene on C−H bonds of the organic compounds used as solvent were observed in low amounts by GC-MS (Scheme 1).

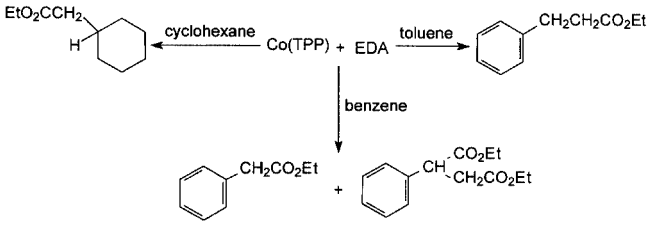

Scheme 1

Intermolecular C−H activation by highly reactive metal carbenoid intermediates formed from diazo compounds has already been reported,[25] but alkylation of a C−H bond as stable as the one in benzene is rare.[26] These reactions will be investigated further.

Mechanistic Studies

The mechanism of the reaction between diazoalkanes and olefins with cobalt-porphyrins as catalysts was investigated by use of styrene as the olefin, EDA as the carbene precursor, and Co(TPP) as the catalyst. We first describe the experimental results and discuss them together in the end.

A series of kinetic measurements was performed; the reactions were followed by IR spectroscopy (disappearance of the absorptions of the diazo group at 2108 cm^{-1}), in benzene as solvent, at 50 °C. Some reactions showed an excellent first order dependence of the rate on the EDA concentration up to its complete consumption, but in several cases deviation from first order was observed after a variable time. We thus decided to calculate the kinetic constants for all reactions by the initial rates method (see also the Exp. Sect.). In all those cases in which first order behavior was observed throughout the reaction, good agreement was observed between the values obtained by the initial rates method and those obtained by fitting log[EDA] versus time for all the data points. The collected data show that the reaction rate is first order in EDA and in the catalyst (Figure 1 and Figure 2, see Exp. Sect.). In the latter case, the straight line in the plot of $k_{obsd.}$ versus the concentration of Co(TPP) showed an intercept on the axis of the concentration. The dependence of the reaction rate on the styrene concentration is more complex and has a bell shape, with styrene concentrations over 0.125 M inhibiting the reaction (Figure 3). Moreover, it has been observed that the diazoalkane is not completely consumed for concentrations of EDA higher than 0.05 mol/L.

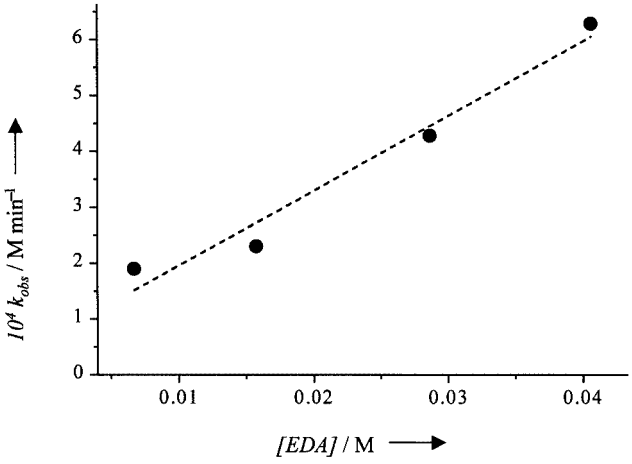

Figure 1. Dependence of the initial reaction rate on the initial EDA concentration; $k_{obsd.} = \{[EDA]_0 - [EDA]_t\}/t$, $R = 0.990$

One of the previously described experiments ($k_{obsd.}$ = 0.0149 min^{-1}) was repeated in the presence of several compounds capable of interfering with the formation of the cyclopropanes. In the presence of diethyl maleate ($k_{obsd.}$ = 0.0139 min^{-1}), diethyl fumarate ($k_{obsd.}$ = 0.0132 min^{-1}), and diethyl succinate ($k_{obsd.}$ = 0.0133 min^{-1}) the reaction rate is about 10% lower, but the reaction is still first order in EDA. This is probably due to the interaction of the metal center with the ester group of the added compound. In the absence of styrene, diethyl maleate reacts with EDA in the presence of Co(TPP) to give the corresponding cyclopropane in low yields. This last reaction is noteworthy, since it has never been reported with other catalytic systems based on metal-porphyrin complexes and it is usually performed with cobalt(0) or nickel(0) complex as catalyst.[27] On the

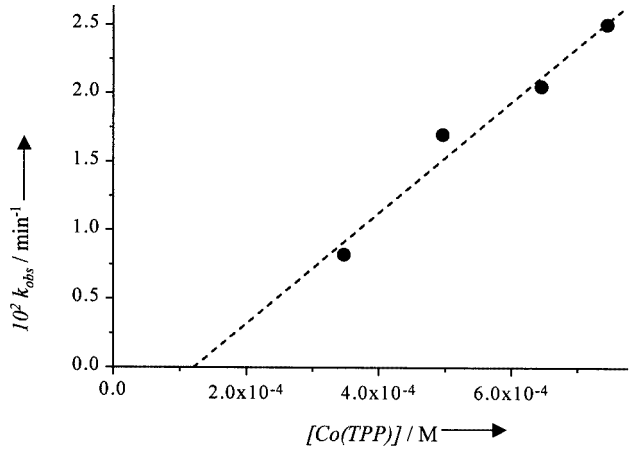

Figure 2. Dependence of the initial reaction rate on the initial Co(TPP) concentration; $k_{obsd.} = \{[EDA]_0 - [EDA]_t\}/[EDA]_0 \cdot t$, $R = 0.982$

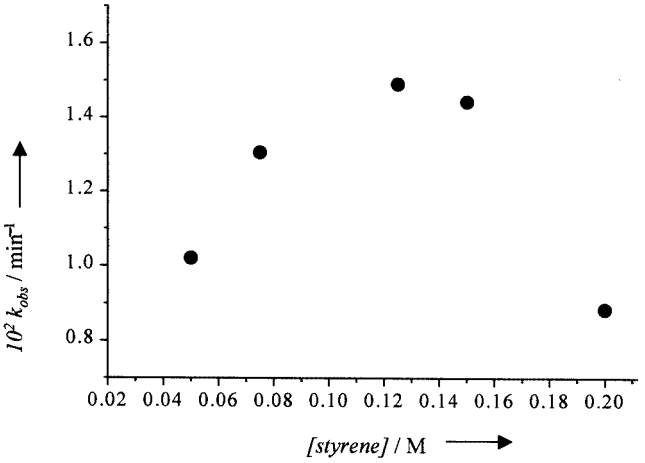

Figure 3. Dependence of the initial reaction rate on the initial styrene concentration; $k_{obsd.} = \{[EDA]_0 - [EDA]_t\}/[EDA]_0 \cdot t$

other hand, when dimethyl fumarate is used as substrate, only the cyclopropane derivative obtained from diethyl maleate (formed by carbene coupling from EDA) is obtained. This result emphasizes the importance of steric effects in this reaction. When we repeated the catalytic cyclopropanation reactions in the presence of the free radical trap TEMPO (2,2,6,6-tetramethylpyperidine-oxyl), we did not observe complete conversion of EDA, and a very slow reaction occurred. Since no irreversible reaction occurs between Co(TPP) and TEMPO alone,[16] this indicates that some intermediates in which unpaired spin density is present on the organic moiety must be formed during the reaction, although this should not be taken as an evidence of the formation of free organic radicals. An analogous outcome was observed for related amination reactions.[15,16]

Several reactions were performed in order to clarify the reaction mechanism. In the absence of the olefin and with use of a Co(TPP)/EDA ratio of 1:100, 35% of the EDA reacts to form diethyl maleate and a complex that has been identified as $Co^{III}(TPP)(CH_2CO_2Et)$ (**7**). A different synthesis of this complex has previously been reported in the literature,[28] but the product was then only characterized spectroscopically. We have now unequivocally characterized complex **7** by X-ray crystallography, and its structure is described in the next section. It is important to note that **7** is inactive as a catalyst. It may be this species that explains why an intercept on the axis of the concentrations is observed on the plot of $k_{obsd.}$ versus the concentration of Co(TPP).

By carrying out the catalytic reaction in a ^1H NMR tube, with a Co(TPP)/EDA/styrene ratio of 1:10:50, we observed that if EDA is added first and then styrene, diethyl maleate is immediately formed, followed by the cyclopropane derivatives. On the other hand, if styrene is added first to the Co(TPP) solution and then EDA, only the cyclopropanes can be detected.

The stoichiometric reaction between Co(TPP) and EDA in the absence of styrene and at 50 °C in benzene was followed by IR spectroscopy, a spectrum being recorded every 10 minutes. It was possible to observe the steady disappearance of EDA ($\nu_{CO} = 1685\ cm^{-1}$) and, after 30 minutes, the formation of an absorption at 1722 cm^{-1}. This new signal is attributable to an unstable intermediate (**8**), since it gradually disappeared and at the end of the reaction only the absorptions due to diethyl maleate ($\nu_{CO} = 1730$, 1750 cm^{-1}) and $Co^{III}(TPP)(CH_2CO_2Et)$ (**7**) ($\nu_{CO} = 1710\ cm^{-1}$) were detected (Figure 4).

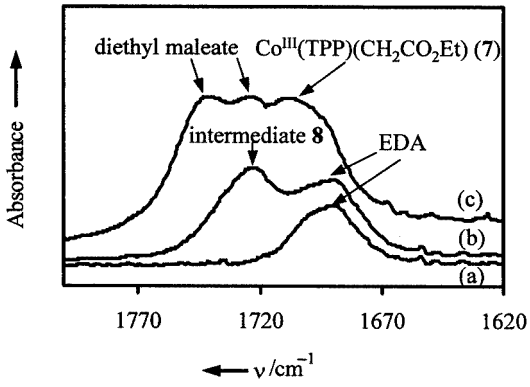

Figure 4. IR spectra of the reaction between Co(TPP) and EDA (stoichiometric ratio = 1:3); a) EDA; b) 30 min after the addition of Co(TPP); c) after 60 min (end of the reaction)

The absorption due to the diazo group at 2108 cm^{-1} gradually disappears, but no shift of this signal was detected. Even spectra subtraction techniques (Figure 5) failed to find any absorption attributable to a diazo group associated with the intermediate absorbing at 1722 cm^{-1}.

When the same reaction was run in C_6D_6 and followed by ^1H NMR spectroscopy, it was possible to observe the formation of a new paramagnetic species of cobalt(II) (δ = 22.2 ppm) in the range from δ = 25 to 10 ppm while the signals of Co(TPP) (13.2, 16.3 ppm) gradually disappeared (Figure 6).

As with the experiment followed by IR spectroscopy, only the signals of $Co^{III}(TPP)(CH_2CO_2Et)$ (**7**) and diethyl maleate were observed at the end of the reaction. From these

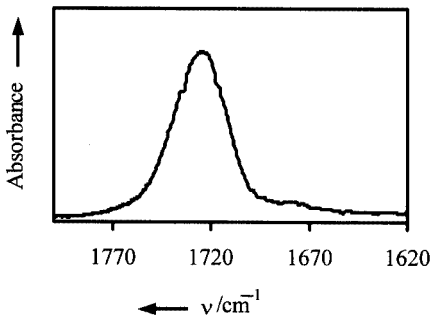

Figure 5. IR spectrum of the intermediate **8** obtained by subtracting spectrum (a) in Figure 4 from spectrum (b)

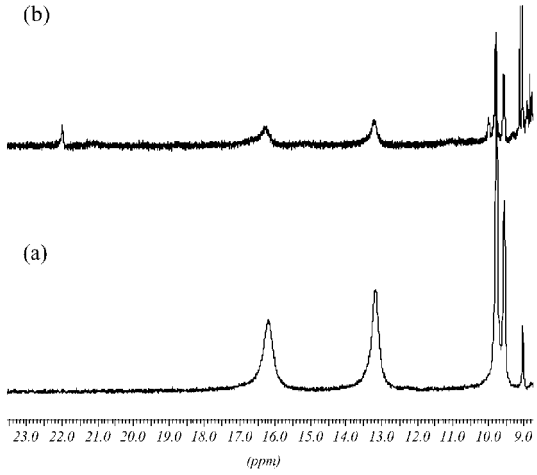

Figure 6. ^{1}H NMR spectrum of the reaction of Co(TPP) with EDA (stoichiometric ratio = 1:5). a) Co(TPP); b) 30 min after the addition of EDA

observations, we suggest that an intermediate carbene complex, $Co^{II}(TPP)(CHCO_2Et)$ (**8**), is formed. However, it was not possible to isolate it, since a fast reaction with EDA (to give diethyl maleate) occurs. We propose that the carbene group should be bridging between the cobalt and a pyrrole nitrogen atom, rather than being terminally bound only to cobalt, because related cobalt(III) complexes display this bonding mode,[20−22] and Tatsumi and Hoffmann's theoretical treatment of metalloporphyrin-carbene complexes[29] shows that an increase in the electron count on the metal stabilizes the bridging mode with respect to the terminal one. The bridging mode should thus be even more favorable for a cobalt(II) complex than for the cobalt(III) analogues. It should be noted that terminal cobalt(II) carbene complexes have been proposed as intermediates in cyclopropanation reactions catalyzed by cobalt Schiff base and dioximato ligands,[17−19] but these are different ligands and the formation of bridged complexes was apparently not taken into consideration.

The kinetic and reactivity data collected is not unequivocal in indicating the correct reaction mechanism. Given the observation of a transient carbene complex **8,** it is very tempting to point to this as the intermediate responsible for the production of both cyclopropane (by reaction with an olefin molecule) and diethyl maleate (by reaction with another EDA molecule). If this is the case, however, it is difficult to explain the bell-shaped dependence of the rate of cyclopropanation with the styrene concentration. The descending part of the curve may be due to competitive formation of a $Co^{II}(TPP)$(styrene) complex (**9**), inactive as catalyst, a mechanism for which there are precedents in related copper chemistry.[2a,30,31] In this case, however, explanation of the ascending part of the curve would require that the reaction between **8** and styrene proceed at a rate slower than, or at least comparable with, that of the formation of **8** itself. If this did not occur and the reaction between **8** and styrene were much faster than the formation of **8** from Co(TPP) and EDA, then the reaction rate should not depend on the styrene concentration and only the previously mentioned inhibiting effect should be observed. However, the assumption of a slow reaction between **8** and styrene contrasts with the failure to observe **8** in the presence of that olefin. We also tried to fit the kinetic data quantitatively to a model of this kind by a multivariate regression, but the results were inconsistent. In recent work in our laboratories[16] we have investigated the mechanism of the amination reaction of benzylic hydrocarbons by aryl azides. It turned out that the species responsible for the activation of the hydrocarbon is a reversibly formed complex in which the aryl azide is still coordinated as such, rather than a nitrene complex. By analogy, we can propose the mechanism shown in Scheme 2 for the cyclopropanation reaction.

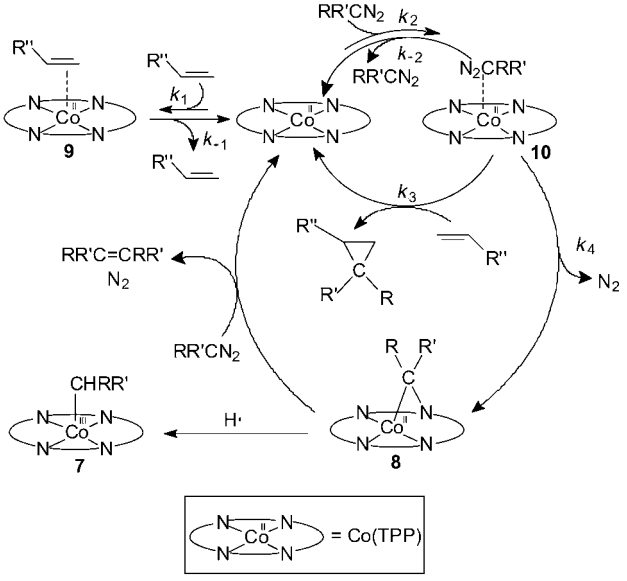

Scheme 2

As shown in Scheme 2, the starting Co(TPP), which is in equilibrium with the catalytically inactive complex **9**, reacts with EDA to form the unstable intermediate **10**. This last complex can either react with the olefin to afford the cyclopropane derivative or lose dinitrogen to give the observed intermediate **8**. This is then responsible for the formation of diethyl maleate by reaction with an additional EDA molecule. The reaction with the olefin is much faster than the

loss of dinitrogen, and the formation of the maleate is unobservable in the presence of an excess of olefin. Both of these reactions regenerate the active Co(TPP). Alternatively, complex **8** can be oxidized to the catalytically inactive Co^{III}(TPP)(CHRR′) (**7**). The source of the "hydrogen radical" necessary to transform **8** into **7** is uncertain, but it may be connected with a decomposition reaction of EDA. Indeed, **7** is formed more easily when a larger amount of EDA is present. We recall that incomplete consumption of the diazoacetate is observed at EDA concentrations higher than 0.05 M. This appears to be related to the formation of the catalytically inactive **7**. In this scenario styrene can either promote the reaction, by trapping the reversibly formed **10**, or inhibit it, by coordinating to Co(TPP) to form **9**. Formation of the cyclopropane even by reaction between the carbene complex **8** and styrene cannot be excluded, but it should not be the only route for its production.

To derive a kinetic equation for the process in Scheme 2 we can make the following assumptions:

a) The steady state approximation can be applied to intermediate **10**.

b) Coordination and de-coordination of the olefin are fast in comparison with the overall reaction. We call $K_{eq} = k_1/k_{-1}$.

c) The total concentration of cobalt at the beginning of the reaction (where data have been determined) is essentially the sum of the concentrations of Co(TPP) and **9**: $[Co]_{tot} = [Co(TPP)] + [\mathbf{9}]$.

d) The process associated with k_4 is slow with respect to that associated with k_3, in agreement with the selectivity data, and so can be neglected.

Under these assumptions the following kinetic equation is derived:

$$-d[EDA]/dt = k_2k_3[Co]_{tot}[EDA][styrene]/(k_{-2} + k_3[styrene])(K_{eq}[styrene] + 1)$$

which is in qualitative agreement with the observed trends, although the number of parameters and the limited number of data points available did not allow a more quantitative fitting.

Although Scheme 2 justifies all of the observed data, we must admit that a quite different mechanism is also consistent with the kinetic data. In this new scenario the intermediate reacting with ethyl diazoacetate would be Co(TPP)(styrene), presumably in equilibrium with both Co(TPP) and an inactive diolefin complex Co(TPP)$(styrene)_2$. A similar mechanism has been shown to operate in the case of a rhodium(III) porphyrin catalyst.[13c,13d] In the case of our system, we view the alternative mechanism as less likely, since no data, either collected by us or reported in the literature, supports the formation of a Co^{II}(porphyrin) complex with two olefins.

X-ray Structure of Co^{III}(TPP)(CH_2CO_2Et) (7)

An ORTEP view of the Co^{III}(TPP)(CH_2CO_2Et) (**7**) molecule with the atom numbering used is shown in Figure 7. Selected interatomic distances and angles are reported in Table 2.

The complex consists of neutral molecules in which the trivalent cobalt atom is pentacoordinate through the four nitrogen atoms of the divalent TPP anion and one carbon atom of the -CH_2CO_2Et moiety, and displays a distorted square-pyramidal coordination geometry. The four nitrogen atoms are coplanar within ± 0.08 Å, and the cobalt atom is displaced from this plane 0.108(1) Å towards the axial −CH_2CO_2Et ligand. The average Co−N bond length is 1.957 Å, and is consistent with the range of nitrogen-cobalt bond lengths observed in five-coordinate organocobalt(III) com-

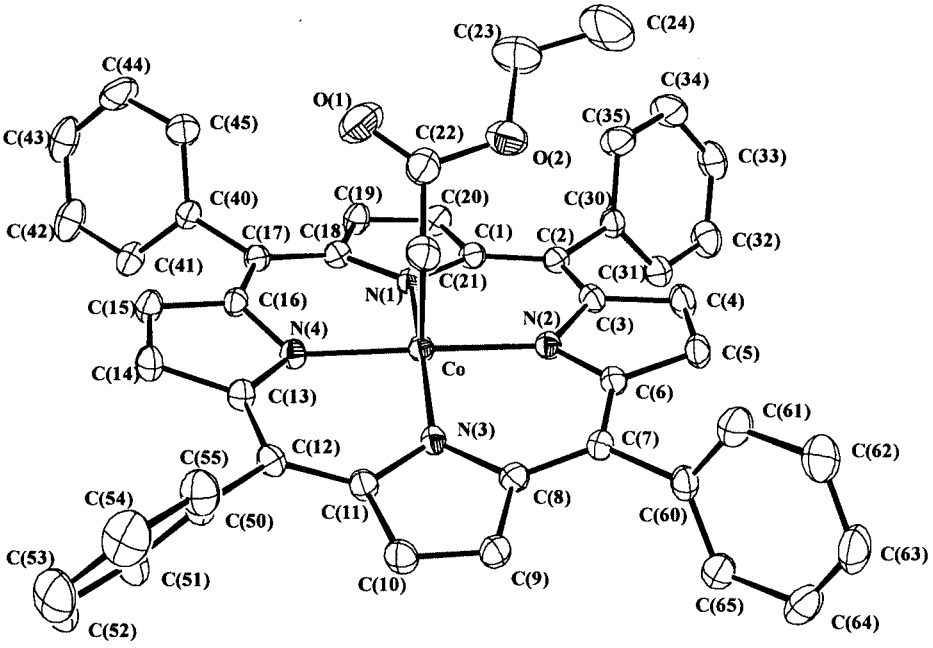

Figure 7. ORTEP drawing of the Co^{III}(TPP)(CH_2CO_2Et) (**7**) molecule; thermal ellipsoids are drawn at 30% probability

Table 2. Selected interatomic distances (Å) and angles (°) for $Co^{III}(TPP)(CH_2CO_2Et)$ (**7**)

Co−N(1)	1.962(2)	Co−N(2)	1.957(2)
Co−N(3)	1.952(2)	Co−N(4)	1.957(2)
Co−C(21)	2.013(3)	O(1)−C(22)	1.201(4)
O(2)−C(22)	1.364(4)	O(2)−C(23)	1.463(4)
N(1)−C(1)	1.389(3)	N(1)−C(18)	1.381(3)
N(2)−C(3)	1.386(3)	N(2)−C(6)	1.385(3)
N(3)−C(8)	1.389(3)	N(3)−C(11)	1.382(3)
N(4)−C(13)	1.383(3)	N(4)−C(16)	1.383(3)
C(1)−C(2)	1.373(4)	C(2)−C(3)	1.384(4)
C(6)−C(7)	1.382(4)	C(7)−C(8)	1.385(4)
C(11)−C(12)	1.383(4)	C(12)−C(13)	1.391(4)
C(16)−C(17)	1.378(4)	C(17)−C(18)	1.387(3)
C(21)−C(22)	1.438(5)	C(23)−C(24)	1.423(6)
N(1)−Co−N(2)	89.6(1)	N(1)−Co−N(3)	168.8(1)
N(1)−Co−N(4)	89.9(1)	N(1)−Co−C(21)	103.6(1)
N(2)−Co−N(3)	90.0(1)	N(2)−Co−N(4)	178.4(1)
N(2)−Co−C(21)	92.1(1)	N(3)−Co−N(4)	90.3(1)
N(3)−Co−C(21)	87.6(1)	N(4)−Co−C(21)	89.5(1)
C(22)−O(2)−C(23)	117.2(3)	Co−N(1)−C(1)	128.1(2)
Co−N(1)−C(18)	127.5(2)	C(1)−N(1)−C(18)	104.4(2)
Co−N(2)−C(3)	127.4(2)	Co−N(2)−C(6)	127.1(2)
C(3)−N(2)−C(6)	104.9(2)	Co−N(3)−C(8)	127.7(2)
Co−N(3)−C(11)	127.6(2)	C(8)−N(3)−C(11)	104.5(2)
Co−N(4)−C(13)	126.6(2)	Co−N(4)−C(16)	126.4(2)
C(13)−N(4)−C(16)	105.1(2)	N(1)−C(1)−C(2)	125.3(3)
N(1)−C(1)−C(20)	109.7(3)	C(2)−C(1)−C(20)	124.9(3)
C(1)−C(2)−C(3)	122.4(3)	C(1)−C(2)−C(30)	119.8(3)
C(3)−C(2)−C(30)	117.7(3)	N(2)−C(3)−C(2)	125.9(3)
N(2)−C(3)−C(4)	109.7(3)	C(2)−C(3)−C(4)	124.3(3)
N(2)−C(6)−C(5)	110.1(3)	N(2)−C(6)−C(7)	125.0(3)
C(5)−C(6)−C(7)	124.5(3)	C(6)−C(7)−C(8)	122.9(3)
C(6)−C(7)−C(60)	118.2(3)	C(8)−C(7)−C(60)	119.0(3)
N(3)−C(8)−C(7)	125.2(3)	N(3)−C(8)−C(9)	110.2(3)
C(7)−C(8)−C(9)	124.4(3)	N(3)−C(11)−C(10)	110.1(3)
N(3)−C(11)−C(12)	125.4(3)	C(10)−C(11)−C(12)	124.2(3)
C(11)−C(12)−C(13)	122.6(3)	C(11)−C(12)−C(50)	119.4(3)
C(13)−C(12)−C(50)	117.9(3)	N(4)−C(13)−C(12)	125.2(3)
N(4)−C(13)−C(14)	109.9(3)	C(12)−C(13)−C(14)	124.9(3)
N(4)−C(16)−C(15)	109.8(3)	N(4)−C(16)−C(17)	125.7(3)
C(15)−C(16)−C(17)	124.4(3)	C(16)−C(17)−C(18)	122.3(3)
C(16)−C(17)−C(40)	118.4(3)	C(18)−C(17)−C(40)	119.3(3)
N(1)−C(18)−C(17)	125.3(3)	N(1)−C(18)−C(19)	110.8(2)
C(17)−C(18)−C(19)	123.8(3)	Co−C(21)−C(22)	110.0(2)
O(1)−C(22)−O(2)	118.6(4)	O(1)−C(22)−C(21)	128.8(4)
O(2)−C(22)−C(21)	112.6(3)	O(2)−C(23)−C(24)	105.0(4)

plexes (1.948−1.969 Å).[32] The porphyrin core shows significant displacements of the atoms from the mean plane of the 24-atom core. The pattern of displacements conforms to an idealized D_{2d} symmetry with the pseudo-twofold axes passing through the methine carbon atoms C(2), C(12) or C(7), C(17) and the pseudo-dihedral mirror planes passing through N(1), Co, N(3) and N(2), Co, N(4).

The Co−C bond is 2.013(4) Å. Tetrahedral geometry is maintained at C(21) with a Co−C(21)−C(22) angle of 110.0(3)°; a significant distortion with respect to the ideal trigonal geometry is observed at C(22), the carbonyl carbon atom [C(21)−C(22)−O(2) 112.6(3)°, C(21)−C(22)−O(1) 128.8(4)°, O(1)−C(22)−O(2) 118.6(4)°], but the four-atom moiety is planar and the plane also includes atom C(23). The conformation of the -CH_2CO_2Et axial appendage is such that the C(21)−C(22) bond almost projects onto the Co−N(1) bond. This orientation produces a C(21)−Co−N(1) angle [103.6(1)°] substantially larger than the other three C(21)-Co-N angles (see Table 2). A similar feature has also been observed in, for instance, (acetonyl)-Co(TPP).[33]

Experimental Section

General Procedures: Unless otherwise specified, all reactions and manipulations were performed under a N_2 atmosphere by use of standard Schlenk apparatus and magnetic stirring. Solvents were dried and distilled by standard procedures and stored under dinitrogen. TPP, *p*-ClTPP, *p*-MeOTPP[34] and their cobalt complexes[35] were synthesized by methods reported in the literature. All other starting materials, including Co(OEP), were commercial products and were used as received. Alkenes, EDA, EDAA, and EDM were purchased from Aldrich. MPhDA[36] was prepared as reported in the literature. Products **1**,[37] **2**,[38] **3**,[39] and **5**[40] have previously been reported in the literature and were characterized by comparison of their analytical data with those reported in the literature or obtained from independently synthesized samples. Gas chromatographic analyses were performed on a Dani 8610 capillary gas chromatograph equipped with a PS 255 column. Ri values (Ri = response factor, relative to naphthalene as an internal standard) were determined by the use of solutions of the compounds of known concentrations. GC-MS analyses were performed on a Shimadzu GCMS-5000 instrument. NMR spectra were recorded on a Bruker AC 300 FT machine (300 MHz) at room temp. IR spectra were recorded on a Bio Rad FTS-7 FT-IR spectrophotometer. Elemental analyses and mass spectra were recorded in the analytical laboratories of Milan University.

Catalytic Reactions

The olefin (6.31 mmol) was added under an inert atmosphere to a solution of the diazo compound (1.26 mmol) and cobalt porphyrin catalyst ($1.26 \cdot 10^{-3}$ mmol) in CH_2Cl_2 (10.0 mL). The solution was heated at reflux with magnetic stirring. The reaction was run to complete consumption of the diazo compound (TLC analysis). The solvent was evaporated in vacuo and the products were purified by flash chromatography on silica gel. The determination of the molar ratio of the two diastereoisomers was carried out by ^{1}H NMR spectroscopy.

Compound 4: ^{1}H NMR (300 MHz, $CDCl_3$): δ = 7.45−7.22 (m, 10 H), 4.31 (q, *J* = 7.2 Hz, 2 H), 2.38 (s, 3 H), 2.21 (s, 1 H), 1.65 (s, 1 H), 1.24 (t, *J* = 7.2 Hz, 3 H)

Compound 6 *cis*: ^{1}H NMR (300 MHz, $CDCl_3$): δ = 7.36−7.20 (m, 5 H), 4.19 (q, *J* = 7.2 Hz, 2 H), 2.40 (s, 3 H), 2.25 (s, 1 H), 1.60 (s, 1 H), 1.27 (s, 3 H), 1.24 (t, *J* = 7.2 Hz, 3 H)

Compound 6 *trans*: ^{1}H NMR (300 MHz, $CDCl_3$): δ = 7.38−7.24 (m, 5 H), 4.02 (q, *J* = 7.2 Hz, 2 H), 2.37 (s, 3 H), 2.10 (s, 1 H), 1.81 (s, 1 H), 1.25 (s, 3 H), 1.21 (t, *J* = 7.2 Hz, 3 H)

Kinetic Measurements

Co(TPP), styrene, and EDA were introduced in that order, under N_2, into a Schlenk flask. The flask was capped with a rubber septum and immediately placed in an oil bath, preheated at 50 °C. The solution was stirred for one minute to dissolve all reagents and a 0.20 mL sample of the solution was withdrawn for IR analysis. The consumption of EDA was monitored by IR spectroscopy (ν_{N2} = 2108 cm^{-1}). The apparent kinetic constants were calculated

by use of the initial rate method. The data for different initial EDA concentrations were fitted to the equation $[EDA]_0 - [EDA]_t = k_{obs}\cdot t$, where $[EDA]_0$ and $[EDA]_t$ are the initial molar concentration of EDA and the molar concentration of EDA at the time t. The data for the series at different Co(TPP) or different styrene concentrations were fitted to the equation: $([EDA]_0 - [EDA]_t)/[EDA]_0 = k_{obs}\cdot t$.

i) Determination of the Kinetic Order with Respect to EDA: Co(TPP) (10.0 mg, $1.49\cdot10^{-2}$ mmol) was dissolved in benzene (30.0 mL) together with EDA (21 μL, 0.20 mmol) and styrene (0.430 mL, 3.75 mmol). The resulting red solution was heated at 50 °C. The consumption of EDA was monitored by recording an IR spectrum every 10 min ($k_{obsd.} = 1.90\cdot10^{-4}$ M min^{-1}). The same reaction was repeated three more times with three different amounts of EDA [a) 50 μL, 0.48 mmol, $k_{obsd.} = 2.30\cdot10^{-4}$ M min^{-1}; b) 90 μL, 0.86 mmol, $k_{obsd.} = 4.28\cdot10^{-4}$ M min^{-1}; c) 128 μL, 1.22 mmol, $k_{obsd.} = 6.29\cdot10^{-4}$ M min^{-1}].

ii) Determination of the Kinetic Order with Respect to Co(TPP): Co(TPP) (15.0 mg, $2.23\cdot10^{-2}$ mmol) was dissolved in benzene (30.0 mL) together with EDA (157 μL, 1.49 mmol) and styrene (0.430 mL, 3.75 mmol). The resulting red solution was heated at 50 °C. The consumption of EDA was monitored by recording an IR spectrum every 10 min ($k_{obsd.} = 2.62\cdot10^{-2}$ min^{-1}). The same reaction was repeated three more times with three different amounts of Co(TPP) [a) 13.0 mg, $1.94\cdot10^{-2}$ mmol, $k_{obsd.} = 1.85\cdot10^{-2}$ min^{-1}; b) 10.0 mg, $1.49\cdot10^{-2}$ mmol, $k_{obsd.} = 1.49\cdot10^{-2}$ min^{-1}; c) 7.0 mg, $1.0\cdot10^{-2}$ mmol, $k_{obsd.} = 0.76\cdot10^{-2}$ min^{-1}].

iii) Determination of the Kinetic Order with Respect to Styrene: Co(TPP) (10.0 mg, $1.49\cdot10^{-2}$ mmol) was dissolved in benzene (30.0 mL) together with EDA (157 μL, 1.49 mmol) and styrene (0.172 mL, 1.50 mmol). The resulting red solution was heated to 50 °C. The consumption of EDA was monitored by recording an IR spectrum every 10 min ($k_{obsd.} = 1.02\cdot10^{-2}$ min^{-1}). The same reaction was repeated four more times with four different amounts of styrene [a) 0.260 mL, 2.25 mmol, $k_{obsd.} = 1.31\cdot10^{-2}$ min^{-1}; b) 0.430 mL, 3.75 mmol, $k_{obsd.} = 1.49\cdot10^{-2}$ min^{-1}; c) 0.520 mL, 4.54 mmol, $k_{obsd.} = 1.44\cdot10^{-2}$ min^{-1}; d) 0.680 mL, 5.94 mmol, $k_{obsd.} = 0.88\cdot10^{-2}$ min^{-1}].

Typical Procedure for the ^{1}H NMR Analysis of the Reaction Progress: Co(TPP) (3.1 mg, $4.6\cdot10^{-3}$ mmol) was dissolved in C_6D_6 (0.75 mL) in an NMR tube. The substrates were added and the solution was then heated to 50 °C inside the probe. An NMR spectrum was recorded every five minutes.

i) EDA (4.7 μL, $4.5\cdot10^{-2}$ mmol) was added to a C_6D_6 solution of Co(TPP), and an NMR spectrum was immediately recorded, showing the presence of diethyl maleate (δ = 5.83 ppm, s 2 H, -*CH*=*CH*-). Styrene (26 μL, $2.3\cdot10^{-1}$ mmol) was then added to the mixture and the reaction was run to complete consumption of EDA. The progress of the reaction has already been described in the results and discussion section.

ii) Styrene (26 μL, $2.3\cdot10^{-1}$ mmol) was added to a C_6D_6 solution of Co(TPP), and an NMR spectrum was immediately recorded. No new peaks were detected, nor was any shift of those of Co(TPP) and styrene. EDA (4.70 μL, $4.47\cdot10^{-2}$ mmol) was then added to the mixture and the reaction was run to complete consumption of EDA. The progress of the reaction has already been described in the results and discussion section.

Stoichiometric Reaction between Co(TPP) and EDA

i) IR Analysis: Co(TPP) (10.0 mg, $1.49\ 10^{-2}$ mmol) and EDA (4.7 μL, $4.5\ 10^{-2}$ mmol) were dissolved in benzene (5 mL) at room temperature. The solution was heated at 50 °C and the consumption of EDA was monitored by recording an IR spectrum every 5 min. The progress of the reaction has already been described in the results and discussion section.

ii) ^{1}H NMR Analysis: Co(TPP) (3.2 mg, $4.8\ 10^{-3}$ mmol) was dissolved in C_6D_6 (0.75 mL) with CH_2Cl_2 (6.0 μL) as an internal standard. EDA (2.5 μL, $2.4\ 10^{-2}$ mmol) was then added to the mixture. The solution was heated at 50 °C and an NMR spectrum was recorded every 5 min. The progress of the reaction has already been described in the results and discussion section.

Preparation of Co^{III}(TPP)(CH_2CO_2Et) (7): EDA (15.7 μL, $1.49\cdot10^{-1}$ mmol) was added under an inert atmosphere to a solution of Co(TPP) (100 mg, $1.49\cdot10^{-1}$ mmol) in CH_2Cl_2 (15.0 mL). The resulting red solution was stirred for 12 h at room temperature, by which time EDA had been completely consumed. The solution was evaporated to dryness under vacuum and the crude product was purified by chromatography on silica gel with CH_2Cl_2/*n*-hexane = 4:6 as eluent (68 mg, 60% yield). The analytical data (^{1}H NMR, IR, elemental analysis) are in agreement with the data reported in the literature.[22] Crystals suitable for X-ray analysis were obtained by crystallization from CH_2Cl_2/*n*-hexane.

X-ray Structure Determination of Co^{III}(TPP)(CH_2CO_2Et) (7): Crystal data: $C_{48}H_{35}CoN_4O_2$, f.w. 758.73, monoclinic, space group $P2_1/c$ (no. 14), $a = 13.098(1)$, $b = 24.840(3)$, $c = 12.552(1)$ Å, β = 116.11(1) °, $Z = 4$, $d_{calc} = 1.374$ Mg·m^{-3}, μ = 5.156 cm^{-1}, $F(000)$ 1576. A crystal sample of dimensions 0.14 × 0.15 × 0.25 mm, obtained by diffusion of *n*-hexane into a CH_2Cl_2 solution of the complex, was mounted on a glass fiber in air at room temperature on a Siemens SMART CCD area-detector diffractometer. Graphite monochromatized Mo-K_α radiation (λ = 0.71073 Å) was used, with the generator working at 50 *k*V and 35 mA. 31789 intensity data were measured in the full sphere (ω scan method) with sample-detector fixed at 5 cm, of which 6648 were independent; 2100 frames (20 s per frame, Δω = 0.3°) were collected and the first 100 frames were recollected for monitoring of crystal decay, which was not observed. An absorption correction was applied by use of the SADABS routine.[41] Transmission factors are in the 0.84−1.00 range. The structure was solved by direct methods (SIR, 97)[42] and refined with full-matrix, least- squares (SHELX93)[43] on the basis of 3113 independent reflections with $I > 2\sigma(I)$; $R = 0.036$, $R_{all} = 0.072$. Anisotropic displacement parameters were assigned to all non-hydrogen atoms. Hydrogens were riding on their carbon atoms. CCDC-190083 contains the supplementary crystallographic data for this paper. These data can be obtained free of charge at www.ccdc.cam.ac.uk/conts/retrieving.html [or from the Cambridge Crystallographic Data Centre, 12, Union Road, Cambridge CB2 1EZ, UK; Fax: (internat.) +44−1223/336−033; E-mail: deposit@ccdc.cam.ac.uk].

Acknowledgments

We thank the MIUR (Programmi di Ricerca Scientifica di Rilevante Interesse Nazionale) for financial support. One of us (A. P.) thanks the University of Milan for a fellowship.

[1] M. P. Doyle, C. D. Forbes, *Chem. Rev.* **1998**, *98*, 911.
[2] [2a] M. M. Díaz-Requejo, A. Caballero, T. R. Belderraín, M. C. Nicasio, S. Trofimenko, P. J. Pérez, *J. Am. Chem. Soc.* **2002**, *124*, 978 and reference therein. [2b] A. Pfaltz, K. M. Lydon, M. A. McKervey, A. B. Charette, H. Label, in *Comprehensive*

Catalysis II E. N. Jacobsen, A. Pfaltz, H. Yamamoto (Eds.) **1999**, chapter 16, p. 513.
[3] M. P. Doyle, M. A. McKervey, T. Ye, in *Modern Catalytic Methods for Organic Synthesis with Diazo Compounds*, John Wiley & Sons, New York, **1998.**
[4] [4a] D. Mansuy, J. P. Mahy, in *Metalloporphyrins Catalyzed Oxidations*, F. Montanari, L. Casella (Eds.), Kluwer Academic Publishers, **1994**, 175, and references therein. [4b] C. G. Hamaker, G. A. Mirafzal, L. K. Woo, *Organometallics* **2001**, *20*, 5171.
[5] A. G. M. Barret, D. C. Braddock, I. Lenoir, H. Tone, *J. Org. Chem.* **2001**, *66*, 8260.
[6] [6a] C. G. Hamaker, J.-P. Djukic, D. A. Smith, L. K. Woo, *Organometallics* **2001**, *20*, 5189. [6b] D. A. Smith, D. N. Reynolds, L. K. Woo, *J. Am. Chem. Soc.* **1993**, *115*, 2511. [6c] L. K. Woo, D. A. Smith, *Organometallics* **1992**, *11*, 2344.
[7] [7a] W.-C. Ho, C.-M. Che, K. F. Cheng, T. C. W. Mok, *Chem. Commun.* **1997**, 1205. [7b] C.-M. Che, J.-S. Huang, F.-W. Lee, Y. Lee, T.-S. Lai, H.-L. Kwong, P.-F. Teng, W.-S. Lee, W.-C. Ho, S.-M. Peng, Z.-Y. Zhon, *J. Am. Chem. Soc.* **2001**, *123*, 4119.
[8] M. Frauenkron, A. Berkessel, *Tetrahedron Lett.* **1997**, *38*, 7175.
[9] [9a] E. Galardon, P. Le Maux, G. Simonneaux, *Chem. Commun.* **1997**, 927. [9b] E. Galardon, P. Le Maux, L. Toupch, G. Simonneaux, *Organometallics* **1998**, *17*, 565. [9c] G. Simonneaux, E. Galardon, C. Paul-Roth, M. Gulea, S. Masson, *J. Organomet. Chem.* **2001**, *617*, 360. [9d] E. Galardon, P. Le Maux, G. Simonneaux, *Tetrahedron* **2000**, *56*, 615. [9e] G. Simonneaux, P. Le Maux, *Coord. Chem. Rev.* **2002**, *228*, 43 and references therein.
[10] [10a] J.-P. Djukic, V. G. Young, Jr., L. K. Woo, *Organometallics* **1994**, *13*, 3995. [10b] C.-M. Che, J.-S. Huang, *Coord. Chem. Rev.* **2002**, *231*, 151 and references therein.
[11] C. J. Ziegler, K. S. Suslick, *J. Organomet. Chem.* **1997**, *528*, 83 and references therein.
[12] Y. Li, J.-S. Huang, Z.-Y. Zhou, C.-M. Che, *J. Am. Chem. Soc.* **2001**, *123*, 4843.
[13] [13a] H. J. Callot, E. Schaeffer, *Nouv. J. Chim.* **1980**, *4*, 311. [13b] J. Maxwell, T. Kodadek, *Organometallics* **1991**, *10*, 4. [13c] J. L. Maxwell, K. C. Brown, D. W. Bartley, T. Kodadek, *Science* **1992**, *256*, 1544. [13d] D. W. Bartley, T. Kodadek, *J. Am. Chem. Soc.* **1993**, *115*, 1656. [13e] J. Robbin Wolf, C. G. Hamaker, J.-P. Djukic, T. Kodadek, L. K. Woo, *J. Am. Chem. Soc.* **1995**, *117*, 9194. [13f] K. C. Brown, T. Kodadek, *J. Am. Chem. Soc.* **1992**, *114*, 8336.
[14] T. Boschi, S. Licoccia, R. Paolesse, P. Tagliatesta, G. Pelizzi, F. Vitali, *Organometallics* **1989**, *8*, 330.
[15] S. Cenini, S. Tollari, A. Penoni, C. Cereda, *J. Mol. Catal. A: Chem.* **1999**, *137*, 135.
[16] [16a] S. Cenini, E. Gallo, A. Penoni, F. Ragaini, S. Tollari, *Chem. Commun.* **2000**, 2265. [16b] F. Ragaini, A. Penoni, E. Gallo, S. Tollari, C. Li Gotti, M. Lapadula, E. Mangioni, S. Cenini, *Chem. Eur. J.,* **2003**, *9*, 249.
[17] [17a] T. Uchida, B. Saha, T. Katsuki, *Tetrahedron Lett.* **2001**, *42*, 2521. [17b] T. Niimi, T. Uchida, R. Irie, T. Katsuki, *Adv. Synth. Catal.* **2001**, *343*, 79. [17c] T. Niimi, T. Uchida, R. Irie, T. Katsuki, *Tetrahedron Lett.* **2000**, *41*, 3647.
[18] [18a] T. Ikeno, M. Sato, H. Sekino, A. Nishizuka, T. Yamada, *Bull. Chem. Soc. Jpn.* **2001**, *74*, 2139. [18b] T. Ikeno, I. Iwakura, T. Yamada, *Bull. Chem. Soc. Jpn.* **2001**, *74*, 2151. [18c] T. Ikeno, I. Iwakura, S. Yabushita, T. Yamada, *Org. Lett.* **2002**, *4*, 517.
[19] [19a] A. Nakamura, A. Konishi, Y. Tatsuno, S. Otsuka, *J. Am. Chem. Soc.* **1978**, *100*, 3443. [19b] A. Nakamura, A. Konishi, R. Tsujitami, M. Kudo, S. Otsuka, *J. Am. Chem. Soc.* **1978**, *100*, 3449.
[20] [20a] A. W. Johnson, D. Ward, P. Batten, A. L. Hamilton, G. Shelton, C. M. Elson, *J. Chem. Soc., Perkin Trans. 1* **1975**, 2076. [20b] A. W. Johnson, D. Ward, *J. Chem. Soc., Perkin Trans. 1* **1977**, 720. [20c] P. Batten, A. L. Hamilton, A. W. Johnson, M. Mahendran, D. Ward, T. King, *J. Chem. Soc., Perkin Trans. 1* **1977**, 1623.
[21] [21a] H. J. Callot, E. Schaeffer, *Tetrahedron Lett.* **1977**, 239. [21b] H. J. Callot, E. Schaeffer, *J. Organomet. Chem.* **1978**, *145*, 91. [21c] H. J. Callot, E. Schaeffer, *Nouv. J. Chem.* **1980**, *4*, 307. [21d] H. J. Callot, E. Schaeffer, *J. Organomet. Chem.* **1980**, *193*, 111. [21e] H. J. Callot, R. Cromer, A. Louati, B. Metz, B. Chevrier, *J. Am. Chem. Soc.* **1987**, *109*, 2946.
[22] [22a] J.-I. Setsune, D. Dolphin, *Organometallics* **1984**, *3*, 440. [22b] J.-I. Setsune, D. Dolphin, *J. Org. Chem.* **1985**, *50*, 2958.
[23] A. Padwa, S. F. Hornbuckle, *Chem. Rev.* **1991**, *91*, 263.
[24] [24a] J. L. Maxwell, S. O'Malley, K. C. Brown, T. Kodadek, *Organometallics* **1992**, *11*, 645. [24b] M. P. Doyle, Q.-L. Zhou, S. H. Simonsen, V. Lynch, *Synlett* **1996**, 697. [24c] H. Ishitani, K. Achiwa, *Synlett* **1997**, 781. [24d] W. J. Seitz, A. K. Saha, M. M. Hossain, *Organometallics* **1993**, *12*, 2604.
[25] H. M. L. Davies, T. Hansen, M. R. Churchill, *J. Am. Chem. Soc.* **2000**, *122*, 3063 and references therein.
[26] [26a] M. A. McKervey, D. N. Russel, M. F. Twohig, *J. Chem. Soc., Chem. Commun.* **1985**, 491. [26b] N. Watanabe, Y. Ohtake, S. Hashimoto, M. Shiro, S. Ikegami, *Tetrahedron Lett.* **1995**, *36*, 1491.
[27] [27a] K. Hiroyoshi, M. Hideki, *J. Mol. Catal.* **1985**, *29*, 157. [27b] K. Hiroyoshi, N. Yoshimasa, M. Hideki, *Bull. Chem. Soc. Jpn.* **1983**, *56*, 1592.
[28] J. Y. Watanabe, J. I. Setsune, *Organometallics* **1997**, *16*, 3679.
[29] K. Tatsumi, R. Hoffmann, *Inorg. Chem.* **1981**, *20*, 3771.
[30] M. Mar Diaz-Requejo, T. R. Belderrain, M. C. Nicasio, F. Prieto, P. Perez, *Organometallics* **1999**, *18*, 2601.
[31] [31a] No stable Co^{II}(porphyrin)(olefin) complex has ever been observed, but some data indicate that interaction between Co^{II}-(porphyrin) complexes and olefins can occur.[31b] Evidence for the formation of cobalt(III) porphyrin complexes with olefins and acetylenes has been provided, although again no stable complex has been isolated.[31c−31g] [31b] M. Tsutsui, R. A. Velapoldi, L. Hoffman, K. Suzuki, A. Ferrari, *J. Am. Chem. Soc.* **1969**, *91*, 3337. [31c] H. Sugimoto, N. Ueda, M. Mori, *Bull. Chem. Soc. Jpn.* **1981**, *54*, 3425. [31d] J.-I. Setsune, Y. Saito, Y. Ishimaru, M. Ikeda, T. Kitao, *Bull. Chem. Soc. Jpn.* **1992**, *65*, 639. [31e] J.-I. Setsune, S. Ito, H. Takeda, Y. Ishimaru, T. Kitao, Y. Saito, M. Sato, H. Ohya-Nishiguchi, *Organometallics* **1997**, *16*, 597. [31f] J.-I. Setsune, H. Takeda, S. Ito, Y. Saito, Y. Ishimaru, K. Fukuhara, Y. Saito, T. Kitao, T. Adachi, *Inorg. Chem.* **1998**, *37*, 2235. [31g] M. Uyemura, T. Aida, *J. Am. Chem. Soc.* **2002**, *124*, 11392.
[32] J. S. Summers, J. L. Petersen, A. M. Stolzenberg, *J. Am. Chem. Soc.* **1994**, *116*, 7189.
[33] M. E. Kastner, W. R. Scheidt, *J. Organomet. Chem.* **1978**, *157*, 109.
[34] R. A. W. Johnstone, M. L. P. G. Nunes, M. M. Pereira, A. M. d'A. Rocha Gonsalves, A. Serra, *Heterocycles* **1996**, *43*, 1423.
[35] [35a] A. Shirazi, H. M. Goff, *Inorg. Chem.* **1982**, *21*, 3420. [35b] A. D. Adler, F. R. Longo, V. Varadi, *Inorg. Synth.* **1976**, *16*, 213.
[36] E. Ciganek, *J. Org. Chem.* **1970**, *35*, 862.
[37] H. Fritschi, U. Leutenegger, A. Pfaltz, *Helv. Chim. Acta* **1988**, *71*, 1553.
[38] W. von E. Doering, L. R. Robertson, E. E. Ewing, *J. Org. Chem.* **1983**, *48*, 4280.
[39] C. J. Sanders, K. M. Gillespie, P. Scott, *Tetrahedron: Asymmetry* **2001**, *12*, 1055.
[40] A. Nakamura, A. Konishi, Y. Tatsuno, S. Otsuka, *J. Am. Chem. Soc.* **1978**, *100*, 3443.
[41] G. M. Sheldrick, *SADABS*, University of Göttingen, Germany, **1996**.
[42] A. Altomare, G. Cascarano, C. Giacovazzo, A. Guagliardi, M. C. Burla, G. Polidori, M. Cavalli, *J. Appl. Crystallogr.* **1994**, *24*, 435.
[43] G. M. Sheldrick, *SHELX93-Program for the refinement of Crystal Structure*, University of Göttingen, **1993**.

Received July 19, 2002
[I02404]

Phosphorus-Selenium Heterocycles from the Tetraphospholane $(PhP)_4CH_2$

Petr Kilian,[a] Pravat Bhattacharyya,[a] Alexandra M. Z. Slawin,[a] and J. Derek Woollins*[a]

Keywords: Phosphanes / Heterocycles / Isomers / Phosphorus / Selenium

Two new heterocyclic and one acyclic species were prepared by reduction/deselenation of the five-membered heterocycle $PhP(Se)CH_2PhP(Se)Se_2$ (containing a $PCPSe_2$ ring sequence). Deselenation with Me_3SiCN led to the four-membered heterocycle $PhP(Se)CH_2PPh(Se)Se$ (containing a PCPSe ring sequence), whereas reaction with Bu_3P afforded the five-membered heterocycle $PhP(Se)CH_2PhP(Se)SePPh$ (ring sequence PCPSeP) and reduction with K metal afforded the dipotassium salt of methylene-bis(diselenophenylphosphinic) acid $[K_2(PhPSe_2)_2CH_2]$. The new compounds were characterised by a combination of NMR, MS and FT IR spectroscopic techniques; their structures were confirmed by single crystal X-ray analyses.

(© Wiley-VCH Verlag GmbH & Co. KGaA, 69451 Weinheim, Germany, 2003)

Introduction

The chemistry of organophosphorus-sulfur and -selenium heterocycles is rich and varied.[1] The common ring sizes are four and five, although larger or smaller rings are not unusual.[2,3] The constitutional variability found in pseudo-binary heterocycles $(RP)_xE_y$ (R = organics, E = S, Se) can be explained by two factors: i) the ease with which their divalent building blocks can rearrange [illustrated, for example, by self-rearrangements of oligomeric $(RP)_5$, $(RP)_4$ and $(RP)_6$], and ii) an ability to form kinetically stable short "homoatomic" chains such as -S-S-, -Se-Se-Se- or, as mentioned above, $(RP)_n$. Cyclophosphanes $(RP)_n$ together with diphosphenes R-P=P-R are important precursors here. In particular, cyclophosphanes with aromatic substituents are frequently studied, due to their stabilizing (kinetic) effect against undesired oxidation or hydrolysis, and, in the case of very bulky organyl groups such as supermesityl, because of their ability to stabilize unusually low phosphorus coordination states.

The chemistry of cyclocarbaphosphanes $[(PR)_x(CR'_2)_y]$ with one or more RP units substituted by carbon functionalities seems to be much less developed than that of the parent cyclophosphanes. Cyclocarbaphosphanes are generally prepared from metallated oligophosphanes and geminal dichloro compounds[4] (Scheme 1); in a similar manner they are also obtained as relatively stable by-products during the synthesis of bifunctional phosphane ligands.[5,6]

Other methods employing Me_3Si-(tBuP)$_4$-$SiMe_3$ [7] or $(i\text{PrPCl})_2CH_2$ [8] have also been reported. Reports on reactions of cyclocarbaphosphanes and related systems with sulfur are scarce (Scheme 2); no report on reactions with selenium was found in the literature.

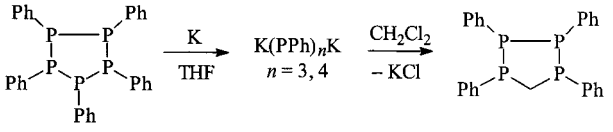

Scheme 1. Synthetically useful route to cyclocarbaphosphanes

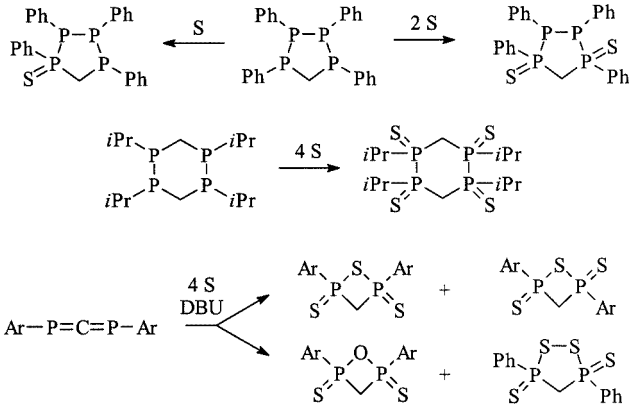

Scheme 2. Reported reactions of carbacyclophosphanes and related systems with sulfur;[9–11] DBU is 1,8-diazabicyclo[5,4,0]undec-7-ene

The results summarised in Scheme 2 show that, unlike the homo-cyclophosphanes $(PR)_x$,[12] the addition of S to $(RP)_x(CH_2)_y$ does not proceed with cleavage of any P–P bond. On the other hand, the treatment of $(PPh)_5$ with vari-

[a] School of Chemistry, University of St. Andrews, St. Andrews, Fife, KY16 9ST, United Kingdom
E-mail: jdw3@st-andrews.ac.uk

ous ratios of grey Se commonly leads to ring rupture and reorganization.[13] Obviously no rules of thumb have been laid down concerning the product structures obtained with varying ratios of $(RP)_n$ or $(RP)_x(CR'_2)_y$ to S/Se, or the effect of the electronic structure of R and R′, thus it seemed interesting to study these − to some extent unpredictable − systems.

We have reported reactions of $(PPh)_4CR_2$ (R = H, Me) with excess sulfur and selenium in a previous communication (Scheme 3).[14]

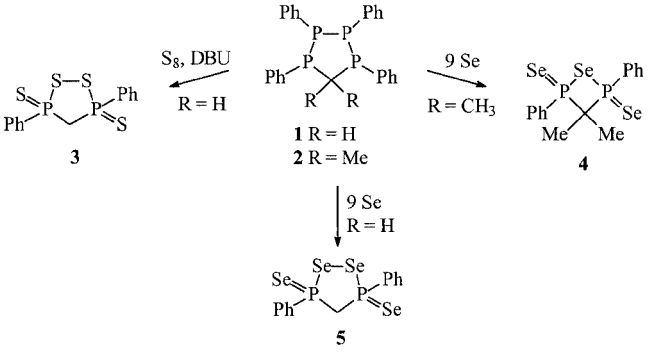

Scheme 3. Heterocycles from $(PPh)_4CR_2$ (R = H, Me)[14]

Herein we report a series of new species obtained by reductive ring-rearrangements of diselenadiphospholane (**5**); as in the case of the products shown in Scheme 3, the P−C−P motif is retained throughout the transformation to the new heterocycles as well as an acyclic dianion.

Results and Discussion

Application of a common strategy − oxidation of tetraphospholane **1** with various ratios of elemental selenium − led in all but one of the ratios studied to complicated mixtures. Attempts to separate these mixtures by flash chromatography on dried silica or alumina as well as by size-exclusion chromatography resulted in poor separation and oxidation/hydrolysis of separated species with deposition of red selenium. The only exception, where a single product was obtained, was the reaction of **1** with an excess of selenium, from which diselenadiphospholane (**5**) was obtained in very good yield and purity without the need for chromatographic separation.[14] This led us to test another tactic for the preparation of products with a lower Se/P ratio; as a starting material heterocycle **5** was used and it was treated with various reducing/deselenating agents such as Ph_3P, nBu_3P, Me_3SiCN and potassium metal. This afforded two new heterocyclic species **6** and **7** and the new dianion **8** (Scheme 4).

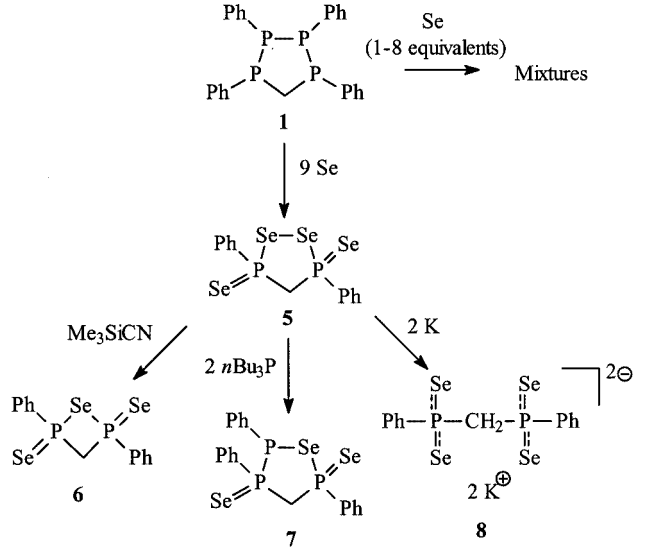

Scheme 4. New P−Se compounds obtained from tetraphospholane **1**

PSePC Heterocycle 6

The ^{31}P NMR spectra of crude reaction mixtures of **1** with seven or eight equivalents of Se indicated that two compounds are present in the solution after heating the two components in toluene. Compound **5** was identified as a major product [singlet with ^{77}Se satellites (2 × AXX′ pattern), δ_P = 43 ppm; ^1J (PSe_{exo}) = 775, ^3J (PSe_{exo}) = 11, ^1J (PSe_{endo}) = 342, ^2J (PSe_{endo}) = 13, ^2J (PP) = 34 Hz], whilst the pattern of the ^{77}Se satellites of a minor singlet at δ_P = −4.1 ppm suggests that the second compound is a four-membered heterocycle **6**. As attempts to separate it from the reaction mixture were unsuccessful, the abstraction of Se from **5** with Ph_3P, nBu_3P or Me_3SiCN was tested. ^{31}P NMR spectroscopy indicated that rather complicated mixtures resulted, although a substantial amount of the four-membered heterocycle **6** was present in the mixtures after the reaction with between one and two equivalents of a reducing agent. Me_3SiCN proved to be the reagent of choice, as the by-product, $Me_3SiCNSe$, is easily removable in vacuo (b.p. 65 °C/20 Torr). However, even after refluxing of **5** with two equivalents of Me_3SiCN in toluene, a small amount of starting material **5** was still present in the mixture, together with the product of further deselenation (vide infra). Attempts to separate the components of the mixture by flash chromatography were unsuccessful. The purification of **6** by recrystallisation was complicated by its similar solubility to **5**, as well as its instability in the solution (substantial decomposition to **5** and further unidentified products was observed when a solution of pure **6** in $CDCl_3$ or toluene was kept for one day at ambient temperature). The ease of self-reorganization of **6** in solution is surprising considering the stability of the dimethyl congener **4**, which was obtained as a sole product by the reaction of **2** with an excess of selenium.[14]

However, a small amount of the pure yellow solid **6** was obtained by repeated crystallisation of the crude product from CH_2Cl_2 and toluene; it was characterised by ^{31}P, ^1H and ^{13}C NMR and IR spectroscopy and EI-MS, the purity was assessed by elemental analysis. The small amount of compound available did not allow its characterisation by ^{77}Se NMR spectroscopy.

The $^{31}P\{^1H\}$ NMR spectrum of **6** (in $CDCl_3$) consists of a singlet (δ_P = −4.1 ppm) with two sets of ^{77}Se satellites,

arising from two distinct isotopomers with one ^{77}Se atom in the *exo*- or *endo*-position of the ring. These two sets are A_2X (Se_{endo}) and AA′X (Se_{exo}) systems (A, A′ = ^{31}P, X = ^{77}Se), the simulation of the latter subspectra allowed the determination of $^1J_{P,P}$ (26 Hz). The magnitudes of $J_{P,Se}$ are as expected (see Exp. Sect.). The ^1H NMR spectrum of **6** consists of the signals of Ph protons and a triplet due to the CH_2 group with $^2J_{H,P}$ = 12.0 Hz, which collapses into a singlet in the $^1H\{^{31}P\}$ spectrum. The $^{13}C\{^1H\}$ NMR spectrum also confirmed the identity of **6**, although the weak signal of the *ipso* carbon was not identified with certainty due to the small amount of sample available. The endocyclic carbon gave a triplet at δ_C = 63.7 ppm with $^1J_{C,P}$ = 32.8 Hz, a similar low magnitude of $^1J_{C,P^v}$ of 27.3 Hz was observed in heterocycle **5**.[14]

Crystallographic analysis (Figure 1, Table 1 and 5) confirms the formation of a four-membered PCPSe heterocycle with a *trans*-geometry of the exocyclic phenyl and seleno substituents. Two independent molecules with approximately the same geometry are present in the asymmetric unit of **6** (Table 1). In both molecules the positions of atoms Se13 and CH_2 group are partially disordered. Each independent molecule possesses only approximate C_2 symmetry, with the C_2 axis passing through the C14 and Se13 atoms. The central four-membered ring is very slightly folded (1.4 and 2.3° along the Se···C diagonal). Despite the symmetric substitution pattern, the geometries at P1 and P2 are slightly different, probably as a result of packing effects.

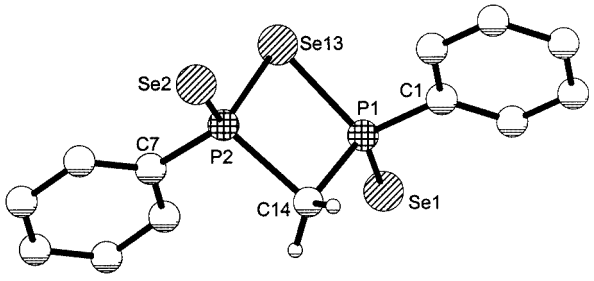

Figure 1. Structure of one of the two independent molecules present in unit cell of **6**; phenyl H atoms are omitted for clarity; the positions of the Se13 atom and CH_2 group are partially disordered

We have published the first structural characterisation of a PCPSe ring (compound **4**) in a recent communication.[14] In contrast to **6**, the presence of two methyl groups bonded to the ring carbon atom in **4** causes significant folding of the heterocycle (17 and 28° along the Se···C diagonal for each of the two molecules in the unit cell). The flattening of the central ring in **6** results in significantly reduced PCP angles in both independent molecules [87.8(2) and 83.3(3)°] with respect to the value found in **4** [96.9(3)°] and, as expected, also to the value found in the five-membered PCPSeSe ring of **5** [116.7(4)°].[14] The terminal Se atoms and the phenyl ring carbon atoms fit an approximate plane, which is nearly perpendicular to the central PCPSe heterocycle.

In summary, an interesting difference in the reactivity of **1** and **2** was observed. Whilst **1** (CH_2 derivative) reacts with a slight excess of selenium in boiling toluene to give the five-membered ring **5** and the formation of only a small amount of the four-membered ring product **6** was observed, compound **2** (CMe_2 derivative), under identical conditions, gives exclusively the four-membered ring product **4**.[14] Furthermore, a spontaneous reorganization of pure **6** in the solution, leading to **5** and unidentified products, was observed. On steric grounds we would predict that **2** should be more likely to give large rings than **1**. We observed the opposite effect and have to conclude that the electronic factors are more significant here. The electron-donating Me groups in **2** appear to favour smaller ring formation.

Table 1. Selected bond lengths (Å) and angles (°) in **6**; values for second independent molecule present in unit cell are in square brackets

P1−Se13	2.262(3) [2.300(4)]
P2−Se13	2.285(4) [2.269(3)]
P1−C14	2.078(7) [2.154(7)]
P2−C14	2.092(6) [2.164(7)]
P1−Se1	2.101(4) [2.099(4)]
P2−Se2	2.087(4) [2.103(4)]
P1−C1	1.792(6) [1.833(6)]
P2−C7	1.818(6) [1.809(6)]
Transannular P···P distance	2.891(5) [2.869(4)]
P1−C14−P2	87.8(2) [83.3(3)]
P1−Se13−P2	78.9(1) [77.8(1)]
C14−P1−Se13	97.2(2) [99.1(2)]
C14−P2−Se13	96.1(2) [99.8(2)]
C1−P1−Se1	116.4(3) [111.6(2)]
C7−P2−Se2	117.6(3) [115.3(2)]
Folding along Se···C diagonal	1.4 [2.3]

P_3CSe Heterocycle (Four Diastereomers 7a-d)

The reaction of **5** with two to three equivalents of nBu_3P or Ph_3P resulted in rather complicated mixtures as shown by $^{31}P\{^1H\}$ NMR spectroscopy. nBu_3P proved to be better suited for the synthetic purposes as the by-product nBu_3PSe is easily removed by washing the oily residue remaining after evaporation of solvent with warm acetonitrile; the separation of Ph_3PSe is not as straightforward. The solid remaining after extraction with acetonitrile was recrystallised from a small amount of toluene, giving a yellow crystalline material. An X-ray analysis was performed at this stage, showing that the product is the toluene-solvated five-membered P_3CSe heterocycle **7a** (Figure 2; a single diastereomer formed from a racemic mixture of its two enantiomers).

The uniformity of shape of the crystals suggested initially that they all consist of one diastereomeric form (**7a**), however the $^{31}P\{^1H\}$ NMR spectrum measured shortly after dissolving the crystalline material was rather complex, although at 121.4 MHz all signals are of first order and are nonfluxional. Following the analysis of spin-spin coupling systems and a P-P COSY experiment the signals were assigned to four distinct diastereomeric forms **7a**−**7d** (Scheme 5), in agreement with the presence of three centres of chirality per molecule (P atoms). The relative amount of isomers changes slightly with time after dissolving in

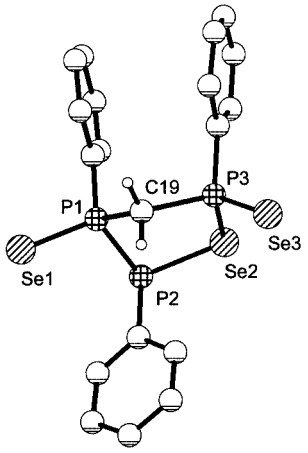

Figure 2. Molecular structure of **7a** (single diastereomer) in the crystal; toluene solvate molecule (0.25 per molecule) and phenyl H atoms are omitted for clarity

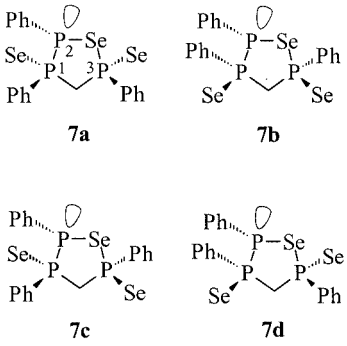

Scheme 5. Structural formulae and numbering of diastereomers **7a**−**7d**

$CDCl_3$, and the equilibrium ratio of 24:26:40:10 was established after several days at ambient temperature. A tentative mechanism explaining the observed inversion of configuration at the P-centres takes into account the fact that a detectable amount of **6** (^{31}P NMR) is always present in the solution as an impurity, even after dissolving crystalline material. We suppose that the change of configuration at the chiral P-centres may involve a ring contraction reaction of the five-membered ring **7a**−**d** to the four-membered ring **6**. The change of configuration may occur during reinsertion of the "PPh" group.

A tentative assignment of the ^{31}P NMR spectroscopic data to the distinct isomers was performed as shown in Table 2 and Scheme 5. Two assumptions were made: (i) that the least abundant isomer in solution possesses the configuration with all Ph substituents positioned in one direction with regard to the central heterocycle (all-*cis*, **7b**); and (ii) that the most abundant isomer in solution will have the least sterically hindered configuration **7c**. This corresponds to the fact that the intensity of signal assigned to **7c** increases steadily with time after preparation of sample until it reaches the major intensity shown above. To assign the remaining two isomers, the most configuration-sensitive chemical shift of P2 was considered. The higher-field P2 signal probably corresponds to isomer **7d**, with a *cis* configuration of Ph groups on atoms P1 and P2 (the same relative configuration as in isomer **7b**).

As expected, the ^1H NMR spectrum (300 MHz) of the mixture of **7a**−**7d** is very complex, and apart from the Ph signals and toluene protons a complicated multiplet ranging from δ = 3.0 to 4.5 ppm arising from CH_2 protons was observed. Employing ^{31}P broadband decoupling of the ^1H NMR spectrum offered partial simplification of the very complex overlapping signals of CH_2 groups from different diastereomers, although an analysis of the coupling constants was still not possible. Nor did measurement of H-P HMQC and H-H COSY experiments allow assignment of these signals to the individual diastereomers. No attempts were made to measure the ^{13}C and ^{77}Se NMR spectra due to the expected complexity.

A molecular ion was observed in the MS spectrum of the mixture of **7a**−**d** using ESI- ionization, whilst pronounced fragmentation was observed in EI+ and CI+ (ionizing gas NH_3) modes, the highest abundant fragments having *m*/*z* values 452 (EI) and 453 (CI).

The solid consisting of **7a**−**d** was further characterised by IR spectroscopy and its purity was assessed by microanalysis.

Crystallographic analysis of **7a** (0.25 toluene solvate, Figure 2, Table 3 and 5) reveals that the central P_3CSe heterocycle in **7a** adopts an envelope conformation with atom P1 lying 0.86 Å out of the plane defined by the other ring atoms (mean deviation of this plane is 0.04 Å), which results in dihedral angles P3−Se2−P2−P1 [19.3(1)°] and Se2−P3−C19−P1 [34.2(1)°]. The bond lengths within the central heterocycle are as expected, although the geometries at P1 and P3 including the inner P−C bond lengths differ slightly as a result of the asymmetry in the molecule. The P−C−P angle in **7a** [109.4(4)°] is slightly lower than the corresponding value [116.6(8)°] found in parent molecule

Table 2. ^{31}P NMR (121.4 MHz, $CDCl_3$) chemical shifts (ppm) and magnitudes of coupling constants (Hz) for four diastereomers **7a**−**7d**; for numbering of atoms see Figure 2 and Scheme 5

Isomer	δ_{P1} [ppm]	δ_{P2} [ppm]	δ_{P3} [ppm]	$^1J_{P1,P2}$ [Hz]	$^2J_{P2,P3}$ [Hz]	$^2J_{P1,P3}$ [Hz]	Abundance[a] [%]
7a	59.4	28.1	46.3	291.4	43.7	0	24
7d	55.8	14.3	49.0	289.9	43.7	3.0	26
7c	55.0	42.3	48.5	295.1	37.8	14.1	40
7b	62.9	−0.5	35.3	252.1	50.4	9.6	10

[a] Approximate relative equilibrium abundance in $CDCl_3$ solution.

1.[12] The phenyl substituents on the neighbouring P1 and P2 atoms alternate above and below the central ring (trans arrangement), all three Ph substituents occupy axial positions. Only two examples of heterocycles with a PPCPSe atomic sequence in cyclic arrangement have been reported previously.[16–18] The first example (**10**, Figure 3), prepared by insertion of Se into a cage phosphane does not offer many structural similarities due to its rigid cage structure.[16] The second known compound containing the PPCPSe ring sequence (**11**, Figure 3) was prepared by the action of carbon disulfide on the product of the reaction of lithium selenide (obtained from $LiHBEt_3$ and Se) with phenyl dichlorophosphane.[18] Interestingly, the substitution pattern as well as the configuration of substituents in **11** is nearly identical to those in **7a** – the P atoms directly bonded to the C atom bear exocyclic Se atoms and the configuration of Ph substituents on two neighbouring P atoms is *trans*. Furthermore, the central heterocycle in **11** adopts an envelope shape, the out-of-plane P atom being the one corresponding to P1 in **7a**. There are differences in the ring conformation in **11** and **7a** though, as the carbon ring atom is formally double bonded in **11** (and there is substantial delocalisation of π-character over all three P–C bonds) to the P atom of the central heterocycle. Thus the dihedral angles corresponding to P3–Se2–P2–P1 and Se2–P3–C19–P1 in **7a** are 30.2 and 8.4 in **11**.

Table 3. Selected bond lengths (Å), angles and torsion angles (°) in **7a**

P1–P2	2.215(3)		
P1–C19	1.897(7)	P3–C19	1.923(8)
P3–Se2	2.280(3)	P2–Se2	2.254(3)
P1–Se1	2.084(2)	P3–Se3	2.094(2)
P1–P2–Se2	97.4(1)	P2–Se2–P3	102.35(9)
Se2–P3–C19	104.4(2)	P3–C19–P1	109.4(4)
C19–P1–P2	104.8(2)		
P3–Se2–P2–P1	19.3(1)	Se2–P3–C19–P1	34.2(1)

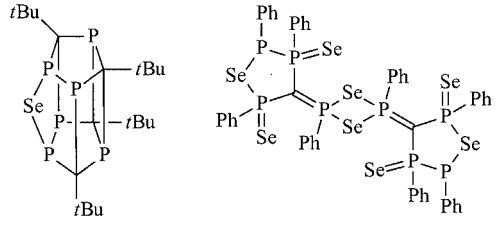

10 **11**

Figure 3. Structural formulae of heterocycles **10** and **11**, related to **7a–d**

Dipotassium Salt 8

The reaction of **5** with two equivalents of potassium metal did not proceed with elimination of potassium selenide as expected, instead a quantitative formation of the dipotassium salt of methylene-bis(diselenophenylphosphinic) acid (**8**) was observed. The colourless solid **8**, isolated by filtration, is surprisingly stable towards water, however on contact with air it slowly decomposes with deposition of red selenium. Recrystallisation of **8** from THF gives crystals of the 0.5THF solvate, as indicated by ^1H NMR spectroscopy. After prolonged drying in vacuo at room temperature partial desolvation took place, as shown by microanalysis data, indicating that the composition changed slightly to give **8** 0.4THF. Compound **8** was fully characterised by ^{31}P, ^1H, ^{13}C and ^{77}Se NMR, IR, ESI-MS (including accurate mass measurement), microanalysis as well as by X-ray crystallography.

The $^{31}P\{^1H\}$ NMR spectrum of **8** in D_2O consists of a singlet (δ_P = 10.7 ppm) with a symmetric set of ^{77}Se satellites. Their analysis allowed determination of magnitudes of $^2J_{P,P}$ (34 Hz), $^1J_{P,Se}$ (588 Hz) and $^3J_{P,Se}$ (2 Hz). The magnitude of $^1J_{PSe}$ was reconfirmed also by measurement of the $^{77}Se\{^1H\}$ NMR spectrum (d, δ_{Se} = 49.9 ppm). The pattern of the ^{31}P and ^{77}Se NMR spectra, together with the magnitudes of $J_{P,Se}$ – lying between the usual values for single and double bonded selenium – clearly indicate that delocalization of the negative charge in the molecule occurs, as shown in the structural formula in Scheme 4. Further, simulation of the C_i second order signal in the $^{13}C\{^1H\}$ NMR spectrum of **8** confirmed the magnitude of $^2J_{P,P}$ (34 Hz); the signal due to the CH_2 group appears in the $^{13}C\{^1H\}$ NMR spectrum as a triplet with $^1J_{C,P}$ = 20 Hz. Dianion **8** represents the first example of the acyclic $Se_2P–C–PSe_2$ moiety; no sulfur analogue is known.

Crystallographic analysis of **8** confirmed the ring-opening reaction of **5** leading to the formation of the potassium salt of the acyclic dianion (Figure 4, Table 4 and 5). Crystals for analysis were grown from acetonitrile, from which compound **8** crystallises as **8**·0.75 MeCN; the position of one of the phenyl substituents is disordered as shown in Figure 4, the angle between Ph planes in the two alternating positions being ca. 45°. Despite the symmetric substitution pattern of the anion, no approximate symmetry element can be found in its structure in the crystal. The low symmetry results mainly from the mutual synclinal configuration of the two P environments, which is adopted by the dianion in order to decrease the steric strain resulting from facing negatively charged bulky Se atoms (the shortest intramolecular Se···Se distance is 3.94 Å). As expected, the P–C–P angle is broader in acyclic **8** [124.4(3)°] than in the parent ring system **5** [116.7(4)°][14] and neutral acyclic $Ph_2P(Se)CH_2P(Se)Ph_2$ [117.9(6)°].[19] The delocalization of the negative charge and π-character in the P–Se bonds was mentioned in the NMR discussion, in the crystal this phenomenon results in the P–Se bond lengths in **8** [2.143(2)–2.165(2) Å] being intermediate between the typical single- and double-bonded P-Se distances [usual distinct values of 2.10 Å (P=Se) and 2.25 Å (P–Se) were found in **5**]. The anion and the K^+ cations interact with the Se atoms with K···Se distances in the range 3.29–3.54 Å; the nitrogen atom of the acetonitrile solvate molecules coordinate to K^+ cations.

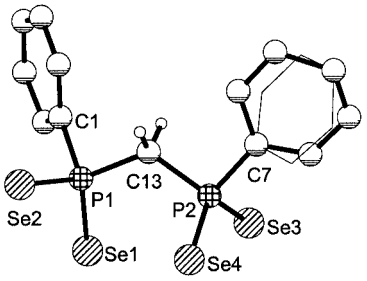

Figure 4. Structure of dianion **8** in the crystal; countercations $2K^+$, acetonitrile solvate molecule (0.75 molecule per dianion) and phenyl H atoms are omitted for clarity; the Ph ring bonded to P2 is disordered, in half of the molecules being in positions as shown in the picture, position in a second half of molecules is indicated by thin lines

Table 4. Selected bond lengths (Å) and angles (°) in **8**

P1−C13	1.848(5)	P2−C13	1.833(6)
Se1−P1	2.143(2)	P1−Se2	2.165(2)
P2−Se3	2.144(2)	P2−Se4	2.150(2)
P1−C1	1.827(6)	P2−C7	1.840(5)
P2−C13−P1	124.4(3)		
C13−P1−Se1	114.9(2)	C13−P1−Se2	110.5(2)
C13−P2−Se3	111.0(2)	C13−P2−Se4	111.1(2)
Se1−P1−Se2	115.60(7)	Se3−P2−Se4	117.07(7)
C13−P1−C1	98.5(3)	C13−P2−C7	100.8(3)

Conclusion

Two new heterocyclic and one acyclic compound with rare structural motifs are reported. In all the products described the P−C−P moiety is preserved. The ^{31}P NMR spectra of the mixtures after heating of $(PhP)_4CH_2$ (**1**) with various ratios of Se indicated that further P−Se heterocycles may exist, however the complexity of mixtures and tendency to reorganization (observed in reported heterocycles **6** and **7a**−**d**) may complicate significantly their isolation in a pure form.

Experimental Section

General Remarks: Compound **1** was prepared from $(PPh)_5$ as described earlier.[4] Compound **5** was prepared by the reaction of **1** with an excess of grey selenium, followed by recrystallisation from hot toluene.[14] All manipulations (unless stated otherwise) were performed under a dry, oxygen-free nitrogen atmosphere using standard Schlenk technique. Solvents and other reagents were dried by standard methods. In vacuo refers to a pressure of ca. 13 Pa. NMR spectra were recorded on Varian Gemini 2000 (300 MHz), Varian Unity (500 MHz) and Bruker Avance (300 MHz) spectrometers and are referred to 85% H_3PO_4 (external reference for ^{31}P) or TMS or deuterated solvent peaks (^1H and ^{13}C). Infrared spectra were recorded as KBr discs.

P_2SeC Heterocycle (4): Me_3SiCN (0.24 mL, 1.80 mmol) and a suspension of **5** (0.50 g, 0.92 mmol) in toluene (10 mL) were heated under reflux for 2 hours. The solvent and volatile by-products were evaporated in vacuo with slight heating. The resulting solid was recrystallised from 3 mL of CH_2Cl_2 and then from hot toluene (2 mL). Further recrystallisations were sometimes needed to obtain product free from starting material **2**. Crystals suitable for an X-ray diffraction study were obtained from dichloromethane. Yield 39 mg (9%). $C_{13}H_{12}P_2Se_3$ (467.1): calcd. C 33.4, H 2.6; found C 33.7, H 2.3. M.p. 183−185 °C. IR (KBr): $\tilde{\nu}$ = 1434vs, 1088vs, 747s, 711s, 563m [ν(P=Se)], 499vs cm^{-1}. ^1H NMR ($CDCl_3$) (300.0 MHz): δ = 5.25 (t, $^2J_{H,P}$ = 12.0 Hz, 2 H, CH_2), 7.60−7.68 (m, 6 H, *m*- and *p*-Ph), 8.50−8.60 (m, 4 H, *o*-Ph) ppm. $^{13}C\{^1H\}$ NMR (75.4 MHz): δ = 63.7 (t, $^1J_{C,P}$ = 32.8 Hz, CH_2), 129.1 (m, *m*-C), 132.6 (m, *o*-C), 133.2 (s, *p*-C) ppm; the small amount of sample available did not allow identification of the *ipso*-C signal. $^{31}P\{^1H\}$ NMR (121.4 MHz): δ = −4.1 (s) ppm; analysis of the ^{77}Se satellites showed $^2J_{P,P}$ = 26, $^1J_{P,Se_{exo}}$ = 810, $^1J_{P,Se_{endo}}$ = 221, $^3J_{P,Se_{exo}}$ = 7 Hz. MS (EI+): *m*/*z* = 470 [M^+], 390 [M − Se], 310 [M − 2Se].

P_3CSe Heterocycle (7a): nBu_3P (1.07 mL, 4.29 mmol) was added with stirring to an externally cooled (0 °C) suspension of **5** (1.00 g, 1.83 mmol) in toluene (20 mL). The mixture was kept at 0 °C for 30 min, then it was left to warm to room temperature and stirred for another 12 hours, followed by filtration and evaporation of the solvents from the filtrate in vacuo. The resulting oil was washed with *n*-hexane (15 mL) and with warm acetonitrile (2 × 10 mL) to remove the nBu_3PSe. The solid obtained was recrystallised from hot toluene (4 mL). Yield 0.23 g (30%) of **7a**−**d** (mixture of diastereomers, each containing approximately half a molecule of toluene) in the form of yellow crystals, some of which were suitable for X-ray analysis. The following analytical and spectroscopic data were obtained from the mixture of four diastereomeric forms **7a**−**d**: $C_{19}H_{17}P_3Se_3 \cdot 1/2C_7H_8$: calcd. C 43.5, H 3.4; found C 43.1, H 3.0. M.p. 143−145 °C. IR (KBr): $\tilde{\nu}$ = 1434s, 1101s, 736vs, 683vs, 567s [ν(P=Se)], 524vs cm^{-1}. ^1H NMR ($CDCl_3$, 300 MHz): δ = 2.25 (s, ≈1.5 H, CH_3 toluene), 4.5−3.0 (set of multiplets, 2 H, CH_2), 8.5−6.9 (set of multiplets, ≈17.5 H, 3.5×Ph) ppm. $^{31}P\{^1H\}$ NMR: see text and Table 2. MS (ESI−): *m*/*z* = 577 [M − H; correct isotopic pattern], 499 [M − Se + 1], 469 [M − P − Se], 299 [PhP_2Se_2, base peak].

Potassium salt (8): Potassium metal (0.07 g, 1.84 mmol) was added to a stirred suspension of **5** (0.50 g, 0.92 mmol) in THF (7 mL). The stirring was continued for 48 hours after which time a white solid precipitated and was filtered off using a sintered glass frit. The product obtained after drying in vacuo was of sufficient purity (assessed by ^{31}P NMR spectroscopy), however it can be recrystallised from cold THF. Yield 540 mg (ca. 85%, before recrystallisation) of 0.5 THF solvated **8** in the form of a colourless solid. Compound **8** is hygroscopic, it is soluble in THF, acetonitrile and water, and decomposes with deposition of red selenium on contact with air. Crystals suitable for X-ray work were obtained from acetonitrile as **8** 0.75MeCN solvate. The following analytical and spectroscopic data were obtained with **8** in the form of its 0.4THF solvate: $C_{13}H_{12}K_2P_2Se_4 \cdot 0.4C_4H_8O$: calcd. C 26.8, H 2.3; found C 26.8, H 2.1. Decomp. above 150 °C. IR (KBr): $\tilde{\nu}$ = 1434vs, 1091s, 738vs, 689s, 524vs, 482vs cm^{-1}. ^1H NMR (D_2O, 300 MHz): δ = 3.68 and 1.82 (2 × m, variable, THF), 4.33 [t, $^2J_{H,P}$ ≈ 11.5 Hz, 2 H, CH_2], 7.31−7.13 (2 × m, 6 H, *m*- and *p*-Ph), 7.79 (m, 4 H, *o*-Ph) ppm. $^{13}C\{^1H\}$ NMR (75.4 MHz): δ = 25.1 (s, THF), 54.8 [t, $^1J_{C,P}$ = 19.5 Hz, CH_2), 68.0 (s, THF), 127.8 [t (virtual), $^3J_{P,C}$ = 6.5 Hz, C_m], 130.6 (s, C_p), 131.5 [t (virtual), $^2J_{P,C}$ = 5.4 Hz, C_o], 136.8 [m (second order), $^1J_{P,C}$ = 62.0, $^3J_{P,C}$ < 2 Hz, C_i] ppm. $^{31}P\{^1H\}$ NMR (121.4 MHz): δ = 10.7 (s) ppm; analysis of ^{77}Se satellites showed $^2J_{P,P}$ = 34.0, $^1J_{P,Se}$ = 588, $^3J_{P,Se}$ = 2.0 Hz;

Table 5. Crystallographic data for **6**, **7a** and **8**

Compound	**6**	**7a**	**8**
Formula	$C_{13}H_{12}P_2Se_3$	$C_{19}H_{17}P_3Se_3$. 0.25[C_7H_8]	$C_{13}H_{12}P_2Se_4K_2$.0.75[C_2H_3N]
M	467.05	597.90	655.00
Crystal habit	yellow prism	yellow prism	colourless prism
Crystal size (mm)	0.12 × 0.1 × 0.1	0.14 × 0.1 × 0.1	0.2 × 0.1 × 0.1
Crystal system	Monoclinic	Monoclinic	Triclinic
Space group	P2(1)	*C*2/*c*	$P\bar{1}$
a (Å)	6.746(1)	14.385(2)	7.778(4)
b (Å)	24.683(3)	10.926(2)	11.201(5)
c (Å)	9.581(1)	31.538(5)	13.044(7)
α (°)	90.00	90.00	99.94(3)
β (°)	101.34(1)	101.41(1)	92.04(3)
γ (°)	90.00	90.00	95.68(3)
Z	4	8	2
ρ_{calcd}	1.983	1.635	1.956
No. of reflections:			
Measured	7737	9982	7398
Independent	3607	3417	5978
Observed [$I > 2\sigma(I)$]	2144	2123	4157
Θ range	2.3- 23.3	2.3−23.3	2.2−32.4
μ (mm^{-1})	7.238	4.743	7.112
Min/max transmission	0.6558/1.0000	0.8696/1.0000	0.7599/1.0000
No. of parameters	277	240	255
R (F^2, obs. data)	0.0787	0.0592	0.0544
wR (F^2, obs. data)	0.1698	0.1351	0.1240

$^{77}Se\{^1H\}$ NMR (57.2 MHz): δ = 49.9 [d, $^1J_{P,Se}$ = 588 Hz] ppm. MS (ESI−): *m*/*z* = 587 [anion + K], 274 [(anion)$^{2-}$], both had correct isotopic pattern; accurate mass measurement on $^{12}C_{13}{}^1H_{12}{}^{39}K^{31}P_2{}^{77}Se_4$ requires 588.6712, found 588.6716 (error of 0.7 ppm).

Crystal Structure Analyses: Data for **6** and **7a** were collected at 293 K on a Bruker SMART CCD diffractometer; data for **8** were collected at the same temperature on a Rigaku Mercury CCD using graphite monochromated Mo-K_α radiation (λ = 0.71073 Å). Absorption corrections were performed on the basis of multiple equivalent reflections. The structures were solved by direct methods. Structural refinements were performed with the full-matrix least-squares method on F^2 using the program SHELXTL (Version 5.10, Bruker AXS, 1997). The non-hydrogen atoms were refined anisotropically, the hydrogen atoms were idealised and refined isotropically using a riding model. CCDC-19036 (**6**), -19037 (**7a**) and -19038 (**8**) contain the supplementary crystallographic data for this paper. These data can be obtained free of charge at www.ccdc.cam.ac.uk/conts/retrieving.html [or from the Cambridge Crystallographic Data Centre, 12, Union Road, Cambridge CB2 1EZ, UK; fax: (internat.) +44-1223/336-033; E-mail: deposit@ccdc.cam.ac.uk].

Acknowledgments

We wish to thank the EPSRC for financial support.

[1] *The Chemistry of Inorganic Homo- and Heterocycles, Vol. 2* (Eds.: I. Haiduc, D. B. Sowerby), Academic Press Harcourt Brace Jovanovich Publishers, London, **1987**.
[2] M. Yoshifuji, N. Higeta, D.-L. An, K. Toyota, *Chem. Lett.* **1998**, 17−18.
[3] M. Yoshifuji, K. Ando, K. Shibayama, N. Inamoto, K. Hirotsu, T. Higuchi, *Angew. Chem. Int. Ed. Engl.* **1983**, *22*, 418−419; *Angew. Chem.* **1983**, *95*, 416−417.
[4] M. Baudler, J. Vesper, P. Junkes, H. Sandmann, *Angew. Chem. Int. Ed. Engl.* **1971**, *10*, 940; *Angew. Chem.* **1971**, *83*, 1019.
[5] S. A. Laneman, F. R. Fronczek, G. G. Stanley, *Phosphorus, Sulfur, and Silicon* **1989**, *42*, 97−102.
[6] K. P. Langhans, O. Stelzer, *Chem. Ber.* **1987**, *120*, 1707−1712.
[7] R. Appel, W. Paulen, *Chem. Ber.* **1983**, *116*, 109−113.
[8] Z. S. Novikova, A. A. Prishchenko, I. F. Lutsenko, *J. Gen. Chem. USSR (Engl. Transl.)* **1979**, *49*, 413−414.
[9] M. Baudler, J. Vesper, B. Kloth, D. Koch, H. Sandmann, *Z. Anorg. Allg. Chem.* **1977**, *431*, 39−48.
[10] Z. S. Novikova, A. A. Prishchenko, I. F. Lutsenko, *J. Gen. Chem. USSR (Engl. Transl.)* **1979**, *49*, 413−414.
[11] K. Toyota, Y. Ishikawa, K. Shirabe, M. Yoshifuji, K. Okada, K. Hirotsu, *Heteroatom Chem.* **1993**, *4*, 279−285.
[12] See for example: M. Baudler, T. Vakratsas, D. Koch, K. Kipker, *Z. Anorg. Allg. Chem.* **1974**, *408*, 225−236.
[13] For a recent review see: M. R. St. J. Foreman, J. D. Woollins, *J. Chem. Soc., Dalton Trans.* **2000**, 1533−1543.
[14] P. Kilian, A. M. Z. Slawin, J. D. Woollins, *Chem. Commun.* **2001**, 2288−2289.
[15] J. Lex, M. Baudler, *Z. Anorg. Allg. Chem.* **1977**, *431*, 49−60.
[16] M. M. Al-Ktaifani, D. P. Chapman, M. D. Francis, P. B. Hitchcock, J. F. Nixon, L. Nyulaszi, *Angew. Chem. Int. Ed.* **2001**, *40*, 3474−3477; *Angew. Chem.* **2001**, *113*, 3474−3477.
[17] P. T. Wood, J. D. Woollins, *Phosphorus, Sulfur and Silicon* **1989**, *41*, 51−56.
[18] J. C. Fitzmaurice, D. J. Williams, P. T. Wood, J. D. Woollins, *J. Chem. Soc., Chem. Commun.* **1988**, 741−743.
[19] P. J. Carroll, D. D. Titus, *J. Chem. Soc., Dalton Trans.* **1977**, 824−829.

Received October 11, 2002
[I02564]

EurJIC
European Journal of Inorganic Chemistry

April 2003
Issue 8
Pages 1469–1644

Papers available ahead of print in Early View at www.interscience.wiley.com

Earliest available Table of Contents:
Automatically, free of charge by e-mail through
www.interscience.wiley.com/alerts

COVER PICTURE

The cover picture shows two views of $Ba_5Fe_4Ti_{10}O_{31}$ type structure. Barium atoms are shown as yellow spheres, iron tetrahedra are depicted in red, iron trigonal bipyramids in gold, and titanium octahedra in blue. On the left side is a full unit cell stack of 18 layers, on the right side, the unique 9-layer repeat unit is shown. Details are discussed in the Microreview by T. Siegrist and T. A. Vanderah on p. 1483 ff.

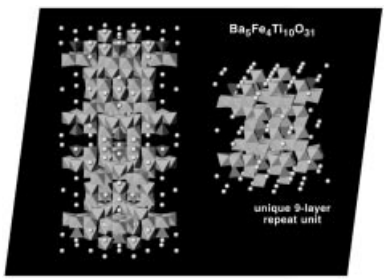

MICROREVIEW

Contents

1483 **T. Siegrist,* T. A. Vanderah**

Combining Magnets and Dielectrics: Crystal Chemistry in the $BaO-Fe_2O_3-TiO_2$ System

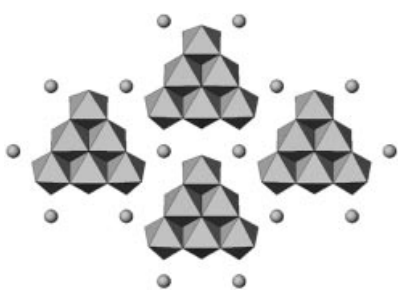

Keywords: Dielectric properties / Magnetic properties / Perovskite phases / Solid-state structures / Titanates / Ferrites

 © WILEY-VCH Verlag GmbH, 69451 Weinheim, Germany, 2003 1434–1948/03/0408–1473 $ 20.00+.50/0

SHORT COMMUNICATIONS

1503 **S. Rau,* B. Schäfer, S. Schebesta, A. Grüßing, W. Poppitz, D. Walther, M. Duati, W. R. Browne, J. G. Vos**

Efficient Energy Transfer in Supramolecular, Hydrogen-Bonded Polypyridylruthenium-Osmium Complexes

Keywords: Ruthenium / Osmium / Supramolecular chemistry / Photosynthesis

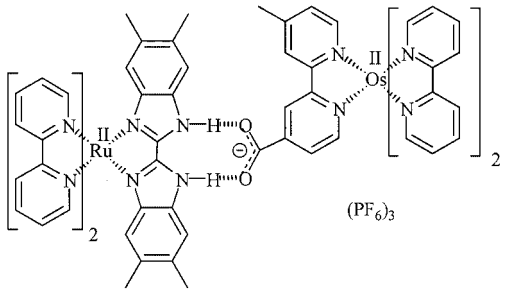

1507 **P. L. Shutov, S. S. Karlov,* K. Harms, O. Kh. Poleshchuk, J. Lorberth,* G. S. Zaitseva**

The First Azaindatrane and Unprecedented Structural Features

Keywords: Azametallatranes / Indium / Tripodal ligands

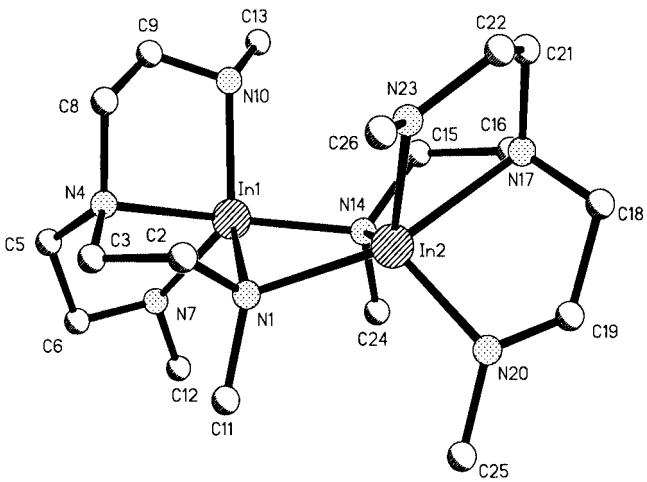

1511 **G. Barberà, F. Teixidor, C. Viñas,* R. Sillanpää, R. Kivekäs**

Sequential Nucleophilic−Electrophilic Reactions Selectively Produce Isomerically Pure Nona-*B*-Substituted *o*-Carborane Derivatives

Keywords: Boron / Clusters / Iodinated compounds / Methylated compounds / Electrophilic reactions

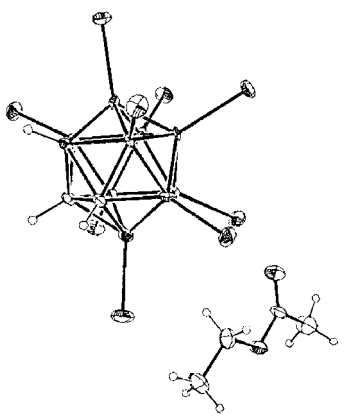

1514 **C.-L. Pan, J.-Q. Xu,* G.-H. Li, D.-Q. Chu, T.-G. Wang**

A Three-Dimensional Framework of Novel Vanadium Clusters Bridged by $[Ni(en)_2]^{2+}$: $Ni(en)_3\{V^{IV}_1V^{V}_5O_{38}Cl\ [Ni(en)_2]_3\}\cdot 8.5H_2O$

Keywords: Polyoxometalates / Hydrothermal synthesis / Cluster compounds / Crystal structure

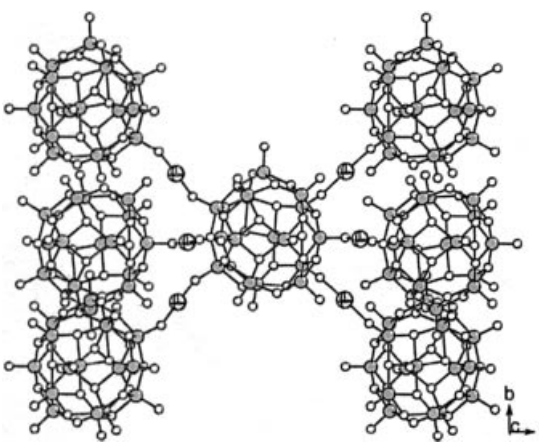

1518 **U. Vogel, P. Sekar, R. Ahlrichs, U. Huniar, M. Scheer***

An Unusual Bonding Situation in a Novel Au^{I}-Phosphido Complex with a Planar Au_3P_3 Framework

Keywords: Metathesis / Cyclopentadienyl ligands / Chromium / P ligands / Gold

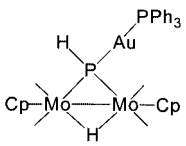

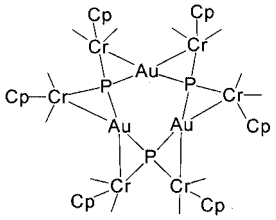

1523 **A. Bacchi,* G. P. Chiusoli, M. Costa,* E. Giacobbi**

Self-Assembly of Supramolecular Structures from Palladium Chloride and Guanidinium Salts of Pyridinecarboxylic Acids − A Dramatic Change on Passing from the *para*- to the *meta*-Substituted Acid

Keywords: Crystal engineering / Hydrogen bonds / Self-assembly / Multicomponent systems

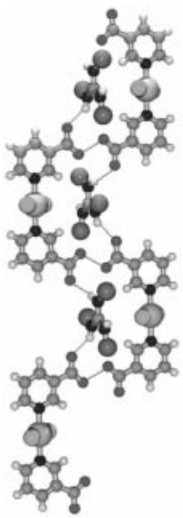

1529 **M. S. Robillard, J. S. Leith, G. A. van der Marel, J. H. van Boom, J. Reedijk***

Application of Gel-Phase ^{195}Pt NMR Spectroscopy in a Novel Solid-Phase Synthesis of a Primary Amine Dichloroplatinum(II) Complex

Keywords: Peptides / Platinum / Solid-phase synthesis / NMR spectroscopy / Bioinorganic chemistry

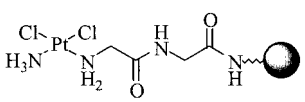

FULL PAPERS

1533 **B. Grüner, B. Štíbr,* J. Holub, I. Císařová**

Metal-Promoted Cage Rearrangements in the Tricarbollide Series: Conversion of Ligand Derivatives 7-L-*nido*-7,8,9-$C_3B_8H_{10}$ (L = H_3N, $tBuH_2N$, Me_2HN) into Neutral 8-R-*nido*-7,8,9-$C_3B_8H_{11}$ (R = H_2N, *t*BuHN, Me_2N) Compounds

Keywords: Boranes / Carboranes / NMR spectroscopy / Rearrangement / N ligands

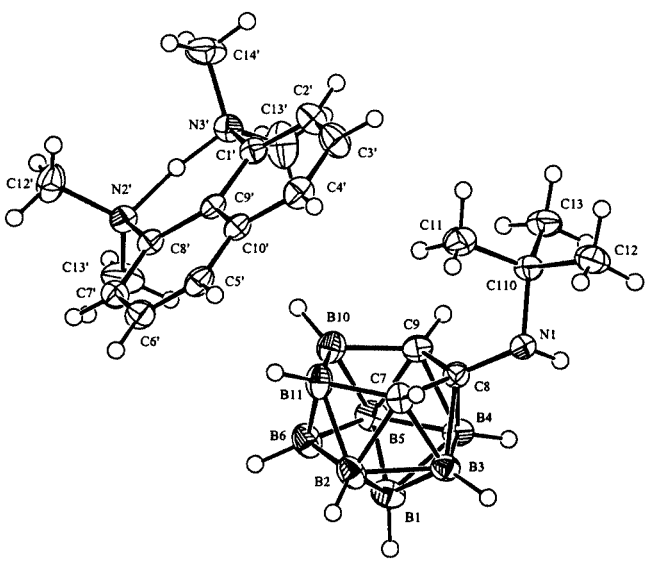

1540 **A. Panja, N. Shaikh, S. Gupta, R. J. Butcher, P. Banerjee***

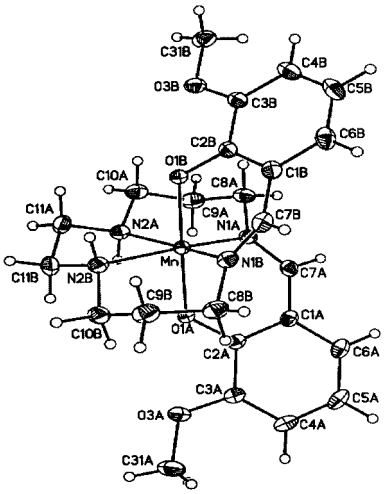

New Mononuclear Manganese(III) Complexes with Hexadentate (N_4O_2) Schiff Base Ligands: Synthesis, Crystal Structures, Electrochemistry, and Electron-Transfer Reactivity towards Hydroxylamine

Keywords: Cyclic voltammetry / Electron transfer / Kinetics / Manganese

1548 **K. Drabent,* Z. Ciunik, P. J. Chmielewski**

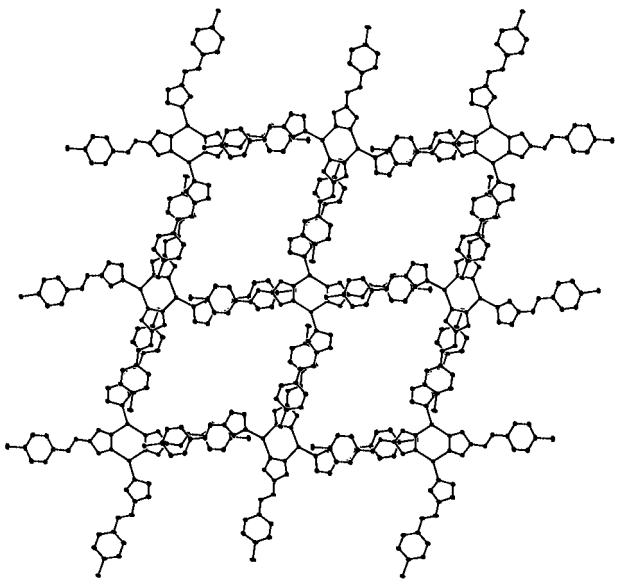

Synthesis, Crystallographic and Spectroscopic Studies of Dimeric Cu^I Complexes with Schiff-Base-Containing Triazole Ligands

Keywords: Copper / Schiff bases / N ligands / Dimers / Self-assembly

1555 **X. Sun, X. Cui, D. P. Arnold,* M. T. M. Choi, D. K. P. Ng, J. Jiang***

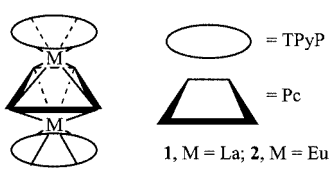

The Electronic Absorption Characteristics of Mixed Phthalocyaninato Porphyrinato Rare Earth(III) Triple-Deckers $M_2(TPyP)_2(Pc)$

Keywords: Phthalocyanines / Porphyrins / Sandwich complexes / Lanthanides

1562 **H. Erras-Hanauer, Z.-W. Mao, G. Liehr, T. Clark,* R. van Eldik***

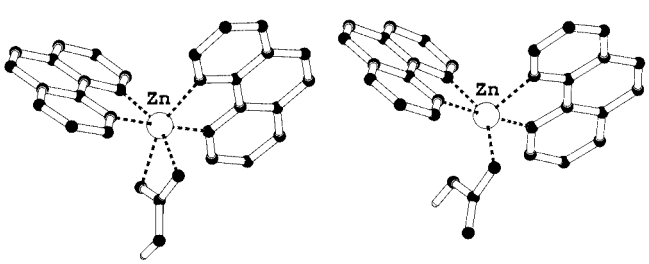

Structures of Carbonato and Bicarbonato Complexes of Bis(1,10-phenanthroline)Zinc(II): Experiment and Theory

Keywords: Density functional calculations / Zinc / Carbonate complexes / Bicarbonate complexes

1570 **D. Zhang, G.-X. Jin,* N.-H. Hu**

Ethylene Polymerization by Self-Immobilized Neutral Nickel Catalysts Bearing Allyl Groups

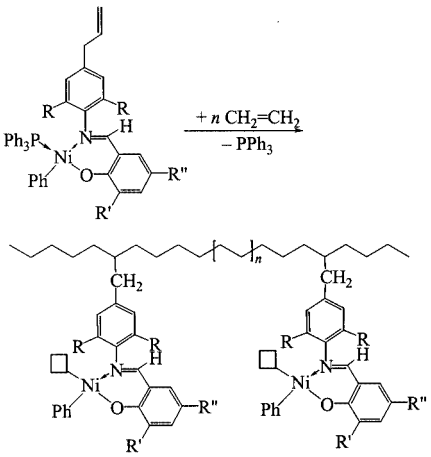

Keywords: Nickel / N,O ligands / Immobilization / Polymerizations

1577 **L. Beneš,* K. Melánová, V. Zima, P. Patrono, P. Galli**

Intercalation of Amino Alcohols into α-Zr-$(HPO_4)_2 \cdot H_2O$

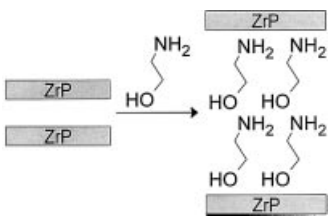

Keywords: Layered compounds / Intercalations / Amino alcohols / Zirconium / Phosphate

1581 **S. V. Kryatov, E. V. Rybak-Akimova,* F. Meyer, H. Pritzkow**

A Study of the Equilibrium and Kinetics of Urea Binding by a Biomimetic Dinickel(II) Complex

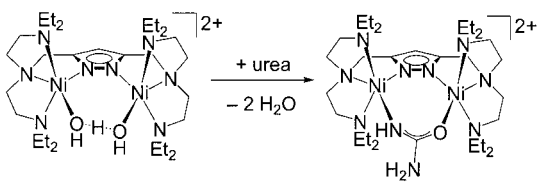

Keywords: Enzyme models / Nickel / N ligands / Kinetics / Thermodynamics

1591 **F. J. Ramos-Lima, A. G. Quiroga, J. M. Pérez, M. Font-Bardía, X. Solans, C. Navarro-Ranninger***

Synthesis and Characterization of New Trans-platinum Complexes Containing Phosphane Groups − Cytotoxic Studies in Cisplatin-Resistant Cells

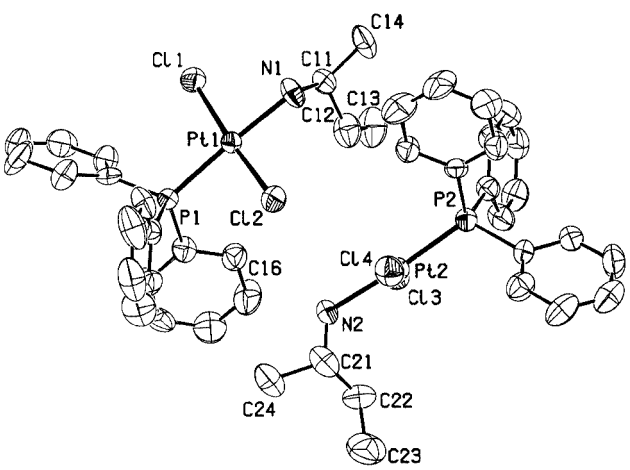

Keywords: Antitumor agents / Bioinorganic chemistry / Crystal structure / Phosphanes / Platinum

1599 **S. Döring, V. V. Kotov, G. Erker,* G. Kehr, K. Bergander, O. Kataeva, R. Fröhlich**

Synthesis and Dynamic Features of (Chloro)zirconocene Cations Stabilised by Pendant (Diarylphosphanyl)alkyl and (Dimethylamino)alkyl Substituents at Their Cyclopentadienyl Ring Systems

Keywords: Cations / Metallocenes / N ligands / P ligands / Zirconium

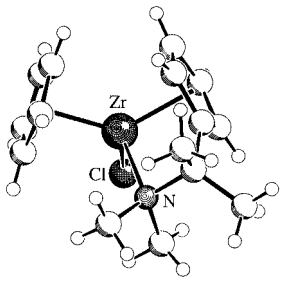

1608 **I. Izquierdo-Barba, A. Asenjo, L. Esquivias, M. Vallet-Regí***

SiO_2-CaO Vitreous Films Deposited onto Ti6Al4V Substrates

Keywords: Thin films / Sol-gel processes / Gels / Glasses / Amorphous materials

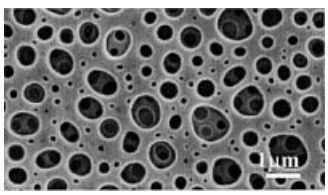

1614 **M. Saoud, A. Romerosa,* S. M. Carpio, L. Gonsalvi, M. Peruzzini***

Ruthenium-Catalysed Selective Transetherification of Substituted Vinyl Ethers To Form Acetals and Aldehydes

Keywords: Ruthenium / Allenylidenes / Vinyl ethers / Homogeneous catalysis / Acetals

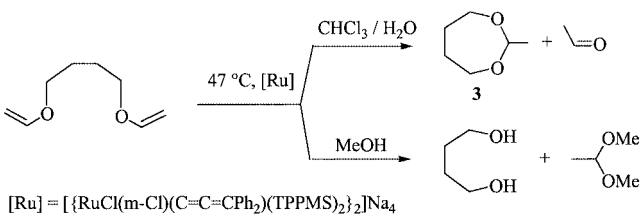

[Ru] = [{RuCl(m-Cl)(C=C=CPh$_2$)(TPPMS)$_2$}$_2$]Na$_4$

1620 **C. Bianchini,* G. Mantovani, A. Meli, F. Migliacci, F. Zanobini, F. Laschi, A. Sommazzi**

Oligomerisation of Ethylene to Linear α-Olefins by new C_s and C_1-Symmetric [2,6-Bis(imino)-pyridyl]iron and -cobalt Dichloride Complexes

Keywords: Cobalt / Ethylene / Iron / N ligands / Oligomerisation

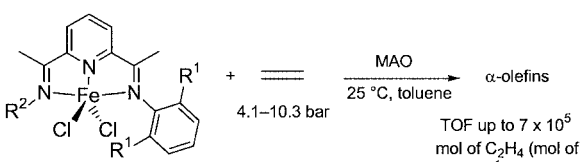

R^1 = Me, *i*Pr; R^2 = cyclohexyl, (*R*)-1-phenylethyl, (*S*)-1-(naphthalen-2-yl)ethyl

1632 **R. Niewa,* Z. Hu, R. Kniep**

Mn and Fe *K*-edge XAS Spectra of Manganese and Iron Nitrido Compounds

Keywords: X-ray absorption spectroscopy / Nitrides / Iron / Manganese

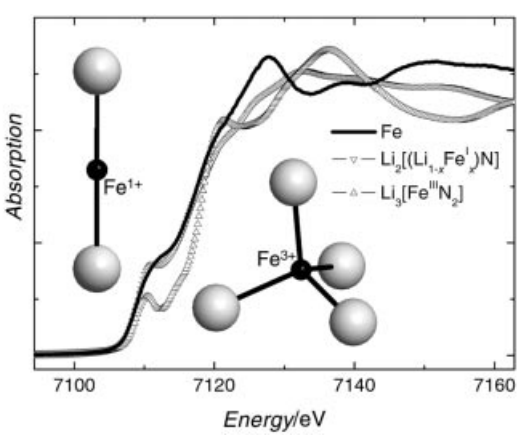

1635

C. D. Antoniadis, G. J. Corban, S. K. Hadjikakou,* N. Hadjiliadis,* M. Kubicki, S. Warner, I. S. Butler

Synthesis and Characterization of $(PTU)I_2$ (PTU = 6-*n*-propyl-2-thiouracil) and $(CMBZT)I_2$ (CMBZT = 5-chloro-2-mercapto-benzothiazole) and Possible Implications for the Mechanism of Action of Anti-Thyroid Drugs

Keywords: Bioinorganic chemistry / Charge transfer / Iodine / S ligands / Nitrogen heterocycles

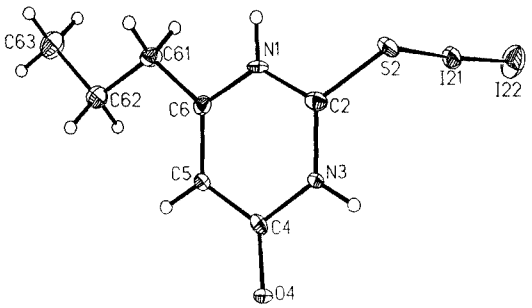

1641

S. Perrier, F. Seela, A. Schwartz, M. Leng, J.-C. Chottard*

The Human Telomeric Sequence $(T_2AG_3)_n$ is Efficiently Cross-Linked by AN1 Binding to the Platinum of a *trans*-$Pt(NH_3)_2$ Chelate of an Antisense Oligo-2′-*O*-Methylribonucleotide

Keywords: Platinum / DNA / RNA / Chelates / Bioinorganic chemistry

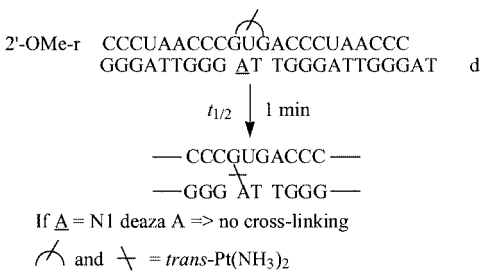

Combining Magnets and Dielectrics: Crystal Chemistry in the $BaO-Fe_2O_3-TiO_2$ System

Theo Siegrist*[a][‡] and Terrell A. Vanderah[b]

Keywords: Dielectric properties / Magnetic properties / Perovskite phases / Solid-state structures / Titanates / Ferrites

Phases observed in the $BaO–Fe_2O_3–TiO_2$ system are classified and described in terms of the framework of close-packed {O,Ba/O} layers, with the transition metal atoms either in octahedral (titanium and iron) or in tetrahedral (iron only) sites. The resulting crystal chemistry features new combinations of structural features intermediate between the magnetic barium hexaferrites and the dielectric barium polytitanates, and thus gives rise to phases with potentially useful magnetic/dielectric properties.

(© Wiley-VCH Verlag GmbH & Co. KGaA, 69451 Weinheim, Germany, 2003)

1. Overview

The crystal chemistry in the $BaO-Fe_2O_3-TiO_2$ phase diagram is surprisingly rich. A recent study of the system found a large number of new phases,[1] with structures featuring moieties from both the polytitanates and hexaferrites, as well as new building blocks showing a mixture of features from both. The observed structural features organize the composition space into regions containing phases with common building units. These regions in the phase diagram, as indicated in Figure 1, include those featuring framework-type structures (e.g., hollandites, indicated in yellow), the perovskite derivatives and polytitanates (light blue), the hexaferrites (dark blue), and intermediate phases with new structural units (red). Magnetic multilayer compounds are in the violet/gray area. The areas are defined by bisecting existing tie lines and are a guide to the eye.

As can be seen, three distinct "structural end members" ($BaO-TiO_2$, $Fe_2O_3-TiO_2$, and $BaO-Fe_2O_3$) dominate along the binary subsystems. The framework-type structures such as hollandite dominate the lower left corner of

[a] Bell Laboratories, Lucent Technologies
600 Mountain Avenue, Murray Hill, NJ 07974, USA
[b] Ceramics Division, Materials Science & Engineering Laboratory, National Institute of Standards and Technology
Gaithersburg, MD 20899, USA
[‡] Second address: Materials Chemistry, Lund University, 22100 Lund, Sweden.

Theo Siegrist was born in Winterthur, Switzerland. He received his diploma in physics (Dipl.-Phys. ETH) from the Federal Institute of Technology (ETH) in Zürich in 1979. He then enrolled in the Ph.D. program at the Laboratory for Solid State Physics at ETH, working in the area of rhenium intermetallic compounds with F. Hulliger. He was awarded the Dr. sc. nat. in 1982. In 1983 he joined the group of F. Holtzberg at the IBM T. J. Watson Research Center as a postdoctoral fellow, working on thin films of semimagnetic semiconductors. In 1985 he became a research associate at the National Research Council of Canada in Ottawa, in the Solid State Chemistry department. There he investigated rare earth intermetallics and heavy fermion uranium compounds. He joined Bell Laboratories in New Jersey, USA in 1986, where he entered the field of high T_c superconductors based on copper oxides. He investigated the crystal chemistry of this new class of compounds and related phases. Further work was done on C_{60} and its compounds, various oxides, and intermetallic phases. From 1998 he spent two years as Professor of Solid State Chemistry at Lund University/Lund Institute of Technology, where he investigated new phases with mixed anion lattices. From 2000 he has once again been at Bell Labs, working on the structural characterization of organic electronic materials and on the crystal chemistry of new phases.

Terrell Vanderah received a B.S. in Chemistry from the University of Maryland in 1977 and a Ph.D. in Inorganic (Solid State) Chemistry from the University of Connecticut in 1985, with Prof. B. L. Chamberland. From 1985 to 1993 she worked as a research chemist at the Naval Weapons Center in China Lake, California, in the area of non-oxide optical ceramics and high-temperature superconductors. In 1994 she moved to the National Institute of Standards and Technology in Gaithersburg to become the group leader for Phase Equilibria. Her research interests include the solid-state chemistry and phase equilibria of oxide systems of electronic interest and the interrelationships of crystal structure, chemical composition, and properties.

MICROREVIEWS: This feature introduces the readers to the author's research through a concise overview of the selected topic. Reference to important work from others in the field is included.

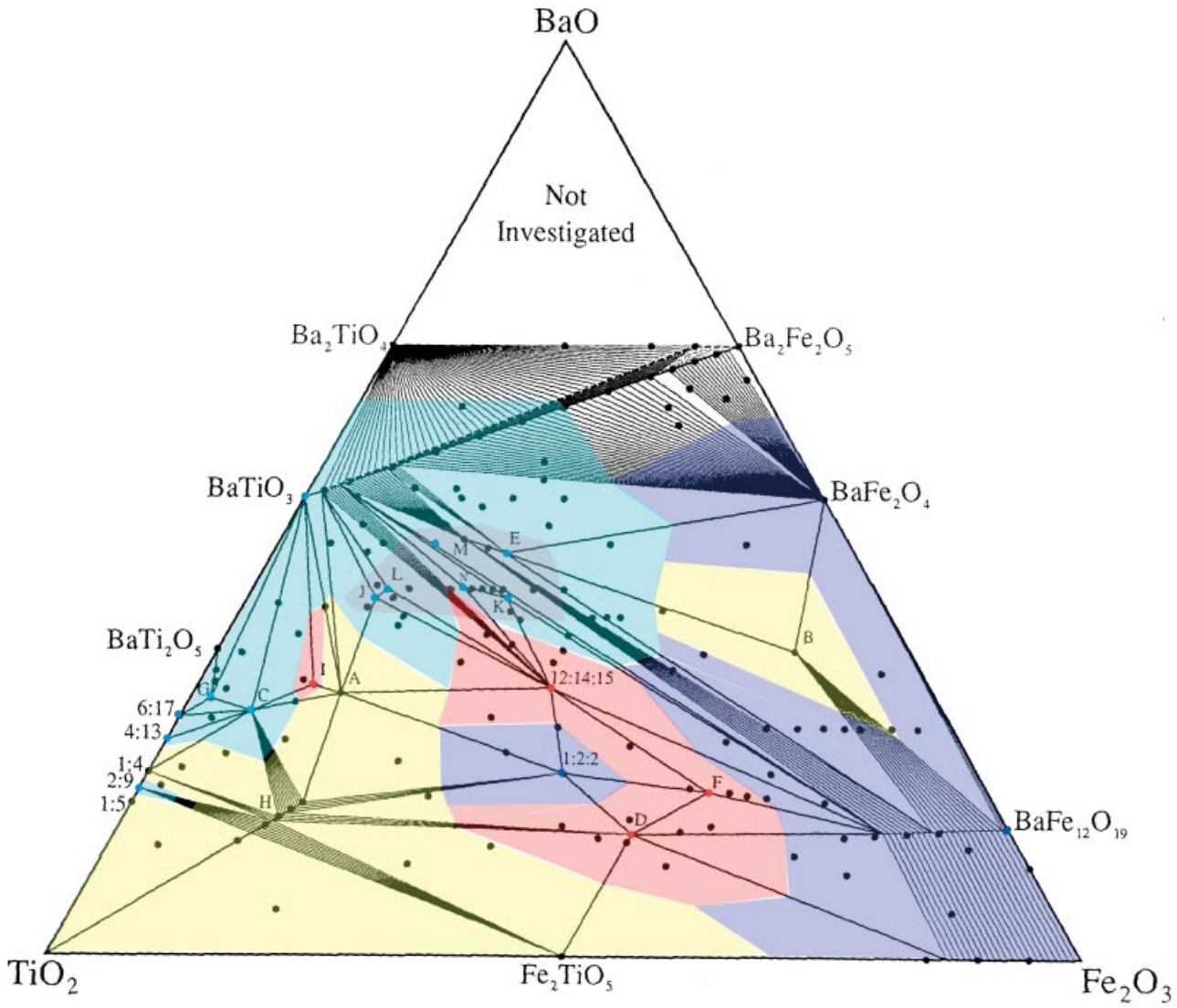

Figure 1. $BaO-Fe_2O_3-TiO_2$ phase diagram with regions of structurally related phases indicated in color; yellow: framework-type phases; light blue: hexagonal polytitanates; dark blue: hexaferrites; violet/gray: magnetic multilayer systems (based on hexagonal perovskite and hexaferrite); red: new "mixed" phases

the phase diagram nearest TiO_2. The other two structural "end members", the polytitanates/perovskites (Ti-rich side) and hexaferrites (Fe-rich side), both feature close-packed {O,Ba/O} layers and would therefore be expected to form numerous "blended" structures. Indeed, in the transition area indicated in red, the phases found are based on seven new types of close-packed {O,Ba/O} layers intermediate between the layers present in the hexaferrites and in the polytitanates. The stacking of the different layers gives rise to a variety of phases, extending from the iron-rich to the titanium-rich side. Phases in this region based on hexagonal $BaTiO_3$ with Fe ordering in distinct layers reveal superstructures with periodicities of around 100 Å. Disorder in stacking is often seen, but their structural features are similar to the other intermediate phases.

Phases indicated in violet/gray include blocks of hexagonal $BaTiO_3$ and often disordered layers mainly comprised of $BaO-Fe_2O_3$.[2] These phases are part of the red area of new structures.

The structural features observed in the $BaO-Fe_2O_3-TiO_2$ system are presented below, and some of the new phases found are discussed. The combination of high dielectric and ferri-/ferromagnetic systems produces potentially useful materials for microwave applications, such as nonreciprocal devices.[3,4] The dielectric properties of some of the phases are discussed in terms of the Clausius–Mosotti theory. Furthermore, the iron valence has to be stabilized at Fe^{3+} to ensure low microwave losses. The phases discussed below are based on Fe^{3+} and Ti^{4+}.

2. Background

High dielectric materials have been key in the miniaturization of microwave devices (i.e. high frequencies of the

order of 50 MHz to 22 GHz). Use of a dielectric material allows the size of a microwave device to be scaled by $\varepsilon^{-1/2}$. Requirements for materials used in microwave applications are a high dielectric constant and low microwave losses, together with a negligible temperature dependence of these properties. Materials in common use are based on mixtures of barium titanates, in which dielectric constants of the order of 28, together with small temperature dependencies, are observed. Furthermore, microwave losses can be reduced such that high-quality filters with Q of the order of 45k and higher can be realized. The loss mechanisms are often related to defects in the material; the presence of reduced titanium, Ti^{3+}, for instance, correlates with increased loss. Careful synthesis of the material to ensure fully oxidized titanium is key to performance.

The addition of a static magnetic field affects the propagation of the electromagnetic wave in such a material, allowing the construction of nonreciprocal devices such as isolators, phase shifters, circulators, etc. Such ceramic magnetic oxides are key components in a wide variety of electronic applications; communication systems, for instance, utilize coaxial circulators and isolators that contain ceramic magnets.[3,4] Materials in current use include spinels, garnets, and hexaferrites, the last of these based on the magnetoplumbite-type structure. Improved materials would exhibit higher dielectric constants and high saturation magnetization, while retaining low-loss behavior in the microwave region. In addition, a small or negligible temperature dependence of the dielectric and magnetic properties is highly desirable. For this reason, a thorough study of the phase equilibria in the $BaO-Fe_2O_3-TiO_2$ system was recently carried out.[1] In particular, combinations of the high dielectric materials based on polytitanates with magnetic Fe_2O_3 were of interest. Since the materials in use today are often based on mixtures of several different crystallographic phases, detailed knowledge of the phase diagram is key to understanding the processing of multicomponent materials with engineered properties. The interface of the barium hexaferrites with the barium polytitanates is discussed below, and the structural relationships emphasized.

The pseudo-binary systems have been examined previously, and corresponding phase diagrams were produced in "Phase Equilibria Diagrams" (formerly "Phase Diagrams for Ceramists"),[5] in Figures 1:208, 4:5130, 91:009, 1:213, 3:4302, 4:5135, 11:9211–13, 93:016, 12:10036, and references cited therein.

The crystal chemistries both of the barium polytitanates[6] and of the barium hexaferrites[7] have been extensively studied in the past. These systems are based on close-packed oxygen lattices, with barium atoms substituting for oxygen atoms while retaining the close-packed arrays. Titanium and iron atoms occupy interstitial sites. The resulting structures obey a metric determined by the close-packed lattice, usually based on a hexagonal unit cell, with layers approximately 2.35 Å thick and in-plane base hexagonal lattice parameters of the order of $a = b = 5.75$ Å. Ordering of the transition metal atoms in interstitial sites and of the barium atoms which are substituted for oxygen atoms often reduces symmetry from hexagonal or rhombohedral to orthorhombic or monoclinic, and correspondingly changes the in-plane lattice parameters. The similar unit cell metrics of the two systems allow the formation of mixed or "blended" phases that would be expected to contain structural motifs both from the polytitanates and from the hexaferrites, giving rise to new structures. Furthermore, new structural motifs combining features of both end systems may also occur.

Only one phase is stable in the pseudobinary $Fe_2O_3-TiO_2$ system: pseudobrookite-type Fe_2TiO_5. It may be regarded as a framework-type structure with edge-sharing octahedra only.

The barium polytitanates may be described as $(BaO)_m(TiO_2)_n$. Of the six phases stable above 1200 °C in the $BaO-TiO_2$ system, $Ba_2Ti_9O_{20}$,[8] $BaTi_4O_9$,[9] $Ba_4Ti_{13}O_{30}$,[10] $Ba_6Ti_{17}O_{40}$,[11] $BaTiO_3$,[12,13] and Ba_2TiO_4,[14] only the last is not based on a close-packed {O,Ba/O} layer system. It contains isolated TiO_4 tetrahedra, making it quite distinct in the series. The phase $Ba_2Ti_5O_{12}$ was found to be stabilized by small amounts of impurities, and is therefore not a true polytitanate.[15] The framework structure of $Ba_4Ti_{11}O_{26}$ is related to the mineral jeppite,[16] but with partial occupancy of titanium to achieve charge balance (also referred to as $Ba_2Ti_{5.5}O_{13}$).[17]

The barium hexaferrite system and spinels differ markedly from the polytitanates in that Fe occupies both octahedral and tetrahedral interstitial sites in the close-packed lattice. This results in sixfold octahedral and fourfold tetrahedral coordination, as well as fivefold trigonal-bipyramidal coordination in the case of the hexaferrites. This last form is obtained when two tetrahedral interstitial sites share a face. The occupying iron atom is usually shifted out of the basal plane into either one of the tetrahedral interstitial sites.

In the case of the hexaferrites, various superstructures based on hexagonal lattices with the *c* axis approaching 1000 Å have been reported.[18] Other phases in the $BaO-Fe_2O_3$ system may adopt structures that are not based on a close-packed lattice. $BaFe_2O_4$, for instance, adopts a "stuffed tridymite"-type structure,[19] while $Ba_2Fe_2O_5$ is reported to occur in a distorted perovskite-type superstructure.[20] $Ba_2Fe_6O_{11}$ may be regarded as intermediate between the tridymite-type structures and the close-packed structures, as a layer of edge-shared octahedra alternate with a partial stuffed tridymite-like framework of tetrahedra.[21]

The spinels and hexaferrites are used in nonreciprocal microwave devices. However, they have considerably lower dielectric constants than the barium polytitanates.

Combinations of the barium polytitanates and barium hexaferrites are of potential interest since they offer the possibility of high dielectric constants in a magnetic system. Depending on the concentration of Fe^{3+}, paramagnetic to ferri- or ferromagnetic systems would be expected. At low iron concentrations, good dielectric materials based on polytitanates, but with weak magnetism, would be likely. In contrast, a high iron concentration would be expected to

Table 1. Crystal structure data for phases

Compound	#L	Stacking sequence	Layer thickness [Å]	Space group	Lattice parameters [Å]	Remarks name (see Figure 1), ref.
$Fe_2O_3-TiO_2$						
Fe_2TiO_5				*Ccmm*	$a = 9.700$, $b = 3.720$, $c = 9.930$	pseudobrookite[44]
$BaO-Fe_2O_3$						
Fe_3O_4	6	$(c)_c$	2.32	$F\bar{4}3m$	$a = 8.384$	S (spinel)[45]
$BaFe_{12}O_{19}$	10	$(hhhcc)_2$	2.32	$P6_3/mmc$	$a = 5.893$, $c = 23.194$	M (hexaferrite)[7,24]
$Ba_2Fe_{14}O_{22}$	18	$(cchhhh)_3$	2.42	$R\bar{3}m$	$a = 5.860$, $c = 43.504$	Y[7]
$BaFe_{18}O_{27}$	14	$(hhhcccc)_2$	2.34	$P6_3/mmc$	$a = 5.880$, $c = 32.845$	W[7]
$Ba_3Fe_{26}O_{41}$	22	$(hhhcchhhcc)_2$	2.38	$P6_3/mmc$	$a = 5.885$, $c = 52.301$	Z (MY)[7]
$Ba_2Fe_{30}O_{46}$	36	$(hhhcchhhcccc)_3$	2.306	$R\bar{3}m$	$a = 5.880$, $c = 84.110$	M_2S[7]
$BaFe_4O_7$	6	$(cch)_2$		$P6_3/m$	$a = 5.160$, $c = 13.811$	[46]
$BaFe_2O_4$	4	$(ch)_2$	2.254	$P6_322$	A = 5.458, $c = 9.016$	[19]
$BaO-TiO_2$						
cubic-$BaTiO_3$	3	$(c)_3$	2.306	$Pm\bar{3}m$	$a = 3.905$	[12]
6H-$BaTiO_3$	6	$(cch)_2$	2.327	$P6_3/mmc$	$a = 5.750$, $c = 14.050$	[13][31]
$Ba_6Ti_{17}O_{40}$	8	$(hcch)_2$	2.340	$C2/c$	$a = 9.883$, $b = 17.080$, $c = 18.920$, $\beta = 98.40°$	[11]
$Ba_4Ti_{13}O_{30}$	6	$(hcc)_2$	2.342	$Cmca$	$a = 17.063$, $b = 9.864$, $c = 14.053$	[10]
$Ba_2Ti_9O_{20}$	6	$(hhc)_2$	2.349	$P\bar{1}$	$a = 14.358$, $b = 14.095$, $c = 7.477$, $\alpha = 95.5°$, $\beta = 100.6°$, $\gamma = 89.9°$	[8]
$BaTi_5O_{11}$	6	$(hcc)_2$	2.337	$P2_1/n$	$a = 7.670$, $b = 14.020$, $c = 7.520$, $\beta = 98.3°$	[47]
$BaTi_6O_{13}$	4	$(h)_4$	2.377	$P\bar{1}$	$a = 7.510$, $b = 9.852$, $c = 7.461$, $\alpha = 105.2°$, $\beta = 118.5°$, $\gamma = 72.3°$	[48]
$Ba_2Ti_{13}O_{22}$	6	$(cch)_2$	2.349	$Cmca$	$a = 10.018$ $b = 11.575$, $c = 14.094$	[30]
$BaTi_2O_5$		–	–	$A2/m$	$a = 9.409$, $b = 3.932$, $c = 16.907$, $\beta = 103.5°$	framework[49]
$BaTi_4O_9$		–	–	$Pmmn$	$a = 14.527$, $b = 3.794$, $c = 6.293$	framework[50]
$Ba_2Ti_6O_{13}$		–	–	$C2/m$	$a = 15.004$, $b = 3.953$, $c = 9.085$, $\beta = 98.01°$	framework[51]
$BaO-Fe_2O_3-TiO_2$						
$Ba_2Fe_2Ti_4O_{13}$		–	–	$C2/m$	$a = 15.216$, $b = 3.898$, $c = 9.135$, $\beta = 98.46°$	A,[52] framework
$Ba_3Fe_{10}TiO_{20}$		–	–	$I2/m$	$a = 15.379$, $b = 11.837$, $c = 5.1845$, $\beta = 91.237°$	B,[32] framework
$BaFe_4Ti_2O_{11}$	6	$(h)_6$	2.264	$P6_3/mmc$	$a = 5.843$, $c = 13.604$	1:2:2[38]
$Ba_{12}Fe_{28}Ti_{15}O_{84}$	8	$(cchc)_2$	2.365	$C2/m$	$a = 9.988$, $b = 17.298$, $c = 19.170$, $\beta = 99.33°$	12:14:15[39]
$Ba_4Fe_2Ti_{10}O_{27}$	8	$(cchh)_2$	2.346	$C2/m$	$a = 19.870$, $b = 11.449$, $c = 9.909$, $\beta = 109.19°$	C[32]
$Ba_6Fe_{45}Ti_{17}O_{106}$	8	$(ch)_4$	2.338	$C2/m$	$a = 19.39$, $b = 20.26$, $c = 10.076$, $\beta = 105.27°$	D[42]
$BaFe_{11}Ti_3O_{23}$	8	$(ch)_4$	2.355	$C2/c$	$a = 19.561$, $b = 8.661$, $c = 10.120$, $\beta = 105.62°$	D′[42]
$Ba_4Fe_4Ti_3O_{16}$	10		2.374		$a = 5.7618$, $c = 23.738$	E
$Ba_4Fe_{28}Ti_5O_{56}$	5	$(chcch)$	2.359	$C2/m$	$a = 10.032$, $b = 17.441$, $c = 12.235$, $\beta = 105.43°$	F[40]
$Ba_4Fe_{28}Ti_5O_{56}$	10	$(chcch)_2$	2.366	$C2/c$	$a = 10.024$, $b = 17.378$, $c = 24.627$, $\beta = 106.15°$	F′[40]
$Ba_{11}Fe_2Ti_{26}O_{66}$	10	$(ccchh)_2$	2.332	$C2/c$	$a = 23.321$, $b = 11.384$, $c = 9.847$, $\beta = 90.09°$	G[34]
$Ba_5Fe_4Ti_{10}O_{31}$	18	$(chhhhhhhc)_2$	2.346	$P6_3/mmc$	$a = 9.9886$, $c = 42.226$	I[41]
$Ba_{27}Fe_{16}Ti_{33}O_{117}$	54	$(cchcchhhhcchhhhcch)_3$	2.354	$R\bar{3}m$	$a = 5.750$, $c = 127.10$	J[37]
$Ba_8Fe_{10}Ti_8O_{39}$	26	–	2.362	–	$a = 9.977$, $c = 61.41$	K[1]
$Ba_6Fe_4Ti_7O_{26}$	42	–	2.353	–	$a = 5.736$, $c = 98.84$	L[1]
$Ba_{11}Fe_8Ti_9O_{41}$	26	$(chcchchcchc)_2$	2.365	$P6_3/mmc$	$a = 5.754$, $c = 61.482$	M[35]
$Ba_2Fe_2Ti_2O_9$		–	–	–	–	N[1]

yield magnets, albeit with reduced dielectric constants. Superexchange, the prevalent magnetic interaction in insulating oxides,[22] produces antiferromagnetic spin alignments, reducing the overall possible magnetic moment of the material. Since the X-ray contrast between Fe and Ti is small, investigations studying the ordering of Fe and Ti may

need the use of synchrotron radiation tuned to the Fe or Ti absorption edge, or neutron diffraction experiments. High-resolution electron microscopy may also be utilized to study the ordering of Fe in such pseudo-quaternary phases.[23]

3. Structural Units

The structural motifs observed in the hexaferrites and the barium polytitanates are few, and so allow classification of the large variety of structures observed in these systems. Stacking sequences, on the other hand, may extend over many layers in one direction. Table 1 compiles the unit cell parameters and stacking sequences for various phases present in the $BaO-Fe_2O_3-TiO_2$ system. The structural motifs observed in the pseudobinary systems are briefly discussed here.

The following color scheme has been adopted for the representation of structures: barium atoms: green or yellow spheres; tetrahedral iron: red tetrahedron; pentagonal iron: gold bipyramid; octahedral iron: dark blue octahedron; octahedral titanium: light blue octahedron.

3.1. Spinel-Type Layers (S-Block)

The spinel-type structure of Fe_3O_4 is based on a close-packed oxygen lattice, with iron present in tetrahedral and octahedral interstitial sites. It should be noted that Fe_3O_4 is a mixed valent system, and so does not meet the criterion of Fe^{3+} ions only. However, since its structural features are prominent, it is described separately here. The layer stacking is $(c)_n$. There are two distinct layers: one with edge-sharing octahedra (sP1 layer), and the other with a 1:2 combination of octahedra and tetrahedra, connected through the corners (sP2 layer) (Figure 2). Three layers, stacked sP2−sP1−sP2, form an "S-block", of Fe_3O_4 stoichiometry with an average layer thickness of 2.33 Å.

3.2. Magnetoplumbite-Type Layers (R-, T-, and Q-Block)

Barium hexaferrite $BaFe_{12}O_{19}$, crystallizes in the magnetoplumbite-type structure,[7,24] containing spinel-type S- and R-blocks. The R-block incorporates pentagonal iron, found in a trigonal bipyramid sandwiched between spinel (sP1) layers. The position of the iron atom in the basal plane of the pyramid is unstable, resulting in displacements that move the iron atom into one of the oxygen tetrahedra in a random way. Two face-sharing FeO_6 octahedra and one barium atom complete the R-block unit. The close-packed oxygen lattice in the R-block has an $(h)_3$ stacking sequence, which gives an overall stacking sequence for the magnetoplumbite-type of $(hhhcc)_2$ (ten-layer structure) with an average layer thickness of 2.318 Å. The individual layers are shown in Figure 2. $BaFe_{12}O_{19}$ is also referred to as hexaferrite M, on the basis of phase diagram studies by Smit and Wijn.[25,7]

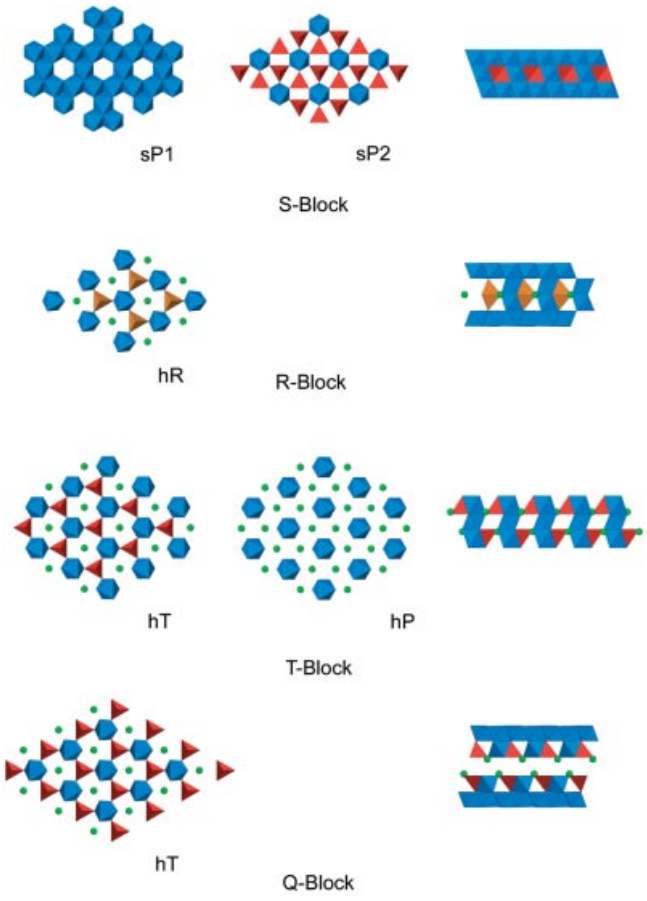

Figure 2. Close-packed layers found in spinel and hexaferrite phases; barium atoms are shown as green spheres, iron octahedra are indicated in dark blue, iron tetrahedra in red, and trigonal bipyramids in gold; the hexaferrites are made up of five different layers only

In hexaferrite Y, $Ba_2Fe_{14}O_{22}$ ($Ba_2Zn_2Fe_{12}O_{22}$),[25] a combination of S-blocks and T-blocks is observed. The T-blocks are made up of three close-packed layers (see Figure 2) containing columns of three face-sharing octahedra. The iron−iron distances in these columns are of the order of 2.84 Å, so iron atoms are moved out of their ideal positions. These iron−iron contacts allow only three face-sharing octahedra, since shifts in a fourth octahedron would be too large. The hT layer (Figure 2) may be regarded as a spinel sP2 layer in which all of the down-pointing tetrahedra have been removed, and a barium atom replaces the apical oxygen. The middle layer hP, containing Ba and octahedra only, is of the same type as observed in the cubic and hexagonal perovskite. The T-block may also be described as a modified R-block, in which the two tetrahedra forming the bipyramids are separated by a layer of octahedra, and are rotated by 60°.

The Q-block, found in iron and chromium ferrites, is related to the T-block in such a manner that the octahedral interstitial sites in the middle layer are not occupied (Figure 2).[26,27] A large number of hexaferrite phases can be described on the basis of the combinations of Q-, R-, S-, and T-blocks. Apart from $BaFe_{12}O_{19}$ (M),[28] for instance,

the hexaferrite phases $BaFe_{18}O_{27}$ (W), $Ba_2Fe_{14}O_{22}$ (Y), $Ba_3Fe_{26}O_{41}$ (Z), and $Ba_2Fe_{30}O_{46}$ (M_2S)[7] have been reported. With the exception of $BaFe_{12}O_{19}$, they show reduced iron valence, and are stabilized by the introduction of divalent atoms such as zinc, magnesium, or cobalt, or of mixtures such as Li^{1+}/Fe^{3+}. Some of these phases, with their stacking sequences and combinations of R-, S-, and T-blocks, are illustrated in Figure 3. For instance, $Ba_2Fe_{30}O_{46}$ is structurally a combination of $BaFe_{12}O_{19}$ and $BaFe_{18}O_{27}$, representing the M2S member, with block arrangement ($RSRS_2$).

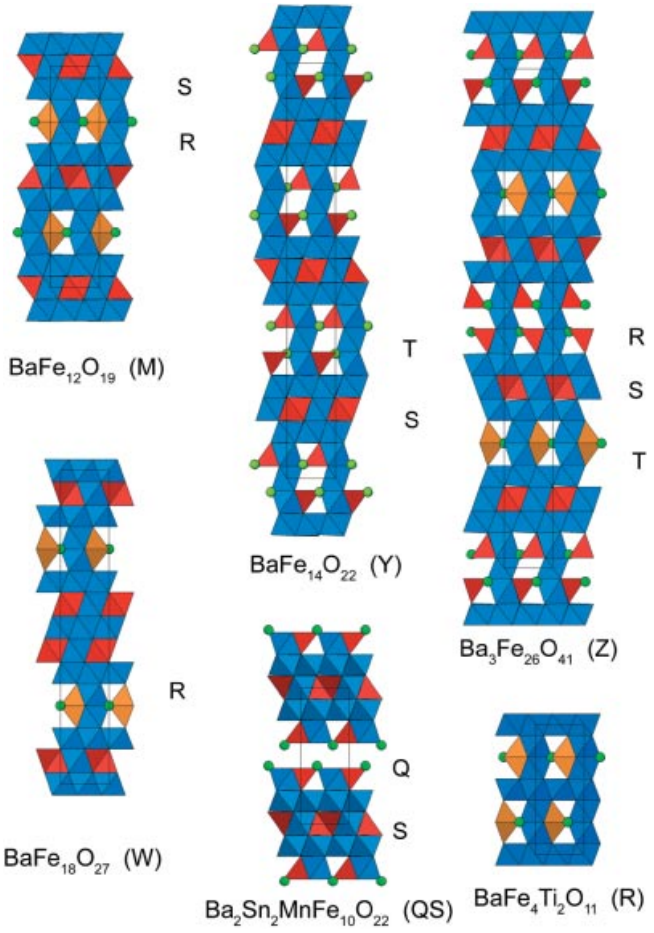

Figure 3. View of stacking sequences of hexaferrite phases M, W, Y, Z, and QS; barium atoms are shown as spheres, iron octahedra are indicated in blue, tetrahedra in red, and bipyramids in gold; hexaferrite building blocks shown in Figure 2 are indicated

The long-period superstructures observed may be described as stacking of different blocks in various ways, combinations, and periodicities.

3.3. Barium Polytitanates

The $BaO-TiO_2$ system contains a large number of phases, nearly all of which feature structures based on close-packed {O,Ba/O} lattices.[6] Mixed-valent barium titanate phases containing Ti^{3+}/Ti^{4+} mixtures have also been prepared and characterized; examples are the hollandite-type $Ba_2Ti_6O_{13}$[29] and the hexagonal 6L $Ba_2Ti_{13}O_{22}$.[22,30]

Only the cubic and hexagonal barium polytitanates are considered below, since these systems are based on close-packed {O,Ba/O} layers and tetravalent titanium in octahedral interstitials. Reduced titanium, Ti^{3+}, detrimentally affects the microwave properties. Barium titanate phases are compiled in Table 1.

The simplest structure present in the $BaO-TiO_2$ system is the well-known cubic perovskite $BaTiO_3$.[12] It may be regarded as a cubic stacking of close-packed layers with a thickness of 2.306 Å, a value expected to be close to the lower limit, since only corner-connected octahedra are present. Projection of the structure along one of the four close-packed stacking directions {111} shows the titanium octahedra well separated by barium atoms (Figure 4), and the same as the hP layer observed in the hexaferrite T-block.

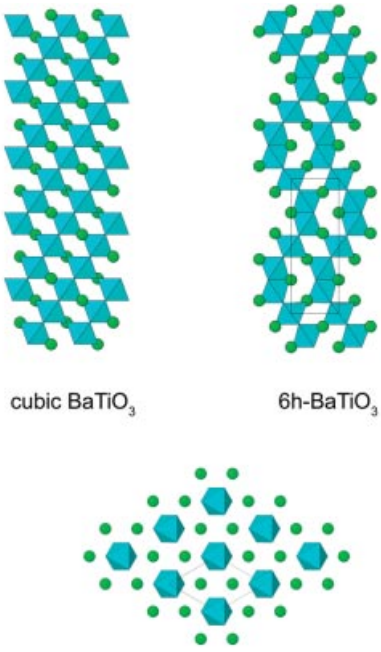

Figure 4. View of the stacking sequence for the cubic and hexagonal perovskite $BaTiO_3$; below is a depiction of a single perovskite layer, common to both structures; barium atoms are shown as green spheres, titanium octahedra are light blue, oxygen is found at the corners of the octahedra

The hexagonal 6H-$BaTiO_3$ structure[13,31] (Figure 4) has a stacking sequence $(cch)_2$ with an average layer thickness of 2.327 Å. It can be viewed as a cubic perovskite type, in which units of three layers are rotated by 180° and stacked on top of the previous layer, resulting in face-sharing titanium octahedra. The titanium−titanium distance in this double layer is increased from 2.327 to 2.69 Å, and so the metal atoms are moved away from the center of the octahedra. In general, face-sharing octahedra in titanates are observed in pairs, unlike in ruthenates, platinates, or nickelates, in which longer face-sharing chains of metal octahedra are found.[22] In an extended face-sharing arrangement, short Ti−Ti contacts of the order of 2.35 Å would be expected from the average layer thickness imposed by the oxygen−oxygen contacts, making such extended systems unstable.

The phases in the $BaO-TiO_2$ system may be written as $(BaO)_m(TiO_2)_n$, with $m = n = 1$ representing the simple $BaTiO_3$, with all tetravalent Ti. Alkaline earth rich titanates are not abundant, with Ba_2TiO_4 being the ($m = 2$, $n = 1$) phase, in which Ti is in tetrahedral coordination.[14] In contrast, a whole series of phases with ($m = 1$, $n = 2$, 4, 5, 6), ($m = 2$, $n = 5$, 9), ($m = 4$, $n = 11$, 13), and ($m = 6$, $n = 17$) have been reported and structurally characterized.[6] Most of these are based on close-packed {O,Ba/O} layers, with Ti in octahedral sites. The octahedra are connected through corners, edges, or faces, giving various stacking sequences. The framework structures of $BaTi_2O_5$, $BaTi_4O_9$, and $Ba_2Ti_{6-x}O_{13}$ (reduced) were discussed further by Tillmanns,[6] and are not considered further here.

Figure 5 shows the different close-packed layers found in $Ba_6Ti_{17}O_{40}$, $Ba_4Ti_{13}O_{30}$, $Ba_2Ti_9O_{20}$, $BaTi_5O_{11}$, and $BaTi_6O_{13}$.[6] The average layer thickness in these compounds is of the order of 2.34 Å. All these systems can be described in terms either of two or of three distinct topological layers. They combine edge- and corner-sharing octahedra only, without any face-sharing octahedra observed. The layers are often complementary in such a way that two or three layers cover an entire plane with octahedra by merging with shear, as for instance in $BaTi_6O_{13}$ and $BaTi_5O_{11}$, thus avoiding face-sharing octahedra.

It is interesting to note that $Ba_4Ti_{13}O_{30}$ [10] is the only phase in which the close-packed layers consist of discrete building blocks that do not form an extended unit. All the other phases have at least one close-packed layer with a one-dimensional chain-type building unit. The discrete building units within each plane are all of the same type; no combination of different units within a plane is observed for the polytitanates.

4. The $BaO-Fe_2O_3-TiO_2$ System

In contrast to the barium polytitanates, the barium hexaferrites show extended, two-dimensionally connected polyhedron arrays, generally resulting in higher symmetry structures. In combinations of the two systems, new types of intermediate structural building blocks would be expected. Indeed, exhaustive study of the $BaO-Fe_2O_3-TiO_2$ phase diagram revealed several new phases.[1] The nomenclature introduced in the phase diagram study is used below (Figure 1).

The five regions identified in the phase diagram are composed of: I. hollandites and framework structures (yellow); II. polytitanate-based systems (light blue); III. magnetic multilayer systems (blended hexagonal perovskite/hexaferrites(violet/gray); IV. hexaferrites and related phases, such as 1:2:2 (dark blue), and V. new family of mixed $BaO-Fe_2O_3-TiO_2$ phases (red).

4.1. Hollandites and Framework Structures (Yellow)

The systems based on framework-type structures are located near the titanium-rich corner of the phase diagram. The hollandite-type phases are in equilibrium with the framework-type phases 1:4 and A, the hexagonal systems 2:9, C and D, the pseudobrookite Fe_2TiO_5, and the hexaferrite-related 1:2:2.

4.2. Polytitanate-Based Systems (Light Blue)

The new phases C and G are in equilibrium with complex polytitanates, such as the phases 6:17 and 4:13, as well as with the cubic and hexagonal perovskites. Furthermore, phases C and G are in equilibrium with each other, which is reflected in the close structural relationship between them.

The layer stacking of phase C, $Ba_4Fe_2Ti_{10}O_{27}$,[32] and phase G,[33] $Ba_{11}Fe_2Ti_{26}O_{66}$,[34] is shown in Figure 6. The 8L structure of $Ba_4Fe_2Ti_{10}O_{27}$ is expanded into the 10L structure of $Ba_{11}Fe_2Ti_{26}O_{66}$ by repetition of the starting layer of every four-layer block. Phase G, $Ba_{11}Ti_{28}O_{66+x}$,[34] containing trivalent Fe, may be written as $Ba_{11}Fe_2Ti_{26}O_{66}$, but is likely to be intermediate, depending on preparation conditions such as oxygen partial pressure. It is easy to see that the close structural relationship of these two systems allows formation of intergrowths. Ordered superstructures based on the regular arrangement of blocks of four and five layers can produce a potentially large number of long-period superstructures. Further electron microscopy studies may reveal the presence of such ordered superstructures. In addition, both phases C and G introduce new close-packed layers in which, unlike in the pseudo-binary systems, two different building blocks are present within a layer. Isolated TiO_6 octahedra coexist with either Ti_5O_9 units or Ti_3O_{14} units.

4.3. Magnetic Super-Lattices (Blended Hexagonal Perovskites/Hexaferrites) (Violet/Gray)

The cubic and hexagonal perovskites $BaTiO_3$ are in equilibrium with the ternary phases A, C, E, G, I, J, K, L, M, N, and 12:14:15, as well as titanium-substituted barium hexaferrite. The new phases E, K, L, M, and N have previously been studied by high-resolution electron microscopy,[2] and further structural information is available for phases J and M. Alternating stacks of hexagonal perovskites and of layers preferentially occupied by Fe are common features in these phases. For instance, phase M, $Ba_{11}Fe_8Ti_9O_{41}$[35] (Figure 7), is a 26L structure with stacking sequence $[(cch)_3(ch)_2]$. As indicated, three hexagonal perovskite (*cch*) stacks alternate with four modified layers consisting of two octahedral layers and two spinel-related layers. All four of these modified layers preferentially contain Fe. Separated by nine hexagonal perovskite layers, this phase forms a natural magnetic super-lattice.[2,36] In the case of phase M, the magnetic layers are located around $z = 1/4$ and 3/4, spaced approximately 30.7 Å apart, with a hexagonal perovskite separation stack of the order of 21 Å in thickness. The iron-rich layers, however, show strong disorder. For instance, the layer containing tetrahedra, octahedra, and Ba may be described as an overlay of the hP and hT layers. The apparent densely packed layer of edge-sharing octahedra shows reduced metal occupancy, and may be regarded as a combination of spinel sP1 and hP layers.

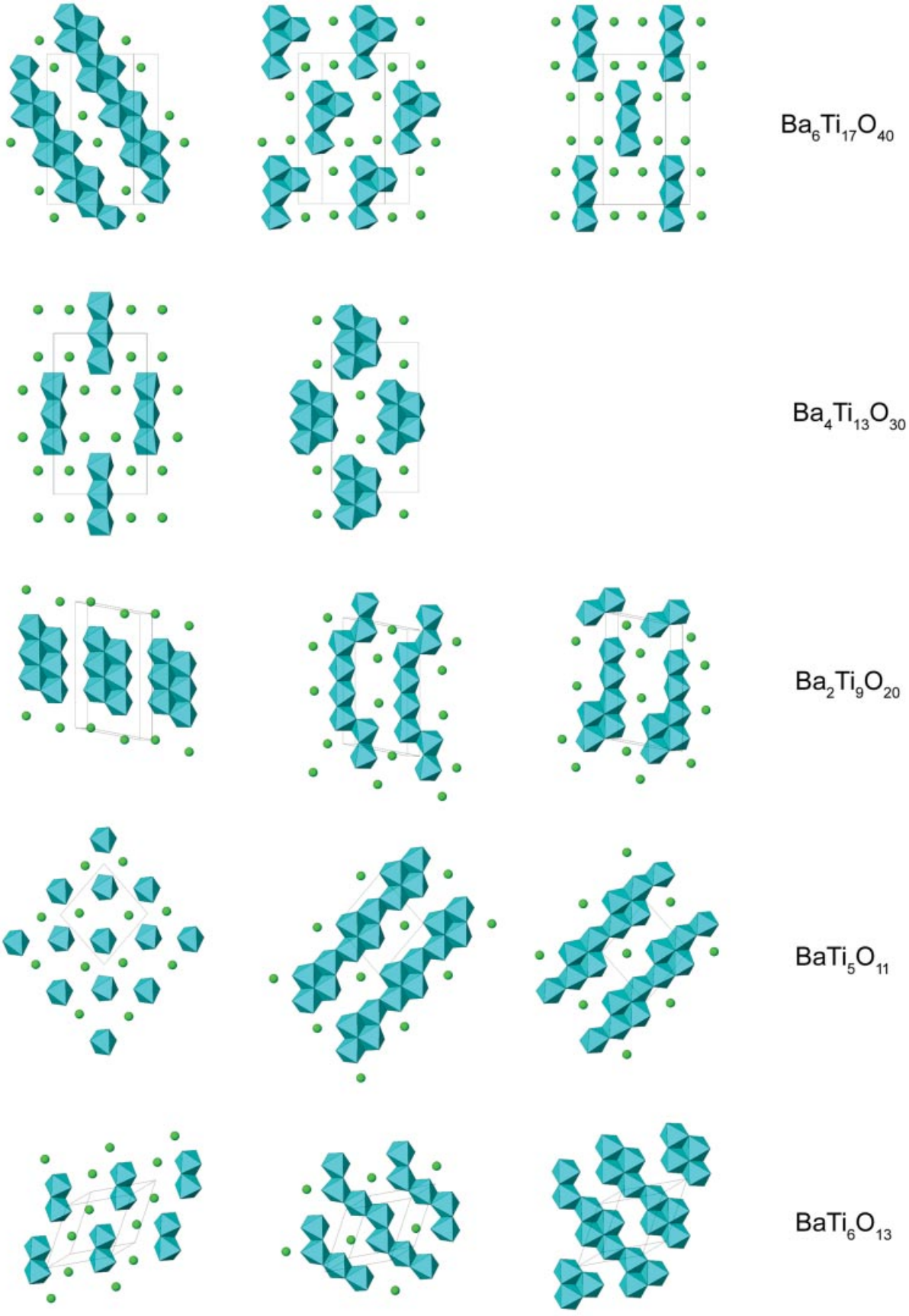

Figure 5. Compilation of the close-packed layers observed in hexagonal polytitanates; titanium octahedra are indicated in light blue and barium atoms are shown as green spheres; only $Ba_4Ti_{13}O_{30}$ has no extended building block

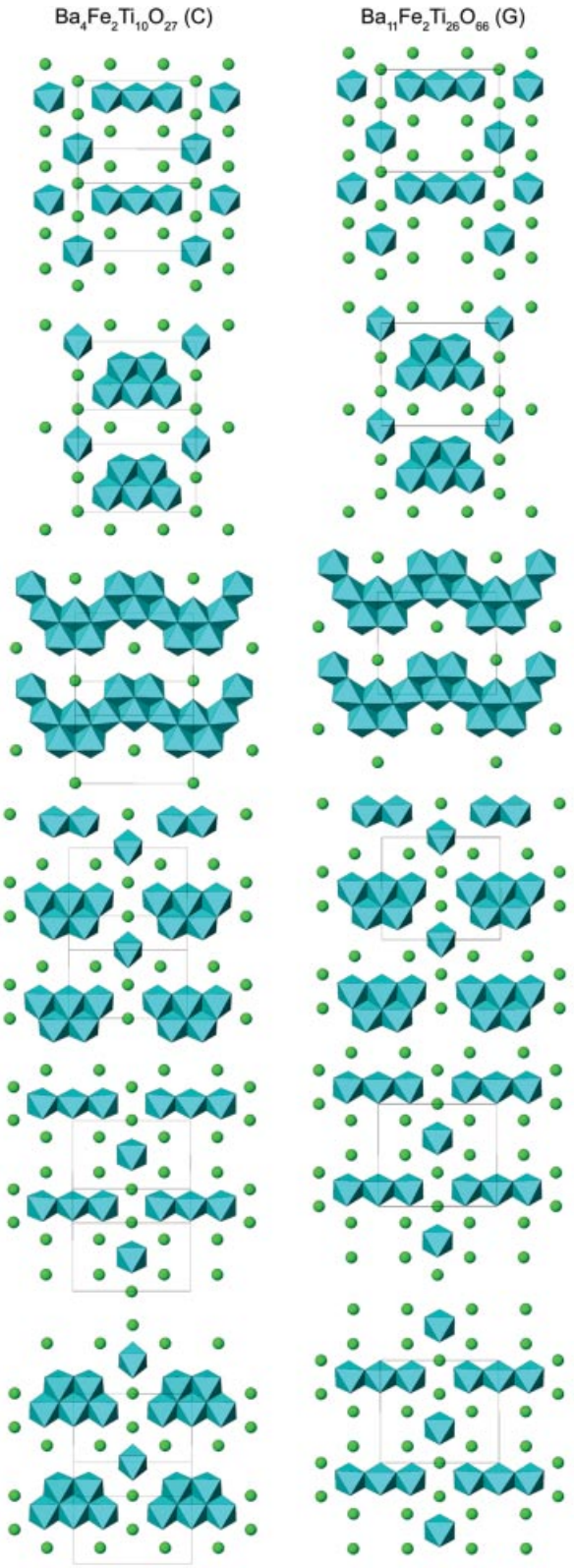

Figure 6. Close-packed layers of $Ba_4Fe_2Ti_{10}O_{27}$ (phase C) and $Ba_{11}Fe_2Ti_{26}O_{66}$ (phase G); the 8L structure of C is expanded into the 10L structure of G by repeating the starting layer in every four-block unit of phase C

Similarly, phase J (Figure 8), $Ba_{27}Fe_{16}Ti_{33}O_{117}$,[37] is based on the same building principle. It is a 54L structure with a $(cchcchhhhcchhhhcch)_3$ stacking sequence, previously described as an 18L monoclinic *C*-centered structure. Like phase M, it is a system with disorder and, to some extent, variable iron stoichiometry. As the stacking sequence indicates, the structure incorporates hexagonal perovskite (*cch*) blocks, alternating with iron-containing nine-layer blocks. Disorder similar to that in M, $Ba_{11}Fe_8Ti_9O_{41}$, is confined to those nine layers.[23,37] Furthermore, diffuse superstructure reflections observed in electron microscopy studies[2,36] indicate a possibly larger supercell.

While the structural characterization of phase E is not yet complete, preliminary investigations show that a hexagonal perovskite unit with a (*cch*) stacking sequence is again present, alternating with iron-containing layers. Furthermore, phases K, L, and N show similar building principles according to electron microscopy studies.[2] While the details of the structures need further elucidation, the overall building principle is well established, producing systems with magnetic iron blocks well separated by hexagonal perovskite blocks. These natural magnetic super-lattices may furthermore produce large supercells in which different blocks may be arranged in various ways. For instance, since J and L, as well as E and M, are in equilibrium, intergrowths are possible for these pairs of phases, giving rise to possible superstructures with *c* axes beyond 100 Å.

4.4. Hexaferrites and Related Phases (Dark Blue)

Phase 1:2:2, $BaFe_4Ti_2O_{11}$, is a hexaferrite-related system consisting of R-blocks only.[38] It is in equilibrium with phase 12:14:15, the framework-type phase A, the hollandites, and phases D and F. Interestingly, the magnetoplumbite $BaFe_{12}O_{19}$ is not in equilibrium with 1:2:2, despite the close structural relationship. Since the iron-only R-block $BaFe_6O_{11}$ has a net charge, the inclusion of two tetravalent titanium atoms renders the block neutral, resulting in the formation of phase 1:2:2. Similar stabilization might be expected from substitution of Zr^{4+} or Hf^{4+} for Fe.

Magnetoplumbite-type $BaFe_{12}O_{19}$ (hexaferrite M) has a solid solution range with TiO_2. It is in equilibrium with $BaFe_2O_4$, a hexagonal phase containing tetrahedral Fe only, Fe_2O_3, phases B, E, M, $Ba(Fe,Ti)O_3$, K, 12:14:15, D, and F. In Figure 1, the connection from the hexaferrites via the magnetic superlattice phases to the hexagonal perovskites is clearly seen. The large number of different types of hexaferrites, however, are not seen in the phase diagram since most of them require slightly reducing conditions upon preparation. The exception is phase 1:2:2, which is neutral. Intergrowths are to be expected on crystal chemical grounds, but are not observed in the phase diagram.

4.5. New Family of Ternary $BaO-Fe_2O_3-TiO_2$ Phases (Red)

New structures are found in the general transition-metal-rich part of the phase diagram, with an iron/titanium ratio ranging approximately from 4:1 to 1:2. These phases are characterized by the presence of fourfold tetrahedral and also fivefold bipyramidal Fe in new arrangements. The

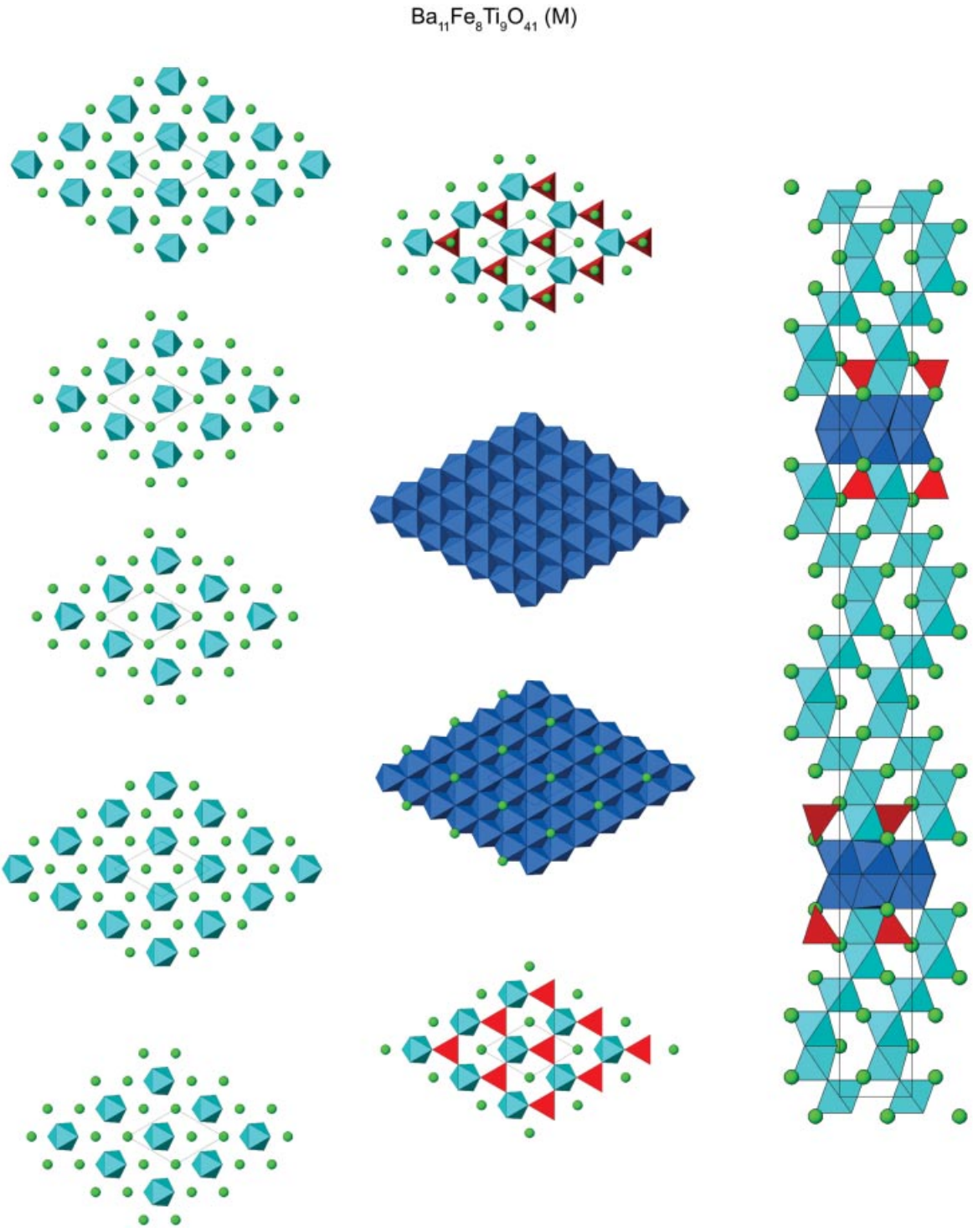

Figure 7. View of the close-packed layers and stacking arrangement of $Ba_{11}Fe_8Ti_9O_{41}$ (phase M), a 26L natural magnetic super-lattice in which iron-containing layers are separated by the hexagonal perovskite motif; disorder is confined to the iron-containing layers only, in which barium atoms randomly replace oxygen atoms; adjacent iron atoms show reduced occupancy corresponding to the barium occupancy factor

structural features show a strong relationship to spinel and magnetoplumbite. In the case of $Ba_{12}Fe_{28}Ti_{15}O_{84}$[39] there are five distinct layers, shown in Figure 9. There is a modified spinel-type layer (sP2) in which two tetrahedra are replaced by barium atoms (layer S1), and one in which five tetrahedra are replaced by barium atoms (layer S2). The latter may also be regarded as an hT layer in which two thirds of the tetrahedra have been removed. Layers containing octahedra only show symmetrical Ti_6O_{22} clusters made up of six edge-sharing octahedra (layer T1). Further,

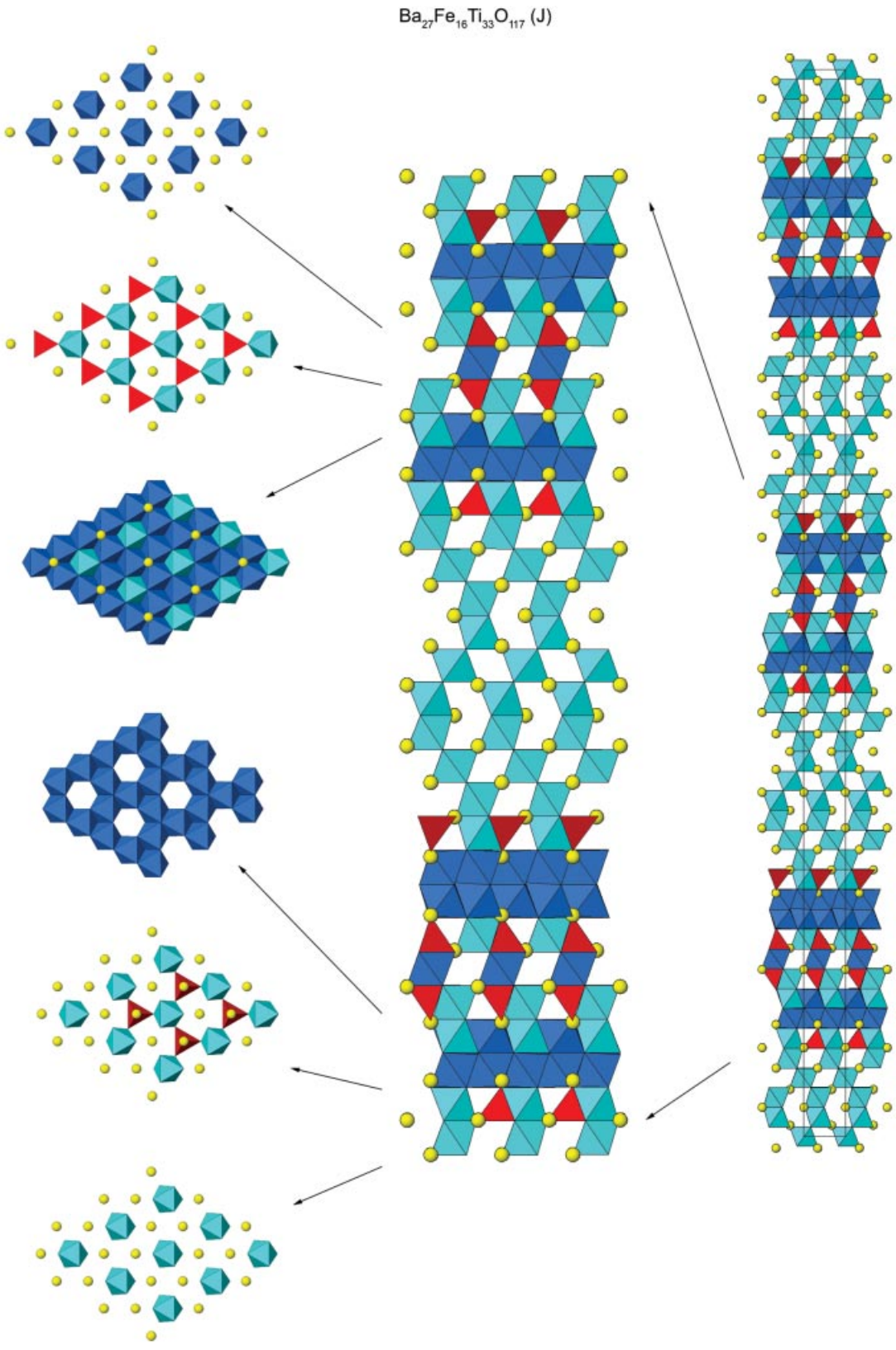

Figure 8. View of the close-packed layers and stacking arrangement of $Ba_{27}Fe_{16}Ti_{33}O_{117}$ (phase J), a 54L natural magnetic super-lattice; the rhombohedral structure has an 18L unique substructure with the hexagonal perovskite motif; disorder similar to that in phase M is observed in the iron-containing layers

layers with extended octahedron frameworks (T2), and finally hP perovskite-type-related layers in which half of the octahedra have been removed (layer P) make up the structure. These five different layer types produce the observed

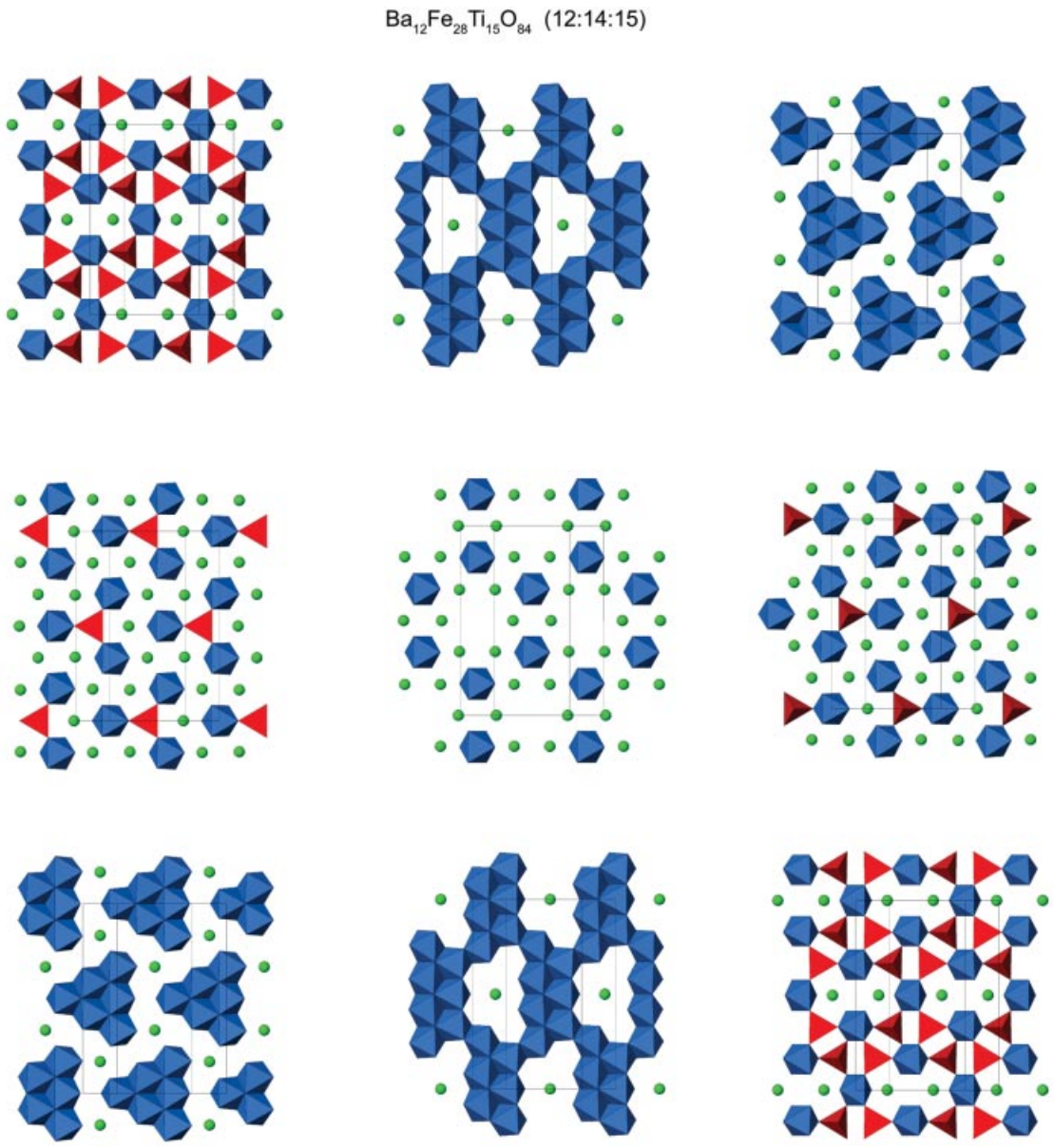

Figure 9. View of the close-packed layers of $Ba_{12}Fe_{28}Ti_{15}O_{84}$ (phase 12:14:15); four new layer types, intermediate between hexaferrite/spinel and polytitanate layers, are observed

8L structure with an {S1−T2−T1−S2−P−S2−T1−T2−S−...} stacking sequence.

The layers S1, T1, and T2 are again present in phase F, $Ba_4Fe_{28}Ti_5O_{56}$ (Figure 10),[40] in an {S1−T2−T1−T1−T2−S1−...} stacking sequence. Two modifications with this stacking were observed, the layers showing different relative orientations. The hexagonal symmetry of the T1 layer allows the orientation of the subsequent T2 layer to be changed by 120°. Superstructures with complicated stacking sequences are therefore possible for these systems. For instance, a more symmetrical unit cell may be produced by the stacking of 15 layers, with subsequent rotation of each five-layer block by 120°. Indeed, a unit cell indicating a 15L structure was previously observed for phase F.[1]

A further layer type is found in phase I, $Ba_5Fe_4Ti_{10}O_{31}$[41] (Figure 11), in equilibrium with $BaTiO_3$ and $Ba_2Fe_2Ti_4O_{13}$, as well as with $Ba_4Fe_2Ti_{10}O_{27}$ (phase C). Phase I is closely related to $Ba_{12}Fe_{28}Ti_{15}O_{84}$, with the S2 and T1 layers present, together with a modified T2′ layer. The T2′ layer derives from the T2 layer by removal of one octahedron to render the layer more symmetric. The combination of the T1 and T2′ layer again shows the principle of full plane coverage with two distinct layers, A new modified R-block of two close-packed layers R1 completes the 9L substructure found in this hexagonal 18L system. The modified R-block R1 shows a similar feature of substitution of barium for a tetrahedron, or, in this case a trigonal bipyramid. The resulting layers show a two-dimensional framework more open than the corresponding hexaferrite R-block.

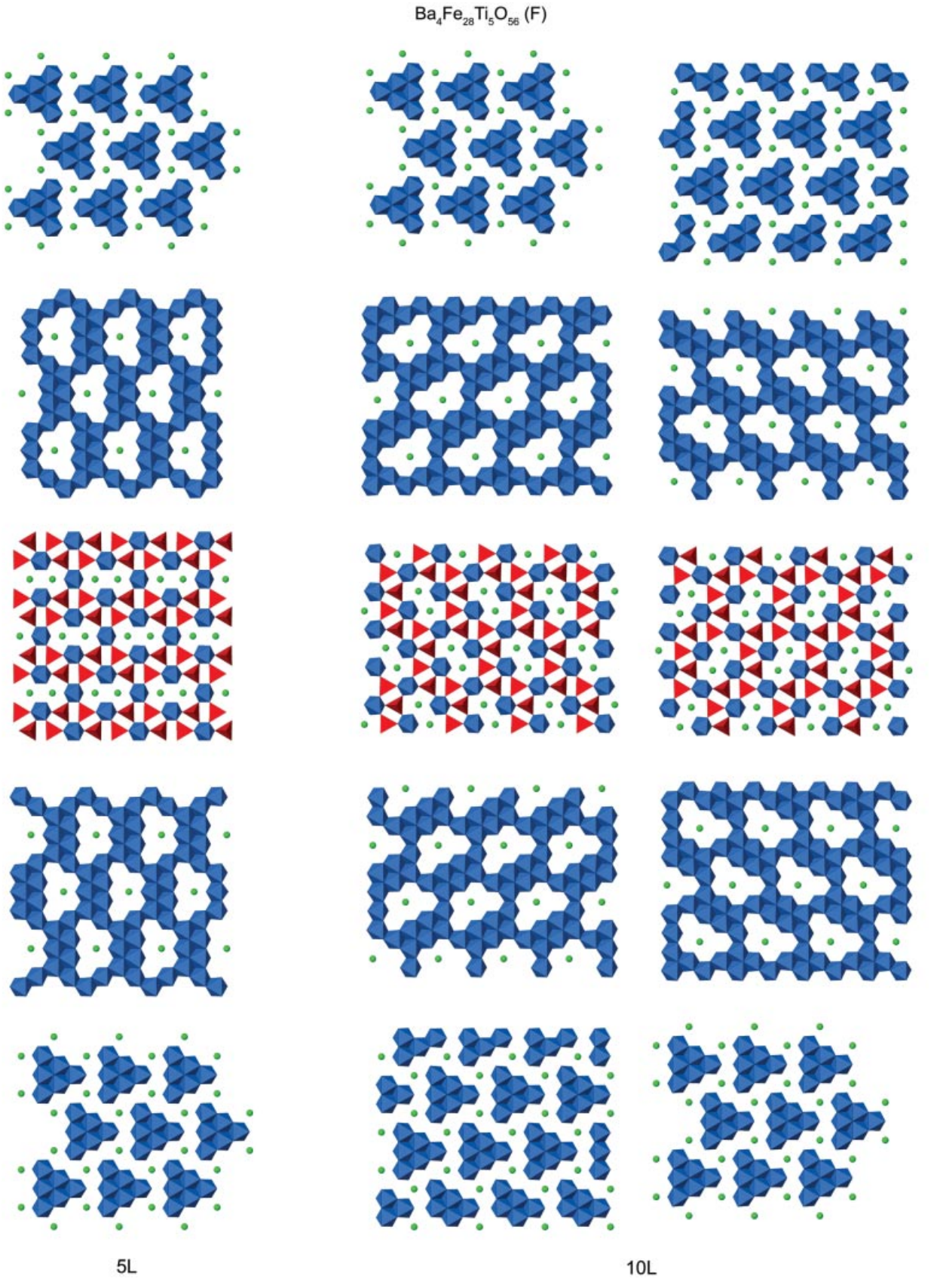

Figure 10. View of the close-packed layers of $Ba_4Fe_{28}Ti_5O_{56}$ (phase F); the 10L superstructure (right) can be derived from the 5L substructure (left) by rotation of the second layer depicted by 120°; only three of the five different layers of $Ba_{12}Fe_{28}Ti_{15}O_{84}$, are present, in the same relative arrangement

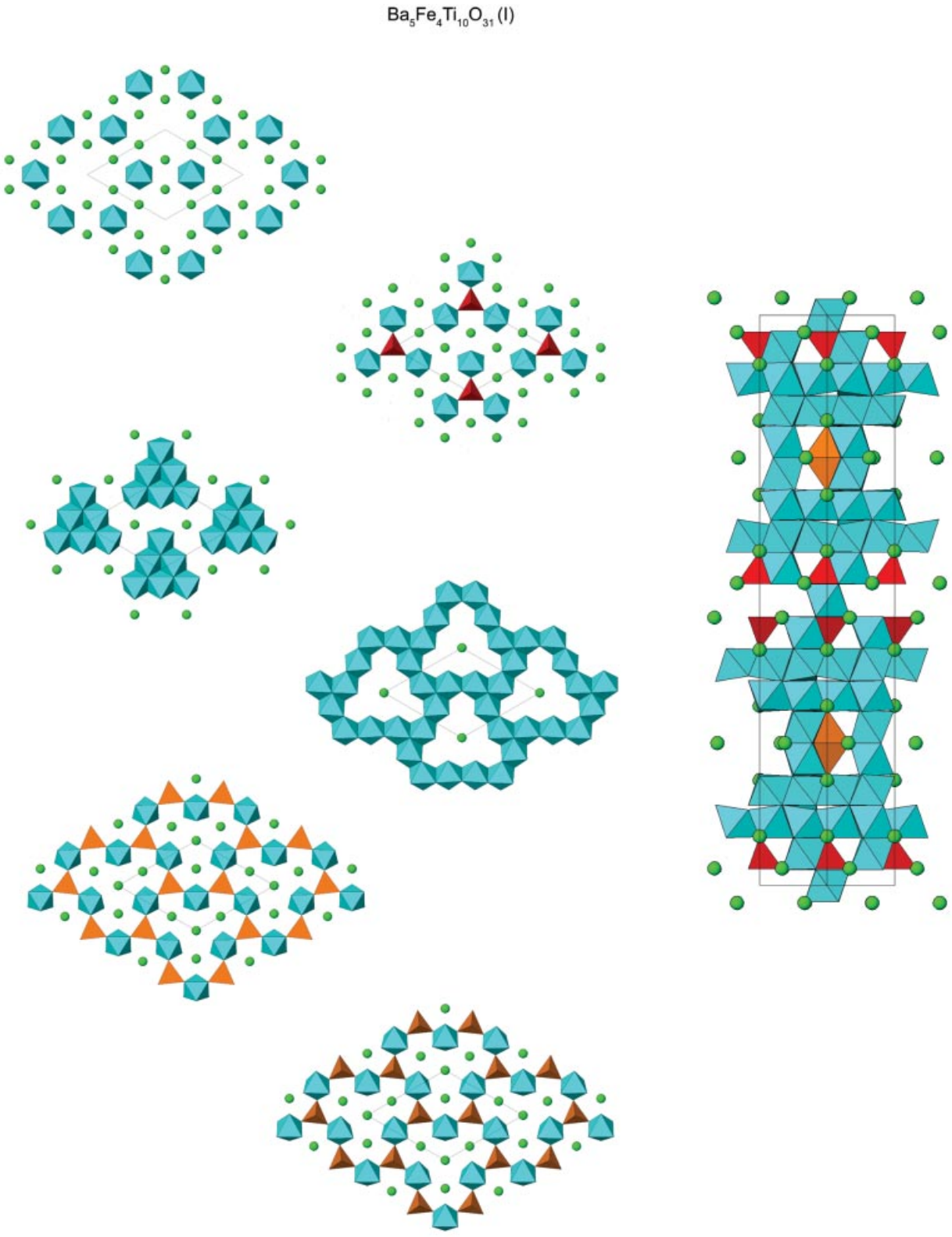

Figure 11. View of the close-packed layers and stacking arrangement of $Ba_5Fe_4Ti_{10}O_{31}$ (phase I); three of the six layers are identical to layers found in $Ba_{12}Fe_{28}Ti_{15}O_{84}$; furthermore, a modified R-block is seen

The stacking sequence in phase I is very similar to that in $Ba_{12}Fe_{28}Ti_{15}O_{84}$. In phase I, it is {P−S2−T1−T2′−R1−T2′−T1−S2−P−...}, in comparison with {P−S2−T1−T2−S1−T2−T1−S2−P−...}. In this respect, phase I ($Ba_5Fe_4Ti_{10}O_{31}$) may be regarded as a modified version of 12:14:15, $Ba_{12}Fe_{28}Ti_{15}O_{84}$. Unlike in

$Ba_{12}Fe_{28}Ti_{15}O_{84}$, the hexagonal symmetry is retained in $Ba_5Fe_4Ti_{10}O_{31}$, due to the higher symmetry of the R1 and T2′ layers, and the absence of the lower symmetric S1 layer. Even though the two structures are closely related in their crystal chemistry, they are not in equilibrium, and so intergrowth of the two would not be expected to occur under the given growth conditions. Interestingly, phase I displays an unusual barium coordination of 9+3 oxygen atoms in which the barium atom is shifted out of the close-packed plane, creating three short bonds of 2.74 Å and three long bonds of 3.50 Å.

A potentially large number of superstructures based on the various S1, S2, T1, T2, T2′, P1, and R1 layers (shown in Figure 12), may be envisioned. Furthermore, possible intergrowth structures produced under different growth conditions allow some degree of stoichiometric variation. Indeed, observed unit cells show lattice parameters up to about 40 Å, and larger superstructures are possible.

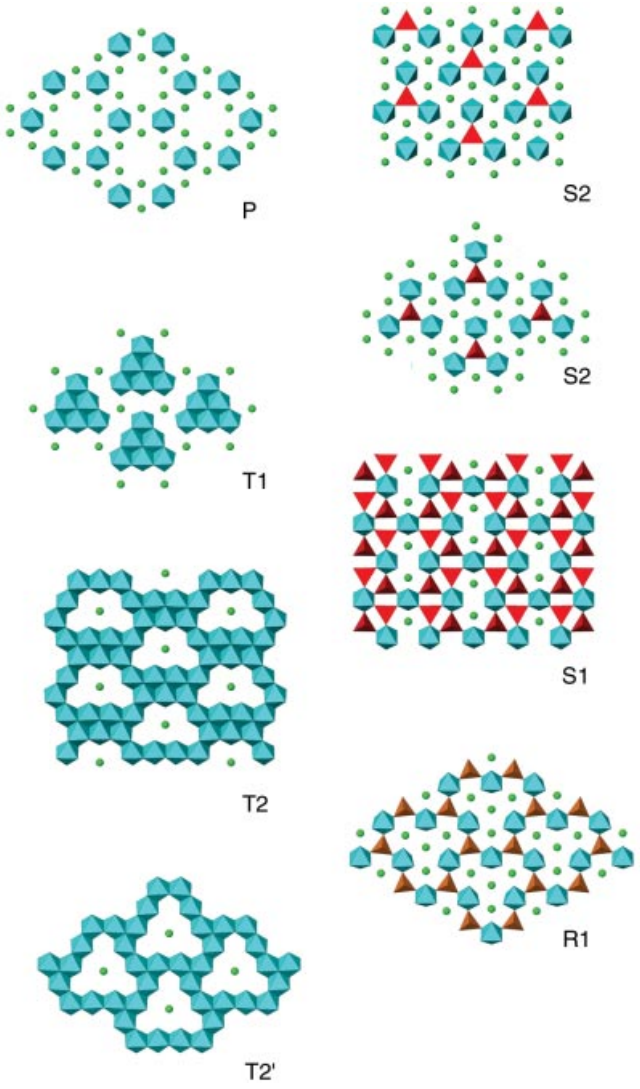

Figure 12. View of the seven different close-packed layers found in the new $BaO-Fe_2O_3-TiO_2$ phases; the close relationship to the T2 and T2′ layers can clearly be seen; the S1 and S2 layers are related to spinel-type layers, as are T2 and T2′ layers; the P and T1 layers are related to perovskite-type layers, and the R1 layers is related to the R-block layers in hexaferrite

Phases D, $Ba_6Fe_{45}Ti_{17}O_{106}$ and D′, $BaFe_{11}Ti_3O_{23}$, which are related,[42] are shown in Figure 13. The two distinct close-packed layers in phase D show a new building principle: the combination of different building units as described above within a single layer. For instance, a hexaferrite T-block layer composed of tetrahedra, octahedra, and Ba is combined with the previously described "ring" structure from a T2′ layer. Every second row of rings in the T2′ layer is split and expanded by the width of one octahedron to accommodate the three tetrahedra around an octahedron and the barium atom. In a similar way, the second layer is made up of the Ti_6O_{22} motif from the T1 layer in combination with the spinel-type sP1 layer of connected octahedra. In this respect, phase D may be regarded as a special intergrowth of the spinel-type structure and phase I, in which the combination is within the close-packed layers.

Phase D′, $BaFe_{11}Ti_3O_{23}$, is also composed only of two distinct layers (Figure 13). The structural motifs are related to the spinel-type structure, in which, in addition to Ba, the sP1 and sP2 layers are combined. As a result, phase D′ contains one-dimensional chains within a close-packed layer based on the substitution of barium for tetrahedra.

5. Dielectric Behavior

The dielectric response of a material may be described by use of the Clausius−Mosotti theory. This approach is valid for frequencies well below typical phonon frequencies in a solid-state material, and far from possible resonances due to magnetic atoms. In the case of the $BaO-Fe_2O_3-TiO_2$ system, Fe does not show resonance behavior up to frequencies of a few GHz. The dielectric constant ε of a material is related to the polarizability α and the molar volume V_m, with α being the sum over all the individual polarizabilities of the atoms in the molar volume ($\alpha = \Sigma_i \alpha_i$), according to Equation (1).

$$\varepsilon = \frac{1+\frac{8\pi\alpha}{3V_m}}{1-\frac{4\pi\alpha}{3V_m}} \quad (1)$$

The individual polarizabilities have been tabulated,[43] and give reasonable values for the dielectric constant ε. To achieve a high dielectric constant, it is therefore necessary to pack large atoms that are easily polarized in as small a volume as possible. As a guide, the value of $(4\pi\alpha/3V_m)$ should be close to 1.0. In the case of cubic $BaTiO_3$, this expression is approximately 0.9975, giving a calculated ε value of 1200. If $(4\pi\alpha/3V_m)$ is exactly 1.0, the expression diverges, giving a nonphysical value, and values larger than 1.0 would result in negative dielectric constants. The temperature dependence of the dielectric constant is related to the thermal expansion coefficient, since, to first order, only

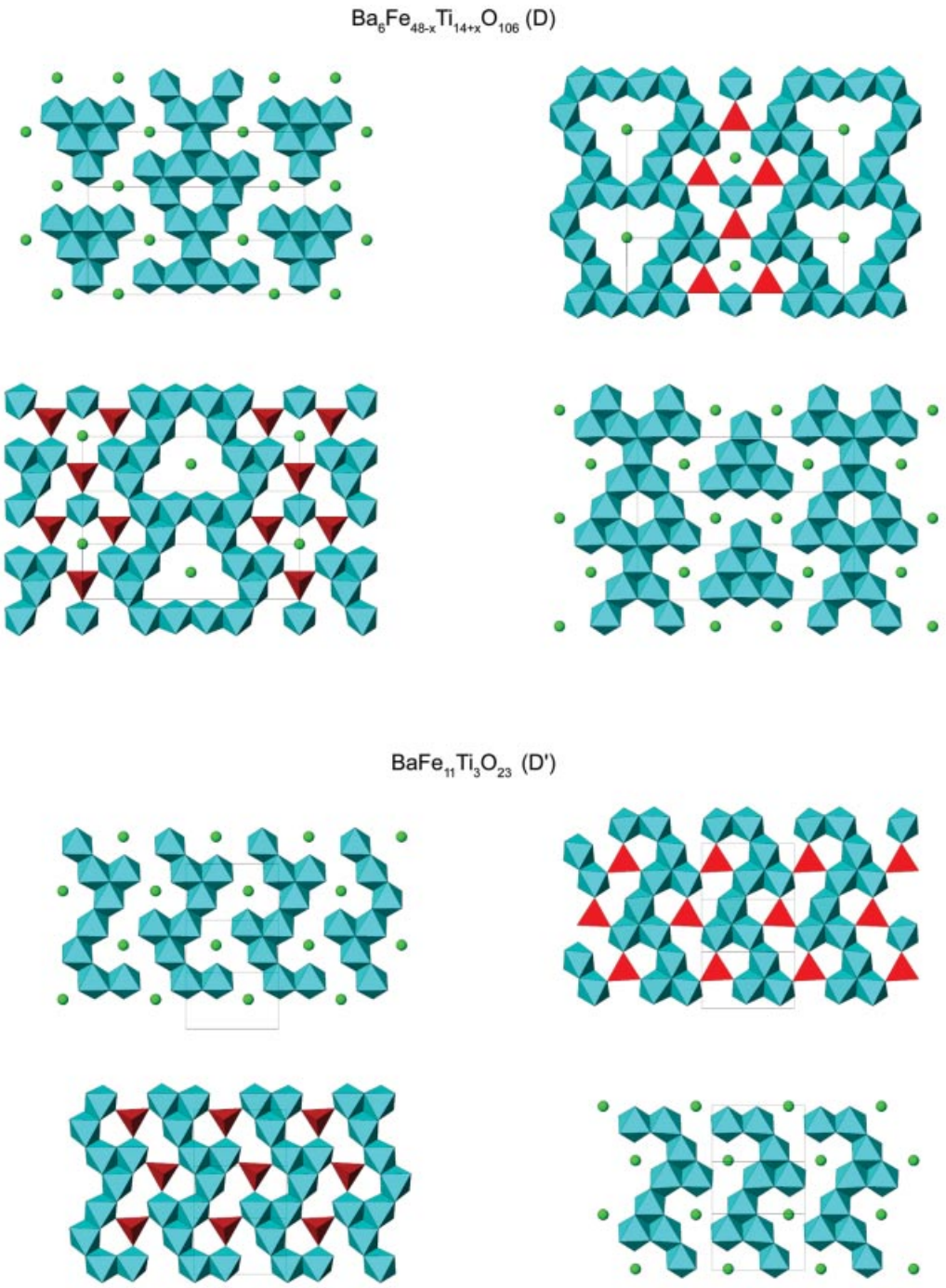

Figure 13. View of the close-packed layers in $Ba_6Fe_{48-x}Ti_{4-x}O_{106}$ (phase D, above) and $BaFe_{11}Ti_3O_{23}$ (phase D′, below); different building blocks are combined within a single close-packed layer; for instance elements of the T1 layer combines with the T2 layers, and elements of the T2′ layer combine with sP1 spinel-type layers in $Ba_6Fe_{48-x}Ti_{14+x}O_{106}$ (phase D); similarly, the combination of spinel-type elements and barium atoms within single layers are also observed for $BaFe_{11}Ti_3O_{23}$

the molar volume V_m has a temperature dependence of the form $V(T) = V_0(1 + \beta T)$. For technological use, a vanishing temperature dependence of ε is desirable, therefore excluding isotropic materials. Lower symmetry systems offer the opportunity of smaller temperature dependence of the molar volume, in which an expansion in one direction may be offset by a contraction in an other direction, resulting in a small or even zero overall thermal volume expansion coefficient. The values for atomic polarizabilities given are:[43] barium (Ba^{2+}) 6.40 Å^3; iron (Fe^{3+}) 2.29 Å^3; titanium (Ti^{4+}) 2.93 Å^3; oxygen (O^{2-}) 2.01 Å^3.

With these values, reasonable estimates of the dielectric constants of the phases found in the $BaO-Fe_2O_3-TiO_2$ system are obtained, assuming that the transition elements are in their expected valence states (i.e., no reduced titanium or reduced/oxidized iron atoms are present).

Estimated dielectric constants ε of a few selected compositions are given in Table 2. The values for the various compounds indicate the expected trend of lower dielectric constant with higher iron concentration, due to the reduced polarizability of iron versus titanium. Furthermore, higher barium concentrations would also be expected to increase the dielectric constant, as is reflected in the higher ε seen in phase M, $Ba_{11}Fe_8Ti_9O_{41}$, for which the estimated ε is of the order of 46. However, these values represent an approximation and do not take into account any loss mechanisms that may arise from mixed iron valence or reduction of titanium during the synthesis of the material.

Table 2. Estimated dielectric constants of selected compositions

Compound	$\varepsilon_{est.}$
$BaFe_4Ti_2O_{11}$ (1:2:2)	30
$Ba_{12}Fe_{28}Ti_{15}O_{84}$ (12:14:15)	26
$Ba_2Fe_2Ti_4O_{13}$ (A)	11
$Ba_3Fe_{10}TiO_{20}$ (B)	10
$Ba_4Fe_2Ti_{10}O_{27}$ (C)	27
$Ba_6Fe_{45}Ti_{17}O_{106}$ (D)	25
$BaFe_{11}Ti_3O_{23}$ (D′)	23
$Ba_4Fe_{28}Ti_5O_{56}$ (F)	23
$Ba_{11}Fe_2Ti_{26}O_{66}$ (G)	31
$Ba_5Fe_4Ti_{10}O_{31}$ (I)	33
$Ba_{27}Fe_{16}Ti_{33}O_{117}$ (J)	46
$Ba_{11}Fe_8Ti_9O_{41}$ (M)	47

It is clear from the above that systems based on channel structures are in general less efficiently packed than close-packed structures, and so polarizabilities per molar volume tend to be smaller for the channel-type structures.

Since the polarizability of barium is roughly twice that of titanium and almost three times that of iron, it is possible to increase the dielectric constant by substituting Ba in place of an iron tetrahedron. This substitution principle has been observed in the phases discussed above, and is reflected in the higher dielectric constants, both estimated and observed, for the barium-rich systems. The highest concentration of Ba would be expected for BaO (cubic rock salt type), but the estimated dielectric constant is only of the order of 15. Here, the molar volume is markedly larger than in comparable $BaO-Fe_2O_3-TiO_2$ phases, due to the lattice contraction (reduction in molar volume) produced by the higher charge on the transition metal atoms in interstitial sites.

6. Magnetic Behavior

The magnetic properties of the new phases in the $BaO-Fe_2O_3-TiO_2$ system are not yet fully established. However, the ferrimagnetic behavior of the hexaferrites is well known and documented.[25]

In the $BaO-Fe_2O_3-TiO_2$ phases as prepared, iron is present as Fe^{3+}, the desired valence state for low loss behavior. Free trivalent Fe is in a $^6S_{5/2}$ state, with a free magnetic moment of 5.92 μ_B. In cases of spinels and hexaferrites, the individual magnetic moments for trivalent iron are the full spin-only moment of 5.92 μ_B, but the magnetic superexchange produces antiferromagnetic coupling between the iron sub-lattices, reducing the net magnetic moment. Superexchange tends to produce antiferromagnetic spin alignments, although more complicated spin structures are possible.[22] Furthermore, the crystal field may produce low-spin iron. All these effects tend to reduce the overall magnetic moment per formula unit. Dilution of iron with nonmagnetic titanium induces changes in the magnetic coupling while reducing the number of spins. In special cases, an increase in the magnetic moment is possible if strong antiferromagnetic coupling is reduced.

At low iron concentrations, paramagnetic behavior with antiferromagnetic interactions would be expected, as observed, for instance, in the case of $Ba_5Fe_4Ti_{10}O_{31}$. Here, paramagnetic behavior was observed at room temperature, with cooperative interactions apparent below 250 K, but without magnetic order at low temperatures.[41] The effective magnetic moment per iron atom, obtained from the high-temperature susceptibility, is 5.12 μ_B, close to the free-atom value. The negative Weiss constant of $\Theta = -190$ K indicates that the dominant interactions are antiferromagnetic in nature. Furthermore, possible magnetic cluster formation is reflected in the behavior of the susceptibility.

Similarly, $Ba_6Fe_{45}Ti_{17}O_{106}$ (phase D) shows Curie–Weiss behavior, with a high-temperature effective magnetic moment of 34 μ_B per formula unit (45 iron atoms), and $\Theta = -806$ K, indicating strong antiferromagnetic interactions. A magnetic transition below 100 K was observed, and was attributed to a small amount of a strongly magnetic impurity, such as $BaFe_{12}O_{19}$. In comparison with $Ba_{12}Fe_{28}Ti_{15}O_{84}$,[39] a phase with less overall iron that shows a ferromagnetic Curie temperature well above room temperature, $Ba_6Fe_{45}Ti_{17}O_{106}$ is an exceptionally weak magnet. Appropriate chemical substitutions would be likely to improve magnetic properties by reducing the antiferromagnetic coupling between different sub-lattices.

The natural magnetic super-lattices found in the regions with low overall iron content merit further investigation, since the iron atoms are preferentially found near to one another. In this way, magnetic interactions within the layers may occur at higher temperatures than might be expected from the overall iron concentration alone. In addition, the two-dimensional character of the structure should be reflected in its magnetic behavior.

7. Conclusions and Outlook

The $BaO-Fe_2O_3-TiO_2$ system shows a wealth of new phases with interesting structural, dielectric, and magnetic properties. The crystal chemistry of a majority of the phases in this system is based on close-packed structures made up of {O,Ba/O} layers. With relatively few distinct types of layers, combining octahedra, tetrahedra, trigonal bipyramids, and barium atoms, a rich variety of stacking sequences with different combinations of the various layers

are found. In the polytitanate-related phases, new types of layers with complexity intermediate between that of the hexaferrites and that of polytitanates form. As in the hexaferrites, superstructures with long periodicities develop, all based on a few common types of layers (Figures 2, 5, and 12). Furthermore, preferential ordering of Fe in distinct layers well separated from each other produces natural magnetic super-lattices. Relationships between structures, based on the stacking arrangement of similar layers in various ways, can be identified in the $BaO-Fe_2O_3-TiO_2$ system. In contrast to the barium polytitanates, which often show low crystallographic symmetry, the mixed barium hexaferrites tend to exhibit higher symmetries based on hexagonal features.

The polarizability of iron is smaller than that of titanium, and substitution of Fe for Ti reduces the overall dielectric constant. This is offset in part by the ability of Fe to occupy tetrahedral interstitial sites, allowing a higher concentration. Phases with high dielectric constants are therefore observed in the mixed iron/titanium systems.

Most microwave materials in use today are composite materials, so knowledge of the phase diagram provides crucial processing information. Combination of hexaferrites and barium polytitanates in a composite process should produce phases described above. Since properties are additive in ceramic composites, knowledge of physical and chemical properties is crucial for tailoring of a material to maximize its performance.

The large number of new phases observed in the $BaO-Fe_2O_3-TiO_2$ phase diagram has produced new insights into the crystal chemistry of these phases. Since the cut of the phase diagram was carried out at 1275 °C, more phases are likely under different preparation conditions. So far, the presence of Fe^{3+} has been needed for microwave applications. However, reduced oxygen pressures may stabilize other new, as yet unknown phases. The rich crystal chemistry observed in this system may be expected to extend into related phases, prepared under different synthesis conditions.

Acknowledgments

We would like to thank L. Schneemeyer, L. Bendersky, and R. S. Roth for valuable discussion and comments.

[1] T. A. Vanderah, J. M. Loezos, R. S. Roth, *J. Solid State Chemistry* **1996**, *121*, 38.
[2] L. A. Bendersky, T. A. Vanderah, R. S. Roth, *Philos. Mag. A* **1998**, *78*, 1299.
[3] G. Geiger, *Am. Ceram. Soc. Bull.* **1994**, *73*, 57.
[4] T. Abraham, *Am. Ceram. Soc. Bull.* **1994**, *73*, 62.
[5] *Phase Equilibria Diagrams* (formerly *Phase Diagrams for Ceramists*), Am. Ceram. Soc., Westerville, OH, **1964**, **1975**, **1981**, **1991**, **1993**, **1995**, **1996**.
[6] E. Tillmanns, W. Hofmeister, W. H. Baur, *J. Solid State Chem.* **1985**, *58*, 14.
[7] P. B. Braun, *Philips Res. Rep.* **1957**, *12*, 491.
[8] E. Tillmanns, W. Hofmeister, W. H. Baur, *J. Am. Ceram. Soc.* **1983**, *66*, 268.
[9] D. H. Templeton, C. H. Dauben, *J. Chem. Phys.* **1960**, *32*, 1515.
[10] E. Tillmanns, W. H. Baur, *Inorg. Nucl. Chem. Lett.* **1971**, *7*, 1169.
[11] E. Tillmanns, W. H. Baur, *Acta Crystallogr., Sect. B* **1970**, *26*, 1645.
[12] H. D. Megaw, *Nature* **1945**, *155*, 484.
[13] H. Blattner, H. Gränicher, W. Känzig, W. Merz, *Helv. Phys. Acta* **1948**, *21*, 341.
[14] K. K. Wu, I. D. Brown, *Acta Crystallogr., Sect. B* **1973**, *29*, 2009.
[15] R. S. Roth, J. J. Ritter, H. S. Parker, D. B. Minor, *J. Am. Ceram. Soc.* **1986**, *69*, 858.
[16] H. Cid-Dresdner, M. Buerger, *Z. Kristallogr., Kristallgeom., Kristallphys., Kristallchem.* **1962**, *117*, 411.
[17] W. Hofmeister, E. Tillmanns, *Fortschr. Mineral.* **1978**, *56*, 42.
[18] A. F. Wells, *Structural Inorganic Chemistry*, Clarendon Press, Oxford, **1975**.
[19] S. Meriani, *Acta Crystallogr., Sect. B* **1972**, *28*, 1241.
[20] X. D. Zou, S. Hovmoeller, M. Parras, J. M. Gonzales-Calbet, M. Vallet-Regi, J. C. Grenier, *Acta Crystallogr., Sect. A* **1993**, *39*, 27.
[21] C. Boivin, D. Thomas, G. Pouillard, P. Perrot, *J. Solid State Chem.* **1979**, *29*, 101.
[22] J. B. Goodenough, J. M. Longo, in: *Landolt-Börnstein*, vol. III/4a new series (Ed.: K.-H. Hellwege), Springer Verlag, Berlin, Heidelberg, New York, **1970**, p. 126.
[23] L. A. Bendersky, T. A. Vanderah, R. S. Roth, *Mat. Res. Soc. Symp. Proc.* **1997**, *453*, 489.
[24] X. Obradors, A. Collomb, M. Pernet, D. Samaras, J. C. Joubert, *J. Solid State Chem.* **1985**, *56*, 171.
[25] J. Smit, H. P. J. Wijn, *Ferrites*, John Wiley & Sons, and Philips Technical Library, New York and Eindhoven, **1959**.
[26] M. C. Cadee, H. J. M. de Groot, L. J. de Jongh, D. J. W. Ijdo, *J. Magn. Magn. Mater.* **1986**, *62*, 367.
[27] I. S. Hagemann, Q. Huang, X. P. A. Gao, A. P. Ramirez, R. J. Cava, *Phys. Rev. Lett.* **2001**, *86*, 894.
[28] W. D. Townes, J. H. Fang, A. J. Perotta, *Z. Kristallogr., Kristallgeom., Kristallphys., Kristallchem.* **1967**, *125*, 11.
[29] W. H. Baur, E. Tillmanns, W. Hofmeister, *Cryst. Struct. Commun.* **1982**, *11*, 2021.
[30] S. Möhr, H. K. Müller-Buschbaum, *J. Alloys Compd.* **1993**, *199*, 203.
[31] I. E. Grey, C. Li, L. M. D. Cranswick, R. S. Roth, T. A. Vanderah, *J. Solid State Chem.* **1998**, *135*, 312.
[32] T. A. Vanderah, W. Wong-Ng, Q. Huang, R. S. Roth, R. G. Geyer, R. B. Goldfarb, *J. Phys. Chem. Solids* **1997**, *58*, 1403.
[33] R. S. Roth, C. J. Rawn, C. G. Lindsay, W. Wong-Ng, *J. Solid State Chem.* **1993**, *104*, 99.
[34] T. Siegrist, T. A. Vanderah, personal communication, **2000**.
[35] T. Siegrist, C. Svensson, T. A. Vanderah, R. S. Roth, *Solid State Sci.* **2001**, *2*, 539.
[36] L. A. Bendersky, J. E. Bonevich, *Philos. Mag. Lett.* **1998**, *77*, 279.
[37] T. Siegrist, T. A. Vanderah, C. Svensson, R. S. Roth, *Solid State Sci.* **2002**, *4*, 911.
[38] F. Haberey, M. Velicescu, *Acta Crystallogr., Sect. B* **1974**, *30*, 1507.
[39] I. E. Grey, A. Collomb, X. Obradors, *J. Solid State Chem.* **1991**, *91*, 131.
[40] T. Siegrist, T. A. Vanderah, personal communication, **2000**.
[41] T. Siegrist, T. A. Vanderah, A. P. Ramirez, R. G. Geyer, R. S. Roth, *J. Alloys Compd.* **1998**, *274*, 169.
[42] T. A. Vanderah, W. Wong-Ng, B. H. Toby, V. M. Browning, R. D. Shull, R. G. Geyer, R. S. Roth, *J. Solid State Chem.* **1999**, *143*, 182.
[43] R. D. Shannon, *J. Appl. Phys.* **1993**, *73*, 348.
[44] M. Hamelin, *Bull. Soc. Chim. Fr.* **1958**, 1559.
[45] W. H. Bragg, *Nature* **1915**, *95*, 516.
[46] S. I. Okamoto, T. Ito, *Acta Crystallogr., Sect. B* **1973**, *29*, 832.

[47] E. Tillmanns, *Acta Crystallogr., Sect. B* **1969**, *25*, 1444.
[48] E. Tillmanns, *Cryst. Struct. Commun.* **1972**, *1*, 1.
[49] E. Tillmanns, *Acta Crystallogr., Sect. B* **1974**, *30*, 2894.
[50] W. Hofmeister, E. Tillmanns, W. H. Baur, *Acta Crystallogr., Sect. B* **1984**, *40*, 1510.
[51] W. Hofmeister, E. Tillmanns, *Acta Crystallogr., Sect. B* **1979**, *35*, 1590.
[52] T. A. Vanderah, Q. Huang, W. Wong-Ng, B. C. Chakoumakos, R. B. Goldfarb, R. G. Geyer, J. Baker-Jarvis, R. S. Roth, A. Santoro, *J. Solid State Chem.* **1995**, *120*, 121.

Received June 21, 2002
[I02338]

Efficient Energy Transfer in Supramolecular, Hydrogen-Bonded Polypyridylruthenium-Osmium Complexes

Sven Rau,*[a] Bernhard Schäfer,[a] Sebastian Schebesta,[a] André Grüßing,[a] Wolfgang Poppitz,[a] Dirk Walther,[a] Marco Duati,[b] Wesley R. Browne,[b] and Johannes G. Vos[b]

Keywords: Ruthenium / Osmium / Supramolecular chemistry / Photosynthesis

Hydrogen bond association between ruthenium bibenzimidazole and carboxylated polypyridylosmium complexes results in stable supramolecular aggregates. The determined stability constant of $\log K \approx 6 \pm 0.3$ allows efficient energy transfer from the ruthenium to the osmium moiety.

(© Wiley-VCH Verlag GmbH & Co. KGaA, 69451 Weinheim, Germany, 2003)

Introduction

Primary processes in natural photosynthesis consist of photon absorption and fast, directional and highly efficient energy transfer along chains of chlorophyll molecules. The efficiency and directionality of the energy-transfer processes are determined by the spatial orientation of the individual chromophores, which is defined by supramolecular forces such as hydrogen bonding and by minute variations of their chemical environment.[1] Artificial systems are most often based on polypyridylruthenium and -osmium complexes, which, due to their photophysical and electrochemical properties, are ideal models. The vast majority of investigations in this area have been generated with covalently linked systems, which are based on highly complicated ligand synthesis.[2] This distinct contrast between natural building principles employing relatively simple components and artificial model components has, to the best of our knowledge, only been overcome in one principle example where hydrogen-bonded ruthenium and osmium complexes have been investigated.[3] The association between both components was accomplished by exploiting the complementary base-pairing of cytosine and guanine, however the complicated ligand synthesis together with relatively low stability constants are serious disadvantages which leave room for considerable improvement. Recently, we have found that the cis diamine moiety of cationic bibenzimidazole ruthenium complexes is an ideal hydrogen bond donor, especially for carboxylate groups.[4] On the basis of this observation it is our intention to develop stable, supramolecular hydrogen-bonded systems where we can study the dependence of the efficiency and directionality of energy-transfer processes on the type of supramolecular association and the modification of the chemical composition of the components. Here we describe the investigation of the first example of these systems based on a novel dicationic ruthenium bibenzimidazole complex as hydrogen-bond donor and a monocationic osmium bipyridine carboxylate[5] as hydrogen-bond acceptor.

Results and Discussion

The investigation was conducted using a bis(2,2′-bipyridine)(4,4′,5,5′-tetramethyl-2,2′-

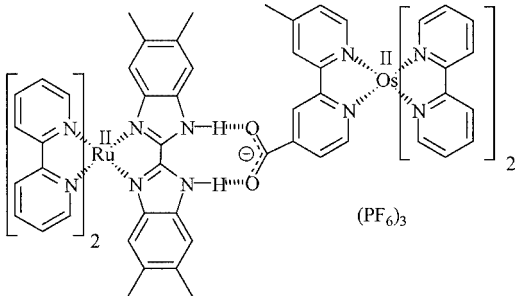

Figure 1. Supramolecular aggregate consisting of bis(2,2′-bipyridine)(4,4′,5,5′-tetramethyl-2,2′-bibenzimidazole)ruthenium(II), Ru(biH_2), and bis(2,2′-bipyridine)(4-carboxy-4′-methyl-2,2′-bipyridine)osmium(II), Os(mcbpy)

[a] Institut für Anorganische und Analytische Chemie, Friedrich-Schiller-University,
07743 Jena, Germany
E-mail: Sven.Rau@uni-jena.de
[b] National Centre for Sensor Research, School of Chemical Sciences, Dublin City University,
Dublin 9, Ireland

Supporting information for this article is available on the WWW under http://www.eurjic.org or from the author.

bibenzimidazole)ruthenium(II) complex, Ru(biH$_2$), as donor and a bis(2,2′-bipyridine)(4-carboxy-4′-methyl-2,2′-bipyridine)osmium(II) complex, Os(mcbpy), as acceptor (Figure 1). It is known that the biimidazole complex is fully protonated in solution and the carboxylate function fully deprotonated,[4,5] which should facilitate the hydrogen bond formation. The synthetic accessibility of the mononuclear components is relatively straightforward and has been described previously.[4,6–9]

In order to investigate the potential of this approach the emission intensity of Ru(biH$_2$) was investigated in the presence of different polypyridylosmium compounds. As reference $[Os(bpy)_3]^{2+}$, containing no carboxylate function, was used. It did not significantly alter the observed emission spectrum of Ru(biH$_2$), as depicted in Figure 2a. In contrast the carboxylated derivative Os(mcbpy) induced a significant decrease in emission intensity of Ru(biH$_2$), which suggested that an intermolecular energy transfer took place, Figure 2b.

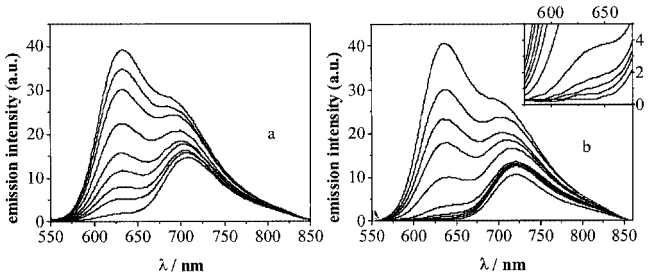

Figure 2. a) Emission spectra of the mixtures of Ru(biH$_2$) and Os(bpy)$_3$ in dichloromethane at various concentrations of Ru(biH$_2$); b) emission spectra of the mixtures of Ru(biH$_2$) and Os(mcbpy) in dichloromethane at various concentrations of Ru(biH$_2$); inset: zoom of region between 575 and 675 nm showing the changes for x between 0.1 and 1 [c(Os complex) = 0.95×10^{-6} mol/L, c[Ru(biH$_2$)] = x * c(Os complex), x = 0.1, 0.33, 0.5. 0.67, 1, 1.5, 2, 2.5, 3, 4]

A more detailed analysis of the obtained data clearly shows that the emission intensities of Ru(biH$_2$) and $Os(bpy)_3^{2+}$ are independent of their respective ratio, whereas the Ru(biH$_2$)-based emission is quiet effectively quenched in the presence of Os(mcbpy). The titration of the luminescence intensities of Ru(biH$_2$) in the presence of Os(mcbpy) yields valuable information about the supramolecular association in solution. The quantity of ruthenium donor was varied, beginning with one-tenth of the Os(mcbpy) concentration to reach, in regular steps, a one to one ratio of donor and acceptor. The concentration of Ru(biH$_2$) was further increased until the final concentration of Ru(biH$_2$) in the last solution was four times higher than the Os(mcbpy) concentration. The results are depicted in Figure 3, all emission spectra consist of the sum of the Ru(biH$_2$)- and Os(mcbpy)-based emissions because a selective excitation of the two fragments is not possible. It is evident from Figure 3 that Os(mcbpy) efficiently quenches the Ru(biH$_2$)-based emission until the concentration of Ru(biH$_2$) exceeds the one to one ratio with respect to Os(mcbpy), whereas $Os(bpy)_3^{2+}$ does not influence the emission of Ru(biH$_2$).

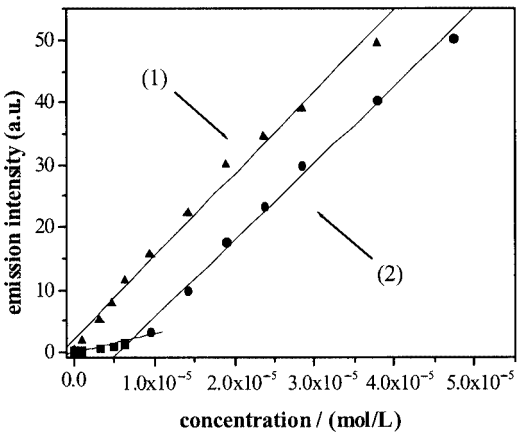

Figure 3. Emission intensity vs. concentration of Ru(biH$_2$) spectra with Os(bpy)$_3$ (1) and Os(mcbpy) (2) in dichloromethane [c(Os complex) = 0.95×10^{-6} mol/L, c[Ru(biH$_2$)] = x * c(Os complex), x = 0.1, 0.33, 0.5. 0.67, 1, 1.5, 2, 2.5, 3, 4]

These results suggest that the ruthenium bibenzimidazole complex interacts with the monocarboxylated osmium complex in such a way that intermolecular energy transfer may occur and that the carboxylate function is essential for this interaction, as depicted in Figure 1.

A careful examination of the obtained data shows that the ruthenium-based phosphorescence in the H-bonded dimer is not completely quenched. One possibility to explain this is a thermodynamic equilibrium between the two free complexes — Ru(biH$_2$) and Os(mcbpy) — and the supramolecular dimer [Ru(biH$_2$)Os(mcbpy)].

On the other hand, it has to be considered that the quenching of the ruthenium-based emission is perhaps not fast enough and, consequently, an emission of a very low intensity level is detected. In order to obtain more detailed information on this process, time-resolved photophysical investigations were performed. Ru(biH$_2$) has an absorption maximum at 482 nm and an emission maximum at 630 nm. Os(mcbpy) has an absorption maximum at 487 nm and an emission maximum at 717 nm. Due to the large separation of nearly 90 nm between both emission maxima it is therefore possible to monitor the emission intensities or lifetimes of the excited states of both complexes independently in the same solution without interference. To gain more insight into this problem luminescence lifetime measurements of the titrated solution were carried out. Figure 4a shows the decay of a one to two mixture of Ru(biH$_2$) and Os(mcbpy) in dichloromethane monitored close to the emission maximum of Ru(biH$_2$) to avoid any Os(mcbpy) signal.

If we compare the decay of the mixture with the decay of the pure donor solution, it is obvious that in the mixture a shorter lived component causes biexponential decay. The lifetime of the short component lies under 10 ns and the unbound Ru(biH$_2$) donor has the same lifetime as in the solution containing no Os(mcbpy) acceptor. Figure 4b depicts the data monitored at the Ru(biH$_2$)-based emission

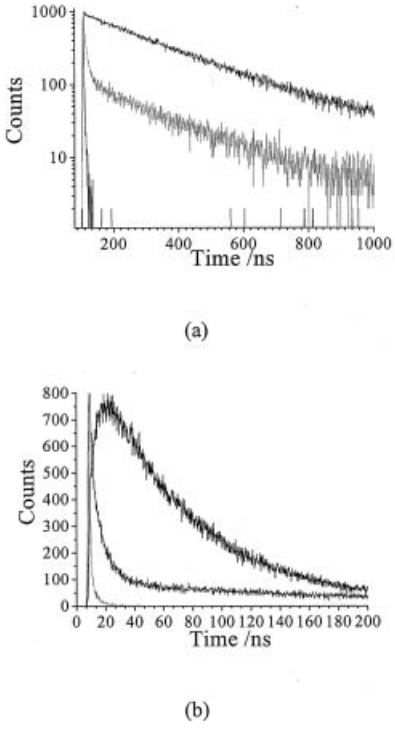

Figure 4. a) Overlay of $Ru(biH_2)$ (top), $Ru(biH_2)$/Os(mcbpy) (ratio 1:2; middle) and IRF (Instrument Response Function; bottom) monitored at 620 nm; b) overlay of $Ru(biH_2)$ (top, monitored at 620 nm) and Os(mcbpy) (middle, monitored at 750 nm) in a 1:2 ratio, IRF (Instrument Response Function; bottom, monitored at 620 nm)

wavelength and at the Os(mcbpy)-based emission. The shape of the Os(mcbpy)-based decay monitored at 750 nm, where $Ru(biH_2)$ does not emit, leads to the conclusion that as long as the short component of $Ru(biH_2)$ dominates its decay for approximately 30 ns the counted number of photons emitted by Os(mcbpy) increases to reach a maximum. After the maximum is passed, the exhibited decay is similar to that observed for free Os(mcbpy). A possible explanation for this behaviour is that the population of the emitting ^{3}MLCT state of Os(mcbpy) is rising. It is evident that the increase of counted photons has to be due to an additional population of these states. A plausible source of this extra population is energy transfer from the $Ru(biH_2)$ ^{3}MLCT state

The obtained results show that a hydrogen-bonded heterodinuclear associate is formed, that efficient energy transfer occurs and that the supramolecular associate is in equilibrium with its unbound components, according to $Ru(biH_2)$ [A] and Os(mcbpy) [B] in equilibrium with Ru(biH_2)Os(mcbpy) [A-B] [Equation (1) and (2)].

$$[A] = ([A_0]\cdot I_Q)/I_{NQ} \quad (1)$$

$$K = ([A_0] - [A])/[A]([B_0] - [A_0] + [A]) \quad (2)$$

Within all these assumptions it is possible to determine the equilibrium constant as $\log K \approx 6 \pm 0.3$ using Equation (2).

Conclusion

The results of the initial investigations presented here clearly show that the perfectly tailored geometrical parameters of the hydrogen-bond interaction groups together with the reduced coulombic repulsion between a monocationic Os(mcbpy) and a dicationic $Ru(biH_2)$ lead to stable supramolecular model compounds for photosynthetic light harvesting complexes. Barigelletti and Ward reported a log(K) $\leq$ 3.7 for the formation of a mixed cytosine-modified ruthenium and guanine-substituted osmium complex exhibiting a detectable change of luminescence properties indicative of Ru $\rightarrow$ Os energy transfer.[3] The difference in the association constants of the system described in this work compared to the one reported by Barigelletti et al. is extraordinarily high. The equilibrium constant is about two to three orders of magnitude higher although there is only a double instead of a triple chelating effect of H-bonding interactions involved within the biimidazole carboxylate system. Furthermore, the structure of the moieties connected by H-bonding in this study appears almost simple in contrast to the synthetic effort made to yield the nucleobase-modified polypyridyl complexes. The application of these construction principles should lead to more advanced compounds which might be used to gain more detailed insight into processes occurring in natural photosynthesis.

Experimental Section

Materials

All solvents used for spectroscopic measurements were of Uvasol (Merck) grade. All other reagents were HPLC grade. *cis*-$[RuCl_2(bpy)_2]\cdot 2H_2O$,[10] *cis*-$[OsCl_2(bpy)_2]\cdot 2H_2O$,[11] and $[Os(mcbpy)(bpy)_2](PF_6)$[6] were prepared by standard procedures. All reagents for synthesis, $RuCl_3\cdot 3H_2O$ (ABCR), 2,2′-bipyridine, trichloroacetic acid, 4,5-dimethyl-1,2-phenylenediamine, and 4,′4-dimethyl-2,2′-bipyridine (Aldrich) were used as received without further purification.

The synthesis of 5,5′,6,6′-tetramethyl-2,2′-bisbenzimidazole was a modification of the method of Reedijk et al.[12] 4-Carboxy-4′-methyl-2,2′-bipyridine was prepared according to literature procedures.[13]

UV/Visible spectra were obtained using a Shimadzu UV 3100 UV/Vis-NIR spectrophotometer. Emission spectra were obtained using a Perkin−Elmer LS50 luminescence spectrometer; at room temperature the measurements were taken using an excitation slide of 10 nm and emission slit of 10 nm. The NMR spectra were recorded on a Bruker 400 MHz spectrophotometer. The mass spectrometry was carried out on a SSQ 170, Finnigan Mat. The Electrospray mass spectrometry was performed on a Finnigan MAT 95 XL double focussing sector field instrument (Thermo Finnigan GmbH, Bremen, Germany) adjusted to a mass resolution of about 2000. The two complexes were first dissolved in a small amount of acetonitrile and then diluted with dichloromethane to a final concentration of 3×10^{-6} M respectively. This solution was introduced into the ion source at a flow rate of 40μL/min. The spray voltage was 4.5 kV and nitrogen was used as sheath gas.

Luminescence lifetime measurements were obtained using an Edinburgh Analytical Instruments (EAI) time-correlated single-photon counting apparatus (TCSPC) comprised of two model J-yA monochromators (emission and excitation), a single photon photomultiplier detection system model 5300, and a F900 nanosecond flashlamp (N2 filled at 1.1 atm pressure, 40 kHz) interfaced with a personal computer via a Norland MCA card. A 500 nm cut-off filter was used in emission to attenuate scatter of the excitation light (337 nm); luminescence was monitored at 640 nm. Data correlation and manipulation was carried out using EAI F900 software version 5.1.3.

Emission lifetimes were calculated using a single-exponential fitting function, Levenberg−Marquardt algorithm with iterative deconvolution (Edinburgh instruments F900 software). The reduced χ^2 and residual plots were used to judge the quality of the fits. Samples were of low concentration (2×10^{-5} M) dissolved in a small amount of dichloromethane at room temperature. The lifetimes of the complexes in equilibrium was measured in aerated dichloromethane. The lifetime errors are estimated to be less than 8%.

The following assumptions were made for the determination of the stability constant *K*. [A_0] [initial concentration of Ru(biH$_2$)] and [B_0] [initial concentration of Os(mcbpy)] of the solutions are determined from the weighted masses of donor and acceptor. The ratio of [*A*] to [A_0] might be expressed by the quotient of the intensities of I_{NQ} to I_Q ($I_{NQ/Q}$ emission intensity for different concentration for not quenched and quenched case) at the maximum of the ruthenium donor (λ_{max} = 630 nm). In order to determine the I_{NQ} correctly the emission intensity of Ru(biH$_2$) was determined in the presence of non-binding $[Os(bpy)_3]^{2+}$. At the monitored emission wavelength of 630 nm the absorption of the two osmium complexes, the binding Os(mcbpy) and $[Os(bpy)_3]^{2+}$, is different. Therefore we have to consider a correcting factor x for I_{NQ}, the concentration [*A*] may therefore be determined using Equation (1) and the corrected I_{NQ}.

Synthesis of [Ru(tmbbiH$_2$)(bpy)$_2$](PF$_6$)$_2$, Ru(biH$_2$): [RuCl$_2$(bpy)$_2$]·2H$_2$O (0.19 mmol) and 5,5′,6,6′-tetramethyl-2,2′-bisbenzimidazole (0.19 mmol) were suspended in a mixture of EtOH/H$_2$O (1:1 v/v, 30 mL) and stirred and refluxed overnight. The reaction mixture was allowed to cool to room temperature and filtered. The volume of the solution was reduced (to ca. 10 mL) by rotary evaporation, and the product was precipitated as the PF$_6$ salt. The crude product was washed with water and diethyl ether, and chromatographed on silica with an eluent formed of THF, CH$_3$CN, KNO$_3$ (saturated aqueous solution) (12:4:0.5, v/v/v). The first peak (main band) contained the desired compound, which was finally obtained by recrystallisation from acetone and water. $[C_{38}H_{34}F_{12}N_8P_2Ru]^{2+}$ (993.7): calcd. C 45.93, H 3.45, N 11.28; found C 46.44, H 3.41, N 10.98. ESI-MS: *m/z* = 704.0 $[C_{38}H_{34}N_8Ru]$, 352.3 $[C_{38}H_{34}N_8Ru]^{2+}$. ^{1}H NMR (CD$_3$CN): δ = 8.54 (d, 2 H), 8.44 (d, 2 H), 8.16 (dd, 2 H), 8.05 (d, 2 H), 7.97 (dd, 2 H), 7.93 (d, 2 H), 7.49 (dd, 2 H), 7.47 (s, 2 H), 7.34 (dd, 2 H), 5.39 (s, 2 H), 2.65 (s, 6 H), 2.15 (s, 6 H) ppm. ^{13}C NMR (CD$_3$CN): δ = 20.37, 20.55, 114.66, 116.07, 124.61, 125.01, 128.08, 128.47, 134.53, 135.46, 137.16, 137.85, 138.34, 141.31, 144.44, 153.70, 154.16, 158.36, 160.07 ppm. UV/Vis (CH$_2$Cl$_2$): λ_{max} = 482 nm (ε = 9200 $M^{-1}cm^{-1}$). Emission (CH$_2$Cl$_2$): λ_{max} = 630 nm. Lifetime of excited state (CH$_2$Cl$_2$): τ = 238 ns.

Acknowledgments

Financial support for this work from the Deutsche Forschungsgemeinschaft (SFB, 436), and the Fonds der Chemischen Industrie is gratefully acknowledged.

[1] [1a] J. Deisenhofer, H. Michel, *Angew. Chem.* **1989**, *101*, 872; *Angew. Chem. Int. Ed. Engl.* **1989**, *28*, 829−847. [1b] R. Huber, *Angew. Chem.* **1989**, *101*, 849; *Angew. Chem. Int. Ed. Engl.* **1989**, *28*, 848−869.
[2] V. Balzani, A. Juris, M. Venturi, S. Campagna, S. Serroni, *Chem. Rev.* **1996**, *96*, 759.
[3] M. D. Ward, F. Barigelletti, *Coord. Chem. Rev.* **2001**, *216−217*, 127−154, and references cited therein.
[4] S. Rau, L. Böttcher, S. Schebesta, M. Stollenz, H. Görls, D. Walther, *Eur. J. Inorg. Chem.* **2002**, *11*, 2800−2809. For other examples see also: S. Fortin, A. L. Beauchamp, *Inorg. Chem.* **2001**, *40*, 105−112.
[5] K. Westermark, H. Rensmo, A. C. Lees, J. G. Vos, H. Siegbahn, *J. Phys. Chem. B.* **2002**, *106*, 10108−10113.
[6] D. A. Buckingham, F. P. Dwyer, H. A. Goodwin, A. M. Sargeson, *Aust. J. Chem.* **1964**, *17*, 325.
[7] M. Haga, *Inorg. Chim. Acta* **1983**, *75*, 29.
[8] D. P. Rillema, R. Sahai, P. Matthews, A. K. Edwards, R. J. Shaver, L. Morgan, *Inorg. Chem.* **1990**, *29*, 167.
[9] S. Rau, T. Büttner, C. Temme, M. Ruben, H. Görls, D. Walther, M. Duati, F. Fanni, J. G. Vos, *Inorg. Chem.* **2000**, *39*, 1621−1624.
[10] B. P. Sullivan, D. J. Salmon, T. J. Meyer, *Inorg. Chem.* **1978**, *17*, 3334.
[11] B. M. Peek, G. T. Ross, S. E. Edwards, G. J. Meyer, T. J. Meyer, B. W. Erickson, *Int. J. Pept. Protein Res.* **1991**, *38*, 114.
[12] E. Müller, G. Bernardinelli, J. Reedijk, *Inorg. Chem.* **1995**, *34*, 5979−5988.
[13] D. G. McCafferty, T. J. Meyer, *Tetrahedron* **1995**, *51*, 1093−1106.

Received December 20, 2002
[I02696]

The First Azaindatrane and Unprecedented Structural Features

Pavel L. Shutov,[a] Sergey S. Karlov,*[b] Klaus Harms,[a] Oleg Kh. Poleshchuk,[c] Jörg Lorberth,*[a] and Galina S. Zaitseva[b]

Keywords: Azametallatranes / Indium / Tripodal ligands

The reaction between $[In(NEt_2)_3]_2$ and $N(CH_2CH_2NMeH)_3$ yields the *N*,*N*′,*N*′′-trimethylazaindatrane dimer $[N(CH_2CH_2NMe)_3In]_2$ (**1**). The composition and structure of **1** were established by ^1H and ^{13}C NMR spectroscopy as well as by an X-ray diffraction study. The X-ray structure shows that both indium atoms are pentacoordinate, with widely differing In–N distances. The structural parameters of **1** were compared with those obtained from a computational study.
(© Wiley-VCH Verlag GmbH & Co. KGaA, 69451 Weinheim, Germany, 2003)

Introduction

Compounds containing intramolecular interactions have found widespread application for the stabilisation of low-valent species or for achieving unusual molecular geometries. Of particular interest are metallatranes of the type $[N(CH_2CH_2Y)_3M-X$, where X = substituent, electron lone pair or nothing and Y = O, NR, CH_2, S] containing tetradentate, c_3-symmetric ligands such as tris(alkoxyamine) groups $[N(CH_2CH_2O)_3]^{3-}$ and tris(amidoamine) groups $[N(CH_2CH_2NR)_3]^{3-}$.[1−3] These ligands bind to various main-group elements or transition metals in a tridentate or tetradentate manner to form complexes. The latter are usually characterised by a transannular N→M interaction. The strength of this N→M interaction depends on the nature of the central atom M and the equatorial substituents Y.

Verkade et al. have recently prepared azametallatranes of boron, aluminium, and gallium,[4−7] but, to the best of our knowledge, no azaindatranes have been reported yet. However, it should be noted that the chemistry of indium-nitrogen compounds, especially indium amides, has been the focus of much interest during the last two decades for their importance in the preparation of nitride ceramic materials and semiconductors.[8]

In this paper we report on the synthesis of the *N*,*N*′,*N*′′-trimethylazaindatrane dimer $[N(CH_2CH_2NMe)_3In]_2$ (**1**). Details of the X-ray crystal and molecular structures of **1** are also described. Our aim was to prepare the first azaindatrane **1** and to compare its structure with the structures of closely related derivatives of Al and Ga (**2** and **3**, respectively).

[a] Fachbereich Chemie, Philipps-Universität Marburg,
Hans-Meerwein-Strasse, 35032 Marburg-Lahn, Germany
Fax: (internat.) +49-6421/282-5642
E-mail: lorberth@chemie.uni-marburg.de
[b] Chemistry Department, Moscow State University,
234 Leninskie Gory, 119899 Moscow, Russia
Fax: (internat.) +7-095/932-8846
E-mail: sergej@org.chem.msu.su
[c] Tomsk Pedagogical University,
Komsomolskii 75, 634041 Tomsk, Russia
E-mail: root@polsh.tomsk.su

Results and Discussion

Treatment of $[In(NEt_2)_3]_2$ with equimolar amounts of $N(CH_2CH_2NMeH)_3$ (Me_3-tren) in toluene afforded azaindatrane **1** in high yield [Equation (1)]. The crystals of compound **1** contain variable amounts of toluene, which could not completely be removed.

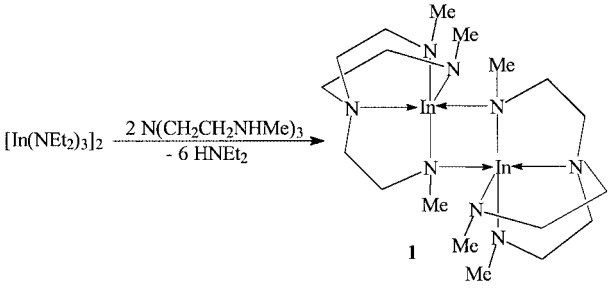

(1)

The NMR spectroscopic data (^1H, ^1H COSY and ^{13}C) of **1** are consistent with its formulation as a dimer $[N(CH_2CH_2NMe)_3In]_2$: compound **1** exists in solution as one of two geometrical isomers of the In_2N_2 core [**A** (cis) and **B** (trans); Scheme 1] analogous to the previously described complexes $[N(CH_2CH_2NMe)_3M]_2$ [M = Al (**2**), Ga (**3**)].[7] This is supported by the appearance of three singlets for the Me groups and 12 partially overlapping multiplets for each of the non-equivalent hydrogens of six methylene groups for both atrane moieties in the ^1H NMR spectrum

of **1**. Nine signals of the atrane skeleton were found in the ^{13}C NMR spectrum of **1**; however, according to Verkade et al. NMR spectroscopy alone is not suitable for the unambiguous attribution of a cis or a trans structure to the $(In-N)_2$ core.[5]

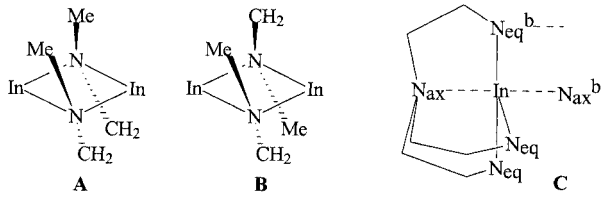

Scheme 1

The dimeric structure of **1** in the solid state was established by an X-ray diffraction study. The molecular structure of **1**·0.5toluene (one of two independent molecules) is shown in Figure 1. Important atomic distances and bond angles are summarised in Table 1. Similarly to both **2** and **3** (M = Al, Ga) molecules of **1** possess a conformation of type **A**, which is unusual for solid-state structures of Group 13 elements.[9] The central $(In-N)_2$ units are non-planar for both independent molecules and form a puckered rectangle (153.0° and 151.1°) with a pseudo-twofold axis through its centre, analogously to both **2** and **3**. The coordination polyhedron of the indium atoms in **1** is a distorted trigonal bipyramid (**C**, Scheme 1).

The transannular bonded nitrogen atoms (N_{ax} and N^b_{ax}) are in axial positions and the covalently bonded nitrogen atoms (two of N_{eq}, and N^b_{eq}) in the equatorial sites. The indium atoms are displaced by 0.36−0.46 Å from a plane defined by the three equatorial nitrogen atoms towards the bridging nitrogen atom of another atrane part of the dimeric structure (N^b_{ax}). The $N_{ax}-In-N^b_{ax}$ angles [150.3(1)−157.77(9)°] are smaller than those for other closely related $[N(CH_2CH_2NMe)_3M]_2$ complexes [average:

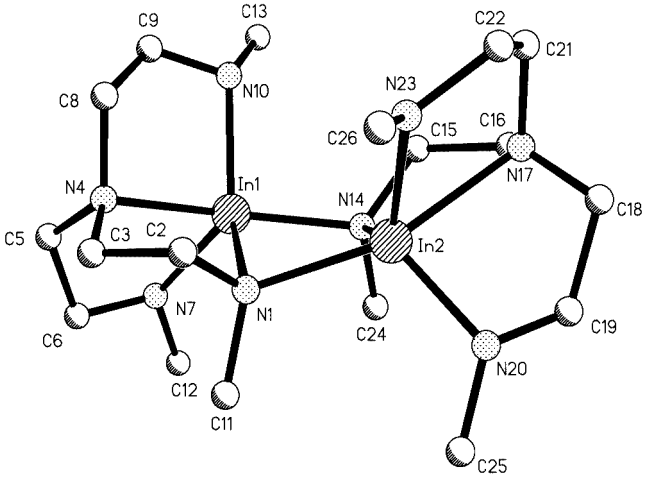

Figure 1. Molecular structure of dimeric azaindatrane **1** (one independent molecule); hydrogen atoms have been omitted for clarity

Table 1. Selected bond lengths (Å) and angles (°) for **1**

	1	**1′**
$In\leftarrow N_{ax}$	In(1)−N(4) 2.099(2)	In(3)−N(30) 2.366(3)
	In(2)−N(17) 2.327(3)	In(4)−N(43) 2.610(3)
$In\leftarrow N^b_{ax}$	In(1)−N(14) 2.063(3)	In(3)−N(46) 2.294(3)
	In(2)−N(1) 2.224(3)	In(4)−N(36) 2.376(3)
$In-N^b_{eq}$	In(1)−N(1) 2.393(3)	In(3)−N(36) 2.174(3)
	In(2)−N(14) 2.456(3)	In(4)−N(46) 2.073(2)
$In-N_{eq}$	In(1)−N(10) 2.083(3)	In(3)−N(27) 2.241(3)
	In(1)−N(7) 2.350(3)	In(3)−N(33) 2.178(3)
	In(2)−N(20) 1.960(3)	In(4)−N(40) 2.103(3)
	In(2)−N(23) 2.208(3)	In(4)−N(49) 2.023(3)
$N_{ax}-In-N^b_{ax}$	N(4)−In(1)−N(14) 150.3(1)	N(30)−In(3)−N(46) 157.77(9)
	N(1)−In(2)−N(17) 153.3(1)	N(36)−In(4)−N(43) 156.34(9)

160.3°, M = Al (**2**) and 162.3°, M = Ga (**3**)].[7] It should be noted that in contrast to both **2** and **3**, there is an unusual set of In−N distances in **1** (Table 1). It is very surprising that the transannular bond lengths In(1)−N(4) and In(1)−N(14) are similar to the values of In−N covalent bonds found in monomeric indium amides [2.02(1)−2.166(4) Å][10,11] and, to the best of our knowledge, these are the shortest transannular In−N distances found to date. Other values of transannular In−N distances in **1** are within the typical range [2.20−2.62 Å],[12,13] although the In(4)-N(43) distance is rather long. Interestingly, values for $In\leftarrow N_{ax}$ distances of three known indium atranes investigated are 2.39(1) Å for $N(CH_2CH_2S)_3In$,[14] 2.386(6) Å for $N(CH_2$-*o*-C_6H_4-$S)_3In$·1-Me-imidazole, 2.345(9) Å for $N(CH_2$-*o*-C_6H_4-$S)_3In$·DMF, and 2.29(1) Å for $N[2\text{-}CH_2$-$(4,6\text{-}Me_2C_6H_2)$-$O]_3In$·$(1\text{-Me-imidazole})_2$.[15]

The nonbridging covalent distances $In-N_{eq}$ in compound **1** are within the range 1.960(3)−2.350(3) Å and are therefore markedly different from those found in indium tris(amides) [2.049(1)−2.130(4) Å].[16,17] In a similar manner, the bridging covalent bonds $In-N^b_{eq}$ in compound **1** also vary from 2.073(2) Å to 2.456(3) Å, the previously reported values lie in the range 2.199(7)−2.305(3) Å.[12,18]

The geometry of the N_{ax} atoms is a distorted tetrahedron with $C-N_{ax}-C$ and $C-N_{ax}-In$ angles ranging from 97.0(2)° to 121.0(3)° for **1**. The same situation was observed for N^b_{eq} [$C-N_{ax}-C$ and $C-N_{ax}-In$: 89.1(1)−121.6(2)°]. The environment of the nonbridged N_{eq} is a pyramid with a sum of bond angles from 334.9° to 352.6°. All five-membered rings of the atrane skeleton in **1** adopt an "envelope"-like conformation. For both **1** and **3**, all carbon atoms in the β-positions to the N_{ax} atom occupy "flap" sites, while the C-α atoms form the base of these envelope planes.

In order to get a better understanding of the structural trends for compound **1** we have carried out a computational study on **1** using the Gaussian 98W program.[19,20] A geometry optimisation of *cis*-**1** leads to the expected parameters of the coordination environment at the indium atoms. Both calculated $N_{ax}-In-N^b_{ax}$ angles (154.9 °) are in good agreement with our X-ray data. The calculated $In\leftarrow N_{ax}$ distances (2.342 Å) are appreciably longer than those in $In\leftarrow N^b_{ax}$ (2.179 Å) and especially than those of covalent

bonds: In−N^{b}_{eq} (2.293 Å) and In−N_{eq} (2.043 and 2.030 Å). Thus, the unusual geometry of the indium atoms in the solid state is probably due to a strong influence of crystal field forces, as is normal in atrane structural chemistry.[21] However, it should be noted that compound **1** may exist as two mesomeric forms (Scheme 2), which could also be a possible reason for the unusual geometry of **1**.

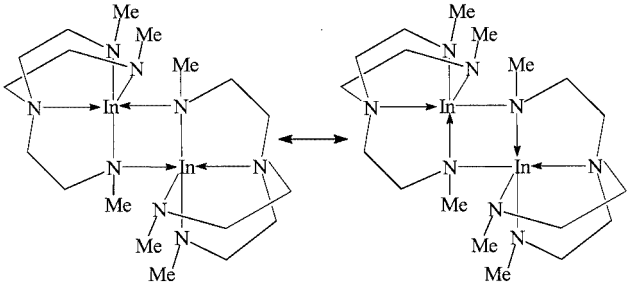

Scheme 2

Conclusion

We have presented the synthesis of *N*,*N*′,*N*′′-trimethylazaindatrane (**1**). Its dimeric structure was confirmed by X-ray diffractometry and by ^{1}H and ^{13}C NMR spectroscopy. The In−N distances in the solid state for this compound show an unusual variety. Further studies on the synthesis of azaindatranes and an investigation of their structure are in progress.

Experimental Section

General Remarks: All manipulations were performed under a dry, oxygen-free argon atmosphere using standard Schlenk techniques. Solvents were dried by standard methods and distilled prior to use. The starting materials Me_3-tren[22] and $[In(NEt_2)_3]_2$ [23] were prepared according to the literature procedures. C_6D_6 was obtained from Deutero GmbH and dried over sodium. ^{1}H and ^{13}C NMR spectra were recorded on a Bruker AC 300 spectrometer. ^{1}H and ^{13}C chemical shifts are reported in ppm relative to Me_4Si as external standard.

***N*,*N*′,*N*′′-Trimethylazaindatrane Dimer (1):** A solution of Me_3-tren (1.92 g, 10.20 mmol) in 15 mL of toluene was added dropwise via cannula within 10 min to a solution of $[In(NEt_2)_3]_2$ (3.38 g, 10.20 mmol) in 15 mL of toluene at room temperature. The reaction mixture was stirred for 48 h and then all volatiles were removed under reduced pressure. The crude product was washed with *n*-pentane (3 × 10 mL). After recrystallisation (toluene/*n*-pentane) **1** (2.23 g, 73%) was obtained as colourless crystals. ^{1}H NMR (C_6D_6, 300.130 MHz): δ = 1.73−3.54 (m, 24 H, $12CH_2$), 2.75 (s, 6 H, $2CH_3$), 3.26 (s, 6 H, $2CH_3$), 2.32 (s, 6 H, $2CH_3$) ppm. ^{13}C NMR (C_6D_6, 75.47 MHz): δ = 42.03, 44.61, 45.56 (CH_3); 48.72, 53.03, 53.34, 54.13, 54.20, 55.90 (CH_2) ppm.

X-ray Crystallographic Study

Crystal Data for 1: $C_{43}H_{93}In_4N_{16}$, M = 1293.61, triclinic, a = 12.4845(7), b = 15.3700(8), c = 15.1624(10) Å, α = 78.938(5), β = 85.708(5), γ = 76.988(4)°, V = 2780.6(3) Å^3, space group $P\bar{1}$, Z = 2, d_{calc} = 1.545 g·cm^{-3}, F(000) = 1318, μ(Mo-K_α) = 1.682 mm^{-1}, colourless block with dimensions ca. 0.45 × 0.45 × 0.30. Total of 36385 reflections (11919 unique, R_{int} = 0.0449) were measured on a Stoe IPDS diffractometer (graphite-monochromated Mo-K_α radiation, λ = 0.71073 Å) at 193(2) K. Data were collected in the range 1.68 < θ < 30.50 (−15 ≤ h ≤ 15, −19 ≤ k ≤ 19, −19 ≤ l ≤ 19). The structure was solved by direct methods[24] and refined by full-matrix least-squares on F^2 [25] with anisotropic thermal parameters for all non-hydrogen atoms. All H atoms were placed in calculated positions and refined using a riding model. The final residuals were: R_1 = 0.0271, wR_2 = 0.0808 for 10623 reflections with I > 2σ(I) and 0.0323, 0.0940 for all data and 607 parameters. Goof = 1.101, maximum shift/e.s.d. = 0.002, maximum Δρ = 0.685 e·Å^{-3}. CCDC-194359 contains the supplementary crystallographic data for this paper. These data can be obtained free of charge at www.ccdc.cam.ac.uk/conts/retrieving.html [or from the Cambridge Crystallographic Data Centre, 12, Union Road, Cambridge CB2 1EZ, UK; Fax: (internat.) +44-1223/336-033; E-mail: deposit@ccdc.cam.ac.uk].

Acknowledgments

We thank Dr. Evgueni Avtomonov and Dr. Andrei Churakov for helpful discussion. We also acknowledge the excellent service offered by the Hochschulrechenzentrum of the Philipps-Universität Marburg. This work was supported by INTAS under Grant No YSF 2001/2-135 for S. S. K. as well as by the Philipps-University Marburg, Chemistry Department, with a grant for P. L. S.

[1] J. G. Verkade, *Coord. Chem. Rev.* **1994**, *137*, 233−295.
[2] S. S. Karlov, G. S. Zaitseva, *Chem. Heterocycl. Comp.* **2001**, *37*, 1325−1357.
[3] R. R. Schrock, *Acc. Chem. Res.* **1997**, *30*, 9−16.
[4] J. Pinkas, B. Gaul, J. G. Verkade, *J. Am. Chem. Soc.* **1993**, *115*, 3925−3931.
[5] J. Pinkas, T. Wang, R. A. Jacobson, J. G. Verkade, *Inorg. Chem.* **1994**, *33*, 4202−4210.
[6] J. Pinkas, J. G. Verkade, *Phosphorus, Sulfur, and Silicon* **1994**, *93−94*, 333−337.
[7] J. Pinkas, T. Wang, R. A. Jacobson, J. G. Verkade, *Inorg. Chem.* **1994**, *33*, 5244−5253.
[8] A. P. Purdy, *Inorg. Chem.* **1994**, *33*, 282−286.
[9] C. J. Carmalt, J. D. Mileham, A. J. P. White, D. J. Williams, J. W. Steed, *Inorg. Chem.* **2001**, *40*, 6035−6038.
[10] H. Sussek, O. Stark, A. Devi, H. Pritzkow, R. A. Fischer, *J. Organomet. Chem.* **2000**, *602*, 29−36.
[11] M. Porchia, F. Benetollo, N. Brianese, G. Rossetto, P. Zanella, G. Bombieri, *J. Organomet. Chem.* **1992**, *424*, 1−13.
[12] J. Kim, S. G. Bott, D. M. Hoffman, *J. Chem. Soc., Dalton Trans.* **1999**, 141−146.
[13] D. C. Bradley, H. Haves, D. M. Frigo, M. B. Hursthouse, M. B. Hussain, *J. Organomet. Chem.* **1987**, *325*, 55−67.
[14] D. J. Rose, J. Zubieta, A. J. Fischman, S. Hillier, J. W. Babich, *Inorg. Chem. Commun.* **1998**, *1*, 164−166.
[15] R. J. Motekaitis, A. E. Martell, S. A. Koch, J. Hwang, D. A. Quarless, M. J. Welch, *Inorg. Chem.* **1998**, *37*, 5902−5911.
[16] M. A. Petrie, K. Ruhlandt-Senge, H. Hope, P. P. Power, *Bull. Soc. Chim. Fr.* **1993**, *130*, 851−855.
[17] J. Kim, S. G. Bott, D. M. Hoffman, *Inorg. Chem.* **1998**, *37*, 3835−3841.
[18] K. A. Aitchison, J. D. J. Backer-Dirks, D. C. Bradley, M. M. Faktor, D. M. Frigo, M. B. Hursthouse, B. Hussain, R. L. Short, *J. Organomet. Chem.* **1989**, *366*, 11−23.
[19] GAUSSIAN 98W. User's Reference, Pittsburgh, Gaussian Inc., 1998, 280.

[20] Ab initio molecular orbital calculations were carried out using the Gaussian 98 program. Geometry optimisations were performed at the HF level of theory. The basis set used in this work was LANL2DZ. This basis set consists of an ecp basis set for the indium atoms and the D95V [T. H. Dunning, P. J. Hay, Modern Theoretical Chemistry, Plenum: New York, 1976.] basis set for another atoms. The LANL2DZ is of double-ζ quality in the valence region.
[21] S. Belyakov, L. Ignatovich, E. Lukevics, *J. Organomet. Chem.* **1999**, *577*, 205−210.
[22] H. Schmidt, C. Lensink, S. K. Xi, J. G. Verkade, *Z. Anorg. Allg. Chem.* **1989**, *578*, 75−80.
[23] G. Rossetto, N. Brianese, A. Camporese, M. Porchia, P. Zanella, R. Bertoncello, *Main Group Met. Chem.* **1991**, *14*, 113−122.
[24] G. M. Sheldrick, *Acta Crystallogr., Sect. A* **1990**, *46*, 467−473.
[25] G. M. Sheldrick, *SHELXL-97, Program for the Refinement of Crystal Structures*, University of Göttingen, Germany, **1997**.
Received November 26, 2002
[I02645]

Sequential Nucleophilic−Electrophilic Reactions Selectively Produce Isomerically Pure Nona-*B*-Substituted *o*-Carborane Derivatives

Gemma Barberà,[a] Francesc Teixidor,[a] Clara Viñas,*[a] Reijo Sillanpää,[b] and Raikko Kivekäs[c]

Keywords: Boron / Clusters / Iodinated compounds / Methylated compounds / Electrophilic reactions

Nine equal substituents on the intensively studied *o*-carborane have been obtained for the first time by a combined nucleophilic-electrophilic reaction sequence. Iodine and methyl groups have been introduced to prove the generality of the method.

(© Wiley-VCH Verlag GmbH & Co. KGaA, 69451 Weinheim, Germany, 2003)

Introduction

During the last decade there has been a great deal of interest in introducing a large number of substituents on boron in icosahedral boranes and heteroboranes.[1−6] The possibility of generating weakly coordinating anions,[3,6,7] X-ray contrast agents,[8] camouflaged boron clusters,[5] the attainment of molecules comparable in size to C_{60} [9] and the generation of stable radicals[4] are some of the goals that have stimulated this research. Substitutions have been achieved with a good degree of success for cluster anions, but there are few examples for the dicarbaboranes. This is surprising considering that the chemistry of the latter has become one of the most intensively investigated areas in the field of boranes and heteroboranes.[10] The paucity of reported examples is in agreement with the relative rates of halogenation, which decrease in the order $[B_{12}H_{12}]^{2-} > [CB_{11}H_{12}]^{-} > C_2B_{10}H_{12}$.[11] Thus, methods to introduce substituents on the well studied *o*-carborane cluster need to be investigated. The *o*-carborane, 1,2-dicarba-*closo*-dodecaborane, contains four distinct types of boron atoms that may be ordered according to their distance from the C atoms, with B(9,12) being the farthest away, followed by B(8,10), B(4,5,7,11), and B(3,6), which are adjacent to both carbon atoms. Those farthest from the carbon atoms are the more electron-rich and those closest are the more electron-poor. It is generally accepted that icosahedral carboranes are aromatic[12] and undergo electrophilic substitution reactions, making this method attractive for the introduction of iodine into the cage molecules.[10] Whereas perfluorination[13] and perchlorination[14] of dicarbaboranes has been achieved, perbromination has not been accomplished. Indeed, only a maximum of four bromine atoms have been incorporated in dicarboranes to date. Periodination of *o*-carborane has not been achieved. Before 1996 the maximum number of iodines in *o*-carborane was two, occupying the 9- and 12-positions.[1,15] Little information exists on higher substitution although reference has been made to 8,9,10,12-tetraiodo-*o*-carboranes.[16] Major progress was recently achieved with the synthesis of the eight iodine 4,5,7,8,9,10,11,12-octaiodo-1,2-dicarba-*closo*-dodecaborane.[8] The carbons adjacent to the B(3,6) positions are resistant to electrophilic methods, although with the extremely powerful electrophiles F^+ and Cl^+ full substitution has been achieved. However, with the milder electrophiles Br^+ and I^+ this has not been possible.

[a] Institut de Ciència de Materials de Barcelona (CSIC), Campus U.A.B.,
08193 Bellaterra, Spain
Fax: (internat.) +34-93/580-5729
E-mail: clara@icmab.es
teixidor@icmab.es
barbera@icmab.es
[b] Department of Chemistry, University of Jyväskylä, 40351 Jyväskylä, Finland
Fax: (internat.) +358-14/260-2501
E-mail: resillan@jyu.fi
[c] Department of Chemistry, University of Helsinki, P. O. Box 55, 00014 Helsinki, Finland
Fax: (internat.) +358-91/915-0198
E-mail: raikkok@saunalahti.fi

Results and Discussion

We based our work on the hypothesis that the first introduced group in the cluster determines the subsequent reactivity of the cluster towards further substitution causing, in cases such as the reaction of *o*-carborane with mild electrophiles, persubstitution to be impossible. To attain such substitution more than one type of reaction is necessary: an

electrophilic reaction for the electron-rich boron atoms and a nucleophilic reaction for the electron-poor B(3,6) atoms. With this aim, we devised the sequence of reactions shown in Scheme 1.

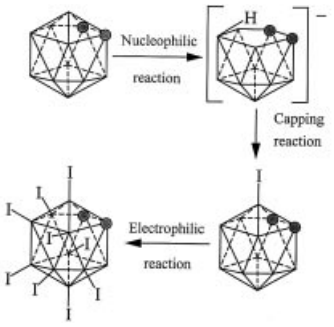

Scheme 1. Synthesis of 3,4,5,7,8,9,10,11,12-nonaiodo-1,2-dicarba-*closo*-dodecaborane (*closo*-**1**) from *o*-carborane

The first step consists of producing 3-I-1,2-$C_2B_{10}H_{11}$. This is achieved by a nucleophilic reaction to remove one boron adjacent to the two carbon atoms followed by a capping reaction with BI_3 to give 3-I-1,2-$C_2B_{10}H_{11}$.[1] The next step consists of an electrophilic reaction with $AlCl_3$ and CH_3I. The presence of one B(3)−I will provide information on the susceptibility of the second boron, B(6), adjacent to both carbons, to electrophilic attack.

In a typical experiment 3-I-1,2-$C_2B_{10}H_{11}$ (3.7 mmol) was mixed with triflic acid[17] (66.5 mmol) and ICl (6.0 mL, 111 mmol). Following heating at 90 °C for three days, and after workup, a 94% yield of 3,4,5,7,8,9,10,11,12-nonaiodo-1,2-dicarba-*closo*-dodecaborane (*closo*-**1**) was obtained. The $^{11}B\{^1H\}$ NMR shows a 2:1:1:1:2:2:1 pattern spanning from δ = −4.2 to −22.1 ppm. Only the resonance at δ = −11.1 ppm, of intensity 1, shows splitting due to proton coupling in the ^{11}B NMR spectrum, indicating that all of the boron atoms, except B(6), have an exo-cluster iodine substituent. This was confirmed by X-ray diffraction analysis of *closo*-**1**·EtOAc (Figure 1).[18] Consequently, the pre-introduced B(3)−I does not labilize B(6)−H.

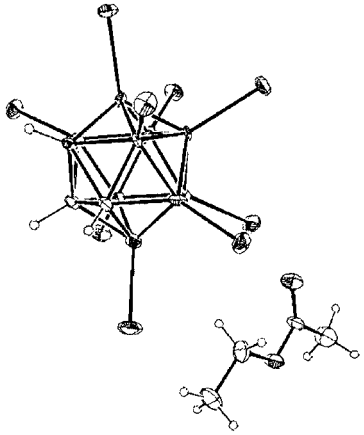

Figure 1. Perspective view of *closo*-**1**·EtOAc with 30% ellipsoids; H atoms have been omitted for clarity; selected bond lengths (Å): C(1)−C(2) 1.637(14), B−I 2.113(6)−2.166(11)

The method is successful for mildly electron-withdrawing elements, posing the question: could it be applicable for the introduction of Me substituents?

A good target was the long sought after 3,4,5,7,8,9,10,11,12-nonamethyl-1,2-dicarba-*closo*-dodecaborane (*closo*-**2**). The strategy for its synthesis was also a combination of nucleophilic and electrophilic attacks, the first producing 3-CH_3–1,2-$C_2B_{10}H_{11}$,[19] followed by reaction with $AlCl_3$ and CH_3I at reflux temperature for two days to produce *closo*-**2** (98%) after subsequent workup. The $^{11}B\{^1H\}$ NMR spectrum shows a 2:1:1:5:1 pattern indicating the geometrical similarity of *closo*-**1** and *closo*-**2**. The B(6) resonance is observed at δ = −17.16 ppm and again shows an exo-terminal proton coupling. As before, the pre-introduced B(3)−CH_3 does not labilize B(6)−H, thus maintaining the *closo* structure.

Conclusion

To summarize, a combined nucleophilic and electrophilic sequential process has allowed for the first time the introduction of nine equal substituents onto the well-studied *o*-carborane species. Iodine and methyl groups have been introduced to prove the generality of the method.

Experimental Section

General Remarks: Elemental analyses were performed using a Carlo Erba EA1108 microanalyser. IR spectra were recorded from KBr pellets on a Shimadzu FTIR-8300 spectrophotometer. ^1H and $^1H\{^{11}B\}$ NMR (300.13 MHz), $^{13}C\{^1H\}$ NMR (75.47 MHz) and ^{11}B NMR (96.29 MHz) spectra were recorded with a Bruker ARX 300 instrument equipped with the appropriate decoupling device. Chemical shift values for ^{11}B NMR spectra were referenced to external $BF_3{\cdot}OEt_2$ and those for ^1H, $^1H\{^{11}B\}$ and $^{13}C\{^1H\}$ NMR spectra were referenced to $SiMe_4$. Chemical shifts are reported in units of parts per million downfield from the reference with all coupling constants in Hz.

Unless otherwise noted, all manipulations were carried out under a dinitrogen atmosphere using standard vacuum line techniques. Iodine monochloride, aluminium trichloride and triflic acid were purchased from Aldrich.

***closo*-1:** Triflic acid (10.0 g, 66.5 mmol) and then ICl (6.0 mL) were added, under nitrogen flow, to 3-iodo-1,2-dicarba-*closo*-dodecaborane (1.0 g, 3.7 mmol). The mixture was heated at 90 °C for three days and then allowed to cool to room temperature. Cold water (10 mL) and then aqueous $NaHSO_3$ were added to the mixture. The resultant precipitate was filtered and then immediately dissolved in 125 mL of hot EtOAc and Zn added until the solution became colourless. The colourless solution was filtered and the solvent evaporated with a water pump. The solid obtained was recrystallized from EtOAc. (4.5 g, 94% yield). $C_2H_3B_{10}I_9$ (1277.1): calcd. C 1.88, H 0.23; found C 1.97, H 0.20. IR: $\tilde{\nu}$ = 3012 ($C_{cluster}$-H), 2650 (B-H) cm^{-1}. ^1H NMR (CD_3COCD_3): δ = 6.98 (br. s, $C_{cluster}$-H, B-H) ppm. ^{11}B NMR (CD_3COCD_3): δ = −4.2 (s, 2B), −9.7 (s, 1B), −11.1 [1B, B(6)], −12.6 (s, 1B), −17.2 (s, 2B), −20.3 (s, 2B), −22.1 (s, 1B) ppm. $^{13}C\{^1H\}$ NMR (CD_3COCD_3): δ = 72.5 (s, $C_{cluster}$) ppm. MALDI-TOF-MS: *m*/*z* = 1277.0 [M^+]. The $^1H\{^{11}B\}$

NMR of crystals of *closo*-**1**·EtOAc was run in CD_3COCD_3: δ = 6.98 (d, $^3J_{H,H}$ = 3.8 Hz, 2 H, $C_{cluster}$-H), 6.98 (br. s, 1 H, B-H), 4.06 (q, $^2J_{H,H}$ = 7.1 Hz, 2 H, CH_2), 3.54 (s, 3 H, CH_3), 1.20 (t, $^2J_{H,H}$ = 7.1 Hz, 3 H, CH_3) ppm.

***closo*-2:** MeI (6.4 mL) was added to a mixture of 3-methyl-1,2-dicarba-*closo*-dodecaborane (0.7 g, 4.4 mmol) and $AlCl_3$ (1.2 g, 8.8 mmol). The mixture was refluxed for 2 days after which the unchanged MeI was distilled off. The residue was hydrolyzed and extracted with pentane. The combined organic phases were treated with $Na_2S_2O_3$ and dried over $MgSO_4$. The final compound was purified by flash silica gel chromatography using pentane as the eluting solvent to give 3,4,5,7,8,9,10,11,12-nonamethyl-1,2-dicarba-*closo*-dodecaborane. (1.2 g, 98% yield). $C_{11}H_{30}B_{10}$ (270): calcd. C 48.89, H 11.11; found C 48.98, H 11.25. IR: $\tilde{\nu}$ = 3056 ($C_{cluster}$-H), 2945, 2905, 2833 (C-H), 2590 (B-H) cm^{-1}. $^1H\{^{11}B\}$ NMR ($CDCl_3$): δ = 0.32 (br. s, 3 H, CH_3), 0.13 (br. s, 6 H, CH_3), 0.05 (br. s, 6 H, CH_3), 0.01 (br. s, 3 H, CH_3), −0.12 (br. s, 3 H, CH_3), −0.23 (br. s, 6 H, CH_3), 2.89 (d, $^3J_{H,H}$ = 43 Hz, 2 H, $C_{cluster}$-H), 1.86 (br. s, 1 H, B-H) ppm. ^{11}B NMR ($CDCl_3$): δ = 5.4 (s, 2B), −2.1 (s, 1B), −4.2 (s, 1B), −8.8 (s, 5B), −17.2 (d, $^1J_{B,H}$ = 161 Hz, 1B) ppm. $^{13}C\{^1H\}$ NMR ($CDCl_3$): δ = −3.02 (br., CH_3), 54.25 (s, $C_{cluster}$) ppm. MALDI-TOF-MS: *m*/*z* = 270.1 [M^+].

X-ray Crystallographic Study: CCDC-185388 contains the supplementary crystallographic data for this paper. These data can be obtained free of charge at www.ccdc.cam.ac.uk/conts/retrieving.html [or from the Cambridge Crystallographic Data Centre, 12, Union Road, Cambridge CB2 1EZ, UK; Fax: (internat.) +44−1223/336−033; E-mail: deposit@ccdc.cam.ac.uk].

Acknowledgments

This work was supported by CICYT (Project MAT01−1575), Generalitat de Catalunya (2001/SGR/00337), and the Academy of Finland (project 41519, RK).

[1] [1a] J. Li, C. M. Logan, M. Jones Jr., *Inorg. Chem.* **1991**, *30*, 4866−4868. [1b] G. Barberà, C. Viñas, F. Teixidor, G. M. Rosair, A. J Welch, *J. Chem. Soc., Dalton Trans.* **2002**, 3647−3648.

[2] [2a] W. Jiang, C. B. Knobler, M. D. Mortimer, M. F. Hawthorne, *Angew. Chem. Int. Ed. Engl.* **1995**, *34*, 1332−1334. [2b] C.-W. Tsang, Q. Yang, E. T.-P. Sze, T. C. W. Mak, D. T. W. Chan, Z. Xie, *Inorg. Chem.* **2000**, *39*, 3582−3589. [2c] B. Grüner, Z. Janousek, B. T. King, J. N. Woodford, C. H. Wang, V. Vsetecka, J. Michl, *J. Am. Chem. Soc.* **1999**, *121*, 3122−3126. [2d] M. D. Mortimer, C. B. Knobler, M. F. Hawthorne, *Inorg. Chem.* **1996**, *35*, 5750−5751. [2e] Z. Zheng, W. Jiang, A. A. Zinn, C. B. Knobler, M. F. Hawthorne, *Inorg. Chem.* **1995**, *34*, 2095−2100. [2f] W. Jiang, C. B. Knobler, C. E. Curtis, M. D. Mortimer, M. F. Hawthorne, *Inorg. Chem.* **1995**, *34*, 3491−3498. [2g] T. Peymann, C. B. Knobler, M. F. Hawthorne, *Inorg. Chem.* **1998**, *37*, 1544−1548. [2h] C. A. Reed, N. L. P. Fackler, K.-C. Kim, D. Stasko, D. Evans, *J. Am. Chem. Soc.* **1999**, *121*, 6314−6315.

[3] B. T. King, Z. Janousek, B. Grüner, M. Trammel, B. C. Noll, J. Michl, *J. Am. Chem. Soc.* **1996**, *118*, 3313−3314.

[4] [4a] T. Peymann, C. B. Knobler, M. F. Hawthorne, *Chem. Commun.* **1999**, 2039−2040. [4b] B. T. King, B. C. Noll, A. J. McKinley, J. Michl, *J. Am. Chem. Soc.* **1996**, *118*, 10902−10903.

[5] A. Herzog, A. Maderna, G. N. Harakas, C. B. Knobler, M. F. Hawthorne, *Chem. Eur. J.* **1999**, *5*, 1212−1217.

[6] [6a] C.-W. Tsang, Z. Xie, *Chem. Commun.* **2000**, 1839−1840. [6b] I. Zharov, B. T. King, Z. Havlas, A. Pardi, J. Michl, *J. Am. Chem. Soc.* **2000**, *122*, 10253−10256. [6c] D. Stasko, C. A. Reed, *J. Am. Chem. Soc.* **2002**, *124*, 1148−1149. [6d] M. J. Ingleson, M. F. Mahon, N. J. Patmore, G. D. Ruggiero, A. S. Weller, *Angew. Chem. Int. Ed.* **2002**, *41*, 3694−3697.

[7] [7a] K. Shelly, C. A. Reed, Y. J. Lee, W. R. Scheidt, *J. Am. Chem. Soc.* **1986**, *108*, 3117−3118. [7b] C. A. Reed, *Acc. Chem. Res.* **1998**, *31*, 133−139. [7c] C. A. Reed, *Acc. Chem. Res.* **1998**, *31*, 325−332. [7d] S. H. Strauss, *Chem. Rev.* **1993**, *93*, 927−942. [7e] S. V. Ivanov, J. J. Rockwell, O. G. Polyakov, C. M. Gaudinsti, O. P. Anderson, K. A. Solntsev, S. H. Strauss, *J. Am. Chem. Soc.* **1998**, *120*, 4224−4225.

[8] R. R. Srivastava, D. K. Hamlin, D. S. Wilbur, *J. Org. Chem.* **1996**, *61*, 9041−9044.

[9] T. Peymann, C. B. Knobler, M. F. Hawthorne, *J. Am. Chem. Soc.* **1999**, *121*, 5601−5602.

[10] [10a] R. N. Grimes, in *Carboranes*, Academic Press, New York, 1970. [10b] V. V. Grushin, V. I. Bregadze, V. N: Kalinin, *J. Organomet. Chem. Lib.* **1988**, *20*, 1. [10c] V. I. Bregadze, *Chem. Rev.* **1992**, *92*, 209−223.

[11] T. Jelínek, J. Plešek, F. Mareš, S. Heřmánek, B. Štíbr, *Polyhedron* **1987**, *6*, 1981−1986.

[12] R. B. King, *Chem. Rev.* **2001**, *101*, 1119−1152.

[13] S. Kongpricha, H. Schroeder, *Inorg. Chem.* **1969**, *8*, 2449−2452.

[14] [14a] H. Schroeder, T. L. Heying, J. R. Reiner, *Inorg. Chem.* **1963**, *2*, 1092−1096. [14b] J. F. Sieckhaus, N. S. Semenuk, T. A. Knowles, H. Schroeder, *Inorg. Chem.* **1969**, *8*, 2449−2452.

[15] L. I. Zakharkin, V. N. Kalinin, *Izv. Akad. Nauk SSSR, Ser. Khim.* **1966**, *3*, 575.

[16] L. I. Zakharkin, V. N. Kalinin, *Izv. Akad. Nauk SSSR, Ser. Khim.* **1969**, *3*, 607.

[17] J. Barluenga, J. M. González, M. A. García-Martín, P. J. Campos, G. Asensio, *J. Org. Chem.* **1993**, *58*, 2058−2060.

[18] Crystal data for *closo*-**1**·EtOAc. $C_6H_{11}B_{10}I_9O_2$, monoclinic, space group $P2_1/n$ (no. 14), *a* = 11.394(3), *b* = 17.549(3), *c* = 14.237(2) Å, β = 100.537(15)°, *U* = 2798.7(10) $Å^3$, *Z* = 4, D_c = 3.240 g cm^{-3}, μ(Mo-K_a) = 9.973 mm^{-1}, *T* = 294 K. *F*(000) = 2360. 4921 Unique reflections were collected by ω/2θ ($2\theta_{max}$ = 50°). The structure was solved by direct methods and refined on F^2 by the SHELX-97 program to *R*1 = 0.0384 (*wR*2 = 0.0774) with a goodness-of-fit of 1.024.

[19] [19a] C. Viñas, G. Barberà, J. Oliva, F. Teixidor, A. J. Welch, G. M. Rosair, *Inorg. Chem.* **2001**, *40*, 6555−6562. [19b] G. Barberà, Doctoral thesis, U. A. B. 2002.

Received November 15, 2002
[I02630]

A Three-Dimensional Framework of Novel Vanadium Clusters Bridged by $[Ni(en)_2]^{2+}$: $Ni(en)_3\{V^{IV}_{11}V^{V}_{5}O_{38}\ Cl\ [Ni\ (en)_2]_3\}\cdot 8.5H_2O$

Cheng-Ling Pan,[a] Ji-Qing Xu,*[a] Guang-Hua Li,[a] De-Qing Chu,[a] and Tie-Gang Wang[a]

Keywords: Polyoxometalates / Hydrothermal synthesis / Cluster compounds / Crystal structure

The hydrothermal reaction of V_2O_5, $H_2C_2O_4\cdot 2H_2O$, KOH, en and $NiCl_2\cdot 6H_2O$ yields a new three-dimensional open-framework solid. The extended structure consists of a three-dimensional network of $[V_{16}O_{38}Cl]^{8-}$ cages, with each cage connected to six other neighboring units through $[Ni(en)_2]^{2+}$ bridging groups.
(© Wiley-VCH Verlag GmbH & Co. KGaA, 69451 Weinheim, Germany, 2003)

The systematic construction of specific architectures from molecular building blocks has been an area of active research over the past few years.[1] Examples range from coordination polymers [2] to larger cluster-based building blocks.[3] The mechanism of the formation of polyoxometalates (POMs) is still not yet fully understood and is often described as self-assembly. What appears to be evident in exploiting suitable molecular building blocks is to employ polyoxoanions linked through some kinds of tethers to form extended structures. While a synthetic method leading to rational design remains a challenging topic, there seems to be an increasing use of a combination of hydrothermal synthesis and structure-directing templates. Small changes in the synthetic technique, such as solvent, pH value or counterion, can lead to different products.[4] However, once structure principles are recognized, the synthesis of targeted species can be designed, as has been demonstrated by the work of Müller and co-works with the large polymolybdates. Zubieta and co-workers have reported one- and two-dimensional polymeric oxometalates in several organic-inorganic hybrid materials.[3a] On-going research has demonstrated that transition metal (e.g. Fe, Co, Ni, Cu, Zn, and Mn) coordination complexes may serve as inorganic bridging ligands linking polyanion clusters into one-, two- and three-dimensional networks.[5]

POMs are an important subclass of metal oxide cluster with an exceptional capacity to form mixed-valence compounds that exhibit rich electronic and magnetic properties and have relevance to catalysis, medicine, and in materials science.[6] Polyoxovanadates have been extensively studied, with many structurally characterized examples now known, such as $[V_4O_{12}]^{4-}$, $[V_5O_{14}]^{3-}$, $[V_6O_{19}]^{8-}$, $[V_{10}O_{28}]^{6-}$, $[V_{12}O_{32}]^{4-}$, $[V_{13}O_{34}]^{3-}$, $[V_{15}O_{36}]^{5-}$, $[V_{15}O_{42}]^{9-}$, $[V_{17}O_{42}]^{4-}$ and $[V_{18}O_{42}]^{12-}$, $[V_{19}O_{49}]^{9-}$ and $[V_{34}O_{82}]^{10-}$.[7] Although polyoxovanadate clusters emerging as discrete ions are common, synthetically prepared examples of extended structures with polyoxoanions are relatively rare. Some new mixed-valance vanadium oxide layers have also been observed in $[Ni(en)_2][V_6O_{14}]$,[8] $[Zn(en)_2][V_6O_{14}]$, $[Cu(en)_2]$-$[V_6O_{14}]$, $[Cu(en)_2][V_{10}O_{25}]$[9] and $[Cd(enMe)_2][V_8O_{20}]$.[10] Khan et al. have reported several three-dimensional frameworks which consist of spherical $[V_{18}O_{42}\ (XO_4)]$ clusters linked by bridging $[M(H_2O)_4]$ groups (X: V, S; M: Fe, Co, Mn, Zn).[5a] At present, we are making a systematic investigation of POMs of group V transition elements for finding the best strategies to design and synthesize metal oxide clusters with new structures. Here, we report an entirely new type of mixed-valence ion $[V_{16}O_{38}Cl]^{8-}$ as a building block, which is bridged by $[Ni(en)_2]^{2+}$ leading to the three-dimensional network $Ni(en)_3\{V^{IV}_{11}V^{V}_{5}O_{38}Cl[Ni(en)_2]_3\}\cdot 8.5H_2O$ (**1**). As far as we are aware, compound **1** is composed of a new type of mixed-valance vanadium-oxygen cluster $[V_{16}O_{38}Cl]^{8-}$ as structural motif, unlike most of the known materials with extended structures, which are composed of well-characterized metal-oxygen cluster types.

The X-ray structure analysis reveals that the extended structure of **1** (Figure 1), consists of a three-dimensional network of $[V_{16}O_{38}Cl]^{8-}$ cages, with each cage connected to six other neighboring units through $[Ni(en)_2]^{2+}$ bridging groups. This generates a network of $\{$-$[V_{16}O_{38}Cl]$-$[Ni(en)_2]$-$[V_{16}O_{38}Cl]$-$\}_n$ arrays running along two mutually non-perpendicular directions, so the overall topology of the six-connected network is simple cubic. The building block in the structure of **1** may be viewed as a "rugby ball"-like $[V_{16}O_{38}Cl]$ shell encapsulating a Cl^- ion at its center, as has been reported by Müller in the polyoxovanadate $[V_{15}O_{36}Cl]^{6-}$.[7g] Indeed, an unusual property of reduced polyoxovanadates is their tendency to form cages encapsulating a guest atom. To the best of our knowledge, there

[a] College of Chemistry and State Key Laboratory of Inorganic synthesis and Preparative Chemistry, Jilin University, Changchun 130023, P. R. China
Fax: (internat.) + 86-431/892-3907
E-mail: pan@mail.jlu.edu.cn
xjq@mail.jlu.edu.cn

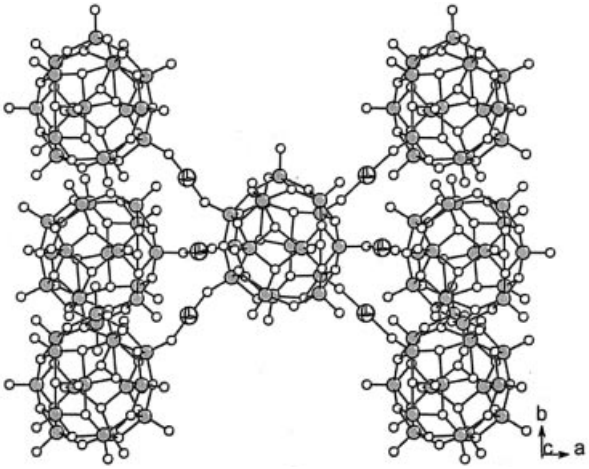

Figure 1. View of the extended structure of $Ni(en)_3\{V_{16}O_{38}Cl[Ni(en)_2]_3\}\cdot 8.5H_2O$, showing nets of $[V_{16}O_{38}Cl]$ clusters interconnected through $[Ni(en)_2]^{2+}$ bridging groups like reticular framework; H_2O, Cl^-, en and $[Ni(en)_3]^{2+}$ groups have been omitted for clarity

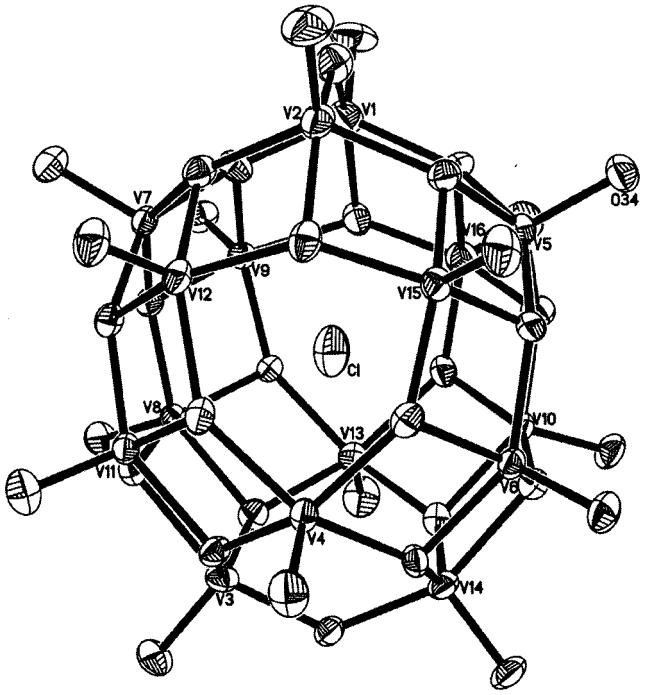

Figure 2. Structure of the $[V_{16}O_{38}Cl]^{8-}$ anion showing a novel cage; selected distances (Å) are as follows: V−O_t 1.584(6)−1.619(6), V−μ_2-O(−Ni) 1.620(5)−1.641(6), V−μ_2-O(−V) 1.760(6)−1.898(7), V−μ_3-O 1.846(5)−2.242(5), Ni−O 2.062(6)−2.131(6)

are no examples where a $[V_{16}O_{38}Cl]$ cage forms a three-dimensional network by $[Ni(en)_2]^{2+}$ bridging.

The $[V_{16}O_{38}Cl]^{8-}$ unit is a novel type of polyoxovanadate cage, as shown in Figure 2. The new vanadium exhibits only one type of coordination i.e. pyramidal. The host shell is made up of 16 VO_5 square pyramids sharing edges through 20 μ_3-oxygen atoms, 8 μ_2-oxygen atoms, and 10 μ_1-oxygen atoms. All the average bond lengths in the cluster are within normal ranges.[7] Fivefold-coordinated VO_5 units are interconnected to form polyoxovanadate $[V_{16}O_{38}]$ units, and the environment around V1 is defined by three μ_3-oxygen groups, a μ_2-O, and an apical O1 moiety. Interestingly, O34 is also bonded to the Ni center of one of the six $Ni(en)_2$ bridges that interlink the other $[V_{16}O_{38}Cl]^{8-}$ clusters; the six-coordination of Ni^{2+} is completed by four N and two O atoms. Furthermore, each surface of the cluster supports six $[Ni(en)_2]^{2+}$ groups which connect different cages by μ_2-oxygen, leading to a three-dimensional network. To the best of our knowledge, the $[V_{16}O_{38}Cl]^{8-}$ cluster in **1** is the first observation of a hexadecavanadium structure containing an included Cl^- anion.

The assignment of the oxidation state of the vanadium is consistent with the coordination geometry and was confirmed by bond valence sum calculations (BVS).[11] The room temperature EPR spectrum of a crystalline sample of compound consists of one signal ($g = 2.002$), indicating the presence of V^{IV}. According to bond valence sum calculations and charge balance, compound **1** is formulated as $Ni(en)_3\{V^{IV}_1V^{V}_5O_{38}Cl[Ni(en)_2]_3\}\cdot 8.5H_2O$.

Each terminal oxygen of the six VO_5 pyramids (V5−V10) in compound **1** is linearly bonded to the nickel(II) center, in contrast to the $[M(en)_2][V_6O_{14}]$ (M = Cu, Zn)[9] structures where the V=O oxygen atoms of the VO_4 tetrahedron are bonded to the metal cations. The octahedral geometry around each nickel is completed by two en groups. The bridging Ni^{2+} ions exhibit strong covalent attachments to the two adjacent clusters with an average Ni−O distance of 2.087 Å, which is much shorter than that in $[M(en)_2][V_6O_{14}]$ (Cu−O: 2.53 Å; Zn−O: 2.54 Å).

The structure of highly reduced polyoxovanadate bridged by $[Ni(en)_2]^{2+}$ in the compound allows us to predict the existence of magnetic exchange coupling. The variable temperature magnetic susceptibility of **1** was measured between 5 and 300 K. The effective magnetic moment of **1** at room temperature (300 K), determined by the equation $\mu_{eff} = 2.83(\chi_M T)^{1/2}$, where χ_M is the molar magnetic susceptibility per formula unit, is 8.72 μ_B, and is therefore smaller than the value expected for the total spin-only value of 11 uncoupled $S = 1/2$ spins of V^{4+} atoms and four uncoupled $S = 1$ spins of Ni^{2+} atoms. Figure 3 shows that the effective magnetic moment of **1** increases as the temperature decreases from 300 to 14 K, which is in agreement with a Weiss constant of $\theta > 0$, indicating the presence of a weak ferromagnetic exchange interaction in compound **1**. In the range 14−5 K, the effective magnetic moment decreases with the temperature decreasing, showing there is antiferromagnetic coupled interaction in **1** in this temperature range. Because no suitable theoretical model is available in the literature[12] for such a complex system, further studies on the magnetic properties of similar systems are ongoing in our lab.

Hydrothermal techniques exploit the principle of "self-assembly" of a metastable solid phase from soluble precur-

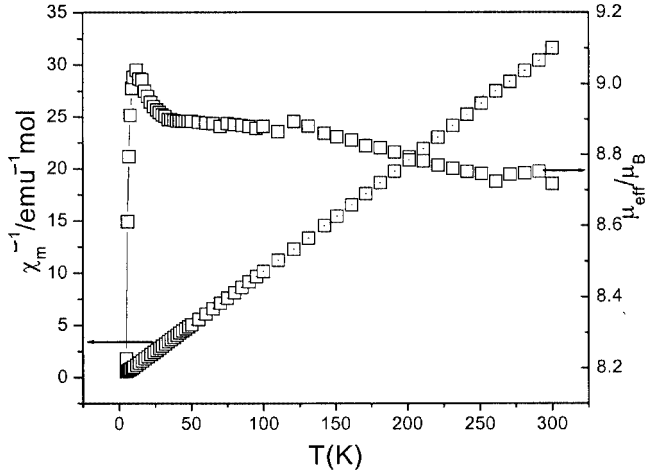

Figure 3. A plot of the effective magnetic moment μ_{eff} and inverse molar susceptibility vs. temperature for compound **1**

sors.[5b] Complex **1** is synthesized from V_2O_5 by exploiting the reducing ability of $H_2C_2O_4{\cdot}2H_2O$ and en. The presence of $H_2C_2O_4$ and en are absolutely essential for product formation. Under more reducing conditions the fully reduced V^{IV} clusters are isolated. V^{IV} and V^{IV}/V^{V} clusters are cryptands and tend to form spherical structures. This feature is evident in the class of reduced and mixed-valence polyoxovanadates described by Zubieta et al.[13] However, this result may originate from the nature of the transition metal ions employed. The nickel ion favors a six-coordinate octahedral geometry. It should be noted that the pH value of the starting mixture has a big influence on the resulting products. Crystals of **1** can only be prepared in a system with pH values in the range from 8.5 to 9.5. The Ni−O−V linkages play a critical role in constructing the chain structure. Although the architecture of a one-, two- and three-dimensional network could not be predicted, we managed to synthesize the compound and obtain high productivity.

Experimental Section

Synthesis of 1: The raw materials used in the synthesis are V_2O_5, $H_2C_2O_4{\cdot}2H_2O$, KOH, $NiCl_2{\cdot}6H_2O$, en, and distilled water. In a typical synthesis of compound **1**, 0.82 g of V_2O_5, 0.5 g of KOH and 1.24 g of $H_2C_2O_4{\cdot}2H_2O$ were first added to 12 mL of distilled water, and then 0.95 g of $NiCl_2{\cdot}6H_2O$ and 0.8 mL of en were added whilst stirring. The reaction mixture, with a pH value about 9.0, was sealed in a 20 mL Teflon-lined autoclave and heated under autogenous pressure at 160 °C for four days. The crystalline product was filtered, washed with distilled water, and dried at ambient temperature to give 0.46 g of **1**. IR: 1582(s) cm^{-1}, 1458(m), 1394(w), 1369(w), 1327(w), 1277(w), 1142(w), 1103(w), 1022(s), 967(s), 650(s), 512(s). $C_{18}H_{89}ClN_{18}Ni_4O_{46.5}V_{16}$ (2387.4): C 9.05, H 3.73, N 10.56; found C 7.36, H 2.08, N 12.94. The TGA of **1** showed that water is lost first, followed by the en molecules in the range 250−469 °C, and a weight gain at 469−583 °C, consistent with the oxidation from V^{IV} to V^{V}.

X-ray Crystallography: Crystal data for $C_{18}H_{89}ClN_{18}Ni_4O_{46.5}V_{16}$, dimensions 0.52 × 0.46 × 0.42 mm, monoclinic, space group $P2_1/n$, a = 21.953(4), b = 15.896(3), c = 25.086(5) Å, β = 109.39(3)°, V = 8258(3) Å^3, Z = 4, Dc = 1.920 g/cm^3, μ(Mo-K_α) = 2.726 mm^{-1}, T = 293(2) K, $R[I < 2\sigma(I)]$ = 0.0754] and the goodness-of-fit on F^2 is 1.007.

CCDC-183112 contains the supplementary crystallographic data for this paper. These data can be obtained free of charge at www.ccdc.cam.ac.uk/conts/retrieving.html [or from the Cambridge Crystallographic Data Centre, 12, Union Road, Cambridge CB2 1EZ, UK; Fax: (internat) +44-1223/336-033; E-mail: deposit@ccdc.cam.ac.uk].

Acknowledgments

This work was supported by National Natural Science Foundation of China (20271021). We also thank Prof. Lin-Hai Hu for the structural analysis.

[1] [1a] M. J. Zaworotko, *Angew. Chem. Int. Ed.* **2000**, *39*, 3052−3054. [1b] M. J. Zaworotko, *J. Chem. Soc. Rev.* **1994**, 283−288.

[2] [2a] O. M. Yaghi, H. Li, *J. Am. Chem. Soc.* **1995**, *117*, 10401−10402. [2b] O. M. Yaghi, H. Li, *J. Am. Chem. Soc.* **1996**, *118*, 295−296. [2c] L. Carlucci, C. Gianfranco, D. M. Prosperio, A. Sironi, *J. Am. Chem. Soc.* **1995**, *117*, 12861−12862. [2d] L. R. MacGillivray, S. Subramanian, M. J. Zaworotko, *J. Chem. Soc., Chem. Commun.* **1994**, 1325−1326.

[3] [3a] P. J. Hagrman, D. Hagrman, J. Zubieta, *Angew. Chem. Int. Ed.* **1999**, *38*, 2638−2684 and references therein. [3b] D. E. Hagram, J. Zubieta, *J. Solid State Chem.* **2000**, *152*, 141−151. [3c] A. Müller, E. Krickemeyer, H. Bogge, M. Schmidtmann, F. Peters, C. Menke, J. Meyer, *Angew. Chem. Int. Ed. Engl.* **1997**, *36*, 484−486. [3d] A. Müller, S. Sarkar, S. Q. N. Shah, H. Bögge, M. Schmidtmann, P. Kogerler, B. Hauptfleisch, A. X. Trautwein, V. Schunemann, *Angew. Chem. Int. Ed.* **1999**, *38*, 3238−3241. [3e] B. T. Holland, P. K. Isbester, C. F. Blanford, E. J. Munson, A. Stein, *J. Am. Chem. Soc.* **1997**, *119*, 6798−6803.

[4] [4a] S. Subramanian, M. J. Zaworotko, *Angew. Chem. Int. Ed. Engl.* **1995**, *34*, 2127−2129. [4b] B. J. S. Johnson, R. C. Schroden, C. Zhu, A. Stein, *Inorg. Chem.* **2001**, *40*, 5972−5978. [4c] R. W. Gable, B. F. Hoskins, R. Robson, *J. Chem. Soc., Chem. Commun.* **1990**, 1677−1678.

[5] [5a] M. I. Khan, *J. Solid State Chem.* **2000**, *152*, 105−112. [5b] J. Lu, Y. Xu, N. K. Goh, L. S. Chia, *Chem. Commun.* **1998**, 2733. [5c] W. M. Bu, G. Y. Yang, L. Ye, J. Q. Xu, Y. G. Fan, *Chem. Lett.* **2000**, 462−463. [5d] C. M Liu, D. Q. Zhang, M. Xiong, D. B. Zhu, *Chem. Commun.* **2002**, 1416−1417.

[6] [6a] M. T. Pope, A. Müller, *Angew. Chem. Int. Ed. Engl.* **1991**, *30*, 34−48. [6b] A. Müller, F. Peters, M. T. Pope, D. Gatteschi, *Chem. Rev.* **1998**, *98*, 239−271. [6c] A. Müller, *Nature* **1991**, *352*, 115−116.

[7] [7a] J. Fuchs, S. Mahjour, J. Pickardt, *Angew. Chem. Int. Ed. Engl.* **1976**, *15*, 374−375. [7b] V. W. Way, W. G. Klemperer, O. M. Yaghi, *J. Am. Chem. Soc.* **1989**, *111*, 4518−4519. [7c] H. K. Chae, W. G. Klemperer, V. W. Day, *Inorg. Chem.* **1989**, *28*, 1423−1424. [7d] V. W. Day, W. G. Klemperer, D. J. Maltbie, *J. Am. Chem. Soc.* **1987**, *109*, 2991−2992. [7e] V. W. Day, W. G. Klemperer, O. M. Yaghi, *J. Am. Chem. Soc.* **1989**, *111*, 5959−5960. [7f] D. Hou, K. S. Hagen, C. L. Hill, *J. Am. Chem. Soc.* **1992**, *114*, 5864−5865. [7g] A. Müller, E. Krickemeyer, M.

Penk, H. J. Walberg, H. Bögge, *Angew. Chem. Int. Ed. Engl.* **1987**, *26*, 1045−1046. [7h] D. Hou, K. S. Hagen, C. L. Hill, *J. Chem. Soc., Chem. Commun.* **1993**, 426−427. [7i] Y. Hayashi, K. Fukuyama, T. Takatera, A. Uehara, *Chem. Lett.* **2000**, 770−771. [7j] G. K. Johnson, E. O. Schlemper, *J. Am. Chem. Soc.* **1978**, 3645−3646. [7k] A. Müller, M. Penk, E. Krickemeyer, H. Bögge, H. J. Wallberg, *Angew. Chem. Int. Ed. Engl.* **1988**, *27*, 1719−1720. [7l] A. Müller, R. Rohlfing, J. Döring, M. Penk, *Angew. Chem. Int. Ed. Engl.* **1991**, *30*, 588−590.

[8] B. Z. Lin, S. X. Liu, *J. Chem. Soc., Dalton Trans.* **2002**, 865−869.

[9] Y. Zhang, J. R. D. DeBord, C. J. O'Connor, R. C. Haushalter, J. Zubieta, *Angew. Chem. Int. Ed. Engl.* **1996**, *35*, 989−991.

[10] L. Zhang, Z. Shi, G. Yang, X. Chen, S. Feng, *J. Chem. Soc., Dalton Trans.* **2000**, 275−278.

[11] I. D. Brown, *Structure and Bonding in Crystals*, Vol. 2 (Eds.: M. O'Keeffe and A. Navrotsky), Academic press, New York, **1981**.

[12] O. Kahn, *Molecular Magnetism*, VCH, New York, **1993**.

[13] M. I. Kahn, Q. Chen, J. Zubieta, *Inorg. Chim. Acta* **1993**, *212*, 199−206.

Received January 7, 2003
[I03009]

An Unusual Bonding Situation in a Novel Au^I-Phosphido Complex with a Planar Au_3P_3 Framework

Ulf Vogel,[a] Perumal Sekar,[a] Reinhart Ahlrichs,[b] Uwe Huniar,[b] and Manfred Scheer*[a]

Dedicated to Professor A. Zschunke on occasion of his 65th birthday

Keywords: Metathesis / Cyclopentadienyl ligands / Chromium / P ligands / Gold

Reaction of the mono-deprotonated derivative of $[\{Cp(CO)_2Mo\}_2(\mu\text{-}PH_2)(\mu\text{-}H)]$ (**1**) leads to the novel complex $[\{Cp(CO)_2Mo\}_2(\mu\text{-}H)\{\mu_3\text{-}P(H)Au(PPh_3)\}]$ (**2**). In contrast the reaction of the analogous Cr derivative $[\{Cp(CO)_2Cr\}_2(\mu\text{-}PH_2)(\mu\text{-}H)]$ (**1a**) leads under identical conditions to a planar Au_3P_3 cluster $[\{CpCr(CO)_2\}_6(P_3Au_3)]$ (**3**). Both complexes were completely structurally and spectroscopically characterised. Density functional calculations have shown that **3** is characterised by P–Cr–Au multicentre and Cr-P multiple bonding.
(© Wiley-VCH Verlag GmbH & Co. KGaA, 69451 Weinheim, Germany, 2003)

Introduction

Polynuclear Au^I complexes are a fascinating field of chemistry[1] as there are, for example, planar, wheel-like mixed metal clusters of the type $[M\{Au(mes)\}_5]X$ (M = Cu, Ag; X = PF_6, ClO_4; mes = 2,4,6-trimethylphenyl)[2] and the larger class of chalcogenido-bridged clusters.[3] Among the latter ones are compounds possessing luminescence properties.[4] However, phosphanido (R_2P^-) substituted Au^I complexes are rare,[5] and for Au^I complexes containing the phosphido (P^{3-}) ligand, only the series of phosphorus-centred homoleptic gold clusters of Schmidbaur et al. exists. These complexes — $P(AuPR_3)_4^+$, $P(AuPR_3)_5^{2+}$, $P(AuPR_3)_6^{3+}$, $(R_3P)_2AuP(AuPR_3)_4^{2+}$, $(R_3PAu)_4PAuP(AuPR_3)_4^{3+}$ — were synthesized by the reaction of PH_3 or $P(SiMe_3)_3$ and $P_2(SiMe_3)_4$, respectively, with R_3PAu^+.[6] Interestingly, due to their instability no X-ray structural analysis exists so far for the tetrahedrally coordinated phosphido complex of the monocation $P(AuPR_3)_4^+$.

Lately, an unusual route to naked[7] phosphorus-containing ligands was presented by Mays et al., who reacted $[\{Cp(CO)_2Mo\}_2(\mu\text{-}PH_2)(\mu\text{-}H)]$ (**1b**)[8] with group 15 trichlorides ECl_3 (E = P, As, Sb) to form the novel mixed group 15 element-containing tetrahedrane complexes $[\{Cp(CO)_2Mo\}_2(\mu,\eta^2\text{-}PE)]$ by elimination of LiCl and HCl.[9] The chromium analogue $[\{Cp(CO)_2Cr\}_2(\mu\text{-}PH_2)(\mu\text{-}H)]$ (**1a**) had not been described in the literature until we found an efficient method for its synthesis by the reaction of $[\{Cp(CO)_2Cr\}_2(\mu,\eta^2\text{-}P_2)]$ with superhydride ($LiBEt_3H$).[10a] Herein we report on the remarkable differences in the reaction behaviour of the corresponding anions of **1a** and **1b** with the transition metal electrophile $[(Ph_3P)AuCl]$ and the formation of the first phosphido-containing mixed metal Au^I complex in an unusual multi-centre bonding situation.

Results and Discussion

Both neutral complexes **1a** and **1b** were converted into the corresponding anions under identical conditions using KH (Scheme 1). Subsequent reaction with $[(Ph_3P)AuCl]$ leads, in the case of the molybdenum complex **1b**, to substitution of a hydrogen atom by a $AuPPh_3$ moiety to form $[\{Cp(CO)_2Mo\}_2(\mu\text{-}H)\{\mu_3\text{-}P(H)Au(PPh_3)\}]$ (**2**). However, for the chromium homologue **1a** a rearrangement of the $[CpCr(CO)_2P]$ units is observed with formation of the novel trinuclear Au cluster **3** with a $Au_3Cr_6P_3$ core.

Complex **2** forms orange and **3** brown crystals, which are slightly soluble in hexane and readily soluble in toluene, CH_2Cl_2 and THF. In their IR spectra the CO stretching frequencies are observed in the typical range for terminal CO ligands. Additionally, a P−H stretching frequency is found for **2** at 2243 cm^{-1}. In the EI mass spectrum of **2** only characteristic fragment ion peaks could be detected, whereas for **3** no such fragments were found. Due to the quadrupolar moment of the ^{197}Au nucleus only two broad singlets at δ = 41.0 and 73.1 ppm are observed in the $^{31}P\{^1H\}$ NMR spectrum of **2** and one for **3** at δ = 38 ppm.

[a] Institut für Anorganische Chemie der Universität Karlsruhe, 76128 Karlsruhe, Germany
Fax: (internat.) +49-(0)721/608-7021
E-mail: mascheer@chemie.uni-karlsruhe.de
[b] Institut für Physikalische Chemie der Universität Karlsruhe, 76128 Karlsruhe, Germany
Fax: (internat.) +49-(0)721/608-7225
E-mail: ramail@tchibm3.chemie.uni-karlsruhe.de

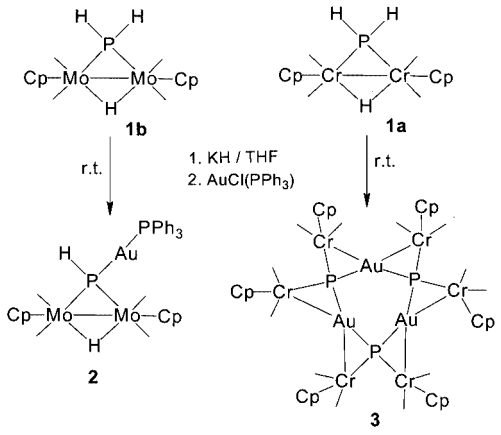

Scheme 1. Different reaction behaviour of dinuclear complexes [{$Cp(CO)_2M$}$_2$(μ-PH_2)(μ-H)] [M = Cr (**1a**), Mo (**1b**)] with $AuCl(PPh_3)$ (CO ligands are represented by bond lines)

The ^{1}H NMR spectrum of **2** shows a characteristic peak at high field ($\delta = -11.73$ ppm) for the bridging hydride ligand. This signal is split into a doublet due to the coupling with the phosphorus atom ($^2J_{H,P} = 29$ Hz). The PH proton also splits into a doublet which is detected at $\delta = 6.12$ ppm ($^1J_{H,P} = 282$ Hz). Two discrete singlets for the Cp protons at $\delta = 4.84$ and 5.04 ppm suggest a *trans* arrangement of the two Cp ligands as found in the solid-state structure of **2**.

The dinuclear [$Mo_2(CO)_4Cp_2$] fragment of **2** (Figure 1) is bridged by a hydrido and a PH($AuPPh_3$) ligand. The Au atom is almost linearly surrounded by its substituents (P1−Au−P2 179.15(7)°]. The Mo−Mo distance is 3.266(2) Å and is similar to that in the neutral complex **1b** [3.282(1) Å].[8b] The Mo−P bond lengths of 2.450(2) and 2.434(2) Å in **2** are only slightly longer than that in the starting material **1b** [2.402(1) Å]. The Au−P distances in **2** are almost identical [Au−P1 2.309(2) Å; Au−P2 2.324(2) Å]. Similar bond lengths are found in the structurally related compounds [$(CO)_8M_2$(μ-H)(μ_3-PCy)Au(PPh_3)] [M = Mn, Re; Cy = cyclohexyl; M = Mn: Au−P1 2.306(1) Å and Au−P2 2.317(1) Å; M = Re: Au−P1 2.313(4) Å, Au−P2 2.303(4) Å].[11]

The X-ray structure analysis of **3** (Figure 2) reveals a planar Au_3P_3 six-membered ring (mean deviation of the atoms from the plane: 0.077 Å), where each of the distorted tetrahedrally surrounded phosphido ligands are bound to two Au atoms as well as to two $CpCr(CO)_2$ moieties. The Au atoms by themselves form an isosceles triangle with the closest distances between the atoms Au2 and Au3 of 3.284(1) Å; the other distances are 3.454(1) and 3.482(1) Å indicating essentially no Au···Au interaction.[6,12] The Au−P bond lengths of **3** are between 2.405(4) Å and 2.440(4) Å and are therefore longer than those found in the square pyramidal-coordinated P atoms of $P(AuPR_3)_5^{2+}$ [13] [2.295(3) Å for the axial P−Au bond and 2.356(3)−2.379(3) Å for the other] and $(R_3PAu)_4PAuP(AuPR_3)_4^{3+}$ [14] [2.293(7) Å (axial) and 2.369(3) Å for the other]. The Au−Cr distances of **3** [2.707(2)−2.748(3) Å] are in the range of those distances found in linear-coordinated

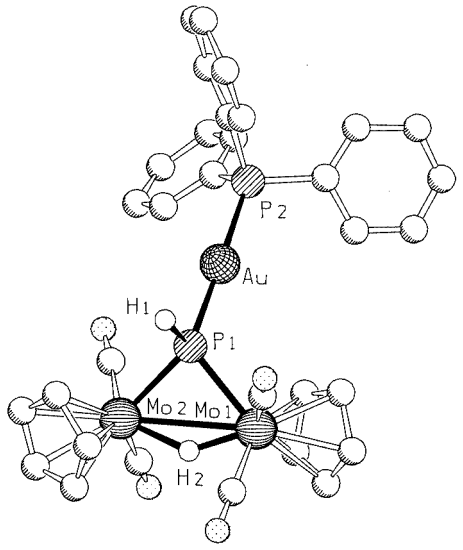

Figure 1. Molecular structure of **2**; hydrogen atoms of the Ph and Cp substituents are omitted for clarity; selected bond lengths [A] and angles [°]: Mo(1)−Mo(2) 3.266(2), Mo(1)−P(1) 2.434(2), Mo(2)−P(1) 2.450(2), Au−P(1) 2.309(2), Au−P(2) 2.324(2); P(1)−Au−P(2) 179.15(7), Mo(1)−P(1)−Mo(2) 83.92(7), Mo(1)−P(1)−Au 119.24(9), Mo(2)−P(1)−Au 127.7(1)

Au−$CrCp(CO)_3$-containing complexes.[15] Significant structural features of **3** are the very short Cr−P bond lengths of 2.135(5)−2.168(4) Å, which are much shorter than the average Cr−P bond lengths in the related complexes [{$Cp(CO)_2Cr$}$_2$(μ-PH_2)$_2$] (2.381 Å),[10b] [$(CO)_4CrP(CH_3)_2$]$_2$ (2.318 Å)[16] and in [{$Cp(CO)_2Cr$}$_2$(μ,η^2-P_2)] (2.409 Å),[17] [{$Cp(CO)_2Cr$}$_2$(μ,η^2-P_2){$Cr(CO)_5$}] (2.405 Å)[18] and [{$Cp(CO)_2Cr$}$_2$(μ,η^2-P_2){$Cr(CO)_5$}$_2$] (2.411 Å).[19] They are

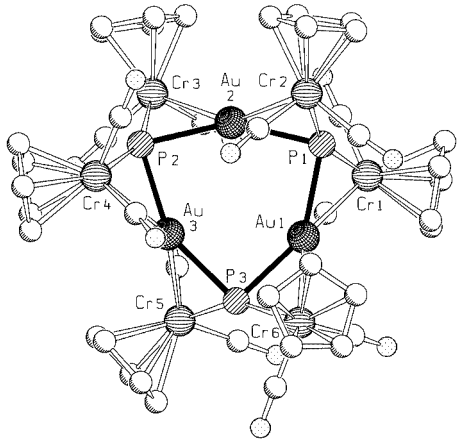

Figure 2. Molecular structure of **3**; hydrogen atoms are omitted for clarity; selected bond lengths [A] and angles [°]: Au(1)−P(1) 2.413(3), Au(1)−P(3) 2.405(4), Au(2)−P(1) 2.399(4), Au(2)−P(2) 2.382(4), Au(3)−P(2) 2.408(4), Au(3)−P(3) 2.440(4), Au(1)−Cr(1) 2.725(3), Au(1)−Cr(6) 2.723(3), Au(2)−Cr(2) 2.730(3), Au(2)−Cr(3) 2.726(2), Au(3)−Cr(5) 2.707(2), Au(3)−Cr(4) 2.748(3), Cr(1)−P(1) 2.135(5), Cr(2)−P(1) 2.154(4), Cr(3)−P(2) 2.168(4), Cr(4)−P(2) 2.163(4), Cr(5)−P(3) 2.167(4), Cr(6)−P(3) 2.171(5); Au(1)−P(1)−Au(2) 91.75(12), Au(2)−P(2)−Au(3) 86.58(12), Au(1)−P(3)−Au(3) 91.96(12), P(1)−Au(1)−P(3) 143.92(13), P(2)−Au(2)−P(1) 153.13(12), P(2)−Au(3)−P(3) 151.00(12), Cr(1)−P(1)−Cr(2) 154.9(2), Cr(4)−P(2)−Cr(3) 154.2(2), Cr(5)−P(3)−Cr(6) 150.8(2)

even shorter than the Cr−P bond length in **1a** [2.266(1) and 2.271(1) Å],[10a] where the Cr−Cr bond is additionally clamped by the μ-H ligand.

Due to these remarkable structural features of **3**, including the unexpected existence of the Au−Cr bonding in this Au^I complex together with the fact that the phosphido atoms of **3** are substituted by only two 15 valence electron $Cp(CO)_2Cr$ units, we first speculated about the existence of additional H bridges between the Au and Cr atoms. Since we found no spectroscopic indication for this, we decided to perform density functional calculations[20] of a hypothetical complex $[\{Cp(CO)_2Cr\}_6(\mu\text{-}H)_6\{(\mu_4\text{-}P)_3Au_3\}]$ (**3a**) with a tentative X-ray structure and various other structures as starting points. This led to a large distribution of hydrogen positions showing Cr−H, Au−H, P−H and Cp−H bonds for different minimum structures of similar energies (some within 20 kJ/mol). The approximate C_3 symmetry of the $(AuP)_3$ ring was always heavily distorted and the bond lengths deviated considerably from the experimental values [d(Au−P) = 2.40−2.72 Å; d(Cr−P) = 2.14−2.39 Å; d(Au−Cr) = 2.75−2.98 Å]. We thus examined the structure of **3** by DFT calculations which resulted in close agreement with the experimental data [d(Au−P) = 2.49−2.56 Å; d(Cr−P) = 2.16−2.19 Å; d(Au−Cr) = 2.75−2.81 Å]. The computed bond lengths exceed the experimental values as is typical for the BP86 functional method, particularly for weak bonds involving Au atoms. The latter are stabilised by attractive dispersion forces, which are not accounted for in DFT.

The bond lengths in **3** and the Cr−P−Cr angle (151−155°) together with the electron count of Cr point to an unusual electronic structure, which is difficult to disentangle due to the low molecular symmetry. Mullikan occupancies[20f] for the valance orbitals 3p(P), 3d(Cr) and 6s(Au) are all close to one (0.8−1.2), which implies that they are all involved in bonding. The three-centre shared electron number[20g,20h] PCrAu = 0.16 indicates pronounced multicentre bonding. These facts may be rationalised by the following simplified picture: the 3p orbitals of (formal) P^{3-} are delocalised to form partial σ- and π-bonds to Cr with π-bonds delocalised into 6s(Au), leading to short P−Cr, relatively long Au−P and weak Au−Cr bonds.

Conclusions

The reported results confirm our observations in the reactivity studies of the tetrahedral P_2-containing complexes $[\{Cp(CO)_2M\}_2(\mu,\eta^2\text{-}P_2)]$ [M = Cr (**4a**), Mo (**4b**)] towards inorganic and organometallic complexes, where we found significant differences due to the lability of the Cr−Cr bond in **4a**[21] in comparison to the more stable Mo−Mo bond of **4b**.[22] Moreover, the molybdenum complex **1b** follows its general reactivity pattern towards transition metal electrophiles of the type $[L_nM'X]$ [X = Cl, Br; L_nM' = $Cp(CO)_3Mo$, $Cp(CO)_3W$, $Cp(CO_2)Fe$, $(CO)_5Mn$] to give complexes of the type $[\{Cp(CO)_2M\}_2(\mu\text{-}H)(\mu_3\text{-}PH)M'L_n]$ in which transition metal phosphorus bonds are formed while retaining the Mo−Mo bond.[23] However, due to the high lability of the Cr−Cr bond in **1a** this complex appears to be a good synthon for the generation of flexible $[PCr(CO)_2Cp]$ units, and thus is a valuable starting material in cluster chemistry.

Experimental Section

General Remarks: All manipulations were performed under an atmosphere of dry N_2 using standard Schlenk techniques. The solvents were dried by common methods and freshly distilled prior to use. The starting materials $[\{Cp(CO)_2Mo\}_2(\mu\text{-}PH_2)(\mu\text{-}H)]$[24] $[\{Cp(CO)_2Cr\}_2(\mu\text{-}PH_2)(\mu\text{-}H)]$[10a] and $[(Ph_3P)AuCl]$[25] were prepared according to literature methods. NMR: Bruker AC 250 (^1H, 250.13 MHz; ^{31}P, 101.256 MHz); standard Me_4Si (^1H), 85% H_3PO_4 (^{31}P). MS: Finnigan MAT 311 ADF at 70 eV. IR: Bruker IFS 28 FT−IR spectrometer.

$[\{Cp(CO)_2Mo\}_2(\mu\text{-}H)(\mu_3\text{-}PH)Au(PPh_3)]$ (2): KH (0.04 g, 1.00 mmol) was added to a solution of $[\{Cp(CO)_2Mo\}_2(\mu\text{-}PH_2)(\mu\text{-}H)]$ (**1b**; 0.35 g, 0.75 mmol) in 25 mL of THF and the solution was stirred at room temperature for 30 minutes. During this time the solution turned deep purple due to the formation of the anion $[\{Cp(CO)_2Mo\}_2(\mu\text{-}PH_2)]^-$. After filtration, $[(Ph_3P)AuCl]$ (0.37 g, 0.75 mmol) was added to the filtrate and the reaction mixture was stirred for another 14 hours. The solvent was then removed completely in vacuo, and the residue was dissolved in a small quantity of CH_2Cl_2. Separation of the reaction mixture by TLC (hexane/CH_2Cl_2 2:1) in a glove box yielded an orange fraction containing a small amount of starting material **1b** and a red fraction of **2**. Recrystallisation from CH_2Cl_2 yielded **2** as orange crystals (0.21 g, 33%). ^1H NMR (300 MHz, [D$_6$]benzene, TMS): δ = −11.73 (d, $^2J_{H,P}$ = 29 Hz, 1 H, MoHMo), 4.84 (s, 5 H, Cp), 5.04 (s, 5 H, Cp), 6.12 (d, $^2J_{H,P}$ = 282 Hz, 1 H; PH), 7.93−7.47 (m, 15 H, PPh_3) ppm. $^{31}P\{^1H\}$ NMR (101 MHz, [D$_6$]benzene, H_3PO_4): δ = 41.0 (s, br), 73.1 (s, br) ppm. MS (EI, 140 °C): *m/z* (%) = 467 (22) $[M^+ - AuPPh_3]$, 443 (1) $[M^+ - AuPPh_3 - CO]$, 406 (9) $[Mo_2(CO)_3Cp_2^+]$, 378 (24) $[Mo_2(CO)_2Cp_2^+]$, 350 (51) $[Mo_2(CO)Cp_2^+]$, 322 (16) $[Mo_2Cp_2^+]$, 262 (100) $[PPh_3^+]$. IR (KBr): ν(PH) = 2243 (w), ν(CO) = 1916 (vs), 1831 (vs) cm^{-1}.

$[\{Cp(CO)_2Cr\}_6\{(\mu_4\text{-}P)_3Au_3\}]$ (3): A solution of $[\{Cp(CO)_2Cr\}_2(\mu\text{-}PH_2)(\mu\text{-}H)]$ (**1a**; 0.46 g, 1.21 mmol) in 15 mL of THF was added to a solution of KH (0.12 g, 3.02 mmol) in 10 mL of THF and the mixture was stirred for 2 h at room temperature. The colour changed from dark green to bluish green due to the formation of the anion $[\{Cp(CO)_2Cr\}_2(\mu\text{-}PH_2)]^-$. The unchanged KH was filtered off and the filtrate was stirred with $[(PPh_3)AuCl]$ (0.6 g, 1.21 mmol) for 3 h. The solvent was then removed in vacuo. Chromatographic separation on a silica gel column (35 × 2.5 cm) with *n*-hexane/toluene (2:1) gave a dark green fraction containing unchanged $[\{Cp(CO)_2Cr\}_2(\mu\text{-}PH_2)(\mu\text{-}H)]$ (**1a**) (0.15 g, 33%). Elution with *n*-hexane/CH_2Cl_2 (1:10) yielded a reddish brown fraction of $[\{Cp(CO)_2Cr\}_6\{(\mu_4\text{-}P)_3Au_3\}]$ (**3**) (0.13 g, 40%). IR (CH_2Cl_2): ν(CO) = 1930 (s), 1903 (vs) cm^{-1}. ^1H NMR (300 MHz, [D$_6$]benzene, TMS): δ = 4.29 (s, 30 H, C_5H_5) ppm. $^{31}P\{^1H\}$ NMR (101 MHz, [D$_6$]benzene, H_3PO_4): δ = 38 ($\omega_{1/2}$ = 1200 Hz) ppm. $C_{42}H_{30}Au_3Cr_6O_{12}P_3$ (1722.49): calcd. C 29.29, H 1.76; found C 28.98, H 1.83.

X-ray Crystallographic Study

2: $C_{32}H_{27}AuMo_2O_4P_2$, M = 926.32, crystal dimensions 0.20 × 0.20 × 0.05 mm^3, triclinic, space group $P\bar{1}$ (No. 2); a = 8.8953(18), b = 13.989(3), c = 14.925(3) Å, α = 63.72(3)°, β = 83.99(3)°, γ = 72.64(3)°, T = 200(1) K, Z = 2, V = 1588.6(6) Å^3, D_c = 1.937 Mg/m^3, μ(Mo-K_α) = 5.519 mm^{-1}, 9502 independent reflexes (R_{int} = 0.1125, $2\theta_{max}$ = 48°), 378 parameters, R_1 = 0.0573 for 4310 observed reflections with $F_o = 4\sigma(F_0)$, wR_2 = 0.1486 for all reflections.

3: $C_{42}H_{30}Au_3Cr_6O_{12}P_3$, M = 1722.47, crystal dimensions 0.08 × 0.04 × 0.02 mm^3, monoclinic, space group $P2_1$ (No. 4); a = 12.268(3), b = 15.996(3), c = 13.010(3) Å, β = 117.32(3)°, T = 193(1) K, Z = 2, V = 2268.4(8) Å^3, D_c = 2.522 Mg/m^3, μ(Mo-K_α) = 11.206 mm^{-1}, 11802 independent reflexes (R_{int} = 0.0621, $2\theta_{max}$ = 51.94°), 591 parameters, R_1 = 0.0474 for 7060 observed with $F_o = 4\sigma(F_0)$, wR_2 = 0.1152 for all reflections.

Crystal structure analyses of **2** and **3** were performed on a STOE IPDS diffractometer with Mo-K_α radiation (λ = 0.71073 Å). The structures were solved by direct methods with the program SHELXS-97,[26a] and full-matrix least-squares refinement on F^2 in SHELXL-97[26b] was performed with anisotropic displacements for non-H atoms, except for the C14 atom of **3**. Hydrogen atoms at the carbon atoms were located in idealised positions and refined isotropically according to the riding model. The hydrogen atoms at the phosphorus and molybdenum atoms of **2** were refined freely. Although different crystals of **3** from different reactions were measured the same results were obtained to refine the data sets of **3** in the acentric space group $P2_1$ as inversion twins in an occupancy ratio of 53:47. All attempts to refine the structure in the centric space groups $P2_1/m$ or $P2_1/c$ failed.

CCDC-194528 (**2**) and CCDC-194529 (**3**) contain the supplementary crystallographic data for this paper. These data can be obtained free of charge at www.ccdc.cam.uk/retrieving.htlm [or from the Cambridge Crystallographic Data Centre, 12, Union Road, Cambridge CB2 1EZ, UK (fax: (internat.) +44-1223/336-033; E-mail: deposit@ccdc.cam.ac.uk].

DFT Calculations

All calculations were carried out using the BP86[20a] functional and the RI-J technique[20b] of the program package TURBOMOLE.[20c] C_1 symmetry and the SV(P)[20d] basis set were used throughout. Calculations with the TZVP[20e] basis set showed similar results.

Acknowledgments

This work was comprehensively supported by the Deutsche Forschungsgemeinschaft and the Fonds der Chemischen Industrie. The authors thank the Degussa AG for the gift of precious metal compounds.

[1] V. W.-W. Yam, E. C.-C. Cheng, *Angew. Chem.* **2000**, *112*, 4410−4412; *Angew. Chem. Int. Ed.* **2000**, *39*, 4240−4242.
[2] E. Cerrada, M. Contel, A. D. Valencia, M. Laguna, T. Gelbrich, M. B. Hursthouse, *Angew. Chem.* **2000**, *112*, 2443−2446; *Angew. Chem. Int. Ed.* **2000**, *39*, 2353−2356.
[3] [3a] D. Fenske, T. Langtepe, M. M. Kappes, O. Hampe, P. Weis, *Angew. Chem.* **2000**, *112*, 1925; *Angew. Chem. Int. Ed.* **2000**, *39*, 1683. [3b] P. A. Bates, J. M. Waters, *Acta Crystallogr., Sect. A* **1987**, *43*, C194. [3c] P. Pyykkö, *Chem. Rev.* **1997**, *97*, 597.
[4] [4a] V. W.-W. Yam, E. C.-C. Cheng, K.-K. Cheung, *Angew. Chem.* **1999**, *111*, 193; *Angew. Chem. Int. Ed.* **1999**, *38*, 197. [4b] V. W.-W. Yam, E. C.-C. Cheng, Z.-Y. Zhou, *Angew. Chem.* **2000**, *112*, 1749; *Angew. Chem. Int. Ed.* **2000**, *39*, 1683. [4c] J. H. K. Yip, J. Prabhavathy, *Angew. Chem.* **2001**, *113*, 2217−2220; *Angew. Chem. Int. Ed.* **2001**, *40*, 2159−2162.
[5] [5a] R. J. Puddephatt, P. J. Thompson, *J. Organomet. Chem.* **1976**, *117*, 395−403. [5b] R. G. Prichard, D. B. Dyson, R. V. Parish, C. A. McAuliffe, B. Beagley, *J. Chem. Soc., Chem. Commun.* **1987**, 371−372. [5c] D. B. Dyson, R. V. Parish, C. A. McAuliffe, R. G. Pritchard, R. Fields, B. Beagley, *J. Chem. Soc., Dalton Trans.* **1989**, 907−914. [5d] H. Schmidbaur, A. A. M. Aly, *Z. Naturforsch., Teil B* **1979**, *34*, 23−26. [5e] H. Schmidbaur, G. Weidenhiller, A. A. M. Aly, O. Steigelmann, G. Müller, *Z. Naturforsch., Teil B* **1989**, *44*, 1503−1508. [5f] J. Vicente, M. T. Chicote, P. G. Jones, *Inorg. Chem.* **1993**, *32*, 4960−4964. [5g] G. A. Carriedo, V. Riera, M. L. Rodriguez, P. G. Jones, J. Lautner, *J. Chem. Soc., Dalton Trans.* **1989**, 639−643. [5h] F. S. Livotto, M. D. Braga, F. Grepioni, *J. Chem. Soc., Dalton Trans.* **1992**, 577−584.
[6] H. Schmidbaur, *Chem. Soc. Rev.* **1995**, 391−400.
[7] Free of any organic substituents or similar fragments like $SiMe_3$, NR_2 and others.
[8] [8a] E. A. V. Ebsworth, A. P. McIntosh, M. Schröder, *J. Organomet. Chem.* **1986**, *312*, C41−C43. [8b] J. E. Davies, M. J. Mays, P. R. Raithby, G. P. Shields, P. K. Tompkin, *Chem. Commun.* **1997**, 361−362.
[9] [9a] J. E. Davies, L. C. Kerr, M. J. Mays, P. R. Raithby, P. K. Tompkin, A. D. Woods, *Angew. Chem.* **1998**, *110*, 1473−1475; *Angew. Chem. Int. Ed.* **1998**, *37*, 1428−1429 . [9b] J. E. Davies, M. J. Mays, P. R. Raithby, G. P. Shields, P. K. Tompkin, A. D. Woods, *J. Chem. Soc., Dalton Trans.* **2000**, 1925−1930.
[10] [10a] P. Sekar, M. Scheer, A. Voigt, R. Kirmse, *Organometallics* **1999**, *18*, 2833−2837. [10b] Average distances of three independent molecules in $[\{Cp(CO)_2Cr\}_2(\mu\text{-}PH_2)_2]$.
[11] [11a] H.-J. Haupt, M. Schwefer, H. Egold, U. Flörke, *Inorg. Chem.* **1995**, *34*, 5461−5467. [11b] H.-J. Haupt, M. Schwefer, U. Flörke, *Z. Anorg. Allg. Chem.* **1994**, *621*, 1098−1105.
[12] P. Pyykkö, N. Runeberg, F. Mendizabal, *Chem. Eur. J.* **1997**, *3*, 1451−1457.
[13] R. E. Bachman, H. Schmidbaur, *Inorg. Chem.* **1996**, *35*, 1399−1401.
[14] H. Schmidbaur, H. Beruda, E. Zeller, *Phosphorus, Sulfur, and Silicon* **1994**, *87*, 245−255.
[15] [15a] P. Braunstein, U. Schubert, M. Burgard, *Inorg. Chem.* **1984**, *23*, 4057−4064. [15b] F. Edelmann, S. Töfke, U. Behrens, *J. Organomet. Chem.* **1986**, *309*, 87−108.
[16] H. Vahrenkamp, *Chem. Ber.* **1978**, *111*, 3472.
[17] L. Y. Goh, C. K. Chu, R. C. S. Wong, T. W. Hambley, *J. Chem. Soc., Dalton Trans.* **1989**, 1951−1956.
[18] L. Y. Goh, R. C. S. Wong, T. C.W. Mak, *J. Organomet. Chem.* **1989**, *373*, 71.
[19] L. Y. Goh, R. C. S. Wong, T. C. W. Mak, *J. Organomet. Chem.* **1989**, *364*, 363.
[20] [20a] J. P. Perdew, *Phys. Rev. B* **1986**, *33*, 8822−8824; J. P. Perdew, *Phys. Rev. B*, **1986**, *34*, 7046; A. D. Becke, *Phys. Rev. A*, **1988**, *38*, 3098−3100. [20b] K. Eichkorn, O. Treutler, H. Öhm, M. Häser, R. Ahlrichs, *Chem. Phys. Lett.* **1995**, *242*, 652−660; K. Eichkorn, F. Weigend, O. Treutler, R. Ahlrichs, *Theo. Chem. Acc.* **1997**, *97*, 119−124. [20c] R. Ahlrichs, M. Bär, M. Häser, H. Horn, C. Kölmel, *Chem. Phys. Lett.* **1989**, *162*, 165−169. [20d] A. Schäfer, H. Horn, R. Ahlrichs, *J. Chem. Phys.* **1992**, *97*, 2571−2577 (SVP). [20e] A. Schäfer, C. Huber, R. Ahlrichs, *J. Chem. Phys.* **1994**, *100*, 5829−5835. [20f] R. S. Mulliken, *J. Chem. Phys.* **1955**, *23*, 1833−1840. [20g] E. R. Davidson, *J. Chem. Phys.* **1967**, *46*, 3320−3324; K. R. Roby, *Mol. Phys.* **1974**, *27*, 81−104. [20h] R. Heinzmann, R. Ahlrichs, *Theor. Chim. Acta* **1976**, *42*, 33−45.
[21] [21a] P. Sekar, S. Umbarkar, M. Scheer, A. Voigt, R. Kirmse, *Eur. J. Inorg. Chem.* **2000**, 2585−2589. [21b] S. B. Umbarkar, P. Sekar, M. Scheer, *Phosphorus, Sulfur and Silicon* **2001**, *169*, 205−208.
[22] J. Bai, E. Leiner, M. Scheer, *Angew. Chem.* **2002**, *114*, 820−823; *Angew. Chem. Int. Ed.* **2002**, *41*, 783−786.

[23] J. E. Davies, M. J. Mays, E. J. Pook, P. R. Raithby, P. K. Tompkin, *J. Chem. Soc., Dalton Trans.* **1997**, 3283−3286.
[24] U. Vogel, PhD thesis, University of Karlsruhe, **2001**.
[25] [25a] C. A. McAuliffe, R. V. Parish, P. D. Randall, *J. Chem. Soc., Dalton Trans.* **1979**, 1730−1735. [25b] W. A. Herrmann, A. Salzer, *Synthetic Methods of Organometallic Chemistry*, Vol. 1, Thieme, Stuttgart **1996**, pp 170.
[26] [26a] G. M. Sheldrick, *SHELXS-97*, University of Göttingen, **1997**. [26b] G. M. Sheldrick, *SHELXL-97*, University of Göttingen, **1997**.

Received January 30, 2003
[I03052]

Self-Assembly of Supramolecular Structures from Palladium Chloride and Guanidinium Salts of Pyridinecarboxylic Acids − A Dramatic Change on Passing from the *para*- to the *meta*-Substituted Acid

Alessia Bacchi,*[a] Gian Paolo Chiusoli,[b] Mirco Costa,*[b] and Emmanuele Giacobbi[b]

Dedicated to the late Prof. Salvatore Castellano

Keywords: Crystal engineering / Hydrogen bonds / Self-assembly / Multicomponent systems

Supramolecular structures **1** and **2** were obtained in the solid state from the reaction between palladium chloride and guanidinium salts of *p*- and *m*-pyridinecarboxylic acid, respectively. The pyridinecarboxylate anions were *trans*-coordinated to palladium dichloride through nitrogen, and the carboxylate groups formed hydrogen bonds with guanidinium cations. The present paper describes a remarkable change in the stoichiometry and structural organization of the solid **3** derived from the *meta*-substituted acid **2**, triggered by the elimination of one guanidine molecule as hydrochloride per molecule of palladium chloride, during crystallization from methanol. The corresponding isonicotinate **1** structure appears to be stable under the same conditions. As shown by the analysis of the crystal structures, the guanidinium nicotinate organic salt **4** turns out to be preorganized to host palladium chloride both in **2** and **3**.
(© Wiley-VCH Verlag GmbH & Co. KGaA, 69451 Weinheim, Germany, 2003)

Interest in the solid-state structures of hybrid materials organised by cooperative interactions of different strength, directionality and range of action (coordinative, electrostatic, lipophilic, hydrogen bonds) is rapidly increasing in the field of crystal engineering.[1] In the framework of a programme aimed at the incorporation of metal salts into supramolecular organic structures, we studied the reaction of palladium chloride with tricyclohexylguanidinium (BH^+) salts of *p*-pyridinecarboxylic acid (isonicotinic acid) or *m*-pyridinecarboxylic acid (nicotinic acid). The formation of supramolecular assemblies self-organized in the solid state according to different stoichiometries showed a hydrogen bond distribution involving both the carboxylic group and the nitrogen base.

Equation (1) indicates the stoichiometry of the reaction of $PdCl_2$ with isonicotinic or nicotinic acids and tricyclohexylguanidine in refluxing acetonitrile, which resulted in the precipitation of yellow solids in both cases. Recrystallisation from a methanol/acetonitrile mixture (1:1) at room temperature led to crystals of the respective palladium complexes (**1** and **2**) of analogous stoichiometry.

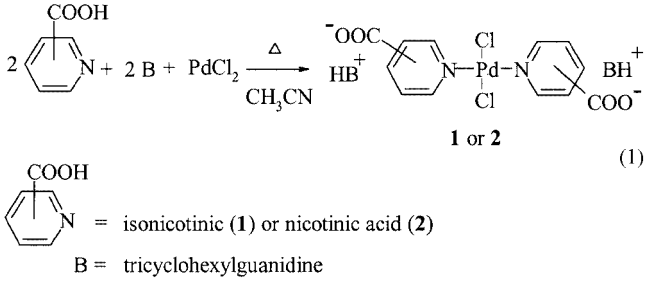

Surprisingly, recrystallisation of **2** from pure methanol gave a crystalline compound (**3**) with one less guanidine molecule per molecule of $PdCl_2$. This behaviour was not observed with complex **1**, which was recovered unchanged from methanol after crystallisation. The proposed course of the reaction leading from **2** to **3** (Scheme 1) is based on the products isolated (see Exp. Sect.). A reasonable interpretation is that during crystallisation one molecule of the Pd^{II} complex is reduced to Pd^0 by methanol (which is oxidized to formaldehyde dimethyl acetal, as confirmed experimentally) with concomitant expulsion of guanidine hydrochloride and nicotinic acid. A second molecule of complex **2** then loses one molecule of guanidine as its nicotinic acid salt, forming complex **3**. It is worth noting that mixing one

[a] Dipartimento di Chimica Generale ed Inorganica, Chimica Analitica, Chimica Fisica, Università di Parma,
Parco Area delle Scienze 17A, 43100 Parma, Italy
Fax: (internat.) +39-0521/905-557
E-mail alessia.bacchi@unipr.it
[b] Dipartimento di Chimica Organica e Industriale, Università di Parma,
Parco Area delle Scienze 17A, 43100 Parma, Italy
Fax: (internat.) +39-0521/905-472
E-mail mirco.costa@unipr.it
Supporting information for this article is available on the WWW under http://www. eurjic.org or from the author.

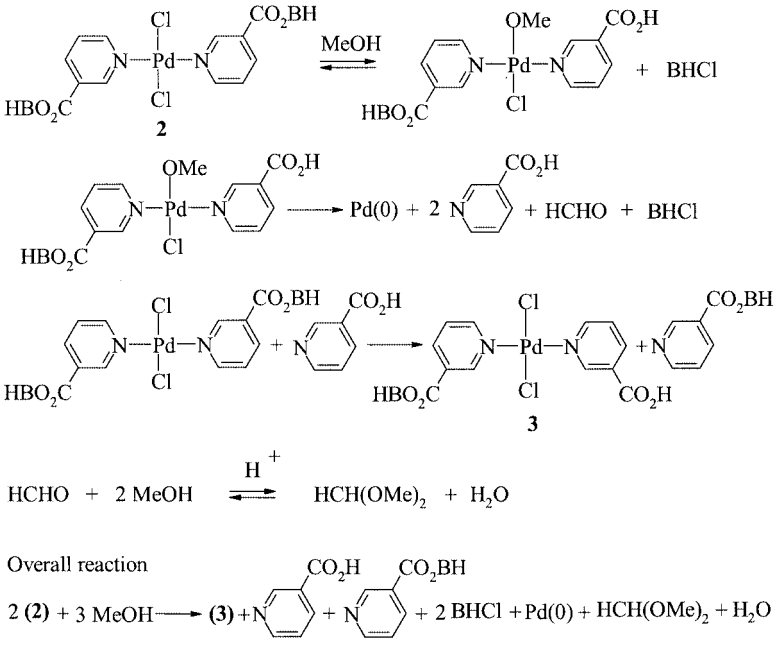

Scheme 1. Proposed course of formation of **3** from **2**

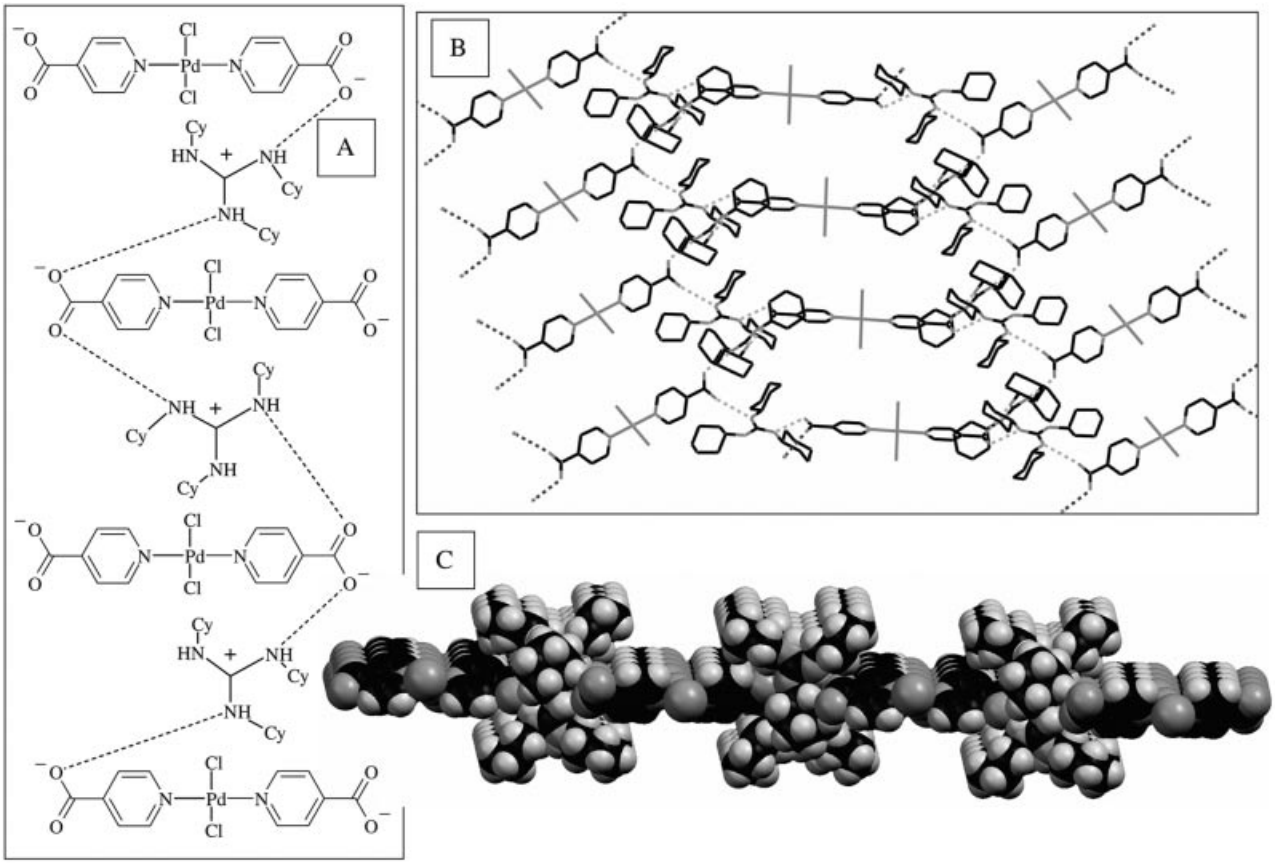

Figure 1. Solid-state arrangement of compound **1**: (A) chains built by NH···O hydrogen bonds between cations and anions, one NH is not involved in the chain formation, Cy = cyclohexyl; (B) the chains are assembled in sheets by coordination of $PdCl_2$ to the dangling pyridinic nitrogen atoms; (C) space-filling view of the section of the sheets; the ridges are formed by the protruding cations; the free NH groups point out of the ridges, to fit in the chlorine array of the adjacent sheets, with consequent staggering of the layers

molecule of guanidine with two molecules of nicotinic acid and one of $PdCl_2$ led to a solid precipitate with stoichiometry corresponding to compound **3**, which was not analysed by X-ray diffraction since its crystallinity was not satisfactory. The direct addition of dry CF_3COOH to **2** also failed to afford suitable crystals, although the stoichiometry of the solid obtained was in agreement with that of complex **3**.

In order to elucidate the structural reasons for the diverse behaviour of the two chemically similar systems **1** and **2**, the crystal structures of **1**, **2** and **3** were determined. In **1** cations and anions are assembled in chains built by $-NH^+\cdots{}^-O_2C-$ hydrogen bonds involving two guanidinic NH donors and both the carboxylate oxygen acceptors [N···O = 2.791(7), 2.935(9) Å] (Figure 1a). The chains are covalently linked in sheets by the inorganic $PdCl_2$ spacers through the pyridinic nitrogens, thus defining a ladder motif in which the rung width, 14 Å, depends on the length of the $[trans\text{-}PdCl_2(i\text{nic-}COO)_2]^{2-}$ spacer. The resulting bidimensional network is formed by meshes with a section of 9 × 20 $Å^2$ (dimensions are expressed as atom-atom distances) rimmed by four anions and four cations (Figure 1b). The sheets are assembled so that the -NH ridges of one sheet match the hollows of the adjacent sheets, corresponding to the $PdCl_2$ sites, thus blocking the development of channels or three-dimensional pores perpendicular to the sheets (Figure 1c).

The local structural perturbation introduced by changing the position of the N donor on the pyridinecarboxylate ring greatly affects the self-assembly of the multicomponent system, showing how the crystal organization depends critically on the shape of the *trans*-$PdCl_2L_2$ unit. With L = nicotinic acid this unit could give rise to a *syn* and an *anti* arrangement (Scheme 2).

Only the latter, however, is present in **2**, where the structural organization of **1** is retained, the only difference being that all the NH groups are involved in intra-chain hydrogen bonds [$NH^+\cdots O^-$ = 2.764(6), 2.901(6), 2.990(6) Å] (Figure 2a). The skew $PdCl_2L_2$ units (length = 13 Å) link paral-

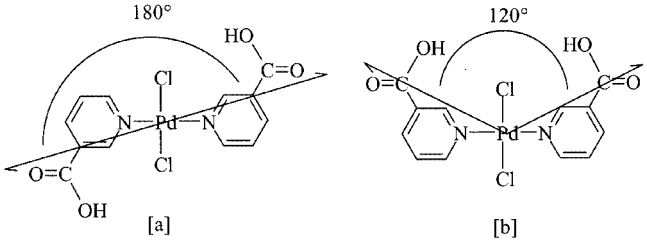

Scheme 2. Geometry and shape of the $PdCl_2L_2$ spacers in: (a) compound **2**, *anti* isomer, linear; and (b) compound **3**, *syn* isomer, bent

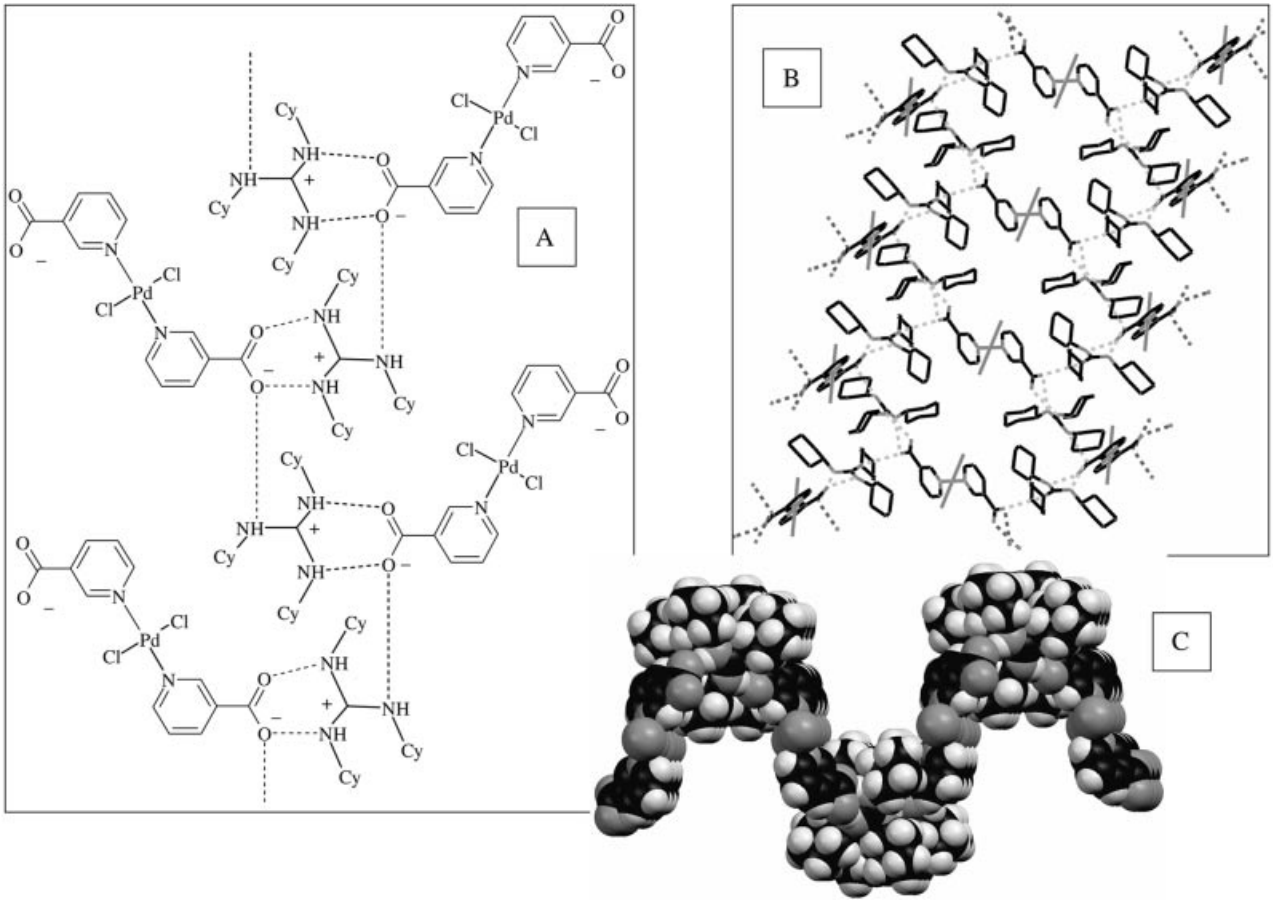

Figure 2. Solid-state arrangement of compound **2**: (A) chains built by NH···O hydrogen bonds as in **1**, all NH groups are involved in the chain formation, Cy = cyclohexyl; (B) sheets organization as in **1**; (C) space-filling view of the section of the sheets; the sheets are corrugated due to the shape of the inorganic spacer

lel chains, forming 10 × 17 Å^2 meshes defined by four anions and four cations (Figure 2b). Due to the shape of the *anti* complex, the sheets are corrugated and assemble in three dimensions in a bump-hollow arrangement (Figure 2c). In both **1** and **2** the bidimensional structural assembly is controlled by coordination bonds and hydrogen bonds resulting in a robust network with wide meshes, promising for the building up of nanometre-sized pores in the third dimension. However, the stacking of the porous sheets is controlled by the close packing principle, and the voids are filled by means of multiple weak dispersive interactions. The largest cavities in structures **1** and **2** are 10 and 33 Å^3, respectively.

A bent *syn*-$PdCl_2L_2$ unit is present in **3**, and this is accompanied by a dramatic change in the stoichiometry and structure of the supramolecular complex, as shown by the X-ray crystal structure. The cations and anions are arranged in hydrogen-bonded chains [N···O = 2.97(1), 2.82(2) Å] generated by translation and the complex is aligned with the direction of the chain (Figure 3a). Only one oxygen on each carboxylate interacts with a nitrogen of the cation, while the other is employed in O−H···O$^-$ strong interactions [O···O = 2.43(2) Å] between chains related by a 2_1 operation (Figure 3b), generating a double-strand motif (Figure 3c). This requires that each complex is monodeprotonated, and causes the observed change in the stoichiometry. The polymeric motif consisting of -CO_2H···$^-$OOC- hydrogen-bonded chains is quite common in the structure of monodeprotonated dicarboxylic acids, and has a stabilising nature.[2] Examples of crystalline salts of monodeprotonated dicarboxylic acids with protonated nitrogen bases where the structure is built through a network of O−H···O$^-$ and N$^+$−H···O$^-$ interactions have recently been reported.[3] In our case the special arrangement of complex **3** is reached through an unusual series of events: protonation of one carboxylate group of **2** (Scheme 1) triggers the supramolecular polymerisation of [$PdCl_2$(nic-COO)(nic-COOH)]$^-$, and induces the precipitation of the *syn*-isomer of the monoanionic complex, which can form chains appropriately arranged in double strands.

The fact that guanidine expulsion occurs with the nicotinic rather than isonicotinic complex points to a favourable arrangement of the former. As a matter of fact the comparison with the structure of guanidinium nicotinate **4** shows that the latter is pre-organised for hosting palladium chloride. The crystal packing of **4** is based on catemers of hydrogen bonds linking cations and anions with the same topology as in **1** and **2** (Figure 4a). The pyridinic N is used to connect adjacent chains through NH···N interactions with the third guanidinium NH. In the crystal, the hydro-

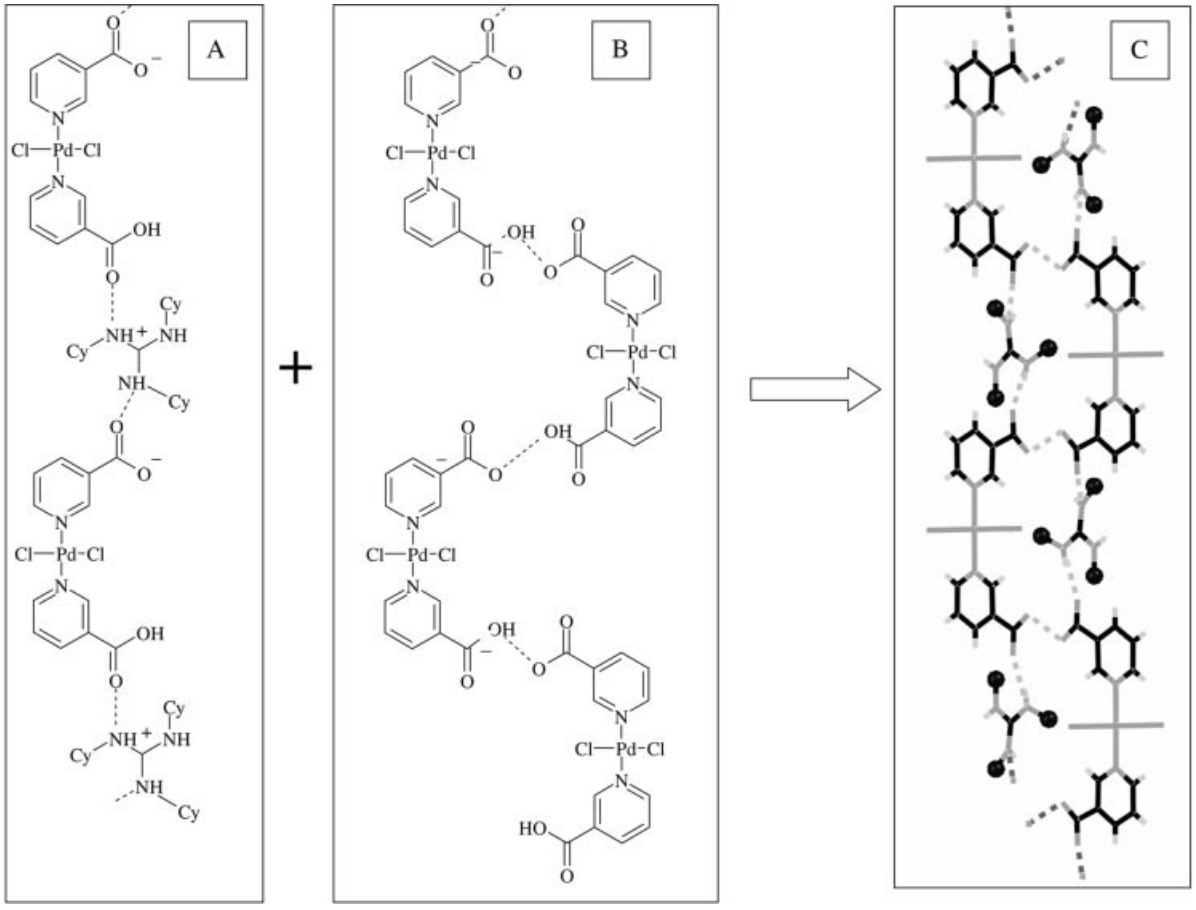

Figure 3. Crystal organization of **3**: (A) chain motif generated by hydrogen bonding between cations and monoanionic complexes, Cy = cyclohexyl; (B) association between pairs of chains via OH···O hydrogen bonds; (C) double strand obtained by assembling a pair of catemers by O−H···O hydrogen bonds; cyclohexyls are represented as solid balls

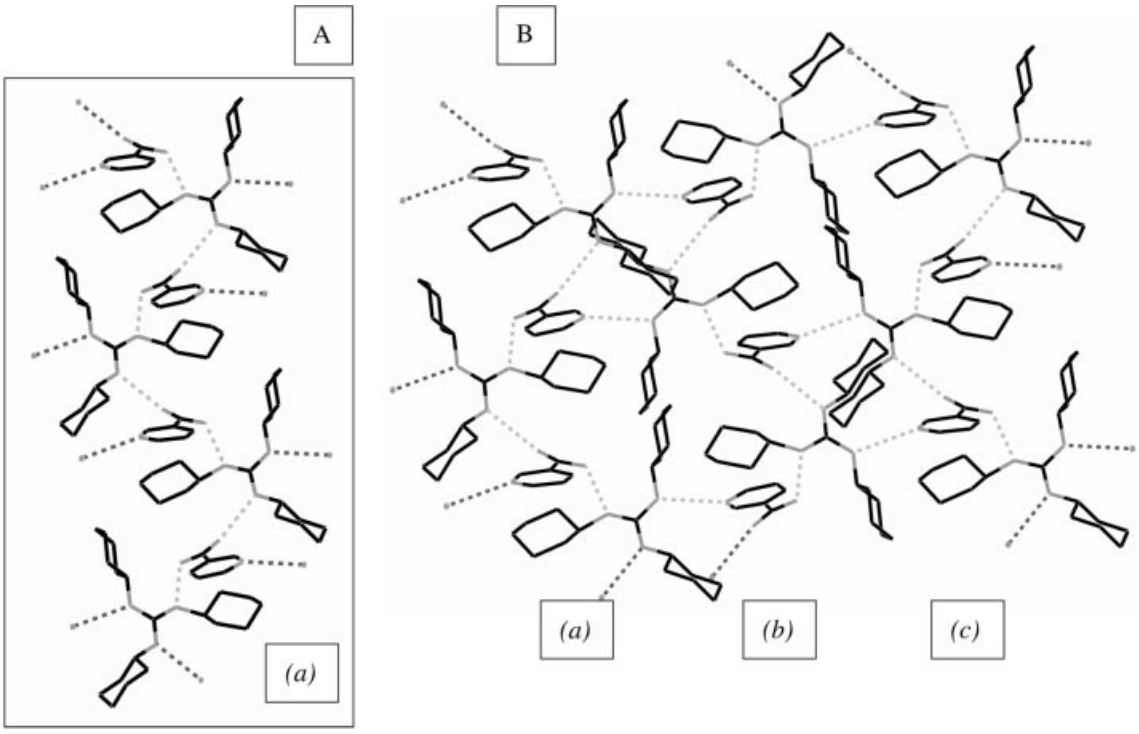

Figure 4. (A) Chain motif in **4**, generated by hydrogen bonds between alternating cations and anions as in **1** and **2**; (B) the chains (*a, b, c*) are arranged in sheets by hydrogen bonding between pyridinic nitrogens and one NH group of the cations

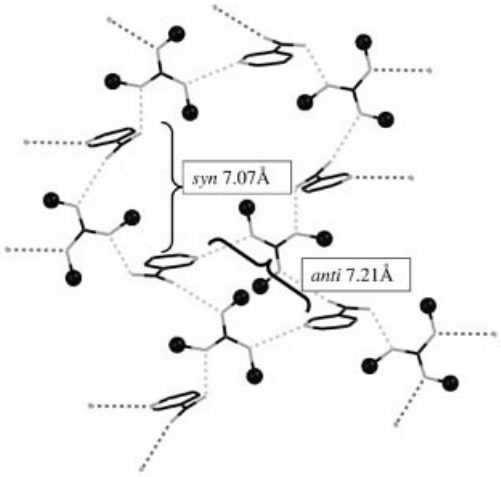

Figure 5. Spatial preorganization of **4** showing how a slight rotation of pyridinic rings can accommodate the $PdCl_2$ unit, giving the structural motif observed either in **2** (*anti* isomer), by sliding of the chains, or in **3** (*syn* isomer) by release of a neutral guanidine; cyclohexyls are represented as solid balls

gen bond of **4** plays the same function as the N−Pd−N covalent link in **1** and **2** in forming bidimensional sheets (Figure 4b). In **2** and **3** the coordination of the incoming Pd requires a concerted rotation of the aromatic rings, to bring the pyridine N atoms into a favourable arrangement. Depending on the mutual position of the pair of pyridinic N atoms, the inorganic spacer orients itself either perpendicular to the organic chains (**2**, *anti* spacer) or parallel to them (**3**, *syn* spacer; Figure 5), in this case causing the release of the guanidine bridging the pair of anions involved in complexation. Guanidine expulsion leaves free -O^- acceptors and -OH donors regularly spaced on the newly formed metal-containing chain, favouring the association of two chains in the observed double strands. The versatile preorganization of the organic salt **4** justifies the remarkable differences in the solid-state organization of the *anti*- and *syn*-spacers and explains how the release of guanidine can occur with a modest expense in terms of structural rearrangement to **3**. Nevertheless guanidine is not expelled spontaneously and liberation of HCl as shown in Scheme 1, is needed.

In conclusion we have reported novel supramolecular arrays held together both by nitrogen coordination to palladium and hydrogen bonds. The structure derived from a guanidine salt of nicotinic acid readily responds to dissolution in methanol by guanidine expulsion and formation of a new structure where the original $NH^+\cdots OOC^-$ bonds are replaced by $NH^+\cdots$OOC-COOH bonds. This type of response can be expected to offer a new tool for working out supramolecular architectures sensitive to chemical stimulation. Work in progress has already shown that similar structures can be obtained with other bi- and tetrasubstituted guanidines.

Experimental Section

Tricyclohexylguanidinium isonicotinate and nicotinate were both prepared in almost quantitative yield by dissolving the pyridinecarboxylic acid (0.73 g, 6 mmol) and tricyclohexylguanidine (1.83 g, 6 mmol) in 20 mL of acetonitrile and refluxing the solution for 6

hours under argon. The corresponding $PdCl_2$ complexes **1** and **2** were prepared in 88% and 86% yield, respectively, by dissolving the guanidinium salt (0.43 g, 1 mmol) and $PdCl_2$ (0.09 g, 0.5 mmol) in 11 mL of acetonitrile. The solutions were refluxed at 70 °C for 6 hours. After cooling and filtering, the precipitates were recrystallised from a 1:1 mixture of methanol and acetonitrile at room temperature to obtain crystals suitable for X-ray analysis. Analogous results were obtained by allowing $PdCl_2$, nicotinic or isonicotinic acid and tricyclohexylguanidine (1:2:2 molar ratio) to react in refluxing CH_3CN for 6 hours. Satisfactory elemental analysis were obtained (available as supporting information).

In order to investigate the process leading from **2** to **3**, complex **2** (0.103 mg 0.1 mmol) dissolved in the smallest quantity of MeOH was left to crystallise. Yellow crystals of complex **3** (24 mg 0.035 mmol) were selected for X-ray analysis. The residue, consisting of crystals of guanidine hydrochloride, nicotinic acid, guanidine nicotinate and palladium(0), was treated with Et_2O to remove formaldehyde dimethylacetal.

The above-described procedure was used for the direct synthesis of complex **3**. Thus $PdCl_2$ (0.044 g, 0.25 mmol), nicotinic acid (0.062 g, 0.50 mmol) and tricyclohexylguanidine (0.076 g 0.25 mmol) were refluxed under argon in dry CH_3CN (4.0 mL) for 6 hours. The mixture was filtered and the yellow precipitate was recrystallised from CH_3OH/CH_3CN (1:1). The solid precipitate gave a satisfactory elemental analysis but was not suitable for single crystal X-ray diffraction.

Treatment of Complex 2 with CF_3COOH: CF_3COOH (0.023 mL, 0.3 mmol) was added to crystals of complex **2** (0.31 g, 0.3 mmol) suspended in dry CH_3CN (6 mL) at 0 °C. After stirring for 2 hours the mixture was filtered and a yellow solid was dried and recrystallised from CH_3CN/CH_3OH (1:1). The solid precipitate gave a satisfactory elemental analysis in agreement with the composition of complex **3**, but was not suitable for single crystal X-ray analysis.

Crystallographic Analysis: Mo-K_α radiation (λ = 0.71073 Å), T = 293 K for **1**, **3** (Siemens AED diffractometer) and **2** (SMART AXS 1000 CCD diffractometer), and Cu-K_α (λ = 1.54178 Å), T = 173 K for **4** (Enraf−Nonius CAD4 diffractometer). Lorentz and polarisation corrections were applied. The structures were solved by direct methods using SIR97[4] and refined by full-matrix least-squares on all F^2 using SHELXL-97.[5] Hydrogen atoms were introduced in calculated positions, and refined riding on their carrier atoms. Anisotropic displacement parameters refined for all non-hydrogen atoms.

1: 0.4 × 0.2 × 0.1 mm, monoclinic, space group $P2_1/c$, a = 12.743(5), b = 9.725(5), c = 22.345(7) Å, β = 105.76(5)°, V = 2665(2) Å^3, ρ = 1.289 Mg·m^{-3}, 5232 unique reflections, 1459 observed [$I > 2\sigma(I)$], 307 parameters, R = 0.0592, R_w = 0.1401. The palladium is on a crystallographic inversion centre.

2: 0.3 × 0.2 × 0.1 mm, monoclinic, space group $P2_1/a$, a = 10.565(2), b = 22.739(3), c = 11.509(2) Å, β = 94.785(2)°, V = 2755.3(1) Å^3, ρ = 1.247 Mg·m^{-3}, 2288 unique reflections, 1636 observed [$I > 2\sigma(I)$], 307 parameters, R = 0.0332, R_w = 0.0823. The palladium is on a crystallographic inversion centre.

3: 0.1 × 0.2 × 0.2 mm, monoclinic, space group $C2/m$, a = 22.786(5), b = 17.730(5), c = 10.405(5) Å, β = 108.31(5)°, V = 3991(2) Å^3, ρ = 1.213 Mg·m^{-3}, 4093 unique reflections, 1077 observed [$I > 2\sigma(I)$], 274 parameters, R = 0.0698, R_w = 0.1825. The metal and the chlorine atoms are on a crystallographic symmetry plane, as well as the carbocationic C atom of guanidinium. The cation is disordered over two equivalent orientations, which do not alter the hydrogen bonding scheme.

4: 0.2 × 0.2 × 0.4 mm, triclinic, space group $P\bar{1}$, a = 16.843(5), b = 14.612(5), c = 11.156(5) Å, α = 66.54(5), β = 103.29(5), γ = 104.70(5)°, V = 2410(1) Å^3, ρ = 1.181 Mg·m^{-3}, 9138 unique reflections, 4436 observed [$I > 2\sigma(I)$], 583 parameters, R = 0.1108, R_w = 0.2668. Two independent molecules are present in the asymmetric unit.

CCDC-189488−189491 (**1**−**4**) contain the supplementary crystallographic data for this paper. These data can be obtained free of charge at www.ccdc.cam.ac.uk/conts/retrieving.html [or from the Cambridge Crystallographic Data Centre, 12, Union Road, Cambridge CB2 1EZ, UK; Fax: (internat.) +44-1223/336-033; E-mail: deposit@ccdc.cam.ac.uk].

Supporting information available (see footnote on the first page of this article): elemental analysis, ORTEP drawings, crystal data and structure refinement tables for **1**−**4**.

[1] [1a] D. Braga, F. Grepioni, G. R. Desiraju, *Chem. Rev.* **1998**, *98*, 1375. [1b] C. B. Aakeroy, A. M. Beatty, *Chem. Commun.* **1998**, 1067. [1c] C. B. Aakeroy, A. M. Beatty, D. S. Leinen, *J. Am. Chem. Soc.* **1998**, *120*, 7383. [1d] C. B. Aakeroy, A. M. Beatty, D. S. Leinen, *Angew. Chem. Int. Ed.* **1999**, *38*, 1815. [1e] A. M. Beatty, *Cryst. Eng. Comm.* **2001**, 51.

[2] Among several examples we recall: [2a] rubidium hydrogen phthalate, R. A. Smith, *Acta Crystallogr., Sect. B* **1975**, *31*, 2347. [2b] 5-aminoisophthalic acid hemihydrate, A. J. Dobson, R. E. Gerkin, *Acta Crystallogr., Sect. C* **1998**, *54*, 1503. [2c] potassium hydrogen oxalate, H. Einspahr, R. E. Marsh, J. Donohue, *Acta Crystallogr., Sect. B* **1972**, *28*, 2194. [2d] For a comment on the stabilising nature of O−H···O$^-$ hydrogen bond, see: P. Macchi, B. BoIversen, A. Sironi, B. C. Chakoumakos, F. K. Larsen, *Angew. Chem. Int. Ed.* **2000**, *39*, 2719.

[3] [3a] J. A. Kaduk, *Acta Crystallogr., Sect. B (Str. Sci.)* **2000**, *56*, 474. [3b] D. Wiechert, D. Mootz, *Angew. Chem. Int. Ed.* **1999**, *38*, 1974.

[4] A. Altomare, G. Cascarano, C. Giacovazzo, A. Guagliardi, M. C. Burla, G. Polidori, M. Camalli, *J. Appl. Cryst.* **1994**, *27*, 435.

[5] SHELXL-97. A program for structure refinement; G. Sheldrick, University of Goettingen, Germany.

Received November 20, 2002
[I02633]

Application of Gel-Phase ^{195}Pt NMR Spectroscopy in a Novel Solid-Phase Synthesis of a Primary Amine Dichloroplatinum(II) Complex

Marc S. Robillard,[a] Jason S. Leith,[a] Gijs A. van der Marel,[a] Jacques H. van Boom,[a] and Jan Reedijk*[a]

Keywords: Peptides / Platinum / Solid-phase synthesis / NMR spectroscopy / Bioinorganic chemistry

Gel-phase ^{195}Pt NMR spectroscopy of dichloroplatinum peptide complexes attached to a solid support is described. The observed ^{195}Pt chemical shifts of the support-bound platinum complexes are in good agreement with the solution-state ^{195}Pt NMR spectra of the soluble and deprotected analogs. This non-destructive analytical method for on-resin-compound analysis was applied in the optimization of the solid-phase synthesis of the primary amine dichloroplatinum complex **6**, which represents a new class of platinum complexes now available via solid-phase synthetic chemistry.
(© Wiley-VCH Verlag GmbH & Co. KGaA, 69451 Weinheim, Germany, 2003)

Introduction

Both combinatorial chemistry and parallel synthesis have embraced solid-phase synthesis (SPS) as one of their fundamental tools. The advantages involved are also likely to pertain to the preparation of libraries of anticancer platinum drugs. Earlier we reported the construction of a dichloroplatinum(II) tripeptide complex (compound **3** in Scheme 1) via a solid-phase approach in nearly quantitative conversion.[1] The rich coordination chemistry of platinum has still not been fully exploited in a solid-phase combinatorial approach. Reactions on a solid support usually require different conditions than in solution, and further explorations in this field would clearly profit from an analytical method that allows the on-resin monitoring of a desired coordination reaction. Standard analytical techniques (MS, HPLC, TLC, NMR) for resin reaction optimization are available once a reaction product is cleaved from the solid support. However, this process is still time consuming, and may alter the desired species or preclude observation of unstable intermediates. This drawback has been widely recognized by solid-phase chemists and, as a result, a plethora of non-destructive analytical methods have been used for on-resin analysis.[2,3] Gel-phase NMR spectroscopy is regarded as one of the more powerful and information rich methods.[4–7] Although on-resin evaluation of metal coordination using NMR spectroscopy, particularly in the field of immobilized catalysts, is of increasing interest,[8–13] only two examples of gel-phase metal NMR spectroscopy have been reported,[12,13] namely for the ^{119}Sn nucleus.

It was envisaged that the diamagnetic ^{195}Pt ($S = 1/2$) nucleus could be applied for monitoring platinum coordination reactions on a solid support using gel-phase NMR spectroscopy. Such an approach would circumvent the need to study the "outer sphere" of an immobilized platinum complex by gel-phase ^{1}H, ^{13}C or ^{31}P NMR spectroscopy, as it is possible to observe the "core" itself.

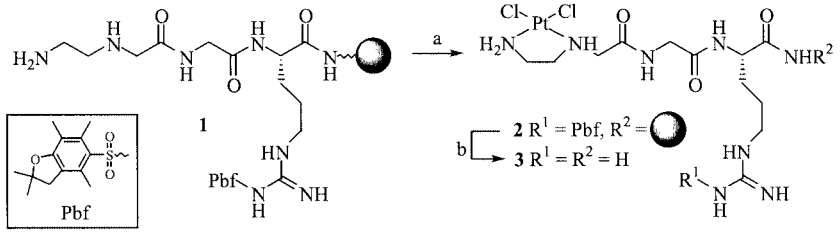

Scheme 1. Solid-phase synthesis of platinum complex **3**; reagents and conditions: a) K_2PtCl_4 (5 equiv., 0.05 M), DMF/H_2O (9:1, v/v), 24 h in the dark; b) TFA/H_2O (95:5, v/v), 1 h

This paper reports on the feasibility of gel-phase ^{195}Pt NMR spectroscopy, using the immobilized dichloroplatinum peptide complex **2** (Scheme 1). The potential of this technique for assessing the success of an unknown com-

[a] Leiden Institute of Chemistry, Gorlaeus Laboratories, Leiden University,
P. O. Box 9502, 2300 RA Leiden, Netherlands
Fax: (internat.) + 31-71/527-4671
E-mail: reedijk@chem.leidenuniv.nl

plexation reaction will be illustrated in a novel solid-phase synthesis of the primary amine dichloroplatinum complex **6** (Scheme 2).

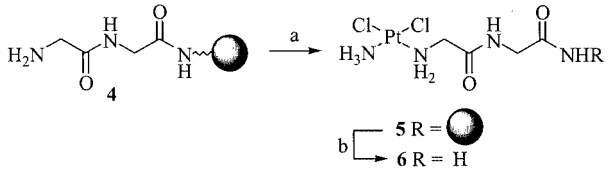

Scheme 2. Solid-phase synthesis of platinum complex **6**; reagents and conditions: a) $[PPh_4][PtCl_3(NH_3)]$ (5 equiv., 0.1 M), DMF/H_2O (9:1, v/v) or DMF, 24 h in the dark; b) TFA, 1 h

Results and Discussion

The immobilized peptide dichloroplatinum complex **2** (Scheme 1) was prepared using our previously published method.[1] Gel-phase ^{195}Pt NMR spectroscopy of **2**, preswollen in [D_7]DMF in a 5 mm NMR tube, using standard solution-state parameters, revealed a clear, albeit broad, signal at $\delta = -2336$ ppm (Figure 1A).

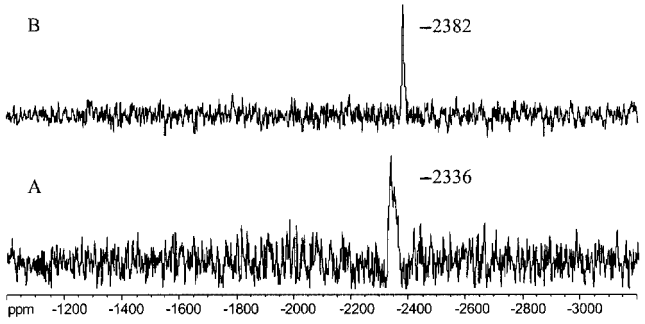

Figure 1. Gel-phase ^{195}Pt NMR spectrum of **2** ([D_7]DMF, 200 mg, 71 μmol) (A), and solution ^{195}Pt NMR spectrum (D_2O) of cleaved and deprotected platinum complex **3** (B)

The gel-phase ^{195}Pt NMR spectrum of **2** not only exhibits a significantly broader signal than the corresponding cleaved and deprotected peptide dichloroplatinum complex **3** dissolved in D_2O (Figure 1B), but is also shifted 46 ppm downfield from the solution-state signal at $\delta = -2382$ ppm. The line width at half-height of **2** is 19.3 ppm, as opposed to a line width at half-height of 6.7 ppm for **3**, indicating that the signal of **2** corresponds to a polymer-bound species. Indeed, when the [D_7]DMF layer was separated from the resin and subjected to ^{195}Pt NMR spectroscopy, no signal appeared. The main factors contributing to line broadening in the gel-phase NMR spectra of polymer-bound species are known to be limited motional freedom, increased correlation time, and magnetic susceptibility variations within the sample.[5,7] The optimal mobility of **2** was attained through the use of DMF, which ensures a high degree of swelling of the polystyrene-based Rink amide resin, as well as solvation of the appended complex with its arginine residue still protected by the apolar Pbf group. Chemical shift studies have indicated that regardless of whether compounds are bound to resins or in solution, the chemical shifts are both virtually identical.[14,15] A conflicting report recently suggested[3] that compounds bound to the solid support exhibit a downfield shift compared to solution-state NMR spectra, due to the high density of aromatic rings within the polymer matrix. However, in the present case the observed, small downfield shift is most likely due to the solvent change, as it has been established that the solvent has a large effect on the chemical shift of platinum (up to a few hundred ppm).[16]

The gel-phase ^{195}Pt NMR technique was subsequently used to optimize the synthesis of a novel type of dichloroplatinum complexes on the solid support. The target molecule **6** (Scheme 2) encompasses a glycine-glycine dipeptide coordinated in a *cis*-configuration to a monoamminedichloroplatinum moiety.

Complex **6** is more cisplatin-like than the dichloroethylenediamineplatinum derivative **3**, as it lacks the ethylene bridge and has a primary amine and a molecule of ammonia as ligands. Gel-phase ^{195}Pt NMR spectroscopy opens the way to investigate whether or not the lack of the ethylenediamine chelating ligand (present in **3**) affects the stability of the primary amine complex on the support. The route of synthesis of target compound **6** (Scheme 2) comprises platination[17,18] of the primary amine of immobilized dipeptide **4** with $[PPh_4][PtCl_3(NH_3)]$, and subsequent release from the solid support with trifluoroacetic acid (TFA). First, dipeptide **4** was reacted with $[PPh_4][PtCl_3(NH_3)]$ (0.1 M, 5 equiv.) in DMF/water (9:1) for one day. The platination conditions were similar to those used for the preparation of **2**, except for the starting platinum salt (K_2PtCl_4 vs. $[PPh_4][PtCl_3(NH_3)]$). After washing the resin with water, DMF, and dichloromethane, a gel-phase ^{195}Pt NMR spectrum was recorded in [D_7]DMF (Figure 2A). The signal at $\delta = -2150$ ppm, with a line width at half-height of 20.9 ppm, corresponds to immobilized **5**, indicating that the solution synthesis method[17,18] is compatible with solid-phase chemistry. However, the signal at $\delta = -1786$ ppm (line width at half-height of 17.8 ppm) was unexpected and is ascribed to hydrolysis of the dichloroplatinum functionality in **5** by the water (10%) present in the reaction mixture.[19] Indeed, subsequent platination in the absence of water afforded a gel-phase ^{195}Pt NMR spectrum devoid of a hydrolysis signal with only the expected $PtCl_2N_2$ chromophore at $\delta = -2147$ ppm (line width at half-height of 15.6 ppm, Figure 2B). This finding indicates that **5** is more susceptible to hydrolysis than the dichloroethylenediamineplatinum derivative **2**, since no hydrolysis signal was observed on the support for the latter after similar reaction conditions. Acidolyis of **5** in TFA and subsequent purification of the product using gel permeation chromatography (HW-40, 0.01 M HCl in water/methanol) gave **6** in 32% yield. The recorded solution-state ^{195}Pt NMR spectrum in D_2O (Figure 2C) shows the $PtCl_2N_2$ chromophore at $\delta = -2200$ ppm, demonstrating roughly the same solvent-induced shift of 53 ppm, as shown for complex **3**.[20] The line width at half-height of **6** (9.6 ppm) is similar to that ob-

served for **3** and considerably smaller than that observed for its immobilized analog **5**.

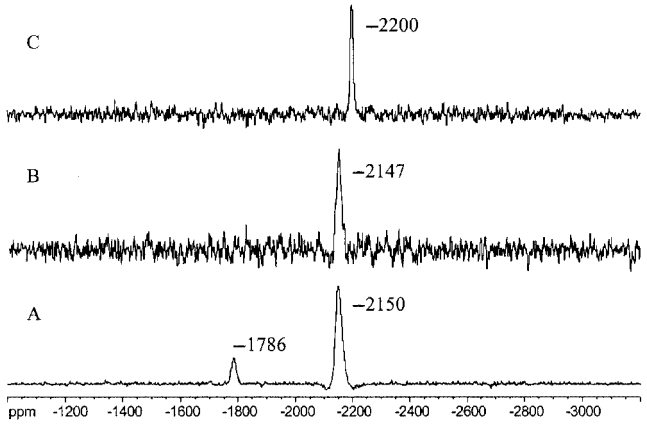

Figure 2. Gel-phase ^{195}Pt NMR spectrum of **5** ([D_7]DMF, 100 mg, 34 μmol) after reaction in DMF/H_2O (9:1) (A), and after reaction in DMF (B); solution-state ^{195}Pt NMR spectrum (D_2O) of cleaved complex **6** (C)

Conclusion

In summary, it has been demonstrated that gel-phase NMR spectroscopy can be applied to the ^{195}Pt nucleus of an immobilized platinum complex. Aided by this technique, the monoamminedichloroplatinum bis-glycine complex **6** has been successfully prepared, representing a new class of platinum complexes now available via solid-phase chemistry. The observed chemical shift of the resin-bound platinum complexes discussed in this paper are in good agreement with the solution-state ^{195}Pt NMR spectra of the soluble and deprotected analogs. As a result of the high receptivity of ^{195}Pt (19.1 times ^{13}C), simple spectra (one signal per nonequivalent Pt) and a wide spectral dispersion (some 15000 ppm, resulting in a high sensitivity to structural perturbations), well-resolved spectra are obtained within hours, without any need for magic-angle spinning. The solvents, polymer backbone and the immobilized ligand are transparent to the technique, eliminating a rigorous drying procedure and suppression techniques. The use of gel-phase ^{195}Pt NMR spectroscopy will be valuable for monitoring a variety of transformations on the resin, aiding the development of novel platinum structures readily available on the solid support, thus facilitating the preparation of new libraries of anticancer platinum complexes.

Experimental Section

General Remarks: All solvents and reagents were of commercial grade and used without purification. Solvents and reagents used in the automated peptide synthesis were of peptide synthesis grade and were purchased from Biosolve. Amino acids and the Rink Amide MBHA resin were purchased from NovaBiochem. K_2PtCl_4 was obtained as a loan from Johnson−Matthey. [PPh_4][$PtCl_3(NH_3)$] was synthesized according to a previously published procedure.[18] Gel permeation chromatography was executed on a HW-40 column (26 mm × 600 mm) at 1.5 mL/min. Mass spectra were recorded on a PE SCIEX API 165 instrument.

NMR Spectroscopy: (Gel-phase) NMR spectra were recorded on a Bruker DPX 300 spectrometer with a 5-mm multi-nucleus probe. The temperature was kept constant at 295 K by a variable temperature unit. ^{1}H NMR spectra were measured using TMS as an external reference at δ = 0 ppm. ^{195}Pt NMR spectra were calibrated with respect to external K_2PtCl_4 at δ = −1614 ppm. Gel-phase ^{195}Pt NMR samples of **2** and **5** were prepared by swelling respectively 200 mg (71 μmol) and 100 mg (34 μmol) of platinated, washed and dried resin in 1 mL of [D_7]DMF in a 5 mm NMR tube. The number of scans used for the gel-phase experiments varied from 89262 to 1243681.

***cis*-Amminedichloro(glycylglycine-NH_2)platinum(II) (6):** Dipeptide **4** was assembled on Rink amide resin with an ABI 433A (Applied Biosystems, division of Perkin−Elmer) peptide synthesizer, employing a FastMoc® peptide synthesis protocol. Immobilized **4** (100.0 mg, 37.9 μmol) was reacted with [PPh_4][$PtCl_3(NH_3)$] (124.6 mg, 189.4 μmol, 0.1 M in DMF) in the dark for one day, washed with water, DMF and dichloromethane and dried in vacuo. Cleavage of the solid support was effected by treatment of **5** with TFA for 1 h, after which the reaction mixture was precipitated with diethyl ether. The resulting solid was washed with diethyl ether, water was added, the mixture was filtered and the resin was washed with water. Subsequently, the combined water fractions were lyophilized, yielding crude **6** as a yellow powder. Purification by gel permeation chromatography (HW-40, 0.01 M HCl in water/methanol, 1:1, v/v) afforded **6** (5.0 mg, 12.0 μmol) in 32% yield, based on **4**. ^{1}H NMR (D_2O): δ = 3.85 (s, 2 H, αGly), 3.83 (s, 2 H, αGly) ppm. ^{195}Pt NMR (D_2O): δ = −2200 ppm. ESI-MS: *m/z* = 449 [M + H + HCl]$^+$.

Acknowledgments

This research was supported by the Council for Chemical Sciences of The Netherlands Organization for Scientific Research (CW-NWO) and by The Netherlands Foundation for Technical Sciences (STW). Support and sponsorship by COST Action D8/00097 and D20/0003 is kindly acknowledged. The authors wish to thank Mr. Cees Erkelens and Dr. Suzanne Kiihne for careful reading of the manuscript and Johnson−Matthey (Reading, UK) for their generous loan of K_2PtCl_4.

[1] M. S. Robillard, A. R. P. M. Valentijn, N. J. Meeuwenoord, G. A. van der Marel, J. H. van Boom, J. Reedijk, *Angew. Chem. Int. Ed.* **2000**, *39*, 3096−3099; *Angew. Chem.* **2000**, *112*, 3226−3229.
[2] M. A. Gallop, W. L. Fitch, *Curr. Opin. Chem. Biol.* **1997**, *1*, 94−100.
[3] P. Grice, A. G. Leach, S. V. Ley, A. Massi, D. M. Mynett, *J. Comb. Chem.* **2000**, *2*, 491−495.
[4] B. J. Egner, M. Bradley, *Drug Discovery Today* **1997**, *2*, 102−109.
[5] P. A. Keifer, *Drug Discovery Today* **1997**, *2*, 468−478.
[6] M. J. Shapiro, J. R. Wareing, *Curr. Opin. Chem. Biol.* **1998**, *2*, 372−375.
[7] G. Lippens, M. Bourdonneau, C. Dhalluin, R. Warras, T. Richert, C. Seetharaman, C. Boutillon, M. Piotto, *Curr. Org. Chem.* **1999**, *3*, 147−169.
[8] S. R. Gilbertson, X. Wang, G. S. Hoge, C. A. Klug, J. Schaefer, *Organometallics* **1996**, *15*, 4678−4680.
[9] E. Lindner, T. Schneller, F. Auer, H. A. Mayer, *Angew. Chem.*

1999, *111*, 2288−2309; *Angew. Chem. Int. Ed.* **1999**, *38*, 2154−2174.
[10] P. Arya, N. V. Rao, J. Singkhonrat, H. Alper, S. C. Bourque, L. E. Manzer, *J. Org. Chem.* **2000**, *65*, 1881−1885.
[11] X. Zhu, B. E. Blough, F. I. Carroll, *Tetrahedron Lett.* **2000**, *41*, 9219−9222.
[12] K. Heinze, *Chem. Eur. J.* **2001**, *7*, 2922−2932.
[13] J. C. Martins, F. A. G. Mercier, A. Vandervelden, M. Biesemans, J.-M. Wieruszeski, E. Humpfer, R. Willem, G. Lippens, *Chem. Eur. J.* **2002**, *8*, 3431−3441.
[14] G. C. Look, C. P. Holmes, J. P. Chinn, M. A. Gallop, *J. Org. Chem.* **1994**, *59*, 7588−7590.
[15] A. Svensson, T. Fex, J. Kihlberg, *Tetrahedron Lett.* **1996**, *37*, 7649−7652.
[16] R. G. Kidd and R. J. Goodfellow, in *NMR and the Periodic Table* (Eds.: R. K. Harris, B. E. Mann), Academic Press, London, **1978**, pp. 249−257.
[17] M. J. Abrams, C. M. Giandomenico, J. F. Vollano, D. A. Schwartz, *Inorg. Chim. Acta* **1987**, *131*, 3−4.
[18] E. G. Talman, W. Brüning, J. Reedijk, A. L. Spek, N. Veldman, *Inorg. Chem.* **1997**, *36*, 854−861.
[19] T. G. Appleton, A. J. Bailey, K. J. Barnham, J. R. Hall, *Inorg. Chem.* **1992**, *31*, 3077−3082.
[20] When crude **6** was dissolved in $[D_7]$DMF and subjected to ^{195}Pt NMR spectroscopy, the $PtCl_2N_2$ chromophore appeared again at $\delta = -2148$ ppm.

Received December 11, 2002
[I02675]

Metal-Promoted Cage Rearrangements in the Tricarbollide Series: Conversion of Ligand Derivatives 7-L-*nido*-7,8,9-$C_3B_8H_{10}$ (L = H_3N, *t*BuH_2N, Me_2HN) into Neutral 8-R-*nido*-7,8,9-$C_3B_8H_{11}$ (R = H_2N, *t*BuHN, Me_2N) Compounds

Bohumír Grüner,[a] Bohumil Štíbr,*[a] Josef Holub,[a] and Ivana Císařová[b]

Keywords: Boranes / Carboranes / NMR spectroscopy / Rearrangement / N ligands

Deprotonation of the eleven-vertex tricarbaborane zwitterions 7-L-*nido*-7,8,9-$C_3B_8H_{10}$ [**1**: L = H_3N (**1a**), *t*BuH_2N (**1b**), Me_2HN (**1c**)], followed by reactions with metal reagents [FeI_2, $NiCl_2$, and $Ni(C_5H_5)_2$] at higher temperatures and in situ acidification, led to the 7 → 8 rearrangement of the *N*-substituted cage carbon atom to yield a series of 8-amino-substituted derivatives of *nido*-7,8,9-$C_3B_8H_{12}$. These were characterized as 8-R-*nido*-7,8,9-$C_3B_8H_{11}$ [**2**: R = H_2N (**2a**), *t*BuHN (**2b**), Me_2N (**2c**)]. A possible rearrangement mechanism for their formation has been proposed. Deprotonation of compound **2a** with proton sponge [PS = 1,8-bis(dimethylaminonaphthalene)] generated the [8-*t*BuHN-*nido*-7,8,9-$C_3B_8H_{10}]^-$ (**2b**$^-$) anion, which can be reprotonated to give the original compound **2b** and not the tautomeric zwitterion 8-*t*BuH_2N-*nido*-7,8,9-$C_3B_8H_{10}$ (**3b**). All compounds were characterized by high-field (^{11}B and ^1H) NMR and IR spectroscopy, and mass spectrometry. The molecular structures of the neutral carbaborane **2b** and its salt PSH$^+$**2b**$^-$were determined by single-crystal X-ray diffraction analyses.

(© Wiley-VCH Verlag GmbH & Co. KGaA, 69451 Weinheim, Germany, 2003)

Introduction

Over the last decade, there has been a growing interest in the chemistry of ten- and eleven-vertex tricarbaboranes.[1−6] The first representatives of the eleven-vertex family (tricarbollides), ligand derivatives 7-L-*nido*-7,8,9-$C_3B_8H_{10}$ (L = amines)[2,6] and the parent tricarbollides *nido*-7,8,9-$C_3B_8H_{12}$ and [*nido*-7,8,9-$C_3B_8H_{11}]^-$, were discovered in 1995.[3,6] An extension of this chemistry has led to the isolation of the isomeric [*nido*-7,8,10-$C_3B_8H_{10}]^-$ anion,[3] its 7-substituted (alkyl and aryl)[4a] and amine-ligand derivatives,[2,4b,4c,6] and finally to the synthesis of isomeric 7-R-*nido*-2,7,10-$C_3B_8H_{11}$ (R = alkyl and aryl)[5] compounds. Later efforts in this area were directed to the exploration of metal complexation properties since $[C_3B_8H_{11}]^-$-type anions can be regarded as cyclopentadienide analogues.[6−12] This research led, in turn, to the isolation of a whole series of metallatricarbollides in which the tricarbaborane core acts as an η^5-coordinating ligand.[6−12] We report herein that, with certain metal reagents, the expected complexation reaction of the [7-R-7,8,9-$C_3B_8H_{10}]^-$ anions (R = H_2N, *t*BuHN, and Me_2N) fails, leading instead to an unexpected 7 → 8 migration of the R−C(cage) carbon atom with the formation of new 8-R-*nido*-7,8,9-$C_3B_8H_{11}$ compounds in moderate to good yields. These are 8-amino-substituted derivatives of *nido*-7,8,9-$C_3B_8H_{12}$ [2,3] and are tautomeric with regards to the nonexistent zwitterions of the 8-L-*nido*-7,8,9-$C_3B_8H_{10}$ compounds. The numbering system for the eleven-vertex compounds used in this work can be seen in Schemes 1 and 2, and in Figures 1−3. The unmarked vertices in Schemes 1 and 2 denote cage BH units.

[a] Institute of Inorganic Chemistry, Academy of Sciences of the Czech Republic (Research Center for New Inorganic Compounds and Advanced Materials, University of Pardubice), 25068, Řež, Czech Republic,
Fax: (internat.) + 420-2/20941502
E-mail: stibr@iic.cas.cz
[b] Faculty of Natural Sciences of Charles University, Hlavova 2030, 12842 Prague 2, Czech Republic
E-mail: cisarova@natur.cuni.cz

Results and Discussion

Syntheses

As shown in Scheme 1, selected zwitterionic compounds of the type 7-L-*nido*-7,8,9-$C_3B_8H_{10}$ [**1**: L = H_3N (**1a**), *t*BuH_2N (**1b**), Me_2HN (**1c**)] were deprotonated in situ at the exoskeletal N site by gentle heating with sodium hydride in DME (1,2-dimethoxyethane) or diethylene glycol dimethyl ether (diglyme) (see Table 1) to give the anions [7-R-*nido*-7,8,9-$C_3B_8H_{10}]^-$ [**1**$^-$: R = H_2N (**1a**$^-$), *t*BuHN (**1b**$^-$), Me_2N (**1c**$^-$)]. These were treated with selected metal reagents [FeI_2, $NiCl_2$, $NiCp_2$ (Cp = $C_5H_5^-$)] at elevated temperatures (95−140 °C, see Table 1) to give the isomeric anions [8-R-*nido*-7,8,9-$C_3B_8H_{10}]^-$ [**2**$^-$: R = H_2N (**2a**$^-$), *t*BuHN (**2b**$^-$), Me_2N (**2c**$^-$)]. Final acidification of the reaction mixture gave a series of neutral compounds of general formulation 8-R-*nido*-7,8,9-$C_3B_8H_{11}$ [**2**: R = H_2N (**2a**), *t*BuHN (**2b**), Me_2N (**2c**)]. As seen from Scheme 1, the net result of

these reactions is, instead of the expected metal complexation, an unusual migration of the amine functionality into the adjacent C-8 position. When compared to structures **1**, compounds **2** thus formed, have lost their original zwitterionic character, being transformed into the tautomeric 8-amino-substituted derivatives of the neutral tricarbaborane *nido*-7,8,9-$C_3B_8H_{12}$.[3] It should be noted that the reactions do not proceed without deprotonation of compounds **1** preceding the reaction with individual metal reagents. The role of the metal reagents is quite obscure, as no sign of complex formation is observed during the reactions, nevertheless, the reactions do not proceed in the absence of the metal reagent. Moreover, the reactions never come to completion (see Table 1) and the starting compounds can easily be recovered by chromatography.

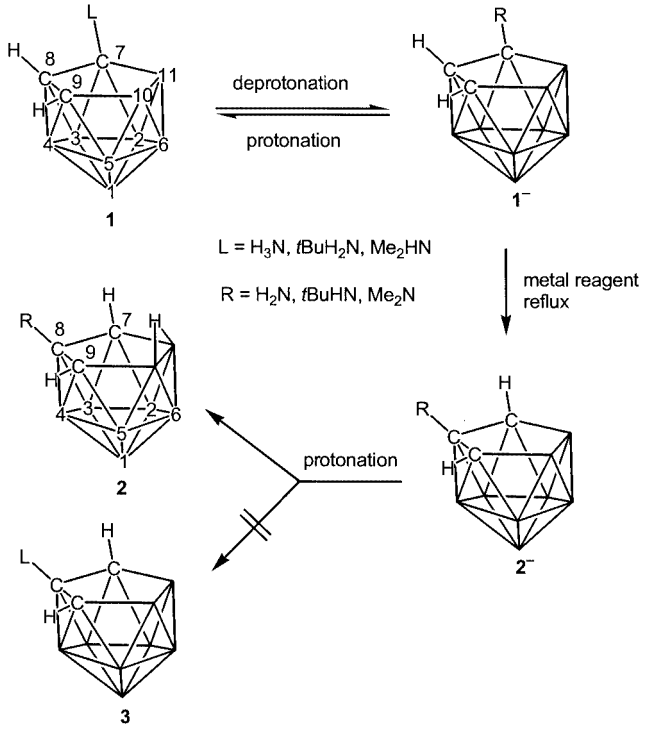

Scheme 1

Although there is no direct evidence on the reaction mechanisms, the formation of anions of type $\mathbf{2}^-$ from anions of type $\mathbf{1}^-$ is consistent with a simple C-7 vertex-swing mechanism outlined in Scheme 2. The mechanism is similar to that proposed recently by Sneddon et al.[5] and involves the formation of two new bonds together with a cleavage of two original bonds around the C-7 vertex. The new system, thus formed, has one of the skeletal carbon atoms in an unfavorable high-connectivity position and is therefore rearranged in a similar manner to the isomeric anions $\mathbf{2}^-$.

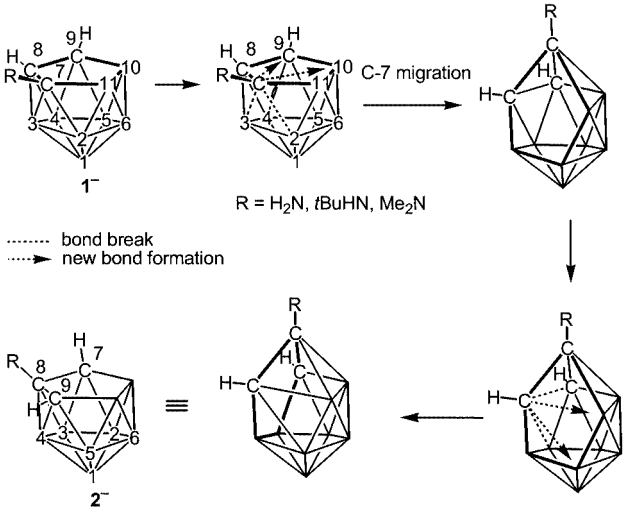

Scheme 2

An interesting aspect is the final protonation of the $\mathbf{2}^-$ anions as there are two ways in which the proton can be added (see Scheme 1). In contrast to the anions $\mathbf{1}^-$, the protonation of $\mathbf{2}^-$does not occur on the exoskeletal nitrogen atom with the anticipated formation of the 8-L-*nido*-7,8,9-$C_3B_8H_{10}$ zwitterions (compounds of type **3**), but exclusively on the open-face B-10−B-11 edge to give the tautomeric 8-R-*nido*-7,8,9-$C_3B_8H_{11}$ (**2**) compounds, 8-substituted derivatives of the parent tricarbollide 7,8,9-$C_3B_8H_{12}$ (**4**).[3]

As demonstrated by a separate experiment, the deprotonation of compound **2b** with PS (see also Scheme 1) proceeds by abstraction of the μ_{10-11} bridging proton with the formation of anion $\mathbf{2b}^-$, which by reprotonation returns to the original compound **2b**, and not the zwitterionic compound **3b**.

Structural Studies

The structures of the neutral compound **2b** and the corresponding salt $PSH^+\mathbf{2b}^-$ were determined by single-crystal

Table 1. Conditions for the formation of 8-amino-substituted derivatives of type **2**

Starting compound	Metal reagent	Conditions	Product	Yield (%)
1a	FeI_2	DME, reflux, 2 h	**2a**	43 (50)[a]
1b	FeI_2	diglyme, 120 °C, 16 h	**2b**	48 (67)[a]
1b	$NiCl_2$	DME, reflux, 16 h	**2b**	51 (64)[a]
1b	$NiCl_2$	diglyme, 140 °C, 16 h	**2b**	60
1b	$NiCp_2$	diglyme, 140 °C, 24 h	**2b**	30
1c	$NiCl_2$	DME, reflux, 42 h	**2c**	18 (66)[a]

[a] Yields based on recovered starting compounds **1** in parentheses.

X-ray diffraction analyses (see Figures 1−3). The molecular structure of the latter salt shows that the arrangement of the substituent at the C8 site and the whole cage remain unaltered by deprotonation. Both structures confirm the adjacent position of all three of the cage carbon atoms in the *nido* cage and the substitution on the central C8 atom. Two symmetrically independent molecules in the unit cell of **2b** differ only slightly in the orientation of the *t*Bu moiety. Selected interatomic distances and angles for both species (see Table 2) show all expected features, with the shortest distances between carbon atoms. The longest interboron distances are those between the open-face B10−B11 vertices. This distance is even more elongated by the presence of the hydrogen bond in **2b** [1.841(3) Å] in comparison with the corresponding separation in PSH^+**2b**$^-$ [1.727(2) Å]. The latter distance is similar to that found for B10−B11 in the zwitterionic compound 7-*t*BuHMeN-7,8,9-$C_3B_8H_{10}$ [1.725(3) Å].[2b]

The structures of all remaining amino derivatives **2a** and **2c** were proposed from the structurally determined com-

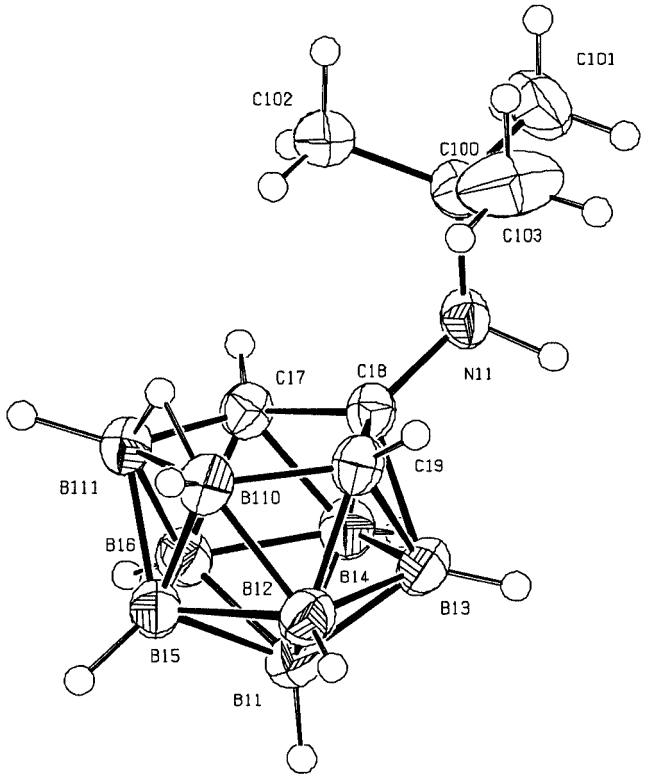

Figure 1. Perspective view of the first molecule of **2b** with atom-numbering scheme (PLATON, displacement ellipsoids at the 50% probability level)

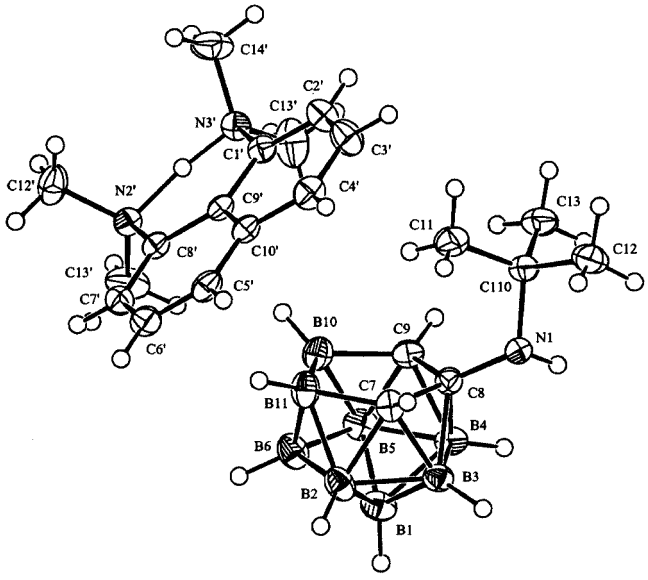

Figure 3. View of the first molecule of PSH^+**2b**$^-$ with atom-numbering scheme (PLATON, displacement ellipsoids at the 50% probability level)

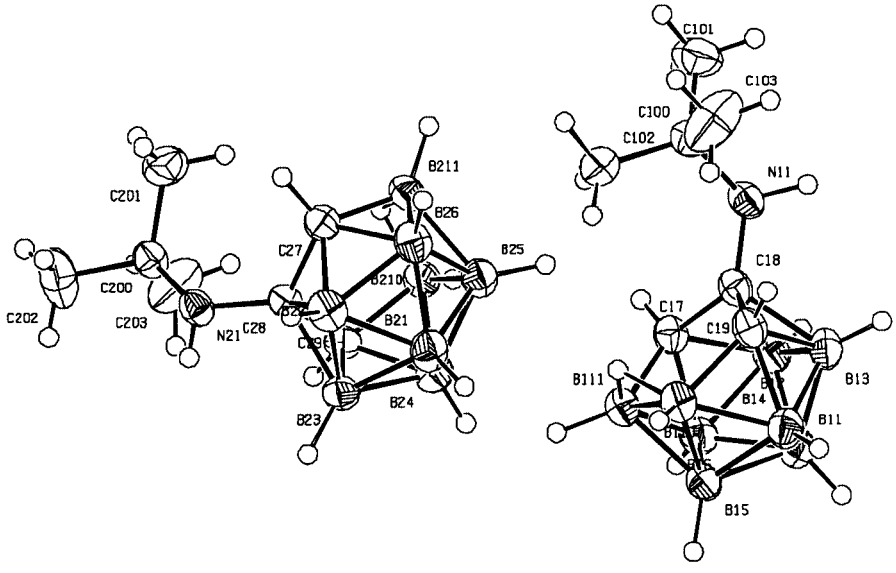

Figure 2. ORTEP representation of two symmetrically independent molecules differing slightly in the orientation of the *t*Bu group present in the unit cell of **2b**

Table 2. Selected interatomic distances [Å] and angles [°] for **2b** and PSH^+**2b**$^-$

Compound	**2b**, molecule 1 * = 1	**2b**, molecule 2 * = 2	PSH^+**2b**$^-$ * = blank
C(*7)−C(*8)	1.529(3)	1.527(3)	1.5283(15)
C(*7)−B(*11)	1.654(3)	1.652(3)	1.6223(18)
C(*8)−N(*1)	1.427(3)	1.419(3)	1.4351(15)
C(*8)−C(*9)	1.536(3)	1.530(3)	1.5359(16)
C(*9)−B(*10)	1.653(3)	1.640(3)	1.6199(19)
B(*10)−B(*11)	1.840(3)	1.841(3)	1.727(2)
N(*1)−C(*10)	1.481(3)	1.506(2)	1.4896(15)
C(*8)−C(*7)−B(*11)	109.92(16)	109.39(16)	111.74(10)
C(*7)−C(*8)−C(*9)	113.86(16)	114.27(16)	109.04(9)
C(*8)−C(*9)−B(*10)	109.86(17)	109.72(16)	111.59(10)
C(*9)−B(*10)−B(*11)	102.69(17)	102.85(16)	103.75(10)
B(*10)−B(*11)−C(*7)	102.78(16)	102.66(16)	103.66(6)
N(*1)−C(*8)−C(*7)	118.32(18)	117.82(17)	117.89(9)
N(*1)−C(*8)−C(*9)	121.20(17)	121.35(17)	124.62(10)
C(*8)−N(*1)−C(*10)	120.70(16)	119.70(15)	119.05(9)
B(*10)−H(*01)	1.28(2)	1.28(2)	
B(*11)−H(*01)	1.16(2)	1.27(2)	

pound **2b**, on the basis of close similarities in their NMR spectroscopic shielding behavior. The comparison revealed (see Figure 4) straightforward similarities between corresponding ^{11}B and ^{1}H resonances for all amino derivatives of **2**. The observed NMR spectroscopic data for this class of compounds (see Exp. Sect.), together with the results of mass spectrometry, are in excellent agreement with their formal descriptions as 8-amino-substituted derivatives of the previously reported parent tricarbaborane **4**.[3] All the cluster ^{11}B and ^{1}H resonances were interrelated by [^{11}B-^{11}B]-COSY[13] and/or ^{1}H{^{11}B(selective)}[14] experiments, which permitted complete assignments and thence comparisons with the known, but isomeric, 7-*t*BuMeN-10-Me-7,8,9-$C_3B_8H_{10}$ and 7-*t*BuMeN-10,11-Me_2-7,8,9-$C_3B_8H_9$ amine derivatives.[2b]

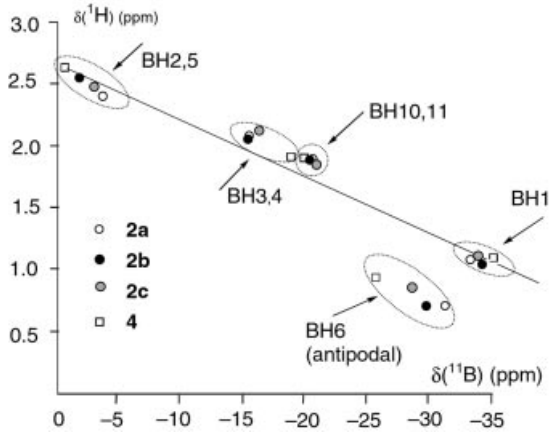

Figure 4. Graphical correlation between the ^{1}H and ^{11}B NMR chemical shifts for compounds **2a**, **2b**, and **2c**, and for the parent tricarbaborane **4**

As shown in Figure 4, the most significant feature of the compounds **2** is the 2:2:2:1:1 patterns of the ^{11}B resonances. These are very similar to those of the parent compound **4**, which is of the same C_s symmetry,[3] the most remarkable feature being the upfield shift of resonances assigned to the antipodal B-6 vertex. A similar effect was also observed in the spectrum of 8-Me-7,8,9-$C_3B_8H_{11}$,[3] the only 8-substituted derivative of **4** isolated so far. The ^{11}B NMR spectrum of PSH^+**2b**$^-$, showing (2+2+1):2:1 patterns of doublets (incidental overlap), is consistent with the same C_s symmetry. As expected, most of the peaks are markedly shifted upfield in comparison with adequate resonances observed for **2b** due to the absence of hydrogen bonding. This correlates closely with the observed bridge effect found in the ^{11}B NMR spectra for the couple of unsubstituted compounds **4** and [7,8,9-$C_3B_8H_{11}$]$^-$ (**4**$^-$).[3] Moreover, ^{1}H NMR spectra of compounds **2a**−**2c** clearly reveal, besides the 7,9-H resonance of intensity 2, a broad high-field singlet due to the presence of the μ_{10-11} bridging proton. As demonstrated graphically in Figure 4, there is an approximately linear correlation between the ^{11}B and ^{1}H chemical shifts for all derivatives of **2**, with the exception of data points for the antipodal B-6-H positions.

Mass spectrometric results along with similar chromatographic and solubility properties are all consistent with the proposed structures of the neutral derivatives of type **2**. Across the series, enhanced solubility in less polar solvents and higher R_f values were observed for **2** in comparison with the corresponding characteristics of the starting zwitterions of structure **1**.

Conclusions

It was shown that the zwitterionic tricarbollides **1** undergo an unusual metal-promoted cage rearrangement upon deprotonation and reaction with some metal reagents to generate isomeric compounds of type **2**. The net result of the rearrangement is a shift of the amine functionality to the adjacent position without changing the configuration of the cage carbon atoms. In contrast to the starting zwitterionic compounds of **1**, the rearranged compounds adopt the tautomeric neutral configuration of **2** and *not* the zwitterionic structure of **3** (see Scheme 1). The relation between structures **2** and **3** falls into the category of H-tautomerism as the two forms differ only in the positioning of the extra hydrogen atom. In structure **2** this hydrogen atom resides in the bridging open-face position, while in the zwitterionic structure **3** it would reside on the exoskeletal nitrogen atom. This interesting aspect of tautomerism in the eleven-vertex tricarbaborane series was encountered for the first time in the 7-substituted series of compounds of the general form 7-*t*BuMeN-10,11-R^1R^2-7,8,9-$C_3B_8H_9$ (R^1, R^2 = H or Me). For R^1 = R^2 = H these compounds exist exclusively in the zwitterionic form 7-*t*BuMeHN-7,8,9-$C_3B_8H_{10}$ (**1d** for L = *t*BuMeHN), while the formally *B*-mono- and *B*,*B*-dimethylated derivatives of **1d**, exist only in the neutral tautomeric forms 7-*t*BuMeN-10-Me-7,8,9-$C_3B_8H_{10}$ and 7-*t*BuMeN-10,11-Me_2-7,8,9-$C_3B_8H_9$.[2b] It seems highly probable that both the electron density on the nitrogen center and the type of substitution of the tricarbaborane core play decisive

roles in determining the preferences for individual tautomeric forms. It is also highly probable that compounds of the general structure **2**, isolated in this work, act as intermediates in the metal complexation reactions of anions of type $\mathbf{1}^-$.[6−12] We are currently studying the aspects of tautomerism and associated rearrangements of tricarbaborane cages occurring during the metal complexation process in more detail. Studies on further interesting rearrangement reactions of compounds of the type **2** and $\mathbf{2}^-$, at high temperatures, are also in progress.

Experimental Section

General Procedures: All reactions were carried out with the use of standard vacuum or inert gas techniques as described by Shriver,[15] although some operations, such as preparative LC, were carried out in air. The starting compounds **1** were prepared according to the literature.[2] The Aldrich DME and diglyme were dried with sodium metal and freshly distilled from sodium diphenylketyl or NaH. Hexane and benzene were dried with CaH_2, CH_2Cl_2 and P_2O_5 and then freshly distilled prior to use. Other chemicals were reagent grade and used as purchased. Preparative liquid chromatography was carried out using Aldrich silica gel (60−230 mesh) as the stationary phase under nitrogen. Analytical TLC on Macherey−Nagel plates with a UV indicator (silica gel on aluminium foil; detection by UV at 254 nm followed by 2% aqueous $AgNO_3$ spray) was used to check the purity of individual chromatographic fractions. Melting points were measured in sealed capillaries and are uncorrected. Elemental analyses were performed in the IIC analytical laboratories using standard procedures. Low-resolution mass spectra were obtained using a Finnigan MAT MAGNUM ion trap quadrupole mass spectrometer equipped with a heated inlet option, as developed by Spectronex AG, Basle, Switzerland (70 eV, EI ionization). Proton (^{1}H) and boron (^{11}B) NMR spectroscopy was performed at 11.75 Tesla with a Varian UNITY-500 instrument. The [^{11}B-^{11}B]-COSY[13] and ^{1}H{^{11}B(selective)}[14] NMR experiments were essentially as described in other related papers from our laboratories.[16] Chemical shifts are given in ppm to high-frequency (low field) of Ξ = 32.083971 MHz (nominally $F_3B{\cdot}OEt_2$ in $CDCl_3$) for ^{11}B (quoted ± 0.5 ppm) and Ξ = 100 MHz ($SiMe_4$) for ^{1}H (quoted ± 0.05 ppm), Ξ being defined as in ref.[17] Residual solvent ^{1}H resonances were used as internal secondary standards. Coupling constants $^1J_{BH}$ are taken from resolution-enhanced ^{11}B NMR spectra with a digital resolution of ± 8 Hz and are given in Hz.

General Conditions for the Synthesis of the 8-R-*nido*-7,8,9-$C_3B_8H_{11}$ Derivatives 2 [R = H_2N (2a), *t*BuHN (2b), Me_2N (2c)]: A slurry of the starting compound **1** (reaction scale 1.5 mmol), NaH (3.15 mmol) and solvent (DME or diglyme, 20 mL) was stirred at room temperature for 1 h and then heated at 90 °C (bath) for an additional hour whilst stirring. Excess metal reagent (see Table 1) (reaction scale 4.5 mmol) was then added and the mixture was stirred under the conditions given in Table 1. The solvent was rotaevaporated and the residue treated with a mixture of Et_2O (20 mL) and water (20 mL), and the aqueous layer was acidified with dilute hydrochloric acid to pH = 3.0 under cooling. The organic layer was then separated and the aqueous phase extracted with additional portions of Et_2O (2 × 20 mL). The combined ethereal extracts were concentrated and the residue treated with CH_2Cl_2 (15 mL) and silica gel (10 g). The solvent was evaporated, the solids were placed on top of a silica gel column (25 × 2 cm) and eluted with a CH_2Cl_2/pentane (1:1, v/v) mixture. The purity of individual fractions was checked by analytical TLC (for R_F values see Table 1). Essentially pure compounds of type **2** were obtained by concentration of the corresponding chromatographic fractions and the products were repurified by crystallization from hexane. Compound **2b** was purified by vacuum sublimation at 120 °C. Subsequent elution with CH_2Cl_2 or its mixtures with CH_3CN (up to 1:1 composition) recovered, in most cases, the starting compounds of type **1**. Reaction conditions for individual derivatives and yields are summarized in Table 1.

2a: R_f (CH_2Cl_2) = 0.40; m.p. 132 °C. ^{11}B NMR ($CDCl_3$): δ = −4.1 (d, $^1J_{B\text{-}H}$ = 159 Hz, 2 B, B-2,5), −15.5 (d, $^1J_{B\text{-}H}$ =171 Hz, 2 B, B-3,4), −20.4 (d, $^1J_{B\text{-}H}$ = 183 Hz, 2 B, B-10,11), −31.4 (d, $^1J_{B\text{-}H}$ = 153 Hz, 1 B, B-6), −32.8 (d, $^1J_{B\text{-}H}$ = 150 Hz, 1 B, B-1) ppm, all theoretical [^{11}B-^{11}B]-COSY cross-peaks observed. ^{1}H{^{11}B} NMR ($CDCl_3$): δ = 2.93 (s, 2 H, 7,9-H), 2.39 (s, 2 H, 2,5-H), 2.16 (br. s, 2 H, NH_2), 2.05 (s, 2 H, 3,4-H), 1.86 (s, 2 H, 10,11-H), 1.18 (s, 1 H, 1-H), 0.62 (s, 1 H, 6-H), −1.92 (s, 1 H, 10,11-μ-H). MS (70 eV, EI): *m*/*z* (%) = 151 (16) $[M]^+$, 150 (100) $[M - H]^+$. $C_3H_{13}B_8N$ (149.6): calcd. B 57.80; found 57.54.

2b: R_f (CH_2Cl_2) = 0.62; m.p. 95 °C. ^{11}B NMR ($CDCl_3$): δ = −1.5 (d, $^1J_{B\text{-}H}$= 162 Hz, 2 B, B-2,5), −15.4 (d, $^1J_{B\text{-}H}$ = 171 Hz, 2 B, B-3,4), −19.9 (d, $^1J_{B\text{-}H}$ = 192 Hz, 2 B, B-10,11), −29.9 (d, $^1J_{B\text{-}H}$ = 147 Hz, 1 B, B-6), −32.6 (d, $^1J_{B\text{-}H}$ = 150 Hz, 1 B, B-1).) ppm, all theoretical [^{11}B-^{11}B]-COSY cross-peaks observed. ^{1}H{^{11}B } NMR ($CDCl_3$): δ = 3.28 (s, 2 H, 7,9-H), 2.66 (s, 2 H, 2,5-H), 2.56 (br. s, 1 H, NH), 2.04 (s, 2 H, 3,4-H), 1.94 (s, 2 H, 10,11-H], 1.19 (s, 9 H, *t*Bu), 1.08 (s, 1 H, 1-H), 0.71 (s, 1 H, 6-H), −2.34 (s, 1 H, 10,11-μ-H) ppm. IR (KBr): $\tilde{\nu}$ = 2579 (B−H) cm^{-1}. MS (70 eV, EI): *m*/*z* = 207 (15) $[M]^+$, 206 (100) $[M - H]^+$. $C_7H_{21}B_8N$ (205.7): calcd. B 42.04, found 41.92.

2c: R_f (CH_2Cl_2) = 0.50; m.p. 75 °C. ^{11}B NMR (CD_3CN): δ = −3.76 (d, $^1J_{B\text{-}H}$ = 158 Hz, 2 B, B-2,5), −16.4 (d, $^1J_{B\text{-}H}$ = 168 Hz, 2 B, B-3,4), −20.6 (d, $^1J_{B\text{-}H}$ = 195 Hz, 2 B, B-10,11), −30.6 (d, $^1J_{B\text{-}H}$ = 140 Hz, 1 B, B-6), −33.6 (d, $^1J_{B\text{-}H}$ = 153 Hz, 1 B, B-1) ppm, all theoretical [^{11}B-^{11}B]-COSY cross-peaks observed. ^{1}H{^{11}B} NMR (CD_3CN): δ = 3.00 (s, 2 H, 7,9-H), 2.43 (s, 2 H, 2,5-H), 2.36 (s, 2 H, 3,4-H), 2.16 (m, 6 H, Me), 1.98 (s, 2 H, 10,11-H), 1.02 (s, 1 H, 1-H), 0.72 (s, 1 H, 6-H), −1.98 (s, 1 H, 10,11-μ-H) ppm. IR (KBr): $\tilde{\nu}$ = 2556 (B−H) cm^{-1}. MS (70 eV, EI): *m*/*z* = 179 (18) $[M]^+$, 178 (100) $[M - H]^+$. $C_5H_{17}B_8N$ (177.7): calcd. B 48.67; found 48.34.

PSH^+[8-*t*BuHN-7,8,9-$C_3B_8H_{10}$]$^-$ (PSH^+2b$^-$): A solution of PS (107 mg, 0.5 mmol) in hexane (15 mL) was added dropwise to a stirred solution of **2b** (100 mg, 0.48 mmol) in hexane (15 mL) over a period of 10 min. The mixture was stirred for an additional 30 min and a white, voluminous precipitate formed. The precipitate was isolated by filtration, washed with hexane (3 × 5 mL) and vacuum-dried to yield 188 mg (92%) of $PSH^+\mathbf{2b}^-$, which was identified by NMR spectroscopy. **PSH^+2b$^-$:** ^{11}B NMR (CD_3CN): δ = −18.5 (d, $^1J_{B\text{-}H}$ = 170 Hz, 2 B, B-10,11), −19.7 (d, $^1J_{B\text{-}H}$ =158 Hz, 5 B, B-2,3,4,5,6), −47.7 (d, $^1J_{B\text{-}H}$ = 139 Hz, 1 B, B-1) ppm, all theoretical [^{11}B-^{11}B]-COSY cross-peaks observed. ^{1}H{^{11}B } NMR (CD_3CN): δ = 18.81 (s, 1 H, PSH^+), 7.35−9.96 (m, 6 H, PS-aromatic), 3.21 (br. s, 6 H, PS-Me), 2.66 21 (br. s, 6 H, PS-Me), 2.17 (s, 2 H, 7,9-H), 1.30, 1.53, 1.80 (s, 1 H, 2 H, 2 H, 2,3,4,5,6-H), 1.13 (s, 9 H, *t*Bu), 0.97 (s, 2 H, 10,11-μ-H), 0.17 (s, 1 H, 1-H) ppm.

Protonation of PSH^+[8-*t*BuHN-7,8,9-$C_3B_8H_{10}$]$^-$ (PSH^+2b$^-$): A solution of $PSH^+\mathbf{2b}^-$ (126 mg, 0.3 mmol) in CH_2Cl_2 (20 mL) was treated with several drops of concentrated H_2SO_4 whilst stirring for 1 h and cooling to 0 °C. The organic layer was then separated and

Table 3. Crystal data and structure refinement for **2b** and $PSH^+\mathbf{2b}^-$

	2b	$PSH^+\mathbf{2b}^-$
Empirical formula	$C_7H_{21}B_8N_1$	$C_7H_{20}B_8N_1\cdot C_{14}H_{19}N_2$
Formula mass	205.75	420.03
Crystal system	monoclinic	monoclinic
Space group	$P2_1/c$	$P2_1/c$
a [Å]	13.9799(4)	13.8910(2)
b [Å]	13.4980(5)	10.1050(2)
c [Å]	13.9760(5)	18.1420(3)
β [°]	100.258(2)	101.127(1)
Z	8	4
V [Å^3]	2595.13(15)	2498.70(7)
μ [mm^{-1}]	0.051	0.060
$D_{calcd.}$ [Mg/m^3]	1.053	1.117
Wavelength [Å]	0.71073	0.71073
F(000)	880	904
θ range [°]	1.51−26	1−27.5
Scan mode	and ω	and ω
h, k, l collected	$-16 \le h \le 17$, $-15 \le k \le 16$, $-16 \le l \le 17$	$-18 \le h \le 18$, $-13 \le k \le 13$, $-23 \le l \le 23$
No. of reflections measured	16548	46448
No. of unique reflections	5209 (R_{int} = 0.048)	5713 (R_{int} = 0.035)
No. of parameters	386	344
GOF[a] all data	1.043	1.065
Final R[a] indices [$I > 2\sigma(I)$]	$R1$ = 0.052, $wR2$ = 0.122	$R1$ = 0.044, $wR2$ = 0.112
R[a] indices (all data)	$R1$ = 0.073, $wR2$ = 0.135	$R1$ = 0.063, $wR2$ = 0.122
w_1/w_2	0.087/0.1561	0.0605/0.4392
Δρ(max./min.) [e Å^{-3}]	0.244/−0.197	0.191/0.180

[a] Definitions: $R(F) = \Sigma||F_o| - ||F_c||/\Sigma|F_o|$; $wR2 = \{\Sigma[w(F_o^2 - F_o^2)^2]/\Sigma[w(F_o^2)^2]\}^{1/2}$; GOF $= \{\Sigma[w(F_o^2 - F_c^2)^2]/(N_{reflns} - N_{params})\}^{1/2}$; weighting scheme $w = [\sigma^2(F_o^2) + (w_1P) + w_2P]^{-1}$; $P = [\max.(F_o^2,0) + 2F_c^2]/3$.

the solvents were evaporated to give 59 mg (96%) of **2b**, which was identified by NMR spectroscopy by comparison with the characteristics of an authentic sample.

X-ray Crystallography: The crystal of **2b** was obtained by slow vacuum sublimation of the tricarbaborane at 120 °C and that of the $PSH^+\mathbf{2b}^-$ salt by slow concentration of the $CHCl_3$ solution in a glass tube. The colorless crystals of **2b** and $PSH^+\mathbf{2b}^-$ of dimensions 0.4 × 0.3 × 0.17 and 0.3 × 0.27 × 0.22 mm, respectively, were mounted on glass fibers with epoxy cement and measured with a four-circle diffractometer Nonius Kappa CCD equipped with a CCD area detector at 150(2) K with Mo-K_α radiation. The crystallographic details for both compounds are summarized in Table 3. The structures were solved by the direct method (SIR97)[18] and that of $PSH^+\mathbf{2b}^-$ was refined by a full-matrix least-squares procedure based on F^2 (SHELXL-97).[19] However, the crystal of **2b** underwent pseudomerohedral twinning, as discovered during the structure solution. The phase problem was therefore solved using the $P2_1$ space group and the model was later transformed into the $P2_1/c$ space group. The symmetry of the diffraction pattern is consistent with the orthorhombic space group $C222_1$ as the result of twinning due the matrix:

h' 0 0 1 h
k' 0 1 0 k
l' 1 0 0 l

The data were corrected accordingly during the refinement by a full-matrix least-squares procedure based on F^2 (SHELXL-97),[19] which yielded a ratio of twin parts 0.472/0.528. The absorption was neglected. All hydrogen atoms, except for those of the methyl groups, were localized on a difference Fourier map and refined isotropically. For $PSH^+\mathbf{2b}^-$, hydrogen positions of the methyl groups and those of the PSH^+ CH moieties were recalculated into idealized positions (riding model) and assigned temperature factors $H_{iso}(H) = 1.2\ U_{eq}$(pivot atom) or $1.5\ U_{eq}$ for the methyl moiety, others were localized on a difference Fourier map and refined isotropically. The final difference maps for both compounds had no peaks of chemical significance. Scattering factors were those implemented in the SHELX programs. CCDC-184057 and -190913 contain the supplementary crystallographic data for compounds **2b** and $PSH^+\mathbf{2b}^-$, respectively. These can be obtained free of charge at www.ccdc.cam.ac.uk/conts/retrieving.html or from the Cambridge Crystallographic Data Centre, 12 Union Road, Cambridge CB2 1EZ, UK [Fax: (internat.) + 44-1223/336-033; E-mail: deposit@ccdc.cam.ac.uk].

Acknowledgments

The authors gratefully acknowledge Drs. J. Fusek, Z. Plzák, and E. Večerníková from the Institute of Inorganic Chemistry, ASCR for providing NMR, mass, and IR spectra. The work was supported by the Ministry of Education of the Czech Republic (project no. LN 00A028) and Grant Agency of the Czech Republic (grant nos. 203/00/1042 and 203/99/M037, the latter is appreciated for the purchase of the Kappa CCD equipment).

[1] [1a] K. Su, B. A. Barnum, P. J. Caroll, L. G. Sneddon, *J. Am. Chem. Soc.* **1992**, *114*, 2730−2731. [1b] C. A. Plumb, L. G. Sneddon, *Organometallics* **1992**, *11*, 1681−1685. [1c] A. Wille, L. G. Sneddon, *Collect. Czech. Chem. Commun.* **1997**, *62*, 1214−1218.

[2] [2a] B. Štíbr, J. Holub, F. Teixido, C. Viñas, *J. Chem. Soc., Chem. Commun.* **1995**, 795−796. [2b] B. Štíbr, J. Holub, I. Císařová, F. Teixidor, C. Viñas, J. Fusek, Z. Plzák, *Inorg. Chem.* **1996**, *35*, 3635−3642. [2c] B. Štíbr, J. Holub, J. Plešek, T. Jelínek, B. Grüner, F. Teixidor, C. Viñas, *J. Organomet. Chem.* **1999**, *582*, 282−285.

[3] J. Holub, B. Štíbr, D. Hnyk, J. Fusek, I. Císařová, F. Teixidor, C. Viñas, Z. Plzák, P. v. R. Schleyer, *J. Am. Chem. Soc.* **1997**, *119*, 7750−7759.
[4] [4a] A. M. Shedlow, P. J. Carroll, L. G. Sneddon, *Organometallics* **1995**, *14*, 4046−4047. [4b] B. Štíbr, J. Holub, I. Císařová, F. Teixidor, C. Viñas, *Inorg. Chim. Acta* **1996**, *245*, 129. [4c] R. Rousseau, E. Canadell, S. Lee, F. Teixidor, C. Viñas, B. Štíbr, *New J. Chem.* **1996**, *20*, 277.
[5] A. M. Shedlow, L. G. Sneddon, *Collect. Czech. Chem. Commun.* **1999**, *64*, 865−882.
[6] B. Štíbr, J. Holub, F. Teixidor, in *Advances in Boron Chemistry* (Ed.: W. Siebert), Royal Society of Chemistry, Cambridge, **1997**, p. 333−340.
[7] B. Štíbr, J. Holub, F. Teixidor, C. Viñas, *Collect. Czech. Chem. Commun.* **1995**, *60*, 2023−2027.
[8] J. Holub, B. Grüner, I. Císařová, J. Fusek, Z. Plzák, F. Teixidor, C. Viñas, B. Štíbr, *Inorg. Chem.* **1999**, *38*, 2775−2780.
[9] B. Grüner, A. Lehtonen, R. Kivekäs, R. Sillanpää, J. Holub, F. Teixidor, C. Viñas, B. Štíbr, *Inorg. Chem.* **2000**, *39*, 2577−2580.
[10] B. Štíbr, B. Grüner, J. Holub, F. Teixidor, F. C. Viñas, A. Lehtonen, R. Sillanpää, R. Kivekäs, in *Contemporary Boron Chemistry* (Eds.: M. G. Davidson, A. K. Hughes, T. B. Marder), Royal Society of Chemistry, Cambridge, **2000**, p. 337−344.
[11] B. Grüner, B. Štíbr, J. Holub, F. Teixidor, C. Viñas, R. Sillanpaa, R. Kivekas, *J. Chem. Soc., Dalton Trans.* **1999**, 3337−3338.
[12] B. Grüner, B. Štíbr, F. Teixidor, C. Viñas, R. Sillanpää, R. Kivekäs, *Inorg. Chem. Commun.* **1999**, *2*, 411−413.
[13] See, for example: [13a] J. D. Kennedy, in *Multinuclear N. M. R.* (Ed.: J. Mason), Plenum Press, New York, **1987**, p. 221. [13b]W. C. Hutton, T. L. Venable, R. N. Grimes, *J. Am. Chem. Soc.* **1984**, *106*, 29. [13c] J. Schraml, J. M. Bellama, *Two-Dimensional NMR Spectroscopy*, Wiley, New York, **1982**, and references therein.
[14] X. L. R. Fontaine, J. D. Kennedy, *J. Chem. Soc., Dalton Trans.* **1987**, 1573.
[15] D. F. Shriver, M. A. Drezdon, *Manipulation of Air Sensitive Compounds*, 2nd ed., John Wiley & Sons, New York, **1986**.
[16] J. Plešek, B. Štíbr, X. L. R. Fontaine, J. D. Kennedy, S. Heřmánek, T. Jelínek, *Collect. Czech. Chem. Commun.* **1991**, *56*, 1618−1635.
[17] W. McFarlane, *Proc. R. Soc. London, Ser. A* **1968**, *306*, 185.
[18] A. Altomore, M. C. Burla, M. Camalli, G. Cascarano, C. Giacovazzo, A. Guagliardi, A. G. G. Molinerni, G. Polidori, R. Spagna, *J. Appl. Crystalogr.* **1999**, *32*, 115.
[19] G. M. Sheldrick, *SHELX97, Program for Crystal Structure Refinement from Diffraction Data*, University of Göttingen, Germany, **1997**.

Received October 10, 2002
[I02558]

New Mononuclear Manganese(III) Complexes with Hexadentate (N_4O_2) Schiff Base Ligands: Synthesis, Crystal Structures, Electrochemistry, and Electron-Transfer Reactivity towards Hydroxylamine

Anangamohan Panja,[a] Nizamuddin Shaikh,[a] Shankareswar Gupta,[a] Ray J. Butcher,[b] and Pradyot Banerjee*[a]

Keywords: Cyclic voltammetry / Electron transfer / Kinetics / Manganese

Four new manganese(III) complexes of hexadentate Schiff base ligand obtained from *N*,*N*′-bis(3-aminopropyl)ethylenediamine and salicylaldehyde, or salicylaldehyde derivatives having N_4O_2 donor sets – [Mn(sal-N-1,5,8,12)]ClO_4 (**1**), [Mn(5-Cl-sal-N-1,5,8,12)]ClO_4 (**2**), [Mn(5-Br-sal-N-1,5,8,12)]-ClO_4 (**3**), and [Mn(3-methoxy-sal-N-1,5,8,12)]ClO_4·H_2O (**4**) – have been synthesized and characterized. The crystal structures of **1** and **4** have been determined, and the kinetics of the electron-transfer reactions between these complexes and hydroxylamine hydrochloride have been followed spectrophotometrically in the 5.5–8.0 pH range. Similar kinetic reactivities of all the complexes towards a particular species of the reductant were noted. Hydrogen-bonded adduct formation between the reactants prior to electron transfer seems to be a possible reaction pathway, according to analysis of the experimental data.
(© Wiley-VCH Verlag GmbH & Co. KGaA, 69451 Weinheim, Germany, 2003)

Introduction

An important area of investigation in the bioinorganic chemistry of manganese is the study of the structures and reactivities of manganese(III) complexes incorporating biologically relevant heteroatom donor ligands. In this regard, syntheses and characterization of manganese(III) complexes with polydentate Schiff base ligands[1–6] have been an ongoing theme. In this communication we report the synthesis of a series of manganese(III) complexes with hexadentate Schiff base ligands possessing N_4O_2 donor sets (Scheme 1): [Mn(sal-N-1,5,8,12)]ClO_4 (**1**), [Mn(5-Cl-sal-N-1,5,8,12)]-ClO_4 (**2**), [Mn(5-Br-sal-N-1,5,8,12)]ClO_4 (**3**), and [Mn(3-methoxy-sal-N-1,5,8,12)]ClO_4·H_2O (**4**). Of these compounds, **1** and **4** have been characterized by X-ray crystallography. A kinetic study of these complexes with hydroxylamine in aqueous solution has been carried out in order to determine the electron-transfer reactivity of these complexes. The mechanistic versatility noted in the reaction behavior of hydroxylamine is attractive in that it can act both as an oxidant or a reductant,[7] and can coordinate through either the N- or the O-end.[8] The estimated bond dissociation energy for the N–H moiety[9] in hydroxylamine (92 kcal·mol^{-1}) is similar to that of the O–H group of tyrosine (85.5 kcal·mol^{-1}),[10,11] and so proton movement – as observed with tyrosine in PSII – may have some relevance to the observed reactions with hydroxylamine.

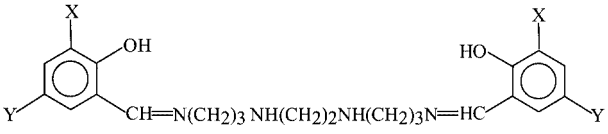

	X	Y	ligand
1	H	H	H_2(sal-N-1,5,8,12) [H_2L^1]
2	H	Cl	H_2(5-Cl-sal-N-1,5,8,12) [H_2L^2]
3	H	Br	H_2(5-Br-sal-N-1,5,8,12) [H_2L^3]
4	OCH_3	H	H_2(3-methoxy-sal-N-1,5,8,12)[H_2L^4]

Scheme 1

Results and Discussion

Crystal Structures of [Mn^{III}sal-N(1,5,8,12)]ClO_4 (1) and [Mn(3-methoxy-sal-N(1,5,8,12)]ClO_4·H_2O (4)

Atom-labeling schemes and molecular views of complex **1** and **4** are shown in Figures 1 and 2, respectively, while selected bond lengths and angles are given in Tables 1 and 2, respectively. In each case the metal is in a hexadentate distorted MnN_4O_2 environment, the two phenolic oxygen

[a] Department of Inorganic Chemistry, Indian Association for the Cultivation of Science,
Kolkata 700 032, India
Fax: (internat.) +91–33/2473 2805
E-mail: icpb@mahendra.iacs.res.in
[b] Department of Chemistry, Howard University,
2400 Sixth Street, NW, Washington, DC 20059, USA
Supporting information for this article is available on the WWW under http://www.eurjic.org or from the author.

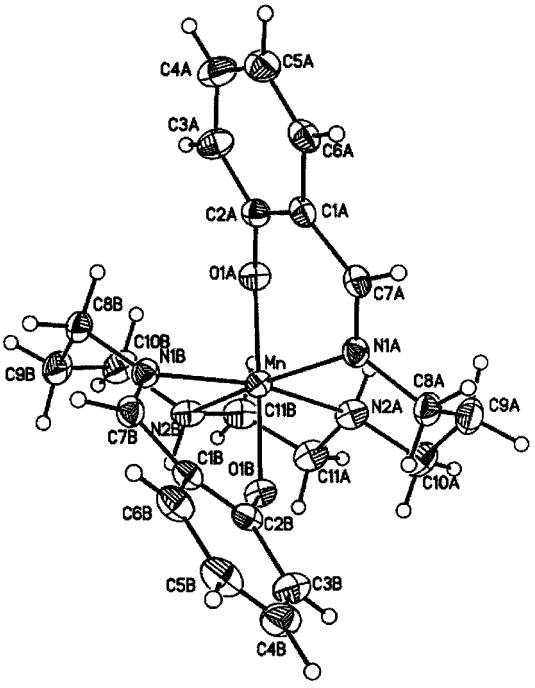

Figure 1. Molecular structure of complex **1** showing atom-labeling scheme

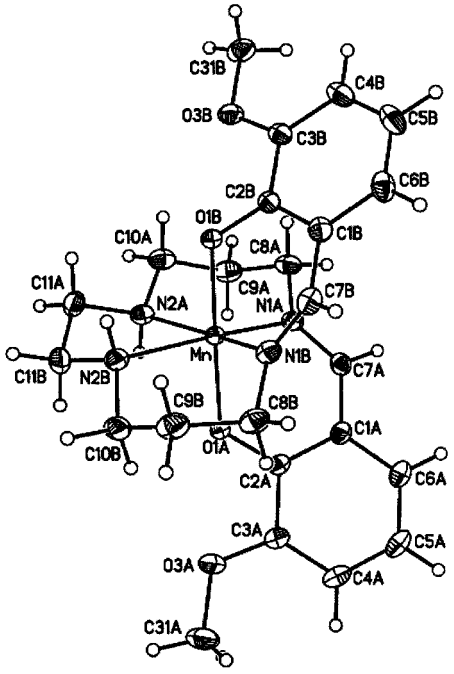

Figure 2. Molecular structure of complex **4** showing atom-labeling scheme

atoms are in a *trans* configuration, and the two coordinating ONN ligand halves are facial. The mean deviations of the manganese atom from the equatorial plane are 0.10 Å in **1** and 0.08 Å in **4**. The bond lengths are quite similar (Tables 1 and 2), the Mn−O(phenolic) lengths being 1.869(4) and 1.878(4) Å in **1** and 1.869(15) and 1.873(15) Å in **4**, the Mn−N(imine) bond lengths being 2.098(4) and 2.102(4) in **1** and 2.054(19) and 2.104(2) Å in **4**, and the Mn−N(amine) lengths being 2.207(4)/2.239(5) and 2.163(2)/2.174(2) Å, respectively. These are consistent with those reported for manganese(III) Schiff base complexes.[1,3−5] Both the lattices are hydrogen bonded, although the hydrogen bonding is less extensive in **1**. The intramolecular hydrogen bonding here involves the N−H moiety and the phenolic oxygen of the ligand and O of the perchlorate anion. The N−H···O(phenolic) distances are 3.199(12) and 3.387(12) Å, whereas N−H···O(perchlorate) is 3.098(18) Å. In **4**, on the other hand, the coordinated water molecule, together with the phenolic oxygen, amine nitrogen (N−H), and perchlorate anion, constitute a network (Figure 3). Both intra- and intermolecular hydrogen bonding are observed, the O(1W)−H···O(phenolic) distances being 2.858(3) and 2.837(7) Å, whereas the O(1W)−H···O(perchlorate) distances are 2.638(10), 3.196(8), and 3.227(7) Å. The amine hydrogen also enters into intramolecular hydrogen bonding with the oxygen of $-OCH_3$ in the aromatic ring, as well as with the H_2O molecule.

Table 1. Selected bond lengths [Å] and angles [°] for complex **1**

Mn−O(1A)	1.869(4)	Mn−O(1B)	1.878(4)
Mn−N(1A)	2.098(4)	Mn−N(1B)	2.102(4)
Mn−N(2B)	2.207(4)	Mn−N(2A)	2.239(5)
O(1A)−Mn−O(1B)	175.50(15)	O(1A)−Mn−N(1A)	87.06(16)
O(1B)−Mn−N(1A)	90.99(17)	O(1A)−Mn−N(1B)	90.41(17)
O(1B)−Mn−N(1B)	86.39(16)	N(1A)−Mn−N(1B)	109.09(17)
O(1A)−Mn−N(2B)	90.37(16)	O(1B)−Mn−N(2B)	92.52(16)
N(1A)−Mn−N(2B)	165.30(17)	N(1B)−Mn−N(2B)	85.38(17)
O(1A)−Mn−N(2A)	95.25(18)	O(1B)−Mn−N(2A)	88.65(18)
N(1A)−Mn−N(2A)	85.77(18)	N(1B)−Mn−N(2A)	164.39(17)
N(2B)−Mn−N(2A)	80.05(18)		

Table 2. Selected bond lengths [Å] and angles [°] for complex **4**

Mn−O(1B)	1.8692(15)	Mn−O(1A)	1.8733(15)
Mn−N(1A)	2.0544(19)	Mn−N(1B)	2.104(2)
Mn−N(2B)	2.163(2)	Mn−N(2A)	2.174(2)
O(1B)−Mn−O(1A)	178.49(7)	O(1B)−Mn−N(1A)	92.42(7)
O(1A)−Mn−N(1A)	86.07(7)	O(1B)−Mn−N(1B)	87.44(8)
O(1A)−Mn−N(1B)	92.98(8)	N(1A)−Mn−N(1B)	104.02(8)
O(1B)−Mn−N(2B)	93.08(7)	O(1A)−Mn−N(2B)	88.40(8)
N(1A)−Mn−N(2B)	169.31(9)	N(1B)−Mn−N(2B)	85.39(9)
O(1B)−Mn−N(2A)	87.56(7)	O(1A)−Mn−N(2A)	92.36(8)
N(1A)−Mn−N(2A)	89.59(8)	N(1B)−Mn−N(2A)	165.69(8)
N(2B)−Mn−N(2A)	81.49(8)		

UV/Visible and IR Spectroscopy

The electronic absorption spectra for all the complexes **1−4** were recorded in acetonitrile, and data are given in Table 3. All the complexes exhibit similar spectral features. There are four important regions in the UV/Vis spectra for this set of complexes. The least intense bands appear in the 630−660 nm range, while another band of higher intensity is observed in the 510−540 nm range. The UV/Vis spectra

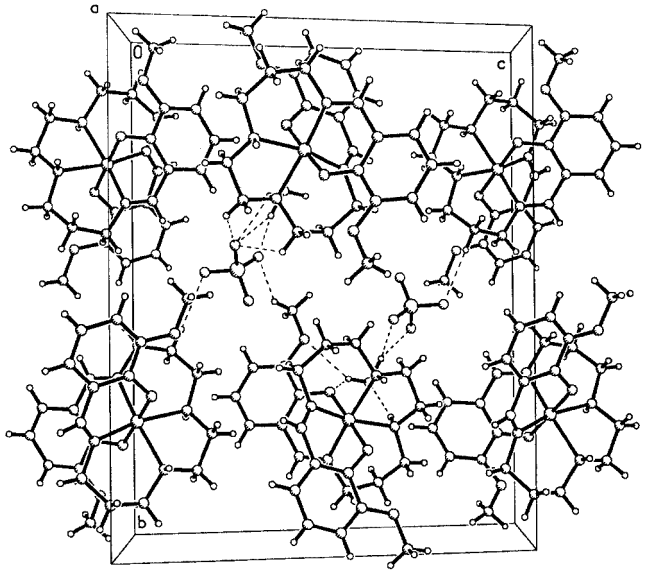

Figure 3. Molecular packing of **4** showing both intra- and intermolecular hydrogen bonding

Table 3. UV/Visible spectroscopic data for the complexes **1**−**4**

Complex	λ_{max}/nm (ε/dm^3 mol^{-1} cm^{-1})
1	640 sh (245), 512 (881), 342 sh (5670), 271 (22390), 226 (36180)
2	653 sh (209), 516 (773), 332 sh (5670), 268 sh (17250), 223 (43580)
3	656 sh (212), 517 (820), 335 sh (6090), 269 sh (17970), 226 (43440)
4	660 sh (403), 534 (1270), 364 sh (5670), 284 (21640), 231 (46260)

of all the complexes show ligand to metal charge-transfer bands in the 330−370 nm region. These bands are similar to those reported for hexacoordinate [Mn^{III}(BBPEN)](PF_6) [H_2BBPEN = *N*,*N*′-bis(2-hydroxybenzyl)-*N*,*N*′-bis(2-methylpyridyl)ethylenediamine] with N_4O_2 donor sets.[12] The intense higher-energy bands in the region 220−280 nm are usually attributed to intraligand π→π* transitions, as observed previously for manganese(III) ions in octahedral environments.[6,12−15] It is interesting to note that all the bands are affected by the benzene ring substitution, which indicates that the frontier molecular orbitals of the high-spin manganese(III) complexes possess significant contribution from the ligands.

In order to provide some insight into the nature of redox and spectroscopically relevant orbitals, extended Hückel MO calculations, using the crystallographic parameters of **1** and **4**, were performed with the aid of the CACAO program (Figure S1 and Figure S2 in the Supplementary Material, see footnote on the first page of this article).[16] The lowest unoccupied molecular orbital (LUMO) of **1** was found to be strongly delocalized, with 61% metal contribution and 29% ligand contribution. The HOMO, on the other hand, is predominantly metal-based (84%), with little contribution from the ligand (6%). The closely spaced (ΔE = 0.036 eV) HOMO-1 also has the same character, but with less contribution from the metal orbitals (72% metal and 17% ligand). In **4**, the LUMO is also strongly delocalized, with a little more contribution from the ligand (58% metal and 33% ligand) relative to **1**. Two closely spaced (ΔE = 0.071 eV) HOMO (83% metal and 7% ligand) and HOMO-1 (64% metal and 30% ligand) orbitals are also delocalized, with a greater contribution from the metal in the former than in the latter.

The EHMO calculations indicate that the frontier molecular orbitals are predominantly metal-based, but with significant contributions from the ligands. The bands in the 630−660 nm range can therefore be assigned as predominantly d-d with some admixed MLCT character. These bands are similar to those reported previously for manganese(III)−Schiff base complexes.[6,12,13,17] The bands in the 510−540 nm range have previously been attributed to phenolato-to-manganese(III) LMCT for similar Mn^{III} complexes.[8,14,15,17] The EHMO calculations, however, indicate that all the frontier MOs are predominantly metal-based with significant contribution from the ligands, so the above assignment is not unambiguous. From the X-ray crystal data, the observed Mn^{III}−O(phenolate) average bond lengths are 1.873 Å for **1** and 1.871 Å for **4**, which is quite short in comparison with the reported values for manganese(III) complexes.[5,14,15,18] The shift of the 510−540 nm bands to much lower energy compared to those (ca. 480−490 nm) reported earlier indicates stronger interaction between the phenolato(O) and manganese(III) center[12] and supports the assignment of the 510−540 nm bands as LMCT from phenolato-to-Mn^{III}.

All the complexes show similar IR spectral features, each exhibiting a strong band attributable to ν(CN) between 1620−1627 cm^{-1}. All of them also show broad unsplit bands at 1081−1095 cm^{-1}, together with bands at 626−627 cm^{-1} indicative of the presence of a noncoordinated perchlorate counterion. As well as these, **4** exhibits a broad band at 3550 cm^{-1} due to the presence of a non-coordinated water molecule in the crystal, which is consistent with the molecular structure.

Electrochemical Studies

Cyclic voltammograms of all the Mn^{III} complexes were recorded in acetonitrile solution with TEAP as supporting electrolyte in the potential range from −1.2 to +1.2 V vs. SCE. The results are summarized in Table 4. As the cyclic voltammetric features of all the complexes are similar, a representative profile for **3** is shown in Figure 4. A notable feature for all the complexes is that an electrochemically quasi-reversible anodic wave and two well defined irreversible cathodic waves are detected. The anodic process corresponds to the Mn^{IV}/Mn^{III} couple, and the peak-to-peak separation lies between 80 mV to 120 mV, slightly above the value expected for a one-electron electrochemically reversible process.[19] The first irreversible cathodic process can be attributed to the Mn^{III}/Mn^{II} couple, in line with previously reported complexes of similar ligand environment.[1,13] The irreversibility of the Mn^{III}/Mn^{II} couple might be due to the

Table 4. Cyclic voltammetric results[a] for manganese(III) complexes at 298 K

Complex[a]	Mn^{IV}/Mn^{III} E_{pa}/V	Mn^{III}/Mn^{II} E_{pc}/V	ΔE_p/V	$(E_{1/2})$/V	E_{pc}/V
1	0.66	0.54	0.12	0.60	−0.60
2	0.78	0.68	0.10	0.67	−0.52
3	0.78	0.70	0.08	0.70	−0.54
4	0.64	0.55	0.09	0.59	−0.58

[a] Solvent: acetonitrile; working electrode: platinum; reference electrode: SCE; E_{pa} and E_{pc} are anodic and cathodic peak potentials respectively; $E_{1/2} = 0.5(E_{pa} + E_{pc})$; $\Delta E_p = E_{pa} - E_{pc}$; scan rate: 50 mV·s^{-1}.

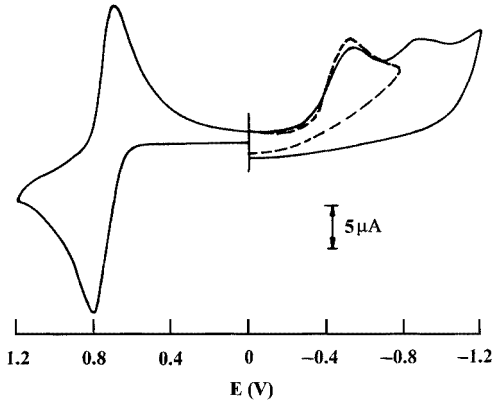

Figure 4. Cyclic voltammogram (scan rate 50 mV·s^{-1}) of complex **3** in acetonitrile at a platinum electrode with ferrocene as internal standard and TEAP as supporting electrolyte

instability of the formally Mn^{II} species.[20] The second cathodic process is very difficult to assign. It has been observed that the cyclic voltammogram of the free ligands features an irreversible reduction at about −1.0 V. The more negative (ca. −0.88 V) cathodic process in the complex is close to that observed for the free ligand. This chemical environment is not suitable to stabilize the Mn(I) state, and Mn^{II}/Mn^{I} couples are not usually observed for this type of complexes.[14] Because of the instability of the formally Mn^{II} species, there might be free ligand (probably protonated) available in the solution, resulting in the second irreversible cathodic wave.[20] The electrochemical results are consistent with those observed previously for manganese(III) complexes.[1,12,21] In the group of complexes at hand, both the E_{pc} and $E_{1/2}$ values are sensitive to substitution, both increasing with increasing electron-withdrawing power of the substituents. The standard extended Hückel MO calculation indicates that the frontier molecular orbitals are predominantly metal-based with significant contribution from the ligands. The ligand contribution both to the HOMO and to the LUMO is reflected in the change in the redox potentials with substitution in the benzene ring.

Electron-Transfer Reactivity

The electron-transfer reactivities of all four complexes were studied in the 5.5−8.0 pH range, with hydroxylamine as the reducing agent. The redox chemistry of hydroxylamine in solution is very complicated, due to its oxidation to various products depending upon the nature of the oxidants. It has been observed that the most common oxidation products of hydroxylamine are N_2O and N_2,[8,22−24] oxidation of hydroxylamine to NO_2^-, NO_3^-, and NO[22−24] being relatively rare.

Stoichiometry

Because of the formation of various products and the complicated redox chemistry involved, variable stoichiometry has usually been encountered for the oxidation of hydroxylamine by various oxidants.[8,22,23] The stoichiometry was therefore examined very carefully in the presence both of excess reductant and of excess oxidant. In the presence of excess hydroxylamine over the complexes, the stoichiometry was determined by bromatometric estimation of the unchanged reductant,[25] whereas in the presence of excess oxidant, the stoichiometry was measured spectrophotometrically with the aid of the known extinction coefficient of the complex (λ_{max} = 517 nm, ε = 820 dm^3 mol^{-1}·cm^{-1} for complex **3**). The results in Table 5 also imply a variable stoichiometry in our system. Thus, under the kinetic reaction conditions, the "putative first step" of the reaction may be given as shown in the following equations.

Table 5. Stoichiometry of the reduction of complex **3** by hydroxylamine hydrochloride (all concentrations are in mmol·dm^{-3}) at 30 °C

[Complex]	pH	$[NH_2OH]$	Δ[complex]/$\Delta[NH_2OH]$
3.00	5.50	30.0	1.05
3.00	5.50	15.0	0.97
20.0	5.50	2.00	1.95
10.0	5.50	2.00	1.75
3.00	8.00	30.0	1.03
3.00	8.00	12.0	1.20
20.0	8.00	2.00	1.98

$$Mn^{III}L + NH_2OH \rightarrow Mn^{II}L + 1/2\ N_2 + H^+ + H_2O \quad (1)$$

and with an excess of Mn^{III}

$$2\ Mn^{III}L + NH_2OH \rightarrow 2\ Mn^{II}L + 1/2\ N_2O + 1/2\ H_2O + 2\ H^+ \quad (2)$$

The appearance of a six-line EPR signal in the g = 2.0 region indicates that at least some complex is in the +2 state in the final form, thus supporting the above mechanism. The electrochemical study shows that the formally $Mn^{II}L$ species formed upon reduction of the parent complexes are unstable and readily decompose. The decomposed species may be hydrated Mn^{2+} ion in aqueous solution, together with free ligand. The formulation of the reduced product as $Mn^{II}L$ is therefore not unambiguous. However, externally added Mn^{2+} ion in the form of

$Mn(ClO_4)_2 \cdot 6H_2O$ was found to exert no effect on the rate of the reactions, indicating that the reduced product of the complexes has no influence on the electron transfer rate.

Kinetics and Mechanism

The kinetics of the oxidation of NH_2OH were observed under pseudo first-order conditions, with the reductant being maintained in large excess over the complex. At a fixed hydrogen ion concentration and ionic strength (pH = 6.0, I = 0.2 mol·dm^{-3} (NaCl), [phosphate] = 0.05 mol·dm^{-3}, temperature = 30 °C and λ = 360 nm), the observed rate constants ($k_{obsd.}$/s^{-1}) [Table 6] follow rate saturation kinetics at higher values of [NH_2OH] for all the complexes **1**−**4**. These observations are consistent with the theoretical rate law in Equation (3).

Table 6. Pseudo-first order rate constants ($k_{obsd.}$/s^{-1}) for the oxidation of NH_2OH by the complexes **1**−**4** at a fixed pH of 6.0 {kinetic conditions: [complex] = 5−6 ×10^{-5} mol·dm^{-3}, I = 0.20 mol·dm^{-3} (NaCl), [buffer] = 0.05 mol·dm^{-3} (phosphate), 30 °C}

10^3 [NH_2OH] [mol·dm^{-3}]	[NaCl][a] [mol·dm^{-3}]	mol % D_2O	10^3 $k_{obsd.}$ [s^{-1}] **1**	**2**	**3**	**4**
0.6		0	2.86	3.88	4.01	1.36
0.6		50	2.85			
0.6		90	2.82			
0.6	0.2		3.22			
0.6	0.4		3.20			
0.6	0.8		3.20			
0.8			3.65	4.19	4.60	1.48
1.0			4.28	4.65	5.00	1.68
3.0			6.63	6.61	7.68	3.25
5.0			7.68	7.99	9.29	3.88
7.0			7.88	8.93	9.57	4.05
10			8.31	9.68	11.1	4.33

[a] I = 1.0 mol·dm^{-3} ($NaNO_3$).

$$k_{obsd.} = (k\,Q\,[NH_2OH])/(1 + Q\,[NH_2OH]) \quad (3)$$

where Q is the association constant between the complex and the reductant prior to the electron-transfer reaction, and the parameters derived by fitting the experimental data to above equation at pH 6.0 are:

(i) k = (9.4±0.1) ×10^{-3} s^{-1} and Q = (791±37) for **1**

(ii) k = (1.03±0.05) ×10^{-2} s^{-1} and Q = (820±130) for **2**

(iii) k = (1.20±0.05) ×10^{-2} s^{-1} and Q = (792±98) for **3**

(iv) k = (5.20±0.1) ×10^{-3} s^{-1} and Q = (527±39.8) for **4**

The effect of pH on the rate of reaction was studied at a constant concentration of NH_2OH (6·10^{-4} mol·dm^{-3}) at which a strict first-order dependence is valid. The observed rate constants decrease with increasing pH (Table 7). Figure 5 shows the plot of k_{ox} vs. [H^+]. The observations are not unprecedented, similar findings having been made in the reaction between this reductant and several mononuclear and polynuclear manganese complexes reported previously,[9,26,27] and have been attributed to the generation of more reactive aquated derivatives of the complexes. The complexes **1**−**4** are octahedral, with all the coordination sites occupied by the four N atoms and the two O atoms of the ligand. An effort was made to examine the electrochemistry of the complex at different pH values in an acetonitrile/water medium, but no variance was seen. There was also no noticeable change in the electronic spectra of the complexes when recorded at different pH values. The conclusion that can be drawn from these observations is that either only one species of the Mn^{III} complexes is present, or that the reactivity of the protonated species is identical to that of the parent species, if one exists, over the pH range studied. The pH variation results are also inconsistent with those expected from the thermodynamic potential values of the reductants. It is well documented that the deprotonated forms of the reductants are more reactive than the protonated species, due to the changed oxidation potential.[28] On protonation, the oxidation potential of the reductant decreases significantly from +3.04 V for NH_2OH to +1.87 V for NH_3OH^+, according to[29]

Table 7. Pseudo-first order rate constants ($k_{obsd.}$/s^{-1}) for the oxidation of NH_2OH by the complexes **1**−**4** at different pH values (kinetic conditions: [NH_2OH] = 6 × 10^{-4} mol·dm^{-3}, [complex] = 5−6 ×10^{-5} mol·dm^{-3}, I = 0.20 mol·dm^{-3} (NaCl), [buffer] = 0.05 mol·dm^{-3} (phosphate), 30 °C)

pH	10^4 $k_{obsd.}$/s^{-1} **1**	**2**	**3**	**4**
5.50	61.3	64.2	69.9	28.8
5.75	41.7	41.1	55.3	19.0
6.00	28.6	40.0	42.7	13.6
6.25	23.5	32.3	31.6	11.2
6.50	19.0	27.9	25.6	9.10
7.00	9.80	14.4	16.7	6.50
7.50	5.50	9.00	4.50	3.00
8.00	3.40	5.00	2.50	1.20

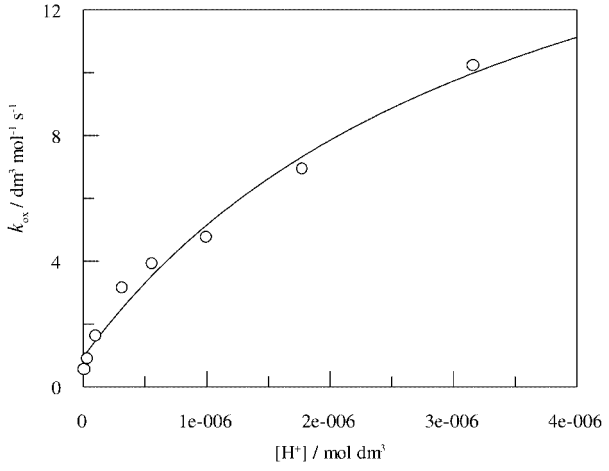

Figure 5. Plot of k_{ox} vs. [H^+] for the oxidation of hydroxylamine by **1** at 30 °C, I = 0.2 mol·dm^{-3} (NaCl), 0.05 mol·dm^{-3} phosphate buffer

$2\,NH_2OH \rightleftarrows N_2 + 2\,H^+ + 2\,H_2O + 2\,e$; E^0 = +3.04 V

$2\,NH_3OH^+ \rightleftarrows N_2 + 4\,H^+ + 2\,H_2O + 2\,e$; E^0 = +1.87 V

It is therefore unlikely that the observed decrease in $k_{obsd.}$ at higher pH values is due to the greater kinetic activity of NH_3OH^+ over NH_2OH. Rate saturation at higher [NH_2OH], however, with high association constant values, and also the leveling off of rates at higher [H^+], are clear indications of some sort of association between the complex and the reductant prior to the electron-transfer act. The self-exchange rate constant of the NH_2OH/NH_2OH^+ couple is very low (5×10^{-13} M^{-1}·s^{-1}), with $E^0 = +0.42$ V.[9,22] In the absence of any accurately determined potential value for the NH_3OH^+/NH_2OH^+ couple the self-exchange rate constant may be taken roughly as that for the NH_2OH/NH_2OH^+ couple.[9] The very low self-exchange rate constant value for the NH_3OH^+/NH_2OH^+ couple and the poor reducing character of the protonated reductant disfavors the outer sphere electron-transfer path. The structure of the complex also discounts the possibility of the formation of a seven-coordinated adduct with the Mn^{III} center, so formation of a hydrogen-bonded adduct (HA) is more reasonable to conceive. The EHMO calculations indicate that the lowest unoccupied molecular orbitals in all the complexes are predominantly metal-based, with significant contribution from the phenoxo ligand. Initial association between the reductant and the complex could involve an interaction with the metal center in addition to hydrogen bonding with the ligand prior to the electron transfer, and would be conducive for an inner sphere mechanism. The following sequence of reactions may be proposed to explain the observed kinetics.

$$NH_2OH + H^+ \overset{K_a}{\rightleftharpoons} NH_3OH^+ \quad (4)$$

$$Mn^{III}L + NH_3OH^+ \overset{Q_1}{\rightleftharpoons} (HA)_1 \xrightarrow{k_1} Mn^{II}L + NH_2O^{\cdot} + 2\,H^+ \quad (5)$$

$$Mn^{III}L + NH_2OH \overset{Q_2}{\rightleftharpoons} (HA)_2 \xrightarrow{k_2} Mn^{II}L + NH_2O^{\cdot} + H^+ \quad (6)$$

The termination of the free radicals for the consumption of a 1:1 ratio was reported to occur as in Equation (7).

$$2\,NH_2O^{\cdot} \xrightarrow{\text{fast}} N_2 + 2\,H_2O \quad (7)$$

The rate law derived from the above sequence of reactions can be given as:

$$k_{ox} = (k'_1\cdot[H^+] + k'_2\cdot K_a)/(K_a + [H^+]) \quad (8)$$

where $k_{ox} = k_{obsd.}/[NH_2OH]$, $k'_1 = k_1Q_1$, and $k'_2 = k_2Q_2$.

The derived kinetic parameters for all the complexes are: $k'_1 = 20.32\pm4.5$ dm^3·mol^{-1}·s^{-1}, $k'_2 = 0.95\pm0.29$ dm^3·mol^{-1}·s^{-1} and $K_a = (3.61\pm0.80) \times10^{-6}$ for **1**; $k'_1 = 13.0\pm1.5$ dm^3·mol^{-1}·s^{-1}, $k'_2 = 1.16\pm0.42$ dm^3·mol^{-1}·s^{-1}, and $K_a = (1.03\pm0.42) \times10^{-6}$ for **2**; $k'_1 = 15.29\pm1.5$ dm^3·mol^{-1}·s^{-1}, $k'_2 = 0.76\pm0.39$ dm^3·mol^{-1}·s^{-1}, and $K_a = (1.18\pm0.45) \times10^{-6}$ for **3**; $k'_1 = 10.00\pm3.4$ dm^3·mol^{-1}·s^{-1}, $k'_2 = 0.56\pm0.18$ dm^3·mol^{-1}·s^{-1}, and $K_a = (4.14\pm0.9) \times10^{-6}$ for **4**.

The pK_a values obtained from kinetic experiments are in good agreement with that reported for NH_2OH (pK_a = 6.0).[30] The composite parameters obtained from the above rate equation are indicative of the similar kinetic reactivity of all the complexes towards a particular species of the reductant. This is also reflected in the potential values of the complexes, which fall in a narrow range. The hydrogen-bonding association between the complex and the reductant species probably occurs through the phenoxo-O of the Schiff base and the hydrogen atom of the reductant. The low association constant ($Q = 5.27 \times 10^2$) encountered in complex **4** is probably a reflection of hindered hydrogen bonding involving the phenoxo-O and the reductant species.

Effect of Chloride Ions

Salem[27] observed that rate of the reaction between hydroxylamine and Mn^{III}-salen complex decreases considerably with increasing chloride ion concentration. It has been claimed that this is due to the lowering of redox potential as well as to the common ion effect, both of which shift the equilibrium according to Equation (9) to the left-hand side.

$$NH_3OH^+Cl^- \rightleftarrows NH_3OH^+ + Cl^- \quad (9)$$

To examine any influence of chloride ions in our systems, we varied its concentration at a fixed ionic strength but no [Cl^-] effect was observed (Table 6). We also carried out some kinetic experiments with hydroxylamine nitrate in place of hydroxylamine hydrochloride; the rate constant values were found to be unaffected. The lowering of redox potential is quite understandable for Mn^{III}-salen complex, since the Cl^- ion can occupy the axial position of Mn^{III} and produce an effect on redox potential, but this is impossible in the hexacoordinate complexes under study.

Solvent Isotope Effect

The rate saturation kinetics and pH dependence on the rate of the reaction indicate the formation of hydrogen-bonded precursor complexes between the Mn^{III} complexes and the reductant prior to the electron-transfer process. These facts prompted us to examine whether the electron-transfer path is coupled with proton movement, as in the case of tyrosine in PS II. We measured the rate constants in aqueous medium partially substituted with D_2O at a fixed concentration of NH_2OH and pH {[NH_2OH] = $6\cdot10^{-4}$ mol·dm^{-3}, pH = 6.0, [buffer] = 0.05 mol·dm^{-3} (phosphate), I = 0.2 mol·dm^{-3} (NaCl) and temp. 25 °C}. The observed rate constants in pure water are almost the same as those in a 90% D_2O/water mixture (Table 6), which rules out proton-coupled electron-transfer paths in this study.

Conclusions

The synthesis and characterization of four new manganese(III) complexes with hexadentate Schiff base ligands

with N_4O_2 donor sets − derived from *N*,*N*′-bis(3-aminopropyl)ethylenediamine and salicylaldehyde, or salicylaldehyde derivatives − are reported. Two of them have been characterized by X-ray crystallography, which shows two phenolic oxygen atoms in *trans* configurations and the two coordinating ONN ligand halves facial. Both the lattices are stabilized through extended hydrogen bonding. The ligand contribution both to the HOMO and to the LUMO is reflected in the change in the redox potentials as well as the shifting of UV/Vis spectra with substitution in benzene ring. The electron-transfer reactivities of all the complexes towards hydroxylamine in the 5.5−8.0 pH range are almost identical, as reflected in the evaluated kinetic parameters. It is also notable that the hydrogen-bonding association between the manganese(III) complexes and the reductant species probably occurs through the phenoxo-O of the Schiff base and the hydrogen atom of hydroxylamine. Chloride ion has no effect on the electron-transfer act, which contrasts with Salem's observations[27] for an almost identical reaction with hydroxylamine. Since the estimated bond dissociation energy for the N−H of hydroxylamine is similar to that of the O−H in tyrosine, an attempt was made to examine the possibility of proton movement during the electron-transfer act. The results of solvent isotope effect studies with variable mixtures of D_2O and water do not indicate any proton-coupled electron-transfer path.

Experimental Section

Materials: Hydroxylamine hydrochloride, *N*,*N*′-bis(3-aminopropyl)ethylenediamine, salicylaldehyde, 5-bromosalicylaldehyde, 5-chlorosalicylaldehyde, and *o*-methoxysalicylaldehyde were of analytical reagent grade (Aldrich) and were used without further purification. All other chemicals − manganese perchlorate hexahydrate, NaCl, NaH_2PO_4, acetonitrile, methanol, sodium hydroxide, and hydrochloric acid − were of reagent grade. Solvent isotope effects were examined with deuterium oxide, 99 atom% D (Aldrich).

Syntheses: All the complexes reported here were synthesized by air oxidation of solutions made up from $Mn(ClO_4)_2{\cdot}6H_2O$ and the Schiff base, by the same general procedure. A typical preparation is outlined below. (***Caution!*** Although no problems have been encountered in this work, perchlorates are potentially explosive and should be handled with care and only in small quantities).

[Mn(sal-N-1,5,8,12)]ClO_4 (1): *N*,*N*′-Bis(3-aminopropyl)ethylenediamine (1.74 g, 0.01 mol) was added to an ethanol (30 cm^3) solution of salicylaldehyde (2.44 g, 0.02 mol). The yellowish orange solution was brought to reflux for 1 h and then allowed to cool to room temperature, which was followed by the dropwise addition of $Mn(ClO_4)_2{\cdot}6H_2O$ (3.61 g, 0.01 mol) dissolved in ethanol (20 cm^3). The resulting dark brown solution was heated at reflux for 30 min. On subsequent cooling to room temperature, a microcrystalline compound separated out and was collected by filtration, washed with cold ethanol and diethyl ether, and dried under vacuum. Yield: 4.54 g, 85%. $C_{22}H_{28}ClMnN_4O_6$ (534.9): calcd. C 49.35, H 5.23, N 10.46; found C 49.21, H 5.26, N 10.28%. FTIR (KBr, cm^{-1}): ν(C=N) 1625, ν(C−O) 1280, ν(ClO_4^-) 1095 and 627. μ_{eff} 4.91 BM.

[Mn(5-Cl-sal-N-1,5,8,12)]ClO_4 (2): Yield: 4.94 g, 82%. $C_{22}H_{26}Cl_3MnN_4O_6$ (603.8): calcd. C 43.74, H 4.31, N 9.28; found C 43.63, H 4.49, N 9.19%. FTIR (KBr, cm^{-1}): ν(C=N) 1624, ν(C−O) 1281, ν(ClO_4^-) 1088 and 626. μ_{eff} 4.89 BM.

[Mn(5-Br-sal-N-1,5,8,12)]ClO_4(3): Yield: 5.54 g, 80%. $C_{22}H_{26}Br_2ClMnN_4O_6$ (692.7): calcd. C 38.13, H 3.75, N 8.09; found C 38.23, H 3.76, N 7.89%. FTIR (KBr, cm^{-1}): ν(C=N) 1627, ν(C−O) 1283, ν(ClO_4^-) 1088 and 627. μ_{eff} 4.94 BM.

[Mn(3-methoxy-sal-N-1,5,8,12)]$ClO_4{\cdot}H_2O$(4): Yield: 5.08 g, 83%. $C_{24}H_{34}ClMnN_4O_9$ (612.9): calcd. C 47.02, H 5.55, N 9.14; found C 47.13, H 5.49, N 9.01%. FTIR (KBr, cm^{-1}): ν(C=N) 1621, ν(C−O) 1281, ν(ClO_4^-) 1082 and 627, ν(O−H) 3550. μ_{eff} 4.92 BM.

Physical Measurements: Microanalysis (CHN) was performed in a Perkin−Elmer 240C elemental analyzer. Magnetic susceptibility measurement was carried out on a PAR 155 vibrating sample magnetometer. The EPR spectra were obtained on a Varian model 109 E-line X-band spectrometer equipped with a low-temperature quartz Dewar for measurements at 77 K. pH measurements were made with a Systronics digital pH meter (model 335, India). The observed pH was corrected by using the relationship, $pH = -\log[H^+] = pH_{obsd.} \pm 0.02$. IR spectra were obtained on a Nicolet, MAGNA-IR 750 spectrometer with samples prepared as KBr pellets. Cyclic voltammetry (scan rate of 0.05 $V{\cdot}s^{-1}$) was performed at a platinum electrode with an EG&G PARC electrochemical analysis system (model 250/5/0) in acetonitrile under dry nitrogen atmosphere in conventional three-electrode configurations.

Kinetic Measurements: Spectral and kinetic measurements were performed in an UV/Vis spectrophotometer (UV-2100, Shimadzu, Japan) with thermostatted cell compartments. The disappearance of the complex peak was monitored at 360 nm as a function of time. All the measurements were made under pseudo first-order conditions with use of an excess of hydroxylamine and a constant ionic strength of 0.2 $mol{\cdot}dm^{-3}$ (NaCl) with 0.05 $mol{\cdot}dm^{-3}$ phosphate buffer at 30 °C. The corresponding rate constants were evaluated by means of a suitable nonlinear curve fit program with data taken for at least three half-lives of the reactions. Every rate constant reported here represents the mean value of at least three determinations that fall within ±5%.

Crystal Structure Determination and Structural Refinements of Complexes 1 and 4: Single crystals of **1** were grown from acetonitrile/ethanol solution, and single crystals of **4** were obtained from acetonitrile/methanol solution. Each crystal was then mounted on an automatic Bruker P4 diffractometer equipped with graphite monochromated Mo-K_α radiation (λ = 0.71073 Å). Unit cell dimensions and intensity data were measured at 296 K. The structure was solved by direct methods and refined by full-matrix, least-squares based on F^2 with anisotropic thermal parameters for non-hydrogen atoms by use of Bruker SHELXTL (data reduction), SHELXS[31] (structure solution), and SHELXL[32] (structure refinement). The hydrogen atoms were included in structure factor calculations in their idealized positions. Information concerning crystallographic data collection and refinement of the structures is compiled in Table 8.

CCDC-191275 and -191276 contain the supplementary crystallographic data for this paper. These data can be obtained free of charge at www.ccdc.cam.ac.uk/conts/retrieving.html [or from the Cambridge Crystallographic Data Centre, 12, Union Road, Cambridge CB2 1EZ, UK; Fax: (internat.) +44−1223/336-033; E-mail: deposit@ccdc.cam.ac.uk].

Table 8. Crystal data and structure refinement for complexes **1** and **4**

Complex	**1**	**4**
Empirical formula	$C_{22}H_{28}ClMnN_4O_6$	$C_{24}H_{34}ClMnN_4O_9$
Molecular mass	534.87	612.94
Crystal system	orthorhombic	monoclinic
Space group	$P2_12_12_1$	$P2_1/c$
a [Å]	7.800(3)	8.056(6)
b [Å]	17.359(8)	20.501(10)
c [Å]	17.891(6)	16.737(9)
β [°]	90.00	101.831(6)
V [Å^3]	2422.5(17)	2705.5(3)
Z	4	4
T [K]	296(2)	296(2)
μ(Mo-K_α) [mm^{-1}]	0.700	0.646
Reflections collected	3957	6871
Independent reflections (R_{int})	3755 (0.0565)	6222(0.013)
Final R_1 wR_2 [$I > 2\sigma(I)$]	0.051 0.121	0.046 0.116

Acknowledgments

A. P. and S. G. gratefully acknowledge financial support from the Council of Scientific and Industrial Research (New Delhi) in the form of research fellowships. P. B. also acknowledges the Council for a research project.

[1] A. Panja, N. Shaikh, R. J. Butcher, P. Banerjee, *Inorg. Chim. Acta*, accepted for publication.
[2] S. K. Chandra, P. Chakraborty, A. Chakravorty, *J. Chem. Soc., Dalton Trans.* **1993**, 863−869.
[3] M. Maneiro, M. R. Bermejo, A. Sousa, M. Fondo, A. M. González, A. Sousa-Pedrares, C. A. McAuliffe, *Polyhedron* **2000**, *19*, 47−54.
[4] C. K. Kipke, M. J. Scott, J. W. Gohdes, W. H. Armstrong, *Inorg. Chem.* **1990**, *29*, 2193−2194.
[5] H. Miyasaka, R. Clerac, T. Ishii, H-C. Chang, Susumu Kitagawa, M. Yamashita, *J. Chem. Soc., Dalton Trans.* **2002**, 1528−1534.
[6] W. M. Coleman, R. K. Boggess, J. W. Hughes, L. T. Taylor, *Inorg. Chem.* **1981**, *20*, 1253−1258.
[7] K. Wieghardt, *Adv. Inorg. Bioinorg. Mech.* **1984**, *3*, 213.
[8] R. A. Scott, G. P. Haight, Jr., J. N. Cooper, *J. Am. Chem. Soc.* **1974**, *96*, 4136−4142.
[9] S. Banerjee, U. R. Choudhury, R. Banerjee, S. Mukhopadhyay, *J. Chem. Soc., Dalton. Trans.* **2002**, 2047−2052.
[10] M. T. Caudle, V. L. Pecoraro, *J. Am. Chem. Soc.* **1997**, *119*, 3415−3416.
[11] M. R. A. Blomberg, P. E. M. Siegbahn, S. Styring, G. T. Babcock, B. Akermark, P. Korall, *J. Am. Chem. Soc.* **1997**, *119*, 8285−8292.
[12] A. Neves, S. M. D. Erthal, I. Vencato, A. S. Ceccato, Y. P. Mascarenhas, O. R. Nascimento, M. Hörner, A. A. Batista, *Inorg. Chem.* **1992**, *31*, 4749−4755.
[13] K. Ramesh, D. Bhuniya, R. Mukherjee, *J. Chem. Soc., Dalton Trans.* **1991**, 2917−2920.
[14] K. Bertoncello, G. D. Fallon, K. Murray, *Inorg. Chim. Acta* **1990**, *174*, 57−60.
[15] X. Li, V. L. Pecoraro, *Inorg. Chem.* **1989**, *28*, 3403−3410.
[16] C. Mealli, D. M. Proserpio, *J. Chem. Educ.* **1990**, *67*, 399.
[17] U. Auerbach, U. Eckert, K. Weighardt, B. Nuber, J. Weiss, *Inorg. Chem.* **1990**, *29*, 938−944.
[18] A. R. Oki, D. J. Hodgson, *Inorg. Chim. Acta* **1990**, *170*, 65−73.
[19] D. H. Evans, K. M. O'Connel, R. A. Petersen, M. J. Kelly, *J. Chem. Educ.* **1983**, *60*, 290−293.
[20] M. Hoogenraad, K. Ramkisoensing, S. Gorter, W. L. Driessen, E. Bouwman, J. G. Hassnoot, J. Reedijk, T. Mahabiersing, F. Hartl, *Eur. J. Inorg. Chem.* **2002**, 377−387.
[21] S. A. Richert, P. K. S. Tsang, D. T. Sawyer, *Inorg. Chem.* **1989**, *28*, 2471−2475.
[22] M.-L. Hung, M. L. McKee, D. M. Stanbury, *Inorg. Chem.* **1994**, *33*, 5108−5112.
[23] R. M. Liu, M. R. McDonald, D. W. Margerum, *Inorg. Chem.* **1995**, *34*, 6093−6099.
[24] G. Rabai, M. T. Beck, *J. Chem. Soc., Dalton. Trans.* **1982**, 573−576.
[25] A. I. Vogel, *A Textbook of Quantitative Inorganic Analysis*, Longmans, London, **1978**, p. 394.
[26] N. Shaikh, M. Ali, P. Banerjee, *Inorg. Chim. Acta* **2002**, *339*, 341−347.
[27] I. A. Salem, *Transition Met. Chem.* **1995**, *20*, 312−315.
[28] A. Chakravorty, *Comments, Inorg. Chem.* **1985**, *4*, 1−16.
[29] J. D. Lee, *Concise Inorganic Chemistry*, 5th ed., Blackwell Science Ltd., Oxford, **1999**, p. 490.
[30] G. Bengtson, *Acta Chem. Scand., Ser. A* **1983**, *37*, 639−645.
[31] G. M. Sheldrick, SHELXS 97, *Acta Crystallogr., Sect. A* **1990**, *46*, 467.
[32] G. M. Sheldrick, SHELXL 97, *Program for Crystal Structure Refinement*, University of Göttingen, **1997**.

Received November 5, 2002
[I02605]

Synthesis, Crystallographic and Spectroscopic Studies of Dimeric Cu^{I} Complexes with Schiff-Base-Containing Triazole Ligands

Krzysztof Drabent,*[a] Zbigniew Ciunik,[a] and Piotr J. Chmielewski[a]

Keywords: Copper / Schiff bases / N ligands / Dimers / Self-assembly

New Cu^{I} complexes of the Schiff-base-containing triazole ligands *N*-[(*E*)-(4-chlorophenyl)methylidene]-4*H*-1,2,4-triazol-4-amine (ClPhtrz) and *N*-[(*E*)-phenylmethylidene]-4*H*-1,2,4-triazol-4-amine (Phtrz) have been synthesised and characterised. Depending on the reaction conditions ClPhtrz forms two different dimeric complexes **1** and **2**. X-ray crystallography revealed that each copper centre exhibits a planar trigonal coordination in **1**, while the tetrahedral coordination sphere of the copper centre in **2** is completed by a solvent molecule. In dimeric complex **3** the tetrahedral coordination of the Cu^{I} ions is formed by two monodentate and two bidentate (bridging) Phtrz ligands. Complexes **1**–**3** are unstable and easily lose coordinating and/or solvating acetonitrile molecules giving **4** (from **1** and **2**) and **5** (from **3**). On the basis of ESI MS and ^{1}H NMR and UV/Vis spectroscopy, it was shown that dimeric complexes **1**–**5** do not survive upon dissolution and dissociate rapidly forming mainly a 1:2 monomeric complex, along with a minor 1:1 complex.
(© Wiley-VCH Verlag GmbH & Co. KGaA, 69451 Weinheim, Germany, 2003)

Introduction

Binuclear and multinuclear transition metal complexes containing two or more metal centres bridged by multidentate ligands have been the subject of great interest in coordination chemistry.[1] Particular interest has been focused on five-membered aromatic nitrogen heterocycles (azoles) as ligands because of their ability to form complexes in which two metal centres are bridged by one, two or three azole groups.[1,2] The most studied bridging ligand of this type is the pyrazolate anion.[3,4] Recently, copper(I) complexes containing pyrazolate ligands have been extensively studied due to their ability to act as selective catalysts in the oxidation of organic substrates such as aliphatic and aromatic amines.[5,6] Different pyrazoles modified by introducing substituents on the heterocyclic ring have been involved in these studies.[5–7] Depending on the ring substituent copper(I) forms a large series of derivatives: neutral 1-D polymers $[Cu(pz)]_{\infty}$ for unsubstituted pyrazole,[8] cyclic trimers $[Cu(pz')]_3$ [pz′ = 3,5-dimethyl-4-nitropyrazole (Hdmnpz),[6] 3,5-dimethylpyrazole (Hdmpz),[9] 3,5-diphenylpyrazole (Hdppz),[10] 3,4,5-trimethylpyrazole (tmpzH)[11]] and cyclic neutral $[Cu(dppz)]_4$ [5] and anionic tetramers $[Cu_4(dmnpz)_6]^{-2}$.[6] However, the most frequently observed structure is a dimer $[Cu_2(pz'')_2X_n]$ [where pz″ = dmpz, dcmpz, dppz, dmnpz (Hdcmpz = 3,5-dicarbomethoxy pyrazole); X = isocyanide, pyridine, PPh_3].[5–8,12] The common feature of all these compounds is that pyrazole ligands are always connected to two adjacent copper(I) ions in an N^1,N^2-bridging mode.

Similar coordination properties could be expected for N^4-substituted 1,2,4-triazole as a ligand. In fact, a number of coordination compounds with this group of ligands coordinated to transition metal ions have been reported.[2] However, to the best of our knowledge, Cu^{I} complexes of N^4-substituted 1,2,4-triazoles are unknown. A limited number of structurally characterised systems based on copper(I) and deprotonated 1,2,4-triazolates have been reported.[13,14] In these systems the nitrogen atoms of the triazolate anion are coordinated to three different Cu^{I} ions, forming polynuclear species; copper(I) complexes with a 1,2,4-triazole moiety as a part of an organic ligand have also been reported.[15–18]

In this work we describe the synthesis of dimeric copper(I) complexes with Schiff-base-containing triazole ligands (Scheme 1). The complexes were characterised by X-ray crystallography. The results are compared with those reported for pyrazole-bridged Cu^{I} dimers. We also report the results of our study on the behaviour of these systems upon dissolution in acetonitrile.

Results and Discussion

Depending on the experimental conditions two products were obtained from the reaction between $[Cu(CH_3CN)_4](ClO_4)$ and *N*-[(*E*)-(4-chlorophenyl)methylidene]-4*H*-1,2,4-triazol-4-amine (ClPhtrz) in acetonitrile. Colourless, needle-shaped crystals of $[Cu_2(ClPhtrz)_4](ClO_4)_2\cdot 2CH_3CN$ (**1**) were grown overnight from a concentrated solution. When the crystallisation was carried on from a very dilute solution light-yellow, prismatic crystals of $[Cu_2(ClPhtrz)_4$-

[a] Faculty of Chemistry, University of Wrocław,
F. Joliot-Curie 14, 50-383 Wrocław, Poland
Fax: (internat.) + 48-71/328-2348
E-mail: drab@wchuwr.chem.uni.wroc.pl

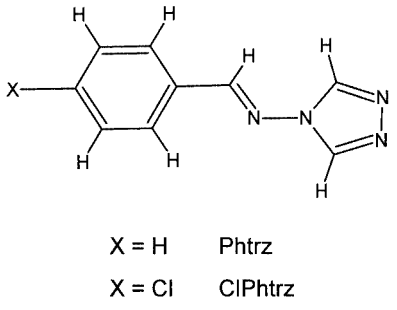

Scheme 1

$(CH_3CN)_2](ClO_4)_2 \cdot CH_3CN$ (**2**) were formed after a much longer time (about 1 month).

The main difference between dimers **1** and **2** is the coordination mode around each copper atom: in **1** the metal ion is coordinated by three triazole ligands whereas in **2** additional coordination of an acetonitrile molecule gives a tetrahedral environment for the copper(I) ion.

The procedure described above is valid for a 1:2 metal-to-ligand ratio or with an excess of ligand in solution. When an excess of metal ion is used only **2** is formed. In the case of $[Cu_2(Phtrz)_6](ClO_4)_2 \cdot 2CH_3CN$ (**3**) the complex is formed in any metal-to-ligand molar ratio. When crystals of **1**−**3** are removed from acetonitrile solution they rapidly lose acetonitrile molecules (within a few minutes; see Exp. Sect.). In this way crystals of **1** and **2** give $[Cu_2(ClPhtrz)_4](ClO_4)_2$ (**4**), whereas **3** gives $[Cu_2(Phtrz)_6](ClO_4)_2$ (**5**). Crystals of **1**−**3** were characterised crystallographically, while complexes **4** and **5** were studied by spectroscopic methods (UV, ^1H NMR, ESI-MS).

Structural Studies

X-ray Structure of 1

The molecular structure of **1** is shown in Figure 1. It consists of a discrete binuclear copper(I) centre bridged by two N^1,N^2-coordinated ClPhtrz ligands. Surprisingly, an additional triazole ligand is bound to the Cu^I ion in a monodentate fashion. This unprecedented coordination mode results in almost *planar* tricoordinate, trigonal coordination environment with a small deviation [0.073(2) Å] of the metal centre from the plane defined by the N11, N12A and N21 atoms. The non-bonding Cu···Cu distance is equal to 3.508(1) Å. A slight deviation from planarity toward a chair-like configuration is observed due to the asymmetric triazole ligands forming a six-membered Cu-$[N\text{-}N]_2$-Cu ring. The copper atoms are located only 0.202(6) Å off the mean plane defined by four triazole nitrogens, well below the value reported for the Cu^I-pyrazole system (0.62 Å).[5] Furthermore, the Cu-N-N-Cu dihedral angle of 13.8(4)° is considerably smaller than that observed (41.7°) for the pyrazole-containing complex $[Cu(dppz)(RNC)]_2$ with the same conformation.[5] In the latter compound it has been suggested that the large value of the dihedral angle is due to the presence of steric interactions between the phenyl groups in the 3,5-positions of the ligand and the cyclohexyl isocyanide groups attached to the copper ions.

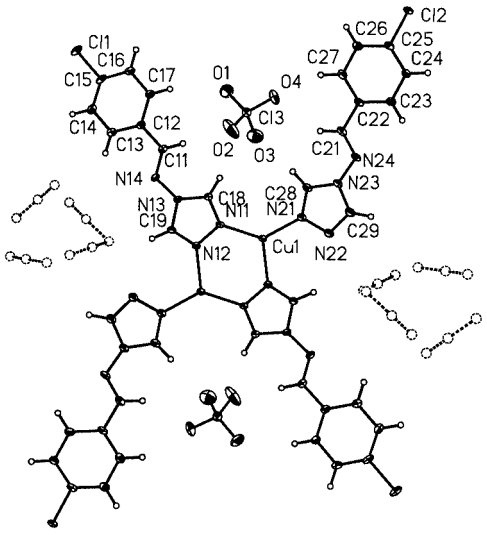

Figure 1. Molecular structure of the dimeric compound **1**; selected bond lengths [Å] and angles [°]: Cu1···Cu1a 3.508(1), Cu1−N11 1.948(3), Cu1−N21 1.937(3), Cu1−N12a 2.012(3); N21−Cu1−N11 131.57(13), N21−Cu1−N12 113.12(13), N11−Cu1−N12 114.89(12), Cu1−N11−N12−Cu1 13.8(4)

Because all the ClPhtrz ligands are coordinated in an almost planar *E* configuration the resulting binuclear unit can be described as an X-shaped dimer. These X-shaped dimers strongly influence the packing of the discrete units in the crystal (Figure 2). The dimers form sheets with an average distance of 3.04 Å between the planes. The chlorine atoms of the ligands (see Scheme 1) are located above and below each copper(I) ion [Cu···Cl = 3.129(1) and 3.242(1) Å, respectively; Cl···Cu···Cl = 158.44(3)°] and are believed to stabilise the packing. As a result rhomboidal channels, defined by the separation of the centre of Cu-$[N\text{-}N]_2$-Cu fragments, are observed parallel to the crystallographic [100] direction with a cross-section of about 15 × 15 Å. The ClO_4^- anions and solvent (acetonitrile) molecules are positioned in these channels (see Figure 2). Location of the non-coordinating solvent molecules in the channels makes them potentially labile and easy to remove from the crystals. The free-pore volume of the unit cell was estimated to be 696 $Å^3$ (25.2% of the total) with the PLATON[19] program (squeeze).

A trigonal environment of Cu^I such as that observed in **1** is rare for dinuclear compounds, but not unknown, and has been reported previously for complexes with pyrazole bridges.[5−7,12,20] However, in all those systems at least one other ligand coordinates to the copper ion. Three-coordinate copper(I) has also been detected in polymeric systems with different ligands.[14,21,22] The dimers derived from tris(pyrazolyl)borate[23] and tris(imidazole)methoxymethane[24] are rare examples of tricoordinate Cu^I complexes without bridges between the metals.

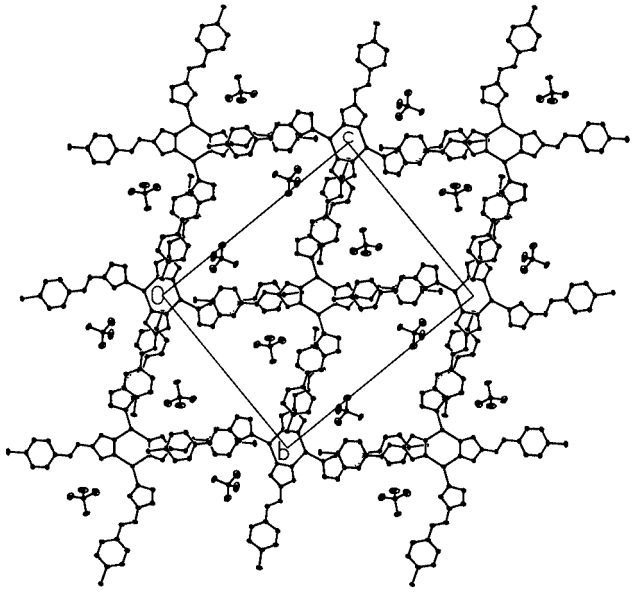

Figure 2. View of **1** along the crystallographic axis *a* illustrating the channels; the disordered acetonitrile molecules have been omitted for clarity

X-ray Structure of 2

When a dilute solution of $[Cu(CH_3CN)_4](ClO_4)$ and ClPhtrz ligand in acetonitrile was allowed to stand for a long time (about one month) light-yellow crystals of **2** were formed. The molecular structure of **2** is shown in Figure 3. The crystals of **2** contain discrete dimeric complexes of Cu^I bridged by two ClPhtrz ligands. Another triazole ligand is bonded in a monodentate fashion to each copper atom, as was observed for **1**. A molecule of acetonitrile completes the distorted tetrahedral coordination geometry. The increased steric crowding around the metal atoms considerably disturbs the planarity of the six-membered cycle defined by two copper and the four nitrogen atoms of bridging ligands. The observed chair-like conformation in **2** is more pronounced than in **1** and the Cu-N-N-Cu torsion angle is 34.2(3)°. The copper atoms are located 0.516(5) Å out of the plane defined by the four nitrogens of the bridging triazole ligands. Each metal ion is moved towards the coordinated acetonitrile molecules. The observed Cu−N distances [1.990(3) to 2.083(3) Å] lie well within the range for tetracoordinate copper(I) complexes[6,25] and are about 0.1 Å longer than the Cu−N bond lengths observed in **1** and other tricoordinate Cu^I structures.[5−8,12] The nonbonding Cu···Cu distance increases from 3.508(1) Å in **1** to 3.685(1) Å in **2**. The same tendency was reported previously for tri- and tetracoordinate pyrazole-containing dimers of Cu^I.[6]

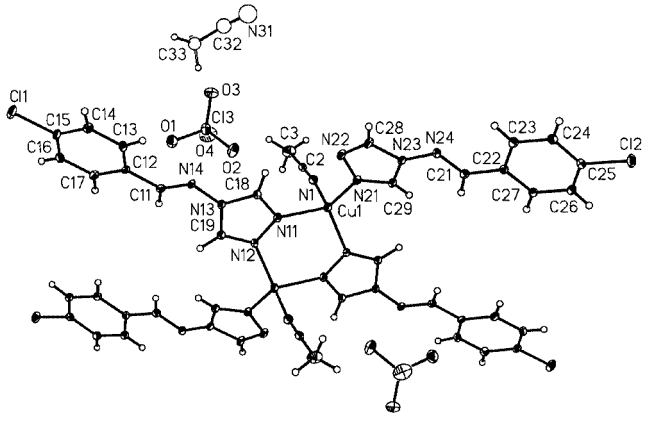

Figure 3. Molecular structure of the dimeric compound **2**; selected bond lengths [Å] and angles [°]: Cu1···Cu1a 3.685(1), Cu1−N11 2.082(3), Cu1−N21 1.991(3), Cu1−N12a 2.028(3), Cu1−N1 2.013(3); N21−Cu1−N1 116.02(11), N21−Cu1−N12 120.68(10), N1−Cu1−N12 102.33(10), N21−Cu1−N11 106.58(10), N1−Cu1−N11 100.12(10), N12−Cu1−N11 109.16(10), Cu1−N11−N12−Cu1 34.2(3)

X-ray Structure of 3

Another tetracoordinate complex **3** was obtained when the 4-chlorophenyl group in the triazole ligand was replaced by a phenyl substituent. A view of the molecule is shown in Figure 4. Compound **3** is a dinuclear Cu^I complex containing two bridging triazole groups as in the case of **1** and **2**. Surprisingly two additional triazole ligands are coordinated to each copper(I) ion in a monodentate fashion to give a coordination number of four, with all four coordination sites being occupied by triazole ligands. The more-regular tetrahedral surrounding of the Cu^I centres causes a less-pronounced chair-like configuration of the Cu-$[N\text{-}N]_2$-Cu ring and, in fact, the copper atoms are located only 0.152(3) Å out of the plane defined by the bridging triazole nitrogens. It is worth noting that this value matches well

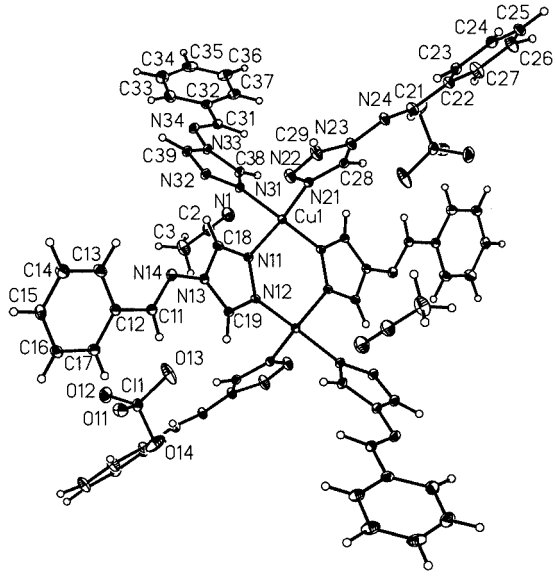

Figure 4. Molecular structure of the dimeric compound **3**; selected bond lengths [Å] and angles [°]: Cu1···Cu1a 3.6606(5), Cu1−N11 2.0737(15), Cu1−N21 2.0376(16), Cu1−N31 2.0220(16), Cu1−N12 1.9923(15); N12−Cu1−N31 119.72(6), N12−Cu1−N21 113.46(6), N31−Cu1−N21 107.02(6), N12−Cu1−N11 112.01(6), N31−Cu1−N11 102.58(6), N21−Cu1−N11 99.71(6), Cu1−N11−N12−Cu1 −10.3(2)

with the value observed in the tricoordinate compound **1**, although the Cu−N bond lengths [1.992(2) to 2.074(2) Å] and the nonbonding Cu···Cu distance [3.6606(5) Å] are closer to those observed in **2**.

Solution Studies

Mass Spectrometry

Formation of monomeric 1:2 and 1:1 complexes from the dimer has been observed by ESI mass spectrometry upon dissolution of original samples of **1**, **2** or **4**. Peaks at *m*/*z* (%) = 475.3 (100), 309.9 (70), 206.6 (10) and 144.5 (10) are observed in the ESI mass spectra independently of the sample used (see above). The isotopic peaks are separated by 1.0 amu, revealing a charge state of +1 for the corresponding ions. Therefore, the peaks at 475.3 and 309.9 correspond to $[Cu(ClPhtrz)_2]^+$ and $[Cu(ClPhtrz)(CH_3CN)]^+$ species, respectively. No peaks characteristic of the dimer entities could be detected in the ESI-MS spectra. The formation of the 1:2 and 1:1 complexes from the pure dimeric complexes should be accompanied by the release of both free ligand and free Cu^{I} cation. Indeed, weak peaks at 206.6 (for $[ClPhtrz]^+$) and at 144.5 (for $[Cu(CH_3CN)_2]^+$) are observed during the ESI-MS analysis.

Unexpected ESI-MS spectra were obtained for complexes **3** and **5**. Despite the different metal to triazole ligand ratio in dimer **3** (2:6) than in dimers **1** and **2** (2:4) the fragmentation led to the same pattern in the mass spectrum, i.e. a monomeric 1:2 species at 406.9 (attributed to $[Cu(Phtrz)_2]^+$) and a 1:1 species at 276.2 (attributed to $[Cu(Phtrz)(CH_3CN)]^+$). Dissociation of the parent dimer results in two additional peaks at 172.2 and 144.1 corresponding to free ligand $[Phtrz]^+$ and solvated copper(I) cation $[Cu(CH_3CN)_2]^+$, respectively

On the basis of the electrospray mass spectrometry results it can be concluded that the dimeric complexes $[Cu_2(ClPhtrz)_4]^{+2}$, $[Cu_2(ClPhtrz)_4(CH_3CN)_2]^{+2}$, and $[Cu_2(Phtrz)_6]^{+2}$ do not survive upon dissolution and dissociate rapidly to mainly form a 1:2 monomeric complex, along with a minor 1:1 complex. Similar phenomena have been observed for other Cu^{I} dimers.[23,24,26]

Spectroscopic Studies

The competitive equilibria related with dissociation of the complexes can also be observed by UV/Vis and ^1H NMR spectroscopy. The UV spectra of **4** or **5** in acetonitrile consist of two major bands: one centred at 210 nm and the other at 283 nm. Both bands contain several shoulders. Comparison of the spectrum obtained for the complex with that of the free ligand reveals a close similarity of the lower energy bands for each of the systems under study. In fact, these spectra are superimposable in this region after normalisation of the absorbance. The band at 210 nm can be reproduced by a superposition of the spectra of an appropriate free ligand and that of $[Cu(CH_3CN)_4]^+$ (Figure 5). Evidently, at the concentration level of electronic spectroscopy the overwhelming excess of acetonitrile ligand causes the complete substitution of Phtrz or ClPhtrz by CH_3CN in the first coordination sphere of the copper(I) ion.

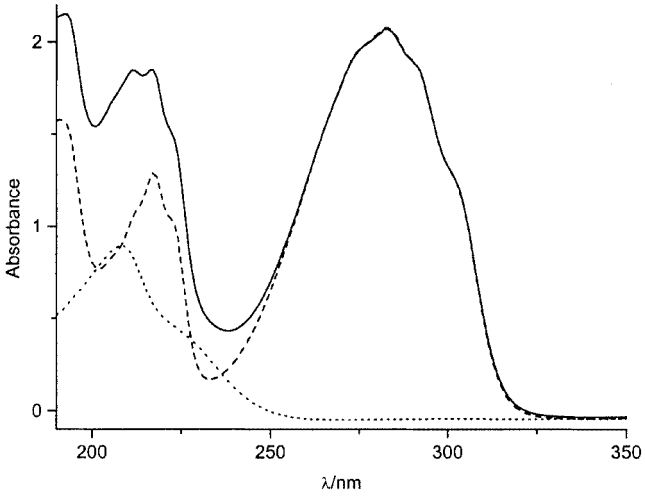

Figure 5. Electronic spectra of acetonitrile solutions of **4** (solid line), ClPhtrz (dashed line), and $[Cu(CH_3CN)_4]ClO_4$ (dotted line)

The ^1H NMR spectra of saturated solutions of the complexes in CD_3CN are consistent with the labile character of the complexes and also reveal the dissociation of the dimers upon dissolution in acetonitrile. The number of signals indicates the degeneracy of the respective resonances, i.e. there is only one peak for the azomethine group (N=CH), the triazole (trz) ring and each type of aryl ring proton (Figure 6). Differentiation of the chemical shifts is expected particularly for these protons that are in the vicinity of the coordination sites if the solid-state structure of the complex is retained in solution. Although the number of peaks is the same for both the complex and for the appropriate free ligand, the positions of the peaks differ considerably [**5** (Phtrz): δ = 8.869 (8.844) ppm (N=CH), 8.864 (8.791) (trz); **4** (ClPhtrz): δ = 8.845 (8.825) (N=CH), 8.838 (8.777) (trz) ppm; CD_3CN, 233 K]. This suggests an equilibrium between coordinated and free ligand in solution. Such an equilibrium, which is fast on the NMR timescale, causes an averaging of the chemical shifts. The considerable broadening of the triazole signal of the complex at low temperature is also consistent with the presence of a fast chemical exchange between coordinated and uncoordinated ligand. Titration of the complex solution with free ligand does not result in the appearance of any additional signals. Instead, it gradually shifts the position of all the peaks to those of the free ligand (Figure 6).

Conclusion

The results discussed here demonstrate that reaction between $[Cu(CH_3CN)_4](ClO_4)$ and Schiff-base-containing triazole ligands in acetonitrile gives various dimeric copper(I) complexes. The composition and geometry of these complexes depend on the reaction conditions (compounds

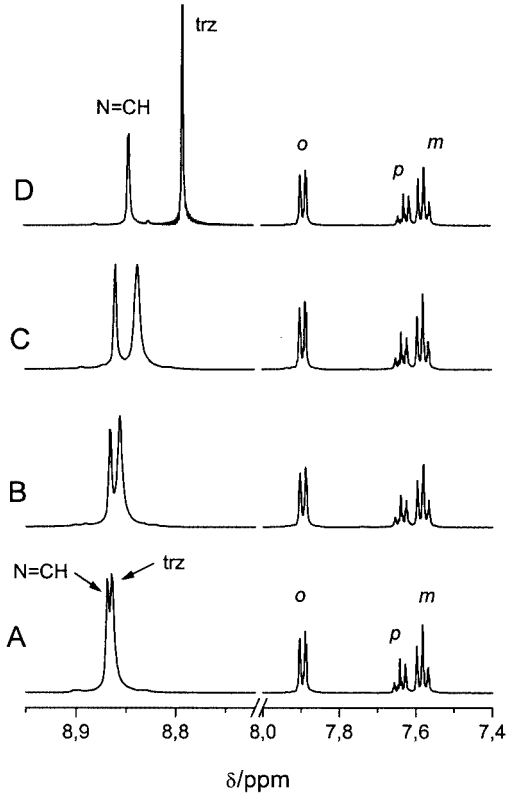

Figure 6. ^{1}H NMR spectra (500 MHz, CD_3CN, 233 K) of a saturated solution of **5** (A), mixtures of **5** and Phtrz (B and C) and Phtrz (D); assignments: N=CH − azomethine proton, trz − triazole protons, *o*, *m*, *p* − *ortho*, *meta*, *para* protons of phenyl substituent

1 and **2**) and/or type of ligand used (**3**), as confirmed by single-crystal X-ray diffraction. Our studies show that Schiff-base-containing triazole ligands coordinate simultaneously in the monodentate and bidentate mode. The latter results in them bridging two metal centres. This is in contrast with pyrazolylcopper(I) complexes, in which a pyrazole molecule acts solely as a bridging ligand. All studied crystals are unstable and lose acetonitrile molecules (coordinated and solvated) forming **4** (from **1** and **2**) and **5** (from **3**). Regardless of the stoichiometry, the complexes dissociate rapidly to form monomeric species upon dissolution, unlike the pyrazole-bridged dimers, which retain their dimeric structure in solution.

Experimental Section

General Remarks: ESI MS were performed on a Finnigan Mat type TSQ700 mass spectrometer. ^{1}H NMR spectra were recorded on a Bruker AM500 spectrometer in CD_3CN. UV spectra were recorded on a Hewlett Packard 8453 diode array spectrophotometer. Elemental analyses were carried out at the Microanalytical Laboratory of this University.

Starting Materials: Commercially available solvents, hydrazine monohydrate, formic acid, 4-chlorobenzaldehyde and benzaldehyde (Fluka) were used without further purification. $[Cu(CH_3CN)_4](ClO_4)$,[27] 4-amino-1,2,4-triazole,[28] and *N*-[(*E*)-(4-chlorophenyl)-methylidene]-4*H*-1,2,4-triazol-4-amine (ClPhtrz)[29] were prepared according to literature procedures. All reactions with Cu^I were carried out under a dry nitrogen atmosphere using standard Schlenk techniques.

Caution. *Perchlorate salts of metal complexes with organic ligands are potentially explosive. Only small quantities of the compound should be prepared and handled with much care!*

***N*-[(*E*)-(phenyl)methylidene]-4*H*-1,2,4-triazol-4-amine (Phtrz):** An ethanolic solution (20 mL) of benzaldehyde (2.12 g, 20 mM) was added to a warm ethanolic solution (25 mL) of 4-amino-1,2,4-triazole (1.69 g, 20 mM) and the resulting solution was refluxed for four hours. The reaction mixture was then cooled to room temperature. The solution was evaporated to dryness under reduced pressure, and the crude product was recrystallised from ethanol/diethyl ether. The resultant white solid was filtered off, washed with diethyl ether and dried under vacuum. Yield 2.55 g, 74%; M.p. 144 °C (subl.). $C_9H_8N_4$ (172.2): calcd. C 62.78, H 4.68, N 32.54; found C 62.71, H 4.66, N 32.54. MS: *m*/*z* = 173 $[MH]^+$. ^{1}H NMR (500 MHz, CD_3CN, 298 K): δ = 8.84 (s, 1 H, N=CH) 8.74 (s, 2 H, triazole) 7.92 (m, 2 H, *ortho*) 7.64 (m, 1 H, *para*) 7.59 (m, 2 H, *meta*) ppm.

$\{[Cu_2(ClPhtrz)_4](ClO_4)_2\}\cdot 2CH_3CN$ (1): A solution of $[Cu(CH_3CN)_4](ClO_4)$ (164 mg, 0.5 mmol) in acetonitrile (5 mL) was added dropwise to an acetonitrile solution (15 mL) of ClPhtrz (207 mg, 1 mmol). The colourless solution was stirred for 15 min, then the volume of the solution was reduced by half over 4 hours in a stream of N_2. The resultant solution was allowed to stand overnight at room temperature, affording colourless, needle-shaped crystals of **1** which were collected by filtration, washed with acetonitrile and diethyl ether. The crystal used in the X-ray structure determination was selected from this sample. The molecular formula for **1** was established on the basis of X-ray crystallographic measurement (see Table 1). Elemental analysis data: vide infra.

$\{[Cu_2(ClPhtrz)_4(CH_3CN)_2](ClO_4)_2\}\cdot CH_3CN$ (2). ***Method A*:** The compound was obtained as described for **1**, but no reduction of solvent volume was done. The colourless solution was allowed to stand at room temperature for about one month. During this time light-yellow, prismatic crystals of **2** were formed.
***Method B*:** The compound was obtained as described in *method A*, but ClPhtrz (104 mg, 0.5 mmol) and $[Cu(CH_3CN)_4](ClO_4)$ (164 mg, 0.5 mmol) were used. After standing overnight at room temp. light-yellow, prismatic crystals were formed. The measured lattice parameters for the crystals obtained by *method B* were identical to those detected for **2** obtained by *method A*. The molecular formula for **2** was established on the basis of X-ray crystallographic measurement (see Table 1). Elemental analysis data: vide infra.

$\{[Cu_2(Phtrz)_6](ClO_4)_2\}\cdot 2CH_3CN$ (3): A solution of $[Cu(CH_3CN)_4](ClO_4)$ (164 mg, 0.5 mmol) in acetonitrile (10 mL) was added to an acetonitrile solution (10 mL) of Phtrz (172 mg, 1 mmol). The resultant light-yellow solution was stirred for 15 min, then about 4 mL of solvent was removed under a stream of dinitrogen. After 4 hours light-yellow crystals of **3** had formed. The crystals were filtered off, washed with acetonitrile and diethyl ether. The molecular formula for **3** was established on the basis of X-ray crystallographic measurement (see Table 1). Elemental analysis data: vide infra.

During the storage of the complexes even in a sealed vial under a dinitrogen atmosphere cracking of the crystals of **1** and **3** was detected, whereas crystals of **2** undergo complete powdering and become white. The analysis of the resulting products **4** and **5** indicated the loss of acetonitrile molecules, either independently solvated (**1** and **3**) or coordinated (**2**).[30] For **4**: $C_{36}H_{28}N_{16}Cl_6Cu_2O_8$ (1152.5):

Table 1. Crystal data and structure refinement

Compound	**1**	**2**	**3**
Empirical formula	$C_{36}H_{28}N_{16}O_8Cl_6Cu_2{\cdot}2H_3CCN$	$C_{40}H_{34}N_{18}O_8Cl_6Cu_2{\cdot}H_3CCN$	$C_{54}H_{48}N_{24}O_8Cl_2Cu_2{\cdot}2H_3CCN$
Molecular weight	1234.63	1275.68	1441.25
T (K)	100(2)	100(2)	100(2)
λ (Å)	0.71073	0.71073	0.71073
Crystal system	Monoclinic	Triclinic	Triclinic
Space group	$P2_1/c$	$P\bar{1}$	$P\bar{1}$
a (Å)	7.0205(8)	9.3882(12)	11.1666(10)
b (Å)	17.9760(14)	11.0484(17)	12.3458(11)
c (Å)	22.0379(17)	13.5942(19)	12.6112(11)
α (°)	90	76.384(13)	68.604(8)
β (°)	96.995(8)	71.686(12)	88.132(7)
γ (°)	90	84.439(12)	80.316(8)
V (Å^3)	2760.5(4)	1300.6(3)	1594.9(2)
Z	2	1	1
D_c (Mg·m^{-3})	1.485	1.629	1.501
μ (mm^{-1})	1.125	1.197	0.827
F(000)	1248	646	740
Crystal size (mm)	0.15 × 0.12 × 0.12	0.17 × 0.15 × 0.13	0.52 × 0.35 × 0.33
θ range for data collection (°)	3.17−28.51	3.35−28.36	3.64−28.37
Ranges of h,k,l	−9→6, −24→23, −29→29	−12→11, −14→8, −18→18	−14→8, −16→16, −16→16
Reflections collected	18818	9065	10983
Independent reflections	6492 (0.0406)	5716 (0.0305)	7019 (0.0200)
Data/parameters	6492/320	5716/414	7019/562
GOF(F^2)	1.099	1.021	1.047
Final R_1/wR_2 indices [$I > 2\sigma(I)$]	0.0579/0.1526	0.0456/0.1077	0.0346/0.0812
Min/max. transmission factor	---	---	0.6731/0.7720
Extinction coefficient	---	---	0.0021(5)
Largest diff. peak/hole (e·Å^{-3})	1.162/−0.462	1.416/−0.983	0.448/−0.500

calcd. C 37.52, H 2.45, N 19.44; (obtained from **1**) C 37.74, H 2.45, N 19.39; (obtained from **2**) C 37.38, H 2.47, N 19.43. For **5**: $C_{54}H_{48}Cl_2Cu_2N_{24}O_8$ (1359.1): calcd. C47.72, H 3.56, N 24.73; found C47.63, H 3.66, N 24.41. The elemental analytical data for **1** and **2** were analogous to that obtained for **4**, while elemental analysis showed that dried **3** and **5** were the same species.

X-ray Crystallographic Study: Crystal data of **1**−**3** are given in Table 1, together with refinement details. All measurements of crystals were performed at low temperature using an Oxford Cryosystem device on a Kuma KM4CCD κ-axis diffractometer with graphite-monochromated Mo-K_α radiation. The crystals were positioned 65 mm from the CCD camera. 612 frames were measured at 0.75° intervals with a counting time in the range 10−20 sec. Accurate cell parameters were determined and refined by least-squares fit of 1900 to 3100 of the strongest reflections. Data reduction and analysis were carried out with the Oxford Diffraction (Poland) (formerly Kuma Diffraction Wrocław, Poland) programs. The data were corrected for Lorentz and polarisation effects. An analytical absorption correction was also applied for **3**. Data reduction and analysis were carried out with the Oxford Diffraction (Poland) Sp. z o. o. (formerly Kuma Diffraction Wrocław, Poland) programs. The structures were solved by direct methods (program SHELXS-97[31]) and refined by the full-matrix least-squares method on all F^2 data using the SHELXL-97[32] programs. In the studied crystals the acetonitrile solvent molecules are disordered, with occupancy parameters of 0.25 in **1**, and 0.5 in **2**, whereas in **3** one molecule has two different orientations in an 0.84:0.16 ratio. The ClO_4^- ion in **3** is also slightly disordered, with two distinct orientations approximately in a 0.93:0.07 ratio. Non-hydrogen atoms were refined with anisotropic displacement parameters except for the disordered solvent molecules in **1** and **2** and the minor components of the disordered acetonitrile molecule and perchlorate ion. Hydrogen atoms were included from the geometry of the molecules and Δρ maps. During refinement their parameters were fixed.
CCDC-198765−198767 (**1**−**3**) contain the supplementary crystallographic data for this paper. These data can be obtained free of charge at www.ccdc.cam.ac.uk/conts/retrieving.html [or from the Cambridge Crystallographic Data Centre, 12, Union Road, Cambridge CB2 1EZ, UK; fax: (internat.) +44-1223/336-033; E-mail: deposit@ccdc.cam.ac.uk].

Acknowledgments

The Authors thank the MENiS for financial support.

[1] P. J. Steel, *Coord. Chem. Rev.* **1990**, *106*, 227−265.
[2] J. G. Haasnoot, *Coord. Chem. Rev.* **2000**, *200*−*202*, 131−185.
[3] S. Trofimenko, *Prog. Inorg. Chem.* **1986**, *34*, 115−210.
[4] G. La Monica, G. A. Ardizzoia, *Prog. Inorg. Chem.* **1997**, *46*, 151−238.
[5] G. A. Ardizzoia, S. Cenini, G. La Monica, N. Masciocchi, M. Moret, *Inorg. Chem.* **1994**, *33*, 1458−1463.
[6] G. A. Ardizzoia, S. Cenini, G. La Monica, N. Masciocchi, A. Maspero, M. Moret, *Inorg. Chem.* **1998**, *37*, 4284−4292.
[7] G. A. Ardizzoia, E. M. Beccalli, G. La Monica, N. Masciocchi, M. Moret, *Inorg. Chem.* **1992**, *31*, 2706−2711.
[8] N. Masciocchi, M. Moret, P. Cairati, A. Sironi, G. A. Ardizzoia, G. La Monica, *J. Am. Chem. Soc.* **1994**, *116*, 7668−7676.
[9] M. K. Ehlert, S. J. Rettig, A. Storr, R. C. Thompson, J. Trotter, *Can. J. Chem.* **1990**, *68*, 1444−1449.
[10] R. G. Raptis, J. P. Fackler, Jr., *Inorg. Chem.* **1988**, *27*, 4179−4182.
[11] M. K. Ehlert, S. J. Rettig, A. Storr, R. C. Thompson, J. Trotter, *Can. J. Chem.* **1992**, *70*, 2161−2173.
[12] G. A. Ardizzoia, M. A. Angaroni, G. La Monica, N. Masciocchi, M. Moret, *J. Chem. Soc., Dalton Trans.* **1990**, 2277−2281.

[13] M. G. B. Drew, P. C. Yates, J. Trocha-Grimshaw, K. P. McKillop, S. M. Nelson, *J. Chem. Soc., Chem. Commun.* **1985**, 262−263.
[14] D. J. Chesnut, A. Kusnetzow, R. Birge, J. Zubieta, *Inorg. Chem.* **1999**, *38*, 5484−5494.
[15] J. G. Haasnoot, T. L. F. Favre, W. Hinrichs, J. Reedijk, *Angew. Chem. Int. Ed. Engl.* **1988**, *27*, 856−858; *Angew. Chem.* **1988**, *100*, 884.
[16] E. Müller, G. Bernardinelli, J. Reedijk, *Inorg. Chem.* **1996**, *35*, 1952−1957.
[17] R-X. Yuan, R-G. Xiong, B. F. Abrahams, G-H. Lee, S-M. Peng, C-M. Che, X-Z. You, *J. Chem. Soc., Dalton Trans.* **2001**, 2071−2073.
[18] G. Gioia Lobbia, M. Pellei, C. Pettinari, C. Santini, B. W. Skelton, N. Somers, A. H. White, *J. Chem. Soc., Dalton Trans.* **2002**, 2333−2340.
[19] A. L. Spek, PLATON, *Acta Crystallogr., Sect. A* **1990**, *46*, C-34.
[20] R. R. Gagne, R. P. Kreh, J. A. Dodge, *J. Am. Chem. Soc.* **1979**, *101*, 6917.
[21] S. Kitagawa, M. Munakata, T. Tanimura, *Inorg. Chem.* **1992**, *31*, 1714−1717.
[22] S. Lopez, S. W. Keller, *Inorg. Chem.* **1999**, *38*, 1883−1888.
[23] C. Maelli, C. S. Arcus, J. L. Wilkinson, T. J. Marks, J. A. Ibers, *J. Am. Chem. Soc.* **1976**, *98*, 711−718.
[24] T. N. Sorrell, A. S. Borovik, *J. Am. Chem. Soc.* **1987**, *109*, 4255−4260.
[25] G. K. Patra, I. Goldberg, *J. Chem. Soc., Dalton Trans.* **2002**, 1051−1057.
[26] A. Ion, M. Buda, J.-C. Moutet, E. Saint-Aman, G. Royal, I. Gautier-Luneau, M. Bonin, R. Zissel, *Eur. J. Inorg. Chem.* **2002**, 1357−1366.
[27] G. J. Kubas, *Inorg. Synth.* **1979**, *19*, 90−92.
[28] R. M. Herbst, J. A. Garrison, *J. Org. Chem.* **1953**, *18*, 872−882.
[29] Z. Ciunik, K. Drabent, *Polish J. Chem.* **2001**, *75*, 1475−1482.
[30] Because of experimental problems (ClO_4^- counteranion) a thermogravimetric analysis of the **1, 2** and **3** could not be performed.
[31] G. M. Sheldrick, SHELXS-97, program for solution of crystal structures, University of Göttingen, 1997.
[32] G. M. Sheldrick, SHELXL-97, *program for crystal structure refinement*, University of Göttingen, 1997.

Received November 29, 2002
[I02662]

The Electronic Absorption Characteristics of Mixed Phthalocyaninato Porphyrinato Rare Earth(III) Triple-Deckers $M_2(TPyP)_2(Pc)$

Xuan Sun,[a] Xuegui Cui,[a] Dennis P. Arnold,*[b] Michael T. M. Choi,[c] Dennis K. P. Ng,[c] and Jianzhuang Jiang*[a]

Keywords: Phthalocyanines / Porphyrins / Sandwich complexes / Lanthanides

Mixed phthalocyaninato tetrakis(4-pyridyl)porphyrinato rare earth triple-decker complexes $M_2(TPyP)_2(Pc)$ [M = La (**1**), Eu (**2**)] have been prepared by condensation between M(TPyP)acac generated in situ and $M(Pc)_2$. Their symmetrical structure (TPyP)M(Pc)M(TPyP) was verified by ^1H NMR (1D and 2D) spectra in $CDCl_3$ solutions. The electronic absorption spectra of these two compounds were recorded in the UV/Vis and near-IR region. A weak absorption in the near-IR region at 860 and 942 nm for **1** and **2**, respectively, was observed as the lowest energy band and is attributed to the electronic transition from HOMO to LUMO for these mono(phthalocyaninato) bis(porphyrinato) rare earth complexes. Their electrochemical properties were investigated by cyclic voltammetry (CV) and differential pulse voltammetry (DPV). Analysis of the relationship between the optical and redox properties of $M_2(TPyP)_2(Pc)$ reveals that the HOMO and LUMO of $M_2(TPyP)_2(Pc)$ have both porphyrin and phthalocyanine character.
(© Wiley-VCH Verlag GmbH & Co. KGaA, 69451 Weinheim, Germany, 2003)

Introduction

Sandwich-type phthalocyaninato and/or porphyrinato metal complexes have been intensively studied.[1−3] These species comprise two or three aromatic macrocyclic ligands held in close proximity by eight-coordinate metal ions in the +3 or +4 oxidation state. They exhibit a wide range of intriguing physical and chemical properties which render them useful in molecular (semi)conductors, molecular electronics and electrochromic displays.[4−5] Although heteroleptic and mixed tetrapyrrole ring complexes containing different phthalocyaninato and porphyrinato ligands have aroused increasing interest in recent years, relatively little is known about their optical, electrochemical and functional properties.[3] As part of our continuing exploration of this novel class of compounds, we have developed several effective pathways for preparing heteroleptic bis(phthalocyaninato) rare earth and mixed (na)phthalocyaninato porphyrinato rare earth double- and triple-deckers and systematically investigated their structural, electrochemical and spectroscopic (both electronic and vibrational) properties.[6−8]

Electronic absorption is one of the most powerful methods to characterize sandwich-type tetrapyrrole metal complexes. With regard to the optical properties of mixed phthalocyaninato porphyrinato rare earth sandwich complexes, it is worth pointing out that we have been intrigued by the significant difference in the appearance of the electronic absorption spectra of $(Por)M^{III}(Pc)M^{III}(Por)$ (for a list of abbreviations, see Table 1) from those of $[M^{III}(Por)(Pc)]^-$ since the very beginning of our research in this field.[9,10]

Table 1. List of abbreviations for ligands

Abbreviation	Ligand
P	general phthalocyaninato or porphyrinato
Pc	phthalocyaninato
Por, Por′	general porphyrinato
TPyP	5,10,15,20-tetrakis(4-pyridyl)porphyrinato
TPP	5,10,15,20-tetraphenylporphyrinato
TClPP	5,10,15,20-tetrakis(4-chlorophenyl)porphyrinato
TBPP	5,10,15,20-tetrakis(4-*tert*-butylphenyl)porphyrinato
TOMPP	5,10,15,20-tetrakis(4-methoxyphenyl)porphyrinato
OEP	2,3,7,8,12,13,17,18-octaethylporphyrinato
Nc	2,3-naphthalocyaninato (linearly annelated tetrabenzophthalocyaninato)

It is well known that an absorption band in the near-IR region is the most prominent feature in the electronic

[a] Department of Chemistry, Shandong University, Jinan 250100, China
Fax: (internat.) + 86-531/856-5211
E-mail: jzjiang@sdu.edu.cn
[b] School of Physical and Chemical Sciences, Queensland University of Technology, G. P. O. Box 2434, Brisbane 4001, Australia
Fax: (internat.) + 61-7/3864-1804
E-mail: d.arnold@qut.edu.au
[c] Department of Chemistry, The Chinese University of Hong Kong, Shatin, N. T., Hong Kong, China
Supporting information for this article is available on the WWW under http://www.eurjic.org or from the author.

absorption spectra of all the neutral homoleptic and heteroleptic tetrapyrrole double-decker rare earth(III) complexes. Such complexes contain an unpaired electron on one ring thus can be depicted as a monoanion radical $P^{\cdot -}$ (P = Por, Pc).[1,2] This near-IR band has been attributed to the ring-to-ring intramolecular charge transfer (RRCT) from the dianion P^{2-} electron donor to the monoanion radical $P^{\cdot -}$ electron acceptor.[3,11] In the spectra of the one-electron reduced form $[M^{III}(Por)(Pc)]^-$, no absorption band has ever been observed in the near-IR region beyond 800 nm, presumably due to the absence of an unpaired electron.[1−3] The reduced mixed ring complexes $[M^{III}(Por)(Pc)]^-$ display electronic absorption features common to both $[M^{III}(Por)_2]^-$ and $[M^{III}(Pc)_2]^-$ or $[M^{IV}(Pc)_2]$.[9,11−13] Thus, except for a weak absorption at ca. 480 nm assigned to a new π-π* transition arising from molecular orbitals delocalized over both rings, the porphyrin Soret band in $Li[M^{III}(TPyP)(Pc)]$ (M = Eu, Gd) appears at ca. 411 nm, whereas the phthalocyanine Soret and Q bands appear at ca. 330 and 584, 635, and 800 nm, respectively.[9]

The electronic absorption spectra of mixed phthalocyaninato porphyrinato rare earth triple-decker compounds $M^{III}_2(Por)_2(Pc)$ [having the constitution (Por)M(Pc)M(Por)] (Por = TPP, TClPP, TBPP, TOMPP) are usually recorded in the region of 300−800 (at most to 900) nm.[10] As these compounds are composed of two $[M^{III}(Por)(Pc)]^-$ moieties, which possess a common Pc^{2-} unit strongly interacting with two outer Por^{2-} rings, their absorption features should be easily understood on the basis of the electronic absorption spectra of $[M^{III}(Por)(Pc)]^-$. However, due to the increased ring-ring separation and consequently decreased ring-ring interaction in triple-deckers $M^{III}_2(Por)_2(Pc)$, all the absorption bands are expected to shift to the red as compared with those in the reduced double-decker counterparts $[M^{III}(Por)(Pc)]^-$. The absorptions at ca. 354 and 420 nm for $Eu_2(Por)_2(Pc)$ (Por = TPP, TClPP, TBPP, TOMPP) can be assigned to the phthalocyaninato and porphyrinato Soret bands, respectively. The band at around 490 nm has been compared to the similar weak absorption at ca. 480 nm for $Li[M^{III}(TPyP)(Pc)]$ (M = Eu, Gd) and similarly assigned to the π-π* transition arising from molecular orbitals delocalized over both rings. The remaining absorptions in the visible region at 539−551 and 603−605 nm for the various $Eu_2(Por)_2(Pc)$ complexes are mainly contributed by the Q bands of the phthalocyanine ring. Apparently, no absorption band similar to that at ca. 800 nm for reduced double-decker $Li[M^{III}(TPyP)(Pc)]$ has been found in the electronic absorption spectra of these triple-deckers. It is this phenomenon that has appeared anomalous to the primary authors of our group for a long time.

Researchers in this field including ourselves have not paid sufficient attention to the characteristic absorption of (Por)-$M^{III}(Pc)M^{III}(Por)$ in the near-IR region beyond 800 nm. One reason for this oversight is the hypothesis that there would be no absorptions in the near-IR region because there is no unpaired electron (hole) in such sandwich triple-deckers. Another reason for overlooking absorption in the near-IR region is the very low intensity of this absorption band (see below), which might be related to the decreased ratio of phthalocyanine to porphyrin in this kind of triple-deckers as well as the generally very weak absorption of porphyrins in the near-IR region. The last reason for missing the near-IR absorption is that the work in mixed phthalocyaninato porphyrinato rare earth triple-deckers thus far has mainly focused on the complexes of Sm, Eu, and Gd,[10] whose lowest energy absorption in the near-IR region is beyond 900 nm.

Our recent work on the 2,3-naphthalocyanine-containing mixed ring sandwiches revealed that $M_2(OEP)_2(Nc)$ $[(OEP)M^{III}(Nc)M^{III}(OEP)]$[8a] complexes exhibit a rather intense near-IR absorption (1000−1100 nm) associated with the HOMO−LUMO electron transition. This encouraged us to re-investigate the electronic absorption characteristics of triple-decker compounds $(Por)M^{III}(Pc)M^{III}(Por)$ and finally led to the discovery of the weak near-IR absorption band in the region of 860−960 nm for the mixed ring triple-decker complexes $M_2(TPyP)_2(Pc)$ (M = La, Eu). Herein we report these results, together with associated electrochemical and NMR characterization data.

Results and Discussion

Synthesis

There are several possible synthetic pathways to rare earth(III) triple-decker complexes with mixed tetrapyrrole ligands $M_2^{III}(Por)_2(Pc)$.[1,3] The most commonly used method involves direct condensation between $H_2(Por)$ and $Li_2(Pc)$ in the presence of $M(acac)_3{\cdot}nH_2O$. However, in addition to the target mixed ring triple-deckers M_2^{III}-$(Por)_2(Pc)$, double-decker $M^{III}(Por)(Pc)$ together with another form of triple-decker $M_2^{III}(Por)(Pc)_2$ were also isolated by this method. The second familiar route is the so-called raise-by-one-story method in which the mono(porphyrinato) compound M(Por)acac generated in situ is treated with mixed ring double-decker M(Por)(Pc). By using this synthetic route, both homo- and heterodinuclear metal triple-deckers $M_2^{III}(Por)_2(Pc)$ or $(Por)M(Pc)M'(Por')$ can be isolated.[14] The third path to $M_2^{III}(Por)_2(Pc)$ developed recently by our group involves the tetramerization of phthalonitriles on the template of mono(porphyrinato) rare earth complex M(Por)acac in *n*-octanol catalyzed by the organic base DBU.[15]

However, it is worth mentioning that none of the above-mentioned procedures works for the tetrakis(4-pyridyl)porphyrin ligand. No $M_2(TPyP)_2(Pc)$ has ever been isolated for rare earths other than cerium thus far. The condensation between H_2TPyP and Li_2Pc with $M(acac)_3{\cdot}nH_2O$ (M = Eu, Gd) usually leads to the formation and isolation of reduced mixed ring double-deckers Li[M(TPyP)(Pc)] together with trace amounts of $M_2(TPyP)(Pc)_2$.[9] In the recent work in which we tried to prepare the mixed ring triple-decker $Eu_2(TPyP)(Pc)_2$ starting with H_2TPyP and $Eu(Pc)_2$ in the presence of $Eu(acac)_3{\cdot}nH_2O$ in refluxing TCB, unexpectedly the triple-decker $Eu_2(TPyP)_2(Pc)$ (**2**) was isolated as the primary product after refluxing the mixture for 18 h. Later it

was found that the other form of triple-decker $Eu_2(TPyP)(Pc)_2$ could only be isolated as the main product after a relatively short reaction time, say less than 12 h. Moreover, pre-preparation of the mono(porphyrinato) compound M(TPyP)acac was found to be unnecessary. More systematic and careful studies revealed that the one-pot reaction of H_2TPyP, $M(Pc)_2$ and $M(acac)_3{\cdot}nH_2O$ could lead directly to the formation of $M_2(TPyP)_2(Pc)$, $M_2(TPyP)(Pc)_2$ and some M(TPyP)(Pc) (M = La, Eu), the relative yields of which were determined by the refluxing time. This indicates that the neutral double-decker M(TPyP)(Pc) produced by degradation of the triple-decker $M_2(TPyP)(Pc)_2$ formed in the first step (Scheme 1) is the intermediate. The neutral double-decker reacts further with M(TPyP)acac formed in situ to generate the mono(phthalocyaninato) bis(porphyrinato) triple-decker compound $M_2(TPyP)_2(Pc)$. This postulate is supported by the isolation of a large amount of $Eu_2(TPyP)(Pc)_2$ when the mixture of H_2TPyP, $Eu(Pc)_2$ and $Eu(acac)_3{\cdot}nH_2O$ is refluxed for a short time (6 h) and relatively high yield of neutral double-decker Eu(TPyP)(Pc) after reflux for a relatively long time (10 h). The fact that Li[M(TPyP)(Pc)] (M = Eu, Gd) could not directly form triple-deckers $M_2(TPyP)_2(Pc)$ seems to suggest that the reduced double-decker Li[M(TPyP)(Pc)] is quite stable and the lithium cation is located on the top of the Pc ring, which prevents the reduced double-decker from reacting further with M(TPyP)acac. The relatively high stability of the reduced form of TPyP-containing double-deckers $[M^{III}(TPyP)(Pc)]^-$ is further confirmed by the isolation of protonated mixed [tetrakis(4-pyridyl)porphyrinato]-(phthalocyaninato) rare earth double-deckers HM^{III}-(TPyP)(Pc) (M = Eu, Gd, Y) formed by tetramerization of phthalonitrile on the template of the mono(porphyrinato) compound M(TPyP)acac.[13]

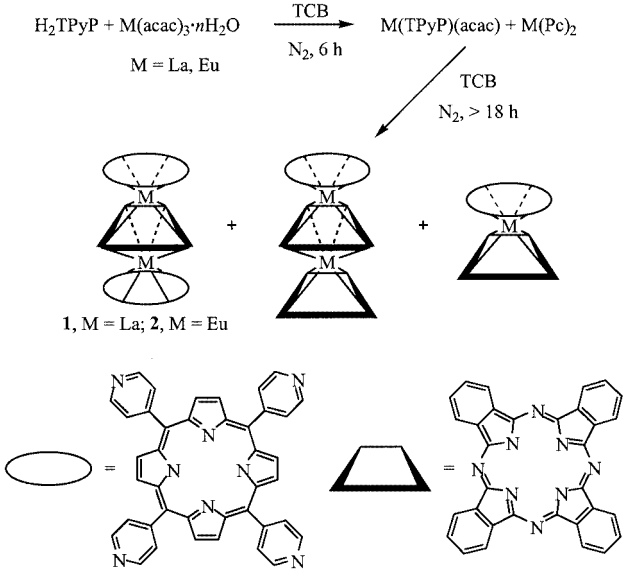

Scheme 1. Synthesis of rare earth triple-deckers

It has been found that among the whole series of rare earth metals, only the lighter rare earths with large enough ionic radius could connect three OEP rings to form homoleptic triple-deckers $M_2(OEP)_3$ (M = La, ..., Tb except for Pm).[1,16,17] This is also true for the formation of mixed ring triple-deckers $M_2(TPyP)_2(Pc)$ as will be detailed elsewhere. The lower yield of $Eu_2(TPyP)_2(Pc)$ (**2**) than $La_2(TPyP)_2(Pc)$ (**1**) is thus rationalized by the smaller ionic size of Eu.

These two compounds were fully characterized by various spectroscopic methods. The MALDI-TOF mass spectrum of **2** and the predicted isotope pattern are shown in the Electronic Supporting Information. However, satisfactory elemental analysis results could not be obtained for these two compounds as is usual for sandwich-type phthalocyaninatoand/or porphyrinato metal complexes and has been reported by different research groups.[15,18]

^{1}H NMR Spectra of $M^{III}_2(TPyP)_2(Pc)$ [M = La (1), Eu (2)]

The molecular structures of the newly prepared triple-decker complexes were clearly demonstrated to be of the form (TPyP)M(Pc)M(TPyP) (M = La, Eu) by their NMR spectra recorded in $CDCl_3$. The chemical shift data for the TPyP β-pyrrole, pyridyl, and Pc α- and β-protons are collected in Table 2, together with the T_1 values for protons in **2**. The assignments of the spectra for both the diamagnetic lanthanum complex and the weakly paramagnetic europium complex were achieved by virtue of the resolved multiplicity in the signals for the Pc α- and β-protons, the availability of spectra for related triple-deckers[10,15,19,20] and the 2D spectra. The positions on the pyridyl rings are labeled *ortho* and *meta* with respect to the bond to the porphyrin *meso*-carbon atom, and the terms *exo* and *endo* refer to the two possible environments with respect to the neighboring (inner) Pc ring. The *exo*/*endo* positions are exchanged by rotation about the bond between the pyridyl *ipso*-carbon atom and the porphyrin *meso*-carbon atom, but at room temperature, rotation is slow enough, as usual for *meso*-tetraarylporphyrins, that the usual AA′XX′ pattern is split into two pairs of signals. We show the ^{1}H NMR spectra of **1** and **2** in Figure 1 and the COSY spectrum of **1** in the Electronic Supporting Information. The sequence of assignments was as follows. The Pc proton signals could be readily identified by their integrals, their characteristic downfield positions, and the double-doublet signals (for **1**) at δ = 9.40 and 8.50 ppm for the α- and β-protons, respectively. The β-porphyrin signal was obvious as a unique 8-proton singlet at δ = 7.35 ppm. The *endo*- and *exo*-*ortho*- and *endo*- and *exo*-*meta*-proton signals appear as broad peaks and were readily assigned as *ortho*/*meta* pairs according to the COSY spectrum. At 30 °C the β-Pc signal overlaps with one of the py signals. For the paramagnetic Eu complex **2**, the assignment of the pair of *ortho*-protons is obvious from measurement of T_1 − faster relaxation is consistent with average proximity to the paramagnetic ion. In addition, an NOESY experiment with short mixing time (150 ms), showed positive cross peaks relating the protons in chemical exchange (EXSY), confirming these assignments. The only remaining ambiguity is the assignment of *exo*/*endo* for each pair of resonances. This has yet to be confirmed and will

Table 2. ^{1}H NMR spectroscopic chemical shifts (T_1 [ms] for Eu complex) for the triple-deckers (TPyP)M(Pc)M(TPyP) in $CDCl_3$ (300 MHz, 30 °C)

Complex[a][b]	Por β	*endo,ortho*	*endo,meta*	*exo,ortho*	*exo,meta*	Pc α	Pc β
1 La,La	7.36 s	9.52 b	9.11 b	6.48 b	8.51 b[c]	9.40 dd	8.50 dd
2 Eu,Eu	3.97 s	11.41 d	10.29 d	4.91 d	8.14 d	12. 56 d	10.73 d
	(150)	(190)	(760)	(190)	(760)	(140)	(390)

[a] Multiplicities: s = singlet, d = doublet, dd = double doublet, b = broad. [b] Assignments of *endo*/*exo* tentative (see text). [c] Signal overlapped with that of the Pc β-proton signals.

require variable-temperature ROESY experiments. The present assignments for **2** are based on the expected strong downfield pseudo-contact shift near the coordinated ion, i.e. on the *endo* side of the py ring. The assignments for **1** have been aligned with those for **2**. In the spectrum of compound **2**, the Pc α- and β-proton signals are less resolved than in analogue **1** because of broadening due to the paramagnetic europium ion. Conversely, the signals of the pyridyl protons of **2** are narrower than those in triple-decker **1** despite the presence of the paramagnetic europium ion. This is attributed to the slower rotation of pyridyl groups about the bond between the pyridyl *ipso*-carbon atom and the porphyrin *meso*-carbon atom associated with the smaller Eu^{III} ion and thus shorter ring−ring distance in compound **2**.

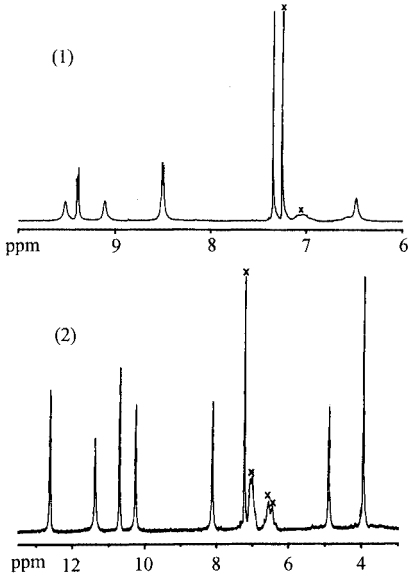

Figure 1. ^{1}H NMR spectra of $La_2(TPyP)_2(Pc)$ (**1**) and $Eu_2(TPyP)_2(Pc)$ (**2**) in $CDCl_3$

$M_2(Por)_2(Pc)$ (Por = TPP, TClPP, TOMPP, TBPP).[10] However, in the near-IR region, a weak absorption band was also observed at 860 and 942 nm for **1** and **2**, respectively. It is noteworthy that re-examination of the electronic absorption spectra of previously reported $M_2(Por)_2(Pc)$ (M = Ce, Sm, Eu, Gd; Por = TPP, TClPP, TOMPP, TBPP) showed that this near-IR absorption at 860−960 nm is common for these mixed ring triple-decker compounds although it had been ignored by most previous studies for the reasons mentioned in the Introduction. After carefully re-examining the documents in this field, the sole work that ever mentioned this absorption before the present report appears to be that of Tran-Thi, who drew the absorption of $Ce_2(TPP)_2(Pc)$ at 890 nm in a schematic representation of the electronic absorption bands for this compound.[12] However, this band was not discussed further.

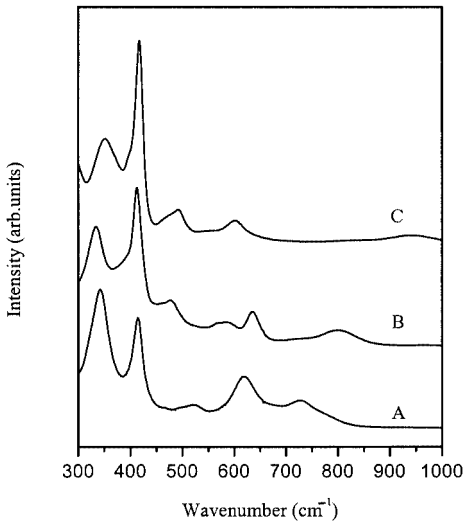

Figure 2. Electronic absorption spectra of (A) $Eu_2(TPyP)(Pc)_2$ in $CHCl_3$, (B) Li[Eu(TPyP)(Pc)] in MeOH, and (C) $Eu_2(TPyP)_2(Pc)$ (**2**) in $CHCl_3$

Electronic Absorption Spectra of $M^{III}_2(TPyP)_2(Pc)$ [M = La (1), Eu (2)]

The electronic absorption spectra of the mixed phthalocyaninato porphyrinato rare earth triple-decker compound **2** together with that of Li[Eu(TPyP)(Pc)] and the related triple-decker $Eu_2(TPyP)(Pc)_2$ are displayed in Figure 2. $M^{III}_2(TPyP)_2(Pc)$ shows similar features in the region from 300 to 800 nm to those of previously reported analogues

As expected, since compound $Eu_2(TPyP)_2(Pc)$ (**2**) consists of two units of $[(TPyP)Eu(Pc)]^-$, **2** indeed exhibits very similar electronic absorption spectrum to the corresponding double-decker Li[Eu(TPyP)(Pc)].[9] The Pc^{2-} and Por^{2-} Soret bands of **2** appear at 351 and 417 nm, respectively. The Pc^{2-} Q bands, which also contain some contributions from the Por ligands, appear at 602 and 942 nm, respectively. The absorption assigned to another π-π* transition

arising from molecular orbitals delocalized over both Pc and Por macrocycles is located at 492 nm. Compared with the spectra of the corresponding double-decker Li[Eu(TPyP)(Pc)], all of the corresponding absorption bands in **2** have been found to red-shift to some extent, indicating the decreased ring-ring interaction in the triple-decker because of the increased ring-ring distance.

For the purposes of comparison, the electronic absorption spectrum of another mixed tetrapyrrole triple-decker species $Eu^{III}_2(TPyP)(Pc)_2$ [(TPyP)Eu(Pc)Eu(Pc)] is also shown in Figure 2. This compound can be regarded as composed of $[(TPyP)Eu(Pc)]^-$ and $[(Pc)Eu(Pc)]^-$. However, the absorption spectrum is not simply a superposition of the spectra of the constituent double-decker species $[(TPyP)Eu(Pc)]^-$ and $[(Pc)Eu(Pc)]^-$, indicating apparent ring−ring interaction between the one Por and the two Pc moieties. The Soret bands of $Eu^{III}_2(TPyP)(Pc)_2$ appear to be composed of two peaks at 340 and 415 nm, which are mainly derived from Pc and TPyP Soret bands, respectively. The prominent Q bands appear at 621 and 740 nm, respectively. Based on similarities in the appearance as well as the relative absorption intensities of these two absorptions to those of phthalocyaninato rare earth triple-decker compounds $M_2(Pc')_3$ at 630−650 and 680−710 nm,[20] these two Q bands are considered to arise mainly from the two neighboring Pc chromophores connected by one europium cation $[(Pc)Eu(Pc)]^-$. Comparison between the electronic absorption spectra of $Eu^{III}_2(TPyP)(Pc)_2$ and $Eu^{III}_2(TPyP)_2$-(Pc) (**2**) clearly reveals that the remaining weak band in the spectrum of the former compound at ca. 520 nm is mainly contributed by $[(TPyP)Eu(Pc)]^-$.

Correlation between Optical and Redox Properties of $M^{III}_2(TPyP)_2(Pc)$ [M = La (1), Eu (2)]

The redox properties of mixed phthalocyaninato porphyrinato rare earth triple-decker compounds $M^{III}_2(Por)_2(Pc)$ [M = La (**1**), Eu (**2**)] were investigated by cyclic voltammetry (CV) and differential pulse voltammetry (DPV) in CH_2Cl_2. The half-wave redox potentials vs. SCE are summarized in Table 3. The cyclic voltammetry of compounds **1** and **2** is similar to that of known analogues.[10] Both these triple-deckers undergo two quasi-reversible one-electron oxidations and two quasi-reversible one-electron reductions under the present conditions. By analogy with the electrochemical properties of related sandwich complexes, especially (na)phthalocyaninato and/or porphyrinato rare earth sandwich complexes, all these processes can be attributed to successive electron removal from or addition to the ligand-based orbitals which are represented by the following five redox states: $[M_2(TPyP)_2(Pc)]/[M_2(TPyP)_2$-$(Pc)]^+$, $[M_2(TPyP)_2(Pc)]^+/[M_2(TPyP)_2(Pc)]^{2+}$, $[M_2(TPyP)_2$-$(Pc)]/[M_2(TPyP)_2(Pc)]^-$, and $[M_2(TPyP)_2(Pc)]^-/[M_2$-$(TPyP)_2(Pc)]^{2-}$.

The potential difference between the first oxidation and the first reduction process, $\Delta E^\circ_{1/2}$(oxd.1−red.1), is an important value for sandwich phthalocyaninato and/or porphyrinato complexes. As the first oxidation step and first reduction step, respectively, involve the HOMO and the LUMO of the molecule, the energy difference between these two redox processes corresponds to the electrochemical molecular band gap. The value $\Delta E^\circ_{1/2}$(oxd.1−red.1) should reflect the energy necessary for the transition of an electron from the HOMO to the LUMO of respective sandwich species and therefore should correlate with the lowest energy optical transition. The equation $\Delta E^\circ_{1/2}$(oxd.1−red.1) − hν = 0.01 eV was established between the redox characteristics and the lowest energy bands of monomeric metalloporphyrins M(Por).[21] According to this equation and the $\Delta E^\circ_{1/2}$(oxd.1−red.1) values of 1.71 and 1.51 V for **1** and **2**, respectively, these two triple-decker compounds should show the lowest energy band at 729 and 827 nm, respectively. However, these results are far away from the observed maxima of 860 and 942 nm for **1** and **2**, respectively, perhaps indicating the significant contribution from the phthalocyanine ring to the frontier orbitals of $M^{III}_2(Por)_2$-(Pc). Moreover, the discrepancy between the experimental and calculated data for these two triple-deckers $M_2(TPyP)_2(Pc)$ is larger than that for double-deckers $[M^{III}(Por)(Pc)]^-$,[11] which seems to suggest that the frontier molecular orbitals of $M_2(TPyP)_2(Pc)$ contain more phthalocyanine contribution. This appears difficult to understand at first glance as the ratio of phthalocyanine to porphyrin in triple-decker $M_2(TPyP)_2(Pc)$ is lower than in double-decker $[M^{III}(Por)(Pc)]^-$. However, this result could be rationalized by the fact that the central Pc ring interrupts direct interaction between the two TPyP ligands in $M_2(TPyP)_2(Pc)$ and the Por and Pc ring-to-ring distance in triple-deckers is larger than in double-deckers. It may also be that such a correlation is inappropriate for sandwich complexes in general. However, it is noteworthy that the maxima of the lowest energy electronic band for naphthalocyanine-containing mixed ring triple-decker analogues $M_2(OEP)_2(Nc)$ correspond well with the calculated values based on their redox data according to the above equation.[8a] This correspondence may well be fortuitous due to the similar redox properties of OEP and Nc rings and is unlikely to mean

Table 3. Electrochemical data for the triple-decker complexes

Compound[a]	$E^\circ_{1/2}$(oxd.2)	$E^\circ_{1/2}$(oxd.1)	$E^\circ_{1/2}$(red.1)	$E^\circ_{1/2}$(red.2)	$\Delta E^\circ_{1/2}$(oxd.1−red.1)
$La_2(TPyP)_2(Pc)$ (**1**)	1.42	0.97	−0.74	−1.27	1.71 V
$Eu_2(TPyP)_2(Pc)$ (**2**)	1.19	0.75	−0.76	−1.27	1.51 V

[a] Recorded with $[Bu_4N][PF_6]$ as electrolyte in CH_2Cl_2 (0.1 M) at ambient temperature. Potentials were determined by cyclic voltammetry with a scan rate of 100 mV s^{-1}, and are expressed as half-wave potentials ($E_{1/2}$) in volts relative to SCE.

that the molecular orbitals, especially the HOMO and LUMO of $M_2(OEP)_2(Nc)$, possess only porphyrin character.

Conclusion

In summary, the HOMO and LUMO of mixed ring triple-deckers $M_2(TPyP)_2(Pc)$ (M = La, Eu) consist of contributions from both macrocycles. However, the research into this subject for mixed phthalocyaninato porphyrinato metal derivatives is relatively undeveloped at this stage due to the lack of systematic investigation into the optical and redox properties of such kinds of compounds. It is clear that the unexpected existence of near-IR absorption for neutral mixed ring triple-deckers warrants further experimental and theoretical attention, and work in this regard is in progress.

Experimental Section

General: $CHCl_3$ and CH_3OH were used as received from Beijing Chemical Reagents. H_2TPyP was purchased from Aldrich. $M(acac)_3{\cdot}nH_2O$[22] and $M(Pc)_2$[23] were prepared according to published procedures. The electronic absorption spectra were recorded with Hitachi U-3300 and Hitachi 3100 spectrophotometers. ^1H NMR spectra were recorded with a Bruker Avance 400 spectrometer at the Centre for Molecular Architecture, Central Queensland University, in $CDCl_3$ solutions at ca. 30 °C. Electrochemical measurements were carried out with a BAS CV-50 W voltammetric analyzer. The cell comprised a platinum-sphere working electrode, a silver-wire counter electrode, and an $Ag/AgNO_3$ (0.1 M in MeCN) reference electrode, which was connected to the solution by a Luggin capillary whose tip was placed close to the working electrode. Typically, a 1.0 mM sample solution containing 0.1 M $[Bu_4N][ClO_4]$ in CH_2Cl_2 was purged with nitrogen for 20 min, then the voltammograms were recorded at ambient temperature. Potentials were referenced to the Ag/Ag^+ couple in MeCN, which was taken as +0.31 V vs. SCE as determined for this system previously using ferrocene as an internal standard.[24]

Preparation of Triple-Decker $La_2(TPyP)_2(Pc)$ (1): A mixture of $La(acac)_3{\cdot}nH_2O$ (15 mg, 0.03 mmol), H_2TPyP (18 mg, 0.03 mmol) and $La(Pc)_2$ (23 mg, 0.02 mmol) in 1,2,4-trichlorobenzene (TCB) (4 mL) was refluxed overnight (> 18 h) under nitrogen to give a dark-blue solution. The volatiles were then removed under reduced pressure and the residue was chromatographed on a silica gel column with $CHCl_3$ to remove trace amounts of unchanged $La(Pc)_2$ as the first fraction. The column was then eluted with $CHCl_3$/MeOH (100:1−5) to elute triple-decker $La_2(TPyP)(Pc)_2$ and the desired triple-decker $La_2(TPyP)_2(Pc)$ as the second and third fractions, respectively. The crude product was repeatedly purified by the same chromatographic procedure, followed by recrystallization from a mixture of $CHCl_3$ and MeOH to afford dark blue microcrystals. Yield 14 mg (47%). MS (MALDI-TOF): an isotopic cluster peaking at m/z = 2025 $[M + H]^+$. IR (KBr): $\tilde{\nu}$ = 1328 cm^{-1} (Pc^{2-}).

Preparation of Triple-Decker $Eu_2(TPyP)_2(Pc)$ (2): This compound was prepared by the above procedure with $Eu(acac)_3{\cdot}H_2O$ (15 mg, 0.03 mmol), H_2TPyP (18 mg, 0.03 mmol) and $Eu(Pc)_2$ (23 mg, 0.02 mmol) as starting materials. Yield 16 mg (51%). MS (MALDI-TOF): an isotopic cluster peaking at m/z = 2051 $[M + H]^+$. IR (KBr): $\tilde{\nu}$ = 1331 cm^{-1} (Pc^{2-}).

Acknowledgments

The authors thank the National Natural Science Foundation of China (Grant no. 20171028), National Ministry of Science and Technology of China (Grant no. 2001CB6105-04), Natural Science Foundation of Shandong Province (Grant no. Z99B03), National Educational Ministry of China, The Science Committee of Shandong Province, Shandong University, Queensland University of Technology, and The Chinese University of Hong Kong for financial support. D. A. thanks the Centre for Molecular Architecture, Central Queensland University for a Visiting Fellowship, and Dr. Martin Johnston for assistance with the NMR measurements.

[1] J. Jiang, K. Kasuga, D. P. Arnold, in *Supramolecular Photosensitive and Electroactive Materials* (Ed.: H. S. Nalwa), Academic Press, New York, **2001**, chapter 2, pp. 113−210.
[2] J. W. Buchler, D. K. P. Ng, in *The Porphyrin Handbook*, vol. 3 (Eds.: K. M. Kadish, K. M. Smith, R. Guilard), Academic Press, San Diego, **2000**, vol. 3, chapter 20, pp. 245−294.
[3] D. K. P. Ng, J. Jiang, *Chem. Soc. Rev.* **1997**, *26*, 433−442.
[4] J. Simon, S. Sirlin, *Pure Appl. Chem.* **1989**, *61*, 1625−1629.
[5] [5a] M. Mardru, G. Guilaud, M. Al. Sadoun, M. Maitrot, C. Clarisse, M. Le Contellec, J.-J. Andre, J. Simon, *Chem. Phys. Lett.* **1987**, *142*, 103−105. [5b] R. Madru, G. Guilaud, M. Al. Sadoun, M. Maitrot, J.-J. Andre, J. Simon, R. Even, *Chem. Phys. Lett.* **1988**, *145*, 343−346.
[6] [6a] J. Jiang, W. Liu, L. Lin, W. F. Law, D. K. P. Ng, *Inorg. Chim. Acta* **1998**, *268*, 49−52. [6b] J. Jiang, J. Xie, M. T. M. Choi, D. K. P. Ng, *J. Porphyrins Phthalocyanines* **1999**, *3*, 322−328.
[7] J. Jiang, M. T. M. Choi, J. Chen, D. K. P. Ng, *Polyhedron* **1998**, *17*, 3903−3908.
[8] [8a] J. Jiang, Y. Bian, F. Furuya, W. Liu, M. T. M. Choi, H. W. Li, N. Kobayashi, Q. Yang, T. C. W. Mak, D. K. P. Ng, *Chem. Eur. J.* **2001**, *7*, 5059−5069. [8b] J. Jiang, W. Liu, K.-L. Cheng, K.-W. Poon, D. K. P. Ng, *Eur. J. Inorg. Chem.* **2001**, 413−417. [8c] F. Furuya, N. Kobayashi, Y. Bian, J. Jiang, *Chem. Lett.* **2001**, 944−945. [8d] J. Jiang, D. Du, D. K. P. Ng, J. Xie, *Chem. Lett.* **1999**, 261−262.
[9] J. Jiang, T. C. W. Mak, D. K. P. Ng, *Chem. Ber.* **1996**, *129*, 933−936.
[10] [10a] J. Jiang, R. L. C. Lau, T. W. D. Chan, T. C. W. Mak, D. K. P. Ng, *Inorg. Chim. Acta* **1997**, *155*, 59−64. [10b] R. L. C. Lau, J. Jiang, D. K. P. Ng, T. W. D. Chan, *J. Am. Soc. Mass Spectrom.* **1997**, *8*, 161−169. [10c] J. Jiang, W. Liu, W.-F. Law, D. K. P. Ng, *Inorg. Chim. Acta* **1998**, *268*, 141−145.
[11] D. Chabach, M. Tahiri, A. De Cian, J. Fischer, R. Weiss, M. El Malouli Bibout, *J. Am. Chem. Soc.* **1995**, *117*, 8548−8556.
[12] T.-H. Tran-Thi, T. A. Mattioli, D. Chabach, A. De Cian, R. Weiss, *J. Phys. Chem.* **1994**, *98*, 8279−8288.
[13] J. Jiang, W. Liu, X. Sun, X. Zhang, D. K. P. Ng, *Chem. Res. Chin. Univ.* **2001**, *17*, 134−142.
[14] D. Chabach, A. De Cian, J. Fischer, R. Weiss, M. El Malouli Bibout, *Angew. Chem. Int. Ed. Engl.* **1996**, *35*, 898−889.
[15] N. Pan, J. Jiang, X. Cui, D. P. Arnold, *J. Porphyrins Phthalocyanines* **2002**, *6*, 347−358.
[16] G. A. Spyroulias, C. P. Raptopoulou, D. de Montauzon, A. Mari, R. Poilblanc, A. Terzis, A. G. Coutsolelos, *Inorg. Chem.* **1999**, *38*, 1683−1696.
[17] [17a] J. W. Buchler, A. De Cian, J. Fischer, M. Kihn-Botulinski, H. Paulus, R. Weiss, *J. Am. Chem. Soc.* **1986**, *108*, 3652−3659. [17b] J. W. Buchler, B. Scharbert, *J. Am. Chem. Soc.* **1988**, *110*, 4272−4276.
[18] T. Gross, F. Chevalier, J. S. Lindsey, *Inorg. Chem.* **2001**, *40*, 4762−4774.
[19] D. P. Arnold, J. Jiang, *Chem. Lett.* **1999**, 483−484.
[20] [20a] W. Liu, J. Jiang, N. Pan, D. P. Arnold, *Inorg. Chim. Acta*

2000, *310*, 140−146. [20b] D. P. Arnold, J. Jiang, *J. Phys. Chem. A* **2001**, *105*, 7525−7533.
[21] J.-H. Fuhrhop, K. M. Kadish, D. G. Davis, *J. Am. Chem. Soc.* **1973**, *95*, 5140−5147.
[22] J. G. Stites, C. N. McCarty, L. L. Quill, *J. Am. Chem. Soc.* **1948**, *70*, 3142−3143.
[23] A. De Cian, M. Moussavi, J. Fischer, R. Weiss, *Inorg. Chem.* **1985**, *24*, 3162−3167.
[24] J. Jiang, W. Liu, K.-W. Poon, D. Du, D. P. Arnold, D. K. P. Ng, *Eur. J. Inorg. Chem.* **2000**, 205−209.

Received December 3, 2002
[I02664]

Structures of Carbonato and Bicarbonato Complexes of Bis(1,10-phenanthroline)Zinc(II): Experiment and Theory

Hans Erras-Hanauer,[a,b] Zong-Wan Mao,[a,c] Günter Liehr,[a] Timothy Clark,*[b] and Rudi van Eldik*[a]

Keywords: Density functional calculations / Zinc / Carbonate complexes / Bicarbonate complexes

We report experimental and theoretical studies on the structure and properties of carbonato and bicarbonato complexes of bis(1,10-phenanthroline)zinc(II). The complex $[Zn(phen)_2O_2CO]$ has been synthesized and DFT calculations have been performed based upon its X-ray structure. The carbonate ligand coordinates in a bidentate binding mode to the metal centre with Zn–O distances of 2.130 and 2.092 Å in the X-ray structure and 2.027 Å for both distances in the calculated gas-phase structure. Because of the fundamental role of (bicarbonato)Zn^{II} complexes, especially in different carbonic anhydrases, the structures and properties of the experimentally unknown bicarbonato complexes of this kind were investigated using DFT with different basis sets up to the Ahlrichs triple zeta basis set with additional polarization functions. The bidentate bicarbonato complex $[Zn(phen)_2O_2C(OH)]^+$ was found to be about 8.2 kcal·mol^{-1} (SHAsvp), 6.4 kcal·mol^{-1} (Ahlrichs triple zeta with polarization functions) and 3.5 kcal·mol^{-1} (Ahlrichs triple zeta) more stable than the quasi-monodentate bicarbonato complex $[Zn(phen)_2O(OH)CO]^+$.
(© Wiley-VCH Verlag GmbH & Co. KGaA, 69451 Weinheim, Germany, 2003)

Introduction

Knowledge of the structures of bicarbonato complexes of Zn^{II} is essential to understand the mechanism of human carbonic anhydrase (HCA),[1−12] an enzyme that catalyzes the hydration of CO_2 and dehydration of HCO_3^- according to the overall reaction given in Equation (1).

$$CO_2 + H_2O \rightarrow HCO_3^- + H^+ \quad (1)$$

Two contrasting structural types have been proposed for these important bicarbonato complexes. The Lindskog structure involves a characteristic monodentate bicarbonate binding mode, i.e., one of the carboxylate oxygen atoms is bound to the zinc ion, whereas the hydroxy oxygen atom is only weakly coordinated to the metal centre. The Lipscomb structure involves a characteristic bidentate bicarbonate binding mode, i.e., both the carboxylate oxygen atoms are utilized as ligands for the zinc centre.[10−12] Two X-ray structures involving monodentate bicarbonate binding to different carbonic anhydrases, i.e. a bicarbonate-HCAI intermediate and a mutant intermediate of bicarbonate-HCAII (Thr-200→His-200), have been determined and taken to support the Lindskog structure.[13,14] However, calculations suggest that the bidentate coordination mode of bicarbonate contributes significantly towards the effective catalytic activity of the enzymes.[15,16] The structure of bicarbonate bound to Co^{II}-substituted carbonic anhydrase closely resembles the bidentate Lipscomb bicarbonate structure with the two bicarbonate oxygen atoms at between 2.3 and 2.5 Å from the Co^{II} ion.[17] However, bicarbonato complexes of Zn^{II} are unstable and have only recently be identified structurally.[18−23]

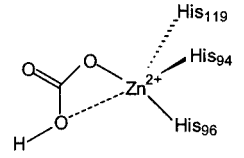

Lindskog structure

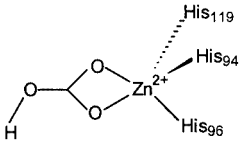

Lipscomb structure

To gain more insight into the possible coordination geometries of bicarbonate to related metal centres, we recently isolated and characterized the first stable bicarbonato complexes of bis(1,10-phenanthroline)copper(II).[24] Two complexes of the type $[Cu(phen)_2OCO_2H]ClO_4$ and $[Cu(phen)_2O_2COH]ClO_4$, in which bicarbonate is bound in monodentate and bidentate modes, respectively, could be characterized (Figure 1). The structures reported resemble

[a] Institute for Inorganic Chemistry, University of Erlangen-Nürnberg,
Egerlandstrasse 1, 91058 Erlangen, Germany
[b] Computer Chemistry Center, University of Erlangen-Nürnberg, Nägelsbachstrasse 25, 91052 Erlangen, Germany
[c] School of Chemistry and Chemical Engineering, Zhongshan University,
510275 Guangzhou, P. R. China

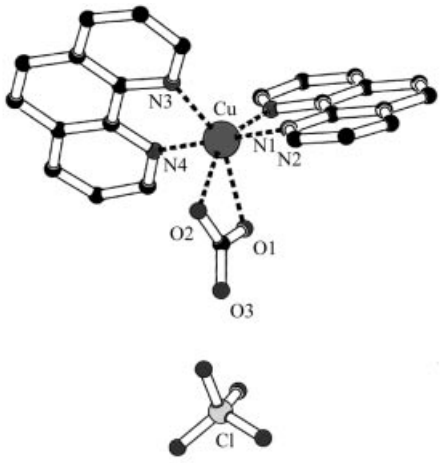

$[Cu(phen)_2O_2COH]ClO_4$

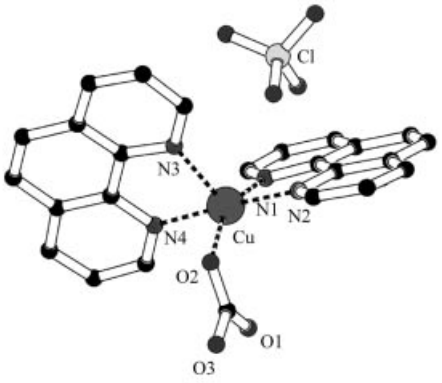

$[Cu(phen)_2OCO_2H]ClO_4$

Figure 1. X-ray structure of the two $Cu(phen)_2$ bicarbonate complexes

Lipscomb- and Lindskog-like intermediates closely with respect to the coordination mode of bicarbonate, but not with respect to the coordination geometry of the metal centre.

We could not isolate similar bicarbonato complexes of Zn^{II}, obtaining instead only $[Zn(phen)_2O_2CO]$ under all experimental conditions. In this structure, carbonate is bound in a bidentate mode − structural details are reported here. Therefore, we have used density functional theory (DFT) to calculate the structures and stabilities of the two possible bicarbonato complexes of Zn^{II}.

Results and Discussion

$[Zn(phen)_2(CO_3)]\cdot 7H_2O$ (1)

Structural and crystallographic data for this complex are reported in Tables 1 and 7. Figure 2 shows that the N_4-coordinated Zn^{II} ion is coordinated by carbonate in a bidentate mode. The bond lengths for Zn−O1 and Zn−O2 are 2.129(2) and 2.091(2) Å, respectively. The coordination polyhedron of the zinc atom can be described as a distorted octahedron. By comparison, in $[Cu(phen)_2(CO_3)]\cdot 7H_2O$ the

Table 1. Selected bond lengths [Å] and angles [°] for $[Zn(phen)_2(CO_3)]\cdot 7H_2O$ (**1**)

Zn−O(2)	2.091(2)	Zn−O(1)	2.129(2)
Zn−N(3)	2.144(2)	Zn−N(1)	2.154(2)
Zn−N(2)	2.160(2)	Zn−N(4)	2.187(2)
C(25)−O(3)	1.254(3)	C(25)−O(1)	1.296(3)
C(25)−O(2)	1.293(3)		
O(2)−Zn−O(1)	62.15(7)	O(2)−Zn−N(3)	99.14(7)
O(1)−Zn−N(3)	94.29(7)	O(2)−Zn−N(1)	92.96(7)
O(1)−Zn−N(1)	97.89(7)	N(3)−Zn−N(1)	165.82(7)
O(2)−Zn−N(2)	149.36(7)	O(1)−Zn−N(2)	89.91(7)
N(3)−Zn−N(2)	95.01(7)	N(1)−Zn−N(2)	77.85(7)
O(2)−Zn−N(4)	106.16(7)	O(1)−Zn−N(4)	164.40(7)
N(3)−Zn−N(4)	76.78(7)	N(1)−Zn−N(4)	92.83(7)
N(2)−Zn−N(4)	103.46(7)	O(3)−C(25)−O(1)	121.8(2)
O(3)−C(25)−O(2)	123.6(2)	O(1)−C(25)−O(2)	114.6(2)

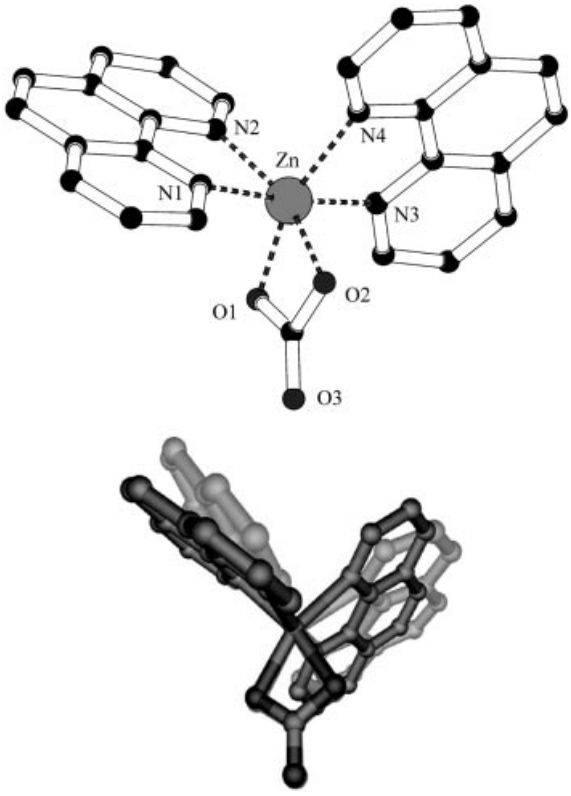

Figure 2. X-ray structure (top) and calculated structure (superimposed on the X-ray structure, bottom) of the $[Zn(phen)_2(O_2CO)]$ complex

Cu−O1 and Cu−O2 bond lengths are 2.421(3) and 1.972(3) Å, respectively,[25] i.e. the carbonate ligand forms a stronger bidentate coordination mode in the Zn^{II} complex than in the corresponding Cu^{II} complex. This behaviour differs from that in monodentate-coordinated nitrate or binuclear carbonate complexes of Zn^{II} reported before.[21,26] Therefore, the bidentate distortion of bicarbonate/carbonate Zn^{II}/Cu^{II} complexes is not only determined by the metal centre, but also by the geometry of the metal complexes.

^{13}C NMR Spectra

^{13}C NMR spectra of the labelled complex **1** were recorded in C_2D_5OD. The $[Zn(phen)_2{}^{13}CO_3]\cdot 7H_2O$ complex revealed a medium peak at $\delta = 171.1$ ppm for the bidentate binding of the carbonate group and a strong peak at $\delta = 163.3$ ppm for free HCO_3^-. Due to the low solubility of complex **1** in water, ^{13}C NMR spectra of 10 mM $[Zn(phen)_2(H_2O)](NO_3)_2$ in the presence of 30 mM $NaH^{13}CO_3$ were also recorded in D_2O/[D_6]DMSO (1:1). The spectra revealed a weak multiplet peak at $\delta = 167.5-171.1$ ppm for the various binding forms of the carbonate group, i.e. polynuclear carbonato complexes, a strong peak at $\delta = 161.5$ ppm for free HCO_3^- and a medium peak at $\delta = 126.4$ ppm for free CO_2. The chemical shift for the bidentate carbonate group lies within the values reported for other (carbonato)zinc complexes.[21,27,28]

Computational Details

Calculations were performed using the Gaussian98[29] program package with the B3LYP[30–32] combination of functionals and both the Schäfer, Horn, Ahlrichs split valence (SHAsv)[33] and the Ahlrichs triple zeta basis sets.[34] These levels of theory are referred to as B3LYP/SHAsv and B3LYP/Ahlrichs_tz, respectively. Calculations with additional polarization functions,[35,36] referred to as SHAsvp and Ahlrichs_tzp, respectively, were also performed. The latter is the highest level of theory used in this study. Due to the large number of basis functions, the use of these basis sets was restricted to the centres of interest, viz. the Zn^{2+} centre, the carbonate ligand and the N atoms of the phenanthroline ligands. For the remaining atoms of the phenanthroline chelates, the SHAsv basis set was used. The following discussion is based on the highest level of calculations, except where stated mentioned. Minimizations used the Berny algorithm along with redundant internal coordinates.[37,38] All structures were verified as local minima on the potential energy hypersurface by frequency analyses, and the zero-point vibrational energies obtained were used unscaled to correct the total energies. The DFT calculations started with the X-ray structure of the $[Zn(phen)_2(CO_3)]$ complex as shown in Figure 2. All geometries of the complexes $[Zn(phen)_2O_2CO]$, $[Zn(phen)_2O(OH)CO]^+$, and $[Zn(phen)_2O_2COH]^+$ were fully optimized without any constraints.

The structure for the carbonate complex was first calculated in C_1 symmetry corresponding to the original X-ray data, followed by further optimization in C_2 symmetry

Table 2. Energies and properties of the calculated structures

		$[Zn(phen)_2O_2CO]$	$[Zn(phen)_2O_2CO]$	$[Zn(phen)_2O_2COH]^+$	$[Zn(phen)_2O(OH)CO]^+$	$[Zn(phen)_2O(OH)CO]^{+\#}$
Basis set	Point group	C_1	C_2	C_1	C_1	C_1
	NImag[a]	0	0	0	0	1
SHAsv	E_{abs}[b]	−3184.843960	−3184.843941	−3185.323211	−3185.340750	–
	ZPE[c]	228.9	228.9	237.7	236.8	–
	E_{rel}[d]	–	–	11.9	0	–
SHAsvp	E_{abs}[b]	–	−3185.225639	−3185.705204	−3185.691203	−3185.645361
	ZPE[c]	–	227.3	236.1	235.6	233.0
	E_{rel}[d]	–	–	0	8.2	37.6
Ahlrichs_tz[e]	E_{abs}[b]	–	−3186.561845	−3187.032820	−3187.028006	–
	ZPE[c]	–	226.1	235.2	234.7	–
	E_{rel}[d]	–	–	0	3.5	–
Ahlrichs_tzp[f]	E_{abs}[b]	−3185.470208	–	−3185.945652	−3185.935461	–
	ZPE[c]	228.9	–	237.5	237.1	–
	E_{rel}[d]	–	–	0	6.4	–

[a] Number of imaginary frequencies (0 for ground states, 1 for transition states). [b] Absolute energy [hartree]. [c] Zero point energy [kcal·mol^{-1}]. [d] Difference in energy between the two bicarbonate complexes [kcal·mol^{-1}]. [e] 6-31G for H (not included in this basis set). [f] SHAsv for C,H (phenanthrolines).

Table 3. Comparision of the X-ray and calculated bond lengths with different basis sets for $[Zn(phen)_2O_2CO]$

Method	C−O3	C−O1	C−O2	Zn−O1	Zn−O2	Zn−N1	Zn−N2	Zn−N3	Zn−N4
X-ray	1.252	1.289	1.296	2.130	2.092	2.146	2.158	2.156	2.189
SHAsv	1.252	1.369	1.369	2.041	2.041	2.147	2.211	2.147	2.211
SHAsvp	1.224	1.345	1.345	2.004	2.004	2.201	2.380	2.201	2.380
Ahlrichs_tz[a]	1.250	1.369	1.369	2.051	2.051	2.184	2.240	2.184	2.240
Ahlrichs_tzp[b]	1.231	1.340	1.341	2.027	2.027	2.185	2.277	2.185	2.278
SHAsvp $[Zn(phen)_2O_2CO] + 2\ H_2O$	1.228	1.338	1.338	2.024	2.024	2.239	2.268	2.239	2.268

[a] 6-31G for H (not included in this basis set). [b] SHAsv for C,H (phenanthrolines).

(SHAsv). Both structures were verified as local minima, and were found to be very similar and practically of the same energy (Table 2). However, the structure with C_2 symmetry was used as the starting structure for the higher level calculations. All calculations were performed for the gas phase, and therefore neither solvent nor crystal effects, nor the influence of counterions was considered. As expected for a molecule in two different states of aggregation, this results in minor structural differences between the calculated and X-ray structures of the unprotonated carbonate complex. Thus, in the calculated structure the carbonate ligand is 0.068 Å closer to the metal centre with a Zn−C distance of 2.437 Å, and the calculated bond lengths for Zn−O1 and Zn−O2 of 2.027 Å are about 0.065 and 0.103 Å shorter than the corresponding bond lengths of 2.092 and 2.130 Å, respectively, found in the X-ray structure. The calculated angle for O1−C−O2 of 112.5° is 2.1° smaller, whereas the O1−Zn−O2 angle is 4.6° larger than in the X-ray structure, viz. 66.7° compared with 62.1°. The C−O1 and C−O2 distances were calculated to be 1.340 and 1.341 Å, respectively, i.e. 0.051 and 0.045 Å longer than in the X-ray structure. A comparison of selected bond lengths from the X-ray and theoretical structures is given in Table 3.

The arrangement of the coordinated phenanthroline ligands depends on the solid or gas phase state of the complex. The dihedral angle between the two ring systems decreases from 125.4° in the crystal to 113.5° in the gas phase structure owing to the more ordered and stacking arrangement of the ligands and the presence of seven water molecules in the crystal structure. Consideration of the two water molecules near the carbonate ligand in the calculations (see below) leads to an almost unchanged dihedral angle of 113.6°. The calculated Zn−N distances show two short Zn−N(1) and Zn−N(3) bonds of 2.185 Å for each, and two long bonds for Zn−N(2) and Zn−N(4) of 2.277 and 2.278 Å. In the X-ray structure a short bond [Zn−N(1) = 2.146 Å] and a long one [Zn−N(4) = 2.189 Å] and two almost equal [Zn−N(2,3) ≈ 2.157 Å] bond lengths for the phenanthroline ligands were found.

In this study the importance of the selected basis set on the bond lengths, especially for Zn^{2+}, could be confirmed. As shown in Table 3, for both basis sets the best agreement between X-ray and calculated structures was obtained without adding additional polarization functions to these basis sets. This paradoxically suggests that these basis sets give larger errors because they cannot reproduce the differences between gas phase and solid state structures. The calculations with the SHAsvp basis set lead to a shortening of between 0.02 and 0.03 Å of all bonds in which O atoms are involved. The corresponding effect on the Zn−N distances is more distinctive. The Zn−N2/N4 bond length is enlarged from 2.211 to 2.380 Å. Thus, with this basis set, the coordination sphere for Zn is strongly distorted in comparison with that found in the X-ray structure. This discrepancy did not occur with the Ahlrichs_tz basis set. The Zn−N bonds are found to be 2.184 and 2.240 Å. All C−O and Zn−O bonds are longer than the SHAsvp results, but almost identical to those found with SHAsv. We included two additional water molecules in our calculations to study their influence on the Zn−O bond lengths, which are too short for all basis sets used. The location of these water molecules was chosen according to the X-ray data. In the optimized structure (Figure 3) the O(carbonate)−O(water) distance averages as 2.643 and 2.648 Å. We used the SHAsvp basis set in a balance between accuracy and computational effort for the optimization. This was performed in C_1 symmetry without any constraints. Summarized bond lengths are given in Table 3. At this level of theory the Zn−O bond length was calculated to be 2.024 Å, which is 0.020 Å (1%) longer than in the corresponding structure without the water molecules. Transferred to the SHAsv and Ahlrichs_tz levels, an elongation of 1% means a Zn−O bond length of about 2.061 and 2.047 Å, respectively, and results in a slightly better agreement with the X-ray structure.

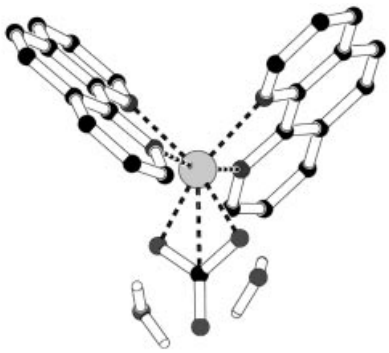

Figure 3. Calculated structure of $[Zn(phen)_2(O_2CO)]$ with two water molecules

The agreement between the X-ray and calculated Ahlrichs_tzp structure is such that the structures and relative energies of the bicarbonate complexes for which experimental data are not available can be satisfactorily calculated. The Lipscomb bicarbonate structure is represented in this model by protonation of O(3) and the Lindskog structure by protonation of O(1). The energies and properties of the calculated structures are summarized in Table 2.

The bicarbonate complex **A** clearly shows a bidentate binding mode with Zn−O bond lengths of 2.156 and 2.228 Å. The former is about 0.2 Å and the latter 0.13 Å shorter than in the related Cu complex,[24] and 0.129 and 0.201 Å, respectively, longer than in the Zn carbonate structure. The C−O(3) distance is elongated to 1.350 Å, whereas the C−O(1) and C−O(2) distances are shortened to 1.267 and 1.260 Å, respectively. As expected, the influence of protonation of O(3) on the structure of the phenanthroline ligands is small. All Zn−N bond lengths decrease to 2.159, 2.169, 2.158, and 2.166 Å, respectively, and the dihedral angle increases by 3.9° on protonation. The coordination sphere of the metal centre is best described as distorted octahedral (Figure 4). Structural details for the different basis sets are given in Table 4. The bicarbonate structure **A** was found to be the most stable bicarbonate complex. Its energy is about 8.2 kcal·mol^{-1} (SHAsvp), 3.5 kcal·mol^{-1} (Ahlrichs_tz) and 6.4 kcal·mol^{-1} (Ahlrichs_tzp) lower

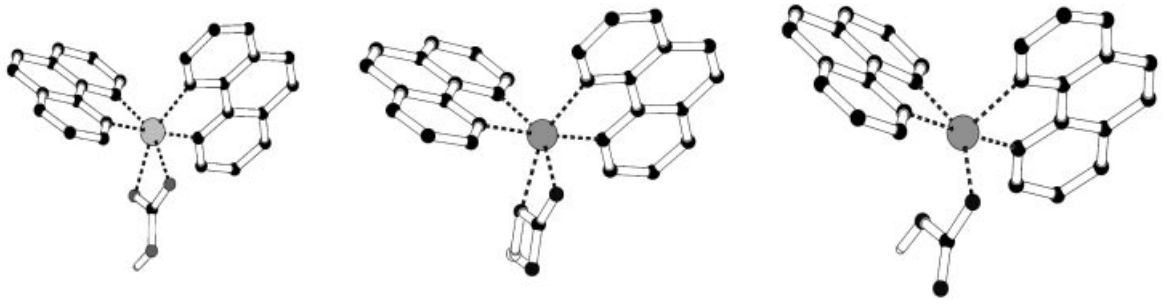

Figure 4. Structures of $[Zn(phen)_2O_2COH]^+$ (**A**), $[Zn(phen)_2O(O\cdots H)CO]^{+\#}$ (transition state for proton transfer), and $[Zn(phen)_2O(OH)CO]^+$ (**B**), respectively

than the bicarbonate complex with the proton bound to O(1) (Table 2).

In the calculated structure of **B**, a strong Zn−O(2) bond of 1.973 Å, which is only 0.051 Å shorter than the 2.024 Å in the bidentate bicarbonate structure, and a weak binding of O(1) to the metal centre with a Zn−O(1) bond length of 2.698 Å, were found. This is consistent with the calculation for the related copper complex (see below). Therefore, the binding mode has a somewhat bidentate character in comparison with the X-ray data of the analogous copper complex, which clearly binds the bicarbonate ligand in a monodentate binding mode. This behaviour shows a distinct dependence on the basis set. The Zn−O(1) distance varies from 2.542 Å (SHAsvp) to 2.980 Å (Ahlrichs_tz). The calculated C−O(1) bond length averages 1.421 Å, whereas the C−O(2) bond length averages 1.283 Å. In terms of the carbonate structure, the third C−O bond, C−O(3), remains, at 1.211 Å, almost unchanged. The structural changes on the phenanthroline ligands concern the Zn−N bond lengths, for which the values are between 2.121 and 2.177 Å, and the dihedral angle of 120.5° is 3.4 and 7.8° larger than in the bicarbonate **A** and in the carbonate structures, respectively. With the SHAsv basis set, in contrast to all other basis sets used, this bicarbonate structure was found to be lower in energy. However, this basis set gives acceptable structures, except for the Zn−O(1) distance, but the calculated energies must be treated with care. Structural details are given in Table 4.

Although, due to the significantly different coordination sphere, these complexes cannot be seen as model complexes for the active site of carbonic anhydrase, the energy of activation for the proton transfer reaction from O1 to O2 is of interest. It was possible to calculate the transition state for this reaction using the QST2 method. In the resulting structure the proton is located almost centrally between O1 and O3 with distances of 1.263 and 1.339 Å, respectively. The binding mode of the bicarbonate ligand changes from monodentate to more bidentate with Zn−O bond lengths of 2.054 and 2.409 Å, respectively. The C−O3 bond is shortened to 1.274 Å, whereas the C−O1 distance remains practically unchanged. Frequency analysis clearly shows a single imaginary frequency almost solely due to the displacement of the hydrogen atom. The activation energy for the proton transfer was calculated to be 37.6 kcal·mol^{-1}, which is close to values found previously for the uncatalyzed proton transfer reactions in related Zn complexes.[39,40]

To validate the methods used here, additional calculations were performed on the related copper bicarbonate complexes for which X-ray data are available.[24] For the $[Cu(phen)_2O(OH)CO]^+$ complex, the structural agreement between experimental and theoretical data is similar to that for the $[Zn(phen)_2(O_2CO)]$ complex. The C−O1 and C−O2 bonds in the calculated structures, viz. 1.295 and 1.397 Å, respectively, are longer than in the X-ray structure (1.264 and 1.364 Å), and the C−O3 bond is 0.012 Å too long. The results for the Cu−O distances are somewhat different. The Cu−O2 bond was calculated to be 1.939 Å, which is 0.059 Å shorter than the X-ray data, but of the same order as found for all metal−O2 bond lengths calculated here for this type of complexes. It was therefore not surprising that the Cu−O1 bond was found to be significantly shorter, viz. 2.720 Å compared with 3.045 Å in the X-ray data, which is similar to the Zn−O1 distances in the $[Zn(phen)_2O(OH)CO]^+$ complex. As already mentioned, this effect depends strongly on the basis set employed. A summary of structural details is given in Table 5. Similar structural differences were obtained between gas phase and solid state structures for the $[Cu(phen)_2O_2COH]^+$ complex. The C_2 symmetry found in the X-ray data is lowered to C_1 in the calculated structure with bond lengths of 1.988 and 2.488 Å, respectively, in contrast to 2.359 Å for both bond lengths in the X-ray structure. In this case, an additional factor to the basis set effects mentioned above is the absence of the perchlorate anion in the calculations. In the X-ray structure, the ClO_4^- anion is positioned like a cap over the bicarbonate ligand with a distance of 2.575 Å between $O(HCO_3^-)$ and $O(ClO_4^-)$. This indicates two hydrogen bonds between the bicarbonate and the perchlorate ions, which leads to a more symmetric arrangement of the bicarbonate ligand with respect to the metal centre. All calculated C−O distances are elongated between 0.037 and 0.103 Å and the Cu−N bonds are in the range of 2.074, 2.098, 2.113, and 2.330 Å. The former values are significantly shorter than those found in the Zn complexes, whereas the last value has the same magnitude as found for the $[Zn(phen)_2(O_2CO)]$ complex (without considering the additional two water molecules). According to our calculations,

Table 4. Comparison of the calculated bond lengths with different basis sets for $[Zn(phen)_2O_2C(OH)]^+$ and $[Zn(phen)_2O(OH)CO]^+$

	$[Zn(phen)_2O_2C(OH)]^+$	$[Zn(phen)_2O(O\cdots H)CO]^+$ #	$[Zn(phen)_2O(OH)CO]^+$
SHAsv:			
C−O3	1.366	−	1.230
C−O1	1.297	−	1.465
C−O2	1.285	−	1.304
Zn−O1	2.224	−	2.570
Zn−O2	2.174	−	1.994
Zn−N1	2.126	−	2.171
Zn−N2	2.152	−	2.151
Zn−N3	2.124	−	2.175
Zn−N4	2.152	−	2.183
O1−H	−	−	1.000
O3−H	0.986	−	−
SHAsvp:			
C−O3	1.341	1.274	1.206
C−O1	1.270	1.263	1.426
C−O2	1.262	1.261	1.286
Zn−O1	2.179	2.409	2.542
Zn−O2	2.135	2.054	1.964
Zn−N1	2.184	2.178	2.195
Zn−N2	2.212	2.194	2.165
Zn−N3	2.184	2.172	2.194
Zn−N4	2.212	2.177	2.194
O1−H	−	1.263	0.975
O3−H	0.974	1.339	−
Ahlrichs_tz:[a]			
C−O3	1.365	−	1.232
C−O1	1.284	−	1.442
C−O2	1.284	−	1.299
Zn−O1	2.322	−	2.980
Zn−O2	2.150	−	1.955
Zn−N1	2.151	−	2.172
Zn−N2	2.149	−	2.118
Zn−N3	2.149	−	2.169
Zn−N4	2.154	−	2.137
O1−H	−	−	0.983
O3−H	0.983	−	−
Ahlrichs_tzp:[b]			
C−O3	1.350	−	1.211
C−O1	1.267	−	1.421
C−O2	1.260	−	1.283
Zn−O1	2.228	−	2.698
Zn−O2	2.156	−	1.973
Zn−N1	2.159	−	2.174
Zn−N2	2.169	−	2.143
Zn−N3	2.158	−	2.177
Zn−N4	2.166	−	2.121
O1−H	−	−	0.977
O3−H	0.977	−	−

[a] 6-31G for H (not included in this basis set). [b] SHAsv for C,H (phenanthrolines).

Table 5. Comparison of the X-ray and calculated bond lengths with the SHAsvp basis set for the Cu bicarbonate complexes

	$[Cu(phen)_2O_2COH]^+$		$[Cu(phen)_2O(OH)CO]^+$	
	X-ray	calculated	X-ray	calculated
C−O3	1.243	1.346	1.197	1.209
C−O1	1.196	1.298	1.364	1.397
C−O2	1.196	1.233	1.264	1.295
Cu−O1	2.359	2.488	1.998	1.939
Cu−O2	2.359	1.988	3.045	2.720
Cu−N1	1.997	2.098	2.052	2.069
Cu−N2	2.119	2.330	1.987	2.122
Cu−N3	1.997	2.074	1.988	2.085
Cu−N4	2.119	2.113	2.173	2.293
O3−H	−	0.975	−	−
O1−H	−	−	−	0.976
Energies:				
E_{abs}[a]	−	−3046.805004	−	−3046.798996
ZPE[b]	−	236.1	−	235.8
E_{rel}[c]	−	0	−	3.8

[a] Absolute energy [hartree]. [b] Zero point energy [kcal·mol^{-1}]. [c] Difference in energy between the two bicarbonate complexes [kcal·mol^{-1}].

the $[Cu(phen)_2O_2COH]^+$ complex is about 3.8 kcal·mol^{-1} more stable than the corresponding $[Cu(phen)_2O(OH)CO]^+$ complex.

Based on the optimized structures obtained with the Ahlrichs_tzp basis set, the ^{13}C NMR shielding factors were calculated using the same basis set and compared with the experimental values obtained for complex **1**. The results (Table 6) demonstrate a good agreement between the experimental and theoretical values. The predicted values for the two bicarbonate complexes demonstrate that protonation of the chelated carbonate ligand (**A**) does not have a significant effect on the chemical shift, in contrast to the ring-opened protonated species (**B**). In fact, in the latter case the chemical shift is very close to that of uncoordinated bicarbonate, suggesting that the bicarbonate ligand is only weakly coordinated to the Zn centre.

The optimized theoretical structures clearly demonstrate the feasibility of stable bicarbonato complexes of bis(phenanthroline)zinc(II), even if these could not be isolated from solution. This, along with the recently identified structures of stable monodentate and bidentate (bicarbonato)Zn^{II} complexes[23] and the results of DFT studies for the conversion of carbon dioxide into bicarbonate with the $[(NH_3)_3Zn(OH)]^+$ model catalyst,[40,41] shows that stable bicarbonato complexes can form part of the overall catalytic cycle of carbonic anhydrase. According to our calculations the ring-closed complex **A** is 8.2 kcal·mol^{-1} (SHAsvp), 6.4 kcal·mol^{-1} (Ahlrichs_tzp), and 3.5 kcal·mol^{-1} (Ahlrichs_tz) more stable than the ring-opened complex **B**. This relatively small difference in energy is in good agreement with reactivity models for a series of zinc complexes.[41]

Experimental Section

$[Zn(phen)_2CO_3]\cdot 7H_2O$ (1): A mixture of (0.284 g, 0.5 mmol) of $[Zn(phen)_2(H_2O)](NO_3)_2$ and (0.336 g, 4.0 mmol) of $NaHCO_3$ was dissolved in 20 mL of water and stirred for 5 min at room temperature. The solution was filtered and allowed to stand in air for slow concentration. After a few days, colourless block crystals (0.212 g; 69.5%) suitable for X-ray analysis were obtained. IR cm^{-1} (KBr pressed pellet): $\tilde{\nu}$ = 1342 (s, CO_3^{2-}). $C_{25}H_{30}N_4O_{10}Zn$ (611.92): calcd. C 49.07, H 4.94, N 9.16; found C 49.05, H 4.88, N 8.96.

Table 6. NMR shielding values for the carbonate and bicarbonate ligands in the Zn phenanthroline complexes

	Calculated (absolute)[a] [ppm]	Calculated (relative to TMS)[a] [ppm]	Experimental [ppm]
TMS	183.3	–	0
$[Zn(phen)_2O_2CO]$	6.9	176.4	171.1
$[Zn(phen)_2O_2COH]^+$	8.6	174.7	–
$[Zn(phen)_2O(OH)CO]^+$	24.7	158.6	–
Free HCO_3^-	20.7	162.6	163.3

[a] Ahlrichs_tzp and SHAsv for C (phenanthrolines) and H.

Spectral Measurements: Infrared spectra were recorded with a Nicolet 5SX instrument using the KBr pellet method. ^{13}C NMR spectra were recorded with a Bruker DPX 300 MHz spectrometer.

X-ray Structure Analysis: Analyses on block single crystals of complex **1** were performed with a Philips PW1100/10 diffractometer. Intensity data were collected using the ω/2θ-scan technique and corrected for Lorentz and polarization effects. The structure of complex **1** was solved by direct methods using the SIR-92 program[42] and refined by full-matrix least-squares methods on F^2 using the SHELXL-93 program.[43] Hydrogen atoms were located partially from a difference synthesis and refined with an overall isotropic thermal parameter. Crystallographic data and data collection parameters are summarized in Table 7, and selected bond lengths and bond angles are given in Table 1. A labelled diagram of **1** is shown in Figure 2. CCDC-175269 for $[Zn(phen)_2(CO_3)]\cdot 7H_2O$ (**1**) contains the supplementary crystallographic data for this paper. These data can be obtained free of charge at www.ccdc.cam.ac.uk/conts/retrieving.html [or from the Cambridge Crystallographic Data Centre, 12 Union Road, Cambridge CB2 1EZ, UK; Fax: (internat.) + 44-1223/336 033; E-mail: deposit@ccdc.cam.ac.uk].

Table 7. Crystallographic details for complex **1**

Empirical formula	$C_{25}H_{30}N_4O_{10}Zn$
Formula mass	611.91
Temperature [K]	293(2)
Wavelength [Å]	0.71069
Space group	$P2_1/c$
a [Å]	9.937(3)
b [Å]	26.414(5)
c [Å]	10.571(3)
α [°]	90
β [°]	105.737(18)
γ [°]	90
V [Å^3]	2671(2)
Z	4
ρ(calcd.) [mg m^{-3}]	1.48
Abs. coeff. [m^{-1}]	0.975
F(000)	1216
Crystal size [mm]	0.68×0.55×0.40
θ range [°]	2.26–25.06
hkl ranges	−11/11, 0/31, −12/5
Reflections collected	6838
Independent reflections	4538
R(int)	0.082
Goodness of fit on F^2	1.03
R_1 [a]	0.066
wR_2[b]	0.153
Largest diff. peak [e·Å^{-3}]	−0.622, 0.53

[a] $R = \Sigma||F_o| - |F_c||/\Sigma F_o$. [b] $wR_2 = [\Sigma w(F_o^2 - F_c^2)^2/\Sigma wF_o^2)^2]^{1/2}$.

Acknowledgments

The authors gratefully acknowledge financial support from the Deutsche Forschungsgemeinschaft through SFB 583 on "Redox Active Metal Complexes", as well as a fellowship to Z.-W. M. from the Alexander von Humboldt Foundation.

[1] W. N. Lipscomb, N. Strater, *Chem. Rev.* **1996**, *96*, 2375–2434.
[2] D. N. Silverman, S. Lindskog, *Acc. Chem. Res.* **1988**, *21*, 30–36.
[3] S. J. Dodgson, R. E. Tashian, G. Gros, N. D. Carter, *The Carbonic Anhydrases*, Plenum Press, New York, **1991**.
[4] D. W. Christianson, *Adv. Protein Chem.* **1991**, *42*, 281–355.
[5] F. Botre, G. Gros, B. T. Storey, *Carbonic Anhydrase*, VCH, Weinheim, **1991**.
[6] E. A. Eriksson, T. A. Jones, A. Liljas, in: *Zinc Enzymes* (Eds.: I. L. C. Bertini, W. Maret, M. Zeppezauer), Birkhäuser, Boston, **1986**, pp. 317–328.
[7] I. Bertini, C. Luchinat, A. Scozzafava, *Struct. Bonding* **1982**, *48*, 45–92.
[8] D. A. Palmer, R. van Eldik, *Chem. Rev.* **1983**, *83*, 651–731.
[9] E. Kimura, K. Koike, M. Shionoya, *Struct. Bonding* **1997**, *89*, 1–28.
[10] W. N. Lipscomb, *Annu. Rev. Biochem.* **1983**, *52*, 17–34.
[11] J.-Y. Liang, W. N. Lipscomb, *Biochemistry* **1987**, *26*, 5293–5301.
[12] S. Lindskog, in: *Zinc Enzymes* (Ed.: G. Spiro), Wiley, New York, **1983**, pp. 77–121.
[13] Y. Xue, J. Vidgren, L. A. Svensson, A. Liljas, B. H. Jonsson, S. Lindskog, *Proteins* **1993**, *15*, 80–87.
[14] V. Kumar, K. K. Kannan, *J. Mol. Biol.* **1994**, *241*, 226–232.
[15] K. M. J. Merz, L. Banci, *J. Am. Chem. Soc.* **1997**, *119*, 863–871.
[16] M. Hartmann, K. M. J. Merz, R. van Eldik, T. Clark, *J. Mol. Model.* **1998**, *4*, 355–365.
[17] K. Hakansson, A. Wehnert, *J. Mol. Biol.* **1992**, *228*, 1212–1218.
[18] E. Kimura, T. Shiota, T. Koike, M. Shiro, M. Kodama, *J. Am. Chem. Soc.* **1990**, *112*, 5805–5811.
[19] R. Alsfasser, S. Trofimenko, A. Looney, G. Parkin, H. Vahrenkamp, *Inorg. Chem.* **1991**, *30*, 4098–4100.
[20] T. Koike, E. Kimura, I. Nakamura, Y. Hashimoto, M. Shiro, *J. Am. Chem. Soc.* **1992**, *114*, 7338–7345.
[21] A. Looney, G. Parkin, *Inorg. Chem.* **1994**, *33*, 1234–1237.
[22] P. M. Schosseler, B. Wehrli, A. Schweiger, *Inorg. Chem.* **1997**, *36*, 4490–4499.
[23] M. Döring, personal communication, **2000**.
[24] Z.-W. Mao, G. Liehr, R. van Eldik, *J. Am. Chem. Soc.* **2000**, *122*, 4839–4840.
[25] Z.-W. Mao, F. Heinemann, G. Liehr, R. van Eldik, *J. Chem. Soc., Dalton Trans.* **2001**, *3652–3562*.
[26] N. Kitajima, S. Hikichi, M. Tanaka, Y. Moro-oka, *J. Am. Chem. Soc.* **1993**, *115*, 5496–5508.
[27] A. Schrodt, A. Neubrand, R. van Eldik, *Inorg. Chem.* **1997**, *36*, 4579–4584.

[28] Z.-W. Mao, G. Liehr, R. van Eldik, *J. Chem. Soc., Dalton Trans.* **2001**, 1593−1600.
[29] M. J. Frisch, G. W. Trucks, H. B. Schlegel, G. E. Scuseria, M. A. Robb, J. R. Cheeseman, V. G. Zakrzewski, J. A. J. Montgomery, R. E. Stratmann, J. C. Burant, S. Dapprich, J. M. Millam, A. D. Daniels, K. N. Kudin, M. C. Strain, O. Farkas, J. Tomasi, V. Barone, M. Cossi, R. Cammi, B. Mennucci, C. Pomelli, C. Adamo, S. Clifford, J. Ochterski, G. A. Petersson, P. Y. Ayala, Q. Cui, K. Morokuma, D. K. Malick, A. D. Rabuck, K. Raghavachari, J. B. Foresman, J. Cioslowski, J. V. Ortiz, B. B. Stefanov, G. Liu, A. Liashenko, P. Piskorz, I. Komaromi, R. Gomperts, R. L. Martin, D. J. Fox, T. Keith, M. A. Al-Laham, C. Y. Peng, A. Nanayakkara, C. Gonzalez, M. Challacombe, P. M. W. Gill, B. Johnson, W. Chen, M. W. Wong, J. L. Andres, C. Gonzalez, M. Head-Gordon, E. S. Replogle, J. A. Pople, *GAUSSIAN 98*, Revision A.5 ed., Gaussian, Inc., Pittsburgh PA, **1998**.
[30] A. D. Becke, *J. Chem. Phys.* **1993**, *98*, 1372−1377.
[31] P. J. Stevens, F. J. Devlin, C. F. Chabalowski, M. J. Frisch, *J. Phys. Chem.* **1994**, *98*, 11623−11627.
[32] C. Lee, W. Yang, R. G Parr, *Phys. Rev. B* **1988**, *37*, 785−789.
[33] A. Schäfer, C. Huber, R. Ahlrichs, *J. Chem. Phys.* **1992**, *97*, 2571−2577.
[34] A. Schäfer, H. Horn, R. Ahlrichs, *J. Chem. Phys.* **1994**, *100*, 5829−5835.
[35] K. Raghavachari, G. W. Trucks, *J. Chem. Phys.* **1989**, *91*, 1062−1065.
[36] S. Huzinaga, *Gaussian Basis Sets for Molecular Calculations*, Elsevier, Amsterdam, **1984**.
[37] H. B. Schlegel, *J. Comput. Chem.* **1982**, *3*, 214−218.
[38] C. Peng, H. B. Schlegel, *Isr. J. Chem.* **1994**, *33*, 449−454.
[39] M. Hartmann, T. Clark, R. van Eldik, *J. Mol. Mod.* **1996**, *2*, 358−361.
[40] M. Mauksch, M. Bräuer, J. Weston, E. Anders, *ChemBioChem* **2001**, *2*, 190−198.
[41] M. Bräuer, J. L. Perez-Lustres, J. Weston, E. Anders, *Inorg. Chem.* **2002**, *41*, 1454−1463.
[42] A. Altomare, G. Cascarano, C. Giacovazzo, A. Guagliardi, M. C. Burla, G. Polidori, M. Camalli, *J. Appl. Crystallogr.* **1994**, *27*, 435−436.
[43] G. M. Sheldrick, *SHELXL-93 ed.,* University of Göttingen, Göttingen, **1993**.

Received July 17, 2002
[I02396]

Ethylene Polymerization by Self-Immobilized Neutral Nickel Catalysts Bearing Allyl Groups

Dao Zhang,[b] Guo-Xin Jin,*[a,b] and Ning-Hai Hu[b]

Dedicated to Professor Fo-Song Wang on the occasion of his 70th birthday

Keywords: Nickel / N,O ligands / Immobilization / Polymerizations

[Ni(Ph)(PPh_3)(N,O)] complexes containing phenylimino-phenolato ligands (N,O) (**1**: N,O = **A**; **2**: N,O = **B**; **3**: N,O = **C**; **4**: N,O = **D**; **5**: N,O = **E**) have been synthesized and characterized. The molecular structure of **4** was determined by single-crystal X-ray analysis. Complexes **2**–**5** bearing allyl groups have been investigated as self-immobilized catalysts for ethylene polymerization without the use of co-catalysts. The high ethylene polymerization activities of ca. 10^5 g·PE mol^{-1} Ni·h^{-1} and high molecular weight ($M_w \approx 10^5$) of polyethylene could be accomplished by changing the ligand structures and reaction conditions. The self-immobilization of catalysts brings about a dramatic increase in the catalytic activities of ethylene polymerization.

(© Wiley-VCH Verlag GmbH & Co. KGaA, 69451 Weinheim, Germany, 2003)

Introduction

The polymerization of ethylene with late-transition-metal catalysts has attracted much interest because they not only catalyze the polymerization or oligomerization of ethylene and α-olefins, but they can also co-polymerize ethylene with α-olefins containing functional groups.[1−12] More recently, Grubbs et al. reported a new family of neutral late-transition-metal catalysts that are capable of polymerizing ethylene to high-molecular-weight linear polyethylene, even in the presence of a broad range of polar additives .[13] At the same time, this new family of catalysts based on neutral Ni^{II} complexes of substituted salicylaldiminato N,O ligands are highly active systems that can polymerize functionalized olefins. More importantly, the neutral, single-component nickel(II) catalysts require no co-catalysts, such as MAO, $B(C_6F_5)_3$ or $Ni(COD)_2$. The substantial cost incurred in the hyper-purification of the monomer feed in the production of polyolefin along with the use of co-catalysts has gone. People have been attracted by the potential for using them as active polymerization catalysts as a result of their low cost and ready availability.[1,2,14,15]

In order to be applied in conventional gas-phase or slurry reactors, homogeneous catalysts have to be heterogenized because soluble catalysts cause "fouling" which means that the polyolefin that is formed is deposited on the reactor walls and causes a "boiler scale effect". Inorganic supports such as silica or alumina[16a] and also organic supports such as polystyrene and starch,[16] have been used to heterogenize soluble polymerization catalysts. Many research groups have reported on the heterogenization of metallocene catalysts.[16] As a different heterogenization strategy, Alt et al. developed the self-immobilization of metallocene catalysts, which is the synthesis of metallocene catalysts with an olefin or alkyne functional group that can be used as a co-monomer in the polymerization process.[17] Recently, our group[18] and also Herrmann et al.[19] reported the self-immobilization of Ni and Fe catalysts, respectively, for olefin polymerization. The homogenous self-immobilized catalyst can be transferred to a heterogeneous catalyst by itself during the ethylene polymerization. Herein, we report on neutral (benzaldehyde-phenylimine)nickel(II) complexes with allyl groups as self-immobilized catalysts, which exhibit excellent activities in ethylene polymerization, without co-catalysts, resulting in linear polymers.

[a] Chemistry Department, Fudan University
220 Handan Road, Shanghai 200433, P. R. China
Fax: (internat.) + 86-21/65641740
E-mail: gxjin@fudan.edu.cn
[b] State Key Laboratory of Polymer Physics and Chemistry, Changchun Institute of Applied Chemistry, Chinese Academy of Sciences
159 Renmin Street, Changchun 130022, P. R. China

Results and Discussion

Synthesis of Nickel Complexes as Self-Immobilized Catalysts

In this study, we utilized nickel complexes that possess phenylimino-phenolato chelate ligands bearing allyl groups. A general synthetic route for these complexes is shown in Scheme 1. The allyl group was introduced in dialkylaniline

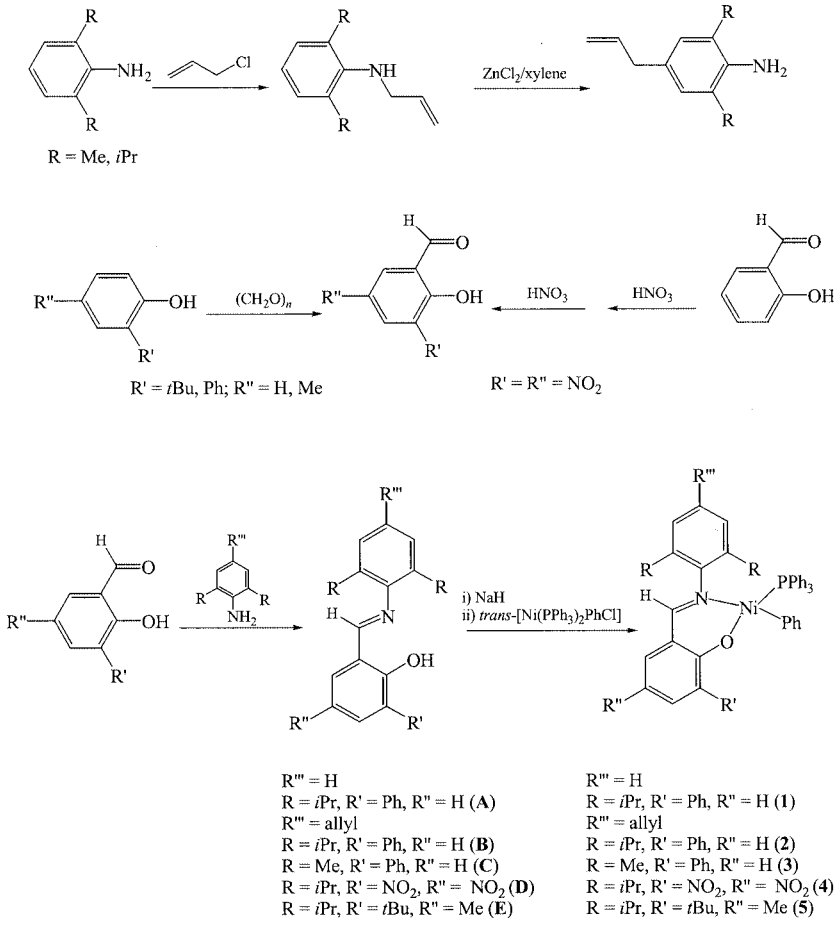

Scheme 1. Preparation of allyl-functionalized (phenylimino-phenolato)nickel complexes

by treating it with allyl chloride, giving *N*-allyl-dialkylaniline. The colorless oil was rearranged to 4-allyl-2,6-dialkylaniline in refluxing xylene in the presence of zinc chloride. Treatment of a phenol derivative with paraformaldehyde in the presence of tin(IV) chloride produced an *ortho*-formylated phenol in high yields. However, phenols containing electron-withdrawing groups barely reacted at all. Dinitrobenzaldehyde was obtained by performing the nitrogenation of benzaldehyde twice.

Ligands **B**−**E** were produced by the condensation of benzaldehyde derivatives with an equimolar amount of the allyl-substituted aniline derivative in alcohol in the presence of formic acid.[15,24,25] All phenylimino-phenolato ligands were characterized by ^{1}H NMR spectroscopy.

The (phenyl)(phenylimino-phenolato)nickel(II) complexes **1**−**5** (Scheme 1) were synthesized according to known procedures.[15,24] The phenylimino-phenolato ligand was dissolved in THF and treated with an excess of NaH. The sodium salt of the corresponding ligand was obtained in benzene and then combined with *trans*-[NiCl(Ph)(PPh_3)$_2$] to form the (benzaldehyde-phenylimine)(phenyl)nickel(II) complex in high yield. The ^{1}H NMR spectroscopic characterization and elemental analyses of complexes **2**−**5** have confirmed the composition of the complexes. The EI mass spectra generally contain the peaks of the molecular ion $[M]^+$. A particularly intense signal is observed for the $[Ni(L)(Ph)]^+$ ion which has lost the two-electron ligand PPh_3.

Molecular Structure

An X-ray crystallographic structure analysis was carried out for catalyst **4** (Figure 1). The unit cell in the solid state contains two crystallographically independent, but chemically similar molecules (**4a** and **4b**) that are related by a non-crystallographic pseudo-inversion center. Table 1 summarizes selected bond lengths and angles.

Complex **4** contains a chelating phenylimino-phenolato ligand, a triphenylphosphane group and a phenyl group. The Ni atoms are arranged in a distorted square-planar geometry made up of four atoms of the ligands (P1, O1, N1, C1 and P2, O6, N4, C47). The PPh_3 group and the imine nitrogen atom are *cis* to one another. The distances between Ni and the imine-N {phenoxy-O} are shorter [1.883(14)−1.967(15) Å] {1.912(12)−1.917(13) Å} than those in other complexes with N−O bidentate ligands [1.926(6)−1.945(4) Å] {1.911(5)−1.931(3) Å}[26b] and N−N bidentate ligands [2.010(5)−2.022(5) Å],[26a] while the distance between Ni and PPh_3 [2.207(5)−2.121(6) Å] is much

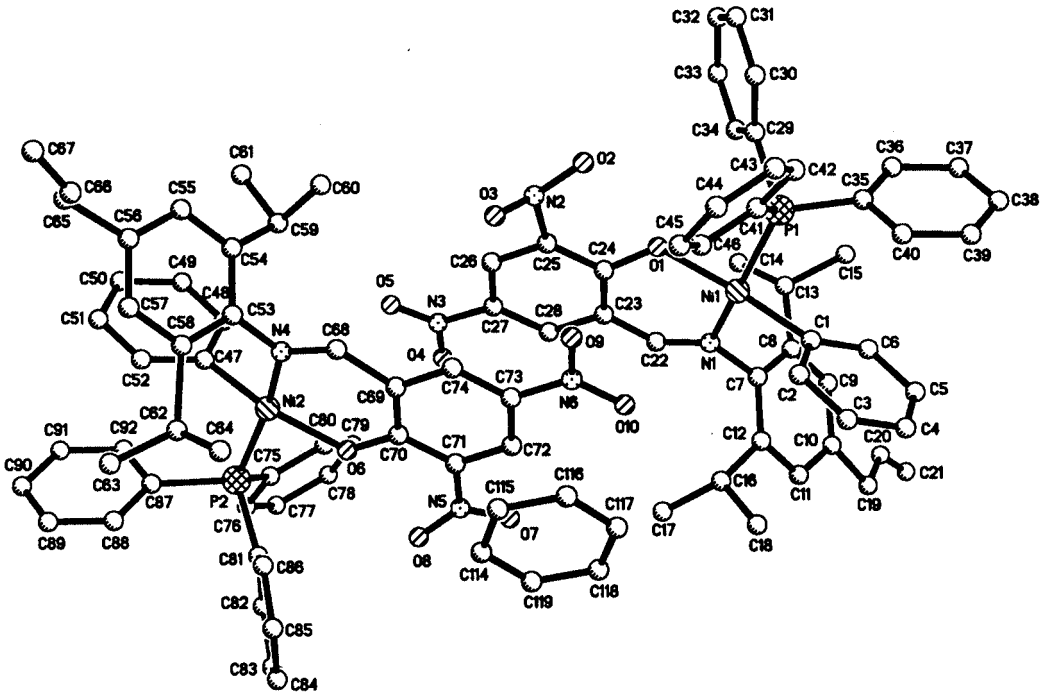

Figure 1. View of the molecular structure of complex **4**; hydrogen atoms have been omitted for clarity

Table 1. Selected bond lengths [Å] and bond angles [°] for **4** (**4a** and **4b**, respectively) with estimated standard deviations

	Bond lengths [Å]			Bond angles [°]	
	4a	**4b**		**4a**	**4b**
Ni−P	2.207(5)	2.121(6)	C(1)−Ni−N(1)	95.1(6)	94.8(6)
Ni−N	1.883(14)	1.967(15)	C(1)−Ni−O(1)	164.9(7)	160.2(6)
Ni−C	1.883(11)	1.857(10)	N(1)−Ni−O(1)	91.9(6)	93.4(6)
Ni−O	1.912(12)	1.917(13)	C(1)−Ni−P	89.0(4)	86.5(4)
N−C(imine)	1.23(2)	1.369(19)	N(1)−Ni−P	164.6(6)	164.3(5)
N−C(Ph)	1.451(16)	1.389(16)	O(1)−Ni−P	87.8(4)	90.5(4)
O−C	1.313(13)	1.324(13)	Ni−N(1)−C(22)	121.0(14)	125.6(13)
C(20)−C(21)	1.182(9)	1.194(9)	Ni−O−C	125.7(9)	130.5(9)

longer than those in other complexes [2.148(2)−2.163(2) Å,[26b] 2.172(2) Å[24]]. However, the dihedral angles defined by the C24 phenyl ring and N3−O4−O5 and also the C69 phenyl ring and N6−O9−O10 are 6.6° and 7.3°, respectively, which indicates that each nitro group is coplanar with its corresponding phenyl ring. At the same time, the dihedral angle of the C24 phenyl ring and C69 phenyl ring is only 4.9° and the distances between the atoms of the nitro groups of **4a** and the phenyl ring plane of **4b** are in the range 3.240−3.510 Å, which means that there is some interaction between the nitro group and the phenyl ring (Figure 2).

Catalysis

The (phenyl)(phenylimino-phenolato)nickel(II) complexes **1**−**5** were tested for ethylene polymerization without any co-catalysts. A significant difference in the activities was observed for the different complexes (Table 2). For example, complex **2** displays an activity of $1.8\cdot10^5$ g PE·mol^{-1} Ni·h^{-1} while complex **5** shows no activity for ethylene polymerization. Attachment of a methyl group (complex **3**), which is sterically smaller than an isopropyl group, at the R position, dramatically decreases the activity. The reason for this is that the bulky substituents surrounding the active center shield the axial faces and retard chain termination. Complex **4**, which contains electron-withdrawing groups such as the nitro groups, shows an enhanced catalytic activity.

As expected a self-immobilization effect,[17−19] similar to that found for metallocenes, could be observed during the polymerization processes. The self-immobilized catalyst **2** bearing allyl substituents displays an ethylene polymerization activity of $1.8\cdot10^5$ g PE·mol^{-1} Ni·h^{-1}, while complex **1**, without allyl group, only exhibits an ethylene polymerization activity of $0.10\cdot10^5$ g PE·mol^{-1} Ni·h^{-1} under the same polymerization conditions. When ethylene was applied

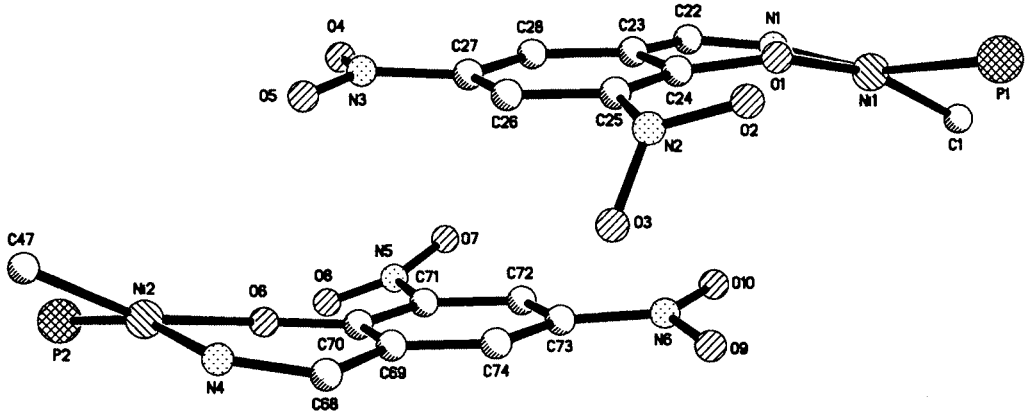

Figure 2. A plot showing the interaction between **4a** and **4b**

Table 2. Results of the ethylene polymerization with complexes **1**−**5**

Complex[a]	Activity[b]	*M*w[c]	*M*w/*M*n[c]
1	0.1	207.0[f]	2.2[f]
2	1.81	66.4	12.8
2[d]	1.32	n.d.[e]	n.d.[e]
3	0.90	121.8	4.6
4	2.90	192.4	32.0
5	0	–	–

[a] Polymerization conditions: 65.4 μmol of the appropriate catalyst, toluene (120 mL), 27 °C, 500-mL autoclave reactor, 4.0 bar ethylene pressure, reaction time 1 h. [b] 10^5 g PE·mol^{-1}Ni·h^{-1}. [c] *M*w ($\times 10^{-3}$) and *M*w/*M*n values were determined by GPC measurement. [d] Polymerization in the presence of 3 mL of methacrylate (MA). [e] Not determined.

to the solution of the self-immobilized catalysts **2**−**5**, the ethylene was polymerized and the catalyst molecules were simultaneously incorporated into the growing chain of polyethylene due to their allyl functions (Scheme 2). At the beginning the color of the reaction mixture became deep and soon a large number of dark-red particles appeared in the polymerization system. These particles still displayed high activities after they were separated to be re-used as heterogeneous catalysts. That is to say, the homogenous catalysts were transformed into heterogeneous systems without any supports. Thus, active centers distributed along the polymer chain prevent catalysts from losing their effectiveness and help to make their catalytic activities more efficient. When complex **1** was used in the polymerization the "self-immobilization" of the nickel catalysts did not occur.

Complex **2** showed a slight drop in activity of ethylene polymerization when 3 mL of methyl acrylate (MA) was added to the polymerization system. This indicates that the self-immobilized neutral nickel catalysts are tolerant towards polar monomers. The IR spectra show that the methyl acrylate was not incorporated into the polymer chain, which suggests that the addition of MA does not destroy the catalytic activity.

Influence of the Polymerization Conditions with Self-Immobilized Catalyst 2

It is well known that the conditions of the polymerization reaction influence the productivity of the self-immobilized catalyst system and the nature of the polymer produced. To study these effects, we carried out polymerization over ranges of catalyst concentration, ethylene pressure, reaction temperature, polymerization time and solvent, employing the self-immobilized catalyst **2**. The results are summarized in Table 3.

To examine the effect of the catalyst concentration on the polymerization of ethylene, we carried out several tests in which the amount of catalyst **2** was systematically varied from 65.4 to 11.3 μmol. At 65.4 μmol of catalyst a broad molecular weight distribution (12.8) was observed, centered at 67213 (M_{pk}s). As the amount of catalyst is decreased to 32.7 μmol, a narrow distribution (9.9) is observed, with an

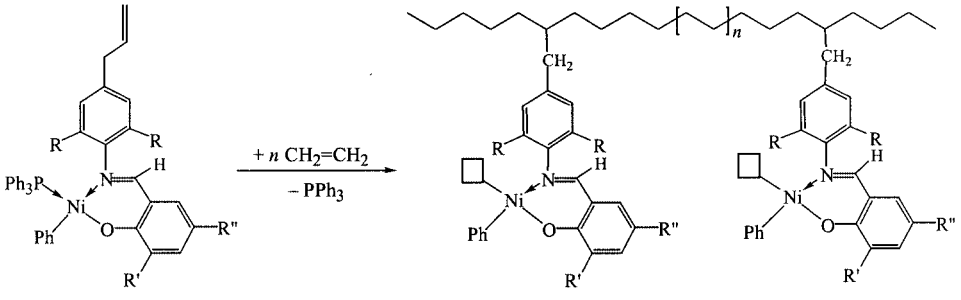

Scheme 2. Self-immobilization of allyl-functionalized (phenylimino-phenolato)Ni^{II} complexes

Table 3. Results of ethylene polymerization with self-immobilized catalyst **2**

No.[a]	Catalyst [μmol]	T [°C]	10^{-5} P [Pa]	Activity[b]	M_v [c]
1	65.4	27	4.0	1.81	82.8
2	65.4	27	3.0	1.30	87.2
3	65.4	27	2.0	0.93	129.3
4	49.1	27	4.0	2.07	31.1
5	32.7	27	4.0	3.14	96.0
6	15.1	27	4.0	2.41	372.4
7	11.3	27	4.0	1.26	196.4
8[d]	11.3	27	4.0	1.14	247.3
9	32.7	27	3.0	0.45	238.0
10[e]	32.7	27	4.0	3.70	171.5
11	32.7	37	3.0	1.81	265.3
12	32.3	47	3.0	2.23	74.2
13	32.7	57	3.0	2.18	11.8
14	32.7	67	3.0	2.00	4.4

[a] Polymerization conditions: 500-mL autoclave reactor, 120 mL of toluene, 800 rpm stirring, reaction time 1 h. [b] 10^5 g PE·mol^{-1}Ni·h^{-1}. [c] M_v ($\times 10^{-3}$) was determined with an Ubbelohde viscometer in decalin at 135±0.1 °C. [d] 120 mL of hexane was used instead of toluene. [e] Reaction time 36 min.

M_{pk}s of 71968. At 15.1 μmol the distribution (3.1) becomes very narrow with an M_{pk}s of 138061.

The ethylene pressure also has an effect on both the activity and the molecular weight distribution of the polyethylene. For example, employing 65.4 μmol of catalyst **2** at 2.0 bar of ethylene, a polymer with a distribution of 7.471 and a peak centered at 73042 was produced. On increasing the pressure to 4.0 bar, a broad distribution (12.8) was observed.

A series of experiments was undertaken to determine the effect of temperature variation on the performance of the catalyst. First, polymerization performed at 47 °C had a higher activity of $2.23 \cdot 10^5$ g PE·mol^{-1} Ni·h^{-1} than those at 27, 37, 57, and 67 °C. These results parallel the effect observed by Grubbs et al.[13] Secondly, with the increase of temperature, the molecular weight M_η varied from 238000 at 27 °C to 4400 at 67 °C, while the molecular weight distribution of PE decreased from 4.2 to 2.3. Moreover, as the reaction time increased from 36 to 60 min the activity decreased slightly from $3.70 \cdot 10^5$ g PE·mol^{-1} Ni·h^{-1} due to partial loss of catalytic activity. The solvent used for the polymerization had a slight influence, for example, when toluene solvent was replaced by hexane the activity decreased from $1.26 \cdot 10^5$ g PE·mol^{-1} Ni·h^{-1} to $1.14 \cdot 10^5$ g PE·mol^{-1} Ni·h^{-1} and M_η increased from 196400 to 247300.

Characterization of the Polyethylene Products

The ^{13}C NMR spectra of polyethylene produced by the self-immobilized catalysts **2**, **3**, and **4** have similar resonances, which can be seen in Table 4. Methyl branches were identified by the resonances at δ = 30.1 (CH_2), 20.1 (CH_3), 30.3 (CH), 37.7 (α-CH_2), 30.5 (γ-CH_2), and 27.6 ppm (β-CH_2).[27,13] The methyl branches were estimated as 0.41% (catalyst **2**), 0.55% (catalyst **3**), and 0.65% (catalyst **4**) in the spectra of PE. No other types of short branches are observed in the ^{13}C NMR spectra. The similar microstructures of polyethylene indicate that the self-immobilized catalysts keep the same arrangement around the active center as that of the original catalysts. The bulk densities of the PE produced by these self-immobilized catalysts are in the range of 0.148−0.278 g·cm^{-3}, which suggests that self-immobilization can improve the morphology of polymer products. The DSC results for the PE produced by catalysts **2**, **3**, and **4**, indicate that the self-immobilized catalysts convert ethylene to linear polyethylene with high crystallinity. The melting point temperatures (Tm [°C]) of the polyethylene produced are 131 °C (catalyst **2**), 130 °C (**3**), and 129 °C (**4**), indicating the high-density nature of the polyethylene.

Conclusion

In this study, we have demonstrated that neutral nickel complexes bearing allyl groups as self-immobilized single-component catalysts display very high ethylene polymerization activities. The activities can be improved by changing the substituents of the benzaldehyde-phenylimine ligand and the polymerization reaction conditions. The results clearly indicate that self-immobilized neutral nickel complexes possess great potential as new olefin polymerization catalysts.

Experimental Section

General: All experiments with metal complexes and phenyliminophenolato ligands were carried out under argon using standard Schlenk and vacuum-line techniques. Solvents were dried by re-

Table 4. ^{13}C NMR spectroscopic data of polyethylene employing self-immobile catalysts **2**, **3**, and **4**

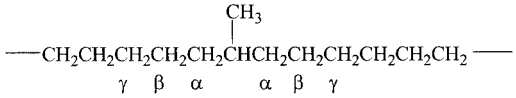

Catalyst	CH_2 (ppm)	CH_3 (ppm)	CH (ppm)	α-CH_2 (ppm)	β-CH_2 (ppm)	γ-CH_2 (ppm)	Branches per 1000 C
2	30.15	20.06	33.36	37.71	27.59	30.53	4
3	30.11	20.06	33.25	37.67	27.55	30.53	6
4	30.11	20.08	33.27	37.71	27.55	30.49	7

fluxing with appropriate drying agents (sodium/benzophenone for toluene, benzene, diethyl ether, THF, and hexane; CaH_2 for dichloromethane; magnesium for methanol) and distilled under argon prior to use. ^1H NMR spectra were recorded with a Varian Unity-400 spectrometer. NMR multiplicities are abbreviated as follows: s = singlet, d = doublet, q = quadruplet, m = multiplet, br = broad. IR spectra of the complexes were measured with a Bio-Rad FTS135 spectrometer. EI-MS spectra were recorded with a Finnigan MAT 8500 spectrometer (electron energy 70 eV) and elemental analyses were performed with a Perkin−Elmer Series II CHN/O Analyzer 2400. The ^{13}C NMR spectroscopic data for polyethylene were obtained using *o*-dichlorobenzene as the solvent with an FX-100 NMR spectrometer at 130 °C. The intrinsic viscosity [η] was measured in decalin at 135 °C using an Ubbelohde viscometer. The viscosity average molecular weight (M_v) was calculated by the following equation $[\eta] = 67.7 \cdot 10^{-3} M_v^{0.67}$. Average molecular weight (M_w) and molecular weight distribution (M_n/M_w) values of polyethylene products were determined using a PL GPC-220 gel permeation chromatograph at 150 °C using a narrow standards calibration and equipped with three PL gel columns (sets of PL gel 10 μm MIXED-B LS). Trichlorobenzene was employed as a solvent at a flow rate of 1.00 mL/min. Melting points were determined by DSC with a Perkin−Elmer 7 Series Thermal Analysis System. The starting materials 3-*tert*-butyl-5-methylbenzaldehyde and 3-phenylbenzaldehyde,[20] 3,5-dinitrobenzaldehyde,[21] 4-allyl-2,6-dimethylaniline,[22] *trans*-[Ni(PPh$_3$)$_2$(Ph)Cl][23] and complex **1**[13] were prepared according to literature procedures and characterized by ^1H NMR spectra. Other commercially available reagents were purchased and used without purification.

General Procedure for Ethylene Polymerization: A 500-mL autoclave was charged with 100 mL of toluene under argon. A solution of the self-immobilized nickel(II) complex (10−65 μmol) in toluene (20 mL) was added. After three times of ethylene gas exchange, the ethylene pressure was raised to the specified value and maintained for a certain time. The polymerization was terminated by the addition of methanol and dilute HCl (10%). The solid polyethylene was filtered, washed with methanol and dried at 40 °C in vacuo.

Preparation of Complex 2. (a) Ligand Synthesis: 4-Allyl-2,6-diisoproylaniline was prepared from 2,6-diisoproylaniline by an analogous method according to ref.[22] The colorless liquid product was collected at 98.5 °C/0.6 Torr in 35% yield. ^1H NMR(400 MHz, $CDCl_3$): δ = 6.85 (s, 2 H, H-Ar), 5.98 (m, 1 H, CH=C), 5.09 (d, 1 H, C=CH$_{(E)}$), 5.03 (d, 1 H, C=CH$_{(Z)}$), 3.6 (br, 2 H, NH_2), 3.30 (d, 2 H, CH_2C=C), 2.92 [m, 2 H, CH(Me)$_2$], 1.26 [d, 12 H, C(CH$_3$)$_2$]. Formic acid (0.25 mL) was added to a methanol solution (5 mL) containing 4-allyl-2,6-diisopropylphenylamine (1.302 g, 6.0 mmol) and 3-phenylbenzaldehyde (1.148 g, 5.8 mmol). After stirring at room temperature for 12 h, the reaction mixture was poured into distilled water (25 mL), extracted with diethyl ether (25 mL × 2), washed with deionized water (25 mL × 2) and dried overnight with anhydrous sodium sulfate. After the solvent was removed by rotary evaporation a yellow solid was separated and dried under vacuum to afford 2.187 g of **B** in 95% yield. ^1H NMR ($CDCl_3$, 400 MHz): δ = 13.68 (s, 1 H, OH), 8.35 (s, 1 H, N=CH), 7.71−7.05 (m, 8 H, Ar−H), 7.00 (s, 2 H, C=N−Ar−H), 6.00 (m, 1 H, CCH=C), 5.11 (q, 2 H, C=CH$_2$), 3.39 (d, 2 H, CH_2C=C), 2.99 (m, 2 H, CHMe$_2$), 1.16 (d, 12 H, CH_3 of *i*Pr). **(b) Complex Synthesis:** Sodium hydride (0.2 g, 5 mmol) was added to a solution of the ligand **B** (0.596 g, 1.5 mmol) in THF (20 mL). The mixture was stirred at room temp. for 2 h, and then centrifuged after which the upper clear solution was transferred and concentrated in vacuo to afford a pale-yellow solid residue. After washing with hexane (20 mL), the sodium salt of the corresponding ligand was obtained. A solution containing the sodium salt of **B** (0.629 g, 1.5 mmol) and *trans*-[Ni(PPh$_3$)$_2$(Ph)Cl] (1.0 g, 1.44 mmol) in benzene (20 mL) was stirred at room temp. After 6 h, the reaction mixture was separated by filtration to remove NaCl. Hexane was slowly added to the top of the filtrate. Complex **2** was obtained as a yellow-orange solid. Yield: 0.95 g (83%). ^1H NMR (400 MHz, C_6D_6): δ = 8.13 (d, 1 H, N=CH), 7.89−6.34 (m, 30 H, Ar-H), 6.02 (m, 1 H, CH=), 5.11 (m, 2 H, =CH$_2$), 4.23 (m, 2 H, CHMe$_2$), 3.32 (d, $J_{H,H}$ = 6.4, 2 H, CH_2), 1.35 (d, $J_{H,H}$ = 6.8 Hz, 6 H, CH_3), 1.27 (d, $J_{H,H}$ = 6.8 Hz, 6 H, CH_3) ppm. EI-MS: *m*/*z* = 717 [M − Ph]$^+$, 455 [M − Ph − PPh$_3$]$^+$. $C_{52}H_{50}NNiOP$ (794.64): calcd. C 78.60, H 6.34, N 1.76; found C 78.88, H 6.22, N 1.73.

Complex 3: Ligand **C** as a yellow solid in 90% yield. ^1H NMR ($CDCl_3$, 400 MHz): δ = 13.71 (s, 1 H, OH), 8.39 (s, 1 H, N=CH), 7.69−7.01 (m, 8 H, Ar-H), 6.93 (s, 2 H, C=N−Ar−H), 5.98(m, 1 H, CCH=C), 5.09(q, 2 H, C=CH$_2$), 3.37(d, 2 H, CH_2C=C), 2.19(s, 6 H, CH_3). **3** as a red crystalline solid. Yield: 0.95 g (86%). ^1H NMR (400 MHz, C_6D_6): δ = 8.07 (d, $J_{P,H}$ = 8.4 Hz, 1 H, N=CH), 7.78−6.44 (m, 30 H, Ar-H), 6.01 (m, 1 H, CH=), 5.10 (d, $J_{H,H}$ = 1.6, 2 H, =CH$_2$), 3.19 (d, $J_{H,H}$ = 6.4 Hz, 2 H, CH_2), 2.53 (s, 6 H, CH_3) ppm. EI-MS: *m*/*z* = 662 [M − Ph]$^+$, 400 [M − Ph − PPh$_3$]$^+$. $C_{48}H_{42}NNiOP$ (738.53): calcd. C 78.06, H 5.73, N 1.90; found C 77.99, H 5.73, N 1.91.

Complex 4: Ligand **D** as yellow-gold crystals in 95% yield. ^1H NMR ($CDCl_3$, 400 MHz): δ = 16.27 (s, 1 H, OH), 9.07 (s, $^4J_{P,H}$ = 3.2 Hz, 1 H, N=CH), 8.50 (s, $^4J_{H,H}$ = 2.8 Hz, 1 H, Ar-H), 8.26 (s, 1 H, Ar-H), 7.10 (s, 2 H, C=N−Ar−H), 5.97 (m, 1 H, CCH=C), 5.16 (q, 2 H, C=CH$_2$), 3.43 (d, 2 H, CH_2C=C), 2.95 (m, 2 H, CHMe$_2$), 1.24 (d, 12 H, CH_3 of *i*Pr). **4** as a red solid. Yield: 1.05 g (90%). ^1H NMR (400 MHz, C_6D_6): δ = 8.34 (d, $J_{H,P}$ = 2.8 Hz, 1 H, N=CH), 7.84−6.34 (m, 24 H, Ar-H), 6.02 (m, 1 H, CH=), 5.12 (m, 2 H, =CH$_2$), 3.96 (m, 2 H, CHMe$_2$), 3.28 (d, $J_{H,H}$ = 6.0, 2 H, CH_2), 1.29 (d, $J_{H,H}$ = 6.8 Hz, 6 H, CH_3), 1.12 (d, $J_{H,H}$ = 6.8 Hz, 6 H, CH_3) ppm. EI-MS: *m*/*z* = 807 [M$^+$], 545 [M − PPh$_3$]$^+$. $C_{46}H_{44}N_3NiO_5P$ (808.53): calcd. C 68.33, H 5.48, N 5.20; found C 68.97, H 5.41, N 5.10.

Complex 5: Ligand **E** as a yellow-green oil in 92% yield. ^1H NMR ($CDCl_3$, 400 MHz): δ = 13.41 (s, 1 H, OH), 8.12 (s, 1 H, N=CH), 7.26−6.98 (m, 4 H, Ar-H), 6.02 (m, 1 H, CCH=C), 5.10 (q, 2 H, C=CH$_2$), 3.39 (d, 2 H, CH_2C=C), 2.99 (m, 2 H, CHMe$_2$), 2.32 (s, 3 H, CH_3Ar), 1.48 (s, 9 H, CH_3 of *t*Bu), 1.16 (d, 12 H, CH_3 of *i*Pr). **5** as a yellow-orange solid. Yield: 0.92 g (81%). ^1H NMR (400 MHz, C_6D_6): δ = 8.10 (d, 1 H, N=CH), 7.90−6.34 (m, 24 H, Ar-H), 6.04 (m, 1 H, CCH=C), 5.11 (q, 2 H, C=CH$_2$), 4.45 (m, 2 H, CH of *i*Pr), 3.32 (d, 2 H, CH_2C=C), 2.32 (s, 3 H, CH_3−Ar), 1.36 (d, 6 H, CH_3 of *i*Pr), 1.36 (d, 6 H, CH_3) 1.26 (d, 12 H, CH_3 of *i*Pr), 1.09 (s, 9 H, CH_3 of *t*Bu) ppm. EI-MS: *m*/*z* = 787 [M]$^+$. $C_{51}H_{56}NNiOP$ (788.67): calcd. C 77.67, H 7.16, N 1.78; found C 77.90, H 7.03, N 1.88.

X-ray Crystal Structure Determination of Complex 4: The crystallographic data for **4** (**4a**/**4b**) are summarized in Table 5. Dark-red single crystals were grown in toluene/hexane (1:1) at −15 °C. The crystal was sealed in a thin-walled glass capillary under argon. The intensity data were collected at 293 K with a Siemens P4 diffractometer using Mo-K_α radiation (λ = 0.71073 Å, graphite monochromator). The stability of the primary beam was controlled by monitoring three check reflections every 100 reflections. Corrections for absorption based on the ψ-scan technique were applied. The structure was solved by direct methods using the SHELXTL-97 program and refined by full-matrix least-squares on F_o^2 using

Table 5. Crystallography data

	4
Empirical formula	$C_{59.50}H_{59}N_3NiO_5P$
Formula mass	985.78
Crystal description	Dark red plate
Crystal size [mm]	0.52 × 0.42 × 0.38
Crystal system	monoclinic
Space group	Cc
a [Å]	38.170(13)
b [Å]	10.477(4)
c [Å]	28.808(4)
β [deg]	102.45(4)
V [Å^3]	11250(6)
Z	8
Density (calcd.) [Mg·m^{-3}]	1.164
Absorption coefficient [mm^{-1}]	0.421
F(000)	4160
θ range for data collection [°]	1.99−22.50
Reflections collected	17155
Data/restraints/parameters	14620/24/791
Independent reflections	14620 (R_{int} = 0.0199)
Final *R* indices [$I > 2\sigma(I)$]	$R1$[a] = 0.0894
	$wR2$[b] = 0.2235
R indices (all data)	$R1$ = 0.2154
	$wR2$ = 0.2669
GOF on F^2	0.820
Absolute structure parameter	0.49(4)
$\rho_{max/min}$ [eÅ^{-3}]	0.821/−0.869

[a] $R1 = \Sigma||F_o| - |Fc||/\Sigma|F_o|$. [b] $wR2 = \{\Sigma[w(F^2_o - F^2_c)]/\Sigma[w(F^2_o)^2]\}^{1/2}$.

SHELXTL-97.[28] All hydrogen atoms were included in idealized positions. CCDC-186490 contains the supplementary crystallographic data for this paper. These data can be obtained free of charge at www.ccdc.cam.ac.uk/conts/retrieving.html [or from the Cambridge Crystallographic Data Centre, 12 Union Road, Cambridge CB2 1EZ, UK; Fax: (internat.) + 44-1223/336-033; E-mail: deposit@ccdc.cam.ac.uk].

Acknowledgments

We would like to thank the National Nature Science Foundation of China (29974029, 29925101) and the Special Funds for Major State Basic Research Projects (G, 1999064800) for financial support.

[1] S. D. Ittle, L. K. Johnson, M. Brookhart, *Chem. Rev.* **2000**, *100*, 469.
[2] G. J. P. Britovesek, V. C. Gibson, D. F. Wass, *Angew. Chem. Int. Ed.* **1999**, *38*, 428.
[3] L. K. Johnson, C. M. Killian, M. Brookhart, *J. Am. Chem. Soc.* **1995**, *117*, 6414.
[4] S. A. Svejda, L. K. Johnson, M. Brookhart, *J. Am. Chem. Soc.* **1999**, *121*, 10634.
[5] D. Tempel, L. K. Johnson, P. S. White, M. Brookhart, *J. Am. Chem. Soc.* **2000**, *122*, 6686.
[6] C. M. Killian, L. K. Johnson, M. Brookhart, *Organometallics* **1997**, *16*, 2005.
[7] S. A. Svejda, M. Brookhart, *Organometallics* **1999**, *18*, 65.
[8] S. J. Mclain, J. Feldman, E. F. McCord, K. H. Gardner, M. F. Teasley, E. B. Coughlin, K. J. Sweetman, L. K. Johnson, M. Brookhart, *Macromolecules* **1998**, *31*, 6705.
[9] B. L. Small, M. Brookhart, A. M. A. Bennett, *J. Am. Chem. Soc.* **1998**, *120*, 4049.
[10] G. J. P. Britovsek, M. Bruce, V. C. Gibson, B. S. Kimerley, P. J. Maddox, S. Mastroianni, S. J. McTavish, C. Redshaw, G. A. Solan, S. Stroemberg, A. J. P. White, D. J. Williams, *J. Am. Chem. Soc.* **1999**, *121*, 8728.
[11] G. J. P. Britovsek, V. C. Gibson, B. S. Kinberley, *Chem. Commun.* **1998**, 849.
[12] E. L. Dias, M. Brookhart, P. S. White, *Organometallics* **2000**, *19*, 4995.
[13] [13a] T. R. Younkin, E. F. Conor, J. I. Henderson, S. K. Friedrich, R. H. Grubbs, D. A. Bansleben, *Science* **2000**, *287*, 460. [13b] D. A. Bansleben, R. H. Grubbs, C Whang, S. Friedrich, T. R. Younkin, R. T. Li, *Meton '98:* "Polymers in transition" June, 10−11, Houston TX, USA, **1998**. [13c] C. Whang, S. Friedrich, T. R. Younkin, R. T. Li, R. H. Grubbs, D. A. Bansleben, M. W. Day, *Organometallics* **1998**, *17*, 3149.
[14] [14a] F. M. Bauers, S. Mecking, *Angew. Chem. Int. Ed.* **2001**, *40*, 3020. [14b] F. M. Bauers, S. Mecking, *Macromolecules* **2001**, *34*, 1165. [14c] S. Mecking, *Angew. Chem. Int. Ed.* **2001**, *40*, 534.
[15] [15a] A. Held, S. Mecking, *Chem. Eur. J.* **2000**, *6*, 4623. [15b] A. Held, F. M. Bauers, S. Mecking, *Chem. Commun.* **2000**, 301.
[16] [16a] K. Soga, M. Kaminaka, *Macromol. Chem. Rapid. Comm.* **1991**, *12*, 367. [16b] K. Soga, M. Kaminaka, *Macromol. Chem. Rapid. Comm.* **1992**, *13*, 22.1. [16c] S. B. Roscoe, J. M. Frechet, J. F. Walzer, A. J. Dias, *Science* **1998**, *280*, 270. [16d] G. G. Hlatky, *Chem. Rev.* **2000**, *100*, 1347 and references therein. [16e] T. R. Boussie, C. Coutard, H. Turner, V. Murphy, T. S. Powers, *Angew. Chem.* **1998**, *110*, 3472−3475; *Angew. Chem. Int. Ed.* **1998**, *37*, 3272−3275.
[17] [17a] H. G. Alt, A. Koppl, *Chem. Rev.* **2000**, *100*, 1205. [17b] H. G. Alt, *J. Chem. Soc., Dalton Trans.* **1999**, 1703.
[18] [18a] D. Zhang, G.-X. Jin, N.-H. Hu, *Chem. Commun.* **2002**, 574. [18b] C. Liu, G.-X. Jin, *New J. Chem.* **2002**, 1485.
[19] F. A. R. Kaul, G. T. Puchta, H. Schneider, F. Bielert, D. Mila-lios, W. A. Herrmann, *Organometallics* **2002**, *21*, 74.
[20] G. Casiraghi, G. Casnati, G. Puglia, G. Sartori, G. Terenghi, *J. Chem. Soc., Perkin Trans.* **1980**, *1*, 1862.
[21] R. Lovert, *J. Chem. Soc.* **1928**, 1978.
[22] M. Elliott, N. F. Janes, *J. Chem. Soc. C* **1967**, 1780.
[23] [23a] P. A. Sehun, *Inorg. Synth.* **1972**, *13*, 124. [23b] M. Hidai, T. Kashiwagi, T. Ikeuchi, Y. Uchida, *J. Organomet. Chem.* **1971**, *30*, 279.
[24] C. Wang, S. Friedrich, T. R. Younkin, R. T. Li, R. H. Grubbs, D. A. Bansleben, M. W. Day, *Organometallics* **1998**, *17*, 3149, supporting information.
[25] S. Chang, L. Jones II, C. Wang, L. M. Henling, R. H. Grubbs, *Organometallics* **1998**, *17*, 3460.
[26] [26a] J. Feldma, S. J. Mclain, A. Parthasarathy, W. J. Marshell, J. C. Calabrese, S. D. Arthur, *Organometallics* **1997**, *16*, 1514. [26b] S. Y. Desjardins, K. J. Cavell, J. L. Hoare, B. W. Skelton, A. N. Sobolev, W. A. White, W. Keim, *J. Organomet. Chem.* **1997**, *544*, 163.
[27] [27a] L. P. Linderman, N. O. Adams, *Anal. Chem.* **1971**, *43*, 1245. [27b] D. E. Dorman, *Macromolecules* **1972**, *5*, 574.
[28] G. M. Sheldrick, University of Göttingen, Germany, **1997**.

Received September 6, 2002
[I02505]

Intercalation of Amino Alcohols into α-$Zr(HPO_4)_2 \cdot H_2O$

Ludvík Beneš,*[a] Klára Melánová,[a] Vítězslav Zima,[a] Pasquale Patrono,[b] and Paola Galli[c]

Keywords: Layered compounds / Intercalations / Amino alcohols / Zirconium / Phosphate

The formation of phases during the intercalation of amino alcohols (2-aminoethanol, 3-aminopropanol, 4-aminobutanol, 5-aminopentanol, and 6-aminohexanol) into α-$Zr(HPO_4)_2 \cdot H_2O$ was studied. The existence of three phases with general formula α-$Zr(HPO_4)_2 \cdot xNH_2(CH_2)_nOH \cdot zH_2O$ (x = 0.5, 1, 2; n = 2–6; z = 0.2–1.2) depends on the molar ratio of the starting compounds in the reaction mixture. The compounds α-$Zr(HPO_4)_2 \cdot 2NH_2(CH_2)_nOH \cdot 1.2H_2O$ (n = 5 and 6) lose water and one molecule of amino alcohol upon heating to about 200 °C, as observed by thermal X-ray diffraction measurements.

(© Wiley-VCH Verlag GmbH & Co. KGaA, 69451 Weinheim, Germany, 2003)

Introduction

α-$Zr(HPO_4)_2 \cdot H_2O$, hereafter α-ZrP, is a layered compound generated by the packing of two-dimensional macromolecular units that interact weakly with each other. Due to the presence of ionogenic P-OH groups on the surface of the layers, and to the easily accessible interlayer region, this compound is able to act as a host for cationic or molecular polar guest species. The host-guest chemistry of α-ZrP has been summarized in several reviews[1–3] and books.[4–6]

The intercalation of strong bases such as alkylamines is driven by the acid-base interaction between the amino group of the amine and the P-OH groups of the layer. The intercalation of aliphatic monoamines and diamines has been investigated by several groups.[7–12] The intercalation process usually occurs in well-defined steps, indicating the presence of two or more solid phases, and the final products contain one water and two monoamine molecules or one water and one diamine molecules per formula unit. The amine is usually protonated during the intercalation.

A homologous series of 1-alkanols or 1,ω-alkanediols with chain lengths ranging from 2 to 18, or 2 to 10 carbon atoms, respectively, was intercalated into α-ZrP, finely dispersed with the guest species, by exposing the reaction mixture to microwave radiation.[13] Thermogravimetric analysis showed that the intercalation compounds contain a maximum of two mols of alkanol or one mol of alkanediol per mol of zirconium phosphate.

The intercalation of amino alcohols was performed by titrating α-ZrP with their aqueous solution.[6] Fully intercalated products contain two molecules of amino alcohol per formula unit, forming a bilayer with the carbon chain axis almost perpendicular to the host layers. These compounds undergo thermal decomposition leading to phases with one and 0.6 amino alcohol molecules per formula unit.

This paper reports on the intercalation of amino alcohols into α-zirconium hydrogenphosphate. The work is focused on a study of phase formation as a function of reaction time and the ratio of the starting compounds (amino alcohol/α-ZrP, hereafter denoted as y).

Results and Discussion

Amino alcohol molecules enter between the host layers and the decrease of concentration of basic amino alcohol molecules in solution is accompanied by a decrease of pH, which can be observed. A plot of the pH value as a function of time is given in Figure 1. 3-Aminopropanol was added to an aqueous suspension of α-ZrP in an amount corresponding to the α-ZrP/aminopropanol ratios of 1:1 and 1:2 at time t = 2 min (see inset in Figure 1). The decrease in the amount of amino alcohol is indicated by an exponential decrease of pH. As is obvious from Figure 1, the decrease of pH proceeds for several hours. This means that a relatively long time is needed to reach equilibrium. This time increases with increasing length of the carbon chains.

[a] Joint Laboratory of Solid State Chemistry of Academy of Sciences of the Czech Republic and University of Pardubice, Studentská 84, 532 10 Pardubice, Czech Republic
Fax: (internat.) +420-46/603-6011
E-mail: ludvik.benes@upce.cz
[b] IMAI-CNR, Area della Ricerca, Via Salaria Km 29.6, 00016 Monterotondo Scalo, Rome, Italy
[c] Dipartimento di Chimica, Universita "La sapienza", P. le Aldo Moro, 5–00185 Rome, Italy

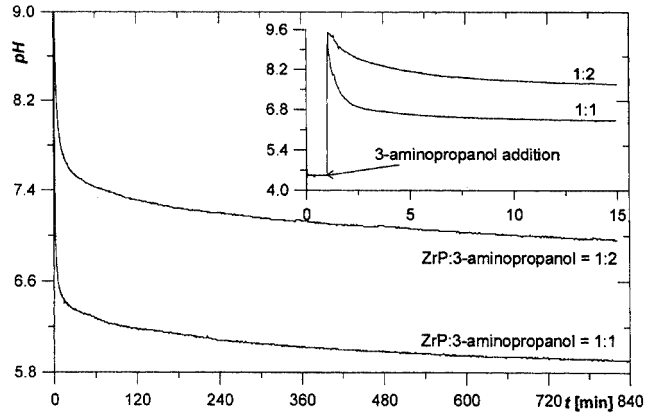

Figure 1. Time course of pH after addition of stoichiometric amount of 3-aminopropanol to an α-ZrP water suspension

For the titration of the aqueous suspensions of α-ZrP, a 100 min time interval between addition of 0.2 mL doses of amino alcohol was chosen, so that a constant pH value was reached (see Figure 2). For the 6-aminohexanol intercalations, 200 min intervals between 0.4 mL doses were used. Titration curves for the titration of α-ZrP with 2-aminoethanol, 3-aminopropanol, 4-aminobutanol, 5-aminopentanol, and 6-aminohexanol are given in Figure 3. In the case of 2-aminoethanol, the reaction occurs in well-resolved steps and plateaus, indicating the presence of three phases. Each step leads to the formation of the given intercalation compound with a characteristic value of the basal spacing that differs from the others in a higher amino alcohol content. The steps become less pronounced for longer amino alcohols.

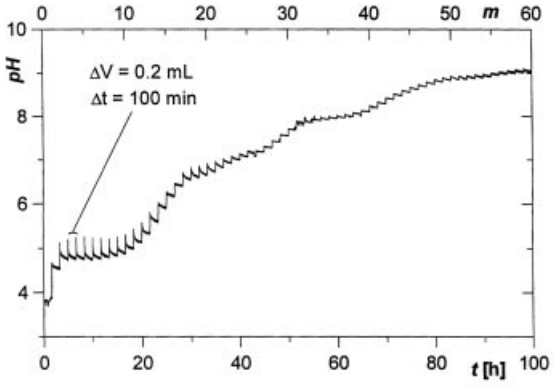

Figure 2. Time dependence of pH during potentiometric titration of an α-ZrP/water suspension with 2-aminoethanol solution; the number of additions of aminoethanol is given in the upper *x* axis

Three phases with different basal spacings were found in the samples during the intercalation (see Figure 4). They are formed consecutively, with a maximum relative ratio at amino alcohol contents *x* of 0.5, 1, and 2 (hereafter denoted as phases 0.5, 1, and 2). The 0.5 phase forms rapidly with amino alcohols having shorter chains (from 2-aminoethanol

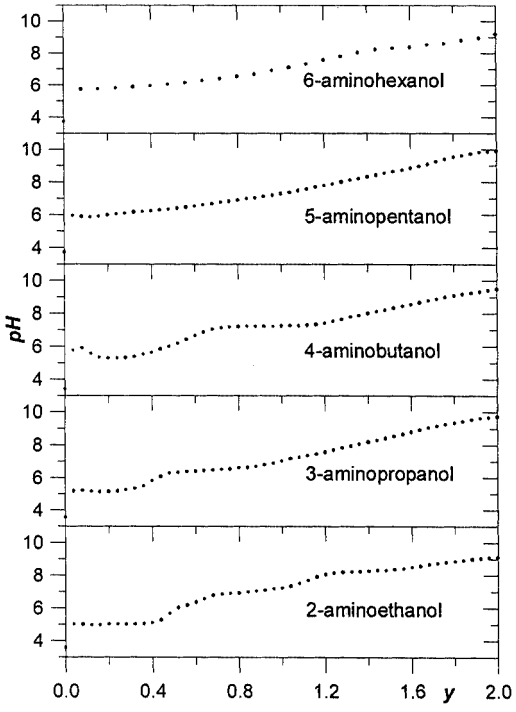

Figure 3. Potentiometric titration curves; *y* = amino alcohol:Zr ratio

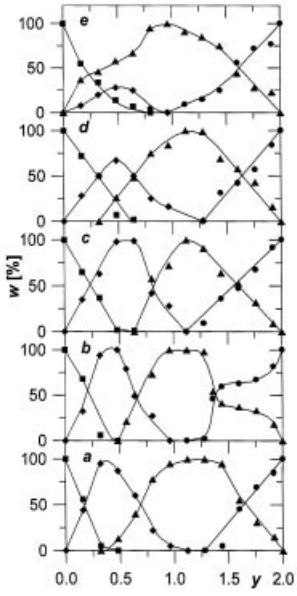

Figure 4. Dependence of relative phase content *w* on stoichiometric quotient *y* of: 2-aminoethanol (a), 3-aminopropanol (b), 4-aminobutanol (c), 5-aminopentanol (d), and 6-aminohexanol (e)

to 4-aminobutanol) and can be prepared in a pure form. In the case of 5-aminopentanol, this phase forms less readily, although it still represents a significant part of the reaction product. On the other hand, only a small amount of the 0.5 phase was observed in the intercalate with 6-aminohexanol, in which it accompanies the 1 phase. While a plateau corresponding to the 1.5 phase is observed on the titration curve for 2-aminoethanol, no such phase was observed for any

amino alcohol in the diffraction spectra of the corresponding intercalates. A moderate consecutive change of the basal spacing of phases 1 and 2 is observed when the ratio of the starting compounds y is changed from 1 to 2. It can be presumed that the amino alcohol content x in these phases is variable within a certain range.

The pure phases $Zr(HPO_4)_2 \cdot xNH_2(CH_2)_nOH \cdot zH_2O$ were prepared by the reaction of α-ZrP with a stoichiometric amount of the corresponding amino alcohol. Their composition was determined by thermogravimetric and elemental analysis. The found compositions (Table 1) are in good agreement with the presumed values ($x = 0.5$, 1.0, and 2.0). The TG curves of all prepared pure intercalate phases of 4-aminobutanol are given in Figure 5. The intercalated water is released up to 200 °C, 4-aminobutanol is released at around 300 °C, and a slow weight decrease at 350−550 °C corresponds to the removal of condensation water and the formation of pyrophosphate ZrP_2O_7. A further slow decrease of the weight is given by the combustion of carbon formed by the decomposition of the amino alcohol. The final product of the heating to 1200 °C is gray and contains some residual carbon.

Table 1. Composition of intercalates $Zr(HPO_4)_2 \cdot xNH_2(CH_2)_nOH \cdot zH_2O$

n	Phase 0.5		Phase 1		Phase 2	
	x	z	x	z	x	z
2	0.46	0.7	0.91	0.4	2.00	1.2
3	0.45	0.9	0.94	1.0	2.00	0.8
4	0.45	1.0	0.86	0.3	1.91	0.7
5	—[a]	—	0.95	1.2	1.90	1.2
6	—[a]	—	0.90	0.2	1.93	1.2

[a] Pure compounds were not prepared.

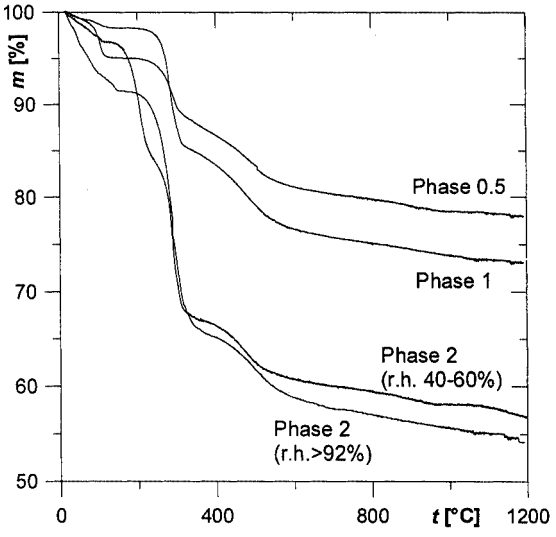

Figure 5. TGA of 4-aminobutanol intercalates

The dependence of the basal spacing of the intercalates prepared on the carbon chain length is given in Figure 6. This dependence is linear for the phases 0.5, with a slope of 0.407.

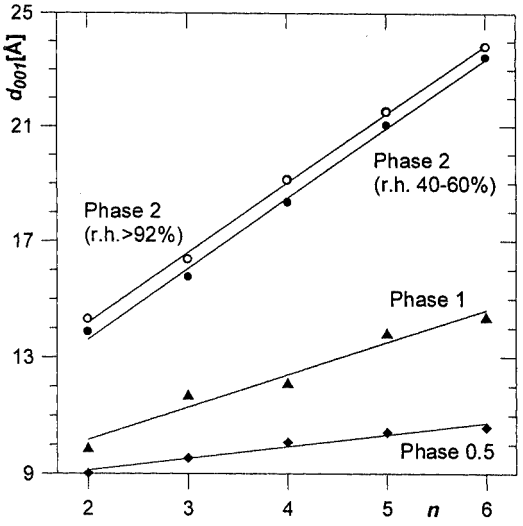

Figure 6. Dependence of the basal spacing d_{001} on the number of carbon atoms n in the amino alcohol chain

For the phases 1, the increment of the basal spacing alternates regularly when a homologous series of amino alcohols is used. The basal spacing increases by about 1.8 Å when going from an amino alcohol with an even number of carbon atoms to an amino alcohol with the chain one carbon atom longer. When we go from an amino alcohol with an odd number of carbon atoms to an amino alcohol with the chain one carbon atom longer, the increase of basal spacing is about 0.5 Å. This alternation can be explained by a different water content in the intercalates (see Table 1). The average increment of the basal spacing is 1.11 Å. As was found by XRD measurements at different relative humidities (*r.h.*), the basal spacing of the 2-aminoethanol, 4-aminobutanol, and 6-aminohexanol intercalates remains constant at *r.h.* > 92% and basal spacing of 3-aminopropanol and 5-aminopentanol intercalates does not change at *r.h.* < 11%. The water content in these intercalates does not depend on the relative humidity of ambient air, as was found by TG measurements.

On the other hand, the water content of the fully intercalated products (phases 2) does depend on the relative humidity. Under ambient conditions (*r.h.* = 40−60%), the intercalates contain about one water molecule per formula unit. The linear dependence of the basal spacing on n has a slope of 2.356. At high relative humidity (*r.h.* > 92%), these intercalates contain two water molecules and their basal spacings increase by about 0.62 Å, although the slope of the dependence of the basal spacing on n is practically the same as under ambient conditions.

The 5-aminopentanol and 6-aminohexanol intercalates (phases 2) were studied by thermal X-ray measurements. A small decrease of the basal spacing (about 0.25 Å) was ob-

served at about 50 °C; this may be caused by water released from the interlayer space. Formation of phases 1 was observed at about 160 °C and the phases 2 disappeared at 200 °C. This is in good agreement with Costantino's results.[6] The temperatures of dehydration and loss of one molecule of amino alcohol determined by TG (79 and 220 °C for 6-aminohexanol) are higher than those determined by XRD. This difference is caused by the insensibility of TG to crystal structure changes which occur during the release of the guest from the interlayer space before its evaporation from the sample.

As follows from the calculated slopes, the molecules of amino alcohols in the interlayer space are less tilted relative to the host layers with an increasing degree of intercalation, so that they form a bimolecular film with chains tilted at an angle of 67° in the fully intercalated phases.

Experimental Section

Well-crystallized α-ZrP, of formula α-$Zr(HPO_4)_2 \cdot H_2O$, was obtained according to the method reported by Alberti and Torracca.[14] A clear solution was prepared by dissolving 10.1 g of $ZrOCl_2 \cdot 8H_2O$, 8 mL of hydrofluoric acid (40% w/w) and 92 mL of H_3PO_4 (85% w/w) in 160 mL of water. The solution was heated at 80 °C for 4 days, maintaining a constant volume by continuously adding water. The α-ZrP precipitate was washed with deionized water and dried in air.

Intercalation of 2-aminoethanol, 3-aminopropanol, 4-aminobutanol, 5-aminopentanol and 6-aminohexanol into α-ZrP was studied. Three types of experiment were carried out:
1) α-ZrP (0.25 g, 0.83 mmol) suspended in 50 mL of H_2O was titrated with a 0.166 M solution of the corresponding amino alcohol. In each step, 0.2 mL of amino alcohol was added at 100 min intervals. The pH values were followed as a function of time.
2) The successive formation of the phases was followed on the samples prepared by the reaction of the suspension of 0.125 g of α-ZrP in 50 mL of H_2O with 0.4, 0.8, 1.2, 1.6, 2.0, 2.4, 2.8, 3.2, 3.6, 4.0, 4.4, 4.8 and 5.0 mL of a 0.166 M solution of the corresponding amino alcohol. After the amino alcohol addition, the samples were stirred for 24 h and the solvents evaporated to dryness at 50 °C.
3) The pure phases $Zr(HPO_4)_2 \cdot xNH_2(CH_2)_nOH \cdot zH_2O$ (x = 0.5, 1.0 and 2.0; z = 0.4−1.2) were prepared by reaction of α-ZrP with a stoichiometric amount of corresponding amino alcohol. The basal spacing and content of water as a function of relative humidity of the atmosphere was followed.

X-ray powder diffraction (XRPD) patterns of the intercalates were obtained with an X-ray diffractometer (HZG-4, Germany) using Ni-filtered Cu-K_α radiation. The Cu-$K_{\alpha 2}$ intensities were removed from the original data. Silicon (a = 5.43055 Å) was used as internal standard. Diffraction angles were measured from 2θ = 1.5° to 2θ = 50°. XRPD patterns at different temperatures, from 20 to 250 °C, were taken on samples heated on a sintered alumina ceramic plate equipped with a thermocouple.[15]

The compositions of the pure phases were calculated from thermogravimetry measurements (Stanton Redcroft STA-801, heating rate 5 °C/min, Pt crucible, Pt-Pt/Rh thermocouples, air flow) and elemental analysis. The weight of the gray residue obtained by heating to 1200 °C was corrected for the carbon remaining in the sample, which was determined by elemental analysis. The difference between the original weight of the sample and the corrected weight of the sample after heating is the weight of the organic substance, hydration water, and condensation water (water released by formation of pyrophosphate ZrP_2O_7). From the corrected weight of the heated sample, the amount of zirconium pyrophosphate was calculated and found to correspond to the amount of condensation water. The amount of hydration water corresponded to the weight loss observed to about 200 °C. The amount of the organic substance was calculated as the difference between the total weight loss and the amount of water. From the amount of the organic substance one can calculate the N, C, and H content of the sample and compare it with the results from elemental analysis. From these considerations the general formula of the intercalation compounds $Zr(HPO_4)_2 \cdot xNH_2(CH_2)_nOH \cdot zH_2O$ was determined.

Acknowledgments

Research was carried out in the framework of the Agreement for Scientific Cooperation between the Italian C.N.R. and the Academy of Sciences of the Czech Republic. K. M., L. B., and V. Z. wish to thank the Grant Agency of the Czech Republic (Grant No. 202/01/0520) for funding.

[1] G. Alberti, M. Casciola, U. Costantino, R. Vivani, *Adv. Mater.* **1996**, *8*, 291−303.
[2] G. Alberti, U. Costantino, *J. Mol. Catal.* **1984**, *27*, 235−250.
[3] A. Clearfield, *Chem. Rev.* **1988**, *88*, 125−148.
[4] G. Alberti, U. Costantino, in *Inclusion Compounds* (Eds.: J. L. Atwood, J. E. D. Davies, D. D. MacNicol), Oxford University Press, Oxford, 1991; Vol. 5, p 136−157.
[5] A. Clearfield, in *Progress in Intercalation Research* (Eds.: W. Müller-Warmuth, R. Schöllhorn) Kluwer Academic Publishers, Dordrecht, 1994; Vol. 17, p 240−252.
[6] A. Clearfield, U. Costantino, in *Comprehensive Supramolecular Chemistry* (Eds.: G. Alberti, T. Bein) Pergamon, Oxford, 1996; Vol 7, p 107−139.
[7] S. Yamanaka, Y. Horibe, M. Tanaka, *J. Inorg. Nucl. Chem.* **1976**, *38*, 323−326.
[8] A. Clearfield, R. M. Tindwa, *J. Inorg. Nucl. Chem.* **1979**, *41*, 871−878.
[9] J. P. Gupta, D. V. Nowell, *J. Chem. Soc., Dalton Trans.* **1979**, 1178−1182.
[10] G. Alberti, U. Costantino, *J. Mol. Catal.* **1984**, *27*, 235−250.
[11] R. M. Tindwa, D. K. Ellis, G.-Z. Peng, A. Clearfield, *J. Chem. Soc., Faraday Trans.* **1985**, *81*, 545−552.
[12] M. Casciola, U. Costantino, L. Di Croce, F. Marmottini, *J. Incl. Phenom.* **1988**, *6*, 291−306.
[13] U. Costantino, R. Vivani, V. Zima, L. Beneš, K. Melánová, *Langmuir* **2002**, *18*, 1211−1217.
[14] G. Alberti, E. Torracca, *J. Inorg. Nucl. Chem.* **1968**, *30*, 317−318.
[15] L. Beneš, *Sci. Pap. Univ. Pardubice Ser. A* **1996**, *2*, 151−155; *Chem. Abstr.* **1997**, *126*, 310616v.

Received September 30, 2002
[I02542]

A Study of the Equilibrium and Kinetics of Urea Binding by a Biomimetic Dinickel(II) Complex

Sergey V. Kryatov,[a] Elena V. Rybak-Akimova,*[a] Franc Meyer,*[b] and Hans Pritzkow[c]

Dedicated to Professor George M. Sheldrick on the occasion of his 60th birthday

Keywords: Enzyme models / Nickel / N ligands / Kinetics / Thermodynamics

The equilibrium and kinetics of urea binding by model dinickel complexes have been studied, which is relevant to the activity of the urease enzyme. The pyrazolate-based, O_2H_3-bridged dinuclear nickel(II) complex $[LNi_2(OH)(H_2O)]^{2+}$ (**1**) binds urea reversibly in organic solvents with the formation of an *N*,*O*-bridged urea anion complex $[LNi_2[OC(NH_2)NH)]^{2+}$ (**2**) and two water molecules. The equilibrium constant has been measured as 4.3(4) in acetone, 2.7(5) in acetonitrile, and 3(1) in methanol at 25 °C. Upon dissolving **1** in anhydrous methanol, the O_2H_3 bridge is substituted for an O_2Me_2H bridge to give $[LNi_2(OMe)(MeOH)]^{2+}$ (**4**),which has been crystallized as **4**·$(ClO_4)_2$ and characterized by X-ray diffraction. Both Ni^{II} ions in **4** are five-coordinate with geometries intermediate between square-pyramidal and trigonal-bipyramidal. The H atom in the Me_2O_2H bridging unit is located in an asymmetric position. The exchange of water and methanol ligands in complexes **1** and **4** is very fast in solution at 25 °C ($k_{obsd.} > 10^3$ s^{-1}). Binding of urea by complexes **1** and **4** are slower reactions ($k_{obsd.} \approx 10^{-1}$ to 10^1 s^{-1} under the concentration conditions used) and can be monitored by stopped-flow techniques. Detailed kinetic studies indicate that binding of urea is a multi-step process. Steady-state intermediates of the tentative formula $[LNi_2(OR)(urea)_n]^{2+}$ (n = 1, 2) are formed in fast preequilibrium with the starting complexes **1** (R = H) and **4** (H = Me), respectively. The bidentate *N*,*O*-coordination and deprotonation of an *O*-bound urea ligand constitute the overall rate-limiting step. The kinetic data suggest that both mono- and bis(urea) complexes participate in the formation of the chelate **2**, and that the latter are substantially more reactive. The bis(urea) pathway was unexpected because only one urea molecule is incorporated into the final product **2**. Reactive intermediates $[LNi_2(OH)(urea)_n]^{2+}$ are close analogs of the reactive intermediate of urease, which also has the hydroxide and urea ligands bound at a dinickel core. However, the reactivities of the intermediates are different. The hydroxide ligand in our model complex acts as a base towards urea, and the urea anion complex **2** is formed. In urease, the hydroxide ligand attacks urea as a nucleophile leading to the hydrolysis of urea.
(© Wiley-VCH Verlag GmbH & Co. KGaA, 69451 Weinheim, Germany, 2003)

Introduction

Urease is an exceptional metallohydrolase that is present in various plants, fungi and bacteria. It contains two proximate nickel ions within its active site and efficiently catalyzes the hydrolysis of urea to finally give carbon dioxide and 2 equiv. of ammonia.[1,2] This is a very remarkable reaction because urea has a very high resonance energy and hence is an extremely stable molecule. In fact, the uncatalyzed hydrolysis of urea has never been observed, while in aqueous solution urea slowly decomposes by an elimination pathway to yield ammonium cyanate.[3] Since the first X-ray crystal structure of microbial urease was published in 1995,[4] accumulating crystallographic evidence has provided a detailed picture of the enzyme active site and a reliable background for understanding its mechanism of catalysis.[5–7] Based on the crystal structures of urease inhibited by either phosphate or diamidophosphate, as well as on the basis of recent model calculations and the mechanistic studies of enzyme inhibition, the process outlined in Scheme 1 now seems most probable.[7,8] It implies that urea first coordinates to one nickel ion through its carbonyl oxygen atom, followed by a transition towards a bridging binding mode and concomitant nucleophilic attack by the bridging hydroxide ligand. The exact sequence of the latter events remains unclear, but work on synthetic model compounds suggests that urea becomes quite acidic (down to pK_a = 3 in aqueous solution) and tends to deprotonate upon *N*-

[a] Department of Chemistry, Tufts University,
Medford, Massachusetts 02155, USA
Fax: (internat.) + 1-617/627-3443
E-mail: elena.rybak-akimova@tufts.edu
[b] Institut für Anorganische Chemie, Georg-August-Universität,
Tammannstrasse 4, 37077 Göttingen, Germany
Fax: (internat.) + 49-551/393063
E-mail: franc.meyer@chemie.uni.goettingen.de
[c] Anorganisch-Chemisches Institut der Universität Heidelberg
Im Neuenheimer Feld 270, 69120 Heidelberg, Germany
Supporting information for this article is available on the WWW under http://www.eurjic.org or from the author.

coordination.[9] This should be even more pronounced upon bidentate *N,O*-binding to two metal ions, thereby rendering the substrate more resistant to hydrolysis under the optimal pH conditions of urease (pH = 4−8).[10] It thus seems likely that one of the Ni−OH bonds is weakened upon initial binding of the substrate, and that formation of the bridging Ni−N_{urea} bond and nucleophilic attack occur simultaneously.[7,8,11]

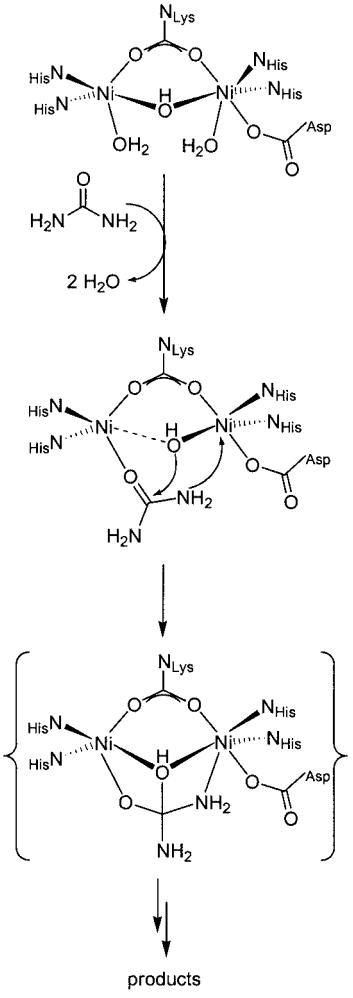

Scheme 1

Several synthetic dinickel model complexes have been prepared to mimic structural or functional features of the urease active site.[11−16] In most model systems where urea coordination has been structurally verified, the substrate is bound through its carbonyl O atom, which is the preferred urea binding mode.[14] In the very few systems showing a dinickel site with a bidentate *N,O*-bridging urea,[11,15,16], the substrate is deprotonated as a ureate anion. Clearly, elucidation of the details of substrate binding is a prerequisite for a comprehensive understanding of urease activity. Likewise, control of urea binding in dinickel model complexes is crucial for achieving urease-like reactivity.

We have therefore carried out an in-depth analysis of the equilibrium and kinetics of urea binding by the active dinickel compound **1**, which was shown to give ureate-bridged **2** in an acid/base reaction according to Scheme 2.[15] The bridging pyrazolate in **1** and **2** was anticipated to most closely resemble the bridging carboxylate of the native enzyme (i.e. a carboxylated lysine residue), since both bridging units are monoanionic and can support similar metal−metal distances (from 3.3 to 4.6 Å for pyrazolate-bridged complexes).[11,12e,13,14d,15,16,17,19,20] Short pendant arms (such as in complex **1**) enforce larger M−M separations. Complex **1** was chosen to specifically investigate the reactivity of an *Ni*-bound hydroxide ligand that can not bridge the two Ni centers. In urease, both terminal and bridging hydroxide ligands are present. Complex **1** possesses an intramolecular O_2H_3 bridge that can be described as a hydrated form of an active *Ni*-bound hydroxide ligand. This terminal hydroxide ligand is expected to be much more reactive as a base compared with a bridging hydroxide ligand. The latter is prevented in **1** due to the large Ni···Ni separation (4.5 Å, as compared to 3.5 Å in urease) enforced by the compartmental pyrazolate ligand scaffold.[13,17] Urea incorporation by the diiron(III) complex $[Fe_2(tpa)_2(\mu\text{-}O)(O_2H_3)]^{3+}$ has recently been shown to proceed by a reversible multistep process.[18] To the best of our knowledge, no quantitative data on the stability of nickel urea complexes or on the kinetics of their formation in solution have been reported.

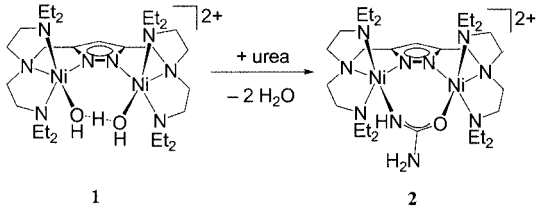

Scheme 2

Results and Discussion

Equilibrium Studies

Initially, the behavior of **1** in various solvents and the equilibrium of urea binding (Scheme 2) were studied by UV/Vis spectroscopy.

Acetone

Complex **1** ($[LNi_2(OH)(H_2O)]^{2+}$) has been shown to react with urea in acetone solution according to Scheme 2,[15] with an equilibrium constant given by K_1 [Equation (1)].

$$[LNi_2(OH)(H_2O)]^{2+} + OC(NH_2)_2 \rightleftarrows [LNi_2\{OC(NH_2)\text{-}NH\}]^{2+} + 2\,H_2O$$
$$K_1 = \{[LNi_2\{OC(NH_2)NH\}][H_2O]^2\}/\{[LNi_2(OH)(H_2O)]\text{-}[OC(NH_2)_2]\} \quad (1)$$

The UV/Vis spectrum of complex **1** in acetone at 25 °C is independent of the water content in the range 0.002−0.2 M H_2O (Table 1). The species $[LNi_2(OH)(H_2O)]^{2+}$ (**1**) ap-

Table 1. UV/Vis data of the complexes

Species	Solvent	λ_{max}/nm (ε/M^{-1}·cm^{-1})[a]
$[LNi_2(OH)(H_2O)]^{2+}$ (**1**)	acetone	405 (290), 653 (65)
1	acetonitrile (0.1 M H_2O)	405 (285), 653 (60)
1	methanol (2 M H_2O)	405 (260), 655 (60)
$[LNi_2\{OC(NH_2)NH\}]^{2+}$ (**2**)	acetone	408 (280), 649 (65)
2	acetonitrile	408 (280), 650 (65)
2	methanol	409 (255), 652 (60)
$[LNi_2(OH)(MeCN)]^{2+}$	acetonitrile	402 (270), 647 (65)
$[LNi_2(OH)(MeOH)]^{2+}$	methanol (0.1 M H_2O)	409 (260), 662 (58)
$[LNi_2(OMe)(MeOH)]^{2+}$ (**4**)	methanol	411 (260), 675 (55)

[a] Absorption coefficient per Ni_2 unit.

pears to be unchanged upon dissolving in such a weakly coordinating solvent as acetone, and no hydration or dehydration occurs in the solution.

Addition of urea to the solution of **1** in acetone elicits a moderate change in the UV/Vis spectrum, with the most sensitive region being 370−470 nm (Figure 1). The absorbance maximum in this region shifts from 405 to 409 nm. The change is cleanly reversed by the addition of water (Figure 2), showing that the reaction between **1** and urea is reversible. Spectrophotometric titrations performed at different concentrations of urea and water showed conserved isosbestic points (at 370 and 410 nm) and conserved extremum points in differential spectra (at 392 and 430 nm; Figure 2), suggesting that only two colored species were at equilibrium. The spectrophotometric titration data obtained in acetone at 25 °C can be fitted satisfactorily by a simple model based on Equation (1) with K_1 = 4.3(4) M, confirming that urea replaces two water molecules in complex **1**.

Acetonitrile

The UV/Vis spectrum of complex **1** in acetonitrile is susceptible to the content of water. The spectrum of **1** in anhydrous acetonitrile (water content < 0.002 M) has an absorbance maximum at 402 nm and is different from that in acetone (Table 1). The addition of water systematically changes the spectrum: the absorbance maximum drifts from

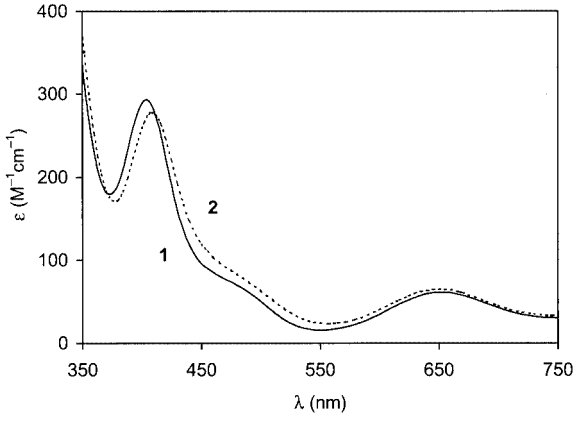

Figure 1. UV/Vis spectra of complexes **1** (solid line) and **2** (dashed line) in acetone

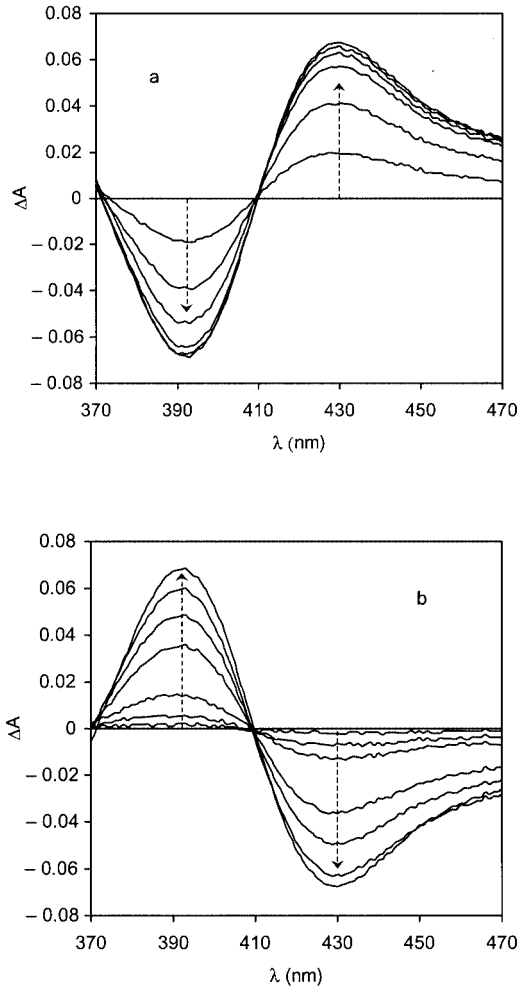

Figure 2. Differential UV/Vis spectra: (a) 2.0 mM solution of **1** in anhydrous acetone titrated with urea: 0.5, 1.0, 1.5, 2.0, 2.5, and 3.0 mM urea; (b) resulting solution titrated with water: 9, 18, 36, 112, 187, 337 mM water, the final line is for the starting complex **1**

402 to 405 nm. At $[H_2O] \geq 0.1$ M the spectrum in acetonitrile is almost congruent to that in acetone. Based on the known reactivity of complex **1** with nitriles,[13] it can be hypothesized that acetonitrile substitutes a molecule of water to form the complex $[LNi_2(OH)(MeCN)]^{2+}$. Such species resemble the crystallographically characterized complex **3**.[19]

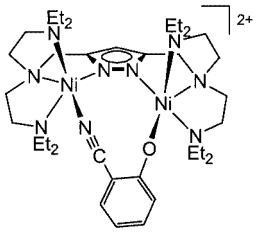

3

The dehydration of complex **1** in acetonitrile solution can be written as Equation (2). The equilibrium constant is estimated as $K_2 = 0.05(2)$ M. It should be noted that regular commercial acetonitrile contains about 0.1 M H_2O, in which medium the dehydration of complex **1** is insignificant.

$$[LNi_2(OH)(H_2O)]^{2+} + MeCN \rightleftarrows [LNi_2(OH)(MeCN)]^{2+} + H_2O$$
$$K_2 = \{[LNi_2(OH)(MeCN)][H_2O]\}/\{[LNi_2(OH)(H_2O)]\} \quad (2)$$
(in MeCN)

Addition of urea to the solution of complex **1** in acetonitrile with controlled water content, $[H_2O] \geq 100$ mM, causes changes in the UV/Vis spectrum that are very similar to those observed in acetone solution (Table 1). With excess urea the spectrum is very similar to that of complex **2** in acetone. The equilibrium constant of Equation (1) in acetonitrile at 25 °C was determined as $K_1 = 2.7(5)$ M, close to that in acetone.

Methanol

The UV/Vis spectrum of complex **1** dissolved in aqueous methanol (> 2 M H_2O) is very similar to those in acetone or aqueous acetonitrile. However, the spectrum is different in anhydrous methanol (Table 1). Spectrophotometric titration of the methanol solution of **1** with water showed two consecutive isosbestic points, suggesting that three species are at equilibrium with significantly different consecutive stability constants. As methanol and water are quite similar as ligands, it is reasonable to assume that these species are $[LNi_2(OH)(H_2O)]^{2+}$ (**1**), $[LNi_2(OH)(MeOH)]^{2+}$ and $[LNi_2(OMe)(MeOH)]^{2+}$ (**4**).

$$[LNi_2(OH)(H_2O)]^{2+} + MeOH \rightleftarrows [LNi_2(OH)(MeOH)]^{2+} + H_2O$$
$$K_3 = \{[LNi_2(OH)(MeOH)][H_2O]\}/\{[LNi_2(OH)(H_2O)]\} \quad (3)$$
(in MeOH)

$$[LNi_2(OH)(MeOH)]^{2+} + MeOH \rightleftarrows [LNi_2(OMe)(MeOH)]^{2+} + H_2O$$
$$K_4 = \{[LNi_2(OMe)(MeOH)][H_2O]\}/\{[LNi_2(OH)(MeOH)]\} \quad (4)$$
(in MeOH)

Indeed, the experimental data can be well fitted to the model based on Equations (3) and (4) with the consecutive equilibrium constants $K_3 = 0.040(5)$ M and $K_4 = 0.6(1)$ M at 25 °C (Scheme 3). Previous work showed that the intramolecular O_2H_3 bridging unit in type **1** complexes is rather labile, allowing for the exchange of water by other ligands, e.g. methanol.[13,20] Formation of complex **4** has been confirmed by its isolation and structural characterization (vide infra).

Addition of urea to the solution of complex **1** in anhydrous methanol elicits changes in the UV/Vis spectrum. The spectrum recorded for large excess of urea is very similar to that of the ureate complex **2** in other solvents (Table 1). Assuming that **4** is the dominant species in the solution of complex **1** in anhydrous methanol, the reaction can be written as Equation (5).

$$[LNi_2(OMe)(MeOH)]^{2+} + OC(NH_2)_2 \rightleftarrows [LNi_2\{OC(NH_2)NH\}]^{2+} + 2\,MeOH$$
$$K_5 = [LNi_2\{OC(NH_2)NH\}]\}/\{[LNi_2(OMe)(MeOH)][OC(NH_2)_2]\} \quad (5)$$
(in MeOH)

Data from spectrophotometric titration fit this assumption well. The equilibrium constant is $K_5 = 130(10)$ M^{-1} at 25 °C. A combination of equilibrium constants K_3, K_4 and K_5 allows us to calculate $K_1 = K_3K_4K_5 = 3(1)$ M in methanol at 25 °C (Scheme 3), which compares well with the values obtained in other solvents (Table 2).

Solid-State Structure of 4

Single crystals of **4**·$(ClO_4)_2$ were obtained by dissolving complex **1**·$(ClO_4)_2$ in anhydrous methanol and subsequent slow diffusion of diethyl ether into the solution. One such crystal was analyzed by X-ray crystallography; the molecular structure of the cation is depicted in Figure 3, together with selected atom distances and bond angles.

The overall structure of **4** is very similar to that of the related O_2H_3-bridged dinickel complex **1**·$(ClO_4)_2$.[20a] As anticipated, complete exchange of water by methanol has occurred, corroborating that the intramolecular O_2H_3 bridge is labile and that binding of substrate molecules should proceed by substitution reactions within the dimetallic pocket of **1**. Both the Ni1···Ni2 and O1···O2 distances are slightly longer in **4** (4.552/2.426 Å in **4** versus 4.380/2.410 Å in **1**[20a]). The coordination is very similar for both Ni1 and Ni2 and is intermediate between square-pyramidal and trigonal-bipyramidal ($\tau = 0.66$ for Ni1 and 0.62 for Ni2; the respective values for complex **1** are 0.38 and 0.82).[21] The bridging hydrogen atom H1, located in the crystallographic analysis, was found in an asymmetric position between the two O atoms with d(O1−H1) = 0.972 Å and d(O2−H1) = 1.457 Å, but the two Ni−O bond lengths are almost identical.

The structure determination of **4** corroborates the conclusions drawn from the solution UV/Vis experiments, i.e. the O_2H_3-bridged complex **1** is transformed into the O_2Me_2H-bridged species **4** in anhydrous methanol.

Kinetic Studies

Initial kinetic experiments were performed on the exchange of methanol and water ligands in complexes $[LNi_2(OR)(ROH)]^{2+}$ (R = H, Me) using rapid-scanning

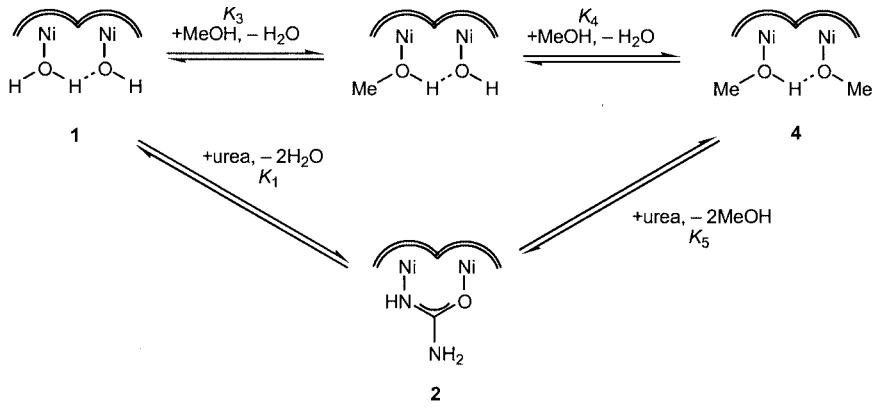

Scheme 3. Equilibrium processes studied

Table 2. Equilibrium constant of urea binding by complex **1** [Equation (1)] in different solvents at 25 °C

Solvent	K_1 [M]
Acetone	4.3(4)
Acetonitrile	2.7(5)
Methanol	3(1)

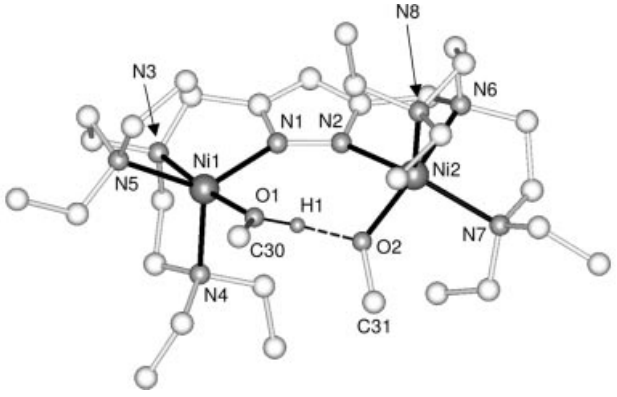

Figure 3. Molecular structure of **4**; in the interests of clarity all hydrogen atoms except H1 have been omitted; selected atom distances [Å] and angles [°]: Ni1–O1 1.987(2), Ni1–N1 2.059(2), Ni1–N3 2.090(2), Ni1–N4 2.120(2), Ni1–N5 2.214(2), Ni2–O2 1.991(2), Ni2–N2 2.072(2), Ni2–N6 2.105(2), Ni2–N7 2.188(2), Ni2–N8 2.155(2), N1–N2 1.380(3), Ni1···Ni2 4.552, O1···O2 2.426; O1–Ni1–N1 93.46(8), O1–Ni1–N3 174.47(8), O1–Ni1–N4 98.22(8), O1–Ni1–N5 100.22(8), N1–Ni1–N3 81.31(8), N1–Ni1–N4 104.21(8), N1–Ni1–N5 134.72(8), N3–Ni1–N4 84.86(8), N3–Ni1–N5 82.41(8), N4–Ni1–N5 116.02(8), O2–Ni2–N2 92.17(8), O2–Ni2–N6 172.39(8), O2–Ni2–N7 101.15(8), O2–Ni2–N8 100.46(8), N2–Ni2–N6 80.87(8), N2–Ni2–N7 135.13(8), N2–Ni2–N8 104.69(8), N6–Ni2–N7 81.92(8), N6–Ni2–N8 84.39(8), N7–Ni2–N8 114.44(8)

stopped-flow spectrophotometry. The solution of complex **4**, $[LNi_2(OMe)(MeOH)]^{2+}$, in anhydrous methanol was mixed with the solutions of water in methanol. Equilibrium studies (vide supra) showed that complex **4** is converted predominantly into $[LNi_2(OH)(MeOH)]^{2+}$ at $[H_2O]$ = 0.1 M and $[LNi_2(OH)(H_2O)]^{2+}$ at $[H_2O]$ = 2 M. The first scan, taken 10 ms after mixing, already revealed the hydrated species upon the introduction of the respective amounts of water (Table 1). In a control experiment, mixing the methanol solution of **4** with the anhydrous solvent did not cause any spectral changes other than dilution. The reaction was reversed, by mixing solutions of **1** and methanol in acetone, and the first spectrum, recorded in 10 ms, was that of $[LNi_2(OH)(MeOH)]^{2+}$ (the formation of **4** in acetone solution could not be observed because of concentration limitations). Thus, the exchange of water and methanol ligands in complexes **1** and **4** is very fast. Substitution of neutral monodentate ligands at high-spin nickel(II) centers is usually a rather quick process, with rate constants on the order of 10^3 to 10^4 s^{-1}.[22]

The reaction between complex **1**, $[LNi_2(OH)(H_2O)]^{2+}$, and urea to form complex **2**, $[LNi_2\{OC(NH_2)NH\}]^{2+}$, proceeds according to Equation (1) in a broad range of reagent concentrations in acetone as a solvent. In acetonitrile and methanol the reaction is complicated by solvation of the starting complex **1**. We performed kinetic studies in both acetone and methanol using single-wavelength stopped-flow spectrophotometry.

Acetone

Wavelengths 392 and 430 nm were chosen as the most susceptible to the transformation of complex **1** into **2** (Figure 2). Mixing the acetone solutions of **1** and urea under conditions of excess urea at 25 °C leads to simple first-order kinetic traces as monitored by spectrophotometry on 3–5 half-lives (Figure 4). Very similar values of the rate constant were observed on the rise and the fall of optical absorbance, at 430 and 392 nm, respectively. The initial and final optical absorbances measured in the kinetic experiments were identical to those determined by conventional spectrophotometry in the equilibrium studies, within the accuracy of determination.

Pseudo-first order rate constants k_{obs} were experimentally determined at 23 different concentrations of urea (0.0080–0.0275 M) and water (0.010–0.100 M). The concentrations were chosen to make the formation of complex **2** almost irreversible [yield > 95% according to Equation (1)].

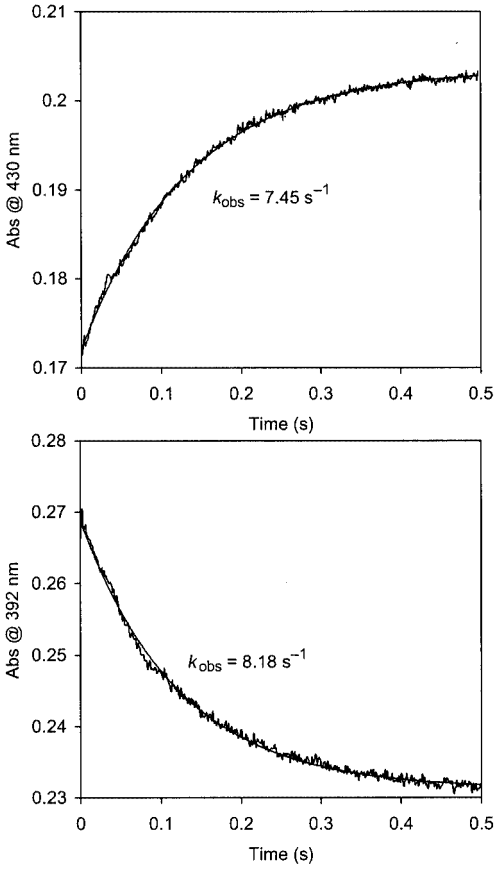

Figure 4. Representative kinetic traces of the reaction between complex **1** and urea in acetone, obtained by stopped-flow spectrophotometry, superimposed with single-exponential fits; conditions: T = 25 °C, $[\mathbf{1}]_0$ = 1.05 mM, $[urea]_0$ = 27.5 mM, and $[H_2O]_0$ = 10 mM

The transformation of complex **1** into complex **2** under these conditions was not a very fast process, with k_{obs} in the range 0.3−8 s^{-1}. The reaction is accelerated by urea and decelerated by water (Figure 5). From the shapes of the concentration dependencies, k_{obs} versus [urea] at constant $[H_2O]$, the reaction order in urea is evidently higher than one. Several kinetic equations were tested to fit the experimental data, and only those with both first- and second-order terms in [urea] gave satisfactory fits (see Supporting Information for details; see also the footnote on the first page of this article). Equation (6) gave the best fit, and also a plausible mechanistic interpretation (vide infra).

$$k_{obs} = \{k'K'[urea] + k''K'K''[urea]^2\}/\{[H_2O] + K'[urea]\} \quad (6)$$

Optimization of Equation (6) by non-linear weighed least-squares method gave k' = 0.39 s^{-1}, K' = 0.29, and $k''K''$ = 650 M^{-1}·s^{-1} with an average relative deviation of 2.7% and a satisfactory coverage of all experimental points (Figure 5).

Additional experiments were made to check if the reaction between **1** and urea is influenced by an external base. Addition of 2,6-dimethylpyridine (1−100 equiv.) to the solution of either complex **1** or **2** in acetone does not change the UV/Vis spectra. Also, the kinetics are constant for the reaction between complex **1** and urea in the presence of up to 10-fold excess of 2,6-dimethylpyridine versus complex **1** in acetone solution.

Methanol

As previously mentioned, complex $[LNi_2(OH)(H_2O)]^{2+}$ (**1**) is converted into $[LNi_2(OMe)(MeOH)]^{2+}$ (**4**) upon dissolution in anhydrous methanol. To minimize the interference from water, solutions of solid **4**·$(ClO_4)_2$ in anhydrous methanol were used. Complex **4** reacts with excess urea to yield complex **2**, as found by the equilibrium studies (vide supra). The formation of **2** from **4** and urea in anhydrous methanol is almost two orders of magnitude slower than from **1** and urea in anhydrous acetone at the same urea concentration. Fortunately, the solubility of urea in methanol is also much higher, allowing a wider range of

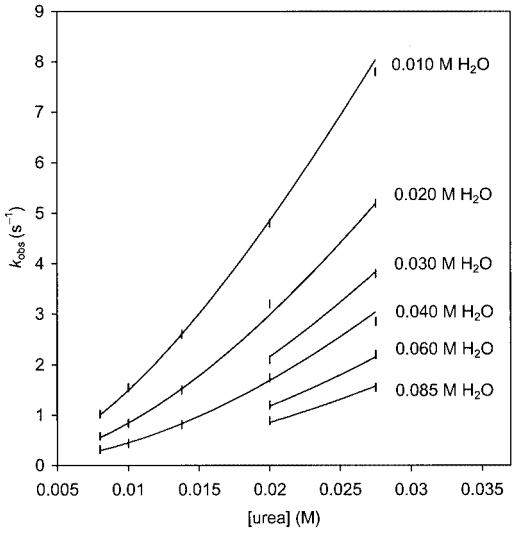

Figure 5. Pseudo first-order rate constants of the reaction between complex **1** and urea in acetone versus urea concentration in the series with constant water concentrations; lines represent the fits with Equation (6)

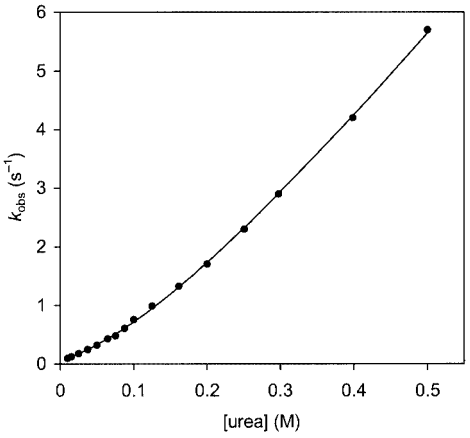

Figure 6. Pseudo first-order rate constants of the reaction between complex **4** and urea in methanol versus urea concentration (T = 25 °C); experimental points superimposed with the fitting line [Equation (7)]

available urea concentrations. Kinetic traces of the reaction between **4** and excess urea fit perfectly with a single-exponential function in all performed experiments. The reaction accelerates with increasing in urea concentration (Figure 6). As in the reaction of **1** with urea in acetone, the kinetic data for the reaction in methanol can be fit satisfactorily only by kinetic equations with both first- and second-order terms in [urea]. Equation (7), which is very similar to Equation (6), gave the best fit for the dependence of k_{obs} versus [urea] and allowed for a similar mechanistic interpretation (vide infra).

$$k_{obs} = \{k'K'[\text{urea}] + k''K'K''[\text{urea}]^2\}/\{1 + K'[\text{urea}]\} \quad (7)$$

Optimization of Equation (7) gave $k' = 1.5\ s^{-1}$, $K' = 2.7\ M^{-1}$, and $k"K'' = 16.5\ M^{-1}\cdot s^{-1}$ with an average relative deviation of 1.1% (Figure 6).

Proposed Mechanism

As mentioned above, the experimental data for the formation of complex **2** in acetone and methanol could be fit satisfactorily only with kinetic equations having both linear and quadratic terms in urea concentration. This result strongly suggests the existence of two reactive pathways, involving one and two urea molecules, respectively. The bis(urea) pathway is dominant at all studied urea concentrations in acetone, and becomes dominant at higher urea concentrations (> 0.08 M) in methanol. The bis(urea) pathway is unexpected, because only one urea molecule is incorporated into the product **2**. A mechanism shown in Scheme 4 can account for the experimental observations.

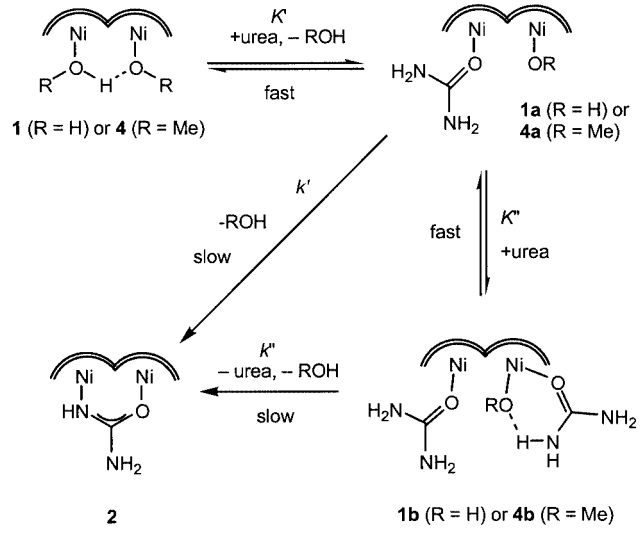

Scheme 4. Kinetic processes studied (formation of **2** was almost irreversible under the concentration conditions used)

The starting complexes **1** (in acetone) or **4** (in methanol) contain easily exchangeable solvent molecules at the LNi_2 core. Therefore, it is reasonable to assume the formation of intermediate urea complexes, $[LNi_2(OR)(urea)]^{2+}$ [**1a** (R = H) or **4a** (R = Me)] and $[LNi_2(OR)(urea)_2]^{2+}$ [**1b** (R = H) or **4b** (R = Me)] in a fast preequilibrium with the starting complex **1** or **4**, respectively (Scheme 4). Fast exchange of monodentate ligands within the LNi_2 core has been observed for water and methanol in this work.

Steady-state mono(urea) intermediates **1a** and **4a** are formed upon the substitution of a neutral coordinated water or methanol molecule for a molecule of urea, which agrees with the kinetic Equations (6) and (7). The Ni^{II} ions in **1a** and **4a** are probably five-coordinate, as found in most complexes with the LNi_2 core and different additional ligands.[13,19] Coordination of the neutral urea ligands in these putative intermediates is most likely *O*-monodentate, as found in most structurally characterized nickel–urea complexes.[12,14] The equilibrium constants for the formation of **1a** and **4a** can be estimated from the kinetic data as $K'_{1a} = 0.30$ (in acetone) and $K'_{4a} = 2.7\ M^{-1}$ (in methanol). These values are reasonable, as urea is generally known to form relatively weak complexes with nickel(II) and other dipositive 3d metal cations.[23] The substitution of a solvent molecule for urea should activate the *Ni*-bound HO^- (or MeO^-, respectively), which in **1** and **4** is present in the stabilized solvated form. The reactivity of the intermediate $[LNi_2(OH)(urea)]^{2+}$ ($k'_{1a} = 0.39\ s^{-1}$) is lower than that of $[LNi_2(OMe)(urea)]^{2+}$ ($k'_{4a} = 1.5\ s^{-1}$), in agreement with the more basic nature of the methoxide ligand. The calculated steady-state yields of intermediates **1a** and **4a** are significant (up to 40%) only at the highest used concentrations of urea, according to the kinetic data (see Supporting Information). An attempt to confirm the rapid formation of intermediate **1a** from **1** in anhydrous acetone at the high urea concentration by rapid scanning spectrophotometry was inconclusive. Upon mixing the acetone solutions of **1** and urea, the first registered spectrum (10 ms) could not be distinguished from that of the starting complex **1**. The spectral changes upon ligand substitution at the LNi_2 core are usually small, and rapid scanning gives UV/Vis spectra of relatively poor quality. Therefore, the formation of intermediates **1a** and **4a** should be considered as the most probable hypothesis.

Intermediates **1b** and **4b** are formed in solution upon binding of a second urea molecule (Scheme 4). Their yield is very small and could not be evaluated from the kinetic data. Because ligand L is quite bulky and usually limits the coordination number of the nickel(II) cations in the LNi_2 core to five,[13,19] intermediates **1a** and **4a** may bind a second urea molecule only weakly (e.g., by sterically unfavorable expansion of the coordination number of a Ni^{II} cation to six, or the substitution of a diethylamino arm of ligand L, or hydrogen bonding). Nevertheless, the bis(urea) pathway is dominant at all studied urea concentrations in acetone and becomes dominant at [urea] > 0.08 M in methanol. Therefore, bis(urea) complexes **1b** and **4b** are much more reactive than their mono(urea) counterparts **1a** and **4a**.

A possible explanation for the unique reactivity of the putative bis(urea) intermediates is as follows. If **1b** and **4b** are formed upon *O*-coordination of two urea molecules to two different Ni^{II} centers at the LNi_2 core, then the HO^- and $OC(NH_2)_2$ ligands bound to the same Ni center may

form an intramolecular hydrogen bond as a part of six-membered pseudo-chelate cycle (Scheme 4). Such O···H−N bonding would make the N atom of urea more nucleophilic than in free or *O*-bound $OC(NH_2)_2$. As a consequence, an intramolecular nucleophilic attack of the urea N atom on the second Ni^{II} cation and a proton transfer from the urea to the HO^- ligand may proceed as simultaneous or closely related events, followed by the loss of water and unproductively bound urea ligands (Scheme 4). The formation of a hydrogen bond between hydroxide and urea ligands bound to different Ni atom in mono(urea) intermediates **1a** and **4a** is less probable. In this picture, the first urea molecule is required to activate the *Ni*-bound HO^- (or MeO^-, respectively) which in **1** and **4** is present in a stabilized solvated form, and the second urea molecule is the actual precursor of the ureate in **2**. The second urea molecule may also cause uncoordination of a diethylamino arm of the dinucleating ligand L,[13,19] in which case the strongly basic free amino arm may play a catalytic role in the intramolecular proton transfer and the formation of the ureate anion at the LNi_2 core. Alternatively, if the second urea molecule is bound to the $[LNi_2(OR)(urea)]^{2+}$ core via hydrogen bonds it may act as a proton shuttle and facilitate the formation of the final ureate complex **2** (see Supporting Information for details).

The rate-limiting step in the formation of **2** for both mono- and bis(urea) pathways involves the bidentate *N*,*O*-coordination and deprotonation of an *O*-coordinated urea. The deprotonation of urea is apparently intramolecular, since Equations (1) and (5) are first-order in the dinickel complexes **1** and **4**, respectively, and the addition of an external base has no influence on the rate of Equation (1). It is not clear whether deprotonation or *N*-coordination of urea occurs first, but these events should be closely related. The amide N-atoms of neutral urea are very poor donors because of their involvement in the resonance with the carbonyl group. However, the N-atoms become very good donors upon deprotonation and the formation of an amide anion. Conversely, *N*-bound urea becomes much more acidic than *O*-bound or free urea, and its deprotonation is facilitated.[9]

In summary, the reactive complexes **1a**, **4a**, **1b**, and **4b** with neutral urea ligands may be formed in solution in a fast preequilibrium and low yield. Formation of the final urea anion complex **2** is different. Thermodynamically, the urea anion $H_2NC(O)NH^-$ has a much higher affinity to the dinickel core than neutral urea, water, methanol, or even hydroxide or methoxide ions, because of the chelate effect and the presence of a deprotonated amide N-donor atom. Kinetically, the formation of **2** is relatively slow, because substitution of several donor atoms at the Ni^{II} centers and a proton transfer are involved. It should be noted that under the concentration conditions used in the kinetic study, the formation of the ureate complex **2** was irreversible (Scheme 4). The bridging *N*,*O*-coordinated urea anion at a dimetal core is quite stable and is not activated for hydrolysis.[11,13,18] Urease avoids the deprotonation of urea at its catalytic dinickel site. In the enzyme, urea undergoes a nucleophilic attack from the hydroxide ligand, which eventually leads to hydrolysis (Scheme 1). This supports the view that nucleophilic attack and *N*-binding of the substrate have to occur simultaneously in urease. The specific action of the enzyme is probably caused by the involvement of additional groups in the stabilization of a tetrahedral intermediate and subsequent general acid/base catalysis.[2,5] Another difference between the reactivity of urease and model complex **1** towards urea is the existence of two parallel reactive pathways for the model complex. While complexes **1** and **2** are not functional models for urease, a detailed investigation of these complexes reveals valuable insight into the binding of urea at a dinickel core.

Conclusion

The equilibrium and kinetics of urea binding by model dinickel complexes have been studied for the first time. Complexes $[LNi_2(OR)(ROH)]^{2+}$ (R = H, Me) with a dinucleating pyrazole-based ligand L react reversibly with urea in solution to form complex $[LNi_2[OC(NH_2)NH)]^{2+}$ with an *N*,*O*-bridging urea anion. Kinetic studies revealed several reaction steps in which, initially, urea substitutes the solvent molecule in $[LNi_2(OR)(ROH)]^{2+}$ to form steady-state intermediates $[LNi_2(OR)(urea)_n]^{2+}$ (n = 1, 2) in a fast pre-equilibrium. The subsequent bidentate *N*,*O*-coordination and deprotonation of an *O*-bound urea ligand constitute the rate-limiting step. Reactive complexes $[LNi_2(OH)(urea)_n]^{2+}$ are close analogs of the reactive intermediate of urease, which also has the HO^- and urea ligands bound at a dinickel core. However, the reactivities of the intermediates are different. In the urease enzyme, the HO^- ligand attacks urea as a nucleophile, leading to the hydrolysis of urea. The HO^- ligand in our model complex acts a base towards urea, and the dinickel complex with urea anion is formed. The present study helps in understanding the factors that govern the pathway of the reaction between the HO^- and urea ligands at a dinickel core, which is a prerequisite for the design of a fully functional synthetic model of urease.

Experimental Section

Caution: Although no problems were encountered, transition metal perchlorate complexes are potentially explosive and should be handled with proper precautions!

General: Complex **1**·$(ClO_4)_2$ was prepared as described previously.[13] Urea (Acros) was recrystallized three times from hot water and dried in vacuo over Drierite for 48 h before use. Anhydrous acetone (Acros), acetonitrile and methanol (Aldrich) were used as received. Solutions of the nickel complexes and urea in the anhydrous solvents were prepared and handled in a dry box. UV/Vis spectra were taken with a Hitachi U-2000 spectrophotometer at 25 °C.

Kinetic Studies: Kinetic experiments were carried out by using a Hi-Tech Scientific (Salisbury, UK) SF-43 stopped-flow apparatus with stainless steel lines. The concentrations of stock solutions were

1−4 mM **1**·$(ClO_4)_2$ in acetone, 8−55 mM urea in acetone, 1−4 mM **4**·$(ClO_4)_2$ in methanol, and 20−1000 mM urea in methanol. The stock solutions of a nickel complex and urea were mixed in a 1:1 ratio. Urea was always taken in at least eightfold excess to allow pseudo first-order conditions.

Urea Solubility: The solubility of urea in acetonitrile and acetone in the range of 0−30 °C was determined by gravimetric measurements. The molar solubility of urea in anhydrous acetonitrile (water content $[H_2O] \leq 0.002$ M) is expressed by $\ln S = 6.2372 - 2615/T$; 0.079 M at 298 K. The molar solubility of urea in anhydrous acetone (water content $[H_2O] \leq 0.002$ M) is expressed by $\ln S = 6.2628 - 2733/T$; 0.055 M at 298 K. The molar solubility of urea in regular commercial acetone (water content $[H_2O] \approx 0.2$ M) can be satisfactorily expressed by $\ln S = 5.6253 - 2465/T$; 0.071 M at 298 K.

Synthesis of 4·$(ClO_4)_2$: A solution of **1**·$(ClO_4)_2$ (0.25 g, 0.84 mmol) in anhydrous MeOH (1 mL) was layered with diethyl ether; green crystals of **4**·$(ClO_4)_2$ gradually formed. To ensure complete replacement of water by methanol, crystallization should be carried out in the presence of predried molecular sieves. $C_{31}H_{68}Cl_2N_8Ni_2O_{10}$ (901.22): calcd. C 41.32, H 7.60, N 12.43; found C 40.40, H 7.45, N 12.41.

X-ray Crystallographic Study: Data collection for **4**·$(ClO_4)_2$ was carried out with a Bruker AXS CCD diffractometer at 173 K by using graphite-monochromated Mo-K_α radiation ($\lambda = 0.71073$ Å). Structures were solved by direct methods (SHELXS-97) and refined by full-matrix least-squares techniques based on F^2 (SHELXL-97).[24] Atomic coordinates and thermal parameters of the non-hydrogen atoms were refined in fully anisotropic models. Hydrogen atoms, except those of the disordered ethyl group, were located in difference Fourier maps and refined isotropically. One of the ethyl groups is disordered over two positions (3:1). $C_{31}H_{68}Cl_2N_8Ni_2O_{10}$, $M = 901.2$, orthorhombic, space group $Pna2_1$, $a = 25.6829(5)$, $b = 13.4179(3)$, $c = 11.9614(2)$ Å, $V = 4122.0(2)$ Å^3, $Z = 4$, $\rho_{calcd.} = 1.452$ g cm^{-3}, μ (Mo-K_α) = 1.104 mm^{-1}, $3.2° < 2\theta < 56.7°$, 40935 measured reflections, 9727 unique ($R_{int} = 0.047$), 8177 observed [$I > 2\sigma(I)$], 743 parameters, final $R1[I > 2\sigma(I)] = 0.032$, $wR2$(all data) = 0.073, goodness of fit on $F^2 = 1.049$, largest diff. peak +0.48/−0.34 e·Å^{-3}. CCDC-191806 contains the supplementary crystallographic data for this paper. These data can be obtained free of charge via www.ccdc.cam.ac.uk/conts/retrieving.html or from CCDC, 12 Union Road, Cambridge CB2 1EZ, UK [Fax: (internat.) + 44-1223/336-033; E-mail: deposit@ccdc.cam.ac.uk].

Acknowledgments

E. R. A. thanks Tufts University, the NSF, and the Research Corporation for financial support. F. M. thanks the Deutsche Forschungsgemeinschaft and the Fonds der Chemischen Industrie for financial support.

[1] [1a] N. E. Dixon, C. Gazolla, R. L. Blakeley, B. Zerner, *J. Am. Chem. Soc.* **1975**, *97*, 4131−4133. [1b] M. A. Halcrow, G. Christou, *Chem. Rev.* **1994**, *94*, 2421−2481. [1c] S. Lippard, *Science* **1995**, *268*, 996−997. [1d] J. C. Fontecilla-Camps, *Struct. Bonding* **1998**, *91*, 1−30. [1e] M. J. Maroney, G. Davidson, C. B. Allan, J. Figlar, *Struct. Bonding* **1998**, *92*, 1−64.

[2] P. A. Karplus, M. A. Pearson, R. P. Hausinger, *Acc. Chem. Res.* **1997**, *30*, 330−337.

[3] R. L. Blakeley, A. Treston, R. K. Andrews, B. Zerner, *J. Am. Chem. Soc.* **1982**, *104*, 612−614.

[4] E. Jabri, M. B. Carr, R. P. Hausinger, P. A. Karplus, *Science* **1995**, *268*, 998−1003.

[5] [5a] E. Jabri, P. A. Karplus, *Biochemistry* **1996**, *35*, 10616−10626. [5b] I.-S. Park, L. O. Michel, M. A. Pearson, E. Jabri, P. A. Karplus, S. Wang, J. Dong, R. A. Scott, P. B. Köhler, M. K. Johnson, R. P. Hausinger, *J. Biol. Chem.* **1996**, *271*, 18632. [5c] M. A. Pearson, L. O. Michel, R. P. Hausinger, P. A. Karplus, *Biochemistry* **1997**, *36*, 8164−8172. [5d] S. Benini, W. R. Rypniewski, K. S. Wilson, S. Ciurli, S. Mangani, *J. Biol. Inorg. Chem.* **1998**, *3*, 268−273. [5e] S. Benini, W. R. Rypniewski, K. S. Wilson, S. Miletti, S. Ciurli, S. Mangani, *J. Biol. Inorg. Chem.* **2000**, *5*, 110−118. [5f] M. A. Pearson, I.-S. Park, R. A. Schaller, L. O. Michel, P. A. Karplus, R. P. Hausinger, *Biochemistry* **2000**, *39*, 8575−8584. [5g] N.-C. Ha, S.-T. Oh, J. Y. Sung, K. A. Cha, M. H. Lee, B.-H. Oh, *Nature Struct. Biol.* **2001**, *8*, 505−509.

[6] S. Ciurli, S. Benini, W. R. Rypniewski, K. S. Wilson, S. Miletti, S. Mangani, *Coord. Chem. Rev.* **1999**, *190−192*, 331−355.

[7] S. Benini, W. R. Rypniewski, K. S. Wilson, S. Miletti, S. Ciurli, S. Mangani, *Structure* **1999**, *7*, 205−216. [7a] S. Benini, W. R. Rypniewski, K. S. Wilson, S. Miletti, S. Ciurli, *J. Biol. Inorg. Chem.* **2001**, *6*, 778−790.

[8] [8a] F. Musiani, S. Arnofi, R. Casadio, S. Ciurli, *J. Biol. Inorg. Chem.* **2001**, *6*, 300−314. [8b] M. J. Todd, R. P. Hausinger, *Biochemistry* **2000**, *39*, 5389−5396.

[9] T. C. Woon, W. A. Wickramasinghe, D. P. Fairlie, *Inorg. Chem.* **1993**, *32*, 2190−2194.

[10] N. E. Dixon, P. W. Riddles, C. Gazzola, R. L. Blakeley, B. Zerner, *Can. J. Biochem.* **1980**, *58*, 1335−1344.

[11] S. Buchler, F. Meyer, E. Kaifer, H. Pritzkow, *Inorg. Chim. Acta* **2002**, *337*, 371−386.

[12] [12a] R. M. Buchanan, M. S. Mashuta, K. J. Oberhausen, J. F. Richardson, *J. Am. Chem. Soc.* **1989**, *111*, 4497−4498. [12b] A. J. Stemmler, J. W. Kampf, M. L. Kirk, V. L. Pecoraro, *J. Am. Chem. Soc.* **1995**, *117*, 6368−6369. [12c] D. Volkmer, A. Hörstmann, K. Griesar, W. Haase, B. Krebs, *Inorg. Chem.* **1996**, *35*, 1132−1135. [12d] D. Volkmer, B. Hommerich, K. Griesar, W. Haase, B. Krebs, *Inorg. Chem.* **1996**, *35*, 3792−3803. [12e] F. Meyer, A. Jacobi, B. Nuber, P. Rutsch, L. Zsolnai, *Inorg. Chem.* **1998**, *37*, 1213−1218. [12f] Hosokawa, H. Yamane, Y. Nakao, K. Matsumoto, S. Takamizawa, W. Mori, S. Suzuki, H. Kimoto, *Inorg. Chim. Acta* **1998**, *283*, 118−123. [12g] D. A. Brown, L. P. Cuffe, O. Deeg, W. Errington, N. J. Fitzpatrick, W. K. Glass, K. Herlihy, T. J. Kemp, H. Nimir, *Chem. Commun.* **1998**, 2433−2434. [12h] M. Arnold, D. A. Brown, O. Deeg, W. Errington, W. Haase, K. Herlihy, T. J. Kemp, H. Nimir, R. Werner, *Inorg. Chem.* **1998**, *37*, 2920−2925. [12i] S. Uozumi, H. Furutachi, M. Ohba, H. Okawa, D. E. Fenton, K. Shindo, S. Murata, D. J. Kitko, *Inorg. Chem.* **1998**, *37*, 6281−6287. [12j] B. Hommerich, H. Schwöppe, D. Volkmer, B. Krebs, *Z. Anorg. Allg. Chem.* **1999**, *625*, 75−82. [12k] A. M. Barrios, S. J. Lippard, *J. Am. Chem. Soc.* **1999**, *121*, 11751−11757. [12l] H. Carlsson, M. Haukka, E. Nordlander, *Inorg. Chem.* **2002**, *41*, 4981−4983.

[13] F. Meyer, E. Kaifer, P. Kircher, K. Heinze, H. Pritzkow, *Chem.-Eur. J.* **1999**, *5*, 1617−1630.

[14] [14a] H. E. Wages, K. L. Taft, S. J. Lippard, *Inorg. Chem.* **1993**, *32*, 4985−4987. [14b] K. Yamaguchi, S. Koshino, F. Akagi, M. Suzuki, A. Uehara, S. Suzuki, *J. Am. Chem. Soc.* **1997**, *119*, 5752−5753. [14c] T. Koga, H. Furutachi, T. Nakamura, N. Fukita, M. Ohba, K. Takahashi, H. Okawa, *Inorg. Chem.* **1998**, *37*, 989−996. [14d] M. Konrad, F. Meyer, A. Jacobi, P. Kircher, P. Rutsch, L. Zsolnai, *Inorg. Chem.* **1999**, *38*, 4559−4566. [14e] A. M. Barrios, S. J. Lippard, *J. Am. Chem. Soc.* **2000**, *122*, 9172−9177. [14f] A. M. Barrios, S. J. Lippard, *Inorg. Chem.* **2001**, *40*, 1060−1064.

[15] F. Meyer, H. Pritzkow, *Chem. Commun.* **1998**, 1555−1556.

[16] F. Meyer, M. Konrad, E. Kaifer, *Eur. J. Inorg. Chem.* **1999**, 1851−1854.

[17] F. Meyer, P. Rutsch, *Chem. Commun.* **1998**, 1037−1038.

[18] S. V. Kryatov, A. Y. Nazarenko, P. D. Robinson, E. V. Rybak-Akimova, *Chem. Commun.* **2000**, 921−922.
[19] F. Meyer, I. Hyla-Kryspin, E. Kaifer, P. Kircher, *Eur. J. Inorg. Chem.* **2000**, 771−781.
[20] [20a] L. Siegfried, T. A. Kaden, F. Meyer, P. Kircher, H. Pritzkow, *J. Chem. Soc., Dalton Trans.* **2001**, 2310−2315. [20b] J. Ackermann, F. Meyer, E. Kaifer, H. Pritzkow, *Chem.-Eur. J.* **2002**, *8*, 247−258.
[21] The angular structural parameter τ is defined as $\tau = (\beta - \alpha)/60$, where α and β represent two basal angles with $\beta > \alpha$. It is a measure for the degree of trigonality: a perfect TB-5 structure is associated with $\tau = 1$, while $\tau = 0$ is expected for an idealized SPY-5 geometry: A. W. Addison, T. N. Rao, J. Reedijk, J. van Rijn, G. C. Verschoor, *J. Chem. Soc., Dalton Trans.* **1984**, 1349−1356.
[22] A. E. Merbach, *Pure Appl. Chem.* **1982**, *54*, 1479−1493.
[23] [23a] A. F. Borina, V. T. Orlova, S. A. Popova, *Zh. Neorg. Khim.* **1991**, *36*, 2617−2622. [23b] V. A. Prokuev, V. V. Zapyshnyi, *Zh. Neorg. Khim.* **1998**, *43*, 810−814.
[24] G. M. Sheldrick, *SHELXS-97, Program for Crystal Structure Solution*, Universität Göttingen, **1997**; G. M. Sheldrick, *SHELXL-97, Program for Crystal Structure Refinement*, Universität Göttingen, **1997**.

Received October 23, 2002
[I02584]

Synthesis and Characterization of New Transplatinum Complexes Containing Phosphane Groups − Cytotoxic Studies in Cisplatin-Resistant Cells

Francisco J. Ramos-Lima,[a] Adoración G. Quiroga,[a] José M. Pérez,[a] Mercé Font-Bardía,[b] Xavier Solans,[b] and Carmen Navarro-Ranninger*[a]

Keywords: Antitumor agents / Bioinorganic chemistry / Crystal structure / Phosphanes / Platinum

In this paper we report the synthesis and characterization of novel *trans* platinum(II) complexes of general formula *trans*-[$PtCl_2$(L)(PPh_3)], where L is $NH_2CH(CH_3)CH_2CH_3$ (complex **1**), (*R*)-$NH_2CH(CH_3)CH_2CH_3$ (complex **2**), (*S*)-$NH_2CH(CH_3)CH_2CH_3$ (complex **3**) and $NH_2CH(CH_3)_2$ (complex **4**). The new complexes contain phosphane ligands *trans* to the amine group. X-ray crystal structure determinations of complexes **1** and **3** confirmed their *trans* configurations. The cytotoxic activity of these complexes have been evaluated and compared with the activity of *trans* platinum complexes already viewed as potential drugs.

(© Wiley-VCH Verlag GmbH & Co. KGaA, 69451 Weinheim, Germany, 2003)

Introduction

Current platinum-based drug research is moving towards the development of new agents capable of overcoming the problem of acquired resistance to cisplatin in order to be active against a wider range of cancer types.[1,2] For decades, platinum complexes of *trans* geometry were not regarded as potential drugs because transplatin is an inactive isomer. Over the last ten years, however, transplatinum complexes have been developed as new drugs.[3,4] We have recently shown that *trans* amino complexes such as *trans*-[$PtCl_2$(dimethylamine)(isopropylamine)] are able to circumvent *cis*-DDP resistance in tumour cells transformed by *ras* oncogenes (Pam212-*ras*), and are also able to kill these cells through apoptosis.[5] In addition, we found in the literature a wide range of active platinum complexes containing aminophosphane,[6,7] triphos ligand[8] and phosphorus derivative ligands.[9] Following these results we thought that the study of the effect of the phosphane in the *trans* configuration could help to extend understanding of the cytotoxic activity of *trans* platinum complexes.

In this paper we report the synthesis and characterization of *trans*-[$PtCl_2$(L)(PPh_3)] complexes, where L is $NH_2CH(CH_3)CH_2CH_3$ (**1**), (*R*)-$NH_2CH(CH_3)CH_2CH_3$ (**2**), (*S*)-$NH_2CH(CH_3)CH_2CH_3$ (**3**) and $NH_2CH(CH_3)_2$ (**4**). As far as we know, these complexes are the first Pt complexes with phosphane groups and chiral amines in *trans* configurations. Moreover, they have chloride leaving groups, which may facilitate comparison with some previously reported *trans* platinum complexes, such as *trans*-[$PtCl_2$(dimethylamine)(isopropylamine)].[4]

[a] Departamento de Química Inorgánica, Universidad Autónoma de Madrid,
28049 Madrid, Spain
[b] Cristalografia, Mineralogia i Dipòsits Minerals, Universitat de Barcelona,
08028 Barcelona, Spain

Results and Discussion

The new *trans*-Pt complexes with phosphane groups are prepared in three different steps. In the first step, K_2PtCl_4 reacts with PPh_3 to produce the *cis* isomer. In a second step, direct treatment of the *cis* isomer with $PtCl_2$ affords the dimer complexes [(μ-Cl)PtCl(PPh_3)]$_2$. Further addition of the desired amine splits the chloro-bridged complex to afford the final *trans* complex *trans*-[$PtCl_2$L(PPh_3)]. A scheme of the synthesis pathway is depicted in Figure 1.

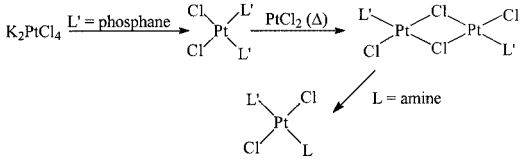

Figure 1. Chart of the synthesis pathway for the complexes **1**, **2**, **3** and **4**

The characterization of these complexes was carried out by IR and ^{195}Pt, ^{31}P, ^{1}H and ^{13}C NMR. The IR spectra show information in the low region in which ν(Pt−Cl) bands are detected.[10] As would be expected for a *trans*-Pt geometry, complexes **1**, **2** and **3** each show only one ν(Pt−Cl) band, at 346 cm^{-1}.[11] Complex **4** also shows a single ν(Pt−Cl) band, but located at 344 cm^{-1}. The ν(Pt−N) band in complexes **1**, **2**, **3** and **4** appears at 430

cm^{-1}. These ν(Pt−N) bands are lower than the ν(Pt−N) band found in *trans*-[$PtCl_2$(dma)(ipa)],[5] probably due to the greater *trans* influence of the phosphorus atom, while the Pt−Cl stretching band is virtually independent of this substitution.[11] This effect is also observed in the X-ray structure discussed below.

The *cis*- and *trans*-platinum complexes can readily be distinguished by comparison of the $^1J(^{31}P\text{-}^{195}Pt)$ values, measured from the ^{195}Pt satellites on the high-field and low-field doublets.[12] We found in the literature that complexes such as *cis*-[$PtCl_2(PPh_3)_2$] show a larger coupling constant than the *trans* isomer between ^{195}Pt and ^{31}P , but any decrease in the covalency of the Pt−P bond will also reduce the coupling.[11] Complexes **1**, **2**, **3** and **4**, in which the P atom is *trans* to the N atom, each show a value of 3600 Hz, normal for a ^{31}P atom *trans* to an N donor.[7,11,13]

The structures of complexes **1** and **3** were determined by X-ray analysis. Selected bond lengths (Å) and angles (°) for complex **1** and **3** are summarized in Table 1 and Table 2, respectively.

Table 1. Selected bond lengths (Å) and angles(°) for complex **1**

Pt−Cl(1)	2.295(3)	Pt−Cl(2)	2.287(3)
Pt−P	2.243(2)	Pt−N	2.144(8)
P−C(5)	1.818(8)	P−C(11)	1.829(9)
P−C(17)	1.823(11)	N−C(1)	1.448(18)
Cl(1)−Pt−Cl(2)	172.72(9)	Cl(1)−Pt−P	96.26(9)
Cl(1)−Pt−N	87.0(3)	Cl(2)−Pt−P	90.06(9)
Cl(2)−Pt−N	87.0(3)	P−Pt−N	173.5(3)
Pt−P−C(5)	113.3(3)	Pt−P−C(11)	116.5(3)
Pt−P−C(17)	110.2(3)	Pt−N−C(1)	115.7(8)

Table 2. Selected bond lengths (Å) and angles(°) for complex **3**

Pt(1)−Cl(1)	2.287 (3)	Pt(2)−Cl(3)	2.312 (3)
Pt(1)−Cl(2)	2.291 (3)	Pt(2)−Cl(4)	2.294 (3)
Pt(1)−P(1)	2.261 (3)	Pt(2)−P(2)	2.211 (3)
Pt(1)−N(1)	2.096 (11)	Pt(2)−N(2)	2.180 (12)
Cl(1)−Pt(1)−Cl(2)	174.62 (13)	Cl(3)−Pt(2)−Cl(4)	169.99 (14)
N(1)−Pt(1)−Cl(1)	87.8 (3)	N(2)−Pt(2)−Cl(3)	84.5 (4)
N(1)−Pt(1)−Cl(2)	87.3 (3)	N(2)−Pt(2)−Cl(4)	85.5 (4)
N(1)−Pt(1)−P(1)	177.3 (3)	N(2)−Pt(2)−P(2)	174.7 (4)
P(1)−Pt(1)−Cl(1)	94.35 (11)	P(2)−Pt(2)−Cl(3)	99.18 (12)
P(1)−Pt(1)−Cl(2)	90.55 (11)	P(2)−Pt(2)−Cl(4)	90.72 (13)

A view of the complex **1**, *trans*-{$PtCl_2[NH_2CH(CH_3)CH_2CH_3](PPh_3)$}, is shown in Figure 2. The space group for the complex **1** is centrosymmetric, so this compound is an equimolar mixture of the *S* and *R* enantiomers. The crystal structure of this compound consists of discrete molecules in which PPh_3 and $NH_2CH(CH_3)CH_2CH_3$ groups are σ bonded to the platinum atom in *trans* configuration. The platinum atom has a square-planar environment with typical angles for square-planar platinum complexes.[4,11,14] The Pt−N distance is similar to that found in complexes with planar amines *trans* to the triethylphosphane ligand, while the Pt−P distance is slightly longer.[14] This difference is probably due to the steric effect of the different bulks and the different electronic effects of the

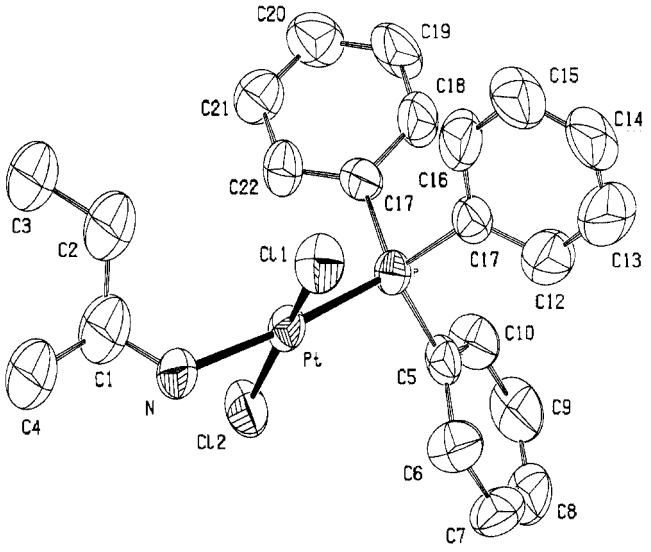

Figure 2. Ortep view of complex **1**

phenyl substituent in the phosphane group.[15] No significant differences in the Pt−Cl *trans* distances are found in comparison with *trans*-[$PtCl_2$(benzoquinoline)(PEt_3)][14] and platinum complexes such as *trans*-[$PtCl_2$(dma)(ipa)].[5] Only the Pt−N distance is significantly longer than those in the complexes mentioned, which is consistent with the greater *trans* influence of phosphane ligands relative to aliphatic amine ones.

The H22(C22)−Pt distance is fairly short [2.97(14) Å] and the distance H2(C2)−Pt is even shorter, in comparison with those found in the references (see Table 3).[12] The data reported in the literature also support the idea of a weak interaction between H and Pt atoms when such a distance is from 2.3 to 2.9 Å, which includes the distance here.[14]

Table 3. Distances (Pt, X) (Å) for complex **1**

d(Pt, X)	Atom X
3.064(13)	C(1)
3.344(9)	C(17)
3.374(13)	C(2)
3.401(8)	C(5)
3.457(12)	C(22)
3.469(8)	C(11)
2.4443	H(1A)
2.8679	H(2)
2.97(14)	H(22)
3.1334	H(1A)
3.1546	H(1)
3.31(6)	H(6)

A view of the complex **3**, which contains the enantiomerically pure amine moiety (*S*)-$NH_2CH(CH_3)CH_2CH_3$, is shown in Figure 3. The crystal structure of this compound consists of two different discrete molecules in which PPh_3 and (*S*)-$NH_2CH(CH_3)CH_2CH_3$ groups are σ bonded to platinum in a *trans* configuration. Although both molecules look like very similar, the main difference between them is the C−H···ring π interaction between C(214)−H(214) and

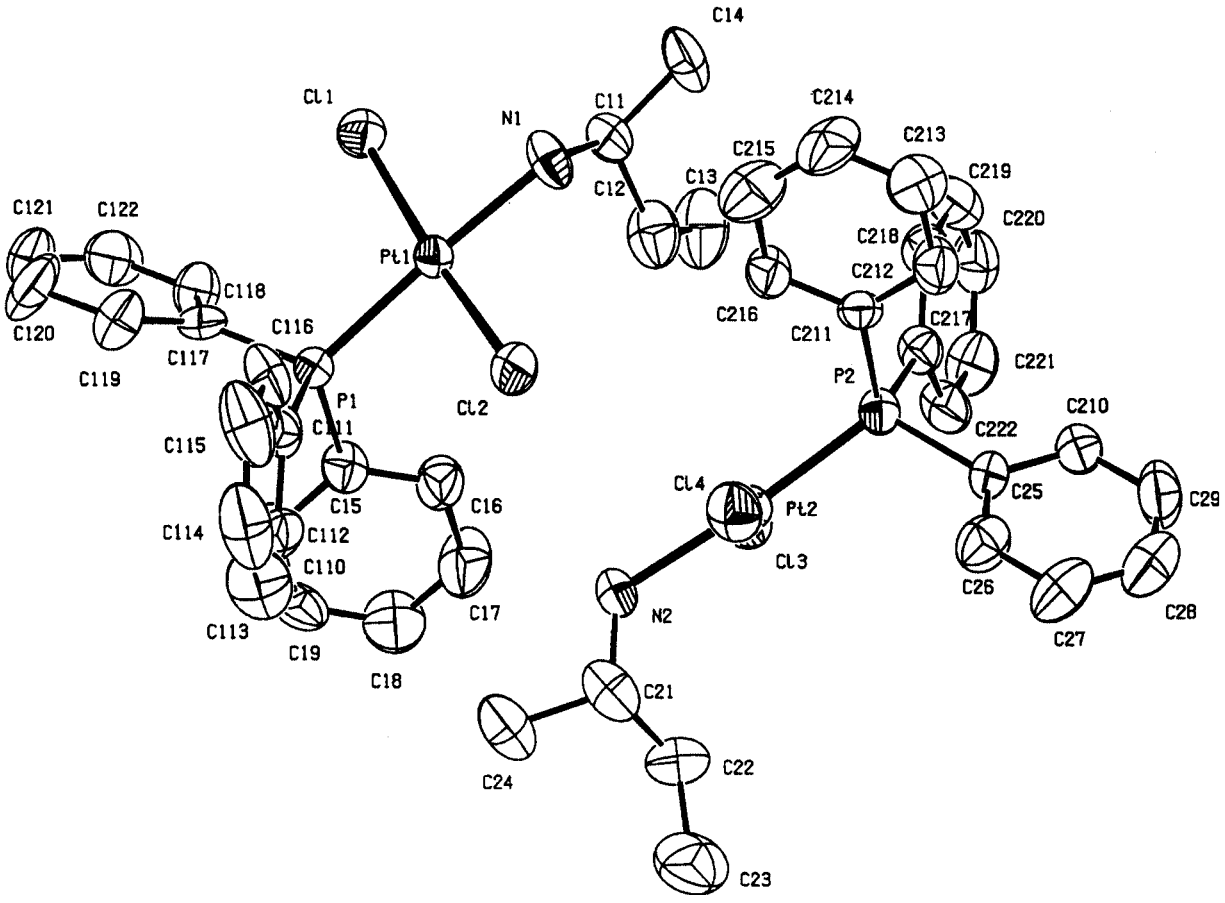

Figure 3. Ortep view of complex **3**

the phenyl represented by C(25), C(26), C(27), C(28), C(29) and C(210) (symmetry code for phenyl ring: $1 + x,y,z$). The distance from H(214) to the aromatic ring centre is 2.635 Å. This π interaction produces a short lengthening of the P(2)−C(25) bond [1.831(12) Å, while this distance is 1.811(12) Å in the equivalent bond in the other molecule] and a shortening of the Pt(2)−P(2) bond [2.211(3) Å, while this value is 2.261(3) Å in the other molecule]. This effect is reflected in the Pt(2)−N(2) distance, which is longer than Pt(1)−N(1) or other bond lengths described in the literature for similar complex such as *trans*[$PtCl_2$(benzoquinoline)-(PEt_3)].[14] These lengthening and shortening interactions could be interpreted in terms of a high *trans* influence in the molecule of Pt(2). The variation in Pt(1)−Cl(1) or Pt(2)−Cl(3) in both structures is related to the value of the Cl(1 or 3)−Pt(1 or 2)−P bond angles. The widening of this angle increases the lengthening of the Pt−Cl bond, so this variation is attributable to steric effects.

The H16(C16)−Pt(1) distance in complex **3a** is fairly short (2.9758 Å) and is similar to the equivalent distance found in complex **1**.

Complex **1** shows a weak hydrogen bond. The hydrogen bonds are: N−H(1A)···Cl(1) (symmetry code for Cl(1) = $1 - x, -y, 1 - z$) with bond lengths N−H = 0.8594 Å, H···Cl = 2.6738 Å, and N···Cl = 3.496(9) Å. On the other hand, hydrogen bonding was not detected for complex **3**, although the only difference with complex **1** is the chirality of the amine.

We determined the cytotoxic activities of complexes **1**, **2**, **3** and **4** against the Pam 212-*ras* line, which are cisplatin-resistant cells through overexpression of H-*ras* oncogene. The cytotoxicities of these complexes were evaluated by using the MTT cell survival assay. The IC_{50} values were defined as the concentration of compound producing 50% of cell death. As shown in Figure 4, the lowest IC_{50} values

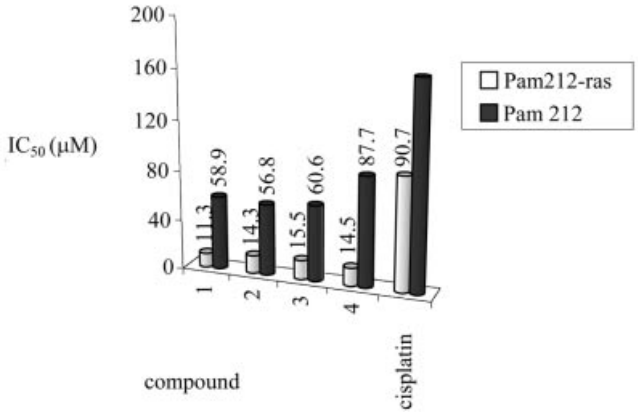

Figure 4. IC_{50} values (μM) for cisplatin and *trans* phosphane platinum derivatives (**1**, **2**, **3** and **4**) in Pam 212 and Pam 212-*ras* cell lines

were obtained with the compounds prepared from the racemic and enantiomerically pure *R* ligand and the *S* isomer (IC_{50} values of 56.84, 58.9 and 60.66 μM). However, the isopropylamine derivative (compound **4**) seems to be less cytotoxic to Pam 212-*ras* cells than compounds **1**, **2** and **3** (IC_{50} value of 87.73 μM) although this compound is still more active than cisplatin (IC_{50} value of 164 μM).

In order to compare the molecular and cellular pharmacological properties of these complexes with those of *trans*-[Pt(dma)(ipa)Cl_2], which is also active against cisplatin-resistant cell lines by induction of apoptotic cell death,[16] we analysed the status of the genomic DNA of Pam 212-*ras* cells after treatment with the novel *trans*-Pt complexes with phosphane ligands. It is known that the final biochemical hallmark of apoptosis is the digestion of genomic DNA into DNA fragments corresponding to multiples of the oligonucleosome unit ("DNA laddering").[17] In addition, it is also known that certain antitumor drugs may achieve a therapeutic index by selective killing of transformed cells without provoking severe toxicity of wild-type cells. Moreover, it has been proposed that this ability may be related with the induction of tumour cell death through apoptosis at drug concentrations lower than those needed to kill normal cells.[18]

Figure 5 shows the electrophoresis in agarose gel of genomic DNA extracted from Pam 212-*ras* cells treated for 24 hours with quantities of complexes **1**, **2**, **3** and **4** corresponding to their IC_{50} or 2 × IC_{50} values. The lanes are: 2 and 3 (complex **2**), 4 and 5 (complex **3**), 6 and 7 (complex **1**) and lane 8 (complex **4**). It may be observed in lanes 2 to 8 that the genomic DNA of Pam 212-*ras* cells appears as a continuous smear and not as a ladder of DNA bands, which would be indicative of apoptosis induction.[17] This leads us to believe that these new platinum complexes have modes of activity against Pam 212-*ras* cells different to those of the previously published isopropylamine derivatives, which induced DNA laddering in these cisplatin-resistant cell lines.[16] It is therefore likely that *trans*-Pt complexes with phosphane ligands may induce cell death through necrotic pathways and/or unfinished apoptotic processes.[19] As reported previously, treatment of Pam 212-*ras* cells with a quantity of *cis*-DDP corresponding to the IC_{50} value did not produce a DNA ladder either, in agreement with the fact that cisplatin is only able to kill this resistant cell line through necrosis and at high drug concentrations.[16]

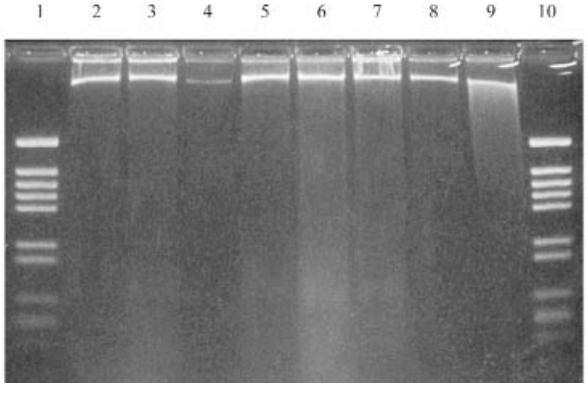

Figure 5. Agarose gel electrophoresis of genomic DNA extracted from Pam 212-*ras* cells treated with quantities corresponding to the IC_{50} values of: complex *R* (**2**), lanes 2 and 3; compound *S* (**3**), lanes 4 and 5; racemic complex (**1**), lanes 6 and 7; complex (**4**), lane 8; and *cis*-DDP, lane 9: − lanes 1 and 10: controls of Φ_{29}-HindIII digested DNA

On the other hand, DNA-binding experiments of complexes **1**, **2**, **3** and **4** with pBR322 plasmid were carried out to determine the molar ratio of bound Pt per nucleotide (r_b) at an input molar ratio of Pt per nucleotide (r_i) of 0.1. Total reflection X-ray fluorescence (TXRF) data showed that binding of compounds **1** to **4** to pBR322 is much lower than that of cisplatin (see Table 4). In fact at r_i = 0.1, the r_b for cisplatin was 0.09, while the r_b values for compounds **1**, **2**, **3** and **4** were 0.002, 0.008, 0.009 and 0.002, respectively, so the binding of complexes **1**−**4** to pBR322 plasmid DNA is 10 to 45 times lower than that of cisplatin.

Table 4. TXRF data for binding of compounds **1** to **4** to pBR322 plasmid DNA. r_i = input molar ratio of Pt per nucleotide; r_b = molar ratio of bound Pt per nucleotide

	r_i	r_b
Cisplatin	0.1	0.09
Complex **1** (racemic)	0.1	0.002
Complex **2** (chiral *R*)	0.1	0.008
Complex **3** (chiral *S*)	0.1	0.009
Complex **4** (isopropylamine)	0.1	0.002

Further experiments with pBR322 showed that complexes **1**−**4** do not alter the electrophoretic mobility either of the oc (open circular) form or of the ccc (covalently closed circular) form of plasmid DNA (see Figure 6). In contrast, we have previously reported that, at r_i = 0.1, both *cis*-DDP and *trans*-[Pt(dma)(ipa)Cl_2] decreases the mobility of the ccc form and increases in the mobility of the oc form in pBR322 DNA.[5] Consequently, the electrophoretic results, in combination with the r_b data obtained by TXRF, suggest that complexes **1**−**4** do not induce relevant structural changes in the double helix, due to their low levels of binding to DNA.

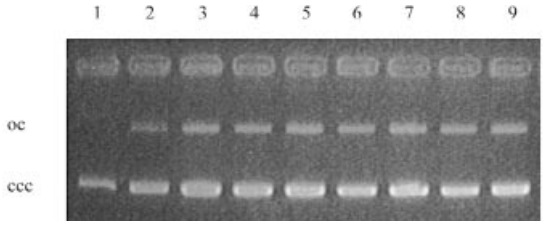

Figure 6. Agarose gel electrophoresis of pBR322 plasmid treated with the *trans* phosphane platinum complexes; lane 1: DNA of control plasmid; lanes 2 to 9, plasmid DNA incubated with complexes **4**, **1**, **2** and **3** at r_i = 0.05 and 0.1 respectively; oc = open circular DNA form; ccc = covalently closed circular DNA form

Conclusions

Replacement of the two amine groups of transplatin by aliphatic amine and phosphane groups results in circumvention of cisplatin resistance. Moreover, these new *trans*-Pt complexes probably achieve this circumvention in a different way from the *trans*-platinum complexes with mixed aliphatic amines that we have previously reported.[5,16] In fact, the *trans*-Pt complexes with phosphane groups do not provoke DNA laddering, which is the final hallmark of the apoptotic process. Overall, the results indicate that, relative to the extent of platinum binding to DNA, these new *trans*-Pt complexes are disproportionately more potent than cisplatin in the induction of cytotoxicity in Pam 212-*ras* cells. As recently suggested for the circumvention of cisplatin resistance by the antitumor drug oxaliplatin, it is likely that the induction of cell death by necrotic pathways and/or unfinished apoptotic programs, possibly enhanced by a contribution of targets other than DNA (such as proteins), may be an important factor in the mechanisms of action of complexes **1−4.** We think that the hydrophobic PPh_3 ligand in complexes **1−4** might also, similarly to the 1,2-diaminecyclohexane ligand in oxaliplatin, direct drug reactivity toward cellular proteins with sulfhydryl groups in hydrophobic pockets that may be poorly reactive with *cis*-DDP, which is polarized.[20]

Experimental Section

Infrared spectra were recorded in Nujol mulls on CsI windows and KBr pellets in the 4000−200 cm^{-1} range with a Perkin−Elmer Model 283 spectrophotometer. NMR spectra were recorded on a Bruker AMX 300 (300 MHz) spectrometer in [D_6]acetone solution. Elemental analysis were performed on a Perkin−Elmer 2400 Series II microanalyzer.

Structural Determination and Refinement of the Complex 1: A prismatic crystal (0.1 × 0.1 × 0.2 mm) was selected and mounted on a MAR345 diffractometer with image plate detector. Unit cell parameters were determined from automatic centring of 5289 reflections ($3 < \theta < 3.1°$) and refined by the least-squares method. Intensities were collected with graphite monochromatized Mo-*K*α radiation. 5329 reflections were measured in the range $2.42 \leq \theta \geq 24.99$, 3170 of which were non-equivalent by symmetry [*R*int(on *I*) = 0.021). 2896 reflections were assumed as observed on application of the condition $I > 2\ \sigma(I)$. Lorentz-polarization and absorption corrections were made. The structure was solved by direct methods, with the SHELXS computer program[21] and refined by the full-matrix, least-squares method, with the SHELX97 computer program,[21] using 3170 reflections (very negative intensities were not assumed). The function minimized was $\Sigma w\ ||F_o|^2 - |F_c|^2|^2$, where $w = [\sigma^2(I) + (0.0723\ P)^2 + 4.1899P]^{-1}$, and $P = (|F_o|^2 + 2\ |F_c|^2)/3$, *f*, *f′* and *f″* were taken from the International Tables of X-ray Crystallography.[22] Ten H atoms were located from a difference synthesis and refined with an overall isotropic temperature factor, and sixteen H atoms were computed and refined with a riding model, with an isotropic temperature factor equal to 1.2 times the equivalent temperature factor of the linked atom. The final *R*(on *F*) factor was 0.042, *wR*(on $|F|^2$) = 0.107 and goodness of fit = 1.082 for all observed reflections. The number of refined parameters was 286. Max. shift/esd = 0.00, Mean shift/esd = 0.00. Max. and min. peaks in final difference synthesis was 0.848 and −0.874 e·Å^{-3}, respectively. The details of the data collected and the structural analyses are summarized in Table 5.

Table 5. Crystal data and structure refinement for *trans*-[$PtCl_2(NH_2CH(CH_3)CH_2CH_3)(PPh_3)$]

Identification code	Complex **1**
Empirical formula	$C_{22}H_{26}Cl_2NPPt$
Molecular mass	601.40
Temperature	293(2) K
Wavelength	0.71069 Å
Crystal system, space group	Triclinic, $P\bar{1}$
Unit cell dimensions	a = 9.7310(10) Å, α = 94.08°
	b = 11.0710(10) Å
	β = 106.8260(10)°
	c = 12.0930(10) Å,
	γ = 112.17°
Vo1ume	1130.68(18) Å^3
Z	2
Calcu1ated density	1.766 Mg/m^3
Absorption coefficient	6.519 mm^{-1}
F(000)	584
Crystal size	0.1 × 0.1 × 0.2 mm
Theta range for data col1ection	2.42 to 24.99 °
Index ranges	$0 \leq h \leq 11$, $-13 \leq k \leq 12$,
	$-14 \leq l \leq 13$
Reflections collected/unique	5329/3170 [*R*int = 0.0216]
Refinement method	Full-matrix, least-squares on F^2
Data/restrains/parameters	3170/18/286
Goodness-of-fit on F^2	1.084
Final R indices [$I > 2\sigma(I)$]	*R*1 = 0.0425, *wR*2 = 0.1074
R indices (all data)	*R*1 = 0.0463, *wR*2 = 0.1117
Largest diff. peak and hole	0.848 and −0.874 e·Å^{-3}

Structural Determination and Refinement of the Complex 3: A prismatic crystal (0.1 × 0.1 × 0.2 mm) was selected and mounted on a MAR345 diffractometer with a image plate detector. Unit cell parameters were determined from automatic centring of 9961 reflections ($3 < \theta < 31°$) and refined by the least-squares method. Intensities were collected with graphite monochromatized Mo-*K*α radiation. 16358 reflections were measured in the range $2.40 \leq \theta \geq 25.01$, 3747 of which were non-equivalent by symmetry [*R*int(on *I*) = 0.038). 3460 reflections were assumed as observed, by application of the condition $I > 2\sigma(I)$. Lorentz-polarization and absorption corrections were made.

The structure was solved by direct methods, with the SHELXS computer program[21] and refined by the full-matrix, least-squares method with the SHELX97 computer program,[21] using 3747 reflections (very negative intensities were not assumed). The function minimized was $\Sigma w\ ||F_o|^2 - |F_c|^2|^2$, where $w = [\sigma^2(I) + (0.0214\ P)^2 + 11.378P]^{-1}$, and $P = (|F_o|^2 + 2\ |F_c|^2)/3$, *f*, *f′* and *f″* were taken from the International Tables of X-ray Crystallography.[22] The chirality of the structure was defined from the Flack coefficient, which is equal to 0.035(12) for the given results.[23] All H atoms were computed and refined with a riding model, with an isotropic temperature factor equal to 1.2 times the equivalent temperature factor of the radiator, which are linked. The final *R*(on *F*) factor was 0.030, *wR*(on $|F_c|^2$) = 0.065 and goodness of fit = 1.083 for all observed reflections. The number of refined parameters was 487. Max. shift/esd = 0.00, Mean shift/esd = 0.00. Max. and min. peaks in final difference synthesis was 0.601 and −0.676 e·Å^{-3},

respectively. The details of the data collected and the structural analyses are summarized in Table 6.

Table 6. Crystal data and structure refinement for *trans*-[$PtCl_2$(*S*-$NH_2CH(CH_3)CH_2CH_3$)(PPh_3)]

Identification code	Complex **3**
Empirical formula	$C_{22}H_{26}Cl_2NPPt$
Molecular mass	601.40
Temperature	293(2) K
Wavelength	0.71069 Å
Crystal system, space group	Monoclinic, $P2_1$
Unit cell dimensions	a = 9.2170(10) Å α = 90° b = 13.7940(10) Å β = 95.107(10)° c = 17.8690(10) Å γ = 90°
Volume	2262.8(3) Å^3
Z	4
Calculated density	1.765 Mg/m^3
Absorption coefficient	6.515 mm^{-1}
F(000)	1168
Crystal size	0.1 × 0.1 × 0.2 mm
Theta range for data collection	2.40 to 25.01°
Index ranges	$0 \le h \le 10$, $0 \le k \le 16$, $-21 \le l \le 21$
Reflections collected/unique	16358/3747 [Rint = 0.0385]
Refinement method	Full-matrix, least-squares on F^2
Data/restraints/parameters	3747/ 1/487
Goodness-of-fit on F^2	1.083
Final R indices [$I > 2\sigma(I)$]	$R1$ = 0.0300, $wR2$ = 0.0654
R indices (all data)	$R1$ = 0.0344, $wR2$ = 0.0676
Absolute structure parameter	0.035 (12)
Largest diff. peak and hole	0.601 and −0.676 e·Å^{-3}

Synthesis and Characterization

***cis*-[$PtCl_2(PPh_3)_2$]:** A PPh_3 (1.263 g, 4.82 mmol) solution in ethanol (2.5 mL) was added to K_2PtCl_4 (1.0 g, 2.4 mmol) solution in water (2.5 mL) and the mixture was stirred in darkness at room temperature for 24 h. The product, a yellow pale precipitate, was collected and washed with water, ethanol and diethyl ether. The solid was then washed with chloroform, and a white precipitate (*cis* isomer) and a yellow solution (*trans* isomer) were obtained. The yellow solution produced a white precipitate on storage in chloroform. This isomerization of yellow *trans*-[$PtCl_2(PPh_3)_2$] to its white *cis* isomer is catalysed by light irradiation.[24]

White solid, yield: 98% (1.859 g). ν(Pt−Cl): 317 cm^{-1} and 292 cm^{-1}, ν(Pt−P): 464 cm^{-1} and 445 cm^{-1}. $C_{36}H_{30}Cl_2P_2Pt$ (790.6): calcd. C 54.60, H 3.82; found C 54.05, H 3.73. ^{1}H NMR (300 MHz, $CDCl_3$, 25 °C) (ppm): 7.49 (m, 6 H, *ortho*); 7.32 (m, 3 H, *para*), 7.25 (m, 6 H, *meta*) ppm. ^{31}P NMR (300 MHz, $CDCl_3$, 25 °C) (ppm): 14.81 (J_{P-Pt}= 3673 Hz)

[(μ-Cl)PtCl(PPh_3)]$_2$: This synthesis was based on F. R. Hartley's method[25] and also on R. J. Goodfellow's method.[26] Goodfellow's method, with some modifications, affords the highest yield.

The complex *cis*-[$PtCl_2(PPh_3)_2$] (0.38 mmol, 0.300 g) and $PtCl_2$ (0.4 mmol, 0.106 g) were finely ground with naphthalene in a mortar. The mixture was transferred into a flask. The mixture was then heated at reflux with stirring at 150 °C for 15 min. After cooling, the solid mixture was transferred to a Soxhlet thimble and washed with light petroleum to remove the naphthalene. The crude product was then extracted with dichloromethane to obtain a yellow-orange solution, which was taken to dryness under reduced pressure. The solid was partially dissolved in chloroform to obtain a orange precipitate and a yellow solution. When the yellow solution was warmed in chloroform it turned orange, with precipitation of the orange isomer (*trans* isomer).

Deep orange solid, yield: 98% (0.394 g). ν(Pt−Cl_μ): 321 and 260 cm^{-1}. ν(Pt−Cl_T): 355 cm^{-1}. $C_{36}H_{30}Cl_4P_2Pt_2$ (1056.6): calcd. C 40.93, H 2.86, Cl 13.47; found C 40.96, H 2.79, Cl 13.36. ^{1}H NMR (300 MHz [D_3]acetonitrile, 25 °C) (ppm): 7.71 (m, 6H), 7.67 (m, 6H), 7.46 (m, 3H).^{31}P NMR (300 MHz [D_3]acetonitrile, 25 °C) (ppm): 3.60 (J_{P-Pt} = 4100.26 Hz)

***trans*-[$PtCl_2$L(PPh_3)]:** Complexes **1**, **2**, **3** and **4** were obtained Chatt's method, with variations.[27] [(μ-Cl)PtCl(PPh_3)]$_2$ (0.142 mmol, 150 mg) was partially dissolved in acetone, together with the stoichiometry quantity of amine ligand (L), at room temperature. A solution was immediately formed, and this was generally accompanied by a lightening in colour. The acetone was removed under reduced pressure. Diethyl ether was added and the *trans*-[$PtCl_2$L(PPh_3)] was dissolved. The solution was filtered to remove the insoluble impurities. The *trans*-[$PtCl_2$L(PPh_3)] solution in diethyl ether produced crystals or a yellow precipitate on storage.

Yellow compounds, yields: 72% (complex **1**, 0.123 g), 61% (complex **2**, 0.104 g) and 50% (complex **3**, 0.085 g). ν(Pt−Cl): 346 cm^{-1}, ν(Pt−P):449 cm^{-1}, ν (Pt−N): 430 cm^{-1}. $C_{22}H_{26}Cl_2NPPt$ (601.4): calcd. C 43.0, H 4.35, N 2.33; found C 43.76, H 4.22, N 2.24. ^{1}H NMR (300 MHz [D_6]acetone, 25 °C) (ppm): 7.70 (m 6 H, *ortho*) 7.44 (m, 9 H, *meta* and *para*), 3.9 (b.s. 2 H, NH_2), 3.36 (sp, 1 H), 1.93 (m, 1 H), 1.60 (m, [$NH_2CH(CH_3)CH_2CH_3$], 1 H, [$NH_2CH(CH_3)CH_2CH_3$]), 1.40 (d, 3 H, [$NH_2CH(CH_3)CH_2CH_3$]), 1.00 (t, 3 H, [$NH_2CH(CH_3)CH_2CH_3$]) ppm. ^{31}P NMR (300 MHz, [D_6]acetone, 25 °C) (ppm): 11.96 (J_{P-Pt}= 3600 Hz) ppm. ^{14}C NMR (300 MHz, [D_6]acetone, 25 °C) (ppm): 135.56(C_{meta}), 131.47(C_{para}), 130.37 (C_{ipso}), 128.64 (C_{ortho}), 52.33 (C−NH_2), 31.50 (CH_2), 21.32 [$CH(CH_3)$], 10.44 [$CH_2(CH_3)$]. $[\alpha]_D^{20}$ = −48.4 (complex **2**), $[\alpha]_D^{20}$ = +48.4 (complex **3**)

***trans*-[$PtCl_2$(ipa)(PPh_3)]:** Yellowish compound. complex **4**. Yield: 90% (0.150 g). ν(Pt−Cl): 344 cm^{-1}, ν(Pt−P): 453 cm^{-1} and 428 cm^{-1}, ν(Pt−N): 430 cm^{-1}. $C_{21}H_{24}Cl_2NPPt$ (587.4): calcd. C.42.94, H 4.12, N 2.38; found C 42.80, H 4.08, N 2.43. ^{1}H NMR (300 MHz [D_6]acetone, 25 °C) (ppm): 7.70 (m, 6 H, C_{ortho}), 7.44 (m, 9 H, *meta* and *para*), 3.97 (b.s., 2 H, NH_2), 3.59 (hp, 1 H, CH), 1.39 (d, 6 H, CH_3, J_H = 7 Hz). ^{31}P NMR (300 MHz [D_6]acetone, 25 °C) (ppm): 11.92 (J_{P-Pt}= 3600 Hz).^{14}C NMR (300 MHz [D_6]acetone, 25 °C) (ppm): 24.5(CH_3), 47.1(CH), 128.6 (C_{ortho}), 130.4 (C_{ipso}), 131.4 (C_{para}), 135.5 (C_{meta}) ppm. ^{195}Pt NMR (300 MHz [D_6]acetone, 25 °C) (ppm): −3792.7 (J_{P-Pt} = 3608 Hz).

Biochemical Probes

Biologicals and Drugs: 100 mm culture and microwell plates were obtained from NUNCLON (Roskilde, Denmark). MTT was purchased from Sigma Co., FCS was supplied by GIBCO-BRL, and ethanol was obtained from Merck. *cis*-Diamminedichloroplatinum(II), cisplatin or *cis*-DDP, was synthesized from K_2PtCl_4 supplied by Johnson Matthey. *cis*-DDP was dissolved in $NaClO_4$ (10 mM). The *trans* platinum phosphane complexes were dissolved in acetone as 1 mg/ml solutions. These solutions were freshly prepared before use.

Cell Lines and Culture Conditions: Pam 212, a normal cell line of murine keratinocytes, and Pam 212-*ras*, a transformed murine keratinocytes cell line overexpressing the H-*ras* oncogene, were cultured in DMEM (Dulbecco modified Eagle's medium), supplemented with FCS (foetal calf serum, 10%), glutamine (2 mM), peni-

cillin (100 units/mL) and streptomycin (100 μg/mL) at 37 °C in an atmosphere of 95% air and 5% CO_2. All cultures were passaged twice weekly, showing a doubling time between 16−24 hours.

Cytotoxicity Assays: Cell survival was evaluated by use of a system based on the tetrazolium compound MTT, which is reduced by living cells to yield a soluble formazan product that can be detected colorimetrically.[28] Cells were platted in 96-well sterile plates at a density of 10^4 cells/well in 100 μL of medium and were incubated for 3−4 h. The compounds were added to final concentrations from 0 to 200 μM in a volume of 100 μL/well. Twenty-four hours later, 50 μL of a MTT solution (1/5 in culture medium) freshly diluted to a concentration of 1 mg/ml were pipetted into each well, and the plate was incubated for 5 h at 37 °C in a humidified 5% CO_2 atmosphere. After the periods specified, the cell viability was evaluated by measurement of the absorbance at 520 nm, by use of a Whittaker Microplate Reader 2001. IC_{50} values (compound concentration that produces 50% of cell growth inhibition) were calculated from curves constructed by plotting (%) cell survival versus drug concentration. The therapeutic index (T.I.) of every compound was calculated as the ratio of the IC_{50} in normal cells versus the IC_{50} in transformed cells. In control experiments it was observed that 10% acetone did not have any effect on cell growth. This was the highest percentage of acetone present in the cell cultures after addition of 200 μM of the compounds. All experiments were made in quadruplicate.

DNA Fragmentation Assay: Pam212-ras cells (5×10^5 cells/mL) were platted in 100 mm sterile dishes. The cells were treated with the compounds for 24 h to a final concentration of the IC_{50} under the conditions described above.[28] The fraction of detached cells was collected by centrifugation of the culture media and washed twice with PBS. The cell pellet was disrupted with 700 μL of lysis buffer (150 mM Tris, tris(hydroxymethyl)aminomethane, pH 8.0; 100 mM NaCl; 100 mM EDTA, ethylenediamine tetracetate). The fraction of non-detached cells was also washed twice with BPS and lysed by addition of 700 μL of lysis buffer to the plate. Both cell fractions were joined and the whole cell lysate was treated with proteinase K (500 μg/mL) for 2 h at 55 °C. Afterwards, samples were exposed to RNase A (50 μg/mL) for 16 h at 37 °C. The DNA was first extracted with phenol, followed by phenol/chloroform/isoamyl alcohol (25:24:1) and a chloroform/isoamyl alcohol (24:1) phase. Subsequently, the DNA was precipitated overnight at −20 °C in 2.5 volumes of cold 100% ethanol/150 mM potassium acetate. After centrifugation at 12,000 rpm for 15 min to recover the precipitated DNA, the supernatant was discarded and the pellet was washed with 70% ethanol. Samples were dried on a SAVANT Speed Vac Concentrator and then resuspended in distilled water. The DNA concentration was calculated by determining the OD_{260}. Electrophoresis of DNA (10 μg/well) was performed for 16 h at 75 V in 1.8% agarose gel with TAE (40 mM Tris-acetate, 1 mM EDTA, pH 8.0) as running buffer. The bands were viewed by ethidium bromide staining for 16 h and UV transillumination. DNA bands were analysed by laser densitometry with a Molecular Dynamics densitometer.

Determination of Platinum Binding to pBR322 Plasmid DNA by TXRF: pBR322 DNA aliquots (50 μg/mL) were incubated with the platinum compounds in a buffer solution containing 50 mM NaCl, 10 mM Tris.HCl (pH 7.4) and EDTA (0.1 mM) at $r_i = 0.1$ (input molar ratio of Pt per nucleotide). Incubations were performed in the dark at 37 °C. After 24 hours of incubation, the DNA of the samples was precipitated with 0.1 volumes of sodium acetate (pH 4.7) and 2.5 volumes of absolute ethanol to eliminate unchanged drug. The DNA content in each sample was measured by UV spectrophotometry at 260 nm in a Shimadzu UV-240 spectrophotometer, and platinum bound to DNA was determined by total reflection X-ray fluorescence (TXRF). Experiments were carried out in triplicate.

TXRF Measurements: The analysis by TXRF was performed with a Seifert Extra-II spectrometer (Seifert, Ahrensburg, Germany). TXRF determinations were carried out by a previously reported procedure.[29] Briefly, a 100 μL sample of the DNA precipitated from the solutions of pBR322 incubated with the platinum complexes was introduced into a 2 mL test tube. This solution was standardised with 100 ng/mL vanadium [Merck (Darmstadt, Germany) ICP vanadium standard solution]. Afterwards, the sample was introduced into a high-purity nitrogen flow concentrator at a temperature of 70 °C until the volume had been reduced five times. An aliquot of 5 μL was then taken, deposited on a clean quartz reflector and dried on a ceramic plate at a temperature of 50 °C. The entire process was carried out in a laminate flow chamber (Model A-100). The samples were analysed by following the X-ray molybdenum line under working conditions of 50 *k*V and 20 mA with a live-time of 1000 s and a dead time of 35%. Spectra were recorded between 0 and 20 keV. The following 15 elements were analysed simultaneously: P, S, K, Ca, V, Fe, Cu, Zn, As, Br, Rb, Sr, Ni, Mn and Pt, in order to obtain a correct deconvolution of profiles associated with the general spectrum. The Pt line was used for Pt quantification. The analytical sensitivity of the TXRF measurements was 0.3 to 22.4 ng Pt in a solution volume of 100 μL, with repeatability between 2 and 8% (the number of determinations was $n = 3$).

Gel Electrophoresis of Drug:pBR322 Complexes: pBR322 DNA aliquots (50 μg/mL) were incubated with the platinum compounds in a buffer solution containing 50 mM NaCl, 10 mM Tris.HCl (pH 7.4) and EDTA (0.1 mM) at several r_i values (0.5 and 0.1). Incubations were performed in the dark at 37 °C. 20 μL aliquots of the drug:DNA complexes containing 1 μg of DNA were subjected to 1.5% agarose gel electrophoresis for 16 h at 25 V in TAE buffer (Tris-acetate 40 mM, EDTA 2 mM pH 8.0). The DNA was stained in the same buffer containing ethidium bromide (0.5 μg/mL). The gels were photographed with a MP-4 Polaroid camera with a 665 Polaroid film and an orange filter.

Acknowledgments

This work was supported by the Spanish CICYT/ SAF 00/0029. Sponsorship by COST Actions D20/001/00 and D20/003/00 is also acknowledged. Johnson Matthey PLC is also acknowledged for their generous gift of K_2PtCl_4.

[1] B. Lippert, *Cisplatin*, Wiley-VCH, Weinheim, **1999**.
[2] L. Kelland, N. Farrell, *Platinum-Based Drugs in Cancer Therapy*, Humana Press, **2000**.
[3] M. V. Beusichem, N. Farrell, *Inorg. Chem.* **1992**, *31*, 934−939.
[4] M. Coluccia, A. Nassi, F. Loseto, A. Boccarelli, M. A. Mariggiò, D. Giordano, F. P. Intini, P. Caputo, G. Natile, *J. Med. Chem.* **1993**, *36*, 510−512.
[5] J. M. Pérez, E. I. Montero, A. M. Gonzalez, X. Solans, M. Font-Bardia, M. A. Fuertes, C. Alonso, C. Navarro-Ranninger, *J. Med. Chem.* **2000**, *43*, 2411−2418.
[6] K. Neplechová, J. Kasparová, O. Vraná, O. Nováková, A. Habtemarian, B. Watchman, P. J. Sadler, V. Brabec, *Mol. Pharm.* **1999**, *56*, 20−30.
[7] N. Margiotta, A. Habtemariam, P. J. Sadler, *Angew. Chem. Int. Ed. Engl.* **1997**, *36*, 1185−1187.
[8] P. Sevillano, A. Habtemariam, S. Parsons, A. Castiñeiras, M. E. García, P. J. Sadler, *J. Chem. Soc., Dalton Trans.* **1999**, *16*, 2861−2870.

[9] W. Henderson, S. R. Alley, *Inorg. Chim. Acta* **2001**, *322*, 106−112.
[10] *Comprehensive Coordination Chemistry*, V5. Late Transition Elements, Eds.: G. Wilkinson, R. D. Gillard, J. A. McCleverty, Pergamon Press, **1987**.
[11] T. G. Appleton, H. C. Clark, L. E. Manzer, *Coord. Chem. Rev.* **1973**, *10*, 335−422.
[12] P. S. Pregosin. In *Phosphorus-31 NMR Spectroscopy in Stereochemical analysis*. Eds.: J. G. Verkade, L. D. Louis, VCH Publishers, New York, pp. 465, **1987**.
[13] A. D. Burrows, M. F. Mahon, M. T. Palmer, *J. Chem. Soc., Dalton Trans.* **2000**, *20*, 3615−3619.
[14] A. Albinati, P. S. Pregosin, F. Wombacher, *Inorg. Chem.* **1990**, *29*, 1812−1817.
[15] M. F. C. Guedes da Silva, E. M. P. R. P. Branco, Y. Wang, J. J. R. Fraústo da Silva, A. J. L. Pombeiro, R. Bertani, R. A. Michelin, M. Mozón, F. Benetollo, G. Bombieri, *J. Organomet. Chem.* **1995**, *490*, 89−99.
[16] E. I. Montero, S. Díaz, A. M. González-Vadillo, J. M. Pérez, C. Alonso, C. Navarro-Ranninger, *J. Med. Chem.* **1999**, *42*, 4264−4268.
[17] A. G. Quiroga, J. M. Pérez, E. I. Montero, D. W. West, C. Alonso, C. Navarro-Ranninger, *J. Inorg. Biochem.* **1999**, *75*, 293−301.
[18] S. W. Lowe, H. E. Ruley, T. Jacks, D. E. Housman, *Cell.* **1993**, *74*, 957−967.
[19] V. M. González, M. A. Fuertes, C. Alonso, J. M. Pérez, *Mol. Pharmacol.* **2001**, *59*, 657−663.
[20] E. Raymond, S. Faivre, S. Chaney, J. Woynarowski, E. Cvitkovic, *Mol. Cancer Ther.* **2002**, *1*, 227−235.
[21] Sheldrick, G. M., A computer program for determination of crystal structure. University of Göttingen, Germany. **1997**
[22] International Tables of X-ray Crystallography, Ed. Kynoch press, Vol. IV, pp 99−100 and 149, **1974.**
[23] H. D. Flack, *Acta Crystallogr., Sect. A* **1983**, *39*, 876− 881.
[24] R. D. Gillard, M. F. Pilbrow, *J. Chem. Soc., Dalton Trans.* **1974**, *21*, 2320−2325.
[25] F. R. Hartley, G. W. Searle, *Inorg. Chem.* **1973**, *12*, 1949−1951.
[26] R. J. Goodfellow, L. M. Venanzi, *J. Chem. Soc.* **1965**, 7533−7534.
[27] J. Chatt, L. M. Venanzi, *J. Chem. Soc.* **1955**, 3858−3864.
[28] M. C. Alley, D. A. Scudiero, A. Monks, M. L. Hursey, M. J. Czerwinski, D. L. Fine, B. J. Abbott, J. G. Mayo, R. H. Shoemaker, M. R. Boyd, *Cancer Res.* **1998**, *48*, 589−601.
[29] R. Fernández-Ruíz, J. D. Tornero, V. M. González, C. Alonso, *Analyst* **1999**, *124*, 583−585.

Received November 29, 2002
[I02406]

Synthesis and Dynamic Features of (Chloro)zirconocene Cations Stabilised by Pendant (Diarylphosphanyl)alkyl and (Dimethylamino)alkyl Substituents at Their Cyclopentadienyl Ring Systems

Steve Döring,[a] Vasily V. Kotov,[a] Gerhard Erker,*[a] Gerald Kehr,[a] Klaus Bergander,[a][‡] Olga Kataeva,[a][‡] and Roland Fröhlich[a][‡‡]

Keywords: Cations / Metallocenes / N ligands / P ligands / Zirconium

Treatment of the substituted (diarylphosphanyl)methyl group-4 metallocene complexes $[(C_5H_4–CR^1R^2–PAr_2)_2ZrCl_2]$ (**2**: R^1/R^2 = CH_3/CH_3, H/CH_3, H/aryl) with $Li[B(C_6F_5)_4]$ in dichloromethane solution results in chloride ligand abstraction (with LiCl precipitation) to yield the complexes $[(C_5H_4–CR^1R^2–PAr_2)_2Zr–Cl^+]$ (**5**), with both phosphanyl groups internally coordinated to the metal centre. Three possible diastereoisomers are observed in the case of **5c** (R^1 = H; R^2 = CH_3), while bulkier R^2 substituents give higher selectivities. The thermally induced (reversible) cleavage of the Zr–phosphane linkage results in dynamic NMR behaviour. Gibbs activation energies of $\Delta G^{\neq}$(298 K) = 14.8 ± 0.5 and 14.5 ± 0.5 kcal/mol were obtained for these intramolecular equilibration processes in the complexes *trans*-**5d** (R^1 = H; R^2 = Ph) and *trans*-**5e** (R^1 = H; R^2 = ferrocenyl), respectively. Treatment of the substituted (dimethylamino)methyl metallocene complexes $[(C_5H_4–CR^1R^2–NMe_2)_2ZrCl_2]$ (**6a**, **6b**) with $Li[B(C_6F_5)_4]$ proceeds analogously to yield the cation systems $[\{C_5H_4–C(CH_3)_2–NMe_2\}_2ZrCl^+]$ (**12a**) and $[\{C_5H_4–CH(CH_3)–NMe_2\}_2ZrCl^+]$ (**12b**, three possible diastereoisomers). Both complexes have their pairs of amino groups coordinated to the metal centre. The complexes exhibit dynamic NMR spectra. Selective equilibration of the diastereotopic $N(CH_3)^A(CH_3)^B$ resonances of complex **12a** is observed [$\Delta G^{\neq}$(233 K) = 11.5 ± 0.2 kcal/mol], whereas the adjacent $C(CH_3)^A(CH_3)^B$ methyl groups remain diastereotopic. The dynamic equilibration of the latter was observed at a markedly higher temperature [$\Delta G^{\neq}$(333 K) = 17.3 ± 0.2 kcal/mol]. Treatment of $[\{C_5H_4–C(CH_3)_2–NMe_2\}CpZrCl_2]$ (**10**) with $Li[B(C_6F_5)_4]$ resulted in the formation of complex $[\{C_5H_4–C(CH_3)_2–NMe_2\}CpZr–Cl^+]$ (**11**), which shows the internal $–N(CH_3)^A(CH)^B$ equilibration proceeding with a markedly higher activation barrier [$\Delta G^{\neq}$(333 K) = 17.6 ± 0.2 kcal/mol] than in **12a**, and a stereochemical memory effect indicative of solvent coordination to the metal centre of the resulting highly electrophilic chlorozirconocene cation intermediate. Complex **11** was characterised by an X-ray crystal structure analysis, which shows the internal Zr←amine coordination.

(© Wiley-VCH Verlag GmbH & Co. KGaA, 69451 Weinheim, Germany, 2003)

Introduction

Alkylzirconocene cations are regarded as the active species in homogeneous Ziegler−Natta olefin polymerisation.[1a−1e] Some of such complexes can very easily be prepared, a typical example being the parent compound $[Cp_2ZrCH_3^+]$ (**1**), readily available from the neutral precursor $[Cp_2Zr(CH_3)_2]$ by a variety of methods.[2a,2b,3−5] The cation **1** is stabilised by tight ion pair formation with its anion.[6] Alternatively, it adds a variety of simple neutral donor ligands such as tetrahydrofuran to form pseudotetrahedral adducts (e.g., $[Cp_2ZrCH_3(THF)^+]$ or its respective "outer-sphere" or "solvent-separated" ion pair).[7,8] $[^RCp_2ZrCl^+]$ complexes are much less stable. Their syntheses are often less straightforward and they require stronger donor ligand stabilisation. A typical example is shown in Scheme 1. Treatment of the (diarylphosphanyl)alkyl-substituted $[^RCp_2Zr(CH_3)_2]$ derivatives with $B(C_6F_5)_3$ as a suitable methyl anion abstractor[9,10] results in the clean formation of the corresponding $[^RCp_2ZrCH_3^+]$ cation (**3**).[11] Treatment of this in turn with a second equivalent of $B(C_6F_5)_3$ in the presence of a chloride source then gives rise to subsequent formation of the doubly internally phosphane-stabilised $[^RCp_2ZrCl^+]$ cation derivative **5** (via **4**, see Scheme 1).[11,12]

It would be interesting to have the corresponding (dimethylamino)alkyl-substituted Cp systems available in order to study the stabilising influence of the tertiary amine donor ligands relative to the stabilising phosphanes. However, their synthesis from **6** by an analogous pathway is precluded by a preferred internal C−H activation process that rapidly takes place at the stage of the intermediate **8** (see Scheme 2).[13−16] We therefore had to devise an alternative pathway to make the (dimethylamino)alkyl−Cp-containing

[a] Organisch-Chemisches Institut der Universität Münster, Corrensstr. 40, 48149 Münster, Germany
[‡] NMR spectroscopy
[‡‡] X-ray structure analyses
Supporting information for this article is available on the WWW under http://www.eurjic.org or from the author.

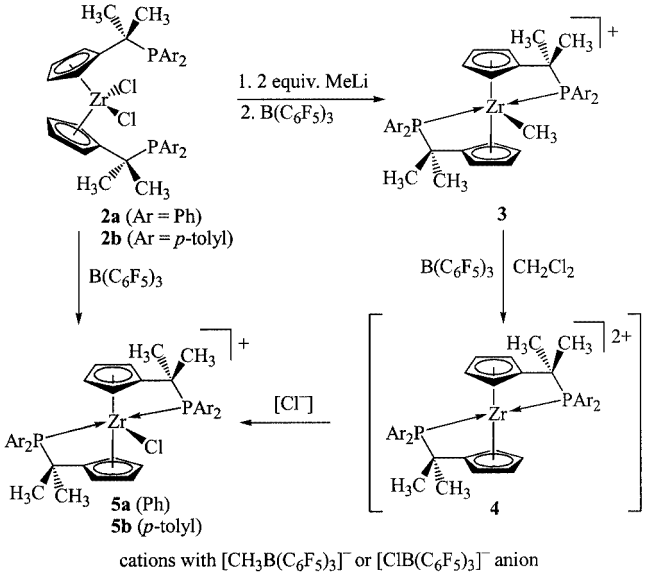

Scheme 1

[$^{R}Cp_2Zr-Cl^+$] cation systems synthetically available. Such a selective preparative route is described in this paper. The dynamic NMR behaviour of the resulting complexes allowed for an estimate of the internal stabilisation of such strongly electrophilic group-4 metallocene cations by tertiary amine donor ligands.

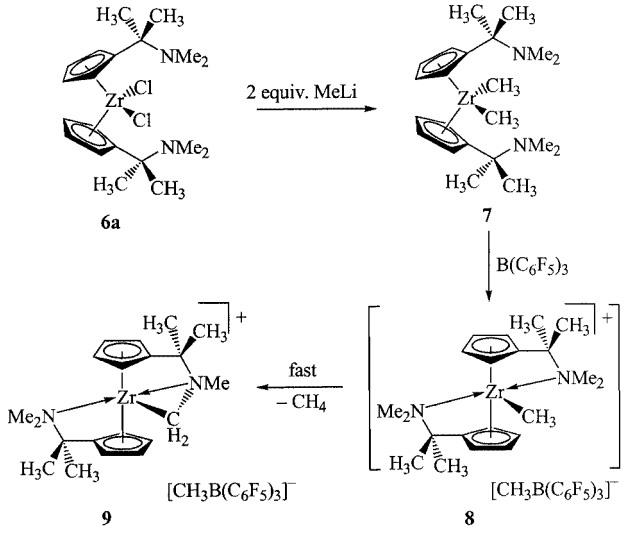

Scheme 2

Results and Discussion

Synthesis and Characterisation of [Chlorobis{[(diarylphosphanyl)alkyl]cyclopentadienyl}zirconium] Cation Complexes

We had previously prepared a series of [{(Ar_2PCMe_2)C_5H_4}$_2$$ZrCl^+$] cation systems by a three-step synthesis via the dication intermediate **4**, as outlined in Scheme 1 [**5a**′: Ar = Ph; **5b**′: Ar = *p*-tolyl, with [$CH_3B(C_6F_5)_3^-$] anion; **5a**′′: Ar = Ph, with [$ClB(C_6F_5)_3^-$] anion].[11] In one case (**5a**′′) we succeeded in preparing the substituted chlorozirconocene cation directly by means of chloride abstraction by the strong organometallic Lewis acid $B(C_6F_5)_3$.[11,12] This result indicated to us that chloride abstraction by more powerful reagents, such as $Li[B(C_6F_5)_4]$,[17,18] might provide a suitable direct route to this general class of internally donor ligand stabilised chlorozirconocene cation systems. Initial tests were therefore carried out with the substituted [{[(diarylphosphanyl)methyl]C_5H_4}$_2$$ZrCl_2$] systems **2a** (Ar = Ph) and **2b** (Ar = *p*-tolyl), which were each treated with 1 mol-equiv. of the $Li[B(C_6F_5)_4]$ reagent in dichloromethane solution at room temperature. After ca. 1 h, the chloride abstraction was complete. The resulting LiCl precipitate was removed by filtration and the corresponding chlorometallocene cation products **5a** and **5b** were isolated in 55 and 67% yields, respectively (both with [$B(C_6F_5)_4^-$] anion, see Scheme 3).

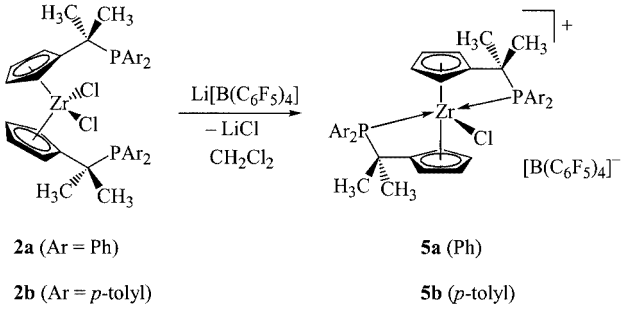

Scheme 3

We have also used the previously described complexes [($C_5H_4-CHR-PAr_2$)$_2$$ZrCl_2$] **2c** (R = CH_3; Ar = Ph), **2d** (R = Ph; Ar = Ph) and **2e** (R = ferrocenyl; Ar = *p*-tolyl)[11,12,30] as neutral substrates for the chloride abstraction reaction with $Li[B(C_6F_5)_3]$ to give the new metallocene cation complexes **5c**−**e** (see Scheme 4).

The complexes **2c**−**e** each contain two stereogenic carbon centres and were each employed in the Cl^- abstraction reaction as ca. 1:1 *meso*-/*rac*-**2(c−e)** mixtures of diastereoisomers. The doubly phosphorus-coordinated products **5c**−**e** can each form three diastereoisomers: two complexes in which the substituents at the pair of stereogenic metallacyclic ring carbon centres are oriented *cis* (*syn*- or *anti*-oriented relative to the Zr−Cl vector,[19] thus giving rise to the formation of compounds *syn-cis*-**5c**−**e** and *anti-cis*-**5c**−**e**, respectively), together with the *trans* diastereoisomers (*trans*-**5c**−**e**) (see Scheme 4).

In the case of **5c** (R = CH_3; Ar = Ph) a near to statistical mixture of the three diastereoisomers was actually obtained (isolated in 54% yield). This is evident from inspection of typical NMR spectra of the organometallic salt **5c**. The ^{31}P NMR spectrum (at 253 K) shows singlets at δ = −36.2 and −45.9 ppm corresponding to the pairs of symmetry-equivalent phosphorus nuclei of the complexes *syn-cis*-**5c** and *anti-cis*-**5c** (no absolute assignment was achieved) and an AB pattern at δ = −38.1 ppm and δ = −47.2 ppm with a $^2J_{P,P}$

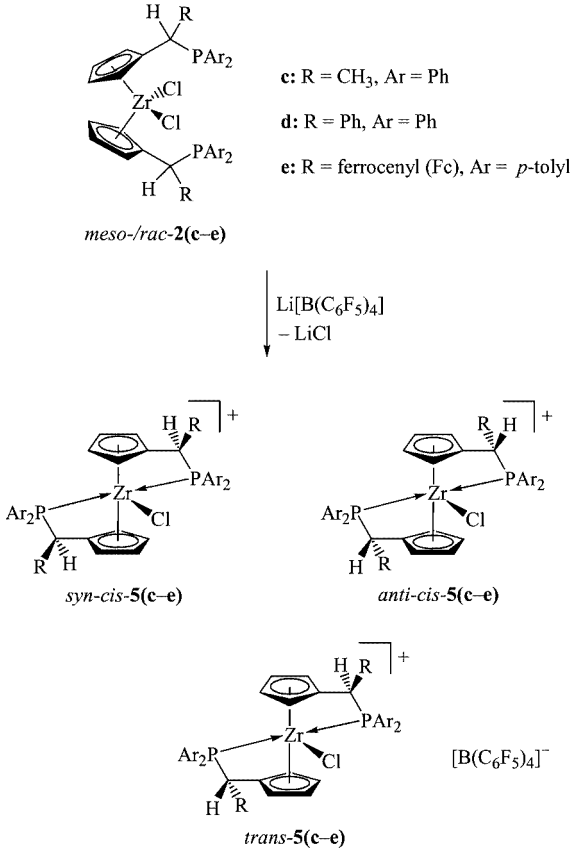

Scheme 4

coupling constant of 110 Hz, attributable to the *trans*-**5c** diastereoisomer (see Figure 1).

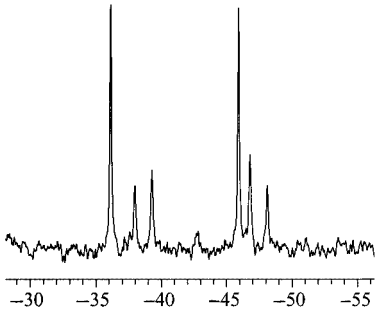

Figure 1. $^{31}P\{^{1}H\}$ NMR spectrum of the close to statistical mixture of the *syn-cis*-**5c**, *anti-cis*-**5c** and *trans*-**5c** diastereomers (in CD_2Cl_2 solution)

As would be expected, each *cis*-**5c** isomer exhibits a set of four methine $^{1}H/^{13}C$ NMR signals of the pair of symmetry-equivalent C_5H_4 ligand units. In contrast, the (C_5H_4−CHMe−[P]) ligands of the *trans*-**5c** isomer are diastereotopic. Consequently, complex *trans*-**5c** shows a set of eight Cp signals of equal intensity (for numerical values see the Exp. Sect.), a pair of C_α−*H* multiplets (δ = 4.21 and 4.47 ppm), each of 1 H relative intensity, and two methyl ^{1}H NMR resonances at δ = 1.25 and 1.50 ppm.

Treatment of complex [(C_5H_4−CHPh−PPh_2)$_2ZrCl_2$] (**2d**) with the Li[$B(C_6F_5)_4$] reagent cleanly resulted in the formation of the chlorozirconocene cation complex **5d**. Again, diastereomeric complexes are formed, but the ^{31}P NMR spectrum of **5d** shows the presence only of the *trans*-**5d** isomer (AB system at δ = −18.4 and −41.8 ppm, $^{2}J_{P,P}$ = 108 Hz) and of *one* of the *cis*-**5d** isomers, in a ca. 1:1 ratio.

Complex *trans*-**5d** shows two ^{1}H NMR Cp−C*H*R signals at δ = 5.65 and 5.57 ppm. An increase in the temperature results in coalescence of the signals of pairwise diastereotopic groups of *trans*-**5d**, including these Cp−C*H*R resonances with a Gibbs activation energy of $\Delta G^{\neq}$(298 K) = 14.8 ± 0.5 kcal/mol.[11,20,21] The NMR signals of the *cis*-**5d** isomers remain unaffected by the dynamic behaviour of *trans*-**5d**. We therefore assign a process as depicted in Scheme 5 to account for this characteristic behaviour, in which a consecutive dissociation of *both* Zr←P linkages takes place in *trans*-**5d**, followed by rotation around the Zr−Cp vector and reformation of the stabilising intramolecular Zr←phosphane interactions.

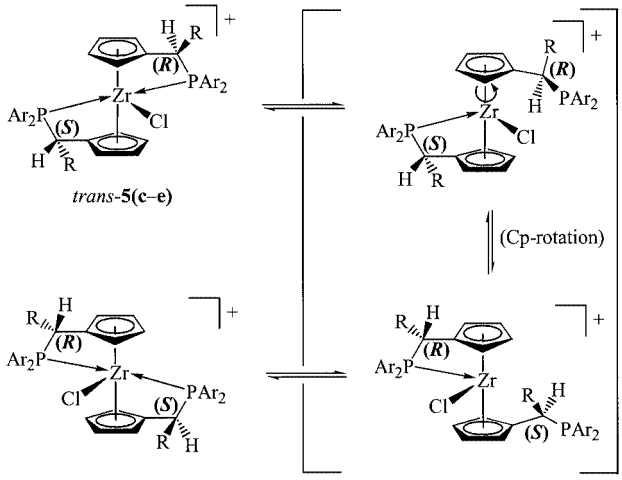

Scheme 5

Complex **5c** shows similar dynamic NMR features at elevated temperatures. We have found indications for an intramolecular equilibration process of *trans*-**5c**, analogous to that described above for **5d**, *and* a separate equilibration between the two *cis*-**5c** isomers. Unfortunately, the coalescence temperatures could not be reached cleanly in this case because of a rapid thermal decomposition of the systems.

Complex **5e** was obtained as a similar mixture of a single *cis*-**5e** diastereomer and the *trans*-**5e** diastereomer. Complex *trans*-**5e** exhibits a total of eight C_5H_4 resonances [at δ = 7.18, 6.92, 6.17, 6.06 ppm (ring A), and δ = 6.65, 6.06, 6.00, 5.94 ppm (ring B)] and a pair of CpC*H*R ^{1}H NMR resonances at δ = 5.06 and 5.12 ppm. From the coalescence of these last two signals at T_c = 298 K, a Gibbs activation energy of $\Delta G^{\neq}(T_c)$ = 14.5 ± 0.5 kcal/mol was obtained. Again, the *cis*-**5e** isomer is not involved in this dynamic process. It shows a single ^{31}P NMR resonance (δ = −18.2

ppm) and four C_5H_4−R ^{1}H NMR multiplets at δ = 7.15, 6.42, 6.35, and 6.22 ppm.

Synthesis and Characterisation of [Chlorobis{[(dimethylamino)alkyl]cyclopentadienyl}zirconocene] Cation Complexes

The starting materials for the preparation of the related [(dimethylamino)alkyl−C_5H_4]zirconium complexes (**6a**,**b** and **10**) were also prepared by a fulvene route,[22] as described previously by us.[14−16] The synthesis started from 6-(dimethylamino)-6-methylfulvene.[23] Hydride addition gave the Li[C_5H_4−CHMe−NMe_2] reagent,[24] which was then transmetallated with zirconium to yield a *meso*/*rac* mixture of [$(C_5H_4$−CHMe−$NMe_2)_2ZrCl_2$] (**6b**). Methyllithium addition to 6-(dimethylamino)-6-methylfulvene[25] gave Li[C_5H_4−CMe_2−NMe_2]. Transmetallation by treatment with [$ZrCl_4(THF)_2$] [26] furnished [$(C_5H_4$−CMe_2−$NMe_2)_2ZrCl_2$] (**6a**), whereas treatment with $CpZrCl_3$ [27] gave [$(C_5H_4$−CMe_2−$NMe_2)CpZrCl_2$] (**10**).

Complex **10** was treated with 1 mol-equiv. of Li[$B(C_6F_5)_4$] in dichloromethane to yield the cation complex **11** (> 70% isolated) (see Scheme 6). Single crystals of **11** suitable for an X-ray crystal structure analysis were obtained when liquid pentane was allowed to diffuse slowly into a CH_2Cl_2 solution of the organometallic salt. Cations and anions of **11** are independent in the solid state. The zirconium atom in **11** is pseudotetrahedrally coordinated by two η^5-cyclopentadienyl rings, the chloride ligand and the nitrogen atom of the pendant −CMe_2−NMe_2 group attached to one of the C_5H_4 ligands (Figure 2). The resulting N−Zr−Cl angle is fairly large at 106.0(1)°, whereas the Zr−N bond length is short at 2.369(3) Å [the respective Zr−N(Me_2) distance in **9**, for example (see Scheme 2), amounts to 2.469(1) Å].[14−16] The framework of the metallacyclic ring system in complex **11** is reasonably unstrained, with bond angles C1−C6−N = 100.7(3)° and C6−N−Zr = 99.6(2) [bond lengths C1−C6 1.528(5) Å, C6−N 1.541(5) Å]. The C1−C6 vector at the C1 to C5 Cp ring is oriented slightly out of the C_5H_4 ring plane toward the zirconium centre (161.5°).

The internal (dimethylamino)alkyl coordination to the electron-deficient zirconium centre also shows up in the ^{15}N NMR shift of **11**.[28] The cation complex **11** exhibits a ^{15}N NMR resonance at δ = −359.8 ppm, which is Δδ > −20 as compared to its neutral precursor **10**,[14−16] for which an open, noncoordinating geometry of the −CMe_2−NMe_2 substituent was found by X-ray diffraction.[14−16]

The *meso*-**6b**/*rac*-**6b** mixture also reacts cleanly with Li[$B(C_6F_5)_4$] in dichloromethane at ambient temperature to yield **12b** (Scheme 7). The NMR spectra at room temperature are quite complicated, due to the dynamics of the system and some signal overlap. At 213 K a clean separation of most resonances is achieved, and it was shown that a ca. 1:2:1 mixture of three diastereoisomers was obtained. These show the same overall characteristics as seen earlier for the related phosphorus complexes (see above). Consequently, it should also be assumed here that two *cis*-configured cation complexes have been obtained, namely *syn*-*cis*-**12b** and *anti*-*cis*-**12b**, and their diastereoisomer *trans*-**12b**. Each of the *cis* complexes shows four ^{1}H/^{13}C NMR methine resonances of their symmetry-equivalent pairs of C_5H_4 ligands, whereas the C_5H_4 ligands of *trans*-**12b** are diastereotopic and hence give rise to the observation of eight respective methine NMR signals. Similarly, we have observed a total of four −C*H*Me− signals in the mixture (one each of *syn*- and *anti*-*cis*-**12b** and two of *trans*-**12b**) as well as four −CH(CH_3)− ^{1}H NMR doublets. Both nitrogen centres in the complexes **12b** are coordinated to the zirconium atom. This follows from the observed ^{1}H and ^{13}C NMR patterns, *and* is clearly demonstrated by the observed *four* ^{15}N NMR resonances[28] (again, two for the pair of *cis*-**12b** isomers and the remaining pair originating from *trans*-**12b**), all of which are charac-

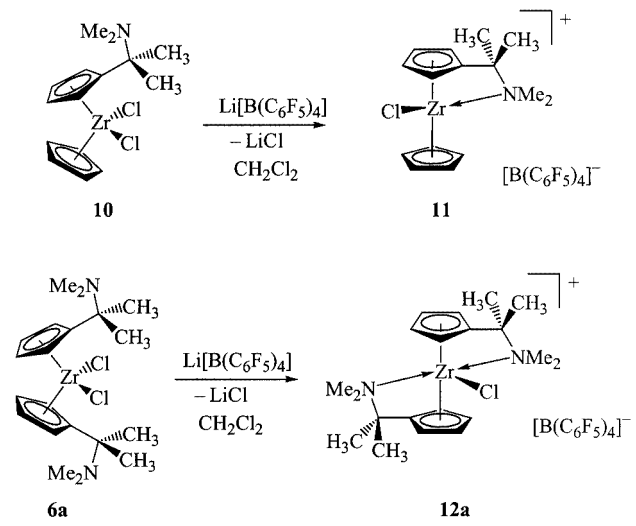

Scheme 6

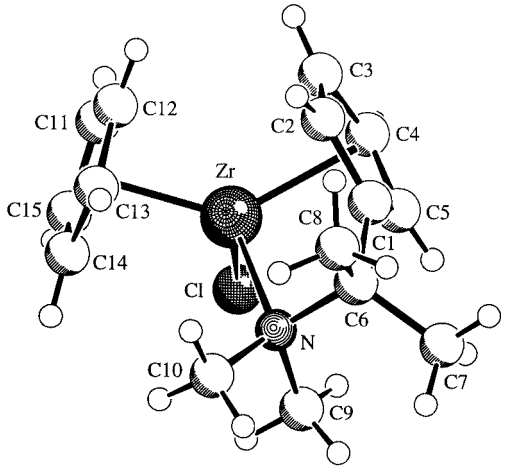

Figure 2. A view of the molecular geometry of **11** in the crystal (only the cation is depicted); selected bond lengths [Å] and angles [°]: Zr−N 2.369(3), Zr−Cl 2.426(1), Zr−C 2.398(4) to 2.502(4), C1−C6 1.528(5), C6−N 1.541(5), C6−C7 1.527(6), C6−C8 1.527(6), N−C9 1.491(5), N−C10 1.480(5); N−Zr−Cl 106.0(1), Zr−N−C6 99.6(2), Zr−N−C9 101.0(2), Zr−N−C10 123.5(2), C9−N−C6 112.8(3), C10−N−C6 115.1(4), C9−N−C10 104.2(3), N−C6−C1 100.7(3), N−C6−C7 112.6(3), N−C6−C8 111.0(4), C7−C6−C1 112.7(4), C8−C6−C1 109.8(4), C7−C6−C8 109.7(4)

teristically shifted to more negative δ values (by $\Delta\delta \approx -30$) relative to the open, noncoordinated amino groups of the starting material **6b** (^{15}N NMR: **12b**: δ = −369.6, −369.3, −364.7, −367.1 ppm vs. **6b**: δ = −337.6 ppm). Because of the complexity of the system, with many overlapping NMR resonances at higher temperature, the dynamic NMR features of the metallocene cation isomers of **12b** were not further analysed.

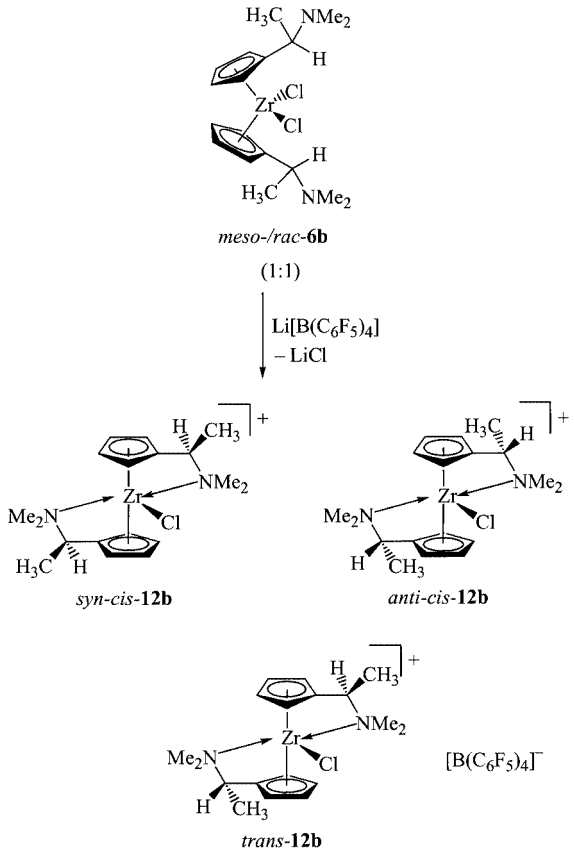

Scheme 7

Treatment of $[(C_5H_4{-}CMe_2{-}NMe_2)_2ZrCl_2]$ (**6a**) with $Li[B(C_6F_5)_4]$ cleanly resulted in chloride abstraction with formation of the complex **12a** (Scheme 6; 78% yield, isolated). Again, the ^{15}N NMR spectra indicate that both $-NMe_2$ groups were coordinated to the central zirconium atom (^{15}N NMR: **12a**: δ = −358.6 vs. **6a**: δ = −337.4 ppm).

The dynamic features of complex **12a** are slightly different from those of the phosphorus-containing cations **5**. At 298 K the ^{1}H NMR spectrum of **12a** shows a 1:1 pair of signals for the $Cp{-}C(CH_3)_2$ methyl groups, indicating their chemical differentiation into *syn*- and *anti*-CH_3 substituents relative to the central Zr−Cl vector. At the same time we observe only a double intensity ^{1}H NMR singlet of the $-N(CH_3)_2$ groups of **12a** at ambient temperature. This indicates that, at room temperature, a rapid equilibration of the diastereotopic methyl groups of the amino function (marked C and D in Scheme 8) is taking place in a process that does not involve a similar exchange of the corresponding (A and B) methyl groups at the adjacent α-carbon atom. This indicates that a rapid dynamic process involving cleavage of the $Zr{-}N(Me)_2$ linkage, inversion at the nitrogen atom, rotation around the $N{-}C(Me_2)$ vector and ring closure by reformation of the Zr−N bond is taking place in the complexes **12**; this process must take place *without* concomitant rotation around the Zr−Cp vector, since no CMe^AMe^B interconversion is observed under these conditions.

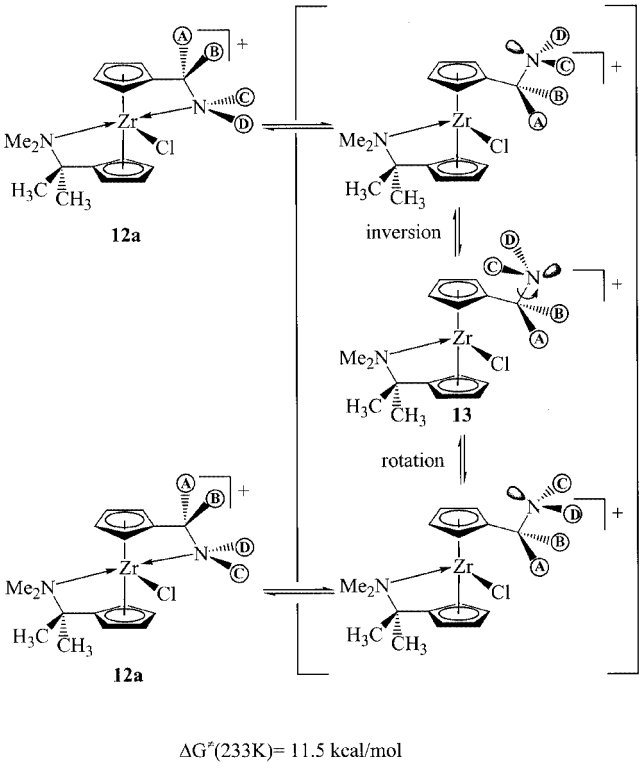

Scheme 8

This isolated dynamic process of the $Zr{-}NMe_2$ moiety in **12a** can be slowed on the ^{1}H NMR timescale and eventually frozen (see Figure 3). Below a decoalescence temperature of T_c = 243 K, a 1:1 pair of $N(CH_3)_2$ ^{1}H NMR resonances is observed, and a Gibbs activation energy of $\Delta G^{\neq}(233\ K) = 11.5 \pm 0.2$ kcal/mol was calculated[20,21] for this characteristic dynamic process of **12a**, which probably involves a rate-determining (reversible) rupture of the zirconium−nitrogen linkage (Scheme 9).

A considerable increase in the monitoring temperature eventually also results in a broadening of the pair of CMe^AMe^B ^{1}H NMR signals and subsequently in their coalescence (see Figure 3). In 1,2-dideuteriotetrachloroethane solvent a Gibbs activation energy of $\Delta G^{\neq}(333\ K) = 17.3 \pm 0.2$ kcal/mol was obtained for this second dynamic process of **12a**. Unlike the "low-temperature" NMe^CMe^D exchange in **12a** (see above), this "high-temperature" intramolecular CMe^AMe^B equilibration requires rupture of *both* Zr−N linkages to take place at some time. We therefore have to assume the involvement of a chlorozirconocene intermedi-

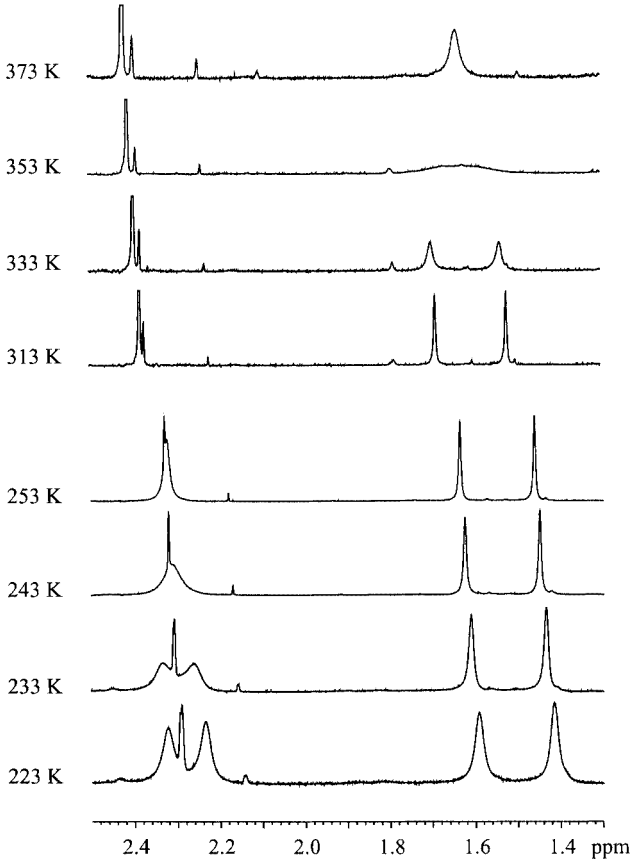

Figure 3. Dynamic ^{1}H NMR spectra of **12a** (600 MHz, $C_2D_2Cl_4$) showing the rapid equilibration of the diastereotopic $-NMe_2$ methyl resonances (left) followed by a markedly slower diastereotopic signal exchange at the adjacent $-CMe_2-$ moieties (right)

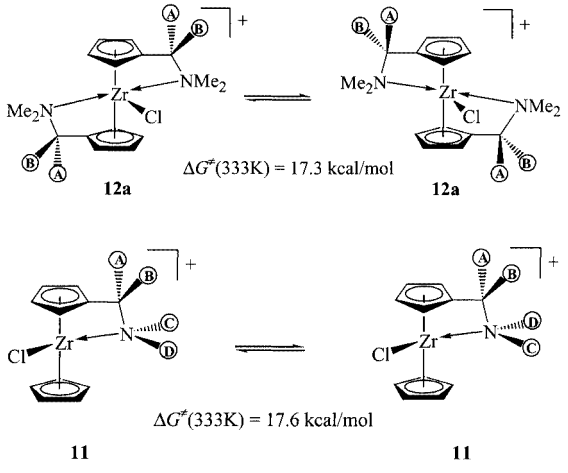

Scheme 9

ate (such as **14**, see Scheme 10) that lacks any favourable internal amine donor stabilisation.

Analogous dynamic behaviour is observed for complex **11**, which at *low* temperature (223 K) shows two $-C(CH_3)-$ ^{1}H NMR singlets (in CD_2Cl_2, 600 MHz) at δ = 1.60 and 1.55 ppm *and* a pair of $-N(CH_3)_2$ singlets (δ = 2.61, 2.33 ppm), of which only the latter displays coalescence with increasing NMR monitoring temperature. This again indicates that rapid (on the NMR timescale) breaking of the Zr−N bond takes place, followed by inversion at the nitrogen atom without equilibration of the remaining groups of signals, but that the activation barrier of this process is substantially higher [**11**: $\Delta G^{\neq}$(333 K) = 17.6 ± 0.2 kcal/mol] than in **12**.

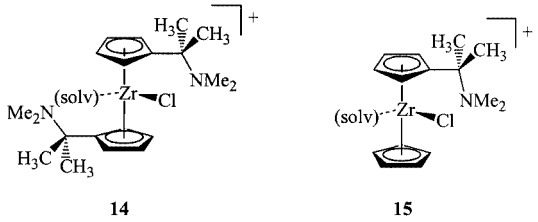

Scheme 10

It is remarkable that the internal NMe^CMe^D equilibration of **11** is observed without a concomitant equilibration of the adjacent CMe^AMe^B moiety. We must assume that the $-NMe_2$ group in the respective intermediate (e.g., **15**; see Scheme 10) is not coordinated to the zirconium atom. Nevertheless, a complete rotation of the $C_5H_4-CMe_2NMe_2$ ligand around the Zr−Cp vector cannot be operative, since this would result in an inversion at the stereogenic zirconium centre,[19] which would be registered as a CMe^AMe^B interconversion on the NMR timescale. This is not observed by dynamic NMR spectroscopy in the experimentally accessible temperature range: the dynamic cation system **11** shows a remarkable stereochemical memory effect. We assume that stereoselective solvent coordination at the reactive intermediate stage (e.g., **15** in Scheme 10) might account for this observation. A similar stabilising solvent coordination of the intermediate **14** derived from the "more symmetrical" system **12a** would in principle also be in accord with the observed dynamic features of that system.

The systems **5a**[11] and **12a** are suitable for comparison of the stabilising features of $-PAr_2$ and $-NMe_2$ groups in a chlorozirconocene cation system, since these two complexes exhibit the same type of dynamic CMe^AMe^B equilibration process requiring rupture of *both* Zr−N/P linkages. Our experiments show that $-NMe_2$ and $-PAr_2$ stabilisation in these [Zr]−Cl^+ systems are about equal, as judged from the respective enantiomerisation barriers of the two systems [$\Delta G^{\neq}_{enant}$(358 K) = 17.5 ± 0.5 kcal/mol (**5a**[11]), $\Delta G^{\neq}_{enant}$(298 K) = 17.3 ± 0.5 kcal/mol (**12a**)]. In addition, comparison of the two nitrogen-stabilised chlorozirconocene cation systems **12a** and **11** shows a fairly substantial difference in the $\Delta G^{\neq}$ values of their internal $-NMe^CMe^D$ equilibration processes. As would be expected, the corresponding activation barrier of **11** is markedly higher because the chloro zirconocene cation resulting from Zr←NR_2- dissociation now lacks any internal stabilisation (but probably benefits from some solvent or anion interaction). In this case, the observed $\Delta G^{\neq}$(**12a**)/$\Delta G^{\neq}$(**11**) differ-

ence of $\Delta\Delta G^{\neq} \approx 6$ kcal/mol for internal $-NMe^{C}Me^{D}$ equilibration should probably be regarded as a lower limit of the stabilisation energy of such an electrophilic zirconocene cation by an amine donor ligand.

Experimental Section

General Remarks: Reactions were carried out under argon in Schlenk-type glassware or in a glovebox. Solvents (including the deuterated solvents used for NMR spectroscopy) were dried and distilled under argon prior to use. The following instruments were used for characterisation of the synthesised compounds: Bruker AC 200 P NMR spectrometer (^{1}H 200 MHz, ^{13}C 50 MHz) at 298 K or a Varian Unity Plus NMR spectrometer (^{1}H 600 MHz, ^{13}C 150 MHz) at variable temperature (most NMR assignments were secured by 2D NMR experiments);[29] a Nicolet 5 DXC FT-IR spectrometer; a Micromass Quattro LC-Z mass spectrometer; elemental analyses were carried out with a Fross−Heraeus CHN-rapid elemental analyser or a Vario El III micro elemental analyser. $[\{C_5H_4(CMe_2)PPh_2\}_2ZrCl_2]$ (**2a**),[11] $[\{C_5H_4(CMe_2)P(tolyl)_2\}_2ZrCl_2]$ (**2b**),[11] $[\{C_5H_4(CHMe)PPh_2\}_2ZrCl_2]$ (**2c**),[12] $[\{C_5H_4(CHPh)PPh_2\}_2ZrCl_2]$ (**2d**),[12] $[\{C_5H_4(CHFc)P(tolyl)_2\}_2ZrCl_2]$ (**2e**),[30] $[\{C_5H_4(CMe_2)NMe_2\}_2ZrCl_2]$ (**6a**),[14−16] $[\{C_5H_4(CHMe)NMe_2\}_2ZrCl_2]$ (**6b**),[14−16] $[\{C_5H_4(CMe_2)NMe_2\}\{Cp\}ZrCl_2]$ (**10**),[14−16] tris(pentafluorophenyl)borane $[B(C_6F_5)_3,]$[9,10] lithium [tetrakis(pentafluorophenyl)borate] $[Li\{B(C_6F_5)_4\}]$[17a][17b,18] were prepared by literature methods.

$[C_5H_4(CHFc)P(tolyl)_2]Li(THF)$:[30] This compound was obtained from (p-tolyl)$_2$PH (2.8 g, 13.0 mmol), nBuLi (8.0 mL, 13.0 mmol) and 6-ferrocenylfulvene (3.9 g, 14.8 mmol), 5.4 g (75%) isolated. ^{1}H NMR (200.1 MHz, C_6D_6/[D$_8$]THF, 298 K): δ = 1.07 (m, 4 H, THF), 1.94, 2.01 (s, each 3 H, Me of p-tolyl), 2.05 (m, 4 H, THF), 3.60, 3.84, 4.05 (m, 4 H, C_5H_4 of Fc), 4.09 (s, 5 H, C_5H_4 of Fc), 4.62 (d, $^2J_{PH}$ = 6.1 Hz, 1 H, CHFc), 6.24 (br. s, 2 H of C_5H_4), 6.30, 6.58 (br. s, each 1 H of C_5H_4), 6.82, 6.89 (m, each 2 H, p-tolyl), 7.31 (m, 2 H, p-tolyl), 7.65 (m, 2 H, p-tolyl) ppm. ^{31}P{^{1}H} NMR (81.0 MHz, C_6D_6/[D$_8$]THF, 298 K): δ = −0.9 ppm.

$[\{C_5H_4(CHFc)P(tolyl)_2\}_2ZrCl_2]$ (2e):[30] **2e** was obtained from $[C_5H_4(CHFc)P(tolyl)_2]Li(THF)$ (5.0 g, 9.0 mmol) and $[ZrCl_4(THF)_2]$ (1.69 g, 4.5 mmol), and isolated as a yellow solid (4.3 g, 81%) as a 1:1 mixture of diastereoisomers. IR (KBr): $\tilde{\nu}$ = 3111, 3091, 2918, 2850, 1595, 1497, 1468, 1456, 1394, 1266, 1185, 1105, 1090, 1039, 1027, 1018, 998, 813, 734, 512, 503, 500, 486, 423 cm^{-1}. ^{1}H NMR (200.1 MHz, C_6D_6, 298 K): δ = 2.02, 2.06 (s, each 6 H, Me of p-tolyl), 3.83 (m, 2 H, Fc), 3.92−3.93 (m, 4 H, Fc), 4.33 (d, J_{PH} = 0.5 Hz, 10 H, Fc), 4.47 (m, 2 H, Fc), 5.04 (d, $^2J_{PH}$ = 1.5 Hz, 2 H, C*H*Fc), 4.65, 4.82, 5.73, 6.32 (m, each 2 H, C_5H_4), 6.83 (pd, $J_{H,H}$ = 8 Hz, 4 H, p-tolyl), 6.93 (pd, $J_{H,H}$ = 7 Hz, 4 H, p-tolyl), 7.10 (pt, $J_{H,H}$ = 8 Hz, 4 H, p-tolyl), 7.46 (dd, $J_{H,H}$ = 6, 8 Hz, 4 H, p-tolyl) ppm. ^{13}C{^{1}H} NMR (50.3 MHz, C_6D_6, 298 K): δ = 21.1, 21.3 (Me of p-tolyl), 42.2 (d, $J_{P,C}$ = 28.9 Hz, *C*HFc), 66.3 (d, $J_{P,C}$ = 2.2 Hz, Fc), 68.2 (Fc), 69.6 (d, $^3J_{P,C}$ = 6.1 Hz, Fc), 70.1 (d, $J_{P,C}$ = 4.4 Hz, Fc), 71.1 (d, $J_{P,C}$ = 5.4 Hz, Fc), 89.9 (d, $J_{P,C}$ = 15.7 Hz, Fc), 105.8, 110.9, 113.8, 125.7 (C, C_5H_4), 129.1 (d, $J_{P,C}$ = 8.8 Hz, p-tolyl), 129.7 (d, $J_{P,C}$ = 4.4 Hz, C, p-tolyl), 131.8 (d, $J_{P,C}$ = 23 Hz, p-tolyl), 131.9 (d, $J_{P,C}$ = 16.6 Hz, C, p-tolyl), 135.7 (d, $J_{P,C}$ = 17.5 Hz, p-tolyl), 137.3 (d, $J_{P,C}$ = 24.5 Hz, p-tolyl), 137.7 (p-tolyl), 138.0 (d, $J_{P,C}$ = 8.8 Hz, C_5H_4), 140.0 (p-tolyl) ppm. ^{31}P{^{1}H} NMR (81.0 MHz, C_6D_6, 298 K): δ = 12.1, 12.8 ppm.

General Procedure for the Preparation of $[\{C_5H_4(CR^1R^2)PAr_2\}_2ZrCl]^+[B(C_6F_5)_4]^-$, $[\{C_5H_4(CR^1R^2)NMe_2\}_2ZrCl]^+[B(C_6F_5)_4]^-$ or $[\{C_5H_4(CMe_2)NMe_2\}\{Cp\}ZrCl]^+[B(C_6F_5)_4]^-$: Dichloromethane (or CD_2Cl_2 or $C_2D_2Cl_4$) was added at room temperature to a mixture of equimolar amounts of the cyclopentadienyl complex (**2a−e, 6a−b, 10**) and the chloride anion abstractor $Li[B(C_6F_5)_4]$. The reaction mixture was stirred for 1 h. The precipitated LiCl was removed by filtration. The filtrate was concentrated in vacuo or used directly. The product was washed twice with pentane and dried in vacuo.

$[\{C_5H_4(CMe_2)PPh_2\}_2ZrCl]^+[B(C_6F_5)_4]^-$ (5a): 5a was obtained from **2a** (3.72 g, 5.0 mmol) and $Li[B(C_6F_5)_4]$ (3.43 g, 5.0 mmol), and isolated as a yellow-brown solid (3.82 g, 55%). IR (KBr): $\tilde{\nu}$ = 3015, 2919, 2856, 1601, 1497, 1443, 1184, 1094, 1018, 802, 514, 492 cm^{-1}. ^{1}H NMR (200.1 MHz, CD_2Cl_2, 300 K): δ = 1.55−2.19 (br. s, 12 H, CH_3), 6.15−6.47 (br. m, 8 H, C_5H_4), 7.32−7.60 (m, 20 H, Ph) ppm. ^{31}P{^{1}H} NMR (81.0 MHz, CD_2Cl_2, 300 K): δ = −29.1 ppm. ^{11}B{^{1}H } NMR (64.2 MHz, CD_2Cl_2, 300 K): δ = −16.6 ($w_{1/2}$ = 32 Hz) ppm. $C_{64}H_{40}BClF_{20}P_2Zr$ (1388.42): calcd. C 55.37, H 2.90; found C 55.33, 3.36.

$[\{C_5H_4(CMe_2)P(tolyl)_2\}_2ZrCl]^+[B(C_6F_5)_4]^-$ (5b): 5b was obtained from **2b** (4.0 g, 5.0 mmol) and $Li[B(C_6F_5)_4]$ (3.43 g, 5.0 mmol), and isolated (2.68 g, 67%) as a beige solid. IR (KBr): $\tilde{\nu}$ = 3030, 3005, 2939, 1621, 1507, 1451, 1287, 1200, 1105, 802, 534 cm^{-1}. ^{1}H NMR (200.1 MHz, CD_2Cl_2, 300 K): δ = 1.55, 1.76 (m, each 6 H, CH_3), 2.41 (s, 12 H, CH_3 of p-tolyl), 6.13, 6.22 (m, each 4 H, C_5H_4), 7.25−7.55 (m, 16 H, p-tolyl) ppm. ^{31}P{^{1}H} NMR (81.0 MHz, CD_2Cl_2, 300 K): δ = −31.0 ppm. ^{11}B{^{1}H} NMR (64.2 MHz, CD_2Cl_2, 300 K): δ = −13.6 ($w_{1/2}$ = 48 Hz) ppm. $C_{68}H_{48}BClF_{20}P_2Zr$ (1444.53): calcd. C 56.54, H 3.35; found C 56.34, 3.72.

$[\{C_5H_4(CHMe)PPh_2\}_2ZrCl]^+[B(C_6F_5)_4]^-$ (5c): 5c was obtained from **2c** (3.58 g, 5.0 mmol) and $Li[B(C_6F_5)_4]$ (3.43 g, 5.0 mmol), and isolated (3.67 g, 54%) as a beige solid. IR (KBr): $\tilde{\nu}$ = 2965, 2810, 1621, 1479, 1453, 1110, 1088, 1015, 802, 685, 554 cm^{-1}. Mixture of three diastereoisomers. ***synlanti-cis*-5c:** ^{1}H NMR (599.9 MHz, CD_2Cl_2, 253 K): δ = 1.23, 1.51 (m, each 3 H, Me), 4.10, 4.33 (m, each 1 H, C*H*Me), 6.20, 6.27, 6.41, 6.88 (br. m, each 2 H, C_5H_4), 7.16−7.65 (m, 20 H, Ph) ppm. ^{13}C{^{1}H} NMR (150.8 MHz, CD_2Cl_2, 253 K): δ = 15.1, 19.6 (Me), 26.5, 38.9 (*C*HMe), 100.6, 102.0, 106.4, 109.0, 112.9, 113.2, 116.2, 120.2 (C_5H_4), 131.0, 133.0 (*ipso*-C of C_5H_4), 129.3−137.0 (Ph) ppm. ^{31}P{^{1}H} NMR (81.0 MHz, CD_2Cl_2, 300 K): δ = −45.9, −36.2 ppm. ***trans*-5c:** ^{1}H NMR (599.9 MHz, CD_2Cl_2, 253 K): δ = 1.25, 1.50 (m, 3 H, Me), 4.21, 4.47 (m, each 1 H, C*H*Me), 5.99, 6.27, 6.46, 6.94 (br. m, each 2 H, C_5H_4), 7.16−7.65 (m, 20 H, Ph) ppm. ^{13}C{^{1}H} NMR (150.8 MHz, CD_2Cl_2, 253 K): δ = 14.4, 19.3 (Me), 26.7, 28.2 (*C*HMe), 100.2, 101.0, 108.6, 108.8, 113.2, 115.3, 115.9, 116.5 (C_5H_4), 132.0, 133.0 (*ipso*-C of C_5H_4), 129.3−137.0 (Ph) ppm. ^{31}P{^{1}H} NMR (81.0 MHz, CD_2Cl_2, 300 K): δ = −47.2 (d, $^2J_{P,P}$ = 110 Hz), −38.1 (d, $^2J_{P,P}$ = 110 Hz) ppm. $[B(C_6F_5)_4]^-$ anion: ^{13}C{^{1}H} NMR (150.8 MHz, CD_2Cl_2, 253 K): δ = 124.0 (br. s, *ipso*-C of C_6F_5), 136.2 (dm, $J_{C,F}$ = 242 Hz, *m*-C_6F_5), 138.1 (dm, $J_{C,F}$ = 242 Hz, *p*-C_6F_5), 148.0 (dm, $J_{C,F}$ = 240 Hz, *o*-C_6F_5) ppm. ^{11}B{^{1}H} NMR (64.2 MHz, CD_2Cl_2, 300 K): δ = −16.6 ($w_{1/2}$ = 33 Hz) ppm. $C_{62}H_{36}BClF_{20}P_2Zr$ (1360.4): calcd. C 54.74, H 2.67; found C 55.34, 3.30.

$[\{C_5H_4(CHPh)PPh_2\}_2ZrCl]^+[B(C_6F_5)_4]^-$ (5d): 5d was obtained from **2d** (4.20 g, 5.0 mmol) and $Li[B(C_6F_5)_4]$ (3.43 g, 5.0 mmol), and isolated (2.74 g, 37%) as a light beige solid. Only the signals of the major *cis*-**5d** isomer are listed. ^{1}H NMR (599.9 MHz, CD_2Cl_2, 253 K): δ = 5.51 (br. m, 2 H, C*H*Ph), 6.38, 6.48, 6.59, 7.10 (m, each 2 H, C_5H_4), 7.2−7.5 (m, 30 H, Ph) ppm. ^{13}C{^{1}H} NMR (150.8 MHz, CD_2Cl_2, 253 K): δ = 39.1 (*C*HPh), 102.0, 109.5,

112.0, 118.0 (C_5H_4), 136.0 (dm, $J_{C,F}$ = 240 Hz, *m*-C_6F_5), 138.0 (*ipso*-C of Ph at P), 138.1 (dm, $J_{C,F}$ = 247 Hz, *p*-C_6F_5), 147.0 (dm, $J_{C,F}$ = 239 Hz, *o*-C_6F_5) ppm; *ipso*-C of C_6F_5, not observed, Ph resonances not listed. $^{31}P\{^1H\}$ NMR (81.0 MHz, CD_2Cl_2, 300 K): δ = −41.8 (d, $^2J_{P,P}$ = 108 Hz), −18.4 (d, $^2J_{P,P}$ = 108 Hz, *trans* isomer), −15.0 (*cis* isomer) ppm. $^{11}B\{^1H\}$ NMR (64.2 MHz, CD_2Cl_2, 300 K): δ = −16.2 ($w_{1/2}$ = 37 Hz) ppm. $C_{72}H_{40}BClF_{20}P_2Zr$ (1484.5): calcd. C 58.25, H 2.72; found C 57.34, 3.48. The coalescence of the CHPh protons of the *trans* isomer was observed at 298 K [^1H NMR (200 MHz, CD_2Cl_2, 243 K): δ = 5.57 and 5.65 ppm; Δν = 17 Hz]: $\Delta G^{\neq}$ = 14.8 ± 0.5 kcal/mol.

[{C_5H_4(CHFc)P(tolyl)$_2$}$_2$ZrCl]$^+$[B(C_6F_5)$_4$]$^-$ (5e): 5e was obtained from **2e** (5.56 g, 5.0 mmol) and Li[B(C_6F_5)$_4$] (3.43 g, 5.0 mmol), and isolated as a beige solid (5.36 g, 61%). IR (KBr): ν̃ = 3019, 2856, 1621, 1491, 1443, 1188, 1088, 1027, 802, 625, 514, 492 cm^{-1}. Two diastereoisomers. ***cis*-5e:** ^1H NMR (599.9 MHz, CD_2Cl_2, 253 K): δ = 2.32 (s, 12 H, CH_3 of *p*-tolyl), 3.96 (s, 10 H, Fc), 3.39, 3.85, 4.07, 4.16 (m, each 2 H, Fc), 6.22, 6.35, 6.42, 7.15 (m, each 2 H, C_5H_4), 7.24−7.43 (m, 16 H, *p*-tolyl) ppm. $^{13}C\{^1H\}$ NMR (150.8 MHz, CD_2Cl_2, 253 K): δ = 35.6 (*C*HFc), 66.9, 67.8, 68.4, 68.7, 84.4 (Fc), 68.6 (Fc), 101.2, 108.2, 111.4, 116.4, 129.3 (C_5H_4), 129.5 (*p*-tolyl) ppm. $^{31}P\{^1H\}$ NMR (81.0 MHz, CD_2Cl_2, 300 K): δ = −18.2. ***trans*-5e:** ^1H NMR (599.9 MHz, CD_2Cl_2, 253 K): δ = 2.26, 2.35 (s, each 6 H, CH_3 of *p*-tolyl), 3.58, 3.88, 3.96, 3.98, 3.99 (s, each 5 H, Fc), 3.58, 3.88, 3.96, 3.99, 4.12, 4.14, 4.16, 4.21 (br. s, each 1 H, Fc), 5.06 (d, J_{PH} = 8.7 Hz, 1 H, C*H*Fc), 5.12 (d, J_{PH} = 5 Hz, 1 H, C*H*Fc), 5.94, 6.00 (m, each 1 H, C_5H_4), 6.06 (m, 2 H, C_5H_4), 6.17, 6.65, 6.92, 7.18 (m, each 1 H, C_5H_4) ppm. $^{13}C\{^1H\}$ NMR (150.8 MHz, CD_2Cl_2, 253 K): δ = 35.9, 36.6 (*C*HFc), 68.9 (2 × Fc), 67.3, 67.7, 68.0, 68.7, 69.0, 69.1, 69.4, 70.3, 83.4, 84.4 (Fc), 101.0, 103.2, 104.0, 109.4, 113.0, 115.6, 115.7, 116.4, 124.2, 129.5 (C_5H_4) ppm; tolyl resonances not listed. $^{31}P\{^1H\}$ NMR (81.0 MHz, CD_2Cl_2, 300 K): δ = −36.1 (d, $^2J_{P,P}$ = 117 Hz), −24.1 (d, $^2J_{P,P}$ = 117 Hz) ppm. [B(C_6F_5)$_4$]$^-$ anion: $^{13}C\{^1H\}$ NMR (150.8 MHz, CD_2Cl_2, 253 K): δ = 124.0 (br. s, *ipso*-C of C_6F_5), 136.6 (dm, $J_{C,F}$ = 240 Hz, *m*-C_6F_5), 138.2 (dm, $J_{C,F}$ = 245 Hz, *p*-C_6F_5), 148.0 (dm, $J_{C,F}$ = 253 Hz, *o*-C_6F_5) ppm. $^{11}B\{^1H\}$ NMR (64.2 MHz, CD_2Cl_2, 300 K): δ = −16.5 ($w_{1/2}$ = 34 Hz) ppm. ESI-MS: *m*/*z* (%) = 1077 (100) [$C_{60}H_{56}ClFeP_2Zr$]. $C_{84}H_{56}BClF_{20}Fe_2P_2Zr$ (1756.46): calcd. C 57.44, H 3.21; found C 56.73, 3.54. The coalescence of the C*H*Fc protons of *trans*-**5e** was observed at 298 K [^1H NMR (599.9 MHz, CD_2Cl_2, 253 K): δ = 5.06 and 5.12 ppm; Δν = 36 Hz]: $\Delta G^{\neq}$ = 14.5 ± 0.5 kcal/mol.

[{C_5H_4(CMe$_2$)NMe$_2$}{Cp}ZrCl]$^+$[B(C_6F_5)$_4$]$^-$ (11): 11 was obtained from **10** (1.89 g, 5 mmol) and Li[B(C_6F_5)$_4$] (3.43 g, 5 mmol), and isolated as a beige solid (3.68 g, 72%). IR (KBr): ν̃ = 3054, 3027, 2985, 1684, 1525, 1464, 1273, 1104, 1020, 985, 805, 745, 590 cm^{-1}. ^1H NMR (599.9 MHz, CD_2Cl_2, 298 K): δ = 1.61, 1.68 (br. s, each 3 H, CMe_2), 2.52 (br. s, 6 H, NMe_2), 6.46, 6.60 (m, each 1 H, C_5H_4), 6.68 (s, 5 H, Cp), 6.75, 6.81 (m, each 1 H, C_5H_4) ppm. ^1H NMR (599.9 MHz, CD_2Cl_2, 223 K): δ = 1.55, 1.60 (br. s, each 3 H, CMe_2), 2.33, 2.61 (s, each 3 H, NMe_2), 6.50, 6.57 (m, each 1 H, C_5H_4), 6.64 (s, 5 H, Cp), 6.69, 6.77 (m, each 1 H, C_5H_4) ppm. $^{13}C\{^1H\}$ NMR (150.8 MHz, CD_2Cl_2, 223 K): δ = 23.0, 25.8 [C(*C*H$_3$)$_2$], 45.3, 47.5, [N(*C*H$_3$)$_2$], 61.1 (*C*Me$_2$), 102.5, 108.7, 114.2, 118.3 (C_5H_4), 120.1 (C_5H_5), 131.3 (*ipso*-C of C_5H_4), 135.7 (dm, $J_{C,F}$ = 245 Hz, *m*-C_6F_5), 137.5 (dm, $J_{C,F}$ = 251 Hz, *p*-C_6F_5), 146.3 (dm, $J_{C,F}$ = 245 Hz, *o*-C_6F_5) ppm, *ipso*-C of C_6F_5 not observed. $^{11}B\{^1H\}$ NMR (64.2 MHz, CD_2Cl_2, 300 K): δ = −16.5 (s, $w_{1/2}$ = 34 Hz) ppm. $C_{39}H_{21}BClF_{20}NZr$ (1021.1): calcd. C 45.88, H 2.07, N 1.37; found C 45.60, H 2.18, N 1.38.

X-ray Crystal Structure Analysis of 11: Empirical formula $C_{15}H_{21}NClZr{\cdot}BC_{24}F_{20}$, *M* = 1021.05, colourless crystal 0.35 × 0.35 × 0.15 mm, *a* = 10.744(1), *b* = 12.990(1), *c* = 13.823(1) Å, α = 96.49(1), β = 91.87(1), γ = 101.02(1)°, *V* = 1878.6(3) Å^3, $\rho_{calcd.}$ = 1.805 g cm^{-3}, μ = 4.97 cm^{-1}, empirical absorption correction by use of SORTAV (0.845 ≤ *T* ≤ 0.929), *Z* = 2, triclinic, space group $P\bar{1}$ (no. 2), λ = 0.71073 Å, *T* = 198 K, ω- and φ-scans, 19488 reflections collected (±*h*, ±*k*, ±*l*), [(sinθ)/λ] = 0.66 Å^{-1}, 8895 independent (R_{int} = 0.036) and 7149 observed reflections [$I \geq 2\sigma(I)$], 572 refined parameters, *R* = 0.050, wR^2 = 0.132, max. residual electron density 1.06 (−0.98) eÅ^{-3}, crystals seem to be partly hydrolysed, the one high peak in the final difference Fourier calculation is 1.90 Å away from Zr, the typical distance for Zr−H_2O, hydrogen atoms calculated and refined as riding atoms. Complex **11** seems to add HCl readily. From the mother liquor of a crystallisation experiment, the "open" HCl adduct [(C_5H_4−CMe$_2$−NHMe$_2$)CpZrCl$_2$] ("**11**+HCl") was characterised by single-crystal X-ray diffraction: Empirical formula $C_{15}H_{22}NCl_2Zr{\cdot}BC_{24}F_{20}$, *M* = 1057.51, colourless crystal 0.40 × 0.15 × 0.05 mm, *a* = 10.746(1), *b* = 13.877(1), *c* = 14.578(1) Å, α = 66.71(1), β = 86.97(1), γ = 85.91(1)°, *V* = 1991.0(3) Å^3, $\rho_{calcd.}$ = 1.764 g cm^{-3}, μ = 5.37 cm^{-1}, empirical absorption correction by SORTAV (0.814 ≤ *T* ≤ 0.974), *Z* = 2, triclinic, space group $P\bar{1}$ (no. 2), λ = 0.71073 Å, *T* = 243 K, ω- and φ-scans, 20597 reflections collected (±*h*, ±*k*, ±*l*), [(sinθ)/λ] = 0.66 Å^{-1}, 9350 independent (R_{int} = 0.031) and 7214 observed reflections [$I \geq 2\sigma(I)$], 585 refined parameters, *R* = 0.044, wR^2 = 0.101, max. residual electron density 0.65 (−0.59) eÅ^{-3}, hydrogen atoms calculated and refined as riding atoms. The data set was collected with a Nonius KappaCCD diffractometer, equipped with a Nonius FR591 rotating anode generator. Programs used: data collection COLLECT (Nonius B.V., **1998**), data reduction Denzo-SMN[31], absorption correction SORTAV[32], structure solution SHELXS-97[33], structure refinement SHELXL-97[34], graphics SCHAKAL[35]. CCDC-184443 for (**11**) and -200138 ("**11**+HCl") contain the supplementary crystallographic data for this paper. These data can be obtained free of charge at www.ccdc.cam.ac.uk/conts/retrieving.html [or from the Cambridge Crystallographic Data Centre, 12 Union Road, Cambridge CB2 1EZ, UK; Fax: (internat.) + 44-1223/336-033; E-mail: deposit@ccdc.cam.ac.uk].

[{C_5H_4(CMe$_2$)NMe$_2$}$_2$ZrCl]$^+$[B(C_6F_5)$_4$]$^-$ (12a): 12 was obtained from **6a** (2.31 g, 5 mmol) and Li[B(C_6F_5)$_4$] (3.43 g, 5 mmol), and isolated as a light beige solid (3.93 g, 71%). IR (KBr): ν̃ = 3031, 3010, 1613, 1520, 1444, 1260, 1101, 1016, 972, 822, 742, 606, 571 cm^{-1}. ^1H NMR (599.9 MHz, CD_2Cl_2, 298 K): δ = 1.53 (s, 6 H, CMe_2), 1.70, 2.40 (s, each 6 H, NMe_2), 6.30, 6.33, 6.35, 6.79 (m, each 1 H, C_5H_4) ppm. ^1H NMR (599.9 MHz, $C_2D_2Cl_4$, 298 K): δ = 1.48 (s, 6 H, CMe_2), 1.65, 2.34 (s, each 6 H, NMe_2), 6.21, 6.26, 6.43, 6.74 (m, each 1 H, C_5H_4) ppm. $^{13}C\{^1H\}$ NMR (150.8 MHz, CD_2Cl_2, 203 K): δ = 24.0, 24.8 [C(*C*H$_3$)$_2$], 45.0, 45.5 [N(*C*H$_3$)$_2$], 59.1 (*C*Me$_2$), 102.2, 107.7, 116.2, 122.1 (C_5H_4), 130.3 (*ipso*-C of C_5H_4Cp), 135.7 (dm, $J_{C,F}$ = 245 Hz, *m*-C_6F_5), 137.5 (dm, $J_{C,F}$ = 251 Hz, *p*-C_6F_5), 143.7 (dm, $J_{C,F}$ = 245 Hz, *o*-C_6F_5) ppm, *ipso*-C of C_6F_5 not observed. $^{11}B\{^1H\}$ NMR (64.2 MHz, CD_2Cl_2, 298 K): δ = −16.5 ($w_{1/2}$ = 33 Hz) ppm. ESI-MS: *m*/*z* (%) = 425 (100) [$C_{20}H_{32}ClN_2Zr$]. $C_{44}H_{32}BClF_{20}N_2Zr$ (1106.2): calcd. C 47.47, H 2.92, N 2.53; found C 47.46, C 3.19, N 2.50.

[{C_5H_4(CHMe)NMe$_2$}$_2$ZrCl]$^+$[B(C_6F_5)$_4$]$^-$ (12b): 12b was obtained from **6b** (2.17 g, 5 mmol) and Li[B(C_6F_5)$_4$] (3.43 g, 5 mmol), and isolated as a beige solid (3.50 g, 65%). IR (KBr): ν̃ = 3021, 2856, 1610, 1512, 1454, 1265, 1078, 1016, 972, 806, 740, 610 cm^{-1}. 1:2:1 mixture of three diastereoisomers: ^1H NMR (599.9 MHz, CD_2Cl_2,

298 K): δ = 1.43−1.54 (m, 24 H, CHCH_3), 2.39 (m, 48 H, NMe_2), 3.74 (q, $^3J_{H,H}$ = 7.2 Hz, 2 H, CHCH$_3$), 3.88 (m, 2 H, CHCH$_3$), 4.06 (q, $^3J_{H,H}$ = 7.2 Hz, 2 H, CHCH$_3$), 4.27 (m, 2 H, CHCH$_3$), 5.88−6.84 (m, 32 H, Cp) ppm. ^{1}H NMR (599.9 MHz, CD_2Cl_2, 213 K): δ = 1.37 (m, 18 H, CHCH_3), 1.46 (m, 6 H, CHCH_3), 2.26, 2.27, 2.35, 2.36 (s, each 12 H, NMe_2), 3.72 (q, $^3J_{H,H}$ = 7.2 Hz, 2 H, CHCH$_3$), 3.83 (q, $^3J_{H,H}$ = 7.2 Hz, 2 H, CHCH$_3$), 3.99 (q, $^3J_{H,H}$ = 7.2 Hz, 2 H, CHCH$_3$), 4.00 (q, $^3J_{H,H}$ = 7.2 Hz, 2 H, CHCH$_3$), 5.95, 6.11, 6.17, 6.19, 6.26, 6.30, 6.31, 6.34, 6.36, 6.45, 6.59, 6.66, 6.70, 6.76, 6.77 (m, each 2 H, C_5H_4) ppm. ^{13}C{^{1}H} NMR (150.8 MHz, CD_2Cl_2, 213 K): δ = 13.5, 13.6, 14.2, 14.4 (CHCH$_3$), 42.3, 44.9, 49.1 (NMe_2), 59.6, 59.8, 59.9, 60.0 (CHCH$_3$), 101.1, 101.2, 101.2, 104.8, 106.6, 106.7,108.2, 108.5, 108.5, 111.3, 114.8, 115.8, 120.6, 121.3, 121.3, 122.2, 122.5, 122.5, 125.7, 128.0 (C_5H_4) ppm. $[B(C_6F_5)_4]^-$ anion: ^{13}C{^{1}H} NMR (150.8 MHz, CD_2Cl_2, 213 K): δ = 135.8 (dm, $J_{C,F}$ = 251 Hz, m-C_6F_5), 137.6 (dm, $^1J_{C,F}$ = 251 Hz, p-C_6F_5), 147.4 (dm, $J_{C,F}$ = 239 Hz, o-C_6F_5) ppm, (*ipso*-C, C_6F_5) not observed. ^{11}B{^{1}H} NMR (64.2 MHz, CD_2Cl_2, 300 K): δ = −16.5 (s, $w_{1/2}$ = 38 Hz) ppm. ESI-MS: *m*/*z* (%) = 397 (100) [$C_{18}H_{28}ClN_2Zr$]. $C_{42}H_{28}BClF_{20}N_2Zr$ (1078.15): calcd. C 46.78, H 2.62, N 2.60; found C 46.99, H 2.92, N 2.50.

Supporting Information: Additional NMR spectroscopic data of complexes **5**, **11** and **12**, and the dynamic ^{1}H NMR spectra of the cation complexes **11** and **12a** in CD_2Cl_2 and $C_2D_2Cl_4$ (see footnote on the first page of this article).

Acknowledgments

Financial support from the Fonds der Chemischen Industrie, the Deutsche Forschungsgemeinschaft, the Alexander von Humboldt Stiftung (V. V. K.) and the NATO (grant no. PST.EV.979160) O. K.) is gratefully acknowledged.

[1] Reviews: [1a] T. J. Marks, *Acc. Chem. Res.* **1992**, *25*, 57−65. [1b] M. Aulbach, F. Küber, *Chem. Unserer Zeit* **1994**, *28*, 197−208. [1c] H.-H. Brintzinger, D. Fischer, R. Mülhaupt, B. Rieger, R. M. Waymouth, *Angew. Chem.* **1995**, *107*, 1255−1283; *Angew. Chem. Int. Ed. Engl.* **1995**, *34*, 1143−1170. [1d] M. Bochmann, *J. Chem. Soc.; Dalton Trans.* **1996**, 255−270. [1e] W. Kaminsky, *J. Chem. Soc., Dalton Trans.* **1998**, 1413−1418.

[2] Reviews. [2a] R. F. Jordan, *Adv. Organomet. Chem.* **1991**, *32*, 325−387. [2b] E. Y.-X. Chen, T. J. Marks, *Chem. Rev.* **2000**, *100*, 1391−1434.

[3] M. Bochmann, A. J. Jaggar, J. C. Nicholls, *Angew. Chem.* **1990**, *102*, 830−832; *Angew. Chem. Int. Ed. Engl.* **1990**, *29*, 780−782.

[4] M. Bochmann, S. J. Lancaster, *J. Organomet. Chem.* **1992**, *434*, C1−C5.

[5] J. C. W. Chien, W.-M. Tsai, M. D. Rausch, *J. Am. Chem. Soc.* **1991**, *113*, 8570−8571.

[6] C. L. Stern, T. J. Marks, *J. Am. Chem. Soc.* **1994**, *116*, 10015−10031.

[7] S. Beck, S. Lieber, F. Schaper, A. Geyer, H.-H. Brintzinger, *J. Am. Chem. Soc.* **2001**, *123*, 1483−1489.

[8] Z. Liu, E. Somsook, C. B. White, K. A. Rosaaen, C. R. Landis, *J. Am. Chem. Soc.* **2001**, *123*, 11193−11207.

[9] X. Yang, C. L. Stern, T. J. Marks, *J. Am. Chem. Soc.* **1991**, *113*, 3623−3625.

[10] [10a] A. G. Massey, A. J. Park, F. G. A. Stone, *Proc. Chem. Soc. London* **1963**, 212. [10b] A. G. Massey, A. J. Park, *J. Organomet. Chem.* **1964**, *2*, 245−250. [10c] A. G. Massey, A. J. Park in *Organometallics Syntheses* (Eds.: R. B. King, J. J. Eisch), Elsevier, New York, **1986**, vol. 3, p. 461−462.

[11] B. E. Bosch, G. Erker, R. Fröhlich, O. Meyer, *Organometallics* **1997**, *16*, 5449−5456.

[12] B. E. Bosch, G. Erker, R. Fröhlich, *Inorg. Chim. Acta* **1998**, *270*, 446−458, and references cited therein.

[13] Reviews: [13a] P. Jutzi, J. Dahlhaus, *Coord. Chem. Rev.* **1994**, *137*, 179−199. [13b] J. Okuda, *Commments Inorg. Chem.* **1994**, *16*, 185−205. [13c] P. Jutzi, U. Siemeling, *J. Organomet. Chem.* **1995**, *500*, 175−185. [13d] H. Butenschön, *Chem. Rev.* **2000**, *100*, 1527−1564.

[14] A. Bertuleit, C. Fritze, G. Erker, R. Fröhlich, *Organometallics* **1997**, *16*, 2891−2899.

[15] J. Pflug, A. Bertuleit, G. Kehr, R. Fröhlich, G. Erker, *Organometallics* **1999**, *18*, 3818−3826.

[16] J. Pflug, G. Erker, G. Kehr, R. Fröhlich, *Eur. J. Inorg. Chem.* **2000**, 1795−1801.

[17] [17a] M. Bochmann, L. M. Wilson, *J. Chem. Soc., Chem. Commun.* **1986**, 1610−1611. [17b] M. Bochmann, L. M. Wilson, M. B. Hursthouse, R. L. Short, *Organometallics* **1987**, *6*, 2556−2563.

[18] [18a] S. Döring, G. Erker, R. Fröhlich, *J. Organomet. Chem.* **2000**, *643−644*, 61−68. [18b] R. E. LaPointe, G. R. Roof, K. A. Abboud, J. Klosin, *J. Am. Chem. Soc.* **2000**, *122*, 9560−9561. [18c] D. Vagedes, G. Erker, R. Fröhlich, *J. Organomet. Chem.* **2002**, *641*, 148−155. [18d] H. S. Strauss, *Chem. Rev.* **1993**, *93*, 927−942.

[19] J. W. Lauher, R. Hoffmann, *J. Am. Chem. Soc.* **1976**, *98*, 1729−1742.

[20] D. A. Kleier, G. Binsch, *D NMR3*, Indiana University, **1970**: D. A. Kleier, G. Binsch, *J. Magn. Reson.* **1970**, *3*, 146−160. K. Marat, *XSIM*, University of Manitoba, **1997**.

[21] M. L. H. Green, L.-L. Wong, A. Sella, *Organometallics* **1992**, *11*, 2660−2668, and references cited therein.

[22] [22a] K. Ziegler, W. Schäfer, *Justus Liebigs Ann. Chem.* **1934**, *511*, 101−109. [22b] K. Ziegler, H.-G. Gellert, H. Martin, K. Nagel, J. Schneider, *Justus Liebigs Ann. Chem.* **1954**, *589*, 91−121. [22c] M. F. Sullivan, W. F. Little, *J. Organomet. Chem.* **1967**, *8*, 277−285. [22d] P. Renaut, G. Tainturier, B. Gautheron, *J. Organomet. Chem.* **1978**, *148*, 43−51. [22e] M. D. Brickhouse, R. R. Squires, *J. Am. Chem. Soc.* **1988**, *110*, 2706−2714. [22f] J. Okuda, *Chem. Ber.* **1989**, *122*, 1075−1077. [22g] R. R. Squires, *Acc. Chem. Res.* **1992**, *25*, 461−467. [22h] T. J. Clark, C. M. Killian, S. Luthra, T. A. Nile, *J. Organomet. Chem.* **1993**, *462*, 247−257.

[23] [23a] K. Hafner, G. Schultz, K. Wagner, *Justus Liebigs Ann. Chem.* **1964**, *678*, 39−53. [23b] K. H. Vöpel, G. Ploss, C. König, *Org. Synth.* **1967**, *47*, 52−54, and references cited therein.

[24] K. Kunz, J. Pflug, A. Bertuleit, R. Fröhlich, E. Wegelius, G. Erker, E.-U. Würthwein, *Organometallics* **2000**, *19*, 4208−4216.

[25] K. J. Stone, R. D. Little, *J. Org. Chem.* **1984**, *49*, 1849−1853.

[26] L. E. Manzer, *Inorg. Synthesis* **1982**, *21*, 135−136.

[27] G. Erker, K. Berg, L. Treschanke, K. Engel, *Inorg. Chem.* **1982**, *21*, 1277−1278.

[28] For other examples of ^{15}N NMR studies of group-4 organometallic systems, see, e.g.: H. G. Alt, K. Föttinger, W. Milius, *J. Organomet. Chem.* **1999**, *572*, 21−30.

[29] S. Braun, H.-O. Kalinowski, S. Berger, *150 and More Basic NMR Experiments*, Wiley-VCH, Weinheim, **1998**, and references cited therein.

[30] B. E. Bosch, doctoral thesis, Univ. Münster, **1997**.

[31] Z. Otwinowski, W. Minor, *Methods Enzymol.* **1997**, *276*, 307−326.

[32] R. H. Blessing, *Acta Crystallogr., Sect. A* **1995**, *51*, 33−37; R. H. Blessing, *J. Appl. Crystallogr.* **1997**, *30*, 421−426.

[33] G. M. Sheldrick, *Acta Crystallogr., Sect. A* **1990**, *46*, 467−473.

[34] G. M. Sheldrick, Universität Göttingen, **1997**.

[35] E. Keller, Universität Freiburg, **1997**.

Received August 13, 2002
[I02460]

SiO_2-CaO Vitreous Films Deposited onto Ti6Al4V Substrates

Isabel Izquierdo-Barba,[a] Agustina Asenjo,[b] Luis Esquivias,[c] and María Vallet-Regí*[a]

Keywords: Thin films / Sol-gel processes / Gels / Glasses / Amorphous materials

A sol-gel dipping method has been utilised to deposit SiO_2-CaO films onto Ti6Al4V alloy substrates. These layers were prepared by the dip-coating technique from a series of precursor solutions with different concentrations of glassy $xSiO_2$-(1 – x)CaO (x = 0.8 mol) diluted with absolute ethanol. The characterisation of the films by a variety of techniques reveals differences in the textural properties and in the films' thicknesses depending on the sol concentration in the precursor solution. Concentrated precursor solutions yield porous layers with a higher thickness and surface roughness than those obtained from the dilute ones.

(© Wiley-VCH Verlag GmbH & Co. KGaA, 69451 Weinheim, Germany, 2003)

Introduction

Titanium and its alloys are widely used in the aerospace, chemical and sporting equipment industries. It was not until the 1960s, however, that Ti6Al4V alloy began to be used as a surgical implant material because of its excellent mechanical properties (tensile strength of 860 MPa and yield strength of 790 MPa), and its lightness (specific gravity of 4.5 g/cm^3). Ti-based alloys are not the best from a biological point of view, however, since they corrode away when implanted; this disadvantage led to the discontinuation of the use of Ti6Al4V alloys for load-bearing applications.[1,2] It is commonly believed that this is due to their poor tribomechanical properties under certain physiological conditions, which could cause a local build-up of low pH acidity and high Cl^- ion concentration.

An interesting alternative for protection of metal surfaces against corrosion phenomena is to employ ceramic coatings. Several attempts have been made in this sense, using sophisticated deposition techniques such as PVD and CVD, ion implantation, reaction-assisted and laser coating.[3−5]

The dipping method is a much simpler, versatile and cost effective option which, combined with the sol-gel chemical method, allows the coating of metal surfaces with ceramic layers. The quality of these coatings is strongly determined by the chemical synthesis of the starting sols. In this initial stage, the control of viscosity, ageing and/or solvent allows the determination, at least indirectly, of the roughness, the porosity and thickness of the deposited ceramic layer.[6,7]

Using this method, layers of hydroxyapatite have been deposited onto metallic substrates of the Ti6Al4V alloy.[8] As an alternative solution to the deposition of hydroxyapatite onto titanium alloys, the deposition of bioactive glasses yields an additional advantage: besides its role as a barrier against corrosion, it could improve the bonding with tissues by means of a bioactive interphase.

The aim of this work is to deposit glassy coatings onto Ti6Al4V alloy. The glass chosen for this type of coating is SiO_2-CaO, which our group produces in bulk forms[9,10] and

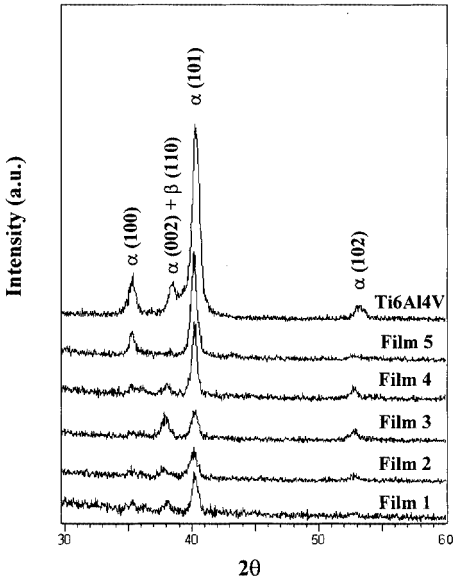

Figure 1. XRD patterns of the Ti6Al4V wafers before and after coating with the different precursor solutions

[a] Departamento de Química Inorgánica y Bioinorgánica, Facultad de Farmacia, Universidad Complutense de Madrid, 28040-Madrid, Spain
E-mail: vallet@farm.ucm.es
[b] Departamento de Física de Materiales, Facultad de Físicas, Universidad Complutense de Madrid, 28040-Madrid, Spain
[c] Departamento de Física de la Materia Condensada, Facultad de Ciencias, Universidad de Cádiz, 11510 Puerto Real (Cádiz), Spain

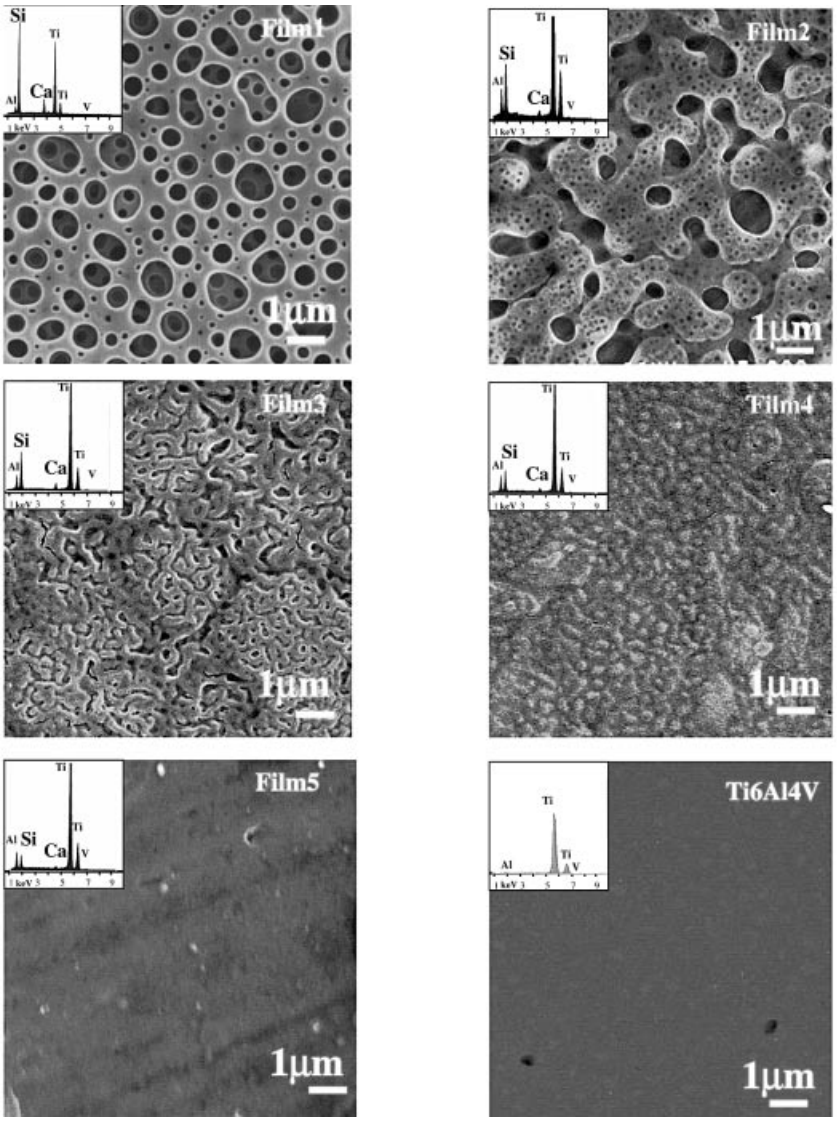

Figure 2. SEM micrographs and EDS spectra of the coatings obtained from the different precursor solutions

where in vitro and in vivo studies have confirmed the bioactivity of such a composition. The films are characterised by X-ray diffraction (XRD), scanning electron microscopy (SEM), X-ray dispersive energy spectroscopy (EDS), reflection ellipsometry and scanning force microscopy (SFM).

It is our purpose to define the production method for these coatings. Their potential applications go beyond the clinical field, and therefore special care is devoted to the control of thickness, roughness and porosity of the deposited layer, through the synthesis conditions, in order to tailor those parameters to the specific application proposed.

Results and Discussion

Five SiO_2-CaO vitreous films were deposited onto Ti6Al4V substrates by the dip-coating method from a series of precursor solutions with different concentrations of glassy $x SiO_2$-$(1-x)$CaO (x = 0.8 mol) diluted with absolute ethanol. The X-ray diffraction patterns show, for all the synthesised films, a broad peak between $15 < 2\theta < 30°$ that could correspond to amorphous silica. Sharp peaks that correspond to the substrate are only observed for 2θ values between 35.1 and 53.0. Figure 1 shows that the intensity of these diffraction maxima decreases as the ethanol volume used in the sol preparation decreases.

SEM, SFM and reflection ellipsometry observations manifest the differences in the textural properties, which depend on to the solution used for coating.

Figure 2 shows the SEM micrographs and EDS spectra of the coatings obtained from the different precursor solutions and the substrate. Film 1 (obtained from the 1:2 sol) presents large pores of different sizes. The pore size ranges between 150 ± 50 nm and 875 ± 50 nm. In film 2 (from the 1:4 sol) the number of pores with a 150 ± 50 nm diam-

eter with regard to those of 875 ± 50 nm is higher than in film 1. The micrograph corresponding to film 3 (1:6 sol) shows a film with a noticeably different structure, consisting of crossed grains. Furthermore, the films 4 (1:8 sol) and 5 (1:12) present a rough structure. Consequently, when the precursor solution has a low ethanol content (films 1 and 2) the films are porous, while as ethanol volume rises the films become more compact (films 3, 4 and 5).

The EDS analyses of the surfaces show that Si and Ca are present in the coatings, while Ti, Al and V, constituents of the substrate, can also be detected. Differences between the relative intensities of substrate (Ti, Al, V) and deposited elements (Ca, Si) are observed. The higher the alcohol content in the precursor solution, the higher the intensity of Ti, Al, V. The Si and Ca content measured by EDS in all cases are 81.2 and 18.8 atom %. These elements have been found homogeneously distributed throughout every sample. These results indicate that the composition does not depend on the sol concentration.

In Figure 3, thickness and refraction indexes of the films obtained by reflection ellipsometry are plotted as a function of the precursor solution concentration. Thickness, ranging from 240 to 1639 nm, decreases as the alcohol content increases as can be expected since the amount of sol drawn also lessens. These data are corroborated by the intensity of the diffraction peaks and EDS observations (see Figure 1 and inset in Figure 2). The refraction index, on the other

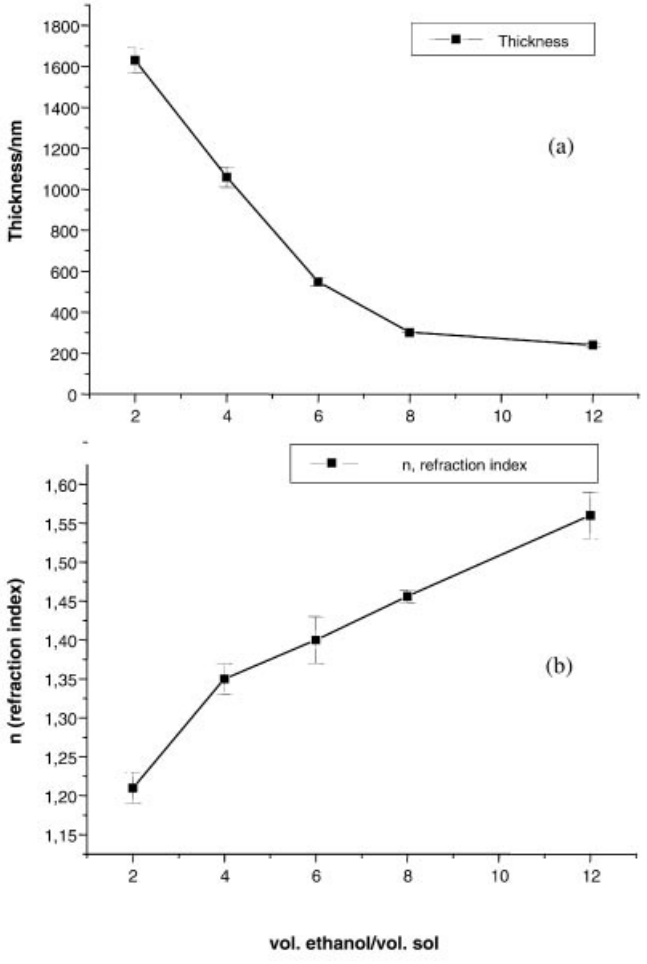

Figure 3. (a) Thickness and (b) refraction index of the films as function of the concentration of the precursor solutions

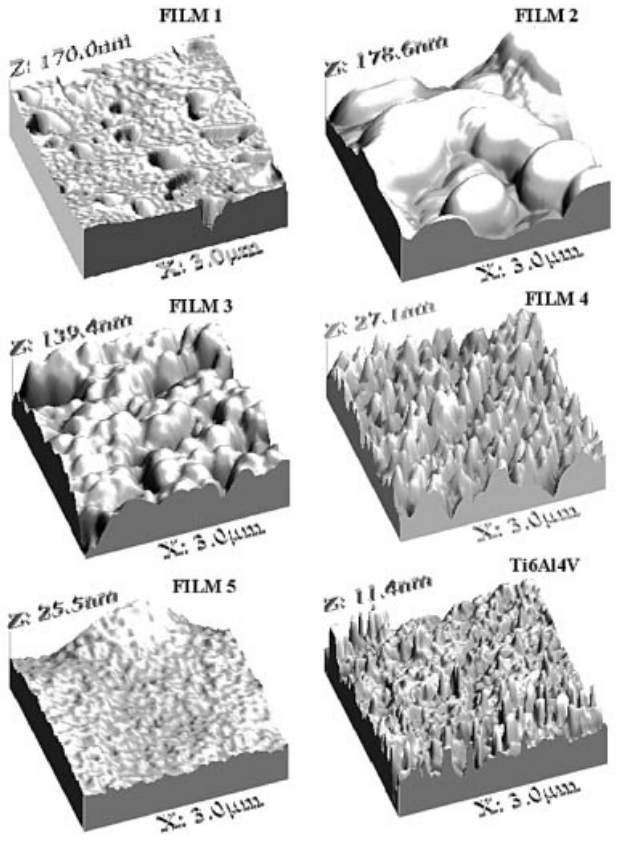

Figure 4. SFM images of the substrate and films; image size: 3 μm × 3 μm

Table 1. Nomenclature, porosity, roughness and grain size of the films obtained

Nomenclature	Precursor solutions (Vol sol:Vol Ethanol)	% Porosity $\rho = (n^2 - n_p^2)/(n^2 - 1)$	Roughness (nm)	Grain size (nm)
Film 1	Sol 1:2	65.6 ± 3.0	25	–
Film 2	Sol 1:4	42.6 ± 3.4	36	800
Film 3	Sol 1:6	34.4 ± 5.3	26	400
Film 4	Sol 1:8	26.2 ± 1.5	6	190
Film 5	Sol 1:12	9.8 ± 6.0	2	90

hand, increases as the precursor concentration decreases. The refraction index, on the other hand, increases as the precursor concentration increases: 1.21 and 1.55 for films 1 and 5, respectively. These results agree with the diminished porosity observed by SEM because the refraction index (n) is related to porosity by the equation shown in the Exp. Sect. Accordingly, n increases as the porosity decreases (see Table 1).

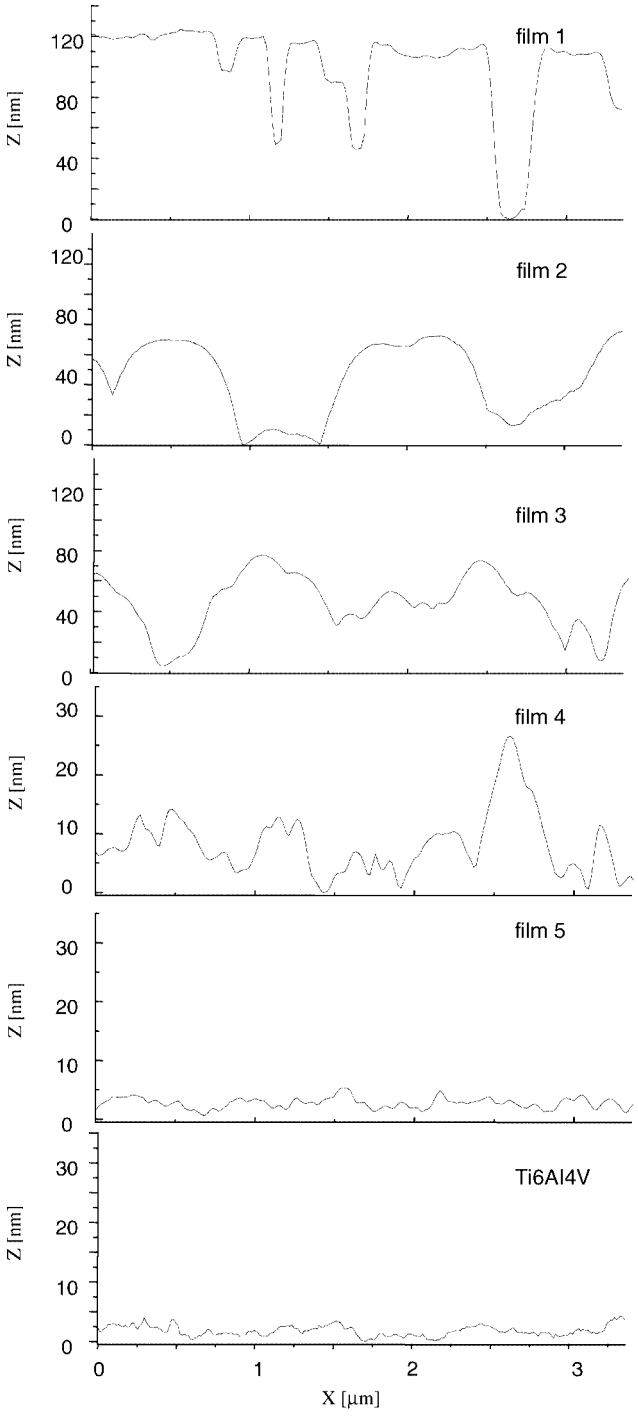

Figure 5. Profiles obtained from the SFM images performed in the different films; note that the profiles corresponding to films 1, 2 and 3 have the same scale, and that the profiles corresponding to films 4, 5 and substrate are presented at a higher magnification

The SFM images shown in Figure 4 are in agreement with the SEM images presented in Figure 2. The advantages in the use of SFM lie in the real 3D information offered, which allows us to study the evolution of the surface roughness versus the precursor concentration. In particular, the roughness (rms) values have been calculated for the different films. The rms values range from 2 nm to 25 nm as shown in Table 1. The lower roughness corresponds to film 5 and an increase of the rms value is observed when the precursor concentration increases. The evolution of the film structure can also be deduced from the analysis of the profiles in Figure 5 obtained from the SFM data. In addition, the SFM images show the increase of the grain size as the precursor concentration increases (see Table 1). Moreover, we have found that, for a precursor concentration of 1:4, the grains start to coalesce, giving an almost continuous film for 1:2 precursor concentrations.

It should also be noted that the structure as well as the roughness of the thicker film, shown in Figure 6, differ from those observed on the other films. This almost continuous film 1 has pores with discrete depth values of 20 nm, 40 nm, 60 nm, 80 nm and 100 nm.

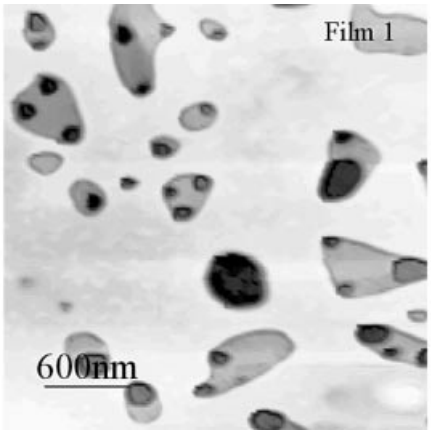

Figure 6. Top view SFM image of film 1; image size: 3 μm × 3 μm

The effect of increasing the alcohol concentration on the sol kinetics is that of slowing down its polymerisation.[6,7,11] Accordingly, the polymerisation of 1:2 sol is faster (and exhibits higher viscosity) than in 1:12 sol. In the latter case, the Si-O-Si aggregates are smaller and easily packed, forming more compact and homogeneous films of lower thickness.

Conclusions

SiO_2-CaO films have been deposited onto Ti6Al4V metal alloy wafers by dip-coating in precursor solutions, a cost-effective and controllable method.

The films are noncrystalline, and are independent of the dipping solution characteristics. In addition, the actual compositions of films do not depend on the precursor solution concentration. However, thickness and texture of surfaces depend on the precursor solution concentration.

The porosity, roughness, grain size and thickness depend on the amount of ethanol present in the dipping solutions. Concentrated dipping solutions yield porous films with higher thickness and surface roughness. Less concentrated precursor solutions produce dense films with higher refraction indexes and lower surface roughness and grain size. The thicker coating shows a continuous film with well-defined pore depths.

In summary, the dip-coating deposition method allows us to tailor the thickness, surface roughness and porosity of the obtained product that can be useful for a variety of applications in the materials science field.

Experimental Section

Dipping Solution Preparation: A SiO_2-CaO, [Si]/[Ca] = 4, sono-sol was elaborated by hydrolysis and polycondensation of tetraethylorthosilane (TEOS) and $Ca(NO_3)_2{\cdot}4H_2O$ under acidic conditions (pH [HNO_3] = 0.5) with R_w = [TEOS]/[H_2O] = 8. Ultrasound waves of 20 MHz were generated by a sonicator device (Sonic & Materials Vibracell), delivering 15 $W{\cdot}cm^{-3}$ of ultrasound power to this liquid mixture for three minutes.

This sol, diluted with different amounts of alcohol (99.99% purity), was distributed in five different containers to obtain the precursor sols named as follow: 1:2 Sol, 1:4 Sol, 1:6 Sol, 1:8 Sol and 1:12 Sol (the figures indicating the sol to ethanol volumes ratio). The sols were aged for 30 days at room temperature before starting to prepare the films.

Films Preparation: Before film deposition, Ti6Al4V metal wafers, provided by IQL (Industrias Quirúrgicas de Levante S.L., Biomet Merck), 13 mm diameter and 1 mm thick, were polished with SiC of 220, 500, 800 and 1200 grit and then with 3−1 μm diamond paste. Finally, the polished discs were washed for 5 min in an ultrasound bath distilled water, alcohol and acetone.

The coating procedure was carried out in a device which allows the control of the substrate extraction at a rate between 50 and 2550 μm/s. Metal substrates were grasped by dipping tweezers, dipped into one of the previously prepared solutions, and then taken out at a constant speed of 1500 μm/s. After muffling the pieces with a thin cloak of sol, they were dried in air at room temperature for 10 minutes and afterwards in an oven at 100 °C for 20 minutes. The samples were stabilised at 550 °C for 10 minutes. This process was repeated six times. Finally, the wafers were washed in an ultrasound bath for five minutes.

Film Characterisation: The resulting films were characterised by X-ray diffraction (XRD), scanning electron microscopy (SEM), X-ray dispersive energy spectroscopy (EDS), reflection ellipsometry and scanning force microscopy (SFM).

X-ray diffraction experiment were carried out using Cu-K_α radiation (λ = 1.54056 Å) in an automatic powder diffractometer (Philips X′Pert MPD) with a thin-film attachment. Scanning measurements at grazing incidence were done in the range $10° < 2\theta < 60°$. The fixed incidence angle was 0.5° for all samples.

SEM and EDS observations were performed on a JEOL 6400 microscope equipped with a Pentajet inper ATW system analyser microscope.

The measurements of reflection ellipsometry were carried out with a PLASMOS SD-2300 automatic ellipsometer with a spot size of 2 mm^2 and a wavelength of 632.8 nm. The ellipsometry angles, Ψ and Δ, were obtained at the same point, under multiple incidence angles (MIA), and are correlated with film thickness and reflective index, n, by means of McCrackins routines[12,13] by interactive calculus with software provided by PLASMOS.

The film porosity, ρ, (as shown in Table 1) was estimated from the refraction indexes calculated by Equation (1),[14]

$$\rho \equiv \frac{n^2 - n_p^2}{n^2 - 1} \quad (1)$$

where n_p is the refraction index of the film measured by reflection ellipsometry and n the refraction index of SiO_2-CaO bulk glass, n = 1.61, calculated as the weighted average of the tabulated indexes for SiO_2 and CaO.[15]

The topography of the samples was obtained by using an Autoprobe-CP SFM from Park Scientific Instruments working in contact mode. Cantilevers with a 0.4 N/m force constant and conical tip were used.

Acknowledgments

Financial support of CICYT (Spain) through Research Project MAT 99-0466 is acknowledged. We thank F. Conde (C.A.I. X-ray Diffraction, UCM) and A. Rodriguez (C.A.I. Electron Microscopy Centre, UCM) for valuable technical and professional assistance. The authors would like to express their gratitude to Industrias Quirúrgicas de Levante S. L., Biomet Merck, which facilitated the titanium alloy.

[1] S. Meassick, H. Champaign, *Surf. Coat. Tech.* **1997**, *93*, 292−296.
[2] J. Gray, *J. Biomed. Mater. Res. Symp.* **1974**, *5*, 27−33.
[3] H. Schimidt, C. Konetschny, U. Fink, *Mater Sci. Tech.* **1998**, *14*, 592−598.
[4] A. Shenhar, I. Gotman, E. Y. Gutmanes, P. Ducheyne, *Mater. Sci. Eng., A* **1999**, *268*, 40−46.
[5] T. M. Yue, J. K. Yu, Z. Mei, H. C. Man, *Mater. Lett.* **2002**, *52*, 206−211.
[6] C. J. Brinker, G. W. Scherer, *Sol-Gel Science. The Physics and Chemistry of Sol-Gel Processing*, Academic Press, Inc., 1990 pp 766−837.
[7] S. Sakka, *J. Sol-Gel Sci. Tech.* **1994**, *2*, 451−455.
[8] W. Weng, *J. Am. Ceram. Soc.* **1999**, *82*, 27−32.
[9] I. Izquierdo-Barba, A. J. Salinas, M. Vallet-Regí, *J. Biomed. Mater. Res.* **1999**, *47*, 243−250.
[10] A. Martinez, I. Izquierdo-Barba, M. Vallet-Regí, *Chem. Mater.* **2000**, *12*, 3080−3088.
[11] T. Peltola, M. Jokinen, H. Rahiala, M. Patsi, J. Heikkila, I. Kangasniemi, A. Yli-Urpo, *J. Biomed. Mater. Res.* **2000**, *51*, 200−208.
[12] F. L. MacCrackins, E. Pasaglia, R. Stromberg, H. L. Steiberg, *J. Res. Natl. Bur. Std.* **1963**, *67*, 363.
[13] F. L. MacCrackins, J. Colson, The symposium of the ellipso-

meter and its use in the measurements of surfaces and thin films, Washington, D. C. **1963**.
[14] G. M. Wu, J. Wang, J. Shen, T. H. Yang, Z. Q. Lai, H. L. Zhang, Q. Y. Zhang, *Chinese, Atomic Energy Science and Technology* **1999**, *33*, 332.
[15] *Handbook of Chemistry and Physics* (Editor in chief: D. R. Lide), 73 rd edition, **1992−1993**, pp 4−39 and 4−95.

Received October 11, 2002
[I02572]

Ruthenium-Catalysed Selective Transetherification of Substituted Vinyl Ethers To Form Acetals and Aldehydes

Mustapha Saoud,[a] Antonio Romerosa,*[a] Sonia Mañas Carpio,[a] Luca Gonsalvi,[b] and Maurizio Peruzzini*[b]

Keywords: Ruthenium / Allenylidenes / Vinyl ethers / Homogeneous catalysis / Acetals

The water-soluble ruthenium allenylidene complex [{RuCl(μ-Cl)(C=C=CPh$_2$)(TPPMS)$_2$}$_2$]Na$_4$ catalyses the selective transformation of substituted linear and cyclic vinyl ethers with MeOH, under mild non acidic conditions, to give acetals, while aldehydes and ketones are obtained in a CHCl$_3$/H$_2$O mixture, which allows for easy recycling of the catalyst. NMR studies showed that the reaction follows a transetherification mechanism rather than simple acid-catalysed hydrolysis.
(© Wiley-VCH Verlag GmbH & Co. KGaA, 69451 Weinheim, Germany, 2003)

Introduction

Unsaturated transition-metal carbene complexes, M=C=(C)$_n$=C, such as vinylidenes (n = 0)[1] and allenylidenes (n = 1),[2] are a ubiquitous class of organometallic compounds whose use in catalysis has gained an increasing consideration during the last decade.[3] In this regard, particular emphasis has been placed on ruthenium vinylidene complexes, which have been shown to catalyze several important processes targeting the elaboration of linear and cyclic organic compounds.[3,4] More recently, ruthenium allenylidene species have also started attracting interest as catalysts or catalyst precursors and have been employed to achieve important metal-mediated reactions such as alkene ring closing metathesis (RCM),[5a−5e] ring opening metathesis polymerisation[5f,5h] and propargylation of aromatic compounds.[6]

In a previous communication we have described the first example of a water-soluble transition metal allenylidene complex of formula [{RuCl(μ-Cl)(C=C=CPh$_2$)-(TPPMS)$_2$}$_2$]Na$_4$ (**1**) [TPPMS = Ph$_2$P{2-OS(O)$_2$-C$_6$H$_4$}$^-$}].[7] As a first exploratory assessment of its catalytic activity, we have demonstrated that this ruthenium(II) complex may be successfully used in the selective ring-opening metathesis (ROM) of cyclic olefins with methylacrylate as chain-transfer reagent. In order to further evaluate the catalytic activity of this water-soluble unsaturated carbene complex, we decided to investigate its behaviour under the conditions of RCM of acyclic dienes,[8−11] a reaction which is well-known with several Grubbs-type ruthenium catalysts,[12,13] including the few that are soluble in water.[14]

However, in spite of our expectations, the reaction of **1** in a biphasic CHCl$_3$/H$_2$O system with representative substrates such as diethyl diallylmalonate and *N*,*N*-diallyltosylamide failed to give any RCM reaction. Thus, when 1,4-butanediol vinyl ether (**2**) was chosen as substrate, we observed that, although not affording RCM products as reported for other Ru-carbene species,[15] complex **1** was still endowed with catalytic activity, bringing about the selective formation of ethanal and 1,4-butandiol, followed by their intermolecular condensation to generate 2-methyl-[1,3]dioxepane (**3**) in almost quantitative yield. When the same reaction was carried out in methanol, the isolated products were 1,1-dimethoxyethane and 1,4-butanediol (Scheme 1). Although this catalytic method is of little synthetic interest, and the reaction under scrutiny can be performed without the need for expensive transition-metal catalysts, this serendipitous discovery nevertheless represents a completely new reaction to the best of our knowledge, and on this basis we decided to study its general applicability and tried to unravel its mechanism.

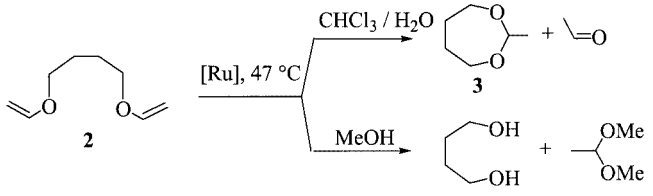

Scheme 1

[a] Área de Quimica Inorganica, Universidad de Almería, 04071, Almería, Spain
Fax: (internat.) +34-950/015-008
E-mail: romerosa@ual.es
[b] Istituto di Chimica dei Composti Organometallici, ICCOM-CNR,
Via Jacopo Nardi 39, 50132 Firenze, Italy
Fax: (internat.) +39-055/247-8366
E-mail: peruz@fi.cnr.it

Results and Discussion

In order to explore the scope of the reaction, we applied our catalytic system to a series of linear and cyclic vinyl ethers bearing different functional groups. The nature of the final products depends strictly on whether the reactions are run under monophasic (MeOH) or biphasic ($CHCl_3$/H_2O) conditions. All the tests were run under very mild conditions (47 °C). The results are summarised in Table 1 and 2 for biphasic and monophasic conditions, respectively. Our protocol is highly specific for vinyl ethers, as diallyl, diethyl, dibenzyl and allylpropargyl ethers were recovered intact after the catalytic tests. This indicates a high tolerance of the method for a wide variety of organic substrates and suggests a potential application for the selective deprotection of masked aldehydes protected as vinyl ethers, such as acid sensitive β-hydroxy aldehydes. However, only trivial products were obtained from the ethers of choice as these were deliberately chosen for screening purposes only.

Table 1. Catalytic reactions of linear and cyclic vinyl ethers in the presence of **1** in $CDCl_3/D_2O$[a]

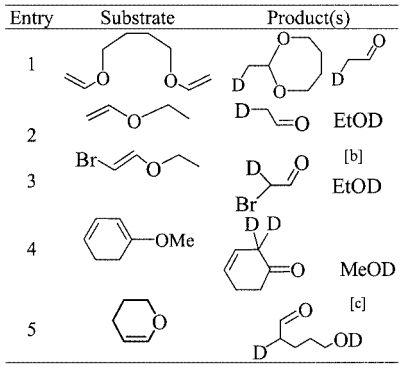

[a] Reaction conditions: substrate (0.1 mmol), **1** (0.005 mmol), $CDCl_3$ (0.5 mL), D_2O (0.5 mL), 47 °C, 2.5 h, in NMR tube (5 mm) under Ar. [b] Bromoacetaldehyde is not stable under the reaction conditions and cyclotrimerizes to 2,4,6-tris(bromodeuteromethyl)-1,3,5-trioxane (see Exp. Sect.). [c] The aldehyde 5-hydroxypentanal intramolecularly condenses to 3-deuterotetrahydro-2*H*-pyran-2-deuterol, equilibrium yield 84% (see Exp. Sect.).

The reactions were carried out on an NMR-tube scale at first and then repeated in bulk to check for reproducibility and to isolate the products. For all reactions the two methods gave similar results, showing that NMR-scale tests can be representative of the actual catalytic test under the same conditions. Under NMR tube reaction conditions, at 47 °C with a 1:1 $CDCl_3/D_2O$ mixture, all vinyl substrates were smoothly converted within three hours, reaching complete selectivity for the products described in Table 1, as determined by NMR spectroscopy and GC-MS techniques. The deep-red coloured catalytically active species remains confined to the water phase and can be recycled up to four times without significant loss of activity (see Exp. Sect.).

An interesting reaction is the selective deuteration of 1-methoxy-1,3-cyclohexadiene to yield 2,2-dideuterocyclohex-3-en-1-one (Table 1, entry 4) where the selective double deuteration at the 2-position follows from H/D exchange via a keto-enol equilibrium (see Scheme 4 in the Exp. Sect.). For linear vinyl ethers the formation of CD_3-diacetals was observed, resulting from the condensation of acetaldehyde and CD_3OD by cleavage of the vinyl carbon-oxygen bond. For example, 2-bromovinyl ethyl ether was converted into 2-bromo-2-deutero-1,1-bis(trideuteromethoxy)ethane (Table 2, entry 8). For cyclic vinyl ethers such as dihydropyran, ring opening and acetalization occur to give the protected 5-trideuteroxy-2-deuteropentan-1-al (Table 2, entry 10). 1-Methoxy1,3-cyclohexadiene was converted into the deuterated OCD_3 analogue (kinetic product) instead of the corresponding diacetal (Table 2, entry 9) which forms only after a week at 47 °C.

Table 2. Catalytic reactions of linear and cyclic vinyl ethers in the presence of **1** in CD_3OD[a]

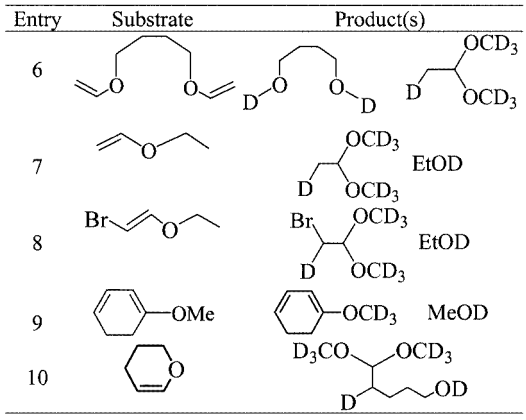

[a] Reaction conditions: substrate (0.1 mmol), **1** (0.005 mmol), CD_3OD (1.0 mL), 47 °C, 17 h, in NMR tube (5 mm) under Ar

We chose 1,4-butanediol vinyl ether (**2**) to test the effect of catalyst concentration on the rate and selectivity of the reaction. In $CDCl_3/D_2O$, the reaction reached completion in 2.5 hours with 5 mol % of catalyst **1**, 8 h with 1 mol % and 20 h with 0.2 mol %, in all cases with selectivity higher than 99%. In CD_3OD, the reaction is slower (17 h) and normally 5 mol % of **1** are required to complete the reaction in a comparable time scale. The nature of the ruthenium precursor was also found to be crucial for the reaction. A series of precursors was tested for the reaction of **2** under standard conditions; the results are summarised in Table 3. Remarkably, while the classic Grubbs catalyst does not work under these reaction conditions, the water-soluble phenylvinylidene complex $[RuCl_2\{C{=}C(H)Ph\}(TPPMS)_2]Na_2$ (**4**)[7] shows a similar reactivity to **1** in promoting the acetalization of **2**. These results are significant and indicate that ruthenium, TPPMS and *unsaturated carbenes* are necessary ingredients in this reaction either as molecular complexes or to form the catalytic species in situ (Table 3, entries 18 and 19). However, catalytic tests with isolated samples of **4** were not systematically evaluated due to the lower stability and difficulty of isolation of **4** compared to **1**.[7]

Table 3. Blank reactions and effect of Ru precursor on the conversion of **2** to 1,4-D-butanediol and 1,1-D-dimethoxy-2-D-ethane[a]

Entry	Precursor	Yield (%)	Time (h)
11	None	–	70
12	TPPMS	–	70
13	$[RuCl_2(CHPh)(PCy_3)_2]$	–	20
14	$[Cp^*Ru(PEt_3)_2Cl]$	–	20
15	$[RuCl_2(PPh_3)_3]$	–	20
16	$[RuCl_2(TPPMS)_2]_2$	80	1 month
17	$[RuCl_2(PPh_3)_3]$ + 4 TPPMS	30	18
18	$[RuCl_2(PPh_3)_3]$ + 4 TPPMS + HC≡CPh	93	16
19	$[RuCl_2(PPh_3)_3]$ + 4 TPPMS + HC≡CC(OH)Ph_2	95	17

[a] Reaction conditions: substrate (0.1 mmol), precursor (0.005 mmol), CD_3OD (1.0 mL), 47 °C, 17 h, in NMR tube (5 mm) under Ar

We obtained evidence for a transetherification mechanism by monitoring the reaction of **2** with **1** in CD_3OD by ^1H and $^{13}C\{^1H\}$ NMR spectroscopy at 47 °C. The decrease in the intensity of the signal at δ = 6.49 ppm (dd, $J_{H,H}$ =

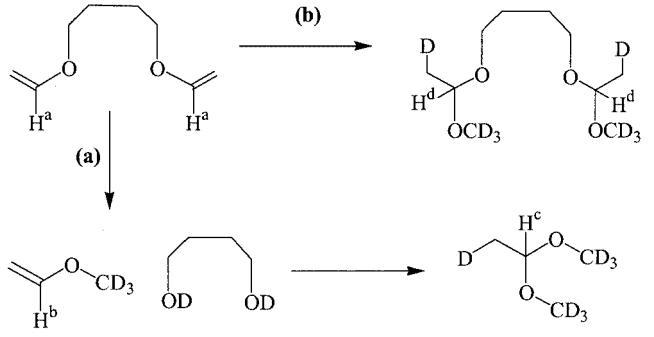

Scheme 2. NMR mechanistic experiments: (a) **2**, 0.1 mmol; **1**, 0.005 mmol. CD_3OD 1.0 cm^3; 47 °C; 24 h, in NMR tube (5 mm) under Ar; (b) **2**, 0.1 mmol; HOTs, 0.01 mmol. CD_3OD 1.0 mL; 47 °C; 24 h, in NMR tube (5 mm) under Ar

14.3, 7.0 Hz) due to the vinyl proton H^a (Scheme 2a) was accompanied by an increase in the intensity of a new signal at δ = 6.51 ppm (dd, $J_{H,H}$ = 14.2, 6.8 Hz) that we attribute to H^b, which in turn decreases in intensity with the appearance of the signal due to H^c at δ = 4.56 ppm (dt, $J_{H,H}$ = 5.2, $J_{H,D}$ = 1.8 Hz) belonging to the final product. A parallel experiment, carried out replacing **1** with HOTs, ruled out the possibility of acid-catalysed hydrolysis of the substrate (Scheme 2b).[16–18] Under these conditions, **2** is immediately converted into a new species that does not contain a vinyl group, is stable and is plausibly the product of addition of CD_3OD to the vinyl double bond as evidenced by the diagnostic H^d signal at δ = 4.66 ppm (dt, $J_{H,H}$ = 5.4, J_{HD} = 1.6 Hz). Although a detailed mechanism cannot be proposed on the basis of the NMR study alone, these latter experiments suggest that the reaction occurs as a two-step transformation of the vinyl substrate by exchange of the ether substituent, followed by addition of alcohol to the C=C double bond with regioselective deuteration of the β-carbon. $^{31}P\{^1H\}$ NMR monitoring of the biphasic reaction shows that **1** quantitatively transforms into an unknown ruthenium species (singlet at δ = 21.4 ppm), which remains catalytically active over more than four runs.

Conclusion

In summary, our study provides an insight into the reactivity of vinyl ethers in the presence of a Ru-allenylidene complex and an alternative method for the production of acetals, aldehydes and ketones from a wide choice of vinyl ether precursors.[19] Although the present method is certainly not convenient for routine applications, it is important to stress that this protocol affords catalytic solvolysis of vinyl ethers under mild conditions at neutral pH in aqueous phase or anhydrous organic phase, with high tolerance for a variety of functional groups. As a consequence, the present ruthenium catalyst might deserve application in particular cases where the vinyl ether functionality is coupled with acid-sensitive groups. We are currently investigating more interesting applications of the catalytic protocol, such as the synthesis of polyacetals[20] and podands. Preliminary experiments showed that our system is active in the selective catalytic synthesis of a variety of linear polyethers by acetalization of vinyl ethyl ether with various glycols.

Experimental Section

General Remarks: Complex **1** was prepared as described previously.[7] ^1H and $^{13}C\{^1H\}$ NMR spectra were recorded on Varian VXR300, or Bruker AVANCE DRX300 spectrometers operating at ca. 300 MHz (^1H) and ca. 75.4 MHz (^{13}C). Peak positions are relative to tetramethylsilane and were calibrated against the residual solvent resonance (^1H) or the deuterated solvent multiplet (^{13}C). $^{31}P\{^1H\}$ NMR spectra were recorded on the same instruments operating at ca. 121 MHz. Chemical shifts were measured relative to external 85% H_3PO_4 with downfield values taken as positive. A Shimadzu GC-14A/GCMS-QP2000 instrument was employed for GC-MS investigations.

Bulk-Scale Experiments: In a typical macro scale experiment, 3 mmol of substrate were added under argon to 2 mL of MeOH together with 0.03 mmol of **1**. After 2 h whilst stirring at 47 °C the solvent was removed giving the 1,1-dimethoxy-substituted product. When a biphasic system was used, 3 mmol of vinyl ether and

0.03 mmol of **1** were dissolved into 1 mL of $CHCl_3$ and 1 mL of H_2O under argon. The mixture was kept at 47 °C for 1 h under vigorous stirring, then the organic phase was separated and dried over $MgSO_4$. The aldehyde or ketone was obtained in nearly quantitative yield by evaporation at reduced pressure of the solvent.

Typical Experimental Procedure for NMR-Tube Tests. (a) Monophasic Conditions: Compound **1** (11 mg, 5×10^{-3} mmol) was introduced into a 5 mm NMR tube, which was repeatedly evacuated and filled with argon. The substrate (20 equiv., typically 15−18 μL) was then added together with 0.5 mL of CD_3OD, to obtain an orange-red homogeneous solution. The tube was kept in an oil bath at 47 °C for typically 15−17 hours after which ^1H and ^{13}C NMR spectra were collected.
(b) Biphasic Conditions: As above, except for solvent (a mixture of $CDCl_3$, 0.5 mL and D_2O, 0.5 mL was used) and reaction time (typically 3 h). The tube was shaken thoroughly after mixing of the reagents and before taking the NMR spectra.

Experimental Procedure for Catalyst Recycling Tests: An NMR tube was charged with **1** (12.5 mg, 5.7×10^{-3} mmol), **2** (18 μL, 0.114 mmol), 0.5 mL of $CDCl_3$ and 0.5 mL of D_2O. The tube containing two separate phases was kept at 47 °C for 3 h, during which time it was shaken approximately every 20 min. After separation of the organic phase, the aqueous phase, which contained the catalyst, was proved to be active in the catalytic reaction during three additional runs carried out by adding 18 μL of **2** to 0.5 mL of $CDCl_3$ (a 100% conversion of **2** was achieved after 2.3 h in the first catalytic run, after 2.5 h in the second catalytic test and after 2.75 h in the third run). Only in the fourth catalytic run was a significant decrease of the catalytic activity observed — the reaction time to transform all of the substrate rose to about 4 h.

NMR and GC-MS Product Characterisation

2-Deuteromethyl-[1,3]dioxepane: (Table 1, entry 1). ^1H NMR (300.13 MHz, $CDCl_3$, room temp.): δ = 1.32 (dt, $J_{H,H}$ = 5.16, $J_{H,D}$ = 1.8 Hz, 2 H, CH_2D), 1.70 (m, 4 H, OCH$_2$CH_2), 3.67 (m, 2 H, OC*H*H), 3.93 (m, 2 H, OCH*H*), 4.95 (t, $J_{H,H}$ = 5.16 Hz, OC*H*O) ppm. $^{13}C\{^1H\}$ NMR (75.47 MHz, $CDCl_3$, room temp.): δ = 28.9 (s, OCH$_2$*C*H$_2$), 66.4 (2 O*C*H$_2$), 100.4 (s, O*C*HO), 31.7 (t, $J_{C,D}$ = 18.5 Hz, *C*H$_2$D) ppm. GC/MS: *m*/*z* (%) = 117 (5) [$C_6H_{11}O_2D$], 101 (43) [$C_5H_9O_2$], 71 (87) [C_4H_7O], 55 (53) [C_4H_7], 43 (100) [C_2H_3O].

Deuteroacetaldehyde: (Table 1, entries 1, 2). ^1H NMR (300.13 MHz, $CDCl_3$, room temp.): δ = 9.79 (br. t, $J_{H,H}$ = 2.80 Hz, 1 H, CHO), 2.19 (dt, $J_{H,H}$ = 2.80, $J_{H,D}$ = 2.25 Hz, 2 H, CH_2D) ppm. $^{13}C\{^1H\}$ NMR (75.47 MHz, $CDCl_3$, room temp.): δ = 200.89 (s, *C*HO), 21.49 (t, $J_{C,D}$ = 19.5 Hz, *C*H$_2$D) ppm. GC/MS: not registered.

Bromodeutero Acetaldehyde: (Table 1, entry 3). Bromoacetaldehyde, which selectively forms from the reaction of **1** with 1-bromo-2-ethoxyethene, is not stable under the reaction conditions and cyclotrimerizes spontaneously to 2,4,6-tris(bromodeuteromethyl)-1,3,5-trioxane (see Scheme 3 below). The NMR analysis of the reaction mixture reveals the presence of both the aldehyde (minor component) and the cyclotrimer. ^1H NMR (300.13 MHz, $CDCl_3$, room temp.): bromoacetaldehyde: δ = 9.55 (d, $J_{H,H}$ = 2.5 Hz, C*H*O), 3.86 (dt, $J_{H,H}$ = 6.8, $J_{H,D}$ = 2.5 Hz, C*H*DBr) ppm; 2,4,6-tris(bromodeuteromethyl)-1,3,5-trioxane: δ = 4.68 (d, $J_{H,H}$ = 5.5 Hz, C*H*OO), 3.61 (dt, $J_{H,H}$ = 5.5, $J_{H,D}$ = 1.9 Hz, C*H*DBr) ppm. $^{13}C\{^1H\}$ NMR (75.47 MHz, $CDCl_3$, room temp.): bromoacetaldehyde: δ = 191.9 (s, *C*HO), 52.2 (t, $J_{C,D}$ = 18.5 Hz, *C*HDBr) ppm. 2,4,6-tris(bromodeuteromethyl)-1,3,5-trioxane: δ = 101.36 (s, *C*HOO), 51.7 (t, $J_{C,D}$ = 18.5 Hz, *C*HDBr) ppm. GC/MS: not registered.

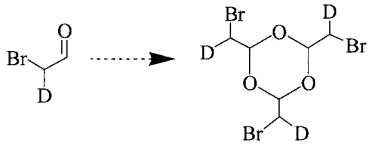

Scheme 3

2,2-Dideuterocyclohex-3-enone: (Table 1, entry 4). The product probably forms by selective incorporation of deuterium in position 2 following H/D exchange. The latter is likely to be promoted by the keto-enol equilibrium depicted in Scheme 4.
^1H NMR (300.13 MHz, $CDCl_3$, room temp.): δ = 2.34 [m, 4 H, $CH_{2(5)}CH_{2(6)}$], 6.03 [dt, $J_{H,H}$ = 10.3, $J_{H,H}$ = 1.9 Hz, 1 H, $CH_{(4)}$], 6.97 [dm, $J_{H,H}$ = 10.3 Hz, 1 H, $CH_{(3)}$] ppm. $^{13}C\{^1H\}$ NMR (75.47 MHz, $CDCl_3$, room temp.): δ = 205.2 [$C_{(1)}$],130.9 [s, $C_{(4)}$], 128.2 [s, $C_{(3)}$], 41.9 [s, $C_{(6)}$], 38.0 [quin., $J_{C,D}$ = 19.7 Hz, $C_{(2)}$], 22.6 [s, $C_{(5)}$] ppm. GC/MS: *m*/*z* (%) = 98 (18) [$C_6H_6D_2O$], 82 (5)[$C_6H_6D_2$], 70 (100%) [$C_5H_6D_2$].

2-Deutero-5-deuteroxypentanal: (Table 1, entry 5). The aldehyde that forms selectively from the cyclic vinyl ether 3,4-dihydro-2*H*-pyran, undergoes acetalization under the present reaction conditions and intramolecularly condenses to yield 3-deuterotetrahydro-2*H*-pyran-2-deuterol. The NMR analysis indicates the formation of an equilibrium mixture with about 84% of the cyclic compound (Scheme 5).
^1H NMR (300.13 MHz, $CDCl_3$, room temp.): 2-deutero-5-deuteroxypentanal: δ = 9.79 (s, 1 H, CHO), 3.46 (m, 2 H, CH_2OD), 1.5−2.1 [m, 5 H, C*H*(D)CH_2CH_2] ppm; 3-deuterotetrahydro-2*H*-pyran-2-deuterol: δ = 4.27 [m, 1 H, OC*H*(OD)], 3.53 (t, $J_{H,H}$ = 7.4 Hz, 2 H, CH_2O), 1.5−2.0 (m, CH_2CH_2 + *C*HD) ppm. $^{13}C\{^1H\}$ NMR (75.47 MHz, $CDCl_3$, room temp.): 2-deutero-5-deuteroxypentanal: δ = 200.1 (s, *C*HO), 62.2 (s, *C*H$_2$OD), 30.4 (t, $J_{C,D}$ = 19.5 Hz, CHD), 27.2 (s, *C*H$_2$CH$_2$OD), 19.6 (s, CHD*C*H$_2$) ppm; 3-deuterotetrahydro-2*H*-pyran-2-deuterol: δ = 94.5 [s, O*C*H(OD)], 62.9 (s, *C*H$_2$O), 29.7 (t, $J_{C,D}$ = 36.3 Hz, CHD), 25.2 (s, *C*H$_2$CH$_2$O), 20.1 (s, *C*H$_2$CHD) ppm. GC/MS: *m*/*z* (%) = 103 (23) [$C_5H_7O_2D_2$], 85 (10) [C_5H_7OD], 58 (100) [C_3H_4OD], 42 (60) [C_3H_4D].

1,4-Butandeuterol: (Table 2, entry 6). ^1H NMR (300.13 MHz, $CDCl_3$, room temp.): δ = 3.67 (m, 4 H, 2 × O*C*H$_2$), 1.64 (m, 4 H,

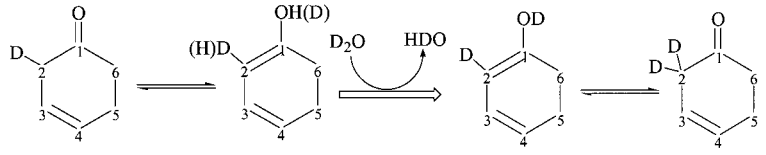

Scheme 4

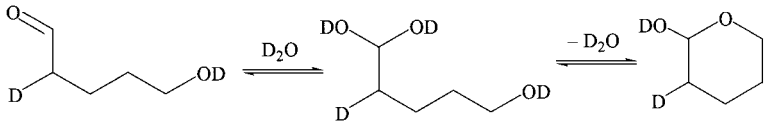

Scheme 5

2 × OCH_2CH_2) ppm. $^{13}C\{^1H\}$ NMR (75.47 MHz, $CDCl_3$, room temp.): δ = 30.2 (s, 2 × OCH_2CH_2), 62.6 (s, 2 × OCH_2) ppm. GC/MS: *m/z* (%) = 92 (2) [$C_4H_8O_2D_2$], 86 (5) [$C_4H_6O_2$], 71 (18) [C_4H_7O], 57 (11) [C_3H_5O], 42 (100) [C_2H_2O].

2-Deutero-1,1-bis(trideuteromethoxy)ethane: (Table 2, entries 6,7). ^1H NMR (300.13 MHz, $CDCl_3$, room temp.): δ = 4.56 [t, $J_{H,H}$ = 5.2 Hz, 1 H, $CH(OCD_3)_2$], 1.26 (dt, $J_{H,H}$ = 5.2, $J_{H,D}$ = 1.8 Hz, 2 H, CH_2D) ppm. $^{13}C\{^1H\}$ NMR (75.47 MHz, $CDCl_3$, room temp.): δ = 101.2 [s, $CH(OCD_3)_2$], 47.5 (sept, $J_{C,D}$ = 21.3 Hz, OCD_3), 17.2 (t, $J_{C,D}$ = 18.7 Hz, CH_2D) ppm. GC/MS: *m/z* (%) = 96 (5) [$C_4H_3O_2D_7$], 81 (53) [$C_3HO_2D_6$], 63 (100) [$C_2HO_2D_3$], 44 (27) [CO_2].

1-Bromo-1-deutero-2,2-bis(trideuteromethoxy)ethane: (Table 2, entry 8). ^1H NMR (300.13 MHz, $CDCl_3$, room temp.): δ = 4.55 [d, $J_{H,H}$ = 5.2 Hz, 1 H, $CH(Ocd_3)_2$], 3.40 (m, 1 H, CHDBr) ppm. $^{13}C\{^1H\}$ NMR (75.47 MHz, $CDCl_3$, room temp.): δ = 103.1 [s, $CH(Ocd_3)_2$], 29.8 (t, $J_{C,D}$ = 23 Hz, CHDBr) ppm. GC/MS: *m/z* (%) = 176 (6) [$C_4H_2O_2D_7Br$], 142 (30) [$C_3H_2OD_4Br$], 108 (5) [C_2H_2DBr], 81 (100) [HBr].

1-Trideuteromethoxy-1,3-cyclohexadiene: (Table 2, entry 9). ^1H NMR (300.13 MHz, $CDCl_3$, room temp.): δ = 5.86 [m, 1 H, $CH_{(3)}$], 5.40 [br. d, $J_{H4,H3}$ = 7.9 Hz, 1 H, $CH_{(4)}$], 4.97 [d, $J_{H,H}$ = 5.1 Hz, 1 H, $CH_{(2)}$], 2.21 [m, 4 H, $CH_{2(5)}CH_{2(6)}$] ppm. $^{13}C\{^1H\}$ NMR (75.47 MHz, $CDCl_3$, room temp.): δ = 127.8 (s, C3), 120.1 (s, C1), 113.4 (s, C4), 76.7 (s, C2), 54.8 (sept, $J_{C,D}$ = 21.3 Hz, OCD_3), 25.1 (s, C5), 22.2 (s, C6) ppm. GC/MS: *m/z* (%) = 114 (40) [$C_8H_7O_2D_7$], 96 (100) [C_6H_8O], 80 (62) [C_6H_8].

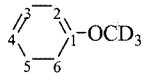

4-Deutero-5,5-bis(trideuteromethoxy)pentan-1-deuterol: (Table 2, entry 10). ^1H NMR (300.13 MHz, $CDCl_3$, room temp.): δ = 4.50 [br. s, 1 H, $CH(OCD_3)_2$], 3.68 (br. t, $J_{H,H}$ = 6.2 Hz, CH_2OD), 1.53−1.80 (m, 5 H, $CHDCH_2CH_2$) ppm. $^{13}C\{^1H\}$ NMR (75.47 MHz, $CDCl_3$, room temp.): δ = 99.8 [s, $CH(OCD_3)_2$], 61.7 (s, CH_2OD), 48.1 (sept, $J_{C,D}$ = 21.8 Hz, OCD_3), 29.8 (t, $J_{C,D}$ = 19.7 Hz, CHD), 18.9 and 25.1 (all s, CH_2CH_2) ppm. GC/MS: *m/z* (%) = [$C_7H_8O_3D_8$] not observed, 120 (30) [$C_6H_6O_2D_5$], 86 (70) [C_5H_8OD], 57 (100) [C_4H_7D], 42 (60) [C_3H_4D].

Acknowledgments

This work was supported by INTAS (00-00018) and NATO (PST-CLG-978521). Thanks are also due to EU through COST D17 Chemistry Action (WGD17/003) for promoting this scientific activity. AR thanks MCYT (Spain) for project PPQ2000-1301 and the Junta de Andalucia for project A29/00. Dr. G. Reginato (ICCOM-CNR) is gratefully acknowledged for helpful discussions.

[1] [1a] M. I. Bruce, *Chem. Rev.* **1991**, *91*, 197−257. [1b] M. C. Puerta, P. Valerga, *Coord. Chem. Rev.* **1999**, *193/195*, 977−1025.
[2] M. I. Bruce, *Chem. Rev.* **1998**, *98*, 2797−2858.
[3] [3a] V. Cadierno, M. P. Gamasa, J. Gimeno, *Eur. J. Inorg. Chem.* **2001**, 571−591. [3b] D. Touchard, P. H. Dixneuf, *Coord. Chem. Rev.* **1998**, *178−180*, 409−429. [3c] H. Werner, *Chem. Commun.* **1997**, 903−910. [3d] C. Bruneau, P. H. Dixneuf, *Chem. Commun.* **1997**, 507−512.
[4] [4a] C. Bruneau, P. H. Dixneuf, *Acc. Chem. Res.* **1999**, *32*, 311−323. [4b] B. M. Trost, *Acc. Chem. Res.* **2002**, *35*, 695−705 and references therein.
[5] [5a] A. Fürstner, M. Picquet, C. Bruneau, P. H. Dixneuf, *Chem. Commun.* **1998**, 1315−1316. [5b] H.-J. Schanz, L. Jafarpour, E. D. Stevens, S. P. Nolan, *Organometallics* **1999**, *18*, 5187−5190. [5c] M. Picquet, D. Touchard, C. Bruneau, P. H. Dixneuf, *New J. Chem.* **1999**, *23*, 141−143. [5d] D. Sémeril, H. Oliver-Borbigon, C. Bruneau, P. H. Dixneuf, *Chem. Commun.* **2002**, 146−147. [5e] D. Sémeril, C. Bruneau, P. H. Dixneuf, *Adv. Synth. Catal.* **2002**, *344*, 585−595. [5f] S. Jung, C. D. Brandt, H. Werner, *New J. Chem.* **2001**, *25*, 1101−1103. [5g] R. Castarlenas, D. Sémeril, A. F. Noels, A. Demonceau, P. H. Dixneuf, *J. Organomet. Chem.* **2002**, in press. [5h] I. A. Abdallaoui, D. Sémeril, P. H. Dixneuf, *J. Mol. Catal. A: Chem.* **2002**, *182−183*, 577−583.
[6] Y. Nishibayashi, M. Yoshikawa, Y. Inada, M. Hidai, S. Uemura, *J. Am. Chem. Soc.* **2002**, *124*, 11846−11847.
[7] M. Saoud, A. Romerosa, M. Peruzzini, *Organometallics* **2000**, *19*, 4005−4007.
[8] T. M. Trnka, R. H. Grubbs, *Acc. Chem. Res.* **2001**, *34*, 18−29.
[9] L. Jafarpour, S. P. Nolan, *J. Organomet. Chem.* **2001**, *617/618*, 17−27.
[10] A. Fürstner, M. Liebl, C. W. Lehmann, M. Picquet, R. Kunz, C. Bruneau, D. Touchard, P. H. Dixneuf, *Chem. Eur. J.* **2000**, *6*, 1847−1857.
[11] A. Fürstner, *Angew. Chem. Int. Ed.* **2000**, *39*, 3013−3043.
[12] G. C. Fu, S. T. Nguyen, R. H. Grubbs, *J. Am. Chem. Soc.* **1993**, *115*, 9856−9857.
[13] E. L. Dias, S. T. Nguyen, R. H. Grubbs, *J. Am. Chem. Soc.* **1997**, *119*, 3887−3897.
[14] T. A. Kirkland, D. M. Lynn, R. H. Grubbs, *J. Org. Chem.* **1998**, *63*, 9904−9909.
[15] C. F. Sturino, J. C. Y Wong, *Tetrahedron Lett.* **1998**, *39*, 9623−9626.
[16] T. Okuyama, T. Fueno, H. Nakatsuji, J. Furukawa, *J. Am. Chem. Soc.* **1967**, *89*, 5826−5831.
[17] G. E. Lienhard, T.-C. Wang, *J. Am. Chem. Soc.* **1969**, *91*, 1146−1153.
[18] A. J. Kresge, H. J. Chen, *J. Am. Chem. Soc.* **1972**, *94*, 2818−2822.

[19] Substituted vinyl ethers can be obtained via Hg^{II}-catalysed alcohol vinylation, see: W. H. Watanabe, L. E. Conlon, *J. Am. Chem. Soc.* **1957**, *79*, 2828−2833; or by Ir-catalysed activation of vinyl acetate in alcohols, see: Y. Okimoto, S. Sakaguchi, Y. Ishii, *J. Am. Chem. Soc.* **2002**, *124*, 1590−1591.
[20] Polyacetals are used as intermediates for the synthesis of heterocycles, as hardeners for poly(vinyl alcohol)s and poly(vinyl acetate) films. Alkyl-, cycloalkyl- and aryl-substituted polyacetals can be obtained from metal-catalysed reaction of vinyl acetate with alkyl orthoesters in the presence of a Lewis acid, see F Bauer, C. Subramaniam, US Patent 6 355 844, **2002**.

Received November 5, 2002
[I02615]

Oligomerisation of Ethylene to Linear α-Olefins by new C_s- and C_1-Symmetric [2,6-Bis(imino)pyridyl]iron and -cobalt Dichloride Complexes

Claudio Bianchini,*[a] Giuseppe Mantovani,[a] Andrea Meli,[a] Fabio Migliacci,[a] Fabrizio Zanobini,[a] Franco Laschi,[b] and Anna Sommazzi[c]

Keywords: Cobalt / Ethylene / Iron / N ligands / Oligomerisation

A new family of C_s- and C_1-symmetric 2,6-bis(imino)pyridyl ligands has been synthesised. These ligands, which differ from their known counterparts in the contemporaneous presence of alkyl and aryl substituent at the ketimine nitrogen atoms, form stable, five-coordinate complexes with $FeCl_2$ and $CoCl_2$. All ligands and catalysts have been fully characterised both in the solid state and in solution. A single-crystal X-ray analysis of $[CoCl_2\{2\text{-}[CMe{=}N\text{–}(2,6\text{-dimethylphenyl})]\text{-}6\text{-}(CMe{=}N\text{–}C_6H_{11})C_5H_3N\}]\cdot H_2O$ shows the metal centre to adopt a highly distorted square-pyramidal geometry. In combination with methylaluminoxane (MAO), both iron and cobalt compounds act as effective and selective (> 99%) catalysts for the oligomerisation of ethylene to a Schulz–Flory distribution of α-olefins, with the α factor ranging from 0.61 to 0.91. The iron catalysts exhibit TOFs as high as $7\cdot10^5$ mol C_2H_4 (mol of cat × h)$^{-1}$ and are much more active than their cobalt analogues. Experiments at different ethylene pressures with the iron catalysts showed that both the propagation rate and the chain transfer rate are first order in ethylene pressure.
(© Wiley-VCH Verlag GmbH, 69451 Weinheim, Germany, 2003)

Introduction

In 1998, Brookhart and Gibson independently discovered that [2,6-bis(arylimino)pyridyl]iron and -cobalt dihalides, when activated by MAO, are effective catalysts for the polymerisation of ethylene to high-density polyethylene (PE) with productivities as high as those of the most efficient metallocenes (Scheme 1).[1]

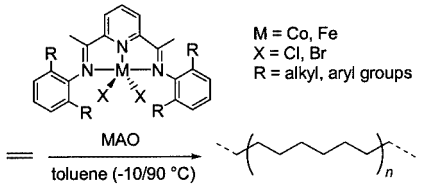

Scheme 1

The advantages of these late transition metal systems over other types of single-site Ziegler–Natta catalysts (e.g., metallocenes, constrained-geometry early transition metal complexes) are multiple, ranging from their ease of preparation and handling to the use of low-cost metals with negligible environmental impact. Another intriguing feature of [bis(arylimino)pyridyl]iron and -cobalt precursors is provided by the facile tuneability of their polymerisation activity by simple modification of the ligand architecture. Indeed, previous studies have shown that the size and regiochemistry of the substituents in the iminoaryl groups are of crucial importance in controlling the polymerisation and oligomerisation of ethylene, and also the isospecific polymerisation of propene.[1–3] In particular, the presence of substituents in both *ortho* positions on each aryl group results in the formation of high molecular weight PE with molecular weights depending upon the size of these substituents.[1] In contrast, the presence of one *ortho* substituent generates catalysts that selectively oligomerise ethylene to Shultz–Flory distributions of α-olefins.[2] Experimental and theoretical studies agree in identifying restricted rotation around the two nitrogen–aryl bonds as the key factor responsible for disfavouring chain transfer over chain propagation.[1,3c,4] Only when the aryl groups are very large (e.g., naphthyl, pyrenyl, 2-benzylphenyl) does restricted rotation apparently operate without the need for two *ortho* substituents, PE being formed.[5]

In this paper we demonstrate that the presence of two arylimino groups in the bis(imino)pyridyl backbone is not a mandatory condition to generate a ligand capable of oligomerising ethylene to α-olefins in conjunction with $FeCl_2$/

[a] Istituto di Chimica dei Composti Organometallici (ICCOM) – CNR,
Via J. Nardi 39, 50132 Firenze, Italy
Fax: (internat.) + 39-055/2478366
E-Mail: bianchin@fi.cnr.it
[b] Dipartimento di Chimica, Università di Siena
Via Aldo Moro, 53100 Siena, Italy
[c] Polimeri Europa, Novara Research Centre, Istituto Guido Donegani,
Via Fauser 4, 28100 Novara, Italy
Fax: (internat.) + 39-0321/447241

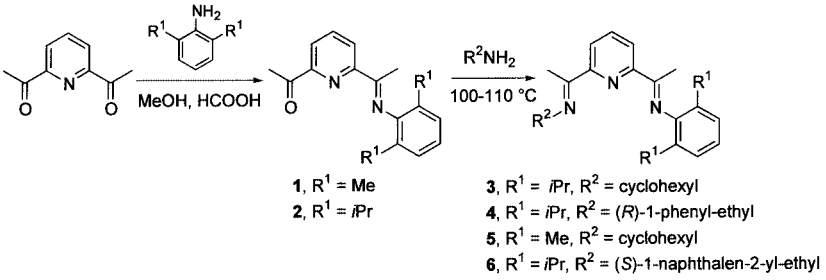

Scheme 2

MAO or $CoCl_2$/MAO. In fact, an aryl group can be replaced by an alkyl group and the resultant [2-(alkylimino)-6-(arylimino)pyridyl]Fe^{II} or -Co^{II} dichloride complexes will oligomerise ethylene as efficiently and selectively as the 2,6-bis(arylimino)pyridyl congeners. It is also shown here that the size of the alkyl group can control both the catalyst productivity and the Schulz−Flory parameters.

Results

Synthesis and Characterisation of Ligands

The 2-(alkylimino)-6-(arylimino)pyridyl ligands **3**−**6** have been synthesised via keto-imine intermediates obtained by treatment of 2,6-diacetylpyridine with the appropriate aniline (0.9 equiv.) in MeOH with formic acid as promoter (Scheme 2).

An important contribution to the selectivity of this reaction was made by the low solubility of the monoimine products, which precipitated upon formation and so suppressed further condensation with the aniline. The bis(imino)pyridine products were indeed obtained in low amounts (2−4%), however, and so the crude reaction products were purified by repeated extraction of the (imino)pyridyl ketones with boiling ethanol. Once purified, these products were treated with the appropriate neat primary amine at 100−110 °C, in the presence neither of solvent nor of acid promoter, to give the expected 2,6-bis(imine)pyridyl ligands. Under these mild conditions, the bis(imino) compounds were obtained selectively.

Synthesis and Characterisation of the Cobalt(II) Complexes

The [2,6-bis(imino)pyridyl]Co^{II} complexes illustrated in Scheme 3 were prepared in acceptable yields by heating of an *n*BuOH solution containing equimolar amounts of anhydrous $CoCl_2$ and ligand at reflux for ca. 10 min. Crystalline compounds were obtained upon cooling to room temperature. Complexes **7** and **9** exhibit C_s symmetry, while complexes **8** and **10** are C_1-symmetric by virtue of the simultaneous presence of 2,6-disubstituted aryl and chiral alkyl groups at the imine nitrogen atoms.

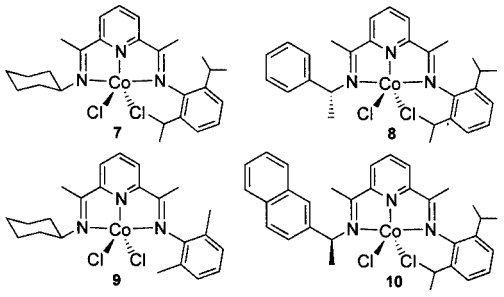

Scheme 3

All complexes are green, crystalline solids and are fairly soluble in polar organic solvents such as THF, dichloromethane, and 1,2-dichloroethane, in which they behave as non-electrolytes. Their solubilities in toluene and other hydrocarbons are very low. All compounds are reasonably thermally stable and air-stable both in the solid state and in solution. For caution's sake, however, their preparation and manipulation in solution were carried out under dry N_2.

Magnetic data at room temperature and relevant IR and UV/Vis absorptions for each complex are reported in the Exp. Sect. The IR spectra of all the compounds each show a red shift of ν(C=N) by ca. 50−60 cm^{-1} relative to the corresponding free ligand, which reflects the coordination of the imine nitrogen atoms to the cobalt atom.

All the complexes are high-spin in the solid state, with μ_{eff} at room temperature ranging from 4.6 to 4.8 BM, which is typical for high-spin cobalt(II) five-coordinate complexes with 2,6-bis(imino)pyridyl ligands.[6] In principle, five-coordinate metal complexes may adopt either square-pyramidal or trigonal-bipyramidal geometries. In idealised C_{4v} and D_{3h} symmetries, a d^7 metal ion may have either a low- or a high-spin configuration, according to whether the energy separation between the two highest orbitals in each symmetry is higher or lower than the spin-pairing energy. A donor atom set consisting of three nitrogen and two chlorine atoms has invariably been found to stabilise the high-spin configuration of cobalt(II).[6] As shown by a single-crystal X-ray analysis on the cyclohexyl/2,6-dimethylphenyl

derivative **9**·H_2O (see below), the presence of the rigid chelating 2,6-bis(imino)pyridyl ligand causes important distortions from the idealised geometries. However, these are apparently not so significant as to favour spin pairing and give a doublet ground state (S = 1/2).

An ORTEP drawing of the molecular structure of **9**·H_2O is shown in Figure 1. Perusal of the bond angles around the metal centre shows that the coordination geometry in **9**·H_2O is greatly distorted from any idealised five-coordinate structure, and may be roughly described as a square pyramid with one chloride ion (Cl1) occupying the apical position. The presence of two chemically different imine nitrogen atoms in **9**·H_2O contributes substantially to the observed stereochemical distortions. Noticeable asymmetries affect the Co−N(imine) distances in fact: Co1−N1 is unusually short [2.185(6) Å] and Co1−N2 is exceedingly long [2.348(6) Å]. These differences are most probably due to the higher nucleophilicity of the alkyl-substituted nitrogen atom N1 relative to the aryl-substituted N2. Indeed, the N1−Co1−N2 angle of 149.3(2)° allows one to invoke *trans* influence effects. In contrast, due to the substantial departures from idealised square-pyramidal geometry, these effects cannot account for the Co−Cl distances, which (although less pronouncedly) are significantly different from one another [Co1−Cl1 2.243(2); Co1−Cl2 2.269(2) Å]. As would be expected,[1d−1e][2b][3c] the M−N(pyridyl) bond [Co1−N3 2.032(6) Å] is shorter than both the M−N(imino) bonds, which have retained the imine C=N double bond character [N1−C1 1.266(10) Å, N2−C3 1.276(9) Å]. The deviation of the metal from the N_3 ligand plane is 0.06 Å. The plane of the 2,6-dimethyl-substituted aryl ring is oriented essentially orthogonally to the plane of the backbone [86.5(2)°].

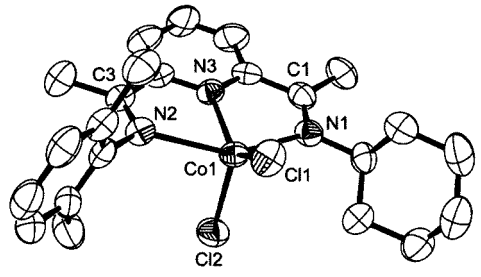

Figure 1. ORTEP drawing of **9**·H_2O (hydrogen atoms omitted); selected bond lengths [Å] and angles [°]: Co1−N1 2.185(6), Co1−N2 2.348(6), Co1−N3 2.032(6), Co1Cl1 2.243(2), Co1−Cl2 2.269(2); N3−Co1−N1 76.7(2), N3−Co1−Cl1 131.87(18), N1−Co1−Cl1 99.91(18), N3−Co1−Cl2 107.58(18), N1−Co1−Cl2 99.80(17), Cl1−Co1−Cl2 120.12(9), N3−Co1−N2 73.4(2), N1−Co1−N2 149.3(2), Cl1−Co1−N1 94.88(15), Cl2−Co1−N2 95.72(16)

The reflectance and solution UV/Vis spectra of the [2,6-bis(imino)pyridyl]Co^{II} complexes are similar to one another, indicating that the primary stereochemistry is the same both in the solid state and in solution: intermediate between the square pyramid and the trigonal bipyramid.[6b] Although the spectra show some changes in band shape and frequency as the substituents at the imine nitrogen atoms vary, these are not sufficient for them to be due to substantial differences in structure. Such differences are probably due to the different steric bulks of the substituents in the complexes.

The presence of three unpaired electrons (S = 3/2) in each complex molecule makes all the Co^{II} compounds X-band-EPR-silent at room temperature both in the solid state and in CH_2Cl_2 solution. A low-temperature EPR study of the X-band was carried out on derivative **8** in CH_2Cl_2 (Scheme 3). At 4 K the spectrum displays a broad and poorly resolved rhombic structure with g_1 = 5.06(8) > g_2 = 3.03(8) > g_3 = 1.95(8) ≠ g_{elect} [<g> = 3.35(8); a_1 40(8) G, a_2 80(8) G, a_3 94(8) G; <a> 71(8) G], which is typical of an "S" = 1/2 fictitious spin (Figure 2). Indeed, the spectrum may be interpreted in terms of an "S" = 1/2 effective spin Hamiltonian occasioned by large Zero Field Splitting (ZFS) effects.[7−11] In fact, we observed a reversible temperature dependence of the signal intensity, which rules out the occurrence of a spin transition. This behaviour is not unusual for $S > 1/2$ paramagnetic metal species affected by important ZFS effects (S = 3/2) as well as noticeable spin-orbit coupling in highly distorted coordination geometries.[7,8,11] All g_i regions show hyperfine structure apparently due to magnetic interaction with the ^{59}Co nucleus (S = 7/2). However, the poor resolution and the presence in each region of more than eight bands, as expected for coupling to cobalt, do not rule out either interactions with other spin-active nuclei in the molecule (e.g., ^{14}N) or the presence of different geometric isomers.

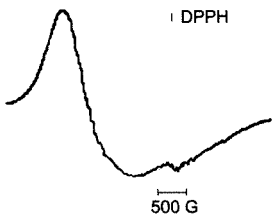

Figure 2. X-band EPR spectrum of cobalt(II) complexes **8** in CH_2Cl_2 at 4 K

The ^1H NMR spectrum of complex **7** was acquired in oxygen-free CD_2Cl_2 solution at 21 °C on a 500 MHz instrument (Figure 3). All protons resonate at chemical shifts significantly different from those of the corresponding protons in the free ligands, which is consistent with the paramagnetic nature of the compound. Analysis of the ^1H NMR resonances suggests that the isotropic shift (i.e., the difference between the observed chemical shift and the reference diamagnetic shift) is almost completely attributable to a Fermi contact contribution.[12] Unambiguous signal assignment was achieved on this basis (Table 1). Overall, the NMR spectrum is similar to that reported by Gibson and co-workers for {2,6-bis[1-(2,6-diisopropylphenylimino)-ethyl]pyridine}cobalt dichloride.[1d] As in the spectrum of this more symmetric complex, the 3-, 4-, and 5-hydrogen atoms of the central pyridine ring and the C*H*Me_2 hydrogen atom exhibit remarkable paramagnetic shifts and line

broadening as well. The strong coordination of the cyclohexyl-substituted imine arm to the cobalt atom, given in evidence in the X-ray structure, is confirmed by the large downfield shift (δ = 143.42 ppm) of the NC*H* resonance as well as its broad linewidth. Similarly, the coordination of both imine nitrogen atoms is demonstrated by the chemical shifts of the N=C*Me* methyl groups. The presence of two signals for the CH*Me* protons is consistent with hindered rotation of the aryl ring about the N−C axis.[1d]

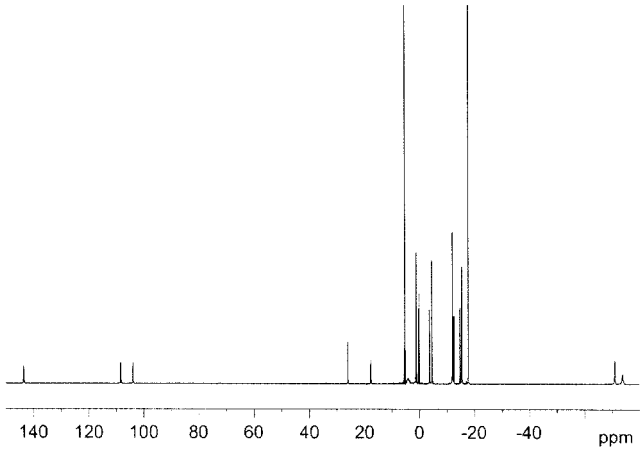

Figure 3. ^{1}H NMR spectrum of **7** (500.13 MHz, 21 °C, CD_2Cl_2)

Table 1. ^{1}H NMR assignments for **7** (CD_2Cl_2, 294 K, 500.13 MHz)

Nucleus	δ [ppm]
3/5-Py	108.18 (s, 1 H); 103.73 (s, 1 H)
4-Py	25.92 (s, 1 H)
N=CCH_3	−4.63 (s, 3 H); −15.41 (s, 3 H)
m-aryl	1.15 (s, 2 H)
p-aryl	−12.69 (s, 1 H)
CH_3 of *i*Pr	−12.14 (br. s, 6 H); −17.81 (s, 6 H)
CH of *i*Pr	−73.80 (br. s, 2 H)
Cy	143.42 (s, 1 H), 17.63 (s, 1 H), 4.1 (br. s, 2 H), 0.25 (s, 1 H), −3.72 (s, 2 H), −14.75 (s, 2 H), −71.05 (s, 2 H)

A cyclic voltammetry study in CH_2Cl_2 was performed on complex **9**, containing cyclohexyl and 2,6-dimethylphenyl groups on the imine nitrogen atoms (Figure 4a). The complex undergoes one irreversible one-electron oxidation at E_p = +1.18 V and another irreversible one-electron reduction at E_p = −0.99 V even at very high scan rates.

Synthesis and Characterisation of the Iron(II) Complexes

Like the cobalt(II) derivatives, the iron(II) complexes could be conveniently prepared by heating of a solution containing anhydrous $FeCl_2$ and 1 equiv. of the ligand at reflux in *n*BuOH for ca. 10 min (Scheme 4). Crystalline compounds were obtained upon cooling to room temperature.

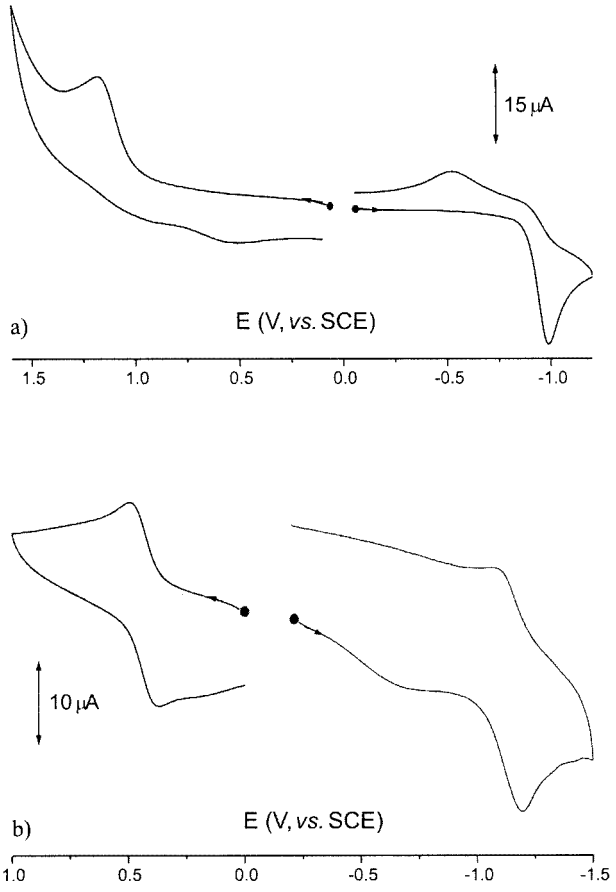

Figure 4. Cyclic voltammograms of the cobalt(II) and iron(II) complexes **9** (a) and **13** (b) in CH_2Cl_2 [$6\cdot10^{-4}$ M, scan rate 0.2 $V\cdot s^{-1}$; Bu_4NPF_6 (0.2 M as supporting electrolyte)]

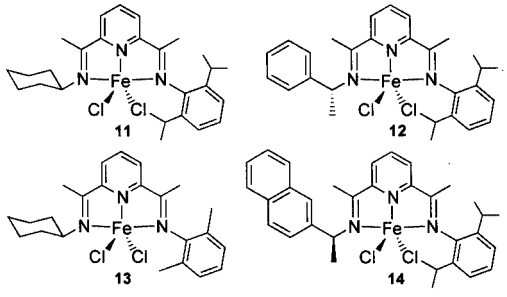

Scheme 4

All compounds are only sparingly soluble in aromatic hydrocarbons, while dissolving fairly well in THF, MeCN, CH_2Cl_2, and 1,2-dichloroethane. In the last of these they behave as non-electrolytes. The solids are fairly air-stable, whereas they decompose in solution unless protected by dinitrogen or argon.

Magnetic data at room temperature and relevant IR absorptions for the [2,6-bis(imino)pyridyl]Fe^{II} compounds are provided in the Exp. Sect. As in the IR spectra of the Co^{II} derivatives, ν(C=N) is generally red-shifted by ca. 50−60 cm^{-1} relative to the corresponding free ligand, reflecting the coordination to the metal centre.

All the compounds are dark blue and exhibit high-spin electronic configurations, as shown by their magnetic moments μ_{eff}, which range from 5.5 to 5.7 BM and are similar to those reported for several high-spin iron(II) five-coordinate complexes with quintuplet ground states.[1,6] The quintuplet ground state makes the complexes EPR-silent even at 4 K and irrespective of the EPR frequency.

Like the [2,6-bis(imino)pyridyl]Co^{II} complexes, the Fe^{II} derivatives might adopt either square-pyramidal or trigonal-bipyramidal structures with various degrees of geometrical distortion. In either geometry, a d^6 metal ion may assume a singlet, a triplet or a quintuplet ground state, depending on the nature of the donor atom set.[14] A donor atom set comprising three nitrogen and two chlorine atoms generally stabilises the high-spin quintuplet configuration for iron(II), as is in fact observed for these bis(imino)pyridyl complexes.[6,13]

None of the [2,6-bis(imino)pyridyl]Fe^{II} complexes described in this work has been studied by X-ray diffraction methods, but the molecular structures of several Fe^{II} derivatives bearing aryl substituents on the imine nitrogen atoms are available from the literature.[1a,1d,2,3c] In most cases the geometry at the iron centre can be described as distorted trigonal-bipyramidal with the pyridyl nitrogen atom and the two chloride ligands forming the equatorial plane; only when the aryl rings on the imine nitrogen atoms bear two bulky substituents − as in {2,6-[2,6-(*i*Pr)$_2$C$_6$H$_3$NCMe]$_2$-C$_5$H$_3$N}iron dichloride − does iron tend to adopt a distorted square-pyramidal coordination geometry.[1c]

The [2,6-bis(imino)pyridyl]Fe^{II} complexes studied here exhibit either C_1 or C_s symmetry by virtue of the simultaneous presence of substituted aryl groups and either chiral [CH(Me)Ph] or cyclic (C_6H_{11}) alkyl groups at the imine nitrogen atoms. The combined action of the ketimine group and the two *o*-alkyl substituents should lock the aryl ring in an orthogonal conformation with respect to the N_3 ligand plane both in the solid state and in solution, while the alkyl group at the other imine nitrogen atom should rotate freely about the C−N axis in solution (vide infra).

Trigonal-bipyramidal structures for all these iron(II) complexes are supported by the UV/Vis spectra in CH_2Cl_2 solution. Some detailed studies of the electronic spectra of five-coordinate Fe^{II} complexes with N_3Cl_2 donor atom sets were reported in the late 1960s, mainly by Ciampolini and coworkers.[14] On the basis of these studies, a band in the 7000−8400 cm^{-1} region, common to all Fe^{II} complexes investigated in this work, can be unambiguously correlated with a spin-allowed transition in trigonal-bipyramidal high-spin Fe^{II} complexes such as [Fe(dienMe)Cl_2] or [Fe(trenMe)Cl]Cl [dienMe = bis(2-dimethylaminoethyl)methylamine; trenMe = tris(2-dimethylaminoethyl)amine].[15] Those complexes also each showed a band at ca. 4000 cm^{-1}, not detectable for our compounds due to the measuring limit of our spectrophotometer. Unlike the trenMe and dienMe complexes, the spectra of **11**−**14** each contain a band at ca. 20000 cm^{-1} that may be attributable to a metal-to-ligand charge transfer (MLCT). Absorption bands at ca. 14500 cm^{-1} have been reported by Gibson for C_{2v}-symmetric [2,6-bis(imino)pyridyl]Fe^{II} complexes and also attributed to MLCT.[1d] In general, MLCT bands fall at higher energy than those observed by Gibson, but a reduction in frequency may occur for highly π-conjugated ligand systems, which may be the case for C_{2v}-symmetric 2,6-bis(imino)pyridyl ligands.[6b]

The reflectance spectra of **11**−**14** are similar to one another and fully comparable with the solution spectra, which indicates that the primary stereochemistry of the Fe^{II} complexes is the same both in the solid state and in solution. As an example, the spectra of **12** in the solid state and in CH_2Cl_2 solution are given in Figure 5.

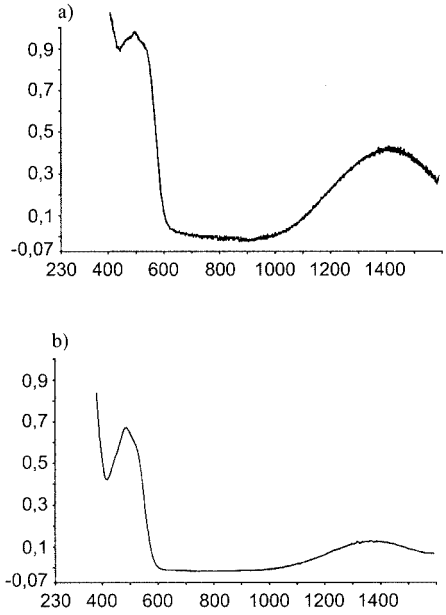

Figure 5. Reflectance spectrum of **12** (a); electronic spectrum of **12** (b) in CH_2Cl_2 solution

The ^{1}H NMR spectrum of **11** was acquired in deaerated CD_2Cl_2 solutions at 21 °C (Figure 6). All protons resonate at chemical shifts significantly different from the corresponding protons in the free ligands, which is consistent with the paramagnetic nature of the compounds. Band assignments are given in Table 2.

Despite the presence of the same ligand, the ^{1}H NMR spectrum of the iron(II) complex **11** is notably different from that of the cobalt(II) analogue **7** (Figure 3), which reflects a structural divergence in solution. In particular, the resonances of four hydrogen atoms of the cyclohexyl group are shifted to high field (ca. −30 and −37 ppm) and have very broad linewidths, which suggests that this cyclohexyl ring is spatially very close to the paramagnetic iron centre on the NMR timescale. No such linewidth broadening for the cyclohexyl resonances was observed for the Co^{II} analogue **7**. The presence of two relatively narrow signals for the *i*Pr groups confirms the hindered rotation of the aryl group.

Unlike the cobalt analogue **9**, the iron complex **13** can be reversibly oxidised ($E^{0\prime}$ = +0.43 V) to give the yellow iron(III) derivative [$FeCl_2${2-[CMe=N(2,6-dimethylphenyl)]-6-(CMe=NC$_6$H$_{11}$)C$_5$H$_3$N}]$^+$, which is stable in CH_2Cl_2

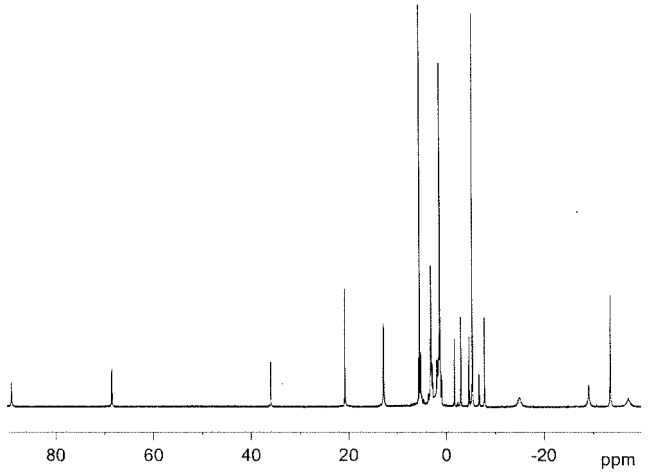

Figure 6. ^{1}H NMR spectrum of **11** (500.13 MHz, 21 °C, CD_2Cl_2)

Table 2. ^{1}H NMR assignments for **11** (CD_2Cl_2, 294 K, 500.13 MHz)

Nucleus	δ [ppm]
3/5-Py	89.11 (s, 1 H); 68.55 (s, 1 H)
4-Py	35.97 (s, 1 H)
N=CCH$_3$	12.79 (s, 3 H); −33.57 (s, 3 H)
m-aryl	20.69 (s, 2 H)
p-aryl	−1.70 (s, 1 H)
CH$_3$ of *i*Pr	3.08 (br. s, 6 H); −5.38 (s, 6 H)
CH of *i*Pr	−14.94 (br. s, 2 H)
Cy	−2.99 (s, 2 H), −7.85 (s, 2 H), −29.10 (s, 2 H), −37.18 (br. s, 2 H), 1.28 (s, 1 H), −4.72 (s, 1 H), −6.74 (s, 1 H)

solution, although no attempt was made to isolate it in the solid state (Figure 4b). Stable C_2-symmetric [2,6-bis(arylimino)pyridyl]Fe^{III} dihalide complexes have been prepared by Gibson and shown to have the same activity as the Fe^{II} precursors in the oligomerisation of ethylene, as a consequence of instantaneous Fe^{III} reduction to Fe^{II} by MAO.[1d,16] Figure 4b also shows that the Fe^{I} derivative, obtained by a partially reversible one-electron reduction of **13** (at $E^{0\prime} = -1.15$ V), has a relatively short lifetime ($t_{1/2}$ = 0.5 s).

Oligomerisation of Ethylene by the Cobalt(II) and Iron(II) Dichloride Complexes, Activated by MAO

The [bis(imino)pyridyl]cobalt (**7**−**10**) and -iron (**11**−**14**) complexes, in combination with the activator MAO, were evaluated as catalysts for the oligomerisation of ethylene in toluene.

Table 3 reports on the results of reactions carried out under a variety of experimental conditions. In all cases the addition of ethylene to the catalyst/co-catalyst mixture resulted in a rapid exothermic event, indicative of no induction period. Initially, all catalysts were tested at 4.1 bar C_2H_4 pressure and 25 °C for 15 min, with 250 equiv. of MAO as both co-catalyst and reactor scavenger. Catalyst activities [mol of C_2H_4 converted (mol of M × h)$^{-1}$] were calculated from the GC readings, by use of extrapolated values for 1-butene.

Table 3. Ethylene oligomerisation with the iron(II) and cobalt(II) catalysts

Entry[a]	Pre-catalyst	Pressure [bar]	TOF [10^{-5}][b]	α	β
1	**11**	4.1	2.4	0.74	0.35
2	**12**	4.1	5.2	0.89	0.12
3	**13**	4.1	3.8	0.66	0.52
4	**14**	4.1	5.6	0.91	0.10
5	**13**	4.8	4.6	0.67	0.49
6	**13**	7.6	6.0	0.67	0.49
7	**13**	10.3	7.4	0.68	0.47
8[c]	**13**	4.1	3.4	0.61	0.63
9	**7**	4.1	< 0.01[d]	–	–
10	**8**	4.1	0.61	0.89	0.12
11	**9**	4.1	< 0.01[d]	–	–
12	**10**	4.1	1.0	0.91	0.10

[a] Reaction conditions: complex (12 μmol), toluene (100 mL), MAO (250 equiv.), 15 min, 25 °C. [b] TOF: mol of C_2H_4 converted (mol of M × h)$^{-1}$. [c] 80 °C. [d] Only butenes.

The four iron complexes **11**−**14** were all active catalysts for the production of α-olefins with Schulz−Flory distributions.[17] No appreciable formation either of internal olefins or of odd carbon oligomers was observed (Figure 7).

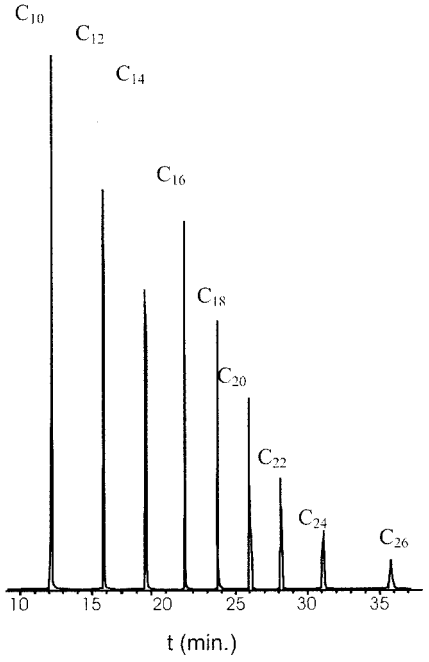

Figure 7. GC trace relative to Entry 1 in Table 3, showing the α-olefins distribution from C_{10} to C_{26}

The catalytic activity increased with the bulkiness of the alkyl substituent at the imine carbon atom (Entries 1, 2, 4), but decreased with the size of the substituents on the aryl ring (Entries 1, 3). The naphthyl group containing catalyst was as active as the C_2-symmetric [2,6-bis(arylimino)pyridyl]iron(II) precursors described by Brookhart and Gibson.[2] Notably, the probability of propagation, indicated by the

Schulz−Flory parameter α,[17] increased steadily with the overall steric hindrance of the imine substituents.

Experiments with precursor **13** in the C_2H_4 pressure range from 4.1 to 10.3 bar showed a linear dependence of activity on the pressure, while the α factor did not vary substantially (Entries 3, 5−7). No isomeric oligomer formed either by alkene isomerisation or by reincorporation of α-olefin products into oligomers later in the reaction was observed. The absence of reincorporation mechanisms was confirmed by independent experiments in which the oligomerisation of ethylene with **13** was carried out in the presence of an excess of 1-undecene. In fact, no odd-numbered carbon oligomer was formed in the temperature range from 25 to 80 °C.[2a] Similarly, these catalysts did not promote head-to-head dimerisation of α-olefins to internal olefins, a reaction that [2,6-bis(arylimino)pyridyl]iron complexes are able to catalyse.[18]

Experiments at relatively high temperature (80 °C) with precursor **13** showed a slight decrease in productivity and α factor as well. Both phenomena have precedent for [2,6-bis(arylimino)pyridyl]iron precursors.[1d] In particular, the decrease in productivity with temperature has been ascribed to the combined effects of faster catalyst degradation and lower ethylene solubility.[1d]

The activities of the cobalt catalysts **7**−**10** (Entries 9−12) were approximately one order of magnitude lower than those of the analogous iron(II) derivatives. The sensitivity to steric effects was even higher for cobalt than for iron, as shown by the catalyst precursors containing the cyclohexyl substituent (Entries 9, 11), which gave only small amounts of 1-butene, indicating a prevalence of chain transfer over chain propagation.

Discussion

The nature and statistical distribution of the α-olefins produced with the [2-(alkylimino)-6-(arylimino)pyridyl]iron and -cobalt catalysts described in this work are consistent with a mechanism involving: (i) metal−alkyl initiators produced by the action of MAO on the dichloride precursors, (ii) propagation by migratory insertion of Co(alkyl)(ethylene) (Cossee−Arlman mechanism), and (iii) termination by chain transfer (Scheme 5).[2,19]

In line with the large majority of catalytic systems for Schulz−Flory oligomerisations of ethylene, the rates of propagation and chain transfer exhibited by the iron catalysts do not differ significantly, the β parameter ($\beta = r_{transfer}/r_{propagation}$) varying between 0.10 and 0.52. It has been found that the activity of the iron catalysts shows a linear dependence on the ethylene pressure, while α is independent of the pressure. Accordingly, both chain propagation and chain transfer are first-order in monomer concentration, as previously observed for [2,6-bis(arylimino)pyridyl]Fe^{II} and -Co^{II} oligomerisation catalysts.[2]

Late transition metal catalysts may undergo chain transfer in ethylene polymerisation by three main mechanisms: β-hydrogen transfer to the metal atom (**A**), β-hydrogen transfer to the monomer (**B**), and chain transfer to aluminium (**C**) (this generally occurs at low pressure) (Scheme 5).[1d,20] The last mechanism can safely be ruled out in the oligomerisation reactions reported here, as only α-olefins were produced, with no saturated hydrocarbon. It is therefore very likely that chain transfer proceeds either by path **A**, involving an associative displacement step followed by β-hydrogen transfer to the metal atom, or by path

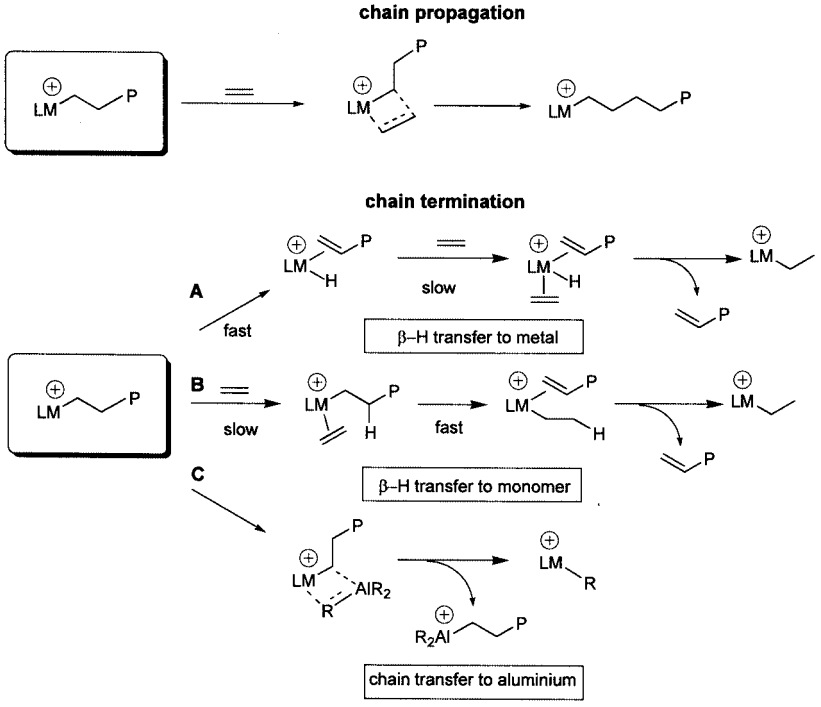

Scheme 5. Chain propagation and chain transfer mechanisms proposed for polymerisation of ethylene by late transition metal catalysts

B, involving direct β-H transfer to the incoming monomer with no formation of metal hydride. The exclusive production of α-olefins with no appreciable formation of internal olefins might be taken as indirect evidence for the occurrence of path **B**, as it does not involve the formation of the metal hydride necessary for isomerisation. Moreover, calculations suggest its involvement in ethylene polymerisation by late transition metal systems.[20] We wish to stress, however, that the chain transfer mechanisms **A** and **B** are kinetically indistinguishable, and so no preference is allowed; nor may one exclude their simultaneous occurrence.

Overall, the performances of these C_s- and C_1-symmetric iron and cobalt catalysts do not diverge substantially from those of the 2,6-bis(arylimino) complexes studied by Brookhart and Gibson, which means that the presence of aryl groups on both ketimine nitrogen atoms is not a necessary condition to produce an ethylene oligomerisation catalyst in conjunction with iron or cobalt dihalides and MAO. Actually, these catalysts polymerise ethylene only when the aryl rings are 2,6-substituted by alkyl groups. As a general trend, α-olefins are produced with one alkyl substituent, while the presence of two alkyl groups results in the formation of PE with molecular weight increasing with the size of these alkyl moieties.[1,2] It has been experimentally and theoretically demonstrated that the steric interaction between the ketimine methyl group and the alkyl substituents increases the barrier to aryl rotation and effectively locks the rings in an orthogonal conformation with respect to the N_3M plane on the timescale of polymerisation.[1d][3c] The steric protection provided by the orthogonal aryl rings contributes to retard the chain transfer, which − irrespective of the mechanism − requires access to the metal centre above or below the N_3M plane.[4] Apparently, one 2,6-substituted aryl moiety is sufficient to slow down the chain-transfer rate and allow oligomer formation. The high α value (0.91) obtained with the naphthyl-substituted catalysts (Table 3, Entries 4 and 12) suggests that polymerisation to high molecular weight PE might be achieved by further increasing the size of the C=N−alkyl group. Studies in this direction are currently being carried out in our laboratory.

The thorough chemical-physical study of the catalyst precursors described in this work suggests that cobalt(II) prefers to be square-pyramidal, while iron(II) prefers to be trigonal-bipyramidal. This behaviour of cobalt(II) and iron(II) metal ions is amply recognised in the literature.[6a,21] With no intention of minimising the importance of electronic effects related to the different d-electron count, it is possible that these structural differences (with implications on the metal spin state),[6a] if maintained during catalysis, may contribute to rendering the cobalt catalysts less active than the iron ones. Square-pyramidal coordination, for example, generally produces less steric congestion at the metal centre than trigonal-bipyramidal coordination and requires less energy to attain the octahedral geometry that seems to feature in relevant transition states in ethylene polymerisation catalysed by five-coordinate [2,6-bis(arylimino)pyridyl]Fe^{II} and -Co^{II} complexes.[4]

Conclusion

C_1- and C_s-symmetric 2-(alkylimino)-6-(arylimino)pyridyl ligands, readily prepared by condensation of chiral and achiral primary amines with 2-(acetyl)-6-(arylimino)pyridine intermediates, coordinate to iron(II) and cobalt(II) dichlorides to give monomeric, paramagnetic complexes. The cobalt complexes adopt distorted square-pyramidal structures both in the solid state and in solution, while the coordination geometries of the iron catalysts can be better described as trigonal-bipyramidal. All the complexes can be activated with MAO to give ethylene oligomerisation catalysts with complete selectivity for α-olefins. Unlike [2,6-bis(arylimino)pyridyl]iron precursors, no head-to-head dimerisation of α-olefins to internal olefins was observed. Iron-based catalysts can be more than one order of magnitude more active than cobalt-based systems. The catalytic activity increases with the bulkiness of the alkyl substituent and decreases with the size of the substituent on the aryl ring. The Schulz−Flory oligomer distribution factor α is not sensitive to the metal centre, but it increases with the size of the alkyl and aryl groups. Both chain propagation and chain transfer are first order in ethylene concentration, and chain transfer proceeds exclusively by β-H transfer.

Experimental Section

General Procedures: All air- and water-sensitive reactions were performed in flame-dried flasks under dinitrogen. Solid compounds were collected on sintered glass frits and washed with appropriate solvents before being dried in a stream of dinitrogen. Anhydrous THF and Et_2O were obtained by distillation from sodium/benzophenone ketyl, while CH_2Cl_2 and MeOH were distilled from CaH_2 and Mg, respectively. All the other reagents and solvents were used as purchased from commercial suppliers. Analytical TLC was performed on pre-coated silica gel 60 F_{254} and/or neutral Al_2O_3 N/UV_{254} plates and developed in an appropriate solvent system. The products were viewed with the aid of UV light (254 nm), I_2 vapour, 2.5% $(NH_4)_6Mo_7O_{24}$ + 1% $(NH_4)_4Ce(SO_4)_4$ in 10% H_2SO_4 and warming. Deuterated solvents for NMR measurements were dried with molecular sieves. ^1H and $^{13}C\{^1H\}$ NMR spectra were obtained with a Bruker ACP 200 instrument working at 200.13 and 50.32 MHz, respectively. All chemical shifts are reported in ppm (δ) relative to tetramethylsilane, referenced to the chemical shifts of residual solvent resonances (^1H and ^{13}C). The multiplicity of the $^{13}C\{^1H\}$ NMR spectra were determined by the DEPT 135 technique and are quoted as: CH_3, CH_2, CH, and C for primary, secondary, tertiary, and quaternary carbon atoms, respectively. Two-dimensional ^1H and ^{13}C NMR spectra were recorded at 21 °C with a Bruker Avance DRX 500 spectrometer operating at 500.132 and 125.77 MHz, respectively, and equipped with a variable-temperature control unit accurate to ±0.1 °C. This instrument was also employed to study the paramagnetic metal complexes. Chemical shifts are relative to 0.03% (v/v) tetramethylsilane. The assignments of the signals was achieved with the aid of 1D spectra, 2D ^1H DQF-COSY, ^1H NOESY, and proton detected ^1H,^{13}C correlations (HMQC and HMBC) using non-spinning samples. 2D NMR spectra were recorded with pulse sequences suitable for phase-sensitive representations by TPPI. ^1H DQF-COSY experiments[22] were recorded with 1024 increments of size 2 K (with 16 scans each) cover-

ing the full range in both dimensions and with a relaxation delay of 1.5 s. ^{1}H NOESY measurements[23] were recorded with 1024 increments of size 2 K (with 16 scans each) covering the full range in both dimensions and with mixing times of 800 ms and a relaxation delay of 1.5 s. ^{1}H,^{13}C HMQC correlations[24] were recorded by use of the standard sequence with no decoupling during acquisition, 1024 increments of size 2 K (with 16 scans each) were collected, covering the full range in both dimensions with a relaxation delay of 1 s. ^{1}H,^{13}C HMBC correlations[25] were recorded by the standard sequence with no decoupling during acquisition and a low-pass *J*-filter to suppress one-bond correlations, 1024 increments of size 2 K (with 32 scans each) were collected, covering the full range in both dimensions, with a relaxation delay of 0.8 s. EPR spectra were recorded for all the compounds at the X-band frequency (9.23 GHz) with a Varian ESR9 spectrometer equipped with a continuous-flow ^{4}He cryostat to work at 4 K. Elemental analyses were performed with a Carlo Erba Model 1106 elemental analyzer. UV/Vis spectra were recorded with a Perkin−Elmer Lamda 9 spectrophotometer. Infrared spectra were recorded with a Perkin−Elmer 1600 Series FT-IR spectrophotometer with samples mulled in Nujol between KBr plates. GC analyses were performed with a Shimadzu GC-14 A gas chromatograph equipped with a flame ionisation detector and a 30-m (0.25 mm i.d., 0.25 μm film thickness) SPB-1 Supelco fused silica capillary column. GC/MS analyses were performed with a Shimadzu QP 5000 apparatus equipped with a column identical to that used for GC analysis. Molar susceptibility analyses were performed with a Sherwood Scientific MSB AUTO balance. Materials and apparatus for electrochemistry have been described elsewhere.[26] Potential values are referred to the Saturated Calomel Electrode (SCE). Under the adopted experimental conditions the one-electron oxidation of ferrocene occurs at $E^{0\prime} = +0.39$ V.

1-{6-[(2,6-Dimethylphenyl)ethanimidoyl]-2-pyridinyl}-1-ethanone (1): Formic acid (50 μL) was added by syringe at 0 °C to a stirred solution of 2,6-diacetylpyridine (0.490 g, 3.0 mmol) and 2,6-dimethylaniline (0.33 mL, 0.327 g, 2.7 mmol) in MeOH (7 mL). Stirring was stopped, and the resulting solution was maintained at 0 °C for 24 h. The desired product precipitated as large, yellow crystals, which were separated by filtration (0.447 g, 1.680 mmol). A second crop (0.148 g, 0.556 mmol) was obtained from the mother liquor after cooling to 0 °C for 48 h. Overall yield 75%. M.p. 117−118 °C. IR: $\nu_{(C=N)}$ 1645 cm^{-1}, $\nu_{(C=O)}$ 1698 cm^{-1}. ^{1}H NMR (200.13 MHz, CD_2Cl_2): δ = 2.02 (s, 6 H, CH_3), 2.22 [s, 3 H, C(NAr)CH_3], 2.76 [s, 3 H, C(O)CH_3], 6.89−6.97 (m, 1 H, CH Ar), 7.05−7.10 (m, 2H CH Ar), 7.96 (m, 1H CH Ar), 8.10 (dd, *J* = 7.7, 1.2 Hz, 1 H, CH Ar), 8.56 (dd, *J* = 7.7, 1.2 Hz, 2 H, CH Ar) ppm. ^{13}C{^{1}H} NMR (50.32 MHz, $CDCl_3$): δ = 17.0 [1 C, C(NAr)*C*H$_3$], 18.6 (2 C, CH_3), 26.4 [1 C, C(O)*C*H$_3$], 123.3 (1 C, CH Ar), 123.9 (1 C, CH Ar), 125.2 (1 C, CH Ar), 126.0 (2 C, C Ar), 128.6 (2 C, CH Ar), 138.0 (1 C, CH Ar), 149.2 (1 C, C Ar), 153.1 (1 C, CH Ar), 156.2 (1 C, C Ar), 167.3 [1 C, *C*(NAr)CH$_3$], 200.7 [1 C, *C*(O)CH$_3$] ppm. $C_{17}H_{18}N_2O$ (266.34): calcd. C 76.67, H 6.81, N 10.53; found C 76.45, H 6.54, N 10.41.

1-{6-[(2,6-Diisopropylphenyl)ethanimidoyl]-2-pyridinyl}-1-ethanone (2): Formic acid (150 μL) was added by syringe at room temperature to a stirred solution of 2,6-diacetylpyridine (1.630 g, 10.0 mmol) and 2,6-diisopropylaniline (1.70 mL, 1.596 g, 9.0 mmol) in MeOH (15 mL). After 12 h, a yellow solid had formed, and this was filtered off and washed with cold (0 °C) MeOH. The precipitate was characterised as a mixture of the expected product (97%) and the corresponding 2,6-bis(imino)pyridyl compound (3%) (^{1}H NMR integration). The solid was suspended in refluxing ethanol and the resulting mixture was filtered while still hot. The solvent was removed from the filtrate under reduced pressure to give pure **1** as pale yellow crystals in 67% yield (2.17 g, 6.73 mmol). M.p. 182−184 °C. IR: $\nu_{(C=N)}$ 1648 cm^{-1}, $\nu_{(C=O)}$ 1698 cm^{-1}. ^{1}H NMR (200.13 MHz, $CDCl_3$): δ = 1.16 [d, *J* = 6.9 Hz, 6 H, CH(CH_3)(CH$_3$)], 1.17 [d, *J* = 6.9 Hz, 6 H, CH(CH$_3$)(CH_3)], 2.28 [s, 3 H, C(NAr)CH_3], 2.74 [sept, *J* = 6.9 Hz, 2 H, C*H*(CH$_3$)(CH$_3$)], 2.81 [s, 3 H, C(O)CH_3], 7.08−7.22 (m, 3 H, C*H* Ar), 7.96 (t, *J* = 7.8 Hz, 1 H, CH Ar), 8.16 (dd, *J* = 7.7, 1.2 Hz, 1 H, CH Ar), 8.58 (dd, *J* = 7.9, 1.2 Hz, 1 H, CH Ar) ppm. ^{13}C{^{1}H} NMR (50.32 MHz, $CDCl_3$): δ = 17.7 [1 C, C(NAr)*C*H$_3$], 23.5 [2 C, CH(*C*H$_3$)(CH$_3$)], 23.9 [2 C, CH(CH$_3$)(*C*H$_3$)], 26.4 [1 C, C(O)*C*H$_3$], 29.0 [2 C, *C*H(CH$_3$)(CH$_3$)], 123.2 (1 C, CH Ar), 123.7 (2 C, CH Ar), 124.4 (1 C, CH Ar), 125.2 (1 C, CH Ar), 136.4 (2 C, C Ar), 138.4 (1 C, CH Ar), 142.9 (1 C, C Ar), 153.1 (1 C, CH Ar), 156.2 (1 C, C Ar), 167.8 [1 C, *C*(NAr)CH$_3$], 200.8 [1 C, *C*(O)CH$_3$] ppm. $C_{21}H_{26}N_2O$ (322.45): calcd. C 78.22, H 8.13, N 8.69; found C 78.39, H 8.17, N 8.84.

***N*-{(*E*)-1-[6-(Cyclohexylethanimidoyl)-2-pyridinyl]ethylidene}-2,6-diisopropylaniline (3):** A mixture of **1** (0.170 g, 0.53 mmol) and cyclohexylamine (0.910 mL, 0.789 g, 7.95 mmol) was heated at 100 °C without stirring for 20 h. Elimination of excess cyclohexylamine by distillation under reduced pressure gave an oily material that was dissolved in 3−4 mL of MeOH and cooled to 0 °C. After 6 h, yellow crystals of the desired product were isolated by filtration (0.153 g, 0.38 mmol, yield 72%). M.p. 186−188 °C. IR: $\nu_{(C=N)}$ 1636 cm^{-1}. ^{1}H NMR: (200.13 MHz, CD_2Cl_2): δ = 1.16 [d, *J* = 6.9 Hz, 12 H, CH(CH_3)$_2$], 1.25−1.95 (m, 10 H, CH_2), 2.26 (s, 3 H, CH_3), 2.45 (s, 3 H, CH_3), 2.77 [sept, 2 H, *J* = 6.9 Hz, C*H*(CH$_3$)$_2$], 3.55−3.66 (m, 1 H, CH), 7.05−7.25 (m, 3 H), 7.81 (t, *J* = 7.8 Hz, 1 H, CH Ar), 8.21 (dd, *J* = 7.8, 1.1 Hz, 1 H, CH Ar), 8.36 (dd, *J* = 7.8, 1.1 Hz, 2 H, CH Ar) ppm. ^{13}C{^{1}H} NMR (50.32 MHz, $CDCl_3$): δ = 14.1 [1 C, C(N-alkyl)*C*H$_3$], 17.8 [1 C, C(N-Ar)*C*H$_3$], 23.6 [2 C, CH(*C*H$_3$)(CH$_3$)], 23.9 [2 C, CH(CH$_3$)(*C*H$_3$)], 25.48 (2 C, CH_2), 25.49 (1 C, CH_2); 28.50 [2 C, *C*H(CH$_3$)(CH$_3$)], 34.1 (2 C, CH_2); 61.0 (1 C, CH), 121.9 (1 C, CH Ar), 122.7 (1 C, CH Ar), 123.7 (2 C, CH Ar), 124.1 (1 C, CH Ar), 136.5 (2 C, C Ar), 147.2 (1 C, CH Ar), 155.4 (1 C, CH Ar), 157.8 (1 C, C Ar), 164.4 [1 C, *C*(N-alkyl)CH$_3$], 167.8 [1 C, *C*(N-Ar)CH$_3$] ppm. $C_{27}H_{37}N_3$ (403.61): calcd. C 80.34, H 9.24, N 10.41; found C 80.54, H 9.37, N 10.39.

2,6-Diisopropyl-*N*-[(*E*)-1-(6-{[(1*R*)-1-phenylethyl]ethanimidoyl}-2-pyridinyl)ethylidene]aniline (4): A mixture of **1** (0.170 g, 0.53 mmol) and (*R*)-(+)-(1-phenylethyl)amine (0.473 mL, 0.450 g, 3.71 mmol) was heated at 100 °C without stirring for 18 h. Elimination of the excess of amine by distillation under reduced pressure gave an oily material that was dissolved in 3−4 mL of MeOH and cooled to 0 °C. After 2 d, yellow microcrystals of the product were isolated by filtration (0.153 g, 0.36 mmol, yield 68%). M.p. 91−93 °C. IR: $\nu_{(C=N)}$ 1633, 1644 cm^{-1}. ^{1}H NMR (200.13 MHz, $CDCl_3$): δ = 1.14−1.19 [m, 12 H, CH(CH_3)$_2$], 1.58 (d, *J* = 6.6 Hz, 3 H, CHCH_3), 2.26 (s, 3 H, CH_3), 2.50 (s, 3 H, CH_3), 2.73 (m, 2 H, CH), 4.97 (q, *J* = 6.6 Hz, 1 H, C*H*CH$_3$), 7.07−7.77 (m, 8 H, CH Ar), 7.85 (m, 1 H, CH Ar), 8.36−8.39 (m, 2 H, CH Ar) ppm. ^{13}C{^{1}H} NMR (50.32 MHz, $CDCl_3$): δ = 14.4 [1 C, C(N-alkyl)*C*H$_3$], 17.9 [1 C, C(N-Ar)*C*H$_3$], 23.6 [2 C, CH(*C*H$_3$)(CH$_3$)], 23.9 [2 C, CH(CH$_3$)(*C*H$_3$)], 25.5 (1 C, CH_3), 29.0 [2 C, *C*H(CH$_3$)(CH$_3$)], 61.0 (1 C, *C*H), 122.2 (1 C, CH Ar), 122.9 (1 C, CH Ar), 123.7 (2 C, CH Ar), 124.2 (1 C, CH Ar), 127.4 (1 C, CH Ar), 127.4 (2 C, CH Ar), 129.1 (2 C, CH Ar), 136.5 (2 C, C Ar), 137.4 (2 C, CH Ar), 146.7 (1 C, CH Ar), 147.3 (1 C, CH Ar), 155.4 (1 C, CH Ar), 157.5 (1 C, C Ar), 165.4 [1 C, *C*(N-alkyl)CH$_3$], 167.8

[1 C, *C*(N-Ar)CH_3] ppm. $C_{29}H_{35}N_3$ (425.62): calcd. C 81.83, H 8.29, N 9.87; found C 82.04, H 8.47, N 9.85.

***N*-{(*E*)-1-[6-(Cyclohexylethanimidoyl)-2-pyridinyl]ethylidene}-2,6-dimethylaniline (5):** A mixture of **2** (0.131 g, 0.49 mmol) and cyclohexylamine (0.485 g, 4.9 mmol) was heated at 100 °C without stirring for 24 h. Elimination of the excess of cyclohexylamine by distillation under reduced pressure gave an oily material that was dissolved in 2 mL of MeOH and cooled to −24 °C. After 3 d, small yellow needles of the product were isolated by filtration (0.13 g, 0.38 mmol, yield 78%). M.p. 98−100 °C. IR: $\nu_{(C=N)}$ 1634 cm^{-1}. ^1H NMR (200.13 MHz, CD_2Cl_2): δ = 1.25−1.95 (m, 10 H, CH_2), 2.01 (s, 6 H, CH_3), 2.20 (s, 3 H, CH_3), 2.42 (s, 3 H, CH_3), 3.55−3.66 (m, 1 H, CH), 6.88−7.08 (m, 3 H, CH Ar), 7.81 (m, 1 H, CH Ar), 8.18 (dd, *J* = 7.7, 1.1 Hz, 1 H, CH Ar), 8.34 (dd, *J* = 7.7, 1.1 Hz, 1 H, CH Ar) ppm. $^{13}C\{^1H\}$ NMR (50.32 MHz, $CDCl_3$): δ = 14.1 [1 C, C(N-alkyl)*C*H_3], 17.8 [1 C, C(N-Ar)*C*H_3], 18.6 (2 C, CH_3), 25.5 (2 C, CH_2), 26.5 (1 C, CH_2); 34.2 (2 C, CH_2); 61.0 (1 C, CH), 121.9 (1 C, CH Ar), 122.8 (1 C, CH Ar), 123.6 (1 C, CH Ar), 126.1 (2 C, C Ar), 128.5 (2 C, CH Ar), 137.3 (1 C, CH Ar), 149.5 (1 C, C Ar), 155.3 (1 C, CH Ar), 157.8 (1 C, C Ar), 164.4 [1 C, *C*(N-alkyl)CH_3], 168.1 [1 C, *C*(N-Ar)CH_3] ppm. $C_{23}H_{29}N_3$ (347.50): calcd. C 79.50, H 8.41, N 12.09; found C 79.78, H 8.65, N 12.15.

2,6-Diisopropyl-*N*-{(*E*)-1-[6-{[(1*S*)-1-(2-naphthyl)ethyl]-ethanimidoyl}-2-pyridinyl]ethylidene}aniline (6): A mixture of **1** (0.170 g, 0.53 mmol) and (*S*)-(−)-(1-naphthalenylethyl)amine (0.33 mL, 0.350 g, 2.04 mmol) was heated at 100 °C without stirring for 17 h. The resulting mixture was diluted with 2−3 mL of MeOH and cooled to 0 °C. After 5 h, pale yellow microcrystals of the product were isolated by filtration (0.118 g, 0.36 mmol, yield 69%). M.p. 66−69 °C. IR: $\nu_{(C=N)}$ 1643 cm^{-1}. ^1H NMR (200.13 MHz, CD_2Cl_2): δ = 1.10−1.17 [m, 12 H, $CH(CH_3)_2$], 1.72 (d, *J* = 6.5 Hz, 3 H, $CHCH_3$), 2.26 (s, 3 H, CH_3), 2.50 (s, 3 H, CH_3), 2.73 [m, 2 H, $CH(CH_3)_2$], 5.67 (q, *J* = 6.5 Hz, 1 H, $CHCH_3$) 7.03−7.20 (m, 3 H, CH Ar), 7.45−7.77 (m, 7 H, CH Ar), 7.88 (m, 1 H, CH Ar), 8.32−8.43 (m, 2 H, CH Ar) ppm. $C_{33}H_{37}N_3$ (475.68): calcd. C 83.32, H 7.84, N 8.83; found C 83.64, H 7.82, N 8.77.

Synthesis of Metal Complexes: All iron(II) and cobalt(II) complexes with the 2,6-bis(imino)pyridyl ligands were prepared by the following procedure. The ligand (1.0 equiv.) was added under nitrogen to a solution of the metal halide (1.2 equiv.) in *n*BuOH and the resulting mixture was heated at reflux for 10 min. After the mixture had cooled to room temperature, a crystalline solid was obtained within 30−60 min. This was filtered through a sintered-glass frit, washed with *n*BuOH and petroleum ether and then dried in a stream of nitrogen.

[*N*-{(*E*)-1-[6-(Cyclohexylethanimidoyl)-2-pyridinyl]ethylidene}-2,6-diisopropylaniline]cobalt Dichloride (7): This complex was obtained as green microcrystals. Yield 70%. IR: $\nu_{(C=N)}$ 1590, 1587 cm^{-1}. μ_{eff} = 4.82 BM (25 °C). Diffuse reflectance spectra (40000−5550 cm^{-1}): 25000 sh, 17000 sh, 15600, 10500, 8200, 5700. Solution spectra (CH_2Cl_2, 28500−6250 cm^{-1}): 25000 sh, 17000 sh, 14950 (ε 830), 11100 (ε 67), 7800 (ε 100). $C_{27}H_{37}Cl_2CoN_3$ (533.45): calcd. C 60.79, H 6.99, N 7.88; found C 60.55, H 7.01, N 8.72.

[2,6-Diisopropyl-*N*-{(*E*)-1-[6-{[(1*R*)-1-phenylethyl]ethanimidoyl}-2-pyridinyl]ethylidene}aniline]cobalt Dichloride (8): This complex was obtained as green crystals. Yield 85%. IR: $\nu_{(C=N)}$ 1590 cm^{-1}. μ_{eff} = 4.95 BM (25 °C). Diffuse reflectance spectra (40000−5550 cm^{-1}): 25000 sh, 17200 sh, 15500, 10500, 8300, 5600. Solution spectra (CH_2Cl_2, 28500−6250 cm^{-1}): 25000 sh, 17100 sh, 14800 (ε 710), 10500 (ε 40), 8000 (ε 75). $C_{29}H_{35}Cl_2CoN_3$ (555.46): calcd. C 62.71, H 6.35, N 7.57; found C 62.80, H 6.29, N 7.60.

[*N*-{(*E*)-1-[6-(Cyclohexylethanimidoyl)-2-pyridinyl]ethylidene}-2,6-dimethylaniline]cobalt Dichloride (9): This complex was obtained as green crystals. Yield 84%. IR: $\nu_{(C=N)}$ 1590 cm^{-1}. μ_{eff} = 4.85 BM (25 °C). Diffuse reflectance spectra (40000−5550 cm^{-1}): 25000 sh, 16950, 15400, 10500, 8150, 5700. Solution spectra (CH_2Cl_2, 28500−6250 cm^{-1}): 25000 sh, 17000 (ε 460), 15450 (ε 740), 11000 (ε 42), 7800 (ε 90). $C_{23}H_{29}Cl_2CoN_3$ (477.34): calcd. C 57.87, H 6.12, N 8.80; found C 57.61, H 6.25, N 8.61.

[2,6-Diisopropyl-*N*-{(*E*)-1-[6-{[(1*S*)-1-(2-naphthyl)ethyl]-ethanimidoyl}-2-pyridinyl]ethylidene}aniline]cobalt Dichloride (10): This complex was obtained as green crystals. Yield 88%. IR: $\nu_{(C=N)}$ 1592 cm^{-1}. μ_{eff} = 4.87 BM (25 °C). Diffuse reflectance spectra (40000−5550 cm^{-1}): 25100 sh, 17400 sh, 15600, 10300, 8000, 5650. Solution spectra (CH_2Cl_2, 28500−6250 cm^{-1}): 25000 sh, 17300 sh, 14900 (ε 700), 10350 (ε 40), 7800 (ε 90). $C_{33}H_{37}Cl_2CoN_3$ (477.34): calcd. C 65.46, H 6.16, N 6.90; found C 65.58, H 6.03, N 6.93.

[*N*-{(*E*)-1-[6-(Cyclohexylethanimidoyl)-2-pyridinyl]ethylidene}-2,6-diisopropylaniline]iron Dichloride (11): This complex was obtained as dark blue microcrystals. Yield 81%. IR: $\nu_{(C=N)}$ 1589, 1580 cm^{-1}. μ_{eff} = 5.72 BM (25 °C). Diffuse reflectance spectra (40000−5550 cm^{-1}): 18200 sh, 7400. Solution spectra (CH_2Cl_2, 28500−6250 cm^{-1}): 20230 (ε 240), 7170 (ε 6). $C_{27}H_{37}Cl_2FeN_3$ (530.36): calcd. C 61.15, H 7.03, N 7.92; found C 60.97, H 6.91, N 7.88.

[2,6-Diisopropyl-*N*-{(*E*)-1-[6-{[(1*R*)-1-phenylethyl]ethanimidoyl}-2-pyridinyl]ethylidene}aniline]iron Dichloride (12): This complex was obtained as a blue powder. Yield 87%. IR: $\nu_{(C=N)}$ 1584 cm^{-1}. μ_{eff} = 5.56 BM (25 °C). Diffuse reflectance spectra (40000−5550 cm^{-1}): 18000 sh, 14600, 8100. Solution spectra (CH_2Cl_2, 28500−6250 cm^{-1}): 20300 (ε 250), 7700 (ε 8). $C_{29}H_{35}Cl_2FeN_3$ (552.37): calcd. C 63.06, H 6.39, N 7.61; found C 62.68, H 6.28, N 7.59.

[*N*-{(*E*)-1-[6-(Cyclohexylethanimidoyl)-2-pyridinyl]ethylidene}-2,6-dimethylaniline]iron Dichloride (13): This complex was obtained as dark blue crystals. Yield 81%. IR: $\nu_{(C=N)}$ 1589 cm^{-1}. μ_{eff} = 5.68 BM (25 °C). Diffuse reflectance spectra (40000−5550 cm^{-1}): 18800 sh, 8330 cm^{-1}. Solution spectra (CH_2Cl_2, 28500−6250 cm^{-1}): 19050 (ε 230), 8350 (ε 12). $C_{23}H_{29}Cl_2FeN_3$ (474.26): calcd. C 58.25, H 6.16, N 8.86; found C 58.13, H 6.29, N 8.68.

[2,6-Diisopropyl-*N*-{(*E*)-1-[6-{[(1*S*)-1-(2-naphthyl)ethyl]-ethanimidoyl}-2-pyridinyl]ethylidene}aniline]iron Dichloride (14): This complex was obtained as blue microcrystals. Yield 79%. IR: $\nu_{(C=N)}$ 1590 cm^{-1}. μ_{eff} = 5.77 BM (25 °C). Diffuse reflectance spectra (40000−5550 cm^{-1}): 18300 sh, 8000. Solution spectra (CH_2Cl_2, 28500−6250 cm^{-1}): 20000 (ε 240), 7900 (ε 8). $C_{33}H_{37}Cl_2FeN_3$ (602.43): calcd. C 65.79, H 6.19, N 6.98; found C 65.90, H 6.10, N 6.84.

Oligomerisation Reactions: A 0.5-L stainless steel reactor was heated at 100 °C under vacuum for 3 h, solid precatalyst (12 μmol) was introduced into the autoclave at room temperature, and the system was evacuated. A solution of oxygen-free toluene (100 mL) and MAO (sol. 10% w/w, 1.6 mL) was then introduced into the reactor and the mixture was stirred at room temperature for 10 min. The system was then heated or thermostatted to the desired temperature, pressurised with ethylene, and stirred at 1500 rpm. The reaction was terminated by cooling to 5 °C and slow depressurisation, followed by addition of MeOH (2 mL) and *n*-heptane (internal standard, 200 μL).

X-ray Structure Determination of 9·H_2O: Single crystals of 9·H_2O were grown by slow diffusion of *n*-hexane into a CH_2Cl_2 solution of **9**. A summary of crystal and intensity data is presented in Table 4.

Experimental data were recorded at 20 °C with an Enraf−Nonius CAD4. A set of 25 carefully centred reflections in the range $8° \leq \theta \leq 10.25°$ was used for determining the lattice constants. As a general procedure, the intensity of three standard reflections were measured periodically every 200 reflections for orientation and intensity control. This procedure did not reveal any appreciable decay in intensities. The data were corrected for Lorentz and polarisation effects. Atomic scattering factors were those tabulated by Cromer and Waber,[27] with anomalous dispersion corrections taken from ref.[28] An empirical absorption correction was applied by use of the program XABS with correction factors in the range 1.3518−0.394. The computational work was carried out by intensive use of the program WINGX. Final atomic coordinates of all atoms and structure factors are available on request from the authors and are provided. A dark green parallelepiped crystal with dimensions 0.375 × 0.300 × 0.225 mm was used for the data collection. The structure was solved by direct methods by use of the SIR97 program.[29] Refinement was performed by full-matrix, least-squares calculations, initially with isotropic thermal parameters and then with anisotropic thermal parameters for all the atoms other than the oxygen atoms. In the final stage of the refinement, two atoms were detected and were assigned as oxygen of solvent molecules and successfully refined. The phenyl ring was treated as a rigid body with D_{6h} symmetry, and the hydrogen atoms were allowed to ride on the attached carbon atoms. Hydrogen atoms were introduced at calculated positions. CCDC-195274 contains the supplementary crystallographic data for this paper. These data can be obtained free of charge at www.ccdc.cam.ac.uk/conts/retrieving.html [or from the Cambridge Crystallographic Data Centre, 12 Union Road, Cambridge CB2 1EZ, UK; Fax: (internat.) + 44-1223/336-033; E-mail: deposit@ccdc.cam.ac.uk].

Table 4. Selected crystallographic data for **9**·H_2O

Empirical formula	$C_{23}H_{31}Cl_2CoN_3O$
Formula mass	495.36
T [K]	293(2)
Crystal system	orthorhombic
Space group	*Pcab* (No. 61)
a [Å]	8.5557(10)
b [Å]	22.0942(17)
c [Å]	27.468(8)
V [Å^3]	5192(2)
Z	8
$\rho_{calcd.}$ [g·cm^{-3}]	1.262
Absorption coefficient [mm^{-1}]	0.884
Crystal size [mm]	0.38 × 0.30 × 0.22
Transmission, min./max.	0.8258/0.7327
2θ range [°]	2.66−24.97
Data/restraints/parameters	4546/0/265
Reflections collected	4546
Independent reflections	4546
$R1$[a]; $wR2$	7.75; 23.09

[a] $I > 2\sigma(I)$.

Acknowledgments

Polimeri Europa and the European Commission (contract no. HPRN-CT-2000-00010, COST Action D17 Working Group 0003/2000) are thanked for financial support. We are grateful to Mr. Dante Masi (ICCOM-CNR) for technical assistance in X-ray data collection and to Prof. Piero Zanello (University of Siena) for CV measurements.

[1] [1a] B. L. Small, M. Brookhart, A. M. A. Bennett, *J. Am. Chem. Soc.* **1998**, *120*, 4049−4050. [1b] G. J. P. Britovsek, V. C. Gibson, B. S. Kimberley, P. J. Maddox, S. J. McTavish, G. A. Solan, A. J. P. White, D. J. Williams, *Chem. Commun.* **1998**, 849−850. [1c] A. M. A. Bennett (DuPont), WO 98/27124. *Chem. Abstr.* **1998**, *129*, 122973x. [1d] G. J. P. Britovsek, M. Bruce, V. C. Gibson, B. S. Kimberley, P. J. Maddox, S. Mastroianni, S. J. McTavish, C. Redshaw, G. A. Solan, S. Strömberg, A. J. P. White, D. J. Williams, *J. Am. Chem. Soc.* **1999**, *121*, 8728−8740. [1e] G. J. P. Britovsek, V. C. Gibson, B. S. Kimberley, S. Mastroianni, C. Redshaw, G. A. Solan, A. J. P. White, D. J. Williams, *J. Chem. Soc., Dalton Trans.* **2001**, 1639−1644.

[2] [2a] B. L. Small, M. Brookhart, *J. Am. Chem. Soc.* **1998**, *120*, 7143−7144. [2b] G. J. P. Britovsek, S. Mastroianni, G. A. Solan, S. P. D. Baugh, C. Redshaw, V. C. Gibson, A. J. P. White, D. J. Williams, M. R. Elsegood, *Chem. Eur. J.* **2000**, *6*, 2221−2231.

[3] [3a] B. L. Small, M. Brookhart, *Polym. Prepr. (Am. Chem. Soc. Div. Polym. Chem.)* **1998**, *39*, 213. [3b] M. Brookhart, B. L. Small (UNC), World Patent Application 98/30612, **1998**. *Chem. Abstr.* **1998**, *129*, 149375r. [3c] B. L. Small, M. Brookhart, *Macromolecules* **1999**, *32*, 2120−2130.

[4] [4a] P. Margl, L. Deng, T. Ziegler, *Organometallics* **1999**, *18*, 5701−5708. [4b] L. Deng, P. Margl, T. Ziegler, *J. Am. Chem. Soc.* **1999**, *121*, 6479−6487. [4c] D. V. Khoroshun, D. G. Musaev, T. Vreven, K. Morokuma, *Organometallics* **2001**, *20*, 2007−2026.

[5] A. S. Abu-Surrah, K. Lappalainen, U. Piironen, P. Lehmus, T. M. Repo, J. Leskelä, *J. Organomet. Chem.* **2002**, *648*, 55−61.

[6] [6a] R. Morassi, I. Bertini, L. Sacconi, *Coord. Chem. Rev.* **1973**, *11*, 343−402. [6b] L. Sacconi, R. Morassi, S. Midollini, *J. Chem. Soc. A* **1968**, 1510−1515. [6c] L. Sacconi, *J. Chem. Soc. A* **1970**, 248−256. [6d] R. Morassi, L. Sacconi, *J. Chem. Soc. A* **1971**, 492−499.

[7] [7a] R. S. Drago, *Physical Methods for Chemists*, Saunders College Publishing, New York, **1992**. [7b] F. E. Mabbs, D. Collison, "Electron Paramagnetic Resonance of d Transition Metal Compounds", in: *Studies in Inorganic Chemistry*, vol. 16, Elsevier Publ., New York, **1992**.

[8] A. Bencini, D. Gatteschi, "ESR spectra of Metal Complexes of the First Transitions Series in Low-Symmetry Environments", in: *Transition Metal Chemistry*, vol. 8, Marcel Dekker Inc., New York, **1982**.

[9] [9a] A. Abragam, B. Bleaney, *Electron Paramagnetic Resonance of Transition Ions*, Dover Publ. Inc., New York, **1970**. [9b] J. E. Wertz, J. R. Bolton, "Electron Spin Resonance: Elementary Theory and Practical Applications", series in: *Advanced Chemistry*, McGraw-Hill Book Company, New York, **1972**.

[10] J. R. Pilbrow, *Transition Ion Electron Paramagnetic Resonance*, Claredon Press, Oxford, **1990**.

[11] R. L. Carlin, *Magnetochemistry*, Springer-Verlag, Berlin, **1986**.

[12] [12a] J. P. Jesson, *NMR of Paramagnetic Molecules: Principles and Applications* (Eds.: G. N. La Mar, W. D. Horrocks, R. H. Holm), Academic Press, New York, **1973**. [12b] R. H. Holm, W. D. Phillips, B. A. Averill, J. J. Mayerle, T. Herskovitz, *J. Am. Chem. Soc.* **1974**, *96*, 2109−2117. [12c] H. M. McConnell, *Proc. Natl. Acad. Sci. U. S. A.* **1972**, *69*, 335−341.

[13] L. Sacconi, *Pure Appl. Chem.* **1968**, *17*, 95−127.

[14] [14a] M. Ciampolini, N. Nardi, *Inorg. Chem.* **1966**, *5*, 1150−1154. [14b] M. Ciampolini, G. P. Speroni, *Inorg. Chem.* **1966**, *5*, 45−49.

[15] M. Ciampolini, *Struct. Bonding* **1969**, *6*, 52−93.

[16] T. M. Kooistra, Q. Knijnenburg, J. M. M. Smits, A. D. Horton, P. H. M. Budzelaar, A. W. Gal, *Angew. Chem.* **2001**, *113*, 4855−4858; *Angew. Chem. Int. Ed.* **2001**, *40*, 4719−4722.

[17] [17a] P. J. Flory, *J. Am. Chem. Soc.* **1940**, *62*, 1561−1565. [17b] G. V. Schulz, *Z. Phys. Chem. Abt. B* **1935**, *30*, 379−385. [17c] G. V. Schulz, *Z. Phys. Chem. Abt. B* **1939**, *43*, 25−31. [17d] G. Henrici-Olivé, S. Olivé, *Adv. Polym. Sci.* **1974**, *15*, 1−19.

[18] B. L. Small, A. J. Marcucci, *Organometallics* **2001**, *20*, 5738−5744.

[19] S. D. Ittel, L. K. Johnson, M. Brookhart, *Chem. Rev.* **2000**, *100*, 1169−1204.
[20] L. Deng, T. K. Woo, L. Cavallo, P. M. Margl, T. Ziegler, *J. Am. Chem. Soc.* **1997**, *119*, 6177−6186.
[21] A. F. Cotton, G. Wilkinson, C. A. Murillo, M. Bochmann, *Advanced Inorganic Chemistry*, 6th ed., Wiley-Interscience, New York, **1999**, pp. 780−786 and 814−822.
[22] A. Derome, M. Williamson, *J. Magn. Res.* **1990**, *88*, 177−186.
[23] [23a] V. Sklener, H. Miyashiro, G. Zon, H. T. Miles, A. Bax, *FEBS Lett.* **1986**, *208*, 94−98. [23b] J. Jeener, B. H. Meier, P. Bachmann, R. R. Ernst, *J. Chem. Phys.* **1979**, *71*, 4546−4553.
[24] A. Bax, R. H. Griffey, B. L. Hawkins, *J. Magn. Reson.* **1983**, *55*, 301−315.
[25] [25a] A. Bax, M. F. Summers, *J. Am. Chem. Soc.* **1986**, *108*, 2093−2094. [25b] M. F. Summers, L. G. Marzilli, A. Bax, *J. Am. Chem. Soc.* **1986**, *108*, 4285−4294.
[26] F. Fabrizi de Biani, F. Laschi, P. Zanello, G. Ferguson, J. Trotter, G. M. O'Riordan, T. R. Spalding, *J. Chem. Soc., Dalton Trans.* **2001**, 1520−1523.
[27] D. T. Cromer, J. T. Waber, *Acta Crystallogr.* **1965**, *18*, 104−109.
[28] *International Tables of Crystallography*, vol. IV, Kynoch Press, Birmingham, UK, **1974**.
[29] A. Altomare, M. C. Burla, M. Camalli, G. Cascarano, C. Giacovazzo, A. Guagliardi, G. Polidori, R. Spagna, *J. Appl. Crystallogr.* **1999**, *32*, 115−119.

Received November 25, 2002
[I02624]

Mn and Fe *K*-edge XAS Spectra of Manganese and Iron Nitrido Compounds

Rainer Niewa,*[a] Zhiwei Hu,[b] and Rüdiger Kniep[a]

Keywords: X-ray absorption spectroscopy / Nitrides / Iron / Manganese

We performed a Mn *K*-edge XAFS study of a number of highly moisture-sensitive nitridomanganates with manganese in different oxidation states and in various surroundings: $Li_2[(Li_{1-x}Mn^{I}_{x})N]$ [x = 0.75(1)], $Li_{24}[Mn^{III}N_3]_3N_2$, and $Li_7[Mn^{V}N_4]$. For reference purposes Mn, MnO and θ-Mn_6N_{5+x} [x = 0.26(1)] were measured. The energy positions of the pre-edge maxima are almost independent of the electronic state of Mn, while the intensity is sensitive to the geometric arrangement of the coordination of Mn. The main-edge is sensitive to the oxidation state – a clear shift to higher energies with increasing oxidation state can be seen. This shift is smaller than the shift observed for the corresponding oxides, due to the lower electronegativity of nitrogen compared to oxygen, and corresponds to a higher covalency of the Mn–N bond. Similar results can be taken from the Fe *K*-edges of $Li_2[(Li_{1-x}Fe^{I}_{x})N]$ with x = 0.20(1) and $Li_3[Fe^{III}N_2]$ in comparison to metallic Fe, $Fe^{II}SO_4\cdot 7H_2O$ and α-$Fe^{III}_2O_3$. The results are consistent with the presence of an unusual oxidation state (+1) for the transition metals in the phases of the general composition $Li_2[(Li_{1-x}M_x)N]$.
(© Wiley-VCH Verlag GmbH & Co. KGaA, 69451 Weinheim, Germany, 2003)

Introduction

XAS spectroscopy at the thresholds is an element-specific tool that can provide valuable information on the oxidation state and the electronic configuration of most atomic components of both crystalline and amorphous materials. The shape and energy position of the absorption spectrum in its near-edge region is closely related to the electronic structure, and is partly also influenced by the magnetic state, the local symmetry, and the coordination environment of the nuclei, while the oscillation observed in the high energy region of the spectrum is associated with the arrangement of the atoms, i.e. the local surrounding.

A wide range of oxidation states is known for Mn: in inorganic oxide compounds manganese covers the whole range of oxidation states from +2 to +7, and in carbonyl complexes the oxidation states −1, 0 and +1 are also known. In nitride chemistry, the highest reported oxidation state for manganese is +5, while the lower oxidation states are predominately stabilized (as generally in 3d nitridometalates):[1] oxidation states below +2 are frequently observed. The oxidation state +5 is known only for $Li_7[MnN_4]$,[2] with a high ratio of electropositive elements to manganese, while in binary manganese nitrides even +3 has not been reached so far. MnN reported in the literature always exhibits a nitrogen deficiency and belongs to the θ-Mn_6N_{5+x} phase region.[3] The situation is similar for lithium nitridoferrates: $Li_3[FeN_2]$ contains iron in its highest oxidation state (+3) observed so far in nitride chemistry.[4] $Li_4[Fe^{II}N_2]$[5] and $Li_2[(Li_{1-x}Fe^{I}_{x})N]$[6,7] are formed as decomposition phases from $Li_3[Fe^{III}N_2]$ at elevated temperatures.

In XAS at the transition metal *K*-edge an M 1s core-electron is excited to the 4p orbitals (dipole allowed), at higher energy the M 1s core-electron is excited to the continuum. In general, XAS spectra of the first-row transition metals have a weak pre-edge structure about 10 eV below the absorption edge, a feature that was assigned as originating from a 1s→3d transition.[8−10] For compounds with the transition metal in a centrosymmetric environment, a 1s→3d transition is electric dipole-forbidden by parity considerations. (The fact, that dipole selection rules hold only in systems with an inversion center is known in spectroscopy as Laporte's rule[11]). However, a weak pre-edge feature is still observed experimentally. In the case of non-centrosymmetric local surroundings M-4p-wavefunctions can mix into the 3d orbitals which provides some electric dipole-allowed 1s→4p character to the transition. All this may lead to a significant pre-edge feature that is more intense for local symmetries lacking an inversion center. In particular, the features in the region of the 1s→3d transition have been shown to be sensitive to the oxidation state and coordination geometry of a 3d transition metal.[10]

X-ray absorption probes the unoccupied part of the electronic structure of the system. Thus, for all discussions it should be mentioned that information on the ground state is concluded from excited states with an M 1s hole, a conclusion which might not be uncritical. This situation is

[a] Max-Planck-Institut für Chemische Physik fester Stoffe, Nöthnitzer Str. 40, 01187 Dresden, Germany
Fax: (internat.) +49-(0)351/4646-3002
E-mail: niewa@cpfs.mpg.de
[b] II. Physikalisches Institut der Universität zu Köln, Zülpicher Str. 77, 50937 Köln, Germany

moderated for metallic compounds, since, as a general rule, the core holes in metals are better screened than in insulators, therefore many-body effects involving both the core hole and the excited electron are less important for metals.[8] We chose to measure *K*-edge spectra, because: i) the relevant energies make it possible to work in transmission mode, hence to use fully encapsulated samples (necessary for the strongly sensitive compounds), and ii) the valence state can be taken directly from the energy shift of the main absorption edge, while in $L_{2,3}$ XAS spectra the edge of oxidized 3d metals can lie at higher or lower energies than those of the corresponding metallic elements. The latter fact is due to strong multiplet interactions in the final state effects.[12,13]

Results and Discussion

The striking features of the presented data are the pre-edge peaks visible for all investigated nitrides, although their shape and their intensity are significantly different. As can be seen from Figure 1, for the manganese compounds the most pronounced and best separated pre-edge features are visible for $Li_7[Mn^{V}N_4]$ and $Li_{24}[Mn^{III}N_3]_3N_2$ around 6539 eV. This pre-edge peak was assigned to a 1s→3d transition.[8–10] In the spectra of the other nitrides the pre-edge is observed only as a shoulder of the main absorption edge, which itself reflects a 1s→4p transition. The positions of the pre-edge feature exhibit only a slight change in energy in the presented data. Therefore, the pre-edge peak becomes more visible when the main absorption edge shifts to higher energies. It was observed earlier that the pre-edge peaks are shifted to higher energy with increasing oxidation state for chromium oxides.[14,15] Such a shift can only be confirmed for the well-separated strong pre-edge signals in the spectra of $Li_7[Mn^{V}N_4]$ and $Li_{24}[Mn^{III}N_3]_3N_2$, indicating the difference in oxidation state (about 1 eV). The intensity of the pre-edge peak can be related directly to the local symmetry of the manganese coordination in the different nitrido compounds: $Li_7[Mn^{V}N_4]$: tetrahedral, lacking centrosymmetry,[2] $Li_{24}[Mn^{III}N_3]_3N_2$: trigonal, slightly non-planar, lacking centrosymmetry,[2] $Li_2[(Li_{1-x}Mn^{I}_x)N]$: linear by N, and thus centrosymmetric, but with Li-Mn disorder in the basal plane perpendicular to the Mn−N bond (second coordination sphere assembled from six Li or Mn) breaking the symmetry,[2] θ-Mn_6N_{5+x}: octahedral, centrosymmetric, but with some degree of N-vacancies breaking the local symmetry.[3]

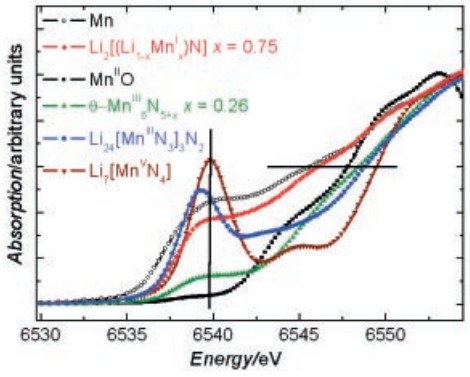

Figure 1. Near-edge XAS spectra of Mn, $Li_2[(Li_{1-x}M_x^{I})N]$ (x = 0.75), $Mn^{II}O$, θ-Mn_6N_{5+x} (x = 0.26), $Li_{24}[Mn^{III}N_3]_3N_2$ and $Li_7[Mn^{V}N_4]$; the strong pre-edge peak for the compounds lacking local centrosymmetry at the Mn-center and the shift of the main absorption edge to higher energies with increasing oxidation state are clearly visible

Unfortunately, the inflection point of the main absorption edge in many spectra is overlapped by the pre-edge feature. However, the general trend of the increasing absorption edge levels at about 0.6 of the full edge jump from elemental Mn and the Mn^{I}-phase $Li_2[(Li_{1-x}Mn^{I}_x)N]$ to $Mn^{II}O$ is still visible (Figure 1). The inflection point of θ-Mn_6N_{5+x} (x = 0.26) lies slightly lower than that of $Li_{24}[Mn^{III}N_3]_3N_2$, indicating the lower oxidation state of Mn in the binary nitride due to the nitrogen deficiency in the crystal structure compared to the ideal composition for a manganese(III) nitride. The edge of $Li_7[Mn^{V}N_4]$ lies at the highest energy, as was to be expected. The absorption edge of $Mn^{II}O$ is much closer to that of the manganese(III) nitrido compounds than to that of the nitridomanganate(I). This is easily understood from the lower electronegativity of the nitrogen ligands compared to oxygen. As observed earlier, the absorption edge is shifted to higher energies with increasing electronegativity of the ligands.[16]

Larger degrees of vacancies and, thus, increased oxidation states of the transition metals in the sense of $Li_{2-y}[(Li_{1-x}M_x)N]$, have been discussed for the analogues substitution series of M = Cu, Ni and Co.[17–19] The small shift of the absorption edge of the manganese(I) compound compared to the manganese foil proves that the oxidation state of manganese in $Li_2[(Li_{1-x}Mn_x)N]$ is close to +1, indicating that the vacancy concentration in this phase (y in $Li_{2-y}[(Li_{1-x}Mn_x)N]$) is small. This is in agreement with our single crystal and magnetic susceptibility investigations.[2] Similar results were also obtained for the M = Cu, Ni, Co substitution phases from XAS spectroscopy, indicating oxidation states close to +1.[20]

The main absorption edge is determined by the threshold of the electron dipole transition from the manganese 1s orbital to the continuum of p-like states above the Fermi energy. The shift of the edge position is correlated with the length of the Mn−N bonds: the shorter it is, the larger the overlap between the electron wavefunctions originating from Mn and N. This results in an increase of the energy of the outer states relative to the energy of the core levels, and thus in a higher-energy shift of the absorption edge. Higher oxidation states generally lead to shorter bond lengths considering the same coordination geometry, thus adding to the effect of the positive edge shift. In our study lower coordination numbers (*CN*) in phases with lower oxidation states of M partly counteract these effects: $\bar{d}$(Mn−N): $Li_2[(Li_{1-x}Mn_x)N]$ [x = 0.75(1)] with *CN*(Mn) = 2: 191 pm;[2] $Li_{24}[MnN_3]_3N_2$ with *CN*(Mn) = 3: 178 pm;[2] $Li_7[MnN_4]$ with *CN*(Mn) = 4: 182 pm;[2] θ-Mn_6N_{5+x} (x = 0.26) with *CN*(Mn) = 5,6: 218 pm[3]. The effect of Li−Mn−disorder, i.e. the size of the substitution parameter

x, on the average bond length $\bar{d}$(Li,Mn−N) in $Li_2[(Li_{1-x}Mn_x)N]$ is negligible.[21]

Figure 2 plots the Fe K-edges of $Li_3[Fe^{III}N_2]$ and $Li_2[(Li_{1-x}Fe^{I}_x)N]$ [x = 0.20(1)] together with reference compounds and the element. As discussed for the manganese compounds, good separation of the pre-edge feature is only reached for $Li_3[Fe^{III}N_2]$ with Fe in tetrahedral (non-centrosymmetric) coordination. The main absorption edge taken at 0.6 of the total edge jump shifts only slightly from metallic Fe to $Li_2[(Li_{1-x}Fe^{I}_x)N]$ [x = 0.20(1)] indicating the oxidation state of iron in the latter phase is close to unity. The absorption edges of $Fe^{II}SO_4{\cdot}7H_2O$ and $Li_3[Fe^{III}N_2]$ nearly coincide for the same reason of electronegativity difference of nitrogen and oxygen as discussed above, while the Fe K-edge of α-$Fe^{III}_2O_3$ is clearly shifted to higher energies.

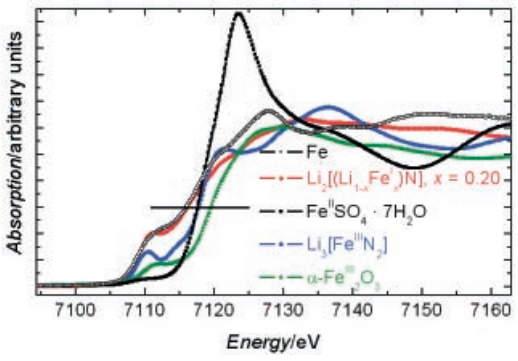

Figure 2. Near-edge XAS spectra of Fe, $Li_2[(Li_{1-x}Fe^{I}_x)N]$ (x = 0.20), $Fe^{II}SO_4{\cdot}7H_2O$, $Li_3[Fe^{III}N_2]$, and α-$Fe^{III}_2O_3$; the shift of the main absorption edge to higher energies with increasing oxidation state is clearly visible

Experimental Section

Samples of the compounds under investigation were prepared and characterized as described previously.[2,3,7,22] For the XAS measurements the air-sensitive compounds $Li_7[Mn^{V}N_4]$, $Li_{24}[Mn^{III}N_3]_3N_2$, $Li_2[(Li_{1-x}Mn^{I}_x)N]$ [x = 0.75(1)], $Li_3[Fe^{III}N_2]$ and $Li_2[(Li_{1-x}Fe^{I}_x)N]$ [x = 0.20(1)] were handled in an Ar-filled glove box with $p(O_2, H_2O) < 1$ ppm. All powder samples were mixed with three times their volume of dry B_4C to produce homogenous absorbers. The air-sensitive samples were loaded in steel capsules equipped with Be windows (0.5 mm). Due to the extreme moisture sensitivity of these samples and the necessary way of handling, thickness effects in the resulting XAS spectra are basically inevitable.[23,24] Non-sensitive samples (MnO, θ-Mn_6N_{5+x}, α-Fe_2O_3) were prepared on mylar films. $Fe^{II}SO_4{\cdot}7H_2O$ was also loaded into a steel capsule to prevent dehydration in vacuo.

The M K-edge measurements were performed in transmission geometry at the E4 bending magnet beamline located at the DORISIII storage ring in the HASYLAB laboratory (Hamburg, Germany). The X-ray beam outgoing from the bending magnet and formed with the toroidal and plane golden mirrors was monochromatized using a double crystal monochromator, equipped with a Si(111) crystal. This resulted in an experimental resolution of about 1.5 eV (FWHM) at the studied thresholds. For detectors ionization chambers were used. The absorption spectra were measured simultaneously with the spectrum of metallic manganese or iron foil, respectively, serving as references for energy calibration. Typical scan times were 30 min with smaller step size and longer measurement times in the range of the main-edge.

Acknowledgments

We wish to thank Dr. K. Klementiev for his support at the E4 beamline.

[1] R. Niewa, *Z. Kristallogr.* **2002**, *217*, 8−23.
[2] R. Niewa, F. R. Wagner, W. Schnelle, O. Hochrein, R. Kniep, *Inorg. Chem.* **2001**, *40*, 5215−5222.
[3] A. Leineweber, R. Niewa, H. Jacobs, W. Kockelmann, *J. Mater. Chem.* **2000**, *10*, 2827−2834.
[4] A. Gudat, R. Kniep, A. Rabenau, W. Bronger, U. Ruschewitz, *J. Less-Common Met.* **1990**, *161*, 31−36.
[5] A. Gudat, R. Kniep, A. Rabenau, *Angew. Chem.* **1991**, *103*, 217−218; *Angew. Chem. Int. Ed. Engl.* **1991**, *30*, 199−200.
[6] J. Klatyk, R. Kniep, *Z. Kristallogr. NCS* **1999**, *214*, 447−448.
[7] J. Klatyk, W. Schnelle, F. R. Wagner, R. Niewa, P. Nowak, R. Kniep, M. Waldeck, V. Ksenofontov, P. Gütlich, *Phys. Rev. Lett.* **2002**, *88*, 207202−1-4.
[8] L. A. Grunes, *Phys. Rev. B* **1983**, *27*, 2111−2131.
[9] F. M. F. de Groot, *J. Electron. Spectrosc. Relat. Phenom.* **1994**, *67*, 529−622.
[10] R. G. Shulman, Y. Yafet, P. Eisenberger, W. E. Blumberg, *Prog. Natl. Acad. Sci. USA* **1976**, *73*, 1384−1388.
[11] See, for example, P. J. Durrant, B. Durrant, *Introduction to Advanced Inorganic Chemistry*, 2nd ed., Longman Group, London, **1970**, p. 976.
[12] R. D. Leapman, L. A. Grunes, *Phys. Rev. Lett.* **1980**, *45*, 397−401.
[13] R. D. Leapman, L. A. Grunes, P. L. Fejes, *Phys. Rev. B* **1982**, *26*, 614−635.
[14] A. Pantelouris, G. Küper, J. Hourmes, C. Feldmann, M. Jansen, *J. Am. Chem. Soc.* **1995**, *117*, 11749−11753.
[15] Z. Hu, G. Kaindl, A. Hayer, D. Reinen, *Z. Anorg. Allg. Chem.* **2001**, *627*, 2647−2653.
[16] Z. Hu, G. Kaindl, G. Meyer, *J. Alloys Comp.* **1997**, *246*, 186−192.
[17] A. G. Gordon, D. H. Gregory, A. J. Blake, D. P. Weston, M. O. Jones, *Int. J. Inorg. Mater.* **2001**, *3*, 973−981.
[18] D. H. Gregory, P. M. O'Meara, A. G. Gordon, D. J. Siddons, A. J. Blake, M. G. Barker, T. A. Hamor, P. P. Edwards, *J. Alloys Comp.* **2001**, *317*, 237−244.
[19] M. T. Weller, S. E. Dann, P. F. Henry, D. B. Currie, *J. Mater. Chem.* **1999**, *9*, 283−287.
[20] R. Niewa, Z.-L. Huang, W. Schnelle, Z. Hu, R. Kniep, Z. Anorg. Allg. Chem. in press.
[21] J. Klatyk, R. Niewa, R. Kniep, *Z. Naturforsch., Teil B* **2000**, *55*, 988−991.
[22] F. Tessier, M. R. Rannade, A. Navrotsky, R. Niewa, F. J. DiSalvo, A. Leineweber, H. Jacobs, *Z. Anorg. Allg. Chem.* **2001**, *627*, 194−200.
[23] D. M. Pease, *Appl. Spectrosc.* **1976**, *30*, 405−410.
[24] F. Szmulowicz, D. M. Pease, *Phys. Rev. B* **1978**, *17*, 3341−3355.

Received January 9, 2003
[I03011]

Synthesis and Characterization of $(PTU)I_2$ (PTU = 6-*n*-propyl-2-thiouracil) and $(CMBZT)I_2$ (CMBZT = 5-chloro-2-mercaptobenzothiazole) and Possible Implications for the Mechanism of Action of Anti-Thyroid Drugs

Constantinos D. Antoniadis,[a] Ghada J. Corban,[a] Sotiris K. Hadjikakou,*[a] Nick Hadjiliadis,*[a] Maciej Kubicki,[b] Stephanie Warner,[c] and Ian S. Butler[c]

Keywords: Bioinorganic chemistry / Charge transfer / Iodine / S ligands / Nitrogen heterocycles

Direct reaction of 6-*n*-propyl-2-thiouracil (PTU), a widely used anti-thyroid drug against hyperthyroidism (Graves' disease), or 5-chloro-2-mercaptobenzothiazole (CMBZTH) with iodine in a molar ratio of 1:1 resulted in the formation of the charge-transfer (CT) complexes $[(PTU)I_2]$ (**1**) or $[(CMBZT)I_2]$ (**2**). All reactions were carried out in dichloromethane and water solutions. Compounds **1** and **2** were characterized by elemental analyses, FT-Raman, FT-IR, UV/Vis and ^1H NMR spectroscopy. The crystal structures of both complexes were determined by X-ray diffraction at 120(1) K (**1**) and 293(2) K (**2**). The charge-transfer nature of the bonds in the adducts **1** and **2** was verified by the lengthening of the I–I bond lengths as compared to the S–I bond lengths and by the characteristic CT bands observed in the UV spectra of the complexes. Compound **1** $[(C_7H_{10}N_2OS)I_2]$ [monoclinic with space group $P2_1/c$ and a = 9.8501(7), b = 10.3101(7), c = 12.0287(8) Å, β = 99.707(6)°, Z = 4] consists of a propylthiouracil ligand bonded with an iodine atom through sulfur. Extended intermolecular N–H···O contacts link the molecules forming a supramolecular assembly. Compound **2** $\{(C_7H_4ClNS_2)I_2\}$ [orthorhombic, space group $P2_12_12_1$, a = 4.1650(10), b = 9.691(2), c = 28.471(6) Å, Z = 4] consists of a 5-chloro-2-mercaptobenzothiazole ligand bonded with an iodine atom through sulfur. An extended intermolecular linkage via I···H–N bonds leads to the formation of an extended structure. Attempts to draw conclusions on the behavior of a thioamide — when used as an anti-thyroidal drug — towards iodine have been made.

(© Wiley-VCH Verlag GmbH & Co. KGaA, 69451 Weinheim, Germany, 2003)

Introduction

The most commonly employed anti-thyroidal drugs for the treatment of hyperthyroidism (Graves' disease) are 6-*n*-propyl-2-thiouracil (PTU), *N*-methylimidazoline-2-thione (methimazole) (MMI) and 3-methyl-2-thioxo-4-imidazoline-1-carboxylate (carbimazole) (CBZ).[1–2] They have been found to inhibit the formation of 3,5,3′-triiodothyronine (T3) and 3,5,3′,5′- tetraiodothyronine (T4) hormones by blocking the metabolism of iodine (Scheme 1).[3] Therefore, there is an increasing interest in the study of charge-transfer (CT) complexes of iodine with thioamides or thiones,[2,4–7] not only for the clarification of the iodine binding mechanism but also for the development of new anti-thyroidal agents.

Although much work has been carried out with these drugs, structural data on their CT complexes with I_2 were only reported very recently for the complex with MMI.[8] Herein we report the structural and spectroscopic characterisation of two new iodine complexes with the heterocyclic thioamides 6-*n*-propyl-2-thiouracil (PTU, I) and 5-chloro-2-mercaptobenzothiazole (CMBZT, II) $[(PTU)I_2]$ (**1**) and $[(CMBZT)I_2]$ (**2**). PTU is used in the treatment of hyperthyroidism while CMBZT was used for comparison purposes.

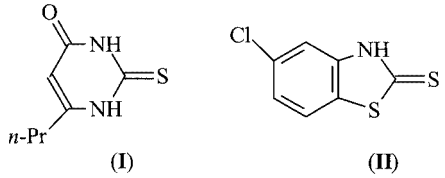

(I) (II)

Results and Discussion

Dark crystals of the complexes, suitable for single crystal analysis by X-ray crystallography, were grown by slow evaporation of the filtrates resulting from the reaction of iodine with the appropriate thioamide in 1:1 or 2:1 molar ratios in

[a] Section of Inorganic and Analytical Chemistry, Department of Chemistry, University of Ioannina, 45110 Ioannina, Greece
Fax: (internat.) +30-26510-44831
E-mail: nhadjil@cc.uoi.gr
[b] Department of Chemistry, A. Mickiewicz, University, ul. Grunwaldzka 6, 60-780 Poznan, Poland
[c] Department of Chemistry, McGill University, 801 Sherbrooke, Montreal Quebec, Canada H2A 2 K6

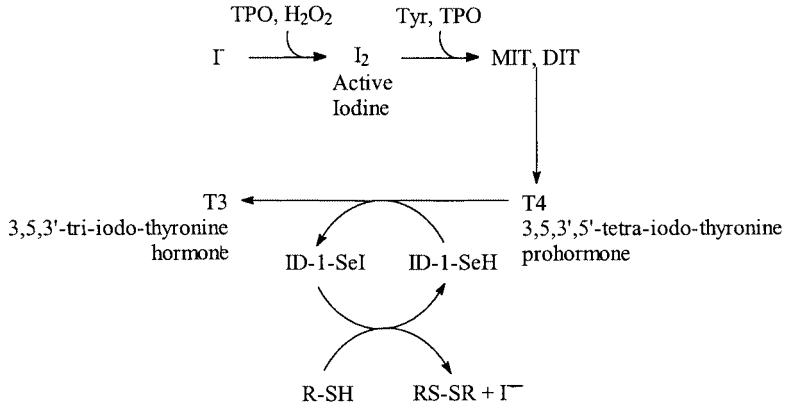

Scheme 1. Mechanism of TPO-catalyzed iodination reactions (MIT = 3-monoiodotyrosine and DIT = 3,5-diiodotyrosine)

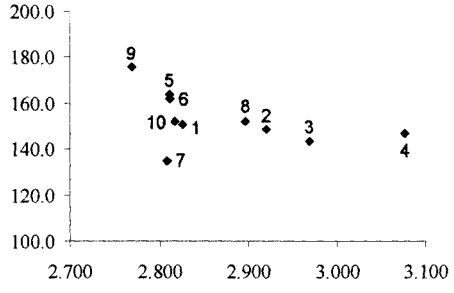

Figure 1. Correlation between ν(I-I) Raman bands of the adducts [{(bztzdtH)I_2}·I_2][7a] (**3**; bztzdtH = benzothiazole-2-thione) ν(I-I)= 143.7 cm^{-1}; [(bztzdtH)I_2][7a] (**4**) ν(I-I) = 147 cm^{-1}, [ptc·I_2][5a] (**5**; ptc = 1,3-dithiacyclohexane-2-thione) ν(I-I)= 164 cm^{-1}; [ttb·I_2][5a] (**6**; ttb = 4,5-ethylenedithio-1,3-dithiole-2-thione) ν(I-I) = 162 cm^{-1}; [mdtt·I_2][5c] [**7**; mdtt = 4,5-bis(methylsulfanyl)-1,3-dithiole-2-thione] ν(I-I) = 136 cm^{-1}; [mbit·I_2][6a] [**8**; mbit = 1,1-methylenebis(3-methyl-4-imidazoline-2-thione)] ν(I-I) = 152 cm^{-1}; [bzoxtH·I_2][6b] (**9**; bzoxtH = benzoxazole-2-thione) ν(I-I) = 176 cm^{-1}; [dmimdtH·I_2][6d] (**10**; dmimdtH = 5,5-dimethylimidazoline-2,4-dithione) ν(I-I) = 152 cm^{-1} and compounds **1** and **2**

dichloromethane. The reactions were also carried out in H_2O. The insoluble dark brown powders obtained were recrystallized from dichloromethane.

The structure of compound **1** shows that the PTU ligand, with anti-thyroidal activity, is able to retain one iodine molecule. The formulae of complexes **1** and **2** were first deduced from elemental analysis and spectroscopic data. Both complexes are highly soluble in organic solvents and their crystals are stable in air, although they were stored in darkness in a refrigerator.

Spectroscopy

Vibrational Spectroscopy

New bands appearing at 153 and 152 cm^{-1} in the far-IR spectra of compounds **1** and **2**, respectively, were assigned to the ν(I−I) stretching vibration modes.[7a] The ν(I−S) bond vibration for the [{(bztzdtH)I_2}·I_2],[7a] [(bztzdtH)I_2][7a] and [{(bzimtH)I_2}$_2$·I_2·H_2O][7a] complexes was observed at 281−280 cm^{-1} and 255−254 cm^{-1}. Here, new bands appear at 250 and 247 cm^{-1} for compounds **1** and **2**, respectively, which can be assigned similarly.

The Raman spectra of complexes **1** and **2**, recorded in the 300−50 cm^{-1} region, show an intense band at 150.9 cm^{-1} for **1** and 148.9, 123.9 cm^{-1} for **2**; these bands are attributed to the ν_1(I−I) vibration of coordinated I_2 moieties.[7a] Iodine gives a band at 180 cm^{-1} ν(I-I) in the solid state.[7a] This shifts to lower frequencies upon coordination to a donor atom because of the reduction of the I−I bond strength. According to Deplano's classification[5a] compound **1** can be classified as being of type **A**, with a weak sulfur-iodine interaction (D···I−I), while compound **2** is of type **B**, with a stronger such interaction (D−I−I). Additionally, complexes **1** and **2** confirm the linear correlation of the d(I−I) bond lengths vs. ν(I-I) FT-Raman frequencies proposed by Deplano et.al.[9] (Figure 1).

UVIVis Spectroscopy

The visible spectra of the thione-iodine adducts in dichloromethane or chloroform exhibit one distinct absorption band at 495−505 nm, assigned to the "blue shift" band of I_2,[6h] which appears at 504 nm in free I_2 in CH_2Cl_2.[6e]

A shoulder in the range 310−360 nm could be assigned to a charge-transfer band from the HOMO of the donor to the iodine LUMO (σ_π*).[2a,5a,5d,6a] It should be noted that the CT (charge transfer) bands are not recognizable for complexes **1** and **2**, as they are most probably covered by the intra-ligand transitions ($\pi^* \leftarrow \pi$ or $\pi^* \leftarrow$ n) occurring at almost the same wavelength. The bands, however, are enhanced in intensity, with increased coefficients, in the complexes. The absorption bands at 285.5 nm in the spectrum of complex **1** and at 336 nm in the case of complex **2** were attributed to intra-ligand ($\pi^* \leftarrow \pi$) transitions.

Thermal Analysis

Thermal analysis in flowing nitrogen shows that complex **2** decomposes in two stages. The TGA and DTA data curves for complex **2** show that the first stage of its decomposition (90−120 °C) is connected with an endothermic effect and involves a 54.7% mass loss consistent with the loss of iodine (calculated mass loss 55.7%). The second stage of its decomposition (180−200 °C) connected

with an endothermic effect and involving a 31.1% mass loss is consistent with the loss of the thione.

Crystal and MolecularStructures of $[(PTU)I_2]$ (1) and $[(CMBZT)I_2]$ (2)

ORTEP diagrams of molecules **1** and **2**, as well as selected bond lengths and angles, are shown in Figure 2 and 3, respectively.

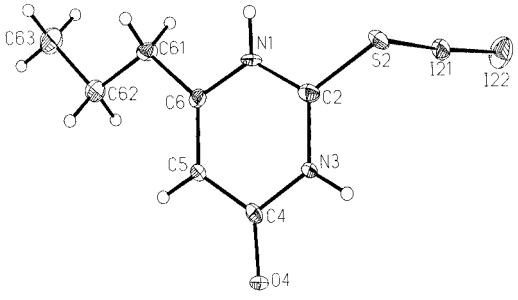

Figure 2. ORTEP diagram of molecule **1** together with the atomic numbering scheme; selected bond lengths (Å), angles [°] and torsion angles [°]: I(21)−I(22) 2.8264(4), S(2)−I(21) 2.7805(10), C(2)−S(2) 1.696(4), C(2)−N(3) 1.358(4), N(1)−C(2) 1.342(5), N(1)−C(6) 1.382(4), N(3)−C(4) 1.396(4) C(4)−O(4) 1.244(4), C(4)−C(5) 1.430(5), C(5)−C(6) 1.362(5); C(2)−S(2)−I(21) 96.05(12), S(2)−I(21)−I(22) 175.85(2), N(3)−C(2)−S(2)−I(21) 85.0(3), N(1)−C(2)−S(2)−I(21) −95.9(3), C(2)−S(2)−I(21)−I(22) −177.0(3)

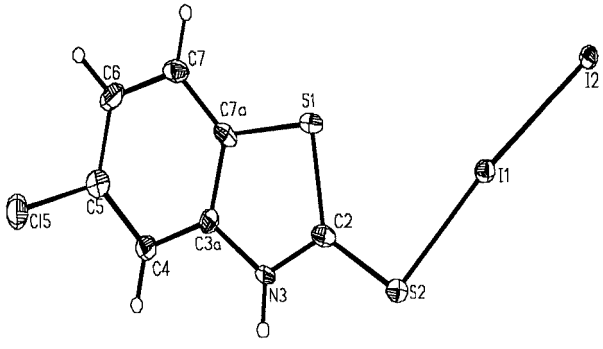

Figure 3. ORTEP diagram of molecule **2** together with the atomic numbering scheme; selected bond lengths (Å), angles [°] and torsion angles [°]: I(1)−I(2) 2.9205(7), I(1)−S(2) 2.634(2), S(2)−C(2) 1.680(6), N(3)−C(2) 1.344(7), S(1)−C(2) 1.746(5), S(1)−C(7A) 1.753(5); S(2)−I(1)−I(2) 173.78(4), C(2)−S(2)−I(1) 105.07(19), I(2)−I(1)−S(2)−C(2) −157.1(4), I(1)−S(2)−C(2)−N(3) 167.9(4), I(1)−S(2)−C(2)−S(1) −13.7(4)

The crystal structures of **1** and **2** consist of a thione ligand bonded to an iodine atom through sulfur, with S−I values of 2.7805(10) Å in **1** (Figure 2), and2.634(2) Å in **2** (Figure 3). The corresponding I−I bond lengths [2.8264(4) Å in **1** and 2.9205(7) Å in **2**] are longer than in iodine itself [gas phase: 2.677 Å;[6e] crystal: 2.715 Å at 110 K[6e]] as a result of the S···I interaction.

Extended intermolecular hydrogen bonding N(1)−H(1)···O(4)#1 [1.96 Å, with N(1)···O(4)#1 = 2.791(4) Å (x, $-y + 1/2$, $z - 1/2$)] and N(3)−H(3)···O(4)#2 [2.02 Å, with N(3)···O(4)#2 = 2.881(4)#2 Å ($-x + 1$, $-y$, $-z + 1$)] is found in complex **1** (Figure 4a). The absence of I···H−N hydrogen bonding in complex (**1**) is due to the perpendicular arrangement of iodine towards the plane of the C=S bond of PTU (vide infra). Since the presence of I···H−N hydrogen bonding in methimazole (MMI) and other related anti-thyroid drugs such as thiazolidine-2-thione (tzdtH) has been shown to play a crucial role in the inhibition[7a,8] this indicates that the inhibition of tyrosil iodination by anti-thyroid drugs should be different in the case of PTU than MMI or thzdtH. In the case of complex **2**, an intermolecular I(2)#2···H(3)−N(3) interaction [2.76 Å, with I(2)#2···N(3) = 3.573(4) Å ($-x + 1$, $y + 1/2$, $-z + 3/2$)] leads to the formation of a supramolecular assembly (Figure 4b).

The X−C=S···I torsion angles for the complexes are N(1)−C(2)−S(2)−I(21) = −95.9(3)° and N(3)−C(2)−S(2)−I(21) = 85.0(3)° for **1**, and I(1)−S(2)−C(2)−S(1) = −13.7(4)° and I(1)−S(2)−C(2)−N(3) = 167.9(4) for **2**. Thus, compound **1** can be considered to contain an almost perpendicular arrangement of iodine atoms with respect to the X−C=S plane. To the best of our knowledge this is the second structurally characterised molecule with such an arrangement, the second being [mbit·I_2].[6a] Examples include {I-S-C-S = −2.3(12)° and I-S-C-N = 174.7(13) in [{(bztzdtH)I_2}·I_2];[7a] I-S-C-S = −15.6(14)° and I-S-C-N = 166.5(15)° in [(bztzdtH)I_2];[7a] I-S-C-N = 3.0(19)° and I-S-C-N′ = −179.7(13)° in [{(bzimtH)I_2}$_2$·I_2·H_2O];[7a] I-S-C-X = −1.5(9)° in [mdtt·I_2];[5c] and I-S-C-X = −96.4(4)° in [mbit·I_2][6a]}. Compound **2**, on the other hand, can be considered as having an almost co-planar arrangement. Finally, the values for the S−I−I angles also imply an almost linear arrangement [S(2)−I(21)−I(22) = 175.85(2)° in (**1**) and S(2)−I(1)−I(2) = 173.78(4)° in (**2**)].

According to the value of the I−I bond order (n) defined by Pauling's equation:[10a]

$$d(\mathrm{I-I}) = d_o - 0.85 \cdot \log(n)$$

where d_o is the I−I bond length of I_2 in the gas phase (2.67 Å),[10b] Bigoli et al.[6a] have classified I_2 adducts into three classes: types **A**, **B** and **C**. When the value of the I−I bond order (n) is greater than or equal to 0.6 [d(I−I) < 2.85 Å] the adduct is classified as type **A**, while if n is less than or equal to 0.4 [d(I−I) > 3.01 Å] the compound is of type **C**;[6a] compounds with intermediate values are of type **B**.[6a] The I−I bond-order values calculated for the complexes studied in this work are 0.654 and 0.507 for complexes **1** and **2**, respectively. Therefore, complex **1** can be classified as type **A**, with a weak S−I interaction, while complex **2** is of type **B**. This is consistent with the classification derived from the spectroscopic data above. Thus, PTU forms a weak CT complex with iodine, in contrast to CMBZT or thiazolidine-2-thione (tzdtH). TzdtH has also been used as anti-thyroidal agent.[1] This molecule reacts with iodine in a molar ratio of 1:2 to form the strong CT

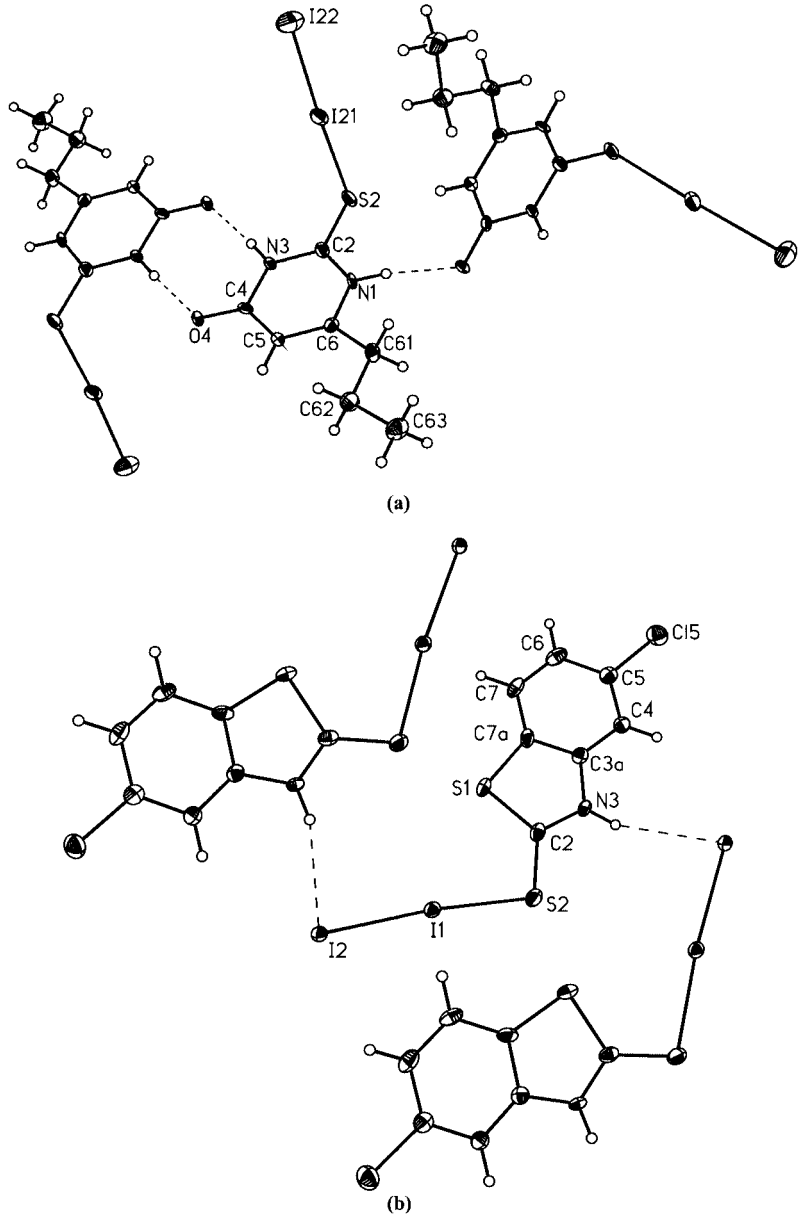

Figure 4. Intramolecular linkages via: (a) N−H···O interactions in **1** and (b) N−H···I interactions in **2**

complex $[\{(tzdtH)_2I^+\}\cdot I_3^-\cdot 2I_2]$,[7a] and is able to retain a total of four iodine molecules per two ligand molecules. On the other hand, MMI reacts with iodine to yield a CT complex which consists of the dication of the disulfite of MMI and I_8^{2-} counteranions $[(C_4H_6N_2S)_2]I_8$.[8] These findings also confirm that the inhibition of tyrosil iodination by anti-thyroid drugs should be different in the case of PTU than MMI or tzdtH, as proposed by Nakataka et.al.[11]

Conclusions

In conclusion, thioamides exhibiting anti-thyroidal activity against hyperthyroidism (Graves' disease) can be classified into two categories: (i) thioamides, such as MMI[8] or tzdtH,[7a] which are strong donors to iodine and form ionic salts, and (ii) thioamides like PTU, which are able to form weak charge-transfer molecules with iodine. Thioamides with intermediate donor activity to iodine — CMBZT, benzothiazole-2-thione (bztdtH)[7a] or benzimidazole-2-thione (bzimtH)[7a] — are able to bind only one I_2 molecule strongly and show no anti-thyroid activity. Thus, it seems that whereas drugs like MMI etc. interfere with the iodination mechanism by forming active iodine species in competition with the tyrosil residues of thyroglobuline[8,12,13] (Scheme 1), drugs like PTU appear to interfere either in the formation of the thyroid peroxide (TPO)-iodonium complex[12,13] or inhibit the activity of iodothyronine deiodinase (ID-1-SeH), an enzyme responsible for the monodeiodination of the **T4** prohormone to the **T3** hormone, as proposed by Berry et al.[13a] and later supported by du Mont et al.[13b] (Scheme 1). This is in agreement with

the proposal of Nakataka et al.,[11] supporting the difference in the inhibition mechanism of these type of drugs.

Experimental Section

Synthesis and Crystallisation of the Molecules: Complexes **1** and **2** were prepared by mixing dichloromethane solutions of iodine with a suspension of the appropriate thione in dichloromethane solution in molar ratios of 1:1 or 2:1, in air, at 0 °C, with continuous stirring, for 24 hours. The mixtures were then filtered and the resulting clear solutions were kept in the refrigerator for several days. Dark crystals of the complexes suitable for single-crystal analysis by X-ray crystallography were then grown and isolated by filtration. The reactions were also carried out in H_2O. The insoluble dark brown powders obtained were recrystallized from dichloromethane to yield the same products as previously.

Complex 1: Yield 0.085 g, (20%); m.p. 144−146 °C. $C_7H_{10}N_2I_2OS$ (424.0): calcd. C 19.83, H 2.37, N 6.61, S 7.56; found C 20.29, H 2.43, N 6.68, S 7.79. UV/Vis (CH_2Cl_2): λ_{max} (logε) = 512.5 nm (3.12), 287.5 (4.25). ^{1}H NMR ($CDCl_3$): δ = 10.05 [s, 1 H, HN(3)−C(2)], 9.74 [s, 1 H, HN(1)−C(2)], 2.41−2.35 [t, 2 H, $H_2C(61)$-C(6) of *n*-Pr], 1.73−1.26 [m, 2 H, $H_2C(62)$-C(61) of *n*-Pr], 1.06−1.00 [t, 3 H, $H_3C(63)$-C(62) of *n*-Pr] ppm.

Complex 2: Yield 0.050 g, (22%); m.p. 160−165 °C. $C_7H_4ClI_2NS_2$ (455.5): calcd. C 18.46, H 0.88, N 3.08, S 14.08; found C 17.90, H 0.63, N 2.80, S 14.07. UV/Vis (CH_2Cl_2): λ_{max} (logε) = 504 nm (2.93), 336 (4.36), 229 (4.41). ^{1}H NMR ($CDCl_3$): δ = 8.02 (s, 2 H, NH), 7.41−7.31 (m, 4 H, aromatic) ppm.

Crystal Data: Data were collected by the ω-scan technique in the $\theta-2\theta$ range 3.53 to 29.30° for **1** and 3.55 to 29.24° for **2** on a KUMA KM4CCD four-circle diffractometer[14a] with CCD detector, using graphite-monochromated Mo-K_α (λ = 0.71073 Å). Cell parameters were determined by a least-squares fit.[14b] All data were corrected for Lorentz-polarization effects and absorption.[14b] The structures were solved by direct methods with SHELXS-97[15] and refined by full-matrix least-squares procedures on F^2. All non-hydrogen atoms were refined anisotropically, hydrogen atoms were located at calculated positions and refined as a "riding model" with isotropic thermal parameters fixed at 1.2-times the U_{eq}'s of the appropriate carrier atom.

1: $C_7H_{10}I_2N_2OS$, mol. wt. = 424.03, monoclinic space group $P2_1/c$, a = 9.8501(7), b = 10.3101(7), c = 12.0287(8) Å, β = 99.707(6)°, V = 1204.09(14) Å^3, Z = 4, T = 120(1) K, ρ(calcd.) = 2.339 g cm^{-3}, μ = 5.365 mm^{-1}, reflections collected 2997. Final R indices [$I > 2\sigma(I)$]: $R1$ = 0.0323, $wR2$ = 0.0745.

2: $C_7H_4ClI_2NS_2$, mol. wt. = 455.48, orthorhombic space group $P2_12_12_1$, a = 4.1650(10), b = 9.691(2), c = 28.471(6) Å, V = 1149.2(4) Å^3, Z = 4, T = 293(2) K, ρ(calcd.) = 2.633 g cm^{-3}, μ = 6.023 mm^{-1}, reflections collected 7301. Final R indices [$I > 2\sigma(I)$]: $R1$ = 0.0275, $wR2$ = 0.0528.

CCDC-189659 (**1**) and -189660 (**2**) contain the supplementary crystallographic data for this paper. These data can be obtained free of charge at www.ccdc.cam.ac.uk/conts/retrieving.html [or from the Cambridge Crystallographic Data Centre, 12, Union Road, Cambridge CB2 1EZ, UK; Fax: (internat.) +44-1223/336-033; E-mail: deposit@ccdc.cam.ac.uk].

Acknowledgments

This work was carried out in partial fulfillment of the requirements for an MSc thesis of C. D. A. (**1**) and G. J. C. (**2**) within the graduate program EPEAEK in Bioinorganic Chemistry financed by the Ministry of Education of Greece and coordinated by Professor N. Hadjiliadis. A NATO grant awarded to N. H. and I. S. B. is also acknowledged.

[1] [1a] Martidale, *The Extra Pharmacopoeia*, 28th edition, The Pharmaceutical Press, London **1982**. [1b] J. Buxeraud, *Traite de Chimie therapeutique*, Tec et Doc Lavoisier, Paris, **1995**, vol 4, ch 18.

[2] [2a] C. Laurence, M. J. El Ghomari, J-Y. Le Questel, M. Berthelot, R. Mokhlisse, *J. Chem. Soc., Perkin Trans.* **1998**, *2*, 1545−1551. [2b] C. Laurence, M. J. El Ghomari, M. Lucon, *J. Chem. Soc., Perkin Trans.* **1998**, *2*, 1159−1162. [2c] C. Laurence, M. J. El Ghomari, M. Berthelot, *J. Chem. Soc., Perkin Trans.* **1998**, *2*, 1163−1166.

[3] [3a] J. Leclerc, J. Orgiazzi, B. Rousser, J. L. Schlienger, J. L. Wemeau, *La Thyroide*, Exapnsion Scientifique Francaise, Paris **1992**. [3b]C. Raby, J. Buxeraud, *Eur. J. Med Chem.* **1980**, *15*, 425−430. [3c] J. Buxeraud, A. B. Absil, J. Claude, C. Raby, G. Catazano, C. Beck, F. Claude, *Eur. J. Med Chem.* **1985**, *20*, 43−50.

[4] [4a] M. Esseffar, W. Bouab, A. Lamsabhi, J. L. M. Abboud, R. Notario, M. Yanez, *J. Am. Chem. Soc.* **2000**, *122*, 2300−2308. [4b] P. D. Boyle, J. Christie, T. Dyer, S. M. Godfrey, I. R. Howson, C. McArthur, B. Omar, R. G. Pritchard, G. R. Williams, *J. Chem. Soc., Dalton Trans.* **2000**, 3106−3112.

[5] [5a] F. Bigoli, P. Deplano, A. Ienco, C. Mealli, M. L. Mercuri, M. A. Pellinghelli, G. Pintus, G. Saba, E. F. Trogu, *Inorg. Chem.* **1999**, *38*, 4626−4636. [5b] F. Demartin, F. A. Devillanova, A. Garau, F. Isaia, V. Lippolis, G. Verani, *Polyhedron* **1999**, *18*, 3107−3113. [5c] N. Bricklebank, P. J. Skabara, D. E. Hibbs, M. B. Hursthouse, K. M. A. Malik, *J. Chem. Soc., Dalton Trans.* **1999**, 3007−3014. [5d] M. C. Aragoni, M. Arca, F. A. Devillanova, A. Garau, F. Isaia, V. Lippolis, G. Verani, *Coord. Chem. Rev.* **1999**, *184*, 271−290.

[6] [6a] F. Bigoli, P. Deplano, M. L. Mercuri, M. A. Pellinghelli, A. Sabatini, E. F. Trogu, A. Vacca, *J. Chem. Soc., Dalton Trans.* **1996**, 3583−3589. [6b] F. Cristiani, F. A. Devillanova, F. Isaia, V. Lippolls, G. Verani, F. Demartin, *Polyhedron* **1995**, *14*, 2937−2943. [6c] F. Demartin, P. Deplano, F. A. Devillanova, F. Isaia, V. Lippolis, G. Verani, *Inorg. Chem.* **1993**, *32*, 3694−3699. [6d] F. Cristiani, F. Demartin, F. A. Devillanova, F. Isaia, G. Saba, G. Verani, *J. Chem. Soc., Dalton Trans.* **1992**, 3553−3560. [6e] F. Freeman, J. W. Zi1ler, H. N. Po, M. C. Keindl, *J. Am. Chem. Soc.* **1988**, *110*, 2586−2591. [6f] F. H. Herbstein, W. Schwotzer, *J. Am. Chem. Soc.* **1984**, *106*, 2367−2373. [6g] F. H. Herbstein, W. Schwotzer, *Angew. Chem. Int. Ed. Engl.* **1982**, *21*, 219. [6h] F. A. Devillanova, G. Verani, *Tetrahedron* **1979**, *35*, 511−514.

[7] [7a] V. Daga, S. K. Hadjikakou, N. Hadjiliadis, M. Kubicki, J. H. Z. dos Santos, I. S. Butler, *Eur. J. Inorg. Chem.* **2002**, 1718−1728. [7b] J. H. Z. dos Santos, I. S. Butler, V. Daga, S. K. Hadjikakou, N. Hadjiliadis, *Spectrochimica Acta Part A* **2002**, *58*, 2725−2735.

[8] M. C. Aragoni, M. Arca, F. Demartin, F. A. Devillanova, A. Garau, F. Isaia, V. Lippolis, G. Verani, *J. Am. Chem. Soc.* **2002**, *124*, 4538−4539.

[9] P. Deplano, F. A. Devillanova, J. R. Ferraro, F. Isaia, V. Lippolis, M. L. Mercuri, *Appl. Spectrosc.* **1992**, *46*, 1625−1629.

[10] [10a] L. Pauling, *The Nature of the Chemical Bond*, 3rd edn, Cornell University Press, Ithaca, New York, **1960**. [10b] H. B. Burgi, *Angew. Chem. Int. Ed. Engl.* **1975**, *14*, 460−473.

[11] A. Nakataka, H. Hidaka, *J. Clin. Endocrinol. Metab.* **1976**, *43*, 152−158.

[12] [12a] D. R. Morris, L. P Hager, *J. Biol. Chem.* **1966**, *241*, 3582−3589. [12b] A. Taurog, *Endocrinology* (Ed.: L. DeGroot), Academic Press, Inc. London, **1979**, vol 1, 331.

[13] [13a] M. J. Berry, J. D. Kieffer, J. W. Harney, P. R. Larsen, *J. Biol. Chem.* **1991**, *266*, 14155−14158. [13b] W. W. du Mont, G.

Mugesh, C. Wismach, P. G. Jones, *Angew. Chem. Int. Ed.* **2001**, *40*, 2486−2489.
[14] [14a] KUMA KM-4CCD user manual, KUMA Diffraction, Wroclaw, Poland 1999. [14b] CrysAlis, for reduction of the data from KUMA CCD diffractometer, KUMA Diffraction, Wroclaw, Poland 1999.
[15] G. M. Sheldrick, SHELXS-97 (Release 97-2), for crystal structure solution, and SHELXL-93, for refinement of crystal structures, Institut fur Anorganische Chemie, University of Göttingen, Germany.

Received November 12, 2002
[I02621]

The Human Telomeric Sequence $(T_2AG_3)_n$ is Efficiently Cross-Linked by AN1 Binding to the Platinum of a *trans*-$Pt(NH_3)_2$ Chelate of an Antisense Oligo-2′-*O*-Methylribonucleotide

Sandrine Perrier,[a] Frank Seela,[b] Annie Schwartz,[c] Marc Leng,[c][†] and Jean-Claude Chottard*[a]

Keywords: Platinum / DNA / RNA / Chelates / Bioinorganic chemistry

In order to irreversibly cross-link an antisense oligonucleotide to the human telomeric sequence $(T_2AG_3)_n$, the inter-strand bridging rearrangement described by Leng et al. was investigated on (21-mer antisense) (20-mer target) duplexes: (G*NG*)(TA) → (G*NG)(TA*), G*NG* being a *trans*-[$Pt(NH_3)_2$\{1,3-(GNG)-*N7*-G,*N7*-G\}] chelate with N = U or T. Three different duplexes were studied, confirming first that for a DNA target strand the rearrangement was faster with a platinated oligo-2′-*O*-methylribonucleotide than with a deoxy oligonucleotide as antisense strand. Second, a telomeric DNA target strand was cross-linked faster than an all-purine oligonucleotide containing a single TA doublet. Accordingly, the half time of formation of the cross-linked hybrid duplex [2′-OMe-r(CCCUAACCCG*UGACCCUAACCC)]·[$d(T_2AG_3)_2(TTA*G_3)(T_2AG_3)$] is one minute, compared with the nine days required for the complete formation of the bridged d(CTCCTG*TGTCTC)·d(GAGATA*AGGAG) duplex. The NMR analysis of the latter showed that the platinum cross-link involves the A*N1 moiety as ligand. The timescale difference between the two reactions raised the question of an eventual kinetic cross-link which might isomerize to the final one observed. This question was addressed using 1-deazaadenine in the TA doublet of the three target strands of this work. No cross-linking reaction was observed, proving that AN1 is the bridging atom in all the cases studied so far.

(© Wiley-VCH Verlag GmbH & Co. KGaA, 69451 Weinheim, Germany, 2003)

Introduction

Transplatin *trans*-diamminedichloroplatinum(II) is clinically ineffective, as opposed to its stereoisomer cisplatin *cis*-diamminedichloroplatinum(II).[1−4] Nevertheless it reacts with both single- and double-stranded DNA. On the former, it gives an intra-strand *trans*-[$Pt(NH_3)_2$\{1,3-d(GNG)-*N7*-G,*N7*-G\}] platinum chelate (named G*NG*) with the sequences d(GNG), N being any nucleotide but G.[5] Such adducts were found to be stable in single-stranded oligonucleotides, except that formed on the d(CG*NG*) sequence, which rearranges into the 1,4-d(C*GNG*)-*N3*-C,*N7*-G chelate.[6,7] Upon pairing with the complementary strands, the G*NG* chelates rearrange into inter-strand adducts. In DNA/DNA duplexes and DNA/RNA hybrids, inter-strand cross-links are formed slowly and involve mainly the N7 atom of the 5′ guanine of the initial chelate and the N3 atom of its complementary cytosine.[8−10]

The discovery of this reaction allowed the conception of a new tool for antisense strategy, although therapeutic applications would require cross-linking reactions with short half times compared to most mRNA half-lives, which are of the order of minutes.[11] An investigation of the influence of the series and of the bases of the antisense and target strands led to the selection of hybrid duplexes between a platinated oligo-2′-*O*-methylribonucleotide and a target RNA containing a 5′-pyrimidine/adenine doublet in place of the triplet complementary to the GNG sequence. In these cases, the inter-strand cross-link is formed between the N7 atom of the 5′-G* of the intra-strand chelate and the facing A on the opposite strand after a few minutes.[12,13] The antisense platinated oligo-2′-*O*-methylribonucleotides can be relatively resistant to nucleases. They can enter the cells where they bind specifically and irreversibly to mRNA. The platinum complex bridging both oligonucleotides resists translating ribosomes and leads to inhibition of mRNA expression.[12,14,15] All these results were obtained with purine-rich target strands, suggesting that the platinated oligonucleotides could also bind irreversibly to the human telomeric sequence $(T_2AG_3)_n$ and therefore become potential inhibitors of telomerase activity.[16−18]

[a] Laboratoire de Chimie et Biochimie Pharmacologiques et Toxicologiques, UMR8601, Université René Descartes, 45 rue des Saints-Pères, 75270 Paris Cedex 06, France
Fax: (internat.) + 33-1/42868387
E-mail: jean-claude.chottard@biomedicale.univ-paris5.fr
[b] Laboratorium für Organische und Bioorganische Chemie, Institut für Chemie, Universität Osnabrück, Barbarastr. 7, 49069 Osnabrück, Germany
[c] Centre de Biophysique Moléculaire, CNRS, Rue Charles Sadron, 45071 Orléans Cedex 2, France
[†] Deceased May 2000

As already reported with target r-UA oligonucleotides,[12,13] we found that the most efficient platinated antisense strands belong to the 2′-*O*-methylribonucleotide series, with the G*NG* triplet facing a d-TA doublet. The fast cross-linking of the platinated ribonucleotide with the telomeric sequence (timescale of a few minutes) compared to that observed in the case of the bridged d(CTCCTG*TGTCTC)·d(GAGATA*AGGAG) duplex (timescale of a few days) raised the question of the possibility of two bridging pathways and/or the existence of a kinetic and a final products. For the cross-linked deoxy duplex, NMR spectroscopy has shown the presence of a *trans*-G*(*N7*)-Pt$(NH_3)_2$-A*(*N1*) bridge.[19] The presence of the 1,3-chelate, the base mismatch, the hybrid pairing and the missing nucleotide on the target strand could allow adenine N7 and/or N1 nucleophilic attack on platinum. This prompted us to check the AN1 involvement in our reactions. We have replaced adenine by 1-deazaadenine (A˙) in the (TA˙) target DNA strand of three duplexes where the G*NG* chelate belongs to DNA or 2′-OMe-RNA strands. No inter-strand cross-link was formed in any of the (G*NG*)(TA˙) duplexes containing 1-deazaadenine, showing the generality of the AN1 involvement (Scheme 1).

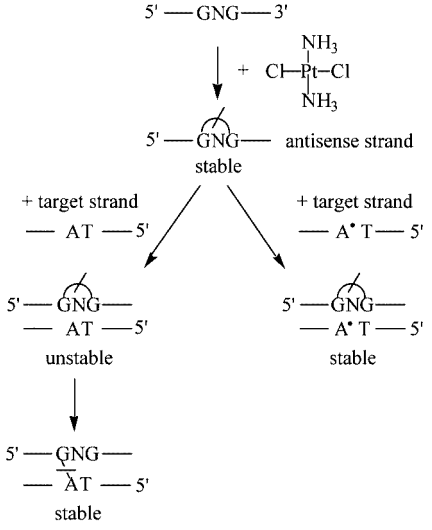

Scheme 1. Inter-strand cross-linking reaction, within a duplex structure, between the adenine of the TA target strand and the platinum atom of the G*NG* intra-strand chelate of the antisense strand; G*NG* = *trans*-[Pt$(NH_3)_2${1,3-(GNG)-*N7*-G,*N7*-G}], G* indicates an *N*7-bound guanine; the bridging reaction is not observed when A in the target strand is replaced by 1-deazaadenine A˙

Results and Discussion

The four antisense oligonucleotides used in this work were 21-mers − either DNA or 2′-OMe-RNA − with a G*NG* intra-strand *trans*-Pt$(NH_3)_2$ chelate in a central position (Figure 1). All of them were ^{32}P labelled at the 5′ position. The (G*NG*) strand was mixed with an equal amount of a (TA) or (TA˙) 20-mer target strand. In two cases, this target strand was the human telomeric $(T_2AG_3)_3$ sequence. Solid-phase synthesis of the oligonucleotides containing 1-deaza-2′-deoxyadenosine was performed in Dr. F. Seela's laboratory (Osnabrück University, Germany). The incorporation of the synthesized 1-deaza-2′-deoxyadenosine was checked by HPLC analysis of the nucleoside composition after enzymatic hydrolysis of the oligomers.[20,21] The duplex oligonucleotides (2 μM) were incubated at 37 °C for 165 minutes. Aliquots were withdrawn at regular time intervals and analyzed by polyacrylamide gel electrophoresis under denaturing conditions. As shown in Figure 2, when the G*NG* chelate is facing the 5′-TA doublet, a new band appears at the expense of that of the platinated single-stranded DNA or 2′-OMe-RNA. This new band migrates slower than that of the antisense strand. It corresponds to the antisense and target strands cross-linked by the *trans*-[Pt$(NH_3)_2${(*N7*-G),d(A)}] bridge as shown by Maxam−Gilbert footprinting, in agreement with previous results.[8,10,13] At the end of the incubation period (165 min), about 90% and 100% of the platinated antisense strand

1	5′ UCUCCUCUG*UG*UCUCCUUCUU AGAGGAGA A T AGAGGAAGAA 5′	2′-OMe-RNA DNA
2	5′ AACCCTAACCCG*TG*ACCCTAA TTGGGATTGGG A T TGGGATT 5′	DNA DNA
3	5′ AACCCUAACCCG*UG*ACCCUAA TTGGGATTGGG A T TGGGATT 5′	2′-OMe-RNA DNA
4	5′ CCCUAACCCG*UG*ACCCUAACCC GGGATTGGG A T TGGGATTGGGATT 5′	2′-OMe-RNA DNA

Figure 1. The paired oligonucleotides **1**−**4** of this study; at the rearrangement site, the intra-strand cross-link G*NG* (G* denotes an *N*7 platinated guanine; N = T or U) faces the 5′-TA doublet; in the text the intra-strand platinated 21-mer is called the (G*NG*) antisense strand, and the target 20-mer either the (TA) or (TA˙) strand according to the presence of adenine or 1-deazaadenine

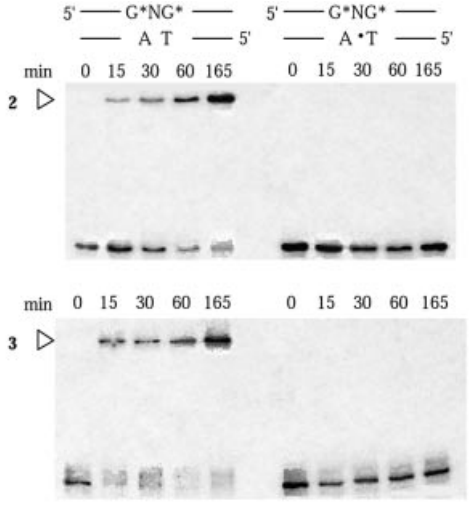

Figure 2. Cross-linking reactions within the DNA/DNA (**2**) and 2′-OMe-RNA/DNA (**3**) duplexes monitored by electrophoresis on a denaturing 20% polyacrylamide gel; the (G*NG*) strands were ^{32}P 5′-end labelled and paired with their complementary telomeric DNA target strand containing either TA or TA˙ (A˙ = 1-deazaadenine); the duplexes were incubated at 37 °C in 150 mM NaCl, 5 mM phosphate buffer, pH 7.5 and 0.2 mM EDTA; incubation times (in minutes) are given above the lanes; the inter-strand adduct is indicated by an arrowhead on the left

were cross-linked to the target strand within the platinated DNA/DNA duplex **2** and 2′-OMe-RNA/DNA hybrids **3** and **4**, respectively (Figure 2), with respective $t_{1/2}$ values of 40 minutes for the former and one minute for the latter two. The half reaction time for the platinated 2′-OMe-RNA/DNA hybrid **1** is 18 minutes. It is noteworthy that the rearrangement is faster when the platinated antisense strand is a 2′-OMe-ribonucleotide (see **2** vs. **3**), as already found.[12,13] Moreover, it is faster when the target deoxyoligonucleotide is the human telomeric sequence $(T_2AG_3)_n$ (see **1** vs. **3** and **4** in Figure 3).

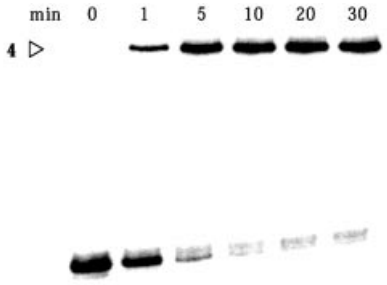

Figure 3. Cross-linking reaction within the 2′-OMe-RNA-(CCCUAACCCG*UG*ACCCUAACCC)/DNA$(T_2AG_3)_4$ hybrid **4**; autoradiogram of a denaturing 20% polyacrylamide gel; the (G*UG*) strand was ^{32}P 5′-end labelled; the hybrid was incubated at 37 °C in 0.2 M NaCl, 5 mM phosphate buffer, pH 7.5 and 0.2 mM EDTA; incubation times (in minutes) are given above the lanes; the inter-strand adduct is indicated by an arrowhead on the left

Replacing the adenine of the TA doublet by a 1-deazaadenine (TA$^{\cdot}$) suppresses the inter-strand cross-linking within any of the three paired sequences **1**−**3**. It must be noted that after 165 minutes, a product migrating like two cross-linked strands was present in a very small amount, accounting for ca. 1% of the total radioactivity for the systems **1** and **2**, and 4% for **3**. This product might result from a slow cross-linking reaction involving the A$^{\cdot}$N7 atom. To check further an eventual rearrangement of the 1,3-intra-strand chelate facing a 1-deazaadenine within the systems studied, the incubation was extended by 48 h for the platinated DNA/DNA duplex **2** (not shown). Some products appeared, with migration similar to that of as two cross-linked strands, and accounting for less than 2% of the total radioactivity. The amount of isolated material was too small to allow any further characterization. These data suggest that the N7 atom of the TA adenine, facing the G*NG* platinum chelate, is not competitive with the N1 atom of the same adenine when binding to the metal and cross-linking the antisense and target strands.

These results agree with the very slow rate of isomerization observed when the UA doublet of a target strand is replaced by UG at the rearrangement site.[12] They also agree with the NMR analysis of the *trans*-Pt(NH_3)$_2$ cross-linked DNA/DNA duplex d(CTCCTG*TGTCTC)·d(GAGATA*AGGAG), which showed that the A*N1 atom is bound to platinum.[19] It is noteworthy that the much longer time needed for the bridging of this duplex (nine days for complete conversion) compared to the speed of our reactions (one minute), shows that the AN1 binding to the platinum is a common feature of all these rearrangements, whatever their efficiency, and can be compared to the (G*NG*)(CN′C) → (G*NG)(CN′C*) cross-linking involving the 3′-CN3 of the target strand. Within a B-DNA the AN1 and CN3 atoms occupy similar positions and this might be retained in the (G*NG*)(CN′C) and (G*NG*)-(TA) duplexes despite the mispairing and the missing nucleotide at the rearrangement core. This could be favored by the stabilizing effect of the 2′-OMe-ribonucleotide nature of the (G*NG*) strand.[13]

In conclusion, we have shown that a platinated 2′-OMe-RNA-antisense strand efficiently cross-links a $(T_2AG_3)_n$ telomeric target with a one minute half-reaction time. This irreversible binding to telomeric sequences might inhibit telomerase activity. Moreover, our results suggest that all the rearrangements involving the G*NG*/TA core involve the AN1 atom of the target strand acting as a bridging ligand to platinum, independently of the nature of the antisense strand and of the cross-linking rate.

Experimental Section

Materials and Methods: The oligodeoxyribonucleotides and oligo-2′-*O*-methyl ribonucleotides (from Eurogentec Belgium) were purified by ion-exchange chromatography (monoQ column, Pharmacia) as described previously.[12,13] The 1-deaza-2′-deoxyadenosine phosphoramidite was synthesized and employed in solid-phase oligonucleotide synthesis.[20−23] The purified oligonucleotides containing 1-deazaadenine were checked by hydrolysis with snake-venom phosphodiesterase followed by alkaline phosphatase yielding the monomeric nucleosides. The presence of the modified nucleotide was controlled by HPLC analysis of the nucleoside composition. The T4 polynucleotide kinase was purchased from Boehringer Mannheim and the radioactive products from Amersham. All other chemicals were purchased from Merck, except *trans*-diamminedichloroplatinum(II), which was a gift of Johnson Matthey (UK).

Platination: The single-stranded oligonucleotides containing a single GNG triplet were reacted with transplatin as described previously.[12,13] The platinated oligonucleotides were incubated in the presence of thiourea to remove the monofunctional adducts[6] and were purified on a monoQ column. The formation of the *trans*-[Pt(NH_3)$_2$\{1,3-(GNG)-*N7*-G,*N7*-G\}] intra-strand chelates was verified by the non-reactivity of the platinated G residues with dimethylsulfate.[10,13]

Linkage Isomerization Reaction: The 5′[^{32}P]-labelled platinated oligonucleotides (2 μM) were mixed at 0 °C with their complementary strands and then incubated at 37 °C in 5 mM phosphate buffer at pH 7.5, 150 mM NaCl and 0.2 mM EDTA. Aliquots were withdrawn at various times and analyzed on electrophoresis gel under denaturing conditions (20% polyacrylamide/7 M urea). The disappearance of the labelled strands containing the intra-strand chelate was monitored by quantitation of the gel bands with a Molecular Dynamics PhosphorImager using ImageQuant software version 3.3 for data processing. The location of the inter-strand cross-link was deduced from Maxam−Gilbert footprinting.[8]

Acknowledgments

We are indebted to the EC Biomed programme "Modulation of gene expression by platinated oligonucleotides" (BMHA CT 97-

2485) and Ministère de la Recherche (doctoral fellowship for S.P.) for financial support. We thank Johnson-Matthey, Inc. for a generous loan of *trans*-diamminedichloroplatinum(II).

[1] A. Eastman, *Pharmacol. Ther.* **1987**, *34*, 155−166.
[2] S. L. Bruhn, J. H. Toney, S. J. Lippard, in *Progress in Inorganic Chemistry: Bioinorganic Chemistry* (Ed.: S. J. Lippard), John Wiley & Sons Inc., New York **1990**, *38*, 477−516.
[3] B. Lippert, *Met. Ions Biol. Syst.* **1996**, *33*, 105−141.
[4] J. M. Malinge, M. Leng, in *Cisplatin, Chemistry and Biochemistry of a Leading Anticancer Drug* (Ed.: B. Lippert), Wiley VCH **1999**, 159−180.
[5] C. A. Lepre, L. Chassot, C. E. Costello, S. J. Lippard, *Biochemistry* **1990**, *29*, 811−823.
[6] K. M. Comess, C. E. Costello, S. J. Lippard, *Biochemistry* **1990**, *29*, 2102−2110.
[7] R. Dalbiès, M. Boudvillain, M. Leng, *Nucleic Acids Res.* **1995**, *23*, 949−953.
[8] R. Dalbiès, D. Payet, M. Leng, *Proc. Natl. Acad. Sci. USA* **1994**, *91*, 8147−8151.
[9] V. Brabec, M. Leng, *Proc. Natl. Acad. Sci. USA* **1993**, *90*, 5345−5349.
[10] M. Boudvillain, R. Dalbiès, C. Aussourd, M. Leng, *Nucleic Acids Res.* **1995**, *23*, 2381−2388.
[11] B. Alberts, D. Bray, J. Lewis, M. Raff, K. Roberts, J. D. Watson, *Molecular Biology of the Cell*, Garland Publishing Inc., New York **1983**, 611−668.
[12] M. Boudvillain, M. Guérin, R. Dalbiès, T. Saison-Behmoaras, M. Leng, *Biochemistry* **1997**, *36*, 2925−2931.
[13] C. Colombier, M. Boudvillain, M. Leng, *Antisense Nucleic Acid Drug Dev.* **1997**, *7*, 397−402.
[14] J. E. Gee, I. Robbins, A. C. Van Der Laan, J. H. Van Boom, C. Colombier, M. Leng, A. M. Raible, J. S. Nelson, B. Lebleu, *Antisense Nucleic Acid Drug Dev.* **1998**, *8*, 103−111.
[15] K. Aupeix-Scheidler, S. Chabas, L. Bidou, J. P. Rousset, M. Leng, J. J. Toulmé, *Nucleic Acids Res.* **2000**, *28*, 438−445.
[16] J. W. Shay, W. E. Wright, *Curr. Opin. Oncol.* **1996**, *8*, 66−71.
[17] C. W. Greider, *Proc. Natl. Acad. Sci. USA* **1998**, *95*, 90−92.
[18] E. Raymond, D. Sun, S. F. Chen, B. Windle, D. D. Von Hoff, *Curr. Opin. Biotechnol.* **1996**, *7*, 583−591.
[19] B. Andersen, E. Bernal-Mèndez, M. Leng, E. Sletten, *Eur. J. Inorg. Chem.* **2000**, *6*, 1201−1210.
[20] F. Seela, T. Wenzel, *Heterocycles* **1993**, *36*, 237−242.
[21] F. Seela, T. Wenzel, *Helv. Chim. Acta* **1994**, *77*, 1485−1499.
[22] G. Cristalli, P. Franchetti, M. Grifantini, S. Vittori, T. Bordoni, C. Geroni, *J. Med. Chem.* **1987**, *30*, 1686−1688.
[23] G. Cristalli, S. Vittori, A. Eleuteri, M. Grifantini, R. Volpini, G. Lupidi, L. Capolongo, E. Pesenti, *J. Med. Chem.* **1991**, *34*, 2226−2230.

Received October 28, 2002
[I02595]

EurJIC
European Journal of Inorganic Chemistry

May 2003
Issue 9
Pages 1645–1828

Papers available ahead of print in Early View at www.interscience.wiley.com

Earliest available Table of Contents:
Automatically, free of charge by e-mail through
www.interscience.wiley.com/alerts

COVER PICTURE

The cover picture shows a schematic illustration of the unusual inorganic-organic hybrid structures (upper right) formed by linking of the inorganic building units through organic linkers. The structures of two different compounds (bottom) containing the inorganic cadmium chloride chains (upper left corner) linked by oxalate and piperazine moieties into two and three dimensions are also shown. Color scheme: Cd – yellow; Cl – green; O – red; N – violet; C – blue. Details are discussed in the article by C. N. R. Rao et al. on p. 1675 ff.

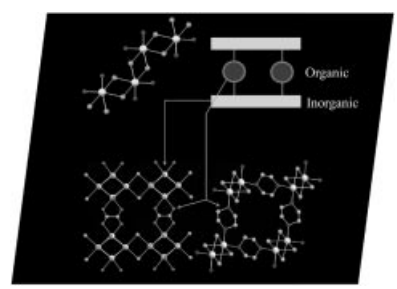

MICROREVIEW

Contents

1659 **C. Graiff, G. Predieri, A. Tiripicchio***

Phosphane-Substituted Selenido–(carbonyl)-iron and –(carbonyl)ruthenium Clusters: Structures, Fluxionality and Reactivity

Keywords: Crystal structures / Fluxional behaviour / Iron clusters / Ruthenium clusters / Selenium compounds

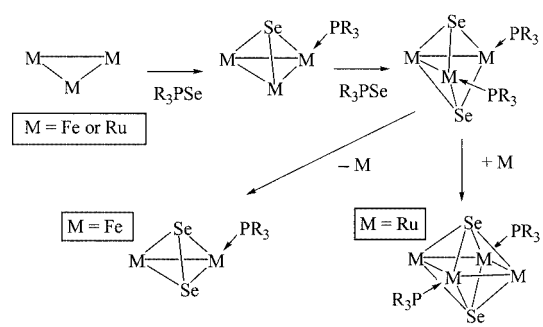

 © 2003 Wiley-VCH Verlag GmbH & Co. KGaA, Weinheim

SHORT COMMUNICATION

1669 **I. A. Koval, D. Pursche, A. F. Stassen, P. Gamez, B. Krebs, J. Reedijk***

The Dicopper(II) Complex of the Novel Asymmetric Dinucleating Ligand Hpy3asym as a Structural Model of Catechol Oxidase

Keywords: Copper / Cyclic voltammetry / Enzyme models / Ligand design / Magnetic properties

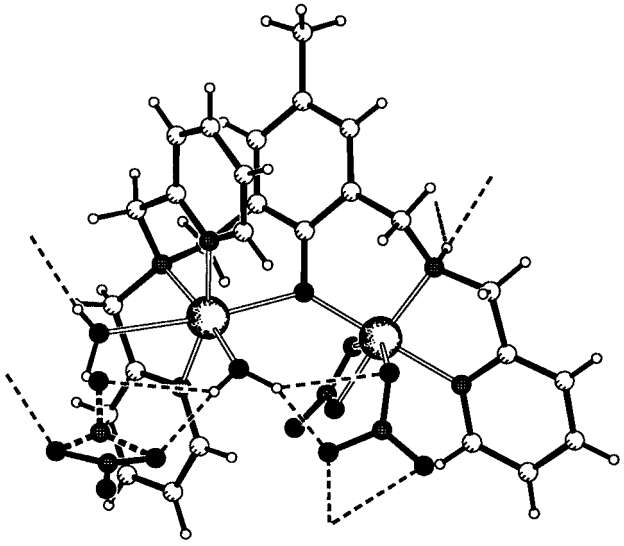

FULL PAPERS

1675 **R. Vaidhyanathan, S. Natarajan, C. N. R. Rao***

Solvothermal Synthesis of a Layered Open-Framework Chlorocadmium Oxalate, $Cd_2(C_2O_4)_{0.5}Cl_3NaCl{\cdot}4H_2O$

Keywords: Materials science / Cadmium / Solvothermal synthesis / Metathesis

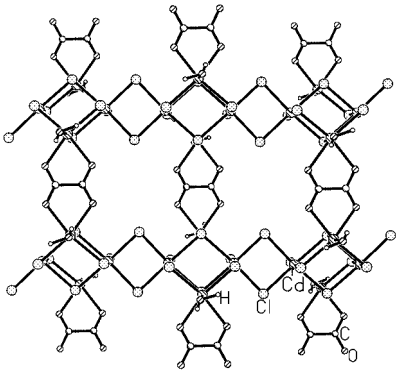

1681 **R. Faissner, G. Huttner,* E. Kaifer, P. Rutsch**

Synthesis of C_1-Symmetric Tripod Ligands Containing a P,P,N Donor Set − η^2-Coordination in d^8-Metal Complexes

Keywords: Mixed donor sets / Nickel / Palladium / Rhodium / Tripodal ligands

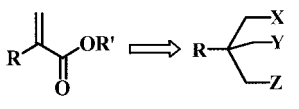

 © 2003 Wiley-VCH Verlag GmbH & Co. KGaA, Weinheim

1694 **C. Conato, W. Kamysz, H. Kozłowski,* M. Łuczkowski, Z. Mackiewicz, F. Mancini, P. Młynarz, M. Remelli,* D. Valensin, G. Valensin**

Cu^{II} Ion Coordination to an Unprotected Pentadecapeptide Containing Two His Residues: Competition Between the Terminal Amino and the Side-Chain Imidazole Nitrogen Donors

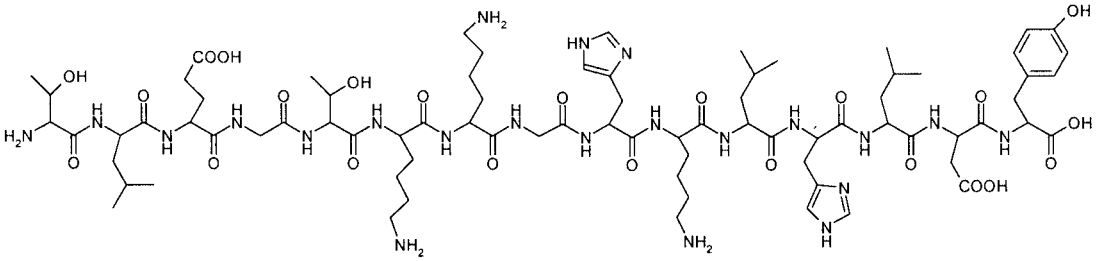

Keywords: Copper / Peptides / Coordination chemistry / Bioinorganic chemistry

1703 **A. Mayboroda, P. Comba,* H. Pritzkow, G. Rheinwald, H. Lang, G. van Koten**

Heterotrinuclear Complexes of the Platinum Group Metals with 2,2′-Biimidazole as a Bridging Ligand

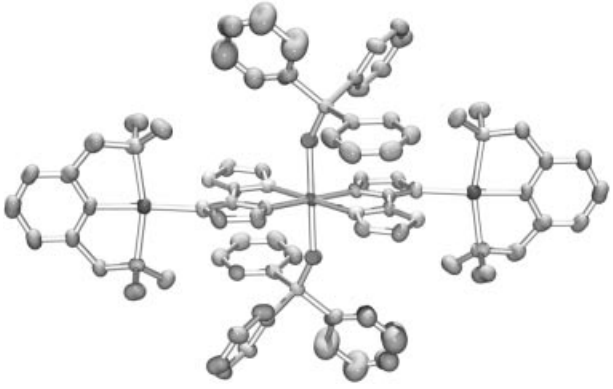

Keywords: Osmium / Platinum / Palladium / Heterometallic complexes / Cyclic voltammetry / Hydrogenation

1711 **P. Comba,* M. Merz, H. Pritzkow**

Catalytic Aziridination of Styrene with Copper Complexes of Substituted 3,7-Diazabicyclo[3.3.1]-nonanones

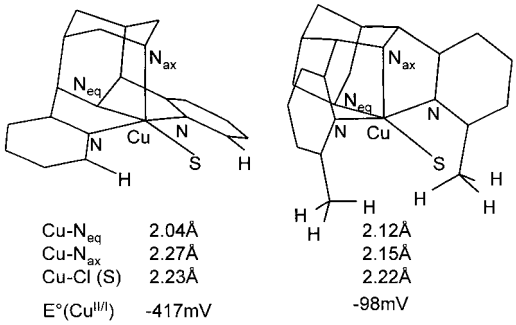

Keywords: Copper / N ligands / Catalysis

1719 **M.-L. Flay, H. Vahrenkamp***

Cyanide-Bridged Oligonuclear Complexes Containing Ni-CN-Cu and Pt-CN-Cu Linkages

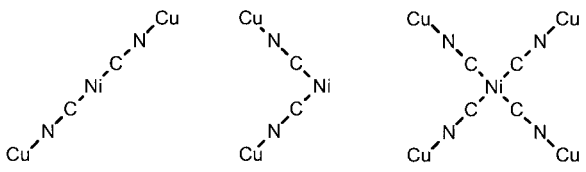

Keywords: Nickel / Platinum / Copper / Cyanide

 © 2003 Wiley-VCH Verlag GmbH & Co. KGaA, Weinheim

1727 **J. Schneider, M. Köckerling, R. Kopitzky, G. Henkel***

Metal-Controlled Stereoselectivity in Complex Formation: Assembly of Tetranuclear Copper(I) Complexes with Four Stereogenic Nitrogen Donor Functions in all-(*R*) and all-(*S*) Configurations

Keywords: Copper / Chirality / N ligands / S ligands / Metal-controlled stereoselectivity

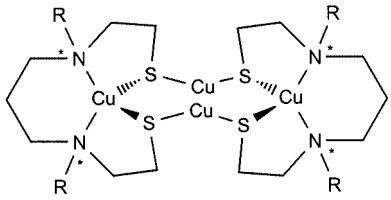

1735 **E. Balogh-Hergovich, G. Speier,* M. Réglier, M. Giorgi, E. Kuzmann, A. Vértes**

Synthesis, Structure, and Catalytic Activity of New μ-Oxo-Bridged Diiron(III) Complexes

Keywords: Iron / Tripodal ligands / Peroxides / Oxidation

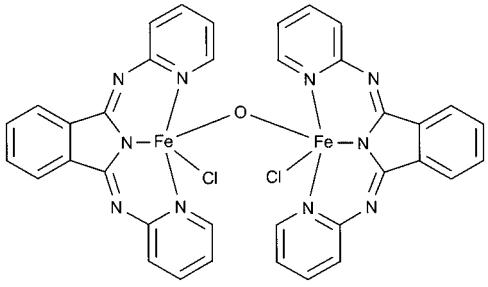

1741 **B. Korybut-Daszkiewicz,* J. Taraszewska,* K. Zięba, K. Woźniak, D. Kamiński**

Cobalt(III) Tetraazamacrocyclic Complexes with Pendant Amino Groups: Synthesis, Structure and Electrochemical Properties

Keywords: Macrocyclic ligands / N ligands / Cobalt / Electrochemistry

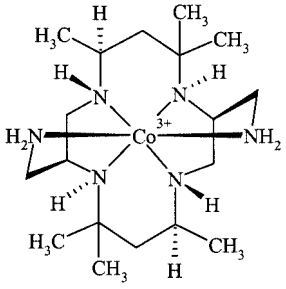

1748 **D. J. Brauer,* K. W. Kottsieper, S. Roßenbach, O. Stelzer**

Novel P,N Ligands Derived from (*R*)- and (*S*)-1-Phenylethylamine with (2*R*,5*R*)-2,5-Dimethylphospholanyl Groups (DuPHAMIN) for Asymmetric Catalysis

Keywords: Asymmetric catalysis / N,P ligands / Rhodium

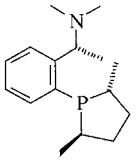

(*R*,*RR*)-**5**

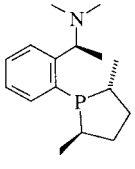

(*S*,*RR*)-**5**

1756 **C. Desplanches, E. Ruiz,* S. Alvarez**

Exchange Coupling in Metal Complexes of the Second Transition Series: A Theoretical Exploration

Keywords: Density functional calculations / Electronic structure / Magnetic properties / Molybdenum / Ruthenium

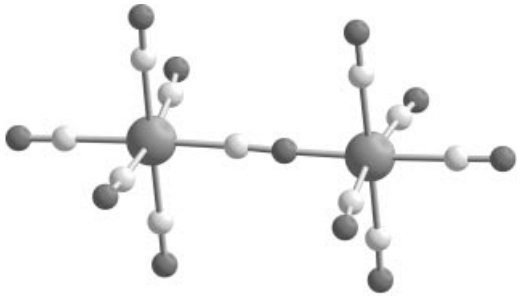

 © 2003 Wiley-VCH Verlag GmbH & Co. KGaA, Weinheim

1761 **A. Galani, M. A. Demertzis, M. Kubicki, D. Kovala-Demertzi***

Organotin-Drug Interactions. Organotin Adducts of Lornoxicam, Synthesis and Characterisation of the First Complexes of Lornoxicam

Keywords: Antitumour agents / Tin / Supramolecular chemistry / Drug delivery

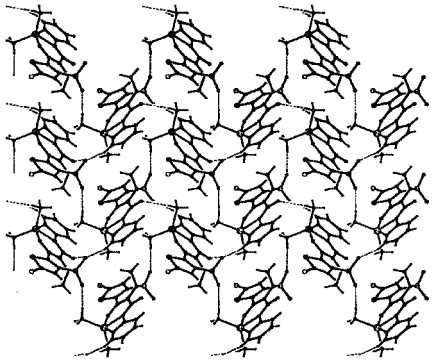

1768 **U. Beckmann, E. Bill, T. Weyhermüller, K. Wieghardt***

Exchange Interactions and Covalency in Dinuclear Complexes of Iron(III) and Gallium(III) Containing the Redox-Noninnocent Ligand 1,2-Bis(3,5-di-*tert*-butyl-2-hydroxyphenyl)oxamide

Keywords: Iron / Gallium / EPR spectroscopy / Moessbauer spectroscopy / Radicals / Magnetic properties / Exchange interactions

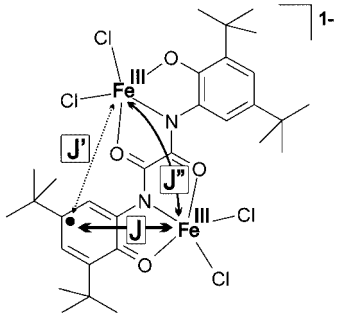

1778 **J. Luo, M. Hong,* R. Wang, R. Cao, Q. Shi, J. Weng**

Self-Assembly of Five Cadmium(II) Coordination Polymers from 4,4′-Diaminodiphenylmethane

Keywords: Cadmium / Coordination polymers / Self-assembly / N ligands

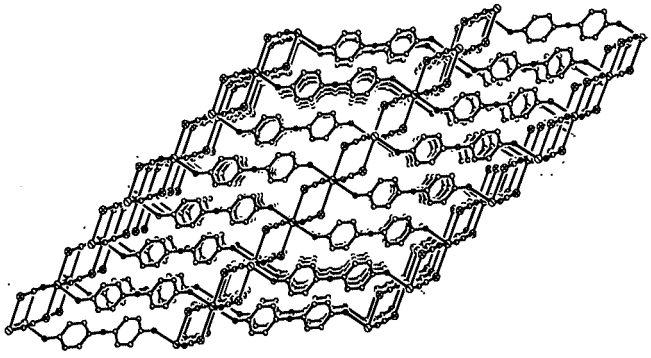

1785 **K. Shimazaki, H. Sekiya, H. Inoue, N. Saeki, K. Ishihara,* K. Matsumoto***

Mechanisms of the Axial Ligand Substitution Reactions of Dinuclear, Head-to-Head α-Pyrrolidonato- and Pivalamidato-Bridged *cis*-Diammineplatinum(III) Complexes with Halide Ions

Keywords: Platinum / Kinetics / Mechanism / α-Pyrrolidone / Pivalamide

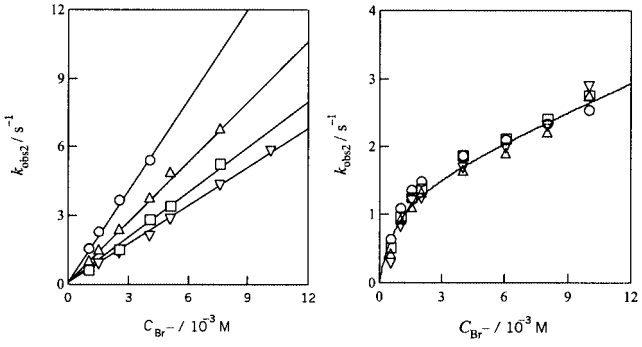

 © 2003 Wiley-VCH Verlag GmbH & Co. KGaA, Weinheim

1794 **S.-M. Zhou,* Y.-S. Feng, L.-D. Zhang**

A Two-Step Route to Self-Assembly of CdS Nanotubes via Electrodeposition and Dissolution

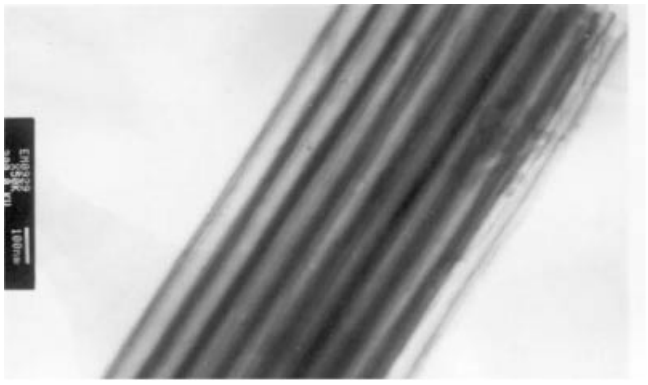

Keywords: Cadmium / Sulfides / Nanotubes / Self-assembly / Electrochemistry

1798 **R.-B. Fu, X.-T. Wu,* S.-M. Hu, J.-J. Zhang, Z.-Y. Fu, W.-X. Du, S.-Q. Xia**

Self-Assembly of Organodiphosphonate, Polyoxomolybdate and Diphenanthrolinecobalt(II) into Two Clusters and One Linear Polymer

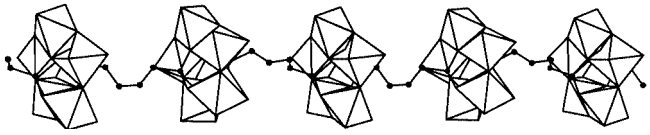

Keywords: Polyoxometalates / Molybdenum / Cobalt / N ligands / Clusters

1802 **A. Zeller, E. Herdtweck, T. Strassner***

Structural Characterization and a New One-Pot Synthesis of *trans*-Chloro(phenyl)bis(triphenylphosphane)nickel(II)

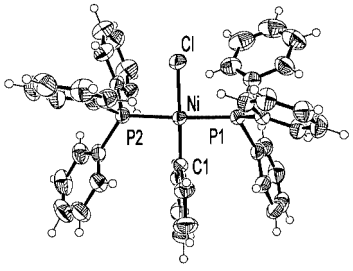

Keywords: Polymerization / Density functional theory calculations / Nickel / Phosphane ligands

1807 **N. d'Alessandro, L. Tonucci, M. Bressan,* L. K. Dragani, A. Morvillo**

Rapid and Selective Oxidation of Metallosulfophthalocyanines Prior to Their Usefulness as Precatalysts in Oxidation Reactions

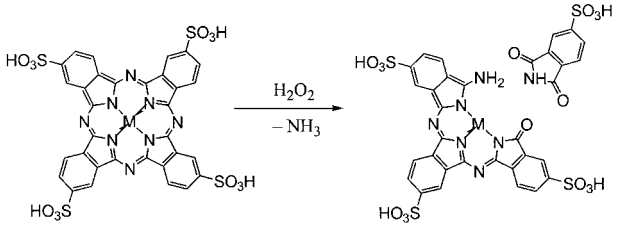

Keywords: Mass spectrometry / Homogeneous catalysis / Inorganic peroxides / Phthalocyanines / Oxidation

 © 2003 Wiley-VCH Verlag GmbH & Co. KGaA, Weinheim

1815 **N. Hoffmann, C. Wismach, L. Ernst, H. Schiebel, P. G. Jones, R. Streubel***

A New Concept for the Efficient Synthesis of Chiral Phosphorus–Nitrogen–Carbon Cage Compounds

Keywords: Azaphospholes / Phosphorus / Cage compounds / Tungsten / Cyclization

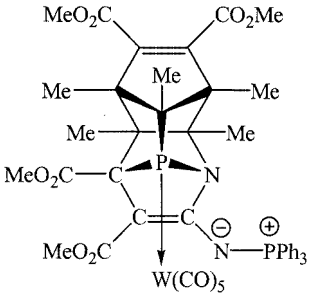

1822 **S. Gao, J. Lu, Y. Zhao, N. Chen, Y. Xie***

The Growth Process, Stability of GaP Nanocrystals and Formation of Ga_3P Nanocrystals under Solvothermal Conditions in Benzene

Keywords: Gallium / Phosphides / Nanostructures / Solvothermal synthesis

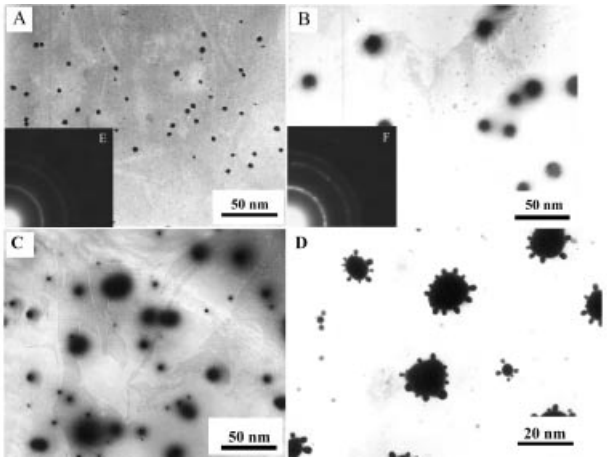

DOI: The fastest way to find an article online is the *Digital Object Identifier* (DOI). Starting in this issue, DOIs will be printed in the footer of the first page of every article. On the WWW, one can find an article for example with a DOI of 10.1002/ejic.200300049 at http://dx.doi.org/10.1002/ejic.200300049. Please use the DOI of the article to link from your home page to the articles in Wiley InterScience. The DOI is a result of a cross-publisher initative to create a system for the persistent identification of documents on digital networks. More information is available from www.doi.org.

Phosphane-Substituted Selenido−(carbonyl)iron and −(carbonyl)ruthenium Clusters: Structures, Fluxionality and Reactivity

Claudia Graiff,[a] Giovanni Predieri,[a] and Antonio Tiripicchio*[a]

Keywords: Crystal structures / Fluxional behaviour / Iron clusters / Ruthenium clusters / Selenium compounds

Selenium-transfer reactions from tertiary phosphane and diphosphane selenides to the carbonyl clusters $[M_3(CO)_{12}]$ (M = Fe or Ru) provide a simple, stepwise synthetic route to phosphane-substituted, mono- and diselenido–(carbonyl)iron and –(carbonyl)ruthenium clusters. Four families of clusters are generally obtained: (*i*) the $M_2Se_2L_6$ tetrahedral species (only for iron), (*ii*) the M_3SeL_{10} capped triangular species, (*iii*) the $M_3Se_2L_9$ square-pyramidal *nido* species (for iron and ruthenium), and (*iv*) the $M_4Se_2L_{11}$ octahedral *closo* species (only for ruthenium), with L being a phosphane or carbonyl ligand. When the tertiary phosphane selenide contains heterocyclic fragments, the reaction is not only limited to the transfer of the selenium atom, but proceeds by P–C and, sometimes, C–H bond cleavages, affording new selenidophosphido carbonyl clusters bearing coordinated heterocyclic fragments. Many clusters show fluxional behaviour in solution because of either ligand mobility or M–M bond migration. Furthermore, dimetallic substituted carbonyl clusters have been prepared by two different synthetic approaches: (1) MM′ + PSe (reactions between preformed dimetallic clusters and tertiary phosphane selenides) and (2) MSeP + M′ [cluster growth reactions from preformed chalcogenido–(carbonyl)metal clusters and suitable organometallic fragments]. In particular, from the tetrahedral clusters $[HMCo_3(CO)_{12}]$ (M = Fe or Ru) monoselenido clusters $[MCo_2(\mu_3\text{-Se})]$ with a tetrahedral core have been obtained. The second type of approach has been applied to the open-triangular *nido* clusters $[Ru_3(\mu_3\text{-Se})_2(CO)_{9-n}L_n]$ (L = tertiary phosphane, n = 1 or 2), which can add zero-s.e.p.'s organometallic fragments, such as $M(CO)_3$ (M = Mo or W), giving the corresponding *closo* clusters $[MRu_3(\mu_4\text{-Se})_2(CO)_{12-n}L_n]$.

(© Wiley-VCH Verlag GmbH & Co. KGaA, 69451 Weinheim, Germany, 2003)

[a] Dipartimento di Chimica Generale ed Inorganica, Chimica Analitica, Chimica Fisica, Università di Parma,
Parco Area delle Scienze 17/A, 43100 Parma, Italy
Fax: (internat.) + 39-0521/905557
E-mail: tiri@unipr.it

I. Introduction

Transition metal species may combine with main group elements or related molecular fragments to afford a variety

Claudia Graiff obtained her PhD degree in chemistry in 1999 at the University of Parma under the supervision of Prof. Giovanni Predieri and Antonio Tiripicchio. Since 1999 she has been a researcher at the University of Parma. Her current research interests concern the synthesis and characterization of chalcogenido−(carbonyl)metal clusters substituted by phosphane ligands.

Giovanni Predieri obtained his degree in Chemistry from the University of Parma in 1972 and was a postdoctoral fellow in 1981 and 1984 at the Laboratoire de Chimie de Coordination of the University of Strasbourg. In 1988 he received the "Arturo Miolati" award from the Italian Chemical Society for his research in Inorganic Chemistry. He is now a full professor of General and Inorganic Chemistry at the Faculty of Science of the University of Parma. His current research interests are in the area of inorganic chemistry, including the synthesis of new transition metal clusters, the design of hybrid organic-inorganic materials by the sol-gel process and, very recently, the production of chelated metal complexes for use in animal nutrition.

Antonio Tiripicchio has been full professor of General and Inorganic Chemistry at the Faculty of Science of the University of Parma since 1980. He is the author of more than 500 papers in international journals and of about 180 communications at national and international symposia and conferences. His current research interests are: synthesis, structure, and reactivity of homo- and heterometallic clusters and their use as precursors of catalysts and materials; characterization of inorganic-organic hybrid materials prepared by sol-gel processes and their use in catalysis; new synthetic routes for the synthesis of organometallic selenides. Presently he is Past-President of the Inorganic Chemistry Division of the Italian Chemical Society of which he was President from 1997 to 1999 and Director of the Interuniversity Consortium on "Chemical Reactivity and Catalysis"

MICROREVIEWS: This feature introduces the readers to the authors' research through a concise overview of the selected topic. Reference to important work from others in the field is included.

of interesting cluster compounds. Apart from their fundamental significance as a class of complexes owning peculiar chemical and structural properties, the growing interest in these species derives from their potential applications as catalysts, electrocatalysts and precursors for semiconductors.[1−3] Very recently, chalcogenido−ruthenium derivatives have shown interesting catalytic activity in oxygen reduction reactions in polymer electrolyte fuel cells (PEMFC),[4−7] suggesting their application as cathodes for these devices. The presence of chalcogenide species, in particular Se, appears to catalyse processes that lead to reduction of oxygen through the formation of selenido−transition metal cluster materials.[8] In addition, it is well known that sulfur and selenium atoms are found in active sites of a large number of proteins.[9]

The availability of substituted chalcogenido−metal clusters offers the opportunity to exert a stoichiometric control in those processes that lead from molecular metal chalcogenides, such as $[M_xE_y(PR_3)_z]$, to extended inorganic solids, like M_xE_y. The stoichiometric control, combined with kinetic control, which derives from low activation energies of these processes, often allows the preparation of otherwise inaccessible solid phases or microinhomogeneous materials, such as nanocomposites.[10]

Different synthetic routes are presently available for the preparation of selenido−transition metal clusters, such as those involving diphenyl diselenide,[11,12] phenylselenyl chloride,[13] selenophene,[14] trialkylsilyl selenides,[15−17] polyselenide anions,[18,19] and phosphane selenides [20−23] as starting materials. Furthermore, small selenido clusters, such as $[M_2(\mu\text{-}Se_2)(CO)_6]$ and $[M_3(\mu_3\text{-}Se)_2(CO)_9]$, can be used conveniently to prepare larger mono- and dimetallic species.[24,25]

II. Synthesis of Selenido Clusters from Phosphane Selenides

The reactions of tertiary phosphane selenides with (carbonyl)metal species provide a simple synthetic procedure to form selenido clusters through transfer of selenium atoms to low-valent metal centres, taking advantage of the frailty of the P=Se bond. Despite the synthetic potential of the phosphane selenides, their reactions with (carbonyl)metal compounds have been explored only to a limited extent prior to the last few years. For this reason, we began studying the reactions of tertiary phosphane and diphosphane selenides with $[M_3(CO)_{12}]$ (M = Fe or Ru)[26,27] with the aim to obtain new phosphane-substituted selenido carbonyl clusters, whose structural characterization, fluxional behaviour and reactivity are the central issues of this Microreview.

The carbonyl clusters $[M_3(CO)_{12}]$ (M = Fe or Ru) react with tertiary phosphane selenides through transfer of selenium atoms to the metal cluster, giving a variety of phosphane-substituted selenido carbonyl clusters, whose structural frameworks are shown in Scheme 1. The open-triangular, variously substituted, *nido* clusters with the M_3Se_2 core are the major products for both metals, but significant amounts of clusters with dinuclear M_2Se_2, trinuclear M_3Se, and tetranuclear M_4Se_2 cores are also obtained. The product distribution is strongly dependent on the reaction conditions, on the nature of the phosphane and on the cluster/phosphane molar ratio. In the case of iron, the reaction takes place rapidly upon gentle warming, whereas, in the case of ruthenium, the presence of Me_3NO as a decarbonylation reagent is required to increase the reaction rate. Most of those clusters are air-stable and can be separated and recognized by silica gel chromatography[28] and recovered by TLC.

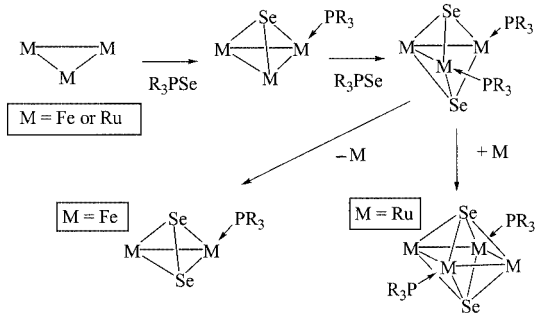

Scheme 1

Moreover, the reactions with bis(diphenylphosphanyl)-methane diselenide ($dppmSe_2$) lead to the formation of other less common compounds, which can be obtained by condensation processes, such as the hexanuclear clusters containing M_6Se_4 cores[29] shown in Scheme 2 and the compound $[Ru_4(\mu_3\text{-}Se)_4(CO)_{10}(dppm)]$, shown in Figure 1, which is the first reported 72-electron Ru_4Se_4 cubane-like cage complex.[30] This complex should be regarded as a secondary product, probably formed by the self-assembly of two dinuclear Ru_2Se_2 groups, derived from *nido*-Ru_3Se_2 by loss of a mononuclear metal fragment. Despite the presence of the bridging diphosphane, the overall geometry of the Ru−Se cubane is very similar to those of the unsubstituted Fe−S and Fe−Se cubanes $[Fe_4E_4(CO)_{12}]$ (E = S, Se).[31,32]

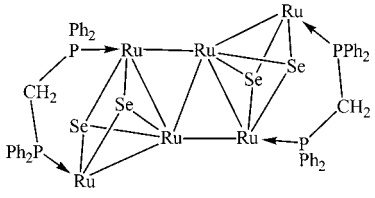

Scheme 2

On the basis of our results we have suggested that the reactions between $[M_3(CO)_{12}]$ and R_3PSe proceeds through two consecutive steps. The monoselenido clusters $[Ru_3(\mu_3\text{-}Se)(\mu_3\text{-}CO)(CO)_8PR_3]$, obtained by the stoichiometry-controlled reaction of phosphane selenide R_3PSe with $[Ru_3(CO)_{12}]$, undergo a second attack by R_3PSe affording the corresponding diselenido derivatives $[Ru_3(\mu_3\text{-}Se)_2(CO)_7(PR_3)_2]$. To demonstrate the stepwise selenium transfer,

 © 2003 Wiley-VCH Verlag GmbH & Co. KGaA, Weinheim

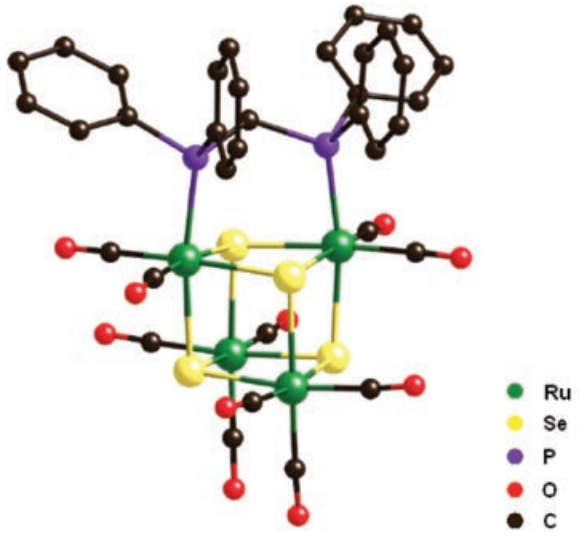

Figure 1. Perspective view of cage compound $[Ru_4(\mu_3\text{-}Se)_4(CO)_{10}(dppm)]$

we have treated the monoselenido clusters with another equivalent of phosphane selenide, obtaining the corresponding diselenido species quantitatively.[33] The process, occurring at 60−70 °C, in the presence of Me_3NO, can be monitored by IR spectroscopy.

The structure of the monoselenido-disubstituted cluster $[Ru_3(\mu_3\text{-}Se)(\mu_3\text{-}CO)(CO)_7(PPh_3)_2]$ is shown in Figure 2. The triangle of ruthenium atoms is capped on one side by a selenium atom and on the other by a carbonyl group. The two PPh_3 ligands coordinate through the P atoms to two Ru atoms in pseudo-equatorial and pseudo-axial positions, respectively. The μ_3-Se ligand is practically equidistant from the three Ru atoms, whereas the μ_3-CO group bridges, in a slightly asymmetrical way, the two shortest Ru−C distances involving the ruthenium atoms coordinated by the two phosphane groups. This slight asymmetry has also been observed in the case of the unsubstituted cluster $[Ru_3(\mu_3\text{-}S)(\mu_3\text{-}CO)(CO)_9]$.[34]

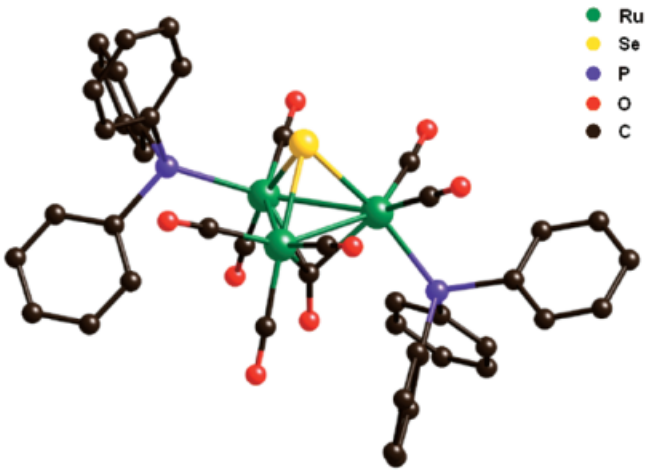

Figure 2. Perspective view of cluster $[Ru_3(\mu_3\text{-}Se)(\mu_3\text{-}CO)(CO)_7(PPh_3)_2]$

The structure of the diselenide cluster $[Ru_3(\mu_3\text{-}Se)_2(CO)_7(dppy)_2]$ [dppy = diphenyl(pyridyl)phosphane] (Figure 3) contains an Ru_3Se_2 core that can be described as a square pyramid with one Ru atom at the apex and two Ru and Se atoms alternating at the base. In this structure, the two phosphane groups coordinate the Ru atoms in pseudo-equatorial and pseudo-axial positions, as in the triphenylphosphane derivative,[35] although, with other ligands, we have obtained analogous clusters with both phosphane groups in equatorial positions.[36] The values of the Ru−P bond lengths, 2.326(3) and 2.371(4) Å, differ remarkably because of the influences of the *trans* Ru−Ru and Ru−Se bonds.

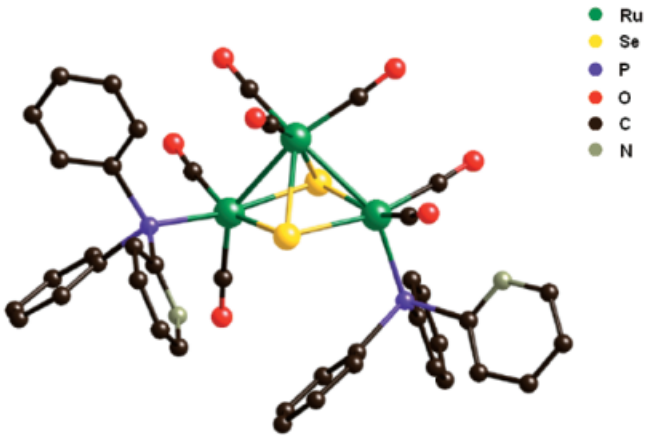

Figure 3. Perspective view of cluster $[Ru_3(\mu_3\text{-}Se)_2(CO)_7(dppy)_2]$

III. Multiple Fragmentation of the Phosphane Selenide Leading to Selenido-Phosphido Clusters

Recently, we observed that tertiary phosphane selenides bearing heterocyclic fragments, such as 2-thienyl (th),[37] 2-pyridyl (py),[38] and 5-(2-pyridyl)-2-thienyl (pyth),[39] (see Scheme 3) can undergo P−C bond cleavage by reaction with (carbonyl)iron and -ruthenium compounds, affording selenido-phosphido clusters. In fact, the heterocyclic moiety was introduced to drive new reactivity patterns in cluster-growing processes, because of the possible release of heterocyclic fragments and the coordinating ability of the heteroatoms.

The cluster $[Ru_3(\mu_3\text{-}Se)(\mu\text{-}PPh_2)(CO)_6(\mu\text{-}\eta^1{:}\eta^2\text{-}C_4H_3S)\{P(C_4H_3S)Ph_2\}]$, obtained by reaction between $[Ru_3(CO)_{12}]$ and diphenyl(2-thienyl)phosphane selenide, was identified only after the determination of its crystal structure by diffraction methods because of its structural singularity. In the structure, shown in Figure 4, the Se atom caps the metal triangle, two sides of which are bridged by a phosphido and a thienyl ligand, which derive from the multiple fragmentation of the parent diphenyl(2-thienyl)-phosphane selenide.

The bonding of the thienyl group is rather unusual, since it interacts through the double bond forming a σ-bond with

 © 2003 Wiley-VCH Verlag GmbH & Co. KGaA, Weinheim

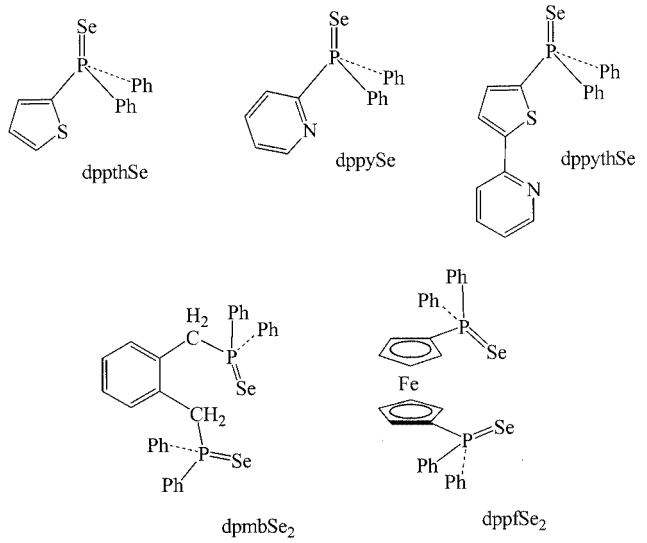

Scheme 3

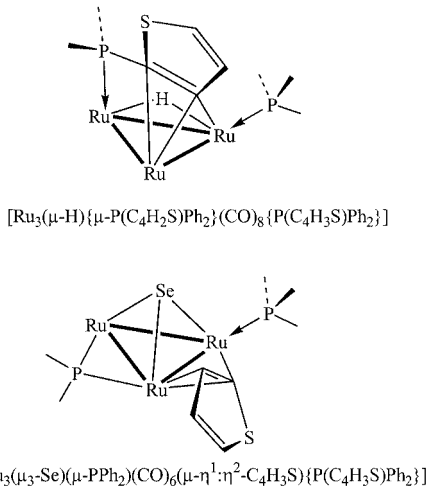

Scheme 4

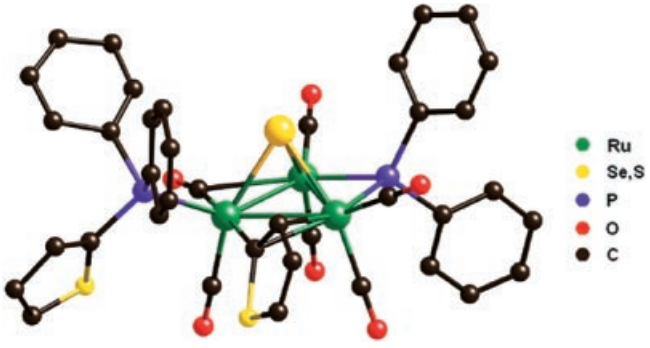

Figure 4. Perspective view of cluster $[Ru_3(\mu_3\text{-}Se)(\mu\text{-}PPh_2)(CO)_6(\mu\text{-}\eta^1{:}\eta^2\text{-}C_4H_3S)\{P(C_4H_3S)Ph_2\}]$

an Ru atom and a π-bond with another Ru atom. The coordination mode (μ-η^1:η^2) of the 2-thienyl fragment is similar to that observed in $[Ru_3(\mu\text{-}H)\{\mu\text{-}P(C_4H_2S)Ph_2\}(CO)_8\{P(C_4H_3S)Ph_2\}]$ for the $Ph_2(C_4H_3S)P$ ligand.[40] The most important difference, however, between the two coordination modes is the position of the bridging thienyl moiety with respect to the metal triangle. In fact, in $[Ru_3(\mu\text{-}H)\{\mu\text{-}P(C_4H_2S)Ph_2\}(CO)_8\{P(C_4H_3S)Ph_2\}]$ the thienyl ring overhangs the metal triangle, whereas in $[Ru_3(\mu_3\text{-}Se)(\mu\text{-}PPh_2)(CO)_6(\mu\text{-}\eta^1{:}\eta^2\text{-}C_4H_3S)\{P(C_4H_3S)Ph_2\}]$ it approaches the triangle laterally, in such a way that the α-carbon atom is almost lying in the cluster plane, as shown in Scheme 4.

The structure of the cluster $[Ru_3(\mu_3\text{-}Se)(\mu\text{-}PPh_2)(CO)_6(\mu\text{-}pyth)\{P(pyth)Ph_2\}]$, obtained by reaction between $[Ru_3(CO)_{12}]$ and diphenyl[5-(2-pyridyl)-2-thienyl]phosphane selenide, is very similar to that with the thienyl ligand.

In the case of the pyridyl group, the ligand $Ph_2(2\text{-}C_5H_4N)PSe$ undergoes multiple fragmentation by reaction with $[Ru_3(CO)_{12}]$ to afford the cluster $[Ru_3(\mu_3\text{-}Se)(\mu\text{-}PPh_2)_2(\mu\text{-}C_5H_4N)(\mu_3\text{-}C_5H_4N)(CO)_6]$ that does not contain any Ru−Ru bond and is built up through the unique synergy of five bridging ligands. The structure of this polynuclear species (Figure 5) is characterized by the presence of a nearly planar array of eleven atoms forming two roughly coplanar fused rings; i.e., the heptaatomic RuPRuPRuCN cycle and one pyridyl ring [dihedral angle 6.9(1)°].

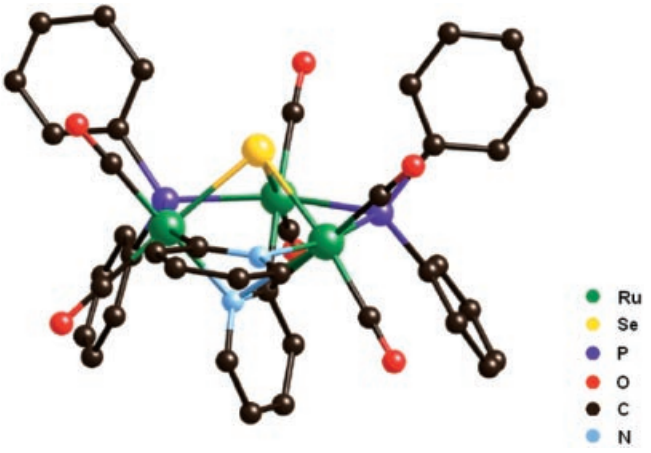

Figure 5. Perspective view of compound $[Ru_3(\mu_3\text{-}Se)(\mu\text{-}PPh_2)_2(\mu\text{-}C_5H_4N)(\mu_3\text{-}C_5H_4N)(CO)_6]$

The μ_3-Se bridging mode, connecting three non-interacting ruthenium atoms, has only a few precedents in other trinuclear ruthenium derivatives.[38] This cluster has been obtained from $Ph_2(2\text{-}C_5H_4N)PSe$ through P=Se and P−C(Py) bond cleavages. It contains two differently bridging pyridyl groups, the former connects two Ru atoms through σ bonds, lying on the plane defined by the three metal atoms, the latter is σ-bonded to the same two Ru atoms, being nearly perpendicular to the metal plane, in such a way that it appears to be involved in a weak π interaction with the third metal atom, which completes its coordination sphere. Moreover, if we consider that the capping pyridyl group donates two π electrons to Ru(1), the whole set of ligands contributes 30 electrons to the structure, attaining the expected count of 54 electrons. This arrange-

 © 2003 Wiley-VCH Verlag GmbH & Co. KGaA, Weinheim

ment would be an unprecedented type of bridging mode for the pyridyl group.

Multiple fragmentations involving P−Se and P−C bond cleavages have been observed also with the two following diphosphane diselenides: the 1,2-bis[(diphenylphosphanyl)-methyl]benzene diselenide[41] ($dpmbSe_2$) and the 1,1′-bis(diphenylphosphanyl)ferrocene diselenide[42] ($dppfSe_2$) (see Scheme 3). The reactions between $[M_3(CO)_{12}]$ (M = Ru or Fe) and the 1,2-bis[(diphenylphosphanyl)methyl]benzene diselenide were carried out with the aim of investigating the use of $dpmbSe_2$ as an effective precursor for selenido−(carbonyl)ruthenium and −(carbonyl)iron clusters containing the scarcely studied 1,2-bis[(diphenylphosphanyl)methyl]benzene ligand. The reaction of $[Ru_3(CO)_{12}]$ with $dpmbSe_2$ in hot toluene affords a variety of phosphane-substituted selenido carbonyl clusters. Along with substituted clusters with Ru_3Se_2, Ru_3Se, and Ru_2Se_2 cores, we have obtained workable amounts of an unprecedented and interesting complex $[Ru_3(\mu_3\text{-}Se)(\mu_3\text{-}H)\{\mu_2\text{-}PPh_2\}(CO)_6(\mu_2\text{-}CHC_6H_4CH_2PPh_2)]$ with an Ru_3Se core bound to phosphido, hydrido, and carbene moieties, whose structure (Figure 6) has been fully elucidated by X-ray diffraction methods.

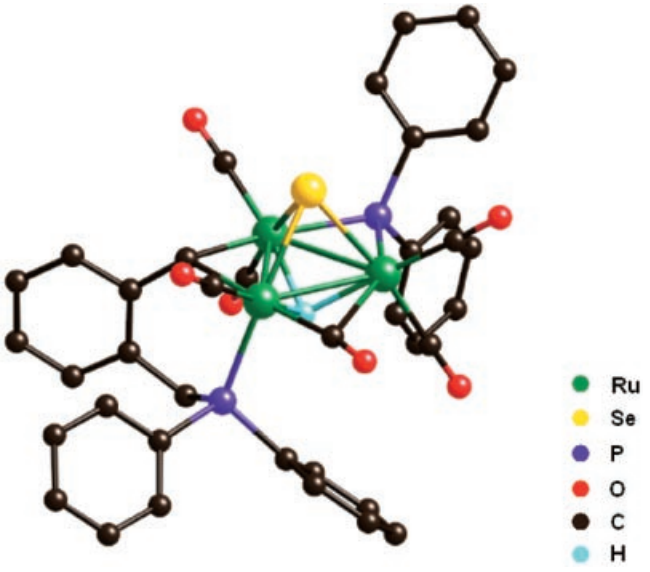

Figure 6. Perspective view of cluster $[Ru_3(\mu_3\text{-}Se)(\mu_3\text{-}H)\{\mu_2\text{-}PPh_2\}(CO)_6(\mu_2\text{-}CHC_6H_4CH_2PPh_2)]$

This cluster is the first example of a triruthenium triangular cluster capped on one side by a μ_3-Se unit and on the other by a μ_3-H atom. The diphosphane has undergone multiple fragmentations, namely P=Se, P−C, and C−H activations. This fragmentation produces a bridging carbene on an Ru−Ru edge resulting from a hydride migration from the Ar-CH_2 group to the cluster. (Carbene)ruthenium complexes have been used widely in the last few years as models, precursors and effective catalysts for olefin metathesis, ring-opening polymerization and alkyne oligomerization.[43] The $^{31}P\{^1H\}$ NMR spectrum, recorded at room temperature, shows two sharp singlets for the σ-coordinated phosphorus atoms and the phosphide group bridging one side of the metal triangle, respectively. The complete proton assignment has been achieved by two-dimensional NMR experiments (COSY, NOESY, TOCSY). The μ_3-hydride signal is found as a doublet of doublets at δ = −14.62 ppm, because of coupling with the two non-equivalent phosphorus atoms. From the 2D NOESY spectrum, a correlation is detected between the hydride and a proton of a methylene group, which, in the solid-state structure, points towards the hydride group at a distance of 2.67(6) Å. The carbene hydrogen atom gives a sharp singlet at δ = 10.13 ppm.

The reactions between $dppfSe_2$ at 60 and 110 °C afford the two isomeric *nido* clusters $[Ru_3(\mu_3\text{-}Se)_2(dppf)(CO)_7]$ (**1**) and $[Ru_3(\mu_3\text{-}Se)_2(\mu\text{-}dppf)(CO)_7]$ (**2**) which contain dppf as chelating and bridging ligand, respectively. Clusters **1** and **2** belong to the family of numerous open-triangular phosphane-substituted Ru_3Se_2 *nido* clusters, which are the primary products of the attack of 2 equiv. of P=Se groups to the starting triangular cluster. The chelated derivative **1**, obtainable under kinetic control, can be converted into the more stable bridged cluster **2** by thermal treatment in toluene solution as shown in Scheme 5. This conversion can be monitored by IR spectroscopy.[42]

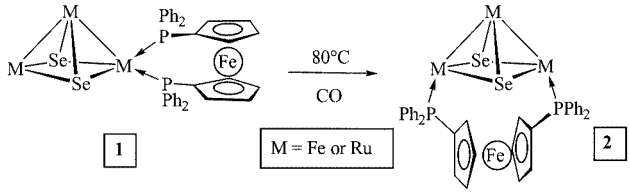

Scheme 5

The cluster $[Ru_3Se\{\mu\text{-}P(Ph)C_5H_4FeC_5H_4PPh_2\}(\mu\text{-}OCPh)(CO)_6]$ (whose structure is depicted in Figure 7) was isolated as a minor product in the reaction between $[Ru_3(CO)_{12}]$ and $dppfSe_2$ at 60 °C.[42] The core consists of a metal triangle capped by a selenium atom and bridged on two sides by a phosphido ligand and by a benzoyl group, respectively, both deriving from multiple fragmentation of dppf diselenide and migratory insertion of a Ph ring into an Ru−C bond of a terminal carbonyl group.

Because of the loss of a phenyl ring, the phosphane-phosphido ligand is coordinated to one side of the Ru−Ru bond in an unusual manner: the phosphido P atom bridges two Ru atoms asymmetrically and participates with the other P atom in the chelation of one of them. The migratory insertion of a phenyl ring into a carbonyl group causes the formation of a benzoyl ligand that bridges two Ru atoms in a $\mu_2\text{-}\eta^1\text{:}\eta^1$-fashion through the C and O atoms. Only few examples are known of a μ_2-benzoyl group bridging two metal atoms in the same $\mu_2\text{-}\eta^1\text{:}\eta^1$-fashion.[42]

IV. Fluxional Behaviour

Two types of fluxional behaviour have been observed: (*i*) ligand mobility and (*ii*) M−M bond migration.

 © 2003 Wiley-VCH Verlag GmbH & Co. KGaA, Weinheim

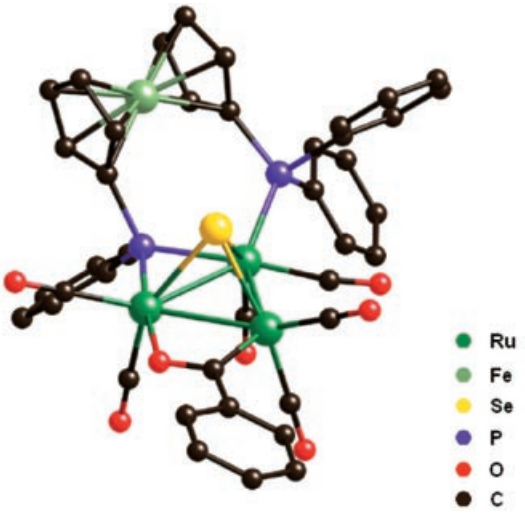

Figure 7. Perspective view of cluster $[Ru_3Se\{\mu\text{-}P(Ph)C_5H_4FeC_5H_4PPh_2\}(\mu\text{-}OCPh)(CO)_6]$

The ferrocenediphosphane ligand can assume different coordination modes in cluster chemistry. This feature derives from the possibility of the cyclopentadienyl rings twisting about their axis. In fact, the P···P separation between the two donor atoms depends on the θ torsional angle, ranging from 3.30 (θ = 0°) to 6.90 Å (θ = 180°). Scheme 6 shows the preferred conformations adopted in the case of chelating (θ = 36°) and in the case of bridging (θ = 72°) over one side of a (carbonyl)metal cluster. To gain an insight into the structures of these molecules in solution, we performed ^{1}H NMR investigations on clusters $[M_3(\mu_3\text{-}Se)_2(\mu\text{-dppf})(CO)_7]$. At room temperature, the proton pattern of $[Fe_3(\mu_3\text{-}Se)_2(\mu\text{-dppf})(CO)_7]$ shows a featureless broad band in the cyclopentadienyl region, suggesting the onset of a fluxional behaviour. At 258 K, four singlets are visible in the same region, which indicate the equivalence of the two cyclopentadienyl rings. It has been demonstrated that the fluxional behaviour consists of the concerted twisting of the two equivalent rings around their axis ($\Delta G^{\ddagger}$ = 58.2 kJ·mol^{-1}, T_c = 303 K)[44] as shown in Scheme 7.

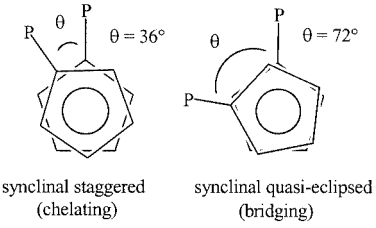

Scheme 6

The pattern of the signals of the protons of the Ru analogue parallels that of the corresponding Fe derivative at 273 °C, indicating that the fluxional behaviour of the ligand, observed for the Fe species, exhibits a higher energy barrier in the Ru congener.

The dynamic behaviour of $[Ru_3(\mu_3\text{-}Se)_2(dppf)(CO)_7]$ (**1**) is quite different (see Scheme 8). At room temperature the

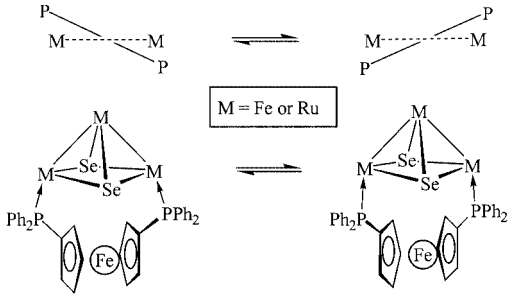

Scheme 7

^{1}H NMR spectrum exhibits four singlets for the Cp protons, indicating the equivalence of the two rings. At 213 K, the two rings become inequivalent, with the proton spectrum showing eight singlets that were assigned by 2D NMR spectra. The fluxional behaviour of **1** consists of the localized scrambling of the chelating ligand around Ru, namely the exchange of the axial and equatorial positions of the two $Ph_2(C_5H_4)P$ moieties. This dynamic behaviour makes the two rings equivalent, but the four protons of each ring remain unequal.[44]

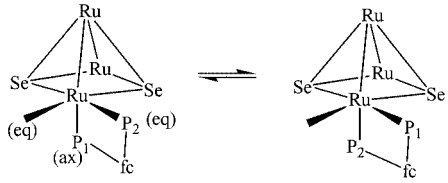

Scheme 8

The cluster $[Ru_3(\mu_3\text{-}Se)_2(\mu\text{-dppm})(CO)_7]$ has the well-known bicapped open-triangular 50-electron core and is the expected primary product of the attack of $dppmSe_2$ on the starting carbonyl cluster. The structure in the solid state is the same as that observed for other phosphane-disubstituted Ru_3Se_2 derivatives, which exhibit two P donor groups coordinated (in axial positions) to the two non-bonded, basal metal atoms. Nevertheless, its NMR spectra in solution suggest fluxional behaviour. In fact, the ^{31}P NMR spectrum shows a singlet and two doublets at lower frequency. The ^{13}C NMR spectra, as well as the ^{77}Se NMR spectra, show a couple of signals, consistent with the presence of two isomers in solution: the first is the symmetrical cluster with the two phosphorus atoms equivalent, as found in the solid state, and the other is that obtained by migration of the M−M bond from a side of the square pyramid to the base, as depicted in Scheme 9.[29]

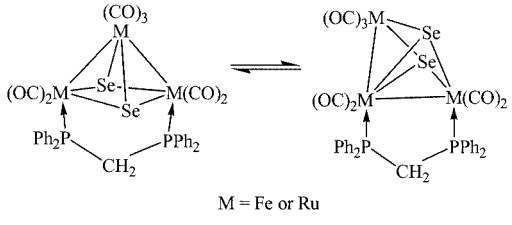

Scheme 9

 © 2003 Wiley-VCH Verlag GmbH & Co. KGaA, Weinheim

Also, the disubstituted Ru_3Se_2 clusters with monophosphanes exhibit ^{31}P NMR spectra in solution indicative of the same fluxional motion observed for the dppm.[35,36]

V. Dimetallic Clusters

Recently, we have extended our interest in the search for new synthetic routes to phosphane-substituted selenido−mixed-metal clusters by considering that the presence of different metals can influence the selectivity of certain processes and can lead to the formation of compounds presenting new, and not always easily predictable, structures.

Two different synthetic strategies have been developed for the synthesis of dimetallic substituted carbonyl clusters: (1) MM′ + PSe (reactions between preformed dimetallic clusters and tertiary phosphane selenides) and (2) MSeP + M′ [cluster growth reactions from preformed chalcogenido−(carbonyl)metal clusters and suitable organometallic fragments].

As a first approach for the synthesis of dimetallic selenido clusters, we have treated different phosphane selenides with the tetrahedral clusters $[HMCo_3(CO)_{12}]$ (M = Fe or Ru) and obtained two classes of products:[45] (*i*) trinuclear selenido clusters possessing an $MCo_2(\mu_3\text{-Se})$ core and (*ii*) tetranuclear hydrido clusters with an $HMCo_3$ core obtained by simple substitution of carbonyl groups by phosphane ligands (Scheme 10).

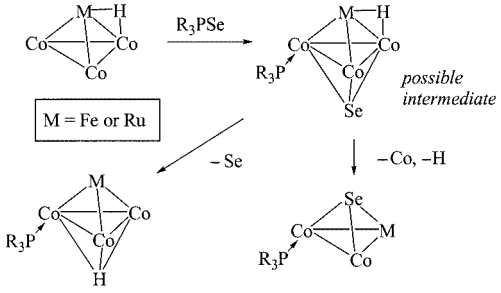

Scheme 10

Both classes are *nido* species and probably are derived from a trigonal-bipyramidal intermediate. While compounds of type (*ii*) have been reported already in the literature, the triangular dimetallic clusters of type (*i*), capped by a μ_3-selenide unit and substituted by a phosphane ligand, have been obtained and fully characterized for the first time. One possible hypothesis for the formation of these clusters is that the reactions proceed first with an addition of the phosphane selenide, giving an intermediate species in which the phosphane group and the selenium atom are coordinated. This intermediate would then loose a cobalt atom and a hydride ligand or a selenium atom to afford type (*i*) or (*ii*), respectively.

As an example of the structure of type (*i*), Figure 8 shows the structure of $[RuCo_2(\mu_3\text{-Se})(CO)_7(\mu\text{-dppy})]$ in which an MCo_2 triangle is capped by a μ_3-Se ligand. The bidentate phosphane ligand bridges the Co−Co edge through the phosphorus and nitrogen atoms. The bidentate bridging phosphane group forms a five-membered ring that is fused with the metal triangle on one side and with the pyridyl ring on the other.

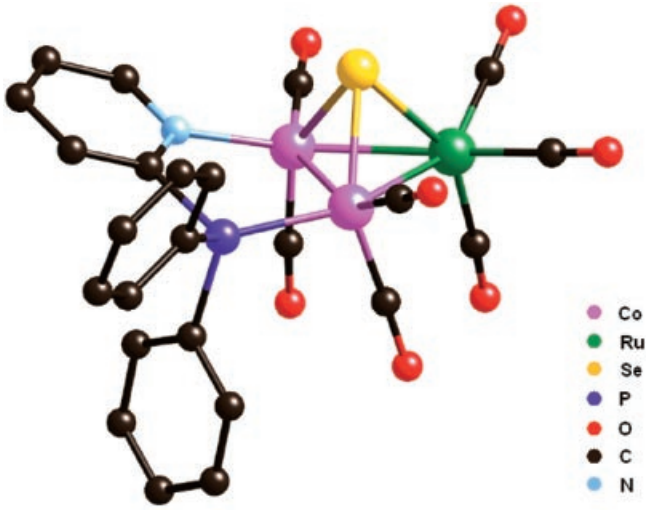

Figure 8. Perspective view of cluster $[RuCo_2(\mu_3\text{-Se})(CO)_7(\mu\text{-dppy})]$

The structure of $[HRuCo_3(CO)_7(\mu\text{-CO})_3(\mu\text{-dppy})]$ (Figure 9) shows a tetranuclear $RuCo_3$ core of type (*ii*) in which two carbonyl groups have been replaced by the dppy ligand bridging two cobalt atoms through the P and N atoms. Perhaps because of the steric hindrance resulting from this coordination, the hydride ligand has migrated from its original μ_3-capping position to the Ru−Co edge.

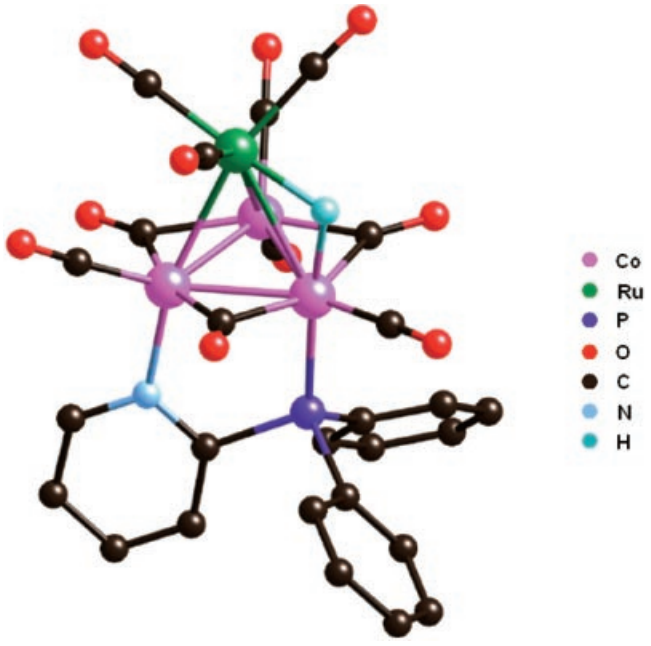

Figure 9. Perspective view of cluster $[HRuCo_3(CO)_7(\mu\text{-CO})_3(\mu\text{-dppy})]$

The linear trinuclear complex $[Pt\{Fe(CO)_3(NO)\}_2(PhCN)_2]$ was chosen for the reaction with phosphane sel-

 © 2003 Wiley-VCH Verlag GmbH & Co. KGaA, Weinheim

enides, by considering that its open geometry and the lability of the PhCN ligands could possibly result in an easy attack of the P=Se moiety to the cluster core. Actually, the reaction of the $PtFe_2$ complex with diphenyl(2-pyridyl)phosphane selenide occurs even at low temperature, affording a variety of compounds.[46] One of them was recognized as the 46-electron cluster $[(CO)_3Fe(\mu_3\text{-}Se)\{Pt(CO)P(2\text{-}C_5H_4N)Ph_2\}_2]$. It exhibits a butterfly framework consisting of two FePtSe wings sharing the common Fe−Se hinge (Figure 10). The value of the Fe−Se bond length, 2.337(1) Å, is slightly smaller than the average one, 2.37 Å, found in several clusters with a *nido*-Fe_3Se_2 core.[27] The two Pt atoms are definitely non-bonded since the Pt···Pt separation is rather large at 3.167(9) Å. By considering the two Fe−Pt bonds, the coordination about the Pt atoms is almost square-planar, with the CO and phosphane ligands being *trans* to the selenium and iron atoms, respectively.

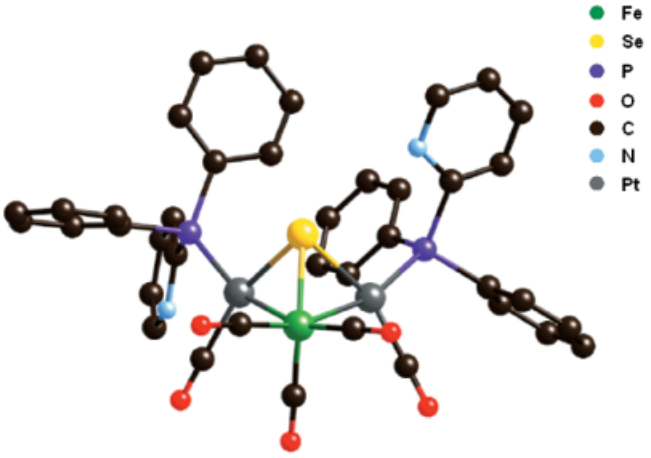

Figure 10. Perspective view of cluster $[(CO)_3Fe(\mu_3\text{-}Se)\{Pt(CO)P(2\text{-}C_5H_4N)Ph_2\}_2]$

There are only a few known examples of the cluster typology found in $[(CO)_3Fe(\mu_3\text{-}Se)\{Pt(CO)P(2\text{-}C_5H_4N)Ph_2\}_2]$. The structure can be described also as a $(CO)_3Fe{\equiv}Se$ group (a legitimate, but unknown, 18-electron species) stabilized by the double bridging interaction with two PtL_2 fragments, a system analogous to the well-understood $L_2M(\mu\text{-acetylene})ML_2$ systems, as shown in Scheme 11.

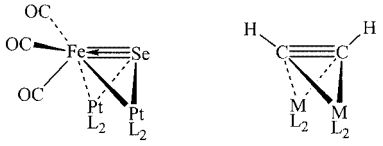

Scheme 11

The chemical bonding in this cluster, and in similar systems, has been analysed through density functional theory (DFT) and qualitative MO approaches, considering the $(CO)_3Fe{\equiv}X$ unit as being equivalent to RC≡CR molecules by isolobal analogy.[46]

The second approach for the synthesis of phosphane-substituted, selenido−mixed-metal clusters consists of the reaction of preformed selenido species with organometallic fragments. This approach was chosen by considering the availability of workable amounts of complexes $[Ru_3(\mu_3\text{-}Se)_2(CO)_{9-n}L_n]$ (n = 1 or 2; L = tertiary phosphane). Compounds of this kind are open-triangular, *nido* clusters with 7 skeletal electron pairs. As a consequence, they could be prone to add a zero-s.e.p. fragment, such as $M(CO)_3$ (M = Mo or W), giving the hypothetical *closo* clusters $[MRu_3(\mu_4\text{-}Se)_2(CO)_{12-n}L_n]$. The reactions of various $[Ru_3(\mu_3\text{-}Se)_2(CO)_7(L)_2]$ clusters with $W(CO)_3(CH_3CN)_3$ afford the dimetallic *closo* clusters $[WRu_3(\mu_4\text{-}Se)_2(\mu\text{-}CO)_4(CO)_6L_2]$,[36] as shown in Scheme 12.

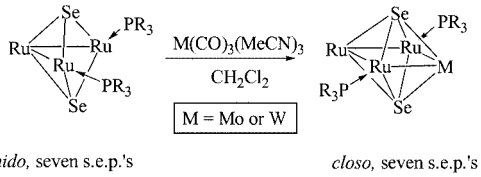

Scheme 12

In their crystal structures, most of these clusters lie on a crystallographic centre, so a disorder exists that involves the mutually opposite Ru and M (M = W or Mo) atoms of the *closo* core of the cluster, resulting in a disordered $Ru_3M(\mu_4\text{-}Se)_2$ cluster core. This disorder caused us to formulate these clusters erroneously in a previous note as $Ru_2W_2Se_2$ electron-deficient species.[47] These complexes belong to the family of diselenide tetranuclear *closo* clusters. They could be described as distorted octahedra in which the three ruthenium atoms and the M atom lie on the basal plane and two selenium atoms at the apices. Two phosphane ligands coordinate the *trans* ruthenium atoms through the phosphorus atoms. Four carbonyl groups bridge the Ru−Ru and Ru−M edges asymmetrically. The crystal structure of compound $[Ru_3M(\mu_4\text{-}Se)_2(\mu\text{-}CO)_4(CO)_6(t4mpp)_2]$ [t4mpp = tris(*p*-methoxyphenyl)phosphane] is reported in Figure 11.

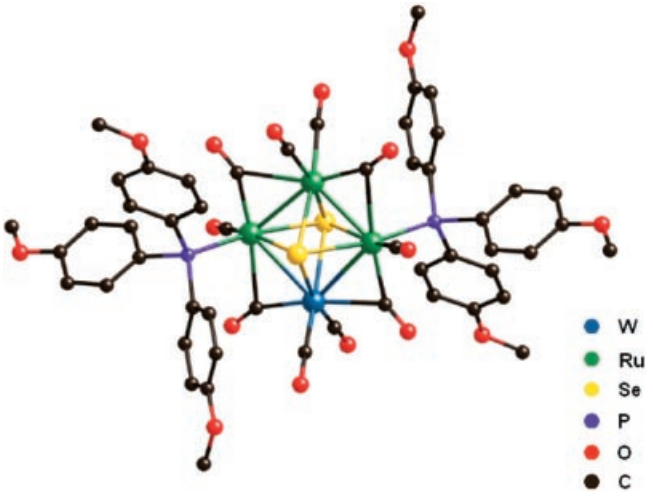

Figure 11. Perspective view of cluster $[Ru_3M(\mu_4\text{-}Se)_2(\mu\text{-}CO)_4(CO)_6(t4mpp)_2]$

 © 2003 Wiley-VCH Verlag GmbH & Co. KGaA, Weinheim

When the starting reagent is the monosubstituted $[Ru_3(\mu_3\text{-}Se)_2(CO)_8L]$ (L = tertiary phosphane) the reaction product is the expected dimetallic *closo* cluster $[WRu_3(\mu_4\text{-}Se)_2(\mu\text{-}CO)_4(CO)_7L]$, which was fully characterized in solution as well as in the solid state. Two isomers were obtained depending on whether the position of the tertiary phosphane on the ruthenium atom is *cis* or *trans* to the tungsten atom (see Scheme 13).

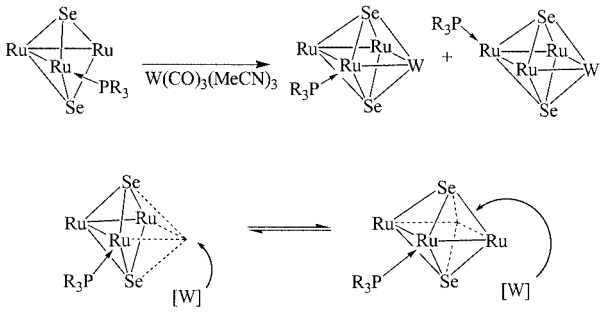

Scheme 13

A possible explanation for the synthesis of the two isomers is derived from the fluxional behaviour of the $Ru_3(\mu_3\text{-}Se)_2$ core clusters: when the Ru−Ru bond is localized on the pyramid edge, the $W(CO)_3$ fragment can fit in the *cis* position with regard to the phosphane ligand; when the Ru−Ru bond is localized on the basal plane, the unique position in which the fragment fits is the *trans* one (see Scheme 13).

In the case of the reaction between $W(CO)_3(MeCN)_3$ and $[Ru_3(\mu_3\text{-}Se)_2(CO)_7(dpbz)_2]$ (dpbz = diphenylbenzylphosphane), the compound $[Ru_3(\mu_3\text{-}Se)(\mu_4\text{-}Se)(CO)_7(dpbz)_2W(CO)_5]$ (Figure 12) was obtained. This cluster can be considered as the product of a donor−acceptor interaction between the fragment $W(CO)_5$ and a selenido atom of $[Ru_3(\mu_3\text{-}Se)_2(CO)_7(dpbz)_2]$.

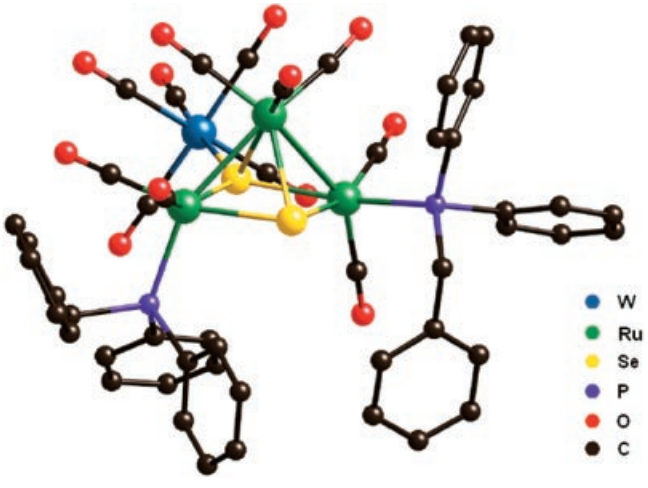

Figure 12. Perspective view of cluster $[Ru_3(\mu_3\text{-}Se)(\mu_4\text{-}Se)(CO)_7(dpbz)_2W(CO)_5]$

A possible mechanism for the production of this compound involves the formation of the labile intermediate $[Ru_3(\mu_3\text{-}Se)(\mu_4\text{-}Se)(CO)_7(dpbz)_2W(CO)_3(CH_3CN)_2]$ (Scheme 14) that could undergo easily the substitution of two acetonitrile groups with two carbonyl groups. If the loss of the two acetonitrile groups is followed by saturation of the coordinative vacancy on the basal plane of the pyramid, the previously described *closo* cluster is obtained.

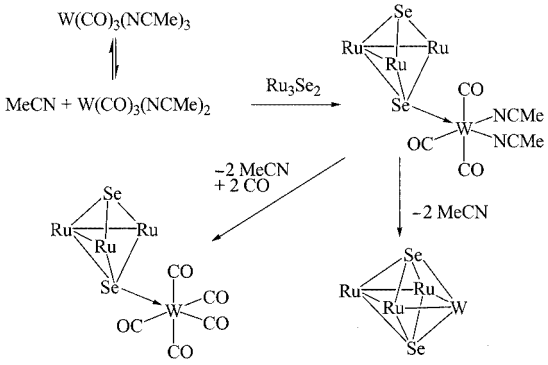

Scheme 14

Concluding Remarks

Systematic investigations on the reactions of tertiary phosphane and diphosphane selenides towards (carbonyl)iron and -ruthenium clusters have achieved the following results: (*i*) The reaction provides a simple, stepwise synthetic route to phosphane-substituted, small-nucleus selenido carbonyl clusters, through transfer of selenium atoms; (*ii*) it leads, in some cases, to the formation of new species, such as the cubane-like cage complex $[Ru_4(\mu_3\text{-}Se)_4(CO)_{10}(\mu\text{-}dppm)]$, that are not easily attainable by other routes; (*iii*) when the tertiary phosphane selenide bears heterocyclic fragments, the reaction is not only limited to the transfer of the chalcogenido atom, but proceeds with P−C and/or C−H bond cleavages, affording selenido-phosphido carbonyl compounds; (*iv*) some clusters display particular physico-chemical characteristics, such as the fluxional behaviour in solution involving ligand exchange as well as M−M bond migration; (*v*) certain compounds exhibit specific activity in cluster-growth reactions, such as the *nido* clusters with the $Ru_3(\mu_3\text{-}Se)_2$ core, which reacts with $M(CO)_3$ fragments (M = Mo or W), leading to the corresponding dimetallic *closo* octahedral species $[Ru_3M(\mu_4\text{-}Se)_2(CO)_{12-n}L_n]$ (L = tertiary phosphane, n = 1 or 2). For the synthesis of dimetallic substituted carbonyl clusters we have also investigated another strategy: treatment of different phosphane selenides with the dimetallic tetrahedral clusters $[HMCo_3(CO)_{12}]$ (M = Fe or Ru) and with the linear trinuclear complex $[Pt\{Fe(CO)_3(NO)\}_2(PhCN)_2]$ obtaining new selenido−mixed-metal clusters substituted by tertiary phosphanes.

Acknowledgments

Financial support from the Ministero dell'Università e della Ricerca Scientifica e Tecnologica (Roma, Cofin 2000) is gratefully

 © 2003 Wiley-VCH Verlag GmbH & Co. KGaA, Weinheim

acknowledged. The facilities of the Centro Interdipartimentale di Misure (Università di Parma) were used to record the NMR and mass spectra.

[1] D. Fenske, G. Longoni, G. Schmid, in: *Clusters and Colloids* (Ed.: G. Schmid), VCH, Weinheim, **1994**, chapter 3, p. 89.
[2] G. Henkel, S. Weissgräber, in: *Metal Clusters in Chemistry* (Eds.: P. Braunstein, L. Oro, P. Raithby), VCH, Weinheim, **1999**, vol. 1, p. 163.
[3] S. Dehnen, A. Eichhöfer, D. Fenske, *Eur. J. Inorg. Chem.* **2002**, 279−317.
[4] F. J. Rodriguez, P. J. Sebastian, *J. New Mater. Electrochem. Syst.* **1999**, *2*, 107−110.
[5] F. J. Rodriguez, P. J. Sebastian, *Surf. Eng.* **2000**, *16*, 43−46.
[6] S. Duron, R. Rivera-Noriega, M. A. Leyva, P. Nkeng, G. Poillerat, O. Solorza-Feria, *J. Solid State Electrochem.* **2000**, *4*, 70−74.
[7] J. Mizutani, K. Matsumoto, *Chem. Lett.* **2000**, *1*, 72−73.
[8] V. Le Rhun, N. Alonso Vante, *J. New Mater. Electrochem. Syst.* **2000**, *3*, 331−336.
[9] T. C. Standtman, *Annu. Rev. Biochem.* **1990**, *59*, 111−127.
[10] M. L. Steigerwald, T. Siegrist, E. M. Gyorgy, B. Hessen, Y.-U. Kwon, S. M. Tanzler, *Inorg. Chem.* **1994**, *33*, 3389−3395.
[11] B. F. G. Johnson, T. M. Layer, J. Lewis, A. Martin, P. R. Raithby, *J. Organomet. Chem.* **1992**, *429*, C41−C45.
[12] T. M. Layer, J. Lewis, A. Martin, P. R. Raithby, W.-T. Wong, *J. Chem. Soc., Dalton Trans.* **1992**, 3411−3417.
[13] T. Chihara, H. Yamazaki, *J. Organomet. Chem.* **1992**, *428*, 169−186.
[14] A. J. Arce, R. Machado, C. Rivas, Y. De Sanctis, A. J. Deeming, *J. Organomet. Chem.* **1991**, *419*, 63−75.
[15] D. Fenske, J. Ohmer, J. Hachgenei, *Angew. Chem. Int. Ed. Engl.* **1985**, *97*, 993−995.
[16] D. Fenske, H. Krautscheid, M. Müller, *Angew. Chem. Int. Ed. Engl.* **1992**, *31*, 321−323.
[17] H. Krautscheid, D. Fenske, G. Baum, M. Semmelmann, *Angew. Chem. Int. Ed. Engl.* **1993**, *32*, 1303−1305.
[18] J. Hsiou Liao, M. G. Kanatzidis, *Inorg. Chem.* **1992**, *31*, 431−439.
[19] J. Hsiou Liao, M. G. Kanatzidis, *J. Am. Chem. Soc.* **1990**, *112*, 7400−7402.
[20] G. Hogarth, N. J. Taylor, A. J. Carty, A. Meyer, *J. Chem. Soc., Chem. Commun.* **1988**, 834−836.
[21] F. Van Gastel, L. Agocs, A. A. Cherkas, J. F. Corrigan, S. Doherty, R. Ramachandran, N. J. Taylor, A. J. Carty, *J. Cluster Sci.* **1991**, *2*, 131−136.
[22] S. M. Stuczynski, Y.-U. Kwon, M. L. Steigerwald, *J. Organomet. Chem.* **1993**, *449*, 167−172.
[23] W. Imhof, G. Huttner, *J. Organomet. Chem.* **1993**, *448*, 247−253.
[24] P. Mathur, Md. M. Hossain, R. S. Rashid, *J. Organomet. Chem.* **1993**, *460*, 83−86.
[25] P. Mathur, Md. M. Hossain, R. S. Rashid, *J. Organomet. Chem.* **1994**, *467*, 245−249.
[26] P. Baistrocchi, D. Cauzzi, M. Lanfranchi, G. Predieri, A. Tiripicchio, M. Tiripicchio Camellini, *Inorg. Chim. Acta* **1995**, *235*, 173−183.
[27] D. Cauzzi, C. Graiff, G. Predieri, A. Tiripicchio, in: *Molecular Clusters in Chemistry*, vol.1, (Eds.: P. Braunstein, L. Oro, P. Raithby), Wiley-VCH, Weinheim, Germany, **1999**, pp. 193−208.
[28] M. Careri, C. Graiff, A. Mangia, P. Manini, G. Predieri, *Rapid Commun. Mass Spectrom.* **1998**, *12*, 225−230.
[29] D. Cauzzi, C. Graiff, G. Predieri, C. Vignali, A. Tiripicchio, *J. Chem. Soc., Dalton Trans.* **1999**, 237−242.
[30] D. Cauzzi, C. Graiff, M. Lanfranchi, G. Predieri, A. Tiripicchio, *J. Chem. Soc., Dalton Trans.* **1995**, 2321−2322.
[31] L. L. Nelson, F. Y.-K. Lo, A. D. Rae, L. Dahl, *J. Organomet. Chem.* **1982**, *225*, 309−329.
[32] L. C. Roof, W. T. Pennington, J. W. Kolis, *Angew. Chem. Int. Ed. Engl.* **1992**, *31*, 913−915.
[33] D. Belletti, D. Cauzzi, C. Graiff, A. Minarelli, R. Pattacini, G. Predieri, A. Tiripicchio, *J. Chem. Soc., Dalton Trans.* **2002**, 3160−3163.
[34] R. D. Adams, J. E. Babin, M. Tasi, *Organometallics* **1988**, *7*, 219−227.
[35] P. Baistrocchi, D. Cauzzi, M. Lanfranchi, G. Predieri, A. Tiripicchio, M. Tiripicchio Camellini, *Inorg. Chim. Acta* **1995**, *235*, 173−183.
[36] D. Belletti, C. Graiff, R. Pattacini, G. Predieri, A. Tiripicchio, results to be published.
[37] D. Cauzzi, C. Graiff, C. Massera, G. Predieri, A. Tiripicchio, *Inorg. Chim. Acta* **2000**, *300−302*, 471−476.
[38] D. Cauzzi, C. Graiff, C. Massera, G. Predieri, A. Tiripicchio, *Eur. J. Inorg. Chem.* **2001**, 721−723.
[39] D. Cauzzi, C. Graiff, C. Massera, G. Predieri, A. Tiripicchio, *J. Cluster Sci.* **2001**, *12*, 259−271.
[40] A. J. Deeming, S. N. Jayasuriya, A. Arce, Y. De Sanctis, *Organometallics* **1996**, *15*, 786−793.
[41] D. Acquotti, D. Belletti, C. Graiff, C. Massera, A. Minarelli, G. Predieri, A. Tiripicchio, results to be published.
[42] F. Fabrizi de Biani, C. Graiff, G. Opromolla, G. Predieri, A. Tiripicchio, P. Zanello, *J. Organomet. Chem.* **2001**, *637−639*, 586−594.
[43] P. Q. Adams, D. L. Davies, A. F. Dyke, S. A. R. Knox, K. A. Mead, P. Woodward, *J. Chem. Soc., Chem. Commun.* **1983**, 222−224, and references therein.
[44] D. Cauzzi, C. Graiff, C. Massera, G. Predieri, A. Tiripicchio, D. Acquotti, *J. Chem. Soc., Dalton Trans.* **1999**, 3515−3521.
[45] P. Braunstein, C. Graiff, C. Massera, G. Predieri, J. Rosè, A. Tiripicchio, *Inorg. Chem.* **2002**, *41*, 1372−1382.
[46] C. Graiff, A. Ienco, C. Massera, C. Mealli, G. Predieri, A. Tiripicchio, F. Ugozzoli, *Inorg. Chim. Acta* **2002**, *330*, 95−102.
[47] D. Cauzzi, C. Graiff, C. Massera, G. Mori, G. Predieri, A. Tiripicchio, *J. Chem. Soc., Dalton Trans.* **1998**, 321−322.

Received November 29, 2002

 © 2003 Wiley-VCH Verlag GmbH & Co. KGaA, Weinheim

The Dicopper(II) Complex of the Novel Asymmetric Dinucleating Ligand Hpy3asym as a Structural Model of Catechol Oxidase

Iryna A. Koval,[a] Daniel Pursche,[b] Arno F. Stassen,[a] Patrick Gamez,[a] Bernt Krebs,[b] and Jan Reedijk*[a]

Keywords: Copper / Cyclic voltammetry / Enzyme models / Ligand design / Magnetic properties

The new asymmetric dinucleating ligand 2-{[bis(2-pyridinylmethyl)amino]methyl}-4-methyl-6-{[(2-pyridinylmethyl)amino]methyl}phenol (Hpy3asym) has been designed in order to model the type-3 active site of the copper proteins. This phenol-based "end-off" compartmental ligand has one tridentate and one didentate arm attached to the 2- and 6-positions of the phenolic ring, respectively. A dinuclear copper(II) nitrate complex with this ligand $[Cu_2(py3asym)(H_2O)_{1.5}(NO_3)_2]NO_3$ has been obtained and structurally characterized. In this complex both copper ions have a distorted octahedral geometry and are endogenously bridged by the phenolic oxygen atom of the deprotonated ligand. The complex shows a donor-atom asymmetry that consists of an N_3O_3 donor set for the Cu1 ion and an N_2O_4 donor set for the Cu2 ion. The electrochemical, magnetic behavior and spectral properties of the complex are discussed.
(© Wiley-VCH Verlag GmbH & Co. KGaA, 69451 Weinheim, Germany, 2003)

Introduction

The copper proteins with the type-3 active site, such as hemocyanins, tyrosinases and catechol oxidases, have attracted the attention of scientists due to their ability to process primary dioxygen under ambient conditions.[1−3] The latter two enzymes use it to perform selective oxidations of organic substrates, such as tyrosine and catechol, to produce various melanins, whereas hemocyanin is the dioxygen transport and storage protein in some arthropods and molluscs.

The type-3 active site is characterized by a dicopper core where each of the metal ions is surrounded by three histidine residues. In the met-Cu^{II}-Cu^{II} form two copper ions are antiferromagnetically coupled via the μ-OH bridge, resulting in an EPR-silent active site.

The determination of the crystal structure of catechol oxidase from sweet potatoes (*Ipomoea batatas*) by some of us[4] offered new insight into the catalytic mechanism of the enzyme with the possibly different functions of the two copper ions. Taking our inspiration from the natural molecule, our attention has turned to the deliberate design of novel model systems of the type-3 active site, where the two copper ions would have distinctively different coordination surroundings. The site specificity of the copper ions may help to answer an important question concerning the binding of the substrate in the natural enzyme, i.e. is the catechol substrate forming a bridge between the two copper(II) centers rather than binding to only one of them?

Dinucleating phenol-based "end-off" compartmental[5] ligands have previously been successfully used for modeling dimetallic biosites.[6−8] In this paper, the synthesis of the novel phenol-based ligand 2-{[bis(2-pyridinylmethyl)-amino]methyl}-4-methyl-6-{[(2-pyridinylmethyl)amino]-methyl}phenol, Hpy3asym, is reported. This dinucleating ligand was designed to hold two copper ions in close proximity and to provide them with different coordination surroundings, thus making one of the two copper ions more readily accessible for the binding of the substrate. This was achieved by substituting the 2- and the 6-positions of the phenol ring by tridentate and didentate arms, respectively, containing nitrogen donor atoms. The reaction of Hpy3asym with copper(II) nitrate yields the new dinuclear asymmetric complex, which is regarded as a structural model of the type-3 active site. The dinuclear copper core exhibits a donor-atom asymmetry in the solid state, comprised of an N_3O_3 donor set for the Cu1 ion and an N_2O_4 donor set for the Cu2 ion. The crystal structure, spectroscopy, electrochemical and magnetic behavior of the complex are reported below.

[a] Leiden University, Leiden Institute of Chemistry,
P. Box 9502, 2300 RA Leiden, Netherlands
Fax: (internat.) +31-71/527-4451
E-mail: reedijk@chem.leidenuniv.nl
[b] Institut für Anorganische und Analytische Chemie der Westfälischen Wilhelms-Universität Münster,
Wilhelm-Klemm-Straße 8, 48149 Münster, Germany
Fax: (internat.) +49-251/833-8366
E-mail: krebs@uni-muenster.de

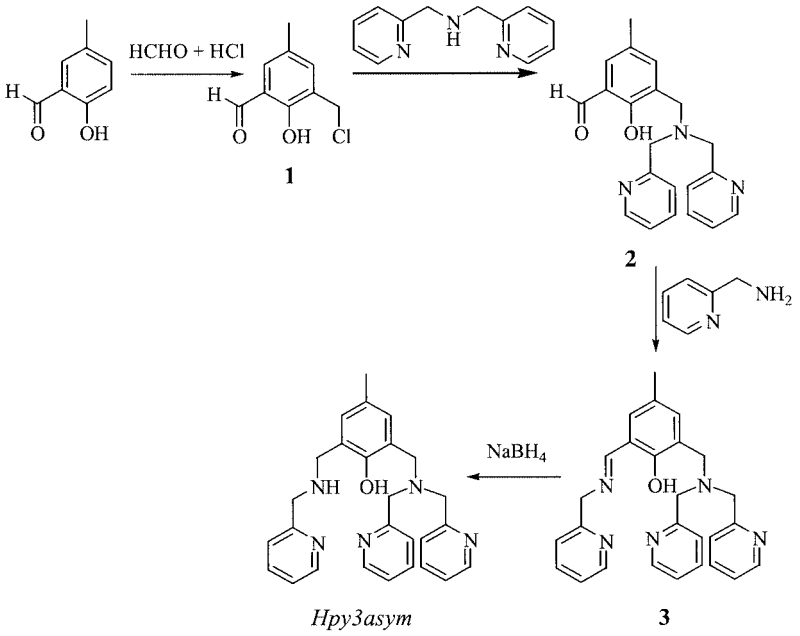

Figure 1. The reaction scheme of the synthesis of the phenol-based compartmental "end-off" ligand Hpy3asym

Results and Discussion

Ligand Design

Hpy3asym was synthesized in three steps (Figure 1) from commercially available 5-methylsalicylaldehyde. The first step includes the introduction of the dichloromethane group in the 3-position of the phenol ring. The chloride atom was subsequently substituted by di(2-picolyl)amine. Finally, the reductive amination of the aldehyde group by 2-aminomethylpyridine and sodium borohydride led to the desired ligand.

Crystal Structure Description

Very small green rectangular crystals of $[Cu_2(py3asym)(H_2O)_{1.5}(NO_3)_2](NO_3)$ were obtained by slow evaporation of the solvent from an acetonitrile solution of the complex. The Platon[9] projection of the complex is depicted in Figure 2. The compound crystallizes in the space group $P2_1/n$. Both copper ions have distinctively different coordination surroundings, showing a donor-atom asymmetry. An endogenous phenolato bridge is present in the dinuclear core, but there is no exogenous bridge. The N_3O_3 coordination sphere around the Cu1 ion can be regarded as a very distorted octahedron. The equatorial plane is formed by the *tert*iary amine nitrogen atom N1 at a distance of 2.0182(18) Å, two *trans* located nitrogen atoms N2 and N3 from two pyridine rings at a distance of 1.9860(17) Å and 1.9760(18) Å, respectively, and the oxygen atom from a water molecule at a distance of 1.9701(16) Å. One of the axial positions is occupied by the bridging phenolate oxygen atom O1 at a relatively long distance of 2.3070(13) Å. The second apical position has a weak O-donor ligand, which was refined for 50% to be water and for 50% a disordered nitrate anion. The oxygen atom O20 (occupancy 0.4886) from the water molecule is at a distance of 2.535(3) Å. The loosely bound oxygen atom O10 (occupancy 0.5114) from the disordered nitrate counteranion [the Cu1−O10a distance is 3.007(6) Å] is at a much larger distance, which, however, still matches the range of bond lengths observed for copper-oxygen bonds along the Jahn−Teller axis.[10−13] The in-plane *cis* angles around the Cu1 ion vary over quite a broad range, viz. 83.92(8)° for the N1−Cu1−N3 angle and 96.92(7)° for the O2−Cu1−N2 angle. Their sum amounts to 357.76°. The O−Cu1−O angle along the Jahn−Teller axis is equal to 173.85(8)° for the O1−Cu1−O20 angle and 165.46(10)° for the O1−Cu1−O10 angle, thus indicating a significant distortion from a regular octahedral geometry.

The coordination sphere around the second copper ion Cu2 can also be described as a distorted octahedron, but with an N_2O_4 donor set. The equatorial plane around the Cu2 ion is formed by two *cis* located nitrogen atoms N4 from the secondary amine [the Cu2−N4 distance is 1.9838(17) Å], N5 from the pyridine ring [the Cu2−N5 distance is 2.0181(17) Å], and two *cis* oxygen atoms, O1 from the bridging phenolate [the Cu2−O1 distance is 1.9353(14) Å] and O3 from the chelating nitrate anion [the Cu2−O3 distance is 1.9910(14) Å]. The second oxygen atom O5 from the chelating nitrate anion and the oxygen atom O6 from the monocoordinated nitrate anion occupy the axial positions, thus adjusting the coordination sphere around the copper ion to a very distorted octahedron [the distances Cu2−O5 and Cu2−O6 are equal to 2.5431(16) Å and 2.5982(16) Å, respectively]. The in-plane *cis* angles vary in the range 87.36°−94.64°. The angle O5−Cu2−O6, which should be equal to 180° in the regular octahedron, is only 157.37(5)°, indicating an even greater distortion from a regular octahedral geometry than observed in the case of the Cu1 ion.

 © 2003 Wiley-VCH Verlag GmbH & Co. KGaA, Weinheim

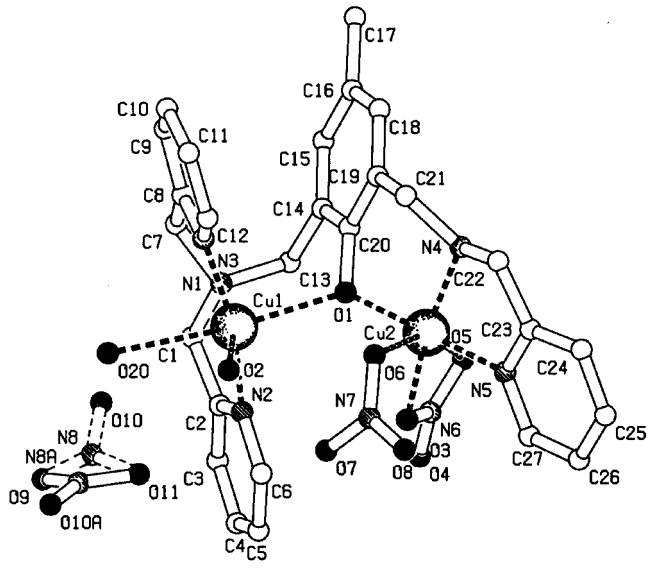

Figure 2. Platon[9] projection of $[Cu_2(py3asym)(H_2O)_{1.5}(NO_3)_2]NO_3$; hydrogen atoms are omitted for clarity; the second axial position at Cu1 ion has a O-donor ligand, which was refined to be 50% water and 50% a disordered nitrate anion

Table 1. Hydrogen bonds (D-H···A) with the distance H···A < r(A) + 2.000 Å and the angle DHA > 110°

D−H	d(D−H), Å	d(H···A), Å	<DHA>, °	d(D···A), Å	A
O2−H2a	0.736	1.971	174.09	2.704	O11
O2−H2a	0.736	2.518	127.91	3.026	O10
O2−H2a	0.736	2.611	155.96	3.296	N8
O2−H2b	0.915	1.802	154.44	2.657	O7
O2−H2b	0.915	2.443	174.95	3.356	N7
O2−H2b	0.915	2.448	145.50	3.245	O6
N4−H4	0.930	2.119	143.16	2.917	O7[a]
N4−H4	0.930	2.574	156.83	3.448	O8[a]
N4−H4	0.930	2.624	156.58	3.497	N7[a]
O20−H20a	0.759	2.087	163.07	2.821	O9[b]
O20−H20b	0.999	2.010	164.96	2.985	O9
O20−H20b	0.999	2.476	145.58	3.348	N8A
O20−H20b	0.999	2.486	127.27	3.191	O11

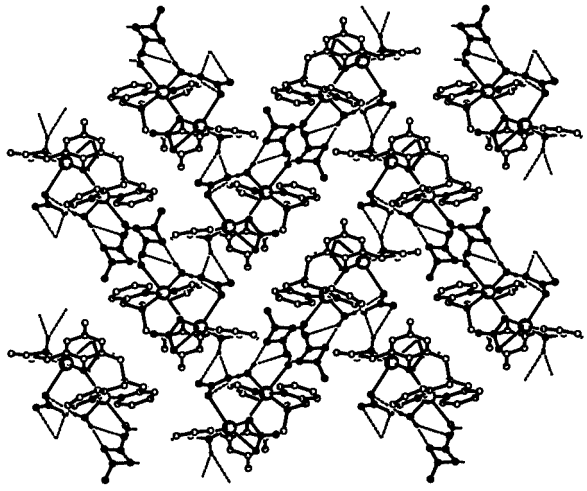

Figure 3. The Platon[9] projection of the "herring bone" packing arrangement along the crystallographic *a* axis; all hydrogen atoms, except for those participating in hydrogen bonding, are omitted

The absence of the exogenous bridge between the two copper ions promotes the large copper-copper separation of 3.9003 Å, which is significantly longer than the distances observed for similar complexes with two types of bridges between the copper ions.[7,8,14] It is interesting to note that potentially bridging nitrate anions are present in the complex; however, they fail to bridge the two copper ions, instead being coordinated as monodentate and didentate chelating ligands. The distribution of charged and neutral ligands in the complex is also remarkable: 1.5 neutral water molecules are coordinated to the Cu1 ion, whereas two charged nitrate anions are coordinated to the Cu2 ion.

The crystal packing is stabilized by an extensive net of intra- and intermolecular hydrogen bonds (see Table 1). In particular, a bifurcated intramolecular hydrogen bonding is realized between the proton H2b of the water molecule coordinated to the Cu1 ion and the two oxygen atoms O6 and O7 of the monodentate nitrate anion coordinated to the Cu2 ion, giving an impression of an exogenous pseudo-bridge between the two copper ions. Furthermore, each formula unit is connected via intermolecular hydrogen bonds to three neighboring units. The Platon[9] projection of the crystal packing along the crystallographic *a* axis is shown in Figure 3. As can be seen, the molecules are assembled by means of hydrogen bonds to form a "herring bone" pattern.

Physical Characterization

Besides the crystal structure determination, the complex was characterized spectroscopically and magnetically. The electrospray mass spectrum (ESI-MS) of the complex performed in acetonitrile reveals one major peak at $m/z = 688$, corresponding to $[Cu_2(py3asym)(NO_3)_2]^+$. The theoretical isotope pattern calculated for the empirical formula $C_{27}H_{28}Cu_2N_7O_7$ is in agreement with the experimentally found one. Thus, the 1.5 water molecules coordinated to the Cu1 ion, observed in the solid state, are lost during the measurement. The UV/Vis spectrum of the solid exhibits two peaks at 456 and 640 nm. The first peak is assigned to an LMCT transition between the bridging phenoxo group and copper ions,[14] whereas the second one is characteristic for Cu^{II} d-d transitions.[15] The positions of these bands do not significantly change when the spectrum of the complex is taken in acetonitrile solution, suggesting no important modifications in the copper-ligand chromophores.

A cyclic voltammogram of the complex recorded in acetonitrile, when scanning towards the negative region of potentials, shows two successive one-electron electrochemical signals. The first one, at −0.13 V vs. Ag/AgCl, is assigned to the $Cu_2^{II,II}/Cu_2^{II,I}$ redox couple. The second one, at −0.33 V, is attributed to the formation of $Cu_2^{I,I}$ species. They both appear to be irreversible. In addition, a very

 © 2003 Wiley-VCH Verlag GmbH & Co. KGaA, Weinheim

broad peak at ca. −0.7 V suggests the reduction of both copper ions to Cu^0 and the deposition of the free metal on the electrode surface. On the reverse scan, an additional sharp anodic peak is observed at −0.27 V. This is the so-called stripping peak, caused by the redissolution of the metallic copper. This peak is absent if the potential sweep is reversed at ca. −0.5 V, before the reduction to Cu^0 can take place. The anodic part of the cyclic voltammogram is characterized by three successive fully irreversible oxidation waves at 1.16, 1.48 and 1.68 V, apparently corresponding to the oxidation of the ligand and/or water molecules.

Magnetic Properties

In Figure 4, the magnetic susceptibility of the complex $[Cu_2(py3asym)(H_2O)_{1.5}(NO_3)_2]NO_3$ is shown, plotted as both χ^{-1} and χ versus the temperature. The compound displays a weak ferromagnetic coupling with a Curie temperature θ of 0.87 K and a Curie−Weiss constant C of 0.39 $cm^3 \cdot K \cdot mol^{-1}$. The value for μ is 1.10 B.M.

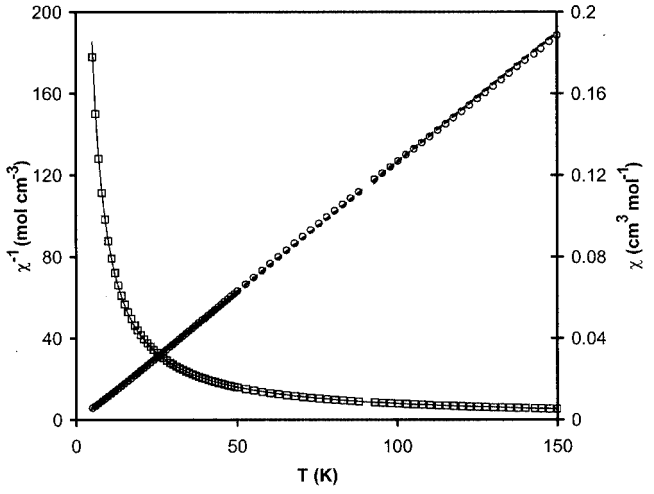

Figure 4. Magnetic susceptibility plotted as χ^{-1} versus T (O) and as χ versus T (□); the dashed line is the Curie−Weiss plot from near field theory and the solid line is the theoretical curve according to the Bleany-Bowers equation

The magnetic properties of this dinuclear copper(II) complex have been interpreted in terms of the Bleaney−Bowers equation [Equation (1)], where g is the magnetic field splitting factor, J is the exchange integral of magnetic theory and N_α is the temperature-independent paramagnetism of one mol of copper(II) ions.[16,17]

$$\chi_M = \frac{g^2 N\beta^2}{3kT}\left(1+\frac{1}{3}e^{J/kT}\right)^{-1} + N\alpha \quad (1)$$

The fit was accomplished by minimization of the reliability factor, defined as $R = \Sigma(\chi_m T_{calc} - \chi_m T_{obs})^2/(\chi_m T_{obs})^2$, by a least-squares procedure. The best fit was obtained for the exchange integral $J = -4.6\ cm^{-1}$, the magnetic field splitting factor $g = 2.02$ and $R = 2.9 \times 10^{-3}$.

Conclusion

The asymmetric phenol-based "end-off" compartmental ligand 2-{[bis(2-pyridinylmethyl)amino]methyl}-4-methyl-6-{[(2-pyridinylmethyl)amino]methyl}phenol forms a dinuclear asymmetric copper(II) nitrate complex which can be regarded as a new structural model of the type-3 active site of the copper proteins. The ligand holds a tridentate and a didentate arms attached to the 2- and 6-positions of the phenol ring. In the solid state the complex possesses donor-atom asymmetry, constituted by an N_3O_3 donor set for the Cu1 ion bound to a tridentate arm, and an N_2O_4 donor set for the Cu2 ion bound to a didentate arm. The magnetic behavior of the complex was interpreted in terms of weak ferromagnetic coupling between the two copper ions, with the exchange integral $J = -4.6\ cm^{-1}$, and a Curie−Weiss temperature θ of 0.87 K.

Experimental Section

General Remarks: Most of the synthetic work was carried out using standard Schlenk techniques. All chemicals were commercially available and used without further purification. 5-Methylsalicylaldehyde was purchased from Fluka, 2-(aminomethyl)pyridine from Acros, and di(2-picolyl)amine from Aldrich. 3-Chloro-5-methylsalicylaldehyde (**1**) was prepared according to the procedure described by Lock.[18] Tetrahydrofuran and methanol were dried by refluxing over sodium. Water was demineralized prior to use. C,H,N determinations were performed on a Perkin−Elmer 2400 Series II analyzer. NMR spectra were recorded on a JEOL FX-200 (200 MHz) FT NMR spectrometer. Solid-state ligand field spectra (300−2000 nm, diffuse reflectance) and in solution were taken on a Perkin−Elmer 330 spectrophotometer equipped with a data station. IR spectra were recorded of pure solids on a Perkin−Elmer FT-IR Paragon 1000 spectrophotometer with a Specac single-reflection diamond ATR P/N 10500, using the diffuse reflectance technique (4000−300 cm^{-1}, res. 4 cm^{-1}). Electrospray mass spectra (ESI-MS) were recorded on the Thermo Finnigan AQA apparatus. Cyclic voltammetry measurements were performed with an Autolab PGSTAT 10 cyclic voltammeter, using a Pt working electrode and a Ag/AgCl reference electrode in acetonitrile (10^{-3} M), with tetrabutylammonium perchlorate as supporting electrolyte, at a scan rate of 0.1 mV/s. DC magnetic susceptibility measurements (5−150 K) were carried out at 0.1 Tesla using a Quantum Design MPMS-5 5T SQUID magnetometer. Data were corrected for magnetization of the sample holder and for diamagnetic contributions, which were estimated from the Pascal constants.[19]

3-{[Bis(2-pyridinylmethyl)amino]methyl}-2-hydroxybenzaldehyde (2): A solution of di(2-picolyl)amine (1.08 g, 5.4 mmol) and triethylamine (1.09 g, 10.8 mmol) in 50 mL of dry THF was added dropwise with stirring to a solution of **1** (1 g, 5.4 mmol) in 250 mL of dry THF under an Ar atmosphere. After completion of the addition, the resulting white suspension was refluxed for two hours and cooled to room temperature. After the removal of the triethylamine hydrochloride salt by filtration, the resulting solution was evaporated under reduced pressure, yielding a yellow oil, from which compound **2** crystallized within a few minutes. Recrystallization from a methanol/diethyl ester mixture gave slightly yellowish crystals of the pure compound **2**. Yield: 1.55 g, 4.5 mmol (82%). ^1H NMR ($CDCl_3$, 200 MHz): δ = 10.42 (s, 1 H, aldehyde proton),

 © 2003 Wiley-VCH Verlag GmbH & Co. KGaA, Weinheim

8.56 (d, 2 H, 6′py-*H*), 7.63 (td, 2 H, 4′py-*H*), 7.40 (t, 2 H, 5′py-*H*), 7.20 (d, 2 H, 3′py-*H*), 7.15 (s, 1 H, 2′phenol-*H*), 7.13 (s, 1 H, 5′phenol-*H*), 3.89 [s, 4 H, N-(CH_2py)$_2$], 3.80 (s, 2 H, phenol-CH_2-N), 2.23 (s, 3 H, CH_3) ppm.

2-{[Bis(2-pyridinylmethyl)amino]methyl}-4-methyl-6-{[(2-pyridinylmethyl)imino]methyl}phenol (3): A solution of 2-pyridylmethylamine (0.39 g, 3.6 mmol) in 50 mL of dry methanol was added dropwise with stirring to a solution of **2** (1.26 g, 3.6 mmol) in 250 mL of dry methanol under argon. After the addition was complete, the resulting bright yellow solution was heated for two hours at 50 °C. The successful formation of the imine derivative was verified by NMR spectroscopy. The imine was reduced in situ to the respective amine with sodium borohydride. ^{1}H NMR (CDCl$_3$, 200 MHz): δ = 8.51 (d, 3 H, 6′py-*H*), 8.34 (s, 1 H, C*H*=N), 7.62 (td, 3 H, 4′py-*H*), 7.33 (t, 3 H, 5′py-*H*), 7.26(d, 2 H, 3′py-*H*), 7.09 (s, 1 H, 3′phenol-*H*), 7.03 (2, 1 H, 5′phenol-*H*), 4.92 (s, 2 H, CH=N-CH_2), 3.88 [s, 4 H, N-(CH_2py)], 3.80 (s, 2 H, phenol-CH_2-N), 2.29 (s, 3 H, CH_3) ppm.

2-{[Bis(2-pyridinylmethyl)amino]methyl}-4-methyl-6-{[(2-pyridinylmethyl)amino]methyl}phenol (Hpy3asym): $NaBH_4$ (0.41 g, 10.9 mmol, 3 equiv./CH=N) was added in situ to a solution of **3** in methanol. After the hydrogen evolution stopped, the resulting colorless solution was refluxed for two hours and the solvent was evaporated under reduced pressure. The residue was dissolved in acidified water and washed three times with dichloromethane. The water layer was made alkaline (pH ≈ 9) by addition of concentrated ammonia. The resulting white suspension was extracted three times with dichloromethane. The organic layers were collected and dried over Na_2SO_4. After evaporation under reduced pressure, the pure compound was obtained as a clear yellow oil. Yield: 1.54 g, 3.5 mmol (96%). ^{1}H NMR (CDCl$_3$, 200 MHz): δ = 8.55 (d, 3 H, 6′py-*H*), 7.59 (td, 3 H, 4′py-*H*), 7.36 (d, 3 H, 3′py-*H*), 7.14 (t, 3 H, 5′py-*H*), 6.93 (s, 1 H, 3′phenol-*H*), 6.84 (s, 1 H, 5′phenol-*H*), 3.95 (s, 2 H, NH-CH_2-py), 3.91 (s, 2 H, phenol-CH_2-NH), 3.85 [s, 4 H, N(CH_2-py)$_2$], 3.75 (s, 2 H, phenol-*N*-CH_2), 2.22 (s, 3 H, CH_3) ppm. ^{13}C NMR (CDCl$_3$, 200 MHz): δ = 159.35, 154.80, 147.32, 136.17, 128.35, 126.35, 124.00, 123.11, 122.85, 121.67, 59.06, 56.12, 54.65, 50.95, 26.22 ppm.

[Cu$_2$(py3asym)(H$_2$O)$_{1.5}$(NO$_3$)$_2$](NO$_3$): The bulk sample was prepared by dissolving Hpy3asym (0.076 g, 0.17 mmol) and Cu(NO$_3$)$_2$·3H$_2$O (0.09 g, 0.37 mmol) in 10 mL of an acetonitrile/water mixture (1:1). The resulting solution was stirred for one hour at room temperature and the solvents evaporated to dryness under reduced pressure. After washing with a small amount of acetone, 0.08 g (0.1 mmol, 59% yield) of the pure compound was obtained as a dark green powder. $C_{27}H_{31}Cu_2N_8O_{11.5}$ (778.68): calcd. C 41.7, H 3.9, N 14.7; found C 41.3, H 4.0, N 14.4. MS(ESI): *m*/*z* = 688 ([Cu$_2$(py3asym)(NO$_3$)$_2$]$^+$). IR: $\tilde{\nu}$ = 3600−3200, broad band (H$_2$O, asymmetric and symmetric OH stretching), 3184 (N−H stretching), 1613 (HOH bending), 1484 (chelating didentate NO$_3^-$, N=O stretching), 1396 (monodentate NO$_3^-$, NO$_2$ asymmetric stretching), 1290 (monodentate NO$_3$-, symmetric NO$_2$ stretching, and chelating didentate NO$_3^-$, asymmetric NO$_2$ stretching).[20]

Single crystals of the complex, suitable for X-ray crystal structure determination, were obtained by slow evaporation of the solvent from an acetonitrile solution containing stoichiometric amounts of Cu(NO$_3$)$_2$·3H$_2$O and the ligand.

X-ray Crystallographic Study: A single crystal of [Cu$_2$(py3asym)(H$_2$O)$_{1.5}$(NO$_3$)$_2$](NO$_3$) was mounted at 100 K on a Bruker AXS SMART 6000 diffractometer equipped with Cu-K_α radiation (λ = 1.54184 Å). $C_{27}H_{31}Cu_2N_8O_{11.5}$, M = 778.68 g mol^{-1}, rectangular green needles, 0.17 × 0.08 × 0.07 mm, a = 10.3731(2), b = 22.1430(4), c = 14.2325(2) Å, β = 105.709(10)°, Z = 4, V = 3146.98(9) Å^3, $\rho_{calcd.}$ = 1.644 g cm^{-3}, μ = 2.322 cm^{-1}, absorption correction: SADABS,[21] monoclinic, space group $P2_1/n$ (no. 14), reflections collected: 18421, independent reflections: 5871 (R_{int} = 0.0314). The structure was solved by direct methods and refined using the SHELX program package.[22,23] All hydrogen atoms were placed at idealized positions riding on the carrier atom, with isotropic thermal parameters, except for two hydrogen atoms located close to O20. They were assigned to rest electron density on the electron density map. The final cycle refinement, including 475 parameters, converted to $R1$ = 0.0312 ($R1$ = 0.0388 all data) and $wR2$ = 0.0800 ($wR2$ = 0.0826 all data) with a maximum (minimum) residual electron density of 0.463 (−0.293) e·Å^{-3}.
CCDC-197305 contains the supplementary crystallographic data for this paper. These data can be obtained free of charge at www.ccdc.cam.ac.uk/conts/retrieving.html [or from the Cambridge Crystallographic Data Centre, 12, Union Road, Cambridge CB2 1EZ, UK; fax: (internat.) +44-1223/336-033; E-mail: deposit@ccdc.cam.ac.uk].

Acknowledgments

Financial support from the NRSC Catalysis (a Research School Combination of HRSMC and NIOK) is kindly acknowledged. Travel and exchange of information and students between Leiden University and Westfälische Wilhelms-Universität Münster through a NWO and DFG grant in the framework of the Joint Graduierten Kolleg is gratefully acknowledged, as is support and sponsorship under COST Action D21/003/2001.

[1] A. Rompel, H. Fischer, D. Meiwes, K. Buldt Karentsopoulos, R. Dillinger, F. Tuczek, H. Witzel, B. Krebs, *J. Biol. Inorg. Chem.* **1999**, 56−63.
[2] C. Gerdemann, C. Eicken, B. Krebs, *Acc. Chem. Res.* **2002**, 183−191.
[3] E. I. Solomon, U. M. Sundaram, T. E. Machonkin, *Chem. Rev.* **1996**, *7*, 2563−2605.
[4] T. Klabunde, C. Eicken, J. C. Sacchettini, B. Krebs, *Nature Structural Biology. Dec* **1998**, *12*, 1084−1090.
[5] H. Adams, D. E. Fenton, S. R. Haque, S. L. Health, M. Ohba, H. Okawa, S. E. Spey, *J. Chem. Soc., Dalton Trans.* **2000**, 1849−1856.
[6] K. Abe, K. Matsufuji, M. Ohba, H. Okawa, *Inorg. Chem.* **2002**, 4461−4467.
[7] N. N. Murthy, M. Mahroof-Tahir, K. D. Karlin, *Inorg. Chem.* **2001**, 628−635.
[8] S. Uozumi, M. Ohba, H. Okawa, D. E. Fenton, *Chem. Lett.* **1997**, 673−674.
[9] A. L. Spek, *PLATON, a multipurpose crystallographic tool*, Utrecht University, The Netherlands, **2002**.
[10] *Comprehensive Coordination Chemistry, Vol. 5* (Ed.: G. Wilkinson), Pergamon Press, Toronto, Canada, **1987**.
[11] B. Barszcz, T. Glowiak, J. Jezierska, *Polyhedron* **1999**, *27*, 3713−3721.
[12] A. C. Rizzi, O. E. Piro, E. E. Castellano, O. R. Nascimento, C. D. Brondino, *Inorg. Chim. Acta* **2000**, 19−25.
[13] P. Manikandan, R. Muthukuraman, K. R. Thomas, B. Varghese, G. V. R. Chandramouli, P. T. Manoharan, *Inorg. Chem.* **2001**, 2378−2389.
[14] S. Torrelli, C. Belle, I. Gautier-Luneau, J. L. Pierre, E. Saint-Aman, J. M. Latour, L. Le Pape, D. Luneau, *Inorg. Chem.* **2000**, 3526−3536.
[15] A. B. P. Lever, *Inorganic Electronic Spectroscopy, Vol. 33*, Elsevier, Amsterdam **1984**.

 © 2003 Wiley-VCH Verlag GmbH & Co. KGaA, Weinheim

[16] M. Kato, H. B. Jonnasen, J. C. Fanning, *Chem. Rev.* **1964**, 99.
[17] N. Figgis, R. L. Martin, *J. Chem. Soc.* **1956**, 3837−3846.
[18] G. Lock, *Ber. Dtsch. Chem. Ges.* **1930**, 551−559.
[19] I. M. Kolthoff, P. J. Elving, *Treatise on Analytical Chemistry, Vol. 4*, Interscience Encyclopedia, Inc., New York **1963**.
[20] K. Nakamoto, *Infrared Spectra of Inorganic and Coordination compounds*, Wiley, New York **1970**.
[21] *SAINT Plus V 6.02*, Bruker AXS Inc., Madison, WI **1999**.
[22] G. M. Sheldrick, *SHELXTL PLUS*, Siemens Analytical X-ray Instruments, **1990**.
[23] G. M. Sheldrick, *SHELXL-97*, Pr*ogram for the refinement of crystal structures*, University of Göttingen, Germany **1997**.
Received November 27, 2002

 © 2003 Wiley-VCH Verlag GmbH & Co. KGaA, Weinheim

Solvothermal Synthesis of a Layered Open-Framework Chlorocadmium Oxalate, $Cd_2(C_2O_4)_{0.5}Cl_3NaCl{\cdot}4H_2O$

R. Vaidhyanathan,[a] Srinivasan Natarajan,[a] and C. N. R. Rao*[a]

Keywords: Materials science / Cadmium / Solvothermal synthesis / Metathesis

The metathesis reaction between $CdCl_2{\cdot}2H_2O$ and sodium oxalate in *n*-hexanol under solvothermal conditions yields a hybrid compound of formula $Cd_2(C_2O_4)_{0.5}Cl_3NaCl{\cdot}4H_2O$. It consists of one-dimensional chains formed by Cd and Cl atoms, containing μ_2(Cl) and μ_3(Cl) bridges, and cross-linked by oxalate units to give a layered structure. The Na^+ ions and water molecules occupy the interlamellar spaces.

(© Wiley-VCH Verlag GmbH & Co. KGaA, 69451 Weinheim, Germany, 2003)

Introduction

A variety of inorganic open-framework compounds containing extra-framework alkali metal ions and other cations have been synthesized in recent years.[1−3] Intercalation of cations and anions in cages and cavities (cryptands, spherands, siderands, coronates) is also well documented in host-guest chemistry.[4] Thus Na^+, K^+, Cl^- and NO_3^- have been incorporated into inorganic host compounds. Interestingly, extended structures of alkali halides such as KCl, RbCl, and CsBr, of varying dimensionalities, have been recently incorporated in host lattices of cadmium oxalate.[5−8] The $NH_4^+Cl^-$ ion-pair has been introduced in the cage formed by the anionic cluster of isopolyvanadate and phenylphosphonate units.[9] The use of solvothermal techniques to prepare hybrid organic-inorganic solids has resulted in materials inaccessible by other means.[10−13] In our efforts to synthesize hybrid open architectures incorporating alkali halides and other inorganic guests by means of solvothermal routes, we have obtained a two-dimensional cadmium oxalate of the composition $Cd_2(C_2O_4)_{0.5}Cl_3NaCl{\cdot}4H_2O$ (**I**), wherein the NaCl unit is accommodated in the cadmium oxalate structure. The synthesis of **I** seems to have become possible because of the solvothermal conditions employed by us with *n*-hexanol as the solvent; **I** is not obtained under hydrothermal conditions.

Results and Discussion

The asymmetric unit of **I** consists of 14 non-hydrogen atoms with two crystallographically distinct, octahedrally coordinated Cd atoms. Whilst Cd(1) is linked by three chlorine atoms, two oxalate oxygens and one bonded water molecule, Cd(2) is connected by six chlorine atoms. The average Cd(1)−O/Cl and Cd(2)−Cl distances are 2.459 Å and 2.631 Å, respectively (Table 1). The framework structure of **I** is formed by linkages involving $Cd(1)O_3Cl_3$, $Cd(2)Cl_6$ and oxalate units. The Cd(2) atoms are connected to each other through chloride bridges, giving rise to infinite one-dimensional chains, and the Cd(1) atoms are connected to these chains by μ_2(Cl)- and μ_3(Cl)-type chloride bridges (Figure 1). These one-dimensional building units are cross-linked by oxalate units giving rise to a layered architecture (Figure 2). Adjacent layers are shifted by 1/2 the unit cell length along the [1 0 1] direction, giving rise to ABAB-type layer stacking. Extra-framework Na^+ ions occupy spaces in the interlamellar regions along with water molecules (Figure 3). The environment around the Na^+ ion in **I** can be considered to be octahedral with five water molecules (av. Na−O = 2.411 Å) and a chloride, which is also attached to two Cd atoms. The Na−Cl distance is 2.999 Å, slightly longer than the distance in bulk NaCl (2.814 Å). Selected bond lengths and angles in **I** are presented in Table 1.

The one-dimensional $CdCl_2$ chain in **I** is similar to the double chain in ABX_3.[14] The structure of **I** can therefore be considered as originating from $CdCl_2$, which under the non-aqueous conditions employed for the synthesis can give rise to $NaCdCl_3$ chains. Cross-linking of the chlorocadmium chains by the oxalate units would then yield the layer present in **I**, the process being somewhat similar to the assembly of molecular metal clusters by organic linkers described by Yaghi and co-workers.[15] The cadmium chloride chains in **I** are also related to the infinite one-dimensional chains formed by the pyramidal β-$[AsS_4]^{3-}$ units observed in the potassium tin thioarsenide compound $KSnAsS_5$.[16] One can visualize the structure of **I** to be arising from the replacement of the $[AsS_4]^{3-}$ units by $[Cd(C_2O_4)Cl_2(H_2O)]^{2-}$ units and simultaneously replacing the Sn^{4+} by Cd^{2+} units, as represented schematically on the next page.

[a] Chemistry and Physics of Materials Unit, Jawaharlal Nehru Centre for Advanced Scientific Research, Jakkur, P. O., Bangalore 560 064, India
E-mail: cnrrao@jncasr.ac.in

Supporting information for this article is available on the WWW under http://www.eurjic.org or from the author.

Table 1. Selected bond lengths and bond angles for $Cd_2(C_2O_4)_{0.5}Cl_3NaCl{\cdot}4H_2O$ (**I**)[a]

Moiety	Distance (Å)	Moiety	Distance (Å)
Cd(1)−O(1)#1	2.292(3)	Cd(2)−Cl(3)#3	2.6756(11)
Cd(1)−O(2)	2.304(3)	Na(1)−O(300)	2.322(5)
Cd(1)−O(10)	2.357(4)	Na(1)−O(100)	2.358(4)
Cd(1)−Cl(1)	2.5303(11)	Na(1)−O(200)	2.382(4)
Cd(1)−Cl(2)	2.5404(11)	Na(1)−O(200)#2	2.421(4)
Cd(1)−Cl(3)	2.7284(10)	Na(1)−O(10)	2.571(4)
Cd(2)−Cl(4)	2.5839(11)	Na(1)−Cl(2)	2.999(2)
Cd(2)−Cl(4)#2	2.5908(11)	C(1)−O(2)	1.249(5)
Cd(2)−Cl(1)#3	2.6199(11)	C(1)−O(1)	1.253(5)
Cd(2)−Cl(2)	2.6479(11)	C(1)−C(1)#1	1.569(8)
Cd(2)−Cl(3)	2.6690(11)		

Moiety	Angle (°)	Moiety	Angle (°)
O(1)#1−Cd(1)−O(2)	72.41(10)	Cl(4)−Cd(2)−Cl(2)	91.02(4)
O(1)#1−Cd(1)−O(10)	88.43(14)	Cl(4)#2−Cd(2)−Cl(2)	92.43(3)
O(2)−Cd(1)−O(10)	93.11(12)	Cl(1)#3−Cd(2)−Cl(2)	176.38(4)
O(1)#1−Cd(1)−Cl(1)	165.68(8)	Cl(4)−Cd(2)−Cl(3)	94.38(3)
O(2)−Cd(1)−Cl(1)	93.93(8)	Cl(4)#2−Cd(2)−Cl(3)	174.67(3)
O(10)−Cd(1)−Cl(1)	96.80(12)	Cl(1)#3−Cd(2)−Cl(3)	90.51(3)
O(1)#1−Cd(1)−Cl(2)	95.39(8)	Cl(2)−Cd(2)−Cl(3)	86.33(3)
O(2)−Cd(1)−Cl(2)	167.08(8)	Cl(4)−Cd(2)−Cl(3)#3	177.46(3)
O(10)−Cd(1)−Cl(2)	90.73(10)	Cl(4)#2−Cd(2)−Cl(3)#3	91.27(3)
Cl(1)−Cd(1)−Cl(2)	97.86(4)	Cl(1)#3−Cd(2)−Cl(3)#3	87.55(3)
O(1)#1−Cd(1)−Cl(3)	86.99(8)	Cl(2)−Cd(2)−Cl(3)#3	90.35(3)
O(2)−Cd(1)−Cl(3)	87.86(8)	Cl(3)−Cd(2)−Cl(3)#3	83.57(3)
O(10)−Cd(1)−Cl(3)	174.79(11)	C(1)−O(1)−Cd(1)#1	116.8(3)
Cl(1)−Cd(1)−Cl(3)	88.24(3)	C(1)−O(2)−Cd(1)	116.3(3)
Cl(2)−Cd(1)−Cl(3)	87.24(3)	O(2)−C(1)−O(1)	125.5(4)
Cl(4)−Cd(2)−Cl(4)#2	90.82(3)	O(2)−C(1)−C(1)#1	117.5(4)
Cl(4)−Cd(2)−Cl(1)#3	90.98(3)	O(1)−C(1)−C(1)#1	117.0(4)
Cl(4)#2−Cd(2)−Cl(1)#3	90.56(4)		

[a] Symmetry transformations used to generate equivalent atoms: #1 $-x+1, y, -z+1/2$; #2 $-x+1, -y+1, -z$; #3 $x, -y+1, z+1/2$; #4 $-x+1/2, -y+1/2, -z$

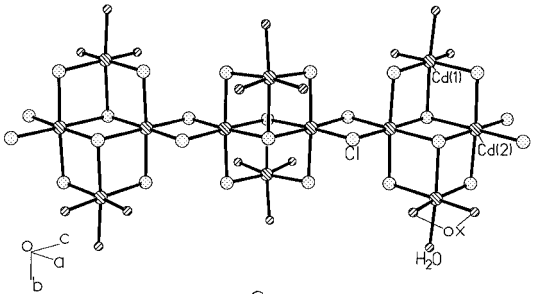

Figure 1. Structure of $Cd_2(C_2O_4)_{0.5}Cl_3NaCl{\cdot}4H_2O$ (**I**) showing the one-dimensional chlorocadmium double chain [note the presence of infinite -(μ_2Cl)- and -(μ_3Cl)- bridges]

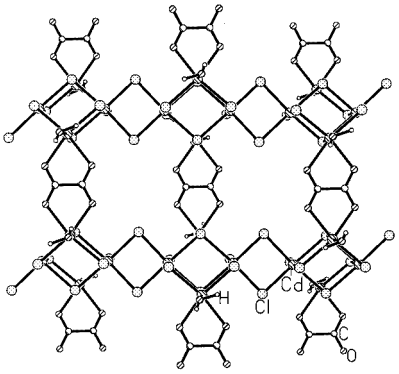

Figure 2. Structure of **I**, showing the two-dimensional chlorocadmium oxalate layer lying in the *ac* plane

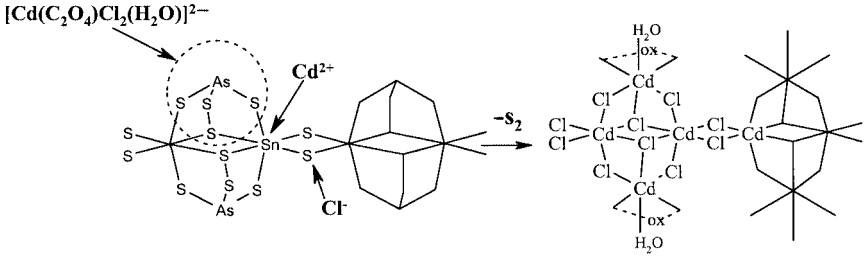

 © 2003 Wiley-VCH Verlag GmbH & Co. KGaA, Weinheim

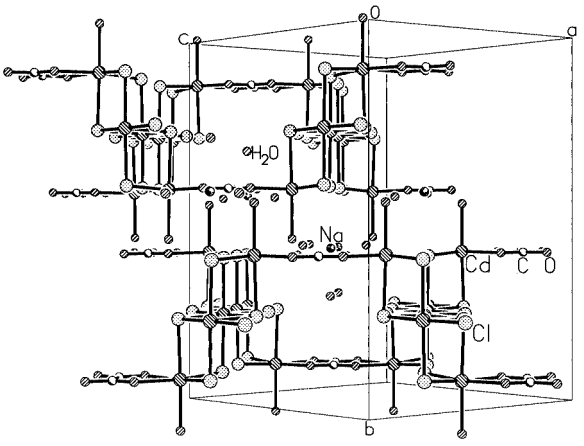

Figure 3. The stacking of the chlorocadmium oxalate layers in **I**; the adjacent layers are shifted by half of the unit cell along the [1 0 1] direction. Note the presence of extra-framework Na^+ ions and water molecules in the interlamellar spaces

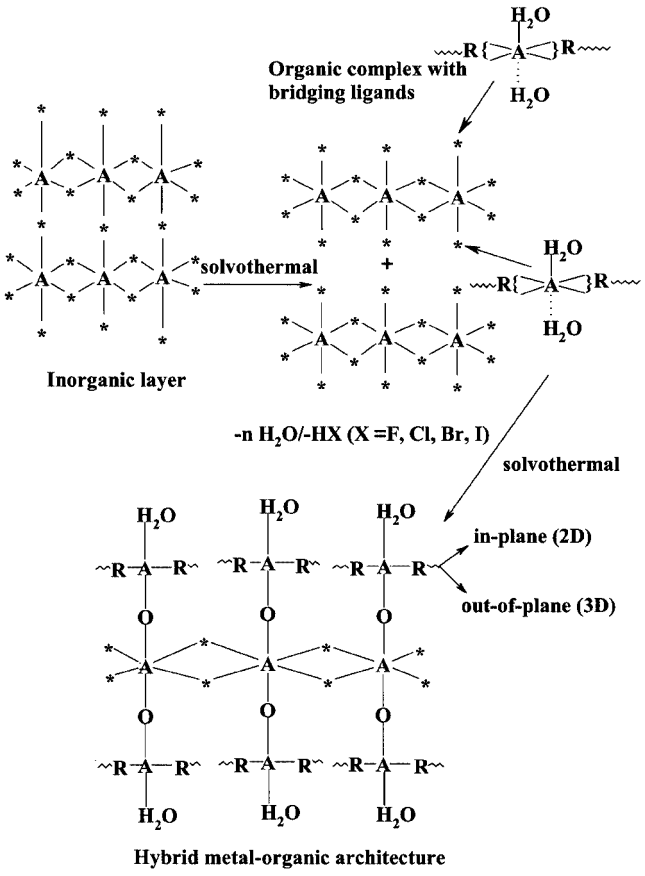

Scheme 1. A general scheme illustrating the building up of complex hybrid metal-organic architectures by aligning the lower-dimensional structures of metal halides/hydroxides by replacing the Cl^- or OH^- ions with metal complexes possessing organic ligands capable of bridging these lower dimensional inorganic structures. Depending on the mode of linking that the organic linkers provide the hybrid metal-organic structures can either be two- or three-dimensional. The probable generation of the low-dimensional structures by the partial disintegration of the higher dimensional parent structure under suitable reaction conditions has also been indicated. A = any metal; * = F, Cl, Br, I, -OH, H_2O; R = dicarboxylate, bipyridyl, nicotinate etc. Note that the one-dimensional inorganic chains can be introduced directly into the reaction medium

The above schematic suggests a new strategy for designing hybrid metal-organic frameworks, wherein one inorganic anion is replaced by another anion possessing an organic ligand, which in turn facilitates the extension of the structure into higher dimensions. A more general schematic representing this notion to illustrate the building up of three-dimensional hybrid metal-organic frameworks by aligning the lower-dimensional structures of metal halides and metal hydroxides by the introduction of metal complexes with organic ligands (dicarboxylate, bipyridyl, nicotinate etc.) capable of bridging the lower dimensional inorganic structures is presented in Scheme 1. Depending on the mode of linking of the organic linkers, the hybrid metal-organic structures can either be two- or three-dimensional. The possibility that the lower-dimensional structures can be generated by the partial disintegration of the higher dimensional parent structure under suitable reaction conditions is also indicated in Scheme 1. This possibility can be realized by observing the close structural relationships among some of the well-known lower-dimensional inorganic structures shown in Scheme 2. A similar notion has been proposed by Wood and co-workers[17−19] to describe the possible building of the cobalt squarate framework from the parent cobalt hydroxide with a brucite structure. Notably, the structural relationship between the Cd(OH)Cl and Cu(OH)Cl to brucite has been noted recently.[20]

It is likely that many such hybrid metal-organic structures with open-architectures can be made by employing other different organic linkers. In this context, we should draw attention to a new three-dimensional, open-framework, neutral and anhydrous chlorocadmium compound $[CdCl_2(C_4H_8N_2)]$ (**II**),[21] synthesized using solvothermal route by us, wherein the amine performs the role of linking the one-dimensional chlorocadmium chains into three-dimensions (Figure 4). Interestingly, in **II**, the channels are hydrophobic and empty. Assembling such predetermined polymeric units via organic pillars or linkers provides an interesting methodology for combining the dimensionality of the electronic exchange pathways and the open frameworks.[22]

The framework structure of **I** has certain unusual features which merit discussion. The position of the chloride, Cl(2), in **I** provides an interesting comparison with the layered chlorocadmium oxalate, $[Rb_2Cd(NO_3)(Cl)(C_2O_4)(H_2O)]$,[6] chlorozinc phosphate, $[C_6NH_{14}][ZnCl(HPO_4)]$[23] and the tin(II) phosphate, $[C_3H_{12}N_2]2[SnPO_4]$.[24] Although the Cl(2) atom in **I** is a bridging chloride its position is similar to that of the pendant Cl atoms in the chlorocadmium oxalate, chlorozinc phosphate and the lone pairs in the Sn^{II} phosphate (Figure 5a−d). The lone-pair of electrons in $[C_3H_{12}N_2]2[SnPO_4]$ and the chlorine atoms in $[C_6NH_{14}][ZnCl(HPO_4)]$ and $[Rb_2Cd(NO_3)(Cl)(C_2O_4)(H_2O)]$ point in a direction perpendicular to the plane of the layer, with the charge-compensating organic amine mol-

 © 2003 Wiley-VCH Verlag GmbH & Co. KGaA, Weinheim

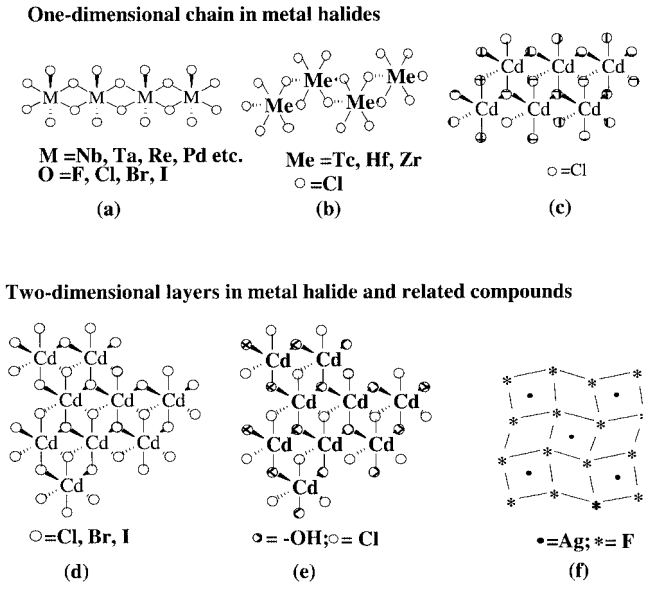

Scheme 2. Some of the low-dimensional structures of metal halogen and related inorganic solids; (a) the *cis*-oriented 1-D chains in NbI_4, $TaCl_4$, WCl_4; (b) the *trans*-oriented 1-D chains in $TcCl_4$, $ZrCl_4$, $PtCl_4$; (c) the $CdCl_3$ double chain present in NH_4CdCl_3; (d) the structure of CdX_2 (X = Cl, Br, I); (e) a layer in Cd(OH)Cl; (f) the layer in AgF. Note the similarity in the structure of the double chain in (c) and the cadmium chloride chain in **I** and also the structural relationship existing among the structures shown here

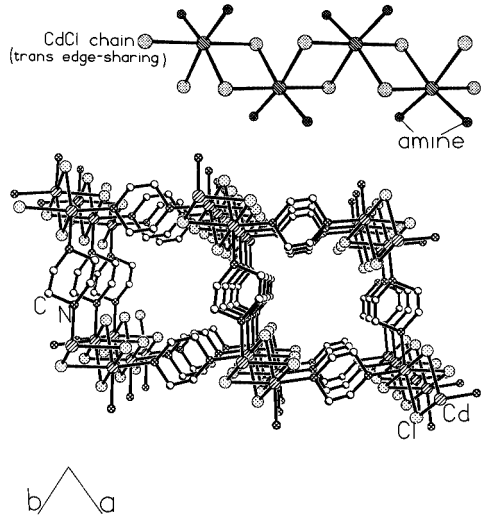

Figure 4. Structure of $[CdCl_2(C_4N_2H_8)]$ (**II**) showing the square hydrophobic channels present along the *a* axis formed by alignment of the Cd-chloro chains by the piperazine units; the inset shows the one-dimensional Cd-chloro chains formed by trans-edge sharing between the $CdCl_4N_2$ octahedra

ecule or the cation situated in the inter-lamellar space. In **I**, Cl(2) points into the inter-lamellar region occupied by the sodium (Figure 5a). Both the Cl atoms and the lone pairs orient themselves perpendicular to the plane of the metal oxalate layer and, satisfying their steric requirements, protrude into the interlayer spaces, making them available for chemical exploitation. Incorporation of halide ions, hydroxy groups or lone pairs in designed compounds, wherein they are made to occupy specific positions with predetermined orientations (based on stereochemical requirements) may enable the formation of materials possessing high chemospecificity.

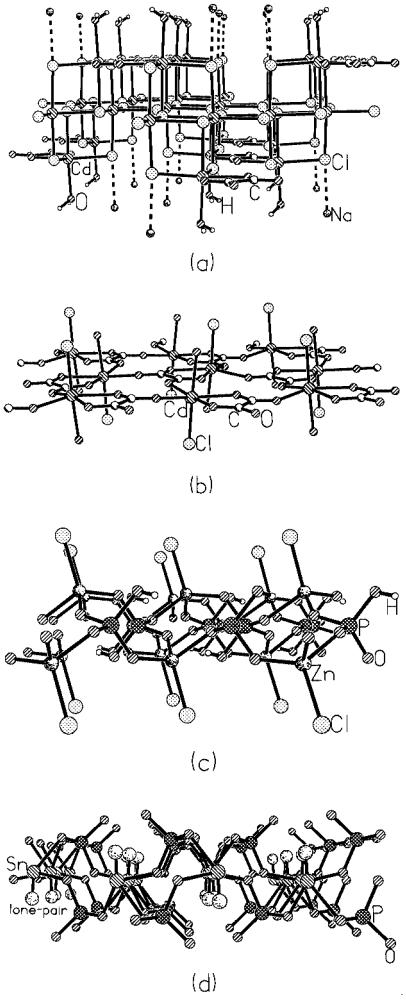

Figure 5. (a) Structure of **I**, showing the Cl(2) atoms pointing to the interlamellar region and the Na···Cl interaction (shown in dotted bonds) between the framework Cl(2) and the guest Na atoms; (b) structure of $[Rb_2Cd(NO_3)(Cl)(C_2O_4)(H_2O)]$, showing the pendant Cl atoms pointing into the interlayer regions; (c) structure of $[C_6NH_{14}][ZnCl(HPO_4)]$, showing the pendant Cl atoms protruding into the interlayer space; (d) structure of $[N_2C_3H_{12}]2[SnPO_4]$, with the pendant Cl atoms protruding into the interlamellar space

The arrangement of the extra-framework Na^+ cations gives rise to certain noteworthy features. The octahedrally coordinated sodium shares an edge with neighboring NaO_5Cl octahedra via bridging water molecules, forming an $Na_2O_8Cl_2$ dimer. These dimers are oriented in such a manner as to form strong O(w)−H···O(w) hydrogen bonds [O(w) = water oxygen] with the adjacent dimer, giving rise to a hydrogen-bond-stabilized one-dimensional ladder (Figure 6). Such low-dimensional structures formed by the guest species, involving weak interactions, contribute to the overall stability of these structures.[25]

In summary, the synthesis and structure of a new open-framework two-dimensional chlorocadmium oxalate compound (**I**) has been achieved. The formation of **I** could be

 © 2003 Wiley-VCH Verlag GmbH & Co. KGaA, Weinheim

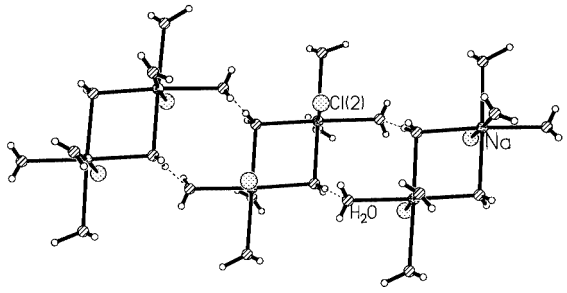

Figure 6. Figure shows the one-dimensional ladder-like structure formed by the $Na_2O_8Cl_2$ dimers *via* O(w)−H···O(w) hydrogen-bond interactions

the result of incomplete dissociation of the starting $CdCl_2$ under solvothermal conditions, facilitating the facile cross-linking by the oxalate units. It is likely that other such unusual structures can be formed under solvothermal conditions by employing other linkers.

Experimental Section

$Cd_2(C_2O_4)_{0.5}Cl_3NaCl{\cdot}4H_2O$ (**I**) was synthesized by the metathesis reaction between $CdCl_2{\cdot}2H_2O$ and sodium oxalate under solvothermal conditions. Typically, sodium carbonate (0.026 g) and oxalic acid (0.1879 g) were dissolved in 3 mL of dry *n*-hexanol. The mixture was stirred for two hours at room temperature. $CdCl_2{\cdot}2H_2O$ (0.20 g) and 0.07 mL of glacial acetic acid were added to the mixture and the contents were stirred to homogeneity (45 mins). The final mixture of the composition $CdCl_2{\cdot}2H_2O$:Na_2CO_3:$H_2C_2O_4{\cdot}2H_2O$:CH_3COOH:*n*-$C_6H_{13}OH$ (1:0.25:1.5:1.2:24) was sealed in a 23 mL PTFE-lined stainless steel autoclave and heated to 150 °C for 60 h. The product — colorless hexagonal plate-like and/or rod-like crystals — was filtered, washed with deionized water and dried under ambient conditions. Both type of crystals with different morphologies were identified to be compound **I**. The role of acetic acid is not clear to us. The water molecules present in **I** could have come from the use of $CdCl_2{\cdot}2H_2O$ and $H_2C_2O_4{\cdot}2H_2O$. The same reaction when carried out in the presence of water (hydrothermally) did not yield **I**. The EDAX studies resulted in an Na:Cd:Cl ratio of 1.0:1.9:4.1, which is in agreement with the calculate values (1.0:2.0:4.0); the elemental microanalysis showed: $Cd_2(C_2O_4)_{0.5}Cl_3NaCl{\cdot}4H_2O$ (**I**): calcd. C 2.4, H 1.6; found C 2.7, H 1.5.

Initial characterization of **I** was carried out by powder X-ray diffraction, thermogravimetric analysis (TGA), IR spectroscopy, elemental microanalysis and EDAX studies. The powder XRD patterns indicated that the products were new materials and were entirely consistent with the structures determined using the single-crystal X-ray diffraction (see Supporting Information). A least-squares fit (Cu-K_α) of the XRD patterns, using the *hkl* indices generated from the single-crystal structure gave the following lattice parameters: a = 12.216(8), b = 17.2104(10), c = 11.834(8) Å, β = 101.507(9) for **I**. IR spectra (KBr pellet) showed characteristic features of the dicarboxylate units.[26] The various bands are: ν_{as}(C=O) at 1646(s) cm^{-1} and ν_s(C=O) at 1417(w) cm^{-1}; ν_s(C-O) + δ(O-C=O) at 1312(s) cm^{-1}; δ(O-C=O)+ ν(MO) at 790(m) cm^{-1}; ν(MO) + ν(C-C) at 516(m) cm^{-1}; ν(MO) + ring def. at 438(w) cm^{-1}. A broad band appears in the 3550−3300 cm^{-1} region due to the presence of water molecules in the structure.

TGA studies of **I** indicate two distinct mass losses. A gradual mass loss in the range 100−300 °C (obsd. 14.3%) due to the loss of four water molecules (14.2%). The second mass loss of 15.7% in the range of 350−450 °C is due to the loss of the oxalate moiety (calcd. 17.4%). Above 500 °C, a gradual loss was observed due to the slow evaporation of the Cd compound.

Single-Crystal Structure Determination: A suitable single crystal of **I** was selected under a polarizing microscope and glued at the tip of a thin glass fiber with cyanoacrylate (superglue) adhesive. Structure determination by X-ray diffraction was performed on a Siemens Smart-CCD diffractometer equipped with a normal focus, 2.4 kW sealed-tube X-ray source (Mo-K_α radiation, λ = 0.71073 Å) operating at 50 kV and 40 mA. A hemisphere of intensity data was collected at room temperature in 1321 frames with ω scans (width of 0.30° and exposure time of 20 s per frame) in the θ range 2.07 to 23.30°. Pertinent experimental details for the structure determinations are presented in Table 2.

The structure was solved and refined by using SHELXTL-PLUS[27] suite of programs. An absorption correction based on symmetry equivalent reflections was applied using the SADABS program.[28] The last cycles of refinement included atomic positions for all the atoms and anisotropic thermal parameters for all the atoms. Full-matrix least-squares structure refinement against $|F^2|$was carried out using the SHELXTL-PLUS package of programs. Details of the crystal data and final refinements are given in Table 2. Selected bond lengths and angles for compound **I** are presented in Table 1. CCDC-203041 (**I**) and CCDC-203042 (**II**) contain the supplementary crystallographic data for this paper. These data can be ob-

Table 2. Crystal data and structure refinement parameters for $Cd_2(C_2O_4)_{0.5}Cl_3NaCl{\cdot}4H_2O$, **I**

Empirical formula	$Cd_2(C_2O_4)_{0.5}Cl_3NaCl{\cdot}4H_2O$
Crystal system	Monoclinic
Space group	*C*2/*c* (No. 15)
Crystal size (mm)	0.10 × 0.0.08 × 0.06
a (Å)	12.2177 (12)
b (Å)	17.2361 (12)
c (Å)	11.8314 (9)
α (°)	90.0
β (°)	101.41 (1)
γ (°)	90.0
Volume (Å^3)	2442.3 (3)
Z	8
Formula mass	505.69
ρ_{calc} (gcm^{-3})	2.750
λ (Mo-K_α) Å	0.71073
μ (mm^{-1})	4.389
θ range (°)	2.07− 23.30
Total data collected	5012
Index ranges	$-13 \le h \le 13$, $-19 \le k \le 19$, $-11 \le l \le 13$
Unique data	1769
Observed data [$I > 2\sigma(I)$]	1477
Refinement method	Full-matrix least-squares on $\|F^2\|$
R_{merg}	0.0411
R indexes [$I > 2\sigma(I)$]	R_1 = 0.0239,[a] wR_2 = 0.0496[b]
R (all data)	R_1 = 0.0304, wR_2 = 0.0515
Goodness of fit ($S_{obs.}$)	1.027
No. of variables	160
Largest difference map peak and hole e·Å^{-3}	0.674 and −0.452

[a] $R_1 = \||F_0| - |F_c|\|/|F_0|$. [b] $wR_2 = \{[w(F_0^2 - F_c^2)^2]/[w(F_0^2)^2]\}^{1/2}$. $w = 1/[\sigma^2(F_0)^2 + (aP)^2 + bP]$, $P = [\max.(F_0^2,0) + 2(F_c)^2]/3$, where a = 0.0103 and b = 0.0000.

 © 2003 Wiley-VCH Verlag GmbH & Co. KGaA, Weinheim

tained free of charge at www.ccdc.cam.ac.uk/conts/retrieving.html [or from the Cambridge Crystallographic Data Centre, 12, Union Road, Cambridge CB2 1EZ, UK; Fax: (internat.) +44−1223/336−033; E-mail: deposit@ccdc.cam.ac.uk].

Supporting Information Available (see footnote on the first page of this article): A figure showing a comparison of the simulated and the experimental powder XRD patterns of **I**.

[1] [1a] A. K. Cheetham, G. Férey, T. Loiseau, *Angew. Chem. Int. Ed.* **1999**, *38*, 3269. [1b] J. M. Thomas, *Angew. Chem. Int. Ed. Engl.* **1994**, *33*, 913. [1c] Dalton Discussion No. 3, Inorganic Crystal Engineering, *J. Chem. Soc., Dalton Trans.* **2000**, 21. [1d] P. Feng, X. Bu, S. Tolber, G. D. Stucky, *J. Am. Chem. Soc.* **1997**, *119*, 2497. [1e] B. A. Adair, G. D. de Delgado, J. M. Delgado, A. K. Cheetham, *J. Solid State Chem.* **2001**, *162*, 150.

[2] [2a] R. Vaidhyanathan, S. Natarajan, C. N. R. Rao, *J. Solid State Chem.* **2001**, *162*, 150. [2b] K. Jayaramn, A. Choudhury, R. Vaidhyanathan, C. N. R. Rao, *New J. Chem.* **2001**, *25*, 1199. [2c] K. Jayaraman, R. Vaidhyanathan, S. Natarajan, C. N. R. Rao, *J. Solid State Chem.* **2001**, *162*, 188.

[3] A. Müller, H. Reuter, S. Dillinger, *Angew. Chem. Int. Ed. Engl.* **1995**, *34*, 2328.

[4] J.-M. Lehn, *Supramolecular Chemistry, Concepts and Perspectives*, VCH, Weinheim, **1995**.

[5] P. A. Prasad, S. Neeraj, S. Natarajan, C. N. R. Rao, *Chem. Commun.* **2000**, 1251.

[6] R. Vaidhyanathan, S. Natarajan, C. N. R. Rao, *J. Solid State Chem.* doi: 10.1006/jssc.**2002**.9530.

[7] R. Vaidhyanathan, S. Neeraj, P. A. Prasad, S. Natarajan, C. N. R. Rao, *Angew. Chem. Int. Ed.* **2000**, *39*, 3470.

[8] R. Vaidhyanathan, S. Natarajan, C. N. R. Rao, *Chem. Mater.* **2001**, *13*, 3524.

[9] A. Müller, K. Hovemeier, R. Rohlfing, *Angew. Chem. Int. Ed. Engl.* **1992**, *31*, 1192.

[10] D. Hagrman, P. J. Hagrman, J. Zubieta, *Angew. Chem. Int. Ed.* **1999**, *38*, 3165.

[11] [11a] P. T. Wood, W. T. Pennington, J. W. Kolis, B. Wu, C. J. O'Connor, *Inorg. Chem.* **1993**, *32*, 129. [11b] M. I. Khan, Y. S. Lee, C. J. O' Connor, R. C. Haushalter, J. Zubieta, *J. Am. Chem. Soc.* **1994**, *116*, 4525. [11c] S. O. H. Gutschke, M. Molinier, A. K. Powell, R. E. P. Winpenny, P. T. Wood, *Chem. Commun.* **1996**, 823.

[12] C. Serre, G. Férey, *Inorg. Chem.* **1999**, *38*, 5370.

[13] W. Bensch, C. Nather, M. Schur, *Chem. Commun.* **1997**, 1773.

[14] A. F. Wells, *Structural Inorganic Chemistry*, Oxford Press, 5th Ed., 1995, p. 450 and references therein.

[15] M. Eddaoudi, D. B. Moler, H. Li, B. Chen, T. M. Reineke, M. O'Keeffe, O. M. Yaghi, *Acc. Chem. Res.* **2001**, *34*, 319 and references therein.

[16] R. G. Iyer, M. G. Kanatzidis, *Inorg. Chem.* **2002**, *41*, 3605.

[17] S. O. H. Gutschke, M. Molinier, A. K. Powell, P. T. Wood, *Angew. Chem. Int. Engl. Ed.* **1997**, *36*, 991.

[18] L. A. Gerrard, P. T. Wood, *Chem. Commun.* **2000**, 2107.

[19] [19a] S. L. Heath, A. K. Powell, *Angew. Chem. Int. Engl. Ed.* **1992**, *31*, 191. [19b] S. L. Heath, P. A. Jordan, I. D. Johnson, G. R. Moore, A. K. Powell, *J. Inorg. Biochem.* **1995**, *59*, 785.

[20] Y. Cudennec, A. Riou, Y. Gerault, A. Lecerf,, *J. Solid State Chem.* **2001**, *162*, 150.

[21] $[CdCl_2(C_4N_2H_8)]$, **II**, M_r = 267.42, monoclinic, space group *C*2/*c* (no.15), a = 9.5500(11), b = 13.601(2), c = 6.6499(8) Å, β = 90.868(2)°; V = 863.6(2) Å^3, Z = 8, μ = 3.069mm^{-1}, D_c = 2.057 g·cm^{-3}. A total of 1770 reflections were collected in the θ range 2.61 to 23.29° of which 585 with $I > 2\sigma(I)$ were considered to be observed. Final R = 0.0513, S_{obs} = 1.014 were obtained for 59 parameters. The average Cd−Cl distance and Cd−N distances are 2.682 and 2.345(4) Å, respectively.

[22] N. Guillou, S. Pastre, C. Livage, G. Férey, *Chem. Commun.* **2002**, 2358 and references therein.

[23] S. Neeraj, S. Natarajan, *J. Mater. Chem.* **2000**, *10*, 1171.

[24] R. Vaidhyanathan, S. Natarajan, *J. Mater. Chem.* **1999**, *9*, 1807.

[25] G. A. Jeffrey, *An Introduction to Hydrogen Bonding*, Oxford University Press, New York, **1997**.

[26] K. Nakamoto, *Infrared and Raman Spectra of Inorganic and Coordination Compounds*, 5th ed., John Wiley, New York, **1997**.

[27] G. M. Sheldrick, SHELXTL-PLUS *Program for Crystal Structure solution and refinement*, University of Göttingen.

[28] G. M. Sheldrick, SADABS *Siemens Area Detector Absorption Correction Program*; University of Göttingen, Göttingen, Germany.

Received November 11, 2002

 © 2003 Wiley-VCH Verlag GmbH & Co. KGaA, Weinheim

Synthesis of C_1-Symmetric Tripod Ligands Containing a P,P,N Donor Set – η^2-Coordination in d^8-Metal Complexes

Ralf Faissner,[a] Gottfried Huttner,*[a] Elisabeth Kaifer,[a] and Peter Rutsch[a]

Dedicated to Professor Horst Kisch on the occasion of his 60th birthday

Keywords: Mixed donor sets / Nickel / Palladium / Rhodium / Tripodal ligands

Tripod ligands $RC(CH_2X)(CH_2Y)(CH_2Z)$ (X, Y, Z = NR_2, PR_2) are accessible from α,β-unsaturated esters $R(=CH_2)COOR'$. The key steps in this synthetic approach are Michael additions of amines and phosphanes to produce $RCH(COOR')(CH_2X)$ (X = NR_2, PR_2) (**2** and **3**), followed by hydroxymethylation with paraformaldehyde to result in $RC(COOR')(CH_2OH)(CH_2X)$ (X = NR_2) (**4**). Standard transformations of this C_1-symmetric precursor allow for the synthesis of tripod ligands such as $PhC(CH_2pz)(CH_2PPh_2)(CH_2PMes)$ (**11**). Coordination of these ligands with d^8-metal ions [nickel(II), palladium(II), rhodium(I)] results in square-planar complexes with the chelate cycles in half-chair, twist-boat or boat conformations, depending on the specific substitution pattern. Coordination through two phosphane donors with the nitrogen donor acting as a dangling arm is generally preferred throughout. Detail preparative procedures and complete characterisation by analytical methods, including X-ray analysis of the coordination compounds, are given.

(© Wiley-VCH Verlag GmbH & Co. KGaA, 69451 Weinheim, Germany, 2003)

Introduction

While tripod ligands $CH_3C(CH_2PR_2)_3$ have been known for a long time,[1] the synthesis of chiral tripodal ligands $CH_3C(CH_2X)(CH_2Y)(CH_2Z)$ (X, Y, Z = donor groups) has only been developed in the last decade.[2,3] Different synthetic procedures were found to allow access to these compounds. It was observed, however, that the introduction of nitrogen donors in one or more of the X, Y, Z positions called for quite specific procedures, dependent both on the specific precursor and on the specific type of the NRR′ function to be introduced.[2b,2d,3g,3h,4] A general drawback of the strategies so far published for the synthesis of $RC(CH_2X)(CH_2Y)(CH_2Z)$ resides in the fact that there is no free choice of the kind of the group R fixed at the backbone of the tripodal ligand. Only ligands with R = H,[5] CH_3,[1–3] and CH_2OR'[6] are easily available by the published routes, while other functions such as benzyl, alkyl or alkenyl groups have to be introduced into appropriate ligand precursors by specific reactions,[7] which do not, however, in general allow for the consequent introduction of three different donor groups X, Y, and Z.

In search of a solution for both of these problems we studied α,β-unsaturated esters $RC(=CH_2)COOR'$ as potential precursors (see Scheme 1). We now report that the transformation of these precursors into tripod ligands is achieved with different kinds of groups R as well as different kinds of donor functions X, Y, Z including NRR′.

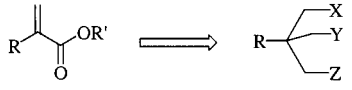

Scheme 1

Results and Discussion

Ligand Synthesis

α,β-Unsaturated esters $RC(=CH_2)COOR'$ are known to undergo 1,4-addition reactions with different types of HX compounds, including RR′NH[8] and R_2PH.[9] By applica-

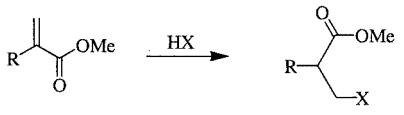

1 **2, 3**

1a R = Ph
1b R = CH_3

2a R = Ph X = $N(CH_2)_5$
2b R = CH_3 X = NEt_2
2c R = CH_3 X = $N(CH_2)_5$
2d R = CH_3 X = pz
3 R = Ph X = PPh_2

Scheme 2

[a] Anorganisch-Chemisches Institut der Universität Heidelberg, Im Neuenheimer Feld 270, 69120 Heidelberg, Germany
Fax: (internat.) + 49-(0)6221/545707
E-mail: g.huttner@indi.aci.uni-heidelberg.de

tion of this strategy, compounds **2** and **3** are obtained from compounds **1** in high yields (see Scheme 2 and Exp. Sect.).

The ester function in compounds **2** offers itself for transformation into a CH_2X' donor entity in later steps of the reaction. In order to obtain tripod ligands, an additional functionalisable CH_2X'' group has to be added to the central position of **2** in such a way that it forms the third "leg" of the desired tripod ligand. Hydroxymethylation is the obvious solution. Reactions of this type are generally quite efficient, but only in the absence of a CH_2NRR' substituent and with aldehyde or ketone functions, rather than an ester function as present in **2**.[10] Unactivated esters of the general type of framework as present in **2** – that is, disubstituted in the α,α′-position – are only rarely found to be suitable precursors for hydroxymethylation.[11] Hydroxymethylation is generally only successful if they are activated by an additional electron-withdrawing group, such as in malonic ester derivatives, and this type of reaction has accordingly been used as a key step for the construction of specific tripod ligands.[3d,7b,7c]

With compound **2**, however, it was found that even substitution under basic conditions by chloromethyl benzyl ether failed (see Scheme 3).

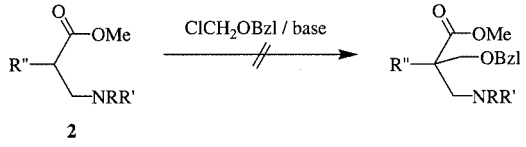

2

Scheme 3

While the direct introduction of a CH_2OH group in the form of formaldehyde or paraformaldehyde is reported to be less efficient[10,12] than the synthesis of its protected form by use of $ClCH_2OBzl$, it still proved possible to find suitable conditions for the synthesis of **4** from **2** by just this route (Scheme 4). The key to obtaining the necessary reactivity was the nature of the deprotonation of **2**; such deprotonation to afford the corresponding enolate is possible with NaH/DMF at 20 °C or LDA/THF at −70 °C. The choice of either one of these bases depends on the nature of R′′ and NRR′ in **2** (see Exp. Sect.), while KO*t*Bu was found to be ineffective in this kind of reaction.

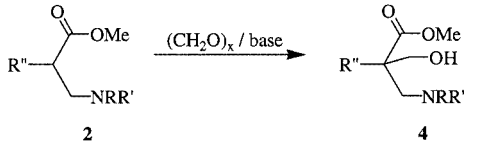

2 **4**

2a R" = Ph NRR' = $N(CH_2)_5$ **4a** R" = Ph NRR' = $N(CH_2)_5$
2b R" = CH_3 NRR' = NEt_2 **4b** R" = CH_3 NRR' = NEt_2
2c R" = CH_3 NRR' = $N(CH_2)_5$ **4c** R" = CH_3 NRR' = $N(CH_2)_5$

Scheme 4

The yields of the transformations of **2** into **4** are between 45 and 65% and correspond well to yields reported for the hydroxymethylation of RCH_2COR' by paraformaldehyde.[10]

In the case of **1a**, Michael addition and hydroxymethylation could be performed in a one-pot reaction with pyrazole as the HNRR′ reagent (see Scheme 5),[13] compound **4d** being obtained in 65% yield in this way. This type of one-pot reaction was, however, only successful with **1a** as the Michael acceptor and pyrazole as the Michael donor, and so only **4d** – and not **4a**–**4c** – is accessible by this simple route.

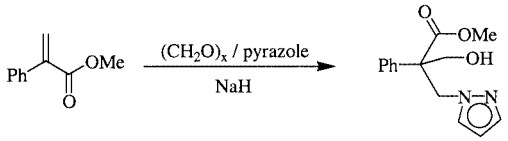

1a **4d**

Scheme 5

The compounds **2**–**4** have been fully characterised by elemental analysis, mass spectrometry and ^1H and ^{13}C NMR spectroscopy (see Tables 4, 6, 7 and Exp. Sect.).

Reduction of the ester function in **4** afforded the diols **5**, which – after activation by mesyl chloride – could be transformed into the diphosphanes **6** (see Scheme 6). These diphosphanes are tripod ligands containing two P and one N donor functions. Their identity was established by their elemental analyses, mass spectra and NMR spectra (see

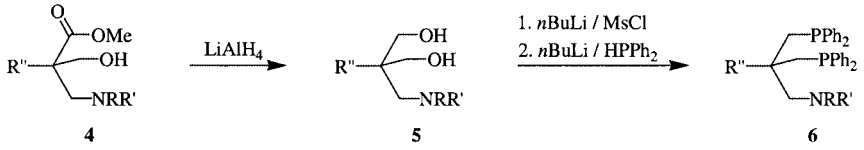

4 **5** **6**

4b R" = CH_3 NRR' = NEt_2 **5a** R" = CH_3 NRR' = NEt_2 **6a** R" = CH_3 NRR' = NEt_2
4d R" = Ph NRR' = pz **5b** R" = Ph NRR' = pz **6b** R" = Ph NRR' = pz

Scheme 6

 © 2003 Wiley-VCH Verlag GmbH & Co. KGaA, Weinheim

Tables 5−7 and Exp. Sect.) and by the formation of tripod metal complexes (see Coordination Chemistry).

Since compounds **4** already contain three different functionalities, their transformation into chiral racemic tripod ligands should be possible. The activation of the OH group of **4** by mesyl chloride was found to be quite inefficient in this respect: either the yields were very low or, as in the case of **4d**, formal elimination of the CH_2pz group occurred, to give **3** as the main product (see Scheme 7).

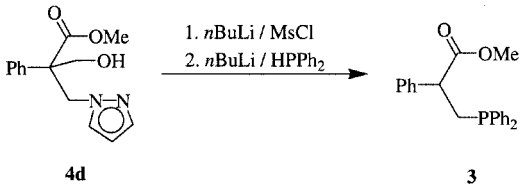

Scheme 7

The mechanism of this reaction has not yet been studied, but $MePPh_2$ and $MeP(=O)Ph_2$ have been observed (^{31}P NMR, GC/MS) as accompanying products.

In contrast, activation by means of the Appel reaction[14] transformed **4** into **7** in fair yields (see Scheme 8). The direct substitution of the chloride function of **7** by diphenylphosphide was successful for **7a**, while with **7b**, with its pyrazolyl functionality, sluggish reactivity, and partial decomposition was observed. For **7a**, with its diethylamine function, a clear transformation into **8** (63% yield) was accomplished (see Scheme 8).

A more general route is based on the reduction of the ester group as the first step. The activation of the resulting alcohol function by mesyl chloride was followed by the substitution of the mesylate by diarylphosphide. The remaining chlorine function could then be substituted by a different diarylphoshide. The reaction sequence has been fully worked out for the transformation **7b** → **9** → **10** → **11** (see Scheme 9). The two phosphide substitution steps give yields normal for this type of process, with an overall yield of **11** of 35% based on **7b**. To avoid unwanted side reactions during these substitution steps (internal cyclization) the reaction temperatures have to be thoroughly controlled (see Exp. Sect., for elemental analysis, NMR spectra, and mass spectra of compounds **7−11**, see Tables 4−7).

Coordination Chemistry

Tripod ligands containing nitrogen and phosphorus donor functions in one and the same ligand are known to form tripodal coordination compounds. This has been demonstrated with $Mo(CO)_3$ as the coordinated entity.[3g,3h] With d^8-ions as the metal constituents, square-planar coordination of the metal ion is generally preferred and is exclusively observed for tripod ligands containing a P,P,N donor set.[4b,15] With this type of η^2-coordination of a tripod ligand containing different types of donor functions, it is not clear a priori which kinds of donor functions will be coordinated.

Compounds **6**, **8**, and **11** offer the opportunity to address this question. The coordination behaviour of this type of compounds with respect to nickel(II), palladium(II), and rhodium(I) was therefore analysed.

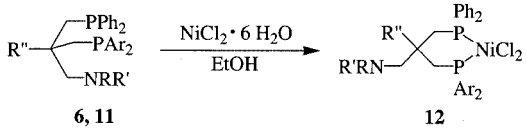

	R"	PAr_2	NRR'
6a	CH_3	PPh_2	NEt_2
6b	Ph	PPh_2	pz
11	Ph	$PMes_2$	pz

	R"	PAr_2	NRR'
12a	CH_3	PPh_2	NEt_2
12b	Ph	PPh_2	pz
12c	Ph	$PMes_2$	pz

Scheme 10

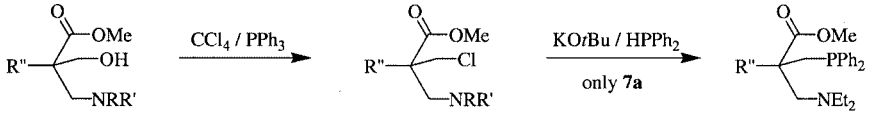

4b R" = CH_3 NRR' = NEt_2
4d R" = Ph NRR' = pz

7a R" = CH_3 NRR' = NEt_2
7b R" = Ph NRR' = pz

R" = CH_3

Scheme 8

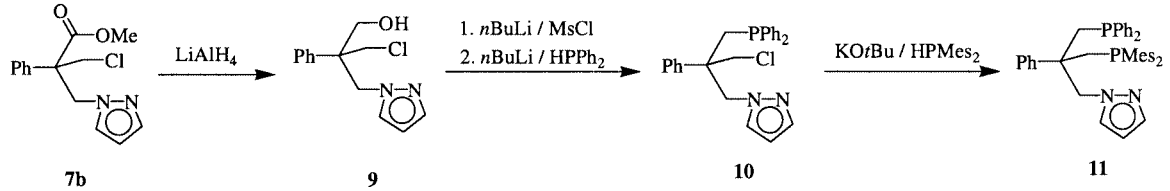

Scheme 9

 © 2003 Wiley-VCH Verlag GmbH & Co. KGaA, Weinheim

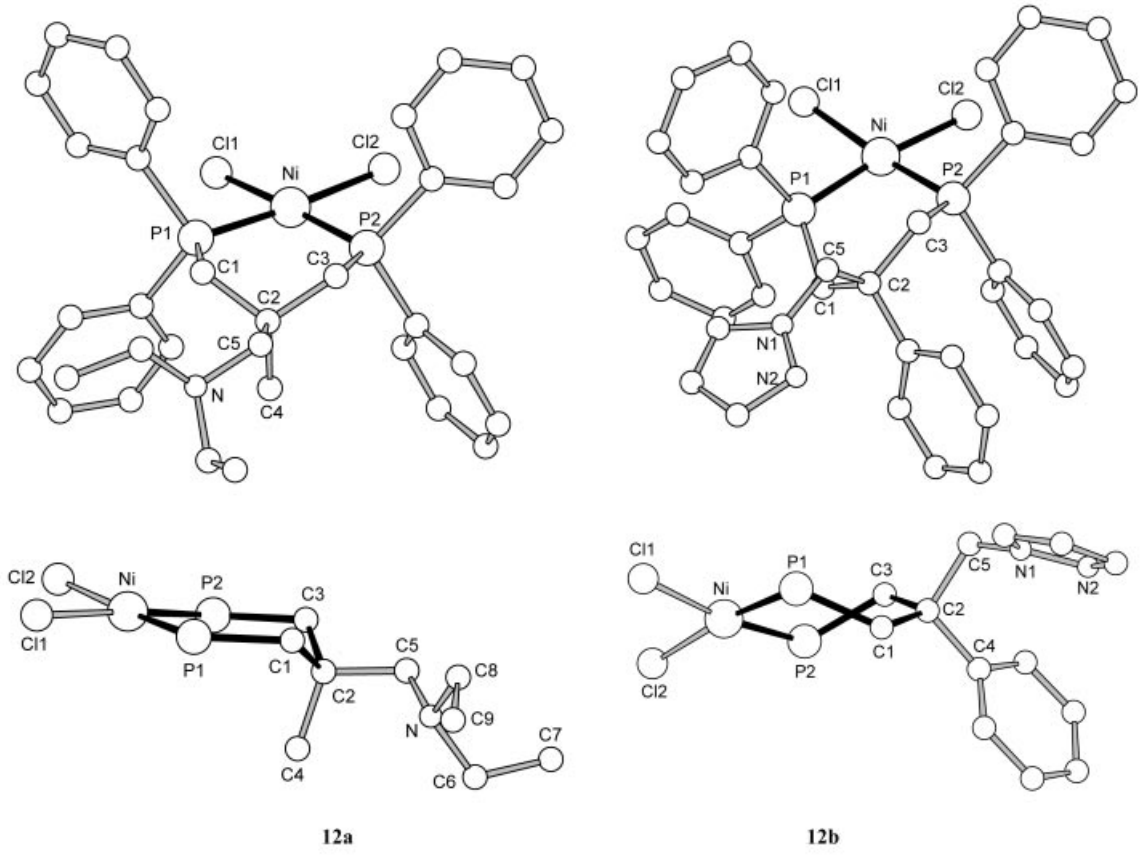

Figure 1. Two views of the X-ray structure of compound **12a** (left, half-chair conformation) and **12b** (right, twist-boat conformation); top: general view; bottom: view showing the conformation of the six-membered chelate cycle (phenyl groups are not shown for the sake of clarity)

Tripod ligands **6a**, **6b**, and **11** each contain a P,P,N donor set. Complexation with aqueous $NiCl_2$ resulted in orange to red, square-planar nickel(II) complexes **12** in which the two phosphane functions are coordinated exclusively while the nitrogen-functionalised "leg" is a dangling substituent (see Scheme 10). The same type of coordination behaviour has already been observed for other ligands of the type $RC(CH_2PPh_2)_2(CH_2X)$. Phosphorus coordination is preferred over coordination of ligand groups X such as NRR′, OH, OMe, and SR.[3e,16]

The structures of **12a** and **12b** as determined by X-ray crystallography are shown in Figure 1.

Interestingly, the conformations of the chelate cycles are different for the two compounds − being a half-chair form in **12a** and a twist-boat form in **12b** (see Table 1). The relative stability of these types of conformations has recently been analysed thoroughly.[17]

Compound **8** has three different potential donor substituents within the tripodal framework: coordination is conceivable for the PPh_2, the NEt_2 and the ester groups. Compound **8** was found to react with $(dme)NiCl_2$ to give a violet, paramagnetic compound, which − due to its insufficient crystallisation properties − could not be obtained in analytically pure form. In contrast, palladium(II), introduced by use of $(cod)PdCl_2$, and rhodium(I), introduced by use of $[(nbd)RhCl]_2$, give the readily crystallised, diamagnetic compounds **13** (yellow) and **14·PF$_6$** (orange) (Scheme 11).

NMR (^1H, ^{13}C, ^{31}P) spectra of **13** reveal the expected resonances as sharp signals even at 30 °C (see Tables 4 and 6). The ethyl groups of the NEt_2 entity are diastereotopic, consistent with the proposed structure. Diastereotopic differentiation of the ethyl groups in **14·PF$_6$** is only observable below −30 °C (see Tables 4 and 6), while above this temperature some dynamic process gives rise to considerable broadening of the peaks such that the diastereotopic differentiation is no longer observable. The dynamic process is presumably due to a change in the conformation of the chelate cycle.[17,18]

X-ray analysis of **13** establishes the square-planar coordination of the palladium atom and reveals that the chelate cycle has a twist-boat conformation (see Figure 2, Table 1). The X-ray structure of **14$^+$** similarly establishes the pseudo-square-planar coordination of the rhodium atom. The chelate cycle is found to have the unconventional boat form, with the sterically more demanding methoxycarbonyl group axial and the methyl group in the equatorial position (see Figure 2, Table 1). The methoxycarbonyl group is orientated such that the normal to its plane points toward the rhodium centre (see Figure 2). The distance between the

 © 2003 Wiley-VCH Verlag GmbH & Co. KGaA, Weinheim

Table 1. Selected bond lengths [pm], bond angles [°] and torsion angles [°] of compounds **12a**, **12b**, **13**, and **14**

	12a [M = Ni][a]	**12b** [M = Ni][a]	**13** [M = Pd][a]	**14·PF$_6$** [M = Rh][a]
M−Cl	219.4(1); 221.6(1)	219.8(1); 219.9(1)	229.8(1)[b]; 239.1(1)[c]	–
M−P	215.8(1); 216.8(1)	215.1(1); 215.7(1)	221.8(1)	228.8(1)
M−N	–	–	213.8(1)	223.8(2)
M−C	–	–	–	210.7(2)[b]; 212.3(2)[b] 223.4(2)[c]; 224.0(2)[c]
P1−M−P2/N	96.1(1)	91.8(1)	93.5(1)	91.1(1)
Cl1−M−Cl2	92.1(1)	94.5(1)	89.9(1)	–
P1−M−Cl1	85.9(1)	87.4(1)	85.6(1)	–
P2/N−M−Cl2	86.2(1)	87.6(1)	92.4(1)	–
P1−M−Cl2	175.1(1)	170.9(1)	167.1(1)	–
P2/N−M−Cl1	176.3(1)	172.4(1)	172.9(1)	–
Chelate cycle[d]	half-chair (2,6 = P)	λ-twist boat (2,6 = P)	λ-twist boat (2 = P, 6 = N)	boat (2 = P, 6 = N)
M−2−3−4	+44.1(4)	+67.9(2)	+59.6(3)	+13.3(2)
2−3−4−5	−72.2(5)	−35.3(2)	−30.8(3)	−74.0(2)
3−4−5−6	+67.2(5)	−30.0(2)	−40.1(4)	+64.2(2)
4−5−6−M	−36.9(4)	+65.0(2)	+71.0(3)	+7.6(2)
5−6−M−2	+8.4(2)	−25.4(1)	−27.6(2)	−48.8(2)
6−M−2−3	−10.8(2)	−25.8(1)	−25.7(1)	+34.7(2)
3−2−6−5	−2.3	−47.7	−51.3	−8.3

[a] Standard deviations in units of the least significant digit are given in each case. [b] *trans* to N. [c] *trans* to P. [d] A consistent numbering scheme (torsion angles) for all the compounds as depicted below is used for the sake of easier comparison:

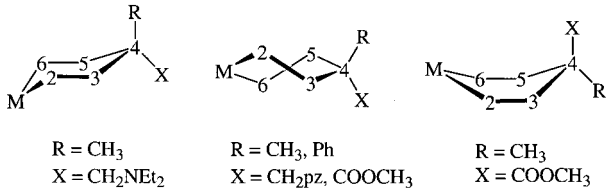

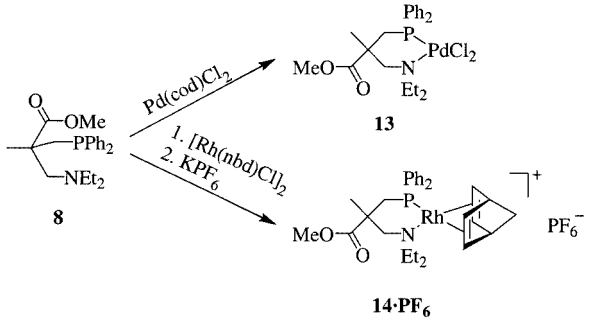

Scheme 11

rhodium atom and the carboxy group (Rh−O: 348.7 pm and 350.2 pm) is too large to be interpreted in terms of any direct bonding between these partners while it is short enough for some type of secondary interaction to be assumed (see Table 2).

Boat conformations as observed for **14**$^+$ have not yet been found in crystal structures of rhodium complexes with six-membered phosphorus-containing saturated chelate cycles, while their inherent relative stability in some cases has been indicated by a thorough molecular dynamics analysis.[17b] With the dynamic behaviour of six-membered phosphorus-containing saturated chelate cycles in mind,[17,18] equilibria between different ring conformations are the most probable explanation for the temperature dependence of the behaviour of the NMR spectra of **14·PF$_6$**.

Conclusion

It has been shown that α,β-unsaturated esters RC(=CH_2)COOR′ may serve as starting materials for the synthesis of tripod ligands RC(CH_2X)(CH_2Y)(CH_2Z). The procedure allows for the incorporation of different types of substituents R in the backbone and also allows the introduction of donor functions X = NR_2 in the presence of different potential phosphorus donor functions (Y, Z).

Ligands of this type − containing a P,P,N donor set − coordinate to d^8-metal ions through their two phosphorus donor groups, resulting in a square-planar coordination with the amine function acting as a dangling arm.

Ligands containing a P,N,O donor set (O = part of a carboxy group) form complexes in which P,N donors serve as ligands in six-membered chelate cycles. For the d^8-metal ions Pd^{II} and Rh^{I} the coordination is square-planar. The O donor is not involved in direct bonding to the metal atom but may engage in secondary interaction with it.

 © 2003 Wiley-VCH Verlag GmbH & Co. KGaA, Weinheim

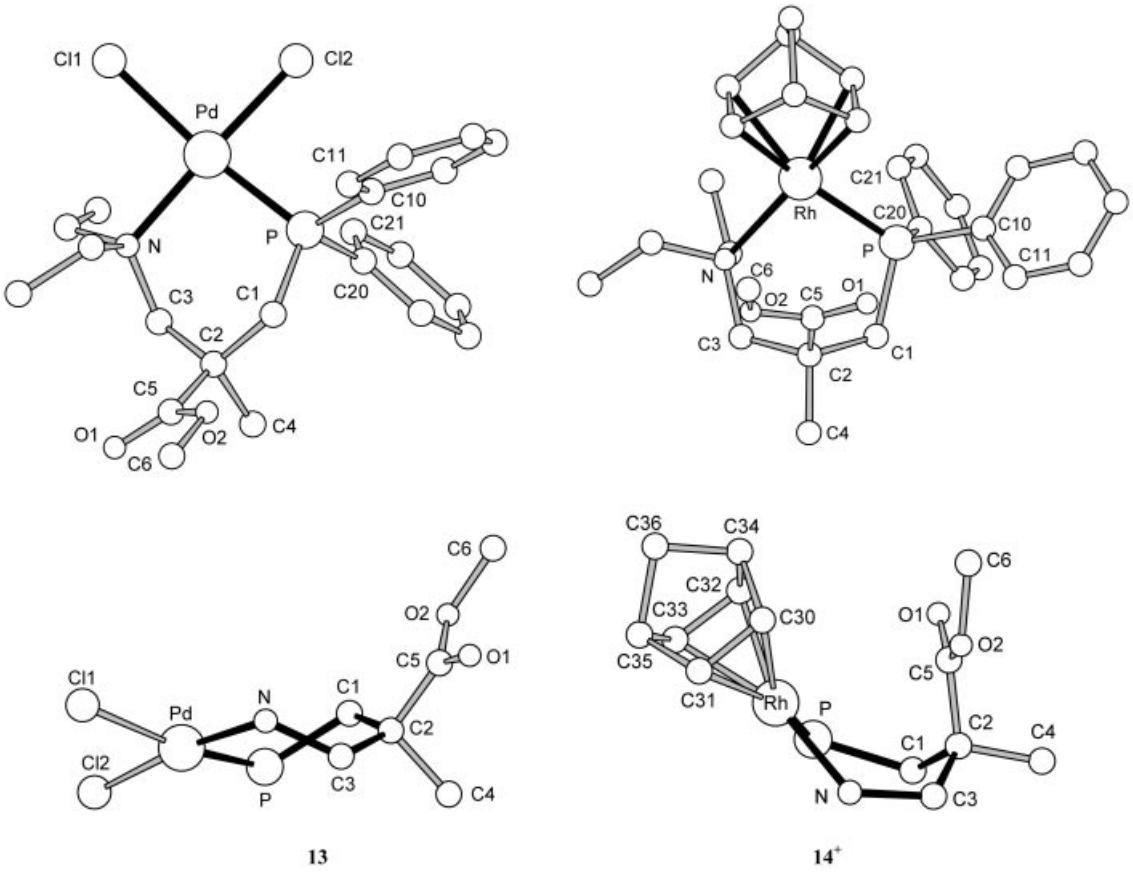

Figure 2. Two views of the X-ray structure of compound **13** (left, twist-boat conformation) and the cation **14**$^+$ (right, boat conformation); top: general view; bottom: view showing the conformation of the six-membered chelate cycle (phenyl groups are not shown for the sake of clarity)

Table 2. Selected bond lengths [pm], bond angles [°] and torsion angles [°] of the ester groups in compounds **13** and **14**

	13 [M = Pd][a]	**14**·PF_6 [M = Rh][a]
C5−O1 (C=O)	119.9(4)	120.0(3)
C5−O2 (C−O)	134.6(4)	133.7(3)
C6−O2 (C−O)	145.8(4)	145.1(3)
M−C5	485.4	313.9
M−O1	559.2	348.7
M−O2	533.3	350.2
C2−C5−O1	124.6(3)	123.9(2)
C2−C5−O2	111.6(3)	112.6(2)
O1−C5−O2	123.6(3)	123.3(2)
C6−O2−C5	116.7(3)	116.6(2)
C6−O2−C5−O1	−3.4(5)	+3.5(3)
C6−O2−C5−C2	−0.1(3)	−8.7(2)

[a] Standard deviations in units of the least significant digit are given in each case.

The conformations of the six-membered chelate cycles comprise the conventional half-chair and twist-boat forms as well as the unconventional boat form.

Experimental Section

General Remarks: All manipulations involving phosphanes were carried out under argon by use of standard Schlenk techniques. All solvents were dried by standard methods[19] and distilled under argon. The solvents $CDCl_3$ and CD_2Cl_2 used for NMR spectroscopic measurements were degassed by three successive "freeze-pump-thaw" cycles and dried over 4 Å molecular sieves. NMR: Bruker Advance DPX 200 at 200.12 MHz (^{1}H); 50.323 MHz (^{13}C{^{1}H}); 81.015 MHz (^{31}P{^{1}H}); T = 303 K unless stated otherwise; chemical shifts (δ) with respect to $CDCl_3$ (^{1}H: δ = 7.27; ^{13}C: δ = 77.0 ppm) and CD_2Cl_2 (^{1}H: δ = 5.32 ppm; ^{13}C: δ = 53.5 ppm) as internal standards. ^{31}P chemical shifts (δ) with respect to 85% H_3PO_4 (^{31}P: δ = 0 ppm) as external standard. FT-IR: Biorad Excalibur FTS 3000 spectrophotometer (samples in solutions between CaF_2 windows). MS: Finnigan MAT 8230. EI (70 eV). FAB (xenon; matrix: 4-nitrobenzyl alcohol). Melting points: Gallenkamp MFB-595010; uncorrected values. Elemental analyses: Microanalytical Laboratory of the Organic-Chemical Institute, University of Heidelberg.

Crystallographic Structure Determinations: Suitable crystals were taken directly out of the mother liquor, immersed in perfluorinated polyether oil, and fixed to a glass capillary. The measurements were carried out with an Enraf−Nonius Kappa CCD diffractometer, with graphite-monochromated Mo-K_α radiation used throughout.

 © 2003 Wiley-VCH Verlag GmbH & Co. KGaA, Weinheim

Table 3. Crystallographic data of compounds **12a**, **12b**, **13**, and **14**

Compound	**12a**	**12b**	**13**	**14·PF$_6$**
Empirical formula (without solvate)	$C_{33}H_{39}Cl_2NNiP_2$	$C_{37}H_{34}Cl_2N_2NiP_2$	$C_{22}H_{30}Cl_2NO_2PPd$	$C_{29}H_{38}F_6NO_2P_2Rh$
Formula mass [g/mol]	641.2	698.2	548.8	711.5
Solvate	1 CH_2Cl_2; 0.5H_2O	–	–	–
Crystal size [mm]	0.15×0.15×0.05	0.10×0.10×0.10	0.10×0.02×0.02	0.20×0.20×0.15
Crystal system	orthorhombic	monoclinic	monoclinic	orthorhombic
Space group	$Pca2_1$ (no. 29)	$P2_1/n$ (no. 14)	$P2_1/n$ (no. 14)	$Pcba$ (no. 61)
Lattice constants:				
a [pm]	2153.9 (4)	1075.6 (2)	1252.3 (3)	2218.7 (4)
b [pm]	1124.4 (2)	1900.5 (4)	1383.4 (3)	1621.6 (3)
c [pm]	1411.8 (3)	1642.5 (3)	1354.3 (3)	1625.7 (3)
β [°]	90	97.54 (3)	92.85 (3)	90
V [10^6·pm^3]	3419 (1)	3328 (1)	2343 (1)	5849 (1)
Z	4	4	4	8
d_X [g·cm^{-3}]	1.426	1.393	1.558	1.616
T [K]	200	200	293	200
Scan range [°]	3.6 ≤ 2θ ≤ 54.9	3.3 ≤ 2θ ≤ 54.0	4.2 ≤ 2θ ≤ 60.2	3.7 ≤ 2θ ≤ 55.8
Method	ω-scan, Δω = 1.0°	ω-scan, Δω =1.0°	ω-scan, Δω =1.0°	ω-scan, Δω =1.0°
Scan speed	30 sec/frame	5 sec/frame	10 sec/frame	10 sec/frame
No. of measured reflections	7860	14564	11921	13968
No. of unique reflections	7544	7251	6845	6966
No. of observed reflections	6782	6095	4985	5451
Observation criterion	$I \geq 2\sigma$	$I \geq 2\sigma$	$I \geq 2\sigma$	$I \geq 2\sigma$
No. of param. refined	348	400	257	409
Resid. el. dens. [10^{-6}e·pm^{-3}]	1.42	0.72	0.89	0.40
R_1/R_w [%] (refinement on F^2)	6.6/15.2	3.7/10.3	4.6/11.4	3.4/8.5

Table 4. Chemical shifts (δ values), integrals [x H], and coupling constants J in the ^{1}H NMR spectra of **4**, **7**, **8**, **13**, and **14**

No.[a]	CH_2N [2 H]	CH_2X [2 H]	OCH_3 [3 H]	C_qCH_3 [3 H]	OH [1 H]	Aryl-H	Others
4a[b]	2.84 d, 3.49 d, $^2J_{H,H}$ = 13.9	4.40 br. s, X = OH	3.70 s	–	6.49 br. s	7.29 m [5 H]	1.38–1.45 m, 1.54 br. s, 2.42–2.69 m [10 H], piperidine-H
4b[b]	2.49 d, 3.02 d, $^2J_{H,H}$ = 14.0	3.61 d, 3.81 d, $^2J_{H,H}$ = 11.3, X = OH	3.63 s	1.04 s	5.44 br. s	–	0.93 t, 2.40–2.60 m [10 H], $^3J_{H,H}$ = 7.1, NEt_2
4c[b]	2.41 d, 3.02 d, $^2J_{H,H}$ = 13.8	3.68 d, 3.91 d, $^2J_{H,H}$ = 11.0, X = OH	3.70 s	1.07 s	5.55 br. s	–	1.36–1.42 m, 1.49–1.52 m, 2.38–2.54 m [10 H], piperidine-H
4d[b]	4.61 d, 5.02 d, $^2J_{H,H}$ = 14.4	3.93 d, 4.17 d, $^2J_{H,H}$ = 12.2, X = OH	3.74 s	–	4.61 br. s	7.33–7.39 m [5 H]	6.22 t, 7.31 d, 7.55 d [3 H], $^3J_{H,H}$ = 2.0, pyrazole-H
7a[b]	2.64 d, 2.73 d, $^2J_{H,H}$ = 14.2	3.69 d, 3.79 d, $^2J_{H,H}$ = 10.8, X = Cl	3.70 s	1.25 s	–	–	0.95 t, 2.53 q [10 H], $^3J_{H,H}$ = 7.1, NEt_2
7b[b]	4.80 d, 5.13 d, $^2J_{H,H}$ = 14.1	4.06 d, 4.34 d, $^2J_{H,H}$ = 10.9, X = Cl	3.81 s	–	–	7.07–7.11 m [2 H], 7.35–7.38 m [3 H]	6.12 t, 6.99 d, 7.52 d [3 H], $^3J_{H,H}$ = 2.0, pyrazole-H
8[b]	2.67 d, 2.85 d, $^2J_{H,H}$ = 13.7	2.35 d, 2.50–2.66 m, $^2J_{H,H}$ = 10.8, X = PPh_2	3.49 s	1.25 s	–	7.35–7.51 m [10 H]	0.97t, 2.50–2.66m [10 H], $^3J_{H,H}$ = 7.1, NEt_2
13[c]	2.77 d, 2.99 d, $^2J_{H,H}$ = 14.3	2.43 d, 3.20 d, $^2J_{H,H}$ = 16.0, X = PPh_2	3.74 s	1.04 s	–	7.45–7.73 m [8 H], 8.13–8.24 m [2 H]	1.44 t, 1.75 t, 2.70–4.30 m [10 H], $^3J_{H,H}$ = 7.1, NEt_2
14[c] [d]	2.26 d, 3.50 d, $^2J_{H,H}$ = 14.7	2.47 d, 3.33 d, $^2J_{H,H}$ = 15.7, X = PPh_2	4.09 s	1.43 s	–	7.32–7.63 m [8 H], 7.86–7.95 m [2 H]	1.03 t, 1.62 t, 2.05–3.10 m [10 H], $^3J_{H,H}$ = 7.1, NEt_2 1.53 br. s,[e] 2.83 br. s,[f] 3.71 br. s,[f] 3.77 br. s,[g] 4.00 br. s,[g] 5.20 br. s,[f] 5.32 br. s,[f] [8 H], norbornadiene-H

[a] s = singlet, d = doublet, t = triplet, m = multiplet, br. s = broad signal; coupling constants in Hz. [b] Solvent $CHCl_3$. [c] Solvent CH_2Cl_2. [d] Measuring temperature −40 °C. [e] CH_2 group. [f] Olefinic CH group. [g] Bridgehead CH group.

The data were processed with the standard Nonius software,[20] and the calculations were performed with the SHELXT PLUS software package. Structures were solved by direct methods with the SHELXS-97 program and refined with the SHELXL-97 program.[21] Graphical handling of the structural data during solution and refinement was performed with XMPA.[22] Atomic coordinates and anisotropic thermal parameters of the non-hydrogen atoms were refined by full-matrix, least-squares calculations. Data relating to the structure determinations are collected in Table 3. Figures 1 and 2 were prepared with WinRay-32.[23] Crystallographic data (excluding structure factors) for the structures reported in this paper have been deposited with the Cambridge Crystallographic Data Centre as supplementary publication nos. CCDC-191480 to -191483. Copies of the data can be obtained free of charge

 © 2003 Wiley-VCH Verlag GmbH & Co. KGaA, Weinheim

Table 5. Chemical shifts (δ values), integrals [*x* H] and coupling constants *J* in the ^{1}H NMR spectra of **5**, **6**, and **9**−**12**

No.[a]	CH_2N [2 H]	CH_2X	CH_2Y	C_qCH_3 [3 H]	OH [2 H]	Aryl-H	Others
5a[b]	2.52 s	3.58 pt [4 H], $^2J_{H,H}$ = 11.3, X = Y = OH		0.79 s	4.97 br. s	−	1.03 t, 2.54 q [10 H], $^3J_{H,H}$ = 7.1, NEt_2
5b[b]	4.72 s	3.90 br. s [4 H], X = Y = OH		−	2.30−3.10 br. s	7.28−7.44 m [5 H]	6.19 t, 7.09 d, 7.55 d [3 H] $^3J_{H,H}$ = 2.0 pyrazole-H
6a[b]	2.54 s	2.45 m [4 H], X = Y = PPh_2		0.98 s	−	7.33−7.50 m [20 H]	0.99 t, 2.64 q [10 H], $^3J_{H,H}$ = 7.0, NEt_2
6b[b]	5.04 s	2.81 d, 2.97 d [4 H], $^2J_{H,H}$ = 14.3, X = Y = PPh_2		−	−	6.86−7.01 m [5 H], 7.17−7.34 m [20 H]	6.06 t, 6.90 d, 7.49 d [3 H], $^3J_{H,H}$ = 2.0, pyrazole-H
9[b]	4.56 d, 4.65 d, $^2J_{H,H}$ = 14.3	3.75 d, 3.94 d [2 H], $^2J_{H,H}$ = 12.0, X = OH	3.80 d, 3.97 d [2 H], $^2J_{H,H}$ = 11.5, Y = Cl	−	4.31 br. s [1H]	7.28−7.39 m [5 H]	6.19 t, 7.15 d, 7.53 d [3 H], $^3J_{H,H}$ = 2.0, pyrazole-H
10[b]	4.57 d, 4.96 d, $^2J_{H,H}$ = 14.0	2.79 br. s [2 H], X = PPh_2	4.07 d, 4.24 d [2 H], $^2J_{H,H}$ = 11.5, Y = Cl	−	−	7.14−7.35 m [15 H]	6.14 t, 7.09 d, 7.53 d [3 H], $^3J_{H,H}$ = 2.0, pyrazole-H
11[b]	4.95 br. s	2.85 d, 2.95 d [2 H], $^2J_{H,H}$ = 14.4, X = PPh_2	3.09 d, 3.36 d [2 H], $^2J_{H,H}$ = 14.4, Y = $PMes_2$	−	−	6.57−6.60 m [4 H], 6.77−7.37 m [15 H]	2.18 br. s [18 H], aryl-CH_3, 6.01 t, 6.77−7.37 m, 7.49 d [3 H], $^3J_{H,H}$ = 2.0, pyrazole-H
12a[c]	2.15 s	2.22 d, 3.80 br. s [4 H], $^2J_{H,H}$ = 15.2, X = Y = PPh_2		0.27 s	−	7.40−7.73 m [16 H], 8.48−8.51 m [4 H]	0.91 t, 2.49 q [10 H], $^3J_{H,H}$ = 7.0, NEt_2
12b[c]	3.87 s	2.74 d, 2.99 d [4 H], $^2J_{H,H}$ = 15.1, X = Y = PPh_2		−	−	6.81−7.13 m [5 H], 7.40−8.20 m [20 H]	5.91 t, 6.40 d, 7.33−7.67 m [3 H], $^3J_{H,H}$ = 2.0, pyrazole-H

[a] s = singlet, d = doublet, t = triplet, m = multiplet, br. s = broad signal, pt = pseudo-triplet; coupling constants in Hz. [b] Solvent $CHCl_3$. [c] Solvent CH_2Cl_2.

on application to the CCDC, 12 Union Road, Cambridge CB2 1EZ, UK [Fax: (internat.) + 44-1223/336033; E-mail: deposit@ccdc.cam.ac.uk].

Materials: Silica gel (Kieselgel 32−63 μm, ICN Biomedicals GmbH) used for chromatography was degassed at 1 mbar for 24 h and saturated with argon. A solution of *n*BuLi in hexane (2.5 M) was used for deprotonations. $HPPh_2$,[24] $HPMes_2$[25] and methyl 2-phenylacrylate (**1a**)[26] were prepared according to or by adaptation of literature procedures. All other chemicals were obtained from commercial suppliers and used without further purification. Boiling range of the petroleum ether used: 40−60 °C. For ^{1}H NMR data see Tables 4 and 5, for ^{13}C NMR data see Table 6, and for analytical data see Table 7.

Ligand Syntheses

General Procedure for the Synthesis of 2: The α,β-unsaturated ester **1a** or **1b** (0.5 mol) was mixed with the secondary amine (1.1 equiv.), and hydroquinone (1.0 g) in the case of **1b**. The solution was heated and, after cooling, the crude product was distilled under reduced pressure through a 15-cm Vigreux column, yielding the β-amino esters **2** as colourless liquids.

Methyl 2-Phenyl-3-(1-piperidino)propanoate (2a): Starting materials: **1a**, piperidine. The mixture was heated to 70 °C for 1 h. Yield: 103.8 g (0.42 mol, 84%), b.p. 84 °C (0.1 mbar). ^{1}H NMR ($CDCl_3$): δ = 1.43−2.61 ppm (m, 10 H, piperidine-H), 2.50−2.61 (m, 1 H, CH_2N), 3.21 (dd, $^2J_{H,H}$ = 12.6, $^3J_{H,H}$ = 10.2 Hz, 1 H, CH_2N), 3.71 (s, 3 H, OCH_3), 3.90 (dd, $^3J_{H,H}$ = 4.6, $^3J_{H,H}$ = 10.2 Hz, 1 H, PhC*H*), 7.31−7.35 (m, 5 H, aromat. H). ^{13}C NMR ($CDCl_3$): δ = 24.8 ppm, 26.5, 55.0 (3 × s, piperidine-C), 50.4 (s, Ph*C*H), 52.3 (s, OCH_3), 62.9 (s, CH_2N), 127.7−138.3 (m, aromat. C), 174.4 (s, C=O).

Methyl 3-(Diethylamino)-2-methylpropanoate (2b): Starting materials: **1b**, diethylamine. The mixture was heated under reflux for 72 h. Yield: 41.6 g (0.24 mol, 48%), b.p. 29 °C (0.2 mbar). ^{1}H NMR ($CDCl_3$): δ = 0.93 ppm (t, 6 H, NCH_2CH_3, $^3J_{H,H}$ = 7.0 Hz), 1.08 (d, 3 H, $CHCH_3$, $^3J_{H,H}$ = 7.1 Hz), 2.30 (dd, $^2J_{H,H}$ = 12.7, $^3J_{H,H}$ = 6.3 Hz, 1 H, CH_2NEt), 2.34 (q, $^3J_{H,H}$ = 7.0 Hz, 4 H, NCH_2CH_3,), 2.50−2.73 (m, 2 H, $CHCH_3$ and CH_2NEt), 3.62 (s, 3 H, OCH_3). ^{13}C NMR ($CDCl_3$): δ = 12.3 ppm (s, NCH_2CH_3), 15.8 (s, $CHCH_3$), 39.4 (s, $CHCH_3$), 47.8 (s, NCH_2CH_3), 51.7 (s, OCH_3), 57.3 (s, CH_2NEt), 177.0 (s, C=O).

Methyl 2-Methyl-3-(1-piperidino)propanoate (2c): Starting materials: **1b**, piperidine. The mixture was heated to 90 °C for 6 h. Yield: 76.0 g (0.41 mol, 82%), b.p. 54 °C (0.2 mbar). ^{1}H NMR ($CDCl_3$): δ = 1.10 ppm (d, $^3J_{H,H}$ = 7.0 Hz, 3 H, $CHCH_3$), 1.35−2.33 (m, 10 H, piperidine-H), 2.21 (dd, $^2J_{H,H}$ = 12.3, $^3J_{H,H}$ = 6.3 Hz, 1 H, CH_2N), 2.53 (dd, $^2J_{H,H}$ = 12.3, $^3J_{H,H}$ = 8.3 Hz, 1 H, CH_2N), 2.62 (sext, 1 H, $^3J_{H,H}$ = 7.1 Hz, $CHCH_3$), 3.63 (s, 3 H, OCH_3). ^{13}C NMR ($CDCl_3$): δ = 16.0 ppm (s, $CHCH_3$), 24.8, 26.3, 55.0 (3 × s, piperidine-C), 38.3 (s, $CHCH_3$), 51.7 (s, OCH_3), 62.7 (s, CH_2N), 177.0 (s, C=O).

Methyl 2-Methyl-3-(1-pyrazolyl)propanoate (2d): Starting materials: **1b**, pyrazole. The mixture was heated under reflux for 60 h. Yield: 68.4 g (0.41 mol, 82%), b.p. 48 °C (0.2 mbar). ^{1}H NMR ($CDCl_3$): δ = 1.07 ppm (d, $^3J_{H,H}$ = 7.1 Hz, 3 H, $CHCH_3$), 3.02 (sext, 1 H, $^3J_{H,H}$ = 7.1 Hz, $CHCH_3$), 3.57 (s, 3 H, OCH_3), 4.08 (dd, $^2J_{H,H}$ = 13.7, $^3J_{H,H}$ = 6.5 Hz, 1 H, CH_2N), 4.34 (dd, $^2J_{H,H}$ = 13.7, $^3J_{H,H}$ = 7.5 Hz, 1 H, CH_2N), 6.11, 7.30, 7.40 (t, 2×d, 3 H, $^3J_{H,H}$ = 2.0 Hz, pyrazole-H). ^{13}C NMR ($CDCl_3$): δ = 15.1 ppm (s, $CHCH_3$), 41.0 (s, $CHCH_3$), 52.2 (s, OCH_3), 54.5 (s, CH_2N), 105.6, 130.2, 140.0 (3 × s, pyrazole-C), 174.9 (s, C=O). For further analytical data of **2a**−**2d**, see Table 7.

Methyl 3-(Diphenylphosphanyl)-2-phenylpropanoate (3): Compound **1a** (1.62 g, 10 mmol) and diphenylphosphane (1.86 g, 10 mmol) were dissolved in DMF (30 mL). NaH (60% dispersion in mineral oil, 200 mg, 5 mmol) was added, and the reaction mixture was stirred at 25 °C for 18 h and then quenched by addition of deoxygenated water (10 mL). The product was extracted with diethyl

 © 2003 Wiley-VCH Verlag GmbH & Co. KGaA, Weinheim

Table 6. Chemical shifts (δ values) and coupling constants J in the $^{13}C\{^1H\}$ NMR spectra of **4**−**14**

No.[a]	CH_2N	CH_2X	CH_2Y	OCH_3	C_qCH_3	C_qCH_3	C=O	Aryl-C	Others
4a[b]	66.9	67.4, X = OH	−	52.6	55.3	−	174.8	126.4−140.4 m	24.1, 26.8, 56.9, piperidine-C
4b[b]	61.0	68.8, X = OH	−	52.1	47.8	20.8	176.9	−	11.7, 48.4, NEt_2
4c[b]	66.2	69.1, X = OH	−	52.2	47.6	21.0	176.8	−	24.1, 26.7, 56.8, piperidine-C
4d[b]	55.5	63.2, X = OH	−	52.9	58.3	−	173.7	126.9−138.9 m	105.8, 131.9, 140.0, pyrazole-C
5a[b]	62.4	68.8, X = Y = OH		−	40.1	19.9	−	−	12.1, 49.3, NEt_2
5b[b]	55.0	66.4, X = Y = OH		−	50.0		−	127.0−140.7 m	105.8, 131.7, 139.8, pyrazole-C
6a[b]	65.5 t, $^3J_{C,P}$ = 7.7	40.2 dd, X = Y = PPh_2, $^1J_{C,P}$ = 15.5; $^3J_{C,P}$ = 8.7		−	41.0 t, $^2J_{C,P}$ = 12.5	26.6 t, $^3J_{C,P}$ = 9.7	−	128.6−141.0 m	12.3, 49.0, NEt_2
6b[b]	59.5 t, $^3J_{C,P}$ = 11.7	39.1 dd, X = Y = PPh_2, $^1J_{C,P}$ = 18.5; $^3J_{C,P}$ = 10.2		−	46.5 t, $^2J_{C,P}$ = 16.2	−	−	126.9−142.0 m	105.3, 131.3, 139.3, pyrazole-C
7a[b]	59.7	49.5, X = Cl	−	52.1	49.7	19.9	175.5	−	12.1, 48.4, NEt_2
7b[b]	54.3	46.6, X = Cl	−	53.2	57.6	−	172.5	126.5−137.9 m	105.7, 131.4, 140.5, pyrazole-C
8[b]	64.3 d, $^3J_{C,P}$ = 9.1	37.6 d, X = PPh_2, $^1J_{C,P}$ = 15.6	−	51.7	48.2 d, $^2J_{C,P}$ = 13.2	22.5 d, $^3J_{C,P}$ = 11.1	177.3	128.7−140.2 m	12.1, 48.5, NEt_2
9[b]	55.8	65.6, X = OH	47.9, Y = Cl	−	50.3	−	−	127.1−139.8 m	106.0, 131.8, 140.1, pyrazole-C
10[b]	57.8 d, $^3J_{C,P}$ = 9.1	38.0 d, X = PPh_2, $^1J_{C,P}$ = 18.1	49.5 d, Y = Cl, $^3J_{C,P}$ = 14.6	−	48.2 d, $^2J_{C,P}$ = 16.1	−	−	127.3−140.2 m	105.6, 131.2, 140.2, pyrazole-C
11[b]	59.8 t, $^3J_{C,P}$ = 11.5	40.9 dd, X = PPh_2, $^1J_{C,P}$ = 16.5, $^3J_{C,P}$ = 8.7	34.7 dd ,Y = $PMes_2$, $^1J_{C,P}$ = 21.0, $^3J_{C,P}$ = 10.1	−	47.9 t, $^2J_{C,P}$ = 20.1	−	−	127.3−140.2 m	21.1 d, $^5J_{C,P}$ = 2.8, *p*-CH_3, 23.2 d, 23.8 d, $^3J_{C,P}$ = 14.5, *o*-CH_3, 105.2, 130.5, 139.2, pyrazole-C
12a[c]	70.4	34.7 br. s, X = Y = PPh_2		−	40.4	24.8	−	128.5−138.6 m	12.1, 49.3, NEt_2
12b[c]	62.9	30.6 br. s, X = Y = PPh_2		−	45.6	−	−	127.2−140.6 m	105.1, 131.2, 139.7, pyrazole-C
13[c]	60.8 d, $^3J_{C,P}$ = 10.7	28.8 d, X = PPh_2, $^1J_{C,P}$ = 26.9	−	53.4	44.5 br. s	28.1 br. s	175.8	128.6−135.9 m	11.7, 13.4, 55.3, 57.9, NEt_2
14[d]	67.2 br. s	32.8 d, X = PPh_2, $^1J_{C,P}$ = 23.9	−	53.7	50.2 br. s	28.3 d, $^3J_{C,P}$ = 14.7	176.1 d, $^3J_{C,P}$ = 4.5	129.2−134.0 m	7.4, 16.0, 52.4, 54.9, NEt_2, 51.8 br. s,[e] 52.2 br. s,[e] 54.9 br. s,[f] 61.1 br. s,[f], 66.7 br. s,[g], 94.6 br. s,[f] 94.7 br. s,[f] norbornadiene-C

[a] All signals are singlets unless otherwise stated; d = doublet, dd = doublet of doublet, t = triplet, m = multiplet, br. s = broad signal; coupling constants in Hz. [b] Solvent $CHCl_3$. [c] Solvent CH_2Cl_2. [d] Measuring temperature −40 °C. [e] Bridgehead CH group. [f] Olefinic CH group. [g] CH_2 group.

ether (4 × 20-mL portions), the organic portion was separated, and solvent was removed in vacuo. The resulting viscous oil was purified by chromatography on silica gel with petroleum ether/diethyl ether (6:1; R_f = 0.43) as eluent to afford **3** (2.30 g, 6.6 mmol, 66%) as a colourless oil. ^1H NMR ($CDCl_3$): δ = 2.59 ppm (d, $^2J_{H,H}$ = 13.6 Hz, 1 H, CH_2P), 2.96 (d, $^2J_{H,H}$ = 13.6 Hz, 1 H, CH_2P), 3.60−3.71 (m, 1 H, PhC*H*), 3.66 (s, 3 H, OCH_3), 7.33−7.48 (m, 15 H, aromat. H). ^{13}C NMR ($CDCl_3$): δ = 33.2 ppm (d, $^1J_{C,P}$ = 14.7 Hz, CH_2P), 49.0 (d, $^2J_{C,P}$ = 19.3 Hz, Ph*C*H), 52.5 (s, OCH_3), 127.9−139.8 (m, aromat. C), 174.3 (d, $^3J_{C,P}$ = 4.6 Hz, C=O). ^{31}P NMR ($CDCl_3$): δ = −20.9 (s). For further analytical data, see Table 7.

Methyl 3-Hydroxy-2-phenyl-2-[(1-piperidino)methyl]propanoate (4a): Compound **2a** (5.00 g, 20 mmol) and paraformaldehyde (2.70 g) were suspended in DMF (100 mL). Upon addition of NaH (60% dispersion in mineral oil, 900 mg) to the cooled (0 °C) suspension, the reaction mixture became clear within minutes. The reaction mixture was allowed to warm up to 25 °C and was stirred for 18 h. The reaction was quenched by the addition of brine (150 mL). The aqueous phase was extracted with diethyl ether (4 × 100-mL portions). The combined organic phases were washed with brine, dried with $MgSO_4$, filtered, and concentrated by rotary evaporation. The resulting viscous oil was purified by chromatography on silica gel with petroleum ether/diethyl ether (1:1; R_f = 0.39, strong tailing) as eluent to afford **4a** (3.60 g, 13.0 mmol, 65%) as a viscous fluid. For analytical data see Tables 4, 6 and 7.

Methyl 2-(Diethylaminomethyl)-3-hydroxy-2-methylpropanoate (4b): A solution of lithium diisopropylamide[27] (110 mmol) in THF (100 mL) was added at −78 °C to a suspension of **2b** (17.3 g, 100 mmol) and paraformaldehyde (10.5 g, 350 mmol) in THF (200 mL). The mixture was stirred for 1 h at −78 °C and then for 4 h at 25 °C, quenched by the addition of water (50 mL) and partitioned between diethyl ether and water. The aqueous layer was extracted with diethyl ether (3 × 50 mL), and the combined organic phases were washed with brine, dried with $MgSO_4$, and concentrated by rotary evaporation. Distillation of the residue under reduced press-

 © 2003 Wiley-VCH Verlag GmbH & Co. KGaA, Weinheim

Table 7. Analytical data of **2**−**14**

No.	Formula	*M* [g/mol]	MS[a] *m*/*z* (%)	$C_{calcd.}/C_{found}$	$H_{calcd.}/H_{found}$	$Cl_{calcd.}/Cl_{found}$	$N_{calcd.}/N_{found}$	$P_{calcd.}/P_{found}$
2a	$C_{15}H_{21}NO_2$	247.3	246 (10), 98 (100)	72.84/72.89	8.56/8.45		5.66/5.59	
2b	$C_9H_{19}NO_2$	173.3	173 (19), 158 (22), 86 (100), 58 (61)	62.39/62.28	11.05/10.90		8.08/8.04	
2c	$C_{10}H_{19}NO_2$	185.3	184 (28), 154 (13), 98 (100), 84 (46), 70 (86), 59 (62), 55 (92)	64.83/64.54	10.34/10.34		7.56/7.55	
2d	$C_8H_{12}N_2O_2$	168.2	168 (36), 137 (18), 109 (67), 81 (100), 69 (45)	57.13/57.14	7.19/7.25		16.66/n.d.	
3	$C_{22}H_{21}O_2P$	348.4	348 (37), 333 (86), 262 (57), 201 (100), 183 (70)	75.85/75.73	6.08/6.08			8.89/n.d.
4a	$C_{16}H_{23}NO_3$	277.4	278 (1), 276 (1), 98 (100)	69.29/69.50	8.36/8.57		5.05/4.83	
4b	$C_{10}H_{21}NO_3$	203.3	203 (1), 86 (100), 58 (16)	59.09/59.37	10.41/10.54		6.89/6.81	
4c	$C_{11}H_{21}NO_3$	215.3	215 (2), 98 (100), 84 (10), 55 (14)	61.37/61.44	9.83/9.74		6.51/6.55	
4d	$C_{14}H_{16}N_2O_3$	260.3	260 (38), 243 (13), 230 (70), 162 (100), 144 (74), 103 (65), 91 (28), 81 (66)	64.60/64.82	6.20/6.42		10.76/10.33	
5a	$C_9H_{21}NO_2$	175.3	175 (2), 86 (100), 58 (15)	61.67/n.d.	12.08/n.d.		7.99/n.d.	
5b	$C_{13}H_{16}N_2O_2$	232.3	232 (3), 184 (75), 144 (100), 134 (37), 103 (55), 91 (51), 81 (80), 77 (52), 69 (38)	67.22/67.43	6.94/7.03		12.06/11.81	
6a	$C_{33}H_{39}NP_2$	511.6	511 (7), 434 (10), 183 (16), 86 (100)	77.47/77.47	7.68/7.84		2.74/2.77	12.11/n.d.
6b	$C_{37}H_{34}N_2P_2$	568.6	568 (12), 491 (100), 383 (10), 301 (14), 262 (17), 183 (20)	78.15/77.54	6.03/6.03		4.93/4.94	10.89/n.d.
7a	$C_{10}H_{20}ClNO_2$	221.7	221 (10), 86 (100), 58 (50)	54.17/53.79	9.09/9.13	15.99/n.d.	6.32/6.33	
7b	$C_{14}H_{15}ClN_2O_2$	278.7	278 (100), 243 (47), 211 (11)	60.33/60.30	5.42/5.45	12.72/12.69	10.05/9.91	
8	$C_{22}H_{30}NO_2P$	371.5	371 (2), 183 (13), 86 (100)	71.14/70.89	8.14/8.30		3.77/3.75	8.34/n.d.
9	$C_{13}H_{15}ClN_2O$	250.7	251 (6), 220 (22), 215 (100), 185 (91), 152 (72), 115 (73), 103 (75), 91 (62), 81 (80), 77 (52)	62.28/62.41	6.03/6.31	14.14/n.d.	11.17/10.65	
10	$C_{25}H_{24}ClN_2P$	418.9	418 (15), 383 (22), 315 (74), 301 (47), 262 (58), 183 (100)	71.68/72.20	5.77/5.89	8.46/8.11	6.69/6.57	7.39/7.67
11	$C_{43}H_{46}N_2P_2$	652.8	653 (45), 533 (100)	79.12/78.89	7.10/7.20		4.29/4.25	9.49/n.d.
12a	$C_{33}H_{39}Cl_2NNiP_2$	641.2	604 (100), 569 (15), 511 (58), 434 (45)	61.81/59.68	6.13/6.52	11.06/n.d.	2.18/2.08	9.66/n.d.
12b	$C_{37}H_{34}Cl_2N_2NiP_2$	698.2	696 (7), 661 (100), 626 (16), 491 (26), 411 (21)	63.65/63.22	4.91/5.15	10.16/9.58	4.01/4.05	8.87/8.70
12c	$C_{43}H_{46}Cl_2N_2NiP_2$	782.4	745 (43), 709 (15), 575 (11), 533 (62), 525 (10), 441 (100)	63.34[b]/63.14	5.74[b]/6.04	12.89[b]/n.d.	3.40[b]/3.36	7.51[b]/n.d.
13	$C_{22}H_{30}Cl_2NO_2PPd$	548.8	512 (100), 477 (59), 370 (71)	48.15/48.18	5.51/5.51	12.92/12.82	2.55/2.61	5.64/5.78
14·PF$_6$	$C_{29}H_{38}F_6NO_2P_2Rh$	711.5	566 (100), 479 (13), 388 (30)	48.96/48.69	5.38/5.39		1.97/2.02	8.71/8.76

[a] Compounds **2**−**11**: EI-MS; compounds **12**−**14**: FAB-MS. [b] Calculated for **12c**·0.5CH_2Cl_2.

 © 2003 Wiley-VCH Verlag GmbH & Co. KGaA, Weinheim

ure afforded **4b** (8.8 g, 43 mmol, 43%) as a colourless liquid, b.p. 62 °C (0.2 mbar). For analytical data, see Tables 4, 6 and 7.

Methyl 3-Hydroxy-2-methyl-2-[(1-piperidino)methyl]propanoate (4c): Starting material: **2c** (18.5 g, 100 mmol). This compound was prepared analogously to **4b**. Yield: 11.1 g (51.6 mmol, 52%), b.p. 99 °C (0.2 mbar). For analytical data, see Tables 4, 6 and 7.

Methyl 3-Hydroxy-2-phenyl-2-[(1-pyrazolyl)methyl]propanoate (4d): Pyrazole (5.10 g, 75 mmol) was deprotonated at 0 °C with sodium hydride (1.00 g, 25 mmol, 60% dispersion in mineral oil) in DMF (50 mL). This solution was slowly added at 0 °C to a mixture of **1a** (8.14 g, 50 mmol) and paraformaldehyde (4.50 g, 150 mmol) in DMF (50 mL). When a clear, colourless solution had formed, the reaction mixture was stirred at 25 °C for 1 h. The reaction was quenched by the addition of brine (150 mL), and the aqueous phase was extracted with diethyl ether (4 × 100-mL portions). The combined organic phases were washed with brine, dried with $MgSO_4$, filtered, and concentrated by rotary evaporation. The resulting viscous oil was purified by chromatography on silica gel with petroleum ether/diethyl ether (1:3; R_f = 0.42) as eluent to afford **4d** (8.10 g, 31.0 mmol, 62%) as a colourless oil. For analytical data, see Tables 4, 6 and 7.

General Procedure for the Synthesis of 5 and 9: A solution of the substituted ester (**4** or **7b**; 20 mmol) in THF (50 mL) was slowly added at 25 °C to a stirred suspension of $LiAlH_4$ (30 mmol per OH group) in THF (200 mL). The mixture was stirred for 15 h and hydrolysed by dropwise addition of water. The precipitate was filtered off and washed five times with ethyl acetate. The combined organic phases were dried with $MgSO_4$ and the solvents were evaporated to dryness to yield the corresponding alcohols.

2-(Diethylaminomethyl)-2-methylpropane-1,3-diol (5a): Starting material: **4b**. Yield: 3.45 g (19.7 mmol, 99%) of a viscous oil.

2-Phenyl-2-[(1-pyrazolyl)methyl]propane-1,3-diol (5b): Starting material: **4d**. Yield: 4.52 g (19.5 mmol, 97%) of a microcrystalline powder, m.p. 86 °C.

2-(Chloromethyl)-2-phenyl-3-(1-pyrazolyl)propan-1-ol (9): Starting material: **7b**. Yield: 4.81 g (19.2 mmol, 96%) of a microcrystalline powder. For further analytical data of **5a**, **5b**, and **9**, see Tables 5−7.

General Procedure for the Synthesis of 6 and 10: The substituted alcohol (**5** or **9**; 10.0 mmol, 1 equivalent) in THF (50 mL) was deprotonated at −30 °C with *n*BuLi (1.2 equiv. per OH group). The resulting solution was then allowed to warm to 25 °C, stirred for 30 min and subsequently recooled to −30 °C. Methanesulfonyl chloride (1.2 equiv. per OH group) was then added slowly, and the reaction mixture was stirred at 0 °C for 2 h. In a separate vessel diphenylphosphane (1.2 equiv. per OH group) in THF (50 mL) was deprotonated with *n*BuLi (1.2 equiv. per OH group). The resulting red lithium diphenylphosphide solution was added to the reaction mixture at −30 °C. After the mixture had been stirred for 15 h at 25 °C, all volatiles were removed in vacuo. The remaining residue was purified by chromatography on silica gel.

{2,2-Bis[(diphenylphosphanyl)methyl]propyl}diethylamine (6a): Starting material: **5a**. Yield: 3.34 g (6.5 mmol, 65%) of a viscous oil, R_f = 0.43 (petroleum ether/diethyl ether, 3:1). ^{31}P NMR ($CDCl_3$): δ = −27.1 ppm (s).

1-{2,2-Bis[(diphenylphosphanyl)methyl]-2-phenylethyl}-1*H*-pyrazole (6b): Starting material: **5b**. Yield: 3.91 g (6.9 mmol, 69%) of a microcrystalline powder, R_f = 0.65 (petroleum ether/diethyl ether/CH_2Cl_2, 2:1:1), m.p. 145 °C. ^{31}P NMR ($CDCl_3$): δ = −26.8 ppm (s).

1-[2-(Chloromethyl)-3-(diphenylphosphanyl)-2-phenylpropyl]-1*H*-pyrazole (10): Starting material: **9**. Yield: 2.32 g (5.5 mmol, 55%) of a microcrystalline powder, R_f = 0.43 (petroleum ether/diethyl ether, 3:1), m.p. 119 °C. ^{31}P NMR ($CDCl_3$): δ = −26.9 ppm (s). For further analytical data of **6a**, **6b**, and **10**, see Tables 5−7.

General Procedure for the Synthesis of 7: A solution of anhydrous PPh_3 (15.7 g, 60 mmol) in CCl_4 (80 mL) was heated under reflux for 90 min, during which the colour of the solution changed from colourless to light red. The substituted β-hydroxy ester **4** (30 mmol), dissolved in CCl_4 (30 mL), was added rapidly to the boiling reaction mixture from a dropping funnel. The solution discoloured immediately and a brown precipitate of $O{=}PPh_3$ was formed. The mixture was heated under reflux for another 12 h and afterwards cooled to 25 °C. The precipitate was filtered off and washed five times with diethyl ether. The combined organic solutions were concentrated by rotary evaporation.

Methyl 2-(Chloromethyl)-3-(diethylamino)-2-methylpropanoate (7a): Starting material: **4b**. Kugelrohr distillation of the residue under reduced pressure afforded **7a** (7.3 g, 32.9 mmol, 55%) as a viscous oil, b.p. 100 °C (0.2 mbar).

Methyl 3-Chloro-2-phenyl-2-[(1-pyrazolyl)methyl]propanoate (7b): Starting material: **4d**. The remaining residue was purified by chromatography on silica gel with petroleum ether/diethyl ether (2:1; R_f = 0.53) as eluent to afford **7b** (9.4 g, 33.7 mmol, 56%) as a colourless powder, m.p. 100 °C. For analytical data of **7a** and **7b**, see Tables 4, 6 and 7.

General Procedure for the Synthesis of 8 and 11: The substituted alkyl chloride (**7b** or **10**; 10 mmol, 1 equiv.) was dissolved in DMSO (25 mL). In a separate vessel, diarylphosphane (1.2 equiv.) in DMSO (40 mL) was deprotonated at 25 °C with KO*t*Bu (1.2 equiv.). The resulting red potassium diarylphosphide solution was stirred for 20 min and then added dropwise to the solution of the alkyl chloride. The reaction mixture was stirred for 15 h and hydrolysed by dropwise addition of water (50 mL). The aqueous phase was extracted with diethyl ether (4 × 40-mL portions). The combined organic phases were washed with brine and dried with $MgSO_4$, and the solvents were evaporated to dryness. The remaining residue was purified by chromatography on silica gel.

Methyl 3-(Diethylamino)-2-[(diphenylphosphanyl)methyl]-2-methylpropanoate (8): Starting material: **7b**. Yield: 2.32 g (6.3 mmol, 63%) of a viscous oil, R_f = 0.43 (petroleum ether/diethyl ether, 3:1). FT-IR (CH_2Cl_2): $\tilde{\nu}$ = 1726 cm^{-1} vs (CO), 1434 m (PPh). ^{31}P NMR ($CDCl_3$): δ = −24.3 ppm (s).

1-{2-[(Dimesitylphosphanyl)methyl]-3-(diphenylphosphanyl)-2-phenylpropyl}-1*H*-pyrazole (11): Starting material: **10**. Yield: 2.32 g (6.3 mmol, 63%) of a microcrystalline powder, R_f = 0.47 (petroleum ether/diethyl ether, 4:1), m.p. 120 °C. ^{31}P NMR ($CDCl_3$): δ = −34.1 ppm (d, $^4J_{P,P}$ = 10 Hz, $PMes_2$), −26.1 (d, $^4J_{P,P}$ = 10 Hz, PPh_2). For further analytical data of **8** and **11**, see Tables 5−7.

Coordination Chemistry Compounds

General Procedure for the Synthesis of 12: A solution of the respective tripod ligand (1.05 mmol) in ethanol (10 mL, with some THF added to increase the solubility if necessary) was added rapidly to a solution of $NiCl_2{\cdot}6H_2O$ (1.0 mmol, 240 mg) in ethanol (10 mL). The colour of the reaction mixture immediately changed to red and within a few minutes the nickel complexes precipitated. After the mixture had been stirred at 25 °C for 1 h, the precipitate was fil-

 © 2003 Wiley-VCH Verlag GmbH & Co. KGaA, Weinheim

tered, washed with diethyl ether (3 × 10-mL portions), and dried in vacuo.

[(6a-κ²*P*)NiCl₂] (12a): Starting material: **6a**. Recrystallisation from CH_2Cl_2/diethyl ether afforded **12a** (525 mg, 0.82 mmol, 82%) in the form of red crystals suitable for X-ray structure analysis, m.p. 212 °C (decomposition). ^{31}P NMR (CD_2Cl_2, −40 °C): δ = 10.7 ppm (s).

[(6b-κ²*P*)NiCl₂] (12b): Starting material: **6b**. Recrystallisation from CH_2Cl_2/diethyl ether afforded **12b** (650 mg, 0.93 mmol, 93%) in the form of red crystals suitable for X-ray structure analysis, m.p. 248 °C (decomposition). ^{31}P NMR (CD_2Cl_2, −40 °C): δ = 15.6 ppm (s).

[(11-κ²*P*)NiCl₂] (12c): Starting material: **11**. Removal of the solvent afforded **12c** (585 mg, 0.75 mmol, 75%) in the form of an orange, microcrystalline solid. ^{1}H NMR and ^{13}C NMR: no sharp signals could be detected, due to a dynamic process. ^{31}P NMR (CD_2Cl_2, −40 °C): δ = −4.5 ppm (d, $^2J_{P,P}$ = 95 Hz, $PMes_2$), 4.0 (d, $^2J_{P,P}$ = 95 Hz, PPh_2).

For crystallographic data of **12a** and **12b**, see Table 3; for further analytical data of **12a**−**12c**, see Tables 5−7.

[(8-κ²*N*,*P*)PdCl₂] (13): A solution of ligand **8** (210 mg, 0.5 mmol) in ethanol (15 mL) was added rapidly to a suspension of (η⁴-cod)$PdCl_2$ (145 mg, 0.5 mmol) in ethanol (10 mL). Within a few minutes the yellow reaction mixture became clear. After the mixture had been stirred at 25 °C for 12 h, all volatiles were removed in vacuo. The residual yellow solid was washed with diethyl ether (3 × 10-mL portions) and dried in vacuo. Recrystallisation from CH_2Cl_2/diethyl ether afforded **13** (180 mg, 0.33 mmol, 66%) in the form of yellow crystals suitable for X-ray structure analysis. FT-IR (CH_2Cl_2): $\tilde{\nu}$ = 1732 cm^{-1} vs (CO), 1438 m (PPh). ^{31}P NMR (CD_2Cl_2): δ = 19.6 ppm (s). For crystallographic data, see Table 3; for further analytical data, see Tables 4, 6 and 7.

[(8-κ²*N*,*P*)(η⁴-nbd)Rh]PF₆ (14·PF₆): [(η⁴-nbd)RhCl]$_2$ (230 mg, 0.5 mmol) was dissolved in acetone (5 mL). In a second flask, potassium hexafluorophosphate (195 mg, 1.05 mmol) was dissolved in acetone (5 mL, 0.1 mL of water added). This solution was added to the orange rhodium(I) solution. A colourless KCl precipitate formed over 5 min, while the colour of the reaction mixture faded. A solution of ligand **8** (370 mg, 1.0 mmol) in CH_2Cl_2 (5 mL) was then added. After the mixture had been stirred at 25 °C for 1 h, all volatiles were removed in vacuo. The residue was taken up in acetone (20 mL) and dried with $MgSO_4$. The insoluble KCl was removed by filtering the solution through Kieselguhr. Removal of the solvent in vacuo and recrystallisation from CH_2Cl_2/diethyl ether afforded **14·PF₆** (640 mg, 0.9 mmol, 90%) in the form of orange crystals suitable for X-ray structure analysis, m.p. 203 °C (decomposition). FT-IR (CH_2Cl_2): $\tilde{\nu}$ = 1725 cm^{-1} vs (CO), 1437 m (PPh). ^{31}P NMR (CD_2Cl_2): δ = −144.2 ppm (sept, $^1J_{P,F}$ = 711 Hz, PF_6^-), 29.8 (d, $^1J_{Rh,P}$ = 174 Hz, PPh_2). For crystallographic data, see Table 3; for further analytical data, see Tables 4, 6 and 7.

Acknowledgments

We are indebted to the Deutsche Forschungsgemeinschaft and the Fonds der Chemischen Industrie for financial support. One of us (R. F.) is indebted to the local Graduiertenkolleg "Selektivität in der organischen und metallorganischen Synthese und Katalyse" for a scholarship. The technical support by T. Jannack (mass spectrometry) and the Microanalytical Laboratory of the Institute of Organic Chemistry is gratefully acknowledged. We are indebted to Dr. J. Scherer and Dr. K. Heinze for their advice and help in solving the crystal structure of **14·PF₆**.

[1] [1a] W. Hewertson, H. R. Watson, *J. Chem. Soc.* **1962**, *84*, 1490−1494. [1b] G. M. Whitesides, C. P. Casey, J. K. Krieger, *J. Am. Chem. Soc.* **1971**, *93*, 1379−1389. [1c] M. J. Burk, J. E. Feaster, R. L. Harlow, *Tetrahedron: Asymmetry* **1991**, *2*, 569−592. [1d] A. Muth, O. Walter, G. Huttner, A. Asam, L. Zsolnai, C. Emmerich, *J. Organomet. Chem.* **1994**, *468*, 149−163.

[2] [2a] S.-T. Liu, C.-L. Tsao, M. C. Cheng, S. M. Peng, *Polyhedron* **1990**, *21*, 2579−2584. [2b] S.-T. Liu, *J. Chin. Chem. Soc.* **1992**, *39*, 611−616. [2c] J. Dale, S. B. Fredriksen, *Acta Chem. Scand.* **1992**, *46*, 271−277. [2d] S.-T. Liu, C.-H. Yieh, H.-P. Dai, *Proc. Natl. Sci. Counc., Repub. China, Part A: Phys. Sci. Eng.* **1995**, *19*, 1−4.

[3] [3a] H. Heidel, G. Huttner, G. Helmchen, *Z. Naturforsch., Teil B* **1993**, *48*, 1681−1692. [3b] H. Heidel, G. Huttner, R. Vogel, G. Helmchen, *Chem. Ber.* **1994**, *127*, 271−274. [3c] T. Seitz, A. Muth, G. Huttner, *Chem. Ber.* **1994**, *127*, 1837−1842. [3d] H. Heidel, G. Huttner, L. Zsolnai, *Z. Naturforsch., Teil B* **1995**, *50*, 729−734. [3e] G. Reinhard, R. Soltek, G. Huttner, A. Barth, O. Walter, L. Zsolnai, *Chem. Ber.* **1996**, *129*, 97−108. [3f] B. Antelmann, U. Winterhalter, G. Huttner, B. C. Janssen, J. Vogelgesang, *J. Organomet. Chem.* **1997**, *545*−*546*, 407−420. [3g] A. Jacobi, G. Huttner, U. Winterhalter, *Chem. Ber./Recueil* **1997**, *130*, 1279−1294. [3h] A. Jacobi, G. Huttner, U. Winterhalter, S. Cunskis, *Eur. J. Inorg. Chem.* **1998**, 675−692. [3i] R. Soltek, G. Huttner, *Eur. J. Inorg. Chem.* **1998**, 1417−1424. [3j] R. Soltek, G. Huttner, L. Zsolnai, A. Driess, *Inorg. Chim. Acta* **1998**, *269*, 143−156. [3k] J. Vogelgesang, G. Huttner, E. Kaifer, P. Kircher, P. Rutsch, S. Cunskis, *Eur. J. Inorg. Chem.* **1999**, 2187−2199.

[4] [4a] S.-T. Liu, C.-Y. Liu, *J. Org. Chem.* **1992**, *57*, 6079−6080. [4b] H.-E. Wang, C.-Y. Liu, M.-C. Cheng, S.-M. Peng, S.-T. Liu, *Phosphorus, Sulfur Silicon Relat Elem.* **1992**, *69*, 201−211.

[5] [5a] C. Sarafidis, U. S. Patent 3.445.540, **1969**; *Chem. Abstr.* **1969**, 30038b. [5b] M. J. Burk, R. L. Harlow, *Angew. Chem.* **1990**, *102*, 1511−1513; *Angew. Chem. Int. Ed. Eng.* **1990**, *29*, 1467−1469. [5c] B. C. Janssen, A. Asam, G. Huttner, V. Sernau, L. Zsolnai, *Chem. Ber.* **1994**, *127*, 501−506.

[6] [6a] T. Seitz, A. Muth, G. Huttner, T. Klein, O. Walter, M. Fritz, L. Zsolnai, *J. Organomet. Chem.* **1994**, *469*, 155−162. [6b] T. Seitz, A. Muth, G. Huttner, *Z. Naturforsch., Teil B* **1995**, *50*, 1045−1049. [6c] T. Seitz, A. Asam, G. Huttner, O. Walter, L. Zsolnai, *Z. Naturforsch., Teil B* **1995**, *50*, 1287−1306. [6d] B. Antelmann, G. Huttner, U. Winterhalter, *J. Organomet. Chem.* **1998**, *553*, 433−441. [6e] P. Schober, R. Soltek, G. Huttner, L. Zsolnai, K. Heinze, *Eur. J. Inorg. Chem.* **1998**, 1407−1415. [6f] J. Vogelgesang, A. Frick, G. Huttner, P. Kircher, *Eur. J. Inorg. Chem.* **2001**, 949−971.

[7] [7a] A. Muth, A. Asam, G. Huttner, A. Barth, L. Zsolnai, *Chem. Ber.* **1994**, *127*, 305−311. [7b] B. C. Janssen, V. Sernau, G. Huttner, A. Asam, O. Walter, M. Büchner, L. Zsolnai, *Chem. Ber.* **1995**, *128*, 63−70. [7c] P. Schober, G. Huttner, L. Zsolnai, A. Jacobi, *J. Organomet. Chem.* **1998**, *571*, 279−288.

[8] E. Rouvier, J.-C. Giacomoni, A. Cambon, *Bull. Soc. Chim. Fr.* **1971**, *5*, 1717−1723.

[9] D. A. Blinn, R. S. Button, V. Farazi, M. K. Neeb, C. L. Tapley, T. E. Trehearne, S. D. West, T. L. Kruger, B. N. Storhoff, *J. Organomet. Chem.* **1990**, *393*, 143−152.

[10] [10a] H. Wurziger, *Kontakte (Darmstadt)* **1988**, *2*, 36−41. [10b] R. Noyori, M. Suzuki, *Angew. Chem.* **1984**, *96*, 854−882; *Angew. Chem. Int. Ed. Engl.* **1984**, *23*, 847−875.

[11] [11a] S. Cacchi, P. G. Ciattini, E. Morera, G. Ortar, *Tetrahedron Lett.* **1988**, *29*, 3117−3120. [11b] L. A. Paquette, G. D. Maynard, *J. Org. Chem.* **1989**, *54*, 5054−5063.

[12] [12a] E. C. Taylor, J. L. La Mattina, *J. Org. Chem.* **1978**, *43*, 1200−1204. [12b] M. P. Moyer, P. L. Feldman, H. Rapoport, *J. Org. Chem.* **1985**, *50*, 5223−5230.

[13] A. Stobie, Intern. Patent WO 9.204.346, **1992**; *Chem. Abstr.* **1992**, *117*, 111614.

 © 2003 Wiley-VCH Verlag GmbH & Co. KGaA, Weinheim

[14] R. Appel, *Angew. Chem.* **1975**, *87*, 863−874; *Angew. Chem. Int. Ed. Engl.* **1975**, *14*, 801−812.
[15] A. Jacobi, G. Huttner, U. Winterhalter, *J. Organomet. Chem.* **1998**, *571*, 231−241.
[16] [16a] S.-T. Liu, G.-J. Liu, C.-H. Yieh, M.-C. Cheng, S.-M. Peng, *J. Organomet. Chem.* **1990**, *387*, 83−94. [16b] H.-E. Wang, M.-C. Cheng, G.-H. Lee, S.-M. Peng, S.-T. Liu, *J. Organomet. Chem.* **1993**, *445*, 171−179.
[17] [17a] A. Frick, V. Schulz, G. Huttner, *Eur. J. Inorg. Chem.* **2002**, 3129−3147. [17b] V. Schulz, A. Frick, G. Huttner, *Eur. J. Inorg. Chem.* **2002**, 3111−3128.
[18] J. Karas, G. Huttner, K. Heinze, P. Rutsch, L. Zsolnai, *Eur. J. Inorg. Chem.* **1999**, 405−420.
[19] *Organikum*, Deutscher Verlag der Wissenschaften, Berlin, **1990**.
[20] *DENZO-SMN, Data Processing Software*, Nonius **1998**; http://www. nonius. com
[21] [21a] G. M. Sheldrick, *SHELXS-97, Program for Crystal Structure Solution*, University of Göttingen, **1997**. [21b] G. M. Sheldrick, *SHELXL-97, Program for Crystal Structure Refinement*, University of Göttingen, **1997**; http://shelx.uni-ac.gwdg.de/shelx/index. html [21c] *International Tables for X-ray Crystallography*, vol. 4, Kynoch Press, Birmingham, U.K., **1974**.
[22] L. Zsolnai, G. Huttner, *XPMA*, University of Heidelberg, **1994**; http://www.rzuser.uni-heidelberg.de/~il1/laszlo/xpm.html
[23] R. Soltek, G. Huttner, *WinRay-32*, University of Heidelberg, **1998**; http://www.uni-heidelberg.de/institute/fak12/AC/huttner/html/winray.html
[24] [24a] R. E. Ireland, D. M. Walba, *Org. Synth. Coll. Vol.* **1988**, *6*, 567−570. [24b] K. Issleib, H. O. Fröhlich, *Z. Naturforsch., Teil B* **1959**, *14*, 349−350.
[25] J. B. Lambert, J. H. So, *J. Org. Chem.* **1991**, *56*, 5960−5962.
[26] [26a] W. Falkenberg, M. Thyes, C. Wenz, U. Schneider (Knoll AG), Ger. Patent DE 19.836.222, **2000**. [26b] A. K. Serelis, G. W. Simpson, *Tetrahedron Lett.* **1997**, *38*, 4277−4280.
[27] [27a] M. W. Rathke, A. Lindert, *J. Am. Chem. Soc.* **1971**, *93*, 2318−2320. [27b] R. J. Cregge, J. L. Herrmann, C. S. Lee, J. E. Richman, R. H. Schlessinger, *Tetrahedron Lett.* **1973**, 2425−2428.

Received August 9, 2002

 © 2003 Wiley-VCH Verlag GmbH & Co. KGaA, Weinheim

Cu^{II} Ion Coordination to an Unprotected Pentadecapeptide Containing Two His Residues: Competition Between the Terminal Amino and the Side-Chain Imidazole Nitrogen Donors

Chiara Conato,[a] Wojciech Kamysz,[b] Henryk Kozłowski,*[c] Marek Łuczkowski,[c] Zbigniew Mackiewicz,[b] Francesca Mancini,[d] Piotr Młynarz,[d][‡] Maurizio Remelli,*[a] Daniela Valensin,[d] and Gianni Valensin[d]

Keywords: Copper / Peptides / Coordination chemistry / Bioinorganic chemistry

The complex-formation equilibria of the pentadecapeptide TLEGTKKGHKLHLDY, the 114–128 protein fragment of SPARC, with the Cu^{II} ion have been investigated, at I = 0.1 mol·dm^{-3} (KNO_3) and T = 298.2 K. Protonation and complex-formation constants have been determined potentiometrically, and formation enthalpies measured by direct solution calorimetry; the complex-formation model and species stoichiometry have been carefully checked by means of UV/Vis absorption, CD and EPR spectroscopy. The structure hypotheses of the complex species are also based on detailed study of the ^{1}H and ^{13}C NMR spectra of the ligand in both the absence and presence of copper ions. The involvement in complex-formation of both the terminal amino and imidazole groups has been suggested and their specific behaviour at different pH values elucidated.

(© Wiley-VCH Verlag GmbH & Co. KGaA, 69451 Weinheim, Germany, 2003)

Introduction

SPARC (Secreted Protein, Acidic and Rich in Cysteine) is a 32 kD calcium-binding matricellular protein[1] secreted by many types of cells. It mediates the cell−matrix interactions without covering any primarily structural role:[2,3] it has counter-adhesive properties, thus altering the cell shape, it modulates growth factor activity and influences the cell-cycle. SPARC is the product of a single-copy gene; its sequence has been highly conserved both during vertebrate evolution and among species.[4] It is highly expressed during embryonic development while its expression in the adult is associated with tissue remodelling or renewal, also in response to injury. SPARC is a major product of many tumours,[5] most likely owing to its activity, and that of its fragments, in angiogenesis,[6] both in their free form and as copper complexes.[7]

Human SPARC consists of 286 amino acids, belonging to three distinct modules.[8] The *N*-terminal module (residues 1−52, after a 17 amino-acid signal sequence) is an acidic region, which binds 5−8 calcium ions with low affinity. It interacts with hydroxyapatite, being involved in the mineralization of cartilage and bones. The second module is a Cys-rich, follistatin-like domain (residues 53−137), in which all the 10 Cys residues are disulfide-bonded. A carbohydrate moiety is *N*-linked at Asn99. This module contains two bioactive peptides (residues 55−74 and 114−130), which enable SPARC to bind the copper ion.[7] The latter fragment, corresponding to the strongest Cu^{II}-binding site of the protein, contains the sequence Gly-His-Lys (GHK) (residues 121−123). GHK, a liver-cell growth factor,[9] is a well recognised Cu^{II} binding peptide;[10] it is present in the human serum and it most likely derives from SPARC hydrolysis.[7] Cu^{II}/GHK complexes proved to have angiogenic activity and to play an important role in wound healing.[9] Module III (residues 138−286) is largely α-helical and contains the extracellular high-affinity calcium binding sites. It is globular and contains two EF-hand motifs.

Recent investigations[11,12] into the complex-formation equilibria of protected $SPARC_{114-128}$ (Ac-TLEGTKKGHKLHLDY-NH_2), $SPARC_{122-126}$ (Ac-HKLHL-NH_2), $SPARC_{121-126}$ (Ac-GHKLHL-NH_2) and

[a] Dipartimento di Chimica, Università di Ferrara
Via L. Borsari 46, 44100 Ferrara, Italy
Fax: (internat.) + 39-0532/240709
E-mail: rmm@unife.it
[b] Faculty of Chemistry, University of Gdansk,
Sobieskiego 18/1, 80-952 Gdansk, Poland
[c] Faculty of Chemistry, University of Wroclaw,
F. Joliot-Curie 14, 50-383 Wroclaw, Poland
E-mail: henrykoz@wchuwr.chem.uni.wroc.pl
[d] Dipartimento di Chimica, Università di Siena,
Via A. Moro, S. Miniato, Siena, Italy
[‡] On leave as research associate at the Department of Chemistry, University of Siena, Italia, funded by the CIRMMP Consortium, CERM, Florence, Italy.
Supporting information for this article is available on the WWW under http://www.eurjic.org or from the author.

 © 2003 Wiley-VCH Verlag GmbH & Co. KGaA, Weinheim **DOI: 10.1002/ejic.200200551**

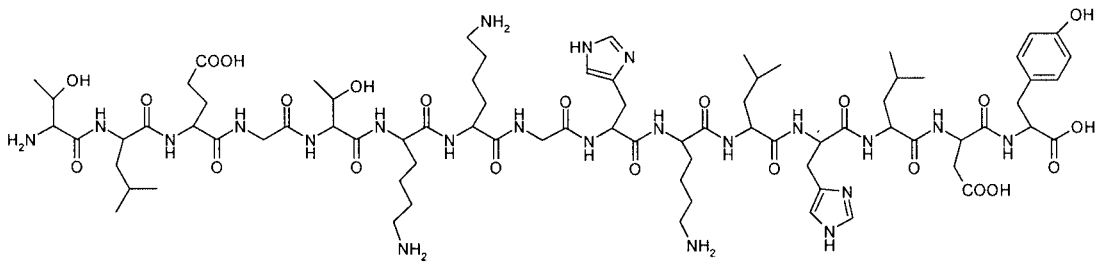

Figure 1. Structure of the ligand TLEGTKKGHKLHLDY.

$SPARC_{120-126}$ (Ac-KGHKLHL-NH_2) fragments with the Cu^{II} ion have shown the central role played by ^{122}His and ^{125}His at acidic pH. The copper-promoted deprotonation of three amido nitrogens has also been reported, at alkaline pH. Here the Cu^{II} complex-formation equilibria of the unprotected TLEGTKKGHKLHLDY pentadecapeptide (see Figure 1) have been investigated, at I = 0.1 mol·dm^{-3} (KNO_3) and T = 298.2 K, to gain new information on the role played in metal ion complexation by His residues belonging to relatively short peptides. In such cases the imidazole nitrogens can compete or cooperate with the terminal amino group for binding copper. In this context, an interesting recent report concerns the Prion Peptide fragment 106−126 ($PrP_{106-126}$),[13] which is neurotoxic in vitro and its activity is highly sensitive to the presence of copper, zinc or iron ions. In that system, the formation of a macrochelate structure at physiological pH has been suggested in which Cu^{II} is bound to both the terminal amino nitrogen and the imidazole ring of the ^{111}His residue. TLEGTKKGHKLHLDY is also a good model for the $PrP_{106-126}$ fragment. Protonation and complex-formation constants have been determined potentiometrically; formation enthalpies have been measured by direct solution calorimetry; complex-formation model and species stoichiometry have been carefully checked by means of UV/Vis absorption, CD and EPR spectroscopy. The proposed structures of the complex species are also based on a detailed study of the ^{1}H and ^{13}C NMR spectra of the ligand both in the absence and in the presence of copper ions.

Results

Ligand protonation constants are shown in Table 1 along with the corresponding thermodynamic quantities determined by calorimetry. It was not possible to distinguish between the two His or the three Lys residues. The terminal carboxylic group is deprotonated over the explored pH range and the corresponding equilibrium is not considered throughout. The thermodynamic results are in good agreement with literature data on analogous ligands,[11,12,14,15] within experimental errors.

Table 1. Protonation and Cu^{II} complex-formation thermodynamic parameters for TLEGTKKGHKLHLDY, at 298.2 K and I = 0.1 mol·dm^{-3} (KNO_3).

Species	Residue	Stoichiometry	logβ	log$K$	$-\Delta G°$ (kJ·mol^{-1})	$-\Delta H°$ (kJ·mol^{-1})	$\Delta S°$ (J·mol^{-1}·K^{-1})
LH	Lys	011	10.95(4)	10.9	62.5(2)	56(7)	20(23)
LH_2	Lys	012	21.61(3)	10.7	123.3(1)	99(2)	83(8)
LH_3	Lys	013	31.78(4)	10.2	181.3(2)	141(4)	136(13)
LH_4	Tyr	014	41.35(5)	9.6	235.9(3)	173(3)	211(11)
LH_5	terminal NH_2	015	48.65(6)	7.3	277.5(3)	209(3)	229(12)
LH_6	His	016	55.22(6)	6.6	315.0(3)	237(3)	261(12)
LH_7	His	017	61.07(6)	5.9	348.4(3)	261(4)	293(13)
LH_8	Glu	018	65.27(7)	4.2	372.3(4)	−	−
LH_9	Asp	019	68.94(7)	3.7	393.3(4)	−	−
MLH_6		116	59.76(9)		341.3(5)	−	−
MLH_5		115	55.21(3)	4.6	315.0(1)	243(5)	240(16)
MLH_4		114	49.85(7)	5.4	284.4(4)	247(4)	125(12)
MLH_3		113	42.37(7)	7.5	241.7(3)	257(4)	−53(15)
MLH_2		112	34.36(6)	8.0	196.0(5)	177(4)	63(14)
MLH		111	25.63(9)	8.7	146.2(6)	145(5)	4(16)
ML	Tyr	110	15.9(1)	9.7	90.9(6)	85(6)	21(21)
MLH_{-1}	Lys	11−1	5.8(1)	10.1	33.3(6)	74(9)	−137(30)
MLH_{-2}	Lys	11−2	−4.8(1)	10.6	−27.2(6)	5(12)	−109(39)
MLH_{-3}	Lys	11−3	−15.7(1)	10.9	−89.8(6)	−36(11)	−180(36)

Uncertainty on the last significant figure in parentheses, as given by the computation program

 © 2003 Wiley-VCH Verlag GmbH & Co. KGaA, Weinheim

Table 1 also shows the whole set of thermodynamic parameters for complex-formation equilibria between the Cu^{II} ion and the pentadecapeptide. Ten mono complexes were detected in the explored pH range; all with different protonation degrees. The corresponding distribution diagram is reported in Figure 2. The ligand starts to bind the Cu^{II} ion at pH 3.5, forming the species MLH_6 and MLH_5. At pH > 4, MLH_4 is formed: it dominates the acidic pH range and is the main species at physiological pH. In the alkaline pH range (7.0−10.5) up to seven protons are subsequently lost by the MLH_4 complex due to deprotonation of some amido nitrogens and of basic side chains of Lys and Tyr residues.

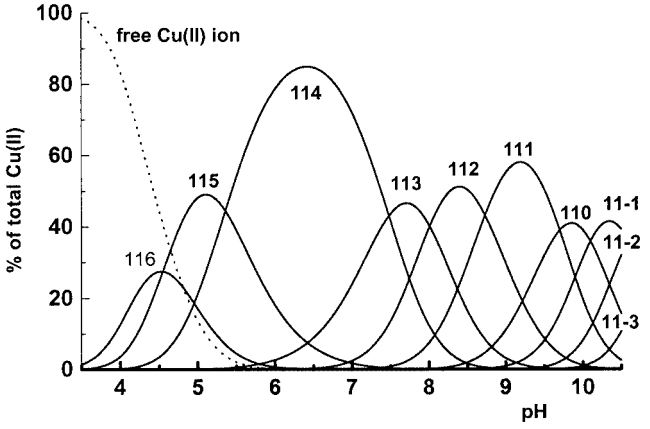

Figure 2. Distribution diagram of Cu^{II}/TLEGTKKGHKLHLDY complexes, at 298.2 K; I = 0.1 mol·dm^{-3} (KNO_3); [Cu^{II}] = 1.0 × 10^{-3} mol·dm^{-3}; [TLEGTKKGHKLHLDY] = 1.2 × 10^{-3} mol·dm^{-3}

Electronic spectra (Figure 3 and Table 2) confirm the presence of a complex species at a pH as low as 4: in fact at pH 4 the wavelength of maximum absorption is already lower than 800 nm. With increasing pH the d−d absorption band shifts towards lower wavelength values. This behaviour is typical of the coordination of successive nitrogen

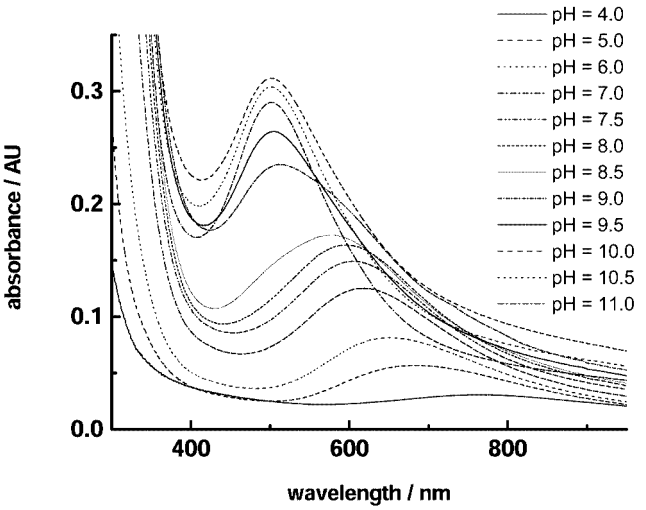

Figure 3. Absorption spectra of Cu^{II}/TLEGTKKGHKLHLDY solutions. [Cu^{II}] = 1.0 × 10^{-3} mol·dm^{-3}, [TLEGTKKGHKLHLDY] = 1.2 × 10^{-3} mol·dm^{-3}, T = 298.2 K, I = 0.1 mol·dm^{-3} (KNO_3).

atoms to the metal ion. A noticeable change in the absorption spectrum is seen between pH 8.0 and 9.5, with the onset of a new absorption band with a maximum close to 500 nm.

The CD spectra show some typical absorption bands (Figure 4 and Table 2). A double band is present in the d−d region, from pH 5 on, which is typical of Cu^{II}/His coordination.[16] The two bands at 250−256 and 350 nm can be ascribed to a charge-transfer transition from imidazole π_2 and π_1 to copper.[17] The positive band at 316−320 nm is most likely due a charge-transfer transition from a deprotonated amido nitrogen to copper:[17] this band is clearly detected from pH 6.0 on.

$A_{\parallel}$ and $g_{\parallel}$ parameters of the EPR spectra are reported in Table 2. At pH 6 they are typical of a 2N complex; at pH 8 those of a 3N complex. From pH 10, the EPR data be-

Table 2. Spectroscopic parameters of Cu^{II}/TLEGTKKGHKLHLDY binary complex formation, at 298.2 K and I = 0.1 mol·dm^{-3} (KNO_3).

pH	UV/Vis λ/nm (ε/ м$^{-1}$cm^{-1})	CD λ/nm (Δε/ м$^{-1}$cm^{-1})	EPR $A_{\parallel}$ ($g_{\parallel}$)
4.0	765 (31)	234 (−1.47); 266 (0.07)	121 (2.50)
5.0	685 (58)	234 (−1.42); 256 (0.33); 670 (−0.11)	121 (2.42); 145 (2.29)
6.0	652 (83)	255 (0.33); 283 (−0.06); 317 (0.06); 699 (−0.17)	121 (2.40); 162 (2.27)
7.0	618 (128)	255 (0.58); 284 (−0.20); 316 (0.32); 701 (−0.20)	167 (2.27); 167 (2.22)
7.5	604 (153)	257 (0.50); 283 (−0.37); 319 (0.60); 350 (sh); 481 (−0.06); 695 (−0.19)	168 (2.27); 168 (2.22)
8.0	596 (168)	259 (sh); 282 (−0.46); 322 (0.89); 350 (sh); 495 (−0.15); 699 (−0.17)	177 (2.22)
8.5	518 (sh); 584 (176)	256 (sh); 282 (−0.42); 321 (1.02); 350 (sh); 504 (−0.37); 610 (0.09); 708 (−0.13)	179 (2.22)
9.0	509 (240); 584 (sh)	252 (sh); 283 (−0.23); 319 (1.05); 350 (sh); 505 (−0.73); 611 (0.23)	177 (2.22)
9.5	504 (271)	251 (sh); 283 (−0.03); 316 (1.26); 350 (sh); 504 (−1.25); 614 (0.37)	186 (2.21)
10.0	502 (319)	245 (sh); 314 (1.23); 505 (−1.38); 615 (0.39)	209 (2.18)
10.5	502 (311)	242 (6.38); 314 (1.31); 505 (−1.54); 616 (0.42)	205 (2.18)
11.0	502 (297)	243 (6.94); 312 (1.34); 505 (−1.66); 618 (0.42)	205 (2.18)
11.5	502 (288)	245 (7.50); 311 (1.27); 506 (−1.71); 620 (0.38)	205 (2.18)

 © 2003 Wiley-VCH Verlag GmbH & Co. KGaA, Weinheim

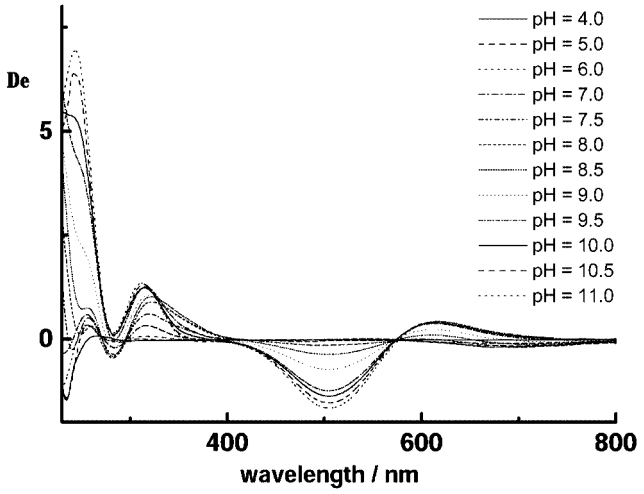

Figure 4. Circular dichroism spectra of Cu^{II}/TLEGTKKGHKLHLDY solutions. $[Cu^{II}] = 1.0 \times 10^{-3}$ mol·dm^{-3}, [TLEGTKKGHKLHLDY] = 1.2×10^{-3} mol·dm^{-3}, $T = 298.2$ K, $I = 0.1$ mol·dm^{-3} (KNO_3).

come typical of a 4N complex characterised by a strong ligand field. No evidence of binuclear species has been found over the whole pH range.

The ^{1}H NMR spectrum of TLEGTKKGHKLHLDY was recorded at both pH ≈ 6 and pH ≈ 10. At pH > 7, most amide protons were removed from the spectrum by chemical exchange. Thus, NMR studies at pH 10.4 were carried out in deuterium oxide (99.95%).

The complete assignment of the peptide at lower pH is reported in the Supplementary Material. None of the NMR spectroscopic data (temperature coefficients of the chemical shifts of amide protons, intramolecular NOEs and HN-H_α coupling constants) was consistent with the presence of secondary structure elements. Only the amide proton of ^{15}Tyr (see Supplementary Material), exhibits a different temperature coefficient compared to the other amide protons ($\Delta\delta/\Delta T = -4.3$ ppb/K), which is very close to values typical of a proton engaged in direct intramolecular or water-mediated hydrogen-bonding (head−tail interaction).

The complete assignment of the ^{13}C NMR spectrum of the peptide, recorded at alkaline pH, is given in the Supporting information (see footnote on the first page of this article).

Upon addition of copper, chemical shifts, line widths and spin−lattice relaxation rates were selectively affected. However, such effects could be observed only at relatively high Cu^{II}/peptide ratios (especially at pH > 7.0), much higher than is usual in NMR experiments on Cu^{II} complexes. As shown in Figure 5, the paramagnetic effects at pH 5.6 were mainly detected on ^{9}His and ^{12}His aromatic protons, on the His H_β and on the ^{14}Asp H_β.

To observe signal broadening at pH 10.4 a large amount of copper was added to the system (Figure 6). The signals that underwent the largest broadening were those of His and ^{1}Thr residues, but, to a lesser extent, the ^{14}Asp, ^{6,7,10}Lys, and ^{15}Tyr residues were also affected. Similarly, the most affected relaxation rates were those of the His resi-

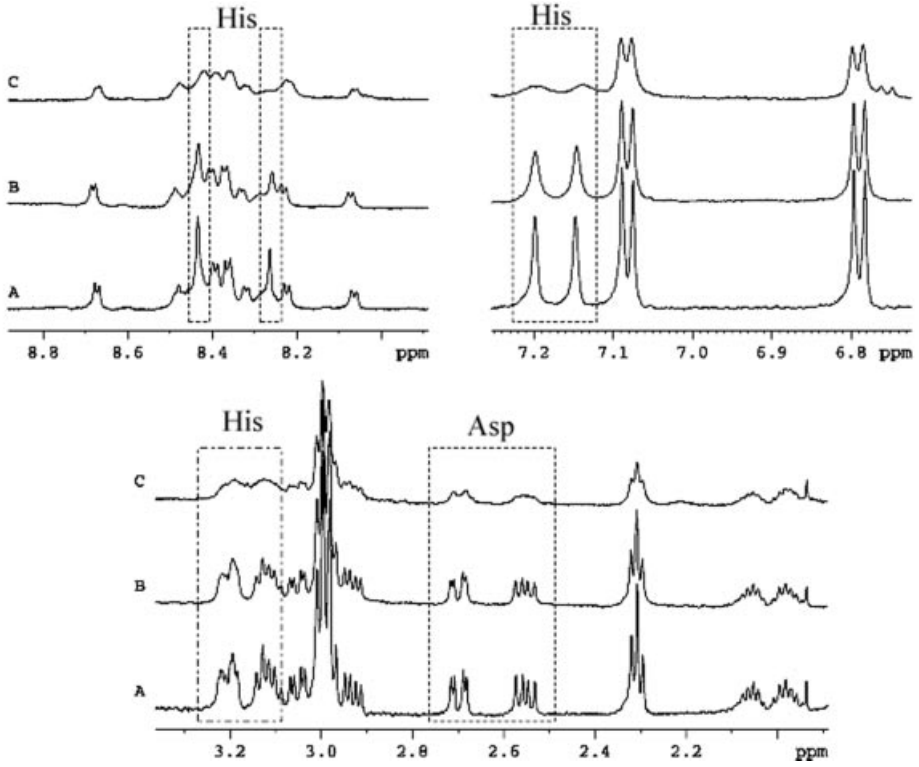

Figure 5. Selected regions of the ^{1}H NMR spectrum of TLEGTKKGHKLHLDY 2.5×10^{-3} mol·dm^{-3} in water at pH 5.6 (A traces) showing the effect of adding Cu^{II} 1.0×10^{-5} mol·dm^{-3} (B traces), $5.0\ 10^{-5}$ mol·dm^{-3} (C traces).

 © 2003 Wiley-VCH Verlag GmbH & Co. KGaA, Weinheim

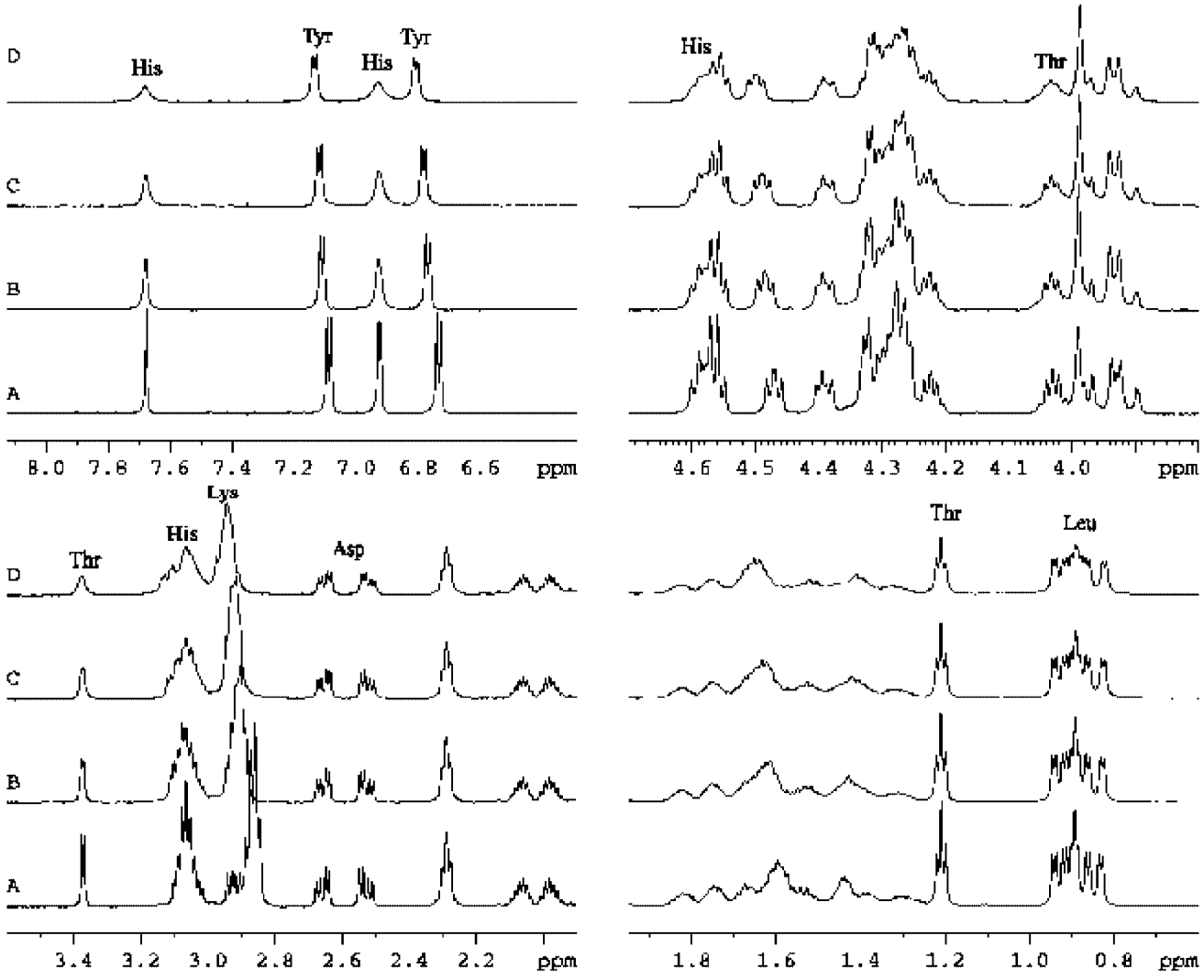

Figure 6. Selected regions of the ^{1}H NMR spectrum of TLEGTKKGHKLHLDY 4.0×10^{-3} mol·dm^{-3} in deuterium oxide at pH 10.4 (A traces) showing the effect of adding Cu^{II}: 1.6×10^{-4} mol·dm^{-3} (B traces), 3.3×10^{-4} mol·dm^{-3} (C traces), 8×10^{-4} mol·dm^{-3} (D traces).

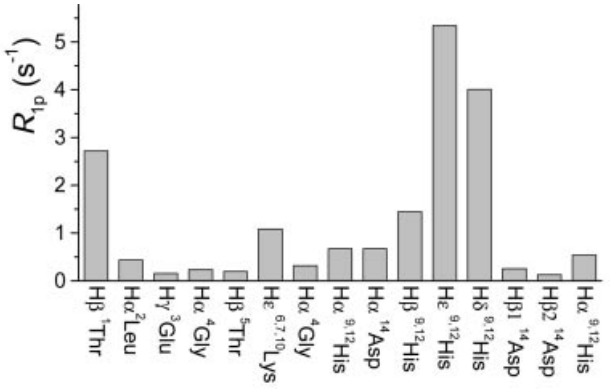

Figure 7. R_{1p} for selected protons of TLEGTKKGHKLHLDY (4.0×10^{-3} mol·dm^{-3}) in deuterium oxide at pH 10.5 after the addition of Cu^{II} (8.0×10^{-4} mol·dm^{-3}).

dues and the H_α, H_β of ^{1}Thr, with slight changes for protons of the ^{14}Asp, ^{6,7,10}Lys and ^{15}Tyr residues (Figure 7). The ^{1}H (Figure 6) and ^{13}C NMR spectra (see Supplementary Material) support the fact that copper perturbs two molecular regions: the *N*-terminal part of the peptide and the His regions. Overlapping ^{1}H NMR signals prevented differentiation of the ^{9}His and ^{12}His residues.

Discussion

TLEGTKKGHKLHLDY contains two different binding sites for copper ions: the terminal amino group and the two side-chain imidazole of its ^{9}His and ^{12}His residues. When the former is protected the two His residues behave as "anchoring" sites for copper at pH < 4.[11,12] Conversely, unprotected peptides can bind copper at approximately the same pH with their terminal amino and neighbouring carbonyl groups.[18] In both cases the metal can promote amido nitrogen ionisation, at pH < 7. The present ligand has both of the above capabilities: the two sites compete to bind copper, and binuclear species could also be formed. How-

 © 2003 Wiley-VCH Verlag GmbH & Co. KGaA, Weinheim

ever, in the present study, where nearly equimolar concentrations of copper and TLEGTKKGHKLHLDY have been used, neither potentiometric nor spectroscopic evidence was found for binuclear species formation. To favour such complexes an excess of copper could have been used, but this was beyond the aim of the present work. However, reports of polynuclear copper/peptide complex formation are common, even in the presence of an excess of ligand.[10]

First of all it is interesting to compare the overall binding ability of the present peptide with that of its protected analogue.[11] The competition diagram reported in Figure 8 shows that the copper complexes with the unprotected peptide are favoured over the whole pH range. This suggests that the terminal amino group plays an important role in determining the behaviour of TLEGTKKGHKLHLDY as a copper ligand. In addition, the wavelength of maximum absorption in the electronic spectra is always slightly lower for the unprotected peptide (Table 2) compared with the protected one,[11] indicating a higher mean coordination number for the former ligand.

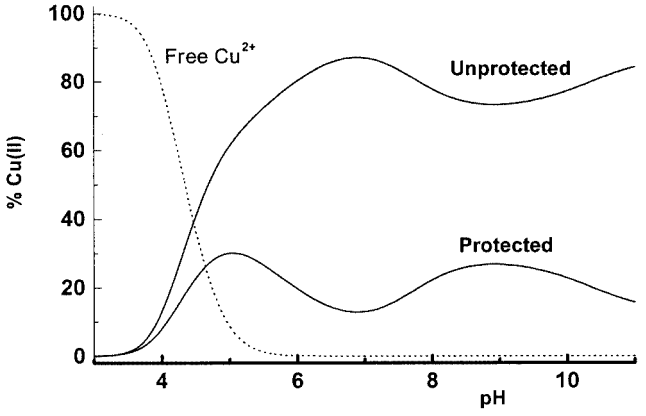

Figure 8. Competition diagram for Cu^{II} complex formation with TLEGTKKGHKLHLDY and Ac-TLEGTKKGHKLHLDY-NH_2. The concentrations were calculated by using the stability constants of Table 1 and ref.[11] at 298.2 K, I = 0.1 mol·dm^{-3} (KNO_3) and identical concentration of the three reagents: 1.0×10^{-3} mol·dm^{-3}.

The species detected at the most acidic pH is the MLH_6 complex (see Figure 2). EPR and UV/Vis data suggest that this is a 1N species where the metal ion is either bound to the terminal NH_2 or to one of the imidazole nitrogens; the three acidic groups (Asp and Glu side chains and terminal carboxylic) are deprotonated. Experimental data favour the second hypothesis. In fact, the computed step constant $\log\beta_{116} - \log\beta_{016} = 4.6$ (see Table 1), corresponding to the coordination of a protonated ligand to the Cu^{II} ion, is very close to that reported for the Cu^{II}/imidazole system (4.2) under the same experimental conditions.[15] Moreover, $\log\beta_{116}$, once the contribution due to terminal-NH_2 protonation has been subtracted (59.8−7.3 = 52.5, Table 1), is very close to the corresponding $\log\beta_{115}$ reported[11] for the protected ligand (52.0). Conversely, a 1N species where the Cu^{II} ion is chelated by the terminal-NH_2 and the neighbouring carbonyl groups could also be hypothesized. However, upon subtracting the constants for protonated sites from $\log\beta_{116}$ a value of 6.0 is obtained (see Table 1), which is significantly higher than the corresponding $\log\beta_{110}$ for the Cu^{II}/penta-alanylamide complex (4.9).[19] Finally, the wavelength of maximum absorption at pH 4 (765 nm, Table 2) is closer to that expected[20] for a $Cu-N_{Im}$ species (758 nm) than the mean value found[20] for a $Cu-N_{amino}$ complex (743 nm).

MLH_5 complex formation starts immediately after that of the MLH_6 species discussed above, at pHs still lower than 4. This complex reaches its highest concentration around pH 5, when it is the most abundant species in solution. The wavelength of maximum absorption in the UV/Vis spectra is blue-shifted with respect to pH 4, and the change in EPR parameters also point to a complex with additional nitrogen atoms bound to copper; the enthalpy of formation, minus the protonation contribution ($\Delta H^\circ_{115} - \Delta H^\circ_{015} = -34$ kJ·mol^{-1}, Table 1), is compatible with a 2N complex. Other structural hypotheses can be put forward for this species, the most likely of which is that TLEGTKKGHKLHLDY binds the metal ion with both imidazole nitrogens, as do its protected analogue[11] and its shorter fragments[12]. The corresponding log$K$ (4.6, Table 1) is close to that already reported for the above systems and is compatible with deprotonation of the second imidazole nitrogen, promoted by the copper ion. CD spectra at pH 5 clearly show a positive band at 256 nm attributable to a π_2 charge-transfer transition from imidazole to copper.[17] The d−d band in the electronic spectra has its maximum at 685 nm (at pH 5), exactly the value expected for a $Cu-(N_{Im})_2$ complex.[20] Subtracting log$K$ for the terminal amino group (7.3, Table 1) from $\log\beta_{115}$ gives 47.9, a value only slightly higher than that reported for the corresponding complex with the protected analogue (47.1).[11] This hypothesis is also in excellent agreement with the NMR spectroscopic data discussed below.

From pH 4.5 on a new species forms in solution: the MLH_4 complex, which reaches its maximum at pH 6.5, when it is almost the only species in solution. It is also the most abundant complex at neutral pH. Even though the EPR data remain those of a 2N complex a relevant blue-shift is registered in the electronic spectra when the pH changes from 5 to 7, suggesting the coordination of a further nitrogen atom, or at least the substitution of one nitrogen donor with another giving a higher ligand field. CD spectra show the onset of two new bands at 283 and 317 nm, which can be ascribed to a π_1 charge-transfer transition from imidazole to copper and to a charge-transfer transition from a deprotonated amido nitrogen to copper, respectively.[17] The log$K$ (5.4, Table 1) is compatible with the deprotonation of both an amido and an amino nitrogen[18] promoted by the copper ion. It is difficult, at this point, to suggest a unique complex structure with the stoichiometry 114 that accounts for all of the above experimental results. EPR data suggest the simultaneous presence of different species with comparable concentrations. One pos-

 © 2003 Wiley-VCH Verlag GmbH & Co. KGaA, Weinheim

sible structure is that already proposed for the corresponding complex formed by Ac-TLEGTKKGHKLHLDY-NH_2:[11] one imidazole and one neighbouring amido nitrogens bound to the equatorial plane of the copper complex. The second N_{Im} should be free, for steric reasons. This would explain the wavelength of maximum absorption in the electronic spectra (652 nm at pH 6, Table 2), which is close to the computed[20] value for this type of coordination (658 nm). This hypothesis also agrees with the EPR results. The complex stoichiometry requires that the terminal amino group is protonated. The $\Delta H°_{114}$ value, once the terminal amino group protonation is subtracted ($-247 + 36 = -211$ kJ·mol^{-1}, Table 1), becomes nearly identical to that found for the protected peptide (-212 kJ·mol^{-1}, ref.[11]). However, the MLH_4 complex formed by the unprotected ligand is much more stable than that reported for the protected peptide.[11] This can deduced by examining the competition diagram of Figure 8 and comparing $\log\beta_{114} - \log K_{amino}$ (42.5, Table 1) with the stability of the corresponding complex with the protected ligand (40.1, ref.[11]). The can be explained by the simultaneous formation, in the present system, of an additional complex species with the same stoichiometry but a different structure, i.e. involving the terminal amino group. The ligand should then form a macrochelate ring with at least one N_{Im} and the terminal amino group simultaneously bound to copper. Such a structure is similar to that previously reported for the $PrP_{106-126}$ peptide.[13]

The first complex to be formed in the alkaline pH range is MLH_3, which becomes the main complex at approximately pH 7.6. Four protons have already been released by the ligand at this stage, in addition to those of the acidic side chains: two from the imidazole side chains, one amido and the terminal amino. EPR data again suggest the presence in solution of two species. The corresponding log*K* (7.5, Table 1) is very close to that found for the protonation of the terminal amino group (7.3, Table 1), but it is also compatible with an amido nitrogen deprotonation, promoted by copper. No new important signal appears in CD spectra when the pH is raised from 6.0 to 7.5; the N_{amido}–copper binding is confirmed by the band at 319 nm. The wavelength of maximum absorption at pH 7.5 (604 nm) is not far from the computed[20] average value for 3N complexes with various combinations of nitrogen atoms bound to copper (581–615 nm). The $-\Delta H°_{113}$ value also suggests a 3N coordination. Again, the simultaneous formation of two complex species with the same MLH_3 stoichiometry best explains the experimental results. One of the complexes should have the metal ion located at the His site of the ligand, as with the protected analogue,[11] with the terminal amino group not protonated and free. The second should be a macrochelate where the terminal amino, one imidazole and one amido nitrogen simultaneously bind the copper ion.

At more basic pHs the complex loses other protons, giving rise to species from MLH_2 to MLH_{-3}. The first two steps (species MLH_2 and MLH) are most likely due to the subsequent deprotonation of two further amido groups which bind the metal ion. The corresponding thermodynamic parameters support this hypothesis. The spectroscopic parameters are typical of a 4N species. The four last protons probably derive from the basic side chains of the ^{15}Tyr, ^{6}Lys, ^{7}Lys and ^{10}Lys residues. The corresponding log*K*s are practically identical to those of the free ligand (Table 1), while the spectroscopic data do not change from pH 10 on. These results suggest that no binding interaction is present in solution between the latter residues and the metal ion, as already found for the protected peptide.[11] It is worth noting that on raising the pH from 9 to 10 big changes are observed in all the registered spectra. In particular, in the CD spectrum the charge-transfer $N_{Im} \rightarrow Cu^{II}$ bands are no longer observed while a new intense band appears at 242–245 nm, which can be ascribed to a charge-transfer transition from the terminal amino group to copper. This result strongly suggests that complex structure in the most alkaline pH range is that typical[20] of any unprotected peptide: "four nitrogens, one amino and three deprotonated peptide nitrogens, occupy the four tetragonal positions about Cu^{2+}". Only weak interactions with other donor atoms should be present in the apical position. In such a structure the two imidazole rings should be free. Once again, the presence of another 4N species, where one N_{Im} and three amido nitrogens are bound to copper, cannot be excluded (see also below). However, this species, the main complex at alkaline pH in the case of the protected peptide,[11] should be present here only in lower amounts.

The effect of paramagnetic Cu^{II} on spin–lattice relaxation rates is measured by the value of the observed relaxation rates R_{1m} in presence of the metal ion. They are defined as:[21]

$$R_{1m} = \frac{p_f}{R_{1f}^{-1}} + \frac{p_b}{R_{1M}^{-1} + \tau_m} \quad (1)$$

where R_{1f} is the rate calculated in the absence of the metal, τ_m is the exchange lifetime from the bound to the free state and p_f and p_b are the molar fraction of the free and bound ligand, the relaxation of which is described by R_{1M}. Since the ligand occurs in the bulk and in the metal coordination sphere, exchange has to be considered. If the metal-bound ligand is much less concentrated than its free form a $p_f \approx$ of **1** can be assumed. Equation (1) can then be reduced:

$$R_{1m} - R_{1f} = R_{1p} = \frac{p_b}{R_{1M}^{-1} + \tau_m} \quad (2)$$

R_{1M} is usually accounted for by the Solomon equation[22] and is proportional to the inverse sixth power of the metal–nucleus distance. The obtained R_{1p} values are consistent with τ_m not dominating Equation (2), but the relatively high Cu^{II}/peptide ratios that can be reached without severe alteration of NMR parameters demonstrate that τ_m contributes to R_{1p} and, therefore, that an intermediate exchange region occurs ($\tau_m \approx R^{-1}{}_{1M}$). Although the NMR spectroscopic data refer to a slight excess of ligand, and they

 © 2003 Wiley-VCH Verlag GmbH & Co. KGaA, Weinheim

cannot be directly transferred to the equimolar solutions discussed above, the distinct effect of Cu^{II} ions on the protons of both His residues (see Figure 5) strongly supports the involvement of two imidazoles in the metal coordination at acidic pHs. The obtained complex is similar to that formed by the protected peptide,[11] except for the involvement of the negatively charged carboxylate of adjacent ^{14}Asp in the coordination sphere. In addition, molecular mechanics calculations[23] performed on the Cu^{II}/TLEGTKKGHKLHLDY complex with the suggested $\{2N_{Im}, O^-\}$ donor set gave the low energy structures shown in Figure 9.

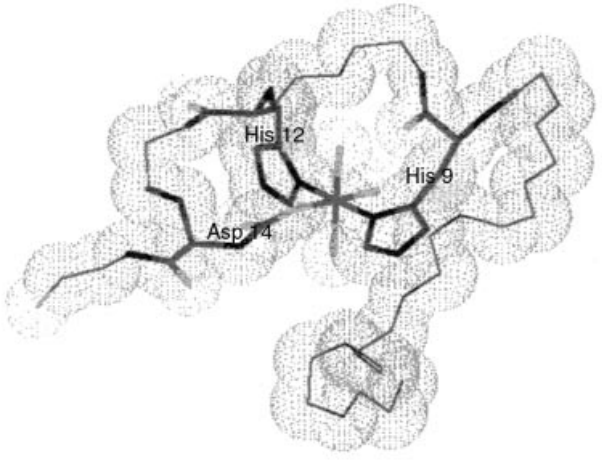

Figure 9. HYPERCHEM structure hypothesis for the Cu^{II}/TLEGTKKGHKLHLDY complex at pH 5.6.

At pH 10.4, ratios as high as 1:25 or 1:5 can be reached, which are consistent with slower off-rates arising from a more complicated exchange process. The observed spin−lattice relaxation rate enhancements (Figure 7) and line broadenings observed on the ^{1}H (Figure 6) and ^{13}C NMR spectra (see Supplementary Material) suggest the presence of two different complexes. In the first complex, copper is bound to ^{9}His and coordination takes place in the *N*-terminal direction, thus involving the ^{8}Gly and ^{7}Lys residues in the same way as with the protected peptide.[11] In the second complex the *N*-terminal group acts as an anchoring point and copper is bound to the amino nitrogen of ^{1}Thr and to the three amide nitrogens of the following residues (^{2}Leu, ^{3}Glu, ^{4}Gly). Moreover the effects measured on R_{1p} of ^{12}His, ^{14}Asp and ^{15}Tyr may result from the accumulation of the negative charges on the C-terminal side of the peptide (Tyr-O^-, Asp-COO^-) and their proximity to paramagnetic centre.

Experimental Section

TLEGTKKGHKLHLDY was synthesised manually on a 0.1 millimol scale by the solid-phase method, using the Fmoc/But amino acids,[24,25] according to the following procedure: (i) 5 and 15 min deprotection steps using 20% piperidine in DMF in the presence of 1% Triton; (ii) coupling reactions carried out with the protected amino acid diluted in DMF/NMP (NMP = *N*-methylpyrrolidone) (1:1, v/v) in the presence of 1% Triton, using DIC (1,3-diisopropylcarbodiimide) as the coupling reagent in the presence of HOBt (Fmoc-AA/DIC/HOBt, 1:1:1) for 1.5 h. The completeness of each coupling reaction was monitored by the chloranil and the ninhydrin tests.[26] The protected peptidyl resin was treated with a mixture of 95% trifluoroacetic acid (TFA), 2.5% water and 2.5% TIS (triisopropylsilane) for 1 h. The cleaved peptide was precipitated with diethyl ether and lyophilised. It was then purified by the solid-phase extraction (SPE) as described previously.[27] The product was homogeneous according to TLC and was judged to be more than 98% pure by HPLC (see Supplementary Material, Figure 3). The molecular weight was checked by FAB MS, using an AMD-604 spectrometer. The ion source was equipped with a Cs^+ gun. The energy of the Cs^+ ions was 12 keV.

Aliquots (2.5 cm^3) of sample solution, containing suitable amounts of the metal ion, the ligand, HNO_3 (when the initial pH value needed to be lowered) and KNO_3 (to adjust the ionic strength to 0.1 $mol{\cdot}dm^{-3}$) were titrated potentiometrically with standard NaOH in a thermostatted potentiometric vessel (pH range: 3.5−11.0; T = 298.2 K). The metal ion concentration was close to $1{\cdot}10^{-3}$ $mol{\cdot}dm^{-3}$ and the metal-to-ligand ratio was 1:1.2. Two pairs of potentiometric titrations, for both protonation and complex-formation, were performed. Further experimental details, equipment and software used are reported elsewhere.[14] Thermodynamic data are given with an estimated accuracy reported as the uncertainty on the last significant figure.

CD, EPR and UV/Vis spectra were recorded on a JASCO J 715, on a Bruker ESP 300E (at, 120 K and 9.4 GHz) and on a Beckman DU 650 spectrometer, respectively. Sample solutions had the same composition as above; the pH was varied by addition of suitable amounts of standard NaOH or HCl, under potentiometric control. Spectra were recorded every 0.5 pH units.

Calorimetric titrations were performed with an Isoperibolic Calorimeter (Tronac) at 298.2 K, by addition of standard HNO_3 to a sample solution (2.5 cm^3) of the same composition as above. For each system two pairs of calorimetric titrations containing not less than 250 experimental points were used to calculate the thermodynamic quantities.

NMR spectra were performed at 14.1 T with a Bruker Avance 600 MHz Spectrometer at controlled temperatures (±0.1 K). Two different peptide solutions were prepared: the first with deionized water containing D_2O (10%), the second with deuterium oxide (99.95% from Merck), and both were carefully deoxygenated through a freezing/vacuum pumping/sealing/thawing procedure. The pH was adjusted to the desired values with either DCl or NaOD, and the required concentration of copper ions was achieved by using a stock solution of copper nitrate (Sigma Chemical Co.) in deuterium oxide. TSP-d_4, 3-(trimethylsilyl)-[2,2,3,3-d_4] propansulfonate, sodium salt, was used as an internal reference standard. The assignment of the spectra was accomplished with TOCSY, COSY, and NOESY 2D experiments. TOCSY spectra were recorded with a total spin-locking time of 75 ms using a MLEV-17 mixing sequence; NOESY spectra were obtained with standard pulse sequences at mixing times ranging between 50 and 400 ms. During all 2D experiments, water suppression was achieved by the Watergate method.[28] The spectral width of homonuclear 2D experiments was typically 6000 Hz in both F_1 and F_2 dimensions. Spin−lattice relaxation rates were measured with inversion recovery pulse sequences. The same sequence was also used to measure the single- or double-selective relaxation rates by means of suitably

 © 2003 Wiley-VCH Verlag GmbH & Co. KGaA, Weinheim

shaped π-pulses instead of the usual non-selective π-pulse. All rates were calculated by regression analysis of the initial recovery curves of longitudinal magnetization components, leading to errors not larger than ±3%. 2D $^{1}H-^{13}C$ shift correlation methods were used to detect and assign ^{13}C NMR spectra at relatively low concentrations. HMBC (multiple-bond heteronuclear multiple-quantum coherence) spectra were obtained with standard pulse sequences, over a spectral width of 6000 Hz in the F_2 dimension and 31700 Hz in the F_1 dimension a total of 1024 points were used in F_2 and 256 in F_1, which was zero filled once before processing; 8 transients were accumulated with a relaxation delay of 2.0 s for each of the 256 increments. A 5-mm broad-band probe was used to perform the ^{13}C NMR spectra, which were acquired with a FID composed of 32768 data points over a spectral width of 28700 Hz (acquisition time 0.570 s), a 90° pulse of 8.5 μs, relaxation delay of 5.0 s; the WALTZ16 broad-band decoupling method was used.[29,30]

Molecular structures were generated by the HYPERCHEM software package[23] implemented on a Pentium 120 MHz PC by using the ZINDO-1 semi-empirical method for charge calculations and the MM+ force field for molecular mechanics and dynamics calculations.

Acknowledgments

Financial support by the University of Ferrara (ex-60%), Polish State Committee for Scientific Research (KBN, 4 TO9A 054 23) and University of Gdansk (BW-8000-5-0290−2) is gratefully acknowledged.

[1] P. Bornstein, *Matrix Biol.* **2000**, *19*, 555−556.
[2] R. A. Brekken, E. H. Sage, *Matrix Biol.* **2000**, *19*, 569−580.
[3] A. D. Bradshaw, E. H. Sage, *J. Clin. Invest.* **2001**, *107*, 1049−1054.
[4] Q. Yan, E. H. Sage, *J. Histochem. Cytochem.* **1999**, *47*, 1495−1505.
[5] T. F. Lane, E. H. Sage, *FASEB J.* **1994**, *8*, 163−173.
[6] E. H. Sage, *Nature Med.* **1997**, *3*, 144−146.
[7] T. F. Lane, M. L. Iruela-Arispe, R. S. Johnson, E. H. Sage, *J. Cell Biol.* **1994**, *125*, 929−943.
[8] E. Hohenester, P. Maurer, R. Timpl, *EMBO J.* **1997**, *16*, 3778−3786.
[9] L. Pickart, J. Freedman, W. J. Loker, J. Peisach, C. M. Perkins, R. E. Stenkamp, B. Weinstein, *Nature* **1980**, *288*, 715−717.
[10] C. Conato, R. Gavioli, R. Guerrini, H. Kozlowski, P. Mlynarz, C. Pasti, F. Pulidori, M. Remelli, *Biochim. Biophys. Acta* **2001**, *1526*, 199−210; and references therein.
[11] C. Conato, W. Kamysz, H. Kozlowski, M. Luczkowski, Z. Mackiewicz, P. Mlynarz, M. Remelli, D. Valensin, G. Valensin, *J. Chem. Soc., Dalton Trans.* **2002**, 3939−3944.
[12] M. Remelli, M. Łuczkowski, A. M. Bonna, Z. Mackiewicz, C. Conato, H. Kozłowski, *New J. Chem.* **2003**, *27*, 245−250.
[13] M. F. Jobling, X. Huang, L. R. Stewart, K. J. Barnham, C. Curtain, I. Volitakis, M. Perugini, A. R. White, R. A. Cherny, C. L. Masters, C. J. Barrow, S. J. Collins, A. I. Bush, R. Cappai, *Biochemistry* **2001**, *40*, 8073−8084.
[14] M. Remelli, C. Conato, A. Agarossi, F. Pulidori, P. Młynarz, H. Kozłowski, *Polyhedron* **2000**, *19*, 2409−2419.
[15] L. D. Pettit, H. K. J. Powell, *The IUPAC Stability Constants Database*, Academic Software and IUPAC, Royal Society of Chemistry, London, **1992−1997**.
[16] P. Młynarz, W. Bal, T. Kowalik-Jankowska, M. Stasiak, M. T. Leplawy, H. Kozłowski, *J. Chem. Soc., Dalton Trans.* **1999**, 109−110.
[17] P. G. Daniele, E. Prenesti, G. Ostacoli, *J. Chem. Soc., Dalton Trans.* **1996**, 3269−3275.
[18] L. D. Pettit, J. E. Gregor, H. Kozlowski, *Persp. Bioinorg. Chem.* **1991**, *1*, 1−41.
[19] W. Bal, M. Dyba, F. Kasprzykowski, H. Kozłowski, R. Łatajka, L. Lankiewicz, Z. Mackiewicz, L. D. Pettit, *Inorg. Chim. Acta* **1998**, *283*, 1−11.
[20] H. Sigel, R. B. Martin, *Chem. Rev.* **1982**, *82*, 385−426.
[21] T. J. Swift, R. E. Connick, *J. Chem. Phys.* **1962**, *37*, 307−320.
[22] I. Solomon, *Phys. Rev.* **1955**, *99*, 559−565.
[23] *HYPERCHEM*, Hypercube release 5.1 Pro for Windows, Hypercube Inc. Waterloo, Canada, **1997**.
[24] R. B. Merrifield, *J. Am. Chem. Soc.* **1963**, *85*, 2149−2154.
[25] G. Barany, R. B. Merrifield, in *The Peptides, Analysis, Synthesis, Biology* (Eds.: E. Gross, J. Meinehofer), Academic Press, New York, **1980**, p.1.
[26] J. E. Kaiser, R. C. Colescott, C. A. Bossinger, D. J. Cook, *Anal. Biochem.* **1970**, *34*, 595−598.
[27] W. Kamysz, B. Kochanska, A. Kędzia, J. Ochocińska, Z. Maćkiewicz, G. Kupryszewski, *Polish J. Chem.* **2002**, *76*, 801−806.
[28] M. Piotto, V. Saudek, J. Sklenàr, *J. Biomol. NMR* **1992**, *2*, 661−665.
[29] A. J. Shaka, J. Keeler, R. Freeman, *J. Magn. Reson.* **1983**, *53*, 274−293.
[30] G. A. Morris, R. Freeman, *J. Magn. Reson.* **1978**, *29*, 433−462.
Received October 7, 2002

 © 2003 Wiley-VCH Verlag GmbH & Co. KGaA, Weinheim

Heterotrinuclear Complexes of the Platinum Group Metals with 2,2′-Biimidazole as a Bridging Ligand

Andrey Mayboroda,[a] Peter Comba,*[a] Hans Pritzkow,[a] Gerd Rheinwald,[b] Heinrich Lang,[b] and Gerard van Koten[c]

Keywords: Osmium / Platinum / Palladium / Heterometallic complexes / Cyclic voltammetry / Hydrogenation

The novel trinuclear complexes $[(Pt\{C_6H_3(CH_2NMe_2\text{-}2,6)_2\})_2(\mu\text{-}Hbiim)_2Os(O{=}PPh_3)_2](NO_3)(SO_3CF_3)_2$ [$C_6H_3(CH_2NMe_2\text{-}2,6)_2$ = pincer ligand, H_2biim = 2,2′-biimidazole] and $[(PdL)_2(\mu\text{-}biim)_2Os(O{=}PPh_3)_2](NO_3)_3$ (L = cod, 1,5-cyclooctadiene or L = en, ethylene-1,2-diamine) were prepared by the reaction of the mononuclear complex $[Os(H_2biim)_2(O{=}PPh_3)_2](NO_3)_3$ with $[Pt\{C_6H_3(CH_2NMe_2\text{-}2,6)_2\}](SO_3CF_3)$, or with $PdL(NO_3)_2$ (L = cod or L = en), in the presence of a base. The exchange reaction between $[Os(Hbiim)_2(O{=}PPh_3)_2](NO_3)_3$ and $[Me_2NH_2][RhCl_4(NHMe_2)]$ led to the formation of $[Os(Hbiim)_2(O{=}PPh_3)_2][RhCl_4(NHMe_2)]$. The solid-state structures of $[Os(Hbiim)_2(O{=}PPh_3)_2][RhCl_4(NHMe_2)]$ and $[(Pt\{C_6H_3(CH_2NMe_2\text{-}2,6)_2\})_2(\mu\text{-}Hbiim)_2Os(O{=}PPh_3)_2](NO_3)(SO_3CF_3)_2{\cdot}4H_2O$ were determined by single-crystal X-ray diffraction. The crystals of $[Os(Hbiim)_2(O{=}PPh_3)_2][RhCl_4(NHMe_2)]$ are triclinic with a space group $P\bar{1}$, with a = 10.4293(5), b = 10.6365(6), c = 13.0287(7) Å, β = 91.6840(10), γ = 109.8540(10)°, V = 1316.14(12) Å^3, Z = 1. The crystals of the complex $[(Pt\{C_6H_3(CH_2NMe_2\text{-}2,6)_2\})_2(\mu\text{-}Hbiim)_2Os(O{=}PPh_3)_2](NO_3)(SO_3CF_3)_2{\cdot}4H_2O$ are triclinic with a space group $P\bar{1}$, with a = 12.604(3), b = 13.471(3), c = 14.347(3) Å, β = 77.530(5), γ = 66.613(4)°, V = 2005.6(7) Å^3, Z = 1. Deprotonation of 2,2′-biimidazole in the mononuclear osmium complex, followed by coordination to an additional transition metal fragment leads to a modification of the ligand field and a variation of the redox properties of the Os^{III} center. $[\{Pd(cod)\}_2(\mu\text{-}biim)_2Os(O{=}PPh_3)_2](NO_3)_3$ shows significant catalytic activity towards hydrogenation of terminal and cyclic alkenes.

(© Wiley-VCH Verlag GmbH & Co. KGaA, 69451 Weinheim, Germany, 2003)

Introduction

Oligonuclear complexes in which the transition-metal centers are bridged by π-conjugated ligands have attracted much attention as model compounds for the study of cooperative effects in, for example, homogeneous catalysis.[1] Mechanisms have been postulated which involve more than one catalytically active metal center within the oligometallic array.[2] Generally, however, only one of the metal centers plays a dominant role in the catalytic cycle, while the other(s) influence the molecular architecture and support the catalytically active center as a donor or acceptor of electron density. An enhancement of the reactivity results from changes in the ligand field or from intramolecular electronic communication between the transition-metal centers.[1b]

Much attention has been focused on the metal-binding ability of the ligand 2,2′-biimidazole (H_2biim) and its derivatives.[3−9] Anionic moieties, e.g. $Hbiim^-$ and $biim^{2-}$, have successfully been used as bridging ligands for the synthesis of homo- and heterometallic oligonuclear complexes. Dinuclear 2,2′-biimidazolate complexes of Rh^I,[3] Ir^I,[3] Cu^{II},[4] Pd^{II},[5,6] Ru^{II},[7] Ru^{II}-Os^{II},[8] and $Ru^{II}-Rh^I$ [9] have been prepared and characterized. An example of a trinuclear heterometallic species of the structural type **A** is $[\{Au(PPh_3)\}_2(\mu\text{-}bbzim)Rh(cod)](ClO_4)$ (bbzim = 2,2′-bibenzimidazole).[9] However, so far there are no examples of trinuclear complexes of types **B** and **C** (Figure 1).

Here, we report on the synthesis and characterization of the $Pt^{II}-Os^{III}-Pt^{II}$ and $Pd^{II}-Os^{III}-Pd^{II}$ complexes, with 2,2′-biimidazolate ($Hbiim^-$, $biim^{2-}$) as the bridging ligands (structural types **B** and **C**). The solid-state structures of $[Os(Hbiim)_2(O{=}PPh_3)_2][RhCl_4\{NH(CH_3)_2\}_2]$ (**2b**) and $[(Pt\{C_6H_3(CH_2NMe_2\text{-}2,6)_2\})_2(\mu\text{-}Hbiim)_2Os(O{=}PPh_3)_2](NO_3)(SO_3CF_3)_2{\cdot}4H_2O$ (**7**) are reported (for the numbering of the complexes, see Scheme 1, cod = 1,5-cyclooctadiene, en = ethylene-1,2-diamine). The electrochemical behavior of compounds **7**−**9** was studied, using cyclic voltammetry, and the catalytic activity of **7**−**9**, in the homogeneous hydrogenation of 1-hexene and cyclohexene, is also reported.

[a] Anorganisch-Chemisches Institut, Universität Heidelberg, Im Neuenheimer Feld 270, 69120 Heidelberg, Germany
E-mail: comba@akcomba.oci.uni-heidelberg.de
[b] Technische Universität Chemnitz, Fakultät für Naturwissenschaften, Institut für Chemie, Lehrstuhl Anorganische Chemie, Straße der Nationen 62, 09111 Chemnitz, Germany
[c] Debye Institute, Department of Metal-Mediated Synthesis, Utrecht University, Padualaan 8, 3584 CH Utrecht, The Netherlands

Supporting information for this article is available on the WWW under http://www.eurjic.org or from the author.

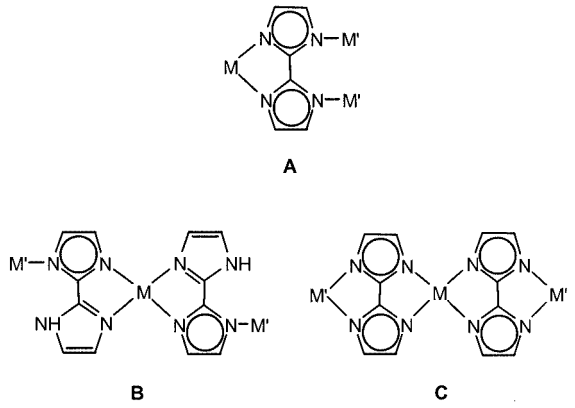

Figure 1. Type **A**−**C** trinuclear complexes with different binding modes between 2,2′-biimidazole and the transition metal centers M and M′

Results and Discussion

Synthesis and Spectroscopy

The mononuclear osmium(III) complex $[Os(H_2biim)_2(O{=}PPh_3)_2](NO_3)_3$ (**1**),[10] was used as a starting material in the synthesis of the trimetallic $OsPt_2$ and $OsPd_2$ complexes **7**−**9**. Complex **1** is a polybasic acid and was successfully deprotonated by KOH, affording $[Os(Hbiim)_2(O{=}PPh_3)_2](NO_3)$ (**2**),[10] and $[Os(biim)_2(O{=}PPh_3)_2]^-$ (**3**, not isolated as a solid). Complexes **2** and **3** are reactive building blocks ("metal complex as the ligand"), which smoothly reacted with various transition-metal complexes, producing the trimetallic compounds **7**−**9** in high yields (Scheme 1). After appropriate workup, complexes **7**−**9** were isolated as red (**7**) or dark green (**8**, **9**) air-stable solids, which gradually decompose at temperatures higher than 150 °C. They are insoluble in tetrahydrofuran, acetone, diethyl ether and aromatic hydrocarbons, only moderately soluble in methanol and dichloromethane, but very soluble in a mixture of these solvents, e.g., in 80% of dichloromethane and 20% of methanol.

We were also interested in the structural properties of mononuclear osmium(III) complexes with a partially deprotonated 2,2′-biimidazolate ligand. Attempts to crystallize $[Os(Hbiim)_2(O{=}PPh_3)_2](NO_3)$ (**2a**) from dichloromethane/methanol were unsuccessful. However, in the presence of the rhodium(III) salt $[Me_2NH_2][RhCl_4\{NH(CH_3)_2\}_2]$ (**10**) single crystals of $[Os(Hbiim)_2(O{=}PPh_3)_2][RhCl_4(NH(CH_3)_2)_2]$ (**2b**), suitable for X-ray structure determination, could be obtained (see below).

The UV/Vis spectra of **7**−**9** have an absorbance maximum at approx. 350 nm, which can be assigned to a metal-to-ligand charge-transfer transition {for comparison, the parent complex $[Os(H_2biim)_2(O{=}PPh_3)_2](NO_3)_3$ (**1**) has two transitions at 360 and 388 nm[10]}. In the visible region, a broad absorbance of low intensity at approx. 550 nm is also observed for **8** and **9**, and these are assigned to d-d transitions. It is worth noting that the mononuclear Os^{III} complex **1**, as well as the Pt^{II} and Pd^{II} complexes **4**−**6**, have no transitions in this region.

The infrared spectrum of 2,2′-biimidazole shows a strong absorption band at around 3100 cm^{-1}, which is assigned to the N−H stretching vibrations. This band is also found in the infrared spectrum of **7** (at 3075 cm^{-1}), however, it is not observed in the infrared spectra of **8** and **9**. This implies that complete deprotonation of the 2,2′-biimidazole bridging ligands occurs in the trinuclear compounds **8** and **9**.

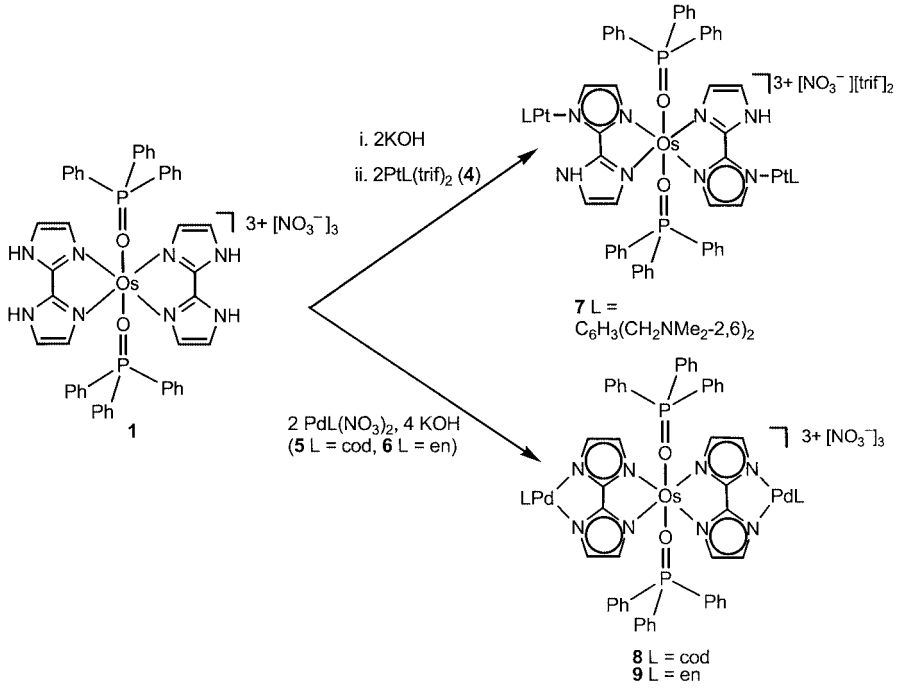

Scheme 1

The effective magnetic moments of the trinuclear complexes [μ_{eff} = 1.87 (**7**), 1.45 (**8**), 1.58 (**9**) BM; powders, 298 K] are as expected for Os^{III} complexes (one unpaired electron, 1.73 BM). Complex **7** could not be characterized by NMR spectroscopy, owing to its magnetic properties. The paramagnetism of complexes **8** and **9** leads to considerable broadening of the NMR signals, but these spectra are sufficiently resolved to be interpreted. The ^1H NMR spectra of [{Pd(cod)}$_2$(μ-biim)$_2$Os(O=PPh$_3$)$_2$](NO$_3$)$_3$ (**8**) and [{Pd(en)}$_2$(μ-biim)$_2$Os(O=PPh$_3$)$_2$](NO$_3$)$_3$ (**9**) show a multiplet between δ = 7.5 and 7.8 ppm, due to the superimposition of the signals resulting from the Ph$_3$PO and biim fragments. The resonance signals at δ = 2.5 and 5.5 ppm, also observed in the ^1H NMR spectrum of **8**, can be assigned to the CH and CH$_2$ groups, respectively, of the coordinated cyclooctadiene. They are slightly shifted to a lower field compared to those in the spectrum of the metal-free ligand. In the spectrum of complex **9**, the resonance signal for the CH$_2$ groups of the en ligands is observed at δ = 2.96 ppm, while in the spectrum of metal-free en, the signal of these protons appears at δ = 2.85 ppm. The carbon resonance signals of the terminal cod (δ = 28.4, 76.4 ppm) and en units (δ = 47.3 ppm), observed in the $^{13}C\{^1H\}$ NMR spectra of **8** and **9**, respectively, are also shifted to a lower field, when compared with the spectra of the corresponding metal-free ligands. As a result of the deprotonation of H$_2$biim and the addition of the PdL complex fragments, the ^{13}C resonances of 2,2′-biimidazole are shifted to a lower field in comparison with **1**. The signal for the C atoms in the 2, 2′-position is observed at δ = 152.1 ppm (**8**) and at δ = 152.6 ppm (**9**), while this resonance is found at δ = 141.2 ppm for **1**. The variation of the terminal ligand coordinated to the palladium center does not affect the chemical shifts of the C atoms in the 2,2′-biimidazolate bridging ligands.

In the $^{31}P\{^1H\}$ NMR spectra of **8** and **9**, the signal for the phosphorus atom of the triphenylphosphane oxide group is seen at δ = 32.6 ppm. Relative to [Os(H$_2$biim)$_2$(O=PPh$_3$)$_2$](NO$_3$)$_3$ (**1**) this ^{31}P signal is shifted to a higher field by approx. 3.8 ppm and this indicates an increase of electron density at the Os^{III} center due to better electron donation of the deprotonated 2,2′-biimidazole ligand.

Electrochemistry

Cyclic voltammetric studies of **1** and **7**−**9** were carried out in methanol at 25 °C. The mononuclear complex [Os(H$_2$biim)$_2$(O=PPh$_3$)$_2$](NO$_3$)$_3$ (**1**) has a reversible one-electron step at $E_{1/2}$ = −1.01 V (vs. $FeCp_2^+/FeCp_2$, Figure 2, a). This is attributed to the Os^{II}/Os^{III} redox couple. Complex **1** also has an irreversible Os^{III}/Os^{IV} oxidation at 0.92 V. In contrast to this, the trinuclear complexes **7**−**9** have a single quasi-reversible voltammetric response (Figure 2, b shows the cyclic voltammogram of **8** as an example). Since [Pt{C$_6$H$_3$(CH$_2$NMe$_2$-2,6)$_2$}](SO$_3$CF$_3$) (**4**), [Pd(cod)(H$_2$biim)](NO$_3$)$_2$ (**5**) and [Pd(en)(H$_2$biim)](NO$_3$)$_2$ (**6**) do not have a cyclic voltammetric response in the potential range −1.2 to +1.2 V, the processes observed in the cyclic voltammograms of **7**−**9** are attributed to the Os^{III}/Os^{IV} redox couple. Electrochemical data are given in Table 1.

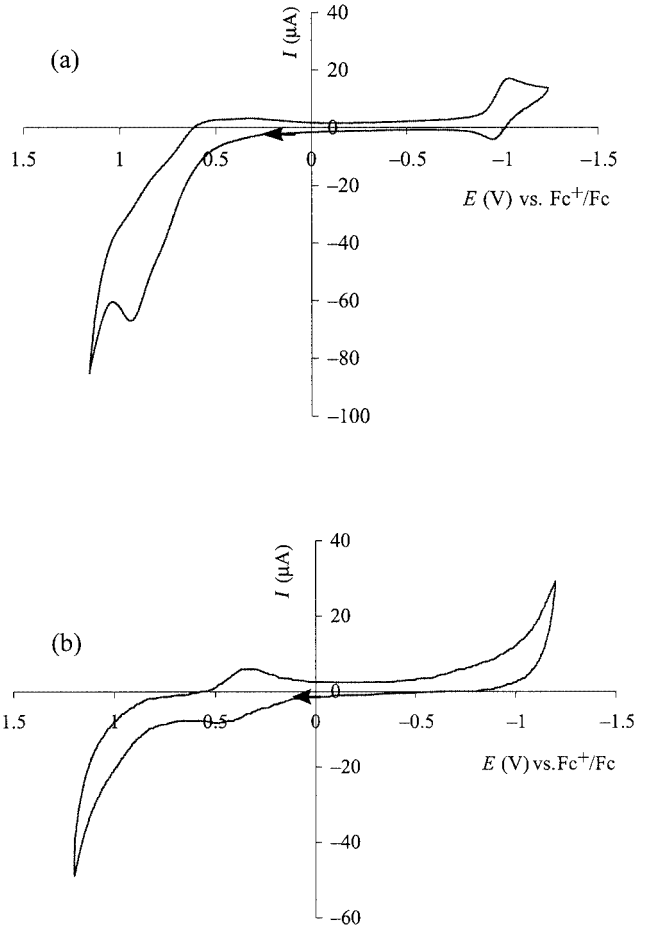

Figure 2. Cyclic voltammograms of (a) [Os(H$_2$biim)$_2$(O=PPh$_3$)$_2$](NO$_3$)$_3$ (**1**) and (b) [{Pd(cod)}$_2$Os(μ-biim)$_2$(O=PPh$_3$)$_2$](NO$_3$)$_3$ (**8**)

Table 1. Electrochemical data of **1** and **7**−**9**

Complex[a]	$E_{1/2}(Os^{III}/Os^{IV})$ [V]
[Os(H$_2$biim)$_2$(O=PPh$_3$)$_2$](NO$_3$)$_3$ (**1**)	0.92
[{Pt[C$_6$H$_3$(CH$_2$NMe$_2$-2,6)$_2$]}$_2$Os(μ-Hbiim)$_2$-(O=PPh$_3$)$_2$](NO$_3$)(SO$_3$SF$_3$)$_2$·4H$_2$O (**7**)	0.53
[{Pd(cod)}$_2$Os(μ-biim)$_2$(O=PPh$_3$)$_2$](NO$_3$)$_3$ (**8**)	0.41
[{Pd(en)}$_2$Os(μ-biim)$_2$(O=PPh$_3$)$_2$](NO$_3$)$_3$ (**9**)	0.23

[a] CH$_3$OH, 25 °C, vs. $E(Fc/Fc^+)$ = 0.00 V.

The addition of transition-metal fragments such as $[Pd(cod)]^{2+}$ or $[Pd(en)]^{2+}$ to **3** leads to a significant cathodic shift of the Os^{III}/Os^{IV} couple (Table 1). For **9**, this occurs at a more negative potential ($E_{1/2}$ = +0.23 V) than that for **8** ($E_{1/2}$ = +0.41 V). However, NMR spectroscopy shows that substitution of cod by en in PdL does not affect the chemical shifts of the C atoms in the biimidazolate bridging

 © 2003 Wiley-VCH Verlag GmbH & Co. KGaA, Weinheim

group, and the chemical shifts of the P atoms in $Ph_3P{=}O$ in **8** and **9** are also almost identical. Therefore, it is not appropriate to attribute the difference in the redox potentials of **8** and **9** to an effect of the terminal ligand (cod, en) on the osmium center. Possible reasons for the shift in the redox potential are a variation of the adsorption properties of the complex cation at the electrode or of the electron transfer between the electrode and the osmium complex as a function of the terminal ligands.

Solid-State Structures

Slow concentration of dichloromethane/methanol solutions of $[Os(Hbiim)_2(O{=}PPh_3)_2][RhCl_4\{NH(CH_3)_2\}_2]$ (**2b**) and $[(Pt\{C_6H_3(CH_2NMe_2\text{-}2,6)_2\})_2(\mu\text{-}Hbiim)_2Os(O{=}PPh_3)_2](NO_3)(SO_3CF_3)_2{\cdot}4H_2O$ (**7**) led to the formation of red crystals of **2b** and pale pink crystals of **7**, respectively. Both **2b** and **7** crystallize in triclinic space groups $P\bar{1}$. The coordination geometry around the osmium center in the two complexes is approximately octahedral. The polyhedron is defined by the four nitrogen atoms of two $Hbiim^-$ ligands and the two oxygen atoms of the $Ph_3P{=}O$ units, which are in the axial positions.

Figure 3 shows the ZORTEP[11] plot of complex **2b**; structural parameters are given in Table 2. The $[Os(Hbiim)_2(O{=}PPh_3)_2]^+$ cation and the $[RhCl_4\{NH(CH_3)_2\}_2]^-$ anion have a center of inversion, located at the osmium and rhodium centers, respectively; the symmetry-generated atoms are identified with the suffix a. The Os(1)−N(1) and Os(1)−N(3) distances in **2b** (bonds to the mono-deprotonated 2,2′-biimidazolate ligands), are nearly identical to those in $[Os(H_2biim)_2(O{=}Ph_3)_2](NO_3)_3$ (**1**) [**2**: Os(1)−N(1) = 2.076(2), Os(1)−N(3) = 2.080(2); **1**: Os(1)−N(1) = 2.0651(19) Å[10]]. The deprotonated imidazolate sites in **2b** are *trans*-oriented. The Os(1)−O(1) bond [2.056(2) Å] is significantly longer than that observed in **1** and in other osmium complexes with a triphenylphosphane oxide, e.g., $[Os(OEP)(O{=}PPh_3)_2]$ (Os−O = 2.036 Å, OEP = octaethylporphyrin).[12] The bite angle N(1)−Os(1)−N(3) [77.78(6)°] is almost identical to that found in **1** [77.14(8)°] and is typical for bite angles in biimidazole and biimidazolato transition-metal complexes, e.g., $[H(CO)(PPh_3)_2Ru(\mu\text{-}biim)Rh(cod)]$ [N−Ru−N = 79.2(2) Å][9] and $[OsCl(\eta^2\text{-}H_2)(H_2biim)_2(P\mathit{i}C_3H_7)_2]Cl$ [N−Os−N = 75.6(3)°] .[13] The Rh^{III} ion in the counterion $[RhCl_4(NHMe_2)_2]^-$ in **2b** has a slightly distorted octahedral coordination geometry, where the chloride ions are situated in the equatorial positions and the amine groups are occupying the axial positions. The Rh(1)−Cl(1) [2.3597(5) Å] and Rh(1)−N(5) [2.106(2) Å] distances are in agreement with the bond lengths observed in similar octahedral Rh^{III} complexes, e.g., $[ImH][RhCl_4(Im)_2]$ (Im = imidazole), with Rh−Cl = 2.326(2) Å and Rh−N = 2.039(4) Å.[14] In the $[RhCl_4(NHMe_2)_2]^-$ anion, the four chloride ligands form an almost ideal quadrangle around the Rh atom [Cl(1)−Rh(1)−Cl(2) = 92.979(2)°].

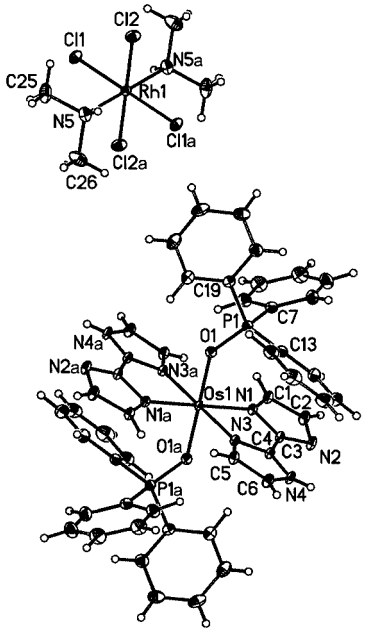

Figure 3. ZORTEP[11] diagram of $[Os(Hbiim)_2(O{=}PPh_3)_2][RhCl_4\{HN(CH_3)_2\}_2]$ (**2b**) (50% probability level); symmetry transformations used to generate equivalent atoms: $a = -x+1, -y+1, -z+1$; $b = -x+2, -y, -z+2$

Table 2. Selected geometric parameters of $[Os(Hbiim)_2(O{=}PPh_3)_2][RhCl_4\{HN(CH_3)_2\}_2]$ (**2b**) and $[(Pt\{(NMe_2)_2CH_2\}_2C_6H_3)_2(\mu\text{-}Hbiim)_2Os(O{=}PPh_3)_2](NO_3)(OTf)_2{\cdot}4H_2O$ (**7**)

	2b	**7**
Distances [Å]		
Os1−O1	2.056(2)	2.030(5)
Os1−N1	2.076(2)	2.060(5)
Os1−N3	2.080(2)	2.076(5)
P1−O1	1.520(2)	1.513(5)
N1−C1	1.373(3)	1.341(9)
N1−C3	1.367(2)	1.362(6)
N2−C2	1.386(3)	1.380(9)
N2−C3	1.334(2)	1.331(8)
N3−C4	1.350(2)	1.341(8)
N3−C5	1.386(2)	1.386(8)
N4−C4	1.341(2)	1.335(8)
N4−C6	1.382(3)	1.366(9)
C1−C2	1.380(3)	1.376(10)
C5−C6	1.368(3)	1.350(9)
Pt1−N2		2.130(6)
Pt1−N5		2.090(6)
Pt1−N6		2.080(6)
Pt1−C25		1.949(6)
Angles [°]		
O1−Os1−N1	97.61(6)	92.0(2)
O1−Os1−N3	94.38(6)	95.32(19)
N1−Os1−N3	77.78(6)	78.3(2)
P1−O1−Os1	138.34(9)	147.4(3)
N2−Pt1−C25		175.2(3)
N5−Pt1−N6		163.1(2)

The crystal structure of **7** consists of the trimetallic $OsPt_2$ cation $[(Pt\{(NMe_2)_2CH_2\}_2C_6H_3)_2(\mu\text{-}Hbiim)_2Os(O{=}PPh_3)_2]^{3+}$ with a nitrate and two triflate counterions and

 © 2003 Wiley-VCH Verlag GmbH & Co. KGaA, Weinheim

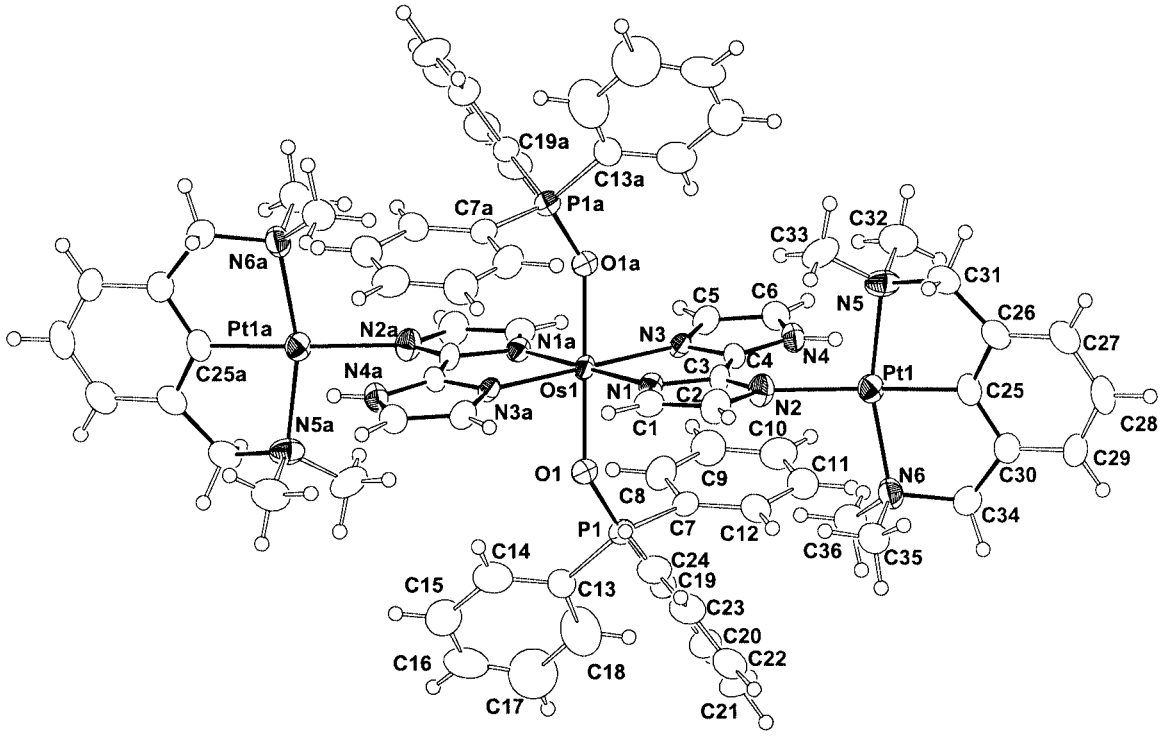

Figure 4. ZORTEP[11] drawing of the complex cation $[(Pt\{C_6H_3(CH_2NMe_2\text{-}2,6)_2\})_2Os(\mu\text{-}Hbiim)_2(O{=}PPh_3)_2]^{3+}$ of **7** (50% probability level; NO_3^-, $SO_3CF_3^-$ and H_2O are omitted for clarity); symmetry transformation used to generate equivalent atoms: $a = -x + 1, -y + 1, -z$; $b = -x + 2, -y, -z$

four water molecules in the unit cell. A plot of the molecular cation with the atom numbering scheme is given in Figure 4, selected bond lengths and angles are listed in Table 2. The molecular cation **7** has a center of inversion situated at the osmium atom; symmetry-generated atoms are identified with the suffix a.

Each $Hbiim^-$ bridging ligand in **7** is planar [root mean squares deviation rms = 0.0547 Å]. The Os(1)−N(1) and Os(1)−N(2) distances are slightly shorter than in **2b**, the bite angles of the Os−biim fragment are, as expected, nearly identical to those in **2b**. However, some changes are observed in the geometry of the triphenylphosphane oxide ligands. The Os(1)−O(1) distance in **7** is shorter than that in **2b** by 0.026 Å, and the P(1)−O(1)−Os(1) angle is larger than that in **2b** by 9.06°. The rigid biimidazole ligand is not affected. The PtL entities are planar [rms deviation = 0.0389 Å, Pt(1)−N(2)−N(5)−N(6)−C(25)] and are *trans*-disposed, similar to the deprotonated sites in $[Os(Hbiim)_2(O{=}PPh_3)_2]^+$ in **2b** (see Figure 3). The platinum centers have a slightly distorted square-planar coordination geometry. The N(5)−Pt(1)−N(6) angle is 163.1(4)°, which is in the typical range for NCN pincer complexes.[15] The PtL units are perpendicular to the imidazole rings [interplanar angle between Pt(1)−N(2)−N(5)−N(6)−C(25) and N(1)−N(2)−C(1)−C(2)−C(3) = 89.14(25)°].

Catalytic Activity

The catalytic properties of the trimetallic complexes **7**−**9** were investigated through the homogeneous hydrogenation of 1-hexene and cyclohexene in dichloromethane solutions at 25 °C, and under a hydrogen pressure of 5 bar. The yields of the catalytic hydrogenation reactions are summarized in Table 3. Complex **7**, as well as its homodinuclear analog $[\{Pt(C_6H_3(CH_2NMe_2\text{-}2,6)_2)\}_2'(\mu\text{-}Hbiim)](SO_3CF_3)_2$ (**11**)

Table 3. Homogeneous hydrogenation of 1-hexene and cyclohexene catalyzed by complexes **1**, **7**−**9** and **11**

Catalyst	Hydrogenation of 1-hexene		Hydrogenation of cyclohexene	
	Time [h]	Yield of hexane (%)	Time [h]	Yield of cyclohexane (%)
$[Os(H_2biim)_2(O{=}PPh_3)_2](NO_3)_3$ (**1**)	10	11	10	0
$[(Pt\{C_6H_3(CH_2NMe_2\text{-}2,6)_2\})_2(\mu\text{-}Hbiim)(SO_3CF_3)_2$ (**11**)	5	2	5	3
$[(Pt\{C_6H_3(CH_2NMe_2\text{-}2,6)_2\})_2(\mu\text{-}Hbiim)_2Os(O{=}PPh_3)_2](NO_3)(SO_3CF_3)_2{\cdot}4H_2O$ (**7**)	5	7	5	3
$[\{Pd(cod)\}_2(\mu\text{-}biim)_2Os(O{=}PPh_3)_2](NO_3)_3$ (**8**)	10	53[a]	10	36
$[\{Pd(en)\}_2(\mu\text{-}biim)_2Os(O{=}PPh_3)_2](NO_3)_3$ (**9**)	5	15	5	10

[a] By-products: 29% 2-hexene, 18% 3-hexene. Note that the formation of by-products in all other experiments was negligible.

 © 2003 Wiley-VCH Verlag GmbH & Co. KGaA, Weinheim

have a low catalytic activity. This is probably due to the inertness of these coordinatively saturated complexes towards ligand exchange. With $[Os(H_2biim)_2(O{=}PPh_3)_2](NO_3)_3$ (**1**) as a catalyst, 11% of hexane was obtained from 1-hexene, but no hydrogenation was observed with cyclohexene. The most active catalyst in the series is $[\{Pd(cod)\}_2Os(\mu\text{-}biim)_2(O{=}Ph_3)_2](NO_3)_3$ (**8**) (Table 3). A probable mechanism for the catalytic cycle involves hydrogenation of 1,5-cyclooctadiene and the formation of a coordinatively unsaturated palladium center as the catalytically active species. This could explain the lower activity of $[\{Pd(en)\}_2Os(\mu\text{-}biim)_2(O{=}PPh_3)_2](NO_3)_3$ (**9**) since the chelating ligand en is not easily substituted by substrate molecules. An attempt to use the mononuclear complex $[Pd(H_2biim)(cod)](NO_3)_2$ (**12**) as a homogeneous catalyst under identical conditions was unsuccessful, as it decomposes under hydrogen with the formation of palladium metal. This adequately demonstrates the increased stability of the Pd(cod) fragment in the trinuclear compound **8** relative to the mononuclear precursor **12**.

Conclusions

Deprotonation of the 2,2′-biimidazole building block in $[Os(H_2biim)_2(O{=}PPh_3)_2](NO_3)_3$ (**1**) provides a powerful route towards the preparation of the trimetallic $Pt^{II}-Os^{III}-Pt^{II}$ and $Pd^{II}-Os^{III}-Pd^{II}$ complexes **7**–**9**. The solid-state structural analysis of $[(Pt\{C_6H_3(CH_2NMe_2\text{-}2,6)_2\})_2(\mu\text{-}Hbiim)_2Os(O{=}PPh_3)_2](NO_3)(SO_3CF_3)_2{\cdot}4H_2O$ (**7**) demonstrates that the two $[Pt\{C_6H_3(CH_2NMe_2\text{-}2,6)_2\}]^+$ moieties are *trans* to each other, as expected from the *trans*-deprotonated sites of the 2,2′-biimidazolato ligands in the starting material, as shown in the solid-state structure of $[Os(Hbiim)_2(O{=}PPh_3)_2][RhCl_4\{NH(CH_3)_2\}_2]$ (**2b**). Cyclic voltammetric studies demonstrate that deprotonation of 2,2′-biimidazole and the coordination to a second metal ion result in a modification of the redox properties of the central osmium ion, and this is probably due to a change in the ligand field. The $OsPd_2$ complex $[\{Pd(cod)\}_2(\mu\text{-}biim)_2Os(O{=}PPh_3)_2](NO_3)_3{\cdot}H_2O$ (**8**) is shown to have considerable catalytic activity towards the homogeneous hydrogenation of linear and cyclic alkenes, e.g. 1-hexene and cyclohexene.

Experimental Section

Materials and Measurements: The complex $[Os(H_2biim)_2(O{=}PPh_3)_2](NO_3)_3{\cdot}H_2O{\cdot}0.5CH_3OH$ (**1**) was prepared by a published method.[10] $[Os(Hbiim)_2(O{=}PPh_3)_2](NO_3){\cdot}2H_2O$ (**2**) was obtained by reaction of **1** with KOH in methanol/dichloromethane.[10] $[Pt\{C_6H_3(CH_2NMe_2\text{-}2,6)_2\}(H_2O)](SO_3CF_3)$ (**4**) was prepared from $[Pt\{C_6H_3(CH_2NMe_2\text{-}2,6)_2\}Cl]$[15] (addition of $AgSO_3CF_3$ in methanol). $[Me_2NH_2][RhCl_4(HNMe_2)_2]$[16] was obtained as described elsewhere. ^1H, $^{13}C\{^1H\}$, and $^{31}P\{^1H\}$ NMR spectra were recorded with a Bruker AC 250 spectrometer, chemical shifts (^1H and ^{13}C) in ppm are quoted relative to $SiMe_4$. ^{31}P chemical shifts are given in ppm with respect to 85% H_3PO_4 (^{31}P: $\delta = 0$) as an external standard. Infrared spectra (KBr pellets) were recorded with a Perkin–Elmer 16PC FT-IR instrument. UV/Vis spectra were obtained with a Cary 1E spectrophotometer. Magnetic measurements were carried out with an Alfa MK 1 magnetic susceptibility balance. Electrochemical measurements (CV) were performed in methanol solutions containing $[nBu_4N]PF_6$ (0.1 mol·dm^{-3}) at 293 K, using a BAS 100B system with a glassy carbon working electrode, a platinum auxiliary electrode and an Ag/AgCl reference electrode. All potentials are referenced to the ferrocene/ferrocenium couple (E = 0.0 V). GC-MS analyses were performed with a Fison GC 8000/MD 800 series instrument, equipped with a ZB-1 (Zebron) column. Melting (decomposition) points were determined with a Gallenkamp MFB 595 010 M melting point apparatus. Organic solvents (methanol, dichloromethane) were freshly distilled before use. Microanalyses were obtained from the microanalytical laboratory of the chemical institutes of the University of Heidelberg or the Technische Universität Bergakademie Freiberg.

X-ray Crystallography: X-ray quality crystals of $[Os(Hbiim)_2(O{=}PPh_3)_2][RhCl_4\{HN(CH_3)_2\}_2]$ (**2b**) and $[(Pt\{C_6H_3(CH_2NMe_2\text{-}2,6)_2\})_2(\mu\text{-}Hbiim)_2Os(O{=}PPh_3)_2](NO_3)(SO_3CF_3)_2$ (**7**) were obtained by slow concentration of solutions of the complexes in a dichloromethane/methanol (4:1) mixture at 25 °C. Experimental crystal data are listed in Table 4 and geometric details are presented in Table 2. X-ray structural data were collected with a Bruker SMART CCD diffractometer. The unit cell parameters were checked for the presence of higher lattice symmetry.[17] Data were corrected for absorption using SADABS.[18] The structures were solved by direct methods (SHELX-97/2).[19] Refinement was carried out by full-matrix least-squares techniques on F^2 (SHELXL-97/2).[19] Hydrogen atoms were located from the difference Fourier map. All hydrogen atoms were fully refined. All non-hydrogen atoms were refined anisotropically.

Catalytic Hydrogenation of 1-Hexene and Cyclohexene: All experiments were performed in a 100-mL stainless steal autoclave with an inner polytetrafluorethylene vessel. In a typical experiment, 0.016 mmol of catalyst was placed as a solid in the autoclave, supplied with a magnetic stirring bar. Under stirring, the catalyst was dissolved in 6 mL of dichloromethane (complexes **7**, **8** and **11**) or in a mixture (90:10, 6 mL) of dichloromethane and methanol (complex **9**). 1-Hexene or cyclohexene (0.16 mmol; purity checked by GC-MS) was added to the solution of the catalyst. The autoclave was evacuated three times and filled with hydrogen. The pressure of hydrogen was increased to 5 bar. The reaction mixture was stirred for 5 h. The autoclave was then degassed and all volatile materials were evaporated from the reaction mixture using an oil-pump vacuum, and condensed (liquid nitrogen). The resulting solution was analyzed by GC-MS.

Synthesis of $[Os(Hbiim)_2(O{=}PPh_3)_2][RhCl_4(HNMe_2)_2]$ (2b): $[Os(Hbiim)_2(O{=}Ph_3)_2](NO_3){\cdot}2H_2O$ (**2**)[10] (100 mg, 0.09 mmol) was treated with $[Me_2NH_2][RhCl_4(HNMe_2)_2]$ (33 mg, 0.09 mmol) in 20 mL of a dichloromethane/methanol (4:1) mixture at 25 °C. Slow evaporation of the solvent resulted in a mixture of solid products. This contained some of the starting materials, $Me_2NH_2NO_3$ and red crystals of **2b**, which were hand-picked and suitable for X-ray crystal structural analysis. Due to the very low yield, no further spectroscopic characterization was possible.

Synthesis of $[(Pt\{C_6H_3(CH_2NMe_2\text{-}2,6)_2\})_2(\mu\text{-}Hbiim)_2Os(O{=}PPh_3)_2](NO_3)(SO_3CF_3)_2{\cdot}4H_2O$ (7): $[Os(Hbiim)_2(O{=}Ph_3)_2](NO_3){\cdot}2H_2O$ (**2**, 200 mg, 0.18 mmol) was dissolved at 25 °C in 15 mL of a dichloromethane/methanol mixture (4:1). $[Pt(\{C_6H_3(CH_2NMe_2\text{-}2,6)_2\}(H_2O)](SO_3CF_3)$ (199 mg, 0.36 mmol), dissolved in methanol (5 mL), was added to the solution. The reac-

 © 2003 Wiley-VCH Verlag GmbH & Co. KGaA, Weinheim

Table 4. Crystal data

	2b	**7**
Empirical formula	$C_{52}H_{54}Cl_4N_{10}O_2OsP_2Rh$	$C_{74}H_{86}F_6N_{13}O_{15}OsP_2Pt_2S_2$
Formula mass [g/mol]	1347.90	2218.00
Crystal system	triclinic	triclinic
Space group	$P\bar{1}$	$P\bar{1}$
a [Å]	10.4293(5)	12.604(3)
b [Å]	10.6365(6)	13.471(3)
c [Å]	13.0287(7)	14.347(3)
α [°]	102.928(1)	63.919(4)
β [°]	91.684(1)	77.530(5)
γ [°]	109.854(1)	66.613(4)
V [Å^3]	1316.1(1)	2005.6(7)
Z	1	1
T [K]	103(2)	173(2)
Radiation used (λ [Å])	Mo-K_α (0.70173)	Mo-K_α (0.70173)
Reflection collected	22971	16683
Independent reflection	8886	11171
R(int)	0.0287	0.428
Linear absorption coefficient [mm^{-1}]	3.040	5.237
R[a] [$I > 2\sigma(I)$]/all	0.0238/0.0275	0.0487/0.1043
$wR2$[b] [$I > 2\sigma(I)$]/all	0.0567/0.0592	0.1008/0.1191
Goodness-of-fit on F^2	1.055	0.958

[a] $R = \Sigma||F_o| - |F_c||/\Sigma|F_o|$. [b] $wR2 = [\Sigma[w(F_o^2 - F_c^2)^2]/\Sigma w(F_o^4)]^{1/2}$.

tion mixture immediately changed from violet to red. The solution was stirred for 2 h, after which the volume was reduced to 4 mL. After 10 h at 25 °C, pale pink crystals of **7** precipitated. The slurry was decanted and the crystalline precipitate was washed twice with acetone (5 mL) and dried using an oil-pump vacuum to afford analytically pure **7**. Yield: 290 mg (0.13 mmol, 73% based on **2**). M.p. 219 °C (dec.). IR (KBr, cm^{-1}): $\tilde{\nu}$ = 1130 $\nu_{(P=O)}$, 1276 $\nu_{(S=O)}$, 1385 $\nu_{a(NO^{3-})}$, 1439 $\nu_{(Ar,C=C)}$, 3075 $\nu_{(NH)}$. Due to paramagnetic line broadening no NMR spectra were recorded [molar magnetic susceptibility (powder, 298 K): 1.49×10^{-3} cm^3·mol^{-1}]. UV/Vis (CH_2Cl_2): λ_{max} (ε, mol^{-1}·dm^3·cm^{-1}) = 548 (6.2×10^2), 375 nm (sh, 7.4×10^3). CV (CH_3OH, 25 °C): $E_{1/2}(Os^{III}/Os^{IV})$ = +0.53 V (ΔE = 200 mV). $C_{74}H_{86}F_3N_{13}O_{15}OsP_2Pt_2S_2$ (2218.00): calcd. C 40.07, H 3.91, N 8.21; found C 40.04, H 3.85, N 8.47.

Synthesis of [{Pd(cod)}$_2$(μ-biim)$_2$Os(O=PPh$_3$)$_2$](NO$_3$)$_3$·2H$_2$O (8): [Os(H_2biim)$_2$(O=Ph$_3$)$_2$](NO$_3$)$_3$ (**1**, (247 mg, 0.2 mmol) was dissolved in dichloromethane/methanol (4:1, 20 mL) at 25 °C. Potassium hydroxide (4.0 mL, 0.2 M in MeOH) was added. After stirring at room temperature for 15 min, [Pd(NO$_3$)$_2$(cod)] {0.40 mmol, prepared in situ by the reaction of [$PdCl_2$(cod)] (120 mg, 0.42 mmol) with $AgNO_3$ (143 mg, 0.84 mmol)} was added. The reaction mixture was stirred for 1 h. All volatile products were then removed using an oil-pump vacuum, and the remaining residue was extracted with dichloromethane (100 mL). The extract was filtered and dichloromethane was removed using an oil-pump vacuum to afford **8** as a dark green solid. Yield: 295 mg (0.178 mmol, 89% based on **1**). M.p.: gradual decomposition at > 150 °C. IR (KBr, cm^{-1}): $\tilde{\nu}$ = 1120 $\nu_{(P=O)}$, 1184 $\nu_{a(NO^{3-})}$, 1436 $\nu_{(Ar,C=C)}$. ^{1}H NMR (CD_3OD): δ = 2.5 (br. s, 16 H, CH_2, cod), 5.5 (br. s, 8 H, CH, cod), 7.5−7.8 (m, 34 H, C_6H_5, H_2-bim) ppm. ^{13}C{^{1}H} NMR (CD_3OD): δ = 28.4 (CH_2, cod), 76.4 (CH, cod), 129.9 (C-2,-2′, biim^{2-}), 130.1 (CH, C_6H_5), 133.1 (CH, C_6H_5), 133.8 (CH, C_6H_5), 136.4 (*i*-C, C_6H_5), 141.3 (C-5,-5′, biim^{2-}), 152.1 (C-4,4′, biim^{2-}) ppm. ^{31}P{^{1}H} NMR (CD_3OD): δ = 32.6 ppm. Molar magnetic susceptibility (powder, 298 K): 8.84×10^{-4} cm^3·mol^{-1}. UV/Vis (CH_2Cl_2): λ_{max} (ε, L·cm^{-1}·mol^{-1}) = 351 (7.7×10^3), 548 nm (3.9×10^3). CV (CH_3OH): $E_{1/2}(Os^{IV}/Os^{III})$ = +0.41 V (ΔE = 280 mV). $C_{64}H_{66}N_{11}O_{13}OsP_2Pd_2$ (1662.28): calcd. C 46.24, H 4.00, N 9.27; found C 45.81, H 4.16, N 9.25.

Synthesis of [{Pd(en)}$_2$(μ-biim)$_2$Os(O=PPh$_3$)$_2$](NO$_3$)$_3$·H$_2$O (9): This complex was prepared from **1** (250 mg, 0.202 mmol) and [Pd(en)(H_2O)$_2$](NO$_3$)$_2$ (132 mg, 0.404 mmol), according to a procedure identical to that for **8**. A dark green solid was isolated. Yield: 270 mg (0.174 mmol, 87% based on **1**). M.p.: gradual decomposition at > 150 °C. IR (KBr, cm^{-1}): $\tilde{\nu}$ = 1118 $\nu_{(P=O)}$, 1384 $\nu_{a(NO^{3-})}$, 1438 $\nu_{(Ar,C=C)}$. ^{1}H NMR (CD_3OD): δ = 2.96 (br. s, 8 H, CH_2, en), 7.6−7.8 (m, 34 H, C_6H_5, H_2bim) ppm. ^{13}C{^{1}H} NMR (CD_3OD): δ = 47.3 (CH_2, en), 129.9 (C-2,-2′, biim^{2-}), 130.0 (CH, C_6H_5), 133.1 (CH, C_6H_5), 133.8 (CH, C_6H_5), 136.7 (*i*-C, C_6H_5), 141.1 (C-5,-5′, biim^{2-}), 152.6 (C-4,4′, biim^{2-}) ppm. ^{31}P{^{1}H} NMR (CD_3OD): δ = 32.6 ppm. Molar magnetic susceptibility (powder, 298 K): 1.07×10^{-3} cm^3·mol^{-1}. UV/Vis (CH_2Cl_2): λ_{max} (ε, L·cm^{-1}·mol^{-1}) = 347 (7.1×10^3), 547 nm (2.7×10^3). CV (CH_3OH): $E_{1/2}(Os^{IV}/Os^{III})$ = +0.23 V (ΔE = 390 mV). $C_{52}H_{56}N_{15}O_{12}OsP_2Pd_2$ (1548.10): calcd. C 40.34, H 3.65, N 13.57; found C 40.48, H 3.72, N 13.15.

Synthesis of [{Pt(C$_6$H$_3$(CH$_2$NMe$_2$-2,6)$_2$)}$_2$(μ-H$_2$biim)](SO$_3$CF$_3$)$_2$ (11): [Pt(C_6H_3(CH_2NMe_2-2,6)$_2$)Cl][15] (100 mg, 0.24 mmol) was dissolved in methanol (20 mL) and treated with $AgOSO_2CF_3$ (61 mg, 0.24 mmol). The reaction mixture was stirred for 12 h and AgCl was removed by filtration 2,2′Biimidazole (16 mg, 0.12 mmol) was added to the filtrate and the reaction mixture was stirred for 10 h. After filtration, methanol was removed using an oil-pump vacuum to afford **11** as a gray solid. Yield: 120 mg {0.1 mmol, 84% based on [Pt(C_6H_3(CH_2NMe_2-2,6)$_2$)Cl]}. M.p. 214 °C (dec.). IR (KBr, cm^{-1}): $\tilde{\nu}$ = 1275 $\nu_{(S=O)}$, 1441 $\nu_{(Ar,\ C=C)}$, 3080 $\nu_{(NH)}$. $C_{32}H_{44}F_6N_8O_6Pt_2S_2$ (1205.02): calcd. C 31.90, H 3.68, N 9.30; found C 31.52, H 4.05, N 8.95.

Acknowledgments

This work was supported in part by the Deutsche Forschungsgemeinschaft, the Fond der Chemischen Industrie and the

 © 2003 Wiley-VCH Verlag GmbH & Co. KGaA, Weinheim

Alexander-von-Humboldt-Stiftung. We thank Mrs. Petra Krämer for help in performing the GC-MS analyses. We also would like to thank Degussa AG (Hanau) for the generous gift of OsO_4 and $RhCl_3$.

[1] [1a] R. Choukroun, D. Gervais, P. Kalck, F. Senocq, *J. Organomet. Chem.* **1987**, *335*, C9−C12. [1b] R. Mutin, C. Lucas, J. Thivole-Cazat, V. Dufand, F. Dany, J. M. Basset, *J. Chem. Soc., Chem. Commun.* **1988**, 896−898. [1c] M. A. Esteruelas, M. P. Garcia, A. M. Lopez, L. Oro, *Organometallics* **1991**, *10*, 127−133. [1d] E. Sola, V. I. Bakhmutov, F. Torres, A. Elduque, J. A. Lopez, F. Lahoz, H. Werner, L. A. Oro, *Organometallics* **1998**, *17*, 683−696.

[2] [2a] P. Kalck, *Polyhedron* **1988**, *7*, 2441−2450. [2b] A. Dedieu, P. Escaffre, J. M. Frances, P. Kalk, A. Thorez, *Nouv. J. Chem.* **1986**, *10*, 631−696.

[3] [3a] S. W. Kaiser, R. B. Saillant, W. M. Butler, P. G. Rasmussen, *Inorg. Chem.* **1976**, *15*, 2681−2687. [3b] S. W. Kaiser, R. B. Saillant, P. G. Rasmussen, *J. Am. Chem. Soc.* **1975**, *97*, 425−426. [3c] S. W. Kaiser, R. B. Saillant, W. M. Butler, P. G. Rasmussen, *Inorg. Chem.* **1976**, *15*, 2688−2694.

[4] M. S. Haddad, D. N. Hendrickson, *Inorg. Chem.* **1978**, *17*, 2622−2630.

[5] R. Usón, J. Gimeno, J. Forniés, F. Martínez, *Inorg. Chim. Acta* **1981**, *50*, 173−177.

[6] A. Maiboroda, G. Rheinwald, H. Lang, *Inorg. Chem. Commun.* **2001**, *4*, 381−383.

[7] P. Majumdar, S.-M. Peng, S. Goswami, *J. Chem. Soc., Dalton Trans.* **1998**, 1569−1574.

[8] M. P. Garcia, A. M. López, M. A. Esteruelas, F. J. Lahoz, L. A. Oro, *Chem. Commun.* **1988**, 793−795.

[9] R. Usón, L. A. Oro, J. Gimeno, M. A. Ciriano, J. A. Cabeza, *J. Chem. Soc., Dalton. Trans.* **1983**, 233−230.

[10] A. Maiboroda, G. Rheinwald, H. Lang, *Eur. J. Inorg. Chem.* **2001**, 2263−2269.

[11] L. Zsolnai, G. Huttner, *ZORTEP*, University of Heidelberg, **1994**.

[12] C. M. Che, T. F. Lai, W. C. Chung, W. F. Schaefer, H. B. Grey, *Inorg. Chem.* **1987**, *26*, 3907−3911.

[13] M. A. Esteruelas, F. J. Lahoz, L. A. Oro, E. Onate, N. Ruiz, *Inorg. Chem.* **1994**, *33*, 787−792.

[14] G. Mesroni, E. Alessio, A. Sessanta o Santi, S. Geremia, A. Bergamo, G. Sava, A. Boccarelli, A. Schettino, M. Coluccia, *Inorg. Chim. Acta* **1998**, *273*, 62−71.

[15] J. Terheijden, G. Van Koten, F. Muller, D. M. Grove, K. Vrieze, E. Nielsen, C. H. Stam, *J. Organomet. Chem.* **1986**, *315*, 401−417.

[16] I. B. Bondarenko, N. A. Buzina, Yu. S. Varshavskii, M. I. Gel'fman, V. V. Razumovskii, T. G. Cherkasova, *Russ. J. Inorg. Chem.* **1971**, *16*, 1629−1672.

[17] A. L. Spek, *Acta Crystallogr., Sect. A* **1990**, *46*, C34.

[18] Area-Detector Absorption Corrections, Siemens Industrial Automation, Inc., Madison, WI, **1996**.

[19] G. M. Sheldrick, *SHELX-97, Programs for Crystal Structure Analysis (Release 97−2)*, University of Göttingen, Germany, **1997**.

Received October 9, 2002

 © 2003 Wiley-VCH Verlag GmbH & Co. KGaA, Weinheim

Catalytic Aziridination of Styrene with Copper Complexes of Substituted 3,7-Diazabicyclo[3.3.1]nonanones

Peter Comba,*[a] Michael Merz,[a] and Hans Pritzkow[a]

Keywords: Copper / N ligands / Catalysis

The copper(II) complexes of five bispidine-type ligands {3,7-diazabicyclo[3.3.1]nonanone; three tetradentate ligands with 2-pyridyl (L^1), 6-methyl-2-pyridyl (L^2) or 2-imidazolyl-3-methyl (L^3) substituents in 2,4-positions; two pentadentate derivatives of L^1 with an additional 2-methylpyridine substituent at N3 (L^4) or N7 (L^5)} have, with one co-ligand (Cl^-), a ligand-enforced square pyramidal ($L^{1,2,3}$) or octahedral ($L^{4,5}$) geometry. The main structural properties of three of the five $[Cu(L)(Cl)]^+$ complexes ($L^{1,2,3}$) are very similar, with Cu–N3 < Cu–N7 and Cu–Cl ≈ 2.25 Å (*trans* to N3); with L^2 Cu–N3 ≈ Cu–N7 and Cu–Cl = 2.22 Å (*trans* to N7); with L^5 Cu–N3 < Cu–N7 and Cu–Cl = 2.72 Å (*trans* to N7). These structural patterns lead to considerable differences in ligand field and electrochemical properties (range of $E°$ of approx. 500mV), and the reactivities of the copper(II) complexes as aziridination catalysts (styrene, PhINTs, CH_3CN) are strikingly different. While the complex with L^2 is very efficient, the activities of those with L^1 and L^3 are reduced to approx. 50% and 30%, respectively, and those with L^4 and L^5 are inactive. The fact that the maximum TON (maximum turnover number) of $Cu^{II}L^2$ (19) is much smaller than the maximum TON of $Cu^{I}L^2$ (47) suggests that in the active form the catalysts are in the Cu^I oxidation state, and that the differences in reduction potentials are of major importance for catalysis. The result that $CuL^{4,5}$ have no activity in the Cu^{II} state and only a small activity in the reduced form indicates that, apart from the reduction potentials, steric effects might also be of importance.
(© Wiley-VCH Verlag GmbH & Co. KGaA, 69451 Weinheim, Germany, 2003)

Introduction

Aziridines, the nitrogen analogues of epoxides, are attractive intermediates in organic synthesis,[1,2] and various aziridine-containing natural products have cytotoxic properties.[3,4] Their synthesis, mediated by copper powder, has been known for many years,[5] and transition metal-catalyzed procedures have recently attracted much attention (Scheme 1).[6] Since their discovery[7–9] copper-catalyzed processes have been studied extensively, and various enantioselective catalysts have been developed.[7–12] PhINTs {[*N*-(*p*-toluenesulfonyl)imino]phenyliodinane} is the most frequently used nitrene source in copper-catalyzed aziridination reactions, but others have also been described.[13–15] An interesting observation is that both copper(I) and copper(II) complexes have been found to be active catalysts. Two possible general mechanisms have been discussed, one which involves the copper complexes as Lewis acid catalysts (activation of the coordinated iodinane without electron transfer) and, in analogy to cyclopropanation, a process with a discrete copper-nitrene intermediate (electron transfer).[11,12] Recent experimental evidence[11,16,17] and theoretical studies[17] indicate that there is a discrete nitrene intermediate, and that the copper(I) complexes are the active catalysts, leading to a copper(I)-nitrene or a copper(III)-imido species; the copper(II) pre-catalysts may enter the catalytic cycle via reduction by PhINTs to the corresponding copper(I) complexes.[17] Interesting questions related to this latter mechanism are the electronic structure, spin state and copper oxidation state of the catalytically active intermediate, i.e., whether it is best formulated as a copper(I)-nitrene or a copper(III)-imido species, and the coordination mode of the nitrene donor, derived from PhINTs, which generally is formulated as a monodentate ligand and recently has been proposed to coordinate as a bidentate with the sulfonyl oxygen atom being an additional donor.[17]

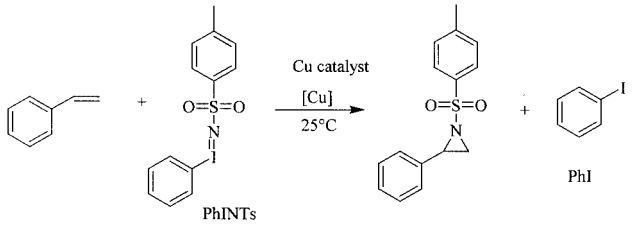

Scheme 1

Copper(II)-catalyzed reactions are of particular interest since, in contrast to copper(I), the catalysts are air-stable. A

[a] Universität Heidelberg, Anorganisch-Chemisches Institut, Im Neuenheimer Feld 270, 69120 Heidelberg
Fax: (internat.) + 49-(0)6226-546617
E-mail: comba@akcomba.oci.uni-heidelberg.de

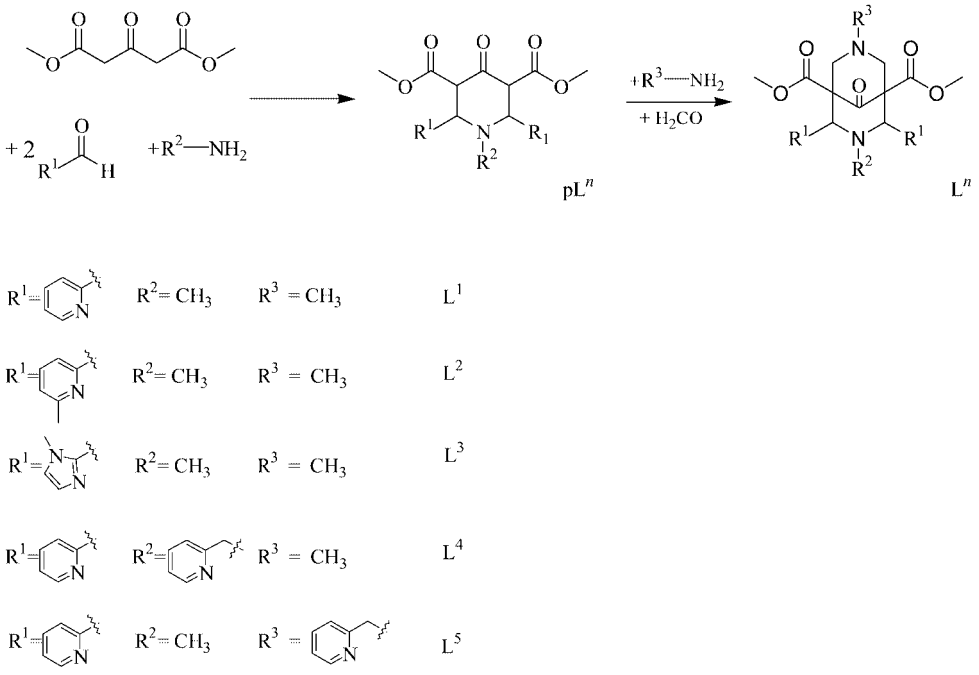

Scheme 2

series of classical copper(II) coordination compounds have recently been reported to efficiently catalyze olefin aziridination.[18–20] Of interest was the observation that the efficiency and, specifically, the reaction rate can be increased significantly when the denticity of the co-ligands is reduced from four to three.[19] The ligands discussed in those studies involve two tertiary amine and one or two pyridine donors, leading to a planar geometry of the putative nitrene intermediate with the copper-nitrene bond in-plane; the reduced reactivity of the tetradentate ligand complexes was believed to be due to a pre-equilibrium, involving copper-pyridine bond breaking.[19,20] This is in agreement with the above mentioned theoretical studies which indicate that the formation of the nitrene intermediate is the rate determining step of the catalytic cycle. Note however that the DFT calculations were done with different and only bidentate ligands.[17]

The copper complexes of the bispidine ligands, reported here (see Scheme 2), are of interest because most of these tetra- and pentadentate ligands enforce an in-plane and strong coordination of the substrate, with one of the tertiary amines as a relatively weak axial donor.[21] This leads to copper complexes with interesting and unprecedented properties,[22–25] and subtle changes in the ligand backbone induce significant structural variation and predictable changes of the redox and electronic properties, as well as the reactivities.[26]

Results and Discussion

Syntheses and Structural Properties: The five bispidone ligands L^{1-5} studied here are all prepared in moderate to high yield, according to the general procedure given in Scheme 2, by variation of the aldehyde and the amine components in the two Mannich condensation steps. As observed before, the coordination to copper(II) leads to hydration of the keto function if the reaction is not done in strictly anhydrous conditions.[22,23,27] The molecular structures of the copper(II) chloro complexes are presented in Figure 1. Table 1 gives selected structural parameters {the structures of $[Cu(L^1)(Cl)]^+$ and $[Cu(L^2)(Cl)]^+$, also included in Figure 1 and Table 1, have been published before[22,23]}.

The bispidine ligands are very rigid. In the present structures this is best seen in the constant N1···N2 distances (N3, N7 according to the IUPAC numbering; the crystallographic numbering used throughout is defined in Figure 1); this is a general feature observed for all transition metal-bispidine complexes.[27] In contrast to this rigidity of the ligand there is a considerable elasticity of the coordination sphere,[26] and this is responsible for appreciable differences in the relative bond lengths, primarily to the tertiary amine donors (see Cu–N1 vs. Cu–N2 in Table 1). This is the result of a dislocation of the copper(II) center within the bispidine cavity, enforced by specific changes at the ligand backbone (see below), and this is a major tool for modifying the properties of the corresponding complexes.

L^1 is highly complementary for copper(II), i.e., $[Cu(L^1)(Cl)]^+$ is a very stable complex {log $K[Cu^{II}(L^1)]$ is approx. 20} ,[28] the stability is similar to that of copper(II) complexes with tetraazamacrocyclic ligands; see also electrochemical and spectroscopic properties below).[21,28,29] An intriguing feature is that the Cu–Cl bond is very short and strong (approx. 2.2 Å vs. approx. 2.5 Å for CuN_4Cl^+ chromophores with axial Cl^-, see also complex with L^5 with a CuN_5Cl^+ chromophore). This is as expected from theoreti-

 © 2003 Wiley-VCH Verlag GmbH & Co. KGaA, Weinheim

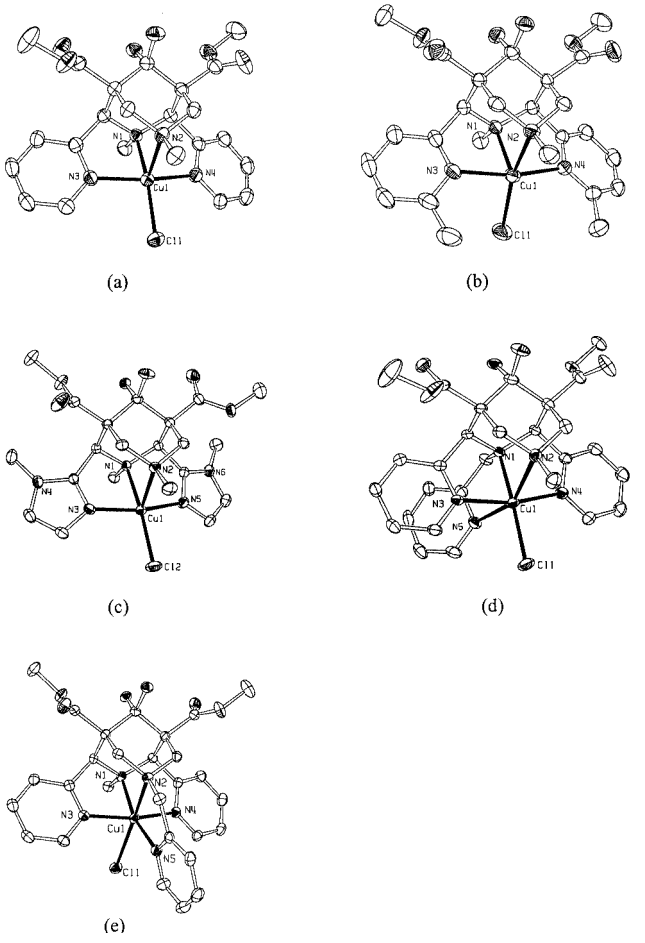

Figure 1. ORTEP[34] plots of (a) $[Cu(L^1)(Cl)]^+$,[19] (b) $[Cu(L^2)(Cl)]^+$,[20] (c) $[Cu(L^3)(Cl)]^+$, (d) $[Cu(L^4)(Cl)]$, (e) $[Cu(L^5)(Cl)]^+$

cal considerations[21] and translates to generally strongly bound and highly activated substrates (peroxide, catecholate)[22–25] and an unprecedented high stability constant for chloride.[29] The main structural features of $[Cu(L^3)(Cl)]^+$ and $[Cu(L^4)(Cl)]^+$ are, as expected, similar to those of $[Cu(L^1)(Cl)]^+$ (see Cu–N1, Cu–N2, Cu–Cl, Figure 1, Table 1). The structural differences of the aromatic five- vs. six-membered ring (L^1 vs. L^3) and the small differences in donor strength between imidazole and pyridine (strong σ-donors, pK_a(pyridine) = 5.3, pK_a(imidazol) = 7.1, weak π-acids) lead only to minor structural variations. The addition of a third pyridine donor *trans* to N2 (L^4, additional pyridine donor in the "Jahn–Teller" axis, 2.5 vs. 2.0 Å) also leads to only small over-all structural changes (Cu–Cl = 2.25 Å, similar to $L^{1,3}$).

More important and interesting are the structural changes enforced by L^2 (α-methyl substitution of the pyridine donors, steric crowding) and L^5 (ligand-enforced coordination of the substrate in the "Jahn–Teller" axis, *trans* to N2). In the latter case (L^5) the structural features are obvious and as expected: the distance to the third pyridine donor is similar to that of the other two (Cu–N3 ≈ Cu–N4 ≈ Cu–N5, note the differences to the structure with L^4), and Cu–Cl = 2.72 Å (in contrast to all the other complexes discussed here, but similar to the usual CuN_5Cl^+ (and CuN_4Cl^+) chromophores, see above).

The most interesting structure, however, is probably that of the complex with L^2. The methyl substitution enforces the coordination of bulky co-ligands (substrates) such as Cl^- *trans* to N2 (note that the sterically less demanding $NCCH_3$ donor is coordinated *trans* to N1[23]). The resulting structure is best described as square pyramidal with the two pyridine donors, Cl^- and N2 in-plane, and N1 as the axial donor (see Figure 2). The main structural differences be-

Table 1. Selected bond lengths (Å) and angles (deg) of the molecular cations of the copper(II) complexes

Bond lengths [Å]	$[Cu(L^1)(Cl)]^+$	$[Cu(L^2)(Cl)]^+$	$[Cu(L^3)(Cl)]^+$	$[Cu(L^4)(Cl)]^+$	$[Cu(L^5)(Cl)]^+$
Cu–N1	2.042(3)	2.147(3)	2.115(2)	2.070(2)	2.036 (2)
Cu–N2	2.272(3)	2.120(3)	2.316(2)	2.478(2)	2.368(2)
Cu–N3	2.020(3)	2.061(3)	1.967(2)	2.011(2)	2.028(2)
Cu–N4	2.024(3)	2.064(3)	1.971(2) [a]	1.987(2)	2.029(2)
Cu–N5	–	–	–	2.544(2)	2.029(2)
Cu–Cl	2.232(1)	2.221(2)	2.2285(6)	2.2546(8)	2.717(6)
N1···N2	2.921	2.930	2.917	2.931	2.915
N3···N4	3.971	4.084	3.869 [a]	3.965	3.995
Valence angles [°]					
N1–Cu–N2	85.02(9)	86.71(12)	82.20(6)	79.70(8)	82.53(6)
N1–Cu–N3	81.25(10)	81.63(13)	80.58(7)	83.62(9)	81.39(7)
N1–Cu–N4	81.15(10)	82.37(13)	80.51(7)[a]	81.74(10)	80.94(7)
N1–Cu–N5	–	–	–	77.95(10)	160.82(7)
N2–Cu–N3	95.95(10)	91.18(13)	91.54(7)	89.39(9)	88.32(6)
N2–Cu–N4	95.35(10)	90.26(13)	95.77(7)[a]	88.27(9)	98.43(6)
N3–Cu–N4	158.13(10)	163.82(13)	158.58(7)[a]	165.36(10)	160.07(7)
N2–Cu–N5	–	–	–	155.11(10)	79.27(7)

[a] For $[Cu(L^3)(Cl)]^+$ N4 in this table corresponds to the crystallographic label N5 (see Figure 1).

 © 2003 Wiley-VCH Verlag GmbH & Co. KGaA, Weinheim

tween $[Cu(L^1)(Cl)]^+$ and $[Cu(L^2)(Cl)]^+$ are then (i) a rotation of the pyridine rings out of the *xy* plane with the methylated ligand L^2; this leads to a destabilization of the entire complex and of the Cu−Cl bond,[21] and (ii) a quenching of the Jahn−Teller-type electronic stabilization due to steric constraints from the bispidine backbone (Cu−N1 ≈ Cu−N2), again leading to destabilization.[26] The stability constant with L^2 is not yet available. However, it is known[30] that differences in the potential of copper(II/I) couples are strongly correlated with the complex stabilities of the corresponding copper(II) complexes. The difference in the reduction potential between $Cu^{II}L^1$ and $Cu^{II}L^2$ of approx. 300 mV (see below) leads to a difference in total energy of approx. 30 kJ·mol^{-1}. The computed energy difference (DFT)[21] is approx. 20 kJ·mol^{-1}, and some of this difference (approx. 10 kJ·mol^{-1}) might be due to the quenching of the Jahn−Teller effect, which was not included in the DFT study (model compound with monodentate ligands).[21] Note, however, that some of these data refer to gas phase calculations and that the co-ligand is not the same in all the studies referred to, i.e., the quoted energies have to be considered with care. Interestingly, the two Cu−Cl bond lengths in the structures with L^1 and L^2 are similar (see Table 2), supporting the interpretation of the structure as square pyramidal with an in-plane Cu−Cl bond, and the short bond is probably also due to less repulsion between Cl^- and the ligand backbone of L^2 (see Figure 2). The theoretically expected decrease in bonding energy[21] is paralleled by a decrease in Cu−Cl stability by an experimentally observed factor of approx. 2.[29]

Also relevant for the aziridination catalysis are the corresponding copper(I) structures. A number of solid state structures have been reported,[23,25,27] and these are similar to the corresponding copper(II) structures. An interesting feature is that with L^1 four- and five-coordinated complexes are known, which differ by one of the pyridine donors (N3 or N4) either being coordinated or not.[23] The dynamics in solution are not yet fully understood but the structural data and a qualitative interpretation of the solution NMR spectra suggest that an equilibrium which also involves a reduced coordination number species is feasible.

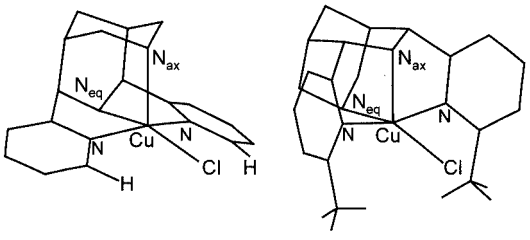

Figure 2. Plots of the crystal structures of $[Cu(L^1)(Cl)]^+$ [22] and $[Cu(L^2)(Cl)]^+$, [23] visualizing the square pyramidal structure of $[Cu(L^2)(Cl)]^+$

Spectroscopy and Electrochemistry: Electronic spectra of the copper(II) complexes of the five bispidine ligands L^{1-5} have been recorded as the chloro complexes (chloride salts) and with a coordinated solvent molecule (tetrafluoroborate salts), each in two different solvents (acetonitrile and methanol), see Table 2. The data of the chloro complexes indicate that chloride remains coordinated, i.e., the spectra are close to identical in the two solvents and different from the spectra of the corresponding tetrafluoroborate salts, which differ for each solvent. This was expected from the strong bonds (see above and ref.[21]), the high stability constants,[29] and is also supported by conductometric experiments with $L^{1,2}$.[25] Worth noting is the strongly different chromophore of the copper(II) complexes with L^4 (generally very weak ligand field), which might be due to the considerable angular distortion of the hexacoordinate complex (N2−Cu−N5 = 155°) and/or subtle changes in π-bonding. The solvent-dependent shift of the dd transitions of the copper(II) complexes with L^2 is much larger than it is for the other complexes and suggests some significant structural changes. For the co-ligands Cl^- and $NCCH_3$ this was expected, i.e., the former coordinates *trans* to N2, the latter *trans* to N1.[23]

Preliminary EPR spectroscopic data are also included in Table 2. The expected trends (*g* vs. ligand field strength, *g* vs. *A*) are observed but the differences are not significant enough, and the lack of resolution in the ligand field spectra, as well as the lack of a thorough assignment do not warrant further interpretation at present. An interesting feature is that, in the EPR spectrum of $[Cu(L^1)Cl]^{2+}$ (in MeOH or DMF/H_2O, frozen solution), there is a well resolved fine-structure in the g_{xy} region of the spectrum; a less well resolved but clearly observable fine-structure is also apparent in the g_z region, and in the g_{xy} region of $[Cu(L^4)Cl]^{2+}$. A more detailed interpretation of these and other spectroscopic features will be given elsewhere.

The reduction potentials are also given in Table 2. These are a measure of the stabilities of the copper(II) complexes

Table 2. Spectroscopic and electrochemical properties of the copper(II) complexes of L^{1-5}

Compound	dd Transitions (nm)				EPR (X = Cl^-[a]/X = CH_3CN[b])			$E°$ (X = CH_3CN)[a]
	X = Cl^- [a]	X = MeOH[b]	X = CH_3CN[b]	X = H_2O[b]	$g_\parallel$	$g_\perp$	$A_\parallel$	(mV vs. $Ag/AgNO_3$)
$[Cu(L^1)(X)]^{n+}$	650 (sh, 700)	660	630	653	2.225/2.245	2.034/2.072	176/172	−417
$[Cu(L^2)(X)]^{n+}$	625 (sh, 740)	785 (sh, 830)	700	625 (sh, 740)	2.245/2.245	2.065/2.085	160/165	−98
$[Cu(L^3)(X)]^{n+}$	640 (sh, 690)	665	650	−	2.230/2.250	2.070/2.070	165/168	−440
$[Cu(L^4)(X)]^{n+}$	720 (sh, 780)	705	665	−	2.255/2.250	2.06/2.08	160/165	−489
$[Cu(L^5)(X)]^{n+}$	640	625	625	−	2.250/2.230	2.060/2.075	170/175	−603

[a] Cl^- salts; identical spectra in CH_3CN, MeOH (and H_2O). [b] BF_4^- salts

 © 2003 Wiley-VCH Verlag GmbH & Co. KGaA, Weinheim

(see above).[30] As expected from the structural data (see above) the electrochemically deduced stabilities of the copper(II) complexes of $L^{1,3,4}$ (coordinated $NCCH_3$) are similar (-489 mV $< E^\circ < -417$ mV). That of the complex with L^5 is significantly larger ($E^\circ = -603$ mV; pentadentate ligand; in L^4 the third pyridine donor is only weakly coordinated and leads to a significant distortion of the chromophore, see spectroscopic data). The difference in E° between the complexes of L^1 and L^4 suggests that in solution the latter remains hexacoordinate. The reduction potential of the complex with L^2 is considerably smaller ($E^\circ = -98$ mV); i.e., the stability of the copper(II) complex is significantly smaller. Note again that, in CH_3CN, the co-ligand with L^2 is coordinated *trans* to N1, while other donors (specifically PhINTs) are expected to coordinate *trans* to N2.

Aziridination Catalysis: The efficiency of the aziridination catalytic reactivity of the copper(II) and copper(I) complexes of L^{1-5} are summarized in Table 3. Note that the aziridines were isolated and their yield determined by weight (see Exp. Sect.). This might lead to a loss of product of up to approx. 5%. The reaction time was not optimized but it appears that the reactions with L^2 and those with copper(I) catalysts are considerably faster than the others.

In a first set of experiments the copper(II) catalysts of L^{1-5} were tested with standard conditions (entries 1,2,5,6,8).[20] Under these conditions, the pentadentate ligands $L^{4,5}$ do not lead to active copper(II) pre-catalysts, and ligands $L^{1,3}$ lead to catalytic systems of similar activities to those observed recently with other tetradentate ligand systems with two tertiary amine and two pyridine donors.[20] An interesting feature is that the activity of the copper(II) catalyst with methyl-substituted pyridine donors (L^2) is enhanced by a factor of at least 2. In a second series of experiments the maximum turnover number (TON) of the most active copper(II) catalyst (L^2) was evaluated (entry 3). A third series of experiments was done to compare the performance of the catalytic systems with copper in the oxidation states (II) and (I) (entries 4,7,9). It appears that the copper(I) forms are generally more efficient. This is supported by the observation that the TONs of the copper(II) systems with the tetradentate ligands L^{1-3} (entries 1,2,5) are qualitatively correlated to the corresponding reduction potentials (Table 2). The fact that ligands $L^{4,5}$ do not lead to active copper(II) pre-catalysts indicates that the ease of reducing the pre-catalysts is not the only property related to the catalytic activity (the reduction potential of $Cu^{II}(L^4)X$ is not much different from those with ligands $L^{1,3}$). Therefore, another important factor might be that the inner-sphere reduction by PhINTs (as proposed in the literature[17]) is, for steric reasons, not possible with the pentadentate ligands. This is supported by the fact that the copper(I) complexes with $L^{4,5}$ show some catalytic activity, but this is marginal.

Based on the current data we assume that electronic and steric effects are both responsible for the observed differences in reactivity. Based on the proposal that the copper(II) pre-catalysts enter the catalytic cycle after reduction by PhINTs to the corresponding copper(I) complexes,[17] the destabilization of the oxidized form by L^2 might be an important driving force for the higher activity (note again here the ambiguity of the site of coordination of substrates to the complex with L^2). PhINTs is a sterically demanding donor, and this is true for a terminal or a chelated copper(I)-nitrene or copper(III)-imido species (with the sulfonyl oxygen atom also coordinated[17]). Therefore, it is not unexpected that its rate-determining formation with the pentadentate ligand L^4 is unfavorable. With L^5, coordination of the substrate to copper(II) is along the Jahn–Teller axis and probably does not lead to a stable interaction, also, this redox potential is extremely negative. Significant differences in steric crowding between the copper-$L^{1,2}$ fragments emerge from Figure 2, the two square pyramidal chromophores are very similar but the L^1 substrate coordination (Cl^- in Figure 2) is hindered by the α-CH groups of the pyridine donors; the corresponding methyl groups are not sterically efficient in L^2. The differences in reactivity between L^1 and L^3 (the repulsion due to the α-CH groups in L^3 is, for geometric reasons, reduced) indicate that electronic factors (reduction potentials) are also of importance in this case.

Conclusion

Subtle changes on the bispidine backbone have been shown to lead to strikingly different structural and electronic properties of the corresponding copper(II) complexes, and these are transferred to strong differences in the activi-

Table 3. Results of the catalytic aziridination of styrene in CH_3CN (for detailed conditions see text)

Entry	Catalyst	[PhINTs] (mol)	[Catalyst] (mol %)	Yield (%)	TON
1	$[Cu^{II}(L^1)](BF_4)_2$	0.4	5	41	9 ± 1
2	$[Cu^{II}(L^2)](BF_4)_2$	0.4	5	94	19 ± 1
3	$[Cu^{II}(L^2)](BF_4)_2$	0.6	3.5	67	19 ± 1
4	$[Cu^{I}(L^2)](BF_4)$	0.9	1.7	80	47 ± 2
5	$[Cu^{II}(L^3)](BF_4)_2$	0.4	5	29	6 ± 0.5
6	$[Cu^{II}(L^4)](BF_4)_2$	0.4	5	0	0
7	$[Cu^{I}(L^4)](BF_4)$	0.4	1.7	7	7.5 ± 1
8	$[Cu^{II}(L^5)](BF_4)_2$	0.4	5	0	0
9	$[Cu^{I}(L^5)](BF_4)$	0.4	1.7	6	5.5 ± 1

 © 2003 Wiley-VCH Verlag GmbH & Co. KGaA, Weinheim

ties of these complexes as aziridination catalysts. It appears that the differences in catalytic activities are due to steric effects and to the destabilization of the copper(II) oxidation state. Bond breaking to one of the pyridine donors in the copper(I) state might facilitate the formation of the copper(I)-nitrene intermediate, and this type of dynamic process with bispidine ligands has been described before.[23] Further ligand modifications might shed more light on the relative importance of all these factors and lead to more efficient catalytic systems.

Experimental Section

Measurements and Materials: Chemicals for the syntheses and solvents were of the highest degree of purity and used without further purification. The piperidone precursors pL^1 for $L^{1,2,5}$, the ligands L^1, L^2, and the corresponding copper(II) complexes (Cl^-, BF_4^- salts) were prepared using published procedures (see Scheme 1).[23]

IR spectra (KBr pellets) were measured with a Perkin−Elmer 16C FT-IR instrument. NMR spectra were recorded with a Bruker AS 300 spectrometer (^1H, 300.13 MHz; ^{13}C, 75.47 MHz); chemical shifts (δ, ppm) are relative to TMS or solvent. Electronic absorption spectra were measured from solutions (approx. 10^{-3} M, CH_3CN), using 1-cm quartz cells, on a Varian Cary 1E instrument. EPR spectra were recorded on a Bruker ELEXSYS E500 spectrometer as approx. 10^{-3} M frozen solutions (liquid nitrogen temperature MeOH, CH_3CN or DMF/H_2O). XSophe, version 1.0.2β, on a Linux workstation was used for the computer simulation of the spectra.[31,32] Electrochemical measurements (cyclic voltammetry, 10−500 mV/s, 2×10^{-3} M complex solutions; 0.1 M tetrabutylammonium hexafluorophosphate in acetonitrile) were obtained from a BAS100B system (data analysis with Digisim) with a glassy carbon working, a Pt-wire auxiliary and a $Ag/AgNO_3$ reference electrode; the potential of the Fc^+/Fc couple at a scan rate of 100 $mV \cdot s^{-1}$ lies at 87 mV with $\Delta E = 64$ mV. Mass spectra were recorded with a Finnigan 8400 spectrometer with a nitrobenzyl alcohol matrix for the FAB spectra. Elemental analyses were obtained from the microanalytical laboratory of the University of Heidelberg.

Ligand Syntheses. Piperidones. pL^3: Methylamine (1.9 mL, 22.7 mmol, 40%, in water) and dimethyl acetonedicarboxylate (3.95 g, 22.7 mmol) were added to a cold solution (4 °C) of 1-methylimidazole-2-carbaldehyde (5.0 g, 45.4 mmol) in methanol (40 mL). After stirring at 4 °C for 4 h a yellowish white solid occurred, which was collected by filtration and washed with methanol. Yield 5.63 g (14.4 mmol, 63%) of a white solid. $C_{18}H_{23}N_5O_5$ (389.4): calcd. C 55.52, H 5.95, N 17.98; found C 55.36, H 5.97, N 17.72. ^1H NMR (300 MHz, $CDCl_3$): δ = 1.79 (s, 3 H, N−CH_3), 3.70 (s, 6 H, N_{Im}−CH_3), 3.72 (s, 6 H, OCH_3), 4.47 (d, $^3J_{H,H}$ = 11.5 Hz, 2 H, CH), 4.84 (d, $^3J_{H,H}$ = 11.4 Hz, 2 H, CH-Im), 6.85 (d, $^3J_{H,H}$ = 1.1 Hz, 2 H, CH_{Im}), 6.92 (d, $^3J_{H,H}$ = 1.1 Hz, 2 H, CH_{Im}) ppm. ^{13}C NMR (75.47 MHz, $CDCl_3$): δ = 30.1 (Im−CH_3), 32.6 (NCH_3), 52.4 (NCH), 53.7 (OCH_3), 59.6 (CH), 122.0 (CH_{Im}), 127.6 (CH_{Im}), 143.8 (C_{Im}), 168.7 (Ester), 199.4 (C=O) ppm. FAB^+MS(NBA): *m*/*z* = 412.2 [M + Na^+], 390.2 [MH^+].

pL^4: The piperidone precursor for L^4 {3,5-dimethyl-2,6-dipyridyl-*N*-[2-(pyridyl)methylene]-4-piperidone-3,5-dicarboxylate} was obtained by a dropwise addition of pyridin-2-aldehyde (9.6 mL, 100 mmol), and then picolylamine (5.1 mL, 50 mmol) to an ice-cold solution of dimethyl acetonedicarboxylate (7.2 mL, 50 mmol) in MeOH (30 mL). After 5 min the orange solution was stored in a freezer (−18 °C). The crystallized product was collected after several days, washed with cold EtOH, and recrystallized from ethanol; a further crop could be obtained by evaporation of the filtrate. Total yield (recrystallized) 19.3 g (42 mmol, 84%).

Bispidones. L^3: An aqueous solution of methylamine (40%, 1.1 mL, 13.0 mmol) and aqueous formaldehyde (37%, 2.1 mL, 26 mmol) were added to a suspension of pL^3 (4.84 g, 12.4 mmol) in ethanol (200 mL) . The suspension was stirred under reflux for 2 h and a clear yellow solution emerged. The solvent was removed under low pressure and the remaining yellow-white solid was recrystallized from ethanol. Yield 3.57 g (8 mmol, 65.2%) of a white solid. $C_{21}H_{28}N_6O_5$ (444.5): calcd. C 56.75 , H 6.35 , N 18.90; found C 56.56 , H 6.48 , N 18.48. ^1H NMR (300.13 MHz, $CDCl_3$): δ = 1.67 (s, 3 H, NCH_3), 2.49 (s, 3 H, NCH_3), 3.62 (s, 6 H, OCH_3), 3.72 (s, 6 H, N_{Im}-CH_3), 3.73 (d, $^2J_{H,H}$ = 13.9 Hz, 2 H, N−CH_2−), 4.03 (s, 2 H, NC*H*), 4.63 (d, $^2J_{H,H}$ = 11.7 Hz, 2 H, N−CH_2−), 6.76 (s, 2 H, Im-*H*), 6.96 (s, 2 H, Im-*H*) ppm. ^{13}C NMR (75.47 MHz, $CDCl_3$): δ = 32.7 (NCH_3), 37.0 (NCH_3), 45.2 (NCH_2), 52.3 (OCH_3), 59.5 ($C_{q,Alkyl}$), 63.6 (N*C*H), 120.9 (Ar-*C*), 127.0 (Ar-*C*), 143.9 (Ar-*C*), 169.9 (ester), 202.0 (C=O) ppm.

L^4: Aqueous methylamine (40%, 4.8 mL, 56.7 mmol) and formaldehyde (37%, 9.2 mL, 113.4 mmol) were added to a suspension of pL^4 (21.79 g, 47.3 mmol) in ethanol (250 mL). The suspension was stirred under reflux for 3 h, and a deep-brown solution occurred. The solvent was removed under low pressure and the remaining brown-green solid was recrystallized from ethanol. Yield 6.58 g (12.7 mmol, 27.5%) of a white solid. $C_{28}H_{29}N_5O_5$ (515.6): calcd. C 65.23, H 5.67, N 13.58; found C 64.86, H 5.60, N 13.41. ^1H NMR (300 MHz, $CDCl_3$): δ = 2.20 (s, 3 H, N−CH_3), 2.56 (d, $^2J_{H,H}$ = 11.8 Hz, 2 H, −CH_2−), 2.98 (d, $^2J_{H,H}$ = 11.8 Hz, 2 H, −CH_2−), 3.72 (s, 8 H, OCH_3 + CH_2-Py), 5.42 (s, 2 H, CH-Py), 6.76 (d, $^3J_{H,H}$ = 7.7 Hz, 1 H, Py-H), 6.97 (t, $^3J_{H,H}$ = 5.7 Hz, 1 H, Py-H), 7.13 (t, $^3J_{H,H}$ = 6.0 Hz, 2 H, Py-H), 7.38 (t, $^3J_{H,H}$ = 7.6 Hz, 2 H, Py-H), 7.68 (t, $^3J_{H,H}$ = 7.6 Hz, 2 H, Py-H), 8.06 (d, $^3J_{H,H}$ = 7.6 Hz, 1 H, Py-H), 8.43 (d, $^3J_{H,H}$ = 4.6 Hz, 1 H, Py-H), 8.47 (d, $^3J_{H,H}$ = 4.4 Hz, 2 H, Py-H) ppm. ^{13}C NMR (75.47 MHz, $CDCl_3$): δ = 44.3 (N−CH_3), 52.3 (O−CH_3), 57.2 (CH_2-Py), 60.7 (CH_2−N), 62.3 (CH-Py), 70.2 ($C_{q,Alkyl}$), 121.5, 122.5, 123.7, 124.3, 135.4, 135.7, 148.9 ($C_{Ar,C-N}$), 149.0 ($C_{Ar,C-N}$), 156.5 ($C_{q,Ar}$), 158.8 ($C_{q,Ar}$), 168.6 (ester), 203.4 (C=O) ppm. FAB^+MS (Nibeol): *m*/*z* = 538.3 [M + Na^+], 516.3 [MH^+].

L^5: 2-(Aminomethyl)pyridine (4.3 g, 39.7 mmol) and aqueous formaldehyde (37%, 6.5 mL, 79.4 mmol) were added to a suspension of pL^1 (12.71 g, 33.1 mmol) in ethanol (200 mL). The suspension was stirred under reflux for 30 min and a clear brown solution occurred. The solvent was removed under low pressure, and the remaining green/brown solid was recrystallized from ethanol. Yield 4.2 g (8.1 mmol, 25.2%) of a white solid. $C_{28}H_{29}N_5O_5$ (515.6): calcd. C 65.23, H 5.67, N 13.58; found C 64.95, H 5.62, N 13.48. ^1H NMR (300 MHz, $CDCl_3$): δ = 1.94 (s, 3 H, N−CH_3), 2.68 (d, $^2J_{H,H}$ = 12.1 Hz, 2 H, −CH_2−), 3.14 (d, $^2J_{H,H}$ = 11.9 Hz, 2 H, −CH−), 3.57 (s, 2 H, CH_2-Py), 3.76 (s, 6 H, OCH_3), 4.66 (s, 2 H, CH-Py), 7.09 (t, $^3J_{H,H}$ = 1.5 Hz, 2 H, Py-H), 7.21 (t, $^3J_{H,H}$ = 6.0 Hz, 1 H, Py-H), 7.33 (d, $^3J_{H,H}$ = 7.6 Hz, 1 H, Py-H), 7.50 (t, $^3J_{H,H}$ = 1.7 Hz, 2 H, Py-H), 7.66 (t, $^3J_{H,H}$ = 7.5 Hz, 1 H, Py-H), 7.92 (d, $^3J_{H,H}$ = 7.8 Hz, 2 H, Py-H), 8.45 (d, $^3J_{H,H}$ = 4.0 Hz, 2 H, Py-H), 8.62 (d, $^3J_{H,H}$ = 4.8 Hz, 1 H, Py-H) ppm. ^{13}C NMR (75.47 MHz, $CDCl_3$): δ = 42.9 (N−CH_3), 52.3 (O−CH_3), 58.5 (CH_2−N), 62.1 (CH-Py), 63.3 (CH_2-Py), 73.6 ($C_{q,Alkyl}$), 122.2, 122.7, 123.6, 124.3, 136.1, 148.9 ($C_{Ar,C-N}$), 149.3 ($C_{Ar,C-N}$), 156.7

 © 2003 Wiley-VCH Verlag GmbH & Co. KGaA, Weinheim

($C_{q,Ar}$), 158.2 ($C_{q,Ar}$), 168.3 (ester), 203.2 (C=O) ppm. FAB^+MS (Nibeol): m/z = 538.3 [M + Na^+], 516.3 [MH^+].

Syntheses of the Copper(II) Compounds. General Method: A solution of the metal salt (1 mmol) in methanol (1 mL) was added to a solution of of the ligand (1 mmol) in acetonitrile (1 mL) . The mixture was stirred for 24 h, the solvent was then evaporated to dryness and the resulting solid washed twice with EtOAc, and dried in vacuo. Note that the ε values given below, specifically for the BF_4^- salts, are not necessarily of pure compounds, with various coordinated solvent molecules, e.g. OH_2, OMe, see text.

[Cu(L^3)(Cl)]Cl: $C_{21}H_{28}Cl_2CuN_6O_5{\cdot}2H_2O$ (614.97): calcd. C 41.01, H 5.24, N 13.63; found C 41.33, H 5.30, N 13.89. FAB^+MS (NBA): m/z = 542.1 ([Cu(L^3)(Cl)]H^+), 560.1 ([Cu(L^3)(Cl)(H_2O)]H^+). IR: ν̃ = 3198 (m, OH), 3096 (w), 2948 (m), 1732 (s), 1540 (w), 1500 (m), 1282 (s), 1272 (s), 1070 (m), 760 cm^{-1} (w). UV/Vis (MeOH): λ (ε, $cm^2{\cdot}mol^{-1}$) = 638 (96), 279 (2520), 237 nm (2340).

[Cu(L^3)](BF_4)$_2$: M.p. 181 °C. $C_{21}H_{28}B_2CuF_8N_6O_5{\cdot}2H_2O$ (717.67): calcd. C 35.14, H 4.49, N 11.71; found C 35.15, H 4.94, N 11.15. FAB^+MS (NBA): m/z = 525.3 ([Cu(L^3)(H_2O)]H^+). $E_{1/2}$ (MeCN) = −440 mV. IR: ν̃ = 3502 (s), 3400 (s), 3136 (m), 2958 (m), 1728 (s), 1544 (w), 1504 (m), 1452 (m), 1274 (s), 1040 (s), 758 cm^{-1} (m). UV/Vis (MeOH): λ (ε, $cm^2{\cdot}mol^{-1}$) = 668 (51), 334 (299), 260 (1088), 237 nm (2289).

[Cu(L^4)(Cl)]Cl: $C_{28}H_{29}Cl_2CuN_5O_5{\cdot}H_2O$ (668.03): calcd. C 49.51, H 4.62, N 10.69; found C 49.53, H 4.89, N 11.05. FAB^+MS (NBA): m/z = 631.2 ([Cu (L^4)(Cl)(OH_2)]H^+). IR: ν̃ = 3376 (s, OH), 3101 (w), 2952 (m), 1724 (s), 1603 (m), 1465 (m), 1423), 1247 (s), 1046 (m), 789 (m), 647 (w), 532 cm^{-1} (w). UV/Vis (MeOH): λ (ε, $cm^2{\cdot}mol^{-1}$) = 714 (29), 260 nm (3035).

[Cu(L^4)](BF_4)$_2$: $C_{28}H_{29}B_2CuF_8N_5O_5{\cdot}2H_2O$ (788.75): calcd. C 42.64, H 4.22, N 8.88; found C 42.86, H 4.32, N 9.01. $E_{1/2}$ = −489 mV in acetonitrile. IR: ν̃ = 3386 (s), 3098 (w), 2952 (m), 1726 (s), 1605 (m), 1465 (m), 1423 (m), 1247 (s), 1046 (m), 786 (m), 645 (w), 534 cm^{-1} (w). UV/Vis (MeOH): λ (ε, $cm^2{\cdot}mol^{-1}$) = 704 (69), 260 nm (3135).

[Cu (L^5)(Cl)]Cl: $C_{28}H_{29}Cl_2CuN_5O_5{\cdot}2H_2O$ (686.04): calcd. C 49.02, H 4.85, N 10.21; found C 49.06, H 4.81, N 10.27. FAB^+MS (NBA): m/z = 631.1 ([Cu(L^5)(Cl)(H_2O)]H^+). UV/Vis (MeOH): λ (ε, $cm^2{\cdot}mol^{-1}$) = 633 (55), 262 (2694), 242 nm (2535).

[Cu(L^5)](BF_4)$_2$: $C_{28}H_{29}B_2CuF_8N_5O_5{\cdot}2H_2O$ (788.75): calcd. C 42.64, H 4.22, N 8.88; found C 42.37, H 4.32, N 8.80. FAB^+MS(NBA): m/z = 596.3 ([Cu(^{5})(OH_2)]H^+).

$E_{1/2}$ (MeCN) = −603 mV. IR: ν̃ = 3444 (s), 3084 (m), 2956 (m), 1730 (s), 1608 (m), 1460 (w), 1438 (m), 1256 (s), 1040 (vs), 764 cm^{-1} (m). UV/Vis (MeOH): λ (ε, $cm^2{\cdot}mol^{-1}$) = 621 (71), 262 (3483), 247 nm (3337).

Catalysis: The aziridination reactions were performed by stirring mixtures of PhINTs (0.4, 0.5, 0.6 mmol), styrene (1.0 mL) and the copper catalyst (5, 3.5, 1.7 mol % vs. PhINTs) in anhydrous CH_3CN (2.0 mL) under a dry argon atmosphere at 25 °C (the catalyst and PhINTs concentrations were varied to determine the maximum TON, see Results and Discussion; all results reported are averages of at least three experiments). For the studies with the Cu^I catalysts care was taken to do the experiments under strictly anaerobic conditions. After 7 h the green solutions were passed through a short column of neutral alumina to remove the copper species, eluted with EtOAc (20 mL), and the elutes were evaporated to yield oily residues. These crude mixtures were recrystallized with hexane to produce the pure aziridine products. $C_{15}H_{15}NO_2S$ (273.3): calcd. C 65.91, H 5.53, N 5.12; found C 65.84, H 5.56 , N 5.14. ^1H NMR (300 MHz, $CDCl_3$): δ = 2.34−2.42 (m, 4 H), 2.98 (d, $^3J_{H,H}$ = 7.2 Hz, 1 H), 3.77 (dd, $^3J_{H,H}$ = 4.7, $^2J_{H,H}$ = 2.3 Hz, 1 H), 7.10−7.34 (m, 7 H), 7.88 (d, $^3J_{H,H}$ = 6.7 Hz, 2 H) ppm.

Crystal Structure Determination: Crystal data and details of the structure determinations are listed in Table 1. Intensity data were collected at low temperature on a Bruker AXS Smart 1000 diffractometer (Mo-K_α, λ = 0.71073 Å, ω-scan). Absorption corrections were performed (multiple scans of equivalent reflections, SADABS). The structures were solved by direct methods and refined by full-matrix least-squares against F^2 of all data, using SHELXTL 5.1.[33]

All non-hydrogen atoms were refined with anisotropic temperature factors. Hydrogen atoms were located in difference Fourier syntheses and refined isotropically. In [Cu(L^3)(Cl)]Cl one of the ester groups (at C-5) of the bispidine ligand is disordered. [Cu(L^4)(Cl)]Cl crystallizes with a disordered acetonitrile molecule.

Table 4. Crystal Data of the copper(II) complexes of $L^{3,4,5}$

	[Cu(L^3)(Cl)]Cl	[Cu(L^4)(Cl)]Cl	[Cu(L^5)(Cl)]Cl
Formula	$C_{21}H_{35}Cl_2CuN_6O_9$	$C_{30}H_{34}Cl_2CuN_6O_6$	$C_{28}H_{33}Cl_2CuN_5O_7$
Formula mass	649.99	709.07	686.03
Space group	$P2_1/c$	$P2_1/c$	$P2_1/n$
a, Å	17.9674(11)	12.3631(11)	13.3492(6)
b, Å	11.9389(7)	23.006(2)	15.6044(7)
c, Å	13.0050(8)	11.1856(10)	14.8385(7)
β, deg	97.030(1)	91.465(2)	110.492(1)
V, Å^3	2768.7(3)	3180.5(5)	2895.4(2)
Z	4	4	4
T, K	190(2)	190(2)	173(2)
$\rho_{calcd.}$, g·cm^{-3}	1.559	1.481	1.574
μ, mm^{-1}	1.042	0.907	0.995
R (F_o)	0.0442	0.0548	0.0351
wR_2 (F_o^2)	0.1323	0.1595	0.0977
μ, mm^{-1}	1.042	0.907	0.995
R (F_o)	0.0442	0.0548	0.0351
wR_2 (F_o^2)	0.1323	0.1595	0.0977

 © 2003 Wiley-VCH Verlag GmbH & Co. KGaA, Weinheim

CCDC 197128−197130 contains the crystallographic data for this paper. This data can be obtained free of charge wire www.ccdc.cam.ac.uk/conts/ or from the Cambridge Crystallographic Data Centre 12 Union Road, Cambridge CB21EZ (Fax: (internat.) +44-1223-336-033; E-mail: depost@ccdc.cam.ac.uk).

Acknowledgments

Generous financial support by the Deutsche Forschungsgemeinschaft (DFG) is gratefully acknowledged. We are grateful to Dr. Lutz Lötzbeyer for measuring the EPR spectra.

[1] D. Tanner, *Angew. Chem. Int. Ed. Engl.* **1994**, *35*, 599.
[2] H. C. Kolb, M. G. Finn, K. B. Sharpless, *Angew. Chem. Int. Ed.* **2001**, *40*, 2004.
[3] S. Shizeki, M. Ohtsuka, K. Irinoda, K. Kukita, K. Nagaoka, T. J. Nakashina, *Antibiot.* **1987**, *40*, 60.
[4] R. S. Coleman, J.-S. Kong, *J. Am. Chem. Soc.* **1998**, *120*, 3538.
[5] H. Kwart, A. A. Kahn, *J. Am. Chem. Soc.* **1967**, *89*, 1950.
[6] P. Müller, *Transition metal-catalyzed nitrene transfer: aziridination and insertion*, vol. *2*, JAI Press Inc., **1997**.
[7] D. A. Evans, M. M. Faul, M. T. Bilodean, *J. Org. Chem.* **1991**, *56*, 6744.
[8] D. A. Evans, M. M. Faul, M. T. Bilodeau, B. A. Anderson, D. M. Barnes, *J. Am. Chem. Soc.* **1993**, *115*, 5328.
[9] D. A. Evans, M. M. Faul, M. T. Bilodeau, *J. Am. Chem. Soc.* **1994**, *116*, 2742.
[10] Z. Li, K. R. Conser, E. N. Jacobsen, *J. Am. Chem. Soc.* **1993**, *115*, 5326.
[11] Z. Li, R. W. Quan, E. N. Jacobsen, *J. Am. Chem. Soc.* **1995**, *117*, 5889.
[12] E. N. Jacobsen, *Aziridiantion*, vol. 2 **1999**.
[13] T. P. Albone, P. S. Aujnla, P. C. Taylor, S. Challenger, A. M. Derrick, *J. Org. Chem.* **1998**, *63*, 9569.
[14] P. Dauban, R. H. Dodd, *J. Org. Chem.* **1999**, *64*, 5304.
[15] A. V. Gontcharov, H. Liu, K. B. Sharpless, *Org. Lett.* **1999**, *1*, 783.
[16] M. M. Diaz-Requejo, P. J. Perez, M. Brookhart, J. L. Templeton, *Organometallics* **1997**, *16*, 4399.
[17] P. Brandt, M. J. Södergren, P. G. Andersson, P.-O. Norrby, *J. Am. Chem. Soc.* **2000**, *122*, 8013.
[18] J. A. Halfen, J. K. Hallman, J. A. Schultz, J. P. Emerson, *Organometallics* **1999**, *18*, 5435.
[19] J. A. Halfen, D. C. Fox, M. P. Mehn, L. Que, *Inorg. Chem.* **2001**, *40*, 5060.
[20] J. A. Halfen, J. M. Uhan, D. C. Fox, M. P. Mehn, L. Que, Jr., *Inorg. Chem.* **2000**, *39*, 4913.
[21] P. Comba, A. Lienke, *Inorg. Chem.* **2001**, *40*, 5206.
[22] H. Börzel, P. Comba, C. Katsichtis, W. Kiefer, A. Lienke, V. Nagel, H. Pritzkow, *Chem. Eur. J.* **1999**, *5*, 1716.
[23] H. Börzel, P. Comba, K. S. Hagen, C. Katsichtis, H. Pritzkow, *Chem. Eur. J.* **2000**, *6*, 914.
[24] H. Börzel, P. Comba, H. Pritzkow, *Chem. Commun.* **2001**, 97.
[25] H. Börzel, P. Comba, K. S. Hagen, M. Kerscher, H. Pritzkow, M. Schatz, S. Schindler, O. Walter, *Inorg. Chem.* **2002**, *41*, 5440.
[26] P. Comba,W. Schiek, *Coord. Chem. Rev.,* in press.
[27] P. Comba, M. Kerscher, M. Merz, V. Müller, H. Pritzkow, R. Remenyi, W. Schiek, Y. Xiong, *Chem. Eur. J.* **2002**, *8*, 5750.
[28] P. Comba, S. Kuwata, G. A. Lawrance, *manuscript in preparation*.
[29] P. Comba, M. Kerscher, A. Roodt, submitted.
[30] E. A. Ambundo, M.-V. Deydier, A. J. Grall, N. Agnera-Vega, L. T. Dressel, T. H. Cooper, N. J. Heeg, L. A. Ochrymowycz, D. B. Rorabacher, *Inorg. Chem.* **1999**, *38*, 4233.
[31] D. Wang, G. R. Hanson, *J. Magn. Reson. A* **1995**, *117*, 1.
[32] D. Wang, G. R. Hanson, *Appl. Magn. Reson.* **1996**, *11*, 401.
[33] G. M. Sheldrick, SHELXTL NT V5.10, Bruker AXS, Madison, Wisconsin, USA, **1999**.
[34] C. K. Johnson, ORTEP, *A Thermal Ellipsoid Plotting Program*, Oak National Laboratories, Oak Ridge, TN, **1965**.

Received November 22, 2002

 © 2003 Wiley-VCH Verlag GmbH & Co. KGaA, Weinheim

Cyanide-Bridged Oligonuclear Complexes Containing Ni-CN-Cu and Pt-CN-Cu Linkages

Marie-Louise Flay[a] and Heinrich Vahrenkamp*[a]

Keywords: Nickel / Platinum / Copper / Cyanide

The central building blocks $Ni(CN)_4^{2-}$ and $Pt(CN)_4^{2-}$ can be combined with one, two or four $Cu^{II}L$ units (L = tren, Me_6tren, tpa) to form di-, tri- and pentanuclear complexes with Ni-CN-Cu and Pt-CN-Cu linkages. Structure determinations of these and the side product [(tren)-Cu–CN–Cu(tren)] $(ClO_4)_2$ reveal mostly linear M-C-N-Cu arrays and *cis*-, *trans*- and star-like arrangements of the CN-Cu units around the central Ni or Pt ions. The $\tilde{\nu}$(CN) IR data for the bridging cyanides show a characteristic hypsochromic effect compared to the data for the free $M(CN)_4^{2-}$ complexes. The absorption bands in the visible spectra of the oligonuclear complexes are shifted to shorter wavelengths than those of the free LCu^{II}-X complexes. The Cu^{II}/Cu^{I} redox steps in the cyclic voltammograms allow the conclusion that there is electronic communication between the external CuL units when they are arranged in a *trans*-orientation at Pt^{II}, but not Ni^{II}, centers.

(© Wiley-VCH Verlag GmbH & Co. KGaA, 69451 Weinheim, Germany, 2003)

Introduction

In a series of papers[1–6] and a review article[7] we have outlined and justified our research work on cyanide-bridged oligonuclear complexes with chain-like arrangements of metal ions and cyanide ligands. This work, which has also been pursued by the research groups of Haim,[8] Connelly,[9] Vogler,[10] Scandola[11] and Denning,[12] originates from the observation that a bridging cyanide is a good conductor of electronic interactions between the metallic groups attached to it. In this context it is not so much the bulk properties like magnetism, luminescence or electrical conductivity that interest us, but the phenomena which result from metal-metal charge transfer like multi-redox steps, mixed valence and long-range electronic interactions.

For this purpose we have synthesized a series of compounds in which the number of cyanide-bridged metal atoms, their ligation patterns and redox properties, the orientation of the bridging ligand (CN versus NC) and the geometry at the interconnected metal atoms (cis, trans, tetrahedral, square planar, octahedral) have been varied. So far we, like others, have been unable to fully characterize chains with more than three CN-linked metal atoms. The best, though not the only, arrangement for long-range metal-metal interactions was found in trans-configured central $M(CN)_2$ or $M(NC)_2$ units derived from square-planar L_2MX_2 or octahedral L_4MX_2 building blocks. Of these, linear arrays M′(μ-CN)Pt(μ-CN)M′ of organometallic L_nM' units attached to $Pt(CN)_2$ centers were the best objects of study due to their inertness and favourable redox properties.[2]

Based on this we have focused our synthetic work on the complexes $[Pt(CN)_4]^{2-}$ and $[Ni(CN)_4]^{2-}$ as starting materials, to which various external redox-active complex units were to be attached. For the present work we chose copper-containing external units in which copper is in a trigonal-bipyramidal ligand environment due to the fact that both Cu^{I} and Cu^{II} are reasonably stable in this environment. The uncharged tripodal ligands tren, Me_6tren and tpa were used to support the trigonal bipyramidal geometry at copper. While the main purpose of the work was to study linear Cu-NC-Ni-CN-Cu and Cu-NC-Pt-CN-Cu arrays, we were also interested in finding out whether all possible modes of attachment of the copper units to the $M(CN)_4$ centers (one to four such units and cis or trans arrays for two of them) could be realized.

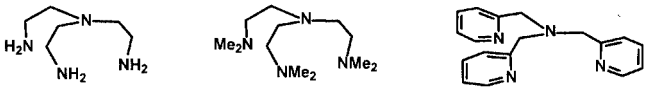

tren Me_6tren tpa

Results and Discussion

$Ni(CN)_4$-Centered Complexes

The first experiments in this series yielded an unexpected result: when $(PPN)_2[Ni(CN)_4]$ was treated with four equiva-

[a] Institut für Anorganische und Analytische Chemie der Universität Freiburg,
Albertstr. 21, 79104 Freiburg, Germany
Fax: (internat.) + 49-(0)761/203-6001
E-mail: vahrenka@uni-freiburg.de

lents of $[Cu(tren)H_2O](ClO_4)_2$ in dimethylformamide, cyanide transfer occurred and the dicopper complex **1** was obtained. It turned out that cyanide transfer is a common feature in these compounds, and could be avoided by using not too polar solvents. Complex **1** with PF_6 counterions has already been described, but not structurally characterized.[13] In addition, the analogous complexes with Me_3tren and Me_6tren ligands have been fully characterized.[14,15]

$$[(tren)Cu-CN-Cu(tren)](ClO_4)_3$$
1

Compound **1** can be considered a reference compound here for structural and spectroscopic comparisons. Its $\tilde{\nu}$(CN) IR absorptions (2182 and 2163 cm^{-1} in KBr) occur at the upper end of the frequency range of all copper compounds described here, and they are also higher than all other reported values for dinuclear M-CN-M′ complexes with organometallic constituents.[1] This means that the $(tren)Cu^{II}$ unit at the C terminus of the cyanide (the only such unit in this paper) is a very poor π-backdonator. The fact that two $\tilde{\nu}$(CN) bands are observed is explained by the existence of two independent complex units in the asymmetric unit of the crystals' unit cell (see below). The spread of the two bands for identical species may serve as a caveat against too detailed discussions of $\tilde{\nu}$(CN) variations in such complexes.

The intended attachment of two L·Cu units to the $Ni(CN)_4$ center could be achieved by adjusting the conditions for (tren)Cu, (Me_6tren)Cu and (tpa)Cu. All three resulting complexes **2**, **3** and **4** were obtained as *trans*-$Ni(CN)_2X_2$ species, i.e. they contain the linear Cu-NC-Ni-CN-Cu arrays. In one case, however, the use of $K_2[Ni(CN)_4]$ instead of $(PPN)_2[Ni(CN)_4]$, and a slight variation of the reaction conditions, yielded a small amount of the *cis*-oriented complex **5**. In contrast to all other new compounds in this paper, which are blue, **5** is blue-green. In one case, namely for L·Cu = (tpa)Cu, the attachment of four L·Cu units was possible: $(PPN)_2[Ni(CN)_4]$ and four equivalents of $[Cu(tpa)CH_3CN](ClO_4)_2$ yielded the pentanuclear complex **6**.

trans-$[L{\cdot}Cu\text{-}NC\text{-}Ni(CN)_2\text{-}CN\text{-}Cu{\cdot}L](ClO_4)_2$
2: L = tren; **3**: L = Me_6tren; **4**: L = tpa

cis-$[(tpa)Cu\text{-}NC\text{-}Ni(CN)_2\text{-}CN\text{-}Cu(tpa)](ClO_4)_2$
5

$[Ni\{CN\text{-}Cu(tpa)\}_4](ClO_4)_6$
6

$Pt(CN)_4$-Centered Complexes

The chemistry of the $Pt(CN)_4$-centered complexes was not fully analogous to that of the $Ni(CN)_4$-centered ones. For platinum the attachment of only one L·Cu unit was possible, resulting in the dinuclear complex **7**. Complex **7** corresponds to several such dinuclear complexes obtained from $L_2Pt(CN)_2$ species and organometallic building blocks. Its low symmetry is reflected by the occurrence of four $\tilde{\nu}$(CN) bands (see Exp. Sect.) of which the highest one at 2179 cm^{-1} can be assigned to the bridging cyanide.

$$[(tpa)Cu\text{-}NC\text{-}Pt(CN)_3]$$
7

The attachment of two L·Cu units to the $Pt(CN)_4$ center occurred in the trans fashion in all three cases, yielding the trinuclear complexes **8**, **9** and **10**. As expected, these complexes have a higher thermal stability than their nickel-containing analogues **2**, **3** and **4**. Attempts to attach three L·Cu fragments to $[Pt(CN)_4]^{2-}$ failed, despite the fact that such complexes with Cp(dppe)Fe and $Cp(PPh_3)_2Ru$ fragments are known.[16] In the case of (tpa)Cu, however, four such units could again be attached, resulting in pentanuclear **11**. As in the nickel case, all these compounds are blue, and despite their high perchlorate content, specifically in **6** and **11**, none of the compounds was found to be explosive.

trans-$[L{\cdot}Cu\text{-}NC\text{-}Pt(CN)_2\text{-}CN\text{-}Cu{\cdot}L](ClO_4)_2$
8: L = tren; **9**: L = Me_6tren; **10**: L = tpa

$[Pt\{CN\text{-}Cu(tpa)\}_4](ClO_4)_6$
11

Structure Determinations

Dinuclear Complexes

The structure of the dinuclear cation of **1** is shown in Figure 1. The asymmetric unit of the orthorhombic crystals contains two independent half-molecules, each of which is related to the other half by a twofold rotation. This makes C and N of the bridging cyanide indistinguishable and a discussion of the bond lengths for the bridging ligand irrelevant. Yet these bond lengths are close to those in the related complexes with Me_3tren and Me_6tren ligands.[14,15] The most notable feature in the structure of **1** is the bending of the Cu-C-N (or Cu-N-C) arrays, which is moderate yet significant, with angles of 164.7(3) and 170.2(3)°.

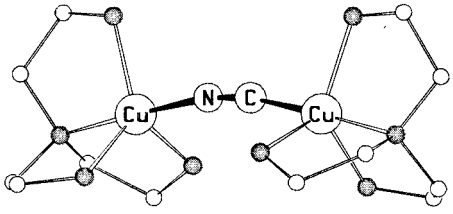

Figure 1. Structure of one of the two independent dinuclear cations of complex **1**; relevant bond lengths: Cu−C or Cu−N 2.008(9) or 1.956(9); C−N 1.134(18) or 1.138(18) Å

The neutral complex **7** also has two formula units in the asymmetric unit and shares the low crystal quality, which is obvious from the high *R* value, and an irregular spread of Pt−C, C−N and Cu−N bond lengths. Thus the structure is mainly a proof of the identity of the complex (Figure 2). Again, there is a slight bending along the Pt-C-N-Cu sequence with Pt−C−N angles of 174(2)° and Cu−N−C angles of 169(2)°. Again there is a closely related and structurally similar reference compound: $[(NH_4)_3Cu\text{-}NC\text{-}Pt(CN)_3]$.[17]

 © 2003 Wiley-VCH Verlag GmbH & Co. KGaA, Weinheim

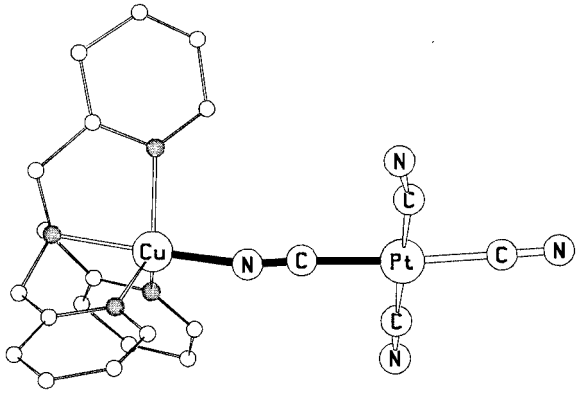

Figure 2. Structure of one of the two independent complex molecules of **7**; relevant bond lengths: Pt−C 1.91(2) and 2.02(2); Cu−N 1.95(2) and 1.94(2); C−N 1.19(3) and 1.09(3) Å.

Trinuclear Complexes

According to our experience the attachment of two ML_n units to $[Ni(CN)_4]^{2-}$ or $[Pt(CN)_4]^{2-}$ leads to trans arrays for steric reasons.[2,16] The *cis*-trinuclear complex **5** is a singular exception to this rule. The complex cation (Figure 3) has twofold symmetry. It is noteworthy that the Ni−C as well as the C−N bond lengths are identical for the terminal and the bridging cyanides. In this complex the bending of the Ni-C-N-Cu array is a means of identifying the C and N atoms of the bridging cyanide: characteristically[1−6] the Ni−C−N angle is close to 180° while the Cu−N−C angle (169°) deviates noticeably from linearity.

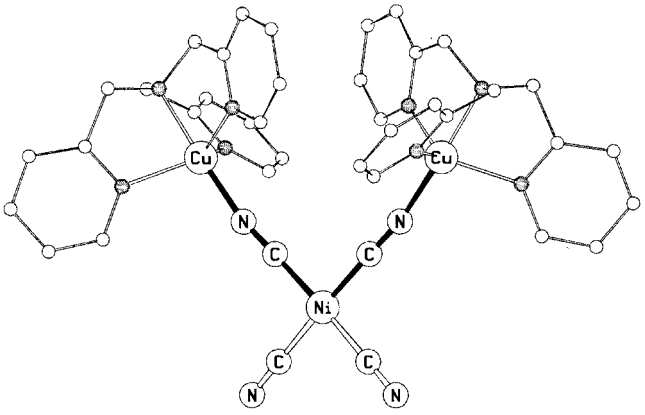

Figure 3. Structure of the trinuclear cation of **5**; relevant bond lengths (Å) and angles (°): Ni−C(term) 1.845(2), Ni−C(br) 1.842(2), C−N(term) 1.163(7), C−N(br) 1.161(7), Cu−N 1.938(5), Ni−C−N(br) 177.5(7), Cu−N−C 168.9(5)

The two $PtCu_2$ complexes **8** and **10** (Figure 4 and 5) can be discussed together. Both contain the Pt center in a virtually ideal square-planar environment, both have the platinum atom on a center of symmetry, both have nearly linear Pt−C−N(bridge) arrays, and in both cases the Cu-N-C array is significantly bent. Again the Pt−C distances are the same for the terminal and the bridging cyanides which seems to indicate that the L·Cu units have rather low σ-acceptor properties. This is reflected by the identical C−N bond lengths for the terminal and bridging cyanides in **10**. These bond lengths differ by 0.08 Å in **8**, which however, like in **7**, may be a reflection of low crystal quality. Most of these features correspond to those of the *trans*-$Pt(CN)_4$ complex with terminal FeCp(dppe) units.[2]

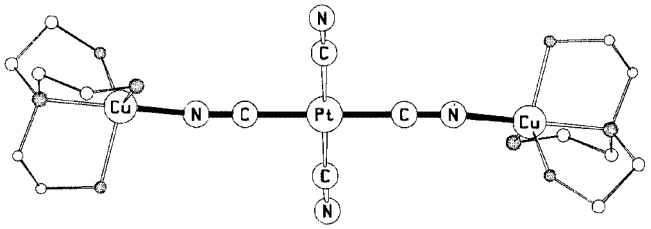

Figure 4. Structure of the trinuclear cation of **8**; relevant bond lengths (Å) and angles (°): Pt−C(term) 1.96(1), Pt−C(br) 1.96(1), C−N(term) 1.12(2), C−N(br) 1.20(2), Cu−N 1.92(1); Pt−C−N(br) 179(1), Cu−N−C 169(1)

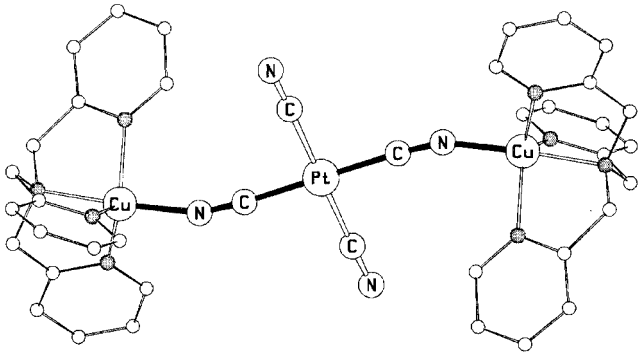

Figure 5. Structure of the trinuclear cation of **10**; relevant bond lengths (Å) and angles (°): Pt−C(term) 1.987(7), Pt−C(br) 1.988(6), C−N(term) 1.142(8), C−N(br) 1.146(8), Cu−N 1.953(5); Pt−C−N(br) 176.0(6), Cu−N−C 160.0(5)

Pentanuclear Complexes

Complexes **6** (Figure 6) and **11** (Figure 7) seem to be the first derivatives of $[Ni(CN)_4]^{2-}$ and $[Pt(CN)_4]^{2-}$ in which all four cyanide ligands are bridging. There are, however, numerous star-like complexes of the type $M(\mu\text{-}CN\text{-}M'L_n)_x$,[7] and the closest relative of **6** and **11** is $[Fe\{CN\text{-}Cu(tpa)\}_6]^{8+}$.[18] While the low crystal quality of **6** renders its structure determination only useful as a product identification, the good crystal quality of **11** allows a meaningful discussion of its molecular dimensions. Complexes **6** and **11** are not isostructural, and only in **6** is the central metal on a center of symmetry. Nevertheless the general appearance of both complexes is quite similar: there is only a small spread of the Ni−C, Pt−C, C−N and Cu−N bond lengths, and these bond lengths correspond closely to those in the trinuclear complexes. There is, however, a variable degree of bending in the Cu-N-C-M-C-N-Cu chains. In **6** one of these chains is linear to a good approximation, the other shows severe bending in a wave-like fashion, as expressed by the

 © 2003 Wiley-VCH Verlag GmbH & Co. KGaA, Weinheim

Cu−N−C angle of 162°. In **11** the Cu−N−C angles vary progressively from 176 to 165°, the Pt−C2−N2−Cu2 array is closest to linearity and the Pt−C1−N1−Cu1 array is most distorted.

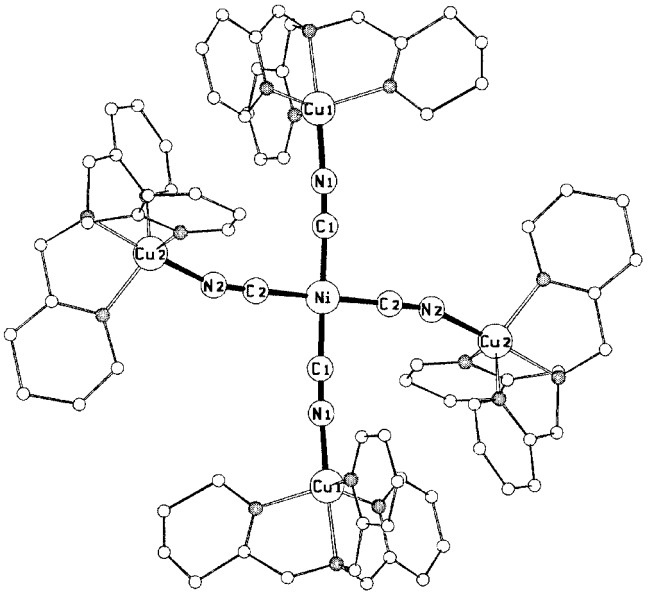

Figure 6. Structure of the pentanuclear cation of **6**; relevant bond lengths (Å) and angles (°): Ni−C1 1.84(2), Ni−C2 1.86(2), C1−N1 1.16(2), C2−N2 1.16(2), Cu1−N1 1.92(2), Cu2−N2 1.94(2); Ni−C1−N1 176.7(14), Ni−C2−N2 178.0(15), Cu1−N1−C1 176.0(18), Cu2−N2−C2 161.9(17)

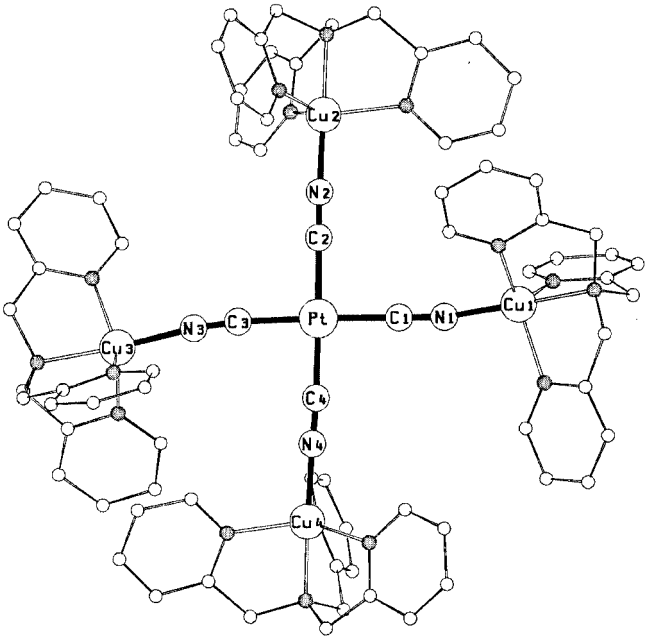

Figure 7. Structure of the pentanuclear cation of **11**; relevant bond lengths (Å) and angles (°): Pt−C1 2.004(6), Pt−C2 1.997(7), Pt−C3 1.995(7), Pt−C4 1.970(7), C1−N1 1.121(8), C2−N2 1.135(8), C3−N3 1.112(8), C4−N4 1.139(8), Cu1−N1 1.940(6), Cu2−N2 1.935(6), Cu3−N3 1.949(6), Cu4−N4 1.948(6); Pt−C1−N1 179.4(7), Pt−C2−N2 179.0(6), Pt−C3−N3 174.0(6), Pt−C4−N4 176.0(7), Cu1−N1−C1 165.2(6), Cu2−N2−C2 176.2(6), Cu3−N3−C3 173.8(6), Cu4−N4−C4 170.4(7)

Altogether it must be stated that the structures of these copper-containing complexes yield only few data for comparative discussions, unlike those of the organometallic complexes that we investigated previously.[1−6] None of the pertinent bond lengths Pt−C, Ni−C, C−N or Cu−N varies significantly with the number of bridging cyanides or the geometry of the complexes. This seems to indicate that the copper(II) ion in those compounds is neither a good π-donor nor a strong σ-acceptor. Thus the Ni−C and Pt−C π-backbonding, which is reflected in the Ni−C, Pt−C and C−N bond lengths, does not vary much, accounting for the similar features of all complexes which were structurally characterized here.

IR Spectroscopy

IR spectroscopy is a more sensitive probe than structure determination for bonding variations in M-CN-M′ arrays. Previously we had observed for $L_2Pt(\text{-CN-M}')_2$ systems with organometallic building blocks M′ that the increase of $\tilde{\nu}$(CN) upon coordination of the second metal (which is a general phenomenon due to the kinematic effect) is modulated in a typical way by the π-donor and σ-acceptor properties of the attached metals.[1,2] As a rule the electron withdrawal by the σ-acceptor at the CN's N terminus is compensated by an increased π-donation from the metal at the C terminus, resulting in a reduction in the increase in $\tilde{\nu}$(CN).[2] Table 1 shows that similar effects are also observed here.

Table 1. IR data for the tri- and pentanuclear complexes [in KBr; $\tilde{\nu}$(CN) in cm^{-1}]

Complex	Backbone	CN_{bridge}	$CN_{term.}$
$[Ni(CN)_4]^{2-}$			2112
$[Pt(CN)_4]^{2-}$			2123
2	*trans*-$Ni(CN\text{-}Cu)_2$	2176	2125
3	*trans*-$Ni(CN\text{-}Cu)_2$	2172	2135
4	*trans*-$Ni(CN\text{-}Cu)_2$	2159	2126
5	*cis*-$Ni(CN\text{-}Cu)_2$	2158	2137, 2126
6	$Ni(CN\text{-}Cu)_4$	2175	
8	*trans*-$Pt(CN\text{-}Cu)_2$	2165	2139
9	*trans*-$Pt(CN\text{-}Cu)_2$	2182	2147
10	*trans*-$Pt(CN\text{-}Cu)_2$	2169	2137
11	$Pt(CN\text{-}Cu)_4$	2196	

For all tri- and pentanuclear complexes the IR bands of the terminal and bridging CN ligands can be clearly discerned. The band positions for the terminal cyanides are only slightly different from those of the $[M(CN)_4]^{2-}$ complexes. In contrast, $\tilde{\nu}$(CN) for the bridging cyanides rises considerably, in fact much more than for the analogous complexes with external organometallic building blocks.[2,16] The number of the CN absorptions corresponds to the symmetry of the complexes. This is also the basis for the assignment of the *trans*-symmetry for **4**, while the *cis*-symmetry of its isomer **5**, which was confirmed by the structure determination, is also reflected in the higher number of its $\tilde{\nu}$(CN) IR bands.

 © 2003 Wiley-VCH Verlag GmbH & Co. KGaA, Weinheim

The $\tilde{\nu}$(CN) values due to the CN bridges can be interpreted satisfactorily by a variable degree of π back-donation from the Ni and Pt centers. Compared to the $[M(CN)_4]^{2-}$ references the values are raised by 42−64 cm^{-1} for the trinuclear and by 63 and 73 cm^{-1} for the pentanuclear complexes. In the pentanuclear complexes the π-backbonding capacity of the central metals has to be shared by four CN ligands and hence their $\tilde{\nu}$(CN) values are lowered to a lesser degree than those of the trinuclear complexes (after the raising due to the kinematic effect). Among the trinuclear complexes those with the Cu(tpa) units have (on average) the lowest $\tilde{\nu}$(CN) values. This sheds light on the origin of the variable π-backdonation: the aromatic tripod tpa provides less electron density to the copper ions than the aliphatic tripods tren and Me_6tren. Hence the Cu(tpa) unit is a better σ-acceptor, which in turn forces the central metal to provide more π back-donation. As mentioned above, these effects are smaller here than for the analogous complexes with organometallic constituents.[2,16] Yet, unlike the data from the structure determinations, they have yielded a consistent interpretation of the electronic situation of the various M-CN-Cu groupings.

Electronic Spectra

Cu^{II} in a trigonal-bipyramidal ligand environment gives rise to two d-d transitions in the visible or NIR range which are the origin of its bluish colours.[19] In practice one broad band at 700−800 nm with a more or less pronounced shoulder on the higher energy side is observed.[20] This is also the case here. Table 2 lists the data for the main absorption bands.

Table 2. Electronic spectra (solvent acetonitrile, λ in nm, ε in $M^{-1}\cdot cm^{-1}$)

Complex	Backbone	$\lambda_{max}(\varepsilon)$
tren complexes		
$[Cu(tren)H_2O](ClO_4)_2$		870(140)
2	*trans*-Ni(CN-Cu)$_2$	815(315)
8	*trans*-Pt(CN-Cu)$_2$	835(315)
Me_6tren complexes		
$[Cu(Me_6tren)H_2O](ClO_4)_2$		850(500)
3	*trans*-Ni(CN-Cu)$_2$	805(1400)
9	*trans*-Pt(CN-Cu)$_2$	830(1100)
tpa complexes		
$[Cu(tpa)CH_3CN](ClO_4)_2$		860(150)
4	*trans*-Ni(CN-Cu)$_2$	755(550)
5	*cis*-Ni(CN-Cu)$_2$	745(670)
10	*trans*-Pt(CN-Cu)$_2$	840(2100)
6 Ni(CN-Cu)$_4$		760(1100)
11 Pt(CN-Cu)$_4$		840(2100)

Three features are noticeable. First, all absorptions for the cyanide-bridged complexes occur at higher energies than those for the cyanide-free L·Cu-X reference compounds. Second, nickel induces a much stronger band shift than platinum. Third, the band positions are independent of the number of L·Cu units attached to the $M(CN)_4$ center. A detailed discussion of these phenomena would require quantum mechanical calculations. Qualitatively, it can be stated, however, that the cyanide ligand, even in its isocyanide orientation, exerts a moderately strong ligand field to the L·Cu unit and that this ligand field is modulated strongly by the central metal. In terms of long-range metal-metal interactions there seems to be no effect, since only the type of connectivity (e.g. Ni-CN-Cu) but not the number of such connectivities determines the energy of the electronic transition.

Considering the fact that the Cu/Pt complexes contain Pt^{II} as a reducing and Cu^{II} as an oxidizing metal, one might envisage the occurrence of a Pt^{II} to Cu^{II} MMCT absorption. Actually the reverse charge transfer, with Pt^{IV} as acceptor, has been observed in related Fe/Pt complexes.[21] However, in the measurement window from 300 to 2500 nm no feature indicative of such a MMCT could be observed.

Electrochemistry

Cyclic voltammetry is the best method for evaluating remote metal-metal interactions in ligand-bridged systems. It has allowed us to show for the first time that there is directionality in such interactions, i.e. in $L_2Pt(CN\text{-}M')$ systems they occur for the linear [*trans*-$Pt(CN)_2$], but not for the bent [*cis*-$Pt(CN)_2$] array.[2] This was one of the reasons for the present study: it could be expected that the inert $[M(CN)_4]^{2-}$ centers would ensure electrochemical stability for their oligonuclear derivatives, and one could hope to obtain isomeric cis and trans complexes. Both expectations were fulfilled, albeit only partially. Table 3 lists the electrochemical data that were obtained.

Table 3. Electrochemical data for the Cu(tpa) complexes (in CH_3CN, scan rate 100 mV/s, potentials vs. Ag/AgCl)

Complex	Backbone	$E_{1/2}$ (red)
$[Cu(tpa)CH_3CN](ClO_4)_2$		−0.05 (rev.)
4	*trans*-Ni(CN-Cu)$_2$	−0.30 (irrev.)
5	*cis*-Ni(CN-Cu)$_2$	−0.24 (irrev.)
10	*trans*-Pt(CN-Cu)$_2$	−0.13, −0.26 (rev.)
6 Ni(CN-Cu)$_4$		−0.10, −0.33 (quasirev.)
11 Pt(CN-Cu)$_4$		−0.10, −0.29 (rev.)

It turned out that the tren and Me_6tren complexes decomposed during the cyclovoltammetric experiments. The tpa complexes yielded satisfying cyclic voltammograms, the most informative of which is shown in Figure 8. All oligonuclear complexes are more difficult to reduce than the mononuclear reference compound, corresponding to the fact that the cyanometalate "ligand" $[M(CN)_4]^{2-}$ increases the electron density at copper. Likewise, the nickel-containing complexes are more difficult to reduce than the platinum-containing ones, which may reflect the different electron-releasing properties of these two metals. Although one might want to discuss cis-trans effects for the two isomeric

 © 2003 Wiley-VCH Verlag GmbH & Co. KGaA, Weinheim

nickel complexes **4** and **5**, the irreversible nature of their redox processes prevents this.

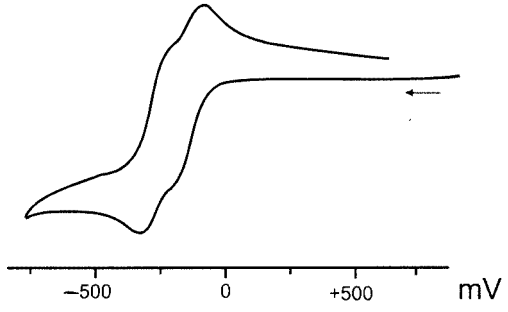

Figure 8. Cyclic voltammogram of complex **10** (in CH_3CN, scan rate 100 mV/s, potentials vs. Ag/AgCl)

The most important observation from the electrochemical measurements is the splitting of the redox wave of the *trans*-Pt(CN-Cu)$_2$ complex **10**. This is proof of the long-range interaction between the two copper ions across two cyanide bridges over a distance of about 10 Å. The number of proven such interactions is still quite small, as they require a redox-inert central metal.[1−12] So far we have observed this interaction only for *trans*-configured trinuclear complexes with central L_2Pt,[2] (Pc)Fe[4] and (salen)M units [M = Cr^{III} or Co^{III}].[6] Like **10**, the pentanuclear complexes **6** and **11** show two redox steps in the reduction of their four Cu(tpa) units. Their separation is larger than the typical one for M′-NC-M-CN-M′ systems (0.05−0.15 V), and the two steps must each represent two-electron reductions. We propose that this again reflects remote metal-metal interactions, both along the two linear Cu-NC-M-CN-Cu arrays, and that the larger potential separation reflects the fact that two electrons are already injected in the first redox step. However, it cannot be excluded that in the first step both copper ions of one linear Cu-NC-M-CN-Cu array are reduced and then the remaining two.

The splitting of the redox waves for **6**, **10** and **11** raised hopes that mixed-valent species might be obtained by partial reduction of the complexes, which might then be investigated for long-range MMCT by UV/Vis-NIR spectroscopy. So far, however, our attempts to achieve this have been unsuccessful.

Conclusions

This work has again shown that square-planar tetracyanometalates are good building blocks for oligonuclear cyanide-bridged complexes that show long-range metal-metal interactions. Between one and four external L·Cu units could be attached to the Ni(CN)$_4$ and Pt(CN)$_4$ centers, and the resulting star-like M(CN-Cu)$_4$ complexes are the first of their kind. The structure determinations have shown that the Cu-NC-M-CN-Cu arrays have a good degree of linearity, but in some cases are noticeably bent at the nitrogen atoms.

The IR absorptions of the C≡N vibrations have allowed some conclusions to be drawn on the electronic situation of the M-CN-Cu arrays. The L·Cu units seem to be both weaker σ-acceptors and π-donors than the organometallic units investigated previously. As a result the kinematic effect is the dominating one in determining the $\tilde{\nu}$(CN) values, and π-backbonding from platinum or nickel to the CN ligands is small, with the effect that the CN IR bands occur at rather high energies.

The electrochemical measurements have again proved the presence of remote metal-metal interactions due to the fact that the complexes containing Cu(tpa) units yield useful cyclic voltammograms. As observed previously, the light central metal (Ni) does not allow the detection of long-range Cu−Cu interactions by means of a splitting of the Cu^{II}/Cu^{I} redox waves. With platinum at the center, however, this splitting occurs. Its order of magnitude corresponds to that previously observed for trinuclear complexes with external organometallic units, thereby supporting the reasonable notion that it is the central and not the external metal unit which controls the long-range metal-metal interactions.

Experimental Section

General: The general working and measuring procedures and the syntheses of the cyanometalates are listed in refs.[1,2] The copper reagents [Cu(tren)H_2O](ClO$_4$)$_2$ (**A**),[22] [Cu(Me$_6$tren)H_2O](ClO$_4$)$_2$ (**B**)[22] and [Cu(tpa)CH_3CN](ClO$_4$)$_2$ (**C**)[23] were prepared as described.

1: A solution of complex **A** (140 mg, 0.33 mmol) in 20 mL of dimethylformamide was added droppwise with stirring into a solution of (PPN)$_2$[Ni(CN)$_4$] (100 mg, 0.08 mmol) in 20 mL of dimethylformamide. The mixture was stirred for 2 h, evaporated to 10 mL and layered with diethyl ether. After one week 45 mg (68%) of **1** had separated as blue crystals, m.p. 180 °C (dec.). $C_{13}H_{36}Cl_3Cu_2N_9O_{12}$·DMF (743.93 + 73.10): calcd. C 23.52, H 5.30, N 17.14; found C 23.48, H 5.28, N 17.18.

2: A solution of complex **A** (96 mg, 0.23 mmol) in 20 mL of methanol was added dropwise with stirring into (140 mg, 0.11 mmol) of (PPN)$_2$[Ni(CN)$_4$] in 20 mL of methanol, upon which a blue precipitate was formed. After 2 h the precipitate was filtered off and washed with dichloromethane and then dissolved in a minimum amount of dimethylformamide. Layering with diethyl ether yielded, within one week, 53 mg (60%) of **2** as a blue powder, m.p. 190 °C (dec.) (the crystalline raw product lost its solvent of crystallization upon drying). $C_{16}H_{36}Cl_2CuN_{12}NiO_8$ (781.23): calcd. C 24.59, H 4.64, N 21.52; found C 24.51, H 4.40, N 21.29.

3: A solution of complex **B** (100 mg, 0.194 mmol) in 20 mL of acetonitrile was added dropwise with stirring to a solution of (PPN)$_2$[Ni(CN)$_4$] (120 mg, 0.97 mmol) in 20 mL of acetonitrile. After 10 h of stirring the solvent was removed in vacuo and the residue washed with dichloromethane. Workup as before for **2** yielded 15 mg (15%) of **3** as a blue powder, m.p. 175 °C (dec.). $C_{28}H_{60}Cl_2Cu_2N_{12}NiO_8$·DMF (949.33 + 73.10): calcd. C 36.41, H 6.60, N 17.80; found C 36.33, H 6.84, N 16.49.

4: A solution of complex **C** (96 mg, 0.16 mmol) in 30 mL of methanol was added dropwise with stirring to a solution of (PPN)$_2$[Ni(CN)$_4$] (100 mg, 0.08 mmol) in 20 mL of methanol at 0

 © 2003 Wiley-VCH Verlag GmbH & Co. KGaA, Weinheim

°C. After 2 h of stirring the resulting precipitate was filtered off and dried in vacuo. Dissolving in acetonitrile and layering with diethyl ether yielded, within one week, 30 mg (35%) of **4** as blue crystals, m.p. 215 °C (dec.). $C_{40}H_{36}Cl_2Cu_2N_{12}NiO_8$ (1069.49): calcd. C 44.92, H 3.39, N 15.71; found C 45.10, H 3.14, N 15.71.

5: A solution of complex **C** (255 mg, 0.43 mmol) in 50 mL of methanol was added dropwise slowly with stirring to a solution of $K_2[Ni(CN)_4]$ (104 mg, 0.43 mmol) in 40 mL of water/methanol (1:1). After 2 h of stirring at 0 °C and subsequent filtration the filtrate was evaporated to dryness. The residue was dissolved in acetonitrile, filtered and the solvents evaporated to dryness again. Dissolving the residue in a minimum amount of acetonitrile and layering with diethyl ether produced, within one week, a mixture of blue-green and colourless crystals. The blue-green crystals were separated manually, and recrystallized again from acetonitrile layered with diethyl ether, resulting in 20 mg (4%) of **5** as blue-green crystals, m.p. 230 °C (dec.). $C_{40}H_{36}Cl_2Cu_2N_{12}NiO_8$ (1069.49): calcd. C 44.92, H 3.39, N 15.71; found C 44.25, H 3.85, N 15.38.

6: Like **4** from $(PPN)_2[Ni(CN)_4]$ (30 mg, 0.24 mmol) and **C** (57 mg, 0.96 mmol). Yield 32 mg (61%) of **6** as blue crystals, m.p. 255 °C (dec.). $C_{76}H_{72}Cl_6Cu_4N_{20}NiO_{24}$ (2175.12): calcd. C 41.97, H 3.34, N 12.88; found C 41.85, H 3.18, N 12.44.

7: A solution of complex **C** (22 mg, 0.04 mmol) in 10 mL of methanol was added dropwise with stirring to a solution of $(PPN)_2[Pt(CN)_4]$ (51 mg, 0.04 mmol) in 10 mL of dichloromethane. After 12 h of stirring the solvent was removed in vacuo, the residue washed with dichloromethane and dried in vacuo. Dissolving in a minimum amount of acetonitrile and layering with diethyl ether yielded, within one week, 9 mg (37%) of **7** as blue crystals, m.p. 204 °C. $C_{22}H_{18}CuN_8Pt$ (653.06): calcd. C 40.46, H 2.78, N 17.16; found C 39.15, H 2.45, N 16.78.

8: A solution of complex **A** (143 mg, 0.34 mmol) in 20 mL of methanol was added dropwise with stirring to a solution of $(PPN)_2[Pt(CN)_4]$ (213 mg, 0.17 mmol) in 20 mL of methanol. After 2 h of stirring the resulting precipitate was filtered off, washed with dichloromethane and dissolved in 5 mL of dimethylformamide, which was layered with diethyl ether. After one week **8** had separated as blue crystals, which crumbled upon drying in vacuo. 100 mg (66%) of solvent-free **8** remained as a blue powder, m.p. 190 °C (dec.). $C_{16}H_{36}Cl_2Cu_2N_{12}O_8Pt$ (917.70): calcd. C 20.94, H 3.95, N 18.32; found C 20.70, H 3.81, N 17.92.

9: Like **3** from **B** (237 mg, 0.45 mmol) and $(PPN)_2[Pt(CN)_4]$ (294 mg, 0.21 mmol). Yield 45 mg (18%) of **9** as a blue powder, m.p. 180 °C (dec.). $C_{28}H_{60}Cl_2Cu_2N_{12}O_8Pt{\cdot}DMF$ (1085.93 + 73.10): calcd. C 32.13, H 5.83, N 15.71; found C 32.41, H 5.73, N 14.47.

10: Like **4** from **C** (129 mg, 0.22 mmol) and $(PPN)_2[Pt(CN)_4]$ (150 mg, 0.11 mmol). Yield 75 mg (57%) of **10** as blue crystals, m.p. 275 °C. $C_{40}H_{36}Cl_2Cu_2N_{12}O_8Pt$ (1205.88): calcd. C 39.84, H 3.01, N 13.94; found C 39.83, H 2.99, N 13.87.

11: Like **4** from **C** (97 mg, 0.16 mmol) and $(PPN)_2[Pt(CN)_4]$ (54 mg, 0.04 mmol). Yield 62 mg (64%) of **11** as blue crystals, m.p. 200 °C (dec.). $C_{76}H_{72}Cl_6Cu_4N_{20}O_{24}Pt{\cdot}2CH_3CN$ (2311.51 + 82.10): calcd. C 40.14, H 3.25, N 12.87; found C 40.05, H 3.13, N 12.85.

Structure Determinations:[24] Crystals were obtained from the reaction mixtures. Diffraction data were recorded at room temp. with a Bruker Smart CCD diffractometer fitted with a molybdenum tube (Mo-K_α, λ = 0.7107 Å) and a graphite monochromator and subjected to empirical absorption corrections. The structures were solved by direct methods and refined anisotropically with the SHELX program suite.[25] Hydrogen atoms were included with fixed distances and isotropic temperature factors 1.5-times those of

Table 4. Crystallographic data

	1	**5**	**6**	**7**	**8**	**10**	**11**
Empirical formula	$C_{13}H_{36}Cl_3Cu_2N_9O_{12}{\cdot}$ DMF	$C_{40}H_{36}Cl_2Cu_2N_{12}NiO_8{\cdot}2CH_3CN$	$C_{76}H_{72}Cl_6Cu_4N_{20}NiO_{24}$	$C_{22}H_{18}CuN_8Pt{\cdot}CH_3CN$	$C_{16}H_{36}Cl_2Cu_2N_{12}O_8Pt{\cdot}6DMF$	$C_{40}H_{36}Cl_2Cu_2N_{12}O_8Pt$	$C_{76}H_{72}Cl_6Cu_4N_{20}O_{24}Pt{\cdot}3CH_3CN$
Molecular mass	743.93 + 73.10	1069.49 + 82.10	2175.12	653.06 + 41.05	917.70 + 438.60	1205.88	2311.51 + 123.15
Crystal size [mm]	0.3 × 0.25 × 0.15	0.4 × 0.2 × 0.1	0.25 × 0.2 × 0.15	0.4 × 0.15 × 0.1	0.8 × 0.6 × 0.5	0.2 × 0.15 × 0.1	0.55 × 0.35 × 0.2
Space group	Pbcn	*C*2/*c*	*C*2/*c*	$P2_1$	$P2_1/c$	$P2_1/c$	$P\bar{1}$
Z	8	4	4	4	4	2	2
a (Å)	11.676(2)	13.010(3)	30.537(3)	9.610(3)	13.012(3)	17.053(13)	11.921(2)
b (Å)	49.142(10)	18.157(4)	17.586(1)	13.381(4)	14.811(3)	9.649(8)	16.979(3)
c (Å)	11.616(2)	21.520(5)	19.568(2)	19.820(5)	15.022(3)	14.511(11)	26.199(4)
α (°)	90	90	90	90	90	90	96.442(3)
β (°)	90	105.056(4)	93.505(2)	92.277(6)	96.88(3)	110.97(2)	100.529(3)
γ (°)	90	90	90	90	90	90	103.784(3)
V (Å^3)	6665(2)	4909(2)	10489(2)	2547(1)	2874(1)	2229(3)	4995(1)
D(calc) (gcm^{-3})	1.62	1.56	1.38	1.81	1.57	1.80	1.62
μ(Mo-K_α) (mm^{-1})	1.59	1.41	1.20	6.35	3.32	4.26	2.48
hkl range	*h:* −13 to 13 *k:* −58 to 58 *l:* −2 to 13	*h:* −17 to 17 *k:* −24 to 24 *l:* −28 to 28	*h:* −33 to 33 *k:* −19 to 19 *l:* −21 to 21	*h:* −6 to 12 *k:* −17 to 14 *l:* −21 to 22	*h:* −14 to 14 *k:* −16 to 0 *l:* −17 to 0	*h:* −12 to 17 *k:* −12 to 2 *l:* −19 to 18	*h:* −15 to 15 *k:* −21 to 21 *l:* −34 to 34
Measured reflections	13571	21722	36160	7737	3566	6436	45719
Independent reflections	5879	5871	7562	7473	3460	4257	23379
Observed refl. [$I > 2\sigma(I)$]	3495	2057	4158	4246	3122	3079	14520
Parameters	400	326	592	617	322	295	1264
Refined reflections	5879	5871	7562	7473	3460	4257	23379
R_1 (obs.refl.)	0.096	0.083	0.149	0.089	0.072	0.038	0.053
wR_2 (all refl.)	0.303	0.171	0.433	0.243	0.244	0.104	0.168
Residual electron density (e/Å^3)	+1.5/−0.8	+0.8/−0.9	+2.1/−0.9	+3.3/−3.1	+1.8/−2.1	+1.5/−1.5	+3.1/−1.9

 © 2003 Wiley-VCH Verlag GmbH & Co. KGaA, Weinheim

their attached atoms. Parameters were refined against F^2. The R values are defined as $R_1 = \Sigma|F_0 - F_c|/\Sigma F_o$ and $wR_2 = \{\Sigma[w(F_0^2 - F_c^2)^2]\Sigma[w(F_0^2)^2]\}^{1/2}$. Drawings were produced with SCHAKAL.[26] Table 4 lists the crystallographic data.

Acknowledgments

This work was supported by the Deutsche Forschungsgemeinschaft (Graduiertenkolleg "Ungepaarte Elektronen") and the Fonds der Chemischen Industrie. We thank Dr. W. Deck for valuable contributions.

[1] N. Zhu, H. Vahrenkamp, *Chem. Ber./Recueil* **1997**, *130*, 1241−1252.
[2] G. N. Richardson, U. Brand, H. Vahrenkamp, *Inorg. Chem.* **1999**, *38*, 3070−3079.
[3] A. Geiß, H. Vahrenkamp, *Inorg. Chem.* **2000**, *39*, 4029−4036.
[4] A Geiß, M. J. Kolm, C. Janiak, H. Vahrenkamp, *Inorg. Chem.* **2000**, *39*, 4037−4043.
[5] Z. N. Chen, R. Appelt, H. Vahrenkamp, *Inorg. Chim. Acta* **2000**, *309*, 65−71.
[6] R. Appelt, H. Vahrenkamp, *Inorg. Chim Acta* in print.
[7] H. Vahrenkamp, A. Geiß, G. N. Richardson, *J. Chem. Soc., Dalton Trans.* **1997**, 3643−3651.
[8] A. Burewicz, A. Haim, *Inorg. Chem.* **1988**, *27*, 1611−1614.
[9] N. G. Connelly, E. M. Hicks, G. R. Lewis, A. G. Orpen, A. J. Wood, *J. Chem. Soc., Dalton Trans.* **2000**, 1637−1643, and references cited therein; K. M. Anderson, N. G. Connelly, N. J. Goodwin, G. R. Lewis, M. T. Moreno, A. G. Orpen, A. J. Wood, *J. Chem. Soc., Dalton Trans.* **2001**, 1421−1427, and references cited therein.
[10] H. Kunkely, V. Pawlowski, A. Vogler, *Inorg. Chim. Acta* **1994**, *225*, 327−330.
[11] C. A. Bignozzi, R. Argazzi, C. Chiorboli, S. Roffia, F. Scandola, *Coord. Chem. Rev.* **1991**, *111*, 261−266; F. Scandola, R. Argazzi, C. A. Bignozzi, C. Chiorboli, M. T. Indelli, M. A. Rampi, *Coord. Chem. Rev.* **1993**, *125*, 283−292.
[12] W. M. Laidlaw, R. G. Denning, *J. Chem. Soc., Dalton Trans.* **1994**, 1987−1994; W. M. Laidlaw, R. G. Denning, *Inorg. Chim. Acta* **1996**, *248*, 51−58.
[13] D. M. Duggan, R. G. Jungst, K. R. Mann, G. D. Stucky, D. N. Hendrickson, *J. Am. Chem. Soc.* **1974**, *96*, 3443−3450.
[14] F. Thaler, C. D. Hubbard, F. W. Heinemann, R. van Eldik, S. Schindler, I. Fábián, A. M. Dittler-Klingemann, F. E. Hahn, C. Orvig, *Inorg. Chem.* **1998**, *37*, 4022−4029.
[15] M. J. Scott, S. C. Lee, R. H. Holm, *Inorg. Chem.* **1994**, *33*, 4651−4662.
[16] G. N. Richardson, H. Vahrenkamp, *J. Organomet. Chem.* **2000**, *597*, 38−41.
[17] I. Escorihuela, L. R. Favello, M. Tomás, *Inorg. Chem.* **2001**, *40*, 636−640.
[18] R. J. Parker, D. C. R. Hockless, B. Moubaraki, K. S. Murray, L. Spiccia, *Chem. Commun.* **1996**, 2789−2790.
[19] C. K. Jørgensen, *Acta Chem. Scand.* **1956**, *10*, 887−910.
[20] M. Duggan, N. Ray, B. Hathaway, G. Tomlinson, P. Briant, K. Plain, *J. Chem. Soc., Dalton Trans.* **1980**, 1342−1348; N. Wei, N. N. Murthy, K. D. Karlin, *Inorg. Chem.* **1994**, *33*, 6093−6100.
[21] M. Zhou, B. W. Pfennig, J. Steiger, D. van Engen, A. Bocarsly, *Inorg. Chem.* **1990**, *29*, 2457−2460.
[22] M. Ciampolini, N. Nardi, *Inorg. Chem.* **1966**, *5*, 1150−1154; S. C. Lee, R. H. Holm, *J. Am. Chem. Soc.* **1993**, *115*, 11789−11798.
[23] S. Fox, A. Nanthakumar, M. Wilkström, K. D. Karlin, N. J. Blackburn, *J. Am. Chem. Soc.* **1996**, *118*, 24−34.
[24] CCDC-199703 (**1**), -199704 (**5**), -199705 (**6**), -199706 (**7**), -199707 (**8**), -199708 (**10**) and -199709 (**11**) contain the supplementary crystallographic data for this paper. These data can be obtained free of charge at www.ccdc.cam.ac.uk/conts/retrieving.html [or from the Cambridge Crystallographic Data Centre, 12, Union Road, Cambridge CB2 1EZ, UK; Fax: (internat.) +44-1223/336-033; E-mail: deposit@ccdc.cam.ac.uk].
[25] G. M. Sheldrick, *SHELX* program suite for the Bruker CCD diffractometer.
[26] E. Keller, *SCHAKAL for Windows*, Universität Freiburg, 2000.

Received December 17, 2002

 © 2003 Wiley-VCH Verlag GmbH & Co. KGaA, Weinheim

Metal-Controlled Stereoselectivity in Complex Formation: Assembly of Tetranuclear Copper(I) Complexes with Four Stereogenic Nitrogen Donor Functions in all-(*R*) and all-(*S*) Configurations

Jörg Schneider,[b,c] Martin Köckerling,[b] Rodion Kopitzky,[b] and Gerald Henkel*[a]

Dedicated to Professor Dieter Sellmann

Keywords: Copper / Chirality / N ligands / S ligands / Metal-controlled stereoselectivity

The reaction of *N*,*N*′-dialkyl-3,7-diazanonane-1,9-dithiolate ($N_2^RS_2$) ligands (R = Me, Et) with monovalent copper resulted in the formation of the chiral complexes $[Cu_4(N_2^{Me}S_2)_2]$ (**1**) and $[Cu_4(N_2^{Et}S_2)_2]$ (**2**) which were characterised by means of X-ray diffraction and spectroscopic techniques. They contain copper atoms in both linear {S–Cu–S} fragments, which act as linkers between mononuclear $[Cu(N_2^RS_2)]^-$ subsites, and in $\{CuS_2N_2\}$ units within these building blocks, which can be described as incomplete coordination octahedra of unusual design. Due to favourable interplay between the spatial demands of the ligand system and the electronic requirements of the copper atom, the nitrogen donor atoms within the $[Cu(N_2^RS_2)]^-$ metallo ligands are restricted to identical absolute configurations. The combination of two $[Cu(N_2^RS_2)]^-$ metallo ligands with two further Cu^I ions to give the tetranuclear complexes **1** or **2** via S–Cu–S bridges underlies stereochemical control, resulting in optically active systems with (*R*,*R*,*R*,*R*) and (*S*,*S*,*S*,*S*) configurations. Consequently, metallo ligands in their enantiomeric forms cannot combine via S–Cu–S bridges to form optically inactive *meso* complexes with the (*R*,*R*,*S*,*S*) configuration.

(© Wiley-VCH Verlag GmbH & Co. KGaA, 69451 Weinheim, Germany, 2003)

Introduction

For most aerobic organisms the enzyme "cytochrome-c oxidase" is involved in the final step of cell respiration. This enzyme contains the heterodimetallic Cu_B-Fe_{a3} and the homodimetallic mixed-valence Cu_A centre. The copper atoms of the latter are coordinated by two bridging cysteinyl groups and one terminally bonded histidine residue each. Additional weakly bonded terminal S(Met) and O(Glu) donor functions complete the coordination spheres around the copper atoms, which are ca. 2.45 Å apart.[1] Dinuclear copper complexes containing N/S donor sets have been synthesised as models for specific properties of the Cu_A centre.[2]

This subject has stimulated our investigations on heteroleptic copper thiolate complexes with ligands containing both sulfur and prochiral nitrogen donor functions.[3] The work described here focuses on the reactions of *N*,*N*′-dialkyl-3,7-diazanonane-1,9-dithiolate ($N_2^RS_2$), which is widely used to stabilise square-planar N_2S_2 [4] or trigonal-bipyramidal N_2S_2S'[5] ligand fields, with Cu^I (a metal known to avoid such coordination situations) resulting in the formation of tetranuclear complexes.

Herein we present the first report of two pathways for the preparation of tetranuclear Cu^I thiolate complexes with $N_2^RS_2$ ligands that stabilise severely distorted pseudo-tetrahedral N_2S_2 ligand fields. Their metal atom frameworks can be derived from the frequently observed regular metal tetrahedron present, for example in $[Cu_4(SCH_2CH_2S)_3]^{2-}$,[6] by elongation of one M−M edge, leading to a completely planar situation yet unknown in copper thiolate chemistry though other derivatives with two elongated edges[7] or with more general rhombohedral[8] or less regular quadrilateral shapes[9] are known. Both $[Cu_4(N_2^{Me}S_2)_2]$ (**1**) and $[Cu_4(N_2^{Et}S_2)_2]$ (**2**), with coordination numbers of 2 and 4 for the metal atoms resulting in CuS_2 and CuN_2S_2 coordination sites, have been synthesised and characterised by means of X-ray structure analysis and spectroscopic techniques.

[a] Universität Paderborn, Department Chemie, Anorganische und Analytische Chemie,
Warburgerstraße 100, 33098 Paderborn, Germany
Fax: (internat.) + 49-(0)5251/60-3423
E-mail: biohenkel@uni-paderborn.de
[b] Gerhard-Mercator-Universität, Fakultät 4, Institut für Chemie, Lotharstr. 1, 47057 Duisburg, Germany
[c] BASF AG Ludwigshafen, Polymer Research, GKD/L − B1, 67056 Ludwigshafen, Germany

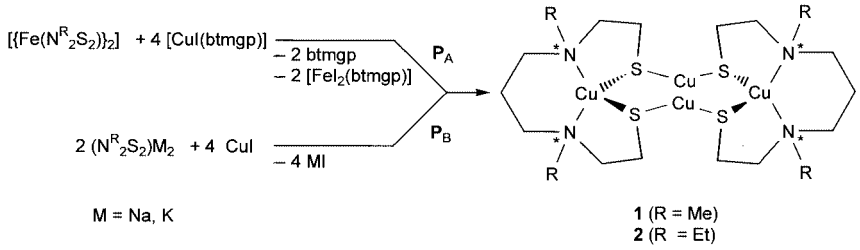

Scheme 1. Pathways for the synthesis of the complexes **1** and **2** [btmgp = 1,3-bis(*N*,*N*,*N*′,*N*′-tetramethylguanidino)propane]

Results and Discussion

Synthetic Pathways

The *N*,*N*′-dialkyl-3,7-diazanonane-1,9-dithiolate ($N^R_2S_2$) ligands used here (R = Me, Et) are accessible from the corresponding diaminodithiols, which can be synthesised by reaction of *N*,*N*′-dialkyl-1,3-diaminopropanes with ethylene sulfide in toluene in sealed glass tubes under strictly anaerobic conditions at high pressure according to the procedure reported by Corbin et al.[10]

The diamino dithiols, isolated after filtration and removal of the solvent, can be purified by distillation before use. A small excess of ethylene sulfide was used to avoid the survival of unchanged diamines. In these reactions, the small amounts of polyethylene thioethers obtained as side products are less soluble and therefore easily removed by filtration. The use of racemic propylene sulfide instead of ethylene sulfide leads to chiral ligands that are reported elsewhere.[3,11]

The $[Cu_4(N^R_2S_2)_2]$ complexes **1** and **2** described here have been prepared by different pathways ($\mathbf{P_A}$ and $\mathbf{P_B}$, Scheme 1).

The reaction of the dinuclear compound $[\{Fe(N^{Me}_2S_2)\}_2]$[5a] with the mononuclear complex [CuI(btmgp)][12] in a molar ratio of 1:4 in MeCN (pathway $\mathbf{P_A}$) leads by ligand exchange to the tetranuclear complex **1** in fairly good yields. In a more straightforward approach (pathway $\mathbf{P_B}$), **2** is accessible by reaction of CuI with $M_2(N^{Et}_2S_2)$ (M = K or Na) in almost quantitative yields. The $M_2(N^R_2S_2)$ precursors are obtained by reaction of sodium or potassium methanethiolate with the diaminodithiol and successive removal of the methane thiol formed in this reaction step.

Both complexes **1** and **2** are soluble in THF and other aprotic solvents such as dichloromethane or chloroform, which allows solution studies (NMR, CV, and UV/Vis). Moreover, the complexes contain four nitrogen donor functions that are chiral centres with identical configurations. Within crystals, both enantiomers [all-(*R*) and all-(*S*)] are present.

Crystal Structures

Complex **1** crystallises together with acetonitrile molecules in a 1:1 molar ratio (Table 1). The molecular structure of **1** within these crystals is shown in Figure 1 [all-(*S*) configuration]. Selected interatomic distances and angles are given in Table 2. The four copper atoms are arranged in a planar rhomboidal fashion with Cu···Cu distances of 2.685 Å for the edges (averaged value) and 2.726 and 4.625 Å for the diagonals. The edges of the rhomb are bridged by thiolate-S atoms (average Cu−S distance: 2.217 Å) that reside in opposite pairs above and below the copper plane at an average distance of 1.369 Å.

Table 1. Crystal data for **1** and **2**

Compound	**1**·CH_3CN	**2**
Empirical formula	$C_{20}H_{43}Cu_4N_5S_4$	$C_{22}H_{48}Cu_4N_4S_4$
Formula mass	736.043	751.098
Crystal system	monoclinic	tetragonal
Space group	$P2_1/c$	$I\bar{4}c2$
a [Å]	15.832(2)	13.910(2)
b [Å]	15.434(1)	
c [Å]	12.729(1)	15.765(4)
β [°]	104.53(2)	
V [Å^3]	3010.9	3050.3
Z	4	4
$D_{calcd.}$ [g·cm^{-1}]	1.624	1.635
T [K]	293	150
λ [Å]	0.71073	0.71073
θ range [°]	1.5−25	1.5−27
Index ranges	*h* 0/+18, *k* −18/0, *l* −15/+14	*h* −17/+17, *k* −17/0, *l* −20/0
Refl. total	5189	3587
Refl. unique	5189	1686
R(int)	−	0.024
Observed [$I > 2\sigma(I)$]	4203	1586
μ(λ) [mm^{-1}]	3.083	3.044
Crystal size [mm]	0.84 × 0.53 × 0.19	0.60 × 0.35 × 0.22
Transmission range	0.111−0.041	0.772−0.703
No. of parameters	299	118
S (F^2)	1.118	1.018
*R*1 (*F*, observed)	0.0446	0.0210
*wR*2 (F^2, all data)	0.1198	0.0477
Final Δ*F* [e$^-$·Å^{-3}]	1.01, −0.39	0.33, −0.32

With the exception of the four methyl and the eight methylene groups bonded to nitrogen atoms, all other non-H atoms of the complex follow in fairly good approximation the symmetry requirements of three twofold rotation axes, two of which pass through the diagonals of the Cu_4 rhomb and the third being normal to this plane. The overall point symmetry of **1** comes very close to C_2 with the twofold axis passing through Cu(2) and Cu(4). Both deprotonated ligand molecules are wrapped around Cu(1) and Cu(3), defining S_2N_2 coordination polyhedra for these two metal atoms, which are neither square-planar nor tetrahedral but

 © 2003 Wiley-VCH Verlag GmbH & Co. KGaA, Weinheim

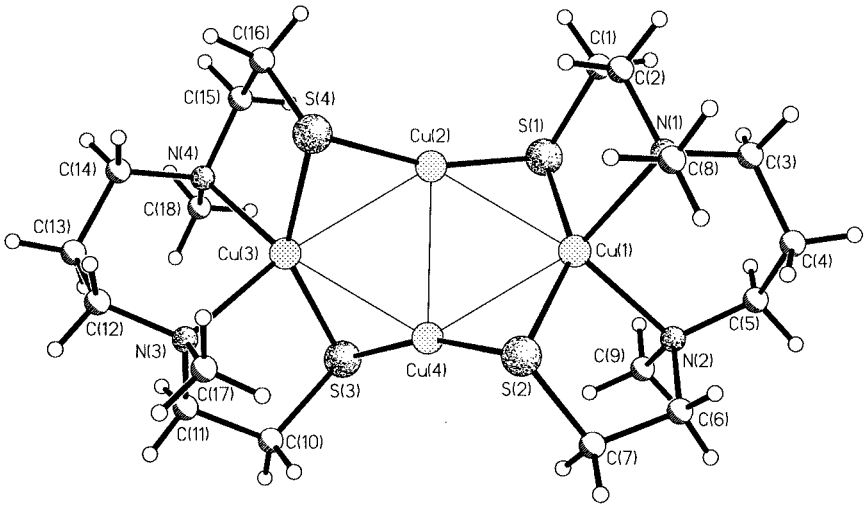

Figure 1. Molecular structure of (*S*,*S*,*S*,*S*)-[$Cu_4(N_2^{Me}S_2)_2$] (**1**)

Table 2. Selected atom distances and angles for **1**

Atoms	Distance [Å]	Atoms	Angle [°]
Cu(1)−Cu(2)	2.678(1)	Cu(2)−Cu(1)−Cu(4)	61.1(1)
Cu(1)−Cu(4)	2.687(1)	Cu(1)−Cu(2)−Cu(3)	118.5(1)
Cu(2)−Cu(3)	2.705(1)	Cu(2)−Cu(3)−Cu(4)	61.0(1)
Cu(3)−Cu(4)	2.669(1)	Cu(1)−Cu(4)−Cu(3)	119.4(1)
Cu(2)−Cu(4)	2.726(1)	S(1)−Cu(1)−S(2)	146.7(1)
Cu(1)−S(1)	2.271(2)	S(1)−Cu(1)−N(1)	88.4(1)
Cu(1)−S(2)	2.268(2)	S(1)−Cu(1)−N(2)	112.5(1)
Cu(1)−N(1)	2.214(5)	S(2)−Cu(1)−N(1)	114.2(1)
Cu(1)−N(2)	2.186(4)	S(2)−Cu(1)−N(2)	89.6(1)
Cu(2)−S(1)	2.167(2)	N(1)−Cu(1)−N(2)	96.9(1)
Cu(2)−S(4)	2.157(2)	S(1)−Cu(2)−S(4)	162.7(1)
Cu(3)−S(3)	2.269(2)	S(3)−Cu(3)−S(4)	144.8(1)
Cu(3)−S(4)	2.262(2)	S(3)−Cu(3)−N(3)	89.9(1)
Cu(3)−N(3)	2.186(4)	S(3)−Cu(3)−N(4)	114.7(1)
Cu(3)−N(4)	2.220(4)	S(4)−Cu(3)−N(3)	115.5(1)
Cu(4)−S(2)	2.169(2)	S(4)−Cu(3)−N(4)	88.0(1)
Cu(4)−S(3)	2.173(2)	N(3)−Cu(3)−N(4)	95.5(1)
		S(2)−Cu(4)−S(3)	163.6(1)

can be derived from a (distorted) $S_2N_2L_2$ octahedron (Figure 1) with sulfur and nitrogen atoms at opposite (slightly bent towards L, mean S−Cu−S angle 145.8°) and neighbouring corners (mean N−Cu−N angle 96.2°), respectively, by removal of L. They are central constituents of mononuclear subunits that act as ligands towards Cu(2) and Cu(4), resulting in slightly bent S−Cu−S coordination sites with valence angles of 162.7(1)° for Cu(2) and 163.6(1)° for Cu(4). As the subunits lack molecular symmetry, the formation of two isomeric forms is possible but only one could be isolated. The other isomer can be obtained by rotating one of the mononuclear subunits of **1** around an axis that passes through Cu(1) and Cu(3). Within the tetranuclear complexes the nitrogen atoms are in identical configurations [all-(*R*) or all-(*S*), respectively]. The average Cu−N distance is 2.202 Å, and the valence angles for Cu(1) and Cu(3) range from 88.0(1)° [S(4)−Cu(3)−N(4)] to 146.7(1)° [S(1)−Cu(1)−S(2)], showing significant distortions if compared with a regular tetrahedron. Moreover, the angles between the planes defined by the CuS_2 and CuN_2 fragments are calculated to be 73.3 and 71.7° for Cu(1) and Cu(3), respectively, demonstrating significant planarisation tendencies within the coordination polyhedra. The methylene groups connecting the nitrogen atoms in the $N_2^{Me}S_2$ ligand fit into six-membered chelate rings that adopt the chair conformation.

In contrast to the methylated complex **1**, the ethylated variant **2** could be isolated in both isomeric forms (**2a** and **2b**, vide supra). Their structures, in the all-(*R*) configurations, are depicted in Figure 2.

Similar to **1**, both isomers are assembled from identical dissymmetric mononuclear subunits with significantly distorted defect-octahedral CuN_2S_2 coordination sites that act as ligands towards additional copper ions. The structure of **2a** (Figure 2, bottom) is closely related to that of **1**. The molecule occupies a twofold rotation axis that passes through Cu(2) and Cu(2a) and is crystallographically imposed. For the other isomeric form (**2b**; Figure 2, top) a twofold rotation axis of crystallographic origin passes through the centre of the Cu_4 rhomb normal to the metal plane. Crystals of **2** contain both isomers in a disordered fashion. The superposition of two conformationally different molecules with twofold rotation axes that are normal to each other results in the crystallographic site symmetry 222. This overall symmetry is reduced towards 2 for the individual complex molecules. The existence of potentially possible conformers with at least one mononuclear subunit possessing twofold symmetry can be excluded from geometric considerations: for all these cases, the valence angle at the central carbon atom of the propylene chain [C(4)] must adopt a value of ca. 132°, which is much too large to be physically meaningful. For both **2a** and **2b**, the Cu···Cu distances are 2.647(1) Å for the edges of the Cu_4 rhomb and 2.675(1) and 4.570(1) Å for the short and long diagonals, respectively. These values compare nicely with those of **1**, as do the Cu−S and Cu−N distances and the overall metal coor-

 © 2003 Wiley-VCH Verlag GmbH & Co. KGaA, Weinheim

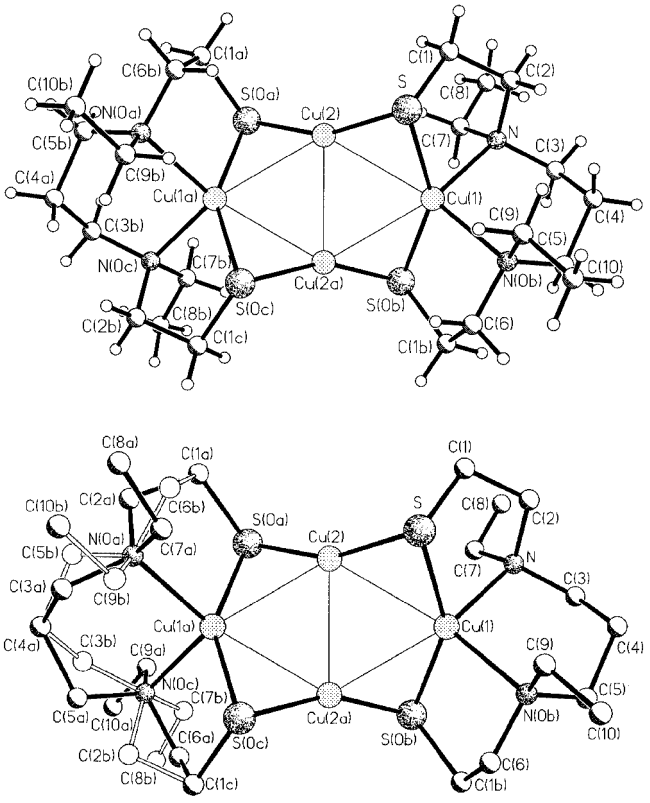

Figure 2. Top: structure of (*R*,*R*,*R*,*R*)-[$Cu_4(N_2^{Et}S_2)_2$] (**2b**); bottom: structure of (*R*,*R*,*R*,*R*)-**2a** with superimposed structure of **2b** (without H atoms; alternative atomic positions shown as open circles)

dination. Selected interatomic distances and angles for both conformers of **2** are given in Table 3.

Table 3. Selected atom distances and angles for **2** (symmetry codes: ′: $y - 1/2, x + 1/2, -z + 2$; ′′: $-x + 1, -y + 2, z$)

Atoms	Distance [Å]	Atoms	Angle [°]
Cu(1)−Cu(2)	2.647(1)	Cu(2)−Cu(1)−Cu(2)′	60.7(1)
Cu(2)−Cu(2)′	2.675(1)	Cu(1)−Cu(2)−Cu(1)′′	119.3(1)
Cu(1)−S	2.273(1)	Cu(1)−Cu(2)−Cu(2)′	59.7(1)
Cu(1)−N	2.196(2)	S−Cu(1)−S′	149.1(1)
Cu(2)−S	2.172(1)	S−Cu(1)−N	88.8(1)
		S−Cu(1)−N′	111.7(1)
		N−Cu(1)−N′	97.9(1)
		S−Cu(2)−S′′	157.8(1)

Spectroscopic Properties

Infrared and Raman Spectra

In the region above 1350 cm^{-1}, the IR spectra of **1** and **2** show strong ν_{as}/ν_s and δ_{as}/δ_s bands of the CH_2 and CH_3 groups. The bands between ca. 1300 cm^{-1} and 1200 cm^{-1} should be attributed to wagging modes of the CH_2 groups, the high intensities being consistent with their great number. A complicated pattern in the range of 1150 to ca. 1000 cm^{-1} with only small differences in frequencies between **1** and **2** is probably a superposition of ν_{C-N} bands, frequencies originating from C−C vibrations and bands associated with the rocking mode of the CH_3 groups (969 cm^{-1}). The bands between 800 and 1000 cm^{-1} can be traced back to C−C stretching and CH_3 rocking vibrations. In the expected region for the ν_{C-S} vibration, four bands are observed. The infrared and Raman spectra of **2** are compared in Figures 3 and 4.

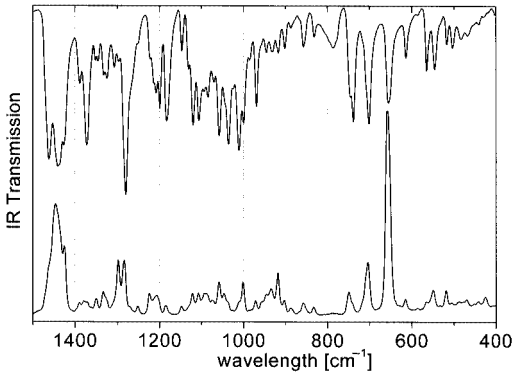

Figure 3. Infrared (top) and Raman (bottom) spectra of **2** (MIR region)

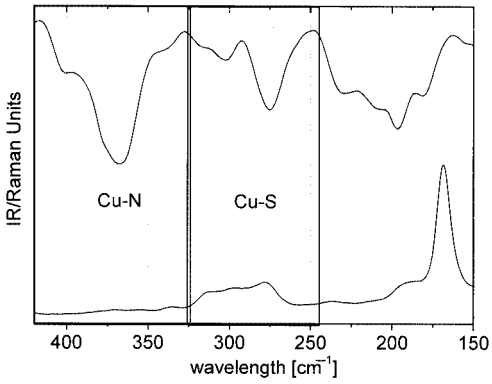

Figure 4. Infrared (top) and Raman (bottom) spectra of **2** (FIR region)

The strong Raman line at 656 cm^{-1} is assigned to the fully symmetric stretch of the C−S groups. This line can be correlated with a weak band in the infrared spectrum which is shifted by 3 cm^{-1}.

As expected for these compounds, in the region down to 400 cm^{-1}, several deformation modes of the heterocyclic five- ($CuSC_2N$) and six-membered ($CuNC_3N$) chelate rings are observed.

Based on the infrared and Raman spectra of **2**, the ν_{Cu-N} and ν_{Cu-S} frequencies can be allocated as illustrated in Figure 4. The ν_{Cu-N} frequencies occur in the range from 325 to 420 cm^{-1} (central frequency at 368 cm^{-1}), whereas the ν_{Cu-S} frequencies are assigned to bands in the range 250−325 cm^{-1} (main frequencies at 276 and 303 cm^{-1}), especially in the Raman spectra. This assignment agrees with the observed relative intensities of the ν_{Cu-S} and the

 © 2003 Wiley-VCH Verlag GmbH & Co. KGaA, Weinheim

ν_{Cu-N} bands, which can be correlated with the higher polarizability of sulfur compared with nitrogen.

NMR Spectra

As a representative example, complex **2** was investigated by NMR spectroscopy. Because different conformers were detected in the crystalline state, a mixture of chemically different states should also be present in solution. Accordingly, the ^{1}H NMR spectrum is very complicated, and so no attempts to allocate signals have been made. Nevertheless, two predominant forms can be identified by different resonances of their methyl groups in accordance with the crystal structure. At room temperature, two overlapping triplets with significant differences in their intensities and coupling constants are resolved ($\Delta^3J \approx 0.2$ Hz), whereas at higher temperatures (333 K) these differences vanish.

Consistent with this assumption, two sets (each of six signals) of carbon atoms are observed in the ^{13}C NMR spectrum for **2**. The signals at $\delta = 8.43$ and 8.54 ppm can be assigned to the methyl groups (positive signal in DEPT-135) of the conformers.

Electrochemistry

Cyclic voltammetry measurements of complex **2**, dissolved in THF, show only irreversible oxidation and reduction events at +610 and −90 mV (vs. GKE), respectively.[13]

Discussion

As the $Cu_4N_4S_4$ cores of the conformers **2a** and **2b** are identical, we shall use **2** here instead of **2a** or **2b**. Both tetranuclear complexes **1** and **2** contain identical mononuclear subunits with the copper atom in a distorted N_2S_2 environment which can be derived from an $N_2S_2L_2$ octahedron by removal of L (vide supra). This spatial arrangement is controlled by the steric requirements of the alkylene spacers connecting the donor functions, which do not allow for a more regular tetrahedral situation. The deviation from tetrahedral symmetry is best reflected by the S−Cu−S valence angle, which is as large as 149.1° in **2** and of comparable size in **1**. Similar analogies between **1** and **2** with respect to other structural features of their $Cu_4N_4S_4$ cores also exist. For clarity, numerical values of **1** are omitted in the following discussion. The vector which passes through the copper atoms of both subunits bisects the S−Cu−S and N−Cu−N triangles. Both CuN_2S_2 polyhedra within each tetranuclear molecule are rotated against each other by ca. 90° around this Cu−Cu vector in such a way that the CuS_2 fragment of one subunit and the CuN_2 fragment of the other are coplanar. As both CuN_2S_2 polyhedra face each other via their S_2 edges, the sulfur atoms form a distorted tetrahedron with opposite edges being 4.382, 4.262 and 4.858 Å in lengths, respectively. The edges that belong to individual CuN_2S_2 polyhedra are bridged by Cu(1). From geometrical considerations, the arrangement of the sulfur atoms should allow for the incorporation of a total of four additional copper atoms into places defined by the centres of the edges of the S_4 tetrahedron that connect the CuN_2S_2 units. For the complexes described here, only one half of these positions are occupied by copper [Cu(2) and Cu(4) in **1**, Cu(2) in **2**] in such a way that planar metal arrangements are formed. This half is associated with the shorter S···S edges of the S_4 tetrahedron, resulting in distorted linear S−Cu−S units. It is noteworthy that these additional copper atoms are shifted from the centres of the S···S edges towards the centroid of the S_4 tetrahedron and approach each other at 2.675 Å, a distance that is only marginally longer than that observed between Cu(2) and Cu(1) (2.647 Å), indicating some degree of attractive Cu···Cu interactions.

As has already been pointed out, the distorted "tetrahedral" CuN_2S_2 coordination sites are characterised by extremely wide S−Cu(1)−S valence angles of 149.1°. This situation can therefore alternatively be regarded as a first-order distorted linear S−Cu−S coordination with additional secondary bonds to nitrogen atoms. In this picture, four of the six edges of the S_4 tetrahedron are occupied by copper atoms, two of which are displaced towards the centroid whereas the remaining ones are shifted in the opposite direction to avoid Cu···Cu interactions that are too short to be stable.

The complex $[Cu_4\{SC_6H_2(i\text{Pr})_3\}_4]$ has recently been identified by Schröter-Schmidt and Strähle as containing a polycyclic Cu_4S_4 framework similar to that of **1** and **2**.[8b] In this case, however, the S_4 tetrahedron is drastically flattened if compared with those in **1** and **2**, and the short diagonal of the Cu_4 rhomb (3.383 Å) is much longer than the edges (2.700 Å). Though secondary Cu−N bonds are lacking in this example, two of the copper atoms are also displaced away from the centroid of the S_4 polyhedron (Cu···Cu 4.207 Å), whereas the others are shifted towards each other at a distance of 3.383 Å. Comparable geometrical features have also been found by Becker et al. and by Block et al. in the tetranuclear thiolate complexes $[Cu_4\{SSi(Ot\text{Bu})_3\}_4]$[8c] and $[Cu_4\{SC_6H_3(2,6\text{-}SiMe_3)_2\}_4]$,[8a] respectively.

Coordination principles in tetranuclear thiolate complexes with planar copper frameworks that are different from those observed in **1** and **2** have been found in $[Cu_4\{SC_6H_2(2,4,6\text{-}i\text{Pr})_3\}_4(\text{bipy})_2]$[14] and $[Cu_4(St\text{Bu})_4(PPh_3)_2]$,[15] respectively. In both cases, two mononuclear $[Cu(SR)_2L]$ subunits with tetrahedral CuN_2S_2 or trigonal-planar $CuPS_2$ coordination sites act as ligands towards "naked" Cu^I ions, forming linear S−Cu−S units within cyclic Cu_4S_4 frames. Due to the non-linearity of the S−Cu−S fragments within the CuN_2S_2 and $CuPS_2$ coordination sites, these frames contain sulfur atoms in planar arrangements. Both frames differ in the magnitude of their Cu-S−Cu angles. For $[Cu_4\{SC_6H_2(2,4,6\text{-}i\text{Pr})_3\}_4(\text{bipy})_2]$,[14] both acute and obtuse angles are present, whereas only acute angles are observed in $[Cu_4(St\text{Bu})_4(PPh_3)_2]$.[15]

Of more general importance is the new finding that ligands derived from 3,7-dialkyl-3,7-diazanonane-1,9-dithiol-

 © 2003 Wiley-VCH Verlag GmbH & Co. KGaA, Weinheim

ate stabilise complexes of coordination number 4 with a nonplanar ligand field. In principle, the spatial arrangement of the ligand donor functions fits perfectly well into a square-planar coordination geometry. This coordination mode has frequently been observed for Ni^{II} and, to a lesser extent, also for Cu^{II} and Pd^{II}.[4] In all these cases, the absolute configurations of the two nitrogen donor atoms are mirror images, resulting in optically inactive *meso* complexes. In contrast, the mononuclear subunits of **1** and **2** should be optically active as the stereogenic nitrogen atoms are in the same absolute configuration. The observed nonplanar arrangement of the N_2S_2 donor set can be derived from a planar case by rotation of the CuS_2 fragment around the bisector of the S−Cu−S angle. This rotation is accompanied by a drastic widening of the S−Cu−S valence angle induced by the restricted S···N bite distance.

To analyse the stereochemical consequences of this rotation with respect to the individual absolute configurations of the nitrogen atoms within the monomeric subunits, we will discuss a hypothetical stepwise mechanism (Scheme 2) starting from the square-planar arrangement.

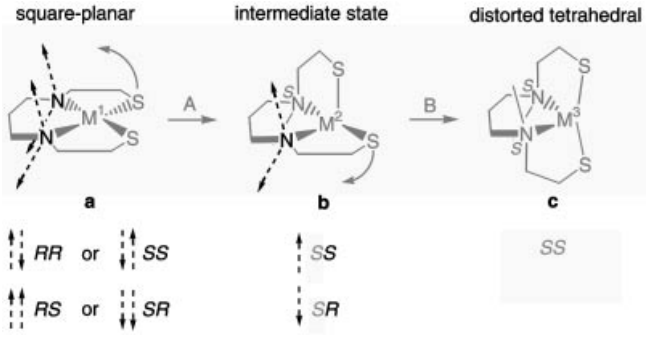

Scheme 2. Metal-controlled stereochemistry (M^1 = Ni^{II}; M^2 = Mn^{II}, Fe^{II}; M^3 = Cu^{I}); the possible positions for the alkyl substituents are indicated by dashed arrows

In this situation (Scheme 2, **a**), each nitrogen atom can, principally, adopt both (*R*) or (*S*) conformations independently. In step A, we shift one of the sulfur atoms into a position such that the Cu−S bond is normal to the remaining CuN_2S plane. Such arrangements have been observed in the dinuclear complexes $[\{Fe(N_2^{Me}S_2)\}_2]$[5] and $[\{Mn(N_2^{Et}S_2)\}_2]$.[5] This procedure has stereochemical consequences with respect to the absolute configuration of the nitrogen atom directly connected with the shifted sulfur atom. If we look from the midpoint of the N···N edge to the copper atom and we shift the sulfur atom of the left-hand side upwards, the nitrogen atom on the same side has to adopt the (*S*) configuration. The absolute configuration of the other nitrogen atom is not restricted by this procedure. Thus, both diastereomeric forms, namely those with (*S*,*S*) and (*R*,*S*) configurations, should be possible (Scheme 2, **b**). In fact, the complex $[\{Fe(N_2^{Me}S_2)\}_2]$[5] is an example of a system which adopts the (*R*,*S*) configuration, whereas in $[\{Mn(N_2^{Et}S_2)\}_2]$,[5] the (*S*,*S*) configuration is observed. In the next step (B), the second sulfur atom is shifted into the opposite direction such that both Cu−S bonds are more or less parallel (Scheme 2, **c**). Both nitrogen atoms are now restricted to adopt the (*S*,*S*) configuration. This situation holds for both **1** and **2**. In the complex $[MoO_2(N_2^{Me}S_2)]$, a related situation has been observed.[16] The same process based on opposite shifts finally leads to the (*R*,*R*) configuration.

As a consequence of the spatial restrictions induced by the alkylene spacers of the polyfunctional ligands, a tetrahedral coordination geometry which requires S−Cu−S valence angles in the order of 109° cannot be achieved, and the rotation process is expected to converge against a limiting angle that is smaller than 90°, in accordance with our observations.

In both complexes **1** and **2** all of the four N atoms of the diamino dithiolate ligands are stereogenic centres with identical absolute configurations. The crystals are racemic mixtures of the two enantiomers [all-(*R*) and all-(*S*)], whereas diastereomers (*R*,*R*,*S*,*S*) have not been observed. The combination of monomeric subunits that are mirror images to tetranuclear complexes (in their *meso* forms) via bridging Cu ions is not possible due to steric requirements of the thiolate-S functions, which cannot form additional S−Cu bonds with suitable geometries. As an important consequence of this spatial control, tetranuclear complexes of the type described above must be optically active, and the assembly of any optically inactive form (with *meso* configuration) is therefore strictly forbidden.

Racemic mixtures of the type described here may play an important role as auxiliaries if it is possible to activate or deactivate one enantiomer selectively by a further chiral component.[17]

Conclusions

Here we have gained control of the stereochemistry of nitrogen donor functions in N_2S_2 ligands by adjusting the spatial demands with metal-specific coordination properties. For Cu^{I}, the coordination of N_2S_2 ligands can only be achieved if both nitrogen atoms adopt the same absolute configuration [(*R*,*R*)or (*S*,*S*)]. These mononuclear chiral CuN_2S_2 units have been found to act pairwise as bifunctional sulfur donor ligands towards monovalent copper ions, forming stable tetranuclear complexes with planar metal frames. The observation that this step is absolutely stereoselective, allowing only combinations of units with identical configurations, should be of more general importance. The stereochemical control can be traced back to an interplay between the coordination properties of the sulfur donor functions of the metallo ligand and the bonding requirements of the bridging copper ions. Consequently, the combination of units with opposite configurations, leading to optically inactive *meso* complexes (*R*,*R*,*S*,*S*), is strictly forbidden. These novel complexes might find applications in chemical and catalytic processes.

Experimental Section

General Remarks: All manipulations were performed under pure dinitrogen using Schlenk techniques or a glove box using abs. sol-

 © 2003 Wiley-VCH Verlag GmbH & Co. KGaA, Weinheim

vents. *N*,*N*′-Diethyl-3,7-diazanonane-1,9-dithiole is readily accessible by procedures described in the literature.[10] The complexes used as starting materials, [{Fe(N_2S_2Me)}$_2$] and [CuI(btmgp)], were synthesised by reaction of [Fe{N[Si(Me)$_3$]$_2$}$_2$] with stoichiometric amounts of *N*,*N*′-diethyl-3,7-diazanonane-1,9-dithiole and addition of btmgp to CuI, respectively.

Physical Measurements: All measurements were performed under strictly anaerobic conditions. IR spectra were obtained using a Bio-Rad FTS-7 (**1**) and a Bruker IFS 66v (**2**) spectrometer. ^{1}H NMR spectra for **2** were obtained with a Bruker Avance DRX 500 spectrometer and solvent signals were used as an internal standard [calibrated on δ = 7.240 (^{1}H), 77.00 (^{13}C)].

X-ray Crystallographic Studies: Single crystals of **1**·MeCN were obtained as yellow blocks by slow cooling of a solution of **1** in MeCN. Suitable yellow crystals of **2** were obtained by slow diffusion of diethyl ether into a MeCN solution of the complex. Crystals were sealed in a glass capillary (**1**) under an inert gas or mounted on top of a glass capillary with silicon grease (**2**). Diffraction data were collected at room temperature (**1**) with a Siemes-Stoe-AED-2 or at 150 K (**2**) with a Siemens P4RA four-circle diffractometer utilizing monochromated Mo-K_α radiation. The data were corrected for absorption (ψ-scan method), as well as for Lorentz and polarisation effects. The structures were solved by direct methods (SHELXS-86).[18] Refinements were done by full-matrix least-squares methods on F^2 with anisotropic thermal displacement parameters for all non-hydrogen atoms using the SHELXL-97 program suite.[19] Hydrogen atoms were fixed on idealised positions and refined with a common isotropic temperature factor. Crystals of **2** are composed of individual complex molecules **2a** and **2b** which occupy the same crystallographic position in a statistical manner. A summary of relevant crystal data is given in Table 1. Crystallographic data (excluding structure factors) for the structures reported in this paper have been deposited with the Cambridge Crystallographic Data Centre as supplementary publication numbers CCDC-203954 (**1**) and -203955 (**2**). Copies of the data can be obtained free of charge on application to CCDC, 12 Union Road, Cambridge CB2 1EZ, UK [Fax: (internat.) + 44-1223/336-033; E-mail: deposit@ccdc.cam.ac.uk].

Preparation of Compounds

[$Cu_4(N_2S_2Me)_2$] (1) (Pathway A): A solution of [CuI(btmgp)] (0.175 g, 0.38 mmol) in MeCN was added dropwise, at room temperature, to a suspension of [{Fe(N_2S_2Me)}$_2$] (0.105 g, 0.19 mmol) in MeCN (15 mL). The mixture was refluxed for 30 min and then filtered. On slow cooling of the filtrate, **1** was obtained as light yellow crystals. Yield: 0.168 g; 60%, based on Cu^{I}. IR (KBr): ṽ = 2957−2920 s, 2841−2799 vs, 2247 m (ν_{CN}), 1458 vs, 1381 m, 1362 m, 1314 m, 1294 s, 1260 m, 1229 s, 1200 vs, 1152 m, 1088 m, 1053 s, 1044 vs, 1032 vs, 993 vs, 959 m, 936 m, 910 m, 893 m, 870 m, 760 vs, 723 vs, 652 m, 600 w, 550 w, 525 w, 467 m, 426 m, 368 m cm^{-1}.

[$Cu_4(N_2S_2Et)_2$] (2) (Pathway B): *N*,*N*′-Diethyl-3,7-diazanonane-1,9-dithiole (0.501 g, 2 mmol) was dissolved in tetrahydrofuran (15 mL) and treated with a slurry of potassium methanethiolate (0.345 g, 4 mmol) in tetrahydrofuran (10 mL). The yellow slurry was stirred at 40 °C for 30 min and the solvent removed in vacuo. The resultant colourless residue was suspended in tetrahydrofuran (20 mL) and again stirred for 30 min at the same temperature. After removal of the solvent under reduced pressure the obtained colourless residue was treated with a solution of copper(I) iodide (0.762 g, 4 mmol) in acetonitrile (25 mL) and the resulting mixture refluxed for 20 min. The solvent was then removed in vacuo and the residue resuspended in tetrahydrofuran (70 mL). After stirring for 16 h, the mixture was filtered and **2** obtained as yellow crystals by slow diffusion of diethyl ether into the clear yellowish filtrate. Yield: 0.413 g; 55%, based on Cu^{I}. $C_{31}H_{59}CuN_6S$ (751.06): calcd. C 35.18, H 6.44, N 7.46, S 17.09; found C 35.31, H 6.45, N 7.48, S 16.92. IR (KBr): ṽ = 2957 vs, 2922 vs, 2824 vs, 1441 s, 1373 m, 1324 m, 1281 vs, 1199 m, 1183 m, 1120 m, 1085 m, 1036 m, 1011 s, 969 m, 917 w, 902 w, 857 w, 787 m, 739 m, 701 m, 656 m, 614 w, 565 m, 503 w, 483 w cm^{-1}. FIR (polyethylene pellet): ṽ = 565 vs, 546 s, 517 m, 503 s, 484 m, 471 m, 451 vw, 438 w, 401 m, 368 vs, 303 w, 276 m, 229 m, 197 s, 181 m, 145 w, 120 m, 110 m, 89 m, 66 m cm^{-1}. Raman (capillary): ṽ = 2922 vs, 2873 m, 2851 m, 2730 w, 1446 w, 1333 vw, 1298 w, 1206 w, 1121 vw, 1093 vw, 1059 w, 1002 w, 934 vw, 918 w, 858 vw, 832 vw, 749 vw, 704 w, 658 m, 615 vw, 550 vw, 519 vw, 471 vw, 425 vw, 278 m, 237 w, 169 m, 120 m, 84 w cm^{-1}. ^{1}H NMR (500 MHz, $CDCl_3$, 298 K): δ = 1.08 (*t*, ^3J = 7.08 Hz, CH_3), 1.10 (*t*, ^3J = 7.26 Hz, CH_3, **2b**), 1.67 ("quint", ^3J = 5.09 Hz, CH_2−CH_2 CH_2−), 2.06 ("quint", ^3J = 6.9 Hz), 2.33 (m), 2.50 (m), 2.64 (m), 2.69 (m), 2.77 (m), 2.93 (*t*, ^3J = 7.08 Hz, H) ppm. ^{13}C NMR (125.75 MHz, $CDCl_3$, 298 K): δ = 8.43 (*C*H$_3$, **2a**), 8.54 (*C*H$_3$, **2b**), 21.89 (C, **2b**), 27.66 (C, **2a**), 27.85 (C, **2b**), 29.18 (C, **2a**), 46.82 (C, **2a**), 50.28 (C, **2b**), 53.09 (C, **2a**), 53.99 (C, **2b**), 56.13 (C, **2a**), 56.87 (C, **2b**) ppm. DEPT-135, ^{1}H^{13}C-COSY, ^{1}H^{1}H-COSY were used for allocation of the signals.

Acknowledgments

This work was supported by the Deutsche Forschungsgemeinschaft and by the Fonds der Chemischen Industrie. J. S. thanks the Stiftung Stipendienfonds des Verbandes der Chemischen Industrie for granting a Kekulé fellowship.

[1] [1a] P. Lappalainen, M. Saraste, *Biochim. Biophys. Acta* **1994**, *222*, 1187. [1b] G. Henkel, A. Müller, S. Weißgräber, G. Buse, T. Soulimane, G. C. M. Steffens, H.-F. Nolting, *Angew. Chem.* **1995**, *107*, 1615; *Angew. Chem. Int. Ed. Engl.* **1995**, *34*, 1488. [1c] S. Itawa, C. Ostermeier, B. Ludwig, H. Michel, *Nature* **1995**, *376*, 660. [1d] T. Tsukihara, H. Aoyana, E. Yamashita, T. Tomizaki, H. Yamaguchi, K. Shinzawa-Itoh, R. Nakashima, R. Yaono, S. Yoshikawa, *Science* **1995**, *269*, 1069.

[2] [2a] R. K. Chadha, R. Kumar, D. G. Tuck, *Can. J. Chem.* **1987**, *65*, 1336. [2b] A. F. Stange, E. Waldhör, M. Moscherosch, W. Kaim, *Z. Naturforsch., Teil B* **1995**, *50*, 115. [2c] R. P. Houser, J. A. Halfen, V. G. Young, Jr., N. J. Blackburn, W. B. Tolman, *J. Am. Chem. Soc.* **1995**, *117*, 10745. [2d] R. P. Houser, V. G. Young, Jr., W. B. Tolman, *J. Am. Chem. Soc.* **1996**, *118*, 2101. [2e] J. Schneider, G. Henkel, *Proc. Int. Conf. Coord. Chem.* **1998**, *33*, 312.

[3] J. Schneider, Dissertation ("Heteroleptische Kupferkomplexe mit Stickstoff- und Chalkogenliganden"), Shaker Verlag, Aachen, **2000**, ISBN 3-8265-8114-8.

[4] For Ni^{II}, see e.g.: J. Schneider, R. Hauptmann, F. Osterloh, G. Henkel, *Acta Crystallogr., Sect. C* **1999**, *55*, 328, and references cited therein. For Cu^{II}, see: [4a] R. P. Houser, W. B. Tolman, *Inorg. Chem.* **1995**, *34*, 1632. [4b] M. Gulotti, L. Casella, A. Pintar, E. Suardi, P. Zanello, S. Mangani, *J. Chem. Soc., Dalton Trans.* **1989**, 1979. For Pd^{II}, see e.g.: M. Y. Darensbourg, T. Tuntullani, J. H. Reibenspies, *Inorg. Chem.* **1995**, *34*, 6287.

[5] For Fe^{II}, see: [5a] W. J. Hu, S. J. Lippard, *J. Am. Chem. Soc.* **1974**, *96*, 2366. [5b] D. K. Mills, Y. M. Hsiao, P. G. Farmer, E. V. Atnip, J. H. Reibenspies, M. Y. Darensbourg, *J. Am. Chem. Soc.* **1991**, *113*, 1421. [5c] G. Musie, C.-H. Lai, J. H. Reibenspies, L. W. Sumner, M. Y. Darensbourg, *Inorg. Chem.* **1998**, *37*, 4086. For Zn^{II}, see: T. Tuntullani, J. H. Reibenspies, P. J. Farmer, M. Y. Darensbourg, *Inorg. Chem.* **1992**, *31*, 3497. For

 © 2003 Wiley-VCH Verlag GmbH & Co. KGaA, Weinheim

Mn^{II}, see: J. Schneider, B. Schnautz, R. Hauptmann, G. Henkel, *Acta Crystallogr.* **1999**, *C55*, 489.
[6] G. Henkel, B. Krebs, P. Betz, H. Fietz, K. Saatkamp, *Angew. Chem.* **1988**, *100*, 1373; *Angew. Chem. Int. Ed. Engl.* **1988**, *27*, 1326.
[7] [7a] J. A. Garcia-Vazquez, J. Romero, R. Castro, A. Sousa, D. J. Rose, J. Zubieta, *Inorg. Chim. Acta* **1997**, *260*, 221. [7b] A. F. Stange, K. W. Klinkhammer, W. Kaim, *Inorg. Chem.* **1996**, *35*, 4087.
[8] [8a] E. Block, H. Kang, G. Ofori-Okai, J. Zubieta, *Inorg. Chim. Acta* **1990**, *167*, 147. [8b] I. Schröter-Schmid, J. Strähle, *Z. Naturforsch., Teil B* **1990**, *45*, 1537. [8c] B. Becker, W. Wojnowski, K. Peters, E.-M. Peters, H. G. von Schnering, *Polyhedron* **1990**, *9*, 1659. [8d] I. G. Dance, L. J. Fitzpatrick, D. C. Craig, M. L. Scudder, *Inorg. Chem.* **1989**, *28*, 1853.
[9] M. A. Khan, R. Kumar, D. G. Tuck, *Polyhedron* **1988**, *7*, 49.
[10] [10a] J. L. Corbin, K. F. Miller, N. Pariyadath, S. Wherland, A. E. Bruce, E. I. Stiefel, *Inorg. Chim. Acta* **1984**, *90*, 41. [10b] F. Osterloh, PhD thesis, Universität Oldenburg, Germany, **1997**.
[11] J. Schneider, A. Heuwing, G. Henkel, manuscript in preparation.
[12] S. Pohl, M. Harmjanz, J. Schneider, W. Saak, G. Henkel, *J. Chem. Soc., Dalton Trans.* **2000**, 3473.
[13] 100 mV/s, tetrabutylammonium hexafluorophosphate, c = 1 mmol/L.
[14] D. Ohlmann, C. M. Marchand, H. Schönberg, H. Grützmacher, H. Pritzkow, *Z. Anorg. Allg. Chem.* **1996**, *622*, 1349.
[15] I. G. Dance, L. J. Fitzpatrick, D. C. Craig, M. L. Scudder, *Inorg. Chem.* **1989**, *28*, 1853.
[16] A. Bruce, J. L. Corbin, P. L. Dahlstrom, J. R. Hyde, M. Minelli, E. I. Stiefel, J. T. Spence, J. Zubieta, *Inorg. Chem.* **1982**, *21*, 917.
[17] [17a] K. Mikami, M. Terada, T. Korenaga, Y. Matsumoto, M. Ueki, R. Angelaud, *Angew. Chem.* **2000**, *112*, 3676; *Angew. Chem. Int. Ed.* **2000**, *39*, 3532. [17b] K. Mikami, T. Korenaga, T. Ohkuma, R. Noyori, *Angew. Chem.* **2000**, *112*, 3854; *Angew. Chem. Int. Ed.* **2000**, *39*, 3707.
[18] G. M. Sheldrick, *SHELXS-86, a program for structure determination*, University of Göttingen, Germany, **1986**.
[19] G. M. Sheldrick, *SHELXL-97, a program for the refinement of crystal structures*, University of Göttingen, Germany, **1997**.
Received October 12, 2002

 © 2003 Wiley-VCH Verlag GmbH & Co. KGaA, Weinheim

Synthesis, Structure, and Catalytic Activity of New μ-Oxo-Bridged Diiron(III) Complexes

Éva Balogh-Hergovich,[a] Gábor Speier,*[b] Marius Réglier,[c] Michel Giorgi,[c] Ernő Kuzmann,[d] and Attila Vértes[d]

Keywords: Iron / Tripodal ligands / Peroxides / Oxidation

The preparation and characterisation of two dinuclear iron(III) complexes with tripodal ligands 1,3-bis(2′-pyridylimino)isoindoline (indH) are presented. The μ-oxo-bridged diiron(III) complex [{FeCl(ind)}$_2$O] (**2**) has been prepared by reacting $FeCl_3 \cdot 6H_2O$ with indH in methanol solution. Compound [{Fe(ind)(OAc)}$_2$O] (**3**) was obtained from the reaction of **2** with CH_3CO_2Ag in THF. Both compounds were characterised by elemental analysis and UV/vis, IR, and Mössbauer spectroscopy. The X-ray structure analysis of [$Fe_2O(ind)_2Cl_2$]·THF (**2**·THF) revealed a distorted trigonal bipyramidal (τ = 0.88) coordination geometry around the iron(III) ion. More importantly, **2** is a good functional model for the activation of small molecules as its 5-coordinate iron ions can easily coordinate such molecules. This is confirmed by the high catalase-like activity of **2**, transforming 87% of the excess of H_2O_2 into O_2 in 1 min. The complexes exhibited monooxygenase-like activity using H_2O_2 as the oxidant and oxidise alkanes to alcohols and ketones in acetonitrile in moderate yields.

(© Wiley-VCH Verlag GmbH & Co. KGaA, 69451 Weinheim, Germany, 2003)

Introduction

Oxo-bridged dinuclear Fe^{III} complexes have been recently extensively studied owing to their presence in a class of non-heme iron proteins that include hemerythrin, ribonucleotide reductase, methane monooxygenase and purple acid phosphatase.[1] The soluble methane monooxygenase, sMMO, isolated from methanotropic organisms catalyses the transformation of methane into methanol using molecular oxygen as the oxidant in the presence of a source of electrons.[2] Several intermediates in the catalytic cycle of sMMO have been characterised but the mechanism of catalytic hydroxylation of unactivated C−H bonds is not fully understood.[3] Spectroscopic studies implicate high-valent (μ-oxo)diiron species as intermediates in the oxidation chemistry of the diiron centres in methane monooxygenase.[4] In the last decade several artificial sMMO systems have been developed using μ-oxo-diiron(III) complexes derived from various supporting ligands, and oxidants such as ROOH,[5] H_2O_2,[6] *m*-chloroperbenzoic acid,[7] and O_2 (+ electron source).[8] For this class of iron complexes the reactivity can be tuned by modifying the ligand around the metal centre.

Hydrogen peroxide may be the best oxidant to functionalise hydrocarbons as it is less expensive, and gives only water as a by-product. However, its use is limited, since a number of diiron complexes have catalase activity.[9]

We report here the preparation and characterisation of μ-oxo-bridged diiron(III) complexes with the tripodal ligand 1,3-bis(2′-pyridylimino)isoindoline (**1**, indH) and their monooxygenase- and catalase-like activity.

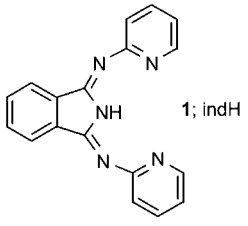

1; indH

Results and Discussion

Synthesis and Characterisation of the Complex [{FeCl(ind)}$_2$O]

Complex [{FeCl(ind)}$_2$O] (**2**) was prepared from equimolar amounts of the ligand and $FeCl_3 \cdot 6H_2O$. In its infrared spectrum the absorptions at 1638 and 1584 cm^{-1} indicate

[a] Research Group for Petrochemistry, Hungarian Academy of Sciences,
8201 Veszprém, Hungary
[b] Department of Organic Chemistry, University of Veszprém,
8201 Veszprém, Hungary
Fax: (internat.) +36-(0)88/427−492
E-mail: speier@almos.vein.hu
[c] Université d'Aix-Marseille 1 et 3, Faculté des Sciences et Techniques de Saint-Jérôme, Chimie, Biologie et Radicaux Libres, UMR CNRS 6517, case 432,
Avenue Escadrille Normandie-Niemen, 13397 Marseille Cedex 13, France
[d] Research Group for Nuclear Techniques in Structural Chemistry, Hungarian Academy of Sciences at Eötvös University Budapest,
Budapest, Hungary

 DOI: 10.1002/ejic.200200575 © 2003 Wiley-VCH Verlag GmbH & Co. KGaA, Weinheim

that the complex contains the deprotonated isoindoline ligand.[10] The band at 792 cm^{-1} is characteristic of the asymmetric stretch of the Fe−O−Fe moiety, while the symmetric stretch occurs at 478 cm^{-1}.[3a,11,12] In the electronic spectrum the band at 238 nm can be assigned to π−π* transitions in the aromatic groups of the ligand, those in the oxo dimer region (388, 473 nm) to a weak oxo-to-iron LMCT transition. The less intense band at 473 nm is assigned to the $^6A_1 \rightarrow (^4A_1, 4E)$ transition and is the signature of the Fe−(μ-O)−Fe motif, independent of the bridging angle.[13,14] Another important characteristic of the μ-oxo core is expected in the 550−700 nm region, which is strongly dependent on the Fe−(μ-O)−Fe angle: the lower the angle, the less energetic and/or the more intense the band.[15] The broad, weak band at 615 nm indicates a bent structure with a low angle, in agreement with X-ray data.

Synthesis and Characterisation of the Complex [{Fe(ind)(OAc)}$_2$O]

Complex [{Fe(ind)(OAc)}$_2$O] (**3**) was prepared by the reaction of [{FeCl(ind)}$_2$O] with CH_3CO_2Ag in THF. Infrared spectrum absorptions at 1638 and 1577 cm^{-1} indicate that the complex contains the deprotonated isoindoline ligand (absence of a strong band at 1100 cm^{-1} and absorptions in the range 1600−1660 cm^{-1}). Complexes with the deprotonated isoindoline ligand exhibit a weak band above 1600 cm^{-1}.[10] The band at 752 cm^{-1} is characteristic of the asymmetric stretch of the Fe−O−Fe moiety, the symmetric stretch occurs at 510 cm^{-1}.[3a,11,12] The ν(CO_2) bands at 1570 and 1430 cm^{-1} suggest a bridged coordination of the acetate groups. In the electronic spectrum of **3**, the band at 237 nm can be assigned to π−π* transitions in the aromatic groups of the ligand, and bands in the oxo dimer region (385, 475 nm) assigned to an oxo-to-iron charge transfer transition. Finally a broad, weak band was observed in the low-energy visible region (720 nm). The considerable red-shift of this band, compared with λ_{max} assigned for the transition in **2**, indicates a smaller Fe−(μ−O)−Fe angle. This supports the binding mode of the acetate as a bidentate bridging ligand between the two iron atoms. From the spectroscopic data for compound **3** the [Fe(ind)(μ-O)(μ-OAc)$_2$(ind)Fe] structure was proposed; however, the [Fe(ind)(OAc)(μ-O)(OAc)(ind)Fe] structure could not be excluded.

Mössbauer Spectroscopy

The Mössbauer spectrum of complex [{FeCl(ind)}$_2$O] is shown in Figure 1 and the parameters are given in Table 1. The relatively low value of the isomer shift (IS) of **2** is due to the high population of 4s orbital of Fe^{III} and it can be explained by the s bonding between Fe^{III} and N(1) and N(6) donor atoms. The large quadrupole splitting (QS) is the consequence of the distorted trigonal bipyramidal geometry around the iron atom.[16,17] The Mössbauer parameters of **3** represent a typical iron(III) with octahedral environment (Table 1). Namely, the higher coordination number results in a higher population of 3d orbital of iron and, at the same time a lower s-electron density at the nucleus of Fe^{III} (higher IS) and a higher symmetry around iron atom than the trigonal bipyramidal coordination in [{FeCl(ind)}$_2$O]. The later effect is the origin of the smaller quadrupole splitting in the complex [{Fe(ind)(OAc)}$_2$O].

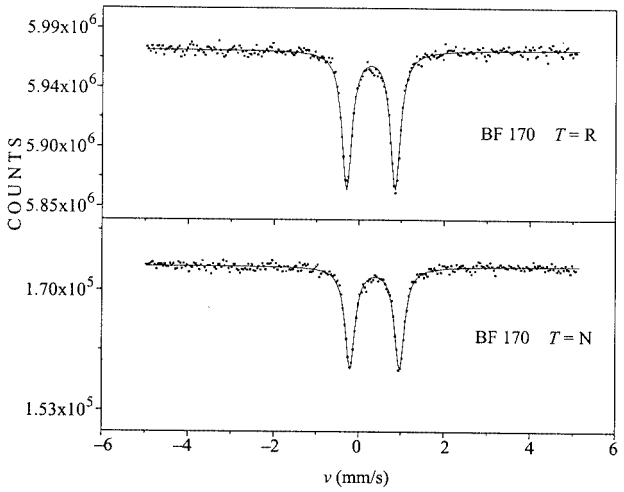

Figure 1. Mössbauer spectra of [{FeCl(ind)}$_2$O]; T_N = temperature of liquid nitrogen

Table 1. Mössbauer parameters for complexes **2** and **3**

	[{FeCl(ind)}$_2$O]		Fe(ind)(OAc)]$_2$O	
	T_N[a]	room. temp.	T_N[a]	room. temp.
IS	0.382	0.279	0.511	0.422
QS	1.164	1.143	0.645	0.617
Line width	0.274	0.284	0.318	0.360

[a] T_N is the temperature of liquid nitrogen.

X-ray Crystal Structure of [{FeCl(ind)}$_2$O]·THF

The molecular structure of complex [{FeCl(ind)}$_2$O]·THF is shown in Figure 2, and selected bond lengths and angles are listed in Table 2. The complex is a μ-oxo dimer, the two iron atoms have a distorted trigonal bipyramidal geometry with $\tau = 0.88$. For perfect square pyramidal and trigonal bipyramidal geometries the values of τ are zero and unity, respectively; τ being an index of the degree of trigonality within the structural continuum between square pyramidal and trigonal bipyramidal geometries.[18] Oxygen and chlorine atoms and one N of the tridentate isoindolinate ligand are in basal positions, while two further N atoms of the ligand occupy apical positions. The metal−metal distance of 3.283 Å is shorter than in other five-coordinated μ-oxo monobridged diiron complexes.[12] Moreover, the Fe−O−Fe angle is significantly shorter than is usually found in similar complexes.[5b,6a,12] These values are close to those in μ-oxo complexes with an additional bridging ligand,[12] and also in dinuclear iron proteins.[1a,1b,3a] The Fe−O bond lengths are within the range reported for (μ-

 © 2003 Wiley-VCH Verlag GmbH & Co. KGaA, Weinheim

oxo)diiron(III) complexes[12] and the Fe−N bond lengths are similar to those obtained for $[FeCl_2(ind)]$.[19] The Fe−N distances involving the pyridine nitrogen atoms, N1 and N3, are significantly longer than for the pyrrole nitrogen atom, N5. The same bond length pattern has been observed in Cu^{II} [20] and Ni^{II} [21] complexes of the isoindolinate ligand. The Fe−Cl bond lengths are similar to those of $[Fe_2O(TPA)_2Cl_2]^{2+}$.[5b]

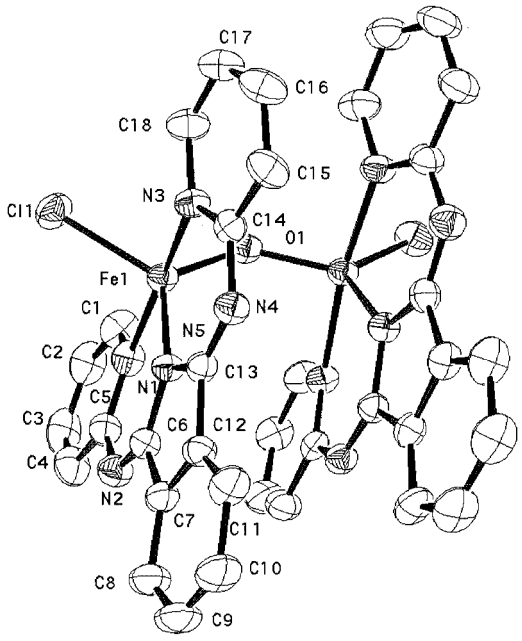

Figure 2. Molecular structure of $[\{FeCl(ind)\}_2O]\cdot THF$

Table 2. Selected bond lengths [Å] and angles [°] for $[\{FeCl(ind)\}_2O]\cdot THF$

Fe(1)−O(1)	1.792(1)	Fe(1)−N(5)	1.998(3)
Fe(1)−Cl(1)	2.272(1)	Fe(1)−N(3)	2.161(3)
Fe(1)−N(1)	2.145(3)	N(3)−C(14)	1.360(4)
N(1)−C(5)	1.341(7)	N(5)−C(13)	1.406(5)
N(1)−C(1)	1.362(5)	N(5)−C(6)	1.384(4)
N(3)−C(18)	1.352(5)		
Fe(1)−O(1)−Fe(1)	131.9(2)	O(1)−Fe(1)−Cl(1)	116.7(1)
N(5)−Fe(1)−Cl(1)	123.4(1)	O(1)−Fe(1)−N(5)	119.8(1)
N(3)−Fe(1)−O(1)	91.2(1)	N(3)−Fe(1)−Cl(1)	92.3(1)
N(1)−Fe(1)−O(1)	96.2(1)	N(1)−Fe(1)−Cl(1)	89.0(1)
N(5)−Fe(1)−N(3)	86.3(1)	N(1)−Fe(1)−N(3)	170.8(1)
N(5)−Fe(1)−N(1)	85.3(1)		

Catalase-Like Activity

The H_2O_2 dismutation activity of complexes **2** and **3** was tested by measuring the dioxygen evolution in acetonitrile with a complex/H_2O_2 ratio of 1:100. As expected, H_2O_2 decomposed to give O_2 gas and water, a reaction competing with the oxidation of cyclohexane. As shown in Figure 3, complex **2** exhibited rather high activity for the decomposition of hydrogen peroxide with about 80 initial turnovers per min at 25 °C (turnover is mmol of O_2 per mmol of complex). The yield of O_2 was 87% based on H_2O_2 after 1 min of reaction. The residual hydrogen peroxide (measured by iodometric titration) was compared with the amount of dioxygen formed and showed good agreement with the stoichiometry of the dismutation reaction. Complex **3** showed much lower dismutation activity.

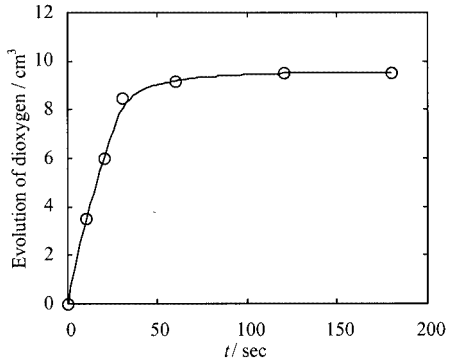

Figure 3. Evolution of dioxygen from H_2O_2 catalysed by $[\{FeCl(ind)\}_2O]$; [**2**] = 1.75 mol·dm^{-3}, $[H_2O_2]$ = 0.175 mol·dm^{-3}

Kinetic measurements of H_2O_2 decomposition in the presence of **2** were performed in acetonitrile at 25 °C under pseudo-first-order conditions. To determine the rate dependence on the two reactants, runs were performed at various $[\{FeCl(ind)\}_2O]$ and H_2O_2 concentrations. The straight line obtained by plotting the initial reaction rate against the initial catalyst concentration indicates a reaction order of one with respect to **2**. The first-order dependence of the reaction rate against $[H_2O_2]$ was established by plotting the initial reaction rate against the $[H_2O_2]$. On the basis of the kinetic data the rate law (1) could be derived. The second-order rate constant k was found to be 9.2 ± 0.6 mol^{-1}·dm^3·s^{-1}.

$$\text{Reaction rate} = k\cdot[H_2O_2][\mathbf{2}] \quad (1)$$

UV/vis spectra of a solution of $[\{FeCl(ind)\}_2O]$ recorded immediately after addition of the oxidant show drastic changes (Figure 4). The final spectrum is very similar to that obtained in the reaction of some other (μ-oxo)diiron(III) complexes with H_2O_2.[6b] This may indicate that in the reaction with hydrogen peroxide the original bent μ-oxo structure decomposes to form a linear μ-oxo type or a mononuclear complex.

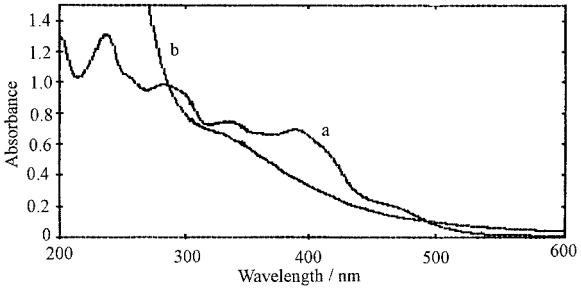

Figure 4. UV/vis spectra of (a) $[\{FeCl(ind)\}_2O]$, (b) **2** with 100 equiv. of H_2O_2 added. [**2**] = 4.02 10^{-5} mol·dm^{-3}, CH_3CN, 25 °C

 © 2003 Wiley-VCH Verlag GmbH & Co. KGaA, Weinheim

Table 3. Oxidation of cyclohexane

Catalyst[a]	Oxidant	Yield [%][b] Cyclohexanol	Cyclohexanone	$tBuO_2$/cyclohexane	*TN*[c][d]
[{FeCl(ind)}$_2$O]	H_2O_2	14.6	14.8	–	29.4
[{FeCl(ind)}$_2$O]	H_2O_2	15.3	13.8	–	29.1[d]
[{FeCl(ind)}$_2$O]	H_2O_2	12.2	13.6	–	25.8[e]
[{Fe(ind)(OAc)}$_2$O]	H_2O_2	4.5	8.4	–	12.9
[$FeCl_2$(ind)]	H_2O_2	4.3	6.6	–	10.9
[{FeCl(ind)}$_2$O]	$tBuO_2H$	7.2	7.2	0.5	14.9
[{Fe(ind)(OAc)}$_2$O]	$tBuO_2H$	7.2	7.4	0.6	15.2

[a] Reaction conditions: cyclohexane (3.5 mmol), oxidant (3.5 mmol), catalyst (35 μmol), acetonitrile (10 cm^3), Ar, 25 °C, 10 h. [b] Based on the oxidant. [c] *TN* (turnover numbers) = mol of product per mol of catalyst. Total yield and TN values take into account that 2 equivalents of oxidant are required to make 1 equivalent of ketone. [d] Under O_2. [e] 1 cm^3 CCl_4 added.

Oxygenation of Alkanes

The monooxygenase-like activity of complexes [{FeCl(ind)}$_2$O] (**2**), [{Fe(ind)(OAc)}$_2$O] (**3**) and [$FeCl_2$(ind)] was tested in the oxidation of alkanes. We checked first the activity of (**2**) in the oxidation of cyclohexane by different oxidants and in different solvents (MeOH, CH_2Cl_2, CH_3CN). Catalytic oxidations were effective only with H_2O_2 and $tBuO_2H$. No oxidation products could be detected with di-*tert*-butyl peroxide and iodosylbenzene. The results (Table 3) show that the best yields were obtained with H_2O_2 in acetonitrile. Under our experimental conditions the molar ratio of iron complex/hydrogen peroxide/substrate is 1:100:100. The oxidation of cyclohexane yielded cyclohexanol and cyclohexanone in a 2:1 ratio. The total turnover number (mmol product per mmol catalyst) was 29.4, and the alcohol + ketone yield was 29.4% after 10 h. In comparison, the yield was 14.9% with $tBuO_2H$ and a small amount of *tert*-butyl cyclohexyl peroxide was also formed. Moreover, the catalyst obtained by replacing the chlorine ligands with acetate was less active. The mononuclear iron(III) complex, [$FeCl_2$(ind)], showed a catalytic activity similar to that of **2**.

As shown in Table 4, complex **2** also catalyses the oxygenation of methylcyclohexane, adamantane, and ethylbenzene. With methylcyclohexane as substrate, the reactivity at the tertiary position is 6 times higher than that at the secondary position, and no oxygenation was observed at the primary position. The normalised reactivity ratio of the tertiary C−H to secondary C−H in the oxygenation of adamantane is 4.0. The adamantane C3/C2 selectivity ratio is in the range found for other systems, including model studies of sMMO by using dinuclear iron complexes,[5a] and also for the MMO enzyme (3.0, normalised).[22] These results show that the regio-selectivity in the alkane hydroxylation catalysed by [{FeCl(ind)}$_2$O] follows the order tertiary > secondary > primary carbon. From the time dependence of the reaction (Figure 5) it seems that cyclohexanone and cyclohexanol were always formed in approximately constant ratios, showing that cyclohexanol is not the precursor of cyclohexanone. Experiments were also performed under dioxygen to elucidate the role of O_2. The almost constant yields of the oxidation products, whether the reaction was carried out under argon or dioxygen, suggest that O_2 is not involved in this reaction (Table 2). When 2,6-di-*tert*-butyl-4-methylphenol, as a free radical trap, was added to the oxidation of cyclohexane prior to H_2O_2 addition in the case of complex **2** there was no significant lowering of the yields of oxidation products. The oxidation reaction of cyclohexane was also performed after addition of CCl_4 to the reaction mixture. No formation of bicyclohexyl and cyclohexyl chloride was observed. Any free cyclohexyl radical present would undergo dimerisation to give bicyclohexyl, and would also abstract Cl from CCl_4 to give cyclohexyl chloride.[23]

Table 4. Oxygenation of alkanes catalysed by [{FeCl(ind)}$_2$O]

Substrate[a]	Product	Yield [%][b]	*TN*[c]
Methylcyclohexane	1-methylcyclohexanol	4.2	
	2-methylcyclohexanol	0.4	
	3-methylcyclohexanol	1.8	15.4
	3-methylcyclohexanone	6.2	
	4-methylcyclohexanone	2.8	
Adamantane[d]	1-adamantanol	9.2	
	2-adamantanol	6.3	16.7
	adamantanone	1.2	
Ethylbenzene	1-phenylethanol	2.5	16.1
	acetophenone	13.6	

[a] Reaction conditions: substrate (3.5 mmol), oxidant (3.5 mmol), **2** (35 μmol), acetonitrile (10 cm^3), Ar, 25 °C, 10 h. [b] Based on the oxidant. [c] *TN* (turnover numbers) = mol of product per mol of catalyst. Total yield and *TN* values take into account that 2 equiv. of oxidant are required to make 1 equiv. of ketone. [d] 20 cm^3 acetonitrile.

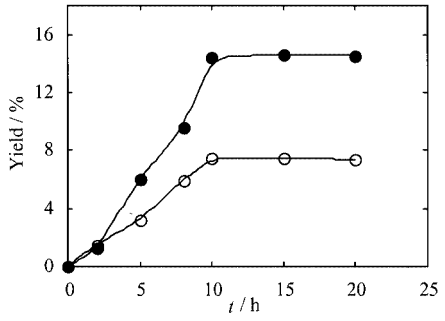

Figure 5. Yields of the products versus reaction time for the oxygenation of cyclohexane, catalyst [{FeCl(ind)}$_2$O]; (•) cyclohexanol, (o) cyclohexanone; [cyclohexane] = 0.35 mol·dm^{-3}, [H_2O_2] = 0.35 mol·dm^{-3}, [**2**] = 3.5 10^{-3} mol·dm^{-3}, CH_3CN 10 cm^3, Ar, 25 °C

 © 2003 Wiley-VCH Verlag GmbH & Co. KGaA, Weinheim

In our study the coordinatively unsaturated iron(III) in [{FeCl(ind)}$_2$O] can easily bind H_2O_2, and an iron-peroxo species, observed also during other H_2O_2 dependent reactions,[24−26] may be a transient precursor of a metal-based oxidative species. Our observations suggest that the reaction proceeds via heterolytic scission of the peroxide bond, resulting in high-valent oxo metal intermediates, rather than via a radical mechanism. The same reaction also occurs with [$FeCl_2$(ind)]. It is likely that the mononuclear [$FeCl_2$(ind)] in solution is converted into the oxo-bridged dimer (**2**), the thermodynamic sink for the Fe^{III} state, and this will be the active catalyst of the reaction. Compound **2** could also be prepared by stirring [$FeCl_2$(ind)] in hot methanol. In [{Fe(ind)(OAc)}$_2$O], obtained by replacing chlorine ligands by acetate bridges, the six-coordinated iron(III) has no vacant site for the coordination of H_2O_2, which results in lower activity. Further spectroscopic studies are needed to elucidate the structure of the intermediate complexes.

Conclusion

Two new μ-oxo-diiron(III) complexes with 1,3-bis(2′-pyridylimino)isoindoline ligands, [{FeCl(ind)}$_2$O] (**2**), [{Fe(ind)(OAc)}$_2$O] (**3**), have been prepared and then characterised by elemental analysis and UV/vis, IR, and Mössbauer spectroscopy. X-ray structure analysis of the complex [Fe_2O(ind)$_2Cl_2$]·THF revealed that the coordination geometry around the iron(III) ion is distorted trigonal bipyramidal ($\tau = 0.88$). In complex **3** the iron(III) has an octahedral environment. Moreover **2** is a good functional model for the activation of small molecules, since each iron ion is five-coordinate and, thus, small substrate molecules can be coordinated easily. Both complexes were effective catalysts for the oxidation of alkanes utilising hydrogen peroxide as oxygen source; however, their use is limited due to their ability to dismutate H_2O_2. Complex **2** exhibits a rather high activity for the decomposition of hydrogen peroxide, transforming 87% of the excess of H_2O_2 into O_2 in 1 min.

Experimental Section

General Remarks: All manipulations were performed under a pure dinitrogen or argon atmosphere unless otherwise stated, using standard Schlenck-type inert-gas techniques.[27] 1,3-Bis(2′-pyridylimino)isoindoline,[28] and [$FeCl_2$(ind)][19] were prepared according to literature methods. Methanol and acetonitrile were purified in the usual manner and stored under argon.[29] All other chemicals were commercial products and were used as received without further purification.

Physical Measurements: Infrared spectra were recorded on a Specord 75 IR (Carl Zeiss) spectrophotometer using samples mulled in Nujol between KBr plates or in KBr pellets. GC analyses were performed on a HP 583OA gas chromatograph equipped with a flame ionisation detector and a 25 m (0.2 mm i.d., 0.25 μm FT) CP-SIL-8CB fused silica capillary column. GC-MS analyses were performed on a HP 5890II/5971 GC/MSD apparatus equipped with a column identical to that used for GC analyses. UV/vis spectra were recorded on a Shimadzu UV-160 spectrophotometer by using quartz cells. The Mössbauer spectroscopy measurements were carried out at room temp. or at liquid nitrogen temperature (T_N) and in zero applied magnetic field using a conventional Mössbauer spectrometer in constant acceleration mode. The γ-rays were provided by a ^{57}Co(Rh) source of 10^9 Bq activity. All isomer shift data are given relative to α-Fe. For the spectrum evaluation we used the MössWinn program package.[30]

Synthesis of [{FeCl(ind)}$_2$O] (2): $FeCl_3$·$6H_2O$ (0.270 g, 1 mmol) was dissolved in methanol (10 cm^3), then 1,3-bis(2′-pyridylimino)isoindoline (0.299 g, 1 mmol) in methanol (20 cm^3) was added and the reaction mixture stirred under argon at 60° for 8 h. After cooling, a dark brown powder of [{FeCl(ind)}$_2$O] precipitated, which was filtered off, washed with acetonitrile and dried under vacuum (0.34 g, 85%). Recrystallisation of the product from THF gave dark brown crystals. M.p. 354−356 °C. IR (KBr): $\tilde{\nu}$ = 1638 w, 1602 w, 1584 s, 1549 m, 1536 s, 1468 s, 1428 m, 1360 w, 1306 w, 1265 m, 1197 m, 1150 w, 1095 w, 1061 s, 1007 m, 898 w, 851 w, 792 m, 783 s, 722 m, 702 m, 641 w, 539 w, 514 w, 478 w, 437 w cm^{-1}. UV/vis (CH_3CN): λ_{max} (log ε/dm^3·mol^{-1}·cm^{-1}) = 238 (4.78), 282 (4.65), 388 (4.51), 473 (3.99), 615 (3.57) nm. $C_{36}H_{24}Cl_2Fe_2N_{10}O$ (795.2): calcd. C 54.36, H 3.04, Cl 8.91, Fe 14.04, N 17.61; found C 54.68, H 3.12, Cl 8.54, Fe 13.44, N 17.34.

Synthesis of [{Fe(ind)(OAc)}$_2$O] (3): [{FeCl(ind)}$_2$O] (1.067 g, 1.34 mmol) in THF (80 cm^3) was treated with CH_3CO_2Ag (0.447 g, 2.68 mmol) at 60 °C for 8 h. The resultant light brown precipitate was filtered off and the solution condensed under vacuum to 30 cm^3. Upon cooling (−10 °C), a dark brown solid was deposited, which was filtered off, washed with acetonitrile and dried under vacuum (0.75 g, 65%). M.p. > 320 °C. IR (KBr): $\tilde{\nu}$ = 1638 w, 1597 w, 1577 s, 1570 s, 1530 s, 1468 s, 1430 s, 1367 w, 1272 m, 1190 m, 1150 w, 1061 s, 1000 m, 878 w, 802 m, 797 s, 752 m, 539 w, 510 w, 430 w cm^{-1}. UV/vis (THF): λ_{max} (log ε/dm^3·mol^{-1}·cm^{-1}) = 237 (4.51), 363 (4.32), 385 (4.35), 409 (4.28), 475 (3.84) 720 (2.45) nm. $C_{40}H_{30}Fe_2N_{10}O_5$ (842.4): calcd. C 57.02, H 3.58, Fe 13.25, N 16.63; found C 56.74, H 3.60, Fe 12.97, N 16.57.

Table 5. Crystallographic data of [{FeCl(ind)}$_2$O]·THF

Empirical formula	$C_{36}H_{24}N_{10}OFe_2Cl_2$·THF
Formula mass	867.36
Crystal size [mm^3]	0.7 × 0.2 × 0.1
Crystal system	orthorhombic
Space group	Pccn
a [Å], α [°]	12.727(1), 90
b [Å], β [°]	13.460(1), 90
c [Å], γ [°]	21.516(1), 90
V [Å^3]	3685.8(4)
Z	4
F(000)	1840
$\rho_{calcd.}$ [g cm^{-3}]	1.621
μ [mm^{-1}]	0.992
$\Theta_{min.}$, $\Theta_{max.}$ [°]	2.90, 26.36
Reflections collected	4014
Reflections total	3632
Reflections unique	2243
Parameters	254
GOF on F^2	1.027
R [$I \geq 2\sigma(I)$] (all data)	0.0502 (0.1028)
R_w (all data)	0.1047 (0.1253)
Max. resd. density [e/Å^3]	0.577

 © 2003 Wiley-VCH Verlag GmbH & Co. KGaA, Weinheim

X-ray Structure Determination of 2: Suitable crystals of [{FeCl(ind)}$_2$O]·THF were obtained from THF. The intensity data were collected with a Nonius Kappa CCD single-crystal diffractometer, using graphite-monochromated Mo-K_α radiation (λ = 0.71073 Å) and φ scan technique at 293 K. Details of the crystal structure determination are shown in Table 5. The structure was solved by direct and difmap methods (SIR92),[31] and refined on F^2 by using full-matrix least-squares methods.[32,33] CCDC-195083 contains the supplementary crystallographic data for this paper. These data can be obtained free of charge at www.ccdc.cam.ac.uk/conts/retrieving.html or from Cambridge Crystallographic Data Centre, 12, Union Road, Cambridge CB2 1EZ, UK [Fax: (internat.) + 44-1223/336-033; E-mail: deposit@ccdc.cam.ac.uk].

Oxidation Reactions: Standard oxidation reactions were carried out under an inert atmosphere of argon. The complex (35 μmol) was dissolved in acetonitrile (10 cm^3) containing 3.5 mmol of substrate. The reaction was then started by adding 3.5 mmol of H_2O_2 or tBuO$_2$H. After stirring for 10 h at 25 °C the products were determined by GC analysis. The structures of the products were confirmed by GC-MS spectrometry, and by comparison with authentic samples.

Catalase-Like Reactions: All reactions were carried out at 25 °C under an argon atmosphere in a thermostatted reactor with stirring. To start the reaction hydrogen peroxide (0.875 mmol, 97 μL) was added through a septum to a stirred solution of the complex (8.75 mmol, 7 mg) in acetonitrile (5 cm^3). The volume of evolved dioxygen was read periodically by using a gas burette. In the kinetic measurements the hydrogen peroxide concentration was first kept constant ([H_2O_2] = 0.175 mol·dm^{-3}) and the concentration of **2** was varied from 0.525 to 3.52 mol·dm^{-3}. To determine the rate dependence on the H_2O_2, the catalyst concentration was kept constant ([**2**] = 1.75 mol·dm^{-3}) and the [H_2O_2] varied in the range 0.0618−0.3088 mol·dm^{-3}.

Acknowledgments

The financial support of the Hungarian National Research Fund (OTKA T-7443, T-016285, T-30400 and T-034839) is gratefully acknowledged.

[1] [1a] D. M. Kurtz, Jr., *J. Biol. Inorg. Chem.* **1997**, *2*, 159−167. [1b] J. B. Vincent, G. L. Olivier-Lilley, B. A. Averill, *Chem. Rev.* **1990**, *90*, 1447−1467. [1c] S. -Y. Choi, P. E. Eaton, D. A. Kopp, S. J. Lippard, M. Newcomb, R. Shen, *J. Am. Chem. Soc.* **1999**, *121*, 12198−12199.

[2] [2a] B. J. Wallar, J. D. Lipscomb, *Chem. Rev.* **1996**, *96*, 2625−2658. [2b] A. C. Rosenzweig, P. Nordlund, P. M. Takahara, C. A. Frederick, S. J. Lippard, *Chem. Biol.* **1995**, *2*, 409−418.

[3] [3a] J. Sanders-Loehr, W. D. Wheeler, A. K. Shiemke, B. A. Averill, T. M. Loehr, *J. Am. Chem. Soc.* **1989**, *111*, 8084−8093. [3b] A. M. Valentine, S. J. Lippard, *J. Chem. Soc., Dalton Trans.* **1997**, 3925−3931. [3c] A. M. Valentine, S. S. Stahl, S. J. Lippard, *J. Am. Chem. Soc.* **1999**, *121*, 3876−3887.

[4] [4a] K. E. Liu, A. M. Valentine, D. Wang, B. H. Huynh, D. E. Edmondson, A. Salifoglou, S. J. Lippard, *J. Am. Chem. Soc.* **1995**, *117*, 10174−10185. [4b] L. Shu, J. C. Nesheim, K. Kauffmann, E. Münck, J. D. Lipscomb, L. Que, Jr., *Science* **1997**, *275*, 515−518.

[5] [5a] R. A. Leising, R. E. Norman, L. Que, Jr., *Inorg. Chem.* **1990**, *29*, 2553−2555. [5b] T. Kojima, R. A. Leising, S. Yang, L. Que, Jr., *J. Am. Chem. Soc.* **1993**, *115*, 11328−11335. [5c] J. M. Vincent, S. Ménage, C. Lambeaux, M. Fontecave, *Tetrahedron Letters* **1994**, *35*, 6287−6290. [5d] M. Costas, K. Chen, L. Que, Jr., *Coord. Chem. Rev.* **2000**, *200−202*, 517−544.

[6] [6a] S. Ito, T. Okuno, H. Matsushima, T. Tokii, Y. Nishida, *J. Chem. Soc., Dalton Trans.* **1996**, 4479−4484. [6b] T. Okuno, S. Ito, S. Ohba, Y. T. Nishida, *J. Chem. Soc., Dalton Trans.* **1997**, 3547−3551.

[7] M. Kodera, H. Shimakoshi, K. Kano, *Chem. Commun.* **1996**, 1737−1738.

[8] S. Ménage, J. B. Galey, J. Dumats, G. Hussler, M. Seité, I. Gautier, G. Chottard, M. Fontecave, *J. Am. Chem. Soc.* **1998**, *120*, 13370−13382.

[9] [9a] R. Tahn, A. Schrodt, L. Westerheide, R. van Eldik, B. Krebs, *Eur. J. Inorg. Chem.* **1999**, 1537−1543. [9b] S. Ménage, J. M. Vincent, C. Lambeaux, M. Fontecave, *J. Chem. Soc., Dalton Trans.* **1994**, 2081−2084.

[10] R. R. Gagné, D. N. Marks, *Inorg. Chem.* **1984**, *23*, 65−74.

[11] J. E. Plowman, T. M. Loehr, C. K. Schauer, O. P. Anderson, *Inorg. Chem.* **1984**, *23*, 3553−3559.

[12] D. M. Kurtz, Jr., *Chem. Rev.* **1990**, *90*, 585−606.

[13] R. Hazell, K. B. Jensen, C. J. McKenzie, H. Toftlund, *J. Chem. Soc., Dalton Trans.* **1995**, 707−717.

[14] R. C. Reem, J. M. McCormick, D. E. Richardson, F. J. Devlin, P. J. Stephens, R. L. Musselman, E. I. Solomon, *J. Am. Chem. Soc.* **1989**, *111*, 4688−4704.

[15] R. E. Norman, R. C. Holz, S. Ménage, C. J. O'Connor, J. H. Zhang, L. Que, Jr., *Inorg. Chem.* **1990**, *29*, 4629−463.

[16] R. R. Berrett, B. W. Fitzsimmons, A. Owusu, *J. Chem. Soc. (A)* **1968**, 1575−1579.

[17] G. M. Bancroft, A. G. Maddock, R. P. Randl, *J. Chem. Soc. (A)* **1968**, 2939−2944.

[18] A. W. Addison, T. N. Rao, J. Reedijk, J. Rijn, van, G. C. Vershoor, *J. Chem. Soc., Dalton Trans.* **1984**, 1349−1356.

[19] É. Balogh-Hergovich, G. Speier, B. Tapodi, M. Réglier, M. Giorgi, *Z. Kristallogr.* **1999**, *214*, 579−580.

[20] É. Balogh-Hergovich, J. Kaizer, G. Speier, G. Huttner, A. Jacobi, *Inorg. Chem.* **2000**, *39*, 4224−4229.

[21] R. J. Letcher, W. Zhang, C. Bensimon, R. J. Crutchley, *Inorg. Chim. Acta* **1993**, *210*, 183−191.

[22] M. Kodera, K. Kano, T. Funabiki, in *Oxygenases and Model Systems* (Ed.: T. Funabiki), Kluwer Academic Publishers, Dordrecht, **1997**, vol. 19, (Catalysis by Metal Complexes), p. 283−343.

[23] R. H. Crabtree, *Chem. Rev.* **1985**, *85*, 245−269.

[24] H. Zheng, S. J. Yoo, E. Münck, L. Que, Jr., *J. Am. Chem. Soc.* **2000**, *122*, 3789−3790.

[25] K. Chen, L. Que, Jr., *J. Am. Chem. Soc.* **2001**, *123*, 6327−6337.

[26] Y. Mekmouche, S. Ménage, C. Toia-Duboc, M. Fontecave, J. B. Galey, C. Lebrun, J. Pécaut, *Angew. Chem. Int. Ed.* **2001**, *40*, 949−952.

[27] D. F. Shriver, M. A. Drezdzon, *The Manipulation of Air-sensitive Compounds*, John Wiley & Sons, New York, **1986**.

[28] W. O. Siegel, *J. Org. Chem.* **1977**, *42*, 1872−1878.

[29] D. D. Perrin, W. L. Armarego, D. R. Perrin, *Purification of Laboratory Chemicals*, 2nd ed., Pergamon, New York, **1990**.

[30] Z. Klencsár, E. Kuzmann, A. Vértes, *J. Rad. Nucl. Chem. Lett.* **1996**, *210*, 105−118.

[31] A. Altamore, G. Cascarano, C. Giacovazzo, A. Guagliardi, M. C. Burla, G. Polidori, M. Camalli, *J. Appl. Cryst.* **1994**, *27*, 435−436.

[32] S. Mackay, C. J. Gilmore, C. Edwards, M. Tremayne, N. Stewart, K. Shankland, *maXus: A Computer Program for the Solution and Refinement of Crystal Structures from Diffraction Data*, University of Glasgow, Scotland, UK, Nonius BV, Delft, The Netherlands and MacScience Co. Ltd., Yokohama, Japan, **1998**.

[33] G. M. Sheldrick, *SHELXL-97: Program for the Refinement of Crystal Structures*, University of Göttingen, Germany, **1997**.

Received October 16, 2002

 © 2003 Wiley-VCH Verlag GmbH & Co. KGaA, Weinheim

Cobalt(III) Tetraazamacrocyclic Complexes with Pendant Amino Groups: Synthesis, Structure and Electrochemical Properties

Bohdan Korybut-Daszkiewicz,*[a] Joanna Taraszewska,*[b] Katarzyna Zięba,[b] Krzysztof Woźniak,[c] and Daniel Kamiński[c]

Keywords: Macrocyclic ligands / N ligands / Cobalt / Electrochemistry

Two isomeric *cis*-2,9-bis(aminomethyl)-5,7,7,12,14,14-hexamethyl-1,4,8,11-tetraazacyclotetradecane (**1** and **2**) and two 2-aminomethyl-2-methyl-1,4,8,11-tetraazacyclotetradecane (**3** and **4**) cobalt(III) complexes have been prepared and characterised. During the synthesis of **2** a minor oxidation product **5** was formed. The structures of **3**, **4** and **5** have been determined by X-ray crystallography, and the UV/Vis spectra of **1**–**5** have been analysed. The average Co–N distances in **1** and **2** have been estimated from the correlation between the average Co–N bond lengths and position of the maximum absorption for hexaamine complexes given in literature. The electrochemical behaviour of **1**–**5** in neutral and acidic solutions has been studied by cyclic voltammetry. In complexes displaying electronic maxima at higher energy, cobalt(III) was reduced at more negative potentials. Small differences in the conformation of ligand between **3** and **4** explain the different behaviour of these complexes in acidic solutions.
(© Wiley-VCH Verlag GmbH & Co. KGaA, 69451 Weinheim, Germany, 2003)

Introduction

Compounds containing the sarcophagine group − consisting of the cyclam unit with a single diamine strap bridging the apical sites of the macrocycle[1] − belong to the most extensively studied Co^{III} macrocyclic hexaamine complexes. In these compounds the hexaaza ligand can completely surround the metal ion coordinated in an octahedral manner. Another approach is realised in pendant arm macrocycles, which usually occupy four equatorial sites around coordinated metal ion, and simultaneously, via pendant coordinating amine groups, are bound at one or both axial positions. The synthesis and physico-chemical properties of macrocyclic Co^{III} tetraamines with pendant amine groups have been extensively studied in recent years.[2−6] Recently Bernhardt et al.[7] synthesised the hexaamine with five secondary amine groups in the macrocyclic ring and one pendant primary amine group to give hexadenate octahedral complexes with Co^{III} and other cations. Macrocyclic Co^{III} tetraamines with one pendant amine group coordinated in one axial position and anion coordinated in the second axial position have also been extensively studied[8−12] Such complexes present a different ligand field environment to that found in the neutral hexaamine complexes.

Here we describe the synthesis, characterisation and electrochemical studies of Co^{III} *C*-functionalised cyclam derivatives containing two or one aminomethyl side arms that are able to interact with the metal ion in the central cavity. In two isomeric Co^{III} complexes of *cis*-2,9-bis(aminomethyl)-5,7,7,12,14,14-hexamethyl-1,4,8,11-tetraazacyclotetradecane (**1** and **2** respectively), the coordination of two pendant amino groups forces the ring to adopt a folded conformation. It was interesting to compare the behaviour of these complexes with their Ni^{II} analogues studied by us recently[13] and with other Co^{III} hexaamine complexes.

The crystallographic data for two isomeric Co^{III} complexes of 2-aminomethyl-2-methyl-1,4,8,11-tetraazacyclotetradecane (**3** and **4**) revealed that both complexes possess the *trans* configuration with the macrocyclic ring occupying the equatorial plane and the apical positions occupied by a pendant NH_2 group and a chloride ion in the *trans* configuration. They differ only in configuration at the secondary amine groups resulting in different conformations of the macrocyclic ring.

A goal of this study was to examine the influence of the macrocyclic ligand conformation on the properties of the synthesised complexes. The structures of the complexes studied are presented in Figure 1.

[a] Institute of Organic Chemistry, Polish Academy of Sciences, Kasprzaka 44/52, 01-224 Warszawa, Poland
Fax: (internat.) +48-(0)22 6326681
E-mail: bkd@icho.edu.pl
[b] Institute of Physical Chemistry, Polish Academy of Sciences, Kasprzaka 44/52, 01-224 Warszawa, Poland
Fax: (internat.) +48-(0)22 6325276
E-mail: jota@ichf.edu.pl
[c] Department of Chemistry, University of Warsaw, Pasteura 1, 02−093 Warszawa, Poland

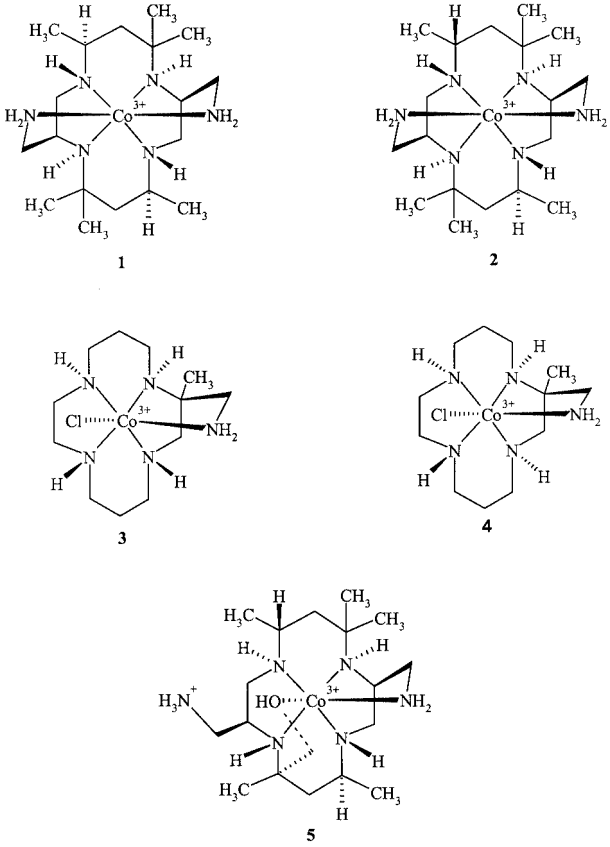

Figure 1. Schematic structures of studied complexes

Results and Discussion

Synthesis and Structure

Cobalt(III) complexes **1** and **2** were prepared by the reaction of free *cis*-2,9-substituted isomeric ligands with $CoCl_2 \cdot 6H_2O$ followed by aerial oxidation. The ^1H and ^{13}C NMR spectra of complexes **1** and **2** are consistent with that expected for the *cis*-fivefolded conformation of ligands – previously observed in their octahedral Ni^{II} complexes.[14]

During the synthesis of **2** (5,12-*trans*) an additional minor oxidation product **5** was formed and isolated by chromatography on a SP Sephadex C-25 column. X-ray analysis (Figure 2) revealed that complex **5** was formed by the oxidation of one of the geminal methyl groups attached to C-5 and located *trans* to the substituents at C-7 and C-10. The macrocyclic ring in complex **5** adopts a *trans*-III planar conformation with the 2-aminomethyl and 5-hydroxymethyl groups coordinated on opposite sides of the macrocycle. The remaining protonated 10-aminomethyl group occupies an equatorial position. A similar dioxygen oxidation of one of the *gem*-dimethyl substituents to a coordinated hydroxymethyl group in *C-meso*-5,7,7,12,12,14-hexamethyl-1,4,8,11-tetrazacyclotetradecane have been reported by House et al.[15]

The *N*-isomeric cobalt(III) complexes **3** and **4** were similarly obtained and separated by chromatography on a Dowex 50WX2 cation-exchange column. Slow evaporation of acetonitrile–methanol (9:1) solutions gave crystals suitable for X-ray crystal analysis.

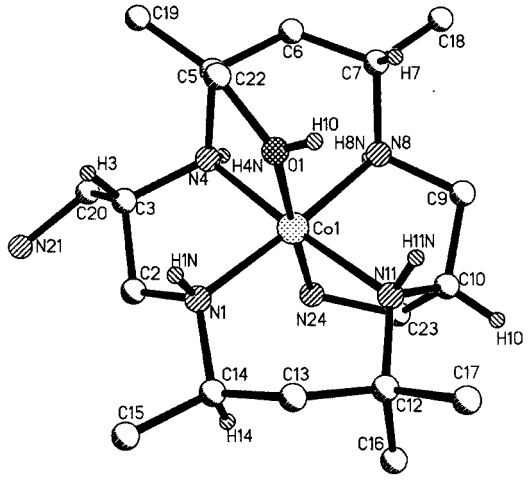

Figure 2. Molecular structure and labelling of atoms for the complex **5**; selected bond lengths (Å) are: Co(1)–O(1) 1.920(3), Co(1)–N(1) 1.957(4), Co(1)–N(4) 1.959(3), Co(1)–N(8) 1.983(3), Co(1)–N(11) 1.961(3), Co(1)–N(24) 1.936(4)

The molecular structures of cations **3** and **4** are shown in Figure 3 and 4, respectively. Both cations have irregular octahedral Co^{III} coordination spheres with the macro-cycle coordinated in a planar conformation and the pendant amino group in the apical position. The sixth coordination position is occupied by a chloride anion; *trans*-III (1*RS*,2*RS*,4*RS*,8*SR*,11*SR*) and *trans*-II (1*RS*,2*RS*,4*SR*,8*RS*,11*RS*) ligand configurations were established for **3** and **4**, respectively. The chloride anion in isomer **4** is coordinated on the same side of the macrocycle as three secondary amino group protons. The Co–Cl bond is longer [2.265(2) and 2.258(3) Å for two independent molecules] in the isomer **4** than in **3** [2.249(2) Å]. The two six-membered endomacrocyclic chelate rings in the cation **3** adopt the chair conformation, whereas one of them in isomer **4** [N(11)–N(1)] exists in the twist-boat conformation. The five-membered chelate rings exist in an envelope conformation in both isomers.

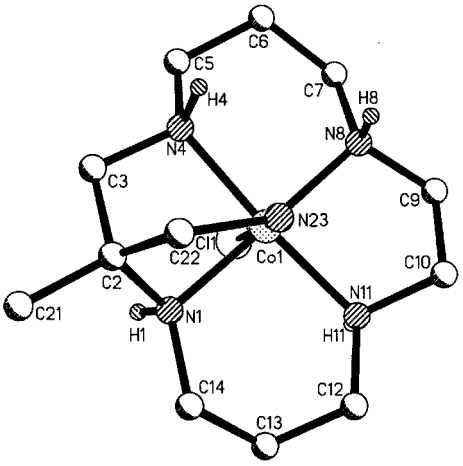

Figure 3. Molecular structure and labelling of atoms for the complex **3**; selected bond lengths (Å) are: Co(1)–Cl(1) 2.249(2), Co(1)–N(1) 1.961(6), Co(1)–N(4) 1.980(7), Co(1)–N(8) 1.965(7), Co(1)–N(11) 1.974(8), Co(1)–N(23) 1.972(6)

 © 2003 Wiley-VCH Verlag GmbH & Co. KGaA, Weinheim

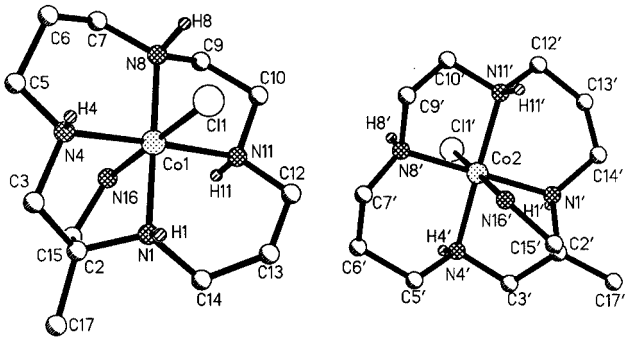

Figure 4. Molecular structure of the two independent cations of complex **4**; selected bond lengths (Å) are: Co(1)−Cl(1) 2.265(2), Co(1)−N(1) 1.942(7), Co(1)−N(4) 1.971(7), Co(1)−N(8) 1.971(8), Co(1)−N(11) 1.988(7), Co(1)−N(16) 1.96(1); Co(2)−Cl(1′) 2.258(3), Co(2)−N(1′) 1.967(7), Co(2)−N(4′) 1.977(7), Co(2)−N(8′) 1.974(7), Co(2)−N(11′) 1.993(7), Co(2)−N(16′) 1.984(8)

Solution Properties

Electronic Spectroscopy of Complexes

The aqueous solution UV/Vis electronic spectra of complexes **1**−**5** are presented in Table 1.

The spectra of complexes **1** and **2** exhibit two spin-allowed d−d transitions characteristic of low-spin d^6 ion in a pseudooctahedral ligand field. The transitions $^1T_{2g}\leftarrow{}^1A_{1g}$ and $^1T_{1g}\leftarrow{}^1A_{1g}$ in both complexes occur at lower energies than those in Co^{III} complexed with *cis*-6,13-dimethyl-1,4,8,11-tetraazacyclotetradecane-6,13-diamine (*cis*-diammac) and other Co^{III} hexaamine complexes.[4] The electronic spectrum of complex **1** displays electronic maxima at higher energies than those of **2**. Spectra of the complexes **3** and **4** exhibit three bands that are similar to those of other complexes of this type.[8,9,11,12] The appearance of the three bands is connected with the lower symmetry of the both complexes in comparison with hexaamine with two pendant NH_2 groups. The transition maxima occur at higher energies for **3** than for **4**. For complexes **1**−**4**, for each pH value, the electronic spectra were unchanged after 5 h, proving the lack of protonation of the amine groups in **1** and **2** and the lack of hydrolysis of the chloro-ligands in the complexes **3** and **4**.

For complex **5** in a neutral solution, the first band was observed as a shoulder at about 340 nm, due to overlap with a strong absorption band in the UV region. The second band appeared at 489 nm. In acidic medium the shoulder and the second band appeared at 338 nm and 469 nm, respectively. This indicates that in neutral solution the pendant amino group substitutes the hydroxy group in the coordination sphere of the central metal ion. In the acidic medium the amino group is protonated and the reverse process takes place.

A correlation has been reported[16] between the Co−N bond length and the position of the absorption maxima in $[Co(N)_6]$ complexes. Unfortunately, for the complexes **1** and **2** we have no crystallographic data. To estimate the average Co−N distance in these complexes we plotted (Figure 5) the λ_{max} values for $^1T_{2g}$ and $^1T_{1g}$ transitions against the average Co−N bond lengths for hexaamine complexes **6**−**12** taken from the literature (Table 1). The structures of complexes **6**−**12** are presented in Figure 6. The open circles and squares in Figure 5 are for complexes **1** and **2**, respectively. The estimated average Co−N distances from this correlation are 1.989 and 2.010 Å for **1** and **2**, respectively.

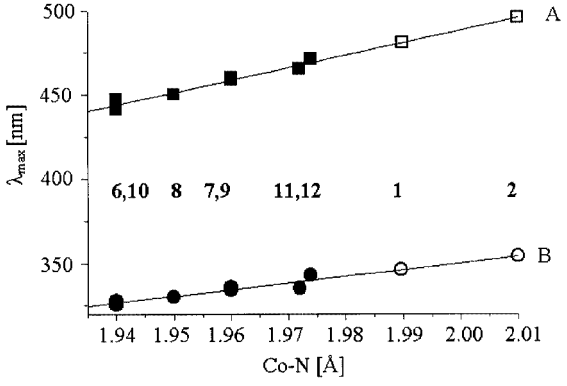

Figure 5. Plot of λ_{max} values against the average Co-N lengths for Co^{III} hexaamine complexes. Open circles and squares refer to complexes **1** and **2**, respectively. A- for $^1T_{1g} \leftarrow {}^1A_{1g}$ and B-for $^1T_{2g}\leftarrow {}^1A_{1g}$ transitions, respectively

Table 1. Electronic absorption spectra, formal potentials and average Co−N distances in cobalt(III) complexes

Complex	E_f [V] vs. MCE	λ_{max}, nm (ε, $dm^3mol^{-1}cm^{-1}$)	Co−N_{av} [Å]	Ref.
1	−0.52	346(92); 481(98)	1.989	this work
2	−0.48	354(121); 496(118)	2.010	this work
3	−0.43	362(94); 454(38); 534(61)	–	this work
4	−0.37	365(118); 461(53.5); 550(85)	–	this work
5	−0.42	338(167); 489(78)	–	this work
6	−0.85	328; 447	1.94	[4]
7	−0.72	334; 459	1.96	[4]
8	−0.86	330; 450	1.95	[4]
9	−0.76	336; 460	1.96	[4]
10	−0.83	325; 441	1.94	[4]
11	−0.71	343; 471	1.974	[4]
12	−0.64	335; 465	1.972	[7]
13	−0.49	350; 516	–	[9]

 © 2003 Wiley-VCH Verlag GmbH & Co. KGaA, Weinheim

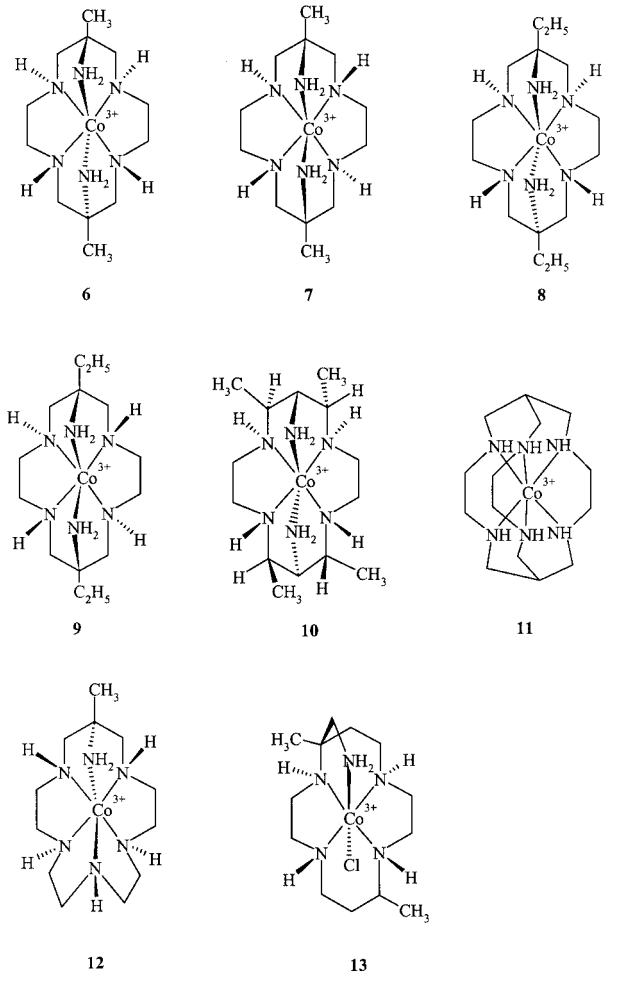

Figure 6. Schematic structures of Co^{III} hexaamine complexes **6**−**11**,[4] **12**[7] and chloro-pentaamine complex **13**[9]

Redox Properties of Complexes and Acid−Base Equilibria

The voltammetric behaviour of **1**−**4** was studied in aqueous solutions containing 0.1 M NaCl as the supporting electrolyte. The redox process Co^{III}/Co^{II} in all complexes was reversible or quasi-reversible. The values of formal potentials E_f, calculated as midpoints between the corresponding cathodic and anodic peaks, are −0.52, −0.48, −0.43 and −0.37 V for complexes **1**−**4**, respectively.

In **1** the ratio i_c/i_a was less than 1 which suggests that the larger Co^{II} ion cannot be well accommodated in the macrocyclic cage and the complex starts decomposing. This is supported by the smaller estimated average Co−N distance for **1** compared with **2**. On the C.V. curves recorded at higher scan rates (1 V s^{-1}) the ratio i_c/i_a was 1.

In comparison with other hexaamine complexes,[4] the redox potentials of the complexes **1** and **2** are shifted to less negative values. Replacement of one -NH_2 group by chloride causes a further positive shift. Comparison of the spectrophotometric and electrochemical parameters for **1**−**5** with those from literature revealed a very good correlation between E_f and λ_{max} (Figure 7). Consequently, for complexes displaying electronic maxima at higher energy, Co^{III} is reduced at more negative potentials. A similar correlation was found for Ni^{II} hexaamine complexes by Gavrish and Lampeka.[17]

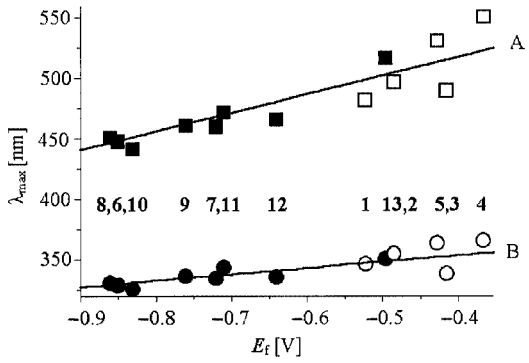

Figure 7. Plots of λ_{max} against formal potentials E_f for Co^{III} complexes **6**−**13**. Open circles and squares refer to complexes **1**−**5**; A for $^1T_{1g} \leftarrow {}^1A_{1g}$ and B for $^1T_{2g} \leftarrow {}^1A_{1g}$ transitions, respectively

The presence of a charged Cl^- donor instead of neutral primary amine group clearly changes both the charge and electronic effects in the complex. As the average Co−N distances in **3** and **4** are similar, the main reason for the difference in E_f values is that the Co−Cl distances are ca. 2.249(2) Å in **3**, and 2.265(2) and 2.258(3) Å in **4**. The longer Co−Cl distance in **4** diminishes the electronic density on the central ion and facilitates reduction of the Co^{III} complex. The shorter Co−NH_2 distance in complex **4** than in **3** seems to play a minor role.

The behaviour of Co^{III} in complexes **1**−**3**, in acidic solutions was similar. Up to the lowest value, pH 1, Co^{III} was reduced at the same potential as in neutral solutions and the reduction currents remained constant, indicating that the pendant NH_2 groups are not protonated. Upon lowering of pH from 7 to 1, the redox process Co^{III}/Co^{II} in **1** and **2** become less reversible ($\Delta E \approx 100$ mV) and the anodic peaks continuously diminished. In **3** up to pH 2.5, the redox process was quasi-reversible with $i_{pa}/i_{pc} = 1$. At lower pHs the anodic current started to diminish due to the protonation of the NH_2 group. The presence of two axial protons from the secondary amino groups in the macrocyclic ring in the neighbourhood of the protonated NH_3^+ group may explain why Co^{II} cannot coordinate either a H_2O molecule or a Cl^- anion. Therefore, this complex is electrochemically inactive. Similarly, the lack of the oxidation of Co^{II} in the protonated form of **2** may be connected with the presence of many methyl groups in the macrocyclic ring, which prevent access of axial ligands.

With increasing solution acidity, the behaviour of the complex **4** was different than that of **3** (Figure 8), indicating that even small differences in structure can significantly influence the electrochemistry. With decreasing pH, the reduction potential of Co^{III} shifts towards less negative values. However, the height of the peak remains constant, which means that the −NH_2 group in this complex is not protonated. The shift of the Co^{III} reduction potential may be connected with the competition between protons from solution and the metal centre for chloride ion, which is at

 © 2003 Wiley-VCH Verlag GmbH & Co. KGaA, Weinheim

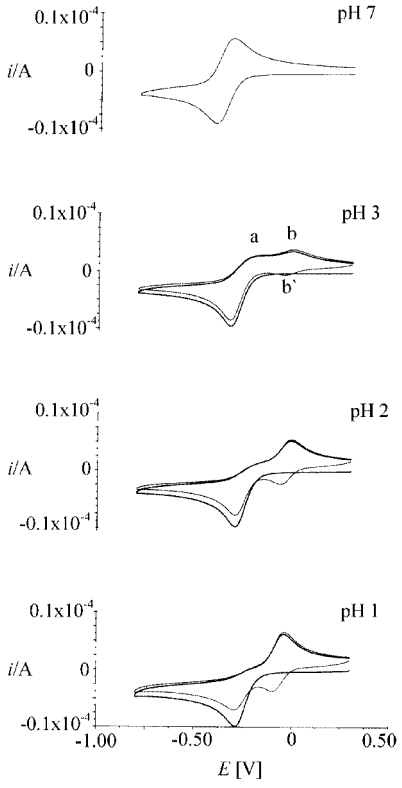

Figure 8. Cyclic voltammograms of 5×10^{-4} M of complex **4** recorded at the GC-20 electrode in aqueous 0.1 M NaCl solution at various pH, scan rate 0.05 V s^{-1}

a longer distance than in **3**. This weakens its coordination ability and decreases the charge density on Co^{III}, making the reduction process easier.

In the anodic scan at pH 3, the anodic peak *a* diminishes as in the other complexes and a new anodic peak *b* appears at about 0.0 V. The product formed at this potential is subsequently reversibly reduced at a potential of peak *b′* in the second scan. The heights of peaks *b* and *b′* increase with lowering pH. The formal potential $E_f = -0.07$ V of this process is similar to that corresponding to the redox process Co^{III}/Co^{II} in $[Co^{III}\text{-cyclam}Cl_2]Cl$[9] (about −0.11 V). Therefore, we can assume that, after protonation of the NH_2 group, Co^{II} in **4** coordinates the Cl^- ion and the second pair of peaks is connected with the Co^{III}/Co^{II} redox process from complex **4** with two chloride ions coordinated to the metal centre. In an experiment performed in 0.1 M $HClO_4$ solution the second pair of peaks appeared at positive potentials (E_f about +0.11 V), which suggests that, after protonation of the -NH_2 group, the ligand at the second apical position was replaced by a water molecule.

In **5**, the reduction potential of Co^{III} is shifted with decreasing pH towards less negative values. For example, from −0.46 V at pH 7 to −0.31 V at pH 1. This is in agreement with the postulated substitution of the coordinated hydroxy group in a neutral solution by the pendant -NH_2 group, protonation of it at low pH values, and subsequent replacement by the OH group.

Conclusion

Structural properties such as ring size and conformation of the ligands studied by us are very selective in the stabilisation of the Co^{II} cations. The effect of the ring size was particularly evident in the case of Co^{II} in the complex **1**. This complex decomposed because Co^{II} could not be well accommodated in the macrocyclic cavity. The redox process in hexaamine complexes **1** and **2** was recorded at more negative potentials than in the complexes **3** and **4** with an axially coordinated Cl donor instead of a neutral primary amine group. The longer Co−Cl distance in complex **4** facilitated the reduction of Co^{III}. Small differences in the ligand conformation between **3** and **4** caused different behaviour of these complexes in acidic solutions.

Experimental Section

Syntheses: The preparation of 2-aminomethyl-2-methyl-1,4,8,11-tetraazacyclotetradecane and isomeric (2*RS*,5*RS*,9*RS*,12*RS*)- and (2*RS*,5*SR*,9*RS*,12*RS*)-2,9-bis(aminomethyl)-5,7,7,12,14,14-hexamethyl-1,4,8,11-tetraazacyclotetradecanes has been described elsewhere.[14]

Instrumentation: Cyclic voltammograms of complexes **1**−**5** were measured at a glassy carbon (GC-20) electrode, with a Pt plate as the counter electrode. The reference electrode, a 1 M NaCl aqueous calomel electrode (MCE), was connected to the electrolytic cell via an intermediate vessel filled with the solution under investigation. Solutions were deaerated by flushing with pure argon. An Autolab (EcoChemie) measuring system was used. Electronic spectra were recorded using a Cary 1 (Varian) spectrophotometer. The NMR spectra were obtained on a Bruker AM 500 spectrometer.

(2*RS*,5*RS*,9*RS*,12*RS*)-2,9-Bis(aminomethyl)-5,7,7,12,14,14-hexamethyl-1,4,8,11-tetraazacyclotetradecanecobalt(III) Trichloride (1): A solution of free ligand (0.34 g, 0.001 mol) in methanol (10 cm^3) was added to a solution of $CoCl_2 \cdot 6H_2O$ (0.24 g, 0.001 mol) in methanol (20 cm^3) and aerated overnight, diluted with water (100 cm^3) and absorbed on the SP Sephadex C-25 column. The column was eluted with a 0.1 M solution of sodium sulfate. The single orange band was collected, absorbed on a Dowex 50WX2 cation-exchange column (H^+ form) that was washed with 1 M HCl and eluted with 3 M HCl. An orange eluate was evaporated to dryness and the residue dissolved in a methanol−acetonitrile mixture. Upon evaporation of methanol, orange crystals were obtained. Yield 0.34 g (70%). $C_{18}H_{42}Cl_3CoN_6 \cdot 2H_2O$ (543.9): calcd. C 39.8, H 8.5, Cl 19.6, N 15.5; found C 39.9, H 8.7, Cl 20.1, N 15.8. ^1H NMR (500.13 MHz, D_2O + DCl): δ = 1.41 (s) and 1.44 (s, 7,14-CH_3), 1.37 (d, 5,12-CH_3), 3.05 (m, 5,12-CH), 2.59 (d) and 3.06 (m, 2,9-CH_2NH_2), 3.54 (m, 2,9-CH), 1.73 (m) and 1.75 (m, 6,13-CH_2) 3.08 (m) and 3.18 (m, 3,10-CH_2), 4.70 (1,8-NH), 5.93 (4,11-NH), 4.92 and 5.49 (NH_2) ppm. ^{13}C NMR (125.8 MHz, D_2O +DCl): δ = 28.0 and 30.8 (7,14-CH_3), 22.0 (5,12-CH_3), 46.9 (2,9-CH_2NH_2), 66.1 (2,9-C), 60.2 (3,10-C), 59.9 (5,12-C), 47.9 (6,13-C), 59.0 (7,14-C) ppm.

(2*RS*,5*SR*,9*RS*,12*RS*)-2,9-Bis(aminomethyl)-5,7,7,12,14,14-hexamethyl-1,4,8,11-tetraazacyclotetradecanecobalt(III) Trichloride (2) and 2-Aminomethyl-9-ammoniummethyl-7-hydroxymethyl-5,7,12,14,14-pentamethyl-1,4,8,11-tetraazacyclotetradecanecobalt(III) Tetrachloride (5): These complexes were obtained from the

 © 2003 Wiley-VCH Verlag GmbH & Co. KGaA, Weinheim

(2*RS*,5*SR*,9*RS*,12*RS*) isomer of the macrocyclic ligand by the same procedure. The minor red ligand oxidation product **5** was isolated as the first band eluted from a SP Sephadex C-25 column. Yield 60% and 8% of **2** and **5**, respectively.

Complex 2: $C_{18}H_{42}Cl_3CoN_6 \cdot 3H_2O$ (561.9): calcd. C 38.5, H 8.6, Cl 18.9, N 14.9; found C 38.9, H 8.2, Cl 18.6, N 14.6. ^{1}H NMR (500.13 MHz, D_2O): δ = 1.35 (s), 1.42 (s), 1.43 (s) and 1.47 (s, 7,14-CH_3), 1.27 (d) and 1.37 (d, 5,12-CH_3), 3.05 (m) and 3.20 (m, 5,12-CH), 2.71 (d), 3.00 (bd) and 2.66 (d), 3.00 (bd, 2,9-CH_2NH_2), 3.53 (t) and 3.59 (t, 2,9-CH), 1.56 (d), 2.16 (dd) and 1.62 (dd), 1.68 (dd, 6,13-CH_2) 3.29 (d), 3.14 (m) and 2.73 (d), 3.12 (m, 3,10-CH_2) ppm. ^{13}C NMR (125.8 MHz, D_2O): δ = 25.3, 27.8, 31.5 and 35.4 (7,14-CH_3), 21.2 and 22.3 (5,12-CH_3), 46.1 and 48.6 (2,9-CH_2NH_2), 64.8 and 64.8 (2,9-C), 50.8 and 61.3 (3,10-C), 52.9 and 59.8 (5,12-C), 45.2 and 47.7 (6,13-C), 59.8 and 61.1 (7,14-C) ppm.

Complex 5: $C_{18}H_{43}Cl_4CoN_6O \cdot 2H_2O$ (596.4): calcd. C 36.3, H 7.9, N 14.1; found C 36.6, H 7.9, N 13.6. ^{1}H NMR (500.13 MHz, D_2O): δ = 1.34 (s), 1.41 s, 1.58 (s) (7,14-CH_3), 1.34 and 1.50 (d, 5,12-CH_3), 3.35 (s, 7-CH_2OH) ppm. ^{13}C NMR (125.8 MHz, D_2O): δ = 20.0, 20.6, 21.3, 25.1, 32.5 (CH_3), 43.0, 47.8, 49.2, 52.1, 53.1, 55.4, 56.9, 57.1, 57.5, 59.7, 62.1, 70.5, 71.3 ppm.

Isomeric 2-Aminomethyl-2-methyl-1,4,8,11-tetraazacyclotetradecanecobalt(III) Trichlorides (3 and 4): A solution of 2-aminomethyl-2methyl-1,4,8,11-tetraazacyclotetradecane (1.0 g, 0.004 mol) in methanol (40 cm^3) was added to solution of $CoCl_2 \cdot 6H_2O$ (1.0 g, 0.004 mol) in methanol (60 cm^3) and aerated overnight, acidified with concentrated HCl (1 cm^3), diluted with water (500 cm^3) and then absorbed on a Dowex 50WX2 cation-exchange column (H^+ form). The column was washed with 1 M HCl and eluted with 2 M HCl. Two deep red bands were separated and the solvents evaporated to dryness. The residues were dissolved in small volumes of methanol and diluted with acetonitrile. Upon evaporation deep red crystals were obtained from both fractions. Yield 0.7 g (41%) of **3** (first fraction) and 0.6 g (35%) of **4** (second fraction).

Complex 3: $C_{12}H_{29}Cl_3CoN_5 \cdot 2H_2O$ (444.72): calcd. C 32.4, H 7.4, Cl 23.9, N 15.8; found C 32.1, H 7.4, Cl 24.5, N 15.8. ^{1}H NMR (500.13 MHz, D_2O + DCl): δ = 1.36 (s, 2-CH_3), 2.78 (m) and 2.86 (m, pendant-CH_2), 4.00 (m), 4.04 (m, NH_2), 6.52 (1-NH), 2.95 (3-CH, ax), 3.00 (3-CH, eq.), 5.56 (4-NH), 3.19 (5-CH, ax), 2.48 (5-CH, eq.), 1.97 (6-CH, ax), 2.05 (6-CH, eq.), 2.67 (7-CH, ax), 2.96 (7-CH, eq.), 6.00 (8-NH), 2.58 (9-CH, ax), 3.06 (9-CH, eq.), 2.56 (10-CH, ax), 3.01 (10-CH, eq.), 6.12 (11-NH), 2.65 (12-CH, ax), 2.85 (12-CH, eq.), 1.82 (13-CH, ax), 2.20 (13-CH, eq.), 2.30 (14-CH, ax), 2.93 (14-CH, eq.) ppm. ^{13}C NMR (125.8 MHz, D_2O +DCl): δ = 16.5 (2-CH_3), 48.8 (pendant-CH_2), 71.4 (2-C), 63.7 (3-C), 48.9 (5-C), 29.2 (6-C), 51.0 (7-C), 54.3 (9-C), 55.9 (10-C), 50.6 (12-C), 28.8 (13-C), 46.1 (14-C) ppm, assignments established on the basis of ^{1}H−^{1}H and ^{1}H−^{13}C correlation experiments.

Complex 4: $C_{12}H_{29}Cl_3CoN_5 \cdot H_2O$ (426.70): calcd. C 33.8, H 7.3, Cl 24.9, N16.4; found C 33.6, H 7.3, Cl 25.2, N 16.1. ^{1}H NMR (500.13 MHz, D_2O + DCl): δ = 1.33 (s, 2-CH_3), 2.67 (m) and 2.88 (m, pendant-CH_2), 3.97 (m, NH_2), 6.27 (bd, 1-NH), 3.34 (m, 3-CH, ax), 2.69 (m, 3-CH, eq.), 6.47 (bt, 4-NH), 2.58 (5-CH, ax), 2.94 (5-CH, eq.), 1.83 (6-CH, ax), 2.17 (bd, 6-CH, eq.), 2.90 (7-CH_2), 6.28 (8-NH), 2.67 (m, 9-CH, ax), 2.98 (m, 9-CH, eq.), 2.45 (m, 10-CH, ax), 3.09 (m, 10-CH, eq.), 5.89 (bt, 11-NH), 2.59 (12-CH, ax), 2.91 (12-CH, eq.), 2.09 (m, 13-CH, ax), 2.25 (m, 13-CH, eq.), 2.53 (14-CH, ax), 2.88 (14-CH, eq.) ppm. ^{13}C NMR

Table 2. Crystal data and structure refinement details for complexes **3**, **4** and **5**

Compound	**3**	**4**	**5**
Empirical formula	$C_{12}H_{29}Cl_3CoN_5 \cdot 2H_2O$	$2C_{12}H_{29}Cl_3CoN_5 \cdot 1.5H_2O$	$C_{18}H_{43}Cl_4CoN_6O \cdot H_2O$
Molecular mass	444.72	844.40	578.33
Temperature [K]	293(2)	293(2)	293(2)
Wavelength [Å]	0.71073	0.71073	0.71073
Crystal system, space group	Orthorhombic, *Pccn*	Monoclinic, $P2_1/c$	Monoclinic, $P2_1/n$
Unit cell dimensions			
a [Å]	18.230(4)	14.855(3)	8.0523(16)
b [Å]	13.650(3)	10.472(2)	19.465(4)
c [Å]	15.770(3)	24.955(5)	17.532(4)
β [°]	90	97.68(3)	95.47(3)
Volume [Å^3]	3924.2(14)	3847.2(13)	2735.4(9)
Z	8	8	4
Calculated density [g·cm^{-3}]	1.505	1.458	1.404
Absorption coefficient [mm^{-1}]	1.30	1.31	1.04
F(000)	1872	1772	1224
Crystal size [mm]	0.2 × 0.2 × 0.4	0.1 × 0.1 × 0.2	0.1 × 0.3 × 0.5
Θ range for data collection [°]	3.19 to 21.00	3.38 to 22.00	3.45 to 21.00
Limiting indices	$-18 \le h \le 18$	$-15 \le h \le 11$	$-6 \le h \le 8$
	$-13 \le k \le 13$	$-10 \le k \le 11$	$-18 \le k \le 19$
	$-8 \le l \le 15$	$-26 \le l \le 26$	$-16 \le l \le 17$
Reflections collected/unique	14029/2073	15455/4681	9775/2906
	R(int) = 0.0627	*R*(int) = 0.1182	*R*(int) = 0.0298
Completeness to Θ = 21.00	98.6%	99.3%	99.0%
Refinement method	Full-matrix least-squares on F^2	Full-matrix least-squares on F^2	Full-matrix least-squares on F^2
Data/restraints/parameters	2073/0/337	4681/0/625	2906/0/461
Goodness-of-fit on F^2	1.197	0.907	1.053
Final *R* indices [$I > 2\sigma(I)$]	*R*1 = 0.0659	*R*1 = 0.0639	*R*1 = 0.0406
	*wR*2 = 0.1420	*wR*2 = 0.1464	*wR*2 = 0.1085
R indices	*R*1 = 0.0673	*R*1 = 0.1221	*R*1 = 0.0448
(all data)	*wR*2 = 0.1427	*wR*2 = 0.1629	*wR*2 = 0.1115
Largest diff. peak and hole [e·Å^{-3}]	0.495 and −0.270	0.801 and −0.426	0.666 and −0.257

 © 2003 Wiley-VCH Verlag GmbH & Co. KGaA, Weinheim

(125.8 MHz, D_2O +DCl): δ = 17.4 (2-CH_3), 49.1 (pendant-CH_2), 72.2 (2-C), 64.0 (3-C), 53.1 (5-C), 25.8 (6-C), 47.1 (7-C), 54.7 (9-C), 56.6 (10-C), 51.0 (12-C), 29.6 (13-C), 42.8 (14-C) ppm, assignments established on the basis of $^1H-^1H$ and $^1H-^{13}C$ correlation experiments.

X-ray Crystallography: Crystal structure data for**3**, **4** and **5** are given in Table 2, together with refinement details. All measurements of crystal were performed on a Kuma KM4CCD κ-axis diffractometer with graphite-monochromated Mo-K_α radiation. The crystal was positioned at 65 mm from the KM4CCD camera. For complex **3**: 4 runs of 575 frames each were measured at 0.2° intervals with a counting time of 37 s. For complex **4**: 4 runs of 153 frames each were measured at 0.75° intervals with a counting time of 30 s. For complex **5**: 4 runs of 153 frames each were measured at 0.75° intervals with a counting time of 30 s. The data were corrected for Lorentz and polarisation effects. No absorption correction was applied. Data reduction and analysis were carried out with the Kuma Diffraction (Wrocław) programs (KM4CCD and KM4RED).

The structures were solved by direct methods[18] and refined using SHELXL.[19] The refinement was based on F^2 for all reflections except those with very negative F^2. Weighted R factors wR and all goodness-of-fit S values are based on F^2. Conventional R factors are based on F with F set to zero for negative F^2. The $F_o^2 > 2s(F_o^2)$ criterion was used only for calculating R factors and is not relevant to the choice of reflections for the refinement. The R factors based on F^2 are about twice as large as those based on F. Most hydrogen atoms were located from differential maps and refined isotropically but some were fixed at ideal geometrical positions. For **4**, we were unable to find one hydrogen atom belonging to the disordered water molecule. One of the water molecules in **4** occupies a special position. Refinement of the solvent molecules is slightly worse. Scattering factors were taken from Tables 6.1.1.4 and 4.2.4.2 in ref.[20]

CCDC-187666, CCDC-187667 and CCDC-187668 contain the supplementary crystallographic data for this paper. These data can be obtained free of charge at www.ccdc.cam.ac.uk/conts/etrieving.html [or from the Cambridge Crystallographic Data Centre, 12, Union Road, Cambridge CB2 1EZ, UK; Fax: (internat.) +44−1223/336−033; E-mail: deposit@ccdc.cam.ac.uk].

Acknowledgments

The X-ray measurements were undertaken at the Crystallographic Unit of the Physical Chemistry Laboratory at the Chemistry Department of the University of Warsaw.

[1] R. J. Geue, T. W. Hambley, J. M. Harrowfield, A. M. Sargeson, M. R. Snow, *J. Am. Chem. Soc.* **1984**, *106*, 5478−5488.
[2] P. V. Bernhardt, G. A. Lawrance, T. W. Hambley, *J. Chem. Soc., Dalton Trans.* **1989**, 1059−1065.
[3] P. V. Bernhardt, P. Comba, T. W. Hambley, *Inorg. Chem.* **1993**, *32*, 2804−2809.
[4] P. V. Bernhardt, L. A. Jones, P. C. Sharpe, *Inorg. Chem.* **1997**, *36*, 2420−2425.
[5] P. Comba, A. F. Sickműller, *Angew. Chem. Ed. Engl.* **1997**, *36*, 2006−2008.
[6] P. V. Bernhardt, L. A. Jones, *Inorg. Chem.* **1999**, *38*, 5086−5090.
[7] P. V. Bernhardt, G. A. Lawrance, M. Napitupulu, G. Wei, *Inorg. Chim. Acta* **2000**, *300−302*, 604−612.
[8] R. W. Hay, M. P. Pujari, B. Korybut-Daszkiewicz, G. Ferguson, B. L. Ruhl, *J. Chem. Soc., Dalton Trans.* **1989**, 85−91.
[9] J. Taraszewska, G. Rosłonek, B. Korybut-Daszkiewicz, *J. Electroanal. Chem.* **1991**, *297*, 245−255.
[10] T. W. Hambley, G. A. Lawrance, M. Martinez, B. W. Skelton, A. H. White, *J. Chem. Soc., Dalton Trans.* **1992**, 1643−1648.
[11] G. A. Lawrance, M. Martinez, B. W. Skelton, A. H. White, *J. Chem. Soc., Dalton Trans.* **1992**, 1649−1652.
[12] Y. Baran, T. W. Hambley, G. A. Lawrance, E. N. Wilkes, *Aust. J. Chem.* **1997**, *50*, 883−888.
[13] B. Korybut-Daszkiewicz, J. Taraszewska, B. Kamieński, *Eur. J. Inorg. Chem.* **2001**, 645−649.
[14] B. Korybut-Daszkiewicz, P. Gluziński, J. Krajewski, A. Kemme, A. Mishniev, *Eur. J. Inorg. Chem.* **1999**, 263−268; A. R. Koliński, B. Korybut-Daszkiewicz, in preparation.
[15] D. A. House, M. Harnett, W. T. Robinson, M. C. Couldwell, *J. Chem. Soc., Chem. Commun.* **1984**, 979−980.
[16] U. Sakaguchi, K. Tomioka, H. Yoneda, *Chem. Lett.* **1984**, 394−352.
[17] S. P. Gavrish, Ya. D. Lampeka, *Russian J. Inorg. Chem.* **1996**, *41*, 1255−1258.
[18] G. M. Sheldrick, *Acta Crystallogr., Sect. A* **1990**, *46*, 467−473.
[19] G. M. Sheldrick, SHELXL-93. *Program for the Refinement of Crystal Structures*, University of Göttingen, Germany.
[20] *International Tables for Crystallography*, (Ed. A. J. C. Wilson), Kluwer: Dordrecht, **1992**, vol. C.

Received June 14, 2002

 © 2003 Wiley-VCH Verlag GmbH & Co. KGaA, Weinheim

Novel P,N Ligands Derived from (*R*)- and (*S*)-1-Phenylethylamine with (2*R*,5*R*)-2,5-Dimethylphospholanyl Groups (DuPHAMIN) for Asymmetric Catalysis

David J. Brauer,*[a] Konstantin W. Kottsieper,[a] Stefan Roßenbach,[a] and Othmar Stelzer[a][†]

Keywords: Asymmetric catalysis / N,P ligands / Rhodium

Novel P,N chelating ligands with three stereogenic centres in positions α to the donor atoms have been prepared in good yields and high enantiomeric purity by a series of reactions beginning with either (*R*)- or (*S*)-1-phenylethylamine. These isomers were first lithiated with *t*BuLi and converted into aminophosphanes **3a** by treatment with $(Et_2N)_2PCl$. They were transformed into the enantiomeric primary phosphanes **4** by quantitative solvolysis with ethanol to give the phosphonous acid esters **3b** and subsequent reduction with $LiAlH_4$. Stepwise treatment of **4** with *n*BuLi and the cyclic sulfate of (*S*,*S*)-2,5-hexanediol gave the isomeric tertiary phosphanes (*R*,*RR*)-**5** and (*S*,*RR*)-**5**. Treatment of the aminophosphane (*R*)-**3a** with (*R*)-2,2′-binaphthol yielded the aminophosphonite (*R*,*R*)-**6** in high yields. Cationic (COD)Rh complexes of **5** were prepared by treatment with $[Rh(COD)Cl]_2$, the PF_6^- salts **7a** being isolated. Analogous (2,5-norbornadiene)Rh complexes **7b** were prepared similarly. The chelate nature of the P,N ligands in these salts is indicated by their NMR spectra in solution and is confirmed by the crystal structures of (*R*,*RR*)-**7a** and (*S*,*RR*)-**7a**. With the exception of (*S*,*RR*)-**7a**, the complexes **7a** and **7b** are shown to catalyse the asymmetric hydrogenation of methyl acetamidocinnamate at room temperature. Differences in the catalytic activity of the complexes are related to the different dynamic behaviour detected by the ^1H EXSY spectra for the COD ligands of **7a**.

(© Wiley-VCH Verlag GmbH & Co. KGaA, 69451 Weinheim, Germany, 2003)

Introduction

Chiral chelates containing phosphorus and an electronically different donor atom can be highly effective coligands in a variety of transition-metal-catalysed asymmetric reactions. The enantioselectivities achieved in these systems[1] may well be comparable with those obtained by use of the established C_2-symmetrical diphosphanes of the DuPHOS type[2] (**1a**), attributed to the electronic asymmetry in the vicinity of the metallic coordination centre. For instance, the different *trans* effects of the coordinating atoms may enhance the steric influence exerted by the chiral substituents on the optical induction. The application of the concept of electronic disparity[3] has in the last decade resulted in the development of novel bidentate P,N hybrid ligands such as **1b**−**1d**[4] for enantioselective catalysis.[5]

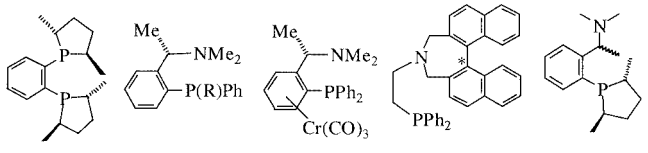

1a **1b** **1c** **1d** **1e**

Ligands of type **1b** are derived from the cheap, commercially available (*R*)- and (*S*)-1-phenylethylamine. We wondered whether it is possible to introduce chiral 2,5-dialkylated phospholane units in place of the P(R)Ph groups of **1b**. Such a synthesis would yield hitherto unknown P,N hybrid ligands **1f** (“DuPHAMIN”) with three stereogenic centres in positions α to the donor atoms P and N. Their catalytic activity would be of particular interest because the interaction of the different types of chiral groups should give “matching” and “mismatching” effects[6] and potentially offer control over stereoselectivity in catalytic reactions.

Results

Lithiation of (*R*)-(+)-**2** with *t*BuLi[7] and subsequent treatment of the organolithium product with $(Et_2N)_2PCl$ gave the aminophosphane (*R*)-(+)-**3a** in 74% yield. (*S*)-(−)-**3a** was analogously derived from (*S*)-(−)-**2**. Solvolysis with ethanol quantitatively formed the corresponding phosphonous acid esters (*R*)-(+)- and (*S*)-(−)-**3b** (Scheme 1). These were reduced with $LiAlH_4$ to yield the two enantiomeric primary phosphanes **4**. The polyphosphane **4b** and the diphosphane **4a** were formed as side products, and these gave further primary phosphane **4** on treatment with potassium and subsequent hydrolysis {(*R*)-**4**: $[\alpha]_D^{20} = 73.3$ (*c* =

[a] Fachbereich 9, Anorganische Chemie, Bergische Universität, Gaußstraße 20, 42097 Wuppertal, Germany
[†] Deceased

 © 2003 Wiley-VCH Verlag GmbH & Co. KGaA, Weinheim **DOI: 10.1002/ejic.200200388**

1.1, CH_2C1_2); (*S*)-**4**: $[\alpha]_D^{20} = -74.4$ (c = 1.1, CH_2C1_2)}. Enantiomers **4** each show a triplet in the $^{31}P\{^1H\}$ NMR spectrum at $\delta_P = -121.95$ ($^1J_{PH}$ = 200.5 Hz). No enantiomerically pure phenylphosphane derivatives of type **4** have previously been reported in the literature. They are synthons of broad applicability for the preparation of chiral P,N ligands by structural variation at the reactive PH_2 group. Thus, stepwise treatment of (*R*)-(+)-**4** with *n*BuLi and cyclic sulfate (*S,S*)-**5a**[8] resulted in the formation of the isomeric tertiary phosphanes (*R,RR*)-**5** in 82% yield, while (*S,RR*)-**5** was obtained analogously in 68% yield. They show singlets at $\delta = -7.10$ or -4.53 ppm, respectively, in the $^{31}P\{^1H\}$ NMR spectrum, no signals that might indicate the presence of additional diastereomers being detected. From the optical purity of the starting materials and the unlikelihood of simultaneous inversion of all three stereogenic centres, the enantiomeric purity of the phosphane ligands of type **5** should exceed 98%. The ^1H NMR spectra of (*R,RR*)-**5** and (*S,RR*)-**5** were analysed completely, and the ^1H NMR spectrum of the phospholane group was simulated as an $ABCDMNQ_3R_3X$ spin system {A, B, C, D = ^1H (C_2H_4); M, N = ^1H [C*H*(Me-P); Q, R = ^1H [CH(*Me*-P)]; X = ^{31}P}. As expected, fifteen resonances were observed in the $^{13}C\{^1H\}$ NMR spectra of both (*R,RR*)-**5** and (*S,RR*)-**5**, in part showing $^nJ_{PC}$ doublet fine structure (n = 1−3) (see Exp. Sect.).

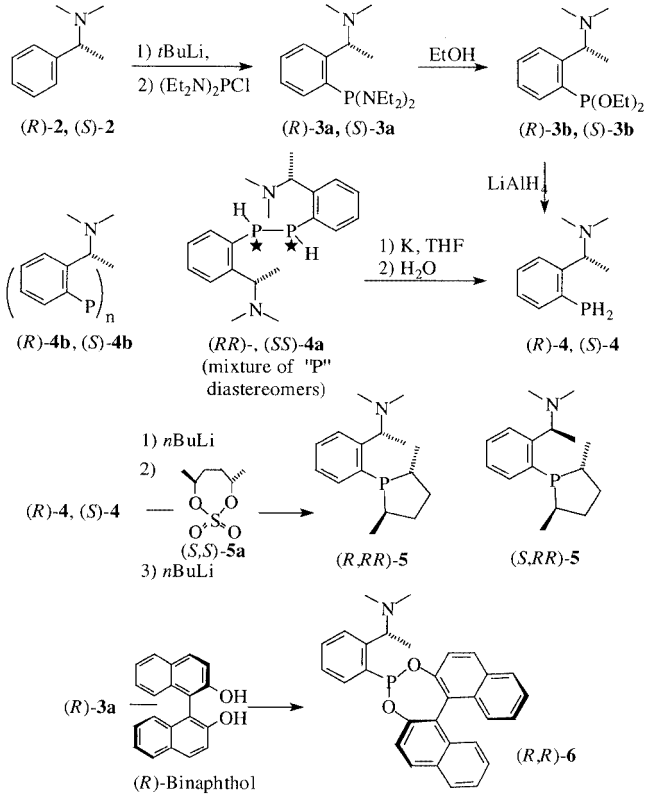

Scheme 1. Syntheses of the chiral P,N ligands

Like (*R*)-**4** and (*S*)-**4**, the aminophosphanes (*R*)-**3a** and (*S*)-**3a** may also be employed as starting materials for the modular synthesis of P,N hybrid ligands based on commercially available (*R*)-and (*S*)-1-phenylethylamine. Treatment of (*R*)-**3a** with (*R*)-2,2′-dihydroxy-1,1′-binaphthyl afforded the novel, axially chiral aminophosphonite ligand (*R,R*)-**6** in high yield.

Treatment of each isomer of **5** with [Rh(1,5-cyclooctadiene)Cl]$_2$ or [Rh(2,5-norbornadiene)Cl]$_2$ and subsequent metathesis with KPF_6 gave the stable Rh^I complexes (*R,RR*)-**7a/b** and (*S,RR*)-**7a/b** (Scheme 2). The observation of two resonances for the diastereotopic Me groups of the NMe_2 unit in the ^1H NMR indicates the P,N coordination of both isomers of **5** in the Rh complexes in solution. This is corroborated by the ^{31}P-^{13}C-coupling fine structure [$^3J_{PC}$ = 2.5 Hz, (*R,RR*)-**7a**; 3.4 Hz, (*S,RR*)-**7a**] of one of the $^{13}C\{^1H\}$ NMR signals of the NMe_2 groups.[9] These observations rule out a rapid dissociation of the N donor of **5** on the NMR time scale.

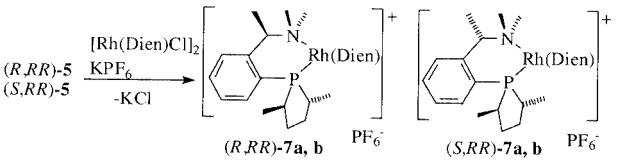

Scheme 2. Syntheses of the complexes (*R,RR*)-**7a**, (*R,RR*)-**7b**, (*S,RR*)-**7a**, and (*S,RR*)-**7b**

Crystal Structures

The crystal structures of (*R,RR*)-**7a** and (*S,RR*)-**7a** have been determined by X-ray diffraction, and drawings of the cations are displayed in Figures 1 and 2. As shown by the distances and angles listed in Tables 1 and 2, good agreement is found for the Rh coordination in the two compounds. The studies confirm the P,N coordination of the novel ligands, the (*R*) configurations of the two carbon atoms α to the phospholane unit and the respective (*R*) and (*S*) configurations of the carbon atom α to the two $CH(Me)NMe_2$ groups.

Inspection of the bottom drawings in Figures 1 and 2 reveals that the inversion of configuration of the benzylic carbon atom is associated with a marked change in the conformation of the $Rh^a-P-C-C-C-N^b$(Rh^a-N^b) chelate ring. Cremer−Pople analysis[10] of their geometries shows that the puckering amplitude of (*S,RR*)-**7a** (0.673 Å) is greater than that of (*R,RR*)-**7a** (0.566 Å). The conformation of the former lies near the half-boat form with the N atom displaced by 0.873(3) Å (rms deviation 0.055 Å) from the plane defined by the other five ring atoms. In contrast, the screw-boat form appears to be the best description of the conformation of the chelate ring in the other isomer, the P1 and α-carbon C1 atoms deviating from the best plane (rms deviation 0.068 Å) of the other four ring atoms by 0.140 and 0.667 Å, respectively.

The methyl group at the α-carbon atom in each structure is found to occupy a pseudoaxial position on the chelate ring, thus avoiding close contact with the neighbouring

 © 2003 Wiley-VCH Verlag GmbH & Co. KGaA, Weinheim

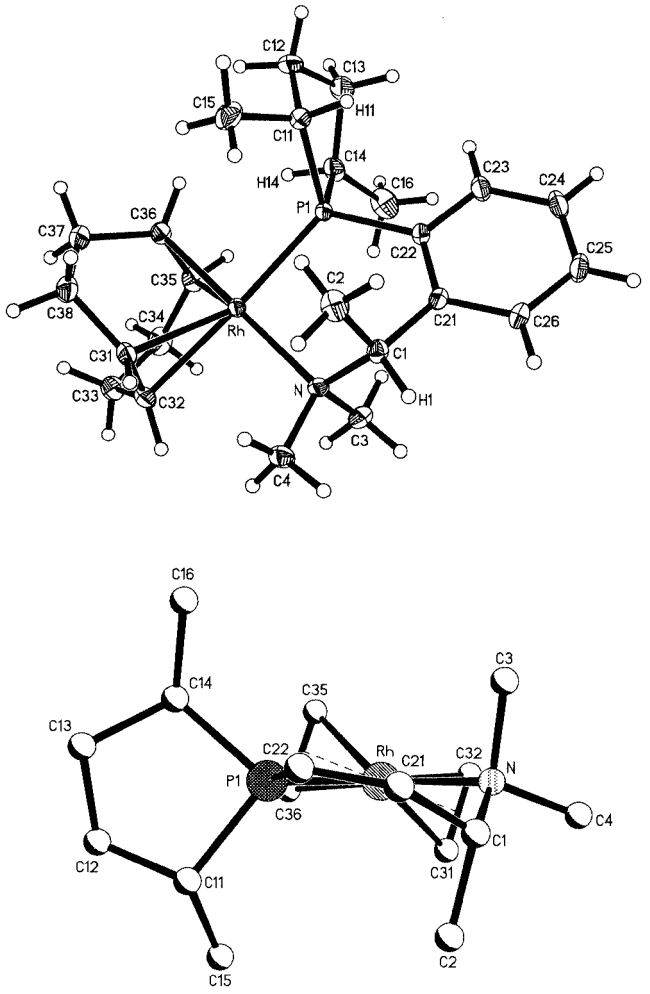

Figure 1. Structure of the cation of (*R*,*RR*)-**7a** (top); front view, showing the orientation of the phospholane group and the chelate ring of (*R*,*RR*)-**7a** (bottom); hydrogen atoms have been omitted for clarity

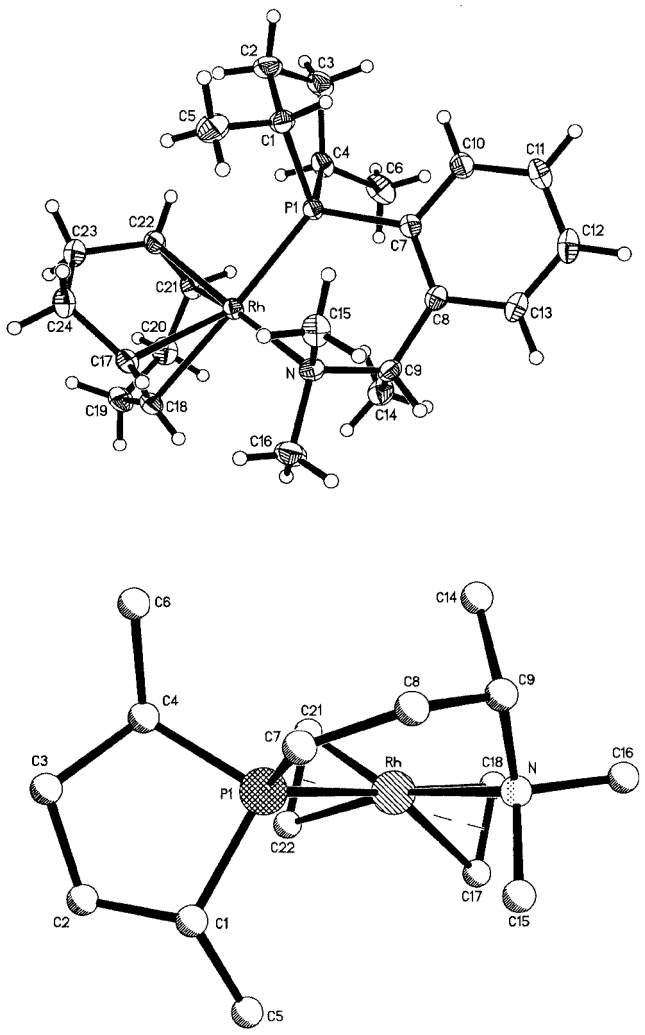

Figure 2. Structure of the cation of (*S*,*RR*)-**7a** (top); front view, showing the orientation of the phospholane group and the chelate ring of (*S*,*RR*)-**7a** (bottom); hydrogen atoms have been omitted for clarity

phenylene hydrogen atom. In (*R*,*RR*)-**7a** this methyl substituent C2 lies on the same side of the chelate ring as the phospholane methyl group C15, which is directed towards the COD ligand. Although these methyl groups are separated by six bonds, they are brought into contact distance [3.823(5) Å] by the screw-boat conformation adopted by the chelate ring. The corresponding methyl groups in (*S*,*RR*)-**7a** lie on opposite sides of the chelate ring. Here, the inwardly directed phospholane methyl group C5 makes a van der Waals contact with the pseudoaxial *N*-methyl group C15 [3.901(8) Å].

The centroids M1 (*trans* to P1) and M2 (*trans* to N) of the C=C double bonds do not lie in the P1−Rh−N plane. The dihedral angle formed by the normals to the M1−Rh−M2 and P1−Rh−N planes is significantly smaller in (*S*,*RR*)-**7a** (14.4°) than in (*R*,*RR*)-**7a** (21.4°). As an inspection of Figures 1 and 2 reveals, the sense of the out-of-plane twist of the COD ligands is the same in the two compounds. Apparently, the orientation of the COD ligands in the solid state reflects the arrangement of the phospholane ring more than it does the disposition of the NMe_2 group. While a similar value was found for this angle in [(COD)Rh{(*R*,*R*)-2,4-bis[(*R*,*R*)-2,5-dimethylphospholano]pentane}]OTf (mean value: 19.3°), a significantly smaller angle (mean 2.6°) was reported for the corresponding (*S*,*S*;*R*,*R*) isomer.[11]

Table 1. Selected distances [Å] and angles [°] in (*R*,*RR*)-**7a**

Rh−P1	2.3065(7)	P1−C22	1.830(3)
Rh−N	2.228(2)	N−C1	1.498(3)
Rh−C31	2.207(3)	C1−C2	1.528(4)
Rh−C32	2.292(3)	C1−C21	1.516(4)
Rh−M1	2.145(3)	C21−C22	1.399(4)
Rh−C35	2.114(3)	C31−C32	1.357(5)
Rh−C36	2.145(3)	C35−C36	1.394(4)
Rh−M2	2.012(3)		
N−Rh−P1	92.33(6)	N−C1−C21	116.1(2)
C22−P1−Rh	115.62(9)	C22−C21−C1	125.8(2)
C1−N−Rh	115.9(2)	C21−C22−P1	121.7(2)

 © 2003 Wiley-VCH Verlag GmbH & Co. KGaA, Weinheim

Table 2. Selected distances [Å] and angles [°] in (*S*,*RR*)-**7a**

Rh−P1	2.3010(10)	P1−C7	1.837(4)
Rh−N	2.209(3)	N−C9	1.508(5)
Rh−C17	2.194(4)	C7−C8	1.392(5)
Rh−C18	2.275(4)	C8−C9	1.516(6)
Rh−M1	2.132(4)	C9−C14	1.526(6)
Rh−C21	2.114(4)	C17−C18	1.344(7)
Rh−C22	2.155(4)	C21−C22	1.376(7)
Rh−M2	2.021(4)		
N−Rh−P1	89.67(9)	N−C9−C8	115.0(3)
C7−P1−Rh	115.51(13)	C7−C8−C9	126.6(3)
C9−N−Rh	109.0(2)	C8−C7−P1	121.6(3)

Catalytic Properties

The hydrogenation of methyl (*Z*)-α-acetamidocinnamate (**8**) at 20 °C is catalysed by (*R*,*RR*)-**7a**. Under a hydrogen pressure of 5 bar, the (*R*) isomer of **9** was formed with 95% *ee*. (Scheme 3). No reaction was observed when (*S*,*RR*)-**7a** was employed as the catalyst under these conditions. At higher temperature (60 °C) the (*R*) isomer of **9** is formed with 60% *ee*.

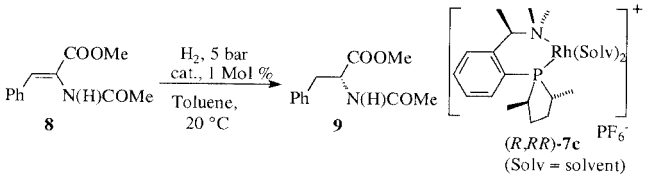

Scheme 3. Hydrogenation of methyl (*Z*)-α-acetamidocinnamate

The difference in the activities of the isomers of **7a** indicates that the catalytically active species **7c** is formed more rapidly in the case of (*R*,*RR*)-**7a**. This is supported by the observation that (*R*,*RR*)-**7a**, on treatment at room temperature with hydrogen, yields cyclooctane, identified by ^{1}H NMR spectroscopy, while (*S*,*RR*)-**7a** did not react. The COD ligand in the latter isomer is obviously bound to the transition metal atom much more tightly than in (*R*,*RR*)-**7a**. This is also indicated by the different dynamic behaviour of the COD ligands in the two isomers as derived from the 400 MHz ^{1}H NOESY spectrum of the olefinic hydrogen atoms. While (*R*,*RR*)-**7a** shows EXSY peaks,[12] these are not observed in the case of (*S*,*RR*)-**7a** (Figure 3). This may be interpreted as a result of diolefin rotation[13] causing a rapid exchange of the CH=CH groups *trans* to the N and P atoms.

A simple mechanism for diolefin rotation at our square-planar d^8 transition metal centre is by cleavage of one Rh−olefin bond, rotation around the remaining Rh−olefin bond and recoordination of the free olefin to Rh either *cis* to the nitrogen atom or *cis* to the phosphorus atom. We assume that the addition of dihydrogen in (*R*,*RR*)-**7a** is favoured only during the short interval in which an olefin either is not coordinated or is in a distorted complex geometry. In this case, addition of dihydrogen to (*S*,*RR*)-**7a** at 20 °C may be much slower than that to the (*R*,*RR*) diastereomer because of the absence of diolefin rotation in the former under these conditions.

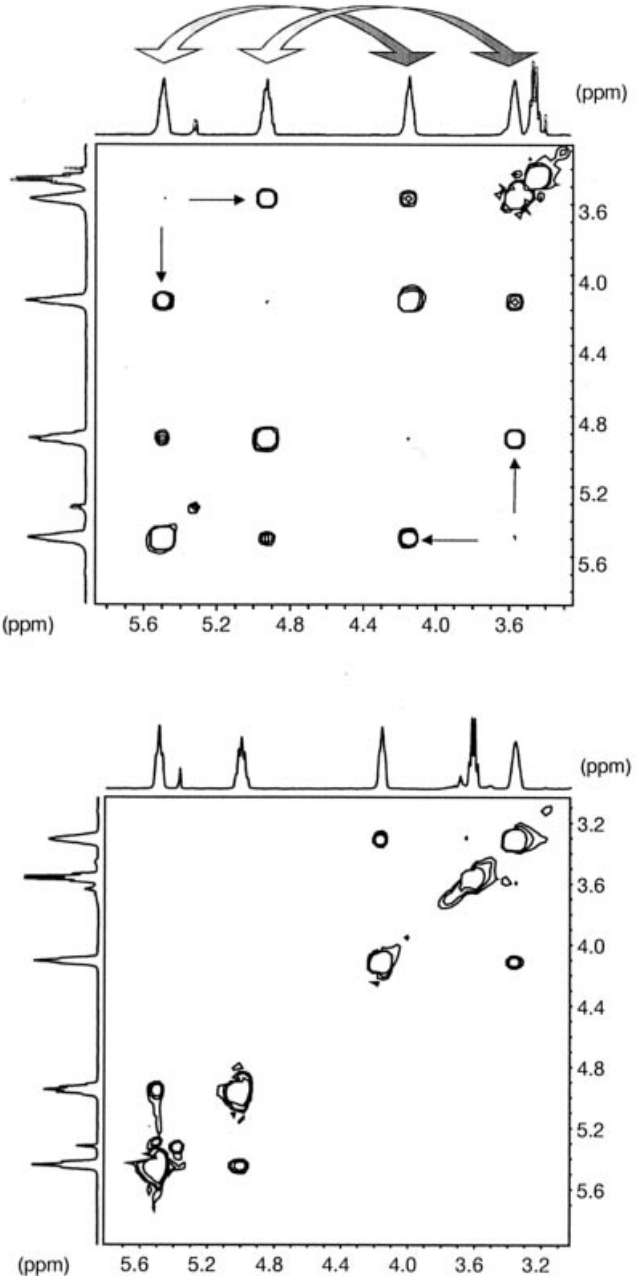

Figure 3. 400 MHz ^{1}H-NOESY spectra at 300 K in CD_2Cl_2 of (*R*,*RR*)-**7a** (top) and (*S*,*RR*)-**7a** (bottom); signals caused by chemical exchange are indicated with arrows; a mixing time of 1.0 s was used

Both norbornadiene complexes (*R*,*RR*)-**7b** and (*S*,*RR*)-**7b** were more active than the corresponding COD complexes. Differences between norbornadiene and COD complexes have also been reported in the literature for related catalytic complexes.[14] With (*R*,*RR*)-**7b** as the pre-catalyst, (*R*)-**9** was formed in 96% *ee*, which is similar to the yield obtained with (*R*,*RR*)-**7a**, while with (*S*,*RR*)-**7b** the hydrogenation product was obtained in only 60% *ee*.

 © 2003 Wiley-VCH Verlag GmbH & Co. KGaA, Weinheim

Experimental Section

General: All reactions were performed under nitrogen by use of standard Schlenk techniques. Diethyl ether and pentane were distilled from $LiAlH_4$, THF and toluene from potassium under nitrogen. Dry CH_2Cl_2, methanol and ethanol were purchased from Aldrich in 99.9% purity and used without further purification. (*S*)- and (*R*)-1-Phenylethylamine (> 98% *ee*) were purchased from Aldrich and converted into the *N*,*N*-dimethyl derivatives by literature methods.[15] Enantiomerically pure (*S*,*S*)-2,5-hexanediol (> 99% *ee*) was purchased from Jülich Fine-Chemicals. The cyclic sulfate was prepared by the method described by Sharpless.[16]

NMR: Spectra were recorded with a Bruker ARX 400 MHz NMR spectrometer with use of standard pulse programs for HH-gs-NOESY measurements, spectra with various mixing times (0.1−1.0 s) being recorded. Positive ^1H, ^{13}C, or ^{31}P NMR chemical shifts are upfield from external Me_4Si or H_3PO_4 (85%).

Synthesis of (*R*)- and (*S*)-4

(*R*)-4: A solution of *t*BuLi (1.6 M, 29.0 mL) was added to a solution of (*R*)-**2** (6.91 g, 46.3 mmol) in *n*-pentane (50 mL) and the mixture was stirred at 20 °C for 14 h. The reaction mixture obtained was added at 0 °C to a solution of chlorobis(diethylamino)phosphane (8.86 g, 42.1 mmol) in dry diethyl ether (30 mL). The LiCl produced was removed by filtration, the solvent was evaporated, and the residue was distilled in vacuo (92 °C, 0.1 mbar). The aminophosphane (*R*)-**3a** (yield: 11.1 g, 74%) was dissolved in EtOH (40 mL) and the solution was heated at 60 °C for 48 h. All volatiles were then evaporated, leaving an oily residue, which was distilled in vacuo (76 °C, 0.1 mbar). Yield: 8.96 g (98%) of (*R*)-**3b**. Compound **3b**, as obtained above, was reduced with $LiAlH_4$ (1.18 g, 31.0 mmol) in THF at −30 to 20 °C. After hydrolytic workup of the reaction mixture with water (10.0 mL), the organic phase was separated and the solvent was evaporated. The remaining residue was dissolved in THF (20 mL), potassium (2.42 g, 62.0 mmol) was added, and the reaction mixture was heated at reflux for 4 h. Methanol (10 mL) was then added and the mixture was stirred for 1 h. All volatiles were removed in vacuo and the residue was distilled in vacuo (69 °C, 0.1 mbar). Yield: 4.59 g (76%), $[\alpha]_D^{20} = 73.3$, $c = 1.14$, CH_2Cl_2. (*S*)-**4** was obtained in an analogous manner from (*S*)-**2** as starting material. Yield: 4.21 g (76.0%). $[\alpha]_D^{20} = -74.4$, $c = 1.1$, CH_2Cl_2. ^1H NMR (C_6D_6): 1.13 (d, $J = 6.7$ Hz, 1 H, Me), 2.01 (s, 6 H, NMe), 3.48 (q, $J = 6.7$ Hz, 3 H, CH), 3.91 (dd, $J = 10.8$, 201.4 Hz, 1 H, PH_2), 4.02 (dd, $J = 10.8$, 198.9 Hz, 1 H, PH_2), 6.94 (m, 1 H, arom. H), 7.09 (m, 1 H, arom. H), 7.23 (m, 1 H, arom. H), 7.41 (m, 1 H, arom. H) ppm. $^{13}C\{^1H\}$ NMR (C_6D_6): δ = 15.14 (Me), 41.20 (NMe), 63.65 (d, $J = 6.1$ Hz, CH), 126.66 (d, $J = 2.0$ Hz, arom. C), 126.92 (d, $J = 3.05$ Hz, arom. C), 128.20 (s, arom. C), 130.66 (d, $J = 11.2$ Hz, arom. C), 136.45 (d, $J = 4.1$ Hz, arom. C), 148.55 (d, $J = 11.2$ Hz, arom. C) ppm. $^{31}P\{^1H\}$ NMR (C_6D_6): δ = −121.95 (d, $J = 200.5$ Hz) ppm. MS (EI): $m/z = 181$ [M^+]. $C_{10}H_{16}NP$ (181.2): calcd. C 66.28, H 8.90, N 7.73; found C 65.62, H 8.70, N 7.60.

Synthesis of (*R*,*RR*)- and (*S*,*RR*)-5

(*R*,*RR*)-5: *n*BuLi (1.6 M solution in *n*-hexane, 10 mL) was added at 0 °C to a solution of (*R*)-**4** (2.87 g, 15.8 mmol) in THF (70 mL) and the reaction mixture was stirred at ambient temperature for 30 min. After addition of (*SS*)-**4a** (2.88 g, 15.8 mmol, dissolved in 10 mL of THF), the mixture was stirred for 30 min. Further *n*BuLi (1.6 M solution in *n*-hexane, 15 mL) was added and the reaction mixture was stirred for another 30 min. To remove excess *n*BuLi, methanol (10 mL) was added to the reaction mixture. All volatiles were then removed in vacuo and the remaining residue was distilled in vacuo (98−101 °C, 0.1 mbar) to afford (*R*,*RR*)-**5** as a colourless liquid. Yield 3.40 g (82%). $[\alpha]_D^{20} = +57.5$, $c = 1.1$, CH_2Cl_2. The isomer (*S*,*RR*)-**5** was synthesised in an analogous manner from (*S*)-**4**. Yield: 1.10 g (68%). $[\alpha]_D^{20} = -158.7$, $c = 1.5$, CH_2Cl_2.

(*R*,*RR*)-5: ^1H NMR (C_6D_6): δ = 0.80 (dd, $J = 6.9$, 9.32 Hz, 3 H, Me), 1.26 (m, $J = 2.8$, 6.3, 9.9, 11.6, −13.1 Hz, 3 H, CH_2), 1.28 (dd, $J = 7.2$, 18.7 Hz, 3 H, Me), 1.29 (d, $J = 6.6$ Hz, 6 H, Me), 1.53 (m, $J = 4.7$, 6.0, 10.5, 11.6, −12.8 Hz, 1 H, CH_2), 1.88 (m, $J = 2.6$, 6.3. 6.5, 8.9, −12.8 Hz, 1 H, CH_2), 2.08 (m, $J = 2.6$, 6.0, 7.3, −13.1, 15.0 Hz, 1 H, CH), 2.21 (s, 6 H, NMe), 2.23 (m, $J = 6.5$, 6.9, 10.5, 23.3 Hz, 1 H, CH), 2.52 (m, $J = 5.9$, 7.2, 7.3, 9.9 Hz, 1 H, CH), 4.68 (dq, $J = 6.6$, 9.1 Hz, 1 H, CH), 7.08 (m, $J = 1.5$, 7.4, 7.8 Hz, 1 H, arom. H), 7.22 (m, $J = 1.4$, 7.3, 7.8 Hz, 1 H, arom. H), 7.36 (m, $J = 1.5$, 1.7, 7.5 Hz, 1 H, arom. H), 7.71 (m, $J = 1.4$, 3.6, 7.9 Hz, 1 H, arom. H) ppm. $^{13}C\{^1H\}$ NMR (C_6D_6): δ = 16.44 (d, $J = 1.5$ Hz, Me), 20.99 (d, $J = 36.1$ Hz, Me), 21.11 (s, Me), 34.84 (d, $J = 13.2$ Hz, CH), 36.63 (d, $J = 3.1$ Hz, CH_2), 37.08 (d, $J = 12.2$ Hz, CH), 37.12 (CH_2), 43.48 (Me), 61.11 (d, $J = 26.4$ Hz, CH), 126.07 (arom. C), 127.53 (d, $J = 5.1$ Hz, arom. C), 129.03 (arom. C), 133.27 (d, $J = 3.1$ Hz, arom. C), 135.92 (d, $J = 31.0$ Hz, arom. C), 152.93 (d, $J = 23.4$ Hz, arom. C) ppm. $^{31}P\{^1H\}$ NMR (C_6D_6): δ = −7.10 ppm. MS (EI): $m/z = 263$ [M^+]. $C_{16}H_{26}NP$ (263.4): calcd. C 72.97, H 9.95, N 5.32, P 11.76; found C 72.74, H 10.00, N 5.31, P 11.51.

(*S*,*RR*)-5: ^1H NMR (C_6D_6): δ = 0.84 (dd, $J = 7.0$, 9.1 Hz, 3 H, Me), 1.27 (dd, $J = 7.2$, 18.6 Hz, 3 H, Me), 1.27 (d, $J = 6.6$ Hz, 3 H, Me), 1.30 (m, $J = 3.4$, 6.1, 9.5, 11.2, −13.0 Hz, 1 H, CH_2), 1.53 (m, $J = 5.6$, 5.8, 9.7, 11.2, −12.6 Hz, 1 H, CH_2), 1.92 (m, $J = 3.4$, 6.1, 6.7, 8.8, −12.6 Hz, 1 H, CH_2), 2.07 (m, $J = 3.4$, 5.8, 7.3, −13.0, 14.7 Hz, 1 H, CH_2), 2.15 (s, 6 H, NMe), 2.34 (m, $J = 6.7$, 7.0, 9.7, 23.6 Hz, 1 H, CH), 2.49 (m, $J = 5.4$, 7.2, 7.3, 9.5 Hz, 1 H, CH), 4.53 (dq, $J = 6.8$, 6.9 Hz, 1 H, CH), 7.09 (m, $J = 1.6$, 7.4, 7.6 Hz, 1 H, arom. H), 7.20 (m, $J = 1.6$, 2.1, 7.7 Hz, 1 H, arom. H), 7.40 (m, $J = 1.5$, 3.8, 7.6 Hz, 1 H, arom. H), 7.64 (m, $J = 1.5$, 3.8, 7.7 Hz, 1 H, arom. H) ppm. $^{13}C\{^1H\}$ NMR (C_6D_6): δ = 17.03 (Me), 17.04 (d, $J = 1.5$ Hz, Me), 20.99 (d, $J = 37.1$, Me), 34.88 (d, $J = 13.7$ Hz, CH), 35.62(d, $J = 10.2$ Hz, CH_2), 36.42 (d, $J = 4.6$ Hz, CH), 37.03 (d, $J = 1.5$ Hz, CH), 42.38 (Me), 61.86 (d, $J = 24.4$ Hz, CH), 126.13 (arom. C), 126.60 (d, $J = 5.1$ Hz, arom. C), 128.74 (d, $J = 1.0$ Hz, arom. C), 133.63 (d, $J = 3.6$ Hz, arom. C), 136.31 (d, $J = 31.0$ Hz, arom. C), 152.47 (d, $J = 21.9$ Hz, arom. C) ppm. $^{31}P\{^1H\}$ NMR (C_6D_6): δ = −4.53 ppm. MS (EI): $m/z = 263$ [M^+]. $C_{16}H_{26}NP$ (263.4): calcd. C 72.97, H 9.95, N 5.32, P 11.76; found C 72.92, H 9.88, N 5.33, P 11.63.

Synthesis of (*R*,*R*)-6: Compound (*R*)-**3a** (1.72 g, 5.34 mmol) was added by syringe to a stirred suspension of (*R*)-2,2′-binaphthol (1.53 g, 5.34 mmol) in dry toluene (30 mL). The mixture cleared immediately and was heated at 80 °C for 2 h. After completion of the reaction, all volatiles were removed in vacuo (0.01 mbar, 40 °C, 12 h) to leave pure (*R*,*R*)-**6** as a colourless, microcrystalline solid. Yield 2.45 g (99%). $[\alpha]_D^{20} = -19.8$ ($c = 0.95$, CH_2Cl_2). ^1H NMR (C_6D_6): δ = 7.75 (m, 2 H), 7.69 (m, 3 H), 7.64 (m, 1 H), 7.59 (m, 1 H), 7.55 (m, 1 H), 7.15 (m, 3 H), 7.02 (m, 4 H), 6.90 (m, 2 H), 6.67 (m, 1 H), 3.89 (q, $J = 6.6$ Hz, 1 H), 2.04 (s, 6 H), 0.95 (qd, $J = 6.6$, 0.9 Hz, 3 H) ppm. $^{13}C\{^1H\}$ NMR (C_6D_6): δ = 152.74 (d, $J = 1.7$ Hz, arom. C), 150.52 (d, $J = 13.6$ Hz), 147.70 (d, $J = 19.5$ Hz, arom. C), 139.20 (d, $J = 48.0$ Hz, arom. C), 133.73 (d, $J = 1.4$ Hz, arom. C), 133.44 (d, $J = 1.5$ Hz, arom. C), 131.66 (d, $J = 0.7$ Hz, arom. C), 131.29 (s, arom. C), 131.25 (d, $J = 2.3$ Hz, arom. C), 130.56 (d, $J = 0.8$ Hz, arom. C), 130.16 (s, arom. C),

 © 2003 Wiley-VCH Verlag GmbH & Co. KGaA, Weinheim

128.94 (d, J = 1.7 Hz, arom. C), 128.78 (s, arom. C), 128.59 (d, J = 0.4 Hz, arom. C), 127.55 (s, arom. C), 127.22 (s, arom. C), 126.80 (s, arom. C), 126.31 (s arom. C), 126.26 (s, arom. C), 125.56 (d, J = 5.7 Hz, arom. C), 25.22 (d, J = 3.2, arom. C), 124.72 (s, arom. C), 124.47 (s, arom. C), 124.36 (d, J = 2.2 Hz, arom. C), 124.00 (s, arom. C), 123.03 (d, J = 1.0 Hz, arom. C), 58.16 (d, J = 7.9 Hz, NMe), 38.38 (d, J = 5.0 Hz, CH), 7.83 (d, J = 3.1 Hz, Me) ppm. $^{31}P\{^1H\}$ NMR (C_6D_6): δ = 150.2 ppm. MS (EI): m/z = 463 [M^+]. $C_{30}H_{26}NO_2P$ (463.5): calcd. C 77.74, H 5.65, N 3.02, P 6.68; found.: C 77.48, H 5.76, N 3.12, P 6.82.

Rh^I Complexes 7a and 7b: Either (*S*,*RR*)-**5** or (*R*,*RR*)-**5** (0.10 g, 0.38 mmol) was added to a solution of [Rh(1,5-cyclooctadiene)Cl]$_2$ (93.7 mg, 0.19 mmol) or [Rh(2,5-norbornadiene)Cl]$_2$ (87.6 mg, 0.19 mmol) in dichloromethane (5 mL). The reaction mixture was stirred at ambient temperature for 20 min. A solution of KPF_6 (105 mg, 0.57 mmol) in water (5 mL) was added with stirring after 1 h. The aqueous phase was separated and the organic phase was washed with three aliquots of water (10 mL). After addition of a tenfold amount of diethyl ether, the Rh complexes were precipitated as red, crystalline solids in 90−95% yield. Crystals of (*S*,*RR*)- and (*R*,*RR*)-**7a** suitable for X-ray structural analysis could be obtained by slow concentration of the dichloromethane solutions.

Isomer (*S*,*RR*)-7a: $[\alpha]_D^{20}$ = 13.7 (c = 1.1, CH_2Cl_2). ^1H NMR (CD_2Cl_2): δ = 0.91 (dd, J = 6.4, 15.0 Hz, 3 H, Me), 1.81 (m, 1 H, CH_2), 1.82 (dd, J = 6.9, 18.1 Hz, 3 H, Me), 1.97 (m, 1 H, CH_2), 2.20 (m, 2 H, CH/CH_2), 2.26 (d, J = 6.5 Hz, 3 H, Me), 2.34 (s, 3 H, NMe), 2.40 (m, 1 H, CH), 2.53 (m, 1 H, CH_2), 2.70 (s, 3 H, NMe), 2.75 (m, 1 H), 2.87 (m, 1 H,), 3.31 (m, 1 H, olef. H), 3.56 (d, J = 6.5 Hz, 1 H, CH), 4.10 (m, 1 H, olef. H), 5.95 (m, 1 H, olef. H), 5.44 (m, 1 H, olef. H), 7.18 (m, 1 H, arom. H), 7.49 (m, 2 H, arom. H), 7.61 (m, 1 H, arom. H) ppm. $^{13}C\{^1H\}$ NMR (CD_2Cl_2): δ =14.05 (d, J = 0.8 Hz, Me), 19.62 (d, J = 9.7 Hz, Me), 23.92 (d, J = 5.6 Hz, Me), 26.03 (d, J = 2.5 Hz, CH_2), 28.90 (d, J = 1.3 Hz, CH_2), 32.47 (s, CH_2), 33.46 (dd, J = 25.9, 1.0 Hz, CH), 35.63 (d, J = 3.8 Hz, CH_2), 36.05 (dd, J = 1.4, 1.4 Hz, CH_2), 38.11 (d, J = 2.3 Hz, CH_2), 44.14 (dd, J = 26.5, 1.3 Hz, CH), 51.57 (d, J =3.4 Hz, NMe), 52.19 (s, NMe), 68.54 (dd, J = 12.1, 1.0 Hz, olef. C), 73.64 (d, J = 6.1 Hz, CH), 81.72 (d, J = 12.5 Hz, olef. C), 100.41 (dd, J = 13.0, 7.1 Hz, olef. C), 106.06 (d, J = 8.4, 6.10 Hz, olef. C), 124.91 (d, J = 23.9 Hz, arom. C), 129.71 (d, J = 4.8 Hz, arom. C), 131.73 (d, J = 8.9 Hz, arom. C), 132.33 (d, J = 2.3 Hz, arom. C), 134.84 (dd, J = 1.1, 1.1 Hz, arom. C), 146.43 (d, J = 14.8 Hz, arom. C) ppm. $^{31}P\{^1H\}$ NMR (CD_2Cl_2): δ = 28.30 (d, J = 150.4 Hz), −143.2 (sept, J = 710.6 Hz) ppm. $C_{24}H_{38}F_6NP_2Rh$ (619.4): calcd. C 46.54, H 6.18, N 2.26, P 10.00; found C 46.70, H 6.32, N 2.39, P 10.38.

Isomer (*R*,*RR*)-7a: $[\alpha]_D^{20}$ = 21.5 (c = 1.0, CH_2Cl_2). ^1H NMR (CD_2Cl_2): δ = 1.29 (dd, 3 H, J = 7.1, 14.2 Hz, Me), 1.49 (m, 1 H, CH_2), 1.70 (dd, 3 H, J = 7.1, 17.3 Hz, Me), 1.83 (d, J = 6.5 Hz, 3 H, Me), 2.09 (m, 2 H, CH_2), 2.23 (m, 1 H, CH_2), 2.41 (m, 1 H, CH), 2.58 (s, 3 H, NMe), 2.60 (m, 1 H, CH), 2.69 (s, 3 H, NMe), 3.47 (q, J = 6.5 Hz, 1 H CH), 3.58 (m, 1 H, olef. H), 4.15 (m, 1 H, olef. H), 4.93 (m, 1 H, olef. H), 5.50 (m, 1 H, olef. H), 7.0 (m, 1 H, arom. H), 7.48 (m, 2 H, arom. H), 7.60 (m, 1 H, arom. H) ppm. $^{13}C\{^1H\}$ NMR (CD_2Cl_2): δ =13.54 (d, J = 1.3 Hz, Me), 18.02 (d, J = 6.6 Hz, Me), 25.89 (d, J = 4.1 Hz, Me), 27.96 (d, J = 2.0 Hz, CH_2), 30.31 (s, CH_2), 31.07 (d, J = 2.5 Hz, CH_2), 33.51 (d, J = 3.1 Hz, CH_2), 35.68 (dd, J = 25.2, 1.0 Hz, CH_2), 35.95 (dd, J = 1.7, 1.7 Hz, CH_2), 38.35 (d, J = 2.0 Hz, CH), 45.93 (dd, J = 25.6, 1.7 Hz, CH), 49.75 (d, J = 2.5 Hz, NMe), 51.11 (s, NMe), 69.52 (dd, J = 11.8, 0.9 Hz, olef. C), 73.15 (d, J = 5.9 Hz, CH), 81.70 (dd, J = 13.1, 0.9 Hz, olef. C), 101.33 (dd, J = 11.6, 7.3 Hz, olef. C), 105.38 (dd, J = 7.9, 7.9 Hz, olef. C), 124.88 (d, J = 23.1 Hz, arom. C), 129.79 (d, J = 5.1 Hz, arom. C), 132.01 (d, J = 2.3 Hz, arom. C), 132.31 (d, J = 8.9 Hz, arom. C), 134.11 (dd, J = 1.0, 1.0 Hz, arom. C), 145.91 (d, J = 14.8 Hz, arom. C) ppm. $^{31}P\{^1H\}$ NMR (CD_2Cl_2): δ = 25.19 (d, J = 150.4 Hz), −141.0 (sept, J = 710.6 Hz) ppm. $C_{24}H_{38}F_6NP_2Rh$ (619.4): calcd. C 46.54, H 6.18, N 2.26, P 10.00; found C 46.55, H 6.11, N 2.37, P 10.36.

Isomer (*S*,*RR*)-7b: $[\alpha]_D^{20}$ = −100.3 (c = 1.1, CH_2Cl_2). ^1H NMR (CD_3COCD_3): δ = 0.89 (dd, J = 6.9, 14.2 Hz, 3 H, Me), 1.41 (m, 1 H, CH_2), 1.55 (m, 1 H, CH_2), 1.65 (m, 1 H, CH_2), 1.84 (dd, 3 H, J = 7.0, 18.2 Hz, Me), 1.91 (m, 1 H, CH_2), 2.07 (m, 1 H, CH), 2.13 (m, 1 H, CH_2), 2.22 (d, J = 6.6 Hz, 3 H, Me), 2.37 (m, 1 H, CH_2), 2.58 (s, 3 H, NMe), 2.86 (m, 1 H, CH), 2.87 (s, 3 H, NMe), 3.74 (dq, J = 1.6, 6.6 Hz, 1 H, CH), 4.02 (m, 1 H, CH), 4.05 (m, 1 H, olef. H), 4.10 (m, 1 H, CH), 4.16 (m, 1 H, olef. H), 5.43 (m, 1 H, olef. H), 5.67 (m, 1 H, olef. H), 7.29 (m, 1 H, arom. H), 7.49 (m, 1 H, arom. H), 7.52 (m, 1 H, arom H), 7.73 (m, 1 H, arom. H) ppm. $^{13}C\{^1H\}$ NMR (CD_3COCD_3): δ = 14.31 (d, J = 2.0 Hz, Me), 18.91 (dd, J = 1.0, 10.7 Hz, Me), 24.35 (d, J = 3.8 Hz, Me), 33.17 (dd, J = 1.8, 28.0 Hz, CH), 36.67 (dd, J = 1.4, 1.4 Hz, CH_2), 38.34 (d, J = 4.3, CH_2), 44.91 (dd, J = 1.4, 26.6 Hz, CH), 50.65 (d, J = 2.8 Hz, NMe), 51.70 (s, NMe), 52.30 (dd, J = 2.0, 2.0 Hz, CH), 53.58 (dd, J = 1.3, 2.8 Hz, CH), 56.28 (d, J = 9.9 Hz, olef. C), 63.74 (d, J = 10.7 Hz, olef. C), 66.61 (dd, J = 1.7, 5.2 Hz, CH_2), 73.34 (d, J = 5.1 Hz, CH), 87.55 (dd, J = 5.3, 10.4 Hz, olef. C), 92.20 (dd, J = 6.2, 8.0 Hz, olef. C), 124.66 (d, J = 24.2 Hz, arom. C), 129.95 (d, J = 5.3 Hz, arom. C), 132.25 (d, J = 9.4 Hz, arom. C), 132.73 (d, J = 2.3 Hz arom. C), 136.08 (dd, J = 1.3, 1.3 Hz, arom. C), 148.52 (d, J = 15.3 Hz, arom. C) ppm. $^{31}P\{^1H\}$ NMR (CD_3COCD_3): δ = 32.43(d,167.9 Hz), −143.0 (sept, J = 707.4 Hz) ppm. $C_{23}H_{34}F_6NP_2Rh$ (603.4): calcd. C 45.78, H 5.68, N 2.32, P 10.27; found C 45.60, H 5.59, N 2.30, P 10.05.

Isomer (*R*,*RR*)-7b: $[\alpha]_D^{20}$ = −78.1 (c = 1.1, CH_2Cl_2). ^1H NMR (CD_3COCD_3): δ = 1.18 (dd, J = 7.2, 14.2 Hz, 3 H, Me), 1.29 (m, 1 H, CH_2), 1.54 (m, 1 H, CH_2), 1.64 (m, 1 H, CH_2), 1.64 (dd, J = 7.1, 17.6 Hz, 3 H, Me), 1.87 (d, J = 0.5 Hz, 3 H, 6.6 Hz, Me), 1.95 (m, 1 H, CH_2), 2.23 (m, 1 H, CH), 2.27 (m, 1 H, CH), 2.54 (s, 3 H, NMe), 2.57 (m, 1 H, CH), 2.59 (s, 3 H, NMe), 2.61 (m, 1 H, CH), 3.64 (dq, J = 1.9, 6.6 Hz, 1 H, CH), 4.03 (m, 1 H, olef. H), 4.05 (m, 1 H, olef. H), 4.21 (m, 1 H, CH.), 4.32 (m, 1 H, CH), 5.38 (m, 1 H, olef. H), 5.58 (m, 1 H, olef. H), 7.30 (m, 1 H, arom. H), 7.48 (m, 1 H, arom. H), 7.52 (m, 1 H, arom H), 7.65 (m, 1 H, arom. H) ppm. $^{13}C\{^1H\}$ NMR (CD_3COCD_3): δ = 14.80 (d, J = 2.53 Hz, Me), 18.15 (dd, J = 1.8, 8.1 Hz, Me), 26.65 (d, J = 3.8 Hz, Me), 35.46 (dd, J = 1.5, 27.0 Hz, CH), 37.11 (dd, J = 1.5, 1.5 Hz, CH_2), 38.51 (d, J = 4.1, CH_2), 46.51 (dd, J = 1.8, 26.2 Hz, CH), 49.64 (d, J = 1.8 Hz, NMe),51.57 (s, NMe), 53.55 (dd, J = 2.0, 2.0 Hz, CH),53.82 (dd, J = 1.3, 2.8 Hz, CH), 56.40 (d, J = 9.9 Hz, olef. C), 65.66 (d, J = 11.2 Hz, olef. C), 67.58 (dd, J = 1.8, 5.3 Hz, CH_2), 72.95 (dd, J = 5.6, CH), 87.22 (dd, J = 5.6, 9.7 Hz, olef. C), 92.01 (dd, J = 6.1, 8.9 Hz, olef. C), 125.17 (d, J = 23.9 Hz, arom. C), 130.73 (d, J = 5.1 Hz, arom. C), 133.13 (d, J = 9.2 Hz, arom. C), 133.20 (d, J = 2.3 Hz, arom. C), 136.38 (dd, J = 1.3, 1.3 Hz, arom. C), 148.80 (d, J = 15.3 Hz, arom. C) ppm. $^{31}P\{^1H\}$ NMR (CD_3COCD_3): δ = 28.74 (d,167.9 Hz), −143.0 (sept, J = 707.4 Hz). $C_{23}H_{34}F_6NP_2Rh$ (603.4): calcd. C 45.78, H 5.68, N 2.32, P 10.27; found C 45.56, H 5.85, N 2.35, P 10.17.

Asymmetric Hydrogenation Reactions: A 100-mL glass autoclave was charged with a solution of methyl (*Z*)-α-acetamidocinnamate (**8**, 0.40 g, 1.8 mmol) in methanol (15 mL). After repeated vacuum/H_2 cycles, the catalyst (ca. 1 mol %) was added and the autoclave was pressurised to 5 bar with hydrogen. The reactions were allowed

 © 2003 Wiley-VCH Verlag GmbH & Co. KGaA, Weinheim

to continue either at 20 °C or at 60 °C and the progress of the hydrogenation was monitored by ^{1}H NMR spectroscopy. After 10−12 h, all volatiles were removed in vacuo, and the residue was dissolved in chloroform (2−3 mL). To remove rhodium catalyst the solutions were filtered through silica gel and the filtrate was concentrated to dryness. Methyl *N*-acetylphenylalaninate (**9**) was obtained as a colourless powder. The *ee* values were determined by HPLC (CHIRACEL, *n*-heptane/2-propanol, flow rate 0.8 mL/h, UV detector) and ^{1}H NMR spectroscopy [chiral shift reagent Eu(hfc)$_3$]. Results are summarised in Table 3.

Table 3. Hydrogenation of methyl (*Z*)-α-acetamidocinnamate (**8**)

Catalyst	*T* [°C]	Time [h]	Yield (%)	*ee* (%)[a]
(*R*,*RR*)-**7a**	20	12	95	96
(*S*,*RR*)-**7a**	60	12	90	60
(*R*,*RR*)-**7b**	20	10	96	95
(*S*,*RR*)-**7b**	20	12	95	60

[a] The (*R*) configuration of **9** was found to be in excess in each case.

X-ray Crystallographic Studies: Crystals were glued to glass fibres and transferred to a Siemens P3 diffractometer, which employed Mo-K_α radiation (0.71073 Å) and was equipped with a graphite monochromator. Intensities were determined at 22 °C by a profile analysis of ω-scans and were corrected for absorption, the correction being made empirically for (*R*,*RR*)-**7a** and by integration for (*S*,*RR*)-**7a**. The structures were solved by direct methods and refined conventionally. Hydrogen atoms were positioned geometrically with the riding model, except for the olefinic hydrogen atoms of (*S*,*RR*)-**7a**, which were refined isotropically. An extinction correction was necessary only for the latter structure. Both structures were solved, refined and depicted with the aid of the SHELXTL program package. Crystal data are summarized in Table 4. Crystallographic data (excluding structure factors) for the structures reported in this paper have been deposited with the Cambridge Crystallographic Data Centre as supplementary publication no. CCDC-166313 and -174251 for (*R*,*RR*)-**7a** and (*S*,*RR*)-**7a**, respectively. Copies of the data may be obtained free of charge on application to CCDC, 12 Union Road, Cambridge CB2 1EZ, UK [Fax: (internat.) + 44-1223/336-033; E-mail: deposit@ccdc.cam.ac.uk].

Table 4. Crystallographic data for (*R*,*RR*)-**7a** and (*S*,*RR*)-**7a**

	(*R*,*RR*)-**7a**	(*S*,*RR*)-**7a**
Empirical formula	$C_{24}H_{38}F_6NP_2Rh$	$C_{24}H_{38}F_6NP_2Rh$
Formula mass	619.40	619.40
Crystal system	orthorhombic	trigonal
Space group	$C222_1$	$P3_112$
a [Å]	9.853(2)	10.1362(13)
b [Å]	17.735(3)	10.1362(13)
c [Å]	29.904(5)	44.621(6)
V [Å^3]	5225.6(15)	3970.3(9)
Z	8	6
D(calcd.) [g cm^{-3}]	1.575	1.554
θ range[°]	2.30−30.00	2.32−25.00
Limiting indices	$-13 \le h \le 13$	$-12 \le h \le 9$
	$-24 \le k \le 24$	$-9 \le k \le 12$
	$-42 \le l \le 42$	$-53 \le l \le 53$
Reflections collected	8374	15557
Unique	7623	4648
R(int)	0.0179	0.0279
Observed [$I > 2\sigma(I)$]	6821	4444
Crystal size [mm]	0.80 × 0.70 × 0.30	0.54 × 0.48 × 0.48
μ [mm^{-1}]	0.833	0.822
Transmission	1.00000−0.80946	0.7539−0.7262
R1 (all data)	0.0361	0.0303
*wR*2 (all data)	0.0727	0.0695
Goodness-of-fit on F^2	0.965	1.043
Parameters	314	350
Δ*F* map [e·Å^{-3}]	0.429 to −0.590	0.379 to −0.391
Extinction parameter	−	0.0049(2)
Flack parameter	−0.02(2)	−0.01(3)

Acknowledgments

This work was supported by the Deutschen Forschungsgemeinschaft and Symyx Technologies, Inc., Santa Clara, CA, USA.

[1] [1a] F. Fache, E. Schulz, M. L. Tommasino, M. Lemaire, *Chem. Rev.* **2000**, *100*, 2159−2232. [1b] G. Helmchen, A. Pfaltz, *Acc. Chem. Res.* **2000**, *33*, 336−345.
[2] [2a] M. J. Burk, J. E. Feaster, W. A. Nugent, R. L. Harlow, *J. Am. Chem. Soc.* **1993**, *115*, 10125−10138. [2b] M. J. Burk, *Acc. Chem. Res.* **2000**, *33*, 363−372.
[3] [3a] T. V. RajanBabu, A. L. Casalnuovo, *J. Am. Chem. Soc.* **1996**, *118*, 6325−6326. [3b] A. Schnyder, L. Hintermann, A. Togni, *Angew. Chem.* **1995**, *107*, 996−998; *Angew. Chem. Int. Ed. Engl.* **1995**, *34*, 931−933. [3c] J. P. Cahill, F. M. Bohnen, R. Goddard, C. Krüger, P. J. Guiry, *Tetrahedron: Asymmetry* **1998**, *9*, 3831−3839. [3d] K. Inoguchi, S. Sakuraba, K. Achiwa, *Synlett* **1992**, 169−178.
[4] [4a] I. Yamada, M. Ohkouchi, M. Yamaguchi, T. Yamagishi, *J. Chem. Soc., Perkin Trans. 1* **1997**, 1869−1874. [4b] D. A. Vasen, A. Salzer, F. Gerhards, H.-J. Gais, R. Stürmer, N. H. Bieler, A. Togni, *Organometallics* **2000**, *19*, 539−546. [4c] H. Kubota, K. Koga, *Tetrahedron Lett.* **1994**, *35*, 6689−6692.
[5] [5a] I. Yamada, M. Yamaguchi, T. Yamagishi, *Tetrahedron: Asymmetry* **1996**, *7*, 3339−3342. [5b] A. Ashimori, B. Bachand, L. E. Overman, D. J. Poon, *J. Am. Chem. Soc.* **1998**, *120*, 6477−6487. [5c] Y. Hayashi, H. Sakai, N. Kaneta, M. Uemara, *J. Organomet. Chem.* **1995**, *503*, 143−146. [5d] A. Lightfoot, P. Schnider, A. Pfaltz, *Angew. Chem.* **1998**, *110*, 3047−3050; *Angew. Chem. Int. Ed.* **1998**, *37*, 2897−2899.
[6] [6a] S. Masamune, W. Choy, J. S. Peterson, L. R. Sita, *Angew. Chem.* **1985**, *97*, 1−31; *Angew. Chem. Int. Ed. Engl.* **1985**, *24*, 1−30. [6b] K. Burgess, M. J. Ohlmeyer, K. H. Whitmire, *Organometallics* **1992**, *11*, 3588−3600. [6c] R. Stranne, J.-L. Vasse, C. Moberg, *Org. Lett.* **2001**, *3*, 2525−2528.
[7] [7a] G. van Koten, J. T. B. H. Jastrzebski, *Tetrahedron* **1989**, *45*, 569−578. [7b] V. M. Dem'yanovich, I. N. Shishkina, K. A. Potekhin, E. V. Balashova, Yu. T. Struchkov, N. S. Zefirov, *Dokl. Chem.* **1998**, *360*, 102−105.
[8] L. Horner, G. Simons, *Phosphorus Sulfur* **1984**, *19*, 65−75.
[9] A similar coupling pattern has been observed for the NMe_2 groups in the Pd^{II} complexes of (*R*,*RR*)-**5a** and (*S*,*RR*)-**5a**: D. J. Brauer, K. W. Kottsieper, S. Roßenbach, O. Stelzer, unpublished results.
[10] D. Cremer, J. A. Pople, *J. Am. Chem. Soc.* **1975**, *97*, 1354−1358.
[11] M. J. Burk, A. Pizzano, J. A. Martin, L. M. Liable-Sands, A. L. Rheingold, *Organometallics* **2000**, *19*, 250−260.
[12] [12a] C. L. Perrin, T. J. Dwyer, *Chem. Rev.* **1990**, *90*, 935−967. [12b] H. Friebolin, *Basic One- and Two-Dimensional NMR Spectroscopy*, 3rd ed., Wiley-VCH, Weinheim, New York, Chichester, Brisbane, Singapore, Toronto, **1998**, p. 276.
[13] [13a] E. Rotondo, G. Battaglia, C. G. Arena, F. Faraone, *J. Or-*

 © 2003 Wiley-VCH Verlag GmbH & Co. KGaA, Weinheim

ganomet. Chem. **1991**, *419*, 399−402. [13b] M. Bortolin, U. E. Bucher, H. Rüegger, L. M. Venanzi, A. Albinati, F. Lianza, S. Trafimenko, *Organometallics* **1992**, *11*, 2514−2521.
[14] [14a] D. Heller, K. Kortus, R. Selke, *Liebigs Ann.* **1995**, 575−581. [14b] D. Heller, S. Borns, W. Baumann, R. Selke, *Chem. Ber.* **1996**, *129*, 85−89.
[15] R. N.Icke, B. B. Wisegarver, *Organic Syntheses Collect. Vol. III*, Wiley, New York, NY, **1962**, p. 723.
[16] Y. Gao, K. B. Sharpless, *J. Am. Chem. Soc.* **1988**, *110*, 7538−7539.

Received January 1, 2002

 © 2003 Wiley-VCH Verlag GmbH & Co. KGaA, Weinheim

Exchange Coupling in Metal Complexes of the Second Transition Series: A Theoretical Exploration

Cédric Desplanches,[a][‡] Eliseo Ruiz,*[a] and Santiago Alvarez[a]

Keywords: Density functional calculations / Electronic structure / Magnetic properties / Molybdenum / Ruthenium

Theoretical methods based on density functional theory using hybrid functionals provide good estimates of the exchange coupling constants for complexes with metals of the second transition series, with accuracy similar to that previously obtained for complexes with lighter transition metals. The influence of the basis set and effective core potentials has been analyzed. The more diffuse nature of the 4d orbitals, in comparison with the 3d ones, considerably modifies the electronic structure and, consequently, the magnetic properties enhancing the antiferromagnetic contributions.
(© Wiley-VCH Verlag GmbH & Co. KGaA, 69451 Weinheim, Germany, 2003)

Introduction

In the field of molecular magnetism, the metals of the second and third transition series have been considered to be less useful than their lighter congeners due to their tendency to form low-spin complexes that in many cases are diamagnetic.[1] The heavier transition metals also tend to form complexes with strong M−M bonds that usually also present diamagnetic behavior.[2] They are also employed because of their large spin-orbit coupling that may give rise to interesting magnetic properties, although rare earth metals have been preferred in this regard.[3] For all these reasons, little is known about the magnetic properties of di- and polynuclear complexes of second and third transition series elements, even if the more diffuse character of the 4d orbitals compared to the 3d ones, the possibility of reaching higher oxidation states and the tendency to adopt larger coordination numbers should make us expect that the heavier metals have very different magnetic behavior.[2] However, during the last five years special attention has been devoted to the magnetic behavior of some complexes, mainly with molybdenum and ruthenium.[4−8]

There have been few theoretical studies of the magnetic properties of these kinds of complexes using ab initio methods. We can mention the work of Bencini et al. devoted to study of the magnetic properties of dioxobenzene-bridged Mo^V complexes using DFT methods.[9] Other open-shell molecules, the d^3-d^3 $[M_2Cl_9]^{3-}$ and $[M_2Cl_{10}]^{4-}$ systems (M = Cr^{3+}, Mo^{3+} and W^{3+}), have been exhaustively studied by Stranger et al. using DFT methods.[10−13] Semiempirical methods have been employed to analyze the exchange coupling through the Hay−Thibeault−Hoffmann model.[14] We can mention one example of complexes with second transition series elements, in this case, Koelle et al., using the extended Hückel method, analyzed the exchange coupling in $[Ru_2(\mu\text{-}Cl)_2Cp_2]$ dinuclear complexes.[15]

During the last years, we have successfully employed theoretical methods based on Density Functional Theory[16] to study the exchange coupling in several complexes containing first transition series metals.[17−20] The goal of this work is to analyze the differences in the magnetic behavior between the complexes of first and second transition series elements and to check if the accuracy in the estimation of the *J* values is similar to that obtained in the case of lighter transition metals.

Computational Methodology

The computational strategy adopted in previous theoretical studies on exchange-coupled dinuclear complexes has been used. For the evaluation of each coupling constant *J*, two separate DFT calculations are carried out, one for the highest spin state and another one for a broken-symmetry singlet state. The *J* values are obtained using Equation (1), where S_1 and S_2 are the total spins of the paramagnetic centers and $S_1 > S_2$ has been assumed for heterodinuclear complexes.[20]

$$E_{HS} - E_{BS} = -(2S_1S_2 + S_2)J \quad (1)$$

The hybrid B3LYP method[21] has been used in all calculations as implemented in Gaussian-98.[22] We have previously found that, among the most common functionals,

[‡] Present address: Institut de Chimie de la Matière Condensée de Bordeaux,
87 avenue du Docteur Albert Schweitzer, 33608 Pessac, France
[a] Departament de Química Inorgànica, and Centre Especial de Recerca en Química Teòrica (CeRQT), Universitat de Barcelona,
Diagonal 647, 08028 Barcelona, Spain

 © 2003 Wiley-VCH Verlag GmbH & Co. KGaA, Weinheim DOI: 10.1002/ejic.200200457

the B3LYP method combined with the broken-symmetry treatment provides the best results for calculating coupling constants.[17,20] We had also found that, when using DFT-based wavefunctions, a reasonable estimate of the low spin state energy can be obtained directly from the energy of a broken-symmetry solution. This fact is due to the inclusion of the non-dynamic correlation effects in the commonly used exchange functionals. If spin projection is applied in addition, a cancellation of such effects results, as discussed recently by Polo et al.[23]

In previous calculations of complexes with transition metal atoms we have usually employed all electron basis sets. Due to the importance of the relativistic effect of the second and third transition series elements, pseudopotentials including relativistic effects are an interesting alternative to the all-electron basis sets. We employed five different basis sets as a benchmark for a dinuclear cyano-bridged Mo^{III} complex, four of them using pseudopotentials for the Mo atoms and one with the double-ζ all-electron basis set proposed by Rappe and Goddard[24] (keyword MSV in the Jaguar code[25]). The four combinations of pseudopotentials and basis sets are as follows: (1) Stoll−Preuss quasi-relativistic pseudopotentials[26] (indicated as SDD in the Gaussian code, we also performed a test calculation with the corresponding nonrelativistic pseudopotentials for molybdenum atoms) combined with the triple-ζ all-electron basis set proposed by Ahlrichs et al.[27] for the other elements; (2) the small-core Hay−Wadt pseudopotential[28] for the Mo atom combined with the D95 all-electron basis set[29] for the first-row elements (indicated in the Gaussian code as LANL2DZ); (3) core potentials proposed by Stevens et al. for all the atoms, using a double-ζ basis set for the valence orbitals[30,31] (called CEP-31G in the Gaussian code) and, (4) the same pseudopotentials as in (3) but with a triple-ζ basis set for the valence shell[30,31] (referred to as CEP-121G in Gaussian). For the other systems with Ru and Mo atoms we have employed option (2) corresponding to the LANL2DZ basis set. Finally, for the calculations of the chromium complex we employed the same basis sets as for the cyano-bridged molybdenum complex along with a triple-ζ all-electron basis set proposed by Ahlrichs (keyword TZV in Gaussian)[27] including two p polarization functions for the chromium atom, usually done by us for first transition series metal atoms.

Results of Benchmark Systems

In order to check the accuracy of the methodology employed previously for complexes with lighter transition metals, we selected a cyano-bridged dinuclear Mo^{III} complex $[Mo_2(CN)_{11}]^{5-}$ with tetraethylammonium as a counterion, recently synthesized by Long et al.[32] (see **1**). This complex is especially interesting because the Mo^{III} cation shows a very unusual octahedral coordination, with $S_1 = S_2 = 3/2$, while Mo^{III} usually adopts structures with coordination numbers of seven or eight with the cyanide ligands.[4]

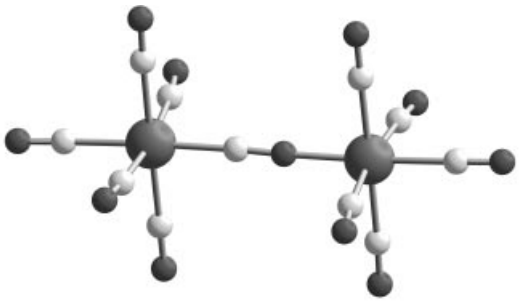

1

The calculated exchange coupling constants for the experimental structure of complex **1** are indicated in Table 1. All calculated values are in excellent agreement with the experimental ones. The all-electron basis set gives results similar to those obtained with effective core potentials (ecp). Thus, it seems that the relativistic corrections incorporated in the ecp are not crucial for the calculation of exchange coupling constants in these types of complexes, probably because we are calculating an energy difference and relativistic corrections of about the same magnitude affect the two spin states. This conclusion is confirmed by the value of -226 cm^{-1} obtained by using the Stoll−Preuss non-relativistic pseudopotentials for molybdenum atoms (and TZV basis set for the other atoms). This also shows the small effect of the relativistic corrections. The values of the exchange coupling constant calculated with the effective core potential are very similar, independent of the quality of the basis set employed.

Table 1. Calculated exchange coupling constants (in cm^{-1}) for complex **1** and for an equivalent symmetric Cr^{III} dinuclear complex with different basis sets and effective core potentials (ecp), together with the available experimental data[32]

	Mo^{III}	Cr^{III}
all-electron MSV	−217	−29
all-electron TZV	–	−31
ecp − SDD + TZV	−242	−27
ecp − LANL2DZ	−225	−25
ecp − CEP-31G	−247	−30
ecp − CEP-121G	−247	−29
exp.	−226	–

One of the goals of this study is to analyze the differences between the complexes of the elements of the first and second transition metal series. For this reason, we performed calculations on a symmetric cyano-bridged Cr^{III} dinuclear complex with a fixed structure (Cr−C = 2.06; Cr−N = 2.14; C−N = 1.14 Å) and the resulting J values can be seen in Table 1. The calculated values using pseudopotentials and an all-electron basis set are very similar as are those of the molybdenum complex, but the most remarkable result is the decrease, by an order of magnitude, of the exchange coupling constant compared to that of the Mo^{III} complex. It is also interesting to point out that the effect of using pseudopotentials is similar for Cr and Mo. Similar Cr^{III} complexes have not been reported in the literature, there

 © 2003 Wiley-VCH Verlag GmbH & Co. KGaA, Weinheim

is only a well-characterized cyano-bridged Cr^{III} dinuclear complex (**2**) having one salycilenealdiminato ligand per Cr^{III} cation and a terminal cyanide ligand to complete an octahedral coordination sphere.[33] We have calculated the exchange coupling constant of this complex using the all-electron basis set to check the accuracy of our calculations, and we obtain a value of $-13.7\ cm^{-1}$ to be compared with the experimental result of $-11.4\ cm^{-1}$. The good agreement makes us confident about the *J* values reported for the Cr^{III} dinuclear model and confirms the weaker coupling of the Cr^{III} complexes compared to the Mo^{III} ones.

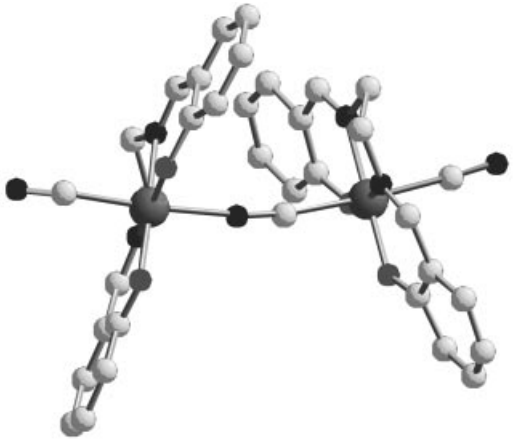

2

In order to rationalize these results, we have analyzed the contributions to the exchange coupling constant by using the Hay−Thibeault−Hoffmann[14] (HTH) and Kahn−Briatt[34,35] (KB) models [Equations (2) and (3), respectively].

$$J = 2K_{ab} - \frac{(\varepsilon_1 - \varepsilon_2)^2}{J_{aa} - J_{ab}} \quad (2)$$

$$J = 2K_{ab} + 4h_{ab}S_{ab} \quad (3)$$

In both models, we can consider, in a rough approximation, that an antiferrromagnetic contribution (second term) depends on the square of the energy gap between the orbitals bearing the unpaired electrons (HTH model) or on the overlap between the "magnetic" orbitals (KB model). We as well as other authors[36,37] have recently shown that such magnetic orbitals are well represented by the localized orbitals of the broken-symmetry solution (we call them BS-OMSO[38]). The overall energy splitting of the six t_{2g}-type orbitals in the high-spin solution is 0.73 eV for the Mo^{III} complex and only 0.32 eV for the Cr^{III} complex. A similar result is found if we employ the KB model: the overlap between each pair of BS-OMSOs directed towards the π-system of the bridging ligand (one of them is shown in Figure 1) is 0.22 for the Mo^{III} complex and 0.05 for the Cr^{III} one. The overlap between the remaining t_{2g} orbital pair is negligible because these orbitals are perpendicular to the exchange pathway. Thus, both models predict a stronger antiferromagnetic contribution for the Mo^{III} complex, if we assume that the other terms in Equations (2) and (3) are similar. The origin of such differences can probably be found in the more diffuse character of the 4d orbitals compared with the 3d ones. To verify this assertion, we have analyzed the overlap integrals between d atomic orbitals of the metal atoms and p atomic orbitals of neighboring carbon or nitrogen atoms. We find that the overlap integrals involving the Mo atom are about one order of magnitude larger than those for Cr, both for the σ- and π-systems.

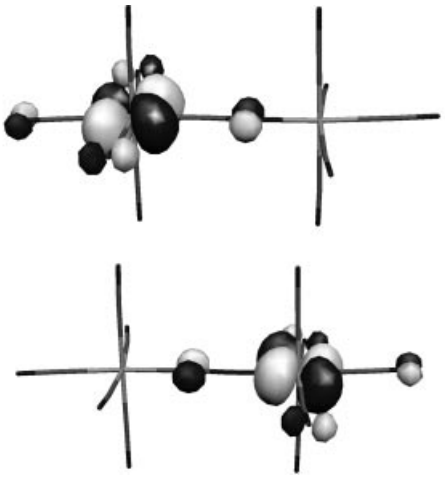

Figure 1. Broken-symmetry orbitals corresponding to one combination of the t_{2g} orbital pairs of $[Mo_2(CN)_{11}]^{5-}$ calculated at the B3LYP level

The spin population distribution also shows significant differences between the complexes of Mo^{III} and Cr^{III}. The spin population at each Mo atom is around 2.8 electrons, but 3.2 at the Cr atoms in the analogous complex. The orbital analysis shows that in both cases there is a small spin population in the formally empty e_g metal orbitals due to spin polarization of the metal−ligand bonding molecular orbitals of the same symmetry,[39] thus accounting for the spin population being larger than the number of unpaired electrons in the Cr compound. The substitution of Cr by Mo, with more diffuse atomic orbitals, results in a larger delocalization that is responsible for a smaller spin population at the molybdenum atoms.

Results of the Full Structures

We have selected two full structures to analyze the accuracy of the DFT methodology proposed for the calculation of the exchange coupling constant. The first structure corresponds to a pyrazino-bridged Ru^{III} dinuclear complex[40] (see **3**) related to the Creutz−Taube mixed-valence complex.[41] The interaction of the π-system of the pyrazine with one of the t_{2g} orbitals produces the largest stabilization due to the π-acid character of the pyrazine ligands while the one that combines slightly with the σ-system remains at an intermediate energy. Each Ru^{III} cation is low-spin d^5, and the unpaired electron is placed in the only t_{2g} orbital that

 © 2003 Wiley-VCH Verlag GmbH & Co. KGaA, Weinheim

interacts neither with the π-system of the bridging ligand, nor with the σ-system (see Figure 2). Therefore, the two combinations of the orbitals bearing the unpaired electron cannot have large contributions towards the bridging ligand and we expect a small energy splitting between the in-phase and out-of-phase combinations of such d orbitals and, consequently, a small exchange coupling constant for this complex. Experimentally, the authors proposed a maximum negative value for the coupling constant of -6 cm^{-1} from magnetic susceptibility measurements,[42] in very good agreement with the presently calculated value at the B3LYP level of -2.6 cm^{-1}.

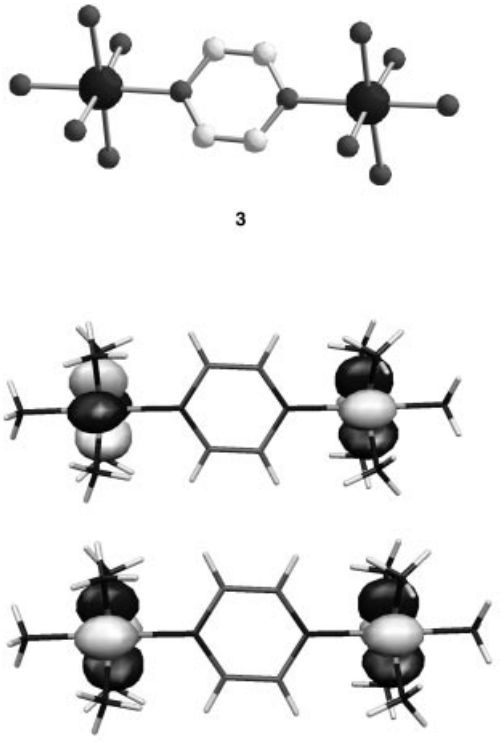

Figure 2. Orbitals bearing the unpaired electrons in the triplet state of the pyrazino-bridged Ru^{III} dinuclear complex **3** calculated at the B3LYP level

The second full structure that we have chosen is a very interesting system because it shows a strong antiferromagnetic exchange coupling between two paramagnetic centers over a long distance. It is an Mo^{V} complex with a very long dipyridylpolyene bridging ligand, complemented with nitrosyl, chloro and tris(pyrazolyl)borato ligands to complete an octahedral coordination sphere at each metal ion (see **4**).[43] The Mo−Mo distance is 20.76 Å and the exchange coupling constant between the two d^1 cations is -82 cm^{-1}, rather large considering the long distance. The authors also proposed a J value of -115 cm^{-1} using the g value obtained from EPR spectroscopy for the fitting of the magnetic susceptibility data. The problem with the experimental data is that it was only measured between 80 and 300 K. We have calculated a somewhat smaller value of -31 cm^{-1}, which nevertheless shows the ability of the present calculations to correctly describe the nature (antiferromagnetic) and approximate magnitude of exchange interactions at very long distances between two Mo^{V} centers.

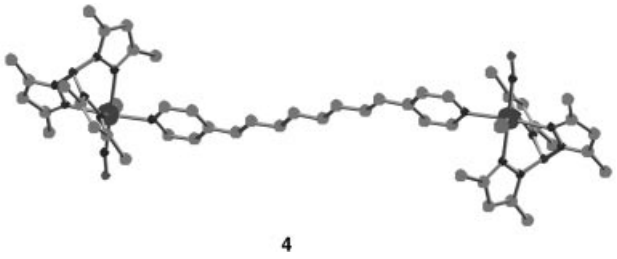

Along the same lines, we have recently predicted with the same methodology that some transition metal complexes with long dicyanamidobenzene-type bridging ligands can show very strong ferromagnetic or antiferromagnetic coupling depending on the isomer and substituents of the bridging ligand.[44] In the same study we have analyzed, from an orbital point of view, the exchange coupling for systems with long conjugated bridging ligands that have usually only been analyzed in terms of the so-called spin polarization mechanism using a McConell model.[45] Our conclusions indicated that usually for a symmetric bridging ligand with an even number of atoms in the exchange pathway, such as that in complex **4**, the two ligand orbitals that combine with the two metal orbitals have different energies. Thus, the two molecular orbitals corresponding to the whole molecule show a sizeable energy splitting, resulting in a large antiferromagnetic contribution, according to the HTH model (see Figure 3). If the bridging ligand has an odd number of atoms, the orbitals remain nearly degenerate and the coupling would be ferromagnetic. For the dipyridylpolyene ligand, the calculated orbital energies are non-degenerate (energy splitting of 0.07 eV equivalent to 550 cm^{-1}) due to different π-bonding or antibonding character at the central C−C bond of the two orbitals, confirming those rules.

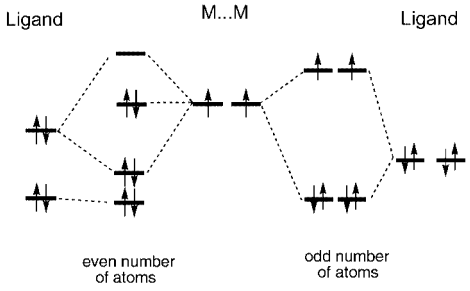

Figure 3. Scheme of the orbital interaction of a dinuclear transition metal complex through a bridging ligand depending on the number of atoms of the bridging ligand

Conclusions

The exchange coupling constants for different complexes of second series transition elements have been calculated using a theoretical method based on density functional theory. The use of the hybrid B3LYP functional, as in previous

 © 2003 Wiley-VCH Verlag GmbH & Co. KGaA, Weinheim

studies devoted to complexes with metals of the first transition series, offers very good results. The influence of the basis set and different effective core potentials on the calculated J value is very small and results obtained with all-electron basis sets or with pseudopotentials are quite similar. The comparative analysis of the electronic structures of the $[Mo_2(CN)_{11}]^{5-}$ and $[Cr_2(CN)_{11}]^{5-}$ complexes reveals the importance of the more diffuse nature of the 4d orbitals of the molybdenum atoms. This fact results in a larger antiferromagnetic contribution that can be understood using the Hay−Thibeault−Hoffmann or Kahn−Briatt models, i.e., a larger energy splitting of the orbitals bearing unpaired electrons or a larger overlap between the localized "magnetic" orbitals, respectively. The study of the spin population distribution also shows a considerably larger delocalization in the case of the Mo^{III} complex due to the more diffuse character of the 4d orbitals.

Acknowledgments

The research has been supported by the Ministerio de Ciencia y Tecnología through project number DGI BQU200298-04033-C02-01. Additional support from Comissió Interdepartamental de Ciència i Tecnologia (CIRIT) through grant 2001SGR-0044 is also acknowledged. The computing resources were generously made available in the Centre de Computació de Catalunya (CESCA) with a grant provided by Fundació Catalana per a la Recerca (FCR) and the Universitat de Barcelona. One of us (C. D.) would like to thank the Programme Improving the Human Research Potential and the Socio-economic Knowledge Base of the European Commission (contract HPMF-CT-2000-00977) for a postdoctoral grant.

[1] O. Kahn, *Molecular Magnetism*, VCH Publishers, New York, **1993**.
[2] F. A. Cotton, G. Wilkinson, C. A. Murielle, M. Bochmann, in *Advanced Inorganic Chemistry*, John Wiley & Sons, New York, **1999**, p. 877.
[3] C. Benelli, D. Gatteschi, *Chem. Rev.* **2002**, *102*, 2369.
[4] O. Kahn, J. Larionova, L. Ouahab, *Chem. Commun.* **1999**, 945.
[5] J. Larionova, B. Mombelli, J. Sanchiz, O. Kahn, *Inorg. Chem.* **1998**, *37*, 679.
[6] J. Larionova, O. Kahn, J. Bartolome, R. Burriel, M. Castro, V. Ksenofontov, P. Gutlich, *Chem. Mater.* **1999**, *11*, 3400.
[7] J. Larionova, O. Kahn, S. Golhen, L. Ouahab, R. Clerac, *Inorg. Chem.* **1999**, *38*, 3621.
[8] J. Larionova, O. Kahn, S. Gohlen, L. Ouahab, R. Clerac, *J. Am. Chem. Soc.* **1999**, *121*, 3349.
[9] A. Bencini, D. Gatteschi, D. Totti, D. N. Sanz, J. A. McCleverty, M. D. Ward, *J. Phys. Chem. A* **1998**, *102*, 10545.
[10] R. Stranger, P. W. Smith, I. E. Grey, *Inorg. Chem.* **1989**, *28*, 1271.
[11] R. Stranger, S. A. Macgregor, T. Lovell, J. E. McGrady, G. A. Heath, *J. Chem. Soc., Dalton Trans.* **1996**, 4485.
[12] R. Stranger, J. E. McGrady, T. Lovell, *Inorg. Chem.* **1998**, *37*, 6795.
[13] R. Stranger, T. Lovell, J. E. McGrady, *Inorg. Chem.* **1999**, *38*, 5510.
[14] P. J. Hay, J. C. Thibeault, R. Hoffmann, *J. Am. Chem. Soc.* **1975**, *97*, 4884.
[15] U. Koelle, H. Lueken, K. Handrick, H. Schilder, J. K. Kurdett, S. Balleza, *Inorg. Chem.* **1995**, *34*, 6273.
[16] W. Koch, M. C. Holthausen, *A Chemist's Guide to Density Functional Theory*, Wiley-VCH Verlag, Weinheim, **2000**.
[17] E. Ruiz, P. Alemany, S. Alvarez, J. Cano, *J. Am. Chem. Soc.* **1997**, *119*, 1297.
[18] E. Ruiz, P. Alemany, S. Alvarez, J. Cano, *Inorg. Chem.* **1997**, *36*, 3683.
[19] E. Ruiz, S. Alvarez, P. Alemany, *Chem. Commun.* **1998**, 2767.
[20] E. Ruiz, J. Cano, S. Alvarez, P. Alemany, *J. Comp. Chem.* **1999**, *20*, 1391.
[21] A. D. Becke, *J. Chem. Phys.* **1993**, *98*, 5648.
[22] M. J. Frisch, G. W. Trucks, H. B. Schlegel, G. E. Scuseria, M. A. Robb, J. R. Cheeseman, V. G. Zakrzewski, J. A. Montgomery, R. E. Stratmann, J. C. Burant, S. Dapprich, J. M. Millam, A. D. Daniels, K. N. Kudin, M. C. Strain, O. Farkas, J. Tomasi, V. Barone, M. Cossi, R. Cammi, B. Mennucci, C. Pomelli, C. Adamo, S. Clifford, J. Ochterski, G. A. Petersson, P. Y. Ayala, Q. Cui, K. Morokuma, D. K. Malick, A. D. Rabuck, K. Raghavachari, J. B. Foresman, J. Cioslowski, J. V. Ortiz, B. B. Stefanov, G. Liu, A. Liashenko, P. Piskorz, I. Komaromi, R. Gomperts, R. L. Martin, D. J. Fox, T. Keith, M. A. Al-Laham, C. Y. Peng, A. Nanayakkara, C. Gonzalez, M. Challacombe, P. M. W. Gill, B. G. Johnson, W. Chen, M. W. Wong, J. L. Andres, M. Head-Gordon, E. S. Replogle, J. A. Pople, *Gaussian98* (revision A.9), Gaussian, Inc, Pittsburgh, PA, **1998**.
[23] V. Polo, E. Kraka, D. Cremer, *Theor. Chem. Acc.* **2002**, *107*, 291.
[24] A. K. Rappé, W. A. Goddard, unpublished results.
[25] *Jaguar 4.1*, Schrödinger, Inc., Portland, **2000**.
[26] D. Andrae, U. Haeussermann, M. Dolg, H. Stoll, H. Preuss, *Theor. Chim. Acta* **1990**, *77*, 123.
[27] A. Schaefer, C. Huber, R. Ahlrichs, *J. Chem. Phys.* **1994**, *100*, 5829.
[28] P. J. Hay, W. R. Wadt, *J. Chem. Phys.* **1985**, *82*, 299.
[29] J. Dunning, T. H., P. J. Hay, in *Modern Theoretical Chemistry*, vol. 3 (Ed.: H. F. Schaefer III), Plenum, New York, **1976**, p. 1.
[30] W. J. Stevens, M. Krauss, H. Basch, P. G. Jasien, *Can. J. Chem.* **1992**, *70*, 612.
[31] W. Stevens, H. Basch, J. Krauss, *J. Chem. Phys.* **1984**, *81*, 6026.
[32] L. G. Beauvais, J. R. Long, *J. Am. Chem. Soc.* **2002**, *124*, 2110.
[33] H. Li, S. J. Zhong, X.-Z. You, W. Chen, *J. Coord. Chem.* **1997**, *42*, 271.
[34] O. Kahn, B. Briat, *J. Chem. Soc. Trans.* **1976**, *72*, 268.
[35] O. Kahn, B. Briat, *J. Chem. Soc. Trans.* **1976**, *72*, 1441.
[36] F. Fabrizi de Biani, E. Ruiz, J. Cano, J. J. Novoa, S. Alvarez, *Inorg. Chem.* **2000**, *39*, 3221.
[37] C. Blanchet-Boiteux, J. M. Mouesca, *Theor. Chem. Acc.* **2000**, *104*, 257.
[38] C. Desplanches, E. Ruiz, A. Rodríguez-Fortea, S. Alvarez, *J. Am. Chem. Soc.* **2002**, *124*, 5197.
[39] J. Cano, E. Ruiz, S. Alvarez, M. Verdaguer, *Comments Inorg. Chem.* **1998**, *20*, 27.
[40] U. Fürholz, S. Joss, H.-B. Bürgi, A. Ludi, *Inorg. Chem.* **1985**, *24*, 943.
[41] C. Creutz, *Prog. Inorg. Chem.* **1983**, *30*, 1.
[42] U. Fürholz, H.-B. Bürgi, F. E. Wagner, A. Stebler, J. H. Ammeter, E. Krausz, R. J. H. Clark, M. J. Stead, A. Ludi, *J. Am. Chem. Soc.* **1984**, *106*, 121.
[43] S. L. W. McWhinnie, J. A. Thomas, T. A. Hamor, C. J. Jones, J. A. McCleverty, D. Collison, F. E. Mabbs, C. J. Harding, L. J. Yellowlees, M. G. Hutchings, *Inorg. Chem.* **1996**, *35*, 760.
[44] E. Ruiz, A. Rodríguez-Fortea, S. Alvarez, submitted for publication.
[45] H. M. McConnell, *J. Chem. Phys.* **1963**, *39*, 1910.

Received August 12, 2002

 © 2003 Wiley-VCH Verlag GmbH & Co. KGaA, Weinheim

Organotin-Drug Interactions. Organotin Adducts of Lornoxicam, Synthesis and Characterisation of the First Complexes of Lornoxicam

Angeliki Galani,[a] Mavroudis A. Demertzis,[a] Maciej Kubicki,[b] and Dimitra Kovala-Demertzi*[a]

Keywords: Antitumour agents / Tin / Supramolecular chemistry / Drug delivery

The synthesis and spectral characterisation of novel organotin complexes [$SnMe_2$(lorn)] (**1**) and [S*n*Bu_2(lorn)] (**2**) of the potent and widely used anti-inflammatory drug lornoxicam, H_2lorn, are reported. Crystal structure determinations of complexes**1** and **2** showed that the ligand is doubly deprotonated at the oxygen and amide nitrogen atoms and is coordinated to the SnR_2 fragment via four- and six-membered chelate rings. The monomers of **1** are linked through intermolecular hydrogen bonds of C–H--O type and through C–H–π intermolecular interactions. There are two similar molecules in the asymmetric unit of **2**. The dimers of **2** are arranged in polymers with a stacking of alternate parallel chains and are linked through intermolecular hydrogen bonds of C–H--O type, and through C–H–π intermolecular interactions. An extended network of Sn–O–Sn, C–H--O and C–H--π contacts lead to aggregation and a supramolecular assembly.

(© Wiley-VCH Verlag GmbH & Co. KGaA, 69451 Weinheim, Germany, 2003)

Introduction

Lornoxicam (6-chloro-4-hydroxy-2-methyl- 2-pyridyl-2*H*-thieno[2,3-*e*]-1,2-thiazine-3- amide-1,1-dioxide) is a new non-steroidal antiflammatory drug (NSAID) with marked analgesic properties that chemically differs from tenoxicam by the presence of a single chloro-substituent in the 8-position.[1] Lornoxicam's principal mode of action is the inhibition of the enzyme cyclooxygenase and thus of prostaglandin synthesis from arachidonic acid.[2] It does not cause shunting of arachidonic acid to the lipoxygenase cascade, and therefore does not increase production of leukotrienes. In vitro experiments have demonstrated that lornoxicam is more than 100 times more potent than tenoxicam and 40 times more potent than piroxicam in its ability to inhibit cyclooxygenase.[1,2] Lornoxicam is a yellow crystalline substance with a pK of 4.7 and a partition coefficient of 1.8 (determined in octanol−phosphate buffer, pH 7.4). The acid−base behaviour of lornoxicam has also been studied and the apparent pK_a-values reported.[3]

Organotin(IV) compounds are important and have received increasing attention in recent years, not only because of their intrinsic interest, but also owing to the importance of tin-based anti-tumour drugs. Some examples find wide applications as catalysts and stabilizers, and certain derivatives are used as biocides, as antifouling agents and for wood preservation. Recent tests on their anti-tumour activity have revealed that several diorganotin adducts, as well as triorganotin species, show potential as antineoplastic and antituberculosis agents.[4,5]

We are interested in the coordination chemistry and anti-inflammatory properties of non-steroidal anti-inflammatory drugs with transition[6] and non-transition metal[7] ions, and report here the interaction of SnR_2O (R is methyl or butyl) with lornoxicam (H_2lorn) and the crystal structure of the complexes [$SnMe_2$(lorn)] and [S*n*Bu_2(lorn)]. These are the first reported structures of a lornoxicam complex.

Results and Discussion

Molecular Structures

The molecular structures of complexes **1** and **2**, along with the atom numbering scheme, are shown in Figure 1 and Figure 2 and crystal data are given in Table 1, together with refinement details. Bond lengths and angles are given in Table 2. Complexes **1** and **2** have a 1:1 Sn/lorn stoichiometry and the doubly deprotonated ligand, lorn, is coordinated as a tridentate ligand via the enolic oxygen O(4) and the amide N(31) and pyridyl N(1′) nitrogen atoms. Two carbon atoms complete the fivefold coordination at the diorganotin(IV) fragments. There are two similar molecules in the asymmetric unit of **2**.

Analysis of the shape-determining angles using the approach of Reedijk and co-workers[8] yields $\tau[(\alpha-\beta)/60]$ val-

[a] Inorganic and Analytical Chemistry, Department of Chemistry, University of Ioannina,
45100 Ioannina, Greece
E-mail: dkovala@cc.uoi.gr
[b] Department of Chemistry, A. Mickiewicz, University, ul. Grunwaldzka 6, 60−78 Poznan, Poland

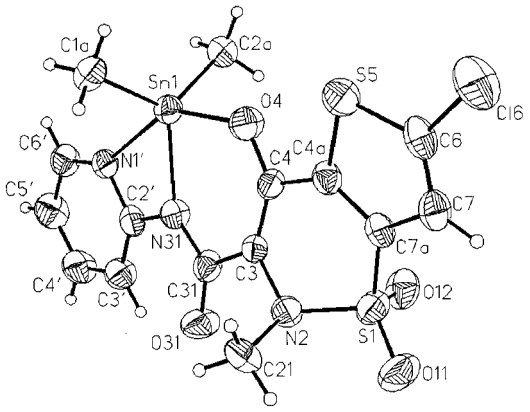

Figure 1. ORTEP representation of **1** with the atom numbering scheme.

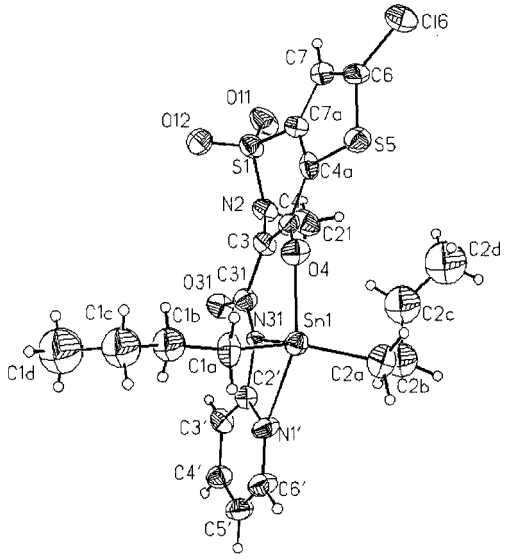

Figure 2. ORTEP representation of **2** with the atom numbering scheme.

ues of 0.01 for both tin centres, Sn(1a) and Sn(1b) for **2**, and 0.29 for **1** (τ = 0.0 and 1.0 for *sp* and *tbp* geometries respectively). The metal coordination geometry is therefore described as square pyramidal with N(31) occupying the apical positions. The donors N(31) are chosen as apices by the simple criterion that neither should be any of the four donor atoms that define the two largest angles, α and β. The coordinated ligand is composed of five rings and the donor atoms NNO are included in three rings, one heterocyclic and two chelates. The heterocyclic ring (I) is planar, the largest deviation from the mean plane being 0.016(6) for C(2′) for **1** and 0.008(12)° for C(5′A) for molecule (1) and 0.015(11) for C(3′B) for molecule (2), respectively, for complex **2**. For **1** the dihedral angles between the planes of the rings I and II, II and III, and I and III are 3.4(3), 3.8(2) and 6.9(2), respectively. For **2** the dihedral angles between the planes of the rings I and II, II and III, and I and III are 0.8(5), 6.1(4) and 6.8(4) for the first molecule Sn(1a), and 2.7(5), 5.2(4) and 7.1(4) for the second molecule Sn(1b), indicating that the ligand as a whole deviates from planarity, the largest deviations arising from the expected puckering of the sulfonamide rings which contain the pyramidal saturated N atoms. The C(31)−O(31) bond lengths indicate strongly that these bonds are ketonic − also supported by the coplanarity of the three bonds to C(31). The di-anionic, tridentate ligand has an *EZZ* configuration about the bonds C(2′)−N(31), N(31)−C(31) and C(31)−C(3) for **1** and **2**. The *EZZ* configuration differs from the *ZZZ* isomer only by a 180° rotation of the pyridyl ring. The deprotonation of amide nitrogen is being one of the principal effects, which favour *EZZ* configuration.

Table 1. Crystal data, data collection and structure refinement

Compound	**1**	**2**
Empirical formula	$C_{15}H_{14}ClO_4N_3S_2Sn$	$C_{21}H_{26}ClN_3S_2Sn$
Molecular mass	518.55	602.71
Crystal system	monoclinic	triclinic
Space group	$P2_1$	$P\bar{1}$
a (Å)	9.0172(13)	12.413(2)
b (Å)	11.797(2)	13.272(2)
c (Å)	9.2567(17)	17.705(2)
α, β, γ (°)	90 108.089(16) 90	78.058(12) 77.058(12) 63.903(16)
V (Å^3)	936.0(2)	2533.1(6)
Z	2	4
D_x (g cm^{-3})	1.84	1.58
F(000)	512	1216
μ (mm^{-1})	1.76	1.31
Crystal size (mm)	0.40 × 0.25 × 0.10	0.30 × 0.20 × 0.150
Θ Range (°)	3.8−25	3.5−26
hkl Range	$-10 \le h \le 10$ $-14 \le k \le 12$ $-11 \le l \le 11$	$-14 \le h \le 14$ $-15 \le k \le 16$ $-21 \le l \le 21$
Reflections:		
collected	7749	12229
unique (R_{int})	2512 (0.040)	7688 (0.047)
Number of parameters	235	505
Weighting scheme:		
A	0.01	0.137
B	0.7	7.996
Extinction parameter *k*	0.00091(10)	
R(*F*)	0.026	0.067
wR(F^2)	0.049	0.169
Goodness of fit	1.14	1.02
max/min Δρ (e·Å^{-3})	0.92/−0.37	2.66/−1.11

Molecules of **2** are joined into dimers in a head-to-tail fashion by intermolecular bonds between tin and the neighbouring ketonic oxygen atom, with distances of Sn(1a)--O(31B)^i 2.954 (2) and Sn(1b)--O(31A)^i 2.971 (2). Intermolecular distances for Sn--O of 2.61−3.02 Å have been confidently reported for intramolecular bonds, indicating Sn−O bonding here.[9b] For **2** the dimers of Sn(1a) and Sn(1b) are arranged in polymers with a stacking of alternate parallel chains. The dimers of Sn(1a) and Sn(1b) are linked through intermolecular hydrogen bonds of the C−H--O type,[9a] O(12B)l···H22A−C(2AA). Inter- and intra- C−H-π molecular interactions[9b] and intra- and intermolecular hydrogen bonds stabilize this structure. For **1** the distance between

 © 2003 Wiley-VCH Verlag GmbH & Co. KGaA, Weinheim

Table 2. Selected bond lengths [Å] and angles [°] for **1** and **2**

	1	**2a**	**2b**
Sn(1)−C(1A)	2.102(6)	2.123(9)	2.118(9)
Sn(1)−C(2A)	2.112(5)	2.104(11)	2.113(11)
Sn(1)−N(31)	2.120(5)	2.133(8)	2.140(8)
Sn(1)−N(1′)	2.400(4)	2.407(8)	2.391(7)
Sn(1)−O(4)	2.094(3)	2.113(6)	2.108(6)
S(1)−O(11)	1.422(4)	1.435(8)	1.444(8)
S(1)−O(12)	1.440(4)	1.413(8)	1.419(8)
S(1)−N(2)	1.624(5)	1.631(8)	1.620(9)
S(1)−C(7A)	1.740(5)	1.735(10)	1.746(10)
C(4)−O(4)	1.315(6)	1.338(10)	1.318(10)
C(4A)−S(5)	1.718(5)	1.729(9)	1.731(9
S(5)−C(6)	1.719(5)	1.738(11)	1.714(10)
C(31)−O(31)	1.221(6)	1.247(11)	1.249(11)
C(31)−N(31)	1.365(7)	1.374(11)	1.384(12)
N(31)−C(2′)	1.394(6)	1.411(11)	1.389(12)
N(1′)−C(6′)	1.335(6)	1.329(12)	1.357(12)
N(1′)−C(2′)	1.351(6)	1.330(11)	1.348(12)
O(4)−Sn(1)−C(1A)	97.1(2)	96.1(4)	97.0(4)
O(4)−Sn(1)−C(2A)	97.19(17)	101.3(4)	99.7(4)
C(1A)−Sn(1)−C(2A)	126.1(2)	142.1(4)	140.6(4)
O(4)−Sn(1)−N(31)	85.09(15)	83.3(2)	83.5(2)
C(1A)−Sn(1)−N(31)	116.2(2)	104.6(3)	105.5(3)
C(2A)−Sn(1)−N(31)	116.63(19)	110.6(4)	111.7(4)
O(4)−Sn(1)−N(1′)	143.79(13)	141.4(2)	141.4(3)
C(1A)−Sn(1)−N(1′)	100.5(2)	92.3(4)	92.5(4)
C(2A)−Sn(1)−N(1′)	97.56(17)	94.6(4)	96.2(4)
N(31)−Sn(1)−N(1′)	58.75(15)	58.2(3)	57.9(3)
N(31)−C(31)−C(3)	115.8(5)	114.1(7)	116.0(8)
N(31)−C(31)−O(31)	122.8(5)	126.2(8)	124.6(9)
O(31)−C(31)−C(3)	121.4(5)	119.6(8)	119.4(8)

Sn(1) and the neighbouring ketonic oxygen atom is 3.562(4), and the monomers of Sn(1) are linked through intermolecular hydrogen bonds of C−H--O type,[9a] O(12)axial···H6′−C(6′), O(11)eq···H13A−C(1A) and O(31)···H23A−C(2A) (Figure 3). Further, C−H−π interactions[9a] and intramolecular hydrogen bonds stabilize the structure. Although the numerous contacts, of many different types, are remarkable, the interactions themselves are consistent with known guidelines for hydrogen bond formation.[9c] In these two cases molecular recognition of the hydrogen bonds and intermolecular contacts lead to aggregation and a supramolecular assembly. These interactions and other close approaches of the type C−H--π, and some intermolecular interactions are listed in Table 3.

The negative charge on the atoms in a molecule with several donor centres can be used to study its formation of a donor−acceptor bond with a metal. In H_2lorn the four oxygen atoms exhibit the maximum electron density and negative charge. The highest effective charge and the highest electron density values for the four oxygen atoms and for the pyridyl and imine nitrogen in **1** and **2** evidently show strong electron-donor properties and could rationalize the coordination scheme and the extended network of inter-, intra- hydrogen, and non-hydrogen bonding. The optimised geometry in the gas phase for H_2lorn the total dipole moment and the enthalpy of formation of neutral, H_2lorn, and double deprotonated lornoxicam, lorn, in the gas state are shown in Figure 4.

Spectral and Electrochemical Characterisation

Infrared Spectroscopy

The ligand, H_2lorn, shows a broad absorption band centred at ca. 3500 and 3400 cm^{-1} that is characteristic of an O−H stretching vibration. The band at 3067 cm^{-1} for lornoxicam is attributed to the N−H stretching vibration. The low frequency of these two bands may be explained by inter- and intramolecular hydrogen bonds involving the nitrogen and two oxygen atoms of the secondary amide group.[11a] The sharp bands observed at 1647, 1619 cm^{-1} and the band at 1596 cm^{-1} in lornoxicam are assigned to the carbonyl ν(C=O) and the ν(C=N) vibrations of the secondary amide group −CO−NH−.[11] The ν(C=O) and the ν(C=N) bands are at lower frequencies in the complexes, at 1619, 1591 and 1567 cm^{-1} for **1** and at 1600, 1599, 1578 and 1549 cm^{-1} for **2**. For compounds **1** and **2**, bands assignable to ν_{asym} and ν_{sym} (Sn−C_2) are observed at 550, 473 and 551, 475 cm^{-1} respectively, indicating a non-linear Sn−C_2 moiety. The bands at 265 and 268 cm^{-1} are assigned to the ν(Sn−N_{pyr}) stretching mode for **1** and **2** respectively; and those at 221 and 215 cm^{-1} for **1**, and at 224 and 211 cm^{-1} for **2**, are assigned to ν(Sn−O) stretching modes.[7,11]

NMR Spectroscopy

^{1}H and ^{13}C NMR spectra were recorded for lornoxicam, **1** and **2**. Peak assignments were based on literature reports.[6,7] The main differences between the ^{1}H NMR spectrum of the free H_2lorn and the complexes are the disappearance of the downfield OH and NH signals. These changes confirm that loss of both hydrogens and metallation occurs, and that the structure of the complexes in the solid state persists in $(CD_3)_2SO$ or $CDCl_3$ solutions. The appearance of the OH peak downfield at δ = 14.02 ppm in $CDCl_3$ for H_2lorn indicates that OH is hydrogen-bonded. In complexes **1** and **2** deshielding of protons H6′, H3′ and the corresponding carbon atoms C(6′), C(3′) is observed, which should be related to the electrophilicity of the tin. A σ-charge donation from the N(1′)-donor to the tin centre removes electron density from the ligand and produces this deshielding, which will attenuate at positions remote from the metal. The upfield shift observed for H4′, H5′ and the corresponding carbon atom C(4′), C(5′) *meta* and *para* to the tin centre could be due to the flow of charge from the tin into the aromatic ring (π-back donation).[7] The signals corresponding to the imino and hydroxyl groups disappear upon interaction with the metal, indicating deprotonation of these atoms and possible coordination to the tin atom. A tridentate coordination via the enolic oxygen, the amide and the pyridyl nitrogen atoms has been recently observed for the first time in a similar complex of piroxicam, $[Bu_2Sn(Pir)]_n$, and tenoxicam, $[Bu_2Sn(ten)]_n$, where the ligand exists also in its doubly deprotonated form.[7] These

 © 2003 Wiley-VCH Verlag GmbH & Co. KGaA, Weinheim

Table 3. Inter-hydrogen bonding, non-hydrogen, π−π and C−H-π interactions

Compound **1**				
D−H···A	*d*(D−H)	*d*(H···A)	*d*(D···A)	<(DHA)
C(2A)−H(2A3)···O(31)^{i}	0.96	2.57	3.380(7)	142.2
C(6′)−H(6′)···O(12)^{i}	0.93	2.39	3.072(7)	130.2
C(1A)−H(1A3)···O(11)^{ii}	0.96	2.51	3.315(8)	141.7
C(1A)−H(1A3)···Cl(6)^{iii}	0.96	3.02	3.821(7)	142.1
Cg(I) (ρ) Cg(J)[a]	Cg−Cg[b]	β≅[c]	CgI-Perp[d]	CgJ-Perp[e]
Cg(5) (ρ) Cg(2)^{iii}	3.798	15.05	3.668	3.461
		H···Cg	X···Cg	C−H···Cg
C(1A) −H(11A) → Cg(3)^{i}		3.382	92.98	3.563
C(1A) −H(12A) → Cg(3)^{i}		2.882	128.81	3.563
C(2A) −H(21A) → Cg(2)^{iv}		3.344	106.61	3.734
Compound **2**				
D−H···A[f]	*d*(D−H)	*d*(H···A)	*d*(D···A)	<(DHA)
C(21A)−H(21B)···Cl(6B)^{v}	0.96	2.93	3.815(12)	154
C(1AB)−H(1A4)···Cl(6B)^{v}	0.97	2.94	3.835(11)	154
C(21B)−H(21E)···Cl(6A)^{vi}	0.96	2.95	3.850(12)	156
C(2AA)−H(2A2)···O(12B)^{vii}	0.97	2.42	3.303(15)	152
Sn(1A)···--O(31B)^{vii}			2.953(7)	
Sn(1B)···--O(31A)^{viii}			2.971(7)	

[a] Where Cg(2), Cg(3) and Cg(5) are referred to the centroids S(5)−C(4A)−C(7A)−C(7)−C(6), O(4)−C(4)−C(3)−C(31)−N(31) and N(1′)−C(2′)−C(3′)−C(4′)−C(5′)−C(6′) for **1** respectively. [b] Cg−Cg is the distance between ring centroids. [c] β is the angle Cg(I)−Cg(J) or Cg(i)−Me vector and normal to plane I (°). [d] CgI-Perp is the perpendicular distance of Cg(I) on ring J. [e] CgJ-Perp is the perpendicular distance of Cg(J) on ring I. [f] D is donor and A is acceptor; symmetry transformations used to generate equivalent atoms, (i) $2-x$, $-1/2+y$, $2-z$; (ii) $-x+2$,$y-1/2$, $-z+1$; (iii) $x-1$, y, z; (iv) x, y $1+z$; (v) $1-x$, $2-y$, $-z$; (vi) $1-x$, $2-y$, $-z$; (vii) $1+x$, $-1+y$, z; (viii) $-1+x$, $1+y$, z.

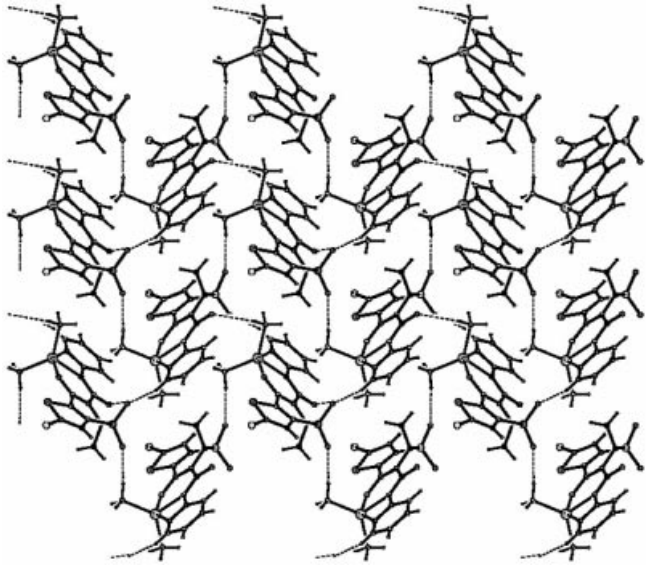

Figure 3. Packing diagram of the complex **1** viewed along the *a* axis of the unit cell, showing intermolecular interactions.

conclusions are confirmed by the ^{13}C NMR spectrum where the signal corresponding to C(4) disappears while the signals to C(3) and C(5) show downfield shift. The bond development of the N(1′) atom with the metal leads to a downfield shift by 6.0 ppm of the C(6′) and C(3′) while the C(4′) and C(5′) shift in the opposite direction by 2.0 ppm.

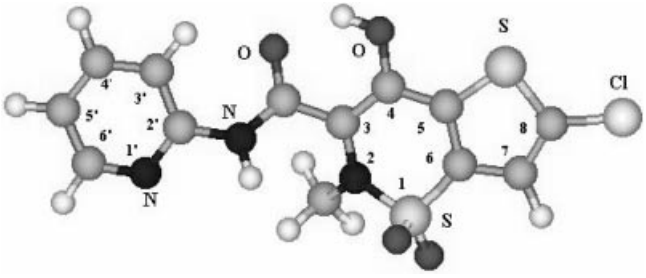

Figure 4. Fully AM1-optimised geometry of the neutral lornoxicam (ΔH_f = −48.28 kcal mol^{-1}; dipole moment = 3.98 Debye) in the gas state (Hyperchem 6.0[10]).

Electronic Spectroscopy

The electronic spectrum of H_2lorn in DMF solution exhibits two broad bands at ca. 398 and 273 nm. The band at 398 nm is assigned to a π → π* and that at 273 nm to a π → π* transition. The very broad band at ca. 400 nm is assignable to a HOMO → LUMO transition. The HOMO orbital (−10.972 eV) is composed of p_z orbitals from Cl 6% (+), C(8)p_z 12% (−), C(5)p_z 12% (+), C(6)p_z 11% (+), C(7)p_z 10% (−), C(4)p_z 6% (−), C(3)p_z 18% (−), N(2)p_z 8% (+) and the LUMO orbital (−9.261) is composed of p_z orbitals from C(6)p_z 5% (+), C(2′)p_z 11% (−), C(4′)p_z 14%

 © 2003 Wiley-VCH Verlag GmbH & Co. KGaA, Weinheim

(+), C(6′)p_z 6% (−), N(1′)p_z 11% (+), C(4) p_z 10% (−),C(10) p_z 17% (+). The HOMO orbital is π-centred on the sulfonamide and thiazine groups and the LUMO orbital is mainly π-centred on the pyridyl ring. H_2lorn and complexes **1** and **2** were studied by the extended-Hückel method using the CACAO PC Beta-Version 5.0 package geometry.[12] The molecular geometry was established by using the crystallographic coordinates of the complexes **1** and **2** and for H_2lorn by using the fully optimised in the gas state. The broad band centred at 376 and 373 nm respectively for **1** and **2** is assigned to a HOMO → LUMO transition. The extended-Hückel calculation using the crystallographic coordinates of **1** gives the following results: the HOMO orbital (−11.354eV) is composed of p_z orbitals from C(l6)p_z 5%(−), C(3)p_z 7%(+), C(6)p_z 9%(+), C(7)p_z 7%(+), C(7a)p_z 7%(−) and of p_y from C(3)p_y 11%(+); the LUMO orbital (−9.294 eV) is composed of p_y from C(4)p_y 10%(−), C(31)p_y 11%(+) and p_z orbitals from C(4) p_z 7%(−), C(7a)p_z 6%(+), C(31)p_z 9%(+). The extended-Hückel calculation using the crystallographic coordinates of **2** gives the following results: the HOMO for (−11.334 eV) is composed of p_x orbitals from C(3)p_x 10%(−), C(4a)p_x 6%(+), C(6)p_x 5%(−), C(7a)p_x 5%(+), C(7)p_x 5%(−) of p_z C(3)p_z 8%(+), C(4a)p_z 11%(−), C(6)p_z 8%(+), C(7a)p_z 5%(−), C(7)p_z 6%(+); the LUMO (−9.322 eV) is composed of p_x from C(4)p_x 10%(−), C(7a)p_x 4%(+), C(31)p_x 13%(+) and p_z orbitals from C(4)p_z 10%(+), C(6)p_z 3%(+), C(7a)p_z 5%(−), C(31)p_z 14%(−). The HOMO energy is isolated, suggesting that the assignment of the lowest energy electronic transition can be assigned to the computed HOMO−LUMO. Also, the similarity of the HOMO−LUMO gap from the calculations (2.060 and 2.012 eV for **1** and for **2** respectively) is reflected in the similarity of the first absorption band energy at ca. 375 nm in the complexes.

The HOMO−n (n = 1−6) levels for **1** are similar in energy, and are more stabilized (by ca. 1.4 eV) relative to the HOMO. The molecular orbital HOMO−6 has components of p_y (7%) and p_z (8%) from Sn, and p atomic orbitals from C(1a) and C(2a). Also, the molecular orbital HOMO-4 for **2** is stabilized by 1.01 eV relative to the HOMO and has components of p_x 6%(−) from Sn and p atomic orbitals from N(1′), C(3′), C(4′), C(5)′ and C(1b) This is consistent with a back donation from the metal to the π* orbitals of the ligand moieties.[13] The broad band at 292 and 295 nm for **1** and **2** is assigned to a combination of π → π* and M → L transitions. It has been found that the interaction of C−Sn σ orbitals and neighbouring p-type orbitals increases the HOMO level, which in turn favours electron transfer. Such σ-π interaction, σ−n and σ−σ interactions enjoy versatile applications in the field of electron transfer.[14]

Electrochemical Measurements

The ability of the complexes to either gain or to lose electrons was studied in anhydrous DMF solution by cyclic voltammetry. The ligand exhibits irreversible reduction peaks at −1.143 and −1.543 V. Irreversible reductions are seen at −0.764 and −1.267 V for **1**, and at −1.135 and 1.792 V for **2**. The electrochemical data suggest that the reduction of **1** and **2** might be regarded as being more or less centred on the ligand system. The electron transfers from the platinum cathode and is directed to the π* LUMO orbital. The reduction potential of **1** is less negative, while that of **2 is** more negative for the corresponding ligand and decreases in the order **1** < **H_2lorn** < **2**, indicating that the reduction process is more easily accomplished for 1 than for either free **H_2lorn** or **2**. The oxidation wave for **H_2lorn** is observed at +0.610 and that for **1** and **2** at 0.483 and 0.842 V, respectively. The oxidation is also associated with a ligand-based process and oxidized products are formed. The oxidation potentials of **1**, **2**, and **H_2lorn** increase in the order **2** > **H_2lorn** > **1**. Thus, both the reduction and oxidation processes in complex **1** are more easily accomplished than in either **2** or the parent drug. However, in the range from +1.5 to −2.5 V additional peaks are observed.

Experimental Section

All the chemicals used were of high purity and purchased from Fluka, Merck and Aldrich. Solvents were purified and dried according to standard procedures. Tenoxicam was a gift from "NYCOMED" NYCOMED DENMARK A/S and was recrystallised twice from ethanol. Elemental analyses were performed on a Carlo Erba EA (model 1108). Infrared and far-infrared spectra were obtained in KBr or polyethylene discs on a Perkin−Elmer Spectrum JX FT-IR spectrophotometer. A Jasco UV/Vis/NIR V 570 series spectrophotometer was used to obtain the electronic absorption spectra. ^{1}H (250.13 MHz) and ^{13}C (62.90 MHz) NMR spectra were recorded with a Bruker AMX-400 spectrometer at room temperature and referenced to DMSO or $CHCl_3$. UV spectra were recorded on a JASCO V-570 spectrophotometer. Electrochemical measurements were made using an AUTOLAB PGSTAT30 potentiostat with a platinum microsphere as working electrode, a platinum wire auxiliary electrode and an Ag/AgCl reference electrode in a three-electrode configuration. Ferrocene was added at the end of each experiment and used as an internal standard. All potentials are reported relative to an Ag/AgCl reference electrode and ferrocenium/ferrocene (Fe^+/Fc, $E_{1/2}$ = 0.173 V in DMF). Experiments were carried out on 1×10^{-3} M solutions of complex, under a nitrogen atmosphere, with Et_4NClO_4 (0.1 M) as supporting electrolyte (scan rate 100 mV s^{-1}).

Preparations

[$SnMe_2$(lorn)]$_n$ (1): $SnMe_2O$ (0.066 g, 0.4 mmol) was added to a solution of lornoxicam (H_2lorn) (0.150 g, 0.4 mmol) in benzene (25 cm^3) and the reaction mixture was refluxed for 7 h under a Dean−Stark trap. The resultant clear solution was rotary evaporated under vacuum to a small volume, chilled and triturated with diethyl ether to give a yellow solid that was redissolved (suspended) in dry diethyl ether and the same procedure was repeated twice. The final yellow product was filtered off and dried in *vacuo* over silica gel. (**1**) m.p. 260−262 °C; Yield 90%. $C_{15}H_{14}ClN_3O_4S_2Sn$ (518.6): calcd. C 34.31, H 2.70, N 8.10, S 9.92; found C 34.88, H 2.65, N 8.30, S 10.3. Crystals of **1** suitable for X-ray analysis were obtained by slow evaporation of a fresh EtOEt/CH_2Cl_2 solution.

[Sn(*n*-C_4H_9)$_2$(Hlorn)$_2$] (2): Sn(*n*-C_4H_9)$_2$O (0.099 g, 0.4 mmol) was added to a solution of lornoxicam (H_2lorn) (0.150 g, 0.4 mmol) in

 © 2003 Wiley-VCH Verlag GmbH & Co. KGaA, Weinheim

benzene (25 cm^3) and the reaction mixture was refluxed for 27 h under a Dean−Stark trap. The resultant clear solution was rotary evaporated under vacuum to a small volume, chilled and triturated with hexane to give a yellow solid that was redissolved (suspended) in hexane and the same procedure was repeated twice. The final light yellow product was filtered off and dried in *vacuo* over silica gel (**1**). M.p. 174−176 °C; Yield 66%. $C_{21}H_{26}ClN_3O_4S_2Sn$ (602.7): calcd. C 41.84, H 4.32, N: 6.97, S 10.65; found C 42.10, H 4.56, N 6.65, S 10.38. Crystals of **2** suitable for X-ray analysis were obtained by slow evaporation of a fresh C_6H_{12}/C_6H_6 solution.

Crystal Structure Determination of Complexes 1 and 2

X-ray diffraction data were collected on a KUMA KM4CCD κ-geometry diffractometer with a CCD detector,[15] by using graphite-filtered Mo-K_α radiation (λ = 0.71073 Å). The unit cell dimensions were calculated from the least-squares fit of 2163 (**1**) and 1450 (**2**) most intense reflections from the whole experiment. Relevant crystallographic data, together with data collection and structure refinement details, are listed in Table 1. The measurements were performed in six separate runs, four runs consisted of 133 frames, and two of 125 frames (ω width of each frame was 0.75°). The θ, κ and angles for the runs were chosen so as to cover the appropriate part of the Ewald sphere. Two reference frames were measured after every 50 frames of experiment; neither the geometry nor the intensity of the reflections in these frames changed significantly during the data collection. Intensity data were corrected for Lorentz and polarisation effects and converted into F^2's. These data were corrected for absorption and averaged with respect to the point group symmetry with SORTAV program.[15b] The structures were solved with SHELXS-97,[16] and SHELXL-97[16] was used for full-matrix least-squares refinement. The function $\Sigma w(0.5F_o1/2^2 - 0.5F_c1/2^2)^2$ was minimised, with $w^{-1} = [\sigma^2(F_o)^2 + A{\cdot}P^2 + B{\cdot}P]$ (where P = [max. (F_o^2, 0) + $2F_c^2$]/3). Final values for A and B are listed in Table 1. In **1** all the non-hydrogen atoms were refined anisotropically, in **2** − due to the large thermal motion of the butyl groups − only the first atoms of these groups (connected to Sn) were refined anisotropically, while the other three atoms from each butyl groups were refined isotropically, with fixed values for U_{iso}. The (relatively weak) constrains were also applied to the geometry of these groups. The attempts to resolve the apparent disorder of butyl groups were not successful. In both structures, hydrogen atoms were placed in calculated positions and refined as "riding mode", i.e. they followed the movements of their carrier atoms. The isotropic displacement parameters for hydrogen atoms were calculated as 1.2 times equivalent displacement parameters for respective carrier non-hydrogen atoms.

Calculations

A computational study with a AM1 parameterization scheme utilizing the Steepest Descent algorithm, as implemented in the HYPERCHEM 6.0 program, was used to investigate the prevailing isomer of free H_2lorn in the gas phase.[10] H_2lorn and the complexes **1** and **2** were studied by the extended-Hückel method using the CACAO PC Beta-Version 5.0 package geometry.[12] The molecular geometry was established by using the crystallographic coordinates of complexes **1** and **2** and for H_2lorn by using the fully optimised in the gas state.[12]

Supplementary Material

CCDC-193499 for **1** and CCDC-193498 for **2** contain the supplementary crystallographic data for this paper. These data can be obtained free of charge at www.ccdc.cam.ac.uk/conts/retrieving.html [or from the Cambridge Crystallographic Data Centre, 12, Union Road, Cambridge CB2 1EZ, UK; Fax: (internat.) +44-1223/336-033; E-mail: deposit@ccdc.cam.ac.uk].

Acknowledgments

We thank NYCOMED DENMARK A/S for the gift of lornoxicam, and also the GSRT for the funding of a bilateral project, Research and Technological Co-operation Greece-Poland, and for the funding support from the research program PENED 99 ED 442. We thank the Centrum of NMR of the University of Ioannina.

[1] J. A. Balfour, A. Fitton, L. B. Barradell, *Drugs* **1996**, *51*, 639.
[2] T. P. Pruss, H. Stroissning, S. Radhofer-Welte, W. Wendtlandt, N. Mehdi, F. Takacs, H. Fellier, *Postgrad. Med. J.* **1990**, *66 (Suppl.* 4), 18.
[3] [3a] R-S. Tsai, P-A. Carrupt, N. El Tayar, Y. Giroud, P. Andrade, B. Testa, F. Brèe, J.-P. Tillement, *Helv. Chim. Acta* **1993**, *76*, 842. [3b] M. R Caira, L. R. Nassimbeni, M. Timme, *J. Pharm. Scienc.* **1995**, *84*, 884. [3c] E. Bernhard, F. Zimmermann, *Arzneim-Forsch. Drug Res.* **1984**, *34*, 647.
[4] [4a] J. J. Zuckerman (Ed.), "*Organotin Compounds: New Chemistry and Applications",* Advances in Chemistry Series, no 157, American Chemical Soc., Washington, **1976**. [4b] C. J. Evans, S. Karpel, "*Organotin Compounds in Modern Technology",* J. Organomet. Chem. Library 16, Elsevier, **1985**. [4c] S. J. Blunden, P. A. Cusack, R. Hill, "*Industrial Uses of Tin Chemicals",* Royal Society of Chemistry. London, **1985**. [4d] A. J. Crowe, in M. Gielen (Ed.), *Metal-Based Antitumour Drugs*, vol. 1, Freund, London, **1989**.
[5] [5a] M. Gielen, *Coord. Chem. Rev.* **1996**, *15*, 41. [5b] D. Kovala-Demertzi, P. Tauridou, U. Russo, M. Gielen, *Inorg. Chim. Acta* **1995**, *239*, 177. [5c] V. Dokorou, Z. Ciunik, U. Russo, D. Kovala-Demertzi, *J. Organom. Chem.* **2001**, *630*, 205. [5d] D. Kovala-Demertzi, V. Dokorou, Z. Ciunik, N. Kourkoumelis, M. A. Demertzis, *Appl. Organom. Chem.* **2002**, *16*, 360.
[6] [6a] D. Kovala-Demertzi, A. Theodorou, M. A. Demertzis, C. Raptopoulou, A. Terzis, *J. Inorg. Biochem.* **1997**, *65*, 151. [6b] A. Theodorou, M. A. Demertzis, D. Kovala-Demertzi, E. A. Lioliou, A. A. Pantazaki, D. A. Kiriakidis, *Biometals* **1999**, *12*, 67. [6c] D. Kovala-Demertzi, *J. Inorg. Biochem.* **2000**, *79*, 153.
[7] [7a] D. Kovala-Demertzi, N. Kourkoumelis, A. Koutsodimou, A. Moukarika, E. Horn, E. R. T. Tiekink, *J. Organomet. Chem.* **2001**, *620*, 194. [7b] M. A. Demertzis, S. K. Hadjikakou, D. Kovala-Demertzi, A. Koutsodimou, M. Kubicki, *Helvet. Chim. Acta* **2000**, *83*, 2787. [7c] S. K. Hadjikakou, M. A. Demertzis, J. R. Miller, D. Kovala-Demertzi, *J. Chem. Soc., Dalton Trans.* **1999**, 663.
[8] A. Addison, R. T. Nageswara, J. Reedijk, J. Van Rijn, G. C. Verschoor, *J. Chem. Soc., Dalton.* **1984**, 1349.
[9] [9a] T. Steiner, B. Lutz, J. van der Maas, A. M. M. Schreurs, J. Kroon, M. Tamm, *Chem. Commun.* **1998**, 171. [9b] T. Steiner, M. Tamm, A. Grzegorzewski, N. Schulte, N. Veldman, A. M. M. Schreurs, J. Kroon, J. van der Maas, B. Lutz, *J. Chem. Soc., Perkin Trans.* **1996**, *2*, 2441. [9c] M. C. Etter, *Acc. Chem. Res.* **1990**, *23*, 120. [9d] G. R. Desiraju, *Acc. Chem. Res.* **1991**, *24*, 290.
[10] Hyperchem, Release 6.01 for Windows, Molecular Modeling System, 2000 Hypercube, Inc.
[11] [11a] L. J. Bellamy, *The Infrared Spectra of Complex Molecules*, Chapman and Hall, London, 1975. [11b] K. Nakamoto, *Infrared and Raman Spectra of Inorganic and Coordination Compounds* 4th ed., John Wiley & Sons, New York, **1980**.
[12] [12a] C. Mealli, D. Proserpio, CACAO PC Beta-Version 5. **1998**. [12b] C. Mealli, D. Proserpio, *J. Chem. Educ.* **1990**, *11*, 440.

 © 2003 Wiley-VCH Verlag GmbH & Co. KGaA, Weinheim

[13] [13a] D. Di Leo, F. Berrettini, R. Cini, *J. Chem. Soc., Dalton Trans.* **1998**, 1993. [13b] D. Kovala-Demertzi, N. Kourkoumelis, M. A. Demertzis, J. R. Miller, C. Frampton, D. X. West, *Eur. J. Inorg. Chem.* **2000**, 727.
[14] J-I Yoshida, K. Nishiwaki, *J. Chem. Soc., Dalton Trans.* **1998**, 2589.
[15] [15a] *CrysAlisRed v. 162*, KUMA Diffraction, Wroclaw, Poland, **2000**. [15b] R. H. Blessing, *J. Appl. Crystallogr.* **1989**, *22*, 396.
[16] [16a] G. M. Sheldrick, *Acta Crystallogr., Sect. A* **1990**, *46*, 467. [16b] G. M. Sheldrick, SHELXL-97, Program for the Refinement of Crystal Structures, University of Göttingen, Germany, **1997**.

Received September 15, 2002

 © 2003 Wiley-VCH Verlag GmbH & Co. KGaA, Weinheim

Exchange Interactions and Covalency in Dinuclear Complexes of Iron(III) and Gallium(III) Containing the Redox-Noninnocent Ligand 1,2-Bis(3,5-di-*tert*-butyl-2-hydroxyphenyl)oxamide

Udo Beckmann,[a] Eckhard Bill,[a] Thomas Weyhermüller,[a] and Karl Wieghardt*[a]

Keywords: Iron / Gallium / EPR spectroscopy / Moessbauer spectroscopy / Radicals / Magnetic properties / Exchange interactions

The dinucleating ligand 1,2-bis(3,5-di-*tert*-butyl-2-hydroxyphenyl)oxamide [H_4(bbpo)] has been synthesized. From its reaction with $GaCl_3$ or $FeCl_3$ in CH_3OH/NaOH the salts $[N(nBu)_4]_2[M_2^{III}(bbpo)Cl_4]$ [M = Ga (**1**), Fe (**2**)] have been isolated as crystalline solids upon addition of $[N(nBu)_4]Cl$. Complexes **1** and **2** have been characterized by single-crystal X-ray crystallography. Cyclic voltammetry established that both species undergo two successive, reversible one-electron oxidations in CH_2Cl_2 {0.10 M $[N(nBu)_4]PF_6$} which are shown to be ligand-centered: one and then two *N*,*O*-coordinated *o*-iminobenzosemiquinonate π-radicals form which couple antiferromagnetically with the high-spin ferric ions in **2**. Thus, the monoanion of **2** has an $S_t = {}^1/_2$ ground state. The complexes have been characterized by Mössbauer, UV/Vis, and EPR spectroscopy.

(© Wiley-VCH Verlag GmbH & Co. KGaA, 69451 Weinheim, Germany, 2003)

1. Introduction

In a recent series of publications[1−6] we have shown that *o*-aminophenolates and their ring-substituted derivatives are redox-noninnocent ligands in coordination chemistry. In particular, we established that high-quality X-ray crystallography allows the unequivocal determination of the protonation and oxidation level of a given *N*,*O*-coordinated ligand in a transition metal complex and that it is possible to discern between an *N*,*O*-coordinated *o*-iminophenolate(−), $(L^{IP})^{2-}$, and its one-electron oxidized form, the *o*-iminobenzosemiquinonate(1−) π-radical, $(L^{ISQ})^{-}$.

When such a radical ligand ($S_{rad} = {}^1/_2$) is coordinated to a paramagnetic transition metal ion with an incompletely filled t_{2g} subshell, very strong intramolecular antiferromagnetic exchange coupling between the radical spin and the t_{2g}^n configuration is observed. Thus, $[Cr^{III}(L^{ISQ})_3]$,[3] containing a Cr^{III} ion with t_{2g}^3 configuration and three $(L^{ISQ})^{1-\cdot}$ radical anions, possesses an $S_t = 0$ ground state, whereas its cobalt(III) analogue[1] (t_{2g}^6) possesses an $S_t = {}^3/_2$ ground state because the three ligand spins couple ferromagnetically.

Here we describe the synthesis of a new dinucleating ligand that contains two *o*-aminophenolate units, which, in principle, should be oxidizable to two *o*-iminobenzosemiquinonate units. The ligand is the tetraanion of 1,2-bis(3,5-di-*tert*-butyl-2-hydroxyphenyl)oxamide [H_4(bbpo)], shown in Scheme 1. If both bound metal ions are paramagnetic, e.g. high-spin Fe^{III}, exchange coupling between these ions and the ligand π-radicals and coupling between the two metal ions containing units, which are bridged by an oxamide unit, should lead to various ground states. As we will show here, this is indeed the case.

[a] Max-Planck-Institut für Strahlenchemie,
Stiftstrasse 34−36, 45470 Mülheim an der Ruhr, Germany

2. Results and Discussion

2.1. Synthesis and Characterization of Complexes 1 and 2

The reaction of 3,5-di-*tert*-butyl-2-(hydroxyamino)benzene (2 equiv.) [7] with oxalyl chloride (1 equiv.) in diethyl ether in the presence of the base triethylamine (2 equiv.) affords the ligand 1,2-bis(3,5-di-*tert*-butyl-2-hydroxyphenyl)oxamide [H_4(bbpo)] in good yields (Scheme 1).

From the reaction of deprotonated H_4(bbpo) in CH_3OH/NaOH solution and 2 equiv. of $GaCl_3$ or $FeCl_3$ the yellow and green crystalline salts of $[N(nBu)_4]_2[M_2^{III}(bbpo)Cl_4]$ [M = Ga^{III} (**1**), Fe^{III} (**2**), respectively] were obtained upon addition of $[N(nBu)_4]Cl$.

In accord with the structures shown in Scheme 1 for the dianions of **1** and **2** the infrared spectra do not show ν(N−H) or ν(OH) stretching frequencies but prominent ν(C=O) stretching frequencies at 1633 cm^{-1} for **1** and at 1611 cm^{-1} for **2**.

The electro spray mass spectra of **1** and **2** in CH_3OH in the negative ion detection mode display peaks at $m/z = 737$ for **1** and at $m/z = 709$ for **2**, corresponding to the monoanions $[M_2^{III}(bbpo)Cl_3]^-$ (M = Ga, Fe, respectively). Both peaks display the correct isotope pattern.

Our attempts to synthesize a pure sample of the paramagnetic heterodinuclear complex $[N(nBu)_4]_2[Ga^{III}$-

 © 2003 Wiley-VCH Verlag GmbH & Co. KGaA, Weinheim DOI: 10.1002/ejic.200200516

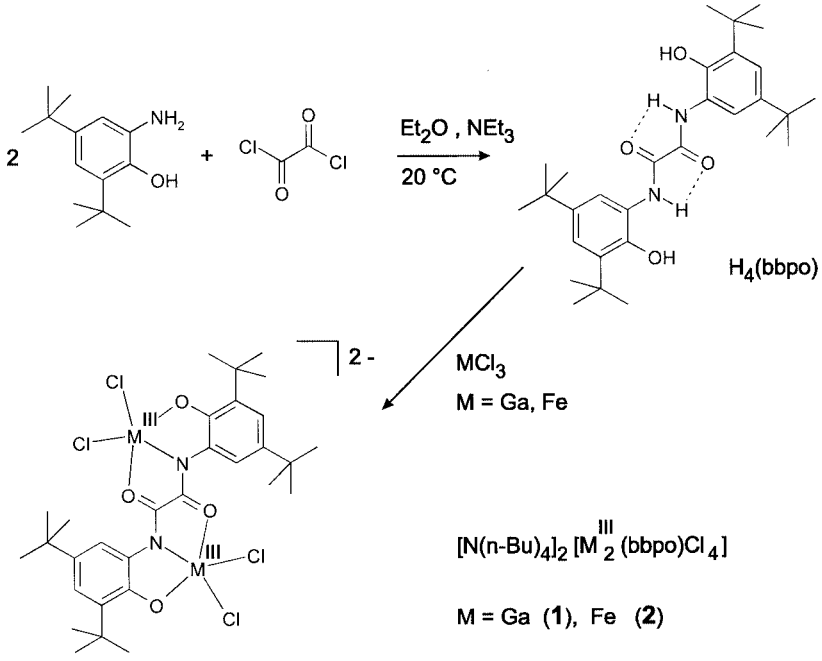

Scheme 1

$Fe^{III}(bbpo)Cl_4$], which would reveal the rhombicity, *E*/*D*, of a single high-spin ferric site in its EPR spectrum, yielded samples contaminated by **1** and **2**. Nevertheless, we found that in equimolar methanolic solutions of **1** [the pure gallium(III) species] and $FeCl_3$ the heterodinuclear species $[Ga^{III}Fe^{III}(bbpo)Cl_4]^{2-}$ is generated as well as **2**. The ESI (negative ion) mass spectra of such solutions clearly show the presence of $[GaFe(bbpo)Cl_3]^-$ at m/z = 724 (Z = 1) and of $[GaFe(bbpo)Cl_4]^{2-}$ at m/z = 379.5 (Z = 2). Both peaks display the correct isotope pattern. The signals of the corresponding homodinuclear monoanions $[M_2^{III}(bbpo)Cl_3]^-$ (M = Ga and Fe) are also present. Addition of $[N(nBu)_4]Cl$ to such solutions initiated the precipitation of a mixture of **1**, **2**, and $[N(nBu)_4]_2$ $[GaFe(bbpo)Cl_4]$. The latter is isomorphous and isostructural with **1** and **2** as was established by X-ray crystallography of a hand-picked, brown single crystal that contained a Ga/Fe ratio of ca. 1:1 (X-ray fluorescence analysis).

2.2. Crystal Structures of 1 and 2

The crystal structures of **1** and **2** have been determined at 100(2) K by single-crystal X-ray crystallography using

Table 1. Crystallographic data for **1**, and **2**

	1	**2**
Empirical formula	$C_{62}H_{112}Cl_4Ga_2N_4O_4$	$C_{62}H_{112}Cl_4Fe_2N_4O_4$
Formula mass	1258.80	1231.06
Space group	$P2_1/c$, no. 14	$P2_1/c$, no. 14
a [Å]	15.493(2)	15.3419(12)
b [Å]	14.182(2)	14.3702(10)
c [Å]	17.059(3)	17.1730(14)
β [°]	111.57(2)	112.29(2)
V [Å]	3485.7(9)	3503.2(5)
Z	2	2
T [K]	100(2)	100(2)
$\rho_{calcd.}$ [g cm^{-3}]	1.199	1.167
Diffractometer used	Nonius Kappa-CCD	Nonius Kappa-CCD
Refl. collected/$2\theta_{max}$ [°]	41071/50.00	60418/60.00
Unique refl./[$I > 2\sigma(I)$]	6137/5087	10221/7783
No. of param./restraints	343/3	382/16
μ(Mo-K_α) [cm^{-1}]	9.70	6.10
$R1$[a]/goodness of fit[b]	0.0945/1.238	0.0465/1.024
$wR2$[c] [$I > 2\sigma(I)$]	0.1982	0.1247

[a] Observation criterion: [$I > 2\sigma(I)$]. $R1 = \Sigma||F_o| - |F_c||/\Sigma|F_o|$. [b] GooF = $\{\Sigma[w(F_o^2 - F_c^2)^2]/(n - p)\}^{1/2}$. [c] $wR2 = \{\Sigma[w(F_o^2 - F_c^2)^2]/\Sigma[w(F_o^2)^2]\}^{1/2}$ where $w = 1/\sigma^2(F_o^2) + (aP)^2 + bP$ and $P = (F_o^2 + 2F_c^2)/3$.

 © 2003 Wiley-VCH Verlag GmbH & Co. KGaA, Weinheim

Mo-K_α radiation. Table 1 gives crystallographic data and Table 2 summarizes selected bond lengths and angles. Figure 1 shows the structure of the dianion in crystals of **2**; the structure of **1** is very similar and not shown.

Table 2. Selected bond lengths [Å] and angles [°] of the dianions in crystals of **1** and **2**

	1	**2**
M−O1	1.921(5)	1.929(2)
M−O2	2.110(5)	2.080(2)
M−Cl1	2.205(2)	2.253(1)
M−Cl2	2.198(2)	2.246(1)
M−N1	1.969(6)	2.049(2)
N1−C7	1.308(9)	1.310(2)
N1−C6	1.402(9)	1.403(2)
O1−C1	1.350(9)	1.340(2)
O2−C7	1.268(8)	1.273(2)
C1−C2	1.41(1)	1.414(3)
C1−C6	1.42(1)	1.414(2)
C2−C3	1.39(1)	1.394(3)
C3−C4	1.39(1)	1.401(3)
C4−C5	1.38(1)	1.391(3)
C5−C6	1.39(1)	1.387(3)
C7−C7*	1.50(1)	1.509(4)
O1−M−N1	83.3(2)	78.8(1)
O1−M−O2*	161.8(2)	154.9(1)
N1−M−O2*	79.5(2)	77.9(1)
O1−M−Cl2	96.6(2)	96.9(1)
N1−M−Cl2	129.1(2)	133.6(1)
O2*−M−Cl2	89.6(1)	92.5(1)
O1−M−Cl1	100.9(2)	101.5(1)
N1−M−Cl1	114.0(2)	108.2(1)
O2*−M−Cl1	91.6(2)	94.5(1)
Cl2−M−Cl1	115.9(1)	117.82(2)

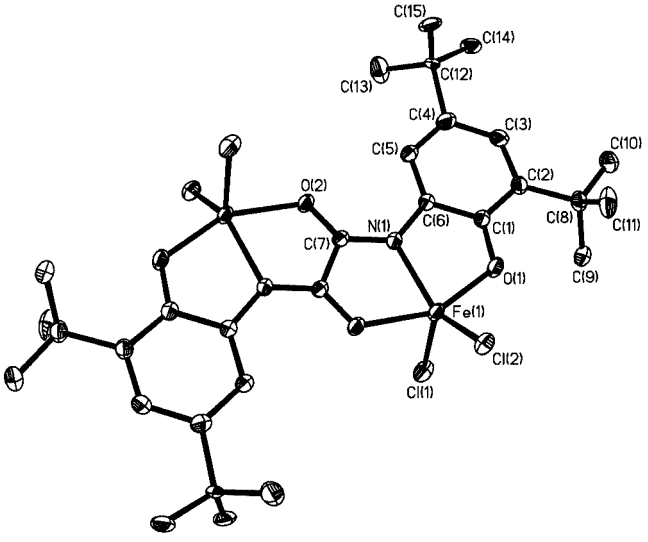

Figure 1. ORTEP representation of the structure of the dianion $[Fe^{III}_2(bbpo)Cl_4]^{2-}$ in crystals of **2**; that of the dianion in **1** is similar and not shown.

Both structures consist of well-separated tetra-*n*-butylammonium cations and dinuclear dianions (ratio 2:1).

The metal ions Ga^{III} and Fe^{III} in **1** and **2**, respectively, are five-coordinate with a distorted trigonal-bipyramidal MCl_2NO_2 polyhedron, where the two chloride ions and the nitrogen donor N1 occupy basal positions whereas the two oxygen donors O1 and O2 are in the remaining two axial sites. The Fe−Cl, Fe−N and Fe−O bond lengths are quite long and indicate a high-spin d^5 configuration at the ferric ions in **2**. The corresponding bonds in **1** are similar since the ionic radii of five-coordinate Ga^{III} and high-spin Fe^{III}, 0.69 and 0.72 Å, respectively, are also similar.[9]

We note that the metrical details of the coordinated *o*-aminophenolate parts of the ligand $(bbpo)^{4-}$ clearly indicate the presence of two *N*,*O*-coordinated *o*-iminophenolato(2−) halves.[5] The six C−C bond lengths of the phenyl rings are, within experimental error, equidistant; no evidence for a quinoid-type distortion typical for *o*-iminobenzosemiquinonato(1−) π-radicals was detected.[1−6] Similarly, the C1−O1 bonds at ca. 1.35 Å are long and typical for phenolates. The two corresponding C6−N1 bonds at 1.40 Å are also long, indicating single bonds.

2.3. Magnetic Properties of 2

The diiron complex **2** has been studied by magnetometry and applied-field Mössbauer spectroscopy. In contrast to the diamagnetic digallium analog **1**, which shows a "normal" ^{1}H NMR spectrum without paramagnetically shifted lines (see Exp. Sect.), the iron compound has a substantial magnetic moment at ambient temperature. Figure 2 (top) displays the temperature dependence of the magnetic moment of solid **2** recorded in the range 2−300 K using a SQUID magnetometer and an external field of 1 T. The molar susceptibilities were corrected for underlying diamagnetism by use of tabulated Pascal constants ($\chi_{dia} = -825 \times 10^{-6}$ cm^3·mol^{-1}). The magnetic moment decreases monotonically from ca. 7 μ_B at 300 K to about 0.5 μ_B at 4 K. The solid line in Figure 2 represents a best fit of the data using the spin Hamiltonian in Equation (1) with $S_1 = S_2 = {}^5/_2$, $J = -9.7 \pm 0.5$ cm^{-1}, $g = 2.016$, $|D| = 1.6 \pm 0.3$ cm^{-1}, and $E/D = 0.33$ for both identical iron sites.

$$H = -2J\,\vec{S}_1 \cdot \vec{S}_2 + \sum_{i=1,2}\{D_i[S^2_{z,i} - \tfrac{1}{3}S_i(S_i+1) + {}^{E}\!/_{D}(S^2_{x,i} - S^2_{y,i})] + g_i\mu_B\vec{S}_i \cdot \vec{B}\} \quad (1)$$

Thus, the spins of the two ferric ions in **2** are weakly antiferromagnetically coupled; the complex possesses an EPR-silent $S_t = 0$ ground state which, however, is not very well isolated from paramagnetic excited states. Thus, the applied field can induce a weak magnetic moment even at 2 K. This is best observed in multi-field measurements with variable-temperature data sampled on a $1/T$ scale (inset of Figure 2). The increasing level of magnetization with increasing field at low temperatures (arrows in the inset) indicates multiplet-mixing by competing exchange and single-ion zero-field splitting (ZFS). Increasing temperature (to the left in the inset) leads to Boltzmann population of the excited S = 1, 2 states and increasing magnetization. The decline of M_{mol} below $\mu_B B/kT = 0.1$ represents the usual $1/T$ behavior

 © 2003 Wiley-VCH Verlag GmbH & Co. KGaA, Weinheim

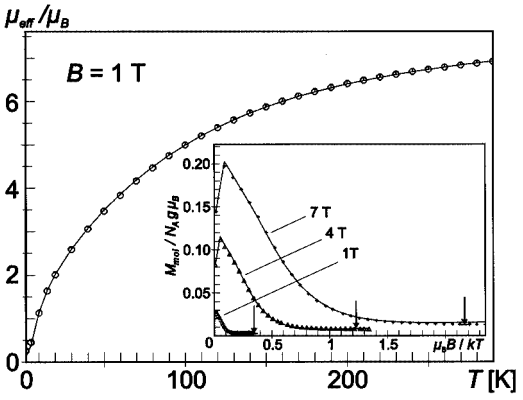

Figure 2. Temperature dependence of the magnetic moment, μ_{eff}, of **2** measured at $B = 1$ T; inset: variable-temperature variable-field plot of magnetization of **2**; the arrows indicate the induced magnetization of "$S_t = 0$" at low temperatures; see text for simulation parameters (solid lines)

at high temperatures due to equal population of the magnetic M_s sublevels. Systematic simulations of the temperature dependence at multiple fields yields a sensitive and unique measure of the exchange coupling constant, $J = -9.7 \pm 0.5$ cm^{-1}, and the ZFS parameter, $|D| = 1.6 \pm 0.3$ cm^{-1}. A similar but weaker antiferromagnetic coupling has been reported for the μ-oxalato-bridged dinuclear species $[Fe^{III}_2(\mu\text{-ox})(ox)_4]^{4-}$, with J established as -3.3 cm^{-1}.[8] The rhombicity parameter E/D in the analysis above was taken from an X-band EPR spectrum of the mixed-metal in complex $[Ga^{III}Fe^{III}(bbpo)Cl_4]^{2-}$ in CH_3OH solution, which selectively probes the Fe^{III} moiety in the bbpo ligand. The spectrum measured at 15 K shows the $g = 4.27$ signal (Figure 3) that is typical of Fe^{III}, $S = {}^5/_2$ with full rhombicity, $E/D = 0.33$. Note that at 15 K both "contaminants" of the Ga/Fe complex, **1** and **2**, are EPR-silent.

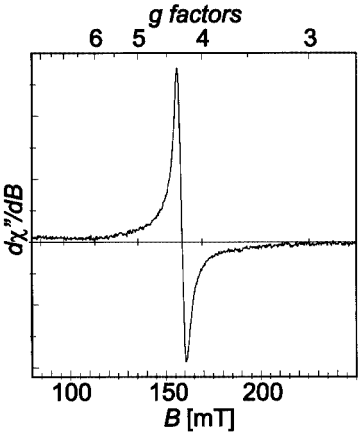

Figure 3. X-band EPR spectrum of $[Ga^{III}Fe^{III}(bbpo)Cl_4]^{2-}$ in CH_3OH solution at 15 K (conditions: frequency 9.4637 GHz; power 20.1 μW; modulation frequency 100 kHz; modulation amplitude 2.49 mT)

The zero-field Mössbauer spectrum of solid **2** at 80 K displays an asymmetric doublet with an isomer shift of 0.45 mm·s^{-1} and a quadrupole splitting of 0.97 mm·s^{-1} that are typical for high-spin ferric ions (Figure 4, top). The lines are broadened by residual spin relaxation close to the limit of fast rates. Magnetically perturbed spectra recorded at 1.8 K with fields of 3 and 7 T applied perpendicular to γ (Figure 4, center and bottom) show almost diamagnetic appearances, as expected for an electronic $S_t = 0$ ground state. The presence of induced magnetization can be visualized from the small but significant deviation of a diamagnetic simulation with "$S = 0$" from experiment (dotted lines). A spin Hamiltonian simulation based on Equation (1) with the above parameters gives a slightly better fit of the 3 and 7 T measurements. As expected, the small internal field in the latter case is opposite to the applied field. The corresponding Mössbauer parameters are summarized in Table 3.

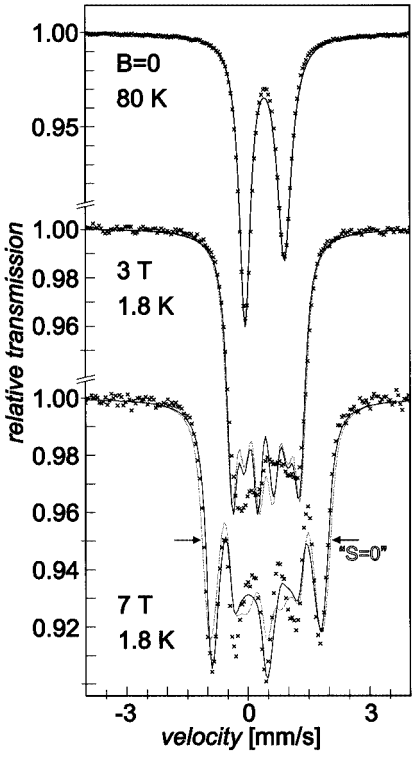

Figure 4. Zero- and applied-field Mössbauer spectra of solid **2**; parameters of the spin-Hamiltonian simulations based on Equation (1) (solid lines) are given in Table 3; the dotted lines represent an alternative diamagnetic simulation ($S = 0$) with the same electric hyperfine parameters

Hence, the magnetic Mössbauer spectra also demonstrate the effect of competing ZFS and exchange interaction for the low-lying spin multiplets of **2**. In addition, the symmetry of the splitting pattern reveals a large asymmetry parameter, $\eta = 0.9 \pm 0.1$, for the electric field gradient (efs) tensor, in agreement with the large rhombicity of the sites. The Mössbauer data agree fully with the electronic structure of **2** consisting of two identical, antiferromagnetically coupled high-spin ferric ions.

2.4. Electro- and Spectroelectrochemistry

The cyclic voltammograms (CV) of complexes **1** and **2** were recorded at 20 °C in CH_2Cl_2 solutions (0.10 M

 © 2003 Wiley-VCH Verlag GmbH & Co. KGaA, Weinheim

Table 3. Mössbauer and spin Hamiltonian parameters for the di- and monoanion of **2**

	$[Fe^{III}_2(bbpo)Cl_4]^{2-}$	$[Fe^{III}_2(bbpo^{ox1})Cl_4]^{1-}$	
		Fe^1	Fe^2
S_{Fe} [a]	$^5/_2$, $^5/_2$	$^5/_2$	$^4/_2$
S_t [b]	0	$^1/_2$	
δ [mm·s^{-1}] at 4.2 K[c]	0.45	0.45	0.49
ΔE_Q [mm·s^{-1}] at 4.2 K[d]	0.98	0.98	−1.15
Γ [mm·s^{-1}] at 4.2 K[e]	0.28	0.28	0.28
$A_{exp}/g_N\beta_N$ [T][f]	21.35	21.35	(21.71, 22.2, 21.67)
$A_{local}/g_N\beta_N$ [T][f]	21.35	21.35	18.73[l]
η[g]	0.9	0.9	0.9
α,β,γ [deg][h]	0; 0; 0	10; 6; 0	11; 65; 0
$\lvert D\rvert$ [cm^{-1}][i]	1.6	1.6	2.4
E/D[j]	0.33	0.33	0.33
J [cm^{-1}][k]	−9.7	−11.5	

[a] Local spin at a single Fe site. [b] Ground state. [c] Isomer shift vs. α-Fe at 298 K. [d] Quadrupole splitting; [e] Line width at half-height. [f] Mössbauer hyperfine coupling constants (isotropic part). [g] Asymmetry parameter; [h] Euler angles. [i] Zero-field splitting parameter from susceptibility measurements of **2**. [j] Rhombicity from the EPR spectrum of $[GaFe(bbpo)Cl_4]^{2-}$. [k] Heisenberg coupling constant from susceptibility measurements of **2**. [l] $A_{local} = {}^6/_7\, A_{exp}$.

$[N(n\mathrm{Bu})_4]PF_6$) at a glassy carbon working electrode and an $Ag/AgNO_3$ reference electrode. Ferrocene was used as an internal standard; all potentials are referenced versus the ferrocenium/ferrocene couple (Fc^+/Fc). Figure 5 displays the CVs of **1** (top) and **2** (bottom).

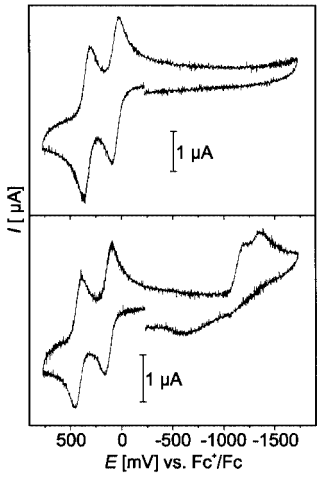

Figure 5. Cyclic voltammograms of **1** (top) and **2** (bottom) in CH_2Cl_2 {0.10 M $[N(n\mathrm{Bu})_4]PF_6$} at 248 K at a scan rate of 100 mV s^{-1} (glassy carbon working electrode; $Ag/AgNO_3$ reference electrode; ferrocene internal standard)

Both **1** and **2** display two reversible one-electron transfer waves in the potential range −0.5 to +0.75 V. The two redox potentials $E^1_{1/2}$ and $E^2_{1/2}$ are observed at +0.077 and +0.354 V for **1**; and at +0.156 and 0.454 V for **2**. Coulometric measurements at appropriately fixed potentials established that both processes correspond to two successive one-electron oxidations of **1** and **2**, respectively, as shown in Equation (2). We will show below that both oxidations are ligand-centered processes that generate the mono- and diradicals $(bbpo^{ox1})^{3-}$ and $(bbpo^{ox2})^{2-}$ shown in Scheme 2.

$$[M^{III}_2(bbpo)Cl_4]^{2-} \underset{+e}{\overset{-e}{\rightleftharpoons}} [M^{III}_2(bbpo)^{ox1\cdot}Cl_4]^{1-} \underset{+e}{\overset{-e}{\rightleftharpoons}} [M^{III}_2(bbpo)^{ox2\cdot-}Cl_4]^{0} \qquad (2)$$
$$E^1_{1/2} \qquad E^2_{1/2}$$

Upon increasing the potential range scanned to −1.7 V the resulting CV of **1** did not show an additional redox process but **2** displayed two successive, irreversible, probably metal-centered reductions: $Fe^{III} \rightarrow Fe^{II}$ at ca. −1.1 and ca. −1.4 V.

Since the coulometric measurements had established that the monoanions, and to a lesser degree the neutral forms of **1** and **2**, are stable in solution their electronic spectra were recorded. The neutral species of **2** proved to be unstable. Figure 6 shows the electronic spectrum of **1** and of its one-electron oxidized form in CH_2Cl_2. As expected, the spectrum of **1** is featureless at $\lambda > 500$ nm but shows an intense absorption at 405 nm (8.6×10^3 M^{-1}·cm^{-1}) which decreases and splits into two bands upon oxidation [393 (7.1×10^3), 412 (7.5×10^3)]. Remarkably, oxidation also yields a broad absorption at 908 nm (730 M^{-1}·cm^{-1}) that is typical for the *o*-iminobenzosemiquinonate(1−) radical.[2]

Electrochemical oxidation the monoanion to the neutral species $[Ga_2(bbpo^{ox2})\ Cl_4]$ is shown in Figure 6 (bottom). Roughly, the absorption maxima of the monoanion double their intensity: 382 sh (7.2×10^3), 402 (8.9×10^3), 414 sh, 421 (9.7×10^3), 466 (3.7×10^3), 506 (2.3×10^3), 727 sh, 874 nm (1.4×10^3 M^{-1}·cm^{-1}), indicating that a second *o*-iminophenolate moiety of the ligand is converted into the corresponding π-radical (Scheme 2). Figure 7 shows the electronic spectra of the di- and monoanions, $[Fe^{III}_2(bbpo)Cl_4]^{2-}$ and $[Fe^{III}_2(bbpo^{ox1})Cl_4]^{-}$, respectively. The spectrum of the dianion displays a typical phenolate-to-iron(III) charge-transfer band at 648 nm (5.0×10^3 M^{-1}·cm^{-1}) and two ligand-based CT bands at 379 (1.5×10^4 M^{-1}·cm^{-1}) and 342 nm (1.7×10^4 M^{-1}·cm^{-1}). The spectrum of the monoanion is similar: 366 sh (1.5×10^4 M^{-1}·cm^{-1}), 406 (1.5×10^4 M^{-1}·cm^{-1}), 492 sh (5.6×10^3 M^{-1}·cm^{-1}), 697 nm (5.0×10^3 M^{-1}·cm^{-1}).

 © 2003 Wiley-VCH Verlag GmbH & Co. KGaA, Weinheim

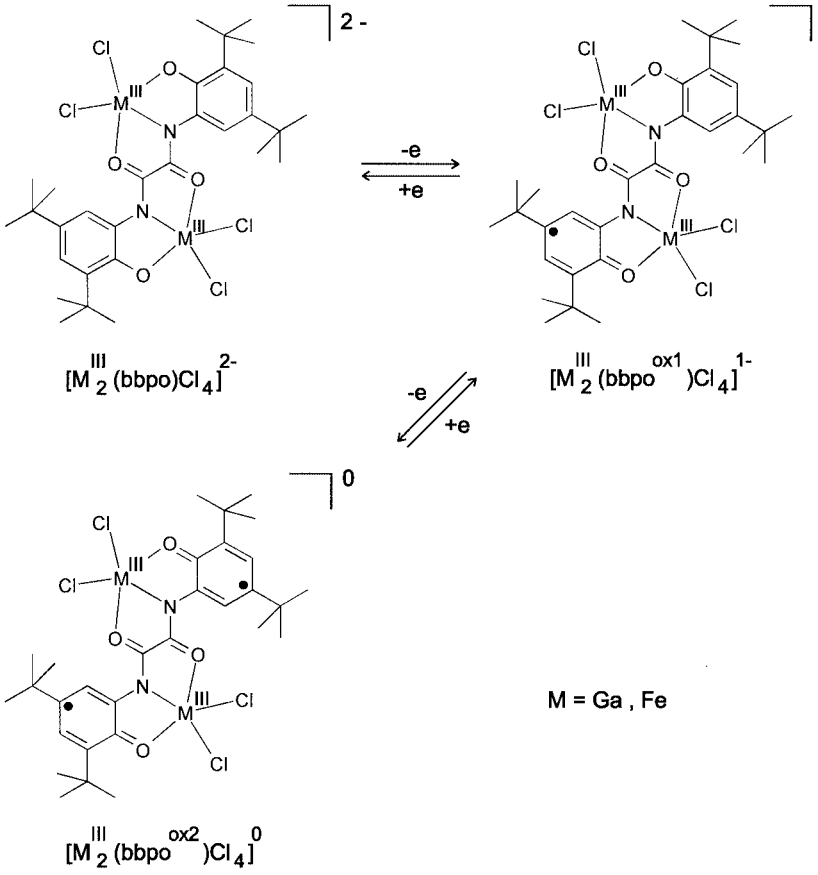

Scheme 2

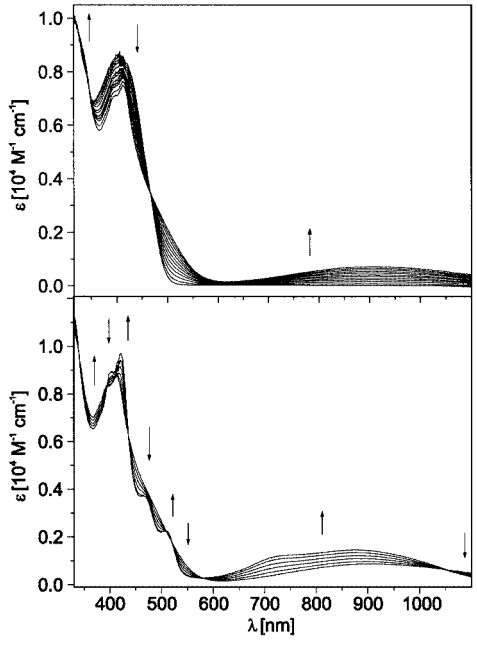

Figure 6. Electronic absorption spectra of **1** and its electrochemically generated one-electron oxidized form (top) at 248 K in CH_2Cl_2 solution {0.10 M $[N(nBu)_4]PF_6$} and of the monoanion and the neutral species (bottom), both of which were electrochemically generated

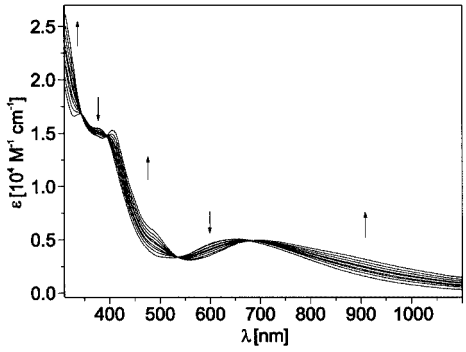

Figure 7. Electronic absorption spectra of **2** and its electrochemically generated one-electron oxidized form at 248 K in CH_2Cl_2 solution {0.10 M $[N(nBu)_4]PF_6$}

2.5. X-band EPR Spectra of *Oxidized* 1 and 2

The X-band EPR spectra of the electrochemically generated monoanion and the neutral complex of **1** have been recorded at 298 K (Figure 8 top and bottom, respectively). Both spectra display typical S = $^1/_2$ signals at g = 2.004 for the monoanion and at g = 2.005 for the neutral species, with clearly discernible Ga hyperfine splitting (I = $^3/_2$) with a_{Ga} = 13.1 MHz for $[Ga_2^{III}(bbpo^{ox1})Cl_4]^{1-}$ and 13.9 MHz

 © 2003 Wiley-VCH Verlag GmbH & Co. KGaA, Weinheim

for $[Ga_2^{III}(bbpo^{ox2})Cl_4]^0$. In both cases the unpaired spin couples only to a single Ga nucleus. This indicates that the spin in the monoanion $[Ga_2^{III}(bbpo^{ox1})Cl_4]^-$ is not delocalized over the whole bridging π-radical ligand $(bbpo^{ox1})^{3-}$ but is localized on one *o*-iminobenzosemiquinonato part. There is no or only very weak electronic coupling through the oxamide C−C bond. This notion is nicely corroborated by the EPR spectrum of the neutral species, which shows virtually the same hyperfine pattern as the monoradical and thus clearly indicates that there are two equivalent (*o*-iminobenzosemiquinonato)gallium(III) ($S = {}^1/_2$) units present without significant exchange interaction. Preliminary simulations (not depicted) suggest that the weak line broadening observed for the diradical species might be consistent with a coupling constant of the order $J = 20$ MHz (7×10^{-4} cm^{-1}).

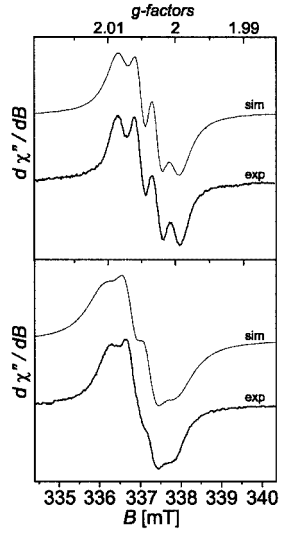

Figure 8. X-band EPR spectra of electrochemically generated monoanion of **1** (top) and of the two-electron oxidized form **1** (bottom) at ambient temperature in fluid solution; simulation parameters are given in the text; conditions: top spectrum (bottom spectrum): frequency 9.4485 GHz (9.4534 GHz); power 7 mW (10 mW); modulation frequency 100 kHz (100 kHz); modulation amplitude 0.08 mT (0.2 mT)

The X-band EPR spectrum of the electrochemically generated monoanion of **2** in frozen CH_2Cl_2 {0.10 M $[N(nBu)_4]PF_6$} at 10 K (Figure 9) clearly establishes that $[Fe_2^{III}(bbpo^{ox1})Cl_4]^-$ possesses an $S_t = {}^1/_2$ ground state since a rhombic signal with $g_x = 1.998$, $g_y = 1.944$, and $g_z = 1.825$ is observed. This $S_t = {}^1/_2$ ground state is assumed to be attained via a relatively strong intramolecular antiferromagnetic coupling, *J*, between an *o*-iminobenzosemiquinonate radical and an high-spin ferric ion, yielding S* = 2, which in turn couples weakly antiferromagnetically to the second high-spin ferric ion, *J′*, as shown in Scheme 3. Electronic coupling between this second ferric ion and the ligand radical is assumed to be either negligibly small or zero.

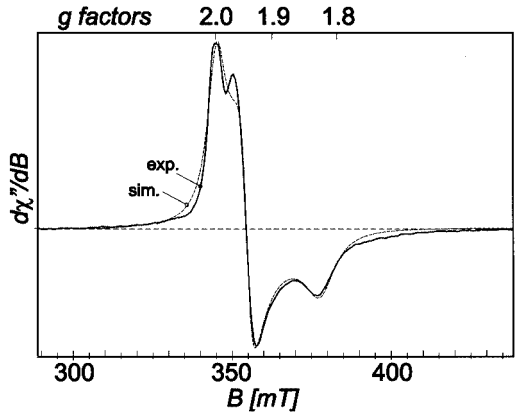

Figure 9. X-band EPR spectrum of electrochemically generated monoanion of **2** in frozen CH_2Cl_2 {0.10 M $[N(nBu)_4]PF_6$} solution at 10 K; the line widths for the simulation are: $W_x = 5.6$; $W_y = 3.4$; $W_z = 13.9$ mT ($g_x = 1.998$; $g_y = 1.944$; $g_z = 1.825$); conditions: frequency 9.6500 GHz; power 100 μW; modulation frequency 100 kHz; modulation amplitude 1.28 mT

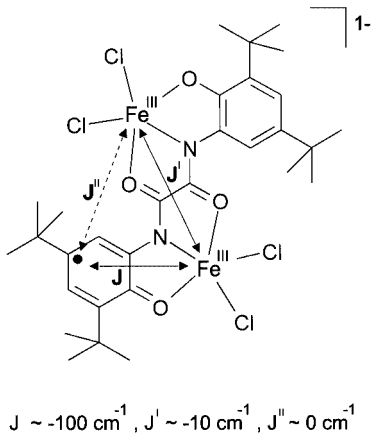

Scheme 3

The *g* values of the $S_t = {}^1/_2$ ground state of oxidized **2** deviate significantly from $g = 2.0$, in contrast to what can be expected from the single-ion properties of the ^6S state of high-spin Fe^{III} or a ligand radical. This does *not* necessarily indicate the formation of Fe^{IV}; the large *g* shifts owe their origin to level mixing of the ground state doublet with excited quadruplet due to competing exchange and ZFS, similar to what was found for **2**. This situation resembles moderately strong coupled high-spin Fe^{III}/Fe^{II} dimers ($S_1 = {}^5/_2$, $S_2 = 2$) as found in the OH-bridged diiron cores of purple-acid phosphatases, methane monooxygenase, and related model compounds[10] where the *g* values span the large range 1.5−2. We achieved a quantitative interpretation of the *g* values of oxidized **2** from a corresponding spin-Hamiltonian approach based on the simplified coupling scheme shown in Scheme 3 by using Equation (1) with $S_1 = {}^5/_2$ for an Fe^{III} site and a fictitious spin $S_2 = S^* = 2$. The latter is the spin of the pair formed by one iron(III) and the very strongly coupled ligand π-radical. This allowed us to probe the effect of ligand oxidation on the electronic properties of

 © 2003 Wiley-VCH Verlag GmbH & Co. KGaA, Weinheim

the respective Fe^{III} site even if their spin coupling is too strong to measure. A reasonable fit of the experimental *g* values was obtained with $D_1 = 1.6\ cm^{-1}$, $E/D_1 = 0.33$ (fixed to the values taken from nonoxidized **2**) and $D_2 = 2.4\ cm^{-1}$, $E/D_2 = 0.33$ (fixed), and $J = -11.5\ cm^{-1}$. (We refrained from introducing local g anisotropies or Euler rotations of the principal axes systems.) The values of D_2 and *J* are convincingly close to what is obtained theoretically for *unperturbed* iron sites by converting the local values of non-oxidized **2** into the oxidized system with $S_2 = S^* = S_{Fe} + S_{rad}$ using spin projection techniques[11]: $D_2 = 2.13\ cm^{-1}$ ($= {}^4/_3\ D_{Fe}$). $E/D_2 = 0.33$, $J = -11.3\ cm^{-1} = {}^7/_6\ J$ ($S_1 = {}^5/_2$, $S_2 = {}^5/_2$). Hence, the unusual EPR *g* values of oxidized **2** are fully consistent with the concept of ligand oxidation and the simplified coupling scheme for the spin ground state with "infinitively" strong Fe^{III}−radical coupling.

2.6. Mössbauer Spectra of *Oxidized* 2

The zero- and applied-field Mössbauer spectra of oxidized **2** were obtained by using the following protocol. The monoanion of **2** was generated coulometrically in CH_2Cl_2 solution {0.10 M $[N(nBu)_4]PF_6$} at 248 K and then frozen to 80 K and transferred to a Mössbauer cup. Subsequently, the solvent CH_2Cl_2 was removed by evaporation under reduced pressure at −30 °C within 2 h and then the sample was rapidly cooled to 80 K. In a parallel experiment the remaining solution was monitored at −30 °C spectrophotometrically to check the redox stability of the monoanion. No decomposition was detected after 2 h.

The zero-field spectrum of $[Fe_2^{III}(bbpo^{ox1})Cl_4]^-$ displays a broad doublet ($\Gamma = 0.82\ mm{\cdot}s^{-1}$, not shown) that could be fitted with two slightly different quadrupole doublets of two non-equivalent ferric sites. The isomer shift and quadrupole splitting parameters of both doublets are similar and are nearly identical to those observed for the dianion (see above). This implies that the one-electron oxidation of **2** is a ligand-centered process. No indication for the presence of Fe^{IV} has been found.

It is interesting and instructive that the applied-field spectra of the monoanion (Figure 10) are significantly more complex than the spectra recorded for the symmetrical dinuclear complex **2** (Figure 4). The magnetic spectra of the monoanion display very broad signals over a large velocity range of ca. $10\ mm{\cdot}s^{-1}$ whereas the analogous spectra of **2** cover only ca. $3\ mm{\cdot}s^{-1}$. The latter were simulated with a single high-spin ferric site, which is definitely not possible for the spectra of the monoanion. Here, the two ferric ions are nonequivalent. We have used the spin coupling Scheme outlined above (and shown in Scheme 3) for the monoanion of **2** where the $S_t = {}^1/_2$ ground state is attained by a strong coupling between one high-spin ferric ion and a ligand π-radical, yielding a fictitious local S* = 2 spin state and, in addition, a weak coupling of this state with the second high-spin ferric ion.

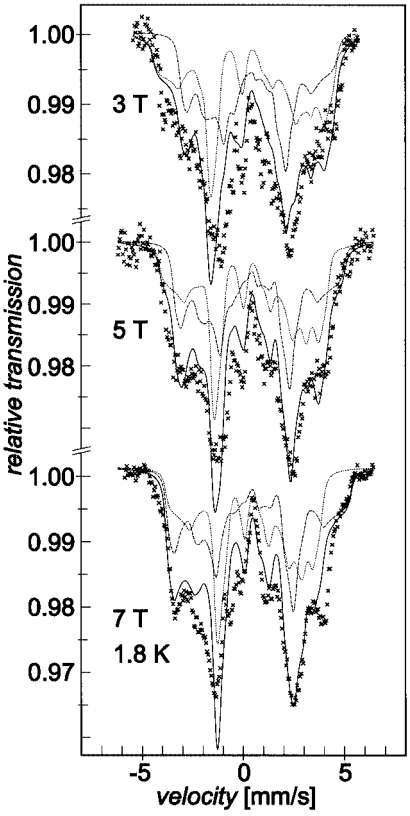

Figure 10. Applied-field Mössbauer spectra of electrochemically generated monoanion of **2** after removal of the solvent CH_2Cl_2 under reduced pressure; simulation parameters are given in Table 3; experimental data are corrected for residual non-oxidized compound **2** by subtracting 10% of the species shown in Figure 4

The same electronic Hamiltonian [Equation (1)] was applied as for the EPR interpretation of oxidized **2**, and the ZFS parameters were taken from the EPR results. Isomer shift, quadrupole splitting, asymmetry parameter and (isotropic) *A* constant of the ferric site could be taken from the data of the diferric starting complex **2**, whereas those of the oxidized S* = 2 site were independently optimized. The results are summarized in Table 3. The experimental *A* value obtained for S* = 2 was converted into a local value for Fe^{III}, $S = {}^5/_2$ by using $A_{Fe} = {}^6/_7\ A_{S^*=2}$.

It is remarkable that the quadrupole splitting and isomer shift of the ferric site with the ligand radical are slightly increased with respect to those of the starting compound or the other ferric site of oxidized **2**, whereas the local hyperfine coupling constant is significantly decreased. Similar systematic trends were indicated previously for the oxidation of iron(III) complexes with phenolate ligands.[12] The variation of the quadrupole splitting (which has no valence contribution for the $3d^5$ configuration) and the increase of the isomer shift reflect the attenuated π-donor capability of the oxidized ligand. The lower covalency of the iron−π-radical bonds for one iron site appears to be the origin of the slight increase of the iron−iron exchange coupling. The reduction of local hyperfine coupling of the ^{57}Fe nucleus at

 © 2003 Wiley-VCH Verlag GmbH & Co. KGaA, Weinheim

the "oxidized" iron site originates from covalent delocalization of radical β-spin density into the α-spin carrying metal d orbitals. The effect corresponds to spin density delocalization onto the central metal ion in radical complexes with *diamagnetic* central ions for which relative strong super hyperfine coupling with the metal nuclei is observed in the EPR spectra. Among others, oxidized compound **1** represents such an example.[1−6] The mechanism of spin delocalization corresponds to that of "*transferred*" or "*super-transferred hyperfine field*" described in solid-state applications of Mössbauer spectroscopy and magnetic materials.[13]

Conclusion

We have shown here that the tetraanion of 1,2-bis(3,5-di-*tert*-butyl-2-hydroxyphenyl)oxamide is a redox-noninnocent dinucleating ligand that reacts with 2 equiv. of $GaCl_3$ or $FeCl_3$ to form the dianionic complexes $[Ga^{III}_2(bbpo)Cl_4]^{2-}$ and $[Fe^{III}_2(bbpo)Cl_4]^{2-}$, respectively. Both dianions undergo, electrochemically, two reversible one-electron oxidations, yielding the monoanions $[M^{III}_2(bbpo^{ox1})Cl_4]^-$ (M = Ga^{III},Fe^{III}) and the neutral species $[M^{III}(bbpo^{ox2})Cl_4]^0$, respectively. The trianion $(bbpo^{ox1})^{3-}$ is a π-radical ($S = {}^1/_2$) whereas the dianion $(bbpo^{ox2})^{2-}$ is a diradical, both of which are of the *o*-iminobenzosemiquinonate type.

The three-spin system of the monoanion $[Fe^{III}_2(bbpo^{ox1})Cl_4]^-$ can be described by a ligand π-radical that couples strongly antiferromagnetically to a high-spin ferric ion, yielding a fictitious S* = 2 state, which in turn couples weakly antiferromagnetically to a second high-spin ferric ion to yield the observed $S_t = {}^1/_2$ ground state. The monoanion $[Ga^{III}_2(bbpo^{ox1})Cl_4]^-$ possesses an $S = {}^1/_2$ ground state whereas the neutral species displays, at room temperature, two uncoupled (*o*-iminobenzosemiquinonate)-gallium(III) units that couple antiferromagnetically at very low temperatures, yielding an $S_t = 0$ ground state. The spin structure provides interesting magnetic properties of long-range coupled systems with competing interactions.

Experimental Section

1,2-Bis(3,5-di-*tert*-butyl-2-hydroxoyphenyl)oxamide [H_4(bbpo)]: To an argon-purged suspension of 2-amino-4,6-di-*tert*-butylphenol[7] (4.4 g, 20 mmol) and triethylamine (2.0 g, 20 mmol) in dry diethyl ether (50 mL), oxalyl chloride (1.3 g, 10 mmol) was added dropwise at 0 °C. After stirring at 0 °C for 30 min, stirring was continued for further 2 h at 20 °C. The resultant colorless precipitate was filtered off and washed with diethyl ether. To the residue was added H_2O (20 mL) and the ligand H_4(bbpo) was filtered off and washed with H_2O until the water was free of chloride. A yellowish powder (3.0 g, 61%) was obtained which was stored under Ar; m.p. 217 °C (uncorrected). ^{1}H NMR (400 MHz, $CDCl_3$, 300 K): δ = 1.29 (s, 18 H, *tert*-butyl), 1.44 (s, 18 H, *tert*-butyl), 7.11 (m, 2 H, *p*-H), 7.28 (m, 2 H, *o*-H), 7.49 (s, 2 H, OH), 9.49 (s, 2 H, NH) ppm. ^{13}C{H} (63 MHz, $CDCl_3$, 300 K): δ = 29.8, 31.4, 34.4, 35.4, 117.7, 123.1, 124.0, 139.7, 143.3, 145.8, 157.2 ppm. MS (EI): *m*/*z* = 496. IR (KBr): $\tilde{\nu}$ = 3342 ν(N−H), 3140 ν(O−H), 1655, 1603, 1530 ν(C=O), ν(C−N) cm^{-1}. $C_{30}H_{44}N_2O_4$ (496.69): calcd. C 72.55, H 8.93, N 5.64; found C 72.8, H 8.7, N 5.4.

[N(*n*Bu)$_4$]$_2$[Ga^{III}_2(bbpo)Cl$_4$] (1): To an argon-purged suspension of the ligand H_4(bbpo) (0.50 g, 1.0 mmol) in dry CH_3OH (20 mL), was added NaOH (2 mL, 1.0 M in CH_3OH). An argon-purged solution of $GaCl_3$ (0.36 g, 2.0 mmol), dissolved in 2−3 mL of CH_3OH was added and upon continuous stirring at 20 °C a yellow precipitate formed. The mixture was then heated to reflux under Ar and [N(*n*Bu)$_4$]Cl (0.56 g, 2.0 mmol) was added. After heating to reflux for a further 4 h, a yellow, microcrystalline precipitate of **1** was obtained. Yield 0.66 g (55%). Recrystallization from CH_3OH solution by diethyl ether diffusion yielded single crystals of **1** suitable for X-ray analysis. $C_{62}H_{112}Cl_4Ga_2N_4O_4$ (1258.85): calcd. C 59.16, H 8.97, Cl 11.27, Ga 11.08, N 4.45; found C 60.0, H 8.7, Cl 11.1, Ga 11.3, N 4.6. MS (ESI-neg. ion): *m*/*z* = 737.1 $\{[Ga_2(bbpo)Cl_3]\}^-$. ^{1}H NMR (250 MHz, [D_4]MeOD, 300 K): δ = 1.02 [t, 24 H, CH_3(TBA)], 1.29 (s, 18 H, *tert*-butyl), 1.40 [m, 16 H, CH_2(TBA)], 1.47 (s, 18 H, *tert*-butyl), 1.65 [m, 16 H, CH_2(TBA)], 3.23 [t, 16 H, CH_2(TBA)], 7.13 (d, ^4J = 2.3 Hz, 2 H), 8.04 (d, ^4J = 2.4 Hz, 2 H) ppm.

[N(*n*Bu)$_4$]$_2$[Fe^{III}_2(bbpo)Cl$_4$] (2): This iron-containing complex was prepared in the same fashion as described above for the synthesis of **1** but using $FeCl_3$ instead of $GaCl_3$. The green microcrystalline product was recrystallized from CH_3OH by diethyl ether diffusion, yielding single crystals of **2** suitable for X-ray crystallography. $C_{62}H_{112}Cl_4Fe_2N_4O_4$ (1231.10): calcd. C 60.49, H 9.17, Cl 11.52, Fe 9.07, N 4.55; found C 60.5, H 9.1, Cl 11.4, Fe 9.1, N 4.6. MS (ESI-neg. ion): *m*/*z* = 709.1.

X-ray Crystallographic Data Collection and Refinement of the Structures: A yellow single crystal of **1** and a black crystal of **2** were coated with perfluoropolyether, picked up with a glass fiber and mounted in the nitrogen cold stream of the diffractometer. Intensity data were collected at 100 K using graphite-monochromated Mo-K_α radiation (λ = 0.71073 Å). The final cell constants were obtained from a least-squares fit of a subset of several thousand strong reflections. Data collection was performed by taking frames at 1.0° (Nonius Kappa-CCD) in ω. Crystallographic data of the compounds are listed in Table 1. The Siemens ShelXTL software package was used for solution, refinement and artwork of the structure.[14,15] The structures were readily solved by direct methods and difference Fourier techniques. All non-hydrogen atoms and hydrogen atoms were placed at calculated positions and refined as riding atoms with isotropic displacement parameters. Split-atom models with restrained C−C distances using the SADI option in SHELX97 were introduced in both structures to account for their disorder by rotation. CCDC-191601 (**1**) and -191602 (**2**) contain the supplementary crystallographic data for this paper. These data can be obtained free of charge at www.ccdc.cam.ac.uk/conts/retrieving.html or from the Cambridge Crystallographic Data Centre, 12 Union Road, Cambridge CB2 1EZ, UK [Fax: (internat.) + 44-1223/336-033; E-mail: deposit@ccdc.cam.ac.uk].

Physical Measurements: Electronic spectra of complexes and spectra of the spectroelectrochemical measurements were recorded with an HP 8452A diode array spectrophotometer (range: 190−1100 nm). Cyclic and square-wave voltammograms and coulometric experiments were performed with an EG&G potentiostat/galvanostat. Temperature-dependent (2−298 K) magnetization data were recorded with a SQUID magnetometer (MPMS Quantum design) in an external magnetic field of 1 T. The experimental susceptibility data were corrected for underlying diamagnetism by use of tabulated Pascal's constants. X-band EPR spectra were re-

 © 2003 Wiley-VCH Verlag GmbH & Co. KGaA, Weinheim

corded with a Bruker ESP 300 spectrometer. Zero- and applied-field Mössbauer spectra were recorded using the equipment described in ref.[16]; programs used for fitting routines have also been described.

Acknowledgments

We thank the Fonds der Chemischen Industrie for financial support.

[1] C. N. Verani, S. Gallert, E. Bill, T. Weyhermüller, K. Wieghardt, P. Chaudhuri, *Chem. Commun.* **1999**, 1747.
[2] P. Chaudhuri, C. N. Verani, E. Bill, E. Bothe, T. Weyhermüller, K. Wieghardt, *J. Am. Chem. Soc.* **2001**, *123*, 2213.
[3] H. Chun, C. N. Verani, P. Chaudhuri, E. Bothe, E. Bill, T. Weyhermüller, K. Wieghardt, *Inorg. Chem.* **2001**, *40*, 4157.
[4] H. Chun, T. Weyhermüller, E. Bill, K. Wieghardt, *Angew. Chem.* **2001**, *113*, 2552; *Angew. Chem. Int. Ed.* **2001**, *40*, 2489.
[5] X. Sun, H. Chun, K. Hildenbrand, E. Bothe, T. Weyhermüller, K. Wieghardt, *Inorg. Chem.* **2002**, *41*, 4295.
[6] H. Chun, P. Chaudhuri, T. Weyhermüller, K. Wieghardt, *Inorg. Chem.* **2002**, *41*, 790.
[7] V. B. Vol'eva, T. I. Prokof'eva, A. I. Prokov'ef, I. S. Belostotskaya, N. L. Komissarova, V. V. Ershov, *Russ. Chem. Bull.* **1995**, *44*, 1720.
[8] D. Armentano, G. DeMunno, J. Faus, F. Lloret, M. Julve, *Inorg. Chem.* **2001**, *40*, 655.
[9] R. D. Shannon, *Acta Crystallogr., Sect. A* **1976**, *32*, 751.
[10] [10a] J. H. Rodriguez, H. Ok, Y.-M. Xia, P. G. Debrunner, B. E. Hinrichs, T. Meyer, N. H. Packard, *J. Phys. Chem.* **1996**, *100*, 6849−6862. [10b] U. Bossek, H. Hummel, T. Weyhermüller, E. Bill, K. Wieghardt, *Angew. Chem.* **1995**, *107*, 2885−2888.
[11] A. Bencini, D. Gatteschi, *EPR of Exchange Coupled Systems*, Springer Verlag, Berlin, **1990**.
[12] M. D. Snodin, L. Ould-Moussa, U. Wallmann, S. Lecomte, V. Bachler, E. Bill, H. Hummel, T. Weyhermüller, P. Hildebrandt, K. Wieghardt, *Chem. Eur. J.* **1999**, *5*, 2554−2565.
[13] F. Granjean, in *Mössbauer Spectroscopy Applied to Inorganic Chemistry* (Ed.: G. J. Long), Plenum Press, New York, **1987**, vol. 2, p. 241−271.
[14] G. M. Sheldrick, Universität Göttingen, **1994**.
[15] ShelXTL V.5, Siemens Analytical X-ray Instruments, Inc., **1994**.
[16] K. Meyer, E. Bill, B. Mienert, T. Weyhermüller, K. Wieghardt, *J. Am. Chem. Soc.* **1999**, *121*, 4859.

Received September 25, 2002

 © 2003 Wiley-VCH Verlag GmbH & Co. KGaA, Weinheim

Self-Assembly of Five Cadmium(II) Coordination Polymers from 4,4′-Diaminodiphenylmethane

Junhua Luo,[a] Maochun Hong,*[a] Ruihu Wang,[a] Rong Cao,[a] Qian Shi,[a] and Jiabao Weng[a]

Keywords: Cadmium / Coordination polymers / Self-assembly / N ligands

Five cadmium(II) coordination polymers formed from dadpm (dadpm = 4,4′-diaminodiphenylmethane), namely, $[Cd(dadpm)(I)_2]_n$ (**1**), $[\{Cd(dadpm)_2(Cl)\}(dca)]_n$ (**2**) [dca = dicyanamide anion, $N(CN)_2^-$], $[\{Cd(dadpm)_2(Br)\}(dca)]_n$ (**3**), $[Cd(dadpm)(SCN)_2]_n$ (**4**) and $[Cd(dadpm)(dca)_2]_n$ (**5**) have been synthesized and characterized by NMR, IR, and fluorescence spectroscopy as well as TG analysis. The ligand dadpm in **1** bridges the metal centers to form a zigzag chain where the halide anion I^- acts as a terminal ligand. Weak Cd···I interactions between adjacent chains extend the zigzag chains into a wave-like layer. Complexes **2** and **3** are isomorphous, the metal centers are bridged by dadpm to generate a double-stranded chain containing the metallacycles of $[Cd_2(dadpm)_2]$, and the halide anions (Cl^- in **2** and Br^- in **3**) link adjacent chains into 2D layer structures in a *trans* mode. Dicyanamide anions in the two complexes lie between the layers as supported anions and link the adjacent layers into 3D structures through hydrogen bonds. In complex **4**, the metal centers are bonded by the thiocyanate anions to form double-stranded chains, which are linked by dadpm in different orientations resulting in a cross-linked 3D structure. In **5**, dicyanamide anions connect the cadmium(II) centers to form a $[Cd(dca)_2]_n$ 2D layer, which contains 24-membered ring units $[Cd_4(\mu_{1,1}\text{-dca-}N,N)_4]$. The dadpm ligand links the adjacent layers into an α-Po-like 3D network structure.

(© Wiley-VCH Verlag GmbH & Co. KGaA, 69451 Weinheim, Germany, 2003)

Introduction

In the research of supramolecular chemistry, much interest has recently been focused on the crystal engineering of coordination frameworks because of their intriguing architectures, fascinating topologies, intertwining phenomena, and potential application in functional materials.[1] Self-assembly based on molecules has emerged as an attractive approach to the fabrication of these new materials, and considerable effort has been made towards the supramolecular networks assembled by covalent and hydrogen bonds or other molecular interactions.[2] The family of metallacyclic nanostructures assembled from transition metal junctions and bridging ligands is now a well-established group of coordination polymers,[3] and the diversity of such coordination nanostructures makes them remarkable examples in the growing library of self-assembled entities.[4] Although many topologically promising architectures have been constructed from building blocks containing nitrogen donors,[5] such as 4,4′-bipyridine,[6] pyrazine,[7] bis(4-pyridyl)ethane,[8] 1,4-bis(4-pyridyl)benzene,[9] 2,4,6-tri(pyridyl)-1,3,5-triazine[10] and 4,4′-azobis(pyridine),[11] few coordination polymers based on bifunctional neutral ligands containing aromatic NH_2 donors are documented. The involvement of oligoaniline in the assembly of supramolecular chemistry is limited because of its instability, as it is easily oxidized in an aqueous solution and/or in air. Although the aromatic diamine ligand dadpm has a poorer donor ability than the corresponding pyridyl-type ligands used before, it can still coordinate to transitional metal ions by one NH_2 group to act as a terminal ligand as in $[Cu_2(C_2H_4N_2O_2)(dadpm)_2(Br)_2]$ [$C_2H_4N_2O_2$ = bis(2-aminoethyl)oxamidato][12a] or two NH_2 groups to act as a bridging ligand as in $\{[Cu(dadpm)(C_3H_4O_4)Cl]Cl\}_2$ ($C_3H_4O_4$ = malonic acid)[12b] and $[Cu_2(dadpm)_2(PyCH_2NHCOCONHCH_2Py)]\cdot 2NO_3\cdot 6H_2O$.[12c] The ligand dadpm may be utilized as a building block for the construction of novel organic/inorganic hybrid materials. In this paper, we report on the self-assembly reactions of dadpm and cadmium(II) halides in the presence of dca^- or SCN^- ions, and the structural characterizations of five coordination polymers, $[Cd(dadpm)(I)_2]_n$ (**1**), $[\{Cd(dadpm)_2(Cl)\}(dca)]_n$ (**2**), $[\{Cd(dadpm)_2(Br)\}(dca)]_n$ (**3**), $[Cd(dadpm)(SCN)_2]_n$ (**4**) and $[Cd(dadpm)(dca)_2]_n$ (**5**).

[a] State Key Laboratory of Structural Chemistry, Fujian Institute of Research on the Structure of Matter, Chinese Academy of Sciences,
Fuzhou, Fujian 350002, China
Fax: (internat.) + 86-591/371-4946
E-mail: hmc@ms.fjirsm.ac.cn

Results and Discussion

Syntheses

During the preparation of the dadpm/Cd complexes, direct treatment of dadpm with various cadmium halides

 © 2003 Wiley-VCH Verlag GmbH & Co. KGaA, Weinheim DOI: 10.1002/ejic.200200540

failed to produce a complex, which may be ascribed to the poor coordination ability of dadpm. As the dicyanamide anion has various coordination modes,[13] and thus can provide a suitable "building block" for assembling novel inorganic/organic hybrid materials, we want to introduce this anion ligand into the Cd halide/dadpm reaction mixture as a co-ligand in order to prepare some novel dadpm−Cd complexes. Mixing of $CdX_2{\cdot}nH_2O$ (X = I, n = 0; X = Br, n = 4; X = Cl, n = 2.5) with 4,4′-diaminodiphenylmethane and sodium dicyanamide in a 1:2:1 ratio in hot aqueous solution resulted in the crystalline complexes **1**, **2** and **3** with 1D to 2D structures. As in our recent report on Cd coordination frameworks,[15] the larger radius of I^- results in the cadmium atom adopting a tetracoordinated geometry upon coordination, while with the halide ions Cl^- and Br^-, the cadmium ion adopts a six-coordinate geometry. The dca^- anion is not incorporated into complex **1**, but acts as a supported anion in both **2** and **3**. The effect of the dca^- anion in the formation of **1** is still unclear. While we changed the reaction sequence, namely, first mixing the Cd salt with the dadpm ligand, then adding the dicyanamide anion to the reaction mixture, complex **5** with an α-P_o-like 3D net structure was obtained, which is completely different from those of **1**, **2** and **3**. Using another anion ligand with a different size and shape, the SCN^- anion, complex **4** with a cross-linked 3D structure was obtained.

Description of the Structures

The X-ray analysis revealed that the cadmium atoms in complex **1** are bridged by a dadpm ligand with the occurrence of an 1D coordination polymeric chain along the *a* axis. An ORTEP view of the chain with atom labeling is shown in Figure 1 (a). Each cadmium atom is tetracoordinated by two nitrogen atoms of two dadpm ligands and two I^- anions with square-planar coordination geometry. The Cd−N(dadpm) bond length is 2.32(2) Å, and the Cd−I distance 2.794(3) Å. The Cd···Cd separation is 13.131 Å through the bridging dadpm ligand. The inter-chains are tightly packed (Cd···Cd = 4.520 Å) by the weak interaction between the Cd^{II} center and the I^- anion belonging to neighbor chains [Cd(E)−I = 3.587 Å, symmetry code: (E) x, y, 1 + z], forming a quasi-2D wave-like sheet as shown in Figure 1 (b). In the sheet structure, there are a four-membered ring and a 28-membered ring, the former contains two cadmium(II) ions and two I^- anions, and the latter two cadmium(II) ions, two I^- anions and two dadpm ligands.

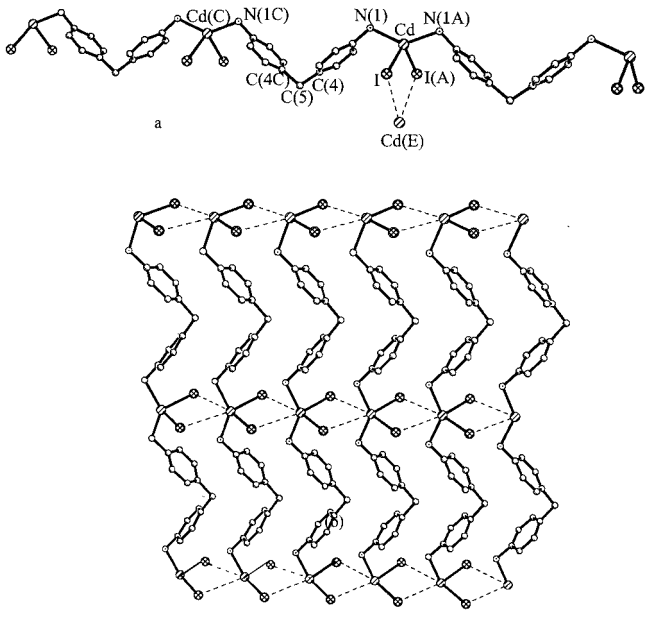

Figure 1. (a) ORTEP drawing of the zigzag chain in **1** with atom numbering scheme, showing the cadmium coordination environment; (b) quasi-two dimensional sheet of **1** formed through weak Cd···I interactions

In the crystal structure of **2**, each cadmium(II) center is bridged by four dadpm ligands to give rise to a double stranded chain as shown in Figure 2 (a). The dadpm adopts a *trans*-gauche conformation and two dadpm ligands bridge two cadmium(II) ions to form a distorted square metallacyclic ring with a Cd−Cd distance of 12.401 Å. In the square ring, each of the two opposite phenyl rings of the two dadpm ligands are parallel and the two adjacent phenyl rings are almost perpendicular with a torsion angle of 89.7°. The dimensions of the ring are approximately 7.15 × 4.15 $Å^2$ based on the distance of the two opposite phenyl rings, which is slightly shorter than those of the $[Cu_2(dadpm)_2]$ macrocycle (8.36 × 4.15 $Å^2$) in $[Cu(dadpm)\{CH_2(COOH)_2Cl\}Cl]_2$.[12b] The cadmium atom is six-coordinate in an elongated octahedral environment. The equatorial plane is defined by four N atoms from four dadpm ligands with two short Cd−N bonds [Cd−N(4A), 2.357(5) Å] and two long Cd−N bonds [Cd−N(5), 2.3852(4) Å]. The four equatorial donor atoms and the central cadmium(II) atom are almost coplanar with a mean deviation of 0.012 Å and N−Cd−N bond angles of 86.1(2) and 93.9(2)°. Two chloride anions are at the axial positions and link the adjacent double-stranded chains into an unprecedented 2D layer with a Cd−Cl bond length of 2.752(6) Å, as shown in Figure 2 (b). The channels are viewed through the metallacycles packing along the *b* axis. The Cl−Cd−N bond angles vary from 80.0(1) to 100.0(1)° and the Cd−Cd separation of adjacent chains is 5.505 Å with a Cd−Cl−Cd bond angle of 180°.

The dicyanamide anion is disordered in the structure. It does not engage in coordination and acts as a supported anion between the 2D layers through the hydrogen bond interactions between the N atoms (N1 and N3) of the dicyanamide anion and the N atoms (N4) of dadpm as in Figure 2 (c) [N3···N4B, 2.821 Å; N1···N4 H, 2.832 Å, symmetry code: (H) $-x$, y, $-1 + z$]. Through these hydrogen bonds, a 32-membered ring constructed by two dadpm ligands, four Cd^{II} centers and two N−C≡N groups of two dca^- anions is formed and the other C≡N groups of the dca^- anions protrude into the cavity of the ring.

An X-ray crystal analysis revealed that complex **3** exhibits a similar structure to that of complex **2** except that **2** has a Br^- bridge instead of a Cl^- bridge. An ORTEP drawing of the molecular structure of **3** with atom labeling is shown in Figure 3 (a). The Cd−N bond lengths [Cd−N(4) 2.38(1)

 © 2003 Wiley-VCH Verlag GmbH & Co. KGaA, Weinheim

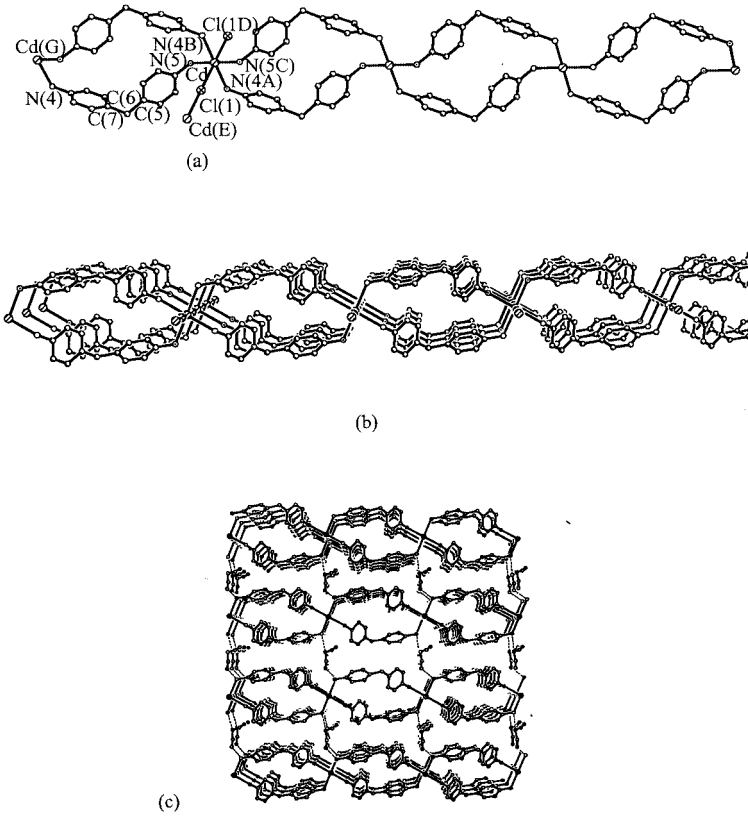

Figure 2. (a) ORTEP drawing of the double-stranded chain in **2** with atom numbering; (b) ORTEP drawing of the layer structure of **2** to view the channels in the *b* axis direction; (c) perspective view of the dicyanamide anion's supported 3D structure of **2**

Å and Cd−N(5A) 2.38(1) Å] in the equatorial plane are slightly longer than those in **2**, and the N−Cd−N bond angles are 85.7(4) and 94.3(4)°. The separation between the two Cd^{II} atoms in the$[Cd_2(dadpm)_2]$ macrocycle is 12.452 Å, similar to that in **2**, and the dimensions of the macrocycle are about 7.25 × 4.06 Å. The Br^- anions coordinate axially with the cadmium centers in a *trans* geometry to link the adjacent chains into a 2D layer with Cd−Br−Cd bond angles of 180°. The Cd−Cd separation of adjacent chains is 5.505 Å, which is larger than the corresponding value in **2** through the Cl^- bridge because of the larger radius of the Br^- ion. Similar to **2** the dicyanamide anions in **3** lie between two adjacent layers acting as supporting anions.

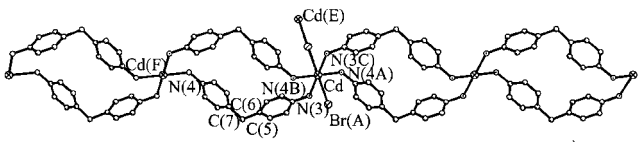

Figure 3. ORTEP drawing of **3** with atom labeling, showing the cadmium coordination environment

An ORTEP view of a Cd center of **4** is shown in Figure 4 (a). Each cadmium(II) atom is located on an inversion center, and coordinated by two thiocyanate nitrogen atoms [Cd−N(SCN), 2.335(7) Å] and two thiocyanate sulfur atoms [Cd−S, 2.746(2) Å] in a *trans* geometry in the equatorial plane, resulting in a chain structure containing eight-membered $[Cd_2(SCN)_2]$ rings as in Figure 4 (a), which have been well documented in Cd^{II}/L/SCN systems.[17] Two nitrogen atoms of two dadpm groups complete the remaining two axial positions around the six-coordinate Cd^{II} center and the distance of Cd−N(dadpm) is slightly longer than Cd−N(SCN) with a bond length of 2.354(6) Å. The cadmium thiocyanate chains are cross-linked by the dadpm with different orientations into a 3D polymer as in Figure 4 (c). The Cd···Cd separation is 13.518 Å through the dadpm ligand. In the 3D structure, four SCN^- ions and four dadpm ligands link eight cadmium ions into a 64-membered ring with dimensions of 30.57 × 6.2 Å, as shown in Figure 4 (b).

Each cadmium(II) center in **5** is in a distorted octahedral environment, being coordinated by four nitrogen atoms of four dca^- ligands in the equatorial plane and two nitrogen atoms of two *trans*-related dadpm ligands at the axial positions as shown in Figure 5 (a). The Cd−N(dadpm) bond length is 2.39(1) Å, and Cd−N(dca) bond lengths are 2.31(1) and 2.33(1) Å. The dca^- ligands and Cd centers are interlinked into a 2D layer, resulting in an hourglass-shaped, 24-membered $[Cd_4(\mu_{1,1}\text{-dca-}N,N)_4]$ metallacycle, as shown in Figure 5 (b), different from other reported Cd−dca coordination polymers in which the Cd centers and dca^- ligands are interconnected into $[Cd(dca)_2]_n$ chains.[18] The Cd···Cd separation through the dca^- ligand in **5** is 7.597 Å. For comparison, $Zn[N(CN)_2]$ features a 2D

 © 2003 Wiley-VCH Verlag GmbH & Co. KGaA, Weinheim

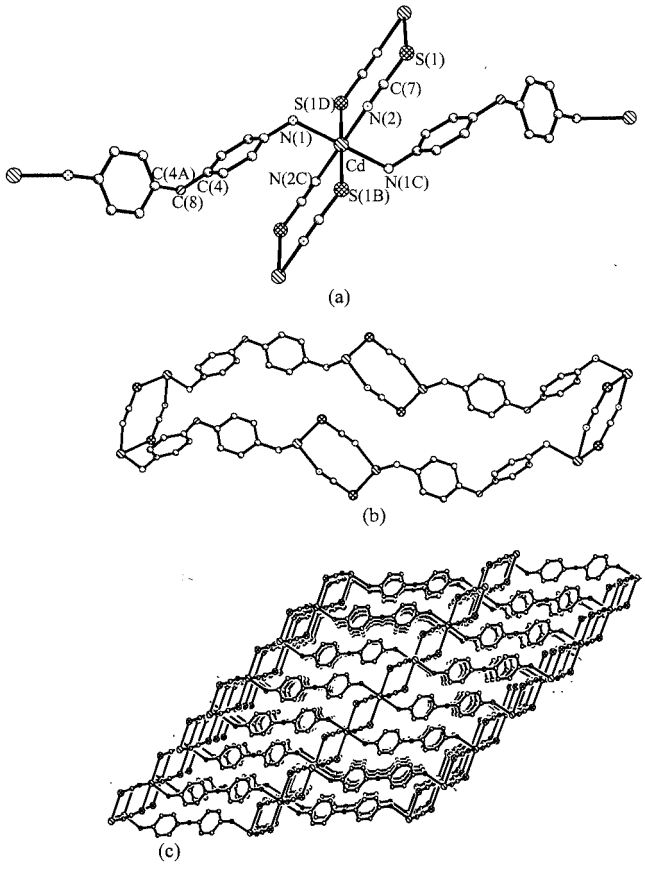

Figure 4. (a) ORTEP drawing of **4** with atom numbering, showing the cadmium coordination environment; (b) perspective of the metallacyle in **4**; (c) view of the 3D structure of **4**

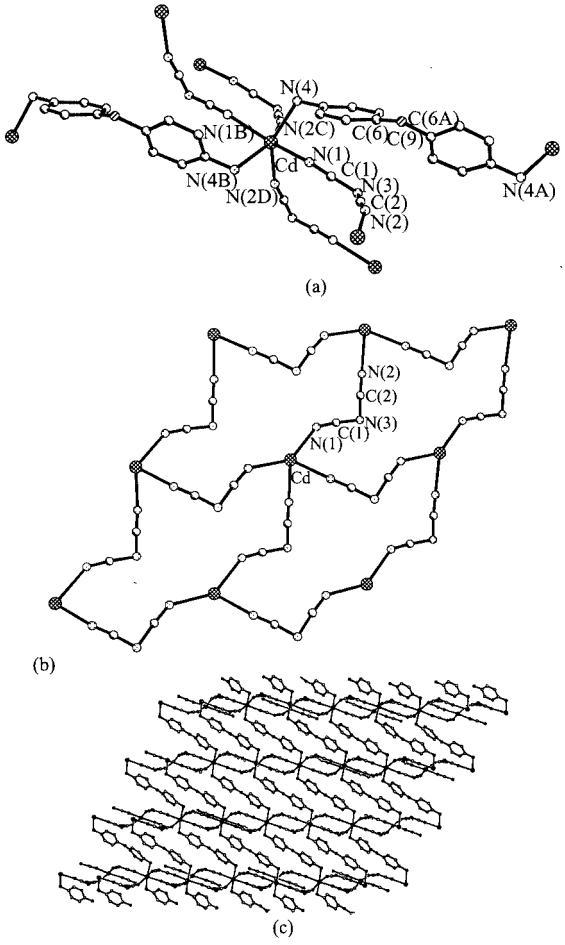

Figure 5. (a) ORTEP drawing of the cadmium(II) coordination in **5** with atom numbering; (b) perspective of the 2D sheet in **5**; (c) view of the α-P_o-like 3D structure of **5**

layer structure with linkages similar to the $[Cd(dca)_2]$ layer in **5**, but the layers are markedly buckled and packed in a staggered fashion due to the tetrahedral configuration of Zn^{II}.[19] To the best of our knowledge, such a $[Cd_4(\mu_{1,1}$-dca-*N*,*N*$)_4]$ arrangement of the metallacycle is unprecedented, and only a few similar structures have been reported, such as $[Mn_4(SCN)_4]$ in $[Mn(EtOH)_2(NCS)_2]$,[20a] $[Mn_4(N_3)_4]$ in $[Mn(4\text{-acpy})_2(N_3)_2]$ (4-acpy = 4-acetylpyridine),[20b] and $[Cd_4(NCS)_4]$ in $[Cd(SCN)_2(3\text{-PyCONH}_2)_2]$ (3-PyCONH$_2$ = nicotinamide).[20c]

As shown in Figure 5 (c), the $[Cd(\mu_{1,1}$-dca-*N*,*N*$)_2]_n$ layers are further linked by the dadpm ligands into an α-P_o-like 3D net as in $[Mn(dca)_2(pz)]$.[21] A 36-membered ring is formed through four cadmium ions linked by two single $\mu_{1,1}$-dca-*N*,*N* bridges and two dadpm ligands. The Cd···Cd distance is 12.328 Å through the bridging dadpm ligand.

The C(Ph)−C−C(Ph) bond angles, the dihedral angles between the two phenyl rings of dadpm and the M···M distances through the dadpm ligand in the five complexes are listed in Table 3. The C(Ph)−C−C(Ph) bond angles show slight differences, which range from 102.0(1)° in **5** to 115.9(1)° in **3**. But the dihedral angles between the two phenyl rings in the dadpm ligand show large differences in the five complexes, ranging from 55.3(2)° in **5**, 57.2(3)° in **4** to 81.6(4)°in **1**, 87.7(6)° in **3** and 89.7(5)° in **2**, which may be ascribed to the different coordination schemes of dadpm. In **1**, **4** and **5** the dadpm ligand links the metal atoms into a zigzag chain, but in **2** and **3**, the dadpm ligand connects the metal atoms into a double-stranded chain. The Cd···Cd distances through the dadpm ligand range from 12.328 Å in **5** to 13.131 Å in **1**. The structural data show the flexibility of the dadpm ligand in the five coordination polymers. The flexibility of dadpm induces a small effective cavity volume of the channels in the five dadpm−Cd complexes and no guest molecules are accommodated in the channels.

IR, ^{1}H NMR and Fluorescent Spectra

All of the five complexes show strong C≡N stretching vibrations of the dca^- or SCN^- ions in the region 2000−2300 cm^{-1}, except complex **1**. The strong C≡N stretching vibration of thiocyanate in **4** at 2116 cm^{-1} suggests a bridging mode.[22] The C≡N stretching vibrations of $[N(CN)_2]^-$ are at 2260, 2210, 2148 cm^{-1} in **2**, and 2258, 2213, 2149 cm$^-$ in **3**, but shifted to 2301, 2248, 2176 cm^{-1} in **5**, which are assigned to $\nu_{sym} + \nu_{asym}$ (C≡N), ν_{asym} (C≡N) and ν_{sym} (C≡N), respectively. Compared with the corresponding spectroscopic data of free $[N(CN)_2]^-$,[23] the

 © 2003 Wiley-VCH Verlag GmbH & Co. KGaA, Weinheim

$[N(CN)_2]^-$ ligand acts as a supported anion in **2** and **3**, but a $\mu_{1,1}$-end-to-end bridge in **5** and **6**, which is consistent with the results of X-ray analyses. The aromatic C−H stretching vibrations are in the region 2800−3000 cm^{-1}. The strong bands in 3100−3350 cm^{-1} are ascribed to ν_{N-H} stretching vibrations in the five complexes.

The ^1H NMR spectra of **1**, **2**, **3**, and **5** show resonance signals at δ = 6.80 and 6.45 [m, 8 H, 2 (C_6H_4)], 4.837 [s, 4 H, 2 (NH_2)] and 3.547 (s, 2 H, CH_2) ppm for the dadpm ligand. The ^1H NMR signals for the NH_2 group protons of all five complexes are slightly shifted downfield relative to the free ligand, while the signals of other protons remain essentially unchanged in the five complexes.

The fluorescent characterization shows that each complex has a strong or medium yellow fluorescent emission[24] [585 (m) in **1**, 590 (s) in **2**, 593 (s) in **3**, 567 (m) in **4**, and 570 nm (m) in **5** and the wavelength at which the complex is excited is 310 nm], which may be ascribed to ligand-to-metal charge transfer (LMCT) bands.

Thermogravimetric Analysis

Thermogravimetric analyses show that all five of the complexes are stable. Complex **1** remains stable up to 190 °C, and then it slowly decomposes with the loss of the ligand dadpm. Complex **2** and **3** are stable up to 153 and 168 °C . The TGA trace displays a gradual weight loss of 11.5% (calculated 10.81%) from 153 to 209 °C for complex **2** and 10.08% (calculated 10.5%) from 168 to 235 °C for complex **3**, which corresponds to the weight loss of one dca^- supported anion. When the temperature exceeds about 250 °C, both of them begin to decompose. Complex **4** decomposes from 220 °C with a weight loss of 49.5% (calculated 44.71%) corresponding to the decomposition of the dadpm ligand. Subsequent weight loss from 350 °C may correspond to the decomposition of the thiocyanate groups. The TG curve of **5** shows that the complex is stable below 238 °C, and that from this temperature the compound decomposes and loses the dadpm and dca ligands almost simultaneously.

Conclusion

In spite of the similarity of the building blocks used, the products display quite different structures. The isolated five coordination compounds include one- or three-dimensional polymeric structures sustained only by coordinative bonds (**1**, **4** and **5**), and three-dimensional arrays connected both by coordinative and hydrogen bonds (**2** and **3**). The variety of the observed structural motifs confirms that rationalization of the resulting topologies is still difficult. Many factors play a role in the formation of the final product: (i) the anions effects (I^-, Cl^- and Br^- in **1**, **2** and **3**, and also dca and SCN^- anions in **4** and **5**); (ii) the conformational flexibility of the dadpm ligand; (iii) the versatility of the metal coordination sphere (the cadmium coordination geometry is tetrahedral in **1**, but octahedral in **2**, **3**, **4** and **5**); and (iv) the reaction sequence (in **2** and **5**). This work demonstrates the feasibility of achieving various polymeric frameworks by self-assembly of the flexible aromatic diamine ligand and metal salts and may provide useful information for crystal engineering.

Experimental Section

General: All chemicals were of an analytical grade and used without further purification. Elemental analyses of C, H N and S were performed with an Elementar Vario ELIII elemental analyzer. IR spectra were recorded as KBr pellets with a Nicolet Magna 750 FT-IR spectrometer in the range of 200−4000 cm^{-1}. Thermogravimetric analyses (TGA) were performed with a NETSCHZ STA-449C thermoanalyzer under N_2 (26−1000 °C range) at a heating

Table 1. Crystallographic data for complexes **1**−**5**

	1	**2**	**3**	**4**	**5**
Empirical formula	$C_{13}H_{14}CdI_2N_2$	$C_{28}H_{28}CdClN_7$	$C_{28}H_{28}BrCdN_7$	$C_{15}H_{14}CdS_2N_4$	$C_{17}H_{14}CdN_8$
Formula mass	564.48	610.42	654.88	428.8	444.74
Crystal system	orthorhombic	triclinic	triclinic	monoclinic	monoclinic
Space group	*Imm*2	$P\bar{1}$	$P\bar{1}$	*C*2/*c*	*C*2/*c*
a [Å]	12.828(4)	5.5052(5)	5.7166(8)	9.411(2)	13.337(2)
b [Å]	13.131(4)	9.9187(9)	9.702(2)	8.059(2)	7.277(1)
c [Å]	4.520(1)	12.166(1)	11.965(2)	20.589(4)	10.214(2)
α [°]	90	88.449(2)	87.302(2)	90	90
β [°]	90	79.453(2)	80.340(2)	93.495(0)	118.557(3)
γ [°]	90	83.843(2)	84.058(2)	90	90
V [Å^3]	761.5(4)	649.3(1)	650.4(2)	1558.5(5)	870.7(3)
Z	4	2	2	8	4
μ [mm^{-1}]	2.737	0.976	2.407	1.669	1.273
No. of reflections:					
total	975	3396	2145	2316	929
unique	508	2270	1222	1375	634
$R[I > 2\sigma(I)]$					
*R*1	0.0546	0.0550	0.0630	0.0603	0.0630
*wR*2	0.1251	0.1538	0.1480	0.1286	0.1788

 © 2003 Wiley-VCH Verlag GmbH & Co. KGaA, Weinheim

rate of 10°/min. NMR spectra were carried out with a Varian 500 spectrometer. Fluorescent spectra were measured with an Edinburgh F900 analytical instrument at Fuzhou University.

Syntheses

$[Cd(dadpm)(I)_2]_n$ (1): Ligand dadpm (0.10 g, 0.5 mmol) was added to an aqueous solution (30 mL) of CdI_2 (0.09 g, 0.25 mmol). After stirring the mixture for about 30 min, a DMF (5 mL) solution of sodium dicyanamide (0.03 g, 0.25 mmol) was added. The above mixture was stirred and heated for 1 h and then filtered while still hot. The filtrate was allowed to stand at room temperature. On concentration for about one week, colorless block crystals of **1** were obtained. Yield: 0.10 g (72%). $C_{13}H_{14}CdI_2N_2$ (564.48): calcd. C 27.64, H 2.48, N 4.96; found C 28.45, H 2.57, N 5.06.

$[\{Cd(dadpm)_2(Cl)\}(dca)]_n$ (2): This compound was prepared as light-yellow block crystals in a similar manner to that of **1** except $CdCl_2{\cdot}2.5H_2O$ was used instead of CdI_2 Yield 0.12 g (78%). $C_{28}H_{28}CdClN_7$ (610.42): calcd. C 55.04, H 4.59, N 16.05; found C 55.14, H 4.66, N 16.14.

$[\{Cd(dadpm)_2(Br)\}(dca)]_n$ (3): This compound was prepared as light-yellow block crystals in a similar manner to that of **1** except $CdBr_2{\cdot}4H_2O$ was used instead of CdI_2. Yield 0.13 g (82%). $C_{28}H_{28}CdBrN_7$ (654.88): calcd. C 51.31, H 4.28, N 14.96; found C 51.42, H 4.26, N 15.04.

$[Cd(dadpm)(SCN)_2]_n$ (4): Sodium thiocyanate (0.05 g, 0.5 mmol) was added to an aqueous (30 mL) solution of $CdCl_2{\cdot}2.5H_2O$ (0.057 g, 0.25 mmol). After stirring of the mixture for about 30 min, a DMF (5 mL) solution of the ligand dadpm (0.05 g, 0.25 mmol) was added. The above mixture was stirred and heated for 1 h and then filtered while still hot. Well-shaped light-yellow crystals of **4** were obtained from the filtrate by slow concentration at room temperature for several days. Yield 0.078 g (73%). $C_{15}H_{14}CdN_4S_2$ (428.8): calcd. C 41.98, H 3.26, N 13.06; found C 42.07, H 3.35, N 13.16.

$[Cd(dadpm)(dca)_2]_n$ (5): This compound was prepared as pale yellow prismatic crystals in a similar manner to that of **4** except that sodium dicyanamide was used instead of sodium thiocyanate. Yield 0.074 g (67%). $C_{17}H_{14}CdN_8$ (444.74): calcd. C 45.87, H 3.15, N 25.18; found C 45.92, H 3.22, N 25.28.

X-ray Crystallography: Colorless crystals of **1** and light-yellow crystals of **2**, **3**, **4** and **5** were selected for diffraction analyses. The data collections were performed with a Siemens Smart CCD diffractometer with graphite-monochromated Mo-K_α radiation (λ = 0.71073 Å) at 298 K. All the structures were solved by direct methods and refined by full-matrix least-squares based on F^2 using the SHELX-97 program.[16] All non-hydrogen atoms were refined anisotropically. Hydrogen atoms were located geometrically. The crystallographic data for compounds **1**−**5** are listed in Table 1, and selected bond lengths and angles in Table 2. Additional crystallographic details and complete listings of the five complexes have been deposited with the Cambridge Crystallographic Data Centre. CCDC-177678 (**1**), -175521 (**2**), -177947 (**3**), -177679 (**4**) and

Table 2. Selected bond lengths [Å] and angles [°] for complexes **1**−**5**; symmetry codes: **1** (A) $-x, -y, z$; (B) $-x, y, z$; (C) $-x, -y-1, z$; **2** (A) $-x, -y, -z+1$; (B) $x+1, y, z-1$; (C) $-x+1, -y, -z$; (D) $x+1, y, z$; (E) $x-1, y, z$; (F) $-x, -y+1, -z$; (G) $x-1, y, z+1$; **3** (A) $x+1, y, z-1$; (B) $-x, -y, -z+1$; (C) $-x+1, -y, -z$; (D) $x+1, y, z$; (E) $x-1, y, z$; (F) $-x, -y+1, -z$; (G) $x-1, y, z+1$; **4** (A) $-x-1, y, -z+1/2$; (B) $x-1/2, y-1/2, z$; (C) $-x, -y, -z+1$; (D) $-x+1/2, -y+1/2, -z+1$; (E) $x+1/2, y+1/2, z$; **5** (A) $-x+1, y, -z+1$; (B) $-x, y, -z$; (C) $x-1/2, y+1/2, z$; (D) $-x+1/2, y+1/2, -z$; (E) $x+1/2, y-1/2, z$)

Complex **1**:			
Cd−N(1)	2.32(2)	Cd−I	2.794(3)
N(1)−Cd−N(1A)	137.0(1)	N(1)−Cd−I(A)	102.8(3)
N(1)−Cd−I	102.8(3)	I−Cd−I(A)	104.9(1)
C(4)−C(5)−C(4C)	109(3)		
Complex **2**:			
Cd−N(4A)	2.357(5)	Cd−N(5)	2.385(4)
Cd−Cl(1)	2.7526(3)		
N(4A)−Cd−N(5)	93.9(2)	N(5)−Cd−Cl(1)	100.0(1)
N(4A)−Cd−Cl(1)	99.4(1)	N(4A)−Cd−N(5C)	86.1(2)
N(4B)−Cd−Cl(1)	80.6(1)	N(5)−Cd−Cl(1D)	80.0(1)
Cl(1D)−Cd−Cl(1)	180.0	Cd(E)−Cl(1)−Cd	180.0
C(5)−C(6)−C(7)	115.8(4)		
Complex **3**:			
Cd−N(3)	2.38(1)	Cd−N(4A)	2.38(1)
Cd-Br	2.8583(4)		
N(3)−Cd−N(4A)	85.7(4)	N(3)−Cd−Br	98.1(3)
N(3)−Cd−N(4B)	94.3(4)	N(3C)−Cd−Br	81.9(3)
N(4B)−Cd−Br	99.0(3)	N(4A)−Cd−Br	81.0(3)
Br−Cd−Br(D)	180.0	Cd(E)−Br−Cd	180.0
C(5)−C(6)−C(7)	116.0(1)		
Complex **4**:			
Cd−N(2)	2.336(7)	Cd−N(1)	2.353(6)
Cd−S(1B)	2.746(2)		
N(1)−Cd−S(1D)	84.0(2)	N(1)−Cd−S(1B)	96.0(2)
N(2)−Cd−N(1C)	91.6(3)	N(2)−Cd−S(1B)	92.4(2)
N(2)−Cd−N(1)	88.4(3)	N(2)−Cd−S(1D)	87.6(2)
N(2)−C(7)−S(1)	177.8(8)	C4−C(8)−C(4A)	114.9(9)
Complex **5**:			
Cd−N(1)	2.32(2)	Cd−N(2C)	2.34(3)
Cd−N(4)	2.38(2)		
N(1B)−Cd−N(1)	144.0(1)	N(2D)−Cd−N(4)	145.8(7)
N(1)−Cd−N(2C)	120.9(7)	N(1)−Cd−N(4B)	89.5(6)
N(1)−Cd−N(2D)	88.0(8)	N(1)−Cd−N(4)	72.1(7)
N(2C)−Cd−N(4)	87.4(8)	N(2D)−Cd−N(2C)	79.4(1)
N(4B)−Cd−N(4)	119.0(1)	C(6)−C(9)−C(6A)	99.3(5)

Table 3. C(Ph)−C−C(Ph) bond angles [°] and the dihedral angles of the two phenyl rings [°], M···M separations through dadpm [Å] for the five complexes

Complex	C(Ph)−C−C(Ph) bond angles	Dihedral angles of the two phenyl rings	M···M separations through dadpm
1	109.5(3)	81.6(4)	13.131
2	115.8(4)	87.7(6)	12.401
3	115.9(1)	89.7(5)	12.452
4	105.5(4)	57.2(3)	12.33
5	102.0(1)	55.3(2)	12.328

 © 2003 Wiley-VCH Verlag GmbH & Co. KGaA, Weinheim

-177680 (**5**), contain the supplementary crystallographic data for this paper. These data can be obtained free of charge at www.ccdc.cam.ac.uk/conts/retrieving.html [or from the Cambridge Crystallographic Data Centre, 12 Union Road, Cambridge CB2 1EZ, UK; Fax: (internat.) + 44-1223/336-033; E-mail: deposit@ccdc.cam.ac.uk].

Acknowledgments

The authors are grateful to the NNSF of China, Chinese Academy of Sciences and State Key Laboratory of Structural Chemistry for financial support.

[1] [1a] S. R. Batten, Robson, *Angew. Chem. Int. Ed.* **1998**, *37*, 1461−1494. [1b] M. J. Zaworotko, *Chem. Soc. Rev.* **1994**, 283. [1c] P. J. Hagrman, D. Hagrman, J. Zubieta, *Angew. Chem. Int. Ed.* **1999**, *38*, 2638−2684. [1d] O. M. Yaghi, H. Li, C. Davis, D. Richardson, T. L. Groy, *Acc. Chem. Res.* **1998**, *31*, 474−484. [1e] S. Noro, S. Kitagawa, M. Kondo, K. Seki, *Angew. Chem. Int. Ed.* **2000**, *39*, 2082−2084. [1f] C. Chen, K. S. Suslick, *Coord. Chem. Rev.* **1993**, *128*, 293−322, and references therein. [1g] M. Kondo, T. Yoshitomi, K. Seki, H. Matsuzaka, S. Kitagawa, *Angew. Chem. Int. Ed. Engl.* **1997**, *36*, 1725−1727. [1h] K. Maruoka, N. Murase, H. Yamamoto, *J. Org. Chem.* **1993**, *58*, 2938−2939. [1i] B. F. Hoskins, H. Robson, *J. Am. Chem. Soc.* **1990**, *112*, 1546−1554. [1j] O. Kahn (Ed.), *Molecular Magnetism, a Supramolecular Function*, Kluwer, Dordrecht, **1996**.

[2] [2a] K. N. Power, T. L. Hennigar, M. J. Zaworotko, *Chem. Commun.* **1998**, 595−600. [2b] O. M. Yaghi, G. Li, H. Li, *Nature (London)* **1995**, *378*, 703−705. [2c] L. Carlucci, G. Ciani, P. Macchi, D. M. Proserpio, *Chem. Commun.* **1998**, 1837−1838. [2d] S. Kawata, S. R. Breeze, S. Wang, J. E. Greedan, N. P. Raju, *Chem. Commun.* **1997**, 717−718. [2e] J. Dai, M. Yamamoto, T. Kuroda-Sowa, M. Maekawa, Y. Suenaga, M. Munakata, *Inorg. Chem.* **1997**, *36*, 2688−2690. [2f] T. Kuroda-Sowa, M. Munakata, H. Matsuda, S. Akiyama, M. Maekawa, *J. Chem. Soc., Daltron Trans.* **1995**, 2201−2208. [2g] M. Ward, *Eur. J. Inorg. Chem.* **1998**, *9*, 52−68.

[3] [3a] B. Olenyuk, A. Fechtenkötter, P. J. Stang, *J. Chem. Soc., Dalton Trans.* **1998**, 1707−1728. [3b] C. Piguet, G. Bernardinelli, G. Hopfgartner, *Chem. Rev.* **1997**, *97*, 2005−2062.

[4] M. C. T. Fyfe, J. F. Stoddart, *Acc. Chem. Res.* **1997**, *30*, 393−401.

[5] [5a] P. J. Stang, B. Olenyuk, *Acc. Chem. Res.* **1997**, *30*, 502−518. [5b] M.-L. Tong, H. K. Lee, X.-M. Chen, R.-B. Huang, T. C. W. Mak, *J. Chem. Soc., Dalton Trans.* **1999**, 3657−3660. [5c] M.-L. Tong, H.-J. Chen, X.-M. Chen, *Inorg. Chem.* **2000**, *39*, 2235−2238. [5d] P. Lightfoot, A. Snedden, *J. Chem. Soc., Dalton Trans.* **1999**, 3549−3552. [5e] L. Carlucci, G. Ciani, D. M. Proserpio, A. Sironi, *Angew. Chem. Int. Ed. Engl.* **1995**, *34*, 1895−1898. [5f] L. Carlucci, G. Ciani, D. M. Proserpio, A. Sironi, *J. Am. Chem. Soc.* **1995**, *117*, 4562−4569. [5g] M.-L. Tong, S.-L. Zheng, X.-M. Chen, *Polyhedron* **2000**, *19*, 1809−1814. [5h] S. Noro, M. Kondo, T. Ishii, S. Kitagawa, H. Matsuzaka, *J. Chem. Soc., Dalton Trans.* **1999**, 1569−1574. [5i] A. J. Blake, N. R. Champness, S. S. M. Chung, M. Schröder, *Chem. Commun.* **1997**, 1675−1676. [5j] L. Carlucci, G. Ciani, P. Macchi, D. M. Proserpio, *Chem. Commun.* **1998**, 1837−1838.

[6] [6a] L. R. MacGillivray, S. Subramanian, M. J. Zaworotko, *J. Chem. Soc., Chem. Commun.* **1994**, 1325−1326. [6b] O. M. Yaghi, H. Li, *J. Am. Chem. Soc.* **1995**, *117*, 10401−10402. [6c] L. Carlucci, G. Ciani, D. M. Proserpio, A. Sironi, *J. Chem. Soc., Dalton Trans.* **1997**, 1801−1804.

[7] [7a] J. S. Haynes, S. J. Retting, J. R. Sams, R. C. Thompson, J. Trotter, *Can. J. Chem.* **1987**, *65*, 420−426. [7b] J. A. Real, G. DeMunno, M. C. Munoz, M. Julve, *Inorg. Chem.* **1991**, *30*, 2701−2704.

[8] A. J. Blake, N. R. Champness, S. S. M. Chung, W. S. Li, M. Schröder, *Chem. Commun.* **1997**, 1005−1006.

[9] M. Fujita, Y. J. Kwon, O. Sasaki, K. Yamaguchi, K. Ogura, *J. Am. Chem. Soc.* **1995**, *117*, 7287−7288.

[10] [10a] B. F. Abraham, S. R. Batten, H. Hamit, B. F. Hoskins, R. Robson, *Angew. Chem. Int. Ed. Engl.* **1996**, *35*, 1690−1692. [10b] S. R. Batten, B. F. Hoskins, R. Robson, *J. Am. Chem. Soc.* **1995**, *117*, 5385−5386.

[11] L. Carlucci, G. Ciani, D. M. Proserpio, *New. J. Chem.* **1998**, 1319−1322.

[12] [12a] Y.-G. Zhang, Mm. Nishiura, J.-M. Li, W. Deng, T. Imamoto, *Inorg. Chem.* **1999**, *38*, 825−827. [12b] H.-X. Zhang, Z.-N. Chen, K.-B. Yu, B.-S. Kang, *Inorg. Chem. Commun.* **1999**, *2*, 223−226. [12c] H.-X. Zhang, B.-S. Kang, Z.-Y. Zhou, A. S. C. Chen, Z.-N. Chen, C. Ren, *J. Chem. Soc., Dalton Trans.* **2001**, *10*, 1664−1669.

[13] [13a] I. Potocnák, M. Dunaj-Jurco, D. Miklos, L. Jäger, *Acta Crystallogr., Sect. C* **1996**, *52*, 1653−1655. [13b] B.-W. Sun, S. Gao, Z.-M. Wang, *Chem. Lett.* **2001**, *1*, 2−3. [13c] J. L. Manson, C. D. Incarvito, A. L. Rheingold, J. S. Miller, *J. Chem. Soc., Dalton Trans.* **1998**, 3705−3706. [13d] J. L. Manson, Q.-Z. Huang, J. W. Lynn, H.-J. Koo, M.-H. Whangbo, R. Bateman, T. Otsuka, N. Wada, D. N. Argyriou, J. S. Miller, *J. Am. Chem. Soc.* **2001**, *123*, 162−172. [13e] J. L. Manson, C. R. Kmety, Q. Huang, J. W. Lynn, G. Bendele, S. Pagola, P. W. Stephens, A. J. Epstein, J. S. Miller, *Chem. Mater.* **1998**, *10*, 2552−2560. [13f] Y. M. Chow, D. Britton, *Acta Crystallogr., Sect. B* **1975**, *31*, 1934−1937.

[14] A. Claramunt, A. Escuer, F. A. Mautner, N. Sanz, R. Vicente, *J. Chem. Soc., Dalton Trans.* **2000**, *15*, 2627−2630.

[15] R. Wang, M. Hong, J. Luo, R. CAO, Q. Shi, J. Weng, *Eur. J. Inorg. Chem.* **2002**, *11*, 2904.

[16] G. M. Sheldrick, *Bruker SHELSTL-PC*, University of Göttingen, Germany, **1997**.

[17] [17a] M. Taniguchi, M. Shimoi, A. Ouchi, *Bull. Chem. Soc. Jpn.* **1986**, *59*, 2299−2302. [17b] M. Taniguchi, Y. Sugita, A. Ouchi, *Bull. Chem. Soc. Jpn.* **1987**, *60*, 1321−1326. [17c] M. Taniguchi, A. Ouchi, *Bull. Chem. Soc. Jpn.* **1987**, *60*, 1192−1194. [17d] G. G. Ram, P. H. William, J. O. Marc, L. B. Andre, *Inorg. Chem.* **1981**, *20*, 3924−3928.

[18] [18a] E. Q. Gao, Z. M. Wang, C. S. Liao, C. H. Yan, *New J. Chem.* **2002**, *26*, 1096−1098. [18b] J. H. Luo, M. C. Hong, J. B. Weng, Y. J. Zhao, R. Cao, *Inorg. Chim. Acta* **2002**, *329*, 59−65. [18c] J.-H. Luo, M.-C. Hong, R. Cao, Y.-C. Liang, Y.-J. Zhao, R.-H. Wang, J.-B. Weng, *Polyhedron* **2002**, *21*, 893−898.

[19] J. L. Manson, D. W. Lee, A. L. Rheingold, J. S. Miller, *Inorg. Chem.* **1998**, *37*, 5966−5967.

[20] [20a] J. N. McElearney, L. L. Balagot, J. A. Muir, R. D. Spence, *Phys. Rev. B.* **1979**, *19*, 306−317. [20b] A. Escuer, R. Vicente, M. A. S. Goher, F. M. Mautner, *Inorg. Chem.* **1996**, *35*, 6386−6391. [20c] G. Yang, H.-G. Zhu, B.-H. Liang, X.-M. Chen, *J. Chem. Soc., Dalton Trans.* **2001**, 580−585.

[21] J. L. Manson, C. D. Incarvito, A. L. Rheingold, J. S. Miller, *J. Chem. Soc., Dalton Trans.* **1998**, 3705−3706.

[22] K. Nakamoto, *Infrared and Raman Spectra of Inorganic and Coordination Compounds*, 4th ed., Wiley, New York, **1986**.

[23] H. Köhler, A. Kolbe, G. Lux, *Z. Anorg. Allg. Chem.* **1977**, *428*, 103−107.

[24] [24a] d^{10} (Cu^{I}, Ag^{I}, Au^{I}, Zn^{II}, Cd^{II}) metal complexes have been found to exhibit intriguing structural and photoluminescent properties: P. D. Havey, H. B. Gray, *J. Am. Chem. Soc.* **1988**, *110*, 2145−2147. [24b] K. R. Kyle, C. K. Ryu, J. A. DiBenedetto, P. C. Ford, *J. Am. Chem. Soc.* **1991**, *113*, 2954−2965. [24c] P. C. Ford, E. Cariati, J. Bourassa, *Chem. Rev.* **1999**, *99*, 3625−3648.

Received September 25, 2002

 © 2003 Wiley-VCH Verlag GmbH & Co. KGaA, Weinheim

Mechanisms of the Axial Ligand Substitution Reactions of Dinuclear, Head-to-Head α-Pyrrolidonato- and Pivalamidato-Bridged *cis*-Diammineplatinum(III) Complexes with Halide Ions

Kazuhiro Shimazaki,[a] Hideo Sekiya,[a] Haruhiko Inoue,[a] Nami Saeki,[a] Koji Ishihara,*[d] and Kazuko Matsumoto*[e]

Keywords: Platinum / Kinetics / Mechanism / α-Pyrrolidone / Pivalamide

The acid dissociation constant of the axial aqua ligand in the Head-to-Head (HH) dinuclear pivalamidato-bridged *cis*-diammineplatinum(III) complex ($[(H_2O)Pt(NH_3)_2(\mu\text{-}C_5H_{10}NO)_2\text{-}Pt(NH_3)_2(H_2O)]^{4+}$) and the formation constants of the successive substitution reactions on the axial sites of the HH α-pyrrolidonato-bridged *cis*-diammineplatinum(III) dinuclear complex and the HH pivalamidato-bridged *cis*-diammineplatinum(III) dinuclear complex with halide ions X^- (X^- = Cl^- and Br^-) to give monohalo and dihalo complexes were determined spectrophotometrically at 25 °C and I = 2.0 M. A kinetic study was also performed for the monohalo and dihalo complex formations. The effect of the bridging ligand upon the axial site reactivity was compared and discussed. The ligand substitution behavior of the monohalo complex was affected by the axial ligand on the opposite Pt site and also by the bridging ligand. For both the α-pyrrolidonato- and the pivalamidato-bridged complexes, the formation of dichloro complexes proceeds only through the simple substitution path (k_2 path), whereas the formation of dibromo complexes proceeds through the two parallel reaction paths: the k_2 and k_3 paths for the former and the k_2 and $k_2^{\#}$ paths for the latter. The difference of the reaction paths is reasonably explained by the different *trans* effect of the halide ion on the opposite axial site for the former complex, but for the latter complex, the reaction paths are not easy to explain.

(© Wiley-VCH Verlag GmbH & Co. KGaA, 69451 Weinheim, Germany, 2003)

Introduction

Head-to-head (HH) amidato-bridged platinum(III) dinuclear complexes containing a metal-metal bond are formed by oxidation of the mixed-valent "platinum blues".[1−11] The two platinum atoms in the dinuclear complexes are nonequivalent: one is coordinated by two ammine nitrogen atoms and two amidate oxygen atoms [$Pt(N_2O_2)$], whereas the other is coordinated by four nitrogen atoms [$Pt(N_4)$], as shown below. The head-to-tail (HT) isomer, in which the two platinum atoms are equivalent, is also known.[4] In our previous reports,[12,13] the kinetics of the axial aqua ligand substitution with halide ions in the HH and HT α-pyridonato-bridged dimers were reported. On both of the HH and HT dimers, the axial ligand substitution occurs in two steps [Equation (1) and (2)].

$$[(H_2O)Pt(NH_3)_2(\mu\text{–}C_5H_4NO)_2Pt(NH_3)_2(H_2O)]^{4+} + X^- \underset{}{\overset{\text{Step 1}}{\rightleftharpoons}} [(H_2O)Pt(NH_3)_2(\mu\text{–}C_5H_4NO)_2Pt(NH_3)_2(X)]^{3+} + H_2O \quad (1)$$

$$[(H_2O)Pt(NH_3)_2(\mu\text{–}C_5H_4NO)_2Pt(NH_3)_2(X)]^{3+} + X^- \underset{}{\overset{\text{Step 2}}{\rightleftharpoons}} [(X)Pt(NH_3)_2(\mu\text{–}C_5H_4NO)_2Pt(NH_3)_2(X)]^{2+} + H_2O \quad (2)$$

In the HT dimer, the first halide substitution occurs at one of the two equivalent Pt^{III} atoms, and the first deprotonation occurs at the H_2O of the other Pt^{III} atom; in the HH dimer, the first deprotonation occurs at the H_2O on the $Pt(N_4)$ atom, and the first halide substitution takes place at the $Pt(N_2O_2)$ atom. These phenomena show that the axial halide exerts a *trans* effect through the Pt−Pt bond to the other axial H_2O ligand after the first substitution in both of the HH and HT dimers. In the second halide substitution at the other Pt atom, the substitution lability is influenced strongly by the first halide ligand on the opposite axial site,

[a] Department of Chemistry, School of Science and Engineering, Waseda University,
3-4-1 Okubo, Shinjuku-ku, Tokyo 169-8555, Japan
Fax: (internat.) + 81-3/3208-2735
E-mail: ishi3719@waseda.jp
kmatsu@waseda.jp
[b] Materials Research Laboratory for Bioscience and Photonics, Graduate School of Science and Engineering, Waseda University,
3-4-1 Okubo, Shinjuku-ku, Tokyo 169-8555, Japan
[c] Advanced Research Institute for Science and Engineering, Waseda University
3-4-1 Okubo, Shinjuku-ku, Tokyo 169-8555, Japan
Supporting information for this article is available on the WWW under http://www.eurjic.org or from the author.

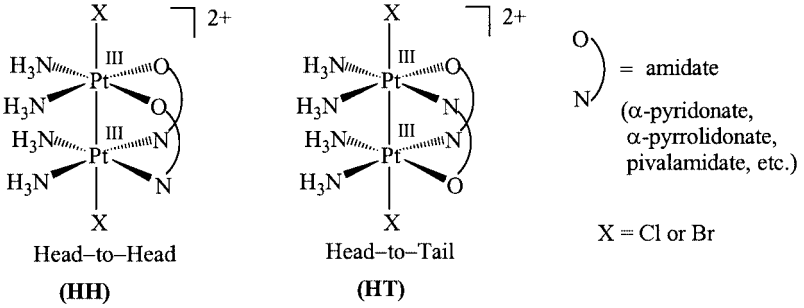

as the charge localization along the Pt−Pt axis is triggered by the first halide ligand, and the extent of the charge localization in the Pt−Pt bond in the dimer {the contribution of HH-$[(X)Pt^{IV}(N_2O_2)\text{-}Pt^{II}(N_4)(H_2O)]^{3+}$ and HT-$[(X)Pt^{IV}(N_3O)\text{-}Pt^{II}(N_3O)(H_2O)]^{3+}$} depends largely on the electron donating ability of the first substituted ligand (X^-).

In this paper we report a kinetic and equilibrium study of the axial aqua ligand substitution with halide ions in the HH α-pyrrolidonato-bridged dinuclear Pt^{III} complex $[(H_2O)Pt(NH_3)_2(\mu\text{-}C_4H_6NO)_2Pt(NH_3)_2(H_2O)]^{4+}$ and the HH pivalamidato-bridged dinuclear Pt^{III} complex $[(H_2O)Pt(NH_3)_2(\mu\text{-}C_5H_{10}NO)_2Pt(NH_3)_2(H_2O)]^{4+}$ (Scheme 1), in order to examine the effect of the bridging ligand on the axial ligand substitution.

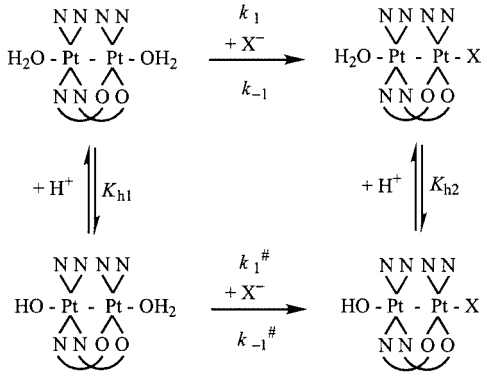

Scheme 1. (X^- = Cl^- or Br^-)

Results

Formation Constants of the HH α-Pyrrolidonato-bridged and the HH Pivalamidato-bridged Monohalo and Dihalo Dimer Complexes

The absorption spectra were measured at I = 2.00 M and 25 °C for solutions with various ratios of halide ion concentration, C_X^-, (X^- = Cl^- or Br^-) to a fixed dimer concentration, C_{HH}, and are shown in Figure 1 and 2. Several distinct isosbestic points are observed. The spectral changes with varying C_X^- are much the same as those for the α-pyridonato-bridged dimers reported previously.[12,13] Therefore, this spectral change corresponds to the following stepwise reactions [Equation (3) and (4)], i.e., the first substitution occurs at the $Pt(N_2O_2)$ atom and the second at the $Pt(N_4)$ atom.

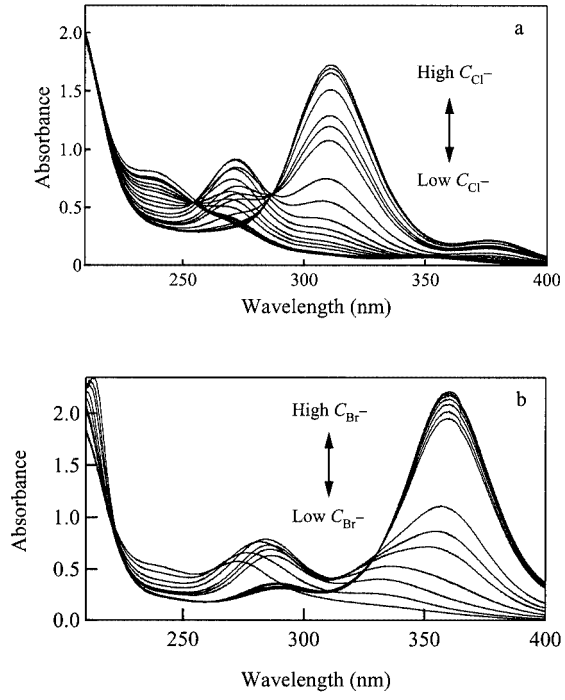

Figure 1. The UV/Vis spectra of the HH α-pyrrolidonato-bridged dimer in acidic aqueous solution with different C_X^- at 25 °C and I = 2.0 M. [H^+] = 1.27 M (a); [H^+] = 0.401 M (b), C_{Cl^-} = 0−4.1 × 10^{-3} M (a); C_{Br^-} = 0−2.1 × 10^{-3} M (b); C_{HH} = 9.6 × 10^{-5} M (a), C_{HH} = 3.9 × 10^{-5} M (b)

$$[H_2O\text{–}Pt(N_4)\text{–}Pt(N_2O_2)\text{–}H_2O]^{4+} + X^- \underset{}{\overset{K_1^X}{\rightleftharpoons}} [H_2O\text{–}Pt(N_4)\text{–}Pt(N_2O_2)\text{–}X]^{3+} + H_2O \quad (3)$$

$$[H_2O\text{–}Pt(N_4)\text{–}Pt(N_2O_2)\text{–}X]^{3+} + X^- \underset{}{\overset{K_2^X}{\rightleftharpoons}} [X\text{–}Pt(N_4)\text{–}Pt(N_2O_2)\text{–}X]^{2+} + H_2O \quad (4)$$

 © 2003 Wiley-VCH Verlag GmbH & Co. KGaA, Weinheim

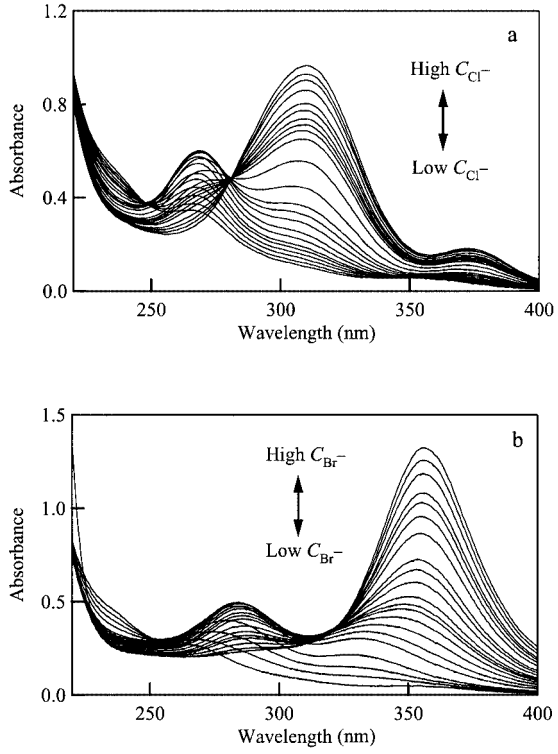

Figure 2. The UV/Vis spectra of the HH pivalamidato-bridged dimer in acidic aqueous solution with different C_X^- at 25 °C and I = 2.0 M. [H^+] = 0.803 M, C_{Cl^-} = 0−1.7 × 10^{-2} M (a); C_{Br^-} = 0−1.1 × 10^{-2} M (b); C_{HH} = 3.9 × 10^{-5} M (a), C_{HH} = 3.2 × 10^{-5} M (b)

The K_1^X and K_2^X values were obtained by simultaneously analyzing the spectra in Figure 1 and 2.

The values of K_{h_1}, the first acid dissociation constant (deprotonation of the H_2O ligand on the $Pt(N_4)$ atom) of the diaqua complex, was also obtained for the pivalamidato-bridged dimer. The obtained values are given in Table 1. The K_1^{Cl} and K_2^{Cl} values agree reasonably with the corresponding values for the reaction of the HH α-pyrrolidonato-bridged dimer with Cl^- (Table 1).

Kinetics for the Formation of the HH α-Pyrrolidonato- and Pivalamidato-Bridged Monohalo Complexes

The formation rate of the monohalo complex (Pt_2X) is given by Equation (5) under the present experimental conditions ($C_{HH} << C_X^-$), in which [HH] is the concentration of the unchanged dimer.

$$d[Pt_2X]/dt = k_{obs1}[HH] \quad (5)$$

The conditional first-order rate constant k_{obs1} is linearly dependent on C_X^- at a given [H^+] as shown in Figure 3, thus, k_{obs1} is expressed as Equation (6):

$$k_{obs1} = k_{f1} C_{HH} \quad (6)$$

It is obvious from Figure 3 that k_{f1} in Equation (6) depends on [H^+]. This [H^+] dependency is similar to that for the HH α-pyridonato-bridged dimer system reported previously,[13] and was successfully analysed according to Equation (7), which was derived based on Scheme 1 for the previous system.

$$k_{obs1} = \frac{k_1 + \frac{k_1^{\#} K_{h1}}{[H^+]}}{1 + \frac{K_{h1}}{[H^+]}} C_{HH} \quad (7)$$

The values of k_1 and $k_1^{\#}$ were obtained by applying a nonlinear least-squares fitting to Equation (7), and are listed in Table 2, together with the related data.

Kinetics for the Formation of the HH α-Pyrrolidonato- and Pivalamidato-Bridged Dihalo Complexes

Under these conditions, $C_{HH} << C_X^-$, the formation rate of the dihalo complex (Pt_2X_2) is expressed as Equation (8), where [HH-X] is the concentration of the monohalo HH dimer.

$$d[Pt_2X_2]/dt = k_{obs2}[HH\text{-}X] \quad (8)$$

The rate constant of the second substitution step, k_{obs2}, depends linearly on C_X^- for the reactions of the α-pyrrolidonato-bridged dimer with Cl^- and the pivalamidato-bridged dimer with Cl^- and Br^-, and nonlinearly for the reaction of the α-pyrrolidonato-bridged dimer with Br^-, as shown in Figure 4.

Table 1. Equilibrium constants for the reaction of the HH amidato-bridged *cis*-diammineplatinum(II) dimer with halide ions determined spectrophotometrically at I = 2.00 M and 25 °C

Bridging ligand	−log K_{h1}	log K_1^{Cl}	log K_2^{Cl}	log K_1^{Br}	log K_2^{Br}
α-Pyridonate[a]	1.71 ± 0.03	5.93 ± 0.02	3.71 ± 0.01	6.20 ± 0.05	4.55 ± 0.01
α-Pyrrolidonate	3.02[b]	5.61 ± 0.03 5.23[c]	3.73 ± 0.01 3.60[c]	5.48 ± 0.02	4.68 ± 0.01
Pivalamidate	2.88 ± 0.01	5.04 ± 0.04	3.21 ± 0.01	5.93 ± 0.01	3.91 ± 0.01

[a] Ref.[13] [b] Ref.[14] [c] Ref.[15]

 © 2003 Wiley-VCH Verlag GmbH & Co. KGaA, Weinheim

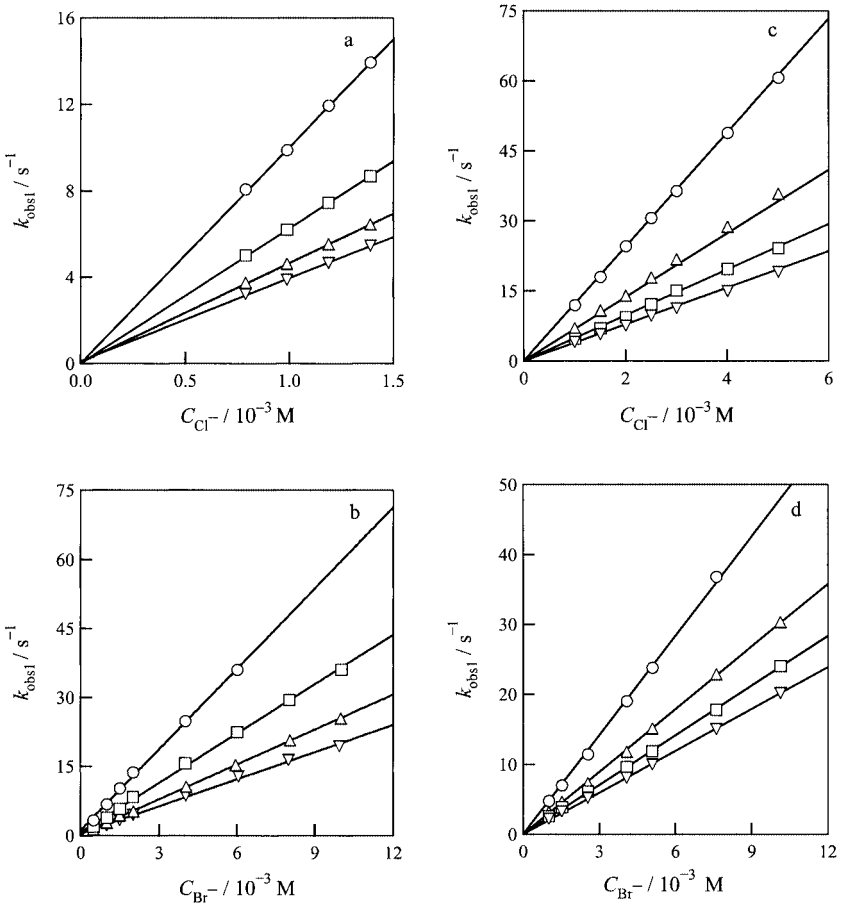

Figure 3. The dependence of k_{obs1} on C_X^- in acidic aqueous solution at 25 °C and I = 2.0 M: (a) the reaction of the HH α-pyrrolidonato-bridged dimer with chloride ion, C_{HH} = 4.0 × 10^{-5} M, [H^+] = 0.208 (circle), 0.401 (square), 0.602 (triangle), 0.803 M (wedge); (b) the reaction of the HH α-pyrrolidonato-bridged dimer with bromide ion, C_{HH} = 4.0 × 10^{-5} M, [H^+] = 0.207 (circle), 0.401 (square), 0.617 (triangle), 0.822 M (wedge); (c) for the reaction of the HH pivalamidato-bridged dimer with chloride ion, C_{HH} = 4.0 × 10^{-5} M, [H^+] = 0.207 (circle), 0.401 (triangle), 0.602 (square), 0.803 M (wedge); (d) for the reaction of the HH pivalamidato-bridged dimer with bromide ion, C_{HH} = 2.0 × 10^{-5} M, [H^+] = 0.401 (circle), 0.803 (triangle), 1.00 (square), 1.20 M (wedge)

Table 2. The rate constants for step 1 of the reactions of the HH amidato-bridged *cis*-diammnineplatinum(III) dimers with halide ions at I = 2.00 M and 25 °C

Ligand	Bridging ligand	Path	k [$M^{-1}s^{-1}$]
Cl^-	α-Pyridonate[a]	k_1	3.1×10^3
		$k_1^{\#}$	4.6×10^5
	α-Pyrrolidonate	k_1	(1.98 ± 0.03)×10^3
		$k_1^{\#}$	(1.70 ± 0.01)×10^6
	Pivalamidate	k_1	(1.12 ± 0.03)×10^3
		$k_1^{\#}$	(1.76 ± 0.07)×10^6
Br^-	α-Pyridonate[a]	k_1	7.2×10^3
		$k_1^{\#}$	2.4×10^5
	α-Pyrrolidonate	k_1	(1.07 ± 0.02)×10^3
		$k_1^{\#}$	(1.00 ± 0.16)×10^6
	Pivalamidate	k_1	(1.12 ± 0.01)×10^3
		$k_1^{\#}$	(1.13 ± 0.01)×10^6

Ref.[13]

The non-linear plot in Figure 4b is very similar to those reported previously for the reactions of HH α-pyridonato-bridged dimer with Cl^- and Br^-, and the reaction of HT α-pyridonato-bridged dimer with Br^-,[12,13] i.e., k_{obs2} increases linearly with C_{Br^-} at lower C_{Br^-}, and it still increases linearly at higher C_{Br^-}, but with a different slope. This fact is explained by the mechanism in Scheme 2.

The linear plots in Figure 4d are dependent on [H^+], and have a close resemblance to those for the reaction of the HT α-pyridonato-bridged dimer with Cl^-. Therefore Scheme 3 can be proposed for the present reaction analogous to the reported α-pyridonato-bridged dimer.

On the other hand, the plots in Figure 4a and 4c have no [H^+] dependency and zero and non-zero intercepts, respectively. These facts correspond to simple substitutions without and with the contribution of the reverse reaction, respectively, as shown in Scheme 4.

In Scheme 2, when the steady-state approximation is applied to the monobromo dimer without an axial ligand at the opposite site, Equation (9) is obtained when the reverse reaction is negligible.

$$k_{obs2} = k_2[Br^-] + \frac{k_3 k_4[Br^-]}{k_{-3} + k_4[Br^-]} \quad (9)$$

 © 2003 Wiley-VCH Verlag GmbH & Co. KGaA, Weinheim

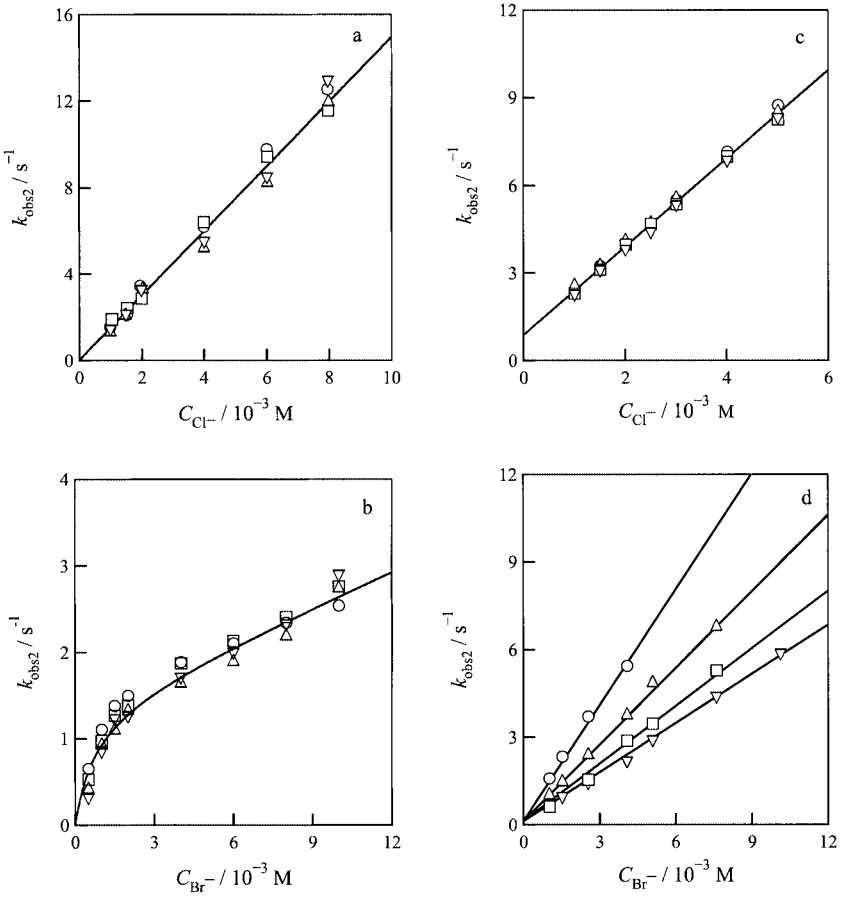

Figure 4. The dependence of k_{obs2} on C_X^- in acidic aqueous solution at 25 °C and I = 2.0 M: (a) the reaction of the HH α-pyrrolidonato-bridged dimer with chloride ion, C_{HH} = 1.0 × 10^{-4} M, [H^+] = 0.207 (circle), 0.401 (square), 0.617(triangle), 0.822 M (wedge); (b) the reaction of the HH α-pyrrolidonato-bridged dimer with bromide ion, C_{HH} = 4.0 × 10^{-5} M, [H^+] = 0.207 (circle), 0.401 (square), 0.617(triangle), 0.822 M (wedge); (c) for the reaction of the HH pivalamidato-bridged dimer with chloride ion, C_{HH} = 4.0 × 10^{-5} M, [H^+] = 0.207 (circle), 0.401 (triangle), 0.602 (square), 0.803 M (wedge); (d) for the reaction of the HH pivalamidato-bridged dimer with bromide ion, C_{HH} = 2.0 × 10^{-5} M, [H^+] = 0.401 (circle), 0.803 (triangle), 1.00 (square), 1.20 M (wedge)

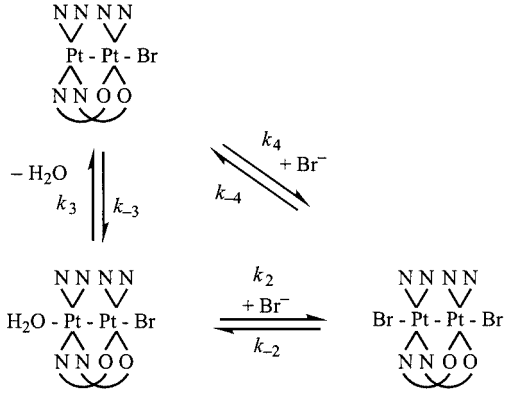

Scheme 2. (HH α-pyrrolidonato-bridged dimer + Br^-)

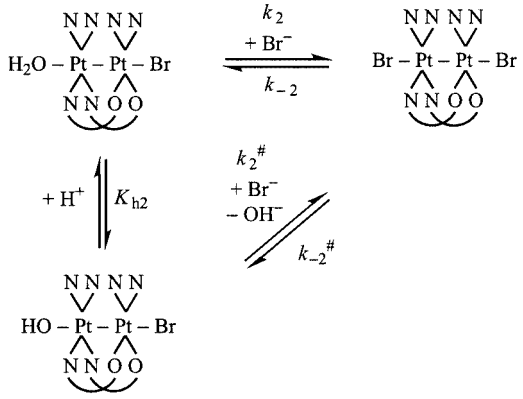

Scheme 3. (HH pivalamidato-bridged dimer + Br^-)

 © 2003 Wiley-VCH Verlag GmbH & Co. KGaA, Weinheim

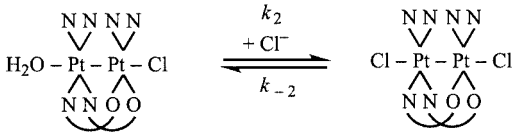

(HH α-pyrrolidonato-bridged dimer + Cl^-)

(HH α-pivalamidato-bridged dimer + Cl^-)

Scheme 4. (HH α-pyrrolidonato-bridged dimer + Cl^-) (HH pivalamidato-bridged dimer + Br^-)

For Schemes 3 and 4, k_{obs2} is represented by Equation (10) and (11), respectively, in which k_{-2} in Equation (11) should be omitted for the reaction of the HH α-pyrrolidonato-bridged dimer with Cl^-.

$$k_{obs2} = \frac{k_2 + \frac{k_2^{\#} K_{h2}}{[H^+]}}{1 + \frac{K_{h2}}{[H^+]}} C_{Br^-} \quad (10)$$

$$k_{obs2} = k_2 C_{Cl^-} + k_{-2} \quad (11)$$

The determined rate constants in Equation (9)−(11) are tabulated in Table 3.

Table 3. The rate constants for step 2 of the reactions of the HH amidato-bridged *cis*-diammnineplatinum(III) dimer with halide ions at I = 2.00 M and 25 °C

Ligand	Bridging ligand	Path	k [$M^{-1}s^{-1}$]
Cl^-	α-Pyridonate[a]	k_2	$(5.50 \pm 0.10)\times10^2$
		k_3 [b]	3.1 ± 0.3
		k_{-3}/k_4 [c]	$(3.7 \pm 0.5)\times10^{-3}$
	α-Pyrrolidonate	k_2	$(1.52 \pm 0.01)\times10^3$
	Pivalamidate	k_2	$(1.51 \pm 0.01)\times10^3$
		k_{-2} [b]	$(8.66 \pm 0.24)\times10^{-1}$
Br^-	α-Pyridonate[a]	k_2	$(4.50 \pm 0.36)\times10^2$
		k_3	4.4 ± 0.8
		k_{-3}/k_4 [c]	$(3.7 \pm 0.8)\times10^{-3}$
	α-Pyrrolidonate	k_2	$(1.36 \pm 0.07)\times10^2$
		k_3	1.39 ± 0.07
		k_{-3}/k_4 [c]	$(7.73 \pm 0.93)\times10^{-4}$
	Pivalamidate	k_2	$(1.01 \pm 0.30)\times10^2$
		k_{-2} [b]	$(1.25 \pm 0.46)\times10^{-2}$
		$k_2^{\#}K_{h2}$ [b]	$(8.52 \pm 0.81)\times10^2$

[a] Ref.[13] [b] In s^{-1}. [c] In M.

Discussion

In view of Table 1, the first acid dissociation constant K_{h1} of the α-pyridonato-bridged dinuclear complex is larger than those of the α-pyrrolidonato- and the pivalamidato-bridged complexes, whose K_{h1}'s are similar. It should be noted that the difference between $\log K_1^{Cl}$ and $\log K_1^{Br}$ for the pivalamidato-bridged system is larger than those for the other two systems, and $\log K_1^{Cl}$ and $\log K_2^{X}$ for the pivalamidato-bridged system are significantly smaller than the corresponding values for the other two systems.

The k_1 values for the reactions of the α-pyridonato-bridged complex with both Cl^- and Br^- are somewhat larger than those for the reactions of the α-pyrrolidonato- and pivalamidato-bridged complexes with the corresponding halide ions, whereas this relation is reversed for the $k_1^{\#}$ values, as shown in Table 2. As mentioned above, in the HH dimer the deprotonation occurs at the H_2O of the $Pt(N_4)$ [H_2O-$Pt(N_2O_2)$-$Pt(N_4)$-OH_2 → H_2O-$Pt(N_2O_2)$-$Pt(N_4)$-OH + H^+], whereas the first ligand substitution takes place at the opposite $Pt(N_2O_2)$ atom [H_2O-$Pt(N_2O_2)$-$Pt(N_4)$-OH_2 + X^- → X-$Pt(N_2O_2)$-$Pt(N_4)$-OH_2 + H_2O]; the second ligand substitution at $Pt(N_4)$ is strongly influenced by the first ligated ligand on the $Pt(N_2O_2)$. So, the k_1 and $k_1^{\#}$ values may reflect that the H_2O-$Pt(N_2O_2)$ bond in the α-pyridonato-bridged diaqua complex is weaker than those in the α-pyrrolidonato- and pivalamidato-bridged complexes, since the H_2O-$Pt(N_4)$ bond in the former complex, which has a larger K_{h1}, is stronger than those in the latter complexes which have smaller K_{h1}, and that once the diaqua complexes are deprotonated, the H_2O-$Pt(N_2O_2)$ bonds in the aquahydroxo complexes become weaker for these complexes, since the opposite HO-$Pt(N_4)$ bonds become stronger in the deprotonated complexes. In the dinuclear complex [X_2-$Pt(N_4)$-$Pt(N_2O_2)$-X_1] the axial bond length [X_1-$Pt(N_2O_2)$, X_2-$Pt(N_4)$, and Pt-Pt] depends on both X_1 and X_2.[13] On the basis of the findings mentioned above, it follows that the bond length (and the extent of the charge localization) also changes depending on the bridging ligand.

The rate constants for step 2 are summarized in Table 3. The rate constants k_2 for the direct substitution of the monohalo complexes with halide ion (see Schemes 2−4) show that the α-pyridonato-bridged monochloro complex is less reactive than the α-pyrrolidonato- and pivalamidato-bridged monochloro complexes, whereas the α-pyridonato-bridged monobromo complex is more reactive than the other monobromo complexes. Thus, the substitution reactivity of the axial sites of the amidato-bridged dinuclear complex is considerably influenced by the bridging ligand.

The formation constant K_2^X ($= k_2/k_{-2}$) for the pivalamidato-bridged dihalo complex, derived from the rate constants (k_2 and k_{-2}) in Table 3, is in excellent agreement with K_2^X in Table 1 obtained by spectrophotometry [$\log K_2^{Cl} = \log(k_2/k_{-2}) = 3.24$; $\log K_2^{Br} = 3.91$], which supports the present kinetic analysis.

The reaction mechanism for step 1 is described in Scheme 1, in which there are two reaction pathways in all the systems under the present conditions: one is the substitution of H_2O at the $Pt(N_2O_2)$ center in the diaqua complex, and the other is also a substitution of H_2O but at the $Pt(N_2O_2)$ center in the aquahydroxo complex. The reaction mechanisms for step 2 are shown in Schemes 2−4. There are three possible pathways for step 2, depending on the axial ligand (X_1) at the $Pt(N_2O_2)$ center, as discussed previously:[12,13] one is the direct substitution path (k_2), the se-

 © 2003 Wiley-VCH Verlag GmbH & Co. KGaA, Weinheim

cond is the path (k_3) via dissociation of the water molecule ligated to the $Pt(N_4)$, and the third is the unusual path ($k_2^{\#}$) of the OH^- replacement at the $Pt(N_4)$. This last path is impossible in mononuclear metal complexes, but can occur in the present complexes, probably due to the contribution of the electron localization of the form $HO\text{-}Pt^{II}\text{-}Pt^{IV}\text{-}X_1$. When X_1 on the $Pt(N_2O_2)$ is less electron donating, the reaction tends to proceed through the k_2 and $k_2^{\#}$ paths,

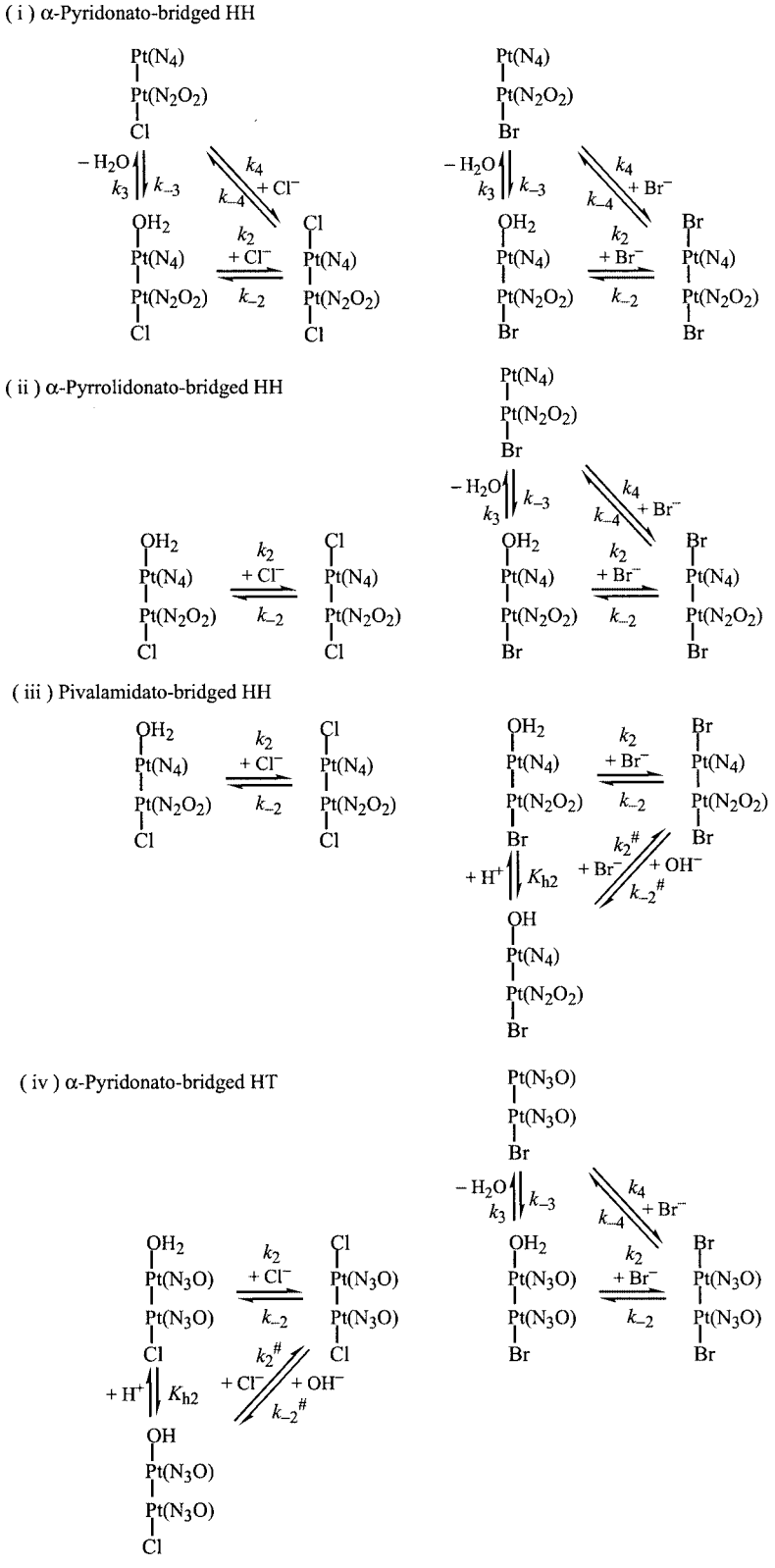

Scheme 5. Reaction pathways of the second step for the reactions of the amidato-bridged Pt^{III} dinuclear complexes with halides

 © 2003 Wiley-VCH Verlag GmbH & Co. KGaA, Weinheim

whereas when X_1 is more electron donating, the k_2 and k_3 paths are preferred. The reaction schemes of step 2 for the reactions of the α-pyrrolidonato- and pivalamidato-bridged complexes are summarized in Scheme 5, together with those for the HH and HT α-pyridonato-bridged dinuclear complexes.[12,13]

The mechanistic difference in the α-pyridonato-bridged HH and HT dinuclear complexes was interpreted as follows: the difference in the HT α-pyridonato-bridged complex + Cl^- and the HT complex + Br^- systems can be reasonably explained by the relative electron donor ability of Cl^- and Br^-. Because the more electron donating Br^- facilitates dissociation of the axial aqua ligand from the opposite Pt atom, the coordinatively unsaturated intermediate is involved in the mechanism [Scheme 5 (iv)]. The charge localization through the Pt−Pt bond would be more pronounced in the HH aquahalo dimer than in the HT aquahalo dimer since the two Pt atoms are not equivalent in the HH diaqua dimer, i.e., the HH aquahalo dimer has greater $Pt^{II}(N_4)$-$Pt^{IV}(N_2O_2)$-X_1 character than the HT aquahalo dimer, and this shifts the mechanism of (iv) to the dissociative mechanism of (i) in Scheme 5. According to these explanations, the extent of charge localization in the α-pyrrolidonato- and pivalamidato-bridged monochloro complexes having only the k_2 path would be intermediate between the HH and HT α-pyridonato-bridged dimers. In the α-pyrrolidonato-bridged monohalo dimer, the charge localization of the monobromo dimer would be more pronounced than that of the monochloro dimer, whereas the opposite tendency is observed for the pivalamidato-bridged monohalo complexes. Therefore, both the bridging ligand and the axial ligand X_1 affect the mechanism. From the viewpoint of the bridging ligand, the order of the electron localization enhancement in the HH monochloro complexes is α-pyridonato-bridged complex > α-pyrrolidonato-bridged complex ≈ pivalamidato-bridged complex, and in the HH monobromo complexes, α-pyridonato-bridged complex ≈ α-pyrrolidonato-bridged complex > pivalamidato-bridged complex. Thus, in the HH amidato-bridged Pt^{III} dinuclear complexes, the effect of X_1 on the substitution reactivity of X_2 is not necessarily as expected from the *trans* effect of the axial ligand X_1, if the bridging ligand is varied.

Conclusion

In α-pyrrolidonato- and pivalamidato-bridged Pt^{III} dinuclear complexes, the first deprotonation occurs from the water molecule on the $Pt(N_4)$ center and the first nucleophilic substitution with X^- ($X^- = Cl^-$ and Br^-) occurs at the $Pt(N_2O_2)$ center. The formation of the HH monohalo complex (step 1) proceeds through two parallel paths: a simple substitution path (k_1) and a path ($k_1^{\#}$) accelerated by the trans-coordinated OH^-. The formation of the HH dihalo complex from the aquahalo complex (step 2) proceeds through only a simple substitution path (k_2) for the reactions of the α-pyrrolidonato- and pivalamidato-bridged complexes with Cl^-, and the mechanism is different from the reactions of the HH and HT α-pyridonato-bridged dimers with Cl^-. Step 2 proceeds through k_2 and a path with dissociation of a water molecule (k_3) for the reaction of the α-pyrrolidonato-bridged dimer with Br^-, and k_2 and a path with OH^- replacement by Br^- at the $Pt(N_4)$ center ($k_2^{\#}$) for the reaction of the pivalamidato-bridged dimer with Br^-. The substitution behavior in step 2 for the pivalamidato-bridged dimer system is quite different from that of the α-pyrrolidonato-bridged dimer and the HH and HT α-pyridonato-bridged dimer systems.

Experimental Section

General Remarks. Reagents: *cis*-$[PtCl_2(NH_3)_2]$ was prepared from $K_2[PtCl_4]$ (Tanaka Kikinzoku Kogyo K.K., Tokyo) according to Dhara's method.[16] Reagent grade α-pyrrolidone (Kanto Chemical Co. Inc., Tokyo) was purified once by vacuum distillation. Pivalamide (98%, Aldrich) was recrystallized twice from water. Sodium chloride (99.99%, Kanto), sodium bromide (99.99%, Aldrich), and perchloric acid (60% UGR for trace analysis, Kanto) were used without further purification. Sodium perchlorate was prepared and purified according to the literature procedure.[17] Head-to-head $[(H_2O)Pt(NH_3)_2(\mu\text{-}C_4H_6NO)_2Pt(NH_3)_2(H_2O)](NO_3)_4{\cdot}2H_2O$ (HH α-Pyrrolidonato-bridged dimer) and Head-to-head $[(H_2O)Pt(NH_3)_2(\mu\text{-}C_5H_{10}NO)_2Pt(NH_3)_2(H_2O)](NO_3)_4{\cdot}2H_2O$ (HH Pivalamidato-bridged dimer) were prepared according to the literature procedures.[18,19]

Measurements: Ionic strength was maintained at 2.00 M with perchloric acid and sodium perchlorate. All the sample solutions were prepared in doubly distilled water just before measurement. Spectrophotometric measurements were performed with rapid-scan/stopped-flow spectrophotometers USP-500 (Unisoku Scientific Instruments, Osaka), RSP601S (Unisoku), and SF-61DX2 (Hi-Tech Scientific, Wiltshire) and spectrophotometers UV-160A (Shimadzu, Kyoto), UV-2200 (Shimadzu), and UV-2400 (Shimadzu). Rate constants were measured by monitoring the absorbance change at 282 nm for the reaction of the HH α-pyrrolidonato-bridged dimer with Cl^- (as NaCl) and at 358 nm for the reaction with Br^- (as NaBr) for k_{obs1}, and at 268 nm for the reaction of the HH pivalamidato-bridged dimer with Cl^-, at 312 nm for the reaction of the HH dimer with Br^- for k_{obs2}, as a function of time after mixing the solutions of the dimer and sodium halide. The formation constants (K_1^X and K_2^X) of the HH monohalo and the dihalo α-pyrrolidonato- and pivalamidato-bridged dimers were determined spectrophotometrically under the following conditions. (a) For the α-pyrrolidonato-bridged dimer: $C_{HH} = 9.6 \times 10^{-4}$ M, $[H^+] = 1.27$ M, $C_{Cl^-} = 0-4.1 \times 10^{-3}$ M for K_1^{Cl} and K_2^{Cl}; $C_{HH} = 3.92 \times 10^{-5}$ M, $[H^+] = 0.401$ M, $C_{Br^-} = 0-2.11 \times 10^{-3}$ M for K_1^{Br} and K_2^{Br}; (b) for the pivalamidato-bridged dimer: $C_{HH} = 3.86 \times 10^{-5}$ M, $[H^+] = 0.803$ M, $C_{Cl^-} = 0-1.7 \times 10^{-2}$ M for K_1^{Cl} and K_2^{Cl}; $C_{HH} = 3.2 \times 10^{-5}$ M, $[H^+] = 0.8037$ M, $C_{Br^-} = 0-1.1 \times 10^{-2}$ M for K_1^{Br} and K_2^{Br}. The acid dissociation constant (K_{h1}) of the HH pivalamidato-bridged dimer was determined spectrophotometrically as described previously[12] under the conditions: $C_{HH} = 1.14 \times 10^{-4}$ M, $[H^+] = 6.69 \times 10^{-5} - 0.115$ M. All the formation and acid dissociation constants were determined with the SPECFIT program.[20] The rate constants k_{obs1} and k_{obs2} for the consecutive reaction [reactions (3) and (4)] were determined simultaneously according to the equation: $A_t = A_e + \alpha\exp(-k_{obs1}t) + \beta\exp(-k_{obs2}t)$, in which A_t and A_e are the absorbances at time t and ∞, respectively, and α and β are composite parameters.[21]

 © 2003 Wiley-VCH Verlag GmbH & Co. KGaA, Weinheim

Acknowledgments

Financial Support from the 21COE "Practical Nano-Chemistry" from MEXT, Japan is gratefully acknowledged.

[1] R. El-Mehdawi, S. A. Bryan, D. M. Roundhill, *J. Am. Chem. Soc.* **1985**, *107*, 6282−6286 and references cited therein.
[2] S. Bryan, M. K. Dickson, D. M. Roundhill, *Inorg. Chem.* **1987**, *26*, 3878−3886 and references cited therein.
[3] R. Faggiani, B. Lippert, C. J. L. Lock, R. A. Speranzini, *J. Am. Chem. Soc.* **1981**, *103*, 1111−1120.
[4] L. S. Hollis, S. J. Lippard, *Inorg. Chem.* **1983**, *22*, 2605−2614.
[5] L. S. Hollis, M. M. Roberts, S. J. Lippard, *Inorg. Chem.* **1983**, *22*, 3637−3644.
[6] T. V. O′Halloran, M. M. Roberts, S. J. Lippard, *Inorg. Chem.* **1986**, *25*, 957−964.
[7] B. Lippert, H. Schoellhorn, U. Thewalt, *Inorg. Chem.* **1986**, *25*, 407−408.
[8] H. Schoellhorn, P. Eisenmann, U. Thewalt, B. Lippert, *Inorg. Chem.* **1986**, *25*, 3384−3391.
[9] B. Lippert, H. Schoellhorn, U. Thewalt, *J. Am. Chem. Soc.* **1986**, *108*, 525−526.
[10] [10a] T. Abe, H. Moriyama, K. Matsumoto, *Chem. Lett.* **1989**, 1857−1860. [10b] T. Abe, H. Moriyama, K. Matsumoto, *Inorg. Chem.* **1991**, *30*, 4198−4204.
[11] K. Matsumoto, K. Sakai, *Adv. Inorg. Chem.* **2000**, *49*, 375−427.
[12] N. Saeki, Y. Hirano, Y. Sasamoto, I. Sato, T. Toshida, S. Ito, N. Nakamura, K. Ishihara, K. Matsumoto, *Eur. J. Inorg. Chem.* **2001**, 2081−2088.
[13] N. Saeki, Y. Hirano, Y. Sasamoto, I. Sato, T. Toshida, S. Ito, N. Nakamura, K. Ishihara, K. Matsumoto, *Bull. Chem. Soc. Jpn.* **2001**, *74*, 861−868.
[14] K. Sakai, T. Tsubomura, K. Matsumoto, *Inorg. Chim. Acta* **1995**, *234*, 157−161.
[15] K. Sakai, Y. Tsuchiya, T. Tsubomura, *Technol. Rep. Seikei Univ.* **1992**, *54*, 77−XXXX.
[16] S. C. Dhara, *Indian J. Chem.* **1970**, *8*, 193−194.
[17] S. Funahashi, K. Haraguchi, M. Tanaka, *Inorg. Chem.* **1977**, *16*, 1349−1353.
[18] [18a] K. Sakai, K. matsumoto, *J. Am. Chem. Soc.* **1989**, *111*, 3074−3075. [18b] K. Sakai, K. Matsumoto, *J. Mol. Catal.* **1991**, *67*, 7−18.
[19] K. Matsumoto, Y. Nagai, J. Matsunami, K. Mizuno, T. Abe, R. Somazawa, J. Kinoshita, H. Shimura, *J. Am. Chem. Soc.* **1998**, *120*, 2900−2907.
[20] SPECFIT Global Analysis System by Robert A. Binstead, Bernhard Jung, Andreas D. Zuberbuhler.
[21] R. G. Wilkins, *Kinetics and Mechanism of Reactions of Transition Metal Complexes*, 2nd ed., VCH, **1991**.

Received October 7, 2002

 © 2003 Wiley-VCH Verlag GmbH & Co. KGaA, Weinheim

A Two-Step Route to Self-Assembly of CdS Nanotubes via Electrodeposition and Dissolution

Shao-Min Zhou,*[a,b] Yi-Si Feng,[a] and Li-De Zhang[a]

Keywords: Cadmium / Sulfides / Nanotubes / Self-assembly / Electrochemistry

Polycrystalline CdS nanotubes (CNTs) were successfully achieved by a two-step treatment, i.e. (CdS+Cd) nanowires (electrodeposition and sulfuration process in anodic alumina membrane) → CNTs (dissolution method of removing Cd in 0.5 M HCl). Having been characterized using X-ray diffraction and scanning electron microscopy, the nanowires, the intermediate products, contain Cd and CdS, and have uniform diameters of about 80 nm and lengths of up to 25 μm, which correspond to the pore size and thickness of the membrane used. The average inner and outer diameters of the as-obtained CNTs are respectively 40 and 80 nm via transmission electron microscopy. Selected area electronic diffraction, X-ray diffraction and X-ray photoelectron energy spectroscopy investigations demonstrate that these CNTs with hexagonal wurtzite polycrystalline structure are pure and stoichiometric. The successful synthesis of these semiconductor CNTs may open up new possibilities for studies of fundamental properties and potential applications of semiconductor nanotubes.

(© Wiley-VCH Verlag GmbH & Co. KGaA, 69451 Weinheim, Germany, 2003)

Introduction

The discovery of free-standing microscopic one-dimensional molecular structures, such as carbon nanotubes, has attracted a great deal of attention in the last decade because of the various interesting properties associated with their small dimensions, high anisotropy, and intriguing tube-like structures. These range from a variety of quantum effects to potentially useful properties such as efficient field-emission and exceptional mechanical strength.[1] A particularly significant breakthrough in WS_2 and MoS_2 nanotubes synthesis was made by Tenne and co-workers[2−4] through the gas-phase reaction between WO_{3-x} or MoO_3 and H_2S in a reducing atmosphere at elevated temperature. Since then many other kinds of nanotubes, such as BN,[5] $NiCl_2$,[6] InS,[7] NbS_2,[8] and Bi,[9] have been reported utilizing various approaches with different growth mechanisms. More recently, Si[10,11] and TiO_2 [12,13] nanotubes were also fabricated and a micro-templated synthesis of CdS nanotubes[14] in aqueous solution at room temperature has also been reported. Although no generalized synthetic method for nanotubes has yet been established, self-assembly growth is a good method for producing nanotubes. For example, Remskar et al.[15] reported the self-assembly of subnanometer-diameter single-wall MoS_2 nanotubes, and rare-earth oxide nanotubes have been formed from dodecylsulfate assemblies.[16] Similarly, Te,[17] NbS_2,[18,19] WS_2,[20] $Cu_{5.5}FeS_{6.5}$,[21] and ReS_2 [22] nanotubes have also been synthesized by self- or induced-assembly. Motivated by these reports, we now report a two-step synthesis of CdS nanotubes based on a self-assembly approach.

Results and Discussion

The CdS nanotubes were synthesized as follows. First, pure metal Cd nanowires were electrodeposited inside the nanochannels of anodic alumina membrane (AAM), and then the outer walls of the Cd nanowires were sulfurized under an atmosphere of sulfur to form a CdS layer under controlled conditions; the (CdS+Cd) nanowires were formed in situ. Secondly, the CdS nanotubes were formed by removal of the Cd, together with AAM, upon dissolution in 0.5 M HCl for 1 hour. Figure 1a shows a typical cross-sectional SEM image, where the intermediate products — the (Cd+CdS) nanowires — consist of a large quantity of wire-like arrays with diameters of about 80 nm and lengths of about 25 μm, corresponding to the pore size and thickness, respectively, of the AAM used. These nanowires are highly ordered and are formed by a template, i.e. they are electrodeposited uniformly and continuously filled into the AAM pores. The composition of the nanowires was confirmed by X-ray diffraction (XRD), as shown in Figure 1b. The peak at 32.15° supports the proposal that there is metallic Cd in the nanowires, whereas no peaks from Al_2O_3 exist due to its amorphous structure at the treatment

[a] Institute of Solid State Physics, Chinese Academy of Sciences, Hefei 230031, P. R. China
Fax: (internat.) + 86-551/559-1434
E-mail: shaominzhou@sohu.com
[b] Lingling University, Yongzhou 425000, P. R. China

 © 2003 Wiley-VCH Verlag GmbH & Co. KGaA, Weinheim **DOI: 10.1002/ejic.200200593**

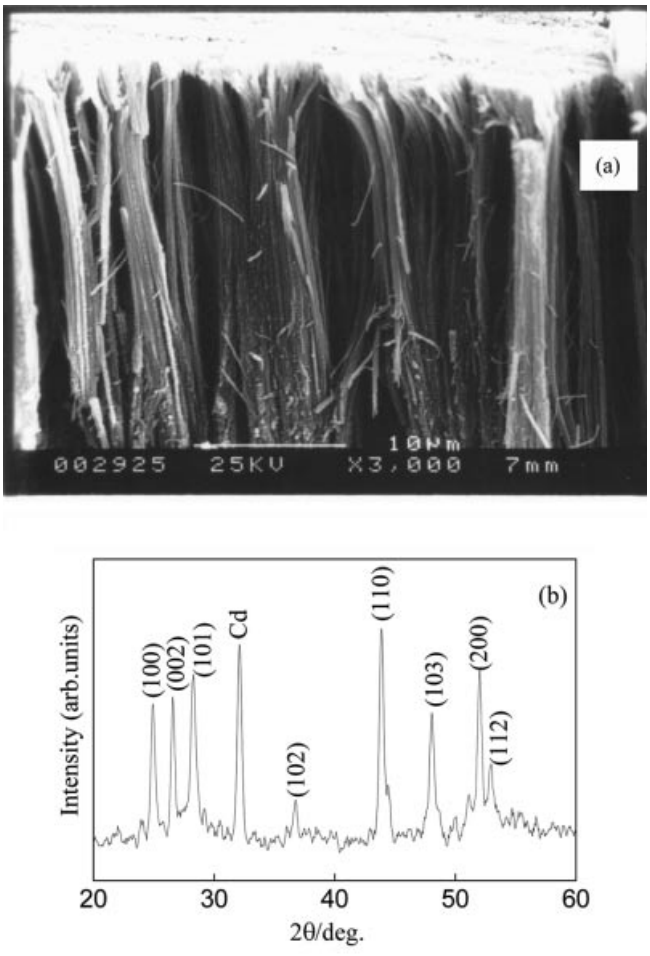

Figure 1. (a) A typical cross-sectional SEM image of (CdS+Cd) nanowires (80 nm in diameters and 25 μm in lengths) and (b) XRD pattern of (Cd+CdS) nanowires

temperature. The Miller indices of the peaks are indicated in Figure 1b where it can be seen that the whole diffractogram can be indexed from the peak positions to a crystalline CdS phase. It is also clear that the XRD pattern of the nanowires exhibits prominent peaks at scattering angles (2θ) of 24.8°, 26.4°, 28.2°, 36.6°, 43.7°, 47.8°, 51.9°, and 52.8°, of the hexagonal CdS crystal lattice (JCPDS Card File, No. 06-0314). After the AAM and the Cd had been completely removed by treatment with 0.5 M HCl for 60 min, we obtained the CdS nanotubes whose typical TEM image is shown in Figure 2a. One can clearly see that these nanotubes appear in alignment and have a hollow structure with a uniform outer diameter of about 80 nm, which is consistent with the results of SEM. A TEM image at higher magnification, taken of the open section of a single nanotube, is presented in Figure 2b; the section marked with a black loop was used for selected area electronic diffraction (SAED) analysis. From this image, it can be seen more clearly that the inner and outer diameters of the nanotube are 40 nm and 80 nm, respectively and its structure is hollow. Moreover, the open section of the nanotube has a rough surface, which might be due to the corrosion by HCl. Because of this, one can suggest that HCl dissolves AAM and Cd in the center of the wire along the nanowire axis, resulting in this kind of hollow structure. An SAED pattern (insert in Figure 2b), taken from the section mentioned above, was recorded with a W electron beam perpendicular to the nanotube axis (other SAED patterns from other sections of the nanotube are essentially identical), which reflects the characteristics of the nanotube structure. The pattern shows that the diffuse diffraction rings in the SAED pattern are due to the polycrystalline structure of the sample. The three rings in the pattern correspond to the [110], [101], and [112] direction; the [110] is the radial direction of the nanotube. Figure 3 shows the XRD pattern of

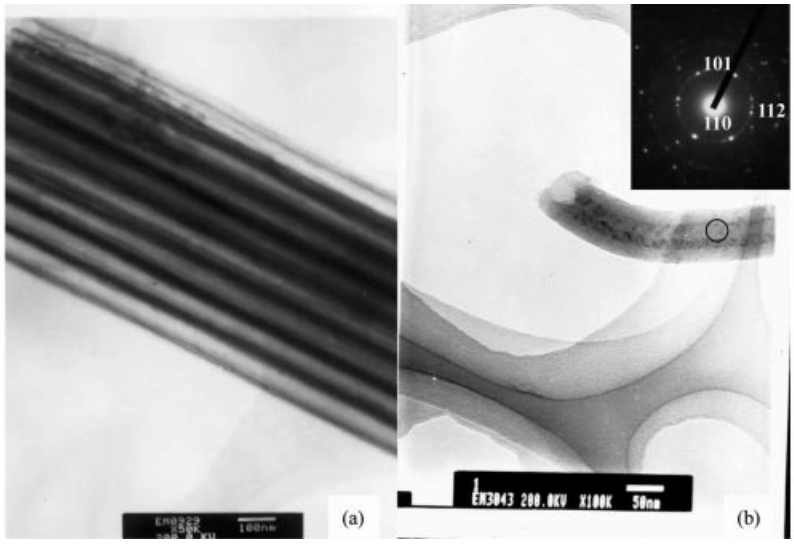

Figure 2. (a) TEM image of CdS nanotube arrays (inside diameter of 40 nm and outside diameter of 80 nm) and (b) a TEM image at higher magnification taken of an individual nanotube; inset: SAED pattern of the CdS nanotube

 © 2003 Wiley-VCH Verlag GmbH & Co. KGaA, Weinheim

the final CdS nanotubes, where all the intense XRD peaks show a wurtzite (hexagonal) structured CdS with lattice constants of $a = 0.413$ nm and $c = 0.671$ nm consistent with the standard values (JCPDS Card File, No. 06-0314) and a previous report.[23] No diffraction peaks from CdO, Cd, S or other impurities have been found in the final products.

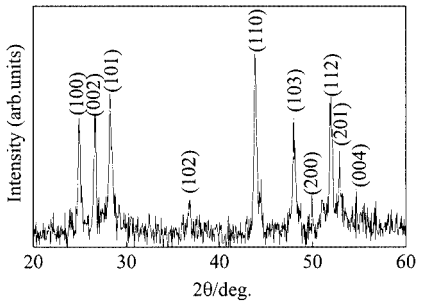

Figure 3. XRD patterns of the CdS nanotubes

A chemical composition analysis of the as-synthesized CdS nanotubes was also performed by X-ray photoelectron energy spectroscopy (XPS). The XPS spectrum (Figure 4) shows that the nanotubes are composed of S and Cd, and quantitative analysis indicates that the atomic ratio of S and Cd is 40:48 within experimental error, which is consistent with stoichiometric CdS (Cd:S = 1:1).

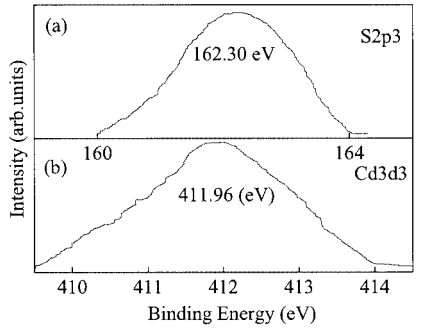

Figure 4. (a) S2p3 XPS spectrum of the CdS nanotubes: the peak binding energy is 162.30 eV and (b) Cd3d3 spectrum of the CdS nanotubes: the peak binding energy is 411.96 eV; the C1s (E= 284.5 eV) level serves as the internal standard

There is one other possible model for the growth of CdS nanotubes: Through the usual template approach, the parameters of Cd nanowires are strongly dependent on the size of the nanochannel in AAM. The mixture of composition CdS + Cd forms through sublimation of sulfur, the residual Cd is dissolved and then the CdS nanotubes appear. This might be a self-assembly process.

$$\text{Cd (electrodeposition nanowire)} \xrightarrow{S} \text{[Cd+CdS]AAM mixed} \xrightarrow{NaOH} \text{CdS (nanotube)}$$

In summary, we have presented a simple, inexpensive, and reasoned method to fabricate CdS nanotubes. They were characterized by SEM, TEM, SAED, XRD, and XPS. The final products formed through self-assembly are pure CdS nanotubes with outside diameters of about 80 nm and inside diameters of about 40 nm. The CdS nanotubes have a uniform hollow structure. The growth mechanism is suggested to be a self-assembly process. The technique may serve as a model for studying the synthesis and properties of other semiconductor nanotubes such as PbS, SnS, ZnS. It is likely that these CdS nanotubes may stimulate technological interest and see many applications in optical fibers or nanodevices.

Experimental Section

The CdS nanotube was formed by a chemical method taking advantage of its low solubility in 0.5 M HCl (Cd and AAMs are readily soluble). In a typical experiment, AAM was prepared via a two-step aluminum anodic oxidation process in a 0.3 M oxalic acid solution, as described previously.[24] The AAM had a diameter of about 80 nm in the pore size and a thickness of 25 μm. Metallic Cd was electrodeposited inside the nanochannels of the AAM with a conventional three-electrode aqueous bath, containing solutions of 0.2 M $CdCl_2$ and 0.1 M H_3BO_3. The deposition potentials were controlled in the range −0.68 to 0.7 V for 240 min at room temperature. Then their surfaces were polished using a 40-nm SiC polishing sandpaper to get rid of Cd particles that had grown excessively and stuck to the surface. The AAM with Cd was washed with distilled water and ethanol, put into a quartz boat and covered with a layer of S powder (99.99%). The boat was placed into the hot zone of a recrystallized alumina tube furnace. The reaction chamber was evacuated with a mechanical pump, and then it was backfilled with high purity Ar gas (0.1 MPa). The reactor was heated to 700 °C from room temperature and held at this temperature for 30 minutes to sulfurize the Cd nanowires. The AAM with CdS membranes was then cleaned with CS_2 to remove the remaining S powder, and washed with ethanol and deionized water. Then, the AAM was immersed in 0.5 M HCl for 60 min and the precipitate was separated from the solution by centrifugation and washed with toluene and absolute ethanol. The semi-finished product [i.e., (CdS+Cd) nanowires] with AAM was firstly characterized by X-ray diffraction (XRD) (PW, 1710 instrument with Cu-K_α radiation, λ = 0.154178 nm at a scanning speed of 0.02°/s in the 2θ range 20−60°). For the SEM analysis (JEOL JSM-63000 instrument) the sample was mounted directly on Cu stubs with conductive gold paint and the AAM was dissolved away. The final products were dried in vacuo at 100 °C for 3 hours and detected by using transmission electron microscopy (TEM) [JEM 200CX equipped with selected area electronic diffraction (SAED), working at 200 kV acceleration voltage], XRD, and X-ray photoelectron energy spectroscopy (XPS) [MKII XPS, employing Mg-K_α, E = 1253.6 eV, the C1s (E = 284.5 eV) level served as the internal standard]. For TEM and SAED, the sample was ultrasonically dispersed in ethanol and a drop of the solution was placed on a Cu grid coated with a holey carbon film. All the chemicals used were of analytical grade and were used without further purification.

Acknowledgments

The authors thank Prof. Dr. W. P. Cai for useful advice. This work is supported by the Natural Science Foundation of China under Grant No 10074064.

 © 2003 Wiley-VCH Verlag GmbH & Co. KGaA, Weinheim

[1] R. Baughman, A. Zakhidov, W. Heer, *Science* **2002**, *297*, 787−792.
[2] R. Tenne, L. Margulis, M. Genut, G. Hodes, *Nature* **1992**, *360*, 444−446.
[3] L. Margulis, G. Salltra, R. Tenne, M. Talianker, *Nature* **1993**, *360*, 144−146.
[4] Y. Feldman, E. Wasserman, J. Srolovita, R. Tenne, *Science* **1995**, *267*, 222−224.
[5] N. Chopra, R. Luyken, K. Cherrey, V. Crespi, M. Cohen, S. Louie, A. Zettl, *Science* **1995**, *269*, 966−967.
[6] R. Hachohen, E. Grunbaum, J. Sloan, L. Hutchison, R. Tenne, *Nature* **1998**, *395*, 336−228.
[7] A. Hollingsworth, M. Pooojary, A. Clearfied, E. Buhro, *J. Am. Chem. Soc.* **2000**, *122*, 3562−3564.
[8] M. Nath, R. Rao, *J. Am. Chem. Soc.* **2001**, *123*, 4841−4843.
[9] Y. Li, J. Wang, Z. Deng, Y. Wu, X. Sun, D. Yu, P. Yang, *J. Am. Chem. Soc.* **2001**, *123*, 9904−9905.
[10] J. Sha, J. Hiu, X. Ma, J. Xu, X. Zhang, Q. Yang, D. Yang, *Adv. Mater.* **2002**, *14*, 1219−1221.
[11] J. Jung, S. shinkai, T. Shimizu, *Nanolett.* **2002**, *2*, 17−20.
[12] T. Kasuga, M. Hiramatsu, A. Hoson, T. Sekino, K. Niihara, *Langmuir* **1998**, *14*, 3160−3162.
[13] T. Kasuga, M. Hiramatsu, A. Hoson, T. Sekino, K. Niihara, *Adv. Mater.* **1999**, *11*, 1307−1309.
[14] M. Shao, F. Xu, Y. Peng, J. Wu, Q. Li, S. Zhang, Y. Qian, *New J. Chem.* **2002**, *26*, 1440−1442.
[15] M. Remskar, A. Mrzel, Z. Skraba, A. Jesih, M. Ceh, J. Demsar, P. Stadelmann, F. Levy, D. Mihailovic, *Science* **2001**, *292*, 479−481.
[16] M. Yada, M. Mihara, S. Mouri, M. Kuroki, T. Kijima, *Adv. Mater.* **2002**, *14*, 309−312.
[17] B. Mayers, Y. Xia, *Adv. Mater.* **2002**, *14*, 279−282.
[18] M. Remskar, A. Mrzel, A. Jesih, F. Levy, *Adv. Mater.* **2002**, *14*, 680−684.
[19] Y. Zhu, W. Hsu, H. Kroto, D. Walton, *J. Phys. Chem. B* **2002**, *106*, 7623−7626.
[20] Y. Li, X. Li, R. He, J. Zhu, Z. Deng, *J. Am. Chem. Soc.* **2002**, *124*, 1411−1416.
[21] Y. Peng, Z. Meng, C. Zhong, J. Lu, L. Xu, S. Zhang, Y. Qian, *New J. Chem.* **2002**, *25*, 1359−1361.
[22] M. Brorson, T. Hansen, C. Jacobsen, *J. Am. Chem. Soc.* **2002**, *124*, 11582−11583.
[23] Y. Chen, Y. Guo, L. Kong, H. Li, *Chem. Lett.* **2002**, *6*, 602−603.
[24] X. Peng, J. Zhang, X. Wang, Y. Wang, L. Zhao, G. Meng, L. Zhang, *Chem. Phys. Lett.* **2001**, *343*, 470−474.

Received October 26, 2002

 © 2003 Wiley-VCH Verlag GmbH & Co. KGaA, Weinheim

Self-Assembly of Organodiphosphonate, Polyoxomolybdate and Diphenanthrolinecobalt(II) into Two Clusters and One Linear Polymer

Rui-Biao Fu,[a] Xin-Tao Wu,*[a] Sheng-Min Hu,[a] Jian-Jun Zhang,[a] Zhi-Yong Fu,[a] Wen-Xin Du,[a] and Sheng-Qing Xia[a]

Keywords: Polyoxometalates / Molybdenum / Cobalt / N ligands / Clusters

[{Co(1,10-phen)$_2$}$_2${(Mo$_4$O$_{12}$)(O$_3$PCH$_2$CH$_2$PO$_3$)}·(H$_2$O)] (**1**), [{Co(1,10-phen)$_2$}$_2${(Mo$_4$O$_{12}$)(O$_3$PCH$_2$CH$_2$CH$_2$PO$_3$)}·(1.5H$_2$O)] (**2**) and [{Co(1,10-phen)$_2$(H$_2$O)$_2$}{Co(1,10-phen)$_2$(H$_2$O)}-{(Mo$_5$O$_{15}$)(O$_3$PCH$_2$CH$_2$CH$_2$CH$_2$PO$_3$)}·(6H$_2$O)] (**3**) were synthesized by self-assembly of H$_2$O$_3$P(CH$_2$)$_n$PO$_3$H$_2$ (n = 2–4), polyoxomolybdate and [Co(1,10-phen)$_2$]$^{2+}$ (1,10-phen = 1,10-phenanthroline) under hydrothermal conditions. Compounds **1** and **2** are novel heterometallic hexanuclear clusters, while compound **3** is a new linear polymer.

(© Wiley-VCH Verlag GmbH & Co. KGaA, 69451 Weinheim, Germany, 2003)

Introduction

Metal-organic units have been successfully introduced into organic-inorganic hybrid systems as charge-compensating motifs, structure-directing components and building blocks to synthesize many new compounds such as micropores.[1−13] In the molybdenum organodiphosphonate system three one-dimensional and two two-dimensional polymers have been produced by incorporating copper-phenanthroline, copper-2,2′-bipyridine and copper-tetra(2-pyridyl)pyrazine as metal-organic subunits.[14−15] In previous work we have successfully used [Co(1,10-phen)$_2$]$^{2+}$ as a metal-organic subunit to synthesize two one-dimensional polymers in the oxovanadium-organodiphosphonate systems.[16] But what the structures will be after self-assembling of different lengths of organodiphosphonate ligands, polyoxomolybdate and [Co(1,10-phen)$_2$]$^{2+}$ as metal-organic subunit together is still unknown. In this paper we report the synthesis and crystal structures of two novel clusters, [{Co(1,10-phen)$_2$}$_2${(Mo$_4$O$_{12}$)(O$_3$PCH$_2$CH$_2$PO$_3$)}·(H$_2$O)] (**1**) and [{Co(1,10-phen)$_2$}$_2${(Mo$_4$O$_{12}$)(O$_3$PCH$_2$CH$_2$-CH$_2$PO$_3$)}·(1.5H$_2$O)] (**2**), and one linear polymer, [{Co(1,10-phen)$_2$(H$_2$O)$_2$}{Co(1,10-phen)$_2$(H$_2$O)}-{(Mo$_5$O$_{15}$)(O$_3$PCH$_2$CH$_2$CH$_2$CH$_2$PO$_3$)}·(6H$_2$O)] (**3**).

[a] State Key Laboratory of Structural Chemistry, Fujian Institute of Research on the Structure of Matter, Chinese Academy of Science,
Fuzhou, Fujian 350002, P. R. China
Fax: (internat.) + 86-591/371-4946
E-mail: wxt@ms.fjirsm.ac.cn

Results and Discussion

The crystal structure of **1** consists of a heterometallic hexanuclear Mo$_4$Co$_2$ cluster built up from an {Mo$_4$O$_{16}$} motif, {PCO$_3$} tetrahedrons and {CoN$_4$O$_2$} octahedrons (Figure 1a). Interestingly, the Mo atoms arrange themselves into a twisted zigzag line in the {Mo$_4$O$_{16}$} motif (Figure 1b), which is composed of four {MoO$_6$} octahedrons. {Mo1O$_6$} shares a face with {Mo2O$_6$} through the O8, O4 and O10 atoms. {Mo2O$_6$} and {Mo3O$_6$} are edge-shared through the O4 and O5 atoms. {Mo3O$_6$} shares a face with {Mo4O$_6$} through the O1, O5 and O6 atoms. Meanwhile {Mo1O$_6$} shares a corner with {Mo3O$_6$} through O4 atoms and {Mo2O$_6$} shares a corner with {Mo4O$_6$} thought O5 atoms. As a result, the Mo1−Mo2, Mo2−Mo3 and Mo3−Mo4 distances are 3.0729(10), 3.2033(10) and 3.0755(11) Å, respectively. The [Mo$_4$O$_{12}$(O$_3$PCH$_2$-CH$_2$PO$_3$)]$^{4-}$ anion is formed by the 1,2-ethylenediphosphonate ligand firmly chelating the Mo1 and Mo4 atoms [Mo1−O14 = 1.981(6), Mo1−O8 = 2.262(5), Mo4−O11 = 2.000(6) and Mo4−O6 = 2.321(5) Å] and linking to the middle two {MoO$_6$} octahedrons [Mo2−O8 = 2.260(6) and Mo3−O6 = 2.277(6) Å] (Figure 1c). Both Co^{II} atoms are in slightly distorted octahedral coordination geometries with four nitrogen atoms from two 1,10-phenanthroline ligands and two oxygen atoms. The {Co1N$_4$O$_2$} octahedron connects to the [Mo$_4$O$_{12}$(O$_3$PCH$_2$CH$_2$PO$_3$)]$^{4-}$ anion by sharing one oxygen atom with an {Mo2O$_6$} octahedron [Co1−O7 = 2.107(6) Å] and another oxygen atom with the {P1CO$_3$} tetrahedron [Co1−O18 = 2.048(6) Å] (Figure 1c). The {Co2N$_4$O$_2$} octahedron is attached to the [Mo$_4$O$_{12}$(O$_3$PCH$_2$CH$_2$PO$_3$)]$^{4-}$ anion through one oxygen atom of the {Mo3O$_6$} octahedron [Co2−O3 = 2.083(6) Å] and another oxygen atom of the {P2CO$_3$} tetrahedron [Co2−O17 = 2.067(6) Å] (Figure 1c). Consequently, each

 © 2003 Wiley-VCH Verlag GmbH & Co. KGaA, Weinheim **DOI: 10.1002/ejic.200200678**

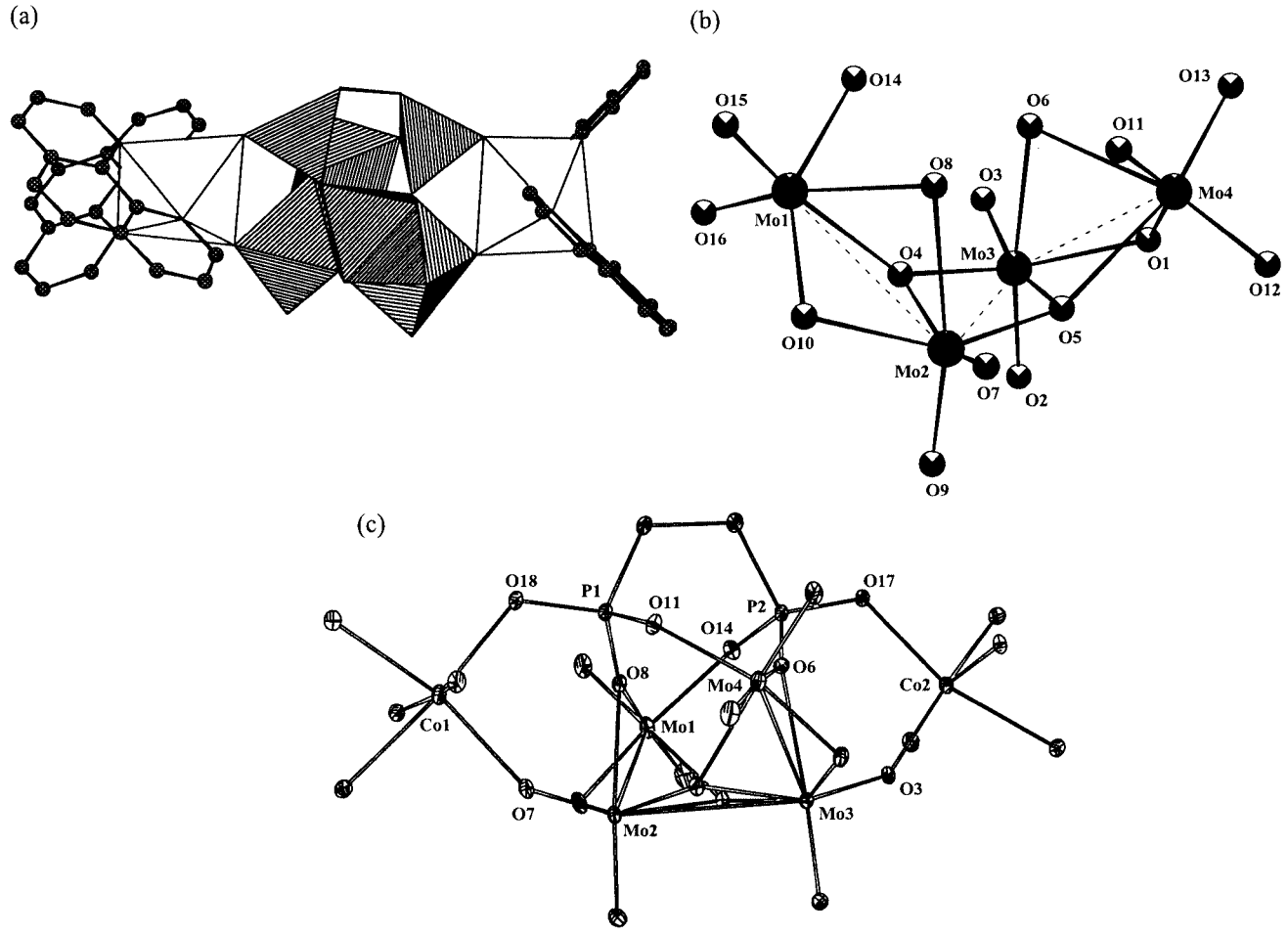

Figure 1. (a) Polyhedron perspective of cluster of **1**; white octahedra: $\{CoN_4O_2\}$; black octahedra: $\{MoO_6\}$; black tetrahedra: $\{PCO_3\}$; hydrogen atoms are omitted for clarity; (b) perspective view of $\{Mo_4O_{16}\}$ motif of **1**; the dotted single lines represent the Mo-Mo bonds; (c) ORTEP view of **1** showing the coordination environments of cobalt, molybdenum and phosphorus (ellipsoids at 10% probability); free water molecules, hydrogen atoms and the carbon atoms of 1,10-phen ligands are omitted for clarity

$\{PO_3\}$ terminus of the 1,2-ethylenediphosphonate group links to one $\{CoN_4O_2\}$ and three different $\{MoO_6\}$ octahedra. The adjacent clusters interact each other through a strong π-π stacking of neighboring parallel 1,10-phen groups at a distance of 3.4−3.5 Å.[6,17,18]

The crystal structure of **2** is almost the same as that of **1** except for the 1,3-propylenediphosphonate ligand (Figure 2).

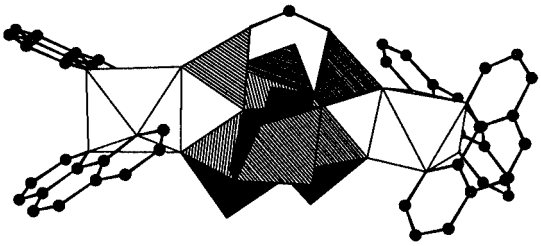

Figure 2. Polyhedron perspective of cluster of **2**; white octahedra: $\{CoN_4O_2\}$; black octahedra: $\{MoO_6\}$; black tetrahedra: $\{PCO_3\}$; hydrogen atoms are omitted for clarity

As expected, the structure of **3** is a linear polymer constructed from an $[Mo_5O_{15}(O_3PCH_2CH_2CH_2CH_2PO_3)]_n^{4n-}$ anionic chain (Figure 3a) and $[Co(1,10\text{-phen})_2(H_2O)_2]^{2+}$ and $[Co(1,10\text{-phen})_2(H_2O)]^{2+}$ fragments (Figure 3b). In the anionic chain, the 1,4-butylenediphosphonate groups bridge the adjacent common $\{Mo_5O_{21}\}$ cyclic clusters.[14,15,19−24] Each $\{PO_3\}$ terminus only coordinates to five Mo^{VI} centers. This is obviously different from $[\{Cu(H_2O)_2(1,10\text{-phen})_2\}\{Cu(1,10\text{-phen})_2\}(Mo_5O_{15})(O_3PCH_2CH_2CH_2PO_3)]\cdot 2.5H_2O$,[14] $[\{Cu(2,2'\text{-bipyridine})_2\}\{Cu(2,2'\text{-bipyridine})(H_2O)\}(Mo_5O_{15})(O_3PCH_2CH_2CH_2CH_2PO_3)]\cdot H_2O$ and $[\{Cu_2(\text{tetra(2-pyridyl)pyprazine})(H_2O)_2\}(Mo_5O_{15})(O_3PCH_2CH_2PO_3)]\cdot 5.5H_2O$.[15] Similar to compounds **1** and **2**, the Co^{II} atoms are also in slightly distorted octahedral coordination geometries with four nitrogen donors from two 1,10-phenanthroline ligands and two oxygen atoms. The $\{Co1N_4O_2\}$ moiety is linked to the anionic chain through an oxo group bridging to the $\{Mo1O_6\}$ octahedron [Co1−O7 = 2.063(5) Å]. While the $\{Co2N_4O_2\}$ octahedron interacts with the anionic chain through hydrogen bonds ($O_{24}\cdots O_{20}$ = 2.703, $O_{23}\cdots O_{18}$ =

 © 2003 Wiley-VCH Verlag GmbH & Co. KGaA, Weinheim

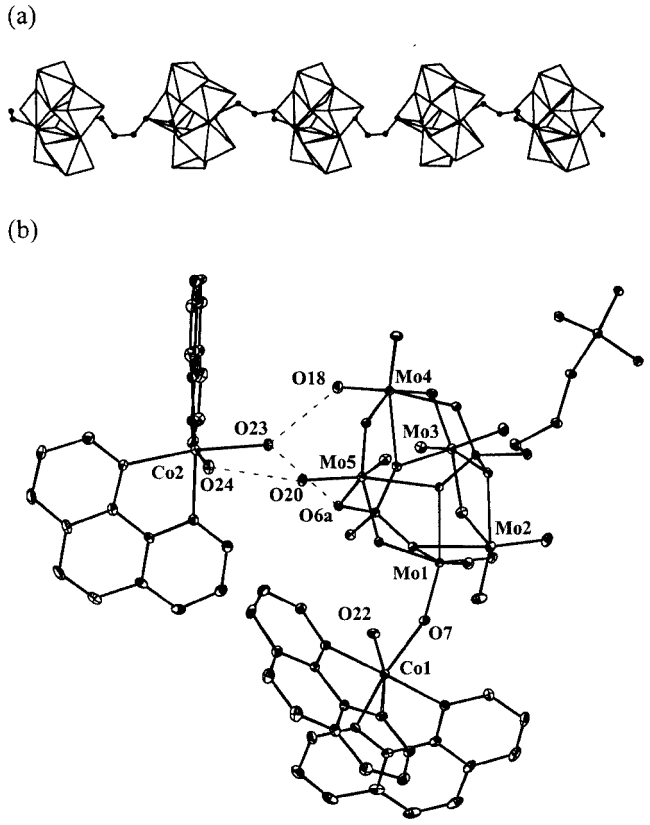

Figure 3. (a) Perspective view of $[Mo_5O_{15}(O_3PCH_2CH_2CH_2PO_3)]_n^{4n-}$ anionic chain of **3**; octahedra: $\{MoO_6\}$; black dots: P and C atoms; hydrogen atoms are omitted for clarity;(b) ORTEP view of **3** showing the coordination geometries of the cobalt, molybdenum and phosphorus atoms (ellipsoids at 10% probability); the dashed lines represent hydrogen bonds; free water molecules and hydrogen atoms are omitted for clarity; symmetry code *a*: $1/2 - x, -1/2 + y, z$.

2.829 and $O_{23}\cdots O_{6a}$ = 2.727 Å). The adjacent chains interact thorough strong π-π stacking of neighboring parallel 1,10-phen groups at a distance of 3.2−3.6 Å.[6,17,18]

Thermogravimetric analysis (TGA) studies were performed on polycrystalline samples under N_2 from room temperature to 1000 °C to study the stability of these compounds. The TGA data show an obvious weight loss starting at about 435 °C for these compounds.

In conclusion, two novel clusters and one linear polymer have been successfully self-assembled under almost identical hydrothermal conditions using $[Co(1,10\text{-phen})_2]^{2+}$ as the metal-organic subunit and organodiphosphonate ligands of different lengths. The structure of **3** differs from **1** and **2**, which may be mainly due to the increased length of the 1,4-butylenediphosphonate ligand.

Experimental Section

1,2-Ethylene-, 1,3-propylene- and 1,4-butylenediphosphonic acids were prepared according to the reported method.[25,26] Other chemicals were of reagent grade quality and obtained from commercial sources without further purification. Compounds **1**, **2** and **3** were synthesized in 25-mL, Teflon-lined, stainless steel vessels under autogenous pressure with a filling capacity of about 40%. The reactants were stirred to homogeneity before heating. CHN analyses were performed with a Vario EL III element analyzer and UV-1100 spectrophotometer. Infrared spectra were obtained on a Nicolet Magna 750 FT-IR spectrometer.

Synthesis

Compound **1**, **2** and **3** were synthesized as red blocks in about 20% (0.1 g), 86.4% (0.357 g) and 40% (0.2 g) yields based on cobalt, respectively, at 180 °C for 48, 144 and 72 h, respectively. Hydrothermal reactions were performed as follows

For **1**: $Co(CH_3COO)_2{\cdot}4H_2O$ (0.1256 g, 0.5043 mmol), $Na_2MoO_4{\cdot}2H_2O$ (0.2408 g, 0.9952 mmol), MoO_3 (0.1446 g, 1.005 mmol), 1,10-phenanthroline·H_2O (0.1999 g, 1.008 mmol), $H_2O_3PCH_2CH_2PO_3H_2$ (0.1955 g, 1.029 mmol) and distilled water (10.0 mL, 555 mmol).

For **2**: $Co(CH_3COO)_2{\cdot}4H_2O$ (0.1254 g, 0.5035 mmol), $Na_2MoO_4{\cdot}2H_2O$ (0.2408 g, 0.9952 mmol), MoO_3 (0.1447 g, 1.005 mmol), 1,10-phenanthroline·H_2O (0.1996 g, 1.007 mmol), $H_2O_3PCH_2CH_2CH_2PO_3H_2$ (0.2010 g, 0.9850 mmol) and distilled water (10.0 mL, 555 mmol).

For **3**: $Co(CH_3COO)_2{\cdot}4H_2O$ (0.1253 g, 0.5031 mmol), $Na_2MoO_4{\cdot}2H_2O$ (0.2419 g, 0.9998 mmol), MoO_3 (0.1435 g, 0.9969 mmol), 1,10-phenanthroline·H_2O (0.1990 g, 1.004 mmol), $H_2O_3PCH_2CH_2CH_2CH_2PO_3H_2$ (0.2182 g, 1.001 mmol) and distilled water (10.0 mL, 555 mmol).

1: $C_{50}H_{38}Co_2Mo_4N_8O_{19}P_2$ (1618.5): calcd. C 37.11, H 2.37, N 6.92; found C 37.03, H 1.74, N 6.43. IR (KBr pellet): $\tilde{\nu}$ = 3500vs cm^{-1}, 3062m, 2904w, 1637w, 1624w, 1581m, 1514s, 1495m, 1423s, 1342w, 1300w, 1225w, 1117s, 1047vs, 982m, 924vs, 901s, 850s, 773m, 729s, 700s, 634s, 584s, 542w.

2: $C_{51}H_{41}Co_2Mo_4N_8O_{19.5}P_2$ (1641.5): calcd. C 37.32, H 2.52, N 6.83; found C 37.40, H 2.09, N 6.82. IR (KBr pellet): $\tilde{\nu}$ = 3500vs cm^{-1}, 3062m, 2893w, 1635w, 1624w, 1579m, 1512s, 1495m, 1452w, 1423s, 1342w, 1225w, 1188w, 1111s, 1049vs, 1028s, 987m, 922vs, 899vs, 860w, 847w, 771m, 727vs, 702vs, 629s, 586s, 567w, 523w.

3: $C_{52}H_{58}Co_2Mo_5N_8O_{30}P_2$ (1934.6): calcd. C 32.38, H 3.02, N 5.79; found C 32.21, H 1.68., N 5.74 IR (KBr pellet): $\tilde{\nu}$ = 3500vs cm^{-1}, 3064m, 2943w, 2899w, 2864w, 1624m, 1579m, 1518s, 1495m, 1427vs, 1344m, 1225w, 1188w, 1146m, 1111s, 1034s, 995m, 943vs, 908vs, 870vs, 762s, 727s, 661m, 590m, 563m, 503m.

X-ray Crystallography: X-ray data of single crystals were collected at a temperature of 293 ± 2 K on a Siemens SMART-CCD diffractometer using graphite-monochromated Mo-K_α radiation (λ = 0.71073 Å). Data were reduced and absorption-corrected with the SMART and SADABS software packages, respectively. The structures were solved by direct methods and refined by full-matrix least-squares techniques on F^2 using SHELXTL-97.[27] All non-hydrogen atoms of the three compounds were treated anisotropically. H_1-H_{26} of **1**, all hydrogen atoms of **2** and H_1-H_{30} of **3** were treated geometrically. $H_{1a}-H_{10a}$ of **1** and $H_{1a}-H_{10a}$ of **3** were identified from the difference Fourier map and fixed with isotropic thermal parameters.

Crystal Data for 1: $C_{50}H_{38}Co_2Mo_4N_8O_{19}P_2$, M = 1618.44, triclinic, $P\bar{1}$, a = 12.2256(6), b = 12.9418(7), c = 18.9455(10) Å, α = 108.7050(10)°, β = 104.4880(10)°, γ = 96.2950(10)°, V = 2699.9(2) $Å^3$, Z = 2, $D_{calcd.}$ = 1.991 g cm^{-3}, T = 293(2) K, μ(Mo-K_α) = 1.645 mm^{-1}. Data were collected on a single crystal with dimensions 0.20 × 0.18 × 0.12 mm. 14204 reflections were measured in the range of $1.19 \leq \theta \leq 25.10°$, 9510 independent reflections

 © 2003 Wiley-VCH Verlag GmbH & Co. KGaA, Weinheim

(R_{int} = 0.0385). Final R_1 = 0.0625 for 7201 observed reflections [$I > 2\sigma(I)$] and wR_2 = 0.1161.

Crystal Data for 2: $C_{51}H_{41}Co_2Mo_4N_8O_{19.5}P_2$, M = 1641.48, triclinic, $P\bar{1}$, a = 12.3372(3), b = 12.7558(3), c = 19.4102(5) Å, α = 108.3930(10)°, β = 102.7940(10)°, γ = 94.6870(10)°, V = 2788.41(12) Å^3, Z = 2, $D_{calcd.}$ = 1.955 g cm^{-3}, T = 293(2) K, μ(Mo-K_α) = 1.595 mm^{-1}. Data were collected on a single crystal with dimensions 0.54 × 0.54 × 0.50 mm. 14616 reflections were measured in the range of 1.15 ≤ θ ≤ 25.06°, 9773 independent reflections (R_{int} = 0.0173). Final R_1 = 0.0301 for 8837 observed reflections [$I > 2\sigma(I)$] and wR_2 = 0.0786.

Crystal Data for 3: $C_{52}H_{58}Co_2Mo_5N_8O_{30}P_2$, M = 1934.56, Orthorhombic, *Pbca*, a = 24.7212(4), b = 19.86320(10), c = 27.2651(2) Å, V = 13388.3(2) Å^3, Z = 8, $D_{calcd.}$ = 1.920 g cm^{-3}, T = 293(2) K, μ(Mo-K_α) = 1.530 mm^{-1}. Data were collected on a single crystal with dimensions 0.48 × 0.34 × 0.26 mm. 41605 reflections were measured in the range of 1.49 ≤ θ ≤ 25.06°, 11783 independent reflections (R_{int} = 0.0513). Final R_1 = 0.0482 for 8884 observed reflections [$I > 2\sigma(I)$] and wR_2 = 0.1117.

CCDC-198179 (**1**), -198180 (**2**) and -198181 (**3**) contain the supplementary crystallographic data for this paper. These data can be obtained free of charge at www.ccdc.cam.ac.uk/conts/retrieving.html [or from the Cambridge Crystallographic Data Centre, 12, Union Road, Cambridge CB2 1EZ, UK; Fax: (internat.) +44-1223/336-033; E-mail: deposit@ccdc.cam.ac.uk].

Acknowledgments

This research was supported by grants from the State Key Laboratory of Structure Chemistry, Fujian Institute of Research on the Structure of Matter, the National Ministry of Science and Technology of China (001CB1089), Chinese Academy of Sciences (CAS), the National Science Foundation of China (20273073 and 90206040), the Science Foundation of CAS and Fujian Province (2002F014).

[1] R. C. Finn, J. Zubieta, *J. Chem. Soc., Dalton Trans.* **2000**, 1821−1823.
[2] R. C. Finn, R. Lam, J. E. Greedan, J. Zubieta, *Inorg. Chem.* **2001**, *40*, 3745−3754.
[3] S. H. Feng, R. R. Xu, *Acc. Chem. Res.* **2001**, *34*, 239−247.
[4] Z. Shi, L. R. Zhang, G. S. Zhu, G. Y. Yang, J. Hua, H. Ping, S. H. Feng, *Chem. Mater.* **1999**, *11*, 3565−3570.
[5] J. Q. Xu, R. Z. Wang, G. Y. Yang, Y. H. Xing, D. M. Li, W. M. Bu, L. Ye, Y. G. Fan, H. Q. Jia, *Chem. Commun.* **1999**, 983−984.
[6] X. M. Zhang, M. L. Tong, X. M. Chen, *Chem. Commun.* **2000**, 1817−1818.
[7] S. S. Y. Chui, S. M. F. Lo, J. P. H. Charmant, A. G. Orpen, I. D. Williams, *Science* **1993**, *283*, 1148−1150.
[8] M. Eddaoudi, D. B. Moler, H. L. Li, B. L. Chen, T. M. Reineke, M. O'Keeffe, O. M. Yaghi, *Acc. Chem. Res.* **2001**, *34*, 319−330.
[9] Z. Shi, S. H. Feng, L. R. Zhang, G. Y. Yang, J. Hua, *Chem. Mater.* **2000**, *12*, 2930−2935.
[10] Z. Y. Fu, X. T. Wu, J. C. Dai, L. M. Wu, C. P. Cui, S. M. Hu, *Chem. Commun.* **2001**, 1856−1857.
[11] C. Z. Lu, C. D. Wu, S. F. Lu, J. C. Liu, Q. J. Wu, H. H. Zhuang, J. S. Huang, *Chem. Commun.* **2002**, 152−153.
[12] H. L. Li, M. Eddaoudi, M. O'Keeffe, O. M. Yaghi, *Nature* **1999**, *402*, 276−279.
[13] S. Y. Yang, L. S. Long, Y. B. Jiang, R. B. Huang, L. S. Zheng, *Chem. Mater.* **2002**, *14*, 3229−3231.
[14] R. C. Finn, J. Zubieta, *Inorg. Chem.* **2001**, *40*, 2467.
[15] R. C. Finn, E. Burkholder, J. Zubieta, *Chem. Commun.* **2001**, 1852−1853.
[16] F. B. Fu, S. M. Hu, Z. Y. Fu, J. J. Zhang, X. T. Wu, *New J. Chem.* **2003**, *27*, 230−232.
[17] S. B. Ferguson, E. M. Sanford, E. M. Seward, F. Diederich, *J. Am. Chem. Soc.* **1991**, *113*, 5410−5419.
[18] W. L. Jorgensen, D. L. Severance, *J. Am. Chem. Soc.* **1990**, *112*, 4768−4774.
[19] W. Kwak, M. T. Pope, T. F. Scully, *J. Am. Chem. Soc.* **1975**, *97*, 5735−5738.
[20] D. G. Lyxell, R. Strandberg, *Acta Crystallogr., Sect. C* **1988**, *44*, 1535−1538.
[21] M. P. Lowe, J. C. Lockhart, W. Clegg, K. A. Fraser, *Angew. Chem. Int. Ed. Engl.* **1994**, *33*, 451−454.
[22] M. P. Lowe, J. C. Lockhart, G. A. Forsyth, W. Clegg, K. A. Fraser, *J. Chem. Soc., Dalton Trans.* **1995**, 145−152.
[23] Y. D. Chang, J. Zubieta, *Inorg. Chim. Acta* **1996**, *245*, 177−198.
[24] W. T. A. Harrison, L. L. Dussack, A. J. Jacobson, *Acta Crystallogr., Sect. C* **1997**, *53*, 856−859.
[25] A. K. Bhattacharya, G. Thyagarajan, *Chem. Rev.* **1981**, *81*, 415−430.
[26] K. Moedritzer, R. R. Irani, *J. Inorg. Nucl. Chem.* **1961**, *22*, 297−304.
[27] G. M. Sheldrick, SHELXT 97, *Program for Crystal Structure Refinement*, University of Göttingen, Germany, **1997**.

Received December 12, 2002

 © 2003 Wiley-VCH Verlag GmbH & Co. KGaA, Weinheim

Structural Characterization and a New One-Pot Synthesis of *trans*-Chloro(phenyl)bis(triphenylphosphane)nickel(II)

Alexander Zeller,[a] Eberhardt Herdtweck,[a] and Thomas Strassner*[a]

Keywords: Polymerization / Density functional theory calculations / Nickel / Phosphane ligands

trans-[NiCl(Ph)(PPh_3)$_2$], the organometallic precursor for a new class of neutral polymerization catalysts, has been synthesized via a new synthetic route. The previously used alkylaluminum compounds are replaced by zinc dust for the reduction of the nickel(II) salt in the presence of triphenylphosphane forming the intermediate Ni(PPh_3)$_4$. In a one-pot reaction, chlorobenzene then adds oxidatively to the intermediate to form the title compound, which was structurally characterized, in high yields. Its geometry is compared to known structures of the higher homologues of group 10. All complexes adopt a distorted square-planar geometry, but the parent structure shows significantly shorter metal-ligand bond lengths than its Pd and Pt congeners, as expected. Density functional theory calculations (B3LYP/6–31G*) on the full structure are in very good agreement with the solid-state structure.

(© Wiley-VCH Verlag GmbH & Co. KGaA, 69451 Weinheim, Germany, 2003)

Introduction

In the almost 50 years since the discovery of transition metal catalysis for olefin polymerization by Ziegler and Natta[1–3] a lot of research activities have been directed towards molecular homogeneous catalytic systems. As a result of this research the zirconocenes and other early transition metal catalysts were found to be extremely active in ethylene polymerization after activation by methylalumoxane (MAO),[4,5] but proved quite sensitive to the presence of air, moisture and polar groups.

Over the past years several new, highly active polymerization catalysts of late transition metals have been developed.[6–8] Compared to catalysts containing early transition metals they exhibit a greater tolerance towards functional groups, which is useful for the copolymerization with polar monomers. They also provide the possibility of making polymers with novel branching structures and thereby new materials with unknown properties.

Recently a new class of neutral polymerization nickel(II) catalysts based on salicylaldimine or anilinotropone ligands has been introduced, which are highly active in the polymerization of olefins (Scheme 1).[9–12] Some of them no longer need to be activated, either by MAO or by other phosphane-binding complexes, and show comparable polymerization activities to early transition metal catalysts. They are even capable of forming polymers in aqueous solutions[13] and produce linear to moderately branched polyethylene.

R = H, *t*Bu, Ph, 9-phenanthroline, 9-anthracene

Scheme 1. Neutral nickel(II) polymerization catalysts

The key intermediate and organometallic precursor for the synthesis of this type of catalysts is *trans*-[NiCl(Ph)(PPh_3)$_2$], which has been mentioned frequently in recent patents.[14–18] Herein we report a new one-pot synthesis of this complex with improved overall yield from readily available and inexpensive reagents. The crystal structure was determined for the first time and is compared to its higher group 10 homologues Pd and Pt, as well as to the results of a DFT calculation for the gas-phase structure.

Results and Discussion

Generally, the divalent complexes [MCl(Ph)(PPh_3)$_2$] (M = Ni, Pd, Pt) result from the oxidative addition of chlorobenzene to the corresponding zerovalent tetraphosphane complex. Accordingly, the title compound can be synthesized by addition of chlorobenzene to Ni(PPh_3)$_4$.[19] A previously published synthesis prepared the latter by reduction of Ni(acac)$_2$ with alkylaluminum compounds.[20] The disad-

[a] Technische Universitaet Muenchen, Anorganisch-chemisches Institut
Lichtenbergstrasse 4, 85747 Garching, Germany
Fax: (internat.) +49-(0)89/289-13473
E-mail: thomas.strassner@ch.tum.de

 © 2003 Wiley-VCH Verlag GmbH & Co. KGaA, Weinheim **DOI: 10.1002/ejic.200200576**

vantage of this reaction is the moderate yield of 55% for the preparation of $Ni(PPh_3)_4$ and the sensitivity of the alkylaluminum compounds.

Another method would be the replacement of weaker ligands, as in the addition of triphenylphosphane to $Ni(COD)_2$, which requires the synthesis of the Ni^0 precursor, usually also carried out by reduction of $Ni(acac)_2$ with trimethylaluminum.[21]

We were able to combine these steps into a one-pot synthesis starting from readily available and inexpensive reagents. The first step is the reduction of $NiCl_2$ by one equivalent of zinc dust in DMF in the presence of triphenylphosphane (Scheme 2), which results in the formation of the brick-red, air sensitive $Ni(PPh_3)_4$.

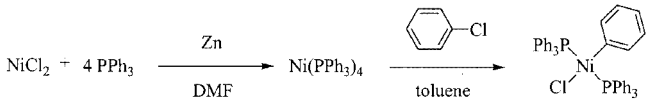

Scheme 2. Synthesis of *trans*-chloro(phenyl)bis(triphenylphosphane)nickel(II)

After removal of DMF and addition of toluene, chlorobenzene was added to the resulting solution. In a previous study of coupling of aryl chlorides, it was reported that an excess amount of zinc in the first reaction step or higher temperatures lead to the decomposition of the oxidative addition product, forming biphenyl and nickel(II) chloride.[22] To suppress this side reaction we changed the solvent to toluene and used only one equivalent of zinc for the reduction of $NiCl_2$ at a reaction temperature of 0 °C for the oxidative addition. We obtained the yellow complex *trans*-$[NiCl(Ph)(PPh_3)_2]$ in good yield (72%). This is much better than the overall yield which can be reached via the two-step synthesis, where the first reaction step (reduction of a Ni^{II} precursor) proceeds with yields of about 60% and the second reaction step (oxidative addition) with about 71%.[19]

Table 1. Selected bond lengths (Å) and angles (°) for the structure of the nickel complex in comparison to the higher homologues and the results of a DFT calculation at the B3LYP/6−31G(d) level

	Pt[27]	Pd[23]	Ni	DFT (Ni)
M−Cl	2.459(1)	2.407(1)	2.2201(6)	2.28
M−C71	2.021(4)	2.016(3)	1.887(2)	1.87
M−P1	2.302(1)	2.316(1)	2.2232(5)	2.25
M−P2	2.295(1)	2.324(1)	2.2151(5)	2.24
P1−M−P2	176.19(6)	177.55(2)	169.29(2)	173.5
C1−M−C71	179.0(2)	179.81(8)	173.07(6)	167.2
P1−M−Cl	87.54(5)	89.75(2)	92.35(2)	90.7
P2−M−Cl	88.83(5)	88.57(2)	88.09(2)	88.2
P1−M−C71	92.38(14)	90.29(7)	88.73(5)	90.7
P2−M−C71	91.23(14)	91.38(7)	92.11(5)	91.7
C72−C71−C76	117.7(5)	117.8(3)	117.4(2)	116.8
Ni−C72	–	–	2.824(2)	2.81
Ni−C76	–	–	2.900(2)	2.93

Yellow crystals of the title compound were obtained by slowly adding hexane to a saturated solution of the complex in toluene. Surprisingly, the X-ray structure was not known up to now even though the X-ray structures of the higher congeners were determined some years ago. The molecular structure is shown in Figure 1. Important bond lengths and angles are given in Table 1, together with the corresponding values for *trans*-$[PdCl(Ph)(PPh_3)_2]$,[23,24] *trans*-$[PtCl(Ph)(PPh_3)_2]$[25−27] and data from a B3LYP/6−31G(d) calculation of the nickel complex.

All the structures show a slightly distorted square-planar geometry, where the two triphenylphosphane ligands, the phenyl group and the chloro ligand bind to the metal center

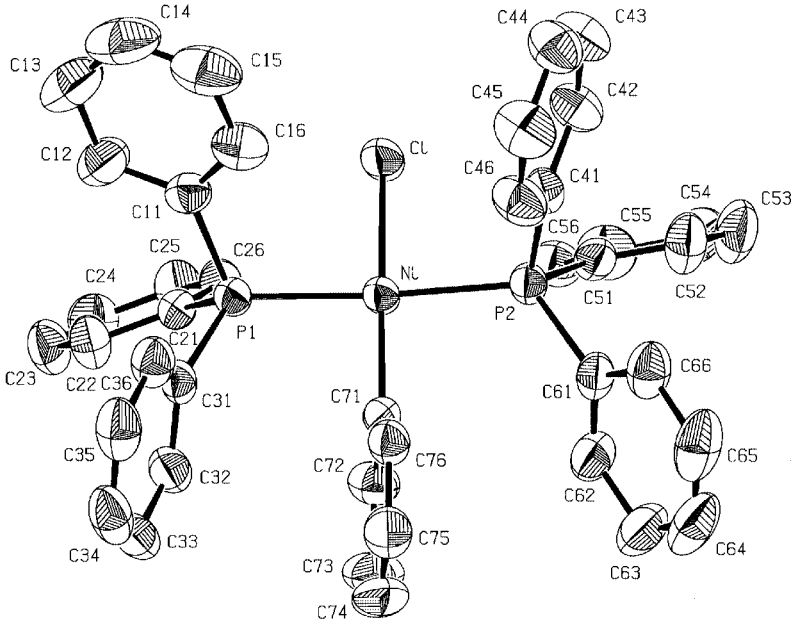

Figure 1. ORTEP representation of *trans*-chloro(phenyl)bis(triphenylphosphane)nickel(II) in the solid state; thermal ellipsoids are drawn at the 50% probability level; hydrogen atoms are omitted for clarity

 © 2003 Wiley-VCH Verlag GmbH & Co. KGaA, Weinheim

in a trans fashion. The trans position of the chloro and phenyl ligands of the nickel compound was already predicted by Hidai et al., based on the frequency of the Ni−Cl stretching vibration in the IR spectra.[19] The nickel-phosphorus distances are 2.2232(5) Å and 2.2151(5) Å, while the nickel-carbon and nickel-chlorine bond lengths are 1.887(2) and 2.2201(6), respectively. The decrease of the metal-ligand bond lengths compared to the higher homologues is within the expected range. The differences between the palladium and platinum structures are small due to relativistic orbital contraction. In all complexes the two metal-phosphorus bonds are slightly asymmetric. The distortion of the square-planar geometry around the metal center can be seen from the P−M−P and C_{71}−M−Cl angles. The largest distortion from the optimum value (180°) is seen in the nickel structure [169.29(2) and 173.07(6)], and the least distortion in the palladium complex [177.55(2) and 179.81(8)°]. The changes in the angles correspond nicely to the changes in the bond lengths and show the steric interaction between all the ligands. In all structures the steric demand of the chlorine atom forces both triphenylphosphane ligands into an almost eclipsed conformation.[23] This conformation seems to be stabilized by π-π interactions between two phenyl rings of the phosphane ligands and the phenyl ring attached to the metal center, which are in a stacked alignment.

The value for the ipso angle around C_{71} (Figure 1) depends on the electronic nature of the substituent: electron-donating groups lead to a decrease of the ipso angle, while electron-deficient groups lead to an increase.[23] In our case the value of the C_{72}−C_{71}−C_{76} angle decreases, even though nickel is more electron donating than palladium. This trend is also apparent from the ^{13}C NMR spectrum, where the signal of the ipso-C atom is observed at a chemical shift of δ = 148.9 ppm compared to δ = 154.0 ppm in the Pd case, indicating a lower deshielding by the metal center.[23,28] The decrease of the ipso angle can be explained by the stronger interaction of the trans chloro ligand, which can be seen in the shorter bond length. This compensates the higher electronegativity of the nickel center.

The density functional theory calculations at the double-ζ level 6−31G(d) show the quality of the electronic structure methods. Even larger transition metal complexes can nowadays be calculated with reasonable effort within acceptable time. All bond lengths are in excellent agreement with the results of the solid-state X-ray structure and show that even metal complexes with two triphenylphosphane ligands and a total of 81 atoms can be treated.

Conclusion

An important precursor for the new class of neutral polymerization catalysts could be synthesized via a new one-pot synthesis with significantly improved yields. The complex *trans*-chloro(phenyl)bis(triphenylphosphane)nickel(II) was structurally characterized by a solid-state single crystal X-ray structure determination. Density functional theory calculations on the complex show that nowadays even first-row transition metals with large ligands can be calculated and that the results are in good agreement with the solid-state structure.

Experimental Section

General Remarks: All manipulations were carried out under Argon using standard Schlenk techniques. Solvents and chlorobenzene were dried and degassed prior to use. NMR spectra were acquired with a JEOL JNM GX 400 spectrometer. Anhydrous nickel(II) chloride and zinc dust were purchased from Merck; triphenylphosphane was purchased from Aldrich. All reagents were used without further purification.

***trans*-Chloro(phenyl)bis(triphenylphosphane)nickel(II):** In a Schlenk flask, anhydrous nickel(II) chloride (1.30 g, 10 mmol), zinc dust (0.66 g, 10 mmol) and triphenylphosphane (11.02 g, 42 mmol) were suspended in DMF (100 mL). The reaction mixture was heated to 50 °C for 2 h and stirred at room temp. for another 15 h after the formation of a brick-red precipitate. The solvent was then evaporated and toluene (200 mL) was added. After adding chlorobenzene (3.10 mL, 25 mmol) the solution was stirred for 3 h at 0 °C. The color changed to a deep brown. After filtration the solution was concentrated to about 70 mL and hexane (100 mL) was added. A yellow solid precipitated which was isolated by filtration, washed twice with hexane (50 mL) and dried for 24 h under high vacuum (5.01 g, 72%). ^{1}H NMR (400 MHz, CD_2Cl_2, 25 °C): δ = 6.15 (br. s, 2 H, *m*-H of Ni-Ph), 6.24 (br. s, 1 H, *p*-H of Ni-Ph), 6.75 (br. s, 2 H, *o*-H of Ni-Ph), 7.28 (br. s, 12 H, *m*-H of PPh_3), 7.37 (br. s, 6 H, *p*-H of PPh_3), 7.57 (br. s, 12 H, *o*-H of PPh_3) ppm. ^{13}C NMR (100.5 MHz, CD_2Cl_2, 25 °C): δ = 120.7 (s, *m*-C of Ph), 126.4 (s, *p*-C of Ni-Ph), 127.7 (t, $J_{C,P}$ = 5.0 Hz, *m*-C of PPh_3), 129.5 (s, *p*-C of PPh_3), 131.8 (t, $J_{C,P}$ = 21.9 Hz, *i*-C of PPh_3), 134.5 (t, $J_{C,P}$ = 5.8 Hz, *o*-C of PPh_3), 137.4 (t, $J_{C,P}$ = 4.2 Hz, *o*-C of Ni-Ph), 148.9 (s, i-C of Ni-Ph) ppm.[29] ^{31}P NMR (161.8 MHz, CD_2Cl_2, 25 °C): δ = 21.6. $C_{42}H_{35}ClNiP_2$ (695.78): calcd. C 72.50, H 5.07; found C 71.88, H 5.04.

Computational Details: The density functional/Hartree−Fock hybrid model Becke3LYP,[30−33] as implemented in Gaussian 98,[34] was used together with the double-ζ basis set 6−31G(d). The geometry was fully optimized.

X-ray Crystallographic Study: Details of the X-ray experiment, data reduction, and final structure refinement calculation are summarized in Table 2. Crystals suitable for an X-ray structure determination were obtained from toluene/hexane. Preliminary examination and data collection were carried out on a kappa-CCD device (Nonius) at the window of a rotating anode (NONIUS FR591; 50 kV; 60 mA; 3.0 kW) and graphite monochromated Mo-K_α radiation (λ = 0.71073 Å).[35] The unit-cell parameters were obtained by full-matrix least-squares refinement of 6718 reflections. Data collection was performed at 293 K with an exposure time of 20 s per frame (7 sets; 980 frames; phi and omega scans; 1.0° scan-width). A total of 74222 reflections were integrated. Raw data were corrected for Lorentz and polarization effects. If necessary, corrections for absorption and decay effects were applied during the scaling procedure.[36] After merging, a sum of 6378 independent reflections remained, and were used for all calculations. The structure was solved by a combination of direct methods[37] and difference-

 © 2003 Wiley-VCH Verlag GmbH & Co. KGaA, Weinheim

Fourier syntheses.[38] All non-hydrogen atoms of the asymmetric unit were refined with anisotropic thermal displacement parameters. All hydrogen atoms were found in the final difference-Fourier maps and refined with isotropic displacement parameters. Full-matrix least-squares refinements were carried out by minimizing $\Sigma w(F_0^2 - F_c^2)^2$ with the SHELXL-97 weighting scheme and stopped at a maximum shift/err of less than 0.001. Neutral-atom scattering factors for all atoms and anomalous dispersion corrections for the non-hydrogen atoms were taken from the *International Tables for Crystallography*. All other calculations (including ORTEP graphics) were done with the program PLATON.[39]

CCDC-195346 contains the supplementary crystallographic data for this paper. These data can be obtained free of charge at www.ccdc.cam.ac.uk/conts/retrieving.html [or from the Cambridge Crystallographic Data Centre, 12, Union Road, Cambridge CB2 1EZ, UK; fax: (internat.) +44−1223/336−033; E-mail: deposit@ccdc.cam.ac.uk].

Table 2. Crystallographic data for *trans*-chloro(phenyl)bis(triphenylphosphane)nickel(II)

Chem. formula	$C_{42}H_{35}ClNiP_2$
Mol. wt.	695.78
Color/shape	Yellow/needle
Cryst size (mm)	0.46 × 0.25 × 0.25
Cryst syst	Monoclinic
Space group	$P2_1/c$ (No. 14)
a (Å)	15.7865(1)
b (Å)	11.9167(1)
c (Å)	20.0396(1)
β (deg)	112.2954(3)
V (Å^3)	3488.07(4)
Z	4
T (K)	293
$\rho_{calcd.}$ (g cm^{-3})	1.325
μ (mm^{-1})	0.754
F_{000}	1448
Θ range (deg)	1.39−25.34
Data collected (h,k,l)	±19, ±14, ±24
No. of reflns collected	74222
No. of indep reflns/R_{int}	6378 (all)/0.041
No. of obsd reflns [$I > 2\sigma(I)$]	5367 (obsd)
No. of params refined	555
R1 (obsd/all)	0.0296/0.0396
wR2 (obsd/all)	0.0737/0.0783
GOF (obsd/all)	1.039/1.039
Max/min $\Delta\rho$ (e·Å^{-3})	+0.28/−0.22

Acknowledgments

We are indebted to Prof. W. A. Herrmann for his generous and continuous support of our work. We are also grateful to the Leibniz-Rechenzentrum for providing computing time.

[1] G. Natta, P. Pino, P. Corradini, F. Danusso, E. Mantica, G. Mazzanti, *J. Am. Chem. Soc.* **1955**, *77*, 1708−1710.
[2] K. Ziegler, E. Holzkamp, H. Breil, H. Martin, *Angew. Chem.* **1955**, *67*, 426.
[3] K. Ziegler, E. Holzkamp, H. Breil, H. Martin, *Angew. Chem.* **1955**, *67*, 541−547.
[4] H. Sinn, W. Kaminsky, H. J. Vollmer, R. Woldt, *Angew. Chem.* **1980**, *92*, 396−402; *Angew. Chem. Int. Ed. Engl.* **1980**, *19*, 390−392.
[5] W. Kaminsky, A. Laban, *Appl. Catal., A General* **2001**, *222*, 47−61.
[6] G. J. P. Britovsek, V. C. Gibson, D. F. Wass, *Angew. Chem.* **1999**, *111*, 448−468; *Angew. Chem. Int. Ed.* **1999**, *38*, 428−447.
[7] S. D. Ittel, L. K. Johnson, M. Brookhart, *Chem. Rev.* **2000**, *100*, 1169−1203.
[8] S. Mecking, *Angew. Chem.* **2001**, *113*, 550−557; *Angew. Chem. Int. Ed.* **2001**, *40*, 534−540.
[9] L. K. Johnson, A. M. A. Bennett, S. D. Ittel, L. Wang, A. Parthasarathy, E. Hauptman, R. D. Simpson, J. Feldman, E. B. Coughlin, et al., in *PCT Int. Appl.* (E. I. Du Pont De Nemours and Co., USA; Johnson, Lynda Kaye; Bennett, Alison Margaret Anne; Ittel, Steven Dale; Wang, Lin; Parthasarathy, Anju; Hauptman, Elisabeth; Simpson, Robert D.), WO 98/30609, **1998**, p. 149 pp.
[10] C. Wang, S. Friedrich, T. R. Younkin, R. T. Li, R. H. Grubbs, D. A. Bansleben, M. W. Day, *Organometallics* **1998**, *17*, 3149−3151.
[11] T. R. Younkin, E. F. Connor, J. I. Henderson, S. K. Friedrich, R. H. Grubbs, D. A. Bansleben, *Science* **2000**, *287*, 460−462.
[12] F. A. Hicks, M. Brookhart, *Organometallics* **2001**, *20*, 3217−3219.
[13] F. M. Bauers, S. Mecking, *Macromolecules* **2001**, *34*, 1165−1171.
[14] A. S. Guram, A. M. Lapointe, H. W. Turner, T. Uno, in *PCT Int. Appl.* (Symyx Technologies, USA), WO 00/20377, **2000**, p. 55 pp.
[15] C. D. Tagge, R. B. Wilson, Jr., in *PCT Int. Appl.* (Sri International, USA)., Wo, **2001**, p. 74 pp.
[16] M. Watanabe, S. Hamura, M. Sato, in *Jpn. Kokai Tokkyo Koho* (Tosoh Corp., Japan), Jp, **2001**, p. 17 pp.
[17] K. Hall, V. Murphy, A. M. Lapointe, J. A. M. Van Beek, G. M. Diamond, in *U. S. Pat. Appl. Publ.*, US 20020034829, **2002**, p. 22 pp.
[18] D. A. Bansleben, S. K. Friedrich, T. R. Younkin, R. H. Grubbs, C. Wang, R. T. Li, in *U. S.* (Cryovac, Inc., USA), US, **2002**, pp. 27 pp., Cont.-in-part of U. S. Ser. No. 822,531, abandoned.
[19] M. Hidai, T. Kashiwagi, T. Ikeuchi, Y. Uchida, *J. Organomet. Chem.* **1971**, *30*, 279−282.
[20] R. A. Schunn, *Inorg. Synth.* **1971**, *13*, 124−126.
[21] R. A. Schunn, S. D. Ittel, M. A. Cushing, *Inorg. Synth.* **1990**, *28*, 94−98.
[22] I. Colon, D. R. Kelsey, *J. Org. Chem.* **1986**, *51*, 2627−2637.
[23] J. P. Flemming, M. C. Pilon, O. Y. Borbulevitch, M. Y. Antipin, V. V. Grushin, *Inorg. Chim. Acta* **1998**, *280*, 87−98.
[24] A. Mentes, R. D. W. Kemmitt, J. Fawcett, D. R. Russeli, *Polyhedron* **1999**, *18*, 1141−1145.
[25] W. Conzelmann, J. D. Koola, U. Kunze, J. Straehle, *Inorg. Chim. Acta* **1984**, *89*, 147−149.
[26] A. Khanna, B. L. Khandelwal, A. K. Saxena, T. P. Singh, *Polyhedron* **1995**, *14*, 2705−2710.
[27] M. G. Crisp, L. M. Rendina, E. R. T. Tiekink, *Z. Kristallogr. NCS* **2001**, *216*, 249−250.
[28] W. A. Herrmann, C. Brossmer, T. Priermeier, K. Oefele, *J. Organomet. Chem.* **1994**, *481*, 97−108.
[29] The triplet of the ipso-C of Ni-Phenyl could only be observed as a singlet due to its very weak intensity.
[30] C. Lee, W. Yang, R. G. Parr, *Phys. Rev. B: Condens. Matter* **1988**, *37*, 785−789.
[31] S. H. Vosko, L. Wilk, M. Nusair, *Can. J. Phys.* **1980**, *58*, 1200−1211.
[32] P. J. Stephens, F. J. Devlin, C. F. Chabalowski, M. J. Frisch, *J. Phys. Chem.* **1994**, *98*, 11623−11627.
[33] A. D. Becke, *J. Chem. Phys.* **1993**, *98*, 5648−5652.
[34] M. J. Frisch, G. W. Trucks, H. B. Schlegel, G. E. Scuseria, M. A. Robb, J. R. Cheeseman, V. G. Zakrzewski, J. A. Montgomery, R. E. Stratmann, J. C. Burant, S. Dapprich, J. M. Millam, A. D. Daniels, K. N. Kudin, M. C. Strain, O. Farkas, J. Tomasi, V. Barone, M. Cossi, R. Cammi, B. Mennucci, C. Pomelli, C. Adamo, S. Clifford, J. Ochterski, G. A. Petersson, P. Y. Ayala, Q. Cui, K. Morokuma, D. K. Malick, A. D. Rabuck, K. Raghavachari, J. B. Foresman, J. Cioslowski, J. V. Ortiz, A. G. Baboul, B. B. Stefanov, G. Liu, A. Liashenko, P. Piskorz, I.

 © 2003 Wiley-VCH Verlag GmbH & Co. KGaA, Weinheim

Komaromi, R. Gomperts, R. L. Martin, D. J. Fox, T. Keith, M. A. Al-Laham, C. Y. Peng, A. Nanayakkara, C. Gonzalez, M. Challacombe, P. M. W. Gill, B. Johnson, W. Chen, M. W. Wong, J. L. Andres, C. Gonzalez, M. Head-Gordon, E. S. Replogle, J. A. Pople, *Gaussian 98*, Revision A.7, Gaussian, Inc., Pittsburgh, PA, **1998**.

[35] Data Collection Software for Nonius KappaCCD devices, Delft, The Netherlands, **2000**.

[36] Z. Otwinowski, W. Minor, *Methods in Enzymology* **1997**, *276*, 307−326.

[37] A. Altomare, G. Cascarano, C. Giacovazzo, A. Guagliardi, M. C. Burla, G. Polidori, M. Camalli, *SIR92, J. Appl. Cryst.* **1994**, *27*, 435.

[38] G. M. Sheldrick, *SHELXL-97*, University of Göttingen, Göttingen, Germany, **1998**.

[39] A. L. Spek, *PLATON A Multipurpose Crystallographic Tool*, Utrecht University, Utrecht, The Netherlands, **2001**.

Received October 16, 2002

 © 2003 Wiley-VCH Verlag GmbH & Co. KGaA, Weinheim

Rapid and Selective Oxidation of Metallosulfophthalocyanines Prior to Their Usefulness as Precatalysts in Oxidation Reactions

Nicola d'Alessandro,[a] Lucia Tonucci,[a] Mario Bressan,*[a] Luana K. Dragani,[b] and Antonino Morvillo[c]

Keywords: Mass spectrometry / Homogeneous catalysis / Inorganic peroxides / Phthalocyanines / Oxidation

Two metallosulfophthalocyanines, RuPcS and FePcS, used in many catalytic oxidation reactions, were readily oxidized by hydrogen peroxide or monopersulfate, under acidic or neutral conditions in water, to form novel metal complexes derived from the facile oxidation of the PcS ring. Meso-nitrogen-oxide derivatives and metal-biliverdin-like derivatives were identified among the products at early reaction times, whereas at longer times fragmentation of the phthalocyanine ring occurred, with formation of sulfophthalimide and metal complexes containing the resulting tridentate ligand. The oxidative degradation of the MPcS complexes has been investigated by ESI-MS, UV/Vis-NIR and ^{1}H, ^{13}C and ^{15}N NMR spectroscopy. These rapidly formed, coordinatively unsaturated complexes represent the dominant species in oxidizing media, at least in the case of the Ru derivative, and must be the real catalyst precursors in previously published oxidation reactions using MPcS complexes. The oxidative degradation reactions occurred with selective mono-denitrogenation of one meso-nitrogen atom and formation of ammonia, thus recalling the celebrated selective degradation of heme to verdoheme and/or biliverdin and CO.

(© Wiley-VCH Verlag GmbH & Co. KGaA, 69451 Weinheim, Germany, 2003)

Introduction

Metalloporphyrins and -phthalocyanines are close structural and functional models for the ubiquitous mono-oxygenase or peroxidase heme enzymes, of principal importance on a global scale for the oxidation of xenobiotics in biological systems. Metalloporphyrins are often very effective systems for the catalytic oxidation of a variety of organic substrates, including alkanes, alkenes and aromatic hydrocarbons.[1] Metallophthalocyanines, despite their cheap and facile preparation, have been studied much less intensively as oxidation catalysts, the main drawback being their extensive insolubility in common organic solvents, which considerably limits the scope of the investigations.[2] Introduction of suitable substituents at the periphery of the molecule can make the metallophthalocyanine complexes soluble, and therefore, suitable for homogeneous catalysis; in this context, tetrasulfonated metallophthalocyanines MPcS (**1** in Scheme 1) are of particular interest, since they make possible catalysis in aqueous media,[3] an obvious green alternative to organic solvents.[4] During the last decade, iron or manganese sulfophthalocyanines have been successfully employed by Meunier et al. for the oxidative dechlorination of chlorophenols[5] and the oxidation of other organic substrates[6] in the presence of hydrogen peroxide and mono-persulfate.

We have also reported on the catalytic activity of ruthenium sulfophthalocyanine, with particular regard to the oxidation of chloro-organics[7,8] and alcohols,[9] and, more recently, of cyclohexanone, cyclohexanol or cyclohexane to adipic acid with hydrogen peroxide and mono-persulfate.[10] During these studies, we become aware that, contrary to common belief, the metallophthalocyanine core does not possess an intrinsic chemical stability in oxidizing media, even under very mild conditions. Indeed, among the few reports found in the literature, we can quote only two examples where the macrocycle is reported to undergo a facile oxidative cleavage in the presence of either oxygen (and sulfite as the sacrificial reductant)[11] or *tert*-butyl hydroperoxide.[12] Many of the MPcS complexes examined during our studies, and particularly the catalytically active ones, were found to be extremely sensitive to oxidants, such as hydrogen peroxide or mono-persulfate, giving rise to dramatic changes in their physical properties, and thus, truly behaving as pre-catalysts. These observations prompted us to conduct a spectroscopic study in aqueous solution, focused on defining the fate of a selected choice of metallosul-

[a] Dipartimento di Scienze, Università "G. d'Annunzio" di Chieti-Pescara,
Viale Pindaro 42, 65127 Pescara, Italy
E-mail: bressan@sci.unich.it
[b] Centro di Salute Ambientale "G. Paone", Consorzio Mario Negri Sud,
66030 Santa Maria Imbaro, Chieti, Italy
[c] Dipartimento di Chimica Inorganica and Centro C.N.R., Università di Padova,
Via Marzolo 1, 35100 Padova, Italy

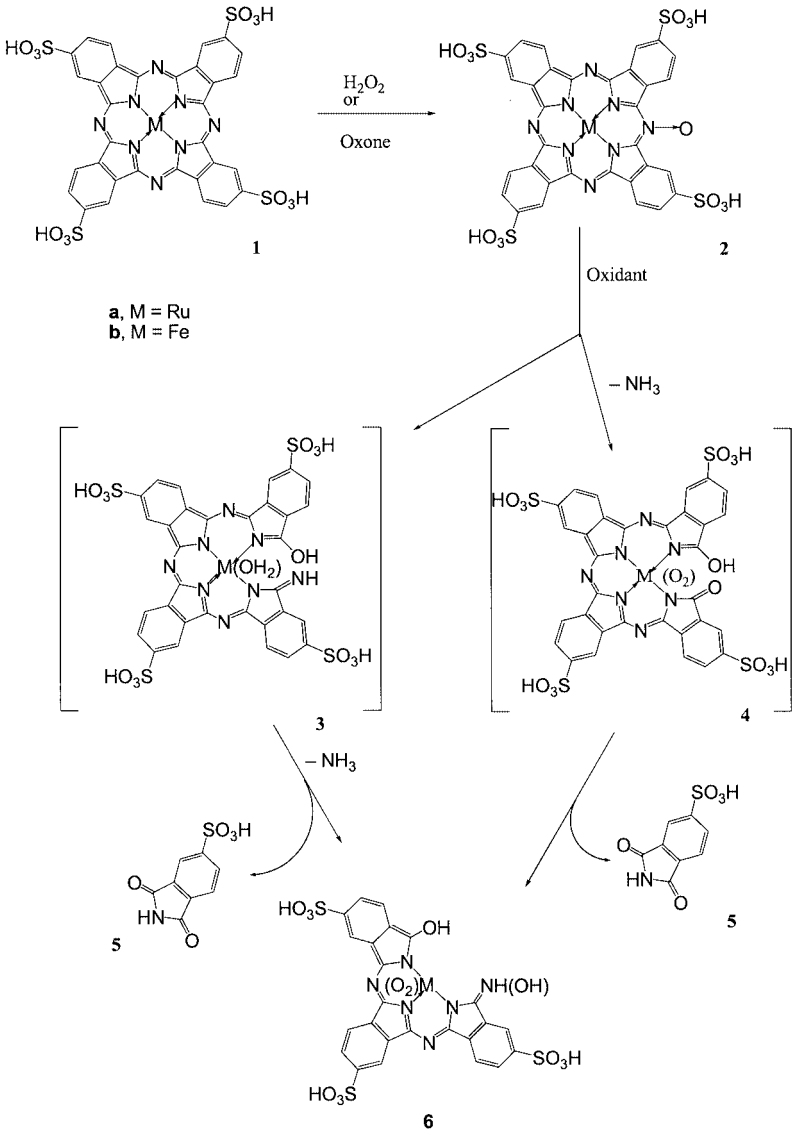

Scheme 1. Proposed pathway for the oxidation of MPcS by H_2O_2 or $KHSO_5$

fophthalocyanines, and the nature of the metal species formed during their mild oxidation by hydrogen peroxide or mono-persulfate.

Results and Discussion

General

The MPcS complexes (M = Fe, Ru and Cu) dissolved in water in the 1−50 mM concentration range were treated with various amounts of H_2O_2 or oxone (from 0.5 to 10 equivalent per mol) in acidic or neutral media and at room temperature. The electronic spectra (300−1500 nm) of the starting MPcS complexes show the diagnostic Q bands in the 620−670 nm region, which arise from the $\pi \rightarrow \pi^*$ transition within the heteroaromatic ring (Table 1). The intensely green/blue solutions became rapidly yellow/colorless (M = Fe and Ru) in the presence of an excess (≥10-fold) of oxidants, with complete disappearance of the corresponding Q band. In most cases, a series of distinct steps could be recognized during the oxidation of the MPcS complexes, leading to the formation of a number of intermediate products, which could be characterized spectroscopic ally. In strongly alkaline media (pH 13), the MPcS complexes, or more likely their hydroxo- and/or oxo-bridged derivatives, are almost insensitive to the oxidizing media, except RuPcS, for which, in the presence of $KHSO_5$ (but not of H_2O_2), a very slow decoloration was observed. The rate of the transformations depends upon the nature of the central ion. The CuPcS complex was found to be completely insensitive to the oxidation, even in acidic media.

The oxidation reactions were followed by ^1H and ^{13}C NMR spectroscopy with the aim of characterizing the metal species resulting from the oxidative degradation. We also recorded the ^{15}N NMR spectra of ^{15}N-RuPcS, but no signals were observed that were attributable to either meso- or metal-coordinating nitrogen atoms, in agreement with literature data, which often report insignificant ^{15}N NMR

 © 2003 Wiley-VCH Verlag GmbH & Co. KGaA, Weinheim

Table 1. Visible spectra of MPcS complexes

Compound	λ_{max}, nm (ε_M)[a]
FePcS	634 (40000)
CuPcS	624 (48000)
RuPcS	638 (26000)

[a] 3.33 μM aqueous solutions at pH 7 (phosphate buffer 0.2 M); the experiments were repeated at pH 2 (H_2SO_4 0.01 M), pH 9 (borate buffer 0.2 M) and pH 12 (NaOH 0.01 M) with no appreciable changes.

spectra for non-symmetrical nitrogen-containing compounds, even if labeled 100%.[13]

ESI-MS spectra, exhibiting the diagnostic isotopic patterns of the metal derivatives, offered the possibility of distinguishing between the metal-containing and purely organic species, and also between monomeric and oligomeric metal-containing species. Quite unexpectedly, the ESI-MS spectra gave clear indications, in all examined cases, of the corresponding molecular ions, when conducted in the positive-ion mode; various sodium-containing clusters, replacing the protons up to complete substitution, were also observed, especially at higher cone voltages (see Exp. Sect.). Under these conditions, peaks at −80 and sometimes at −160 amu were detected, indicative of a loss of SO_3. Clearly, cleavage of the S-benzene bond occurs to give the corresponding trisulfophthalocyanine derivative [M − 80], although the S-aromatic bond was not as easily cleaved as the S-aliphatic analog; the fact that this fragmentation was observed only at very high cone voltages suggests strongly that this event is an example of collision induced dissociation (CID).[14]

All attempts to isolate solid compounds from the oxidized reaction mixtures were unsuccessful and evaporation in vacuo resulted in intractable waxy solids, which did not yield solid materials.

RuPcS

RuPcS is diamagnetic both in the solid state (Gouy's method) and in aqueous solution (Evans' method), in agreement with a low-spin configuration of ruthenium(II) (d^6). The visible spectra in water show the diagnostic Q band at 638 nm, and also exhibit a definite shoulder, at higher energies, indicative of aggregation in aqueous solution.[15] The intensely green solutions of RuPcS become rapidly yellow in the presence of oxone or H_2O_2, with complete disappearance of the Q band, whereas no other absorptions are detected in the visible or in the near infrared regions, up to 1500 nm, which represents the upper wavelength for aqueous solutions containing peroxides. Simple demetalation, a rare event for metallophthalocyanine complexes,[16] can be ruled out on the basis of direct experiments, since the UV spectra of an organic phase, purposely added to the reaction mixtures, do not exhibit the absorptions at 310 and 385 nm that are diagnostic for RuO_4, the expected dominant species for free ruthenium in acidic oxidizing media. The diamagnetism of the aqueous solutions of the starting RuPcS complex is maintained in the presence of excess of oxidant, whereas the ^{1}H NMR spectra, showing for the starting RuPcS only a broad signal in the δ = 8 ppm region, exhibit well resolved signals at δ = 8.1 and 7.9 ppm upon oxidation, clearly indicative of the expected AMX patterns of the 1,2,4-aromatic proton system, thus suggesting extensive removal of the strong intermolecular interaction occurring in polar media (stacking) that is probably responsible for the broad NMR signal.

The ^{1}H NMR spectra of the acidic reaction mixtures with mono-persulfate also exhibit three more signals, centered at δ = 7 ppm (J = 51 Hz), which, in the case of the ^{15}N-RuPcS derivative, were replaced by a doublet with $J(^1H\text{-}^{15}N)$ = 74 Hz; significantly, the ^{15}N NMR spectra (DEPT-45) exhibit five signals centered at δ = −360 ppm, having the same $J(^1H\text{-}^{15}N)$ reported above. These findings are diagnostic of the presence of ammonium ions, which, on the basis of the measured intensity ratios between benzene and ammonium protons, are found in a 1:1 molar ratio with the regards to the complex, even after longer reaction times (Table 2). Hydrogen peroxide in acidic media behaves similarly, giving rise to the ^{1}H NMR signals of the ammonium ion. In this case, however, because of the presence of oxygen, continuously formed upon dismutation of the oxidant, quantitation of the ammonia produced was performed with an ion-selective electrode; again, the quantity of ammonia never exceeded the 1:1 molar ratio (Table 2).

Table 2. Production of ammonia by oxidation of MPcS complexes

Compound	Time, h	NH_4^+ produced	
		$KHSO_5$[a]	H_2O_2[b]
RuPcS	1	1.1	1.1
	18	1.1	1.03
FePcS	1.5	n.d.	0.45
	16	n.d.	0.73
CuPcS	16	0	0

[a] mol/mol of MPcS; ^{1}H NMR measurements. Reaction conditions: aqueous solution of MPcS, 1 mM, and $KHSO_5$, 0.5 M; pH ca. 2; 20 °C. [b] mol/mol of MPcS, electrochemical measurements. Reaction conditions: aqueous solution of MPcS, 1 mM, and H_2O_2, 2 M; pH ca. 2 (H_2SO_4); 20 °C.

It should be noted that the oxidation appears to be highly selective, involving only one of the eight nitrogen atoms of the macrocycle: further treatment of the oxidized RuPcS complex with sodium hydroxide under strongly alkaline conditions and refluxing led to complete denitrogenation of the compound, with formation of ammonia in the expected 8:1 molar ratio. The oxidative denitrogenation of amines to ammonia is a known process in biochemistry, where it is catalyzed by amine oxidase, a non-heme copper-containing enzyme, and is also reported to occur in the presence of a biomimetic copper complex.[17]

The ^{13}C NMR spectrum of the RuPcS complex (60 mM) shows the expected eight signals, which arise from the three tertiary [δ = 121, 125 and 132 ppm (aromatic CH carbons)] and the five quaternary carbon atoms [δ = 133 and 135 ppm (β-C with respect to N); δ = 144 ppm (sulfonate-

 © 2003 Wiley-VCH Verlag GmbH & Co. KGaA, Weinheim

bonded carbon); δ = 174 and 179 ppm (α-C)]. The oxidized solutions exhibit closely related eight-signal ^{13}C NMR spectra, whose differences in chemical shift from the untreated samples are scarcely significant, although they do confirm the integrity of the organic backbone. Also, 3-sulfophthalimide exhibits a related ^{13}C NMR spectrum (see Exp. Sect.), with almost imperceptible differences in the positions of each signal, including those from the α-C's, and is therefore independent of the nature of the bonded heteroatoms (oxygen or nitrogen).

The ESI spectra of RuPcS were found to be highly sensitive to the applied cone voltage, thus making the interpretation of the data complicated (Figure 1). Under medium cone voltage (50−100 V), the penta-protonated species $Ru^{II}PcSH_5^+$ (*m*/*z* = 935), showing the diagnostic isotopic (metal) pattern of the monomer, is the dominant species (Figure 2). By further increasing the applied voltage, and therefore under very drastic conditions, significant changes of the fine structure of the signal were observed, with the peak at *m*/*z* = 934 (−1 amu) gaining intensity and thus pointing to the formation of the $Ru^{III}PcSH_4^+$ species, produced in the capillary tip upon the one-electron oxidation of the central metal ion. At lower cone voltage (5−50 V), the main feature is the appearance of a new species that is still monomeric, but with *m*/*z* = 969. This species becomes dominant at very low voltage; the observed *m*/*z* value fit with a Ru^{IV} species, such as $Ru^{IV}(OH)_2PcSH_5^+$, which might arise from an oxidation in the capillary tip, is rather surprising because it occurrs under such mild conditions. The ^{15}N-RuPcS complex gives the expected ESI signal at *m*/*z* = 943, i.e. +8 amu with respect to the unlabelled derivative, and at lower voltage than the above Ru^{IV} species at *m*/*z* = 977−979 (the presence of small amount of ^{14}N in the labeled compound led to some loss of the conventional isotopic pattern of ruthenium).

Upon treatment with the oxidants, a series of distinct intermediate species could be detected by ESI-MS spectra. At low oxidant-to-metal ratios (ca. 1:1), a new signal appears at *m*/*z* = 951 − an increase of 16 amu with respect to the starting species − that still retains the diagnostic isotopic pattern of the monomer; the ^{15}N-RuPcS derivative behaves similarly, leading to the appearance of an ion at *m*/*z* = 959.

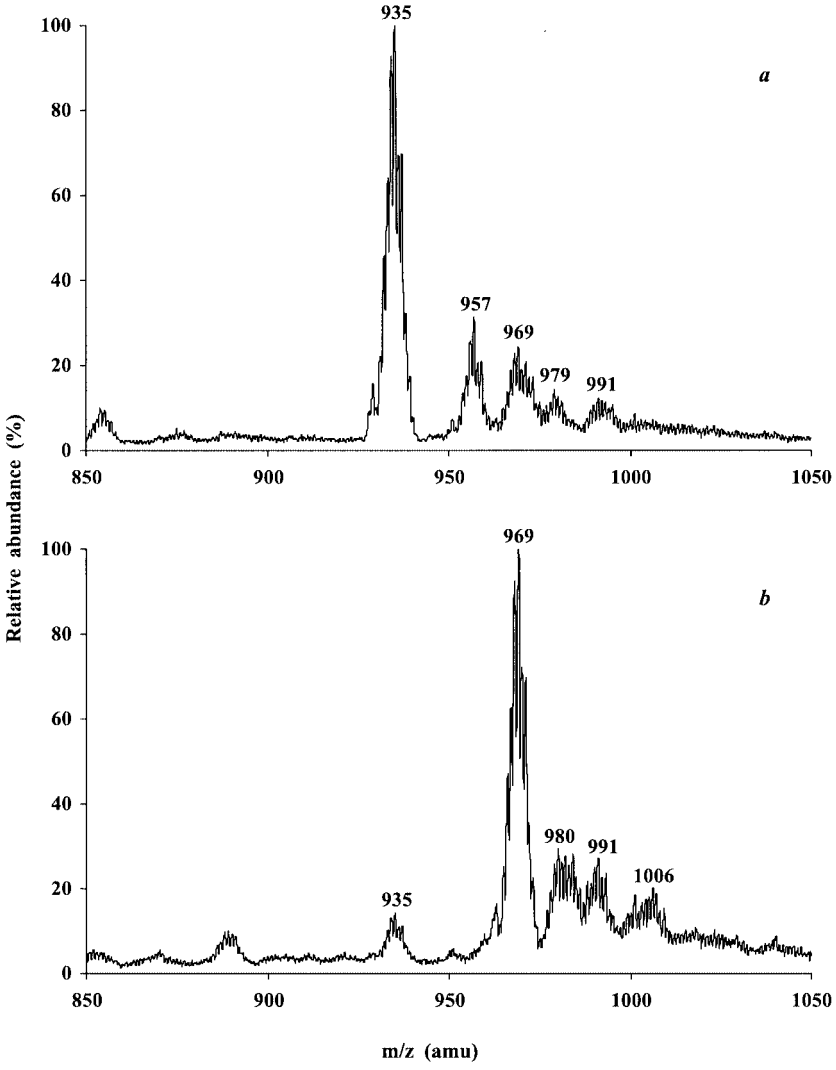

Figure 1. ESI-MS spectra of aqueous 5 mM solution of RuPcS, at high (150 V) (a) and low (30 V) (b) cone voltage

 © 2003 Wiley-VCH Verlag GmbH & Co. KGaA, Weinheim

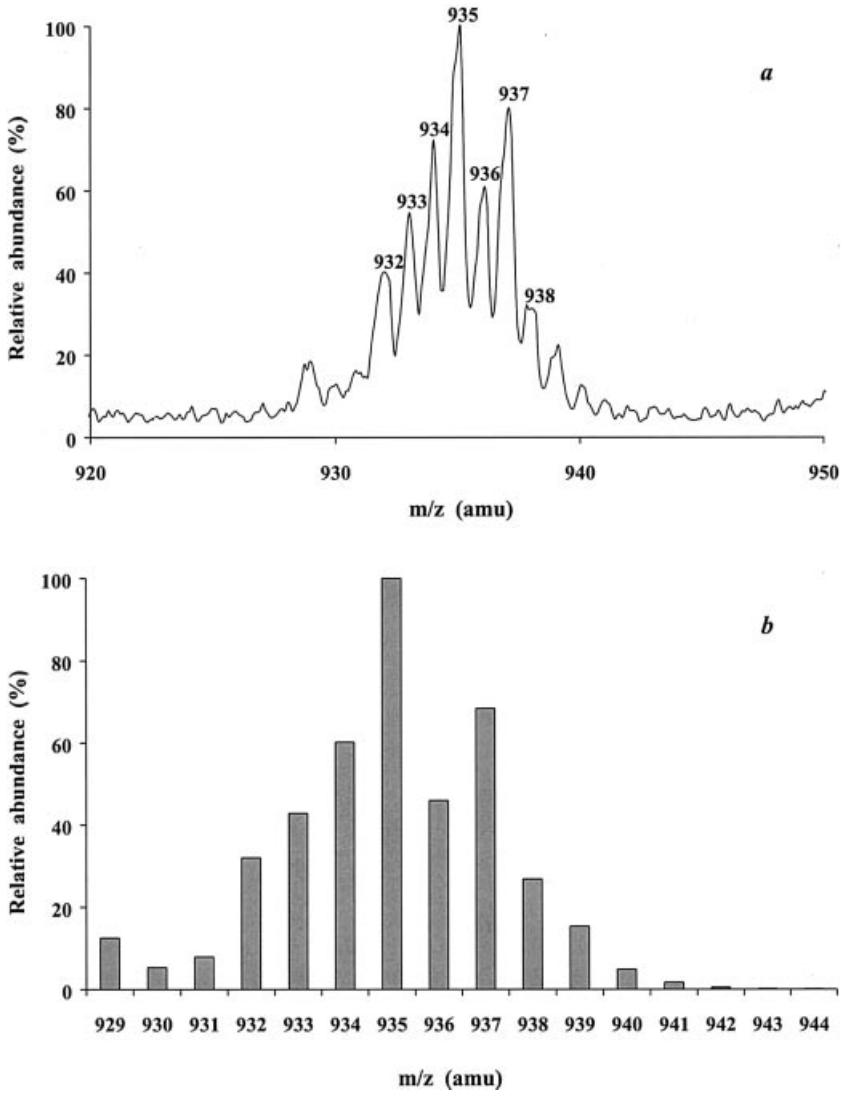

Figure 2. Fine structure of m/z = 935 peak of RuPcS (50 V) (a) vs. calculated isotopic pattern (b)

As in the case of the starting RuPcS discussed above, these signals are replaced at lower voltage by a signal at m/z = 985 (993 for the labeled derivative), again attributed to oxidation of the complex at the capillary tip. Both signals could be detected in the ESI spectra, when the measurements were performed at intermediate voltage, in order to achieve maximum sensitivity (Figure 3). The species detected at m/z = 951 (959 for ^{15}N) and clearly incorporating one oxygen atom, can be attributed to either an oxometal derivative Ru^{IV}(O)PcS or, more likely, a complex with a mono-oxygenated ligand, where the metal is still in a lower oxidation state, for example a Ru^{II}PcOS species (**2a** in Chart 1), where PcOS is the mono-nitrogen-oxide derivative in the meso position of the PcS ligand. An immediate explanation for the ready formation of the nitrogen-oxide derivative could be provided by the conventional chemistry of nitrogen-containing heteroaromatics towards inorganic peroxidic reagents.[18] However, the fact that some of the MPcS derivatives, such as CuPcS, are totally resistant to the oxidative treatment, suggests a direct involvement of the central metal atom in the oxygenation process, rather than an uncatalyzed attack by the peroxidic oxidant on a meso-nitrogen atom of the PcS ring. Under this hypothesis the oxygenation of a meso-nitrogen is highly reminiscent of the first step of the oxidation of heme (to hydroxyheme).[19]

Upon addition of further oxidant to RuPcS (up to 10:1), a fast and almost complete disappearance of the oxygenated species occurred; the ESI-MS spectra shows the presence of strong signals both at higher (m/z around 1003, 1022 and 1040) and lower molecular weights (m/z around 778, 796, 814 and 833), most of them apparently lacking the diagnostic isotopic pattern of ruthenium and possibly indicating the presence of closely related ions differing by a few amu. At longer reaction times, only the species with lower molecular weights were observed (Figure 3). ^{15}N-RuPcS behaved similarly, leading to the formation of ions with m/z centered at ca. 1010, 1030 and 1048 and at 784, 802, 817 and 838 amu. A direct comparison of the masses of the ions from the ^{14}N or the ^{15}N samples might make possible, in principle, an evaluation of the nitrogen content of the various species; unfortunately most of the signals did not exhibit the standard isotopic pattern of ruthenium, and therefore the exact

 © 2003 Wiley-VCH Verlag GmbH & Co. KGaA, Weinheim

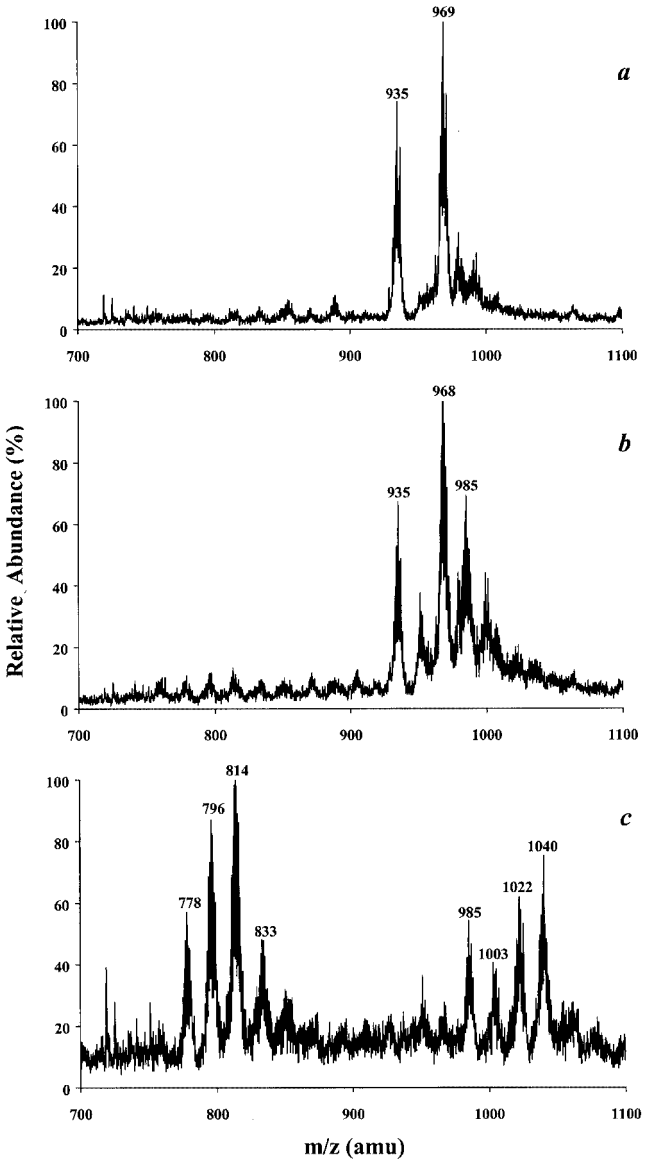

Figure 3. ESI-MS spectra of aqueous 5 mM solution of RuPcS (50 V) (a) and after addition of $KHSO_5$: in equimolar amount (50 V) (b) and twofold molar excess (50 V) (c); (in both cases reaction time 10 min)

masses were too uncertain to allow unequivocal conclusions. The intermediate species around *m*/*z* = 1003, 1022 and 1040 (1010, 1030 and 1048 for the ^{15}N-labeled derivative) were tentatively attributed to the aqua clusters (mono-, di- and tri-) of ions from compounds **3a** or **4a**, i.e., dioxoruthenium(VI) complexes with biliverdin-like ligands, either containing all the starting nitrogen atoms or lacking one of them, respectively; on this basis, the corresponding non-aquated cations might come at *m*/*z* = 985 and 986, respectively (992 and 993 for the ^{15}N-labeled derivative), and are therefore superimposed on the species formed in the initial stages of the reaction and discussed previously. Biliverdin- and verdoheme-like derivatives of phthalocyanines have been reported in the literature, although they were prepared upon photolysis of a triazatetrabenzocorrole and not directly from a phthalocyanine ring;[20] significantly, these derivatives were reported to lack not only the diagnostic Q-band, but also other absorptions of comparable intensity, and are thus in agreement with the observed quenching of the $\pi\rightarrow\pi^*$ bands in oxidized RuPcS complexes. The peaks at *m*/*z* = 778, 796, 814 and 833 (784, 802, 817 and 838 for the ^{15}N-labeled derivative) fit well with a series of aquated cations (from none to three molecules of water) from compound **6a**, i.e., a dioxoruthenium(VI) complex of a tridentate ligand formed upon fragmentation of the PcS ring (Scheme 1). Accordingly, the resulting organic fragment 3-sulfophthalimide (**5**) was detected as a single peak at *m*/*z* = 228 (positive ionization mode; 229 for the ^{15}N-labeled derivative) or at *m*/*z* = 227 (negative ionization mode); an original sample of the compound exhibited the same spectral behavior. One molecule of ammonia was also produced, during either the first or the second step (Scheme 1); to the best of our knowledge, fragmentation of a phthalocyanine ring with production of ammonia has never been reported.

FePcS

In the presence of small amounts of added mono-persulfate or hydrogen peroxide (1:1 molar ratio), a distinct shift of the Q-band of FePcS towards lower energies was observed, whose blue solutions (λ_{max} = 634 nm) turned green (λ_{max} = 670 nm; Figure 4) and finally, in the presence of increasing amounts of the oxidant (10-fold), almost colorless. The oxidized solutions became paramagnetic almost immediately (Evans' method), whereas, and quite surprisingly, the starting paramagnetic (Gouy's method) iron(II) (d^6) derivative,[21] was apparently diamagnetic by Evans' method, once dissolved in water. If it is conceivable that the expected strong stacking of the MPcS moieties occurring in the aqueous solutions does not allow reliable measurements of the magnetic moments by the Evans method, the fact that the oxidized complex was found to be clearly paramagnetic also points to an extensive removal of stacking upon oxidation. The benzene protons were still observed as a large unstructured signal at δ = 8−10 ppm (^1H NMR spectra), but most significantly, and as in the ruthenium case

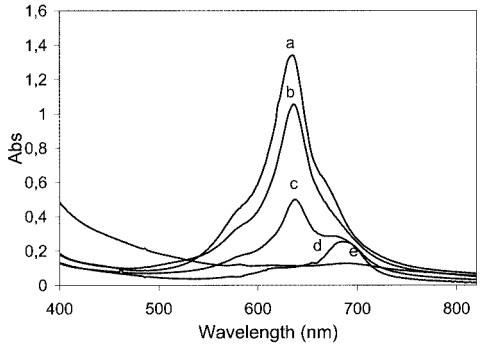

Figure 4. Vis spectra of aqueous 3.33 μM solution of FePcS (a) and after addition of $KHSO_5$: in equimolar amount (b); threefold molar excess (c); fourfold molar excess (d); 10-fold molar excess (e). In all the experiments no difference was observed between 1 and 10 minutes of wait before the recording, following the dilution, of the spectra

 © 2003 Wiley-VCH Verlag GmbH & Co. KGaA, Weinheim

discussed above, ammonia was produced upon oxidation, again, at least with hydrogen peroxide, in a 1:1 molar ratio with the metal (Table 2). In the presence of oxone the ammonia signals were also clearly detected by ^{1}H NMR spectroscopy, although accurate quantitation was not possible neither by NMR measurements, because of the paramagnetism of the solution, or by electrochemical measurements, since the selective ion electrode requires a constant ionic strength. Furthermore, in the presence of increasing amounts of the oxidants (10-fold), almost colorless solutions were obtained.

The oxidized solution showed, even during the early stages of the reaction, the complete disappearance of the ESI-MS signal (positive pattern) of the starting complex at m/z = 888 and the diagnostic isotopic pattern of an iron monomer, which corresponds to a $Fe^{III}PcSH_4^+$ ion, probably because of an easy oxidation of iron(II) to iron(III) in the capillary tip of the spectrometer. However, and unlike RuPcS, no important peaks were detected in the ESI spectra of the oxidized solutions, although the visible spectra gave clear evidence of transformation products: instead, only very weak and confusing signals were observed in the 700−750 and 500−550 amu regions, even under milder ionization conditions, together with sharp signals at m/z = 228 and 250, clearly attributable to sulfophthalimide (**5**) and the corresponding sodium cluster. These results suggest a very fast and extensive fragmentation of the oxidation products, indicative of a high sensitivity of the system either to the ionization conditions or to the chemical oxidation itself.

Conclusions

The most important finding in these experiments is that it is clearly evident that the rapid and irreversible oxidative degradation of the MPcS complexes studied with H_2O_2 or mono-persulfate occurs under very mild conditions, and prior to any role as precatalysts for oxidation reactions. A mechanism is tentatively proposed, involving the initial formation of oxidizing metal species in higher oxidation states, followed by a selective intra- (or inter) molecular attack at one meso-nitrogen atom of the phthalocyanine ring, with formation of a mono N-oxide derivative (compound **2**). As a consequence of the disruption of the aromaticity of the PcS macrocycle, a facile hydrolysis can be envisaged with ring opening and production of ammonia (compounds **3** and **4**). These biliverdin-like complexes then undergo further oxidative fragmentation, with loss of sulfophthalimide (detected) or 3-iminosulfoisoindoline (not detected), to tridentate ligands (compound **6**) that are still coordinated to the metal ions. It is fairly conclusive that this event results in the in situ formation of coordinatively unsaturated metal complexes, now thought to be candidate precatalysts for the oxidation reactions previously reported.[5a,7] Although the efficacy of each precatalyst also depends upon the intrinsic reactivity of the metal species towards the specific substrate, it is interesting to note that the different catalytic behaviors of the two MPcS complexes strictly reflect the degree of degradation in the oxidizing media. RuPcS gave rise to relatively long-lived coordinatively unsaturated metal species and was indeed shown to be an effective and efficient precatalyst in the $KHSO_5$ oxidation of caprolactone to adipic acid; in contrast, FePcS, which underwent fast and extensive demetalative fragmentation, provided to be a far less effective catalyst.[10] The fast and quantitative transformation of the MPcS complexes into catalytically active species, when in oxidizing media, could be a new paradigm for the general behavior of related classes of metallomacrocycles in oxidation catalysis.

Experimental Section

General Procedures: The reactions were typically carried out at 20 °C in a 5 mL vial, by stirring magnetically 2 mL of an aqueous solution containing the complexes (0.1−10 mM) and suitable amounts of H_2O_2 or $KHSO_5$ (from 0.5:1 to 10:1). Ammonia analysis was performed electrochemically (Orion, model 420A) with an ion-selective electrode (Orion, model 95−12; a glass electrode with a gas diffusion membrane); calibration curve was performed by a 1 M solution of NH_4Cl.

Materials: RuPcS[8] was prepared by template synthesis starting from $RuCl_3{\cdot}3H_2O$, sodium 4-sulfophthalate and urea, following early general procedures for the synthesis of metallosulfophthalocyanines.[21] The ^{15}N-RuPcS derivative was prepared similarly, starting from commercially available ^{15}N-urea (99% isotopic purity, Isotec Inc.). $FePcS{\cdot}3H_2O$ (monosodium salt) and CuPcS (tetrasodium salt) were purchased from Aldrich.

NMR Measurements: NMR spectra were recorded on a Bruker Avance 300 MHz (Karlsruhe, Germany) equipped with a BBO 5 mm probe; the frequencies of the observed nuclei were 300.13, 75.47 and 30.42 MHz respectively for ^{1}H, ^{13}C and ^{15}N. In the case of ^{1}H spectra a water suppression (Bruker made − zgcppr) pulse sequence was used; in addition a reference consisting of a co-axial capillary, inside the NMR tube, filled with a 30 mM D_2O solution of the sodium salt of 3-(trimethylsilyl)propionic acid-2,2′,3,3′-d_4 (TSP) was used.

FTIR spectra were acquired on a Perkin−Elmer Spectrum 2000 equipped with an MIR source and a MIR-TDGS detector; to record the spectra the samples were suspended in anhydrous KBr pellets; spectral width, for all the experiments, was 5000−370 cm^{-1}.

Vis spectra was carried out on a Perkin−Elmer Lambda 2 series 3300; the spectral window was 350−800 nm.

ESI-MS Measurements: The HPLC apparatus used was a Perkin−Elmer series 200 quaternary pump system (Norwalk, CT, USA). Analyses were performed at room temperature using a reversed phase Supelcosil LC-PAH column (250 × 4.6 mm; 5 μm) purchased from Supelco (Bellefonte, PA, USA). Samples were automatically injected using a Perkin−Elmer series 200 autosampler (thermostatted at 4 °C) with a 20 μL injection-loop. Isocratic separations were carried out using a mobile phase consisting of methanol (50%) and water (50%), both with 0.5% of formic acid at the flow rate of 200 μL/min. The HPLC system was connected to a Perkin−Elmer mod. 785A UV/Vis detector (Norwalk, CT, USA) set at the wavelength 280 nm and then to a PE Sciex Turboionspray source (2.1 L/min NEB gas). Acquisitions were carried out in positive ion mode over the mass range 700−1100 amu (or

 © 2003 Wiley-VCH Verlag GmbH & Co. KGaA, Weinheim

100−1500 amu when the detection of 3-sulfophthalimide was necessary), using a step size of 0.1 amu and a dwell time of 0.350 ms. The nebulizer gas (air) and the curtain gas (N_2) flows were set at 1.7 L/min and 2.7 L/min, respectively. The ionization voltage was set at +5200 V and the orifice and ring potentials were normally set at +50 V and +280 V, respectively; higher and lower voltage condition are referred to orifice potentials varied between 5 and 180 V and ring potentials between 100 and 360 V. Instrument control and data acquisition were performed with Macintosh System 7600/132 (Apple, Copertino, CA, USA) using Masschrom 1.1.1 software (PE Sciex, Foster City, CA, USA). The Mass Spectrometer was calibrated with polypropylene glycol (PPG) obtained from PE Sciex and the resolution was set in the range 0.6−0.8 amu.

Magnetic Moments Measurements: Magnetic moments were measured by Gouy's method (solid state) or Evans' method, performed as follows: a coaxial NMR tube (5 mm i.d.) was filled with a 0.31 M solution of *tert*-butanol in D_2O (tube) and with a 0.31 M solution of *tert*-butanol also containing ca. 30 mM of the MPcS complexes in D_2O (external capillary); the calculations for the susceptivity were performed according to the literature.[22]

Synthesis of 3-Sulfophthalimide (5): 3-Sulfophthalic acid (30 g, 0.122 mol) was heated at 150 °C in vacuo for 3 h; after cooling, urea (3.6 g, 0.06 mol) was added under nitrogen atmosphere and the mixture heated again to 130 °C until evolution of gas had finished (yield: 2.5%). ^{1}H NMR (300.13 MHz, D_2O, 25 °C: δ = 8.08 (d, 1 H, 1-CH), 7.93 (dd, 1 H, 3-CH), 7.77 (d, $J_{3,4}$ = 7.9, $J_{1,3}$ = 1.7 Hz, 1 H, 4-CH) ppm. ^{13}C NMR (75.47 MHz, D_2O, 25 °C): δ = 126.4, 129.1, 129.7 (CH); 132.4, 135.4 (β-C); 145.4 (sulfonate-C); 171.0, 172.0 (α-C) ppm. IR (KBr film): double peak at $\tilde{\nu}$ = 1714−1738 cm^{-1} (C=O). $C_8H_5NO_5S{\cdot}2.5H_2O$ (272.2): C 36.03, H 3.68, N 5.17, S 11.76; found C 35.14, H 3.16, N 5.16%, S 12.46.

Acknowledgments

The authors thank Mr. A. Ravazzolo, C. N. R., Padova, for technical assistance.

[1] J. T. Groves, *J. Porphyrins Phthalocyanines* **2000**, *4*, 350−352, and references therein.
[2] A. B. Sorokin, A. Tuel, *Catalysis Today* **2000**, *57*, 45−49.
[3] X. Tao, W. Ma, T. Zhang, J. Zhao, *Chem. Eur. J.* **2002**, *8*, 1321−1326.
[4] [4a] *Aqueous-Phase Organometallic Catalysis. Concepts and Applications* (Eds.: B. Cornils and W. A. Herrmann), Wiley-VCH, Weinheim, **1998**. [4b] *Aqueous Organometallic Chemistry and Catalysis* (Eds.: I. T. Horvàth and F. Joò), NATO ASI Series, Kluwer, Dordrecht, **1995**.
[5] [5a] A. Sorokin, J.-L. Seris, B. Meunier, *Science* **1995**, *268*, 1163−1166. [5b] A. Sorokin, S. De Suzzoni-Dezard, D. Poullain, J.-P. Noel, B. Meunier, *J. Am. Chem. Soc.* **1996**, *118*, 7410−7411. [5c] A. Sorokin, B. Meunier, *Chem. Eur. J.* **1996**, *2*, 1308−1317. [5d] B. Meunier, A. Sorokin, *Acc. Chem. Res.* **1997**, *30*, 470−476. [5e] A. Hadasch, A. Sorokin, A. Rabion, B. Meunier, *New J. Chem.* **1998**, *22*, 45−51.
[6] [6a] A. Sorokin, L. Fraisse, A. Rabion, B. Meunier, *J. Mol. Catal. A: Chemical* **1997**, *117*, 103−114. [6b] A. Sorokin, B. Meunier, *Eur. J. Inorg. Chem.* **1998**, 1269−1281. [6c] R. Song, A. Robert, J. Bernadou, B. Meunier, *Inorg. Chim. Acta* **1998**, *272*, 228−234. [6d] A. Hadasch, B. Meunier, *Eur. J. Inorg. Chem.* **1999**, 2319−2325.
[7] M. Bressan, N. d'Alessandro, L. Liberatore, A. Morvillo, *Coord. Chem. Rev.* **1999**, *185−186*, 385−402.
[8] M. Bressan, N. Celli, N. d'Alessandro, L. Liberatore, A. Morvillo, L. Tonucci, *J. Organomet. Chem.* **2000**, *593−594*, 416−420.
[9] N. d'Alessandro, L. Liberatore, L. Tonucci, A. Morvillo, M. Bressan, *J. Mol. Catal.* **2001**, *175*, 83−90.
[10] N. d'Alessandro, L. Liberatore, L. Tonucci, A. Morvillo, M. Bressan, *New J. Chem.* **2001**, *25*, 1319−1324.
[11] W. Pasiuk-Bronikowska, M. Ktajewska, I. Flis-Kabulska, *Polyhedron* **1998**, *18*, 561−569.
[12] E. M. Gaigneaux, R. Maggi, P. Ruiz, B. Delmon, *J. Mol. Catal. A* **1996**, *109*, 67−74.
[13] S. Berger, S. Braun, H. O. Kalinowski, in *NMR Spectroscopy of the Non-Metallic Elements*, John Wiley & Sons, Chichester, **1997**, p 111−318.
[14] C. L. Gatlin, F. Tureček, in *Electrospray Ionization Mass Spectrometry* (Ed.: R. B. Cole), John Wiley & Sons, Inc. New York, **1997**, 527−570.
[15] Y. C. Yang, J. R. Ward, R. P. Seiders, *Inorg. Chem.* **1985**, *24*, 1765−1769.
[16] P. A. Stuzhin, O. G. Khelevina, B. D. Berezin, in *Phthalocyanines. Properties and Applications, Vol. 4* (Eds.: C. C. Leznoff and A. B. P. Lever), VCH, New York, **1996**, p. 19−79, and references therein.
[17] M. Hess, T. Weyhermuller, K. Wieghardt, P. Chauduri, *7th International Symposium on Dioxygen Activation and Homogeneous Catalytic Oxidation*, York, **1999**, C4.
[18] [18a] J. G. Robke, E. J. Behrman, *J. Chem. Res. (S)* **1993**, 412−413. [18b] P. Thellend, W. Battioni, W. Sanderson, D. Mansuy, *Synthesis* **1997**, *12*, 1387−1388. [18c] S. L. Jain, B. Sain, *Chem. Commun.* **2002**, 1040−1041.
[19] [19a] T. Yoshida, C. Taiko Migita, *J. Inorg. Biochem.* **2000**, *82*, 33−41. [19b] I. Spasojevic, I. Batinic-Haberle, R. D. Stevens, P. Hambright, A. N. Thorpe, J. Grodwoski, P. Neta, I. Fridovich, *Inorg. Chem.* **2001**, *40*, 726−739. [19c] L. Avila, H.-W. Huang, J. C. Rodriguez, P. Moenne-Loccoz, M. Rivera, *J. Am. Chem. Soc.* **2000**, *122*, 7618−7619.
[20] J. Li, L. R. Subramanian, M. Hanack, *Chem. Commun.* **1997**, 679−680.
[21] J. H. Weber, D. H. Busch, *Inorg. Chem.* **1965**, *4*, 469−471.
[22] S. Braun, H. O. Kalinowski, S. Berger, in *150 and More Basic NMR Experiments: a Practical Course*, Wiley-VCH, Weinheim, **1998**, pp 285−287.

Received October 25, 2002

 © 2003 Wiley-VCH Verlag GmbH & Co. KGaA, Weinheim

A New Concept for the Efficient Synthesis of Chiral Phosphorus−Nitrogen−Carbon Cage Compounds

Nils Hoffmann,[a] Catleen Wismach,[a] Ludger Ernst,[b] Hans-Martin Schiebel,[b] Peter G. Jones,[a] and Rainer Streubel*[a]

Keywords: Azaphospholes / Phosphorus / Cage compounds / Tungsten / Cyclization

A new concept for the efficient synthesis of a chiral phosphorus-nitrogen-carbon cage-compound is reported, which is comprised of a high-yield three-step procedure starting from a *P*-Cp*-substituted 2*H*-azaphosphirene complex. Thermolysis of a solution of the latter complex in the presence of Ph_3PNCN and DMAD afforded the *P*-Cp*-substituted 2*H*-1,2-azaphosphole complex **11** in a clean reaction; a further reaction at 75 °C with DMAD produced complex **12** via an *intermolecular* Diels–Alder reaction of the Cp* group. A subsequent *intramolecular* Diels–Alder reaction of **12**, at 120 °C, yielded the title compound, complex **13,** in quantitative yields. Elemental analyses and detailed (solution) NMR spectroscopic and MS investigations confirmed all complexes. Furthermore, solid state structures of complexes **11** and **13** were established by X-ray single crystal structure analyses.

(© Wiley-VCH Verlag GmbH & Co. KGaA, 69451 Weinheim, Germany, 2003)

Introduction

The development − or better, constant search − of new and effective synthetic methods of rigid chiral trivalent phosphorus(III) compounds, which might offer improved performance in asymmetric catalysis, is one of the current challenges in Organophosphorus Chemistry, as pointed out recently by Mathey.[1] Early findings by Shell scientists in 1966 showed that cyclic phosphanes perform better in hydroformylation processes than tributyl-phosphane.[2] Burk[3] then showed in 1990 that phospholane-based C_2-symmetric chelating ligands, dubbed as DuPHOS, are important in the catalytic hydrogenation of functional alkenes. Mathey[4] and Réau[5] reported the use of the 1-phosphanorbornadiene **1**, obtained by [4+2] cycloaddition reactions of a transient 2*H*-phosphole and tolane,[6] in hydrogenation[4] and hydroformylation[5] reactions. The same ligand system was modified by Herrmann and co-workers and introduced as NORBOS **2** in the biphasic hydroformylation of propene.[7] It was Mathey again, who developed BIPNOR[8] as a new bidentate ligand and employed it e.g. in the asymmetric isomerization of a cyclic diene, in which it proved to be far superior to BINAP.[9]

In view of this background and the great variety of established structures of polycyclic phosphanes[10] and phosphorus-carbon cage compounds[10,11] with a ring junction phosphorus atom, it is surprising − at first sight − that studies of their use as cocatalysts have remained scarce. The problem is that most often their synthesis relies, at one stage or another, on the employment of phosphaalkyne derivatives, which are not readily accessible, e.g. in the case of **3**,[12] and/or because of the lack of straightforward high-yield synthetic methodologies. One of the few exceptions may be **4** (Scheme 1), which was obtained by a ligand-centered reaction as a coordination compound in quantitative yields.[13]

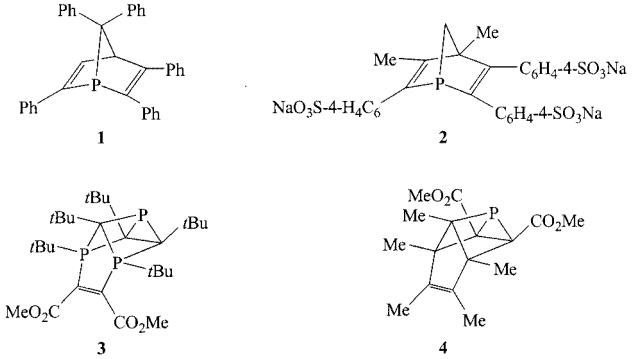

Scheme 1. Unusual bicyclic phosphanes (**1**, **2**) and phosphorus−carbon cage compounds (**3**, **4**)

For the same aforementioned reasons the selective synthesis of phosphorus-nitrogen-carbon cage compounds such as **5**[14] and **6**[15] aroused interest (Scheme 2); the latter was obtained as a coordination compound. Grützmacher demonstrated that **5** is surprisingly stable under oxidative

[a] Institut für Anorganische und Analytische Chemie der Technischen Universität Braunschweig,
Postfach 3329, 38023 Braunschweig Germany
Fax: (internat.) + 49-(0)531/391-5387
E-mail: r.streubel@tu-bs.de
[b] Institut für Organische Chemie der Technischen Universität Braunschweig,
Postfach 3329 38023 Braunschweig Germany

conditions and thus showed that such ligand systems might have additional advantageous properties associated with their unusual small valence bond angle sums at phosphorus (Σ°P), which are below 270°, e.g. Σ°P·255° (**5**) and Σ°P·263° (**6**). He also showed that **5** can be used successfully as a new ligand system in catalytic hydrosilylations.[16] It is also remarkable that unusual properties of phosphanes with valence bond angle sums at phosphorus below 270° were predicted theoretically by Orpen and Connely some years ago.[17]

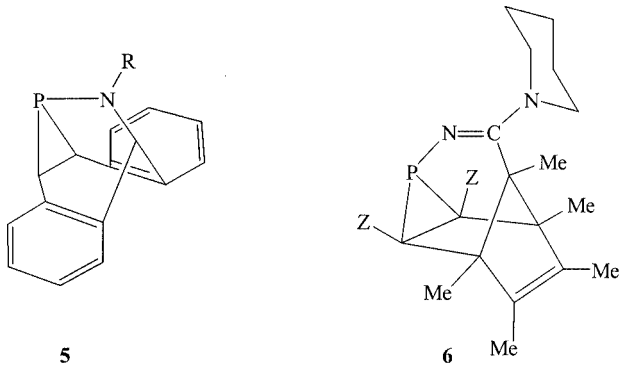

Scheme 2. Unusual phosphorus−nitrogen−carbon cage compounds **5** and **6**

Because of our long-standing interest in the synthesis of new mono- and polycyclic unsaturated phosphorus-nitrogen heterocycles[18] using 2*H*-azaphosphirene complexes[19] as precursors, we recently decided to return to the unresolved problem of the surprising instability of the exocyclic P−C bond of the *P*-pentamethylcyclopentadienyl-substituted 2*H*-1,2-azaphosphole complex **7**.[20] Upon heating in benzonitrile, complex **7** decomposed in the presence of dimethyl acetylenedicarboxylate (DMAD), forming the bicyclic heterocycle **8**, the first 7-aza-1-phosphanorbornadiene complex (Scheme 3).

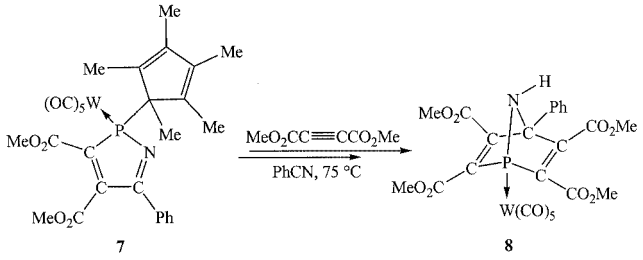

Scheme 3. Formation of 7-aza-1-phosphanorbornadiene complex **8** via thermolysis of the 2*H*-1,2-azaphosphole complex **7** in the presence of DMAD

Results and Discussion

In an attempt to synthesize new functional derivatives of **8**, we have now achieved selective synthesis of 2*H*-1,2-azaphosphole complex **11** using the *P*-Cp*-substituted 2*H*-azaphosphirene complex **9**[21] and Ph_3PNCN[22] (**10**) in *o*-xylene at 75 °C (Scheme 4). Surprisingly, complex **11** showed no signs of decomposition up to temperatures as high as 120 °C! Since the only difference between **7** and **11** is the replacement of a phenyl by the Ph_3PN group, clearly the new substituent is responsible for this dramatic effect − but the reason is not immediately apparent.

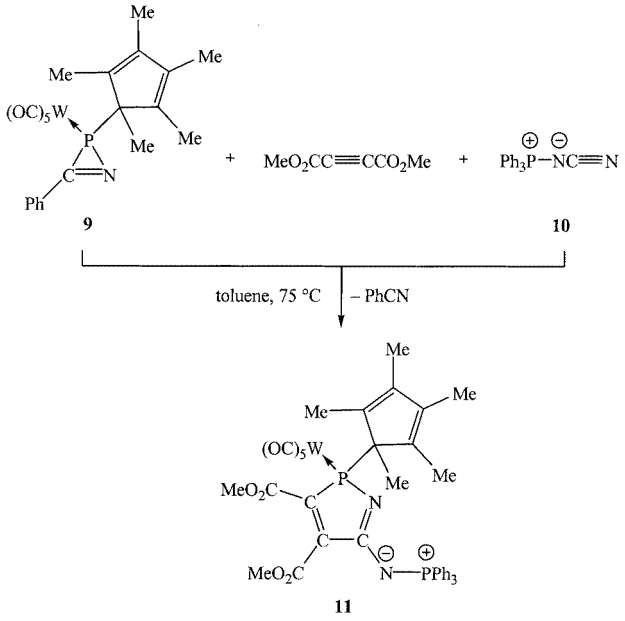

Scheme 4. Synthesis of 2*H*-1,2-azaphosphole complex **11**

We were also able to carry out a clean *intermolecular* Diels−Alder reaction of **11** with DMAD at 75 °C, which yielded complex **12** in high yields, just by strictly controlling the reaction times for the first (**9** → **11**) and the second chemical transformations (**11** → **12**). Further studies of the thermal stability of complex **12** led to another surprisingly high-yield and unprecedented cycloaddition reaction in azaphosphole chemistry. Upon heating an *o*-xylene solution of complex **12** at 120 °C an *intramolecular* Diels−Alder reaction of the aza-1,3-diene unit of the 2*H*-1,2-azaphosphole ring with the dimethyl-substituted ethylene unit of the norbornadiene substituent selectively furnished complex **13**, which contains a new phosphorus−nitrogen−carbon cage compound as the ligand system (Scheme 5).

It is remarkable that the ^{31}P resonance of the ring junction phosphorus atom in **13** at δ = 158.4 ppm [$J(^{183}W,P)$ = 269.9 Hz] is much more deshielded than the phosphorus nuclei in **11** and **12**, although it now has a more conventional chemical environment. Therefore, this deshielding might be explained in terms of ring strain in **13**.[23] Furthermore, the exocyclic phosphorus atom in **13** experiences a significant shielding in comparison with **11** and **12** and resonates at δ = 1.3 [**11**: δ(P) = 18.1 and **12**: δ(P) = 18.4 ppm].

Discussion of Selected ^1H and ^{13}C NMR Spectroscopic and Mass Spectrometric Data

The ^1H and ^{13}C NMR spectra of complexes **11**−**13** were assigned as fully as possible by the use of two-dimensional shift correlation experiments (HSQC and HMBC). One-di-

 © 2003 Wiley-VCH Verlag GmbH & Co. KGaA, Weinheim

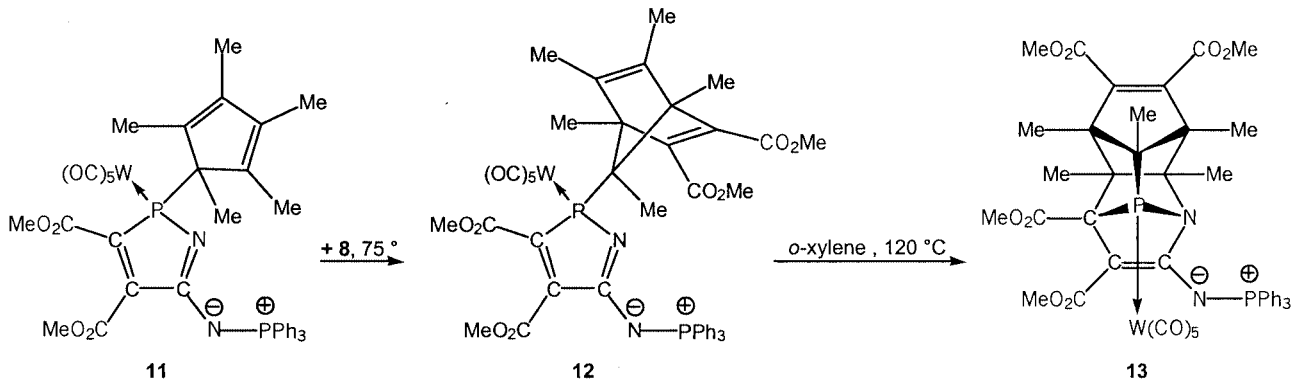

Scheme 5. Synthesis of complexes **12** and **13** using inter- and intramolecular Diels–Alder reactions

mensional ^{1}H and ^{13}C NMR spectra were recorded at magnetic field strengths of both 4.7 T and 9.4 T so that, for closely lying lines, one could unequivocally decide which line distances corresponded to coupling constants involving ^{31}P and which ones to small chemical shift differences.

The ^{1}H and ^{13}C NMR signals of the PPh_3 groups of **11–13** are assigned in a straightforward manner and need not be discussed. In the spectra of **11** the ^{13}C and ^{1}H signals belonging to the same ester groups can be identified by the correlation spectra. But as the ester nuclei do not show any correlations to 'outside' nuclei, it is not clear which ester group gives rise to which signals. Assignment of the signals of the Cp* moiety starts from the large $^{3}J_{P,H}$ coupling constant (15.0 Hz) of the protons of the methyl group at the quaternary sp^3 carbon (Cp*-C-1). By exploiting the $^{2}J_{C,H}$ and $^{3}J_{C,H}$ correlations, the ^{1}H and ^{13}C signals of the Cp* group are fully assigned. The vicinity of the chiral phosphorus atom causes chemical nonequivalence of C-2 and C-5, of C-3 and C-4 and of their attached methyl groups. It may be noted that three-bond C,H-correlations are found across the double bonds of the Cp* group but not across the C-3/C-4 single bond, i.e. there is no crosspeak for C-3/4-Me or C-4/3-Me. The carbon atoms of the 2*H*-1,2-azaphosphole ring show no HMBC correlations to any protons. They are tentatively assigned on account of their chemical shifts and coupling constants with phosphorus. Hence, the most deshielded carbon (δ_C = 166.5 ppm) is assumed to be C-5 because of its amidine character. Of the remaining ring carbon atoms, C-4 has $^{2}J_{P,C}$ and $^{3}J_{P,C}$ couplings, while C-3 experiences $^{1}J_{P,C}$ and $^{4}J_{P,C}$ interactions. The values of 18.9 or 26.1 Hz associated with δ_C = 149.4 ppm are believed to be too large for $^{4}J_{P,C}$. Thus C-3 is assigned to δ_C = 151.6 ppm with its *J* values of 4.4, 2.7 Hz.

The spectral assignments for **12** were similar to those described for **11**. The two ester groups at the 2*H*-1,2-azaphosphole ring are distinguished from those at the norbornadiene moiety by the coupling of their carbonyl carbon nuclei with the phosphorus atom. Assignment of the pentamethylnorbornadiene atoms started with the protons of the 7-methyl group which were again identified by their coupling with ^{31}P. The protons of one of the bridgehead methyl groups were found to be strongly shielded (δ = 0.08 ppm), while their counterparts show a more normal ^{1}H chemical shift of δ = 1.59 ppm. Possible causes for this shielding are the aromatic rings of the triphenylphosphane-iminyl group or one or several of the carbonyl groups of the $W(CO)_5$ substituent. The unknown geometry of **12** does not permit a definite conclusion. Finally, the extreme deshielding of the carbon C-7 from the norbornadiene bridge (δ = 90.5 ppm), an sp^3 carbon atom with a phosphorus atom as the only somewhat polar substituent, is in line with the large chemical shift in norbornadiene itself (δ = 75.1 ppm),[24] which is further increased by the presence of one α- and two β-methyl groups.

For compound **13**, all ^{13}C and ^{1}H chemical shifts of the central 1-aza-11-phosphatetracyclo[6.2.1.1^{3,6}.0^{2,7}]dodeca-4,9-diene system were assigned from the crosspeaks in the HSQC and HMBC spectra. Apart from the methyl carbons (*C*-methyl and ester *O*-methyl) and the $W(CO)_5$ group, only the carbon nuclei of the 9,10-double bond showed no correlations with distant protons. These carbon atoms have widely different chemical shifts (δ = 159.8 ppm and 98.6) which are characteristic of a push-pull substituted double bond.

A common feature of the EI-mass spectra of **11**, **12** and **13** is the cleavage of the P,N ylidic bond, thus generating $[Ph_3P]^{+\cdot}$ and neutral species such as nitrenes. The further degradation of $[Ph_3P]^{+\cdot}$ has been reported previously[25] and was very recently observed in the case of *P*-bis(trimethylsilyl)methyl-substituted 2*H*-1,2-azaphosphole complexes.[26] Another important fragmentation process is the cleavage of the exocyclic P–C bond of the complexes **11** and **12.** Furthermore, all complexes lose the $W(CO)_5$ fragment upon ionization. In the case of complex **13** the main fragmentation includes a rearrangement of the polycyclic ring system by formation of a substituted pyridine radical cation.

Discussion of Selected Structural Data

We were able to confirm the molecular structures of complexes **11** (Figure 1) and **13** (Figure 3 and 4) for the solid state by X-ray single crystal structure analyses (Table 1). The almost planar 2*H*-1,2-azaphosphole ring of complex **11** (mean deviation of 0.02 Å) showed no unusual atom dis-

 © 2003 Wiley-VCH Verlag GmbH & Co. KGaA, Weinheim

tances when compared to complex **14** (Figure 2),[15] the only known structure of a *P*-Cp*-substituted phosphole[27,28] or heterophosphole.[29] As a common structural motif in diester-substituted 2*H*-1,2-azaphosphole rings[25] the ester group at C16 almost shows an in-plane orientation, whereas the ester group at C-17 is oriented out-of-plane. The torsion angle of N(1)−C(18)−N(2)−P(2) is 0.3° and, therefore, should enable electronic interactions between the substituent and the ring system. The planes of the two five-membered rings in **11** are partially eclipsed, in contrast to **14**, where the respective planes adopt a conformation in which they have an opposite orientation along the exocyclic P−C bond. However, this does not greatly effect the corresponding P−C distances [**11**: P(1)−C(6) 1.886(3) Å and **14**: P(1)−C(8) 187.7(2) Å]. A comparison of the azaphospholene moiety of the molecular structure of complex **13** (Figure 3 and 4) with compounds **15**[30] and **16**[31] (Figure 5), which also have azaphospholene ring structures with a C−C double bond, reveals the uniqueness of **13**. The C(7)−C(8) distance of 1.373(2) Å is that of an elongated C-C double bond [**15**: 1.290(3) Å;[30] **16**: 1.329 Å[31]], which might be caused by the electronic interaction with the Ph_3PN group [N(1)−C(8)−N(2)−P(2): −29.8 °]. It is also remarkable that the P(1)−C(6) and P(1)−N(1) distances of 1.8925(15) and 1.7706(13) Å, respectively, are fairly long [**15**: 1.818(2) and 164.5(2) Å;[30] **16**: 180.0 and 171.6 pm[31]]. This is associated with a long P(1)−C(13) distance of 1.8968(15) Å and a short P(1)−W distance of 2.4744(4) Å. The valence bond angle sum of Σ°P(1)·273 °, which very much resembles the situation of compound **8** in its transition metal-coordinated form.

Table 1. Crystal data and structure refinement[34] of complexes **11** and **13**

Complex	**11**	**13**
Empirical formula	$C_{41}H_{46}N_3O_9P_2W$	$C_{47}H_{50}Cl_2N_2O_{13}P_2W$
M_r	970.60	1167.58
Crystal size (mm)	0.21 × 0.14 × 0.05	0.31 × 0.30 × 0.08
Crystal system	triclinic	monoclinic
Space group	$P(-1)$	$P2_1/n$
Unit cell dimensions		
a (Å)	11.9636(12)	17.4060(10)
b (Å)	13.8639(14)	12.3286(6)
c (Å)	14.5331(14)	22.1482(12)
α (°)	93.959(3)	90
β (°)	90.407(3)	101.746(3)
γ (°)	113.490(3)	90
V (Å^3)	2203.9(4)	4653.3(4)
Z	2	4
$D_{calcd.}$ (Mg·m^{-3})	1.463	1.667
μ (mm^{-1})	2.747	2.734
Transmissions	0.7119−0.8622	0.6192−0.8622
F(000)	978	2352
T (K)	133(2)	133(2)
$2\theta_{max}$	60	60
No. of reflections		
measured	47472	84792
unique	13346	14181
R_{int}	0.0434	0.0339
Parameters	541	613
Restraints	9	102
wR (F^2, all reflections)	0.0694	0.0564
R [F, $I > 2\sigma(I)$]	0.0313	0.0205
S	0.781	1.011
max. Δρ (e·Å^{-3})	2.161	1.153

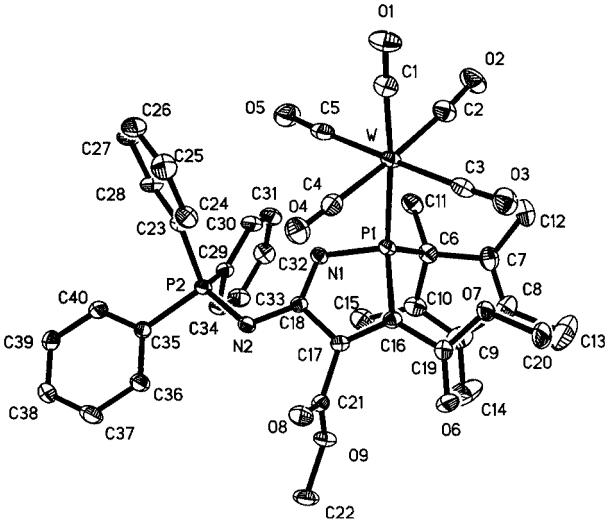

Figure 1. Molecular structure of **11** from the crystal (ellipsoids represent 50% probability levels; hydrogen atoms are omitted for clarity); selected bond lengths [Å] and angles [°] (values for both molecules are given): W−C1 2.004(3), W−P1 2.5338(7), P1−N1 1.691(2), N1−C18 1.306(3), C16−C17 1.338(3); W−P1−C6 118.79(8), C18−N1−P1 111.15(17), C16−C17−C18 112.7(2). The following short contacts are observed in **11**: C37−H37···O8 Å (operator $-x$, $-y + 1$, $-z + 2$); C28−H28···O2 (operator $-x + 1$, $-y + 1$, $-z + 1$); C11−H11C···O99 (operator $-x + 1$, $-y + 1$, $-z + 1$); C26−H26···O99 (operator $-x + 1$, $-y + 1$, $-z + 1$)

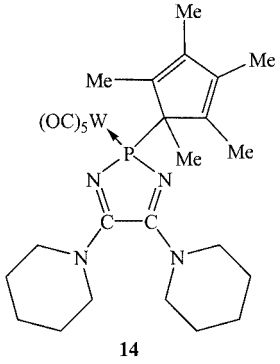

14

Figure 2. 2*H*-1,2-azaphosphole complex **14**[15]

Because studies of a so called[31] "dimer" of compound **16** have shown an excellent performance (up to 95% *ee* at −70 °C) in hydrovinylation reactions of styrene,[32] we are currently trying to liberate the new polycyclic phosphane ligand of **13**.

 © 2003 Wiley-VCH Verlag GmbH & Co. KGaA, Weinheim

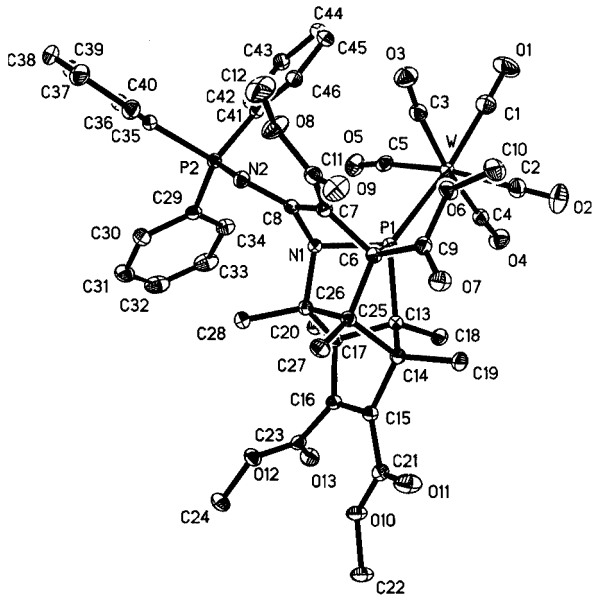

Figure 3. Molecular structure of **13** from the crystal (ellipsoids represent 50% probability levels; hydrogen atoms are omitted for clarity); selected bond lengths [A] and angles [°] (values for both molecules are given): W−P1−C6 125.82(5), N1−P1−C13 92.77(6), P1−N1−C8 106.15(9), N1−C8−C7 110.37(13), C6−C7−C8 110.90(13), C7−C6−P1 99.88(10). Specified hydrogen bonds (with esds except fixed and riding H): D−HH···AD···A<(DHD) 0.952.553.393(2)147.3C(32)−H(32)···O(11), 0.952.493.403(2)161.9C(37)−H(37)···O(13)

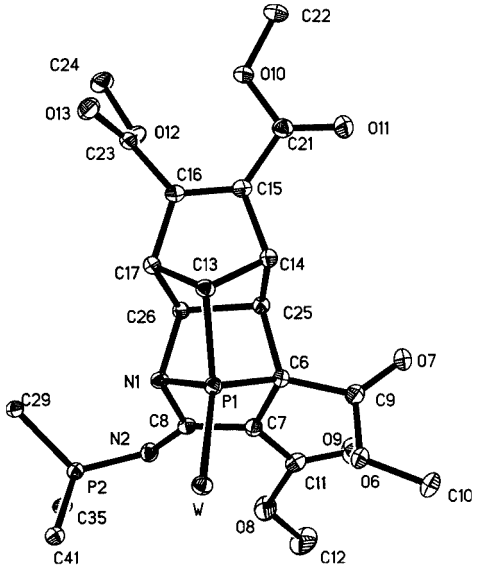

Figure 4. Reduced molecular structure of **13** (top-view)

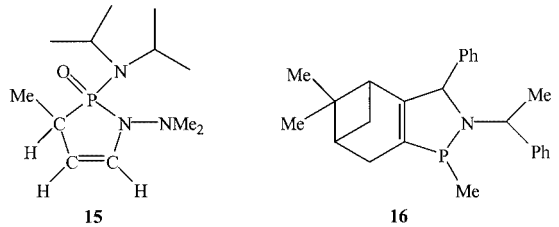

Figure 5. Azaphospholenes **15**[30] and **16**.[31]

Conclusions

We have shown that the stability of *P*-Cp*-substituted 2*H*-1,2-azaphosphole complexes can be significantly enhanced by choosing the right substituent and that they are now available for further investigations − two new reactions were presented here. Furthermore, this example can be regarded as a blueprint for the synthesis of other phosphorus-carbon and phosphorus-nitrogen-carbon cage compounds thus underlining once more the usefulness of *P*-Cp*-substituted 2*H*-azaphosphirene complexes in the construction of new and unusual polycyclic phosphane ligands.

Experimental Section

General Procedures: All reactions and manipulations were carried out under an atmosphere of deoxygenated dry nitrogen, using standard Schlenk techniques with conventional glassware, and solvents were dried according to standard procedures. The NMR spectra were obtained on the Bruker spectrometers Avance DRX400 and Avance DPX200 at operation frequencies of 400 MHz (^{1}H), 101 MHz (^{13}C), 161 MHz (^{31}P) and of 200 MHz (^{1}H), 50 MHz (^{13}C), 81 MHz (^{31}P), respectively. Chemical shifts were referenced to internal tetramethylsilane (^{1}H, δ = 0.00 ppm), $CDCl_3$ (^{13}C, δ = 77.0 ppm) and to the frequency of virtual external 85% orthophosphoric acid (^{31}P, δ = 0.0 ppm). The latter frequency was determined independently from a concentric capillary of H_3PO_4 in neat $CDCl_3$. DEPT-135 spectra were carried out to determine the degree of substitution of the carbon atoms. The spectrometer software used was XWin NMR version 2.6. The manufacturer's pulse programs 'invigstp' (gradient-selected phase-sensitive HSQC) and 'inv4gslplrnd' (gradient-selected HMBC) controlled the two-dimensional NMR spectroscopic experiments[33]. The 2D experiments were optimized for coupling constants of 145 Hz [$^1J_{C,H}$] and 7.7 Hz [$^{2,3}J_{C,H}$]. Digital resolutions were chosen to be small enough in both dimensions to permit the resolution of closely lying chemical shifts. All coupling constants reported involve ^{31}P unless otherwise specified. Electron impact (EI) (70 eV), chemical ionization (CI) (ammonia), and fast atom bombardment (FAB) (Xenon, NBA) mass spectra were recorded on a double focusing mass spectrometer Finnigan MAT-8430; Exact mass resolution R = 10000 (10%-valley-definition). Infrared spectra were recorded on a Biorad FT-IR 165 (selected data given). UV/vis spectra were recorded on a Hewlett Packard HP 8452. Melting points were obtained on a Büchi 535 capillary apparatus. Elemental analyses were performed by using a Carlo Erba analytical gas chromatograph. The κP-notation in the nomenclature is intended to differentiate between *P*- and *N*-coordination of the appropriate heterocycle to the metal.

[Pentacarbonyl{3,4-bis(methoxycarbonyl)-2-pentamethylcyclopentadienyl-5-(*N*-triphenylphosphonioimidoyl)-2*H*-1,2-azaphosphole-κP}tungsten(0)] (11): Carbonitrile **10** (0.9 mmol) and DMAD (0.85 mmol) were added to a solution of 2*H*-azaphosphirene complex **9** (0.51 g, 0.86 mmol), dissolved in toluene (5 mL). The solution was heated at 75 °C for 25 min while stirring slowly and was controlled by ^{31}P NMR spectroscopy. All volatile components were then removed in vacuo (ca. 0.01 mbar) and the products separated by low-temperature column chromatography (SiO_2, −10 °C, 10 × 2 cm, *n*-pentane/diethyl ether, 50:50). Evaporation of the third fraction yielded complex **11** as a yellow solid.

 © 2003 Wiley-VCH Verlag GmbH & Co. KGaA, Weinheim

Yield: 620 mg, 77%; m.p. 87 °C (decomp.). ^{1}H NMR: δ = 0.83 (d, *J* = 15.0 Hz, 3 H, cp*-1-Me), 1.25 (br. s, 3 H, cp*-5-Me), 1.52 (br. s, 3 H, cp*-2-Me), 1.660 (dd, *J* = 4.2, 1.2 Hz, 3 H, cp*-4-Me), 1.673 (dd, *J* = 4.3, 1.2 Hz, 3 H, cp*-3-Me), 3.74 (s, 3 H, 4- or 3-azaphosphole(azap)-COO*Me*), 3.94 (s, 3 H, 3- or 4-azap-*COOMe*), 7.44 (m_c, 6 H, H-*meta* of PPh_3), 7.55 (m_c, 3 H, H-*para* of PPh_3), 7.80 (m, 6 H, H-*ortho* of PPh_3) ppm. ^{13}C NMR: δ = 11.16 (d, *J* = 1.5 Hz, cp*-4-Me), 11.22 (d, *J* = 0.7 Hz, cp*-5-Me), 11.4 (d, *J* = 1.5 Hz, cp*-3-Me), 12.2 (d, *J* = 1.6 Hz, cp*-2-Me), 13.7 (d, *J* = 0.9 Hz, cp*-1-Me), 52.1 (s, azap-4- or 3-COO*Me*), 52.5 (s, azap-3- or 4-COO*Me*), 62.6 (dd, *J* = 6.1, 0.5 Hz, cp*-C-1), 127.3 (d, *J* = 100.7 Hz, C-*ipso* of PPh_3), 128.7 (d, *J* = 12.5 Hz, C-*meta* of PPh_3), 132.5 (d, *J* = 2.9 Hz, C-*para* of PPh_3), 133.4 (d, *J* = 10.1 Hz, C-*ortho* of PPh_3), 137.1 (s, cp*-C-5), 137.2 (d, *J* = 3.0 Hz, cp*-C-2), 139.4 (d, *J* = 6.7 Hz, cp*-C-3), 140.0 (d, *J* = 5.9 Hz, cp*-C-4), 149.4 (dd, *J* = 26.1, 18.9 Hz, azap-C-4), 151.6 (dd, *J* = 4.4, 2.7 Hz, azap-C-3), 163.8 (dd, *J* = 10.7, 2.3 Hz, azap-4- or 3-*C*OOMe), 165.4 (dd, *J* = 14.5, 1.0 Hz, azap-3- or 4-*C*OOMe), 166.5 (dd, *J* = 11.7, 5.5 Hz, azap-C-5), 196.5 (d, *J* = 7.4, *J*(^{183}W,C) = 126.5 Hz, WCO-*cis*), 199.5 (d, *J* = 25.4 Hz, WCO-*trans*) ppm. ^{31}P NMR: δ = 18.1 (d, *J* = 1.2 Hz, PPh_3), 105.0 [br. s, *J*(^{183}W,P) = 256.0 Hz, azap-P] ppm. UV/Vis (CH_3CN): λ (lg ε) = 228 (4.90), 248 (4.64), 274 (4.15), 300 (3.86), 324 (3.84), 360 (3.71), 380 (3.52) nm. IR (KBr): ṽ = 2069 (vs, CO), 1980 (vs, CO), 1931 (s, CO), 1741 (vs, CO_2), 1719 (vs, CO_2) cm^{-1}. MS (EI, ^{184}W): *m*/*z* = 934 (1) $[M]^{+\cdot}$, 903 (1) $[M - OCH_3]^+$, 799 (100) $[M - Cp^*]^{+\cdot}$, 771 (18) $[M - Cp^*\text{-}CO]^{+\cdot}$, 743 (45) $[M - Cp^*\text{-}2CO]^{+\cdot}$, 687 (40) $[M - Cp^*\text{-}4CO]^{+\cdot}$, 659 (90) $[M - Cp^*\text{-}5CO]^{+\cdot}$, 631 (35) $[M - Cp^*\text{-}6CO]^{+\cdot}$, 262 (20) $[PPh_3]^{+\cdot}$, 183 (30) $[PPh_2]^+$. $C_{40}H_{36}N_2O_9P_2W$ (934.5): calcd. C 51.41, H 3.88, N 3.00; found C 51.26, H 4.23, N 3.20.

{Pentacarbonyl[2,3-bis(methoxycarbonyl)-2-(1,4,5,6,7-pentamethylnorborna-2,5-dien-7-yl)-3,4-bis(methoxycarbonyl)-5-(*N*-triphenylphosphonioiminoyl)-2*H*-1,2-azaphosphole-κP]tungsten(0)} (12): Carbonitrile **10** (1 mmol) and DMAD (2 mmol) were added to a toluene (6 mL) solution of 2*H*-azaphosphirene complex **11** (0.6 g, 1 mmol). The solution was heated at 75 °C for 20 h while stirring slowly and was controlled by ^{31}P NMR spectroscopy. All volatile components were then removed in vacuo (ca. 0.01 mbar) and the products separated by low-temperature column chromatography (SiO_2, −10 °C, 10 × 2 cm, *n*-pentane/diethyl ether, 20:80). Evaporation of the third fraction yielded complex **12** as a yellow solid. Yield: 850 mg, 79%; m.p. 152 °C (decomp.). ^{1}H NMR: δ = 0.08 [s, 3 H, norbornadiene(nor)-4-Me], 1.37 (d, *J* = 15.7 Hz, 3 H, nor-7-Me), 1.45 (s, 3 H, nor-5-Me), 1.49 (s, 3 H, nor-6-Me), 1.59 (s, 3 H, nor-1-Me), 3.63 (s, 3 H, 3- or 2-nor-COO*Me*), 3.66 (s, 3 H, 2- or 3-nor-COO*Me*), 3.82 [s, 3 H, 4- or 3-azaphosphole(azap)-COO*Me*], 3.98 (s, 3 H, 3- or 4-azap-COO*Me*), 7.46 (m_c, 6 H, H-*meta* of PPh_3), 7.57 (m_c, 3 H, H-*para* of PPh_3), 7.80 (m_c, 6 H, H-*ortho* of PPh_3) ppm. ^{13}C NMR: δ = 9.0 (s, nor-4-Me) 11.36 (d, *J* = 4.0 Hz, nor-1-Me) 11.44 (s, nor-5-Me), 12.4 (s, nor-6-Me), 16.4 (d, *J* = 18.4 Hz, nor-7-Me), 51.6 (s, 3- or 2-nor-COO*Me*), 51.7 (s, 2- or 3-nor-COO*Me*), 52.3 (s, 4- or 3-azap-COO*Me*), 52.5 (s, 3- or 4-azap-COO*Me*), 66.0 (d, *J* = 8.6 Hz, nor-C-1), 68.3 (d, *J* = 4.6 Hz, nor-C-4), 90.5 (d, *J* = 5.5 Hz, nor-C-7), 126.8 (d, *J* = 100.3 Hz, C-*ipso* of PPh_3), 128.6 (d, *J* = 12.5 Hz, C-*meta* of PPh_3), 132.5 (d, *J* = 2.9 Hz, C-*para* of PPh_3), 133.4 (d, *J* = 10.1 Hz, C-*ortho* of PPh_3), 145.3 (dd, *J* = 26.1, 19.1 Hz, ap-C-4), 146.3 (s, nor-C-6), 147.7 (s, nor-C-5), 149.0 (d, *J* = 7.4 Hz, nor-C-2), 151.0 (dd, *J* = 3.7, 2.8 Hz, azap-C-3), 156.5 (d, *J* = 5.5 Hz, nor-C-3), 161.9 (dd, *J* = 11.9, 2.3 Hz, 4- or 3-azap-*C*OOMe), 165.1 (d, *J* = 1.2 Hz, 2- or 3-nor-*C*OOMe), 165.4 (dd, *J* = 14.8, 0.9 Hz, 3- or 4-azap-*C*OOMe), 165.8 (dd, *J* = 9.1, 5.7 Hz, azap-C-5), 166.0 (s, 3- or 2-nor-*C*OOMe), 197.2 [d, *J* = 6.8, *J*(^{183}W,C) = 127.3 Hz, WCO-*cis*], 199.8 (d, *J* = 23.6 Hz, WCO-*trans*) ppm. ^{31}P NMR: δ = 18.5 (d, *J* = 1.3 Hz, PPh_3), 97.0 [d, *J* = 1.3, *J*(^{183}W,P) = 242.6 Hz, PW] ppm. UV/Vis (CH_3CN): λ (lg ε) = 230 (4.89), 258 (4.48), 272 (4.30), 284 (4.17), 296 (4.10), 316 (3.89), 340 (3.65), 360 (3.39) nm. IR (KBr): ṽ = 2079 (vs, CO), 1988 (vs, CO), 1939 (s, CO), 1735 (vs, CO_2), 1724 (vs, CO_2) cm^{-1}. MS (EI, ^{184}W): *m*/*z* = 1076 (7) $[M]^{+\cdot}$, 752 (30) $[M - W(CO)_5]^{+\cdot}$, 277 (100) [Nor.]$^+$, 262 (78) $[PPh_3]^{+\cdot}$, 183 (55) $[PPh_2]^+$. $C_{46}H_{42}N_2O_{13}P_2W$ (1076.6): calcd. C 51.32, H 3.93, N 2.60; found C 49.77, H 4.04, N 2.54.

[Pentacarbonyl{4,5,8,9-tetrakis(methoxycarbonyl)-2,3,6,7,12-pentamethyl-10-triphenylphosphonioiminoyl-1-aza-11-phosphatetracyclo[6.2.1.1^{3,6}.0^{2,7}]dodeca-4,9-diene-κP}tungsten(0)] (13): 12 (0.37 g, 0.00034 mol) was dissolved in *o*-xylene (1.8 mL) and heated at 120 °C for 100 min while stirring slowly. All volatile components were then removed in vacuo (ca. 0.01 mbar) and the products separated by low-temperature column chromatography (SiO_2, −10 °C, 10 × 2 cm, *n*-pentane/diethyl ether, 10:30). Evaporation of the second fraction and recrystallization from diethyl ether yielded complex **13** as pale a yellow solid.

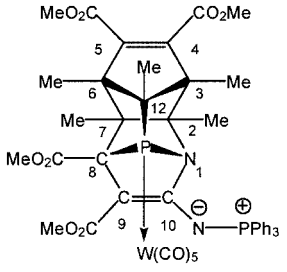

Yield: 200 mg, 53%; m.p. 142 °C (decomp.). ^{1}H NMR: δ = 0.65 (s, 3 H, 3-Me), 0.74 (s, 3 H, 2-Me), 1.00 (d, *J* = 15.4 Hz, 3 H, 12-Me), 1.07 (s, 3 H, 6-Me), 1.35 (s, 3 H, 7-Me), 3.55 (s, 3 H, 8- or 9-COO*Me*), 3.68 (s, 3 H, 4- or 5-*COOMe*), 3.73 (s, 3 H, 5- or 4-*COOMe*), 3.74 (s, 3 H, 9- or 8-COO*Me*), 7.47 (m_c, 6 H, H-*meta* of PPh_3), 7.56 (m_c, 3 H, H-*para* of PPh_3), 7.82 (m, 6 H, H-*ortho* of PPh_3) ppm. ^{13}C NMR: δ = 9.2 (d, *J* = 14.8 Hz, 12-Me), 10.7 (s, 3-Me), 13.3 (v. br. s, 6-Me), 13.8 (br. d, *J* = 4.8 Hz, 7-Me), 15.5 (br. d, *J* = 4.1 Hz, 2-Me), 50.3 (s, 8- or 9-COO*Me*), 51.3 (d, *J* = 0.7 Hz, 9- or 8-COO*Me*), 51.96 (s, 4- or 5-COO*Me*), 52.02 (s, 5- or 4-*COOMe*), 61.4 (br. d, *J* = 13.6 Hz, C-7), 68.6 (d, *J* = 1.3 Hz, C-3), 68.9 (s, C-6), 73.7 (d, *J* = 13.6 Hz, C-12), 74.5 (dd, *J* = 11.0, 1.5 Hz, C-8), 85.6 (br. d, *J* ≈ 1.3 Hz, C-2), 98.6 (dd, *J* = 14.1, 7.5 Hz, C-9), 128.6 (d, *J* = 12.8 Hz, C-*meta* of PPh_3), 130.3 (d, *J* = 105.7 Hz, C-*ipso* of PPh_3), 132.1 (d, *J* = 3.0 Hz, C-*para* of PPh_3), 132.9 (d, *J* = 10.7 Hz, C-*ortho* of PPh_3), 141.7 (d, *J* = 4.2 Hz, C-4), 142.6 (br. d, *J* = 4.8 Hz, C-5), 159.8 (dd, *J* = 4.3, 1.2 Hz, C-10), 164.8 (d, *J* = 0.4 Hz, 5- or 4-*C*OOMe), 165.0 (s, 4- or 5-*C*O-OMe), 166.1 (dd, *J* = 5.3, 1.1 Hz, 8- or 9-*C*OOMe), 169.3 (br. s, 9- or 8-*C*OOMe), 195.5 [d, *J* = 7.8, *J*(^{183}W,C) = 125.4 Hz, WCO-*cis*], 197.8 (d, *J* = 29.9 Hz, WCO-*trans*) ppm. ^{31}P NMR: δ = 1.3 (s, $Ph_3P{=}N$), 158.4 [s, *J*(^{183}W,P) = 269.9 Hz, $C_2P{-}N$] ppm. UV/Vis (CH_3CN): λ (lg ε) = 232 (4.93), 252 (4.51), 264 (4.35), 276 (4.22), 300 (4.09), 318 (3.92), 332 (3.85), 356 (3.76) nm. IR (KBr): ṽ = 2074 (s, CO), 1990 (s, CO), 1939 (vs, CO), 1929 (vs, CO), 1742 (s, CO_2), 1732 (s, CO_2) cm^{-1}. MS (EI, ^{184}W): *m*/*z* = 1076 (10) $[M]^{+\cdot}$, 934 $[M - DMAD]^{+\cdot}$, 752 (15) $[M - W(CO)_5]^{+\cdot}$, 277 (30) $[HNPPh_3]^+$, 262 (48) $[PPh_3]^{+\cdot}$, 183 (46) $[PPh_2]^+$, 28 (100) [CO]. MS (*pos.*-DCI, ^{35}Cl, ^{184}W): *m*/*z* = 1077 (22) $[M + H]^+$. MS (*neg.*-DCI, ^{35}Cl, ^{184}W): = *m*/*z* = 1076 (12) $[M]^{-\cdot}$, 814 (38) $[M - PPh_3]^{-\cdot}$, 324 (62) $[W(CO)_5]^{-\cdot}$. $C_{46}H_{42}N_2O_{13}P_2W$ (1076.6) : calcd. 1074.1644; found 1074.1652 (δ = −0.7 ppm).

 © 2003 Wiley-VCH Verlag GmbH & Co. KGaA, Weinheim

CCDC-193063 and -193064 contain the supplementary crystallographic data for this paper. These data can be obtained free of charge at www.ccdc.cam.ac.uk/conts/retrieving.html [or from the Cambridge Crystallographic Data Centre, 12, Union Road, Cambridge CB2 1EZ, UK; Fax: (internat.) +44−1223/336−033; E-mail: deposit@ccdc.cam.ac.uk].

Acknowledgments

We are grateful to the Fonds der Chemischen Industrie and the Deutsche Forschungs-gemeinschaft for financial support.

[1] F. Mathey, in *Phosphorus-carbon heterocyclic chemistry: the rise of a new domain* (Ed. F. Mathey), Pergamon, Amsterdam, **2001**, ch. 7, p. 753.
[2] Shell Internationale, Research N. V. Maatschappij, *Neth. Pat. 6 516 164*, **1966**, *Chem. Abstr.* **1967**, *66*, 28392r.
[3] M. J. Burk, J. E. Feaster, R. L. Harlow, *Organometallics* **1990**, *9*, 2653.
[4] F. Mathey, D. Neibecker, A. Brèque, *Fr. Pat.* 2 588 197, **1987**, *Chem. Abstr.* **1987**, *107*, 219468v.
[5] D. Neibecker, R. Réau, *Angew. Chem.* **1989**, *101*, 479, *Angew. Chem. Int. Ed. Engl.* **1989**, *28*, 500.
[6] F. Mathey, F. Mercier, C. Charrier, J. Fischer, A. Mitschler, *J. Am. Chem. Soc.* **1981**, *103*, 4595.
[7] W. A. Hermann, C. W. Kohlpainter, R. B. Manetsberger, H. Bahrmann, H. Kottmann, *J. Mol. Catal.* **1995**, *97*, 65.
[8] M.-O. Bevierre, F. Mercier, L. Ricrad, F. Mathey, *Bull. Soc. Chim. Fr.* **1992**, *129*, 1.
[9] T. Faitg, J. Soulié, J.-Y. Lallemand, F. Mercier, F. Mathey, *Tetrahedron* **2000**, *56*, 101.
[10] J. C. Tebby, in *Phosphorus-carbon heterocyclic chemistry: the rise of a new domain* (Ed.: F. Mathey), Pergamon, Amsterdam, **2001**, ch. 6.2, p. 671.
[11] R. Streubel, *Angew. Chem.* **1995**, *107*, 478; *Angew. Chem. Int. Ed. Engl.* **1995**, *34*, 436.
[12] P. Binger, S. Leininger, M. Regitz, U. Bergsträßer, J. Bruckmann, C. Krüger, *J. Organomet. Chem.* **1997**, *529*, 215.
[13] U. Rohde, F. Ruthe, P. G. Jones, R. Streubel, *Angew. Chem.* **1999**, *111*, 158; *Angew. Chem. Int. Ed.* **1999**, *38*, 215.
[14] J. Liedtke, H. Rüegger, S. Loss, H. Grützmacher, *Angew. Chem.* **2000**, *112*, 2596; *Angew. Chem. Int. Ed.* **2000**, *39*, 2479.
[15] R. Streubel, U. Schiemann, N. Hoffmann, Y. Schiemann, P. G. Jones, D. Gudat, *Organometallics* **2000**, *19*, 475.
[16] J. Liedtke, S. Loss, C. Widauer, H. Grützmacher, *Tetrahedron* **2000**, *56*, 143.
[17] A. G. Orpen, N. G. Connelly, *Organometallics* **1990**, *9*, 1206.
[18] R. Streubel, *Top. Curr. Chem.* in press.
[19] R. Streubel, *Coord. Chem. Rev.* **2002**, *227*, 172.
[20] R. Streubel, H. Wilkens, U. Rohde, A. Ostrowski, J. Jeske, F. Ruthe, P. G. Jones, *Eur. J. Inorg. Chem.* **1999**, 1567.
[21] R. Streubel, U. Rohde, J. Jeske, F. Ruthe, P. G. Jones, *Eur. J. Inorg. Chem.* **1998**, 2005.
[22] S. Bittner, M. Pomerantz, Y. Assaf, P. Krief, S. Xi, M. K. Witczak, *J. Org. Chem.* **1988**, *53*, 1.
[23] T. Wettling, J. Schneider, O. Wagner, C. Kreutzer, M. Regitz, *Angew. Chem.* **1989**, *101*, 1035; *Angew. Chem. Int. Ed. Engl.* **1989**, *28*, 1013.
[24] T. Wettling, J. Schneider, O. Wagner, C. Kreutzer, M. Regitz, *Angew. Chem.* **1989**, *101*, 1035; *Angew. Chem. Int. Ed. Engl.* **1989**, *28*, 1013.
[25] J. M. Miller, PhD Thesis, Cambridge University, **1966**.
[26] R. Streubel, N. Hoffmann, H.-M. Schiebel, F. Ruthe, P. G. Jones, *Eur. J. Inorg. Chem.* **2002**, 957.
[27] L. D. Quin, in *Phosphorus-carbon heterocyclic chemistry: the rise of a new domain* (Ed.: F. Mathey), Pergamon, Amsterdam, **2001**, ch. 4.2.1, p. 219.
[28] L. D. Quin, G. S. Quin, in *Phosphorus-carbon heterocyclic chemistry: the rise of a new domain* (Ed. F. Mathey), Pergamon, Amsterdam, **2001**, ch. 4.2.2, p. 307.
[29] A. Schmidpeter, in *Phosphorus-carbon heterocyclic chemistry: the rise of a new domain* (Ed. F. Mathey), Pergamon, Amsterdam, **2001**, ch. 4.3, p. 363.
[30] A. M. Arif, A. H. Cowley, R. M. Kren, D. L. Wetstmoreland, *Heteroat. Chem.* **1990**, *1*, 117.
[31] K. Angermund, A. Eckerle, F. Lutz, *Z. Naturforsch., Teil B* **1995**, *50*, 488.
[32] G. Wilke, *Angew. Chem.* **1998**, *100*, 189, *Angew. Chem. Int. Ed. Engl.* **1988**, *27*, 185.
[33] S. Braun, H.-O. Kalinowski, S. Berger: *150 and More Basic NMR Experiments.* 2nd ed. Wiley-VCH, Weinheim, **1998**, ch. 12, p. 476.
[34] G. M. Sheldrick, SHELXL-97, *Program for crystal structure refinement*, University Göttingen, **1997**.

Received November 27, 2002

 © 2003 Wiley-VCH Verlag GmbH & Co. KGaA, Weinheim

The Growth Process, Stability of GaP Nanocrystals and Formation of Ga_3P Nanocrystals under Solvothermal Conditions in Benzene

Shanmin Gao,[a] Jun Lu,[a] Yan Zhao,[a] Nan Chen,[a] and Yi Xie*[a]

Keywords: Gallium / Phosphides / Nanostructures / Solvothermal synthesis

The growth process, stability of GaP nanocrystals and the formation of Ga_3P nanocrystals under solvothermal conditions were investigated. At moderate reaction times and temperature, the growth process is mainly in accordance with the Ostwald ripening mechanism, which is the dissolving of the smaller GaP crystallites and growth into larger ones. However, GaP nanocrystallites become unstable under increasing reaction temperatures or prolonged reaction times. EDAX and XRD were used to identify the new Ga_3P phase.

(© Wiley-VCH Verlag GmbH & Co. KGaA, 69451 Weinheim, Germany, 2003)

Introduction

Semiconductor nanocrystals have attracted considerable interest since they exhibit a wide variety of intriguing size-dependent properties, such as the blue shift of the optical absorption and photoluminescence, electronic and nonlinear optical effects and fast relaxation times. These properties result from a quantum confinement effect in systems with small dimensions; these dimensions are sensitive to the fabrication method.[1−2] Research on the applications of semiconductor nanometer materials, such as biological fluorescence marking[3] and optoelectronic devices, has also been greatly promoted.[4−5] In addition, the high surface area and the specific growth kinetics can also influence the interior structure of nanocrystals. In order to use these effects, however, it is important to control the size and the size distribution, as well as the stability of the particles against conglomeration. The structural, physical, electronic and magnetic properties may be controlled by changing the synthetic method.

Increasing progress has been made on the research and development of semiconductor nanometer materials.[6] Among the semiconductor materials, the group II−VI compounds have been studied the most widely. Much work has been done on them, especially on aspects of their preparation and properties.[7−10] The core/shell nanostructures of the II−VI materials have also been studied because the shell type and shell thickness provide further control for tailoring the optical, electronic, electrical, and chemical properties of semiconductor nanocrystals.[11−14] In contrast, III−V semiconductor nanoscale materials are less well studied because the II−VI semiconductors are easier to prepare, for a number of reasons.[15] Current interest has focused on the synthesis and characterization of III−V semiconductor nanocrystals and the optical properties of quantum size particles.[16−18] III−V semiconductor nanowires have attracted much interest in recent years for their potential application in high-electron-mobility nanoelectronic devices and full-color flat panel displays.[19] Several approaches have been successfully developed for the fabrication of these nanowires.[20−24] The morphology, microstructure and the growth mechanism of the nanowires has been investigated in detail.

The most important route for the formation of the III−V semiconductor nanocrystals involves organometallic reagents.[25−29] The solvothermal synthetic route has been studied extensively and has proven to be a powerful route for the preparation of new materials,[30−32] in particular for the preparation of III−V semiconductor nanocrystals.[33−36] The advantage of this method is the effective prevention of the oxidation of the products, with the result that the isolated crystalline materials do not need subsequent treatment at high temperatures. In addition, organometallic precursors are not required. However, since the reaction takes place in a sealed system, relatively little work has been done with regards to the growth process and the stability of the product in the solvothermal process, which in fact influences their application directly.[37]

GaP is an indirect-gap semiconductor and has many important uses in microelectronic devices. A few reports have been published on the synthesis and properties of GaP nanocrystals[25,38−39] and nanowires.[28,29] In previous work, we have reported on the factors that affect the particle size of GaP nanocrystals in the reactions of both $GaCl_3{\cdot}Et_2O$ and $GaCl_3$·benzene with Na_3P, where the GaP nanorods and nanospheres were synthesized under solvothermal conditions in benzene.[40,41] It is necessary to study the growth

[a] Structure Research Laboratory and Department of Chemistry, University of Science and Technology of China, Hefei, Anhui 230026, P. R. China
Fax: (internat.) + 86-551/360-3987
E-mail: yxielab@ustc.edu.cn

 © 2003 Wiley-VCH Verlag GmbH & Co. KGaA, Weinheim **DOI: 10.1002/ejic.200200647**

mechanism and the stability of nanoparticles under different synthetic conditions in order to determine the best method of synthesis. As far as we are aware, the synthesis of Ga_3P nanocrystals has not been reported previously, although the electronic state of Ga_3P clusters has been studied theoretically.[42] It is clear that in the smaller clusters the P−P bond plays a more decisive role in the structure and bonding, however, as the cluster size increases beyond four atoms, the magic stability of P_4 can be overcome by the Ga−P bonds and thus a mixed cluster is expected to exhibit greater stability. We have previously studied the stability of GaP nanocrystals under solvothermal conditions in benzene,[43] but the growth process and the formation mechanism were not discussed.

In this paper, the growth process and stability of GaP nanocrystals under solvothermal conditions in benzene are investigated in detail. A method for controlling the reaction process and improving the uniformity of the GaP grains is presented, as well as the formation of the Ga_3P nanocrystals.

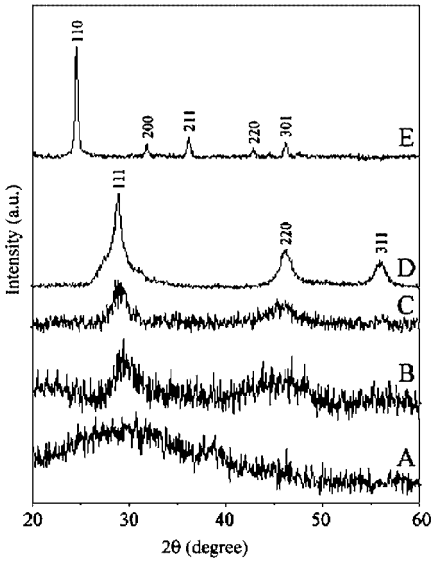

Figure 1. XRD patterns of samples obtained at 300 °C for different reaction times of the mixture: 0 h (A), 3 h (B), 7 h (C), 12 h (D), 24 h (E)

Results and Discussion

The Formation and Growth of GaP Nanocrystals

The reaction was carried out at 300 °C and a series of changes was experienced over different time periods. Figure 1 (A) shows the XRD pattern of the product obtained from mixing the starting materials Na_3P and $GaCl_3$ in a benzene solution, at room temperature. A bump centered at 29° can clearly be seen, which corresponds to the (111) diffraction peak of the GaP crystal with a zincblende structure, indicating the existence of many GaP particles that are small in size. As the reaction proceeds, the bump center becomes weaker from B to D, whereas the three diffraction peaks corresponding to (111), (220) and (311) of the zincblende GaP grow stronger and narrower. However, when the reaction time is increased to 24 h, a new phase appears, indicating that GaP nanoparticles have undergone a chemical change [Figure 1 (E)]. The average size of the GaP crystallites of samples A, B, C and D were calculated to be about 2, 8, 11 and 48 nm, respectively, by the Scherrer equation, which indicates that the particle size enlarges with increasing reaction time.

In order to study the grain size distribution and its change during the reaction, the absorption spectra of samples A, B, C and D were analyzed, which are shown in Figure 2. The absorption peak positions and shape reflect the particle sizes and granularity distribution. The spectrum of sample A is only an inconspicuous peak at about 400 nm, indicating the amorphous nature of A. The absorption spectra of samples B and C show several broad peaks, indicating that there is a broad granularity distribution of GaP nanocrystallites. The absorption edge shifts progressively to the red due to the growth of grains during the reaction process. Although the XRD data indicate larger average particle sizes, this could not be verified by UV/Vis studies. Because there is a broad granularity distribution of GaP nanocrystallites, large numbers of the GaP nanocrystallite particles are smaller than the Bohr radius of the exciton in GaP. So, in the absorption spectra of samples B and C, the broad excitonic peaks arise due to the quantum confinement effect Definitive evidence of the nanoscale dimensions of the quantum particles was obtained from our TEM studies.

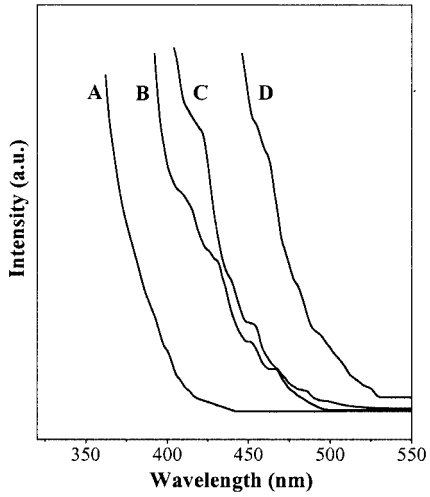

Figure 2. Optical absorption spectra of samples A, B, C and D of Figure 1; sample dispersion in benzene

The morphology of the as-prepared nanoparticles was studied by Transmission Electron Microscopy (TEM), as shown in Figure 3. Figure 3 (A) shows the morphology of the product of sample A. In sample B there are very few large crystallites but a large amount of smaller ones. Compared with sample B, the proportion of large crystallites increases in sample C and the granularity distribution is irregular, although many smaller particles also exist. The

 © 2003 Wiley-VCH Verlag GmbH & Co. KGaA, Weinheim

shape of these nanoparticles is nearly spherical with diameters ranging from 5 to 10 nm for sample B and 8 to 16 nm for sample C, in accordance with the average size estimated from the XRD patterns. Because there are so many smaller particles, the excitonic peaks arise in our UV/Vis studies for samples B and C. The proportion of smaller crystallites in sample D is reduced and the grains become uniform. As in sample C, the GaP particles are essentially spherical and the average diameter is nearly 46 nm, which is also consistent with the calculated crystallite sizes from XRD patterns. Figure 3 (E and F) represent the selected area electron diffraction (SAED) of samples A and D, respectively. Figure 3 (E) shows one electron diffraction ring and (F) shows three electron diffraction rings corresponding to the zincblende phase. The SAED results are consistent with the XRD results. Figure 3 (E) indicates that the diffraction bump centered at 29° in Figure 1 (A) corresponds to the (111) diffraction peak of a GaP crystal with a zincblende structure.

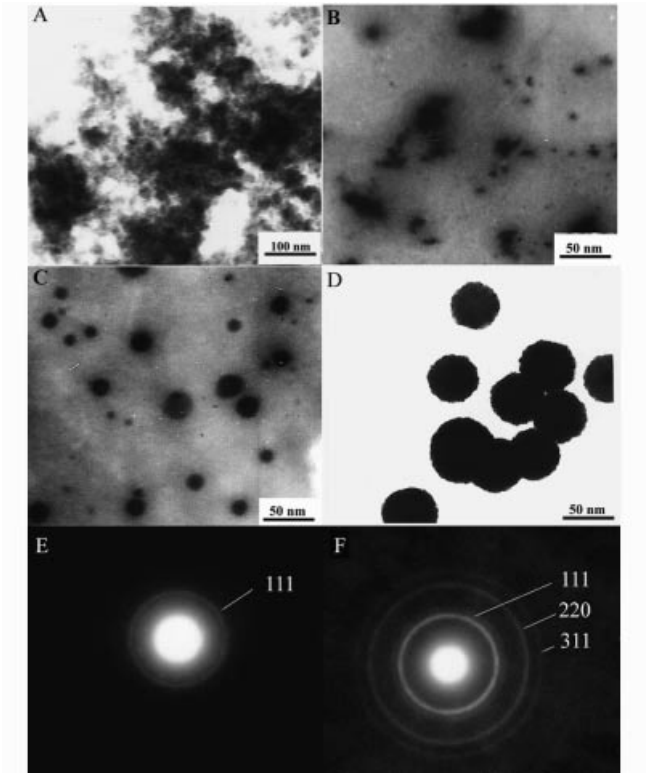

Figure 3. TEM images for GaP nanocrystals prepared at 300 °C for different reaction times of the mixture: 0 h (A), 3 h (B), 7 h (C), 12 h (D); E and F are the SAED patterns of samples A and D

From the XRD, UV/Vis absorption spectra and TEM images, it is clear that samples B and C consist mainly of smaller crystallites with few large ones present. A mass transport process should exist between these crystallites under high-temperature-high-pressure (HTHP) solvothermal conditions in benzene. This phenomenon can be explained as follows, according to the Kelvin equation [Equation (1)], (where P_0 and P_r are the equilibrium vapor pressure of constituents on the surface of the bulk crystal and nanocrystals with radius r, respectively, σ is the surface tension, ρ is the density of nanocrystals, R is a constant, T is absolute temperature and M is the molecular mass) it is obvious that P_r increases rapidly with a decrease of r.

$$P_r = P_0 \exp\left(\frac{2\sigma M}{\rho R T r}\right) \quad (1)$$

P_r on the surface of the smaller GaP crystallites is larger than it is for the larger crystallites. The different values of P_r for crystallites with different radii is the driving force for the transport of Ga and P from the surface of smaller crystallites to the larger ones. For GaP nanocrystallites, the smaller grains dissolve because of the unsaturation condition near the surface, while the larger grains increase in size due to the supersaturation condition.

From the discussion mentioned above, we propose a method for controlling the transport of the constituents and improving the uniformity of the grain size. As we know, at high monomer concentration the smaller particles grow faster than the larger ones and, as a result, the size distribution becomes more uniform. Therefore, we can raise the concentration of Ga and P in the reaction system to create supersaturation of Ga and P at the surface of the small crystallites as well as the large ones. Assuming that the additional concentration of Ga and P are $[Ga]_{av}$ and $[P]_{av}$, the equilibrium concentrations of the corresponding constituents on the surface of the large crystallites are $[Ga]_{le}$ and $[P]_{le}$, and the values on the surface of the small crystallites are $[Ga]_{se}$ and $[P]_{se}$. The real concentrations of Ga and P are as follows:

Small crystallites: $[Ga]_s = [Ga]_{se} + [Ga]_{av}$, $[P]_s = [P]_{se} + [P]_{av}$

Large crystallites: $[Ga]_l = [Ga]_{le} + [Ga]_{av}$, $[P]_l = [P]_{le} + [P]_{av}$

It is obvious that $[Ga]_l < [Ga]_s$ and $[P]_l < [P]_s$. For the reaction Ga + P $\rightleftarrows$ GaP, the speed (v) is described in Equation (2), where v is the growth speed of crystallites and k is a constant.

$$v = k\,[Ga] \times [P] \quad (2)$$

Thus, the growth speed of the smaller crystallites is faster than that of the larger ones. As a result, the uniformity of the grains improves. This ability to control the uniformity of the semiconductor nanocrystalline grains affords an opportunity to further test theories of quantum confinement and yields samples with desirable optical characteristics suitable for practical application. More experiments were performed to provide further evidence in order to draw better conclusions. Samples A and B are obtained when the concentrations of the precursors are twice those of the first experiments, at 300 °C for 4 h and 6 h, respectively. TEM images of the above samples are shown in Figure 4 (A and B). Figure 4 (C and D) are the images, under the same experimental conditions, where the concentrations of the pre-

 © 2003 Wiley-VCH Verlag GmbH & Co. KGaA, Weinheim

cursors are the same as those of the first experiments. It can be seen from the images of samples A and B that the grain size is more uniform than in the samples formed at 300 °C for 4 h and 6 h at lower concentrations. From the TEM images of samples C and D one can see the aggregation of the particles, confirming our previous assumptions. This phenomenon is in accordance with the results obtained from the absorption spectra. The absorption spectra of samples A and B were analyzed and the results are shown in Figure 5. The absorption spectra are regular, with a single absorption peak indicating the uniformity of the particle sizes. The particle sizes of samples A and B are about 5 and 9.5 nm, respectively. The Bohr radius of the exciton is reported to be 55 Å (a diameter of 11 nm) in GaP.[44] The absorbance peaks at 380 nm [Figure 5 (A)] and 416 nm [Figure 5 (B)] correspond to approximately 5 and 9 nm GaP crystallites, respectively, which is consistent with the TEM results.

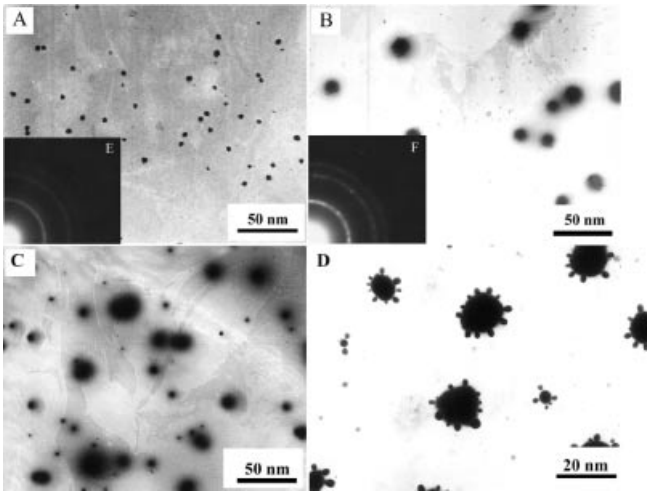

Figure 4. TEM images for GaP nanocrystals prepared at 300 °C at twice the precursor concentrations for 4 h (A), 6 h (B); C and D are the TEM images for GaP nanocrystals prepared at four times the precursor concentrations for 4 h and 6 h; the insets E and F are the SAED pattern of samples A and B

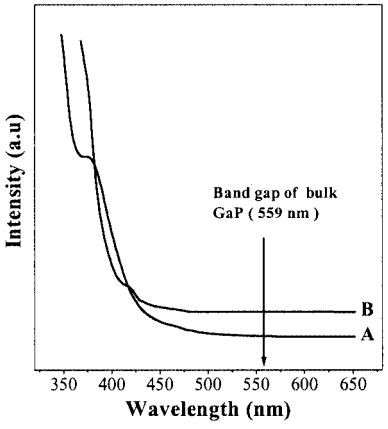

Figure 5. Optical absorption spectra of samples A and B of Figure 4

The Stability of GaP Nanoparticles and the Formation of Ga_3P Nanocrystals

In the previous section it could be seen that a new phase was obtained after Na_3P and $GaCl_3$ reacted at 300 °C for 24 h. The XRD pattern of this new phase is shown in Figure 1 (E). An Energy Dispersive X-ray Diffraction (EDAX) analysis study was performed in order to determine the composition of sample E, obtained at 300 °C over 24 h. Figure 6 shows the EDAX spectrum, in which both P and Ga bands are detected when the electron beam is focused on one of the particles. Na and Cl were also detected because the sample was not properly washed and so an extremely small amount of by-product (NaCl) is present. Because of the low concentration of NaCl and the small particle size, direct determination of the NaCl by X-ray diffraction is difficult; no NaCl diffraction peaks appear in Figure 1 (E). The insert in Figure 6 indicates the results of the elemental analysis. From the EDAX and element analysis, we conclude that the new compound is Ga_3P. Moreover, all the reflections shown in Figure 1 (E) can be indexed to the tetragonal Ga_3P phase and the average crystallite sizes of Ga_3P were found to be about 55 nm, as estimated from the Scherrer formula.

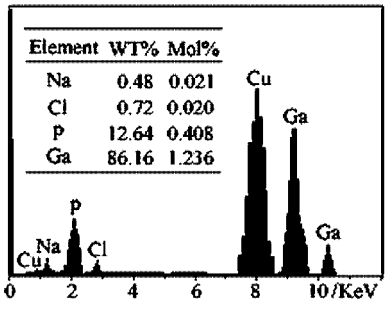

Figure 6. The EDAX results of Ga_3P at 300 °C for 24 h; inset: elemental analysis result of sample E

From the above discussion it can be seen that Ga_3P is obtained from the reaction of Na_3P and $GaCl_3$ at 300 °C for 24 h, indicating that GaP is in fact metastable in the solvothermal process. In order to confirm this metastability, a further series of experiments was performed. All products were identified from the XRD patterns. Figure 7 shows the XRD patterns of the samples that were prepared at 420 °C for 12 h (A), 400 °C for 14 h (B) and 340 °C for 20 h (C). The relationship between the reaction conditions and products is summarized in Table 1. Figure 8 shows the TEM images of Ga_3P, from which one can see that at 420 °C for 12 h (A) or at 400 °C for 14 h (B), Ga_3P nanocrystallites have a high crystallinity and are well distributed. This is better than the results for Ga_3P obtained at 340 °C for 20 h (C) or at 300 °C for 24 h (D). The size distribution of the sample obtained at 300 °C for 20 h is irregular: the largest particle size is 75 nm but the smallest is only 20 nm. This result is consistent with the average particle sizes from the

 © 2003 Wiley-VCH Verlag GmbH & Co. KGaA, Weinheim

XRD patterns. Figure 8 (E and F) are the ED patterns of samples A and D. The diffraction intensity gives more proof of the crystallinity of the samples at different temperatures and times.

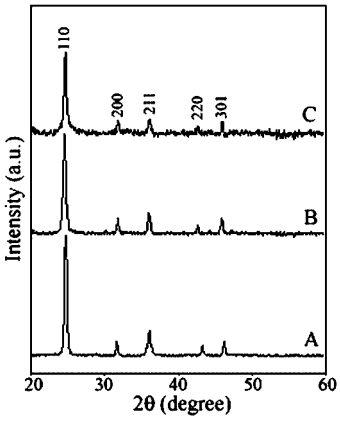

Figure 7. XRD patterns of Ga_3P at 420 °C/12 h (A), 400 °C/14 h (B), 340 °C/20 h (C)

Table 1. Relation between reaction conditions and products

Temp. [°C]	Time [h]	Product
300	7	GaP
	12	GaP
	20	GaP (major), Ga_3P (minor)
	24	Ga_3P
340	8	GaP
	12	GaP (major), Ga_3P (minor)
	20	Ga_3P
380	8	GaP
	12	GaP (major), Ga_3P (minor)
400	8	Ga_3P (major), GaP (minor)
	14	Ga_3P
420	8	Ga_3P (major), GaP (minor)
	12	Ga_3P

In the current system, GaP was formed by the reaction $Na_3P + GaCl_3 \rightarrow GaP + 3\ NaCl$, but upon prolonging the reaction time or increasing the reaction temperature, the products turned into Ga_3P. Careful observation showed that, after heating at 300 °C for between 3 and 12 h, the autoclave was filled with a blue-green benzene solution and a gray-black powder (GaP), whereas when the heating time reached 24 h at 300 °C, 20 h at 340 °C, 14 h at 400 °C or 12 h at 420 °C, the autoclave was filled with a yellow or light-brown benzene solution and a gray-white powder (Ga_3P). Upon removing some of the yellow or light-brown benzene solution and dripping it onto filter paper in air, spontaneous combustion takes place, indicating that white phosphorus is dissolved in the yellow or light-brown benzene solutions. In our experiments the Na_3P and $GaCl_3$ molar ratio is 1:1, so we believe that under solvothermal conditions in benzene, the decomposition of GaP should take place when the reaction time is prolonged or the reaction temperature is increased as shown in Equation (3).

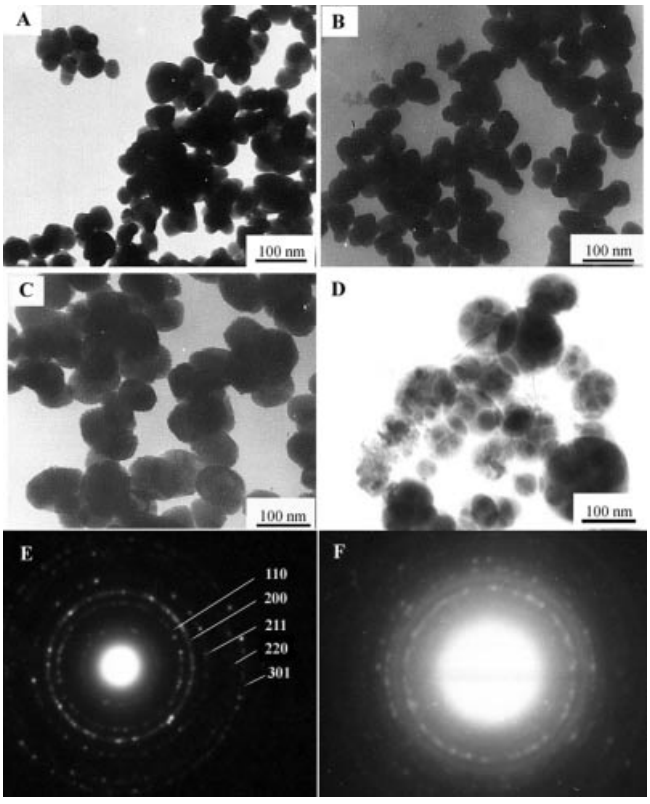

Figure 8. TEM images of Ga_3P at 420 °C/12 h (A), 400 °C/14 h (B), 340 °C/20 h (C), 300 °C/24 h (D); E and F are the SAED pattern of samples A and D

$$6\ GaP \rightarrow 2\ Ga_3P + P_4 \quad (3)$$

In order to study the reaction mechanism, more experiments were performed. A purified sample of GaP was placed into an autoclave, under the same solvothermal conditions; the results differed from the above-mentioned results. Thus, either NaCl or unchanged Na_3P is necessary for the decomposition process to occur.[45−47]

Experimental Section

Preparation and Growth of GaP Nanocrystals: All analytical grade solvents used in our experiments were dried with sodium chips and distilled under a flow of N_2. All reagents were analytical grade or better and used without any purification, except for Na_3P, which was prepared according to the literature (small pieces of sodium and an excess of white phosphorus were mixed in benzene, heated to the melting point of sodium, and stirred and refluxed for 10−12 h).[48] A typical experimental procedure is as follows: Na_3P powder and a benzene solution of $GaCl_3$ were placed in a stainless steel autoclave and benzene was added to raise its ratio to 70−85%. After the air in the solution was expelled by N_2 (99.999% pure), the autoclave was sealed and heated to 300 °C over different time

 © 2003 Wiley-VCH Verlag GmbH & Co. KGaA, Weinheim

periods, and then allowed to cool to room temperature. The products were filtered off and washed with benzene, absolute ethanol and distilled water. Finally, the products were dried under vacuum at room temperature for 2 h. In order to study the growth and stability of GaP nanoparticles the as-prepared GaP was treated at different temperatures and times under the same conditions.

Characterization of the Products: The phases of the products were detected at a scanning rate of $0.02°s^{-1}$ in the 2θ range from 20 to 60° by using a *D*/max-γA X-ray diffractometer with Ni-filtered Cu-K_α radiation. Optical absorption spectra were recorded with a Hitachi 340 UV/Vis/NIR recording spectrophotometer at room temperature. The absorption cell used was a 1-cm quartz cuvette. A blank solution of benzene was used as the reference. TEM images of the samples were obtained from a Hitachi model H800 transmission electron microscope using an accelerating voltage of 200 kV. To prepare the TEM samples, the colloids were briefly ultrasonicated, and then a drop of the colloidal suspension was applied to a copper mesh covered with a carbon film for 30 s.

Acknowledgments

Financial support from the National Natural Research Foundation of China and Chinese Ministry of Education is gratefully acknowledged. We are indebted to Prof. G. E. Zhou and Dr. X. M. Liu for their help with the XRD and TEM analyses.

[1] C. B. Murray, C. R. Kagan, M. G. Bawnedi, *Annu. Rev. Mater. Sci.* **2000**, *30*, 545 and references therein.
[2] U. Banin, Y. W. Cao, D. Katz, O. Millo, *Nature* **1999**, *400*, 542.
[3] G. P. Mitchell, C. A. Mirkin, R. L. Letsinger, *J. Am. Chem. Soc.* **1999**, *121*, 8122.
[4] M. C. Schlamp, X. G. Peng, A. P. Alivisatos, *J. Appl. Phys.* **1997**, *82*, 5837.
[5] D. L. Klein, R. Richard, A. K. L. Lin, A. P. Alivisatos, P. L. McEuen, *Nature* **1997**, *389*, 699.
[6] T. Trindade, P. O'Brien, N. L. Pickett, *Chem. Mater.* **2001**, *13*, 3843 and references therein.
[7] X. Peng, M. C. Schlamp, A. V. Kadavanich, A. P. Alivisatos, *J. Am. Chem. Soc.* **1997**, *119*, 7019.
[8] A. P. Alivisatos, P. F. Barbara, A. W. Castleman, J. Chang, D. A. Dixon, M. L. Klein, G. L. McLendon, J. S. Miller, M. A. Ratner, P. J. Rossky, S. I. Stupp, M. E. Thompson, *Adv. Mater.* **1998**, *10*, 1297.
[9] A. L. Rogach, S. V. Kershaw, M. G. Burt, M. T. Harrison, A. Kornowski, A. Eychmüller, H. Weller, *Adv. Mater.* **1999**, *11*, 552.
[10] M. A. Anderson, S. Gorer, R. M. Penner, *J. Phys. Chem. B* **1997**, *101*, 5895.
[11] M. T. Harrison, S. V. Kershaw, A. L. Rogach, A. Kornowski, A. Eychmuller, H. Weller, *Adv. Mater.* **2000**, *12*, 123.
[12] Y. W. Cao, U. Banin, *Angew. Chem. Int. Ed.* **1999**, *38*, 3692.
[13] B. Schreder, T. Schmidt, V. Ptatschek, U. Winkler, A. Materny, E. Umbach, M. Lerch, G. Müller, W. Kiefer, L. Spanhel, *J. Phys. Chem. B* **2000**, *104*, 1677.
[14] D. Hagrman, C. Zubieta, D. J. Rose, J. Zubieta, R. C. Haushalter, *Angew. Chem. Int. Ed. Engl.* **1997**, *36*, 873.
[15] J. R. Heathand, J. J. Shiang, *Chem. Soc. Rev.* **1998**, *27*, 65.
[16] A. Manz, A. Birkner, M. Kolbe, R. A. Fischer, *Adv. Mater.* **2000**, *12*, 569.
[17] O. I. Micic, S. P. Ahrenkiel, D. Bertram, A. J. Nozik, *Appl. Phys. Lett.* **1999**, *75*, 478.
[18] O. I. Micic, H. M. Cheong, H. Fu, A. Zunger, J. R. Spragus, A. Mascarenhas, A. J. Nozik, *J. Phys. Chem. B* **1997**, *101*, 4904.
[19] X. F. Duan, Y. Huang, Y. Cui, J. F. Wang, C. M. Lieber, *Nature* **2001**, *409*, 66.
[20] W. S. Shi, Y. F. Zheng, N. Wang, C.-S. Lee, S.-T. Lee, *Adv. Mater.* **2001**, *13*, 591.
[21] C.-C. Chen, C.-C. Yeh, *Adv. Mater.* **2000**, *12*, 738.
[22] X. Duan, J. Wang, C. M. Lieber, *Appl. Phys. Lett.* **2000**, *76*, 1116.
[23] X. Duan, C. M. Lieber, *Adv. Mater.* **2000**, *12*, 298.
[24] M. S. Gudiksen, C. M. Lieber, *J. Am. Chem. Soc.* **2000**, *122*, 8801.
[25] R. J. Jouet, R. L. Wells, A. L. Rheingold, C. D. Incarvito, *J. Organomet. Chem.* **2000**, *601*, 191.
[26] X. Peng, J. Wickham, A. P. Alivisatos, *J. Am. Chem. Soc.* **1998**, *120*, 5343.
[27] M. Green, P. O'Brien, *Chem. Commun.* **1998**, 2459.
[28] R. Cohen, L. Kronik, A. Shanzer, D. Cahen, A. Liu, Y. Rosenwaks, J. K. Lorenz, A. B. Ellis, *J. Am. Chem. Soc.* **1999**, *121*, 10545.
[29] A. Manz, A. Birkner, M. Kolbe, R. A. Fischer, *Adv. Mater.* **2000**, *12*, 8.
[30] W. S. Sheldrick, M. Wachhold, *Angew. Chem. Int. Ed. Engl.* **1997**, *36*, 206.
[31] J. Yang, J. H. Zeng, S. H. Yu, L. Yang, G. E. Zhou, Y. T. Qian, *Chem. Mater.* **2000**, *12*, 3259.
[32] A. Holllingsworth, D. M. Poojary, A. Clearfield, W. E. Buhro, *J. Am. Chem. Soc.* **2000**, *122*, 3562.
[33] L. Grocholl, J. J. Wang, E. G. Gillan, *Chem. Mater.* **2001**, *13*, 4290.
[34] S. D. Dingman, N. P. Rath, P. D. Markowitz, P. C. Gibbons, W. E. Buhro, *Angew. Chem. Int. Ed.* **2000**, *39*, 1470.
[35] Y. Xie, Y. Qian, W. Wen, S. Zhang, Y. Zhang, *Science* **1996**, *272*, 1926.
[36] J. Jegier, S. McKernan, A. P. Purdy, W. L. Gladfelter, *Chem. Mater.* **2000**, *12*, 1003.
[37] C. C. Chen, A. B. Herhold, C. S. Johnson, A. P. Alivisatos, *Science* **1997**, *276*, 398.
[38] S. S. Kher, R. L. Wells, *Chem. Mater.* **1994**, *6*, 2056.
[39] O. I. Micic, J. R. Sprague, C. J. Curtis, K. M. Jones, J. L. Machol, A. J. Nozik, H. Giessen, B. Fluegel, G. Mohs, N. Peyghambarian, *J. Phys. Chem.* **1995**, *99*, 7754.
[40] S. M. Gao, D. L. Cui, B. B. Huang, M. H. Jiang, *J. Cryst. Growth* **1998**, *192*, 89.
[41] S. M. Gao, Y. Xie, J. Lu, G. A. Du, W. He, D. L. Cui, B. B. Huang, M. H. Jiang, *Inorg. Chem.* **2002**, *41*, 1850.
[42] P. Y. Feng, K. Balasubramanian, *Chem. Phys. Lett.* **1998**, *288*, 1.
[43] C. Y. Xin, S. M. Gao, D. L. Cui, B. B. Huang, X. Y. Qin, M. H. Jiang, *Acta Phys.-Chim. Sin.* **1999**, *15*, 105.
[44] M. V. Ramakrishna, R. A. Friesner, *J. Chem. Phys.* **1991**, *95*, 8309.
[45] D. S. Tin, T. Miller, T. C. Chiang, *Phys. Rev. B* **1991**, *44*, 10719.
[46] H. Ishida, K. Terakura, *Phys. Rev. B* **1989**, *40*, 11519.
[47] R. Ramfrez, *Phys. Rev. B* **1989**, *40*, 10144.
[48] D. J. Peterson, Y. J. Logan, *J. Inorg. Nucl. Chem.* **1966**, *28*, 53..

Received November 25, 2002

 © 2003 Wiley-VCH Verlag GmbH & Co. KGaA, Weinheim

EurJIC
European Journal of Inorganic Chemistry

May 2003
Issue 10
Pages 1829–2000

Papers available ahead of print in Early View at www.interscience.wiley.com

Earliest available Table of Contents:
Automatically, free of charge by e-mail through
www.interscience.wiley.com/alerts

COVER PICTURE

The cover picture shows a schematic view of part of a novel complex that undergoes reversible dioxygen binding. The complex is a zig-zag oligomer formed in sublimed layers of [*meso*-triphenyl(4-pyridyl)porphyrinato]cobalt(II) and is depicted here with molecular dioxygen coordinated at each cobalt centre. The relatively open, microporous structure of the oligomer arises as a result of pyridine coordination, which inhibits closer-packed structures (e.g. with parallel contiguous porphyrin rings), and ensures facile transport of molecular oxygen to the coordination site. The zig-zag chain also inhibits the formation of dioxygen-bridged centres, with the result that this basic structure is relatively stable. On warming, the Co–dioxygen link may be broken, with the evolution of dioxygen, which can readily diffuse through the microporous structure, leaving the zig-zag oligomer chain effectively intact. Details are discussed in the article by T. S. Kurtikyan et al. on p. 1861 ff.

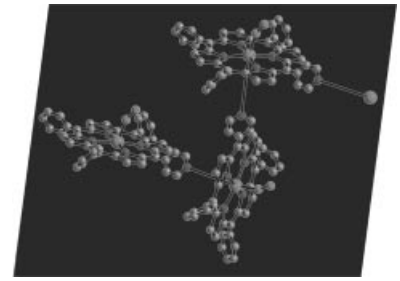

MICROREVIEW

Contents

1843 **L. Weber**

The Quest for Isophosphaalkynes (Isophosphocyanides) C≡P–R – Still an Elusive Class of Compounds

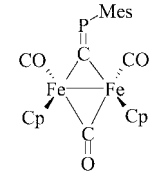

Keywords: Isophosphaalkynes / Phosphaalkynes / Phosphorus / Synthetic methods

 © 2003 Wiley-VCH Verlag GmbH & Co. KGaA, Weinheim

SHORT COMMUNICATION

1857 **T. Chivers,* T. J. Clark, M. Krahn, M. Parvez, G. Schatte**

Cubane Complexes with Two (or More) Group 14−Group 16 Double Bonds: Synthesis and X-ray Structures of $Sn_4Se_2(NtBu)_4$ and $Ge_4Se_3(NtBu)_4$

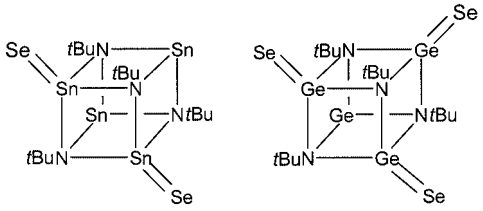

Keywords: Germanium / Main group elements / Multiple bonds / Selenium / Tin

FULL PAPERS

1861 **T. S. Kurtikyan,* J. S. Ogden, R. K. Kazaryan, V. N. Madakyan**

IR Study of the Interaction of Dioxygen with [*meso*-Triphenyl(4-pyridyl)porphyrinato]cobalt(II)

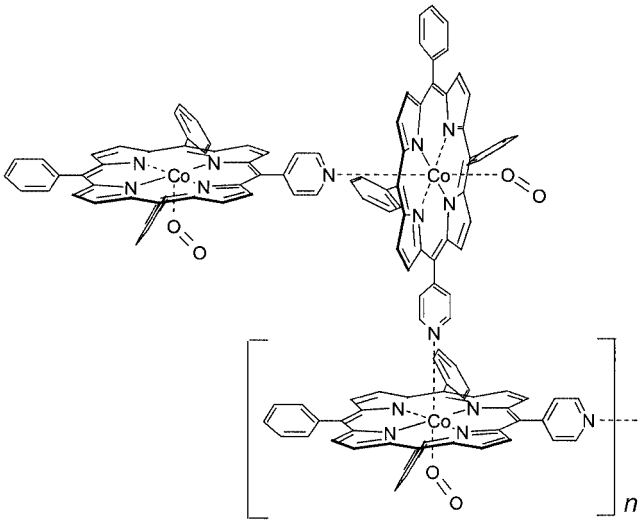

Keywords: Cobalt / Porphyrins / Matrix isolation / IR spectroscopy / Microporous materials

1866 **S. Willemin, J. Larionova,* R. Clérac,* B. Donnadieu, B. Henner, X. F. Le Goff, C. Guérin**

Crystal Structures and Intercalation Reactions of Three-Dimensional Coordination Polymers $[M(H_2O)_2]_2[Mo(CN)_8]\cdot 4H_2O$ (M = Co, Mn)

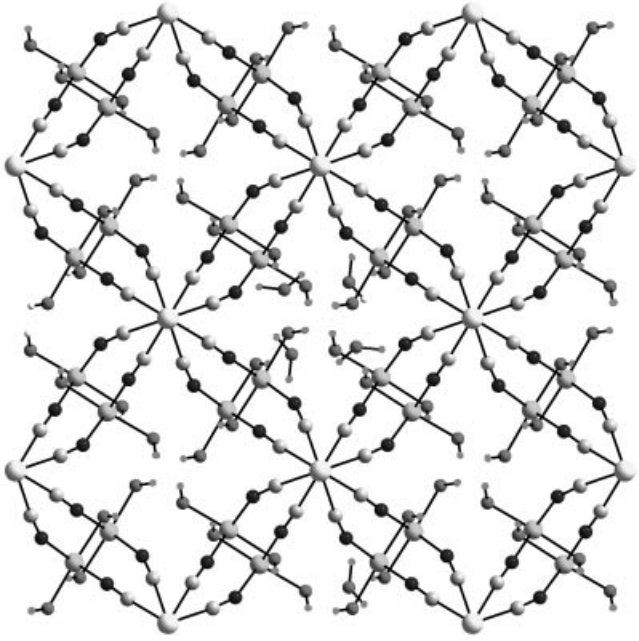

Keywords: Bridging ligands / Cyanides / Molybdenum / Intercalations / Cobalt / Manganese

1873 **R. Stodt, S. Gencaslan, I. M. Müller, W. S. Sheldrick***

Preparation, Reactivity and Peptide Labelling Properties of (η^6-Arene)ruthenium(II) Complexes with Pendant Carboxylate Groups

Keywords: Ruthenium / Amino acids / Peptides / Bioinorganic chemistry

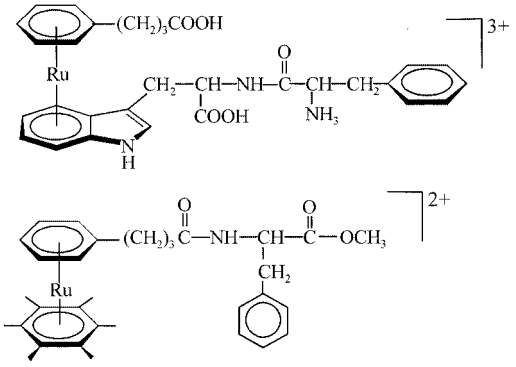

1883 **C. M. Standfest-Hauser, K. Mereiter, R. Schmid, K. Kirchner***

Formation of Ruthenium−Aminocarbene Complexes from Aldimines and Aminals

Keywords: Carbenes / Density functional calculations / N ligands / Ruthenium

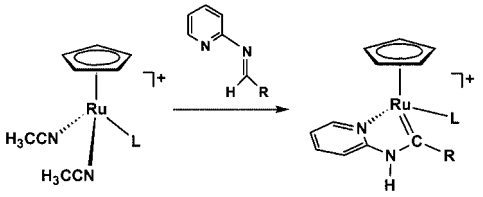

1893 **V. Comte, J. P. Tranchier, F. Rose-Munch,* E. Rose, D. P. P. Richard, C. Moïse**

Reactivity of Metallophosphide Anions with Electrophilic (Arene)tricarbonylmetal Complexes

Keywords: Anions / Carbonyl ligands / Arene ligands / Manganese / Chromium / Iron

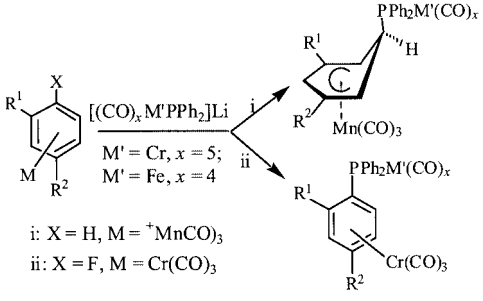

1900 **K. E. Berg, Y. Pellegrin, G. Blondin, E. Anxolabéhère-Mallart, W. Leibl, A. Aukauloo***

A Rigid Molecular Scaffold Affixing a (Polypyridine)ruthenium(II)- and a Nickel(II)-Containing Complex: Spectroscopic Evidence for a Weakly Coupled Bichromophoric System

Keywords: Ruthenium / Nickel / Polynuclear complexes / Rigid heteroditopic ligands / Redox chemistry / Photophysical studies

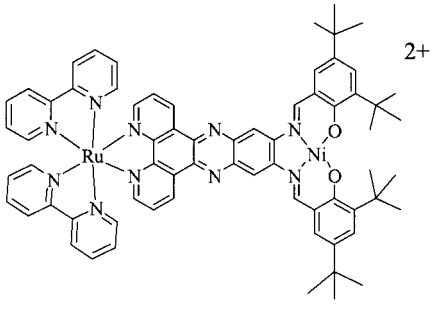

 © 2003 Wiley-VCH Verlag GmbH & Co. KGaA, Weinheim

1911 J. H. Espenson,* S. M. Nabavizadeh

Kinetic and Equilibrium Studies of Reactions of N-Heterocycles with Dimeric and Monomeric Oxorhenium(V) Complexes

Keywords: Rhenium / N ligands / Kinetics / Linear free-energy relationships

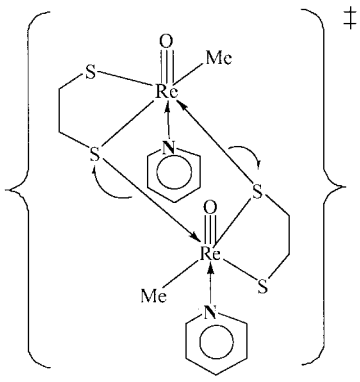

1917 A. Klein,* J. van Slageren,* S. Záliš

Co-Ligand Involvement in Ground and Excited States of Electron-Rich (Polypyridyl)Pt^{II} Complexes

Keywords: Emission / Platinum / N ligands / Photophysics / Optical spectroscopy / Theoretical calculations / DFT / Crystal structure

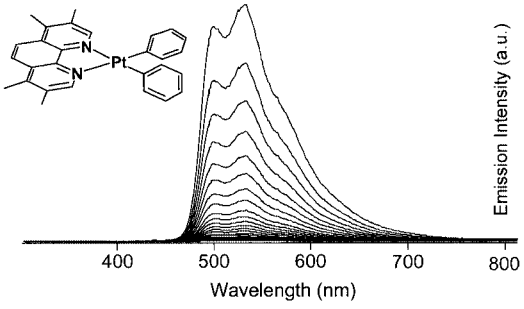

1929 K. R. Flower,* R. G. Pritchard, J. E. Warren

Synthesis of [RuX(CO){η^2-*C*,*N*-$C_6H_4C(H)$=NC_6H_4-4-NO_2}$(PPh_3)_2$] (X = F, Cl, Br, I): Evidence of Non-Conventional Ru−X Hydrogen Bonds Leading to Octahedral Coordination at the Halide Atom

Keywords: Ruthenium / Cyclometallated ligands / Charge transfer / Hydrogen bonds / Pi interactions

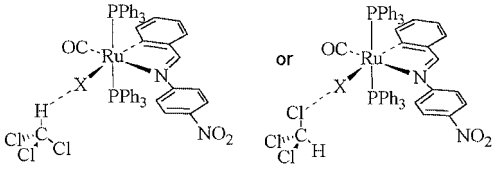

1939 M. C. Aragoni, M. Arca,* T. Cassano, C. Denotti, F. A. Devillanova, R. Frau, F. Isaia, F. Lelj, V. Lippolis, L. Nitti, P. Romaniello, R. Tommasi, G. Verani

NIR Dyes Based on [M(R,R′timdt)$_2$] Metal-Dithiolenes: Additivity of M, R, and R′ Contributions To Tune the NIR Absorption (M = Ni, Pd, Pt; R,R′timdt = Monoreduced Form of Disubstituted Imidazolidine-2,4,5-trithione)

Keywords: S ligands / Nickel / Palladium / Platinum / Density functional calculations / Nonlinear optics

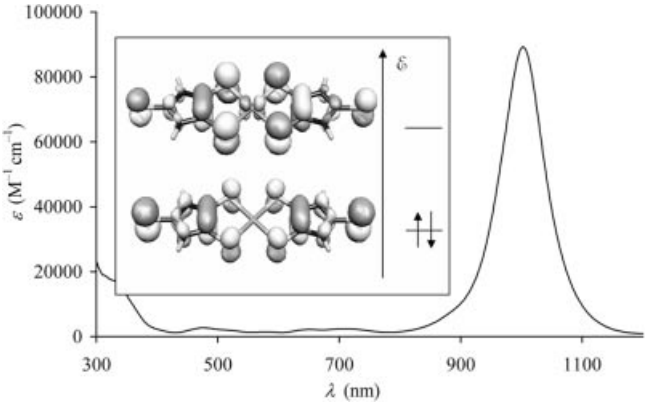

 © 2003 Wiley-VCH Verlag GmbH & Co. KGaA, Weinheim

1948 **C. Comuzzi,* A. Melchior, P. Polese, R. Portanova, M. Tolazzi***

Thermodynamics of Complex Formation of Silver(I), Cadmium(II) and Cobalt(II) with Open-Chain Polyamines in Dimethyl Sulfoxide and Molecular Dioxygen Binding to Cobalt(II) Complexes

Keywords: Amine complexes / Cadmium / Cobalt / Dioxygen / Silver / Thermodynamics

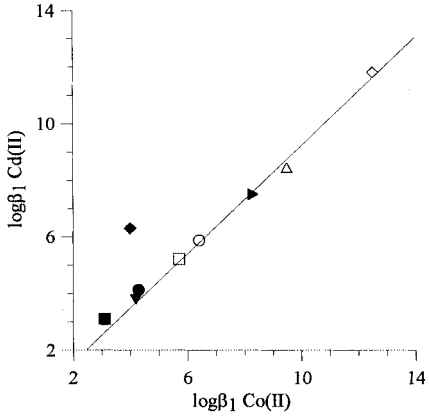

1956 **S. Mukherjee, T. Weyhermüller, E. Bothe, P. Chaudhuri***

Structural, Magnetochemical and Electrochemical Studies of Dinuclear Complexes Containing the $[V^{V}O]_2$, $[V^{IV}O]_2$, Cr_2^{III}, Mn_2^{III} and Fe_2^{III} Cores of a Potentially Pentadentate Phenol-Containing Ligand with (O,N,O,N,O)-Donor Atoms

Keywords: N,O ligands / Transition metals / Magnetic properties / Radicals / Electrochemistry

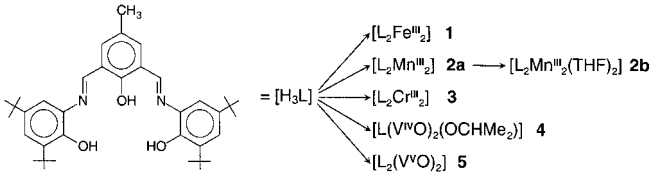

1966 **M. P. Maurya,* S. Khurana, Shailendra, A. Azam, W. Zhang, D. Rehder***

Synthesis, Characterisation and Antiamoebic Studies of Dioxovanadium(V) Complexes Containing ONS Donor Ligands Derived from *S*-Benzyldithiocarbazate

Keywords: Medicinal chemistry / S ligands / Potassium / Vanadium

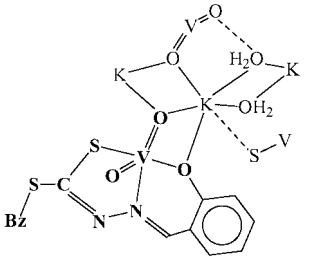

1974 **C. Bazzicalupi, A. Bencini,* E. Berni, A. Bianchi,* P. Fornasari, C. Giorgi, B. Valtancoli**

Zn^{II} Complex with a Phenanthroline-Containing Macrocycle as Receptor for Amino Acids and Dipeptides − Hydrolysis of an Activated Peptide Bond

Keywords: Macrocyclic ligands / Zinc / Amino acids / Enzyme models / Stacking interactions

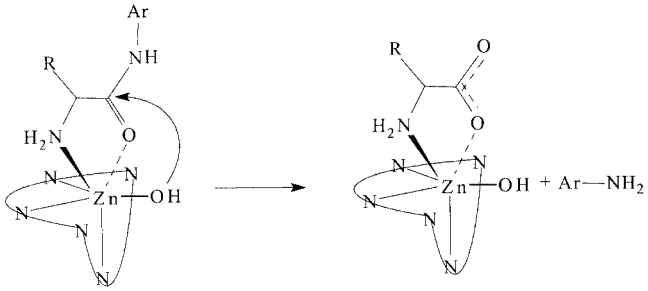

 © 2003 Wiley-VCH Verlag GmbH & Co. KGaA, Weinheim

1984 **M. Soibinet, I. Déchamps-Olivier,* E. Guillon, J.-P. Barbier, M. Aplincourt, F. Chuburu, M. Le Baccon, H. Handel**

XAS, ESR and Potentiometric Studies of Three Dinuclear *N*,*N*′-*para*-Xylylenebis(tetraazamacrocycle)copper(II) Complexes − X-ray Crystal Structure of [*N*,*N*′-*p*-Xylylenebis(cyclen)]-copper(II)

Keywords: Copper / ESR spectroscopy / Macrocyclic ligands / Potentiometry / X-ray studies

1995 **A. M. Madalan, V. Voronkova, R. Galeev, L. Korobchenko, J. Magull, H. W. Roesky,* M. Andruh***

Exchange Interactions at the Supramolecular Level − Synthesis, Crystal Structure, Magnetic Properties, and EPR Spectra of $[Mn(MAC)(TCNQ)_2]$ (MAC = Pentaaza Macrocyclic Ligand; $TCNQ^{\cdot -}$ = Radical Anion of 7,7,8,8-Tetracyano-*p*-quinodimethane)

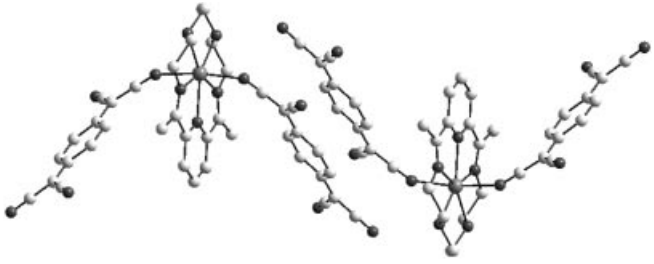

Keywords: Manganese / N ligands / Stacking interactions / Magnetic properties / EPR spectroscopy / Radicals

DOI: The fastest way to find an article online is the *Digital Object Identifier* (DOI). The DOIs will be printed in the footer of the first page of every article.
On the WWW, one can find an article for example with a DOI of 10.1002/ejic.200300049 at http://dx.doi.org/10.1002/ejic.200300049.
Please use the DOI of the article to link from your home page to the articles in Wiley InterScience.
The DOI is a result of a cross-publisher initative to create a system for the persistent identification of documents on digital networks. More information is available from www.doi.org.

The Quest for Isophosphaalkynes (Isophosphocyanides) C≡P−R — Still an Elusive Class of Compounds

Lothar Weber*[a]

Dedicated to Professor Heinrich Nöth on the occasion of his 75th birthday

Keywords: Isophosphaalkynes / Phosphaalkynes / Phosphorus / Synthetic methods

This review gives an account on the quest for isophosphaalkynes, a class of compounds that still resists isolation and/or spectroscopic detection. Synthetic attempts toward this target are reported. On the other hand, a number of coordination compounds featuring isophosphaalkyne ligands have been prepared, the syntheses, structures, and chemistry of which are discussed.

1. Introduction

The concepts of isolobal compounds and the diagonal relationship between carbon and phosphorus in the periodic table of elements have proven exceedingly fruitful for the development of the chemistry of phosphorus in low coordination states.[1] Accordingly, alkynes **A** are closely related to diphosphorus **B**, which exists only in the gas phase, as well as to phosphaalkynes **C** and to isophosphaalkynes **D** (Scheme 1).

The chemistry of phosphaalkynes has been well developed and has been documented comprehensively in a series of review articles and text books.[2] In contrast, our knowledge of their isomers of type **D** is scarce. At a first glance this lack of examples is surprising, especially if one formally extends the relationship of phosphaalkynes and isophosphaalkynes to their nitrogen homologues, the cyanides (nitriles) R−C≡N (**E**) and isocyanides R−N≡C (**F**). Both classes of compound are familiar to the chemist as versatile and useful reagents in organic[3] and coordination chemis-

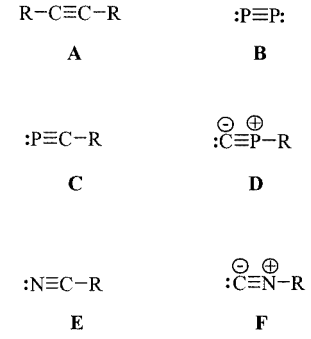

Scheme 1. Isoelectronic compounds featuring triple bonding

[a] Fakultät für Chemie der Universität Bielefeld, Universitätsstraße 25, 33615 Bielefeld, Germany

Lothar Weber was born in 1944 in Langenöls in Schlesien. He studied at the Universität Marburg and received his doctorate there under the direction of Professor Günter Schmid in 1973. Afterwards, he carried out postdoctoral studies with Professor Barry M. Trost at the University of Wisconsin in Madison, USA. On his return to Marburg, he began the experimental work leading to his Habilitation, which was completed in 1982 at the Universität Essen. His work focussed on the coordination chemistry of sulfur ylides. In 1985, he became a C2 Professor and then joined the Fakultät für Chemie der Universität Bielefeld. His research interests include the chemistry of compounds with low-coordinate elements of the fifth main group, the synthesis of homo- and heterocycles with heavy elements, as well as new aspects in boron chemistry.

MICROREVIEWS: This feature introduces the readers to the author's research through a concise overview of the selected topic. Reference to important work from others in the field is included.

 DOI: 10.1002/ejic.200200674 © 2003 Wiley-VCH Verlag GmbH & Co. KGaA, Weinheim

try.[4] At this point, it should be mentioned that the comparison of species of type **C** with alkynes **A**, rather than cyanides **E**, usually is given preference on the grounds of their polarity, their MO sequences and, consequently, their reactivity. In this account, both kinds of relationships are addressed where appropriate.

2. Attempted Syntheses of Isophosphaalkynes

The most prominent synthetic principle for preparing isophosphaalkynes is based upon the α-elimination of lithium halides from phosphaalkenylidene carbenoids **G** (Scheme 2).

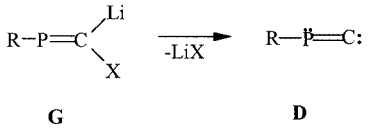

Scheme 2. Synthesis of isophosphaalkynes by α-elimination of lithium halides from phosphavinylidene carbenoids **G**

The reactive precursors may be synthesized by several routes. The outcome of their decomposition, however, strongly depends on the nature of the halide substituent as well as on the stereochemistry about the P=C double bond. The (*E*)-configured 2-chloro-1-(2,4,6-tri-*tert*-butylphenyl)-1-phosphaethene (**1a**) was lithiated in THF at −58 °C with a slight excess of *tert*-butyllithium to result in the complete conversion of **1a** into the corresponding *cis*-lithium compound **2a** (Scheme 3). Warming of the mixture to −48 °C completed the formation of **4a** within 10 min. No intermediates were detected by ^{31}P NMR spectroscopy. The identity of *cis*-**2a** was further substantiated by quenching the compound with methyl iodide at low temperature to give the (*E*)-configured phosphaalkene **5a**. Similar reactions were observed with the 2,4,6-tri-*tert*-pentylphenyl group as a substituent at the phosphorus atom[5a][5b] or with Mes* P=C(Br)Cl as a precursor.[5c]

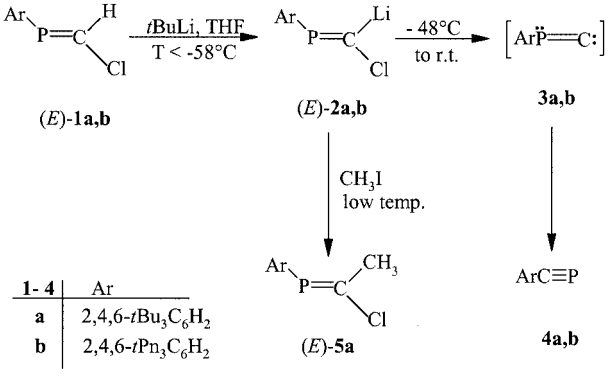

Scheme 3. Generation of phosphaalkynes **4a**,**b** and phosphaalkene (*E*)-**5a** from phosphavinylidene carbenoids (*E*)-**2a**,**b**

In contrast to this reactivity, the (*Z*)-configured phosphaalkylidene carbenoid (*Z*)-**2a**, obtained either by deprotonation of (*Z*)-2-chloro-1-(2,4,6-tri-*tert*-butylphenyl)-1-phosphaethene [(*Z*)-**1a**] with *tert*-butyllithium or by a chlorine/lithium exchange of Mes*P=CCl$_2$ (**6**, Scheme 4) with *n*-butyllithium in THF at −78 °C, did not produce **4a** upon warming. Quenching of (*Z*)-**2a** with methyl iodide at any temperature gave (*E*)-**5a**.[5a]

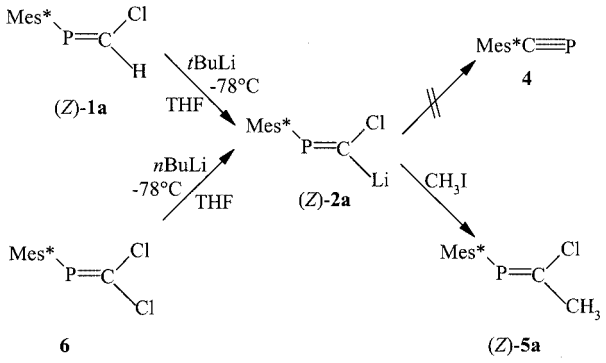

Scheme 4. Preparation and methylation of phosphavinylidene carbenoid (*Z*)-**2a**

It was assumed that solvation about the lithium atom in (*E*)-**2a** destabilizes the molecule, because of steric congestion between the bulky supermesityl group and the solvents coordinated around the lithium atom, which, thus, facilitates the α-elimination and formation of **4a**. Such a severe steric crowding should be absent in (*Z*)-**2a**, which increases its thermostability.[5a] In line with this assumption, single crystals of (*Z*)-Mes*−P=C(Cl){Li(dme)$_2$} were grown from a 1,2-dimethoxyethane solution at −60 °C and were subjected to an X-ray structure determination.[6] Lithium compound (*Z*)-**2a** served as a valuable precursor for the syntheses of interesting organophosphorus species, such as 1,4-diphosphabutatriene **7**, 1,4-diphosphabutadiene **8**,[7] and 1,3-diphosphacyclobutane-2,4-diyl[8] **9** (Scheme 5). From a formal point of view, compound **7** may be envisaged as a dimerization product of isophosphaalkyne **3a**, although synthetic routes are conceivable that circumvent the free vinylidene-like **3a**.

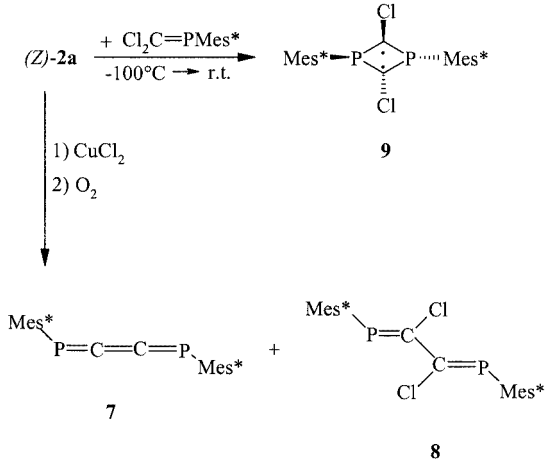

Scheme 5. Synthesis of **7**, **8**, and **9** from phosphavinylidene carbenoid (*Z*)-**2a**

 © 2003 Wiley-VCH Verlag GmbH & Co. KGaA, Weinheim

A different reaction pattern has been observed with 2-bromo-1-(2,4,6-tri-*tert*-butylphenyl)-1-phosphaethenyllithium, which was obtained as an (*E*)/(*Z*) mixture (1:5) by treatment of Mes*−P=CBr_2 with *n*-butyllithium in THF at −78 °C (Scheme 6).

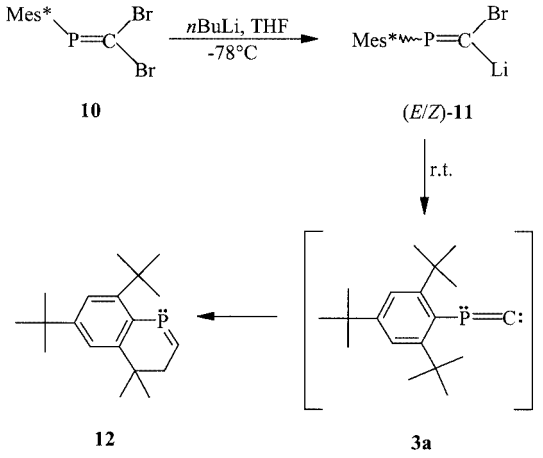

Scheme 6. Synthesis of 3,4-dihydro-1-phosphanaphthalene **12** from Mes*P=CBr_2

Warming of the reaction mixture to room temperature led to the formation of the 3,4-dihydro-1-phosphanaphthalene derivative **12** in 17% yield. None of the compounds Mes*P≡C (**3a**) or Mes*C≡P (**4a**) was detected in the reaction mixture. It is conceivable that **12** resulted from an intramolecular C−H insertion reaction of transient **3a**. Attempts to trap the isophosphaalkyne with cyclohexene or tetracyanoethylene, however, failed. The contrasting behavior of (*E*/*Z*)-**11** was attributed to the increased tendency of the bromide ion to act as a leaving group, which allows the smooth liberation of **3a** at lower temperatures.[9] Interestingly, the preparation of **12** from precursor **10** via intermediate (*E*/*Z*)-**11** also depends on the nature of the organolithium compound employed. The reaction of dibromophosphaethene **10** with 2 equiv. of *tert*-butyllithium, instead of *n*-butyllithium, in THF at −78 °C afforded (*E*/*Z*)-**11**, and slow warming to ambient temperature yielded 1,3,6-triphosphafulvene **13** (18% yield) in addition to small amounts of Mes*(H)P−C≡C−Mes*, Mes*C≡P (**4a**), and 1-phospha-3,4-dihydronaphthalene **12**.[10] As indicated before, triphosphafulvene **13** was not observed in the corresponding reaction of Br_2C=PMes* with *n*-butyllithium. The mechanism proposed for the formation of **13** involves the liberation of **4a** from (*E*/*Z*)-**11** and the subsequent addition of a second equivalent of **11** to the phosphaalkyne. Addition of the resulting 1,3-diphosphabutadienyllithium **14** to Mes*C≡P should give the 1,3,5-triphosphahexatrienyllithium **15**, which then cyclizes to form the final product (Scheme 7).[10]

Treatment of Mes*P=CI_2 with 2 equiv. of *n*-butyllithium at −120 °C yielded exclusively (*E*)-Mes*P=C(I)Li (**16**), which is stable to ca. −100 °C. At ca. −85 °C, **16** fragmented into Mes*C≡P (**4a**) with a half-life of roughly 4 h. No ^{31}P NMR spectroscopic signals were observed other then those of **16** and **4a**. This result led to the assumption

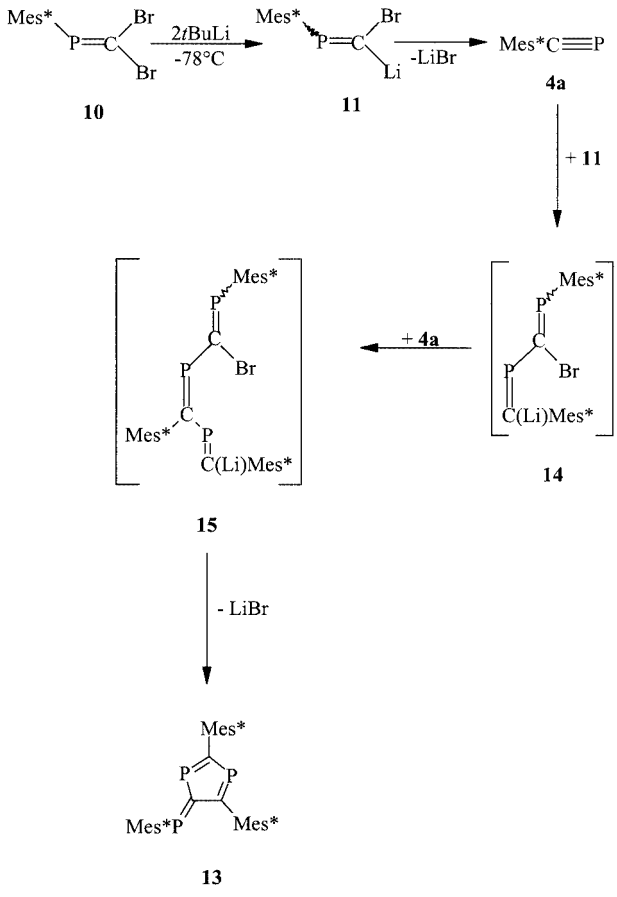

Scheme 7. Synthesis of triphosphafulvene **13** from Mes*P=CBr_2

that the rearrangement of **3a** into **4a** at this low temperature must be extremely rapid, or that the migration of the supermesityl group from the phosphorus atom to the carbon atom occurs concomitantly with the extrusion of lithium iodide,[11] which circumvents the intermediacy of free **3a**.

3. Theoretical Studies

The failure to synthesize isophosphaalkynes, or at least to obtain reliable proof of their existence as reactive intermediates, has been rationalized on the basis of qualitative considerations as well as detailed quantum chemical considerations. Phosphorus is a high main group element and, thus, it is reluctant to undergo s−p mixing of the valence orbitals.[12a] In other words, phosphorus suffers from "orbital nonhybridization."[12b] This effect has the further consequence that phosphorus, in contrast to its first-row analog nitrogen, prefers structures in which an inert s-orbital contains two nonbonding electrons. While this state is well documented in white phosphorus, its consequence for the formation of linear triple bonds is also apparent. Such an unfavorable sp-hybrid would exist in the isophosphaalkyne, HPC. On the other hand, such a bonding situation is not observed in the phosphaalkyne, HCP. The phosphorus

 © 2003 Wiley-VCH Verlag GmbH & Co. KGaA, Weinheim

atom here can constitute a nonbonding s-orbital that is not forced to participate in bonding with the neighboring carbon atom.

These qualitative considerations[12a] find support in detailed quantum chemical calculations. According to the ab initio calculations for the HCP/HPC system, the linear HPC and HCP isomers correspond to the energy maximum and energy minimum, respectively, on the energy surface of the singlet ground state, and the relative energy between them is 83.9 kcal/mol at the MP4/6-31g** level.[13a,13b] The existence of a slightly bent HPC structure, however, in which the nonbonding s-orbital at the phosphorus atom is partly freed, is conceivable by other calculations. These calculations predict a local energy minimum that is merely 2.3 kcal/mol below the transition state for the rearrangement to HCP.[13c] In contrast to this prediction, the first-row analog HNC is a stable energy minimum on the electronic hypersurface, since a nitrogen atom can form an sp-hybrid orbital suitable for a linear arrangement of the three atoms in the isocyanide. According to electron-correlated ab initio calculations, the energy difference between the two structures HCN and HNC is ca. 14 kcal/mol.[14]

A further hint at the stability of the isophosphaalkyne has been given by quantum chemical considerations. Electronegative substituents (e.g., fluorine) tend to withdraw p-electrons from a bond. As a consequence, a fluorine atom stabilizes, to a considerable extent, the isophosphaalkyne form, RPC (R = F). For the reasons mentioned above, this stability occurs to a larger extent than that for the corresponding phosphaalkyne form, RCP. Ab initio calculations agree with these considerations.[13b] Although the energy barrier for the rearrangement from FPC to FCP is increased (13−17 kcal/mol), so far FPC has not been characterized experimentally. Principally, it is conceivable that the compound could be observed in an inert matrix at low temperature.[13b]

4. Isosphosphaalkyne Complexes

It is obvious that the facile α-elimination of lithium halides from *C*-lithiated *C*-halophosphaalkenes and the marked propensity to rearrangement of the initial products has thwarted the detection and isolation of isophosphaalkynes. Metallation of the dihalophosphaalkenes by transition metal complexes through oxidative addition processes, however, should lead to coordination compounds featuring isophosphaalkyne ligands. A model reaction, in which an isocyanide dichloride was converted into an isocyanide ligand at a transition metal center was reported in the mid-1970s (Scheme 8).[4h]

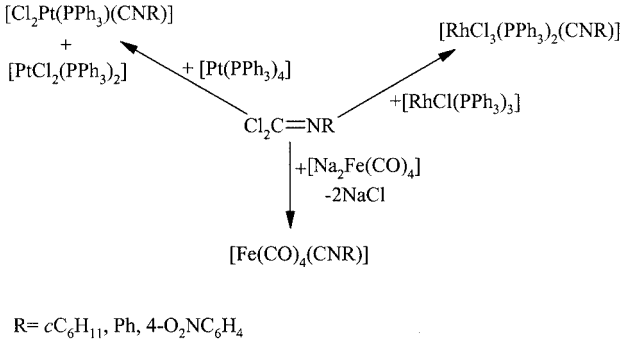

Scheme 8. Formation of isocyanide complexes from isocyanide dichlorides

The first examples of stable (arylisophosphaalkyne)metal complexes **18a**,**b** were prepared by reaction of *trans*-[(X)(PEt$_3$)$_2$Pt{C(=PMes*)X}] (**17a**,**b**) with [Pt(PEt$_3$)$_4$] in benzene (or in hexanes) at room temperature (Scheme 9). This oxidative addition-type reaction was complete within 24 h and afforded **18a**,**b** as the only products. The key compounds **17a**,**b** were available either by an oxidative addition of X$_2$C=PMes* (X = Cl, Br) onto [Pt(PEt$_3$)$_4$] in benzene at 25 °C or, in the case of **17a**, by treatment of *trans*-[PtCl$_2$(PEt$_3$)$_2$] with LiC(Cl)=PMes* in THF at −78 °C.[15]

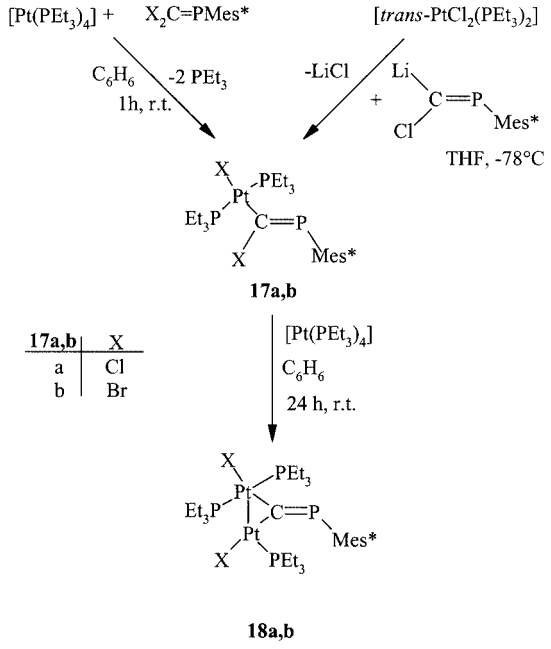

Scheme 9. Synthesis of (μ-isophosphaalkyne)diplatinum complexes **18a**,**b**

The direct synthesis of red, crystalline **18a**,**b** from the dihalophosphaalkenes and 2 equiv. of [Pt(PEt$_3$)$_4$] was also possible, albeit in much lower yield (Scheme 10).[15] A plausible mechanism for the generation of the μ-isophosphaalkyne complexes invokes the intermediacy of the doubly *C*-metalated phosphaalkenes **19a**,**b**, which extrude 1 equiv. of PEt$_3$ under Pt−Pt bond formation.

An X-ray diffraction study reveals **18a** as a dinuclear complex in which a Pt−Pt single bond of 2.6751(5) Å is nonsymmetrically bridged by the isophosphaalkyne ligand (Figure 1). The Pt−C bond lengths between the two inequivalent metal atoms and the bridging ligand are markedly different. The distance Pt(2)−C(1) of 1.86(1) Å is shorter than Pt(1)−C(1) [2.107(9) Å] by 0.22 Å.

 © 2003 Wiley-VCH Verlag GmbH & Co. KGaA, Weinheim

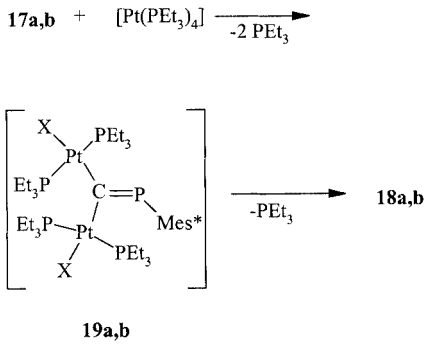

Scheme 10. Proposed mechanism for the formation of **18a**,**b**

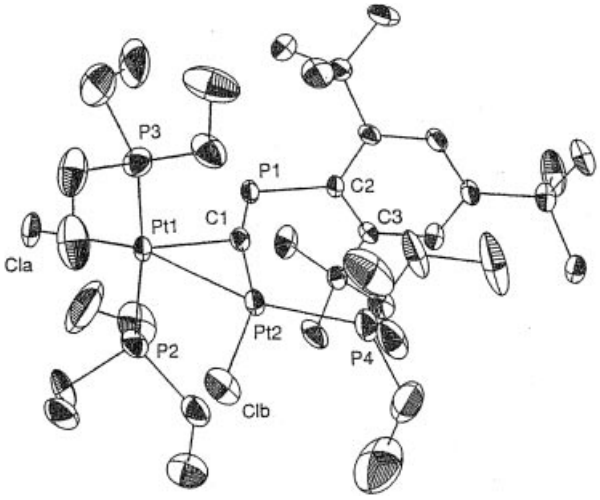

Figure 1. Molecular structure of [(Cl)(PEt_3)Pt(μ-C=PMes*)-Pt(PEt_3)$_2$(Cl)](*Pt*−*Pt*) (**18a**) in the crystal; selected bond lengths [Å] and angles [°]: Pt(1)−Pt(2) 2.6751(5), Pt(1)−C(1) 2.107(9), Pt(2)−C(1) 1.89(1), P(1)−C(1) 1.67(1), P(1)−C(2) 1.89(1); C(1)−P(1)−C(2) 110.7(5), Pt(1)−C(1)−Pt(2) 83.8(4), Pt(1)−C(1)−P(1) 112.0(5), Pt(2)−C(1)−P(1) 164.1(6)

The Pt−C(1)−P(1) angles also differ significantly. The angle Pt(2)−C(1)−P(1) of 164.1(6)° is close to linearity, whereas the angle Pt(1)−C(1)−P(1) of 112.0(5)° is sharply bent. The separation between Pt(1) and P(1) of 3.15 Å excludes any bonding interaction. The bond length C(1)−P(1) of 1.67(10) Å falls in the typical range for a P−C double bond (1.65−1.72 Å), as determined from numerous phosphaalkenes without π-donating substituents at the tricoordinate carbon atom. Therefore, the most reasonable description of the organophosphorus ligand is that of a semibridging group that is strongly coordinated to Pt(2) and interacts more weakly with Pt(1). At this point, it should be mentioned that solutions of the pure key compounds **17a** and **17b** in nonpolar solvents (C_6D_6, hexanes) are stable at ambient temperature under argon for at least one week. In polar solvents, such as CH_2Cl_2, $CHCl_3$, or THF, however, they decompose rapidly to the phosphaalkyne Mes*C≡P (**4a**) and [X_2Pd(PEt_3)$_2$] via the intermediate **20**, the identity of which was authenticated in one case by an X-ray structural analysis (Scheme 11). The propensity for this conversion depends on the metal (Pt < Pd), the halide (Cl < Br) and the phosphane ligand (PEt_3 < PPh_3). At no stage of this transformation is free isophosphaalkyne involved.[15c,15d] In the light of this finding, it is clear that the dechlorination of Cl_2C=PMes* by [Pd(PPh_3)$_4$] to give Mes*C≡P and *trans*-[$PdCl_2$(PPh_3)$_2$] cannot involve free C≡P−Mes* as was claimed in the respective communication.[16]

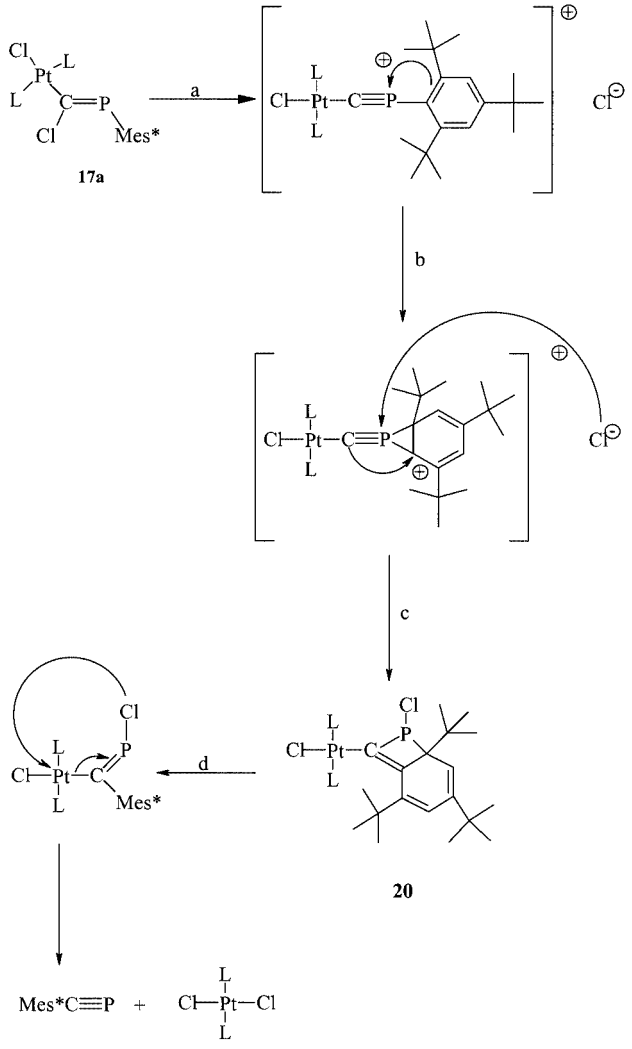

Scheme 11. Proposed mechanism for the decomposition of *C*-platiniophosphaalkene **17a** in polar solvents

One might even speculate that the conversion of Li(Cl)C=PMes* into Mes*C≡P proceeds by a similar mechanism, where lithium plays the role of the platinum center. At this point, it is clear that the synthetic principle realized in Scheme 9 for producing μ-isophosphaalkyne complexes is also limited by the stability of the respective *C*-metallo-*C*-halophosphaalkenes. To be certain of this effect would require a more thorough study concerning the particular role of the metal atom, the halogen atom, the ancillary ligands and the substituents at the phosphorus atom in the process. A first step toward this study was to change the metal complex, which by reaction with precursor metal-

 © 2003 Wiley-VCH Verlag GmbH & Co. KGaA, Weinheim

lophosphaalkenes **17a**,**b**, should furnish heterodimetallic analogs of **18a**,**b** as products. When [Pt(PEt_3)$_4$] was replaced by [Pd(PEt_3)$_4$], however, the reaction with **17a**,**b** proceeded in a completely different manner.

After stirring the reaction solution of **17a**,**b** and [Pd(PEt_3)$_4$] for 24 h at ambient temperature, complexes **22a**,**b** and [*trans*-Pd(X)(Mes*)(PEt_3)$_2$] were observed as the only products (Scheme 12). The latter compounds could be separated easily from the mixture by fractional crystallization and were characterized by an X-ray diffraction analysis. Although stable in solution for at least one week, all attempts to isolate **22a**,**b** without decomposition failed and the identification of **22a**,**b** was confined to spectroscopy. The ^{31}P NMR spectroscopic resonance of the unprecedented terminal phosphocyanide ligand was assigned to a triplet at δ = 68.0 ppm (J_{pp} = 9.2 Hz) resulting from coupling to the two equivalent P nuclei of the PEt_3 ligands. Moreover, **22a**,**b** could be trapped by reaction with [Pt(PEt_3)$_4$] to yield the dinuclear complexes **23a**,**b** featuring a bridging phosphocyanide ligand in an η^1:η^2-mode of coordination. Complex **23a** was also accessible by treatment of the *C*-palladiophosphalkene **17c** with 1 mol-equiv. of [Pt(PEt_3)$_4$] under similar reaction conditions.[15b]

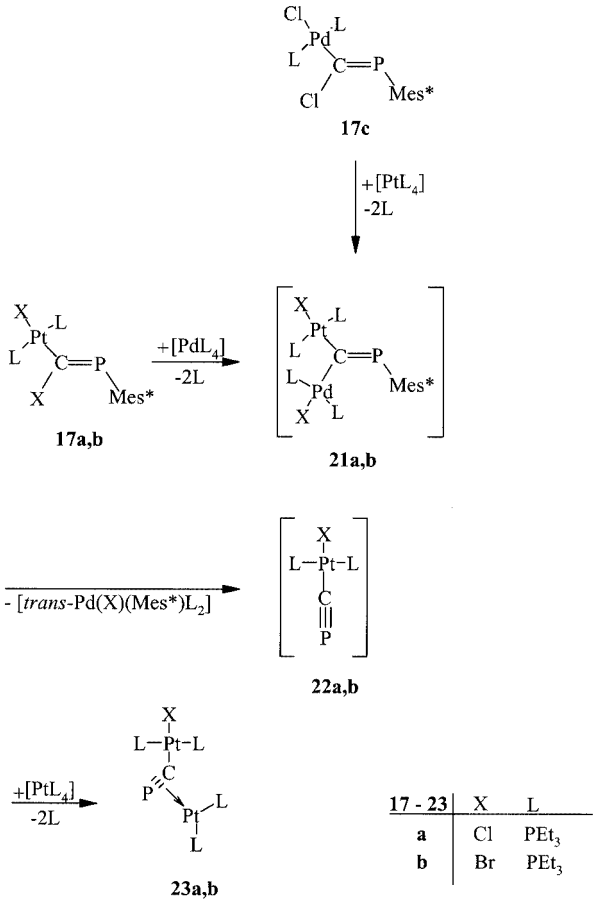

Scheme 12. Synthesis of μ-η^1:η^2-phosphocyanide complexes **23a**,**b**

The X-ray analysis of **23a** shows a dinuclear complex containing a bridging C≡P ligand that is η^1-*C*-bonded to Pt(1) and η^2-*C*,*P*-bonded to Pt(2) (Figure 2). The distance between both platinum centers [3.7868(3) Å] eliminates any likelihood of significant bonding occurring between the metal atoms. The atoms Cl, Pt(1), C(1), P(1), Pt(2), P(4), and P(5) are nearly coplanar (to within 0.061 Å), while P(2) and P(3) are located 2.292 and 2.279 Å above and below this plane, respectively. The C(1)−P(1) bond length of 1.666(6) Å compares well to that in [η^2-(*t*BuC≡P)Pt(PPh_3)$_2$] [1.67(2) Å] and is quite typical for η^2-ligated phosphaalkynes. As mentioned above, the preparation of dinuclear complexes with bridging isophosphaalkyne ligands, according to the method devised in Scheme 9, seems to be limited by the nature of the metal atom. Moreover, an additional limitation is given by the few examples of dichlorophosphaalkenes that are available to date and by the demand for bulky substituents that have to be present in these reagents. In a very recent study, the dichlorophosphaalkene $(Me_3Si)_2N-P=CCl_2$ was utilized as an additional candidate for the oxidative addition to two platinum metal centers. The reaction of [Pt(PEt_3)$_4$] with $Cl_2C=PN(SiMe_3)_2$ in THF or hexanes at −50 °C immediately and quantitatively produced the η^1-phosphaalkenyl complex *cis*-[Cl(Et_3P)$_2$Pt{C(Cl)=PN($SiMe_3$)$_2$}] (*cis*-**24**) by oxidative addition of one of the C−Cl bonds. A quantitative *cis*/*trans* isomerization to give *trans*-**24** occurred at 0 °C (Scheme 13).[17]

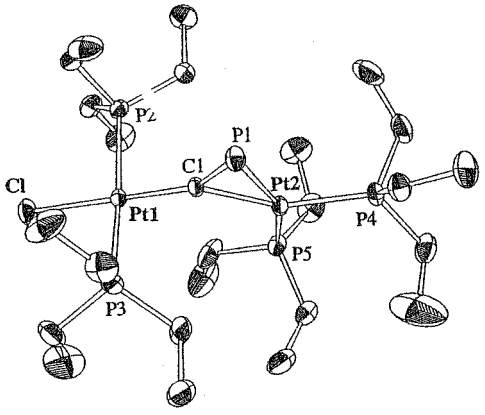

Figure 2. Molecular structure of **23a** in the crystal; selected bond lengths [Å] and angles [°]: Pt(1)−C(1) 1.950(6), Pt(1)−Cl 2.412(2), Pt(1)−P(2) 2.302(2), Pt(1)−P(3) 2.297(2), Pt(2)−C(1) 2.083(5), Pt(2)−P(1) 2.337(2), Pt(2)−P(4) 2.269(2), Pt(2)−P(5) 2.277(2), C(1)−P(1) 1.666(6); Pt(1)−C(1)−P(1) 144.0(3), Pt(1)−C(1)−Pt(2) 139.7(3), C(1)−Pt(2)−P(1) 43.8(2)

Although the molecular structure and the ^{31}P NMR spectrum of *trans*-**24** are very similar to those of *trans*-[Cl(Et_3P)$_2$Pt{C(Cl)=PMes*}] (**18a**), both species differ significantly in their reactivities. In contrast to **18a**, which in THF solution completely decomposed to Mes*C≡P and [Pt(PEt_3)$_2$Cl$_2$] within 24 h, THF solutions of *trans*-**24** are stable for weeks. Treatment of the latter compound with a 2nd equiv. of [Pt(PEt_3)$_4$] did not yield the anticipated μ-isophosphaalkyne complexes, but resulted in decomposition to a mixture of unidentified materials. Complex *trans*-**24** proved, however, to be an excellent precursor reagent for preparing the μ-η^1:η^2-phosphocyanide complex **23a**. Thus,

 © 2003 Wiley-VCH Verlag GmbH & Co. KGaA, Weinheim

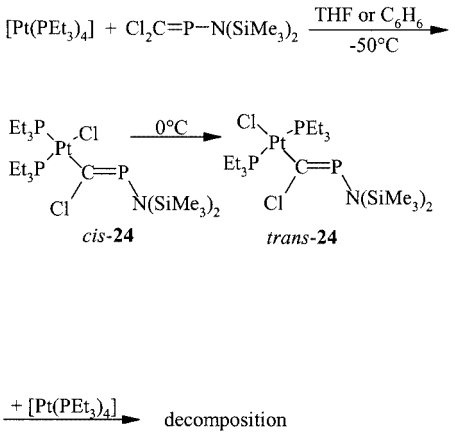

Scheme 13. Generation of *C*-platiniophosphaalkenes *cis*- and *trans*-**24**

reduction of an equimolar mixture of **24** and $[Pt(PEt_3)_2Cl_2]$ with 3 equiv. of sodium benzophenone ketyl in THF afforded pure crystalline **23a** in 79% yield. This reaction was performed on a scale of several grams without a decrease in yield or purity of the product. It was crucial for the success of this process that the reducing agent be added to the mixture of both metal complexes. This requirement was rationalized by the need to trap the in situ generated dicoordinate complex $[Pt(PEt_3)_2]$ by π-coordination to the P=C double bond of **24** (Scheme 14). To date, this transformation is limited to using PEt_3 as a ligand in the platinum halide complex. Compound **24** remained unaffected in solution in similar reduction experiments with $[PtCl_2(PPh_3)_2]$, $[PtCl_2\{PiPr_3\}_2]$, $[PtCl_2(PCy_3)_2]$, and $[PtCl_2(depe)]$.

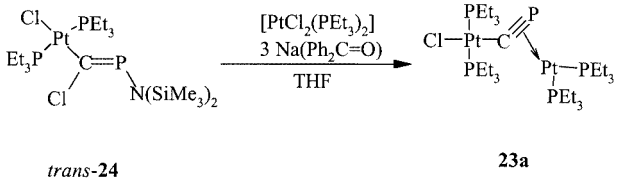

Scheme 14. Conversion of *trans*-**24** into **23a**

The availability of larger quantities of complex **23a** allowed a thorough investigation of its chemical reactivity to be made. Like classical η^2-phosphaalkyne complexes, the molecule exhibits significant nucleophilicity at the phosphorus atom of the C–P ligand. In keeping with this nucleophilicity, the treatment of **23a** with 3 equiv. of methyl iodide in THF for 12 h at ambient temperature resulted in the formation of the methyl isophosphaalkyne complex $[(Cl)(Et_3P)Pt(\mu\text{-}C{=}PMe)Pt(PEt_3)_2I](Pt{-}Pt)$ (**27**), with $(MePEt_3)I$ as a byproduct (Scheme 15).

Most likely this reaction was initiated by the methylation of the phosphorus atom of the C≡P bond to afford the cationic η^1-*C*:η^2-*C*,*P*-isophosphaalkyne complex **25**. Attack of the iodide ion at the zero-valent platinum center gave complex **26**, which may be regarded formally as a *C*,*C*-dimetallophosphaalkene. Extrusion of PEt_3 and Pt–Pt bond formation eventually afforded product **27**. Evidence for this

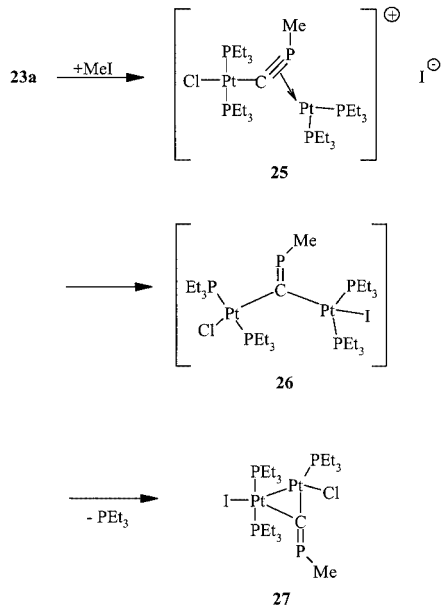

Scheme 15. Synthesis of μ-isophosphaalkyne complex **27** from **23a** and methyl iodide

proposal was taken from the clean methylation of **23a** with methyl triflate to give salt $\mathbf{25}^+OTf^-$. The latter salt was converted into **27** by treatment with a tenfold amount of NaI. Moreover, comparison of the NMR spectroscopic data of the triflate of $\mathbf{25}^+$ with the related platinum and tungsten adducts **28** and **29** adds further support for **25** being the initial product of the methylation reaction (Scheme 16).

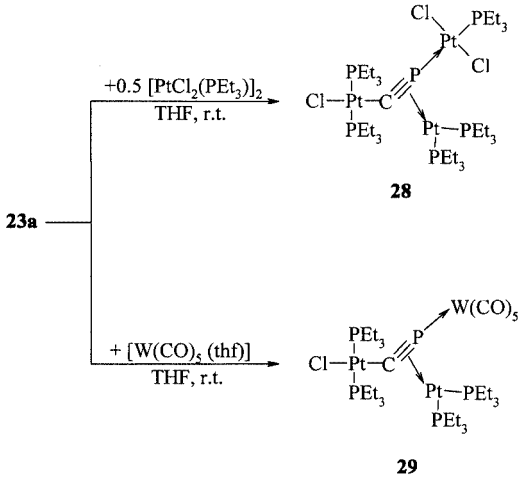

Scheme 16. Phosphocyanide as an η^1:η^1:η^2-ligand in trinuclear complexes **28** and **29**

For a successful alkylation, the synthetic sequence depicted in Scheme 15 could represent a more general access to (μ-isophosphaalkyne)diplatinum complexes. More importantly, this approach would no longer be dependent on sterically demanding groups. To evaluate this concept, alkylation of **23a** was performed with benzyl bromide, isopropyl iodide, alkyl bromide, and 2,4,6-tri-*tert*-butylbenzyl bromide under the same conditions as for the methylation. Ac-

 © 2003 Wiley-VCH Verlag GmbH & Co. KGaA, Weinheim

cording to ^{31}P NMR spectroscopic observations, however, only the reactions with benzyl bromide and isopropyl iodide yielded μ-isophosphaalkyne complexes analogous to **27**. Unfortunately, the benzyl derivative could not be isolated in a pure state, and the isopropyl derivative decomposed during the course of the alkylation.[17] In a recent paper, the dichlorophosphaalkenes $Cl_2C{=}PN(SiMe_3)_2$ and $Cl_2C{=}$PMes* were treated with zero-valent nickel complexes,[18] which produced interesting and novel organophosphorus compounds instead of the anticipated isophosphaalkyne complexes. The reaction of 0.5 equiv. of $Cl_2C{=}PN(SiMe_3)_2$ with $[(Ph_3P)_2Ni(C_2H_4)]$ in toluene in the range between −78 °C and room temperature produced $[Ni_2Cl_2(PPh_3)_2\{\mu\text{-}\eta^2{:}\eta^2\text{-}C(PPh_3){=}PN(SiMe_3)_2\}]$ (**31**) in 74% yield. Low-temperature (−30 °C) ^{31}P NMR spectroscopic monitoring showed complex **30** as the only observable intermediate in this reaction. A stoichiometric reaction of $[(Ph_3P)_2Ni(C_2H_4)]$ with $Cl_2C{=}PN(SiMe_3)_2$ at −30 °C yielded **30** quantitatively. This compound could not be isolated because of decomposition, but the addition of a 2nd equiv. of $[(Ph_3P)_2Ni(C_2H_4)]$ to the reaction mixture led to oxidative addition of the remaining C−Cl bond in **30** to $[(Ph_3P)_2Ni(C_2H_4)]$ to give **31** (Scheme 17). The latter complex can be viewed as a triphenylphosphane-stabilized $\eta^2{:}\eta^2$-isophosphaalkyne complex. Attempts to remove the phosphane from **31** with 9-borabicyclo[3,3,1]nonane resulted in complete decomposition.

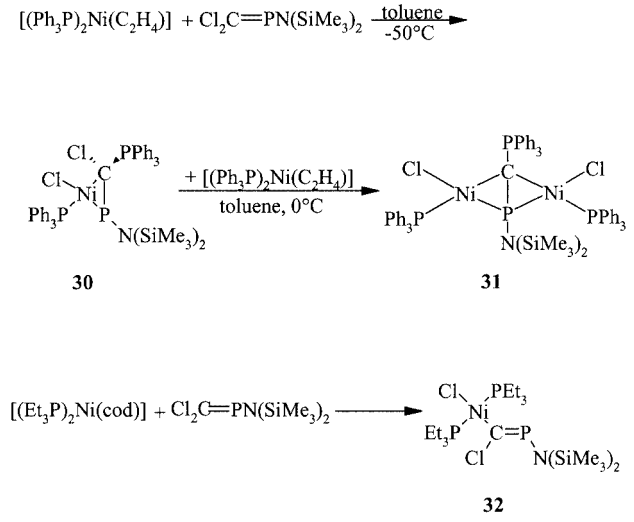

Scheme 17. Reaction of zero-valent nickel complexes with $(Me_3Si)_2NP{=}CCl_2$

In contrast to the reaction in Scheme 17 with PPh_3 as a ligand in the nickel complex precursor, the treatment of a 1:2 mixture of $[Ni(cod)_2]$ and PEt_3 with $Cl_2C{=}PN(SiMe_3)_2$ afforded the nickeliophosphaalkene **32**, which is formally analogous to the *Pt*-functionalized species **24**. This compound did not rearrange to an analog of **30**, and it did not react further with an excess of Ni^0 complexes to molecules like **31** or to μ-isophosphaalkene complexes. In solution, compound **32** decomposed to nontractable materials within 1 d. In contrast to this finding, the dihalophosphaalkenes $X_2C{=}P{-}Mes^*$ (X = Cl, Br) were dehalogenated by 2 equiv. of $[Ni(cod)_2]/2PR_3$ mixtures to give the metalloheterocycles **33** in moderate yields (Scheme 18).

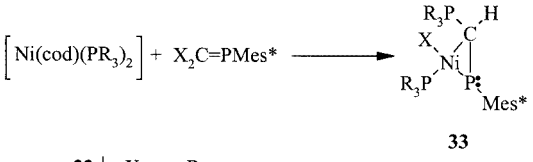

33	X	R
a	Cl	Ph
b	Br	Ph
c	Br	Cy

Scheme 18. Preparation of metalloheterocycle **33**

A completely different approach to dinuclear complexes with bridging μ-isophosphaalkyne ligands **37a−c** made use of the condensation of the cationic (μ-carbyne)diiron complex **34** with the secondary aryl(silyl)phosphanes **35a−d** in acetonitrile in the presence of 1,8-diazabicyclo[5.4.0]undec-7-ene (DBU) (Scheme 19).[19a,19b]

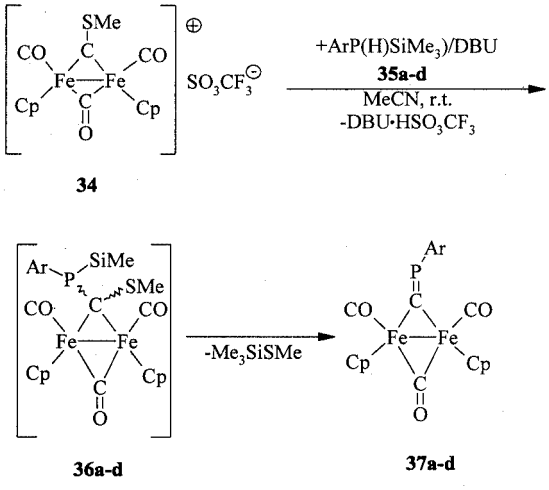

35-37	Ar
a	2,4,6-$Me_3C_6H_2$
b	2,4,6-$i Pr_3C_6H_2$
c	2,4,6-$t Bu_3C_6H_2$
d	2,4,6-$(CF_3)_3C_6H_2$

Scheme 19. Synthesis of (μ-isophosphaalkyne)diiron complexes **37a−d**

Complexes **37a−c** were isolated in moderate yields as dark-red, air-stable crystals after column chromatography. Thermolabile derivative **37d**, however, had to be converted into its stable $[Cr(CO)_5]$ adduct **38d** by treatment with (cyclooctene)$Cr(CO)_5$ immediately after isolation.[19b] It is conceivable that the generation of **37a−d** was initiated by the nucleophilic attack of phosphanes **35a−d** at the bridging carbyne carbon atom, with subsequent deprotonation of the resulting phosphonium salt. Alternatively, the nucleophilic attack of anions $[P(SiMe_3)Ar]^-$ is also possible. Evi-

 © 2003 Wiley-VCH Verlag GmbH & Co. KGaA, Weinheim

dence for the intermediates **36** is given by ^{31}P NMR spectroscopic signals at δ = 8.3 (**36a**) and 2.1 ppm (**36c**) at the beginning of the process. Elimination of Me_3SiSCH_3 from **36a–d** afforded the final products. The presence of P=C double bonds was indicated by ^{31}P NMR spectroscopic resonances at δ = 200–258 ppm and doublets in the $^{13}C\{^1H\}$ NMR spectra at very low field (δ = 333.8–345.8 ppm).

The X-ray structure analysis of **37a** shows a dinuclear complex, the Fe–Fe bond of which [2.527(5) Å] is symmetrically bridged by a μ-CO ligand [Fe(1,2)–C(12) = 1.954(16), 1.927(15) Å] and a μ-C=P–Mes* ligand [Fe(1,2)–C(13) = 1.903(16), 1.927(16) Å] (Figure 3). The P–C bond length of 1.683(17) Å is consistent with a double bond. The angles Fe(1)–C(13)–P(1) [147.2(10)°] and Fe(2)–C13)–P(1) [129.7(9)°] differ significantly, but not as much as in the diplatinum complex **18a** [164.1(6)° and 112.0(5)°]. The condensation discussed here for the construction of the P=C bond of an μ-isophosphaalkyne complex is independent from the existence of a phosphaalkene precursor. This method, however, also lacks generality. Thus, reaction of **34** with an equimolar amount of *t*BuP(H)$SiMe_3$ in acetonitrile in the presence of DBU afforded complex **40** within 2 d at room temperature[19c] (Scheme 20).

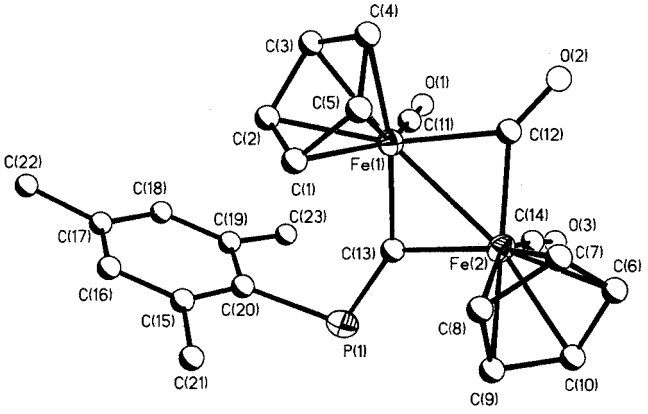

Figure 3. Molecular structure of **37a**; selected bond lengths [Å] and angles [°]: Fe(1)–Fe(2) 2.527(5), Fe(1)–C(12) 1.954(16), Fe(2)–C(12) 1.927(15), Fe(1)–C(13) 1.903(16), Fe(2)–C(13) 1.927(16), P(1)–C(13) 1.683(17); Fe(1)–C(13)–P(1) 147.2(10), Fe(2)–C(13)–P(1) 129.7(9), Fe(1)–C(12)–O(2) 138.3(13), Fe(2)–C(12)–O(2) 140.4(13), C(13)–P(1)–C(20) 104.5(7)

The reaction of **34** with *i*$PrPH_2$ or $(Me_3Si)_3CP(H)SiMe_3$ did not yield tractable products. The identity of **40** was deduced from elemental analyses and spectroscopic evidence. The ^{31}P NMR spectrum revealed a doublet of decets at δ = −6.0 ppm ($^1J_{PH}$ = 265, $^3J_{PH}$ = 14 Hz), whereas in the $^{13}C\{H\}$ NMR spectrum a doublet at δ = 420.0 ppm ($^1J_{PH}$ = 83 Hz) is diagnostic of a μ-phosphanylcarbyne ligand. Monitoring of the course of the reaction by $^{31}P\{H\}$ NMR spectroscopy showed, before DBU was added, only the resonance of *t*BuP(H)$SiMe_3$ at δ = −85.5 ppm. After the addition of the base, this resonance was replaced by a singlet at δ = 20.6 ppm, which in the proton-coupled experiment became a doublet of multiplets ($^1J_{PH}$ = 383.1 Hz). This signal is attributed to intermediate **38**. After 14 h at 20 °C, the spectrum displayed two singlets at δ = −7.9 and −17.4 ppm in addition to the resonance for **38**. After 2 d, only the singlet at δ = −7.9 ppm of the final product **40** remained. The signal at δ = −17.4 ppm was due to intermediate **39**, which was isolated after 2 h of reaction and fully characterized by an X-ray diffraction study (Figure 4).[19c]

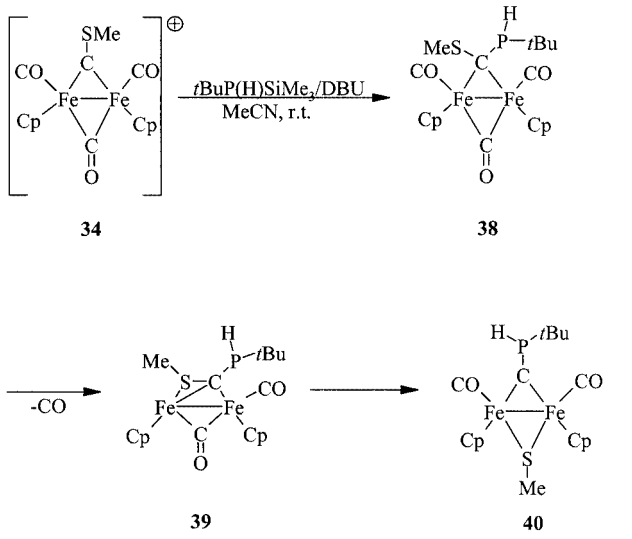

Scheme 20. Synthesis of μ-phosphanylcarbyne complex **40**

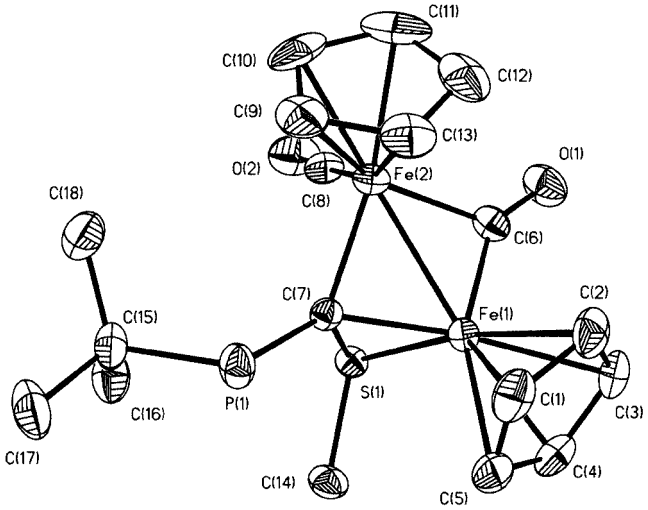

Figure 4. Molecular structure of **39** in the crystal; selected bond lengths [Å] and angles [°]: Fe(1)–Fe(2) 2.5015(7), Fe(1)–C(7) 1.910(3), Fe(2)–C(7) 1.975(3), Fe(1)–S(1) 2.2309(8), S(1)–C(7) 1.800(3), P(1)–C(7) 1.807(3), P(1)–C(15) 1.885(3); Fe(2)–C(7)–P(1) 124.34(14), C(7)–P(1)–C(15) 108.37(14), S(1)–C(7)–P(1) 125.4(2), Fe(1)–C(7)–P(1) 126.8(2), Fe(1)–C(7)–Fe(2) 80.14(10)

The most interesting feature of the molecule is that the *tert*-butylphosphanyl(methylthiolato)methylidene ligand bridges the Fe–Fe unit via the distorted tetrahedral carbon atom C(7) [Fe(1,2)–C(7) = 1.910(3), 1.975(3) Å]. In addition, the sulfur atom of the thiolato substituent is coordinated to Fe(1) [Fe(1)–S(1) = 2.231(1) Å]. The distances

 © 2003 Wiley-VCH Verlag GmbH & Co. KGaA, Weinheim

P(1)−C(7) [1.807(3) Å] and S(1)−C(7) [1.800(3) Å] are consistent with single bonds. The attempted condensation of the metallodisilylphosphanes **41a−d** with μ-carbyne complex **34** resulted in the formation of the dinuclear complexes **45a−d** featuring μ-η^1-*P*:η^2-*C*,*P*-metallophosphaalkene ligands instead of the anticipated trinuclear C≡P complexes **46** (Scheme 21).[19d]

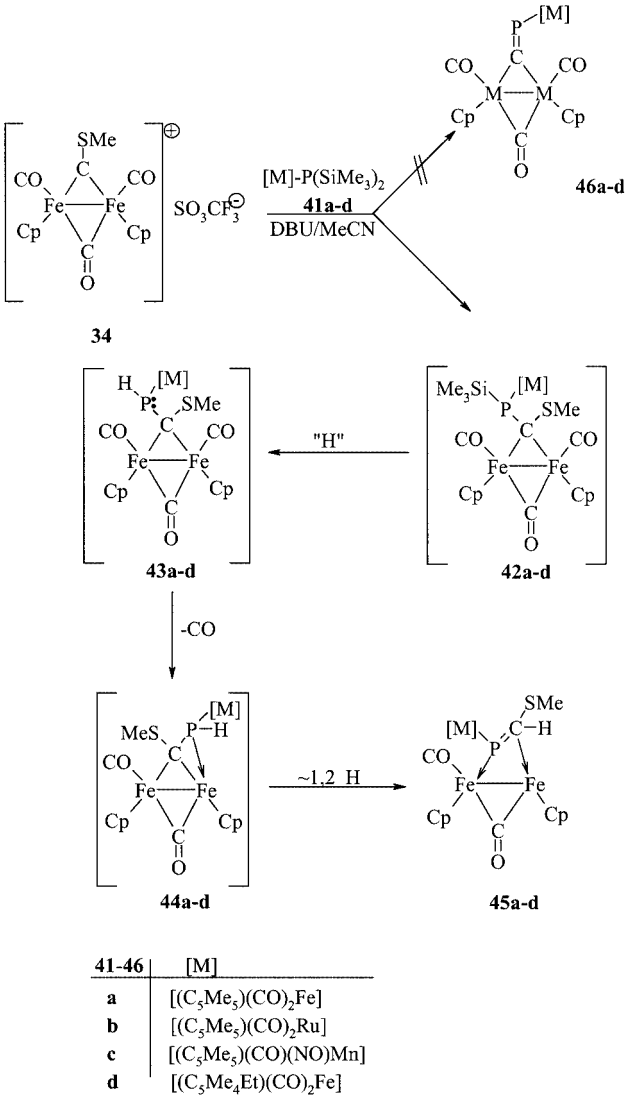

Scheme 21. Synthesis of μ-η^1:η^2-metallophosphaalkene complexes **45a−d**

It is reasonable to propose that the synthesis of compounds **45** is initiated by the nucleophilic attack of metallo(-silyl)phosphide {P[M](SiMe$_3$)}$^-$ at the carbyne bridge of **34** to give the μ-alkylidene complex **42**. The replacement of the Me$_3$Si group in **43** by a hydrogen atom was unexpected. Since traces of moisture are excluded from the reaction, the source of the hydrogen atom might be DBU itself. An intramolecular replacement of CO by the phosphane function in **43** results in intermediate **44**. A 1,2-hydrogen shift and a second Fe−P contact leads to the final product **45**. It is worth mentioning that the preparation of **45** failed when NEt$_3$ was used as the base instead of DBU. In a control experiment, (η^5-C$_5$Me$_5$)(CO)$_2$FePH$_2$, **34**, and DBU afforded **45a** with a slightly improved yield (39%, cf. 28%). The difference in reactivity between aryl−PH(SiMe$_3$) or aryl−PH$_2$ and [M]PH(SiMe$_3$) or [M]PH$_2$ towards **34** may be rationalized by regarding the common intermediate **42**. Obviously, activation by the aryl group at the phosphorus atom promotes the 1,2-eliminations of Me$_3$SiSMe or HSMe to give **37**, whereas the electron-releasing metallo group enhances the phosphane's nucleophilicity, favoring the intramolecular CO displacement instead of the 1,2-elimination. The chemistry of the (μ-isophosphaalkyne)diiron complexes **37** largely resembles that of classical phosphaalkenes. Thus, the synthesis of the pentacarbonylchromium complexes **47a**,**d** and of the [Fe(CO)$_4$] adduct **48a** was accomplished by reaction of **37a**,**d** with pentacarbonyl(cyclooctene)chromium or nonacarbonyldiiron, respectively, with the organophosphorus moiety acting as an η^1-ligand through the lone pair of electrons at the P atom (Scheme 22).[19b]

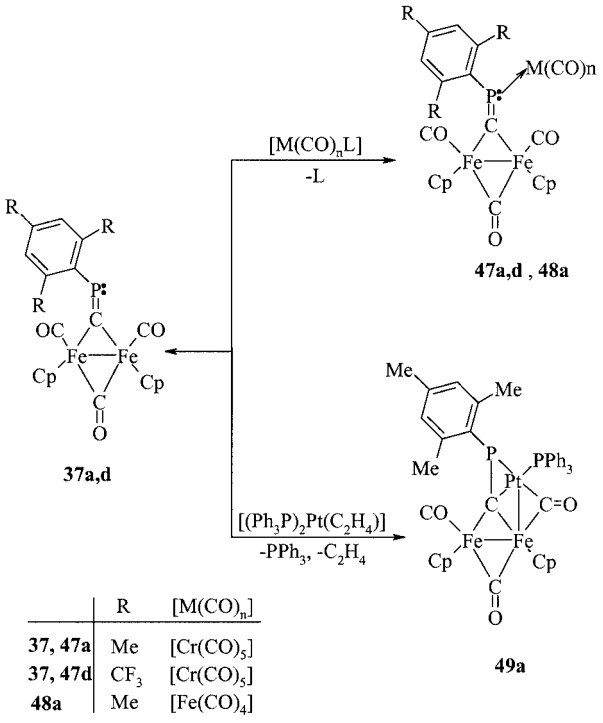

Scheme 22. Preparation of the trinuclear complexes **47a**,**d**, **48a**, and **49a** featuring bridging isophosphaalkyne ligands

The η^1-ligation of the phosphorus atom of **37a**,**d** to an [M(CO)$_n$] fragment in **47c**,**d** and **48a** was accompanied by the typical shielding of the ^{31}P NMR spectroscopic signal ($\Delta\delta^{31}$P = 25.0−74.3 ppm). The black crystalline complex **49a**, isolated from the reaction between **37a** and [(Ph$_3$P)$_2$Pt(C$_2$H$_4$)] displayed, in the ^{31}P NMR spectrum, two doublets at δ = 129.9 and 44.15 ppm ($^2J_{P,P}$ = 9.8 Hz) for the ^{31}P nuclei of the isophosphaalkyne and PPh$_3$ ligands. The increased high-field shift upon coordination (Δδ = 125.6 ppm) and the $^1J_{P,Pt}$ coupling constant of only

 © 2003 Wiley-VCH Verlag GmbH & Co. KGaA, Weinheim

63 Hz suggest a π-interaction between the platinum atom and the P−C unit.[19b]

The X-ray diffraction study of **47a** (Figure 5) shows a pentacarbonylchromium complex that is attached to ligand **37a** via the lone pair of electrons at the P atom [Cr(1)−P(1) = 2.412(8) Å]. The geometry of **37a** is not significantly perturbed by the [$Cr(CO)_5$] fragment. The bonds and angles of the [Fe_2(μ-CO)(μCPMes)] unit of **47a** are shorter and smaller than those in the precursor molecule. Atoms C(15) and P(1) have trigonal-planar geometries. The exocyclic angles Fe(1)−C(15)−P(1) [139.0(13)°] and Fe(2)−C(15)−P(1) [140.3(14)°] in **47c** are nearly identical, whereas in **37a** they differ markedly [147.2(10) and 129.7(9)°, respectively].[19b]

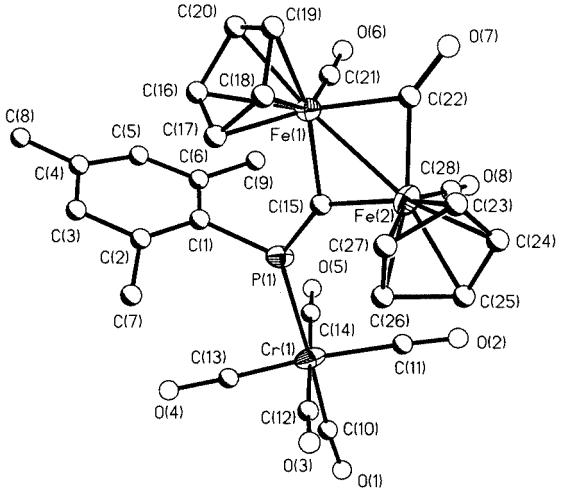

Figure 5. Molecular structure of **47a** in the crystal; selected bond lengths [Å] and angles [°]: Fe(1)−Fe(2) 2.500(6), Fe(1)−C(15) 1.958(21), Fe(2)−C(15) 1.908(21), Fe(1)−C(22) 1.953(26), Fe(2)−C(22) 1.912(25), P(1)−C(15) 1.632(21), P(1)−C(1) 1.836(23), P(1)−Cr(1) 2.412(8); Fe(1)−C(15)−P(1) 139.0(13), Fe(2)−C(15)−P(1) 140.3(14), C(15)−P(1)−Cr(1) 132.7(9), Cr(1)−P(1)−C(1) 118.1(7), Fe(1)−C(15)−Fe(2) 80.6(8)

The molecular structure of **49a** (Figure 6) shows a μ-isophosphaalkyne complex acting as an η^3-ligand towards a [$Pt(PPh_3)$] fragment. Thereby, the skeleton of **37a** remains mainly unaffected. The trigonal-planar donor atom C(12) of the isophosphaalkyne bridges both iron atoms symmetrically [Fe(1)−C(12) = 1.915(9), Fe(2)−C(12) = 1.918(10) Å]. The Fe−Fe bond [2.519(4) Å] is similar to that in **37a** [2.527(5) Å]. The π-coordination to the Pt atom causes an elongation of the P=C bond to 1.737(10) Å, with a Pt−C bond of 2.162(9) Å and a relatively long Pt−P(2) contact of 2.471(2) Å. The Pt(1)−P(1) bond to the PPh_3 ligand has a length of only 2.240(2) Å. Compound **49a** may be regarded as either a [$Pt(PPh_3)$] complex of an η^3-1-ferra-3-phosphaallyl ligand or, in line with the Wade−Mingos rules, as an *arachno* cluster constructed of the atoms Pt(1), P(2), C(12), and Fe(1). The polyeder skeleton electron count gives only 40 valence electrons (v.e.) instead of the theoretically required 42. This agrees with the fact that Pt^0 complexes often acquire only 16 v.e. instead of the familiar 18 v.e. shell.

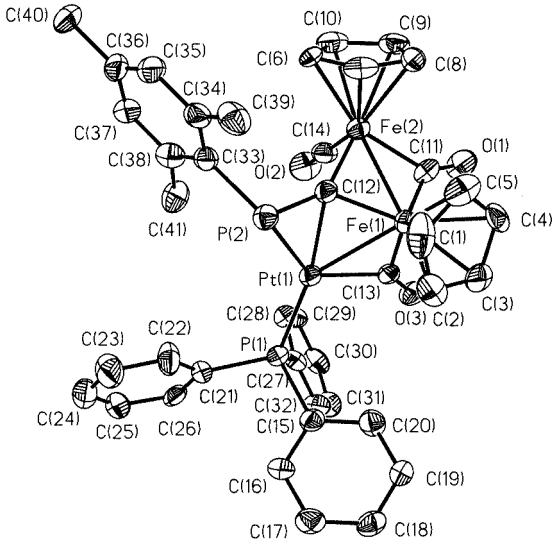

Figure 6. Molecular structure of **49a** in the crystal; selected bond lengths [Å] and angles [°]: Pt(1)−Fe(1) 2.577(2), Pt(1)−P(1) 2.240(2), Pt(1)−P(2) 2.471(2), Pt(1)−C(12) 2.162(9), Pt(1)−C(13) 1.997(2), Fe(1)−C(11) 1.879(10), Fe(1)−C(12) 1.915(9), Fe(1)−C(13) 1.951(9), Fe(1)−Fe(2) 2.518(4), Fe(2)−C(11) 1.952(9), Fe(2)−C(12) 1.918(10), P(2)−C(12) 1.737(10), P(2)−C(33) 1.862(10); Fe(1)−C(12)−Fe(2) 82.4(4), Fe(2)−C(12)−P(2) 146.5(5), Fe(1)−C(12)−P(2) 130.6(5), C(12)−P(2)−C(33) 105.9(4)

The oxidation of the μ-isophosphaalkyne complex **37a** with an equimolar amount of sulfur or an excess of grey selenium in benzene at 20 °C led to the formation of the methylene(thioxo)-λ^5,σ^3-phosphorane **50a** ($\delta^{31}P$ = 159.4 ppm) and the methylene(selenoxo)-λ^5,σ^3-phosphorane **50b** ($\delta^{31}P$ = 128.0 ppm) as orange-brown microcrystalline solids[19c] (Scheme 23). Methylation at the phosphorus atom of **37a** to give red microcrystalline **51** ($\delta^{31}P$ = 108.8 ppm) was effected by reaction with methyl triflate. The (μ-phosphanylalkylidene)diiron derivative **52** resulted from the subsequent reduction of salt **51** with $NaBH_4$ (Scheme 24).[19c]

Despite the existence of complexes with μ-isophosphaalkyne ligands, coordination compounds with terminal isophosphaalkyne ligands are still unknown and, thus, remain a challenge for the experimental chemist. A possible approach to these targets was stimulated by inspection of the electronic structures of aminocarbyne complexes, such as **53**,[20,21] or of the methanidocarbyne complex **54**,[22] where limiting structures such as **53′** and **54′** contribute significantly to the ground states of the molecules. In line with the diagonal relationship between C and P atoms, it is conceivable that structure **55′**, which features a terminal isophosphaalkyne ligand, also may be significant for the adequate description of the phosphidocarbyne complexes **55** (Scheme 25).

The chlorocarbyne complexes [Tp*$(CO)_2$M≡C−Cl] [**56**: M = Mo; **57**: M = W; Tp* = $HB(3,5\text{-}Me_2HC_3N_2)_3$][23] and inverse phosphaalkenes $Me_3SiP{=}C(NR_2)_2$ (**58a**: R=Me; **58b**: Et), the P−C bonds of which are strongly polarized ($P^{\delta-}C^{\delta+}$), were envisioned as suitable precursors for the

 © 2003 Wiley-VCH Verlag GmbH & Co. KGaA, Weinheim

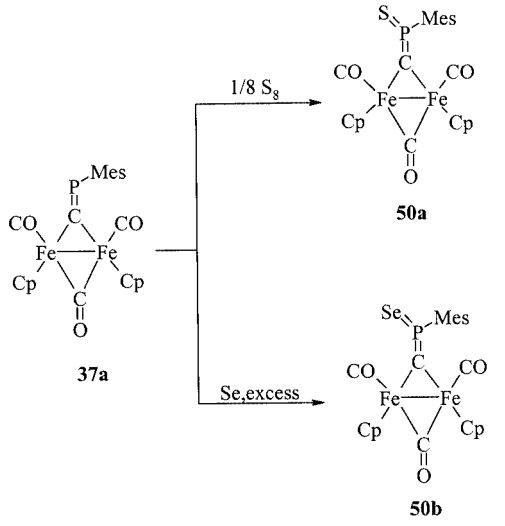

Scheme 23. Oxidation of μ-isophosphaalkyne complex **37a** by sulfur and selenium

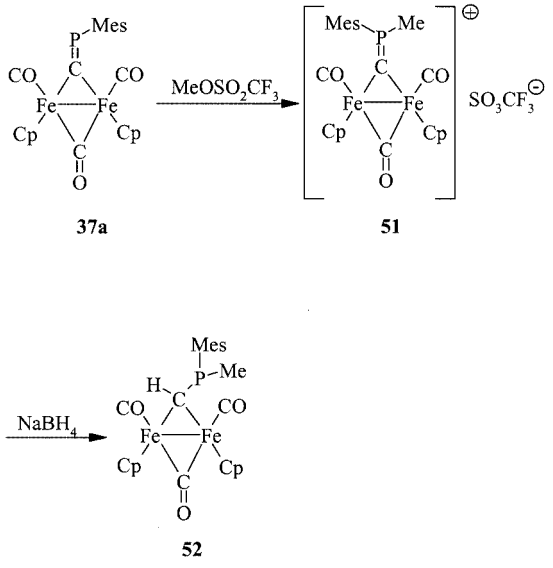

Scheme 24. Synthesis of μ-phosphanylcarbene complex **52**

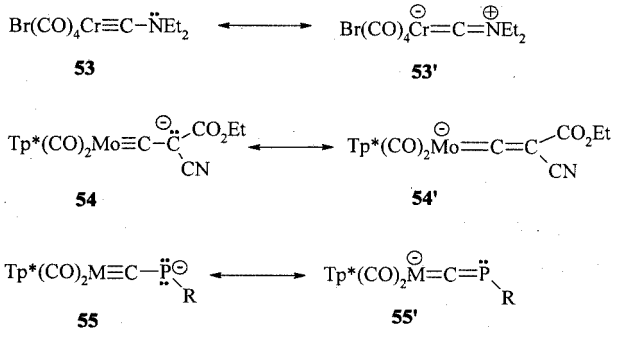

Scheme 25. Limiting structures of the formally related carbyne complexes **53**, **54**, and **55**

synthesis of complexes **55**.[24] Reaction of the carbyne complexes **56** and **57** with 2 mol-equiv. of phosphaalkene **58a** in CH_2Cl_2 at 20 °C led to precipitation of the red compounds **59a** and **60a** within 2 h. The analogous conversion of **56** and **57** to the corresponding complexes **59b** and **60b** by treatment with $Me_3SiP{=}C(NEt_2)_2$ required 15−18 h to reach completion (Scheme 26).[25]

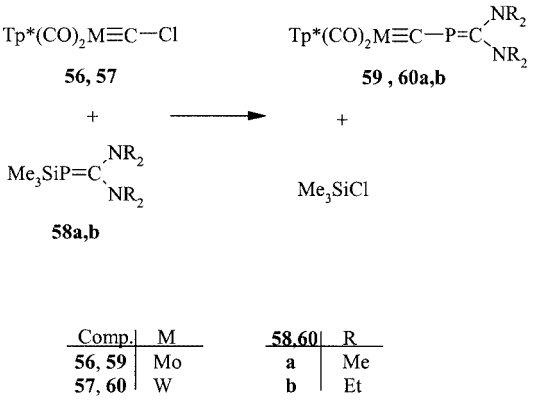

Comp.	M
56, 59	Mo
57, 60	W

58,60	R
a	Me
b	Et

Scheme 26. Synthesis of complexes **59a**,**b** and **60a**,**b**

On the basis of IR and ^1H, ^{13}C, and ^{31}P NMR spectroscopic evidence, three resonance structures were chosen to fully describe the bonding situation in **59** and **60** (Scheme 27).

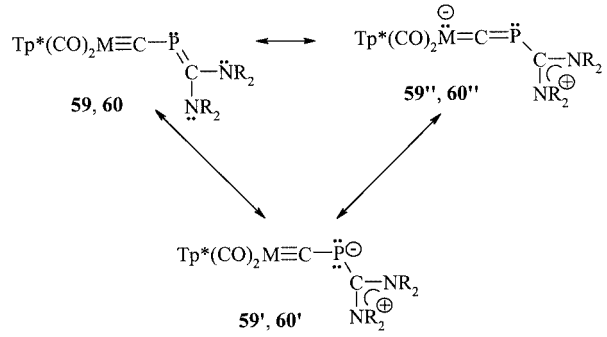

Scheme 27. Limiting structures of complexes **59** and **60**

Since the interpretation of the spectroscopic data is not unambiguous, however, an X-ray structual analysis of **60b** was carried out (Figure 7).

The most informative feature of the molecule is the geometry of the organophosphorus ligand. The bond length W(1)−C(3) of 1.838(6) Å compares well with that of the corresponding bond length in $[Tp^*(CO)_2W{\equiv}C{-}PMe_2Ph]PF_6$ [1.821(9) Å][26] and must be regarded as a metal−carbon triple bond. Accordingly, it is better to consider the ligand in **60b** as a phosphaalkenyl-functionalized methylidyne than as the anticipated terminal isophosphaalkyne ligand as depicted in structural formulas **59**′′ and **60**′′. The valence angle W(1)−C(3)−P(1) of 167.9(4)° deviates only slightly from linearity, which is in line with it having an sp-hybridized donor carbon atom. The bonds between the two-coordinate phosphorus atom and carbon atoms C(3) and C(4) are of equal length [1.759 Å]. Considering the different hybridizations at C(3) (sp) and C(4) (sp^2), and

 © 2003 Wiley-VCH Verlag GmbH & Co. KGaA, Weinheim

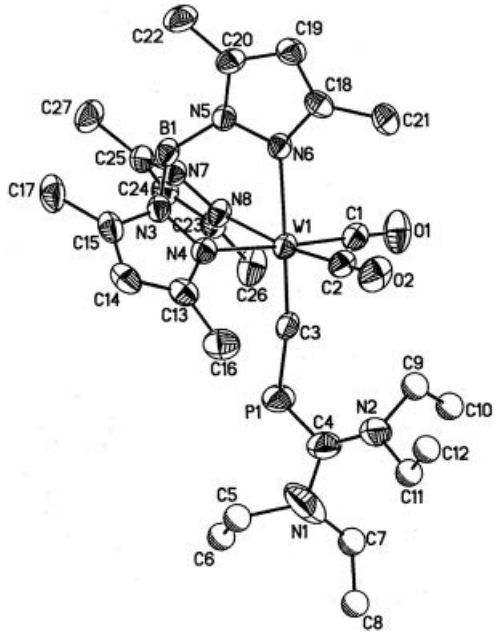

Figure 7. Molecular structure of **60b** in the crystal; selected bond lengths [Å] and angles [°]: W(1)−C(3) 1.838(6), P(1)−C(3) 1.759(7), P(1)−C(4) 1.759(9), N(1)−C(4) 1.362(11), N(2)−C(4) 1.354(10); W(1)−C(3)−P(1) 167.9(4), C(3)−P(1)−C(4) 105.7(3), P(1)−C(4)−N(1) 115.1(7), P(1)−C(4)−N(2) 127.9(7), N(1)−C(4)−N(2) 117.0(8)

in view of the P−C (sp) bond length in [Tp*$(CO)_2W{\equiv}C{-}PMe_2Ph]^+$ [1.741(9) Å], the bond P(1)−C(1) may be designated as a single bond, whereas the bond length P(1)−C(1) compares well with the P=C double bond in the inversely polarized phosphaalkene $HP{=}C(NMe_2)_2$ [1.740(1) Å].[27] Atom C(4) has a trigonal-planar environment with shortened carbon−nitrogen bonds N(2)−C(4) [1.354(10) Å and N(1)−C(4) [1.362(11) Å] because of π-conjugation.

In a more recent paper, another attempt was described at the synthesis of a molybdenum alkylidynephosphanide complex of type **55** (Scheme 25). In contrast to the synthesis of **59** and **60**, where the C−P bond was formed between a positively polarized alkylidyne carbon atom and a negatively polarized phosphorus atom, the approach to anion **63** was based on the reaction of anion **61** and $PhPCl_2$. Reduction of the phosphanylalkylidyne complex **62** with sodium amalgam afforded complex **63**, which features the MoCPPh arrangement expected for a complex with a terminal isophosphaalkyne (phosphoisocyanide) ligand (Scheme 28).

Inspection of the molecular structure obtained from an X-ray diffraction study showed a molybdenum−carbon distance Mo−C(1) of 1.762(5) Å, which has to be regarded again as a triple bond. The bond length P−C(1) of 1.771(5) Å in **63** is similar to that in **60b** [1.759(7) Å], but markedly longer than the P−C single bond in [Tp*$(CO)_2W{\equiv}C{-}PMe_2Ph]^+$ [1.741(9) Å]. Obviously, the P−C bond shortening is mainly the result of an sp-hybridized carbon atom, rather than resulting from a significant amount of C−P multiple bonding. The angles

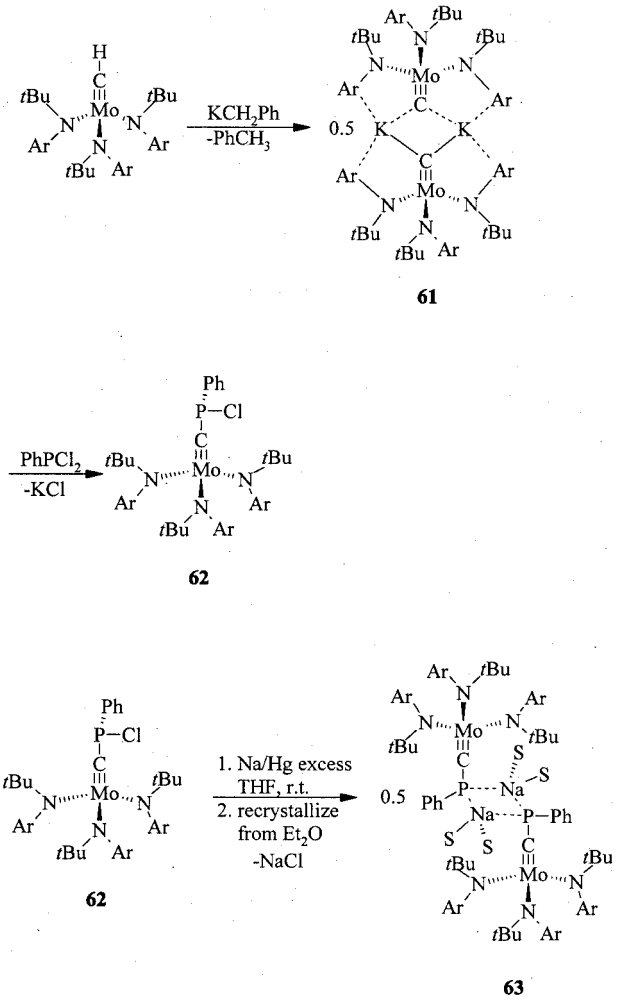

Scheme 28. Synthesis of the dimeric sodium phosphanidocarbyne complex **63**; S = ether or THF

Mo−C(1)−P [171.0(3)°] and C(1)−P−C(41) [106.0(2)°] are similar to the corresponding values in **60b** [W−P−C = 167.9(4)°; C−P−C = 105.7(3)°].[28] In conclusion, the bonding situation in the anion of **63** is similar to those of the previously reported complexes **59** and **60**, and are better interpreted in terms of alkylidyne complexes that are functionalized at the sp-hybridized carbon atom by either a $[PPh]^-$ unit or a phosphaalkenyl group, and not, as claimed by the authors, as a P-analog **55** of complexes with terminal isocyanide ligands.

5. Conclusions

What have we learnt about isophosphaalkynes? Firstly, the rich chemistry displayed by organic isocyanides is not mirrored by their phosphorus analogs. All attempts to synthesize these molecules have met with failure. In many instances the more stable isomers, the well-known phosphaalkynes, were isolated instead. Moreover, all experiments attempting to trap these molecules to provide some evidence for their transient existence have been unsuccessful. From mechanistic work with (isophosphaalkyne)plati-

 © 2003 Wiley-VCH Verlag GmbH & Co. KGaA, Weinheim

num complexes, it might even be concluded that the degradation of phosphavinylidene carbenoids of the type R−P=C(X)Li to phosphaalkynes RCP and lithium halide circumvents the occurrence of free isophosphaalkynes. Quantum-chemical calculations predict isophosphaalkynes as maxima on the energy surface in the system HPC/HCP with energies of ca. 80 kcal/mol above the ground state. In contrast to these findings, the chemistry of dinuclear and trinuclear complexes with bridging phosphaalkyne ligands seems to be more promising for their synthesis. Here, however, it must be stated that the successful preparation of these compounds lacks generality. Product formation is governed sensitively by the nature of the transition metal, its ancillary ligands and the substituents at the dicoordinate phosphorus atom.

To date, no coordination compounds featuring terminal isophosphaalkyne ligands are known. Recently prepared complexes with the required atomic array MCP−R display C−P bond orders of unity only.

In summary, the synthesis of free isophosphaalkynes still remains a challenge. Future approaches to a satisfactory solution may involve sterically encumbering substituents, such as *m*-terphenyl units, at the P atom that could prevent 1,2-P−C migrations and that enclose the C=P terminus in a protective environment. Another possible method to add stability to isophosphaalkynes involves employing highly electronegative substituents at the phosphorus atom. Likewise, the search for complexes with terminal isophosphaalkyne ligands still awaits a solution.

Acknowledgments

The author is grateful to Prof. W. W. Schoeller for valuable discussions and for his assistance in composing the section on the theoretical studies.

[1] [1a] *Multiple Bonds and Low Coordination in Phosphorus Chemistry* (Eds.: M. Regitz, O. J. Scherer), Thieme, Stuttgart, **1990**. [1b] K. B. Dillon, F. Mathey, J. F. Nixon, *Phosphorus: The Carbon Copy*, Wiley, Chichester, **1998**.

[2] [2a] M. Regitz, *Chem. Rev.* **1990**, *90*, 191−213. [2b] M. Regitz, P. Binger, *Angew. Chem.* **1988**, *100*, 1541−1565; *Angew. Chem. Int. Ed. Engl.* **1988**, *27*, 1484. [2c] M. Regitz in ref.[1a], pp. 58−89. [2d] Ref.[1b], pp. 41−86. [2e] L. Weber, *Adv. Organomet. Chem.* **1997**, *41*, 1−67.

[3] Reviews: [3a] M. P. Perisiamy, H. M. Walborsky, *Org. Prep. Proced. Int.* **1979**, *11*, 293−311. [3b] M. P. Perisiamy, H. M. Walborsky, in: *The Chemistry of Triple Bonded Functional Groups* (Eds.: S. Patai, Z. Rappoport), Wiley, Chichester, **1983**, supplement C, part 2, pp. 835−887. [3c] P. Hoffmann, D. Marquarding, H. Kliimann, in: *The Chemistry of the Cyano Group* (Ed.: Z. Rappoport), Wiley, London, **1970**, pp. 853−883. [3d] I. Ugi, *Isonitrile Chemistry*, Academic Press, New York, **1971**.

[4] Reviews: [4a] L. Malatesta, *Prog. Inorg. Chem.* **1959**, *1*, 283. [4b] L. Malatesta, F. Bonati, *Isocyanide Complexes of Transition Metals*, John Wiley & Sons, New York, **1969**. [4c] P. M. Treichel, *Adv. Organomet. Chem.* **1973**, *11*, 21. [4d] F. Bonati, G. Minghetti, *Inorg. Chem. Acta* **1974**, *9*, 95. [4e] Y. Yamamoto, *Coord. Chem. Rev.* **1980**, *32*, 193. [4f] E. Singleton, H. E. Oosthuizen, *Adv. Organomet. Chem.* **1983**, *22*, 209. [4g] L. Weber, *Angew. Chem.* **1998**, *110*, 1597−1598; *Angew. Chem. Int. Ed.* **1998**, *37*, 1515−1517. [4h] W. P. Fehlhammer, A. Mayr, B. Olgemüller, *Angew. Chem.* **1975**, *87*, 290; *Angew. Chem. Int. Ed. Engl.* **1975**, *14*, 369. [4i] M. V. Barybin, V. G. Young, Jr., J. E. Ellis, *J. Am. Chem. Soc.* **2000**, *122*, 4678−4691.

[5] [5a] M. Yoshifuji, H. Kawayami, Y. Kawai, K. Toyota, M. Yasunami, T. Niitsu, N. Inamoto, *Chem. Lett.* **1992**, 1053−1056. [5b] M. Yoshifuji, T. Niitsu, N. Inamoto, *Chem. Lett.* **1988**, 1733−1734. [5c] R. Appel, M. Immenkeppel, *Z. Anorg. Allg. Chem.* **1987**, *553*, 7−14.

[6] E. Niecke, M. Nieger, O. Schmidt, D. Gudat, W. W. Schoeller, *J. Am. Chem. Soc.* **1999**, *121*, 519−522.

[7] S. Ito, K. Toyota, M. Yoshifuji, *J. Organomet. Chem.* **1998**, *553*, 135−140.

[8] E. Niecke, A. Fuchs, F. Baumeister, M. Nieger, W. W. Schoeller, *Angew. Chem.* **1995**, *107*, 640−642; *Angew. Chem. Int. Ed. Engl.* **1995**, *34*, 555−557.

[9] S. Ito, K. Toyota, M. Yoshifuji, *Chem. Commun.* **1997**, 1637−1638.

[10] S. Ito, H. Sugiyama, M. Yoshifuji, *Angew. Chem.* **2000**, *112*, 2892−2894, *Angew. Chem. Int. Ed.* **2000**, *39*, 2781−2783.

[11] S. J. Goede, F. Bickelhaupt, *Chem. Ber.* **1991**, *124*, 2677−2684.

[12] [12a] W. W. Schoeller, in ref.[1a], pp. 5−32. [12b] W. W. Schoeller, T. Dabisch, T. Busch, *Inorg. Chem.* **1987**, *26*, 4383.

[13] [13a] K. K. Lehman, S. C. Ross, L. L. Lohr, *J. Chem. Phys.* **1985**, *82*, 4460−4469. [13b] M. T. Nguyen, T.-K. Ha, *J. Mol. Struct. Theochem* **1986**, *139*, 145−152. [13c] E. Goldstein, S. Jin, R. Carillo, R. J. Cave, *J. Comput. Chem.* **1993**, *14*, 186.

[14] P. K. Pearson, H. F. Schäfer, U. Wahlgren, *J. Chem. Phys.* **1975**, *62*, 350.

[15] [15a] H. Jun, V. G. Young, Jr., R. J. Angelici, *J. Am. Chem. Soc.* **1991**, *113*, 9379−9380. [15b] H. Jun, R. J. Angelici, *Organometallics* **1994**, *13*, 2454−2460. [15c] H. Jun, R. J. Angelici, *Organometallics* **1993**, *12*, 4265−4266. [15d] H. Jun, V. G. Young, Jr., R. J. Angelici, *Organometallics* **1994**, *13*, 2444−2453. [15e] H. Jun, V. G. Young, Jr., R. J. Angelici, *J. Am. Chem. Soc.* **1992**, *114*, 10065−10066.

[16] V. D. Romanenko, M. Sanchez, T. V. Sarina, M. R. Mazieres, R. Wolf, *Tetrahedron Lett.* **1992**, *21*, 2981.

[17] W. V. Konze, V. G. Young, Jr., R. J. Angelici, *Organometallics* **1999**, *18*, 258−267.

[18] W. V. Konze, V. G. Young, Jr., R. J. Angelici, *Organometallics* **1998**, *17*, 1569−1581.

[19] [19a] L. Weber, I. Schumann, T. Schmidt, H.-G. Stammler, B. Neumann, *Z. Anorg. Allg. Chem.* **1993**, *619*, 1759−1764. [19b] L. Weber, I. Schumann, H.-G. Stammler, B. Neumann, *Chem. Ber.* **1994**, *127*, 1349−1353. [19c] L. Weber, I. Schumann, M. H. Scheffer, H.-G. Stammler, B. Neumann, *Z. Naturforsch., Teil B* **1997**, *52*, 655−662. [19d] L. Weber, I. Schumann, H.-G. Stammler, B. Neumann, *Organometallics* **1995**, *14*, 1626−1631. [19e] L. Weber, V. Zanotti, unpublished results

[20] [20a] E. O. Fischer, G. Huttner, W. Kleine, A. Frank, *Angew. Chem.* **1975**, *87*, 781; *Angew. Chem. Int. Ed. Engl.* **1975**, *14*, 760. [20b] E. O. Fischer, W. Kleine, G. Kreis, F. R. Kreißl, *Chem. Ber.* **1978**, *111*, 3542−3551

[21] N. M. Kostic, R. F. Fenske, *Organometallics* **1982**, *1*, 489−496.

[22] S. Chaona, F. J. Lalor, G. Ferguson, M. M. Hunt, *J. Chem. Soc., Chem. Commun.* **1988**, 1606−1608.

[23] T. Desmond, F. J. Lalor, G. Ferguson, M. Parvez, *J. Chem. Soc., Chem. Commun.* **1983**, 457−459.

[24] [24a] L. N. Markovskii, V. D. Romanenko, T. I. Pidvarko, *Zh. Obshch. Khim.* **1982**, *52*, 1925−1926 (*Chem. Abstr.* **1982**, *97*, 216330h). [24b] L. Weber, O. Kaminski, *Synthesis* **1995**, 158.

[25] L. Weber, G. Dembeck, R. Boese, D. Bläser, *Chem. Ber./Recueil* **1997**, *130*, 1305−1308.

[26] G. M. Jamison, P. S. White, J. L. Templeton, *Organometallics* **1991**, *10*, 1954−1959.

[27] A. N. Chernega, A. V. Ruban, V. D. Romanenko, L. N. Markovskii, A.-A. Korkin, M. Y. Antipin, Y. T. Struchkov, *Heteroatom Chem.* **1991**, *2*, 229−241, and references cited therein.

[28] T. Agapie, P. L. Diaconescu, C. C. Cummins, *J. Am. Chem. Soc.* **2002**, *124*, 2412−2413.

Received January 1, 2002

 © 2003 Wiley-VCH Verlag GmbH & Co. KGaA, Weinheim

Cubane Complexes with Two (or More) Group 14−Group 16 Double Bonds: Synthesis and X-ray Structures of $Sn_4Se_2(NtBu)_4$ and $Ge_4Se_3(NtBu)_4$

Tristram Chivers,*[a] Timothy J. Clark,[a] Mark Krahn,[a] Masood Parvez,[a] and Gabriele Schatte[a]

Keywords: Germanium / Main group elements / Multiple bonds / Selenium / Tin

Monomeric complexes with two or three terminal M=Se bonds, $Sn_4Se_2(NtBu)_4$ or $Ge_4Se_3(NtBu)_4$, respectively, are produced by oxidation of $(MNtBu)_4$ (M = Sn, Ge) with selenium in hot toluene.

(© Wiley-VCH Verlag GmbH & Co. KGaA, 69451 Weinheim, Germany, 2003)

The varied uses of binary Group 14−16 compounds as semiconductors, in thermoelectric devices and for optoelectronic materials,[1] have provided a stimulus for investigations of potential single-source precursors.[2,3] In addition to these practical applications, there is a fundamental interest in compounds containing a formal double bond between heavier Group 14 and 16 elements.[4] These highly reactive functionalities may be stabilized either by attaching two extremely bulky groups to the Group 14 element to give a three-coordinate ketone analogue[5] or by intramolecular heteroatom coordination leading to four- or five-coordinate metal centers.[6] Although there have been impressive advances in the range and diversity of these so-called "heavy ketones",[4] no examples of compounds containing more than one Group 14-Group 16 double bond have been reported.

Recently we described the unexpected formation and X-ray structure of the stannatellone $[t\text{BuNSn}(\mu\text{-N}t\text{Bu})_2\text{TeN}t\text{Bu}](\mu_3\text{-SnTe})$ in which the Sn=Te functionality is stabilized by three *t*BuN ligands.[7] This finding prompted us to investigate the oxidation of divalent tin or germanium in the cubic molecules $(MNtBu)_4$ (M = Sn, Ge)[8] by chalcogens as a source of complexes containing several terminal M=E bonds (E = S, Se, Te). In this communication we report the synthesis and X-ray structures of **2** and **3**, which contain two or three M=Se bonds, respectively, as well as the monochalcogenides **1a** and **1c**.

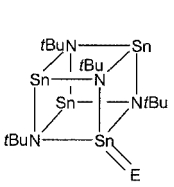

1a, E = S
1b, E = Se
1c, E = Te

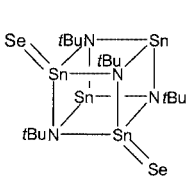

2

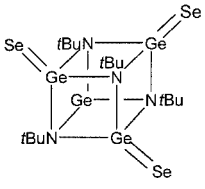

3

The reaction of $(SnNtBu)_4$ with one equivalent of sulfur in toluene at 85 °C produces **1a** in 87% yield. The use of an excess of sulfur in this reaction yields insoluble products, suggesting the formation of polymers involving bridging, rather than terminal, sulfide ligands, upon further oxidation of **1a** with sulfur. Richeson et al. have shown that there is a delicate balance between the formation of terminal and bridging SnS bonds in the case of the amidinate complexes $[SSn\{CyNC(R)NCy\}_2]_n$.[6c] A monomeric structure ($n = 1$) is observed for R = *t*Bu, whereas a dimer ($n = 2$) with bridging sulfide ligands is found for R = Me.

The reaction of $(SnNtBu)_4$ with four equivalents of selenium in boiling toluene yields the distannaselone **2b** in 64% yield whereas the monostannatelone **1c** is obtained in 68% yield from the reaction of $(SnNtBu)_4$ with an excess of tellurium under similar conditions. The lack of formation of the distannatellone presumably reflects the weaker oxidizing power of tellurium compared to that of selenium. The compounds **1a**, **1c** and **2** were characterized by ^{1}H NMR spectra, X-ray crystallography[9−11] and, in the case of **1c** and **2**, by CHN analyses. The stannathione **1a** exhibits a molecular ion in the FAB mass spectrum.

The molecular structures of **1c** and **2**, accompanied by pertinent metrical parameters, are depicted in Figure 1 and 2, respectively. The structure of **1a** resembles that of **1c** and

[a] Department of Chemistry, University of Calgary
Calgary, Alberta T2N 1N4, Canada
Fax: (internat.) + 1-403/289-9488
E-mail: chivers@ucalgary.ca

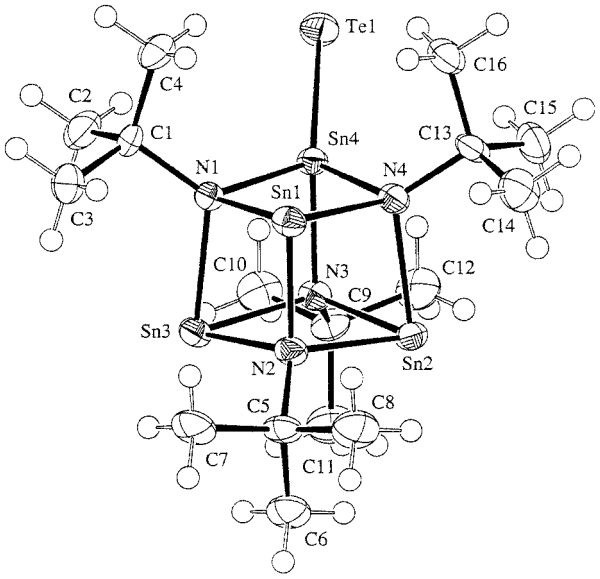

Figure 1. X-ray structure of **1c**; selected bond lengths (Å) and bond angles (deg): Sn(4)−Te(1) 2.589(1), |Sn^{IV}−N| 2.124(4) range 2.116(4)−2.130(4), |Sn^{II}−N| 2.217(5), range 2.191(5)−2.229(5), |N−Sn^{IV}−N| 85.0(2), |N-Sn^{II}−N| 80.6(2); selected bond lengths (Å) and bond angles (deg) for **1a**: Sn(1)−S(1) 2.262(3), Sn(4)−S(2) 2.255(3), |Sn^{IV}−N| 2.114(8), range 2.112(6)−2.142(8), |Sn^{II}−N| 2.217(9), range 2.186(5)−2.229(6), |N−Sn^{IV}−N| 85.2(3), |N−Sn(2)−N| 80.5(3)

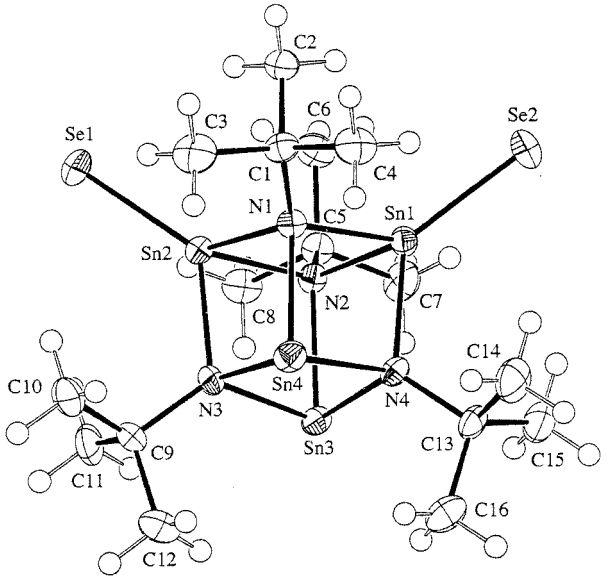

Figure 2. X-ray structure of **2**; selected bond lengths (Å) and bond angles (deg): Sn(1)−Se(2) 2.372(1), Sn(2)−Se(1) 2.363(1), |Sn^{IV}−N| 2.141(5), range 2.122(5) − 2.157(5), |Sn^{II}−N| 2.233(5) range 2.206(5)−2.253(5), b|N−Sn^{IV}−N| 84.3(2), |N-Sn^{II}−N| 80.0(2)

selected bond lengths and bond angles are given in the caption to Figure 1. All three structures contain terminal Sn=E bonds (E = S, Se or Te) and the framework of the $(SnNtBu)_4$ cube is maintained. There are no significant intermolecular contacts. The Sn=S bond length of 2.262(3) Å in **1a** is similar to the value of 2.280(5) Å found in the five-coordinate amidinate complex [S=Sn{CyNC(*t*Bu)-NCy}$_2$].[6c] The Sn=Te bond length of 2.589(1) Å in **1c** is indistinguishable from the value of 2.592(1) Å found for [*t*BuNSn(μ-N*t*Bu)$_2$TeN*t*Bu](μ$_3$-SnTe) in which the tin atom is in an identical four-coordinate environment.[7] The mean Sn=Se bond length of 2.367(7) Å in **2** can be compared with values of 2.398(1) Å[6d] or 2.394(1) Å[6f] for related five-coordinate complexes. Two general trends are evident from the structural data for these three complexes. First, the mean Sn^{IV}−N bond length is 0.09 Å shorter than the mean Sn^{II}−N distance, reflecting the higher ionic character in the Sn^{IV}−N bonds. Secondly, the mean bond angle N−Sn^{IV}−N is about 4.5° larger than the value of N−Sn^{II}−N, suggesting that the stereochemical influence of the Sn=E bonding electrons is less pronounced than that of the lone pair of electrons on the Sn^{II} centres.

The ^{1}H NMR spectrum of **1a** in C_6D_6 at 23 °C shows two resonances at δ = 1.47 and 1.25 ppm, attributable to N*t*Bu groups, with the expected 3:1 relative intensities. By contrast, the ^{1}H NMR spectra of **1c** and **2** in C_6D_6 at 23 °C both exhibit singlets at δ = 1.42 ppm. These observations imply fluxional behaviour involving rapid exchange of chalcogen substituents between Sn^{II} and Sn^{IV} sites in **1c** and **2**. Similar observations have been reported for the *bis* adduct $(SnNtBu)_4{\cdot}2AlCl_3$, which exhibits a singlet at δ = 1.32 ppm in the ^{1}H NMR spectrum (in C_7D_8) at 28 °C.[12] The low solubility of these imidotin chalcogenides precluded further investigation of this phenomenon by low temperature NMR spectroscopy. We note, however, that selenium exchange is approximately two orders of magnitude faster than sulfur exchange for (porphyrinato)tin(II) complexes.[13] The solid-state ^{119}Sn NMR spectrum for **2** shows the expected two resonances for Sn^{II} and Sn^{IV} sites at δ = +1347 and −111 ppm, respectively [cf. δ = +1142 for $(SnNtBu)_4$].

These findings indicate that the oxidation of the remaining Sn^{II} centers becomes more difficult after the initial oxidation of one or two Sn^{II} sites in $(SnNtBu)_4$, presumably as a result of the electron-withdrawing effect of the chalcogen substituents. Consequently, we also investigated the chalcogen oxidation of the germanium(II) cube $(GeNtBu)_4$,[8] which should be more easily oxidized than the Sn^{II} analogue.

The reaction of $(GeNtBu)_4$ with four equivalents of tellurium in boiling toluene for one day produces $Ge_4Te(NtBu)_4$, the germanium analogue of **1c**, in 42% yield.[14,15] By contrast, oxidation with selenium under similar conditions yields the trigermaselone $Ge_4Se_3(NtBu)_4$ (**3**) as yellow air-sensitive crystals in about 60% yield. An X-ray structural determination of **3** (Figure 3)[16] revealed three Ge=Se double bonds with a mean bond length of 2.187(1) Å [cf. 2.196(4) Å and 2.2212(3) Å in the amidinate complexes [CyNC(R)NCy)$_2$Ge=Se (R = Me, *t*Bu), in which the germanium centers are also four-coordinate].[6b] The mean Ge^{IV}−N bond length is 0.11 Å shorter than the mean Ge^{II}−N distance and the bond angle N−Ge^{IV}−N is 4.8° larger than the value of N-Ge^{II}−N. The ^{1}H NMR spectrum of **3** in C_6D_6 at 23 °C shows two resonances with the expected 1:3 relative intensities, implying that any selenium exchange is slow on the NMR time scale. However, limited

 © 2003 Wiley-VCH Verlag GmbH & Co. KGaA, Weinheim

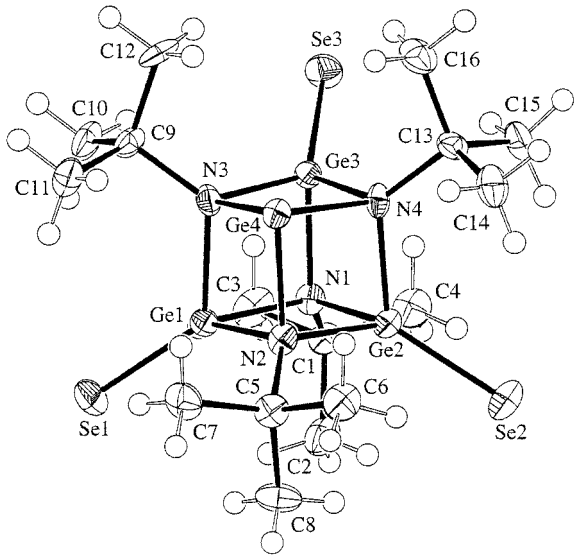

Figure 3. X-ray structure of **3**; selected bond lengths (Å) and bond angles (deg): Ge(1)−Se(1) 2.1852(13), Ge(2)−Se(2) 2.1872(13), Ge(3)−Se(3) 2.1871(13), |Ge^{IV}−N| 1.958(7), range 1.944(7)−1.985(7), |Ge^{II}−N| 2.068(7), range 2.064(7)−2.071(7), |N−Ge^{IV}−N| 85.8(3), |N-Ge^{II}−N| 81.0(3)

solubility precluded the measurement of the ^{77}Se NMR spectrum.

In summary, the oxidation of the cubic systems $(MNtBu)_4$ with selenium provides a facile route to the first complexes containing more than one Group 14-Group 16 double bond. Tetraselones $[M_4Se_4(NR)_4]$ (M = Sn, Ge) would be of particular interest as potential single-source precursors to binary semi-conductors such as SnSe, via the thermodynamically favoured elimination of RN=NR. Achievement of this goal will require either a more easily oxidized imidotin(II) cubane, for example $(SnNPh)_4$,[17] or a more reactive source of selenium.

Experimental Section

1a: The reagents $(SnNtBu)_4$ [18] and $Ge(NtBu)_4$ [8] were prepared from $M(NMe_2)_2$ and *tert*-$BuNH_2$ by modifications of the literature procedures. A mixture of $(SnNtBu)_4$ (0.400 g, 0.527 mmol) and cyclooctasulfur (0.017 g, 0.530 mmol) in toluene was heated at 85 °C for one day. The yellow solution was filtered and solvent was removed under vacuum to give yellow crystals of **1a** (0.361 g, 0.456 mmol, 87%). ^{1}H NMR (C_6D_6, 23 °C): δ = 1.47 (s, 27 H, *t*Bu), 1.25 (s, 9 H, *t*Bu) ppm. MS (FAB): *m*/*z* = 792 $[M + H]^+$.

1c: A mixture of $(SnNtBu)_4$ (0.362 g, 0.477 mmol) and tellurium powder (0.243 g, 1.90 mmol) in toluene (30 mL) was heated at 125 °C for two days. The orange solution was removed by cannula from unchanged tellurium. Orange crystals of **1c** (0.287 g, 0.324 mmol, 68%) were obtained after one day at −23 °C. $C_{16}H_{36}N_4Sn_4Te$ (886.92): calcd. C 21.67, H 4.09, N 6.32; found C 20.60, H 4.10, N 5.65. ^{1}H NMR (C_6D_6, 23 °C): δ = 1.42 (s) ppm.

2: A mixture of $(SnNtBu)_4$ (0.406 g, 0.535 mmol) and grey selenium powder (0.169 g, 2.14 mmol) in toluene (40 mL) was heated at 125 °C for one day. The yellow solution was decanted by cannula from unchanged selenium. Yellow crystals of **2** (0.314 g, 0.342 mmol, 64%) were obtained after one day at −23 °C. **2**·C_7H_8, $C_{23}H_{43}N_4Se_2Sn_4$ (1009.3): calcd. C 27.37, H. 4.39, N 5.55; found C 26.64, H 4.58, N 5.46. ^{1}H NMR (C_6D_6, 23 °C): δ = 1.42 (s) ppm.

3: A mixture of $(GeNtBu)_4$ (0.030 g, 0.052 mmol) and grey selenium powder (0.016 g, 0.203 mmol) was heated at 130 °C in toluene (20 mL) for one day. The yellow-orange solution was decanted from unchanged selenium and stored at −16 °C for one day to give yellow crystals of **3** (0.025 g, 0.031 mmol, 59%). ^{1}H NMR (C_6D_6, 23 °C): δ = 1.67 (s, 9 H, *t*Bu), 1.33 (s, 27 H, *t*Bu) ppm. **3**·C_7H_8.

X-ray quality crystals of **1a**·0.5C_7H_8, **1c**·0.5C_7H_8, **2**·C_7H_8 and **3**·C_7H_8 were obtained by recrystallization from toluene at −23 °C.

X-ray data were collected on a Nonius Kappa CCD diffractometer using Mo-K_α radiation (λ = 0.71073 Å) at 170 K. All of the structures contained disordered toluene molecules in the lattice.

Acknowledgments

The authors gratefully acknowledge financial support from the Natural Sciences and Engineering Research Council (Canada).

[1] For the synthesis of Sn^{II} chalcogenides, see: [1a] S. Schlecht, M. Budde, L. Kienle, *Inorg. Chem.* **2002**, *41*, 6001. [1b] S. Schlecht, L. Kienle, *Inorg. Chem.* **2001**, *40*, 5719. [1c] Y. Li, Z. Wang, Y. Ding, *Inorg. Chem.* **1999**, *38*, 4737.

[2] [2a] P. Boudjouk, M. P. Remington Jr., D. G. Grier, W. Triebold, B. R. Jarabek, *Organometallics* **1999**, *18*, 4534. [2b] P. Boudjouk, D. J. Seidler, S. R. Bahr, G. J. McCarthy, *Chem. Mater.* **1994**, *6*, 2108.

[3] A. L. Seligson, J. Arnold, *J. Am. Chem. Soc.* **1993**, *115*, 8214.

[4] For reviews see: [4a] N. Tokitoh, R. Okazaki, in *The Chemistry of Organic Germanium, Tin and Lead Compounds*, Vol. 2, Part 1, (Ed.: Z. Rapoport), Wiley, Chichester, U. K., **2002**, p. 843. [4b] N. Tokitoh, R. Okazaki, *Adv. Organomet. Chem.* **2001**, *47*, 121−166. [4c] R. Okazaki, N. Tokitoh, *Acc. Chem. Res.* **2000**, *33*, 625. [4d] P. P. Power, *Chem. Rev.* **1999**, *99*, 3463−3502.

[5] For examples, see: [5a] T. Matsumoto, N. Tokitoh, R. Okazaki, *J. Am. Chem. Soc.* **1999**, *121*, 8811. [5b] M. Saito, N. Tokitoh, R. Okazaki, *J. Am. Chem. Soc.* **1997**, *119*, 11124. [5c] N. Tokitoh, T. Matsumoto, R. Okazaki, *J. Am. Chem. Soc.* **1997**, *119*, 2337.

[6] For examples, see: [6a] S. R. Foley, G. P. A. Yap, D. S. Richeson, *J. Chem. Soc., Dalton Trans.* **2000**, 1663. [6b] S. R. Foley, R. Bensimon, D. S. Richeson, *J. Am. Chem. Soc.* **1997**, *119*, 10359. [6c] Y. Zhou, D. S. Richeson, *J. Am. Chem. Soc.* **1996**, *118*, 10850. [6d] W-P. Leung, W-H. Kwok, L. T. C. Law, Z-Y. Zhou, T. C. W. Mak, *Chem. Commun.* **1996**, 505. [6e] M. C. Kuchta, G. Parkin, *J. Chem. Soc., Chem. Commun.* **1994**, 1351. [6f] M. C. Kuchta, G. Parkin, *J. Am. Chem. Soc.* **1994**, *116*, 8377. [6g] M. Veith, S. Becker, V. Huch, *Angew. Chem. Int. Ed. Engl.* **1989**, *28*, 1237; *Angew. Chem.* **1989**, *101*, 1287.

[7] T. Chivers, G. Schatte, *Chem. Commun.* **2001**, 2264.

[8] M. Veith, M. Grosser, *Z. Naturforsch., Teil B* **1982**, *37*, 1375.

[9] Crystal data for **1a**·0.5C_7H_8: crystal size 0.27 × 0.15 × 0.18 mm, orthorhombic, *Pnma*, *a* = 22.0498(1) Å, *b* = 10.9784(3) Å, *c* = 23.7983(4) Å, *V* = 5760.9(2) Å^3, *Z* = 8. The asymmetric unit is composed of two half molecules of the complex lying on a mirror plane and a half molecule of toluene of solvation. Least-squares refinement on F^2 based on 6836 unique reflections [5754 reflections with $I > 2\sigma(I)$] gave a final R_1 of 0.051.

[10] Crystal data for **1c**·0.5C_7H_8: crystal size 0.12 × 0.12 × 0.06 mm, monoclinic, $P2_1/n$, *a* = 12.9436(3) Å, *b* = 13.3315(3) Å, *c* = 18.0675(5) Å, β = 104.7156(8)°, *V* = 3015.4(1) Å^3, *Z* = 4. Least squares refinement on F^2 based on 7454 unique reflections [4771 reflections with $I > 2\sigma(I)$] gave a final R_1 of 0.043.

 © 2003 Wiley-VCH Verlag GmbH & Co. KGaA, Weinheim

[11] Crystal data for **2**·C_7H_8: crystal size 0.20 × 0.08 × 0.07 mm, orthorhombic, $P2_12_12_1$, a = 10.6423(2) Å, b = 13.3534(2) Å, c = 23.3413(3) Å, V = 3317.05(9) Å^3, Z = 4. The Se atoms are disordered with occupancy factors of 0.958(2); the remaining fraction Se(12) with occupancy factor 0.085(3) is bonded to Sn(4). Least-squares refinement on F^2 based on 7383 unique reflections [6823 reflections with $I > 2\sigma(I)$] gave a final R_1 of 0.032.

[12] M. Veith, W. Frank, *Angew. Chem. Int. Ed. Engl.* **1985**, *24*, 223; *Angew. Chem.*, **1985**, *97*, 312.

[13] L. M. Berreau, L. K. Woo, *J. Am. Chem. Soc.* **1995**, *117*, 1314.

[14] The formation of the germanium monosulfide $Ge_4S(NtBu)_4$ from the reaction of $\{Li_2[S(NtBu)_3]\}_2$ has been reported, but no synthetic or structural details were given. R. Fleischer, D. Stalke, *Organometallics* **1998**, *17*, 832.

[15] An X-ray structural determination revealed d(Ge=Te) = 2.4240(4) Å, M. Parvez, private communication [cf. 2.398(1) and 2.466(1) Å for germatellurones containing three- and five-coordinate germanium, respectively].[5c,6e]

[16] Crystal data for **3**·C_7H_8: $C_{23}H_{44}Ge_4N_4Se_3$, M = 903.86, colourless prisms (0.05 × 0.05 × 0.02 mm), orthorhombic, space group $P2_12_12_1$, a = 10.4013(3), b = 13.4568(3), c = 22.9765(8) Å, V = 3216.0(2) Å^3, Z = 4, $\rho_{calcd.}$ = 1.867 g cm^{-3}, μ(Mo-K_α) = 7.12 mm^{-1}. Least squares refinement on F^2 based on 3186 unique reflections [2605 reflections with $I > 2.00\ \sigma(I)$] gave a final R_1 = 0.036. The carbon atoms of the disordered toluene molecule were allowed isotropic displacement parameters. CCDC-198992 (**1a**), -198993 (**1c**), -198994 (**2**), -198995 (**3**) contain the supplementary crystallographic data for this paper. These data can be obtained free of charge via www.ccdc.cam.ac.uk/conts/retrieving.html (or from the Cambridge Crystallographic Data Centre, 12, Union Road, Cambridge CB2 1EZ, UK; fax: (internat.) +44-1223/336-033; or E-mail: deposit@ccdc.cam.ac.uk).

[17] From cyclic voltammetry the oxidation potential of $(SnNPh)_4$ is +0.63V (vs. Fe/Fe^{2+}) cf. +1.00 V for $(SnNtBu)_4$. D. R. Armstrong, F. Benevelli, A. D. Bond, N. Feeder, E. A. Harron, A. D. Hopkins, M. McPartlin, D. Moncrieff, D. Sáez, E. A. Quadrelli, A. D. Woods, D. S. Wright, *Inorg. Chem.* **2002**, *41*, 1492.

[18] R. E. Allan, M. A. Beswick, N. L. Cromhout, M. A. Paver, P. R. Raithby, A. Steiner, M. Trevithick, D. S. Wright, *Chem. Commun.* **1996**, 1501.

Received February 6, 2003

 © 2003 Wiley-VCH Verlag GmbH & Co. KGaA, Weinheim

IR Study of the Interaction of Dioxygen with [*meso*-Triphenyl(4-pyridyl)-porphyrinato]cobalt(II)

Tigran S. Kurtikyan,*[a,b] J. Steven Ogden,[c] Robert K. Kazaryan,[d] and Valery N. Madakyan[d]

Keywords: Cobalt / Porphyrins / Matrix isolation / IR spectroscopy / Microporous materials

The interaction of O_2 ($^{18}O_2$) with [*meso*-triphenyl(4-pyridyl)-porphyrinato]cobalt(II) [Co(MPyTPP)] has been investigated by means of IR spectroscopy under matrix-isolation conditions and by the action of dioxygen on thin sublimed layers. These studies have led to the characterisation of two dioxygen adducts: (1) a very unstable dioxygen adduct similar to that observed earlier for the closely related [*meso*-tetraphenylporphyrinato]cobalt(II) Co(TPP), and (2) a new type of coordinated O_2 ($^{18}O_2$) complex which is formed after warming Co(MPyTPP) either in pure oxygen matrices, or as sublimed layers in the presence of oxygen. The $\nu(O_2)$ vibration in this second species is more than 100 cm^{-1} lower than in the first, and the dioxygen adduct thus formed is thermally stable at 200 K. This adduct is identified as a six-coordinate dioxygen complex, with one coordination site occupied by the pyridyl group of an adjacent Co(MPyTPP) molecule. In the sublimed layers, the capacity for self-assembly of Co(MPyTPP) oligomers leads to the formation of microporous solids containing coordinatively unsaturated metal ions which have the ability to bind oxygen reversibly upon storage at ambient conditions.

(© Wiley-VCH Verlag GmbH & Co. KGaA, 69451 Weinheim, Germany, 2003)

Introduction

Some metalloporphyrins (MP) are known to be efficient oxygen carriers and have been studied for potential applications in the fields of artificial hemoglobin, oxygen-permselective membranes, catalytically active electrode coatings, selective O_2 adsorbents and sensors.[1−6] Co^{II} porphyrins attract special attention due to the reversible character of their O_2 binding,[7] and their thin films are promising in applications which depend on specific chemoresponsive properties of materials.[8]

In order to generate selective chemoresponsive materials, molecularly sized binding sites or pores must be created, and pyridylporphyrins have recently become a focus of attention due to their ability to form microporous self-assembling arrays.[9] Very interesting results in this area are now available for Zn, Ru and Os porphyrins. However, the potential for the self-assembly of biologically important Co, Fe and Mn pyridylporphyrins has surprisingly received very little attention. This may be due to the ease of oxidation and the ability to form five- and six-coordinate species, including dioxygen-bridged and μ-oxo structures.

The construction of microporous materials containing coordinatively unsaturated metal ions in their network promises to be an attractive tool for tailoring materials with useful chemoresponsive properties. As was shown earlier, low temperature sublimed layers of MTPP (M = metal dication; TPP = *meso*-tetraphenylporphyrinato dianion), which exhibit ligand-binding properties in the amorphous state lose this ability upon crystallization during storage at ambient conditions.[10] This occurs as a result of the dramatically decreased cross-section of the pores in the absence of solvated or ligand molecules in these solids.[11] In contrast, pyridylporphyrins are now widely explored as building blocks for constructing nanoporous materials.[12] In these studies the pyridyl groups of the porphyrins are usually coordinated to the metal centre of another complex.[9,13] It is reasonable, however, to expect that metallopyridylporphyrins containing metal ions capable of axial coordination can form self-assembled arrays, as was observed for Zn(MPyTPP) (MPyTPP = *meso*-monopyridyltriphenylporphyrinato dianion).[14,15] Lin[16] observed such self-assembly in the course of the hydrothermal synthesis of MTPyP (M = Co, Mn; TPyP = *meso*-tetrapyridylporphyrin) leading to unique metalloporphyrin hexamers with large cavities. In these assemblies, however, the metal ions

[a] Molecular Structure Research Center,
Azatutyan av.26, 375014, Yerevan, Armenia
E-mail: tkurt@msrc.am
[b] Institute of Applied Chemistry, (ARIAC),
Bagratunyats st. 70, 375029, Yerevan, Armenia
[c] Department of Chemistry, University of Southampton,
Highfield, Southampton SO17 1BJ, UK
[d] Medical State University,
Koryun st. 5, 375025, Yerevan, Armenia

are coordinatively saturated. The same pattern was observed in sublimed films of CoT4PyP [T4PyP = *meso*-tetrakis(4-pyridyl)porphyrin][17] and CoT3PyP [T3PyP = *meso*-tetrakis(3-pyridyl)porphyrin],[18] which, although porous, slowly lose their O_2-binding ability due to the formation of coordinatively saturated structures. It could be expected that in the metal-*meso*-pyridyltriphenylporphyrin compounds, in which the number of metal ions and pyridyl groups is equal, the probability of formation of six-coordinate saturated structures might be diminished.

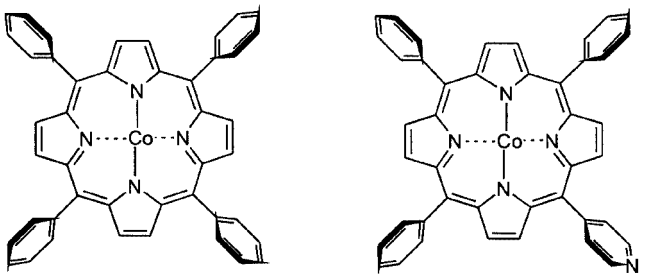

A **B**

In this paper the interaction of Co(MPyTPP) (**B**) with O_2 is studied under matrix isolation and solid-state conditions, and it is shown that this interaction differs significantly from that of the closely related Co(TPP) (**A**).

Results and Discussion

As expected from the closely related structures, the IR spectrum of Co(MPyTPP) (Figure 1a) in an Ar matrix is very similar to that of Co(TPP) reported elsewhere.[19] Isolation of this compound in a pure oxygen matrix ($^{16}O_2$) leads to the immediate appearance of a new band at 1286 cm^{-1} (Figure 1b), which has a counterpart at ca. 1208 cm^{-1} when $^{18}O_2$ is used (Figure 1c). From the value of this isotopic shift, and by analogy with previous work,[19] these bands are readily assigned to coordinated dioxygen in the adducts Co(MPyTPP)($^{16}O_2$) and Co(MPyTPP)($^{18}O_2$).

It is interesting to note that experiments using pure oxygen matrices showed clear evidence of the intramolecular O-O stretching mode [ca. 1551 ($^{16}O_2$) and 1460 cm^{-1} ($^{18}O_2$)]. This stretching mode is technically forbidden in IR spectra and appears only very weakly in deposits of pure solid oxygen. Its apparent enhancement here may be connected with a possible interaction of the O_2 molecule with the π-cloud of the porphyrin macrocycle or with the coordinated dioxygen adduct. The latter interpretation seems to be more probable, in view of the polar nature of coordinated O_2 and of the high sensitivity of its stretching band to the environment. For example, in our experiments the ν(O_2) of coordinated dioxygen was observed at 1286, 1279 and 1251 cm^{-1} in an O_2 matrix, an Ar matrix and in the sublimed layer, respectively.

In contrast to previous studies on Co(TPP), slow warming of matrix-isolated samples up to 200 K results in disappearance of the 1286 cm^{-1} band, indicating decomposition of this species, and the appearance of a new band at about

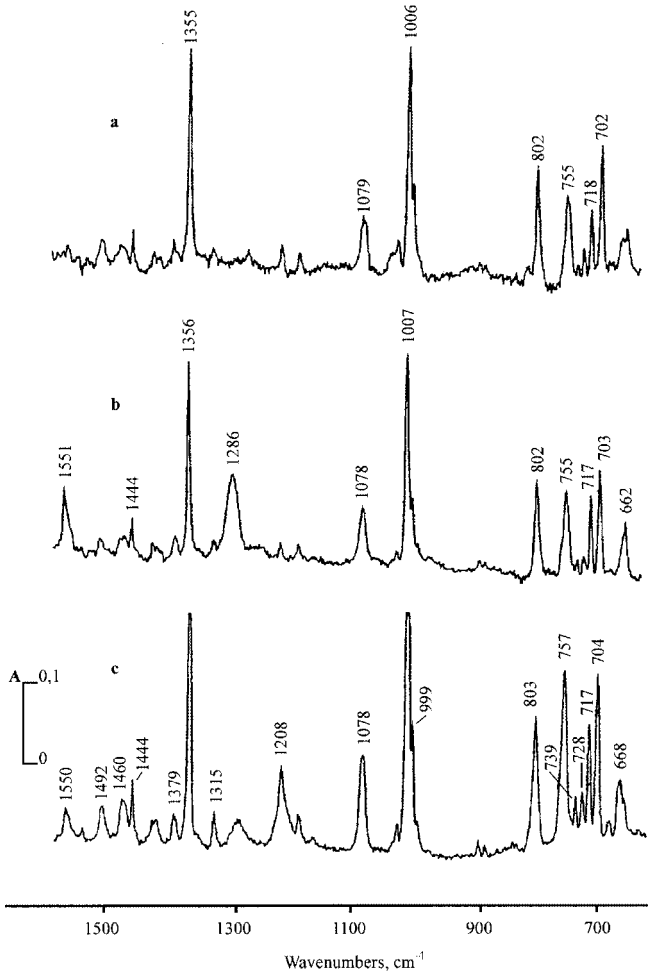

Figure 1. IR spectra of Co(MPyTPP) isolated in Ar (a), $^{16}O_2$ (b), and $^{18}O_2/^{16}O_2$ = 7/3 (c) matrices at 12 K

1170 cm^{-1} (Figure 2a) in the same spectral region where a triad of porphyrin bands may be found in the solid state (Figure 4a). The same procedure with isotopically enriched $^{18}O_2$ samples leads to the appearance of a new band at 1103 cm^{-1} (Figure 22b). This isotopic dependence confirms its assignment as a dioxygen stretching mode, and indicates the formation of another type of complex.

We believe that this band should be assigned to the six-coordinate dioxygen complex in which one coordination site is occupied by the pyridyl group of an adjacent Co(MPyTPP) molecule. In this process, the slow warming of the dioxygen matrix results in the slow elimination of free O_2, and the formation of coordination links with adjacent molecules to form the six-coordinate dioxygen complex represented in Figure 3.

It is to be anticipated that this type of coordination involving a base ligand in an axial position (*trans* to dioxygen) would shift ν(O_2) to markedly lower frequency, while the ν(Co-O_2) band should shift upward. Such a ligand would increase the amount of electron donation to the metal d orbitals, thus enhancing the M-O_2 bond strength (and hence the thermal stability of the complex) but would consequently weaken the O−O bond by increasing the net

 © 2003 Wiley-VCH Verlag GmbH & Co. KGaA, Weinheim

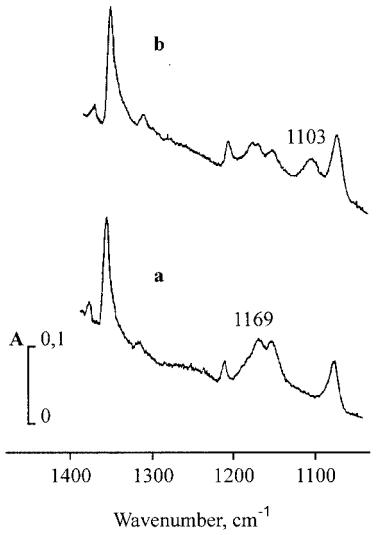

Figure 2. IR spectra of Co(MPyTPP) initially isolated in $^{16}O_2$ matrix at 12 K, warmed to 200 K and recooled (a); (b) the same as (a) with an isotopic mixture $^{18}O_2/^{16}O_2$ of 7/3

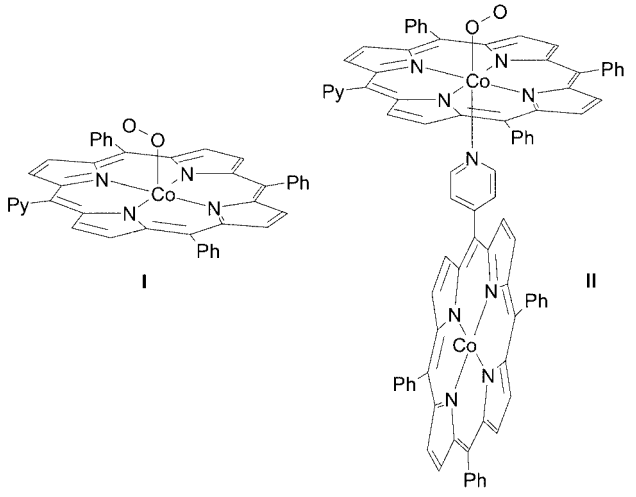

Figure 3. Schematic view of dioxygen complexes of Co(MPyTPP) produced in an O_2 matrix (I) and after elimination of O_2 by warming of sample to 200 K (II)

occupancy of the antibonding $\pi_g^*(O_2)$ orbitals. This effect has been quantitatively demonstrated by Nakamoto and co-workers for a series of Co(TPP)(base)(O_2) complexes, where the $\nu(O_2)$ frequency decreases linearly as the pK_a of the base increases.[20] It is also worth noting that in the Raman spectra of the six-coordinate (O_2)Co(TPP)(B) complexes (where B is a nitrogen base), the $\nu(O_2)$ bands are observed in the vicinity of 1160 cm^{-1}.[20]

The ability of Co-*meso*-aryl-substituted porphyrins to bind dioxygen is inherent not only for the isolated molecules (i.e. matrix-isolated or solvated molecules) but is also found in the layers obtained by sublimation onto a low-temperature (77 K) substrate. These layers are both amorphous and microporous,[10] with the result that interacting gases can easily diffuse into the bulk of the layers. The adducts thus formed can be studied by IR spectroscopy without solvent interference.

A study of thin layers of Co(MPyTPP) obtained by sublimation onto a support cooled with liquid nitrogen in the presence of 60 Torr O_2 reveals two new IR bands at 1251

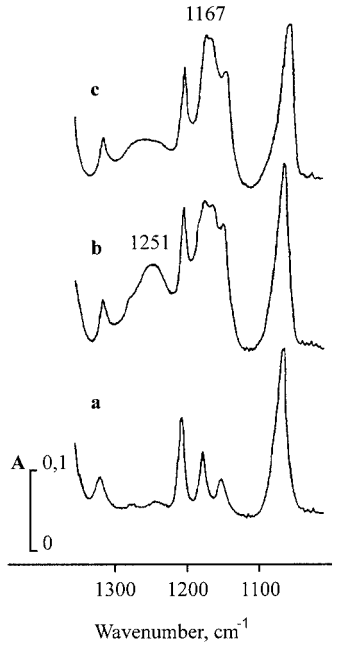

Figure 4. IR spectra of CoMPyTPP sublimed layer at 80 K (a), after exposure to 60 Torr O_2 and annealing in the cycle 80 K→ 120 K → 80 K (b); (c): the same as (b) with the layer obtained by sublimation onto a room temperature substrate

and 1167 cm^{-1} (Figure 4b). After the support is heated to room temperature, both bands disappear and the initial spectrum is restored. On admission of new portions of O_2, these bands appear again, but the intensity of the low-frequency band increases at the expense of the high frequency band.

When oxygen gas is admitted to layer samples prepared at 77 K and stored for one day at room temperature, the IR spectrum again shows a relatively weak band at 1251 cm^{-1}, with the band at 1167 cm^{-1} substantially increased in intensity. The same pattern is observed for the layers obtained by sublimation onto a room-temperature substrate (Figure4c).

These results can be interpreted as follows. In the related Co(TPP) system, the reversible nature of dioxygen binding by sublimed layers has been shown previously,[10] and the band at 1250 cm^{-1} has been attributed to $\nu(O_2)$ of the Co(TPP)(O_2) adduct, with the assignment confirmed by experiments with $^{18}O_2$. In similar experiments with the *meso*-tetrapyridyl-substituted derivatives CoT4PyP[17] and CoT3PyP[18] the $\nu(O_2)$ bands of bound dioxygen appear in the 1160 cm^{-1} region (ca. 1100 cm^{-1} for $^{18}O_2$) and the adducts obtained are thermally much more stable than those produced with Co(TPP). These differences were explained in terms of formation of coordinatively linked polymers and formation of a six-coordinate dioxygen adduct with the pyridyl base in the *trans* axial position.

In this work there is additional spectral evidence of such coordination links in Co-pyridyl porphyrins. The single medium-intensity band of Co(TPP) at ca. 1600 cm^{-1}, which

 © 2003 Wiley-VCH Verlag GmbH & Co. KGaA, Weinheim

corresponds to the C=C stretching of the phenyl groups in Co(MPyTPP) gains intensity, and becomes complex due to mixing with the C=N stretching of the pyridyl group. This band exhibits well-defined changes upon annealing of the

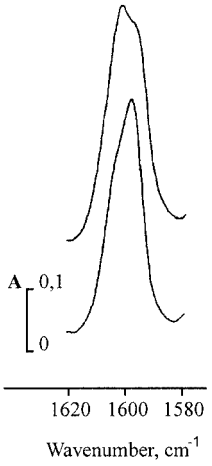

Figure 5. IR spectra of Co(MPyTPP) sublimed layer in the region of the skeletal vibrations of aryl substitutes at 80 K: after deposition onto a low temperature substrate (lower curve); after warming to room temperature and recooling (upper curve)

layer (Figure 5). The high frequency shoulder in the low temperature sublimate gains intensity after annealing and, as a result, the peak maximum shifts to higher wavenumbers (by about 8 cm^{-1}). This observation is consistent with the increasing number of coordinated pyridyl groups, since it is known[21] that coordination of pyridine to metal ions leads to a high frequency shift of this mode. The same spectral pattern represented in the upper spectrum of Figure 6. This same structure has been observed for $[Zn(MPyTPP)]_n$, for which X-ray analysis established that the pyridyl group of the porphyrin periphery is bound to the metal centre of an adjacent porphyrin, thereby creating a polymer with a long chain and a zigzag conformation.[14,15]

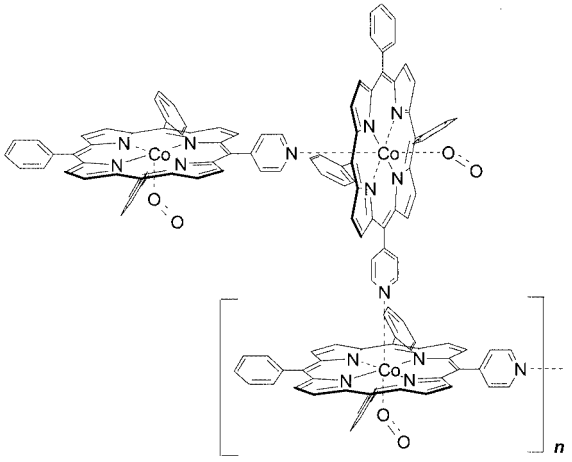

Figure 6. Schematic view of a coordination oligomer produced in sublimed layers of Co(MPyTPP) and its dioxygen adducts

ure 6 is observed when a sublimed layer is formed by deposition onto a room-temperature substrate.

On the basis of these results it can therefore be concluded that both the warming of a low-temperature Co(MPyTPP) sublimed layer and the deposition of Co(MPyTPP) onto a room-temperature substrate lead to the formation of one-dimensional coordination oligomers as represented in Figure 6. This same structure has been observed for $[Zn(MPyTPP)]_n$, for which X-ray analysis established that the pyridyl group of the porphyrin periphery is bound to the metal centre of an adjacent porphyrin, thereby creating a polymer with a long chain and a zigzag conformation.[14,15]

As a result of their low-temperature O_2-binding ability, sublimed layers of Co(MPyTPP) may therefore offer major advantages over the previously investigated systems Co(TPP), Co(T4PyP) and Co(T3PyPP). As mentioned above sublimed layers of Co(TPP) lose their O_2-binding ability upon storage at room temperature. Co(T4PyP) and Co(T3PyP) layers stored in vacuo for a week under the same experimental conditions bind only 50% of the initial quantities. In contrast, the amount of bound dioxygen in Co(MPyTPP) layers stored at room temperature for one month decreases by less than 20%, based on the decreased intensity of the 1167 cm^{-1} $\nu(O_2)$ band. It worth noting that this capability for low-temperature O_2-binding is also retained for the layers stored in air. Apparently the zigzag conformation of oligomer chain prevents the formation of dioxygen-bridged structures, which leads to the irreversible oxidation of the metal ions.

Conclusions

[*meso*-Triphenyl(4-pyridyl)porphyrinato]cobalt(II) Co(MPyTPP) binds dioxygen both under matrix isolation conditions and in the solid state. The self assembly of Co(MPyTPP) in sublimed layers lead to the formation of one-dimensional coordination oligomers containing coordinatively unsaturated Co^{II} in its chains. Similar to other pyridyl-porphyrin arrays the layers have a microporous structure and their low-temperature O_2-binding ability is conserved on storing in air.

The areas in which this property can be used are now the primary focus of our attention. Preliminary data indicate, for instance, that sublimed layers of CoMPyTPP can selectively bind dioxygen from CO/O_2 mixtures and can therefore serve as a device for the purification of CO by removing trace quantities of O_2.

Experimental Section

Co(MPyTPP) was obtained from H_2MPyTPP, which was synthesised according to a previously reported procedure.[22] NMR and UV/Vis spectra were in good agreement with reported data.[22] In a typical experiment, Co(MPyTPP) was placed in a Knudsen cell and was first heated to about 400 K under high vacuum ($P < 10^{-6}$ Torr) to remove solvent molecules.[11] The CsI substrate of the optical cryostat was then cooled to ca. 12 K using a closed-cycle Displex refrigeration system. The matrix-isolation apparatus and general methodology used have been described elsewhere.[23] Co(MPyTPP) was sublimed at ca. 520 K together with a large excess of Ar (BOC, 99.999%), Ar/O_2, or pure O_2 (BOC, 99, 999%). O-18 enriched samples were obtained using a mixture of $^{18}O_2 + {}^{16}O_2$ in the mol ratio 7:3, as established by mass spectrometry.

 © 2003 Wiley-VCH Verlag GmbH & Co. KGaA, Weinheim

The interaction of O_2 with sublimed layers of Co(MPyTPP) was carried out in the optical cryostat, such that the deposited film was obtained by sublimation on the low (77 K) or room-temperature substrate according to published procedures.[10] In a typical procedure, thoroughly dried and pre-cooled oxygen was slowly fed into the cryostat from a vessel attached to a mercury gauge for measurements of O_2 pressure. The sublimed layer was then stored for 30 min while the temperature was alternated in the following sequence: 80 → 120 → 80 K. The oxygen gas was then pumped off and IR spectra obtained over a range of temperatures.

Infrared spectra were recorded using Perkin−Elmer PE983G and Specord M-80 instruments, linked to appropriate data-handling systems. UV/Visible spectra were obtained on a Specord M-40 spectrophotometer, and $CDCl_3$ − solution NMR spectra were obtained on a Varian Mercury instrument.

Acknowledgments

This work was supported by INTAS (Grant # 911).

[1] E. Tsuchida, *Artificial Red Cells*, Wiley, New York, **1995**.
[2] H. Nishide, X.-S. Chen, E. Tsuchida, *Functional Monomers and Polymers*, New York, **1997**, Ch. 6, 173−207.
[3] H. Nishide, Y. Tsukahara, E. Tsuchida, *J. Phys. Chem. B* **1998**, *102*, 8766−8770.
[4] D. M. Oglesby, B. T. Upchurch, B. D. Leighty, J. P. Collman, X. Zhang, P. C. Hermann, *Anal. Chem.* **1994**, *66*, 2745−2751.
[5] F. D'Souza, Y.-Y. Hsieh, G. R. Deviprasad, *Chem. Commun.* **1998**, 1027−1028.
[6] B. G. Maiya, *J. Porphyrins Phthalocyanines* **2000**, *4*, 393−397.
[7] R. D. Jones, D. A. Summerville, F. Basolo, *Chem. Rev.* **1979**, *79*, 139−179.
[8] K. S. Suslick, N. A. Rakow, M. E. Kozal, J.-H. Chou, *J. Porphyrins Phthalocyanines* **2000**, *4*, 407−413.
[9] T. Imamura, K. Fukushima, *Coord. Chem. Rev.* **2000**, *198*, 133−156.
[10] T. S. Kurtikyan, A. V. Gasparyan, G. G. Martirosyan, G. H. Zhamkochyan, *J. Appl. Spectr. (Rus.)*. **1995**, *62*, 62−66.
[11] M. P. Byrn, C. J. Curtis, Y. Hsiou, S. I. Khan, P. A. Sawin, S. K Tendick, A. Terzis, C. E. Strouse, *J. Am. Chem. Soc.* **1993**, *115*, 9480−9497.
[12] M. E. Kosal, K. S. Suslick, *J. Solid State Chem.* **2000**, *152*, 87−98.
[13] E. Iengo, E. Zangrando, R. Minatel, E. Alessio, *J. Am. Chem. Soc.* **2002**, *124*, 1003−1008.
[14] A. M. Shachter, E. B Fleischer, R. C. Haltiwanger, *J. Chem. Soc., Chem. Commun.* **1988**, 960−961.
[15] E. B. Fleicher, A. M. Shachter, *Inorg. Chem.* **1991**, *30*, 3763−3769.
[16] K.-J. Lin, *Angew. Chem. Int. Ed.* **1999**, *38*, 2730−2732.
[17] T. S. Kurtikyan, V. N. Madakyan, *Russ. J. Coord. Chem. (Rus)*. **1992**, *2*, 139−143.
[18] T. S. Kurtikyan, V. N. Madakyan, *Russ. J. Coord. Chem. (Rus)*. **1992**, *8*, 869−874.
[19] M. Kozuka, K. Nakamoto, *J. Am. Chem. Soc.* **1981**, *103*, 2162−2168.
[20] J. R. Kincaid, L. M. Proniewicz, K. Bajdor, K. Nakamoto, *J. Am. Chem. Soc.* **1985**, *107*, 6775−6781.
[21] N. S. Gill, R. H. Nutal, D. F. Scaife, D. W. Sharp, *J. Inorg. Nucl. Chem.* **1961**, *18*, 79−87.
[22] G. N. Williams, R. F. X. Williams, A. Lewis, P. Hambright, *J. Inorg. Nucl. Chem.* **1979**, *41*, 41−44.
[23] A. K. Brisdon, R. A. Gomme, J. S. Ogden, *J. Phys. Chem.* **1991**, *95*, 2927−2930.

Received November 16, 2002

 © 2003 Wiley-VCH Verlag GmbH & Co. KGaA, Weinheim

Crystal Structures and Intercalation Reactions of Three-Dimensional Coordination Polymers $[M(H_2O)_2]_2[Mo(CN)_8]\cdot 4H_2O$ (M = Co, Mn)

Stéphanie Willemin,[a] Joulia Larionova,*[a] Rodolphe Clérac,*[b] Bruno Donnadieu,[c] Bernard Henner,[a] Xavier Fréderic Le Goff,[b] and Christian Guérin[a]

Keywords: Bridging ligands / Cyanides / Molybdenum / Intercalations / Cobalt / Manganese

Two coordination polymers $[M^{II}(H_2O)_2]_2[Mo^{IV}(CN)_8]\cdot 4H_2O$ [M^{II} = Co (**1**), Mn (**2**)] were prepared as monocrystals and structurally characterised. These compounds crystallise in the tetragonal systems *I*4/*m* (**1**) and *I*4/*mcm* (**2**) and form three-dimensional networks containing channels occupied by two types of water molecules, i.e. coordinated to M^{II} and crystallised ones. The dehydration of these materials occurs topochemically to give $[M^{II}(H_2O)]_2[Mo^{IV}(CN)_8]$ compounds having an open metal coordination site on the M^{II} ions that may be accessible to coordination by other species and serve as a reaction site. The intercalation of water, ammonia and amines has been studied.
(© Wiley-VCH Verlag GmbH & Co. KGaA, 69451 Weinheim, Germany, 2003)

Introduction

One of the challenges of contemporary chemistry is the molecular design of materials to achieve specific properties. An interesting group of compounds that has attracted considerable attention from material chemists and crystal engineers is two- and three-dimensional coordination polymers able to absorb and/or desorb guest molecules, which exhibit potential applications in the areas of separation and catalysis.[1] A very successful approach to these materials involves the deliberate design by self-assembly of two- and three-dimensional host-guest supramolecular architectures containing relatively large channels, cavities, or windows. Zeolites, which contain channels and cavities because of rigid three-dimensional frameworks and clays, via intercalation between two-dimensional layers, are natural prototypes of such architectures and are currently used. However, it is relatively difficult to modify and derivatise them in a systematic way in comparison with coordination polymers. Numerous examples already exist of inorganic[2] and metal-organic[3,4] zeolite and clay mimics which reversibly incorporate small molecules or organic guests. The structural flexibility of the molecular frameworks and their different nature compared to zeolites and clays may provide novel complementary properties, for example, optical, electronic or magnetic for such "porous" materials.[5] Some of these coordination polymers act as hosts in intercalation reactions since a vacant site for coordination of others species may have been created.

In recent years, a large number of structurally characterised host-guest open framework solids have been obtained by a self-assembly of systems containing cyanometalate units as building blocks.[6−13] As a matter of fact, the multidimensional structure formed by the successive −M−CN−M′− linkages affords a void with a shape and/or a size appropriate to the intercalation of a guest molecule in order to stabilise the crystal structure. This stabilisation can also be provided by the coordination of labile ligands at M′ (for instance, H_2O, NH_3, aliphatic and aromatic amines, etc.) which can be exchanged by intercalation. Two- and three-dimensional Hoffman-like frameworks containing linear and bent $[Ag(CN)_2]^-$ or $[Au(CN)_2]^-$ twofold coordination,[7] trigonal and pyramidal $[Cu(CN)_3]_2^-$ threefold coordination,[8] tetrahedral[9] $[Cd(CN)_4]^{2-}$ and square-planar[10] $[Ni(CN)_4]^{2-}$ fourfold coordination and also sixfold coordination[11] $[M(CN)_6]^{n-}$ building blocks, combined with a different metallic or organometallic coordination centre, have already been reported.

The eightfold-coordinated building blocks $[M(CN)_8]^{4-}$ (M^{IV} = Mo, W, Nb) offering eight bridging cyano ligands potentially able to form tightly connected architectures, have attracted some attention in recent years because of their magnetic[12f] and photomagnetic properties.[12a−12e] Nevertheless, structurally characterised polynuclear coordination polymers based on the use of $[M(CN)_8]^{4-}$ (M = Mo

[a] Laboratoire de Chimie Moléculaire et Organisation du Solide, UMR 5637, Université Montpellier II,
Place E. Bataillon, 34095 Montpellier cedex 5, France
Fax: (internat.) + 33-4/67143852
E-mail: joulia@univ-montp2.fr
[b] Centre de Recherche Paul Pascal (CRPP), UPR CNRS 8641, 33600 Pessac, France,
E-mail: clerac@crpp.u-bordeaux.fr
[c] Laboratoire de Chimie de Coordination, UPR CNRS 8241, 31077 Toulouse, France
Supporting information for this article is available on the WWW under http://www.eurjIc.org or from the author.

 © 2003 Wiley-VCH Verlag GmbH & Co. KGaA, Weinheim **DOI: 10.1002/ejic.200200583**

or W) as building blocks are still rare. In fact, as far as we are aware, structural reports of cyano-bridged $M^{II}M^{IV}$ (M = Mo or W) dimetallic compounds are very recent and concern the following examples: the chain $[\{Mn_2(L)_2(H_2O)\}]\{Mo(CN)_8\}]\cdot 5H_2O$,[12c] the two-dimensional mixed-valence compound $[\{Mn(L)\}_6\{Mo^{III}(CN)_7\}\{Mo(CN)_8\}_2]\cdot 19.5H_2O$[12d] {L = 2,13-dimethyl-3,6,9,12,18-pentaazabicyclo[12.3.1]octadeca-1(18),2,12,14,16-pentaene} and the three-dimensional compound $[Fe(H_2O)_2]_2[Mo(CN)_8]$.[12e] Furthermore, to the best of our knowledge, the intercalation behaviour of these compounds has never been studied. As a matter of fact, the $[M(CN)_8]^{4-}$ building block has also been employed in combination with the organometallic $[(CH_3)_3Sn]^+$ cation in order to design three-dimensional coordination polymers $[\{(CH_3)_3Sn\}_4M^{IV}(CN)_8]$ (M^{IV} = Mo, W) containing THF guest molecules in the channels.[13] However, after removal of the guest molecules by heating, no reabsorption of THF or absorption of others solvent molecules has been observed.

In this context, this paper is devoted to the synthesis and the crystal structures of two three-dimensional networks based on the $[Mo(CN)_8]^{4-}$ building block and M^{II} = Co, Mn metal ions. The title compounds were prepared for the first time as single crystals and their crystal structures were resolved. The presence of labile ligands coordinated to an M^{II} ion, i.e., H_2O molecules, opens the possibility for substitution reactions. In principle, this strategy should offer a means of incorporating various guest molecules in the network and thus modulate both structural and physical properties of these compounds.

Results and Discussion

Synthesis and Crystal Structures of $[M(H_2O)_2]_2[Mo(CN)_8]\cdot 4H_2O$ (M = Mn, Co)

The slow diffusion in an H-shaped tube of two 10^{-4} M aqueous solutions containing $K_4[Mo(CN)_8]\cdot 2H_2O$[10] and $[M(H_2O)_6](NO_3)_2$, allows yellow (M^{II} = Mn) or orange (M^{II} = Co) crystalline plates to be obtained. The complexes have been fully characterised by elemental analyses, IR spectroscopy, and X-ray crystallography (Table 1).

Infrared C−N stretches for both compounds [2144 (s) cm^{-1}] are shifted to higher frequencies than those of $K_4[Mo(CN)_8]\cdot 2H_2O$ [2125 (s), 2102 (s) cm^{-1}], clearly showing a coordination of all the CN groups to M^{II}.

The X-ray crystallographic study at 160 K reveals that these compounds $[M(H_2O)_2]_2[Mo(CN)_8]\cdot 4H_2O$ [M = Co^{II} (**1**), Mn^{II} (**2**)] have three-dimensional structures. Although, these two compounds are not strictly isostructural, the organisation of the three-dimensional structures and their cell parameters are similar. The compounds crystallise in a tetragonal system with space groups *I*4/*m* for **1** and *I*4/*mcm* for **2**. The structures possess one molybdenum (Mo^{IV}) site and one M^{II} (M^{II} = Co or Mn) site. Eight −C−N−M linkages surround the Mo atom forming a perfect square antiprism environment, as shown in Figure 1. Thus, the geometry of $[Mo(CN)_8]^{4-}$ unit is changed from the dodecahedral one in the starting $K_4[Mo(CN)_8]\cdot 2H_2O$ compound[14] to square-antiprismatic in the final products. It should be noted that such a geometrical rearrangement is characteristic for two- and three-dimensional compounds containing $[M(CN)_8]^{4-}$ units which have already been reported.[12,13] The Mo−C bond lengths are equal to 2.160(7) and 2.168(6) Å for **1** and 2.153(4) Å for **2**. The C−N bond lengths are equal to 1.145(9), 1.141(9) Å for **1** and 1.150(5) Å for **2**. Four N−C−Mo linkages and two water molecules in the *trans* configuration surround the M^{II} sites (Figure 1). The sites adopt a perfect octahedral environment. The M−N bond lengths are equal to 2.124(6), 2.158(6) Å for **1** and 2.207(3) Å for **2**. The M−O1 and M−O2 bond lengths are equal to 2.051(9) and 2.099(8) Å for **1** and 2.283(8) and 2.231(8) Å for **2**, respectively. It should be noted that all of the Mo−C−N bonded angles are close to 180° [Mo−C1−N1 175.2(6)°; Mo−C2−N2 174.3(5)° for **1** and

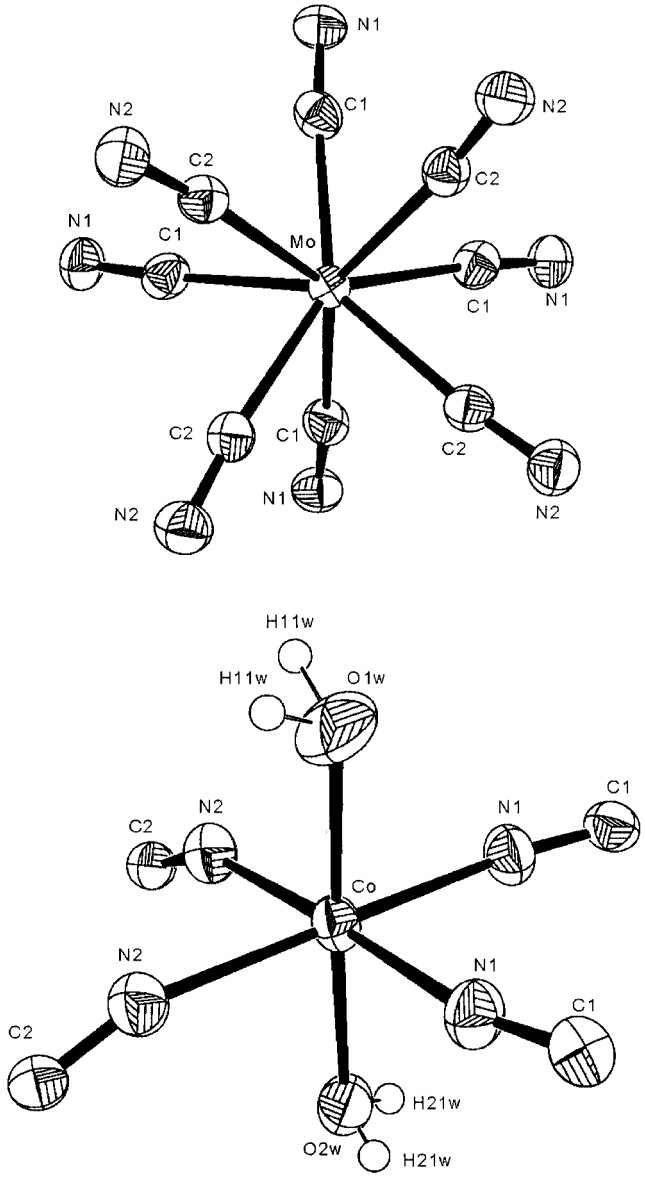

Figure 1. ORTEP drawing of local coordination environment of Mo and Co sites for compound **1**

 © 2003 Wiley-VCH Verlag GmbH & Co. KGaA, Weinheim

178.5(3)° for **2**], while the M−N−C bonded angles deviate significantly from 180° [165.9(6)°, 155.2(6)° for **1** and 162.5(3)° for **2**].

The structural arrangement may be described as a centrosymmetrical $\{MoC2N2MN2C2\}_2$ lozenge motif which is linked to four other identical motifs by C2N2 bridges to form corrugated grid-like sheet layers, as shown in Figure 2 for **1**. The three-dimensional organisation may be described as interconnected perpendicular layers parallel to {[110], [111]} and {[011], [010]} planes. Each Mo atom belongs to two perpendicular layers and is a node of the three-dimensional network. This arrangement results in channels running along the *c* axis occupied by coordinated and crystallised water molecules as shown in a whole view of the structure of **1** viewed in the *ab* plane (Figure 3).

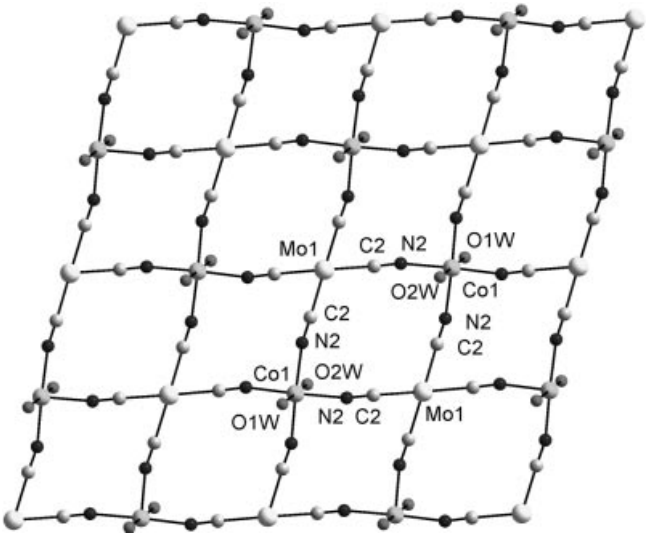

Figure 2. A view of the structure in the {[110], [111]} plane, showing a corrugated grid-like plan for compound **1**; hydrogen atoms are omitted for clarity

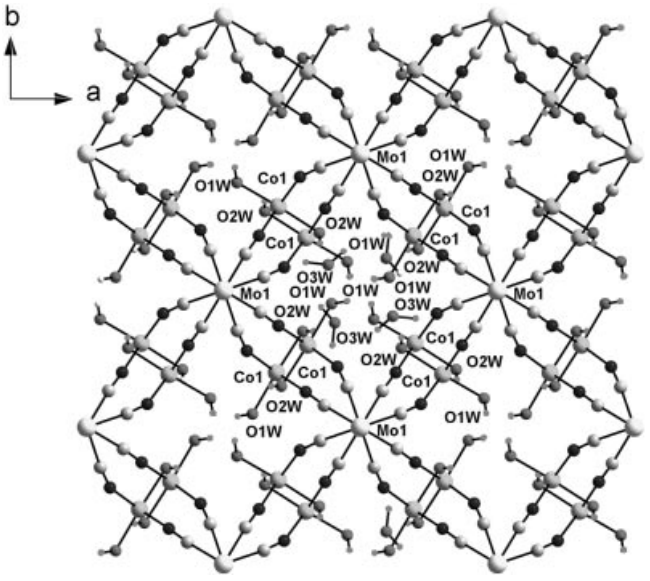

Figure 3. Global view of the crystal structure of **1** in the *ab* plane; the crystallised water molecules are only shown in one channel for clarity

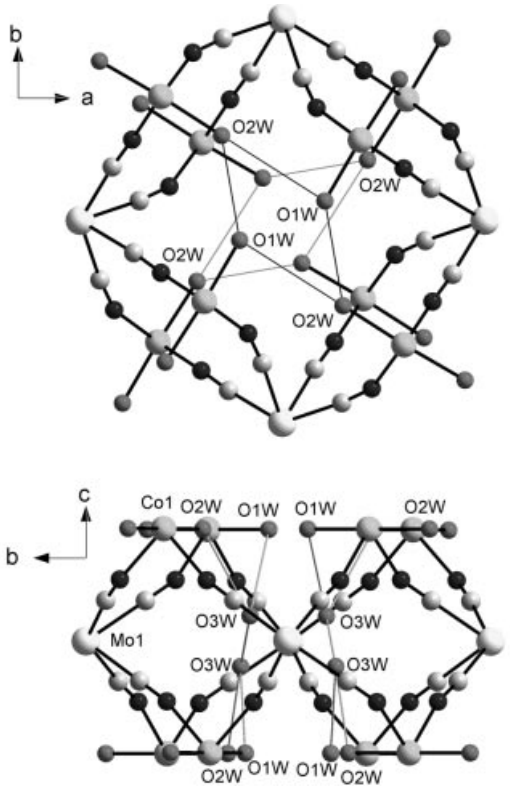

Figure 4. Top: fragment of the crystal structure of **1** along the *c* axis showing the cavity with a hydrogen bonding network coordinated between Co^{II}-coordinated water molecules; bottom: fragment of the crystal structure of **1** along the *b* axis showing the hydrogen bonding between the Co^{II}-coordinated and crystallised water molecules

As can be seen in Figure 4 (top), each of the four water molecules coordinated to the M^{II} ions situated in the *ab* plane are linked by means of hydrogen bonds forming a non-centrosymmetrical lozenge $\{O1WO2W\}_2$ in the centre of the channel [3.089(12) Å for O1···O2 and 3.554(13) Å for O2···O1] (dashed lozenge). Another identical lozenge (greg lozenge) is placed behind that of the first and turned by 90° in the *ab* plane. The two types of lozenges alternate along the *c* axis. Additionally, in each water lozenge at the centre of the cavity the O1 and O2 atoms are linked by hydrogen bonds to the O3 W atoms of the crystallised water molecule [2.894(9) Å for O2···O3 and 3.030(9) Å for O1···O3], resulting in columns of water molecules inserted in the channels delimited by the cavities along the *c* direction [Figure 4 (bottom)]. The cavity size may be estimated as 5.98 × 6.02 Å (or as the cavity volume of 133.4 $Å^3$), which leads to the possibility of intercalation of the appropriated molecules.

Magnetic Properties of $[M(H_2O)_2]_2[Mo(CN)_8]\cdot 4H_2O$ [M = Co (1), Mn (2)]

The temperature dependence of the magnetic susceptibility (χ_M) for polycrystalline samples of **1** and **2** were recorded under an applied field of 1000 Oe. For compound **2**, χ_M can be fitted using the Curie−Weiss law [$\chi_M = C/(T$

 © 2003 Wiley-VCH Verlag GmbH & Co. KGaA, Weinheim

$-\theta)]$ with $C = 8.58$ emu·K·mol^{-1} and $\theta = -1.4$ K, down to 1.8 K. The Curie constant (C) is in agreement with the expected value for two Mn^{2+} ions with $S = 5/2$ and $g = 1.98\pm0.05$. The negative sign of the Weiss constant obtained from the Curie−Weiss fitting, reveals the presence of weak antiferromagnetic interactions between the Mn^{II} ions through the diamagnetic NC−Mo^{IV}−CN bridges. The $\chi_M T$ value at room temperature for **1** is equal to 5.3 emu·K·mol^{-1}, which corresponds to the calculated spin value for two Co^{II} ions ($S = 3/2$, $g = 3.36$), since Mo^{IV} is diamagnetic. The decrease in $\chi_M T$ at low temperature may have two origins, spin−orbit coupling and antiferromagnetic interactions between the Co^{II} ions. Nonetheless, no theoretical model exists for the three-dimensional lattice, taking both factors into account.

Dehydration of 1 and 2 and Intercalation Reactions of $[M(H_2O)]_2[Mo(CN)_8]$ [M = Co (1), Mn (2)]

The thermogravimetric analysis (TGA) of **1** and **2** was performed under argon from room temperature up to 700 °C. The TGA curves exhibit four well-pronounced weight losses as the temperature was increased at a heating rate of 1 °C·min^{-1}, as shown in Figure 5 (top). The first and second weight-loss steps can be determined by inflection points at 88 and 131 °C, respectively; the third step contains two poorly pronounced inflexion points at 260 and 484 °C; the fourth step has an inflexion point at 575 °C.

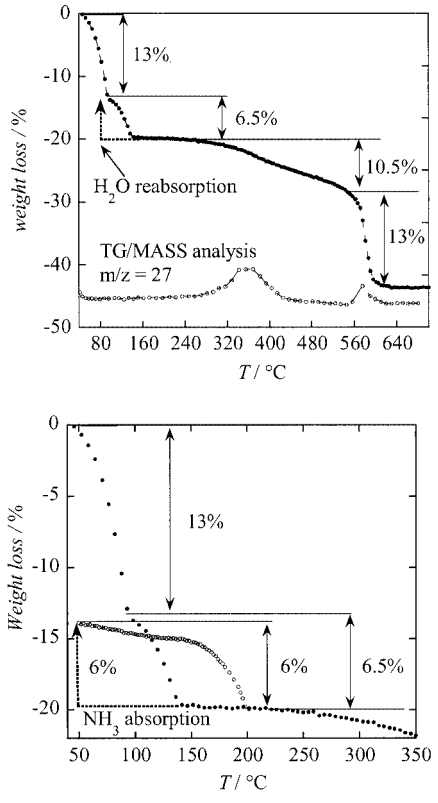

Figure 5. Top: TGA and TGA/MASS curves for $[Mn(H_2O)_2]_2[Mo(CN)_8]\cdot 4H_2O$; heating rate 1 °C/min; bottom: TGA and ammonia absorption curves for $[Mn(H_2O)_2]_2[Mo(CN)_8]\cdot 4H_2O$

The first and second weight-loss steps of 13.0 and 6.5%, respectively, are consistent with the loss of the four crystallized and the two coordinated water molecules, leading to $[Co(H_2O)]_2[Mo(CN)_8]$ (**1a**) and $[Mn(H_2O)]_2[Mo(CN)_8]$ (**2a**). After heating at 150 °C, the compounds retain their crystallinity and appear to be isomorphous with their corresponding hydrated phases based on X-ray powder diffraction pattern. The coordination number decreases upon dehydration as evidenced in the case of the cobalt derivative, which undergoes a colour change from orange-yellow, with $\lambda = 410$ nm, to green, with $\lambda = 590$ nm, according to the UV/Vis spectra. The M^{2+} ions are in an octahedral environment in **1** and **2** with two water molecules (O1 and O2) occupying two coordination sites in the *trans* positions (Figure 1). The heating of these compounds, up to 150 °C, leads to the loss of one of these coordinated water molecules and to five-coordinate metal ions. It should be outlined that this unusual change of the coordination number from six to five has already been observed for metal phosphonates $Co(O_3PCH_3)\cdot H_2O$.[16] The magnetic moment of the dehydrated cobalt compound **1** decreased from 5.3 emu·K·mol^{-1} to 4.7 emu·K·mol^{-1}, which indicated a decrease in coordination number, as previously reported by Cunningham.[16c] However, it is difficult to indicate which water molecule (O1W or O2W) is leaving. It should also be noted that the infrared C−N stretch (2154 cm^{-1}) for both dehydrated phases are reversibly shifted toward higher frequencies from those of the hydrated phases (2144 cm^{-1}) showing a reversible change in the symmetry of $[M^{II}(H_2O)]_2[Mo(CN)_8]$ fragments upon heating.

The third weight-loss step of 10.5% could be attributed to the simultaneous loss of the last two coordinated water molecules (6.4%) and one CN^- group (4.6%). The TGA/MASS analysis of the gas evolved during this weight loss step indicates the presence of the water (ionic current $m/z = 18$ for H_2O^+) and the cyanide (ionic current $m/z = 27$ for HCN^+) (Figure 5). Such losses of cyano ligands upon heating around 350 °C has also been observed for the precursor $K_4[Mo(CN)_8]\cdot 2H_2O$[17a] and for octacyanometallates of alkaline metals.[17b] The X-ray powder pattern for the title compounds heated to 500 °C indicated decomposition of the original structures.

The generation of an open metal coordination site on the M^{II} ions implies that the dehydration reaction should be reversible. After heating of samples **1** and **2** up to 150 °C under argon, the exposure of the dehydrated powders to air moisture at 25 °C leads to intercalation/coordination of two water molecules [Figure 5 (top)]. As a result, the X-ray powder pattern of the rehydrated sample was restored and the colour of the cobalt-containing compound recovered its original orange-yellow colour.

In a similar approach, the behaviour towards an intercalation/coordination of ammonia and amines was studied. The intercalation of NH_3 gas was observed at room temperature for samples **1** and **2** that had originally been outgassed at 150 °C. As shown in Figure 5 (bottom), it is possible to approximate the amount of NH_3 molecules that have intercalated. The mass gain (6.0%) is in good agree-

 © 2003 Wiley-VCH Verlag GmbH & Co. KGaA, Weinheim

ment with the calculated value (5.9%) for $[M(H_2O)(NH_3)]_2[Mo(CN)_8]$. Further evidence for the formation of $[Co(H_2O)(NH_3)]_2[Mo(CN)_8]$ and $[Mn(H_2O)(NH_3)]_2[Mo(CN)_8]$ was obtained from thermogravimetric, elemental and FTIR analyses. As shown in Figure 5 (bottom), the loss of NH_3 (inflexion point at 181 °C) occurs at 50 °C higher than the temperature of water loss in the hydrated compounds (inflexion point at 131 °C). The weight loss between 30 and 200 °C constitutes 6% of the total mass and the theoretical value calculated by assuming the formula $[M(H_2O)(NH_3)]_2[Mo(CN)_8]$ is 5.9%. In addition, the elemental analysis shows good agreement between the calculated and experimental values. IR data provide strong evidence that the NH_3 molecule occupies the empty coordination site created upon dehydration. The IR spectra of both compounds $[Co(H_2O)(NH_3)]_2[Mo(CN)_8]$ and $[Mn(H_2O)(NH_3)]_2[Mo(CN)_8]$ show the antisymmetric and symmetric NH_3 stretching in the 3400−3000 cm^{-1} region; NH_3 deformation is observed in the 1612 cm^{-1} region with symmetric deformation taking place at 1401 and 1221 cm^{-1}. Finally, rocking vibrations occur at 950−595 cm^{-1}.[18]

A remarkable feature of the amine intercalation reactions of $[M(H_2O)]_2[Mo(CN)_8]$ is their selectivity with respect to shape and size. Experiments in which $[M(H_2O)]_2[Mo(CN)_8]$ (M^{II} = Mn, Co) were subjected to methyl-, ethyl-, and dodecylamines for prolonged reaction times showed the formation of intercalation compounds with all primary amines except dodecylamine. The formation of compounds having a general formula $[M(H_2O)(amine)]_2[Mo(CN)_8]$ have been observed. The intercalation reactions were surveyed by thermogravimetric analyses and the final compounds were characterised by IR spectra. In addition, in the case of bulkier amines such as pyridine no intercalation reaction was observed. This selectivity with respect to shape and size may be accounted for by considering the structural environment of the water molecule in $[M(H_2O)_2]_2[Mo(CN)_8]$, which is assumed to occupy the amino coordination site. Its cavity size (71.1 $Å^3$) can obviously limit the accessibility to the open coordination site.

Conclusion

In summary, two new coordination polymers $[M(H_2O)_2]_2[Mo(CN)_8]\cdot 4H_2O$ ($M = Co^{II}$ and Mn^{II}) have been prepared and crystallised. These compounds form three-dimensional networks containing channels occupied by coordinated and crystallised water molecules. The title compounds can easily be dehydrated to yield $[M(H_2O)]_2[Mo(CN)_8]$ compounds. The dehydration is reversible and both derivatives readily reabsorb moisture from the atmosphere. Furthermore, the dehydration reaction leaves an empty coordination site on the bivalent metal ion, which has been exploited by reaction with ammonia and primary amines upon exposure to a flow of respective gases in order to form intercalation compounds. Since the interaction of inserted molecules with the dehydrated compounds takes place mainly through coordination to the M^{II} ions, the porosity should not be regarded as a prerequisite for reversible absorption.[24] Studies concerning intercalation reactions of coordination polymers presenting ferromagnetic ordering, and the influence of this on the magnetic properties, are currently in progress.

Experimental Section

Syntheses: Unless otherwise noted, all manipulations were performed at ambient temperature using reagents and solvents as received. The precursor $K_4[Mo(CN)_8]\cdot 2H_2O$ was prepared as already described.[15,16]

$[M^{II}(H_2O)_2]_2[Mo(CN)_8]\cdot 4H_2O$ [M^{II} = Co (1) or Mn (2)]: $[M^{II}(H_2O)_6](NO_3)_2\cdot 4H_2O$ (2.0 mmol) (M^{II} = Mn or Co) in water (30 mL) was added to a solution of $K_4[Mo(CN)_8]\cdot 2H_2O$ (1.0 mmol) in water (30 mL, natural pH), which immediately led to a precipitation of orange-yellow (**1**) or yellow (**2**) products. The solids were washed three times with water and then and dried in air with ethanol. Yield: 0.45 g, 82%. **1**: $C_8H_{16}Co_2MoN_8O_8$: calcd. C 16.96, H 2.82, Co 20.82, Mo 16.94, N 19.78; found C 17.26, H 3.54, Co 20.41, Mo 17.23, N 20.36. IR (KBr): $\tilde{\nu}$ = 3404(sh), 2144, 1616, 537, 431 cm^{-1}. **2**: $C_8H_{16}Mn_2MoN_8O_8$: calcd. C 17.20, H 2.87, Mn 19.68, Mo 17.19, N 20.07; found C 17.63, H 3.85, Mn 20.16, Mo 17.27, N 19.87. IR (KBr): $\tilde{\nu}$ = 3404(sh), 2145, 1616, 537, 431 cm^{-1}. The crystals, suitable for X-ray analysis, were obtained by slow diffusion in an H-shaped tube with two 10^{-4} M aqueous solutions containing $K_4[Mo(CN)_8]\cdot H_2O$ and $[M(H_2O)_6](NO_3)_2$, respectively. After two months, yellow (M = Mn^{II}) and orange-red (M = Co^{II}) crystalline plates were obtained. The crystals were insoluble in most common solvents and stable in air. The composition of the crystalline compound was also established by single-crystal X-ray diffraction at 160 K.

Dehydration of $[M^{II}(H_2O)_2]_2[Mo(CN)_8]\cdot 4H_2O$ [M^{II} = Co (1) or Mn (2)] and Intercalation of Ammonia and Amines into the Resulting Product: Both manganese- and cobalt-containing compounds were dehydrated by heating under argon at 150 °C for 1 h. Dehydrated samples **1a** and **2a** were stored in a drybox prior to use. **1a** (after heating at 150 °C): $C_8H_4Co_2MoN_8O_2$: calcd. C 20.98, Co 25.73, Mo 20.95, N 24.47; found C 20.51, Co 25.47, Mo 20.67, N 24.64. IR (KBr): $\tilde{\nu}$ = 3604, 3411, 3224, 2145, 1616, 537, 431 cm^{-1}. **2a** (after heating at 150 °C): $C_8H_4Mn_2MoN_8O_2$: calcd. C 21.35, Mn 24.42, Mo 21.32, N 24.90; found C 21.45, Mn 24.89, Mo 21.01, N 24.47. IR (KBr): $\tilde{\nu}$ = 3606, 3417, 3190, 2145, 1616, 537, 431 cm^{-1}. The intercalation of ammonia and primary amines was carried out by exposing the dehydrated compounds to a flow of ammonia or corresponding amine gases at 150 °C. For the dehydrated cobalt-containing compound **1**, the reaction appeared to be complete in 5 min, as evidenced by a colour change from green (dehydrated) to orange-yellow and by mass-gain measurements determined by thermogravimetry analysis [Figure 5 (insert)]. To ensure complete reaction, the compounds dehydrated at 150 °C were usually exposed to ammonia or amine gas for 30 min. Longer exposure to the flow of ammonia or amine gas did not produce different results. In the case of dodecylamine (b.p. 247 °C), **1a** or **2a** was added to the dodecylamine and the mixture was stirred for 30 min. The solid was filtered, washed three times with cyclohexane and dried under vacuum. $[Co(H_2O)(NH_3)]_2[Mo(CN)_8]$: $C_8H_{10}Co_2MoN_{10}O_2$: calcd. C 19.53, Co 23.95, Mo 19.50, N 28.47; found C 19.70, Co 23.41, Mo 19.36, N 28.63. IR (KBr): $\tilde{\nu}$ = 3607, 3371, 3283, 3199, 2138, 1615, 1400, 1220, 1096, 1021, 807, 593, 461 cm^{-1}.

 © 2003 Wiley-VCH Verlag GmbH & Co. KGaA, Weinheim

Table 1. Crystal data and structure refinement for **1** and **2**

Empirical formula	$C_2H_4N_2O_2Co_{0.5}Mo_{0.25}$ (**1**)	$CH_2NOMo_{0.13}Mn_{0.25}$ (**2**)
Formula mass	141.5	75.6
Temperature [K]	160(2)	160(2)
Wavelength [Å]	0.71073	0.71073
Crystal system	tetragonal	tetragonal
Space group	*I*4/*m* (87)	*I*4/*mcm* (140)
Unit cell dimensions [Å]	$a = b$ =11.748(2)	$a = b$= 11.679(2)
	c = 13.022(3)	c = 13.276(3)
Volume [Å^3]	1797.2(6)	1810.83(60)
Z	16	32
Calculated density [Mg/m^3]	2.092	1.988
Absorption coefficient [mm^{-1}]	2.568	2.109
F(000)	1120	1040
2θ range for data collection [°]	3.3−51.86	3.3−48.75
Reflections collected/unique	2794/866 [R(int) = 0.0620]	6999/412 [R(int) = 0.0263]
Completeness to 2θ	25.93°, 94.1%	24.36°, 96.3%
Refinement method	full-matrix least squares on F^2	full-matrix least squares on F^2
Data/restraints/parameters	866/0/83	412/0/39
Absorption correction:	semiempirical (DIFABS)[18]	semiempirical (DIFABS)[18]
$T_{min} - T_{max}$	0.238−0.699	0.460−0.824
Goodness-of-fit on F^2	1.148	1.270
Weight [$P = (F_o^2 + 2F_c^2)/3$]	$1/[\sigma^2(F_o^2) + (0.0628P)^2 + 19.361P]$	$1/[\sigma^2(F_o^2) + (0.0292P)^2 + 21.012P]$
Final R indices [$I > 2\sigma(I)$]	$R1$ = 0.0530, $wR2$ = 0.1355	$R1$ = 0.0325, $wR2$ = 0.0869
R indices (all data)	$R1$ = 0.0589, $wR2$ = 0.1391	$R1$ = 0.0325, $wR2$ = 0.0869
Largest diff. peak/hole [e·Å^{-3}]	0.830/−0.861	0.513/−0.632

$[Mn(H_2O)(NH_3)]_2[Mo(CN)_8]$: $C_8H_{10}Mn_2MoN_{10}O_2$: calcd. C 19.85, Mn 22.70, Mo 19.82, N 28.94; found C 19.55, Mn 22.97, Mo 19.06, N 28.20. IR (KBr): $\tilde{\nu}$ = 3609, 3380, 3290, 3099, 2146, 1611, 1400, 1220, 1038, 600, 468, 436 cm^{-1}. $[Co(H_2O)(CH_3NH_2)]_2[Mo(CN)_8]$: $C_{10}H_{14}Co_2MoN_{10}O_2$: calcd. C 23.09, Co 22.66, Mo 18.45, N 26.93; found C 24.20, Co 22.41, Mo 18.36, N 26.69. IR (KBr): $\tilde{\nu}$ = 3600, 3325, 3268, 3182, 2725, 2695, 2114, 1611, 1402, 1220, 1036, 595, 461, 436 cm^{-1}. $[Mn(H_2O)(CH_3NH_2)]_2[Mo(CN)_8]$: $C_{10}H_{14}Mn_2MoN_{10}O_2$: calcd. C 23.44, Mn 21.46, Mo 18.74, N 27.36; found C 23.67, Mn 21.97, Mo 18.06, N 27.20. IR (KBr): $\tilde{\nu}$ = 3609, 3380, 3290, 3099, 2146, 1611, 1400, 1220, 1038, 600, 468, 436 cm^{-1}. $[Co(H_2O)(C_2H_5NH_2)]_2[Mo(CN)_8]$: $C_{12}H_{18}Co_2MoN_{10}O_2$: calcd. C 26.29, Co 21.50, Mo 17.50, N 25.55; found C 24.80, Co 21.41, Mo 17.36, N 25.50. IR (KBr): $\tilde{\nu}$ = 3372, 3268, 3182, 2974, 2137, 1682, 1608, 1502, 1470, 1384, 1215, 1035, 840, 582, 461, 436 cm^{-1}. $[Mn(H_2O)(C_2H_5NH_2)]_2[Mo(CN)_8]$: $C_{12}H_{18}Mn_2MoN_{10}O_2$: calcd. C 26.68, Mn 20.34, Mo 17.76, N 25.93; found C 26.73, Mn 20.97, Mo 17.06, N 25.20. IR (KBr): $\tilde{\nu}$ = 3370, 3270, 3185, 2974, 2137, 1682, 1608, 1502, 1470, 1384, 1215, 1035, 846, 580, 465, 430 cm^{-1}.

X-ray Crystallography and Structure Solution: For **1** and **2**, data were collected at a low temperature (T = 160 K) with a Stoe Imaging Plate Diffraction System (IPDS), equipped with an Oxford Cryosystems Cryostream Cooler Device and using a graphite-monochromated Mo-K_α radiation (λ = 0.71073 Å). Final unit cell parameters were obtained by means of a least-squares refinement of a set of 8000 well-measured reflections, and a crystal decay was monitored during data collection by measuring 200 reflections per image, no significant fluctuations of intensities were observed (Table 1). Structures were solved by means of Direct Methods using the program SIR92,[19] and subsequent difference Fourier maps, models were refined by least-squares procedures on F^2 by using SHELXL-97[20] integrated in the package WINGX version 1.64.[21] For complex **1** hydrogen atoms connected to the H_2O molecules were located on a difference Fourier map and isotropically refined. For compound **2**, owing to the symmetry operators on which H_2O molecules were located, hydrogen atoms were statistically disordered and consequently could not be located. For compounds **1** and **2** a semiempirical correction absorption was applied[22] and all non-hydrogen atoms were anisotropically refined; in the last cycles of refinement a weighting scheme was used, where weights are calculated from the following formula: $w = 1/[\sigma^2(F_o^2) + (aP)^2 + bP]$ where $P = (F_o^2 + 2F_c^2)/3$. CCDC-194778 and -194779 contain the supplementary crystallographic data for this paper. These data can be obtained free of charge at www.ccdc.cam.ac.uk/conts/retrieving.html [or from the Cambridge Crystallographic Data Centre, 12 Union Road, Cambridge CB2 1EZ, UK; Fax: (internat.) + 44-1223/336-033; E-mail: deposit@ccdc.cam.ac.uk].

Physical Measurements: Infrared spectra were recorded using KBr disks or Nujol mulls between NaCl plates with a Nicolet Model 510P spectrophotometer. UV/Vis spectra were recorded with a Cary-17D spectrometer. Thermogravimetry (TG) analyses were performed using a Netzsch STA 409 instrument under argon, from 30 to 700 °C, at a heating rate of 1 °C·min^{-1}; volatiles were determined using a Balzers QMG 421 quadruple Mass Spectrometer coupled with ATG equipment. Magnetic susceptibility data were collected with a Quantum Design MPMS-XL SQUID magnetometer. The compounds were measured on finely grounded polycrystalline samples between 1.8 and 320 K at 1000 G. The data were corrected for the sample holder and the diamagnetism contributions calculated from Pascal's constants.[23] Powder X-ray data were recorded with a Bruker D5000 diffractometer using a Bragg−Brentano geometry; a Cu target and a back monochromator were used ($K_{\alpha1} + K_{\alpha2}$); 2θ range 5−88°; 2θ steps 0.02°.

[1] [1a] P. J. Hagrman, D. Hagrman, J. Zubieta, *Angew. Chem. Int. Ed.* **1999**, *38*, 2638−2684. [1b] C. Janiak, *Angew. Chem. Int. Ed. Engl.* **1997**, *36*, 1431−1434. [1c] A. J. Blake, N. R. Champness, P. Hubberstey, W.-S. Li, A. Withersby, M. Schroeder, *Coord. Chem. Rev.* **1999**, *183*, 117−138. [1d] M. Eddaoudi, H. Li, O. M. Yaghi, *J. Am. Chem. Soc.* **2000**, *122*, 1391−1397.

 © 2003 Wiley-VCH Verlag GmbH & Co. KGaA, Weinheim

[2] [2a] U. Müller, *Angew. Chem. Int. Ed.* **2000**, *39*, 502−504. [2b] A. Müller, H. Reuter, S. Dillinger, *Angew. Chem. Int. Ed. Engl.* **1995**, *34*, 2311−2327. [2c] P. Losier, M. Zaworotko, *Angew. Chem. Int. Ed. Engl.* **1996**, *35*, 2779−2782. [2d] L. C. Tabares, J. A. R. Navarro, J. M. Salas, *J. Am. Chem. Soc.* **2001**, *123*, 383−387.

[3] [3a] H. Li, C. E. Davis, T. L. Groy, D. G. Kelley, O. M. Yaghi, *J. Am. Chem. Soc.* **1998**, *120*, 2186−2187. [3b] O. M. Yaghi, G. Li, H. LI, *Nature* **1995**, *378*, 703−704. [3c] D. Venkataraman, G. B. Gardner, S. Lee, J. S. Moore, *J. Am. Chem. Soc.* **1995**, *117*, 11600−11601. [3d] G. K. H. Shimizu, G. D. Enright, C. I. Ratcliffe, J. A. Ripmeester, D. D. Wayner, *Angew. Chem. Int. Ed.* **1998**, *37*, 1407−1409. [3e] M. Fujita, Y. J. Kwon, S. Washiju, K. Ogura, *J. Am. Chem. Soc.* **1994**, *116*, 1151−1152.

[4] [4a] M. Kondo, T. Yoshitomi, K. Seki, H. Matsuzaka, S. Kitagava, *Angew. Chem. Int. Ed. Engl.* **1997**, *36*, 1725−1727. [4b] P. Brunet, M. Simard, J. D. Wuest, *J. Am. Chem. Soc.* **1997**, *119*, 2737−2738. [4c] K. Endo, T. Ezuhara, M. Koyanagi, H. Masuda, Y. Aoyama, *J. Am. Chem. Soc.* **1997**, *119*, 499−505. [4d] A. W. Coleman, S. G. Bott, S. D. Morley, C. M. Means, K. D. Robinson, H. Zhang, J. L. Atwood, *Angew. Chem. Int. Ed.* **1998**, *37*, 1361−1363.

[5] [5a] D. Armentano, G. De Munno, F. Lloret, M. Julve, *Inorg. Chem.* **1999**, *38*, 3744−3747. [5b] G. De Munno, D. Armentano, M. Julve, F. Lloret, R. Lescouëzec, J. Faus, *Inorg. Chem.* **1999**, *38*, 2234−2237. [5c] G. De Munno, M. Julve, F. Nicolo, F. Lloret, J. Faus, R. Ruiz, E. Sinn, *Angew. Chem. Int. Ed. Engl.* **1993**, *32*, 613−615. [5d] V. Niel, J. M. Martinez-Agudo, M. C. Munoz, A. B. Gaspar, J. A. Real, *Inorg. Chem.* **2001**, *40*, 3838−3839.

[6] T. Iwamoto, in: *Comprehensive Supramolecular Chemistry*, vol.6 (Eds.: J. L. Atwood, J. E. D. Davies, D. D. MacNicol, F. Vögtle, J.-M. Lehn), Pergamon, New York, **1996**, pp. 643−675.

[7] [7a] D. B. Leznoff, Bao-Yu Xue, B. O. Patrick, V. Sanchez, R. C. Tompson, *Chem. Commun.* **2001**, 259−260. [7b] B. F. Hoskins, R. Robson, N. V. Y. Scarlett, *J. Chem. Soc., Chem. Commun.* **1994**, 2025−2026. [7c] T. Soma, T. Iwamoto, *Chem. Lett.* **1995**, 271−272. [7d] T. Soma, T. Iwamoto, *Chem. Lett.* **1994**, 821−822. [7e] T. Soma, H. Yuge, T. Iwamoto, *Angew. Chem. Int. Ed. Engl.* **1994**, *33*, 1765−1765. [7f] S. C. Abrahams, J. L. Bernstein, R. Liminga, E. T. Eisenmann, *J. Chem. Phys.* **1980**, *73*, 4585−4587. [7g] G. Bowmaker, B. J. Kennedy, J. C. Reid, *Inorg. Chem.* **1998**, *37*, 3969−3974.

[8] [8a] D. W. Knoeppel, J. Liu, E. A. Meyers, S. G. Shore, *Inorg. Chem.* **1998**, *37*, 4828−4837. [8b] D. J. Chesnut, J. Zubieta, *Chem. Commun.* **1998**, 1707−1708. [8c] A. K. Brimah, E. Siebel, R. Dieter Fischer, N. A. Davies, D. C. Apperley, R. K. Harris, *J. Organomet. Chem.* **1994**, *475*, 85−94.

[9] [9a] T. Iwamoto, D. F. Shriver, *Inorg. Chem.* **1972**, *11*, 2570−2572. [9b] H. Yuge, T. Iwamoto, *J. Chem. Soc., Dalton. Trans.* **1993**, 2841−2843. [9c] T. Kitazawa, T. Kikuyama, M. Takeda, T. Iwamoto, *J. Chem. Soc., Dalton. Trans.* **1995**, 3715−3718. [9d] T. Kitazawa, M. Takeda, *J. Chem. Soc., Chem. Commun.* **1993**, 309−310. [9e] T. Kitazawa, M. Akiyama, M. Takahashi, M. Takeda, *J. Chem. Soc., Chem. Commun.* **1993**, 1112−1113. [9f] S. Nishikori, C. I. Ratecliffe, J. A. Rimpeester, *J. Am. Chem. Soc.* **1992**, *114*, 8590−8595.

[10] [10a] K.-M. Park, R. Kuroda, T. Iwamoto, *Angew. Chem. Int. Ed. Engl.* **1993**, *32*, 884−886. [10b] E. Ruiz, S. Alvarez, R. Hoffmann, J. Bernstein, *J. Am. Chem. Soc.* **1994**, *116*, 8207−8221. [10c] E. Ruiz, S. Alvarez, *Inorg. Chem.* **1995**, *34*, 3260−3269. [10d] S. Nishikori, T. Iwamoto, *Inorg. Chem.* **1986**, *25*, 788−794. [10e] H. Yuge, T. Iwamoto, *J. Chem. Soc., Dalton Trans.* **1994**, 1237−1239. [10f] B. F. Hoskins, R. Robson, *J. Am. Chem. Soc.* **1990**, *112*, 1546−1554.

[11] [11a] M. Ohaba, H. Okawa, N. Fukita, Y. Hashimoto, *J. Am. Chem. Soc.* **1997**, *119*, 1011−1019. [11b] H. Miyasaka, H. Okawa, A. Miyazaki, T. Enoki, *Inorg. Chem.* **1998**, *37*, 4878−4883. [11c] H. Miyasaka, N. Matsumoto, N. Re, E. Gallo, C. Floriani, *Inorg. Chem.* **1997**, *36*, 670−676. [11d] H. Miyasaka, N. Matsumoto, H. Okawa, N. Re, E. Gallo, C. Floriani, *J. Am. Chem. Soc.* **1996**, *118*, 981−994. [11e] H. Miyasaka, H. Ieda, N. Matsumoto, N. Re, R. Crescenzi, C. Floriani, M. Font-Bardia, *Inorg. Chem.* **1998**, *37*, 255−263. [11f] M. Ohba, N. Usuki, N. Fukita, H. Okawa, *Angew. Chem. Int. Ed.* **1999**, *38*, 1795−1798. [11g] T. Niu, X. Wang, A. J. Jacobson, *Angew. Chem. Int. Ed.* **1999**, *38*, 1934−1937. [11h] M. P. Shores, L. G. Beauvais, J. R. Long, *J. Am. Chem. Soc.* **1999**, *121*, 775−779. [11i] E. Colacio, J. M. Dominguez-Vera, M. Ghazi, R. Kivekäs, F. Lloret, J. M. Moreno, H. Stoeckli-Evans, *Chem. Commun.* **1999**, 987−988. [11j] S. Ferlay, T. Mallah, J. Vaissermann, F. Bartolomé, P. Veillet, M. Verdaguer, *Chem. Commun.* **1996**, 2481−2482. [11k] E. Colacio, J. M. Dominguez-Vera, M. Gazi, R. Kivekäs, J. M. Moreno, A. Pajunen, *J. Chem. Soc., Dalton. Trans.* **2000**, 505−509. [11l] T. Niu, X. Wang, A. J. Jacobson, *Angew. Chem. Int. Ed.* **1999**, *38*, 1934−1937. [11m] T. Niu, A. J. Jacobson, *Inorg. Chem.* **1999**, *38*, 5346−5350. [11n] T. Niu, J. Lu, X. Wang, J. D. Korp, A. J. Jacobson, *Inorg. Chem.* **1998**, *37*, 5324−5328.

[12] [12a] G. Rombaut, M. Verelst, S. Golhen, L. Ouahab, C. Mathonière, O. Kahn, *Inorg. Chem.* **2000**, *39*, 1025−1030. [12b] G. Rombaut, S. Golhen, L. Ouahab, C. Mathonière, O. Kahn, *J. Chem. Soc., Dalton. Trans.* **2000**, 3609−3614. [12c] G. Rombaut, C. Mathonière, Ph. Guionneau, S. Golhen, L. Ouahab, M. Verelst, P. Lecante, *Inorg. Chimica Acta* **2001**, *326*, 27−29. [12d] A. K. Sra, M. Andruh, O. Kahn, S. Golhen, L. Ouahab, J. V. Yakhmi, *Angew. Chem. Int. Ed.* **1999**, *38*, 2606−2609. [12e] A. K. Sra, G. Rombaut, F. Lahitête, S. Golhen, L. Ouahab, C. Mathonière, J. V. Yakhmi, O. Kahn, *New J. Chem.* **2000**, *24*, 871−874. [12f] P. Franz, L. Keller, M. Pilkington, J. Ensling, S. Decurtins, *Mid-Term Conference on the ESF Programme "Molecular Magnets"* Davos, **2001**, H4.

[13] J. Lu, W. T. A. Harrison, A. J. Jacobson, *Angew. Chem. Int. Ed. Engl.* **1995**, *34*, 2557−2559.

[14] [14a] J. L. Hoard, H. H. Nordsieck, *J. Am. Chem. Soc.* **1939**, *61*, 2853−2857. [14b] E. L. Muetterties, C. M. Wright, *Q. Rev., Chem. Soc.* **1967**, 109−123. [14c] E. L. Muetterties, L. J. Guggenberger, *J. Am. Chem. Soc.* **1974**, *96*, 1748−1756.

[15] B. Sieklucka, J. Szklarzewicz, T. J. Kemp, W. Errington, *Inorg. Chem.* **2000**, *39*, 5156−5158.

[16] [16a] K. J. Frink, R.-Ch. Wang, J. L. Colon, A. Clearfield, *Inorg. Chem.* **1991**, *30*, 1438−1441. [16b] G. Cao, T. E. Mallouk, *Inorg. Chem.* **1991**, *30*, 1434−1438. [16c] D. Cunningham, P. J. D. Hennelly, T. Deeney, *Inorg. Chim. Acta* **1979**, *37*, 95−97.

[17] [17a] S. Willemin, J. Larionova, B. Henner, C. Guérin, unpublished results. [17b]N. B. Vrecena, B. I. Chernjk, P. V. Novosad, *Koord. Chim.* **1988**, *14*, 855.

[18] K. Nakamoto, *Infrared and Raman Spectra*, John Wiley and Sons Inc., New York, **1986**, p. 191.

[19] *SIR92 Program for automatic solution of crystal structures by direct methods:* A. Altomare, G. Cascarano, G. Giacovazzo, A. Guagliardi, M. C. Burla, G. Polidori, M. Camalli, *J. Appl. Cryst.* **1994**, *27*, 435−443.

[20] *SHELX97 (includes SHELXS-97, SHELXL-97, CIFTAB) − Programs for Crystal Structure Analysis (Release 97−2)*: G. M. Sheldrick, Institut für Anorganische Chemie der Universität, Tammanstrasse 4, 3400 Göttingen, Germany, **1998**.

[21] *WINGX:* L. J. Farrugia, *J. Appl. Crystallogr.* **1999**, *32*, 837−847.

[22] *DIFABS:* N. Walker, D. Stuart, *Acta Crystallogr., Sect. A* **1983**, *39*, 1−22.

[23] E. A. Boudreaux, L. N. Mulay, *Theory and Applications of Molecular Paramagnetism*, John Wiley and Sons, New York, **1976**.

[24] [24a] M. Albrecht, M. Lutz, A. L. Spek, G. van Koten, *Nature* **2000**, *406*, 970−974. [24b] E. Colacio, F. Lloret, R. Kivekäs, J. Suares-Varela, M. R. Sundberg, *Chem. Commun.* **2002**, 592−593.

Received October 27, 2002

 © 2003 Wiley-VCH Verlag GmbH & Co. KGaA, Weinheim

Preparation, Reactivity and Peptide Labelling Properties of (η^6-Arene)ruthenium(II) Complexes with Pendant Carboxylate Groups

Ralf Stodt,[a] Susan Gencaslan,[a] Iris M. Müller,[a] and William S. Sheldrick*[a]

Keywords: Ruthenium / Amino acids / Peptides / Bioinorganic chemistry

(η^6-Arene)ruthenium(II) complexes of the type [{[η^6-$C_6H_5(CH_2)_nCOOH$]Ru(μ-Cl)Cl}$_2$] (**2a**, n = 1; **3**, n = 3) with tethered carboxylate groups can be obtained by dehydrogenation of the appropriate cyclohexadiene with $RuCl_3 \cdot 3H_2O$. Formation of a κ*O*-coordinated chelate in weakly acidic solution is observed by means of a ^{1}H NMR titration for both [{η^6-$C_6H_5(CH_2)_3COOH$}Ru(aq)](OTf)$_2$ (**3a′**) and [{η^6-$C_6H_5(CH_2)_3COOH$}Ru(phen)(aq)](OTf)$_2$ (**5′**). Sandwich complexes of the type [{η^6-$C_6H_5(CH_2)_3COOH$}Ru(η^6-amino acid)](OTf)$_2$ [amino acid = AcpheOH (**6**), ActyrOEt (**7**), ActrpOH (**8**)] can be prepared by treating [{η^6-$C_6H_5(CH_2)_3COOH$}Ru(acetone)$_3$](OTf)$_2$ with the appropriate aromatic bioligand in CF_3COOH (**6**/**8**) or CH_2Cl_2 (**7**). Chemospecific η^6-labelling of the *C*-terminal indole function is observed for the peptide HphetrpOH in the analogous complex **9**. Quantitative formation of **8** can also be achieved in aqueous solution in the presence of a 3:1 excess of the {η^6-$C_6H_5(CH_2)_3COOH$}Ru^{II} fragment. This can also be employed for the *N*-terminal labelling of amino acids and peptides in its sandwich complex [(η^6-C_6Me_6)Ru{η^6-$C_6H_5(CH_2)_3$-COOH}](OTf)$_2$ (**10**). Coupling reactions by the carbodiimide method with EDC afford water-stable complexes of the type [(η^6-C_6Me_6)Ru{η^6-$C_6H_5(CH_2)_3C(O)R$}](OTf)$_2$ [R = trpOMe (**11**), pheOMe (**12**), glyglyOEt (**13**)] in good yields. X-ray structures of [(η^6-$C_6H_5CH_2COOC_2H_5$)RuCl(phen)](OTf) (**4b′**) and **10** are reported.

(© Wiley-VCH Verlag GmbH & Co. KGaA, 69451 Weinheim, Germany, 2003)

Introduction

Current interest in (η^6-arene)ruthenium(II) complexes with heteroatom donors tethered to the η^6-arene moiety has primarily been motivated by their potential as homogeneous catalysts.[1,2] Examples of chelating side-chains have included amines,[1] alcohols,[1−3] thioethers,[4] and phosphanes.[1,5−9] Chloro-bridged complexes of the type [{(η^6-arene)Ru(μ-Cl)Cl}$_2$] with *N*-terminal protected derivatives of phenylglycine ethyl ester as the functionalised arene ligand have also been reported recently.[10] In comparison to the analogous dimeric ruthenium(II) compounds with η^6-coordinated benzene or cymene ligands,[11,12] these η^6-phenylglycine complexes exhibit a strongly enhanced solubility in polar solvents. Their ensuing decomposition in solution may well be due to participation of side-chain donor atoms in the metal coordination sphere[10] and apparently renders them unsuitable for possible further application, e.g. for the labelling of peptides or proteins as previously reported for the CpRu^{II}, Cp*Ru^{II} and (η^6-cymene)Ru^{II} fragments.[13−18]

Given that they have an adequate stability in polar solvents, (η^6-arene)ruthenium(II) complexes with pendant free carboxylate groups should be of interest not only for the chemospecific η^6-labelling of tryptophan, tyrosine or phenylalanine residues but also for the more general *N*-terminal labelling of peptides. Furthermore, the recent report that [{η^5-$C_5H_4(CH_2)_2NH_2$-κ*N*}Ru(CH_3CN)$_2$](PF_6) with its tethered amine side-chain can quantitatively label the phenylalanine side-chain of the hormone secretin[19] suggests that a hemilabile carboxylate coordination might also enhance the π-complexing ability of (η^6-arene)ruthenium(II) complexes in aqueous solution. We have, therefore, prepared compounds of the type [{[η^6-C_6H_5-$(CH_2)_n$COOH]Ru(μ-Cl)Cl}$_2$] (n = 1, 3) and studied their reactivity and peptide labelling properties.

Results and Discussion

(η^6-Arene)ruthenium(II) complexes with tethered carboxylate groups (n = 1, 3) can be obtained by dehydrogenation of the appropriate cyclohexadiene with $RuCl_3 \cdot 3H_2O$ in accordance with the general method of Bennett et al.[11,12] 2,5-Dihydrophenylacetic acid[20] and 2,5-dihydro-4-phenylbutyric acid (**1**) were prepared for this purpose by a Birch reduction of phenylacetic acid (paa) and 4-phenylbutyric acid (pba), respectively. Treatment of 3-phenylpropionic acid (ppa) with sodium in ammonia solution leads, in contrast, to reduction not only of the phenyl moiety but also of the carboxylate function. Employment of the ethyl ester of ppa affords 2,5-dihydro-3-phenylpropanol[21,22] in high yield (74%). As 3-phenylpropanol has already been studied as a functionalised η^6-arene ligand by Kurosawa et

[a] Lehrstuhl für Analytische Chemie, Ruhr-Universität Bochum, 44780 Bochum, Germany
Fax: (internat.) + 49-234/32-14742
E-mail: William.Sheldrick@ruhr-uni-bochum.de

al.[1−3] our own investigations have concentrated on the coordination behaviour of the (η^6-ppa)Ru^{II} and (η^6-pba)Ru^{II} fragments.

Treatment of 2,5-dihydrophenylacetic acid or 2,5-dihydro-4-phenylbutyric acid with ruthenium(III) trichloride in an acetone/water solution at reflux leads to the formation of [{(η^6-paa)Ru(μ-Cl)Cl}$_2$] (**2a**) and [{(η^6-pba)Ru(μ-Cl)Cl}$_2$] (**3**), respectively, in high yields (Scheme 1). Use of ethanol as the solvent affords ethyl esters such as [{(η^6-$C_6H_5CH_2COOC_2H_5$)}Ru(μ-Cl)Cl}$_2$] (**2b**), which can subsequently be hydrolysed with NaOH at pH = 12 to provide the chloro-bridged η^6-complexes of the free carboxylic acids. Interestingly, the reaction of 2,5-dihydrophenylacetic acid with $RuCl_3 \cdot 3H_2O$ takes only 20 min to reach completion in refluxing ethanol in comparison to 4 h for 1,3-cyclohexadiene or α-phellandrene.[11,12] This suggests that initial rapid κ*O*-coordination by the tethered carboxylate function may facilitate subsequent η^4-coordination of the neighbouring cyclohexadiene ring. η^6-Coordination of the phenyl moieties in **2a**, **2b**, and **3** is confirmed by the pronounced upfield ^{1}H NMR shifts of their aromatic protons in comparison to the parent carboxylic acids. For instance complex **3** exhibits resonances at δ = 5.44 (d, 2 H), 5.68 (t, 2 H) and 5.61 ppm (t, 1 H) for its phenyl *ortho*, *meta*, and *para* protons in acetonitrile solution. The esterification of the carboxylate function in **2b** is indicated by the observation of a strong ν(CO) band at 1749 cm^{-1} in its IR spectrum. In contrast, **2a** and **3** display typical CO valence absorptions for free carboxylic acids at 1704 and 1711 cm^{-1}, respectively.

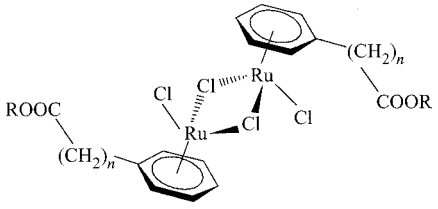

2a, n = 1, R = H; **2b**, n = 1, R = C_2H_5; **3**, n = 3, R = H

Scheme 1

Aqueous solutions of **2a**, **2b**, and **3** are stable for a period of several weeks over a wide pH range (2 ≤ pH ≤ 12). As a result of their free carboxylate groups, **2a** and **3** exhibit enhanced solubility in water or methanol in comparison to the ester complex **2b**. The extent of any participation of the tethered arm in the metal coordination sphere may be expected to be dependent both on the arm length and on the pH value of an aqueous solution of **2a** or **3**. In order to study the possibility of carboxylate κ*O*-coordination, aqueous solutions of [{η^6-$C_6H_5(CH_2)_3COOH$}Ru(aq)](OTf)$_2$ (**2a′**) and [{η^6-$C_6H_5(CH_2)_3COOH$}Ru(aq)](OTf)$_2$ (**3′**) were prepared by addition of 2 equiv. of Ag(OTf) to **2a** and **3**, respectively, followed by filtration of the resulting precipitated AgCl. A pH titration of **2a′** in the range of 1.53 ≤ pH* ≤ 12.12 (Figure 1a) provides no evidence for the presence of new species in comparison with those of the type [{(η^6-arene)Ru}$(H_2O)_3]^{2+}$, [{(η^6-arene)-Ru(μ-OH)(H_2O)}$_2]^{2+}$, and [{(η^6-arene)Ru}$_2$(μ-OH)$_3]^+$ observed for [(η^6-C_6H_6)Ru(aq)]$^{2+}$.[23,24] In Figure 1a MH refers to [(η^6-$C_6H_5CH_2COOH$)Ru$(H_2O)_3]^{2+}$, M to [(η^6-$C_6H_5CH_2COO$)Ru$(H_2O)_3]^+$, M_2H_{-2} to [{(η^6-$C_6H_5CH_2COO$)Ru(μ-OH)(H_2O)}$_2$], and M_2H_{-3} to [{(η^6-$C_6H_5CH_2COO$)Ru}$_2$(μ-OH)$_3]^-$. The formation of the dinuclear species M_2H_{-3} in weakly acidic and alkaline solutions is indicated by characteristic highfield shifts of ca. 0.6 ppm for the aromatic protons. Figure 1a suggests that the tethered carboxylate group of the short side-chain in **2a′** does not participate in intramolecular κ*O*-coordination to any significant degree. The presence of the intermediate hydroxy-bridged complex M_2/M_2H_{-2} leads to an additional set of ^{1}H NMR signals in the range 3.6 ≤ pH* ≤ 6.2.

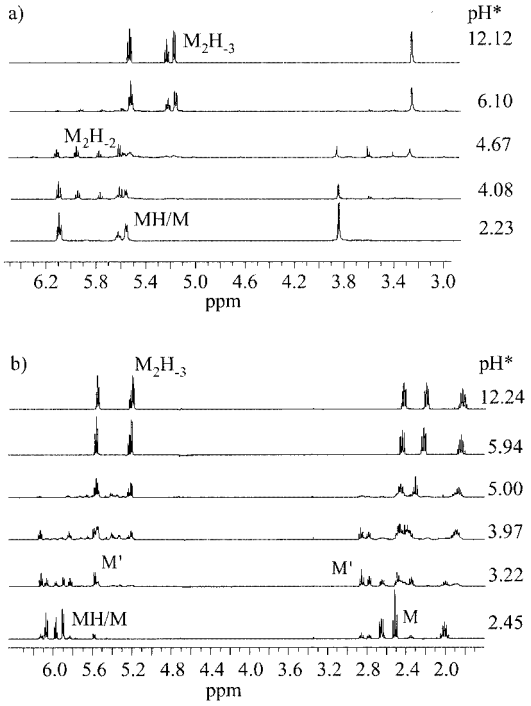

Figure 1. pH dependence of the ^{1}H NMR spectra of (a) [(η^6-$C_6H_5CH_2COOH$)Ru(aq)]$^{2+}$ (**2a′**) and (b) [{η^6-$C_6H_5(CH_2)_3$-COOH}Ru(aq)]$^{2+}$ (**3′**); the species nomenclature is based on the assignment of MH to [(η^6-$C_6H_5CH_2COOH$)Ru$(H_2O)_3]^{2+}$ in (a) and [(η^6-$C_6H_5(CH_2)_3COOH$) Ru$(H_2O)_3]^{2+}$ in (b)

A comparison of Figure 1a and b indicates that the lengthening of the side-chain in [{η^6-C_6H_5-$(CH_2)_3COOH$}Ru(aq)](OTf)$_2$ (**3′**) enables the formation of a new distinct species M′ (or possibly a dinuclear species M′$_2$ in the range 2.4 ≤ pH* ≤ 5.5). The pronounced low-field shifts of the side-chain α−γ-methylene protons and the opposite highfield shifts of the phenyl *ortho* and *meta* protons are characteristic of this complex. As deprotonation of the carboxylate group will be expected in the range 4 ≤ pH* ≤ 5, it is reasonable to postulate that the tethered arm must participate in the ruthenium(II) coordination sphere in this species, i.e. that M′ will probably be [{η^6-

$C_6H_5(CH_2)_3COO$-κ*O*} $Ru(H_2O)_2]^+$. Since intermolecular κ*O*-carboxylate coordination cannot be ruled out, the alternative dinuclear species [{[η⁶-$C_6H_5(CH_2)_3COO$-κ*O*]$Ru(H_2O)_2$}$_2$] (M′$_2$) must also be taken into consideration.

To simplify the analysis of the pH-titration data for (η⁶-arene)ruthenium(II) complexes with functionalised arene moieties, it is helpful to block two of the three potential κ*O*-coordination sites with the bidentate ligand 1,10-phenanthroline (1,10-phen). The light-brown mononuclear complexes **4a**, **4b**, and **5** of the type [(η⁶-arene)RuCl(1,10-phen)]$^+$ were prepared for this purpose by reaction of the chloro-bridged dinuclear compounds **2a**, **2b**, and **3** with 1,10-phen in ethanol at reflux (Scheme 2). Bidentate κ²*N*,*N*′-coordination of 1,10-phenanthroline leads to characteristically pronounced downfield shifts of the signals for the *ortho* and *meta* protons of the η⁶-arene moiety, e.g. 0.60 ppm for **4b** in CD_3OD solution in comparison to 0.49 ppm for **2b** in CD_3CN. In contrast, the signals of the *para* protons are only shifted by 0.16 ppm to the lower field for the **2b**/**4b** pair. The ^{1}H NMR signal for the benzyl protons of **4b** can be observed at δ = 3.67 ppm in acetonitrile (or CD_3OH) but disappears within 5 min in D_2O or CD_3OD. The responsible rapid H/D exchange in the latter solvents is clearly a consequence of the relatively high acidity of the methylene protons in **4b** as a result of both the η⁶-coordination of the phenyl group[25,26] and the presence of a neighbouring carboxylate group. A similar H/D exchange is also observed for **4a** in CD_3OD but not for the η⁶-phenylbutyric acid complex **5** with its longer side-chain. The formation of the neutral enol form of the acetic acid side-chain in **4a**/**4b**, following the loss of a methylene proton and concomitant addition of a deuteron to the carboxylate C=O double bond, is apparently of importance in rate determining for the H/D exchange.

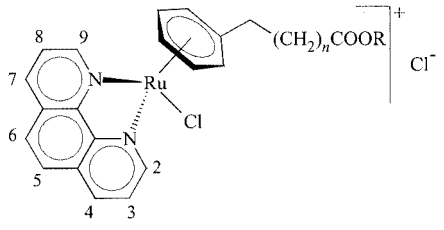

4a, *n* = 1, R = H; **4b**, *n* = 1, R = C_2H_5; **5**, *n* = 3, R = H

Scheme 2

After addition of 1 equiv. of Ag(OTf) to **4b** and filtration of the precipitated AgCl, crystals of the resulting complex, [(η⁶-$C_6H_5CH_2COOC_2H_5$)RuCl(phen)](OTf) (**4b**′), were grown by gas diffusion of diethyl ether into a methanol solution of the complex. As depicted in Figure 2, the complex cation of **4b**′ displays an effectively eclipsed conformation for its substituent methylene carbon atom C17 relative to N21 of the bidentate 1,10-phen ligand. This is in accordance with the expectations for half-sandwich complexes of the general type [(η⁶-arene)]$ML_3]^{n+}$ with a +I substituent in the η⁶-arene moiety and electron donor ligands L.[27] Interestingly both of the relatively acidic methylene protons participate in the formation of C−H···O hydrogen bonds to the triflate oxygen atoms. Respective C···O/H···O distances of 3.448/2.480 and 3.440/2.472 Å are observed for these interactions.

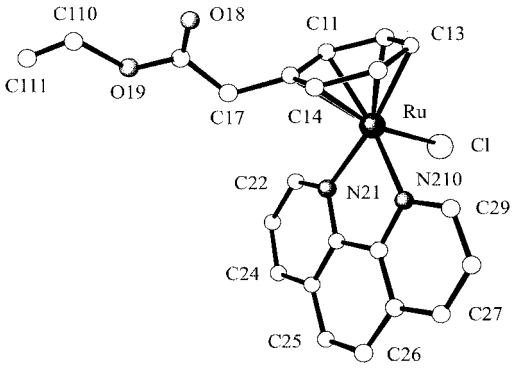

Figure 2. Molecular structure of the cation of [(η⁶-$C_6H_5CH_2COOC_2H_5$)RuCl(phen)](OTf) (**4b**′); selected bond lengths [Å] and angles [°]: Ru−N21 2.096(5), Ru−N210 2.097(5), Ru−Cl 2.398(9); N21−Ru−N210 77.7(2), N21−Ru−Cl 84.1(1), N210−Ru−Cl 85.4(9)

Aqueous solutions of [(η⁶-$C_6H_5CH_2COOH$)Ru(phen)(aq)](OTf)$_2$ (**4a**′) and [{η⁶-$C_6H_5(CH_2)_3COOH$}Ru(phen)(aq)](OTf)$_2$ (**5**′) were prepared by addition of 2 equiv. of Ag(OTf) to **4a** and **5** and subsequent filtration of the resulting precipitated AgCl. Selected ^{1}H NMR spectra in D_2O are depicted in Figure 3 for **5**′ in the range 3.40 ≤ pH* ≤ 11.46. The aqua complex [{η⁶-$C_6H_5(CH_2)_3COOH$}$Ru(OH_2)(phen)]^{2+}$ (MH) predominates at low pH* (2.48, Figure 4) and exhibits two deprotonation steps to afford [{η⁶-$C_6H_5(CH_2)_3COO$}Ru(OH$_2$)(phen)]$^+$ (M) and subsequently [{η⁶-$C_6H_5(CH_2)_3COO$}Ru(OH)(phen)] (MH_{-1}). The latter hydroxy complex predominates in alkaline solution at pH* = 11.46. Initial loss of the side-arm carboxylate protons leads to modest lowfield shifts for the 1,10-phen protons H2/H9 and the η⁶-pba aromatic protons in the approximate range 3.5 ≤ pH* ≤ 5.5, which are then followed by more pronounced upfield shifts on deprotonation of the aqua ligand between pH* values of ca. 6.5 and 8.5.

The presence of a second monocation M′ in acid or weakly alkaline solution (ca. 3 ≤ pH* ≤ 8) is indicated by the appearance of a second set of ^{1}H NMR signals for the protons of the η⁶-pba ligand at pH* = 3.40. The side chain resonances are recorded at a lower field to those of M, as was previously observed for the analogous protons in [{η⁶-$C_6H_5(CH_2)_3OH$-κ*O*}Ru(phen)](BF$_4$).[1] This suggests that the deprotonated carboxylate group of the tethered arm in **5**′ must also coordinate the ruthenium(II) atom in species M′ (Figure 4). A dimeric structure in which the phenylbutyric acid ligands adopt an η⁶:κ*O*-bridging mode cannot be

 © 2003 Wiley-VCH Verlag GmbH & Co. KGaA, Weinheim

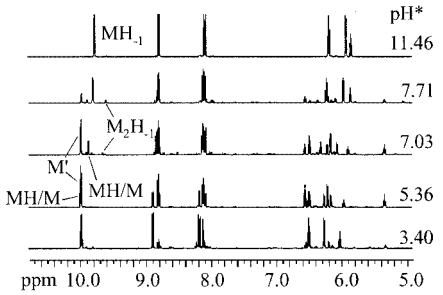

Figure 3. pH dependence of the ^{1}H NMR spectra of [{η-$C_6H_5(CH_2)_3COOH$}Ru(aq) (phen)](OTf)$_2$ (**5′**), where MH represents [(η^6-pba)Ru(H_2O)(phen)]$^{2+}$

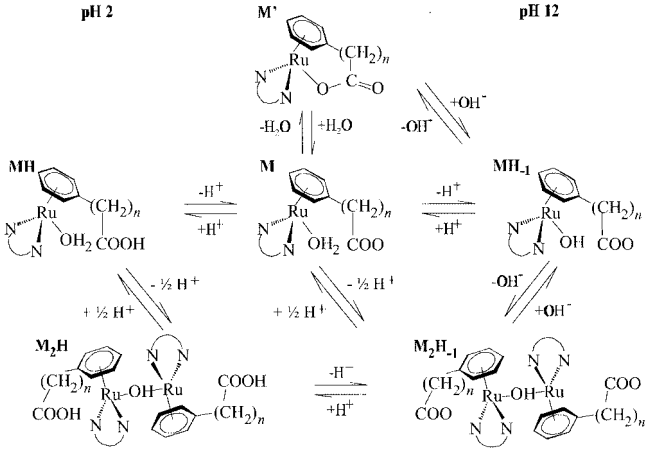

Figure 4. Proposed structures for the species MH/M/MH$_{-1}$, M′, and M_2H/M_2H_{-1} formed by **5′** in aqueous solutions

ruled out with certainty but would appear to be improbable. Neither M′ nor the minor hydroxy-bridged dinuclear species M_2H_{-1} can undergo deprotonation and their ^{1}H NMR signals therefore exhibit no significant shifts in the range $6.5 \leq pH^* \leq 8.5$.

Using the ^{1}H NMR integral values for the 1,10-phen H2/H9 signals it is possible to establish the pH dependence of the individual microspecies MH/M/MH$_{-1}$, M′ and M_2H/M_2H_{-1}. As depicted in Figure 5, the tethered arm chelate M′ clearly predominates in weakly acidic solutions and reaches a concentration maximum at $pH^* \approx 5.5$. The general pH dependence of the macrospecies MH, M/M′, M_2H_{-1}, and MH$_{-1}$ was confirmed by potentiometric pH titrations (Figure 6). Although signals for an analogous tethered arm chelate M′ could also be observed in the ^{1}H NMR spectra of **4b′** in the range $3 \leq pH^* \leq 8$, the concentration of this microspecies is much lower than for that of **5′**. The aqua complex [(η^6-$C_6H_5CH_2COO$)Ru(OH_2)(phen)]$^+$ (M) predominates for **4b′** in weakly acidic solution and even at its concentration maximum the microspecies M′ only accounts for ca 8% of the (η^6-arene)Ru^{II} complexes in solution.

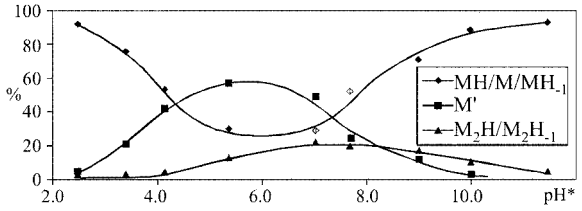

Figure 5. pH-dependent microspecies distribution for **5′** on the basis of the ^{1}H NMR titration data

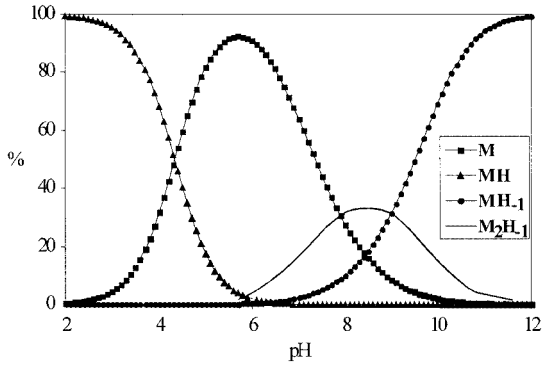

Figure 6. pH-dependent macrospecies distribution for **5′** as determined by potentiometric titration; the following stability constants were obtained from the least-squares refinement with HYPERQUAD:[27] logβ (MH) = 4.40(1), logβ (MH$_{-1}$) = −8.62(1), logβ (M_2H_{-1}) = −4.42(8) for a goodness-of-fit S = 4.6

Amino Acid and Peptide Labelling

We have previously reported the suitability of [(η^6-cymene)Ru(acetone)$_3$]$^{2+}$ for the labelling of aromatic amino acids and their residues in peptides.[17,18] In contrast to the tris(acetonitrile) complex cation [(η^5-C_5Me_5)Ru(CH_3CN)$_3$]$^+$, which delivers the entropically favoured sandwich complex as an insoluble product on treatment with the free aromatic acids phenylalanine (HpheOH), tyrosine (HtyrOH), and tryptophan (HtrpOH) in THF,[15,16] the analogous reaction of [(η^6-cymene)Ru(acetone)$_3$]$^{2+}$ leads predominantly to κ^2*N*,*O*-chelates in CH_2Cl_2 or H_2O. η^6-Coordination of the half-protected or free amino acids can, however, be achieved for the (η^6-cymene)Ru^{II} fragment by employing CF_3COOH as the reaction medium. The protonation of the amino and carboxylato groups under such strongly acidic conditions prevents their incorporation into the Ru^{II} coordination sphere. (η^6-paa)Ru^{II} and (η^6-pba)Ru^{II} sandwich complexes of aromatic amino acids can also be obtained in high yields under analogous reaction conditions and the complexes **6**−**9** are presented as typical examples for η^6-labelling.

The characteristic ^{1}H and ^{13}C NMR spectroscopic data for these sandwich complexes are similar to those of the analogous (*p*-cymene)Ru^{II} complexes.[17,18] For instance, the ^{1}H NMR signals for the aromatic protons of **6** (Scheme 3) all lie in the narrow range δ = 7.00−7.19 ppm. This means that, whereas the pba phenyl proton resonances are shifted downfield by up to ca. 1.2 ppm, the phenylalanine aromatic

 © 2003 Wiley-VCH Verlag GmbH & Co. KGaA, Weinheim

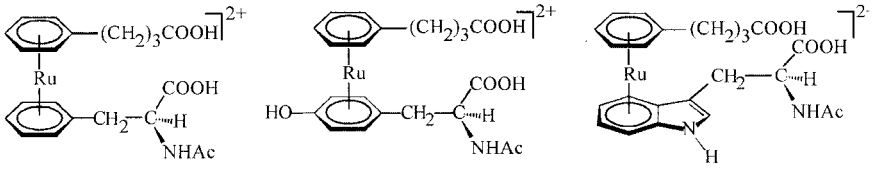

6 **7** **8**

Scheme 3

resonances experience only modest upfield shifts (ca. 0.2 ppm) relative to those of the uncoordinated ligands.[17] η^6-Labelling of tyrosine derivatives leads to a marked enhancement in the acidity of the *p*-hydroxy function, that is effectively fully deprotonated in polar solvents.[18] The associated increase in shielding for the *N*-acetyltyrosine ethyl ester aromatic protons in **7** causes their ^{1}H NMR resonances to move upfield to δ = 6.49/6.57 (*ortho*) and 6.00 (*meta*) in CD_3OD solution. Evidence for the stabilisation of the ketonic form of the η^6-coordinated tyrosine moiety of **7** in polar solvents is also provided by the upfield shift of ca 15 ppm observed for the ^{13}C NMR signal of the *para* carbon atom on going from a [D_3]nitromethane to a [D_4]methanol solution. The possibility of facial chirality leads to the formation of diastereomers of the η^6-ActrpOH sandwich complex **8** in a ca. 1:1 ratio. The pronounced lowfield ^{1}H NMR shifts, for the signals of the pyrrolic protons H5 to δ = 8.24 and 8.28 ppm, are characteristic for the η^6-coordination of the indole moieties in these isomers.

Koefod and Mann[29] demonstrated that kinetically controlled η^6-coordination of the Cp*Ru^{II} moiety leads to a preference for partially localised arene π-systems (e.g. indole) over highly delocalised arenes (e.g. phenyl). This kinetically derived chemospecificity was also observed by us for the reaction of [(η^6-cymene)Ru(acetone)$_3$]$^{2+}$ with the dipeptide HphetrpOH.[18] Exclusive η^6-indole coordination was confirmed during this work for [{η^6-$C_6H_5(CH_2)_3COOH$}Ru(η^6_{ind}-HphetrpOH)]-$(OTf)_2$·CF_3COOH (**9**, Scheme 4), which was obtained in good yield by stirring a 1:1 mixture of [{η^6-$C_6H_5(CH_2)_3COOH$}Ru(acetone)$_3$](OTf)$_2$ with the dipeptide in CF_3COOH solution for 4 h at room temperature. Formation of a mononuclear complex was confirmed by FAB MS and elemental analysis, which also indicated that **9** contains a third counter anion (CF_3COO^-), i.e. that its peptide amino function must be protonated. Both the characteristic lowfield shifts of the indole H5 protons to δ = 8.25 and 8.30 ppm in two diastereomers and the unchanged values of the five phenylalanine aromatic protons (δ = 7.37 ppm) are in accordance with chemospecific tryptophan labelling.

As a result of competitive coordination by amino and/or carboxylate functions and the stability of the predominant hydroxy-bridged dimer [{(η^6-arene)Ru}$_2$(μ-OH)$_3$]$^+$, yields of sandwich complexes of aromatic amino acids are relatively low for [(η^6-cymene)Ru(aq)]$^{2+}$ in weakly acid or alkaline aqueous solution. This state of affairs is illustrated in Figure 7 for the reaction of [(η^6-cymene)Ru(aq)]$^{2+}$ with *N*-

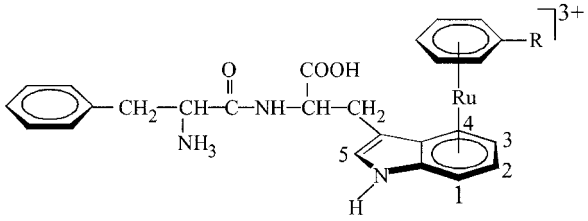

9, R = $(CH_2)_3COOH$

Scheme 4

acetyltryptophan (ActrpOH) in D_2O at pH* = 5.0 and T = 60 °C. Formation of the sandwich complex [(η^6-cymene)Ru(η^6-ActrpOH)]$^{2+}$ was monitored by ^{1}H NMR spectroscopy using the integral values of its characteristic lowfield indole H5 resonances. After 18 h, no further change was observed for the integral ratio of the combined η^6-coordinated indole signals at $\delta \approx$ 8.2 ppm to that at $\delta \approx$ 7.5 ppm for free ActrpOH. The final value corresponds to a 15% yield of the amino acid sandwich complex. Formation of the macrochelates [(η^6-pbaH$_{-1}$-κO)Ru(H_2O)$_2$]$^+$ and [(η^6-pbaH$_{-1}$-κO)Ru(OH)(H_2O)] in weakly acidic solution (see Figure 1b) significantly reduces the concentration of the bis(hydroxy)-bridged species M_2H_{-2} in comparison to the (η^6-cymene)Ru^{II} fragment. Furthermore, intramolecular charge neutralisation in these pendant-arm species should also disfavour competitive κO coordination by amino acid carboxylato functions. Taken together both factors would be expected to lead to an increased level of η^6-labelling as is indeed confirmed in Figure 7 for ActrpOH. A 37% yield of the sandwich complex [(η^6-pba)Ru(η^6-ActrpOH)]$^{2+}$ (**8**) was indicated by the ratio of the indole H5 integral values at ca. 8.2 and δ = 7.5 ppm after 18 h. Employment of a 3:1 excess of [(η^6-pba)Ru(aq)]$^{2+}$ leads to an effectively quantitative η^6-labelling of the aromatic amino acid. This observed water tolerance for direct derivatisation of ActrpOH is analogous to that reported for [{η^5-$C_5H_4(CH_2)_2NH_2$-κN}Ru($CH_3CN)_2$]$^+$ by Grotjahn.[19] The applicability of the (η^6-pba)Ru^{II} fragment to peptide labelling will be the subject of further studies.

Given the presence of suitable functional groups and an adequate stability for classical peptide synthetic conditions, organometallic fragments can be introduced at either the N or C terminus of the bioligand. A range of sandwich complexes have been prepared for this purpose in recent years including the ferrocenylmethyl[30,31] and [(η^5-Cp*)M{η^6-

 © 2003 Wiley-VCH Verlag GmbH & Co. KGaA, Weinheim

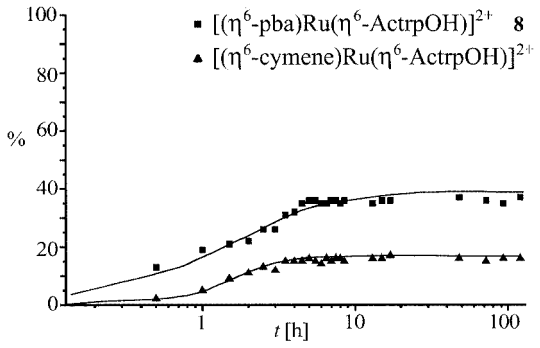

Figure 7. Time dependence for the η^6-labelling of *N*-acetyltryptophan with (a) (η^6-pba)Ru^{II} and (b) (η^6-cymene)Ru^{II} in D_2O solution at pH* = 5.0 and T = 60 °C

$CH_3OC_6H_4(CH_2)_2COOR\}]^{n+}$ (R = *N*-succinimide; M = Ir, n = 2; M = Ru, n = 1) fragments.[32,33] We, therefore, prepared both $[(\eta^6\text{-}C_6Me_6)Ru(\eta^6\text{-ppa})](OTf)_2$ and $[(\eta^6\text{-}C_6Me_6)Ru(\eta^6\text{-pba})](OTf)_2$ (**10**) as potential *N*-terminal labels for peptides. However, preliminary reactivity studies indicated that yields of coupling products for the former complex would be at best very low, as also observed for $[(\eta^5\text{-Cp*})Ir(\eta^6\text{-}CH_3OC_6H_4CH_2COOR)](BF_4)_2$ (R = *N*-succinimide)[32] which also only has one CH_2 group in its pendant arm. Further investigations were, therefore, restricted to the 4-phenylbutyric acid complex **10**, which was prepared by reaction of $[(\eta^6\text{-pba})Ru(acetone)_3](OTf)_2$ with C_6Me_6 in trifluoroacetic acid.

The X-ray structure of the dication of **10** is depicted in Figure 8. Its butyric acid side chain adopts an almost perpendicular position relative to the η^6-coordinated phenyl ring, as indicated by the torsion angle of −93.8(6)° for C11−C16−C17−C18. The asymmetric unit also contains a methanol molecule, whose oxygen atom O51 participates in O111−H···O51 and O51−H51···O hydrogen bonds of length 2.607(4) and 2.741(4) Å, respectively, to neighbouring sandwich cations and OTf^- anions.

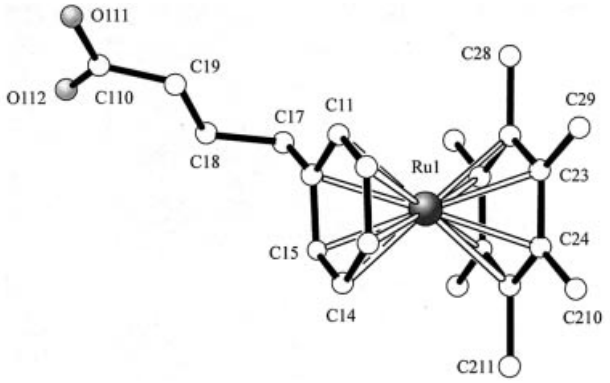

Figure 8. Molecular structure of the cation of $[\{\eta^6\text{-}C_6H_5(CH_2)_3COOH\}Ru(\eta^6\text{-}C_6Me_6)](OTf)_2{\cdot}CH_3OH$ (**10**)

N-Terminal coupling reactions were performed for **10** with HtrpOMe, HpheOMe, and HglyglyOEt by the carbodiimide method in the presence of *N*-[3-(dimethylamino)-propyl]-*N*′-ethylcarbodiimide EDC. The resulting labelled amino acids and peptides were separated in good yields (46−73%) from the reaction mixture by semi-preparative reversed-phase HPLC with pentafluoropropionic acid as an ion-pairing agent. $[(\eta^6\text{-}C_6Me_6)Ru\{\eta^6\text{-}C_6H_5(CH_2)_3C(O)trpOMe\}](OTf)_2$ (**11**), $[(\eta^6\text{-}C_6Me_6)Ru\{\eta^6\text{-}C_6H_5(CH_2)_3C(O)pheOMe\}](OTf)_2$ (**12**), and $[(\eta^6\text{-}C_6Me_6)Ru\{\eta^6\text{-}C_6H_5(CH_2)_3C(O)glyglyOEt\}](OTf)_2$ (**13**) were characterised by FAB MS and $^1H/^{13}C$ NMR spectroscopy (Scheme 5).

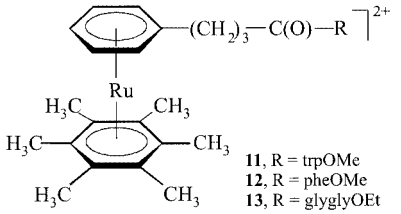

Scheme 5

As depicted for **12** and **13** in Figure 9 the resonances of the five aromatic pba protons at δ ≈ 6.7−6.8 ppm lie in the characteristic spectral window for amino acids and peptides (δ = 4.8−6.8 ppm) and should therefore allow for the adequate quantitative estimates of such labelled peptides in biological systems. Compounds **11**−**13** are soluble in a range of polar solvents and exhibit long-term stability in aqueous solution.

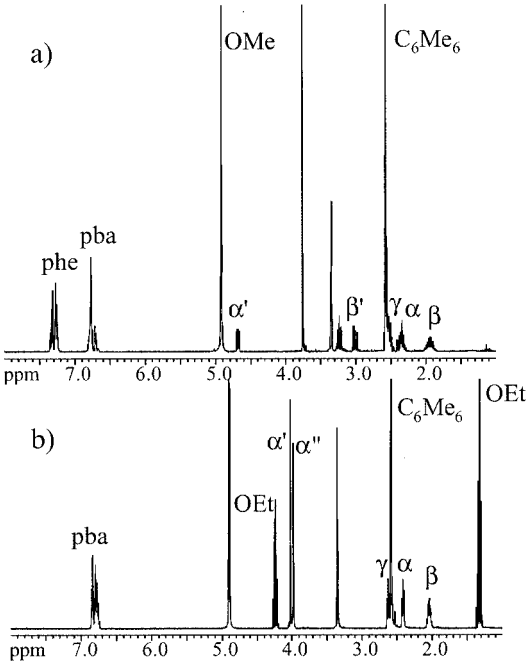

Figure 9. ^1H NMR spectra of (a) $[(\eta^6\text{-}C_6Me_6)Ru\{\eta^6\text{-}C_6H_5(CH_2)_3C(O)pheOMe\}](OTf)_2$ (**12**) and (b) $[(\eta^6\text{-}C_6Me_6)Ru\{\eta^6\text{-}C_6H_5(CH_2)_3C(O)glyglyOEt\}](OTf)_2$ (**13**)

In summary, our present work demonstrates that the pendant-arm fragment $\{\eta^6\text{-}C_6H_4(CH_2)_3COOH\}Ru^{II}$ is eminently suitable for both η^6- and *N*-terminal labelling of amino acids and peptides. The formation of κ*O*-coordinated

 © 2003 Wiley-VCH Verlag GmbH & Co. KGaA, Weinheim

species involving the tethered carboxylate function may, as shown for ActrpOH, favour markedly higher yields of the former type of complex in aqueous solution in comparison with (η^6-cymene)Ru^{II}.

Experimental Section

General: All manipulations and reactions were performed under argon in carefully dried solvents using standard Schlenk techniques. FTIR: Perkin−Elmer 1760X as KBr discs. FAB MS: Fisons VG Autospec with 3-nitrobenzyl alcohol as the matrix. ^1H and ^{13}C NMR spectroscopy: Bruker DRX 400 with chemical shifts reported as δ values relative to the signal of the deuterated solvent. ^{13}C NMR signals for the $CF_3SO_3^-$ anions are observed in the range δ = 121.8−122.8 ppm (q) and are not given for individual complexes. Elemental analyses: Vario EL of Elementar Analysensysteme GmbH. 2,5-Dihydrophenylacetic acid[20] and 2,5-dihydro-3-phenylpropanol[21,22] were prepared as for 2,5-dihydro-4-phenylbutyric acid by Birch reduction of the appropriate phenyl-substituted acid. $RuCl_3·3H_2O$ was purchased from Chempur, amino acids and peptides from Bachem and carboxylic acids from Acros. Potentiometric titrations were performed with a fully automated microprocessor-controlled pH-titration unit (Metrohm 691 with Dosimat 665) in a thermostatted vessel at 25±1 °C under Ar with carbonate-free 0.1 mol·dm^{-3} NaOH. A constant background ionic strength of 0.1 mol·dm^{-3} KNO_3 (p.a.) was employed for all titrations. Further details of the experimental procedure are given in ref.[34] pH* values for ^1H NMR spectra in D_2O were not corrected for deuterium isotope effects. Semipreparative HPLC separations were carried out at an eluent flow rate of 15−25 mL·min^{-1} with a Knauer 64 pump, A0258 sample injector and Merck L-4000A UV detector using columns (25 × 2 cm i.d.) packed with Nucleosil 100-C_{18} (d_p = 10 μm).

2,5-Dihydro-4-phenylbutyric Acid (1): A solution of 4-phenylbutyric acid (9.85 g, 0.06 mol) in diethyl ether (100 mL) was added to a solution of sodium (14.80 g, 0.6 mol) in ammonia (400 mL) at −78 °C. Ethanol (112 mL, 1.80 mol) was added dropwise over 90 min and the solution was stirred until its original blue colour disappeared. After removal of NH_3 and addition of water (200 mL), the product was extracted with diethyl ether following an adjustment to pH = 2 with hydrochloric acid. The diethyl ether phase was then washed with water and dried with $MgSO_4$ before removal of the solvent in vacuo to afford **1**. Yield 8.57 g (86%). $C_{10}H_{14}O_2$ (166.2): calcd. C 72.3, H 8.5; found C 71.7, H 8.2. FAB MS: *m/z* (%) = 166 (38) $[M]^+$, 106 (38) $[M - C_2H_4O_2]^+$, 79 (100) $[M - C_4H_8O_2]^+$. ^1H NMR (CD_3Cl): δ = 1.70 (m, $^3J_{H,H}$ = 7.5 Hz, 2 H, β-CH_2), 2.28 (t, $^3J_{H,H}$ = 7.5 Hz, 2 H, α-CH_2), 2.56 (m, 4 H, CH_2 dihydrophenyl), 5.37 (m, 1 H, CH), 5.63 (m, 2 H, CH), 10.90 (br., 1 H, COOH) ppm. ^{13}C NMR (CD_3Cl): δ = 22.2, 26.7, 28.7, 34.4, 36.6, 119.4, 124.2, 124.2, 133.7, 180.1 ppm.

[{(η^6-$C_6H_5CH_2COOH$)Ru(μ-Cl)Cl}$_2$ (2a): 2,5-Dihydrophenylacetic acid (2.24 g, 16.20 mmol) was added to a solution of $RuCl_3·3H_2O$ (1.06 g, 4.05 mmol) in acetone/water (5:1, 48 mL) and the reaction mixture heated at reflux with stirring for 6 h. After removal of acetone, the deep-red aqueous solution was left to stand at 4 °C to afford a red precipitate of **2a** within 12 h, which was washed with diethyl ether and dried in vacuo. Yield 1.08 g (86%). $C_{16}H_{16}Cl_4O_4Ru_2$ (616.3): calcd. C 31.2, H 2.6, O 10.4; found C 31.0, H 2.6, O 10.7. FAB MS: *m/z* (%) = 580 (16) $[M - Cl]^+$, 546 (10) $[M - 2\ Cl]^+$, 458 (100) $[M - 2\ Cl, - 2\ CO_2]^+$. ^1H NMR (CD_3CN): δ = 3.59 (s, 4 H, α-CH_2), 5.54 (d, $^3J_{H,H}$ = 5.5 Hz, 4 H, *ortho*-H), 5.67 (t, $^3J_{H,H}$ = 5.5 Hz, 2 H, *para*-H), 5.74 (t, $^3J_{H,H}$ = 5.5 Hz, 4 H, *meta*-H) ppm. ^{13}C NMR (CD_3CN): δ = 39.0, 83.0, 84.5, 86.6, 97.3, 175.1 ppm. IR: $\tilde{\nu}$ = 1704 vs. (CO) cm^{-1}. **2a** can also be prepared by alkaline hydrolysis of **2b** at pH = 12.

[{(η^6-$C_6H_5CH_2COOC_2H_5$)Ru(μ-Cl)Cl}$_2$] (2b): 2,5-Dihydrophenylacetic acid (1.68 g, 12.15 mmol) was added to a solution of $RuCl_3·3H_2O$ (1.00 g, 4.05 mmol) in ethanol (60 mL) and the reaction mixture heated at reflux while stirring for 20 min. The resulting red precipitate was filtered, washed with ethanol, and dried in vacuo. Yield 1.34 g (98%). $C_{20}H_{24}Cl_4O_4Ru_2$ (672.4): calcd. C 35.7, H 3.6, O 9.5; found C 35.3, H 3.5, O 9.7. FAB MS: *m/z* (%) = 637 (100) $[M - Cl]^+$. ^1H NMR (CD_3CN): δ = 1.22 (t, $^3J_{H,H}$ = 7.0 Hz, 6 H, OEt), 3.59 (s, 4 H, α-CH_2), 4.14 (dd, $^3J_{H,H}$ = 7.0 Hz, 4 H, OEt), 5.55 (d, $^3J_{H,H}$ = 5.0 Hz, 4 H, *ortho*-H), 5.69 (t, $^3J_{H,H}$ = 5.5 Hz, 2 H, *para*-H), 5.74 (t, $^3J_{H,H}$ = 5.0, 5.5 Hz, 4 H, *meta*-H) ppm. ^{13}C NMR (CD_3CN): δ = 14.4, 39.3, 62.1, 83.2, 84.6, 86.4, 95.6, 170.5 ppm. IR: $\tilde{\nu}$ = 1749 vs. (CO) cm^{-1}.

[{(η^6-$C_6H_5(CH_2)_3COOH$)Ru(μ-Cl)Cl}$_2$] (3): 2,5-Dihydrophenylbutyric acid (2.02 g, 12.15 mmol) was added to a solution of $RuCl_3·3H_2O$ (1.06 g, 4.05 mmol) in acetone/water (5:1, 48 mL) and the reaction mixture heated at reflux while stirring for 6 h. After removal of acetone, the deep-red aqueous solution was left to stand at 4 °C to afford a red precipitate of **3** within 12 h, that was washed with diethyl ether and dried in vacuo. Yield 1.20 g (88%). $C_{20}H_{24}Cl_4O_4Ru$ (672.4): calcd. C 35.7, H 3.6, O 9.5; found C 35.7, H 3.6, O 9.6. FAB MS: *m/z* (%) = 637 (100) $[M - Cl]^+$ 602 (65) $[M - 2\ Cl]^+$. ^1H NMR (CD_3CN): δ = 1.90 (m, $^3J_{H,H}$ = 7.4, 7.0 Hz, 4 H, β-CH_2), 2.38 (t, $^3J_{H,H}$ = 7.4 Hz, 4 H, α-CH_2), 2.56 (t, $^3J_{H,H}$ = 7.0 Hz, 4 H, γ-CH_2), 5.44 (d, 4 H, *ortho*-H), 5.61 (t, 2 H, *para*-H), 5.68 (t, 4 H, *meta*-H) ppm. ^{13}C NMR (CD_3CN): δ = 25.4, 33.3, 33.6, 82.5, 83.1, 84.1, 86.6, 174.5 ppm. IR: $\tilde{\nu}$ = 1711 vs. (CO) cm^{-1}.

[(η^6-$C_6H_5CH_2COOH$)RuCl(1,10-phen)]Cl (4a): 1,10-Phenanthroline (0.441 g, 1.575 mmol) and **2a** (0.462 g, 0.75 mmol) were stirred in ethanol (75 mL) at reflux for 1 h. After cooling, the light-brown product was precipitated by addition of diethyl ether (40 mL) washed with ethanol and diethyl ether and dried in vacuo. Yield 0.610 g (83%). $C_{20}H_{16}Cl_2N_2O_2Ru$ (488.3): calcd. C 49.2, H 3.3, N 5.7, O 6.6; found C 47.6, H 3.2, N 5.4, O 6.7. FAB MS: *m/z* (%) = 453 (100) $[M - Cl]^+$. ^1H NMR (CD_3OD): δ = 5.83 (t, $^3J_{H,H}$ = 6.5 Hz, 1 H, *para*-H), 6.04 (d, $^3J_{H,H}$ = 6.5 Hz, 2 H, *ortho*-H), 6.37 (t, $^3J_{H,H}$ = 6.5 Hz, 2 H, *meta*-H), 8.11 (dd, 2 H, phen H3/8), 8.22 (s, 2 H, phen H5/6), 8.85 (dd, 2 H, phen H4/7), 9.88 (dd, 2 H, phen, H2/9) ppm. ^{13}C NMR (CD_3OD): δ = 39.4, 85.0, 91.3, 107.5, 127.8, 129.0, 132.4, 140.3, 147.7, 157.2, 179.1 ppm. IR: $\tilde{\nu}$ = 1702 vs. (CO) cm^{-1}.

[(η^6-$C_6H_5CH_2COOC_2H_5$)RuCl(1,10-phen)]Cl (4b): Preparation as for **4a** with **2b** (0.504 g, 0.75 mmol) and a reaction time of 2.5 h. Yield of light-brown **4b** 0.651 g (84%). $C_{22}H_{20}Cl_2N_2O_2Ru$ (516.4): calcd. C 51.2, H 3.9, N 5.4, O 6.2; found C 50.5, H 4.0, N 5.4, O 6.9. FAB MS: *m/z* (%) = 481 (100) $[M - Cl]^+$. ^1H NMR (CD_3OD): δ = 1.25 (t, $^3J_{H,H}$ = 7.0 Hz, 3 H, Et), 4.13 (q, $^3J_{H,H}$ = 7.0 Hz, 2 H, Et), 5.99 (t, $^3J_{H,H}$ = 6.0 Hz, 1 H, *para*-H), 6.31 (d, $^3J_{H,H}$ = 6.0 Hz, 2 H, *ortho*-H), 6.38 (t, $^3J_{H,H}$ = 6.0 Hz, 2 H, *meta*-H), 8.12 (dd, 2 H, phen H3/8), 8.22 (s, 2 H, phen H5/6), 8.86 (dd, 2 H, phen H4/7), 9.90 (dd, 2 H, phen H2/9) ppm. ^{13}C NMR (CD_3OD): δ = 14.7, 39.2, 62.9, 85.0, 87.8, 89.5, 100.0, 127.8, 129.0, 132.4, 140.4, 147.6, 157.3, 171.0 ppm. IR: $\tilde{\nu}$ = 1752 vs. (CO) cm^{-1}.

[(η^6-$C_6H_5(CH_2)_3COOH$)RuCl(1,10-phen)]Cl (5): Preparation as for **4a** with **3** (0.504 g, 0.75 mmol) and a reaction time of 1 h. Yield of light-brown **5** 0.712 g (92%). $C_{22}H_{20}Cl_2N_2O_2Ru$ (516.4): calcd. C 51.2, H 3.9, N 5.4, O 6.2; found C 50.4, H 3.8, N 5.2, O 6.4. FAB MS: *m/z* (%) = 481 (100) $[M - Cl]^+$. ^1H NMR (CD_3OD): δ =

 © 2003 Wiley-VCH Verlag GmbH & Co. KGaA, Weinheim

2.01 (m, $^3J_{H,H}$ = 7.1, 7.5 Hz, 2 H, β-CH_2), 2.45 (t, $^3J_{H,H}$ = 7.1 Hz, 2 H, α-CH_2), 2.71 (t, $^3J_{H,H}$ = 7.5 Hz, 2 H, γ-CH_2), 5.91 (t, 1 H, *para*-H), 6.13 (d, 2 H, *ortho*-H), 6.36 (t, 2 H, *meta*-H), 8.13 (dd, 2 H, phen H3/8), 8.23 (s, 2 H, phen H5/6), 8.86 (dd, 2 H, phen H4/7), 9.88 (dd, 2 H, phen H2/9) ppm. ^{13}C NMR (CD_3OD): δ = 26.3, 34.1, 34.4, 83.5, 85.4, 90.5, 99.7, 127.8, 129.0, 132.5, 140.3, 147.6, 157.2, 175.8 ppm. IR: $\tilde{\nu}$ = 1707 vs. (CO) cm^{-1}.

[{η^6-$C_6H_5(CH_2)_3COOH$}Ru(η^6-AcpheOH)]$(CF_3SO_3)_2$ (6): Ag(OTf) (103 mg, 0.4 mmol) was added to a solution of **3** (67.2 g, 0.1 mmol) in acetone (5 mL) and the solution stirred for 20 min. After centrifugation of the precipitated AgCl and removal of acetone, CF_3COOH (5 mL) was added to the resulting [{η^6-$C_6H_5(CH_2)_3COOH$}Ru(acetone)$_3$](OTf)$_2$ and the solution stirred with *N*-acetylphenylalanine (41.4 mg, 0.2 mmol) in CF_3COOH (5 mL) at 50 °C for 5 h. The solution was reduced in volume to 3 mL and the yellow product precipitated with diethyl ether (10 mL), washed with methanol/diethyl ether and dried in vacuo. Yield 140.1 mg (91%). $C_{23}H_{25}F_6NO_{11}RuS_2$ (770.6): calcd. C 35.7, H 3.3, N 1.8, S 8.3; found C 35.5, H 3.0, N 1.5, S 8.2. FAB MS: *m*/*z* (%) = 621 (3) [M − OTf]$^+$, 472 (100) [M − 2 OTf]$^+$. ^{1}H NMR (CD_3OD): δ = 2.01 (s, 3 H, Ac), 2.03 (m, 2 H, β-CH_2 pba), 2.53 (t, $^3J_{H,H}$ = 7.0 Hz, 2 H, α-CH_2 pba), 2.84 (t, $^3J_{H,H}$ = 7.5 Hz, 2 H, γ-CH_2 pba), 3.11, 3.36 (dd, $^2J_{H,H}$ = 14.0, $^3J_{H,H}$ = 7.3 Hz, 2 H, β-CH_2 AcpheOH), 4.81 (dd, $^3J_{H,H}$ = 7.3 Hz, 1 H, α-CH AcpheOH), 7.00−7.15 (mm, 9 H, phenyl), 7.19 (m, 1 H, phenyl) ppm. ^{13}C NMR (CD_3OD): δ = 22.7, 26.4, 33.6, 34.1, 37.6, 54.0, 95.3, 95.6, 96.0, 96.3, 96.4, 96.9, 97.3, 114.8, 119.0, 172.5, 173.7, 176.4 ppm. IR: $\tilde{\nu}$ = 1657, 1701, 1739 vs. (CO) cm^{-1}.

[(η^6-$C_6H_5(CH_2)_3COOH$)Ru(η^6-ActyrOEt)]$(CF_3SO_3)_2$ (7): Preparation as for **6** with *N*-acetyltyrosine ethyl ester (50.3 mg, 0.2 mmol) and 3 h of refluxing in CH_2Cl_2 (10 mL) instead of CF_3COOH. The resulting solid was dissolved in methanol and the product precipitated by addition of diethyl ether. Drying in vacuo afforded the yellow complex **7**. Yield 148.9 mg (91%). $C_{25}H_{29}F_6NO_{12}RuS_2$ (814.7): calcd. C 36.9, H 3.6, N 1.7, S 7.8; found C 36.4, H 3.2, N 1.5, S 8.0. FAB MS: *m*/*z* (%) = 664 (5) [M − OTf]$^+$, 516 (100) [M − 2 OTf]$^+$. ^{1}H NMR (CD_3OD): δ = 1.32 (t, $^3J_{H,H}$ = 7.3 Hz, 3 H, OEt), 2.02 (s, 3 H, Ac), 2.00 (m, 2 H, β-CH_2 pba), 2.53 (t, $^3J_{H,H}$ = 7.0 Hz, 2 H, α-CH_2 pba), 2.68 (t, $^3J_{H,H}$ = 7.4 Hz, 2 H, γ-CH_2 pba), 2.94, 3.14 (dd, $^2J_{H,H}$ = 14.4, $^3J_{H,H}$ = 7.5 Hz, 2 H, β-CH_2 ActyrOEt), 4.26 (q, $^3J_{H,H}$ = 7.3 Hz, 2 H, OEt), 4.77 (dd, $^3J_{H,H}$ = 7.5 Hz, 1 H, α-CH ActyrOEt), 6.00 (m, 2 H, *meta*-H tyr), 6.49, 6.57 (m, 2 H, *ortho*-H tyr), 6.62 (t, 1 H, pba), 6.67 (t, 2 H, pba), 6.76 (d, 2 H, pba) ppm. ^{13}C NMR (CD_3OD): δ = 14.7, 22.7, 26.5, 33.6, 33.8, 36.7, 54.4, 63.5, 81.5, 93.0, 93.4, 94.1, 96.7, 96.9, 103.6, 114.3, 156.8, 171.5, 173.7, 175.2 ppm. IR: $\tilde{\nu}$ = 1629, 1708, 1756 vs. (CO) cm^{-1}.

[{η^6-$C_6H_5(CH_2)_3COOH$}Ru(η^6-ActrpOH)]$(CF_3SO_3)_2$ (8): Preparation as for **6** with *N*-acetyltryptophan (49.26 mg, 0.2 mmol) and 3 h of stirring at 50 °C. Yield 136.0 mg (84%). $C_{25}H_{26}F_6N_2O_{11}RuS_2$ (809.7): calcd. C 37.1, H 3.2, N 3.5, S 7.9; found C 37.5, H 3.5, N 3.2, S 8.1. FAB MS: *m*/*z* (%) = 660 (9) [M − OTf]$^+$, 511 (100) [M − 2 OTf]$^+$. ^{1}H NMR (CD_3OD): δ = 1.90 (m, 2 H, β-CH_2 pba), 2.02, 2.05 (2 s, 3 H, Ac), 2.32 (m, 2 H, α-CH_2 pba), 2.47 (t, $^3J_{H,H}$ = 7.0 Hz, 2 H, γ-CH_2 pba), 3.23 (2 d, 1 H, β-CH_2 ActrpOH), 3.43 (2 dd, 1 H, β-CH_2 ActrpOH), 4.81 (m, 1 H, α-CH ActrpOH), 6.53 (t, 1 H, pba), 6.60−6.70 (m, 5 H, pba/trp), 6.75 (dd, 1 H, trp), 7.74−7.82 (mm, 2 H, trp), 8.24, 8.28 (2 s, 1 H, trp) ppm. ^{13}C NMR (CD_3OD): δ = 22.7, 22.9, 26.1, 27.7, 28.1, 32.5, 33.7, 53.6, 53.7, 82.0, 82.1, 87.4, 87.5, 88.4, 88.5, 88.9, 91.8, 93.0, 93.4, 93.8, 94.7, 104.1, 107.4, 114.0, 114.1, 115.4, 115.5, 144.4, 173.6, 174.0, 176.5 ppm. IR: $\tilde{\nu}$ = 1668, 1748 vs. (CO) cm^{-1}.

[{η^6-$C_6H_5(CH_2)_3COOH$}Ru(η$^6_{ind}$-HphetrpOH)]$(CF_3SO_3)_2$·CF_3COOH (9): Preparation as for **6** with HphetrpOH (70.8 mg, 0.2 mmol) and 4 h of stirring at room temperature. Yield 160.6 mg (78%). $C_{32}H_{33}F_6N_3O_{11}RuS_2$·$CF_3COOH$ (1028.8): calcd. C 39.7, H 3.3, N 4.1, S 6.2; found C 39.4, H 3.7, N 4.0, S 6.4. FAB MS: *m*/*z* (%) = 766 (4) [M − OTf, − CF_3COOH]$^+$, 616 (100) [M − 2 OTf, − CF_3COOH]$^+$. ^{1}H NMR (CD_3OD): δ = 1.98 (m, 2 H, β-CH_2 pba), 2.36 (2 t, 2 H, α-CH_2 pba), 2.47 (2 t, 2 H, γ-CH_2 pba), 3.12 (2 dd, 1 H, β-CH_2 HphetrpOH), 3.44 (2 dd, 1 H, β′-CH_2 HphetrpOH), 4.28 (2 dd, 1 H, α-CH_2 HphetrpOH), 4.81 (m, 1 H, α′-CH_2 HphetrpOH), 6.50−6.78 (mm, 7 H), 7.37 (m, 5 H, phenyl), 7.77 (2 d, 1 H, trp), 7.82 (2 d, 1 H, trp), 8.25, 8.30 (2 s, 1 H, trp) ppm. ^{13}C NMR (CD_3OD): δ = 26.2, 27.7, 27.9, 32.6, 32.7, 33.7, 38.7, 38.8, 53.8, 54.0, 55.8, 55.9, 82.0, 82.1, 87.5, 87.6, 88.4, 88.5, 88.9, 92.0, 93.0, 93.5, 93.8, 94.0, 94.7, 104.0, 104.1, 112.7, 114.0, 114.1, 115.0, 115.1, 129.2, 130.4, 130.9, 135.6, 144.6, 144.7, 170.1, 173.4, 176.6 ppm.

[(η^6-C_6Me_6)Ru{η^6-$C_6H_5(CH_2)_3COOH$}]$(CF_3SO_3)_2$ (10): Preparation as for **6** by stirring [{η^6-$C_6H_5(CH_2)_3COOH$}Ru(acetone)$_3$](OTf)$_2$ (1 mmol) with C_6Me_6 (162 mg, 1 mmol) in CF_3COOH (50 mL) at reflux for 2 h. Yield 701 mg (97%). $C_{24}H_{30}F_6O_8RuS_2$ (725.7): calcd. C 39.7, H 4.2, S 8.8; found C 39.6, H 3.7, S 8.6. FAB MS: (*m*/*z*) (%) = 427 (100) [M − 2 OTf]$^+$. ^{1}H NMR (CD_3OD): δ = 2.00 (m, $^3J_{H,H}$ = 7.0, 8.3 Hz, 2 H, β-CH_2 pba) 2.51(t, $^3J_{H,H}$ = 7.0 Hz, 2 H, α-CH_2 pba), 2.59(s, 18 H, CH_3 C_6Me_6), 2.62 (t, $^3J_{H,H}$ = 8.3 Hz, 2 H, δ-CH_2 pba), 6.72−6.81 (m, 5 H, pba) ppm. ^{13}C NMR (CD_3OD): δ = 17.8, 27.8, 32.1, 33.5, 95.7, 96.3, 96.9, 111.1, 115.2 ppm.

[(η^6-C_6Me_6)Ru{η^6-$C_6H_5(CH_2)_3C(O)trpOMe$}]$(CF_3SO_3)_2$ (11): Compound **10** (108 mg, 0.15 mmol) was added to a solution of HtrpOMe·HCl (42 mg, 0.165 mmol) in CH_2Cl_2 (8 mL). After cooling to −15 °C, EDC (33 mg, 0.165 mmol) and triethylamine (30.7 mg, 0.30 mmol) were added to the suspension which was stirred at this temperature for 12 h and then at room temp. for 4 h. After removal of the solvent, the resulting solid was dissolved in CH_3OH (15 mL) and the product **11** separated by ion-pairing reversed-phase semi-preparative HPLC (Nucleosil 100-C18, d_p = 10 μm; eluent 45% CH_3OH/55% H_2O, 0.1% PFP, 20 mL/min; t_R = 16.9 min). Recrystallisation from CH_3OH afforded 93.0 mg (67%) of **11**. $C_{36}H_{42}F_6N_2O_9S_2Ru$ (925.2): calcd. C 46.7, H 4.6, N 3.0, S 6.9; found C 46.9, H 4.6, N 2.9, S 6.7. FAB MS: (*m*/*z*) (%) = 777 (3) [M − OTf]$^+$, 627 (100) [M − 2 OTf]$^+$. ^{1}H NMR (CD_3OD): δ = 1.91 (m, 2 H, β-CH_2 pba), 2.35 (m, 2 H, α-CH_2 pba), 2.44 (m, 2 H, γ-CH_2 pba), 2.52 (s, 18 H, CH_3 C_6Me_6), 3.22 (dd, 1 H, β′-CH_2 trp), 3.37 (dd, 1 H, β′-CH_2 trp), 3.77 (s, 3 H, OMe), 4.73 (dd, 1 H, α′-CH_2 trp), 6.61 (m, 3 H, pba), 6.72 (2 t, 2 H, bpa), 7.08 (t, 1 H, trp), 7.16 (t, 1 H, trp), 7.19 (s, 1 H, trp), 7.40 (dd, 1 H, trp), 7.58 (dd, 1 H, trp) ppm. ^{13}C NMR (CD_3OD): δ = 17.7, 27.7, 28.5, 32.3, 34.9, 53.2, 55.4, 95.9, 96.0, 96.9, 97.1, 111.2, 111.3, 112.8, 115.0, 119.5, 120.3, 122.9, 125.0, 129.0, 138.4, 174.6, 174.9 ppm.

[(η^6-C_6Me_6)Ru{η^6-$C_6H_5(CH_2)_3C(O)pheOMe$}]$(CF_3SO_3)_2$ (12): Preparation as for **11** with HpheOMe·HCl (33 mg, 0.17 mmol) and **10** (108 mg, 0.15 mmol) as starting compounds. HPLC separation was performed with a 50% CH_3OH/50% H_2O, 0.1% PFP eluent mixture (t_R = 13.1 min). Yield 61.1 mg (46%). $C_{34}H_{41}F_6NO_9S_2Ru$ (886.9): calcd. C 46.0, H 4.7, N 1.6, S 7.2; found C 45.9, H 4.8, N 1.4, S 7.2. FAB MS: (*m*/*z*) (%) = 588 (100) [M − 2 OTf]$^+$. ^{1}H NMR (CD_3OD): δ = 1.94 (m, 2 H, β-CH_2 pba), 2.23 (m, 2 H, α-CH_2 pba), 2.54 (m, 2 H, γ-CH_2 pba), 2.57 (s, 18 H, CH_3 C_6Me_6), 3.00 (dd, 1 H, β′-CH_2 phe), 3.22 (dd, 1 H, β′-CH_2 phe), 3.76 (s, 3 H, OMe), 4.68 (dd, 1 H, α′-CH_2 phe), 6.70 (t, 1 H, pba), 6.77 (m, 4 H, pba), 7.29 (m, 5 H, phe) ppm. ^{13}C NMR (CD_3OD): δ = 17.8,

 © 2003 Wiley-VCH Verlag GmbH & Co. KGaA, Weinheim

27.9, 32.5, 34.9, 38.4, 53.1, 55.8, 96.0, 96.1, 96.2, 97.1, 111.4, 115.0, 128.3, 129.9, 130.5, 138.6, 168.6, 175.0 ppm.

[(η⁶-C_6Me_6)Ru{η⁶-$C_6H_5(CH_2)_3C(O)glyglyOEt$}]$(CF_3SO_3)_2$ (13): Preparation as for **11** with HglyglyOEt·HCl (46.1 mg, 0.165 mmol) and **10** (108 mg, 0.15 mmol) as starting materials. HPLC separation was performed with a 15% CH_3OH/85% H_2O, 0.1% PFP eluent mixture (t_R =20.1 min). Yield 93.4 mg (73%). $C_{30}H_{40}F_6N_2O_{10}S_2Ru$ (867.8): calcd. C 39.9, H 4.8, N 3.3, S 7.6; found C 39.9, H 4.7, N 3.1, S 7.5. FAB MS: (*m*/*z*) (%) = 546 (100) $[M - 2\ OTf]^+$, 379 (29) $[M - 2\ OTf, - glyglyOEt]^+$, 263(26) $[M - 2\ OTf, - C_6H_5(CH_2)_3C(O)glyglyOEt]^+$. ^1H NMR (CD_3OD): δ = 1.32 (t, $^3J_{H,H}$ = 7.6 Hz, 3 H, OEt), 2.04 (2 t, 2 H, β-CH_2 pba), 2.42 (t, $^3J_{H,H}$ = 7.0 Hz, 2 H, α-CH_2 pba), 2.59 (s, 18 H, CH_3 C_6Me_6), 2.62 (t, $^3J_{H,H}$ = 7.9 Hz, 2 H, γ-CH_2 pba), 3.98, 4.01 (2 s, 4 H, α′-,α"-CH_2 gly), 4.24 (q, 2 H, OEt), 6.78 (m, 3 H, pba), 6.84 (m, 2 H, pba) ppm. ^{13}C NMR (CD_3OD): δ = 14.8, 17.8, 27.9, 32.3, 35.0, 42.5, 45.3, 62.7, 96.0, 96.2, 97.1, 111.4, 115.2, 171.7, 172.3, 175.4 ppm.

X-ray Structural Analyses of 4b′ and 10: Crystal and refinement data are summarised in Table 1. Unit cell constants were obtained from least-squares fits to the settings of 25 reflections centred with a Siemens P4 diffractometer. Intensities were collected with the diffractometer at varied speeds using the ω-scan mode for Mo-K_α radiation. Monitored control reflections exhibited no significant alterations in intensity during data collection. Semi-empirical absorption corrections were performed for **4b′** on the basis of ψ scans and the structures solved by direct methods. Refinement against F^2 was performed by SHELX-97[35] with anisotropic temperature factors for non-hydrogen atoms and protons at geometrically calculated positions. Compound **10** contains a methanol molecule in its asymmetric unit. CCDC-195945 and -195946 (**4b′** and **10**) contain the supplementary crystallographic data for this paper. These data can be obtained free of charge at www.ccdc.cam.ac.uk/conts/retrieving.html [or from the Cambridge Crystallographic Data Centre, 12 Union Road, Cambridge CB2 1EZ, UK; Fax: (internat.) + 44-1223/336-033; Email: deposit@ccdc.cam.ac.uk].

Table 1. Crystal and refinement data for **4b′** and **10**

	4b′	**10**·CH_3OH
Empirical formula	$C_{23}H_{20}ClF_3N_2O_5RuS$	$C_{25}H_{34}F_6O_9RuS_2$
M	630.0	757.7
Crystal system	monoclinic	monoclinic
Space group	$P2_1/c$	$P2_1/c$
a [Å]	8.134(5)	13.006(2)
b [Å]	18.878(4)	14.891(2)
c [Å]	15.953(3)	16.091(2)
β [°]	90.00(3)	94.81(6)
V [$Å^3$]	2449.8(8)	3105.4(8)
Z	4	4
F(000)	1264	1544
$P_{calcd.}$ [g/cm^3]	1.708	1.621
Crystal size [mm]	0.39·0.15·0.14	0.60·0.38·0.28
Radiation	Mo-K_α	Mo-K_α
μ [mm^{-1}]	0.895	0.723
$2\theta_{max}$ [°]	25	25
h, *k*, *l* range	9/−0, 0/22, −18/18	−1/14, −1/17, −19/19
Collected reflections	4808	6659
Unique reflections	4313	5388
No. of variables	326	403
R_1 [$I > 2\sigma(I)$]	0.059	0.038
wR_2 (all data)	0.115	0.098
S (goodness-of-fit)	1.005	1.025
max./min. Δρ [e·$Å^3$]	0.38/−0.38	0.40/−0.49

[1] Y. Miyaki, T. Onishi, H. Kurosawa, *Inorg. Chim. Acta* **2000**, *300*, 369−377.
[2] Y. Miyaki, T. Onishi, S. Ogoshi, H. Kurosawa, *J. Organomet. Chem.* **2000**, *616*, 135−139.
[3] T. Ohnishi, Y. Miyaki, H. Asano, H. Kurosawa, *Chem. Lett.* **1999**, 809−810.
[4] M. A. Bennett, L. Y. Goh, A. C. Willis, *J. Chem. Soc., Chem. Commun.* **1992**, 1180−1182.
[5] B. Therrien, T. R. Ward, M. Pilkington, C. Hoffmann, F. Gilardoni, J. Weber, *Organometallics* **1998**, *17*, 330−337.
[6] P. D. Smith, A. H. Wright, *J. Organomet. Chem.* **1998**, *559*, 141−147.
[7] A. Fürstner, M. Liebl, C. W. Lehmann, M. Picquet, R. Kunz, C. Bruneau, D. Touchard, P. H. Dixneuf, *Chem. Eur. J.* **2000**, *6*, 1847−1857.
[8] M. A. Bennett, A. J. Edwards, J. R. Harper, T. Khimyak, A. C. Willis, *J. Organomet. Chem.* **2001**, *629*, 7−18.
[9] J. H. Nelson, K. Y. Ghebreyessus, V. C. Cook, A. J. Edwards, W. Wielandt, S. B. Wild, A. C. Willis, *Organometallics* **2002**, *21*, 1727−1733.
[10] H. Dialer, P. Mayer, K. Polborn, W. Beck, *Eur. J. Inorg. Chem.* **2001**, 1051−1055.
[11] M. A. Bennett, A. K. Smith, *J. Chem. Soc., Dalton Trans.* **1974**, 233−241.
[12] P. Pertici, P. Salvadori, A. Biasci, G. Vitulli, M. A. Bennett, L. A. P. Kane-Maguire, *J. Chem. Soc., Dalton Trans.* **1988**, 315−320.
[13] K. Severin, R. Bergs, W. Beck, *Angew. Chem. Int. Ed.* **1998**, *37*, 1634−1654.
[14] D. B. Grotjahn, *Coord. Chem. Rev.* **1999**, *190*, 1125−1141.
[15] W. S. Sheldrick, A. J. Gleichmann, *J. Organomet. Chem.* **1994**, *470*, 183−187.
[16] A. J. Gleichmann, J. M. Wolff, W. S. Sheldrick, *J. Chem. Soc., Dalton Trans.* **1995**, 1549−1554.
[17] J. M. Wolff, W. S. Sheldrick, *J. Organomet. Chem.* **1997**, *531*, 141−149.
[18] J. M. Wolff, W. S. Sheldrick, *Chem. Ber./Recueil* **1997**, *130*, 981−988.
[19] D. B. Grotjahn, C. Joubran, D. Combs, D. C. Brune, *J. Am. Chem. Soc.* **1998**, *120*, 11814−11815.
[20] H. S.-I. Chao, G. A. Berchthold, *J. Org. Chem.* **1981**, *46*, 1191−1194.
[21] D. Johnson, J. W. Smart, J. K. Sutherland, *J. Chem. Soc., Chem. Commun.* **1977**, 497−498.
[22] B. B. Snider, T. C. Kirk, *J. Am. Chem. Soc.* **1983**, *105*, 2364−2368.
[23] M. Stebler-Röthlisberger, A. Ludi, *Polyhedron* **1986**, *5*, 1217−1221.
[24] M. Stebler-Röthlisberger, W. Hummel, P.-A. Pittet, H.-B. Bürgi, A. Ludi, A. E. Merbach, *Inorg. Chem.* **1988**, *27*, 1358−1363.
[25] F. C. Pigge, J. J. Coniglio, *Curr. Org. Chem.* **2001**, *5*, 757−784.
[26] J. R. Miura, J. B. Davidson, G. C. Hincapié, D. J. Burkey, *Organometallics* **2002**, *21*, 584−586.
[27] E. L. Muetterties, J. R. Bleeke, E. J. Wucherer, T. A. Albright, *Chem. Rev.* **1982**, *82*, 499−525.
[28] A. Sabatini, A. Vacca, P. Gans, *Talanta* **1996**, *43*, 1739−1753.
[29] R. S. Koefod, K. R. Mann, *J. Am. Chem. Soc.* **1990**, *112*, 7287−7923.
[30] D. Freiesleben, K. Polborn, C. Robl, K. Sünkel, W. Beck, *Can. J. Chem.* **1995**, *73*, 1164−1174.

 © 2003 Wiley-VCH Verlag GmbH & Co. KGaA, Weinheim

[31] A. Hess, J. Sehnert, T. Weyhermüller, N. Metzler-Nolte, *Inorg. Chem.* **2000**, *39*, 5437−5443.
[32] H. El Amouri, M. Gruselle, J. Vaissermann, M. McGlinchey, G. Jaouen, *J. Organomet. Chem.* **1995**, *485*, 79−84.
[33] H. El Amouri, S. Canceil, Y. Besace, L. Richard, *Organometallics* **1996**, *15*, 2303−2307.
[34] W. Wirth, J. Blotevogel-Baltronat, U. Kleinkes, W. S. Sheldrick, *Inorg. Chim. Acta* **2002**, *339*, 14−26.
[35] G. M. Sheldrick, *SHELX-97, program for structure solution and refinement*, Göttingen, Germany, **1997**.

Received October 29, 2002

 © 2003 Wiley-VCH Verlag GmbH & Co. KGaA, Weinheim

Formation of Ruthenium−Aminocarbene Complexes from Aldimines and Aminals

Christina M. Standfest-Hauser,[a] Kurt Mereiter,[b] Roland Schmid,[a] and Karl Kirchner*[a]

Keywords: Carbenes / Density functional calculations / N ligands / Ruthenium

Specific pyridine-based aldimines and aminals act as chelating ligands towards the RuCpL and RuTpL (Tp = hydrido trispyrazolylborate) fragments giving κ^2N,N'-coordinated cyclic imine complexes. Under particular conditions, as elucidated in this paper, these complexes rearrange into cyclic aminocarbene complexes. Thus, the reaction of $[RuCp(L)(CH_3CN)_2]PF_6$ (L = CH_3CN, PMe_3, $SbPh_3$) with 1 equiv. of py–N=CHR [R = Ph (phenyl), Fc (ferrocenyl), Np (naphthyl)] affords the cyclic aminocarbene complexes $[RuCp(L)(=C(R)NH–py)]PF_6$, whereas when L = PPh_3, P*i*Pr_3, and CO the reaction stops at the stage of the imine complex $[RuCp(L)(\kappa^2N,N'$-py–N=CHR$)]PF_6$. Analogously, [RuTp(COD)Cl] (COD = 1,5-cyclooctadiene) also reacts readily with the imines py–N=CHR (R = Ph, *p*$MeOC_6H_4$, Np) at elevated temperatures to yield the aminocarbene complexes [RuTp{=C(R)NH–py}Cl]. This process may open a new synthetic route for obtaining carbene complexes. The mechanism of the imine–aminocarbene conversion was analyzed by DFT/B3LYP calculations. Accordingly, the operation of a direct 1,2 hydrogen shift can be ruled out; the reaction seems to involve hydrido iminoacyl intermediates resulting from C–H bond activation and deprotonation/protonation steps.
(© Wiley-VCH Verlag GmbH & Co. KGaA, 69451 Weinheim, Germany, 2003)

Introduction

It is highly fascinating to witness the vast and diversified varieties of rearrangements within and between molecules ligated to a transition metal center. In a recent communication,[1] we reported the conversion of an aldimine to an amino carbene (Scheme 1, top). This conversion is analogous to the rearrangement of a coordinated olefin to a carbene (Scheme 1, bottom).[2] Both of these processes involve a formal 1,2 hydrogen shift whose intimate mechanism remains unknown. For the olefin−carbene conversion, the presence of a heteroatom X featuring a strong π-donor group is of crucial importance. In fact, if X = H, alkyl, or aryl, the reverse process is more favorable.[3]

In a previous report,[1] we reacted the complex $[RuCp(L)(CH_3CN)_2]PF_6$, where L = CH_3CN, PMe_3, PPh_3, or CO, with (*E*)-*N*-(phenylmethylene)-2-pyridine amine (py−N=CHPh). The outcome of the reaction varied with the nature of the co-ligand L. Whereas [RuCp(L){=C(Ph)NH−py}]PF_6 was obtained when CH_3CN and PMe_3 were employed, the reaction stops at the stage of the imine complex $[RuCp(L)(\kappa^2N,N'$-py−N=CHR$)]PF_6$ with L = PPh_3 and CO. Similarly, [RuTp(COD)Cl] (Tp = hydrido trispyrazolylborate, COD = 1,5-cyclooctadiene) reacts readily with py−N=CHPh at elevated temperatures to give the aminocarbene complex [RuTp{=C(Ph)NH−py}Cl].

Our goal was to extend the scope of the above reactions to better understand the reasons for the intriguing imine−aminocarbene conversion. Towards this goal, we have used other imines with the general structure py−N=CHR, viz. R = ferrocenyl (Fc) and naphthyl (Np), and also py−CH_2−N=CHPh. Furthermore, we also used pyridine-based aminals which are known to be capable of forming amino carbenes by C−N and N−H bond cleavage and amine elimination.[4,5] We have included also P*i*Pr_3 and $SbPh_3$ as co-ligands to see whether the ligand size changes the reaction outcome. Finally, DFT/B3LYP calculations were performed to back up the mechanistic suggestions.

[a] Institute of Applied Synthetic Chemistry, Vienna University of Technology,
Getreidemarkt 9, 1060 Vienna, Austria
Fax: (internat.) + 43-1/58801-15499
E-mail: kkirch@mail.zserv.tuwien.ac.at
[b] Institute of Chemical Technologies and Analytics, Vienna University of Technology,
Getreidemarkt 9, 1060 Vienna, Austria

Results and Discussion

Synthesis and Characterization

Treatment of $[RuCp(L)(CH_3CN)_2]PF_6$ [L = CH_3CN (**1**), PMe_3 (**2a**)] with 1 equiv. of py−N=CHR [R = Ph (phenyl), Fc (ferrocenyl), Np (naphthyl)] afforded the aminocarbene

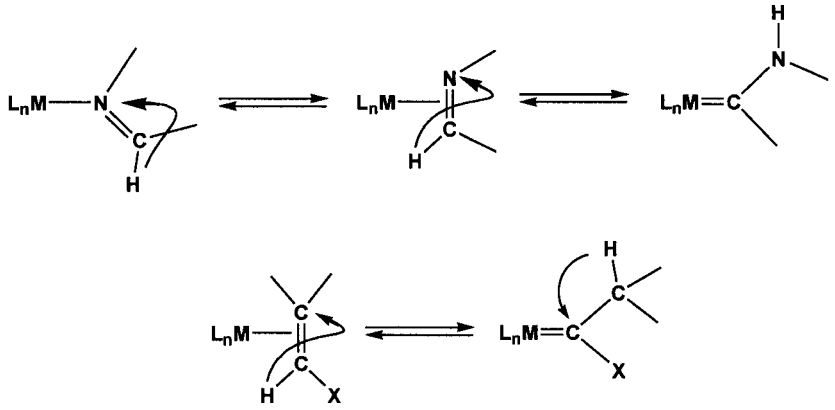

Scheme 1

complexes [RuCp(L){=C(R)NH−py}]PF_6 (**8a−c**, **9a−c**) in high yields (Scheme 2). A similar transformation between [RuCp($SbPh_3$)(CH_3CN)$_2$]PF_6 (**3**) and py−N=CHFc leads to the aminocarbene complex [RuCp($SbPh_3$){=C(Fc)-NH−py}]PF_6 (**10**). Analogously, [RuTp(COD)Cl] (**5**) also readily reacts with the imines py−N=CHR (R = Ph, *p*Me-OC_6H_4, Np) at elevated temperatures to yield the aminocarbene complexes [RuTp{=C(R)NH−py}Cl] (**11a−c**) (Scheme 3). The ferrocenyl-based imine py−N=CHFc was not stable under the reaction conditions. We note that no carbene complexes were obtained from **1−3** by reaction with monodentate aldimines RN=CHR′ (R = Ph, *i*Pr; R′ = Ph, *i*Pr).

All of the carbene complexes formed are air-stable, in both solution and in the solid state, with the exception of **8a−c**, and were characterized by ^1H, $^{13}C\{^1H\}$, and $^{31}P\{^1H\}$ NMR spectroscopy and elemental analysis. In the $^{13}C\{^1H\}$ NMR spectra of **8−10**, the carbene moiety is identified by downfield signals in the range of δ = 263.2 to 281.4 ppm. Other spectral changes accompanying the transformation to aminocarbene complexes include a characteristic broad resonance between δ = 11.8 and 13.2 ppm assignable to the NH proton.

The solid-state structure of **11a** was determined by single-crystal X-ray diffraction. An ORTEP diagram is depicted in Figure 1 with some bond lengths reported in the caption.

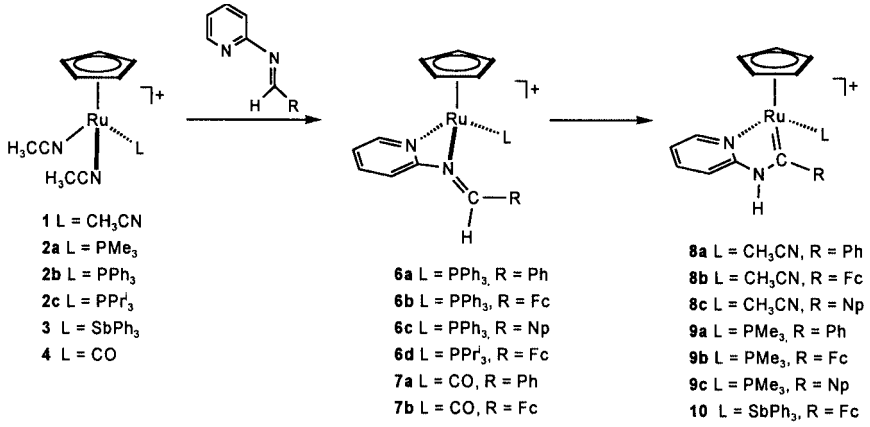

Scheme 2

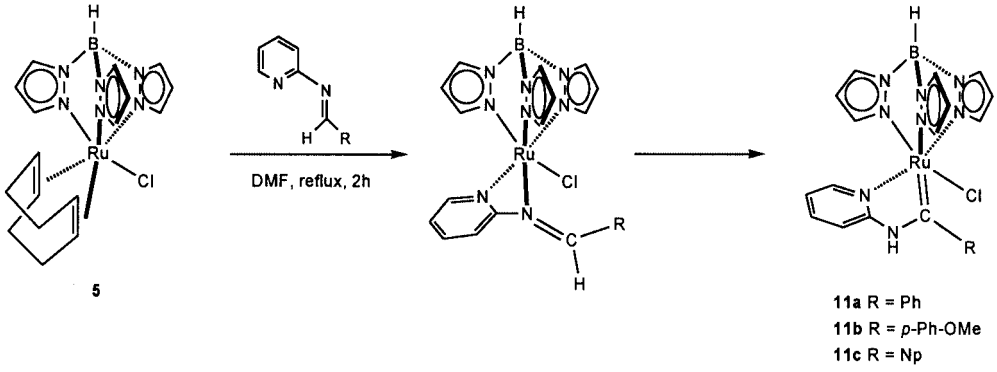

Scheme 3

 © 2003 Wiley-VCH Verlag GmbH & Co. KGaA, Weinheim

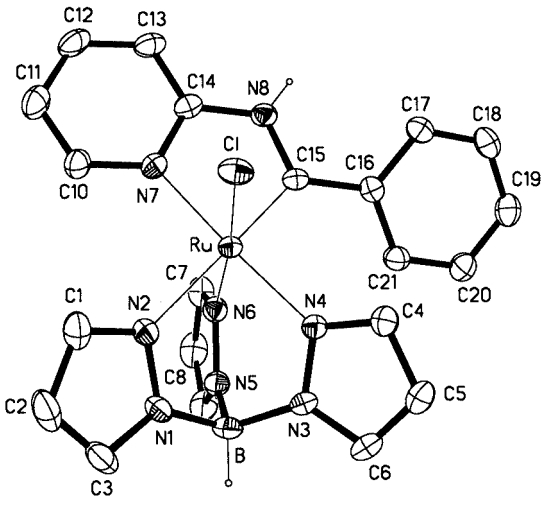

Figure 1. Structural view of **11a** showing 20% thermal ellipsoids (aromatic H atoms omitted); selected bond lengths (Å) and angles (°): Ru−N(2) 2.210(3), Ru−N(4) 2.074(3), Ru−N(6) 2.048(3), Ru−N(7) 2.046(3), Ru−Cl 2.414(1), Ru−C(15) 1.915(3), C(15)−Ru−N(7) 79.7(1), C(15)−Ru−N(6) 92.8(1), C(15)−Ru−N(4) 92.2(1), C(15)−Ru−N(2) 176.6(1), C(15)−Ru−Cl 94.1(1)

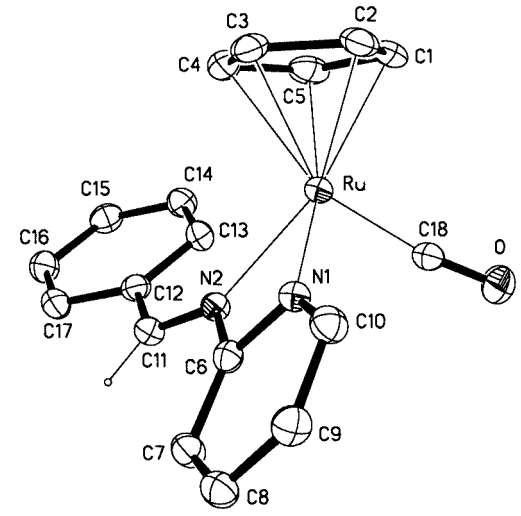

Figure 3. Structural view of **7a** showing 50% thermal ellipsoids (aromatic H atoms and PF_6^- ions omitted for clarity); selected bond lengths (Å) and angles (°): Ru−C(1−5)$_{av}$ 2.201(2), Ru−C(18) 1.876(2), Ru−N(1) 2.125(2), Ru−N(2) 2.167(2), N(2)−C(11) 1.288(3), C(18)−O 1.144(2), N(1)−Ru−N(2) 62.8(1), Ru−C(18)−O 171.6(1)

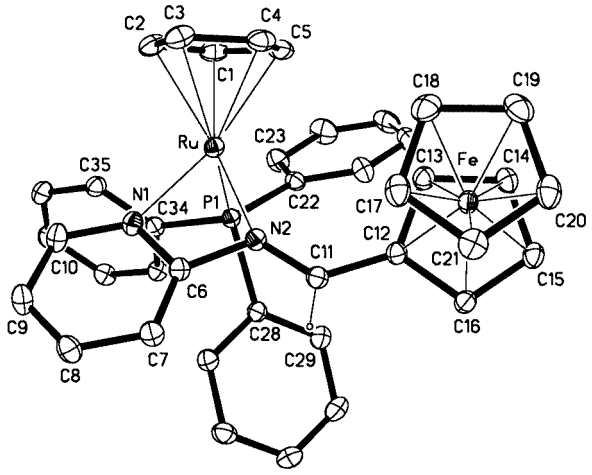

Figure 2. Structural view of **6b**·$(CH_3)_2CO$ showing 40% thermal ellipsoids [aromatic H atoms, PF_6^- and $(CH_3)_2CO$ omitted for clarity]; selected bond lengths (Å) and angles (°): Ru−C(1−5)$_{av}$ 2.186(2), Ru−P(1) 2.310(1), Ru−N(1) 2.104(1), Ru−N(2) 2.168(1), N(2)−C(11) 1.294(2), N(1)−Ru−N(2) 62.2(1)

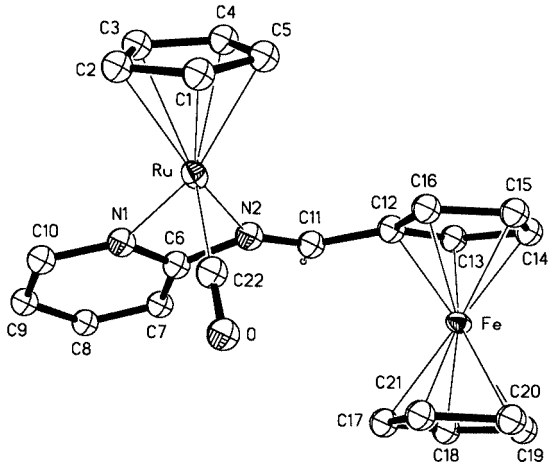

Figure 4. Structural view of **7b** showing 50% thermal ellipsoids (aromatic H atoms and PF_6^- ions omitted for clarity); selected bond lengths (Å) and angles (°): Ru−C(1−5)$_{av}$ 2.174(11), Ru−C(22) 1.846 (10), Ru−N(1) 2.080(9), Ru−N(2) 2.133(8), N(2)−C(11) 1.267(11), C(22)−O 1.139(11), N(1)−Ru−N(2) 60.3(3), Ru−C(22)−O 176.1(11)

The coordination geometry is distorted octahedral with all angles at ruthenium between 79 and 98° and 172 and 176°. The two Ru−N(Tp) bond lengths cis to the carbene moiety are significantly shorter [Ru−N(4) = 2.074(3) Å, Ru−N(6) = 2.048(3) Å] than that trans to the carbene moiety [Ru−N(2) = 2.210(3) Å]. The Ru−N(py) and Ru−Cl bond lengths are 2.046(3) and 2.414(1) Å. The Ru−C(15) bond length is 1.915(3) Å, which is similar to that in other heteroatom-stabilized ruthenium carbene complexes (cf. 1.959(1) Å in **9a**[1]). The C(15)−Ru−N(7) angle is 79.1(1)°.

If the ligand L in $[RuCp(L)(CH_3CN)_2]PF_6$ is relatively bulky, such as PPh_3 or P*i*Pr$_3$, or if it is a relatively strong π acceptor, as in the case of CO, the reaction with py−N=CHR does not result in the formation of aminocarbene complexes. Instead, and in keeping with previous results,[1] the complexes $[RuCp(L)(\kappa^2N,N'\text{-py}-N{=}CHR)]PF_6$ (**6a**−**d**, **7a**,**b**) are obtained according to Scheme 2. In view of the strained four-membered N−Ru−N−C ring system, it is noteworthy that no rearrangement to carbene complexes is observed, even at elevated temperature for 24 h. Complexes **6** and **7** were characterized by NMR spectroscopy and elemental analysis. In addition, the structures of **6b**, **7a**, and **7b** were determined by X-ray crystallography and are presented in Figure 2, Figure 3 and Figure 4. The overall structures are very similar and they can be described as three-legged piano stool conformations with the two N atoms of the imine ligand and the PPh_3 and CO ligands, respectively, as the legs. The N−Ru−N angles in **6b**, **7a**, and **7b** are

 © 2003 Wiley-VCH Verlag GmbH & Co. KGaA, Weinheim

62.2(1), 62.8(1), and 60.3(3)°, respectively. The four-membered N−Ru−N−C ring system is essentially planar with torsion angles of 2.5(1), −2.1(1), and −1.4(5)°.

Notwithstanding these stable structures, the relief of the strain of the four-membered N−Ru−N−C ring might be a factor that favors the rearrangement of the κ^2NN imine into the aminocarbene complex. In fact, the imine complex derived from py−CH_2−N=CHR, rather than py−N=CHR, that features a five-membered N−Ru−N−C−C ring instead of a four-membered one, does not convert into the aminocarbene, even if kept for long times at elevated temperatures. This lack of reactivity is the case for [RuCp(CH_3CN)(κ^2*N*,*N*′-py−CH_2−N=CHPh)]PF_6 (**12**) and [RuTp(κ^2*N*,*N*′-py−CH_2−N=CHPh)Cl] (**13**) that are obtained from **1** and **5**, respectively (Schemes 4 and 5). A structural view of **12** is given in Figure 5 with selected bond lengths reported in the caption. This complex can be described in terms of a three-legged piano stool conformation with the two N atoms of the imine ligand and the N atom of the CH_3CN ligand as the legs. It is worth noting that the N−Ru−N angle [77.8(1)°] is considerably larger than those in **6b**, **7a**, and **7b**.

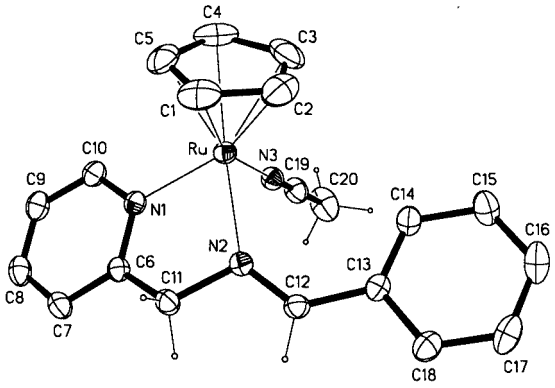

Figure 5. Structural view of **12** showing 50% thermal ellipsoids (aromatic H atoms and PF_6^- ions omitted for clarity); selected bond lengths (Å) and angles (°): Ru−C(1−5)$_{av}$ 2.153(3), Ru−N(1) 2.104(1), Ru−N(2) 2.117(1), Ru−N(3) 2.077(1), N(1)−Ru−N(2) 77.8(1), Ru−N(3)−C(19) 178.9(3)

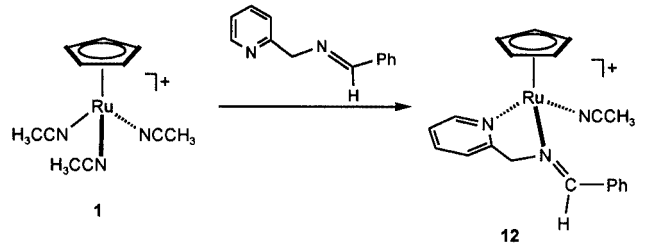

Scheme 4

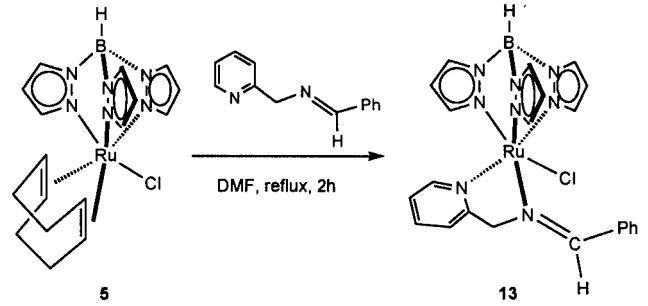

Scheme 5

The generality of cyclic aminocarbene construction is further implied by the finding that aminals also react with the RuCpL and RuTpL fragments to form the corresponding aminocarbene complexes. In these reactions, the aminal at first obviously transforms back into the starting aldimines and amines. Thus, **1** and **2** react with *N*,*N*′-bis(2-pyridyl)-1,1-propanediamine [py−NHCH(Et)NH−py] and *N*,*N*′-bis(2-picolyl)-1,1-propanediamine [pyMe-NHCH(Et)-NH−pyMe] to form [RuCp(py−NH_2){=C(NH−py)Et}]-PF_6 (**14a**), [RuCp(pyMe-NH_2){=C(NH−pyMe)Et}]PF_6 (**14b**), and [RuCp(PMe_3)(=C(NH−py)Et]PF_6 (**15**) in high yields (Scheme 6). Interestingly, with **2b** the reaction does not stop at the aminocarbene stage, but proceeds further to give the olefin complex **16**. Such a mode of rearrangement is a common decomposition pathway of electron-deficient carbene complexes.[3] A structural view of **16**, determined

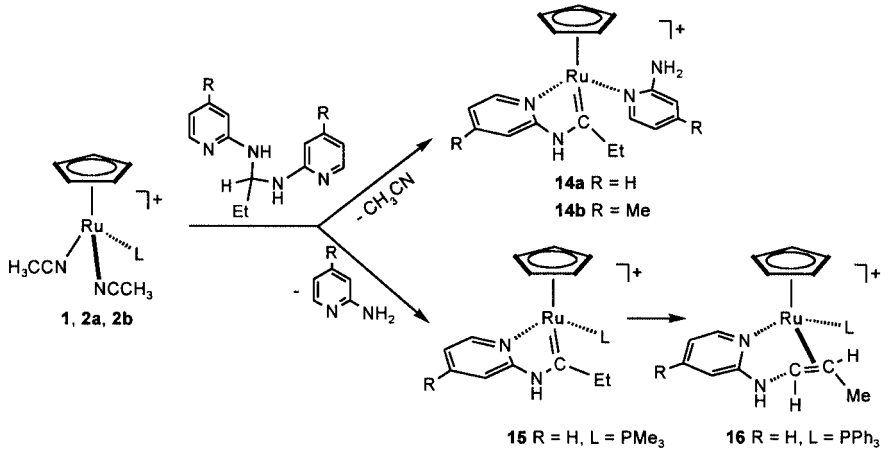

Scheme 6

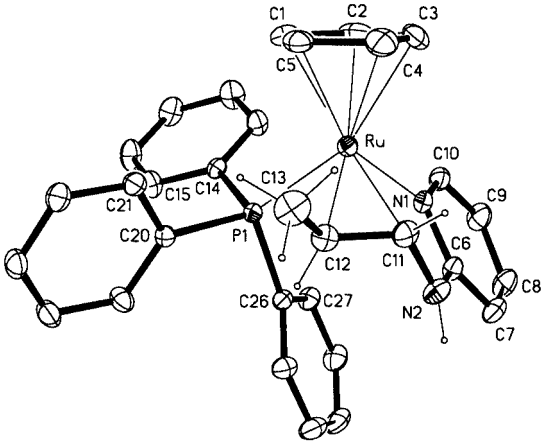

Figure 6. Structural view of **16** showing 20% thermal ellipsoids (aromatic H atoms and PF_6^- ions omitted for clarity); selected bond lengths (Å) and angles (°): Ru−C(1−5)$_{av}$ 2.224(4), Ru−P(1) 2.348(1), Ru−N(1) 2.122(1), Ru−C(11) 2.171(3), Ru−C(12) 1.272(3), C(11)−C(12) 1.383(5), N(1)−Ru−C(11) 76.1(1)

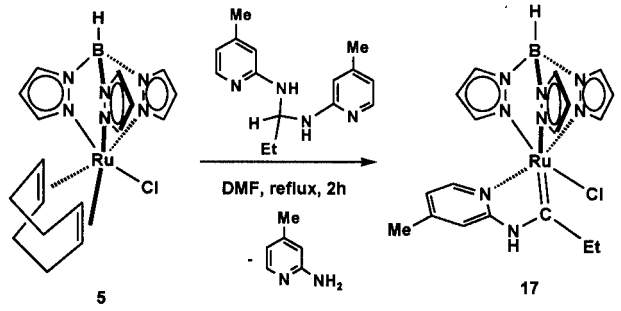

Scheme 7

by X-ray crystallography, is shown in Figure 6 with selected bond lengths reported in the caption. Similarly, [RuTp(COD)Cl] (**5**) reacts with pyMe-NHCH(Et)NH-pyMe to give [RuTp{=C(NH−pyMe)Et}Cl] (**17**) as shown in Scheme 7. These reactions involve both C−H and C−N activation steps, which thereby release a 2-aminopyridine molecule. It may be pertinent to note that **2b** does not react with py−N=CHPh to form an aminocarbene complex or a rearrangement product thereof.

Mechanistic Aspects

In the absence of detectable intermediate products on the way from the κ^2NN-imine to the aminocarbene complexes, we performed DFT (B3LYP) calculations using py−N=CH_2 and HCN as model ligands. Along these lines, several key intermediates can be proposed and these are depicted in Scheme 8 (energy in kcal/mol). The overall reaction is exothermic by 8.0 kcal/mol. The reliability of the computational method (details in the Exp. Sect.) is supported by the good agreement between the calculated geometries of **A** and **F** (Figure 7) with the X-ray structures for the related complexes (**6a**, **6b**, **7a**, **7b**, and **9a**).

At first, the imine moiety of the κ^2N,N'-py−N=CH_2 complex **A** becomes side-on coordinated (**B**). The endothermic nature of this step (8.3 kcal/mol) points to the preference for end-on coordination, although the activation barrier is relatively low (12.8 kcal/mol). Next, an agostic C−H bond is formed (**C**) that is energetically unfavorable by 4.9 kcal/mol. In proceeding from **A** to **C**, a rotation about the −N=CH_2 bond takes place that moves the substituent (hydrogen in the model system) from a syn position to an anti one, with respect to the metal center. Subsequent C−H bond activation leads eventually to the hydrido iminoacyl intermediate **D**.[6−8] This process is slightly endothermic by 1.2 kcal/mol and has a small activation barrier (2.3 kcal/mol). Such types of intermediates have been suggested recently for the reaction of [RuHCl(P*i*Pr$_3$)$_2$]$_2$ also

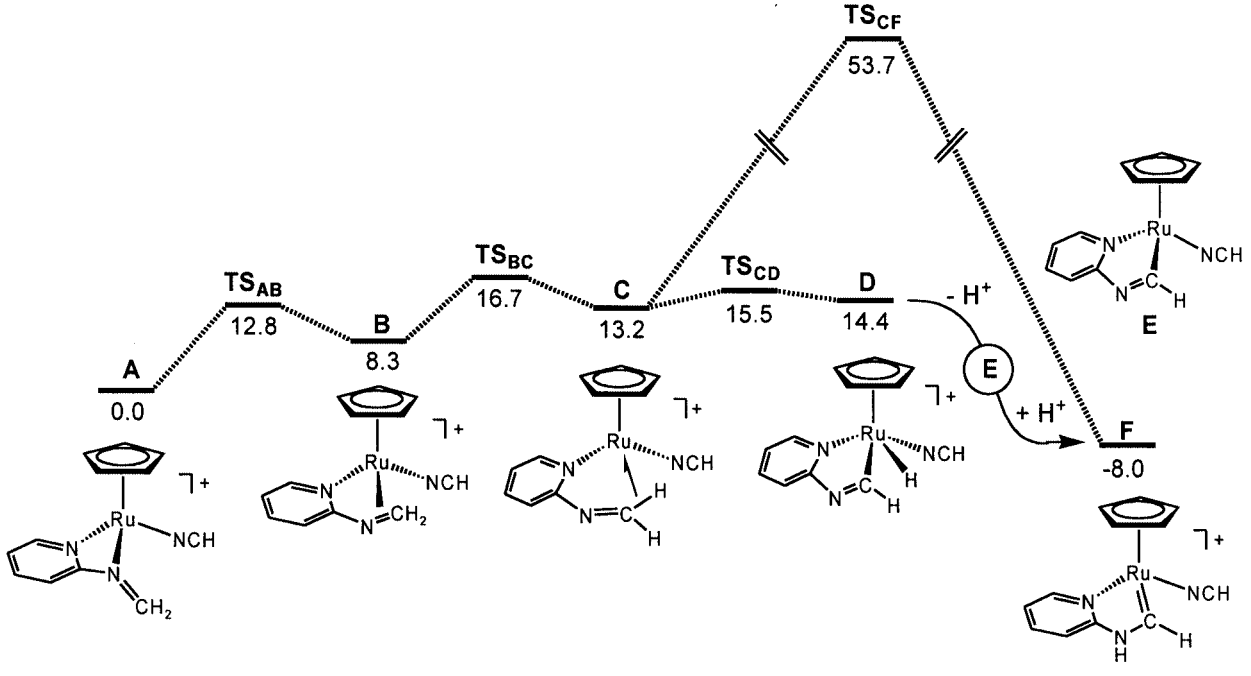

Scheme 8

 © 2003 Wiley-VCH Verlag GmbH & Co. KGaA, Weinheim

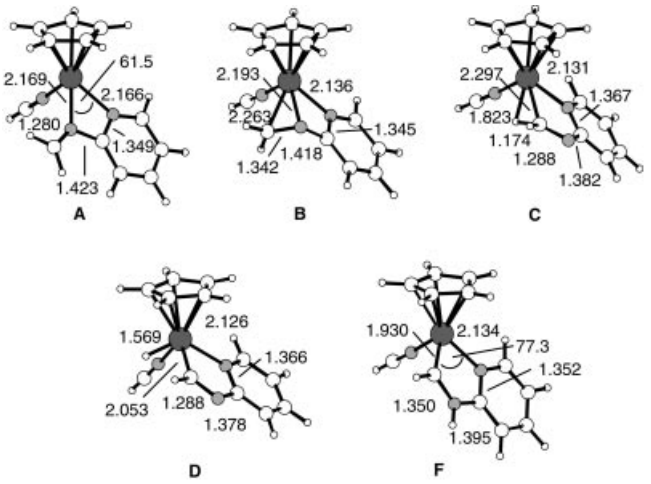

Figure 7. Optimized B3LYP geometries of the equilibrium structures **A**, **B**, **C**, **D**, and **F** (distances in Å and angles in deg)

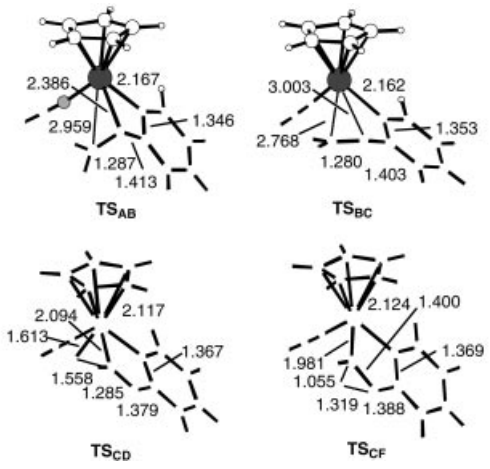

Figure 8. Optimized B3LYP geometries of the transition states TS_{AB}, TS_{BC}, TS_{CD}, and TS_{CF} (distances in Å)

with imines, in which case, however, isocyanides are formed and not aminocarbenes.[9]

It appears that the step from **C** to **D** involving C−H activation/oxidative addition, is particularly crucial to the overall imine-to-aminocarbene transformation. The reactivity of the imine complex is arguably lessened in the case of sterically demanding co-ligands like PPh_3 in **2b** and P*i*Pr$_3$ in **2c**. Note that the cone angle[10] increases in the order $CH_3CN < PMe_3 < SbPh_3 < PPh_3 < PiPr_3$. Alternatively, the presence of a strongly π-accepting co-ligand, such as CO, in **4** may prevent the oxidative addition step. The structures of the entities **A**−**F** as well as the corresponding transition states TS_{AB}−TS_{CF} are shown in Figure 7 and Figure 8.

The mechanism that is least clear is that for the onward reaction from **D** to **F**. According to our DFT calculations, a direct 1,2 hydrogen shift has a barrier as high as 53.7 kcal/mol and, thus, it is safe to exclude it. Alternative possibilities include the intermediacy of a neutral imino acyl complex **E** or, more appealingly, deprotonation/protonation assisted by adventitious water, counterion, or solvent. We favor a hydrogen-transfer pathway based on the implication of water as depicted in Scheme 9. Such a process, though in need of verification, would be consistent with the proton-transfer catalysis of water molecules arranged in cyclic aggregates that have been suggested, for example, for the dehydration of carbonic acid[11] or the hydration of sulfur trioxide.[12]

Conclusion

The factors that contribute to the present imine-to-aminocarbene rearrangement are summarized as follows. (i) The reaction is chelate assisted with the presence of the pyridine moiety being essential for the coordination of the imine to the metal center. (ii) In the four-membered N−Ru−N−C ring, the chelated imine ligand is under steric strain. (iii) The five-membered ring system N−Ru−C−N−C, arising from the rearrangement, interacts with the planar pyridine ring and can be considered as a 10-π-electron metallacycle that benefits from aromatic stabilization. (iv) Heteroatom stabilization seems to be an important factor too. (v) The co-ligand L should not be too bulky and only a moderate π acceptor.

The reaction of pyridine-based aldimines and aminals with both RuCp and RuTp complexes could furnish alternative and simple preparation methods for special carbene complexes without the use, for example, of diazoalkanes.

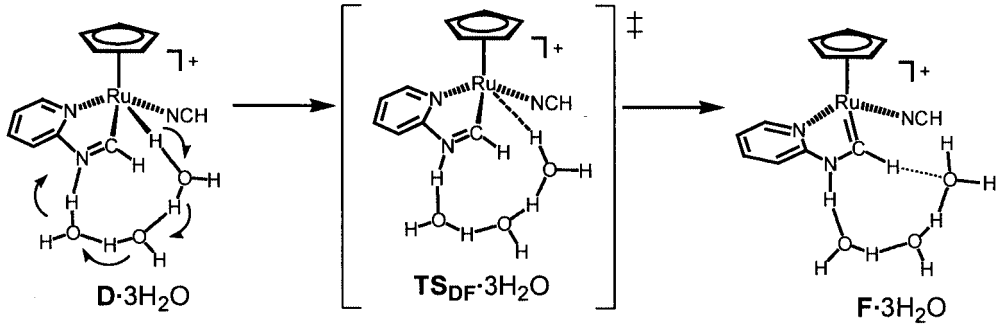

Scheme 9

 © 2003 Wiley-VCH Verlag GmbH & Co. KGaA, Weinheim

Experimental Section

General: All manipulations were performed under an inert atmosphere of argon by using Schlenk techniques. All chemicals were standard reagent grade and used without further purification. The solvents were purified according to standard procedures.[13] The deuterated solvents were purchased from Aldrich and dried over 4-Å molecular sieves. $[RuCp(CH_3CN)_3]PF_6$ (**1**),[14] $[RuCp(PMe_3)(CH_3CN)_2]PF_6$ (**2a**), $[RuCp(PPh_3)(CH_3CN)_2]PF_6$ (**2b**), and $[RuCp(P\mathit{i}Pr_3)(CH_3CN)_2]PF_6$ (**2c**),[15] $[RuCp(SbPh_3)(CH_3CN)_2]PF_6$ (**3**),[16] $[RuCp(CO)(CH_3CN)_2]PF_6$ (**4**) and $[RuTp(COD)Cl]$ (**5**),[17] $[RuCp(PPh_3)(\kappa^2\mathit{N},\mathit{N}'\text{-py−N=CHPh})]PF_6$ (**6a**), $[RuCp(CO)(\kappa^2\mathit{N},\mathit{N}'\text{-py−N=CHPh})]PF_6$ (**7a**), $[RuCp(CH_3CN)\{=C(Ph)NH-py\}]PF_6$ (**8a**), $[RuCp(PMe_3)\{=C(Ph)NH-py\}]PF_6$ (**9a**), $[RuTp\{=C(Ph)NH-py\}Cl]$ (**11a**), $[RuCp(py-NH_2)\{=C(NH-py\}Et)]PF_6$ (**12a**), $[RuCp(PMe_3)\{=C(NH-py)Et\}]PF_6$ (**13**), and $[RuCp(PPh_3)(py-NH-\eta^2\text{-}CH=CHMe)]PF_6$ (**14**)[1] were prepared according to literature procedures. ^1H, $^{13}C\{^1H\}$, and $^{31}P\{^1H\}$ NMR spectra were recorded on a Bruker AVANCE-250 spectrometer and were referenced to $SiMe_4$ and H_3PO_4 (85%), respectively. ^1H and $^{13}C\{^1H\}$ NMR signal assignments were confirmed by ^1H-COSY, 135-DEPT, and HMQC(^1H-^{13}C) experiments.

$[RuCp(PPh_3)(\kappa^2\mathit{N},\mathit{N}'\text{-py−N=CHFc})]PF_6$ (6b): (*E*)-*N*-(Ferrocenylmethylene)-2-pyridineamine (py−N=CHFc) (44 mg, 0.152 mmol) was added to a solution of **2b** (100 mg, 0.152 mmol) in CH_2Cl_2 (5 mL). After the mixture was stirred at room temperature for 9 h, the solvent was evaporated under vacuum and the resulting red solid was collected on a glass frit and washed twice with diethyl ether (10 mL). Yield: 105 mg (80%). $C_{39}H_{34}F_6FeN_2P_2Ru$ (863.57): calcd. C 54.24, H 3.97; found C 54.29; H 4.04. ^1H NMR ([D$_6$]acetone, 20 °C): δ = 9.20 (s, 1 H, N=C*H*Fc), 8.52 (d, $J_{H,H}$ = 4.42 Hz, 1 H, py^6), 7.77 (vt, $J_{H,H}$ = 7.84 Hz, 1 H, py^4), 7.55−7.15 (m, 17 H, PPh$_3$, py^3, py^5), 5.26−5.17 (m, 1 H, FeCp^s), 5.06−4.99 (m, 1 H, FeCp^s), 4.97−4.87 (m, 2 H, FeCp^s), 4.69 (s, 5 H, RuCp), 4.26 (s, 5 H, FeCp) ppm. $^{13}C\{^1H\}$ NMR ([D$_6$]acetone, 20 °C): δ = 169.7 (1C, py^6), 164.5 (1C, py^2), 151.9 ($J_{C,P}$ = 1.4 Hz, 1C, N=*C*HFc), 138.1 (1C, py^4), 133.7 ($J_{C,P}$ = 40.6 Hz, 3C, Ph^1), 133.3 ($J_{C,P}$ = 11.0 Hz, 6C, Ph^{2,6}), 130.1 ($J_{C,P}$ = 2.2 Hz, 3C, Ph^4), 128.5 ($J_{C,P}$ = 9.9 Hz, 6C, Ph^{3,5}), 123.9 (1C, py^3), 109.2 (1C, py^5), 75.8 (1C, FeCp^{s1}), 74.8 (1C, FeCp^s), 74.7 (1C, FeCp^s), 74.5 (5C, RuCp), 74.5 (1C, FeCp^s), 71.9 (1C, FeCp^s), 70.2 (5C, FeCp) ppm. $^{31}P\{^1H\}$ NMR ([D$_6$]acetone, 20 °C): δ = 49.7 (*P*Ph$_3$), −144.2 ($^1J_{PF}$ = 719.5 Hz, *P*F$_6$) ppm.

$[RuCp(PPh_3)(\kappa^2\mathit{N},\mathit{N}'\text{-py−N=CHNp})]PF_6$ (6c): An NMR tube was charged with **2b** (50 mg, 0.080 mmol) and *N*-(naphthylmethylene)-2-pyridine amine (py−N=CHNp) (23 mg, 0.080 mmol), and when they were dissolved in [D$_6$]acetone (0.5 mL), the color changed from yellow to dark red. After 12 h at room temperature NMR spectra were taken indicating quantitative formation of **6c**. ^1H NMR ([D$_6$]acetone, 20 °C): δ = 10.24 (s, 1 H, N=C*H*Np), 9.27 (d, $J_{H,H}$ = 7.31 Hz, 1 H, py^6), 8.64 (td, $J_{H,H1}$ = 5.28, $J_{H,H2}$ = 0.80 Hz, 1 H, py^4), 8.15−7.99 (m, 1 H, py^3), 7.90−7.80 (m, 1 H, py^5), 7.78−7.58 (m, 7 H, Np), 7.47−7.16 (m, 15 H, PPh$_3$), 4.76 (d, $J_{H,H}$ = 0.16 Hz, 5 H, RuCp) ppm. $^{13}C\{^1H\}$ NMR ([D$_6$]acetone, 20 °C): δ = 162.9 (1C, py^6), 164.0 (1C, py^2), 152.1 (1C, N=*C*HNp), 138.4 (1C, py^4), 136.9, 135.5, 134.0 (3C, Np), 133.3 ($J_{C,P}$ = 41.5 Hz, 3C, Ph^1), 133.2 ($J_{C,P}$ = 11.5 Hz, 6C, Ph^{2,6}), 132.3 (1C, Np), 130.2 ($J_{C,P}$ = 2.2 Hz, 3C, Ph^4), 129.3, 128.7 (2C, Np), 128.5 ($J_{C,P}$ = 9.9 Hz, 6C, Ph^{3,5}), 128.0, 127.1, 125.6, 124.8 (4C, Np), 122.2 (1C, py^3), 110.2 (1C, py^5), 75.3 ($J_{C,P}$ = 2.1 Hz, 5C, RuCp) ppm. $^{31}P\{^1H\}$ NMR ([D$_6$]acetone, 20 °C): δ = 49.7 (*P*Ph$_3$), −144.1 ($^1J_{PF}$ = 719.5 Hz, *P*F$_6$) ppm.

$[RuCp(P\mathit{i}Pr_3)(\kappa^2\mathit{N},\mathit{N}'\text{-py−N=CHFc})]PF_6$ (6d): This compound was prepared analogously to **6b** by using **2c** (50 mg, 0.090 mmol) and py−N=CHFc (26 mg, 0.090 mmol) as the starting materials. Yield: 49 mg (71%). $C_{30}H_{40}F_6FeN_2P_2Ru$ (761.52): calcd. C 47.32, H 5.29; found C 47.41, H 5.33. ^1H NMR ([D$_6$]acetone, 20 °C): δ = 9.64 (s, 1 H, N=C*H*Fc), 8.64 (d, $J_{H,H1}$ = 5.03 Hz, 1 H, py^6), 7.96 (t, $J_{H,H}$ = 7.99 Hz, 1 H, py^4), 7.66 (d, $J_{H,H}$ = 8.45 Hz, 1 H, py^3), 7.41 (dd, $J_{H,H1}$ = 7.54, $J_{H,H2}$ = 5.25 Hz, 1 H, py^5), 5.31−5.22 (m, 1 H, FeCp^s), 5.09−5.01 (m, 1 H, FeCp^s), 5.00−4.90 (m, 2 H, FeCp^s), 4.72 (s, 5 H, RuCp), 4.45 (s, 5 H, FeCp), 2.26 (m, J_{PH} = 7.27 Hz, 3 H, CH), 1.14 (ddd, $J_{H,H1}$ = 12.90, $J_{H,H2}$ = 7.20, $J_{H,H3}$ = 2.43 Hz, 18 H, CH$_3$) ppm. $^{13}C\{^1H\}$ NMR ([D$_6$]acetone, 20 °C): δ = 170.1 (1C, py^6), 165.5 (1C, py^2), 153.0 (1C, N=*C*HFc), 138.5 (1C, py^4), 124.1 (1C, py^3), 108.5 (1C, py^5), 76.0 (1C, FeCp^{s1}), 74.9 (1C, FeCp^s), 74.6 (1C, FeCp^s), 73.2 (1C, FeCp^s), 72.9 (1C, FeCp^s), 71.7 ($J_{C,P}$ = 1.35 Hz, 5C, RuCp), 70.4 (5C, FeCp), 26.8 ($J_{C,P}$ = 18.9 Hz, 3C, P[*C*H(CH$_3$)$_2$]$_3$), 19.5 [6C, P[CH(*C*H$_3$)$_2$]$_3$] ppm. $^{31}P\{^1H\}$ NMR ([D$_6$]acetone, 20 °C): δ = 52.2 (P*i*Pr$_3$), −144.1 ($^1J_{PF}$ = 708.1 Hz, *P*F$_6$).

$[RuCp(CO)(\kappa^2\mathit{N},\mathit{N}'\text{-py−N=CHFc})]PF_6$ (7b): This compound was prepared analogously to **6b** by using **4** (50 mg, 0.090 mmol) and py−N=CHFc (26 mg, 0.090 mmol) as the starting materials. Yield: 132 mg (89%). $C_{22}H_{19}F_6FeN_2OPRu$ (629.29): calcd. C 41.99, H 3.04; found C 41.87; H 3.10. ^1H NMR ([D$_6$]acetone, 20 °C): δ = 9.67 (s, 1 H, N=C*H*Fc), 8.53 (d, $J_{H,H}$ = 5.18 Hz, 1 H, py^6), 8.14 (dt, $J_{H,H1}$ = 8.14, $J_{H,H2}$ = 1.27 Hz, 1 H, py^4), 7.80 (d, $J_{H,H}$ = 8.38 Hz, 1 H, py^3), 7.52 (dd, $J_{H,H1}$ = 7.54, $J_{H,H2}$ = 5.41 Hz, 1 H, py^5), 5.38 (s, 5 H, RuCp), 5.14−4.92 (m, 4 H, FeCp^s), 4.47 (s, 5 H, FeCp) ppm. $^{13}C\{^1H\}$ NMR ([D$_6$]acetone, 20 °C): δ = 200.7 (1C, CO), 171.0 (1C, py^6), 166.0 (1C, py^2), 152.7 (1C, N=*C*HFc), 140.4 (1C, py^4), 124.2 (1C, py^3), 109.9 (1C, py^5), 81.9 (1C, FeCp^s), 81.1 (5C, RuCp), 76.4 (1C, FeCp^s), 76.3 (1C, FeCp^s), 75.7 (1C, FeCp^s), 74.6 (1C, FeCp^{s1}), 71.0 (5C, FeCp) ppm.

$[RuCp(CH_3CN)(=C(Fc)NH-py)]PF_6$ (8b): Compound py−N=CHFc (133 mg, 0.461 mmol) was added to a solution of **1** (200 mg, 0.461 mmol) in CH_2Cl_2 (7 mL). After the mixture was stirred at room temperature for 24 h, the solvent was evaporated under vacuum and the resulting purple solid was collected on a glass frit and washed twice with diethyl ether (10 mL). Yield: 152 mg (85%). $C_{23}H_{22}F_6FeN_3PRu$ (642.33): calcd. C 43.01, H 3.45; found C 43.11; H 3.47. ^1H NMR ([D$_6$]acetone, 20 °C): δ = 11.90 (br. s, 1 H, NH), 9.10 (d, $J_{H,H}$ = 5.63 Hz, 1 H, py^6), 7.95 (ddd, $J_{H,H1}$ = 8.45, $J_{H,H2}$ = 7.23, $J_{H,H3}$ = 1.37 Hz, 1 H, py^4), 7.72 (dd, $J_{H,H1}$ = 8.38, $J_{H,H2}$ = 0.83 Hz, 1 H, py^3), 7.22 (ddd, $J_{H,H1}$ = 7.23, $J_{H,H2}$ = 5.86, $J_{H,H3}$ = 1.29 Hz, 1 H, py^5), 5.28−5.18 (m, 1 H, FeCp^s), 5.16−5.10 (m, 1 H, FeCp^s), 4.86 (s, 5 H, RuCp), 4.84−4.78 (m, 2 H, FeCp^s), 4.30 (s, 5 H, FeCp), 2.34 (s, 3 H, CH$_3$CN) ppm. $^{13}C\{^1H\}$ NMR ([D$_6$]acetone, 20 °C): δ = 264.6 (1C, Ru=*C*), 159.0 (1C, py^2), 155.8 (1C, py^6), 138.7 (1C, py^4), 127.2 (1C, CH$_3$*C*N), 119.7 (1C, py^3), 112.3 (1C, py^5), 87.9 (1C, FeCp^{s1}), 80.7 (5C, RuCp), 75.1 (1C, FeCp^s), 74.2 (1C, FeCp^s), 73.8 (1C, FeCp^s), 70.3 (5C, FeCp), 68.2 (1C, FeCp^s), 3.1 (1C, *C*H$_3$CN) ppm.

$[RuCp(CH_3CN)(=C(Np)NH-py)]PF_6$ (8c): This compound was prepared analogously to **8b** by using **1** (100 mg, 0.230 mmol) and py−N=CHNp (64 mg, 0.276 mmol) as the starting materials. Yield: 111 mg (83%). $C_{23}H_{20}F_6N_3PRu$ (584.47): calcd. C 47.27, H 3.45; found C 47.33; H 3.40. ^1H NMR ([D$_6$]acetone, 20 °C): δ = 12.86 (s, 1 H, NH), 9.21 (ddd, $J_{H,H1}$ = 5.73, $J_{H,H2}$ = 1.54, $J_{H,H3}$ = 0.75 Hz, 1 H, py^6), 8.14−7.99 (m, 4 H, Np, py^4), 7.94−7.85 (m, 1 H, Np), 7.78−7.69 (m, 2 H, Np), 7.67 (d, $J_{H,H}$ = 8.06 Hz, 1 H, py^3), 7.63−7.53 (m, 1 H, Np), 7.41 (ddd, $J_{H,H1}$ = 7.31, $J_{H,H2}$ = 5.80, $J_{H,H3}$ = 1.38 Hz, 1 H, py^5), 4.74 (s, 5 H, RuCp), 2.47 (s, 3 H,

 © 2003 Wiley-VCH Verlag GmbH & Co. KGaA, Weinheim

CH_3CN) ppm. $^{13}C\{^1H\}$ NMR ([D$_6$]acetone, 20 °C): δ = 269.5 (1C, Ru=*C*), 158.4 (1C, py^2), 155.7 (1C, py^6), 138.9 (1C, py^4), 136.9, 135.1, 133.7, 129.8, 128.9, 128.6, 128.4, 126.5, 125.3, 125.1 (10C, Np), 124.6 (1C, CH_3*C*N), 120.5 (1C, py^3), 113.2 (1C, py^5), 82.1 (5C, RuCp), 2.9 (1C, *C*H$_3$CN) ppm.

[RuCp(PMe$_3$){=C(Fc)NH−py}]PF$_6$ (9b): This compound was prepared analogously to **8b** by using **2a** (50 mg, 0.107 mmol) and py−N=CHFc (31 mg, 0.107 mmol) as the starting materials. Yield: 68 mg (94%). $C_{24}H_{28}F_6FeN_2P_2Ru$ (677.36): calcd. C 42.56, H 4.17; found C 42.61; H 4.19. ^1H NMR ([D$_6$]acetone, 20 °C): δ = 11.89 (br. s, 1 H, NH), 8.97 (dd, $J_{H,H1}$ = 5.94, $J_{H,H2}$ = 0.69 Hz, 1 H, py^6), 7.88 (m, 1 H, py^4), 7.76 (d, $J_{H,H}$ = 8.07 Hz, 1 H, py^3), 7.12 (ddd, $J_{H,H1}$ = 7.16, $J_{H,H2}$ = 5.79, $J_{H,H3}$ = 1.37 Hz, 1 H, py^5), 5.20 (d, J_{PH} = 0.30 Hz, 5 H, RuCp), 5.15−5.05 (m, 1 H, FeCp^s), 4.94−4.87 (m, 1 H, FeCp^s), 4.83−4.74 (m, 2 H, FeCp^s), 4.33 (s, 5 H, FeCp), 1.09 (d, J_{PH} = 9.90 Hz, 9 H, PMe$_3$) ppm. $^{13}C\{^1H\}$ NMR ([D$_6$]acetone, 20 °C): δ = 263.2 ($J_{C,P}$ = 12.1 Hz, 1C, Ru=*C*), 157.9 (1C, py^6), 155.7 ($J_{C,P}$ = 1.9 Hz, 1C, py^2), 137.5 (1C, py^4), 119.2 (1C, py^3), 113.0 (1C, py^5), 88.0 (1C, FeCp^{s1}), 83.0 (5C, RuCp), 76.8 (1C, FeCp^s), 73.7 (1C, FeCp^s), 73.0 (1C, FeCp^s), 70.6 (5C, FeCp), 66.9 (1C, FeCp^s), 17.5 ($J_{C,P}$ = 31.8 Hz, 3C, PMe$_3$) ppm. $^{31}P\{^1H\}$ NMR ([D$_6$]acetone, 20 °C): δ = 6.2 (*P*Me$_3$), −144.2 ($^1J_{PF}$ = 708.4 Hz, *P*F$_6$) ppm.

[RuCp(PMe$_3$){=C(Np)NH−py}]PF$_6$ (9c): This compound was prepared analogously to **8b** by using **2a** (50 mg, 0.107 mmol) and py−N=CHNp (25 mg, 0.107 mmol) as the starting materials. Yield: 59 mg (91%). $C_{24}H_{17}F_6N_2P_2Ru$ (610.42): calcd. C 47.22, H 2.81; found C 47.17; H 2.78. ^1H NMR ([D$_6$]acetone, 20 °C): δ = 12.66 (br. s, 1 H, NH), 9.08 (d, $J_{H,H}$ = 5.79 Hz, 1 H, py^6), 8.20−7.47 (m, 9 H, Np, py^4, py^3), 7.32 (ddd, $J_{H,H1}$ = 7.23, $J_{H,H2}$ = 5.86, $J_{H,H3}$ = 1.37 Hz, 1 H, py^5), 4.94 (d, J_{PH} = 0.30 Hz, 5 H, RuCp), 1.34 (d, J_{PH} = 9.90 Hz, 9 H, PMe$_3$) ppm. $^{13}C\{^1H\}$ NMR ([D$_6$]acetone, 20 °C): δ = 268.8 ($J_{C,P}$ = 9.7 Hz, 1C, Ru=*C*), 157.6 (1C, py^2), 155.8 (1C, py^6), 147.4 (1C, Np), 137.8 (1C, py^4), 133.7 (1C, Np), 129.4 (1C, Np), 128.5 (2C, Np), 126.9 (1C, Np), 126.7 (1C, Np^q), 126.5 (1C, Np), 125.3 (2C, Np), 119.9 (1C, py^3), 113.6 (1C, py^5), 84.1 (5C, RuCp), 17.5 ($J_{C,P}$ = 32.3 Hz, 3C, PMe$_3$) ppm. $^{31}P\{^1H\}$ NMR ([D$_6$]acetone, 20 °C): δ = 5.4 (*P*Me$_3$), −144.2 ($^1J_{PF}$ = 719.5 Hz, *P*F$_6$) ppm.

[RuCp(SbPh$_3$){=C(Fc)NH−py}]PF$_6$ (10): This compound was prepared analogously to **6b** by using **3** (80 mg, 0.107 mmol) and py−N=CHFc (31 mg, 0.107 mmol) as the starting materials. Yield: 89 mg (87%). $C_{39}H_{34}F_6FeN_2PSbRu$ (954.35): calcd. C 49.08, H 3.59; found C, 49.12, H 3.62. ^1H NMR ([D$_6$]acetone, 20 °C): δ = 11.76 (br. s, 1 H, NH), 9.19 (d, $J_{H,H}$ = 5.18 Hz, 1 H, py^6), 7.67 (dt, $J_{H,H1}$ = 7.73, $J_{H,H2}$ = 0.91 Hz, 1 H, py^4), 7.53−7.12 (m, 16 H, SbPh$_3$, py^3), 6.98 (ddd, $J_{H,H1}$ = 6.62, $J_{H,H2}$ = 6.24, $J_{H,H3}$ = 0.46 Hz, 1 H, py^5), 5.36 (s, 5 H, RuCp), 5.07−4.94 (m, 2 H, FeCp^s), 4.86−4.73 (m, 2 H, FeCp^s), 4.27 (s, 5 H, FeCp) ppm. $^{13}C\{^1H\}$ NMR ([D$_6$]acetone, 20 °C): δ = 263.4 (1C, Ru=*C*), 157.4 (1C, py^2), 155.9 (1C, py^6), 135.2 (1C, py^4), 134.9 (6C, Ph$_3^{2,6}$), 132.2 (3C, Ph$_3^1$), 130.2 (3C, Ph$_3^4$), 129.3 (6C, Ph$_3^{3,5}$), 118.6 (1C, py^3), 113.0 (1C, py^5), 87.6 (1C, FeCp^{s1}), 79.3 (5C, RuCp), 76.5 (1C, FeCp^s), 74.3 (1C, FeCp^s), 73.7 (1C, FeCp^s), 70.2 (5C, FeCp), 67.1 (1C, FeCp^s) ppm.

[RuTp{=C(C$_6$H$_4$OMe*p*)NH−py)Cl] (11b): A solution of **5** (100 mg, 0.218 mmol) and *N*-(*p*-methoxyphenylmethylene)-2-pyridineamine (py−N=CHC$_6$H$_4$OMe*p*) (92.5 mg, 0.436 mmol) in DMF (4 mL) was heated under reflux for 2.5 h. After evaporation of the solvent under reduced pressure, the brown product was washed with pentane (2 × 5 mL), and dried under vacuum. Yield: 94.4 mg (77%). $C_{22}H_{22}BN_8ClORu$ (561.81): calcd. C 47.04, H 3.95; found C, 47.11, H 3.89. ^1H NMR ([D$_6$]DMSO, 20 °C): δ = 13.17 (s, 1 H, N*H*), 8.33 (d, $J_{H,H}$ = 5.5 Hz, 1 H, py^6), 8.11 (br. s, 1 H, Tp), 8.05 (d, $J_{H,H}$ = 2.2 Hz, 1 H, Tp), 7.89 (d, $J_{H,H}$ = 2.4 Hz, 1 H, Tp), 7.85 (d, $J_{H,H}$ = 2.2 Hz, 1 H, Tp), 7.83−7.68 (m, 2 H, py^{3,4}), 7.16 (t, $J_{H,H}$ = 6.3 Hz, 1 H, py^5), 6.77 (s, 4 H, Ph), 6.64 (br. s, 1 H, Tp), 6.50 (vt, 1 H, $J_{H,H}$ = 1.8 Hz, Tp), 6.00 (vt, 1 H, $J_{H,H}$ = 2.0 Hz, Tp), 5.94 (vt, 1 H, $J_{H,H}$ = 2.1 Hz, Tp), 5.88 (d, $J_{H,H}$ = 1.6 Hz, 1 H, Tp), 3.71 (s, 3 H, OC*H*$_3$) ppm. $^{13}C\{^1H\}$ NMR ([D$_6$]DMSO, 20 °C): δ = 276.9 (1C, Ru=*C*), 161.1 (1C, py^2), 160.7 (1C, Ph^4), 151.2 (1C, py^6), 149.6 (1C, Ph^1), 146.2 (1C, Tp), 143.0 (1C, Tp), 142.4 (1C, Tp), 137.2 (1C, Tp), 137.1 (1C, py^4), 135.8 (1C, Tp), 135.5 (1C, Tp), 128.0 (2C, Ph^{3,5}), 115.3 (1C, py^5), 113.8 (1C, Ph^{2,6}), 112.3 (1C, py^3), 106.8 (2C, Tp), 105.9 (1C, Tp), 56.1 (1C, O*C*H$_3$) ppm.

[RuTp{=C(Np)NH−py}Cl] (11c): This compound was prepared analogously to **11b** by using **5** (100 mg, 0.218 mmol) and py−N=CHNp (61 mg, 0.262 mmol) as the starting materials. Yield: 87.9 mg (69%). $C_{25}H_{22}BN_8ClRu$ (581.84): calcd. C 51.61, H 3.81; found C 51.57, H 3.78. ^1H NMR ($CDCl_3$, 20 °C): δ = 12.30 (s, 1 H, N*H*), 8.85−5.66 (m, 21 H, py$^{2-6}$, Np, Tp) ppm. $^{13}C\{^1H\}$ NMR ($CDCl_3$, 20 °C): δ = 281.4 (1C, Ru=*C*), 159.7 (1C, py^2), 151.0 (1C, py^6), 142.2 (1C, Tp), 141.1(1C, Tp), 136.9 (1C, py^4), 136.2 (1C, Tp), 135.7 (1C, Tp), 135.4 (1C, Tp), 134.6 (1C, Tp), 129.1−124.8 (m, 10C, Np), 118.7 (1C, py^5), 105.9 (1C, py^3), 105.9 (3C, Tp) ppm.

[RuCp(CH$_3$CN)(κ^2*N*,*N*′-py−CH$_2$−N=CHPh)]PF$_6$ (12): This compound was prepared analogously to **6b** by using **1** (100 mg, 0.230 mmol) and *N*-(phenylmethylene)-2-picolylamine (py−CH$_2$−N=CHPh) (50 mg, 0.253 mmol) as the starting materials. Yield: 90 mg (74%). $C_{20}H_{20}F_6N_3PRu$ (548.44): calcd. C 43.80, H 3.68; found C 43.85, H 3.71. ^1H NMR ([D$_6$]acetone, 20 °C): δ = 9.19 (d, $J_{H,H}$ = 5.05 Hz, 1 H, py^6), 9.11 (d, $J_{H,H}$ = 1.26 Hz, 1 H, N=C*H*Ph), 8.50−8.48 (m, 2 H, py^4, Ph), 7.98 (dt, $J_{H,H1}$ = 7.78, $J_{H,H2}$ = 1.53 Hz, 1 H, py^3), 7.68−7.56 (m, 4 H, Ph), 7.44 (vt, 1 H, $J_{H,H}$ = 6.56 Hz, py^5), 5.62 (d, 1 H, $J_{H,H1}$ = 17.69 Hz, CH$_2$), 5.43 (d, $J_{H,H}$ = 17.69 Hz, 1 H, CH$_2$), 4.28 (s, 5 H, Cp), 2.19 (s, 3 H, CH$_3$CN) ppm. $^{13}C\{^1H\}$ NMR ([D$_6$]acetone, 20 °C): δ = 173.0 (1C, py^6), 160.5 (1C, py^2), 155.2 (1C, N=*C*HPh), 137.7 (1C, py^4), 134.3 (1C, Ph^1), 132.5 (1C, Ph^4), 130.2 (2C, Ph^{2,6}), 128.8 (2C, Ph^{3,5}), 125.9 (1C, CH$_3$*C*N), 124.3 (1C, py^3), 120.6 (1C, py^5), 74.6 (1C, CH$_2$), 70.5 (5C, Cp), 2.7 (1C, *C*H$_3$CN) ppm.

[RuTp(κ^2*N*,*N*′-py−CH$_2$−N=CHPh)Cl] (13): This compound was prepared analogously to **11b** by using **5** (100 mg, 0.218 mmol) and py−CH$_2$−N=CHPh (47 mg, 0.240 mmol) as the starting materials. Yield: 87.9 mg (64%). $C_{22}H_{22}BN_8ClRu$ (545.81): calcd. C 48.41, H 4.06; found C 48.49, H 4.13. ^1H NMR ($CDCl_3$, 20 °C): δ = 9.05 (s, 1 H, N=C*H*), 8.12 (d, $J_{H,H}$ = 5.8 Hz, 1 H, py^6), 7.89 (d, $J_{H,H}$ = 2.4 Hz, 1 H, Tp), 7.83 (d, $J_{H,H}$ = 1.9 Hz, 1 H, Tp), 7.73 (d, $J_{H,H}$ = 2.2 Hz, 1 H, Tp), 7.61 (d, $J_{H,H}$ = 1.4 Hz, 1 H, Tp), 7.57 (d, $J_{H,H}$ = 2.2 Hz, 1 H, Tp), 7.4 −7.37 (m, 3 H, Ph), 7.33 (d, $J_{H,H}$ = 2.1 Hz, 1 H, Tp), 7.23−7.13 (m, 2 H, Ph), 7.02 (t, $J_{H,H}$ = 7.6 Hz, 1 H, py^4), 6.74 (t, $J_{H,H}$ = 7.5 Hz, 1 H, py^5), 6.61 (d, $J_{H,H}$ = 14.9 Hz, 1 H, C*H*$_2$), 6.44 (d, $J_{H,H}$ = 7.9 Hz, 1 H, py^3), 6.26 (vt, $J_{H,H}$ = 2.1 Hz, 1 H, Tp), 6.03 (vt, $J_{H,H}$ = 2.1 Hz, 1 H, Tp), 5.67 (vt, $J_{H,H}$ = 2.0 Hz, 1 H, Tp), 5.23 (d, $J_{H,H}$ = 16.0 Hz, 1 H, C*H*$_2$) ppm. $^{13}C\{^1H\}$ NMR ($CDCl_3$, 20 °C): δ = 171.4 (1C, N=*C*HPh), 162.4 (1C, py ^{2}), 153.6 (1C, py ^{6}), 145.1 (1C, Tp), 144.3 (1C, Tp), 141.7 (1C, Tp), 136.6 (1C, Tp), 135.4 (1C, Tp), 134.9 (1C, Tp), 134.4 (1C, py ^{4}), 133.7 (1C, Ph^1), 130.0 (1C, Ph^4), 128.2 (2C, Ph^{2,6}), 128.0 (2C, Ph^{3,5}), 123.2 (1C, py ^{5}), 119.2 (1C, py ^{3}), 106.8 (1C, Tp), 106.6 (1C, Tp), 106.2 (1C, Tp), 75.2 (1C, CH$_2$) ppm.

[RuCp(pyMe-NH$_2$){=C(NH−pyMe)Et}]PF$_6$ (14b): A solution of **1** (100 mg, 0.230 mmol) and *N*,*N*′-bis(2-picolyl)-1,1-propanediamine

 © 2003 Wiley-VCH Verlag GmbH & Co. KGaA, Weinheim

Table 1. Details for the crystal structure determinations of complexes **6b**·$(CH_3)_2CO$, **7a**, **7b**, **11a**, **12**, and **16**

	6b·$(CH_3)_2CO$	**7a**	**7b**	**11a**	**12**	**16**
Empirical formula	$C_{42}H_{40}F_6FeN_2OP_2Ru$	$C_{18}H_{15}F_6N_2OPRu$	$C_{22}H_{19}F_6FeN_2OPRu$	$C_{21}H_{20}BClN_8Ru$	$C_{20}H_{20}F_6N_3PRu$	$C_{31}H_{30}F_6N_2P_2Ru$
Formula mass	921.62	521.36	629.28	531.78	548.43	707.58
Crystal size, mm	0.45 × 0.35 × 0.10	0.75 × 0.07 × 0.05	0.40 × 0.06 × 0.06	0.32 × 0.22 × 0.18	0.64 × 0.20 × 0.12	0.70 × 0.04 × 0.02
space group	$P\bar{1}$ (No. 2)	$P2_1/n$ (No. 14)	$P2_1/n$ (No. 14)	$C2/c$ (No. 15)	$P2_1/n$ (No. 14)	$P2_1/n$ (No. 14)
a, Å	11.035(1)	10.485(1)	10.820(7)	27.131(7)	10.167(2)	13.469(2)
b, Å	14.187(2)	13.966(2)	13.369(9)	11.152(3)	11.840(2)	15.052(3)
c, Å	14.450(2)	12.698(2)	30.38(2)	15.546(4)	18.149(3)	14.808(3)
α, deg	74.574(3)					
β, deg	70.554(3)	90.338(3)	93.17(2)	106.24(1)	96.803(3)	100.60(1)
γ, deg	67.939(3)					
V, Å^3	1951.2(4)	1859.2(4)	4387(5)	4516(2)	2169.3(6)	2950.7(9)
Z	2	4	8	8	4	4
$\rho_{calcd.}$, g cm^{-3}	1.569	1.863	1.905	1.564	1.679	1.593
T, K	173(2)	123(2)	123(2)	297(2)	183(2)	297(2)
μ, mm^{-1} (Mo-*Kα*)	0.906	1.000	1.493	0.839	0.859	0.703
F(000)	936	1032	2496	2144	1096	1432
Absorption corr.	multi scan	multi scan	none	multi scan	multi scan	multi scan
θ_{max}, deg.	30	30	25	25	30	30
No. of reflections measd.	24939	12429	23139	22327	30388	40569
No. of unique reflections	10853	5172	7627	3937	6244	8421
no. of reflections $I > 2\sigma(I)$	9168	3956	4022	3140	5260	6841
No. of params	515	262	367	289	295	379
R_1 $[I > 2\sigma(I)]$[a]	0.031	0.028	0.080	0.033	0.032	0.045
R_1 (all data)	0.041	0.047	0.162	0.048	0.041	0.058
wR_2 (all data)	0.082	0.062	0.219	0.092	0.091	0.134
Diff. Four. peaks, min./max., e·Å^{-3}	−0.63/0.83	−0.42/0.56	−1.09 /1.86	−0.55/0.92	−0.86/0.85	−0.74/1.51

[a] $R_1 = \Sigma F_o - F_c / \Sigma F_o$, $wR_2 = [\Sigma[w(F_o^2 - F_c^2)^2]/\Sigma[w(F_o^2)^2]]^{1/2}$.

[pyMe−NHCH(Et)NH−pyMe] (59 mg, 0.20 mmol) in CH_2Cl_2 (8 mL) was stirred at room temperature for 3 h. The volume of the solution was then reduced to about 1 mL. Upon addition of diethyl ether, a brick-red solid was obtained that was collected on a glass frit, washed with diethyl ether, and dried under vacuum. Yield: 98 mg (75%). $C_{20}H_{25}F_6N_4PRu$ (567.48): calcd. C 42.33, H 4.44; found C 43.27, H 4.40. ^{1}H NMR ([D$_6$]acetone, 20 °C): δ = 12.70 (br. s, 1 H, NH), 9.15 (d, $J_{H,H}$ = 6.00 Hz, 1 H, py), 8.16 (d, $J_{H,H}$ = 6.16 Hz, 1 H, py), 7.39 (m, 1 H, py), 7.15 (d, $J_{H,H}$ = 5.53 Hz, 1 H, py), 6.49 (m, 1 H, py), 6.30 (br. s, 2 H, NH_2), 6.19 (d, $J_{H,H}$ = 5.05 Hz, 1 H, py), 4.98 (s, 5 H, Cp), 4.07 (m, $J_{H,H}$ = 7.27 Hz, 1 H, CH_2), 3.87 (m, $J_{H,H}$ = 7.31 Hz, 1 H, CH_2), 2.43 (s, 3 H, py−Me), 2.08 (s, 3 H, py−Me), 1.43 (t, $J_{H,H}$ = 7.50 Hz, 3 H, CH_3) ppm. ^{13}C{^{1}H} NMR ([D$_6$]acetone, 20 °C): δ = 276.6 (1C, Ru=*C*), 162.6 (1C, py^q), 158.6 (1C, py^q), 154.7 (1C, py), 151.5 (1C, py), 150.5 (1C, py^q), 150.0 (1C, py^q), 121.5 (1C, py), 115.1 (1C, py), 112.4 (1C, py), 109.9 (1C, py), 82.1 (5C, Cp), 45.5 (1C, *C*H$_2$CH$_3$), 20.5 (1C, py−Me), 20.0 (1C, py−Me), 12.2 (1C, CH$_2$*C*H$_3$) ppm.

[RuTp{=C(NH−pyMe)Et}Cl] (17): This compound was prepared analogously to **11b** by using **5** (100 mg, 0.218 mmol) and pyMe-NHCH(Et)NH-pyMe (72.5 mg, 0.283 mmol) as the starting materials. Yield: 65.6 mg (61%). $C_{18}H_{22}BN_8ClRu$ (497.76): calcd. C 43.43, H 4.46; found C 43.39, H 4.49. ^{1}H NMR ([D$_6$]DMSO, 20 °C): δ = 13.06 (s, 1 H, N*H*), 8.15 (d, $J_{H,H}$ = 5.8 Hz, 1 H, py^6), 8.06 (d, $J_{H,H}$ = 1.7 Hz, 1 H, Tp), 7.98 (d, $J_{H,H}$ = 2.2 Hz, 1 H, Tp), 7.87 (d, $J_{H,H}$ = 2.2 Hz, 1 H, Tp), 7.82−7.70 (m, 2 H, 2Tp), 7.44 (s, 1 H, py^3), 6.98 (dd, J_1 = 6.0, J_2 = 1.3 Hz 1 H, py^5), 6.45 (vt, $J_{H,H}$ = 2.0 Hz, 1 H, Tp), 6.28 (vt, $J_{H,H}$ = 2.0 Hz, 1 H, Tp), 5.88 (vt, $J_{H,H}$ = 2.1 Hz, 1 H, Tp), 5.79 (d, $J_{H,H}$ = 1.9 Hz, 1 H, Tp), 3.47−3.15 (m, 2 H, C*H*$_2$), 2.07 (s, 3 H, py−Me), 0.77 (t, $J_{H,H}$ = 7.7 Hz, 3 H, C*H*$_3$) ppm. ^{13}C{^{1}H} NMR ([D$_6$]DMSO, 20 °C): δ = 290.3 (1C, Ru=*C*), 160.0 (1C, py^2), 150.7 (1C, py^6), 148.5 (1C, py^4), 145.1 (1C, Tp), 142.7 (1C, Tp), 141.6 (1C, Tp), 136.6 (1C, Tp), 135.7 (1C, Tp), 135.6 (1C, Tp), 120.7(1C, py^5), 111.9 (1C, py^3), 106.6 (1C, Tp), 106.5 (1C,Tp), 106.3 (1C, Tp), 39.6 (1C, *C*H$_2$), 21.5 (1C, *C*H$_3$−CH$_2$), 10.9 (1C, py−Me) ppm.

Crystallographic Structure Determinations: Crystals of **6b**·$(CH_3)_2CO$, **7a**, **7b**, **11a**, **12**, and **16** were obtained by vapor diffusion of Et_2O into either CH_2Cl_2 or acetone solutions. Crystal data and experimental details are given in Table 1. All X-ray data were collected on a Bruker Smart CCD area detector diffractometer (graphite-monochromated Mo-K_α radiation, λ = 0.71073 Å, 0.3° ω-scan frames covering either hemispheres (**7a**, **7b**) or complete spheres of the reciprocal space, Bruker Kryoflex cooling unit). Corrections for Lorentz and polarization effects, for crystal decay, and for absorption were applied (multi-scan method with the program SADABS[18]). All structures were solved by direct methods using the program SHELXS-97.[19] Structure refinements on F^2 were carried out with program SHELXL-97.[20] All non-hydrogen atoms were refined anisotropically. Hydrogen atoms were inserted in idealized positions and were refined riding on the atoms to which they were bonded. Critical hydrogen atoms were refined in positional parameters without such restraints.

CCDC-200230 to -200235 contain the supplementary crystallographic data for this paper. These data can be obtained free of charge at www.ccdc.cam.ac.uk/conts/retrieving.html [or from the Cambridge Crystallographic Data Centre, 12, Union Road, Cam-

 © 2003 Wiley-VCH Verlag GmbH & Co. KGaA, Weinheim

bridge CB2 1EZ, UK; Fax: (internat.) + 44-1223/336-033; E-mail: deposit@ccdc.cam.ac.uk].

Computational Details: All calculations were performed using the Gaussian98 software package on the Silicon Graphics Origin 2000 of the Vienna University of Technology.[21] The geometry and energy of the model complexes and the transition states were optimized at the B3LYP level[22] with the Stuttgart/Dresden ECP (SDD) basis set[23] to describe the electrons of the ruthenium atom. For the C, N, and H atoms the 6-31g** basis set was employed.[24] A vibrational analysis was performed to confirm that the structures of the model compounds have no imaginary frequencies. The transition-state structure was relaxed after applying a small perturbation to ensure that it is connected to the corresponding reactant and product. A vibrational analysis was also performed to confirm that it has only one imaginary frequency. The geometries were optimized without constraints (C_1 symmetry).

Acknowledgments

Financial support by the "Fonds zur Förderung der wissenschaftlichen Forschung" (Project No. P14681-CHE) is gratefully acknowledged. Support from the EC through the COST D17 Action is also acknowledged.

[1] C. M. Standfest-Hauser, K. Mereiter, R. Schmid, K. Kirchner, *Organometallics* **2002**, *21*, 2001.
[2] [2a] J. N. Coalter, G. J. Spivak, H. Gerard, E. Clot, E. R. Davidson, O. Eisenstein, K. G. Caulton, *J. Am. Chem. Soc.* **1998**, *120*, 9388. [2b] J. N. Coalter, J. C. Bollinger, J. C. Huffman, U. W. Zwanziger, K. G. Caulton, E. R. Davidson, H. Gerard, E. Clot, O. Eisenstein, *New J. Chem.* **2000**, *24*, 9.
[3] [3a] T. Bodnar, A. R. Cutler, *J. Organomet. Chem.* **1981**, *213*, C31. [3b] C. Casey, W. H. Miles, H. Tukada, *J. Am. Chem. Soc.* **1985**, *107*, 2924. [3c] R. S. Bly, R. K. Bly, *J. Chem. Soc., Chem. Commun.* **1986**, 1046.
[4] For the conversion of aminals to aminocarbene ligands on clusters, see: R. D. Adams, *Chem. Rev.* **1989**, *89*, 1703.
[5] For a related acetal rearrangement, see: D. B. Grotjahn, H. C. Lo, *Organometallics* **1996**, *15*, 2860.
[6] A. Ohtaka, N. Kato, H. Kurosawa, *Organometallics* **2002**, *21*, 5464.
[7] For related reactions of this ligand, see: [7a] C. -H Jun, C. W. Moon, D.-Y. Lee, *Chem. Eur. J.* **2002**, *8*, 2422. [7b] J. W. Suggs, *J. Am. Chem. Soc.* **1979**, *101*, 489.
[8] For hydrido-acyl-hydroxycarbene rearrangements, see: [8a] C. P. Casey, C. J. Czerwinski, K. A. Fusie, R. Hayashi, *J. Am. Chem. Soc.* **1997**, *119*, 3971. [8b] D. Steinborn, M. Gerisch, C. Bruhn, J. A. Davies, *Inorg. Chem.* **1999**, *38*, 680.
[9] J. N. Coalter, J. C. Huffman, K. G. Caulton, *Organometallics* **2000**, *19*, 3569.
[10] C. A. Tolman, *Chem. Rev.* **1977**, *77*, 313.
[11] T. Loerting, C. Tautermann, R. T. Kroemer, I. Kohl, A. Hallbrucker, E. Mayer, K. Liedl, *Angew. Chem. Int. Ed.* **2000**, *39*, 891.
[12] C. A. Pommerening, S. M. Bachrach, L. S. Sunderlin, *J. Phys. Chem. A* **1999**, *103*, 1214.
[13] D. D. Perrin, W. L. F. Armarego, *Purification of Laboratory Chemicals*, 3rd Ed., Pergamon, New York, **1988**.
[14] T. P. Gill, K. R. Mann, *Organometallics* **1982**, *1*, 485.
[15] E. Rüba, W. Simanko, K. Mauthner, K. M. Soldouzi, C. Slugovc, K. Mereiter, R. Schmid, K. Kirchner, *Organometallics* **1999**, *18*, 3843.
[16] E. Becker, C. Slugovc, E. Rüba, C. Standfest-Hauser, K. Mereiter, R. Schmid, K. Kirchner, *J. Organomet. Chem.* **2002**, *649*, 55.
[17] C. Gemel, G. Trimmel, C. Slugovc, S. Kremel, K. Mereiter, R. Schmid, K. Kirchner, *Organometallics* **1996**, *15*, 3998.
[18] G. M. Sheldrick, *SADABS: Program for Absorption Correction*, University of Göttingen, Germany, **1996**.
[19] G. M. Sheldrick, *SHELXS-97: Program for the Solution of Crystal Structures*, University of Göttingen, Germany, **1997**.
[20] G. M. Sheldrick, *SHELXL-97*: *Program for Crystal Structure Refinement*, University of Göttingen, Germany, **1997**.
[21] M. J. Frisch, G. W. Trucks, H. B. Schlegel, G. E. Scuseria, M. A. Robb, J. R. Cheeseman, V. G. Zakrzewski, J. A. Montgomery, Jr., R. E. Stratmann, J. C. Burant, S. Dapprich, J. M. Millam, A. D. Daniels, K. N. Kudin, M. C. Strain, O. Farkas, J. Tomasi, V. Barone, M. Cossi, R. Cammi, B. Mennucci, C. Pomelli, C. Adamo, S. Clifford, J. Ochterski, G. A. Petersson, P. Y. Ayala, Q. Cui, K. Morokuma, D. K. Malick, A. D. Rabuck, K. Raghavachari, J. B. Foresman, J. Cioslowski, J. V. Ortiz, A. G. Baboul, B. B. Stefanov, G. Liu, A. Liashenko, P. Piskorz, I. Komaromi, R. Gomperts, R. L. Martin, D. J. Fox, T. Keith, M. A. Al-Laham, C. Y. Peng, A. Nanayakkara, C. Gonzalez, M. Challacombe, P. M. W. Gill, B. Johnson, W. Chen, M. W. Wong, J. L. Andres, C. Gonzalez, M. Head-Gordon, E. S. Replogle, J. A. Pople, Gaussian, Inc., Pittsburgh PA, **1998**. *Gaussian 98*, revision A.7 Gaussian, Inc.: Pittsburgh, PA, **1998**.
[22] [22a] A. D. Becke, *J. Chem. Phys.* **1993**, *98*, 5648. [22b] B. Miehlich, A. Savin, H. Stoll, H. Preuss, *Chem. Phys. Lett.* **1989**, *157*, 200. [22c] C. Lee, W. Yang, G. Parr, *Phys. Rev. B* **1988**, *37*, 785.
[23] [23a] U. Haeusermann, M. Dolg, H. Stoll, H. Preuss, *Mol. Phys.* **1993**, *78*, 1211. [23b] W. Kuechle, M. Dolg, H. Stoll, H. Preuss, *J. Chem. Phys.* **1994**, *100*, 7535. [23c] T. Leininger, A. Nicklass, H. Stoll, M. Dolg, P. Schwerdtfeger, *J. Chem. Phys.* **1996**, *105*, 1052.
[24] [24a] A. D. McClean, G. S. Chandler, *J. Chem. Phys.* **1980**, *72*, 5639. [24b] R. Krishnan, J. S. Binkley, R. Seeger, J. A. Pople, *J. Chem. Phys.* **1980**, *72*, 650. [24c] A. H. Wachters, *Chem. Phys.* **1970**, *52*, 1033. [24d] P. J. Hay, *J. Chem. Phys.* **1977**, *66*, 4377. [24e] K. Raghavachari, G. W. Trucks, *J. Chem. Phys.* **1989**, *91*, 1062. [24f] R. C. Binning, L. A. Curtiss, *J. Comput. Chem.* **1995**, *103*, 6104. [24g] M. P. McGrath, L. Radom, *J. Chem. Phys.* **1991**, *94*, 511.

Received December 20, 2002

 © 2003 Wiley-VCH Verlag GmbH & Co. KGaA, Weinheim

Reactivity of Metallophosphide Anions with Electrophilic (Arene)tricarbonylmetal Complexes

Virginie Comte,[a] Jean Philippe Tranchier,[b] Françoise Rose-Munch,*[b] Eric Rose,[b] Danièle Perrey,[a] Philippe Richard,[a] and Claude Moïse[a]

Keywords: Anions / Carbonyl ligands / Arene ligands / Manganese / Chromium / Iron

Reaction of metallophosphide anions $[(CO)_xM'PPh_2]^-$ (M′ = Cr, Fe) with neutral tricarbonyl(η^6-fluoroarene)chromium and cationic (η^6-arene)tricarbonylmanganese complexes give rise to the formation of dinuclear complexes. These complexes are obtained either by substitution of the fluoride anion in the (arene)chromium complexes, or by addition to the ring in the (arene)manganese complexes. The X-ray structure of one homodimetallic (Cr–Cr) complex was obtained and compared with its solution structure.

(© Wiley-VCH Verlag GmbH & Co. KGaA, 69451 Weinheim, Germany, 2003)

Introduction

Arenes coordinated to electrophilic neutral $Cr(CO)_3$ or cationic $Mn(CO)_3$ groups undergo a large variety of transformations that would otherwise not be feasible with the free arenes.[1] Among them, nucleophilic additions, followed by acidic and (or) oxidative treatment, provide efficient access to functionalized arenes or cyclohexadienes.[1,2] A wide range of carbon nucleophiles have been shown to react with (η^6-arene)tricarbonylchromium and -manganese complexes,[1] but relatively few investigations have been carried out using organometallic derivatives as the nucleophiles.

In the Mn series, benzylic and homobenzylic organometallic carbanions have been used as nucleophiles. Beck et al., for example, described the reactivity of Mn complexes with deprotonated diphenylmethane or benzothiophene coordinated to $Cr(CO)_3$,[3] as well as with carbonylosmate,[4] carbonylrhenate[5] and anionic alkynyl complexes.[6] More recently, Sweigart et al.[7] demonstrated that a weak nucleophile such as $[Pt(PPh_3)_2(C_2H_4)]$ could cleave a strained C−C bond in the four-membered ring of biphenylene coordinated to an $Mn(CO)_3^+$ fragment, giving the insertion product. Similarly, metal insertion into the C−S and C−O bonds of benzothiophene and benzofuran, respectively, was also observed [the carbocyclic rings of the benzothiophene and the benzofuran were coordinated to $Mn(CO)_3^+$ entities].[8] Metal insertion into the C−Cl bond of cationic tricarbonyl(chloroarene)manganese complexes was also seen.[9a]

Our own contribution in this field has been aimed at studying the reactivity of Fischer-type carbene anions[10] and of deprotonated (alkoxy-substituted arene)tricarbonylchromium complexes[11] towards (η^6-arene)tricarbonylmanganese complexes. These reactions result in the formation of heterodi- or -polymetallic complexes.

In the Cr series, strongly nucleophilic organometallic anions [such as $Fe(CO)_4^{2-}$, $M(CO)_5^{2-}$, M = Cr, W, $CpFe(CO)_2^-$] reacted with $[(C_6H_5X)Cr(CO)_3]$, allowing the formation of dinuclear complexes, which arise as a result of halogen substitution by the organometallic anions.[12]

This has led us to investigate the reaction of metallophosphide anions with (η^6-arene)metal complexes, and for this purpose we have selected the $[(CO)_xM'PPh_2]^-$ anions. These metallophosphide anions are, for example, able to achieve Cp substitution in neutral molybdenocene and tungstenocene dichlorides.[13] The presence of *tert*-butyl or trimethylsilyl groups on the cyclopentadienyl rings does not affect the site of substitution, and products with 1,3-disubstituted Cp-ring[13d] (Scheme 1) are obtained.

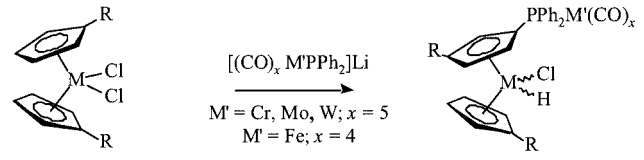

R = H, CMe_3, $SiMe_3$
M = Mo, W

Scheme 1. Reaction of metallophosphide anions with metallocene dichlorides

[a] Laboratoire de Synthèse et d'Electrosynthèse Organométalliques, UMR CNRS 5632, Faculté des Sciences Gabriel,
21000 Dijon, France
[b] Laboratoire de Synthèse Organique et Organométallique, UMR CNRS 7611, Université Pierre et Marie Curie, Tour 44 − 1er étage,
4, Place Jussieu, 75252 Paris Cedex 05, France
rosemun@ccr.jussieu.fr

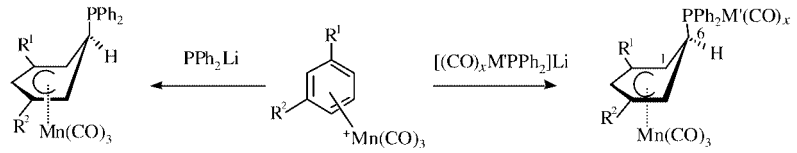

2 1 3

	1a	1b	1c	2a	3aCr]	3a[Fe]	3b[Cr]	3b[Fe]	3c[Cr]
R^1	H	OCH_3	OCH_3	H	H	H	OCH_3	OCH_3	OCH_3
R^2	H	H	OCH_3	H	H	H	H	H	OCH_3
M'					Cr	Fe	Cr	Fe	Cr
x					5	4	5	4	5

Scheme 2. Reaction of metallophosphide anions with $(\eta^6\text{-arene})Mn(CO)_3^+$ complexes

This unexpected reactivity led us to believe that metallophosphide anions are rather good nucleophiles.

In this paper, we describe the reactivity of two metallophosphide anions towards several substituted (η^6-arene)manganese and -chromium complexes (complexes **1**, Scheme 2; and **4**, Scheme 3). The conformational study of one of the resulting dinuclear complexes in the solid state and in solution is also presented.

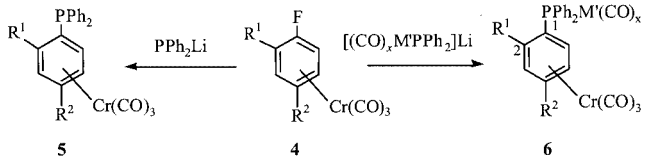

5 4 6

	4a	4b	4c	5a	5b	5c	6a[Cr]	6b[Cr]	6b[Fe]	6c[Cr]	6c[Fe]
R^1	H	CH_3	H	H	CH_3	H	H	CH_3	CH_3	H	H
R^2	H	H	CH_3	H	H	CH_3	H	H	H	CH_3	CH_3
M'							Cr	Cr	Fe	Cr	Fe
x							5	5	4	5	4

Scheme 3. Reaction of metallophosphide anions with (η^6-arene)-$Cr(CO)_3$ complexes

Results and Discussion

The starting (arene)tricarbonylmanganese (**1a**−**c**) and -chromium (**4a**−**c**) complexes were prepared according to literature procedures.[14,15]

Reactivity towards $[(\eta^6\text{-Arene})Mn(CO)_3]^+$ Complexes

In a preliminary experiment, treatment of a suspension of $[(\eta^6\text{-}C_6H_6)Mn(CO)_3](PF_6)$ (**1a**) in THF with PPh_2Li[16] at −80 °C resulted in the formation of the addition product, the η^5-cyclohexadienyl complex **2a**[17] in a 40% yield, according to Scheme 2.

It is worth noting that when PPh_2Li was added to bent metallocenes $[(\eta^5\text{-}C_5H_5)_2MCl_2]$ (M = Mo, W), the complexity of the reaction mixture did not permit isolation of the desired product.[18a] Similarly, treatment of complex **1a** with $[(CO)_xM'PPh_2]Li$ afforded the neutral complexes **3a[Cr]** and **3a[Fe]** in 55 and 35% yields, respectively. If the reaction was performed with anisole and the 1,3-dimethoxybenzene complexes, **1b** and **1c**, dimetallic derivatives **3b[Cr]**, **3b[Fe]** and **3c[Cr]**[18b] were recovered in 55, 55 and 65% yields, respectively (Scheme 2). It is important to emphasize the *meta* regioselectivity[19] of the nucleophilic addition with respect to the methoxy group in the cases of **1b** and **1c**.

The ^{1}H NMR spectra of the resulting neutral addition complexes (Table 1) features the characteristic signals for the η^5-cyclohexadienyl groups, the 1-H and 5-H protons display low-frequency resonances (between δ = 3.00 and 3.57 ppm), the 2-H and 4-H protons show resonances at almost the same frequency (δ = 4.85−5.07 ppm), and the 3-H protons give signals at the highest frequency (δ = 5.04−5.47 ppm) for the dinuclear complexes **3a[Cr]**, **3a[Fe]**, **3b[Cr]**, **3b[Fe]**, and **3c[Cr]** (Entries 2−6, Table 1), and at

Table 1. ^{1}H NMR spectroscopic data of 6-substituted tricarbonyl[(η^5-1,2,3,4,5)-cyclohexadienyl]manganese complexes

Entry	Complex[a]	1-H, 5-H	2,4-H	3-H	6-H	Ph
1	**2a**	3.16[b] (dd)	5.04[b] (dd)	6.06[b] (t)	3.73 (m)	7.36 (m)
2	**3a[Cr]**	3.56[b] (dd)	4.85[b] (dd)	5.18[b] (t)	4.30[c] (td)	7.54 (m)
3	**3a[Fe]**	3.57[b] (dd)	4.99[b] (dd)	5.47[b] (t)	4.36 (m)	7.59 (m)
4	**3b[Cr]**[d]	3.39[d] (m), 3.56[b] (dd)	4.90[b] (dd)	5.11[b] (d)	4.39 (m)	7.55 (m)
5	**3b[Fe]**[d]	3.00(m), 3.56[b] (dd)	5.07[b] (dd)	5.42[b] (d)	4.47 (m)	7.55 (m)
6	**3c[Cr]**[e]	3.00 (m), 3.56[b] (dd), 3.40 (m)	−	5.04[f] (t)	4.38[g] (dt)	7.55 (m)

[a] CD_3COCD_3, multiplicity is given in parentheses. [b] $^3J_{H,H}$ = 5.9 Hz. [c] $^3J_{H,H} = {}^2J_{HP}$ = 5.9 Hz. [d] OMe: δ = 3.39. [e] OMe: δ = 3.44. [f] $^4J_{H,H}$ = 2 Hz. [g] $^2J_{HP}$ = 9.3 Hz; $^3J_{H,H}$ = 5.6 Hz.

 © 2003 Wiley-VCH Verlag GmbH & Co. KGaA, Weinheim

even higher frequency (δ = 6.06 ppm) for the mononuclear complex **2a** (Entry 1, Table 1).

The resonance for 6-H in the mononuclear complex **2a** presents a signal at δ = 3.73 ppm, in agreement with that previously observed for the product obtained after addition of phosphate to coordinated $[(arene)Mn(CO)_3]^+$ cations.[19c] The signals for the 6-H protons of the dinuclear complexes (Entries 2−6), which can be used as a probe for the coordination of PPh_2 to the $M'(CO)_x$ entity, display a high-frequency shift, δ = 4.30−4.47 ppm. This is consistent with the coordination of a phosphorus atom to a metal center.

Reactivity Towards (η⁶-Arene)Cr(CO)₃ Complexes

The tricarbonyl(η⁶-haloarene)chromium complexes **4a**, **4b** and **4c** reacted with PPh_2Li in THF in the presence of freshly distilled HMPT; derivatives **5a**,[20] **5b** and **5c**, respectively, were obtained in 60% yields (Scheme 3).

No reaction takes place in the absence of HMPT (which increases the nucleophilicity of the anions), emphasizing the low electrophilic nature of the Cr complexes. The easy formation of **5b** shows that steric effects, due to the presence of the *ortho*-methyl group, play no part. These metallophosphane complexes could lead to many μ-phosphido-bridged heteropolymetallic complexes. For example, we were able to synthesize such a dimetallic system incorporating a group-8 metallocene derivative.[21]

Similarly, by using $[(CO)_xM'PPh_2]Li$ (x = 5, M′ = Cr and x = 4, M′ = Fe), dimetallic complexes **6a[Cr]**, **6b[Cr]**, **6b[Fe]**[18b] (Scheme 3) were isolated in 85, 80 and 60% yields, respectively. Their ^1H NMR spectroscopic data (Entries 1, 2, 4−6, Table 2) are consistent with *ipso*-nucleophilic aromatic substitution occurring at the carbon atom bearing the fluoride atom. The same regioselectivity was clearly observed when using the *para*-disubstituted complex **4c** as the starting material. This afforded the new *para*-disubstituted complexes **5c**, **6c[Cr]** and **6c[Fe]** (Scheme 3). No *cine*- or *tele*-S_NAr was observed.[1d]

It is important to note the influence of the PPh_2 or the $PPh_2M'(CO)_x$ unit on the conformation of the $Cr(CO)_3$ tripod. Indeed the 4-H protons, *para* to the phosphanyl residue, display signals at the highest frequency (between δ = 5.80 and 6.12 ppm; Entries 1, 2, 4−6, Table 2).

This is in agreement with an *anti*-eclipsed conformation of the tripod, with respect to the bulky phosphanyl group.[1g] Similarly, the eclipsed 2-H and 6-H protons present signals at a high frequency. The biggest difference in the chemical shifts observed for two adjacent protons (3-H and 4-H) is δ = 0.92 ppm for complex **5b**. This is due to the synergic effect of the electron-donating methyl group, which favors an eclipsed conformation, and the phosphanyl group, whose steric hindrance favors an *anti*-eclipsed conformation. This confirms that the main conformation of the tripod in solution is eclipsed, with respect to the methyl group.[1d]

The IR spectra of $Cr(CO)_3$ present two well-resolved stretching modes, in accordance with the C_{3v} symmetry.[22] The absorptions are assigned to a nondegenerate symmetry vibration A1, and a doubly degenerate asymmetric vibration E.[22]

In order to evaluate the effect of complexation of the phosphorus atom by the $M'(CO)_x$ metal fragment, we compared some selected IR and ^1H NMR spectroscopic data of the mononuclear and dinuclear complexes of this chromium series (Table 3).

In all cases, a shift to higher wavenumbers is observed for the carbonyl stretching vibrations of the $Cr(CO)_3$ entity for the dimetallic complexes. This is in agreement with a stronger CO force constant, and with a decrease in the retro-donation of the chromium towards the carbonyl groups. In the NMR spectra, the 6-H protons (β to the phosphorus atom) of the dinuclear complexes present signals at a much higher frequency than those of the mononuclear complexes, e.g. the $\Delta\delta$(6-H) [$\delta(6\text{-H}_{dinuclear}) - \delta(6\text{-H}_{mononuclear})$] could reach δ = 0.57 ppm for **6c[Fe]** (Entry 8, Table 3).

In order to know more about the conformation of these complexes in the solid state, an X-ray analysis was performed on crystals of complex **6b[Cr]**. Two views of the ORTEP diagram are presented in Figure 1.

First of all, the two metallic moieties lie on both sides of the arene ring. The $Cr(CO)_3$ moiety adopts an eclipsed conformation relative to the methyl group. It is worth not-

Table 2. ^1H NMR spectroscopic data of tricarbonyl[η⁶-(1-substituted arene)]chromium complexes

Entry	Complex[a]	2-H	3-H	4-H	5-H	6-H	Ph
1	**5a**	5.56[b] (dd)	5.40[c] (dd)	5.80[c] (t)	5.40[c] (dd)	5.56[b] (dd)	7.50 (m)
2	**5b**[d]	–	4.91 (m)	5.83[c] (dd)	5.50 (m)	5.36[b] (dd)	7.50 (m)
3	**5c**[e]	5.45 (m)	5.45 (m)	–	5.45 (m)	5.45 (m)	7.55 (m)
4	**6a[Cr]**	5.86[b] (dd)	5.50[c] (dd)	6.06[c] (t)	5.50[c](dd)	5.86[b] (dd)	7.75 (m)
5	**6b[Cr]**[f]	–	5.41 (m)	6.10[c] (dd)	5.45 (m)	5.63[b] (dd)	7.70 (m)
6	**6b[Fe]**[g]	–	5.37 (m)	6.12 (m)	5.37 (m)	5.45 (m)	7.70 (m)
7	**6c[Cr]**[h]	5.90[i] (dd)	5.44[j] (d)	–	5.44[j] (d)	5.90[i] (dd)	7.55 (m)
8	**6c[Fe]**[k]	6.02[j] (dd)	5.54[j] (d)	–	5.80[j] (d)	5.98[i] (dd)	7.60 (m)

[a] CD_3COCD_3, multiplicity is given in parentheses. [b] $^3J_{H,H} = {}^3J_{PH} = 5.9$ Hz. [c] $^3J_{H,H}$=5.9 Hz. [d] Me: δ = 2.26. [e] Me: δ = 2.23. [f] Me: δ =2.11. [g] Me: δ = 2.16. [h] Me: δ = 2.33. [i] $^3J_{H,H} = {}^3J_{PH} = 6.4$ Hz. [j] $^3J_{H,H} = 6.4$ Hz. [k] Me: δ = 2.35.

 © 2003 Wiley-VCH Verlag GmbH & Co. KGaA, Weinheim

Table 3. Selected IR and ^{1}H NMR spectroscopic data for (arene)chromium complexes

Entry[a][b]	Complex	ν(Cr−CO), A1 mode	ν(Cr−CO), E mode	$\Delta\nu_{A1}$, $\Delta\nu_{E}$	δ(6-H)	Δδ(6-H)
1	**5a**	1969	1899		5.56	
2	**6a[Cr]**	1978	1909	+9[c], +6[c]	5.86	+0.30
3	**5b**	1971	1895			
4	**6b[Cr]**	1972	1898	+1[d], +3[d]		
5	**6b[Fe]**	1972	1897	+1[e], +2[c]		
6	**5c**	1970	1900		5.45	
7	**6c[Cr]**	1973	1901	+3[f], +1[f]	5.90	+0.45
8	**6c[Fe]**	1976	1901	+6[g], +1[g]	6.02	+0.57

[a] IR spectra in THF [cm^{-1}]. [b] NMR spectra in $CDCl_3$ [ppm]. [c] Δν = ν**6a[Cr]** − ν**5a**. [d] Δν = ν**6b[Cr]** − ν**5b**. [e] Δν = ν**6b[Fe]** − ν**5b**. [f] Δν = ν**6c[Cr]** − ν**5c**. [g] Δν = ν**6c[Fe]** − ν**5c**.

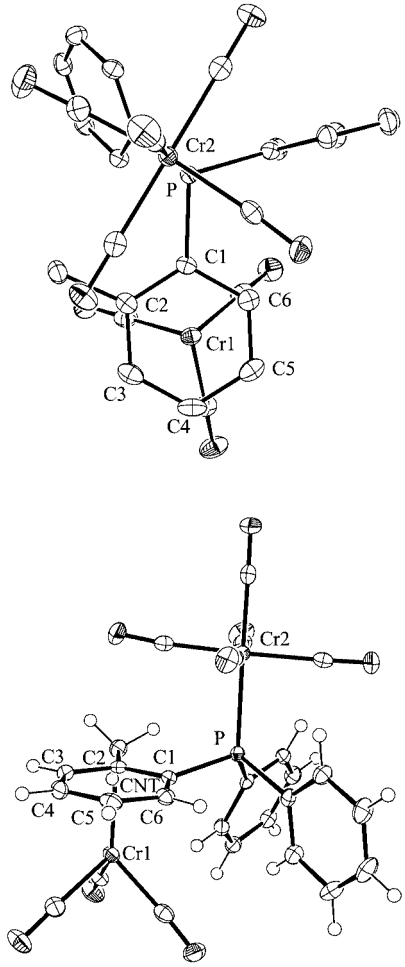

Figure 1. Two views of the ORTEP diagram of **6b[Cr]**; thermal ellipsoids are drawn at the 50% probability level; selected parameters: CNT−Cr1 1.724(2), C1−P 1.843(2), Cr2−P 2.4107(5), C1−P−Cr2 108.19(6)

ing that the longest chromium−carbon bond length is seen for Cr−C1 [2.268(2) Å], for the carbon atom substituted by the phosphane group, whereas the chromium−carbon bond length Cr−C2, for the carbon atom substituted by the methyl group, is 2.255(2) Å. The four other bond lengths are in the range 2.204−2.222 Å. Furthermore, the phosphorus atom, whose C1−P bond length is 1.843(2) Å, displays a shift of 0.471(2) Å out of the mean-aromatic plane, away from the Cr center.[23] The metal-to-ring distance is 1.724(2) Å. It is interesting to compare this structure with the tricarbonyl[(diisopropylphosphanyl)benzene]chromium structure (complex **A**), which presents a partially eclipsed conformation of the $Cr(CO)_3$ entity (midway between eclipsed and staggered, relative to the η^6-phenyl ring).[20a] In Table 4, selected bond lengths of complexes **A** and **6b[Cr]** are reported for comparison; coordination of the phosphorus substituent to $Cr(CO)_5$ does not seem to significantly affect these values. However, a small increase in the Cr−C1 bond length is induced.

Table 4. Selected bond lengths [Å] of complexes **A**[20a] and **6b[Cr]**

Complexes	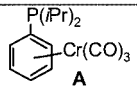 **A**	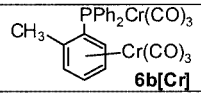 **6b[Cr]**
Cr–C1	2.231(2)	2.2682(17)
Cr–C2	2.197(3)	2.2550(17)
Cr–C3	2.211(3)	2.2120(19)
Cr–C4	2.218(3)	2.2116(19)
Cr–C5	2.206(3)	2.2219(18)
Cr–C6	2.209 (2)	2.2039(18)
C1–P	1.840(3)	1.8431(18)
Cr–Ar	1.71	1.724(2)

Conclusion

Metallophosphide anions readily react with electrophilic (η^6-arene)tricarbonylmanganese (by nucleophilic additions) and chromium complexes (by *ipso*-nucleophilic substitutions), and allow the easy formation of neutral dinuclear complexes, one of which has been fully characterized by X-ray analysis. Both types of reactions are useful in the synthesis of highly functionalized arylphosphane complexes, and they might therefore complement the methods previously described where nucleophilic arene derivatives are treated with electrophilic phosphanes XPR_2.

 © 2003 Wiley-VCH Verlag GmbH & Co. KGaA, Weinheim

Experimental Section

General Comments: All reactions were carried out under purified argon. The solvents and eluents were dried by an appropriate procedure and distilled under argon from sodium and benzophenone immediately before use. Standard Schlenk techniques and conventional glass vessels were employed. Column chromatography was performed under argon with silica gel (70−230 mesh). Elemental analyses were carried out with an EA 1108 CHNS-O FISONS Instruments. ^{1}H (200 MHz), ^{31}P (81 MHz) and ^{13}C (50 MHz) spectra were collected with a Bruker AC 200 spectrometer. Chemical shifts are relative to internal TMS (^{1}H, ^{13}C) or external H_3PO_4 (^{31}P). IR spectra were recorded with a Nicolet 205 IR-FT. The lithium reagent $[(CO)_xM'PPh_2]Li$ (x = 5, M′ = Cr; x = 4, M′ = Fe) was prepared according to a literature method,[24] using low-chloride methyllithium (Janssen). The manganese complexes were prepared according to two different procedures, using $[BrMn(CO)_5]$ with $AlCl_3$ or $AgBF_4$ and the free arenes.[14] The syntheses of the chromium complexes were achieved by heating $[Cr(CO)_6]$ and the free arene in a 9:1 mixture of di-*n*-butyl ether and THF.[15]

(Arene)manganese Complexes. General Procedure: 5 mL of a THF solution of PPh_2Li or $[(CO)_xM'PPh_2]Li$ (1 mmol) was added dropwise to a suspension of $[(\eta^6\text{-}C_6H_4\text{-}2\text{-}R^1\text{-}4\text{-}R^2)Mn(CO)_3](PF_6)$ (1 mmol) in THF (15 mL) at −80 °C. The stirred mixture was gradually warmed to room temperature for about 5 h, and THF was then removed in vacuo. With $R^3 = PPh_2$, the crude product was dissolved in Et_2O and filtered through Celite. For the dimetallic systems [$R^3 = (CO)_xM'PPh_2$], the residue was washed with pentane and chromatographed (eluent: toluene) to give an orange-yellow powder. All complexes $[(\eta^5\text{-}C_6H_3\text{-}2\text{-}R^1\text{-}4\text{-}R^2\text{-}6\text{-}R^3)Mn(CO)_3]$ were isolated after recrystallization from toluene.

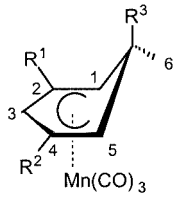

$[(\eta^5\text{-}C_6H_6\text{-}6\text{-}R^3)Mn(CO)_3]$ ($R^3 = PPh_2$: 2a): Yellow crystals (60 mg, 40% yield). IR (νCO, THF): $\tilde{\nu}$ = 2014 (w), 1935 (s) cm^{-1}. ^{1}H NMR (CD_3COCD_3): see Table 1. ^{31}P{^{1}H} NMR (CD_3COCD_3): δ = 9.9 (s) ppm. $C_{21}H_{16}MnO_3P$ (402.3): calcd. C 62.70, H 4.01; found C 62.44, H 4.14. **{$R^3 = PPh_2Cr(CO)_5$: 3a[Cr]}:** Yellow crystals (326 mg, 55% yield). IR (νCO, THF): $\tilde{\nu}$ = 2061 (m), 2020 (s), 1982 (w), 1940 (s) cm^{-1}. ^{1}H NMR (CD_3COCD_3): see Table 1. ^{31}P{^{1}H} NMR (CD_3COCD_3): δ = 62.8 (s) ppm. $C_{26}H_{16}CrMnO_8P$ (594.3): calcd. C 52.55, H 2.71; found C 52.97, H 2.77. **{$R^3 = PPh_2Fe(CO)_4$: 3a[Fe]}:** Yellow crystals (199 mg, 35% yield). IR (νCO, THF): $\tilde{\nu}$ = 2053 (m), 1978 (w), 1943 (s) cm^{-1}. ^{1}H NMR (CD_3COCD_3): see Table 1. ^{31}P{^{1}H} NMR (CD_3COCD_3): δ = 77.4 (s) ppm. $C_{25}H_{16}FeMnO_7P$ (570.2): calcd. C 52.67, H 2.83; found C 52.95, H 2.58.

$[(\eta^5\text{-}C_6H_5\text{-}2\text{-}OMe\text{-}6\text{-}R^3)Mn(CO)_3]$ {$R^3 = PPh_2Cr(CO)_5$: 3b[Cr]}: Yellow crystals (343 mg, 55% yield). IR (νCO, THF): $\tilde{\nu}$ = 2061 (m), 2019 (s), 1980 (w), 1940 (s) cm^{-1}. ^{1}H NMR (CD_3COCD_3): δ = 3.39 (m, 4 H, OMe and 1-H) ppm, see Table 1. ^{31}P{^{1}H} NMR (CD_3COCD_3): δ = 63.4 (s) ppm. $C_{27}H_{18}CrMnO_9P$ (624.3): calcd. C 51.92, H 2.88; found C 52.20, H 2.98. **{$R^3 = PPh_2Fe(CO)_4$: 3b[Fe]}:** Not recrystallized (329 mg, 55% yield). IR (νCO, THF): $\tilde{\nu}$ = 2053 (m), 2018 (f), 1978 (m), 1940 (s) cm^{-1}. ^{1}H NMR (CD_3COCD_3): δ = 3.39 (s, 3 H, OMe) ppm; see Table 1. ^{31}P{^{1}H} NMR (CD_3COCD_3): δ = 77.3 (s) ppm.

$[(\eta^5\text{-}C_6H_4\text{-}1\text{-}OMe\text{-}3\text{-}OMe\text{-}5\text{-}R^3)Mn(CO)_3]$ {$R^3 = PPh_2Cr(CO)_5$: 3c[Cr]}: Yellow crystalline powder (425 mg, 65% yield). IR (νCO, THF): $\tilde{\nu}$ = 2061 (m), 2018 (s), 1983 (w), 1937 (s) cm^{-1}. ^{1}H NMR (CD_3COCD_3): δ = 3.44 (s + m, 8 H, OMe, 1-H + 5-H) ppm; see Table 1. ^{31}P{^{1}H} NMR (CD_3COCD_3): δ = 61.3 (s) ppm. $C_{28}H_{20}CrMnO_{10}P$ (654.4): calcd. C 51.39, H 3.08; found C 52.17, H 3.79.

(Arene)chromium Complexes. General Procedure: 5 mL of a THF solution of PPh_2Li or $[(CO)_xM'PPh_2]Li$ (1 mmol) was added dropwise at −80 °C to a solution of $[(\eta^6\text{-}C_6H_3\text{-}1\text{-}F\text{-}2\text{-}R^1\text{-}4\text{-}R^2)Cr(CO)_3]$ (1 mmol) in THF (15 mL) in the presence of freshly distilled HMPT (1 mmol). The stirred mixture was gradually warmed to room temperature for about 5 h, and THF was then removed in vacuo. With $R^3 = PPh_2$, the crude product was dissolved in toluene and filtered through Celite. For the dimetallic systems [$R^3 = (CO)_xM'PPh_2$], the residue was washed with pentane and chromatographed (eluent: toluene) to give a yellow powder. All complexes $[(\eta^6\text{-}C_6H_3\text{-}1\text{-}R^3\text{-}2\text{-}R^1\text{-}4\text{-}R^2)Cr(CO)_3]$ were isolated as yellow crystals after recrystallization from acetone.

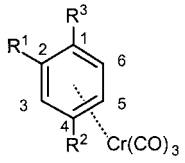

$[(\eta^6\text{-}C_6H_5\text{-}1\text{-}PPh_2)Cr(CO)_3]$ (5a): Yellow crystals (238 mg, 60% yield). IR (νCO, THF): $\tilde{\nu}$ = 1969 (s), 1899 (s) cm^{-1}. ^{1}H NMR (CD_3COCD_3): see Table 2. ^{31}P{^{1}H} NMR ($CDCl_3$): δ = −1.8 (s) ppm. $C_{21}H_{15}CrO_3P$ (398.3): calcd. C 63.32, H 3.80; found C 62.93, H 4.08.

$[(\eta^6\text{-}C_6H_4\text{-}1\text{-}PPh_2\text{-}2\text{-}Me)Cr(CO)_3]$ (5b): Not recrystallized (247 mg, 60% yield). IR (νCO, THF): $\tilde{\nu}$ = 1971 (s), 1895 (s) cm^{-1}. ^{1}H NMR (CD_3COCD_3): δ = 2.26 ppm (s, 3 H, Me); see Table 2. ^{31}P{^{1}H} NMR (CD_3COCD_3): δ = −9.8 (s) ppm.

$[(\eta^6\text{-}C_6H_4\text{-}1\text{-}PPh_2\text{-}4\text{-}Me)Cr(CO)_3]$ (5c): Yellow crystals (247 mg, 60% yield). IR (νCO, THF): $\tilde{\nu}$ = 1970 (s), 1900 (s) cm^{-1}. ^{1}H NMR (CD_3COCD_3): δ = 2.23 (s, 3 H, Me), ppm; see Table 2. ^{31}P{^{1}H} NMR ($CDCl_3$): δ = −2.9 (s) ppm. $C_{22}H_{17}CrO_3P$ (412.3): calcd. C 64.08, H 4.16; found C 63.73, H 3.81.

$[(\eta^6\text{-}C_6H_5\text{-}1\text{-}R^3)Cr(CO)_3]$ {$R^3 = PPh_2Cr(CO)_5$: 6a[Cr]}: Yellow crystals (501 mg, 85% yield): IR (νCO, THF): $\tilde{\nu}$ = 2065 (w), 1978 (m), 1943 (s), 1909 (s) cm^{-1}. ^{1}H NMR (CD_3COCD_3): see Table 2. ^{31}P{^{1}H} NMR (CD_3COCD_3): δ = 61.5 (s) ppm. ^{13}C{^{1}H} NMR ($CDCl_3$): δ = 232 [s, Cr(*C*O)$_3$], 221.4 [d, J = 6.4 Hz, Cr(*C*O)$_5$ *trans*], 216.7 [d, J = 12.8 Hz, Cr(*C*O)$_5$ *cis*], 136.1 (d, J = 36.7 Hz, Ph *ipso*), 133.1 (d, J=11 Hz, Ph *ortho*), 131.4 (s, Ph *para*), 129.5 (d, J = 9.2 Hz, Ph *meta*), 101.5 (d, J = 24.8 Hz, C-1), 99.4 (d, J = 10 Hz, C-2 and C-6), 96.2 (s, C-4), 87.9 (d, J = 6.4 Hz, C-3 and C-5) ppm. $C_{26}H_{15}Cr_2O_8P$ (590.4): calcd. C 52.90, H 2.56; found C 52.98, H 2.69.

$[(\eta^6\text{-}C_6H_4\text{-}1\text{-}R^3\text{-}2\text{-}Me)Cr(CO)_3]$ {$R^3 = PPh_2Cr(CO)_5$: 6b[Cr]}: Yellow crystals (483 mg, 80% yield). IR (νCO, THF): $\tilde{\nu}$ = 2067 (w), 1972 (m), 1944 (s), 1898 (s) cm^{-1}. ^{1}H NMR (CD_3COCD_3): δ = 2.11 (s, 3 H, Me) ppm; see Table 2. ^{31}P{^{1}H} NMR (CD_3COCD_3): δ = 60.21 (s) ppm. ^{13}C{^{1}H} NMR ($CDCl_3$): δ = 232.5 [s, Cr(*C*O)$_3$], 221.5 (d, J=5.5 Hz, Cr(*C*O)$_5$ *trans*), 216.8 (d, J = 12 Hz, Cr(*C*O)$_5$

 © 2003 Wiley-VCH Verlag GmbH & Co. KGaA, Weinheim

cis), 134.9 (d, J = 12 Hz, Ph *ortho*), 133.9 (d, J = 36 Hz, Ph *ipso*), 133.1 (d, J = 12 Hz, Ph *ortho*), 133.0 (d, J = 35 Hz, Ph *ipso*), 131.9 (s, Ph *para*), 131.4 (s, Ph *para*), 129.7 (s, Ph *meta*), 129.5 (s, Ph *meta*), 112.7 (d, J = 8.3 Hz, C-2), 104.7 (d, J = 20 Hz, C-1), 97.9 (d, J = 14.7 Hz, C-6), 97.1 (s, C-4), 92.4 (d, J = 4.6 Hz, C-5), 87.5 (d, J = 6.5 Hz, C-3), 22.4 (s, CH_3) ppm. $C_{27}H_{17}Cr_2O_8P$ (604.4): calcd. C 53.66, H 2.84; found C 53.57, H 3.02. **{R^3 = $PPh_2Fe(CO)_4$: 6b[Fe]}:** Not recrystallized (348 mg, 60% yield). IR (νCO, THF): $\tilde{\nu}$ = 2051 (w), 1972 (s), 1943 (s), 1897 (s) cm^{-1}. ^1H NMR (CD_3COCD_3): δ = 2.16 (s, 3 H, Me) ppm; see Table 2. $^{31}P\{^1H\}$ NMR (CD_3COCD_3): δ = 74.0 (s) ppm.

[(η⁶-C_6H_4-1-R^3-4-Me)$Cr(CO)_3$] {R^3 = $PPh_2Cr(CO)_5$: 6c[Cr]}: Yellow crystals (362 mg, 60% yield). IR (νCO, THF): $\tilde{\nu}$ = 2066 (w), 1973 (m), 1943 (s), 1901 (s) cm^{-1}. ^1H NMR (CD_3COCD_3): δ = 2.33 (s, 3 H, Me) ppm; see Table 2. $^{31}P\{^1H\}$ NMR (CD_3COCD_3): δ = 60.5 (s) ppm. $^{13}C\{^1H\}$ NMR ($CDCl_3$): δ = 231.4 [s, $Cr(CO)_3$], 221.4 (d, J = 6.5 Hz, $Cr(CO)_5$ *trans*), 216.7 (d, J = 12 Hz, $Cr(CO)_5$ *cis*), 136.5 (d, J = 37 Hz, Ph *ipso*), 133.0 (d, J = 10.5 Hz, Ph *ortho*), 131.3 (s, Ph *para*), 129.4 (d, J = 9 Hz, Ph *meta*), 111.9 (s, C-4), 99.9 (d, J = 14.7 Hz, C-2 and C-6), 99.4 (d, J = 27 Hz, C-1), 89.3 (d, J = 6.5 Hz, C-3 and C-5), 21.3 (s, CH_3). $C_{27}H_{17}Cr_2O_8P$ (604.4): calcd. C 53.66, H 2.84; found C 53.80, H 2.99. **{R^3 = $PPh_2Fe(CO)_4$: 6c[Fe]}:** Yellow crystals (330 mg, 57% yield). IR (νCO, THF): $\tilde{\nu}$ = 2051 (w), 1976 (s), 1942 (s), 1901 (s) cm^{-1}. ^1H NMR (CD_3COCD_3): δ = 2.35 (s, 3 H, Me) ppm; see Table 2. $^{31}P\{^1H\}$ NMR (CD_3COCD_3): δ = 78.1 (s) ppm. $C_{26}H_{17}CrFeO_7P$ (580.2): calcd. C 53.82, H 2.95; found C 54.30, H 2.99.

Crystal Structure of 6b[Cr]: Single crystals of **6b[Cr]** were obtained by recrystallization from acetone. Intensity data were collected with a Nonius Kappa CCD at 110 K. The structure was solved with a Patterson search program and refined with full-matrix least-squares methods based on F^2(SHELXL-97)[25] with the aid of the WINGX program.[26] All non-hydrogen atoms were refined with anisotropic thermal parameters. Hydrogen atoms were included in their calculated positions or found in the final difference Fourier maps and refined with a riding model. CCDC-187419 contains the supplementary crystallographic data for this paper. These data can be obtained free of charge at www.ccdc.cam.ac.uk/conts/retrieving.html [or from the Cambridge Crystallographic Data Centre, 12 Union Road, Cambridge CB2 1EZ, UK; Fax: (internat.) + 44-1223/336-033; E-mail: deposit@ccdc.cam.ac.uk].

Acknowledgments

We thank the CNRS and the European Community TMR program no. FMRX-CT98-0166 and COST D14 program for financial support (J. P. T., F. R. M. and E. R.).

[1] [1a] F. Mc Quillin, D. G. Parker, G. R. Stephenson, *Transition Metal, Organometallics for Organic Synthesis*, Cambridge University Press, Cambridge, **1991**, p. 429. [1b] M. F. Semmelhack, *Comprehensive Organometallic Chemistry* (Eds.: W. Abel, F. G. A. Stone, G. Wilkinson), Pergamon, Oxford, **1995**, vol. 12, chapter 9, p. 979. [1c] K. F. McDaniel, *Comprehensive Organometallic Chemistry* (Eds.: E. W. Abel, F. G. A. Stone, G. Wilkinson), Pergamon, Oxford, **1995**, vol. 6, chapter 4, p. 93. [1d] F. Rose-Munch, V. Gagliardini, C. Renard, E. Rose, *Coord. Chem. Rev.* **1998**, *178–180*, 249. [1e] R. D. Pike, D. A. Sweigart, *Coord. Chem. Rev.* **1999**, *187*, 183. [1f] D. Astruc, *Chimie Organométallique*, Ed. EDP Sciences, Les Ulis, France, **2000**, p. 111. [1g] F. Rose-Munch, E. Rose, *Eur. J. Inorg. Chem.* **2002**, *6*, 1269. [1h] F. Rose-Munch, E. Rose, *Modern Arene Chemistry* (Ed.: D. Astruc), Wiley-VCH, Weinheim, **2002**, chapter 11, p. 368.

[2] [2a] A. R. Pape, K. P. Krishna, E. P. Kündig, *Chem. Rev.* **2000**, *100*, 2917. [2b] G. Bernardinelli, S. Gillet, E. P. Kündig, L. Ronggang, A. Ripa, L. Saudan, *Synthesis* **2001**, *13*, 2040.

[3] J. Breimair, M. Wieser, W. Beck, *J. Organomet. Chem.* **1992**, *441*, 429.

[4] B. Niemer, J. Breimair, T. Völkel, B. Wagner, K. Polborn, W. Beck, *Chem. Ber.* **1991**, *124*, 2237.

[5] B. Niemer, M. Steinmann, W. Beck, *Chem. Ber.* **1988**, *121*, 1767.

[6] J. Milke, K. Sünkel, W. Beck, *J. Organomet. Chem.* **1997**, *543*, 39.

[7] X. Zhang, G. B. Carpenter, D. A. Sweigart, *Organometallics* **1999**, *18*, 4887.

[8] H. Li, G. B. Carpenter, D. A. Sweigart, *Organometallics* **2000**, *19*, 1823.

[9] [9a] For insertion of a Pd entity into the C−Cl bond of cationic Mn complexes, see: J. F. Carpentier, Y. Castanet, J. Brocard, A. Mortreux, F. Rose-Munch, C. Susanne, E. Rose, *J. Organomet. Chem.* **1995**, *493*, C22. [9b] For insertion of a Pd entity into the C−Cl bond of Cr complexes, see for example: J. F. Carpentier, F. Petit, A. Mortreux, V. Dufaud, J. M. Basset, J. Thivolle-Cazat, *J. Mol. Cat.* **1993**, *81*, 1.

[10] F. Rose-Munch, C. Susanne-Lecorre, F. Balssa, E. Rose, J. Vaissermann, E. Licandro, A. Papagni, S. Maiorana, W. Meng, R. Stephenson, *J. Organomet. Chem.* **1997**, 545.

[11] C. Renard, R. Valentic, F. Rose-Munch, E. Rose, J. Vaissermann, *Organometallics* **1998**, *17*, 1587.

[12] [12a] J. A. Heppert, M. E. Thomas-Miller, P. N. Swepston, M. W. Extine, *J. Chem. Soc., Chem. Commun.* **1988**, 280. [12b] J. A. Heppert, M. E. Thomas-Miller, F. Takusagawa, M. A. Morgenstern, M. R. Shaker, *Organometallics* **1989**, *8*, 1199. [12c] G. B. Richter-Addo, A. D. Hunter, N. Wichrowska, *Can. J. Chem.* **1990**, *68*, 41.

[13] [13a] S. Rigny, J.-C. Leblanc, C. Moïse, *New J. Chem.* **1995**, *19*, 145. [13b] S. Rigny, J.-C. Leblanc, C. Moïse, B. Nuber, *New J. Chem.* **1997**, *21*, 469. [13c] S. Rigny, V. I. Bakhmutov, B. Nuber, J.-C. Leblanc, C. Moïse, *Inorg. Chem.* **1996**, *35*, 3202. [13d] V. Comte, O. Blacque, M. M. Kubicki, C. Moïse, *Organometallics* **2001**, *20*, 5432.

[14] [14a] For the preparation of **1a** see: A. M. Munro, P. L. Pauson, *Z. Anorg. Allg.* **1979**, *458*, 211. [14b] For preparation of **1b**, see: P. L. Pauson, J. A. Segal, *J. Chem. Soc.* **1975**, 1677. [14c] For the preparation of **1c**, see: F. Balssa, V. Gagliardini, F. Rose-Munch, E. Rose, *Organometallics* **1996**, *15*, 4373.

[15] For the preparation of **4a**, see: [15a] C. A. L. Mahaffy, *J. Organomet. Chem.* **1984**, *262*, 33. For the preparation of **4b** and **4c**, see: [15b] G. Winkhaus, L. Pratt, G. Wilkinson, *J. Chem. Soc.* **1961**, 3807.

[16] PPh_2Li was prepared from PPh_2H and butyllithium. PPh_2H was prepared by a published procedure: V. D. Bianco, S. Doronzo, *Inorg. Synth.* **1976**, *16*, 162.

[17] The reaction of PPh_2Li with $[(C_6H_6)Mn(CO)_3]^+$ was already described: P. J. C. Walker, A. J. Mawby, *Inorg. Chim. Acta* **1973**, *7*, 621. However, the corresponding addition product was obtained in a very small amount which, according to the authors, rendered impossible complete characterisation of the complex which decomposed during attempted purification.

[18] [18a] S. Rigny, Thesis, Université de Bourgogne, **1995**. [18b] We were unable to purify complexes **3c[Fe]** and **6a[Fe]** for stability reasons.

[19] Such a regioselectivity has been observed for other nucleophiles adding *meta* to the MeO substituent of the arene ring, see for example: [19a] A. J. Pearson, I. C. Richards, *J. Organomet. Chem.* **1983**, *258*, C41. [19b] R. P. Alexander, G. R. Stephenson, *J. Organomet. Chem.* **1986**, *314*, C73. [19c] Y. K. Chung, H. K. Bae, I. N. Jung, *Bull. Korean Chem. Soc.* **1988**, *9*, 349. [19d] A. J. Pearson, P. R. Bruhn, F. Gouzoules, S. H. Lee, *J. Chem. Soc., Chem. Commun.* **1989**, 659. [19e] W. H. Miles, P. M. Smiley, H. R. Brinkman, *J. Chem. Soc., Chem. Commun.* **1989**, 1897. [19f]

 © 2003 Wiley-VCH Verlag GmbH & Co. KGaA, Weinheim

F. Balssa, V. Gagliardini, C. Lecorre-Susanne, F. Rose-Munch, E. Rose, J. Vaissermann, *Bull. Soc. Chim. Fr.* **1997**, *134*, 537.
[20] Complex **5a** has already been synthesised by treating the lithium derivative of (benzene)tricarbonylchromium complexes with chloro(diphenyl)phosphane: [20a] W. R. Cullen, S. J. Rettig, H. Zhang, *Can. J. Chem.* **1996**, *74*, 2167. Alternative: transmetallation of a stannous derivative of (benzene)tricarbonylchromium complexes with *n*BuLi followed by treatment with chloro(diphenyl)phosphane: [20b] W. E. Wright, L. Lawson, B. T. Baker, D. C. Rae, *Tetrahedron* **1993**, *11*, 323.
[21] V. Comte, C. Moïse, F. Rose-Munch, E. Rose, unpublished results.
[22] F. Van Meurs, J. M. A. Baas, H. Van Bekkum, *J. Organomet. Chem.* **1976**, *113*, 353.
[23] J. P. Djukic, F. Rose-Munch, E. Rose, J. Vaissermann, *Eur. J. Inorg. Chem.* **2000**, 1295 and references therein.
[24] M. J. Breen, P. M. Shulman, G. L. Geoffroy, A. L. Rheingold, W. C. Fultz, *Organometallics* **1984**, *3*, 782.
[25] G. M. Sheldrick, *SHELX97, Programs for Crystal Structure Analysis* (includes SHELXS-97, SHELXL-97), release 97-2, University of Göttingen, Germany, **1998**.
[26] L. J. J. Farrugia, *Appl. Crystallogr.* **1999**, *32*, 837.

Received September 19, 2002

 © 2003 Wiley-VCH Verlag GmbH & Co. KGaA, Weinheim

A Rigid Molecular Scaffold Affixing a (Polypyridine)ruthenium(II)- and a Nickel(II)-Containing Complex: Spectroscopic Evidence for a Weakly Coupled Bichromophoric System

Yann Pellegrin,[a] Katja E. Berg,[a] Geneviève Blondin,[a] Elodie Anxolabéhère-Mallart,[a] Winfried Leibl,[b] and Ally Aukauloo*[a]

Keywords: Ruthenium / Nickel / Polynuclear complexes / Rigid heteroditopic ligands / Redox chemistry / Photophysical studies

The synthesis of Dppz*t*BuSalH$_2$ (**7**), a rigid conjugated ditopic ligand containing a Dppz (dipyrido[3,2-*a*:2′,3′-*c*]phenazine) skeleton and a salophen-type chelate, is reported. The complexes Dppz*t*BuSalNi (**10**), [Ru(bpy)$_2$(Dppz*t*BuSalH$_2$)]$^{2+}$ (**11**), and [Ru(bpy)$_2$(Dppz*t*BuSalNi)]$^{2+}$ (**12**) have been prepared and characterised using common spectroscopic methods. Electrochemical, UV/Vis spectroelectrochemical and EPR studies were conducted on compounds **7**, **10**, **11**, and **12**. The singly reduced radical forms of **7** and **10** can be generated electrochemically, with the lone electron located on the low-lying phenazine π*-molecular orbital. Complexes **11** and **12** show several reduction waves and electronic and EPR data obtained for the electrogenerated singly reduced species show them to be closely related to the radical species **7**$^{\bullet-}$ and **10**$^{\bullet-}$, respectively. The presence of nickel(II) in compound **12** renders the addition of the second electron on the phenazine group reversible. Both **11** and **12** show common features on the cathodic side of their cyclic voltammograms, with reversible one-electron ruthenium-centred oxidation. An additional low-potential reversible-oxidation wave is observed for **12**, and this is ascribed to oxidation of the nickel(II) ion. The combined spectroscopic data best describe the ruthenium-containing complexes as weakly coupled bichromophoric systems. Photophysical studies attest to the formation of a charge-separated state for **11**, whereas a strong quenching is detected for **12**.

(© Wiley-VCH Verlag GmbH & Co. KGaA, 69451 Weinheim, Germany, 2003)

Introduction

Ruthenium complexes such as [Ru(bpy)$_3^{2+}$], which contain α,α′-diimine ligands, have repeatedly intrigued chemists due to their unique photophysical properties.[1] These lumophores have been widely used in studies of photochemically or electrochemically induced multielectron or energy transfers.[2] More recently, a wide variety of complexes bearing the Ru(bpy)$_3^{2+}$ unit have been designed with the aim of devising a new class of anion and cation sensors.[3] In such "molecular reconnaissance machines" the response is triggered by a modification of the luminescence and/or electrochemical properties of the photoactive core in the presence of the substrate. Molecular switches using this lumophore take advantage of this fundamental characteristic of the [Ru(bpy)$_3^{2+}$] core.[4] In general, the recent extensive developments in the area of inorganic photochemistry can be credited to the well-known metal-to-ligand charge transfer (MLCT) bands of [Ru(bpy)$_3^{2+}$]; excitation of this complex at wavelengths corresponding to these bands leads to the formation of the lowest-energy excited state corresponding to [Ru^{III}(bpy)$^{\bullet-}$(bpy)$_2$]$^{2+}$.[5] This energetic excited state has been exploited to serve both as an electron-transfer reductant and an oxidant.[6] In this respect, research on mixed-metal dimetallic systems containing both ruthenium and a first-row transition metal ion was triggered due to their potential in the study of electron transfer[7] and in the development of novel photocatalysts.[8] At the forefront of this research is the design of suitable ligands capable of coordinating the ruthenium centre and the transition metal ion. A great number of homoditopic ligands and complexes thereof have been synthesised, and electron and energy transfers have been studied in relation to the chemical nature of the complexes and the intermetallic separation provided by the spacer.[9] The 2,2′-bipyridine ligand has been extensively used as the starting point in the synthesis of a considerable number of functionalised heterotopic ligands.[10] In most cases however, bipyridine is covalently linked to an ancillary ligand by a flexible arm. In such systems, the distance between, and the orientation of, the electron donor and acceptor, parameters which are essential in electron transfer studies, are not known precisely.[11] In addition, it has been shown that photophysical properties are a function of the

[a] Laboratoire de Chimie Inorganique, UMR 8613, Université de Paris-Sud,
91405 Orsay, France
E-mail: aukauloo@icmo.u-psud.fr
[b] Service de Bioénergétique, CEA Saclay,Bât. 532,
91191 Gif-sur- Yvette CEDEX, France

Supporting information for this article is available on the WWW under http://www.eurjic.org or from the author.

 © 2003 Wiley-VCH Verlag GmbH & Co. KGaA, Weinheim **DOI: 10.1002/ejic.200200561**

position of the pendant ligand on the bipyridine moiety.[12] With these considerations in mind, we have devoted our attention to the synthesis of rigid conjugated hybrid ligands capable of holding the two protagonist metal ions with known intermetallic distances.[13] We report here the synthesis of the novel heteroditopic ligand Dppz*t*BuSalH_2 (**7**) based on the Dppz[14] (dipyrido[3,2-*a*:2′,3′-*c*]phenazine) skeleton which contains a salophen-type cavity. This ligand can be viewed as a fused ring system of bipyridine, phenazine and salophen.

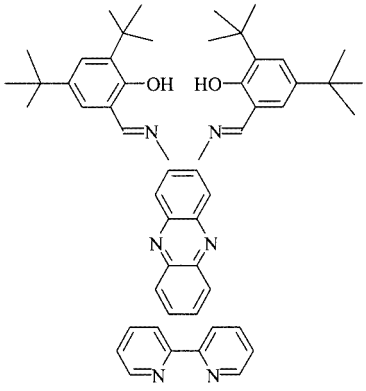

The coordinating ability of **7** is demonstrated by the stepwise metallation of both anchoring sites leading to a new ruthenium/nickel complex. Electrochemical studies coupled with UV/Vis/NIR and EPR techniques have been used to elucidate the redox behaviour and nature of the electrogenerated species derived from the complexes $[Ru(bpy)_2(Dppz\textit{t}BuSalH_2)]^{2+}$ (**11**) and $[Ru(bpy)_2(Dppz\textit{t}BuSalNi)]^{2+}$ (**12**). These results have been corroborated by comparative studies carried out on the unmetallated ligand **7** and the mononuclear nickel(II) complex [Dppz*t*BuSalNi] (**10**), in which the phenanthroline end of the ligand is metal-free. The synthesis of this latter complex and the study of its electronic properties were necessary in order to shed light on the actual contribution of each chromophore in the dinuclear ruthenium/nickel complex. The results of these studies suggest a weakly coupled bichromophoric complex, and that the ligand participates actively in the electrochemical processes of the mono- and dinuclear compounds. Finally, results from preliminary photophysical studies are given.

Results and Discussion

Synthesis

The synthetic pathway for **7** is shown in Scheme 1. Condensation of phendione **1** with 1,2-diamino-4,5-bis(*p*-tosylamino)benzene (**2**) in refluxing methanol gave **5** in quantitative yield. Deprotection of the tosyl groups was carried out in concentrated sulfuric acid to give **6** in near quantitative yield. Our synthetic approach leading to **6** differs from the one described by Lehn et al[20] in that no further purification was necessary prior to use. Bearing in mind the solubility problems encountered with rigid conjugated systems, we intentionally synthesised the corresponding Schiff base by condensation of 2 equiv. of 3,5-di-*tert*-butylsalicylaldehyde in the presence of triethyl orthoformate in boiling ethanol. Selective metallation (Scheme 2) of the different coordinating sites of **7** was achieved by initially coordi-

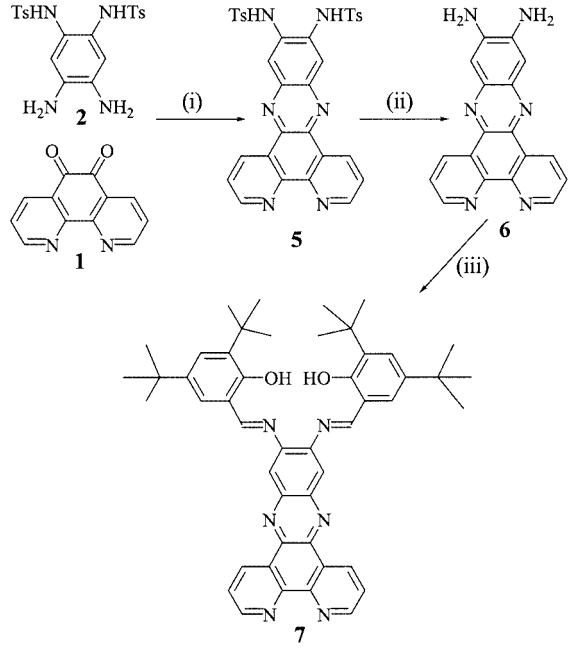

Scheme 1. Synthetic route for the preparation of the ligand Dppz*t*BuSalH_2 (**7**); conditions: (i) reflux in MeOH; (ii) concd. H_2SO_4, room temp., Na_2CO_3; (iii) reflux in EtOH/$HC(OEt)_3$

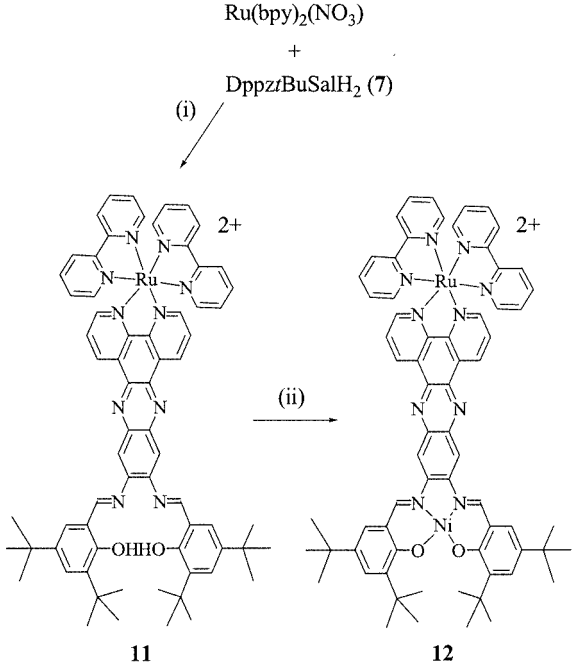

Scheme 2. Selective metallation of Dppz*t*BuSalH_2; (i) reflux in MeOH, NH_4PF_6 (aq); (ii) Ni(acetate)$_2$·4H_2O reflux in MeOH, NH_4PF_6 (aq)

 © 2003 Wiley-VCH Verlag GmbH & Co. KGaA, Weinheim

nating the phenanthroline end to $[Ru(bpy)_2]^{2+}$. The salophen cavity of the resulting complex $[Ru(bpy)_2(DppztBuSalH_2)^{2+}]$ (**11**) was easily metallated using nickel(II) acetate according to usual procedures.[36] Compounds **11** and **12** were purified for photophysical measurements, by chromatography on a neutral alumina column using dichloromethane/methanol (95:5 and 90:10, respectively) as eluents, and the desired compounds were collected as the first major fraction in both cases.

The synthetic pathway for **7** is shown in Scheme 1.

A different synthetic strategy was required to prepare [DppztBuSalNi] (**10**), the complex containing Ni^{II} in the salophenic cavity (see Scheme 3). Direct complexation of the salophenic cavity was discarded as it results in the formation of polynuclear Ni^{II} complexes and purification of the mixture was arduous and gave only low yields. As an alternative we used the well-known template synthesis to prepare the Ni^{II} complex **8** in almost quantitative yield.[21] Reduction of the nitro groups was carried out under hydrogen in the presence of Pd/C as catalyst. Complex **10** was synthesised in good yield following the condensation of the diamino derivative **9** with phendione **1** in refluxing methanol.

^{1}H NMR Spectra

^{1}H NMR spectroscopy was used to monitor the stepwise metallation of **7**. Attachment of the N−N chelating site of the phenanthroline end to the diamagnetic Ru^{II} showed, as expected, a downfield shift of the phenanthroline protons and certain bipyridine protons.[22−23] This phenomenon was even more pronounced when the Ni^{II} ion was bound in the tetracoordinating salophen cavity, with a downfield shift of as much as $\delta = 0.95$ ppm for the signal of the imine hydrogen atoms. Evidence for the coordination of nickel(II) to the salophen cavity was also obtained from ^{1}H NMR spectroscopy, with loss of the signal from the phenol protons.

Infrared Spectra

The sequential binding of the different metal ions was also monitored by infrared spectroscopy. Coordination of ruthenium was characterised by aliphatic C−H vibrations of the *tert*-butyl groups in the region of 2950 cm^{-1}, together with intense absorption bands at about 1585−1610 cm^{-1} corresponding to the imino C=N stretch. Nickel(II) insertion to yield **12** was indicated by a red shift of about 30 cm^{-1} for the band of the imino groups.[24]

Mass Spectrometry

Mass spectra of the ruthenium complexes **11** and **12** were obtained by Electrospray Ionisation Mass Spectrometry. Parent ion peaks minus one or two accompanying anions were detected. In both cases, the doubly charged species appeared as the major peak. The experimental and the simulated spectra for the doubly charged complex [**12** − 2 PF_6]$^{2+}$ are given in Figure 1.

UV/Vis Spectroscopy

The absorption spectra of **7**, **10**, **11** and **12** in CH_2Cl_2 are shown in Figure 2, and the absorption maxima together with their extinction coefficients given in Table 1. Figure 2 (a) shows the electronic perturbation that occurs upon metallation of the salophenic N_2O_2 cavity of **7** with Ni^{II}. Strong π-π* transitions at 310 and 430 nm characterise the extended delocalised π-system of the DppztBuSalH_2 skeleton. Spectral modifications for the mononuclear Ni^{II} complex are noticed in both the high- and low-energy regions compared to the free ligand. The prominent feature is the MLCT band at 500 nm typical of Ni−salophen complexes. The dissymmetric nature of this band may suggest the presence of π-π* intra-ligand transitions which undergo a bathochromic shift relative to that of the free ligand. This shift

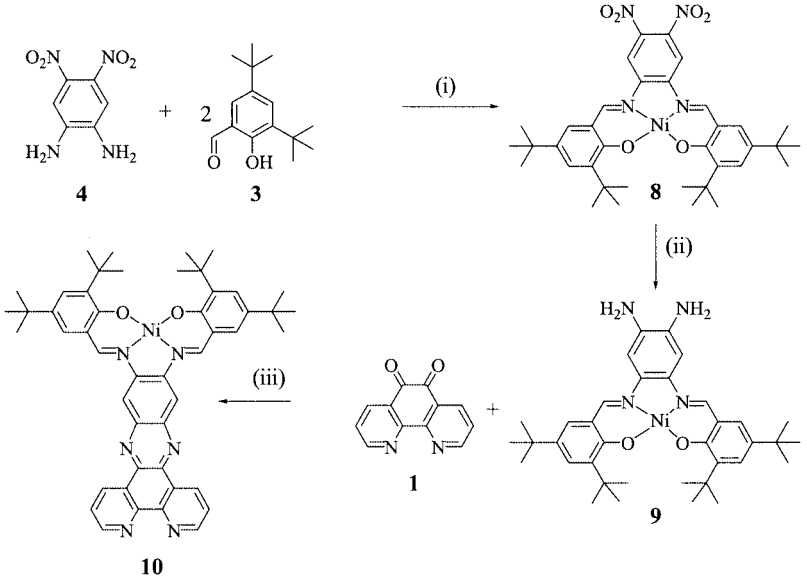

Scheme 3. Synthetic steps for DppztBuSalNi (**10**); (i) $NiCl_2{\cdot}6H_2O$, reflux in dry ethanol/$HC(OEt)_3$; (ii) H_2 40 atm, Pd/C in MeOH; (iii) reflux in MeOH

 © 2003 Wiley-VCH Verlag GmbH & Co. KGaA, Weinheim

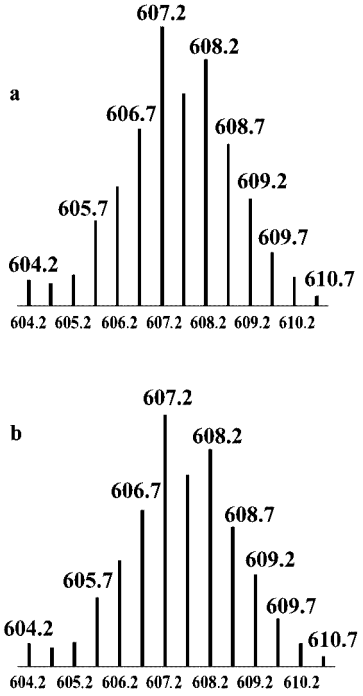

Figure 1. ESI-MS of $[Ru(bpy)_2DppztBuSalNi]^{2+}$ (**12**); (a) experimental and (b) simulated spectrum

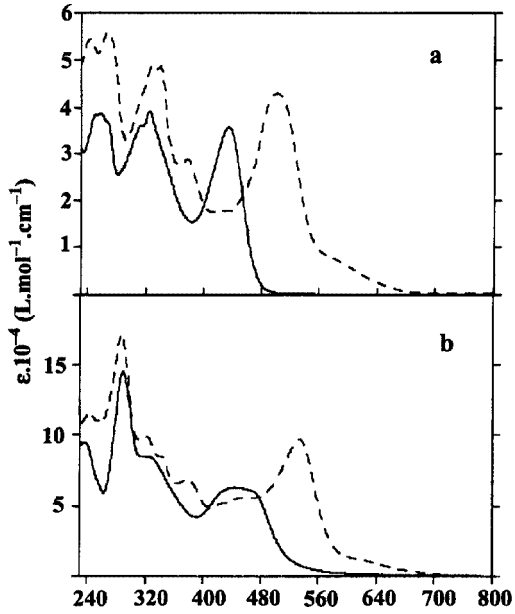

Figure 2. Absorption spectra in CH_2Cl_2; a) $DppztBuSalH_2$ (**7**) (solid line) and DppztBuSalNi (**10**) (dotted line); b) spectra of $[Ru(bpy)_2DppztBuSalH_2]^{2+}$ (**11**) (solid line) and $[Ru(bpy)_2DppztBuSalNi]^{2+}$ (**12**) (dotted line)

can be attributed to a diminution of the HOMO−LUMO gap upon metallation. The weak absorption band observed at the base of the MLCT transition at 620 nm corresponds to a d-d transition for Ni^{II} sitting in a square-planar coordination site.[25]

UV/Vis spectra of **11** and **12** are depicted in Figure 2 (b). The electronic absorption spectrum of **11** contains spectral features due to both $[Ru(bpy)_3]^{2+}$ and $DppztBuSalH_2$. Two intense bands are observed at higher energy, one for the usual intense spin-allowed ligand-centred transitions of the bpy ligands at 290 nm characteristic of (polypyridine)-ruthenium complexes[1,5] and a band at 325 nm attributed to intra-ligand transitions of **7**. A broad, asymmetric absorption band extending from 390 to 550 nm is accounted for by the superposition of low-energy π-π* intra-$DppztBuSalH_2$-ligand transitions and an admixture of dπ(Ru)-π*(bpy) together with dπ(Ru)-π* (bpy′) (where bpy′ denotes the bipyridine moiety of the ligand **7**) MLCT transitions. This agrees with previous findings for (polypyridine)ruthenium(II) complexes containing extended delocalised π-systems, where it has been shown that the low-lying orbitals confined on the central part of the rigid aromatic ligand are decoupled from the metal t_{2g}-type orbitals[26] due to the nearly non-existent orbital contribution from the nitrogen atoms of the coordinating imino groups. Hence, the optical properties of **11** suggest a bichromophoric character for the complex. Metallation of the salophen cavity with Ni^{II} induces a significant change in the appearance of the electronic absorption spectrum as shown in Figure 2 (b). The position and intensity of the π-π* transitions due to the bpy moieties are almost unaffected. A series of three bands between 320 and 380 nm, probably originating from intra-ligand π-π* transitions together with charge transfer transitions from Ni^{II} to the ligand, is observed. This explanation is supported by the observation of these bands in the spectrum of complex **10**. Ruthenium charge transfer transitions towards π*-orbitals of the ligands are detected as a shoulder at 460 nm on a more intense MLCT band from the salophen−Ni part of the dinuclear Ru/Ni complex **12**. The observation of a weak band at ca. 620 nm, characteristic of a d-d transition for a d^8 square-planar Ni^{II} complex, provides further evidence for metallation of the salophen cavity.

Spectroelectrochemical Properties and EPR Spectroscopy

Electrochemical studies on $[Ru(diimine)_3^{2+}]$ complexes are widely used to characterise the π*-orbital energies of

Table 1. UV/Vis/NIR data for $DppztBuSalH_2$ (**7**), DppztBuSalNi (**10**), $[Ru(bpy)_2DppztBuSalH_2]^{2+}$ (**11**) and $[Ru(bpy)_2DppztBuSalNi]^{2+}$ (**12**)

	λ [nm] (ε [10^{-3} L·mol^{-1}·cm^{-1}])							
$DppztBuSalH_2$ (**7**)	250 (38.4)	260 (38.7)	265 sh	310 (36.3)	325 (39.1)	345 sh	430 (35.8)	
DppztBuSalNi (**10**)	245 (54.6)	265 (55.7)	330 (49)	340 (48.8)	375 (28.6)	430 sh	500 (42.8)	
$[Ru(bpy)_2(DppztBuSalH_2)]^{2+}$ (**11**)	240 (94.4)	290 (145)	325 sh	445 (63.1)	465 sh			
$[Ru(bpy)_2(DppztBuSalNi)]^{2+}$ (**12**)	245 (116)	290 (172)	320 (99.1)	340 (85.1)	380 (68.6)	455 sh	535 (97.3)	620 sh

 © 2003 Wiley-VCH Verlag GmbH & Co. KGaA, Weinheim

Table 2. Half-wave potentials E for the oxidation (^{ni}E) and the reduction (^{n}E) of DppzBuSalH$_2$ (**7**), [DppzBuSalNi] (**10**), [Ru(bpy)$_2$DppzBuSalH$_2$]$^{2+}$ (**11**) and [Ru(bpy)$_2$DppzBuSalNi]$^{2+}$ (**12**) (from cyclic voltammetry at 100 mV/s; $E = 1/2(E_{pa} + E_{pc})$ in V vs. SCE in the presence of TBAClO$_4$)

	^{V}E	^{IV}E	^{III}E	^{II}E	^{I}E	^{i}E	^{ii}E	^{iii}E
DppzBuSalH$_2$ (**7**)[a]				−1.40[b]	−1.11	+1.18	+1.29[c]	+1.58[c]
[DppzBuSalNi] (**10**)[a]				−1.43[b]	−0.99	+1.13		
[Ru(bpy)$_2$(DppzBuSalH$_2$)]$^{2+}$ (**11**)[d]		−2.0[b]	−1.63	−1.45	−0.88	+1.26[c]	+1.43[e]	
[Ru(bpy)$_2$(DppzBuSalNi)]$^{2+}$ (**12**)[d]	−1.88[b]	−1.64	−1.44	−1.27	−0.81	+1.07	+1.29[c]	+1.42[e]

[a] Measured in dichloromethane. [b] Measured in acetonitrile. [c] Partly irreversible step, cathodic peak given. [d] Irreversible step, anodic peac given. [e] Adsorption and desorption phenomena observed under our experimental conditions, anodic peak given.

Table 3. UV/Vis/NIR data for the electrogenerated species (from spectroelectrochemistry)

	λ [nm] (ε [10^{-3} L·mol^{-1}·m^{-1}])								
DppzBuSalH$_2^{\cdot-}$ (**7**$^{\cdot-}$)	300 (32.5)	381 (32.4)	455 (18.1)	545 sh	750 sh	840 (10)			
[DppzBuSalNi]$^{\cdot-}$ (**10**$^{\cdot-}$)	308 (36.3)	326 (35.8)	372 (42.4)	390 sh	490 sh	517 (38.1)	613 (10.5)	820 sh	917 (17.1)
[Ru(bpy)$_2$(DppzBuSalH$_2$)]$^{\cdot+}$ (**11**$^{\cdot+}$)	245 (95.4)	291 (145)	382 (73.8)	470 (56.2)	550 sh	750 (14.7)	880 sh		
[Ru(bpy)$_2$(DppzBuSalNi)]$^{\cdot+}$ (**12**$^{\cdot+}$)	244 (135)	289 (169)	353 (79)	388 (82.3)	475 sh	515 (80)	622 sh	800 sh	865 (23.4)

the ligands linked to Ru^{II}. In addition, the redox potential of the Ru$^{III/II}$ metal centre gives, in general, a clear indication of the nature of the interaction with the coordinated ligands. Furthermore, electrochemical data coupled with other spectroscopic information are currently used to rationalise the modifications in the absorption and emission spectra of [Ru(diimine)$_3^{2+}$] derivatives.[1b,14c,27] The electrochemical properties of **7**, **10**, **11** and **12** were investigated by cyclic voltammetry (CV) and these data are summarised in Table 2. Electronic data for the electrochemically generated species are given in Table 3. In what follows, we analyse the electrochemical behaviour of **7** and **10** and discuss the spectroscopic characterisation of the electrogenerated species. These results are then correlated to the Ru^{II}-containing complexes.

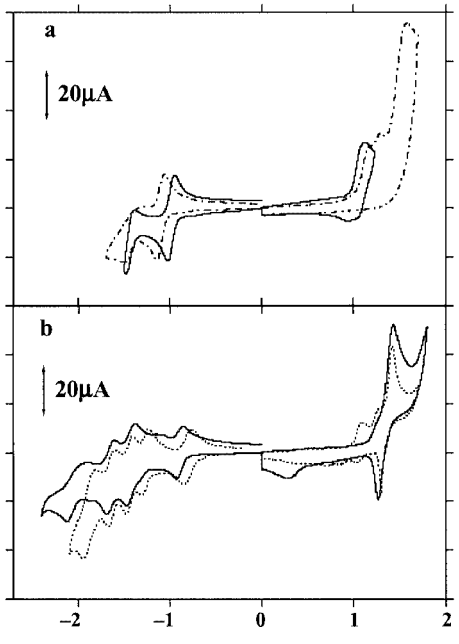

Figure 3. Cyclic voltammograms in CH_2Cl_2 (10^{-3} M solutions, room temperature, sweep rate 100 mV·s^{-1}, Ag/AgClO$_4$ electrode as reference, 0.1 M TBAClO$_4$ as supporting electrolyte); a) DppzBuSalH$_2$ (**7**) (dotted line) and DppzBuSalNi (**10**) (solid line); b) [Ru(bpy)$_2$DppzBuSalH$_2$]$^{2+}$ (**11**) (solid line) and [Ru(bpy)$_2$DppzBuSalNi]$^{2+}$ (**12**) (dotted line)

Ligand DppzBuSalH$_2$ (7) and Complex [DppzBuSalNi] (10)

The cyclic voltammograms of the free ligand **7** and its Ni^{II} complex **10** are shown in Figure 3 (a). Owing to the poor solubility of these species in acetonitrile, cyclic voltammograms of **7** and **10** were run in dry dichloromethane. Two waves are observed upon reduction of **7**, one reversible and a second quasi-irreversible at −1.1 and −1.39 V vs. SCE, respectively. The reversible one-electron reduction wave at −1.1 V falls in the range of potentials typical for phenazine-containing moieties.[27] No reversible waves are observed upon oxidation, even when scanning up to +1.7 V. However, two consecutive poorly resolved waves at +1.18 and +1.29 V vs. SCE are attributed to oxidation of the phenol groups. Compared to the first reduction of Dppz, an anodic shift of about 100 mV indicates the uptake of the first electron by the "modified" phenazine framework which contains imino π-accepting groups. The second electron addition occurs at a more positive potential than that of Dppz [−1.4 vs. −2.0 V (SCE), respectively]. The fact that salophen lacks a reduction wave within this potential range clearly implies that this electron-transfer process involves the phenazine part of the ligand. As reported earlier, the doubly reduced form of the Dppz ligand leads to a considerable increase in charge at the nitrogen atoms, thus enhancing its protonation aptitude. In the case of **7**, the same phenomenon will be occurring and this explains the flat-

 © 2003 Wiley-VCH Verlag GmbH & Co. KGaA, Weinheim

tened nature of the corresponding anodic peak.[28] Redox properties of **10** are illustrated in Figure 3 (a, solid line); in comparison to **7** only minor changes are observed upon reduction. A shift of about 120 mV towards less negative potential is noticed for the first reversible reduction wave. The increased ease of reduction of the nickel(II) complex confirms the lowering in energy of the ligand LUMO upon metallation. In contrast to the ligand, a reversible oxidation wave is observed at +1.13 V vs. SCE, which is attributed to the formation of a nickel(III) complex. Such a potential is consistent with the $Ni^{III/II}$ redox couple of Ni−salophen.[29]

Spectroelectrochemical studies were carried out to investigate the stability and the spectroscopic signatures of electroreduced **7** and **10** after the first reduction wave. UV/Vis/NIR spectral changes of **7** and **10** were monitored at room temperature by using a thin-layer cell in dry dichloromethane in the presence of 0.1 M $TBAPF_6$ at −1.2 and −1.0 V, respectively. The electronic response of **7** is strongly modified upon addition of the first electron, as shown in Figure 4 (a). New high-intensity broad bands spanning the range 600−950 nm and another broad band at 380 nm are observed. These new spectral features are also found for singly reduced phenazine-containing compounds.[27] The double-hump band observed for $Dppz^-$ (547 and 570 nm) is shifted to lower energy for $\mathbf{7}^{\cdot-}$ with the maxima at 765 and 840 nm, indicating that the unpaired electron is localised on a more extended π-system.

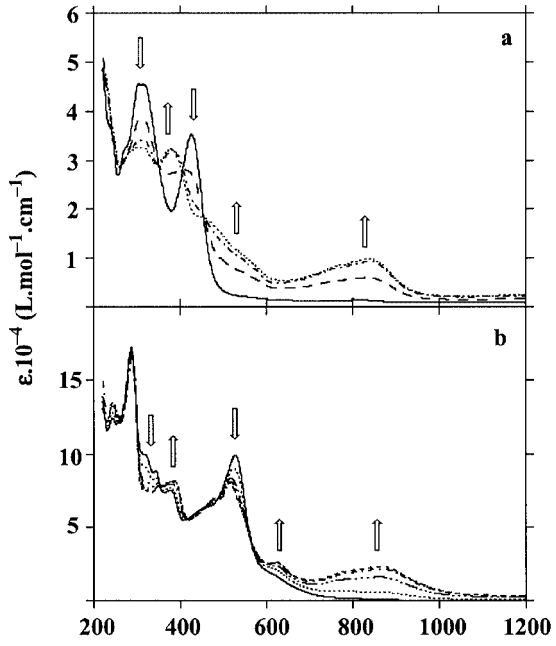

Figure 4. Electronic absorption spectra upon electrolysis at controlled potential in CH_2Cl_2 (10^{-3} M solutions, room temperature, SCE as reference, 0.1 M $TBAClO_4$ as supporting electrolyte); a) $DppztBuSalH_2$ (**7**) upon reduction at −1.3 V/SCE; b) $[Ru(bpy)_2DppztBuSalNi]^{2+}$ (**12**) upon reduction at − 0.96 V/SCE

The complete recovery of the initial spectrum upon reoxidation, together with the observation of several isosbestic points (265, 350, 405 and 450 nm), confirmed the presence of only two species in equilibrium at all times during the electrochemical study, showing the reversible nature of this electron-transfer process under our experimental conditions. The singly reduced species was also generated by a controlled potential bulk electrolysis at −30 °C. The EPR spectrum of the electrolysed solution showed an isotropic signal at $g = 2.007$, indicating the presence of an organic radical species with a peak to trough line width of 0.75 mT. In contrast to the paramagnetic singly reduced Dppz species, where well-resolved EPR signals have been observed,[27] the smooth EPR signal registered for $\mathbf{7}^{\cdot-}$ confirms the delocalisation of the electron on a more delocalised π-system, hence resulting in the interaction of the single electron with a larger number of nuclear spins.

The spectroelectrochemical behaviour of **10** was monitored using identical techniques as for **7**. The changes in the electronic spectrum of **10** upon the addition of one electron are similar to those of **7,** at least in the low-energy region. However, the maxima of these broad bands are shifted to lower wavenumbers (ca. 1040 cm^{-1}) indicating a smaller energy difference between the HOMO and LUMO when Ni^{II} is inserted into the N_2O_2 coordinating cavity. These absorption bands resemble those observed for the monoanion radical of **7** which favours localisation of the added electron on the phenazine part of the metallo complex. No substantial change in the d-d transition of the Ni^{II} centre at 620 nm is observed, but this band becomes more apparent in the electrolysed species. The one-electron process for this reduction wave was confirmed by bulk electrolysis at a controlled potential, and a reverse cyclic voltammogram on the electrolysed solution indicates the presence of only one species at the same potential as the initial complex. The frozen solution EPR spectrum of the electrolysed compound is shown in Figure 5. The signal is slightly anisotropic and is best simulated with values of $g_\perp = 2.0055$ and $g_{//} = 2.0012$. This weak anisotropy can be explained by a partial delocalisation of the lone electron in a d_π-type orbital of the nickel centre.[30] The lack of hyperfine coupling is most probably due to extensive overlap of a large number of signals with small EPR coupling constants, resulting from interaction with neighbouring atoms.

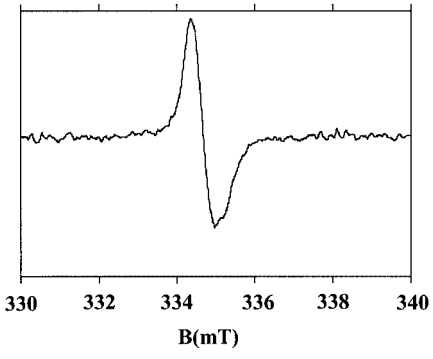

Figure 5. EPR spectra of $[DppztBuSalNi]^{\cdot-}$ ($\mathbf{10}^{\cdot-}$) at 100 K after bulk electrolysis at −1.2 V vs. SCE in dry dichloromethane and $TBAClO_4$ as supporting electrolyte

 © 2003 Wiley-VCH Verlag GmbH & Co. KGaA, Weinheim

$[Ru(bpy)_2Dppz tBuSalH_2]^{2+}$ and $[Ru(bpy)_2Dppz tBuSalNi]^{2+}$ Complexes

Electrochemical properties of the ruthenium-containing complexes have been studied in both dichloromethane and acetonitrile in the presence of 0.1 M TBAP as supporting electrolyte, and the corresponding data are given in Table 2. Electrochemical studies of $[Ru(diimine)_3^{2+}]$ complexes are indeed crucial in evaluating the relative energy of the ligand π*-orbitals, especially for heteroleptic complexes, and also the nature of the interactions of the ligands with the metal centre. The first reductive process for the metal complex is often informative regarding the energy levels of the π*-orbitals of the ligands linked to the ruthenium(II) ion, whereas the first oxidation process is indicative of the metal t_{2g}-orbital energy. However, this is only true if the processes of reduction and oxidation are as in Equations 1 and 2, respectively.[31]

$$[M^{II}L_3]^{2+} + e^- \rightarrow [M^{II}L_2(L^{\cdot -})]^+ \quad (1)$$

$$[M^{II}L_3]^{2+} \rightarrow [M^{III}L_3]^{3+} + e^- \quad (2)$$

Cyclic voltammograms of **11** and **12** are given in Figure 3 (b). The electrochemical behaviours of **11** and **12** may be regarded as the superposition of each of **7** and **10** together with the $[Ru(bpy)_3^{2+}]$ chromophore, respectively. On the cathodic side of the CV of **11**, both reduction waves for the ligands are observed at −0.89 and −1.3 V vs. SCE, followed by the sequential addition of one electron to the bipyridine co-ligands. The oxidation wave for the $Ru^{III/II}$ couple is observed at +1.4 V vs. SCE and is probably masking the oxidation wave for the phenol groups. The fact that the oxidation potential for the Ru^{II} ion remains unchanged when compared to $[Ru(bpy)_3^{2+}]$ supports the idea that the phenazine moiety together with the bis(salicylidene)diimine groups have very little electronic influence on the metal centre. One can thus envision $[Ru(bpy)_2Dppz tBuSalH_2]^{2+}$ as consisting of two chromophores with little electronic communication between them. Complex **12** displays similar electrochemical behaviour; an almost identical pattern is observed on the cathodic part of the CV while on oxidation, a reversible wave is observed at +1.07 V vs. SCE followed by another wave at 1.42 V vs. SCE corresponding to oxidation of the phenol group, which is detected as a shoulder on the oxidation wave for the $Ru^{III/II}$ couple. It should be noted that, when scanning up to 1.8 and 1.7 V for **11** and **12**, respectively, we observed irreversible cathodic waves at 0.28 V for **11** and 0.37, 0.70 and 0.86 V for compound **12**. These waves probably originate from chemically altered species as no such waves are present when scanning to a potential just beyond the $Ru^{III/II}$ couple. The intensities of the corresponding waves for the $Ru^{III/II}$ couple suggest that adsorption and desorption phenomena are taking place at the surface of the vitreous carbon electrodes.

Singly Reduced Forms of $[Ru(bpy)_2Dppz tBuSalH_2]^{2+}$ (11) and $[Ru(bpy)_2Dppz tBuSalNi]^{2+}$ (12)

The first reduction potential for **11** occurs at −0.99 V which is very close to that of the free ligand under the same conditions (−1.11 V) [^1E(complex) − ^1E(ligand) = 0.12 V].[26,27] This implies that the coordination of ligand **7** to the Ru^{II} ion has little influence on the uptake of the first electron. Another way to describe this result is to consider that the singly occupied molecular orbital (SOMO) is developed mainly on the phenazine together with the bis(salicylidene)diimine framework. Moreover, the displacement of this wave to a more positive potential can be related to the dipositive charge of the complex of ligand **7**. Spectroelectrochemically, the uptake of the first electron is characterised by the growth of intense bands in the region of 600 to 950 nm and at 380 nm, attributable to the coordinated $Dppz tBuSalH_2$. Similarly to **7**, a fall in intensity of the π-π* intra-ligand charge-transfer transitions at 325 and 440 nm for **11** also underpins the proposed site of reduction. In addition, no alteration in either the Ru^{II} to bpy MLCT transitions at about 460 nm or the internal transition of the bound bpy ligands in their neutral form at 290 nm is observed, thus providing further evidence for the reduction site.[32]

EPR of a frozen solution of the singly reduced complex $\mathbf{11}^{\cdot +}$ generated electrochemically showed an isotropic signal with a *g* factor of 2.007. The negligible change in the observed *g* values for the free ligand $\mathbf{7}^{\cdot -}$ and the ruthenium complex $\mathbf{11}^{\cdot +}$ reflects the feeble interaction of the unpaired electron with the metal ion. It should be noted that the observed *g* values for other $[Ru(bpy)_2(L^{\cdot -})]^{2+}$ species, where L is a diimine-type ligand, deviate markedly from the *g* value of the metal-free ligand anion radical; this is mainly due to a strong interaction of the unpaired electron with the Ru^{II} ion.[33] Thus, the EPR spectrum of $\mathbf{11}^{\cdot +}$ is consistent with the single electron being confined to a molecular orbital located predominantly on part of the ligand skeleton, with a weak contribution from the Ru^{II} centre and the ligating diimine part of the corresponding ligand. As observed in the case of the radical species of the free ligand, no hyperfine structure is observed for $\mathbf{11}^{\cdot +}$, probably for the same reason as mentioned above.

The electrochemical response of **12** in acetonitrile is given in Figure 3 (b). Five reversible one-electron reduction waves at room temperature are observed in the potential range scanned. Of particular interest is the approximately 200 mV shift of the first reduction wave to more positive potential relative to **11** and **10**. Such a shift of the redox potential clearly denotes the stabilisation of the LUMO predominantly localised on the phenazine skeleton of the spacer ligand **7**.[34] The change in the electronic spectrum of **12** upon addition of one electron is shown in Figure 4 (b). The singly reduced species is characterised by the same bands in the low-energy region as those already observed for compounds **7**, **10** and **11** for the same electron transfer process. The spectral modification of **12** is closely related to that of **10**, again confirming the same position for the unpaired elec-

 © 2003 Wiley-VCH Verlag GmbH & Co. KGaA, Weinheim

tron of the heterodimetallic complex. No appreciable alteration of the π-π* transition of the chelated bipyridine moieties at 290 nm is observed, and the Ru^{II}-to-ligand charge-transfer transitions at 460 nm are present as shoulders on the pronounced MLCT transitions of the Ni−salophen chromophore. Decisive spectroscopic characterisation of the first reduction process comes from the EPR spectrum of an electrolysed solution of **12**. An isotropic signal with a *g* factor of 2.013 and a line-to-line width of 0.75 mT typical of a radical species was detected. Here too, no hyperfine coupling is apparent. An interesting feature in the CV of **12** is the presence of a second reversible wave at −1.27 V (in acetonitrile vs. SCE). While no apparent shift has been detected for the second wave of **7** upon metallation of only one end of the heterotopic ligand (i.e. for compounds **10** and **11**), a marked displacement of about 260 mV to more anodic potential is observed in the case of the dimetallic complex. The more reversible nature of the uptake of the second electron on the bridging ligand reflects the gain in stability of the doubly reduced species in the case where both ends of the ligand contain a divalent ion.

Singly Oxidised Form of 12

The Ru^{II}/Ni^{II} complex exhibits three oxidation waves in the positive potential region at +1.07, +1.29 and +1.42 V vs. SCE, respectively. When compared to the first oxidation process of **10**, where only the salophen cavity is occupied by Ni^{II}, a small cathodic shift of ca. 60 mV is noted. The observed potential falls within the range expected for the $Ni^{III/II}$ couple of a salophen-type complex. Even the small shift observed for **12** is surprising, as a more positive potential for the oxidation of the Ni^{II} centre would be expected for this dicationic complex.[29] We tentatively rationalise this observation by noting the more π-accepting character of the bridging ligand when both extremities of the latter are metallated. Hence, a stronger ligand field is exerted on the Ni^{II} centre, thereby enhancing its propensity to oxidise. Few changes were observed spectroelectrochemically upon the removal of the first electron. The frozen-solution X-band EPR spectrum of the electrochemically generated Ru^{II}/Ni^{III} complex at 15 K shows a rhombic symmetry, with a large *g* tensor anisotropy (g_x = 2.289, g_y = 2.232, g_z = 2.022), which is commonly observed for Ni^{III} complexes in salophen-type environments.[29] Upon addition of degassed pyridine to the electrolysed solution and subsequent freezing, we obtained the EPR spectrum shown in Figure 6. The new adduct still exhibits a rhombic-type spectrum with superhyperfine couplings in all *g* regions. The best agreement between the experimental spectrum and the simulated one was obtained using the following parameters: g_x = 2.1986, g_y = 2.1645, g_z = 2.0265; $A_x = 16.34 \times 10^{-4}$ cm^{-1}, $A_y = 16.10 \times 10^{-4}$ cm^{-1}, $A_z = 20.43 \times 10^{-4}$ cm^{-1}. Simulation was realised using a Gaussian profile and line widths of 0.8, 0.7 and 0.6 mT for the *x*, *y* and *z* peaks, respectively. In addition, a signal at g = 2.0038 was detected, and attributed to the phenoxyl radical generated during the electrolysis, due to the close proximity of the two oxidation waves (Ni^{III}/Ni^{II} and $PhO^{\cdot+}$/PhO). The well-resolved quintuplet at higher magnetic field is the fingerprint of a six-coordinate Ni^{III} species, with two pyridine rings in axial positions and an axial repartition of the spin density on the Ni^{III} centre.

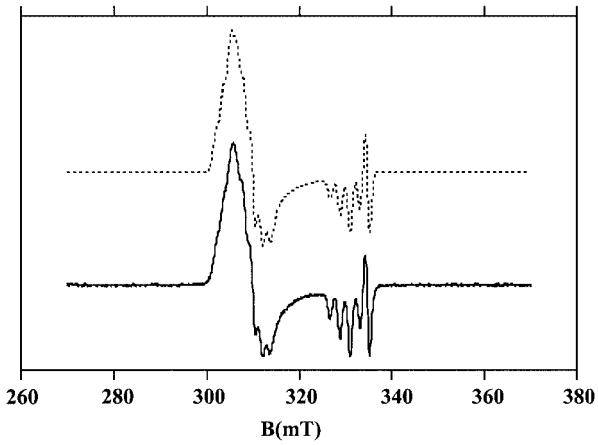

Figure 6. EPR spectrum of $[Ru(bpy)_2DppztBuSalNi]^{3+}$ ($\mathbf{12}^{3+}$) at 15 K, generated by electrolysis at 1.11 V/SCE in dry degassed acetonitrile and 0.1 M $TBAClO_4$ as supporting salt in the presence of pyridine (solid line); the dotted line shows the simulated spectrum

Preliminary Photophysical Studies

Upon excitation of the mononuclear ruthenium complex **11** at 532 nm (MLCT Ru^{II}→bipyridine moiety) in degassed ethanol at room temperature, fluorescence emission was observed around 610 nm. The observed fluorescence lifetime (minor of 40 ps is much shorter than that of $[Ru(bpy)_3^{2+}]$, which indicates rapid quenching of the excited state. Time-resolved absorption spectroscopy revealed that the transient species generated by photoexcitation at 532 nm displays an absorption at around 820 nm, a wavelength similar to that of the electrochemically singly reduced $[Ru(bpy)_2(DppztBusalH_2^{\cdot-})]^{2+}$ species (Figure 4, a). This is a strong indication that the quenching of the excited state is due to internal photoinduced electron transfer, probably forming the charge-separated state $Ru^{III}(bpy)_2(DppztBusalH_2^{\cdot-})^{2+}$. The lifetime observed for this transient species was about 400 ns. In contrast, the dinuclear complex **12** exhibits a very efficient quenching of the excited state which is not accompanied by absorption changes in the near infrared. The most likely explanation is that fast energy transfer to the Ni^{II} ion occurs in this complex where the excited state is efficiently quenched before internal charge separation can occur. We are currently investigating the photophysical behaviour of **10** and **12** in more detail.

Conclusion

Based on the X-ray structure of **10**[35] an approximate distance of 12.5 Å between the Ru^{II} and Ni^{II} ions is expected. This separation thus falls within the desired distance for electron or energy transfer studies in these model

 © 2003 Wiley-VCH Verlag GmbH & Co. KGaA, Weinheim

complexes. Spectroelectrochemical studies suggest a weak electronic coupling between the different chromophores in our system, a prerequisite in the design of supramolecular systems containing a photoactive site. We believe that our approach to building novel heteroditopic ligands will be a source of inspiration for the synthesis of novel ancillary ligands on anchoring molecules such as phenanthroline.

Experimental Section

General: Electrochemical measurements were performed with an EGG PAR (model 273A) electrochemical workstation. The solvents were distilled under nitrogen in the presence of dry calcium chloride and the solution [1 mmol·L^{-1} for complexes and ligand and 0.1 mol·L^{-1} of tetrabutylammonium perchlorate ($TBAClO_4$)] introduced within an argon-purged heart-shaped cell. Cyclic voltammetry was performed using a glassy carbon electrode (3 mm in diameter) as the working electrode, a platinum grid as the counter electrode and an $Ag/AgClO_4$ (0.01 M) electrode in acetonitrile as the reference (E_{ref} = 0.3 V/ECS). Electrolyses were carried out at controlled potentials in a three-electrode cell, using a platinum gauze as the working electrode, a platinum grid as the counter electrode and an $Ag/AgClO_4$ (0.01 M) electrode in acetonitrile as the reference. Low-temperature electrolyses were run using 0.2 M $TBAClO_4$. UV/Vis/NIR spectra were obtained using 1-cm quartz cells with a Varian Cary 5E spectrophotometer (200−1500 nm). Spectroelectrochemical data were obtained by a combination of a three-electrode thin cell (0.5 mm) mounted in a UV/Vis/NIR spectrophotometer. IR spectra were obtained with a Perkin−Elmer 1000 spectrometer, using KBr matrix pellets. NMR spectra were obtained using Bruker AC 200 (200 MHz) and AC 250 (250 MHz) spectrometers. The solvents used were $CDCl_3$ or $[D_6]$DMSO. EPR spectra were recorded with an X-band Elexsys (Bruker) spectrometer at 15, 77 or 100 K. Elemental analyses were carried out at the Services de Microanalyse, ICSN-CNRS, Gif-sur-Yvette. Mass spectra were recorded with a Finnigan Mat Mat95S in a *BE* configuration at low resolution. Flash-absorption and fluorescence transients were measured with setups of local design. All measurements were taken at 296 K. For absorption transients the measuring light was provided by a 150-W tungsten-halogen lamp, and the wavelength was selected with interference filters placed before and after the 10 × 1 mm sealed cuvette containing the sample. The sample was excited at 90° to the measuring beam by a flash from a frequency-doubled Nd:YAG laser (532 nm, duration 5 ns, ca. 2 mJ/cm^2; Surelight, Continuum). Absorbance changes were detected with a silicon photodiode and signals were amplified by a wideband preamplifier (model 5185, EG&G) before they were recorded by a digital oscilloscope (TDS, 744A, Tektronix). For fluorescence transients, excitation was achieved by a flash from a frequency-doubled picosecond Nd:YAG laser (532 nm, duration 25 ps, ca. 300 μJ/cm^2; Continuum). The detection wavelength was selected by an interference filter centred at 610 nm and signals were detected with a microchannel plate photomultiplier tube (R2566 U, Hamamatsu) and a 7-GHz digitising oscilloscope (IN7000, Intertechnique). Ruthenium trichloride was purchased from the Aldrich Chemical Company. 2,2′-Bipyridine (bpy) and 1,10-phenanthroline (phen) were obtained from the Janssen Chemical Company. 1,10-Phenanthroline-5,6-dione (phendione, **1**),[15] 1,2-diamino-4,5-bis(*p*-toluenesulfamido)benzene (**2**),[16] 3,5-di-*tert*-butylsalicylaldehyde (**3**),[17] 4,5-diamino-1,2-dinitrobenzene (**4**),[18] and $[Ru(bpy)_2Cl_2]$[19] were synthesised as described in the literature.

Synthesis of 11,12-Bis(*p*-tosylamino)dipyrido[3,2-*a*:2′,3′-*c*]phenazine (5): 1,2-diamino-4,5-bis(*p*-tosylamino)benzene (**2**) (2.23 g, 5 mmol) was added to a suspension of phendione (**1**) (1.55 g, 5 mmol) in methanol (50 mL) , and the mixture was refluxed for 1 h. The hot suspension was filtered while hot to give a beige solid which was washed with cold methanol and dried under vacuum. Yield: 2.92 g (94%). IR: $\tilde{\nu}$ = 3436 (N−H), 3034, 2820 (C−H), 1619 (C=N), 1580 (C=N) cm^{-1}. ^1H NMR ($[D_6]$DMSO): δ = 9.48 (d, 2 H), 9.16 (d, 2 H), 7.93 (dd, 2 H), 7.86 (s, 2 H), 7.78 (d, 2 H), 7.36 (d, 2 H), 2.28 (s, 6 H) ppm. $C_{32}H_{24}N_6O_4S_2$ (620.7): calcd. C 61.92, H 3.90, N 13.54; found C 61.88, H 3.82, N 13.42.

Synthesis of 11,12-Diaminodipyrido[3,2-*a*:2′,3′*c*]phenazine (6): Deprotection of the tosyl group was achieved by treating **5** (1.24 g, 2 mmol) with concentrated sulfuric acid (10 mL) at room temperature for 4 h. The deep violet solution was then added dropwise to ice-cold water and the brown solid was filtered off. After treatment with a concentrated solution of sodium carbonate (20 mL), the yellow solid was collected by filtration and washed with the minimum amount of water. The compound was then dried under vacuum. Yield: 0.54 g (86%). IR: $\tilde{\nu}$ = 3390 (N−H), 1630 (C=N) cm^{-1}. ^1H NMR ($[D_6]$DMSO): δ = 7.84 (d, 2 H), 7.63 (d, 2 H), 7.27 (dd, 2 H), 7.15 (s, 2 H), 6.33 (s, 4 H) ppm. $C_{18}H_{12}N_6$ (312.33): calcd. C 69.22, H 3.87, N 26.91; found C 69.17, H 4.01, N 26.75.

Synthesis of Dppz*t*BuSalH$_2$ (7): The diamino derivative **6** (94 mg, 0.3 mmol) and 3,5-di-*tert*-butylsalicylaldehyde (**3**) (188 mg, 0.8 mmol) were suspended in dry ethanol (30 mL) together with a few drops of triethyl orthoformate. The mixture was heated under reflux for 2 h and the yellow precipitate was separated by filtration. The solid was washed with diethyl ether and dried under vacuum. Yield: 192 mg (86%). IR: $\tilde{\nu}$ = 2950−2905 (C−H, aliph), 1610 (C=N) cm^{-1}.^1H NMR ($CDCl_3$): δ = 13.26 (s, 2 H), 9.63 (dd, 2 H), 9.30 (dd, 2 H), 8.93 (s, 2 H), 8.07 (s, 2 H), 7.82 (dd, 2 H), 7.54 (d, 2 H), 7.35 (d, 2 H), 1.48 (s, 18 H), 1.37 (s, 18 H) ppm. $C_{48}H_{52}N_6O_2$ (744.97): calcd. C 77.39, H 7.04, N 11.28; found C 77.12, H 7.17, N 11.36.

Synthesis of [DN*t*BuSalNi] (8): A solution of $NiCl_2·6H_2O$ (0.480 g, 2 mmol) in ethanol (10 mL) was added to a solution containing 4,5-diamino-1,2-dinitrobenzene (**4**) (396 mg, 2 mmol) and 3,5-di-*tert*-butylsalicylaldehyde (**3**) (936 mg, 4 mmol) in ethanol (100 mL). The resulting mixture was then heated to reflux with constant stirring for 2 h. The dark precipitate was then filtered off, washed with ethanol and dried under vacuum. Yield: 1.1 g (80%). IR (KBr): $\tilde{\nu}$ = 2955 (aliphatic CH), 1619 (C=N), 1358 and 1338 cm^{-1} (NO_2). ^1H NMR ($CDCl_3$): δ = 8.23 (s, 2 H), 8.21 (s, 2 H), 7.48 (d, 2 H), 7.14 (d, 2 H), 1.43 (s, 9 H), 1.30 (s, 9 H) ppm. $C_{36}H_{46}N_4NiO_7·H_2O$ (705.47): calcd. C 61.29, H 6.57, N 7.94; found C 60.96, H 6.62, N 7.89.

Synthesis of [DA*t*BuSalNi) (9): A slurry of compound **8** (690 mg, 1 mmol) and Pd/C (10%, 100 mg) in dry THF was maintained under hydrogen (40 bar) with stirring for 12 h. The mixture was filtered through a bed of Celite and then washed twice with THF (2 × 40 mL). The solvents were removed under reduced pressure and the red solid was sonicated in cold methanol (10 mL). The residue was filtered off, washed with the minimum amount of methanol and dried under vacuum. Yield: 440 mg. (70%). IR (KBr): $\tilde{\nu}$ = 3330 (NH), 2950 (aliphatic CH), 1614−1596 cm^{-1} (C=N). ^1H NMR ($CDCl_3$): δ = 7.88 (s, 2 H), 7.34 (d, 2 H), 7.02 (d, 2 H), 6.95 (s, 2 H), 3.49 (s, 4 H), 1.43 (s, 9 H), 1.37 (s, 9 H) ppm. $C_{36}H_{48}N_4NiO_2$ (627.49): calcd. C 68.91, H 7.71, N 8.93; found C 69.16, H 7.84, N 8.77.

 © 2003 Wiley-VCH Verlag GmbH & Co. KGaA, Weinheim

Synthesis of DppzᵗBuSalNi (10): A slurry of compound **9** (628 mg, 1 mmol) in methanol (30 mL) was added dropwise to a refluxing solution of phendione (**1**) (210 mg, 1 mmol) in methanol (20 mL) with constant stirring. After the addition was complete, the mixture was heated to reflux for 2 h, whereby a red solid formed. The hot mixture was filtered and the solid was washed with methanol and dried under vacuum. Yield: 680 mg (85%). IR (KBr): $\tilde{\nu}$ = 3330 (NH), 2950 (aliphatic CH), 1614−1596 cm^{-1} (C=N). ^1H NMR ($CDCl_3$): δ = 9.49 (dd, 2 H), 9.22 (dd, 2 H), 8.39 (s, 4 H),7.68 (dd, 2 H), 7.45 (d, 2 H), 7.14 (d, 2 H), 1.46 (s, 9 H), 1.34 (s, 9 H) ppm. $C_{48}H_{50}N_6NiO_2{\cdot}0.5CH_2Cl_2$ (844.1): calcd. C 69.01, H 6.09, N 9.96; found C 68.90, H 6.15, N 9.82.

Synthesis of $[Ru(bpy)_2(DppzᵗBuSalH_2)](PF_6)_2$ (11): *cis*-$[Ru(bpy)_2Cl_2]{\cdot}2H_2O$ (52 mg, 0.1 mmol) and $AgNO_3$ (34 mg, 0.2 mmol) were suspended in methanol (20 mL). The mixture was stirred magnetically for 2 h under argon and a white precipitate of AgCl was filtered off. $DppzᵗBuSalH_2$ (**7**) (74 mg, 0.1 mmol) was added to the clear red solution followed by a few drops of triethyl orthoformate. The reaction mixture was heated to reflux under argon with constant stirring for 2 h. The reddish solution was filtered to remove any insoluble material and then concentrated in a rotary evaporator. An orange solid was precipitated upon addition of a concentrated aqueous solution of NH_4PF_6. The precipitate was collected by filtration and washed with diethyl ether. Yield: 70 mg (47%). A pure sample of **11** for photophysical measurements was obtained by chromatography on neutral alumina using a mixture of dichloromethane/methanol (95:5) (R_f = 0.58). IR: $\tilde{\nu}$ = 2950−2905 (C−H, aliph), 1585−1610 (C=N) cm^{-1}. ^1H NMR ([D$_6$]DMSO): δ = 13.48 (s, 2 H), 9.57 (d, 2 H), 9.33 (s, 2 H), 8.88 (m, 4 H), 8.49 (s, 2 H), 8.23 (m, 4 H), 8.14 (m, 2 H), 8.05 (m, 2 H), 7.83 (m, 2 H), 7.78 (m, 2 H), 7.67 (s, 2 H), 7.60 (m, 2 H), 7.48 (s, 2 H), 7.39 (m, 2 H), 1.41 (s, 18 H), 1.33 (s, 18 H) ppm. ES-MS: *m*/*z* = 579.2 [**11**]. $C_{68}H_{68}F_{12}N_{10}O_2P_2Ru{\cdot}0.33NaPF_6$ (1504.35): calcd. C 54.29, H 4.56, N 9.31; found C 54.3, H 4.7, N 9.35.

Synthesis of $[Ru(bpy)_2(DppzᵗBusalNi)](PF_6)_2$ (12): Metallation of the salophen cavity was carried out following established procedures. Ni(acetate)$_2{\cdot}4H_2O$ (6 mg, 0.24 mmol) was added to compound **11** (58 mg, 0.2 mmol) dissolved in methanol (20 mL) and the mixture was stirred for 2 h. The deep red solution was concentrated under reduced pressure and a solid was precipitated on addition of a concentrated aqueous solution of NH_4PF_6. The red solid was filtered off, washed with water and dried under vacuum. Yield: 26 mg (85%). A pure sample of **12** for photophysical measurements was obtained by chromatography on neutral alumina using a mixture of dichloromethane/methanol (90:10) (R_f = 0.61). IR: $\tilde{\nu}$ = 2950−2905 (C−H, aliph), 1605−1640 (C=N), 845 cm^{-1} (PF_6). ^1H NMR ([D$_6$]DMSO): δ = 9.52 (d, 2 H), 9.33 (s, 2 H), 9.19 (s, 2 H), 8.88 (dd, 4 H), 8.22 (m, 4 H), 8.14 (m, 2 H), 8.06 (dd, 2 H), 7.82 (d, 2 H), 7.77 (d, 2 H), 7.64 (d, 2 H), 7.60 (m, 2 H), 7.41 (d, 2 H), 7.39 (m, 2 H), 1.41 (s, 18 H), 1.32 (s, 18 H) ppm. ES-MS: *m*/*z* = 607.2 [**12**]. $C_{68}H_{66}F_{12}N_{10}NiO_2P_2Ru$ (1505.01): calcd. C 54.27, H 4.42, N 9.31; found C 54.05, H 4.31, N 9.29.

Acknowledgments

The authors wish to thank Professor Jean-Jacques Girerd for fruitful discussions. This work was supported by the CNRS (Programme Energie, PRI4) and the CEA for the LRC project (LRC-CEA no. 33V). K. B. wishes to acknowledge the European TMR program and STINT (The Swedish Foundation for International Cooperation in Research and Higher Education) for financial support.

[1] [1a] K. Kalyanasundaran, *Coord. Chem. Rev.* **1992**, *46*, 159−244. [1b] A. Juris, V. Balzani, F. Barigelletti, S. Campagna, P. Belser, A. von Zelewsky, *Coord. Chem. Rev.* **1988**, *84*, 85−277. [1c] J.-P. Sauvage, J.-P. Collin, J.-C. Chambron, S. Guillerez, C. Coudret, V. Balzani, F. Barigelletti, L. De Cola, L. Flamigni, *Chem. Rev.* **1994**, *94*, 993−1019.

[2] [2a] J. R. Winkler, H. B. Gray, *Chem. Rev.* **1992**, *92*, 369−379. [2b] H. B. Gray, J. R. Winkler, *Annu. Rev. Biochem.* **1996**, *65*, 537−561. [2c] D. Mandler, I. Willner, *J. Am. Chem. Soc.* **1984**, *106*, 5352−5353. [2d] K. A. Maxwell, M. Sykora, J. M. De Simone, T. J. Meyer, *Inorg. Chem.* **2000**, *39*, 71−75. [2e] L. De Cola, P. Belser, *Coord. Chem. Rev.* **1998**, *177*, 301−346. [2f] C. Chiorboli, C. A. Bignozzi, F. Scandola, E. Ishow, A. Gourdon, J.-P. Launay, *Inorg. Chem.* **1999**, *38*, 2402−2410. [2g] M. D Ward, F. Barigelletti, *Coord. Chem. Rev.* **2001**, *216*, 127−154. [2h] F. Barigelletti, L. Flamigni, *Chem. Soc. Rev.* **2000**, *29*, 1−12.

[3] [3a] P. D. Beer, J. Cadman, *Chem. Rev.* **2000**, *205*, 131−155 and references therein. [3b] A. P. de Silva, H. Q. N. Gunaratne, T. Gunnlaugsson, A. J. M. Huxley, C. P. McCoy, J. T. Rademacher, T. E. Rice, *Chem. Rev.* **1997**, *97*, 1515−1566. [3c] T. Mizuno, W.-H. Wei, L. R. Eller, J. L. Sessler, *J. Am. Chem. Soc.* **2002**, *106*, 1134−1135. [3d] F. Bolletta, I. Costa, L. Fabbrizzi, M. Licchelli, M. Montalti, P. Pallavicini, L. Prodi, N. Zaccheroni, *J. Chem. Soc., Dalton Trans.* **1999**, 1381−1385.

[4] [4a] J. Otsuki, M. Tsujino, T. Lizaki, K. Araki, M. Seno, K. Takatera, T. Watanabe, *J. Am. Chem. Soc.* **1997**, *119*, 7895−7896. [4b] S. Fraysse, C. Coudret, J.-P. Launay, *Eur. J. Inorg. Chem.* **2000**, 1581−1590.

[5] K. Kalyanasundaran, *Photochemistry of Polypyridine and Porphyrin Complexes*, Academic, New York, **1992**.

[6] [6a] N. Kitamura, H.-B. Kim, S. Sumio, S. Tazuke, *J. Phys. Chem.* **1989**, *93*, 5750−5756. [6b] H.-B. Kim, N. Kitamura, Y. Kawanishi, S. Tazuke, *J. Phys. Chem.* **1989**, *93*, 5757−5764.

[7] [7a] G. M. Brown, N. Sutin, *J. Am. Chem. Soc.* **1979**, *101*, 883−892. [7b] M. A. Augustin, J. K. Yandell, *Inorg. Chem.* **1979**, *18*, 577−583. [7c] H. B. Gray, J. R. Winkler, *Electron Transfer in Chemistry* (Ed.: V. Balzani), Wiley-VCH, Weinheim, **2001**, vol 3, p. 3−23.

[8] [8a] R. Langen, I.-J. Chang, J. P. Germanas, J. H. Richards, J. R. Winkler, H. B. Gray, *Science* **1995**, *268*, 1733−1735. [8b] L. Sun, L. Hammarström, B. Akermark, S. Styring, *Chem. Soc. Rev.* **2001**, *30*, 36−49. [8c] D. Burdinski, K. Wieghardt, S. Steenken, *J. Am. Chem. Soc.* **1999**, *121*, 10781−10787. [8d] D. Burdinski, E. Bothe, K. Wieghardt, *Inorg. Chem.* **2000**, *39*, 105−116. [8e] E. Fujita, S. J. Milder, B. S. Brunschwig, *Inorg. Chem.* **1992**, *30*, 2079−2035. [8f] E. Kimura, X. Bu, M. Shionoya, S. Wada, S. Maruyama, *Inorg. Chem.* **1992**, *31*, 4542−4546.

[9] [9a] V. Balzani, A. Juris, M. Venturi, S. Campagna, S. Serroni, *Chem. Rev.* **1996**, 759−833. [9b] L. DeCola, V. Balzani, F. Barigelletti, L. Flamigni, P. Belser, S. Bernhard, *Recl. Trav. Chim. Pays Bas.* **1995**, *114*, 534. [9c] V. Balzani, F. Barigelletti, P. Belser, S. Bernhard, L. DeCola, L. Flamigni, *J. Phys. Chem.* **1996**, *100*, 16786−16788. [9d] P. Belser, S. Bernhard, C. Blum, A. Beyeler, L. DeCola, V. Balzani, *Coord. Chem. Rev.* **1999**, *192*, 155−169. [9e] A. Yoshimura, K. Nozaki, N. Ikeda, T. Ohno, *J. Phys. Chem.* **1996**, *100*, 1630. [9f] P. T. Gulyas, T. A. Smith, M. N. Paddon-Row, *J. Chem. Soc., Dalton. Trans.* **1999**, 1325−1335. [9g] R. Ziessel, M. Hissler, A. El-ghayoury, A. Harriman, *Coord. Chem. Rev.* **1998**, *177*, 1251. [9h] F. Scandola, C. Chiorboli, M. T. Indelli, M. A. Rampi, *Electron Transfer in Chemistry* (Ed.: V. Balzani), Wiley-VCH, Weinheim, **2001**, vol 3, p. 337−408.

[10] C. Kaes, A. Katz, M. W. Hosseini, *Chem. Rev.* **2000**, *100*, 3553−3590 and references therein.

[11] [11a] A. Helms, D. Heiler, G. Mc Lendon, *J. Am. Chem. Soc.* **1991**, *113*, 4325−4327. [11b] J. Kroon, A. M. Oliver, M. N. Paddon-Row, J. W. Verhoeven, *J. Am. Chem. Soc.* **1990**, *112*, 4868−4873. [11c] E. H. Yonemoto, G. B. Saupe, R. H. Schmehl,

 © 2003 Wiley-VCH Verlag GmbH & Co. KGaA, Weinheim

S. M. Hubig, R. L. Riley, B. L. Iverson, T. E. Mallouk, *J. Am. Chem. Soc.* **1994**, *116*, 4786−4795.

[12] N. H. Damrauer, T. R. Boussie, M. Devenney, J. K. McKusker, *J. Am. Chem. Soc.* **1997**, *119*, 8253−8268.

[13] [13a] C. R. Rice, A. Guerrero, Z. R. Bell, R. L. Paul, G. R. Motson, J. C. Jeffery, M. D. Ward, *New. J. Chem.* **2001**, *25*, 185−187. [13b] V. W.-W. Yam, V. W.-M. Lee, F. Ke, K.-W. M. Siu, *Inorg. Chem.* **1997**, *36*, 2124−2129. [13c] N. Komatsuzaki, Y. Himeda, M. Goto, K. Kasuga, H. Sugihara, H. Arakawa, *Chem. Lett.* **1999**, 327−328. [13d] K. E. Berg, Y. Pellegrin, G. Blondin, X. Ottenwaelder, Y. Journaux, M. M. Canovas, T. Mallah, S. Parsons, A. Aukauloo, *Eur. J. Inorg. Chem.* **2002**, 323−325.

[14] [14a] J. Fees, M. Ketterle, A. Klein, J. Fiedler, W. Kaim, *J. Chem. Soc., Dalton Trans.* **1999**, 2595−2599. [14b] A. E. Friedman, J.-C. Chambron, J.-P. Sauvage, N. J. Turro, J. K. Barton, *J. Am. Chem. Soc.* **1990**, *112*, 4960−4962. [14c] J. C. Chambron, J.-P. Sauvage, E. Amouyal, P. Koffi, *Nouv. J. Chim.* **1985**, *9*, 527−529.

[15] S. Bodige, F. M. MacDonnell, *Tetrahededron Lett.* **1997**, *38*, 8159−8160.

[16] F. E. Arnold, *J. Polym. Sci. Polym. Chem. Ed.* **1970**, *8*, 2079−2089.

[17] J. F. Larrow, E. N. Jacobsen, Y. Gao, Y. Hong, X. Nie, C. M. Zepp, *J. Org. Chem.* **1994**, *54*, 1939−1942.

[18] G. W. H. Cheeseman, *J. Chem. Soc.* **1962**, 1170−1176.

[19] B. P. Sullivan, T. J. Meyer, *Inorg. Chem.* **1978**, *17*, 3334−3341.

[20] K. Wärnmark, J. A. Thomas, O. Heyke, J. M. Lehn, *Chem. Commun.* **1996**, 701−702.

[21] F. Averseng, P. G Lacroix, I. Malfant, G. Lenoble, P. Cassoux, K. Nakatani, I. MalteyFanton, J. A. Delaire, A. Aukauloo, *Chem. Mater.* **1999**, *11*, 995−1002.

[22] F. H. Allen, O. Kennard, R. Taylor, *Acc. Chem. Res.* **1983**, *16*, 146−153.

[23] L. DeCola, V. Balzani, F. Barigelletti, L. Flamigni, P. Belser, A. von Zelewsky, M. Frank, F. Vögtle, *Inorg. Chem.* **1993**, *32*, 5228−5238.

[24] K. Nakamoto, *Infrared and Raman Spectra of Inorganic and Coordination Compounds*, 5th ed., John Wiley & Sons, New York, **1997**.

[25] [25a] A. B. P. Lever, *Inorganic Electronic Spectroscopy*, 2nd ed., Elsevier, New York, **1984**. [25b]C. Freire, B. de Castro, *J. Chem. Soc., Dalton Trans.* **1998**, 1491−1497.

[26] [26a] S. D. Ernst, W. Kaim, *J. Am. Chem. Soc.* **1986**, *108*, 3578−3586. [26b] S. D. Ernst, W. Kaim, *Inorg. Chem.* **1989**, *28*, 1520−1528. [26c] J. Bolger, A. Gourdon, E. Ishow, J. P. Launay, *Inorg. Chem.* **1996**, *35*, 2937−2944. [26d] E. Ishow, A. Gourdon, J. P. Launay, C. Chiorboli, F. Scandola, *Inorg. Chem.* **1999**, *38*, 1504−1510. [26e] L. Flamigni, S. Encinas, F. Barigelletti, F. M. MacDonnell, K-J. Kim, F. Puntoriero, S. Campagna, *Chem. Commun.* **2000**, 1185−1186. [26f] M-J. Kim, R. Konduri, H. Ye, F. M. MacDonnell, F. Puntoriero, S. Serroni, S. Campagna, T. Holder, G. Kinsel, K. Rajeshwar, *Inorg. Chem.* **2002**, *19*, 2471−2476. [26g] R. Konduri, H. Ye, F. M. MacDonnell, S. Serroni, S. Campagna, K. Rajeshwar, *Angew. Chem.* **2002**, *17*, 3315−3317, *Angew. Chem. Int. Ed.* **2002**, *41*, 3185−3187.

[27] J. Fees, W. Kaim, M. Moscherosch, W. Matheis, J. Klima, M. Krejcik, S. Zalis, *Inorg. Chem.* **1993**, *32*, 166−174.

[28] W. Kaim, *Angew. Chem.* **1983**, *95*, 201−220; *Angew. Chem. Int. Ed. Engl.* **1983**, *22*, 171−190.

[29] B. de Castro, C. Freire, *Inorg. Chem.* **1990**, *29*, 5113−5119.

[30] [30a] A. Aukauloo, X. Ottenwaelder, R. Ruiz, Y. Journaux, S. Poussereau, B. Cervera, M. C. Muñoz, *Eur. J. Inorg. Chem.* **1999**, 1067−1071. [30b] F. V. Lovecchio, E. S. Gore, D. H. Busch, *J. Am. Chem. Soc.* **1974**, *96*, 3109−3118.

[31] M. N. Ackermann, L. V. Interrante, *Inorg. Chem.* **1984**, *23*, 3904−3911.

[32] [32a] G. A. Heath, L. J. Yellowlees, P. S. Braterman, *J. Chem. Soc., Chem. Commun.* **1981**, 287−289. [32b] R. M. Berger, *Inorg. Chem.* **1990**, *29*, 1920−1924.

[33] [33a] D. E. Morris, K. W. Hanck, M. K. DeArmond, *J. Am. Chem. Soc.* **1983**, *105*, 3032−3038. [33b] W. Kaim, S. Ernst, V. Kasack, *J. Am. Chem. Soc.* **1990**, *112*, 173−178.

[34] [34a] M. M. Richter, K. J. Brewer, *Inorg. Chem.* **1992**, *31*, 1594−1598. [34b] M. M. Richter, K. J. Brewer, *Inorg. Chem.* **1993**, *32*, 2827−2834.

[35] The X-ray structure of the mononuclear Ni^{II} complex **10** was obtained on a microcrystal by Dr. D. Flot and Dr. C. Philouze at the ESRF facility, Grenoble, France. Owing to some disorder, an *R* factor of only 25% was obtained.

[36] R. H. Holm, A. Chakravorty, L. J. Theriot, *Inorg. Chem.* **1966**, *5*, 625−635.

Received October 7, 2002
[I02561]

 © 2003 Wiley-VCH Verlag GmbH & Co. KGaA, Weinheim

Kinetic and Equilibrium Studies of Reactions of N-Heterocycles with Dimeric and Monomeric Oxorhenium(v) Complexes

James H. Espenson*[a] and S. Masoud Nabavizadeh[a]

Keywords: Rhenium / N ligands / Kinetics / Linear free-energy relationships

Equilibrium constants have been evaluated for the reaction $\{MeReO(edt)\}_2 + 2\ L \rightarrow 2\ MeReO(edt)L$, where edt is 1,2-ethanedithiolate and L is any of 13 N-donor heterocyclic ligands. The values of K range from $1.37(27)\times10^{-2}$ for pyrimidine to $1.95(6)\times10^{6}$ for imidazole at 25 °C in chloroform. A successful correlation of log$K$ with log (K_a) of HL^+ was realized except in the case of the 2-substituted ligands 2-picoline and quinoline, where steric effects make K smaller than expected from the proton basicity of L. The kinetics of the same reactions were studied; the rate law for the reaction in the forward direction is given by $-d[\{MeReO(edt)\}_2]/dt = \{k_a + k_b[L]\}[L] \times [\{MeReO(edt)\}_2]$. Except for 2-picoline and quinoline, the major pathway is provided by the term that shows the quadratic dependence on [L]. Values of log (k_b) also correlate with log K, and therefore necessarily with log (K_a).

Introduction

We have studied the interaction of N-heterocycles with certain high-valent oxorhenium complexes. Our studies encompass the evaluation of equilibrium constants and rate constants for complexes of the core composition [MeRe(O)-(dithiolate)]. Actually, that core, with coordination number four, is never a detectable species, not even as a reaction intermediate. The stable species all show five-coordination as depicted in Scheme 1. The complexes of interest comprise dimers, $\{MeRe(O)(dithiolate)\}_2$,[1,2] and monomers, $\{MeRe(O)(dithiolate)L\}$,[3,4] where L is pyridine (**1**) or any of the other N-heterocycles shown in Scheme 2.

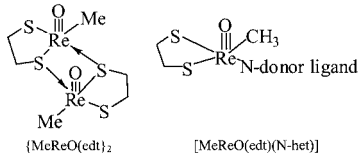

Scheme 1. Structural formulas of methyl(oxo)rhenium(v) complexes

These complexes have soft metal centers; the chelating dithiolate is never displaced and (phosphane)rhenium complexes, although not a subject of this study, are more stable than those with hard bases such as pyridines.[4] We have explored correlations between the equilibrium and rate constants for experimental studies carried out in chloroform.

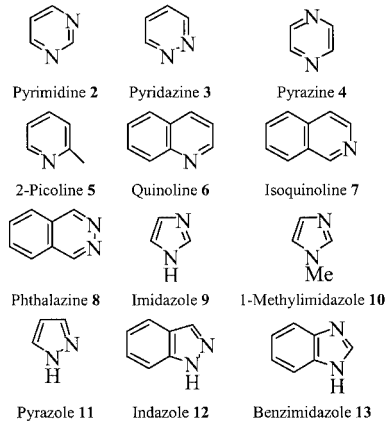

Scheme 2. Structural formulas of N-heterocycles

In addition, the equilibrium constants for the coordination of N-heterocycles (L) were correlated with the aqueous pK_a values of HL^+.

One finds in the literature values of stability constants for 1:1 complexes of several imidazoles with many divalent metal ions.[5−7] A correlation was identified between the equilibrium constants and pK_a values, except for benzimidazole (**13**), which could be attributed to the steric hindrance this particular ligand poses for coordination to a metal site. Complexes of the general formula $[M(CN)_5L]^{n-}$ offer the advantage that there is but a single open coordination site. Their coordination chemistry — including structure, spectroscopy and kinetics — have been reported for M = Fe, Ru, and Os.[8] Because of the particular steric effects of 2-substituted imidazole ligands, their interactions have been the subject of a separate investigation.[9] In addition, rate constants for the formation and dissociation of

[a] Department of Chemistry, Iowa State University
Ames, IA 50011, USA
Fax: (internat.) + 1-515/294-5233
E-mail: espenson@iastate.edu
Supporting information for this article is available on the WWW under http://www.eurjic.org or from the author.

 DOI: 10.1002/ejic.200200601 © 2003 Wiley-VCH Verlag GmbH & Co. KGaA, Weinheim

$[Ru^{II}(CN)_5L]^{3-}$ ions (L = Py, ImH etc.) have been reported.[10]

Results

Equilibrium Studies

Values of the equilibrium and rate constants have been evaluated for the reactions represented by Equation (1).

$$\{MeReO(edt)\}_2 + 2L = 2\ MeReO(edt)L \quad K = \frac{[MeReO(edt)L]^2}{[\{MeReO(edt)\}2] \times [L]^2} \qquad (1)$$

The absorbance of a solution at equilibrium is the sum of the larger component from the monomer and the smaller one from the dimer [Equation (2)].

$$Abs_{eq} = \varepsilon_D[\{MeReO(edt)\}_2]_{eq} + \varepsilon_{ML}[MeReO(edt)L]_{eq} = \varepsilon_D[D]_{eq} + \varepsilon_{ML}[ML]_{eq} \qquad (2)$$

Mass balance for rhenium must also be maintained [Equation (3)].

$$[Re]_T = 2 \times [\{MeReO(edt)\}_2]_{eq} + [MeReO(edt)L]_{eq} = 2 \times [D]_{eq} + [ML]_{eq} \qquad (3)$$

The simultaneous solution of these equations, which is presented in the Supporting Information (see footnote on page 1 of this article), affords an exact expression for the equilibrium absorbance in which the indicated equilibrium is sustained [Equation (4)], where [L] represents the equilibrium ligand concentration.[4]

$$Abs_{eq} = \varepsilon_D[D]_0 + \left(\varepsilon_{ML} - \frac{\varepsilon_D}{2}\right) \times \left[\frac{-K + \sqrt{K^2 + \frac{16K[D]_0}{[L]^2}}}{4/[L]^2}\right] \qquad (4)$$

The values of K were determined for most of the ligands by fitting the equilibrium absorbances to Equation (4) by the method of nonlinear least squares. Such solutions contained L at a known concentration because $[L]_T \approx [L]_{eq} >> [Re]_T$. Figure 1 presents repetitive scan spectra showing the equilibrium progression from D to ML for L = pyridine (**1**), with increasing ligand concentration. Tight isosbestic points were found, showing that only the two rhenium species were present throughout the set of experiments. The inset of Figure 1 shows the fit to Equation (4) of the absorbance values at one wavelength, 364 nm. For L = pyridine, the value of K so determined is $1.04(16) \times 10^4$ L·mol^{-1} in chloroform at 25.0 °C.

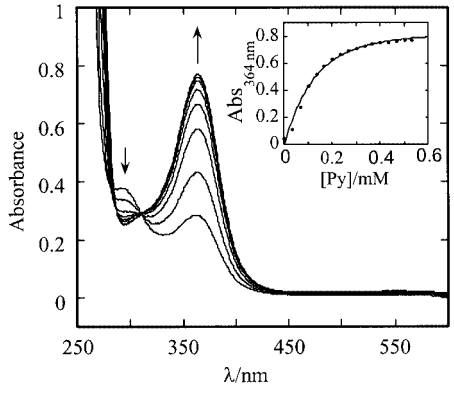

Figure 1. Absorbance changes as a solution of $[MeReO(edt)]_2$ was titrated with pyridine; isosbestic points were noted at 283 and 311 nm; the inset shows the analysis of the spectrophotometric data to evaluate the equilibrium constant according to Equation (4)

A more complex situation arises when K is quite large, as was the case for imidazole, 1-methylimidazole, and benzimidazole. Then, $[L]_T$ must not be $>> [Re]_T$ in order to realize the balance between D and ML needed for the evaluation of K. That is, $[L]_T \neq [L]_{eq}$. This situation requires an iterative solution. To do so, we made use of the program PSEQUAD.[11] The data for **11** were checked by both methods of calculation, and the agreement in the values of K was within the experimental error: 96±7 and 95±3 by nonlinear least-squares and by using the program PSEQUAD, respectively. The values of the equilibrium constants by the method most appropriate for the given complex are summarized in Table 1. The Supporting Information lists the initial concentration of $[MeReO(edt)]_2$ and the range of each ligand L used in the determination of the values of K.

Kinetic Studies

In many of the kinetics experiments, the reaction proceeded to completion. The gauge of this is whether the given [L] used for a particular experiment and the value of K inherent to it satisfied the condition $K[L]_{eq} >> 1$. In such cases, the data were analyzed by first-order kinetics. In terms of absorbance this is given by Equation (5) , where Abs_0 and Abs_∞ are the respective initial and final absorbance and k_{for} is the pseudo-first-order rate constant for the forward reaction.

$$Abs_t = Abs_\infty + (Abs_0 - Abs_\infty)\exp(-k_{for}t) \qquad (5)$$

It was not always feasible to drive the reaction to completion at an attainable ligand concentration, particularly when K is small. Additionally, for ligands with intermediate values of K, some reactions proceeded to completion, for which Equation (5) applies, but other experiments at lower [L] did not. The data in these cases require treatment by a kinetic model that takes into account the opposing rates of the forward and reverse reactions, which appear as a rate *difference*. In general, the apparent rate *constants* for equilibration are the *sum* of those for the forward and reverse reactions. The data could thus be treated by Equation (6), in which the designations k^Ψ indicate rate constants that depend on [L].[4,15]

$$Abs_t = Abs_\infty + \frac{(1+q)\cdot[Abs_0 - Abs_\infty]\cdot e^{-k_e t}}{1+q\cdot e^{-k_e t}}$$

$$\text{where } k_e = k^\Psi_{for} + 4k^\Psi_{rev}[M-L]_\infty,\ q = \frac{4k^\Psi_{rev}[ML]_\infty}{2k^\Psi_{for} + 4k^\Psi_{rev}[ML]_\infty} \text{ and } k^\Psi_{for} = k_e \times \frac{1-q}{1+q}. \qquad (6)$$

 © 2003 Wiley-VCH Verlag GmbH & Co. KGaA, Weinheim

Table 1. Kinetic and equilibrium data for monomerization with N-heterocycles at 25 °C in $CHCl_3$

Ligand	K_{eq}/L mol^{-1} [a]	k_a/L mol^{-1}s^{-1}	k_b/L^2 mol^{-2} s^{-2}	pK_a [b]	λ/nm[c]
1	$1.04(16)\times10^4$	–	$1.35(1)\times10^5$	5.23 (25 °C)	364
2	$1.37(27)\times10^{-2}$	$4.1(1)\times10^{-2}$	$9.9(8)\times10^{-1}$	1.23 (20 °C)	390
3	$1.12(10)\times10^1$	$5.2(10)\times10^{-1}$	$3.21(16)\times10^2$	2.24 (20 °C)	422
4	$7.71(77)\times10^{-2}$	$7.3(80)\times10^{-4}$	1.06(2)	0.65 (20 °C)	410
5	$5.7(6)\times10^{-2}$	$5.7(16)\times10^{-3}$	$4.9(9)\times10^{-2}$	5.97 (20 °C)	360
6	9×10^{-2}	$1.99(10)\times10^1$	–	4.90 (20 °C)	390
7	$3.00(34)\times10^2$	1.07(59)	$6.73(49)\times10^3$	5.40 (20 °C)	390
8	$1.04(10)\times10^2$	$5.3(9)\times10^{-1}$	$9.9(5)\times10^2$	3.47 (20 °C)	420
9	$1.95(6)\times10^6$	$3.49(18)\times10^4$	$6.98(2)\times10^6$	6.99 (25 °C)	365
10	$1.32(5)\times10^6$	$1.92(99)\times10^2$	$4.3(2)\times10^6$	6.95 (25 °C)	365
11	$9.58(72)\times10^1$	$8.44(82)\times10^1$	$4.34(1)\times10^4$	2.49 (25 °C)	362
12	3.35(13)	$1.96(42)\times10^1$	4.47(78)	1.25 (25 °C)	350
13	$5.0(3)\times10^4$	$5.6(64)\times10^{-1}$	$1.18(7)\times10^4$	5.53 (25 °C)	360

[a] K was evaluated by use of the nonlinear least-squares method except for ligands **9**, **10**, and **13** for which the program PSEQUAD was used. [b] K_a applies to the reaction $HL^+ = H^+ + L$ in aqueous solution at the specified temperature. Data are from refs.[12–14] [c] λ specifies the wavelength used for fitting data from equilibrium and kinetics studies.

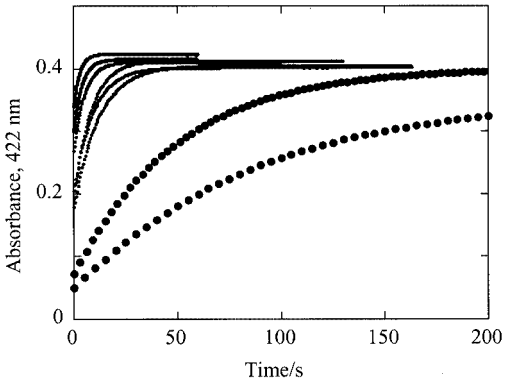

Figure 2. Absorbance-time curves for the reaction of $\{MeReO(edt)\}_2$ with pyridazine (**3**) in chloroform at 25.0 °C; data are shown for experiments with $[L]_0$ in the range 4.6–32.1 mM

The increase in absorbance for one typical family of kinetic experiments with L = pyridazine, **3**, is presented in Figure 2. The values of the pseudo-first-order rate constants for the reactions in the forward direction were determined as a function of [L]. The rate law in the general case contains two terms [Equation (7)], although in any specific case a contribution from one of the terms may be absent within the experimental error.

$$-\frac{d[\{MeReO(edt)\}_2]}{dt} = \{k_a[L] + k_b[L]^2\} \times [\{MeReO(edt)\}_2] \quad (7)$$

Because this is the rate equation for the forward reaction, that for the reverse reaction follows from it [Equation (8)].

$$v_{rev} = \left\{k_{-a}[L]^{-1} + k_{-b}\right\}[MeReO(edt)L]^2 \quad (8)$$

That is, one term of the reverse rate law shows inhibition by L. This feature is already incorporated in Equation (6). As a consequence of the equilibrium situation, we also have, by microscopic reversibility, the relation according to Equation (9).

$$K = \frac{k_a}{k_{-a}} = \frac{k_b}{k_{-b}} \quad (9)$$

The weighted nonlinear least-squares fitting of the values of k^{Ψ}_{for} to Equation (7) is presented in Figure 3 for the same L. Values of k_a and k_b so obtained are also given in Table 1.

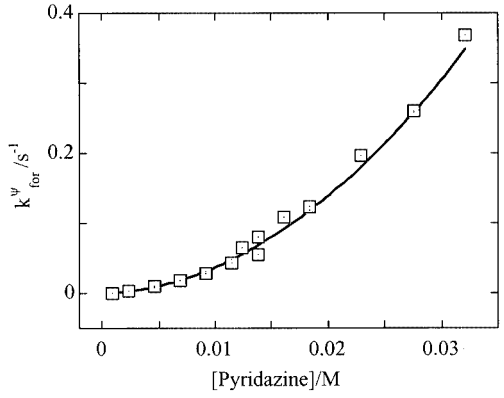

Figure 3. A representative set of kinetic data for L = pyridazine (**3**) depicting the weighted nonlinear least-squares fit to Equation (7), with linear and quadratic dependencies on [L]

Interpretation and Discussion

Correlation of Lewis and Brønsted Basicities

Figure 4 displays a plot of log$K$ for the reaction according to Equation (1) versus logK_a, for the acid ionization of HL^+.[12–14] Except for ligands **5** and **6**, a good correlation was found; the slope of the line in Figure 4 is -1.08 ± 0.09. Exceptions for those two ligands are logical as well, in that they present a steric barrier for coordination to the rhenium

 © 2003 Wiley-VCH Verlag GmbH & Co. KGaA, Weinheim

center which is absent in the proton basicity. No deviation was found for benzimidazole (**13**), where a steric effect for the rhenium center might have been expected to exist. That steric effect would be smaller than the ones for **5** and **6**, because the bond angle between N, the ring C, and the C in the 2-position is 132° in **13** and 120° in **5** and **6**.

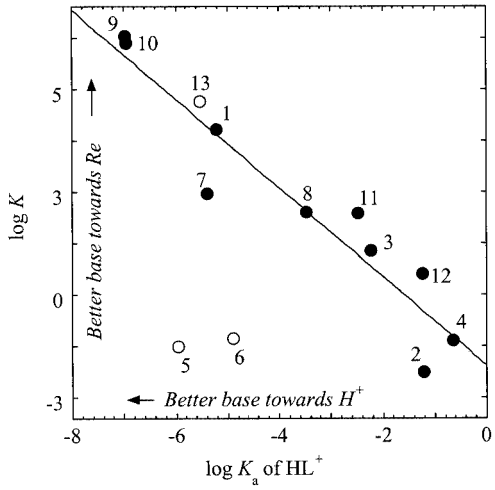

Figure 4. Plot showing a correlation between the equilibrium constants for monomerization of $[MeReO(edt)]_2$ by different ligands L in chloroform and the aqueous acid ionization constants of the same ligands, both on logarithmic scales; ligands **5**, **6**, and **13** were omitted from the linear fit

A study from the literature reported that **13** does indeed coordinate less strongly to Cu^{2+} and Zn^{2+} in aqueous solution than do the other members of a series of ligands all of which were imidazoles that lacked a substituent in the 2-position.[6] Aside from **13**, a good correlation between K and K_a exists except for N-heterocycles substituted in the 2-position.

One might raise an objection to the correlation presented in Figure 4, in that the y axis refers to data for a dirhenium species that incorporates two ligands in the equilibrium whereas the x axis refers to a single L. To address this point, we have used K values for two ligands to derive values of K' that refer to this reaction [Equation (10)].

$$MeReO(edt)L + L' = MeReO(edt)L' + L \quad (10)$$

It is immaterial which L one chooses as the constant reference point because other ligands then constitute L′. We have arbitrarily selected MeIm as L. The value of K' for Equation (10) is given by Equation (11).

$$K' = \sqrt{\frac{K(L')}{K(MeIm)}} \quad (11)$$

We then constructed a plot of logK' against log$K$ for proton transfer, as in the reaction $MeImH^+ + L' \rightleftarrows MeIm + HL'^+$. The result is shown in Figure 5. The correlation is fully acceptable, excluding the ligands with steric effects for coordination. The slope of the line in Figure 5, drawn without reference to such ligands is 0.54±0.07. That is, the equilibrium of ligand exchange at the rhenium center is less sensitive to the ligand than is ligand protonation.

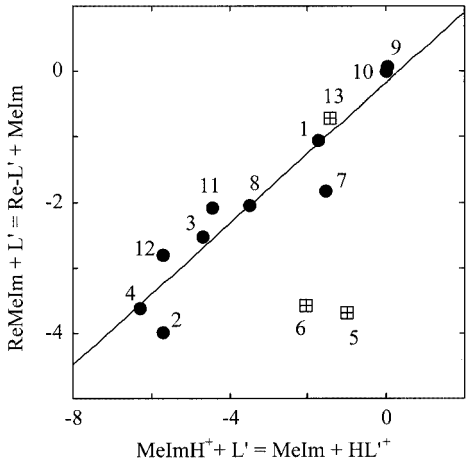

Figure 5. Correlation of the equilibrium constants for exchange of ligands at a rhenium center versus the equilibrium constants for proton exchange, both on logarithmic scales

Linear-Free Energy Correlations of Rate Constants

Two approaches will be explored. First, we ask whether there is a correlation between the equilibrium constants and the rate constants. Figure 6 depicts a plot of K versus k_b, which establishes that a reasonable correlation exists except for ligands **5** and **13**, where steric issues intrude most strongly. We take this to mean that the equilibrium and kinetic processes, both of which establish two new Re−N bonds, are governed by related factors. The same approach for log$K$ versus logk_a is less satisfactory, probably because a single Re−N bond is made in this kinetic step and because the k_a values are less precise, this being the minor kinetic pathway.

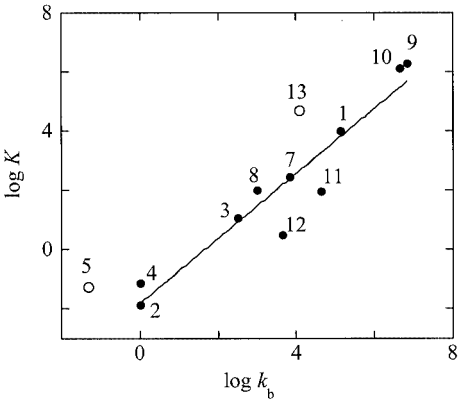

Figure 6. The linear-free energy correlation of equilibrium and kinetic data for the reaction according to Equation (1)

Mechanism

The kinetic data lead us to formulate the reaction steps that are consistent with the kinetic data by the model pre-

 © 2003 Wiley-VCH Verlag GmbH & Co. KGaA, Weinheim

sented in Scheme 1. The ligands are shown as attacking the Re^{V} atom at the vacant coordination position trans to the Re≡O multiple bond. This is not generally a site for stable coordination, in that the binding constant for a sixth ligand is small. Indeed, in our studies such metastable transient species never accumulated to a concentration level at which they could be detected. Nonetheless, once one or two nucleophiles attack the Re^{V} atom, then further events rapidly ensue. In particular, either or both of the weaker S→Re coordinate bonds is released as the entering ligand L enters an equatorial position on the monomeric reaction product. This equation follows from Scheme 1 [Equation (12)].

$$-\frac{d[D]}{dt} = \frac{1}{2}\frac{d[ML]}{dt} = \left(\frac{k_3K_1[L] + k_4K_1K_2[L]^2}{1 + K_1[L] + K_1K_2[L]^2}\right)[D] \quad (12)$$

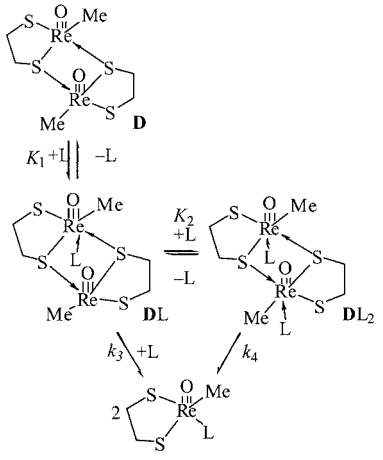

Scheme 1. Kinetic scheme for monomer formation

Equation (7) is a limiting form of Equation (12), when $K_l[L] + K_1K_2[L]^2 << 1$, according to which $k_a = k_3K_1$ and $k_b = k_4K_1K_2$. Further resolution is not possible; the values of the equilibrium constants K_1 and K_2 are too small to allow **D**L and **D**L_2 to attain concentrations that are significant compared to that of **D**. This, of course, is the basis for the inequality given.

In our original study of the monomerization of [MeReO(dithiolate)]$_2$ with a series of phosphane and pyridine ligands,[4] a rate law with linear and quadratic dependencies on [L] was found, just as in Equation (7) [see also Equation (12)]. We formulate the quadratic pathway in terms of an attack of two ligands, one on each rhenium atom. Following that, monomerization occurs as the coordinate S→Re bonds within the dimer are broken. The transition state for this pathway can be drawn as in the right-hand pathway of Scheme 1. On the other hand, our original assignment for the k_a pathway no longer seems credible. We no longer claim that the k_a pathway represents a scheme that generates equal amounts of the product MeReO(edt)L and an intermediate four-coordinate intermediate MeReO(edt). In none of our studies on catalysis or coordination chemistry has such a species been detected. Rather, we postulate that one of the S→Re coordinate bonds in the dimer has been broken, generating a half-opened dirhenium intermediate that reacts subsequently but rapidly with a second L. This idea is formulated in the pathway that is shown on the left-hand side of Scheme 1. The further advantage of the revised proposal is that it maintains a coordination number of five about both oxorhenium(v) atoms, which is the preferred geometry.

Conclusion

Equilibrium constants for reactions in which a series of N-heterocyclic ligands react with a dimeric oxorhenium(v) complex, leading to its monomerization, have been evaluated. Rate constants for the same reactions have been determined. The values of *K* and *k* correlate with one another and with the proton basicity of the ligands.

Experimental Section

The compound methyltrioxorhenium ($MeReO_3$ or MTO) was synthesized according to a literature procedure.[16] It was then used to prepare the rhenium complex that is the focus of this study, the dimer [MeReO(edt)]$_2$, which was known from previous research.[17] A new and more efficient synthetic procedure has since been devised.[18] MTO (1.0 mmol) was added to a stirred solution of PPh_3 (1.0 mmol) in toluene (10 mL), containing a catalytic amount of diphenylacetylene. After 5 min, 1,2-ethanedithiol (1.0 mmol) was added. The resulting mixture was stirred at room temperature for 6 h and layered with hexane (20 mL). After 2 d, a brown-black solid deposited, which was collected by washing with hexane. Further material could be obtained by concentrating the mother liquor and recrystallizing the residue from CH_2Cl_2/hexanes.The isolated compound was characterized by comparing its NMR and UV/Vis spectra with those of the previously prepared material, which had also been characterized by X-ray diffraction.[17] Other reagents, including the N-heterocyclic ligands, were purchased from commercial sources (Aldrich, except for pyridine, Fisher Scientific). They were used without further purification. Certain ligands that might have been included in the study were not reactive or were insufficiently soluble (2,5-dimethylpyrrole and 1,2,4-triazolo[1,5-*a*]pyrimidine). Chloroform was used as the solvent in these studies and the data were obtained at 25 °C. Spectrophotometric methods were used throughout. For equilibrium studies of the reaction according to Equation (1) and for the slower kinetics experiments, a Shimadzu Model 3101 instrument was used. Faster reactions were studied by stopped-flow spectrophotometry with an OLIS apparatus equipped with a rapid scanning monochromator. Absorbance-time data were extracted at single wavelengths for further analysis. Reagent-grade chloroform was used as the solvent for these studies. The ethanol stabilizer that accompanies the commercial solvent has no effect. Supporting Information (see footnote on the first page of this article) for this article comprises the derivation of Equation (4) and the list of concentrations used in the evaluation of *K*.

Acknowledgments

This research was supported by grant CHE-9982004 from the National Science Foundation. S. M. N. also wishes to acknowledge

 © 2003 Wiley-VCH Verlag GmbH & Co. KGaA, Weinheim

support from the Ministry of Science, Research and Technology of Iran. Some experiments were conducted with the use of the facilities of the Ames Laboratory. We are grateful to Dr. Gábor Lente for assistance in the use of the PSEQUAD program.

[1] J. Jacob, I. A. Guzei, J. H. Espenson, *Inorg. Chem.* **1999**, *38*, 1040−1041.
[2] G. Lente, X. Shan, I. A. Guzei, J. H. Espenson, *Inorg. Chem.* **2000**, *39*, 3572−3576.
[3] J. Jacob, G. Lente, I. A. Guzei, J. H. Espenson, *Inorg. Chem.* **1999**, *38*, 3762−3763.
[4] G. Lente, I. A. Guzei, J. H. Espenson, *Inorg. Chem.* **2000**, *39*, 1311−1319.
[5] L. E. Kapinos, B. Song, H. Sigel, *Chem. Eur. J.* **1999**, *5*, 1794−1802.
[6] L. E. Kapinos, B. Song, H. Sigel, *Inorg. Chim. Acta* **1998**, *280*, 50−56.
[7] H. Sigel, A. Saha, N. Saha, P. Carloni, L. E. Kapinos, R. Griesser, *J. Inorg. Biochem.* **2000**, *78*, 129−137.
[8] L. M. Baraldo, P. Forlano, A. R. Parise, L. D. Slep, J. A. Olabe, *Coord. Chem. Rev.* **2001**, *219−221*, 881−921.
[9] E. M. Sabo, R. E. Shepherd, M. S. Rau, M. G. Elliott, *Inorg. Chem.* **1987**, *26*, 2897−907.
[10] J. M. A. Hoddenbagh, D. H. Macartney, *Inorg. Chem.* **1986**, *25*, 380−383.
[11] L. Zékány, I. Nagypál, in: *Computational methods for the determination of formation constants* (Ed.: D. Leggett), Plenum Press, New York, **1985**.
[12] R. M. Smith, A. E. Martell, *Critical Stability Constants*, Plenum Press, New York, **1974**.
[13] D. R. Lide, Editor-in-Chief, *CRC Handbook of Chemistry and Physics*, 81st ed., CRC Press, Boca Raton, **2000**.
[14] J. Catalan, R. M. Claramunt, J. Elguero, J. Laynez, M. Menendez, F. Anvia, J. H. Quian, M. Taagepera, R. W. Taft, *J. Am. Chem. Soc.* **1988**, *110*, 4105−11.
[15] E. L. King, *Int. J. Chem. Kinet.* **1982**, *14*, 1285.
[16] W. A. Herrmann, R. M. Kratzer, R. W. Fischer, *Angew. Chem. Int. Ed. Engl.* **1997**, *36*, 2652−2654.
[17] J. H. Espenson, X. Shan, Y. Wang, R. Huang, D. W. Lahti, J. Dixon, G. Lente, A. Ellern, I. A. Guzei, *Inorg. Chem.* **2002**, *41*, 2583−2591.
[18] X. Shan, J. H. Espenson, unpublished results.

Received October 31, 2002

 © 2003 Wiley-VCH Verlag GmbH & Co. KGaA, Weinheim

Co-Ligand Involvement in Ground and Excited States of Electron-Rich (Polypyridyl)Pt^{II} Complexes

Axel Klein,*[a] Joris van Slageren,*[b][‡] and Stanislav Záliš[c]

Keywords: Emission / Platinum / N ligands / Photophysics / Optical spectroscopy / Theoretical calculations / DFT / Crystal structure

The electronic absorption and luminescence properties of electron-rich organometallic platinum(II) complexes with aromatic α-diimine ligands [(α-diimine)PtR$_2$] (R = alkyl, alkynyl, Ph or Mes, Mes = 2,4,6-trimethylphenyl) were examined. The crystal and molecular structures of [(bpy)PtMe$_2$], [(tap)PtPh$_2$] and [(tmphen)PtMes$_2$] were determined from single-crystal XRD and discussed in view of intermolecular interactions that influence the emission behaviour. The combination of theoretical calculations (DFT) and spectroscopic techniques (absorption and emission) revealed the character of electronic transitions and excited states. In particular they showed that the co-ligand involvement in the frontier orbitals is small for R = Me, but large in case of R = alkynyl, Ph or Mes. Depending on the chelate ligand and its substitution pattern, the emission efficiencies of the complexes cover a wide range from strong emission in fluid solution at ambient temperature to very weak emission in rigid matrices (glasses) at low temperatures with no emission at ambient temperature. The emission lifetimes, determined at low temperature in solvent glasses, mainly depend on the chelate ligand and not on the co-ligands. The emission quantum yields of the complexes in solution at room temperatures are much larger for R = Mes than for R = Ph or Me. The emission bands for the complexes with unsaturated co-ligands show slight structuring at low temperatures in contrast to the alkyl-substituted ones.
(© Wiley-VCH Verlag GmbH & Co. KGaA, 69451 Weinheim, Germany, 2003)

Introduction

Platinum(II) complexes with α-diimine ligands and their photophysical properties have been the subject of much interest in the last three decades.[1−21] Their square-planar geometry provides the possibility to introduce selectively properly designed α-diimine ligands and suitable co-ligands in a coplanar arrangement and thus allows the tailoring of molecules for potential application as photosensitizers or photocatalysts.[16,22−24] The platinum centre itself provides relatively high stability against isomerisation or thermal decomposition. Electronic transitions in such complexes span a broad range depending on both the diimine ligand and the co-ligand(s) (see Scheme 1). Ligand field (LF or d−d) transitions occur as the lowest transition in case where the diimine ligand is a weak acceptor and the co-ligand is a relatively weak σ donor. When choosing the z axis coincident with the main symmetry axis (in C_{2v} symmetry), the highest occupied MOs are $d_{x^2-y^2}$ or d_{z^2}, while d_{yz} is the LUMO (Scheme 1, case A). In this case metal-to-ligand charge transfer (MLCT) transitions lie at higher energies. Examples of this situation are [(bpy)PtX$_2$] (X = Cl, Br, I).[6,8,11,18] If the π and π* orbitals of the diimine ligand are higher and lower in energy than the filled and empty d(Pt) orbitals, respectively, the lowest-energy electronic transitions are of intraligand (π-π*) character (Scheme 1, B). This situation was found for [(bpy)Pt(en)]$^{2+}$,[11] and is caused by the stronger ligand field of the en ligand compared to X. If the diimine ligand is a good π acceptor, its

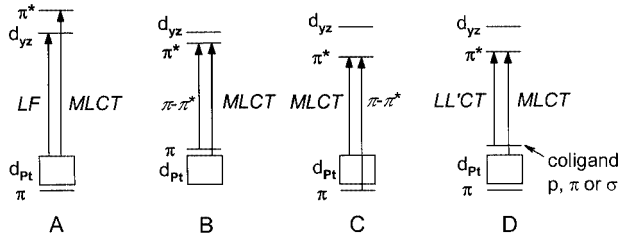

Scheme 1. Qualitative MO scheme for (diimine)platinum complexes assuming C_{2v} symmetry; note that the z axis coincides with the (main) C_2 axis and the x axis is perpendicular to the coordination plane

[a] Institut für Anorganische Chemie, Universität Stuttgart, Pfaffenwaldring 55, 70569 Stuttgart, Germany
E-mail: aklein@iac.uni-stuttgart.de
[b] Institute of Molecular Chemistry, Universiteit van Amsterdam, Nieuwe Achtergracht 166, 1018 WV Amsterdam, The Netherlands
[c] J. Heyrovský Institute of Physical Chemistry, Academy of Sciences of the Czech Republic, Dolejškova 3, 18000 Prague 8, Czech Republic
[‡] Present address: 1. Physikalisches Institut, Universität Stuttgart, Pfaffenwaldring 57, 70550 Stuttgart, Germany
E-mail: slageren@pi1.physik.uni-stuttgart.de
Supporting information for this article is available on the WWW under http://www.eurjic.org or from the author.

π* level lies lower than d_{yz} and the lowest-energy transition is the "classical" metal-to-ligand charge transfer (MLCT or d→π*) transition (Scheme 1, C). The same situation is encountered if a weakly π-accepting chelate ligand is combined with co-ligands of medium to high donor strength such as in [(bpym)Pt(CN)$_2$] (bpym = 2,2′-bipyrimidine),[17] [(bpy)Pt(pz)$_2$] (pz = pyrazolates),[6] or [(terpy)Pt(X)]$^+$ (terpy = 2,2′:6′2′′-terpyridine, X = Cl, OH, SCN,[24−26] or alkynyl).[27]

If the co-ligands are no longer innocent, as assumed for the previous cases, but provide high-lying, filled p or π orbitals, the HOMO may have significant to dominating co-ligand contributions, admixed to platinum 5d orbitals, and the resulting lowest transition is assigned to a ligand-to-ligand charge transfer (L′LCT) (Scheme 1, D).[28] Since the HOMO has mixed metal/ligand character, it is also referred to as "mixed metal/ligand-to-ligand" charge transfer (MML′LCT).[7] Examples are the well-known dithiolate complexes such as [(bpy)Pt(mnt)] (mnt = malonitriledithiolate), where the HOMO is mainly formed by the p orbitals of the sulfur ligator atoms.[5,7,29−31] The same situation occurs when the co-ligands are unsaturated hydrocarbons such as phenyl or alkynyl. The π orbitals of the unsaturated system might act as the HOMO (Scheme 1, D). On the other hand back-bonding from Pt to the π* orbitals of the substituents should lower the electron density at the platinum atom with resulting destabilisation of the d orbitals. The situation then approaches case C. So far lowest absorption bands of such compounds containing aryl or alkynyl substituents have been assigned to "classical" MLCT transitions with no contribution from the π orbitals other than (small) π back-bonding.[1,3,27] The MLCT assignment is based on the fact that the absorption maxima increase with increasing energy of the diimine π*-orbital, E_{max} (complex): tmphen > dmphen > phen > bpy > dppz > tap. In the series of an individual diimine ligand the absorption energy increases slightly from methyl to mesityl and markedly from mesityl to phenyl. This parallels the electron donating ability of the substituents, upon which the platinum d orbitals are destabilised, decreasing the energies of the absorption maxima. However, we recently reported on a series of electron rich organoplatinum complexes with diazabutadiene ligands [(R′-DAB)PtR$_2$] (R′-DAB = *N*,*N*′-disubstituted 1,4-diazabutadienes, R′ = aryl or alkyl, R = alkyl, aryl or alkynyl) which were proven to exhibit low-lying L′LCT transitions.[19] It was shown, that the lowest transition gradually changes character from MLCT to L′LCT due to the contribution of the co-ligands to the HOMO. With increasing electron-donating ability of the alkyl co-ligands, the character of the lowest transition gradually obtains partial σ-bond-to-ligand (SBLCT or σ→π*) character with consequent photolability of such complexes. The corresponding aryl and alkynyl complexes have much larger contributions of the co-ligand to the highest filled orbitals and the lowest transitions therefore have mixed MLCT/L′LCT character.

An appropriate choice of diimine chelate ligand and co-ligands should therefore allow predetermination of the characters of the lowest energy transitions and lowest emitting states in such molecules.

This paper reports a combined experimental and theoretical study including absorption and emission spectroscopy together with quantum chemical calculations to determine the character of electronic transitions in a broad series of electron-rich platinum complexes of the type [(N^N)PtR$_2$] with R = alkyl, alkynyl, phenyl or mesityl (2,4,6-trimethylphenyl). The diimine ligands (N^N) range from the very good accepting aliphatic diimine ligands R′-DAB (*N*,*N*′-disubstituted diazabutadienes) to relatively electron-rich ones such as 1,10-phenanthroline (phen) and derivatives. The aim was to ascertain the extent to which the co-ligands contribute to the frontier orbitals and hence to the excited state, and, secondly, if emission spectroscopy can give a clue as to the excited state character.

Results and Discussion

The dimethylplatinum complexes were chosen as a means to render the platinum centre electron-rich without the possibility of π-electron contribution. Phenyl, mesityl and the alkynyl co-ligands C≡CR (R = *t*Bu or Ph) can potentially interact with the diimine ligands via their π systems. A special reason to use mesityl co-ligands comes from the fact that they provide steric shielding of the complexes axial positions and therefore prevent stacking or dimer formation, which simplifies assignment. Earlier, we reported that they emit light much more effectively than their diphenyl or dimethyl analogues,[21] which was recently used by Kane−Maguire and Wright to study energy- and electron-transfer processes in such systems.[2] The diimine ligands which were chosen are depicted in Scheme 2. Complexes of phenanthroline ligands are known to exhibit more long-lived emissions compared to their bpy analogues and the diazabutadienes (DAB), due to their rigidity which leads to decreased vibrational overlap between ground and excited states and concurrent slow nonradiative decay.[32] Introduction of the methyl substituent to phenanthroline increases the electron density in these ligands (4,7-dmphen and tmphen). Substitution on the 2,9-positions gives additionally rise to steric interactions (repulsions) with the bulky mesityl groups and yields the highly distorted complex [(2,9-dmphen)PtMes$_2$]. Its molecular structure, as determined from X-ray crystallography, shows marked deviation from the square-planar environment of the metal atom.[33] The use of the tap ligand [34−38] was motivated by the aim to decrease the electron density by the introduction of two further nitrogen atoms, but at the same time maintain the above described rigidity of a phenanthroline type of ligand. The dppz ligand is known to form emissive transition metal complexes which display different types of lowest excited states depending on the metal fragment (^{3}MLCT or $^3\pi-\pi^*$).[39] Furthermore such complexes can intercalate between DNA base pairs and might be used as DNA sensors.[40−42] The crystal structure of [(dppz)PtMes$_2$] was recently reported and shows π-stacking of pairs of two molecules in the unit cell.[43]

 © 2003 Wiley-VCH Verlag GmbH & Co. KGaA, Weinheim

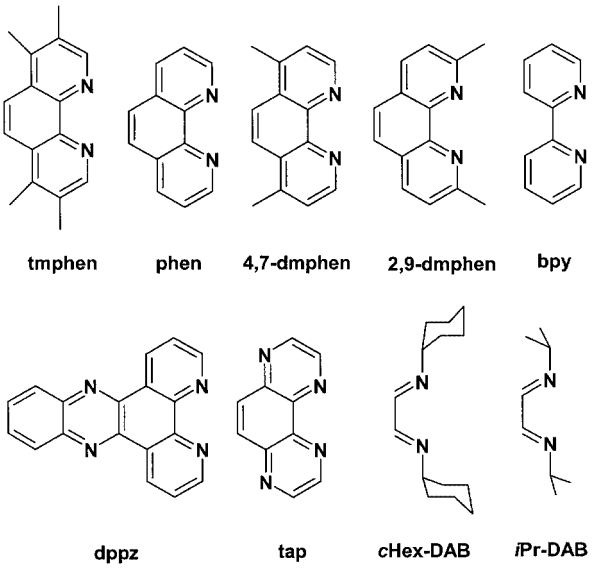

Scheme 2. Representation and nomenclature of the diimine ligands used: tmphen = 3,4,7,8-tetramethyl-1,10-phenanthroline, phen = 1,10-phenanthroline, 4,7-dmphen = 4,7-dimethyl-1,10-phenanthroline, 2,9-dmphen = 2,9-dimethyl-1,10-phenanthroline, bpy = 2,2′-bipyridine, dppz = dipyrido[3,2-*a*:2′,3′-*c*]phenazine, tap = 1,4,7,10-tetrazazaphenanthrene (pyrazino[2,3-*f*]quinoxaline), *c*Hex-DAB = *N*,*N*′-dicyclohexyl-1,4-diazabutadiene (*N*,*N*′-dicyclohexyl-1,2-ethanediimine), *i*Pr-DAB = *N*,*N*′-diisopropyl-1,4-diazabutadiene (*N*,*N*′-diisopropyl-1,2-ethanediimine)

Crystal Structure Determination of [(tmphen)PtMes$_2$], [(tap)PtPh$_2$], and [(bpy)PtMe$_2$]

The molecular structure and intermolecular phenomena such as Pt−Pt interaction or π−π stacking of the aromatic diimine ligands have a strong impact on the emission properties of molecules of the type which is presently under study.[10,12,44] Therefore, the results are discussed of a single-crystal X-ray diffraction study on [(tmphen)PtMes$_2$] (Figure 1), [(tap)PtPh$_2$] (Figure 2) and [(bpy)PtMe$_2$] (Figure 3),

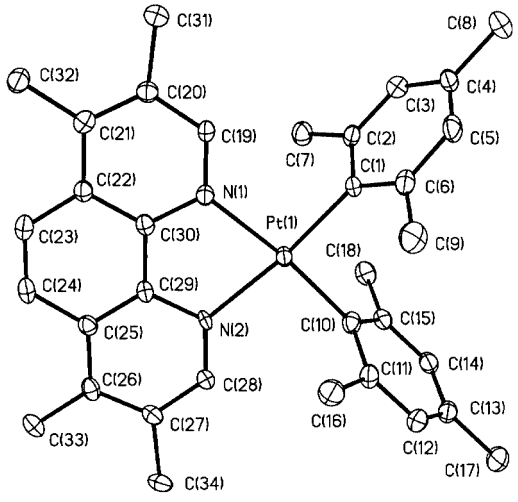

Figure 1. View of [(tmphen)PtMes$_2$] from crystal structure determination (with numbering); the atoms are represented by 50% thermal ellipsoids

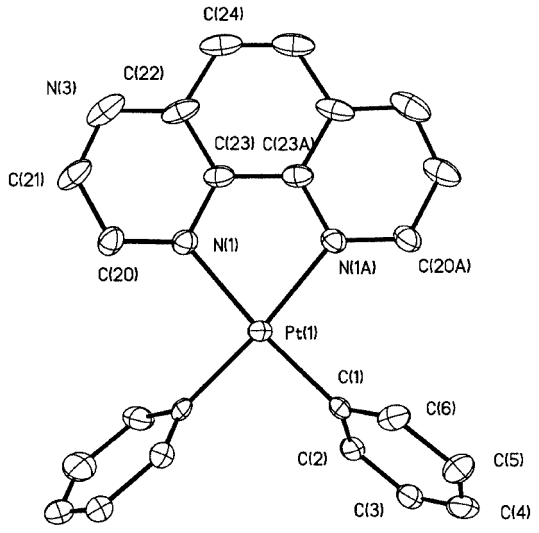

Figure 2. View of [(tap)PtPh$_2$] from crystal structure determination (with numbering); the atoms are represented by 50% thermal ellipsoids

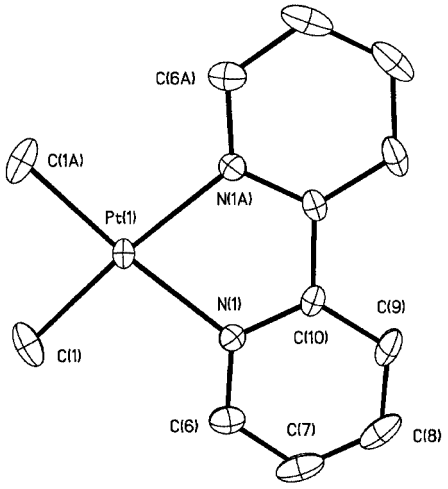

Figure 3. View of [(bpy)PtMe$_2$] from crystal structure determination (with numbering); the atoms are represented by 50% thermal ellipsoids

of which the first two are previously unpublished structures. The structures were solved and refined with the results shown in the Supporting Information (see also the footnote on the first page of this article). Table 1 lists some selected structural parameters of these complexes.

The molecular structures of all three complexes are quite similar. That of the tmphen complex fits into the series of other dimesitylplatinum complexes so far characterized by X-ray diffraction such as [(bpy)PtMes$_2$],[45] or [(phen)PtMes$_2$],[46] and [(dppz)PtMes$_2$].[43] The crystal and molecular structure of [(bpy)PtMe$_2$] (Figure 6) has been reported before,[47] our results being essentially the same but more precise. The chelate "bite" angle in all these compounds lies between 78 and 79° and the Pt−N distances and other structural parameters within the chelate ligands do not vary significantly. The aryl substituents in the mesityl and phenyl complexes show a tilt angle towards the co-

 © 2003 Wiley-VCH Verlag GmbH & Co. KGaA, Weinheim

Table 1. Selected structural parameters for [(tmphen)$PtMes_2$], [(tap)$PtPh_2$] and [(bpy)$PtMe_2$]

[(tmphen)$PtMes_2$]		[(tap)$PtPh_2$]		[(bpy)$PtMe_2$]	
	Distance [Å]		Distance [Å]		Distance [Å]
Pt1−C1	2.031(7)	Pt−C1	1.995(9)	Pt1−C1	2.040(6)
Pt1−C10	2.024(7)		−	−	
Pt1−N1	2.103(5)	Pt−N1	2.113(7)	Pt1−N1	2.094(4)
Pt1−N2	2.111(6)		−	−	
C29−C30	1.427(9)	C23−C23A	1.43(2)	C10−C10A	1.477(8)
C23−C24	1.340(11)	C24−C24A	1.33(3)		−
$C_{Mes}-C_{Mes}$[a]	1.394(10), 1.402(11)	$C_{Ph}-C_{Ph}$[a]	1.39(2)		−
Pt1−C_{ortho} [b]	3.268(10), 3.282(10)				
	Angle [°]		Angle [°]		Angle [°]
C10−Pt1−C1	90.7(3)	C1−Pt−C1A	91.0(6)	C1−Pt−C1A	87.8(5)
N1−Pt1−N2	78.6(2)	N1−Pt−N1A	79.4(4)	N1−Pt−N1A	78.2(2)
C10−Pt1−N1	173.6(2)	C1−Pt−N1	174.2(3)	C1−Pt−N1	175.1(2)
C1−Pt1−N1	95.1(2)	C1−Pt−N1A	94.8(4)	C1−Pt−N1A	97.0(3)
	Dihedral angle [°]		Dihedral angle [°]		Dihedral angle [°]
Mes/co-plane[c]	70.2, 68.7	Ph/co-plane	68.7		−
Mes/Mes	81.7	Ph/Ph	86.3		−
Py/Py[d]	2.0	Pz/Pz[d]	1.2	Py/Py[d]	2.0

[a] Averaged values for $C_{aryl}-C_{aryl}$ distances. [b] Closest contacts to *ortho*-C atoms of the two mesityl substituents. [c] The coordination plane as defined by C1, C10, N1, N2 and Pt1. [d] Defined by the six-membered rings which form (approximately) half the ligand.

ordination plane of about 68−70°. Similar tilt angles were also found for [(dpp)$PtPh_2$] [dpp = 2,3-bis(2-pyridyl)pyrazine].[13] This means, that the aryl tilt angle is not governed by the steric strain from the methyl substituent. Furthermore in view of the above-mentioned similar structures which exhibit different symmetry, space groups and packing of the molecules it is unlikely that the tilt angle has its origin in crystal packing effects, but is indeed the optimal molecular geometry. Recent calculations showed, that this tilt angle is crucial for the calculated energies and characters of the MOs and hence the electronic transitions in such complexes[19,33,48] The only difference between the mesityl and the phenyl complexes is the shorter Pt−N bond of the phenyl derivative. A similar observation was made for the complex [(2,9-dmphen)$PtPh_2$] in comparison to the mesityl analogue.[33]

Intermolecular interactions are of importance for optical spectroscopy. Therefore we examined the crystal structures of the complexes in that respect. In square-planar platinum(II) complexes, two intermolecular interactions are important, namely π interactions of the aromatic α-diimine ligands and Pt···Pt interactions. The tmphen complex forms dimers in the unit cell, which are π-stacked in a non-graphite-like fashion, with an interplanar distance of 3.52(1) Å (Figure 4). Perhaps due to their methyl substituents the ligands are not ordered back-to-back but offset. For the [(dppz)$PtMes_2$] complex a graphite-like stacking with the formation of dimers was observed with a interplanar distance of 3.427(2) Å,[43] not very different from that of the chloro derivative [(dppz)$PtCl_2$] of about 3.45 Å[49] and

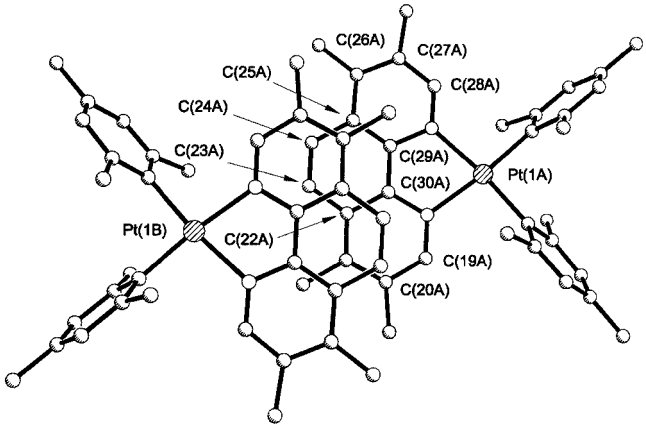

Figure 4. View of two molecules packing in [(tmphen)$PtMes_2$]

graphite (3.354 Å). In [(tap)$PtPh_2$] again a different π-stacking is observed (Figure 5). The ligand planes intersect much more and there is no diagonal offset like for the tmphen complex. Also in contrast to the tmphen complex the molecules form indefinite stacks along the crystallographic *c* axis, with the interplanar distance being only 3.056(2) Å. Although the structure of [(bpy)$PtMe_2$] was published,[47] the crystal packing was not discussed. In fact, the complex exhibits quite a complex stacking behaviour (Figure 6). The distance between the planes of the ligand is 3.45(1) Å. Interestingly, this behaviour does not resemble that of the dichloro complex [(bpy)$PtCl_2$] which occurs either in the red form with strong Pt···Pt interaction (*d* = 3.45 Å) but no π

 © 2003 Wiley-VCH Verlag GmbH & Co. KGaA, Weinheim

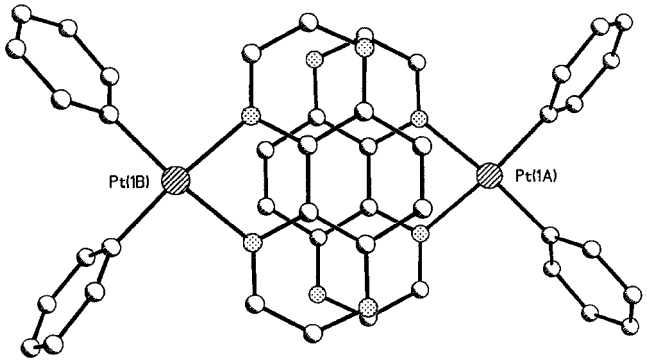

Figure 5. View of two molecules packing in [(tap)$PtPh_2$]

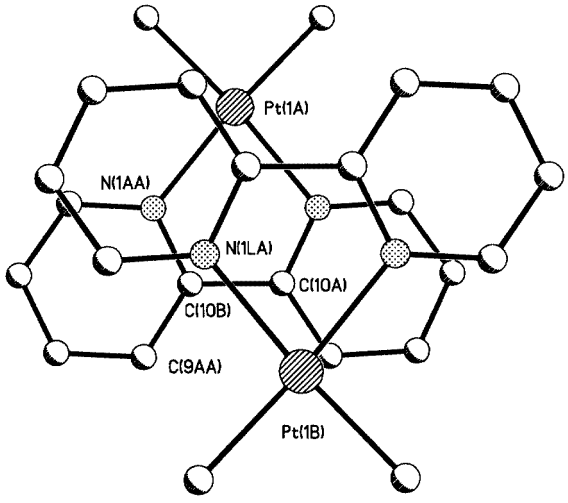

Figure 6. View of two molecules packing in [(bpy)$PtMe_2$]

interaction [50] or the yellow form with longer Pt···Pt distances of 4.5 Å and stacking of each one pyridyl unit.[51] These two polymorph types are also found in a series of (diimine)platinum complexes with Cl, CN, NCS, NCO as substituents.[44]

The Pt···Pt distances vary from complex to complex. In the tmphen complex, it is 9.331(3) Å within the dimer, and the shortest Pt···Pt distance with 6.465(3) Å is found between adjacent stacks. In case of the dppz complex the shortest Pt···Pt distance is 7.784(4) Å. The tap complex, in which the molecules are not diagonally offset like in the tmphen derivative, the Pt···Pt distance within the stacks is slightly shorter at 7.673(2) Å. The shortest Pt···Pt distance is between adjacent stacks [6.465(3) Å]. The Pt···Pt distance in the bpy complex is 5.496(3) Å, longer than the distances in either form of the dichloro complex.

From these data we can conclude that no strong Pt···Pt interactions are present in the molecules in their crystalline form, and the only possible intermolecular interaction is that of π stacking. This type of interaction can cause excimer formation. This will be further discussed in the emission spectroscopy section (see below). The DFT-calculated bond lengths and angles fit the experimentally obtained ones for [(bpy)$PtMes_2$],[45] and [(bpy)$PtMe_2$] well.

Absorption Spectroscopy and Calculations

The complexes [(α-diimine)PtR_2] (R = Me, Ph, or Mes) exhibit broad and partly structured long-wavelength absorption bands (Figure 7).[2,19−21,52] These bands show negative solvatochromism, indicating their charge transfer character (Table 2). The absorption bands of the complexes can be divided into two sets, one in the visible and one in the near UV, which are denoted by CT(1) and CT(2), respectively. For the corresponding R′-DAB (DAB = 1,4-diaza-butadiene) complexes it was shown that the various absorptions within one set are due to the presence of several electronic transition rather than vibronic structuring.[19] CT(1) always consists of several components which are all of moderate to weak intensity. The second band system [CT(2)] is always stronger than the first one and less structured. The energies of the absorption maxima increase with the diimine π*-level energy, and decrease with increasing electron-donating abilities of the co-ligands.

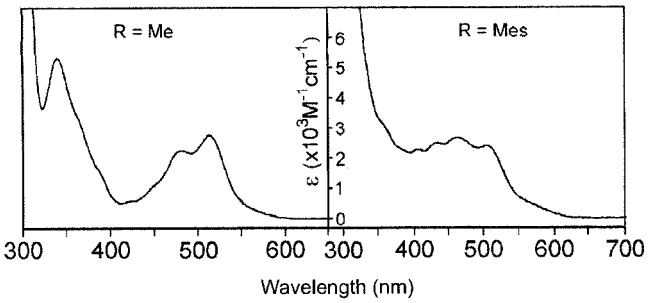

Figure 7. Absorption spectra of [(bpy)$PtMe_2$] (left) and [(bpy)$PtMes_2$] (right) in toluene solution

In order to assign the absorption bands, and in particular to determine the co-ligand contributions to the highest occupied MOs (HOMO), DFT calculations were performed on two complexes, namely [(bpy)$PtMe_2$] and [(bpy)$PtMes_2$]. As expected, the lowest unoccupied MOs (LUMO) are calculated to be almost exclusively located on bpy, even more so than in the case of the corresponding *i*Pr-DAB complexes (Tables 3 and 4).[19] This is due to the lower electron density on the coordinating nitrogen atoms in the case of bpy which limits delocalization of the frontier orbitals. The methyl contribution to the highest occupied MOs is quite limited (Table 3), making them almost purely metal-centred in character.

For the mesityl derivative the calculations yield a markedly changed situation. The HOMO 47a has mixed Pt-5d/mesityl-π orbital character and the following HOMOs are of almost pure π_{Mes} character and only one more or less pure d_{Pt} orbital has remained. Hence, like in the case of the *i*Pr-DAB complexes, also the highest occupied MOs of arylplatinum(II) complexes of aromatic α-diimines have predominant co-ligand character. This is at variance with the metal character which is generally assumed in literature.

The TD-DFT-calculated lowest transitions of [(bpy)$PtMe_2$] can be described as having mainly d_{Pt}-π*(bpy) (MLCT) character in agreement with the "classical" assign-

 © 2003 Wiley-VCH Verlag GmbH & Co. KGaA, Weinheim

Table 2. Long-wavelength absorption maxima of platinum complexes

Compound[a]	CT(2)			CT(1)	
	λ_5 (ε)	λ_4 (ε)	λ_3 (ε)	λ_2 (ε)	λ_1 (ε)
[(*c*Hex-DAB)$PtMe_2$]	402 (3.4)	471sh (0.3)	498 (1.2)	535 (2.1)	577 (2.6)
[(*c*Hex-DAB)$PtMes_2$]	361 (3.6)	467 (3.4)	508 (3.5)	542 (3.6)	602sh (2.5)
[(bpy)$PtMe_2$]	340 (5.2)	423 (0.9)	454sh	482 (2.64)	513 (2.81)
[(bpy)$PtMes_2$]	352 (3.1)	406 (2.31)	432 (2.48)	459 (2.69)	504 (2.46)
[(bpy)$PtPh_2$]	341 (3.79)	388 (1.90)	416 (1.46)	454 (2.43)	480 (3.12)
[(tmphen)$PtMe_2$]	324 (4.98)	–	360sh (2.0)	450 (3.77)	477 (3.68)
[(tmphen)$PtMes_2$]	331 (4.12)	345 (3.38)	398 (3.71)	444 (3.38)	469 (3.06)
[(tmphen)$PtPh_2$]	336 (2.59)	346 (2.36)	384 (2.1)	428sh (2.8)	448 (2.98)
[(phen)$PtMe_2$]	330 (5.04)	364 (2.41)	450 (2.96)	470 (3.15)	509 (3.62)
[(phen)$PtMes_2$]	336sh (3.0)	–	420 (3.62)	447 (3.04)	500 (2.80)
[(phen)$PtPh_2$]	395 (2.26)	–	–	459sh (3.01)	477 (3.54)
[(dppz)$PtMe_2$]	362 (13.1)[b]	377 (12.3)[b]	450 (2.96)	480 (3.05)	521 (3.42)
[(dppz)$PtMes_2$]	362 (12.9)[b]	378 (12.3)[b]	436 (3.84)	471sh (3.12)	513 (2.75)
[(dppz)$PtPh_2$]	363 (12.1)[b]	379 (12.3)[b]	–	463 (2.79)	483 (2.83)
[(TAP)$PtMe_2$]	385 (2.34)	–	480 (2.43)	508sh (2.3)	554 (2.45)
[(TAP)$PtMes_2$]	375sh (3.4)	408 (3.02)	470 (3.31)	498 (3.42)	567 (2.83)
[(TAP)$PtPh_2$]	–	432 (2.38)	454sh (2.2)	503sh (2.1)	533 (2.51)
[(2,9-dmphen)$PtMes_2$]	274 (28)[b]	293 (16.7)[b]		418 (2.45)	497 (2.13)
[(2,9-dmphen)$PtPh_2$]	273 (29)[b]		384 (3.08)	438 (2.56)	461 (2.59)
[(4,7-dmphen)$PtMes_2$]	268 (26)[b]	338 sh	406 (2.96)	448 (2.69)	481 (2.50)

[a] Absorption maxima in wavelength [nm] from measurements in toluene solution. The molar extinction coefficients ε are given in parentheses [1000 $M^{-1}cm^{-1}$]. [b] Intraligand transitions.

Table 3. ADF/BP calculated one-electron energies and percentage composition of selected highest occupied and lowest unoccupied molecular orbitals of [(bpy)$PtMe_2$] expressed in terms of composing fragments

MO	*E* [eV]	Prevailing character	Pt	Me	bpy
Unoccupied					
$7a_2$	−2.18	π* bpy	3 (d_{xy})	–	97
$10b_1$	−2.45	π* bpy	3 (d_{xz})	–	96 (π*)
$9b_1$	−3.14	π* bpy	9 (d_{xz})	–	90 (π*)
Occupied					
$21a_1$	−4.53	d_{Pt}	24 (s), 54 ($d_{x^2-y^2}$), 14 (d_{z^2})	8	–
$6a_2$	−4.60	d_{Pt}	85 (d_{xy})	8	6
$8b_1$	−4.98	d_{Pt}	76 (d_{xz})	6	17
$20a_1$	−5.02	d_{Pt}	15 ($d_{x^2-y^2}$), 63 (d_{z^2})	18	3
$17b_2$	−6.04	sp^3 (Me)	18 (d_{yz}), 1 (p_y)	46	31
19a1	−6.15	sp^3 (Me)	5 (s), 3 (p_z), 15 ($d_{x^2-y^2}$)	59	18
$5a_2$	−6.66	π bpy	–	–	99

ment. The calculated energies agree only moderately with the experimentally found ones (Table 5). One reason is the strong solvatochromism of the compounds, as displayed by the shift of the experimental energies going from toluene to pentane as solvent. However, they agree at least qualitatively, showing a number of low energy transitions of weak to moderate intensity which can be found in the range of 420−520 nm in the spectra, and a stronger transition which

Table 4. ADF/BP-calculated one-electron energies and percentage composition of selected highest occupied and lowest unoccupied molecular orbitals of [(bpy)$PtMes_2$] expressed in terms of composing fragments

MO	*E* [eV]	Prevailing character	Pt	Mes	bpy
Unoccupied					
48b	−0.65	Mes + Pt	6 (p_y), 16 (d_{yz})	64	13
49a	−1.33	π* bpy	–	1	98
48a	−2.50	π* bpy	2 (d_{xy})	–	98
47b	−2.75	π* bpy	2 (d_{xz})	–	97 (π*)
46b	−3.51	π* bpy	6 (d_{xz})	–	93 (π*)
Occupied					
47a	−4.62	Mes + Pt	3 (s), 2 (d_{xy}), 19 ($d_{x^2-y^2}$), 9 (d_{z^2})	67	–
46a	−5.03	d_{Pt}	19 (s), 37 ($d_{x^2-y^2}$), 28 (d_{z^2})	15	–
45b	−5.14	π (Mes)	10 (d_{xz})	88	2
44b	−5.26	π (Mes)	2 (d_{xz})	98	–
45a	−5.35	Mes	6 (d_{xy})	93	–
44a	−5.45	d_{Pt}	79 (d_{xy}), 3 (d_{z^2})	11	6
43b	−5.74	d_{Pt}	70 (d_{xz})	19	11
43a	−6.53	Mes	2 (s), 2 (p_z), 3 ($d_{x^2-y^2}$), 8 (d_{z^2})	68	16
42a	−6.81	d_{Pt} + Mes	1 (s); (p_z), 21 ($d_{x^2-y^2}$), 26 (d_{z^2})	52	–
37a	−6.98	π bpy	–	–	99

 © 2003 Wiley-VCH Verlag GmbH & Co. KGaA, Weinheim

Table 5. Selected calculated lowest TD-DFT singlet excitation energies [eV] for [(bpy)$PtMe_2$] compared to experimental absorption data

State	Main character [%]	ADF/BP		Experiment		
		Transiton energy [eV]	Osc. strength	Transiton energy [eV][a]	Transition energy [eV][b]	Extinction coeff. [M^{-1} cm^{-1}][b]
$^1A_1$	75 ($8b_1 \rightarrow 9b_1$), 16 ($6a_2 \rightarrow 7a_2$),	2.17	0.017	2.22	2.42	2810
$^1B_2$	97 ($6a_2 \rightarrow 10b_1$)	2.42	0.010	2.42	2.57	2640
$^1B_2$	95 ($8b_1 \rightarrow 7a_2$)	2.96	0.036	3.10	3.26	2410(sh)
$^1A_1$	40 ($8b_1 \rightarrow 10b_1$), 30 ($6a_2 \rightarrow 7a_2$), 20 ($8b_1 \rightarrow 9b_1$)	3.15	0.152	3.53	3.65	5200
$^1A_1$	92 ($6a_2 \rightarrow 8a_2$);	3.65	0.041	4.43	4.13	5800(sh)

[a] Measured in pentane. [b] In toluene.

Table 6. Selected calculated lowest TD-DFT singlet excitation energies [eV] for [(bpy)$PtMes_2$] compared to experimental absorption data

State	Main character [%]	ADF/BP		Experiment[a]	
		Transition energy [eV]	Osc. strength	Transition energy [eV]	Extinction coeff. [M^{-1} cm^{-1}]
^1A	48 ($44b \rightarrow 47b$), 36 ($43b \rightarrow 46b$)	2.50	0.011	2.46	2460
^1A	44 ($44b \rightarrow 47b$), 30 ($43b \rightarrow 46b$)	2.56	0.031	2.70	2690
^1B	67 ($44a \rightarrow 47b$), 28 ($44b \rightarrow 48a$)	2.75	0.006	2.87	2480
^1A	46 ($43b \rightarrow 47b$), 32 ($44a \rightarrow 48a$), 10 ($43b \rightarrow 46b$)	3.39	0.172	3.52	3100

[a] Measured in toluene.

can be recognized in the dominant band at about 340 nm in the spectra.

As a consequence of the mixed-metal/co-ligand character of the highest occupied MOs of [(bpy)$PtMes_2$], its electronic transitions have mixed L′LCT/MLCT character, where both contribute in roughly equal measures (Table 6). Interestingly, these are directed towards different π* orbitals of bpy. Again, the transition energies and oscillator strengths show only qualitative agreement with the observed values as above.

Emission Spectroscopy

Most of the assignments of excited states and electronic transitions in (diimine)platinum complexes are based on emission studies,[1,3,6−8,12,18,27] since the collected data, such as emission lifetimes, quantum yields, apparent Stokes shifts etc., allow easy discrimination between ligand-field (LF), intra-ligand (π-π*) and charge-transfer excited states. Here we use emission spectra both at room temperature and in low-temperature solvent glasses to probe for any differences in excited-state properties between the methyl complexes on one side and the aryl derivatives on the other. The room-temperature emission data of the complexes are reported in Table 7. None of the DAB or tap complexes proved to be emissive in fluid solution at room temperature. Furthermore, only two of the methyl complexes (tmphen and dppz) showed luminescence under these conditions. For all other complexes emission was observed as broad unstructured bands, albeit with low quantum yields between 10^{-5} and 10^{-3}. The excitation spectra (Figure 8) show that the observed emission bands are indeed due to the complexes. Comparing the three different types (Me, Mes, and Ph) of complexes it can be seen that the methyl complexes are the poorest emitters, followed by the phenyl complexes, which have quantum yields that are a by factor of 3−5 higher. The mesityl complexes show the highest luminescence efficiency with quantum yields of a factor of 5−10 higher than those of the corresponding methyl complexes. Considering the low quantum yield, the excited-state decay is mainly governed by nonradiative processes, which are apparently more efficient for the methyl complexes than for the aryl ones. Transient absorption and time-resolved emission measurements under these conditions showed that the lifetimes were shorter than our instrument resolution (5 ns). Another interesting observation is that while for both the methyl and mesityl complexes the apparent Stokes shifts are mostly above 6000 cm^{-1}, those of the phenyl complexes are much lower at around 3000 cm^{-1}. Apparently, the phenyl complexes are much less distorted in their excited states than the other ones. Decrease in excited state distortion should lead to slower nonradiative decay by decrease of vibrational overlap. However no increase in quantum yield, which would be the consequence, was observed for the phenyl derivatives.

Apart from these general observations, some interesting peculiarities can be observed. The sterically overcrowded complex [(2,9-dmphen)$PtMes_2$] emits only very weakly at rather high energy with a resulting Stokes shift of 3000

 © 2003 Wiley-VCH Verlag GmbH & Co. KGaA, Weinheim

Table 7. Luminescence quantum yields at 298 K

Compound[a]	$\lambda_{abs,max}$	λ_{em}	Stokes shift [cm^{-1}]	Φ[b]
[(tmphen)$PtMe_2$]	464	714	7550	0.00071
[(dppz)$PtMe_2$]	505	760	6650	0.00060
[(tmphen)$PtMes_2$]	457sh, 436	620	5750	0.00984
[(dppz)$PtMes_2$]	492sh, 424	765	7250	0.00210
[(4,7-dmphen)$PtMes_2$]	466sh, 438	657	6240	0.00542
[(phen)$PtMes_2$]	482	688	6220	0.00258
[(bpy)$PtMes_2$]	481	687	6230	0.00227
[(2,9-dmphen)$PtMes_2$]	472	550	3005	0.00073
[(dppz)$PtPh_2$][c]	483	605	4175	0.02710
[(dppz)$PtPh_2$]	464	517	2210	0.00255
[(dppz)$PtPh_2$]	464	760	8350	0.00171
[(dppz)$PtPh_2$][d]	464	550	3370	—[e]
[(tmphen)$PtPh_2$]	442	518	3320	0.00239
[(phen)$PtPh_2$]	456	524	2850	0.00123
[(bpy)$PtPh_2$]	453	522	2920	0.00107
[(2,9-dmphen)$PtPh_2$]	445	516	3090	0.00024

[a] From measurements in THF solution. $\lambda_{(abs,max)}$ = long-wavelength absorption maximum [nm]. $\lambda_{(ex)}$ = excitation wavelength. [b] Φ = emission quantum yield relative to $[(bpy)_3Ru]^{2+}$ in MeCN solution ($\Phi = 0.062$).[61] [c] In toluene solution. [d] Dilute. [e] Not determined.

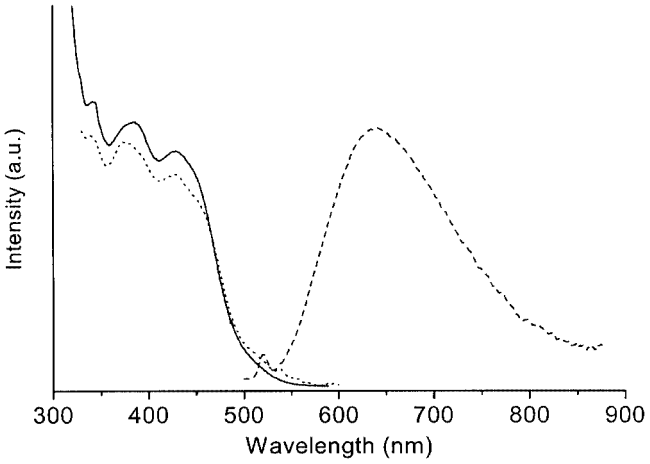

Figure 8. Absorption (——), emission (----) and excitation spectrum (····) of [(tmphen)$PtMes_2$] in CH_2Cl_2 solution

cm^{-1}. Methyl substitution of phenanthroline ligand increases the emission energies and the quantum yields of the mesityl complexes as demonstrated by the series phen < 4,7-dmphen < tmphen, which can be attributed to the energy gap law. The compound [(dppz)$PtPh_2$] exhibits a complex behaviour. In THF solution, at a concentration of 10^{-5} mol/L, two emission maxima were observed at 517 and 760 nm, respectively. After dilution to approx. 10^{-6} mol/L, the 760-nm band disappeared and a weak band was observed at 550 nm with the 517-nm band more or less unchanged. The band at 550 nm seems to be similar to those of the other complexes and we therefore assign the very-long-wavelength emission at 760 nm to excimer emission. The high-energy component at 517 nm might originate from a ligand-centered ($^3\pi$-π^*) state. In toluene solution also an emission at rather low energy is observed with a relatively high quantum yield. No change in emission maximum was observed on dilution. Most probably the excited molecule interacts with toluene molecules. This is in accordance with the observation that dppz complexes readily form dimeric π stacks,[43] and also strongly interact with aromatic solvent molecules such as toluene.[43] Possibly the deviating behaviour of this complex can be traced to its different excited state character (see below).

At low temperature (90 K) in glassy frozen 2-MeTHF, all the examined mesityl- and methylplatinum complexes, upon irradiation into their lowest absorption bands, show broad emissions with lifetimes of mostly some μs (Table 8). They were only very slightly structured. As an example the time-resolved spectra of [(tmphen)$PtPh_2$] are depicted in Figure 9. The Stokes shifts were all in the same range (4000−6000 cm^{-1}). The DAB complexes have the shortest emission lifetimes. This and the highest Stokes shift in the series reflect the high flexibility of the R′-DAB ligand, which allows rapid non-radiative decay. Similar differences have been recently observed for tetramethylplatinum(IV) complexes, where the tmphen derivative exhibited an enormously increased lifetime (9.3 μs) compared to the *c*Hex-DAB analogue (44 ns).[32] The lowest-energy emissions of all other complexes have lifetimes which are all in the same range. Solid-state data for the mesityl complexes of bpy (τ = 0.9 μs), phen (1.8 μs) and tmphen (2.1 μs) have been reported in literature, which compare well with the present numbers.[2] Interestingly, no differences are observed between the methyl complexes on one hand, and the aryl ones on the other. This means that the difference in excited-state character is not reflected in emission lifetimes. For [(dppz)$PtPh_2$] the lowest excited state is clearly of intra-ligand (phenazine) character. This might account for the peculiar behaviour at ambient temperature. In some cases on higher energy excitation longer-lived emission bands are observed at higher energies. These are often quite structured and we assign them to intraligand (IL) emissions. The fact that in some cases the lifetime is not much longer than that of the lowest-energy emission can be explained by the observation that even if the lowest excited state has IL character, its lifetime is of the same order of magnitude. For example, the emission of the yellow form of [(bpy)$PtCl_2$] in the solid state which is assigned to an $^3\pi$-π^* excited state has also a comparably low lifetime of only 3.5 μs compared to the phenanthroline analogue with 13.3 μs (both measured at 10 K).[8] Emission from higher excited states has been observed for other complexes at low temperatures, e.g. in (diimine)tungsten complexes.[53] Apparently, in all these cases radiative decay from a higher excited state is in competition with internal conversion or intersystem crossing to the lowest excited state.

The fact that the low-temperature lifetimes are not affected by the nature of the co-ligand, suggests that the differences in room-temperature emission quantum yield are due

 © 2003 Wiley-VCH Verlag GmbH & Co. KGaA, Weinheim

Table 8. Low-temperature luminescence data

Compound[a]	Absorption: λ_{abs} [nm]	Excitation: λ_{exc} [nm]	Emission: λ_{em} [nm]	Stokes shift [cm^{-1}]	τ
[(N^N)PtMe$_2$]					
(*c*Hex-DAB)	370, 382, 474sh, 506, *542*	532	761	5310	8.3 ns
(*c*Hex-DAB)	370, 382, 474sh, 506, *542*	355	492, 525, *577*, 624sh	1120	1.7 μs
(bpy)	345sh, 427sh, 452, *484*	532	631	4810	3.1 μs
(bpy)	345sh, 427sh, 452, *484*	440	*523*, 559, 600sh	1540	8.0 μs
(tmphen)	352sh, 430, *460*	460	620	5610	2.5 μs
(dppz)	341, 359, 377, 462, *496*	450	640	4540	2.7 μs
[(N^N)PtMes$_2$]					
(*p*Tol-DAB)	485, 544, *588*	532, 355	815	4740	11 ns
(*c*Hex-DAB)	391, 407, 476 *506*	532	658sh, *734*	6140	68 ns
(*c*Hex-DAB)	391, 407, 476, *506*	532, 355	*584*, 607	2640	1.3 μs
(*i*Pr-DAB)	391, 407, 476, *506*	532	*737*, 796 sh	6190	51 ns
(tap)	429, 459, *522*, 591sh	532	684	4540	270 ns
(dppz)	414, 441, *475*, 532	440	*540*, 584, 635	2530	699 μs
(dppz)	414, 441, *475*, 532	532	582sh, *618*	4870	1.3 μs
(bpy)	366, 388, 411, 440, *472*	532	*584*, 607	4060	1.3 μs
(phen)	367, 388, 412, 441, *470*	532	*583*, 606	4120	1.4 μs
(tmphen)	391, 374, 388, 424, *449*	532, 440	*548*, 565	4023	2.7 μs
[(N^N)PtPh$_2$]					
(tmphen)	334sh, 408, *432*	440	501, *533*, 564sh	4390	7.9 μs
(dppz)	359, 374sh, 431, *456*	455	*540*, 584, 635	3410	782 μs

[a] From measurements at 90 K in glassy frozen 2-MeTHF solutions. The most intense component of the absorption or emission spectra is in italics and serves to calculate the Stokes shift. τ is the excited state lifetime as calculated from time-resolved measurements.

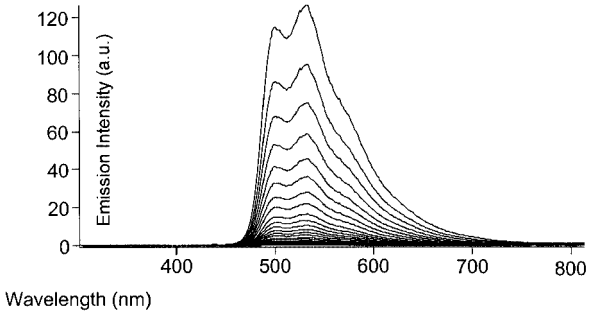

Figure 9. Time-resolved emission spectra of [(tmphen)PtPh$_2$] in MTHF glass at 110 K; λ_{exc} = 440 nm, *P* = 6.9 mJ, time delay between the spectra: 2000 ns

to thermally activated processes rather than traceable to the difference in excited-state character. It has been suggested that the rotation around the *o*-Me group in (α-diimine)mesitylplatinum(II) complexes could be such a thermally excited decay pathway. In the methyl and phenyl complexes clearly additional pathways must be present.

No differences between the methyl and aryl complex lifetimes at low temperature were found to indicate a difference in excited-state character. For example, the MLCT state of [(bpy)PtMe$_2$] has a lifetime of 3.1 μs at low temperatures, while that of the corresponding mesityl complex is slightly shorter at 1.3 μs. However, closer inspection of literature data reveals that in square-planar (α-diimine)platinum(II) complexes, the excited-state lifetime depends only weakly on the excited-state character. The excited states of [(3,3′-(CH$_3$OCO)$_2$bpy)PtCl$_2$] (τ = 1.1 μs),[8] and [(dmbpy)Pt(pz)$_2$] (dmbpy = 4,4′-dimethyl-2,2′-bipyridine; pz = dimethyl- or tetramethylpyrazole; τ = 1.8 or 0.4 μs, respectively)[6] were assumed to have MLCT character. However, the observed twist angle of 64(3)° of the pyrazolate groups relative to the binding plane in the above-mentioned complexes,[54] suggests that the π system of these pyrazolates may contribute significantly to the highest MOs. Alkynylplatinum(II) complexes have similar lifetimes, e.g. [(tmbpy)Pt(C≡C*p*Tol)$_2$] (τ = 1.3 μs, tmbpy = 4,4′,5,5′-tetramethyl-2,2′-bipyridine).[1] There is a number of indications that the alkynyl moiety is significantly involved in the excited state. Thus, DFT calculations on [(*i*Pr-DAB)Pt(C≡CH)$_2$] show over 60% participation of the alkynyl groups in the highest MOs. In addition, the excited state IR spectra of [(R′-bpy)Pt(C≡CR)$_2$] (R = Aryl, R′-bpy = alkyl-substituted bpy) shows a clear upward shift of the ν(C≡C) frequency of about 25−35 cm^{-1} compared to the ground states.[1] And finally, it was remarked that the photophysical behaviour of [(4,4′-*t*Bubpy)Pt(C≡CNMe)$_2$] "does not fit with the model of a lowest ^{3}MLCT excited state".[1] Other complexes which have excited states that are clearly different from purely MLCT, such as the (α-diimine)platinum(II) dithiolate complexes, which have ^{3}MML′LCT (^{3}L′LCT) lowest-excited

 © 2003 Wiley-VCH Verlag GmbH & Co. KGaA, Weinheim

states, also have comparable emission lifetimes.[5] Finally, the IL emission of the above-mentioned yellow form of [(bpy)$PtCl_2$] has again a similar emission lifetime, namely 3.5 μs.

The only difference between the MLCT emissions of the methyl complexes and the L′LCT/MLCT emissions of the aryl complexes is the partial structuring of the emission bands of the latter complexes. This is rather unusual for ^{3}MLCT emissions of (diimine)platinum complexes.[3,5,8,18] Such structuring was also observed for the before-mentioned complexes [(dmbpy)$Pt(pz)_2$],[6] or [(tmbpy)Pt-(C≡CTol)$_2$],[1] which most probably have similar mixed L′LCT/MLCT excited states.

Conclusions

The DFT calculations showed that the lowest excited states of the methyl-substituted (α-diimine)platinum(II) complexes have virtually pure MLCT character. In contrast those of the corresponding phenyl and mesityl complexes were revealed to have mixed L′LCT/MLCT character. This is supported by the molecular structures from single-crystal XRD which show an optimum tilt angle for the aryl groups for effective ligand(aryl)-to-ligand(diimine) interaction. From the emission data, there were two differences in excited-state behaviour between these two types of complexes. Firstly, the room-temperature quantum yields are up to 10 times larger for the mesityl complexes, compared to the methyl derivatives. Secondly, a slight structuring of the emission bands was visible for the aryl derivatives, which could not be found for the methyl derivatives. The low-temperature emission lifetimes, however, do not depend on the nature of the co-ligand. It must therefore be concluded that emission spectroscopy is not a very sensitive tool to determine the excited-state character in (α-diimine)platinum(II) complexes. Techniques such as time-resolved IR spectroscopy are more promising in that respect. Furthermore, we have found from the combination of single-crystal XRD and concentration-dependent emission behaviour that for these electron-rich (diimine)platinum(II) complexes with alkyl, aryl or alkynyl ligand intermolecular Pt···Pt interactions do not occur and intermolecular π-stacking does only play a very minor role in sharp contrast to corresponding complexes with halide or pseudohalide ligands.

Experimental Section

Preparations: All preparations and manipulations were carried out under argon or nitrogen. The synthesis of the complexes [(*i*Pr-DAB)PtR_2] (R = alkyl, alkynyl or aryl) was recently described.[19] Other dimethyl and dimesityl complexes were prepared from [$(Me_2Pt(\mu\text{-}SMe_2)_2PtMe_2]$,[55] or [$(dmso)_2PtMes_2$],[56] respectively, as recently described for the DAB complexes.[20] The diphenylplatinum complexes were prepared from [(COD)$PtPh_2$],[57] as reported for various diimine ligands.[58] The compounds were thoroughly recrystallised to ensure the absence of impurities. They gave correct elemental analyses and ^{1}H NMR spectroscopy proved their identity and purity (see Supporting Information).

General Procedures for Crystal Structure Analyses: Suitable crystals of the complexes were obtained by slow concentration of saturated toluene solutions. For all three compounds, the data collection was performed at T = 183(2) K with a Siemens P4 diffractometer using Mo-K_α radiation (λ = 0.71073 Å). The absorption correction was done by ψ-scans. The structures were solved using the SHELXTL-PLUS package,[59] and refinement was carried out with SHELXL-97 employing full-matrix least-squares methods on F^2.[60] All non-hydrogen atoms were treated anisotropically, and hydrogen atoms were included by using appropriate riding models. Additional details on crystal data and structure refinement of [(tmphen)$PtMes_2$], [(tap)$PtPh_2$] and [(bpy)$PtMe_2$] can be found in the Supporting Information. CCDC-204746 [(bpy)$PtMe_2$], -204747 [(tap)$PtPh_2$], and -204748 [(tmphen)$PtMes_2$] contain the supplementary crystallographic data for this paper. These data can be obtained free of charge at www.ccdc.cam.ac.uk/conts/retrieving.html [or from the Cambridge Crystallographic Data Centre, 12, Union Road, Cambridge CB2 1EZ, UK; Fax: (internat.) + 44-1223/336-033; E-mail: deposit@ccdc.cam.ac.uk].

Instrumentation: ^{1}H NMR spectra for analytical purposes were recorded with a Bruker AC 250 spectrometer. UV/Vis absorption spectra were recorded with Bruins Instruments Omega 10, Hewlett−Packard 8453 Diode Array, or Varian Cary 4E spectrometers. Steady-state emission spectra were recorded with Spex Fluorolog or Spex Fluorolog 3 emission spectrophotometers, equipped with Peltier-cooled Hamamatsu 928 and 636−10 photomultiplier detectors, respectively. The solutions were deaerated by Ar purging for at least 20 min prior to measurement. The quantum yields were determined by comparison to [$(bpy)_3Ru]^{2+}$ in acetonitrile solution (Φ = 0.062),[61] and were found to be generally lower by the factor of 100 or more compared to this standard. Time-resolved emission spectra of samples in 2-MeTHF glasses (90 K) were recorded in an Oxford Instruments cryostat, using Spectra Physics GCR3 Nd:YAG or Coherent Infinity XPO lasers as excitation sources and an OMA detection system described elsewhere.[62] The solutions were prepared under nitrogen and freeze-pump-thaw-degassed three times before measurements.

Theoretical Calculations: The ground-state electronic-structure calculations on complexes [(bpy)PtR_2] (R = Me, Mes) were performed on the base of density functional theory (DFT) methods by using the ADF2000.2,[63,64] and Gaussian 98[65] program packages. The lowest excited states of the closed-shell complexes were calculated by the time-dependent DFT (TD-DFT) method (both ADF and G98 programs). Within the ADF program, Slater-type orbital (STO) basis sets of triple-ζ quality with polarization functions were employed, except for the methyl groups on the Mes ligands, which were described by basis sets of double-ζ quality with polarization functions. The inner shells were represented by frozen-core approximation (1s for C, N and 1s−4d for Pt were kept frozen). The following density functionals were used within ADF: the local density approximation (LDA) with VWN parametrisation of electron gas data or the functional including Becke's gradient correction[66] to the local exchange expression in conjunction with Perdew's gradient correction[67] to the LDA expression (ADF/BP). The scalar relativistic (SR) zero order regular approximation (ZORA) was used within this study.[68] Within Gaussian-98 Dunning's polarized valence double-ζ basis sets [69] were used for C, N and H atoms and quasirelativistic effective core pseudopotentials and corresponding optimized set of basis functions[70] for Pt. The hybrid Becke's three-parameter functional with the Lee, Yang and Parr correlation func-

 © 2003 Wiley-VCH Verlag GmbH & Co. KGaA, Weinheim

tional (B3LYP) [71] was used in Gaussian 98 calculations (G98/B3LYP). Gaussian 98 was used for the calculations of the vibrations at G98/B3LYP optimised geometries. The calculations on [(bpy)$PtMe_2$] and [(bpy)$PtMes_2$] were performed in C_{2v} or C_2 constrained symmetries, respectively. The z axis was taken coincident with C_2 symmetry axis, while the platinum atom and bpy ligand lie in the yz plane. All results discussed correspond to optimised geometries.

Acknowledgments

This work was carried out in the framework of the COST D14 action. A. K. would like to thank Prof. D. J. Stufkens (University of Amsterdam) for the opportunity to do research in his group and also for fruitful discussions and Prof. W. Kaim is acknowledged for financial support. We are also grateful for a loan of K_2PtCl_4 by Johnson Matthey (JM). S. Z. thanks the Ministry of Education of the Czech Republic (OC.D14.20) for the financial support.

[1] C. E. Whittle, J. A. Weinstein, M. W. George, K. S. Schanze, *Inorg. Chem.* **2001**, *40*, 4053−4062.
[2] K. E. Dungey, B. D. Thompson, N. A. P. Kane-Maguire, L. L. Wright, *Inorg. Chem.* **2000**, *39*, 5192−5196.
[3] M. Hissler, W. B. Connick, D. K. Geiger, J. E. McGarrah, D. Lipa, R. J. Lachicotte, R. Eisenberg, *Inorg. Chem.* **2000**, *39*, 447−457.
[4] M. Hissler, J. E. McGarrah, W. B. Connick, D. K. Geiger, S. D. Cummings, R. Eisenberg, *Coord. Chem. Rev.* **2000**, *208*, 115−137.
[5] W. B. Connick, D. Geiger, R. Eisenberg, *Inorg. Chem.* **1999**, *38*, 3264−3265.
[6] W. B. Connick, V. M. Miskowski, V. H. Houlding, H. B. Gray, *Inorg. Chem.* **2000**, *39*, 2585−2592.
[7] W. Paw, S. D. Cummings, M. A. Mansour, W. B. Connick, D. K. Geiger, R. Eisenberg, *Coord. Chem. Rev.* **1998**, *171*, 125−150.
[8] V. M. Miskowski, V. H. Houlding, C.-M. Che, Y. Wang, *Inorg. Chem.* **1993**, *32*, 2518−2524.
[9] V. H. Houlding, V. M. Miskowski, *Coord. Chem. Rev.* **1991**, *111*, 145−152.
[10] V. M. Miskowski, V. H. Houlding, *Inorg. Chem.* **1991**, *30*, 4446−4452.
[11] V. M. Miskowski, V. H. Houlding, *Inorg. Chem.* **1989**, *28*, 1529−1533.
[12] W. Lu, M. C. W. Chan, K.-K. Cheung, C.-M. Che, *Organometallics* **2001**, *20*, 2477−2486.
[13] Y.-Y. Ng, C.-M. Che, S.-M. Peng, *New J. Chem.* **1996**, *20*, 781−789.
[14] C.-W. Chan, L.-K. Cheng, C.-M. Che, *Coord. Chem. Rev.* **1994**, *132*, 87−97.
[15] N. Chaudhury, R. J. Puddephatt, *J. Organomet. Chem.* **1975**, *84*, 105−115.
[16] A. Von Zelewsky, P. Belser, P. Hayoz, R. Dux, X. Hua, A. Suckling, H. Stoeckli-Evans, *Coord. Chem. Rev.* **1994**, *132*, 75−85.
[17] J. Biedermann, G. Gliemann, U. Klement, K.-J. Range, M. Zabel, *Inorg. Chem.* **1990**, *29*, 1884−1888.
[18] M. Maestri, D. Sandrini, V. Balzani, L. Chassot, P. Jolliet, A. Von Zelewsky, *Chem. Phys. Lett.* **1985**, *122*, 375−379.
[19] A. Klein, J. van Slageren, S. Záliš, *Inorg. Chem.* **2002**, *41*, 5216−5225.
[20] W. Kaim, A. Klein, S. Hasenzahl, H. Stoll, S. Záliš, J. Fiedler, *Organometallics* **1998**, *17*, 237−247.
[21] W. Kaim, A. Klein, *Organometallics* **1995**, *14*, 1176−1186.
[22] V. Balzani, A. Credi, M. Venturi, *Coord. Chem. Rev.* **1998**, *171*, 3−16.
[23] J. E. McGarrah, Y.-J. Kim, M. Hissler, R. Eisenberg, *Inorg. Chem.* **2001**, *40*, 4510−4511.
[24] J. A. Bailey, M. G. Hill, R. E. Marsh, V. M. Miskowski, W. P. Schaefer, H. B. Gray, *Inorg. Chem.* **1995**, *34*, 4591−4599.
[25] D. R. McMillin, J. J. Moore, *Coord. Chem. Rev.* **2002**, *229*, 113−121.
[26] J. F. Michalec, S. A. Bejune, D. G. Cuttell, G. C. Summerton, J. A. Gertenbach, J. S. Field, R. J. Haines, D. R. McMillin, *Inorg. Chem.* **2001**, *40*, 2193−2200.
[27] Q.-Z. Yang, L.-Z. Wu, Z.-X. Wu, L.-P. Zhang, C.-H. Tung, *Inorg. Chem.* **2002**, *41*, 5653−5655.
[28] A. Vogler, H. Kunkely, *Comments Inorg. Chem.* **1990**, *9*, 201−220.
[29] J. A. Weinstein, N. N. Zheligovskaya, M. Y. Mel′nikov, F. Hartl, *J. Chem. Soc., J. Chem. Soc., Dalton Trans.* **1998**, *15*, 2459−2466.
[30] Z. Hao, Z. Tang, Q. Shi, *Inorg. Chim. Acta* **1999**, *284*, 112−115.
[31] M. T. Cocker, R. E. Bachman, *Inorg. Chem.* **2001**, *40*, 1550−1556.
[32] J. van Slageren, D. J. Stufkens, S. Záliš, A. Klein, *J. Chem. Soc., Dalton Trans.* **2002**, 218−225.
[33] A. Klein, E. J. L. McInnes, W. Kaim, *J. Chem. Soc., Dalton Trans.* **2002**, 2371−2378.
[34] K. Karlsson, C. Moucheron, A. Kirsch-De Mesmaeker, *New J. Chem.* **1994**, *18*, 721−729.
[35] A. Kirsch-De Mesmaeker, R. M. D. Nasielski-Hinkens, D. Pauwels, J. Nasielski, *Inorg. Chem.* **1984**, *23*, 377−379.
[36] L. Jacquet, J. M. Kelly, A. Kirsch-De Mesmaeker, *J. Chem. Soc., Chem. Commun.* **1995**, 913−914.
[37] S. Ernst, C. Vogler, A. Klein, W. Kaim, *Inorg. Chem.* **1996**, *35*, 1295−1300.
[38] A. Klein, C. Vogler, W. Kaim, *Organometallics* **1996**, *15*, 236−244.
[39] M. R. Waterland, K. C. Gordon, J. J. McGarvey, P. M. Jayaweera, *J. Chem. Soc., J. Chem. Soc., Dalton Trans.* **1998**, 609−616.
[40] R. E. Holmlin, J. A. Yao, J. K. Barton, *Inorg. Chem.* **1999**, *38*, 174−189.
[41] R. M. Hartshorn, J. K. Barton, *J. Am. Chem. Soc.* **1992**, *114*, 5919−5925.
[42] H. D. Stoeffler, N. B. Thornton, S. L. Temkin, K. S. Schanze, *J. Am. Chem. Soc.* **1995**, *117*, 7119−7128.
[43] A. Klein, T. Scheiring, W. Kaim, *Z. Anorg. Allg. Chem.* **1999**, *625*, 1177−1180.
[44] W. B. Connick, R. E. Marsh, W. P. Schaefer, H. B. Gray, *Inorg. Chem.* **1997**, *36*, 913−922.
[45] A. Klein, H.-D. Hausen, W. Kaim, *J. Organomet. Chem.* **1992**, *440*, 207−217.
[46] A. Klein, W. Kaim, E. Waldhoer, H.-D. Hausen, *J. Chem. Soc., Perkin Trans. 2* **1995**, 2121−2126.
[47] S. Achar, V. J. Catalano, *Polyhedron* **1997**, *16*, 1555−1561.
[48] A. Klein, J. van Slageren, S. Záliš, *J. Organomet. Chem.* **2001**, *620*, 202−210.
[49] M. Kato, C. Kosuge, S. Yano, M. Kimura, *Acta Crystallogr., Sect. C* **1998**, *54*, 621−623.
[50] R. S. Osborn, D. Rogers, *J. Chem. Soc., Dalton Trans.* **1974**, 1002−1004.
[51] M. Textor, H. R. Oswald, *Z. Anorg. Allg. Chem.* **1974**, *407*, 244−256.
[52] S. Hasenzahl, H.-D. Hausen, W. Kaim, *Chem. Eur. J.* **1995**, *1*, 95−99.
[53] I. R. Farrell, J. van Slageren, S. Záliš, A. Vlček, Jr., *Inorg. Chim. Acta* **2001**, *315*, 44−52.
[54] W. P. Schaefer, W. B. Connick, V. M. Miskowski, H. B. Gray, *Acta Crystallogr., Sect. C* **1992**, *48*, 1776−1778.
[55] J. D. Scott, R. J. Puddephatt, *Organometallics* **1983**, *2*, 1643−1648.
[56] C. Eaborn, K. Kundu, A. Pidcock, *J. Chem. Soc., Dalton Trans.* **1981**, 933−938.
[57] H. C. Clark, L. E. Manzer, *J. Organomet. Chem.* **1973**, *59*, 411−428.

 © 2003 Wiley-VCH Verlag GmbH & Co. KGaA, Weinheim

[58] C. Vogler, B. Schwederski, A. Klein, W. Kaim, *J. Organomet. Chem.* **1992**, *436*, 367−378.
[59] G. M. Sheldrick, *SHELXTL-PLUS: An Integrated System for Solving, Refining and Displaying Crystal Structures from Diffraction Data*; Siemens Analytical X-ray Instruments Inc., Madison, WI, **1989**.
[60] G. M. Sheldrick, *SHELXL-97: A program for Crystal Structure Determination*; Universität Göttingen, Göttingen, **1997**.
[61] E. M. Kober, J. L. Marshall, W. J. Dressick, B. P. Sullivan, J. V. Caspar, T. J. Meyer, *Inorg. Chem.* **1985**, *24*, 2755−2763.
[62] C. J. Kleverlaan, D. J. Stufkens, I. P. Clark, M. W. George, H. van Willigen, A. Vlček, Jr., *J. Am. Chem. Soc.* **1998**, *120*, 10871−10879.
[63] C. Fonseca Guerra, J. G. Snijders, G. te Velde, E. J. Baerends, *Theor. Chim. Acta* **1998**, *99*, 391−403.
[64] S. J. A. van Gisbergen, J. G. Snijders, E. J. Baerends, *Comput. Phys. Commun.* **1999**, *118*, 119−138.
[65] M. J. Frisch, G. W. Trucks, H. B. Schlegel, G. E. Scuseria, M. A. Robb, J. R. Cheeseman, V. G. Zakrzewski, J. A. Montgomery, Jr., R. E. Stratmann, J. C. Burant, S. Dapprich, J. M. Millam, A. D. Daniels, K. N. Kudin, M. C. Strain, O. Farkas, J. Tomasi, V. Barone, M. Cossi, R. Cammi, B. Mennucci, C. Pomelli, C. Adamo, S. Clifford, J. Ochterski, G. A. Petersson, P. Y. Ayala, Q. Cui, K. Morokuma, D. K. Malick, A. D. Rabuck, K. Raghavachari, J. B. Foresman, J. Cioslowski, J. V. Ortiz, A. G. Baboul, B. B. Stefanov, G. Liu, A. Liashenko, P. Piskorz, I. Komaromi, R. Gomperts, R. L. Martin, D. J. Fox, T. Keith, M. A. Al-Laham, C. Y. Peng, A. Nanayakkara, C. Gonzalez, M. Challacombe, P. M. W. Gill, B. G. Johnson, W. Chen, M. W. Wong, J. L. Andres, M. Head-Gordon, E. S. Replogle, J. A. Pople, *Gaussian 98 (Revision A.6)*, Gaussian, Inc., Pittsburgh, PA, **1998**.
[66] A. D. Becke, *Phys. Rev. A* **1988**, *38*, 3098−3100.
[67] J. P. Perdew, *Phys. Rev. B* **1986**, *33*, 8822−8824.
[68] E. van Lenthe, A. Ehlers, E. J. Baerends, *J. Chem. Phys.* **1999**, *110*, 8943−8953.
[69] D. E. Woon, T. H. J. Dunning, *J. Chem. Phys.* **1993**, *98*, 1358−1371.
[70] D. Andrae, U. Haeussermann, M. Dolg, H. Stoll, H. Preuss, *Theor. Chim. Acta* **1990**, *77*, 123−141.
[71] P. J. Stephens, F. J. Devlin, C. F. Cabalowski, M. J. Frisch, *J. Phys. Chem.* **1994**, *98*, 11623−11627.

Received November 8, 2002

 © 2003 Wiley-VCH Verlag GmbH & Co. KGaA, Weinheim

Synthesis of [RuX(CO){η²-*C*,*N*-$C_6H_4C(H)=NC_6H_4$-4-NO_2}$(PPh_3)_2$] (X = F, Cl, Br, I): Evidence of Non-Conventional Ru−X Hydrogen Bonds Leading to Octahedral Coordination at the Halide Atom

Kevin R. Flower,*[a] Robin G. Pritchard,[a] and John E. Warren[a]

Keywords: Ruthenium / Cyclometallated ligands / Charge transfer / Hydrogen bonds / Pi interactions

Treatment of [RuCl(CO){η²-*C*,*N*-$C_6H_4C(H)=NC_6H_4$-4-NO_2}$(PPh_3)_2$] (**4-Cl**) with Ag[BF_4] in acetone/CH_2Cl_2 gives the cationic complex [Ru{O=$C(CH_3)_2$}(CO){η²-*C*,*N*-$C_6H_4C(H)=NC_6H_4$-4-NO_2}$(PPh_3)_2$][BF_4] (not isolated), which then reacts with NaX (X = F, Br, I) to afford the new compounds [RuX(CO){η²-*C*,*N*-$C_6H_4C(H)=NC_6H_4$-4-NO_2}$(PPh_3)_2$] (X = F, Br, I) (**4-F**, **4-Br**, and **4-I**). All of the new compounds have been characterised by elemental analysis (C, H, and N), ^{1}H, $^{13}C\{^1H\}$, $^{31}P\{^1H\}$ NMR spectroscopy and IR spectroscopy. The IR data support the hypothesis that the fluoride ligand is the strongest halogen π-donor to the metal centre. In addition, the compounds **4-Br**·1.5$CHCl_3$, **4-Cl**·1.5$CHCl_3$, **4-F**·2$CDCl_3$, and **4-I**·1.5$CHCl_3$ have been characterised by single-crystal X-ray diffraction studies; all show Ru–X···$HCCl_3$ interactions with the Ru–F interaction being the strongest. In addition, there is evidence for the presence of competing RuX···$ClCHCl_2$ (X = Cl, Br) interactions in compounds **4-Br** and **4-Cl**; these appear to be charge transfer in nature. The generality of these interactions has been probed using searches of the Cambridge Crystallographic Database and the data obtained suggests that these interactions have some, but limited, precedence.
(© Wiley-VCH Verlag GmbH & Co. KGaA, 69451 Weinheim, Germany, 2003)

Introduction

There was an initial reluctance to accept the possibility of the hydrogen bond, from its first mention in 1902,[1] based upon the chemical dogma that hydrogen has a valence of one.[2] The hydrogen bond first reached the mainstream in Pauling's book *The Nature of the Chemical Bond*[3] in which the electrostatic nature of the interaction was emphasised. In 1960 Pimentel and McClellan modified the definition of a hydrogen bond to: "A hydrogen bond is said to exist when (1) there is evidence of a bond, and (2) there is evidence that this bond sterically involves a hydrogen atom involved in a bond to another atom."[4] Conventionally, hydrogen bonds involved hydrogen atom interactions with electronegative elements and donor groups such as N−H, O−H, halogen−H, with conventional acceptors based upon the same atoms in different hybridisation states.[5] Non-conventional interactions recognise the potential of, for example, C−H, P−H, M−H systems, to act as donors and π-systems (aryl, acetylenic) and C−F, for example, to act as acceptors. These and other secondary intermolecular interactions that influence solid-state structures are currently of much interest, with hydrogen bonding of particular note, due to its importance in biological systems,[6] non-covalent synthesis,[7] crystal engineering,[8] catalysis,[9,10] and anion recognition,[11] to name but a few. A recent review of hydrogen bonding in the solid state has also recently appeared.[12] In addition to the hydrogen bond it has been recognised[13] that the halogens, Cl, Br, and I, may also interact with electronegative atoms via weak secondary interactions. The nature of these interactions has been subject to much debate. It has been shown that covalently bound halogen atoms do not occupy spherical volumes in space but are ellipsoidal due to the anisotropic distribution of electron density about their nucleus.[14,15] This leads to a non-uniform van der Waals radius that is shorter in the C−X bond direction. This so-called polar flattening has been used to explain why there are close intermolecular halogen···halogen contacts. Allen et al. have shown, however, that intermolecular contacts between the halogen (Cl, Br, and I) and the electronegative (O, N) atoms can exist,[16] and strong intermolecular halogen···halogen interactions have been reported, for example, for chlorine monofluoride.[17]

Based on methodology developed by Roper and Wright[18] we recently reported[19,20] the preparation of some cycloruthenated azobenzene-containing complexes of the type [RuX(CE)(η²-*C*,*N*-$C_6H_4N=NC_6H_5$)$(PPh_3)_2$] (X = Cl, Br, I; E = O, S) and subsequently extended the methodology to the preparation[21] of complexes of the type [RuCl(CO){η²-*C*,*N*-$C_6H_4C(H)=NC_6H_4$-4-R}$(PPh_3)_2$] (**1-Cl**, **2-Cl**, **3-Cl**, **4-Cl**; R = NMe_2, Me, I, NO_2) which contain cycloruthenated 2-(phenylimino)phenyl ligands (Figure 1). The structural and spectroscopic characteristics of these

[a] Department of Chemistry, UMIST,
P. O. Box 88, Manchester M60 1QD, United Kingdom
Fax: (internat.) + 44-161/200-4559
E-mail: k.r.flower@umist.ac.uk

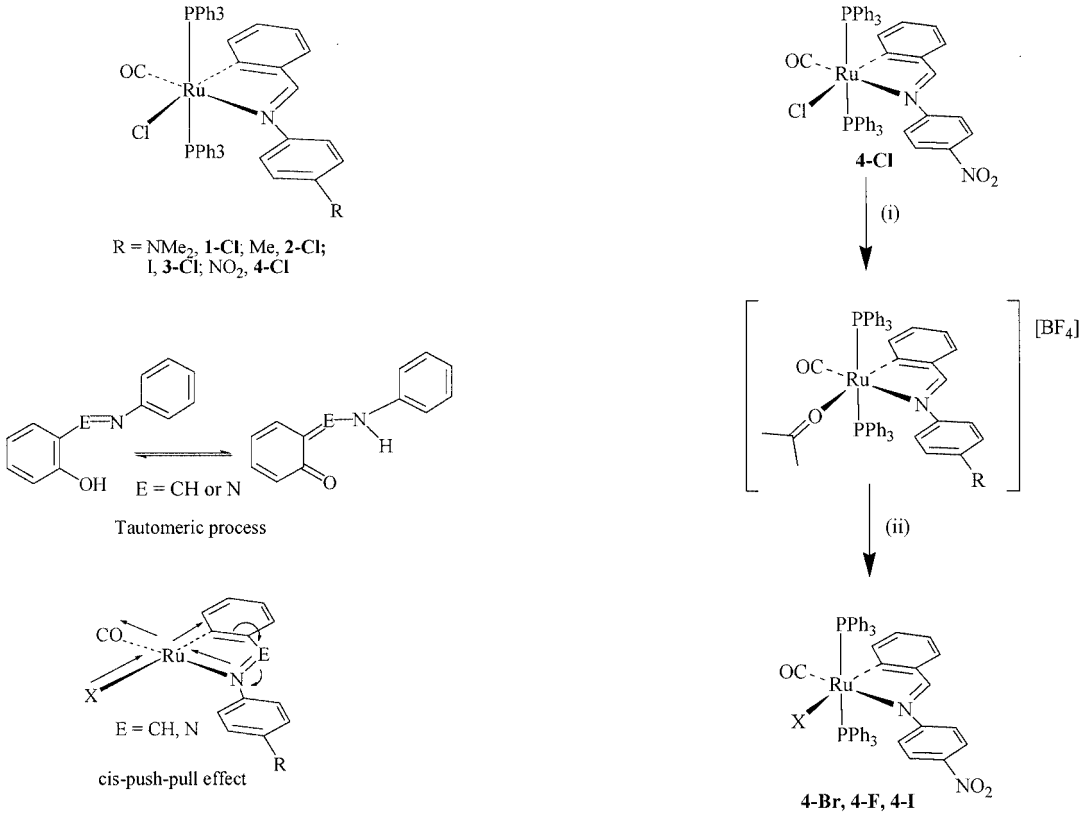

Figure 1. The analogy between the *cis*-push-pull effect and the tautomerisation in *ortho*-(hydroxy)azobenzenes and analogous Schiff bases

Scheme 1. (i) $Ag[BF_4]$, CH_2Cl_2, $OC(CH_3)_2$, 20 min; (ii) NaX, H_2O, EtOH, 1 h

Table 1. Physical, analytical and IR data for **4-Br**, **4-Cl**, **4-F**, and **4-I**

Compound[a][b]	Color	Yield (%)	C, H, N microanalysis: found (calcd.)			IR: ν(CO) [cm^{-1}]
4-Br [RuBr(CO){η²-*C*,*N*-$C_6H_4C(H)=NC_6H_4$-4-NO_2}$(PPh_3)_2$]·1.5$CHCl_3$	orange	93	54.7 (54.4)	3.9 (3.6)	2.9 (2.5)	1938
4-Cl [RuCl(CO){η²-*C*,*N*-$C_6H_4C(H)=NC_6H_4$-4-NO_2}$(PPh_3)_2$]·1.5$CHCl_3$	red	94	56.9 (56.6)	3.8 (3.7)	2.3 (2.6)	1929
4-F [RuF(CO){η²-*C*,*N*-$C_6H_4C(H)=NC_6H_4$-4-NO_2}$(PPh_3)_2$]·2$CHCl_3$	red	95	55.3 (55.0)	3.7 (3.6)	2.7 (2.5)	1923
4-I [RuI(CO){η²-*C*,*N*-$C_6H_4C(H)=NC_6H_4$-4-NO_2}$(PPh_3)_2$]·1.5$CHCl_3$	orange	96	52.4 (52.2)	3.7 (3.4)	2.8 (2.4)	1940

[a] Calculated values in parentheses. [b] Spectra recorded as Nujol mulls between KBr discs, all bands strong.

Table 2. $^{31}P\{^1H\}$ NMR and ^1H NMR data for compounds **4-Br**, **4-Cl**, **4-Br**, **4-F**, **and 4-I**

Compound[a]	^{31}P (δ)	^1H (δ)
4-Br	27.4	8.13 (t, J_{HP} = 1.6, 1 H, CH=N), 7.56 (d, $J_{H,H}$ = 9.2, 2 H, aryl-H),7.48−7.04 (m, 31 H, aryl-H), 6.56 (m, 2 H, aryl-H), 6.23 (d, $J_{H,H}$ = 9.2 Hz, 2 H, aryl-H), 6.10 (t, $J_{H,H}$ = 7.0 Hz, 1 H, aryl-H)
4-Cl	28.2	8.15 (t, J_{HP} = 2.0, 1 H, CH=N), 7.59 (d, $J_{H,H}$ = 9.0, 2 H, aryl-H),7.48−7.04 (m, 31 H, aryl-H), 6.60 (m, 2 H, aryl-H), 6.33 (d, $J_{H,H}$ = 9.0, 2 H, aryl-H), 6.12 (t, $J_{H,H}$ = 7.0 Hz, 1 H, aryl-H)
4-F	26.9 (d, J_{PF} = 15.3)	8.20 (t, J_{HP} = 1.7, 1 H, CH=N), 7.69 (d, $J_{H,H}$ = 9.0, 2 H, aryl-H),7.48−7.04 (m, 31 H, aryl-H), 6.93 (d, $J_{H,H}$ = 9.0 Hz, 2 H, aryl-H), 6.74 (d, $J_{H,H}$ = 9.0, 1 H, aryl-H), 6.55 (t, $J_{H,H}$ = 7.0 Hz, 1 H, aryl-H), 6.23 (t, $J_{H,H}$ = 7.4 Hz, 1 H, aryl-H)
4-I	26.4	8.09 (t, J_{HP} = 1.7, 1 H, CH=N), 7.55 (d, $J_{H,H}$ = 8.8, 2 H, aryl-H),7.46−7.04 (m, 31 H, aryl-H), 6.59 (m. 2 H, aryl-H), 6.15 (t, $J_{H,H}$ = 7.6 Hz, 1 H, aryl-H), 6.08 (d, $J_{H,H}$ = 8.8 Hz, 2 H, aryl-H)

[a] Spectra recorded in $CDCl_3$ at 293 K; coupling constants (*J*) in Hz; s = singlet, d = doublet, t = triplet, m = multiplet.

 © 2003 Wiley-VCH Verlag GmbH & Co. KGaA, Weinheim

Table 3. $^{13}C\{^1H\}$ NMR data for **4-Br**, **4-Cl**, **4-F**, and **4-I**

Compound[a]	CO	C1	C2	C3	C4	C5	C6	C7	C8	C9	C10	C11	C12	C13	C14	C15
4-Br	206.9 (t, J = 16.4)	191.9 (t, J = 9.2)	141.1	130.7	120.3	131.6	142.4	175.2	154.8	125.4	122.3	145.1	133.5 (t, J = 21.2)	134.1 (t, J = 5.0)	127.6 (t, J = 4.3)	129.3
4-Cl	206.7 (t, J = 16.3)	191.9 (t, J = 9.1)	141.1	130.8	120.1	131.3	142.3	174.9	154.9	125.2	122.5	145.0	133.3 (t, J = 21.1)	134.0 (t, J = 5.3)	127.6 (t, J = 4.3)	129.3
4-F	206.4 (t, J = 16.9)	192.9 (t, J = 10.2; t[b], J = 33.3)	141.1	130.4	119.8	131.2	142.7	172.1	154.6	124.4	123.2	144.9	132.8 (t, J = 21.7)	133.6 (t, J = 5.3)	127.7 (t, J = 4.3)	129.4
4-I	207.6 (t, J = 15.0)	192.7 (t, J = 9.2)	141.1	130.7	120.5	131.9	142.8	175.6	154.7	125.8	122.2	145.1	133.7 (t, J = 21.8)	134.3 (t, J = 4.8)	127.5 (t, J = 4.8)	129.3

[a] Spectra recorded in $CDCl_3$ at 298 K; all resonances singlets unless otherwise stated; all $J = J_{PC}$ [Hz] except: [b] $J = J_{FC}$ [Hz].

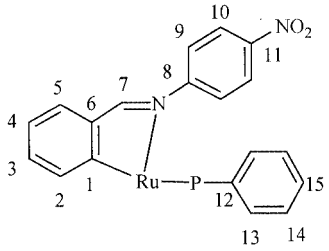

Figure 2. Numbering scheme for $^{13}C\{^1H\}$ NMR spectroscopic data

compounds afforded evidence for a *cis*-push-pull effect between the halide ligand and the CO ligand, which is moderated by the cyclometallated ligand. This effect was clearly shown by comparison of the solid-state structures (X-ray) and $^{13}C\{^1H\}$ NMR spectroscopic data obtained for **1-Cl**, **2-Cl**, **3-Cl**, and **4-Cl** with that obtained from previous studies concerned with the tautomeric process undergone by *ortho*-(hydroxy)azobenzene and [*ortho*-(hydroxy)phenylimino]-phenyl Schiff bases[22−24]. The effect was shown to be dependent on the *para* substituent of the phenylimino ring. We were then interested to see if the magnitude of the effect could be moderated by the π-donor strength of the halogen ligand. Herein we report that chloride/halogen exchange in **4-Cl** is readily facilitated by treatment with Ag^+ followed by the reaction with NaX (X = F, Br, I) and that the spectroscopic evidence shows that the fluoride ligand is the strongest π-donor. Furthermore, the solid-state structures

Table 4. Crystal data and data collection and refinement details for **4-Br**, **4-Cl**, **4-F** and **4-I**

	4-Br	**4-Cl**	**4-F**	**4-I**
Empirical formula	$C_{51.5}H_{40.5}BrCl_{4.5}N_2O_3P_2Ru$	$C_{51.5}H_{40.5}Cl_{5.5}N_2O_3P_2Ru$	$C_{52}H_{41}Cl_6FN_2O_3P_2Ru$	$C_{51.5}H_{40.5}Cl_{4.5}IN_2O_3P_2Ru$
Formula mass	1137.80	1093.34	1136.58	1184.79
T [K]	150(2)	150(2)	150(2)	120(2)
Crystal size [mm]	0.10 × 0.10 × 0.10	0.10 × 0.10 × 0.10	0.20 × 0.10 × 0.10	0.40 × 0.18 × 0.08
λ(Mo-K_a) [Å]	0.71073	0.71073	0.71073	0.71073
Crystal system	monoclinic	monoclinic	monoclinic	monoclinic
Space group	*P*21/*n*	*P*21/*n*	*P*21/*n*	*P*21/*n*
a [Å]	10.9721(2)	11.0466(2)	12.03500(10)	10.9441(2)
b [Å]	27.3926(6)	27.4903(5)	24.3670(3)	27.3627(6)
c [Å]	16.0903(5)	15.8580(2)	18.0200(2)	16.3220(3)
β [°]	90.8460(10)	90.00(1)	110.5450(10)	90.8640(10)
V [Å^3]	4835.5(2)	4815.67(14)	5021.09(9)	4887.23(17)
Z	4	4	4	4
d(calcd.) [Mg/m^3]	1.563	1.508	1.504	1.610
F(000)	2292	2220	2304	2364
2θ range [°]	2.97−27.47	1.28−29.14	2.57−7.43	2.91−27.69
Total number of reflections collected	29592	38523	36273	35796
Independent reflections	10347	11221	11256	11000
R(int)	0.0849	0.0809	0.0421	0.1057
Compl. to θ (%)	93.3	86.6	98.1	96.1
Data/restraints/parameter	10347/34/656	11221/29/648	11256/0/768	11000/12/748
GOF	1.021	1.024	1.031	1.033
$R1$ [$I > 2\sigma(I)$]	0.0593	0.0531	0.0355	0.0524
$wR2$	0.1302	0.1134	0.0816	0.1345
$R1$ (all data)	0.1113	0.0872	0.0489	0.0767
$wR2$	0.1487	0.1274	0.0889	0.1472

 © 2003 Wiley-VCH Verlag GmbH & Co. KGaA, Weinheim

of **4-Br**, **4-Cl**, **4-F**, and **4-I** display some interesting weak secondary interactions; in particular, the presence of Ru−X···$HCCl_3$ (X = F, Cl, Br, I) and Ru−X···$ClCCl_2H$ (X = Cl, Br) contacts, as well as hydrogen bonds to both the triphenylphosphane and cyclometallated ligands leading to essentially octahedrally coordinated halogen atoms.

Results and Discussion

The compounds [RuX(CO){η^2-*C*,*N*-$C_6H_4C(H)=NC_6H_4$-4-NO_2}$(PPh_3)_2$] (X = Br, F, I) (**4-Br**, **4-F**, **4-I**) were prepared, in essentially quantitative yield, according to the method illustrated in Scheme 1; i.e. treatment of **4-Cl** with a stoichiometric amount of Ag[BF_4] followed by, after filtration to remove AgCl, addition of a slight excess of NaX (X = F, Br, I).

The new compounds **4-Br**, **4-F**, and **4-I** were all characterised by elemental analysis (C, H, N) and IR spectroscopy (Table 1), ^1H and $^{31}P\{^1H\}$ NMR spectroscopy (Table 2), and $^{13}C\{^1H\}$ NMR spectroscopy (Table 3, see Figure 2 for the numbering scheme).

Compounds **4-Cl**, **4-Br**, **4-F**, **4-I** have also been characterised by single-crystal X-ray diffraction studies, see Table 4 for data collection and processing parameters, Table 5 for

Table 5. Selected bond lengths [Å] and angles [°] for **4-Br, 4-Cl, 4-F** and **4-I**

	4-Br	**4-Cl**	**4-F**	**4-I**
Ru(1)−X	2.6609(4)	2.5116(4)	2.1224(13)	2.8427(3)
Ru(1)−C(1)	2.050(3)	2.0527(13)	2.033(2)	2.059(3)
Ru(1)−N(1)	2.236(3)	2.2239(11)	2.2001(18)	2.241(2)
Ru(1)−C(14)	1.832(4)	1.8285(14)	1.823(2)	1.839(3)
C(14)−O(1)	1.156(4)	1.1554(17)	1.158(3)	1.143(4)
C(7)−N(1)	1.293(4)	1.3077(18)	1.295(3)	1.307(4)
C(1)−Ru(1)−X	169.90(10)	169.21(4)	166.42(7)	171.07(8)
C(1)−Ru(1)−N(1)	78.07(12)	78.31(5)	79.02(8)	77.97(10)
N(1)−Ru(1)−C(14)	167.05(12)	167.70(5)	171.58(9)	166.95(10)
N(1)−Ru(1)−X	92.54(7)	91.80(3)	87.40(6)	93.71(6)
C(14)−Ru(1)−X	100.18(10)	100.72(4)	100.09(8)	99.21(8)
C(14)−Ru(1)−C(1)	89.37(14)	89.39(6)	93.47(9)	89.24(11)
X−Ru(1)−P(1)	87.73(2)	86.816(12)	91.05(4)	89.462(18)
X−Ru(1)−P(2)	91.50(2)	91.452(12)	87.74(4)	90.529(18)
P(1)−Ru(1)−P(2)	173.57(3)	173.491(13)	174.59(2)	174.05(3)
Ru(1)−X(1)−H(51)	145.29(5)	145.22(6)	176.59(5)	142.4(4)
H(9)−X(1)−H(40)	149.90(5)	156.84(4)	169.03(4)	143.2(5)
H(26)−X(1)−H(46)	143.77(4)	146.39(7)	154.02(6)	137.9(4)

Table 6. Hydrogen bond data, distances [Å] and angles [°] for **4-Br**, **4-Cl**, **4-F**, **4-I**

Compound	Interaction	D−H	H···A	D···A	D−H···A
4-Br	C(51)−H(51)-Br(1)	1.00	3.02(3)	4.02(4)	173.1(3)
	C(9)−H(9)−Br(1)	0.95(3)	2.92(3)	3.385(5)	111.6(2)
	C(26)−H(26)−Br(1)	0.95(4)	2.81(4)	3.483(3)	128.7(5)
	C(40)−H(40)−Br(1)	0.95(4)	2.90(3)	3.536(3)	125.2(3)
	C(46)−H(46)−Br(1)	0.95(5)	2.76(3)	3.652(3)	157.3(4)
4-Cl	C(51)−H(51)-Cl(L1)	1.00	2.98(3)	3.963(2)	167.1(3)
	C(9)−H(9)−Cl(L1)	0.95(4)	2.79(3)	3.2935(14)	113.9(3)
	C(26)−H(26)−Cl(L1)	0.95(4)	2.68(3)	3.3617(15)	129.0(2)
	C(40)−H(40)- Cl(L1)	0.95(3)	2.79(3)	3.4534(14)	127.1(2)
	C(46)−H(46)−Cl(L1)	0.95(4)	2.71(4)	3.5934(15)	154.7(4)
4-F	C(51)−D(51)−F(1)	1.00(3)	1.81(3)	2.799(3)	172(3)
	C(9)−H(9)−F(1)	0.95(3)	2.32(3)	2.857(3)	115.1(19)
	C(26)−H(26)−F(1)	0.93(3)	2.24(3)	3.031(3)	143(2)
	C(40)−H(40)−F(1)	0.96(4)	2.23(3)	3.019(3)	139(2)
	C(46)−H(46)−F(1)	0.91(4)	2.59(3)	3.314(3)	141(9)
	C(7)−H(7)−O(1)	0.94(3)	2.63(3)	3.471(3)	169.3(4)
	C(17)−H(17)−O(2)	0.94(3)	2.581(3)	3.414(4)	149(20
	C(3)−H(3)−O(3)	0.93(3)	2.46(3)	3.327(3)	156(3)
4-I	C(51)−H(51)−I(1)	1.05(2)	3.02(3)	4.053(3)	167.3(4)
	C(9)−H(9)- I(1)	1.00(2)	3.176(4)	3.553(2)	104(3)
	C(26)−H(26)−I(1)	1.02(3)	3.030(4)	3.60(3)	116.5(3)
	C(40)−H(40)−I(1)	1.00(3)	2.999(3)	3.647(2)	123.3(3)
	C(46)−H(46)−I(1)	0.95(3)	2.85(3)	3.737(2)	154.7(4)

 © 2003 Wiley-VCH Verlag GmbH & Co. KGaA, Weinheim

selected bond lengths [Å], angles [°], Table 6 for hydrogen-bond data, Table 7 for halogen···halogen interaction data and Table 8 for selected torsion angles. ORTEP[25] representations of the molecular structures of **4-Br**, **4-Cl**, **4-F**, **4-I** are presented as Figures 3−6, respectively (all the structures have the same numbering scheme, which is fully illustrated for **4-F**). For **4-Cl** and **4-Br** there are two representations as one chloroform solvate interacts with the Ru−X bond in two different ways. The chloroform molecules and hydrogen atoms not involved in hydrogen bonding have been omitted for clarity. All of the structures are best considered as octahedral about a central ruthenium atom with two PPh_3 ligands mutually *trans* and axial with the *ortho*-metallated imine, carbonyl and halide ligands in the equatorial plane. For a more detailed discussion see later.

Table 7. Halogen−halogen interaction, distances [Å] and angles [°] data for **4-Br** and **4-Cl**

Compound	C(51)−Cl(1)	Cl(1)···X	C(51)···X	C(51)−Cl(1)···X
4-Br	1.665(5)	3.21(4)	4.966(5)	169.1(4)
4-Cl	1.710(4)	3.218(4)	4.916(4)	171.5(5)

Table 8. Selected torsion angles [°] for **4-Br**, **4-Cl**, **4-F**, **4-I**

Compound	Ru−P(1)−C(21)−C(26)	Ru−N(1)−C(8)−C(9)	Ru−P(2)−C(39)−C(40)	Ru−P(2)−C(45)−C(46)
4-Br	5.0(3)	−54.5(4)	0.9(3)	52.4(3)
4-Cl	6.21(14)	−52.87(18)	−1.94(14)	53.05(13)
4-F	13.4(2)	−41.7(3)	−16.7(2)	61.25(19)
4-I	1.5(3)	−56.6(4)	5.9(3)	53.0(3)

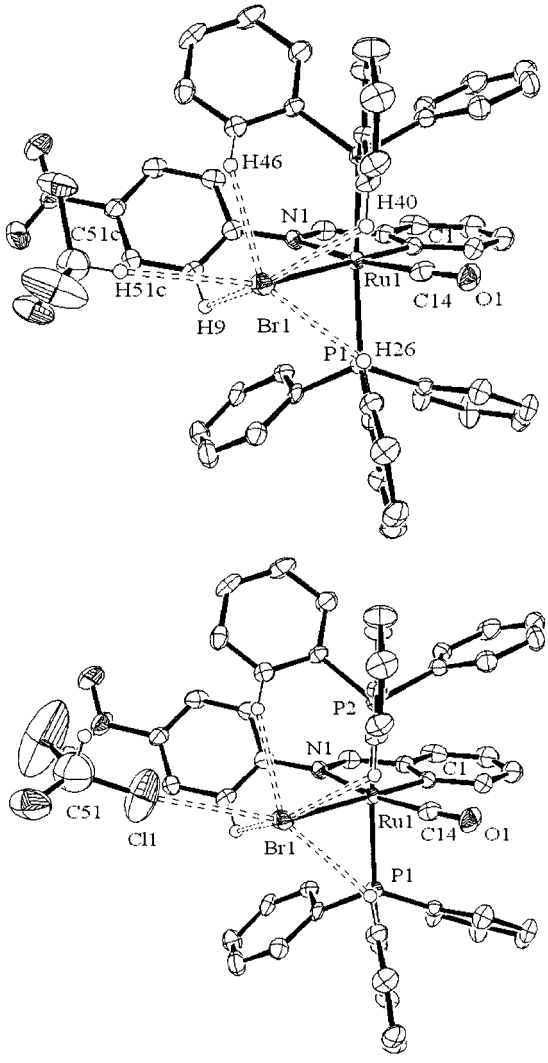

Figure 3. ORTEP representation of **4-Br** showing non-conventional interactions at the bromide ligand; thermal ellipsoids at 50%

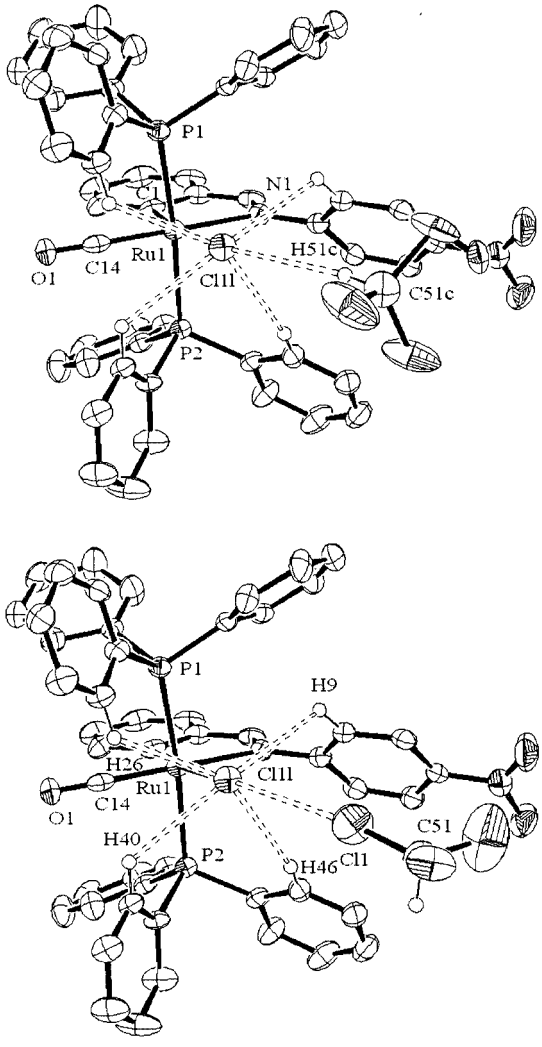

Figure 4. ORTEP representation of **4-Cl** showing non-conventional interactions at the chloride ligand; thermal ellipsoids at 50%

 © 2003 Wiley-VCH Verlag GmbH & Co. KGaA, Weinheim

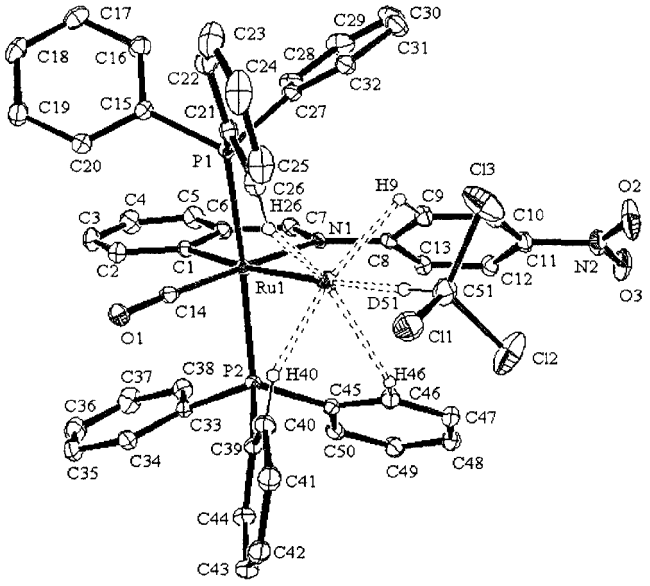

Figure 5. ORTEP representation of **4-F** showing non-conventional interactions at the fluoride ligand; thermal ellipsoids at 50%

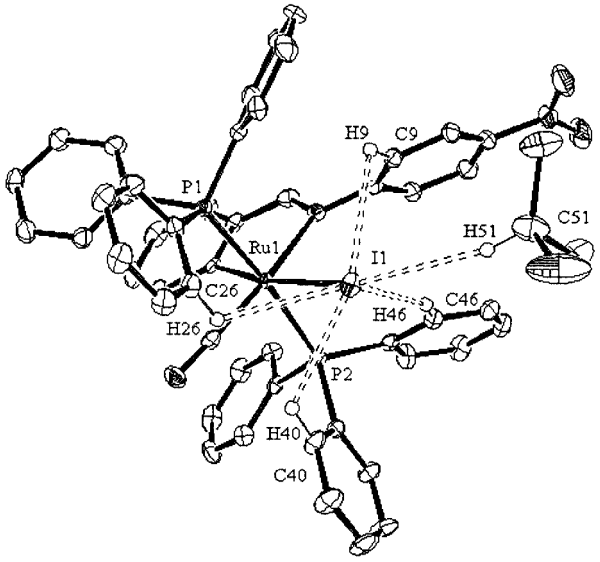

Figure 6. ORTEP representation of **4-I** showing non-conventional interactions at the iodide ligand; thermal ellipsoids at 50%

The IR spectra (Table 1) for **4-Cl**, **4-Br**, **4-F**, **4-I** all show a single strong ν(CO) band between 1923 (**4-F**) and 1940 cm^{-1} (**4-I**). In a previous report[21] describing the synthesis of [RuCl(CO){η^2-*C*,*N*-$C_6H_4C(H)=NC_6H_4$-4-R}$(PPh_3)_2$] (R = NMe_2, Me, I, NO_2) **1-Cl**, **2-Cl**, **3-Cl**, **4-Cl** we were able to correlate the metallated carbon $^{13}C\{^1H\}$ resonance with the Hammet σ^+ parameter[26] which confirmed that the remote *para* substituent influences the *cis* push-pull effect (Figure 1); however, the trend in ν(CO) stretching frequencies was consistent with the $^{13}C\{^1H\}$ NMR spectroscopic data, but not conclusive due to the narrow frequency separation across the series of 6 cm^{-1}. For compounds **4-Cl**, **4-Br**, **4-F**, **4-I**, where the expected π-donor strength of the halide follows the trend F > Cl > Br > I with a constant *para* substituent (NO_2), the ν(CO) decreases across the series I > Br > Cl > F. This observation is consistent with the fluoride ligand being the strongest π-donor, Table 1 (note: the wavenumber separation across the whole series is 17 cm^{-1}). It should also be remembered that the orthogonal halide p-orbital will be involved in *cis*-π-donation to the CO ligand, in this case mediated by a metal d_π-orbital, not the cyclometallated ligand.[27] It must therefore be a combination of both processes that accounts for the differences in the observed ν(CO) values observed for **4-Cl**, **4-Br**, **4-F**, **4-I**. Compelling evidence for this trend in π-donor strength for the halides (F > Cl > Br > I) to transition metal centres has been noted previously.[28]

The compounds **4-Cl**, **4-Br**, **4-I** all show the expected singlet resonance in their $^{31}P\{^1H\}$ NMR spectra Table 1, whereas for **4-F** a doublet is observed with $J_{P,F}$ = 15.3 Hz. The resonance position is barely perturbed on halogen exchange.

The ^1H NMR spectroscopic data are consistent with the formulation of **4-Cl**, **4-Br**, **4-F**, **4-I**. All the compounds show a triplet resonance for the imine CH proton (coupling to the mutually *trans*-phosphane ligands). The presence of solvents of crystallisation is often seen in the ^1H NMR spectra due to the propensity of these compounds to entrain solvent in the crystal lattice. For example, recrystallisation[21] of **4-Cl** from CH_2Cl_2 and EtOH afforded **4-Cl**·$1.5CH_2Cl_2$, indeed the rapidity of recrystallisation process can affect the amount of solvent incorporated and microanalytical data need to be correlated with the NMR spectroscopic data. This is equally true for compounds **1-Cl**, **2-Cl** and **3-Cl**.[21]

The $^{13}C\{^1H\}$ NMR spectra were assigned with the aid of DEPT-135 spectra substituent effects[29] and the data previously reported[21] for **1-Cl**, **2-Cl**, **3-Cl**, **4-Cl**, and are consistent with the formulation of **4-Br**, **4-Cl**, **4-F**, **4-I**.

The Solid-State Structures of 4-Br, 4-Cl, 4F, 4-I

The presence of conventional N−H or O−H hydrogen bonds to high-valent metal fluoride complexes is well documented,[30] as is the presence of both conventional and non-conventional hydrogen bonds to organometallic complexes containing a fluoride ligand.[31] A search of the CDS[32] revealed only one other example[33] of a chloroform molecule hydrogen-bonding to a transition metal fluoride. In this case, to a fluoro−iron−porphyrin [C−H···F, C−H 0.96(5); H···F 2.11(5); C−H···F 136(4)]. This interaction is considerably longer (17%) than that observed in **4-F** (Table 6). The shorter nature of the hydrogen bond interaction in **4-F** is presumably because the interaction, in this case, is with the radially less diffuse sp lone pair of the fluoride ligand. Work by others[34,35] on M−Cl systems, however, has shown a preference for the p-type lone pair to be more basic and interact with a hydrogen-bond donor (angular preference 100−110°).[35] This type of donor approach is ruled out in this system because of the steric bulk of the ancillary ligand set. Further analysis[36] of the crystallographic data revealed that four non-conventional intramolecular hydrogen bonds from the ancillary ligand phenyl ring hydrogen atoms H(9), H(26), H(40) and H(46) to the fluoride ligand

 © 2003 Wiley-VCH Verlag GmbH & Co. KGaA, Weinheim

complete an essentially octahedral environment about the fluorine atom. In addition to these intramolecular hydrogen bonds the presence of three intermolecular hydrogen bonds was also observed: one to each of the carbonyl and nitro group oxygen atoms (Table 6, Figure 7).

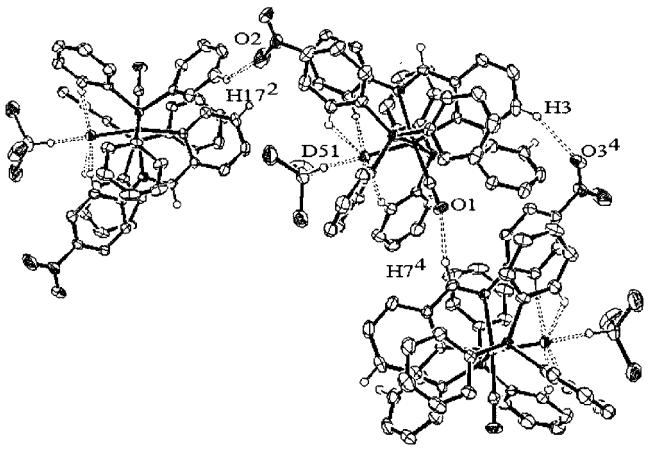

Figure 7. ORTEP representation of **4-F** showing both inter- and intramolecular hydrogen bonds; thermal ellipsoids at 50%

Since perusal of CDS[32] suggested that no complete series of M−X···$HCCl_3$ (X = F, Cl, Br, I) hydrogen bond interactions had been reported to-date **4-Br**, **4-Cl**, **4-I** were recrystallised under conditions identical to those used to obtain the crystals of **4-F**. In each case crystals suitable for an X-ray diffraction study were obtained.

On solving the X-ray data for **4-Br**, **4-Cl**, **4-I** it was found that the three structures are isostructural, but different from **4-F**. The difference is essentially due to the incorporation of 2 mol-equiv. of $CDCl_3$ of crystallisation into the lattice of the latter, compared to 1.5 into the former three. For **4-Br**, **4-Cl**, **4-I** one $CHCl_3$ of crystallisation interacts with the Ru−X bond and a second (half occupancy) is located on a crystallographic inversion site; the latter will not be discussed.

For compound **4-I**, an Ru−I···$HCCl_3$ hydrogen bond is clearly present (Figure 6, Table 6); however, for compounds **4-Br** and **4-Cl** this is not explicitly the case. The $CHCl_3$ solvent molecule located close to the Ru−X (X = Cl, Br) moiety is disordered. When the disorder was modelled for **4-Cl** it was found that there were two principal orientations of the $CHCl_3$ molecule and when this model was used (allowing for variable occupancy) to decipher the disorder observed in **4-Br** it was found that the disorder is identical, save that the relative occupancies of the orientations differ. Thus, in addition to the Ru−X···$HCCl_3$ hydrogen bond illustrated in Figures 3 and 4, an Ru−X···$ClCCl_2H$ (X = Cl, Br) interaction, substantially less than the sum of the van der Waals radii,[37] was found to be present for both compounds (Figures 3 and 4, Table 7). The Ru−X···$ClCCl_2H$ (X = Cl, Br) interaction is present for **4-Cl** 39% and for **4-Br** 76% of the time. Since the same disorder model is applicable to both cases it appears that certain orientations of the $CHCl_3$ molecule are preferred and there must be some explanation for this. The Ru−X···$HCCl_3$ interaction is perfectly understandable; however, the Ru−X···$ClCHCl_2$ is not immediately so. The proposed Ru−X···$ClCCl_2H$ interaction observed for compounds **4-Br** and **4-Cl** is unlikely to be electrostatic in nature since both the Ru−X and $HCCl_3$ chlorine atoms would be expected to carry partial negative charges. The X···ClC interaction in compounds **4-Br** and **4-Cl** [X = Br 169.1(4); X = Cl 171.5(5) °] is "essentially linear" and one possible explanation would be that charge transfer (n → σ*) from the Ru−X moiety to the C−Cl bond could be responsible for these interactions. Since this type of interaction seemed unusual to us a search of the CDS database was carried out to discover if there was any generality to such interactions in the solid state. The initial searches carried out were generic and considered the possibility of any transition metal halide interaction with a chloro-containing hydrocarbon within the sum of the van der Waals radii. The results of these searches were as follows: for the transition metal chlorides 226 hits, metal bromides 32 hits, and transition metal iodides 17 hits. These data are presented as scatter plots, Figures 8−10; there were no metal fluoride interactions. What is striking, however, is the number of hits and the mean of X−Cl−C (X = Cl, Br, I) with angles of 155.1, 163.1 and 164.8°, respectively. It is important to note here that no restrictions were put on the searches, so both inter- and intramolecular contacts are represented in the plots. On further narrowing the search to just interactions between a chloroform molecule chlorine atom and a transition metal bound chlorine atom, 44 (Cl) and 5 (Br) hits, respectively, were obtained. Scatter plots of the data are presented as Figures 11 and 12. For the TM−Cl···$ClCHCl_2$ system the angular range is generally greater than 150°, with one exception KOMFIB, which has an interaction angle of 75°. The Cl···Cl approach is only 3.9% less than the sum of the van der Waals radii and, due to the nonspherical nature of van der Vaals radii, it is unlikely that this is a noteworthy contact and can be ignored.

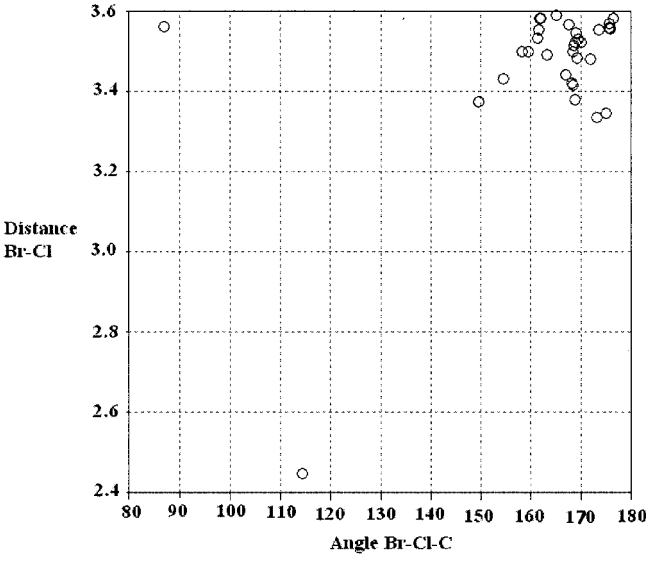

Figure 8. Scatter plot of TMBr···ClCR distance [Å] versus Cl···ClCR angle [°]

 © 2003 Wiley-VCH Verlag GmbH & Co. KGaA, Weinheim

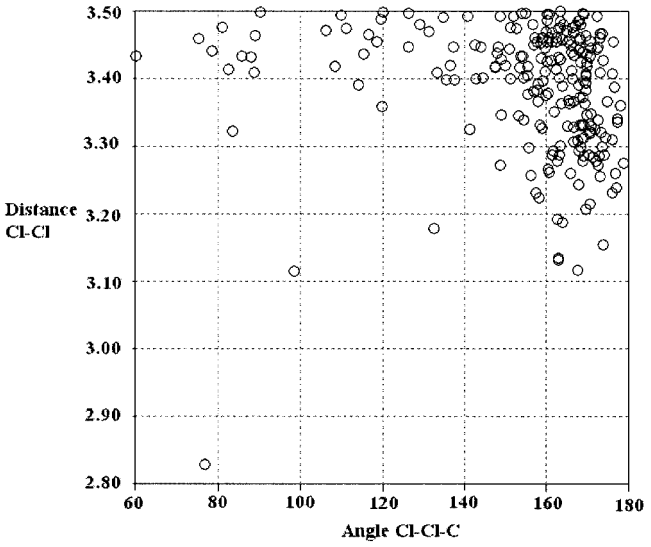

Figure 9. Scatter plot of TMCl···ClCR distance [Å] versus Cl···ClCR angle [°]

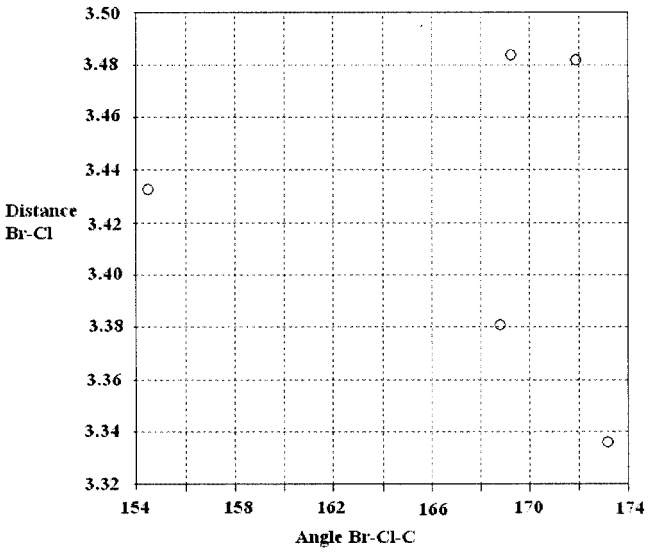

Figure 11. Scatter plot of TMBr···$ClCHCl_2$ distance [Å] versus Cl···ClCR angle [°]

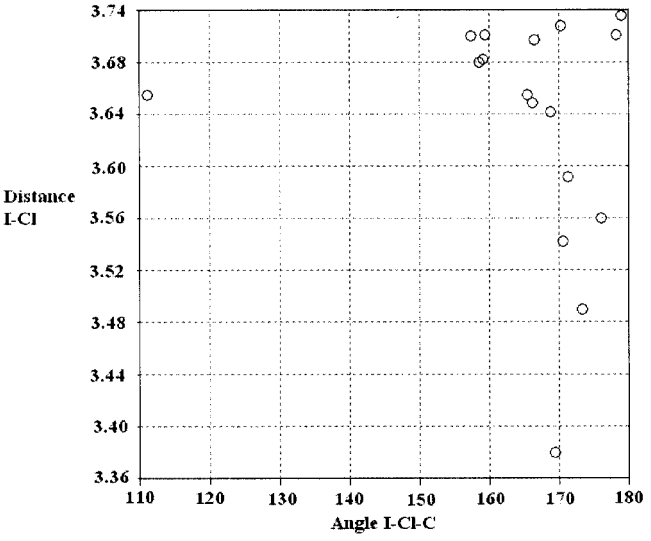

Figure 10. Scatter plot of TMI···ClCR distance [Å] versus Cl···ClCR angle [°]

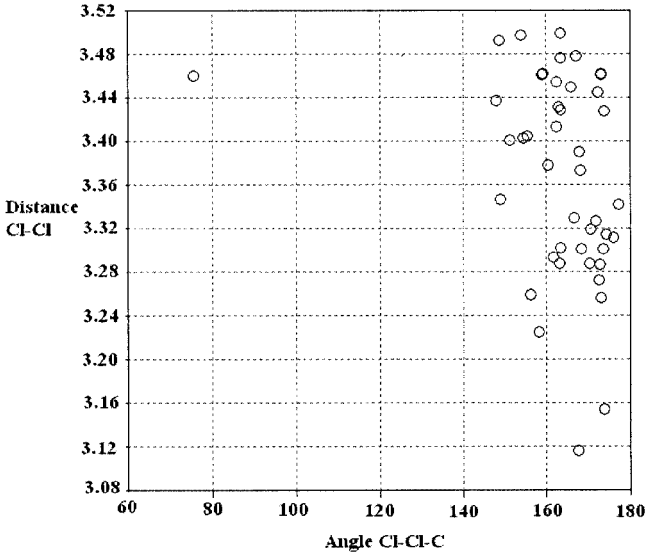

Figure 12. Scatter plot of TMCl···$ClCHCl_2$ distance [Å] versus Cl···ClCR angle [°]

For the TM−Br···$ClCHCl_2$ system the angular range is greater than 154°, with four interactions greater than 169°. These plots show then that the chloroform interaction with the metal halide has mean X−Cl−C (X = Br, Cl) angles of 167.5 and 162.9°, respectively, which are very close to linear. All the points are also comfortably within the sum of the van der Waals radii (3.75 and 3.60 Å),[37] with the Ru−X···$ClCCl_2H$ (X = Br, Cl) interaction observed for **4-Br** and **4-Cl** towards the shorter ends of the observed ranges (Figures 11 and 12). This would suggest that the Ru−X···Cl (X = Cl, Br) interactions observed in this system are real, supported at least by the presence of other comparable interactions present in the CDS, and qualitatively, at least, of comparable strength to the Ru−X···H (X = Br, Cl) interaction. The "linear" nature of these interactions is consistent with the idea that that the interaction is charge-transfer in nature [Ru−X to the C−Cl bond (n → σ*)].

An alternative interpretation could be put forward based upon polar flattening. To invoke this argument a van der Waals radius approximately 0.25 Å less than the accepted value for each atom would be required if the interaction was to fall outside the sum of the van der Waals radii. When considered in conjunction with the following: compounds **4-F** and **4-I** form exclusively hydrogen-bonded interactions with the chloroform solvate; the strength of the hydrogen bond Ru−X···$HCCl_3$ would be expected to follow the trend X = F > Cl > Br > I; the "disorder" is the same, save for relative occupancy, for **4-Br** and **4-Cl** (suggesting a preference for the chloroform's orientation); it tends to make this approach less attractive in this case.

 © 2003 Wiley-VCH Verlag GmbH & Co. KGaA, Weinheim

In addition to the electronic effects the increasingly bulky halide ligand exacts steric influences on the surrounding ligands, which manifests itself clearly in the orientation of the phenyl rings bearing the hydrogen atoms H(9), H(26), H(40) and H(46) that are involved in hydrogen bonding to the Ru−X halogen atoms. They all twist as expected to accommodate the increasing volume requirements of the halogen atom, or alternatively twist in to encapsulate the smaller halogen atom. Further, as a result of the increasing Ru−X bond length, not surprisingly, the octahedral coordination nature of the halogen atom becomes increasingly distorted on going from fluoride to iodide.

Conclusion

We have readily effected halogen exchange in the compound [RuCl(CO){η²-*C*,*N*-$C_6H_4C(H)=NC_6H_4$-4-NO_2}(PPh_3)$_2$] to generate the family of compounds [RuX(CO){η²-*C*,*N*-$C_6H_4C(H)=NC_6H_4$-4-NO_2}(PPh_3)$_2$] (X = F, Cl, Br, I) and shown that the fluoride ligand is the strongest π-donor. Further, on recrystallisation of the compounds **4-Br**, **4-Cl**, **4-F**, **4-I** from chloroform the Ru−X moiety forms a hydrogen bond to the chloroform of crystallisation and it is apparent that the strongest interaction, as expected, is to the fluorine atom. Unexpectedly, a competing Ru−X···$ClCHCl_2$ (X = Cl, Br) interaction has been observed. In conjunction with data from a series CDS searches, this interaction has been shown to have precedence and is possibly charge-transfer in nature. Further, intramolecular hydrogen bonds from phenyl ring hydrogen atoms of the PPh_3 and the cyclometallated imine ligands to the halogen atom were observed in all of the compounds. This leads to essentially octahedral coordination about the halogen atom. The presence of these ancillary ligand phenyl−hydrogen interactions may well have implications for results obtained from theoretical calculations where, for example, the PPh_3 ligand is simplified to PH_3 as in a recent report detailing the mechanism of protonation of the η²-allene ligand in [ReCl(η²-$H_2C=C=CH_2$)(dppe)$_2$] using the model compound [ReCl(η²-$H_2C=C=CH_2$)(PH_3)$_4$]. In this study initial protonation was suggested to occur at the chloride ligand, but took no account of potentially competing hydrogen bond interactions from the dppe phenyl ring hydrogen atoms.[38]

Experimental Section

General Remarks: All solvents, except alcohols, were dried by refluxing in the presence of an appropriate drying agent (toluene, Na; CH_2Cl_2, P_4O_{10}; hexane, NaK) and distilled prior to use. [RuHCl(CO)(PPh_3)$_3$][39] and [RuCl(CO){η²-*C*,*N*-$C_6H_4CH=NC_6H_4$-4-NO_2}(PPh_3)$_2$][21] were prepared according to literature procedures. All other chemicals were obtained from commercial sources and used as received except for $RuCl_3$ which was loaned by Johnson Matthey. Infrared spectra were recorded as nujol mulls between KBr plates with a Nicolet 5PC spectrometer. ^1H NMR (200.2 MHz) and $^{31}P\{^1H\}$ NMR (81.3 MHz) were recorded with a Bruker DPX200 spectrometer and $^{13}C\{^1H\}$ NMR (100.55 MHz) were recorded with a Bruker DPX400 spectrometer. ^1H and $^{13}C\{^1H\}$ NMR spectra were referenced to $CHCl_3$ (δ = 7.26 ppm) and $CHCl_3$ (δ = 77.0 ppm) and $^{31}P\{^1H\}$ NMR spectra were referenced externally to 85% H_3PO_4 (δ = 0.0 ppm). Elemental analyses were performed by the Microanalytical Service, Department of Chemistry, UMIST; solvates of crystallisation were confirmed by repeated elemental analysis and confirmed by ^1H NMR spectroscopy. The syntheses of all complexes were carried out under dinitrogen using standard Schlenk techniques. Workups were generally carried out in the open unless otherwise stated.

[RuF(CO){η²-*C*,*N*-$C_6H_4CH=NC_6H_4$-4-NO_2}(PPh_3)$_2$]·2$CHCl_3$ (4-F): Ag[BF_4] (0.022 g, 0.11 mmol) was added to [RuCl(CO){η²-*C*,*N*-$C_6H_4CH=NC_6H_4$-4-NO_2}(PPh_3)$_2$] (0.1 g, 0.11 mmol), dissolved in CH_2Cl_2/acetone (1:1, 10 mL) under a stream of dry N_2. After 20 min, the solution was filtered to remove AgCl, and NaF (0.05 g, 1.2 mmol), dissolved in H_2O (0.2 mL), was added followed by enough EtOH to generate a homogeneous solution. After 20 min, the organic solvent was removed under reduced pressure precipitating crude **4-F**. Collection by filtration and recrystallisation from $CHCl_3$ afforded **4-F**·2$CHCl_3$ (0.118 g, 96%). Compounds **4-Br**, **4-Cl**, **4-I** were prepared in an analogous fashion; see Table 1 for physical and analytical data.

X-ray Crystallographic Study: All of the crystals were grown by the slow evaporation of chloroform from a 20-mg sample, initially dissolved in 0.5 mL of solvent in a lightly capped 5-mm NMR tube. All measurements were carried out with a Nonius Kappa CCD diffractometer using graphite-monochromated Mo-K_α radiation (λ = 0.71073 Å) at 150 K for **4-Br**, **4-Cl**, **4-F** and 120 K for **4-I** at the National Crystallographic Service, University of Southampton, England. The structures were solved by direct methods using SHELXL-97[40] and subjected to full-matrix least-squares refinement on F^2. In **4-Br** and **4-Cl** the $CHCl_3$ which interacts with the halogen ligand is disordered and was modelled using the same geometric restraints and with variable atomic site occupancies. Additionally for **4-Br**, **4-Cl** and **4-I**, the lattice $CHCl_3$ is disordered about a crystallographic inversion point and was also modelled using geometric restraints, but in this case the atomic site occupancies were set to 0.5. In this case the disorder in **4-Br** and **4-Cl** was not the same. The crystallographic details are presented in Table 4. CCDC-172276, -172277, -172278, -1772279 (**4-F** to **4-I**) contain the supplementary crystallographic data for this paper. These data can be obtained free of charge at www.ccdc.cam.ac.uk/conts/retrieving.html [or from the Cambridge Crystallographic Data Centre, 12 Union Road, Cambridge CB2 1EZ, UK; Fax: (internat.) + 44-1223/336-033; E-mail: deposit@ccdc.cam.ac.uk].

Acknowledgments

We thank the EPSRC National Crystallographic Service for data collections project number 01XR10, the EPSRC for the award of a postgraduate studentship to J. E. W. and Johnson Matthey for the kind loan of $RuCl_3$.

[1] A. Werner, *Justus Liebigs Ann. Chem.* **1902**, *322*, 261−297.
[2] J. C. Speakman, *The Hydrogen Bond and Other Intermolecular Forces* (Monographs for Teachers, no. 27), The Chemical Society, London, **1975**, p. 8.
[3] L. Pauling, *The nature of the chemical bond*, Cornell University Press, Ithaca, New York, **1939**.
[4] G. C. Pimentel, A. L. McClellan, *The hydrogen bond*, W. H. Freeman, San Francisco, **1960**.

 © 2003 Wiley-VCH Verlag GmbH & Co. KGaA, Weinheim

[5] G. R. Desirauju, T. Steiner, *The Weak Hydrogen Bond in Structural Chemistry and Biology*, Oxford University Press, Oxford, **1999**.
[6] G. A. Jeffrey, W. Saenger, *Hydrogen Bonding In biological Structures*, Springer-Verlag, Berlin, **1991**.
[7] L. J. Prins, D. N. Reinhoudt, P. Timmerman, *Angew. Chem.* **2001**, *113*, 2446−2492; *Angew. Chem. Int. Ed.* **2001**, *40*, 2382.
[8] G. R. Desirajau, *Crystal Engineering: the Design of Organic Solids*, Elsevier, Amsterdam, **1991**.
[9] E. J. Corey, T. W. Lee, *Chem. Commun.* **2001**, 1321−1329.
[10] M. Yamakawa, I. Yamada, R. Noyori, *Angew. Chem.* **2001**, *113*, 2900−2903; *Angew. Chem. Int. Ed.* **2001**, *40*, 2818−2821.
[11] P. D. Beer, P. A. Gale, *Angew. Chem.* **2001**, *113*, 502−532; *Angew. Chem. Int. Ed.* **2001**, *40*, 486−516.
[12] T. Steiner, *Angew. Chem.* **2002**, *114*, 58−80; *Angew. Chem. Int. Ed.* **2002**, *41*, 48−76.
[13] N. Ramasubbu, R. Parthasarathy, P. Murry-Rust, *J. Am. Chem. Soc.* **1986**, *108*, 4308−4314.
[14] S. C. Nyburg, W. Wong-Ng, *Proc. R. Soc. London A* **1979**, *367*, 29−45.
[15] S. L. Price, A. J. Stone, J. Lucus, R. S. Rowland, A. E. Thornley, *J. Am. Chem. Soc.* **1994**, *116*, 4910−4918.
[16] J. P. M. Lommerse, A. J. Stone, R. Taylor, F. H. Allen, *J. Am. Chem. Soc.* **1996**, *118*, 3108−3116.
[17] R. Boese, A. D. Boese, D. Bläser, M. Yu, A. Ellerern, K. Seppelt, *Angew. Chem.* **1997**, *109*, 1538−1541; *Angew. Chem. Int. Ed. Engl.* **1997**, *36*, 1489 and refs therein.
[18] W. R. Roper, L. J. Wright, *J. Organomet. Chem.* **1977**, *142*, C1−C6.
[19] W. I. Cross, K. R. Flower, R. G. Pritchard, *J. Organomet. Chem.* **2000**, *601*, 164−171.
[20] K. R. Flower, R. G. Pritchard,, *J. Organomet. Chem.* **2001**, *620*, 60−68.
[21] K. R. Flower, V. J. Howard, R. G. Pritchard, J. E. Warren, *Organometallics* **2002**, *21*, 1184−1189.
[22] K. Venkataraman, *Synthetic Dyes*, vol. 1, Academic Press, New York, **1952**.
[23] H. Zollinger, *Azo and Diazo Chemistry*, Wiley-Interscience, New York, **1961**.
[24] L. Antonov, W. M. F. Fabian, D. Nedeltcheva, F. S. Kamounah, *J. Chem. Soc., Perkin Trans. 2* **2000**, 1173−1179.
[25] C. K. Johnson, Report ORNL-5138, Oakridge National Laboratory, Tennessee, USA, **1976**.
[26] J. March, *Advanced Organic Chemistry, Structure, Reaction, and Mechanisms*, 4th ed. Wiley Interscience, New York, **1992**, p. 28.
[27] K. G. Caulton, *New J. Chem.* **1994**, *18*, 25−41.
[28] K. Fagnou, M. Lautens, *Angew. Chem.* **2002**, *114*, 26−49; *Angew. Chem. Int. Ed.* **2002**, *41*, 26−47.
[29] H. O. Kalinowski, S. Berger, S. Braun, *Carbon-13 NMR Spectroscopy*, Wiley-Interscience, New York, **1988**.
[30] W. Massa, D. Babel, *Chem. Rev.* **1988**, *88*, 275−296.
[31] T. G. Richmond, *Coord. Chem. Rev.* **1990**, *105*, 221−250.
[32] F. H. Allen, J. E. Davies, O. J. Johnson, O. Kennard, C. F. Macrae, G. F. Mitchell, J. M. Smith, D. Watson, *J. Chem. Inf. Compt. Sci.* **1991**, *31*, 187−204.
[33] S. C. Lee, R. H. Holm, *Inorg. Chem.* **1993**, *32*, 4745−4753.
[34] G. P. A. Yap, A. L. Rheingold, P. Das, R. H. Crabtree, *Inorg. Chem.* **1995**, *34*, 3474−3476.
[35] G. Aullón, D. Bellamy, L. Brammer, E. A. Bruton, A. G. Orpen, *Chem. Commun.* **1998**, 653−654.
[36] A. L. Spek, *Platon (C)*, Utrecht University, Padualaan 8, 3584 CH, Utrecht, The Netherlands, **1900−2002**.
[37] A. Bondi, *J. Phys. Chem.* **1964**, *68*, 441−451.
[38] M. L. Kuznetsov, J. L. Pombeiro, A. I. Dement'ev, *J. Chem. Soc., Dalton Trans.* **2000**, 4413−4421.
[39] N. Ahmad, J. J. Levison, S. D. Robinson, M. J. Uttley, *Inorg. Synth.* **1974**, *15*, 48−49.
[40] G. M. Sheldrick *Programs for crystal structure analysis* (release 97-2), University of Göttingen, **1998**.

Received September 18, 2002

 © 2003 Wiley-VCH Verlag GmbH & Co. KGaA, Weinheim

NIR Dyes Based on [M(R,R′timdt)$_2$] Metal-Dithiolenes: Additivity of M, R, and R′ Contributions To Tune the NIR Absorption (M = Ni, Pd, Pt; R,R′timdt = Monoreduced Form of Disubstituted Imidazolidine-2,4,5-trithione)

M. Carla Aragoni,[a] Massimiliano Arca,*[a] Tiziana Cassano,[b] Carla Denotti,[a] Francesco A. Devillanova,[a] Romina Frau,[a] Francesco Isaia,[a] Francesco Lelj,[c] Vito Lippolis,[a] Luigi Nitti,[b] Pina Romaniello,[c] Raffaele Tommasi,[b] and Gaetano Verani[a]

Keywords: S ligands / Nickel / Palladium / Platinum / Density functional calculations / Nonlinear optics

With the aim of preparing new dyes for Q-switching and/or mode-locking Nd-based lasers, such as Nd:YLF and Nd:YAG (emission wavelengths 1053 and 1064 nm, respectively), the syntheses of about 30 new neutral dithiolenemetal complexes belonging to the class [M(R,R′timdt)$_2$] have been carried out [M = Ni (**4a–c**; **4g–j**), Pd (**5a–j**), Pt (**6a–j**); R,R′timdt = monoreduced form of disubstituted imidazolidine-2,4,5-trithione]. The examination of the effects induced on the intense NIR absorption by changing M, R, and R′ has allowed for the recognition of the additive contributions ($\Delta\lambda$) of the central metal ion and of the substituents to the $\lambda_{max}^{M,R,R'}$ position of the NIR absorption maximum, which is in the region of 1000 nm. The high $\Delta\lambda$ values due to aromatic substituents have been elucidated by means of Hybrid-DFT calculations performed on the model compound [Ni(H$_2$timdt)(Ph,H-timdt)]. Both the $\lambda_{max}^{M,R,R'}$ values and the molar extinction coefficients vary with the solvent. Complex **5f** [M = Pd, R = *p*-F-C$_6$H$_4$, R′ = *m*,*m*,*p*-(MeO)$_3$-C$_6$H$_2$] shows that it has been possible to exactly match the emission wavelength of the Nd:YLF and Nd:YAG lasers in chloroform and toluene, respectively (by choosing the appropriate combination of metal ion and substituents). The highest extinction coefficient ever observed for a metal-dithiolene (120000 $M^{-1}\cdot cm^{-1}$ at 1034 nm in toluene) is also reported for complex **6g** [M = Pt, R = *p*-F-C$_6$H$_4$, R′ = naphthyl]. Time-resolved absorption dynamics measurements on **5f** have also been carried out by means of pump-probe experiments, with a picosecond Nd:YAG Q-switched and mode-locked laser.
(© Wiley-VCH Verlag GmbH & Co. KGaA, 69451 Weinheim, Germany, 2003)

Introduction

The tuning of specific molecular properties by means of chemical modifications is of current interest in material chemistry and engineering.[1] During the past years, the design of organic chromophores with specific optical properties has been made possible thanks to the discovery of well-defined structure-property relationships (SPRs).[2−4] Nevertheless, the relationships between the structural factors and the nonlinear optical properties of inorganic materials are still not well understood.[1,5] In particular, this applies to the search for materials which can be used in laser applications, such as Q-switching or mode-locking. In order to be exploited as saturable absorbers, dyes have to satisfy several criteria. In particular, (i) the fundamental absorption should exhibit a very high cross-section at the laser emission wavelength, (ii) no excited-state absorption should be present at the same wavelength, and (iii) the molecules should be very stable when exposed to light. Moreover, in order to prevent damage to laser optics, the dyes must be quite soluble in inert solvents. Most materials used in laser applications are based on organic substrates, but these are generally photochemically not as stable as required.

Bis-dithiolene complexes of d^8 metals have been used for Q-switching near-infrared (NIR) lasers since the early 1970s,[6−8] and have also been used as materials for molecular magnets, conductors, and superconductors.[9,10] These complexes exhibit a high degree of π-electron delocalization,[11−13] involving the organic framework as well as the metal center,[14] which confers peculiar and unique molecular properties, such as planarity, optical non-

[a] Dipartimento di Chimica Inorganica ed Analitica, Complesso Universitario di Monserrato, S. S.
554 bivio per Sestu, 09042 Monserrato (Cagliari), Italy
Fax: (internat.) + 39-070/675-4456
E-mail: marca@unica.it
[b] DETO, Dipartimento di Fisica and INFM,
Via G. Amendola 173, 70126 Bari, Italy
[c] Dipartimento di Chimica,
Via N. Sauro 85, 85100 Potenza, Italy

linearity,[15] high thermal and photochemical stabilities, along with the ability to have a variable charge, which in some cases can vary reversibly from −2 to +2. The possibility of applying dithiolenes to laser technology relies on the unique property that these complexes feature an intense Vis/NIR absorption in the neutral state, due to a singlet[16] $\pi \rightarrow \pi^*$ transition between the HOMO and LUMO,[17] at frequencies which depend on the nature of the substituents at the carbon atoms of the dithiolene moiety.[6] In particular, donor substituents shift the position of this absorption to energies lower[9,17] than those found in the dithiolenes which are derived from the edt ligand {[$M(edt)_2$]; edt = ethylenedithiolato, M = Ni (**1**), λ_{max} = 720 nm; M = Pd (**2**), λ_{max} = 785 nm; M = Pt (**3**), λ_{max} = 680 nm}.[18−20] Obviously, among the various dithiolenes, only a few compounds meet all the requirements. Since 1995,[21] a series of papers has reported on the synthesis, spectroscopic and structural characterization,[22−24] reactivity[25,26] and photophysical properties[27−29] of the new class of dithiolenes [$M(R,R'timdt)_2$] [R,R′timdt = disubstituted monoreduced imidazolidine-2,4,5-trithione; M = Ni (**4**), Pd (**5**), Pt (**6**)]. The most striking property of these dithiolenes is the unusually intense absorption at about 1000 nm, with extinction coefficients in chloroform as high as 80000 $M^{-1}\cdot cm^{-1}$. This absorption is assigned to a $\pi-\pi^*$ singlet transition and has been confirmed by TD-DFT calculations.[27,28] The application of these dithiolenes to Nd-based lasers,[21,27] such as Nd:YLF and Nd:YAG (emission wavelengths 1053 and 1064 nm, respectively), was prevented by their very low solubility. Therefore, it was necessary to look for new substituents, with the aim of both increasing the solubility, and of simultaneously shifting the position of the absorption to values as close as possible to the emission wavelengths of the Nd lasers.

Here we report on the syntheses of almost 30 new dithiolenes belonging to the title class. By referring to the NIR spectral properties of all the dithiolenes synthesized so far, the present work shows that there is an additive effect of the metal ion and of the substituents on the maximum NIR absorption wavelength, and that it is possible to quantify these contributions to the position of the NIR absorption band. In particular, the high contribution by the aromatic groups is elucidated on the basis of DFT calculations. The absorption saturation temporal dynamics of the dithiolene **5f**, which exactly matches the emission wavelength of the Nd:YLF and Nd:YAG lasers in chloroform and toluene, respectively, has been investigated using the picosecond pump-probe technique. The physical processes responsible for the dynamics have been explained using multi-level rate equations,[27,28] supported by relativistic time-dependent density functional calculations.

Results and Discussion

In order to apply [$M(R,R'timdt)_2$] dithiolenes successfully to Q-switch or mode-lock Nd-based lasers, two main goals were to be achieved: a) to significantly increase their solubility in common organic solvents, such as chloroform or dichloromethane; and b) to ensure that the wavelength of the maximum in the NIR absorption is as close as possible to the target laser emission wavelength. The change in the central metal ion and in the substituents R and R′ at the nitrogen atoms enables both objectives to be met. In fact, from the NIR spectra of the first series of synthesized Ni, Pd, and Pt complexes belonging to this class,[24] it could be seen that both the solubility and the position of the NIR absorption depend on the metal ion and on the R and R′ substituents; e.g., aromatic substituents shift the position of the absorption in the desired direction, however, the solubility in low-polar solvents is greatly reduced. With the aim of obtaining a satisfactory solubility, and in order to match the positions of the NIR absorption maxima with the laser emission wavelengths, several new [$M(R,R'timdt)_2$] dithiolenes have been prepared with alkyl and aryl substituents, in particular with the introduction of fluorine atoms or fluorine-rich groups into the phenyl ring.

Synthesis

According to the well-established route summarized in Scheme 1,[24] approximately 30 new Ni-, -Pd-, and Pt-dithiolenes, containing different types of substituents (**4a−c** and **4g−j**, **5a−j**, **6a−j** for Ni, Pd, and Pt, respectively), have been synthesized by the sulfuration of the corresponding disubstituted 2-thioxoimidazolidine-4,5-diones (**7a−j**) with Lawesson's reagent (**8**; 1,3,2,4-dithiadiphosphetane 2,4-disulfide).[30] Unfortunately, with the only exception of **4g**, the syntheses of the Ni complexes that are derived from the 2-thioxoimidazolidine-4,5-diones with a *p*-fluorophenyl substituent (**4d−f**) have not been successful. All the new compounds have been fully characterized by conventional methods, confirming the properties already reported for this class of neutral complexes.[23,24] In particular, the melting points are very high, generally over 250 °C, thus confirming their outstanding thermal stabilities. Among the synthesized dithiolenes, those with phenyl substituents are, in general, not very soluble. However, the solubility increases when naphthyl or *p*-CF_3O-C_6H_4 groups are present.

NIR-Spectroscopy

Effect of M, R, and R′

Considering the new dithiolenes and those previously reported,[24] the typical NIR absorption maximum in $CHCl_3$ ($\lambda_{max}^{M,R,R'}$) spans over 60 nm between 991 (M = Ni; R = R′ = Me) and 1053 nm (**5f**). The molar extinction coefficients in the same solvent are in some cases higher than the previously reported[24] maximum value of 80000 $M^{-1}\cdot cm^{-1}$. For example, among the new most soluble complexes, **6c**, **6g**, and **6h** have values of 91000, 105000, and 110000 $M^{-1}\cdot cm^{-1}$, respectively, which are by far the highest values ever reported for dithiolene complexes.

The qualitative observation that the $\lambda_{max}^{M,R,R'}$ values depend on both the central metal ion and the substituents R and R′ has now been quantified, due to the great number

 © 2003 Wiley-VCH Verlag GmbH & Co. KGaA, Weinheim

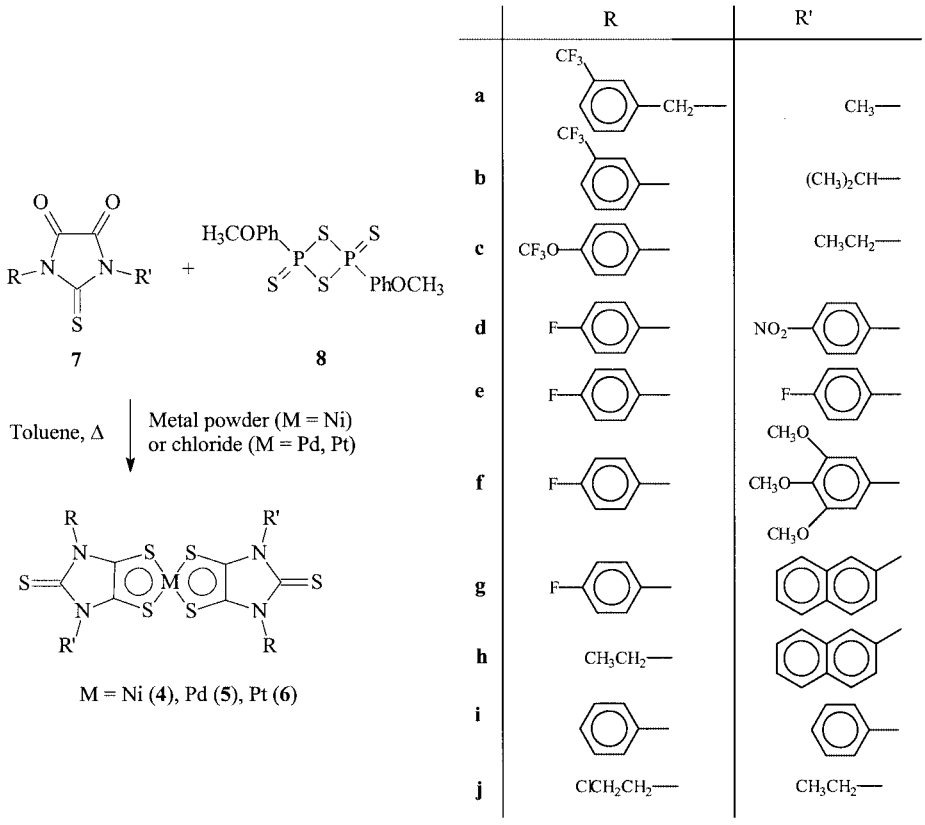

Scheme 1. Overall reaction path in the syntheses of dithiolenes **4**−**6**

(about 60) of synthesized dithiolenes, according to the relationship

$$\lambda_{max}^{M,R,R'} = \lambda_{max}^{Ni,Me,Me} + \Delta\lambda^{M} + \sum_{j=1}^{4}\Delta\lambda_{j}^{R}$$

where $\lambda_{max}^{Ni,Me,Me}$ represents the absorption wavelength recorded for [Ni(Me$_2$timdt)$_2$] ($\lambda_{max}^{Ni,Me,Me}$ = 991 nm), which can be considered the simplest member of this class of compounds. A least-squares fit (R = 0.97) of the experimental values listed in Table 1 has allowed for the evaluation of the contribution of the metal ion ($\Delta\lambda^{M}$) and of each substituent ($\Delta\lambda^{R}$). The goodness of such a regression (Figure 1) can be used to predict the absorption wavelength position of a particular dithiolene with a peculiar metal ion and substituent. As reported in Table 1, the central metal ion Pd confers a remarkable contribution ($\Delta\lambda^{Pd}$ = 20.59 nm) to $\lambda_{max}^{M,R,R'}$, compared with Ni and Pt ($\Delta\lambda^{M}$ = 0.00 and 1.62 nm for M = Ni and Pt, respectively). The bathochromic shift is influenced by the electron-releasing ability of the substituents; thus, for alkyl substituents, the shift increases with the length of the chain ($\Delta\lambda^{R}$ = 1.52, 1.86, 2.93, 3.72 nm for R = Et, *i*Pr, pentyl and nonyl, respectively) in agreement with an increasing $+I$ effect. The bathochromic effect due to the phenyl ring is more effective, and depends on the presence of groups bonded to the phenyl ring [$\Delta\lambda^{R}$ = 7.86, 5.36, 8.86 and 12.95 nm for R = phenyl, *p*-F-C$_6$H$_4$, *p*-Cl-C$_6$H$_4$, and *m*,*m*,*p*-(MeO)$_3$-C$_6$H$_2$, respectively]. Unexpectedly, the extension of π-aromaticity in the ligand (π-aromaticity extends from phenyl to naphthyl substituents) does not significantly increase the $\lambda_{max}^{M,R,R'}$ values ($\Delta\lambda^{R}$ = 7.86, 8.38 nm for R = phenyl, naphthyl, respectively).

Theoretical Calculations

The assignment of the intense low-energy Vis/NIR transition to a singlet π−π* HOMO−LUMO excitation,[16] peculiar to bis-dithiolenes, was also confirmed for [M(R,R′timdt)$_2$], based on Hybrid-DFT[24] and TD-DFT[28] calculations performed on the [M(H$_2$timdt)$_2$] complexes [M = Ni (**4^H**), Pd (**5^H**), Pt(**6^H**)], i.e. on the hypothetical complexes with four hydrogen atoms instead of the four organic substituents. These calculations accounted for the trends found on changing the central metal ion, not only in the [M(R,R′timdt)$_2$] complexes, but also in those derived from the edt ligand.[18−20,24] Since it is very interesting to understand the origin of the remarkable bathochromic shift observed in the presence of aromatic substituents, Hybrid-DFT calculations at the same level of theory as those carried out on **4^H**−**6^H** have now been extended to the mixed-ligand [Ni(H$_2$timdt)(H,Ph-timdt)] model complex (**9**, Figure 2), where a phenyl ring has been introduced as a substituent at the nitrogen atom of the nickel complex. In addition, in order to evaluate the influence of the ring orientation with respect to the molecular plane, the geometry was optimized at different frozen C(9)−N(13)−C(21)−C(22) dihedral angles (θ) correspond-

 © 2003 Wiley-VCH Verlag GmbH & Co. KGaA, Weinheim

Table 1. Experimental NIR absorption maxima $\lambda_{exp}^{M,R,R'}$ [nm] for neutral [M(R,R′timdt)$_2$] dithiolenes, compared with the $\lambda_{max}^{M,R,R'}$ [nm] estimated on the basis of the additive coefficients $\Delta\lambda^M$ and $\Delta\lambda^R$: $\Delta\lambda^M$ = 0.00 (Ni), 20.59 (Pd), 1.62 (Pt) nm; $\Delta\lambda^R$ = 0.00 (Me), 1.52 (Et), 1.86 (*i*Pr), 2.93 (pentyl), 3.72 (nonyl), 2.72 ($ClCH_2CH_2$), 7.86 (Ph), 5.36 (*p*-F-C_6H_4), 8.86 (*p*-Cl-C_6H_4), 8.98 (*p*-O_2N-C_6H_4), 9.05 (*p*-MeO-C_6H_4), 8.01 (*p*-F_3CO-C_6H_4), 6.65 (*m*-F_3C-C_6H_4), 12.95 [*m*,*m*,*p*-$(MeO)_3$-C_6H_2], 8.38 (naphthyl) nm

M	R	R′	Ref.	$\lambda_{exp}^{M,R,R'}$	$\Delta\lambda^M + \sum_{i=1}^{4}\Delta\lambda_i^R$	$\lambda_{max}^{M,R,R'}$
Ni	Et	*p*-CF_3O-C_6H_4	[a] **(4c)**	1010	19.04	1010
Ni	Et	$ClCH_2CH_2$	[a] **(4j)**	1001	8.46	999
Ni	Et	Et	[b]	996	6.06	997
Ni	Et	naphthyl	[a] **(4h)**	1007	19.78	1011
Ni	Et	pentyl	[b]	998	8.89	1000
Ni	Et	Ph	[b]	1010	18.75	1010
Ni	*p*-F-C_6H_4	naphthyl	[a] **(4g)**	1019	27.48	1018
Ni	Me	*m*-F_3C-$C_6H_4CH_2$	[a] **(4a)**	992	2.72	994
Ni	Me	*p*-MeO-C_6H_4	[b]	1009	18.00	1009
Ni	Me	*p*-Cl-C_6H_4	[b]	1008	17.72	1009
Ni	Me	Me	[b]	991	0.00	991
Ni	Me	nonyl	[b]	996	7.43	998
Ni	Me	pentyl	[c]	997	5.86	997
Ni	Me	Ph	[c]	1010	15.72	1007
Ni	Me	*i*Pr	[b]	996	3.73	995
Ni	Ph	Ph	[a] **(4i)**	1023	31.44	1022
Ni	*i*Pr	*m*-F_3C-C_6H_4	[a] **(4b)**	1008	17.03	1008
Pd	Et	*p*-CF_3O-C_6H_4	[a] **(5c)**	1032	39.43	1030
Pd	Et	$ClCH_2CH_2$	[a] **(5j)**	1027	42.57	1034
Pd	Et	Et	[b]	1017	26.45	1017
Pd	Et	naphthyl	[a] **(5h)**	1033	40.17	1031
Pd	Et	pentyl	[b]	1019	29.28	1020
Pd	Et	Ph	[b]	1030	39.14	1030
Pd	*p*-F-C_6H_4	*m*,*m*,*p*-$(MeO)_3$-C_6H_2	[a] **(5f)**	1052	56.88	1048
Pd	*p*-F-C_6H_4	*p*-F-C_6H_4	[a] **(5e)**	1027	41.84	1033
Pd	*p*-F-C_6H_4	naphthyl	[a] **(5g)**	1047	47.87	1039
Pd	*p*-F-C_6H_4	*p*-O_2N-C_6H_4	[a] **(5d)**	1040	49.11	1040
Pd	Me	*m*-F_3C-$C_6H_4CH_2$	[a] **(5a)**	1017	23.11	1014
Pd	Me	*p*-MeO-C_6H_4	[b]	1030	38.39	1029
Pd	Me	*p*-Cl-C_6H_4	[b]	1030	38.11	1029
Pd	Me	Me	[b]	1010	20.39	1011
Pd	Me	*p*-O_2N-C_6H_4	[b]	1030	38.39	1029
Pd	Me	nonyl	[b]	1020	27.82	1019
Pd	Me	pentyl	[c]	1017	26.25	1017
Pd	Me	*i*Pr	[b]	1013	24.11	1015
Pd	Ph	Ph	[a] **(5i)**	1042	51.83	1043
Pd	*i*Pr	*m*-F_3C-C_6H_4	[a] **(5b)**	1028	37.42	1028
Pt	Et	*p*-F_3CO-C_6H_4	[a] **(6c)**	1010	20.51	1012
Pt	Et	$ClCH_2CH_2$	[a] **(6j)**	1006	9.94	1001
Pt	Et	Et	[b]	998	7.54	999
Pt	Et	naphthyl	[a] **(6h)**	1011	21.26	1012
Pt	Et	pentyl	[b]	1004	10.37	1001
Pt	Et	Ph	[b]	1012	20.22	1011
Pt	*p*-F-C_6H_4	*m*,*m*,*p*-$(MeO)_3$-C_6H_2	[a] **(6f)**	1025	37.96	1029
Pt	*p*-F-C_6H_4	*p*-F-C_6H_4	[a] **(6e)**	1015	22.93	1014
Pt	*p*-F-C_6H_4	naphthyl	[a] **(6g)**	1021	28.95	1020
Pt	*p*-F-C_6H_4	*p*-O_2N-C_6H_4	[b]	1021	30.20	1021
Pt	Me	*m*-F_3C-$C_6H_4CH_2$	[a] **(6a)**	994	4.19	995
Pt	Me	*p*-MeO-C_6H_4	[b]	1010	19.47	1010
Pt	Me	*p*-Cl-C_6H_4	[b]	1010	19.20	1010
Pt	Me	Me	[b]	993	1.47	992
Pt	Me	*p*-O_2N-C_6H_4	[b]	1010	19.47	1010
Pt	Me	nonyl	[b]	1001	8.91	1000
Pt	Me	pentyl	[c]	999	7.33	998
Pt	Me	*i*Pr	[b]	997	5.20	996
Pt	Ph	Ph	[a] **(6i)**	1022	32.91	1024
Pt	*i*Pr	*m*-F_3C-C_6H_4	[b]	1010	18.50	1010

[a] This work. [b] Taken from ref.[24] [c] Unpublished results.

 © 2003 Wiley-VCH Verlag GmbH & Co. KGaA, Weinheim

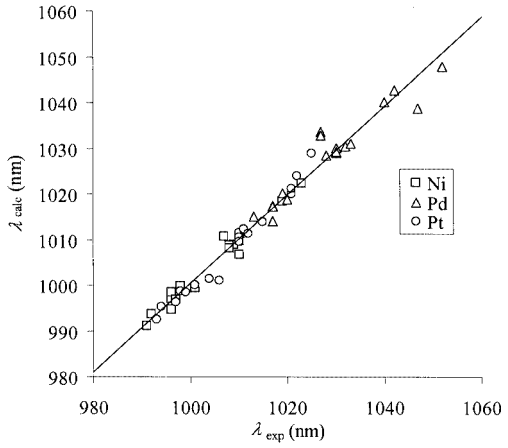

Figure 1. Linear correlation ($R = 0.97$) between experimental (λ_{exp}) and calculated (λ_{calc}) NIR absorption maxima wavelengths; λ_{calc} values have been evaluated by fitting with respect to the $\Delta\lambda^M$ and $\Delta\lambda^R$ parameters

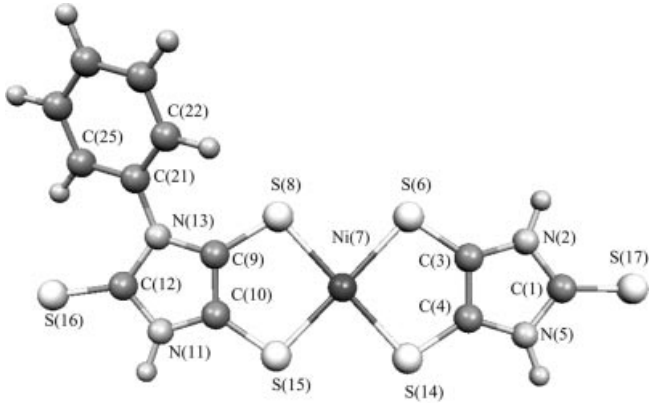

Figure 2. Drawing and atom numbering scheme of the model dithiolene **9**

ing to the rotation of the phenyl ring around the C(21)−N(13) bond. On passing from θ = 0° to θ = 180°, two local minima in the total electronic energy are found at 60 and 120°, respectively, while the maxima are found when the ring lies in the molecular plane (Table 2, Figure 3), the

Table 2. Relative total electronic DFT energy variation Δ*E*, Kohn−Shan energies for the HOMO and the LUMO (E^{HOMO} and E^{LUMO}, respectively), HOMO−LUMO energy gap ΔE, calculated for **9** at different torsional angles θ (0° ≤ θ ≤ 90°)

θ [°]	Δ*E* [kcal/mol][a]	E^{HOMO} [eV]	E^{LUMO} [eV]	ΔE [eV]
0	7.752	−5.287	−4.199	1.088
10	5.638	−5.271	−4.188	1.083
20	3.544	−5.249	−4.169	1.079
30	1.880	−5.225	−4.150	1.077
40	0.763	−5.206	−4.131	1.075
50	0.169	−5.187	−4.112	1.075
60	0.000	−5.170	−4.095	1.076
70	0.108	−5.157	−4.082	1.077
80	0.224	−5.148	−4.071	1.078
90	0.325	−5.146	−4.065	1.079

[a] ΔE = 1.078 eV for **4^H**.

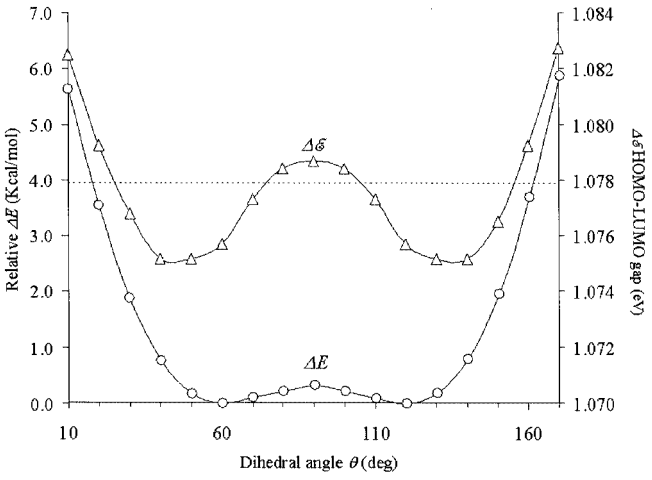

Figure 3. Relative total electronic energy variation Δ*E* (circles) and Kohn−Shan HOMO−LUMO energy gap ΔE (triangles) compared with the ΔE value calculated for **4^H** at the same level of theory (dotted line), calculated for **9** as a function of the phenyl rotation (θ)

difference between the two extremes being about 8 kcal/mol. The rotation around the C(21)−N(13) bond does not affect the nature of the main frontier orbitals. The calculated Kohn−Shan HOMO and LUMO are depicted in Figure 4. The former is a π-orbital extended over the whole molecule, with the contribution of the p_z atomic orbitals of all the atoms, with the exception of the metal center and the carbon atoms of the terminal thioxo groups. All the atoms contribute to the π*-LUMO; the metal ion is directly involved through its nd_{xz} atomic orbitals. In Figure 3, the differences between the HOMO and LUMO energies, ΔE, calculated by varying the dihedral angle θ (Table 2), are also reported and compared with the energy calculated[24] for **4^H** at the same level of theory. The minima in the HOMO−LUMO energy gap are found when the phenyl ring is twisted by about 45° with respect to the dithiolene molecular plane, a value which is close to those calculated for the total electronic energy minima. Therefore, at θ values corresponding to a total electronic energy lower than 1 kcal/mol (40° ≤ θ ≤ 140°), the HOMO−LUMO energy gap in **9** is lower than the gap calculated for **4^H**. This is in agreement with the NIR bathochromic shift measured in the presence of phenyl rings, and in general, of aromatic substituents. Contrary to our expectations, it should be

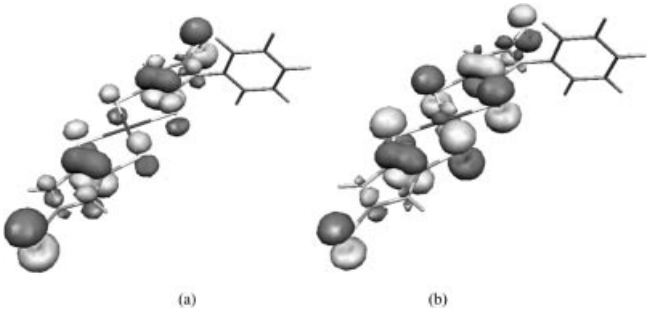

Figure 4. Sketches of Kohn−Shan HOMO (a) and LUMO (b) calculated for **9** at θ = 60° (contour value 0.05)

 © 2003 Wiley-VCH Verlag GmbH & Co. KGaA, Weinheim

noted that such a shift is not directly due to the conjugation between the molecular electronic π-system and that of the phenyl ring, since the minima in the total electronic energy and those in the HOMO−LUMO energy gap, ΔE, are found at 45 and 60°, respectively. This also accounts for the $\Delta\lambda^{R}$ value of the naphthyl group (8.58 nm), which does not differ significantly from that estimated for the phenyl ring (7.86 nm).

Solvatochromic Effect

The UV/Vis/NIR spectra of the [M(R,R′timdt)$_2$] dithiolenes were recorded in solvents of varying polarity, ranging from CCl_4 (dielectric constant $\varepsilon_d = 2.2$) to dimethyl sulfoxide ($\varepsilon_d = 47.2$). As previously observed for different neutral nickel-dithiolenes,[31] both the $\lambda_{max}^{M,R,R'}$ and the molar extinction coefficient values depend on the nature of the solvents. Thus, the solvent is another factor that can be used to modulate the position of the NIR maximum. For solvents having dielectric constants of up to about 35, a continuous decrease in $\lambda_{max}^{M,R,R'}$ is observed on increasing ε_d; for solvents with high ε_d values (nitrobenzene, dimethylformamide, dimethyl sulfoxide: $\varepsilon_d = 35.7, 38.3, 47.2$) the trend is roughly reversed. This does not depend on the nature substituents R and R′, since it has been observed for all dithiolenes, and the change in the solvent does not affect the trend in $\Delta\lambda^{R}$: consequently, the λ_{max} values recorded in different solvents are linearly correlated (see Figure 5 for chloroform and toluene). The values recorded for [Pt(naphthyl,*p*-F-C_6H_4-timdt)$_2$] (**6g**) and [Pt(pentyl,Et-timdt)$_2$] are reported as an example in ref.[32], and in Figure 6 the NIR spectra of **6g** recorded in MeCN, $CHCl_3$, and toluene are superimposed (λ_{max}^{6g} = 1002, 1019 and 1034 in MeCN, $CHCl_3$ and toluene, respectively). As can be seen, the bathochromic shift is accompanied by an increase in the absorption extinction coefficients (90000, 105000 and 120000 $M^{-1}\cdot cm^{-1}$ in MeCN, $CHCl_3$, and toluene, respectively). It is worth noting that one of the proposed goals has been reached, since the NIR absorption maxima of **5f** in chloroform and toluene exactly match the emission wavelengths of the Nd:YLF and Nd:YAG lasers.

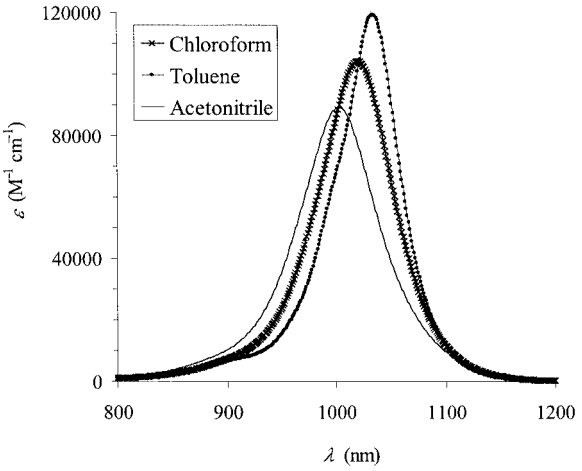

Figure 6. Vis/NIR spectra of **6g** ($c = 1.51 \times 10^{-5}$ M) recorded in acetonitrile, chloroform, and toluene

Photophysical Measurements

The thermal and photochemical stabilities of [Ni(*i*Pr$_2$-timdt)$_2$] had been previously tested in CH_2Cl_2 solution under the action of the FT-Raman spectrometer (0.5 W; 24 h).[22] Since an actual application implies much higher energies, the three dithiolenes **4c**−**6c** were dispersed in polythene pellets and exposed to the action of an Nd:YAG Q-switched mode-locked laser delivering 30-ps (FWHM) pulses at a 10 Hz repetition rate (λ_{em} = 1064 nm) for 9 h (324000 shots, power density 110 MW/cm^2). A comparison of the transmittance before and after the exposure reveals no change. The same test was performed on a commercially available Q-switching dye,[33] which showed a 30% decrease

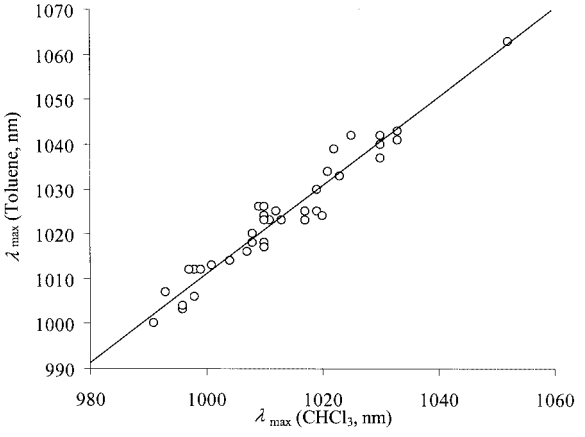

Figure 5. Linear relationship between the λ_{max} values found in chloroform and in toluene for Ni-, Pd-, and Pt-dithiolenes (R = 0.94)

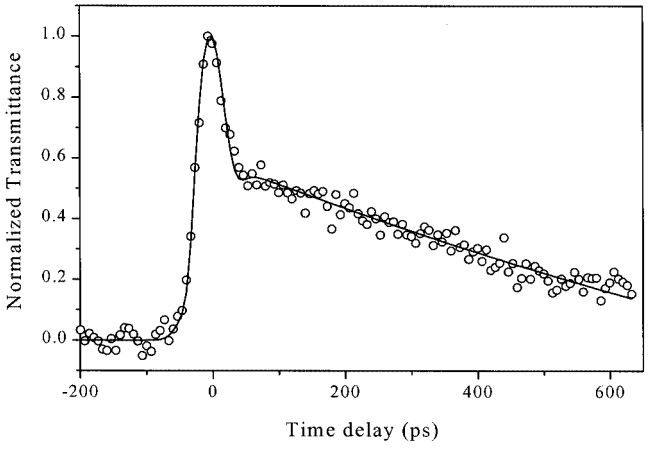

Figure 7. Experimental $\Delta T/T$ (dots) measured as a function of the pump-probe time delay in a chloroform solution of **5f** (λ = 1064 nm); the solid line is the least-squares fit of the experimental data

 © 2003 Wiley-VCH Verlag GmbH & Co. KGaA, Weinheim

in transmittance after exposure for 1 h. The intense absorption of complex **5f** in toluene at the exact emission wavelength of the Nd:YAG laser suggested the investigation of its absorption saturation properties in this spectral region. Unfortunately, the low solubility in this solvent prevented pump-probe measurements, which were therefore performed in chloroform solution. The experimental results are reported in Figure 7. A fast increase in the transient normalized transmittance $\Delta T/T$ is observed, followed by a decay similar to those found[27] in other dithiolenes belonging to the same series. It has been shown that the decay depends on both the central metal ion and the substituents R and R′.[27] Based on TD-DFT calculations performed on the model complexes $\mathbf{4^H}-\mathbf{6^H}$, the six-level model reported in Figure 8 was proposed to account for the absorption dynamics.[27,28] According to this model, excitation from the ground state S_0 to the first dipole-allowed state S_2 occurs, which can decay to S_1. Since the transition to S_0 is dipole-forbidden, decay from S_1 to T_1 occurs through intersystem crossing. In addition, absorption from S_1 and T_1 to higher excited states S_n and T_k, resonant with the $S_0 \rightarrow S_2$ excitation, may be allowed. The numerical solution of the first-order differential equations reported in Figure 8 allows a least-squares fit of the experimental data (solid lines in Figure 7). The measured signal recovery that corresponds to the recovery of the absorption saturation, exhibits two components with different temporal dynamics. The fast decay is almost time-resolution-limited, and has essentially been assigned to the $S_2 \rightarrow S_1$ transition ($\tau_{32} \approx 4$ ps). On the contrary, the slower component decreases with a time constant ($\tau_{25} \approx 122$ ps) that is roughly inversely proportional to the spin-orbit coupling constant for the metal ion, indicating a large contribution of the intersystem crossing process $S_1 \rightarrow T_1$, to dynamics at long time delays. It should be mentioned that the absorption cross-sections for the $S_1 \rightarrow S_n$ and $T_1 \rightarrow T_k$ transitions are proportional to those relating to $S_0 \rightarrow S_2$, through γ_1 and γ_2 (see Figure 8), which have been considered as fitting parameters.

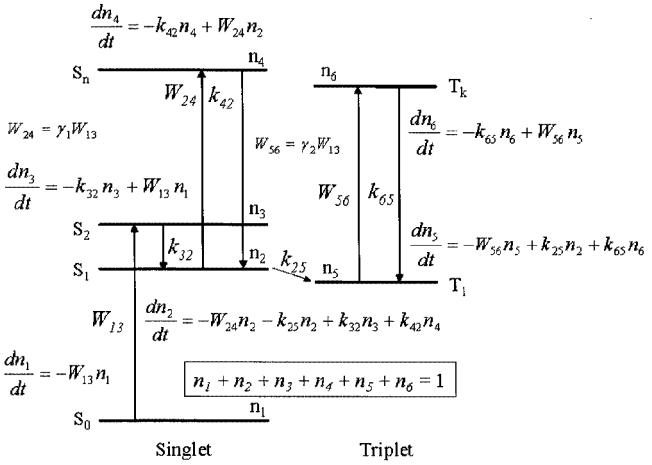

Figure 8. Scheme of the six-level model for the investigated complexes; the equations used as a model for the fitting of the pump-probe experiments are also reported; for **5f**, the main fit parameters are: $\tau_{32} = 4$ ps, $\tau_{25} = 122$ ps; $\gamma_1 = 1.9$; $\gamma_2 = 1.9$

Conclusions

The very high thermal and photochemical stabilities accompanied by the unprecedented intensities in the NIR absorption around 1000 nm show that the [M(R,R′timdt)$_2$] class of neutral dithiolenes is among the most promising classes of molecular materials for NIR laser applications. In addition, this class of complexes shows another interesting advantage compared with other dithiolenes, such as those derived from the dmit ligand, since a never-ending number of compounds can be synthesized by structurally modifying the substituents R and R′. Thus, the change in the central metal ion and the introduction of suitable polar groups in the substituents R and R′, along with the choice of a suitable solvent, allowed us to overcome solubility problems, as well as to modify the position of the NIR absorption maximum. In fact, the additivity of the contributions $\Delta\lambda^M$ and $\Delta\lambda^R$ in determining the $\lambda_{max}^{M,R,R'}$ position, accompanied by the solvatochromic effect depending on the dielectric constant of the solvent, allows for the tuning of the value of $\lambda_{max}^{M,R,R'}$ in a fairly wide range of wavelengths. Among the dithiolenes reported in this paper, compound **5f** [M = Pd, R = *p*-F-C$_6$H$_4$, and R′ = *m*,*m*,*p*-(MeO)$_3$-C$_6$H$_2$] matches the emission wavelengths of the Nd:YLF and Nd:YAG lasers exactly in chloroform and toluene, respectively. Moreover, the influence of the solvent on the molar extinction coefficient has allowed for the measurement of a value of 120000 $M^{-1}\cdot cm^{-1}$ for compound **6g** in toluene, the highest value ever encountered for a dithiolene complex. Through DFT calculations, it had been demonstrated that the metal ion contributes to the Kohn−Shan LUMO through its nd_{xy} atomic orbital (n = 3, 4, 5 for Ni, Pd, Pt), which depends on n. In this study, the DFT calculations have shown that the effect of the substituents arises mainly as a result of the inductive and/or steric factors, and not as a result of the extension of the π-aromaticity of the dithiolene system to the substituents, thus justifying the similar $\Delta\lambda^R$ contributions estimated for the phenyl and naphthyl groups. Finally, the behavior of these complexes as saturable absorbers has been proven, and the picosecond saturation dynamics for compound **5f** has been studied by a pump-probe technique, supporting future applications in the field of Nd-based lasers.

Experimental Section

Procedures and Methods: All solvents and reagents were Aldrich products used as purchased. All operations were carried out under dry nitrogen. The purity of each compound has been checked by CHNS and TLC analyses. Elemental analyses were performed with a FISONS EA-1108 CHNS-O instrument. FT-IR and FT-Raman spectra were collected as previously reported.[23,24] UV/Vis/NIR spectra were recorded using a 1-cm path-length cell, with a Varian Cary 5 spectrophotometer at 20 °C in a thermostatted compartment.

Disubstituted 2-Thioxoimidazolidine-4,5-diones 7a−j: These products were prepared according to literature methods by treating an

 © 2003 Wiley-VCH Verlag GmbH & Co. KGaA, Weinheim

appropriate *N*,*N*′-dialkylthiourea or *N*-alkyl-*N*′-arylthiourea with oxalyl chloride in a CH_2Cl_2 solution,[23] and were recrystallized from CH_2Cl_2 or diethyl ether.

[Ni(R,R′timdt)$_2$] (4a−j): As previously pointed out,[24] both nickel powder and nickel chloride can be used in these syntheses, although higher yields are generally obtained starting from the metal powder. A general synthesis consists of refluxing the disubstituted 2-thioxoimidazolidine-4,5-dithione **7a−j** (about 5 mmol) with a slight excess (about 10%) of Lawesson's reagent (**8**) in 100 mL of previously degassed toluene for a time varying between 20 min and 1 h, depending on the substituents. After concentration of the reaction mixture, EtOH was added to lower the solubility of the complex and the dithiolene was filtered off. Starting from imidazolidine **7d−f**, the formation of the dithiolene complexes has not been proven. Yields % (mg, starting from 5 mmol of the corresponding 2-thioxoimidazolidine-4,5-dione): **4a**, 14 (255); **4b**, 15 (283); **4c**, 11 (209); **4g**, 8 (165); **4h**, 11 (190); **4i**, 5 (86); **4j**, 20 (282). Nickel-dithiolenes were recrystallized from chloroform/ethanol mixtures.

[Pd(R,R′timdt)$_2$] (5a−j): Compounds **5a−j** were synthesized according to the previously described procedure,[23,24] starting from compounds **7a−g** and using $PdCl_2$. Yields % (mg, starting from 5 mmol of the corresponding 2-thioxoimidazolidine-4,5-dione): **5a**, 42 (814); **5b**, 25 (502); **5c**, 18 (363); **5d**, 17 (381); **5e**, 21 (424); **5f**, 35 (834); **5g**, 22 (480); **5h**, 18 (333); **5i**, 48 (882); **5j**, 20 (306).

[Pt(R,R′timdt)$_2$] (6a−g): The syntheses of **6a−g** were very similar to those for the Pd analogues, starting from $PtCl_2$ instead of $PdCl_2$. Yields % (mg, starting from 5 mmol of the corresponding 2-thioxoimidazolidine-4,5-dione): **6a**, 32 (691); **6b**, 17 (379); **6c**, 24 (538); **6d**, 22 (493); **6e**, 21 (470); **6f**, 38 (990); **6g**, 33 (794); **6h**, 4 (83); **6i**, 66 (1360); **6j**, 65, (1139).

Elemental analyses of all synthesized dithiolenes correspond to the expected values.

Photophysical Measurements: A saturated solution of complex **5f** in chloroform was filtered and placed in a 1-mm quartz optical cell. The temporal dynamics of the saturable absorption was investigated using a picosecond time-resolved pump-probe technique. The ps Nd:YAG laser beam was divided into two parts using a beam splitter to create the pump and probe pulses. The pump beam was focused on a spot ca. 200 μm in diameter, in order to obtain a peak irradiance of about 20 GW/cm^2. The probe beam was focused on a smaller spot (ca. 50 μm) to reduce the effect of excitation spatial inhomogeneity, and its peak irradiance was always kept at about 0.1% of that of the pump. All the experiments were performed at $T = 295$ K. The experimental data were fitted according to a previously outlined procedure.[27]

Computations: Quantum chemical calculations were carried out by using the commercially available suite of programs Gaussian 98 package.[34] Density functional calculations (DFT)[35,36] regarding the model dithiolene **9** were performed using the hybrid Becke3LYP functional (which uses a mixture[37] of Hartree−Fock and DFT exchange, along with DFT correlation, the Lee−Yang−Parr correlation functional,[38] together with Becke's gradient correction[39]). The basis set for all calculations was the Schafer, Horn, and Ahlrichs pVDZ basis[40] for C, H, N, and S, while for Ni, Hay−Wadt LANL2DZ basis sets together with ECP sets[41] were employed. After scanning the potential energy surface by rotating the phenyl ring in dithiolene **9** by 10° between 0 and 180°, single optimization calculations were performed at each rotational step to calculate the orbital compositions and the Kohn−Shan orbital energies. All the results were elaborated with the Molekel 4.2 program.[42] The values of $\Delta\lambda^M$ and $\Delta\lambda^R$ were estimated by an iterative least-squares fit minimizing the squared sum

$$\sum_{i}^{N}\left|\lambda_{max}^{M,R,R'}(i)-\lambda_{max}^{Ni,Me,Me}-\Delta\lambda^{M(i)}-\sum_{j}^{4}\Delta\lambda^{R(i,j)}\right|^2$$

of the differences between experimental $\lambda_{max}^{M,R,R'}$ and estimated values for each of the N synthesized dithiolenes, where $\lambda_{max}^{Ni,Me,Me}$ is the NIR absorption wavelength recorded for [Ni(Me$_2$timdt)$_2$].

Acknowledgments

This project was carried out as part of a MIUR (Ministero dell'Istruzione dell'Università della Ricerca) project. CINECA (Centro Interuniversitario Nord Est Calcolo Automatico) is also acknowledged for computational facilities. We wish to thank Dr. Antonio Masello for the help in the syntheses of compounds **4j−6j**.

[1] K. Base, M. T. Tierney, A. Fort, J. Muller, M. W. Grinstaff, *Inorg. Chem.* **1999**, *38*, 287−289.
[2] S. R. Marder, C. B. Gorman, F. Meyers, J. W. Perry, G. Bourhill, J. L. Bredas, B. M. Pierce, *Science* **1994**, *265*, 632−635.
[3] S. R. Marder, D. N. Beratan, L. T. Cheng, *Science* **1991**, *252*, 103−106.
[4] F. Meyers, S. R. Marden, B. M. Pierce, J. L. Bredas, *J. Am. Chem. Soc.* **1994**, *116*, 10703−10714.
[5] S. D. Cummings, L.-T. Cheng, R. Eisemberg, *Chem. Mater.* **1997**, *9*, 440−450.
[6] U. T. Mueller-Westerhoff, B. Vance, D. I. Yoon, *Tetrahedron* **1991**, *47*, 909−932.
[7] U. T. Mueller-Westerhoff, K. H. Drexhage, *IEEE J. Quantum Electron. QE-8* **1972**, 759−763.
[8] U. T. Mueller-Westerhoff, K. H. Drexhage, US Patent 3,743,964, **1973**.
[9] P. Cassoux, *Coord. Chem. Rev.* **1999**, *185−186*, 213−232.
[10] E. Canadell, *Coord. Chem. Rev.* **1999**, *185−186*, 629−651.
[11] G. N. Schrauzer, V. P. Mayweg, *J. Am. Chem. Soc.* **1966**, 3235−3242.
[12] D. C. Olson, V. P. Mayweg, G. N. Schrauzer, *J. Am. Chem. Soc.* **1966**, 4876−4882.
[13] M. D. Ward, J. A. McCleverty, *J. Chem. Soc., Dalton Trans.* **2002**, 275−288.
[14] R. Williams, E. Billig, J. H. Waters, H. B. Grey, *J. Am. Chem. Soc.* **1966**, *88*, 43−50.
[15] S. N. Oliver, S. V. Kershaw, A. E. Underhill, C. A. S. Hill, A. Charlton, *Nonlinear Opt.* **1995**, *10*, 87−99.
[16] W. L. Tan, W. Ji, J. L. Zuo, J. F. Bai, X. Z. You, J. H. Lim, S. Yang, D. J. Hagan, E. W. Van Stryland, *Appl. Phys. B* **2000**, *70*, 809−812.
[17] U. T. Mueller-Westerhoff, B. Vance, in *Comprehensive Coordination Chemistry*, 1st ed., Pergamon Press, Oxford, England, **1987**, vol. 2, p. 595−631.
[18] K. W. Browall, T. Bursh, L. V. Interrante, *Inorg. Chem.* **1972**, *11*, 1800−1806.
[19] K. W. Browall, L. V. Interrante, *J. Coord. Chem.* **1973**, *3*, 27−38.
[20] G. N. Schrauzer, V. P. Mayweg, *J. Am. Chem. Soc.* **1965**, *87*, 3585−3592.
[21] F. Bigoli, P. Deplano, F. A. Devillanova, V. Lippolis, P. J. Lukes, M. L. Mercuri, M. A. Pellinghelli, E. F. Trogu, *J. Chem. Soc., Chem. Commun.* **1995**, 371−372.
[22] F. Bigoli, P. Deplano, F. A. Devillanova, J. R. Ferraro, V. Lippolis, P. J. Lukes, M. L. Mercuri, M. A. Pellinghelli, E. F. Trogu, J. M. Williams, *Inorg. Chem.* **1997**, *36*, 1218−1226.
[23] M. Arca, F. Demartin, F. A. Devillanova, A. Garau, F. Isaia, F. Lelj, V. Lippolis, S. Pedraglio, G. Verani, *J. Chem. Soc., Dalton Trans.* **1998**, 3731−3736.

 © 2003 Wiley-VCH Verlag GmbH & Co. KGaA, Weinheim

[24] M. C. Aragoni, M. Arca, F. Demartin, F. A. Devillanova, A. Garau, F. Isaia, F. Lelj, V. Lippolis, G. Verani, *J. Am. Chem. Soc.* **1999**, *121*, 7098−7107.
[25] F. Bigoli, P. Deplano, M. L. Mercuri, M. A. Pellinghelli, G. Pintus, E. F. Trogu, G. Zonnedda, H. H. Wang, J. Williams, *Inorg. Chim. Acta* **1998**, *273*, 175−183.
[26] F. Bigoli, S. Curreli, P. Deplano, L. Leoni, M. L. Mercuri, M. A. Pellinghelli, A. Serpe, E. F. Trogu, *J. Chem. Soc., Dalton Trans.* **2002**, 1985−1991.
[27] T. Cassano, R. Tommasi, L. Nitti, M. C. Aragoni, M. Arca, C. Denotti, F. A. Devillanova, F. Isaia, V. Lippolis, F. Lelj, P. Romaniello, *J. Chem. Phys.*, in press.
[28] P. Romaniello, M. C. Aragoni, M. Arca, T. Cassano, C. Denotti, F. A. Devillanova, F. Isaia, F. Lelj, V. Lippolis, R. Tommasi, *J. Phys. Chem.*, submitted.
[29] M. C. Aragoni, M. Arca, T. Cassano, C. Denotti, F. A. Devillanova, F. Isaia, V. Lippolis, D. Natali, L. Nitti, M. Sampietro, R. Tommasi, G. Verani, *Inorg. Chem. Commun.* **2002**, *5*, 869−872.
[30] S. Sheibe, B. J. Pedersen, S.-O. Lawesson, *Bull. Soc. Chim. Belg.* **1978**, *87*, 229−240.
[31] W. Freyer, *J. Prakt. Chem.* **1986**, *328*, 253−260.
[32] NIR absorption maxima [nm] recorded for [Pt(naphthyl,*p*-F-C_6H_4-timdt)$_2$] and [Pt(pentyl,Et-timdt)$_2$] in various solvents (dielectric constants ε_d in paretheses): THF (7.52) 1024, 1004; CCl_4 (2.24) 1032, 1013; benzene (2.28) 1034, 1015; *p*-xylene (2.4) 1034, 1014; toluene (2.4) 1034, 1015; $CHCl_3$ (4.8) 1021, 1004; CH_2Cl_2 (9.08) 1017, 1001; MeCN (37.5) 1002, 986; ethyl acetate (6.02) 1015, 996; MeOH (32.6) 1001, 985; EtOH (24.3) 1009, 994; 1,4-dioxane (2.2) 1024, 1005: 1,2-dichloroethane (16.7) 1022, 1006; DMF (38.3) 1027, 1006; DMSO (47.2) 1036, 1015; nitrobenzene (35.7) 1037, 1009. The two sets of data are linearly correlated ($R = 0.95$).
[33] 6-Methyl-8-[5-(6-methyl-2,4-diphenyl-6,7-dihydro-5*H*-chromen-8-yl)penta-2,4-dienylidene]-2,4-diphenyl-5,6,7,8-tetrahydro-2*H*-chromenium perchlorate.
[34] M. J. Frisch, G. W. Trucks, H. B. Schlegel, G. E. Scuseria, M. A. Robb, J. R. Cheeseman, V. G. Zakrzewski, J. A. Montgomery, R. E. Stratmann, J. C. Burant, S. Dapprich, J. M. Millam, A. D. Daniels, K. N. Kudin, M. C. Strain, O. Farkas, J. Tomasi, V. Barone, M. Cossi, R. Cammi, B. Mennucci, C. Pomelli, C. Adamo, S. Clifford, J. Ochterski, G. A. Petersson, P. Y. Ayala, Q. Cui, K. Morokuma, D. K. Malick, A. D. Rabuck, K. Raghavachari, J. B. Foresman, J. Cioslowski, J. V. Ortiz, B. B. Stefanov, G. Liu, A. Liashenko, P. Piskorz, I. Komaromi, R. Gomperts, R. L. Martin, D. J. Fox, T. Keith, M. A. Al-Laham, C. Y. Peng, A. Nanayakkara, C. Gonzalez, M. Challacombe, P. M. W. Gill, B. G. Johnson, W. Chen, M. W. Wong, J. L. Andres, M. Head-Gordon, E. S. Replogle, J. A. Pople, *Gaussian 98* (Revision A.7), Gaussian, Inc., Pittsburgh, PA, **1998**.
[35] E. S. Kryachko, E. V. Ludeña, *Energy Density Function Theory of Many Electron Systems*, Kluwer Academic Publisher, Dortrecht, Boston, **1990**.
[36] B. Miehlich, A. Savin, H. Stoll, H. Preuss, *Chem. Phys. Lett.* **1989**, *157*, 200−206.
[37] A. D. Becke, *J. Chem. Phys.* **1993**, *98*, 1372−1377.
[38] C. Lee, W. Yang, R. G. Parr, *Phys. Rev. B* **1988**, *37*, 785−789.
[39] A. D. Becke, *J. Chem. Phys.* **1993**, *98*, 5648−5652.
[40] A. Schafer, H. Horn, R. Ahlrichs, *J. Chem. Phys.* **1992**, *97*, 2571−2577.
[41] P. J. Hay, W. R. Wadt, *J. Chem. Phys.* **1985**, *82*, 270−298.
[42] S. Potmann, H. P. Lüthi, *Chimia* **2000**, *54*, 766−769.

Received November 11, 2002

 © 2003 Wiley-VCH Verlag GmbH & Co. KGaA, Weinheim

Thermodynamics of Complex Formation of Silver(I), Cadmium(II) and Cobalt(II) with Open-Chain Polyamines in Dimethyl Sulfoxide and Molecular Dioxygen Binding to Cobalt(II) Complexes

Clara Comuzzi,*[b] Andrea Melchior,[a] Pierluigi Polese,[a] Roberto Portanova,[a] and Marilena Tolazzi*[a]

Keywords: Amine complexes / Cadmium / Cobalt / Dioxygen / Silver / Thermodynamics

Ag^{I}, Cd^{II} and Co^{II} complex formation with the primary and tertiary tetraamines 1,4,7,10-tetraazadecane (trien) and 1,1,4,7,10,10-hexamethyltriethylenetetraamine (hmtrien) has been studied at 298 K in the aprotic solvent dimethyl sulfoxide (DMSO) and in an ionic medium set to 0.1 mol·dm^{-3} with Et_4NClO_4 under anaerobic conditions. UV/Vis spectrophotometric and calorimetric measurements have been carried out to obtain the thermodynamic parameters for the systems investigated. Mononuclear 1:1 complexes are formed for all systems. In addition, trien also forms the ML_2 mononuclear complex and a polynuclear M_2L_3 species with M = Cd^{2+} and Co^{2+}. All the complexes are enthalpy stabilized, whereas the entropy changes counteract the complex formation. The results are discussed in terms of the different basicities, steric requirements and solvation both of the ligands and of the complexes formed. The influence of *N*-alkylation on the selectivity of the ligands towards metal ions is analysed. In the case of the Co^{II} complexes, their ability to take up dioxygen has also been studied by voltammetric and UV/Vis measurements and gasometric absorption.
(© Wiley-VCH Verlag GmbH & Co. KGaA, 69451 Weinheim, Germany, 2003)

Introduction

A comparison of the properties of transition-metal complexes with primary, secondary and tertiary amine ligands reveals several remarkable effects of *N*-alkylation of the ligands on the thermodynamics and kinetics[1−5] of complex formation and on ligand substitution reactions.

In a very recent work[3] it was shown that *N*-alkylation causes several contradictory effects: on one hand, the nitrogen atoms become better σ-donors as a consequence of the introduction of electron-donating substituents, which shifts the redox potential of the $M^{n+1}L_m/M^nL_m$ couples cathodically, while on the other hand, solvation and steric effects shift the potential anodically. As the solvation effects are larger, *N*-alkylation stabilizes low-valent transition metal complexes and the redox potentials of the couples are shifted anodically for L = tertiary amines.[1,3,5,6]

In addition, the stability constants of the complexes with the tertiary amines are smaller than those with primary and secondary amines,[3,5−9] this behaviour mainly being attributed to outer-sphere solvation effects and to ligand strain energy.[5c,5e,5g,5h]

In the last few years, a variety of polyamine structures have been investigated in water[9−18] and in non-aqueous solvents[8,19−25] with the aims both of improving knowledge of the coordination chemistry of soft and hard metal ions and of studying how basicities and steric effects may affect the selectivity pattern in metal coordination.

As examples of the great interest in these ligands and their application it should be remembered that they show potential for use as sequestering agents for metal ions of environmental importance,[18] both toxic and essentials, such as Cd^{II}, Pb^{II}, or Ca^{II}, Mg^{II}, Zn^{II}, Mn^{II}, Fe^{III}, Cu^{II}, and employment as models for carrier molecules,[6,15,18,26−31] such as in Cu^{I} or Co^{II} complexes.

In this context, the papers published by our group concerning the complexation of transition-metal ions such as Ag^{I}, Cd^{II} and Co^{II}[8,22a−22d] have shown that nitrogen functionalization strongly influences not only the stoichiometry and the nature of all the metal ion complexes formed, but also, very interestingly, the selectivity of these ligands towards metal ions.[8c] In fact, while − for example − dien shows a higher affinity for the borderline soft/hard divalent Cd^{II} than for the very soft univalent Ag^{I} ion, the opposite is true with regard to pmdien. As far as cobalt(II) complexes are concerned, different *N*-alkylation of polyamines also has important effects on the dioxygen affinity of these complexes:[6] electron transfer between the metal centre and di-

[a] Dipartimento di Scienze e Tecnologie Chimiche, Università di Udine,
Via Cotonificio 108, 33100 Udine, Italy
Fax: (internat.) + 39-0432/558803
E-mail: tolazzi@dstc.uniud.it
[b] Dipartimento di Scienze e Tecnologie Chimiche, Università di Udine,
Via Cotonificio 108, 33100 Udine, Italy
Fax: (internat.) + 39-0432/558803
E-mail: comuzzi1@dstc.uniud.it

 © 2003 Wiley-VCH Verlag GmbH & Co. KGaA, Weinheim **DOI: 10.1002/ejic.200200685**

oxygen should depend on the available electron density at the central metal ion, which is in turn greatly affected by the electron-donor properties of the ligands in the coordination sphere.[26,27]

As an extension of previous works we report here on results concerning the complex formation of Ag^{I}, Cd^{II} and Co^{II} with the differently *N*-methylated polyamines 1,4,7,10-tetraazadecane (trien) and 1,1,4,7,10,10-hexamethyltriethylenetetraamine (hmtrien) in the aprotic solvent dimethyl sulfoxide (DMSO). For silver(I), data relating to trien complexation in DMSO had been published previously.[22d]

Especially interesting comparisons between the monovalent d^{10} acceptor silver(I), of very soft character, and the divalent and mildly soft Cd^{2+} should be possible. In addition, although the complex formation of Cd^{II} has been extensively studied in the past[32–34] and in more recent[7,17,33] years, nevertheless few thermodynamic data concerning its ability to coordinate simple open-chain N-donor ligands are available.[7,8c,34f,35] Moreover, Co^{II} model compounds are of great interest since they may provide a better understanding of biological molecules and assist in the study of new homogeneous catalysts for selective oxidations under mild conditions.[26–31]

The values of the stability constants of the various systems investigated were determined by different techniques. Direct potentiometric techniques were used for Ag^{I} and Cd^{II} (see Exp. Sect., potentiometric measurements), whereas for the Co^{II}/polyamine systems, UV/Vis spectroscopic measurements were employed, with the use of Cd^{II} as auxiliary metal ion[36] for reasons discussed in a previous paper.[8b] The enthalpy values were obtained by direct calorimetric titrations. In the case of the Co^{II} complexes, their ability to take up dioxygen was also studied by voltammetric and UV/Vis measurements and by gasometric absorption. All measurements were performed at 298 K and in an ionic medium adjusted to 0.1 mol·dm^{-3} with Et_4NClO_4 as neutral salt.

Results

Computer treatment of the potentiometric experimental data shows that the best fit is obtained when the polynuclear species M_2L_3 (M = Cd, Co) is considered in addition to ML and ML_2 mononuclear ones for metal(II)/trien systems, whereas the ML species is the only one formed in all other cases. The overall stability constants obtained from the potentiometric data minimization procedures, with the corresponding limits of error, are listed in Table 1 for the reactions $i\ M^{n+} + j\ L \rightleftarrows M_iL_j^{n+}$ (M = Ag^{I}, Cd^{II}, Co^{II}, L = trien and hmtrien). Figure 1 gives the distributions of Cd^{2+} and Co^{2+} among the various species. Figure 2 gives Δh_v, the total molar enthalpy change, as a function of $R_c = c_L/c_M$ (total ligand/total metal concentration) for the Cd^{2+}/trien and Co^{2+}/trien systems.

Some conclusions about the prevalent coordinated species formed can be drawn from examination of the shapes of the curves, which are fully consistent with the information obtained from analysis of the potentiometric data.

Table 1. Overall stability constants and thermodynamic functions for the reaction reactions $i\ M^{n+} + j\ L \rightleftarrows M_iL_j^{n+}$ (M = Ag^{I}, Cd^{II}, Co^{II}, L = trien and hmtrien) in DMSO at 298 K and I = 0.1 mol·dm^{-3} and in water;[7,15] the errors quoted correspond to three standard deviations

Ligand	Complex	logβ_{ij}	$-\Delta G°_{\beta ij}$ [kJmol^{-1}]	$-\Delta H°_{\beta ij}$ [kJmol^{-1}]	$-T\Delta S°_{\beta ij}$ [kJmol^{-1}]
trien	AgL[a]	10.32	58.91	91.5	32.6
	AgL(water)[b]	7.7	43.9	–	–
	CdL	11.81(0.04)	67.4(0.2)	79(2)	11.6
	Cd_2L_3	30.9(0.1)	176.4(0.7)	249(7)	72.6
	CdL_2	17.00(0.08)	97.0(0.5)	138(3)	41
	CdL(water)[b]	11.12	63.5	41	–22.5
	CoL	12.50(0.06)	71.3(0.3)	86(1)	14.7
	Co_2L_3	33.2 (0.3)	189(2)	273(9)	84
	CoL_2	18.2(0.3)	104(2)	149(4)	45
	CoL(water)[b]	11.31	64.5	44.3	–20.3
hmtrien	AgL	7.82(0.04)	44.6(0.2)	69.3(0.6)	24.7
	CdL	6.30(0.02)	36.0(0.1)	68(4)	32
	CoL	4.0(0.2)	23(1)	42(4)	19
	CoL(water)[c]	8±1			

[a] Ref.[22d] [b] Ref.[7], I = 1.00 mol·dm^{-3}. [c] Ref.[15], estimated value, medium unknown.

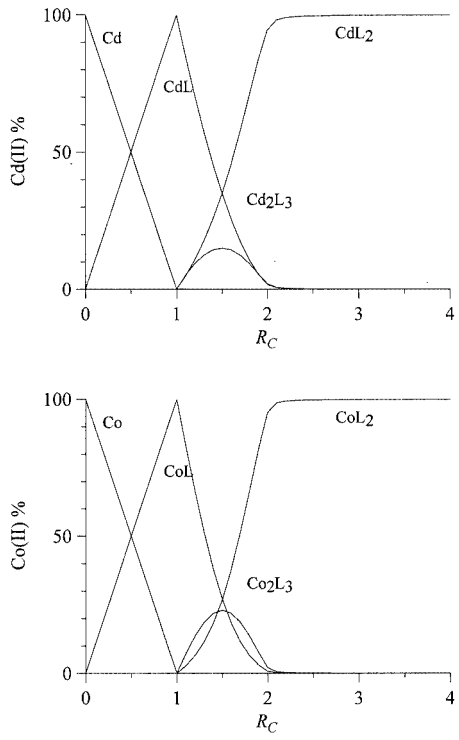

Figure 1. The percent distribution of the species in the Cd^{II}/trien and Co^{II}/trien systems in DMSO at c_M = 10 mmol·dm^{-3}

The slope change at R_c = 1 is connected with the formation of the very stable mononuclear ML complex. As c_L increases, a slope change is observed at R_c = 1.5, a separation of the curves at various concentrations is then shown until R_c = 2, and then no heat is released. This agrees with the formation of a very stable M_2L_3 and a subsequent, less

 © 2003 Wiley-VCH Verlag GmbH & Co. KGaA, Weinheim

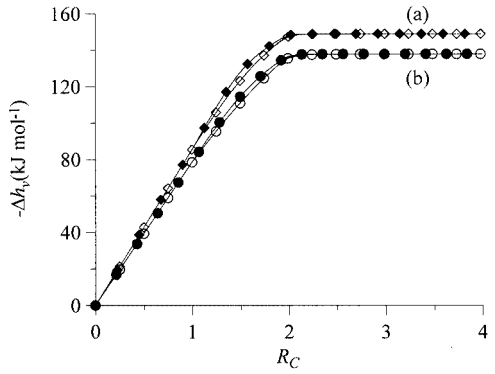

Figure 2. The total molar enthalpy changes, Δh_n, as a function of $R_c = c_L/c_M$ for Cd^{II}/trien and Co^{II}/trien systems in DMSO: (a) 5.05 (open circles), 19.91 (filled circles) mmol·dm^{-3} in Cd^{2+}; (b) 5.04 (open squares), 20.01 (filled squares) mmol·dm^{-3} in Co^{2+}; the solid lines have been calculated from the values of β_{ij} and $\Delta H°_{\beta ij}$ in Table 1

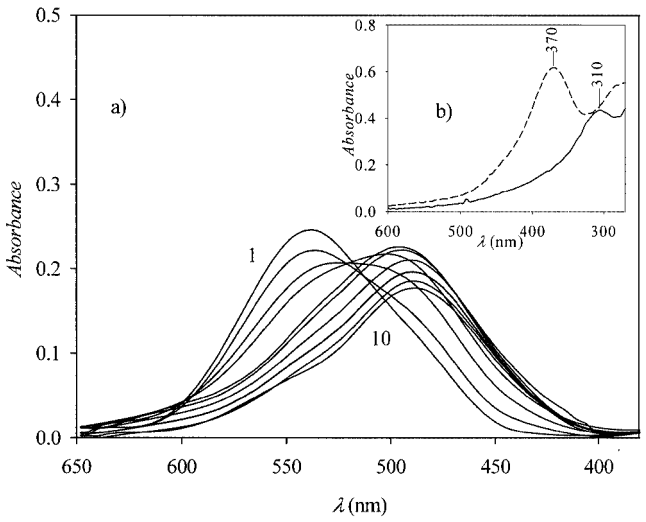

Figure 3. (a) Spectral changes observed during the reaction between Co^{2+} and trien in DMSO: calcd. $c°_{Co}$ = 21.8 mmol·dm^{-3}, $c°_{Cd}$ = 21.6 mmol·dm^{-3} (spectrum 1); $c°_{trien}$ varied from 0 (spectrum 1) to 54.5 (spectrum 10) mmol·dm^{-3}; (b) UV/Vis spectrum of a solution of [Co(trien)$^{2+}$] = 0.2 mmol·dm^{-3} under nitrogen with 4% O_2 after 9 s of exposure and after 30 min of exposure (dotted line); the spectrum remains unchanged after 6−8 h of exposure

stable, ML_2 complex according to the reaction steps in Equations (1) and (2).

$$2\,ML + L \rightleftharpoons M_2L_3 \quad (1)$$

log β = 7.28 and 8.2, $\Delta H°$ = −91 and −101, $T\Delta S°$ = −49.4 and −54.6 kJ·mol^{-1} for M = Cd and Co, respectively

$$M_2L_3 + L \rightleftharpoons 2\,ML_2 \quad (2)$$

log β = 3.1 and 3.2, $\Delta H°$ = −27 and −25, $T\Delta S°$ = −9.4 and −6 kJ·mol^{-1} for M = Cd and Co

No more complexes are formed beyond ML_2. The fit between experimentally determined and calculated curves (full lines in Figure 2) is quite good.

Figure 3 (a) shows the spectral changes observed during reactions between Co^{2+} and trien, in the presence of Cd^{2+} as competitor, in terms of absorbances vs. wavelengths. Figure 3 (b) also shows (inserted) the spectral modification due to dioxygen uptake for the $[Co(trien)]^{2+}$ species. Figure 4 shows log β_{1Cd} plotted as a function of log β_{1Co} to provide a better illustration of the behaviour of the two ions.

The O_2 absorption by the $[Co(trien)]^{2+}$ adduct was measured at constant pressure by use of a standard apparatus containing a thermostatted gas burette in order to determine the stoichiometry of the dioxygenated complex. Figure 5 gives the dioxygen binding curve, $R_{O2} = n_{O_2}/n_{[Co(trien)]^{2+}}$ vs. time.

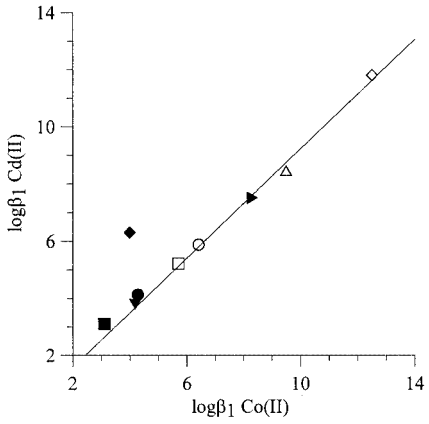

Figure 4. log β_{1Cd} as a function of logβ_{1Co} for ethylenediamine (en; open circle); *N*,*N*′-dimethylenediamine (dmen; open square); *N*,*N*,*N*′-trimethylenediamine (trmen; filled circle); *N*,*N*,*N*′*N*′-tetramethylenediamine (tmen; filled square); diethylenetriamine (dien; open triangle); *N*,*N*′′-dimethyldiethylenetriamine (dmdien; filled triangle); *N*,*N*,*N*′,*N*′′,*N*′′-pentamethyldiethylenetriamine (pmdien; filled triangle next to filled circle); 1,4,7,10-tetraazadecane (trien; open diamond), 1,1,4,7,10,10-hexamethyltriethylenetetraamine (hmtrien; filled diamond)

Discussion

All the complexes are formed in strongly exothermic reactions, whereas the entropy terms oppose the reactions (Table 1). The negative enthalpy and entropy values are typical of reactions involving complexation of metal ions by neutral ligands in aprotic solvents.[3,6,19] Data in water solutions are also available for all the trien systems,[7] whereas analogous data for the Co^{II}/hmtrien system are reported only as estimated values. It should be remembered that Cd^{2+} and Co^{2+} are hexasolvated in both solvents, with the solvent molecules in a regular octahedral arrangement, whereas silver(I) is tetrahedrally solvated both in DMSO and in water.[8b,19]

The complexes are characterized by lower stabilities in water than in DMSO. In addition, they are always more enthalpy-stabilized in DMSO than in water, while in the latter solvent the entropy terms are favourable. It has already been found that this trend is inconsistent with what would be expected on the basis of the thermodynamic parameters of transfer of the metal ions investigated here from water to DMSO,[6,37] and should be associated with greater solvation, through hydrogen bonding, of primary and secondary amines in water than in DMSO.[38] This was also

 © 2003 Wiley-VCH Verlag GmbH & Co. KGaA, Weinheim

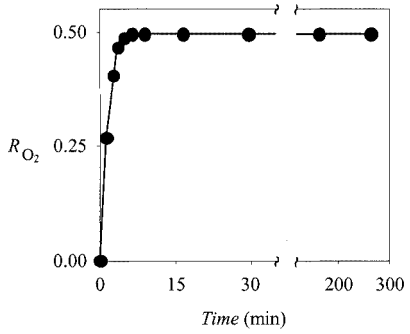

Figure 5. Plot of the ratio R_{O2} = moles O_2/moles complex vs. time measured for a 30 mM solution of $[Co(trien)]^{2+}$ complex in pure oxygen

confirmed by the fact that the opposite has been observed for the complexes with tertiary amines, as these are more stable in water than in DMSO,[6,8b,8c] *N*-methylation inhibiting the formation of hydrogen bonds of the type M−*N*−H···O with the solvent and the higher solvation of the metal ion in DMSO therefore prevailing in governing the trend of the stabilities.

Silver(I)/hmtrien System

A comparison with the thermodynamic functions previously determined for the Ag^{I}/trien system[22d] (also shown in Table 1), in which the ligand was shown to behave as tetradentate ligand, shows that hmtrien is also able to tetracoordinate Ag^{I}, forming three fused five-membered chelate rings.

The drop in $\log\beta_1$, of about two orders of magnitude, on going from primary to tertiary amino groups should be associated with: (i) the different basicities of the amino groups, which decrease in the order $-NH_2 > -NHR > -NR_2$ in DMSO,[38] (ii) steric hindrance, which results in elongation of the metal−nitrogen bonds,[1,3,5c,5e,5g,5h] and (iii) the absence of M−*N*−H···O hydrogen bonds, which are responsible for a decrease in outer-sphere solvation energy, thus increasing the hydrophobic nature of the complexes,[16] and of a decrease in the nitrogen σ-donating properties, which reverses the trend found in the gas phase, in which it has been shown that tertiary amine ligands are better σ-donors.[3] Effects (i) and (ii) in particular are also responsible for the decreased enthalpy gain for hmtrien complexation. Effect (iii) transforms the central cation into a harder acid.[3] As far as point (ii) is concerned, some authors have recently proposed, on the basis of X-ray results and molecular-mechanics calculations (MM), that nonbonded repulsions between the *N*-methyl groups are the primary cause of the observed elongation of the M−N bonds.[5c,5e,5g,5h]

Cd^{II}/Tetraamine Systems

Trien certainly behaves as tetradentate ligand in the CdL complex, as shown by the trend in the thermodynamic functions in relation to those of the $[Cd(dien)]^{2+}$ system [diethylenetriamine (dien), $\log\beta_1 = 8.46$, $\Delta H°_1 = -65.3$, $T\Delta S°_1 = -17$ kJ·mol^{-1} [8c]], in which dien is known to act as terdentate ligand; this was confirmed by independent FT-IR measurements run on a 1:1 Cd/trien solution, in which the bands due to free secondary (at 3313 cm^{-1}) and primary (at 3360 and 3300 cm^{-1}) amino groups were not present.

The huge drop in stability and exothermicity observed on going from trien to hmtrien was similarly observed for other analogous primary and tertiary polyamines; from the thermodynamic values it therefore seems reasonable to suppose that hmtrien also acts as tetradentate ligand, the trend in the data being greatly influenced, as in the case of the silver(I) system, by the different basicities and steric requirements of the ligands.

The Cd^{II} ion is certainly hexacoordinate in the ML_2 complex with trien, according to its tendency to bind polyamines, exhausting all coordinative positions.[8c,39] This is clearly indicated by the values of the thermodynamic functions for the stepwise reaction according to Equation (3), which are of the same order of magnitude as those found for the CdL complex formation with the diamine ethylenediamine (en) ($\log\beta_1 = 5.88$, $\Delta H°_1 = -52.2$, $T\Delta S°_1 = -19$ kJ·mol^{-1} [8c]).

$$CdL + L \rightleftharpoons CdL_2 \quad (3)$$
$$\log K_2 = 5.19,\ \Delta H_{K_2} = -59,\ T\Delta S_{K_2} = -29.4\ \text{kJ·mol}^{-1}$$

The more favourable enthalpy gain (with respect to that of the 1:1 Cd/en system) reported for Equation (3), despite one of the nitrogen atoms of the second entering trien being secondary, is due to the observed fact[8c] that in Cd^{II} − as well as in Co^{II} − complexation with polyamines, the desolvation of the species involved occurs mainly in the first step of complexation.[6,8b,8c] This is also confirmed by the less favourable entropy term.

A real novelty for the Cd^{II} system is the formation of an appreciable amount of a Cd_2L_3 species (Table 1 and Figure 1), which is formed despite the dielectric constant of DMSO (46.4[19]) and enhances the importance of electrostatic repulsion in the case of polynuclear species formation. The high stability of this complex is due to the enthalpic factors, as the entropy value strongly counteracts the complex formation. Unfortunately, it was not possible to obtain unambiguous information about the number of coordinated amino groups by spectroscopic (NMR, FT-IR or UV/Vis) measurements, as Cd_2L_3 (and also Co_2L_3, see below) is present in solution together with both the mononuclear CdL and, even worse, the CdL_2 species. Nevertheless, two reasonable coordination modes may be hypothesized: (i) that in which the exhaustive hexacoordination of the metal ions is achieved, and (ii) that in which two ML tetracoordinate complexes are bridged by another trien ligand, which coordinates only with the two primary amino groups. As a large number of thermodynamic data relating to complex formation of Cd^{II} with differently methylated mono-, di- and triamines are available,[8c] an attempt to draw some conclusions about the coordination mode described above has been made by use of a chemometric approach based on a multiple linear least-squares regression. The contribution

 © 2003 Wiley-VCH Verlag GmbH & Co. KGaA, Weinheim

of each bonded nitrogen atom to the total value of the thermodynamic functions has therefore been calculated.

The calculated values of $\Delta G°$ and $\Delta H°$ (and their errors) expected for the coordination of one single primary and secondary N groups in chain (not methylated) are, respectively:
$\Delta G_{Cd} = -15.7(0.6)$ and $-14.6(1.0)$;
$\Delta H_{Cd} = -25.1(0.7)$ and $-15.7(1.1)$ kJ·mol^{-1}
[for Co^{II} the calculated values are, respectively, $\Delta G_{Co} = -16.6(0.6)$ and $-15.0(1.0)$; $\Delta H_{Co} = -27.5(1.0)$ and $-17.9(1.5)$ kJ·mol^{-1} [6,8b]]

According to the $\Delta G°$ and $\Delta H°$ values calculated above, expected values for Cd_2L_3 should be:
$\Delta G_{Cd} = -182.1(8.7)$ (logβ = 31.9) and
$\Delta H_{Cd} = -245(9.5)$ in the case of formation of species (i) and
$\Delta G_{Cd} = 152.8(8.1)$ (logβ= 26.7) and
$\Delta H_{Cd} = -213.4(8.9)$ kJ·mol^{-1} for the species (ii)

From comparison with the experimental results in Table 1, one can suggest that hypothesis (i) seems to be more reasonable**.**

The 1:1 complex stability with trien is greater than that of the corresponding Ag^I complex and reflects the higher affinity of the N atom for the borderline soft/hard divalent acceptor Cd^{II} than for the very soft univalent Ag^I ion. As far as hmtrien is concerned, the selectivity towards the metal ions is reversed. This agrees with other experimental evidence[8c] explained in terms of the more difficult arrangement that a bulky ligand may suffer when octahedrally rather than tetrahedrally coordinated.[8c,35b] The decreasing hard nature of the ligand[1] is also responsible for this behaviour.

Co^{II}/Tetraamine System

Co^{II} forms the same complexes as Cd^{II} with trien; the trend in the thermodynamic functions, together with analysis of the data obtained previously for other di- and triamines,[6,8b] suggest conclusions very similar to those reported here for the Cd^{II}/trien system (see above).

Better, comparison between the two systems shows that a higher stability (and exothermicity) is associated with Co^{II}/trien complex formation than that of the analogous situation with Cd^{II}, and this was also observed for other primary and secondary polyamines (see Figure 4, in which, for the sake of simplicity, only the logβ_1 values for CdL polyamine systems are reported as a function of the logβ_1 values for the analogous Co^{II} complexes). The harder Co^{II} is in fact characterized by stronger affinity than the medium/soft Cd^{II} towards the $-NH_2$ and $-NHR$ groups.

In addition, in the polynuclear M_2L_3 complex, it is likely that the larger Cd^{II} ions may be closer to each other than Co^{II} ions, and its stability should therefore be more dependent on electrostatic repulsions (see Table 1 for comparison).

With regard to *N*-alkylated hmtrien, the trend is completely reversed, the value of the stability constant being about two orders of magnitude less than the value found for the analogous Cd^{II}/hmtrien and much of the same order of magnitude as found for the Co^{II}/bidentate pmdien (pmdien = *N*,*N*,*N*′,*N*′′,*N*′′-diethylenetriamine) system.

This value was surprisingly low in comparison with that, though uncertain, available for the same Co^{II}/hmtrien system in water (Table 1). Unfortunately, data on hmtrien coordination to Cd^{II} in water are not known and so no comparison between the Δlogβ_1 values of Cd^{II}/- and Co^{II}/primary and tertiary tetraamine complexes in water is possible. On the other hand, a considerable drop in stability is also seen when considering the complex formation of the borderline[19] Cu^{II} ion, the chemical behaviour of which is, in certain aspects, similar to that of Co^{II} with trien and hmtrien in water (from 20.1 to 12.60[16]).

Other experimental techniques − direct UV/Vis titration of Co^{II} solutions and potentiometric titrations with Ag^I as competitor ion − were therefore also performed on the Co/hmtrien system, and the value reported in Table 1 was fully confirmed.

An analysis of all data so far reported for the two Cd^{II}/- and Co^{II}/polyamine systems in DMSO may provide an explanation for this behaviour. From Figure 4 it can be inferred that: (i) the drop in complex stability on *N*-methylation is more evident for Co^{II} than for Cd^{II}, and (ii) this drop, especially for Co^{II}, is more important on going from secondary to tertiary N groups. This can probably be explained by taking into account that: (i) large metal ions such as Cd^{II} can better minimize steric hindrances when bulky $-N(CH_3)_2$ moieties are involved in complex formation,[8c] and (ii) the increasingly soft nature of the nitrogen donors accounts for the difficulty encountered by tertiary amines in exhausting the coordination sites in Co^{II} complexation, whereas they are able to do it when the Cd^{II} ion is involved. This is confirmed in particular by analysis of the data in Figure 4 for the amines containing tertiary amino groups; they show similar stabilities with Co^{II}, whereas their CdL complex stabilities increase gradually with the increase in the number of probably coordinated nitrogen atoms. With Co^{II} a maximum of two nitrogen atoms are found to be able to coordinate the hard central ion, when tertiary polyamines are considered. As far as this last point is concerned, it has already been shown that the severe steric strain present in tertiary *N*-methylated amines, also confirmed by MM calculations, does not allow formation of a hexaamine complex when all N donors are tertiary, whereas this does occur when the degree of *N*-methylation is decreased.[5c,5g,5h]

The electron densities on the metal ions in the complexes, and therefore their dioxygen affinities, would be expected to be significantly lowered when the Co^{II}/hmtrien complex is formed, in relation to its Co^{II}/trien analogue.

With the aim of improving knowledge of correlation between electrochemical properties of the complexes and their dioxygen affinities, voltammetric measurements were carried out on both 1:1 Co^{II}/trien and Co^{II}/hmtrien systems.

The results obtained showed that the signals relative to the $Co^{II}L_j/Co^{III}L_j$ couples, and therefore to the reaction according to Equation (4) were not visible for the two systems

 © 2003 Wiley-VCH Verlag GmbH & Co. KGaA, Weinheim

investigated, probably for the reasons explained previously.[6]

$$Co^{II}L_j \rightarrow Co^{III}L_j + e \quad (4)$$

The values of E_{pc}, the cathodic potential at maximum diffusion current, for the reaction according to Equation (5) are, on the other hand, easily evaluated for the two systems investigated and are −1.65 and − 1.50 V for the trien and hmtrien system, respectively.

$$Co^{II}L_j + 2e \rightarrow Co(0) + jL \quad (5)$$

By taking into account that the dioxygen uptake by a given complex represents the formation of a charge-transfer complex, a correlation between E_{pc} and Co^{II} charge density and therefore $Co^{II}L_j$ dioxygen affinity, should be observed. The higher the charge density, the more difficult the reduction process to Co^0 should be, and the more negative the E_{pc} value;[6] the E_{pc} value for the tertiary amine is in fact shifted anodically. That confirms how steric aspects of ligand design might be used to produce desired redox properties.[40]

It is of interest to note that the critical value of −1.54 V proposed in ref.[6] is not reached by the Co^{II}/hmtrien complex and that therefore, on the basis of the correlation between electrochemical properties and $Co^{II}L$ dioxygen affinity (see ref.[6] for details), we should predict that this adduct should not be able to bind dioxygen.

This is confirmed by the fact that no changes are observed in the spectra of deaerated and aerated solutions of the Co^{II}/hmtrien system, whereas for the Co^{II}/trien 1:1 species the aerated spectrum shows the very rapid (Figure 3, b) appearance of a charge-transfer band at 310 nm, to which a second band at 370 nm is added within a few minutes. The intensity of the latter band increased for about 60 min when the O_2 concentration was 4%, the kinetic behaviour being dependent on the initial dioxygen concentration. This band then remained constant for at least 6 h. This development seems to be consistent with the formation of two different dioxygenated species formed by different kinetic and thermodynamic pathways; the thermodynamically stable species seems not to undergo autoxidation, at least within the first 6 h. In addition, the dioxygen uptake is likely to be irreversible, as the UV absorption did not decrease with N_2 bubbling

A confirmation of this qualitative interpretation, together with an indication of the stoichiometry of the CoL/O_2 species, is provided by the O_2 absorption, which shows a quick uptake of dioxygen and then a plateau reached at R_{O2} = 0.5 (Figure 5), suggesting the formation of a μ-peroxo complex in which the dioxygen molecule bridges two metal ions; the dinuclear μ-superoxo complex is not considered, as the maximum of the charge-transfer band is located here at 325 nm, whereas normally the electronic spectrum of the green μ-superoxo adduct shows an additional band around 710 nm.[26,41] The 2:1 CoL/O_2 adduct formation agrees with the general tendency of Co^{II} complexes with simple polyazaalkanes to form dinuclear dioxygen species in dipolar solvents rather than end-on species, which normally requires superstructured ligands able to form a protective cavity around the metal ion.[26,31,41] Detailed thermodynamic and kinetic studies on this system are in progress.[42]

Conclusions

The *N*-functionalization of the ligands has a strong influence on the stoichiometry and the nature of the complexes formed, as well as, much more interestingly, on the selectivities of the ligands towards metal ions, as suggested by the behaviour of primary and secondary amines with respect to the tertiary ones. The former pair show the general stability trend increasing in the order $Ag^{I} < Cd^{II} < Co^{II}$, the latter reverse this trend and the complex stability increases in the order $Co^{II} < Cd^{II} < Ag^{I}$. The Cd^{II} ion generally coordinates all the donor sites of the nitrogen ligands, whereas Co^{II} does not when tertiary amino groups are involved.

The decreasingly hard nature of the nitrogen donors is mainly responsible for the fact that *N*-alkylation of trien prevents the Co/hmtrien system from being able to take up dioxygen. The E_{pc} value of −1.50 V allows this behaviour to be predicted, on the basis of all of the reported data, and provides additional insights into the correlation between electrochemical properties, number of methyl substituents and consequent dioxygen affinity of the anaerobic Co^{II} complexes.

Finally, it is suggested that a 2:1 $[Co(trien)_2]^{2+}/O_2$ complex is formed under aerobic conditions.

Experimental Section

General Remarks: $Co(ClO_4)_2 \cdot 6DMSO$ and $Cd(ClO_4)_2 \cdot 6DMSO$ were prepared and purified as described.[8b] Anhydrous silver perchlorate was obtained from $AgClO_4 \cdot H_2O$ (Fluka; puriss) as described previously.[22a] Dimethyl sulfoxide (Fluka; > 99%) was purified by distillation according to the described procedures,[22a] degassed by a pumping-freezing procedure, and stored in the presence of 4-Å molecular sieves. The ligands trien and hmtrien (Aldrich; > 97%) were purified by fractional distillation.[43] Stock perchlorate solutions of Cd^{II} and Co^{II} ions were prepared by dissolution of weighed amounts of the adducts in anhydrous degassed DMSO, and their concentrations were determined by titration with EDTA.[44] The solutions of $AgClO_4$ were prepared and standardized as before.[22a] The background salt Et_4NClO_4 was recrystallized twice from methanol and dried at 110 °C. Solutions of the ligands were prepared by dissolution of weighed amounts in DMSO and standardized by thermometric titration with standard $HClO_4$ solutions. All standard solutions were prepared and stored in an MB Braun 150 glovebox under a controlled atmosphere containing less than 1 ppm of water and less than 1 ppm of oxygen. The water content in the solutions, typically 10−20 ppm, was determined with the aid of a Metrohm 684 KF Coulometer.

Potentiometric Measurements: All measurements were carried out under dry, oxygen-free nitrogen in an MB Braun-150 glovebox, in a thermostatted cell maintained at 298.0 ± 0.1 K. The experimental data required for the determination of the stability constants of the Ag^{I}/hmtrien and the Cd^{II}/trien and Cd^{II} /hmtreien systems were

 © 2003 Wiley-VCH Verlag GmbH & Co. KGaA, Weinheim

the equilibrium concentrations of the silver and cadmium ions, respectively, obtained from the electromotive force (emf) data of a galvanic cell similar to that reported previously.[22a] The emf values were measured with the aid of an Amel 338 pHmeter equipped with a Metrohm 6.0328.000 silver electrode as a working electrode and a Metrohm 6.0718.000 silver electrode as a reference in the first case and with a Weiss WCD1001 Cd ion selective electrode as working electrode and a Methrom 6.0718.000 silver electrode as reference one in the second case. Aliquots of ligand solutions of known concentrations were first added to the cell containing only solutions of metal (metal = Ag^{I} or Cd^{II}) perchlorate ($2.00 < c^{\circ}_{Metal} < 30.00$ mmol·dm^{-3}) of exact known concentration and the free metal ion concentration was measured after each titrant addition. Some titrations were carried out in duplicate to verify the reproducibility of the system. Equilibrium was typically reached in 2−5 min. The Nernstian response of the Ag and Cd electrodes were obtained in the range 10^{-7} < metal ion < 10^{-2} mmol·dm^{-3}. The computer program Hyperquad[45] was used for calculation of the stability constants.

Spectrophotometric Measurements: UV/Vis spectra were recorded with a Varian Cary 50 Spectrophotometer directly inside the glovebox, by use of optic fibre probes and a quartz cuvette with a pathlength of 1 cm (117.100 Bracco cell). The data were recorded over the wavelength range 300−650 nm. Different types of titrations were carried out in order to obtain the best competition between Cd^{II} and Co^{II} for the same ligand and/or to provide evidence of possible formation of mixed or polynuclear species. The absorption maximum for $Co(ClO_4)_2$ in DMSO occurs at 535 nm, with an extinction molar coefficient $\varepsilon = 11.9$ mol^{-1}·dm^3·cm^{-1}. The absorption maximum of CoL_j complexes are shifted to lower wavelengths, in line with an increase in the ligand field strength. The fact that equilibrium was attained was supported by the observation that addition of titrant solution produce an immediate spectral change with no further change noted after several hours. The absorbance data at about 20 different wavelengths in the 450−550-nm range were analysed and the formation constants of the Co_iL_j complexes ($i = 1$, $j = 1$ for L = hmtrien; $i = 1$, $j = 1$, 2 and $i = 2$, $j = 3$ for L = trien) were determined, together with the molar extinction coefficients of the complexes at each relevant wavelength, by use of the Hyperquad program.[45] The UV/Vis measurements for dioxygen uptake were carried out by use of an analogous apparatus with the aid of optic fibre probes (Hellma) of 1-cm length dipped directly into the reaction vessel.

Calorimetric Measurements: A Tronac model 87−558 precision calorimeter was employed to measure the heats of reaction. The calorimeter was checked by titration of tris(hydroxymethyl)aminomethane (tham) with a standard solution of HCI in water. The experimental value of the heat of neutralization of tham was found to be $\Delta H^{\circ} = -47.59$ kJ·mol^{-1}, in good agreement with the accepted value of -47.53 ± 0.13 kJ·mol^{-1}.[7] The calorimetric titrations were performed at 298.00 ± 0.02 K by addition of known volumes of ligand solutions ($50 < c^{\circ}_{L} < 400$ mmol·dm^{-3}) to 20 mL of metal ion (Ag^{I}, Cd^{II}, Co^{II}) solutions ($2.00 < c^{\circ}_{Metal} < 30.0$ mmol·dm^{-3}). For each titration run, n experimental values of the total heat produced in the reaction vessel were calculated as a function of the added titrant. These values were corrected only for the heat of dilution of the titrant, which was determined separately. The heat of dilution of the titrate was found to be negligible in the metal ion concentration range used. The quantity Δh_n, total heat per mol of metal ion, was defined and calculated by dividing the net reaction heat by the number of mol of metal ion in the calorimetric vessel. The least-squares computer program Letagrop Kalle[46] was used for the calculation of the enthalpy changes.

FT-IR Spectroscopy: The FT-IR spectra were obtained with a Bio-Rad FTS 40 spectrometer (maximum resolution 4 cm^{-1}; 16 scans). A cell with barium fluoride windows (thickness of 25 μm) was used. The cells were filled and closed in the glovebox and quickly transferred to the spectrometer. The c°_{Co} and c°_{trien} values in the DMSO solutions were about 50 mmol·dm^{-3}.

Cyclic Voltammetry: The cyclic voltammograms of CoL_1 complexes were carried out with an EG&G Princetown Applied Research Model 263A potentiostat controlled by a Win/PC-based program. A saturated Ag/AgCl electrode was employed as reference and a Pt electrode was used as working electrode, with a Pt wire being present as auxiliary electrode. The measurements were carried out with a scan rate of 100 mV/s.

O_2 Absorption: Measurement of O_2 absorption was performed with the aid of a gas burette connected to a vessel containing 0.6 mmol of total cobalt(II) in 20 mL of DMSO ($I = 0.1$ M) in the presence of 0.6 mmol of trien. The system was thermostatted at 298.0 K with a water circulating bath. The solution was vigorously stirred to minimize diffusion effects.

Acknowledgments

This work was supported by the Ministero dell'Università e della Ricerca Scientifica e Tecnologica (MURST, Rome) within the program PRIN 2000.

[1] D. Meyerstein, *Coord. Chem. Rev.* **1999**, *185−186*, 141−147, and refs. cited therein.
[2] Z.-L. Lu, M. S. A. Hamza, R. van Eldik, *Eur. J. Inorg. Chem.* **2001**, 503−510.
[3] T. Clark, M. Hennemann, R. van Eldik, D. Meyerstein, *Inorg. Chem.* **2002**, *41*, 2927−2935.
[4] N. Navon, A. Burg, H. Cohen, R. van Eldik, D. Meyerstein, *Eur. J. Inorg. Chem.* **2002**, 423−429.
[5] [5a] P. V. Bernhardt, P. Comba, T. W. Hambley, *Inorg. Chem.* **1993**, *32*, 2804−2809. [5b] P. V. Bernhardt, A. M. T. Bygott, R. J. Geue, A. J. Hendry, B. R. Korybut-Daszkiewicz, P. A. Lay, J. R. Pladziewicz, A. M. Sargeson, A. C. Willis, *Inorg. Chem.* **1994**, *33*, 4559−4561. [5c] V. Bernhardt, J. M. Harrowfield, D. C. R. Hockless, A. M. Sargeson, *Inorg. Chem.* **1994**, *33*, 5659−5670. [5d] P. V. Bernhardt, K. A. Byriel, C. H. L. Kennard, P. C. Sharpe, *Inorg. Chem.* **1996**, *35*, 2045−2052. [5e] P. V. Bernhardt, *J. Am. Chem. Soc.* **1997**, *119*, 771−774. [5f] P. V. Bernhardt, l. A. Jones, *J. Chem. Soc., Dalton Trans.* **1998**, 1757−1761. [5g] P. Comba, *Coord. Chem. Rev.* **1999**, *182*, 345−371. [5h] P. Comba, *Coord. Chem. Rev.* **1999**, *185−186*, 81−98. [5i] P. V. Bernhardt, G. A. Lawrence, M. Napitupulu, G. Wei, *Inorg. Chim. Acta* **2000**, *300−302*, 604−612.
[6] C. Comuzzi, A. Melchior, P. Polese, R. Portanova, M. Tolazzi, *Eur. J. Inorg. Chem.* **2002**, 2194−2201 and references therein.
[7] [7a] R. M. Smith, A. E. Martell, in *Critical Stability Constants*, Plenum Press, New York, **1989**, vol. 6, 2nd supplement. [7b] A. E. Martell, R. M. Smith, R. J. Motekaitis, *Critically Selected Stability Constants of Metal Complexes Database*, version 5.0, **1998**.
[8] [8a] C. Comuzzi, V. Novelli, R. Portanova, M. Tolazzi, *Supramol. Chem.* **2001**, *13*, 455−460. [8b] C. Comuzzi, M. Grespan, P. Polese, R. Portanova, M. Tolazzi, *Inorg. Chim. Acta* **2001**, *321*, 49−55. [8c] C. Comuzzi, M. Grespan, A. Melchior, R. Portanova, M. Tolazzi, *Eur. J. Inorg. Chem.* **2001**, 3087−3094. [8d] C. Comuzzi, V. Novelli, R. Portanova, M. Tolazzi, *Polyhedron* **2002**, *21*, 1337−1342.
[9] D. Kuppert, J. Sander, C. Roth, M. Wörle, T. Weyhermüller, G. J. Reiss, U. Schilde, I. Müller, K. Hegetschweiler, *Eur. J. Inorg. Chem.* **2001**, 2525−2542.

 © 2003 Wiley-VCH Verlag GmbH & Co. KGaA, Weinheim

[10] R. M. Clay, S. Corr, M. Micheloni, P. Paoletti, *Inorg. Chem.* **1985**, *24*, 3330−3336.
[11] R. Hancock, A. E. Martell, *Chem. Rev.* **1989**, *89*, 1875−1914.
[12] A. Bencini, A. Bianchi, P. Paoletti, *Coord. Chem. Rev.* **1992**, *120*, 51.
[13] F. C. J. M. van Veggel, W. Verboom, D. N. Reinhoudt, *Chem. Rev.* **1994**, *94*, 279−299.
[14] C. Bazzicalupi, A. Bencini, A. Bianchi, V. Fusi, E. Garcia-Espana, P. Paoletti, P. Paoli, B. Voltancoli, *Inorg. Chem.* **1993**, *32*, 4900−4908.
[15] I. Bertini, L. Messori, G. Golub, H. Cohen, D. Meyerstein, *Inorg. Chim. Acta* **1995**, *235*, 5−8.
[16] G. Golub, H. Cohen, P. Paoletti, A. Bencini, D. Meyerstein, *J. Chem. Soc., Dalton Trans.* **1996**, 2055−2060.
[17] G. Crisponi, A. Diaz, V. M. Nurchia, T. Pivetta, M. J. Tapia Este'vez, *Polyhedron* **2002**, *21*, 1319−1327.
[18] A. Bencini, A. Bianchi, P. Fornasari, C. Giorgi, P. Paoletti, B. Valtancoli, *Polyhedron* **2002**, *21*, 1329−1335.
[19] S. Ahrland, in *The Chemistry of Non-aqueous Solvents* (Ed.: J. J. Lagowsky), Academic Press, New York, **1978**, vol. 5a and references therein.
[20] B. G. Cox, J. Garcia-Rosas, H. Schneider, *J. Am. Chem. Soc.* **1981**, *103*, 1384−1389.
[21] H. K. Chantooni, I. M. Kolthoff, *J. Solut. Chem.* **1985**, *14*, 1−12.
[22] [22a] A. Cassol, P. Di Bemardo, P. L. Zanonato, R. Portanova, M. Tolazzi, *J. Chem. Soc.* **1987**, 657−660. [22b] A. Cassol, P. Di Bemardo, P. L. Zanonato, R. Portanova, M. Tolazzi, G. Tomat, *J. Chem. Soc., Dalton Trans.* **1988**, 1781−1784. [22c] A. Cassol, P. Di Bemardo, P. L. Zanonato, R. Portanova, M. Tolazzi, G. Tomat, V. Cucinotta, D. Sciotto, *J. Chem. Soc., Faraday Trans. 1* **1989**, *85*, 2445−2452. [22d] A. Cassol, P. Di Bemardo, P. L. Zanonato, R. Portanova, M. Tolazzi, G. Tomat, *J. Chem. Soc., Faraday Trans.* **1990**, *86*, 2841−2845. [22e] A. Cassol, P. Di Bemardo, R. Portanova, M. Tolazzi, G. Tomat, P. L. Zanonato, *J. Chem. Soc., Dalton Trans.* **1992**, 469−474. [22f] Z. Wang, G. R. Choppin, P. di Bemardo, P. L. Zanonato, R. Portanova, M. Tolazzi, *J. Chem. Soc., Dalton Trans.* **1993**, 2791−2796. [22g] A. Cassol, G. R. Choppin, P. Di Bemardo, R. Portanova, M. Tolazzi, G. Tomat, P. L. Zanonato, *J. Chem. Soc., Dalton Trans.* **1993**, 1695−1698. [22h] P. Di Bernardo, G. R. Choppin, R. Portanova, P. L. Zanonato, *Inorg. Chim. Acta* **1993**, *207*, 85−91. [22i] A. Cassol, P. Di Bernardo, R. Portanova, M. Tolazzi, P. L. Zanonato, *Inorg. Chim. Acta* **1997**, *262*, 1−8.
[23] F. Arnaud-Neu, *Chem. Soc. Rev.* **1994**, 235−241.
[24] N. Heidari, A. Thaler, H. Schneider, B. G. Cox, *Inorg. Chim. Acta* **1998**, *279*, 186−191.
[25] A. Thaler, N. Heidari, B. G. Cox, H. Schneider, *Inorg. Chim. Acta* **1999**, *286*, 160−168.
[26] [26a] A. F. Martell, D. T. Sawyer, *Oxygen Complexes and Oxygen Activation by Transition Metals*, Plenum, New York, **1988**. [26b]G. Mc Lendon, A. E. Martell, *J. Chem. Soc., Chem. Commm* **1975**, 223−225.
[27] H. Sugimoto, T. Nagayama, S. Maruyama, S. Fujinami, Y. Yasuda, M. Suzuki, A. Uehara, *Bull. Chem. Soc. Jpn.* **1998**, *71*, 2267−2279.
[28] R. D. Jones, D. A. Summerville, F. Basolo, *Chem. Rev.* **1979**, *79*, 139−179.
[29] T. D. Smith, J. T. Pilbrow, *Coord. Chem. Rev.* **1981**, *39*, 295−383.
[30] E. C. Niederhoffer, J. H. Timmons, A. Martell, *Chem. Rev.* **1984**, *84*, 137−203.
[31] L. I. Simandi, in *Dioxygen Activation and Homogeneous Catalytic Oxidation*, Elsevier, Amsterdam, **1991**.
[32] S. Ahrland, I. Persson, *Acta Chem. Scand., Ser. A* **1980**, *34*, 645.
[33] S.-I. Ishiguro, K. Ozutsumi, *Inorg. Chem.* **1990**, *29*, 1117−1123.
[34] [34a] S. Ahrland, N.-O. Bjork, *Acta Chem. Scand., Ser. A* **1974**, *28*, 823−828. [34b] M. Sandstrom, I. Persson, S. Ahrland, *Acta Chem. Scand., Ser. A* **1978**, *32*, 607−625. [34c] M. Kodama, E. Kimura, *J. Chem. Soc., Dalton Trans.* **1978**, 1081−1085. [34d] S. Ahrland, E. Avsar, T. Berg, *J. Organomet. Chem.* **1979**, *181*, 17. [34e] S. Ahrland, S.-I. Ishiguro, A. Marton, I. Persson, *Acta Chem. Scand., Ser. A* **1985**, *39*, 227−240. [34f] S.-I. Ishiguro, K. Ozutsumi, H. Ohtaki, *Bull. Chem. Soc. Jpn.* **1987**, *60*, 531−538. [34g] I. Persson, B. Schneider, *Inorg. Chim. Acta* **1989**, *158*, 245−248. [34h] R. Bhula, P. Osvath, D. C. Weatherburn, *Coord. Chem. Rev.* **1988**, *91*, 89−213.
[35] [35a] A. Bencini, A. Bianchi, P. Paoletti, P. Paoli, *Coord. Chem. Rev.* **1992**, *120*, 29. [35b] M. Koide, H. Suzuki, S.-I. Ishiguro, *J. Chem. Soc., Faraday Trans.* **1995**, *91*, 3851−3858. [35c] H. Adams, R. Bastida, D. E. Fenton, A. Macias, S. E. Spey, L. Valencia, *J. Chem. Soc., Dalton Trans.* **1999**, 4131−4138. [35d] P. Arranz-Mascaros, R. Lopez-Garzou, M. D. Gutierrez-Valero, M. L. Godino-Salido, J. M. Moreno, *Inorg. Chim. Acta* **2000**, *304*, 137−143. [35e] D. J. R. Brook, S. Fornell, J. E. Stevens, B. Noll, T. H. Koch, W. Eisfeld, *Inorg. Chem.* **2000**, *34*, 562−567. [35f] G. J. Grant, M. W. Jones, K. D. Loveday, D. G. VanDerveer, W. T. Pennington, C. T. Eagle, L. F. Mehne, *Inorg. Chim. Acta* **2000**, *300−302*, 250−263. [35g] C. Bazzicalupi, A. Bencini, A. Bianchi, V. Fedi, C. Giorgi, P. Paoletti, L. Tei, B. Voltancoli, *Inorg. Chim. Acta* **2000**, *300−302*, 653−660. [35h] M. Di Vaira, F. Mani, P. Stoppiani, *Inorg. Chim. Acta* **2000**, *303*, 61−69. [35i] M. B. Inouoe, I. C. Muñoz, M. Inouoe, Q. Fernando, *Inorg. Chim. Acta* **2000**, *300−302*, 206−211. [35j] G. Park, N. Ye, R. D. Rogers, M. W. Brechbiel, R. P. Plonalp, *Polyhedron* **2000**, *19*, 1155−1161.
[36] F. J. C. Rossotti, H. Rossotti, in *The determination of Stability Constants*, McGraw-Hill, New York, **1968**.
[37] C. Halidas, G. Heffer, Y. Marcus, *Chem. Rev.* **2000**, *100*, 819−852.
[38] A. Mucci, R. Domain, R. L. Benoit, *Can. J. Chem.* **1980**, *58*, 953−958.
[39] E. Bartoszak-Adamska, R. Bregier-Jarzebowska, L. Lechoslaw Lomozik, *Polyhedron* **2002**, *21*, 739−744.
[40] T. W. Hambley, *Inorg. Chem.* **1988**, *27*, 2496−2501.
[41] [41a] S. Cabani, N. Ceccanti, M. R. Tine′, *Pure Appl. Chem.* **1991**, *63*, 1455−1464. [41b] S. Cabani, *React. Funct. Polym.* **1996**, *28*, 167−182.
[42] C. Comuzzi, A. Melchior, P. Polese, R. Portanova, M. Tolazzi, *Inorg. Chim. Acta*, accepted.
[43] D. D. Perrin, W. L. F. Annarego, D. R. Perrin, in *Purification of Laboratory Chemicals*, 2nd ed., Pergamon, Oxford, **1980**.
[44] A. I. Vogel's, in *Textbook of Quantitative Chemical Analysis*, 5th ed., Longman Group, London, UK, **1989**.
[45] P. Gans, A. Sabatini, A. Vacca, *Talanta* **1996**, *43*, 1739−1753.
[46] R. Arnek, *Ark. Kemi* **1970**, *32*, 81−88.

Received December 16, 2002

 © 2003 Wiley-VCH Verlag GmbH & Co. KGaA, Weinheim

Structural, Magnetochemical and Electrochemical Studies of Dinuclear Complexes Containing the $[V^{V}O]_2$, $[V^{IV}O]_2$, Cr^{III}_2, Mn^{III}_2 and Fe^{III}_2 Cores of a Potentially Pentadentate Phenol-Containing Ligand with (O,N,O,N,O)-Donor Atoms

Soumen Mukherjee,[a] Thomas Weyhermüller,[a] Eberhard Bothe,[a] and Phalguni Chaudhuri*[a]

Keywords: N,O ligands / Transition metals / Magnetic properties / Radicals / Electrochemistry

Dinuclear complexes $[L_2Fe^{III}_2]$ (**1**), $[L_2Mn^{III}_2]$ (**2a**), $[L_2Mn^{III}_2(THF)_2]$ (**2b**), $[L_2Cr^{III}_2]$ (**3**), $[L(V^{IV}O)_2(OCHMe_2)]$ (**4**) and $[L_2(V^{V}O)_2]$ (**5**) with a pentadentate phenol-containing ligand H_3L (= $C_6H_2(CH_3)(OH)\{[C(CH_3)_3]_2(OH)NCH\}_2$) bearing the N_2O_3 donor atoms have been synthesized and the X-ray structures of **1**, **2b**, **4** and **5** are reported. The compounds were characterized by IR, UV/Vis and Mössbauer spectroscopy, mass spectrometry, electrochemical and variable-temperature (2–295 K) magnetic susceptibility measurements. Analysis of the susceptibility data demonstrates antiferromagnetic interactions between the metal centers establishing diamagnetic ground states for complexes **1**–**4**. The electrochemical results suggest the generation of ligand-centered oxidation processes attributable to the phenoxyl radicals, rather than the formation of unusually high oxidation states at the central metal centers. The ligand H_3L has the potential to act in a multidentate fashion as evidenced by the X-ray structures of **2b** and **5**. In compound **2b** the central phenolate oxygen of the *p*-cresol ring does not function as a bridging atom between two manganese centers, whereas in **5** the ligand is tetradentate with one noncoordinating nitrogen atom.
(© Wiley-VCH Verlag GmbH & Co. KGaA, 69451 Weinheim, Germany, 2003)

Introduction

This work stems from our ongoing interest[1] in phenol-containing ligands, and their one-electron oxidation products, i.e. phenoxyl radicals. The widespread occurrence of tyrosine radicals[2] in metalloproteins involving oxygen-dependent enzymatic radical catalysis has prompted inorganic chemists to model tyrosine by using phenolate ligands.[3] In an earlier paper[4] we described a dinucleating Schiff-base ligand H_3L, obtained by the condensation (1+2) of 2,6-diformyl-4-methylphenol with 6-amino-2,4-di-*tert*-butylphenol. This ligand can be used to prepare complexes containing Cu^{II}_2, Cu^{II}_4, Ni^{II}_2 and Ni^{II}_4 cores, which have been spectroscopically and structurally characterized and reported.[4] This paper is a continuation of our investigations with the ligand H_3L and describes coordination of the ligand with the Fe^{III}, Mn^{III}, Cr^{III}, (V^{IV}=O) and (V^{V}=O) ions. The compounds described here are given below with their labels.

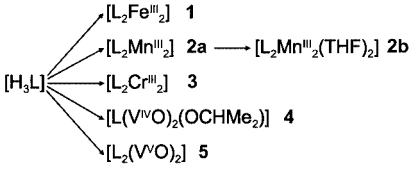

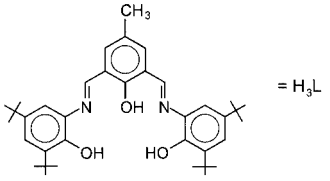

Results and Discussion

Reactions of metal salts with the ligand H_3L in the presence of triethylamine afforded complexes **1**–**5** in moderate yield. The dinuclear complexes were easily isolated and characterized by different methods. Remarkably $[L_2Mn^{II}_2]$ (**2a**), which is considered to possess an identical coordination sphere and atom connectivity as the structurally characterized $[L_2Fe^{III}_2]$ (**1**), yields on recrystallization from THF $[L_2Mn^{III}_2(THF)_2]$ (**2b**), in which the phenolate-bridging between two manganese centers prevailing in **2a** does not persist any more, thus resulting in a comparatively long Mn···Mn separation (6.45 Å).

[a] Max-Planck-Institut für Strahlenchemie,
Stiftstrasse 34–36, 45470 Mülheim an der Ruhr, Germany
E-mail: Chaudh@mpi-muelheim.mpg.de

 © 2003 Wiley-VCH Verlag GmbH & Co. KGaA, Weinheim **DOI: 10.1002/ejic.200200594**

Selected IR spectroscopic data for complexes **1**−**5** are given in the Exp. Sect. The sharp peaks in the solid state FTIR spectrum due to ν(OH) of the ligand H_3L occur at 3523, 3492 and 3348 cm^{-1}. These bands are missing in **1**−**5**, indicating that on complexation the phenol-character of the ligand has been lost. There are several peaks in the region 3000−2800 cm^{-1} due to the *tert*-butyl groups along with the other ν(C−H), ν(C=C), ν(C=N) and ν(C−O) vibrations found in the normal range for these types of linkages. For **4** the sharp strong-band at 990 cm^{-1} is associated with the ν(V=O) vibration. The corresponding band for **5** occurs at 996 cm^{-1}.

The EI mass spectrum of **1** exhibits the molecular ion peak centered around *m*/*z* = 1247 with the expected isotopic distribution pattern, unambiguously indicating the composition to be Fe_2L_2. For **2a** the parent ion peak corresponds to a small peak centered around *m*/*z* = 1244; the peaks with the greatest intensities are observed at *m*/*z* = 206, 351 and 568. EI-MS unambiguously indicates the presence of THF in **2b**. Compound **3** shows the main peak at *m*/*z* = 1239 in the MS-ESI (positive) spectrum in CH_2Cl_2, indicating the composition to be Cr_2L_2, similar to that of **1**. In the EI mass spectrum of **4,** the parent ion peak with an abundance of ≈21% is observed at *m*/*z* = 760 with the expected isotopic distribution pattern. The peak at *m*/*z* = 718 with an abundance of 100% corresponding to the V_2O_3L species is also observed. In addition there are other peaks including one at *m*/*z* = 702 corresponding to the V_2O_2L species. EI-MS for **5** does not leave any doubt about the composition being $V_2O_2L_2$, with the molecular ion peak at *m*/*z* = 1268; the base peak (100%) with *m*/*z* = 1251 corresponds to V_2L_2O. The other significant peaks at *m*/*z* = 1236 and 618 are attributed to the $V_2L_2^{+}$ and $V_2L_2^{2+}$ ions.

Single Crystal X-ray Diffraction Studies

Structure of $[L_2Fe_2^{III}]\cdot 2.5CH_3CN$ (1)

Although H_3L is particularly suited to the formation of dinuclear complexes, and the analytical and spectroscopic data are in agreement with the presence of a dinuclear Fe_2L_2 unit as the smallest unit in **1**, an X-ray analysis was undertaken to remove any doubt regarding connectivity. Indeed, the structural analysis shows the presence of two six-coordinate iron(III) centers within the $Fe_2O_6N_4$ coordination unit. An ORTEP drawing of the molecule is shown in Figure 1 with selected bond lengths and angles provided in Table 1.

The iron atoms, Fe(1) and Fe(2), are in distorted octahedral environments with FeN_2O_4 coordination spheres. The two octahedra share a common edge and are bridged by two phenolate oxygen atoms O(50) and O(10). The six oxygen atoms of two ligands are roughly coplanar with the two Fe atoms. Thus, for the two iron centers, the Fe(1)O(1)O(41)O(50)O(10) and Fe(2)O(62)O(22)O(50)O(10) atoms constitute the equatorial planes. Each iron center is coordinated to two nitrogen atoms, e.g. Fe(1)−N(7) and Fe(1)−N(47), which are *trans* to each other with an angle

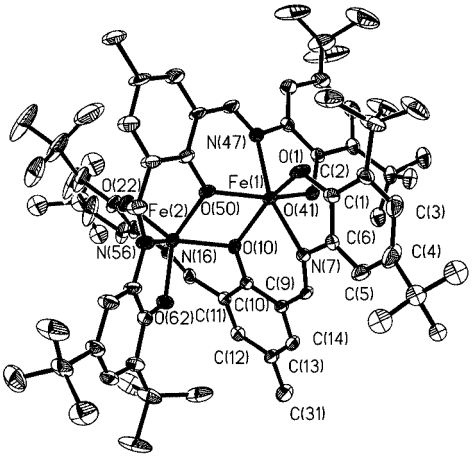

Figure 1. An ORTEP drawing of the neutral molecule $[L_2Fe_2^{III}]\cdot 2.5CH_3CN$ (**1**)

Table 1. Selected interatomic distances (Å) and angles (degrees) in $[Fe_2^{III}L_2]\cdot 2.5CH_3CN$ (**1**)

Fe(1)−O(1)	1.913(4)	Fe(1)···Fe(2)	3.32(1)
Fe(1)−O(41)	1.914(3)		
Fe(1)−O(10)	2.042(4)		
Fe(1)−O(50)	2.044(4)		
Fe(1)−N(47)	2.161(4)		
Fe(1)−N(7)	2.166(4)		
Fe(2)−O(62)	1.920(4)		
Fe(2)−O(22)	1.927(4)		
Fe(2)−O(50)	2.041(4)		
Fe(2)−O(10)	2.044(3)		
Fe(2)−N(16)	2.167(5)		
Fe(2)−N(56)	2.174(5)		
O(1)−Fe(1)−O(41)	100.2(2)	O(62)−Fe(2)−O(22)	122.5(2)
O(1)−Fe(1)−O(10)	150.9(2)	O(62)−Fe(2)−O(50)	135.4(2)
O(41)−Fe(1)−O(10)	99.8(2)	O(22)−Fe(2)−O(50)	94.3(2)
O(1)−Fe(1)−O(50)	99.9(2)	O(62)−Fe(2)−O(10)	93.4(2)
O(41)−Fe(1)−O(50)	150.8(2)	O(22)−Fe(2)−O(10)	135.9(2)
O(10)−Fe(1)−O(50)	71.1(2)	O(50)−Fe(2)−O(10)	71.2(2)
O(1)−Fe(1)−N(47)	89.6(2)	O(62)−Fe(2)−N(16)	88.8(2)
O(41)−Fe(1)−N(47)	79.1(2)	O(22)−Fe(2)−N(16)	77.2(2)
O(10)−Fe(1)−N(47)	114.9(2)	O(50)−Fe(2)−N(16)	126.3(2)
O(50)−Fe(1)−N(47)	80.0(2)	O(10)−Fe(2)−N(16)	79.1(2)
O(1)−Fe(1)−N(7)	79.2(2)	O(62)−Fe(2)−N(56)	77.6(2)
O(41)−Fe(1)−N(7)	89.9(2)	O(22)−Fe(2)−N(56)	88.9(2)
O(10)−Fe(1)−N(7)	79.9(2)	O(50)−Fe(2)−N(56)	79.1(2)
O(50)−Fe(1)−N(7)	114.6(2)	O(10)−Fe(2)−N(56)	126.3(2)
N(47)−Fe(1)−N(7)	162.7(2)	N(16)−Fe(2)−N(56)	151.3(2)

N(47)−Fe(1)−N(7) of 162.7(2)°, and which belong to two different L^{3-} ligands.

The non-bridging Fe−O bond lengths [Fe(1)−O(1), Fe(1)−O(41) av. 1.913(4) and Fe(2)−O(62), Fe(2)−O(22) av. 1.923(7) Å] are distinctly different from the bridging Fe−O bond lengths [Fe(1)−O(10), Fe(1)−O(50) av. 2.043(5) and Fe(2)−O(10), Fe(2)−O(50) av. 2.043 Å]. The symmetry in the bridging bond lengths in the nearly planar Fe_2O_2 rhomboid is noteworthy. Although the Fe−O−Fe angle of 108.9(2)° in **1** falls into the range of 105−110° observed for previously structurally characterized $Fe_2^{III}(OPh)_2$ bridges, the Fe···Fe separation of 3.32 Å is one of the longest yet found for complexes with this bis(phenox-

 © 2003 Wiley-VCH Verlag GmbH & Co. KGaA, Weinheim

ide) bridge.[5−8] In the previously reported complex $[Fe_2^{III}(salmp)_2]$,[8] where salmp^{3-} is the pentadentate ligand 2-bis(salicylidenamino)methylphenolate, the Fe−O−Fe angle of 97° is the smallest yet found. Primarily because of the differences in the Fe−O−Fe angles, the magnetic properties of **1** differ considerably from those of $[Fe_2^{III}(salmp)_2]$, although **1** and $[Fe_2^{III}(salmp)_2]$ are otherwise very similar. The Fe−N and Fe−O bond lengths are consistent with a high-spin electron configuration for both Fe^{III} centers in **1** with imine nitrogen and phenolate oxygen donor ligands. The d^5 high spin electron configuration has also been confirmed both by Mössbauer spectroscopy and magnetic susceptibility measurements.

Molecular Structure of $[Mn_2^{III}L_2(THF)_2]\cdot 4CH_3CN$ (2b)

Deep orange single crystals of **2b** were obtained by slow evaporation of a tetrahydrofuran solution of **2a**. The structure of **2b** is shown in Figure 2 with selected bond lengths and angles provided in Table 2. The molecule is based on two MnO_4N_2 octahedra, in which two triply deprotonated ligands $[O^{\cap}N^{\cap}O^{\cap}N^{\cap}O]^{3-}$ span between the two manganese centers. The pentadentate ligand $[O^{\cap}N^{\cap}O^{\cap}N^{\cap}O]$ acts as a tridentate (*O*,*N*,*O*)-donor ligand to one manganese center, whilst the residual two donor atoms *N*,*O* coordinate to the second manganese center. Thus, each of the manganese centers attains only pentacoordination through the ligand. The sixth coordination site of each manganese center is occupied by the oxygen atom of a tetrahydrofuran molecule. That the manganese centers are in the +III oxidation state is evident from the axial elongation of the octahedra along the N(47)−Mn(1)−O(80) and the N(16)−Mn(2)−O(90) axes, as expected for a Jahn−Teller distorted high-spin d^4 ion. The atoms Mn(1)N(7)O(1)O(41)O(14) and Mn(2)N(56)O(54)O(22)O(62) comprise the equatorial planes for each octahedron around the Mn(1) and Mn(2) centers respectively. The $MnNO_3$ fragment is essentially planar, the maximum deviation from the mean plane being 0.01 Å. Of note is the axial position of each coordinated tetrahydrofuran molecule. The average equatorial Mn−O and Mn−N distances of 1.896(16) and 2.006(3) Å respectively, fall in the range reported for other structurally characterized d^4 Mn^{III} complexes,[9] and is also consistent with the susceptibility measurements. The smallest acute bite angle between the phenolate O atom and the N atom of the L^{3-} ligand has been found for the Mn(1) center with the angle O(41)−Mn(1)−N(47) being 77.2(1)°.

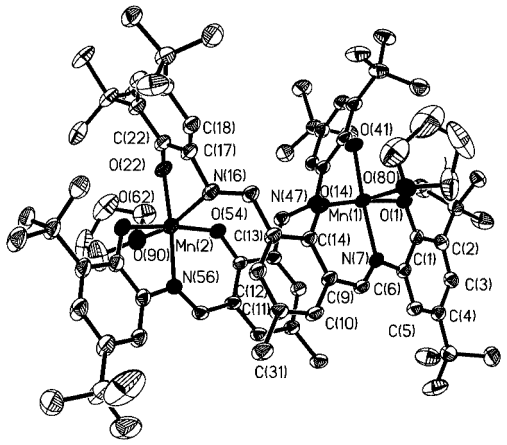

Figure 2. Molecular structure of $[L_2Mn_2^{II}(THF)_2]\cdot 4CH_3CN$ (**2b**)

Table 2. Selected bond lengths (Å) and angles (deg) for $[Mn_2^{III}L_2(THF)_2]\cdot 4CH_3CN$ (**2b**)

Mn(1)−O(1)	1.879(2)
Mn(1)−O(41)	1.899(2)
Mn(1)−O(14)	1.907(2)
Mn(1)−N(7)	2.005(2)
Mn(1)−O(80)	2.291(3)
Mn(1)−N(47)	2.310(3)
Mn(2)−O(62)	1.888(2)
Mn(2)−O(22)	1.896(2)
Mn(2)−O(54)	1.906(2)
Mn(2)−N(56)	2.008(3)
Mn(2)−O(90)	2.271(3)
Mn(2)−N(16)	2.341(3)
O(1)−Mn(1)−O(41)	89.79(9)
O(1)−Mn(1)−O(14)	174.17(9)
O(41)−Mn(1)−O(14)	95.98(9)
O(1)−Mn(1)−N(7)	82.77(10)
O(41)−Mn(1)−N(7)	172.21(10)
O(14)−Mn(1)−N(7)	91.49(10)
O(1)−Mn(1)−O(80)	94.12(10)
O(41)−Mn(1)−O(80)	94.36(10)
O(14)−Mn(1)−O(80)	84.60(10)
N(7)−Mn(1)−O(80)	88.51(10)
O(1)−Mn(1)−N(47)	92.67(10)
O(41)−Mn(1)−N(47)	77.16(10)
O(14)−Mn(1)−N(47)	89.46(10)
N(7)−Mn(1)−N(47)	100.79(10)
O(80)−Mn(1)−N(47)	169.12(9)
O(62)−Mn(2)−O(22)	90.85(10)
O(62)−Mn(2)−O(54)	173.90(10)
O(22)−Mn(2)−O(54)	95.21(9)
O(62)−Mn(2)−N(56)	82.45(10)
O(22)−Mn(2)−N(56)	173.02(10)
O(54)−Mn(2)−N(56)	91.52(10)
O(62)−Mn(2)−O(90)	93.88(10)
O(22)−Mn(2)−O(90)	88.62(10)
O(54)−Mn(2)−O(90)	85.61(10)
N(56)−Mn(2)−O(90)	93.79(11)
O(62)−Mn(2)−N(16)	91.94(10)
O(22)−Mn(2)−N(16)	76.16(10)
O(54)−Mn(2)−N(16)	90.17(10)
N(56)−Mn(2)−N(16)	101.98(11)
O(90)−Mn(2)−N(16)	163.78(10)
Mn(1)···Mn(2)	6.448(2)

Compound **2b** is a rare example of a complex bearing a dinucleating ligand containing the central *p*-cresol group,[10] in which the central phenolate oxygen, O(54) or O(14), of the cresol ring does not coordinate as a bridging atom between two metal centers.

Molecular Structure of $[L(V^{IV}{=}O)_2OCHMe_2]\cdot CH_3CN$ (4)

The structure of **4** (Figure 3) shows a divanadyl(IV) complex with a bridging isopropoxide originating from the vanadium isopropoxide starting material. The atoms V(1) and V(2) are additionally bridged by a phenolate oxygen O(10). The pentacoordination of each vanadium atom is achieved

 © 2003 Wiley-VCH Verlag GmbH & Co. KGaA, Weinheim

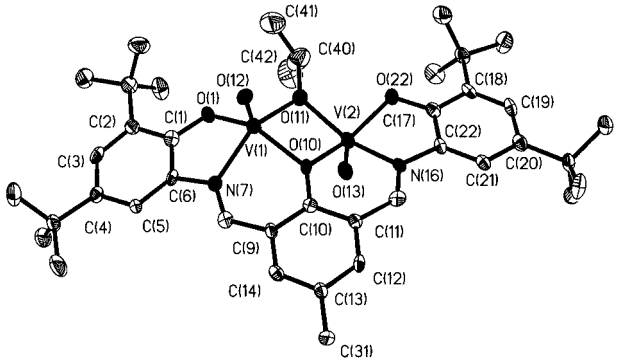

Figure 3. Molecular structure of $[L(V^{IV}{=}O)_2(OCHMe_2)]{\cdot}CH_3CN$ (**4**)

by oxygen atoms O(12) and O(13), with V(1)−O(12) and V(2)−O(13) distances of 1.586(3) and 1.588(3) Å respectively, indicating their double-bond character. The V=O groups are *trans* to each other in the di-vanadium complex. The coordination polyhedra for the vanadium centers are distorted square pyramidal with O(1)N(7)O(11)O(10) for V(1) and O(22)N(16)O(11)O(10) for V(2) forming the basal planes, in which both V(1) and V(2) are located 0.60 Å out of the equatorial planes. The ring V(1)O(11)V(2)O(10) is not planar, the dihedral angle being 10.3°. The distances V−O and V−N are in the ranges reported for comparable complexes[11] and are in agreement with the d^1 electron configuration for the vanadium centers. This electronic structure has also been confirmed by the magnetic susceptibility measurements. The separation V(1)···V(2) of 3.063 Å necessitates consideration of a direct interaction between the metal centers. Selected interatomic distances and bond angles are listed in Table 3.

Table 3. Selected bond lengths (Å) and angles (deg) for $[L(V{=}O)_2(OCHMe_2)]{\cdot}CH_3CN$ (**4**)

V(1)−O(12)	1.586(3)
V(1)−O(1)	1.905(3)
V(1)−O(11)	1.970(3)
V(1)−O(10)	1.995(3)
V(1)−N(7)	2.066(4)
V(2)−O(13)	1.588(3)
V(2)−O(22)	1.919(3)
V(2)−O(11)	1.953(3)
V(2)−O(10)	1.994(3)
V(2)−N(16)	2.065(4)
O(12)−V(1)−O(1)	109.3(2)
O(12)−V(1)−O(11)	110.6(2)
O(1)−V(1)−O(11)	95.45(13)
O(12)−V(1)−O(10)	107.86(14)
O(1)−V(1)−O(10)	142.13(14)
O(11)−V(1)−O(10)	77.92(12)
O(12)−V(1)−N(7)	102.6(2)
O(1)−V(1)−N(7)	80.16(14)
O(11)−V(1)−N(7)	146.03(14)
O(10)−V(1)−N(7)	85.12(13)
O(13)−V(2)−O(22)	107.3(2)
O(13)−V(2)−O(11)	110.9(2)
O(22)−V(2)−O(11)	94.61(13)
O(13)−V(2)−O(10)	106.1(2)
O(22)−V(2)−O(10)	146.22(13)
O(11)−V(2)−O(10)	78.36(12)
O(13)−V(2)−N(16)	105.7(2)
O(22)−V(2)−N(16)	79.87(14)
O(11)−V(2)−N(16)	142.89(14)
O(10)−V(2)−N(16)	86.15(13)
V(2)−O(10)−V(1)	100.30(13)
V(2)−O(11)−V(1)	102.65(14)
V(1)···V(2)	3.063(1)

Structure of $[L_2(VO)_2]{\cdot}2CH_3CN$ (5)

Crystals of $[L_2(VO)_2]{\cdot}2CH_3CN$, obtained by crystallizing **5** from an acetonitrile solution, were subjected to a single-crystal X-ray diffraction study at 100 K. Figure 4 shows a perspective view and the atom-labeling scheme for **5**. Selected bond parameters are listed in Table 4.

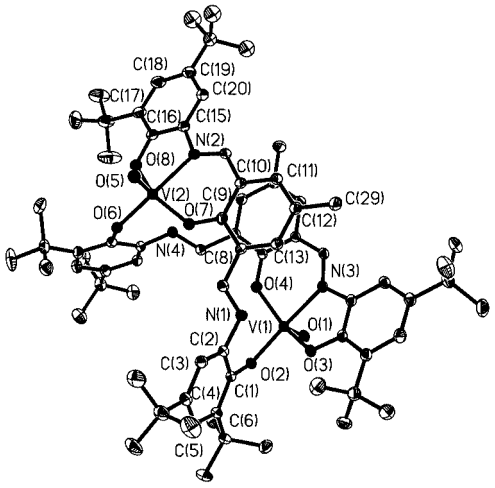

Figure 4. A perspective view of the neutral complex $[L_2(V^{V}O)_2]{\cdot}2CH_3CN$ (**5**)

In the distorted square pyramidal VO_4N coordination spheres, the metal atoms are displaced toward the O(1) or O(5) atoms from the equatorial planes O(2)O(3)N(3)O(4) for V(1) and O(6)O(7)N(2)O(8) for V(2) by 0.33 and 0.31 Å respectively. The V(1)−O(1) and V(2)−O(5) distances of 1.603(2) and 1.595(2) Å correspond to vanadium−oxygen multiple bonds and closely resemble vanadium(v) complexes containing a single V=O group.[12] Each ligand with its five donor atoms spans between two vanadium(v) centers but one N atom, N(1) or N(4), does not coordinate to any of the metal centers, making each of the ligands tetradentate. *Such behaviour for ligands based on 2,6-diformyl-p-cresol has not been observed before.* A schematic drawing of the coordination sphere is shown below to highlight the tetradentate coordination of the ligand.

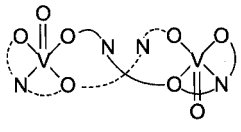

The V−O and V−N bond lengths (Table 4) are similar to those seen in vanadium(v) complexes bearing monooxo- and *cis*-dioxo-vanadium moieties.[13] The C−O (average 1.34 Å) and the aromatic C−C (average 1.40 Å) bond

 © 2003 Wiley-VCH Verlag GmbH & Co. KGaA, Weinheim

Table 4. Selected bond lengths (Å) and angles (deg) for $[L_2(VO)_2]\cdot 2CH_3CN$ (**5**)

V(1)−O(1)	1.603(2)
V(1)−O(2)	1.8202(13)
V(1)−O(4)	1.8787(14)
V(1)−O(3)	1.883(2)
V(1)−N(3)	2.108(2)
V(2)−O(5)	1.595(2)
V(2)−O(6)	1.8340(14)
V(2)−O(7)	1.874(2)
V(2)−O(8)	1.875(2)
V(2)−N(2)	2.124(2)
O(1)−V(1)−O(2)	100.01(7)
O(1)−V(1)−O(4)	101.12(7)
O(2)−V(1)−O(4)	102.23(6)
O(1)−V(1)−O(3)	105.51(7)
O(2)−V(1)−O(3)	88.66(6)
O(4)−V(1)−O(3)	148.96(7)
O(1)−V(1)−N(3)	93.26(7)
O(2)−V(1)−N(3)	163.17(7)
O(4)−V(1)−N(3)	85.14(6)
O(3)−V(1)−N(3)	77.78(6)
O(5)−V(2)−O(6)	98.01(7)
O(5)−V(2)−O(7)	100.17(8)
O(6)−V(2)−O(7)	102.69(6)
O(5)−V(2)−O(8)	104.38(8)
O(6)−V(2)−O(8)	89.26(7)
O(7)−V(2)−O(8)	150.87(7)
O(5)−V(2)−N(2)	95.41(7)
O(6)−V(2)−N(2)	163.20(7)
O(7)−V(2)−N(2)	84.75(6)
O(8)−V(2)−N(2)	77.61(7)

lengths are in the expected range. The ligand is thus chelated in the trianionic phenolate form and the compound is correctly described with a formal oxidation state of +v for the vanadium ion with a d^0 electron configuration. The diamagnetism and ^{51}V NMR spectroscopic data for **5** corroborate this assignment

Mössbauer Isomer Shifts and Quadrupole Splitting

The Mössbauer spectrum of **1** at 80 K in a zero applied magnetic field and the nonlinear least-squares fit are shown in Figure 5. The spectrum was fitted with a single quadrupole split doublet with an isomer shift of $\delta = 0.518$ mm·s^{-1} and a quadrupole splitting of $\Delta E_Q = 0.754$ mm·s^{-1}. This isomer shift is consistent with those observed for high spin iron(III) ions in an octahedral or distorted octahedral environment.[14] The magnitude of the quadrupole splitting is a reflection of the unsymmetrical electric field gradient about each high-spin iron(III) site, although the two metal sites are equivalent.

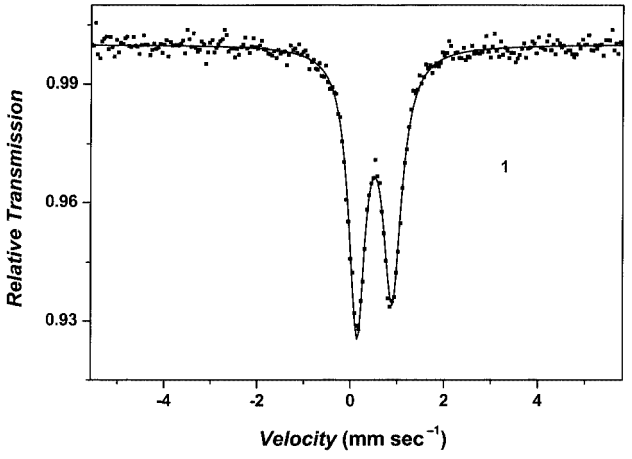

Figure 5. Mössbauer spectrum of **1** at 80 K in an applied zero-field

Magnetic Susceptibility Measurements

Variable temperature solid-state magnetic susceptibility measurements were performed on powdered samples of **1**−**4** over the temperature range 2−290 K in an applied magnetic field of 1 T (Figure 6). We used the Heisenberg spin Hamiltonian in the form $H = -2J\hat{S}_1\cdot\hat{S}_2$ for an isotropic exchange coupling between the two spins S_1 and S_2. The experimental magnetic data were simulated (shown as solid lines in Figure 6) by using a least-squares fitting computer program with a full-matrix diagonalization of exchange coupling, Zeeman splitting and axial single-ion zero-field interactions (DS_z^2), if necessary.

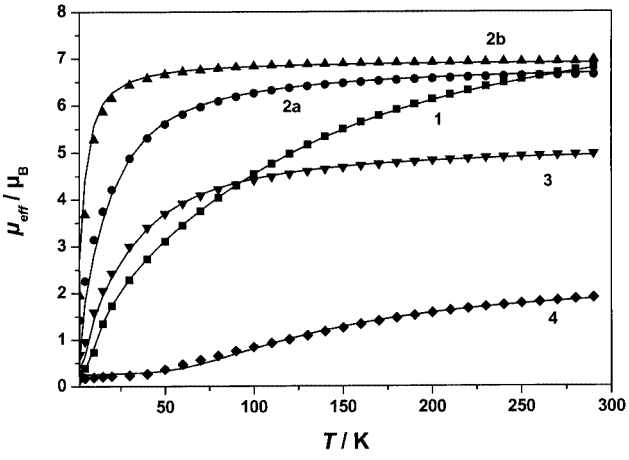

Figure 6. Plots of μ_{eff} vs. T for solid **1**−**4**. The solid lines represent the best fits of the data to the exchange coupling models

The magnetic behavior of $[Fe_2^{III}L_2]$ (**1**), is characteristic of an antiferromagnetically coupled dinuclear complex. At 290 K the μ_{eff} value of 6.784 μ_B ($\chi_M\cdot T = 5.755$ cm^3·K·mol^{-1}) decreases monotonically with decreasing temperature until it reaches a value of 0.274 μ_B ($\chi_M\cdot T = 9.380 \times 10^{-3}$ cm^3·K·mol^{-1}) at 2 K. This is a clear indication of exchange coupling between two paramagnetic Fe^{III} centers ($S_{Fe} = {}^5/_2$) with a resultant $S_t = 0$ ground state. The solid line in Figure 6 represents the best fit with the following parameters: $J = -12.7$ cm^{-1}, $g = 2.00$ (fixed) and PI ($S = {}^5/_2$) = 0.003. The calculated antiparallel exchange is in keeping with the range observed for comparable diphenoxo-bridged ferric dimers.[1,6,7]

Two semi-empirical magnetostructural correlations relating the magnitude of the exchange coupling to the iron-

 © 2003 Wiley-VCH Verlag GmbH & Co. KGaA, Weinheim

oxygen bond length in exchange coupled phenoxo-, alkoxo- and hydroxo-bridged dinuclear iron(III) compounds have been proposed.[5,7] By using the empirical relationship $J = -10^7 \exp(-6.8d)$,[7] where d is the averaged iron−oxygen distance, 2.043 Å for **1**, the J value for **1** can be calculated to be -9.25 cm^{-1}, which differs from the experimentally observed value of -12.7 cm^{-1}. The second equation[5] leads to a calculated value of -5.1 cm^{-1}. Regrettably, none of these two correlations can satisfactorily reproduce the exchange interaction in **1**.

The magnetic moment, μ_{eff}/molecule, for $[L_2Mn_2^{III}]$ (**2a**) of 6.636 μ_B ($\chi_M{\cdot}T$ = 5.507 cm$^3{\cdot}$K$\cdot$mol^{-1}) at 290 K decreases monotonically with decreasing temperature until it reaches a value of 1.421 μ_B ($\chi_M{\cdot}T$ = 0.2523 cm$^3{\cdot}$K$\cdot$mol^{-1}) at 2 K. This temperature dependence of μ_{eff} is a clear indication of an antiferromagnetic exchange coupling between two paramagnetic Mn^{III} (S_{Mn} = 2) centers. A least-squares fit, shown as the solid line in Figure 6, with $J = -2.95$ cm^{-1} and g = 1.98 was obtained. Thus a weak exchange coupling is operating between the Mn^{III} centers through the diphenoxo-bridge and, as expected, the exchange interaction is weaker in **2a** than that in **1**. The exchange coupling operating in **2b** is even weaker than that in **2a**, as evidenced from the temperature-dependence of μ_{eff} for **2b**. The magnetic moment μ_{eff} varies only slightly (μ_{eff} = 6.94 to 6.54 μ_B) in the temperature range 290−40 K, but then starts to decrease monotonically reaching a value of 1.94 μ_B at 2 K. Simulation of the experimental magnetic data yields $J = -0.66$ cm^{-1} and g = 1.995 (the solid line in Figure 6). The antiferromagnetic coupling in **2b** which is weaker than in **2a** is in agreement with the dimeric solid state structure of **2b** in which the manganese(III) centers are 6.45 Å apart.

The experimental magnetic moment of **3** decreases from 4.95 μ_B ($\chi_M{\cdot}T$ = 3.064 cm$^3{\cdot}$K$\cdot$mol^{-1}) at 290 K to an essentially diamagnetic value of μ_{eff} = 0.677 μ_B ($\chi_M{\cdot}T$ = 0.05736 cm$^3{\cdot}$K$\cdot$mol^{-1}) at 2 K, resulting from the antiferromagnetic interaction between the two Cr^{III} ions bridged by a diphenoxo group. The solid line in Figure 6 represents the best fit with the following parameters: $J = -7.6$ cm^{-1}, g = 1.893 and PI (S = $^3/_2$) = 0.01. The calculated antiparallel exchange falls in the range observed for comparable phenoxo-alkoxo-bridged chromium(III) dimers.[15−16]

The temperature dependence of the molar magnetic susceptibility χ_M for **4** shows a clear maximum around 230 K, consistent with the presence of significant antiferromagnetic coupling. Increases in χ_M at low temperatures ($\leq$ 30 K) have often been seen in strongly antiferromagnetically coupled systems and arise from a small amount of paramagnetic impurity in the sample. The magnetic moment of **4** is 1.83 μ_B ($\chi_M{\cdot}T$ = 0.4197 cm$^3{\cdot}$K$\cdot$mol^{-1}) at 290 K, which is significantly lower than the spin-only value of 2.45 μ_B for two uncoupled S = $^1/_2$ spins. Furthermore μ_{eff} gradually decreases on decreasing the temperature, reaching 0.15 μ_B at 2 K. The data were fitted using the following parameters: $J = -128.5$ cm^{-1}, g = 1.90, PI (S = $^1/_2$) = 0.018, TIP = 80 $\times 10^{-6}$ cm$^3{\cdot}$mol^{-1} and $\theta = -3.0$ K. The antiferromagnetic coupling constant of -128.5 cm^{-1} lies in the range of values found for other dinuclear vanadyl(IV) complexes[11,17] containing phenoxo, alkoxo and hydroxo-bridging ligands.

^{51}V NMR Measurements

Compound **5** containing V^V with a d^0 electron configuration is diamagnetic and was examined by ^{51}V NMR spectroscopy[18] with $VOCl_3$ in C_6D_6 as an internal standard. The compound gives rise to a single signal at $\delta = -420$ ppm, suggesting that there is only one species in solution, as in the solid state (vide infra).

Electrochemistry and Spectroelectrochemistry

The electrochemical properties of complexes **1** (Fe^{III}), **2a** (Mn^{III}) and **3** (Cr^{III}) were investigated in CH_2Cl_2 solutions containing 0.1 M TBA(PF_6). Voltammetric experiments (cyclic voltammetry, CV and square wave voltammetry, SQW) reveal that all three compounds can undergo three consecutive oxidations.

Figure 7 shows representative examples of the electrochemical measurements. The respective redox potentials vs. the Fc^+/Fc couple are compiled in Table 5. The first two oxidations are reversible on the time scale of cyclic voltammetry (scan rates 0.05−0.5 V/s). The peak positions are almost independent of the scan rates and the peak separations are close to the values observed for ferrocene under the same conditions (0.08 V). The third oxidations are

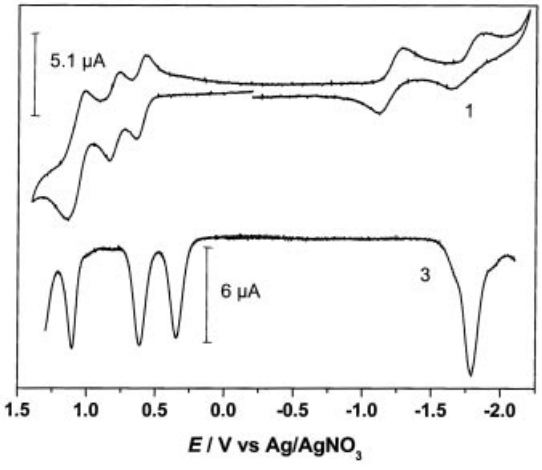

Figure 7. Cyclic voltammogram (50 mV/s) of **1** (top) and square wave voltammogram at 25 Hz of **3** (bottom) in CH_2Cl_2 [0.1 M nBu$_4$NPF$_6$]

Table 5. Redox potentials ($E_{1/2}$ in Volt vs. Fc^+/Fc) for reduction and oxidation of complexes **1−3**

	$E_{1/2}$ (ox3)[a][b]	$E_{1/2}$ (ox2)	$E_{1/2}$ (ox1)	$E_{1/2}$ (red1)	$E_{1/2}$ (red2)
1 (Fe^{III})	+0.870	+0.586	+0.390	−1.42	−1.95
2a (Mn^{III})	+0.860[c]	+0.542	−0.060	−1.30	
3 (Cr^{III})	+0.905[c]	+0.410	+0.144	−1.99[c]	

[a] CV and SQW in CH_2Cl_2 solutions containing 0.1 M nBu$_4$NPF$_6$; working electrode: 2-mm glassy carbon disk. [b] Fc^+/Fc in CH_2Cl_2 vs. Ag/AgNO$_3$: $E_{1/2}$ = 0.216 V for **1**, 0.240 V for **2b** and 0.203 V for **3**. [c] Chemically irreversible; square wave peak potentials are given.

 © 2003 Wiley-VCH Verlag GmbH & Co. KGaA, Weinheim

either chemically irreversible (**2a** and **3**; no reverse peaks observable) or contain an irreversible component (**1**; oxidation peak at all scan rates twice as high as the peak of re-reduction and of the reversible peaks).

The redox potentials of the second and third oxidations are very similar for all three compounds irrespective of the nature of the central metal ion. This provides firm evidence that these oxidations are ligand centered and give rise to phenoxyl radicals.

The redox potentials of the first oxidations are spread over a somewhat larger range (Table 5). In particular, the redox potential of **2a** is low and could be due to formation of the Mn^{IV} oxidation state. We therefore performed spectroelectrochemical measurements at −25 °C and found that the spectral changes upon the first oxidation of **2a** show the fingerprints for phenoxyl radical formation.[19] In the difference spectra a new peak with a maximum at 417 nm developed together with a broad band which extends from 650−950 nm and has a maximum at ≈800 nm. Therefore, the first oxidation of **2a** can be clearly assigned to phenoxyl radical formation. In spectroelectrochemical experiments with **1** and **3**, an increase in absorption at 350−450 nm and at >700 nm was observed during the first oxidation, as expected for formation of phenoxyl radicals. However, the maxima of the difference spectra were at 350−370 nm rather than at 400−420 nm. It is most likely that these spectra are distorted by small oxidation-induced shifts in the very intense charge-transfer bands of the complexes (the ε-values of the starting material are ten times higher than those of phenoxyl radicals at the respective wavelengths). In view of the similarity of the redox potentials of **1** and **3** we therefore conclude that in these complexes the first oxidations also represent formation of phenoxyl radicals.

The reductions at potentials of less than −1 V are either electrochemically quasi-reversible (**1** and **2a**; peak separation 0.15−0.25 V at 0.2 V/s scan rate) or chemically irreversible (**3**; high peak current and lack of reverse peak). They were not further investigated and are most likely metal-centered reductions to the M^{2+} oxidation states.

A few experiments were done with the Vanadium V^V compound $[L_2(V{=}O)_2]$ (**5**). The square wave voltammogram exhibits three oxidations in the accessible potential range, two reversible ones at −0.136 V and +0.226 V and one irreversible at +1.02 V. These oxidations, which occur in the same potential range as those of **1**−**3**, we also tentatively assign to phenoxyl radical formation. Reductions also occur in the potential range −0.7 to −0.9 V and these are most likely to be metal-centered reductions to the V^{IV} oxidation state. The square wave voltammogram, however, exhibits complex multiple peak formations and therefore accurate redox potentials cannot be evaluated.

Concluding Remarks

The structural analysis of a series of transition metal complexes derived from the pentadentate ligand H_3L demonstrates the ability of this dinucleating ligand to form complexes of metal ions of the first transition series mostly in a six-coordinate fashion. As evidenced by the square-pyramidal five-coordinate V^{IV} **4** and V^V **5** complexes, this may be overcome by electronic factors, e.g. the Jahn−Teller effect and absence of LFSE. The fact that this ligand can adapt itself to various metal ion sizes to yield dinuclear complexes makes it a versatile building block for the construction of bimetallic complexes, which might be useful for the study of biologically relevant dinuclear complexes.

From the X-ray data above and particularly those of **2b** and **5**, it is clear that within a family of complexes it is possible to obtain a variety of coordination environments. Complexes of Schiff base ligands have been in the literature for over 150 years and rigid chelating environments for the metals have been proposed for complexes of this type. The present ligand H_3L, also a Schiff-base ligand, demonstrates how the local environment around the metal becomes distorted to accommodate the increasing internal chelate ring and how the ligand itself adjusts from originally pentadentate to tetradentate in a complex. The realization that the present ligand H_3L has the potential to switch between different chelating modes highlights the prospect of designing a generic ligand system which should have a rich, interesting and independent chemistry worthy of greater exploration. Overall this Robson-type ligand with *tert*-butyl substituents has offered a new chelating flexibility.

The electrochemical results suggest the generation of ligand-centered oxidation processes attributable to the phenoxyl radicals, rather than the formation of unusually high oxidation states at the central metal centers.

Experimental Section

Materials and Physical Measurements: Reagent or analytical grade materials were obtained from commercial suppliers and used without further purification, except those for electrochemical measurements. Elemental analyses (C,H,N) were performed by the Microanalytical Laboratory Dornis & Kolbe, Mülheim, Germany. Fourier transform infrared spectra in KBr discs were recorded on a Perkin−Elmer 2000 FT-IR instrument. Electronic absorption spectra in solution were measured on a Perkin−Elmer Lambda 19 spectrophotometer. Magnetic susceptibilities of powdered samples were recorded on a SQUID magnetometer in the temperature range 2−295 K with an applied field of 1 T. Experimental susceptibility data were corrected for the underlying diamagnetism using Pascal's constants and for the TIP contributions. Cyclic voltammetric and coulometric measurements were performed on EG&G equipment (potentiostat/galvanostat model 273A). Mass spectra were recorded with either a Finnigan MAT 8200 (electron ionization, EIMS) or a MAT 95 (electrospray ESI-MS) instrument. A Bruker DRX 400 instrument was used for NMR spectroscopy.

Preparations

H_3L: The ligand H_3L was prepared as described earlier.[4]

$[L_2Fe_2^{II}]$ (1): To a degassed solution of the ligand H_3L (0.29 g; 0.5 mmol) and NEt_3 (0.12 mL) in an acetonitrile/dichloromethane solvent mixture (10 ml:15 mL) was added $Fe(ClO_4)_2{\cdot}6H_2O$ (0.18 g; 1 mmol) and the resultant solution was heated to reflux for 0.5 h under argon, then cooled and stirred in air for an hour. The result-

 © 2003 Wiley-VCH Verlag GmbH & Co. KGaA, Weinheim

ant deep reddish-brown solution was kept at ambient temperature for crystallization. After 2 d red-brown microcrystals were collected by filtration and air-drying. Yield: 0.14 g (45%). $C_{74}H_{94}Fe_2O_6N_4$: calcd. C 71.26, H 7.60, Fe 8.95, N 4.49; found C 71.3, H 7.6, Fe 9.0, N 4.5. EI-MS: *m*/*z* = 1247 [M^+]. IR (KBr disk): $\tilde{\nu}$ =2953 s cm^{-1}, 2865 m, 1610 m, 1591 m, 1565 m, 1471 s, 1443 s, 1408 m, 1255 s, 1163 m, 834 m, 537 m, 492 m. UV/Vis (CH_2Cl_2): λ_{max} ($\varepsilon/M^{-1}\cdot cm^{-1}$) = 560 sh (≈7800), 421 nm (34200).

X-ray quality crystals of **1**·2.5CH_3CN were grown from an acetonitrile solution.

[$L_2Mn_2^{III}$] (2a): A methanolic solution (25 mL) of the ligand H_3L (0.29 g; 0.5 mmol), manganese(III) acetate (0.13 g; 0.2 mmol) and tetrabutylammonium methoxide (0.2 mL) was heated to reflux for 1 h. Red-brown microcrystals of **2a** were formed on cooling to room temperature. The solid was collected by filtration and air-dried. Yield: 70 mg (≈23%). $C_{74}H_{94}Mn_2N_4O_6$: calcd. C 71.36, H 7.61, Mn 8.82, N 4.50; found C 71.50, H 7.5, Mn 8.7, N 4.5. EI-MS: *m*/*z* = 1242−1246 [M^+]. IR (KBr disk): $\tilde{\nu}$ =2953 s cm^{-1}, 2866 m, 1610 m, 1587 m, 1472 m, 1442 m, 1406 m, 1360 m, 1246 s, 1161 m, 836 m, 561 m, 537 m. UV/Vis (CH_2Cl_2): λ_{max} ($\varepsilon/M^{-1}\cdot cm^{-1}$) = 470 nm (22000).

[$L_2Mn_2^{III}(THF)_2$] (2b): X-ray quality crystals of **2b**·4CH_3CN were obtained by crystallizing **2a** from a tetrahydrofuran/acetonitrile solution. $C_{82}H_{110}Mn_2N_4O_8$·4CH_3CN: calcd. C 69.57, H 7.91, Mn 7.07, N 7.21; found C 69.7, H 7.9, Mn 7.3, N 6.7.

[$L_2Cr_2^{III}$] (3): A solution of the ligand (0.29 g; 0.5 mmol), NEt_3 (0.1 mL) and $CrCl_2$ (0.12 g; 0.5 mmol) in tetrahydrofuran (25 mL) was heated to reflux under argon for 15 min and then in air for a further 1 h. The resultant deep-red solution was filtered and the filtrate was evaporated to dryness using a rotary evaporator. The solid obtained was dissolved in of THF (5 mL) and the solution was filtered to remove any solid. After addition of acetonitrile (2 mL) to the filtrate, slow evaporation at room temperature yielded **3** as an orange-red microcrystalline solid. Yield: 0.13 g (42%). $C_{74}H_{94}Cr_2N_4O_6$: calcd. C 71.70, H 7.64, Cr 8.39, N 4.52; found C 71.4, H 7.6, Cr 8.3, N 4.5. EI-MS (pos., CH_2Cl_2): *m*/*z* = 1239−1246 [M^+]. IR (KBr disk): $\tilde{\nu}$ = 2953 s cm^{-1}, 2905 m, 2867 m, 1598 m, 1565 m, 1474 s, 1445 s, 1406 m, 1256 s, 1162 m, 832 m, 569 m, 539 m, 517 m. UV/Vis (CH_2Cl_2): λ_{max} ($\varepsilon/M^{-1}\cdot cm^{-1}$) = 458 (16450), 337 sh nm (≈16000).

[$L(V^{IV}{=}O)_2\mu$-$OCH(CH_3)_2$] (4): A solution of the ligand H_3L (0.29 g; 0.5 mmol), vanadyltris(isopropoxide) (0.25 ml; 1 mmol) and Et_3N (0.3 mL) in a deoxygenated acetonitrile/dichloromethane solvent mixture (10 ml:10 mL) was heated to reflux under argon for 1 h and then stirred in air for a further 1 h. The solution was filtered to remove any solid particles and the filtrate was allowed to evaporate slowly at ambient temperature to provide deep red crystals. Yield: 0.18 g (47%). $C_{40}H_{54}N_2O_6V_2$: calcd. C 63.15, H 7.15, N 3.68, V 13.39; found C 63.1, H 7.1, N 3.6, V 13.5. EI-MS: *m*/*z* = 760 (20.8%) [M^+], 718 (100%) [$M^+ - C_3H_7$], 703 (54%) [$M^+ - C_3H_7O$]. IR (KBr disk): $\tilde{\nu}$ = 2953 s cm^{-1}, 2867 m, 1614 m, 1569 m, 1476 s, 1446 m, 1362 m, 1250 s, 1161 s, 990 vs, 948 m, 831 s, 567 m, 546 s. UV/Vis (CH_2Cl_2): λ_{max} ($\varepsilon/M^{-1}\cdot cm^{-1}$) = 363 (14900), 470 nm (10500).

X-ray quality crystals of **4**·CH_3CN were obtained by recrystallization of **4** from acetonitrile.

Table 6. Crystallographic data for [$L_2Fe_2^{III}$]·2.5 CH_3CN (**1**), [$L_2Mn_2^{II}(THF)_2$]·4 CH_3CN (**2b**), [$L(VO^{IV})_2(OCHMe_2)$]·CH_3CN (**4**) and [$L_2(VO^{V})_2$]·2 CH_3CN (**5**)

	1	**2b**	**4**	**5**
Empirical formula	$C_{74}H_{94}Fe_2N_4O_6$·2.5CH_3CN	$C_{82}H_{110}Mn_2N_4O_8$·4CH_3CN	$C_{42}H_{59}N_3O_6V_2$	$C_{74}H_{94}N_4O_8V_2$·2CH_3CN
Formula mass	1349.87	1553.84	803.80	1351.52
Temperature	100(2) K	100(2) K	100(2) K	100(2) K
Wavelength (Mo-K_α)	0.71073 Å	0.71073 Å	0.71073 Å	0.71073 Å
Crystal system	Triclinic	Triclinic	Triclinic	Triclinic
Space group	$P\bar{1}$	$P\bar{1}$	$P\bar{1}$	$P\bar{1}$
Unit cell dimensions	*a* = 16.887(2) Å	*a* = 11.6088(8) Å	*a* = 8.456(1) Å	*a* = 14.8895(8) Å
	b = 17.026(2) Å	*b* = 12.6390(8) Å	*b* = 16.087(2) Å	*b* = 16.047(1) Å
	c = 17.040(2) Å	*c* = 31.802(2) Å	*c* = 16.685(2) Å	*c* = 16.881(1) Å
	α = 115.63(2)°	α = 79.41(1)°	α = 71.35(2)°	α = 77.47(1)°
	β = 113.09(2)°	β = 83.17(1)°	β = 89.26(2)°	β = 79.50(1)°
	γ = 90.69(2)°	γ = 72.87(1)°	γ = 79.26(2)°	γ = 81.47(1)°
Volume (Å^3); *Z*	3964.7(8); 2	4372.7(5); 2	2110.2(4); 2	3846.5(4); 2
Density (calcd.) Mgm^{-3}	1.131	1.180	1.265	1.167
Absorp. coeff. (mm^{-1})	0.417	0.346	0.490	0.298
F(000)	1442	1664	852	1440
Crystal size (mm)	0.39 × 0.37 × 0.34	0.44 × 0.36 × 0.24	0.33 × 0.14 × 0.09	0.35 × 0.11 × 0.10
θ range for data collect.	1.69 to 26.00°	2.31 to 27.11°	2.16 to 22.50°	4.21 to 32.50°
Reflections collected	26505	31923	13369	44652
Independent reflect.	13350 [*R*(int.) = 0.0419]	18622 [*R*(int.) = 0.0482]	5434 [*R*(int.) = 0.0852]	27516 [*R*(int.) = 0.0452]
Absorpt. correction	SADABS	Gaussian, face indexed	Gaussian, face indexed	Gaussian, face indexed
Data/restraints/param.	13308/36/805	18622/6/1000	5430/0/479	27259/34/839
Goodness-of-fit on F^2	1.057	1.065	1.012	1.014
Final *R* indices	*R*1 = 0.0862,	*R*1 = 0.0747,	*R*1 = 0.0527,	*R*1 = 0.0681,
[$I > 2\sigma(I)$]	*wR*2 = 0.2532	*wR*2 = 0.1899	*wR*2 = 0.1194	*wR*2 = 0.1539
R indices (all data)	*R*1 = 0.1223,	*R*1 = 0.0933,	*R*1 = 0.0963,	*R*1 = 0.1102,
	*wR*2 = 0.2875	*wR*2 = 0.2020	*wR*2 = 0.1345	*wR*2 = 0.1814

 © 2003 Wiley-VCH Verlag GmbH & Co. KGaA, Weinheim

$[L_2(V^V{=}O)_2]$ (5): A deoxygenated solution of the ligand (0.29 g; 0.5 mmol) and Et_3N (0.25 mL) in a solvent mixture of acetonitrile/dichloromethane (30 ml:10 mL) was charged with $V(THF)_3Cl_3$ (0.19 g; 0.5 mmol) and the resultant solution was heated to reflux under argon for 1 h and then stirred in air for a further 1 h. The clear solution was kept at room temperature for slow evaporation of the solvents. After 3 d the dark-brown crystals were collected by filtration. Yield: 0.2 g (63%). $C_{74}H_{94}N_4O_8V_2$: calcd. C 70.01, H 7.46, N 4.41, V 7.99; found C 69.83, H 7.35, N 4.40, V 7.95. EI-MS: m/z = 1266−1269 [M^+], 1251−1254 [$M^+ - CH_3$], 618 [LV^+]. IR (KBr disk): $\tilde{\nu}$ = 3442 m cm^{-1}, 2954 s, 2904 s, 2867 s, 1616 m, 1591 m, 1544 s, 1476 s, 1443 s, 1361 s, 1244 s, 996 s, 838 m. UV/Vis (CH_2Cl_2): λ_{max} (ε/M^{-1}·cm^{-1}) = ca. 414 sh (≈25600), 659 nm (5200). ^{51}V NMR: δ = −420 ppm.

X-ray quality crystals of **5**·$2CH_3CN$ were obtained from an acetonitrile solution of **5**.

X-ray Crystallographic Data Collection and Refinement of the Structures: Single crystals of **1** (orange-red), **2b** (red), **4** (orange-red) and **5** (orange-red) were coated with perfluoropolyether, picked up with glass fibers and mounted on a Kappa-CCD diffractometer equipped with a nitrogen cold stream at 100 K. Graphite-monochromated Mo-K_α radiation (λ = 0.71073 Å) was used. Crystallographic data of the compounds are listed in Table 6. Cell constants were obtained from a least-squares fit of the diffraction angles of several thousand strong reflections. Intensity data were corrected for Lorentz and polarization effects. The Siemens ShelXTL software package (G. M. Sheldrick, Universität Göttingen) was used for solution, refinement, and artwork of the structures, and the neutral atom scattering factors of the program were used. All structures were solved and refined by direct methods and difference Fourier techniques. Non-hydrogen atoms were refined anisotropically, and hydrogen atoms were placed at calculated positions and refined as riding atoms with isotropic displacement parameters.

CCDC-195241 (**1**), -195242 (**2b**), -195243 (**4**)and -195244 (**5**) contain the supplementary crystallographic data for this paper. These data can be obtained free of charge at www.ccdc.cam.ac.uk/conts/retrieving.html [or from the Cambridge Crystallographic Data Centre, 12, Union Road, Cambridge CB2 1EZ, UK; Fax: (internat.) +44-1223/336-033; E-mail: deposit@ccdc.cam.ac.uk].

Acknowledgments

Financial support from the DFG (Grant: Priority Program Ch111/2−1), the Max-Planck Society and Fonds der Chemischen Industrie is gratefully acknowledged. Thanks are due to Mrs. H. Schucht, Mrs. P. Höfer, Mr. A. Göbels, Mr. B. Mienert for skilful technical assistance.

[1] See for example: T. Weyhermüller, T. K. Paine, E. Bothe, E. Bill, P. Chaudhuri, *Inorg. Chim. Acta* **2002**, *337*, 344.

[2] *Chem. Rev.* **1996**, *96; Metal Ions in Biological Systems*, (Eds.: H. Sigel, A. Sigel, Marcel-Dekker), New York, **1994**, vol. 30; G. T. Babcock, M. Espe, C. Hoganson, N. Lydakis-Simantiris, J. McCracken, W. Shi, S. Styring, C. Tommas, K. Warncke, *Acta Chem. Scand.* **1997**, *51*, 533; M. M. Fontecave, J. L. Pierre, *Bull. Soc. Chim. Fr.* **1996**, *133*, 653; D. P. Goldberg, S. J. Lippard, *Adv. Chem. Ser.,* **1995**, *246*, 59; J. Stubbe, W. A. van der Donk, *Chem. Rev.* **1998**, *98*, 705.

[3] For example: J. A. Halfen, B. A. Jazdzewski, S. Mahapatra, L. M. Berreau, E. C. Wilkinson, L. Que, Jr, W. B. Tolman, *J. Am. Chem. Soc.* **1997**, *119*, 8217; Y. Wang, T. D. P. Stack, *J. Am. Chem. Soc.* **1996**, *118*, 13097; D. Zurita, I. Gautier-Luneau, S. Menage, J. L. Pierre, E. Saint-Aman, *J. Biol. Inorg. Chem.* **1997**, *2*, 46; E. Bill, J. Müller, T. Weyhermüller, K. Wieghardt, *Inorg. Chem.* **1999**, *38*, 5795 and references therein; M. A. Halcrow, L. M. Lindy Chia, X. Liu, E. J. L. McInnes, L. J. Yellowlees, F. E. Mabbs, I. J. Scowen, M. McPartlin, J. E. Davies, *J. Chem. Soc., Dalton Trans.* **1999**, 1753; S. Itoh, S. Takayama, R. Arakawa, A. Furuta, M. Komatsu, A. Ishida, S. Takamuku, S. Fukuzumi, *Inorg. Chem.* **1997**, *36*, 1407; K. Yamato, T. Inada, M. Doe, A. Ichimura, T. Takui, Y. Kojima, T. Kikunaga, S. Nakamura, N. Yanagihara, T. Onaka, S. Yano, *Bull. Chem. Soc. Jpn.* **2000**, *73*, 903; Y. Shimazaki, S. Huth, A. Odani, O. Yamauchi, *Angew. Chem. Int. Ed. Engl.* **2000**, *112*, 1666; M. Vaidyanathan, M. Palaniandavar, *Proc. Indian Acad. Sci. (Chem. Sci)*, **2000**, *112*, 223; C. N. Verani, E. Bothe, D. Burdinski, T. Weyhermüller, U. Flörke, P. Chaudhuri, *Eur. J. Inorg. Chem.* **2001**, 2161.

[4] S. Mukherjee, T. Weyhermüller, E. Bothe, K. Wieghardt, P. Chaudhuri, *Eur. J. Inorg. Chem.* **2003**, *5*, 863.

[5] S. M. Gorun, S. J. Lippard, *Inorg. Chem.* **1991**, *30*, 1625.

[6] A. Elmali, Y. Elerman, I. Svoboda, *Z. Naturforsch., Teil B* **2001**, *56*, 897.

[7] R. Werner, S. Ostrovsky, K. Griesar, W. Haase, *Inorg. Chim. Acta* **2001**, *326*, 78 and references therein.

[8] B. Snyder, G. S. Patterson, A. J. Abrahamson, R. H. Holm, *J. Am. Chem. Soc.* **1989**, *111*, 5214 and references therein.

[9] For example: S. B. Yu, C. P. Wang, E. P. Day, R. H. Holm, *Inorg. Chem.* **1991**, *30*, 4067.

[10] H. Okawa, H. Furutachi, D. E. Fenton, *Coord. Chem. Rev.* **1998**, *174*, 51 and references cited therein.

[11] For example: C. J. Carrano, C. M. Nunn, R. Quan, J. A. Bonadies, V. L. Pecoraro, *Inorg. Chem.* **1990**, *29*, 944; S. L. Castro, M. E. Cass, F. J. Holländer, S. L. Bartley, *Inorg. Chem.* **1995**, *34*, 466; S. Burojevic, I. Shweky, A. Bino, D. A. Summers, R. C. Thompson, *Inorg. Chim. Acta* **1996**, *251*, 75; W. Plass, *Z. Anorg. Allg. Chem.* **1997**, *623*, 1290; Y. Sun, M. Melchior, D. A. Summers, R. C. Thompson, S. J. Rettig, C. Orvig, *Inorg. Chem.* **1988**, *37*, 3119; A. S. Cecato, A. Neves, M. A. de Brito, S. M. Drechsel, A. S. Mangrich, R. Werner, W. Haase, A. J. Bortoluzzi, *J. Chem. Soc., Dalton Trans.* **2000**, 1573.

[12] Selected examples: D. C. Crans, H. Chen, O. P. Anderson, M. M. Miller, *J. Am. Chem. Soc.* **1993**, *115*, 6769; M. Bashipoor, H. Schmidt, C. Schutzke, D. Rehder, *Chem. Ber.* **1997**, *130*, 651; M. Moon, M. Pyo, Y. C. Myoung, C. I. Ahn, M. S. Lah, *Inorg. Chem.* **2001**, *40*, 554; M. S. Palacios, M. J. Rocio, S. Dominguez, P. Gill, C. Ruiz-Perez, F. V. Rodriguez-Romero, J. M. Dance, *Polyhedron* **1997**, *16*, 1143; W. Plass, *Z. Anorg. Allg. Chem.* **1997**, *623*, 461; B. Baruah, S. Das, A. Chakravorty, *Inorg. Chem.* **2002**, *41*, 4502.

[13] C. R. Cornman, G. J. Colpas, J. D. Hoeschele, J. Kampf, V. L. Pecoraro, *J. Am. Chem. Soc.* **1992**, *114*, 9925; A. Neves, W. Walz, K. Wieghardt, B. Nuber, J. Weiss, *Inorg. Chem.* **1988**, *27*, 2484.

[14] P. Gütlich, "*Mössbauer Spectroscopy*", (Ed. U. Gonser), Springer-Verlag, Berlin, Heidelberg, New York, **1975**; N. N. Greenwood, T. C. Gibb, "*Mössbauer Spectroscopy*", Chapman and Hall, London, **1971**.

[15] E. D. Estes, R. P. Scaringe, W. E. Hatfield, D. J. Hodgson, *Inorg. Chem.* **1976**, *15*, 1179; H. R. Fischer, D. J. Hodgson, E. Pedersen, *Inorg. Chem.* **1984**, *23*, 4755; A. Bencini, M. D. Vaira, F. Manni, *J. Chem. Soc., Dalton Trans.* **1991**, 41; M. Nakahanda, T. Fujihara, A. Fuyuhiro, S. Kaizaki, *Inorg. Chem.* **1992**, *31*, 1316; A. Böttcher, H. Elias, J. Gleurup, M. Neuburg, C. E. Olsen, J. Springborg, H. Weihe, M. Zehnder, *Acta Chem. Scand.,* 1994, **48**, 981; M. Ardon, A. Bino, K. Michelsen, E. Pedersen, *J. Am. Chem. Soc.* **1987**, *109*, 5855; U. Bossek, K.

 © 2003 Wiley-VCH Verlag GmbH & Co. KGaA, Weinheim

Wieghardt, B. Nuber, J. Weiss, *Angew. Chem. Int. Ed. Engl.* **1990**, *29*, 1055; N. Arulsamy, J. Gleurup, D. J. Hodgson, *Inorg. Chem.* **1994**, *23*, 2066.
[16] T. K. Paine, T. Weyhermüller, K. Wieghardt, P. Chaudhuri, *Inorg. Chem.* **2002**, *41*, 6538.
[17] A. P. Ginsberg, E. Koubeck, H. J. Williams, *Inorg. Chem.* **1966**, *5*, 1656; E. F. Hasty, T. J. Colburn, D. N. Hendrickson, *Inorg. Chem.* **1973**, *12*, 2414; K. Wieghardt, U. Bossek, K. Volckmar, W. Swiridoff, J. Weiss, *Inorg. Chem.* **1984**, *23*, 1387; E. Solari, A. Klose, C. Floriani, N. Re, A. Chiesi-Villa, C. Rizzoli, *Polyhedron* **1996**, *15*, 4103; N. S. Dean, M. R. Bond, C. J. O′Connor, C. J. Carrano, *Inorg. Chem.* **1996**, *35*, 7643.
[18] D. Rehder, *Angew. Chem. Int. Ed. Engl.* **1991**, *30*, 148.
[19] C. N. Verani, E. Bothe, D. Burdinski, T. Weyhermüller, U. Flörke, P. Chaudhuri, *Eur. J. Inorg. Chem.* **2001**, 2161.

Received October 24, 2002

 © 2003 Wiley-VCH Verlag GmbH & Co. KGaA, Weinheim

Synthesis, Characterisation and Antiamoebic Studies of Dioxovanadium(V) Complexes Containing ONS Donor Ligands Derived from *S*-Benzyldithiocarbazate

Mannar R. Maurya,*[a] Shilpa Khurana,[a] Shailendra,[b] Amir Azam,[b] Wenjian Zhang,[c] and Dieter Rehder*[c]

Keywords: Medicinal chemistry / S ligands / Potassium / Vanadium

Three new dioxovanadium(V) compounds, $[K(H_2O)][VO_2(sal\text{-}sbdt)]$ (**1**), $[K(H_2O)_2][VO_2(Clsal\text{-}sbdt)]$ (**2**), and $[K(H_2O)_2][VO_2(Brsal\text{-}sbdt)]$ (**3**) (where H_2sal-sbdt are the Schiff bases formed between salicylaldehyde and dithiocarbazates) have been synthesised, and the structures of **1** and **2** revealed by X-ray diffraction analyses. The ligands coordinate in the tridentate *ONS* fashion out of the enethiolate tautomeric form. The potassium counterions, coordinated to water molecules, the phenolate-O, the oxo groups on vanadium and, in the case of **1**, to the thiolate, provide interlinkages between the anions and thus a complex supramolecular network, further reinforced by intermolecular hydrogen bonds between oxo groups and water molecules. In vitro tests of the antiamoebic activity against the protozoan parasite *Entamoeba histolytica* showed comparable (**1** and **2**) or substantially better (**3**) amoebocidal action than metronidazole, a commonly used drug against amoebobiasis.

(© Wiley-VCH Verlag GmbH & Co. KGaA, 69451 Weinheim, Germany, 2003)

Introduction

Amoebobiasis, a world-wide disease due to protozoan parasites and affecting more than 10% of the world's population is responsible for approximately 100,000 deaths annually, placing it second to malaria in mortality of infectious diseases.[1,2] Nitroimidazole drugs such as metronidazole [1-(2-hydroxyethyl)-2-methyl-5-nitroimidazole] are presently the most effective antiamoebic medications. Side effects are, however, common:[3] mutagenic effects have been established for bacteria, and high doses in rodents can cause carcinoma.[4] As a result of this and also taking into account the possibility of the development of resistant strains of the amoeba against metronidazole, a search for new effective amoebicidal agents is required in order to provide a new dimension in the therapy of amoebiasis.

Schiff base and related metal complexes have experienced long standing applications in biology and medicine,[5,6] as well as in the catalysis of chemical and petrochemical processes.[7,8] Our interest in studies of complexes containing these ligands with sulfur and nitrogen functions arises from their significant antifungal, antiprotozoal, antibacterial, and anticancer activity.[9] More recently, an in vitro insulinmimetic potential of these compounds has been established.[10] Carcinostatic activities have been found for metal complexes of dithiocarbazoic acid and the Schiff bases derived from its *S*-methyl ester.[5] The ruthenium(II) and palladium(II) complexes of Schiff bases derived from *S*-alkyldithiocarbazates have also shown antiamoebic activity.[11,12] In this overall context, vanadium complexes are of specific physiological interest because of their redox activity (V^{IV}/V^{V}): The redox potential can be tuned by the choice of the ligand set so as to provide redox interaction with oxygen species such as peroxide and superoxide. The superoxide radical anion generated in the process $V^{V} + O_2^{2-} \rightarrow V^{IV} + O_2^{-}$ can trigger further physiological events.[13,14]

The potential of vanadium(V) complexes as antiamoebic agents has thus far only been marginally explored.[15] In order to obtain information on the biological activity of dioxovanadium(V) complexes with Schiff base ligands derived from dithiocarbazates, we report here on the synthesis, characterisation, structure elucidation and in vitro screening of the antiamoebic activity of VO_2^{+} complexes with an *ONS* donor set as represented in Scheme 1. In vitro

[a] Department of Chemistry, Indian Institute of Technology Roorkee,
Roorkee 247 667, India
E-mail: rkmanfcy@iitr.ernet.in
[b] Department of Chemistry, Jamia Milia Islamia, Central University,
New Delhi 110 025, India
[c] Institut für Anorganische und Angewandte Chemie, Universität Hamburg,
Martin-Luther-King-Platz 6, 20146 Hamburg, Germany
E-mail: dieter.rehder@chemie.uni-hamburg.de

 © 2003 Wiley-VCH Verlag GmbH & Co. KGaA, Weinheim **DOI: 10.1002/ejic.200200642**

testing was carried out with the HM1:1MSS strain of *Entamoeba histolytica*.

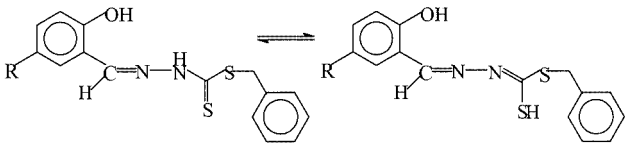

Scheme 1. R = H: H_2sal-sbdt, R = Cl: H_2Clsal-sbdt, R = Br: H_2Brsal-sbdt

Results and Discussion

Synthesis and Thermogravimetric Properties

$[VO(acac)_2]$ reacts with the potassium salt of H_2Rsal-sbdt, H_2L (cf. Scheme 1) under mild basic conditions to give dioxovanadium(v) complexes, $K[VO_2L]$. The probable reaction pathway is given by Equations (1) to (3).

$$[VO(acac)_2] + K_2L \rightarrow [VOL] + 2\ acacK \quad (1)$$

$$2\ [VOL] + 1/2\ O_2 + 2\ MeOH \rightarrow 2\ [VOL(OMe)] + H_2O \quad (2)$$

$$[VOL(OMe)] + 2\ KOH \rightarrow K[VO_2L] + MeOK + H_2O \quad (3)$$

This reaction scheme is based on the fact that H_2sal-sbdt under aerobic conditions gives [VO(OEt)(sal-sbdt)] in ethanol which, in the presence of NaOH, is ultimately oxidised to $[VO_2(sal\text{-}sbdt)]^-$.[16] The orange-yellow compounds **1**−**3** are soluble in methanol, ethanol, acetonitrile, DMF, and DMSO. Lowering the pH of the methanolic solution of **1**−**3** with HCl dissolved in methanol gave brown, incompletely characterised complexes, which are also obtained on using one equivalent (instead of two) of KOH during the synthesis. As shown by, inter alia, thermogravimetric analysis, the complexes contain one (**1**) or 2 water molecules per formula unit (**2** and **3**). The loss of water in the temperature range 120−180 (**1**) and 120−220 °C (**2** and **3**) indicates covalently although not particularly strongly bonded water. On further heating of **1**, the anhydrous complex $K[VO_2(sal\text{-}sbdt)]$ loses the $SCH_2C_6H_5$ group between 180 and 320 °C, followed by the loss of an SCN group between 320 and 600 °C. The remaining residue decomposes to yield KVO_3 as the end product at ca. 670 °C. A very similar decomposition pattern had been observed previously for $[VO_2(acpy\text{-}sbdt)]$ (Hacpy-sbdt = Schiff base derived from acetylpyridine and *S*-benzyldithiocarbazate).[17] The anhydrous forms of **2** and **3** lose $SCH_2C_6H_5$ in the temperature range 220−390 °C, while thermal removal of SCN and other residues is not discernible in these complexes. However, the total weight loss corresponds to the remaining organic residue less one oxygen. The percent weight loss of the end product (i.e. KVO_3) in both complexes compares well with the expected values.

IR and Electronic Spectra

A list of selected IR and electronic spectroscopic data is presented in Table 1. The Schiff bases exhibit a strong band between 1030 and 1041 cm^{-1} due to the ν(C=S), thus indicating the thione (thiocarbonyl, cf. Scheme 1, left) nature of the uncoordinated ligands. This is further supported by the absence of an IR band at ca. 2500 cm^{-1} for ν(SH) and the presence of a band at ca. 3100 cm^{-1} for ν(NH) of the hydrazide moiety. The disappearance of both, the ν(C=S) and ν(NH) bands, in the spectra of the complexes suggests the thioenolisation of the C=S group (Scheme 1, right) and coordination of the enethiolate sulfur to vanadium. This is further supported by the appearance of a new band at 709−776 cm^{-1} due to the ν(C−S) stretch. A strong band associated with the ν(C=N) (azomethine) stretch appears at 1615−1622 cm^{-1} in the free ligands, and this band undergoes a bathochromic shift by 18−21 cm^{-1} in the complexes, thereby indicating the participation of the azomethine nitrogen in coordination. A broad band appears around 3400 cm^{-1} in the ligands and is assigned to the ν(OH) (phenolic) stretch. For the complexes, a broad band associated with water molecules governs this region. In addition, all complexes display two sharp bands at 888−930 and 921−954 cm^{-1}, corresponding to the ν_{sym}(*cis*-VO_2) and ν_{as}(*cis*-VO_2) modes, respectively.

The electronic absorption spectrum of **1** is dominated by an intense band at 392 nm, which is assigned to the $PhO^- \rightarrow V(d\pi)$ ligand to metal charge transfer (LMCT) band. Substitution by Cl or Br in the *para* position of the phenolate shifts this band to higher wavelengths. Two additional bands appearing in the UV region are due to intraligand transitions.

NMR Spectra

The coordination modes of the ligands were also confirmed by recording ^1H NMR spectra of the free ligands and the complexes. As presented in Table 2, all ligands display two sharp resonances in the δ = 10.25 to 13.45 ppm region, indicating the presence of NH (and thus the thionic nature of the free ligands) and phenolic OH protons. In contrast, the absence of these signals in the spectra of the complexes shows that bonding occurs through the phenolic oxygen and enethiolate sulfur atoms. A significant downfield shift of ca. 0.5 ppm for the azomethine (−CH=N−) proton signal in the complexes relative to the corresponding free ligands supports the coordination of the azomethine nitrogen atom. Aromatic and CH_2 protons resonate in the expected region in the spectra of the ligands and the complexes. These results are consistent with those previously obtained for dioxomolybdenum(vi) complexes.[18]

Table 3 contains ^{13}C NMR spectroscopic data of the ligands and complexes. Assignments of the signals are based on the chemical shifts and intensity patterns, and coordination induced shifts Δδ = [δ(complex) − δ(free ligand)] of the signals for carbon atoms in the vicinity of the coordinating functions. Δδ values are provided in parentheses in Table 3. A large Δδ was observed for the azomethine carbon

 © 2003 Wiley-VCH Verlag GmbH & Co. KGaA, Weinheim

Table 1. IR and electronic spectroscopic data

Compound	IR (cm^{-1})[a] ν(C=S/C−S)	ν(C=N)	ν (VO_2)	$\lambda_{max}(\varepsilon)$
H_2sal-sbdt	1041	1622		
[K(H_2O)][VO_2(sal-sbdt)] **1**	766	1601	921, 888	214.5(58300), 293.5(42910), 391.5(13370)
H_2Clsal-sbdt	1036	1618		
[K(H_2O)$_2$][VO_2(Clsal-sbdt)] **2**	697	1600	937, 902	234.5(43170), 294.5(31050), 401(10370)
H_2Brsal-sbdt	1030	1615		
[K(H_2O)$_2$][VO_2(Brsal-sbdt)] **3**	709	1595	954, 930	227(53030), 295(39998), 401(13180)

[a] ν(C=S) for the ligands and ν(C−S) for the complexes.

Table 2. ^{1}H NMR spectroscopic data

Compound	OH	NH	−CH=N−	CH_2	Aromatic
H_2sal-sbdt	13.40 (s, 1 H)	10.24 (s, 1 H)	8.55 (s, 1 H)	4.50 (s, 2 H)	6.89 (m, 2 H), 7.28 (m, 4 H), 7.40 (d, 2 H), 7.64 (d, 1 H)
[K(H_2O)][VO_2(sal-sbdt)] (**1**)			9.07 (s, 1 H)	4.40 (s, 2 H)	6.86 (q, 2 H), 7.23 (q, 1 H), 7.32 (t, 2 H), 7.43 (q, 3 H), 7.65 (d, 1 H)
H_2Clsal-sbdt	13.42 (s, 1 H)	10.51 (s, 1 H)	8.49 (s, 1 H)	4.51 (s, 2 H)	6.93 (d, 1 H), 7.33 (m, 4 H), 7.42 (d, 2 H) 7.61 (d, 1 H)
[K(H_2O)$_2$][VO_2(Clsal-sbdt)] (**2**)			9.09 (s, 1 H)	4.41 (s, 2 H)	6.86 (d, 1 H), 7.44 (m, 6 H), 7.79 (d, 1 H)
H_2Brsal-sbdt	13.45 (s, 1 H)	10.55 (s, 1 H)	8.47 (s, 1 H)	4.50 (s, 2 H)	6.86 (d, 1 H), 7.30 (m, 3 H), 7.41 (m, 3 H), 7.73 (d, 1 H)
[K(H_2O)$_2$][VO_2(Brsal-sbdt)] (**3**)			9.09 (s, 1 H)	4.41 (s, 2 H)	6.82 (d, 1 H), 7.33 (m, 3 H), 7.47 (m, 3 H), 7.91 (d, 1 H)

(C7), the carbon atom bearing the phenolate oxygen (C1) and the enethiolate sulfur (C8), thus confirming the coordination mode deduced from the IR and ^{1}H NMR spectra. Other signals appear at nearly identical positions in the free and complexed ligands (for numbering scheme see Scheme 2).

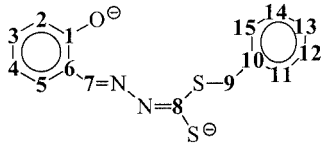

Scheme 2

The ^{51}V NMR spectra exhibit one strong resonance between δ = −465.9 and −468.0 ppm, well within the range of dioxovanadium(v) complexes where a soft thio functionality participates in coordination in addition to the *O* and *N* atoms.[19] The brown solid isolated by using only one equivalent of KOH during the synthesis of **1** gave a signal at δ = −404.6 ppm in addition to that of authentic **1** (δ = −468.0 ppm). Of the two resonances, the less intense resonance at δ = −404.6 ppm is close to the one reported for [VO(OEt)(sal-sbdt)] (δ = −399 ppm).[16] This further supports the proposed pathway for the formation of **1** through [VO(OMe)(sal-sbdt)] as shown by Equations (1) to (3).

Reactivity of 2 Towards HCl

Addition of methanol saturated with HCl gas to [K(H_2O)$_2$][VO_2(Clsal-sbdt)] (**2**) dissolved in MeOH leads to a darkening of the solution and a progressive drop in the intensities of the 400 and 295 nm bands. As the methoxo complex [VO(OMe)(sal-smdt)] (H_2sal-smdt is the Schiff base from salicylaldehyde and *S*-methyldithiocarbazate) exhibits very similar electronic absorptions (400, 307, and 238 nm),[20] the dioxo complex **2** apparently slowly changes

Table 3. ^{13}C NMR spectroscopic data

Compound[a]	C1[b]	C6	C7[b]	C8[b]	C9	C10	C2 − C5/C11 − C15
H_2sal-sbdt	157.3	119.1	144.9	195.5	37.7	136.8	116.4, 119.7, 127.3, 127.4 128.5, 129.3, 132.3
[K(H_2O)][VO_2(sal-sbdt)] (**1**)	165.0, (7.7)	119.0	159.3, (14.4)	173.6, (−21.9)	36.3	137.7	117.6, 119.6, 127.0, 128.3, 129.0, 133.6
H_2Clsal-sbdt	156.0	121.0	142.6	196.2	37.6	136.9	118.3, 123.4, 125.4, 127.3, 128.5, 129.3, 131.6
[K(H_2O)$_2$][VO_2(Clsal-sbdt)] (**2**)	161.9, (5.9)	120.5	156.5, (13.9)	173.2, (−23.0)	34.6	135.9	119.0, 119.4, 125.3, 126.6, 127.3, 130.1, 131.3
H_2Brsal-sbdt	156.5	121.6	142.5	196.1	37.6	136.9	110.9, 118.7, 127.3, 128.3, 128.5, 129.3, 134.4
[K(H_2O)$_2$][VO_2(Brsal-sbdt)] (**3**)	163.8, (7.3)	121.3	158.0, (15.5)	174.6, (−21.5)	36.0	137.4	107.7, 126.7, 128.1, 128.8, 134.4, 135.5

[a] Numbering scheme see Scheme 2. [b] Coordination shifts are given in parentheses

 © 2003 Wiley-VCH Verlag GmbH & Co. KGaA, Weinheim

to the corresponding methoxo complex. An increase of the amount of added HCl causes the disappearance of the 400 nm band, accompanied by a broadening and finally splitting of the 295 nm band into two components (310 and 282 nm); Figure 1. On the basis of ^{1}H and ^{51}V NMR spectroscopic studies, it has been suggested that there is an equilibrium between [VO(OEt)(sal-sbdt)] and [VO(OH)(sal-sbdt)] in $CDCl_3$.[16] A similar equilibrium may also be considered here, which should move towards the formation of [VO(OH)(Clsal-sbdt)] with the addition of more HCl. An oxo-hydroxo species has been generated on acidification of $K[VO_2(sal\text{-}inh)H_2O]$ (where H_2sal-inh is *N*-isonicotinamido-2-hydroxyphenylimine),[21] and even of the dimeric dioxo complex $[VO_2L]_2$ {where H_2L = *N*-[(*o*-hydroxyphenyl)methyl]-*N*′-(2-hydroxyethyl)ethylenediamine} in solution.[22] An oxo-hydroxo complex, viz. $[VO(OH)Tp(H_2O)]$ [Tp = *tris*(3,5-diisopropyl-1-pyrazolyl)borate] has recently been structurally characterised.[23] On allowing the above solution to stand overnight, or on addition of KOH dissolved in methanol, the solution acquires the original pattern, i.e. the reaction is reversible and gives the spectrum of **2**. The reversibility of such a reaction is an important observation in the context of the vanadate-dependent haloperoxidases, for which a hydroxo group in an apical position has been proposed on the basis of X-ray diffraction analysis.[24]

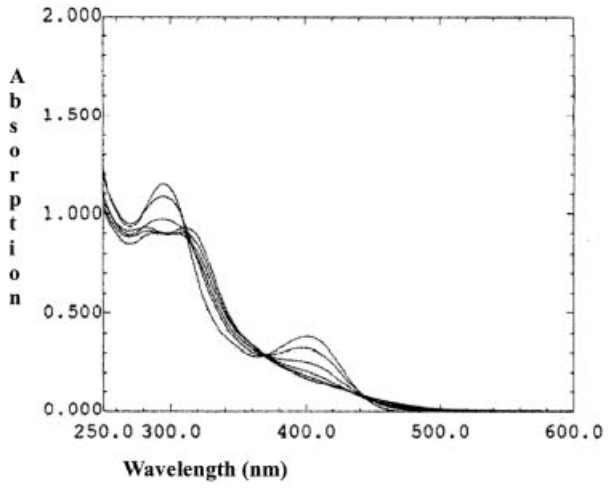

Figure 1. Electronic absorption spectra of the titration of compound **2** (maxima at 400 and 295 nm) with methanolic HCl, showing the formation of [VO(OH)(Clsal-sbdt)] (new bands at 310 and 282 nm)

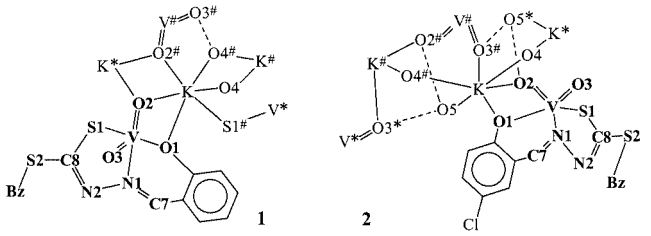

Figure 2. Schematic representations of the coordination environments of vanadium (bold) and potassium, and numbering schemes of **1** and **2**. O3 is the apical oxo group, O4 and O5 are water molecules; Bz = benzyl. # and * refer to atoms not belonging to the formula unit.

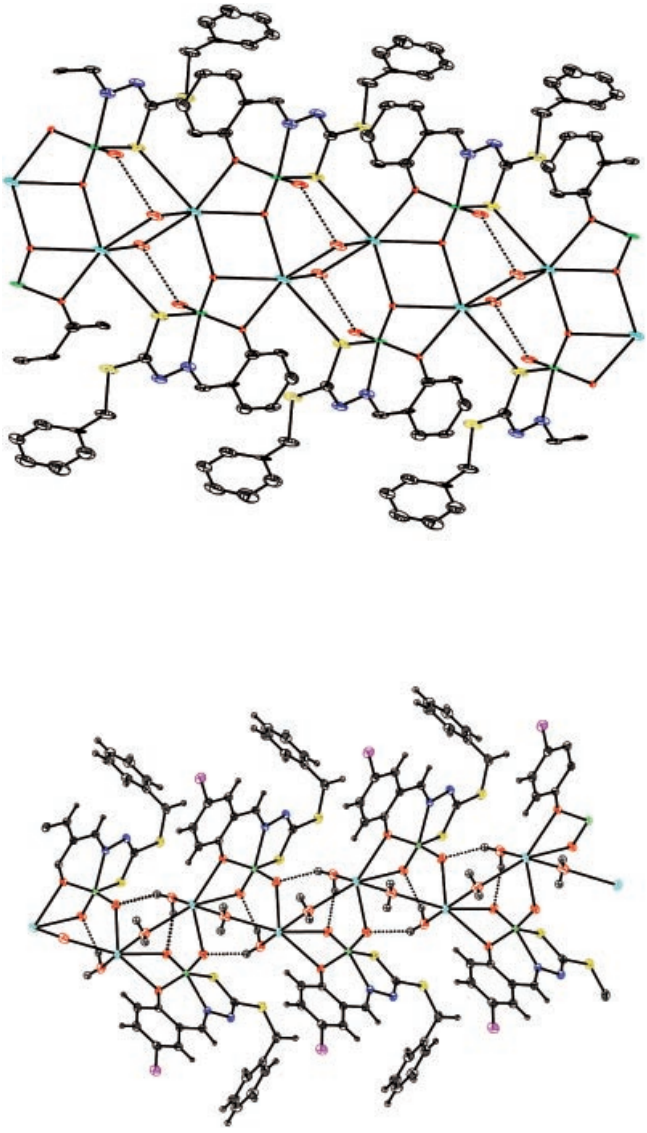

Figure 3. ORTEP drawings (50% probability level), representing sections of the supramolecular arrangements in **1** and **2**. Colour code: V (green), K (light blue), O (red), N (dark blue), S (yellow).

Description of the Structures

Schematic drawings of the coordination environments of vanadium and potassium in **1** and **2** are shown in Figure 2, ORTEP representations of the networks interlinking anions and cations in Figure 3. Table 4 provides a synopsis of selected structure parameters.

In compound **1**, vanadium is in a square pyramidal environment with one of the oxo groups (O3) in the apex and the second oxo group (O2) plus three atoms of the tridentate ligand (O1, N1, S1) forming the plane. Vanadium is 0.0953 Å above this plane. The distance to the nitrogen *trans* to O2, *d*(V−N1), is somewhat elongated with respect to the average V−N(azomethine) bond lengths.[17,25] While

 © 2003 Wiley-VCH Verlag GmbH & Co. KGaA, Weinheim

Table 4. Selected bond lengths [Å] and angles [°] for **1** and **2** (#: refers to the coordination sphere of an adjacent cation or anion)

	$[K(H_2O)]$-$[VO_2(sal\text{-}sbdt)]$, **1**	$[K(H_2O)_2]$-$[VO_2(Clsal\text{-}sbdt)]$, **2**
V−O	11.881(6)	1.9040(10)
V−O	21.660(6)	1.6598(11)
V−O	31.606(6)	1.6223(11)
V−N	12.205(7)	2.1791(12)
V−S	12.370(3)	2.3716(4)
N1−N	21.405(9)	1.4046(16)
S1−C	81.783(8)	1.7370(15)
N2−C	81.251(10)	1.2923(18)
K−O	12.806(6)	2.7789(11)
K−O	22.769(6)	2.7935(12)
K−O2#	2.7586(6)	
K−O3#		2.7469(12)
K−O4	2.765(6)	2.8243(14)
K−O4#	2.751(6)	2.8342(14)
K−O5		2.7488(17)
K···S1#	3.467(3)	
O3···O4	2.887	
O2···O5		2.867
O3···O5		2.861
O1−V−S	1141.4(2)	143.04(4)
O1−V−O2	97.3(3)	96.36(5)
O1−V−N1	82.2(3)	83.23(4)
O2−V−S1	87.0(2)	87.36(4)
O2−V−N1	152.1(3)	151.91(5)
N1−V−S1	76.9(2)	76.98(3)
O3−V−S1	107.1(2)	104.67(4)
O3−V−O1	107.6(3)	109.04(5)
O3−V−O2	108.9(3)	107.68(6)
O3−V−N	197.7(3)	98.86(5)

the apical V=O bond, d(V−O3) = 1.606(6) Å is in the expected range, the basal d(V−O2) = 1.660(6) Å is widened as a consequence of covalent bonding contacts to two K^+ ions. Each potassium ion is thus coordinated to two basal oxo groups (O2, and O2# of a second vanadium centre), the phenolate-O (O1), and to two bridging water molecules (O4 and O4#). In addition, there is a weak bond of 3.467 Å to the S1 of the thiolate group (sum of covalent radii: 2.98, sum of van der Waals radii: 4.60 Å). The potassium ions form an endless zigzag chain via alternate $\{K(\mu\text{-}H_2O)\}_2^{2+}$ and $\{K(\mu\text{-}OVO)\}_2$ links. This chain is "layered" by the ligand fragments of the vanadate anion, with the benzyl rings attached to S2 forming the outer sphere. Adjacent anions in these layers are connected to each other through O2/O1−K−S1 links. Connection of two anions *across* the chain occurs through $\{K(\mu\text{-}VO_2)\}_2$ links; the apical oxo groups of the two $[VO_2(sal\text{-}sbdt)]^-$ anions oppose each other.

On the molecular level, the structure of **2** compares to that of **1**. In **2**, both the basal (O2) *and* the apical (O3) oxo groups of the VO_2 moiety are involved in binding to the K^+ ion. The resulting elongation of d(V−O3) = 1.622(1) is, however, less pronounced than that of d(V−O2) = 1.660(1) Å. The coordination environment of the counterion of **2** differs from that in **1** in that an additional − terminal − water molecule replaces the thiolate group. On the supra-molecular level, anions and cations again arrange so as to form a band structure with a central $\{K(H_2O)(\mu\text{-}H_2O)\}_n$ zigzag chain and an envelope formed by the ligands of the complex anion, with the hydrophobic benzyl fragments exposed to the outside. Additional linkages for the K^+ ion along the chain are bridging VO_2^+ moieties. Coordination of the K^+ ion to the phenolate-O group (O1), and H-bonds formed between both oxo groups (O2 and O3) and terminal H_2O molecule (O5) at the potassium ion provide interconnections between the anions *across* the chain.

Biological Activity

A quantification of drug action was obtained by determining the approximate concentration causing a 50% reduction in the number of cells of *E. histolytica* relative to a control. TYIS-33 medium was used as a control to estimate 100% live confluence of amoeba cells. The inhibition concentration (IC_{50}) of the ligands (H_2sal-sbdt**,** H_2Clsal-sbdt and H_2Brsal-sbdt, c.f. Scheme 1) and their complexes (**1**, **2**, and **3**) are indexed in Table 5. All the compounds screened for anti-amoebic activity in vitro had IC_{50} values of clearly less than 10 μM. IC_{50} value < 20 μM are usually considered significant in amoebicidal action.[26] The high activity of compounds **1**, **2**, and **3**, surmounting that of the ligands, showed that complexation of the organic ligands to vanadium substantially enhances the activity. This behaviour, which is particularly pronounced for H_2Brsal-sbdt (IC_{50} = 4.2) vs. complex **3** (1.35 μM), may be explained by Tweedy's theory,[27] according to which chelation reduces the polarity of the ligand due to partial sharing of its negative charge with the metal, favouring transportation of the complexes across the lipid layer of the cell membrane. In an earlier communication,[15] we had introduced dioxovanadium complexes with bidentate *ON* ligands, showing activity in the range of 2.4−9.6 μM as compared to metronidazole (IC_{50} 2.1 μM). The use of ligands containing a sulfur functionality, as in the case of **1**, **2**, and **3**, apparently improves the activity.

Table 5. In vitro screening for amoebicidal activity of the ligands and their vanadium complexes against an HM1:1MSS strain of *E. histolytica*

Compound	IC_{50} (μM)	S.D.[a]
H_2sal-sbdt	5.19	0.95
$[K(H_2O)][VO_2(sal\text{-}sbdt)]$ **1**	2.67	0.52
H_2Clsal-sbdt	3.57	0.57
$[K(H_2O)_2][VO_2(5\text{-}Clsal\text{-}sbdt)]$ **2**	2.23	0.43
H_2Brsal-sbdt	4.19	0.78
$[K(H_2O)_2][VO_2(5\text{-}Brsal\text{-}sbdt)]$ **3**	1.35	0.26
Metronidazole	2.05	0.31

[a] Standard deviation.

A similar observation holds for Pd^{II}, Pt^{II}, and Ru^{II} complexes of *SN* donor ligands derived from *S*-alkyldithiocarbazate,[11,12,28] as compared to the corresponding complexes with *ON* ligands, suggesting that sulfur attains a general

 © 2003 Wiley-VCH Verlag GmbH & Co. KGaA, Weinheim

role in activity enhancement. This can be compared with the natural product allicin, a sulfinothioc acid [−S(O)−S−] derivative isolated from garlic (*Allium sativum*),[29] which is very active as an antimicrobial agent, possibly due to its specific interference with sulfhydryl enzymes. An additional important feature in these biologically active metal complexes may be imparted by the tridentate ligand system.[30] The binding of the chelated metals to the nitrogen bases of DNA and RNA, and the inhibition of DNA synthesis through the blockage of the enzyme ribonucleotide diphosphate reductase (RBD) have been suggested as possible mechanisms of action.[30,31] What is evident at this stage, however, is that the general mechanisms of operation of these compounds and their complexes, whether in their action as cytotoxic,[30] antibacterial or antifungal agents,[32−34] is still eluding researchers.

Conclusion

Three new anionic dioxovanadium complexes containing an *ONS* ligand set have been prepared, where *O* is a phenolate, *N* an imine, and *S* a thiolate function from a ligand system obtained by condensation of salicylaldehyde and dithiocarbazate. The dianionic ligand coordinates out of its enethiolate tautomeric form. The potassium counterion is in a coordination environment provided by six *O* atoms (**1**) or five *O* atoms [plus a weak K···S(thiolate) bond] (**2**), from water, and phenolate plus the doubly bonded oxo groups on vanadium. The aquapotassium ions form zigzag chains interconnecting adjacent complex anions. The complexes exhibit anti-amoebal in vitro activity towards *Entamoeba histolytica* similar to or, in the case of **3**, better than metronidazole, a medication commonly used in amoebobiasis

Experimental Section

Materials and Measurements: V_2O_5 (Loba Chemie, India), benzyl chloride (Spectrochem, India), salicylaldehyde (E. Merck, India) and acetylacetone (Aldrich, U.S.A.) were used as obtained. 5-Chlorosalicylaldehyde,[35] *S*-benzyldithiocarbazate,[36] and [VO(acac)$_2$] [acac = acetylacetonate(1−)][37] were prepared according to methods reported in the literature. The ligands H_2sal-sbdt and H_2Brsal-sbdt were prepared as described.[38]

The Central Drug Research Institute, Lucknow, India, carried out elemental analyses. ^{1}H NMR spectra were obtained with a Bruker 200 MHz spectrometer, ^{13}C and ^{51}V NMR spectra with a Bruker AM-360 spectrometer at 90.56 and 94.73 MHz, respectively, in [D$_6$]DMSO with the usual parameter settings. All ^{51}V NMR spectroscopic values are referenced relative to $VOCl_3$ as external standard. UV/Vis spectra were recorded in acetonitrile and methanol on a UV-1601 PC UV/Visible spectrophotometer, IR spectra as KBr pellets using a Perkin−Elmer model 1600 FT-IR spectrometer. The Scientific Instrumentation Centre of the Indian Institute of Technology, Roorkee, carried out thermogravimetric analyses, in static air.

Crystal Structure Determinations: Data were collected on a Bruker SMART Apex CCD diffractometer using a graphite monochromator and Mo-K_α radiation (λ = 0.71073 Å) at 153(2) K. Hydrogen atoms were placed into calculated positions and included in the last cycles of refinement. Crystal data and details of the data collection and refinement are collated in Table 6. The program systems SHELXS 86 and SHELXL 93 were used throughout.[39]

CCDC-198451 (**1**) and CCDC-198450 (**2**) contain the supplementary crystallographic data for this paper. These data can be obtained free of charge at www.ccdc.cam.ac.uk/conts/retrieving.html [or from the Cambridge Crystallographic Data Centre, 12, Union Road, Cambridge CB2 1EZ, UK; Fax: (internat.) +44-1223/336-033; E-mail: deposit@ccdc.cam.ac.uk].

The morphology of the crystals of **1** (thin plates) did not allow for a high quality data set ($R1$ = 0.068).

In vitro Tests Against *E. histolytica*: The ligands and their metal complexes were screened in vitro for antiamoebic activity against a (HM1:1MSS) strain of *Entamoeba histolytica* by the microdilution method.[40] *E. histolytica* trophozoites were cultured in TYIS-33 growth medium as described previously[41] in wells of 96-well microtiter plates (Costar). ca. 1 mg of the compounds subjected to the tests were dissolved in DMSO (40 μL), and culture medium was added so as to obtain a concentration of 1 mg/mL (corresponding to ca. 2.8 mM for the ligands and 2.2 mM for the complexes). Dissolution was facilitated by mild sonication in a sonicleaner bath for a few minutes. As evidenced by a comparison of UV/Vis spectra of the complexes dissolved in DMSO on the one hand, and DMSO + TYIS-23 medium on the other hand, the complexes preserve their integrity under biological conditions. Stock solutions were prepared by further dilution of the culture medium to 0.1 mg/mL. Under these conditions, the complexes are stable and no inhibition of amoeba occurs.[42,43] Twofold serial dilutions were made in wells of 96-well microliter plates in 170 μL of medium. Each test included metronidazole as a standard amoebicidal drug, control wells (culture medium plus amoebae), and a blank (culture medium only). The control wells were prepared from a confluent culture by pouring off the medium, adding 2 mL of fresh medium and chilling the culture on ice to detach the organisms from the flask wall. The number of amoeba per mL was estimated with a haematocytometer, and trypan blue exclusion was used to confirm viability. Fresh culture medium was added to dilute the suspension to 10^5 organism/mL, and 170 μL of this suspension was added to the test and control wells so that the wells were completely filled (total volume 340 μL) An inoculum of $1.7 \cdot 10^4$ organisms/well was chosen in order to ascertain confluent − but not excessive − growth in the control wells. The plates were sealed with expanded polystyrene, secured with tape, placed in a modular incubation chamber and gassed for 10 min with nitrogen before incubation at 37 °C for 72 h.

After incubation, the growth of amoebae in the plates was checked with a low power microscope. The culture medium was removed by inverting the plate and shaking gently. The plate was then immediately washed once in sodium chloride solution (0.9%) at 37 °C. This procedure was completed quickly, and the plates were not allowed to cool in order to prevent the detachment of amoebae. After drying at room temperature, the amoebae were fixed with methanol and, when dry, stained with 0.5% aqueous eosin for 15 min. The stained plates were washed once with tap water and then twice with distilled water and allowed to dry. A 200 μL portion of a 0.1 M sodium hydroxide solution was added to each well to dissolve the protein and release the dye. The optical density of the resulting solution in each well was determined at 490 nm with a microplate reader. The % inhibition of amoebal growth was calculated from the optical densities of the control and test wells, and plotted against the logarithm of the dose of the drug tested. Linear

 © 2003 Wiley-VCH Verlag GmbH & Co. KGaA, Weinheim

Table 6. Crystal data and structure refinement for $[K(H_2O)][VO_2(sal\text{-}sbdt)]$ (**1**) and $[K(H_2O)_2][VO_2(Clsal\text{-}sbdt)]$ (**2**)

Empirical formula	$C_{15}H_{14}KN_2O_4S_2V$	$C_{15}H_{15}KN_2O_5S_2ClV$
Formula mass [g mol^{-1}]	440.4	492.9
Crystal system, space group	monoclinic, $P2_1/c$	monoclinic, $P2_1/c$
Unit cell dimensions	17.282(12)	6.2843(2)
a [Å]	7.309(5)	37.3447(11)
b [Å]	14.162(10)	8.7230(3)
c [Å]	94.933(12)	107.2450(10)
β [°]	1782(2)	1955.13(11)
Cell volume [Å^3]	4	4
Z	1.642	1.675
Calculated density [g cm^{-3}]	1.047	1.100
Absorption coefficient [mm^{-1}]	896	1000
F(000)	0.40 × 0.15 × 0.10	0.8 × 0.5 × 0.3
Crystal size [mm]	2.37 to 25.05	1.09 to 32.57
θ range for data collection [°]	$-13 \leq h \leq 20, -8 \leq k \leq 8,$	$-8 \leq h \leq 9, -31 \leq k \leq 56,$
Limiting indices	$-16 \leq l \leq 16$	$-13 \leq l \leq 12$
Reflections collected/unique	9280/3133	28486/7088
R(int)	0.2204	0.0286
Parameters refined	216	260
Goodness of fit on F^2	0.786	1.174
R indices, $[I > 2\sigma(I_0)]$: $R1$, $wR2$	0.0685, 0.1445	0.0359, 0.0947
R indices (all data): $R1$, $wR2$	0.1654, 0.1741	0.0408, 0.1010
Largest diff. peak/hole [e·Å^{-3}]	0.727/−0.710	0.605/−0.544

regression analysis was used to obtain the best-fitting straight line from which the IC_{50} value was determined.

Preparation of Complexes: Spectroscopic data are collated in Table 1 (IR and UV/Vis), Table 2 (^{1}H NMR), and Table 3 (^{13}C NMR) in the Results and Discussion section.

$[K(H_2O)][VO_2(sal\text{-}sbdt)]$ (1): H_2sal-sbdt (0.604 g, 2 mmol) was dissolved in methanol (30 mL) containing KOH (0.056 g, 1 mmol), and $[VO(acac)_2]$ (0.53 g, 2 mmol) was added to this solution. The reaction mixture was refluxed on a water bath under aerobic condition for 6 h. After cooling to room temperature, 1 mmol of additional KOH was added, and the solution was kept for 2 days at ambient temperature to allow for slow evaporation of the solvent. The yellow precipitate thus obtained was filtered, washed with cold methanol and finally recrystallised from methanol to afford 0.40 g (45%) of crystalline complex **1**. $C_{15}H_{14}KN_2O_4S_2V$ (440 g·mol^{-1}): calcd. C 40.91, H 3.18, N 6.36; found C 40.89, H 3.23, N 6.42. ^{51}V NMR ([D$_6$]DMSO): δ = −468.0 ppm.

$[K(H_2O)_2][VO_2(Clsal\text{-}sbdt)]$ (2), and $[K(H_2O)_2][VO_2(Brsal\text{-}sbdt)]$ (3): Complexes **2** (0.439 g, 50% yield) and **3** (0.45 g, 42% yield) were prepared analogously to **1**, replacing H_2sal-sbdt by H_2Clsal-sbdt or H_2Brsal-sbdt. Both complexes were also recrystallised from methanol. Data for **2**: $C_{15}H_{15}ClKN_2O_5S_2V$ (492.5 g·mol^{-1}): calcd. C 36.55, H 3.05, N 5.69; found C 36.67, H 3.11, N 5.53. ^{51}V NMR: δ = −467.3 ppm. Data for **3**: $C_{15}H_{15}BrKN_2O_5S_2$ (537 g·mol^{-1}): calcd. C 33.52, H 2.79, N 5.21; found C 33.38, H 2.83, N 5.16. ^{51}V NMR: δ = −465.9 ppm.

Acknowledgments

This work was supported by the Department of Science and Technology of the IIT Roorkee, the Government of India, the Deutsche Forschungsgemeinschaft and the Fonds der Chemischen Industrie.

[1] WHO, Report of the expert consultation on amoebiasis, *WHO Epidemiol. Record* **1997**, *14*, 4.
[2] J. A. Walsh, *Rev. Infect. Dis.* **1986**, *8*, 228−238.
[3] P. A. Martinez, *Biology of Entamoeba histolytica* in: *Amoebiasis* (Ed.: P. A. Martinez), Elsevier, Amsterdam, **1986**, pp. 12−43.
[4] C. E. Voogd, J. J. van der Stel, J. J. A. A. Jacobs, *Mutat. Res.* **1974**, *26*, 483−490.
[5] M. A. Ali, S. E. Livingstone, *Coord. Chem. Rev.* **1974**, *13*, 101−132.
[6] D. K. Johnson, T. B. Murphy, N. J. Rose, W. H. Goodwin, L. Pickart, *Inorg. Chim. Acta* **1982**, *67*, 159−165.
[7] K. Srinivasan, S. Perrier, *J. Mol. Catal.* **1986**, *36*, 297.
[8] P. K. Bhattacharya, *Proc. Ind. Acad. Sci. (Chem. Sci.)* **1990**, *102*, 247−254.
[9] A. Saxena, J. K. Koacher, J. P. J. Tandon, *Antibact. Antifung. Agents* **1981**, *9*, 435−438.
[10] D. Rehder, J. Costa Pessoa, C. F. G. C. Geraldes, M. M. C. A. Castro, T. Kabanos, T. Kiss, B. Meier, G. Micera, L. Pettersson, M. Rangel, A. Salifoglou, I. Turel, D. Wang, *J. Biol. Inorg. Chem.* **2002**, *7*, 384−396.
[11] N. Bharti, M. R. Maurya, F. Naqvi, A. Bhattacharya, S. Bhattacharya, A. Azam, *Eur. J. Med. Chem.* **2000**, *35*, 481−486.
[12] N. Bharti, M. R. Maurya, F. Naqvi, A. Azam, *Bioorg. Med. Chem. Lett.* **2000**, *10*, 2243−2245.
[13] J. M. McCord, I. Fridovich, *Superoxide and Superoxide Dismutases*, Academic Press, New York, **1977**.
[14] D. T. Sawyer, J. S. Valentine, *Acc. Chem. Res.* **1981**, *14*, 393−400.
[15] N. Bharti, Shailendra, M. T. G. Garza, D. E. Cruz-Vega, J. Castro Garza, K. Saleem, F. Naqvi, M. R. Maurya, A. Azam, *Bioorg. Med. Chem. Lett.* **2002**, *12*, 869−871.
[16] D. Wang, M. Ebel, C. Schulzke, C. Grüning, S. K. K. Hazari, D. Rehder, *Eur. J. Inorg. Chem.* **2001**, 935−942.
[17] M. R. Maurya, S. Khurana, W. Zhang, D. Rehder, *Eur. J. Inorg. Chem.* **2002**, 1749−1760.
[18] A. Syamal, M. R. Maurya, *Trans. Met. Chem.* **1986**, *11*, 255−258.
[19] D. Rehder, C. Weidemann, A. Duch, W. Priebsch, *Inorg. Chem.* **1988**, *27*, 584−587.
[20] S. K. Dutta, S. B. Kumar, S. Bhattacharyya, E. R. T. Tiekink, M. Chaudhury, *Inorg. Chem.* **1997**, *36*, 4954−4960.
[21] M. R. Maurya, S. Khurana, C. Schulzke, D. Rehder, *Eur. J. Inorg. Chem.* **2001**, 779−788.
[22] G. J. Colpas, B. J. Hamstra, J. W. Kampf, V. L. Pacoraro, *Inorg. Chem.* **1994**, *33*, 4669−4675.
[23] M. Kosugi, S. Hikichi, M. Akita, Y. Moro-oka, *Inorg. Chem.* **1999**, *38*, 2567−2578.

 © 2003 Wiley-VCH Verlag GmbH & Co. KGaA, Weinheim

[24] S. Macedo-Ribeiro, W. Hemrika, R. Renirie, R. Wever, A. Messerschmidt, *J. Biol. Inorg. Chem.* **1999**, *4*, 209−219.

[25] [25a] C. R. Cornman, G. J. Colpas, J. D. Hoeschele, J. Kampf, V. L. Pecoraro, *J. Am. Chem. Soc.* **1992**, *114*, 9925−9933. [25b] D. Wang, M. Ebel, C. Schulzke, C. Grüning, S. K. S. Hazari, D. Rehder, *Eur. J. Inorg. Chem.* **2001**, 935−942.

[26] S. J. Marshall, P. F. Russell, C. W. Wright, M. M. Anderson, J. D. Phillipson, G. C. Kirby, D. C. Warhurst, P. L. Schiff, *Antimicrob. Agent. Chemoth.* **1994**, *38*, 96−103.

[27] B. G. Tweedy, *Phytopathology* **1964**, *55*, 910.

[28] Shailendra, N. Bharti, F. Naqvi, A. Azam, *Helv. Chim. Acta* **2002**, *85*, 2713−2720.

[29] S. Ankri, T. Miron, A. Rabonkov, M. Wilchek, D. Mirelman, *Antimicrob. Agent. Chemoth.* **1997**, *41*, 2286−2288.

[30] J. Garcia-Tojal, M. K. Urtiaga, R. Cortés, L. Lezama, M. I. Arriortua, T. Rojo, *J. Chem. Soc., Dalton Trans.* **1994**, 2233−2238, and references therein.

[31] M. A. Ali, K. K. Dey, M. Nazimuddin, F. E. Smith, R. J. Butcher, J. P. Jasinski, J. M. Jasinski, *Polyhedron* **1996**, *15*, 3331−3339.

[32] P. Souza, A. I. Matesanz, V. Fernández, *J. Chem. Soc., Dalton Trans.* **1996**, 3011−3013.

[33] L. Mishra, *J. Ind. Chem. Soc.* **1999**, *76*, 175−181.

[34] F. J. Baerlocher, R. F. Langler, M. U. Frederiksen, N. M. Georges, R. D. Witherell, *Aust. J. Chem.* **1999**, *52*, 167−172.

[35] F. J. Welcher, *Organic Analytical Reagents*, D. Van Nostrand Co., New York, **1947**, vol. 3, p. 254.

[36] M. A. Ali, M. T. H. Tarafder, *J. Inorg. Nucl. Chem.* **1977**, *39*, 1785−3339.

[37] R. A. Row, M. M. Jones, *Inorg. Synth.* **1957**, *5*, 113.

[38] A. Syamal, M. R. Maurya, *Trans. Met. Chem.* **1986**, *11*, 255.

[39] [39a] G. M. Sheldrick, *SHELXS 86*, University of Göttingen, **1986**. [39b] G. M. Sheldrick, *SHELXS 93*, University of Göttingen, **1993**.

[40] C. W. Wright, M. J. O'Neill, J. D. Phillipson, D. C. Warhurst, *Antimicrob. Agents Chemother.* **1988**, *32*, 1725−1729.

[41] L. S. Diamond, D. R. Harlow, C. C. Cunnick, *Trans. R. Soc. Trop. Hyg.* **1978**, *72*, 431−432.

[42] F. D. Gillin, D. S. Reiner, M. Suffness, *Antimicrob. Agents Chemother.* **1982**, *22*, 342−345.

[43] A. T. Keene, A. Harris, J. D. Phillipson, D. C. Warhurst, *Planta Med.* **1986**, *52*, 278−284.

Received November 26, 2002

 © 2003 Wiley-VCH Verlag GmbH & Co. KGaA, Weinheim

Zn^{II} Complex with a Phenanthroline-Containing Macrocycle as Receptor for Amino Acids and Dipeptides − Hydrolysis of an Activated Peptide Bond

Carla Bazzicalupi,[a] Andrea Bencini,*[a] Emanuela Berni,[a] Antonio Bianchi,*[a] Patrizia Fornasari,[a] Claudia Giorgi,[a] and Barbara Valtancoli[a]

Keywords: Macrocyclic ligands / Zinc / Amino acids / Enzyme models / Stacking interactions

The interaction between several L-amino acids and dipeptides and the Zn^{II} complex with ligand L, a macrocycle containing a triamine chain linking the 2,9 positions of a phenanthroline moiety, has been studied by means of potentiometric and ^1H NMR spectroscopic measurements in aqueous solutions. In the $[ZnL]^{2+}$ complex, the metal ion displays an unsaturated coordination environment and the metal can act as a binding site for these substrates. Amino acids and dipeptides in their neutral (zwitterionic) form bind to Zn^{II} through the carboxylate function and, when in their anionic form, through the amine group. In this case the carbonyl of the amide function is probably also involved in metal coordination. Amino acids containing aromatic pendants form the most stable complexes, due to hydrophobic and/or π-stacking interactions between the aromatic subunits of the substrates and the phenanthroline moiety of the metal receptor. The hydrolytic properties of the Zn^{II} complex with L, involving the cleavage of the peptide bond, have been tested by using L-leucine-*p*-nitroanilide (LNA), which contains an activated peptide bond. This substrate forms stable $[ZnL(LNA)]^{2+}$ and $[ZnL(OH)(LNA)]^{+}$ complexes. The formation of the $[ZnL(OH)(LNA)]^{+}$ complex is followed by LNA hydrolysis, through a nucleophilic attack of the Zn–OH function on the peptide bond.
(© Wiley-VCH Verlag GmbH & Co. KGaA, 69451 Weinheim, Germany, 2003)

Introduction

Over the years a great deal of interest has focused on the role of metal ions in the active centers of hydrolytic metalloenzymes (e.g. phosphatase, amino- and carboxypeptidase, carbonic anhydrase, P1-nuclease).[1−15] Hydrolytic metalloenzymes generally contain one or more Zn^{II} ions in their active site. The catalytic role of zinc is generally ascribed to two main functions: i) binding and activation of the substrates, and ii) deprotonation of Zn^{II}-coordinated water molecules to give Zn−OH functions, which can act as nucleophiles in the hydrolytic mechanism. The catalytic site is often lodged in a hydrophobic pocket, which may contribute to substrate binding and can also assist in the formation of the nucleophilic Zn^{II}−OH functions.

Aminopeptidases are one of the Zn^{II} enzymes and contain either one or two zinc ions per active site and specifically hydrolyze the *N*-terminal residue of polypeptide chains, through a catalytic mechanism which involves coordination of the peptide function to zinc, followed by a nucleophilic attack of a Zn−OH group on the carbonyl carbon and cleavage of the peptide bond.[4,5,7,12−15]

As one of the approaches to the study of Zn^{II} enzymes, a number of synthetic Zn^{II} complexes have recently been used as simple model systems for hydrolytic enzymes.[16−50] Examples of functional models for aminopeptidases are less common, due to the marked hydrolytic inertness of the peptide bond to hydrolysis. Examples of Cu^{II},[17,18,51−53] Pt^{II},[54] Pd^{II},[55−57] Co^{III} [18,58] and Ce^{IV} [59] complexes able to cleave the peptide bond in aqueous solutions are known; peptide bond cleavage induced by Zn^{II} complexes has rarely been observed,[40] and occurs only at high temperature in aqueous solution, due to the low tendency of Zn^{II} to hydrolyze the amide bonds. As a matter of fact, binding of free Zn^{II} to peptides may even inhibit the cleavage of the peptide bond.[37]

We have recently reported on the synthesis of a series of phenanthroline-containing polyamine macrocycles,[60,61] such as L (Figure 1), able to form stable Zn^{II} complexes in aqueous solutions.[62]

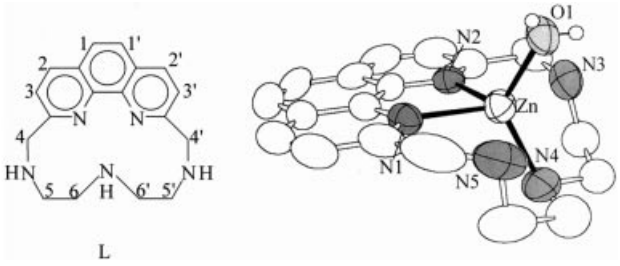

Figure 1. L drawing (with atom labelling used in NMR spectroscopic experiments) and crystal structure of the $[ZnL(H_2O)]^{2+}$ cation.

[a] Dipartimento di Chimica, Polo Scientifico, Università di Firenze,
Via della Lastruccia 3, 50019 Sesto Fiorentino, Firenze, Italy
E-mail: andrea.bencini@unifi.it

 © 2003 Wiley-VCH Verlag GmbH & Co. KGaA, Weinheim **DOI: 10.1002/ejic.200200648**

The rather high stability of the complexes is mainly due to the heteroaromatic nitrogens, which can offer an optimal binding site for the metal ion. At the same time, the rigidity of the phenanthroline unit does not allow for the involvement of all the aliphatic amine groups in the metal binding. Actually, the crystal structure of the $[ZnL(H_2O)]^{2+}$ cation (Figure 1) shows a Zn^{II} coordination environment not saturated by the ligand donors, since the two benzylic nitrogens are not involved in metal binding.[62] A water molecule is coordinated to Zn^{II}, to give an almost tetrahedral coordination environment for the metal. The presence of "free" binding sites at the Zn^{II} ion makes this complex a promising metallo-receptor for substrate molecules.

A solution study showed that the coordinated water molecule deprotonates at a slightly alkaline pH to give a $Zn^{II}-OH$ function. A dihydroxo complex $[ZnL(OH)_2]$ is also formed at an alkaline pH. Finally, phenanthroline can generate a rather hydrophobic environment for the metal. These characteristics make this complex a potential candidate for a model system of hydrolytic enzymes.

With this in mind, we decided to investigate the effective binding properties of this complex for amino acids and dipeptides as well as its hydrolysis of a peptide bond. The substrates involved in this study, along with the atom labeling used in the NMR spectroscopy experiments, are shown in Scheme 1.

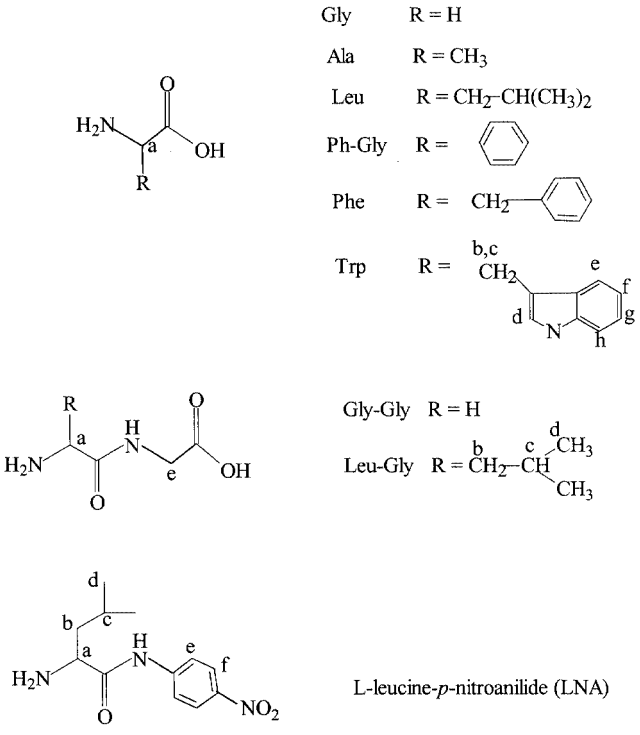

Scheme 1

Results and Discussion

Crystal Structure of $[ZnL(HGly)]_2(ClO_4)_4 \cdot 1.5H_2O$

The crystal structure consists of $[ZnL(HGly)]^{2+}$ cations, perchlorate anions and water solvent molecules. The $[ZnL(HGly)]^{2+}$ cation contains the amino acid in its neutral form, herein indicated by HGly. The asymmetric unit contains two $[ZnL(HGly)]^{2+}$ independent cations. The ORTEP[63] drawings of the two $[ZnL(HGly)]^{2+}$ cations (herein indicated A and B) with atom labelling are shown in Figure 2 and Table 1 lists selected bond angles and distances for the coordination sphere of Zn^{II}. The coordination environment for the Zn^{II} ion is almost equal in both the A and B cations and can be described as a distorted tetrahedron. In complex A, the Zn1 ion is coordinated by the N1 and N2 heteroaromatic nitrogens, the central N4 amine of the aliphatic chain and the O1g oxygen of the carboxylate group of the amino acid.

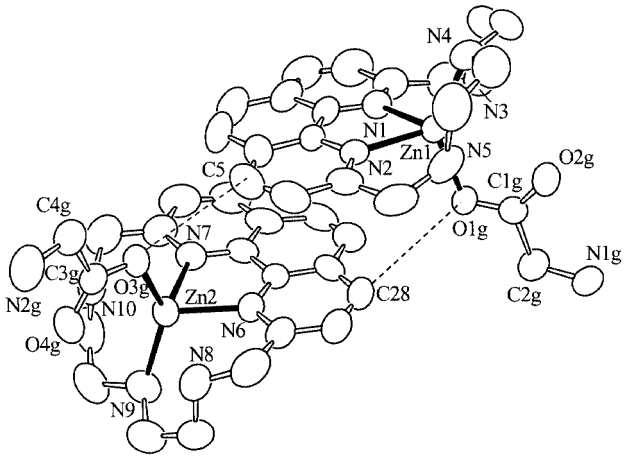

Figure 2. ORTEP drawing of the $[ZnL(HGly)]^{2+}$ complex, representing the A and B independent units coupled by π-stacking and C–H···O hydrogen bond interactions

Table 1. Bond lengths [Å] and angles [°] for the metal coordination environment in the A and B cations of $[ZnL(HGly)]_2(ClO_4)_4 \cdot 1.5H_2O$

A Unit			
Zn1–O1g	1.989(4)	Zn1–N1	2.165(5)
Zn1–N2	2.171(5)	Zn1–N4	2.094(6)
O1g–Zn1–N1	103.79(19)	N1–Zn1–N2	74.64(19)
O1g–Zn1–N2	104.79(17)	N4–Zn1–N1	110.5(2)
O1g–Zn1–N4	135.5(2)	N4–Zn1–N2	110.9(2)
B unit			
Zn2–O3g	1.990(4)	Zn2–N7	2.167(5)
Zn2–N6	2.150(5)	Zn2–N9	2.095(6)
O3g–Zn2–N6	104.83(18)	N6–Zn2–N7	75.0(2)
O3g–Zn2–N7	104.42(19)	N9–Zn2–N6	110.7(2)
O3g–Zn2–N9	136.1(2)	N9–Zn2–N7	109.0(2)

The Zn–N bond lengths are in the range 1.99–2.17 Å. Their values are typical for Zn^{II} complexes with polyamine compounds. The benzylic nitrogens N3 and N5 are not coordinated, lying far apart from the metal ion [Zn1···N3 2.440(6) Å, Zn1···N5 2.448(7) Å].

In complex B, the Zn2 ion is coordinated by three donor atoms of the ligand molecule (N6, N7 and N9) and the

 © 2003 Wiley-VCH Verlag GmbH & Co. KGaA, Weinheim

O3g oxygen atom of glycine, while the N8 and N10 benzylic nitrogen atoms are not coordinated (Table 1).

It is worth noting that, in both $[ZnL(HGly)]^{2+}$ independent cations, the amino acid is in its zwitterionic form. In both A and B complexes, the C−O bond lengths of the carboxylic group of HGly are equal within their e.s.d. [C1g−O1g 1.234(8) Å, C1g−O2g 1.238(8) Å, C3g−O3g 1.259(7) Å, C3g−O4g 1.226(8) Å], indicating that this group is in its anionic form. The unbound amine group is therefore protonated. Such a monodentate binding mode of Gly is rather common for amino acids in their zwitterionic form.[24−26,35−37,64]

In both A and B, the coordination geometry of the metal ion is very similar to that found in the crystal structure of $[ZnL(H_2O)](ClO_4)_2$. Actually, in the present structure an oxygen donor of the carboxylate unit simply replaces the Zn^{II}-coordinated water molecule of $[ZnL(H_2O)](ClO_4)_2$. The overall conformation of the ligand is also similar in the two complexes. As already found in $[ZnL(H_2O)]^{2+}$, the ligand is folded along the line connecting the benzylic nitrogen atoms, giving rise to dihedral angles of 82.4(3)° (A complex) and 84.5(3)° (B complex) between the mean planes defined respectively by the benzylic nitrogen atoms and the aromatic unit (max deviations 0.15(1) Å for C8 in the A complex and 0.154(8) Å for C25 in the B complex) and by the three secondary nitrogen atoms of the aliphatic chains.

Inspection of the crystal packing reveals the presence of π-stacking interactions between the phenanthroline moiety of the two independent cations. As shown in Figure 2, the two heteroaromatic groups are almost parallel [the dihedral angle between the planes containing the aromatic groups is 7.1(2)°] and lie 3.55 Å apart from each other. In addition, two H-bonding interactions between a C−H aromatic carbon atom of each complex and a carboxylate oxygen atom belonging to the other [C5···O3g 3.34(1) Å and C28···O1g 3.412(9) Å] contribute to the molecular pairing.[65]

Binding of L-Amino Acids and L-Dipeptides to the Zn^{II} Complex Containing L

The binding of the amino acids glycine (HGly), L-phenylglycine (Hph-Gly), L-alanine (HAla), L-phenylalanine (HPhe), L-leucine (HLeu) and L-tryptophan (HTrp) to the $[ZnL]^{2+}$ complex was studied by means of potentiometric and ^1H NMR spectroscopic measurements in aqueous solutions; the results of the potentiometric investigation are reported in Table 2.

Table 2. Equilibrium constants for the addition of L-amino acids to the Zn^{II} complex with the ligand L (NMe_4NO_3 0.1 M, 298 K).

Reaction	log *K*					
	Gly	*ph-Gly*	*Ala*	*Phe*	*Leu*	*Trp*
$[ZnL]^{2+} + A^- = [ZnL(A)]^+$	2.96(4)	3.61(3)	2.95(4)	3.83(4)	2.11(4)	5.12(6)
$[ZnL]^{2+} + AH = [ZnL(AH)]^{2+}$	2.58(4)	2.71(5)	2.43(2)	2.79(3)	−	3.71(3)
$[ZnL(OH)]^+ + A^- = [ZnL(OH)(A)]$						5.02(6)

All of the amino acids under investigation, with the exception of leucine, interact with the $[ZnL]^{2+}$ complex, both in their neutral and deprotonated forms, herein indicated as HA and A^-, respectively, to give the $[ZnL(HA)]^{2+}$ and $[ZnL(A)]^+$ species (Table 2). Among the six amino acids, leucine gives the weakest interaction, and only the complex with its deprotonated form is formed in aqueous solutions. On the contrary, tryptophan gives the strongest interaction with $[ZnL]^{2+}$. Figure 3 shows the distribution diagram of complexes formed by tryptophan in the presence of our Zn^{II} complex. The formation of the complex with the zwitterionic form of the amino acid $[ZnL(HTrp)]^{2+}$ occurs at an acidic pH and is followed by deprotonation of the amino acid at neutral pH to give the [ZnL(Trp)] complex. In this case a third species, $[ZnL(Trp)OH]^+$, is found at an alkaline pH.

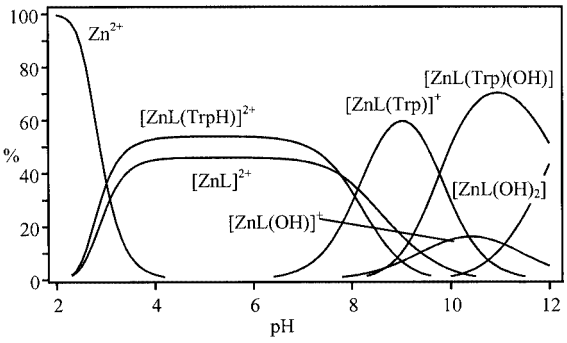

Figure 3. Species distribution diagram for the system $[ZnL]^{2+}$/Trp in 1:1 molar ratio (NMe_4NO_3 0.1 M, 298 K).

The data in Table 2 clearly outline that the stability of the complexes of our metallo-receptor with the neutral form of amino acids (HA) is lower than that found with their anionic form (A^-). A similar behavior was found for the addition of amino acids to the "free" Zn^{II} ion; it is generally accepted that coordination to Zn^{II} involves the anionic carboxylate function in the $[Zn(HA)]^{2+}$ complex and both the carboxylate and the amine groups, with the formation of a six-membered chelate ring, in the deprotonated $[Zn(A)]^+$ complex.[35−37,47,64] To shed further light on the binding mode of amino acids to our Zn^{II} complex we recorded ^1H NMR spectra at different pH values. Figure 4 (a) shows the pH dependence of the Trp signals in the presence and in the absence of our Zn^{II} complex, while Figure 4 (b) shows the ^1H NMR spectrum of a D_2O solution containing $[ZnL](ClO_4)_2 \cdot H_2O$ and tryptophan in a 1:1 molar ratio at pH 9.3, where the $[ZnL(Trp)]^+$ is the prevalent species in solution, compared with those of deprotonated tryptophan (Trp^-) and $[ZnL]^{2+}$.

As shown in Figure 4(a), the formation of the $[ZnL(HTrp)]^{2+}$ complex in the pH range 3−7 does not lead to a significant variation in the chemical shifts of the ^1H NMR signals of the protons in the α-position to the carboxylate and the amine function (*a* in Scheme 1) with respect to the same signals of the amino acid HA (prevalent in solution in the pH range 3−8), where the acidic proton is located on the amine group. This would indicate that in

 © 2003 Wiley-VCH Verlag GmbH & Co. KGaA, Weinheim

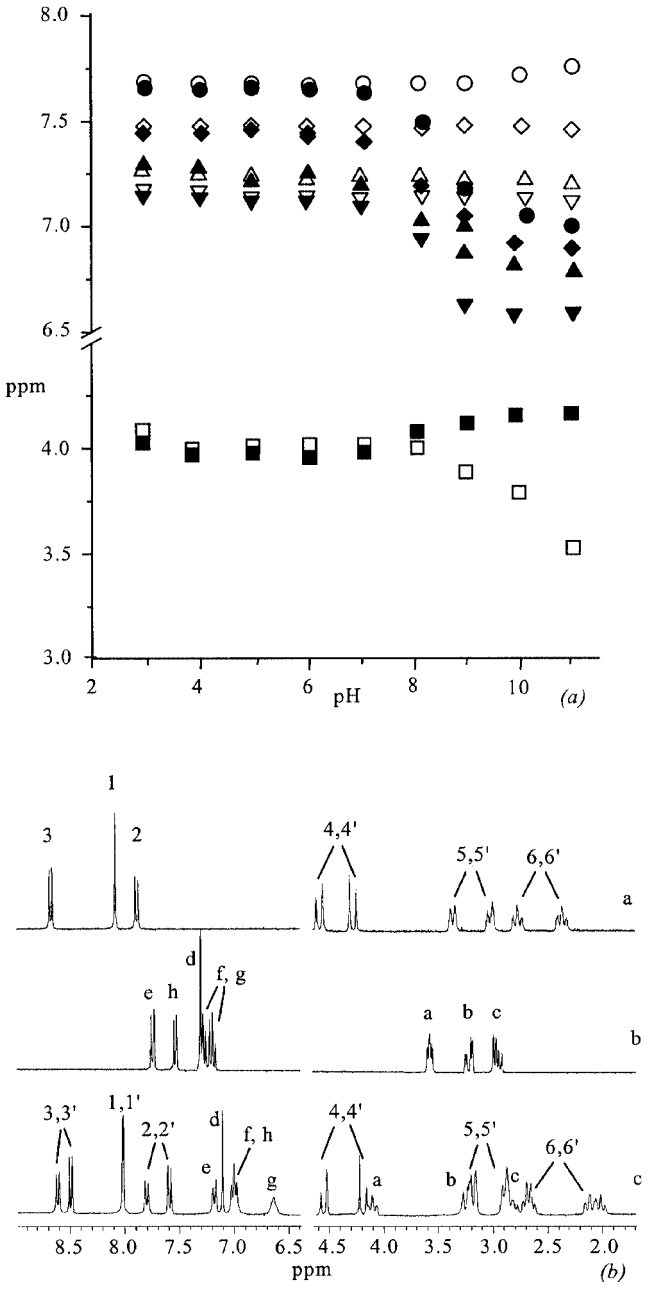

Figure 4. (*a*): pH dependence of the ^1H NMR chemical shifts of selected protons of Trp in the absence (□: a proton; ▽: g; △: f; ◇: h; ○: e). and in the presence of the Zn^{II} complex with L (■: *a* proton; ▼: *g*; ▲: *f*; ◆: *h*; ●: *e*). The signals of the protons *b*, *c* and *d* are omitted for clarity. (*b*): ^1H NMR spectra of $[ZnL]^{2+}$ (a), Trp^- (b) and $[ZnL(Trp)]^+$ (pH, 9.3) (c). See Scheme 1 and Figure 1 for the labelling used.

$[ZnL(HA)]^{2+}$ the acidic proton localization is not changed by HA binding to zinc and, therefore, HA coordination takes place through the carboxylate group, while the amine remains protonated. This hypothesis is corroborated by the crystal structure of the $[ZnL(HGly)]^{2+}$ cation, which shows the metal coordinated by one oxygen atom of the carboxylate function, while the amine group is protonated.

At an alkaline pH, the *a* signal of tryptophan alone shifts upfield, due to deprotonation of the amine group. On the contrary, the formation of the $[ZnL(Trp)]^+$ complex above pH 7 leads to a minor, but significant, downfield shift of the *a* resonance [Figure 4 (a)]. Similar downfield shifts for the signal of the *a* protons are also found for all the amino acids under investigation [up to 0.4 ppm in the case of Trp, see Figure 4 (b)]. This indicates the involvement of the NH_2 group in Zn^{II} binding. However, a bidentate coordination mode of the deprotonated amino acids, involving both the amine and the carboxylate functions, has generally been found in binary and ternary Zn^{II} complexes with these substrates,[24−26,35−37,47,64] and can be presumed to a reasonable extent in the present case.

The most interesting finding in Table 2 is the higher stability of the adducts with amino acids containing an aromatic side arm. In particular, tryptophan, which contains the largest aromatic subunit, indole, shows addition constants to the $[ZnL]^{2+}$ complex that are two orders of magnitude higher than Gly, Ala or Leu. This is rather surprising, since the addition constants of Gly or Ala to the "free" Zn^{II} ion are somewhat higher than those reported for ph-Gly, Phe and Trp.[66] Figure 4 (a) also shows that the formation of the $[ZnL(Trp)]^+$ complex remarkably affects the spectrum of the indole units, with a marked upfield shift of the signals of the aromatic protons with respect to the corresponding signals of "free" Trp^-. At the same time, the phenanthroline subspectrum displays a dramatic loss of symmetry. Besides the downfield shift of the *a* signal of the $[ZnL(Trp)]^+$ complex, discussed above, Figure 4 (b) displays a splitting into two doublets of each signal of the protons 2 and 3. The singlet attributed to 1 is also split into a doublet. Similarly to the indole resonances, the signals of the phenanthroline protons show a marked upfield shift with respect to the corresponding signals in $[ZnL]^{2+}$.

These spectral characteristics account for the presence of π-stacking interactions between phenanthroline and the aromatic pendant arm of Trp (Scheme 2), which can contribute to the stability of the complex.

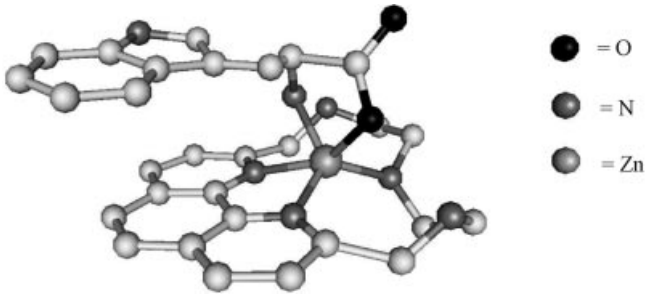

Scheme 2

In the case of Phe and ph-Gly, substrate complexation by $[ZnL]^{2+}$ is also accompanied by upfield shifts of the resonances of the aromatic protons of the substrates and phenanthroline. The shifts, however, are generally smaller (ca. 0.1−0.2 ppm) than those observed for Trp and no loss of symmetry was found for the phenanthroline unit. This accounts for a reduced π-stacking pairing between the phenyl units and phenanthroline. Accordingly, the stability of the Phe and ph-Gly complexes is lower than that of the Trp complex.

 © 2003 Wiley-VCH Verlag GmbH & Co. KGaA, Weinheim

Interestingly, no significant shift of the signals of the aromatic protons are observed at acidic pH, where the complexes with the protonated forms (HA) of the amino acids are present in solution [Figure 4(a)]. This experimental observation points out that the pairing between the two aromatic moieties is disrupted by coordination to Zn^{II} through the carboxylate function, due to protonation of the amine group in the $[ZnL(HA)]^{2+}$ complex.

Similar π-stacking interactions have already been observed by Sigel et al. in the case of ternary metal complexes[67,68] involving Trp and dipyridine or ATP. In the latter case the indole unit of Trp and the adenine moiety of the nucleotide are paired *via* π-stacking.[67] Yamauchi et al. also found intramolecular stacking interactions in Cu^{II} ternary complexes with Trp and dipyridine or phenanthroline, both in solution and in the solid state.[47][69−72]

In conclusion, our Zn^{II} complex may behave as a multifunctional receptor for amino acids, presenting two distinct binding sites, i.e., the metal center, which forms coordination bonds with amino acids, and the heteroaromatic unit, which can give stabilizing hydrophobic and/or π-stacking interactions with the aromatic portion of the substrates. These interactions lead to an unusual selectivity pattern in amino acid binding by our Zn^{II} complex, since the amino acids with aromatic pendant arms are strongly bound with respect to the aliphatic amino acids Gly or Ala.

In order to evaluate the effective binding properties of our complex towards the peptide amide group, we decided to extend our analysis to dipeptides. Unfortunately, most of the dipeptides tested, such as tryptophan-containing dipeptides, form low soluble complexes with $[ZnL]^{2+}$. Our study was therefore limited to L-glycylglycine (HGly-Gly) and L-leucylglycine (HLeu-Gly). Table 3 reports the equilibrium constants for the addition of these dipeptides to the $[ZnL]^{2+}$ complex in aqueous solution.

Table 3. Equilibrium constants for the addition of Gly-Gly and Leu-Gly to the Zn^{II} complex with the ligand L (NMe_4NO_3 0.1 M, 298 K).

Reaction	log *K*	
	Gly-Gly	*Leu-Gly*
$[ZnL]^{2+} + A^- = [ZnL(A)]^+$	2.84(9)	3.91(4)
$[ZnL]^{2+} + HA = [ZnL(AH)]^{2+}$	1.9(1)	3.06(2)
	pK_a	
$[ZnL(A)]^+ + H_2O = [ZnL(A)(OH)] + H^+$	8.77(6)	8.95(3)

The formation of the complex with the neutral form of the dipeptide ($[ZnL(HLeu\text{-}Gly)]^{2+}$) at acidic pH is followed by deprotonation of the substrate to give $[ZnL(Leu\text{-}Gly)]^+$ at a slightly alkaline pH. A further deprotonation step is monitored above pH 9. This process could be attributed, in principle, to deprotonation of the amide function to give the $[ZnL(Leu\text{-}GlyH_{-1})]^+$ complex or to deprotonation of a coordinated water to give a hydroxylated ternary complex. Gly-Gly shows similar binding features towards $[ZnL]^{2+}$ (Table 3). As already found in the case of binding amino acids, the addition constants of the deprotonated dipeptides to the $[ZnL]^{2+}$ complex are about one order of magnitude higher than those of the dipeptides in their neutral (zwitterionic) form. To clarify the binding mode of these dipeptides to Zn^{II}, we decided to record ^1H NMR spectra on solutions containing the dipeptides in the presence of $[ZnL]^{2+}$ at different pH values. The formation of the $[ZnL(HLeu\text{-}Gly)]^{2+}$ complex at pH 5 does not significantly change the spectrum of the dipeptide in its neutral form, which contains a protonated amine and a carboxylate group in its anionic form. Only a minor shift (ca. 0.05 ppm) of the CH_2 protons in the α-position to the carboxylate group is observed. As in the case of amino acids, this may suggest that in $[ZnL(HLeu\text{-}Gly)]^{2+}$ the dipeptide is coordinated to Zn^{II} through the carboxylate group, while the amine group still remains protonated. On the contrary, the comparison of the ^1H NMR spectra of the anionic form of the Leu-Gly dipeptide in the absence and in the presence of our $[ZnL]^{2+}$ complex at pH 8.5 shows that the formation of the $[ZnL(Leu\text{-}Gly)]^+$ species leads to a marked upfield shift of the signal of the proton in the α-position (*a* in Scheme 1) to the carbonyl carbon atom and the deprotonated NH_2 group (Figure 5).

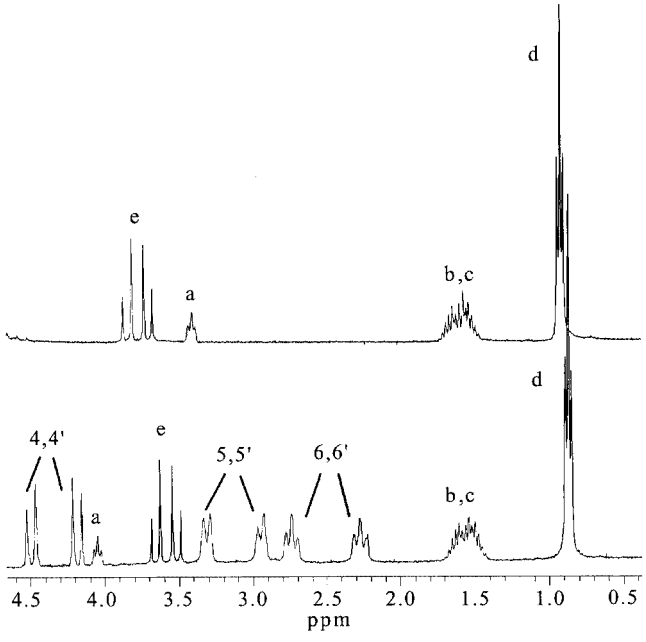

Figure 5. ^1H NMR spectra of Leu-Gly$^-$ (a) and $[ZnL(Leu\text{-}Gly)]^+$ (pH, 8.5) (b). (See Scheme 1 and Figure 1 for the labelling used).

A similar behavior is also found in the case of Gly-Gly. As already proposed in the case of amino acids, the potentiometric and ^1H NMR spectroscopic data suggest that Leu-Gly, in its anionic form, binds to Zn^{II} by using the amine group. However, the coordination of the amide carbonyl function in metal binding can also be supposed, in agreement with the binding mode generally found for dipeptides to Zn^{II} alone as well as in ternary Zn^{II} complexes.[35−37] The deprotonation process observed in the pH range 9−12 does not significantly alter the ^1H NMR spectrum of coordinated Leu-Gly$^-$, suggesting that the de-

 © 2003 Wiley-VCH Verlag GmbH & Co. KGaA, Weinheim

protonation process involves a coordinated water molecule to give a [ZnL(Leu-Gly)(OH)] complex.

The latter complex contains both a Zn^{II}-coordinated dipeptide and a Zn−OH function, as a potential nucleophile in a hydrolytic process. On the other hand, dipeptide hydrolysis in the presence of our model complex is too slow to be confidently followed at a physiological temperature. This observation prompted us to test the effective hydrolytic ability of our Zn^{II} complex by using L-leucine-*p*-nitroanilide (LNA), a substrate containing an activated peptide bond.

L-Leucine-*p*-nitroanilide (LNA) Binding and Hydrolysis by the Zn^{II} Complex Containing L

LNA, a substrate generally used to test the hydrolytic ability of leucine-aminopeptidases involving the *N*-terminal peptide bond,[73] behaves as a weak base (log K = 7.37(3) for the equilibrium LNA + H^+ = $LNAH^+$ at 308.1 K) and can also cause deprotonation at a strongly alkaline pH to give a $[LNA(H_{-1})]^-$ species (pK_a = 10.6).

LNA binding by $[ZnL]^{2+}$ was studied by means of potentiometric and ^1H NMR spectroscopic experiments at 308.1 K.[74] The $[ZnL]^{2+}$ complex forms rather stable adducts with this substrate, with a log K value of 5.55 for the equilibrium $[ZnL]^{2+}$ + LNA = $[ZnL(LNA)]^{2+}$. A small interaction is also detected with the protonated form of the substrate $HLNA^+$ {log K = 2.1 for the equilibrium $[ZnL]^{2+}$ + $HLNA^+$ = $[ZnL(HLNA)]^{3+}$}. Finally, the potentiometric measurements show that the $[ZnL(LNA)]^{2+}$ complex releases a single proton at pH > 8 to give a deprotonated species.[74] Once again, this process could be ascribed to deprotonation of the amide group of LNA, giving a complex, or a metal-bound water molecule, yielding, respectively, a $[ZnL(LNAH_{-1})]^+$ or a $[ZnL(LNA)(OH)]^+$ species. The distribution diagram, derived from the potentiometric measurements (Figure 6) shows that the formation of the $[ZnL(LNA)]^{2+}$ complex, in the pH range 4−7, is followed by complex deprotonation in the pH range 8−10.

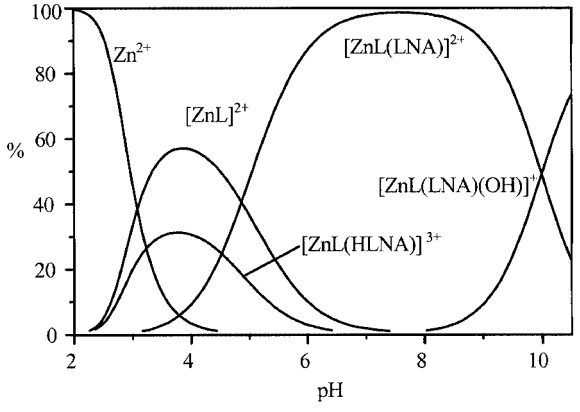

Figure 6. Species distribution diagram for the system $[ZnL]^{2+}$/LNA in 1:1 molar ratio (NMe_4NO_3 0.1 M, 308.1 K).

Figure 7 (a) displays the ^1H chemical shifts of selected protons of LNA in the presence and in the absence of the Zn^{II} complex with L at different pHs, while Figure 7 (b) shows the ^1H NMR spectroscopic chemical shift of the $[ZnL(LNA)]^{2+}$ complex, compared with those of LNA and $[ZnL]^{2+}$.

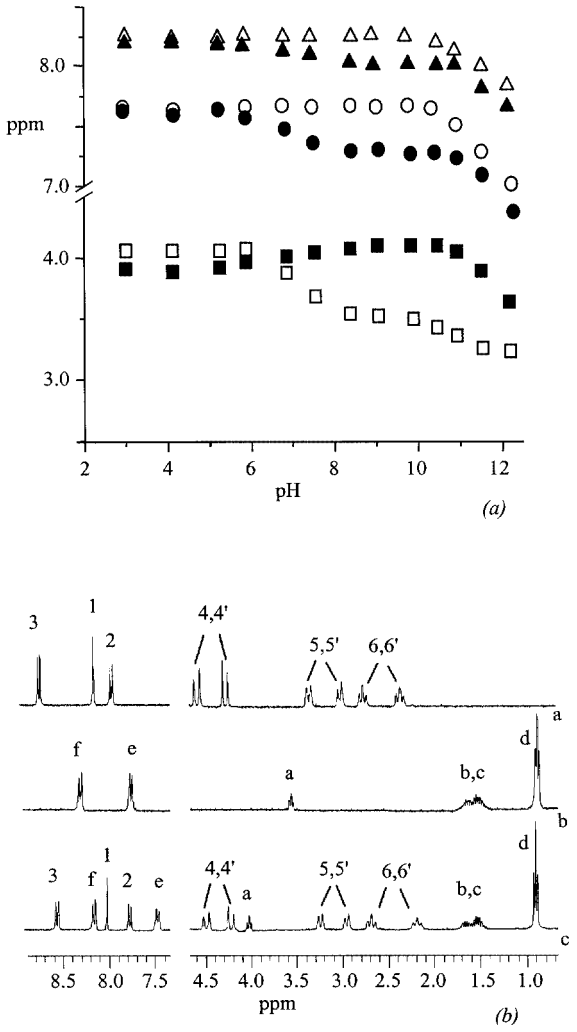

Figure 7. (*a*) pH dependence of the ^1H NMR chemical shifts of selected protons of LNA in the absence (□: *a* proton; △: f; ○: e). and in the presence of the $[ZnL]^{2+}$ complex (■: *a* proton; ▲: *f*; ●: *e*). The signals of protons *b*, *c* and *d* are omitted for clarity. Their chemical shift does not significantly change in the pH range investigated. (*b*) ^1H NMR spectra of $[ZnL]^{2+}$ (a), LNA (b) and $[ZnL(LNA)]^{2+}$ (pH, 7.5) (c). (see Scheme 1 and Figure 1 for the labelling used).

The signal of the *a* proton of "free" LNA displays an upfield shift in the pH range 6−8.5, resulting from the deprotonation of the amine group of $HLNA^+$ to give the neutral LNA form. The ^1H signals of the aromatic protons, on the other hand, do not significantly shift, up to pH 10. LNA deprotonation above pH 10 yields the $[LNA(H_{-1})]^-$ anion, which is accompanied by a marked upfield shift of the aromatic protons *e* and *f*. [Figure 7 (a)]. In the presence of Zn^{II}, the formation of the $[ZnL(LNA)]^{2+}$ complex in the pH range 4−7 (see Figure 6) gives rise to a slight, but significant, downfield shift of the *a* resonance. Actually, the *a* signal in $[ZnL(LNA)]^{2+}$ is ca 0.5 ppm downfield shifted with respect to that of unbound LNA [Figure 7 (b)].

These observations are indicative of the involvement of the amine group in metal coordination. Although these

 © 2003 Wiley-VCH Verlag GmbH & Co. KGaA, Weinheim

NMR spectroscopic data do not allow conclusions to be inferred as to the role of the peptide bond in metal binding, the rather high value of the equilibrium constant for the addition of LNA to the Zn^{II} complex and the analogies of the LNA structure with amino acids and dipeptides, leads to the supposition that the carbonyl oxygen of the amide function is also involved, or partially involved, in Zn^{II} binding, with the formation a stabilizing six-membered chelate ring. Figure 7 (a and b) also shows that both the phenanthroline and phenyl protons are upfield shifted above pH 5, where the $[ZnL(LNA)]^{2+}$complex occurs, due to π-stacking and hydrophobic interactions between the aromatic units of metallo-receptor and substrate. Therefore, as already observed in the binding of the amino acids, our Zn^{II} complex behaves as a multifunctional binding site for LNA, since both coordination bonds and supramolecular interactions contribute to the complex stability.

According to Figure 6, the $[ZnL(LNA)]^{2+}$ complex deprotonates in the pH range 8−10; the ^1H NMR signals of coordinated LNA do not shift appreciably in this pH region [Figure 7(a)], indicating that deprotonation occurs on a coordinated water molecule, with the formation of the $[ZnL(LNA)(OH)]^{+}$ hydroxo complex.

Although the potentiometric measurements do not reveal the formation of other complexes between LNA and $[ZnL]^{2+}$in the pH range investigated (2.5−10.5), the analysis of the ^1H NMR spectra of LNA recorded at a strongly alkaline pH (pH >10.5) in the presence of $[ZnL]^{2+}$ reveals a marked upfield shift of the signals of the *a*, *e* and *f* protons [Figure 7 (a)]. A similar upfield shift is also observed at a strongly alkaline pH for the corresponding signals of "free" LNA, due to deprotonation of the amide function to give the *N*-deprotonated $[LNA(H_{-1})]^{-}$ species. This comparison suggests that the $[ZnL(LNA)(OH)]^{+}$ complex undergoes deprotonation in strongly alkaline solutions to give a neutral $[ZnL(LNAH_{-1})(OH)]$ complex. A similar complex, containing a *N*-deprotonated LNA unit coordinated to a Zn^{II} complex has recently been characterized by Vahrenkamp et al.[26] Our attention, however, was focused on the $[ZnL(LNA)(OH)]^{+}$ complex, which contains a Zn^{II}-coordinated neutral LNA molecule and a Zn−OH function, in close proximity, as a potential nucleophile for cleavage of the peptide bond.

Indeed, the $[ZnL(LNA)(OH)]^{+}$ complex promotes LNA hydrolysis in aqueous solution at 308.1 K to give L-leucine and *p*-nitroanilide. The hydrolysis products were identified by means of ^1H NMR spectroscopic measurements. Pseudo-first order rate constants k_{LNA} have been determined at different pH values for the complex. In Figure 8 k_{LNA} values for the Zn-L complexes are reported as a function of pH, together with the distribution curve of the $[ZnL(LNA)(OH)]^{+}$ species at 308.1 K. A good fit between the k_{LNA} values and the distribution curve of the $[ZnL(LNA)(OH)]^{+}$ was found. No promoted hydrolysis was observed below pH 8, where the $[ZnL(LNA)(OH)]^{+}$ is absent from the solution. Accordingly, it can be concluded that the $[ZnL(LNA)(OH)]^{+}$ is the kinetically active species. We can propose a two-step hydrolytic mechanism where LNA is bound to the Zn^{II} complex, probably in a bidentate binding mode, which involves the peptide bond. Hydrophobic interactions also contribute to complex stabilization. Coordination of the peptide bond to the electrophilic Zn^{II} ion would activate the amide carbon atom leading to the subsequent intramolecular nucleophilic attack of the Zn-bound hydroxide or to intermolecular attack of hydroxide from the medium. On the other hand, the nucleophilic character of a Zn−OH function is only slightly lower than that of hydroxide.[75] At the same time, in $[ZnL(LNA)(OH)]^{+}$ the metal-bound hydroxide is close to the substrate. This suggests that the peptide bond cleavage occurs via an intramolecular pathway, as sketched in Scheme 3.

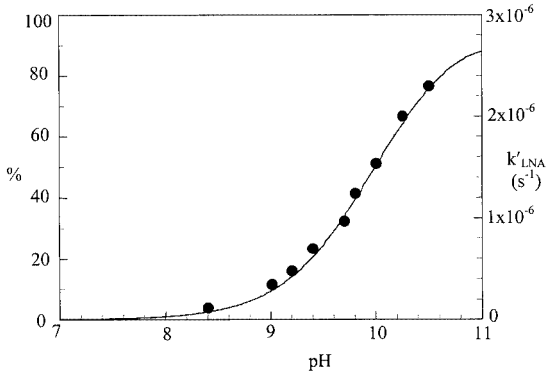

Figure 8. Plot of the distribution curve of $[ZnL(LNA)(OH)]^{+}$ (solid line, right *y* axis) and k_{LNA} values (●, left *y* axis) as a function of pH (0.1 M NMe_4NO_3, 308.1 K).

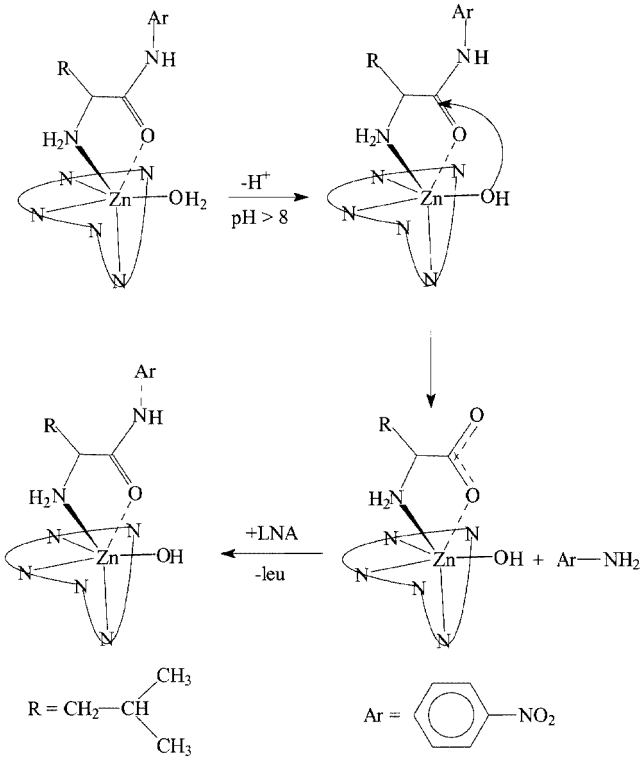

Scheme 3

 © 2003 Wiley-VCH Verlag GmbH & Co. KGaA, Weinheim

The $[ZnL(LNA)(OH)]^+$ complex is formed in a yield of 70% percentage, at most, in the pH range used in the kinetic measurements (Figure 8). As a consequence, the first order rate constants, k'_{LNA}, have been determined from the maximum k_{LNA} value by using the following equation:

$$v = k_{LNA}[\text{total } Zn^{II} \text{ complex}] = k'_{LNA}\,[ZnL(LNA)(OH)^+]$$

By using this expression, a k'_{LNA} value of $3.0 \cdot 10^{-6}$ s^{-1} can be calculated. The hydrolysis rate is much lower than those reported for aminopeptidases,[73] but, at the same time, almost two orders of magnitude higher than the rate constant for spontaneous hydrolysis of LNA.

The addition constant of LNA to the $[ZnL]^{2+}$ is ca 3100 times higher than the corresponding constant of Leu; this consideration implies that LNA hydrolysis promoted by our Zn^{II} is free, for the major part, of inhibiting agents generated by its own hydrolysis, due to the replacement of Leu by the strongly bound LNA substrate in the coordination sphere of $[ZnL]^{2+}$.

The hydrolytic process is too slow at 308.1 K to determine the reaction turnover. However, an experiment carried out at 343.1 K and pH 9.7, with an excess of substrate showed that 1 equiv. of the complex can completely cleave as many as 11 equiv. of LNA.

Conclusion

The particular molecular topology of the phenanthroline-containing macrocycle L leads to an unsaturated coordination sphere of the metal in the $[ZnL]^{2+}$ complex. Therefore, the metal ion can behave as a binding site for substrate molecules and anions. Actually, the $[ZnL]^{2+}$ forms stable complexes with amino acids and dipeptides in their zwitterionic or anionic forms. The phenanthroline moiety can act as a further binding site for substrates containing aromatic pendants, through stacking and/or hydrophobic interactions, giving a peculiar selectivity pattern in amino acid binding. In some cases, a [ZnL(A)OH] species is also formed in aqueous solution. This species contains, in close proximity, both a coordinated substrate and a $Zn^{II}-OH$ unit, a potential nucleophile towards cleavage of the peptide bond. Our complex is indeed able to hydrolyze the peptide bond of the activated substrate L-leucine-*p*-nitroanilide (LNA). The cleavage process occurs in two successive steps i) substrate binding, through coordination bonds to Zn^{II} and stacking interactions and ii) nucleophilic attack of a Zn−OH function, formed at alkaline pH values. Although hydrolysis only occurs at alkaline pH values, this mechanism resembles that proposed for peptide hydrolysis by aminopeptidases.

In particular, selective recognition of amino acids, due to stabilizing π-stacking interactions, is a striking result; it could be used, in principle, for anchoring the complex onto a specific peptide bond of polypeptide chains. This effect, coupled with the hydrolytic properties of the Zn−OH function, encourage the development of other metal complexes with phenanthroline-containing ligands, with the purpose to generate more strongly nucleophilic M−OH functions in aqueous solutions.

Experimental Section

General Remarks: Ligand L and its Zn^{II} complex $[ZnL(H_2O)](ClO_4)_2$ were prepared as already described.[61][62] 300.07 MHz ^1H spectra in D_2O solutions at different pH values were recorded at 298.1 K in a Varian Unity 300 MHz spectrometer. Peak positions are reported relative to HOD at δ = 4.79 ppm. ^1H-^1H and ^1H-^{13}C 2D correlation experiments were performed to assign the signals. Small amounts of 0.01 mol dm^{-3} NaOD or DCl solutions were added to solutions containing the substrates and $[ZnL(H_2O)](ClO_4)_2$ to adjust the pD. The pH was calculated from the measured pD values using the following relationship:[76] pH = pD − 0.40

UV/Vis spectra were recorded on a Shimadzu UV-2101PC spectrophotometer.

Potentiometric Measurements: All the pH metric measurements (pH = −log $[H^+]$) were carried out in degassed 0.1 mol·dm^{-3} NMe_4NO_3 solutions, at 298.1 or 308.1 K, by using the equipment and procedure that have already been described.[60] The combined Ingold 405 S7/120 electrode was calibrated as a hydrogen concentration probe by titrating known amounts of HCl with CO_2-free NMe_4OH solutions and determining the equivalent point by the Gran's method[77][78] which allows for the determination of the standard potential E^o, and the ionic product of water (pK_w = 13.83(1) at 298.1 K and 13.40(1) at 308.1 K in 0.1 mol·dm^{-3} NMe_4NO_3). All equilibria involved in the studied systems were determined, or redetermined,[79] under the present experimental conditions in order to obtain a consistent set of data. The concentration of $[ZnL(H_2O)](ClO_4)_2$ was 1×10^{-3} mol·dm^{-3} in all experiments, while the concentrations of the substrates were varied in the range $1 \times 10^{-3}-4 \times 10^{-3}$ mol·dm^{-3}. At least three measurements (about 150 data points for each) were performed for each system in the pH range 2.5−10.5 and the relevant e.m.f. data were treated by means of the computer program HYPERQUAD[79] that furnished the relevant equilibrium constants reported in Table 2 and 3.

Kinetics of Leucine-*p*-Nitroanilide (LNA) Hydrolysis: The hydrolysis rate of LNA in the presence of the Zn^{II} complexes with L to give Leu and *p*-nitroaniline was measured by an initial slope method following the increase in the 405 nm absorption of the released *p*-nitroaniline at 308.1 K. The molar absorbance of *p*-nitroaniline was determined at the pH of each measurement. The ionic strength was adjusted to 0.1 M with NMe_4NO_3. TAPS (pH, 7.8−8.9), CHES (pH, 8.9−9.7) and CAPS (9.7−10.5) buffers were used (50 mM). In a typical experiment, with LNA (2−5 mM) and $[ZnL(H_2O)](ClO_4)_2$ (0.5 mM) in aqueous solutions at the appropriate pH (the reference experiment does not contain the Zn^{II} complex) were mixed, the UV absorption decay was recorded immediately and was followed until 5% of *p*-nitroaniline had been formed.

At a given pH value, a plot of the hydrolysis rates vs. $[ZnL(LNA)(OH)^+]$ concentration, calculated at the different LNA concentrations, gave a straight line, allowing for the determination of the pseudo-first order rate constants k_{LNA} from the slope of the line. Errors on k_{LNA} values were about 5%.

X-ray Crystallographic Study: Crystals of $[ZnL(HGly)]_2(ClO_4)_4 \cdot 1.5H_2O$ were obtained by slow evaporation of an aqueous solution containing $[ZnL(H_2O)](ClO_4)_2$ and HGly in a 1:1 molar

 © 2003 Wiley-VCH Verlag GmbH & Co. KGaA, Weinheim

ratio at pH 5. Crystal data: $C_{40}H_{55}Cl_4N_{12}O_{21.5}Zn_2$, MW = 1320.50; a = 18.520(1) Å, b = 15.171(1) Å, c = 19.884(2) Å, β = 106.107(7)°; Z = 4, calculated density 1.634 Mg/m^3, monoclinic, $P2_1/a$. Data Collection: P4 SIEMENS X-ray diffractometer, λ = 1.54178 Å (Cu-$K\alpha$), graphite monochromated, 0.3 × 0.2 × 0.15 mm, θ−2θ up to θ = 60° at room temperature, 7885 reflections collected, 6637 symmetry-independent reflections, $I > 2\sigma(I)$, μ = 3.710 mm^{-1}, Psi-Scan method, transmission factors 0.44−0.57. Structural analysis and refinement: direct method of the SIR97 program;[81] full-matrix least-squares method of SHELXL-97;[82] All the non-hydrogen atoms were anisotropically refined. The hydrogen atoms were introduced in calculated positions and their coordinates and thermal factors refined in agreement with those of the linked atoms. Parameter/F_o ratio = 0.11, final agreement factors $R1$ = 0.0701, $wR2$ = 0.1908 [$I > 2\sigma(I)$]; $R1$ = 0.0790, $wR2$ = 0.2013(all data).

CCDC-198421 contains the supplementary crystallographic data for this paper. These data can be obtained free of charge at www.ccdc.cam.ac.uk/conts/retrieving.html [or from the Cambridge Crystallographic Data Centre, 12, Union Road, Cambridge CB2 1EZ, UK; Fax: (internat.) +44−1223/336−033; E-mail: deposit@ccdc.cam.ac.uk].

Acknowledgments

Financial support by the Italian Ministero dell'Università e della Ricerca Scientifica e Tecnologica (COFIN 2000) is gratefully acknowledged.

[1] *Zinc Enzymes*, Birkauser: Boston, MA, **1986**, I. Bertini, C. Luchinat, W. Marek, M. Zeppezauer (Eds.).
[2] E. E. Kim, H. W. Wyckoff, *J. Mol. Biol.* **1991**, *218*, 449−464.
[3] J. E. Coleman, *Annu. Rev. Biophys. Biomol. Struct.* **1992**, *21*, 441−483.
[4] W. N. Lipscomb, N. Sträter, *Chem. Rev.* **1996**, *96*, 2375−2434.
[5] D. E. Wilcox, *Chem. Rev.* **1996**, *96*, 2435−2458.
[6] H. Steinhagen, G. Helmchem, *Angew. Chem. Int. Ed. Engl.* **1996**, *35*, 2339−2342.
[7] N. Sträter, W. N. Lipscomb, T. Klabunde, B. Krebs, *Angew. Chem. Int. Ed. Engl.* **1996**, *35*, 2024−2055.
[8] S. J. Dodgson, R. E. Tashian, G. Gros, N. D. Carter, *The Carbonic Anhydrases*, Plenum Press: New York, **1991**.
[9] D. W. Christianson, *Adv. Protein Chem.* **1991**, *41*, 281−355;
[10] D. N. Silverman, S. Lindskog, *Acc. Chem. Res.* **1988**, *21*, 30−36;
[11] F. Botrè, G. Gros, B. T. Storey, *Carbonic Anhydrases*; VCH, Weinheim, Germany, **1991**.
[12] S. K. Burley, P. R. David, W. N. Lipscomb, *Proc. Nat. Acad. Sci. USA* **1990**, *88*, 6916−6920.
[13] S. K. Burley, P. R. David, R. M. Sweet, A. Taylor, W. N. Lipscomb, W. N, *J. Mol. Biol.* **1992**, *224*, 113−140.
[14] N. Sträter, W. N. Lipscomb, *Biochemistry* **1995**, *34*, 14792−14800.
[15] R. C. Holz, *Coord. Chem. Rev.* **2002**, *232*, 5−26.
[16] A. Blasko, T. C. Bruice, *Acc. Chem. Res.* **1999**, *32*, 475−484 and refs. therein.
[17] E. L. Hegg, J. N. Burstyn, *Coord. Chem. Rev.* **1999**, *173*, 133−165 and refs. Therein.
[18] R. Krämer, *Coord. Chem. Rev.* **1999**, *173*, 243−261 and refs. therein.
[19] S. H. Gellman, R. Petter, R. Breslow, *J. Am. Chem. Soc.* **1986**, *108*, 2388−2394.
[20] E. Kimura, *Tetrahedron* **1992**, *30*, 6175−6217.
[21] E. Kimura, T. Koike, *Chem. Commun.* **1998**, 1495−1500.
[22] E. Kimura, *Acc. Chem. Res.* **2001**, 171−179, and refs. therein.
[23] S. Aoki, E. Kimura, *Rev. Mol. Biotech.* **2002**, 90, 129−155, and refs. therein.
[24] H. Vahrenkamp, *Acc. Chem. Res.* **1999**, *32*, 589−596. and refs. therein.
[25] P. Gockel, R. Vogler, M. Gelinsky, A. Meiszner, H. Albrich, H. Vahrenkamp, *Inorg. Chim. Acta* **2001**, *323*, 16−22.
[26] M. Rombach, M. Gelinsky, H. Vahrenkamp, *Inorg. Chim. Acta* **2002**, *334*, 25−33.
[27] S. Hikichi, M. Tanaka, Y. Moro-oka, N. Kitajima, *J. Chem. Soc., Chem. Commun.* **1992**, 814−815.
[28] M. Yashiro, A. Ishikubo, M. Komiyama, *J. Chem. Soc., Chem. Commun.* **1995**, 1793−1794.
[29] M. Yashiro, A. Ishikubo, M. Komiyama, *Chem. Commun.* **1997**, 83−84.
[30] S. Matsuda, M. Yashiro, A. Kuzuka, A. Ishikubo, M. Komiyama, *Angew. Chem. Int. Ed. Eng.* **1998**, *37*, 3284−3286.
[31] P. Molenveld, J. F. J. Engbersen, D. N. Reinhoudt, *Chem. Soc. Rev.* **2000**, *29*, 75−86.
[32] B. Altava, M. I. Burguete, S. V. Luis, J. F. Miravet, E. Garcia-España, V. Marcelino, C. Soriano, *Tetrahedron* **1997**, *57*, 4751−4762.
[33] A. M. Barrios, S. J. Lippard, *Inorg. Chem.* **2001**, *40*, 1060−1064.
[34] D. Lee, P.-L. Hung, B. Spingler, S. J. Lippard, *Inorg. Chem.* **2002**, *41*, 521−531, and refs. therein.
[35] H. Sigel, *Coord. Chem. Rev.* **1990**, *100*, 453−489.
[36] H. Sigel, in *Metal Ion in Biological System*s, Amino Acids and Derivatives as Ambivalent Ligands (H. Sigel, Ed.), vol. 9, Marcel Dekker, NY, **1979**.
[37] H. Sigel, R. B. Martin, *Chem. Rev.* **1982**, *82*, 385−426.
[38] J. Chin, *Acc. Chem. Res.* **1991**, *24*, 145−152.
[39] P. Jurek, A. E. Martell, *Inorg. Chim. Acta* **1999**, *287*, 47−51.
[40] M. T. B. Luiz, B. Szpoganicz, M. Rizzoto, M. G. Basallote, A. E. Martell, *Inorg. Chim. Acta* **1999**, *287*, 134−141.
[41] D. Kong, A. E. Martell, J. Reibenspies, *Inorg. Chim. Acta* **2002**, *333*, 7−14.
[42] P. Chadhuri, C. Stockheim, K. Wieghardt, W. Deck, R. Gregorzik, H. Vahrenkamp, B. Nuber, J. Weiss, *Inorg. Chem.* **1992**, *31*, 1451−1457.
[43] W. H. Chapman, R. Breslow, *J. Am. Chem. Soc.* **1995**, *117*, 5462−5469.
[44] R. Breslow, N. Nesnas, *Tetrahedron Lett.* **1999**, *40*, 3335−3338.
[45] K. G. Ragunathanm, H.-J. Schneider, *Angew. Chem. Int. Ed. Engl.* **1996**, *35*, 1219−1220.
[46] M. Bräuer, J. L. Perez-Lustres, J. Weston, J. Anders, *Inorg. Chem.* **2002**, *41*, 1454−1463.
[47] O. Yamauchi, A. Odani, M. Takani, *J. Chem. Soc., Dalton Trans.* **2002**, 3411−3421 and refs therein.
[48] C. Bazzicalupi, A. Bencini, A. Bianchi, V. Fusi, G. Giorgi, P. Paoletti, B. Valtancoli, D. Zanchi, *Inorg. Chem.* **1997**, *36*, 2784−2790.
[49] C. Bazzicalupi, A. Bencini, E. Berni, A. Bianchi, V. Fedi, V. Fusi, G. Giorgi, P. Paoletti, B. Valtancoli, *Inorg. Chem.* **1999**, *38*, 4115−4122.
[50] C. Bazzicalupi, A. Bencini, E. Berni, A. Bianchi, G. Giorgi, P. Paoletti, B. Valtancoli, *Inorg. Chem.* **1999**, *38*, 6323−6325.
[51] E. L. Hegg, J. N. Burstyn, *J. Am. Chem. Soc.* **1995**, *117*, 7015−7016.
[52] M. T. B. Luiz, B. Szpoganicz, M. Rizzoto, M. G. Basallote, A. E. Martell, *Inorg. Chim. Acta* **1997**, *254*, 345−351.
[53] J. Yan, R. Breslow, *Tetrahedron Lett.* **2000**, *41*, 2059−2062.
[54] I. E. Burgeson, N. M. Kostic, *Inorg. Chem.* **1991**, *30*, 4299−4305.
[55] T. N. Parac, N. M. Kostic, *J. Am. Chem. Soc.* **1996**, *118*, 51−58.
[56] T. N. Parac, N. M. Kostic, *J. Am. Chem. Soc.* **1996**, *118*, 5946−5951.
[57] N. M. Milovic, N. M. Kostic, *J. Am. Chem. Soc.* **2002**, *124*, 4759−4769.
[58] A. Shepartz, D. Breslow, *J. Am. Chem. Soc.* **1987**, *109*, 1814−1826.
[59] M. Yashiro, T. Takarada, S. Miyama, M. Komiyama, M. ;, *Chem. Commun.* **1994**, 1757−1758.

 © 2003 Wiley-VCH Verlag GmbH & Co. KGaA, Weinheim

[60] C. Bazzicalupi, A. Bencini, V. Fusi, G. Giorgi, P. Paoletti, B. Valtancoli, *Inorg. Chem.* **1998**, *37*, 941−948.
[61] C. Bazzicalupi, A. Bencini, V. Fusi, G. Giorgi, P. Paoletti, B. Valtancoli, *J. Chem. Soc., Dalton Trans.* **1998**, 393−399.
[62] C. Bazzicalupi, A. Bencini, A. Bianchi, G. Giorgi, B. Valtancoli, M. A. Bernardo, F. Pina, *Inorg. Chem.* **1999**, *38*, 3806−3813.
[63] C. K. Johnson, ORTEP, Report ORNL-3794, Oak Ridge National Laboratory, Oak Ridge, TN, **1971.**
[64] H. C. Freeman, in Inorganic Biochemistry, vol. 1, Eichhorn G. L. (Ed.) Elsevier, Amsterdam, **1973**, 121−166.
[65] C···O distances ranging between 3 and 3.8 Å are generally considered as hydrogen bond contacts (see, for instance, G. T. Desiraju, *Acc. Chem. Res.* **1991**, *24*, 290−296; G. T. Desiraju *Acc. Chem. Res.* **2002**, *35*, 565−573 and refernces therein; R. Taylor, O. Kennard, *J. Am. Chem. Soc.*, **1982**, *104*, 5063−5068. Some authors, however, classify this interaction as hydrogen bond only if the C···O distance is lower than 3.25 Å (F. A. Cotton, L. M. Daniels, G. T. Jordan, C. A. Murrillo, *Chem. Commun.* **1997**, 1673−1674; J. Donohue, in Structural Chemistry and Molecular Biology, A. Rich, N. Davidson (Eds.), Freeman: San Francisco, **1968**, 443−465.)
[66] R. M. Smith, A. E. Martell, *NIST Stability Constants Database,* Version 4.0, National Institute of Standard and Technology: Washington, DC, **1997**.
[67] H. Sigel, C. F. Naumann, *J. Am. Chem. Soc.* **1976**, *98*, 730−739.
[68] H. Sigel, *Angew. Chem. Int. Ed. Engl.* **1982**, *2*, 389−391. H. Sigel, *Pure Appl. Chem.* **1989**, *61*, 923−931.
[69] O. Yamauchi, A. Odani, *J. Am. Chem. Soc.* **1985**, *107*, 5938−5945.
[70] T. Sugimori, H. Masuda, N. Ohata, K. Koiwai, A. Odani, O. Yamauchi, *Inorg. Chem.* **1997**, *36*, 576−583.
[71] T. Sugimori, H. Masuda, A. Odani, O. Yamauchi, *Inorg. Chim. Acta* **1991**, *180*, 73−79.
[72] O. Yamauchi, A. Odani, T. Kohzuma, H. Masuda, K. Toriumi, K. Saito, *Inorg. Chem.* **1989**, *28*, 4066−4068.
[73] C. Stamper, B. Bennett, T. Edwards, R. C. Holz, D. Ringe, G. Petsko, *Biochemistry* **2001**, *40*, 7035−7046, and references therein.
[74] Stability constants of the Zn^{II} complexes with **L** and addition constants of LNA to the $[ZnL]^{2+}$ complex (potentiometrically determined in $NMeNO_3$ 0.1 M at 308.1 K): $Zn^{2+} + L = [ZnL]^{2+}$, log K = 15.98; $[ZnL]^{2+} + OH^- = [ZnL(OH)]^+$, log$K$ = 4.64; $[ZnL(OH)]^+ + OH^- = [ZnL(OH)_2]$, log$K$ = 2.95; $[ZnL]^{2+} + LNA = [ZnL(LNA)]^{2+}$, log$K$ = 5.55; $[ZnL]^{2+} + HLNA^+ = [ZnL(HLNA)]^{3+}$, log$K$ = 2.1; $[ZnL(LNA)]^{2+} + H_2O = [ZnL(LNA)(OH)]^+ + H^+$, log$K$ = 10.0.
[75] I. Bertini, H. B. Gray, S. J. Lippard, J. S. Valentine, *Bioinorganic Chemistry*, Univeristy Science Books: Sausalito, CA, **1994**.
[76] A. K. Covington, M. Paabo, R. A. Robinson, R. G. and Bates, *Anal. Chem.* **1968**, *40*, 700−706.
[77] G. Gran, *Analyst* (London), **1952**, *77*, 661−663.
[78] F. J. Rossotti, H. Rossotti, *J. Chem. Educ.* **1965**, *42*, 375−378.
[79] Protonation and Zn^{II} addition constant for amino acids and dipeptides (A) determined in the present work (potentiometrically determined in $NMeNO_3$ 0.1 M at 298.1 K): Gly, log $K^{HA}{}_A$ = 9.52(1), log $K^{AH2}{}_{HA}$ = 2.37(1), log $K^{ZnA}{}_A$ = 4.94(1), log $K^{ZnA2}{}_{ZnA}$ = 4.38(1); Ala, log $K^{HA}{}_A$ = 9.66(1), log $K^{AH2}{}_{HA}$ = 2.38(1), log $K^{ZnA}{}_A$ = 4.54(3), log $K^{ZnA2}{}_{ZnA}$ = 4.45(4); PhGly, log $K^{HA}{}_A$ = 8.87(1), log $K^{AH2}{}_{HA}$ = 1.97(1), log $K^{ZnA2}{}_{2A}$ = 8.20(2); Phe, log $K^{HA}{}_A$ = 9.03(1), log $K^{AH2}{}_{HA}$ = 2.31(1), log $K^{ZnA2}{}_{2A}$ = 8.94(2); Try: log $K^{HA}{}_A$ = 9.50(2), log $K^{AH2}{}_{HA}$ = 2.23(3), log $K^{ZnA2}{}_{2A}$ = 9.70(3); Gly-Gly, log $K^{HA}{}_A$ = 8.00(1), log $K^{AH2}{}_{HA}$ = 3.12(1), log $K^{ZnA}{}_A$ = 3.48(9), log $K^{ZnA2}{}_{ZnA}$ = 3.18(8); Leu-Gly log $K^{HA}{}_A$ = 7.99(3), log $K^{H2A}{}_{HA}$ = 3.28(2), log $K^{ZnA}{}_A$ = 2.84(3), log $K^{ZnA2}{}_{ZnA}$ = 2.77(2), where $K^{AB}{}_A$ = [AB]/[A][B] and $K^{AB2}{}_{AB}$ = $[AB_2]$/[AB][B].
[80] P. Gans, A. Sabatini, A. Vacca, *J. Chem. Soc., Dalton Trans.* **1985**, 1195−1200.
[81] A. Altomare, M. C. Burla, M. Camalli, G. L. Cascarano, C. Giacovazzo, A. Guagliardi, A. G. G. Moliterni, G. Polidori, R. Spagna, *J. Appl. Crystallogr.* **1999**, *32*, 115.
[82] G. M. Sheldrick, *SHELXL-97*, Göttingen, **1997**.

Received November 27, 2002

 © 2003 Wiley-VCH Verlag GmbH & Co. KGaA, Weinheim

XAS, ESR and Potentiometric Studies of Three Dinuclear *N,N′-para*-Xylylenebis(tetraazamacrocycle)copper(II) Complexes − X-ray Crystal Structure of [*N,N′-p*-Xylylenebis(cyclen)]copper(II)

Mathieu Soibinet,[a] Isabelle Déchamps-Olivier,*[a] Emmanuel Guillon,[a] Jean-Pierre Barbier,[a] Michel Aplincourt,[a] Françoise Chuburu,[b] Michel Le Baccon,[b] and Henri Handel[b]

Keywords: Copper / ESR spectroscopy / Macrocyclic ligands / Potentiometry / X-ray studies

Dicopper complexes with *N,N′-p*-xylylenebis(cyclam or cyclen) and with the heteroditopic *N,N′-p*-xylylenebis(cyclam-cyclen) were synthesized. An X-ray study of the *N,N′-p*-xylylenebis(cyclen)dicopper complex showed that the copper(II) ion is five-coordinate with an H_2O molecule in apical position. With this ligand, a polymeric chain was also obtained in the presence of KSCN. The terminal donor atoms of the bridging NCS^- anion are coordinated in apical position to the square-pyramidal copper(II) ion. Two alternating kinds of Cu_2L^{4+} moieties are present in the chain, the first with two N_4S chromophores and the second with two N_5 chromophores. EXAFS and XANES results are in agreement with a five-coordinate copper ion in the cyclen unit and a six-coordinate copper ion in the cyclam unit. Thermodynamic constants were determined by potentiometry. The existence of dinuclear Cu_2L^{4+} species (ligand/metal ratio < 1) and mononuclear $CuLH_n^{(2+n)+}$ species (ligand/metal ratio > 1) were confirmed by an ESR study at variable pH.
(© Wiley-VCH Verlag GmbH & Co. KGaA, 69451 Weinheim, Germany, 2003)

Introduction

Since the early 1960s, homodinuclear macrocyclic complexes have been studied extensively.[1] The interest in such dinuclear complexes stems from different particularities. Fundamentally, the presence of two metal centres not too far away from one another can induce interactions that can influence the complex's magnetic or redox properties. These complexes have been used in the development of two-centred metal catalytic reagents.[2] Moreover, these dimacrocyclic complexes may serve as models for the charge transfer, electron transport, and allosteric behaviour found in many metal-containing biochemical systems.[3,4] Besides their fundamental interest, these ligands and complexes are also used in anti-HIV drugs, in particular, the *m*- or *p*-xylylenebis(cyclam)[5−7] (referred to as AMD 2986 and AMD 3100, respectively) and the *p*-xylylenebis(cyclen)dizinc complexes[8] are implicated in the inhibition of particular HIV strains with low levels of cytotoxicity.

The coordination of bis(macrocycles) containing two covalently, potentially chelating subunits has been studied intensively in recent years.[9] Cyclam and cyclen are involved in compounds with linkages between two nitrogen atoms or two carbon atoms. The bridge (alkanediyl chain or xylylene group) can modify the intermetallic distance and the orientation of the macrocyclic ring. Our purpose is the investigation of the copper(II) coordination with the little studied *p*-xylylenebis(*N,N′*-cyclam) or -bis(*N,N′*-cyclen) (Scheme 1).

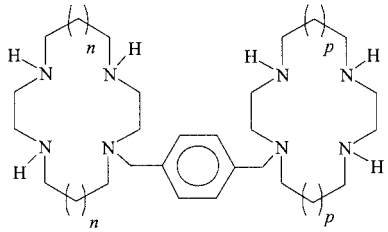

*para*cyclen	$n = p = 0$
*para*cyclam-cyclen	$n = 1$ and $p = 0$
*para*cyclam	$n = p = 1$

Scheme 1

Except for the dizinc complex used in anti-HIV drugs, the metal complexes with these ligands have seldom been studied. With the *p*-xylylenebis(tetraazamacrocycles) ligands, the copper complexes have been described; Fabbrizzi et al.[10] only studied the mutual copper interaction by electrochemistry, while the intermetallic distances were esti-

[a] GRECI, Université de Reims Champagne-Ardenne, B. P. 1039, 51687 Reims Cedex 2, France
Fax: (internat.) + 33-3/26913243
E-mail: isabelle.dechamps@univ-reims.fr
[b] UMR CNRS 6521, Université de Bretagne Occidentale, B. P. 809, 29285 Brest Cedex, France

 © 2003 Wiley-VCH Verlag GmbH & Co. KGaA, Weinheim **DOI: 10.1002/ejic.200200517**

mated by Guilard et al.[11] by ESR spectroscopy. These authors demonstrated the influence of different spacers linked to the two macrocycles on the electrochemical properties and on the Cu−Cu distances in these bis(tetraazamacrocycle) complexes. In addition, electrochemical aqueous solution studies and UV/Vis and ESR spectroscopic investigations have been carried out on other (tetraazamacrocycle)copper complexes such as bis(isocyclam)[12] and spirocyclam.[13] Kinetic phenomena are always present when a metallic ion is incorporated in a tetraazamacrocycle[14] or in the tetraaza units of a bis(macrocycle).[15] Solution studies therefore have to be performed carefully, taking the kinetic of complexation of the tetraaza rings into account. Crystallographic data for this type of compounds are very scarce, and to the best of our knowledge, only the structure of a dinuclear copper(II) complex with two 1,4,7,10-tetraazacyclododecane units *N,N′*-bridged by 2,6-dimethyl-1-methoxybenzene[16] has been described in the literature.

In order to understand the behaviour of a ligand implicated in anti-HIV drugs, it was interesting to investigate the complexation of these ligands with a biologically interesting cation such as copper(II). These studies were made by combining potentiometry and ESR spectra, and taking kinetic phenomena into account. A heteroditopic bis(macrocyclic) ligand was also studied (see Scheme 1, *para*cyclam-cyclen ligand). Solid compounds were also prepared, but only complexes with *para*cyclen give crystals suitable for X-ray studies. The structures of monomeric (*para*cyclen)$Cu_2(ClO_4)_4$ and polymeric $[(para\text{cyclen})Cu_2]_2(SCN)_8$ chains induced by the potentially bidentate thiocyanate anion, have been reported. XAS results permitted the determination of the environment around the copper cation when a cyclam unit is present in the ligand.

Results and Discussion

Solution Studies

Ligand Protonation Constants

Protometric study of the three ligands allowed us to determine the protonation constants given in Table 1.

For each ligand, the first four constants follow the usual order, their values decreasing from K_1 to K_4; for the last one (K_4), both macrocycles are diprotonated. As far as the values of the last four constants (K_5 to K_8) are concerned, only some of them could be calculated, the others being too weak to be given with sufficient accuracy. In the case of the ligand *para*cyclam-cyclen, one inversion among these constants' values is observed ($K_7 > K_5$ and K_6).

Such an inversion in the order of the values of protonation constants has been reported previously[18] for cyclam, K_4 being greater than K_3 (Table 1). We also determined the protonation constants of cyclam, and our values are in good agreement with those previously obtained[18] especially if we take the differences in experimental conditions (ionic strength, temperature) into account. The inversion of the K_3 and K_4 constant values was attributed to a conformational modification of the cyclam accompanying its third protonation.[18] Consequently, whereas the addition of the third proton is difficult because of energetic requirements accompanying to the geometrical change, the addition of the fourth one is facilitated.

The same interpretation can be proposed for the successive protonations of *para*cyclam-cyclen. Constants K_5 and K_6 correspond to the attachment of a third proton on each of the two cycles, whereas constant K_7 corresponds to the attachment of a fourth proton on the cyclam cycle. As with the cyclam, the third protonation is difficult, which explains why the constant value K_5 is below that of K_7.

Copper Complexation Studies

The complexation kinetics of the macrocycles cyclen and cyclam are well-known pH-dependent phenomena. As a result, the batch method is often used in order to study the formation of the complexes in solution. However, we did not use this method in our experiments, since it requires a large quantity of product. We thus performed classical titrations, all our measures being made after waiting times, at constant initial pH, of 60, 90, and 120 d between the preparation of the solutions and the beginning of the titrations. All the titrations gave identical results.

Protometric titrations in the presence of copper were monitored by ESR at 150 K. Whatever the pH of the solution may have been, for ratios R = [ligand]/[metal] greater than 1, ESR spectra each give a signal of four equidistant lines, characteristic of the presence of mononuclear species. The obtained spectroscopic parameters $g_{\|}$ and $A_{\|}$ are very close to those of complexes formed with cyclam or cyclen[19]

Table 1. Logarithms of successive protonation constants

	$\log K_1$ [a]	$\log K_2$	$\log K_3$	$\log K_4$	$\log K_5$	$\log K_6$	$\log K_7$	$\log K_8$
*para*cyclen	11.1 (0.1)	10.5 (0.1)	9.44 (0.04)	8.75 (0.06)				
*para*cyclam	12.3 (0.1)	11.1 (0.1)	9.80 (0.05)	8.9 (0.1)	2.90 (0.07)	ca. 1		
*para*cyclam-cyclen	12.5 (0.2)	10.95 (0.1)	9.7 (0.1)	8.86 (0.04)	2.76 (0.07)	1.7 (0.3)	2.9 (0.3)	
cyclen	11.13 (0.01)	10.17 (0.06)	1.51(0.09)					
cyclen[b]	10.97	9.87	< 2					
cyclam	11.72 (0.01)	10.57 (0.01)	1.91 (0.08)	2.7 (0.1)				
cyclam[c]	11.6	10.6	1.61	2.42				

[a] Values in parentheses represent 2σ standard deviation. $\log K_n$ refers to the equilibrium $LH_{n-1} + H^+ \leftarrow\!\!\rightarrow LH_n$. [b] Ref.[17] [c] Ref.[18]

 © 2003 Wiley-VCH Verlag GmbH & Co. KGaA, Weinheim

Table 2. ESR parameters of copper complexes in aqueous solution

		$g_{\parallel}$	$A_{\parallel}$ [10^{-4} cm^{-1}]	$g_{\perp}$	$A_{\perp}$ [10^{-4} cm^{-1}]
*para*cyclen[a]	$CuLH_n^{(2+n)+}$	2.20	180	2.05	10
	Cu_2L^{4+}	2.19	92	2.06	10
*para*cyclam[a]	$CuLH_n^{(2+n)+}$	2.19	192	2.06	10
	Cu_2L^{4+}	2.19	95	2.06	10
*para*cyclam-cyclen[a]	$CuLH_n^{(2+n)+}$	2.19	192	2.06	10
	Cu_2L^{4+}	2.19	93	2.06	10
cyclen[b]	CuL^{2+}	2.198	184	2.057	24.1
cyclam[b]	CuL^{2+}	2.186	205	2.049	38.7

[a] Values obtained by simulation. [b] Ref.[19]

(Table 2). For ratios R smaller than 1, the obtained ESR spectra each show a signal with seven equidistant lines, characteristic of the formation of dinuclear species.[11] The values of the $g_{\parallel}$ parameter are identical to those of the previous complexes, whereas the values of $A_{\parallel}$ are half those obtained for mononuclear complexes (Table 2). The complexes formed are therefore different, given the experimental conditions of the preparation of the solutions, but the copper environments in mono- or dinuclear complexes are similar to those of the copper ion in the cyclen or the cyclam complexes.

The stability constants of the complexes were calculated, taking only mononuclear species into account for ratios R greater than 1, and only dinuclear species for ratios R less than 1. This is in agreement with the ESR study. The values of the global constants of formation are presented in Table 3.

Table 3. Logarithms of overall stability constants

	$CuLH_2^{4+}$ log β_{112} [a]	$CuLH^{3+}$ log β_{111}	CuL^{2+} log β_{110}	Cu_2L^{4+} log β_{210}
*para*cyclen	39.4 (0.4)	30.4 (0.4)	19.6 (0.2)	39.2 (0.3)
*para*cyclam	42.3 (0.1)	33.8 (0.3)	23.5 (0.5)	44.0 (0.3)
*para*cyclam-cyclen	42.4 (0.1)	33.7 (0.2)	22.3 (0.3)	42.3 (0.3)
cyclen[b]			23.3	
cyclam[b]			26.5	

[a] Values in parentheses represent 2σ standard deviation. [b] Ref.[17]

In the case of the dinuclear species Cu_2L^{4+}, on the one hand, the complexation of two copper(II) ions by the four nitrogen atoms of each cycle induces the complete deprotonation of the ligand. On the other hand, in the case of mononuclear complexes $CuLH_n^{(n+2)+}$, the copper ion is engaged only in one macrocycle, and we obtain three complexation constants, corresponding to the formation of $CuLH_2^{4+}$ and then to the deprotonation of two nitrogen atoms from the non-complexed cycle (see distribution curves Figure 1).

The stability constants obtained are all very high, so the complexes formed are very stable. The values of the logarithms of the constants β_{110} of the complexes CuL^{2+} formed

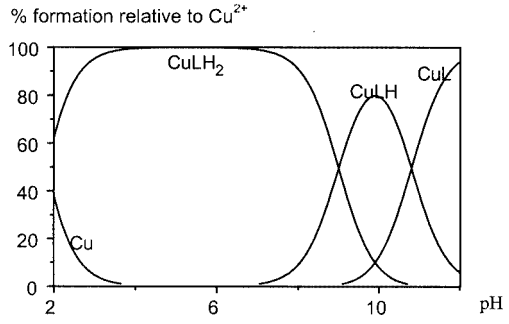

Figure 1. Distribution curves for the mononuclear (*para*cyclen)copper(II) complexes (R = [ligand]/[metal] > 1)

with the three bis(macrocycles) are in the same range as those of complexes CuL^{2+} formed with cyclen or cyclam. Similarly, we observe that the values of the logarithms of the constants β_{210} of the dinuclear complexes Cu_2L^{4+} are twice as high as those of the CuL^{2+} complexes. As a result, the two macrocyclic cavities of the ligands indeed seem to be independent of one another with regard to the complexation phenomenon. Lastly, in the case of mononuclear complexes formed with the *para*cyclam-cyclen ligand, the ESR spectra and the values of the stability constants of the complexes do not allow us to locate the metallic cation in the cyclen or cyclam cavity.

For each ligand, the electronic spectra of solutions with different ratios (R = 2, 1, and 0.5) were plotted between pH = 2 and 11. For the *para*cyclen and *para*cyclam ligands, the spectra of the mono- and dinuclear complexes each show only one absorption band, the position of which remains unchanged whatever the pH may be.

In the case of *para*cyclen, the band is located at a wavelength (λ = 594 nm) very close to that noted for the complex $[Cu(cyclen)(H_2O)]^{2+}$ (λ = 599 nm).[20] The geometries of the complexes formed with cyclen and *para*cyclen are identical; they are pentacoordinated complexes with square-base-pyramidal geometries. The four nitrogen atoms of the macrocycle form the base of each pyramid, whereas a water molecule occupies the fifth position.[19]

For the complex formed with *para*cyclam, the position of the band (λ = 528 nm) is similar to those in complexes formed with different ligands derived from cyclam (512 nm

 © 2003 Wiley-VCH Verlag GmbH & Co. KGaA, Weinheim

$< \lambda <$ 550 nm).[19,21] This value is typical of the square-planar CuN_4 chromophore with a strong ligand field.[22] However, the 14-membered cyclam has a ring large enough to surround a range of metal ions, and its complexes generally adopt the strain-free, thermodynamically more stable *trans*-III (*R*,*S*,*S*,*R*) conformation, in which the metal ion is indeed inside the ring of the macrocycle in a square-planar structure, with two adjacent NH hydrogen atoms directed towards one side of the macrocycle plane and the other two in the opposite direction.[23]

In the case of the *para*cyclam-cyclen ligand, the spectra obtained for the dinuclear complex Cu_2L^{4+} ($R < 1$) show only one wide band at $\lambda = 578$ nm, a position intermediary between those noted for the cyclam and cyclen complexes. The spectrum calculated as the sum of the spectra of the *para*cyclen and *para*cyclam complexes also presents an absorption maximum at 578 nm. When the ratio *R* increases, the position of the band changes (Figure 2). The formation of the complexes was monitored by addition of *para*cyclam-cyclen to a solution of copper ions (10^{-3} mol·L^{-1}). For the addition of ligand quantity greater than the quantity of copper ions, the position of the absorption maximum moves closer to $\lambda = 540$ nm and the ESR spectrum is characteristic of a mononuclear species. This value of the absorption maximum indicates that the copper ion is mostly engaged in the cyclam cavity.

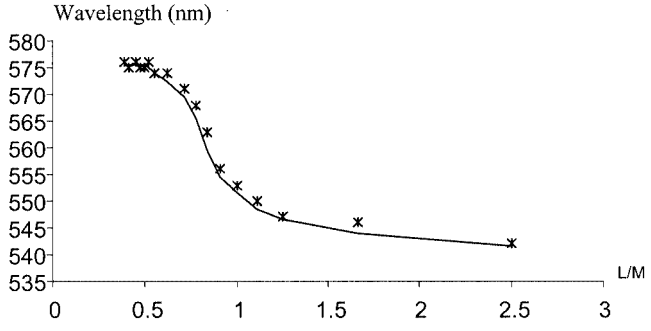

Figure 2. Variation of the wavelength of the maximum of absorbance as a function of the ratio R = L/M in acidic medium (pH ≈ 2); L = *para*cyclam-cyclen, M = Cu; [Cu^{2+}] = 10^{-3} mol·L^{-1}

Solid Complexes Studies

Only dinuclear complexes have been isolated in the solid state. When the ligand was a hydrochloride salt (*para*cyclam and *para*cyclam-cyclen), chloride anions were present in the solid complex. Only *para*cyclen complexes have been obtained as monocrystals suitable for X-ray diffraction. Conversely, structures of monocyclen compounds are scarce.

X-ray Diffraction Studies

(*para*cyclen)$Cu_2(ClO_4)_4$·$4H_2O$

The structure of Cu_2L^{4+} moieties is given in Figure 3, structural data in Table 4, and interatomic distances and angles in Table 5.

Figure 3. ORTEP drawing of the cation [(*para*cyclen)Cu_2]$^{4+}$

The two five-coordinate copper ions are located in square-pyramidal coordination environments. The base is formed by the four nitrogen atoms of the tetraazamacrocycle and an H_2O molecule is bonded in apical position. The two metal centres are always located on each side of the planar xylylene spacer so that the intramolecular Cu−Cu distance is the greatest (Scheme 2).

The Cu^1-N distances, in the 2.020−2.052 Å range generally found for $Cu-N_{amine}$ coordination bonds, and the $N-Cu^1-N$ (85.8−86.8°) and O^1-Cu^1-N angles (101.5−107.5°) indicate geometry close to an ideal square-pyramidal coordination environment for the first copper cation. The Cu^2-N distances (2.006−2.068 Å) and the O^2-Cu^2-N angles (98.2−111.6°), however, indicate a slight distortion of the square-pyramidal geometry. For the two copper ions, $Cu-N_{substituted}$ bonds ($Cu-N^4$ and $Cu-N^5$) are slightly longer than the other $Cu-N_{amine}$ values, as is generally observed.

The monoclinic cell contains four Cu_2L^{4+} moieties (Figure 4), which are stacked with the xylylene groups along an axis, the dihedral angle between two xylylene planes being nearly 90°. We can also note that the copper atoms appear in straight lines. Two neighbouring Cu_2L^{4+} moieties are perpendicular, the tops of the two square-pyramidal moieties point in opposite directions (Scheme 3); this molecular stacking produces intermolecular Cu−Cu distances (9.352, 7.993, or 6.059 Å) shorter than the intramolecular distance (11.540 Å) (Scheme 2). A complete stacking pattern (Figure 4) suggests that hydrogen bonds exist between water molecules, perchlorate ions and amine groups and thus stabilize the crystal lattice of the complex.

[(*para*cyclen)Cu_2]$_2$$(SCN)_8$·$7H_2O$

The structure of the polymeric chain is given in Figure 5, structural data in Table 4, and interatomic distances and angles in Table 6.

The chain is made up of Cu_2L^{4+} moieties linked by a bidentate thiocyanate anion. The terminal S and N donor atoms are coordinated in apical positions, taking the place of the water molecule present in the monomer complex. The copper atom is five-coordinate, and two alternating kinds of Cu_2L^{4+} moieties are present in the chain, the first with two N_4S chromophores (copper atom denoted Cu^1) and the second with two N_5 chromophores (copper atom denoted Cu^2). The Cu^2-N_{SCN} and Cu^1-S distances are 2.054 and 2.482 Å, respectively. The thiocyanate is collinear with the

 © 2003 Wiley-VCH Verlag GmbH & Co. KGaA, Weinheim

Table 4. Crystal data and details of the structure determination of (*para*cyclen)$Cu_2(ClO_4)_4{\cdot}4H_2O$ and $[(para\text{cyclen})Cu_2]_2(SCN)_8{\cdot}7H_2O$

	(*para*cyclen)$Cu_2(ClO_4)_4{\cdot}4H_2O$	$[(para\text{cyclen})Cu_2]_2(SCN)_8{\cdot}7H_2O$
Empirical formula	$C_{24}H_{54}N_8O_{20}Cl_4Cu_2$	$C_{56}H_{106}N_{24}O_7S_8Cu_4$
Formula mass	1043.63	1738.3
Temperature [K]	173	173
Crystal system	monoclinic	triclinic
Space group	*P*21/c	$P\bar{1}$
Colour	blue	blue
a [Å]	14.4414(2)	10.5352(3)
b [Å]	28.8197(5)	13.9086(4)
c [Å]	10.5005(2)	14.2432(5)
α [°]	90	78.037(5)
β [°]	110.184(5)	71.201(5)
γ [°]	90	87.741(5)
Volume [Å^3]	4101.9(1)	1932.0(1)
Z	4	1
$D_{calcd.}$ [g·cm^{-3}]	1.69	1.49
Absorption coefficient [mm^{-1}]	1.384	1.366
F(000)	2160	910
λ(Mo−K_α) [Å]	0.71073	0.71073
No of independent reflections	9356	8778
No of reflections [$I > 3.0\sigma(I)$]	4592	5292
*R*1	0.057	0.054
*wR*2	0.070	0.074
Goodness-of-fit on F^2	1.046	1.050

Table 5. Bond lengths [Å] and angles [°] in the (*para*cyclen)-$Cu_2(ClO_4)_4{\cdot}4H_2O$ complex

Cu1−O1	2.189(5)	O1−Cu1−N1	101.5(2)
Cu1−N1	2.020(6)	O1−Cu1−N2	103.9(2)
Cu1−N2	2.021(6)	O1−Cu1−N3	107.5(2)
Cu1−N3	2.018(6)	O1−Cu1−N4	105.2(2)
Cu1−N4	2.052(5)	N1−Cu1−N2	86.8(2)
Cu2−O2	2.139(5)	N1−Cu1−N3	85.8(2)
Cu2−N5	2.068(5)	N1−Cu1−N4	153.3(2)
Cu2−N6	2.006(6)	N2−Cu1−N3	148.5(2)
Cu2−N7	2.028(6)	N2−Cu1−N4	86.4(2)
Cu2−N8	2.025(6)	N3−Cu1−N4	86.6(2)
		O2−Cu2−N5	107.6(2)
		O2−Cu2−N6	111.6(2)
		O2−Cu2−N7	98.2(2)
		O2−Cu2−N8	99.3(2)
		N5−Cu2−N6	86.7(2)
		N5−Cu2−N7	86.2(2)
		N5−Cu2−N8	152.9(3)
		N6−Cu2−N7	150.1(3)
		N6−Cu2−N8	86.5(3)
		N7−Cu2−N8	86.5(3)

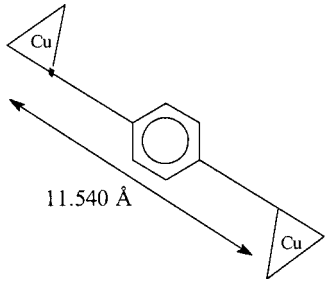

Scheme 2. Intramolecular Cu−Cu distance

Cu−N apical bond and practically perpendicular (93.7°) to the Cu−S apical bond. The Cu−N_{cyclen} distances, in the 2.021−2.059 Å range, and the angles around the copper ion indicate a regular geometry around the metal centre. The polymerisation does not affect the packing of the Cu_2L^{4+} moieties; the intramolecular Cu−Cu distances (11.575 Å) are very close to those observed in the monomer (11.539 Å) and the distance between the two copper ions bridged by the thiocyanate anion (5.810 Å) is also very close to the shortest intermolecular distance obtained in the monomer (6.061 Å). The crystal packing is stabilized by the uncoordinated thiocyanate ion and crystallization water molecules.

X-ray Absorption Spectroscopy (XAS)

The lack of single crystals of (*para*cyclam)Cu_2 and (*para*-cyclam-cyclen)Cu_2 complexes, and their poor crystallinity, prevented from obtaining structural information by the common X-ray diffraction techniques. We therefore decided to study the X-ray absorption near-edge structure (XANES) and the extended X-ray absorption fine structure (EXAFS) spectra of these two compounds with the (*para*cyclen)Cu_2 complex as a model. To the best of our knowledge, the use of XAS techniques in the structural study of bis-(macrocyclic) compounds is new. Only a few uses of XAS for (monocyclam)copper(II) complexes have been reported.[24,25]

A comparison of the XANES spectra for the compounds and the reference [(*para*cyclen)Cu_2 complex] is shown in Figure 6a, with the corresponding first derivatives in Figure 6b. The three spectra seem almost identical with respect to their shape and transition energies. They are typical of copper(II) complexes, each with a very weak 1s→3d pre-

 © 2003 Wiley-VCH Verlag GmbH & Co. KGaA, Weinheim

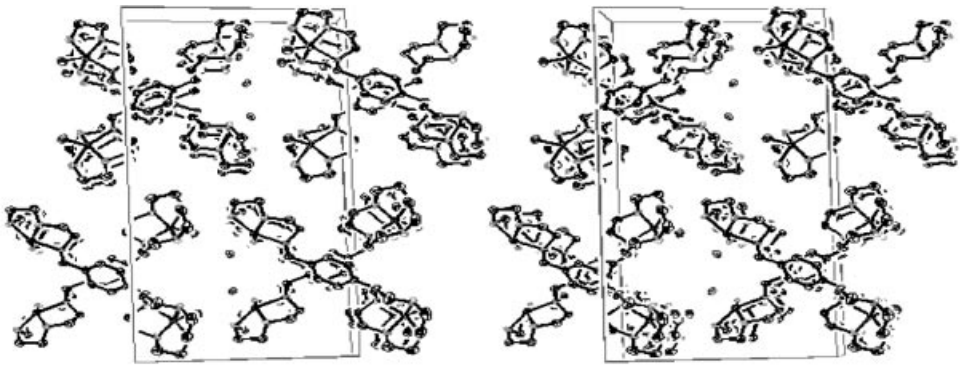

Figure 4. Crystal packing of the unit cell of $[(para\text{cyclen})Cu_2]^{4+}$

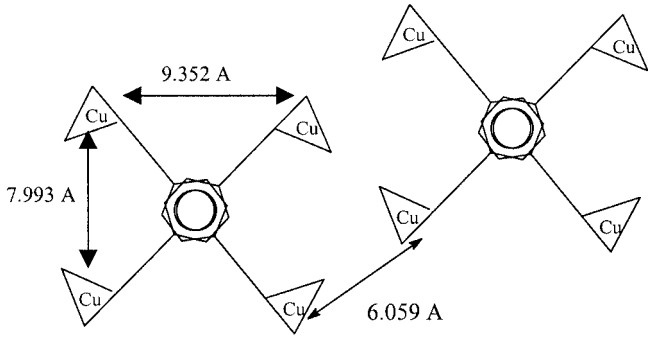

Scheme 3. Intermolecular Cu−Cu distances

edge feature and an absorption edge centred around 8990 eV. Furthermore, each spectrum has the characteristic shoulder (α) of copper(II) in elongated tetragonal surroundings on the low-energy side of the edge.[26] The energy gap between this shoulder (α) and the pre-edge (β) is equal to 6.5 eV for (*para*cyclen)Cu_2 and 6.9 eV for (*para*cyclam)Cu_2. For the (*para*cyclam-cyclen)Cu_2 complex, we can observe a small shoulder on the β peak of the first derivative, and the gaps between α and these two "peaks" are equal to 6.5 and 6.9 eV, which confirms that the copper(II) ion is held in two different geometries arising from the two macrocyclic cavities (cyclam and cyclen). Indeed, the copper(II) ion is in a C_{4v} square-pyramidal environment in the cyclen macrocyclic cavity, and in an O_h or D_{4h} geometry in the cyclam.

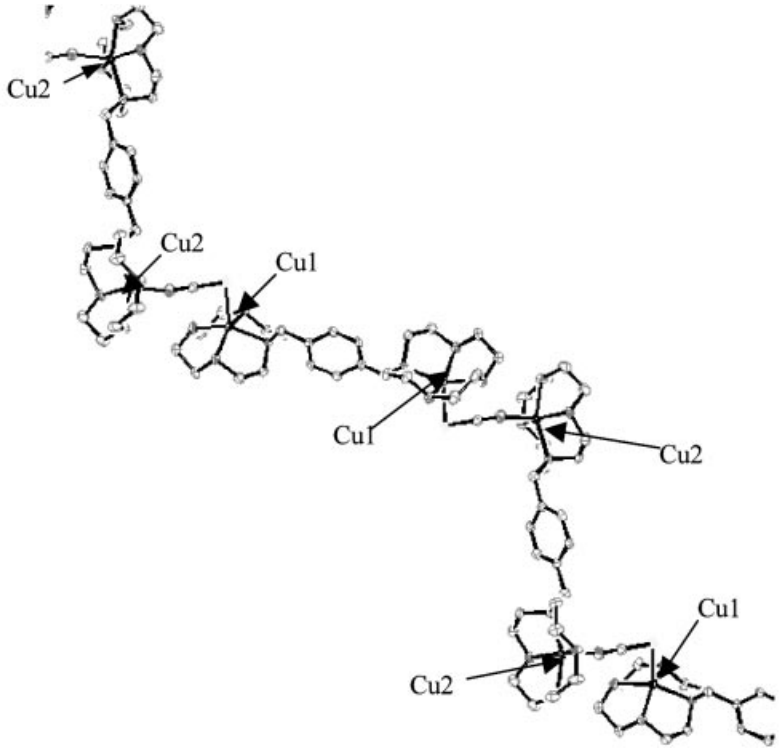

Figure 5. ORTEP drawing of the crystallographic repeating unit of the polymeric chain $[(para\text{cyclen})Cu_2]_2(SCN)_8 \cdot 7H_2O$

 © 2003 Wiley-VCH Verlag GmbH & Co. KGaA, Weinheim

Table 6. Bond lengths [Å] and angles [°] in [(*para*cyclen)Cu_2]$_2$(SCN)$_8$·7H_2O

Cu1−N1	2.059(4)	N1−Cu1−N2	86.5(2)
Cu1−N2	2.029(5)	N1−Cu1−N3	150.9(2)
Cu1−N3	2.033(4)	N1−Cu1−N4	85.8(2)
Cu1−N4	2.035(4)	N2−Cu1−N3	85.5(2)
Cu1−S1	2.482(5)	N2−Cu1−N4	147.1(2)
Cu2−N5	2.055(4)	N3−Cu1−N4	85.8(2)
Cu2−N6	2.021(4)	S1−Cu1−N1	106.0(2)
Cu2−N7	2.023(5)	S1−Cu1−N2	100.6(2)
Cu2−N8	2.040(4)	S1−Cu1−N3	102.9(2)
Cu2−N9	2.054(5)	S1−Cu1−N4	112.2(2)
C25−N9	1.172(7)	N5−Cu2−N6	85.4(2)
S1−C25	1.646(6)	N5−Cu2−N7	150.6(2)
		N5−Cu2−N8	86.(2)
		N6−Cu2−N7	85.4(2)
		N6−Cu2−N8	147.2(2)
		N7−Cu2−N8	86.4(2)
		N5−Cu2−N9	107.8(2)
		N6−Cu2−N9	104.0(2)
		N7−Cu2−N9	101.6(2)
		N8−Cu2−N9	108.7(2)
		Cu1−S1−C25	93.7(5)
		Cu2−N9−C25	162.3(5)
		N9−C25−S1[a]	178.8(6)

[a] The bridging NCS^- is indexed N9−C25−S1.

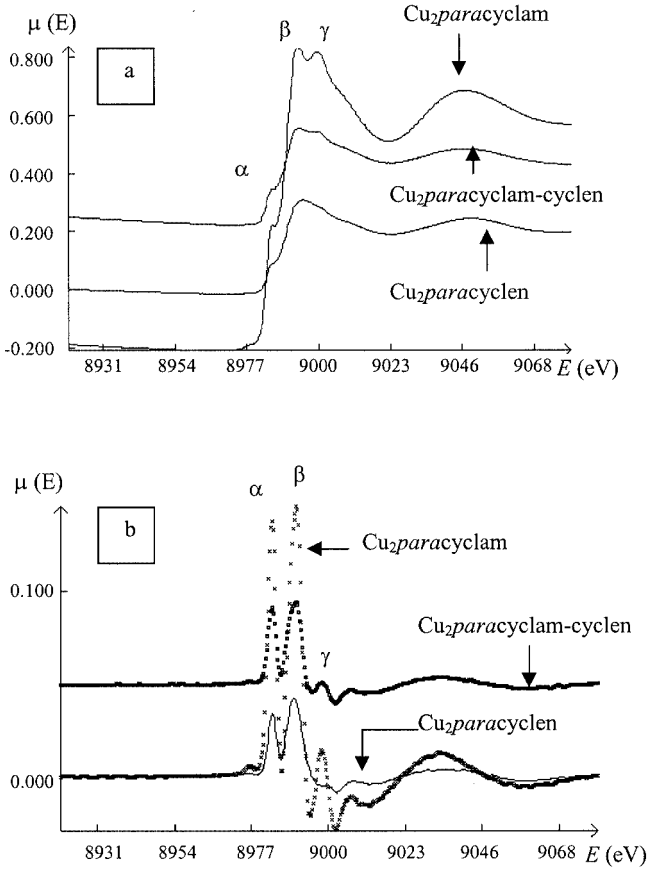

Figure 6. (a) Normalised XANES spectra (pre- and near-edge region) of (*para*cyclam)Cu_2, (*para*cyclam-cyclen)Cu_2, and (*para*cyclen)Cu_2; (b) comparison of their first derivatives

This value provides an estimate for the destabilisation of the $4p_z$ metal orbital, z being the elongation axis.[26,27] Our values are smaller than those (between 8 and 9 eV) found for copper(II) complexes in which the axial ligands are remote from the metal centre, giving rise to a D_{4h} square-planar environment.[27,28] These results are consistent with a distorted octahedral geometry for (*para*cyclam)Cu_2, and a mixed distorted octahedral-square-pyramidal one for (*para*cyclam-cyclen)Cu_2. The main transition, termed β, is attributed to the $1s\rightarrow4p_\pi$ transition, and is mainly affected by axial ligands as discussed above. On the other hand, the γ transition, corresponding to the $1s\rightarrow4p_s$ transition, is mainly sensitive to the equatorial ligands. This transition, centred at 8998 eV in the three compounds, indicates that the bond strengths between central metal ion and ligands are identical, and can be estimated from the (*para*cyclen)Cu_2 reference at approximately 2.35 Å.

The *k*-space experimentally determined and fitted EXAFS spectra $k\chi(k)$ vs. k for (*para*cyclam)Cu_2 and (*para*cyclam-cyclen)Cu_2, at the copper *K*-edge, and the corresponding Fourier transforms are given in Figure 7.

The two experimentally determined $k\chi(k)$ values and their Fourier transforms (FTs) are very similar, and allow us to assume that the local structures of the Cu^{II} ions are nearly the same. The slight differences can be attributed to the size of the macrocyclic cavity, which is greater for cyclam (ten carbon atoms) than for cyclen (eight carbon atoms). Actually, the two (*para*cyclam)Cu_2 and (*para*cyclam-cyclen)Cu_2 compounds differ only by one macrocyclic cavity. The amplitudes of the EXAFS oscillations appear nearly unchanged, indicating the almost identical numbers of nearest neighbours around each metal ion. The Fourier transform spectra are composed of three main peaks. From the expected structures for these complexes, it can be proposed that the first peak should correspond to the four nitrogen atoms of the macrocyclic cavity, and the second to one or two axial water oxygen atoms. The third peak, above 2.7 Å, should correspond to the eight or ten carbon atoms belonging to the cyclen or cyclam cavity.

The number and postulated nature of neighbours, the inter-neighbour distances, the Debye−Waller factors, and the energy threshold resulting from quantitative analysis of EXAFS data for the three first coordination shells of the (*para*cyclam)Cu_2 and (*para*cyclam-cyclen)Cu_2 compounds at the copper *K*-edge are given in Table 7.

The goodness of fit from the fits of the EXAFS functions and the corresponding FTs can be seen in Figure 7. For the (*para*cyclam)Cu_2 complex, the first shell was best fit with four nitrogen atoms per copper(II) ion at an average distance of 2.02 Å from the absorbing copper atom. These four atoms are positioned in the equatorial plane of a Jahn−Teller distorted, elongated octahedron. Actually, the two axial oxygen atoms, of water molecules, of the octahedron are found at 2.78 Å from the Cu^{II} ions, similarly to the arrangement described for $Cu(OH)_2$.[29] The third shell of neighbouring atoms was best fitted with ten carbon atoms at an average distance of 3.12 Å. Taking these values into account, the most likely structural interpretation is that

 © 2003 Wiley-VCH Verlag GmbH & Co. KGaA, Weinheim

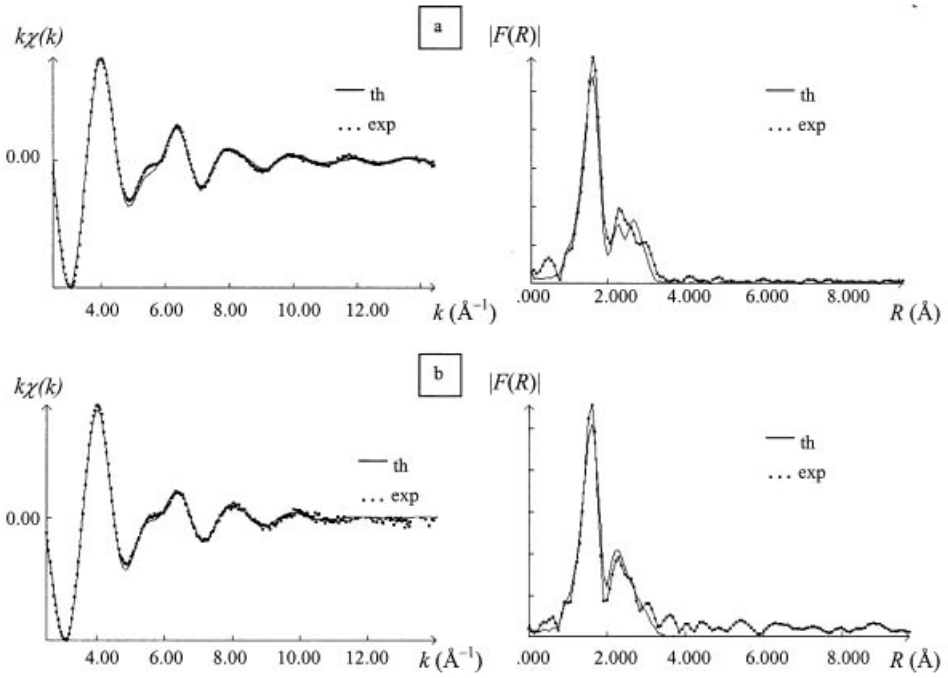

Figure 7. Experimentally measured and fitted k^3-weighted EXAFS spectra and the corresponding Fourier transforms of (*para*cyclam)Cu_2 (a) and (*para*cyclam-cyclen)Cu_2 (b)

Table 7. EXAFS results at the Cu-*K*-edge for the (*para*cyclam)Cu_2 and (*para*cyclam-cyclen)Cu_2 complexes

		N	*R* [Å]	σ [Å^{-1}]	ΔE_0 [eV]
(*para*cyclam)Cu_2	Cu−N	4	2.02	0.023	0.15
	Cu−O	2	2.78	0.007	0.02
	Cu−C	10	3.12	0.055	0.83
(*para*cyclam-cyclen)Cu_2	Cu−N	4	2.04	0.016	0.42
	Cu−O_{cyclam}	2	2.72	0.010	1.02
	Cu−O_{cyclen}	1	2.24	0.068	0.24
	Cu−C_{cyclam}	10	3.13	0.070	0.67
	Cu−C_{cyclen}	8	2.77	0.148	5.61

the two cyclam macrocyclic cavities are located in the equatorial plane with all four nitrogen donor atoms involved in chelating and remaining water of hydration of the first coordination sphere occupying axial positions. This structure agrees well with Ohtaka and Seki's findings[24] for the (monocyclam)copper(II) complex in solution by SAX (Cu−N and Cu−O bond lengths were found to be 2.01 and 2.77 Å), and also those of Tasker and Sklar[30] for the same complex by X-ray diffraction (Cu−N 2.02 Å, distorted octahedral geometry).

Fitting of the EXAFS data for the first coordination shell of the (*para*cyclam-cyclen)Cu_2 complex resulted in a very slight increase in the Cu−N bond length from 2.02 to 2.04 Å. This is consistent with the size of the macrocyclic cavities. Actually, in the cyclam one, the copper(II) ion is in the same plane as the four nitrogen atoms (*trans* N−Cu−N angle around 180°),[31] whereas in the cyclen cavity the metal ion is slightly above (Table 5: *trans* N−Cu−N angle around 150°), increasing the Cu−N bond length. The second and third shells of (*para*cyclam-cyclen)Cu_2 have been fitted for both cyclen and cyclam cavities. The results obtained for the latter are the same as in the (*para*cyclam)Cu_2 complex. For the cyclen cavity the results agree with our X-ray crystallographic data for (*para*cyclen)$Cu_2(ClO_4)_4{\cdot}4H_2O$. However, the more distant carbon atoms give rise to high thermal disorder with a high Debye−Waller factor for these atoms (around 0.15 Å^{-1}). In summary, XAS techniques have been shown to be a good alternative to X-ray diffraction for obtaining structural and geometrical information.

ESR Experiments

The frozen aqueous solution ESR spectra (150 K) of mononuclear complexes show the typical four-line patterns expected for coupling of the electron to the 3/2 spin of a copper(II) nucleus. The hyperfine coupling constants and *g* values are very close to those found for the copper complexes with cyclen or cyclam (Table 2, Figure 8).

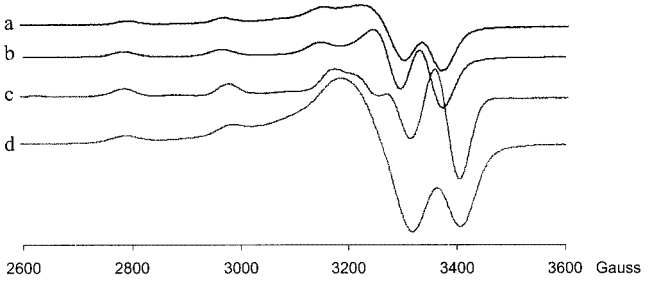

Figure 8. EPR spectra of mononuclear CuL^{2+} complexes at 150 K: (a) (*para*cyclen)Cu, (b) simulation of (*para*cyclen)Cu, (c) (*para*cyclam)Cu, (d) (*para*cyclam-cyclen)Cu

 © 2003 Wiley-VCH Verlag GmbH & Co. KGaA, Weinheim

The ESR spectra of the three dinuclear complexes obtained at 150 K in a H_2O/glycerol mixture or in DMF (Figure 9) present a septuplet around 3000 G and a signal at half field, in agreement with those described by Guilard et al.[11] The existence of seven equidistant lines corresponding to the two allowed transitions ($\Delta M_S = 1$) and that of a signal at half field assigned to a forbidden transition ($\Delta M_S = 2$) are characteristic of a dicopper compound with intramolecular exchange between the two copper ions ($I_{Cu} = 3/2$).[32] Unfortunately, the forbidden transition is poorly defined and it is not possible to estimate the Cu−Cu distance from the ratio of the intensity of the forbidden transition to the intensity of the allowed transition.[32]

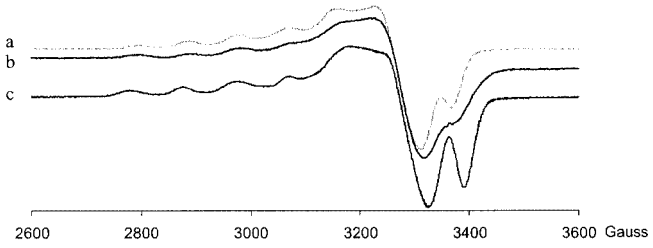

Figure 9. EPR spectra of dinuclear Cu_2L^{4+} complexes at 150 K: (a) (*para*cyclen)Cu_2, (b) (*para*cyclam-cyclen)Cu_2, (c) (*para*cyclam)Cu_2

The *g* values (Table 2) for *para*cyclen and *para*cyclam compounds are similar to those of (cyclen)- and (cyclam)-copper complexes. The hyperfine splittings in the spectra of the dinuclear complexes are approximately half of those characteristic of mononuclear copper(II) complexes in tetragonally distorted octahedral environments for cyclam compounds, and square-pyramidal geometries for cyclen compounds. The $A_{\|}$ values are indicative of a very weak *D* parameter in these dinuclear complexes.[32]

In the dinuclear *para*cyclam-cyclen complex, the copper coordination environment dictated by the macrocyclic holes is different and so the distances between two lines are irregular. However, this effect is insufficient to resolve the two sets of seven lines, the parameters of cyclen and cyclam complexes being too close.

Although the polymeric thiocyanate complex shows two different dinuclear *para*cyclen moieties with CuN_5 and CuN_4S chromophores, respectively, the signal is close to that of (*para*cyclen)$Cu_2(ClO_4)_4$.

Conclusion

In summary, only pure dinuclear complexes were isolated in the solid state. In the case of mononuclear compounds, their isolation was carried out by use of an ion-exchange method with a solution of NaCl as eluent. Unfortunately, sodium chloride could not be completely separated from these complexes.

Among the dinuclear compounds, two complexes formed with the *para*cyclen ligand were obtained as monocrystals suitable for X-ray diffraction. The first is a monomeric compound in which the two five-coordinate copper atoms are located in a square-pyramidal environment (chromophore N_4O), the second, obtained in the presence of an excess of KSCN, is a polymeric chain with two kinds of Cu_2L^{4+} moieties alternately present in the chain (one with two N_4S chromophores, the other with two N_5 chromophores).

With the two other ligands, *para*cyclam and *para*cyclam-cyclen, the complexes were not obtained as monocrystals. They were therefore studied by XAS, which is a good alternative to X-ray diffraction to obtain structural information. In the case of the *para*cyclam ligand, the complex formed is an elongated octahedron (four equatorial N atoms and two axial O atoms of water molecules). With the ligand *para*cyclam-cyclen, the copper atom in the cyclam cavity is six-coordinate (chromophore N_4O_2) and that in the cyclen cavity is five-coordinate (chromophore N_4O).

With regard to the study in solution, the results of the potentiometric titrations, the ESR experiments and the electronic spectra are in good agreement. When the ratio R = ligand/metal is higher than 1, mononuclear complexes $CuLH_n^{(2+n)+}$ ($0 < n < 3$) are formed, and when R is lower than 1, the formation of the dinuclear compounds Cu_2L^{4+} is emphasised. The complexes are very stable and the two macrocyclic cavities of the ligands seem to be independent of one another regarding the complexation phenomenon.

Experimental Section

Spectroscopic Measurements: Electronic spectra in aqueous solution were all measured in the 300−900 nm range with a Lambda 6 Perkin−Elmer spectrophotometer. The ESR spectra were obtained at 150 K with a Bruker ELEXSYS 500 spectrophotometer in the X-band at 9.40 GHz. Simulations were carried out with the software Simfonia.

Potentiometric Measurements: To determine the protonation constants of the ligands and the stability constants of the copper(II) complexes, potentiometric titrations were carried out with an automatic titrator consisting of a Metrohm dosimat 665 microprocessor burette and a Metrohm 713 pH meter connected to a computer. The titration procedure was fully automated.[33] All measurements were performed within a cell thermoregulated at 20.0±0.1 °C under a nitrogen stream to avoid the dissolution of carbon dioxide. the ionic strength was adjusted to 1 with potassium nitrate. The combined type "U" glass electrode Metrohm used had a very low alkaline error. Solutions of ligand (1.10^{-3} to 3.10^{-3} mol·L^{-1}) and ligand/copper nitrate mixture (ligand/metal ratios [L]/[M] in the range 0.5−2) were titrated with a 0.1 mol·L^{-1} KOH solution. The stability constants were calculated and refined with PROTAF.[34] The fitted global formation constants β_{mlh} are defined for the equilibrium (except for the proton, the charges are not shown for clarification):

$$\beta_{mlh} = \frac{[M_m L_l H_h]}{[M]^m [L]^l [H^+]^h}$$

$$m\,M + l\,L + h\,H^+ \rightleftharpoons M_m L_l H_h$$

A negative *h* value refers to the hydroxide ion.

 © 2003 Wiley-VCH Verlag GmbH & Co. KGaA, Weinheim

Crystal Structure Determination: The crystal data were collected at 173 K with a Kappa CCD diffractometer using monochromated Mo-K_α radiation (λ = 0.71073Å). The structures were solved by direct methods. After refinement of the non-hydrogen atoms, difference-Fourier maps revealed maxima of residual electron density close to the positions expected for hydrogen atoms. Hydrogen atoms were introduced as fixed contributors at calculated positions [C−H = 0.95 Å; B(H) = 1.3B_{eqv}]. Final difference maps revealed no significant maxima. All calculations used the Nonius OpenMoleN package.[35] Neutral atom scattering factor coefficients and anomalous dispersion coefficients were taken from a standard source.[36] Crystallographic data (excluding structure factors) for the structures reported in this paper have been deposited with the Cambridge Crystallographic Data Centre as supplementary publication nos. CCDC-187962 [(*para*cyclen)$Cu_2(ClO_4)_4$·$4H_2O$] and -187961 {[(*para*cyclen)Cu_2]$_2$$(SCN)_8$·$7H_2O$}. Copies of the data can be obtained free of charge on application to CCDC, 12 Union Road, Cambridge CB2 1EZ, UK [Fax: (internat.) + 44-1223/336-033; E-mail: deposit@ccdc.cam.ac.uk].

X-ray Absorption Data Collection and Processing: The XANES (X-ray absorption near-edge structure) and EXAFS (extended X-ray absorption fine structure) data were collected at the Laboratoire d'Utilisation du Rayonnement Electromagnétique (LURE), Paris-Sud University, with the XAS4 beam line of the storage ring DCI with an energy of 1.85 GeV and a mean intensity of 300−200 mA. The measurements were carried out at the copper *K*-edge in the transmission mode with an Si(111) for EXAFS, and Si(311) for XANES channel-cut monochromator at room temperature. The detector were low-pressure (ca. 0.2 atm) air-filled ionisation chambers. The photon energy was calibrated from the spectrum of a copper foil, 8979 eV being assigned to the pre-edge peak. Each spectrum was the sum of three recordings in the 8830−9830 eV range for EXAFS, and the 8920−9080 eV range for XANES, including the copper *K*-edge (ca. 8979 eV). The XANES spectra were recorded step-by-step, every 0.3 eV with a 2 s accumulation time per point. The spectrum of a 5 μm copper foil was recorded just behind the sample to check the energy calibration, thus ensuring an energy accuracy of 0.25 eV. The EXAFS spectra were recorded with sampling steps of 2 eV, and an integration time of 2.0 s per point was used. The EXAFS data analysis was performed with the "EXAFS pour le Mac" and EXAFS98 programs.[37] The $\chi(k)$ functions were extracted from the data[38] with a linear pre-edge background, a combination of polynomials (of order 5) and spline atomic-absorption background, and normalised by the Lengeler−Eisenberger method.[39] The energy threshold, E_0, was taken at the half maximum of the absorption edge. Radial distribution functions $F(R)$ were calculated by Fourier transforms of $k^3w(k)\mu(k)$ in the 2−14 Å^{-1} range; $w(k)$ is a Kaiser−Bessel apodization window with a smoothness coefficient τ = 3 (k is the photoelectron wavenumber). The peaks corresponding to the successive atomic shells were then isolated and back-Fourier-transformed into k space to determine the mean coordination number N, the bond length R, and the Debye−Waller factor σ by a least-squares fitting procedure using the standard EXAFS formula, without multiple scattering:

$$\chi(k) = S_0^2 \sum_i \left[\frac{N_i}{R_i^2} A_i(k) e^{-2\sigma_i^2 k^2} e^{-2R_i/\lambda(k)} \sin(2kR_i + \Phi_i(k)) \right]$$

The experimental phase $\Phi_i(k,R_i)$ and amplitude $A_i(k,R_i)$ have been extracted from the model compounds of known crystallographic structure, Cu(1,4,8,11-tetraazacyclotetradecane),[24] and (*para*cyclen)Cu_2.

Syntheses: The metal salts were purchased from Aldrich. The other reagents were used as the highest grade commercially available without further purification. The three ligands were synthesized by a new method described by Handel et al.,[40] with an aminal as intermediate.

(*para*cyclen)$Cu_2(ClO_4)_4$·$4H_2O$ (1): The neutral ligand ($5.2\cdot10^{-5}$ mol) was dissolved in distilled water (10 mL) and a copper(II) perchlorate solution in ethanol ($1.17\cdot10^{-4}$ mol) was added dropwise. The blue solution was stirred at room temperature for 7 d and was then concentrated under vacuum. The violet solid was washed twice with absolute ethanol. The complex was recrystallized from saturated aqueous $NaClO_4$ solution. $C_{24}H_{54}Cl_4Cu_2N_8O_{20}$ (1043.1): calcd. C 27.61, H 5.18, N 10.74; found C 27.55, H 5.20, N 10.26.

(*para*cyclam)$Cu_2Cl_2(ClO_4)_2$·H_2O (2): Solid NaOH ($1.75\cdot10^{-3}$ mol) was added to a suspension of ligand hydrochloride ($8.2\cdot10^{-5}$ mol) in absolute ethanol (10 mL). After elimination of NaCl and NaOH in excess, a copper(II) perchlorate solution in methanol ($1.74\ 10^{-4}$ mol) was added dropwise in order to obtain 60 mL of a mauve solution. After stirring at room temperature for 24 h, the blue mauve solid was filtered and washed twice with ethanol. $C_{28}H_{56}Cl_4Cu_2N_8O_9$ (917.1): calcd. C 37.37, H 6.01, N 12.41; found C 36.98, H 6.22, N 12.35.

(*para*cyclam-cyclen)$Cu_2Cl_2(ClO_4)_2$·$2H_2O$ (3): This complex was prepared by the same procedure as used for compound **2**. $C_{26}H_{54}Cl_4Cu_2N_8O_{10}$ (907.1): calcd. C 34.10, H 5.95, N 12.35; found C 34.41, H 6.00, N 11.79.

(*para*cyclen)$Cu_2(SCN)_4$·H_2O (4): After the neutral ligand ($2\cdot10^{-4}$ mol) had been dissolved in methanol (50 mL), an aqueous solution of copper nitrate ($4.2\cdot10^{-4}$ mol) was added. The solution was heated at reflux for 1 h and the solvents were evaporated under vacuum. The crude solid was dissolved in water and a blue solid was precipitated with an excess of KSCN. This solid was filtered and washed with ethanol. $C_{28}H_{48}Cu_2N_{12}O_1S_4$ (823.1): calcd. C 40.72, H 6.06, N 20.36 found C 41.13, H 5.75, N 20.01. Attempted recrystallization in water with an excess of KSCN produced another compound [(*para*cyclen)Cu_2]$_2$$(SCN)_8$·$7H_2O$, a monocrystal suitable for X-ray study.

Synthesis of Mononuclear Complexes: These complexes were very difficult to isolate because of the presence of small amounts of dinuclear compounds or uncomplexed ligands. The isolation of mononuclear compounds could be carried out with an ion-exchange column (SP Sephadex C 25)[41] and an NaCl solution ($0.4\cdot mol\cdot L^{-1}$) as eluent. Unfortunately, sodium chloride could not be completely separated from the complexes.

Acknowledgments

We thank Dr. A. De Cian (Université Louis Pasteur, Strasbourg, France) for the single-crystal X-ray analyses. The Region Champagne-Ardenne is acknowledged for a grant to M. S.

[1] T. A Kaden, *Coord. Chem. Rev.* **1999**, 190−192; T. A Kaden, *Coord. Chem. Rev.* **1999**, 371−389.
[2] M. S. Young, J. J. Chen, *J. Am. Chem. Soc.* **1995**, *117*, 10577−10578.
[3] P. A. Vigato, S. Tamburini, D. E. Fenton, *Coord. Chem. Rev.* **1990**, *106*, 25−170.
[4] [4a] *Copper Coordination Chemistry: Biochemical and Inorganic*

 © 2003 Wiley-VCH Verlag GmbH & Co. KGaA, Weinheim

Perspectives (Eds. K. Karlin, J. Zubieta), Academic Press, New York, **1983**. [4b] *Biological and Inorganic Copper Chemistry, vol. I and II perspectives* (Eds. K. Karlin, J. Zubieta), Academic Press, New York, **1986**.
[5] G. J. Bridger, R. T. Skerlj, S. Padmanabhan, S. A. Martellucci, G. W Henson, M. J. Abrams, H. C. Joao, M. Witvrouw, K. De Vreese, R. Pauwels, E. De Clercq, *J. Med. Chem.* **1996**, *39*, 109−119.
[6] E. De Clercq, *Mol. Pharmacol.* **2000**, *57*, 833−839.
[7] K. De Vreese, V. Kofler-Mongold, C. Leutgeb, V. Weber, K. Vermeire, S. Schacht, J. Anne, E. De Clercq, R. Datema, G. Werner, *J. Virol.* **1996**, *70*, 689−696.
[8] E. Kimura, M. Kikuchi, H. Kitamura, T. Koike, *Chem. Eur. J.* **1999**, *5*, 3113−3123.
[9] D. Chartres, L. F. Lindoy, G. V. Meehan, *Coord. Chem. Rev.* **2001**, 216−217; D. Chartres, L. F. Lindoy, G. V. Meehan, *Coord. Chem. Rev.* **2001**, 249−286.
[10] M. Ciampolini, L. Fabbrizzi, A. Poggi, B. Seghi, F. Zanobini, *Inorg. Chem.* **1987**, *26*, 3527−3533.
[11] S Brandes, C. Gros, F. Denat, P. Pullumbi, R. Guilard, *Bull. Soc. Chim. Fr.* **1996**, *133*, 65−73.
[12] R. Schneider, A. Riesen, T. Kaden, *Helv. Chim. Acta* **1986**, *69*, 53−61.
[13] A. McAuley, S. Subramanian, M. J. Zaworotko, K. Biradha, *Inorg. Chem.* **1999**, *38*, 5078−5085.
[14] H. Elias, *Coord. Chem. Rev.* **1999**, *187*, 37−73.
[15] L. Siegfried, A. Urfer, T. A. Kaden, *Inorg. Chim. Acta* **1996**, *251*, 177−183.
[16] Q. Xu, M. Du, R.-H. Zhang, H.-Y. Shen, X.-H. Bu, W.-M. Bu, *Chinese J. Chem.* **2000**, *18*, 357−363.
[17] A. Bianchi, M. Micheloni, P. Paoletti, *Coord. Chem. Rev.* **1991**, *110*, 17−113.
[18] R. D. Hancock, R. J. Motekaitis, J. Mashishi, I. Cukrowski, J. H. Reibenspies, A. E. Martell, *J. Chem. Soc., Perkin Trans. 2* **1996**, 1925−1929.
[19] K. Miyoshi, H. Tanaka, S. Tsuboyama, S. Murata, H. Shimizu, K. Ishizu, *Inorg. Chim. Acta* **1983**, *78*, 23−30.
[20] M. Gaspar, R. Grazina, A. Bodor, E. Farkas, M. A. Santos, *J. Chem. Soc., Dalton Trans.* **1999**, 799−806.
[21] [21a] A. E. Goeta, J. A. K. Howard, D. Maffeo, H. Puschmann, J. A. G. Williams, D. S. Yufit, *J. Chem. Soc., Dalton Trans.* **2000**, 1873−1880. [21b] R. Buxtorf, T. A. Kaden, *Helv. Chim. Acta* **1974**, *57*, 1035−1042. [21c] M. R. Oberholzer, M. Neuburger, M. Zehnder, T. A. Kaden, *Helv. Chim. Acta* **1995**, *78*, 505−513.
[22] B. J. Hathaway, *J. Chem. Soc., Dalton Trans.* **1972**, 1196−1199.
[23] M. T. S. Amorim, S. Chaves, R. Delgado, J. R. Frausto da Silva, *J. Chem. Soc., Dalton Trans.* **1991**, 3065−3071.
[24] H. Ohtaki, H. Seki, *J. Macromol. Sci. Chem.* **1990**, *A27*, 1305−1319.
[25] J. H. Choy, B. W. Kim, J. B. Yoon, J. C. Park, *Mol. Cryst. Liq. Cryst.* **1998**, *311*, 303−311.
[26] N. Kosugi, T. Yokoyama, K. Asakuna, H. Kuroda, *Chem. Phys.* **1984**, *91*, 249−258.
[27] C. Surville-Barland, R. Ruiz, A. Aukauloo, Y. Journeaux, I. Castro, B. Cervera, M. Julve, F. Lloret, F. Sapina, *Inorg. Chim. Acta* **1998**, *278*, 159−169.
[28] C. Mangenay, J. C. Lacroix, K. I. Chane-Ching, M. Jouini, F. Villain, S. Ammar, N. Jouini, P. C. Lacaze, *Chem. Eur. J.* **2001**, *7*, 5029−5040.
[29] M. Magini, *J. Chem. Phys.* **1981**, *74*, 2523−2529.
[30] P. A. Tasker, L. Sklar, *J. Cryst. Mol. Struct.* **1975**, *5*, 329−338.
[31] T. H. Lu, T. H. Tahirov, Y. L. Liu, C. S. Chung, C. C. Huang, Y. S. Hong, *Acta Crystallogr., Sect. C* **1996**, *52*, 1093−1099.
[32] [32a] S. S. Eaton, K. M. More, B. M. Sawant, G. R. Eaton, *J. Am. Chem. Soc.* **1983**, *105*, 6560−6567. [32b] S. S. Eaton, *J. Am. Chem. Soc.* **1982**, *104*, 5002−5003.
[33] I. Déchamps-Olivier, J. P. Barbier, M. Aplincourt, N. Oget, F. Chuburu, H. Handel, *Helv. Chim. Acta* **1999**, *82*, 790−795.
[34] [34a] R. Fournaise, C. Petitfaux, *Talanta* **1987**, *34*, 385−395. [34b] R. Fournaise, C. Petitfaux, *Analysis* **1990**, *18*, 242−249.
[35] OpenMoleN, *Interactive Structure Solutions*, Nonius B. V., Delft, The Netherlands, **1997**.
[36] D. T. Cromer, J. T. Waber, *International Tables for X-ray Crystallography*, The Kyonoch Press, Birmingham, **1974**, vol. IV, tables 2.2b, 2.3.1.
[37] [37a] A. Michalowicz, in: *Logiciels pour la Chimie*, Société Française de Chimie, Paris, **1991**, p. 102. [37b]A. Michalowicz, *J. Chem. Phys. IV* **1997**, *7*, 235−245.
[38] [38a] B. K. Teo, in: *Inorganic Chemistry Concepts, EXAFS: Basic Principles and Data Analysis*, Springer-Verlag, Berlin, **1986**, p. 9. [38b] D. C. Königsberger, R. Prins, in: *X-ray Absorption Principles, Applications, Techniques of EXAFS, SEXAFS and XANES*, John Wiley, New York, **1988**. [38c] F. W. Lytle, D. E. Sayers, E. A. Stern,, *Physica* **1989**, *B158*, 701−704 (“Co-Chairmen Report of the International Workshop on Standards and Criteria in X-ray Absorption Spectroscopy”).
[39] B. Lengeler, P. Eisenberger, *Phys. Rev.* **1980**, *B21*, 4507−4518.
[40] M. Le Baccon, F. Chuburu, L. Toupet, H. Handel, M. Soibinet, I. Déchamps-Olivier, J. P. Barbier, M. Aplincourt, *New J. Chem.* **2001**, 1168−1174.
[41] L. Fabbrizzi, L. Montagna, A. Poggi, T. A. Kaden, L. C. Siegfried, *J. Chem. Soc., Dalton Trans.* **1987**, 2631−2687.

Received September 16, 2002

 © 2003 Wiley-VCH Verlag GmbH & Co. KGaA, Weinheim

Exchange Interactions at the Supramolecular Level − Synthesis, Crystal Structure, Magnetic Properties, and EPR Spectra of [Mn(MAC)(TCNQ)$_2$] (MAC = Pentaaza Macrocyclic Ligand; TCNQ$^{\cdot-}$ = Radical Anion of 7,7,8,8-Tetracyano-*p*-quinodimethane)

Augustin M. Madalan,[a,b] Violeta Voronkova,[c] Ravil Galeev,[c] Ludmila Korobchenko,[c] Jörg Magull,[a] Herbert W. Roesky,*[a] and Marius Andruh*[b]

Dedicated to Professor Achim Müller on the occasion of his 65th anniversary

Keywords: Manganese / N ligands / Stacking interactions / Magnetic properties / EPR spectroscopy / Radicals

The reaction between [Mn(MAC)(H$_2$O)$_2$]Cl$_2$·4H$_2$O and LiTCNQ (MAC = 2,13-dimethyl-3,6,9,12,18-pentaazabicyclo[12.3.1]octadeca-1(18),2,12,14,16-pentaene) affords a complex with the formula [Mn(MAC)(TCNQ)$_2$] (**1**), whose crystal structure has been determined. Its structure consists of neutral mononuclear entities. The manganese(II) ion is heptacoordinated, with a pentagonal bipyramidal geometry. The apical positions are occupied by the TCNQ$^{\cdot-}$ radicals, while the macrocyclic ligand is coordinated at the equatorial positions. The seven Mn–N distances range from 2.273(3) to 2.301(6) Å. The strong intermolecular π–π stacking interactions between the TCNQ radicals (3.2 Å) leads to weave-like infinite chains, which propagate along the crystallographic *c* axis. The cryomagnetic investigation of **1** revealed a weak intermolecular antiferromagnetic coupling of the Mn^{2+} ions (J = −0.18 cm^{-1}), which is mediated by the diamagnetic $(TCNQ)_2^{2-}$ pairs resulting from the stacking interactions in the crystal. The intermolecular exchange interaction between the Mn^{2+} ions was further confirmed by variable temperature EPR spectroscopic measurements [$|J|$ = 0.15(5) cm^{-1}], which have been carried out in both the X and Q bands.
(© Wiley-VCH Verlag GmbH & Co. KGaA, 69451 Weinheim, Germany, 2003)

Introduction

Since the pioneering work of Melby et al.,[1] the TCNQ$^{\cdot-}$ radical has been widely used as a building-block for the construction of molecular solids with exciting physical properties.[2] Among these the magnetic ordering,[3] as well as the electrical conductivity are particularly attractive.[4] The neutral TCNQ molecule acts as a strong acceptor due to its low reduction potential to form the radical anion, TCNQ$^{\cdot-}$. The reaction between various metallocenes, [M(Cp*)$_2$] (Cp* = C$_5$Me$_5$) with TCNQ leads to a family of charge transfer complexes, [M(Cp*)$_2$]$^{\cdot+}$[TCNQ]$^{\cdot-}$, with strong magnetic interactions between the spin carriers. Some of these compounds are molecular magnets.[5]

Due to its high σ-donor character towards transition-metal ions, the TCNQ$^{\cdot-}$ ion can act as a ligand generating a rich coordination chemistry.[6,7] The synthetic approach consists of the reaction of transition-metal complexes with LiTCNQ. The TCNQ$^{\cdot-}$ radical coordinates at a vacant site on the metal centre, or replaces a weakly coordinated ligand in the coordination sphere of the metal ion. Most of these complexes have the general formula [M(N$_4$)(TCNQ)$_2$], where (N$_4$) denotes various polyamine ligands (e.g. tetraazamacrocyclic ligands, open tetraamines, two ethylenediamine molecules, etc.) and M^{2+} = Fe^{2+},[8] Ni^{2+},[9] Cu^{2+},[10] and Co^{2+}.[10a] Using TCNQ$^{\cdot-}$ as a ligand, we have recently synthesised the first coordination compound containing three different types of spin carriers: 2p (TCNQ$^{\cdot-}$), 3d (Cu^{2+}) and 4f (Gd^{3+}).[11] The TCNQ$^{\cdot-}$ species coordinates to both Cu^{2+} and Gd^{3+} ions.

As a part of our research program on the exchange interactions mediated by π−π stacking, we report here the synthesis, crystal structure, magnetic and EPR spectroscopic properties of a new Mn^{2+}−TCNQ$^{\cdot-}$ compound, [Mn(MAC)(TCNQ)$_2$], where MAC stands for the pentaazamacrocyclic ligand (2,13-dimethyl-3,6,9,12,18-pentaazabicyclo[12.3.1]octadeca-1(18),2,12,14,16-pentaene).

[a] Institut für Anorganische Chemie der Universität, Tammannstr. 4, 37077 Göttingen, Germany
E-mail: hroesky@gwdg.de
[b] Inorganic Chemistry Laboratory, Faculty of Chemistry, University of Bucharest,
Str. Dumbrava Rosie nr. 23, 70254 Bucharest, Romania
E-mail: marius.andruh@dnt.ro
[c] Zawoisky Physical-Technical Institute of the Russian Academy of Sciences, Department of Chemical Physics, Laboratory of Molecular Photochemistry,
Sibirsky Trakt 10/7, Kazan, Russia

Results and Discussion

Description of the Structure

The structure of compound **1** consists of mononuclear entities with the TCNQ·- anions coordinated to the metal ion (Figure 1). The manganese(II) ion exhibits a coordination number of seven with a pentagonal bipyramidal geometry. The $TCNQ^{\cdot -}$ groups are coordinated in the apical positions, while the equatorial positions are occupied by the nitrogen atoms of the macrocyclic ligand. The seven Mn−N distances range from 2.273(3) to 2.301(6) Å. The shortest Mn−N distance corresponds to the Mn−pyridyl nitrogen bond. Selected bond lengths and angles are given in Table 1. The values of the interatomic distances in the TCNQ species are diagnostic of their electronic nature. In the case of compound **1**, the carbon−carbon distances fall in the range expected for $TCNQ^{\cdot -}$ anions.[2,4c]

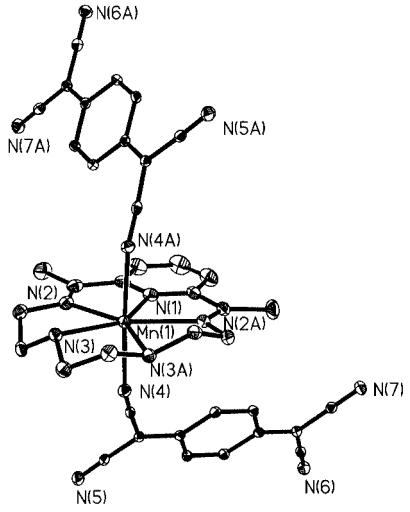

Figure 1. Molecular structure of $[Mn(MAC)(TCNQ)_2]$ and the atom numbering scheme.

Table 1. Selected bond lengths (Å) and angles (°) (symmetry codes i: $2 - x$, y, $2.5 - z$)

Mn1−N1	2.273(3)		
Mn1−N4^i	2.285(6)		
Mn1−N4	2.285(6)		
Mn1−N3	2.297(3)		
Mn1−N3^i	2.297(3)		
Mn1−N2^i	2.301(6)		
Mn1−N2	2.301(6)		
N1−Mn1−N4^i	86.21(6)	N1−Mn1−N4	86.21(6)
N4^i−Mn1−N4	172.42(8)	N1−Mn1−N3	142.27(6)
N4^i−Mn1−N3	91.17(8)	N4−Mn1−N3	94.82(8)
N1−Mn1−N3^i	142.27(6)	N4^i−Mn1−N3^i	94.82(8)
N4−Mn1−N3^i	91.17(8)	N3−Mn1−N3^i	75.46(8)
N1−Mn1−N2^i	69.47(6)	N4^i−Mn1−N2^i	87.01(8)
N4−Mn1−N2^i	90.34(8)	N3−Mn1−N2^i	148.05(8)
N3^i−Mn1−N2^i	72.92(8)	N1−Mn1−N2	69.47(6)
N4^i−Mn1−N2	90.34(8)	N4−Mn1−N2	87.01(8)
N3−Mn1−N2	72.92(8)	N3^i−Mn1−N	2148.05(8)
N2^i−Mn1−N2	138.94(8)		

An analysis of the packing diagram reveals interesting interactions at the supramolecular level. The small separations between anionic radicals arising from different $[Mn(MAC)(TCNQ)_2]$ units (3.2 Å) indicate the occurrence of strong π−π interactions. Consequently, the overlap of the $TCNQ^{\cdot -}$ π clouds generates weave-like chains propagating along the crystallographic *c* axis (Figure 2). The distance between the manganese atoms within the supramolecular chain is 13.03 Å. Consequently, the structure can be described as consisting of 1-D infinite chains:

···−[Mn(MAC)]−$(TCNQ)_2$−[Mn(MAC)]−$(TCNQ)_2$−[Mn(MAC)]−$(TCNQ)_2$−···

in which the [Mn(MAC)] moieties are connected through dimerized $TCNQ^{\cdot -}$ ligands.

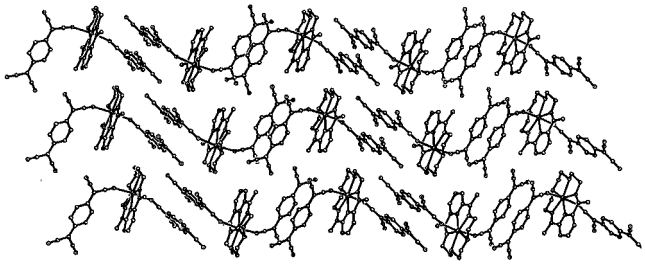

Figure 2. Packing diagram showing the formation of chains through the π−π stacking interactions between the TCNQ radicals.

Magnetic Measurements

The magnetic properties of compound **1** are shown in the form of an $\chi_M T$ versus T plot (Figure 3). The value of the $\chi_M T$ product at room temperature (4.2 $cm^3\ mol^{-1}K$) is lower than expected for the two types of spin carriers: Mn^{2+} ($S = 5/2$) and two $TCNQ^{\cdot -}$ radicals (each one with $S = 1/2$). In fact, the room temperature value corresponds exactly to $S = 5/2$, that is, only to one Mn^{2+} (indeed, the expected value of the $\chi_M T$ product for $S = 5/2$ is 4.37 $cm^3\ mol^{-1}K$). The lower value of the $\chi_M T$ product at room temperature for **1** can be explained by the strong antiferromagnetic coupling between the stacked $TCNQ^{\cdot -}$ radicals connecting the $[Mn(MAC)]^{2+}$ entities. This phenomenon has been observed with other compounds, where the stacking interactions between $TCNQ^{\cdot -}$ radicals lead to diamagnetic $(TCNQ)_2^{2-}$ dimers.[2,9] As the temperature is lowered $\chi_M T$ remains constant down to 70 K, then decreases abruptly, reaching a value of 1.9 $cm^3\ mol^{-1}$ K at 2.0 K. Considering the $TCNQ^{\cdot -}$ ions do not contribute to the magnetic moment of **1**, the magnetic properties can be simulated by taking into account only the $[Mn(MAC)]^{2+}$ units. The decrease of $\chi_M T$ in the lower temperature range can be due to the zero-field splitting (D) of the manganese(II) ion and/or to a weak intermolecular antiferromagnetic interaction between the local spins mediated by the π−π stacking interactions. A least-squares fit of the susceptibility data, taking into account the zero field splitting, led to $D = 5.1$ cm^{-1}, a value which is too high for a manganese(II) complex. We recall that for the parent compound,

 © 2003 Wiley-VCH Verlag GmbH & Co. KGaA, Weinheim

$[Mn(MAC)(H_2O)_2]Cl_2{\cdot}4H_2O$, the value of the D parameter obtained from EPR spectroscopic measurements was found to be 0.07 cm^{-1}.[12] The alternative way of rationalizing the magnetic behaviour is to consider only the exchange interactions of the manganese(II) ions within the supramolecular chain. The exchange pathway is provided by the diamagnetic $(TCNQ)_2^{2-}$ dimers. Consequently the magnetic data can be analysed using the Hamiltonian: $\boldsymbol{H} = -J\Sigma S_i S_{i+1}$. The temperature dependence of the magnetic susceptibility is given by Equation (1) and Equation (2):[14]

$$\chi_M^{chain} = \{Ng^2\beta^2 S_{Mn}(S_{Mn}+1)/3kT\}\{(1+u)/(1-u)\} \quad (1)$$

(Fisher's infinite chain model) with:

$$u = \coth[JS_{Mn}(S_{Mn}+1)/kT] - [kT/JS_{Mn}(S_{Mn}+1)] \quad (2)$$

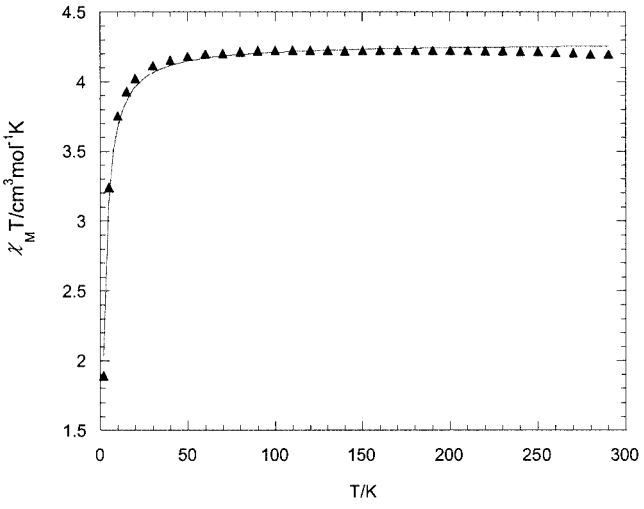

Figure 3. Temperature dependence of the $\chi_M T$ product. The solid line represents the best fit curve.

The least-squares fit of the data leads to $J = -0.18$ cm^{-1} and $g = 1.99$. The low J value is quite reasonable, since the distance between the manganese(II) ions within a chain is large (13.03 Å).

By fitting the data using the Curie–Weiss law, $\chi_M{}^{-1} = (T-\theta)/C$, we obtained $\theta = -0.7$ K, $C = 4.230$ $cm^3mol^{-1}K$ and $g = 1.98$. Given that $\theta = zJ'S(S+1)/3k$ and $S = 5/2$, it follows that $zJ' = -0.34$ cm^{-1}. As the packing diagram shows, $z = 2$ and consequently $J' = -0.17$ cm^{-1}, in good agreement with Fisher's model.

EPR Measurements

EPR spectra have been recorded on powder samples. Both X-band and Q-band (Figure 4) spectra consist of a single signal centred at $g = 2.028(5)$. The shape and the peak-to-peak linewidth of the signal, ΔB, are frequency-dependent. A slight asymmetry of the signal with ΔB=945 Oe is observed in the X-band at room temperature, the shape of the signal being intermediate between Lorentzian and Gaussian. As the frequency is increased, the asymmetry disappears and ΔB decreases to 595 ± 50 Oe at room temperature (Figure 4). As the temperature is decreased, the linewidth of the signal increases. The measurements in the X-band show that this increase occurs mainly in the range of 100–300 K, and at $T = 12$ K ΔB increases to 1590 ± 20 Oe. The temperature dependence of the spectrum in the Q-band shows that as the temperature is decreased, the linewidth increases from 595±50 Oe at room temperature to 1120 ± 100 Oe at 4.2 K.

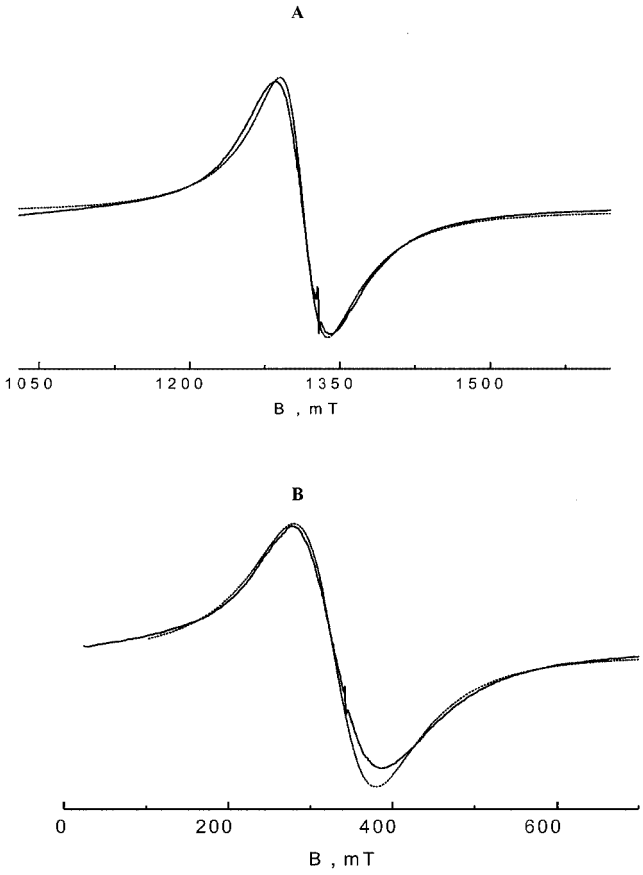

Figure 4. Experimental (solid lines) and simulated (dotted lines) EPR spectra at the Q-band (A) and at X-band (B) of compound **1** at room temperature. A narrow signal in the Q-band spectrum is due to the radical placed in the resonator for measuring the frequency.

The decrease in linewidth as a function of frequency is known as the "10/3" effect.[15] The frequency dependence of the linewidth of the signal has been previously observed for some compounds of Mn^{2+}.[16] This effect was interpreted using the Kuba and Tomita equation obtained for a simple cubic lattice composed of $S = 1/2$ ions,[17] in which the frequency dependence of the linewidth of the signal is described as the frequency dependence of its dipole contribution. Our estimation of the dipole contribution to the linewidth of compound **1** shows that it is not determinant and cannot describe the frequency dependence observed for this compound.

 © 2003 Wiley-VCH Verlag GmbH & Co. KGaA, Weinheim

The powder spectra of compound **1** do not show the fine and hyperfine structures due to the dipole−dipole and exchange interactions between neighbouring manganese(II) ions. It is known that if the exchange interaction, $-JS_iS_{i+1}$, exceeds the dipole-dipole and other interactions, an exchange-narrowed line is observed. The form of the EPR spectrum of the studied compound and its change with frequency and temperature were interpreted by supposing that the main contribution to the linewidth is due to the unresolved fine structure and not to the dipole−dipole interaction.

The frequency dependence of the EPR spectra was analysed using a simulation program that was written taking into account the fine structure [due to the zero-field splitting of manganese(II) ion] and the hyperfine structure for $S = 5/2$, the exchange interaction, and by averaging these structures according to the kinetic equations given in ref.[18] The linewidth of each component of the hyperfine structure was chosen by taking into account the dipole-dipole contribution. The value of the D parameter was taken as 0.07 cm^{-1}.[12] In the absence of the exchange interaction, the form of the spectrum of a polycrystalline Mn^{2+} sample in the X-band would be asymmetric. In the Q-band the form of the spectrum changes because the ratio between the fine structure parameter and the Zeeman energy changes. The exchange interaction averages out the fine structure but some differences in the X- and Q-bands remain. The observation of these differences enables us to estimate the J value. The asymmetry observed in the X-band is the manifestation of the incomplete averaging of the fine structure. The adjustment of the simulated and observed spectra at room temperature at the two frequencies allowed us to estimate the value of the exchange interaction $|J|$ as 0.15(5) cm^{-1}, which is in reasonably good agreement with the value obtained through cryomagnetic measurements. In our model, the temperature dependence of the spectrum in the X-band can be explained by the change in either of the parameters D or J. The assumption about the change in the D parameter, which shows a certain change in the distortion of the nearest environment of Mn^{2+}, agrees with the EPR spectroscopic data of $[Mn(MAC)(H_2O)_2]Cl_2{\cdot}4H_2O$.[12] The increase of the linewidth in the Q-band, however, can be described only by a decrease in the J parameter. The EPR spectroscopic data therefore enable us to suppose that the exchange interaction decreases weakly as the temperature is decreased.

In conclusion, we have shown by means of two independent techniques (magnetic susceptibility and EPR spectroscopic measurements) that the intermolecular π−π stacking of the $TCNQ^{\cdot-}$ ligands, which leads to diamagnetic $(TCNQ)_2^{2-}$ dimers, is able to mediate weak exchange interactions between the manganese(II) ions.

Experimental Section

Preparation of [Mn(MAC)(TCNQ)$_2$] (1): The manganese precursor, $[Mn(MAC)(H_2O)_2]Cl_2{\cdot}4H_2O$, was synthesised according to the literature.[12] LiTCNQ was obtained according to ref.[1] The reaction was carried out under oxygen-free nitrogen, using standard Schlenk techniques and degassed solvents. A solution of LiTCNQ (0.4 g, 1.9 mmol) in methanol/acetonitrile (1:1, 10 mL) was added dropwise to a solution of $[Mn(MAC)(H_2O)_2]Cl_2{\cdot}4H_2O$ (0.44 g, 0.9 mmol) dissolved in methanol/acetonitrile (30 mL). The resultant mixture was allowed to stand at room temperature. After several hours, red crystals resulted, which were filtered off and washed with methanol/acetonitrile (1:1). IR data (KBr, cm^{-1}): $\tilde{\nu}$ = 3247 m, 2188 vs, 2166 s, 1580 s, 1499 s, 1341 s, 1170 s, 1103 w, 937 w, 914 w, 818 m, 718 w, 476 w. $C_{39}H_{29}MnN_{13}$ (734.68): calcd. C 63.76, H 3.98, N 24.78; found C 63.5, H 4.3, N 24.3.

Crystallographic Data Collection and Structure Determination: The diffraction intensities for compound **1** were collected on a STOE Image Plate IPDS II-System. The structures was solved by direct methods and refined against F^2 by using SHELXL-97.[13] Heavy atoms were refined anisotropically. Hydrogen atoms were included using the riding model with U_{iso} tied to U_{iso} of the parent atoms. Crystallographic data and other pertinent information are summarised in Table 2. CCDC-196351 contains the supplementary crystallographic data for this paper. These data can be obtained free of charge at www.ccdc.cam.ac.uk/conts/retrieving.html [or from the Cambridge Crystallographic Data Centre, 12, Union Road, Cambridge CB2 1EZ, UK; Fax: (internat.) +44-1223/336-033; E-mail: deposit@ccdc.cam.ac.uk].

Table 2. Crystal data and structure refinement for compound **1**

Empirical formula	$C_{39}H_{29}MnN_{13}$
Formula mass	734.68
Crystal system	monoclinic
Space group	*C*2/*c*
a (Å)	10.6960(7)
b (Å)	15.8054(13)
c (Å)	21.2076(16)
β (°)	93.93(1)
V (Å^3)	3576.81(15)
Z	4
$D_{calcd.}$ (g cm^{-3})	1.364
R_1 [$F_o > 4\sigma(F_o)$]	0.0478
R_1 (all data)	0.0546

Other Measurements: IR spectra (KBr pellets) were recorded on a BIO-RAD FTS 135 spectrometer. Magnetic susceptibility measurements were carried out using a SQUID magnetometer (MPMS Quantum Design). EPR measurements of the powder samples were carried out on ERS-230 and Varian spectrometers in the temperature range 300−10 K (X-band), 300−100 K and at 4.2 K (Q-band).

Acknowledgments

A. M. M. and M. A. are grateful to the Alexander von Humboldt Foundation for financial support of this work. Support from the INTAS Program (Project 2000−00375) and the Deutsche Forschungsgemeinschaft is gratefully acknowledged. We thank Professor K. Wieghardt for the magnetic measurements and Professor K. M. Salikhov for helpful discussions. Support from the Russian Foundation for Basic Research No. 01−03−32270 is greatly appreciated.

[1] L. R. Melby, R. J. Herder, W. Mahler, R. E. Benson, W. E. Mochel, *J. Am. Chem. Soc.* **1962**, *84*, 3374.
[2] L. Ballester, A. Gutiérrez, M. F. Perpiñán, M. T. Azcondo, *Coord. Chem. Rev.* **1999**, *190−192*, 447.

 © 2003 Wiley-VCH Verlag GmbH & Co. KGaA, Weinheim

[3] [3a] A. H. Reis Jr., L. D. Preston, J. M. Williams, S. W. Peterson, G. A. Candela, L. J. Schwartzendruber, J. S. Miller, *J. Am. Chem. Soc.* **1979**, *101*, 2756. [3b] W. E. Broderick, J. A. Thompson, E. P. Day, B. M. Hoffman, *Science* **1990**, *249*, 401. [3c] W. E. Broderick, B. M. Hoffman, *J. Am. Chem. Soc.* **1991**, *113*, 6334.
[4] [4a] J. B. Torrance, *Acc. Chem. Res.* **1979**, *12*, 79. [4b] M. T. Azcondo, L. Ballester, E. Coronado, A. M. Gil, C. Gómez, A. Gutiérrez, M. F. Perpiñán, J. Ramos, A. E. Sánchez, *Synth. Met.* **1997**, *86*, 1833. [4c] L. Ballester, A. M. Gil, A. Gutiérrez, M. F. Perpiñán, M. T. Azcondo, A. E. Sánchez, U. Amador, J. Campo, F. Palacio, *Inorg. Chem.* **1997**, *36*, 5291.
[5] J. S. Miller, A. J. Epstein, *Angew. Chem. Int. Ed. Engl.* **1994**, *33*, 385.
[6] H. Endres, in J. S. Miller (Ed.), *Extended Linear Chain Compounds*, vol. 3, Plenum, New York, **1983**, p. 263.
[7] W. Kaim, M. Moscherosch, *Coord. Chem. Rev.* **1994**, *129*, 157.
[8] P. Kundeler, P. J. Koningsbruggen, J. P. Cornelissen, A. N. van der Host, A. M. van der Kraan, A. L. Spek, J. A. Haasnoot, J. Reedijk, *J. Am. Chem. Soc.* **1996**, *118*, 2190.
[9] [9a] L. Ballester, M. C. Barral, A. Gutiérrez, A. Monge, M. F. Perpiñán, C. Ruiz Valero, A. Sánchez-Pelaez, *Inorg. Chem.* **1994**, *33*, 2142. [9b] L. Ballester, A. Gutiérrez, M. F. Perpiñán, U. Amador, M. T. Azcondo, A. E. Sánchez, C. Bellitto, *Inorg. Chem.* **1997**, *36*, 6390. [9c] L. Ballester, A. M. Gill, A. Gutiérrez, M. F. Perpiñán, M. T. Azcondo, A. E. Sánchez, E. Coronado, C. J. Gómez-García, *Inorg. Chem.* **2000**, *39*, 2837.
[10] [10a] J. P. Cornelissen, J. H. van Diemen, L. R. Groeneveld, J. G. Haasnoot, A. L. Speck, J. Reedijk, *Inorg. Chem.* **1992**, *31*, 198. [10b] M. T. Azcondo, L. Ballester, A. Gutiérrez, M. F. Perpiñán, U. Amador, C. Ruiz-Valero, C. Bellitto, *J. Chem. Soc., Dalton Trans.* **1996**, 3015.
[11] A. M. Madalan, H. W. Roesky, M. Andruh, M. Noltemeyer, N. Stanica, *Chem. Commun.* **2002**, 1638.
[12] O. Jiménez-Sandoval, D. Ramírez-Rosales, M. del Jesús Rosales-Hoz, M. E. Sosa-Torres, R. Zamorano-Ulloa, *J. Chem. Soc., Dalton Trans.* **1998**, 1551.
[13] G. M. Sheldrick, SHELXL-97, *Program for Crystal Structure Refinement*, University of Göttingen, Germany, **1997**.
[14] [14a] O. Kahn, *Molecular Magnetism*, VCH Publishers, New York, **1993**, p. 258. [14b] M. E. Fisher, *Am. J. Phys.* **1964**, *32*, 343.
[15] P. W. Anderson, P. R. Weiss, *Rev. Mod. Phys.* **1953**, *25*, 269.
[16] E. Pleau, G. Kokoszka, *J. Chem. Soc., Faraday Trans. 2* **1973**, *69*, 355.
[17] R. Kubo, K. Tomita, *J. Phys. Soc.* **1954**, *9*, 888.
[18] Yu. N. Molin, K. M. Salikhov, K. I. Zamaraev, *Spin Exchange Principles and Application in Chemistry and Biology*, Springer, Berlin, **1980**.

Received November 11, 2002

 © 2003 Wiley-VCH Verlag GmbH & Co. KGaA, Weinheim

EurJIC
European Journal of Inorganic Chemistry

June 2003
Issue 11
Pages 2001–2184

Papers available ahead of print in Early View at www.interscience.wiley.com

Earliest available Table of Contents:
Automatically, free of charge by e-mail through
www.interscience.wiley.com/alerts

COVER PICTURE

The cover picture shows two isomers of a carbonylcopper(I) complex of the new ligand tris(pyrazolyl)methanesulfonate (Tpms). This new class of ligands contains three nitrogen donor atoms and in addition a sulfonate group which makes the ligands more hydrophilic. The sulfonate group can act as a competing donor centre. Therefore Tpms ligands are ambidentate ligands, that can adapt their coordination modes according to the electronic preferences of the metal centre. In solution, e.g., carbonylcopper(I) and zinc halide complexes show an equilibrium between the N,N,N- and N,N,O-coordination mode. Synthesis, characterization and the dynamic stereochemistry of Tpms and Tpms^{tBu} complexes are presented in the article by W. Kläui et al. on p. 2059 ff. We thank B. Kugel and P. Kunz for their help with the cover picture.

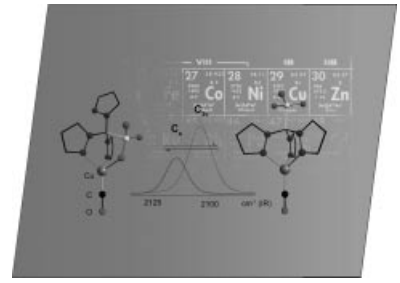

MICROREVIEW

Contents

2017 **A. Jutand**

The Use of Conductivity Measurements for the Characterization of Cationic Palladium(II) Complexes and for the Determination of Kinetic and Thermodynamic Data in Palladium-Catalyzed Reactions

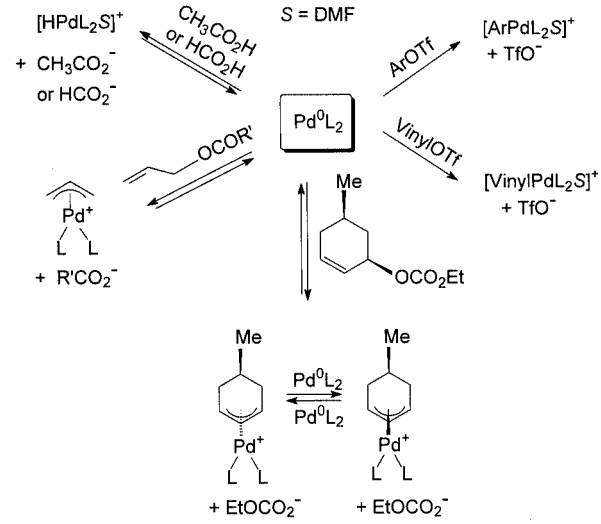

Keywords: Cationic complex / Conductivity / Kinetics / Mechanism / Palladium

 © 2003 Wiley-VCH Verlag GmbH & Co. KGaA, Weinheim

SHORT COMMUNICATIONS

2041 **A. V. Usatov,* E. V. Martynova, I. S. Neretin, Yu. L. Slovokhotov, A. S. Peregudov, Yu. N. Novikov**

The First Mononuclear η^2-C_{60} Complex of Osmium: Synthesis and X-ray Crystal Structure of $[(\eta^2\text{-}C_{60})Os(CO)(t\text{BuNC})(PPh_3)_2]$

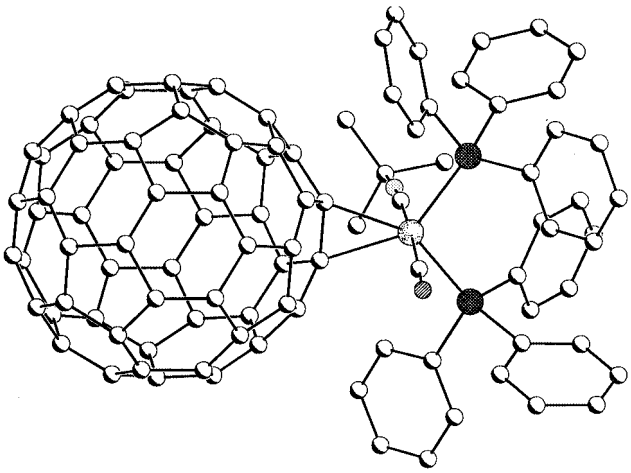

Keywords: Fullerenes / Olefins / Osmium / Pi interactions

2045 **S. Aime,* E. Gianolio, A. Barge, D. Kostakis, I. C. Plakatouras, N. Hadjiliadis**

Modulation of the Prototropic Exchange Rate at the Water Molecule Coordinated to a Gd^{III} Ion

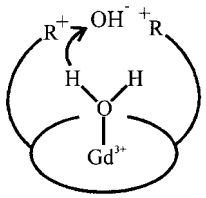

Keywords: Gadolinium / Chelates / Basicity / Neighbouring-group effects / Prototropic exchange / Imaging agents

2049 **M. Scheibitz, J. W. Bats, M. Bolte, M. Wagner***

P−B Adducts of 3,4-Dimethyl-1-phosphaferrocene with Bromoboranes

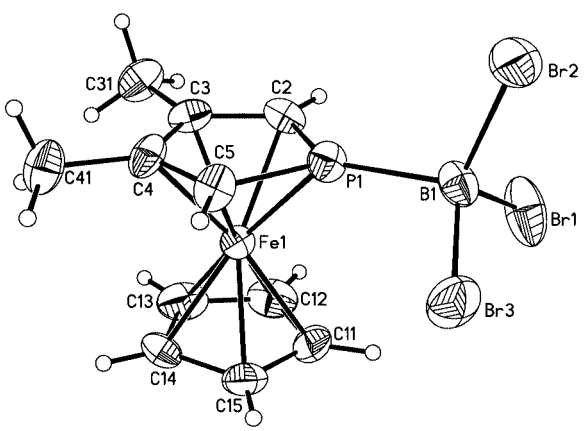

Keywords: Boranes / Donor-acceptor systems / Metallocenes / P ligands / X-ray diffraction

© 2003 Wiley-VCH Verlag GmbH & Co. KGaA, Weinheim

2054 **X. Xu, S. Gou,* W. Huang, Y. Ma, Y. Li**

Assembly of Seven Nickel(II) Metals by Chiral, Salen-Type Ligands with μ_3-OH Bridges

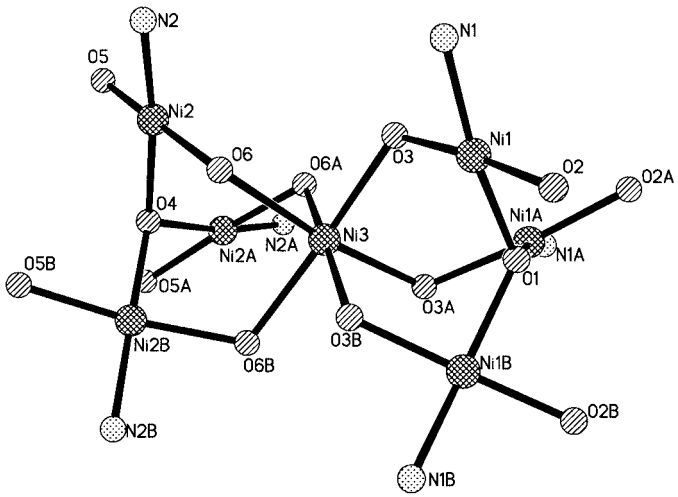

Keywords: Nickel / Chirality / Bridging ligands

FULL PAPERS

2059 **W. Kläui,* M. Berghahn, W. Frank, G. J. Reiß, T. Schönherr, G. Rheinwald, H. Lang**

Tris(pyrazolyl)methanesulfonates: More Than Just Analogues of Tris(pyrazolyl)borate Ligands; N,N,N-, N,N,O-, and Other Coordination Modes

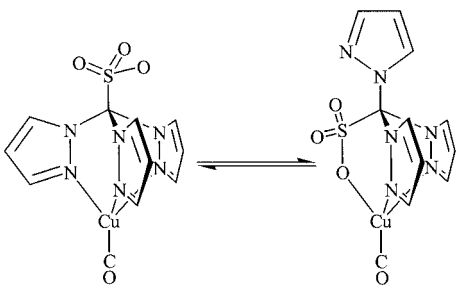

Keywords: Enzyme models / N,O ligands / Transition metals / Tripodal ligands

2071 **C. Redshaw,* M. R. J. Elsegood**

Tungsten(VI) Complexes Derived from Calix[6]- and -[8]arenes: Oxo and Oxychloride Species

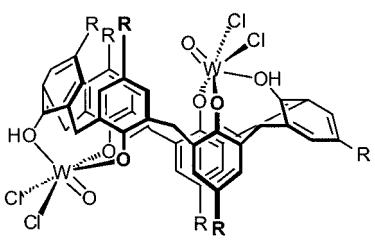

Keywords: Tungsten / Calixarenes / Oxo ligands

2075 **M. Sivák,* M. Mad'arová, J. Tatiersky, J. Marek**

First (Peroxo)vanadium(V) Complex with Heteroligand Formed in Reaction System − Synthesis, Structure and Reactivity of K[$VO(O_2)$(*omeida*)]·H_2O {*omeida* = *N*-[2-(2-oxomorpholine-4-yl)ethyl]iminodiacetato(2−)}

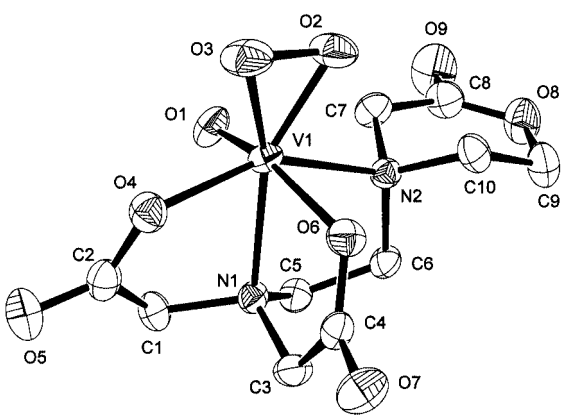

Keywords: Vanadium / Peroxo ligands / δ-Lactones / ^{51}V NMR spectroscopy / *N*-acetyl-L-cysteine

 © 2003 Wiley-VCH Verlag GmbH & Co. KGaA, Weinheim

2082 **T. Pintauer, U. Reinöhl, M. Feth, H. Bertagnolli, K. Matyjaszewski***

Extended X-ray Absorption Fine Structure Study of Copper(I) and Copper(II) Complexes in Atom Transfer Radical Polymerization

Keywords: EXAFS spectroscopy / Copper / Radical reactions / Polymerizations

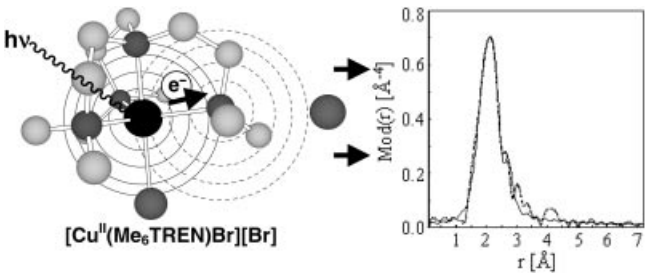

2095 **C. B. Perry, M. A. Fernandes, K. L. Brown, X. Zou, E. J. Valente, H. M. Marques***

Probing the Nature of the Co^{III} Ion in Cobalamins − Spectroscopic and Structural Investigations of the Reactions of Aquacobalamin (Vitamin B_{12a}) with Ambident Nucleophiles

Keywords: Cobalamins / Ambidentate ligands / Cobalt / Bioinorganic chemistry / X-ray diffraction

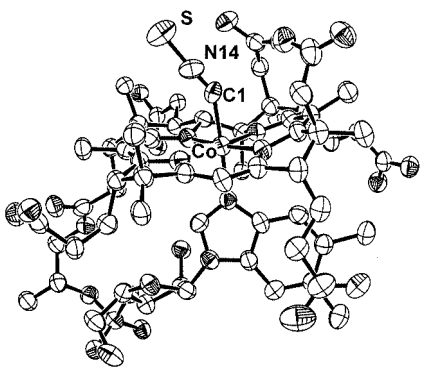

2108 **L. Garlaschelli,* F. Greco, G. Peli, M. Manassero,* M. Sansoni, R. Gobetto,* L. Salassa, R. Della Pergola**

Synthesis, Solid-State Structure and Multinuclear NMR Studies of the New Polyhydrido Iridium Carbonyl Cluster $Ir_4H_4(\mu\text{-}H)_4(CO)_4(PPh_3)_4$

Keywords: Cluster compounds / Iridium / Hydride ligands / NMR spectroscopy / P ligands

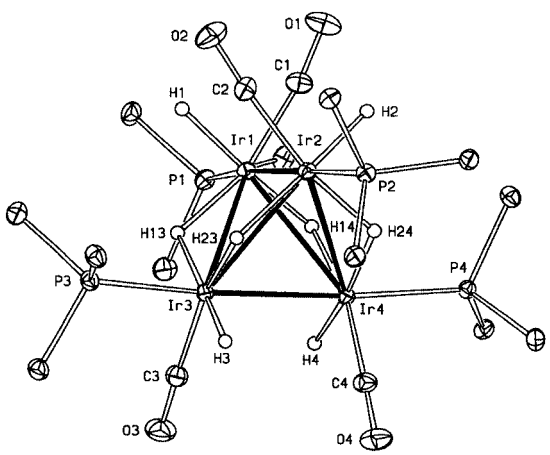

2113 **T. Jakusch, A. Dörnyei, I. Correia, L. Rodrigues, G. K. Tóth, T. Kiss,* J. Costa Pessoa,* S. Marcão**

Interaction of $V^{IV}O$, $V^{V}O_2$ and Cu^{II} with a Peptide Analogue

Keywords: Vanadium / Copper / Peptides / Speciation / Spectroscopy / Bioinorganic chemistry

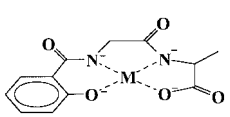

 © 2003 Wiley-VCH Verlag GmbH & Co. KGaA, Weinheim

2123 **P. Gómez-Saiz, J. García-Tojal,* M. Maestro, J. Mahía, L. Lezama, T. Rojo**

Coordination Modes in a (Thiosemicarbazone)-copper(II)/Oxalato System − Structures of $[\{Cu(L)\}_2(ox)]\cdot 2H_2O$, $[Cu(HL)(ox)(H_2O)]$, $[\{Cu(HL)\}_2(ox)][Cu(ox)_2]\cdot 2H_2O$ and $[\{Cu(HL)\}_2(ox)](NO_3)_2$ − Ferro- vs. Antiferromagnetic Behavior in Dinuclear Compounds

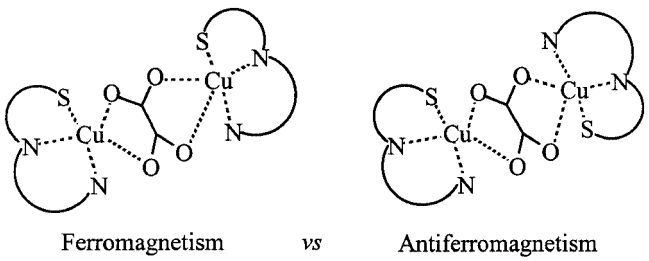

Keywords: Copper / Carboxylate ligands / Magnetic properties / Thiosemicarbazone complexes

2133 **W. Malisch,* D. Schumacher, B. Schmiedeskamp, H. Jehle, D. Eisner, W. W. Schoeller, M. Nieger**

Iron-Fragment-Substituted Heterosiloxanes of Gallium $[Cp(OC)_2Fe{-}SiR_2OGaR'_2]_2$ (R, R′ = Alkyl, Aryl) − Structures of $[Cp(OC)_2Fe\text{-}SiR_2{-}OGaMe_2]_2$ (R = Me, Ph)

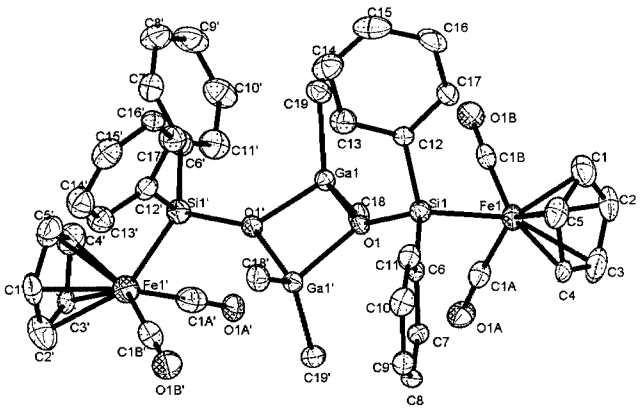

Keywords: Gallium / Iron / Silanols / Silicon / Siloxanes

2139 **H. Provendier, C. C. Santini,* J.-M. Basset, L. Carmona**

Surface Organometallic Chemistry on Oxides: The First Well-Defined Selenium(IV) Derivative Grafted onto Silica

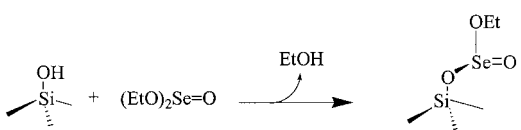

Keywords: Acetaldehyde / Oxidation / Selenium / Supported catalysis / Surface chemistry

2145 **M. T. Gamer, P. W. Roesky***

Bridged Aminotroponiminate Complexes of Zinc

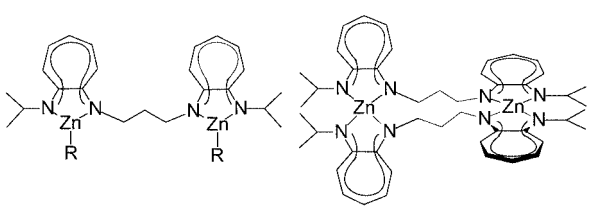

Keywords: Aminotroponiminate / Coordination chemistry / N ligands / Zinc

 © 2003 Wiley-VCH Verlag GmbH & Co. KGaA, Weinheim

2149 **Y. Steudel, R. Steudel***

Structures and Thermodynamics of the Sulfuranes SF_3CN and $SF_2(CN)_2$ as well as of the Persulfurane $SF_4(CN)_2$ − An ab initio MO Study by the G3(MP2) Method

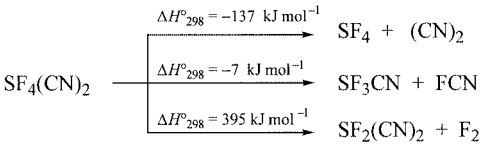

Keywords: Sulfuranes / Sulfur / Cyanides / Fluorides / Transition states / Reaction mechanisms

2153 **H.-J. Himmel**

Calculated Enthalpies for Dimerisation of Binary, Unsaturated, Main-Group Element Hydrides as a Means to Analyse Their Potential for Multiple Bonding

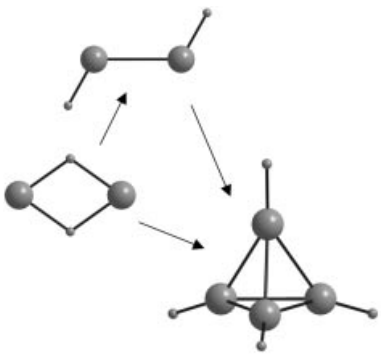

Keywords: Main-group element hydrides / Dimerization / Enthalpy / Multiple bonding / Calculations

2164 **L.-C. Song,* P.-C. Liu, Q.-M. Hu, Z. Lin, Y.-B. Wang**

Synthesis and Characterization of Pentaarylated [60]Fullerene Coordinated Complexes [(η^2-$Ar_5C_{60}H$)$M(PPh_3)_2$] (M = Pt, Pd) and an ab initio Study on Their Isomerism

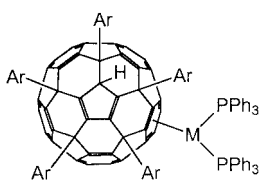

Keywords: Ab initio calculations / Fullerenes / Isomerism / Palladium / Platinum

2170 **M. Burgos, O. Crespo, M. C. Gimeno, P. G. Jones, A. Laguna***

Gold, Silver and Palladium Complexes with the 2,2′-Dipyridylamine Ligand

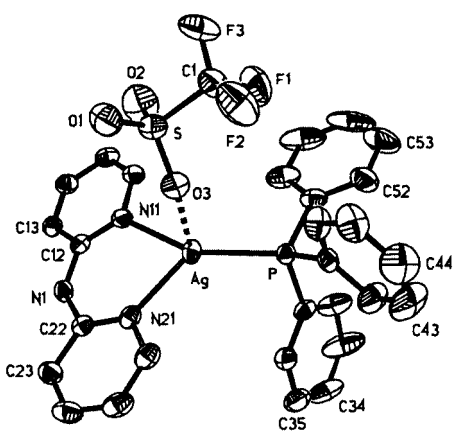

Keywords: Gold / N Ligands / Palladium / Silver

 © 2003 Wiley-VCH Verlag GmbH & Co. KGaA, Weinheim

2175 **X. Zheng, G. E. Herberich***

New Alkali Metal Boratabenzenes: Structures of K([18]-Crown-6)(C_5H_5BMe), of the Tetrahydropyran Solvate K(3,5-$Me_2C_5H_3B-NMe_2$)$(THP)_2$, and of Two THF Solvates of K[3,5-Me_2-$C_5H_3B-N(SiMe_3)_2$]

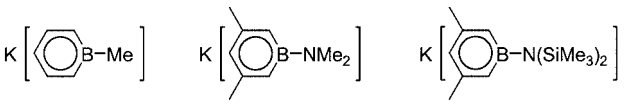

Keywords: Alkali metal salts / Borabenzene / Boratabenzene / Boron

CORRECTION

2183 **P. Paredes, D. Miguel, F. Villafañe***

Synthesis of (η^3-Allyl)bromodicarbonylbis(pyrazole)molybdenum(II) and Reactivity towards [Au(acac)PPh_3]: Structure and Dynamic Behavior of the Monometallic Pyrazole and Heterometallic Pyrazolate Complexes

Keywords: Molybdenum / Gold / Heterometallic complexes / N ligands / Fluxionality

 © 2003 Wiley-VCH Verlag GmbH & Co. KGaA, Weinheim

The Use of Conductivity Measurements for the Characterization of Cationic Palladium(II) Complexes and for the Determination of Kinetic and Thermodynamic Data in Palladium-Catalyzed Reactions

Anny Jutand[a]

Keywords: Cationic complex / Conductivity / Kinetics / Mechanism / Palladium

This review illustrates how conductivity measurements are used to characterize the *cationic* character of aryl-, vinyl-, hydrido-, and (η^3-allyl)palladium(II) complexes generated by oxidative addition of aryl and vinyl triflates, acetic/formic acid, and allylic carboxylates/carbonates, respectively, with palladium(0) complexes in DMF. These cationic palladium(II) complexes have been postulated as key intermediates in Stille, Heck, Tsuji–Trost, and Trost reactions, but most of them have never been characterized in the context of real oxidative additions, i.e., with the counteranion delivered by the reagent (triflates, carboxylates, and carbonates). The role of chloride ions has been examined and the mechanistic consequences are reported. Conductivity measurements are also used to obtain thermodynamic and kinetic data on the formation of cationic palladium(II) complexes and, consequently, to gain a deeper insight into the mechanism of palladium-catalyzed reactions. The *reversibility* of oxidative additions of acetic/formic acid and allylic carboxylates/carbonates with Pd^0 complexes has been established and equilibrium constants have been determined. The isomerization of cyclic *trans*/*cis* cationic (η^3-allyl)palladium(II) complexes is evidenced by a rate constant that depends on the Pd^0 precursor: kinetic evidence for an S_N2 mechanism that is responsible for the loss of stereoselectivity observed in catalytic reactions. Under conditions in which the oxidative additions are irreversible, the *kinetics* of the formation of cationic (η^3-allyl)palladium(II) complexes has been monitored by conductivity measurements for the determination of the rate constants. By comparing the rate of disappearance of Pd^0, it has been shown that oxidative additions of allylic carboxylates proceed in two steps with the detection of intermediate neutral, kinetic Pd^0 complexes ligated to the allylic carboxylate unit. As an example of its application, the mechanism of a Stille reaction has been investigated by conductivity measurements of an ionic by-product in DMF.

© Wiley-VCH Verlag GmbH & Co. KGaA, 69451 Weinheim, Germany, 2003

Introduction

Many palladium-catalyzed reactions involve cationic palladium(II) complexes generated in the first step of the catalytic cycle. In Heck reactions[1] with aryl triflates (ArOTf, Tf = SO_2CF_3),[1,2] [Equation (1)], cationic arylpalladium(II) complexes are formed in the oxidative addition of aryl triflates to Pd^0 complexes [Equation (2), L = monodentate ligand or L_2 = bidentate ligand].

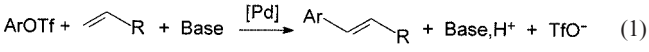

(1)

(2)

In Tsuji−Trost reactions [Equation (3)], cationic (η^3-allyl)palladium(II) complexes are formed in the oxidative addition of allylic carboxylates (or carbonates) to Pd^0 complexes [Equation (4)].[3]

[a] Ecole Normale Supérieure, Département de Chimie, UMR CNRS 8640,
24, Rue Lhomond, 75231 Paris Cedex 5, France
Fax: (internat.) + 33-1/44323325
E-mail: Anny.Jutand@ens.fr

Anny Jutand was born in France in 1948. She studied chemistry at the Ecole Nationale Supérieure de Chimie de Paris (MS degree, University Paris VI, 1971). She obtained her Doctorate under the direction of Professor J. F. Fauvarque at the University Paris XIII in Villetanneuse. After a postdoctoral stay with Professor B. Åkermark at the Royal Institute of Technology in Stockholm, she moved back to the University Paris XIII. In 1984, she joined Dr. C. Amatore's group at the Ecole Normale Supérieure in Paris. She became Research Director at CNRS (a position equivalent to a full Professor) in 1992. Her current research interests are centered on the investigation of the mechanism of transition metal catalyzed reactions and the development of reactions that require activation by both a transition metal and electron transfer.

MICROREVIEWS: This feature introduces the readers to the authors' research through a concise overview of the selected topic. Reference to important work from others in the field is included.

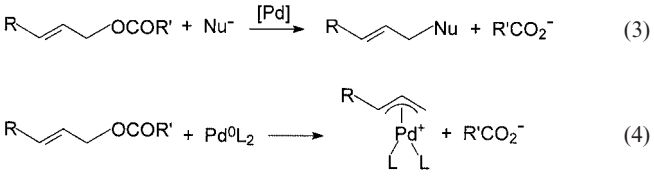

Most cationic complexes postulated, however, as key intermediates have not been characterized under the conditions of real oxidative additions. This review illustrates how, by using conductivity measurements,[4,5] cationic palladium(II) complexes formed in oxidative additions may be detected and characterized[6] under the real conditions of a catalytic reaction. Moreover, since the conductivity of free ionic species is proportional to their concentration,[5] this technique can also be used to obtain thermodynamic and kinetic data for the formation of cationic palladium(II) complexes and, consequently, to obtain a deeper insight into the mechanism of palladium-catalyzed reactions.

I. Observation by Conductivity Measurements of Cationic Arylpalladium(II) Complexes in the Oxidative Addition of Aryl Triflates to Neutral Pd^0 Complexes

Since 1984, aryl (or vinyl) triflates often have been used, instead of aryl (or vinyl) halides, in palladium-catalyzed Heck reactions [Equation (1)][2] or Stille reactions [Equation (5)].[7]

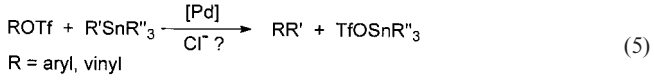

Such reactions, however, are greatly affected by the presence of chloride ions, which are added in large excess relative to the palladium catalyst. Extra chloride ions are always required in the case of Stille reactions involving vinyl triflates [Equation (5)].[7a,7b] A mechanistic investigation of the oxidative addition of vinyl triflates to $Pd^0(PPh_3)_4$, reported by Scott and Stille in 1986,[7b] revealed that undefined unstable complexes were formed in THF, whereas stable, well-characterized neutral $(\eta^1\text{-vinyl})Pd^{II}Cl(PPh_3)_2$ complexes were generated when the oxidative addition was performed in the presence of chloride ions. The undefined complexes were postulated to be unstable cationic complexes $[(\eta^1\text{-vinyl})Pd^{II}(PPh_3)_n]^+TfO^-$ (n = 2 or 3). In 1989, Stang et al. established that well-characterized cationic complexes $[(\eta^1\text{-vinyl})Pt^{II}(PPh_3)_3]^+TfO^-$ are formed in the oxidative addition of vinyl triflates to $Pt^0(PPh_3)_4$ in toluene.[8]

To explain the effect of chloride ions on the efficiency of palladium-catalyzed Stille reactions involving aryl triflates, Echavarren and Stille[7c] proposed in 1987 that neutral complexes $ArPdCl(PPh_3)_2$ were produced when the oxidative addition of $Pd^0(PPh_3)_4$ was performed in the presence of chloride ions, whereas decomposition took place in the absence of chloride ions. To characterize cationic complexes $[ArPd(PPh_3)_n]^+$ that would be formed in the oxidative addition of aryl triflates to $Pd^0(PPh_3)_4$, the reaction was reinvestigated by Farina et al. in 1993 in the polar solvent NMP. The authors could not conclude, however, what the structure is of the arylpalladium(II) complex formed in the absence of chloride ions in NMP.[9]

Until 1995, none of the complexes $[ArPdL_n]^+TfO^-$ or $[(\eta^1\text{-vinyl})PdL_n]^+TfO^-$ had been characterized in the oxidative addition of aryl or vinyl triflates, respectively, to Pd^0 complexes.

I.1 Evidence from Conductivity Measurements for the Formation of Cationic *trans*-$[ArPdL_2S]^+$ Complexes in the Oxidative Addition of Aryl Triflates to Neutral Pd^0 Complexes in DMF

In 1995, the cationic character of $[ArPd^{II}(PPh_3)_2S]^+$ complexes, formed in the oxidative addition of aryl triflates to a halide-free Pd^0 complex such as $Pd^0(PPh_3)_4$, was established by conductivity measurements in DMF [Equation (6), L = PPh_3, S = solvent].[10]

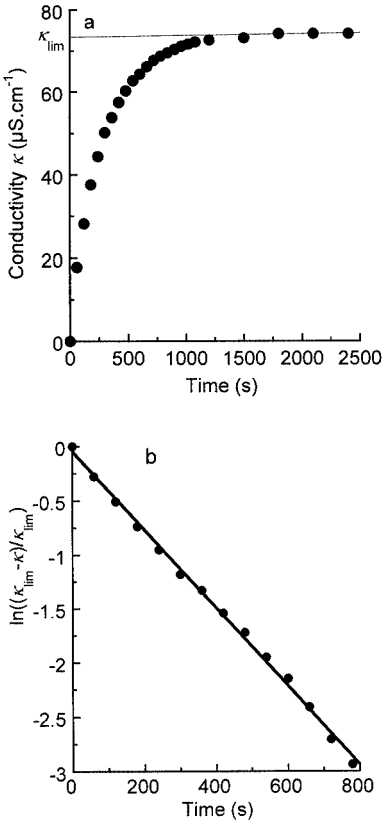

Figure 1. Kinetics of the formation of *trans*-[4-$O_2NC_6H_4Pd(PPh_3)_2(DMF)]^+TfO^-$ in the oxidative addition of 4-$O_2NC_6H_4OTf$ (10 mM) to $Pd^0(PPh_3)_4$ (2 mM) in DMF at 20 °C: (a) variation of the conductivity versus time; $\kappa = \kappa_{exp} - \kappa_0$ (κ_{exp}: experimental conductivity at t; κ_0: initial residual conductivity of 2 $\mu S \cdot cm^{-1}$); (b) variation of $\ln[(\kappa_{lim} - \kappa)/\kappa_{lim})]$ versus time; κ: conductivity at t; κ_{lim}: final conductivity

 © 2003 Wiley-VCH Verlag GmbH & Co. KGaA, Weinheim

$$ArOTf + Pd^0L_4 \xrightarrow{k_{app}} ArPdL_2S^+ + TfO^- + 2\,L \quad (6)$$

Indeed as is shown in Figure 1 (a), the conductivity (κ) of a solution of $Pd^0(PPh_3)_4$ (2 mM) in DMF (residual conductivity: $\kappa_0 = 2\ \mu S{\cdot}cm^{-1}$) increased upon addition of an aryl triflate (4-$O_2NC_6H_4OTf$) to reach a final, constant conductivity, κ_{lim}. This limiting value was obtained after the oxidative addition was complete, as confirmed by the total disappearance of $Pd^0(PPh_3)_4$, monitored simultaneously by amperometry.[10] This experiment shows that ionic species are formed in the oxidative addition. Moreover, such ionic species are rather stable, as is attested by the observed constant limiting value, κ_{lim} (Figure 1, a).

Cationic complexes were then isolated after an oxidative addition performed in a toluene/DMF solution. Analyses by FAB and electrospray mass spectrometry delivered values of *m*/*z* corresponding to the $[ArPd(PPh_3)_2]^+$ cations (Ar = 4-ClC_6H_4 and 4-$O_2NC_6H_4$) with the predicted isotope pattern expected for the Pd atom. The TfO^- anion was also characterized by FAB spectrometry.[10] Additionally, these complexes were characterized by ^{31}P NMR spectroscopy performed in DMF. The observation of one singlet in the ^{31}P NMR spectrum, even in the presence of excess PPh_3 released from $Pd^0(PPh_3)_4$ [Equation (6)], establishes that the cationic complex contains only two phosphane ligands. Moreover, those two phosphane ligands sit in a relative *trans* orientation on the Pd^{II} atom, with the fourth position being occupied by the solvent as in compound **1**.[10] Consequently, the cationic complexes $[ArPd(PPh_3)_3]^+TfO^-$ are not generated in DMF.

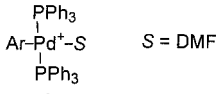

1

The association of the cations *trans*-$[ArPdL_2S]^+$ with the anion TfO^- was studied by observing the variation of their conductivities versus their concentration. In DMF, the conductivity of the ionic species, determined by the value of κ_{lim} (as in Figure 1, a), varied linearly with the palladium concentration in the range $0.5-3 \times 10^{-3}$ M (Figure 2, a).[10] This study established that free ions, *trans*-$[ArPdL_2(DMF)]^+$ and TfO^-, are formed in DMF [Equation (7), L = PPh_3].

$$ArOTf + Pd^0L_4 \xrightarrow{DMF} \underset{trans}{ArPdL_2(DMF)^+} + TfO^- + 2\,L \quad (7)$$

The molar conductivity Λ_M of these ions was calculated in DMF at 20 °C. The values are indicative of 1:1 electrolytes in solution in DMF:[6]

$\Lambda_M = 35\ (\pm 2)\ S{\cdot}cm^2{\cdot}mol^{-1}$ for *trans*-$[4\text{-}O_2NC_6H_4Pd(PPh_3)_2(DMF)]^+TfO^-$

$\Lambda_M = 57\ (\pm 2)\ S{\cdot}cm^2{\cdot}mol^{-1}$ for *trans*-$[4\text{-}ClC_6H_4Pd(PPh_3)_2(DMF)]^+TfO^-$

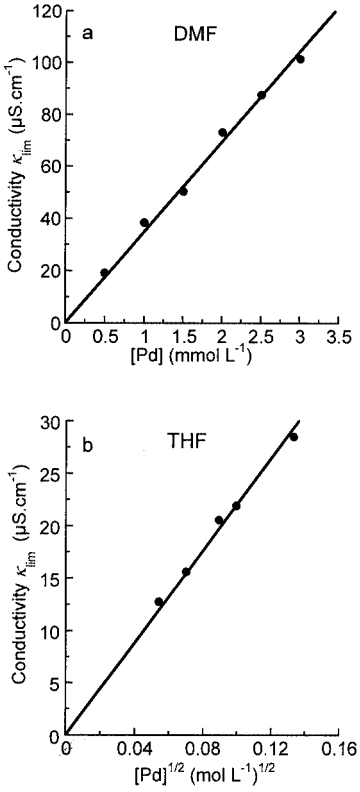

Figure 2. (a) Variation of the conductivity of *trans*-$[4\text{-}O_2NC_6H_4Pd(PPh_3)_2(DMF)]^+TfO^-$ in DMF, determined by the value of κ_{lim} (Figure 1, a) versus the concentration of Pd initially introduced as $Pd^0(PPh_3)_4$ before reaction with 4-$O_2NC_6H_4OTf$, at 20 °C; (b) variation of the conductivity of *trans*-$[4\text{-}O_2NC_6H_4Pd(PPh_3)_2(THF)]^+TfO^-$ in THF (determined as in Figure 2, a) versus the square root of the Pd concentration, at 20 °C

In THF, the conductivity of the ionic species formed in the oxidative addition was lower than that observed in DMF. Moreover, the conductivity varied linearly with the square root of the palladium concentration (Figure 2, b).[10] This observation establishes that free ions *trans*-$[ArPd(PPh_3)_2(THF)]^+$ and TfO^- are formed in THF,[11] but they are involved in an equilibrium with the neutral complex $[ArPd(OTf)(PPh_3)_2]$.[13]

The effect of additives (chloride or acetate ions) on the structure of the cationic complexes has been tested. Addition of chloride ions, from nBu_4NCl (2 mM), to a solution of *trans*-$[4\text{-}O_2NC_6H_4Pd(PPh_3)_2(DMF)]^+TfO^-$ (2 mM) in DMF resulted in a conductivity lower than the sum of the intrinsic conductivities of *trans*-$[4\text{-}O_2NC_6H_4\text{-}Pd(PPh_3)_2(DMF)]^+TfO^-$ and $nBu_4N^+Cl^-$.[10] This observation is indicative of the formation of a neutral complex, which was identified as *trans*-4-$O_2NC_6H_4PdCl(PPh_3)_2$ [Equation (8), L = PPh_3] by comparison with an authentic sample.

$$ArPdL_2(DMF)^+ + TfO^- + nBu_4N^+ + Cl^- \longrightarrow ArPdClL_2 + TfO^- + nBu_4N^+ \quad (8)$$

 © 2003 Wiley-VCH Verlag GmbH & Co. KGaA, Weinheim

It has also been observed that the oxidative addition in DMF of aryl triflates to the anionic Pd^0 complex $[Pd^0(PPh_3)_2Cl]^-$, generated by addition of chloride ions to $Pd^0(PPh_3)_4$ or by the electrochemical reduction of $PdCl_2(PPh_3)_2$,[14] gave the neutral *trans*-$ArPdCl(PPh_3)_2$ (Scheme 1).[10,15]

Scheme 1. Oxidative addition of aryl triflates to anionic Pd^0 complexes

Similarly, the oxidative addition in DMF of aryl triflates to the anionic Pd^0 complex $[Pd^0(PPh_3)_2(OAc)]^-$, generated from $Pd(OAc)_2$ and 3 equiv. of PPh_3,[16] led to neutral complexes *trans*-$ArPd(OAc)(PPh_3)_2$ (Scheme 2).[15] At low concentrations, some *trans*-$[ArPd(PPh_3)_2(DMF)]^+$ may still coexist with *trans*-$ArPd(OAc)(PPh_3)_2$ since the partial dissociation of the latter to the cationic complex and AcO^- has been established independently ($K_{diss} = 1.3 \times 10^{-3}$ M).[16b,16c]

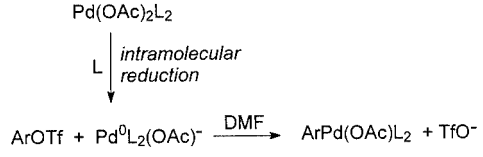

Scheme 2. Oxidative addition of aryl triflates to anionic Pd^0 complexes

Consequently, in the case of the *monodentate phosphane* PPh_3, cationic complexes *trans*-$[ArPdL_2(DMF)]^+$ (TfO^- counteranion) are generated in the oxidative addition of aryl triflates to neutral Pd^0 complexes in DMF, whereas neutral complexes *trans*-$[ArPdXL_2]$ (X = Cl, OAc) are formed in the oxidative addition to anionic Pd^0 complexes ligated by chloride or acetate ions.

The oxidative addition of aryl triflates to Pd^0 complexes ligated to *bidentate bis(phosphane)* (P,P) ligands has also been investigated. When the oxidative addition of aryl triflates [Ar = 4-$O_2NC_6H_4$, 3,5-$(CF_3)_2C_6H_3$, C_6H_5] to $Pd^0(dppf)(\eta^2\text{-}CH_2{=}CHCO_2Me)$ was performed in THF, the resulting cationic $[ArPd(dppf)(THF)]^+$ complexes were not stable at room temperature.[17] Stable, neutral ArPdCl(dppf), ArPdI(dppf) and ArPd(OAc)(dppf) complexes were obtained, however, when the oxidative additions were performed in the presence of chloride, iodide or acetate ions, respectively.[17] Recently, Alcazar–Roman and Hartwig reported data on the oxidative addition of phenyl triflate to $Pd^0(BINAP)_2$ in THF. A stable cationic complex was obtained only in the presence of an amine: $[PhPd(BINAP)(NH_2R)]^+TfO^-$ (R = alkyl).[18]

Oxidative additions, however, of aryl triflates to Pd^0 ligated to bis(phosphane) (P,P) ligands are sluggish reactions.[17–19] To bypass this problem, chemists interested in the mechanism of reactions involving cationic $[ArPd(P,P)S]^+TfO^-$ complexes (supposedly formed in the oxidative addition of aryl triflates) have synthesized such complexes by treating ArPdX(P,P) (X = I, Br, Cl) with AgOTf.[18–21] Using this strategy, Brown and Hii characterized complexes $[ArPd(dppf)(THF)]^+TfO^-$ [Ar = Ph, 4-$CH_3OC_6H_4$, 3,5-$(CF_3)_2C_6H_3$] in THF at low temperatures ($\leq$ 0 °C); they found that [{3,5-$(CF_3)_2C_6H_3$}Pd(dppf)(DMF)]$^+TfO^-$ is stable at room temperature in DMF.[20b] In a similar manner, Espinet et al. reported that stable complexes $[ArPd(dppe)(THF)]^+TfO^-$ (Ar = C_6F_5, $C_6Cl_2F_3$) can be synthesized in THF.[19] These complexes have been characterized by conductivity measurements.[19,20b] Ludwig et al. have synthesized complexes $[PhPd(P,P)(DMF)]^+TfO^-$ (P,P = dppe, dppp, dcpe), which are stable at 0 °C.[21]

Consequently, polar solvents such as DMF (and, to lesser extent, THF) and amines appear to be good coordinating solvents and ligands, respectively, for the stabilization of cationic complexes $[ArPdL_2S]^+TfO^-$ [L = monophosphane or L_2 = bis(phosphane), *S* = solvent or amine] formed in the oxidative addition of aryl triflates to neutral Pd^0 complexes.

I.2 Kinetics of the Formation of Cationic $[ArPd(PPh_3)_2S]^+$ Complexes in the Oxidative Addition of Aryl Triflates to Neutral Pd^0 Complexes in DMF Monitored by Conductivity Measurements – Influence of Chloride Ions

Any oxidative addition performed using $Pd^0(PPh_3)_4$ involves $SPd^0(PPh_3)_2$ [22] as the reactive complex generated from $Pd^0(PPh_3)_3$ [23] in an endergonic and fast equilibrium (Scheme 3).

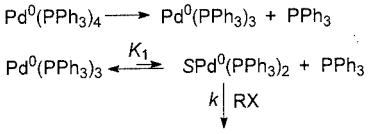

Scheme 3. Mechanism of oxidative additions from $Pd^0(PPh_3)_4$ (*S* = solvent)

The oxidative addition of aryl triflates with $Pd^0(PPh_3)_4$ [Equation (6)] is then an overall reaction that proceeds via $SPd^0(PPh_3)_2$ and k_{app} is the apparent rate constant of the overall reaction ($k_{app} = K_1k/[PPh_3]$).[22]

Since the conductivity κ of $[ArPd(PPh_3)_2(DMF)]^+TfO^-$ in DMF is proportional to its concentration, the evolution of the conductivity κ with time, as observed in Figure 1 (a), characterizes the kinetics of the formation the cationic complex $[ArPd(PPh_3)_2(DMF)]^+$ in the oxidative addition of ArOTf to $Pd^0(PPh_3)_4$. The variation of $\ln[(\kappa_{lim} - \kappa)/\kappa_{lim}]$ versus time was linear (Figure 1, b): $\ln[(\kappa_{lim} - \kappa)/\kappa_{lim}] = -k_{app}[ArOTf]t$.[10] The slope of the line gives the value of the rate constant for the formation of the cationic complex (0.35 ± 0.02 $M^{-1}s^{-1}$ for 4-$O_2NC_6H_4OTf$ in DMF at 20 °C). This rate constant is very similar to the rate constant of the disappearance of the Pd^0 complex monitored independently by amperometry ($k_{app} = 0.32 \pm 0.02$ $M^{-1}s^{-1}$).[10] This observation shows that, if the oxidative addition involves the

 © 2003 Wiley-VCH Verlag GmbH & Co. KGaA, Weinheim

Table 1. Accelerating effect of chloride ions [added as nBu$_4$NCl to Pd^0(PPh$_3$)$_4$ prior to the addition of ArOTf] on the rate of the oxidative addition of aryl triflates to Pd^0(PPh$_3$)$_4$ (c_0 = 2 mM) in DMF at 20 °C (Scheme 4)

ArOTf	4-O$_2$NC$_6$H$_4$OTf		C$_6$H$_5$OTf		1-Naphthyl−OTf	
Cl$^-$ equiv./[Pd^0(PPh$_3$)$_4$]	0	150	0	150	0	150
k_{app}^{Cl} [M^{-1}·s^{-1}]	0.32	0.59	1.7×10^{-3}	33×10^{-3}	7.5×10^{-2}	43×10^{-2}

formation of an intermediate neutral complex, ArPd(OTf)L$_2$, then the ionization of this neutral complex in DMF to [ArPdL$_2$(DMF)]$^+$ and TfO$^-$ is faster than the oxidative addition step. Consequently, the affinity of the anion TfO$^-$ for the Pd^{II} in DMF is very low.

Since chloride ions play an important role in the efficiency of palladium-catalyzed reactions performed from aryl triflates,[7d−7f,9] it was of interest to investigate a possible kinetic effect of chloride ions in the oxidative addition of aryl triflates. This effect cannot be monitored by conductivity measurements because of the high conductivity of nBu$_4$NCl when added in relatively large amounts. This problem was solved by investigating the kinetics of the oxidative addition of aryl triflates by amperometry.[10,22] This technique allows monitoring of the decay of the Pd^0 concentration in the oxidative addition by recording the decay of its oxidation current (which is proportional to its concentration) versus time, after addition of the aryl triflate. As summarized in Table 1, the effect of chloride ions [added as nBu$_4$NCl to Pd^0(PPh$_3$)$_4$ prior to the addition of the aryl triflate] is to accelerate the rate of the oxidative addition,[10] as a consequence of the formation of anionic [Pd^0(PPh$_3$)$_2$Cl]$^-$ complexes.[14] Addition of a rather large amount of chloride ions, relative to Pd^0(PPh$_3$)$_4$, is required to observe a significant accelerating effect with highly reactive triflates. The effect is more pronounced when poorly reactive aryl triflates are considered (Table 1).

Consequently, the chloride ions play a dual role in the oxidative addition of aryl triflates to Pd^0(PPh$_3$)$_4$: (i) acceleration of the oxidative addition and (ii) formation of neutral *trans*-ArPdCl(PPh$_3$)$_2$ complexes (Scheme 4).[10]

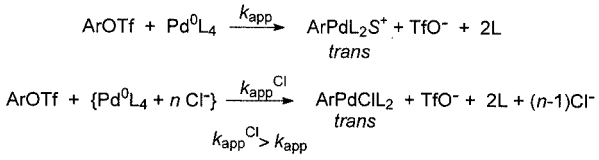

Scheme 4. Effect of chloride ions on the oxidative addition of aryl triflates to Pd^0(PPh$_3$)$_4$ in DMF

Since aryl triflates may supplant aryl halides in palladium-catalyzed reactions, it was of interest to compare their reactivity in oxidative additions to Pd^0(PPh$_3$)$_4$ (c_0 = 2 mM). The following order of reactivity in DMF was established: PhI >> PhOTf > PhBr >> PhCl, with rate constants at 20 °C of 17, 0.0017, and 0.001 M^{-1}s^{-1} for PhI, PhOTf and PhBr, respectively.[10] In DMF, the complexes *trans*-PhPdI(PPh$_3$)$_2$ and *trans*-PhPdBr(PPh$_3$)$_2$, formed by the oxidative additions of PhI and PhBr, respectively, partly dissociate to generate the cationic complexes *trans*-[PhPd(PPh$_3$)$_2$(DMF)]$^+$ [Equation (9), $K_I = 5.8 \times 10^{-4}$ M, $K_{Br} = 2.8 \times 10^{-4}$ M at 25 °C].[24] Since the values of the equilibrium constants K_I and K_{Br} are low, the degree of dissociation will be significant only at low concentrations.

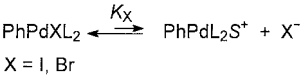

(9)

Conductivity measurements have also been used to characterize cationic complexes formed in the oxidative addition of aryl iodides to (P,N,P)Pd^0(dba) complexes in DMSO.[25] The ionic character found for complexes [ArPd(P,N,P)]$^+$ indicates that the (P,N,P) ligands behave as *tridentate* ligands for the Pd^{II} complex [Equation (10)]. The kinetics of formation of the cationic complexes has been monitored by conductivity measurements that have allowed determination of the rate constant k_{app} [Equation (10)].[25] The effect that the N-bearing substituent and the aryl group have on the rate of the oxidative addition was then investigated.

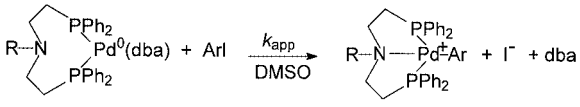

(10)

R= Ph, *t*Bu, 4-MeO-C$_6$H$_4$; Ar = Ph, 4-MeO-C$_6$H$_4$, 4-NO$_2$-C$_6$H$_4$

I.3 Conclusion and Mechanistic Consequences in Palladium-Catalyzed Stille and Heck Reactions: Cationic versus Neutral Arylpalladium(II) Complexes as Key Intermediates

On the basis of the kinetic data and the structures of arylpalladium complexes reported above, the mechanisms of palladium-catalyzed reactions involving aryl triflates (ArOTf) may differ from those involving aryl halides (ArX). On one hand, aryl triflates are less reactive than aryl iodides and so the oxidative addition (first step of the catalytic cycles) may become rate-determining when using aryl triflates. On the other hand, the formation of cationic *trans*-[ArPdL$_2$*S*]$^+$TfO$^-$ complexes from aryl triflates versus neutral *trans*-ArPdXL$_2$ from aryl halides may affect their reactions with nucleophiles: transmetallation with organostannanes in the case of Stille reactions [Equation (11)] and carbopalladation with alkenes in the case of Heck reactions [Equation (12)]. Moreover, the presence of chloride ions in reactions performed using aryl triflates[7a−7f,9,12] introduces

 © 2003 Wiley-VCH Verlag GmbH & Co. KGaA, Weinheim

some complexity, since chloride ions accelerate the rate of the slow oxidative addition of aryl triflates and affect the structure of the arylpalladium(II) complex involved in the reaction with the nucleophile by formation of neutral *trans*-$ArPdClL_2$ complexes.

I.3.1 Stille Reactions

With regard to these observations, Espinet et al. have analyzed the puzzling role, positive or negative, depending on ligand and solvent, of chloride ions in Stille reactions involving aryl triflates (aryl = C_6F_5 or $C_6Cl_2F_3$) and CH_2=$CHSnBu_3$ [Equation (11)].[12]

$$ArOTf + RSnR'_3 \xrightarrow[Cl^- ?]{[Pd]} ArR + TfOSnR'_3 \quad (11)$$

In THF, whatever the ligand (PPh_3 or $AsPh_3$), neutral *trans*-$ArPdClL_2$ complexes are formed in the presence of chloride ions. When the palladium atom is ligated by $AsPh_3$, the transmetallation of CH_2=$CHSnBu_3$ with *trans*-$ArPdCl(AsPh_3)_2$ is fast and the oxidative addition of aryl triflates to $Pd^0(AsPh_3)_4$ is rate-determining. Thus, the positive role of chloride ions in this Stille reaction arises from an acceleration of the oxidative addition. When the palladium atom is ligated by PPh_3, the transmetallation with *trans*-$[ArPdCl(PPh_3)_2]$ becomes rate-determining. In this case, the inhibiting role of chloride ions in the Stille reaction arises from a deceleration of the transmetallation, which is even slower with neutral *trans*-$ArPdCl(PPh_3)_2$ complexes than with cationic complexes $[ArPdX'(PPh_3)_2]^+$ (X′ = PPh_3 or *S*) formed in the absence of chloride ions.[12]

I.3.2 Heck Reactions

The question of the reactivity of neutral versus cationic arylpalladium(II) complexes is also crucial in Heck reactions performed with aryl triflates [Equation (12)].[2]

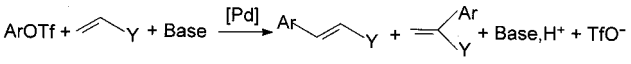

(12)

The simultaneous use of aryl triflates and *bidentate ligand* (P,P) may affect the reactivity, regioselectivity and enantioselectivity of the reactions. Indeed, the catalytic reactions work well with electron-rich alkenes (Y = OR, ...) and allow the unusual substitution by the aryl group at the more-substituted carbon atom of the alkene (α-arylation).[2] An "ionic" mechanism has been proposed by Cabri et al.[2a,2d,2f] and Hayashi et al.[2b,2c,2e] (Scheme 5). Cationic complexes $[ArPd(P,P)S]^+$ generated in the oxidative addition have a labile coordination site *cis* to the Ar group and easily react with electron-rich alkenes. The carbopalladation step (also called an insertion step) gives a cationic alkylPd^{II} complex in which the aryl group and the electron-donor group Y are attached to the same C atom (Scheme 5).

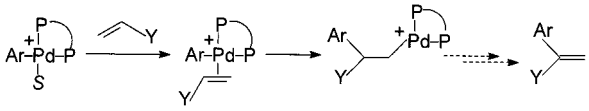

Scheme 5. Mechanism of the carbopalladation step from *cationic* arylpalladium(II) complexes ligated to bidentate (P,P) ligands

This mechanism will also operate with aryl halides, provided that silver[26a] or thallium[26b] salts are present to abstract the halide ion from ArPdX(P,P) to generate the cationic complexes $[ArPd(P,P)S]^+$.[20]

The mechanism of the formation of the arylated alkene from the intermediate cationic alkylPd^{II} complex[20b,27] is still under debate (Scheme 5). In the absence of a base, Brown and Hii have characterized by ^1H NMR spectroscopy the cationic alkylPd^{II} complex formed from $[PhPd(dppf)(THF)]^+$ and CH_2=$CHCO_2Me$ in THF at low temperatures (Scheme 6).[20b] The arylated alkene was formed by a β-hydride elimination (Scheme 6, path A). Neither $[HPd(P,P)S]^+$ nor $Pd^0(P,P)$ were detected, but a new cationic alkylPd^{II} species was observed to have formed by addition of the transient $[HPd(P,P)S]^+$ ion to the alkene CH_2=$CHCO_2Me$ (Scheme 6, path A). Consequently, no Pd^0 complex was generated from $[HPd(P,P)S]^+$ in the absence of a base. On the basis of DFT calculation, Deeth et al. have proposed the existence of a β-agostic hydrogen atom (Scheme 6, path B) because of the cationic character of the alkylpalladium(II) species formed in the carbopalladation step.[27a] Consequently, in the presence of a base, the Pd^0 complex would not be generated via a cationic palladium hydride formed by the traditional β-hydride elimination, but instead by deprotonation by the base of the acidic agostic proton (Scheme 6, path B).

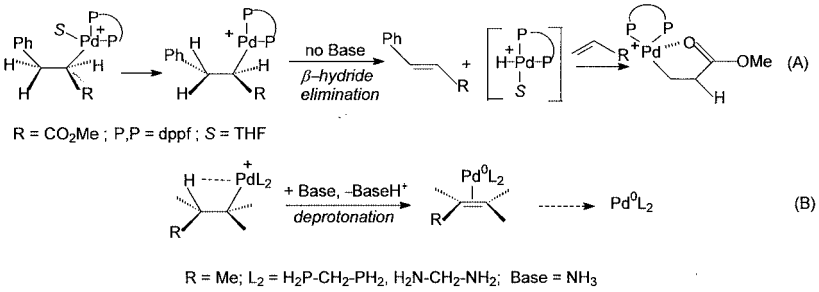

Scheme 6. Mechanism of the formation of an arylated alkene from *cationic* alkylpalladium(II) complexes ligated by bidentate ligands

 © 2003 Wiley-VCH Verlag GmbH & Co. KGaA, Weinheim

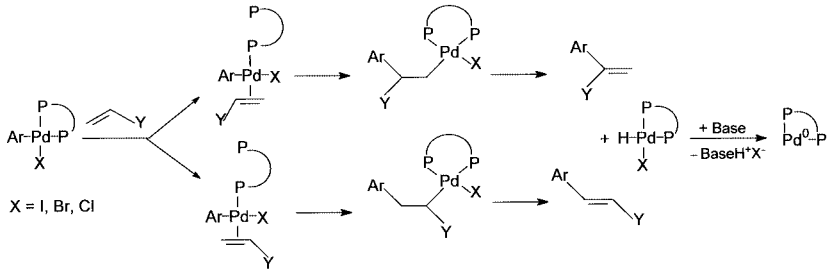

Scheme 7. Mechanism of the carbopalladation step from *neutral* arylpalladium(II) complexes ligated to bidentate (P,P) ligands, followed by β-hydride elimination and formation of a Pd^0 complex

A "neutral" mechanism is proposed when neutral ArPdX(P,P) complexes are generated in the oxidative addition of aryl halides (X = I, Br, Cl) or of aryl triflates in the presence of chloride ions (X = Cl).[2a,2d,2f] The neutral complexes would be less reactive than the cationic ones because the complexation of the alkene requires the unfavorable deligation of one P atom of the bis(phosphane) ligand. Moreover, such Heck reactions lead to nonselective α- and β-arylation (Scheme 7).[2a,2d,2f]

Although the "ionic" mechanism is supposed to induce better enantioselectivity in intramolecular Heck reactions,[2b,2c,2e,27b] Overman et al. have observed that the enantioselectivity is improved under the conditions of the "neutral" mechanism, i.e., from aryl iodides or from aryl triflates in the presence of chloride ions.[28] They propose the deligation of the halide as the key step responsible of this enantioselectivity, rather than deligation of one P atom of the bis(phosphane) via a pentacoordinate Pd^{II} transition state (Scheme 8).

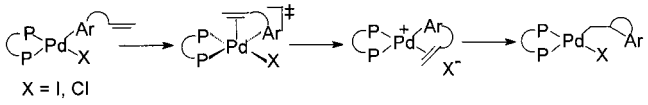

Scheme 8. Mechanism of the intramolecular carbopalladation step

As far as monodentate ligands (L) are concerned, cationic *trans*-$[ArPdL_2S]^+$ complexes appear to be more reactive than neutral *trans*-$ArPdXL_2$ (X = I) ones; they are, however, less reactive than *trans*-$ArPd(OAc)L_2$ complexes. The following order of reactivity with styrene has been observed in DMF:[16b,16c] *trans*-$PhPd(OAc)(PPh_3)_2$ > *trans*-$[PhPd(PPh_3)_2S]^+$ > *trans*-$PhPdI(PPh_3)_2$.

Because of the labile coordination site in the cationic complex *trans*-$[ArPdL_2S]^+$, no phosphane dissociation is required. The coordination of the alkene leads, however, to a *trans* complex, *trans*-$[ArPd(\eta^2\text{-alkene})L_2]^+$, which must reorganize to the *cis* complex (a thermodynamically unfavorable process) to allow alkene insertion into the Ar−Pd bond (Scheme 9). The evolution of the cationic alkylPd^{II} complex may then follow the mechanism proposed in Scheme 6 (path B) for bidentate ligands.

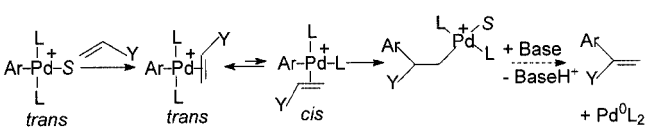

Scheme 9. Mechanism of the carbopalladation step from *cationic* arylpalladium(II) complexes ligated to monodentate ligands

The carbopalladation step from neutral *trans*-$ArPdXL_2$ complexes requires dissociation of one phosphane unit, which must be rate-determining when PPh_3 is considered (Scheme 10).

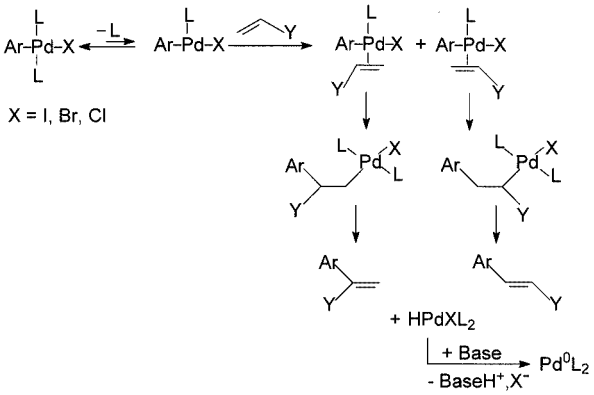

Scheme 10. Mechanism of the carbopalladation step from *neutral* arylpalladium(II) complexes ligated to monodentate ligands, followed by β-hydride elimination

When the Pd^0 precursor is $Pd(OAc)_2$ and PPh_3, *trans*-$ArPd(OAc)(PPh_3)_2$ complexes are generated in the oxidative addition of aryl triflates (Scheme 2)[15] or iodides.[16] The higher reactivity of *trans*-$ArPd(OAc)(PPh_3)_2$ compared to that of *trans*-$ArPdI(PPh_3)_2$ may be understood as a result of an easier displacement of the phosphane by the acetate, which may behave as a bidentate ligand[16c] {Scheme 11, see Sect. III for the existence of cationic $[HPdL_2(DMF)]^+$ formed in the β-hydride elimination step}.

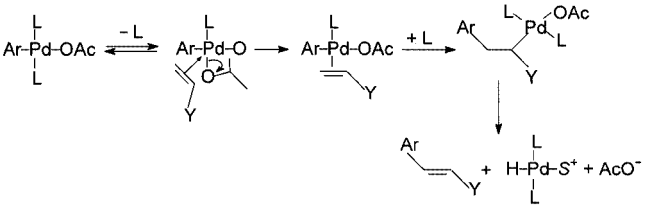

Scheme 11. Mechanism of the carbopalladation step from $ArPd(OAc)(PPh_3)_2$ complexes followed by β-hydride elimination in DMF

 © 2003 Wiley-VCH Verlag GmbH & Co. KGaA, Weinheim

II. Formation of Cationic Palladium(II) Complexes in the Oxidative Addition of Vinyl Triflates or Benzoic Anhydride to $Pd^0(PPh_3)_4$ in DMF Observed by Conductivity Measurements

II.1 Formation of Cationic $[VinylPd(PPh_3)_2S]^+$ Complexes in the Oxidative Addition of Vinyl Triflates to Neutral Pd^0 Complexes in DMF Monitored by Conductivity Measurements

Since DMF appears to be a good coordinating solvent for cationic palladium(II) complexes, this property prompted us to investigate the mechanism of the oxidative addition of vinyl triflates to $[Pd^0(PPh_3)_4]$ in DMF. Cationic complexes *trans*-$[(\eta^1\text{-vinyl})Pd^{II}(PPh_3)_2(DMF)]^+TfO^-$ were generated and characterized by conductivity measurements (Figure 3), NMR spectroscopy, and electrospray mass spectrometry [Equation (13)].[29]

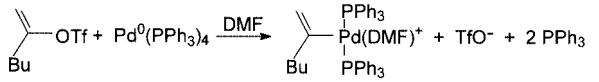

(13)

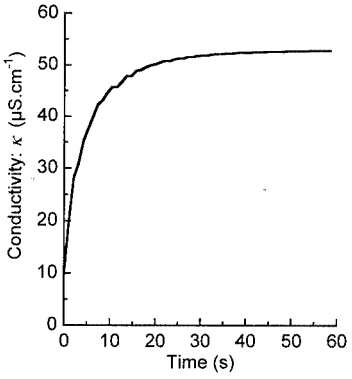

Figure 3. Kinetics of the formation of $[CH_2{=}C(n\text{Bu})Pd(PPh_3)_2(DMF)]^+TfO^-$ in the oxidative addition of $CH_2{=}C(n\text{Bu})OTf$ (2 mM) to $[Pd^0(PPh_3)_4]$ (2 mM) in DMF at 10 °C; variation of the conductivity κ versus time; $\kappa = \kappa_{exp} - \kappa_0$ (κ_{exp}: experimental conductivity at t; κ_0: initial residual conductivity of 3 $\mu S{\cdot}cm^{-1}$)

The oxidative addition was considerably faster than that of aryl triflates. Cationic vinylic complexes, however, were less stable than *trans*-$[ArPd(PPh_3)_2(DMF)]^+TfO^-$ since a slow degradation took place that gave the phosphonium salt $[vinylPPh_3]^+TfO^-$ together with a Pd^0 complex that was detected when the oxidative addition was performed under stoichiometric conditions [Equation (14)].[29]

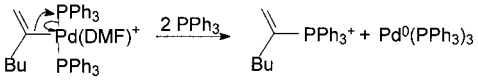

(14)

To date, in the vinylic series, the only stable cationic complexes characterized by conductivity measurements in CH_3NO_2 have been $[(\eta^1\text{-vinyl})Pt(PPh_3)_3]^+TfO^-$ formed in the oxidative addition of vinyl triflates to $Pt^0(PPh_3)_4$ in toluene, as reported by Stang et al.,[8] in which, in the absence of any coordinating solvent, a phosphane ligand occupies the fourth coordination site on the Pd^{II} center.

II.2 Formation of Cationic $[AcylPd(PPh_3)_2S]^+$ Complexes in the Oxidative Addition of Benzoic Anhydride to Neutral Pd^0 Complexes Monitored by Conductivity Measurements in DMF

Aromatic carboxylic anhydrides $(ArCO)_2O$ were introduced by Sakamoto et al. as *acylating* agents in palladium-catalyzed cross-coupling reactions (m = ZnX),[30a] and they have been used recently by Yamamoto et al. in Susuki-type reactions [m = $B(OH)_2$] [Equation (15)].[30b]

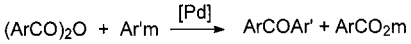

(15)

Recently, these compounds were used by de Vries et al. as *arylating* agents in palladium-catalyzed Heck reactions [Equation (16)].[31]

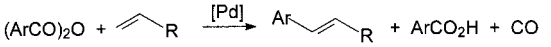

(16)

The mechanism of the oxidative addition of the benzoic anhydride to $Pd^0(PPh_3)_4$ (2 mM) has been investigated in DMF. Two $acylPd^{II}$ complexes have been identified (Scheme 12). The cationic complex *trans*-$[(PhCO)Pd(PPh_3)_2(DMF)]^+$, with $PhCO_2^-$ as the counteranion, was detected by conductivity measurements.[32]

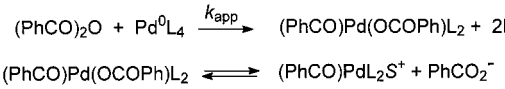

Scheme 12. Oxidative addition of benzoic anhydride to $Pd^0(PPh_3)_4$ in DMF ($k_{app} = 3 \times 10^{-3}\ M^{-1}s^{-1}$)

The neutral and cationic $acylPd^{II}$ complexes did not undergo any decarbonylation, which would have generated $phenylPd^{II}$ complex(es), a process required in the Heck reaction [Equation (16)]. Exchanging the two monodentate PPh_3 units with one bidentate ligand, dppp, gave a mixture of $[(PhCO)Pd(dppp)(DMF)]^+PhCO_2^-$ and (PhCO)Pd(OCOPh)(dppp) without any detectable decarbonylation process occurring.[32] Consequently, this reaction excludes the use of phosphane ligands in Heck reactions performed with $(PhCO)_2O$ that are, indeed, efficient with Pd^0 precursors consisting of Pd^{II} salts in the absence of any phosphane ligand.[31]

III. Reversible Formation of Cationic Palladium(II) Hydride Complexes *trans*-$[HPd(PPh_3)_2(DMF)]^+$ in the Oxidative Addition of Carboxylic Acids to $Pd^0(PPh_3)_4$ Observed by Conductivity Measurements in DMF

As developed by Trost et al.,[33] palladium-catalyzed reactions involving alkynes (e.g., cycloisomerization of enynes,

 © 2003 Wiley-VCH Verlag GmbH & Co. KGaA, Weinheim

isomerization of alkynes to 1,3-dienes) are initiated by the reaction of a carboxylic acid HA (acetic or formic acid) with a Pd^0L_n complex (L = monophosphane ligand). A stoichiometric amount of formic acid is required in the Pd-catalyzed hydrocarboxylation of alkynes,[34] or hydrocarbonylation of aryl halides.[35]

The reaction of a carboxylic acid HA with Pd^0L_n was supposed to generate a hydridopalladium complex $[HPd^{II}AL_{n'}]$ [Equation (17)][36] that initiates the catalytic cycle by a *syn*-hydropalladation of the alkyne to form an (η^1-vinyl)palladium(II) complex as a key intermediate for further steps [Equation (18)].[33a,33b]

$$Pd^0L_n + HA \longrightarrow HPdAL_{n'} + (n\text{-}n')L \quad (17)$$

$$HPdAL_{n'} + R{-}\equiv \longrightarrow \begin{matrix} R \\ \diagdown \\ PdAL_{n'} \end{matrix} \!\!=\!\!\begin{matrix} \\ \diagup \\ H \end{matrix} \quad (18)$$

When weak carboxylic acids are considered (acetic or formic acid), the reaction is considered as an oxidative addition, i.e., insertion of Pd^0 into the H−A bond [Equation (17)].[33a,33b] Initially, it was not clear, however, whether the anion A^- remained ligated to the Pd^{II} atom or not. In 1993, Zargarian and Alper proposed the formation of cationic palladium hydride complexes $[HPd(PR_3)_2(\eta^2\text{-alkyne})]^+HCO_2^-$ in the Pd-catalyzed hydrocarboxylation of alkynes in the presence of formic acid.[34] In 1998, Trost proposed in a review the involvement of cationic complexes $[HPdL_{n''}]^+$ (rather than $[HPd(OAc)L_{n'}]$) "undoubtedly formed to some extent, albeit in an unfavorable equilibrium".[33c] Neither $HPd(OAc)L_{n'}$ nor $[HPdL_{n''}]^+$ was characterized in this context.

III.1 Evidence for the Formation of *trans*-$[HPd(PPh_3)_2(DMF)]^+A^-$ ($A^- = CH_3CO_2^-$, HCO_2^-) by Conductivity Measurements in DMF

The reaction of $Pd^0(PPh_3)_4$ with acetic acid in DMF at 25 °C was monitored by conductivity measurements.[37] The conductivity κ of a solution of $Pd^0(PPh_3)_4$ (2 mM) increased after addition of *n* equiv. of acetic acid ($n > 1$) and reached a limiting value (named κ_{equil} in Figure 4) that increased when *n* was increased up to 100. The limiting values were lower in the presence of excess PPh_3 (Figure 4).

The conductivity of acetic acid (a weak acid in DMF, $pK_a = 13.5$) was measured independently in DMF at 25 °C and was found to be negligible (e.g., 6.9 μS·cm^{-1} at 200 mM) compared to that observed when acetic acid was added to $Pd^0(PPh_3)_4$ in DMF (Figure 4).

These experiments establish that the reaction of $Pd^0(PPh_3)_4$ with acetic acid gives ionic species, which are observed to be involved in an equilibrium with the reagents because the concentration of the ionic species increased with the concentration of acetic acid. PPh_3 was involved in the backward reaction of this equilibrium. Since $Pd^0(PPh_3)_3$ is the major complex in solution,[23] the overall equilibrium observed is described in Equation (19). The inhibiting effect of PPh_3 indicates that $SPd^0(PPh_3)_2$ is the reactive species,

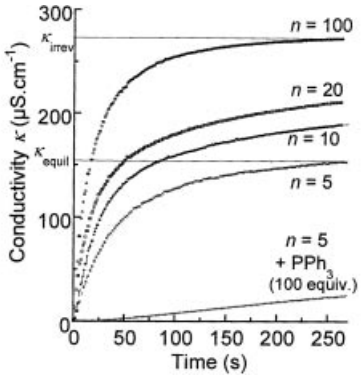

Figure 4. Conductivity in DMF of $[HPd(PPh_3)_2(DMF)]^+AcO^-$ generated in the reaction of $Pd^0(PPh_3)_4$ (2 mM) with *n* equiv. of acetic acid: $n = 100$, 20, 10, and 5 in the absence of PPh_3, or $n = 5$ in the presence of 100 equiv. of PPh_3 (as indicated in the Figure) at 25 °C

since it occurs in regular oxidative additions [Equations (20) and (21)].[22]

$$Pd^0L_3 + HA \underset{k_b}{\overset{k_f}{\rightleftharpoons}} HPdL_2S^+ + A^- + L \qquad K \quad (19)$$

$$Pd^0L_3 \rightleftharpoons SPd^0L_2 + L \quad (20)$$

$$SPd^0L_2 + HA \rightleftharpoons HPdL_2S^+ + A^- \quad (21)$$

The structure of the cationic complex *trans*-$[HPd^{II}(PPh_3)_2(DMF)]^+$ was established by NMR spectroscopy (Table 2).[37] The very negative ^1H NMR spectroscopic chemical shift suggests a hydride character for the H atom ligated to the Pd^{II} atom. The unique ^{31}P NMR spectroscopic singlet indicates that the Pd^{II} center is ligated by only two equivalent PPh_3 units that are situated in a relative *trans* position and that the fourth coordination site is occupied by the solvent. This situation differs from that of $[HPd(PPh_3)_3]^+[CH(SO_2CF_3)_2]^-$ generated in nonpolar solvents such as toluene,[38] or $[HPd(PPh_3)_3]^+CF_3CO_2^-$ generated in aqueous CF_3CO_2H, in which the palladium(II) species is ligated by three phosphane units.[39]

The reaction of $Pd^0(PPh_3)_4$ with formic acid was also monitored by conductivity measurements.[35] the experiments were performed, however, at 0 °C because of a lack of stability observed at 25 °C.[40] The reaction gave the cationic complex *trans*-$[HPd(PPh_3)_2(DMF)]^+$, with HCO_2^- as the counteranion, by a reversible process (Table 2). The overall equilibrium, expressed in Equation (19), was fully positioned to its right-hand side in the presence of 70 equiv. of formic acid.

Consequently, a cationic palladium(II) hydride *trans*-$[HPd(PPh_3)_2(DMF)]^+$ is formed in a reversible reaction, either from acetic acid or from formic acid [Equation (19)]. The molar conductivity Λ_M was calculated for the two complexes $[HPd(PPh_3)_2(DMF)]^+CH_3CO_2^-$ and $[HPd(PPh_3)_2(DMF)]^+HCO_2^-$ (Table 2).

 © 2003 Wiley-VCH Verlag GmbH & Co. KGaA, Weinheim

Table 2. Characterization of the cationic hydridopalladium(II) complex $[HPd(PPh_3)_2(DMF)]^+$ formed in the oxidative addition of carboxylic acids AH to $Pd^0(PPh_3)_4$ (c_0 = 2 mM) in DMF, as well as equilibrium and rate constants [Equation (19)]

AH	Molar conductivity Λ_M [S·cm^{-2}·mol^{-1}]	^{1}H NMR [ppm][a]	^{31}P NMR [ppm][b]	K	k_f [M^{-1}·s^{-1}] (k_b) [M^{-2}·s^{-1}]
CH_3CO_2H	$[HPdL_2(DMF)]^+$, $CH_3CO_2^-$ 135 (± 5)[c]	−7.48 (br. s)	20.77 (s)	0.5×10^{-3}[c]	0.28[c] (560)[c]
HCO_2H	$[HPdL_2(DMF)]^+$, HCO_2^- 110 (± 5)[d]	−7.28 (br. s)	20.97 (s)	10^{-3}[d]	0.012[d] (12)[d]

[a] 400 MHz; shifts are referred to TMS. Solvent: $CDCl_3$ containing 10% of DMF. [b] 163 MHz; shifts are referred to H_3PO_4 as an external reference. Solvent: DMF containing 10% [D_6]acetone. [c] 25 °C. [d] 0 °C.

III.2 Determination of the Equilibrium and Rate Constants of the Oxidative Addition of Acetic or Formic Acid to $Pd^0(PPh_3)_4$ in DMF by Conductivity Measurements

III.2.1 Determination of the Equilibrium Constant K

The reaction of acetic or formic acid (n equiv.) with $Pd^0(PPh_3)_4$ obeys the general Equation (19). The equilibrium constant K was determined from the conductivity data, since the limiting values of the conductivity κ_{equil} (Figure 4) provide the thermodynamic concentration of $[HPd(PPh_3)_2(DMF)]^+$ and AcO^- at various concentrations of acetic acid.[37]

$$K = [HPdL_2(DMF)^+][A^-][L]/[Pd^0L_3][HA] = c_0 \cdot x_{equil}^2(1 + x_{equil})/(1 - x_{equil})(n - x_{equil})$$

c_0: initial concentration of $Pd^0(PPh_3)_4$; $x_{equil} = \kappa_{equil}/\kappa_{irrev}$; κ_{equil}: final conductivity measured when the equilibrium is fully established in the presence of n equiv. of HA ($t > 250$ s, Figure 4); κ_{irrev}: final conductivity measured when the equilibrium is fully positioned on its right-hand side, $n = 100$ for CH_3CO_2H (Figure 4), $n = 70$ for HCO_2H.

Identical values for K were found, whatever concentration range was investigated for each carboxylic acid ($0 < n < 100$ for acetic acid and $0 < n < 70$ for formic acid). This result establishes that the cation and anion are free ions in DMF.[37] The values of the equilibrium constants K for acetic and formic acid are gathered in Table 2. Even though they were determined at slightly different temperatures, one notices that, at identical concentrations of acids, the equilibrium lies more in favor of the cationic palladium hydride for formic acid than it does for acetic acid, which is in agreement with the fact that formic acid is slightly more acidic than acetic acid.

III.2.2 Determination of Rate Constants k_f and k_b

Acetic acid is a weak acid in DMF and the concentration of protons is negligible (vide supra) when compared to the Pd^0 concentration. This situation, however, does not exclude the possibility of a direct protonation of $Pd^0(PPh_3)_2$ to form $[HPd(PPh_3)_2S]^+$. The two pathways — (i) direct protonation of $Pd^0(PPh_3)_2$ by H^+ or (ii) oxidative addition of acetic acid to $Pd^0(PPh_3)_2$ to form $HPd(OAc)(PPh_3)_2$ followed by a fast ionization step — may be discriminated by determining the reaction order in acetic acid for the forward reaction [Equation (19)]. That is to say, a reaction order of 1/2 for CH_3CO_2H would suggest the protonation route and a reaction order of 1 for CH_3CO_2H would suggest the oxidative addition route.

The equilibrium in Equation (19) was completely shifted towards the cationic complex $[HPdL_2(DMF)]^+$ when 100 equiv. of acetic acid were treated with $Pd^0(PPh_3)_4$ (c_0 = 2 mM) in DMF. Consequently, the uppermost curve in Figure 4 is representative of the rate of formation of the cationic complex $[HPdL_2(DMF)]^+$. This kinetic curve did not exhibit any induction period, which would result in a significant accumulation of a neutral intermediate species. Moreover, the reaction was found to be faster when the concentration of acetic acid was increased (vide infra). Consequently, the intermediate neutral complex $HPd(OAc)(PPh_3)_2$, if formed in the reaction of acetic acid with $Pd^0(PPh_3)_2$, did not accumulate. Thus, the ionization of $HPd(OAc)(PPh_3)_2$ to $[HPd(PPh_3)_2(DMF)]^+$ and AcO^- was faster than its formation from $Pd^0(PPh_3)_4$, and the rate of formation of the ionic species was the same as that of the disappearance of the Pd^0 complex. Consequently, the rate constant of the forward reaction [k_f in Equation (19)] was determined using the conductivity data of the uppermost curve in Figure 4 ($n = 100$ for CH_3CO_2H). When starting from $Pd^0(PPh_3)_4$, the concentration of PPh_3 was not constant [Equation (20)] and the kinetic law is: $2\ln(1 - x_t) + x_t = -k_{obsd.} \cdot t = -k_f \cdot [HA]^\alpha t$ ($x_t = \kappa_t/\kappa_{irrev}$; κ_t = conductivity at time t; κ_{irrev} = final conductivity; α = reaction order in HA). The values of $k_{obsd.}$ were calculated for acetic acid (Figure 5, a) and formic acid from the slope of the regression line obtained by plotting $[2\ln(1 - x_t) + x_t]$ against time (Figure 5, b).[37]

The reaction of $Pd^0(PPh_3)_4$ with acetic acid was rather fast (uppermost curve in Figure 4) and, consequently, only two concentrations of acetic acid could be tested ($n = 100$: $k_{obsd.} = 0.057$ s^{-1}; $n = 200$: $k_{obs} = 0.104$ s^{-1}). From these results, it appears that the reaction order α in acetic acid is close to 1 ($k_{obsd.} = k_f \cdot [HA]$), which favors the pathway of an oxidative addition of acetic acid to $SPd^0(PPh_3)_2$ followed by a fast ionization step of the neutral complex $HPd(OAc)(PPh_3)_2$. The values of k_f were then determined for acetic and formic acid (Table 2).[37] The values of the

 © 2003 Wiley-VCH Verlag GmbH & Co. KGaA, Weinheim

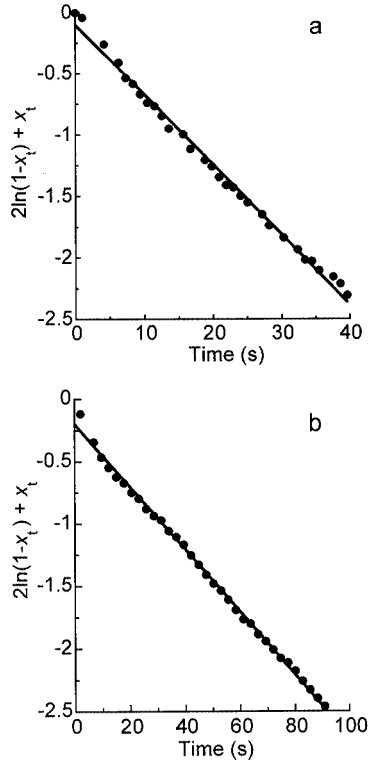

Figure 5. Kinetics of the oxidative addition of $Pd^0(PPh_3)_4$ (2 mM) in DMF to: (a) acetic acid (0.2 M) at 25 °C; (b) formic acid (0.2 M) at 0 °C; in both figures, plot of $[2\ln(1 - x_t) + x_t]$ versus time; $x_t = \kappa_t/\kappa_{irrev}$; κ_t = conductivity at t; κ_{irrev} = final conductivity, under conditions where the reactions were irreversible (see uppermost curve in Figure 4 for acetic acid)

rate constants of the backward reaction [k_b in Equation (19)] were then deduced from the values of the equilibrium constant $K = k_f/k_b$ (Table 2).

The overall equilibrium in Equation (19) may be then considered as the successive equilibria shown in Equation (22), which involve a reversible oxidative addition as the very first step (L = PPh_3).

$$Pd^0L_2 + HA \rightleftharpoons \underset{cis}{HPdAL_2} \rightleftharpoons \underset{trans}{HPdAL_2} \rightleftharpoons \underset{trans}{HPdL_2S^+} + A^- \quad (22)$$

III.3 Conclusion and Mechanistic Consequences

The results above illustrate how conductivity data may be used efficiently (i) to characterize ionic complexes formed in the reaction between a carboxylic acid and a Pd^0 complex, (ii) to establish the reversibility of this reaction and to determine its equilibrium constant, (iii) to determine the rate constant of the forward and backward reactions of the equilibrium, and (iv) to delineate the mechanism by discriminating between oxidative addition and protonation.

It has been established that a cationic palladium hydride $[HPd(PPh_3)_2(DMF)]^+$ is generated by oxidative addition of weak carboxylic acids (acetic or formic acid) and $Pd^0(PPh_3)_4$ in a coordinating solvent as DMF. However, it is generated in an unfavorable equilibrium. Consequently, as predicted by Trost,[33c] if a high concentration of the key intermediate $[HPdL_2S]^+$ is needed, a large excess of the carboxylic acid is required and use of formic acid is more efficient than acetic acid.[41]

In Heck reactions, when the precursor of the Pd^0 catalyst is $Pd(OAc)_2$ associated with phosphane ligands L, the active Pd^0 complex in the oxidative addition with PhI is the anionic species $[Pd^0L_2(OAc)]^-$, and $ArPd(OAc)L_2$ is formed in the oxidative addition of aryl iodides[16] or triflates.[15] The carbopalladation of the alkene by $ArPd(OAc)L_2$ is followed by β-hydride elimination (Scheme 11) that, according to the results just reported above, should not generate the neutral $HPd(OAc)(PPh_3)_2$ in DMF, but instead the cationic palladium hydride $[HPd(PPh_3)_2(DMF)]^+$ with AcO^- as the counteranion (Scheme 11). Since the reversibility of the oxidative addition of the acetic acid with $Pd^0(PPh_3)_2$ has been established [Equation (22)], however, the complex $[HPd(PPh_3)_2(DMF)]^+AcO^-$ must be involved in an equilibrium with acetic acid and Pd^0L_2, so that the Pd^0L_2 complex should be generated in the absence of a base. The role of the base would then be devoted to its reaction with acetic acid to generate AcO^- as a key ligand for the active complexes $[Pd^0L_2(OAc)]^-$ and $ArPd(OAc)L_2$.[16]

IV. Reversible Formation of Cationic $[(\eta^3\text{-allyl})PdL_2]^+$ Complexes in the Oxidative Addition of Allylic Carboxylates or Carbonates to Pd^0 Complexes Observed by Conductivity Measurements in DMF

Palladium complexes are efficient catalysts for Tsuji−Trost reactions, i.e., nucleophilic substitutions on allylic carboxylates[3] or carbonates[42] (R′ = OR′′) [Equation (23)].

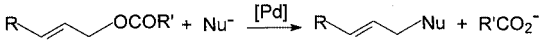

(23)

The first step of the catalytic cycle is an oxidative addition of the allylic derivative, allylOCOR′, to a lowly ligated Pd^0 complex, Pd^0L_2 (L = monodentate phosphane ligand or L_2 = bidentate phosphane ligand) [Equation (24)], which is believed to proceed in two successive steps.[3]

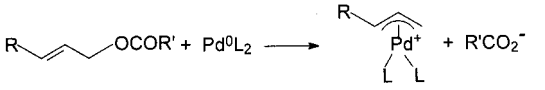

(24)

The first of these steps is a reversible complexation of the C=C double bond of the allylic derivative to Pd^0L_2 [Equation (25)]; the second step is the oxidative addition (commonly named the "ionization step") in which a cationic $[(\eta^3\text{-allyl})Pd^{II}L_2]^+$ complex is formed with the leaving group $R'CO_2^-$ as the counteranion [Equation (26)].

 © 2003 Wiley-VCH Verlag GmbH & Co. KGaA, Weinheim

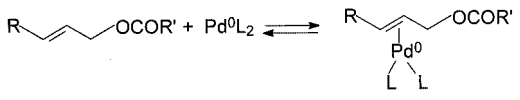

(25)

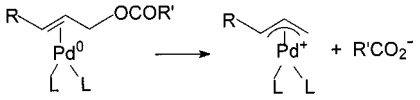

(26)

The mechanism of the next step, the nucleophilic attack onto the cationic $[(\eta^3\text{-allyl})PdL_2]^+$ complex has been widely investigated [Equation (27)].[3] Such reactions have been usually performed, however, on cationic palladium(II) complexes that were not generated in the oxidative addition of Equation (24),[43] but instead independently synthesized from dimeric $Pd_2(\eta^3\text{-allyl})_2(\mu\text{-Cl})_2$ complexes[43b] by addition of monodentate or bidentate phosphanes and abstraction of the chloride ion by MY (M = K, Na, Ag; Y = BF_4, BPh_4, OTf) [Equation (28)].[43b,44a] Under such conditions, the counteranion is BF_4^-, BPh_4^- or TfO^-, but not $R'CO_2^-$ as it would be in the oxidative addition performed from allylOCOR′. The complex [(2-methylallyl)$Pd(PPh_3)_2]^+BF_4^-$ has been characterized by conductivity measurements in aqueous acetone;[44a] the conductivity of related complexes in THF is very low.[44b] A few complexes [(1,3-diphenyl-η^3-allyl)Pd(P,P)]$^+AcO^-$ (P,P: ferrocenylphosphane ligands) have been synthesized from $Pd_2(\eta^3\text{-allyl})_2(\mu\text{-OAc})_2$, but at low temperatures.[45]

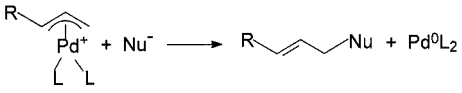

(27)

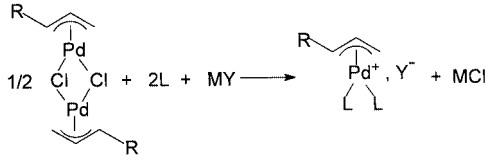

(28)

Consequently, until 1999 the cationic character of $[(\eta^3\text{-allyl})PdL_2]^+$ complexes, generated in the oxidative addition of allylic acetates with AcO^- as counteranion [Equation (24)], had never been established. Such complexes have recently been characterized by conductivity measurements in DMF with monodentate and bidentate phosphane ligands.[46−50] In addition, the reversibility of the oxidative addition has also been established by conductivity measurements in conjunction with other analytical techniques (vide infra).[46−50]

The Pd^0 precursor investigated was $Pd^0(dba)_2$ (dba: *trans*,*trans*-dibenzylideneacetone) associated with either 2 equiv. of a monophosphane ligand (L = PPh_3)[51] or with 1 equiv. of a bidentate bis(phosphane) (P,P) ligand {dppb [1,4-bis(diphenylphosphane)butane] or dppf [1,4-bis(diphenylphosphanyl)ferrocene)}[52] which are catalytic precursors for the Tsuji−Trost reactions.[3,51]

IV.1 Reversible Formation of Cationic $[(\eta^3\text{-allyl})PdL_2]^+$ Complexes in the Oxidative Addition of Allyl Acetate to Pd^0 Complexes Ligated by a Monophosphane Ligand

The reaction of $Pd^0(dba)_2$ with 2 equiv. of PPh_3 in DMF or THF gives the major complex $Pd^0(dba)(PPh_3)_2$. The species is involved in an equilibrium with the minor complex $SPd^0(PPh_3)_2$, the usual active species in oxidative additions (Scheme 13).[53]

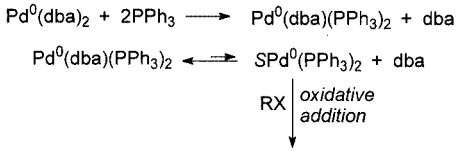

Scheme 13. Mechanism of the oxidative addition of an electrophile RX with the Pd^0 complex generated from the catalytic precursors $Pd^0(dba)_2$ and PPh_3 (2 equiv.) in DMF or THF

Conductivity measurements were performed on a solution of $Pd^0(dba)_2$ (c_0 = 2 mM) and 2 equiv. of PPh_3 in DMF after addition of 6.2 equiv. of $CH_2{=}CHCH_2OAc$. The conductivity κ increased with time to reach a plateau (κ_{equil}) whose value increased upon successive additions of allyl acetate (Figure 6, a).[46] This observation establishes that ionic species were formed that were involved in an equilibrium with the starting reagents [Equation (29)] because their concentration increased upon increasing the allyl acetate concentration. The conductivity κ_{equil} decreased when the concentration of dba was increased (Figure 6, b). Consequently, dba is involved in the reverse reaction of the equilibrium [Equation (29)].[46]

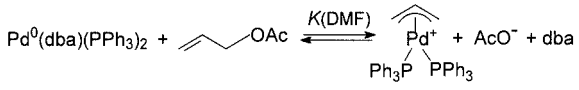

(29)

The complex $[(\eta^3\text{-}CH_2CHCH_2)Pd(PPh_3)_2]^+$ formed in the reaction was identified by a singlet in the ^{31}P NMR spectrum at δ = 24.06 ppm; by comparison, an authentic sample of $[(\eta^3\text{-}CH_2CHCH_2)Pd(PPh_3)_2]^+BF_4^-$ has δ = 24.08 ppm.[44a] The reversibility of the equilibrium in Equation (29) was established independently by treating $[(\eta^3\text{-}CH_2CHCH_2)Pd(PPh_3)_2]^+BF_4^-$ with 1 equiv. of nBu_4NOAc in the presence of 2 equiv. of dba. The complex $Pd^0(dba)(PPh_3)_2$ formed in the backward reaction was characterized by ^{31}P NMR spectroscopy when the reaction was performed in DMF, whereas $CH_2{=}CHCH_2OAc$ was characterized by ^1H NMR spectroscopy when the reaction was performed in $CDCl_3$.[46]

The equilibrium constant K_{DMF} [Equation (29)] could have been determined using the conductivity data of Figure 6 (a), as was accomplished for $[HPd(PPh_3)_2(DMF)]^+AcO^-$ (see Sect. III.2.1). The full shift, however, of the equilibrium towards the ionic species required a larger amount of allyl acetate ($n >> 100$) than that used in Figure 6 (a). Consequently, the intrinsic con-

 © 2003 Wiley-VCH Verlag GmbH & Co. KGaA, Weinheim

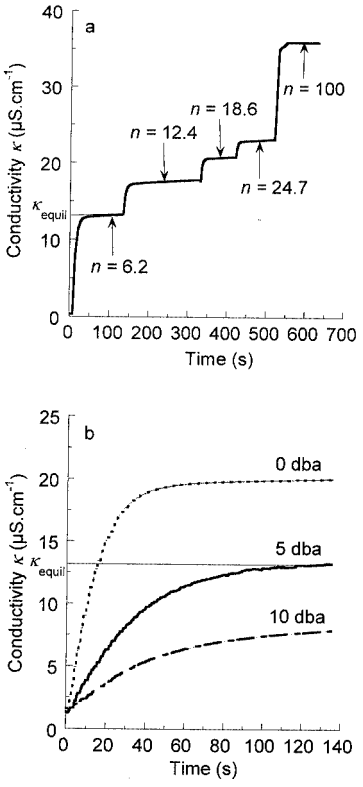

Figure 6. (a) Conductivity in DMF of $[(\eta^3\text{-}CH_2CHCH_2)Pd(PPh_3)_2]^+AcO^-$ formed in the reaction of the Pd^0 complex generated from $Pd^0(dba)_2$ (2 mM) and PPh_3 (4 mM) with $CH_2{=}CHCH_2OAc$ added successively at 20 °C; as indicated, n is the cumulative number of equiv. of $CH_2{=}CHCH_2OAc$; (b) conductivity of $[(\eta^3\text{-}CH_2CHCH_2)Pd(PPh_3)_2]^+AcO^-$ generated in the reaction of $Pd^0(dba)_2$ (2 mM) and PPh_3 (4 mM) with $CH_2{=}CHCH_2OAc$ (0.1 M) at 20 °C, in the presence of various amounts of dba, which was added to $Pd^0(dba)_2$ and PPh_3 prior the introduction of $CH_2{=}CHCH_2OAc$

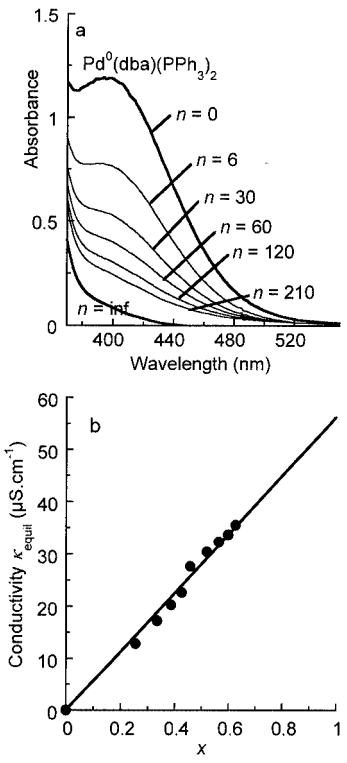

Figure 7. (a) UV spectrum performed in a 1-mm path cell of a solution of $Pd^0(dba)_2$ (1 mM) and PPh_3 (2 mM) in the presence of n equiv. of $CH_2{=}CHCH_2OAc$ in DMF at 20 °C; (b) plot of the conductivity κ_{equil}, measured for various values of n in Figure 6 (a), versus the corresponding molar fraction x calculated from the value of the equilibrium constant K [Equation (29)]; the molar conductivity Λ_M of $[(\eta^3\text{-}CH_2CHCH_2)Pd(PPh_3)_2]^+AcO^-$ was determined by extrapolation to $x = 1$

ductivity κ of $[(\eta^3\text{-}CH_2CHCH_2)Pd(PPh_3)_2]^+$ and AcO^- could not be determined from Figure 6 (a). The equilibrium constant $K_{DMF} = [(\eta^3\text{-}C_3H_5)PdL_2^+][AcO^-][dba]/[Pd^0(dba)L_2][CH_2{=}CHCH_2OAc]$ was determined easily by UV spectroscopy, taking advantage of the absorbance of $Pd^0(dba)(PPh_3)_2$ (λ_{max} = 396 nm) in DMF (Figure 7, a).

Successive additions of the allyl acetate resulted in successive additional decays of the absorbance of $Pd^0(dba)(PPh_3)_2$ (Figure 7, a), which provides further evidence for the equilibrium in Equation (29). At a given wavelength, the thermodynamic concentration of $Pd^0(dba)(PPh_3)_2$ was given by the ratio $(D_{equil} - D_{inf})/(D_0 - D_{inf})$ at different allyl acetate concentrations with $(D_{equil} - D_{inf})$ being the absorbance of $Pd^0(dba)(PPh_3)_2$ at the equilibrium position and $(D_0 - D_{inf})$ being the initial absorbance of $Pd^0(dba)(PPh_3)_2$.[46]

$K_{DMF} = 3.5\ (\pm\ 0.4) \times 10^{-5}$ M (20 °C)

One notices in Figure 7 (a) that more than 100 equiv. of allyl acetate were required to completely shift the equilibrium towards the cationic complex. From the value of K_{DMF}, the molar fraction x of the cationic complex could be calculated for each value of n used in the conductivity measurements of Figure 6 (a). The plot of κ_{equil} (determined in Figure 6, a) versus x was linear (Figure 7, b), which confirms the formation of the free ions $[(\eta^3\text{-}CH_2CHCH_2)Pd(PPh_3)_2]^+$ and AcO^- in DMF. The molar conductance was determined by extrapolation to $x = 1$.

$\Lambda_M = 56\ (\pm\ 2)$ S·cm^{-2}·mol^{-1} for
$[(\eta^3\text{-}CH_2CHCH_2)Pd(PPh_3)_2]^+AcO^-$ in DMF at 20 °C

No conductivity was observed in THF, but clearly the reaction took place since the UV absorbance of $Pd^0(dba)(PPh_3)_2$ (λ_{max} = 394 nm) decreased stepwise upon successive additions of the allyl acetate, as had been observed in DMF. Moreover, the resulting cationic complex $[(\eta^3\text{-}CH_2CHCH_2)Pd(PPh_3)_2]^+$ was characterized by ^{31}P NMR spectroscopy (δ = 24.5 ppm) in THF. Consequently, non-dissociative ion pairs $[(\eta^3\text{-}CH_2CHCH_2)\text{-}Pd(PPh_3)_2{}^+AcO^-]$ are formed in THF [Equation (30)], whereas free ions were formed in DMF [Equation (29)]. The equilibrium constant K_{THF} was determined by UV spectroscopy.

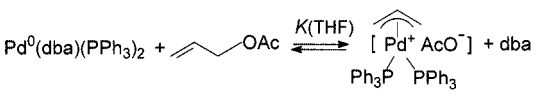

(30)

$K(THF) = 1\ (\pm\ 0.4) \times 10^{-3}$ (20 °C)

 © 2003 Wiley-VCH Verlag GmbH & Co. KGaA, Weinheim

One notices that for the same concentration of Pd^0 (c_0 = 1 mM), the equilibrium lies more in favor of the cationic complex in DMF than it does in THF.[46]

In both solvents, DMF and THF, we observe an overall equilibrated reaction from $Pd^0(dba)(PPh_3)_2$, but it is a multistep process (Scheme 14, R′ = Me). Indeed, the three initially sharp signals in the ^1H NMR spectrum of the allyl ligand of $[(\eta^3\text{-}CH_2CHCH_2)Pd(PPh_3)_2]^+BF_4^-$ observed in $CDCl_3$ became broad after addition of 1 equiv. of nBu$_4$NOAc and 2 equiv. of dba, and sharp signals of CH_2=$CHCH_2OAc$ (formed by attack of acetate ions on the allyl ligands) appeared. The presence of both broad and sharp signals in the same ^1H NMR spectrum indicates that different equilibria are operating with different equilibration rates. Consequently, the oxidative addition involves at least two steps and probably proceeds via the intermediate postulated in the literature, complex $Pd^0(\eta^2\text{-}CH_2$=$CHCH_2OAc)(PPh_3)_2$, which could not be detected when PPh_3 is the ligand for the palladium center. Clear-cut evidence for the intermediates is provided in the reactions with allylic benzoates or with bidentate ligands (see Sect. IV.3 and IV.2, respectively).

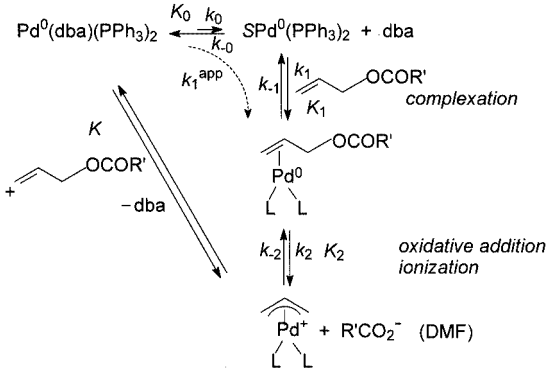

Scheme 14. Mechanism of the reversible reaction of allyl carboxylates with the Pd^0 complexes generated from $Pd^0(dba)_2$ and PPh_3 (2 equiv.) in DMF

Consequently, the overall equilibrium between $Pd^0(dba)(PPh_3)_2$, CH_2=$CHCH_2OAc$ and the cationic complex $[(\eta^3\text{-}CH_2CHCH_2)Pd(PPh_3)_2]^+AcO^-$ involves three successive equilibria (Scheme 14, R′ = Me) with K = $K_0{\cdot}K_1{\cdot}K_2$.

Compared to the postulated mechanisms in Equations (25) and (26), we now have clear evidence that the reaction of an allyl acetate with a Pd^0 complex is a reversible reaction, which leads to a cationic $[(\eta^3\text{-allyl})Pd(PPh_3)_2]^+$ complex with AcO^- as the counteranion. This result demonstrates unambiguously that the true oxidative addition (ionization step) is a reversible reaction (with K_2 as its equilibrium constant, Scheme 14, R′ = Me). Consequently, the acetate ion is not an "innocent" leaving group since it reacts with the cationic $[(\eta^3\text{-allyl})Pd(PPh_3)_2]^+$ complex to give back the allylic acetate and a Pd^0 complex.[46]

This conclusion is in agreement with a few reports in the literature that have suggested that the oxidative addition step is reversible. Indeed, in the absence of any nucleophile, isomerization of the C=C bond of allylic acetates had been observed as well as isomerization at the allylic position in substituted cyclic allylic acetates.[54]

IV.2 Reversible Formation of Cationic $[(\eta^3\text{-allyl})PdL_2]^+$ Complexes in the Oxidative Addition of the Allyl Acetate to Pd^0 Complexes Ligated by Bidentate Bis(phosphanes)

The reaction of $Pd^0(dba)_2$ with 1 equiv. of a bidentate P,P ligand in DMF or THF gives the major complex $Pd^0(dba)(P,P)$. This complex is involved in an equilibrium with the minor complex SPd^0(P,P), which is the more reactive species in oxidative additions (Scheme 15).[53b,55]

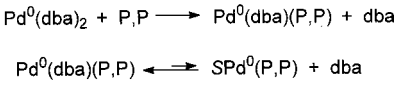

Scheme 15. Pd^0 complexes generated from $Pd^0(dba)_2$ and 1 equiv. of a bidentate P,P ligand in DMF or THF

The reaction of CH_2=$CHCH_2OAc$ with the Pd^0 complexes generated from $Pd^0(dba)_2$ (c_0 = 2 mM) and dppb (2 mM) in DMF was monitored by conductivity measurements to characterize the formation of ionic species.[47] The conductivity increased with time after addition of 5 equiv. of allyl acetate and reached a limiting value (Figure 8, a). This limiting value increased slightly after addition of a further 5 equiv. of allyl acetate, but remained unchanged after addition of yet another 5 equiv. of allyl acetate. The limiting conductivity (κ_{equil}) decreased upon successive additions of dba (Figure 8, a). These experiments establish that ionic species form that are involved in an equilibrium with the starting reagents, whereas dba is involved in the backward reaction [Equation (31)].

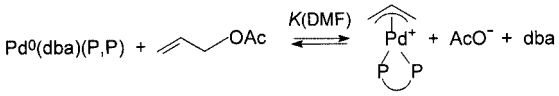

(31)

The complex formed in the oxidative addition was characterized by ^{31}P NMR spectroscopy [δ = 21.5 ppm (s)] and its structure was assigned to the cationic complex $[(\eta^3\text{-}CH_2CHCH_2)Pd(dppb)]^+AcO^-$ by comparison with an authentic sample of $[(\eta^3\text{-}CH_2CHCH_2)Pd(dppb)]^+BF_4^-$ [δ = 21.7 ppm (s)]. The molar conductance Λ_M of $[(\eta^3\text{-}CH_2CHCH_2)Pd(dppb)]^+AcO^-$ was determined from the value of κ_{irrev} (Figure 8, a) obtained when the equilibrium was fully shifted to the side of formation of the ionic species (15 equiv. allyl acetate). At this point, its concentration was c_0 = 2 mM, i.e., the initial Pd^0 concentration.

Λ_M = 42 (± 2) S·cm^{-2}·mol^{-1} for $[(\eta^3\text{-}CH_2CHCH_2)Pd(dppb)]^+AcO^-$ in DMF at 25 °C

The backward reaction of the equilibrium in Equation (31) was monitored by UV and ^{31}P NMR spectroscopy.

 © 2003 Wiley-VCH Verlag GmbH & Co. KGaA, Weinheim

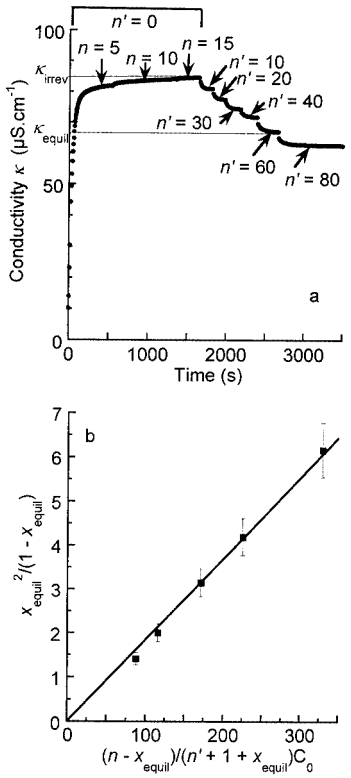

Figure 8. (a) Conductivity in DMF of $[(\eta^3\text{-}CH_2CHCH_2)Pd(dppb)]^+AcO^-$ formed in the reaction of the Pd^0 complex, generated from $Pd^0(dba)_2$ (2 mM) and dppb (2 mM), with $CH_2{=}CHCH_2OAc$ added successively ($0 < t < 1500$ s) at 25 °C; as indicated by the arrows, n is the cumulative number of equiv. of $CH_2{=}CHCH_2OAc$; this addition is followed by successive additions of dba ($t > 1500$ s); as indicated by the arrows, n' is the cumulative equiv. of added dba; (b) determination of the equilibrium constant K [Equation (31)] using the conductivity data of Figure 8 (a); plot of $[x^2_{equil}/(1 - x_{equil})]$ versus $[(n - x_{equil})/(n' + 1 + x_{equil})c_0]$. The value of $x_{equil} = \kappa_{equil}/\kappa_{irrev}$ [κ_{equil}: conductivity measured when the equilibrium in Equation (31) is fully established in the presence of n equiv. of $CH_2{=}CHCH_2OAc$ and n' equiv. of dba ($n = 5$ with $n' = 0$; $n = 15$ with $10 \le n' \le 80$; κ_{irrev}: conductivity when the equilibrium in Equation (31) is totally displaced towards its right-hand side in the absence of added dba ($n = 15$, $n' = 0$)]; K is determined from the slope

The UV spectrum of a solution of $[(\eta^3\text{-}CH_2CHCH_2)Pd(dppb)]^+BF_4^-$ (2 mM) in DMF exhibited, after addition of 5 equiv. of dba and 5 equiv. of nBu$_4$NOAc, an absorption band at $\lambda_{max} = 385$ nm that is characteristic of $Pd^0(dba)(dppb)$. Two broad signals in the ^{31}P NMR spectrum of $Pd^0(dba)(dppb)$ were also observed ($\delta = 21.17$ and 18.0 ppm).[55] These experiments provide clear evidence that the acetate ions react with the cationic complex $[(\eta^3\text{-}CH_2CHCH_2)Pd(dppb)]^+$ to generate a Pd^0 complex.[47]

IV.2.1 Determination of the Equilibrium Constant in DMF by Conductivity Measurements

The equilibrium constant K_{DMF} of the overall equilibrium [Equation (31)] was determined using the conductivity measurements of Figure 8 (a). The molar fraction x of the cationic complex in the equilibrium is given by $x_{equil} = \kappa_{equil}/\kappa_{irrev}$ for various values of n (equiv. of allyl acetate) and n' (equiv. of added dba).

$$K_{DMF} = [(\eta^3\text{-}CH_2CHCH_2)Pd(dppb)^+][AcO^-]\text{-}[dba]/[Pd^0(dba)(dppb)][CH_2{=}CHCH_2OAc]$$

$$K_{DMF} = c_0{\cdot}x^2_{equil}(n' + 1 + x_{equil})/(1 - x_{equil})(n - x_{equil})$$

Plotting $[x^2_{equil}/(1 - x_{equil})]$ versus $[(n - x_{equil})/(n' + 1 + x_{equil})c_0]$ gave a straight line with K_{DMF} as the slope (Figure 8, b): $K_{DMF} = 1.8 \times 10^{-2}$ M at 25 °C (Table 3, Entry 19). The equilibrium constant K was similarly calculated for the reaction involving the ligand dppf (Table 3, Entries 16, 17).[47]

Table 3. Effect of the leaving group $-OCOR'$ on the kinetics and thermodynamics of the reaction of allyl carboxylates[a] with the Pd^0 complexes generated from $Pd^0(dba)_2$ ($c_0 = 1$ mM) and 2 equiv. of PPh_3 (Scheme 14) or $Pd^0(dba)_2$ ($c_0 = 2$ mM) and 1 equiv. of dppf or dppb (Scheme 16) in DMF; comparative equilibrium constants K and rate constants k_1^{app}, K_0k_1, and k_2

Entry	$CH_2{=}CHCH_2{-}OCOR'$	Ligand	T [°C]	$10^3 \times K$ [M]	k_1^{app} [$M^{-1}s^{-1}$]	K_0k_1 [s^{-1}]	k_2 [s^{-1}]
1	$-OCO_2Et$	PPh_3	20	irrev.	> 100[b]	> 0.1	n.d.[c]
2	$-OCO_2Et$	PPh_3	–15	irrev.	1.5	0.0015	> 0.015
3	$-OCOCF_3$	PPh_3	–10	irrev.	40[d]	0.004	>> 1
4	$-OCOCF_3$	PPh_3	20	irrev.	> 100[b]	> 0.1	n.d.[c]
5	$-OCOCH_2Cl$	PPh_3	20	280	> 100[b]	> 0.1	n.d.[c]
6		PPh_3	20	150	> 100[b]	> 0.1	n.d.[c]
7		PPh_3	10	n.d.	80	0.08	0.5
8		PPh_3	20	8.6	62	0.062	n.d.
9		PPh_3	10	n.d.	30	0.03	0.17
10	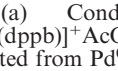	PPh_3	20	2	n.d.	n.d.	n.d.
11		PPh_3	10	n.d.	25	0.025	0.15
12	$-OCOCH_3$	PPh_3	20	0.035	n.d.	n.d.	n.d.
13	$-OCOCF_3$	dppf	16	340	> 100[b]	> 0.2	n.d.
14	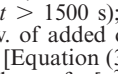	dppf	16	180	> 100[b]	> 0.2	0.021
15	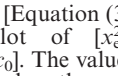	dppf	16	14	94	0.19	0.01
16	$-OCOCH_3$	dppf	16	1.1	4.8	0.019	0.018
17	$-OCOCH_3$	dppf	25	0.7	8.4	0.017	n.d.
18	$-OCOCF_3$	dppb	25	52	n.d.[c]	n.d.[c]	n.d.[c]
19	$-OCOCH_3$	dppb	25	18	26	0.1	0.025

[a] For a given ligand, the leaving groups are classified, when going down the table, in the order of their decreasing ability to leave. [b] Fast reaction: 100 $M^{-1}{\cdot}s^{-1}$ is the maximum value of the rate constant that could be determined by UV spectroscopy under our experimental conditions ($t_{1/2} = 2$ s for $c_0 = 1$ mM and [allylOCOR′] = 5 mM). [c] Not determined because the reaction is too fast. [d] For concentrations of $CH_2{=}CHCH_2OCOCF_3$ smaller than 0.02 M.[50]

Therefore, as for PPh_3, the reaction of the allyl acetate with the Pd^0 complex formed from $Pd^0(dba)_2$ and 1 equiv. of either dppb or dppf is a reversible reaction that generates cationic complexes $[(\eta^3\text{-}CH_2CHCH_2)Pd(P,P)]^+$ with AcO^- as the counteranion. The overall equilibrium, however, lies considerably more in favor of the cationic (η^3-allyl)palladium complex for the bidentate ligands dppb and dppf than it does for PPh_3 (compare the values of K in Table 3, Entries 12, 17, 19).[46,47]

IV.2.2 Determining the Rate Constants of the Complexation and Ionization Steps: Kinetic Evidence for Intermediate Neutral Complexes [$Pd^0(\eta^2\text{-}CH_2{=}CHCH_2OAc)(P,P)$]

As seen in Figure 8 (a), the overall equilibrium in Equation (31) could easily be fully displaced towards the side of the cationic complex. With 5 equiv. of $CH_2{=}CHCH_2OAc$,

 © 2003 Wiley-VCH Verlag GmbH & Co. KGaA, Weinheim

the overall reaction could be considered as being almost irreversible. Under such conditions, the kinetics of the formation of the cationic complex $[(\eta^3\text{-}CH_2CHCH_2)Pd(dppb)]^+$ with AcO^- as the counteranion could be monitored by conductivity measurements in DMF (curve C in Figure 9, a). The disappearance of $Pd^0(dba)(dppb)$ was monitored by UV spectroscopy at $\lambda_{max} = 385$ nm in DMF (curve A in Figure 9, a). The rate of disappearance of $Pd^0(dba)(dppb)$ was faster ($t_{1/2} = 8$ s) than the rate of formation of the cationic complex $[(\eta^3\text{-}CH_2CHCH_2)Pd(dppb)]^+$ ($t_{1/2} = 25$ s) whose kinetic curve C was S-shaped initially (Figure 9, a). Consequently, an intermediate neutral complex was generated before the formation of the cationic complex $[(\eta^3\text{-}CH_2CHCH_2)Pd(dppb)]^+$, presumably $Pd^0(\eta^2\text{-}CH_2{=}CHCH_2OAc)(dppb)$ where the Pd^0 atom is ligated to the C=C bond of the allyl acetate, as has been postulated in the literature.[3] The evolution of this neutral complex over time was deduced from the kinetic curves A and C (curve B in Figure 9, a). The neutral complex could not be characterized spectroscopically because it has too short a lifetime, but this was the first kinetic evidence for its formation.

Consequently, the reaction of allyl acetate with the Pd^0 complex, formed from $Pd^0(dba)_2$ and 1 equiv. of dppb, is a reversible one [Equation (31)] that proceeds through three reversible steps (Scheme 16, R′ = Me) with $K = K_0{\cdot}K_1{\cdot}K_2$.[47]

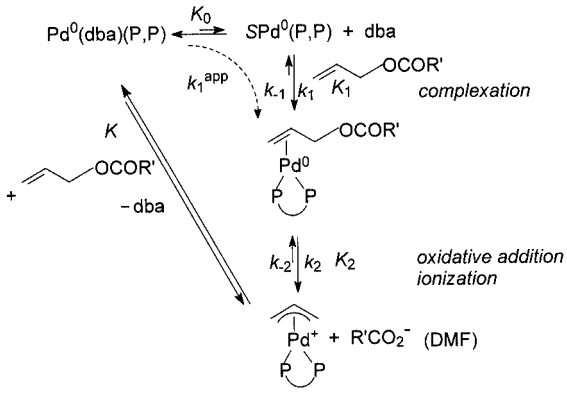

Scheme 16. Mechanism of the reversible reaction in DMF of allyl carboxylates with the Pd^0 complex formed from $Pd^0(dba)_2$ and 1 equiv. of (P,P) ligand (dppb, dppf)

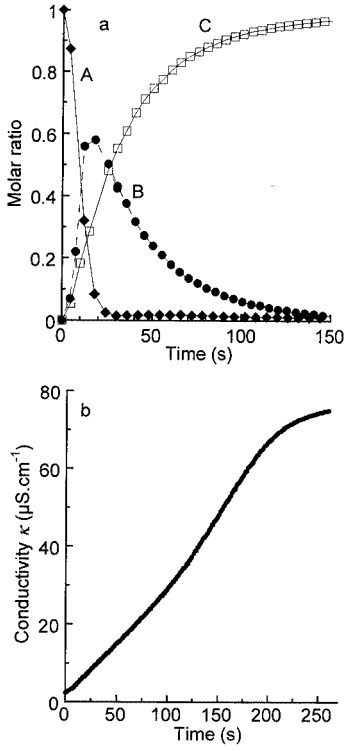

Figure 9. (a) Kinetics of the reaction of $CH_2{=}CHCH_2OAc$ (10 mM) with the Pd^0 complex formed from $Pd^0(dba)_2$ (2 mM) and dppb (2 mM) in DMF at 25 °C: A (filled diamonds): molar ratio of $Pd^0(dba)(dppb)$ versus time, determined by UV spectroscopy at 425 nm; B (filled circles): molar ratio of the neutral intermediate complex $(\eta^2\text{-}CH_2{=}CHCH_2OAc)Pd^0(dppb)$ versus time, determined from curves A and C [B = 1 − (A + C)]; C (empty squares): molar ratio of the cationic complex $[(\eta^3\text{-}CH_2CHCH_2)Pd(dppb)]^+AcO^-$ versus time, determined by conductivity measurements; (b) kinetics of the reaction of $CH_2{=}CHCH_2OAc$ (10 mM) with the Pd^0 complex formed from $Pd^0(dba)_2$ (2 mM) and dppf (2 mM) in DMF at 16 °C, monitored by conductivity measurements of the cationic complex $[(\eta^3\text{-}CH_2CHCH_2)Pd(dppf)]^+AcO^-$

Curve A in Figure 9 (a) represents the kinetics of the overall complexation step in which $Pd^0(dppb)(\eta^2\text{-}CH_2{=}CHCH_2OAc)$ is formed from $Pd^0(dba)(dppb)$ via $SPd^0(dppb)$. The values of $K_0{\cdot}k_1$ (Scheme 16) and the apparent rate constant of the overall complexation step, $k_1^{app} = K_0{\cdot}k_1/c_0$, were determined (Table 3, Entry 19).[47] A reaction order of +1 in allyl acetate was found for this step.[47]

Curve C in Figure 9 (a) represents the kinetics of the formation of the cationic complex $[(\eta^3\text{-}CH_2CHCH_2)Pd(dppb)]^+AcO^-$. Since this step is slower than the overall complexation step, the rate constant of the oxidative addition/ionization step (k_2 in Scheme 16) can be readily obtained from curve C, which is established by conductivity measurements, when $t > 30$ s (Table 3, Entry 19).[47] The rate of formation of the cationic $[(\eta^3\text{-}CH_2CHCH_2)Pd(dppb)]^+$ complex did not depend on the concentration of allyl acetate when it was in the range 0.02−0.1 M ($10 < n < 50$). This observation confirms a posteriori that the complexation and oxidative addition/ionization steps proceed successively on different timescales, with the oxidative addition/ionization step being slower (rds) than the overall complexation step. The term $k_1^{app}[CH_2{=}CHCH_2OAc] > k_2$ as soon as $[CH_2{=}CHCH_2OAc] > 1$ mM in DMF at 25 °C.[47]

Similar results were obtained when the Pd^0 precursor was formed from $Pd^0(dba)_2$ and 1 equiv. of dppf. The S-shaped curve, representative of the kinetics of formation of $[(\eta^3\text{-}CH_2CHCH_2)Pd(dppf)]^+AcO^-$, was, however, amplified (Figure 9, b) because of a smaller difference in the timescales of the complexation and ionization steps at the concentration of allyl acetate investigated here (0.1 mM). Determination of k_1^{app}, $K_0{\cdot}k_1$ and k_2 (Table 3, Entries 16, 17)

 © 2003 Wiley-VCH Verlag GmbH & Co. KGaA, Weinheim

showed that $k_1^{app}[CH_2{=}CHCH_2OAc] > k_2$ as soon as $[CH_2{=}CHCH_2OAc] = 4$ mM in DMF at 16 °C.[47]

Therefore, by means of two different analytical techniques — UV spectroscopy for the complexation step and conductivity measurements for the ionization step — kinetic evidence for the formation of the intermediate complex $Pd^0(\eta^2\text{-}CH_2{=}CHCH_2OAc)(P,P)$ (P,P = dppb, dppf) has been obtained for the first time.

IV.3 Influence of the Leaving Group on the Kinetics and Thermodynamics of the Reaction of Allyl Carboxylates with Pd^0 Complexes in DMF

The influence of the leaving group $R'CO_2^-$ on the equilibrium and rate constants of the reaction of allyl carboxylates or carbonates with Pd^0 complexes has been investigated. The equilibrium constant $K = K_0{\cdot}K_1{\cdot}K_2$ of the overall equilibrium between $Pd^0(dba)L_2$ (L = PPh_3 or L_2 = dppb or dppf), allyl carboxylates or carbonates, and the ionic species, was determined by UV spectroscopy, as reported above for the case of allyl acetate, $CH_2{=}CHCH_2OAc$ (Schemes 14 and 16; Table 3).[50] The overall reaction may be irreversible in the case of very reactive allyl carboxylates, or by using a large excess of them. Under conditions of irreversibility, the apparent rate constant $k_1^{app} = K_0{\cdot}k_1/c_0$ of the overall complexation step (Schemes 14 and 16) was determined by UV spectroscopy, which provided kinetic data on the disappearance of the Pd^0 complex. The rate of formation of the cationic complex $[(\eta^3\text{-allyl})PdL_2]^+$ was monitored by conductivity measurements. The rate constant, k_2 (Schemes 14 and 16), was determined when the ionization step was rate-determining. The data are gathered in Table 3.[50]

The reaction of allyl carboxylates $CH_2{=}CHCH_2OCOR'$ was irreversible when considering very good OCOR′ leaving groups, such as carbonate and trifluoroacetate (Table 3, Entries 1−4), whatever the conditions (large excess of dba or at low temperatures). The rate constants of the chemical steps, k_1^{app} and k_2 (Scheme 14), were too fast to be determined with high precision at 20 °C. Thus, the kinetics were monitored below 0 °C (Table 3, Entries 2, 3). For $OCOCF_3$, at −10 °C, the kinetic curve of the formation of the cationic complex was exponential (not S-shaped) with a rate of formation equal to that of the rate of disappearance of $Pd^0(dba)(PPh_3)_2$. This observation means that ionization of the intermediate complex $Pd^0(\eta^2\text{-}CH_2{=}CHCH_2OCOCF_3)(PPh_3)_2$ was faster than its formation, which was, thus, rate-determining: $k_1^{app}[CH_2{=}CHCH_2OCOCF_3] < k_2$.[50] Under such conditions, monitoring the rate of formation of the cationic complex by conductivity measurements did not provide the value of k_2, but, instead, that of k_1^{app}. A reaction order of +1 was found at low concentrations of $CH_2{=}CHCH_2OCOCF_3$ whereas the reaction order was zero at higher concentrations (> 0.2 M). This observation means that at high concentrations of $CH_2{=}CHCH_2OCOCF_3$, the reaction rate was no longer determined by the complexation of $CH_2{=}CHCH_2OCOCF_3$, but by the step that delivered the reactive species $SPd^0(PPh_3)_2$ from $Pd^0(dba)(PPh_3)_2$; i.e., the forward reaction with k_0 of the first equilibrium (Scheme 14). This result allowed the determination of $k_0 = 0.17\ M^{-1}{\cdot}s^{-1}$ (DMF, −10 °C).[50] Therefore, a fast oxidative addition may be limited by a decomplexation step (here dba) that delivers the reactive lowly ligated Pd^0 complex.[18]

For less effective leaving groups, such as chloromethyl acetate, benzoates, and acetate (Table 1, Entries 5−12, 14−17, 19), the overall reaction was equilibrated and, as expected, the better the leaving group, the higher the value of *K*. Indeed, a good leaving group will favor the two forward reactions, i.e., the complexation step, because the C=C bond becomes less electron-rich, and the oxidative addition step, in which the leaving group is released. A good leaving group will also disfavor the backward reaction of the last step (rate constant k_{-2}) because of its poor ability as a nucleophile. Thus, it is a consistent observation that, for a given ligand, the rate constants k_1^{app} (or $K_0{\cdot}k_1$) and k_2 increase with increasing leaving-group ability (Table 3, Entries 7,9,11 and 15, 14).[50]

In the benzoate series ($CH_2{=}CHCH_2OBz$), the rate constants k_1^{app} and k_2 were determined at 10 °C (Table 3, Entries 7, 9, 11).[50] The kinetic curves for the formation of the cationic complexes were S-shaped for appropriate concentrations of allyl benzoates (ca. 10 mM). This observation is again evidence for the formation of the intermediate complexes $Pd^0(\eta^2\text{-}CH_2{=}CHCH_2OBz)(PPh_3)_2$ with the overall complexation step being slightly faster than the ionization step: $k_1^{app}[CH_2{=}CHCH_2OBz] > k_2$.

Therefore, the ionization step is faster than the complexation step for good leaving groups (carbonate, trifluoroacetate) and the ionization step is rate-determining for poor leaving groups (acetate, benzoates).

IV.4 Reversible Formation of Cationic $[(\eta^3\text{-allyl})PdL_2]^+$ in the Oxidative Addition of Allylic Carbonates to Pd^0 Complexes Observed by Conductivity Measurements

The palladium-catalyzed reaction of allylic carbonates may be performed with neutral pronucleophiles NuH [Equation (32)].[42]

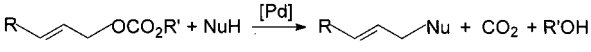

(32)

Indeed, the anion $EtOCO_2^-$, formed in the oxidative addition of the allylic carbonate to Pd^0 complexes, may decarboxylate to generate the basic EtO^- ion that is able to deprotonate NuH. As was found for allylic acetates, the oxidative addition of the allylic carbonate to Pd^0 complexes was supposed in the literature to give ionic species, i.e., a cationic $(\eta^3$-allyl)palladium(II) complex with the unstable $EtOCO_2^-$ counteranion.[56]

 © 2003 Wiley-VCH Verlag GmbH & Co. KGaA, Weinheim

IV.4.1 Evidence from Conductivity Measurements in DMF for the Reversible Formation of a Cationic [(η³-allyl)PdL₂]⁺ Complex in the Oxidative Addition of a Cyclic Allylic Carbonate to Pd⁰ Complexes

Conductivity measurements were performed in DMF at 20 °C on a solution of $Pd^0(dba)_2$ (2 mM) and 2 equiv. of PPh_3 by successive addition of various amounts of the allylic carbonate *cis*-**2** (formula in Scheme 17).[57] The conductivity κ increased with time to reach a limiting value that increased when the concentration of the allylic carbonate was increased (Figure 10, a). From these experiments, it was established that ionic species are formed in an equilibrium with the allylic carbonate and $Pd^0(dba)(PPh_3)_2$. On the other hand, the conductivity decreased when dba was added (Figure 10, a), which establishes that dba is involved in the backward reaction of the equilibrium. The allylic protons of the Pd^{II} complex were characterized by ^1H NMR spectroscopy in $CDCl_3$, as were those of the $EtOCO_2^-$ anion. This anion remained unchanged after 1 h, which proves its relative stability in chloroform[56] with regards to its decarboxylation. Consequently, it is assumed that the allylic carbonate *cis*-**2** reacts with the Pd^0 complex through an overall reversible reaction with formation of a cationic complex **3** with $EtOCO_2^-$ as the counteranion [Equation (33)].[57] This complex should be a priori *trans*-**3** (left part of Scheme 17) since the overall reaction always proceed with inversion of the configuration.[3]

$$Pd^0(dba)L_2 + \underset{\mathbf{2}}{allyl\text{–}OCO_2Et} \overset{K}{\rightleftharpoons} \underset{\mathbf{3}}{(\eta^3\text{–}allyl)PdL_2^+} + EtOCO_2^- + dba \qquad L = PPh_3 \qquad (33)$$

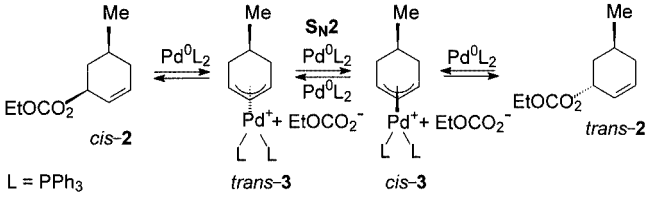

Scheme 17. Mechanism of the oxidative addition of a cyclic allylic carbonate to Pd^0L_2, whose precursor is either Pd^0L_4 or $Pd^0(dba)_2$ plus 2 equiv. of L in DMF (the solvent on Pd^0L_2 has been omitted voluntarily)

As was done with the allyl acetate (see Sect. IV.1), the equilibrium constant *K* was determined by UV spectroscopy. Indeed, addition of *n* equiv. of *cis*-**2** to $Pd^0(dba)(PPh_3)_2$ (c_0 = 1 mM), formed from $Pd(dba)_2$ and 2 equiv. of PPh_3, in DMF resulted in a fast decay of the absorbance of $Pd^0(dba)(PPh_3)_2$, which reached a constant value (Figure 10, b). Successive additions of *cis*-**2** resulted in related additional decays of the absorbance of $Pd^0(dba)(PPh_3)_2$, thus confirming that $Pd^0(dba)(PPh_3)_2$ and *cis*-**2** were involved in an equilibrium with the cationic complex **3**, dba, and $EtOCO_2^-$ [Equation (33)]. The UV spectroscopic data in Figure 10 (b) provided the thermodynamic

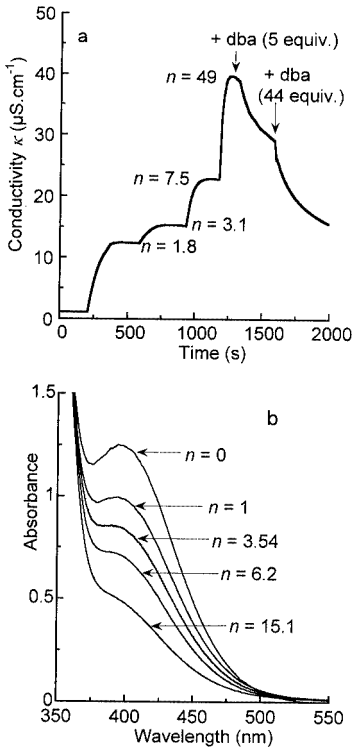

Figure 10. (a) Conductivity in DMF of the cationic complex $[(\eta^3\text{-allyl})Pd(PPh_3)_2]^+EtOCO_2^-$ (**3**) generated in the reaction of the Pd^0 complex formed from $Pd^0(dba)_2$ (2 mM) and PPh_3 (4 mM), with the cyclic allylic carbonate *cis*-**2** added successively ($0 < t < 1250$ s) (*n*: cumulative number of equiv.), followed by the successive addition of dba at 20 °C; (b) UV spectrum of $Pd^0(dba)(PPh_3)_2$, generated from $Pd^0(dba)_2$ (1 mM) and PPh_3 (2 mM) in the presence of *n* equiv. of *cis*-**2** at 20 °C, performed in DMF in a 1-mm path cell

concentration of $Pd^0(dba)(PPh_3)_2$ at different concentrations of *cis*-**2** and, thus, allowed the determination of *K*.[57]

$K = 1.4 (\pm 0.1) \times 10^{-4}$ M (DMF, 20 °C)

IV.4.2 Evidence for the Isomerization at the Allylic Position in the Oxidative Addition of Allylic Carbonate to Pd⁰ Complexes by an S_N2 Mechanism

The isomerization of *cis*-**2** to *trans*-**2** in the presence of a catalytic amount of $Pd^0(PPh_3)_4$ in THF at room temperature has been observed by Moreno-Mañas et al.[58] This reaction was reinvestigated in DMF, with $Pd^0(dba)_2$ and 2 equiv. of PPh_3, to compare the rate of isomerization as a function of the $SPd^0(PPh_3)_2$ precursor, all the while keeping in mind the fact that any oxidative addition performed from $Pd^0(PPh_3)_4$ [via $SPd^0(PPh_3)_2$] is faster than that performed from $Pd^0(dba)_2$ and 2 equiv. of PPh_3 [via $SPd^0(PPh_3)_2$] because of the higher concentration (ca. tenfold) of the reactive complex $SPd^0(PPh_3)_2$ in its equilibrium with $Pd^0(PPh_3)_3$ (Scheme 3) than in its equilibrium with $Pd^0(dba)(PPh_3)_2$ (Scheme 13).[53]

 © 2003 Wiley-VCH Verlag GmbH & Co. KGaA, Weinheim

The *cis*-**2**/*trans*-**2** isomerization was observed by ^{1}H NMR spectroscopy by treating $Pd^0(dba)_2$ and 2 equiv. of PPh_3 with a stoichiometric amount of *cis*-**2** in $CDCl_3$.[57] The thermodynamic ratio (40:60)[58] was obtained after 1 h. Therefore, the reaction of the cyclic allylic carbonate *cis*-**2** with $Pd^0(dba)(PPh_3)_2$ [via $SPd^0(PPh_3)_2$] affords two cationic complexes, *cis*-**3** and *trans*-**3** (characterized by ^{31}P NMR spectroscopy), by an overall equilibrium [Equation (33)] that is established in less than 20 min, as observed by UV spectroscopy and conductivity measurements, while the overall *cis*-**2**/*trans*-**2** isomerization requires a much longer time to occur.[57]

When the same series of experiments was conducted with $Pd^0(PPh_3)_4$ in DMF, the thermodynamic ratio was reached already after 15 min. Consequently, the rate of *cis*-**2**/*trans*-**2** isomerization is faster when the precursor of $SPd^0(PPh_3)_2$ is $Pd^0(PPh_3)_4$ rather than $Pd^0(dba)_2$ and 2 equiv. of PPh_3; i.e., when the concentration of $SPd^0(PPh_3)_2$ is relatively higher. This situation supports an isomerization of the *trans*-**3** and *cis*-**3** cationic complexes proceeding through an S_N2 mechanism induced by $SPd^0(PPh_3)_2$ (Scheme 17), followed by nucleophilic attack of the ethyl carbonate anion. Thus, kinetic evidence is now available that favors the S_N2 mechanism already proposed[59a,59b] and established in the literature.[59c−59e]

One hypothesis for the *trans*-**3**/*cis*-**3** isomerization proceeding by the S_N2 mechanism is given in Scheme 18. The cationic (η^3-allyl)Pd^{II} complex *trans*-**3** would be involved in equilibrium with the cationic (η^1-allyl)Pd^{II} complex *trans*-**4**, which may be considered as an allylic derivative with the PdL_2^+ moieties as the leaving group. As classically reported for any allylic activation by a Pd^0 complex,[3] the incoming Pd^0L_2 species would first coordinate the C=C bond in an *anti* position relative to the η^1-ligated $Pd^{II}L_2^+$ moieties (complex **5**). Activation of the allylic Pd−C bond would then proceed with formation of the complex *cis*-**3** and release of Pd^0L_2, which results in an overall exchange of the $Pd^{II}L_2$ unit of the complex *trans*-**3** by the incoming Pd^0L_2 unit with inversion of the configuration to produce *cis*-**3**.

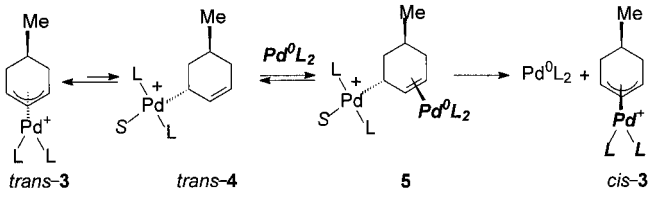

Scheme 18. Tentative explanation for the isomerization by the so-called S_N2 mechanism

It results from this mechanistic investigation that the loss of stereoselectivity in nucleophilic substitutions on the cyclic allylic carbonate *cis*-**2**, reported by Moreno-Mañas et al.,[58] arises from the isomerization of the intermediate cationic (η^3-allyl)palladium(II) complexes.

IV.5 Formation of Neutral (η^1-Allyl)(chloro)palladium Complexes in the Presence of Chloride Ions in DMF and THF

In DMF or THF, the cationic (η^3-allyl)palladium complex $[(\eta^3\text{-}CH_2CHCH_2)Pd(PPh_3)_2]^+Cl^-$ was not formed from $[Pd(\eta^3\text{-}CH_2CHCH_2)(\mu\text{-}Cl)]_2$ by addition of 4 equiv. of PPh_3 in the absence of any chloride scavenger. Indeed, the neutral complex (η^1-CH_2=$CHCH_2$)$PdCl(PPh_3)_2$ was isolated and characterized (Scheme 19).[60a] The latter complex was also generated upon addition of 1 equiv. of chloride ions (from nBu_4NCl) to the cationic $[(\eta^3\text{-}CH_2CHCH_2)Pd(PPh_3)_2]^+BF_4^-$ in DMF or THF (Scheme 19).[60a]

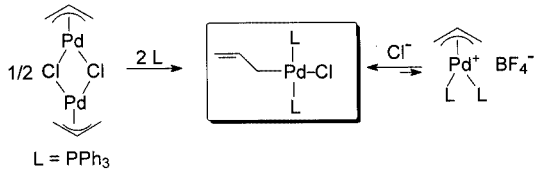

Scheme 19. Formation of (η^1-allyl)(chloro)palladium complexes

The neutral complex (η^1-CH_2=$CHCH_2$)$PdCl(PPh_3)_2$ was also generated in an oxidative addition of allyl acetate to Pd^0 complexes in the presence of voluntarily added chloride ions.[60a] This result emphasizes the crucial role of the presumably "innocent" ligands, such as chloride ions, which do not behave simply as counteranions of cationic (η^3-allyl)palladium(II) complexes, but may modify the chemical structure of the reactive intermediates by formation of neutral (η^1-allyl)(chloro)palladium(II) complexes. Consequently, the catalytic precursors of Tsuji−Trost reactions,[3] i.e., $[Pd(\eta^3\text{-}CH_2CHCH_2)(\mu\text{-}Cl)]_2$ plus 4 equiv. of PPh_3 or $[(\eta^3\text{-}CH_2CHCH_2)Pd(PPh_3)_2]^+BF_4^-$ are not equivalent. In the presence of chloride ions coming from the precursor or added in the catalytic reactions, the intermediate that is prone to react with the nucleophile might be not the cationic (η^3-allyl)palladium(II) complex, as usually considered, but the neutral (η^1-allyl)(chloro)palladium(II) species. Consequently, the presence of chloride ions might affect the regioselectivity of the catalytic reaction as well as its enantioselectivity.[61] Preliminary results on the influence of chloride ions on the reactivity of morpholine with $[(\eta^3\text{-}CH_2CHCH_2)Pd(PAr_3)_2]^+BF_4^-$ (Ar = 4-ClC_6H_4) show that the rate of nucleophilic attack is decelerated upon increasing the concentration of chloride ions. The reaction involves both cationic $[(\eta^3\text{-}CH_2CHCH_2)Pd(PAr_3)_2]^+$ and neutral (η^1-CH_2=$CHCH_2$)$PdCl(PAr_3)_2$ complexes as reactive species.[60b]

IV.6 Conclusion and Mechanistic Consequences

By means of conductivity measurements, the mechanism of the first step of the Tsuji−Trost reactions, i.e., the reaction of allylic carboxylates or carbonates with Pd^0 com-

 © 2003 Wiley-VCH Verlag GmbH & Co. KGaA, Weinheim

plexes, has been more deeply established. Indeed, whether the phosphane ligand examined here is monodentate (L) or bidentate (L_2), we have used conductivity measurements to (i) characterize the cationic $[(\eta^3\text{-allyl})PdL_2]^+$ complexes formed in the reaction, with the corresponding counteranion being either carboxylates or carbonate, (ii) give evidence for the reversibility of this reaction and subsequently determined the equilibrium constants, and (iii) investigate the kinetics of formation of the cationic $[(\eta^3\text{-allyl})PdL_2]^+$ complexes.

The combination of UV spectroscopy, used to monitor the kinetics of disappearance of the Pd^0 complex, with conductivity measurements, used to monitor the kinetics of formation of the cationic complex, provides kinetic evidence that the overall reaction proceeds in two steps: first a complexation step with formation of intermediate neutral complexes $Pd^0(\eta^2\text{-}CH_2{=}CHCH_2OCOR')L_2$ ($R' = CH_3$, L_2 = dppb, dppf; $R' = Ar$, $L = PPh_3$), followed by the formation of a cationic $[(\eta^3\text{-allyl})Pd^{II}L_2]^+$ complex with $R'CO_2^-$ as the counteranion (ionization step). The better the leaving group OCOR′, the higher the concentration of the cationic complex. For good leaving groups (carbonate, trifluoroacetate), the ionization step is faster than the complexation step, whereas the ionization step is rate-determining for poorer leaving groups (acetate, benzoates).

The reaction of a cyclic allylic carbonate was found to proceed with isomerization at the allylic position when the monodentate PPh_3 ligand was considered. This finding is a consequence of the *trans*/*cis* isomerization of the cyclic $[(\eta^3\text{-allyl})Pd(PPh_3)_2]^+$ complexes by an S_N2 mechanism induced by $Pd^0(PPh_3)_2$. This mechanism, which has already been established in the literature, was confirmed kinetically by evidence that the rate of isomerization depends on the concentration of Pd^0 and its precursor. This mechanism is not restricted to cyclic allylic carbonates since we have recently observed that the reaction of a cyclic allylic benzoate also proceeds with isomerization at the allylic position, and with kinetics that are dependent on the Pd^0 precursor.[62]

This study establishes definitively that the role of the leaving group in Tsuji−Trost reactions is certainly more intricate than it is usually considered to be. Since the leaving group's concentration increases as the catalytic reaction proceeds, it may play a significant kinetic role in competing with the nucleophiles (whose concentration decreases along the catalytic reaction) in the attack on the cationic $[(\eta^3\text{-allyl})PdL_2]^+$ species. The degree of reversibility of the overall oxidative addition (which is dependent on the nature of the leaving group) controls the concentration of the available Pd^0L_2 species and, consequently, may affect the stereoselectivity of catalytic reactions performed on cyclic allylic carbonates or carboxylates by isomerization of the intermediate cyclic cationic $[(\eta^3\text{-allyl})PdL_2]^+$ complexes. The stereoselectivity may be affected also by the nature of the Pd^0 precursors, which control the concentration of available Pd^0L_2, or by the presence of chloride ions, which determine the structure of the complex reacting with the nucleophile, i.e., cationic $[(\eta^3\text{-allyl})PdL_2]^+$ or neutral $(\eta^1\text{-allyl})PdClL_2$ complexes.

V. Miscellaneous Use of Conductivity Measurements for the Investigation of the Mechanism of a Stille Reaction: Ionization of $ISnBu_3$ in DMF

When a Stille reaction is performed using an aryl iodide [Equation (34)], $ISnBu_3$ is formed quantitatively as a by-product.[7e,7f,63,64]

$$PhI + CH_2{=}CH\text{-}SnBu_3 \xrightarrow{Pd^0(dba)_2 + 2AsPh_3} Ph\text{-}CH{=}CH_2 + ISnBu_3 \quad (34)$$

Taking advantage of the fact that $ISnBu_3$ dissociates into the free ions I^- and Bu_3Sn^+ in DMF, the mechanism of the transmetallation step — reaction of $CH_2{=}CHSnBu_3$ with $PhPdI(AsPh_3)_2$ [formed in the fast oxidative addition of PhI to the Pd^0 complex generated from $Pd^0(dba)_2$ and 2 equiv. of $AsPh_3$][65] — has been investigated in DMF by conductivity measurements [Equation (35)].[66]

$$PhPdIL_2 + CH_2{=}CH\text{-}SnBu_3 \xrightarrow{DMF} Ph\text{-}CH{=}CH_2 + I^- + {}^+SnBu_3 + Pd^0L_2 \quad (35)$$
$$L = AsPh_3$$

The objective was to discriminate between the reaction of $CH_2{=}CHSnBu_3$ with $PhPdI(AsPh_3)_2$ (**6**) (Scheme 20, path **A**) or with $PhPdI(AsPh_3)(DMF)$ (**7**) (Scheme 20, path **B**), generated by the partial dissociation of $PhPdI(AsPh_3)_2$ in DMF (observed in a previous study).[65] The mechanism in path **A** has been established by Casado and Espinet for $ArPdI(AsPh_3)_2$ (Ar = C_6F_5, $C_6Cl_2F_3$) in THF,[64] whereas the mechanism in path **B** has been proposed by Farina and Krishnan for $PhPdI(AsPh_3)_2$ in THF.[63] Whatever the mechanism, the nucleophilic attack of $CH_2{=}CHSnBu_3$ gives the common complex **8**[63,64] which evolves to generate complex **9** together with I^- and Bu_3Sn^+ in DMF. Styrene is then formed by a rapid reductive elimination from **9**. Consequently, the rates of formation of styrene and of the ionic species I^- and Bu_3Sn^+ are the same and the investigation of the rate of formation of I^- and Bu_3Sn^+ by conductivity measurements will provide the rate of the overall transmetallation step and the mechanistic pathway.

In DMF, the conductivity of a solution of $PhPdI(AsPh_3)_2$ (2 mM) increased with time after addition of 10 equiv. of $CH_2{=}CHSnBu_3$ (Figure 11, a). The final conductivity was identical ($\kappa_{lim} = 76 \pm 5$ μS·cm^{-1} at 25 °C) to that measured for an authentic sample of $ISnBu_3$ (2 mM) in DMF (κ = 75 μS·cm^{-1} at 25 °C), indicating that I^- and Bu_3Sn^+ were produced quantitatively. The kinetics of formation of I^- and Bu_3Sn^+ was accelerated upon increasing the concentration of $CH_2{=}CHSnBu_3$ (reaction order of +1) and was retarded by an excess of $AsPh_3$ (Figure 11, a),[66] which is indicative of a decomplexation of the $AsPh_3$ ligand in the transmetallation step, either before of after reaction with $CH_2{=}CHSnBu_3$.

 © 2003 Wiley-VCH Verlag GmbH & Co. KGaA, Weinheim

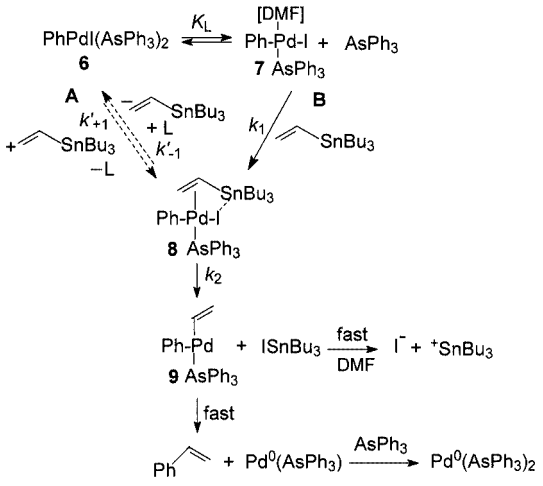

Scheme 20. Mechanism of the transmetallation step in a Stille reaction in DMF [Equation (35)]

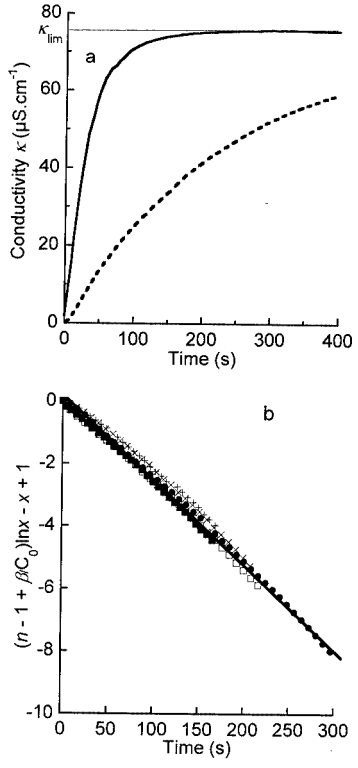

Figure 11. (a) (—) Kinetics of the reaction of CH_2=$CHSnBu_3$ (20 mM) with $PhPdI(AsPh_3)_2$ (2 mM) in DMF at 25 °C, as monitored by conductivity measurements of I^- and Bu_3Sn^+; value of $\kappa = \kappa_{exp} - \kappa_0$ (κ_{exp}: experimental conductivity at t; κ_0: initial residual conductivity of 3 $\mu S \cdot cm^{-1}$; κ_{lim}: conductivity of an authentic sample of $ISnBu_3$ (2 mM) in DMF; (---) kinetics in the presence of 5 equiv. of added $AsPh_3$; (b) influence of the concentration of $AsPh_3$ on the kinetics of the reaction of CH_2=$CHSnBu_3$ (20 mM) with $PhPdI(AsPh_3)_2$ (2 mM) in DMF at 25 °C; plot of $[(n - 1 + \beta/c_0)\ln x - x + 1]$ versus time [Equation (40)] with n = 3 (++), 4 (filled squares), 5 (empty squares), 6 (××), 7 (filled circles) [$x = (\kappa_{lim} - \kappa)/\kappa_{lim}$; κ: conductivity of I^- and Bu_3Sn^+ at t; κ_{lim}: final conductivity, determined as in Figure 11 (a)]

The kinetic laws for paths **A** and **B** (Scheme 20) are given by Equation (36) and (37), respectively (L: $AsPh_3$; Sn: CH_2=$CHSnBu_3$).[63]

$$d[I^-]/dt = d[^+SnBu_3]/dt = -d[\mathbf{6}]/dt = \frac{k'_{+1}k_2[\mathbf{6}][Sn]([L] + K_L)}{(k'_{-1}[L] + k_2)[L]} \quad (36)$$

$$d[I^-]/dt = d[^+SnBu_3]/dt = -d[\mathbf{6}]/dt = \frac{k_1K_L[\mathbf{6}][Sn]}{[L] + K_L} \quad (37)$$

Taking into account the value of $K_L = 3.1 \times 10^{-4}$ M in DMF,[65] Equation (36) simplifies into Equation (38) at high concentrations of L ([L] > 6 mM) so that paths **A** and **B** could not be distinguished on the basis of the observed rate law at high concentrations of L. Both laws can be expressed as Equation (39) with $\alpha = k_1 \cdot K_L$ and $\beta = K_L$ for Equation (37) and $\alpha = k_2 \cdot K'_1$ and $\beta = k_2/k'_{-1}$ for Equation (38).

$$-d[\mathbf{6}]/dt = \frac{k_2K'_1[\mathbf{6}][Sn]}{[L] + k_2/k'_{-1}} \quad (38)$$

$$-d[\mathbf{6}]/dt = \frac{\alpha[\mathbf{6}][Sn]}{[L] + \beta} \quad (39)$$

Because of the limiting solubility of $AsPh_3$ in DMF (14 mM), $AsPh_3$ could not be added in large excess. Therefore, the concentration of $AsPh_3$ was not constant during the reaction and the integration of Equation (39) gives Equation (40) with $x = (\kappa_{lim} - \kappa)/\kappa_{lim}$ (determined as in Figure 11, a) and n being the initial number of equiv. of $AsPh_3$ added to $Pd^0(dba)_2$ before addition of 1 equiv. of PhI, which generates $PhPdI(AsPh_3)_2$.

$$(n - 1 + \beta/C_0)\ln x - x + 1 = -\frac{\alpha[Sn]t}{C_0} \quad (40)$$

A value of $\beta = 3.2 \times 10^{-4}$ was determined, so that the plot of $(n - 1 + \beta/c_0)\ln x - x + 1$ versus time was linear whatever the value of n (Figure 11, b) in agreement with Equation (40), which is then valid over the whole range of concentrations of $AsPh_3$ added to $PhPdI(AsPh_3)_2$ (2–10 mM). Consequently, the experimental kinetics of the transmetallation step are in agreement with the mechanism of path **B** in Scheme 20; this conclusion would not be the case for the mechanism of path **A**, since Equation (38) is valid only for high concentrations of $AsPh_3$ (> 6 mM). Since $\beta = K_L$ [Equations (37) and (39)], a second method to determine $K_L = 3.2 \pm 0.1 \times 10^{-4}$ M (DMF, 25 °C) is available and is in agreement with the value of $K_L = 3.1 \times 10^{-4}$ M (DMF, 25 °C) determined in a previous study.[65]

Since $\alpha = k_1 \cdot K_L$, then $k_1 = 8.3 \pm 0.5$ $M^{-1}s^{-1}$. A similar value of $k_1 = 7.5$ $M^{-1}s^{-1}$(DMF, 25 °C) was determined by treating CH_2=$CHSnBu_3$ with $PhPdI(AsPh_3)$(DMF) generated by the fast dissociation of the dimer $Ph_2Pd_2(\mu\text{-}I)_2(AsPh_3)_2$ (**10**) in DMF.[66] The kinetics of this system were also monitored by conductivity measurements of I^- and Bu_3Sn^+ generated in the reaction.[66]

Therefore, K_L has been determined independently by two different strategies: (i) from the partial dissociation of

 © 2003 Wiley-VCH Verlag GmbH & Co. KGaA, Weinheim

$PhPdI(AsPh_3)_2$ to $PhPdI(AsPh_3)(DMF)$ observed in DMF,[65] and (ii) from the kinetics of the transmetallation step performed with $PhPdI(AsPh_3)_2$ [66] (vide supra). Similarly, the same value of k_1, which characterizes the reactivity of $PhPdI(AsPh_3)(DMF)$ with $CH_2{=}CHSnBu_3$, has been determined independently by two different strategies: (i) from the kinetics of the transmetallation step performed with $PhPdI(AsPh_3)_2$ (vide supra)[66] and (ii) from the kinetics of the reaction of $CH_2{=}CHSnBu_3$ with $PhPdI(AsPh_3)(DMF)$ generated by the fast dissociation of the dimer **10** in DMF.[66]

This result definitively proves that, in DMF, the transmetallation step involves the reaction of $CH_2{=}CHSnBu_3$ with $PhPdI(AsPh_3)(DMF)$ generated by dissociation of $PhPdI(AsPh_3)_2$ (path **B** in Scheme 20). This study illustrates how to take advantage of conductivity measurements, used to monitor the kinetics of the formation of a by-product, to gain a deeper insight into the mechanism of a palladium-catalyzed reaction that does not involve any ionic palladium complexes as intermediates.

Conclusion

Taking advantage of the fact that DMF is a good solvent for dissociating and coordinating cationic palladium(II) complexes, conductivity measurements have proved to be efficient for characterizing the cationic nature of palladium(II) complexes that have already been postulated in the literature, but not characterized in the context of a real oxidative addition, such as (i) $[(aryl)PdL_2(DMF)]^+TfO^-$ or $[(vinyl)PdL_2(DMF)]^+TfO^-$ ($L = PPh_3$) generated in oxidative additions of aryl or vinyl triflates, respectively, to Pd^0 complexes, (ii) $[HPdL_2(DMF)]^+RCO_2^-$ ($R = CH_3$, H; $L = PPh_3$) generated in oxidative additions of acetic or formic acid to Pd^0 complexes, and (iii) $[(\eta^3\text{-allyl})PdL_2]^+R'CO_2^-$ (R' = alkyl, aryl, OEt; $L = PPh_3$ or L_2 = dppe, dppf) in oxidative additions of allylic carboxylates (or carbonates) to Pd^0 complexes. In all cases, the cationic palladium(II) complex and its counteranion were generated as free ions. Such cationic complexes are key intermediates in Stille, Heck, and Tsuji–Trost reactions. The role of chloride ions has been investigated with the formation of neutral complexes $ArPdClL_2$ and $(\eta^1\text{-allyl})PdClL_2$ ($L = PPh_3$). The cationic and neutral character of the intermediate Pd^{II} complexes is of crucial importance because it determines their reactivities with nucleophiles in Heck, Stille, and Tsuji–Trost reactions.

Conductivity measurements have also been used to gather thermodynamic data on the formation of cationic palladium(II) complexes. Indeed, the reversibility of oxidative additions of allylic carboxylates (or carbonates) to Pd^0 complexes has been established as well as that of acetic and formic acid, and the equilibrium constants have been determined. The reversible oxidative addition of a cyclic allylic carbonate generates cyclic *cis* and *trans* $[(\eta^3\text{-allyl})PdL_2]^+EtOCO_2^-$ complexes. The *cis*/*trans* isomerization proceeds by an S_N2 mechanism induced by the Pd^0L_2 complex.

Conductivity measurements have also been used to gather kinetic data on the formation of cationic palladium(II) complexes. Under conditions where the oxidative additions were irreversible, the rates of formation of the cationic palladium(II) complexes (monitored by conductivity measurements) were compared to those of the disappearance of the palladium(0) complex (monitored by UV spectroscopy). Kinetic evidence has been obtained for the formation of neutral intermediate complexes $Pd^0(\eta^2\text{-allyl-OCOR}')L_2$ ($R' = CH_3$, L_2 = dppb, dppf; $R' = Ar$, $L = PPh_3$) in the oxidative addition of allylic carboxylates to palladium(0) complexes, establishing that two successive reactions are involved (complexation and ionization steps) whose relative rates depend on the nature of the leaving group $-OCOR'$. Thus, the effect of the leaving group has been clarified.

As a somewhat unrelated application of this method, monitoring the formation of an ionic by-product (I^-, $^+SnBu_3$) by conductivity measurements has brought about a deeper insight into the mechanism of the transmetallation step of a Stille reaction, which does not involve any ionic intermediate palladium complexes, by establishing the involvement of $PhPdI(AsPh_3)(DMF)$ as the species that reacts with an organotin derivative.

Acknowledgments

The author wishes to express her gratitude to the students who have greatly contributed to the research work summarized here: S. Gamez, A. Mosleh, A. Ndedi Ntepe, C. Orthwein as well as Dr. G. Meyer and Prof. C. Amatore. Drs. I. Chiarotto, K. K. Hii, R. Pleixats, Profs. J. B. Brown, I. Carelli, M. Moreno-Mañas and J. G. de Vrieze are thanked for fruitful collaborations. S. Négri is also thanked for technical assistance. The financial support from CNRS, ENS (MNRT) and University Paris VI is gratefully acknowledged. Johnson Matthey is thanked for a generous loan of sodium tetrachloropalladate.

[1] [1a] A. de Mejeire, F. E. Meyer, *Angew. Chem. Int. Ed. Engl.* **1994**, *33*, 2379–2411. [1b] G. T. Crisp, *Chem. Soc., Rev.* **1998**, *27*, 427–436. [1c] I. P. Beletskata, A. V. Cheprakov, *Chem. Rev.* **2000**, *100*, 3009–3066. [1d] M. Larhed, A. Hallberg, *Handbook of Organopalladium Chemistry for Organic Synthesis* (Ed.: E. Negishi), Wiley-Interscience, New York, **2002**, vol. I, chapter IV.2, p. 1133–1178.

[2] For Heck reactions from aryl triflates, see: [2a] W. Cabri, I. Candiani, S. DeBernardinis, F. Francalanci, S. Penco, R. Santi, *J. Org. Chem.* **1991**, *56*, 5796–5800. [2b] F. Ozawa, A. Kubo, T. Hayashi, *J. Am. Chem. Soc.* **1991**, *113*, 1417–1419. [2c] T. Hayashi, A. Kubo, F. Ozawa, *Pure Appl. Chem.* **1992**, *64*, 421–427. [2d] W. Cabri, I. Candini, A. Bedeschi, R. Santi, *J. Org. Chem.* **1992**, *57*, 3558–3563. [2e] F. Ozawa, A. Kubo, Y. Matsumoto, T. Hayashi, *Organometallics* **1993**, *12*, 4188–4196. [2f] W. Cabri, I. Candini, *Acc. Chem. Res.* **1995**, *28*, 2–7.

[3] [3a] J. Tsuji, *Palladium Reagents and Catalysts*, John Wiley & Sons, Chichester, **1996**, p. 290. [3b] S. A. Godleski, in *Comprehensive Organic Synthesis*, vol. 4 (Eds: B. M. Trost, I. Flemming, M. F. Semmelhack), Pergamon, Oxford, **1991**. [3c]G. Consiglio, R. Waymouth, *Chem. Rev.* **1989**, *89*, 257–276. [3d] C. G. Frost, J. Howard, J. M. J. Williams, *Tetrahedron: Asymmetry* **1992**, *3*, 1089–1122. [3e] A. Pfaltz, *Acc, Chem. Rev.* **1993**, *26*, 339–345. [3f] B. M. Trost, *Acc. Chem. Res.* **1996**, *29*, 355–364. [3g] B. M. Trost, D. L. Van Kanken, *Chem. Rev.* **1996**, *96*, 395–422.

 © 2003 Wiley-VCH Verlag GmbH & Co. KGaA, Weinheim

[4] P. W. Atkins, *Physical Chemistry*, 5th ed., Oxford University Press, **1994**, p. 834−839.

[5] Modern conductivity meters (e.g., CDM210 Radiometer Analytical) deliver the conductivity κ of solutions containing ionic species. $\kappa = kG$ where G is the conductance ($G = 1/R$; R: resistance of the solution containing the ionic species) expressed in Siemens (S; 1 S = 1 Ω^{-1}) and k is the cell constant expressed in cm^{-1} (the value of k is usually close to 1 cm^{-1}). The measured conductivity κ is expressed in $S{\cdot}cm^{-1}$. Considering a strong electrolyte with c_i being the concentration of one ion, z_i its charge and λ_i its equivalent conductivity, the overall conductivity is expressed as $\kappa = \Sigma\lambda_i z_i c_i$ if the solution behaves ideally. In the case of a 1:1 electrolyte at a concentration c, $\kappa = (\lambda_+ + \lambda_-)c = \Lambda_M c$. The molar conductivity Λ_M of the electrolyte is usually expressed in $S{\cdot}cm^2{\cdot}mol^{-1}$ when the concentration C is expressed in $mol{\cdot}L^{-1}$.[4] The conductivity can be recorded versus time using a computerized home-made program.

[6] For a review on the characterization of coordination compounds by conductivity measurements, see: W. J. Geary, *Coord. Chem. Rev.* **1971**, *7*, 81−122.

[7] [7a] W. J. Scott, G. T. Crisp, J. K. Stille, *J. Am. Chem. Soc.* **1984**, *106*, 4630−4632. [7b] W. J. Scott, J. K. Stille, *J. Am. Chem. Soc.* **1986**, *108*, 3033−3040. [7c] A. M. Echavarren, J. K. Stille, *J. Am. Chem. Soc.* **1987**, *109*, 5478−5486. [7d] A. M. Echavarren, J. K. Stille, *J. Am. Chem. Soc.* **1988**, *110*, 1557−1565. [7e] V. Farina, G. P. Roth, *Adv. Metalorg. Chem.* **1996**, *5*, 1−53. [7f] V. Farina, V. Krishnamurthy, W. J. Scott, *Org. React.* **1997**, *50*, 1−339.

[8] P. J. Stang, M. H. Kowalski, M. D. Schiavelli, D. Longford, *J. Am. Chem. Soc.* **1989**, *111*, 3347−3356.

[9] V. Farina, B. Krishnan, D. R. Marshall, G. P. Roth, *J. Org. Chem.* **1993**, *58*, 5434−5444.

[10] A. Jutand, A. Mosleh, *Organometallics* **1995**, *14*, 1810−1817.

[11] The oxidative addition of 4-$O_2NC_6H_4OTf$ to $Pd^0(PPh_3)_4$ in THF was monitored by ^{31}P NMR spectroscopy at room temperature. The spectrum exhibits a singlet at δ = 22.2 ppm attesting that only *trans*-[4-$O_2NC_6H_4Pd(PPh_3)_2(THF)]^+TfO^-$ was formed and not [4-$O_2NC_6H_4Pd(PPh_3)_3]^+TfO^-$. Espinet et al. have reported that $[C_6F_5Pd(PPh_3)_3]^+TfO^-$ was generated as a minor complex in the oxidative addition of C_6F_5OTf to $Pd^0(PPh_3)_4$ in THF at 20 °C.[12]

[12] A. L. Casado, P. Espinet, A. M. Gallego, *J. Am. Chem. Soc.* **2000**, *122*, 11771−11782.

[13] Espinet et al. have reported that a related neutral complex *trans*-$(C_6Cl_2F_3)Pd(OTf)(PPh_3)_2$ predominates in the equilibrium with the ionic *trans*-$[(C_6Cl_2F_3)Pd(PPh_3)_2(THF)]^+$ and TfO^- at low temperatures in THF, but had almost disappeared above room temperature. The cationic complex was then predominant.[12]

[14] C. Amatore, M. Azzabi, A. Jutand, *J. Am. Chem. Soc.* **1991**, *113*, 8375−8384.

[15] A. Jutand, A. Mosleh, *J. Org. Chem.* **1997**, *62*, 261−274.

[16] [16a] C. Amatore, A. Jutand, M. A. M'Barki, *Organometallics* **1992**, *11*, 3009−3013. [16b] C. Amatore, E. Carré, A. Jutand, M. A. M'Barki, G. Meyer, *Organometallics* **1995**, *14*, 5605−5614. [16c] C. Amatore, A. Jutand, *Acc. Chem. Res.* **2000**, *33*, 314−321.

[17] A. Jutand, K. K. Hii, M. Thornton-Pett, J. M. Brown, *Organometallics* **1999**, *18*, 5367−5374.

[18] L. M. Alcazar-Roman, J. F. Hartwig, *Organometallics* **2002**, *21*, 491−502.

[19] A. L. Casado, P. Espinet, A. M. Gallego, J. M. Martínez-Ilarduya, *Chem. Commun.* **2001**, 339−340.

[20] [20a] J. M. Brown, J. J. Pérez-Torrente, N. W. Alcock, H. J. Clase, *Organometallics* **1995**, *14*, 207−213. [20b] J. M. Brown, K. K. Hii, *Angew. Chem. Int. Ed. Engl.* **1996**, *35*, 657−659.

[21] M. Ludwig, S. Strömberg, M. Svensson, B. Åkermark, *Organometallics* **1999**, *18*, 970−975.

[22] J. F. Fauvarque, F. Pflüger, M. Troupel, *J. Organomet. Chem.* **1981**, *208*, 419−427.

[23] B. E. Mann, A. Musco, *J. Chem. Soc., Dalton Trans.* **1968**, *14*, 5605−5614.

[24] C. Amatore, E. Carré, A. Jutand, *Acta Chem. Scand.* **1998**, *52*, 100−106.

[25] K. K. Hii, M. Thornton-Pett, A. Jutand, R. P. Tooze, *Organometallics* **1999**, *18*, 1887−1896.

[26] [26a] K. Karabelas, C. Westerlund, A. Hallberg, *J. Org. Chem.* **1985**, *50*, 3896−3900. [26b] W. Cabri, I. Candiani, A. Bedeshi, R. Santi, *Tetrahedron Lett.* **1991**, *32*, 1753−1756.

[27] [27a] R. J. Deeth, A. Smith, K. K. Hii, J. M. Brown, *Tetrahedron Lett.* **1998**, *39*, 3229−3232. [27b] K. K. Hii, T. D. W. Claridge, J. M. Brown, *Angew. Chem. Int. Ed. Engl.* **1997**, *36*, 984−987.

[28] L. E. Overman, D. J. Poon, *Angew. Chem. Int. Ed. Engl.* **1997**, *36*, 518−521.

[29] A. Jutand, S. Négri, submitted.

[30] [30a] T. Sakamoto, Y. Kondo, N. Mutura, H. Yamanaka, *Tetrahedron* **1993**, *49*, 9713−9720. [30b] R. Kakino, S. Yasumi, I. Shimizu, A. Yamamoto, *Bull. Chem. Soc. Jpn.* **2002**, *75*, 137−148.

[31] M. S. Stephan, A. J. J. M. Teunissen, G. K. M. Verzijl, J. G. de Vries, *Angew. Chem. Int. Ed.* **1998**, *37*, 662−664.

[32] A. Jutand, S. Négri, J. G. de Vries, *Eur. J. Inorg. Chem.* **2002**, 1711−1717.

[33] [33a] B. M. Trost, W. Pfrengle, H. Urabe, J. Dumas, *Acc. Chem. Res.* **1990**, *23*, 34−42. [33b] B. M. Trost, M. J. Krische, *Synlett* **1998**, 1−16. [33c] B. M. Trost, *Chem. Eur. J.* **1998**, *4*, 2405−2412.

[34] D. Zargarian, H. Alper, *Organometallics* **1993**, *12*, 712−724.

[35] I. Carelli, I. Chiarotto, S. Cacchi, P. Pace, C. Amatore, A. Jutand, G. Meyer, *Eur. J. Org. Chem.* **1999**, 1471−1473.

[36] For a review on hydrido complexes of palladium, see: V. V. Grushin, *Chem. Rev.* **1996**, *96*, 2011−2033.

[37] C. Amatore, A. Jutand, G. Meyer, I. Carelli, I. Chiarotto, *Eur. J. Inorg. Chem.* **2000**, 1855−1859.

[38] A. R. Siedle, R. A. Newmark, W. B. Gleason, *Inorg. Chem.* **1991**, *30*, 2005−2009.

[39] V. N. Zudin, V. D. Chinakov, V. M. Nekipelov, V. A. Likholobov, Y. I. Yermakov, *J. Organomet. Chem.* **1985**, *289*, 425−430.

[40] The conductivity did not stabilize, but instead it increased continually with time at 25 °C. The degradation probably arose from a side reaction induced by the formate ion, i.e., the partial decarboxylation of the neutral intermediate HPd(OCHO)$(PPh_3)_2$ (formed in the very first step of the reaction) before ionization. This well-known decarboxylation of formate gave $HPdH(PPh_3)_2$, leading to H_2 and Pd^0L_2 that again underwent a reaction with HCO_2H. A similar degradation has been proposed by Zargarian and Alper.[34]

[41] If, however, the catalytic reactions are carried out in benzene, a non-coordinating and non-ionizing solvent, the neutral complexes $HPdA(PPh_3)_2$ (A = $OCOCH_3$ or OCHO)[33a,33b] must be formed, but in low concentration because they are involved in an endergonic equilibrium with the carboxylic acid and the Pd^0 complex.

[42] J. Tsuji, *Tetrahedron* **1986**, *42*, 4361−4401.

[43] Few cationic (η^3-allyl)palladium(II) complexes formed by an oxidative addition of an allylic acetate have been reported with acetate as the counter anion. See: [43a] T. Yamamoto, O. Saito, A. Yamamoto, *J. Am. Chem. Soc.* **1981**, *103*, 5600−5602. [43b] P. R. Auburn, P. B. Mackenzie, B. Bosnich, *J. Am. Chem. Soc.* **1985**, *107*, 2033−2046. [43c] A cationic (η^3-allyl)palladium(II) complex has been synthesized by oxidative addition of an allylic acetate to a Pd^0 complex, but with BF_4^- as the counteranion because of treatment of the complex with $NaBF_4$ before isolation. See: T. Hayashi, T. Hagihara, M. Konishi, M. Kumada, *J. Am. Chem. Soc.* **1983**, *105*, 7767−7768. [43d] T. Hayashi, A. Yamamoto, T. Hagihara, *J. Org. Chem.* **1986**, *51*, 723−727.

[44] [44a] J. Powell, B. L. Shaw, *J. Chem. Soc. A* **1968**, 774−777. [44b] B. Åkermark, G. Åkermark, L. S. Hegedus, K. Zetterberg, *J. Am. Chem. Soc.* **1981**, *103*, 3037−3040.

[45] T. Hayashi, A. Yamamoto, Y. Ito, E. Nishioka, H. Miura, K. Yanagi, *J. Am. Chem. Soc.* **1989**, *111*, 6301−6311.

 © 2003 Wiley-VCH Verlag GmbH & Co. KGaA, Weinheim

[46] C. Amatore, A. Jutand, G. Meyer, L. Mottier, *Chem. Eur. J.* **1999**, *5*, 466−473.
[47] C. Amatore, S. Gamez, A. Jutand, *Chem. Eur. J.* **2001**, *7*, 1273−1280.
[48] C. Amatore, S. Gamez, A. Jutand, *J. Organomet. Chem.* **2001**, *624*, 217−222.
[49] C. Amatore, S. Gamez, A. Jutand, G. Meyer, L. Mottier, *Electrochim. Acta* **2001**, *46*, 3237−3244.
[50] N. Agenet, C. Amatore, S. Gamez, H. Gérardin, A. Jutand, G. Meyer, C. Orthwein, *ARKIVOC* **2002**, 92−101 (http://www.arkat-usa.org/).
[51] For seminal works on the use of $Pd(dba)_2$ with monodentate phosphane ligands in allylic substitutions, see: D. Ferroud, J. P. Genêt, J. Muzart, *Tetrahedron Lett.* **1984**, *25*, 4379−4382.
[52] For seminal works on the use of $Pd(dba)_2$ with bidentate phosphane ligands in allylic substitutions, see: J. C. Fiaud, H. de Gournay, M. Larchevêque, H. B. Kagan, *J. Organomet. Chem.* **1978**, *154*, 175−185.
[53] [53a] C. Amatore, A. Jutand, F. Khalil, M. A. M'Barki, L. Mottier, *Organometallics* **1993**, *12*, 3168−3178. [53b] C. Amatore, A. Jutand, *Coord. Chem. Rev.* **1998**, *178−180*, 511−528.
[54] [54a] B. M. Trost, T. R. Verhoeven, J. F. Fortunak, S. M. McElvain, *Tetrahedron Lett.* **1979**, *25*, 2301−2304. [54b] B. M. Trost, T. R. Verhoeven, *J. Am. Chem. Soc.* **1980**, *102*, 4730−4743. [54c] J.-E. Bäckvall, R. E. Nordberg, J. Vagberg, *Tetrahedron Lett.* **1983**, *24*, 411−412.
[55] C. Amatore, G. Broeker, A. Jutand, F. Khalil, *J. Am. Chem. Soc.* **1997**, *119*, 5176−5185.
[56] For stable cationic complexes $[(\eta^3\text{-allyl})PdL_2]^+$ (L = PMe_3, PMe_2Ph, $PMePh_2$) with ethyl carbonate as the counteranion, see: F. Ozawa, T. Son, S. Ebina, K. Osakada, A. Yamamoto, *Organometallics* **1992**, *11*, 171−176.
[57] C. Amatore, S. Gamez, A. Jutand, G. Meyer, M. Moreno-Mañas, L. Morral, R. Pleixats, *Chem. Eur. J.* **2000**, *6*, 3372−3376.
[58] M. Moreno-Mañas, L. Morral, R. Pleixats, *J. Org. Chem.* **1998**, *63*, 6160−6166.
[59] [59a] T. Takahashi, Y. Jinbo, K. Kitamura, J. Tsuji, *Tetrahedron Lett.* **1984**, *25*, 5921−5924. [59b] P. B. Mackenzie, J. Whelan, B. Bosnich, *J. Am. Chem. Soc.* **1985**, *107*, 2046−2054. [59c] H. Kurosawa, S. Ogoshi, N. Chatani, Y. Kawasaki, S. Murai, I. Ikeda, *Chem. Lett.* **1990**, 1745−1748. [59d] J-E. Bäckvall, K. L. Granberg, A. Heumann, *Isr. J. Chem.* **1991**, *31*, 17−24. [59e] K. L. Granberg, J.-E. Bäckvall, *J. Am. Chem. Soc.* **1992**, *114*, 6858−6863.
[60] [60a] C. Amatore, A. Jutand, M. A. M'Barki, G. Meyer, L. Mottier, *Eur. J. Inorg. Chem.* **2001**, 873−880. [60b] T. Cantat, A. Jutand, G. Meyer, submitted.
[61] [61a] G. C. Lloyd-Jones, S. C. Stephen, *Chem. Commun.* **1998**, 2321−2322. [61b] G. C. Lloyd-Jones, S. C. Stephen, *Chem. Eur. J.* **1998**, *4*, 2539−2549. [61c] B. M. Trost, F. D. Toste, *J. Am. Chem. Soc.* **1999**, *121*, 4545−4555.
[62] C. Amatore, J. C. Fiaud, A. Jutand, L. Mensah, G. Meyer, unpublished results.
[63] V. Farina, B. Krisnan, *J. Am. Chem. Soc.* **1991**, *113*, 9585−9595.
[64] A. L. Casado, P. Espinet, *J. Am. Chem. Soc.* **1998**, *120*, 8978−8985.
[65] C. Amatore, A. Bucaille, A. Fuxa, A. Jutand, G. Meyer, A. Ndedi Ntepe, *Chem. Eur. J.* **2001**, 2134−2142.
[66] C. Amatore, A. Bahsoun, A. Jutand, G. Meyer, A. Ndedi Ntepe, L. Ricard, *J. Am. Chem. Soc.*, **2003**, *115*, 4212−4222.

Received February 4, 2003

 © 2003 Wiley-VCH Verlag GmbH & Co. KGaA, Weinheim

The First Mononuclear η^2-C_{60} Complex of Osmium: Synthesis and X-ray Crystal Structure of $[(\eta^2\text{-}C_{60})Os(CO)(t\text{BuNC})(PPh_3)_2]$

Alexander V. Usatov,*[a] Ekaterina V. Martynova,[a] Ivan S. Neretin,[a] Yuri L. Slovokhotov,[a] Alexander S. Peregudov,[a] and Yurii N. Novikov[a]

Keywords: Fullerenes / Olefins / Osmium / Pi interactions

The interaction of C_{60} fullerene with the *cis*-dihydride osmium complex $[OsH_2(CO)(PPh_3)_3]$ (**I**) in the presence of *t*BuNC gives a novel metal complex $[(\eta^2\text{-}C_{60})Os(CO)(t\text{BuNC})(PPh_3)_2]$ (**II**) as the first mononuclear osmium complex with an η^2-coordinated fullerene ligand. Complex **II** was isolated and characterized by elemental analysis, UV, IR, ^1H and ^{31}P NMR spectroscopy. An X-ray diffraction study of **II** as its dichlorobenzene solvate revealed a distorted trigonal bipyramidal coordination of the Os atom, with a 6/6 bond of C_{60} and two PPh_3 ligands in the equatorial plane and CO and *t*BuNC as axial ligands.

(© Wiley-VCH Verlag GmbH & Co. KGaA, 69451 Weinheim, Germany, 2003)

A large number of mononuclear complexes of fullerenes with transition metals, with general formula $(\eta^2\text{-}C_n)ML$ (where L stands for any ligand environment of M metal), with an olefin-like π-coordinated fullerene moiety have been obtained and structurally characterized for most metals of the platinum family, including Ru,[1] Rh,[2−4] Ir,[5,6] Pd,[7,8] and Pt.[9−11] Based on their structures and spectroscopic properties, $(\eta^2\text{-}C_n)$ fullerene ligands in such mononuclear complexes are believed to be analogues of acceptor η^2-olefins with electron-withdrawing substituents (e.g. tetrafluoroethylene or tetracyanoethylene).[12,13] However, no mononuclear η^2-derivatives of fullerenes with osmium have been reported to date, notwithstanding the fact that an exopolyhedrally coordinated osmate complex of C_{60}, $(\sigma,\sigma\text{-}C_{60})O_2OsO_2(4\text{-}tert\text{-butylpyridine})_2$, was the first fullerene derivative studied by single-crystal X-ray diffraction.[14] Meanwhile, a number of osmium tri-[15−17] and pentanuclear clusters,[17,18] with the C_{60} moiety connected to a cluster core in an η^2- [in $Os_3(CO)_{11}(\eta^2\text{-}C_{60})$[15]], $\eta^1{:}\eta^2{:}\eta^1$-,[16] $\eta^2{:}\eta^2$- [17] or $\eta^2{:}\eta^2{:}\eta^2$-mode,[15,17,18] have been obtained and structurally characterised by X-ray methods.

In this paper we report the synthesis of the first mononuclear π-complex of osmium with buckminsterfullerene as an η^2-ligand and its structural characterization by single-crystal X-ray diffraction. To reach this goal, we have used the method recently developed by us for a synthesis of the mixed-ligand η^2-C_{60} and σ-carboranyl derivative of iridium $[(\eta^2\text{-}C_{60})Ir(o\text{-}HCB_{10}H_9CCH_2PPh_2\text{-}B,P)(t\text{BuNC})_2]$.[6] This approach is based on the interaction of the C_{60} molecule with a coordinatively unsaturated reactive intermediate, generated in situ from the corresponding metal *cis*-dihydride complex and *tert*-butyl isocyanide. The *t*BuNC ligand, having both π-acceptor and σ-donor properties, plays a dual role in the synthesis: as a strong π-acceptor it promotes the reductive elimination of a dihydrogen molecule from the initial dihydride complex after ligand substitution, to give a low-valent intermediate, whereas as a σ-donor it enhances the electron density at the metal center facilitating the effective coordination of the bulky and electron-deficient fullerene ligand.

As a starting *cis*-dihydride complex, the well-known and readily available $[OsH_2(CO)(PPh_3)_3]$[19] (**I**), which does not react directly with C_{60}, was chosen. However, when C_{60} and **I** are refluxed together in toluene with *t*BuNC, a substitution of triphenylphosphane ligand for isocyanide occurs, accompanied by elimination of dihydrogen, giving rise to a new $[(\eta^2\text{-}C_{60})Os(CO)(t\text{BuNC})(PPh_3)_2]$ complex (**II**) (Scheme 1).

The product **II**, obtained in analytically pure form by chromatography, was characterized by microanalysis and spectroscopy data (UV/Vis, IR, ^1H and ^{31}P NMR). The UV/Vis pattern of **II** is rather typical for transition metal η^2-C_{60} complexes.[3,6,20] The presence of a strong ν(CO) band at 1953 cm^{-1} and a strong single ν(NC) band at 2153 cm^{-1} in the IR spectrum of **II** reveals both isocyanide and carbonyl ligands to be present in the molecule, pointing to a specific substitution of the triphenylphosphane ligand. According to the ^1H NMR spectroscopic data, complex **II** contains two PPh_3 and one *t*BuNC ligand, whereas the presence of only one singlet resonance at $\delta = 7.9$ ppm in the $^{31}P\{^1H\}$ NMR corresponds to the existence of only one isomer, with two equivalent PPh_3 ligands, in solution. The latter may be considered as evidence of metal-fullerene coordination by the 1−2 bond (see discussion in ref.[20]).

[a] A. N. Nesmeyanov Institute of Organoelement Compounds, Russian Academy of Sciences,
Vavilov St. 28, Moscow 119991, Russia
Fax: (internat.) +7-095/135-5085

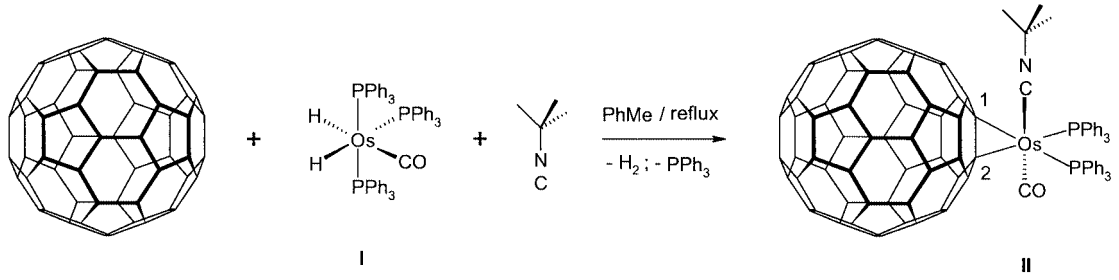

Scheme 1

The analytical data for **II** (C, H P, Os) correspond unequivocally to a monoadduct such as $[(C_{60})Os(CO)(t\text{-BuNC})(PPh_3)_2]$. However, the available spectroscopic data do not allow us to distinguish between the possible equatorial (with carbonyl and *t*BuNC as axial ligands) and *trans*-axial positions of the two equivalent PPh_3 ligands. Notwithstanding a close resemblance of the spectroscopic data for **II** with those of the related complex $[Os(C_2F_4)(CO)\{(p\text{-Tolyl})NC\}(PPh_3)_2]$ [ν(CO) = 1968 cm^{-1}, ν(NC) = 2160 cm^{-1}; δ_P = 3.5 ppm],[21] with two equivalent equatorial PPh_3 ligands and strong preference of equatorial location of bulky PPh_3 and fullerene ligands due to the steric repulsion, no decisive evidence was obtained in favor of one of the two possible isomers from the spectroscopic data.

To determine the molecular geometry of **II** unequivocally and to analyze its structural features, we grew a single crystal of **II** from *o*-dichlorobenzene solution and performed an X-ray diffraction study.

The molecular structure of $\mathbf{II}\cdot 2.5C_6H_4Cl_2$ with selected geometric parameters (bond lengths and bond angles) is shown in Figure 1. The molecule $[(\eta^2\text{-}C_{60})Os(CO)(t\text{-BuNC})(PPh_3)_2]$ has an ordered C_{60} moiety with a normal olefin-type π-coordination to the osmium atom. A trigonal bipyramidal ligand environment of Os in **II** is completed by two equatorial PPh_3 ligands, with one isocyanide and one CO ligand in the axial positions. Most of the bond lengths and angles (see Figure 1) have their normal values. However, the bond angles P(1)−Os−P(2) [109.58(5)°], P(1)−Os−C_{60} [120.3(1)°] and P(2)−Os−C_{60} [130.1(1)°] in the equatorial plane of the trigonal bipyramid (where C_{60} denotes a center of the coordinated 6/6 bond) display a substantial asymmetry due to intramolecular C−H···C steric repulsion between one Ph substituent at P(2) and C_{60} (shortest H···C distances at 2.64−2.87 Å are slightly less than the sum of their van der Waals radii). Metal-fullerene bonding leads to elongation of η^2-coordinated 6/6 bonds to 1.498(7) Å from the normal value of 1.39 Å in pristine C_{60} and a more pyramidal environment of the C atoms [the spherical excess (spherical excess is 360° − Σ(all CCC bond angles) of the carbon environment, which is a good quantitative measure of pyramidalization,[22] is 12° in pristine C_{60}, 23.2 and 24.0° at these atoms of **II**, 7.4−8.6° at their neighbors and 10.5−13.5° at all other C atoms].

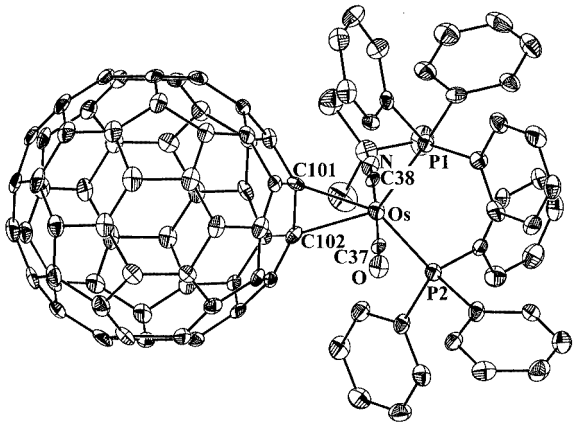

Figure 1. Molecule **II** with atomic numbering in the coordination environment of the Os atom (hydrogen atoms not shown); bond lengths (A): Os−P(1) 2.347(2), Os−P(2) 2.351(1) Os−C(37) 1.898(2), Os−C(38) 2.011(2), Os−C(101) 2.193(5), Os−C(102) 2.193(5), C(37)−O(1) 1.146(4), C(38)−N(1) 1.169(6), C(101)−C(102) 1.479(7); bond angles (°): P(1)−Os−P(2) 109.58(5), P(1)−Os−C(37) 88.52(8), P(2)−Os−C(37) 92.41(7), P(1)−Os−C(38) 96.13(8), P(2)−Os−C(38) 84.26(7), C(37)−Os−C(38) 175.0(1), Os−C(37)−O 178.0(2), Os−C(38)−N 173.9(2)

It is interesting to note that only two mononuclear phosphane π-complexes of osmium with η^2-coordinated olefins having electron acceptor substituents, viz. $[(Ph_3P)_2Os(CO)_2(\eta^2\text{-}C_4H_2O_3)]$[21] (with maleic anhydride) and $[(iPr_3P)_2OsH(OH)(CO)(\eta^2\text{-}CH_2{=}CHCOOMe)]$[23] (with methylmetacrylate) are found in the last (2002) version of the Cambridge Structural Database (CSD). Mononuclear π-complexes of Ru with electron-accepting olefins, which have been studied in more detail, include derivatives of tetrafluoroethylene $[(Ph_3P)_2Ru(CO)_2(\eta^2\text{-}C_2F_4)]$,[21] maleic anhydride $[(Ph_3P)_2Ru(CO)\{(p\text{-Tolyl})NC\}(\eta^2\text{-}C_4H_2O_3)]$,[24] and buckminsterfullerene $[(Ph_3P)_2RuCl(NO)(\eta^2\text{-}C_{60})]$.[1] The main geometric molecular parameters of these complexes are compared with the corresponding parameters of **II** in Table 1.

The Os−C(C_{60}) bond lengths [2.193(5) Å] in **II** are typical for mononuclear complexes with π-coordinated acceptor

 © 2003 Wiley-VCH Verlag GmbH & Co. KGaA, Weinheim

Table 1. Geometric parameters of the pentacoordinate metal environment in **II** and several closely related complexes

Complex	M−P (Å)	M−CO (Å)	M−C(π) (Å)	P−M−P (deg.)	C_2(π)−M-L (deg.)	Ref.
$[(Ph_3P)_2Os(CO)(t\text{BuNC})(\eta^2\text{-}C_{60})]$ (**II**)	2.35	1.90	2.19	109.6	120.3 130.3	[a]
$[(Ph_3P)_2Os(CO)_2(\eta^2\text{-}C_4H_2O_3)]$[b]	2.43	1.91	2.18	99.3[c]	86.1 117.4[c]	[21]
$[(i\text{Pr}_3P)_2OsH(OH)(CO)(\eta^2\text{-}CH_2{=}CHCO_2Me)]$[d]	2.40	1.84	2.19	144.3[e]	104.3 109.0	[23]
$[(Ph_3P)_2RuCl(NO)(\eta^2\text{-}C_{60})]$	2.45	–	2.22	113.2	122.3 124.3	[1]
$[(Ph_3P)_2Ru(CO)[(p\text{-Tolyl})NC](\eta^2\text{-}C_4H_2O_3)]$[b]	2.37	1.85	2.19	107.0	117.3 135.6	[24]
$[(Ph_3P)_2Ru(CO)_2(\eta^2\text{-}C_2F_4)]$	2.43	1.92	2.09	101.4	127.5 131.1	[21]

[a] Two PPh_3 and two CO ligands in equatorial and axial positions, respectively. [b] η^2-Methyl methacrylate. [c] Hydride H atom between two equatorial PPh_3 ligands. [d] η^2-Methyl methacrylate. [e] Hydride H atom between two equatorial PPh_3 ligands.

olefins (see Table 1), and are almost identical to the Os−C(olefin) distances in $[(Ph_3P)_2Os(CO)(\eta^2\text{-}C_2H_4)_2]$ (2.15−2.19 Å).[25] In a disordered structure of $[Os_3(CO)_{11}(\eta^2\text{-}C_{60})]$, η^2-coordination to one of three Os atoms in a triangular cluster is accompanied by larger distances (2.22−2.27 Å)[15] that lie within the usual range (2.21−2.32 Å) for a multicenter Os_3-(η^2: η^2:η^2-C_{60}) coordination.[15,17,18] A planar trigonal arrangement of two phosphanes and the center of the coordinated 6/6 bond of the η^2-C_{60} ligand in the equatorial plane around the Os atom in **II** is similar to other mononuclear fullerene derivatives like $[(PPh_3)_2Pd(\eta^2\text{-}C_{60})]$,[7] $[(PPh_3)_2Pd(\eta^2\text{-}C_{70})]$,[8] $[(DIOP)_2Pt(\eta^2\text{-}C_{60})]$,[11] $[(PPh_3)_2RuCl(NO)(\eta^2\text{-}C_{60})]$,[1] $[(PPh_3)_2RhH(CO)(\eta^2\text{-}C_{60})]$,[2] and $[L_2IrCl(CO)(\eta^2\text{-}C_n)]$ (where L is a phosphane ligand).[13] Unlike the symmetric L_2M-(6/6 bond) fragment in all these complexes, the P−Os−C_{60} angles in **II** differ by 10°. However, in the related pentacoordinate complex $[(PPh_3)_2Ru(CO)[(p\text{-tolyl})NC](\eta^2$-malonic anhydride)] with carbonyl and isocyanide axial ligands,[24] which is the closest non-fullerene analogue of **II**, the P−Ru(olefin) angles in the equatorial plane differ by 18.3° (see Table 1). Even the large angle difference in mononuclear $[(Ph_3P)_2Os(CO)_2(\eta^2\text{-}C_4H_2O_3)]$ is due to the axial position of one PPh_3 ligand,[21] whereas in $[(i\text{Pr}_3P)_2OsH(OH)(CO)(\eta^2\text{-}CH_2{=}CHCOOMe)]$ a hydride ligand is situated between two $i\text{PPr}_3$ groups in the equatorial plane.[23] Such asymmetry of the flexible metal coordination probably refers to an interplay of interligand repulsion and molecular packing forces in the crystal.

Thus, we have shown that the interaction of fullerene with *cis*-dihydride transition metal complexes in the presence of isocyanide gives a rather convenient and general synthetic route to (η^2-C_{60}) metal complexes. It allowed us to obtain the first mononuclear osmium fullerene complex $[(\eta^2\text{-}C_{60})Os(CO)(t\text{BuNC})(PPh_3)_2]$ whose crystal and molecular structure was completely characterized by single-crystal X-ray diffraction.

Experimental Section

General: All manipulations were performed under oxygen-free argon in dry degassed solutions. IR spectra were obtained on a Specord M80 spectrometer. ^{1}H NMR spectra (400.3 MHz) and $^{31}P\{^1H\}$ NMR spectra (160.02 MHz) were recorded on a Bruker AMX-400 spectrometer and are quoted relative to residual signals of the solvent (internal standard) and 85% H_3PO_4 (external standard), respectively. $[OsH_2(CO)(PPh_3)_3]$ was prepared by a standard literature procedure.[19b]

Synthesis of $[(\eta^2\text{-}C_{60})Os(CO)(t\text{BuNC})(PPh_3)_2]$ (II): $[OsH_2(CO)(PPh_3)_3]$ (**I**) (0.0699 g, 0.069 mmol) and *t*BuNC (17.2 μL, 0.153 mmol) were added to a solution of C_{60} (0.050 g, 0.069 mmol) in toluene (50 mL), with stirring, and the reaction mixture was refluxed for 24 h. After cooling the reaction mixture to room temperature, a small quantity (0.013 g) of insoluble precipitate (not further unidentified) was filtered off, and the solution was concentrated to 5 mL and then diluted with pentane. The precipitate was filtered, washed with pentane, dissolved in 1 mL of $CHCl_3$ and chromatographed on a short column packed with alumina, eluting with a $CHCl_3$/hexane mixture (1:1). A green fraction was collected, solvents were removed under reduced pressure and the residue was washed with pentane, and dried in vacuo at 60 °C to give 41 mg (38%) of **II**. $C_{102}H_{39}NOOsP_2$ (1546.6): calcd. C 79.21, H 2.54, Os 12.30, P 4.00; found C 78.47, H 2.64, Os 12.77, P 4.35. UV/Vis (THF): λ = 259, 333, 394 (sh), 444, 671 nm. IR (KBr pellet): $\tilde{\nu}$ = 2153 cm^{-1} (NC), 1953 (CO). ^{1}H NMR ($CDCl_3$): δ = 0.86 (s, 9 H, *t*Bu), 7.32 (m, 18 H, Ph), 7.58 (m, 12 H, Ph) ppm. $^{31}P\{^1H\}$ NMR ($CDCl_3$): δ = 7.9 ppm.

X-ray Structure Determination of II: Dark green crystals of **II**·2.5(*o*-$C_6H_4Cl_2$) were grown by slow diffusion of heptane into an *o*-dichlorobenzene solution of complex **II** at room temperature. The crystals are triclinic, space group $P\bar{1}$, a = 13.254(3), b = 16.753(4), c = 18.642(4) Å, α = 87.575(5)°, β = 74.626(5)°, γ = 73.672(5)°, V = 3828(1) Å^3, Z = 2, $d_{calcd.}$ = 1.661 g/cm^3, and μ(Mo-K_α) = 19.52 mm^{-1}. The intensities of 21936 unique reflections (R_{int} = 0.063) were measured at 110(2) K on a Bruker SMART 1000 CCD diffractometer (graphite monochromated Mo-K_α radiation, λ = 0.71073 Å, ω and scan technique with a 0.3° step in ω and 10 s per frame exposure, θ ≤ 30.15°). Reflection intensities were integrated using the SAINT software[26] and corrected for absorption

 © 2003 Wiley-VCH Verlag GmbH & Co. KGaA, Weinheim

semiempirically (SADABS program)[26] based on multiple measurements of identical reflections and equivalents. The structure was solved by direct methods and refined by full-matrix least-squares against F^2. Two molecules of *o*-dichlorobenzene were located in general positions, and one more such molecule, disordered about the inversion center, was found in the difference Fourier map. One of the two *o*-dichlorobenzene molecule appeared to be disordered. All disordered atoms in the crystal structure of **II** were refined with isotropic thermal parameters. All H atoms were placed geometrically and included in the refinement using a riding model. The refinement converged to $wR_2 = 0.1074$ and $GOF = 0.733$ for all independent reflections ($R_1 = 0.0543$ was calculated against F for a total of 10492 observed reflections with $I > 2\sigma(I)$]; the number of refined parameters was 1127. All calculations were performed with SHELXTL-97.[27]

CCDC-202941 contains the supplementary crystallographic data for this paper. These data can be obtained free of charge at www.ccdc.cam.ac.uk/conts/retrieving.html [or from the Cambridge Crystallographic Data Centre, 12, Union Road, Cambridge CB2 1EZ, UK; Fax: (internat.) +44-1223/336-033; E-mail: deposit@ccdc.cam.ac.uk].

Acknowledgments

This work was supported by the Russian Foundation for Basic Research (Projects Nos. 00-03-32807, 02-03-33225 and 02-03-06419), the Russian Federation State Research Program "Fullerenes and atomic clusters" [Contr. No. 107-14 (00)-P], and by the Russian Federation Ministry of Industry, Science, and Technology Sub-Program "Fundamental Problems of Modern Chemistry" [Contr. No. 402-19.6/22.3/23.1 (00)-P]. The authors are grateful to Prof. Mikhail Yu. Antipin for access to the equipment of the Center for X-ray Structural Studies, Institute of Organoelement Compounds.

[1] A. N. Chernega, M. L. H. Green, J. Haggitt, A. H. H. Stephens, *J. Chem. Soc., Dalton Trans.* **1998**, 755−767.
[2] A. L. Balch, J. W. Lee, B. C. Noll, M. M. Olmstead, *Inorg. Chem.* **1993**, *32*, 3577−3578.
[3] Y. Ishii, H. Hoshi, Y. Hamada, M. Hidai, *Chem. Lett.* **1994**, 801−804.
[4] H. Song, K. Lee, J. T. Park, I.-H. Suh, *J. Organomet. Chem.* **1999**, *584*, 361−365.
[5] A. L. Balch, V. J. Catalano, J. W. Lee, *Inorg. Chem.* **1991**, *30*, 3980−3981.
[6] A. V. Usatov, E. V. Martynova, F. M. Dolgushin, A. S. Peregudov, M. Yu. Antipin, Yu. N. Novikov, *Eur. J. Inorg. Chem.* **2002**, 2565−2567.
[7] V. V. Bashilov, P. V. Petrovskii, V. I. Sokolov, S. V. Lindeman, I. A. Guzey, Yu. T. Struchkov, *Organometallics* **1993**, *12*, 991−992.
[8] M. M. Olmstead, L. Hao, A. L. Balch, *J. Organomet. Chem.* **1999**, *578*, 85−90.
[9] P. J. Fagan, J. C. Calabrese, B. Malone, *Science* **1991**, *252*, 1160−1161.
[10] M. Iyoda, Y. Ogawa, H. Matsuyama, H. Ueno, K. Kikuchi, I. Ikemoto, Y. Achiba, *Fullerene Sci. Technol.* **1995**, *3*, 1−9.
[11] V. V. Bashilov, P. V. Petrovsky, V. I. Sokolov, F. M. Dolgushin, A. I. Yanovsky, Yu. T. Struchkov, *Russ. Chem. Bull.* **1996**, *45*, 1207−1213.
[12] P. J. Fagan, J. C. Calabrese, B. Malone, *Acc. Chem. Res.* **1992**, *25*, 134−142, and references therein.
[13] A. L. Balch, M. M. Olmstead, *Chem. Rev.* **1998**, *98*, 2123−2165, and references therein.
[14] J. M. Hawkins, A. Meyer, T. A. Lewis, S. Loren, F. J. Hollander, *Science* **1991**, *252*, 312−313.
[15] J. T. Park, H. Song, J.-J. Cho, M.-K. Chung, J.-H. Lee, I.-H. Suh, *Organometallics* **1998**, *17*, 227−236.
[16] H. Song, K. Lee, C. H. Lee, J. T. Park, H. Y. Chang, M.-G. Choi, *Angew. Chem. Int. Ed.* **2001**, *40*, 1500−1502; *Angew. Chem.* **2001**, *113*, 1548−1550.
[17] K. Lee, C. H. Lee, H. Song, J. T. Park, H. Y. Chang, M.-G. Choi, *Angew. Chem. Int. Ed.* **2000**, *39*, 1801−1804; *Angew. Chem.* **2000**, *112*, 1871−1874.
[18] H. Song, K. Lee, J. T. Park, M.-G. Choi, *Organometallics* **1998**, *17*, 4477−4483.
[19] [19a] N. Ahmad, S. D. Robinson, M. F Uttley, *J. Chem. Soc., Dalton Trans.* **1972**, 843−847. [19b] N. Ahmad, J. J. Levison, S. D. Robinson, M. F Uttley, *Inorg. Synth.* **1974**, *15*, 54−55.
[20] A. V. Usatov, K. N. Kudin, E. V. Vorontsov, L. E. Vinogradova, Yu. N. Novikov, *J. Organomet. Chem.* **1996**, *522*, 147−153.
[21] A. K. Burrell, G. R. Clark, C. E. F. Rickard, W. R. Roper, D. C. Ware, *J. Organomet. Chem.* **1990**, *398*, 133−158.
[22] I. S. Neretin, K. A. Lyssenko, M. Yu. Antipin, Yu. L. Slovokhotov, O. V. Boltalina, P. A. Troshin, A. Yu. Lukonin, L. N. Sidorov, R. Taylor, *Angew. Chem. Int. Ed.* **2000**, *39*, 3273−3276; *Angew. Chem.* **2000**, *112, 18*, 3283−3283.
[23] A. J. Edwards, S. Elipe, M. A. Esteruelas, F. J. Lahoz, L. A. Oro, C. Valero, *Organometallics* **1997**, *16*, 3828−3836.
[24] C. E. F. Rickard, W. R. Roper, L. J. Wright, L. Young, *J. Organomet. Chem.* **1989**, *364*, 391.
[25] G.-Y. Kiel, J. Takats, F.-W. Grevels, *J. Am. Chem. Soc.* **1987**, *109*, 2227−2229.
[26] SMART and SAINTPLUS, Area detector control and integration software, Ver. 6.01. Bruker Analytical X-ray Systems, Madison, Wisconsin, U. S. A, **1999**.
[27] SHELXTL, An integrated system for solving, refining and displaying crystal structures from diffraction data, Ver. 5.10. Bruker Analytical X-ray Systems, Madison, Wisconsin, U. S. A, **1997**.

Received February 11, 2003

 © 2003 Wiley-VCH Verlag GmbH & Co. KGaA, Weinheim

Modulation of the Prototropic Exchange Rate at the Water Molecule Coordinated to a Gd^{III} Ion

Silvio Aime,*[a] Eliana Gianolio,[a] Alessandro Barge,[a] Dimitrios Kostakis,[b] Ioannis C. Plakatouras,[b] and Nick Hadjiliadis[b]

Keywords: Gadolinium / Chelates / Basicity / Neighbouring-group effects / Prototropic exchange / Imaging agents

The aim of this work is to assess whether it is possible to control the rate of the prototropic exchange in a class of DTPA bis-amide Gd^{III} complexes.

(© Wiley-VCH Verlag GmbH & Co. KGaA, 69451 Weinheim, Germany, 2003)

In the last decade much attention has been devoted to the understanding of the determinants of the water-exchange process in Gd^{III} complexes because their successful application as MRI contrast agents is related to the occurrence of a suitable exchange lifetime (τ_M) of the coordinated water.[1−4] The latter parameter inversely affects the inner-sphere relaxation term (R_{1p}^{is}) and is often the main determinant of the overall relaxivity of a paramagnetic Gd^{III} complex. The R_{1p}^{is} contribution is given by Equation (1):

$$R_{1p}^{is} = \frac{q[C]}{55.5(T_{1M} + \tau_M)} \quad (1)$$

where [*C*] is the molar concentration of the paramagnetic agent, *q* is the number of coordinated water molecules and T_{1M} is the relaxation time of their protons. Thus, as long as τ_M is shorter than T_{1M} the paramagnetic relaxation effect can be efficiently transferred to the bulk water solvent.

Bis-amide derivatives of Gd-DTPA (DTPA = diethylenetriamine pentaacetic acid) display relatively long exchange lifetimes of the coordinated water,[5−8] therefore their relaxivity is usually smaller than expected. However, such a drawback has been exploited in order to assess the rate of prototropic exchange at the coordinated water molecule. The latter process is pH-dependent and becomes significantly high either at acidic or basic pH, to overcome the "quenching" effect of the slow exchanging water, thus allowing the system to raise the relaxivity expected on the basis of its T_{1M} value.

[a] Dipartimento di Chimica IFM, Università di Torino,
Via P. Giuria 7, 10125 Torino, Italy,
Fax: (internat.) +39-011/670-7855
E-mail: silvio.aime@unito.it
[b] University of Ioannina, Department of Chemistry,
Ioannina 45110, Greece

Thus, τ_M in Equation (1) can be replaced by Equation (2):

$$\tau_M = \left[\left(\tau_M^0\right)^{-1} + \left(k_{ex} \frac{k_W}{[H_3O^+]} \right) \right]^{-1} \quad (2)$$

where k_{ex} is the prototropic exchange rate. Although the prototropic exchange is either acid or base catalysed, its assessment, in the case of bis-amide derivatives of Gd-DTPA, is preferentially pursued under basic conditions because the limited thermodynamic stability of these complexes may cause some release of Gd^{III} ions upon protonation of the acetic arms at acidic pH. Typically the determination of k_{ex} is then carried out by fitting the pH-dependent curve of the relaxivity in the pH range between 3 and 10.

The aim of this work is to assess whether it is possible to control the rate of the prototropic exchange in this class of Gd^{III} complexes.

Six novel bis-amide derivatives of Gd-DTPA have been synthesised (Scheme 1). These ligands were obtained according to the previously reported procedure[9] based on the reaction of DTPA bis-anhydride with the amine group of the entering R substituent. Compounds **1** and **2** were obtained by hydrolyzing the ester functionalities of **3** and **4**, respectively.

The corresponding Gd^{III} complexes were obtained by reacting equimolar amounts of any given ligand and $GdCl_3$ at pH 6. The eventual excess of uncomplexed Gd^{III} ions was precipitated as the hydroxide as the pH of the solution was brought to basic values, and separated by ultracentrifugation.

At neutral pH and 298 K, the relaxivity (measured at 20 MHz) shown by all six complexes is very similar (ca. 5 ± 0.4 $mM^{-1}s^{-1}$). In all cases the relaxivity increases as the temperature is increased. This is an unambiguous symptom of the occurrence of a slow water-exchange that "quenches"

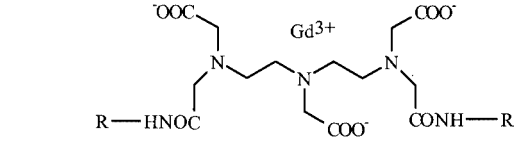

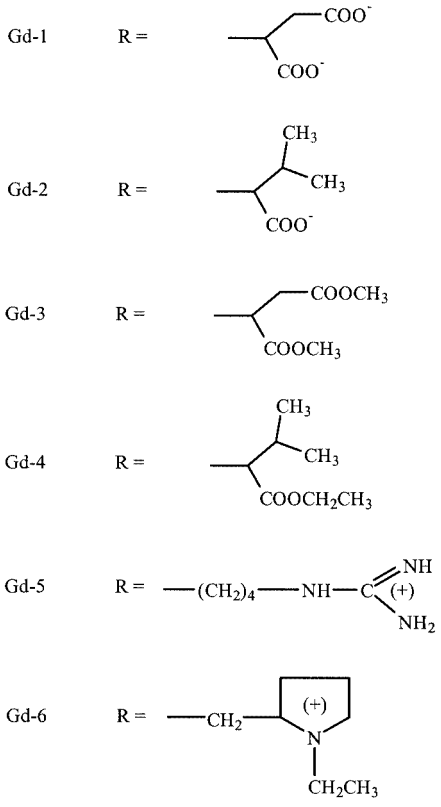

Scheme 1. Schematic representation of the structures of the six bisamide DTPA derivatives

the attainable relaxivity in analogy with previous observations in a number of related Gd-bisamide DTPA systems.[10−12] ^{17}O-R_{2p} measurements at variable temperature yield accurate values for the exchange rate of the coordinated water (Table 1) applying a well-established fitting procedure to the theoretical values obtained from the Swift−Connick equation.[13]

Table 1. Relaxometric and dynamic prameters for Gd^{III} complexes

Complexes	r_{1p} (mM^{-1} s^{-1}) at pH 7	τ_M^O (μs)[a]	T_{1M} (s)[b]	k_{ex} (M^{-1} s^{-1})
Gd-1	5	2.36	3.8×10^{-6}	4.6×10^{8}
Gd-2	5.3	1.98	3.6×10^{-6}	2.7×10^{9}
Gd-3	4.6	2.56	5.2×10^{-6}	7.5×10^{9}
Gd-4	5.1	2.22	3.8×10^{-6}	4.2×10^{9}
Gd-5	5.3	2.2	3.95×10^{-6}	1.2×10^{10}
Gd-6	5.3	2.66	3.1×10^{-6}	8.6×10^{10}

[a] Values calculated from the fitting of ^{17}O NMR profiles (pH 7 and 298 K). [b] Values calculated from the fitting of NMRD profiles recorded at basic pH.

The proton relaxivity measurements, in the pH range from 6 to 12, display the expected increase as the prototropic exchange-rate becomes fast enough to remove the limit of the slow-exchange of the coordinated water. It has been very interesting to observe that the increase of r_{1p} takes place at significantly different pH values; for instance, pH 10 for **Gd-1** and pH 7 for **Gd-6** (Figure 1). The observed behaviour clearly reflects the occurrence of different prototropic exchange rates as a function of the R substituents. The accurate determination of the prototropic exchange rates was performed by fitting the observed pH-dependent relaxivity curves according to Equation (1) modified as in Equation (2) and using T_{1M} values obtained from NMRD profiles measured at pH 12 (Table 1) and $\tau \cong \tau_M^O$ values calculated from ^{17}O NMR profiles.

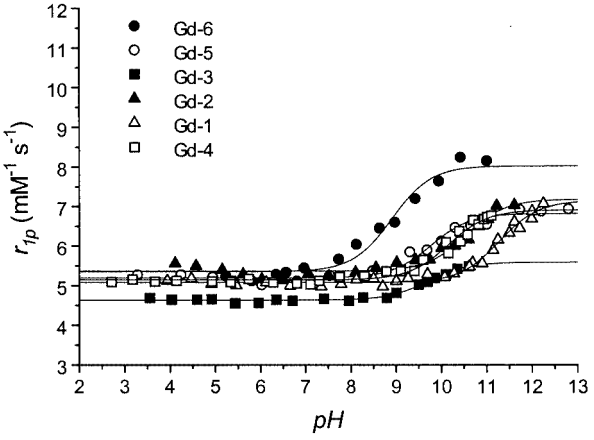

Figure 1. Effect of $[OH^-]$ catalysis on the prototropic exchange as assessed from the increase of r_{1p} as a function of pH. The continuous lines represent the theoretical values calculated according to Equations (1) and (2) for the evaluation of R_{1p}^{is}. R_{1p} is the sum of R_{1p}^{is} + R_{1p}^{os} (outer sphere) and R_{1d}. R_{1p}^{os} was obtained by fitting NMRD profiles. R_{1d} was set equal to 0.38 s^{-1}

Although not proven, we discarded any significant contribution from the exchange of amide protons.[14] When, in related complexes, saturation transfer experiments were carried out by irradiating the NH moieties in Eu^{III} complexes, k_{ex} values were found to be ca. 8×10^5 mM^{-1} s^{-1} around pH 10. Such values do not have significant effects on the R_{1p}^{is} of Gd^{III} complexes [Equation (1): T_{1M} calculated for NH protons, at a distance from the metal ion of 4.2 Å, is 3.6×10^{-5}].

From these data one draws the conclusion that the base catalysis of the prototropic exchange takes place in this series of related complexes with remarkable differences, being fastest for **Gd-6** and slowest for **Gd-1** (Figure 2). The observed behaviour is easily rationalised in terms of the accessibility of OH^- ions to the coordinated water molecule. The positively charged substituents in **Gd-5** and **Gd-6** promote the access of the negatively charged hydroxyl ions to the water coordination site. On the other hand the negatively charged carboxylate moieties in **Gd-1** and **Gd-2** hamper the approach of the hydroxyl groups, thus causing an overall decrease of the prototropic exchange. On passing from **Gd-1** to **Gd-3** and from **Gd-2** to **Gd-4**, the esterifi-

 © 2003 Wiley-VCH Verlag GmbH & Co. KGaA, Weinheim

cation of these substituents removes the residual negative charge, with a consequent increase of the base catalysis of the prototropic exchange.

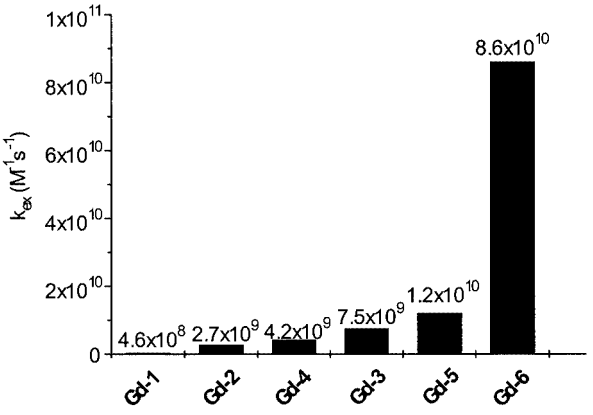

Figure 2. Prototropic exchange rates at the coordinated water molecule in Gd^{III} complexes of a series of bis-amide DTPA ligands

These observations unambiguously indicate that it is possible to control the rate of the prototropic exchange by introducing suitable substituents on the surface of the ligand coordination cage of the Gd^{III} ion. As far as OH^- catalysis is concerned it is apparent that the main determinant is the overall residual charge.

In principle, one may expect that the prototropic exchange rate is also affected by the solution structure of the investigated complex. Actually, the lanthanide(III) complexes of bis-amide DTPA ligands are present in solutions as mixtures of four pairs of interconverting isomers[15−17] and it is likely that the nature of the R substituents could affect the isomer distribution. However, if this were the case, the results reported here indicate that such effects are not of primary importance in the determination of OH^- catalysis of the prototropic exchange of the coordinated water.

Experimental Section

Synthesis of 1−4: Ligands **1**−**4** were prepared by adding DTPA-bisanhydride (1 mmol) in portions to a stirring solution of distilled DMF (15 cm^3) containing 2 mmol of HCl·Asp, HCl·Val, $Asp(OMe)_2$·HCl, or ValOEt·HCl. The reaction mixture was heated for 36 h at 80 °C, the solution was allowed to cool and the solvent was removed under vacuum to result in an oil that solidified upon addition of acetone/diethyl ether (30:70; 300 cm^3). The white solid was dried under reduced pressure over $CaCl_2$.

Synthesis of 5: Diethylenetriamine-*N*,*N*′′-bis(4-guanidinobutyl)-*N*,*N*′,*N*′′-triacetic acid (5) was prepared by adding DTPA-bisanhydride (4.2 g, 0.012 mol) in portions to a stirring solution of distilled DMF (70 cm^3) containing agmatine (3.27 g, 0.025 mol; previously purified from the sulfate by extraction with 1-butanol from water at pH 13). The reaction mixture was heated for 4 h at 50 °C, and 20 h at room temperature. The solution was then allowed to cool and the solvent was removed under vacuum to result in an oil that solidified on addition of acetone/diethyl ether (30:70; 50 cm^3). The white solid was dried under reduced pressure over $CaCl_2$.

Synthesis of 6: Diethylenetriamine-*N*,*N*′′-bis(2-aminomethylethylpyrrolidine)-*N*,*N*′,*N*′′-triacetic acid (6) was prepared by adding DTPA-bisanhydride (0.582 g 0.002 mol) in portions to a stirring solution of distilled DMF (10 cm^3) containing 2-aminomethylethylpyrrolidine (0.418 g, 0.003 mol). The reaction mixture was heated for 24 h at 50 °C, the solution was allowed to cool and the solvent was removed under vacuum to give an oil that solidified on addition of acetone/diethyl ether (30:70; 50 cm^3). The white solid was dried under reduced pressure over $CaCl_2$.

Synthesis of Gd^{III} Complexes: The general procedure for the synthesis of the gadolinium complexes consists of the addition of equimolar amounts of the corresponding ligand (2 mmol) and $GdCl_3·6H_2O$ (2 mmol) in deionized water (20 cm^3), followed by adjustment of the pH to 6.0 by adding KOH.

The longitudinal water proton relaxation rate was measured by using a Stelar Spinmaster (Mede, Pavia, Italy) spectrometer operating at 20 MHz, by means of the standard inversion-recovery technique (16 experiments, 2 scans). A typical 90° pulse width was 3.5 μs and the reproducibility of the T_1 data was ±0.5%. The temperature was controlled with a Stelar VTC-91 air-flow heater equipped with a copper-constantan thermocouple (uncertainty ±0.1 °C).

Variable temperature ^{17}O NMR measurements were recorded at 2.1 T on a JEOL EX-90 spectrometer, equipped with a 5 mm probe, by using a D_2O external lock. Experimental settings: spectral width 10000 Hz, 90° pulse (7 μs), acquisition time 10 ms, 1000 scans and no sample spinning. Aqueous solutions containing 2.6% of ^{17}O isotope (Yeda, Israel) were used. The observed transverse relaxation rates (R^O_{2obs}) were calculated from the signal width at half-height ($\Delta\nu_{1/2}$): $R^O_{2obs} = \pi\,\Delta\nu_{1/2}$.

[1] S. Aime, M. Botta, M. Fasano, S. Geninatti Crich, E. Terreno, *Coord. Chem. Rev.* **1999**, 321−333.
[2] E. Tóth, O. M. Ni Dhubhghaill, G. Besson, L. Helm, A. E. Merbach, *Magn. Res. Chem.* **1999**, 701−708.
[3] S. Aime, M. Botta, S. Geninatti Crich, G. B. Giovenzana, R. Pagliarin, M. Piccinini, M. Sisti, E. Terreno, *J. Biol. Inorg. Chem.* **1997**, 470−479.
[4] S. Hajela, M. Botta, S. Giraudo, J. D. Xu, K. N. Raymond, S. Aime, *J. Am. Chem. Soc.* **2000**, 11228−11229.
[5] S. Aime, M. Botta, M. Fasano, S. Paoletti, E. Terreno, *Chem. Eur. J.* **1997**, 1499−1504.
[6] D. Pubanz, G. Gonzalez, D. H. Powell, A. E. Merbach, *Inorg. Chem.* **1995**, *34*, 4447−4453.
[7] H. Lammers, F. Maton, D. Pubanz, M. W. Van Laren, H. Van Bekkum, A. E. Merbach, R. N. Muller, J. A. Peters, *Inorg. Chem.* **1997**, *36*, 2527−2538.
[8] E. Toth, L. Helm, A. E. Merbach, R. Hedinger, K. Hegetschweiler, A. Janossy, *Inorg. Chem.* **1998**, *37*, 4104−4113.
[9] S. Aime, M. Fasano, S. Paoletti, E. Terreno, *Gazz. Chim. Ital.* **1995**, 125.
[10] D. H. Powell, O. M. Ni Dhubhghaill, D. Pubanz, L. Helm, Y. S. Lebedev, W. Schlaepfer, A. E. Merbach, *J. Am. Chem. Soc.* **1996**, *118*, 9333−9346.
[11] M. Periasamy, D. Whitye, L. DeLearie, D. Moore, R. Wallace, W. Lin, J. Dunn, W. Hirth, W. Cacheris, *Invest. Radiol.* **1991**, *26*, S217−S220.
[12] S. W. A. Bligh, A. H. M. S. Chowdhury, M. McPartlin, I. J. Scowen, R. A. Bulman, *Polyhedron* **1995**, *14*, 567−569.
[13] T. J. Swift, R. E. J. Connick, *J. Chem. Phys.* **1962**, 307.

 © 2003 Wiley-VCH Verlag GmbH & Co. KGaA, Weinheim

[14] S. Aime, A. Barge, J. I. Bruce, M. Botta, J. A. K. Howard, J. M. Moloney, D. Parker, A. S. de Sousa, M. Woods, *J. Am. Chem. Soc.* **1999**, *121*, 5762−5771.
[15] S. Aime, F. Benetollo, G. Bombieri, S. Colla, M. Fasano, S. Paoletti, *Inorg. Chim. Acta* **1997**, 63−70.
[16] C. Geraldes, A. M. Urbano, M. A. Hoefnagel, J. A. Peters, *Inorg. Chem.* **1993**, *32*, 2426−2432.
[17] C. Geraldes, A. M. Urbano, M. C. Alpoim, M. A. Hoefnagel, J. A. Peters, *J. Chem. Soc., Chem. Commun.* **1991**, 656−658.
Received March 18, 2003

 © 2003 Wiley-VCH Verlag GmbH & Co. KGaA, Weinheim

P−B Adducts of 3,4-Dimethyl-1-phosphaferrocene with Bromoboranes

Matthias Scheibitz,[a] Jan W. Bats,[b][‡] Michael Bolte,[b][‡] and Matthias Wagner*[a]

Dedicated to Prof. Dr. Herbert Wagner on the occasion of his retirement

Keywords: Boranes / Donor-acceptor systems / Metallocenes / P ligands / X-ray diffraction

The crystalline adducts FcP–BBr_3 (**2**) and FcP–BBr_2Fc (**3**), which are very rare examples of *P*-bonded complexes between phosphaferrocene and a main-group metal atom, were obtained by the reaction of 3,4-dimethyl-1-phosphaferrocene (FcP) with BBr_3 and $FcBBr_2$ (Fc: ferrocenyl). According to X-ray crystallography, the Fe–P bond length in **2** is 0.085 Å shorter than in the parent phosphaferrocene. All structural changes resulting from P–B acid–base pairing follow the same qualitative trend, but are significantly larger than those occurring from the formation of transition metal complexes of phosphaferrocene. In contrast to **2**, NMR spectroscopy reveals **3** to be almost completely dissociated in $CDCl_3$ solution at room temperature.

(© Wiley-VCH Verlag GmbH & Co. KGaA, 69451 Weinheim, Germany, 2003)

Introduction

Oligonuclear transition metal complexes are receiving great attention because of their numerous applications both in homogeneous catalysis[1] and in materials science.[2] The sandwich complex ferrocene has proven to be a particularly important building block in this context. 1,2-Disubstituted ferrocene derivatives give access to chelate ligands possessing planar chirality that have been employed successfully in asymmetric catalysis.[3−5] In the field of materials science, Manners et al. took advantage of the ring-opening polymerisation of strained *ansa*-ferrocenes for the generation of poly(ferrocenylene)s that exhibit interesting optical and electronical properties.[6] Phosphaferrocenes **A**[7] and 1,1′-diphosphaferrocenes **B**[8] (Figure 1), which became available from the work of Mathey et al., were soon recognized to form stable κ-*P* complexes with various transition metals.[9] Ganter et al. developed appropriately substituted derivatives of **A** as a new class of chiral chelate ligands,[10,11] while **B** was used as bridging unit in the formation of heterotrimetallic aggregates.[12]

Our group recently reported a convenient approach to ferrocene-containing macromolecules that benefits from the facile formation of Lewis acid−base adducts. For example, the reaction of the diborylated ferrocene 1,1′-fc(BMe_2)$_2$ [fc = (C_5H_4)$_2$Fe] with selected difunctional Lewis bases (e.g., pyrazine) gives access to polymeric materials in high yield and under very mild conditions (e.g., **C**, Figure 1).[13−15] We decided to investigate whether the or-

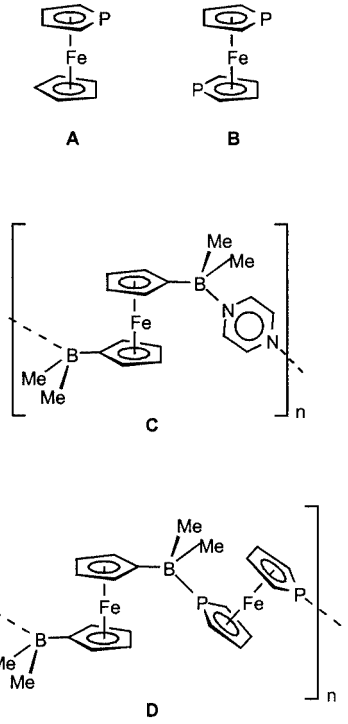

Figure 1. Phosphaferrocene **A**, 1,1′-diphosphaferrocene **B** (only the parent molecules are shown as representatives of the whole class of derivatives), a B−N-bonded charge-transfer coordination polymer **C**, and the final target molecule **D**

[a] Institut für Anorganische Chemie, J. W. Goethe-Universität Frankfurt,
Marie-Curie-Strasse 11, 60439 Frankfurt (Main), Germany
Fax: (internat.) + 49-69/79829260
E-mail: Matthias.Wagner@chemie.uni-frankfurt.de
[b] Institut für Organische Chemie, J. W. Goethe-Universität Frankfurt,
Marie-Curie-Strasse 11, 60439 Frankfurt (Main), Germany
[‡] X-ray crystallography

ganic linker in **C** can be replaced by the redox-active organometallic template ligand **B** to generate target molecules like **D** (Figure 1).

A particular challenge is offered by the fact that despite the plethora of well-characterized complexes of phosphaferrocene and transition metals, no adducts of **A** and only one adduct of **B**[16] with main-group Lewis acids has been isolated so far. In contrast to the related azaferrocene, which is readily quaternized by methyl iodide,[17] diphosphaferrocene **B** was found to react only at elevated temperature, even in neat benzyl bromide. The reaction leads to the decomposition of the phosphaferrocene moiety with liberation of *P*,*P*-dibenzylphospholium bromide.[18] Acetylations, formylations and carboxylations of phosphaferrocenes occur selectively at the α-carbon atoms of the coordinated phospholyl ring.[8,18,19] Moreover, treatment of **A** or **B** with trifluoromethanesulfonic acid leads to protonation on the iron atom, rather than on the phosphorus atom.[20] In summary, the P atom of phosphaferrocenes possesses an energetically low-lying lone pair of electrons and consequently acts as a rather poor σ donor. The LUMO, on the other hand, has pronounced p_z character on the phosphorus atom and is well suited to accept π-electron density.[9,11] The stability of phosphaferrocene-κ-*P*−ML_n complexes is, therefore, expected to grow with an increasing degree of back bonding from electron-rich ML_n fragments. Thus, the fact that main-group elements are not able to have $d_\pi-p_\pi$ interactions with **A** or **B** might explain why corresponding κ-*P* η^1-adducts are virtually unknown up to now. One report on the reaction of phosphaferrocene with $BF_3{\cdot}OEt_2$ has been published that provides evidence for the existence of a phosphorus-bonded adduct in solution (^{31}P NMR spectroscopic control).[20] Moreover, the hypothetical P−B complex $\mathbf{A}{\cdot}BH_3$ has been studied theoretically using DFT methods.[21] Mathey et al. recently reported the reaction of octa-*n*-propyldiphosphaferrocene with $GaCl_3$, which leads to the formation of a tetrahedral gallium(III) complex featuring a chelating diphosphaferrocene ligand.[16] Here, we describe the synthesis, isolation and structural characterization of two P−B adducts of 3,4-dimethyl-1-phosphaferrocene (**1**, Scheme 1).

Results and Discussion

Synthesis and Spectroscopic Characterization

The phosphaferrocene derivative **1** (Scheme 1) was chosen for our investigation because it is accessible in high yield by an established procedure.[7,22] When **1** is treated with the strong Lewis acid BBr_3 in $CDCl_3$ (stoichiometric ratio: 1:1), no obvious reaction takes place since the resulting clear mixture still possesses the orange colour of the initial phosphaferrocene solution. NMR spectroscopy at ambient temperature, however, reveals significant shifts of some characteristic resonances. The phosphorus nucleus in **2** [$\delta(^{31}P) = -13.2$ ppm, $h_{1/2} = 30.1$ Hz] is deshielded by 69.3 ppm compared to that of the free ligand **1** [$\delta(^{31}P) = -82.5$ ppm, $h_{1/2} = 6.5$ Hz]. A strong downfield shift of the

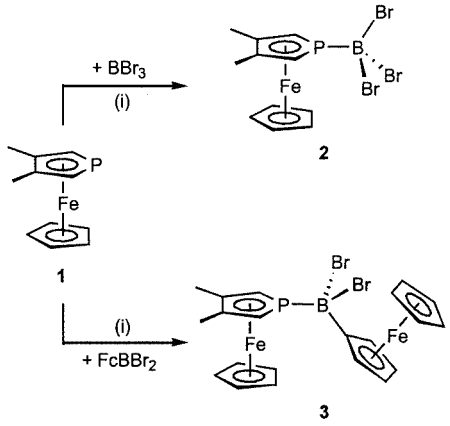

Scheme 1. Synthesis of the P−B-bonded phosphaferrocene adducts **2** and **3**; (i) ambient temperature, C_6H_6

^{31}P NMR signal is also generally observed upon complexation of phosphaferrocenes with transition metal ions.[9] No signal is detectable in the ^{11}B NMR spectrum, which is most likely due to severe line broadening resulting from a dynamic adduct equilibrium. In the ^1H NMR spectrum of **2**, and with respect to parent 3,4-dimethyl-1-phosphaferrocene [**1**: $\delta(^1H) = 3.74$ ($^2J_{P,H} = 36.3$ Hz, phospholyl α-C*H*), 4.15 (C_5H_5) ppm], the resonances of the phospholyl α-protons [**2**: $\delta(^1H) = 4.18$ ($^2J_{P,H} = 29.1$ Hz) ppm] and the cyclopentadienyl ring [**2**: $\delta(^1H) = 4.55$ ppm] are shifted to lower field by 0.44 ppm and 0.40 ppm, respectively. Moreover, the $^2J_{P,H}$ coupling constant decreases by 7.2 Hz. Both the ^{31}P and ^{11}B NMR spectra were recorded also at −50 °C ($CDCl_3$). Under these conditions, the ^{31}P NMR resonance appears at $\delta = -12.9$ ppm as a well-resolved quadruplet with intensity ratios of 1:1:1:1 and a coupling constant of $^1J_{P,B} = 138.5$ Hz ($^1J_{P,B}$ values have been reported within a range of 10−180 Hz[23]). The ^{11}B NMR signal possesses a chemical shift value of $\delta = -20.9$ ppm (d, $^1J_{P,B} = 138.5$ Hz). Consequently, at −50 °C the solution contains mainly the adduct **2**, rather than free **1** and BBr_3.

The ^{11}B and ^1H NMR spectra of an equimolar mixture of **1** with $FcBBr_2$ in $CDCl_3$ at ambient temperature show only negligible differences to the NMR spectra of the individual components. In the ^{13}C NMR spectrum of **1**/$FcBBr_2$, the doublet of the phospholyl α-carbon atoms is broad, while the other signals remain unchanged. The chemical shift of the ^{31}P NMR resonance is the same in **1**/$FcBBr_2$ as in the case of **1**, but the width at half height increases from $h_{1/2} = 6.5$ Hz (**1**) to $h_{1/2} = 165.6$ Hz (**1**/$FcBBr_2$). Thus, NMR spectroscopy reveals the Lewis acid−base pair **1**/$FcBBr_2$ to be almost completely dissociated at room temperature in $CDCl_3$ solution. Slow evaporation of an equimolar mixture of **1** and $FcBBr_2$ in benzene, however, yielded X-ray-quality crystals of the desired P−B-bonded dinuclear species **3**.

X-ray Crystal Structure Determination

The phosphaferrocene−borane adducts **2** and **3** crystallize from benzene in the space groups *Pna*2_1

 © 2003 Wiley-VCH Verlag GmbH & Co. KGaA, Weinheim

(orthorhombic) and $P2_1/c$ (monoclinic), respectively (Table 1). A comparison of the molecular geometries of **1**, **2** (Figure 2) and **3** (Figure 3) reveals remarkable structural changes as a result of P−B bond formation (Table 2). The Fe(1)−P(1) bond length in the BBr_3 adduct **2** possesses a value of 2.199(2) Å, which is 0.085 Å shorter than the iron−phosphorus bond in the parent 3,4-dimethyl-1-phosphaferrocene (**1**) [2.284(1) Å].[24] $FcBBr_2$ is known to be a weaker Lewis acid than BBr_3 because the ferrocenyl substituent acts as an electron donor towards the formally empty p orbital of the boron atom.[25] Consequently, the length of the Fe(1)−P(1) bond in **3** [2.216(1) Å] is intermediate between the values determined for **1** and **2**. These findings are consistent with the general trend observed for transition metal complexes of phosphaferrocenes. A search of the Cambridge Structural Database (CSD, Version 5.24, November 2002)[26] reveals the average Fe−P bond length in monophosphaferrocene derivatives to be 2.285(13) Å (10 structures). This value is reduced to 2.238(16) Å in the corresponding phosphorus-bonded transition metal complexes (22 structures). Interestingly, the effect of Fe−P bond contraction is larger in the borane adducts **2** and **3** than in the corresponding transition metal complexes. P−B acid−base pairing also has a pronounced influence on the C(2)−P(1)−C(5) angle, which is stretched from 88.9(2)° in **1** to 94.7(4)° in **2**, and to 92.7(2)° in **3**. Again, these findings are in good qualitative agreement with the structural features obtained for phosphaferrocene−transition metal aggregates [C−P−C angle in free phosphaferrocene (mean value of 10 derivatives): 89(1)°; C−P−C angle in phosphaferrocene−transition metal complexes (mean value of 22 structures): 92(1)°]. Thus, in all phosphaferrocene derivatives investigated so far (including **2** and **3**), a long Fe−P bond appears to be associated with a small C−P−C angle. It has to be noted that the degree of phospholyl ring puckering is largely unaffected by P−B bond formation. In the case of **1**, the P atom is located at a position 0.048(1) Å above the C(2)C(3)C(4)C(5) plane, while in **2** this displacement is only slightly reduced to a value of 0.043(1) Å. Thus, the phosphorus atom is not just pulled toward the iron centre upon coordination of BBr_3, which would result in a flattening of the phospholyl ligand, but rather it moves toward the C(3)−C(4) bond along a line almost parallel to the C(2)C(3)C(4)C(5) plane {**1**: *d*[P(1)···MP] = 2.589 Å; **2**: *d*[P(1)···MP] = 2.504 Å; MP: midpoint of the C(3)−C(4) bond}. As a result, the P−Fe bond, as well as the P−C bonds, become shorter [cf. **1**: P(1)−C(2) = P(1)−C(5) = 1.774(3) Å; **2**: P(1)−C(2) = P(1)−C(5) = 1.745(8) Å], the C−P−C angle increases, and the adjacent P−C−C angles decrease [cf. **1**: P(1)−C(2)−C(3) = 113.9(2)°, P(1)−C(5)−C(4) = 114.0(2)°; **2**: P(1)−C(2)−C(3) = 109.0(5)°, P(1)−C(5)−C(4) = 110.0(5)°]. The differences observed between the geometrical parameters of **1** and **3** are rather similar to those described above for **1** and **2** and, thus, do not merit further discussion. The P(1)−B(1) bond in **2** [1.972(9) Å] is 0.051 Å shorter than in **3** [2.023(4) Å]. The bond angles around the boron atoms cover a range between P(1)−B(1)−Br(3) = 104.9(4)° and Br(1)−B(1)−Br(3) = 112.2(4)° in the case of **2**, and P(1)−B(1)−Br(1) = 102.9(2)° and C(21)−B(1)−Br(1) = 114.2(2)° in the case of **3**. The relevant Br−B−Br angles of 110.9(4)°, 111.9(4)°, and 112.2(4)° in **2** are slightly larger than the value expected for an sp^3-hybridized boron atom with ideal tetrahedral geometry (109.5°). In **3**, the boron centre is somewhat less pyramidalized, which, together with the longer P(1)−B(1) bond, again indicates a weaker acid−base interaction as is the case in **2**. This interpretation is in agreement with the conclusions drawn from our NMR spectroscopic studies (see above). The BBr_3 adduct **2** features a torsion angle C(2)−P(1)−B(1)−Br(2) of 85.4(5)°. A similar conformation is observed in **3** for the BBr_2P fragment with respect to the ferrocenyl substituent [C(22)−C(21)−B(1)−P(1) = −87.9(3)°], whereas, com-

Table 1. Selected crystallographic data for **2** and **3**

Compound	**2**	**3**
Formula	$C_{11}H_{13}BBr_3FeP$	$C_{21}H_{22}BBr_2Fe_2P$
M	482.57	587.69
Crystal system	orthorhombic	monoclinic
Space group	$Pna2_1$	$P2_1/c$
a [Å]	14.1040(10)	10.561(3)
b [Å]	15.5060(10)	22.221(5)
c [Å]	6.9450(9)	8.8365(17)
β [°]	90	97.366(14)
V [$Å^3$]	1518.8(2)	2056.5(8)
Z	4	4
D_c [g cm^{-3}]	2.110	1.898
T [K]	173(2)	144(2)
μ(Mo-K_α) [mm^{-1}]	8.965	5.378
$2\theta_{max.}$ [°]	56.56	65.42
Measured reflections	25504	36221
Unique reflections (R_{int})	3772 (0.083)	7009 (0.072)
Observed reflections [$I > 2\sigma(I)$]	3174	4777
Parameters refined	157	246
*R*1 [$I > 2\sigma(I)$]	0.051	0.051
*wR*2 [$I > 2\sigma(I)$]	0.121	0.080
GOOF on F^2	1.031	1.074
Largest diff. peak/hole [e·$Å^{-3}$]	0.74/−0.83	1.13/−0.65

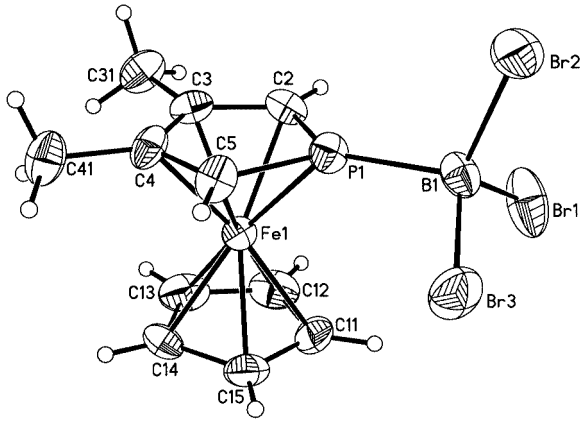

Figure 2. Molecular structure and numbering scheme of compound **2**; thermal ellipsoids shown at the 50% probability level

 © 2003 Wiley-VCH Verlag GmbH & Co. KGaA, Weinheim

pared to compound **2**, the phosphaferrocene moiety is rotated by almost 180° about the P(1)−B(1) bond [C(2)−P(1)−B(1)−C(21) = −90.8(3)°]. This conformation results in a short intramolecular C−H···π interaction between the C(11)−H(11) bond and the cyclopentadienyl ring C(21)C(22)C(23)C(24)C(25) [H(11)···Cg = 2.68 Å, C(11)−H(11)···Cg = 152°; Cg: centroid of the cyclopentadienyl ligand]. Both the ferrocene and phosphaferrocene groups have approximately eclipsed conformations. In **3**, the angle between the planes of the five-membered rings is 1.7° for the ferrocenyl group and 4.2° for the phosphaferrocene moiety.

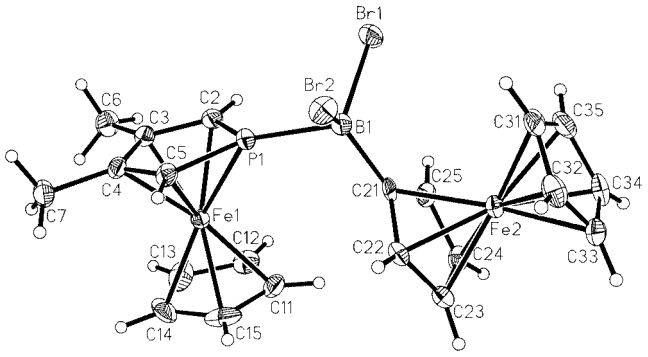

Figure 3. Molecular structure and numbering scheme of compound **3**; thermal ellipsoids shown at the 50% probability level

Table 2. Selected bond lengths [Å], angles [°] and torsion angles [°] of **1**,[24] **2** and **3**; Note: The atom labels of compound **1** have been adapted to the numbering scheme of **2** and **3**

Compound	**1** (T = 74 K)	**2** (T = 173 K)	3 (T = 144 K)
Fe(1)−P(1)	2.284(1)	2.199(2)	2.216(1)
Fe(1)−C(2)	2.072(2)	2.075(7)	2.076(3)
Fe(1)−C(3)	2.057(2)	2.070(7)	2.066(3)
Fe(1)−C(4)	2.054(2)	2.073(7)	2.062(3)
Fe(1)−C(5)	2.060(2)	2.095(7)	2.075(3)
P(1)−C(2)	1.774(3)	1.745(8)	1.744(3)
P(1)−C(5)	1.774(3)	1.745(8)	1.741(3)
C(2)−C(3)	1.424(4)	1.441(11)	1.420(4)
C(3)−C(4)	1.436(3)	1.438(10)	1.427(4)
C(4)−C(5)	1.422(4)	1.431(10)	1.419(4)
P(1)−B(1)	−	1.972(9)	2.023(4)
C(2)−P(1)−C(5)	88.9(2)	94.7(4)	92.7(2)
P(1)−C(2)−C(3)	113.9(2)	109.0(5)	110.9(2)
P(1)−C(5)−C(4)	114.0(2)	110.0(5)	111.1(2)
C(2)−C(3)−C(4)	111.6(2)	113.7(6)	112.7(3)
C(5)−C(4)−C(3)	111.6(2)	112.6(6)	112.7(3)
C(2)−P(1)−B(1)−Br(2)	−	85.4(5)	−
C(2)−P(1)−B(1)−C(21)	−	−	−90.8(3)

Conclusion

In contrast to the rich chemistry that has been developed for complexes between phosphaferrocene and transition metals, examples of *P*-bonded adducts between phosphaferrocene and main-group Lewis acids remained unknown until recently.[16] We have shown that adducts FcP−BBr_3 (**2**) and FcP−BBr_2Fc (**3**) are readily obtained from the reaction of 3,4-dimethyl-1-phosphaferrocene (FcP) with BBr_3 and $FcBBr_2$, respectively (Fc: ferrocenyl). NMR spectroscopy using $CDCl_3$ solutions reveals a considerable amount of adduct **2** to be present in the equilibrium at ambient temperature while **3** is largely dissociated even at −50 °C (cf. theory predicts a small P−B bond-dissociation energy in **A**·BH_3 of D_e = 17.4 kcal·mol^{-1}; B3LYP/6−31G* level).[21] In the solid state, however, **1** binds not only to BBr_3, but also to $FcBBr_2$. All structural changes resulting from P−B acid−base pairing follow the same qualitative trend as those that occur in the formation of complexes of phosphaferrocene with transition metals. The experimental results obtained for **1** and **2** are also in good agreement with the theoretical calculations on **A** and **A**·BH_3. For example, the Fe−P bond is contracted by 0.085 Å upon going from **1** to **2** and by 0.050 Å upon going from **A** to **A**·BH_3. Moreover, the P(1)−B(1) bond length in **2** possesses a value of 1.972(9) Å, which is in good agreement with the theoretically predicted bond length of 1.987 Å in **A**·BH_3.[21]

The dinuclear ferrocenyl aggregate **3** contains all the key structural motifs underlying the target compound **D** (Figure 1). Work is currently in progress to synthesise corresponding coordination polymers from 1,1′-diphosphaferrocene derivatives and 1,1′-diborylferrocenes.

Experimental Section

General Remarks: All reactions and manipulations of air-sensitive compounds were carried out in dry, oxygen-free argon using standard Schlenk glassware. Solvents were freshly distilled under argon from Na/benzophenone (C_6H_6) or passed through a 4-Å molecular sieve column ($CDCl_3$) prior to use. NMR: Bruker AMX 250, AMX 400, DPX 250; abbreviations: s = singlet, d = doublet, vtr = virtual triplet, q = quadruplet, n.r. = multiplet expected in the NMR spectrum, but not resolved; n.o. = signal not observed. ^{11}B [^{31}P] NMR spectra are reported relative to external BF_3·Et_2O [H_3PO_4, 85% in water]. 3,4-Dimethylphosphaferrocene (**1**)[7,22] and dibromoborylferrocene[27] were synthesized according to literature procedures.

Syntheses

2: A solution of BBr_3 (14 mg, 0.056 mmol) in $CDCl_3$ (0.25 mL) was added in an NMR tube to a frozen solution of **1** (13 mg, 0.056 mmol) in $CDCl_3$ (0.25 mL). The reaction mixture was warmed to ambient temperature within 30 min and investigated by NMR spectroscopy. When the same quantities of BBr_3 and **1** were mixed together in toluene at −78 °C, **2** was obtained as a microcrystalline solid. Yield: 21 mg (78%). X-ray-quality crystals of **2** were grown from a highly dilute benzene solution by slow evaporation of the solvent. ^{1}H NMR (250.1 MHz, $CDCl_3$, 303 K): δ = 2.23 (s, 6 H, CH_3), 4.18 (d, $^2J_{P,H}$ = 29.1 Hz, 2 H, α-CH), 4.55 (s, 5 H, C_5H_5) ppm. ^{13}C NMR (62.9 MHz, $CDCl_3$, 303 K): δ = 15.9 (CH_3), 75.2 (C_5H_5), n.o. (C-α), n.o. (*C*CH_3) ppm. ^{11}B NMR (80.3 MHz, $CDCl_3$, 303 K): n.o. (BBr_3). ^{11}B NMR (80.3 MHz, $CDCl_3$, 223 K): δ = −20.9 (d, $^1J_{P,B}$ = 138.5 Hz, BBr_3) ppm. ^{31}P NMR (101.3 MHz, $CDCl_3$, 303 K): δ = −13.2 (n.r., $h_{1/2}$ = 30.1 Hz, phospholyl-P) ppm. ^{31}P NMR (101.3 MHz, $CDCl_3$, 223 K): δ = −12.9 (q, $^1J_{P,B}$ = 138.5 Hz, phospholyl-P) ppm.

 © 2003 Wiley-VCH Verlag GmbH & Co. KGaA, Weinheim

3: 1 (13 mg, 0.056 mmol) and $FcBBr_2$ (20 mg, 0.056 mmol) were dissolved in $CDCl_3$ (0.50 mL) at ambient temperature and the resulting mixture was sealed in an NMR tube. X-ray-quality crystals of **3** were grown from a benzene solution by slow evaporation of the solvent. Yield: 31 mg (94%). ^1H NMR (250.1 MHz, $CDCl_3$, 303 K): δ = 2.18 (s, 6 H, CH_3), 3.78 (d, $^2J_{P,H}$ = 35.5 Hz, 2 H, α-CH), 4.19, 4.23 (2 × s, 2 × 5 H, 2 × C_5H_5), 4.52, 4.91 (2 × vtr, 2 × 2 H, $^3J_{H,H}$ = $^4J_{H,H}$ = 1.8 Hz, C_5H_4) ppm. ^{13}C NMR (100.6 MHz, $CDCl_3$, 303 K): δ = 16.4 (CH_3), 71.5 (2 × C_5H_5), 78.1 (br. d, $^1J_{P,C}$ = 57.3 Hz, C-α), n.o. (*C*CH_3), 77.1, 78.2 (C_5H_4) ppm. ^{11}B NMR (80.3 MHz, $CDCl_3$, 303 K): δ = 46.1 (s, $h_{1/2}$ = 119.0 Hz, BBr_2) ppm. ^{11}B NMR (80.3 MHz, $CDCl_3$, 223 K): δ = 45.1 (s, $h_{1/2}$ = 466.2 Hz, BBr_2) ppm. ^{31}P NMR (101.3 MHz, $CDCl_3$, 303 K): δ = −81.9 (s, $h_{1/2}$ = 165.6 Hz, phospholyl-P) ppm. ^{31}P NMR (101.3 MHz, $CDCl_3$, 223 K): δ = −80.4 (s, $h_{1/2}$ = 252.8 Hz, phospholyl-P) ppm.

X-ray Crystallographic Studies

2: A single crystal (red needle; 0.06 × 0.07 × 0.31 mm) was analysed with a STOE IPDS II two-circle diffractometer with graphite-monochromated Mo-K_α radiation. An empirical absorption correction was performed using the MULABS option[28] in PLATON;[29] the minimum and maximum transmissions were 0.1676 and 0.6153, respectively. The structure was determined by direct methods using the program SHELXS[30] and refined against F^2 with full-matrix least-squares techniques using the program SHELXL-97.[31] The data/parameter ratio was 24.0. All non-hydrogen atoms were refined with anisotropic displacement parameters. Hydrogen atoms were located by difference Fourier synthesis and refined using a riding model.

3: A single crystal (orange block; 0.19 × 0.24 × 0.45 mm) was analysed with a SIEMENS SMART CCD diffractometer; repeatedly measured reflections remained stable. An empirical absorption correction using the program SADABS[32] gave a correction factor between 0.674 and 1.000. Equivalent reflections were averaged (R_{int} = 0.072). The structure was determined by direct methods using the program SHELXS.[30] Hydrogen atoms were geometrically positioned and treated as riding atoms. All non-hydrogen atoms were refined with anisotropic thermal parameters. The structure was refined on F^2 values using the program SHELXL-97.[31]

CCDC-203030 and -203031 contain the supplementary crystallographic data for this paper. These data can be obtained free of charge at www.ccdc.cam.ac.uk/conts/retrieving.html [or from the Cambridge Crystallographic Data Centre, 12 Union Road, Cambridge CB2 1EZ, UK; Fax: (internat.) + 44-1223/336-033; E-mail: deposit@ccdc.cam.ac.uk].

Acknowledgments

M. W. is grateful to the Deutsche Forschungsgemeinschaft (DFG) for financial support. M. S. wishes to thank the Fonds der Chemischen Industrie (FCI) and the Bundesministerium für Bildung und Forschung (BMBF) for a PhD grant.

[1] B. Cornils, W. A. Herrmann, *Applied Homogeneous Catalysis with Organometallic Compounds − A Comprehensive Handbook*, 2nd ed., Wiley-VCH, Weinheim, Germany, **2002**.
[2] D. W. Bruce, D. O'Hare, *Inorganic Materials*, 2nd ed., John Wiley & Sons, Chichester, UK, **1996**.
[3] A. Togni, T. Hayashi, *Ferrocenes*, Wiley-VCH, Weinheim, Germany, **1995**.
[4] I. Ojima, *Catalytic Asymmetric Synthesis*, Wiley-VCH, Weinheim, Germany **2000**.
[5] E. N. Jacobsen, A. Pfaltz, H. Yamamoto, *Comprehensive Asymmetric Catalysis*, vol. I−III, Springer, New York, USA, **1999**.
[6] P. Nguyen, P. Gómez-Elipe, I. Manners, *Chem. Rev.* **1999**, *99*, 1515−1548.
[7] F. Mathey, A. Mitschler, R. Weiss, *J. Am. Chem. Soc.* **1977**, *99*, 3537−3538.
[8] G. de Lauzon, B. Deschamps, J. Fischer, F. Mathey, A. Mitschler, *J. Am. Chem. Soc.* **1980**, *102*, 994−1000.
[9] F. Mathey, *Coord. Chem. Rev.* **1994**, *137*, 1−52.
[10] C. Ganter, L. Brassat, C. Glinsböckel, B. Ganter, *Organometallics* **1997**, *16*, 2862−2867.
[11] C. Ganter, *J. Chem. Soc., Dalton Trans.* **2001**, 3541−3548.
[12] B. Deschamps, F. Mathey, J. Fischer, J. H. Nelson, *Inorg. Chem.* **1984**, *23*, 3455−3462.
[13] M. Fontani, F. Peters, W. Scherer, W. Wachter, M. Wagner, P. Zanello, *Eur. J. Inorg. Chem.* **1998**, 1453−1465; M. Fontani, F. Peters, W. Scherer, W. Wachter, M. Wagner, P. Zanello, *Eur. J. Inorg. Chem.* **1998**, 2087.
[14] M. Grosche, E. Herdtweck, F. Peters, M. Wagner, *Organometallics* **1999**, *18*, 4669−4672.
[15] R. E. Dinnebier, M. Wagner, F. Peters, K. Shankland, W. I. F. David, *Z. Anorg. Allg. Chem.* **2000**, *626*, 1400−1405.
[16] X. Sava, M. Melaimi, N. Mézailles, L. Ricard, F. Mathey, P. Le Floch, *New. J. Chem.* **2002**, *26*, 1378−1383.
[17] K. K. Joshi, P. L. Pauson, A. R. Quazi, W. H. Stubbs, *J. Organomet. Chem.* **1964**, *1*, 471−475.
[18] G. de Lauzon, B. Deschamps, F. Mathey, *Nouv. J. Chim.* **1980**, *4*, 683−685.
[19] F. Mathey, *J. Organomet. Chem.* **1977**, *139*, 77−87.
[20] R. M. G. Roberts, J. Silver, A. S. Wells, *Inorg. Chim. Acta* **1986**, *119*, 165−169.
[21] G. Frison, F. Mathey, A. Sevin, *J. Phys. Chem. A* **2002**, *106*, 5653−5659.
[22] A. Breque, F. Mathey, P. Savignac, *Synthesis* **1981**, 983−985.
[23] S. Berger, S. Braun, H.-O. Kalinowski, *NMR-Spektroskopie von Nichtmetallen*, vol. 3 ("^{31}P- NMR-Spektroskopie"), Thieme Verlag, Stuttgart, Germany, **1993**.
[24] R. Wiest, B. Rees, A. Mitschler, F. Mathey, *Inorg. Chem.* **1981**, *20*, 2966−2970.
[25] A. Appel, F. Jäkle, T. Priermeier, R. Schmid, M. Wagner, *Organometallics* **1996**, *15*, 1188−1194.
[26] F. H. Allen, *Acta Crystallogr., Sect. B* **2002**, *58*, 380−388.
[27] T. Renk, W. Ruf, W. Siebert, *J. Organomet. Chem.* **1976**, *120*, 1−25.
[28] R. H. Blessing, *Acta Crystallogr., Sect. A* **1995**, *51*, 33−38.
[29] A. L. Spek, *Acta Crystallogr., Sect. A* **1990**, *46*, C34.
[30] G. M. Sheldrick, *Acta Crystallogr., Sect. A* **1990**, *46*, 467−473.
[31] G. M. Sheldrick, *SHELXL-97 − A Program for the Refinement of Crystal Structures*, Universität Göttingen, Göttingen, Germany, **1997**.
[32] G. M. Sheldrick, *SADABS*, Universität Göttingen, Göttingen, Germany, **2000**.

Received February 14, 2003

 © 2003 Wiley-VCH Verlag GmbH & Co. KGaA, Weinheim

Assembly of Seven Nickel(II) Metals by Chiral, Salen-Type Ligands with μ_3-OH Bridges

Xuan Xu,[a] Shaohua Gou,*[a] Wei Huang,[a] Yonglin Ma,[a] and Yizhi Li[a]

Keywords: Nickel / Chirality / Bridging ligands

A chiral heptanuclear nickel(II) complex $[Ni^{II}(Ni^{II}_2L)_3(\mu_3\text{-}OH)_2]\cdot 3H_2O$ [H_4L = (2*R*,3*R*)-1,4-bis(3,5-di-*tert*-butylsalicylideneamino)-2,3-butanediol], containing two μ_3-OH bridges, has been prepared and structurally characterized; its thermal and magnetic properties were investigated.

(© Wiley-VCH Verlag GmbH & Co. KGaA, 69451 Weinheim, Germany, 2003)

Introduction

Polynuclear complexes have recently attracted much attention in molecular assembly, with one of the major goals being to try to obtain single-molecule magnets by designing discrete polynuclear entities with high-spin ground states that exhibit useful magnetic properties.[1] Among these multinuclear systems, OH^-, RO^-, RCO_2^- and other groups are often used as bridging ligands.[2] In our research of transition metal complexes, some new salen-type ligands with optically active diamino moieties have been prepared to bind metals in the same manner as in Jacobson's catalysts.[3] Considering the flexibility of the ligands and the known bridging ability of hydroxyl groups, we have chosen (2*R*,3*R*)-1,4-diamino-2,3-butanediol to react with salicylaldehyde derivatives to get a number of Schiff bases as chiral ligands. Herein we report the first preparation and crystal structure of an unusual heptanuclear nickel(II) complex, $[Ni^{II}(Ni^{II}_2L)_3(\mu_3\text{-}OH)_2]\cdot 3H_2O$, together with its magnetic and thermal behavior.

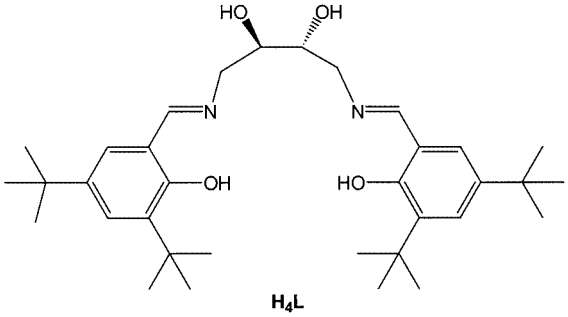

H_4L

[a] State Key Laboratory of Coordination Chemistry, Nanjing University
Nanjing 210093, China
Fax: (internat.) +86-25/331-4502
E-mail: sgou@nju.edu.cn

Results and Discussion

Preparation and Characterization

The title complex was synthesized by reaction of H_4L with $NiCl_2\cdot 6H_2O$ in methanol in the presence of triethylamine. The ligand was prepared by the Schiff-base condensation of 3,5-di-*tert*-butylsalicylaldehyde with (2*R*,3*R*)-1,4-diamino-2,3-butanediol, which was, in turn, obtained by hydrolization of (4*R*,5*R*)-4,5-bis(aminomethyl)-2-isopropyl-1,3-dioxolane.[4] The tetra-deprotonated ligand was formed in situ in the presence of the metal ions.

The crystal structure of the complex is shown in Figure 1. It is a heptanuclear nickel(II) compound with three water molecules of crystallisation. The structure is composed of three dinuclear $[Ni_2L\cdot 1/3(\mu_3\text{-}OH)_2]$ units, with a six-coordinate Ni^{II} moiety in the center (Figure 2). In the structure, there is a threefold symmetry axis containing Ni(3), O(1) and O(4). The three units are obtained by symmetry operations. Thus, the whole system has D_3 symmetry. Each ligand has six ligating groups which are evenly divided into two groups to encapsulate two nickel atoms in two open compartments, where each metal is coordinated by a phenolic oxygen anion, an imine nitrogen atom and an alkyloxy anion of the ligand, as well as a bridging OH^- group. It is noted that there are two hydroxy anions in the molecule and each of them functions as a bridge to connect three metal atoms bound by three ligands. In comparison to quite a number of examples of μ_3-hydroxo bridges in six-coordinate polynuclear nickel(II) complexes,[5] the current example, where three nickel(II) ions in a square-planar geometry are linked by one μ_3-OH^- bridge, is rare. It is also interesting to note that the RO^- anion in the ligand works as a bridging group to connect two metal atoms, whereas the PhO^- anion does not. Consequently, there are three types of "O" donor atoms in this heptanuclear compound.

 © 2003 Wiley-VCH Verlag GmbH & Co. KGaA, Weinheim **DOI: 10.1002/ejic.200300113**

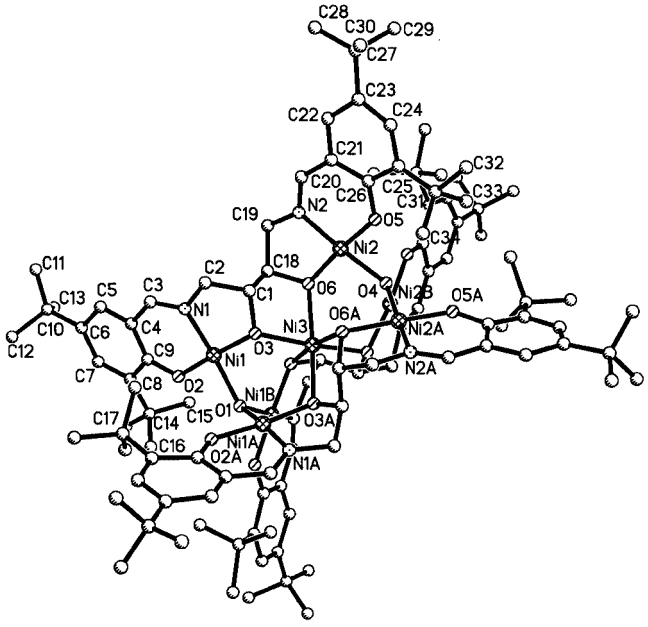

Figure 1. View of the heptanuclear complex, crystalline water molecules are omitted (the labels A and B indicate that these atoms are obtained by symmetry operations)

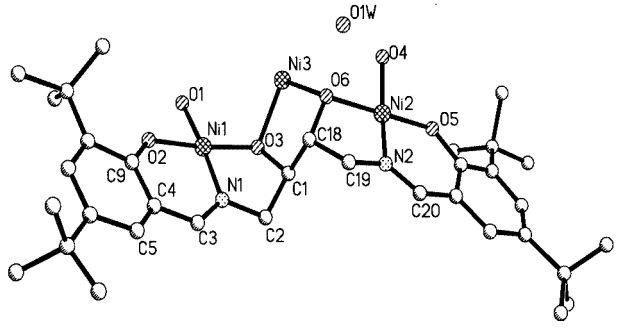

Figure 2. Structure of the dinuclear unit $[Ni_2L{\cdot}1/3(\mu_3\text{-}OH)_2]{\cdot}H_2O$ (50% probability ellipsoids)

More significantly, three dinuclear units share a central nickel atom coordinated by six alkyloxy groups from three ligands, whose 2+ charge is balanced by two μ_3-OH^- anions. The geometry of the central Ni atom is distorted octahedral, and the Ni−O distances are in agreement with normal values.[5] In the $[Ni_2L]$ unit, each metal atom is in a configuration of a distorted square plane consisting of N(1)O(1)O(2)O(3) or N(2)O(4)O(5)O(6); the deviation from the appropriate plane is 0.0410 Å for Ni(1) and 0.0279 Å for Ni(2). The average bond lengths for PhO−Ni (1.82 Å) and N−Ni (1.83 Å) are similar to the values reported for mononuclear salen Ni^{II} complexes.[6] For RO−Ni bonds, the mean distance is 1.87 Å, which is shorter than the usual Ni−O distance in six-coordinate Ni^{II} complexes[7] and close to those in a planar Ni^{II} coordination geometry.[8] In addition, the μ_3-HO-Ni distance of 1.90 Å here is also shorter than the reported values in six-coordinate Ni^{II}.[5]

The seven metal atoms adopt the topology of two tetrahedra sharing a common apex at Ni(3). Ni(1), Ni(1A) and Ni(1B) form an equilateral triangle (Ni−Ni distance: 3.209 Å), which is parallel to its counterpart composed of Ni(2), Ni(2A) and Ni(2B) (Ni−Ni distance: 3.216 Å). Ni(3) is located in the center of the two triangular planes, forming a trigonal prismatic structure (Figure 3). The distance between two triangular planes is 5.538 Å, and that of Ni(3) to these two planes are 2.754 Å and 2.784 Å, respectively. Although a few heptanuclear nickel(II) compounds have recently been reported,[9] our complex is the first example of a heptanuclear nickel(II) complex of a chiral ligand.

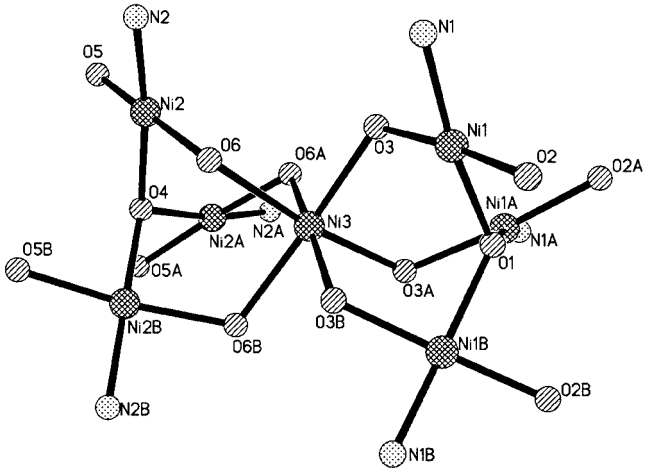

Figure 3. A view of the coordination environments around the nickel atoms; pertinent bond lengths (Å) and angles (°): Ni(1)−O(2) 1.806(3), Ni(1)−N(1) 1.831(4), Ni(1)−O(3) 1.860(3), Ni(1)−O(1) 1.895(13), Ni(2)−N(2) 1.826(4), Ni(2)−O(5) 1.838(3), Ni(2)−O(6) 1.884(3), Ni(2)−O(4) 1.9025(13), Ni(3)−O(3) 2.066(3), Ni(3)−O(6) 2.124(3), N(1)−Ni(1)−O(1) 170.19(16), O(2)−Ni(1)−O(3) 174.55(15), N(2)−Ni(2)−O(4) 171.21(16), O(5)−Ni(2)−O(6) 172.87(15), O(3)−Ni(3)−O(6)B 171.68(12), O(3)−Ni(3)−O(6) 81.54(11), Ni(1)−O(3)−Ni(3) 115.38(15), Ni(2)−O(6)−Ni(3) 113.10(15) (the labels A and B mean these atoms are obtained by symmetry operations)

The variable magnetic susceptibilities of the title complex in the range 77 to 300 K have been measured, and the related $\chi_m T$ vs. T curve is shown in Figure 4. As the temperature decreases, the $\chi_m T$ value is essentially constant (Curie-like behavior). The room temperature magnetic moment of the complex is 3.15 BM (300 K), compatible with that of a free single nickel(II) ion. This result indicates that the magnetic behavior of the compound is characterized as one paramagnetic nickel(II) ion. This is consistent with the six-coordinate Ni^{II} atom being in an octahedral configuration in the structure; the other six Ni^{II} atoms in a square-planar configuration make no contribution to the system.

A TGA analysis of the compound showed that it loses 3.29% of its weight between 15 °C and 67 °C, which can be accounted for by the loss of three waters of crystallisation together with another water molecule probably resulting from the conversion of the $Ni(OH)_2$ part of the compound to NiO and H_2O. The compound then decomposes gradually in the range from 67 °C to 310 °C, followed by a rapid weight loss in the range 310−580 °C, indicating the decomposition of the organic ligand. The residue (ca. 24% of

 © 2003 Wiley-VCH Verlag GmbH & Co. KGaA, Weinheim

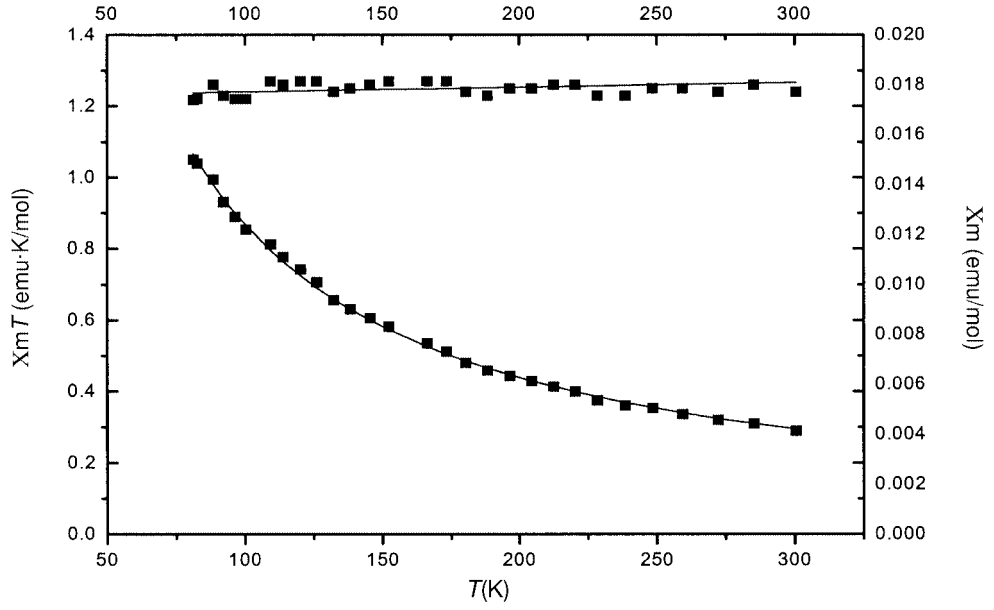

Figure 4. $\chi_m T$ product and χ_m vs. T for the complex; solid lines represent the best fit to the result in agreement with Curie law.

the original weight) is due to the formation of NiO, compatible with the theoretical value of 23.5%.

Experimental Section

Materials and General Methods: All solvents and chemicals were of analytical grade and used without further purification. Elemental analyses were measured with a Perkin−Elmer 1400C analyzer. Infrared spectra (4000−400 cm^{-1}) were recorded on a Nicolet FT-IR 170X spectrophotometer. Electrospray ionization (ES) mass spectra were performed in CH_3CN/CH_3OH on a Finnigan MAT SSQ 710 mass spectrometer in the scan range 300−1200 amu.

$[Ni^{II}(Ni^{II}{}_2L)_3(\mu_3\text{-}OH)_2]\cdot 3H_2O$ (1): The ligand **L** was prepared by a Schiff-base condensation. The title complex was obtained by the following method. $NiCl_2\cdot 6H_2O$ (0.120 g, 0.5 mmol) and the ligand (0.140 g, 0.25 mmol, 1 equiv.) were dissolved in methanol (20 mL). After stirring the resultant solution for thirty minutes, Et_3N (2 equiv.) was added. The mixture was kept refluxing for an hour, then cooled down to room temperature. The brown precipitate was filtered off and dried (Yield: 15%). Single crystals for crystal determination were obtained by slow evaporation of the solvent at room temperature. $C_{102}H_{152}N_6Ni_7O_{17}$ (2145.3): calcd. C 57.02, H 7.26, N 3.85; found C 57.23, H 7.16, N 3.93. IR (KBr): $\tilde{\nu}$ = 3442 cm^{-1} (O−H), 1619 (C=N), 1439 (phenyl),1172(C−O). ESI-MS: *m*/*z* (%) = 553.5 (100) $[H_5L]^+$, 609.5 (26)$[NiH_3L]^+$. $[\alpha]_D^5 = -98.7$ (c = 0.1, $CHCl_3$).

X-ray Crystallography Study: $C_{102}H_{152}N_6Ni_7O_{17}$, M = 2145.27, trigonal, space group $P321$, a = 17.9182(12), b = 17.9182(12), c = 22.363(3) Å, V = 6218.0(10) Å^3, Dc = 1.146 g cm^{-3}, Z = 2, μ = 1.091 mm^{-1}, S = 1.016, $F(000)$ = 2276, T = 293(2) K, $2\theta_{max}$ = 49.98°, 7343 unique data, final $R1$ = 0.0543, $wR2$ = 0.1141 for 5789 observed reflections [$I > 2\sigma(I)$] with 403 variables. A single crystal was mounted on a glass fiber for measurement. Data were collected on a SMART 4 K CCD diffractometer with graphite-monochromated Mo-K_α radiation (λ = 0.71073 Å). The collected data were reduced with the program SAINT, and empirical absorption corrections were done with the SADABS program. The structure was solved by direct methods and refined by least-squares method on F^2_{obs} with the SHELXTL-PC97 software package.
CCDC-198224 contains the supplementary crystallographic data for this paper. These data can be obtained free of charge at www.ccdc.cam.ac.uk/conts/retrieving.html [or from the Cambridge Crystallographic Data Centre, 12, Union Road, Cambridge CB2 1EZ, UK; fax (internat.) +44-1223/336-033; E-mail: deposit@ccdc.cam.ac.uk].

Acknowledgments

The authors are grateful to the National Natural Science Foundation of China for a research project (20271026). This work is also funded in part by Jiangsu Province Science & Technology Department (BK2001031). SG wants to thank the Third World Academy of Science (TWAS) for a research grant to support this project.

[1] [1a] R. Sessoli, D. Gatteschi, A. Caneschi, M. A. Novak, *Nature* **1993**, *365*, 141−143. [1b] Z. Sun, D. Ruiz, E. Rumberger, C. D. Incarnito, K. Folting, A. L. Rheingold, G. Christou, D. N. Hendrickson, *Inorg. Chem.* **1998**, *37*, 4758−4759. [1c] D. Gatteschi, A. Müller, F. Peters, M. Pope, *Chem. Rev.* **1998**, *98*, 239−271.
[2] G. Christou, D. Gatteschi, D. N. Hendrickson, R. Sessoli, *MRS Bull.* **2000**, *25*, 66−71.
[3] [3a] W. Zhang, J. L. Loebach, S. R. Wilson, E. N. Jacobsen, *J. Am. Chem. Soc.* **1990**, *112*, 2801−2803. [3b] R. Irie, K. Noda, Y. Ito, N. Matsumoto, T. Katsuki, *Tetrahedron Lett.* **1990**, *31*, 7345−7348. [3c] L. Canali, D. C. Sherrington, *Chem. Soc. Rev.* **1999**, *28*, 85−93. [3d] E. N. Jacobsen, *Acc. Chem. Res.* **2000**, *33*, 421−431. [3e] T. Katsuki, *Adv. Synth. Catal.* **2002**, *344*, 131−147.
[4] D. K. Kim, G. Kim, J. Gam, Y. B. Cho, H. T. Kim, J. H. Tai, K. H. Kim, W. S. Hong, J. G. Park, *J. Med. Chem.* **1994**, *37*, 1471−1485.
[5] [5a] Y. Sunatsuki, H. Shimada, T. Matsuo, M. Nakamura, F. Kai, N. Matsumoto, N. Re, *Inorg. Chem.* **1998**, *37*, 5566−5574. [5b] J. M. Clemente-Juan, B. Chansou, B. Donnadieu, J. P. Tuchagues, *Inorg. Chem.* **2000**, *39*, 5515−5519. [5c] H. Adams, S. Clunas, D. E. Fenton, D. N. Towers, *J. Chem. Soc., Dalton Trans.* **2002**, 3933−3935.

 © 2003 Wiley-VCH Verlag GmbH & Co. KGaA, Weinheim

[6] A. Haikarainen, J. Sipilä, P. Pietikäinen, A. Pajunen, I. Mutikainen, *J. Chem. Soc., Dalton Trans.* **2001**, 991−995.
[7] H. Adams, S. Clunas, D. E. Fenton, *Chem. Commun.* **2002**, 418−419.
[8] P. Werndrup, S. Gohil, V. G. Kessler, M. Kritikos, L. G. Hubert-Pfalzgraf, *Polyhedron* **2001**, *20*, 2163−2169.
[9] [9a] S. Y. Lai, C. C. Wang, Y. H. Chen, C. C. Lee, Y. H. Liu, S. M. Peng, *J. Chin. Chem. Soc.* **1999**, *46*, 477−485. [9b] P. M. Forster, A. K. Cheetham, *Angew. Chem. Int. Ed.* **2002**, *41*, 457−459. [9c] D. Gaynor, Z. A. Starikova, S. Ostrovsky, W. Haasec, K. B. Nolan, *Chem. Commun.* **2002**, 506−507.

Received February 26, 2003

 © 2003 Wiley-VCH Verlag GmbH & Co. KGaA, Weinheim

Tris(pyrazolyl)methanesulfonates: More Than Just Analogues of Tris(pyrazolyl)borate Ligands; N,N,N-, N,N,O-, and Other Coordination Modes

Wolfgang Kläui,*[a] Michael Berghahn,[a] Walter Frank,[a] Guido J. Reiß,[a] Thomas Schönherr,[b] Gerd Rheinwald,[c] and Heinrich Lang[c]

Dedicated to Professor Rüdiger Mews on the occasion of his 60th birthday

Keywords: Enzyme models / N,O ligands / Transition metals / Tripodal ligands

The thallium(I) salts of tris(pyrazolyl)methanesulfonate (Tpms) and tris(3-*tert*-butylpyrazolyl)methanesulfonate (Tpms^{tBu}) have been used to prepare the following complexes: [(Tpms^{tBu})ZnX] [X = Cl (**1a**), Br (**1b**), I (**1c**), Et (**3**), OAc (**5a**)], [(Tpms^{tBu})NiX] [X = Cl (**2a**), Br (**2b**)], [(Tpms^{tBu})-CoCl(Hpz^{tBu})] (**3**), [(Tpms^{tBu})Zn(μ-OAc)(μ-OH)Zn(Tpms^{tBu})] (**5b**), [(Tpms^{tBu})Cu(CO)] (**6a**), and [(Tpms)Cu(CO)] (**6b**). The solid-state structures of **1b**, **2a**, **3**, and **5b** have been determined by X-ray analysis. The optical spectra of **2a** and **3** were investigated by means of the angular overlap model to elucidate their electronic structures in view of the underlying molecular geometries. Variable-temperature NMR and IR spectroscopic studies show that Tpms and Tpms^{tBu} can act as N,N,N and N,N,O ligands. Both coordination modes are present in solution for the zinc complexes **1a**,**b** and the copper carbonyl complexes **6a**,**b**. The N,N,O bonding mode is entropically favoured in solution. For the nickel complexes **2a**,**b**, the Tpms^{tBu} ligand acts as a tripodal nitrogen ligand in the solid state and in solution. For the dinuclear zinc complex **5b**, one of the Tpms^{tBu} ligands acts as an N,N,O ligand and one as an N,O ligand. Complex **5b** is one of the very few structural models of the dinuclear zinc enzymes phospholipase C and phosphotriesterase.

(© Wiley-VCH Verlag GmbH & Co. KGaA, 69451 Weinheim, Germany, 2003)

Introduction

Recently we reported the synthesis of the tris(pyrazolyl)-methanesulfonates (Tpms), a novel class of ligands.[1] These ligands were designed by analogy to the well-known tris-(pyrazolyl)borate (Tp) ligands.[2] They have the same nitrogen-donor set as the Tp ligands, but in addition they bear a sulfonate group to make the ligands more hydrophilic.

Herein we describe the coordination behaviour of the sterically demanding ligand tris(3-*tert*-butylpyrazolyl)methanesulfonate (Tpms^{tBu}) (Figure 1) towards zinc(II), nickel(II), cobalt(II), and copper(I) ions, as well as the structural flexibility and the dynamic stereochemistry of this ligand.

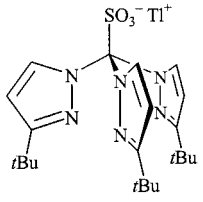

Figure 1. Schematic structure of the thallium salt of the Tpms^{tBu} ligand

Results and Discussion

1. The Complexes [(Tpms^{tBu})ZnX] (1) and [(Tpms^{tBu})NiX] (2) (X = Halide)

The complexes [(Tpms^{tBu})MX] were synthesised by reaction of TlTpms^{tBu} with the appropriate metal halide at room temperature [Equation (1)]. In contrast to the analogous Tp^{tBu} complexes,[3] these Tpms^{tBu} complexes have good solubility in polar solvents like wet methanol.

$$TlTpms^{tBu} + MX_2 \longrightarrow [Tpms^{tBu}MX] + TlX \quad (1)$$

[a] Institut für Anorganische Chemie und Strukturchemie der Universität Düsseldorf,
Universitätsstraße 1, 40225 Düsseldorf, Germany
E-mail: klaeui@uni-duesseldorf.de
[b] Institut für Theoretische Chemie der Universität Düsseldorf,
Universitätsstraße 1, 40225 Düsseldorf, Germany
[c] Lehrstuhl für Anorganische Chemie, Technische Universität Chemnitz,
Straße der Nationen 62, 09107 Chemnitz, Germany

The Solid-State and Solution Structures of [(Tpms^{tBu})ZnX] [X = Cl (1a), Br (1b), I (1c)]

The sterically demanding ligand Tp^{tBu} stabilises almost exclusively ions with coordination number four ("tetrahedral enforcer"[4]) and forms complexes with the composition [Tp^{tBu}MX]. In the case of **1a**−**c**, the analogous composition [(Tpms^{tBu})ZnX] is found, but the ^{1}H NMR spectra in $CDCl_3$ do not show the expected pattern of signals. Three different sets of pyrazolyl signals are found for **1a** and **1b**.

Variable-temperature NMR studies of **1a** and **1b** show that two of the three sets of signals occur in an intensity ratio of 1:2 at all temperatures (Figure 2). This ratio indicates that an equilibrium between two different species exists in solution: the expected C_{3v}-symmetrical complex and a C_s-symmetrical complex (Scheme 1). In the C_s-symmetrical species, Tpms^{tBu} coordinates with two nitrogen atoms and one oxygen atom of the sulfonate group, i.e. the ligand acts as an N,N,O ligand.

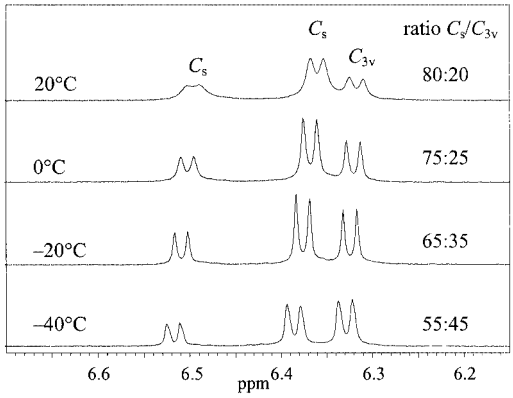

Figure 2. ^{1}H NMR spectra (200 MHz) of **1a** (pyrazolyl 4-*H* region) in $CDCl_3$ in the temperature range −40 to +20 °C

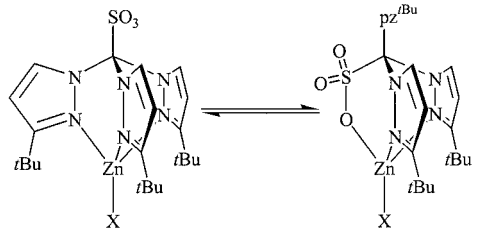

Scheme 1. Equilibrium between a C_{3v}- and a C_s-symmetrical zinc halide complex in solution (X = Cl, Br)

The ^{1}H NMR spectrum of **1c** shows only the signals for the C_s-symmetrical complex. Even at low temperatures the C_{3v}-symmetrical complex cannot be detected.

Obviously the sulfonate group, which was introduced to increase the solubility in polar solvents, is a competing donor centre. This result was surprising since the sulfonate unit is regarded as a weakly coordinating group, especially in comparison with nitrogen atom donors.[5]

Having the results of the variable-temperature studies at hand, we calculated the equilibrium constant $K = c[C_s]/c[C_{3v}]$ for **1a**. The enthalpy and entropy of the transformation of the C_{3v}-symmetrical into the C_s-symmetrical species were determined from a van't Hoff plot. In chloroform, the C_{3v}-symmetrical species is favoured enthalpically ($\Delta H = +8.0$ kJ·mol^{-1}), but the entropy of the transformation is positive: $\Delta S = +40$ J·K^{-1}·mol^{-1}. As a result, the C_s-symmetrical complex is the dominant isomer in the studied temperature range. The C_s isomer is favoured entropically per se because of its lower symmetry. We assume, however, that the rather large positive entropy is a result of the smaller dipole moment of the C_s-symmetrical complex, which allows the solvent to be more disordered.

Compound **1b** crystallises from THF/pentane in the monoclinic space group $P2_1/c$. The asymmetric unit of the crystal structure contains two complexes with very similar structures and one molecule of THF. The ZORTEP plot given in Figure 3 shows one of the symmetry-independent complexes. Selected bond lengths and angles are summarised in Table 1.

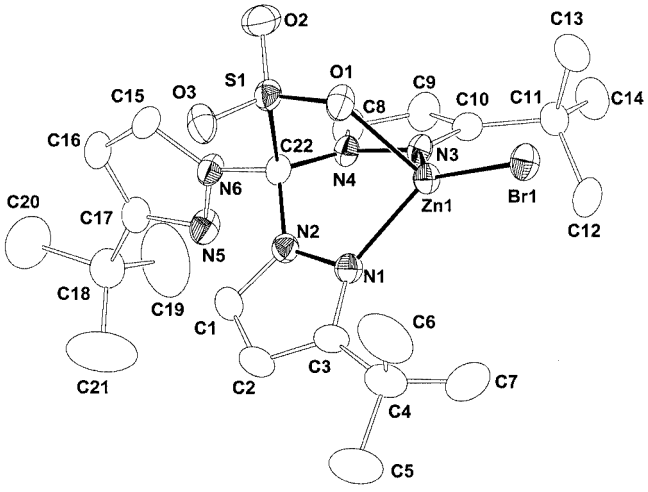

Figure 3. ZORTEP plot of [(Tpms^{tBu})ZnBr] (**1b**)

The zinc atom is coordinated in a distorted tetrahedral geometry. In the solid state, the Tpms^{tBu} ligand coordinates as an N,N,O ligand.

Recently, Burzlaff published the structure of a zinc complex containing a similar monoanionic N,N,O ligand derived from bis(pyrazolyl)acetic acid. It is a model compound for zinc enzymes with the facially coordinating 2-His-1-carboxylate triad, such as thermolysin and carboxypeptidase.[6] The Zn−O bond lengths show that the sulfonate group is a weaker donor than the carboxylate group. Burzlaff observed a Zn−O bond length of 1.990(2) Å, which is significantly shorter than in **1b** [2.017(2) Å]. The Zn−O distances in thermolysin (2.08 Å) and carboxypeptidase (2.2 Å) are very similar to the Zn−O distance of compound **1b**.[6]

 © 2003 Wiley-VCH Verlag GmbH & Co. KGaA, Weinheim

Table 1. Selected bond lengths [Å] and angles [°] in [(Tpms^{tBu})ZnBr] (**1b**)

Zn1−N3	2.014(2)	Zn2−N9	2.025(2)
Zn1−O1	2.017(2)	Zn2−O4	2.032(2)
Zn1−N1	2.048(2)	Zn2−N7	2.054(2)
Zn1−Br1	2.2905(4)	Zn2−Br2	2.2778(5)
S1−O2	1.426(2)	S2−O5	1.431(2)
S1−O3	1.435(2)	S2−O6	1.437(2)
S1−O1	1.463(2)	S2−O4	1.470(2)
S1−C22	1.885(3)	S2−C44	1.880(3)
N3−Zn1−O1	91.73(9)	N9−Zn2−O4	92.89(9)
N3−Zn1−N1	90.42(9)	N9−Zn2−N7	89.39(10)
O1−Zn1−N1	91.13(9)	O4−Zn2−N7	91.25(9)
N3−Zn1−Br1	131.13(7)	N9−Zn2−Br2	134.66(7)
O1−Zn1−Br1	108.04(6)	O4−Zn2−Br2	108.55(6)
N1−Zn1−Br1	131.74(7)	N7−Zn2−Br2	128.08(7)
O2−S1−O3	117.88(14)	O5−S2−O6	117.37(14)
O2−S1−O1	112.35(13)	O5−S2−O4	113.41(13)
O3−S1−O1	112.81(14)	O6−S2−O4	112.25(14)
O2−S1−C22	105.27(14)	O5−S2−C44	104.76(13)
O3−S1−C22	103.17(13)	O6−S2−C44	104.63(13)
O1−S1−C22	103.48(12)	O4−S2−C44	102.50(12)

Structural Studies on [(Tpms^{tBu})NiX], X = Cl (2a), Br (2b)

To see the influence of the nature of the metal ion on the coordination behaviour of the Tpms^{tBu} ligand, we prepared the nickel complexes [(Tpms^{tBu})NiX] (**2a**: X = Cl; **2b**: X = Br) by analogy to the zinc complexes **1a**−**c**. The crystal structure of **2a** was determined. The complex crystallises from THF/pentane in the monoclinic space group $P2_1/n$. Figure 4 shows an ORTEP plot of **2a**. Selected bond lengths and angles are summarised in Table 2.

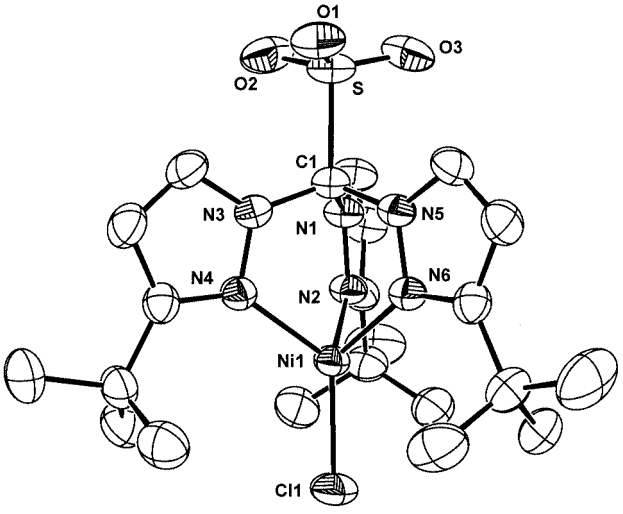

Figure 4. ORTEP plot of [(Tpms^{tBu})NiCl] (**2a**)

In contrast to the above-mentioned zinc complexes, Tpms^{tBu} coordinates to the nickel ion through the three pyrazolyl nitrogen atoms and forms a complex with C_{3v}-symmetry. This coordination is the same N,N,N mode as observed in the C_s-symmetrical trigonal-bipyramidal rhodium complex [(Tpms)Rh(nbd)], the structure of which we have recently determined.[7]

Table 2. Selected bond lengths [Å] and angles [°] in [(Tpms^{tBu})NiCl] (**2a**)

Ni1−N2	2.0088(13)	N2−Ni1−N6	90.06(5)
Ni1−N6	2.0105(14)	N2−Ni1−N4	90.12(5)
Ni1−N4	2.0105(13)	N6−Ni1−N4	89.66(5)
Ni1−Cl1	2.1746(6)	N2−Ni1−Cl1	124.24(4)
S1−O1	1.4380(15)	N6−Ni1−Cl1	125.30(4)
S1−O2	1.4433(16)	N4−Ni1−Cl1	126.35(4)
S1−O3	1.4452(15)	O1−S1−O2	115.04(10)
S1−C1	1.9283(15)	O1−S1−O3	115.98(9)
		O2−S1−O3	115.92(9)
		O1−S1−C1	102.44(8)
		O2−S1−C1	102.26(8)
		O3−S1−C1	101.96(8)

The nickel centre is coordinated in a trigonally distorted tetrahedral geometry. This arrangement is apparent from the N−Ni−Cl angles [124.24(4)−126.35(4)°] and in the smaller N−Ni−N angles [89.66(5)−90.12(5)°]. The distortion is similar to that observed for the [Tp^{tBu}MX] complexes.[8] The UV/Vis spectra of **2a** in dichloromethane and tetrahydrofuran solution, and in the solid state, are identical, and therefore we propose the same coordination mode of the Tpms^{tBu} ligand in solution as is observed in the solid state. The spectrum of **2b** in solution is slightly shifted bathochromically, but shows the same pattern as the spectrum of **2a**; therefore, an analogous structure can be assumed for **2b**. Both compounds are intensively red, an unusual colour for tetrahedral nickel(II) complexes. To obtain a better understanding of their colour, we have analysed the UV/Vis spectra in terms of the Angular Overlap Model (AOM) (see below).

2. Structural Studies on [(Tpms^{tBu})CoCl(Hpz^{tBu})] (3), a Five-Coordinate Cobalt(II) Complex

In bioinorganic chemistry it is often possible to probe the metal environment in zinc-containing enzymes with a cobalt ion as a substitute for the native zinc ion. This substitution can be misleading, however, because of the slightly different tendencies of cobalt(II) and zinc(II) ions to prefer tetrahedral vs. trigonal-bipyramidal coordination.[9] We wanted, therefore, to compare the coordination behaviour of Tpms^{tBu} towards zinc and cobalt chloride.

The reaction of TlTpms^{tBu} with cobalt chloride leads to a blue complex with the composition [(Tpms^{tBu})CoCl(Hpz^{tBu})] (**3**). The UV/Vis spectrum of this compound in dichloromethane exhibits its major band in the range 520−603 nm with an absorption coefficient ε_{max} = 402 $M^{-1}\cdot cm^{-1}$. This band shows the same pattern as the major band of the five-coordinate complex [Tp^{tBu}Co(η^2-NO_3)] (517−600 nm, ε_{max} = 212 $M^{-1}\cdot cm^{-1}$ in THF) published by Parkin.[8] Obviously a five-coordinate complex has formed rather than the expected four-coordinate halide complex.

Complex **3** crystallises from THF/pentane in the monoclinic space group $P2_1/n$ and the asymmetric unit of the crystal structure contains one molecule of THF. The ORTEP plot is given in Figure 5. Selected bond lengths and angles are summarised in Table 3.

 © 2003 Wiley-VCH Verlag GmbH & Co. KGaA, Weinheim

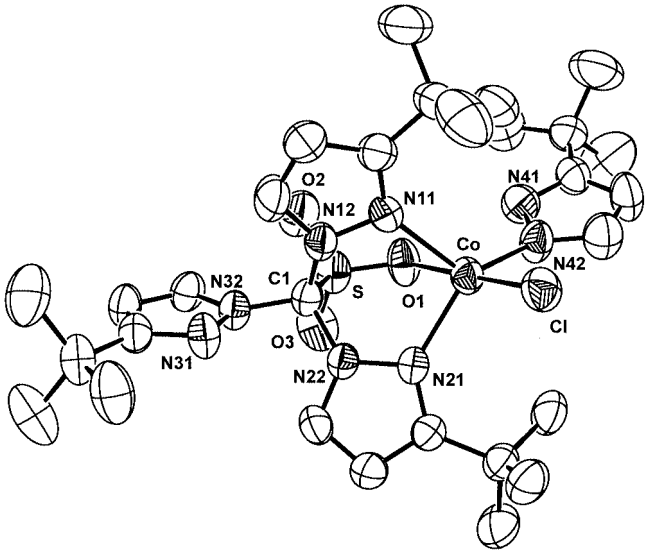

Figure 5. ORTEP plot of [(Tpms^{tBu})CoCl(Hpz^{tBu})] (**3**)

Table 3. Selected bond lengths [Å] and angles [°] in [(Tpms^{tBu})-CoCl(Hpz^{tBu})] (**3**)

Co−N42	2.035(3)	N42−Co−C1	97.49(10)
Co−N21	2.051(3)	N21−Co−C1	103.89(8)
Co−N11	2.094(3)	N11−Co−C1	103.88(8)
Co−C1	2.2738(12)	N42−Co−O1	78.51(11)
Co−O1	2.355(2)	N21−Co−O1	77.94(10)
S−O3	1.421(3)	N11−Co−O1	79.52(10)
S−O2	1.430(3)	Cl−Co−O1	175.81(7)
S−O1	1.453(2)	O3−S−O2	116.62(19)
S−C1	1.879(3)	O3−S−O1	113.99(18)
		O2−S−O1	113.61(18)
N42−Co−N21	28.33(12)	O3−S−C1	103.67(16)
N42−Co−N11	123.07(11)	O2−S−C1	104.43(16)
N21−Co−N11	96.63(10)	O1−S−C1	102.28(14)

The Tpms^{tBu} ligand coordinates in the N,N,O mode. The coordination sphere is completed by a chloro ligand and a pyrazole ligand, which derives from partial hydrolysis of the Tpms^{tBu} ligand. This hydrolysis cannot be avoided, even by using thoroughly dried anhydrous cobalt(II) chloride. This observation is noteworthy because the hygroscopic $ZnCl_2$ used for the synthesis of **1a** contained significant amounts of water, but in this case no hydrolysis occurred. The formation of **3** shows the different reactivity of cobalt and zinc ions. We have observed a similar difference in the coordination behaviour of cobalt and zinc ions towards the Tp^{Ph} ligand.[9]

The crystal structure analysis shows that the cobalt(II) ion in **3** has a distorted trigonal-bipyramidal coordination geometry. The coordinated oxygen atom of the tripodal ligand and the chloro ligand occupy the axial positions. Two pyrazolyl rings of the Tpms^{tBu} ligand and the free pyrazole are in the equatorial positions. The Co−O bond [2.355(2) Å] is significantly longer than those of Co^{II}−sulfonate complexes cited in the Cambridge Crystallographic Database [coordination number (CN) 5: 2.06 Å; CN 6: 1.94−2.22 Å].[10]

As the sulfonate group is less bulky than a *tert*-butylpyrazolyl group, Tpms^{tBu} does not prevent coordination numbers higher than four from forming when it acts as an N,N,O ligand. This effect allows the additional coordination of a ligand such as the *tert*-butylpyrazol unit.

The five-coordinate cobalt(II) complex **3** has the intensive blue colour that we had expected for a four-coordinate cobalt(II) complex. Since no ligand-field analysis of the novel ligand Tpms^{tBu} has been carried out until now, we analysed the UV/Vis spectrum of the cobalt complex **3** together with the spectrum of the tetrahedral nickel complex **2a** (see above) in terms of the Angular Overlap Model, hoping for a consistent picture of the ligand-field properties of this ligand.

3. AOM Analysis of the UV/Vis Spectra of the (Tpms^{tBu})Ni^{II} and -Co^{II} Complexes 2a and 3

The Angular Overlap Model (AOM) has been shown to be a powerful tool for rationalising d^n-level splittings in low-symmetry transition metal complexes.[11] Its advantage over the conventional ligand-field theory emerges from explicitly accounting the specific angular geometry of the chromophore, as well as involving peculiarities of the metal−ligand bonding. The latter is achieved by introducing *local* metal−ligand interaction parameters of σ and π type, which are often transferable between similar transition metal complexes. In this section we investigate the optical spectra of [(Tpms^{tBu})NiCl] (**2a**) and [(Tpms^{tBu})-CoCl(Hpz^{tBu})] (**3**) by means of the AOM to elucidate their electronic structures in view of the underlying molecular geometries.

[(Tpms^{tBu})NiCl] (2a)

In a tetrahedral ligand field, the d^8 system of Ni^{II} gives rise to a $^3T_1$ (^3F) ground state and $^3T_2$ (^3F), $^3A_2$ (^3F), and $^3T_1$ (^3P) excited states. The optical spectrum is dominated by the spin-allowed transition $^3T_1$ (^3F) → $^3T_1$ (^3P), typically located in the region 14000−17000 cm^{-1}, whereas the other triplets are expected in the near-infrared (4000−11000 cm^{-1}).[12] As so far, the present complex **2a** shows the typical absorption pattern, which is depicted in Figure 6, though the band maxima are significantly shifted to lower wavelengths. This observation is particularly true when compared with the closely related complex [Tp^{tBu}NiCl]:[8] The main absorption, which reflects the respective colour of a complex, is shifted from 505 nm (purple) to 475 nm (red), the latter being a rather uncommon colour for tetrahedrally coordinated nickel(II) complexes. The reason for the hypsochromic shift is not clear at first glance.

To elucidate this situation, we have measured spectra of microcrystalline powders, where a better resolved band structure was obtained on cooling down to liquid helium temperatures. Band maxima, on the other hand, are only slightly shifted, which excludes a solvent effect being responsible for the red colour of [(Tpms^{tBu})NiCl]. A deeper

 © 2003 Wiley-VCH Verlag GmbH & Co. KGaA, Weinheim

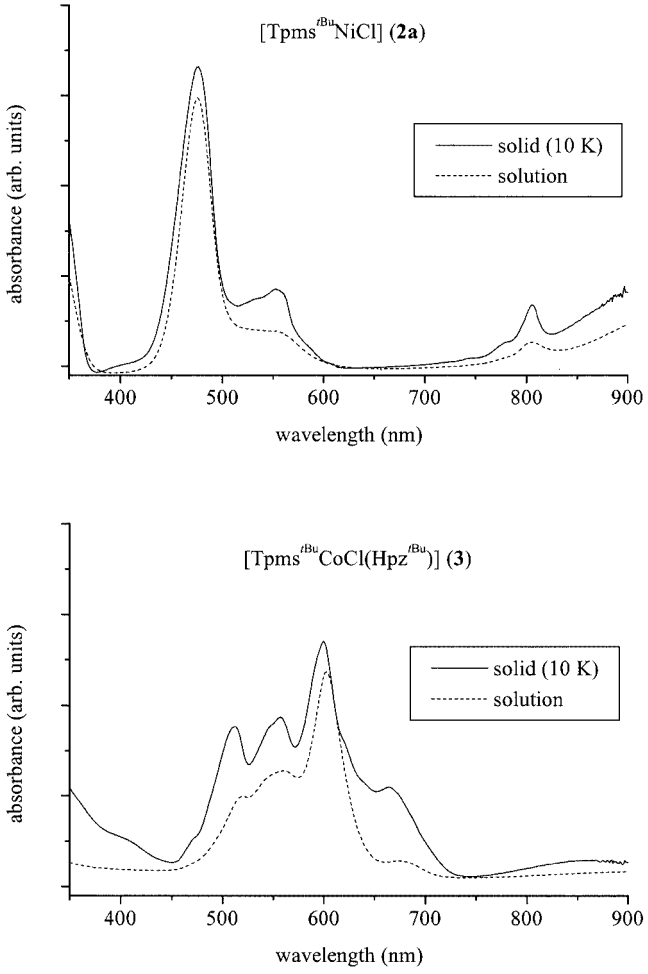

Figure 6. UV/Vis spectra of [(Tpms^{tBu})NiCl] (**2a**) and [(Tpms^{tBu})-CoCl(Hpz^{tBu})] (**3**) in solution (dichloromethane) and in the solid state

look into the electronic structure reveals that the underlying trigonal symmetry is the reason for the higher transition energies according to $^3T_1$ (^3F) → $^3T_1$ (^3P) and $^3T_1$ (^3F) → $^3A_2$ (^3F). We note that further band splittings are expected by the effect of spin-orbit coupling present in Ni^{II} complexes. Such information, however, is not available, even from the better resolved low-temperature spectrum. Moreover, from our AOM calculations, we have found such splittings and band shifts to be significantly smaller than those resulting from the geometrical effect. Therefore we restrict the following discussion to the analysis of the LS states.

The orbitally triply degenerate states split under the influence of the local trigonal symmetry, which is reflected, for example, in the large splitting of about 3000 cm^{-1} for the intense $^3T_1$ (^3P) band. A deconvolution of the band shape yields maxima at 474 nm and 556 nm, which are due to the transitions $^3A_2$ (^3F) → $^3A_2$ (^3P) and $^3A_2$ (^3F) → ^3E (^3P), respectively (in the notation of the C_{3v} group). The transition into $^3A_2$ (^3F) is located at 805 nm (12400 cm^{-1}), again somewhat higher in energy than observed for other pseudo-tetrahedrally coordinated nickel compounds. Besides these absorptions, the low-temperature spectrum exhibits several spin-forbidden transitions into singlet states that result from ^1D (^1E, $^1T_2$) and the higher ^1G ($^1T_2$, $^1A_1$, $^1T_1$, ^1E) multiplets. This manifold of experimentally available data provides a sound base for a reliable AOM analysis of the d-states involved. It turns out that the hypsochromic band shift has a simple geometrical background: When comparing the angular structure of the chromophore of [(Tpms^{tBu})NiCl] determined here with those of the related complexes [Tp^{tBu}MCl] (M = Zn, Cu, Ni, Fe, Co),[8,13] we recognize larger angles Cl−M−N for the complex under investigation (close to 125°) than for any of the Tp^{tBu} compounds (mean values around 121°). The trigonal elongation causes the considerable splitting of the orbitally degenerate triplet states together with a lowering of the ground-state energy that is responsible for the higher transition energies in [(Tpms^{tBu})NiCl]. To prove this result, we performed a complete analysis for all the d-states, which are accessible from the low-temperature absorption spectrum. In the optimization procedure, all underlying AOM parameters, i.e. e_σ^{Cl}, e_σ^{pz}, e_π^{Cl}, $e_{\pi\perp}^{pz}$, were freely optimized as were also the Racah parameters *B* and *C* that describe the electron−electron interaction.[14] While anisotropic π interaction requires, in general, two independent AOM parameters ($e_{\pi\|}$ and $e_{\pi\perp}$) for considering contributions parallel and perpendicular to the chelate plane, the in-plane π interaction with the pyrazole group is small and can be reasonably neglected here as for ammine and sp^2-hybridized amine complexes ($e_{\pi\|}^{pz} = 0$). All calculations were performed with the AOMX programme,[14] which is available in the internet (www.aomx.de). The result of our optimization procedure is presented in Table 4. Herein we used different weighting factors to distinguish spin-allowed from spin-forbidden transitions, since the band maxima of the latter have been located by a deconvolution procedure. The underlying electronic parameters are collected in Table 5. For identifying the eigenstates, the geometry was kept trigonal by taking a value of 125° for all three Cl−Ni−N angles. This restriction does not weaken the analysis, because further splittings of degenerate E states are not observed in the low-temperature absorption spectrum [the small absorption at 13500 cm^{-1} may be due to spin-orbit effects and/or the low-symmetry splitting of ^1E (^1D)].

In summary, the AOM analysis clearly demonstrates that all details obtained from the optical spectrum can be rationalized. The derived parameter values are reasonable and their positive values prove the expected antibonding behaviour. Because of an unfavorable relationship between experimental data (eight) and fitted parameters (six), clear-cut decisions about the presented parameter values should not be made on this stage. They may, nevertheless, serve as a useful estimation for future investigations of similar compounds.

[(Tpms^{tBu})CoCl(Hpz^{tBu})] (3)

The situation with the cobalt compound is rather different. The structural investigation exhibits coordination number five and a strongly distorted geometry with absence of

 © 2003 Wiley-VCH Verlag GmbH & Co. KGaA, Weinheim

Table 4. Experimental and calculated d−d transition energies for [(Tpms^{tBu})NiCl] (**2a**) (in cm^{-1})

Excited state (C_{3v})	Parent state (T_d)	Energy (exp.)	Energy (calcd.)	Difference	Weight
$^3A_2$ [a]	$^3T_1$ (^3F)	0[a]	0[a]		
^3E	$^3T_1$ (^3F)		5240		
$^3A_1$	$^3T_2$ (^3F)		7690		
^3E	$^3T_2$ (^3F)		10100		
^3A	**$^3A_2$ (^3F)**	**12420**	**12350**	**70**	**1.0**
^1E	^1E (^1D)	12830[b]	12390	440	0.2
^1E	$^1T_2$ (^1D)	17250	17130	120	0.2
^3E	**$^3T_1$ (^3P)**	**18050**	**18060**	**10**	**1.0**
$^1A_1$	$^1T_2$ (^1D)	18500	18360	140	0.2
$^1A_1$	$^1T_2$ (^1G)	19300	19790	49	0.2
^3A	**$^3T_1$ (^3P)**	**21100**	**21090**	**10**	**1.0**
^1E	$^1T_2$ (^1G)	sh [c]	22070		
$^1A_1$	$^1A_1$ (^1G)	sh [c]	23260		
$^1A_1$	$^1T_1$ (^1G)	25200	25010	190	0.2
^1E	$^1T_1$ (^1G)	25200	25580	380	0.2
^1E	^1E (^1G)		29430		

[a] Ground state. [b] The small absorption at 13500 cm^{-1} may be due to spin-orbit effects and/or the low-symmetry splitting of ^1E (^1D). [c] Shoulder.

Table 5. AOM bonding and interelectronic Racah parameters (in cm^{-1}, rounded) for [(Tpms^{tBu})NiCl] (**2a**) and [(Tpms^{tBu})-CoCl(Hpz^{tBu})] (**3**) as obtained from the analysis of d−d transitions in the optical absorption spectra

	e_σ^{pz}	$e'_{\pi\perp}{}^{pz}$	e_σ^{Cl}	e_π^{Cl}	e_σ^{O}	e_π^{O}	B	*C*/*B*
2a	5400	400	4500	350	–	–	690	5.3
3	5300	800	4700	400	5800	1000	450	5.8

symmetry or any useful pseudo-symmetry. Moreover, since Tpms^{tBu} coordinates in the N,N,O mode, additional parameters for the Co−OSO$_2$ group have to be considered when applying the AOM. This situation demands substantial spectroscopic information, which is deduced, once more, from the low-temperature spectrum obtained from microcrystalline powders. As can been seen in Figure 6, the overall band pattern again is not changed, while the spectral resolution is largely improved on cooling down to T = 10 K.

To elucidate the complicated absorption structure, we proceeded as follows. First, we asked what would a simple electrostatic ligand field calculation, where all ligators are assumed to contribute by the same potential, predict for this particular geometry (Figure 5). It turns out that such a point charge approximation may already explain the overall band pattern. The present high-spin d^7 system exhibits a quartet ground term and nine more higher quartet states, which, unfortunately, cannot be related to parent states arising from any higher symmetric fivefold coordination. Under the reasonable assumption that the more intense transitions are due to spin-allowed transitions, we performed an optimization under the restrictions given above. This procedure results in a reasonable fit, whereby the expected quartet transition energies vary in the optical spectrum from 14000 to 20000 cm^{-1}, which is in line with the experimental findings. This result demonstrates that the geometrical structure of the chromophore is the main reason for the colour of **3**. In a second step, we have distinguished between σ- and π-bonding peculiarities and allowed free variation for the e_σ parameters involved. The AOM calculation then leads to a significantly better result, with the differences between calculated and observed spin-allowed transitions, obtained from a band deconvolution, becoming ca. 1000 cm^{-1} or less. The reliability of the subsequent assignments is confirmed by the parameter values derived from the fitting procedure, which show, for example, the expected trend for the σ donors: $e_\sigma^{O} > e_\sigma^{N} > e_\sigma^{Cl}$.[11]

Though keeping in mind the problem of overparametrization, a more-convincing band fit can be achieved when absorptions located around 18000 cm^{-1} are assigned to transitions into doublet states. Such spin-forbidden bands gain intensity by low symmetry and by the relatively large spin-orbit coupling present in cobalt(II) complexes. Under these assumptions, the AOM allows us to fit the absorption band pattern fairly well. It follows that the main peaks at 511, 597 and 633 nm represent quartet bands, whereby the latter broader bands cover two spin-allowed transitions each. All the other spectral features should arise from spin-forbidden transitions into doublet states. Spin-orbit coupling, however, mixes quartet and doublet states and causes further band shifts and level splittings.[15] Therefore, clear-cut assignments to be used in the optimization procedure cannot be made, which prevents the evaluation of definite AOM parameter values. In Table 5 we present an estimation only for the underlying model parameters. Nevertheless, it can certainly be concluded that the optical spectrum is due to metal-localized d−d transitions, which can be reasonably described by the AOM. We show that the distinct geometric arrangement of ligator atoms causes the specific spectral

 © 2003 Wiley-VCH Verlag GmbH & Co. KGaA, Weinheim

pattern, rather then bonding peculiarities of the various ligating groups.

4. Zinc−Acetate Complexes of Tpms^{tBu}

Tl(Tpms^{tBu}) reacts with diethylzinc in tetrahydrofuran to give [(Tpms^{tBu})ZnEt] (**4**). The instability of ethylthallium leads to the precipitation of metallic thallium, which can be separated easily by centrifugation. The reaction of **4** with acetic acid yields acetato complexes. Varying the stoichiometric ratio results in two different products. With 1 equiv. of acetic acid, the expected acetato complex [(Tpms^{tBu})-ZnOAc] (**5a**) is formed. The reaction of **4** with 0.5 equiv. of acid, surprisingly, generates a dinuclear Tpms^{tBu} complex with a bridging acetato and a bridging hydroxo ligand (**5b**) (Scheme 2). The origin of the hydroxo ligand is unclear, it is probably due to traces of water in the solvent.

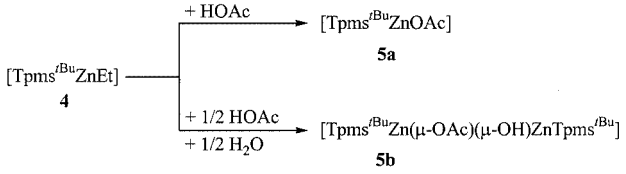

Scheme 2. Synthesis of the acetato complexes **5a** and **5b**

The complexes **5a** and **5b** can easily be distinguished spectroscopically. On the one hand, the intensity ratios of the pyrazolyl signals to the methyl signal of the acetato group in the ^{1}H NMR spectra are different. On the other hand, the OH valence stretching vibration of **5b** is clearly identified as a sharp band at 3620 cm^{-1} in the IR spectrum. It is a very sensitive probe for the non-associated OH group.

Table 6 displays the carboxylate stretching vibrations $\nu_{as}(CO_2)$ and $\nu_s(CO_2)$ of **5a** and **5b**. The position of $\nu_{as}(CO_2)$ and the difference $\Delta\nu(CO_2) = \nu_{as}(CO_2) - \nu_s(CO_2)$ are useful probes for determining the coordination mode of the acetato ligand.[16] The position of $\nu_{as}(CO_2)$ and the large value of $\Delta\nu(CO_2)$ in the case of **5a** indicates a monodentate coordination. This η^1-coordination was proven for [Tp^{tBu}ZnOAc] by Parkin through a crystal structure analysis[17] and is well known for other Tp^{R}Zn−carboxylato complexes.[9] The band for the asymmetric valence stretching $\nu_{as}(CO_2)$ of **5b** is shifted to smaller wavenumbers and the decrease of $\Delta\nu(CO_2)$ is typical for a bridging acetato ligand.[16]

Table 6. Carboxylate stretching vibrations (cm^{-1}) for **5a** and **5b** in the solid state

Compound	$\nu_{as}(CO_2)$	$\nu_s(CO_2)$	$\Delta\nu(CO_2)$
5a	1592	1331	261
5b	1573	1437	136

The crystal structure analysis of **5b** confirmed the spectroscopic results suggesting the bridging nature of the acetato and hydroxo ligands. Complex **5b** crystallises from diethyl ether in the monoclinic space group *I*2a, and the asymmetric unit of the crystal structure contains one molecule of diethyl ether. Figure 7 shows an ORTEP plot of **5b**. Selected bond lengths and angles are summarised in Table 7.

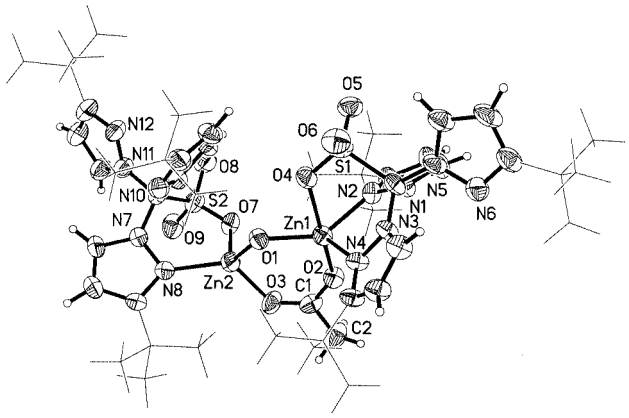

Figure 7. ORTEP plot of [(Tpms^{tBu})Zn(μ-OAc)(μ-OH)Zn-(Tpms^{tBu})] (**5b**)

Table 7. Selected bond lengths [Å] and angles [°] in [(Tpms^{tBu})Zn(μ-OAc)(μ-OH)Zn(Tpms^{tBu})] (**5b**)

Zn1−O1	1.938(3)	O1−Zn1−O2	95.74(12)
Zn1−O2	2.029(3)	O1−Zn1−N2	138.49(14)
Zn1−N2	2.064(4)	O2−Zn1−N2	94.64(14)
Zn1−N4	2.116(4)	O1−Zn1−N4	119.83(14)
Zn1−O4	2.273(3)	O2−Zn1−N4	107.16(13)
Zn2−O1	1.930(3)	N2−Zn1−N4	94.90(16)
Zn2−O3	1.939(3)	O1−Zn1−O4	82.19(11)
Zn2−O7	2.002(3)	O2−Zn1−O4	170.55(12)
Zn2−N8	2.053(4)	N2−Zn1−O4	81.13(13)
S1−O5	1.428(3)	N4−Zn1−O4	81.72(13)
S1−O6	1.442(3)	O1−Zn2−O3	101.98(13)
S1−O4	1.458(3)	O1−Zn2−O7	115.72(13)
S1−C3	1.888(5)	O3−Zn2−O7	98.45(14)
S2−O8	1.428(4)	O1−Zn2−N8	118.04(13)
S2−O9	1.437(3)	O3−Zn2−N8	126.15(16)
S2−O7	1.482(3)	O7−Zn2−N8	95.11(15)
S2−C25	1.861(5)	Zn2−O1−Zn1	123.12(14)
O2−C1	1.293(5)	O3−C1−O2	125.4(5)

It was surprising to us that the two zinc atoms have different coordination numbers in the solid state: four and five. One Tpms^{tBu} ligand coordinates in the known N,N,O mode, whereas the other acts as a bidentate N,O ligand. These different coordination modes are due to the asymmetrical bridge between the zinc atoms. Because of the short hydroxo bridge, the structure of **5b** is folded and the sterically demanding *tert*-butyl groups prevent the coordination of the second pyrazolyl ring.

NMR spectroscopic studies on **5b** ($CDCl_3$ and CD_2Cl_2) at room temperature show that all the pyrazole rings are equivalent in solution; i.e., the pyrazole rings undergo dynamic exchange. This exchange is fast on the NMR spectroscopic time scale, even at 203 K (CD_2Cl_2).

The dinuclear complex **5b** is an excellent structural model of dinuclear centres of the zinc enzymes phospholipase C and phosphotriesterase. Both of these enzymes contain a

 © 2003 Wiley-VCH Verlag GmbH & Co. KGaA, Weinheim

dinuclear zinc centre with N,N,O binding motifs with the zinc ions connected by a bridging hydroxo and a bridging carboxylato ligand (phosphotriesterase: carbamylated lysin).[18] The Zn−Zn distance in the enzymes is 3.3 Å, which is nearly the same as in our model complex **5b** [Zn−Zn: 3.4008(8) Å].

5. Studies on Carbonylcopper(I) Complexes

To compare the donor abilities of Tpms^{tBu} with that of other tripodal ligands, we synthesised carbonylcopper(I) complexes. The CO stretching frequency strongly correlates with the electronic properties of the metal centre.

[(Tpms^{tBu})Cu(CO)] (**6a**) was obtained by the reaction of Tl(Tpms^{tBu}) and copper(I) chloride in dichloromethane under a carbon monoxide pressure of 3−4 bar. In addition, we synthesised [(Tpms)Cu(CO)] (**6b**) by the reaction of KTpms with a carbon monoxide saturated solution of [Cu(MeCN)$_4$]PF$_6$ in methanol. The IR spectra in dichloromethane (Figure 8) show that in solution both carbonyl complexes exist in two isomeric forms, like the zinc complexes **1a** and **1b** (Scheme 3)

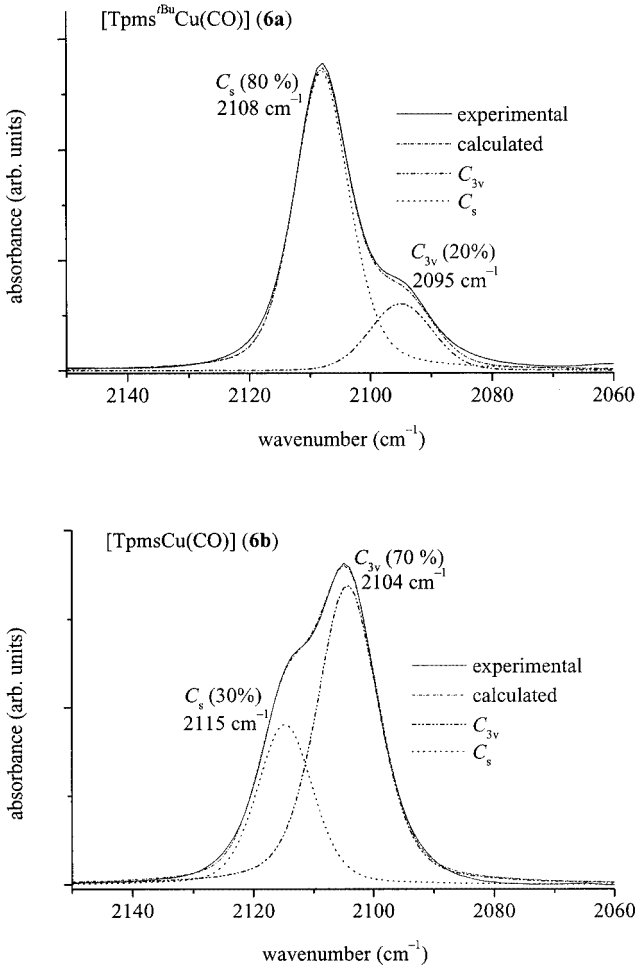

Figure 8. Analysis of the IR spectra (CO stretching bands) of the carbonyl complexes **6a** and **6b** in dichloromethane solution

From variable-temperature NMR spectroscopic studies we know that in the case of [(Tpms^{tBu})Cu(CO)] (**6a**) the C_s-symmetrical species is the preferred isomer, and, therefore, the more intense CO band (2108 cm^{-1}) is assigned to this isomer. [(Tpms)Cu(CO)] (**6b**) favours the N,N,N coordination mode in solution, and, therefore, the more intense CO band (2104 cm^{-1}) is assigned to the C_{3v}-symmetrical complex. The different behaviour of the Tpms^{tBu} ligand, compared to the Tpms one, may be a consequence of the repulsion between the *tert*-butyl groups and the carbonyl ligand.

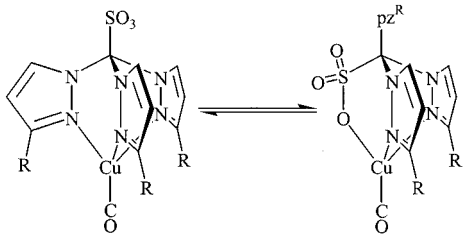

Scheme 3. Equilibrium between the N,N,N mode (C_{3v}) and the N,N,O mode (C_s) (R = H, *t*Bu)

Table 8 displays a comparison of CO stretching vibrations of tripodal nitrogen ligand complexes of the type [(ligand)Cu(CO)].

Table 8. CO stretching vibrations (cm^{-1}) of carbonylcopper(I) complexes of the type [(ligand)Cu(CO)] in the solid state

Ligand	ν(CO)	Ligand	ν(CO)	Ligand	ν(CO)
Tpms	2101	Tp	2083[a] [23]	HC(pz^{Me,Me})$_3$	2113[24]
Tpms^{tBu}	2093/2088	Tp^{tBu}	2069[25]	HC(pz^{tBu})$_3$	2100[24]
		Tp^{Me,Me}	2060[26]		
		Tp^{iPr,iPr}	2056[27]		

[a] In light petroleum ether.

In the Tp complexes, the CO stretching vibrations are shifted towards lower energies compared to those of **6a** and **6b**. Thus, the Tpms ligands are weaker donors than the Tp ligands. The anionic Tpms ligands are stronger donors compared to the neutral tris(pyrazolyl)methane ligands.

From the IR spectra measured in the temperature range from −10 to +83 °C, we have determined the equilibrium constants for the two isomeric forms of [(Tpms^{tBu})Cu(CO)] (**6a**) in toluene. With a van't Hoff plot we calculated the enthalpy and entropy of the transformation of the C_{3v}-symmetrical species into the C_s-symmetrical one. The resulting values are $\Delta H = +6$ kJ·mol^{-1} and $\Delta S = +35$ J·K^{-1}·mol^{-1}. Variable-temperature ^{1}H NMR measurements in CD_2Cl_2 (−70 to +5 °C) yield the same values. They are very similar to the thermodynamic parameters of [(Tpms^{tBu})ZnCl] (**1a**) (see above).

Conclusion

The thallium salt of the sterically demanding ligand Tpms^{tBu} is a convenient starting material for halide com-

 © 2003 Wiley-VCH Verlag GmbH & Co. KGaA, Weinheim

plexes of zinc(II), nickel(II) and cobalt(II) ions, as well as for alkylzinc and carbonylcopper(I) complexes. Tpms^{tBu} can act as a tripodal N,N,N ligand, as a tripodal N,N,O ligand and as a bipodal N,O ligand. In Rh^{I} complexes, we have observed Tpms to exhibit bipodal N,N coordination.[7] From the CO stretching vibrations of **6a** and **6b** we conclude that the tripodal Tpms ligands are weaker donors than are tris(-pyrazolyl)borate ligands. The equilibrium between C_{3v}- and C_s-symmetrical complexes in solution (**1a**, **1b**, **6a**, **6b**) indicates that, in the solvents that we have used here, there is no significant difference in the stabilities of the N,N,N and the N,N,O coordination modes. The equilibration between the two isomeric forms is slow on the NMR spectroscopic time scale. The formation of **3** shows that hydrolysis of the Tpms^{tBu} ligand occurs in the presence of certain metal ions; we have not yet observed this behaviour with the unsubstituted Tpms ligand. The coordination number of the Tpms complexes is not restricted to four. In the sterically less demanding N,N,O coordination mode the ligand allows also a coordination number of five (**3**, **5b**). All in all, this feature demonstrates that Tpms^{tBu} is a structurally flexible ligand that can adapt to the preferences of the metal centre. The complexes described here are soluble in polar solvents, like wet methanol. This solubility should allow reactivity studies of metalloenzyme model compounds with Tpms ligands to be carried out under more realistic conditions than with model compounds containing the highly hydrophobic Tp ligands.

Experimental Section

General Remarks: The compound KTpms was synthesised according to a published procedure.[1] All other reagents were commercial samples and were used as received. All reactions were carried out under nitrogen using standard Schlenk techniques, unless stated otherwise. Solvents were purified and degassed by standard procedures. Filtration was carried out using 1-μm membrane filters (regenerated cellulose, Schleicher & Schuell). Centrifugation was carried out using a Hettich Rotina 46 Schlenk tube centrifuge. ^1H and ^{13}C NMR spectra were recorded with Bruker DRX 200 (at 293 K) or Bruker DRX 500 (at 298 K) spectrometers. Chemical shifts (δ) are given in ppm referenced to the solvent peak.[19] Infrared spectra were recorded with a Bruker IFS 66 FT spectrometer. FAB mass spectra were recorded with a Finnigan MAT 8200 instrument (Ar, 8 kV, matrix: NBA unless stated otherwise). Elemental analyses were performed with a Perkin−Elmer CHN-2400/II elemental analyser. The absorption spectra of **2a** and **3**, dissolved in dichloromethane, were recorded with a Analytik Jena Specord S 100 spectrometer. Microcrystalline powders of both compounds were embedded in polyethylene pellets and their transmission was measured with a Cary 4 spectrometer. Temperatures down to 10 K were achieved by using a commercial flow-cryostat technique.

Tl(Tpms^{tBu}): Under cooling to −65 °C, a solution of *n*-butyllithium (1.6 M, 42 mL) was added to a solution of tris(3-*tert*-butylpyrazolyl)methane[20] (21 g, 54 mmol) in diethyl ether (60 mL). The solution immediately turned red and later became brown. After 40 min, sulfur trioxide−trimethylamine complex (8.4 g, 60 mmol) was added at −35 °C. Under constant stirring, the resulting suspension was warmed to room temperature overnight. The solvent was then evaporated. To remove excess tris(3-*tert*-butylpyrazolyl)methane, the residue was treated with dichloromethane, stirred for 1 h, filtered and washed with pentane, to yield an off-white powder (15 g). Recrystallisation from boiling toluene (400 mL) yielded colourless crystals of Li(Tpms^{tBu}) (8.9 g, 19 mmol, 36%). The thallium salt was obtained by adding a solution of $TlNO_3$ (10 g, 37 mmol) in a methanol/water mixture (3:7, 100 mL) to a solution of Li(Tpms^{tBu}) (8.9 g, 19 mmol) in a methanol/water mixture (7:3, 100 mL) in a beaker. Tl(Tpms^{tBu}) precipitated as a white solid. The precipitate was washed with water and dried under reduced pressure at room temperature. Yield: 8.6 g, 68%. ^1H NMR (200 MHz, $CDCl_3$): δ = 1.31 (s, 27 H, CH_3), 6.27 (d, $^3J_{H,H}$ = 2.7 Hz, 3 H, pyrazolyl 4-*H*), 7.43 (d, $^3J_{H,H}$ = 2.7 Hz, 3 H, pyrazolyl 5-*H*) ppm. $^{13}C\{^1H\}$ NMR (500 MHz, $CDCl_3$): δ = 31.4 [s, C(*C*H_3)$_3$], 33.1 [s, (CH$_3$)$_3$*C*], 97.1 (s, *C*SO_3), 105.2 (s, pyrazolyl *C*-4), 134.3 (s, pyrazolyl *C*-5), 165.2 (s, pyrazolyl *C*-3) ppm. IR (KBr): $\tilde{\nu}$ = 3155, 3124 [w, ν(C−H)], 2959 [vs, ν(C−H), CH_3], 1530 [m, ν(C=C)], 1481, 1463 [m, δ_{as}(*t*Bu)], 1397, 1363 [vs, δ_s(*t*Bu)], 1033 [(vs, ν_s(SO)], 636 [s, ν(C−S] cm^{-1}. MS (FAB$^+$): *m*/*z* = 871 [M + Tl]$^+$, 667 [M + H]$^+$, 381 [M − SO_3Tl]$^+$. $C_{22}H_{33}N_6O_3STl$ (665.99): calcd. C 39.7, H 5.0, N 12.6; found C 39.7, H 4.9, N 12.7.

[(Tpms^{tBu})MX] Complexes: The preparation of [(Tpms^{tBu})ZnCl] (**1a**) is described in detail as a representative example of this type of complex. Workup procedures and spectroscopic data for the analogous complexes are described below.

[(Tpms^{tBu})ZnCl] (1a): A stirred solution of Tl(Tpms^{tBu}) (0.92 g, 1.4 mmol) in methanol (20 mL) was treated with $ZnCl_2$ (0.19 g, 1.4 mmol) at room temperature. After 1 h of stirring, the precipitated TlCl was filtered and the solvent was evaporated under reduced pressure. The colourless residue was dissolved in a small amount of dichloromethane, filtered and the product was precipitated with pentane. The white powder was washed with pentane and dried at 40 °C for 24 h under reduced pressure (yield: 0.54 g, 70%). ***C*$_s$-Symmetrical Complex:** ^1H NMR (200 MHz, $CDCl_3$): δ = 1.46 (s, 9 H, CH_3), 1.51 (s, 18 H, CH_3), 6.36 (d, $^3J_{H,H}$ = 2.8 Hz, 2 H, pyrazolyl 4-*H*), 6.49 (d, $^3J_{H,H}$ = 2.5 Hz, 1 H, pyrazolyl 4-*H*), 6.85 (d, $^3J_{H,H}$ = 2.8 Hz, 2 H, pyrazolyl 5-*H*), 8.78 (d, $^3J_{H,H}$ = 2.5 Hz, 1 H, pyrazolyl 5-*H*) ppm. ***C*$_{3v}$-Symmetrical Complex:** ^1H NMR (200 MHz, $CDCl_3$): δ = 1.34 (s, 27 H, CH_3), 6.32 (d, $^3J_{H,H}$ = 3.0 Hz, 3 H, pyrazolyl 4-*H*), 9.07 (d, $^3J_{H,H}$ = 3.0 Hz, 3 H, pyrazolyl 5-*H*) ppm; ratio C_s:C_{3v} = 3.4:1. $^{13}C\{^1H\}$ NMR (500 MHz, CD_2Cl_2): δ = 30.0, 30.1, 30.3 [s, C(*C*H$_3$)$_3$], 32.6, 32.7, 32.9 [s, *C*(CH$_3$)$_3$], 94.5 (s, *C*SO_3), 104.3, 105.1, 106.3 (s, pyrazolyl *C*-4), 136.1, 136.5, 137.2 (s, pyrazolyl *C*-5), 167.3, 168.2 (s, pyrazolyl *C*-3) ppm. IR (KBr): $\tilde{\nu}$ = 3163 [w, ν(C−H)], 2969 [vs, ν(C−H)], CH_3], 1526 [m, ν(C=C)], 1401, 1368[vs, δ_s(*t*Bu)], 1036[vs, ν_s(SO)], 652[vs, ν(C−S)] cm^{-1}. MS (FAB$^+$): *m*/*z* = 561 [M + H]$^+$, 525 [M − Cl]$^+$, 463 [Tpms^{tBu} + 2H]$^+$, 381 [C(pz^{tBu})$_3$]$^+$, 259 [C(pz^{tBu})$_2$ + H]$^+$, 57 [*t*Bu]$^+$. $C_{22}H_{33}ClN_6O_3SZn$ (562.45): calcd. C 47.0, H 5.9, N 14.9, found C 47.4, H 6.2, N 14.3.

[(Tpms^{tBu})ZnBr] (1b): $ZnBr_2$ (0.16 g, 0.73 mmol), Tl(Tpms^{tBu}) (0.47 g, 0.71 mmol), yield: 0.28 g (65%) of a white powder. Crystals suitable for X-ray analysis were obtained by diffusion of pentane in a concentrated solution of **1b** in THF. ***C*$_s$-Symmetrical Complex:** ^1H NMR (200 MHz, $CDCl_3$): δ = 1.35 (s, 9 H, CH_3), 1.53 (s, 18 H, CH_3), 6.36 (d, $^3J_{H,H}$ = 3.0 Hz, 2 H, pyrazolyl 4-*H*), 6.50 (d, $^3J_{H,H}$ = 2.7 Hz, 1 H, pyrazolyl 4-*H*), 6.84 (d, $^3J_{H,H}$ = 3.0 Hz, 2 H, pyrazolyl 5-*H*), 8.79 (d, $^3J_{H,H}$ = 2.7 Hz, 1 H, pyrazolyl 5-*H*) ppm. ***C*$_{3v}$-Symmetrical Complex:** ^1H NMR (200 MHz, $CDCl_3$): δ = 1.48 (s, 27 H, CH_3), 6.33 (d, $^3J_{H,H}$ = 3.1 Hz, 3 H, pyrazolyl 4-*H*), 9.09 (d, $^3J_{H,H}$ = 3.1 Hz, 3 H, pyrazolyl 5-*H*) ppm; ratio C_s/C_{3v} = 10:1. $^{13}C\{^1H\}$ NMR (500 MHz, CD_2Cl_2): δ = 30.0, 30.5 [s, C(*C*H$_3$)$_3$],

 © 2003 Wiley-VCH Verlag GmbH & Co. KGaA, Weinheim

32.9 [s, $C(CH_3)_3$], 94.5 (s, CSO_3), 104.5, 105.2, 106.3 (s, pyrazolyl *C*-4), 136.2, 136.5, 137.2 (s, pyrazolyl *C*-5), 167.4, 168.2 (s, pyrazolyl *C*-3) ppm. IR (KBr): $\tilde{\nu}$ = 3163 [w, ν(C−H)], 2969 [vs, ν(C−H), CH_3], 1525 [m, ν(C=C)], 1401, 1369 [vs, δ_s(*t*Bu)], 1036 [vs, ν_s(SO)], 652 [vs, ν(C−S)] cm^{-1}. MS (FAB^+): *m*/*z* = 607 $[M + H]^+$, 525 $[M - Br]^+$, 463 $[(Tpms^{tBu}) + 2\ H]^+$, 381 $[C(pz^{tBu})_3]^+$, 259 $[C(pz^{tBu})_2 + H]^+$, 57 $[tBu]^+$. $C_{22}H_{33}BrN_6O_3SZn$ (606.90): calcd. C 43.5, H 5.5, N 13.8, found C 43.7, H 5.6, N 13.4.

[(Tpms^{tBu})ZnI] (1c): ZnI_2 (0.29 g, 0.91 mmol), Tl(Tpms^{tBu}) (0.61 g, 0.91 mmol), yield: 0.36 g (52%) of a white powder. ^1H NMR (200 MHz, $CDCl_3$): δ = 1.34 (s, 9 H, C*H*$_3$), 1.56 (s, 18 H, C*H*$_3$), 6.35 (d, $^3J_{H,H}$ = 2.7 Hz, 2 H, pyrazolyl 4-*H*), 6.49 (br. s, 1 H, pyrazolyl 4-*H*), 6.83 (d, $^3J_{H,H}$ = 2.7 Hz, 2 H, pyrazolyl 5-*H*), 8.80 (br. s, 1 H, pyrazolyl 5-*H*) ppm. $^{13}C\{^1H\}$ NMR (500 MHz, CD_2Cl_2): δ = 30.2, 31.0 [s, C(*C*H$_3$)$_3$], 32.9 [s, *C*(CH$_3$)$_3$], 94.5 (s, *C*SO$_3$), 105.3, 106.2 (s, pyrazolyl *C*-4), 136.2 (s, pyrazolyl -*C*5), 167.6, 168.3 (s, pyrazolyl *C*-3) ppm. IR (KBr): $\tilde{\nu}$ = 3163 [w, ν(C−H)], 2969 [vs, ν(C−H), CH_3], 1525 [m, ν(C=C)], 1400, 1369 [vs, δ_s(*t*Bu)], 1035 [vs, ν_s(SO)], 652 [vs, ν(C−S)] cm^{-1}. MS (FAB^+): *m*/*z* = 653 $[M + H]^+$, 525 $[M - I]^+$, 515 $[M - SO_3 - tBu]$, 381 $[C(pz^{tBu})_3]^+$, 259 $[C(pz^{tBu})_2 + H]^+$, 57 $[tBu]^+$. $C_{22}H_{33}IN_6O_3SZn\cdot 1/2CH_2Cl_2$ (696.37): calcd. C 38.8, H 4.9, N 12.1, found C 39.0, H 5.0, N 12.3.

[(Tpms^{tBu})NiCl] (2a): $NiCl_2\cdot 6H_2O$ (0.23 g, 0.97 mmol), Tl(Tpms^{tBu}) (0.64 g, 0.96 mmol). Diffusion of pentane into a concentrated solution of the crude product in THF yielded dark red crystals (0.13 g, 25%) suitable for X-ray analysis. IR (KBr): $\tilde{\nu}$ = 3169 [w, ν(C−H)], 2975 [vs, ν(C−H), CH_3], 1527 [m, ν(C=C)], 1397, 1364 [vs, δ_s(*t*Bu)], 1055 [vs, ν_s(SO)], 619 [s, ν(C−S)] cm^{-1}. MS (FAB^+): *m*/*z* = 643 $[M - Cl + Hpz^{tBu}]^+$, 519 $[M - Cl]^+$, 463 $[M - Cl - SO_3]^+$, 381 $[C(pz^{tBu})_3]^+$, 259 $[C(pz^{tBu})_2 + H]^+$. UV/Vis (CH_2Cl_2): λ_{max} (ε_{max}) = 475 nm (370 $M^{-1}\cdot cm^{-1}$). $C_{22}H_{33}ClN_6NiO_3S$ (555.75): calcd. C 47.6, H 6.0, N 15.1, found C 47.6, H 5.8, N 15.3.

[(Tpms^{tBu})NiBr] (2b): $NiBr_2\cdot 3H_2O$ (0.08 g, 0.29 mmol), Tl(Tpms^{tBu}) (0.19 g, 0.29 mmol). Diffusion of pentane into a concentrated THF solution of the crude product yielded red crystals (0.03 g, 17%). IR (KBr): $\tilde{\nu}$ = 3156 [(w, ν(C−H)], 2969 [vs, ν(C−H), CH_3], 1526 [m, ν(C=C)], 1400, 1368 [vs, δ_s(*t*Bu)], 1030 [vs, ν_s(SO)], 619 [s, ν(C−S)] cm^{-1}. MS (FAB^+): *m*/*z* = 643 $[M - Br + Hpz^{tBu}]^+$, 519 $[M - Br]^+$, 463 $[M - Br - SO_3]^+$, 381 $[C(pz^{tBu})_3]^+$, 259 $[C(pz^{tBu})_2 + H]^+$. UV/Vis (CH_2Cl_2): λ_{max} (ε_{max}) = 485 nm (450 $M^{-1}\cdot cm^{-1}$). $C_{22}H_{33}BrN_6NiO_3S\cdot 1/2C_4H_8O$ (636.26): calcd. C 45.3, H 5.9, N 13.2, found C 45.1, H 6.0, N 13.1.

[(Tpms^{tBu})CoCl(Hpz^{tBu})] (3): A stirred solution of $CoCl_2$ (0.16 g, 1.2 mmol) (dried at 150 °C under reduced pressure for 8 h) in methanol (5 mL) was treated with a solution of Tl(Tpms^{tBu}) (0.67 g, 1.0 mmol) in methanol (15 mL) at room temperature. The precipitated TlCl was separated after 15 min and the solvent was evaporated under reduced pressure. The blue residue was dissolved in dichloromethane (10 mL) and the solution was filtered. Evaporation of the solvent and then washing the residue with pentane yielded a blue powder (0.45 g, 0.66 mmol, 55%). Analytically pure crystals suitable for X-ray analysis were obtained by diffusion of pentane into a concentrated solution of **3** in THF. Yield: 0.18 g (24%). UV/Vis (CH_2Cl_2): λ_{max} (ε_{max}) = 520 nm (167 $M^{-1}\cdot cm^{-1}$), 558 (214), 603 (402), 674 (48). IR (KBr): $\tilde{\nu}$ = 3380 [s, ν(N−H)], 3159 [w, ν(C−H)], 2965 [vs, ν(C−H), CH_3], 1530 [s, ν(C=C)], 1397, 1365 [s, δ_s(*t*Bu)], 1042 [s, ν_s(SO)], 644 [s, ν(C−S)] cm^{-1}. MS (FAB^+): *m*/*z* = 644 $[M - Cl]^+$, 520 $[M - Cl - Hpz^{tBu}]^+$, 440 $[M - Cl - Hpz^{tBu} - SO_3]^+$, 381 $[C(pz^{tBu})_3]^+$, 259 $[C(pz^{tBu})_2 + H]^+$. $C_{29}H_{45}ClCoN_8O_3S\cdot C_4H_8O$ (752.29): calcd. C 52.7, H 7.1, N 14.9, found C 51.7, H 7.0, N 14.6.

[(Tpms^{tBu})ZnEt] (4): A solution of Tl(Tpms^{tBu}) (1.7 g, 2.5 mmol) in THF (30 mL) was added dropwise at room temperature to a solution of $ZnEt_2$ (1 M solution in hexane, 3.0 mL, 3.0 mmol) in THF (20 mL). The precipitated thallium metal was separated by centrifugation. The colourless supernatant solution was concentrated until the onset of crystallisation and then left to stand at −30 °C. After 2 d, colourless crystals (1.0 g, 64%) were collected by filtration. ^1H NMR (200 MHz, C_6D_6): δ = 1.00 (q, $^3J_{H,H}$ = 8.0 Hz, 2 H, C*H*$_2$), 1.15 [s, 27 H, C(C*H*$_3$)$_3$], 1.72 (t, $^3J_{H,H}$ = 8.0 Hz, 3 H, C*H*$_3$), 5.73 (br. s, 2 H, pyrazolyl 4-*H*), 5.94 (br. s, 1 H, pyrazolyl 4-*H*), 6.74 (br. s, 2 H, pyrazolyl 5-*H*), 9.24 (br. s, 1 H, pyrazolyl 5-*H*) ppm. $^{13}C\{^1H\}$ NMR (500 MHz, C_6D_6): δ = 5.6 (s, *C*H$_2$CH$_3$), 12.7 (s, CH$_2$*C*H$_3$), 30.8, 31.0 [s, C(*C*H$_3$)$_3$], 32.9, 33.3 [s, *C*(CH$_3$)$_3$], 95.4 (s, *C*SO$_3$), 104.7, 106.0 (s, pyrazolyl *C*-4), 135.8, 137.9 (s, pyrazolyl *C*-5), 166.9 (s, pyrazolyl *C*-3) ppm. IR (KBr): $\tilde{\nu}$ = 3163 [w, ν(C−H)], 2964 [vs, ν(C−H), CH_3], 1524 [s, ν(C=C)], 1399, 1367 [vs, δ_s(*t*Bu)], 1043 [vs, ν_s(SO)], 649 [vs, ν(C−S)] cm^{-1}. MS (FAB^+; matrix: NPOE): *m*/*z* = 649 $[M - Et + Hpz^{tBu}]^+$, 555 $[M + H]^+$, 525 $[M - Et]^+$, 445 $[M - SO_3 - tBu]$, 381 $[C(pz^{tBu})_3]^+$, 57 $[tBu]^+$. $C_{24}H_{38}N_6O_3SZn\cdot C_4H_8O$ (628.17): calcd. C 53.5, H 7.4, N 13.4, found C 53.1, H 7.5, N 13.5.

[(Tpms^{tBu})ZnOAc] (5a): A solution of **4** (0.61 g, 0.97 mmol) in THF (10 mL) was treated with acetic acid (55 μL, 0.97 mmol). After 10 min of stirring at room temperature, the solution was concentrated under reduced pressure and the product was precipitated with hexane. Yield: 0.11 g (20%) of a white powder. ^1H NMR (200 MHz, C_6D_6): δ = 1.24 [s, 27 H, C(C*H*$_3$)$_3$], 1.96 (s, 3 H, acetate C*H*$_3$), 5.89 (d, $^3J_{H,H}$ = 2.8 Hz, 3 H, pyrazolyl 4-*H*) 7.66 (br. s, 3 H, pyrazolyl 5-*H*) ppm. $^{13}C\{^1H\}$ NMR (500 MHz, C_6D_6): δ = 23.7 (s, *C*H$_3$CO$_2$), 30.8 [s, C(*C*H$_3$)$_3$], 33.2 [s, *C*(CH$_3$)$_3$], 96.6 (s, *C*SO$_3$), 105.8 (s, pyrazolyl *C*-4), 136.3 (s, pyrazolyl *C*-5), 166.7 (s, pyrazolyl *C*-3), 182.3 (s, CH$_3$*C*O$_2$) ppm. IR (KBr): $\tilde{\nu}$ = 3126 [w, ν(C−H)], 2966 [vs, ν(C−H), CH_3], 1592 [vs, $\nu_{as}(CO_2)$], 1532 [s, ν(C=C)], 1403, 1366 [s, δ_s(*t*Bu)], 1331 [s, $\nu_{as}(CO_2)$], 1036 [vs, ν_s(SO)], 647 [vs, ν(C−S)] cm^{-1}. MS (FAB^+): *m*/*z* = 381 $[C(pz^{tBu})_3]^+$, 259 $[C(pz^{tBu})_2 + H]^+$, 57 $[tBu]^+$. $C_{24}H_{36}N_6O_5SZn$ (586.04): calcd. C 49.2, H 6.2, N 14.3, found C 49.1, H 6.3, N 14.1.

[(Tpms^{tBu})Zn(μ-OAc)(μ-OH)Zn(Tpms^{tBu})] (5b): A solution of **4** (0.32 g, 0.51 mmol) in benzene (5 mL) was treated with acetic acid (19 μL, 0.34 mmol). After 10 min of stirring at room temperature, the solvent was evaporated under reduced pressure. The residue was treated with a small amount of diethyl ether and filtered, and then the colourless solution was stored at −30 °C overnight. Analytically pure crystals suitable for X-ray analysis were collected by filtration. Yield: 0.05 g (16%). ^1H NMR (200 MHz, $CDCl_3$): δ = 1.33 [s, 54 H, C(C*H*$_3$)$_3$], 2.02 (s, 3 H, acetate C*H*$_3$), 6.34 (d, $^3J_{H,H}$ = 2.9 Hz, 6 H, pyrazolyl 4-*H*), 7.45 (d, $^3J_{H,H}$ = 2.9 Hz, 6 H, pyrazolyl 5-*H*) ppm. $^{13}C\{^1H\}$ NMR (500 MHz, CD_2Cl_2): δ = 25.1 (s, *C*H$_3$CO$_2$), 30.3 [s, C(*C*H$_3$)$_3$], 32.6 [s, *C*(CH$_3$)$_3$], 95.3 (s, *C*SO$_3$), 105.5 (s, pyrazolyl *C*-4), 135.1 (s, pyrazolyl *C*-5), 166.6 (s, pyrazolyl *C*-3), 181.3 (s, CH$_3$*C*O$_2$) ppm. IR (KBr): $\tilde{\nu}$ = 3619 [m, sharp, ν(O−H)], 3155 [w, ν(C−H)], 2966 [vs, ν(C−H), CH_3], 1573 [vs, $\nu_{as}(CO_2)$], 1531 [s, ν(C=C)], 1437 [m, $\nu_{as}(CO_2)$], 1401, 1365 [s, δ_s(*t*Bu)], 1050 [s, ν_s(SO)], 646 [s, ν(C−S)] cm^{-1}. MS (FAB^+): *m*/*z* = 381 $[C(pz^{tBu})_3]^+$, 259 $[C(pz^{tBu})_2 + H]^+$. $C_{46}H_{70}N_{12}O_9S_2Zn_2\cdot C_4H_{10}O$ (1204.17): calcd. C 49.9, H 6.7, N 14.0, found C 49.9, H 6.7, N 13.9.

[(Tpms^{tBu})Cu(CO)] (6a): A solution of Tl(Tpms^{tBu}) (0.35 g, 0.52 mmol) in dichloromethane (5 mL) was saturated with carbon monoxide in a Schlenk tube equipped with a Teflon seal and valve. After 10 min, CuCl (0.10 g, 1.0 mmol) was added, the suspension was pressurized with 3−4 bar of carbon monoxide and stirred for 48 h at room temperature. Thereafter, the precipitated TlCl and

 © 2003 Wiley-VCH Verlag GmbH & Co. KGaA, Weinheim

remaining CuCl was filtered off and the product was precipitated with hexane under carbon monoxide. The colourless product was isolated by filtration and washed with pentane. Yield: 0.14 g (50%). ^{1}H NMR (200 MHz, $CDCl_3$): δ = 1.33 (s, 9 H, C*H*$_3$), 1.49 (s, 18 H, C*H*$_3$), 6.25 (br. s, 2 H, pyrazolyl 4-*H*), 6.39 (br. s, 1 H, pyrazolyl 4-*H*), 6.74 (br. s, 2 H, pyrazolyl 5-*H*), 8.87 (br. s, 1 H, pyrazolyl 5-*H*) ppm. IR (KBr): $\tilde{\nu}$ = 3177, 3136 [w, ν(C−H)], 2972 [vs, ν(C−H), CH_3], 2093/2088 [vs, ν(CO)], 1528 [s, ν(C=C)], 1483, 1458 [m, δ_{as}(*t*Bu)], 1390, 1365 [s, δ_s(*t*Bu)], 1053 [vs, ν_s(SO)], 621 [vs, ν(C−S)] cm^{-1}. MS (FAB$^+$): *m*/*z* = 525 [M − CO + H]$^+$, 445 [M − SO_3 − CO + H]$^+$, 387 [M − SO_3 − CO − *t*Bu]$^+$, 381 [C(pz$^{t\mathrm{Bu}}$)$_3$]$^+$, 321 [M − SO_3 − CO − pz$^{t\mathrm{Bu}}$]$^+$, 57 [*t*Bu]$^+$. $C_{23}H_{33}CuN_6O_4S$ (553.17): calcd. C 49.9, H 6.0, N 15.2, found C 49.8, H 5.8, N 15.4.

[(Tpms)Cu(CO)] (6b): [Cu(MeCN)$_4$]PF_6 (259 mg, 0.7 mmol) was dissolved in methanol (10 mL). The colourless solution was saturated with carbon monoxide, stirred at room temperature for 20 min and then KTpms (229 mg, 0.7 mmol) was added. A white precipitate had formed within seconds. The mixture was stirred under CO for 1 h and then the precipitate was filtered off, washed with a small portion of methanol and dried for 4 h in a stream of dry N_2. Yield: 0.09 g (34%). ^{1}H NMR (200 MHz, CD_2Cl_2): δ = 6.41 (dd, $^3J_{H,H}$ = 1.7, 2.8 Hz, 3 H, pyrazolyl 4-*H*), 7.81 (d, $^3J_{H,H}$ = 1.7 Hz, 3 H, pyrazolyl 3-*H*), 8.45 (br. s, 3 H, pyrazolyl 5-*H*) ppm. ***C*$_s$-Symmetrical Complex:** ^{1}H NMR ($CDCl_3$, 200 MHz, 213 K) δ = 6.50 (dd, $^3J_{H,H}$ = 2.0, 2.6 Hz, 2 H, pyrazolyl 4-*H*), 6.64 (dd, $^3J_{H,H}$ = 1.9, 2.1 Hz, 1 H, pyrazolyl 4-*H*), 6.88 (d, $^3J_{H,H}$ = 2.6 Hz, 2 H, pyrazolyl 5-*H*), 7.91 (s, 2 H, pyrazolyl 3-*H*), 7.99 (s, 1 H, pyrazolyl 3-*H*), 8.9 (overlapped, 3 H, pyrazolyl 5-*H*) ppm. ***C*$_{3v}$-Symmetrical Complex:** ^{1}H NMR (200 MHz, $CDCl_3$): δ = 6.39 (dd, $^3J_{H,H}$ = 1.7, 2.8 Hz, 3 H, pyrazolyl 4-*H*), 7.75 (d, $^3J_{H,H}$ = 1.7 Hz, 3 H, pyrazolyl 3-*H*), 8.90 (d, $^3J_{H,H}$ = 2.8 Hz, 3 H, pyrazolyl 5-*H*) ppm; ratio C_s/C_{3v} = 1:3. IR (KBr): $\tilde{\nu}$ = 3180, 3127 [s, ν(C−H)], 2101 [vs, ν(CO)], 1524 [s, ν(C=C)], 1052 [vs, ν_s(SO)], 621 [vs, ν(C−S)] cm^{-1}. $C_{11}H_9CuN_6O_4S$ (384.84): calcd. C 34.3, H 2.4, N 21.8, found C 34.2, H 2.4, N 22.0.

X-ray Crystallographic Study: Crystals of compounds **1b**, **2a**, **3** and **5b** suitable for X-ray study were investigated with area-detector diffractometers using graphite-monochromated Mo-K_α radiation (λ = 0.71073 Å). Unit cell parameters were determined by least-squares refinements on the positions of 18000, 1953, 7998 and 2000 reflections in the range 2° < θ < 30.5°, 3° < θ < 27.5°, 2° < θ < 25° and 2° < θ < 25°, respectively. Space groups of type no. 14 were uniquely determined in the cases of **1b**, **2a** and **3**. In the case of **5b**, systematic extinctions were consistent with space groups *Ia* and *I*2/*a*, but the latter proved to be the correct one in the course of structure refinement. Lp corrections were applied to all the intensity data. In the case of **1b**, empirical absorption corrections have been performed ($T_{min.}$ = 0.175; $T_{max.}$ = 0.250), and in the case of **2a**, an empirical extinction parameter was refined. The structures were solved by direct methods[21] and the positions of all hydrogen atoms were found in the case of **1b**, **2a** and **5b**. In the case of **3**, the hydrogen atom positions of the tetrahydrofuran molecule were calcu-

Table 9. Crystallographic data for compounds **1b**, **2a**, **3** and **5b**

	1b	**2a**	**3**	**5b**
Empirical formula	$C_{48}H_{74}Br_2N_{12}O_7S_2Zn_2$	$C_{22}H_{33}ClN_6NiO_3S$	$C_{33}H_{25}ClCoN_8O_4S$	$C_{50}H_{79}N_{12}O_{10}S_2Zn_2$
Molecular mass	1285.87	555.76	751.27	1203.11
Crystal system	monoclinic	monoclinic	monoclinic	monoclinic
Space group	$P2_1/c$	$P2_1/n$	$P2_1/n$	$I2/a$
a [Å]	20.2171(3)	9.775(2)	12.010(2)	30.245(2)
b [Å]	15.6790(2)	17.935(4)	19.330(4)	11.0222(5)
c [Å]	21.0561(3)	15.186(3)	16.920(3)	38.801(3)
β [°]	115.8650(10)	95.67(3)	90.50(3)	98.508(10)
V [Å^3]	6005.83(15)	2649.3(9)	3927.9(13)	12792.6(14)
Z	4	4	4	8
F(000)	2656	1168	1592	5080
$D_{calcd.}$ [Mg·m^{-3}]	1.422	1.393	1.270	1.249
μ(Mo-K_α) [mm^{-1}]	2.254	0.946	0.603	0.874
Crystal size [mm]	0.45 × 0.40 × 0.25	0.51 × 0.34 × 0.33	0.30 × 0.25 × 0.20	0.72 × 0.33 × 0.28
Diffractometer	Bruker SMART CCD	Stoe IPDS	Stoe IPDS	Stoe IPDS
Monochromator	graphite	graphite	graphite	graphite
T [K]	173(2)	293(2)	293(2)	293(2)
Data-collecting mode	Ω scans	Φ scans	Φ scans	Φ scans
θ range [°]	1.12−30.46	2.27−27.50	2.00−25.01	1.85−25.00
hkl ranges	−28 ≤ *h* ≤ 16	−12 ≤ *h* ≤ 12	−14 ≤ *h* ≤ 14	−35 ≤ *h* ≤ 35
	−21 ≤ *k* ≤ 20	−23 ≤ *k* ≤ 23	−22 ≤ *k* ≤ 22	−13 ≤ k ≤ 13
	−28 ≤ *l* ≤ 28	−19 ≤ *l* ≤ 19	−20 ≤ *l* ≤ 20	−46 ≤ l ≤ 46
No. of reflns. measd.	46966	33151	43565	81477
No. of unique reflns.	16305	6031	6925	11243
No. of reflns. obsd. [$I > 2\sigma(I)$]	10093	5275	4754	3772
No. of param./restraints	925/0	317/0	481/0	706/0
Refinement method	Full-matrix least squares on F^2	Full-matrix least squares on F^2	Full-matrix least squares on F^2	Full-matrix least squares on F^2
Final *R* indices [$I > 2\sigma(I)$], wR_2 [a]	0.0445, 0.0787	0.0336, 0.0938	0.0524, 0.1091	0.0477, 0.0687
R indices (all data), wR_2 [a]	0.0978, 0.0957	0.0375, 0.0955	0.0716, 0.1121	0.1476, 0.0746
Max./min. Δρ [e·Å^{-3}]	0.519/−0.492	0.391/−0.349	0.476/−0.213	0.326/−0.246
Goodness-of-fit on F^2	1.007	1.024	1.165	0.735

[a] As defined in SHELXL 97-2.

 © 2003 Wiley-VCH Verlag GmbH & Co. KGaA, Weinheim

lated. Refinements by full-matrix least-squares calculations[22] on F^2 converged to the indicators given in Table 9. Anisotropic displacement parameters were refined for all atoms heavier than hydrogen. All atomic coordinates and isotropic displacement parameters were refined for the hydrogen atoms of **1b**. Idealised bonds lengths and angles for CH_3, CH_2 and CH groups were used for the other compounds; the riding model was applied for their hydrogen atoms. In addition, the hydrogen atoms of the CH_3 groups were allowed to rotate around the neighbouring C−C bonds. The isotropic displacement parameters of the H atoms were kept equal to 150, 120 and 120% of the equivalent isotropic displacement parameters of the parent primary, secondary and "aromatic" carbon atoms, respectively. Scattering factors, dispersion corrections and absorption coefficients were taken from International Tables for Crystallography (**1992**, Vol. C, Tables 6.1.1.4, 4.2.6.8 and 4.2.4.2). CCDC-197748 to -197751 contain the supplementary crystallographic data for this paper. These data can be obtained free of charge at www.ccdc.cam.ac.uk/conts/retrieving.html [or from the Cambridge Crystallographic Data Centre, 12 Union Road, Cambridge CB2 1EZ, UK; Fax: (internat.) + 44-1223/336-033; E-mail: deposit@ccdc.cam.ac.uk].

Acknowledgments

We thank the Fonds der Chemischen Industrie for the continual support of our work.

[1] W. Kläui, M. Berghahn, G. Rheinwald, H. Lang, *Angew. Chem.* **2000**, *112*, 2590−2592; *Angew. Chem. Int. Ed.* **2000**, *39*, 2464−2466.
[2] The nomenclature used for Tp is based on the one described: S. Trofimenko, *Chem. Rev.* **1993**, 943−980.
[3] S. Trofimenko, J. C. Calabrese, J. S. Thompson, *Inorg. Chem.* **1987**, 1507−1514.
[4] S. Trofimenko, J. C. Calabrese, P. J. Domaille, J. S. Thompson, *Inorg. Chem.* **1989**, 1091−1101.
[5] B. J. Hathaway in *Comprehensive Coordination Chemistry* (Eds.: G. Wilkinson, R. D. Gillard, J. A. McCleverty), Pergamon Press, Oxford, **1987**, vol. 2 ("Ligands").
[6] A. Beck, B. Weibert, N. Burzlaff, *Eur. J. Inorg. Chem.* **2001**, 521−527.
[7] W. Kläui, D. Schramm, W. Peters, G. Rheinwald, H. Lang, *Eur. J. Inorg. Chem.* **2001**, 1415−1424.
[8] R. Han, A. Looney, K. McNeill, G. Parkin, A. L. Rheingold, B. S. Haggerty, *J. Inorg. Biochem.* **1993**, *49*, 105−121.
[9] A. Kremer-Aach, W. Kläui, R. Bell, A. Strerath, H. Wunderlich, D. Mootz, *Inorg. Chem.* **1997**, 1552−1563.
[10] Cambridge Structural Database, Version 5.22, October **2001**.
[11] T. Schönherr, *Top. Curr. Chem.* **1997**, *191*, 87−152.
[12] A. B. P. Lever, *Inorganic Electronic Spectroscopy*, 2nd ed., Elsevier, Amsterdam, **1984**.
[13] T. R. Belderraín, M. Paneque, E. Carmona, E. Gutiérrez-Puebla, M. Angeles Monge, C. Ruiz-Valero, *Inorg. Chem.* **2002**, 425−428 and references therein.
[14] H. Adamsky, M. Atanasov, T. Schönherr, *Comprehensive Coordination Chemistry II* (Eds.: T. J. Meyer, J. A. McClaverty), Elsevier, vol. 1 ("Fundamentals"), in press.
[15] The spin-orbit coupling constant of the free Co^{II} is fairly large (515 cm^{-1}), although it is somewhat reduced in the complex: B. N. Figgis, M. A. Hitchman, *Ligand Field Theory and Its Applications (Special Topics in Inorganic Chemistry)*, John Wiley & Sons, New York, **2000**.
[16] K. Nakamoto, *Infrared and Raman Spectra of Inorganic and Coordination Compounds*, 4th ed., John Wiley & Sons, New York, **1986**.
[17] R. Han, I. B. Gorell, A. Looney, G. Parkin, *J. Chem. Soc., Chem. Commun.* **1991**, 717−719.
[18] [18a] E. Hough, L. K. Hansen, B. Birkness, K. Jynge, S. Hansen, A. Hordvik, C. Little, E. Dodson, Z. Derewenda, *Nature* **1989**, *338*, 357−360. [18b] J. L. Vanhooke, M. M. Benning, F. M. Raushel, H. M. Holden, *Biochemistry* **1996**, *35*, 6020−6025.
[19] H. Günther, *NMR Spectroscopy*, 2nd ed., John Wiley & Sons, New York, **1994**.
[20] D. L. Reger, J. E. Collins, D. L. Jameson, R. K. Castellano, *Inorg. Synth.* **1998**, *32*, 63−65.
[21] G. M. Sheldrick, *SHELXS-97, Program for the Solution of Crystal Structures*, University of Göttingen, Germany, **1990**.
[22] G. M. Sheldrick, *SHELXL-97, Program for the Refinement of Crystal Structures*, University of Göttingen, Germany, **1997**.
[23] M. I. Bruce, A. P. P. Ostazewski, *J. Chem. Soc., Chem. Commun.* **1972**, 1124−1125.
[24] D. L. Reger, J. E. Collins, A. L. Rheingold, L. M. Liable-Sands, *Organometallics* **1996**, *15*, 2029−2032.
[25] C. E. Ruggiero, S. M. Carrier, W. E. Antholine, J. W. Whittaker, C. J. Cramer, W. B. J. Tolman, *J. Am. Chem. Soc.* **1993**, *115*, 11285−11298.
[26] C. Mealli, C. S. Arcus, J. L. Wilkinson, T. J. Marks, J. A. Ibers, *J. Am. Chem. Soc.* **1976**, *98*, 711−718.
[27] N. Kitajima, K. Fujisawa, C. Fujimoto, Y. Moro-oka, S. Hashimoto, T. Kitagawa, K. Toriumi, K. Tatsumi, A. Nakamura, *J. Am. Chem. Soc.* **1992**, *114*, 1277−1291.

Received November 5, 2002

 © 2003 Wiley-VCH Verlag GmbH & Co. KGaA, Weinheim

Tungsten(VI) Complexes Derived from Calix[6]- and -[8]arenes: Oxo and Oxychloride Species

Carl Redshaw*[a] and Mark R. J. Elsegood[b]

Keywords: Tungsten / Calixarenes / Oxo ligands

Treatment of *p-tert*-butylcalix[6]areneH_6 (H_6L) or *p-tert*-butylcalix[8]areneH_8 (H_8L^1) with 2 equiv. of [$WOCl_4$] in refluxing toluene affords, after workup, the complexes [$(WOCl_2)_2LH_2$] (**1**) and [{$WO(NCMe)$}$_2L^1$] (**2**), respectively. The molecular structures of **1** and **2** have been determined and reveal conformationally constrained macrocyclic rings.
(© Wiley-VCH Verlag GmbH & Co. KGaA, 69451 Weinheim, Germany, 2003)

Introduction

The coordination chemistry of the calix[*n*]arene ring systems has attracted considerable attention during the last decade.[1] Attention has focused primarily on calix[4]arene transition metal species, however despite this activity, only a limited number of oxometal species have been reported.[2] Such oxo species have attracted attention due, in part, to their tendency to self-assemble into columnar structures.[3] In certain cases, this has resulted in liquid crystalline properties. For the group-VI metals, the contributions of the groups of Floriani and Young are particularly relevant. Crystallographic studies of species derived from the oxychloride precursors [$MOCl_4$] (M = Mo, W) reveal monomeric complexes with octahedrally coordinated metal centres.[2c,2g] By contrast, oxometal species for the larger ring systems ($n > 4$) are extremely rare and no structural data have been reported.[4] As part of an ongoing programme[5] investigating the coordination environments afforded by the medium-sized calix[*n*]arene rings (n = 6, 8), we here describe the synthesis and molecular structures of novel tungsten(VI) complexes (see **I** and **II** in Scheme 1) bearing either oxo or both oxo and chloro ligands via the interaction of the parent calix[6 and 8]arene$H_{6,8}$ with the metal oxytetrachloride complex [$WOCl_4$]. The molecular structures of the two new calixarene tungsten species have been determined and reveal conformationally constrained macrocyclic rings.

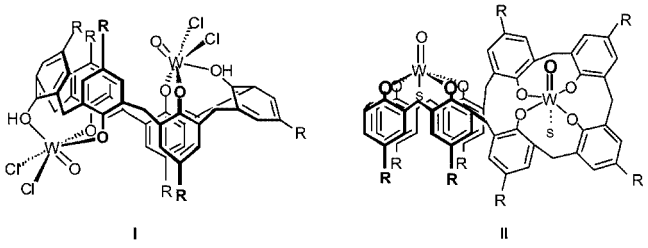

Scheme 1. R = *t*Bu; S = solvent (CH_3CN)

Results and Discussion

Reaction of H_6L with 2 equiv. of [$WOCl_4$] in refluxing toluene affords, after workup, large red-purple prisms of the complex [$(WOCl_2)_2LH_2$] (**1**) in ca. 60% yield. Stoichiometrically, **1** is formed by loss of 2 equiv. of HCl per tungsten centre. In the IR spectrum of this compound, a band is observed for ν(W=O) at 941 cm^{-1} {cf. 999 and 1006 cm^{-1} reported for the 1,3-dialkoxy-*p-tert*-butylcalix[4]-areneH_2 (R_2calH_2) complexes [$Et_2calWOCl_2$] and [$Me_2calWOCl_2$], respectively},[2g] whilst a broad feature at 3181 cm^{-1} is assigned to ν(OH). The ^1H NMR spectrum is consistent with the solid-state structure: two singlets in the *tert*-butyl region in a 2:1 ratio. The methylene protons appear as two doublets and a singlet (each integrating to 4 H), for which the latter is assigned to the CH_2 groups on the "fold" of the pinch (see Figure1, b). A broad singlet (integrating to 2 H) appears at δ_{OH} = 9.28 ppm.

Crystals of **1**·8MeCN suitable for an X-ray determination were grown from a hot, saturated solution of acetonitrile on slow cooling to ambient temperature. The asymmetric unit comprises one molecule of **1** and eight molecules of acetonitrile, one of which is disordered, with two others H-bonded to the calix[6]arene oxygen atoms O(2) and O(5). The molecular structure is shown in Figure 1 (a and b) to-

[a] Wolfson Materials and Catalysis Centre, School of Chemical Sciences and Pharmacy, University of East Anglia
Norwich, NR4 7TJ, U.K.
E-mail: carl.redshaw@uea.ac.uk
[b] Chemistry Department, Loughborough University, Loughborough, Leicestershire, LE11 3TU, U.K.

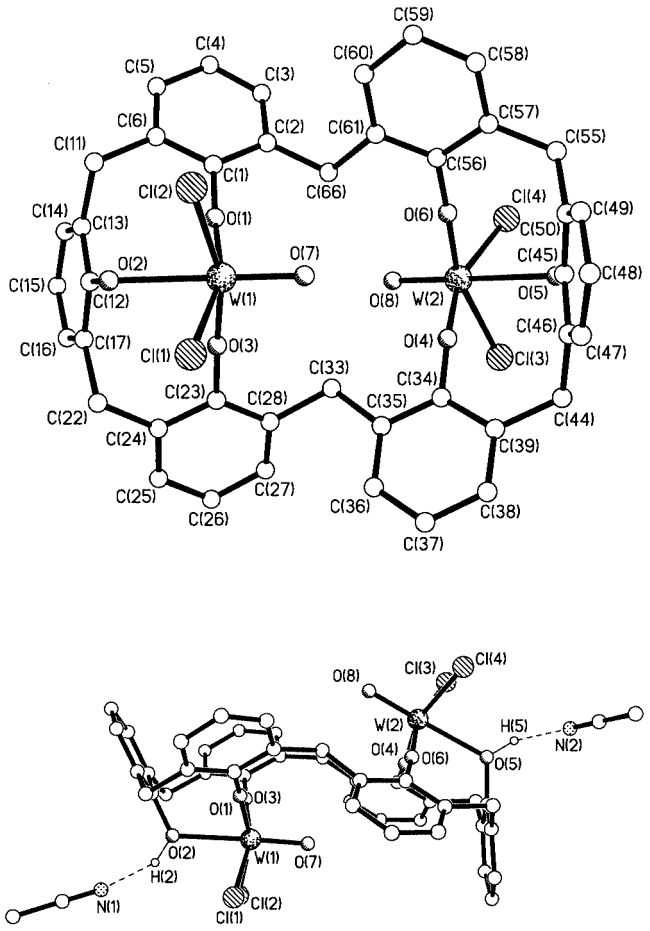

Figure 1. (a, top) Molecular structure of **1**; H atoms and calixarene *t*Bu groups omitted for clarity; (b, bottom) view of **1** emphasising pinched conformation; C*H* atoms and calixarene *t*Bu groups omitted for clarity; selected bond lengths [Å] and angles [°]: W(1)−Cl(1) 2.344(4), W(1)−Cl(2) 2.369(4), W(1)−O(1) 1.847(8), W(1)−O(2) 2.332(8), W(1)−O(3) 1.842(8), W(1)−O(7) 1.706(9), W(2)−Cl(3) 2.380(3), W(2)−Cl(4) 2.345(3), W(2)−O(4) 1.858(7), W(2)−O(5) 2.335(7), W(2)−O(6) 1.845(8), W(2)−O(8) 1.688(8); Cl(1)−W(1)−Cl(2) 85.95(18), O(7)−W(1) − Cl(1) 97.3(3), O(7)−W(1) − Cl(2) 96.6(3), O(1)−W(1)−O(7) 100.8(4), O(93) − W(1)−O(7) 100.0(4), W(1)−O(1)−C(1) 164.3(8), W(1)−O(2)−C(12) 119.0(6), W(1)−O(3)−C(23) 170.5(7)

gether with selected bond lengths and angles. The calix[6]arene ligand remains doubly protonated and adopts a pinched conformation to accommodate the two facially coordinated tungsten centres, one lying above and one below the plane of the macrocyclic ring (as emphasised in Figure 1, b). The geometry about each tungsten centre is best described as pseudo-octahedral with the oxo ligand lying *trans* to the elongated W−OH bond [W(1)−O(2) 2.332(8), cf. W(1)−O(1) 1.847(8); W(1)−O(3) 1.842(8) Å]. Interestingly, the OH binding site in **1** is equivalent to that occupied by the OR groups for the complexes [R_2calMOCl_2] (M = Mo, R = Et; M = W, R = Me) reported by Young et al.[2g] Furthermore, in these 1,3-dialkoxy-*p*-*tert*-butylcalix[4]arene systems, the W=O grouping leads to the adoption of an unusual nonconical conformation. Similarly, in **1** the W=O groups push other groups away (VSEPR) and this is thought to lead to the adoption of the pinched conformation. The W−O−C angles are also indicative of deprotonation at O(1) and O(3), viz. W(1)−O(1)−C(1) 164.3(8)°, W(1)−O(3)−C(23) 170.5(7)°, cf. W(1)−O(2)−C(12) 119.0(6)°. The W=O bond lengths (av. 1.70 Å) are typical of those observed in other oxotungsten(VI) complexes[6] and is in good agreement with that observed for the calix[4]areneH$_4$ (calH$_4$) complex [calWO(CH$_3$CO$_2$H)] [1.698(4) Å];[2c] that observed for [R_2calWOCl_2] is slightly longer [1.673(3) Å].[2g]

We then targeted the calix[8]arene (H_8L^1) species {[WO(NCMe)]$_2L^1$} (**2**), using a procedure similar to that for **1**. As expected, four molecules of HCl are lost per tungsten centre. The NMR signals/integrals are consistent with the expected target complex: eight distinct doublets for the *endo*- and *exo*-methylene groups together with four signals (each of 18 H) for the *tert*-butyl groups. In the IR spectrum of **2**, a strong band at 969 cm^{-1} is assigned to the ν(W=O) stretch. Crystals suitable for an X-ray determination were grown from an acetonitrile solution at room temperature; they incorporate two noncoordinated molecules of acetonitrile per molecule of the complex. The molecular structure is shown in Figure 2 together with selected bond lengths and angles. The calix[8]arene twists to accommodate the two [W=O] fragments in a manner similar to that observed previously for the organoimido complex {[Mo(NAr)(NCMe)]$_2L^1$} (Ar = C$_6$H$_3$*i*Pr$_2$-2,6).[5a] In **2**·2MeCN, each tungsten centre adopts a pseudo-octahedral geometry with the tungsten atoms an average of 0.30 Å out of the plane of the calixarene oxygen atoms. The W=O bond lengths (ca. 1.70 Å) are similar to those observed in **1** and elsewhere.[6] A molecule of acetonitrile binds to each tungsten centre *trans* to the oxo function and each is surrounded by three calixarene phenoxide sub-units.

The analogous reactions using [MoOCl_4] appear to be more sensitive to reduction, and deep blue solutions are readily formed. However, we note with interest that in the

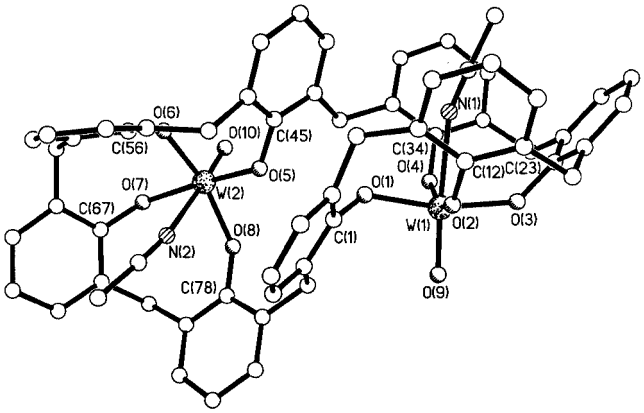

Figure 2. Molecular structure of **2**; H atoms and calixarene *t*Bu groups omitted for clarity; selected bond lengths [Å] and angles [°]: W(1)−O(1) 1.922(3), W(1)−O(2) 1.921(3), W(1)−O(3) 1.927(3), W(1)−O(4) 1.891(2), W(1)−O(9) 1.703(3), W(1)−N(1) 2.402(3), W(2)−O(5) 1.913(3), W(2)−O(6) 1.912(3), W(2)−O(7) 1.935(3), W(2)−O(8) 1.903(3), W(2)−O(10) 1.699(3), W(2)−N(2) 2.413(3); O(9)−W(1)−N(1) 176.15(12), O(9)−W(1)−O(1) 99.29(12), O(9)−W(1)−O(2) 99.74(12), O(9)−W(1)−O(3) 95.23(12), O(9)−W(1)−O(4) 103.24(12)

 © 2003 Wiley-VCH Verlag GmbH & Co. KGaA, Weinheim

case of *p-tert*-butylcalix[4]areneH$_4$ (*t*BucalH$_4$), reaction with [MoOCl$_4$] affords a blue, diamagnetic complex of stoichiometry [(*t*BucalH$_4$)(*t*Bucal)MoO·2CH$_2$Cl$_2$].[2a]

In conclusion, we have demonstrated that the oxychloride complex [WOCl$_4$] readily reacts with medium-sized calix[*n*]arene ring systems (n = 6 or 8) to afford highly crystalline products. In each case, the calixarene ligands are flexible enough to accommodate two tungsten centres possessing oxo or chloro ligands or combinations thereof.

Experimental Section

General: All manipulations were carried out under nitrogen using standard Schlenk and cannula techniques or in a conventional nitrogen-filled glove-box. Solvents were refluxed in the presence of an appropriate drying agent, and distilled and degassed prior to use. Elemental analyses were performed by the microanalytical services of the School of Chemical Sciences and Pharmacy at the University of East Anglia. NMR spectra were recorded with a Varian VXR 400 S spectrometer at 400 or a Gemini at 300 MHz (^{1}H) at 298 K; chemical shifts are referenced to the residual protio impurity of the deuterated solvent. IR spectra (nujol mulls, KBr windows), Perkin−Elmer 577 and 457 grating spectrophotometers. [WOCl$_4$] was prepared by the method of Gibson;[7] the ligands *p-tert*-butylcalix[6]arene H$_6$ (H$_6$L) and *p-tert*-butylcalix[8]arene (H$_8$L′) were prepared from *p-tert*-butylphenol and formaldehyde.[8] All other chemicals were obtained commercially and used as received, unless stated otherwise.

[(WOCl$_2$)$_2$L] (1): [WOCl$_4$] (1.0 g, 2.94 mmol) and H$_6$L (1.4 g, 1.44 mmol) were refluxed in toluene (40 mL) for 12 h. After cooling to room temperature, the volatiles were removed under reduced pressure and the residue extracted with MeCN (30 mL). Prolonged standing at ambient temperature afforded large red/purple prisms of **1**·8MeCN. (1.55 g, 58%). C$_{82}$H$_{104}$Cl$_4$N$_8$O$_8$W$_2$·CH$_3$CN (1880.3): calcd. C 52.6, H 5.4, N 0.9;[9]found C 52.3, H 5.3, N 1.1. IR: $\tilde{\nu}$ = 2359 w, 1608 m, 1302 m, 1268 m, 1205 s, 1122 m, 1096 w, 993 s, 941 m, 898 w, 881 m, 812 w, 806 w, 752 w, 730 w cm^{-1}. ^{1}H NMR (300 MHz, CD$_3$CN): δ = 9.28 (br. s, 2 H, OH), 7.60−7.14 (3 × m, 12 H, aryl H), 4.86 (d, $^2J_{H,H}$ = 13.5 Hz, 4 H, *endo*-CH$_2$), 4.66 (s, 4 H, *endo*/*exo*-CH$_2$), 3.66 (d, $^2J_{H,H}$ = 13.5 Hz, 4 H, *exo*-CH$_2$), 1.40 [s, 36 H, C(CH$_3$)$_3$], 1.29 [s, 18 H, C(CH$_3$)$_3$] ppm.

[{WO(NCMe)}$_2$L^1] (2): [WOCl$_4$] (1.0 g, 2.94 mmol) and H$_8$L^1 (1.86 g, 1.43 mmol) were refluxed in toluene (40 mL) for 12 h. After cooling to room temperature, the volatiles were removed under reduced pressure and the residue extracted with MeCN (30 mL). Prolonged standing at ambient temperature afforded orange prisms (1.13 g, 41%). C$_{92}$H$_{110}$N$_2$O$_{10}$W$_2$·4CH$_3$CN (1935.7): calcd. C 62.0, H 6.3, N 4.3; found C 61.6, H 6.3, N 4.1.[9] IR: $\tilde{\nu}$ = 2393 w, 2359 w, 2307 w, 2280 w, 2256 w, 1600 w, 1586 w, 1293 s, 1259 s, 1242 m, 1200 s, 1182 s, 1113 s, 1027 s, 968 s, 941 w, 916 m, 855 m, 838 s, 821 m, 795 s, 786 m, 760 w, 727 w, 675 w cm^{-1}. ^{1}H NMR (400 MHz, CDCl$_3$): δ = 7.45 (d, $^4J_{H,H}$ = 2.4 Hz, 2 H, aryl H), 7.31 (t, $^4J_{H,H}$ = 2.6 Hz, 4 H, aryl H), 7.18 (d, $^4J_{H,H}$ = 2.3 Hz, 2 H, aryl H), 7.09 (d, $^4J_{H,H}$ = 2.3 Hz, 2 H, aryl H), 6.96 (d, $^4J_{H,H}$ = 2.3 Hz, 2 H, aryl H), 6.87 (d, $^4J_{H,H}$ = 1.8 Hz, 2 H, aryl H), 6.70 (d, $^4J_{H,H}$ = 2.2 Hz, 2 H, aryl H), 5.44 (d, $^2J_{H,H}$ = 16.6 Hz, 2 H, *endo*-CH$_2$), 4.77 (d, $^2J_{H,H}$ = 12.9 Hz, 2 H, *endo*-CH$_2$), 4.61 (d, $^2J_{H,H}$ = 12.5 Hz, 2 H, *endo*-CH$_2$), 4.28 (d, $^2J_{H,H}$ = 16.7 Hz, 2 H, *endo*-CH$_2$), 3.43 (d, $^2J_{H,H}$ = 13.0 Hz, 2 H, *exo*-CH$_2$), 3.24 (d, $^2J_{H,H}$ = 12.6 Hz, 2 H, *exo*-CH$_2$), 2.58 (d, $^2J_{H,H}$ = 15.4 Hz, 2 H, *exo*-CH$_2$), 2.31 (d, $^2J_{H,H}$ = 15.1 Hz, 2 H, *exo*-CH$_2$), 1.95 (br. s, 9 H, 3 MeCN), 1.34 [s, 18 H, C(CH$_3$)$_3$], 1.27 [s, 18 H, C(CH$_3$)$_3$], 1.16 [s, 18 H, C(CH$_3$)$_3$], 1.02 [s, 18 H, C(CH$_3$)$_3$] ppm.

X-ray Crystallography: Measurements for **1**·8MeCN and **2**·2MeCN were carried out with a Bruker AXS SMART 1 K CCD area detector diffractometer equipped with Mo-K_α radiation (λ = 0.71073 Å) at 160 K. Narrow-frame exposures (0.3° in ω) were employed. Cell parameters were refined from all strong reflections in each data set. Intensities were corrected semiempirically for absorption, based on symmetry-equivalent and repeated reflections. The structures were solved by direct methods and refined by full-matrix least squares on F^2 values for all unique data. All non-hydrogen atoms were refined anisotropically. H atoms were included in a riding model with U_{iso} set to be 1.2 times (1.5 times for methyl-H) U_{eq} of the carrier atom. Crystal data for **1**·8MeCN: C$_{66}$H$_{80}$Cl$_4$O$_8$W$_2$·8CH$_3$CN, M = 1839.23, monoclinic, space group $P2_1/c$, a = 12.4800(6), b = 24.8091(12), c = 28.1016(14) Å, V = 8696.2(7) Å^3, Z = 4, F(000) = 3728, $D_{calcd.}$ = 1.405 g·cm^{-3}, μ (Mo-K_α) = 2.821 mm^{-1}, 60614 data measured of which 15280 were unique, R_{int} = 0.0358, wR = 0.1866 (on F^2), R = 0.0779 [for 14455 data with $F^2 > 2\sigma(F^2)$]. Largest difference map features within ±4.3 e·Å^{-3}. Two calixarene *t*Bu groups and one CH$_3$CN molecule of crystallisation were disordered over two sets of positions. Crystal Data for **2**·2MeCN: C$_{92}$H$_{110}$N$_2$O$_{10}$W$_2$·2CH$_3$CN, M = 1853.63, triclinic, space group $P\bar{1}$, a = 15.7724(6), b = 16.3034(6), c = 18.2020(6) Å, α = 101.005(2), β = 90.436(2), γ = 93.838(2)°, V = 4583.2(3) Å^3, Z = 2, F(000) = 1896, $D_{calcd.}$ = 1.343 g·cm^{-3}, μ (Mo-K_α) = 2.565 mm^{-1}, 34801 data measured of which 20907 were unique, R_{int} = 0.0273, wR = 0.0906 (on F^2), R = 0.0348 [for 15392 data with $F^2 > 2\sigma(F^2)$]. Largest difference map features within ±1.6 e·Å^{-3}. One calixarene *t*Bu group was disordered over two sets of positions and two CH$_3$CH molecules of crystallisation were refined at half occupancy. Programs used were Bruker AXS SHELXTL[10] for structure solution, refinement, and molecular graphics, Bruker AXS SMART (control) and SAINT (integration), and local programs.[11] CCDC-203411 and -203412 contain the supplementary crystallographic data for this paper. These data can be obtained free of charge at www.ccdc.cam.ac.uk/cont/retrieving.html [or from the Cambridge Crystallographic Data Centre, 12 Union Road, Cambridge, CB2 1EZ, UK; Fax: (internat.) + 44-1223/336-033; E-mail: deposit@ccdc.cam.ac.uk].

Acknowledgments

The University of East Anglia and Professor V. C. Gibson (Imperial College, U.K.) are thanked for financial support.

[1] [1a] C. D. Gutsche, *Calixarenes*, Royal Society of Chemistry, Cambridge, **1989**. [1b] D. M. Roundhill, *Prog. Inorg. Chem.* **1995**, *43*, 553. [1c] C. Wieser, C. B. Dielman, D. Matt, *Coord. Chem. Rev.* **1997**, *165*, 93. [1d] A. Ikeda, S. Shinkai, *Chem. Rev.* **1997**, *97*, 1713. [1e] C. D. Gutsche, *Calixarenes Revisited*, Royal Society of Chemistry, Letchworth, **1988**. [1f] J. L. Atwood, L. J. Barbour, M. J. Hardie, C. L. Raston, *Coord. Chem. Rev.* **2001**, *222*, 3. [1g] *Calixarenes 2001* (Eds.: Z. Asfari, V. Böhmer, J. Harrowfield, J. Vicens), Kluwer, Dordrecht, **2001**. [1h] W. Sliwa, *Croat. Chim. Acta* **2002**, *75*, 131. [1i] P. D. Harvey, *Coord. Chem. Rev.* **2002**, *233−234*, 289.

[2] [2a] F. Corazza, C. Floriani, A. Chiesi-Villa, C. Guatini, *J. Chem. Soc., Chem. Commun.* **1990**, 640. [2b] F. Corazza, C. Floriani, A. Chiesi-Villa, C. Guatini, *J. Chem. Soc., Chem. Commun.* **1990**, 1083. [2c] F. Corazza, C. Floriani, Chiesi-Villa, C. Rizzoli, *Inorg. Chem.* **1991**, *30*, 4465. [2d] B. Castellano, E. Solari, C. Floriani, R. Scopelliti, N. Re, *Inorg. Chem.* **1999**, *38*,

 © 2003 Wiley-VCH Verlag GmbH & Co. KGaA, Weinheim

3406. [2e] S. Dovesi, E. Solari, R. Scopelliti, C. Floriani, *Angew. Chemie. Int. Ed.* **1999**, *38*, 2388. [2f] A. Caselli, E. Solari, R. Scopelliti, C. Floriani, *J. Am. Chem. Soc.* **1999**, *121*, 8296. [2g] A. J. Millar, J. M. White, C. J. Doonan, C. G. Young, *Inorg. Chem.* **2000**, *39*, 5151. [2h] A. Lehtonen, R. Sillanpää, *Polyhedron* **2000**, *17*, 3327. [2i] U. Radius, *Inorg. Chem.* **2001**, *40*, 6637.

[3] [3a] P. D. Hampton, C. E. Daitch, T. M. Alam, E. A. Pruss, *Inorg. Chem.* **1997**, *36*, 2879. [3b] B. Xu, T. M. Swager, *J. Am. Chem. Soc.* **1993**, *115*, 1159.

[4] [4a] G. E. Hofmeister, F. E. Halm, S. F. Pedersen, *J. Am. Chem. Soc.* **1989**, *111*, 2318. [4b] G. E. Hofmeister, E. Alvarado, J. A. Leary, D. I. Yoon, S. F. Pedersen, *J. Am. Chem. Soc.* **1990**, *112*, 8843.

[5] [5a] V. C. Gibson, C. Redshaw, W. Clegg, M. R. J. Elsegood, *J. Chem. Soc., Chem. Commun.* **1995**, 2371. [5b] V. C. Gibson, C. Redshaw, W. Clegg, M. R. J. Elsegood, *Chem. Commun.* **1997**, 1605. [5c] V. C. Gibson, C. Redshaw, W. Clegg, M. R. J. Elsegood, *Polyhedron* **1997**, *16*, 4385. [5d] V. C. Gibson, C. Redshaw, W. Clegg, M. R. J. Elsegood, *Chem. Commun.* **1998**, 1969. [5e] C. Redshaw, M. R. J. Elsegood, *Inorg. Chem.* **2000**, *39*, 5164. [5f] C. Redshaw, M. R. J. Elsegood, *Polyhedron* **2000**, *19*, 2657. [5g] V. C. Gibson, C. Redshaw, M. R. J. Elsegood, *J. Chem. Soc., Dalton Trans.* **2001**, 767. [5h] V. C. Gibson, C. Redshaw, M. R. J. Elsegood, *New J. Chem.* **2002**, *26*, 16. [5i] V. C. Gibson, C. Redshaw, M. R. J. Elsegood, *Chem. Commun.* **2002**, 1200.

[6] W. Clegg, R. J. Errington, P. Kraxner, C. Redshaw, *J. Chem. Soc., Dalton Trans.* **1992**, 1431 and references therein.

[7] V. C. Gibson, T. P. Kee, A. Shaw, *Polyhedron* **1988**, *7*, 579.

[8] A. Arduini, A. Casnati in: *Macrocycle Synthesis* (Ed.: D. Parker), Oxford University Press, **1996**, chapter 6.

[9] Samples for microanalysis were freshly crystallised from acetonitrile. We have observed during X-ray crystallography that the amount of acetonitrile of crystallisation in calix[6 and 8]arene ligands often varies: M. R. J. Elsegood, C. Redshaw, unpublished results.

[10] G. M. Sheldrick, *SHELXTL user manual, version 5*, Bruker AXS Inc., Madison, WI, **1994**.

[11] *SMART and SAINT software for CCD diffractometers*, Bruker AXS Inc., Madison, WI, **1994**.

Received February 14, 2003

 © 2003 Wiley-VCH Verlag GmbH & Co. KGaA, Weinheim

First (Peroxo)vanadium(V) Complex with Heteroligand Formed in Reaction System − Synthesis, Structure and Reactivity of K[VO(O$_2$)(*omeida*)]·H$_2$O {*omeida* = *N*-[2-(2-oxomorpholine-4-yl)ethyl]iminodiacetato(2−)}

Michal Sivák,*[a] Mariana Mad'arová,[a] Jozef Tatiersky,[a] and Jaromír Marek[b]

Keywords: Vanadium / Peroxo ligands / δ-Lactones / ^{51}V NMR spectroscopy / *N*-acetyl-L-cysteine

The crystalline peroxo complex of vanadium(V), K[VO(O$_2$)(*omeida*)]·H$_2$O, where *omeida* is a δ-lactone derivative, *N*-[2-(2-oxomorpholine-4-yl)ethyl]iminodiacetate(2−), has been obtained by reaction of vanadate with H$_2$O$_2$ and *N*-(2-hydroxyethyl)ethylenediaminetriacetic acid (*HEDTA*) in acidic aqueous solution at pH = 3 and 278 K. X-ray analysis revealed a distorted pentagonal-bipyramidal coordination around the vanadium atom, with a typical *cis* arrangement of oxo and peroxo ligands in apical and equatorial positions, respectively. Two amino nitrogen atoms of the tetradentate *omeida*(2−)-N^1,N^2,O^1,O^2 ligand occupy the neighbouring equatorial positions of the pentagonal plane, and two oxygen atoms of carboxymethyl groups bound to the same N1 nitrogen atom are in equatorial and apical positions. The six-membered lactone ring in *omeida* was formed in the reaction solution from carboxy and hydroxy groups not involved in coordination with the vanadium atom. The ^{51}V NMR spectra of K[VO(O$_2$)(*omeida*)]·H$_2$O, and of peroxovanadate/*HEDTA*/H$_2$O and vanadate/*HEDTA*/H$_2$O solutions, as well as the ^{1}H NMR spectrum of *HEDTA*, proved that lactone ring closure proceeds only in peroxovanadate but not vanadate solutions. Spectroscopic investigation of the oxygen transfer reaction from the peroxo ligand in [VO(O$_2$)(*omeida*)]$^-$ to the thiolato sulfur atom in [Co(*en*)$_2${S(CH$_2$)$_2$NH$_2$}]$^{2+}$ or [Co(*en*)$_2$(*cyst*)]$^+$, and of the oxidation of *N*-acetyl-L-cysteine by K[VO(O$_2$)(*omeida*)]·H$_2$O, revealed much more complicated reaction mechanisms than those of other (amino-polycarboxylato)monoperoxo complexes of vanadium(V).
(© Wiley-VCH Verlag GmbH & Co. KGaA, 69451 Weinheim, Germany, 2003)

Introduction

Monoperoxo complexes of vanadium(V) with polydentate heteroligands *L* providing an N$_x$O$_y$ donor set[1−7] are structural and functional models for the peroxo form of vanadium haloperoxidase, and are also studied for the insulin mimetic properties of vanadium(IV,V) complexes. They are useful models for the peroxo form of the enzyme despite the differing coordination numbers of the vanadium atom in the enzyme and in synthesized monoperoxo complexes. In the active site of the peroxo form, the five-coordinate vanadium atom, in a distorted tetragonal-pyramidal arrangement, is bound to the imidazole nitrogen atom of His496, two non-protein oxygen atoms and two peroxo oxygen atoms of the η^2-peroxo ligand.[8] In previous structurally characterized neutral, anionic or cationic monoperoxo complexes with predominantly seven-coordinate vanadium atom, [VO(O$_2$)*L*], and in anionic diperoxo complexes with six- or seven-coordinate vanadium atom, [VO(O$_2$)$_2$*L*]$^{n-}$, the mono- or polydentate heteroligand *L* used in the synthesis and the ligand bound to the vanadium atom are identical. We describe here the first (peroxo)vanadium(V) complex with heteroligand formed in situ. The reaction of vanadate(V) with H$_2$O$_2$ and *HEDTA* (**1**) in acidic aqueous solution did not result, as expected, in the formation and isolation of an oxo(peroxo)(*hedta*) complex of vanadium(V), but the monoperoxo complex with coordinated *N*-[2-(2-oxomorpholine-4-yl)ethyl]iminodiacetate(2−) (*omeida*) (**2**), K[VO(O$_2$)(*omeida*)]·H$_2$O, crystallized out.

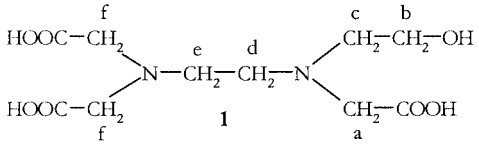

1

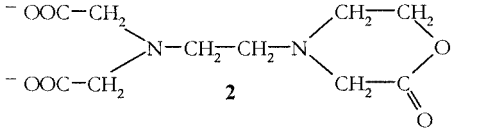

2

The reactivity of (peroxo)vanadium(V) complexes as oxidants can be studied in the reaction with a thiolato or cysteinato complex of Co^{III}, in which the peroxo oxygen atom is transferred to the coordinated sulfur atom, while a sulfen-

[a] Department of Inorganic Chemistry, Faculty of Natural Sciences, Comenius University,
Mlynská dolina, 84215 Bratislava 4, Slovakia
E-mail: sivak@fns.uniba.sk
[b] Laboratory of Functional Genomics and Proteomics, Faculty of Sciences, Masaryk University,
Kotlárská 2, 611 37 Brno, Czech Republic

ato complex is formed. We have previously determined the rate constants for this reaction using a series of structurally characterized monoperoxo complexes of vanadium(v) that have single-signal ^{51}V NMR spectra in aqueous solution.[6]

The interaction of vanadate with *HEDTA* in the absence of hydrogen peroxide was investigated by Crans et al.[9] Based on ^{51}V and ^{13}C NMR measurements they found that two species exist in aqueous vanadate/*HEDTA* solutions, in which the tetradentate *hedta* ligand coordinates to the vanadium atom either via two amino nitrogen atoms, and carboxylic and alkoxy oxygen atoms in alkaline solutions, or via nitrogen atoms and two carboxylic oxygen atoms in acidic or slightly alkaline solutions.

Results and Discussion

The IR spectrum of K[$VO(O_2)$(*omeida*)]·H_2O exhibits the characteristic bands observed for mono(peroxo)vanadium(v) complexes with coordinated deprotonated polycarboxylato ligands:[3,6,10–12] $\nu(V-O_p)$ at 562 (O_p = peroxo oxygen atom), $\nu(O_p\text{-}O_p)$ at 928, $\nu(V=O)$ at 947, $\nu_s(COO^-)$ at 1399, $\nu_{as}(COO^-) + \delta(H_2O)$ at 1616–1670 cm^{-1}. Moreover, it contains a sharp intense band at 1754 cm^{-1}, which is too high for the stretching vibration in uncoordinated COOH groups (1700–1720 cm^{-1}) – strongly indicating the presence of a "new" short C=O bond in the complex. This was confirmed by X-ray structure analysis which, surprisingly, showed that the heteroligand bound in the complex is not the anion of **1** but a derivative of morpholin-2-one (**2**). Thus, the IR band at 1754 cm^{-1}, which corresponds with the range 1747–1737 cm^{-1} reported for free δ-lactones,[13] and with 1750 cm^{-1} for 4-methylmorpholin-2-one,[14] can be assigned to a C=O stretching vibration in the coordinated *omeida* ligand [*d*(C8–O9) = 1.203(3) Å, Table 1].

Figure 1 illustrates the molecular structure of the [$VO(O_2)$(*omeida*)]$^-$ anion and Table 1 lists selected bond lengths and angles. The structure of [$VO(O_2)$(*omeida*)]$^-$ is mononuclear, with a distorted pentagonal-bipyramidal arrangement around the vanadium atom. The *omeida* dianion is coordinated as tetradentate ligand, providing an N_2O_2 donor set, and forming three five-membered chelate rings. Two carboxylate oxygen atoms, O4 and O6, are in *cis* positions of the bipyramid. Unlike in the [$VO(O_2)$(H*edta*)]$^{2-}$ ion,[15] these deprotonated and coordinated carboxylic oxygen atoms originate from carboxymethyl groups bound to the same N1 nitrogen atom. The pentagonal plane is formed by O2, O3 oxygen atoms of the η^2-peroxo ligand, N1, N2 nitrogen atoms occupying the *cis* positions, and carboxylic O4 oxygen atom. The apical positions of the bipyramid are occupied by doubly bonded oxo ligand O1 and deprotonated carboxylic O6 oxygen atoms. The average standard deviation of atoms from the pentagonal plane is 0.0515 Å. The vanadium atom is displaced from the plane towards the apical O1 oxygen atom by 0.2045(9) Å. This is less than the average value, 0.236 Å, found for other mono(peroxo)vanadium(v) complexes with polydentate aminopolycarboxylates.[3,6,16,17]

Table 1. Selected bond lengths [Å] and angles [°] for K[$VO(O_2)$(*omeida*)]·H_2O

In coordination polyhedron:			
V1–O1	1.605(2)	O1–V1–O3	104.98(9)
V1–O3	1.866(2)	O1–V1–O2	104.40(9)
V1–O2	1.868(2)	O3–V1–O2	45.08(8)
V1–O4	2.048(2)	O1–V1–O4	95.85(8)
V1–O6	2.106(2)	O1–V1–O6	164.80(8)
V1–N1	2.197(2)	O3–V1–O6	89.98(8)
V1–N2	2.282(2)	O2–V1–O6	87.98(8)
O2–O3	1.431(3)	O4–V1–O6	83.78(7)
		O1–V1–N1	88.63(8)
		O4–V1–N1	74.98(7)
		O6–V1–N1	76.57(7)
		O1–V1–N2	88.23(8)
		O6–V1–N2	85.24(7)
		N1–V1–N2	77.53(7)
In coordinated 2-oxomorpholine:			
O8–C8	1.339(3)	C8–O8–C9	120.8(2)
O8–C9	1.460(3)	C10–N2–C7	106.2(2)
O9–C8	1.203(3)	N2–C7–C8	115.9(2)
N2–C10	1.484(3)	O9–C8–O8	118.6(3)
N2–C10	1.484(3)	O9–C8–C7	120.7(3)
N2–C7	1.486(3)	O8–C8–C7	120.6(2)
C7–C8	1.511(4)	O8–C9–C10	113.5(2)
C9–C10	1.510(4)	N2–C10–C9	111.3(2)

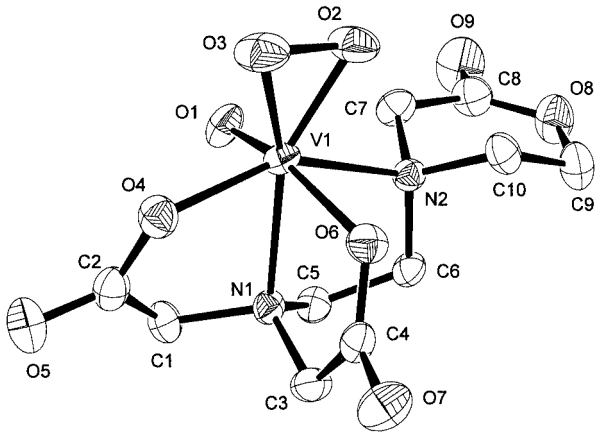

Figure 1. X-ray crystal structure of the anionic complex [$VO(O_2)$(*omeida*)]$^-$, showing the atomic numbering scheme; hydrogen atoms are omitted for simplicity; the ORTEP plot is drawn at a 50% probability

The generally observed *trans* effect, i.e. the elongation of the apical V–O6 bond *trans* to the short V–O1 bond when compared with the equatorial V–O4 distance, given by $\Delta d(V-O)$ = 0.058 Å, is also much less significant than in other polycarboxylato complexes with ligands that provide an NO_3 donor set [$\Delta d(V-O)$ = 0.073–0.200 Å],[6] and even in the (carboxymethyl)histidinato(2–) complex, K[$VO(O_2)$(*cmhist*)]·H_2O,[18] with $\Delta d(V-O)$ = 0.099 Å. The latter complex was previously the only structurally well-characterized peroxo complex with the same arrangement of N_2O_2 donor set atoms around the vanadium atom as in the complex studied here. Both in K[$VO(O_2)$(*cmhist*)]·H_2O and K[$VO(O_2)$(*omeida*)]·H_2O, the N2 atoms are from the heterocycles imidazole and morpholin-2-one, respectively.

 © 2003 Wiley-VCH Verlag GmbH & Co. KGaA, Weinheim

The pentagonal bipyramid in $[VO(O_2)(omeida)]^-$ is not symmetric: the O2, O3 peroxo oxygen atoms deviate from the O1,V1,N1,O6 plane by 0.6354(29) and 0.7952(29) Å, respectively. Two glycinate rings, the almost planar "apical" one formed by V1, N1, C3, C4, O6 atoms (deviation of fitted atoms 0.0725 Å) and the "equatorial" one formed by V1, N1, C1, C2, O4 atoms (deviation of fitted atoms 0.2318 Å), are perpendicular (89.92°). Only one hydrogen bond between the oxygen atom of a water molecule and the uncoordinated O7 carboxylic oxygen atom with $d(H_w-O7)$ = 1.990(60) and $d(O_w-O7)$ = 2.797(3) Å has been found. Similarly, as in the (carbamoylethyl)iminodiacetato complex, $K[VO(O_2)(ceida)]\cdot 2H_2O$,[6] the potassium cation in $K[VO(O_2)(omeida)]\cdot H_2O$ is coordinated by seven oxygen atoms, one of a water molecule, three end-bonded carboxylic oxygen atoms (O5, O5, O7) of three different anions, and two carboxylic (O4, O6) and an O3 peroxo oxygen atoms coordinated to the same vanadium atom. The K−O distances range from 2.667(2) to 3.007(2) Å. The distance to the eighth oxygen atom, 3.428 Å, exceeds the 3.25 Å of any other higher coordination number.[19]

^{51}V NMR Measurements

All ^{51}V NMR spectra were measured at 278 K, the same temperature at which $K[VO(O_2)(omeida)]\cdot H_2O$ was synthesized. The ^{51}V NMR spectrum of a 0.015 M aqueous solution of $K[VO(O_2)(omeida)]\cdot H_2O$ (Figure 2, a), measured 7 min after dissolution, exhibits a single peak at δ = −515 ppm ($W_{1/2}$ = 450 Hz). This shift is unusually low for a heteroligand mono(peroxo)vanadate and it occurs in the region where, mostly, the chemical shifts for heteroligand dioxo complexes of vanadium(v) are observed.[20−23] However, the UV/Vis spectrum of the same solution exhibits the peroxo-to-vanadium CT band at λ_{max} = 439 nm (ε = 357 $mol^{-1}\cdot dm^3\cdot cm^{-1}$), which is within the 410−460 nm range typical for monoperoxo complexes of vanadium(v).[24,25] The chemical shift δ = −515 ppm can thus be assigned to the $[VO(O_2)(omeida)]^-$ ion **I** (Scheme 1). The presence of a single peak allows us to suggest that the molecular structure of the complex anion is maintained on dissolution. After 24 h, 95% of the vanadium is still in solution in the form of **I**, as well as a minor species with $\delta(^{51}V)$ = −567 ppm ($W_{1/2} \approx$ 260 Hz) (Figure 2, b), which we assign to an isomeric peroxo(*omeida*) complex **II**, because no absorbance decrease due to peroxo ligand decomposition was observed in the UV/Vis spectrum. The smaller $W_{1/2}$ value for **II** is in accordance with its higher symmetry when compared with **I** (Scheme 1). Further evidence for the assignment of **I** and **II** was provided by the ^{51}V NMR spectra of aqueous peroxovanadate/*HEDTA*, vanadate/*HEDTA* and peroxovanadate/*HEDTA*/*OMEIDA* solutions (*OMEIDA* = *N*-[2-(2-oxomorpholin-4-yl)ethyl]iminodiacetic acid), measured at the same pH as used in the synthesis.

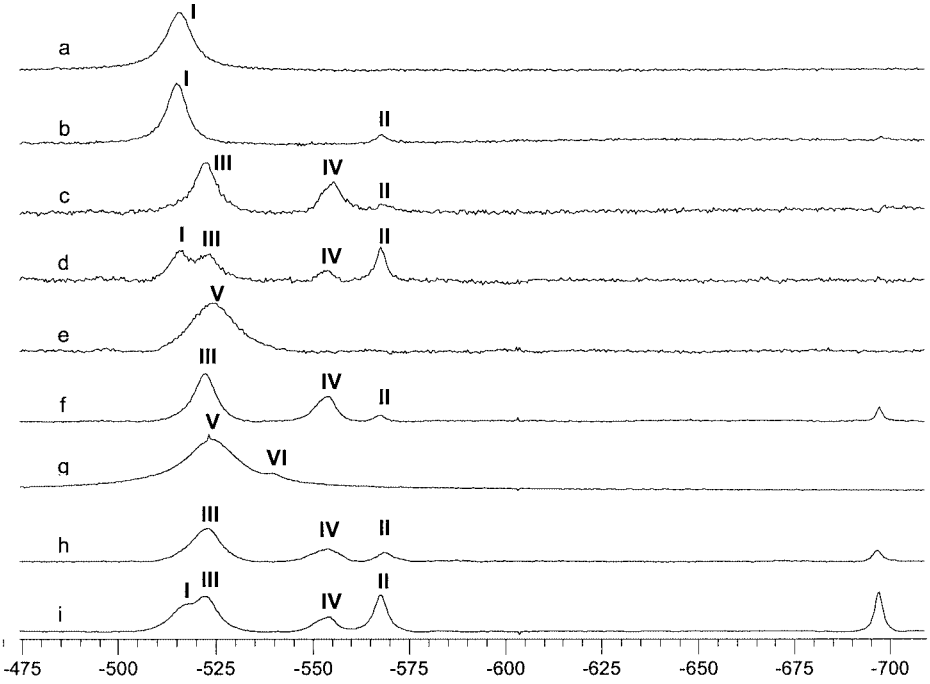

Figure 2. Selected ^{51}V NMR spectra of aqueous solutions at 278 K; a, b: 0.015 M $K[VO(O_2)(omeida)]\cdot H_2O$, (a) 7 min, (b) 24 h after dissolution; c, d: peroxovanadate/*HEDTA* solutions, (c) 15 min, (d) 5 d after preparation, concentrations: see Table 2; e, f: vanadate/*HEDTA* solutions, (e) 8 min to 70 h after preparation, (f) after addition of 1 mmol H_2O_2 to the solution (e) prepared 70 h before addition; g: vanadate/*HEDTA*/*OMEIDA* solutions, c(**3**ii) = 0.15 M, $c(KVO_3)$ = 0.075 M; h: peroxovanadate/*HEDTA*/*OMEIDA* (**3**i) solutions, c(**3**i) = 0.15 M, $c(KVO_3)$ = 0.075 M, $c(H_2O_2)$ = 0.225 M; i: peroxovanadate/*HEDTA*/*OMEIDA* (**3**ii) solutions, c(**3**ii) = 0.15 M, $c(KVO_3)$ = 0.075 M, $c(H_2O_2)$ = 0.225 M; pH(c−i) = 3.0

 © 2003 Wiley-VCH Verlag GmbH & Co. KGaA, Weinheim

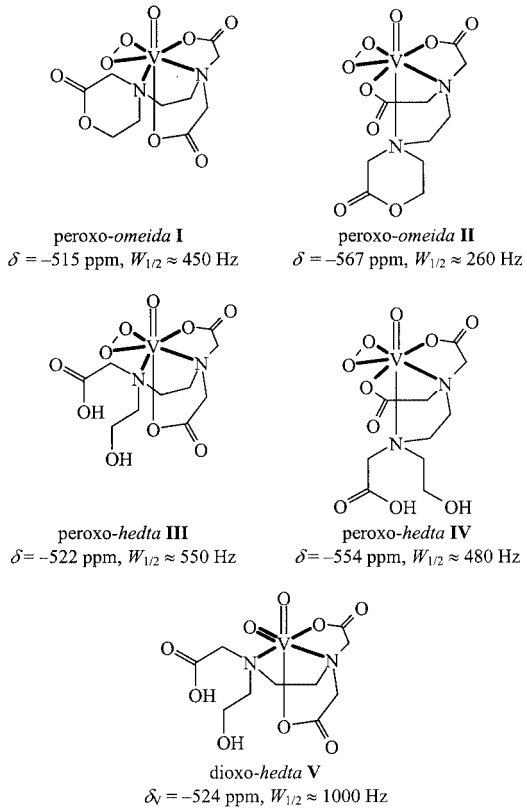

Scheme 1. ^{51}V NMR spectral characteristics and proposed structures of dioxo(*hedta*)-, monoperoxo(*hedta*)- and monoperoxo(*omeida*)vanadates formed in vanadate/*HEDTA*/H_2O and peroxovanadate/*HEDTA*/H_2O solutions

Peroxovanadate/HEDTA/H_2O Solutions (pH = 3)

Preparation: 0.225 mmol of H_2O_2 (0.022 mL, w = 30%) was added to 0.15 mmol of KVO_3, dissolved in H_2O (5 mL), and 0.3 mmol of *HEDTA* was then dissolved in the resultant solution. Before making up to the total volume of 10 mL, the pH was adjusted with 0.5 M KOH. Changes in the ^{51}V NMR spectrum of the peroxovanadate/*HEDTA*/H_2O solution with time allowed us to observe the formation of the peroxo(*hedta*) species and their subsequent transformation into the peroxo(*omeida*) complexes **I** and **II**. The spectrum measured 15 min after preparation of the solution (Figure 2, c) exhibits shifts of two dominant species at δ = −522 ppm (**III**) (I_{rel} = 63%, $W_{1/2}$ ≈ 550 Hz) and −554 ppm (**IV**) (I_{rel} = 31%, $W_{1/2}$ ≈ 480 Hz), and two minor species with shifts at δ = −567 ppm (I_{rel} ≈ 3%) and −697 ppm, the latter being the shift of the heteroligand-free diperoxo ion $[VO(O_2)_2(H_2O)_x]^-$.[26,27] We assign the major species **III** and **IV**, to isomeric monoperoxo(*hedta*) complexes (Scheme 1) formed immediately after mixing the solutions, which then undergo the lactone ring closure, while the monoperoxo(*omeida*) complexes **I** and **II** are formed. After 20 h, the peak at δ = −515 ppm corresponding to complex **I**, with known solid structure, appeared (I_{rel} = 11%), which after 5 d became the predominant species (I_{rel} = 40%). The increase of I_{rel}(**I** + **II**) for the monoperoxo(*omeida*) species with time is proportional to the decrease of I_{rel}(**III** + **IV**) for the monoperoxo(*hedta*) complexes (Table 2). This indicates that lactone formation under such mild conditions proceeds on the ligand coordinated to the $VO(O_2)^+$ moiety. Under same conditions, free *HEDTA* does not undergo cyclization, as evidenced by its unchanged ^{1}H NMR spectrum.

Table 2. Dependence of I_{rel} on time for monoperoxo(*omeida*) (**I**, **II**) and monoperoxo(*hedta*) (**III**, **IV**) complexes formed in peroxovanadate/*HEDTA*/H_2O solutions at pH = 3; conditions: T = 278 K, concentrations: 0.015 M vanadate, 0.03 M *HEDTA*, 0.023 M H_2O_2

Species	δ [ppm]	$W_{1/2}$ [Hz]	I_{rel} [%][a]					
			15 min	90 min	20 h	24.5 h	2 d	5 d
I	−515	ca. 520	–	–	11[b]	12[b]	19.5[b]	40[b]
II	−567	ca. 260	3	5.5	13	15.5	19	22.5
III	−522	550	63	60	48[b]	45[b]	39[b]	23[b]
IV	−554	480	31	29	24	20	18.5	13

[a] Difference between the sum of I_{rel} for **I**−**IV** and 100% corresponds to I_{rel} for $[VO(O_2)_2(H_2O)x]^-$. [b] Values obtained by deconvolution.

Vanadate/HEDTA/H_2O Solutions (pH = 3)

Preparation: 1 mmol of *HEDTA* was dissolved in 0.1 M KOH (4 mL), 0.5 mmol of KVO_3 (1 mL, 0.5 M) and 0.5 M KOH (0.4 mL) were added, and the total volume made up to 10 mL. Relevant data on the formation of the dioxo- and monoperoxo(*omeida*) complexes were also provided by changes in the ^{51}V NMR spectra of the vanadate/*HEDTA*/H_2O solutions with time, and spectra of the same solutions to which 1 mmol of H_2O_2 (0.1 mL, w = 30%) was added just before NMR measurements. The spectrum of the vanadate/*HEDTA*/H_2O solution, measured 8 min to 70 h after preparation of the solutions, remained unchanged (Figure 2, e). It exhibits a very broad single peak with δ = −524 ppm ($W_{1/2}$ ≈ 1200 Hz), which is similar to data observed for the $[VO_2(Hedta)]^{2-}$ ion (δ = −518 ppm, $W_{1/2}$ ≈ 1000 Hz).[23] We consider the species with δ = −524 ppm to be the dioxo(*hedta*) complex **V**, $[VO_2(hedta)]^{n-}$, which is identical to the species found by Crans[9] in vanadate/*HEDTA* solutions at 298 K in the pH range 5−9 (δ = −520 ppm, $W_{1/2}$ = 710 Hz). The shift by 4 ppm and the signal broadening (710 → 1200 Hz) is caused by the lower temperature in our measurements. In the complex **V**, the *hedta* ligand was proposed to be bound via two amino nitrogen atoms and two carboxylic oxygen atoms.[9] However, when H_2O_2 was added after 8 min, or after 8, 24 and 70 h to the prepared vanadate/*HEDTA*/H_2O solutions, the spectra (Figure 2, f) exhibited, besides the shift of $[VO(O_2)_2(H_2O)_x]^-$ (I_{rel} ≈ 4%), three peaks with identical chemical shifts and $W_{1/2}$ values to those for **II**, **III** and **IV** (Table 2). The small change in chemical shifts (−524 → −522 ppm) but the significant change in $W_{1/2}$ (1200 → 540 Hz), both evidently occurring in all spectra after the addition of H_2O_2, confirmed the formation of the dioxo- and peroxo(*hedta*) species before and after the addition of hydrogen peroxide, respectively. The relative intensities for

 © 2003 Wiley-VCH Verlag GmbH & Co. KGaA, Weinheim

II−**IV** do not significantly change with the time of addition of H_2O_2, and were approx. 62% for **II**, 29% for **III**, and 5% for **IV**. Monoperoxo(*omeida*) complex **I** was not observed, even when H_2O_2 was added after 70 h to the vanadate/*HEDTA*/H_2O solution, i.e. after a time when a significant amount of **I** has formed in the peroxovanadate/*HEDTA*/H_2O solution (Table 2). Thus, lactone ring closure and the formation of peroxo(*omeida*) complex **I** from *HEDTA* is, under the given conditions, a slow process that proceeds only in the peroxovanadate solution.

Alkaline Solution of K[VO(O$_2$)(omeida)]·H$_2$O (pH = 8.5)

Preparation: 0.5 M KOH (0.2 mL) was added to 0.15 mmol of the complex, dissolved in H_2O (8 mL), and the volume made up to 10 mL. Generally, lactone rings open in alkaline media and, indeed, ring opening was observed in the NMR spectrum of a 15 mM aqueous solution of K[$VO(O_2)$(*omeida*)]·H_2O measured just 12 min after preparation. The spectrum's six peaks correspond to monoperoxo(*omeida*) complexes **I**, **II** (I_{rel} = 67, 7.5%, respectively), monoperoxo(*hedta*) complexes **III**, **IV** (I_{rel} = 11, < 1%, respectively), and two minor species with signals at δ = −499 ppm (I_{rel} = 3.5%) and −750 ppm (I_{rel} = 6%). The δ = −499 ppm shift corresponds to $[VO_2(hedta)]^{n-}$, with *hedta* coordinated in alkaline solutions (pH = 7−11) via the alkoxy group,[9] and the δ = −750 ppm shift to the diperoxovanadate species which exhibit, over a wide pH range (0.5−11), a strong pH dependence of δ values (−690 to −765 ppm).[26,28] After 8 h, I_{rel}(**I** + **II**) decreased to 33% and I_{rel}(**III** + **IV**) increased to 61%, whereas I_{rel} for the diperoxovanadate remained almost constant. These and previous measurements show that the pH change between 3.0 and 8.5 has no influence on the chemical shifts for **I**−**IV**. These constant chemical shifts over a wide pH range provide an additional indirect confirmation of the assignment for **III** and **IV**, because the shifts for mono- or dimeric vanadates with chemical shifts δ = −550 to −570 ppm, which could be also present in solution as uncomplexed vanadium forms, exhibit a pH dependence in the region discussed.[26]

Vanadate/HEDTA/OMEIDA/H$_2$O and Peroxovanadate/HEDTA/OMEIDA/H$_2$O solutions (pH = 3)

In a further series of experiments that confirmed the above conclusions, we measured the ^{51}V NMR spectra of vanadate and peroxovanadate solutions with *HEDTA*/*OMEIDA* heteroligand solution (**3**) prepared by: (i) refluxing for 20 h the 0.7 M aqueous solution of *HEDTA* (pH = 1, acidified with 1 M $HClO_4$) or (ii) refluxing the same solution for 25 h after it had stood for 3 weeks at room temperature. In such solutions, the formation of *OMEIDA* is expected, as the cyclization of chelating aminopolycarboxylic acids is favored by higher temperature and lower pH.[29] The vanadate/*HEDTA*/*OMEIDA*/H_2O solution for NMR measurements was prepared as follows; to avoid, in the absence of H_2O_2, the formation of $H_xV_{10}O_{28}^{(6-x)-}$ ions which have a poor complex formation ability, solution **3** (2 mL, 0.7 M) was mixed with 1.5 mL of alkalized 0.5 M KVO_3 (prepared by dissolving the metavanadate in 0.1 M KOH). The pH of the resulting solution was then adjusted to 3 by addition of 0.2 mL of 0.5 M KOH. The spectrum of vanadate/*HEDTA*/*OMEIDA*/H_2O solution prepared from **3**(i) exhibits a single shift at δ = −524 ppm ($W_{1/2}$ ≈ 1200 Hz). The spectrum of the same solution, however, prepared using the heteroligand solution **3**(ii) (Figure 2, g) gave on deconvolution two shifts, at δ = −524 ppm ($W_{1/2}$ ≈ 1250 Hz, I_{rel} = 86%) due to dioxo(*hedta*) complex **V**, and at δ = −539 ppm ($W_{1/2}$ ≈ 355 Hz, I_{rel} = 14%), which we assign to a dioxo(*omeida*) complex **VI**, $[VO_2(omeida)]^-$. The spectra of the peroxovanadate/*HEDTA*/*OMEIDA*/H_2O solutions (prepared in the same way but with addition of 0.23 mL of 30% H_2O_2) showed (Figure 2, h and i) that, with increased reaction time for lactone formation in **3**(i), with respect to **3**(ii), the sum of I_{rel} for monoperoxo(*omeida*) complexes (**I**, **II**) increased from 12 to 43%, while I_{rel} for the monoperoxo(*hedta*) species (**III**, **IV**) decreased from 81 to 41%. These results showed that *HEDTA* in solutions **3** was not completely transformed into *OMEIDA*, i.e. the lactone closure does not proceed easily in the absence of peroxovanadate even at high temperatures and long reaction times. *OMEIDA* has not yet been synthesized as a pure solid; only its dimethyl and diethyl esters are known.[30]

Reactivity of K[VO(O$_2$)(*omeida*)]·H$_2$O

Previously,[6,31] we investigated the kinetics of oxygen transfer reaction from the peroxo ligand in a series of (amino-polycarboxylato)- or (pyridinecarboxylato)monoperoxovanadates, $[VO(O_2)L]$, to the thiolato sulfur atom in $[Co(en)_2\{S(CH_2)_2NH_2\}]^{2+}$ as a pseudo-monomolecular reaction in excess of the vanadium complex [Equation (1)].

$$[VO(O_2)L] + [Co(en)_2\{S(CH_2)_2NH_2\}]^{2+} \rightarrow VO_2L + [Co(en)_2\{SO(CH_2)_2NH_2\}]^{2+} \quad (1)$$

The first-order rate constants at 298 K lead to the following sequence of increasing reactivity: $[VO(O_2)(ada)]^- < [VO(O_2)(ceida)]^- < [VO(O_2)(nta)]^{2-} < [VO(O_2)(quin)_2]^{3-} < [VO(O_2)(H_2O)_2(pic)]$, which correlates with the charge-transfer energy and temperature of active oxygen release. However, Equation (1) with $[VO(O_2)(omeida)]^-$ as oxidant provided some unexpected results. Under both pseudo-mono- and bimolecular reaction conditions, a linear increase of the sulfenato complex concentration with time was found, as is known for zero-order reactions. The same course of concentration change was also observed in a reaction solution from which dissolved dioxygen was bubbled out by nitrogen, and also in a solution kept out of the cell compartment, i.e. not irradiated by 371 nm light. The participation of molecular oxygen in the reaction, or photochemical effects, can thus be excluded. Even the 1:1 reaction of $[VO(O_2)(omeida)]^-$ with the cysteinato complex, $[Co(en)_2(cyst)]^+$, could not be evaluated as a bimolecular reaction, as the relationship between absorbance and time is given by $1/A = a - b \times \ln t$ (Figure 3).

 © 2003 Wiley-VCH Verlag GmbH & Co. KGaA, Weinheim

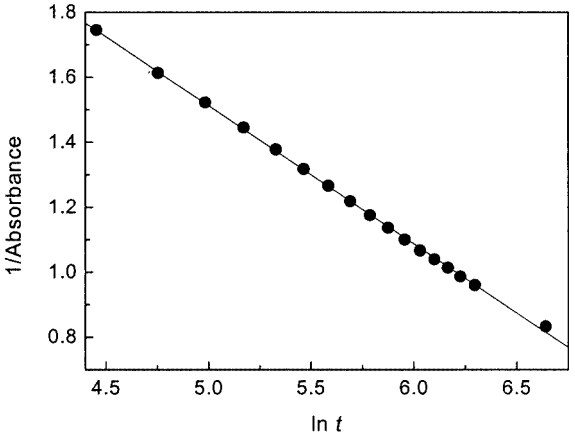

Figure 3. Reciprocal absorbance at 371 nm vs. ln[function of time] for 1:1 aqueous solution of $[VO(O_2)(omeida)]^-$ (**I**) and $[Co(en)_2(cyst)]^+$; c = 0.0007 M, T = 298.2 K, measured in a closed 1-cm cell under nitrogen

We further investigated the interaction of $[VO(O_2)(omeida)]^-$ with *N*-acetyl-L-cysteine at 37 °C. This is of interest with respect to the insulin mimetic properties of vanadium(IV) and -(V) complexes, which include (carboxymethyl)aspartato(3−) complex, $K_2[VO(O_2)(cmaa)(H_2O)]$, prepared according to the literature[32,33] and which have been recently studied in vitro by Rehder et al.[34] The biological activity of *N*-acetyl-L-cysteine, which, for example, inhibits the phosphorylation of tyrosine in cellular proteins caused by peroxovanadates,[35] has an important effect in chronic bronchitis[36] or improves by increased oxygen delivery the survival of patients with hepatic failure.[37] The changes in the UV/Vis spectrum of a 1:5 solution of $[VO(O_2)(omeida)]^-$ and N-acetyl-L-cysteine with time showed that about one-third of the $[VO(O_2)(omeida)]^-$ was decomposed in 6 h. The concentration decrease with time is linear even in this reaction (Figure 4).

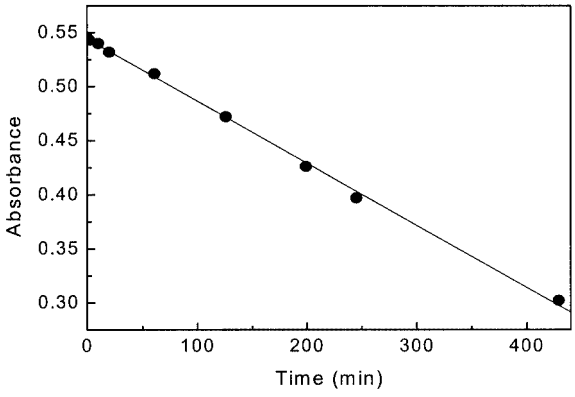

Figure 4. Absorbance at 440 nm vs. time for 1:5 aqueous solution of $[VO(O)_2(omeida)]^-$ (**I**) and *N*-acetyl-L-cysteine; c = 0.0015 and 0.0075 M, respectively; T = 310 K, measured in closed 1-cm cell under nitrogen

The absorbance changes linearly up to a high degree of conversion, i.e. for more than just the initial phase of reaction, where linearity of the measured property is common. These reactions obviously exhibit "mixed kinetics", i.e. the observed absorbance change corresponds to several reaction types. The mechanism of oxidation, both of Co^{III} complexes and *N*-acetyl-L-cysteine by $[VO(O_2)(omeida)]^-$, is thus more complicated than that found for other heteroligand monoperoxo complexes of vanadium(V).[31] A detailed kinetic study is needed to elucidate the reaction mechanism.

Conclusions

The reaction of aqueous peroxovanadate with *HEDTA* resulted in the formation and isolation of a crystalline monoperoxo complex of vanadium(V) with the dianion of *OMEIDA*, $K[VO(O_2)(omeida)]\cdot H_2O$. The crystal structure determination revealed that the vanadium atom in $[VO(O_2)(omeida)]^-$ is in a typical distorted pentagonal-bipyramidal arrangement, and is coordinated by oxygen atoms of the oxo and η^2-peroxo ligands, and by N_2O_2 donor set atoms of the tetradentate *omeida* heteroligand. ^{51}V NMR measurements showed that the heteroligand is formed in situ (pH = 3, 278 K) only in peroxovanadate but not vanadate solutions. The ^{51}V NMR spectra revealed two isomeric monoperoxo(*hedta*) complex anions and their transformation into isomeric monoperoxo(*omeida*) complexes. The $VO(O_2)(omeida)]^-$ ion as oxidant in the reaction with thiolato or cysteinato complexes of Co^{III} and with *N*-acetyl-L-cysteine, both under pseudo-mono- or bimolecular conditions, showed unusual kinetic behaviour: linear concentration changes with time. The elucidation of the reaction mechanism requires a further kinetic study.

Experimental Section

General Remarks: The FT IR spectrum (Nujol mull) was registered with a Nicolet Magna 750 spectrometer. The NMR spectra were recorded with a Varian Gemini 2000 spectrometer (300 MHz for ^1H). ^{51}V NMR spectra were recorded at 78.879 MHz in a 5-mm diameter NMR vial and with a capillary with D_2O immersed in the measured aqueous solution. Typical parameters were: sweep width 32 kHz, line broadening factor 20 Hz, acquisition time of 63 ms with a relaxation delay 10 ms. The chemical shifts are related to $VOCl_3$ as external standard. The V NMR 6.1 program was used to deconvolute spectra between δ = −490 and −530 ppm. The ^1H NMR spectra in D_2O were obtained by using standard parameters. The UV/vis spectral and kinetic measurements were performed with a Hewlett−Packard 8452 spectrometer with a thermostatted (±0.1 °C) compartment. ^1H NMR data of *HEDTA*: (278 K, c = 0.01 M): δ = 3.873 (s, a), 3.831 (t, b), 3.495 (t, c), 3.337 (t, e), 3.723 (s, f) (lettered according to formula **1**).

Synthesis of $K[VO(O_2)(omeida)]\cdot H_2O$: KVO_3 (0.28 g, 2 mmol), prepared from V_2O_5 and KOH at pH ≈ 8, was dissolved under heating in water (10 mL). The solution was then ice-cooled and H_2O_2 (0.3 mL, 30%; Slavus, Slovakia) was added. To the resulting red peroxovanadate solution, *HEDTA* (0.56 g, 2 mmol; Aldrich) was added in small portions whilst stirring. The pH was adjusted to 3.0 with 2 M KOH, and ethanol (15 mL) was added dropwise to initiate the crystallization. The small amount of initially formed orange

 © 2003 Wiley-VCH Verlag GmbH & Co. KGaA, Weinheim

precipitate dissolved within 24 h. From the refrigerated solution (5 °C), kept in closed vessel, very dark red crystals of K[VO(O_2)(*omeida*)]·H_2O crystallized out within 2 weeks. Yield: 0.26 g, 31.5%. Monocrystals suitable for X-ray analysis were obtained by crystallization from the first filtrate. After isolation, the product was washed with cooled ethanol (5 °C) and dried over silica gel at 5 °C. The peroxo complex formed is very stable in the reaction solution: we have obtained identical products even on subsequent crystallization from the mother solution within three months. The repeated CHN analysis and IR spectra showed that the solid complex is stable for several months when kept at 5 °C. $C_{10}H_{16}KN_2O_{10}V$ (414.3): calcd. C 28.96, H 3.89; K 9.44, N 6.76, O_2^{2-} 7.72; found C 28.66, H 3.77, K 8.98, N 6.44, O_2^{2-} 7.62. C, H and N contents were determined with a Carlo−Erba 1106 analyzer, peroxide by iodometric titration and potassium by flame photometry (Flapho 4, Zeiss Jena). IR: $\tilde{\nu}$ = 422 vw, 431 w, 494 m, 530 m, 562 s, 596 w, 657vw, 730 m, 743 m, 814 m, 883 s, 928 vs, 947 vs, 972 w, 987 m,1010 w, 1077 w, 1064 w, 1064 vw, 1094 s, 1115 w,1129 vw, 1167 vw, 1222 s, 1248 w, 1265 s, 1283 m, 1300s, 1318 s, 1339 m, 1353 s, 1399 vs, 1488 w, 1616 vs, 1643 vs, 1671 vs sh, 1731 m, 1754 vs, 3367 s, 3544 m cm^{-1}.

Kinetic Measurements: Oxidation of the thiolato and cysteinato complexes, $[Co(en)_2\{S(CH_2)_2NH_2\}]^{2+}$ and $[Co(en)_2(cyst)]^+$, was monitored at 371 nm, corresponding to absorption maximum for the sulfenato complex formed. $[Co(en)_2\{S(CH_2)_2NH_2\}](ClO_4)_2$ and $[Co(en)_2(cyst)]ClO_4$ were synthesized according to published procedures.[38,39] The reaction with *N*-acetyl-L-cysteine was monitored at the wavelength of absorption maximum for $[VO(O_2)(omeida)]^-$ (440 nm).

X-ray Crystallographic Study: The X-ray measurements were taken at 293 K with a KUMA CCD diffractometer with graphite-monochromated Mo-K_α radiation by using the ω-2θ scan technique. No significant decay of the intensity was observed. The data were not corrected for absorption effects. Some 2246 reflections with $I > 2\sigma_I$, of all unique reflections obtained, were classified as observed. Crystallographic data for K[VO(O_2)(*omeida*)]·H_2O: dark red crystals, 293(2) K, $KVC_{10}H_{16}N_2O_{10}$, M_r = 414.29, monoclinic, a = 18.0558(12), b = 6.9241(4), c = 12.0978(8) Å, β = 99.695°, V = 1490.9(2) $Å^3$, Z = 4, space group $P2_1/c$, $D_{calcd.}$ = 1.846 g/cm^3, λ = 0.71073 Å, $R1$ = 0.0323, $wR2$ = 0.0866, $R1 = F_o - F_c/F_o$, $wR2 = \{[w(||F_o|^2 - |F_c|^2|)^2]/[w(F_o^4)]\}^{1/2}$. CCDC-178735 contains the supplementary crystallographic data for this paper. These data can be obtained free of charge at www.ccdc.cam.ac.uk/conts/retrieving.html [or from the Cambridge Crystallographic Data Centre, 12 Union Road, Cambridge CB2 1EZ, UK; Fax: (internat.) + 44-1223/336-033; E-mail: deposit@ccdc.cam.ac.uk].

Acknowledgments

This work was financially supported by the Ministry of Education of the Slovak Republik (Grant No.1/8201/01).

[1] G. J. Colpas, B. J. Hamstra, J. W. Kampf, V. L. Pecoraro, *J. Am. Chem. Soc.* **1994**, *116*, 3627−3628.
[2] G. J. Colpas, B. J. Hamstra, J. W. Kampf, V. L. Pecoraro, *J. Am. Chem. Soc.* **1996**, *118*, 3469−3478.
[3] M. Sivák, J. Tyršelová, F. Pavelcík, J. Marek, *Polyhedron* **1996**, *15*, 1057−1062.
[4] F. W. B. Einstein, R. J. Batchelor, S. J. AngusDunne, A. S. Tracey, *Inorg. Chem.* **1996**, *35*, 1680−1684.
[5] K. Kanamori, K. Nishida, N. Miyata, K. Okamoto, *Chem. Lett.* **1998**, 1267−1268.
[6] M. Sivák, V. Suchá, L'. Kuchta, J. Marek, *Polyhedron* **1999**, *18*, 93−99.
[7] M. Casný, D. Rehder, *Chem. Commun.* **2001**, 921−922.
[8] A. Messerschmidt, L. Prade, R. Wever, "X-ray Structures of Native andPeroxo Form Reveal Vanadium Chemistry in Vanadium Haloperoxidases", in: *Vanadium Compounds, Chemistry, Biochemistry and Therapeutical Applications* (Eds.: A. S. Tracey, D. Crans), *ACS Symp. Ser.* **1998**, *711*, 186−201, *Biol. Chem.* **1997**, *378*, 309−315.
[9] D. C. Crans, P. K. Shin, *J. Am. Chem. Soc.* **1994**, *116*, 1305−1315.
[10] M. Sivák, D. Joniaková, P. Schwendt, *Transition Met. Chem.* **1993**, *18*, 304−308.
[11] P. Schwendt, M. Sivák, A. E. Lapshin, Y. I. Smolin, Y. F. Shepelev, D. Gyepesová, *Transition Met. Chem.* **1993**, *19*, 34−36.
[12] L'. Kuchta, M. Sivák, J. Marek, F. Pavelcík, M. Casný, *New. J. Chem.* **1999**, 43−46.
[13] R. N. Jones, B. S. Gallagher, *J. Am. Chem. Soc.* **1959**, 5242−5251.
[14] S.-I. Murahashi, T. Naota, K. Ito, Y. Maeda, H. Taki, *J. Org. Chem.* **1987**, *52*, 4319−4327.
[15] A. E. Lapshin, Y. I. Smolin, Y. F. Shepelev, P. Schwendt, D. Gyepesová, *Kristallografiya* **1992**, *37*, 1415−1423.
[16] L'. Kuchta, M. Sivák, F. Pavelcík, *J. Chem. Res.* **1993**, (S) 393 and (M) 2801.
[17] A. E. Lapshin, Y. I. Smolin, Y. F. Shepelev, M. Sivák, D. Gyepesová, *Acta Crystallogr., Sect. C* **1993**, *49*, 867−870.
[18] K. Kanamori, K. Nishida, N. Miyata, K. Okamoto, *Chem. Lett.* **1998**, 1267−1268.
[19] *International Tables for X-ray Crystallography*, Kynoch Press, Birmingham, **1968**, vol. III, p. 258.
[20] D. C. Crans, P. K. Shin, *J. Am. Chem. Soc.* **1994**, *116*, 1305−1319.
[21] K. Elvingston, M. Fritzsche, D. Rehder, L. Petterson, *Acta Chem. Scand.* **1994**, *48*, 878−885.
[22] D. C. Crans, H. Holst, D. Keramidas, D. Rehder, *Inorg. Chem.* **1995**, *34*, 2524−2534.
[23] S. J. Angus-Dunne, R. J. Batchelor, A. S. Tracey, F. W. B. Einstein, *J. Am. Chem. Soc.* **1995**, *117*, 5292−5296.
[24] M. Sivák, P. Schwendt, *Transition Met. Chem.* **1989**, *14*, 273−276.
[25] M. Sivák, *Chem. Papers* **1987**, *41*, 311−319.
[26] I. Andersson, S. AngusDunne, O. W. Howarth, L. Petterson, *J. Inorg. Biochem.* **2000**, *80*, 51−58.
[27] O. W. Howarth, J. R. Hunt, *J. Chem. Soc., Dalton Trans.* **1979**, 1388−1391.
[28] V. Conte, F. di Furia, S. Moro, *J. Mol. Catal.* **1994**, *94*, 323−333.
[29] Y. Shi, J. A. Campbell, *J. Radioanal. Nucl. Chem.* **2000**, *245*, 293−300.
[30] J. R. Geigy A.-G., Brit. 950,666 (*Chem. Abstr.* **1964**, *61*, 4367e).
[31] O. Vollarová, J. Benko, M. Sivák, *Collect. Czech. Chem. Commun.* **1996**, *61*, 574−588.
[32] M. Sivák, P. Schwendt, *Proc. 13th Conf. Coord. Chem.*, Smolenice, Slovakia, **1991**, p. 259−260.
[33] M. Casný, Thesis, Comenius University Bratislava, **1999**.
[34] D. Rehder, J. C. Pessoa, C. F. G. C. Geraldes, M. M. C. A. Castro, Th. Kabanos, T. Kiss, B. Meier, G. Micera, L. Petterson, M. Rangel, A. Salifoglou, I. Turel, D. Wang, *J. Biol. Inorg. Chem.* **2002**, 384−396.
[35] J. Park, A. Y. C. Liu, *J. Cell. Physiol.* **2000**, *185*, 348−357.
[36] E. M. Grandjan, P. Berthet, K. Ruffmann, P. Leuenberger, *Pharmacol. Res.* **2000**, *42*, 39−50.
[37] Z. Ben-Ari, H. Vaknin, R. Tur-Kaspa:, *Hepato-Gastroenterol.* **2000**, *47*, 786−789.
[38] D. L. Nosco, E. Deutsch, *Inorg. Synth.* **1982**, *21*, 19−23.
[39] C. P. Sloan, J. H. Krueger, *Inorg. Chem.* **1975**, *14*, 1481−1485.

Received July 12, 2002

 © 2003 Wiley-VCH Verlag GmbH & Co. KGaA, Weinheim

Extended X-ray Absorption Fine Structure Study of Copper(I) and Copper(II) Complexes in Atom Transfer Radical Polymerization

Tomislav Pintauer,[a] Ulrich Reinöhl,[b] Martin Feth,[b] Helmut Bertagnolli,[b] and Krzysztof Matyjaszewski*[a]

Keywords: EXAFS spectroscopy / Copper / Radical reactions / Polymerizations

Extended X-ray Absorption Fine Structure (EXAFS) spectroscopy has been used to investigate structural features of Cu^{I}-Br and $Cu^{II}Br_2$ complexes with dNbpy, PMDETA, Me_6TREN, tNtpy, and Me_4CYCLAM in various solvents {dNbpy = 4,4′-bis(5-nonyl)-2,2′-bipyridine, PMDETA = *N*,*N*,*N*′,*N*′′,*N*′′-pentamethyldiethylenetriamine, Me_6TREN = tris[2-(dimethylamino)ethyl]amine, tNtpy = 4,4′,4′′-tris(5-nonyl)-2,2′:6′,2′′-terpyridine, Me_4CYCLAM = 1,4,8,11-tetramethyl-1,4,8,11-tetraazacyclotetradecane}. The structures of the Cu^{I} and Cu^{II} complexes were found to depend on the solvent polarity and the number of nitrogen atoms in the ligand. Generally, in non-polar media and with monomers typically used in ATRP, Cu^{I} complexes preferred a tetracoordinate geometry, and were either ionic as observed in $[Cu^{I}(dNbpy)_2]^+[Cu^{I}Br_2]^-$ (Cu^{I}–N_{AV} = 2.00 Å, Cu^{I}–Br_{AV} = 2.25 Å) and $[Cu^{I}(Me_4CYCLAM)]^+[Cu^{I}Br_2]^-$ (Cu^{I}–N_{AV} = 2.06 Å, Cu^{I}–Br_{AV} = 2.23 Å), or neutral as in $[Cu^{I}$(PMDETA)Br] (Cu^{I}–N_{AV} = 2.12 Å, Cu^{I}–Br_{AV} = 2.33 Å), and $[Cu^{I}$(tNtpy)Br] (Cu^{I}–N_{AV} = 2.03 Å, Cu^{I}–Br_{AV} = 2.29 Å). The EXAFS analysis of $Cu^{II}Br_2$ complexes indicated a preference for a coordination number of five, such as in $[Cu^{II}(dNbpy)_2Br]^+[Br]^-$ (Cu^{II}–N_{AV} = 2.03 Å, Cu^{II}–Br_{AV} = 2.43 Å), $[Cu^{II}(PMDETA)Br_2]$ (Cu^{II}–N_{AV} = 2.03 Å, Cu^{II}–$Br_{1,AV}$ = 2.44 Å, Cu^{II}–$Br_{2,AV}$ = 2.64 Å) and $[Cu^{II}(Me_6TREN)Br]^+[Br]^-$ (Cu^{II}–N_{AV} = 2.09 Å, Cu^{II}-Br_{AV} = 2.39 Å), with the exception of the neutral tetracoordinate $[Cu^{II}(dNbpy)Br_2]$ (Cu^{II}–N_{AV} = 2.02 Å, Cu^{II}–Br_{AV} = 2.36 Å), which has been observed in non-polar media. Additionally, polar media were found to favor bromide dissociation in $[Cu^{II}(Me_6TREN)Br]^+[Br]^-$ and $[Cu^{II}(PMDETA)Br_2]$, as indicated by a decrease in the Br and Cu coordination numbers at the Cu- and Br-*K*-edges, respectively.

(© Wiley-VCH Verlag GmbH & Co. KGaA, 69451 Weinheim, Germany, 2003)

Introduction and Background

The synthesis of macromolecules with well-defined compositions, architectures, and functionalities represents an ongoing effort in the field of polymer chemistry. Over the past few years, atom transfer radical polymerization (ATRP) has emerged as a very powerful and robust technique to meet these goals.[1−6] The basic working mechanism of ATRP (Scheme 1) involves a reversible switching between two oxidation states of a transition metal complex.[3,7,8] Typically, a copper(I) halide is used in conjunction with a nitrogen-based ligand (Scheme 2).[9,10]

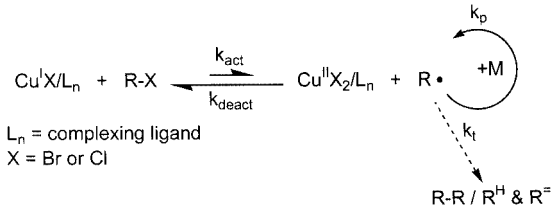

Scheme 1. Proposed mechanism for ATRP

Homolytic cleavage of the alkyl halide bond (R−X) by the Cu^{I} complex generates an alkyl radical R· and the corresponding Cu^{II} complex. The radical R· can either (a) propagate with a propagation rate constant k_p, by adding across the double bond of a vinyl monomer, (b) terminate by either coupling or disproportionation (k_t), or (c) be reversibly deactivated by the Cu^{II} complex (k_{deact}). Since the position of equilibrium is strongly shifted towards the dormant species ($k_{act} << k_{deact}$), radical termination is suppressed. As a result of the persistent radical effect,[11,12] polymers with predictable molecular weights, narrow molecular-weight distributions and high functionalities have been synthesized.[13]

Structural and mechanistic studies are crucial in understanding this mechanism further and are inherently part of the future developments of ATRP. Correlation of the catalyst structure[14−19] with reaction parameters such as the activation and deactivation rate constants[20−24] can lead to a development of more active catalysts and controlled polymerization of less reactive monomers (e.g. vinyl esters). Furthermore, systematic evaluation of the concurrent reac-

[a] Department of Chemistry, Carnegie Mellon University, 4400 Fifth Avenue, Pittsburgh, PA 15213, USA
Fax: (internat.) + 1-412/268-6897
E-mail: km3b@andrew.cmu.edu
[b] Institut für Physikalische Chemie, Universität Stuttgart, Pfaffenwaldring 55, 70569, Stuttgart, Germany
Fax: (internat.) + 49-711/685-4443
E-mail: h.bertagnolli@ipc.uni-stuttgart.de

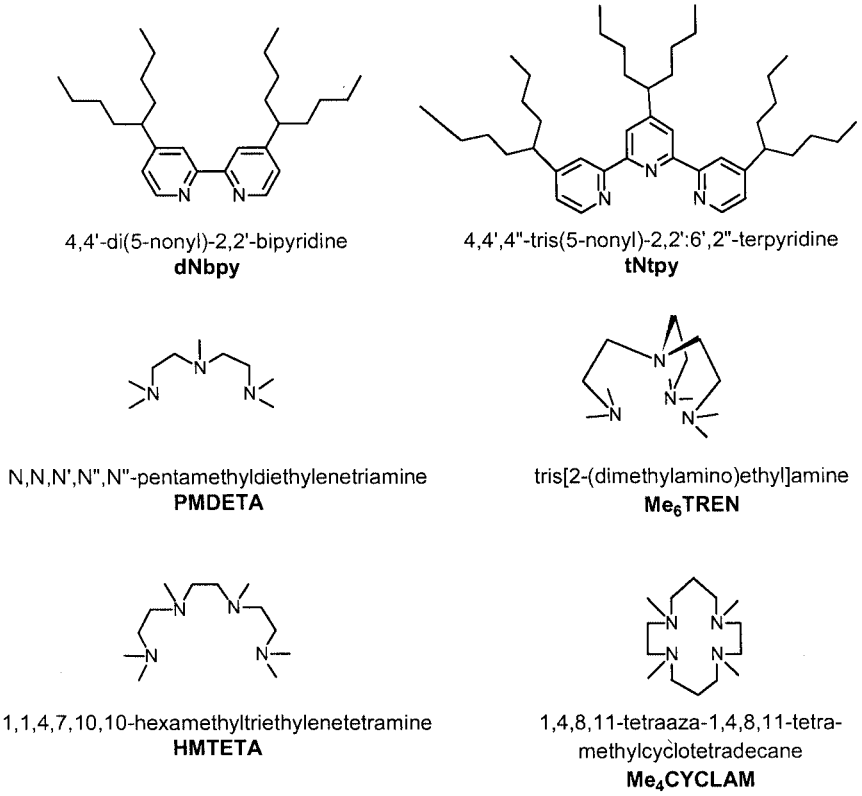

Scheme 2. Nitrogen-based ligands typically used in copper-mediated ATRP

tions that might occur in ATRP such as radical, monomer or solvent coordination[25] to the active catalysts, as well as transfer reactions associated with the ligand,[26−28] can provide much needed information about how to extend polymerization control to even higher molecular weight polymers, and generally improve the overall catalytic process.

Extended X-ray Absorption Fine Structure (EXAFS) spectroscopy has been shown to be a powerful technique for determining the structures of transition metal complexes in both the solid state and in solution.[29−32] An analysis of the EXAFS spectrum provides information on the bond lengths, the coordination number and the nature of the scattering atoms surrounding an excited atom.[33,34] In this paper, we report the results of an EXAFS spectroscopic study of $Cu^{I}Br$ and $Cu^{II}Br_2$ complexes with 4,4′-bis(5-nonyl)-2,2′-bipyridine (dNbpy), 4,4′,4′′-tris(5-nonyl)-2,2′:6′,2′′-terpyridine (tNtpy), *N*,*N*,*N*′,*N*′′,*N*′′-pentamethyldiethylenetriamine (PMDETA), tris[2-(dimethylamino)ethyl]amine (Me_6TREN) and 1,4,8,11-tetramethyl-1,4,8,11-tetraazacyclotetradecane (Me_4CYCLAM) in various solvents. The structures reported by EXAFS spectroscopy are primarily based on the interatomic distances around the absorber and their comparison with the structurally isolated and characterized model compounds. Due to the inherent errors in determination of the coordination numbers, the reported structures might also represent the average structures in solution. Therefore the possibility of the presence of other species that might co-exist in equilibrium cannot be excluded.

Results and Discussion

Model Complexes

In order to test the applicability and accuracy of EXAFS spectroscopic analysis in determining the structures of $Cu^{I}Br$ and $Cu^{II}Br_2$ complexes with nitrogen-based ligands, we have conducted measurements at Cu- and Br-*K*-edges for a series of complexes in the solid state for which the molecular structures are known. Table 1 shows the comparison between experimental bond lengths from EXAFS measurements at room temperature with distances derived from the single-crystal X-ray structures of $Cu^{I}Br$ and $Cu^{II}Br_2$ complexes with nitrogen-based ligands. Solid-state samples of $[Cu^{I}(bpy)_2]^{+}[ClO_4]^{-}$ [35] were used to model tetrahedral complexes, $[Cu^{I}(Me_6TREN)]^{+}[ClO_4]^{-}$ [36] for trigonal-bipyramidal complexes, $[Cu^{I}(bpy)Br]_2$[37] for bridged complexes, and $[N(C_4H_9)_4]^{+}[Cu^{I}Br_2]^{-}$ [38] for linear Cu^{I} complexes. Additionally, $[Cu^{II}(bpy)_2Br]^{+}[BF_4]^{-}$ [39] and $[Cu^{II}Br(Me_6TREN)]^{+}[Br]^{-}$ [40] were used as model compounds for trigonal-bipyramidal complexes, whilst $[Cu^{II}(PMDETA)Br_2]$[41] and $[Cu^{II}(terpy)Br_2]$[14,42] were used to model distorted square-pyramidal Cu^{II} complexes. As shown in Table 1, a good agreement has been observed between the distances determined by EXAFS and X-ray crystallography, confirming the accuracy of the EXAFS analysis.

The corresponding coordination numbers were also determined by iterative fitting. Typically, the error for the coordination number is about 10−15% when the peaks in the Fourier-transformed spectra are well resolved and separated

 © 2003 Wiley-VCH Verlag GmbH & Co. KGaA, Weinheim

Table 1. Comparison of experimental bond lengths [Å] from EXAFS measurements at room temperature with distances in the single-crystal X-ray structures; coordination numbers were fixed to the crystallographically derived values

Complex	Cu−N_{AV} [Å] EXAFS	Cu−N_{AV} [Å] X-ray	Cu−Br_{AV} [Å] EXAFS	Cu−Br_{AV} [Å] X-ray
$[Cu^{I}(bpy)_2]^+[ClO_4]^-$ [35]	1.98	2.02		
$[Cu^{I}(Me_6TREN)]^+[ClO_4]^-$ [36]	2.13	2.16		
$[Cu^{I}(bpy)Br]_2$ [37]	2.10	2.09	2.44	2.44
			2.25	2.23
$[N(C_4H_9)_4]^+[Cu^{I}Br_2]^-$ [38]				
$[Cu^{II}(bpy)_2Br]^+[BF_4]^-$ [39]	2.01	2.04	2.41	2.42
$[Cu^{II}Br(Me_6TREN)]^+[Br]^-$ [40]	2.09	2.11	2.39	2.39
$[Cu^{II}(PMDETA)Br_2]$[41]	2.09	2.10	2.44, 2.64	2.45, 2.64
$[Cu^{II}(terpy)Br_2]$[42]	2.02	2.01	2.45	2.49

{e.g. in $[Cu^{I}(bpy)_2]^+[ClO_4]^-$ $CN(N)_{fit}$ = 3.7, r_{fit} = 1.98 Å, $CN(N)_{X\text{-}ray}$ = 4.0, $r_{X\text{-}ray}$ = 1.98 Å}. In the case of significant overlapping of the peaks, the error in the coordination number can amount to 30% {e.g. in $[Cu^{II}(bpy)_2Br]^+[BF_4]^-$ $CN(N)_{fit}$ = 2.7, r_{fit} = 2.00 Å, $CN(N)_{X\text{-}ray}$ = 4.0, $r_{X\text{-}ray}$ = 2.01 Å and $CN(Br)_{fit}$ = 0.7, r_{fit} = 2.40 Å, $CN(Br)_{X\text{-}ray}$ = 1.0, $r_{X\text{-}ray}$ = 2.41 Å}. However, the distances determined either by iterative fitting or fitting with fixed coordination numbers agree within 1% with the distances measured by X-ray crystallography. Therefore, since the error range for the coordination numbers is significantly larger than the accuracy of the distances, the interpretation of the following systems is mainly based on the determined distances and their comparison with the model compounds.

$Cu^{I}Br$ and $Cu^{II}Br_2$ Complexes with the dNbpy Ligand

Unsubstituted 2,2′-bipyridine was the first ligand used in copper-mediated ATRP.[9] Alkyl substitutions in the 4- and 4′-positions of the bipyridine ring, such as in dNbpy (Scheme 2) further improved the solubility of the catalyst in non-polar media, which resulted in higher conversions with very low polydispersities.[43] Table 2 shows the summary of room-temperature EXAFS spectroscopic measurements, in different solvents, of $Cu^{I}Br$ and $Cu^{II}Br_2$ complexes with the dNbpy ligand.

The EXAFS spectrum of the $Cu^{I}Br$ complex with 1 equiv. of dNbpy in styrene is well fit using the structural model in which the Cu^{I} center is coordinated by 3.8 nitro-

Table 2. Structural parameters of $Cu^{I}Br$ and $Cu^{II}Br_2$ complexes with dNbpy ligand, determined by EXAFS measurements under ambient conditions at the Cu- and Br-*K*-edge; MA = methyl acrylate

Complex[a]	Solvent	Backscatt.	N	*r* [Å]	σ [Å]	ΔE_0 [eV]	*k* [$Å^{-1}$]	Fit index
$Cu^{I}Br$/dNbpy	styrene	Cu−N	3.8	2.01	0.096	18.7	3.8−12.5	27.6
		Cu−Br	1.1	2.25	0.078			
		Br−Cu	0.8	2.24	0.074	21.8	4.1−12.6	27.8
	MA	Cu−N	3.7	1.99	0.100	13.6	4.0−12.5	29.6
		Cu−Br	1.3	2.26	0.090			
		Br−Cu	1.0	2.26	0.100	18.5	4.3−12.0	19.6
$Cu^{I}Br$/2dNbpy	styrene	Cu−N	2.9	2.03	0.105	19.0	4.1−12.0	36.2
		Cu−Br	1.4	2.25	0.105			
		Br−Cu	0.8	2.24	0.087	21.2	4.3−12.5	29.6
	MA	Cu−N	2.8	2.01	0.100	21.9	4.2−12.5	20.7
		Cu−Br	1.3	2.26	0.090			
		Br−Cu	0.8	2.25	0.100	14.5	4.2−12.0	34.5
$Cu^{II}Br_2$/2dNbpy	MA	Cu−N	1.4	2.01	0.071	17.2	4.0−13.7	29.1
		Cu−Br	1.5	2.37	0.071			
		Cu−C	2.0	2.94	0.049			
		Br−Cu	0.9	2.37	0.059	13.5	4.1−14.0	31.6
	toluene	Cu−N	1.8	2.03	0.051	15.0	4.1−15.1	20.1
		Cu−Br	2.1	2.37	0.074			
		Cu−C	1.6	2.93	0.049			
		Br−Cu	1.1	2.35	0.062	18.8	4.2−14.1	16.5
	MeOH	Cu−N	2.8	2.03	0.071	17.8	4.2−14.8	27.0
		Cu−Br	0.6	2.43	0.063			
		Br−Cu	0.30	2.42	0.067	19.4	4.2−14.1	56.9

[a] *N* = coordination number, *r* = absorber−backscatterer distance, σ = Debye−Waller factor. Inherent errors are approximately 10−30% for coordination numbers and Debye−Waller factors and 1% for distances.

 © 2003 Wiley-VCH Verlag GmbH & Co. KGaA, Weinheim

gen atoms at a distance of 2.01 Å and 1.1 bromine atoms at a distance of 2.25 Å. The results in methyl acrylate are analogous, indicating similar structural features for the complex. Furthermore, when 2 equiv. of dNbpy were used relative to $Cu^{I}Br$, the average $Cu^{I}-N$ and $Cu^{I}-Br$ distances did not change significantly, although the coordination number of nitrogen appears to be lower than in solutions that contained only 1 equiv. of dNbpy. Taking into account the inherent error of 10−30% for the coordination numbers and 1% for the distances, the most plausible species in non-polar media is the ionic complex $[Cu^{I}(dNbpy)_2]^+[Cu^{I}Br_2]^-$. The neutral complex $[Cu^{I}(dNbpy)Br]_2$ can be ruled out since $Cu^{I}-Br$ bond lengths in Br-bridged Cu^{I} complexes are typically 2.4−2.5 Å (Table 1).[37] The average $Cu^{I}-N$ bond length in the $[Cu^{I}(dNbpy)_2]^+$ cation (2.01 Å) is consistent with the average $Cu^{I}-N$ bond lengths in bpy derivatives such as $[Cu^{I}(bpy)_2]^+[ClO_4]^-$ [35] (2.021 Å), $[Cu^{I}(6,6'\text{-}Me_2\text{-}bpy)_2]^+[BF_4]^-$ [44] (2.032 Å) and $[Cu^{I}(4,4'\text{-}Me_2\text{-}bpy)_2]^+[Br]^-$ [45] (2.035 Å). Furthermore, the $Cu^{I}-Br$ bond length in the linear $[Cu^{I}Br_2]^-$ anion (2.25 Å) is similar to that seen in related complexes such as $[N(C_4H_9)_4]^+[Cu^{I}Br_2]^-$ [38] (2.226 Å), $[P(C_6H_5)_4]^+[Cu^{I}Br_2]^-$ [46] (2.214 Å) and $[Cu^{I}(phen)_2]^+[Cu^{I}Br_2]^-$ [47] (2.216 Å).

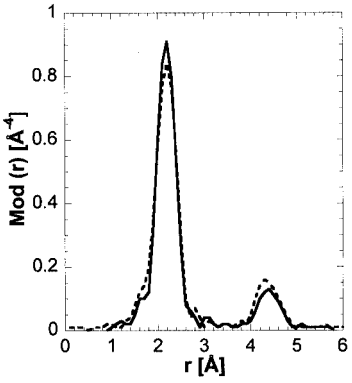

Figure 1. Comparison of the experimental Fourier transformed $k^3\chi(k)$ functions at the Br-*K*-edge of $Cu^{I}Br$/dNbpy in toluene (solid line) and $[N(C_4H_9)_4][Cu^{I}Br_2]$ in the solid state (broken lines)

Figure 1 shows the Fourier transformations of the EXAFS functions at the Br-*K*-edge of the $Cu^{I}Br$/2dNbpy complex in toluene and of $[N(C_4H_9)_4]^+[Cu^{I}Br_2]^-$ in the solid state. The similarity of the two spectra further suggests the presence of $[Cu^{I}Br_2]^-$ anions in the $Cu^{I}Br$/(2)dNbpy complex in non-polar media, which is consistent with the proposed species $[Cu^{I}(dNbpy)_2]^+[Cu^{I}Br_2]^-$.

We have investigated the complexation between $Cu^{I}Br$ and dNbpy in non-polar media previously by Electrospray Ionization Mass Spectrometry (ESI-MS)[48] and EXAFS spectroscopy.[15] ESI-MS spectra of $Cu^{I}Br$ complexed with 1 or 2 equiv. of dNbpy in toluene, methyl acrylate, or styrene showed only the presence of the $[Cu^{I}(dNbpy)_2]^+$ cation and the $[Cu^{I}Br_2]^-$ anion, which is consistent with the proposed species, $[Cu^{I}(dNbpy)_2]^+[Cu^{I}Br_2]^-$. Furthermore, the EXAFS analysis at the Cu-*K*-edge also indicated the presence of $[Cu^{I}(dNbpy)_2]^+[Cu^{I}Br_2]^-$. Recently, the molecular structure of a related bpy-based ATRP active catalyst, $[Cu^{I}(dNEObpy)_2]^+[Cu^{I}Br_2]^-$ (dNEObpy = 4,4′-bis{[dimethyl(neophyl)silyl]methyl}-2,2′-bipyridine) further confirmed this unusual 1:1 stoichiometry in non-polar media between $Cu^{I}Br$ and bpy based ligands.[17]

Taking into account the inherent error in determining the coordination numbers by EXAFS spectroscopy (10−30%), $[Cu^{I}(dNbpy)_2]^+[Cu^{I}Br_2]^-$ might not be the only complex present in solution. Consequently, the possibility of more than one species co-existing in equilibrium cannot be excluded. Depending on the temperature, solvent polarity, and the amount of dNbpy, the substitution of Br in $[Cu^{I}Br_2]^-$ by dNbpy may lead to the formation of $[Cu^{I}(dNbpy)_2]^+[Br]^-$ (Scheme 3).

A similar equilibrium has been proposed earlier for $[Cu^{I}(dNEObpy)_2]^+[Cu^{I}Br_2]^-$.[17] Additionally, solvent and monomer coordination to the Cu^{I} center[49] cannot be ruled out due to the limited sensitivity of EXAFS measurements.[32] More experimental evidence is therefore needed to further characterize this system.

The results of the EXAFS spectroscopic analysis of the $Cu^{II}Br_2$ complex with 2 equiv. of dNbpy in methyl acrylate (Table 2) indicate that the coordination sphere around the Cu^{II} center consists of 1.4 N atoms at a distance of 2.01 Å and 1.5 Br atoms at a distance of 2.37 Å (a carbon backscatterer was used in the analysis in order to increase the accuracy of the fit). In toluene, the average $Cu^{II}-N$ and $Cu^{II}-Br$ distances did not change significantly, but the coordination numbers of N and Br increased to 1.8 and 2.1, respectively. In a more polar solvent, such as methanol, the coordination number of N increased even further to 2.8, and that of Br decreased to 0.6. Furthermore, the decrease

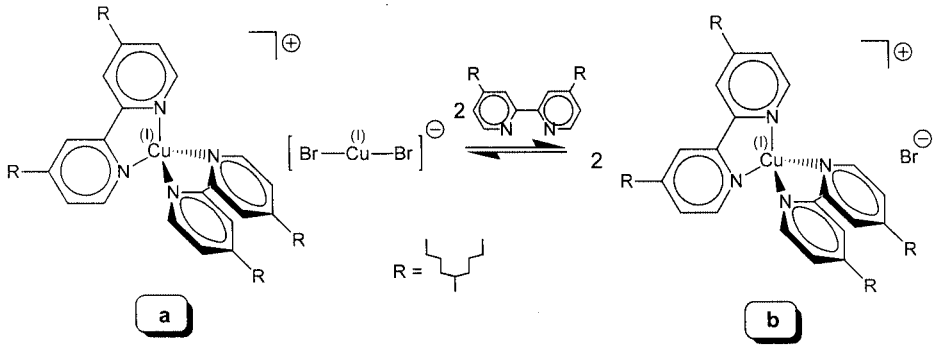

Scheme 3. Proposed structures for the $Cu^{I}Br$/(2)dNbpy complex in (a) non-polar and (b) polar media

 © 2003 Wiley-VCH Verlag GmbH & Co. KGaA, Weinheim

in the Br coordination number was accompanied by an increase in the average $Cu^{II}-Br$ bond length from 2.37 to 2.43 Å. In non-polar media such as toluene and methyl acrylate, the results of the EXAFS spectroscopic measurements are consistent with the neutral complex $[Cu^{I}-{}^{I}(dNbpy)Br_2]$ which has been isolated and characterized previously.[16] In the solid state, $[Cu^{II}(dNbpy)Br_2]$ has a distorted square-planar geometry. The Cu^{II} center is coordinated by the two nitrogen atoms of a single dNbpy ligand ($Cu^{II}-N_{AV}$ = 2.017 Å) and to two bromine atoms ($Cu^{II}-Br_{AV}$ = 2.359 Å). $[Cu^{II}(dNbpy)Br_2]$ undergoes bromide substitution by dNbpy to form the ionic complex $[Cu^{II}(dNbpy)_2Br]^+[Br]^-$, which is strongly favored a in more polar medium such as methanol (Scheme 4).

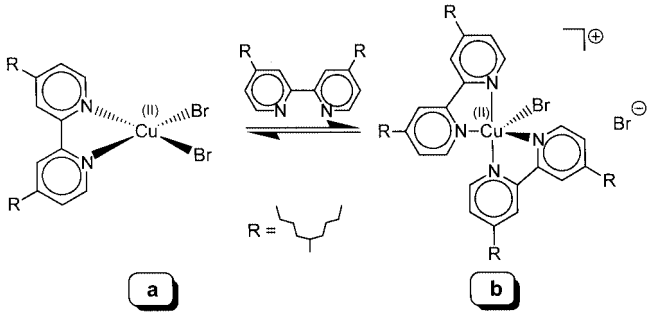

Scheme 4. Proposed structures for the $Cu^{II}Br_2$/(2)dNbpy complex in (a) non-polar and (b) polar media based on EXAFS measurements

The average $Cu^{II}-N$ (2.03 Å) and $Cu^{II}-Br$ (2.43 Å) bond lengths of $[Cu^{II}(dNbpy)_2Br]^+[Br]^-$ in methanol, as determined by EXAFS, are in good agreement with the average distances in the structurally characterized compounds $[Cu^{II}(bpy)_2Br]^+[Br]^-$ [50] ($Cu^{II}-N_{AV}$ = 2.034 Å, $Cu^{II}-Br$ = 2.429 Å), $[Cu^{II}(bpy)_2Br]^+[PF_6]^-$ [39] ($Cu^{II}-N_{AV}$ = 2.044 Å, $Cu^{II}-Br$ = 2.467 Å) and $[Cu^{II}(dNbpy)_2Br]^+[Cu^{I}Br_2]^-$ [14] ($Cu^{II}-N_{AV}$ = 2.016 Å, $Cu^{II}-Br$ = 2.426 Å). Additionally, as ΔH and ΔS for the equilibrium reaction in Scheme 4 were found to be negative, an increase in the temperature favors formation of the neutral complex $[Cu^{II}(dNbpy)Br_2]$. It was determined that under the typical initial reverse ATRP conditions [$T \geq 90$ °C and total copper(II) concentration in the range 1.0×10^{-2} to 1.0×10^{-1} M], the $Cu^{I}-{}^{I}Br_2$ complex and 2 equiv. of dNbpy will predominantly form the neutral complex $[Cu^{II}(dNbpy)Br_2]$.[16]

We have previously investigated the complexation between $Cu^{II}Br_2$ and dNbpy in non-polar media, including monomers that are typically used in ATRP. Based on the EXAFS[15] and ESI-MS[48] study, we proposed the formation of a 1:1 complex, $[Cu^{II}(dNbpy)_2Br]^+[Cu^{II}Br_3]^-$. The structure was primarily based on the relative intensities of the absorbance peaks in the ESI-MS spectra since both species have, on average, the same atomic distances as derived from the EXAFS measurements. The absence of the charge in $[Cu^{II}(dNbpy)Br_2]$ may be responsible for its weak intensity. This could consequently lead to the wrong conclusion about the most probable structure in solution.

Table 3. Structural parameters of $Cu^{I}Br$ and $Cu^{II}Br_2$ complexes with PMDETA ligand, determined by EXAFS measurements under ambient conditions at the Cu- and Br-*K*-edge

Complex[a]	Solvent	Backscatt.	N	*r* [Å]	σ [Å]	ΔE_0 [eV]	*k* [$Å^{-1}$]	Fit index
$Cu^{I}Br$/PMDETA	MA	Cu−N	2.9	2.12	0.114	15.6	4.3−13.6	15.7
		Cu−Br	1.2	2.33	0.084			
		Cu−C	5.1	2.94	0.120			
		Br−Cu	1.0	2.32	0.063	19.1	4.2−14.1	19.6
	styrene	Cu−N	2.7	2.14	0.109	14.5	4.4−13.6	11.4
		Cu−Br	1.2	2.33	0.089			
		Cu−C	5.9	2.97	0.118			
		Br−Cu	1.0	2.33	0.063	19.1	4.2−14.1	19.6
	toluene	Cu−N	2.5	2.10	0.097	19.0	4.5−13.6	27.7
		Cu−Br	1.0	2.30	0.091			
		Cu−C	6.2	2.91	0.116			
		Br−Cu	1.3	2.29	0.097	24.7	4.4−14.9	25.6
	MeOH	Cu−N	2.8	2.13	0.105	15.6	4.4−14.0	21.4
		Cu−Br	1.1	2.35	0.095			
		Cu−C	6.0	2.94	0.118			
		Br−Cu	1.0	2.33	0.093	23.0	4.2−14.4	24.7
$Cu^{II}Br_2$/PMDETA	toluene/	Cu−N	3.6	2.13	0.099	12.5	4.4−14.0	29.1
	MeOH	Cu−Br	1.0	2.42	0.084			
	(4:1 vol.)	Cu−C	7.4	2.99	0.107			
		Br−Cu	0.5	2.39	0.074	20.7	4.2−12.0	27.0
	MeOH	Cu−N	3.1	2.09	0.087	16.5	3.8−15.0	23.3
		Cu−Br	1.1	2.41	0.087			
		Cu−C	7.0	2.94	0.107			
		Br−Cu	0.4	2.39	0.077	13.2	3.8−12.0	21.7
	H_2O	Cu−N	4.0	2.06	0.081	15.3	3.9−14.8	40.9
		Cu−C	6.0	2.91	0.093			

[a] *N* = coordination number, *r* = absorber−backscatterer distance, σ = Debye−Waller factor. Inherent errors are approximately 10−30% for coordination numbers and Debye−Waller factors and 1% for distances.

 © 2003 Wiley-VCH Verlag GmbH & Co. KGaA, Weinheim

$Cu^{I}Br$ and $Cu^{II}Br_2$ Complexes with the PMDETA Ligand

Apart from substituted bipyridines, other linear and cyclic amines were successfully used as ligands in the formation of ATRP catalysts.[51−55] In particular, commercially available tridentate PMDETA (Scheme 2) showed a high potential for the controlled polymerization of a variety of monomers. Typically, the ligand/copper(I) halide ratio used in the polymerization was 1:1. Shown in Table 3 is a summary of the room-temperature EXAFS measurements of $Cu^{I}Br$ and $Cu^{II}Br_2$ complexes with 1 equiv. of PMDETA in different solvents, including monomers typically used in ATRP. The typical experimental and calculated Fourier transformations of the EXAFS spectra for the $Cu^{I}Br$/PMDETA and $Cu^{II}Br_2$/PMDETA complexes are shown in Figures 2 and 3, respectively.

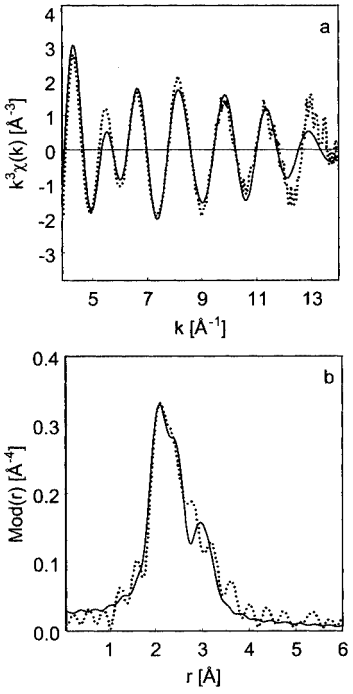

Figure 2. Experimental (dotted line) and calculated (solid line) $k^3\chi(k)$ functions (a) (k range: 3.90−14.0 Å^{-1}) and their Fourier transformations (b) at the Cu-K-edge for $Cu^{I}Br$/PMDETA in toluene at room temperature (see Table 3 for fit parameters)

The results of the EXAFS spectroscopic analysis of $Cu^{I}Br$/PMDETA in methyl acrylate, styrene, toluene, and methanol (Table 3) indicate similar structural features for the complex in these solvents. In all solvents, the EXAFS data are well fit by a structural model that includes 3.0 nitrogen atoms at a distance of 2.12 Å and 1.0 bromine atoms at a distance of 2.33 Å.

The average $Cu^{I}-N$ bond length is in agreement with those in other Cu^{I} complexes with similar nitrogen-based chromophores.[56] Additionally, the $Cu^{I}-Br$ bond length indicates covalent bonding to the Cu^{I} center. Based on these results, one structure that is consistent with the EXAFS analysis is the neutral complex [Cu^{I}(PMDETA)Br]. However, other structures might also co-exist in equilibrium and are shown in Scheme 5.

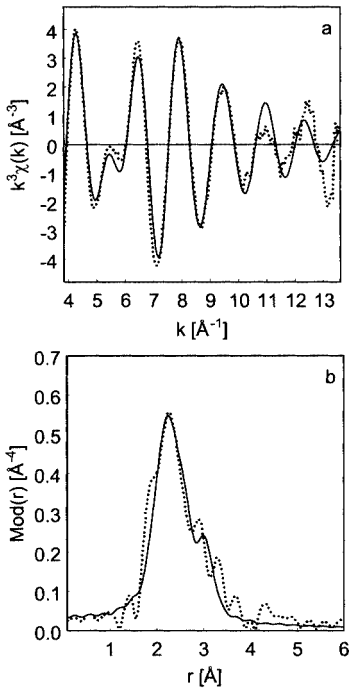

Figure 3. Experimental (dotted line) and calculated (solid line) $k^3\chi(k)$ functions (a) (k range: 3.80−14.1 Å^{-1}) and their Fourier transformations (b) at the Cu-K-edge for $Cu^{II}Br_2$/PMDETA in toluene/methanol mixture (80%/20% v/v) at room temperature (see Table 3 for fit parameters)

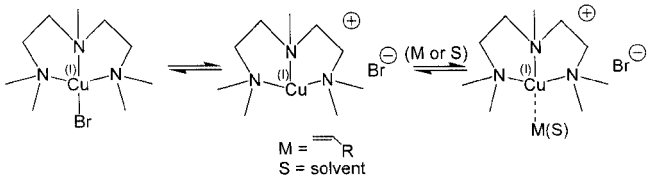

Scheme 5. Proposed structures for the $Cu^{I}Br$/PMDETA complex

Based on the solvent polarity and temperature, the dissociation of bromide could lead to the formation of the ionic complex [Cu^{I}(PMDETA)]$^+$[Br]$^-$. The coordinatively unsaturated [Cu^{I}(PMDETA)]$^+$ cation can be further coordinated by solvent (S) or monomer leading to the formation of [Cu^{I}(PMDETA)(S)]$^+$[Br]$^-$ and [Cu^{I}(PMDETA)(M)]$^+$[Br]$^-$, respectively. We were recently able to isolate and structurally characterize [Cu^{I}(PMDETA)(π-styrene)]$^+$[BPh_4]$^-$ and [Cu^{I}(PMDETA)(π-MA)]$^+$[BPh_4]$^-$ which model the monomer coordination to [Cu^{I}(PMDETA)]$^+$.[57] The monomer coordination occurred via π-bond formation, with a significant contribution from Cu^{I} π-back donation, as manifested in the strong shielding of the vinyl protons. Similar coordination has also been observed previously in [Cu^{I}(dien)(π-1-hexene)]$^+$[BPh_4]$^-$ (dien = diethylenetriamine).[58] A more detailed characterization of the $Cu^{I}Br$/PMDETA catalytic system in ATRP is under investigation.

Room temperature EXAFS measurements of the $Cu^{II}Br_2$ complex with 1 equiv. of PMDETA are shown in Table 3. The study was limited to relatively polar media, due to the poor solubility of the complex in typical non-polar ATRP solutions.

 © 2003 Wiley-VCH Verlag GmbH & Co. KGaA, Weinheim

In a toluene/MeOH mixture (4:1 vol.), the EXAFS spectrum was fit reasonably well by assuming that the Cu^{II} center is coordinated by 3.6 nitrogen atoms at a distance of 2.13 Å and 1.0 bromine atoms at a distance of 2.42 Å. In more polar methanol, the average $Cu^{II}-N$ and $Cu^{II}-Br$ bond lengths did not change significantly. On the other hand, the EXAFS spectrum in H_2O indicated the absence of a $Cu^{II}-Br$ bond, which was also confirmed by measurements at the Br-*K*-edge. The structure of the $Cu^{II}Br_2$ complex with 1 equiv. of PMDETA has been recently reported. In the solid state, the complex exists as $[Cu^{II}(PMDETA)Br_2]$ with a distorted square-pyramidal coordination sphere.[14] The Cu^{II} center is coordinated by three nitrogen atoms of the PMDETA ligand ($Cu^{II}-N_{AV}$ = 2.098 Å) and two bromine atoms ($Cu^{II}-Br_{AV}$ = 2.545 Å). The $Cu^{II}-Br$ bond length in the apical position (2.644 Å) is much longer than the $Cu^{II}-Br$ bond length in the basal position (2.446 Å). This was attributed to the relatively small energy differences between the trigonal bipyramidal and square-pyramidal geometries of pentacoordinate Cu^{II} complexes. The average $Cu^{II}-N$ bond lengths determined by EXAFS spectroscopy in toluene/MeOH (2.13 Å), MeOH (2.09 Å) and H_2O (2.06 Å) are in good agreement with the average $Cu^{II}-N$ bond length in $[Cu^{II}(PMDETA)Br_2]$ (2.098 Å). However, the average $Cu^{II}-Br$ bond lengths in toluene/MeOH (2.42 Å) and MeOH (2.41 Å) are inconsistent with the average bond length in $[Cu^{II}(PMDETA)Br_2]$ (2.545 Å). Taking into account the coordination number of Br at the Cu- and Br-*K*-edges, the structural features of the $Cu^{II}Br_2$ complex with PMDETA determined by EXAFS can be explained in terms of bromide dissociation from $[Cu^{II}(PMDETA)Br_2]$. In toluene/MeOH and MeOH, the EXAFS data suggest the presence of $[Cu^{II}(PMDETA)Br]^+[Br]^+$. In H_2O, additional dissociation of bromide could result in the formation of $[Cu^{II}(PMDETA)]^{2+}[Br]_2^-$. Since Cu^{II} complexes prefer a pentacoordinate geometry,[56] the vacant coordination sites in $[Cu^{II}(PMDETA)Br]^+[Br]^-$ and $[Cu^{II}(PMDETA)]^{2+}[Br]_2^-$ are likely to be occupied by solvent molecules (MeOH or H_2O) (Scheme 6).

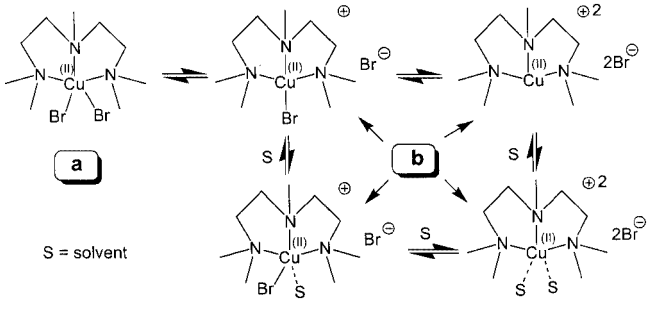

Scheme 6. Proposed structures for the $Cu^{II}Br_2$/PMDETA complex in (a) non-polar and (b) polar media based on EXAFS measurements

This has been demonstrated in the solid state with X-ray studies of the structures of the related complexes $[Cu^{II}(PMDETA)(H_2O)]^{2+}[ClO_4]_2^-$ [59] and $[Cu^{II}(PMDETA)(H_2O)_2]^{2+}[BF_4]_2^-$.[60] The replacement of bromide via π-bond formation with a monomer is less likely to occur with Cu^{II} complexes because the binding constants are typically very low.[61] However, substitution can potentially occur with functionalized olefins because they can additionally coordinate to the Cu^{II} complexes via functional groups (S, O, N etc.).[62]

Dissociation of halide anions from Cu^{II} complexes has been the subject of numerous investigations.[63–65] The equilibrium constants were found to strongly depend on the temperature and polarity of the reaction medium. Furthermore, polar and protic solvents such as MeOH and H_2O were found to favor halide anions dissociation, an observation which was most likely due to solvation effects. High values of the equilibrium constant for halide dissociation from $[Cu^{II}(L)-X]^+$ (X = Br^- or Cl^-) complexes could explain the fast ATRP reactions in polar media. The halide dissociation from $[Cu^{II}(L)-X]^+$ shifts the position of the ATRP equilibrium (see Scheme 1), resulting in an increase in radical concentration. Our recent measurements determined that the equilibrium constant for bromide dissociation from $[Cu^{II}(PMDETA)Br_2]$ in H_2O at room temperature was K = 0.18 mol·L^{-1}.[66] Using this value, one can estimate that under typical conditions of the EXAFS experiment (room temperature, $[Cu^{II}Br_2]_0$ = $[PMDETA]_0 \approx 0.05$ M) approximately 80% of the $Cu^{II}Br_2$/PMDETA complex in H_2O contains dissociated bromide anions. This further supports the results of the EXAFS analysis and structures proposed in Scheme 6. A more detailed study of the effect of halide dissociation from other ATRP active Cu^{II} complexes is currently being carried out.

$Cu^{I}Br$ and $Cu^{II}Br_2$ Complexes with the Me_6TREN Ligands

Tris[2-(dimethylamino)ethyl]amine (Me_6TREN, Scheme 2) is a tetradentate nitrogen-based ligand that has been successfully used in ATRP. Typically, the ligand/$Cu^{I}Br$ ratio was 1:1. This catalytic system showed a very high activity, enabling fast and controlled polymerization of methyl acrylate at ambient temperature.[52] The results of EXAFS measurements of $Cu^{I}Br$ and $Cu^{II}Br_2$ complexes with Me_6TREN in different solvents are summarized in Table 4.

The Cu-*K*-edge EXAFS spectrum of the $Cu^{I}Br$ complex with 1 equiv. of Me_6TREN in styrene can be best modeled by assuming that the coordination sphere around the Cu^{I} center is occupied by 3.0 nitrogen atoms at a distance of 2.15 Å and 1.2 bromine atoms at a distance of 2.33 Å. The results in methyl acrylate and toluene (Figure 4) are analogous, indicating similar structural features of the complex in those solvents.

Taking into account the 18-electron rule and the tetradentate nature of Me_6TREN, one would expect that the most probable structure of the $Cu^{I}Br/Me_6TREN$ complex in solution would be $[Cu^{I}(Me_6TREN)]^+[Br]^-$. The average $Cu^{I}-N$ bond lengths in styrene (2.15 Å), methyl acrylate (2.15 Å) and toluene (2.14 Å) are in agreement with the

 © 2003 Wiley-VCH Verlag GmbH & Co. KGaA, Weinheim

Table 4. Structural parameters of $Cu^{I}Br$ and $Cu^{II}Br_2$ complexes with Me_6TREN ligand, determined by EXAFS measurements under ambient conditions at the Cu- and Br-*K*-edge; MA = methyl acrylate

Complex[a]	Solvent	Backscatt.	N	*r* [Å]	σ [Å]	ΔE_0 [eV]	*k* [$Å^{-1}$]	Fit index
$Cu^{I}Br/Me_6TREN$	styrene	Cu−N	3.0	2.15	0.114	14.8	4.2−15.6	15.4
		Cu−Br	1.2	2.33	0.080			
		Cu−C	4.0	2.95	0.105			
		Br−Cu	1.0	2.32	0.071	19.1	3.6−14.0	17.1
	MA	Cu−N	2.8	2.15	0.110	15.3	4.2−15.4	12.3
		Cu−Br	1.1	2.33	0.077			
		Cu−C	5.9	2.94	0.116			
		Br−Cu	1.0	2.32	0.077	18.6	4.2−13.1	14.6
	toluene	Cu−N	2.8	2.14	0.100	18.6	4.2−14.6	20.8
		Cu−Br	1.3	2.31	0.084			
		Cu−C	5.4	2.91	0.118			
		Br−Cu	1.2	2.31	0.086	21.8	3.8−14.0	18.0
$Cu^{II}Br_2/Me_6TREN$	MeOH	Cu−N	3.2	2.13	0.100	18.8	4.2−15.0	19.9
		Cu−Br	1.4	2.38	0.081			
		Cu−C	8.7	2.94	0.114			
		Br−Cu	0.9	2.38	0.087	14.8	4.1−14.4	32.0
	H_2O	Cu−N	4.1	2.06	0.105	21.1	4.4−13.0	31.4
		Cu−Br	0.30	2.42	0.074			
		Cu−C	8.0	2.89	0.105			
		Br−Cu	0.0					

[a] *N* = coordination number, *r* = absorber−backscatterer distance, σ = Debye−Waller factor. Inherent errors are approximately 10−30% for coordination numbers and Debye−Waller factors and 1% for distances.

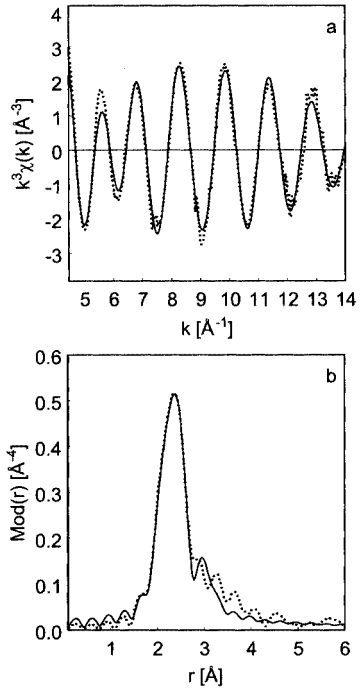

Figure 4. Experimental (dotted line) and calculated (solid line) $k^3\chi(k)$ functions (a) (*k* range: 4.20−14.6 $Å^{-1}$) and their Fourier transformations (b) at the Cu-*K*-edge for $Cu^{I}Br/Me_6TREN$ in toluene at room temperature (see Table 4 for fit parameters)

previously characterized complex $[Cu^{I}(Me_6TREN)]^{+}$-$[ClO_4]^{-}$ (2.161 Å).[36] However, the coordination number of N appears to be rather low for the tetradentate Me_6TREN ligand. Additionally, the presence of a Br backscatterer in the spectrum of the Cu-*K*-edge indicates covalent bonding to the Cu^{I} center. This evidence contradicts the presence of the solely ionic species $[Cu^{I}(Me_6TREN)]^{+}[Br]^{-}$.

The presence of a Cu^{I}−Br absorbance in the EXAFS spectrum of $Cu^{I}Br/Me_6TREN$ could suggest the presence of linear $[Cu^{I}Br_2]^{-}$ anions, as described earlier in the case of $[Cu^{I}(dNbpy)_2]^{+}[Cu^{I}Br_2]^{-}$. However, the average Cu^{I}−Br bond lengths in styrene (2.33 Å), methyl acrylate (2.33 Å), and toluene (2.31 Å) appear to be longer than the Cu^{I}−Br bond length in other Cu^{I} complexes with $[Cu^{I}Br_2]^{-}$ anions (2.206−2.232 Å).[17,38,46,47] The elongation of the Cu^{I}−Br bond in $[Cu^{I}Br_2]^{-}$ anions is possible, but was not observed in the structurally related complex $[Cu^{I}(HMTETA)]^{+}[Cu^{I}Cl_2]^{-}$ (HMTETA = 1,1,4,7,10,10-hexamethyltriethylenetetramine), in which the Cu^{I}−Cl bond length was found to be similar to those seen in other Cu^{I} complexes with linear $[Cu^{I}Cl_2]^{-}$ anions.[36]

The structure of the $Cu^{I}Br/Me_6TREN$ complex consistent with the EXAFS analysis is likeley to be the neutral $[Cu^{I}(Me_6TREN')Br]$ (Me_6TREN' denotes a tricoordinate Me_6TREN). Similar structures were proposed earlier for copper[67] and cobalt[68] complexes with the Me_6TREN ligand in order to explain the kinetics of ligand substitution reactions. Furthermore, the dissociation of one "amine" arm in Cu^{II} complexes with other tetradentate nitrogen-based ligands has also been reported.[69,70]

Due to the sensitivity of EXAFS measurements, inherent errors in coordination numbers (10−30%), and also the possibility of the co-existence of more than one species in equilibrium means that all complexes discussed above could be present in solution. The proposed structures are shown in Scheme 7. More experimental evidence is needed to confirm the proposed structures, relative proportions of each species and more importantly their activity in the $Cu^{I}Br/Me_6TREN$ catalytic system in ATRP.

 © 2003 Wiley-VCH Verlag GmbH & Co. KGaA, Weinheim

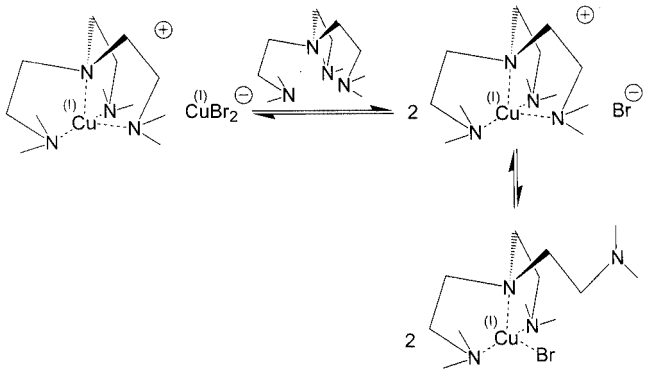

Scheme 7. Proposed structures for the $Cu^{I}Br/Me_6TREN$ complex

Room-temperature EXAFS data for the $Cu^{II}Br_2$ complex with 1 equiv. of Me_6TREN are summarized in Table 4. In methanol, the EXAFS spectrum of the Cu-*K*-edge (Figure 5) was reasonably well fit using the structural model that includes 3.2 nitrogen atoms at a distance of 2.13 Å and 1.4 bromine atoms at a distance of 2.38 Å. These data are consistent with $[Cu^{II}(Me_6TREN)Br]^+[Br]^-$ which was isolated and characterized previously.[40] $[Cu^{II}(Me_6TREN)Br]^+[Br]^-$ has a distorted trigonal-bipyramidal geometry. The Cu^{II} center is coordinated by 4 nitrogen atoms of the Me_6TREN ligand ($Cu^{II}-N_{AV}$ = 2.116 Å) and 1 bromine atom ($Cu^{II}-Br$ = 2.393 Å). As indicated in Table 4, there is a significant decrease in the coordination number of Br in the more polar H_2O. This result points to the bromide dissociation as discussed previously in the case

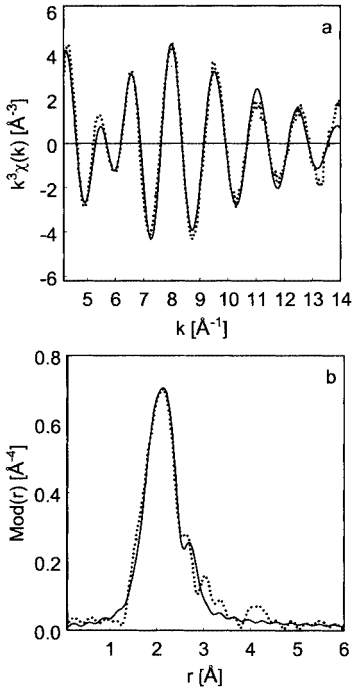

Figure 5. Experimental (dotted line) and calculated (solid line) $k^3\chi(k)$ functions (a) (k range: 4.00−14.2 $Å^{-1}$) and their Fourier transformations (b) at the Cu-*K*-edge for $Cu^{II}Br_2/Me_6TREN$ in methanol at room temperature (see Table 4 for fit parameters)

of $[Cu^{II}(PMDETA)Br_2]$. The proposed equilibrium is shown in Scheme 8.

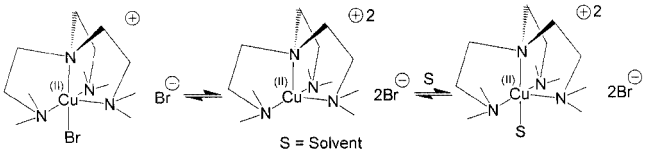

Scheme 8. Proposed structures for the $Cu^{II}Br_2/Me_6TREN$ complex

The vacant coordination site in $[Cu^{II}(Me_6TREN)]^{2+}[Br]_2^-$ is most likely occupied by the solvent molecule (H_2O or MeOH), as demonstrated in the structurally related complex $[Cu^{II}(Me_6TREN)(H_2O)]^{2+}[ClO_4]_2^-$.[70] The equilibrium constant for the dissociation of Br^- from the $[Cu^{II}(Me_6TREN)Br]^+$ chromophore has been determined spectrophotometrically in H_2O.[63,64] Under typical EXAFS conditions ($[Cu^{II}Br_2]_0$ = $[Me_6TREN]_0$ = 0.05 M), the equilibrium constant of 0.23 $mol\cdot L^{-1}$ would indicate that approximately 85% of the complex has dissociated with formation of bromide anions. This further supports the results of the EXAFS analysis and structures proposed in Scheme 8.

$Cu^{I}Br$ Complexes with the $Me_4CYCLAM$ and tNtpy Ligands

The substituted terpyridine (tNtpy)[71] and cyclic tetradentate amine ($Me_4CYCLAM$)[52] were also used in the ATRP of various monomers (Scheme 2). The polymerization of methyl acrylate and styrene catalyzed by $Cu^{I}Br$/tNtpy was controlled and the resultant polymers had relatively low polydispersities (M_w/M_n < 1.2). ATRP using $Cu^{I}Br/Me_4CYCLAM$ resulted in fast and uncontrolled polymerizations, which was attributed to a low deactivation rate constant.[14,72,73] Table 5 shows the summary of EXAFS-determined structural data for $Cu^{I}Br$ complexes with the tNtpy and $Me_4CYCLAM$ ligands.

The Cu-*K*-edge EXAFS spectrum of the $Cu^{I}Br/Me_4CYCLAM$ complex in methyl acrylate (Figure 6) is well fit using the structural model in which Cu^{I} is coordinated by 3.8 nitrogen atoms at a distance of 2.06 Å and 1.7 bromine atoms at a distance of 2.23 Å. In a more polar medium (MA/MeOH = 3:1, v/v), the signal due to the coordinated bromine atoms disappears and only nitrogen backscatterers are visible in the FT Cu-*K*-edge EXAFS spectrum. The average $Cu^{I}-N$ bond lengths for the $Cu^{I}Br/Me_4CYCLAM$ complex in methyl acrylate (2.06 Å) and methyl acrylate/MeOH (3:1, v/v) (2.05 Å) are shorter than the average $Cu^{I}-N$ bond lengths in the related complexes $[Cu^{I}(HMTETA)]^+[Cu^{I}Cl_2]^-$ ($Cu^{I}-N_{AV}$ = 2.111 Å)[36] and $[Cu^{I}(Me_6TREN)]^+[ClO_4]^-$ ($Cu^{I}-N_{AV}$ = 2.161 Å).[74] The shortening of the average $Cu^{I}-N$ bond length in $Cu^{I}Br/Me_4CYCLAM$ could be due to the steric strain imposed by the cyclic $Me_4CYCLAM$ ligand as described in the literature.[75,76] Copper(I) complexes with $Me_4CYCLAM$ are therefore expected to adopt a square-planar geometry as

 © 2003 Wiley-VCH Verlag GmbH & Co. KGaA, Weinheim

Table 5. Structural parameters of $Cu^{I}Br$ complexes with Me_4CYCLAM and tNtpy ligands, determined by EXAFS measurements under ambient conditions at the Cu- and Br-*K*-edge; MA = methyl acrylate

Complex[a]	Solvent	Backscatt.	N	*r* [Å]	σ [Å]	ΔE_0 [eV]	*k* [$Å^{-1}$]	Fit index
$Cu^{I}Br$/	MA	Cu−N	3.8	2.06	0.112	17.0	4.2−11.6	49.7
		Cu−Br	1.7	2.23	0.114			
		Cu−C	4.1	2.93	0.114			
Me_4cyclam	MA/	Cu−N	4.1	2.05	0.093	16.4	4.2−13.4	37.3
	MeOH	Cu−C	3.0	2.83	0.104			
	(3:1 vol.)	Cu−C	4.0	3.44	0.094			
		Cu−Br	0.0					
$Cu^{I}Br$/tNtpy	MA	Cu−N	2.7	2.03	0.099	12.6	3.9−14.9	32.9
		Cu−Br	1.0	2.29	0.101			
		Cu−C	3.1	2.94	0.102			
	styrene	Cu−N	2.6	2.03	0.114	17.6	4.0−11.1	27.6
		Cu−Br	0.7	2.29	0.081			
		Cu−C	2.9	2.96	0.102			
		Br−Cu	0.9	2.29	0.102			

[a] *N* = coordination number, *r* = absorber−backscatterer distance, σ = Debye−Waller factor. Inherent errors are approximately 10−30% for coordination numbers and Debye−Waller factors and 1% for distances.

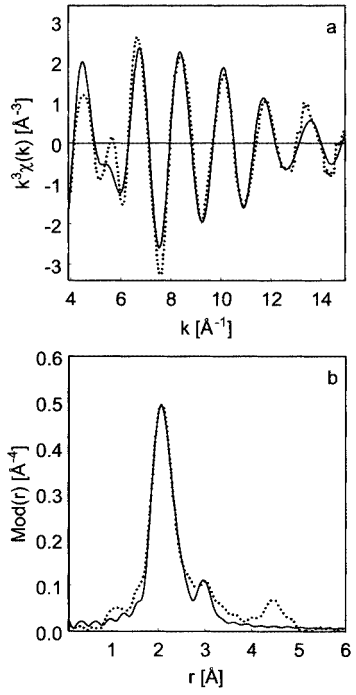

Figure 6. Experimental (dotted line) and calculated (solid line) $k^3\chi(k)$ functions (a) (*k* range: 3.90−14.9 $Å^{-1}$) and their Fourier transformations (b) at the Cu-*K*-edge for $Cu^{I}Br$/Me_4CYCLAM in methyl acrylate at room temperature (see Table 5 for fit parameters)

opposed to tetrahedral and square-pyramidal structures observed in $[Cu^{I}(HMTETA)]^{+}[Cu^{I}Cl_2]^{-}$ and $[Cu^{I}(Me_6TREN)]^{+}[ClO_4]^{-}$, respectively. The average $Cu^{I}-Br$ bond length and coordination number of Br in $Cu^{I}Br$/Me_4CYCLAM in methyl acrylate are consistent with Cu^{I} complexes containing $[Cu^{I}Br_2]^{-}$ anions (2.206−2.232 Å).[17,38,46,47] Similar to $Cu^{I}Br$/Me_6TREN discussed earlier, the EXAFS results of $Cu^{I}Br$/Me_4CYCLAM in methyl acrylate are consistent with $[Cu^{I}(Me_4CYCLAM)]^{+}[Cu^{I}Br_2]^{-}$. In more polar media, the complex predominantly exists as $[Cu^{I}(Me_4CYCLAM)]^{+}[Br]^{-}$ (Scheme 9). The 1:1/2 stoichiometry in $[Cu^{I}(Me_4CYCLAM)]^{+}[Cu^{I}Br_2]^{-}$ indicates the presence of free Me_4CYCLAM in the ATRP system since the catalyst is typically prepared by mixing $Cu^{I}Br$ with an equimolar amount of Me_4CYCLAM. Consequently, the free ligand can participate in chain transfer reactions which limit the control of the polymerization at higher molecular weights, as observed previously in the case of PMDETA.[26,27]

The EXAFS-determined structural data of the $Cu^{I}Br$ complex with tNtpy (Table 5) in methyl acrylate indicate that the coordination sphere around the Cu^{I} center is occupied by 2.7 nitrogen atoms at a distance of 2.03 Å and 1.0 bromine atoms at a distance of 2.29 Å. The coordination numbers and distances in styrene indicate similar structural features of the complex. The EXAFS data in methyl acrylate and styrene are consistent with the neutral complex $[Cu^{I}(tNtpy)Br]$. However, as discussed earlier in the case of the $Cu^{I}Br$ complex with tridentate PMDETA, other species might co-exist in equilibrium. The proposed structures are shown in Scheme 9, and are subject to further investigation.

The structures of the $Cu^{II}Br_2$ complexes with tNtpy and Me_4CYCLAM in solution, although not investigated by EXAFS, are expected to be similar to the complexes with PMDETA and Me_6TREN as discussed above. In the solid state, the $Cu^{II}Br_2$ complex with tNtpy exists as neutral $[Cu^{II}(tNtpy)Br_2]$.[14] The Cu^{II} center has a distorted square-bipyramidal geometry and is coordinated by 3 nitrogen atoms of the tNtpy ligand ($Cu^{II}-N_{AV}$ = 2.027 Å) and 2 bromine atoms ($Cu^{II}-Br_{AV}$ = 2.467 Å). Analogous to the molecular structure of $[Cu^{II}(PMDETA)Br_2]$, the $Cu^{II}-Br$ bond in the apical position (2.528 Å) was found to be longer than the $Cu^{II}-Br$ bond in the basal position (2.407 Å). Moreover, the $Cu^{II}Br_2$ complex with Me_4CYCLAM has been isolated as ionic $[Cu^{II}(Me_4CYCLAM)Br]^{+}[Br]^{-}$.[14] The Cu^{II} center in the complex is distorted square-pyramidal with the average $Cu^{II}-N$ and $Cu^{II}-Br$ bond lengths

 © 2003 Wiley-VCH Verlag GmbH & Co. KGaA, Weinheim

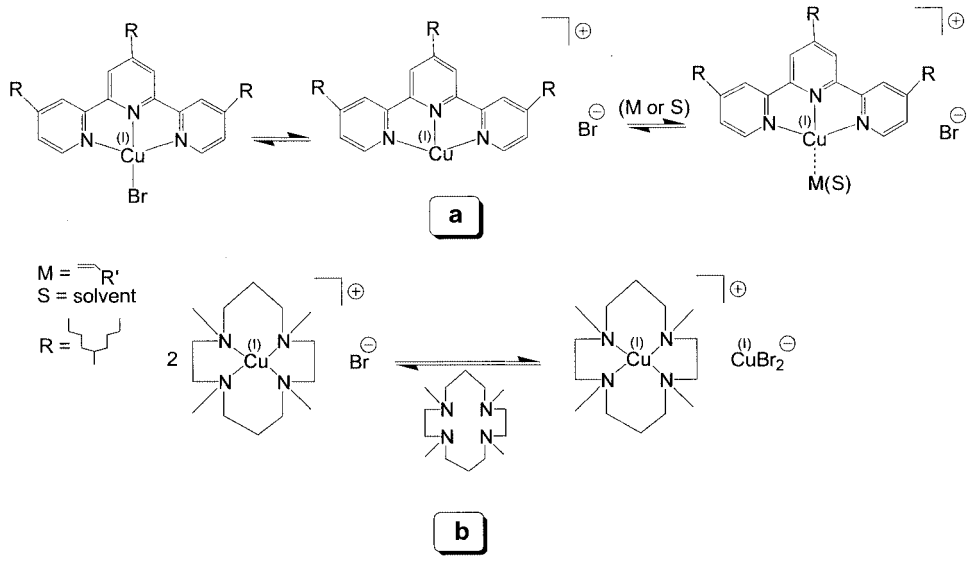

Scheme 9. Proposed structures for the (a) Cu^IBr/tNtpy and (b) $Cu^IBr/Me_4CYCLAM$ complexes

being 2.087 and 2.809 Å, respectively. The complex is expected to undergo bromide substitution in polar media such as H_2O and MeOH, similar to the previously discussed PMDETA- and Me_6TREN-based complexes.

Conclusions

In summary, EXAFS has been used to investigate the structural features of Cu^IBr and $Cu^{II}Br_2$ complexes with dNbpy, PMDETA, Me_6TREN, tNtpy, and Me_4CYCLAM in various solvents, including styrene and methyl acrylate which are monomers typically used in ATRP. The structures reported by EXAFS were primarily based on the interatomic distances around the absorber, due to the inherent error in the coordination numbers. In non-polar media, the EXAFS spectroscopic analysis of the Cu^IBr complex with dNbpy at room temperature indicated the presence of $[Cu^I(dNbpy)_2]^+[Cu^IBr_2]^-$ {Cu^I-N_{AV} = 2.01 Å (styrene), 1.99 Å (MA), Cu^I-Br_{AV} = 2.25 Å (styrene), 2.26 Å (MA)}. In polar media, such as MeOH, $[Cu^I(dNbpy)_2]^+[Br]^-$ was the preferred species (Cu^I-N_{AV} = 2.01 Å). Similarly, the EXAFS spectra of the $Cu^{II}Br_2$ complex of dNbpy in nonpolar and polar media were consistent with the presence of $[Cu^{II}(dNbpy)Br_2]$ {$Cu^{II}-N_{AV}$ = 2.01 Å (MA), 2.03 Å (toluene), $Cu^{II}-Br_{AV}$ = 2.37 Å (MA), 2.37 Å (toluene)} and $[Cu^{II}(dNbpy)_2Br]^+[Br]^-$ {$Cu^{II}-N_{AV}$ = 2.03 Å (MeOH), $Cu^{II}-Br_{AV}$ = 2.43 Å (MeOH)}, respectively. The EXAFS-determined structural data of Cu^IBr complexes with the tridentate ligands PMDETA and tNtpy in methyl acrylate indicated the presence of neutral $[Cu^I(PMDETA)Br]$ (Cu^I-N_{AV} = 2.12 Å, Cu^I-Br_{AV} = 2.33 Å) and $[Cu^I(tNtpy)Br]$ (Cu^I-N_{AV} = 2.03 Å, Cu^I-Br_{AV} = 2.29 Å), respectively. The coordination numbers and distances indicated similar structural features to those of the complexes in toluene and styrene. The results of the EXAFS analysis of the Cu^IBr/Me_6TREN complex in methyl acrylate, styrene, and toluene were well fit by a structural model that included 3 nitrogen atoms at a distance of 2.15 Å and 1 bromine atom at 2.32 Å, which potentially indicated the presence of several species namely $[Cu^I(Me_6TREN)]^+[Br]^-$, $[Cu^I(Me_6TREN)]^+[Cu^IBr_2]^-$, and $[Cu^I(Me_6TREN')Br]$ (Me_6TREN' denotes a tricoordinate Me_6TREN). The decrease in the coordination number of N was not observed in the Cu^IBr complex with tetradentate Me_4CYCLAM, which in a non-polar medium such as methyl acrylate, predominantly exist as $[Cu^I(Me_4CYCLAM)]^+[Cu^IBr_2]^-$ (Cu^I-N_{AV} = 2.06 Å, Cu^I-Br_{AV} = 2.23 Å). In more polar media, the structure changed to $[Cu^I(Me_4CYCLAM)]^+[Br]^-$ (Cu^I-N_{AV} = 2.05 Å). Additionally, the $Cu^{II}Br_2$ complexes with PMDETA and Me_6TREN, namely $[Cu^{II}(PMDETA)Br_2]$ ($Cu^{II}-N_{AV}$ = 2.09 Å, $Cu^{II}-Br_{1,AV}$ = 2.44 Å, $Cu^{II}-Br_{2,AV}$ = 2.64 Å) and $[Cu^{II}(Me_6TREN)Br]^+[Br]^-$ ($Cu^{II}-N_{AV}$ = 2.09 Å, $Cu^{II}-Br_{AV}$ = 2.39 Å), respectively, were found to undergo bromide dissociation in MeOH and H_2O, as indicated by a decrease in the Br/Cu coordination number the latter being determined by analysis of the EXAFS spectra at the Cu- and Br-*K*-edges.

Experimental Section

Materials: Cu^IBr (99.999%), $Cu^{II}Br_2$ (99.999%), $Cu^{II}(CF_3SO_3)_2$ (99%), and $[N(C_4H_9)_4]^+[Br]^-$ (98%) were purchased from Aldrich and used as received. *N,N,N′,N″,N″*-Pentamethyldiethylenetriamine (PMDETA) (99%, Aldrich) was distilled under nitrogen. 2,2′-Bipyridine (99%, Aldrich) was recrystallized from methanol. Tris[2-(dimethylamino)ethyl]amine (Me_6TREN)[77] and 4,4′-bis(5-nonyl)-2,2′-bipyridine (dNbpy)[78] were prepared according to literature procedures. All solvents were distilled and deoxygenated prior to use. Unless otherwise noted, experiments were performed under nitrogen in a dry box or using a Schlenk line. Elemental analyses for C, H, and N were performed by Chemisar Laboratories Inc., Guelph, Ontario, Canada.

 © 2003 Wiley-VCH Verlag GmbH & Co. KGaA, Weinheim

Model Compounds: $[Cu^{I}(bpy)_2]^+[ClO_4]^-$,[35] $[Cu^{I}(bpy)Br_2]$,[37] $[N(C_4H_9)_4]^+[Cu^{I}Br_2]^-$,[38] $[Cu^{II}(terpy)Br_2]$,[14,42] $[Cu^{II}(Me_6TREN)Br]^+[Br]^-$,[40] $[Cu^{II}(PMDETA)Br_2]$,[41] and $[Cu^{II}(dNbpy)Br_2]$[16] were synthesized according to literature procedures. $[Cu^{II}(dNbpy)_2Br]^+[Y]^-$ (Y = Br^-, PF_6^-, and $CF_3SO_3^-$) were prepared in CH_3CN according to the procedures for $[Cu^{II}(bpy)_2Br]^+[Br]^-$,[50] $[Cu^{II}(bpy)_2Br]^+[PF_6]^-$,[39] and $[Cu^{II}(bpy)_2Br]^+[CF_3SO_3]^-$ [79] but using dNbpy instead of bpy.

EXAFS Measurements and Data Analysis: The EXAFS measurements of the samples were performed at the beamline 2−3 at the SSRL, a division of SLAC, which is operated by Stanford University (USA). For the measurements at the Cu- *K*-edge (8982.5 eV) and Br-*K*-edge (13474.0 eV) an Si(111) double crystal monochromator was used. A synchrotron beam current up to 100 mA was used (electron energy 3.00 GeV). All experiments were carried out under ambient conditions. The tilt of the second monochromator crystal was set to 30% harmonic rejection. Energy resolution was estimated to be about 2 eV for the Cu-*K*-edge and 4 eV for the Br-*K*-edge. Data were collected in transmission mode with ion chambers. All ion chambers were filled with nitrogen in the case of the measurements at the Cu-*K*-edge, and the second and third chamber with argon in the case of the measurements at the Br-*K*-edge. Energy calibration was performed with the corresponding metal foils in the case of Cu, and lead metal foil (Pb L_{III}-edge) in the case of Br. The samples in the solid state were embedded in a polyethylene matrix and pressed into pellets. Liquid samples were measured in a specially designed transmission sample cell for liquids which was filled under nitrogen. The concentration of all samples was adjusted to yield an absorption jump of $\Delta\mu \approx 1.5$. Data evaluation started with background absorption removal from the experimental absorption spectrum by subtraction of a Victoreen-type polynomial. The background-subtracted spectrum was then convoluted with a series of increasingly broader Gauss functions and the common intersection point of the convoluted spectra was taken as the energy E_0.[80,81] To determine the smooth part of the spectrum, corrected for pre-edge absorption, a piecewise polynomial was used. It was adjusted in such a manner that the low-*R* components of the resultant Fourier transformation were minimal. After division of the background-subtracted spectrum by its smooth part, the photon energy was converted into photoelectron wave numbers *k*. The resultant EXAFS function was weighted with k^3. Data analysis in *k* space was performed according to the curved wave multiple scattering formalism of the program EXCURV92 with XALPHA phase and amplitude functions.[82] The mean free path of the scattered electrons was calculated from the imaginary part of the potential (VPI was set to −4.00) and an overall energy shift (ΔE_0) was assumed. The Amplitude Reduction Factor (AFAC) was set to a value of 0.8 in the case of the Cu-*K*-edge as well as the Br-*K*-edge. The fitting of the spectra at the Cu-*K*-edge was typically performed by using Br and N backscatterers. For some complexes, a C backscatterer was also used in order to improve the accuracy of the fit.

Acknowledgments

Financial support from the CMU CRP Consortium and an NSF grant (CHE-0096601) is greatly appreciated. The authors also acknowledge the SSRL for the kind support of synchrotron radiation facilities.

[1] K. Matyjaszewski (Ed.), *Controlled Radical Polymerization*, vol. 685, ACS Symposium Series, Washington, DC, **1998**.
[2] K. Matyjaszewski (Ed.), *Controlled/Living Radical Polymerization: Progress in ATRP, NMP and RAFT*, vol. 768, ACS Symposium Series, Washington, DC, **2000**.
[3] K. Matyjaszewski, J. Xia, *Chem. Rev.* **2001**, *101*, 2921−2990.
[4] M. Kamigaito, T. Ando, M. Sawamoto, *Chem. Rev.* **2001**, *101*, 3689−3745.
[5] K. Matyjaszewski, T. P. Davis, *Handbook of Radical Polymerization*, John Wiley & Sons, Inc., Hoboken, **2002**.
[6] M. Qinggao, K. L. Wooley, *J. Polym. Sci. Part A: Polym. Chem.* **2000**, *38*, 4805−4820.
[7] K. Matyjaszewski, *Chem. Eur. J.* **1999**, *5*, 3095−3102.
[8] T. E. Patten, K. Matyjaszewski, *Acc. Chem. Res.* **1999**, *32*, 895−903.
[9] J.-S. Wang, K. Matyjaszewski, *J. Am. Chem. Soc.* **1995**, *117*, 5614−5615.
[10] T. E. Patten, J. Xia, T. Abernathy, K. Matyjaszewski, *Science* **1996**, *272*, 866−868.
[11] H. Fischer, *Chem. Rev.* **2001**, *101*, 3581−3610.
[12] H. Fischer, *J. Polym. Sci. Part A: Polym. Chem.* **1999**, *37*, 1885−1901.
[13] V. Coessens, T. Pintauer, K. Matyjaszewski, *Prog. Polym. Sci.* **2001**, *26*, 337−377.
[14] G. Kickelbick, T. Pintauer, K. Matyjaszewski, *New. J. Chem.* **2002**, *26*, 462−468.
[15] G. Kickelbick, U. Reinohl, T. S. Ertel, A. Weber, H. Bertagnolli, K. Matyjaszewski, *Inorg. Chem.* **2001**, *40*, 6−8.
[16] T. Pintauer, J. Qiu, G. Kickelbick, K. Matyjaszewski, *Inorg. Chem.* **2001**, *40*, 2818−2824.
[17] A. T. Levy, M. M. Olmstead, T. E. Patten, *Inorg. Chem.* **2000**, *39*, 1628−1634.
[18] D. M. Haddleton, A. J. Clark, D. J. Duncalf, A. M. Heming, D. Kukulj, A. J. Shooter, *J. Chem. Soc., Dalton Trans.* **1998**, 381−385.
[19] D. M. Haddleton, D. J. Duncalf, D. Kukulj, M. C. Crossman, S. G. Jackson, S. A. F. Bon, A. J. Clark, A. J. Shooter, *Eur. J. Inorg. Chem.* **1998**, 1799−1806.
[20] K. Matyjaszewski, H.-j. Paik, P. Zhou, S. J. Diamanti, *Macromolecules* **2001**, *34*, 5125−5131.
[21] A. Goto, T. Fukuda, *Macromol. Rapid Commun.* **1999**, *20*, 633−636.
[22] K. Ohno, A. Goto, T. Fukuda, J. Xia, K. Matyjaszewski, *Macromolecules* **1998**, *31*, 2699−2701.
[23] K. Matyjaszewski, *J. Macromol. Sci., Pure Appl. Chem.* **1997**, *A34*, 1785−1801.
[24] T. Pintauer, P. Zhou, K. Matyjaszewski, *J. Am. Chem. Soc.* **2002**, *124*, 8196−8197.
[25] D. M. Haddleton, S. Perrier, S. A. F. Bon, *Macromolecules* **2000**, *33*, 8246−8251.
[26] F. Schon, M. Hartenstein, A. H. E. Muller, *Macromolecules* **2001**, *34*, 5394−5397.
[27] M. Bednarek, T. Biedron, P. Kubisa, *Macromol. Chem. Phys.* **2000**, *201*, 58−66.
[28] K. Matyjaszewski, K. A. Davis, T. E. Patten, M. Wei, *Tetrahedron* **1997**, *53*, 15321−15329.
[29] P. A. Lee, P. Citrin, P. Eisenberger, B. M. Kincaid, *Rev. Mod. Phys.* **1980**, *53*, 769−806.
[30] H. Bertagnolli, T. S. Ertel, *Angew. Chem. Int. Ed. Engl.* **1994**, *33*, 45−66.
[31] B. K. Teo, *Acc. Chem. Res.* **1980**, *13*, 412−419.
[32] J. E. Penner-Hahn, *Coord. Chem. Rev.* **1999**, *190−192*, 1101−1123.
[33] E. A. Stern, *Phys. Rev. B* **1974**, *10*, 3027−3037.
[34] F. W. Lytle, D. E. Sayers, E. A. Stern, *Phys. Rev. B* **1975**, *11*, 4825−4835.
[35] M. Munakata, S. Kitagawa, A. Asahara, H. Masuda, *Bull. Chem. Soc. Jpn.* **1987**, *60*, 1927−1929.
[36] M. Becker, F. W. Heinemann, F. Knoch, W. Donaubauer, G.

 © 2003 Wiley-VCH Verlag GmbH & Co. KGaA, Weinheim

Liehr, S. Schindler, G. Golub, H. Cohen, D. Meyerstein, *Eur. J. Inorg. Chem.* **2000**, 719−726.
[37] B. W. Skelton, A. F. Waters, A. H. White, *Aust. J. Chem.* **1991**, *44*, 1207−1215.
[38] M. Asplund, S. Jagner, M. Nilsson, *Acta Chem. Scand., Ser. A* **1983**, *37*, 57−62.
[39] R. J. Crutchley, R. Hynes, E. J. Gabe, *Inorg. Chem.* **1990**, *29*, 4921−4928.
[40] M. D. Vaira, P. L. Orioli, *Acta Crystallogr., Sect. B* **1968**, *24*, 595−599.
[41] S. R. Breeze, S. Wang, *Inorg. Chem.* **1996**, *35*, 3404−3408.
[42] M. I. Arriortua, J. L. Mesa, T. Rojo, T. Debaerdemaeker, D. Beltran-Porter, H. Stratemeier, D. Reinen, *Inorg. Chem.* **1988**, *27*, 2976−2981.
[43] K. Matyjaszewski, T. E. Patten, J. Xia, *J. Am. Chem. Soc.* **1997**, *119*, 674−680.
[44] P. J. Burke, D. R. McMillin, W. R. Robinson, *Inorg. Chem.* **1980**, *19*, 1211−1214.
[45] R. D. Willett, G. Pon, C. Nagy, *Inorg. Chem.* **2001**, *40*, 4342−4352.
[46] S. Anderson, S. Jagner, *Acta Chem. Scand., Ser. A* **1985**, *39*, 297−305.
[47] P. C. Healy, L. M. Engelhardt, V. A. Patrick, A. H. White, *J. Chem. Soc., Dalton Trans.* **1985**, 2541−2545.
[48] T. Pintauer, C. B. Jasieczek, K. Matyjaszewski, *J. Mass. Spectrom.* **2000**, *35*, 1295−1299.
[49] H. Masuda, K. Machida, *J. Chem. Soc., Dalton Trans.* **1988**, 1907−1910.
[50] M. A. Khan, D. G. Tuck, *Acta Crystallogr., Sect. B* **1981**, *B37*, 1409−1412.
[51] J. Xia, K. Matyjaszewski, *Macromolecules* **1997**, *30*, 7697−7700.
[52] J. Xia, S. G. Gaynor, K. Matyjaszewski, *Macromolecules* **1998**, *31*, 5958−5959.
[53] J. Xia, K. Matyjaszewski, *Macromolecules* **1999**, *32*, 2434−2437.
[54] J. Xia, X. Zhang, K. Matyjaszewski, in: *Transition Metal Catalysis in Macromolecular Design*, vol. 760 (Eds.: L. S. Boffa, B. M. Novak), Am. Chem. Soc., Washington, D. C., **2000**, pp. 207−223.
[55] K. Matyjaszewski, B. Gobelt, H. Paik, C. P. Horwitz, *Macromolecules* **2001**, *34*, 430−440.
[56] G. Wilkinson, *Comprehensive Coordination Chemistry*, Pergamon Press, New York, **1987**, vol. 5, pp. 539−551.
[57] T. Pintauer, N. V. Tsarevsky, G. Kickelbick, K. Matyjaszewski, *Polym. Prepr. (Am. Chem. Soc., Div. Polym. Chem.)* **2002**, *43*, 221−222.
[58] M. Pasquali, C. Floriani, A. Gaetani-Manfredotti, A. Chiesi-Villa, *Inorg. Chem.* **1979**, *18*, 3535−3542.
[59] M. J. Scott, R. H. Holm, *J. Am. Chem. Soc.* **1994**, *116*, 11357−11376.
[60] S. J. Barlow, S. J. Hill, J. E. Hocking, P. Hubberstey, W.-S. Li, *J. Chem. Soc., Dalton Trans.* **1997**, *24*, 4701−4704.
[61] F. R. Hartley, *Chem. Rev.* **1973**, *73*, 163−190.
[62] R. Jones, *Chem. Rev.* **1968**, *68*, 785−807.
[63] G. Golub, A. Lashaz, H. Cohen, P. Paoletti, A. Bencini, B. Valtancoli, D. Meyerstein, *Inorg. Chim. Acta* **1997**, *255*, 111−115.
[64] G. Golub, H. Cohen, P. Paoletti, A. Bencini, L. Messori, I. Bertini, D. Meyerstein, *J. Am. Chem. Soc.* **1995**, *117*, 8353−8361.
[65] S.-J. Ishiguro, L. Nagy, H. Ohtaki, *Bull. Chem. Soc. Jpn.* **1987**, *60*, 2053−2058.
[66] T. Pintauer, B. McKenzie, K. Matyjaszewski, *Polym. Prepr. (Am. Chem. Soc., Div. Polym. Chem.)* **2002**, *43*, 217−218.
[67] F. Thaler, C. D. Hubbard, F. W. Heinemann, R. Eldik, S. Schindler, I. Fabian, A. M. Dittler-Klingemann, F. E. Hahn, C. Orvig, *Inorg. Chem.* **1998**, *37*, 4022−4029.
[68] Z.-L. Lu, M. S. A. Hamza, R. Eldik, *Eur. J. Inorg. Chem.* **2001**, 503−510.
[69] J. H. Coates, P. R. Collins, S. F. Lincoln, *J. Chem. Soc., Faraday Trans.* **1979**, *75*, 1236−1244.
[70] J. H. Coates, P. R. Collins, S. F. Lincoln, *Aust. J. Chem.* **1980**, *33*, 1381−1387.
[71] G. Kickelbick, K. Matyjaszewski, *Macromol. Rapid Commun.* **1999**, *20*, 341−346.
[72] J. Gromada, K. Matyjaszewski, *Macromolecules* **2001**, *34*, 7664−7671.
[73] J. Gromada, K. Matyjaszewski, *Macromolecules* **2002**, *35*, 6167−6173.
[74] M. Becker, F. W. Heinemann, S. Schindler, *Chem. Eur. J.* **1999**, *5*, 3124−3129.
[75] M. Pasquali, C. Floriani, G. Venturi, A. G. Mandredotti, A. Chiesi-Villa, *J. Am. Chem. Soc.* **1982**, *104*, 4092−4099.
[76] L. M. Engelhardt, R. A. Papsergio, A. H. White, *Aust. J. Chem.* **1984**, *37*, 2207−2213.
[77] M. Ciampolini, N. Nardi, *Inorg. Chem.* **1966**, *5*, 41−44.
[78] T. B. Hadda, H. L. Bozec, *Polyhedron* **1988**, *7*, 575−577.
[79] C. O′Sullivan, G. Murphy, B. Murphy, B. Hathaway, *J. Chem. Soc., Dalton Trans.* **1999**, *11*, 1835−1844.
[80] T. S. Ertel, H. Bertagnolli, S. Huckmann, U. Kolb, D. Peter, *Appl. Spectrosc.* **1992**, *46*, 690−698.
[81] M. Newville, P. Livins, Y. Yakoby, J. J. Rehr, E. A. Stern, *Phys. Rev. B: Condens. Matter Mater. Phys.* **1993**, *47*, 14126−14131.
[82] S. J. Gurman, N. Binsted, I. Ross, *J. Phys. C* **1984**, *17*, 143−151.

Received September 5, 2002

 © 2003 Wiley-VCH Verlag GmbH & Co. KGaA, Weinheim

Probing the Nature of the Co^{III} Ion in Cobalamins − Spectroscopic and Structural Investigations of the Reactions of Aquacobalamin (Vitamin B_{12a}) with Ambident Nucleophiles

Christopher B. Perry,[a] Manuel A. Fernandes,[a] Kenneth L. Brown ,[b] Xiang Zou,[b] Edward J. Valente,[c] and Helder M. Marques*[a]

Keywords: Cobalamins / Ambidentate ligands / Cobalt / Bioinorganic chemistry / X-ray diffraction

The rate of substitution of the H_2O β-ligand in aquacobalamin (vitamin B_{12a}) is surprisingly fast for Co^{III}. This may arise as a result of transfer of electron density to Co^{III} by the corrin, conferring on the metal atom a softer and more labile character, and would require electronic communication between the equatorial ligand and the axial coordination sites of the metal atom. We have substituted H_2O in B_{12a} with the ambidentate nucleophiles SCN^-, $SeCN^-$, NO_2^- and $S_2O_3^{2-}$, examined the UV/Vis spectra of the resultant complexes, crystallised them, and determined their structures by X-ray diffraction methods. The UV/Vis spectra of these complexes, as well as those of H_2OCbl^+, SO_3Cbl^- and MeCbl, were fitted by Gaussian functions. The principal bands move to lower energy in response to an increase in donation of electron density from the axial ligand, demonstrating direct electronic communication between the axial and the equatorial ligands. In the solid state, the thiocyanato ligand in SCNCbl is coordinated through N, although ^{13}C NMR spectroscopy shows that the complex exists as a mixture of two linkage isomers in solution. $SeCN^-$, NO_2^- and $S_2O_3^{2-}$ are coordinated through the softer available donor in each case (Se, N and S, respectively). There is a regular ground-state *trans* effect such that as the donor power of the β-ligand increases, the *trans* $Co–N_{ax}$ bond length increases. A survey of the structures available in the CSD shows that this preference for the softer donor atom in ambidentate nucleophiles is not unusual in Co^{III} complexes. The Co–N bond length in SCNCbl is marginally long for coordination to Co^{III}, but the axial bond lengths of the other complexes are as expected. Hence, whereas the corrin macrocycle clearly imparts lability on Co^{III}, presumably by transfer of electron density onto the metal atom, this is insufficient to have a major effect on the ground-state structures of its complexes.

(© Wiley-VCH Verlag GmbH & Co. KGaA, 69451 Weinheim, Germany, 2003)

Introduction

We have previously[1] studied the kinetics of the ligand substitution reactions of coordinated H_2O in aquacobalamin (H_2OCbl^+, vitamin B_{12a}, Figure 1) by a series of small anionic ligands ($S_2O_3^{2-}$, SCN^-, NO_2^-, NCO^-, $SeCN^-$, N_3^-) and determined the second-order rate constants, k_{II}, corresponding to the bimolecular reaction of Equation (1), where bzm is the base 5,6-dimethylbenzimidazole that occupies the lower (α) coordination site of aquacobalamin, N_4 represents the equatorial corrin ligand, and charges are omitted for convenience. We calculated the activation parameters $\Delta H^{\ddagger}$ and $\Delta S^{\ddagger}$ from the temperature dependence of k_{II} and the Mulliken charge population of the donor atoms from semiempirical molecular orbital calculations using the PM3 model.[2,3]

$$\text{bzm-Co(N}_4\text{)-OH}_2 + \text{L} \xrightarrow{k_{II}} \text{bzm-Co(N}_4\text{)-L} + \text{H}_2\text{O} \quad (1)$$

If we assumed, irrespective of the thermodynamically preferred product, that (i) SCN^- reacts through N, (ii) NO_2^- reacts through N, (iii) NCO^- reacts through O, (iv) $S_2O_3^{2-}$ reacts through S and (v) $SeCN^-$ reacts through Se in the microscopic process that determines the magnitude of the activation parameters, then a three-dimensional plot of $\Delta H^{\ddagger}$ as a function of the energy, E_σ, of the frontier orbital with σ symmetry on the donor atom, and the Mulliken population (MP) of that atom, yielded a planar surface ($r^2 = 0.81$; $f = 6.30$; 92% confidence that the correlation is not due to random chance) that showed that $\Delta H^{\ddagger}$ decreases, and the reactions speed up, as the MP and E_σ decreased. A similar correlation with $\Delta S^{\ddagger}$ was observed ($r^2 = 0.95$; $f =$

[a] Molecular Sciences Institute, School of Chemistry, University of the Witwatersrand,
P. O. Wits, Johannesburg 2050, South Africa
Fax: (internat.) + 27-11/717-6749
E-mail: hmarques@aurum.chem.wits.ac.za
[b] Department of Chemistry and Biochemistry, Ohio University, Athens, OH 75701, United States of America
[c] Department of Chemistry, Mississippi College, Clinton, MS 39058, United States of America
Supporting information for this article is available on the WWW under http://www.eurjic.org or from the author.

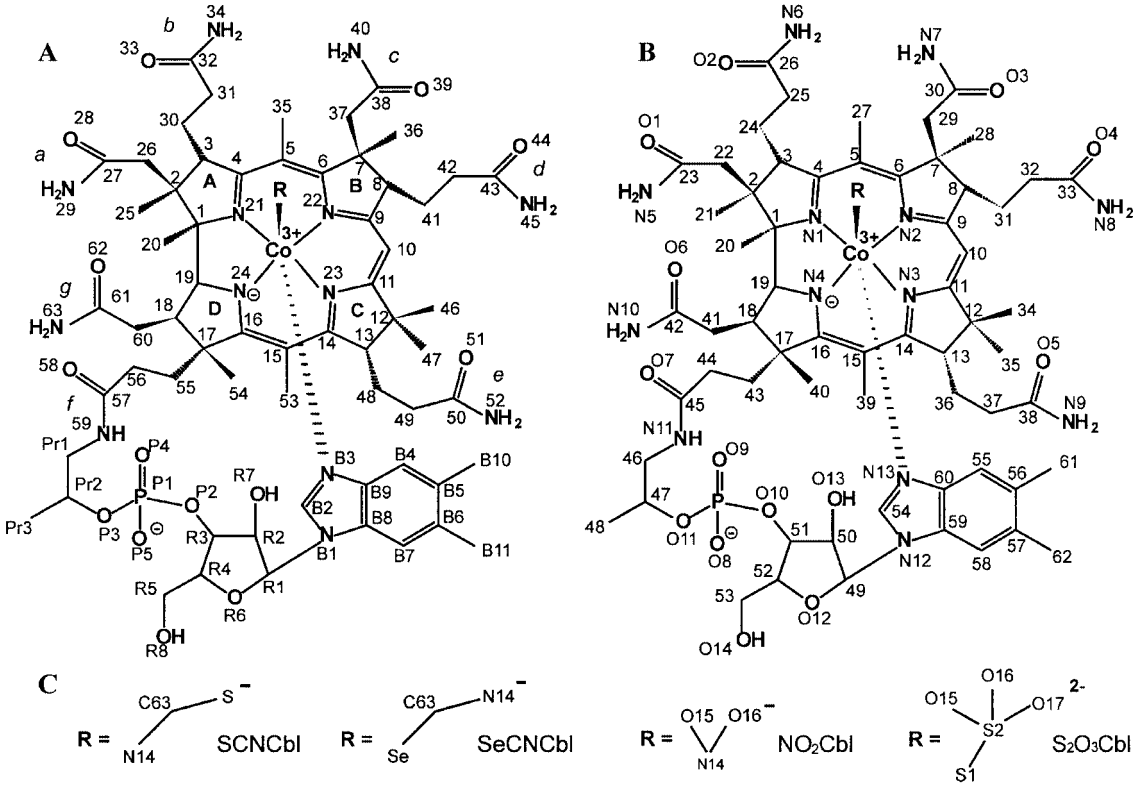

Figure 1. (A) The common numbering scheme and standard view of the cobalt corrinoids; aquacobalamin (vitamin B_{12a}) has a Co^{III} ion coordinated in the equatorial plane by the macrocyclic ligand corrin; the equatorial ligand on the lower (α) face is 5,6-dimethylbenzimidazole (bzm), whilst that on the upper (β) face is R = H_2O; coordinated H_2O is readily replaced by ligands from solution in reactions that are surprisingly fast for Co^{III}; in this view, the C13···C17 portion of the molecule is known as the southern quadrant, C7···C13 as the eastern quadrant, and so on; (B) and (C) show the crystallographic numbering scheme used in this work

26.6; > 99% confidence that the correlation is not due to random chance), with $\Delta S^{\ddagger}$ decreasing and the reaction becoming slower with decreasing MP and E_{σ}. There is therefore a compensating effect between $\Delta H^{\ddagger}$ and $\Delta S^{\ddagger}$, the origin of which, related to the density of states in the transition state, was discussed.

Co^{III} usually behaves as a hard (class a) metal ion.[4] The curious mixture of the kinetically favoured donor atom in the reactions of B_{12a} with ambident nucleophiles (the harder of the two donors is preferred in the reaction with SCN^- and NCO^-, but the softer donor in the case of $S_2O_3^{2-}$, NO_2^- and $SeCN^-$), may be evidence of a somewhat softer metal ion character due to a transfer of electron density from the corrin ring. It has previously been pointed out[5,6] that the rates of ligand substitution reactions at the Co^{III} centre in the cobalamins are surprisingly fast for Co^{III}, which is a classic example of an inert transition metal ion. Thus, the lability ratio of the metal ion towards substitution in corrin, porphyrin, cobaloxime and macrocyclic saturated ammine systems is 10^9:10^6:10^4:1 (Figure 2). We suggest that this considerable *cis*-labilising effect of the corrin is due to the transfer of electron density from the macrocycle to the metal ion, conferring on the metal atom some element of labile character characteristic of Co^{II}. For this

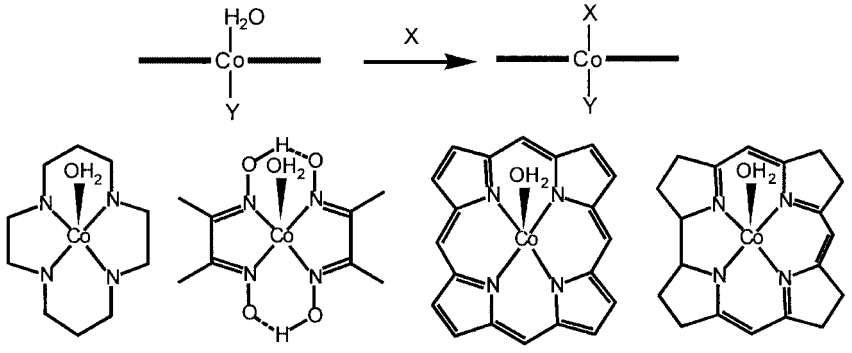

Figure 2. Changing the equatorial ligand system from (left to right) ammine to cobaloxime to porphyrin and corrin causes the rate of substitution of the axial H_2O to increase approximately in the ratio 1:10^4:10^6:10^9 [5]

 © 2003 Wiley-VCH Verlag GmbH & Co. KGaA, Weinheim

to be a feasible explanation for the kinetic behaviour, direct electronic communication between the corrin ring and the axial coordination site of Co^{III} is required. To this end, we have shown[5] that substitution of the H centre at the C10 position with Cl (Figure 1), and an increase in the donor power of the axial ligand ($H_2O < CN^- < Me$) increased the C10−Cl bond length as well. Moreover, Mulliken charges obtained from semiempirical MO calculations using the ZINDO/1 model[7,8] (which correlate well with ^{13}C NMR chemical shifts and which may therefore be used to determine the pattern of electron distribution in these complexes) confirmed that the charge density on the metal ion, on the N donor atoms of the corrin, and on the corrin C atoms is affected by the donor power of the axial ligand. We have also shown recently[9] that if the H atom at C10 is replaced by an electron-withdrawing NO group, the metal ion is deactivated towards ligand substitution, i.e., 10-NO-H_2OCbl^+ is inert towards substitution of the axial H_2O molecule by pyridine and N_3^-, and reacts only slowly with CN^-.[10] The conferring of some labile character on the metal atom may be an important aspect of the biological chemistry of coenzyme B_{12} (AdoCbl, adenosylcobalamin; R = 5′-deoxyadenosyl in Figure 1,) since the first step in AdoCbl-catalysed enzymatic reactions is homolysis of the Co−C bond to produce Co^{II} and an alkyl radical,[11−13] a process that is catalysed by a factor of 10^{12} or higher.[14−16] There is a clear mechanistic advantage from increasing the electron density on the metal atom and increasing its lability. It has been shown, for example, that reduction of methylcobalamin to Co^{II} results in a $> 10^{15}$ rate enhancement of thermal homolysis of the Co−C bond[17] and Co^{II} corrinoids are either five-coordinate[18,19] or, at most, the β-ligand interacts very weakly with the metal centre.[18] It is an attractive hypothesis that the corrin transfers significant electron density onto Co^{III}, in effect conferring some labile Co^{II}-like character to it, and that the protein, on binding the coenzyme B_{12} cofactor and perhaps the substrate, modulates this effect further thereby activating the Co−C bond towards homolysis.

The axial Co−N bonds to the bzm base tend to be long (2.26−1.95 Å),[20] whereas the Co−N bond lengths in the equatorial plane of Co^{III} are similar to those in Co^{III}−ammine complexes (1.96−1.99 Å), as Lenhert pointed out.[21] This may be merely a consequence of the steric demands of bzm (and, in particular, the clashing of the B4 proton with the corrin ring), rather than a structural response to low-spin Co^{II}-like character of the metal atom. In this regard it is probably significant that the Co−N(imidazole) bond in Co-β-cyanoimidazolylcobamide, where the bzm base has been replaced by a sterically much less demanding imidazole,[22] is "normal", with a distance of 1.97 Å. In methionine synthase[23] and in methylmalonyl CoA mutase[24] the bzm base is replaced by an imidazole residue from the protein. The $Co-N_{ax}$ bond length in the former is not unusual (2.2 ± 0.2 Å), although the resolution is relatively low. In the latter, the B_{12} cofactor is present as Co^{II}, and there is a long $Co-N_{ax}$ bond (2.5 ± 0.1 Å), despite attempts to constrain this bond length to more normal values during the refinement process.[25] There is no crystal structure of imidazolylcob(II)amide, but a comparison of the $Co-N_{ax}$ bond lengths of cyanocobalamin and cyanoimidazolylcobamide strongly suggests[26] that the $Co-N_{ax}$ bond length is as much as 0.4 Å longer when the cofactor is bound to the protein.

The very rich chemistry of organocobalamins is further evidence that the Co^{III} ion in the cobalamins behaves very differently from a classical, hard and inert d^6 ion. As mentioned, the first step in the AdoCbl-catalysed enzymatic reactions is formation of Co^{II} and a radical (i.e., the Co−C bond could be formulated as $Co^{II} + R^{\cdot}$). Both UV/Vis and resonance Raman spectroscopic results suggest that an alkylcobalamin is best viewed as a compound intermediate between Co^{III} and a carbanion.[27] The transfer of a methyl group from methylcobalamin to homocysteine produces Co^{I}, which then acts as a powerful nucleophile towards the methyl group donor, N5-methyltetrahydrofolate,[28] i.e. the Co−C bond could be formulated as $Co^{I} + R^{+}$.

In this paper we investigate the *cis* influence (to demonstrate the electronic communication between the axial coordination site and the corrin ring) and *trans* influences (to extend further the well-established *trans* influence in the cobalamins to the compounds under investigation) and then explore further the nature of the Co^{III} ion by addressing two questions. Firstly, when offered an ambident nucleophile with two donor atoms of different hardness, what is the thermodynamically favoured product? Secondly, is there any evidence in the solid state for an elongation of the axial bond to such a nucleophile? To this end, we have displaced H_2O in B_{12a} with $S_2O_3^{2-}$, SCN^-, NO_2^-, and $SeCN^-$ and crystallised the resultant compounds in order to determine their structures by X-ray diffraction analysis. We have been unable to crystallise CNOCbl, which slowly decomposes to CNCbl. Pertinent to this work is a report by Randaccio[29] and co-workers on the crystal structures of sulfitocobalamin, SO_3Cbl^-. This was found to be *S*-bound with a Co−S bond length of 2.134(7) Å. We are currently using NMR-restrained molecular modelling techniques to examine the structures of these compounds in solution and will report on those results elsewhere.

Results

UV/Vis Spectra

The UV/Vis spectra of H_2OCbl^+, NO_2Cbl, SCNCbl, $S_2O_3Cbl^-$, SeCNCbl, SO_3Cbl^- and MeCbl are shown in Figure 3. The spectrum of, for example, H_2OCbl^+ with its well-defined γ-band (the prominent band around 350 nm), has been referred to as a "typical" cobalamin spectrum, whereas that of MeCbl (for example), where the γ-band is apparently less well defined, and a greater number of bands are discernible especially in the shorter wavelength region, has been termed an "atypical" spectrum.[30] On this basis, one would classify the spectra of H_2OCbl^+, NO_2Cbl and SCNCbl as "typical" and those of $S_2O_3Cbl^-$, SeCNCbl, SO_3Cbl^- and MeCbl as "atypical".

 © 2003 Wiley-VCH Verlag GmbH & Co. KGaA, Weinheim

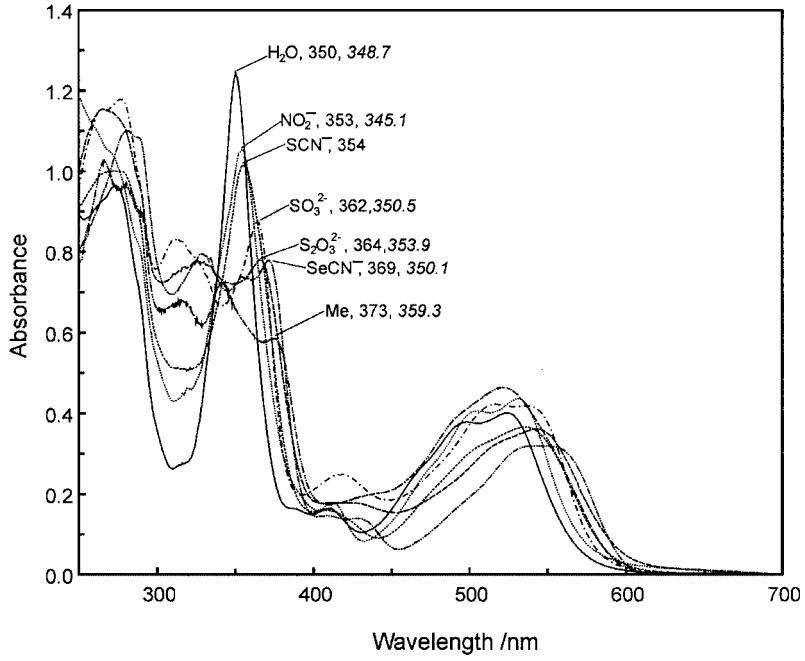

Figure 3. The UV/Vis spectra of cobalamin complexes; the identity of the β-axial ligand is given in each case, as is the observed position [nm] of the maximum absorption in the γ-band region of the spectrum; the γ-band envelope consists of three overlapping transitions, as shown by a Gaussian analysis of the spectra (see text, and Figure 4); the mean position of these three transitions is given in italics

An example of the fitting of the spectra under discussion with a series of Gaussian functions is shown in Figure 4. Either 11 (H_2OCbl^+, NO_2Cbl), 12 ($S_2O_3Cbl^-$, SeCNCbl, SO_3Cbl^-) or 13 (MeCbl) Gaussian functions were required to adequately fit the spectra. The results are listed in Table S1 of the Supporting Information. The γ-band of the corrins is best modelled as the overlap of three transitions, as are the αβ-bands (in the 450−600 nm region). In the case of NO_2Cbl, two of the components of the γ-band region overlap closely, and the region can only be resolved into two component Gaussian functions.

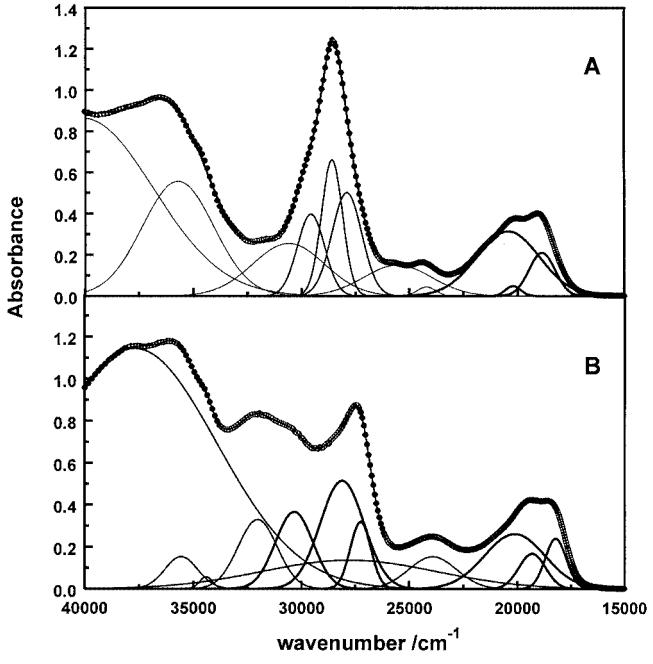

Figure 4. Resolved UV/Vis spectra of (A) H_2OCbl^+ and (B) SeCNCbl; The γ-band in each case is best fitted by three Gaussian functions (shown as bold lines); the circles are the experimental data and the line through the circles is the sum of the individual Gaussian bands

Structure of SCNCbl

SCNCbl crystallises in the orthorhombic space group $P2_12_12_1$ (R_1 = 8.75%, Figure 5). The experimental data are summarised in Table 1. The thiocyanato ligand is coordinated through N [Co−N = 1.954(11) Å] in a bent fashion [Co−N−C = 146.2(11)°], and positioned over C15 (Figure 6). Some of the bond lengths and bond angles involving the metal ion are summarised in Table 2.

As is usually found in the crystal structures of cobalt corrinoids, several solvent water molecules are incorporated, and they are extensively hydrogen-bonded to the amide side chains of the corrin. Possible hydrogen bonds were identified by standard methods.[31] An amide proton of N40 in the *c* side chain appears to be hydrogen-bonded to the N atom of coordinated SCN^- (N40···NCS = 3.309Å, N40−H−NCS = 161°). N52 of the *e* side chain amide group is hydrogen-bonded to N45 of the *d* side chain of a neighbouring molecule, whilst O51 acts as a hydrogen bond acceptor to N63 of the *g* side chain. The second N63 proton is hydrogen-bonded to O33 of the *b* side chain of a neighbouring molecule. Both hydroxy groups of the ribose act as hydrogen bond donors towards solvent water molecules.

Structure of SeCNCbl

SeCNCbl crystallises in the orthorhombic space group $P2_12_12_1$ (R_1 = 7.46%, Figure 5). The experimental data are

 © 2003 Wiley-VCH Verlag GmbH & Co. KGaA, Weinheim

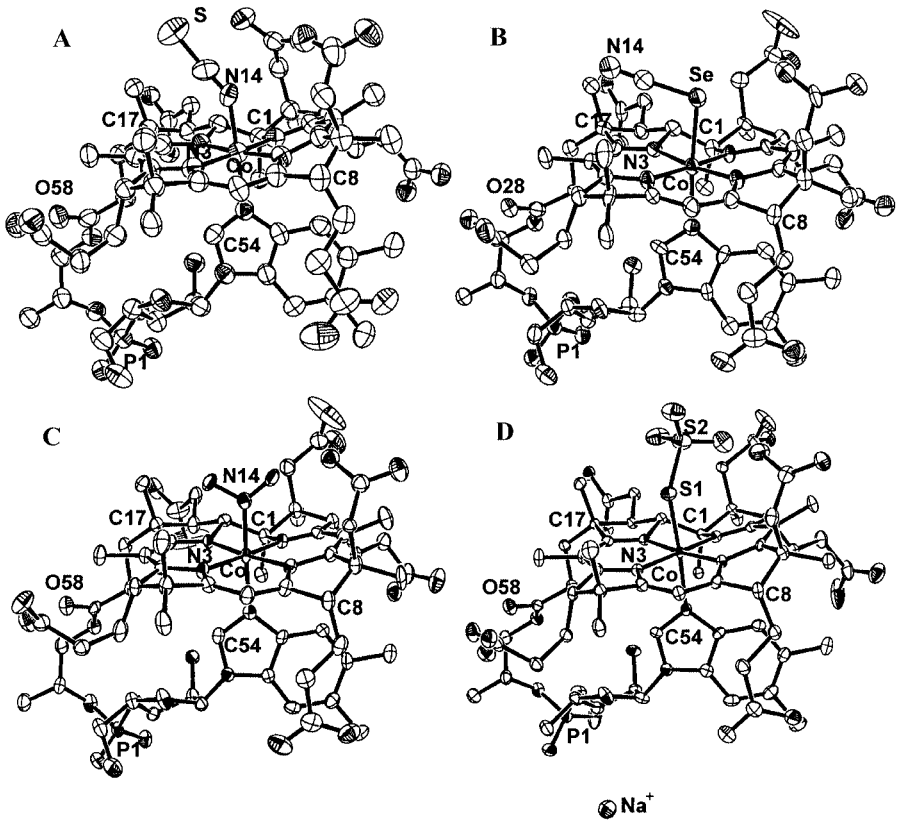

Figure 5. ORTEP diagram of (A) SCNCbl (25% probability contours), (B) SeCNCbl (50% probability contours), (C) NO_2Cbl (50% probability contours, with disorder in the orientations of the NO_2 ligand, and the *c* and *e* side chains removed for clarity), (D) $Na^+S_2O_3Cbl^-$ (50% probability contours)

summarised in Table 1. The selenocyanato ligand is coordinated through Se [Co−Se = 2.394(2) Å] in a bent fashion [Co−Se−C = 104.3(3)°] and the ligand is orientated over the southern quadrant of the molecule (Figure 6). Some of the bond lengths and bond angles involving the metal ion are summarised in Table 2. We were also able to grow crystals rapidly by using a near-saturated solution of B_{12a} in the presence of 0.05 mol·dm^{-3} KSeCN (crystals were obtained in a few hours). Although the crystal quality was poor, the diffraction data (not shown) were good enough for refinement to a level that showed unambiguously an *Se*-bound selenocyanato ligand.

The amide NH groups of the *a*, *b*, *c*, *d*, *e* and *f* side chains act as hydrogen bond donors towards solvent water molecules, whilst the *d* and *e* amide groups are also hydrogen-bonded to the carbonyl group of the *a* side chains of neighbouring molecules. The *g* side chain is hydrogen-bonded to the *b* and *e* side chains of neighbouring molecules. The R7 and R8 hydroxy groups [see Figure 1(A)] are hydrogen-bonded to solvent water molecules.

Structure of NO_2Cbl

NO_2Cbl crystallises in the orthorhombic space group $P2_12_12_1$ (R_1 = 7.16%, Figure 5). The experimental data are summarised in Table 1. The nitro ligand is coordinated through N [Co−N = 1.941(5) Å] and the ligand is disordered over two positions (Figure 6). In the first position [0.82(10) occupancy], the two oxygen atoms point towards C10 and the C1−C19 bond [N−O−N = 121.6(5)°]. In the second position [0.18(10) occupancy] they are virtually orthogonal to this, pointing towards C5 and C15 [N−O−N = 111.2(15)°]. Some of the bond lengths and bond angles involving the metal ion are summarised in Table 2.

As with the other structures, there is extensive hydrogen bonding of the amide side chains. One of the *c* side chain amide protons is hydrogen-bonded to the N atom of the coordinated NO_2 ligand. Hydrogen bonding occurs between the amide protons of the *e*, *d* and *g* side chains of one molecule, and the *a* side chain of one neighbouring molecule and the *a* and *b* side chains of a second neighbouring molecule, respectively. The amide proton of the *a* side chain is hydrogen-bonded to the O atom of the acetone solvent molecule in the same unit cell, whilst one of the *d* side chain amide protons is hydrogen-bonded to a neighbouring acetone molecule. The amide groups of the *b*, *c*, *e*, *f* and *g* side chains are hydrogen-bonded to water molecules.

Structure of $S_2O_3Cbl^-$

$Na^+S_2O_3Cbl^-$ crystallises in the orthorhombic space group $P2_12_12_1$ (R_1 = 5.88%, Figure 5). The experimental data are summarised in Table 1. The thiosulfate ligand is coordinated through S [Co−S = 2.2861(11) Å]. The ligand points towards C1 and comes within van der Waals contact with the *a* side chain (Figure 6); as a consequence, the li-

 © 2003 Wiley-VCH Verlag GmbH & Co. KGaA, Weinheim

Table 1. Experimental data for the crystal structure determination of XCbl; X = SCN^-, $SeCN^-$, NO_2^-, $S_2O_3^{2-}$ (* excludes solvate molecules)

	SCNCbl	SeCNCbl	$S_2O_3Cbl^-$	NO_2Cbl
CCDC-	-185962	-185963	-185964	-185965
Empirical formula*	$C_{63}H_{88}CoN_{14}O_{14}PS$	$C_{63}H_{88}CoN_{14}O_{14}PSe$	$C_{62}H_{88}CoN_{13}NaO_{32}PS_2$	$C_{62}H_{88}CoN_{14}O_{16}P$
Molecular mass	1387.4	1434.3	1375.4	1432.4
Temperature [K]	173(2)	123(2)	123(2)	123(2)
Wavelength [Å]	0.71073	0.71073	0.71073	0.71073
Crystal system	orthorhombic	orthorhombic	orthorhombic	orthorhombic
Space group	$P2_12_12_1$	$P2_12_12_1$	$P2_12_12_1$	$P2_12_12_1$
Unit cell dimensions [Å]	a = 16.353(4) b = 20.823(5) c = 23.933(6)	a = 15.955(6) b = 21.338(7) c = 23.646(8)	a = 16.020(3) b = 20.922(3) c = 24.722(4)	a = 16.120(4) b = 20.974(6) c = 23.309(6)
Volume [$Å^3$]	8150(3)	8050(5)	8286(2)	7881(4)
Z	4	4	4	4
Density (calcd.) [gcm^{-3}]	1.352	1.406	1.437	1.394
Absorption coefficient [mm^{-1}]	0.342	0.772	0.374	0.328
F(000)	3540	3608	3816	3530
Crystal size [mm]	0.36 × 0.20 × 0.20	0.34 × 0.17 × 0.16	0.44 × 0.34 × 0.30	0.40 × 0.22 × 0.22
θ range for data collection [°]	1.30−23.25	1.29−24.99	1.51−28.01	1.31−25.50
Index ranges	$-17 \le h \le 17$ $-22 \le k \le 22$ $-5 \le l \le 26$	$-18 \le h \le 18$ $-25 \le k \le 23$ $-28 \le l \le 22$	$-20 \le h \le 10$ $-26 \le k \le 27$ $-29 \le l \le 30$	$-19 \le h \le 18$ $-15 \le k \le 25$ $-28 \le l \le 25$
Reflections collected	27133	35010	48888	38172
Independent reflections	10141 [R(int) = 0.0804]	13094 [R(int) = 0.0826]	17883 [R(int) = 0.0275]	14186 [R(int) = 0.0380]
Completeness to θ	23.25°, 90.3%	24.99°, 95.5%	28.01°, 91.8%	25.50°, 98.5%
Absorption correction	semiempirical from equivalents	semiempirical from equivalents	semiempirical from equivalents	semiempirical from equivalents
Max./min. transmission	0.9347/0.8867	0.8864/0.7792	0.8960/0.8527	0.9313/0.8799
Refinement method	full-matrix least squares on F^2	full-matrix least squares on F^2	full-matrix least squares on F^2	full-matrix least squares on F^2
Data/restraints/parameters	10141/1/1001	13094/7/988	17883/39/1063	14186/81/1043
Goodness-of-fit on F^2	1.047	1.049	1.085	1.069
Final R indices [$I > 2\sigma(I)$]	R_1 = 0.0875, wR_2 = 0.2041	R_1 = 0.0746, wR_2 = 0.1675	R_1 = 0.0589, wR_2 = 0.1672	R_1 = 0.0716, wR_2 = 0.1878
R indices (all data)	R_1 = 0.1453, wR_2 = 0.2605	R_1 = 0.1246, wR_2 = 0.2030	R_1 = 0.0661, wR_2 = 0.1732	R_1 = 0.0843, wR_2 = 0.1959
Absolute structure parameter	−0.10(4)	−0.014(16)	0.012(13)	0.04(2)
Largest diff. peak/hole [e·$Å^{-3}$]	0.017/−0.015	0.104/−0.110	1.382/−1.073	1.081/−0.536

gand bends away [the NB3−Co−S angle is 167.05(9)°]. The coordinated $S_2O_3^{2-}$ ion is hydrogen-bonded to the amide group of the *a* side chain (through one of the O atoms) and to the amide group of the *c* side chain (through the donor S atom). Selected bond lengths and bond angles involving the metal ion are summarised in Table 2. The Na^+ counterion is in close contact with the R8 hydroxy group and a cluster of four solvent water molecules.

The *a* side chain amide group is hydrogen-bonded to a solvent water molecule in addition to the coordinated $S_2O_3^{2-}$ ion as described above. The *b* side chain is hydrogen-bonded to the phosphate group of a neighbouring molecule. The *d* and *e* side chains are hydrogen-bonded to the *a* side chains of two different neighbours, whilst the *g* side chain hydrogen-bonds to the *e* and *b* side chains of two different neighbours. The R7 hydroxy group is involved in an intramolecular hydrogen bond to the phosphate group.

In addition to these hydrogen bonds, the cobalamin molecules are also connected to each other through the Na^+ counterion [Na−O3: 2.327(4) Å; Na−O14 (1/2 − x, −y, 1/2 + z): 2.367(4) Å]. This reinforces the interactions between molecules related by the twofold screw axis parallel to *c* as shown in Figure 7.

Solid-State Packing

The majority of cobalamins crystallise in the $P2_12_12_1$ space group.[20,29] Kratky and co-workers have shown that most of the crystal structures of cobalamins belonging to this space group can be assigned to one of four packing types. Types I−III are classified according to the *c*/*a* and *b*/*a* cell axis ratios. More recently, Randaccio et al.[29] discovered a fourth packing type, IV. The four packing types differ in the way the cobalamin molecules stack in the solid state. From the *c*/*a* and *b*/*a* cell axis ratios we have found that all four structures reported here belong to packing type I.

The Corrin Fold

The corrin fold angle (the angle between the mean planes through N21−C4−C5−C6−N22−C9−C10 and C10−C11−N23-C14−C15−C16-N24[32]) in SCNCbl is

 © 2003 Wiley-VCH Verlag GmbH & Co. KGaA, Weinheim

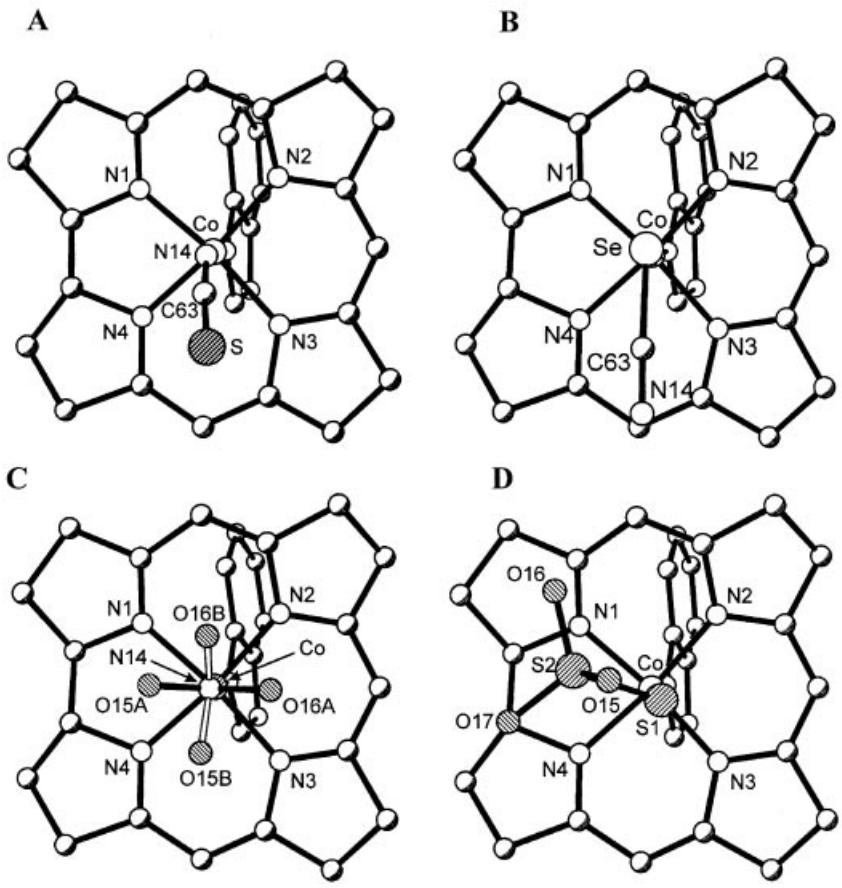

Figure 6. View of the upper face of the four corrins showing the orientation of the axial liagnds; for clarity, only the β-ligand, the corrin core, and the bzm ligand are shown

large (22.4°); of the cobalt corrinoid structures reported to date only cyano-13-*epi*-cobalamin[33] has a larger fold angle (23.7°). The fold angle in SeCNCbl is much smaller (13.7°), close to the average corrin fold angle of about 14°.[26] The fold angle is 14.5° in NO_2Cbl and somewhat larger (17.2°) in $S_2O_3Cbl^-$.

Coordinated bzm

In all the structures studied, the bzm ligand is coordinated off-vertical to the corrin ring, with a tilt angle (the angle between the mean plane through the 9 heavy atoms of the aromatic core of the bzm ligand, and the normal to the mean plane through the 24 heavy atoms of the corrin core) of 15° in SeCNCbl, 8° in NO_2Cbl, 13° in SCNCbl and 10° in $S_2O_3Cbl^-$. In each case the tilt is towards the eastern quadrant of the molecule and probably reflects the steric strain inherent in the nucleotide loop which attaches the bzm ligand to the *f* side chain through a ribose and an aminopropanol moiety (Figure 1).

Discussion

cis and *trans* Influences in Cobalamin Chemistry

The Co−NB3 bond is quite short in SCNCbl [1.958(9) Å], somewhat longer in NO_2Cbl [2.008(4) Å], and significantly longer in $S_2O_3Cbl^-$ [2.078(3) Å], SeCNCbl [2.102(7) Å] and[29,32] SO_3Cbl^- [2.134(4) Å or 2.156(5) Å] (Table 2). An examination of the Co−NB3 bond lengths in eleven cobalamins RCbl where the β-ligand is an alkyl group [adenylpropyl,[34] CF_3,[35] CH_3,[36] (*R*)- and (*S*)-2,3-dihydroxypropyl,[37] adenosyl (four separate determinations),[21,38] 2′,5′-dideoxy-5′-adenosyl and 2′,3′,5′-trideoxy-5′-adenosyl[39]] shows that the average Co−NB3 bond (2.23 ± 0.05 Å) is significantly longer than the average for the three structures XCbl (1.97 ± 0.04 Å) where the β-ligand is an inorganic moiety (X = Cl^-, N_3^- and[40] H_2O[41]). With cyanide as the *trans* ligand, the Co−NB3 bond is longer than in the XCbl systems, but shorter than in the RCbl systems (2.008 Å in CNCbl[42] and 2.023 Å in CNCbl-*b*-carboxylate[43]). There is clearly a ground-state *trans* influence; a soft or polarisable ligand in the β-position (alkyl, S- or

 © 2003 Wiley-VCH Verlag GmbH & Co. KGaA, Weinheim

Table 2. Bond lengths and bond angles of the coordination sphere of Co^{III} in cobalamin complexes with ambidentate nucleophiles

Co−X−Y	SCNCbl X = N; Y = C	SeCNCbl X = Se; Y = C	NO_2Cbl X = N; Y = O	$S_2O_3Cbl^-$ X = S; Y = O	SO_3Cbl^- [a] X = S; Y = O
Co−N21	1.890(9)	1.892(6)	1.888(4)	1.881(3)	1.870(3) 1.883(5)
Co−N22	1.916(8)	1.921(7)	1.917(4)	1.915(3)	1.913(2) 1.901(5)
Co−N23	1.909(9)	1.928(7)	1.922(4)	1.915(3)	1.890(3) 1.904(5)
Co−N24	1.872(8)	1.909(6)	1.906(4)	1.893(3)	1.886(4) 1.901(5)
Co−NB3	1.955(9)	2.100(7)	2.008(4)	2.078(3)	2.134(4) 2.156(5)
Co−X	1.955(11)	2.394(2)	1.941(5)	2.2861(11)	2.231(1) 2.241(2)
N21−Co−N22	91.0(4)	89.9(3)	90.30(18)	90.33(13)	
N24−Co−N23	89.9(4)	89.6(3)	90.23(18)	90.54(13)	
N21−Co−N23	172.4(4)	173.0(3)	173.18(18)	172.83(13)	
N22−Co−N24	172.6(4)	172.7(3)	173.06(18)	172.77(13)	
N21−Co−N24	82.6(4)	83.8(3)	83.09(17)	82.92(13)	
N22−Co−N23	96.6(4)	96.9(3)	96.43(19)	96.32(13)	
N24−Co−NB3	94.5(3)	96.3(3)	95.46(18)	95.43(12)	
N21−Co−NB3	91.9(4)	91.5(3)	90.84(17)	90.80(12)	
N22−Co−NB3	89.2(4)	87.6(3)	86.69(17)	87.24(12)	
N23−Co−NB3	87.4(4)	87.1(3)	88.47(18)	86.87(12)	
N24−Co−X	87.6(4)	91.3(2)	90.31(18)	91.94(9)	
N21−Co−X	92.1(4)	90.6(2)	92.13(18)	100.67(9)	
N22−Co−X	89.1(3)	85.0(2)	87.85(18)	86.73(9)	
N23−Co−X	88.9(4)	91.6(2)	89.22(19)	82.43(9)	
NB3−Co−X	175.4(4)	172.3(2)	173.79(18)	167.07(9)	
Co−X−Y	145.7(11)	104.1(3)	121.2(4); 117.1(4) (A),[b] 129.1(11); 119.5(10) (B)[b]	122.33(6)	

[a] For comparison from Randaccio et al.[29] The reported values are for $[(SO_3)Cbl](NH_4)$. There is a more recent determination of the structure of $[(SO_3)Cbl](NH_4)$·glycerol using synchotron radiation,[63] and the results from that determination are given in italics. [b] Two positions of the NO_2 ligand.

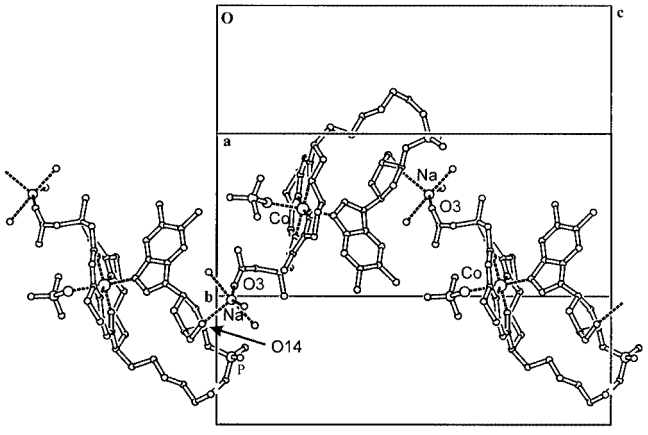

Figure 7. There is an interaction between the Na^+ counterion and oxygen atoms on neighbouring cobalamin molecules related by the twofold screw axis parallel to the *c* axis in the $S_2O_3Cbl^-$ structure; portions of the cobalamin molecules have been omitted for clarity

Se-donor as in $S_2O_3Cbl^-$ and SeCNCbl, respectively) causes an elongation of the Co−NB3 bond. The thiocyanato ligand, coordinated through N acts as a typical hard inorganic moiety, whilst coordinated NO_2^- has a similar ground-state *trans* structural influence as CN^-.

The large corrin fold angle of 22.4° in SCNCbl (the average fold angle of cobalamins in about 14°) is probably a consequence of the short Co−NB3 bond. Kratky and co-workers[20] have shown that as the axial Co−NB3 bond length decreases, the corrin fold angle increases. This is because the bzm ligand, and the B4 proton in particular, interact with the corrin ring and the corrin folds upwards towards the β-ligand in response. The corrin angles of SeCNCbl, NO_2Cbl and $S_2O_3Cbl^-$ are significantly smaller (see above).

The complexity of the UV/Vis spectra of the cobalamins makes it difficult to unambiguously determine the band positions. A plot of the apparent position of the γ-band maximum (a measure of the *cis* influence[30]) against the Co−NB3 bond length (a measure of the *trans* influence,[20] see above) shows the two parameters are correlated, albeit poorly ($r^2 = 0.58$, $n = 6$) (Figure 8, A), and the band moves to longer wavelength as the softness of the axial ligand increases. The spectrum of SCNCbl is excluded, because SCNCbl exists in solution as a mixture of the two linkage isomers, see below.

The origin of the transitions in the electronic spectrum of the corrinoids has been reviewed.[44] Kuhn and co-workers[45] used a one-dimensional free-electron model of the

 © 2003 Wiley-VCH Verlag GmbH & Co. KGaA, Weinheim

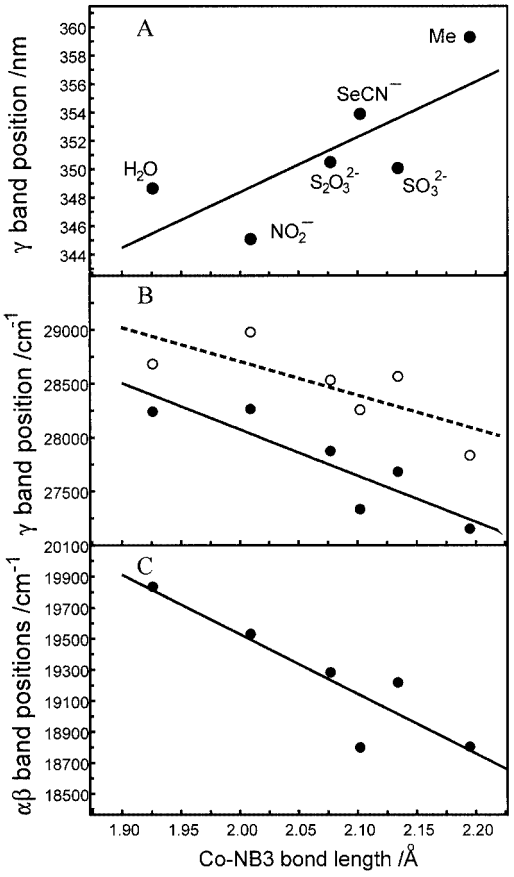

Figure 8. (A) Dependence of the apparent position of the γ-band (see Figure 3) on the Co−NB3 bond length; (B) relationship between the mean position of the three Gaussian components of the γ-band (open circles) and the two lowest-energy Gaussian components of the γ-band (filled circles) and the Co−NB3 bond length: (C) relationship between the mean position of the three components of the αβ-absorption envelope (see Figure 3) and the Co−NB3 bond length

open chain analogue of the 13-atom corrin chromophore (1,5,9,13-tetraazatrideca-1,3,5,7,9,11-pentaene) coordinated to Co^{III} to model the corrin and assign the principal bands in the electronic spectrum. In this model, the 7 lowest-energy levels of the π-electron system are occupied, and the γ-band is a symmetry-allowed transition between two states mixed by configurational interactions, $\pi_6 \rightarrow \pi_8$ and $\pi_7 \rightarrow \pi_9$. As has been noted,[46] the γ-band may be split into at least two components. The αβ-bands were assigned to the forbidden $\pi_7 \rightarrow \pi_8$ transition (the lower energy α-band) and its vibrational fine structure (the β-band). The interaction of this system with the axial ligands has been studied using an iterative extended Hückel molecular orbital method,[47] and it was shown that the main effect of the axial ligands is to change the energy of the π_7 orbital. Hence, transitions involving π_7 should shift to longer wavelength as the strength of the axial ligand field increases. Unlike the models used, the corrinoids are asymmetric with respect to rotation in the plane of the macrocycle. Since this asymmetry is expected to split these transitions, this may be the reason why both the γ- and the α,β-regions are modelled best by three Gaussian functions (Figure 4).

The three components of the γ-band were plotted against the length of the *trans*-Co−NB3 bond. Whilst the two lower energy components move to lower energy as the Co−NB3 bond length increased, there was no obvious correlation with the position of the highest-energy component, which suggests (but does not prove) that this component may not involve transitions from the π_7-molecular orbital of the corrin and may indeed not be part of the transitions that make up the γ-band. A plot of the mean position of the three Gaussian functions, and of the mean position of the two lowest-energy Gaussian functions, against the Co−NB3 bond length is shown in Figure 8, B. The latter gives a better correlation ($r^2 = 0.79$) than the former ($r^2 = 0.58$). In either case, the mean position of the components of the γ-band move to lower energy as the polarisability of the β ligand increases and the *trans*-Co−NB3 bond length increases. Similarly, all three components of the αβ-absorption envelope move to longer wavelengths as the Co−NB3 bond length increases, Figure 8, C ($r^2 = 0.81$).

This analysis indicates that there is no fundamental difference, apart from more transitions in the shorter wavelength region becoming observable, between the "typical" spectra of H_2OCbl^+, NO_2Cbl and SCNCbl, and the "atypical" spectra of $S_2O_3Cbl^-$, SeCNCbl, SO_3Cbl^- and MeCbl. The apparent differences in the γ-region stem from the components that constitute the γ-band moving apart in response to an increase in donation of electron density from the axial ligand field.

The results presented in Figure 8 are evidence for a correlation (albeit weak) between the ground-state *cis* and *trans* influences in the cobalamins. As the polarisability of the β-ligand increases, the *trans*-Co−NB3 bond length increases (*trans* influence), a consequence of the increasing electron density on the metal atom. This is transferred into the delocalised π-electron system of the corrin ring and the mean positions of the γ- and the αβ-transitions move to longer wavelength. The *trans* influence effect noted here is a further demonstration of the occurrence of a regular *trans* influence in the cobalamins as recently demonstrated by Randaccio and co-workers[32] who used DFT calculations to show that shortening of the Co−S bond in cobalamins with S-donor β-ligands causes the *trans*-Co−NB3 bond to lengthen.

The Corrin Fold

As noted above, the corrin ring in SCNCbl is considerably more folded than in SeCNCbl, NO_2Cbl or $S_2O_3Cbl^-$ (the fold angles are 22.4°, 13.7°, 14.5° and 17.2°, respectively). Examination of an overlay of the structures of SCNCbl and SeCNCbl shows that the principal reason for this is the Co−X−C−Y bond angle. When X = Se and Y = N, the small angle (104.3°) brings the axial ligand snugly between, and in close van der Waals contact with, C46 and C54 and very near the C15−C53 moiety. This forces the southern quadrant to be considerably flatter than when NCS^- is coordinated. In that case, the Co−X−C−Y (X = N, Y = S) angle is considerably larger (146.2°), and the bent axial group stands proud of C46, C54 and

 © 2003 Wiley-VCH Verlag GmbH & Co. KGaA, Weinheim

C15−C53. The mean Co−N−O angle in NO_2Cbl is 121.7° and the oxygen atoms of the ligand are not in van der Waals contact with the corrin or its substituents, with the exception of the hydrogen bond formed with the *c* side chain amide group. In S_2O_3Cbl$^-$ the coordinated ligand lies along the C10···C1/C19 fold axis. Despite this, the corrin is quite folded, since the Co−S−S angle is large due to the van der Waals contacts of the ligand with the substituents in the western portion of the molecule as noted above.

The Nature of the Co^{III} Ion in Cobalamins

We have found that SCN^- coordinates to Co^{III} in SCNCbl through N. Cobalt complexes with *N*-bound thiocyanate ions are common. A survey of the Cambridge Structural Database (CSD)[48] shows that there are 37 structures containing *N*-bound SCN^- to Co^{III} with a mean Co−N bond length of 1.93 ± 0.05 Å, but only three structures with *S*-bound SCN^- (d_{Co-S} = 2.29 ± 0.03 Å). In the case of Co^{II}, 86 structures have *N*-bound NCS^-, d_{Co-N} = 2.01 ± 0.07 Å, and there is only one structure [a low-spin dicobalt(II) compound of a Schiff-base marcrocycle with four bound thiocyanato ligands, two *N*-bound and two *S*-bound[49]] with *S*-bound SCN^- (d_{Co-S} = 2.584 Å). Hence, irrespective of the oxidation state of the metal ion, there is a strong preference for the thiocyanate ion to coordinate through N.

As expected, NO_2^- forms a longer bond to low-spin d^7 Co^{II} than it does to low-spin d^6 Co^{III}. The Co−NCS bond of 1.954(11) Å in SCNCbl is marginally long for coordination to Co^{III} (mean 1.93 ± 0.05 Å, see above), but short for coordination to Co^{II} (mean 2.01 ± 0.07 Å). It could be argued that the crowded β-face of the corrin ring contributes to Co−N bond lengthening. However, the Co−N−C angle is 146.2(11)°, which is close to the smallest angle (140.7°) found in the CSD for *N*-bound SCN^- to Co^{III} (the range is 140.7−178.8°, with an average value of 168 ± 8°). The analogous data for Co^{II} are 137.4−179.5°, 166 ± 8°. One would expect the angle to be considerably larger if there was a significant steric effect. The slightly long Co−N bond to NCS^- in SCNCbl is not due to steric reasons and could be the result of some partial Co^{II} character of the metal ion.

There is a report[50] of a crystal structure of SCNCbl in which the thiocyanato ligand is bound through S. The ^{1}H and ^{13}C NMR data of a solution containing B_{12a} and sufficient SCN^- for complete complex formation (the formation constant of the thiocyanato complex is log *K* = 3.1[51]) at 25 °C contains two sets of peaks close to each other, indicative of two different but related species in solution, which we assumed to be the linkage isomers. The peaks in the ^{1}H NMR spectrum due to the C10 and C13 protons are relatively free of overlap and were integrated, giving ratios of 1:0.75 and 1:0.86, respectively. (We have not been able to assign the individual resonances to each of the two linkage isomers.) SCNCbl clearly exists in solution as a mixture of the *N*- and the *S*-bound isomers and it is perhaps fortuitous that we obtained the *N*-bound isomer.

Addition of excess KSeCN to a solution of B_{12a} results in the immediate formation of a purple solution which, over time, changes to a solution with a more distinctly red colour. The initial ^{1}H and ^{13}C NMR spectra are consistent with a single product, and there is an apparently smooth transition to a second product with a half-life of about 2 d. The UV/Vis and ^{13}C NMR spectra of the final product are identical to those of CNCbl. Analysis of the X-ray diffraction of crystals obtained from the aged solution confirmed that the product is CNCbl (data not reported). This process occurs both under aerobic and anaerobic conditions. Since the crystal structure of the initial compound shows the ligand to be *Se*-bound, and there is no evidence for linkage isomerism in the ^{1}H and ^{13}C NMR spectra, we conclude that the selenocyanato complex decomposes slowly with extrusion of Se to form CNCbl. To date we have made no attempt to explore the mechanism of this reaction, but we note a report that [Ru(bmipy)(dcbpy)I]$^-$ [dcbpy^{2-} = 4,4′-dicarboxy-2,2′-bipyridyl; bmipy = 2,6-bis(1-methylbenzimidazol-2-yl)pyridyl] reacts with $SeCN^-$ to form a mixture of the *Se*- and the *N*-bound complexes. Prolonged reaction produces only the *N*-bound isomer which then rapidly yields the cyano complex with extrusion of Se.[52] Also, when *cis*-L_2Ru$(NCS)_2$ (L_2 = diethyl 2,2′-bipyridyl-4,4′-dicarboxylate) is oxidised to Ru^{III}, S is eliminated and the dicyanato complex is produced.[53] These workers noted that the reaction mechanism is complex, and postulated that extrusion of S occurs through a cyclic intermediate and rearrangement from *N*- to *C*-bound cyanide ion. Since $SeCN^-$ is coordinated to cobalamin in a bent fashion, an analogous cyclic intermediate appears to be feasible in the Se extrusion pathway.

There is only one example of a Co^{III}−selenocyanate complex in the CSD (a diselenocyanato cobaloxime complex[54]) and no complexes of Co^{II}. The Co^{III} compound has the ligand *Se*-bound to the metal atom with a Co−Se bond length of 2.383 Å, a Co−Se−C angle of 106.2° and an Se−N−C angle of 175.5°. Hence, the geometry is quite similar to that of SeCNCbl where the analogous parameters are 2.394 Å, 104.3° and 176.2°. Thus, the cobalt ions in the cobalamins behave like Co^{III} towards $SeCN^-$.

The great majority of NO_2^- complexes of Co^{III} reported in the CSD (148 structures) have the ligand bonded through the softer N donor with a mean Co−N bond length of 1.94(3) Å, an N−O bond length of 1.22(3) Å, a Co−N−O bond angle of between 112° and 132° [mean 120(2)°] and an O−N−O angle of between 92° and 135° [mean 119(3)°]. There are only two structures with *O*-bound NO_2^- [the mean Co−O bond length is 1.90(4) Å]. The two available structures of NO_2^- complexes of Co^{II} both have the ligand bonded through N. The Co−N bond lengths vary between 1.889 and 1.944 Å [mean 1.92(6) Å]. Surprisingly, the average Co^{II}−N bond is somewhat shorter than the average Co^{III}−N bond and this may be indicative of some metal-to-ligand back-bonding. The NO_2Cbl structure is therefore typical for coordination of NO_2^- to Co^{III} [the results for the major occupied site has Co−N = 1.941(5) Å, N−O = 1.230(2) Å, Co−N−O = 121.1(4)° and 117.2(4)° and

 © 2003 Wiley-VCH Verlag GmbH & Co. KGaA, Weinheim

O−N−O = 121.6(5)°]. The ^1H and ^{13}C NMR spectra indicate the presence of a single compound in solution and the kinetic data (see Introduction) are consistent with reaction through N. There is therefore no evidence for the nitrito isomer.

Although there are relatively few structures of complexes containing $S_2O_3^{2-}$ coordinated to cobalt (there is one with Co^{II}, and six with Co^{III}), those which have been reported are all *S*-bonded. There are significant differences in the lengths of the Co−S bonds: 2.488 Å in the *cis*-bis(thiosulfato)tetraaquacobalt(II) ion[55] and, on average, 2.28(3) Å in the Co^{III} complexes. In the latter, the average Co−S−S bond angle is 112(2)°. Therefore, the observed bond length of 2.286(1) Å in $S_2O_3Cbl^-$ is consistent with coordination to a Co^{III} centre. The somewhat large Co−S−S bond angle of 122.35(6)° is probably a consequence of close steric contact with the *a* side chain.

Conclusion

The lability of the formally low-spin Co^{III} centre in cobalamins, a notable feature of B_{12} chemistry (see Figure 2), is clearly conferred by the equatorial corrin ligand. There is clear evidence of electronic communication between the equatorial ligand system and the axial coordination sites of the metal ion. Thus, the principal transitions in the electronic spectra of the cobalamins shift to longer wavelengths as the donor power of the β-ligand increases (Figures 3 and 8). In addition to this *cis* influence, there is a normal *trans* influence as the Co−NB3 bond length responds to the donor ability of the β-ligand (Figure 8).

The structures of four cobalamin complexes obtained by the displacement of the axial H_2O molecule of B_{12a} with ambident nucleophiles (SCN^-, $SeCN^-$, NO_2^- and $S_2O_3^{2-}$) have been determined by X-ray diffraction methods. Our results show that Co^{III} in the complexes studied usually binds to the softer of the two available donor atoms (Se rather than N in $SeCN^-$, N rather than O in NO_2^- and S rather than O in $S_2O_3^{2-}$), but SCN^- is found to be *N*-bound in the solid state. However, there is a previous report of an *S*-bound complex and SCNCbl exists as a mixture of the two linkage isomers in solution. This preference for the softer donor atom in ambidentate nucleophiles is not unusual for cobalt complexes. An examination of the structures available in the CSD shows that irrespective of the oxidation state of the Co centre (+2 or +3), there is a strong preference for the thiocyanate ion to coordinate to the cobalt atom through N. The only example of a Co^{III}−selenocyanato complex in the CSD has the ligand bound through Se. NO_2^- usually coordinates to Co^{III} through N. The two Co^{II} structures available with NO_2^- as a ligand also have the ligand *N*-bound. There are relatively few structures of $S_2O_3^{2-}$ coordinated to Co^{II} and Co^{III}; all are *S*-bound.

If the metal ion in the cobalamins had significant Co^{II}-like character, then the bond to the β-axial ligand should be long, consistent with population of d_{z^2} in a pseudo-octahedral ligand field; in Co^{II} corrinoids the β-ligand is either absent or, at most, interacts very weakly with the metal centre. The Co−N bond in SCNCbl is marginally long for coordination to Co^{III} [$d_{Co^{III}-N}$ = 1.93 ± 0.05 Å; 1.954(11) Å observed in SCNCbl]. However, the other complexes have bond lengths expected for coordination to Co^{III}. Therefore, the increase in electron density that the corrin undoubtedly imparts to the metal atom has no significant effect on the ground-state structures of these complexes.

Experimental Section

UV/Vis Studies: UV/Vis spectra were recorded using a Cary 3E spectrophotometer with the cell compartment thermostatted by a water-circulating bath. These spectra, as well as those of SO_3Cbl^- and CH_3Cbl, the crystal structures of which have been reported by others, were analysed by Gaussian analysis, as we have done previously for iron porphyrins.[56] Each spectrum was converted into a plot of absorbance against wavenumber and fitted to the sum of the minimum number of Gaussian bands [Equation (2)] using non-linear least squares.[57] In Equation (2), A_T is the total absorbance, λ the measured wavenumber, λ_j the wavenumber at which the *j*th Gaussian component reaches a maximum absorbance, α_j the intensity of the *j*th peak and Δ_j the half-width of the *j*th band at 0.607 of the maximum intensity.

$$A_T = \sum_{j=1}^{n} \alpha_j \exp\left[\frac{-(\lambda - \lambda_j)^2}{2\Delta_j^2}\right] \quad (2)$$

Single Crystal X-ray Structure Determinations: Crystals were grown by dissolving hydroxocobalamin (approximately 50 mg, Roussel, > 99% pure, HPLC) in deionised water (700 μL) . To this was added an excess of the salt of the ligand. The solution was gently heated to ensure dissolution. The crystals were grown in H-tubes in a refrigerator, by vapour diffusion of acetone into the aqueous solution. Crystals usually appeared after about a week. A suitable crystal was selected after visual examination under a microscope. Intensity data were collected with a Bruker SMART 1 K CCD area detector diffractometer with graphite-monochromated Mo-K_α radiation (50 kV, 30 mA). The collection method involved ω-scans of 0.3° width. Data reduction was carried out using the program SAINT+[58] and absorption corrections were made using the program SADABS.[59] The crystal structures were solved by direct methods using SHELXS-97.[60] All non-hydrogen atoms of the cobalamin were first refined isotropically followed by anisotropic refinement by full-matrix least-squares calculations based on F^2 with SHELX-97 until convergence was achieved. Hydrogen atoms were positioned geometrically and allowed to ride on their respective parent atoms. In most cases it was not possible to locate the hydrogen atoms on the water molecules. These have been included in the formula sum, however. Diagrams and publication material were generated using WinGX[61] and PLATON.[62] CCDC-185962 to -185965 contain the supplementary crystallographic data for this paper. These data can be obtained free of charge at www.ccdc.cam.ac.uk/conts/retrieving.html [or from the Cambridge Crystallographic Data Centre, 12 Union Road, Cambridge CB2 1EZ, UK; Fax: (internat.) + 44-1223/336-033; E-mail: deposit@ccdc.cam.ac.uk].

X-ray Structure Determination of SCNCbl: SCNCbl was found to contain some disordered guest water molecules. These were mod-

 © 2003 Wiley-VCH Verlag GmbH & Co. KGaA, Weinheim

elled over two positions by either fixing their occupancies, or by assigning their occupancies to a free variable and allowing the free variable to be refined.

X-ray Structure Determination of SeCNCbl: All the solvent molecules in SeCNCbl were refined anisotropically with full occupancies.

X-ray Structure Determination of NO_2Cbl: Disordered atoms in the main body of the NO_2Cbl structure were refined independently with individual isotropic temperature factors. Disordered moieties included the NO_2 ligand and the *c* and *e* side chains. The NO_2 ligand was modelled over two orientations, with a site occupancy ratio of 0.82:0.18. The *c* and *e* side chains were both modelled over two orientations in 0.63:0.37 and 0.61:0.39 site occupancy ratios, respectively. Soft SADI restraints were used to ensure that all the bond lengths between the same atoms in each orientation were similar. The unit cell of NO_2Cbl contained a solvent acetone molecule in addition to several water solvent molecules. All C−C bonds, and the C−O bond in the acetone molecule were restrained to 1.50(2) and 1.24(2) Å, respectively, and a FLAT restraint was used to ensure that all the atoms were planar. Many of the water molecules in the NO_2Cbl structure were found to be disordered, or partially present. These were refined independently with individual isotropic thermal factors if the refinement was unstable.

X-ray Structure Determination of NaS_2O_3Cbl: The acetone solvent molecule in the $S_2O_3Cbl^-$ structure was refined isotropically, and all C−C and C−O bonds were restrained to 1.50(2) and 1.24(2) Å, respectively. All atoms in the acetone molecule were kept in a plane with the FLAT restraint. As with the previous structures, some of the solvent water molecules were refined and fixed with partial occupancies or, if they were disordered, modelled over two orientations. These solvent molecules were refined isotropically if anisotropic refinements resulted in unstable thermal parameters. ISOR restraints were applied to some of the solvent water molecules to approximate their U_{ij} values to isotropic behaviour.

Acknowledgments

This work was sponsored by the National Research Foundation, Pretoria, the University of the Witwatersrand through the Molecular Sciences Institute (H. M. M.) and the National Institute of Health (USA), grant GM48858 (K. L. B.).

[1] H. M. Marques, L. Knapton, *J. Chem. Soc., Dalton Trans.* **1997**, 3827−3833.
[2] J. J. P. Stewart, *J. Comput. Chem.* **1989**, *10*, 209−220.
[3] J. J. P. Stewart, *J. Comput. Chem.* **1989**, *10*, 221−264.
[4] R. G. Pearson, *J. Am. Chem. Soc.* **1963**, *85*, 3533−3539.
[5] K. L. Brown, S. Cheng, X. Zou, J. D. Zubkowski, E. J. Valente, L. Knapton, H. M. Marques, *Inorg. Chem.* **1997**, *36*, 3666−3675.
[6] C. K. Poon, *Coord. Chem. Rev.* **1973**, *10*, 1−35.
[7] A. D. Bacon, M. C. Zerner, *Theor. Chim. Acta* **1979**, *53*, 21−54.
[8] W. P. Anderson, W. D. Edwards, M. C. Zerner, *Inorg. Chem.* **1986**, *25*, 2728−2732.
[9] H. M. Marques, L. Knapton, X. Zou, K. L. Brown, *J. Chem. Soc., Dalton Trans.* **2002**, 3195−3200.
[10] H. M. Marques, L. Knapton, unpublished results.
[11] R. G. Finke, D. A. Schiraldi, B. J. Mayer, *Coord. Chem. Rev.* **1984**, *54*, 1−22.
[12] J. Halpern, *Science (Washington, DC, U. S.)* **1985**, *227*, 869−875.
[13] R. Banerjee, S. Chowdhury, in *Chemistry and Biochemistry of B_{12}* (Ed.: R. Banerjee), Wiley, New York, **1999**, pp. 707−729.
[14] R. G. Finke, B. P. Hay, *Inorg. Chem.* **1984**, *23*, 3041−3043.
[15] B. P. Hay, R. G. Finke, *J. Am. Chem. Soc.* **1986**, *108*, 4820−4829.
[16] K. L. Brown, S. Cheng, J. D. Zubkowski, E. J. Valente, *Inorg. Chem.* **1997**, *36*, 1772−1781.
[17] B. D. Martin, R. G. Finke, *J. Am. Chem. Soc.* **1992**, *114*, 585−592.
[18] B. Kräutler, W. Keller, M. Hughes, C. Caderas, C. Kratky, *J. Chem. Soc., Chem. Commun.* **1987**, 1678−1680.
[19] B. Kräutler, W. Keller, C. Kratky, *J. Am. Chem. Soc.* **1989**, *111*, 8936−8938.
[20] K. Gruber, G. Jogl, G. Klintschar, C. Kratky, in *Vitamin B_{12} and B_{12} Proteins* (Eds.: B. Kräutler, D. Arigoni, B. T. Golding), Wiley-VCH, New York, **1998**, pp. 335−347.
[21] P. G. Lenhert, *Proc. Royal Soc., London* **1968**, *A303*, 45−84.
[22] B. Kräutler, R. Konrat, E. Stupperich, G. Färber, K. Gruber, C. Kratky, *Inorg. Chem.* **1994**, *33*, 4128−4136.
[23] C. L. Drennan, S. Huang, J. T. Drummond, R. G. Matthews, M. L. Ludwig, *Science (Washington, DC, U. S.)* **1994**, *226*, 1669−1674.
[24] F. Mancia, N. H. Keep, A. Nakagawa, P. F. Leadlay, S. McSweeny, B. Rasmussen, P. Bosecke, O. Diat, P. R. Evans, *Structure* **1996**, *4*, 339−350.
[25] M. L. Ludwig, P. R. Evans, in *Chemistry and Biochemistry of B_{12}* (Ed.: R. Banerjee), Wiley, New York, **1999**, pp. 595−632.
[26] C. Kratky, B. Kräutler, in *Chemistry and Biochemistry of B_{12}* (Ed.:R. Banerjee), Wiley, New York, **1999**, pp. 9−41.
[27] J. M. Pratt, in *Chemistry and Biochemistry of B_{12}* (Ed.: R. Banerjee), Wiley, New York, **1999**, pp. 73−112.
[28] R. T. Taylor, in *B_{12}* (Ed.: D. Dolphin), Wiley, New York, **1982**, vol. 2, pp. 307−355.
[29] L. Randaccio, S. Geremia, G. Nardin, M. Slouf, I. Srnova, *Inorg. Chem.* **1999**, *38*, 4087−4092.
[30] J. M. Pratt, in *Chemistry and Biochemistry of B_{12}* (Ed.: R. Banerjee), Wiley, New York, **1999**, pp. 113−164.
[31] M. Nardelli, *J. Appl. Crystallogr.* **1995**, *28*, 659−659.
[32] J. P. Glusker in *B_{12}* (Ed.:D. Dolphin), Wiley, New York, **1982**, vol. 1, pp. 23−106.
[33] K. L. Brown, D. R. Evans, J. D. Zubkowski, E. J. Valente, *Inorg. Chem.* **1996**, *35*, 415−423.
[34] T. G. Pagano, L. G. Marzilli, M. M. Flocco, C. Tsai, H. L. Carrell, J. P. Glusker, *J. Am. Chem. Soc.* **1991**, *113*, 531−542.
[35] K. L. Brown, X. Zou, *Inorg. Chim. Acta* **1998**, *267*, 305−308.
[36] M. Rossi, J. P. Glusker, L. Randaccio, L. G. Marzilli, *J. Am. Chem. Soc.* **1985**, *107*, 1729−1738.
[37] N. W. Alcock, R. M. Dixon, B. T. Goulding, *J. Chem. Soc., Chem. Commun.* **1985**, 603−605.
[38] F. J. Savage, P. F. Lindley, J. L. Finney, P. A. Timmins, *Acta Crystallogr., Sect. B* **1987**, *43*, 280−295.
[39] B. Kräutler, in: "Organic Reactivity: Physical and Biological Aspects" (Eds.: B. T. Golding, R. J. Griffin, H. Maskill), *Spec. Publ. - R. Soc. Chem.* **1995**, 148, 209−214. Coordinates supplied by: C. Kratky, Karl-Franzens-Universität, Graz, Austria.
[40] L. Randaccio, S. Geremia, M. Furlan, M. Slouf, *Inorg. Chem.* **1998**, *37*, 5390−5393.
[41] C. Kratky, G. Fäber, K. Gruber, K. Wilson, Z. Dauter, H.-F. Nolting, R. Konrat, B. Kräutler, *J. Am. Chem. Soc.* **1995**, *117*, 4654−4670.
[42] B. Kräutler, R. Konrat, E. Stupperich, G. Fäber, K. Gruber, C. Kratky, *Inorg. Chem.* **1994**, *33*, 4128−4139.
[43] J. M. Waters, T. N. M. Waters, *Proc. Indian Acad. Sci.* **1984**, *93*, 219−234.
[44] C. Giannotti, in *B_{12}* (Ed.: D. Dolphin), Academic Press, New York, **1982**, pp. 393−430.
[45] H. Kuhn, K. H. Drexhage, H. Martin, *Proc. R. Soc.* **1965**, *288*, 348−351.

 © 2003 Wiley-VCH Verlag GmbH & Co. KGaA, Weinheim

[46] P. O. Offenhartz, B. H. Offenhartz, M. M. Fung, *J. Am. Chem. Soc.* **1970**, *92*, 2966−2973.
[47] G. N. Schrauzer, *Naturwissenschaften* **1966**, *53*, 459−463.
[48] Version 5.22, Oct. 2001 release: F. H. Allen, *Acta Crystallogr., Sect. B* **2002**, *58*, 380−388.
[49] S. Brooker, P. G. Plieger, B. Moubaraki, K. S. Murray, *Angew. Chem. Int. Ed.* **1999**, *38*, 408−410.
[50] Personal communication with D. C. Hodgkin, quoted by J. M. Pratt, *Inorganic Chemistry of B_{12}*, Academic Press, London, **1972**, p. 152.
[51] J. M. Pratt, *Inorganic Chemistry of B_{12}*, Academic Press, London, **1972**, p. 58.
[52] O. Kohle, S. Ruile, M. Grätzel, *Inorg. Chem.* **1996**, *35*, 4779−4787.
[53] G. Wolfbauer, A. M. Bond, D. R. MacFarlane, *Inorg. Chem.* **1999**, *38*, 3836−3846.
[54] I. D. Samus, N. V. Belov, *Dokl. Akad. Nauk SSSR* **1970**, *193*, 333−336.
[55] A. Carter, M. G. B. Drew, *Polyhedron* **1999**, *18*, 1445−1453.
[56] O. Q. Munro, H. M. Marques, *Inorg. Chem.* **1996**, *35*, 3768−3779.
[57] G. Brink, *FIT, a computer program for non-linear least-squares fitting using the Marquard algorithm*, University of the Witwatersrand, Johannesburg, South Africa, **1992**.
[58] *SAINT+*, Version 6.02 (includes XPREP and SADABS), Bruker AXS Inc., Madison, Wisconsin, USA, **1999**.
[59] G. M. Sheldrick, *SADABS*, University of Göttingen, Germany, **1996**.
[60] G. M. Sheldrick, *SHELXS-97*, release 97-2, University of Göttingen, Germany, **1997**.
[61] WinGX, Version 1.63.01: L. J. Farrugia, *J. Appl. Crystallogr.* **1999**, *32*, 837−838.
[62] A. L. Spek, *Acta Crystallogr., Sect. A* **1990**, *46*, C34−C34.
[63] L. Randaccio, S. Geremia, M. Stener, D. Toffoli, E. Zangrando, *Eur. J. Inorg. Chem.* **2002**, 93−103.

Received October 31, 2002

 © 2003 Wiley-VCH Verlag GmbH & Co. KGaA, Weinheim

Synthesis, Solid-State Structure and Multinuclear NMR Studies of the New Polyhydrido Iridium Carbonyl Cluster $Ir_4H_4(\mu\text{-}H)_4(CO)_4(PPh_3)_4$

Luigi Garlaschelli,*[a] Francesco Greco,[a] Giulia Peli,[a] Mario Manassero,*[b] Mirella Sansoni,[b] Roberto Gobetto,*[c] Luca Salassa,[c] and Roberto Della Pergola[d]

Keywords: Cluster compounds / Iridium / Hydride ligands / NMR spectroscopy / P ligands

The carbonyl hydride cluster $Ir_4H_8(CO)_4(PPh_3)_4$ (**1**) has been formed in high yield and purity by heating a mixture of $Ir_4(CO)_{12}$ and PPh_3 in toluene at 90 °C under hydrogen at atmospheric pressure. The product has been characterised by microanalysis, spectroscopy (IR, ^1H and ^{31}P NMR) and X-ray diffraction. In the solid state one hydrogen, one CO and one triphenylphosphane ligand are terminally bonded to each iridium atom, whereas four hydride ligands are bridging. All the hydrogen atoms were directly located by X-ray analysis at an average H–Ir distance of 1.55 Å (for the terminal H) and 1.75 Å (for the μ-H). As shown by ^1H and ^{31}P NMR spectra, two isomeric forms (**1A** and **1B**) of the cluster are present in CD_2Cl_2 solution at room temperature, and they do not interconvert in the explored temperature range. However, if a solid sample of the cluster is dissolved at 188 K, only **1A** is detected by NMR spectroscopy. The structure of **1B** could be proposed on the basis of the T_1 relaxation times of the various hydrides: it results by localised exchange of H and CO around two vertices of the tetrahedral frame.

(© Wiley-VCH Verlag GmbH & Co. KGaA, 69451 Weinheim, Germany, 2003)

Hydrogen atoms are common ligands in transition metal chemistry[1] and can be bound to the cluster framework in a variety of ways.[2] Beside the most common terminal, bridging, and face-capping modes,[3] they can also occupy an interestitial coordination mode site, with up to six H-metal interactions.[4,5]

The hydride ligands in many clusters are abstracted from the solvent in which the cluster is prepared.[6] However, hydrides can also be introduced using a rational synthetic route, commonly acidification of an anionic cluster,[5,7,8] or hydrogenation of a suitable precursor.[9] Alternatively, the precursor might have contained hydrides and these are carried over into the cluster product.[10]

Owing to their low scattering factors, hydride ligands are difficult to locate by X-ray crystallography, and frequently neutron diffraction studies must be undertaken.[4,11,12] NMR spectroscopy is a powerful tool for determining the position of the hydrides in solution (especially when the cluster contains other nuclei with spin 1/2, such as ^{31}P, ^{103}Rh or ^{195}Pt).[13] A few cases of solid-state ^1H NMR studies have also been reported.[14]

In the present work we report the spectroscopic characterisation and the solid-state structure of the new cluster $[Ir_4H_8(CO)_4(PPh_3)_4]$, which can be obtained in a one-pot synthesis directly from $Ir_4(CO)_{12}$, PPh_3 and hydrogen. Among the huge number of tetrahedrally substituted iridium clusters,[12,15–17] the compound described here is peculiar in several aspects: the simplicity of the synthesis, the highly symmetric structure, its straightforward dynamic behaviour, and the large number of ligands around a small tetrahedral core. As one half of the ligands are hydrides, the compound can model the dissociative chemisorption of hydrogen on small iridium particles.[18]

$[H_2Ir_4(CO)_{10}]^{2-}$, with two terminal hydrides,[15] and $[HIr_4(CO)_{11}]^-$, with a bridging hydride located from neutron diffraction,[12] are other examples of hydrido-carbonyl clusters of iridium; $[HIr_4(CO)_{10}PPh_3]^-$ [19] and $[HIr_4(CO)_{10}PPh_2]$,[20] are tetranuclear clusters containing both hydride and P-donor ligands.

[a] Dipartimento di Chimica Inorganica, Metallorganica e Analitica dell'Università di Milano,
Via G. Venezian 21, 20133 Milano, Italy
Fax: (internat.) + 39-02/5031-4405
E-mail: luigi.garlaschelli@unimi.it
[b] Dipartimento di Chimica Strutturale e Stereochimica Inorganica dell'Università di Milano,
Via G. Venezian 21, 20133 Milano, Italy
E-mail: m.manassero@istm.cnr.it
[c] Dipartimento di Chimica Inorganica, Chimica Fisica e Chimica dei Materiali dell'Università di Torino,
Via P. Giura 7, 10125 Torino, Italy
E-mail: roberto.gobetto@ch.unito.it
[d] Dipartimento di Scienze dell'Ambiente e del Territorio dell'Università degli Studi di Milano Bicocca,
Piazza della Scienza 1, 20126 Milano, Italy

Supporting information for this article is available on the WWW under http://www.eurjic.org or from the author.

 © 2003 Wiley-VCH Verlag GmbH & Co. KGaA, Weinheim **DOI: 10.1002/ejic.200200690**

Results

Synthesis and Chemical Characterisation

While trying to synthesise an iridium cluster containing an interestitial phosphido atom, $Ir_4(CO)_8(PPh_3)_4$ [17] (**2**) was heated in refluxing toluene under a hydrogen atmosphere. The infrared spectrum of the brownish-yellow solution suggested the formation of a mixture. Attempts to separate the main products by preparative TLC or column chromatography failed, and therefore we sought milder conditions in order to increase the selectivity of the reaction. Eventually, a two-step, one-pot synthesis was devised, which is more simple and more selective: the first step is the carbonyl substitution of $Ir_4(CO)_{12}$ accomplished in refluxing toluene, with PPh_3 and $Ir_4(CO)_{12}$ in a 4:1 molar ratio. In the second step, the mixture of partially substituted clusters is placed under hydrogen and heated gently at a temperature below 90 °C until the infrared spectrum shows complete conversion (usually 24 hours). The product was crystallised from CH_2Cl_2/cyclohexane and was formulated as $Ir_4H_8(CO)_4(PPh_3)_4$ (**1**), by means of microanalysis, NMR spectroscopy, and X-ray analysis.

The poor reactivity of **1** is evidence of its stability. Despite the large number of hydride ligands, **1** cannot be deprotonated by base: when it was dissolved in THF, with an excess of Na_2CO_3 or KOH, the IR spectrum did not show any modification. A toluene solution of $Ir_4H_8(CO)_4(PPh_3)_4$ was placed under a carbon monoxide atmosphere at room temperature and no reaction was detected after three hours. However, heating the same solution at 110 °C for four hours resulted in the transformation into a mixture of $Ir_4(CO)_9(PPh_3)_3$ and **2**.

Solid-State Structure

The solid-state structure of **1**, and the numbering scheme, are shown in Figure 1. Relevant distances and angles are collected in Table 1. The metallic framework is tetrahedral, but the (idealised) molecular symmetry is S_4, with the unique axis intersecting the two unbridged Ir−Ir bonds. Thus, the four equivalent iridium vertices are coordinated by one triphenylphosphane, one terminal CO, one terminal and two bridging hydride ligands. The cluster is only slightly distorted by the presence of four μ-H ligands: the unbridged edges measure 2.726 Å and the bridged ones 2.919 Å. The five ligands are arranged in a square-based pyramidal coordination, with the PPh_3 ligands in the axial positions. The P-donors are almost perfectly mutually *trans*, separated by an unbridged Ir−Ir bond, and *cis* to the bridging hydride (with corresponding P−Ir−Ir angles of 115°) and therefore the metal atoms are octahedrally surrounded. The average distances between metals and ligands of different nature are well within the normal range for iridium clusters,[12,16,19,20] and are collected in Table 1. The Ir−H bond lengths are obviously affected by high standard deviations (0.03−0.04 Å) and therefore differences of 0.1 Å are of little significance; however, constant trends for the Ir−(μ-H)−Ir bond lengths seem to suggest some asymmetry, with long bonds *trans* to the carbonyl and short bonds *trans* to the terminal hydride, a pattern contrasting with the "structural" trans effect in octahedral metal complexes, being smaller for CO than for H.[21]

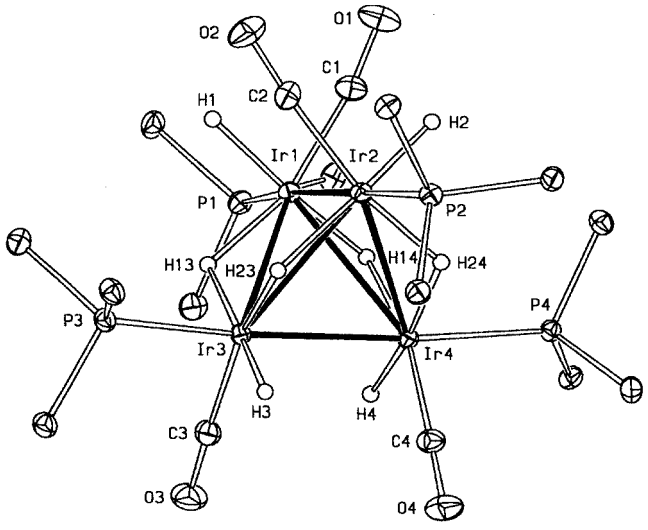

Figure 1. The solid state structure of **1**; for clarity, only the *ipso* carbon atoms of the phenyl rings are indicated; ellipsoids are drawn at 30% probability

Table 1. Selected distances (Å) and angles (deg.) in $[Ir_4H_8(CO)_4(PPh_3)_4]$ (**1**) with estimated standard deviations (esd's) on the last figure in parentheses; term = terminal; br = edge bridging; tr = *trans*

Ir1−Ir2	2.721(1)	Ir1−C1	1.846(3)
Ir1−Ir3	2.925(1)	Ir2−C2	1.847(3)
Ir1−Ir4	2.916(1)	Ir3−C3	1.854(3)
Ir2−Ir3	2.906(1)	Ir4−C4	1.855(3)
Ir2−Ir4	2.931(1)		
Ir3−Ir4	2.732(1)	Ir1−P1	2.305(1)
Ir1−H1	1.62(4)	Ir2−P2	2.315(1)
Ir2−H2	1.58(3)	Ir3−P3	2.315(1)
Ir3−H3	1.51(4)	Ir4−P4	2.320(1)
Ir4−H4	1.51(4)		
Ir1−H13	1.71(3)	Ir3−H13	1.80(3)
Ir1−H14	1.60(4)	Ir3−H23	1.69(4)
Ir2−H23	1.82(3)	Ir4−H14	1.87(4)
Ir2−H24	1.63(4)	Ir4−H24	1.86(3)
Average distances		**Average angles**	
C−O	1.143	P−Ir−H_{br}	88
Ir−P	2.314	H_{br}−Ir−H_{br}	102
Ir − CO	1.850	H_{term}−Ir−CO	86
Ir-H_{term}	1.55	H_{term}−Ir−P	89
Ir−H_{br}	1.75	P−Ir−CO	96
		P−Ir−Ir_{tr}	175
		P−Ir−Ir_{cis}	115
		Ir−C−O	174

Multinuclear VT NMR Spectroscopy

When a sample of **1** is dissolved at low temperature in CD_2Cl_2 the ^1H NMR spectrum shows only two absorptions in the hydride region, at δ = −15.24 and −17.25 ppm

 © 2003 Wiley-VCH Verlag GmbH & Co. KGaA, Weinheim

respectively, in agreement with the presence of the terminal and bridging hydride ligands of the highly symmetric structure determined by X-ray analysis. As the temperature is increased three new resonances appear in the proton spectrum at $\delta = -14.82$, -16.11 and -18.89 ppm, respectively, in the relative ratio 2:1:1. The intensity of these new absorptions is temperature dependent, as shown in Figure 2.

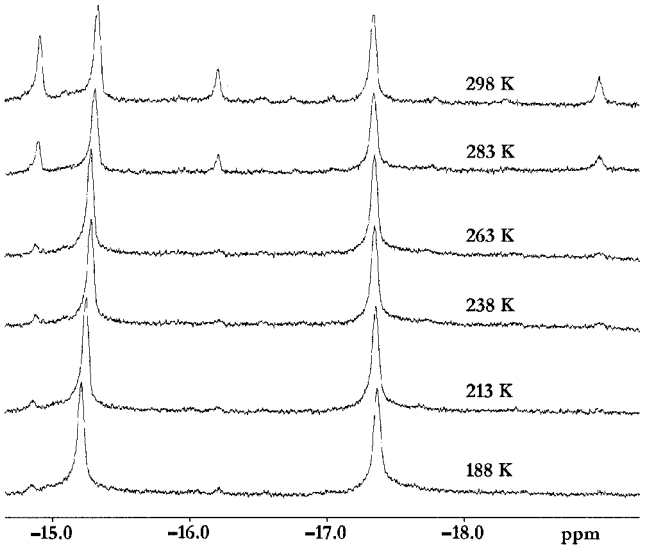

Figure 2. The ^{1}H NMR spectrum of **1**, recorded in CD_2Cl_2, at variable temperature

The high-field resonance can readily be assigned to a terminal hydride, whereas the two lower field signals are consistent with the formation of two distinct bridging hydride absorptions.

The same process has also been examined by ^{31}P and ^{13}C NMR spectroscopy. Monitoring the VT ^{31}P NMR spectrum in the same range of temperature, one can easily see that at 188 K only one ^{31}P signal is present at $\delta = 3.5$ ppm, whereas upon increasing the temperature a second absorption is observed at $\delta = 4.2$ ppm; at room temperature the spectrum shows two signals. Similarly, only a single resonance is detected in the ^{13}C NMR spectrum for the sample dissolved at 188 K in CD_2Cl_2, whereas a second absorption can be observed in the carbonyl region when the temperature is increased ($\delta = 166.78$ and 165.80 ppm).[22] Obviously the new resonances in the ^{1}H, ^{13}C, and ^{31}P NMR spectra must be associated with the formation of a second isomer (**1B**; Scheme 1), different from that found in the solid state (**1A**), which increases in concentration at higher temperature. The two resonances in the ^{31}P NMR spectrum were unambiguously assigned to **1A** ($\delta = 3.5$ ppm) and **1B** ($\delta = 4.2$ ppm) by running a ^{1}H-^{31}P 2D experiment. It is worth noting that if the sample is recrystallised again and a new experiment is performed with the previously reported procedure the same results are obtained. However, if the solution containing **1A** and **1B** at equilibrium is cooled to 188 K, both isomers are present; thus, the rate of exchange between the two isomers is slow on the NMR timescale.

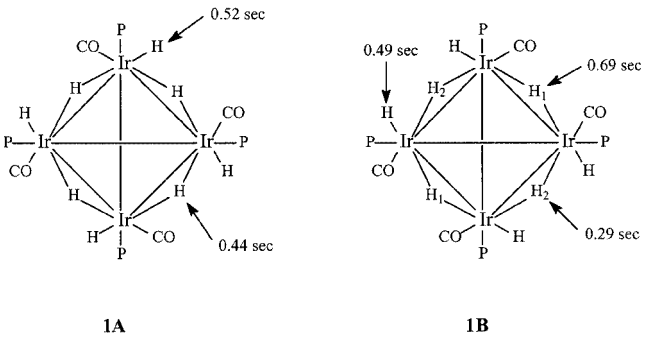

Scheme 1. The structure of isomers **1A** and **1B**, with the T_1 relaxation times of the different hydride ligands

On the basis of the spectroscopic results it is reasonable to suggest that the second structure is also highly symmetric and the difference with respect to the former one is due to the position of the hydride ligands on the metal framework.

In order to assign the structure of the isomer **1B** an evaluation of the longitudinal relaxation times (T_1) of the hydride resonances has been performed. It has previously been demonstrated that this technique provides a suitable method for the determination of the structures of polyhydridic cluster systems[23] due to the dependence of T_1 on the relative interproton distances.[24]

The T_1 values obtained for the hydride ligands of the two isomers at room temperature are reported in Scheme 1, and are proposed on the basis of the relaxation and symmetry data.

The difference between the two isomers is the reciprocal orientation of CO and terminal H around the tetrahedron: by inverting the position of these ligands at two iridium vertices the molecular symmetry is lowered from S_4 to D_2. The T_1 values of the terminal hydrides are similar in both isomers, whereas the bridging hydrides show substantial changes. In particular, the relaxation time for the higher-field signal of **1B** is substantially shorter than the others, indicating a closer proximity of these hydrides to other hydride ligands in the cluster. On this basis it is straightforward to assign the resonance at $\delta = -18.89$ ppm (having shorter T_1) to the H_2 hydride in the structure. All the other attributions are summarised in Figure 3.

The complex spin system of twelve ^{31}P and ^{1}H nuclei, further complicated by chemical exchange, could not be examined in details. As a matter of fact, the observed bands are so broadened (either by chemical exchange or by low resolution at 188 K) that no hyperfine structure was observed at all (expected values for $^2J_{P,H} = 5-10$ Hz).[19,20]

Experimental Section

General: All the solvents were purified and dried by conventional methods and stored under nitrogen. All the reactions were carried out under an oxygen-free nitrogen atmosphere using standard Schlenk-tube techniques.[25] $Ir_4(CO)_{12}$ was prepared by literature methods.[26]

 © 2003 Wiley-VCH Verlag GmbH & Co. KGaA, Weinheim

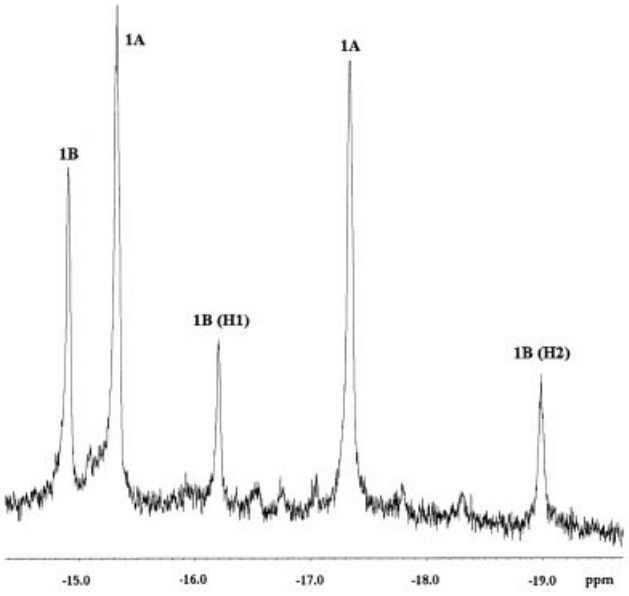

Figure 3. The ^1H NMR spectrum of **1**, recorded in CD_2Cl_2, at room temperature, with the assignments of the peaks

NMR experiments were performed on a JEOL EX 400 spectrometer (^1H operating frequency 399.78 MHz); non-selective inversion recovery was used to obtain ^1H T_1 values. Samples for T_1 measurements were prepared in the absence of O_2 by using standard freeze-pump-thaw techniques. Temperature calibration was carried out with a standard methanol ^1H thermometer. Errors in the reported T_1 values were estimated to be in the range ±2%.

Synthesis of $Ir_4H_8(CO)_4(PPh_3)_4$: $Ir_4(CO)_{12}$ (0.55 g, 0.50 mmol) and PPh_3 (0.52 g, 2 mmol) were suspended in 40 mL of toluene. The mixture was refluxed for 7 hours, and the IR spectrum of the yellow solution showed bands consistent with a mixture of tri- and tetra-substituted derivatives of $Ir_4(CO)_{12}$. The inert atmosphere was removed and the Schlenk was refilled with hydrogen. The solution was heated at 80 °C for about 24 hours and the colour changed from the yellow to pale yellow. After cooling, the solution was filtered, and the solvent was removed in vacuo. The residue was dissolved in dichloromethane and layered with cyclohexane. Yellow prismatic crystals were obtained in 65% yield (0.63 g). IR: ν(CO): 2121w 1993s cm^{-1} in CH_2Cl_2. $C_{76}H_{68}Ir_4O_4P_4$ (1938.1): calcd. C 47.1, H 3.5 found C 47.2, H 3.6.

X-ray Data Collection and Structure Determination: Crystal data are summarised in Table 2; other experimental details are listed in the supporting information. The diffraction experiment was carried out on a Bruker SMART CCD area-detector diffractometer at 223 K. No crystal decay was observed, so that no time-decay correction was needed. The collected frames were processed with the software SAINT,[27] and an absorption correction was applied (SADABS)[28] to the collected reflections. The calculations were performed using the Personal Structure Determination Package[29] and the physical constants tabulated therein.[30] The structure was solved by direct methods (SHELXS)[31] and refined by full-matrix least-squares using all reflections and minimising the function $\Sigma w(F_o^2 - kF_c^2)^2$ (refinement on F^2). Anisotropic thermal factors were refined for all the non-hydrogen atoms. The eight hydridic hydrogen atoms were refined with isotropic thermal factors. The remaining hydrogen atoms were placed in their ideal positions (C−H = 0.97 Å), with the thermal parameter B 1.10-times that of the carbon atom to which they are attached and not refined. In the final difference Fourier map the maximum residual was 1.88(81) e·Å^{-3} at 0.81 Å from Ir(2). CCDC-199711 contains the supplementary crystallographic data for this paper. These data can be obtained free of charge at www.ccdc.cam.ac.uk/conts/retrieving.html [or at Cambridge crystallographic Data Centre, 12 Union Road, Cambridge CB2 1EZ, UK; Fax: (internat.) +44-1223/336-033; E-mail: deposit@ccdc.cam.ac.uk].

Table 2. Crystallographic data

Formula	$C_{76}H_{68}Ir_4O_4P_4$
M	1938.08
Colour	pale yellow
Crystal system	monoclinic
Space group	$P2_1/c$ (no.14)
a/Å	15.196(1)
b/Å	24.237(2)
c/Å	18.949(2)
α/°	90
β/°	106.13(1)
γ/°	90
V/Å^3	6704.3(9)
Z	4
F(000)	3696
D_c/g cm^{-3}	1.92
T/K	223
Crystal dimensions (mm)	0.29 × 0.41 × 0.58
μ (Mo-K_α)/cm^{-1}	80.28
Min. and max. transm. factors	0.50−1.00
Scan mode	ω
Frame width/°	0.30
Time per frame/sec	10
No. of frames	3650
Detector-sample distance/cm	4.00
θ-range/°	3−26
Reciprocal space explored	full sphere
No. of reflections (total; independent)	164038; 20468
R_{int}	0.039
Final R_2 and R_{2w} indices[a] (F^2, all reflections)	0.034, 0.060
Conventional R_1 index [$I > 2\sigma(I)$]	0.022
Reflections with $I > 2\sigma(I)$	17033
No. of variables	825
Goodness of fit[b]	1.00

[a] $R_2 = [\Sigma(|F_o^2 - kF_c^2|/\Sigma F_o^2]$, $R_{2w} = [\Sigma w(F_o^2 - kF_c^2)^2/\Sigma w(F_o^2)^2]^{1/2}$. [b] $[\Sigma w(F_o^2 - kF_c^2)^2/(N_o - N_v)]^{1/2}$, where $w = 4F_o^2/\sigma(F_o^2)^2$, $\sigma(F_o^2) = [\sigma^2(F_o^2) + (0.04F_o^2)^2]^{1/2}$, N_o is the number of observations and N_v the number of variables.

Supporting Information: The ^{13}C NMR spectra for this article are available (see footnote on the first page of this article).

Acknowledgments

This work was funded by MIUR.

[1] *Recent Advances in Hydride Chemistry* (Eds.: M. Peruzzini and R. Poli), Elsevier, Amsterdam (The Netherlands) **2001**.
[2] A. P. Humpries, H. D. Kaesz, *Prog. Inorg. Chem.* **1979**, *25*, 145−222.
[3] A. Albinati, L. M. Venanzi, *Coord. Chem. Rev.* **2000**, *200−202*, 687−715.
[4] R. Bau, M. H. Drabnis, L. Garlaschelli, W. T. Klooster, Z. Xie, T. F. Koetzle, S. Martinengo, *Science* **1997**, *275*, 1099−1102.
[5] D. W. Hart, R. G. Teller, C.-Y. Wei, R. Bau, G. Longoni, S. Campanella, P. Chini, T. F Koetzle, *Angew. Chem. Int. Ed. Engl.* **1979**, *18*, 80−81.

 © 2003 Wiley-VCH Verlag GmbH & Co. KGaA, Weinheim

[6] [6a] A. J. Amoroso, B. F. G. Johnson, J. Lewis, P. R. Raithby, W. T. Wong, *J. Chem. Soc., Chem. Commun.* **1991**, 814−815. [6b] P. J. Bailey, M. A. Beswick, B. F. G. Johnson, J. Lewis, M. McPartlin, P. R. Raithby, M. C. Ramirez de Arellano, *J. Chem. Soc., Dalton Trans.* **1996**, 3515−3520.
[7] [7a] M. Manassero, M. Sansoni, G. Longoni, *J. Chem. Soc., Chem. Commun.* **1976**, 919−920. [7b] R. Della Pergola, C. Bandini, F. Demartin, E. Diana, L. Garlaschelli, P. L. Stanghellini, P. Zanello, *J. Chem. Soc., Dalton Trans.* **1996**, 747−754.
[8] A. Ceriotti, R. Della Pergola, L. Garlaschelli, F. Laschi, M. Manassero, N. Masciocchi, M. Sansoni, P. Zanello, *Inorg. Chem.* **1991**, *30*, 3349−3357.
[9] [9a] S. A. R. Knox, J. W. Koepke, M. A. Andrews, H. D. Kaesz, *J. Am. Chem. Soc.* **1975**, *97*, 3942−3952. [9b] L. M. Bavaro, P. Montangero, J. B. Keister, *J. Am. Chem. Soc.* **1983**, *105*, 4977−4981.
[10] [10a] R. Della Pergola, L. Garlaschelli, F. Demartin, M. Manassero, N. Masciocchi, G. Longoni, *J. Organomet. Chem.* **1988**, *352*, C59−C62. [10b] G. Ciani, M. Moret, A. Sironi, P. Antognazza, T. Beringhelli, G. D'Alfonso, R. Della Pergola, A. Minoja, *J. Chem. Soc., Chem. Commun.* **1991**, 1255−1257. [10c] C. S. Yang, C. P. Cheng, *J. Chem. Soc., Dalton Trans.* **1994**, 2011−2014.
[11] A. Bashall, L. H. Gade, J. Lewis, B. F. G. Johnson, G. J. McIntyre, M. McPartlin, *Angew. Chem. Int. Ed. Engl.* **1991**, *30*, 1164−1166.
[12] R. Bau, M. Chiang, C.-Y. Wei, L. Garlaschelli, S. Martinengo, T. F. Koetzle, *Inorg. Chem.* **1984**, *23*, 4758−4762.
[13] [13a] S. Martinengo, B. T. Heaton, R. J. Goodfellow, P. Chini, *J. Chem. Soc., Chem. Commun.* **1977**, *2*, 39−40. [13b] T. Beringhelli, A. Ceriotti, G. D'Alfonso, R. Della Pergola, G. Ciani, M. Moret, A. Sironi, *Organometallics* **1990**, *9*, 1053−1059. [13c] M. J. Davis, R. Roulet, *Inorg. Chim. Acta* **1992**, *197*, 15−20.
[14] [14a] S. Aime, P. J. Barrie, D. F. Brougham, R. Gobetto, G. E. Hawkes, *Inorg. Chem.* **1995**, *34*, 3557−3559. [14b] T. Eguchi, B. T. Heaton, R. Harding, K. Miyagi, G. Longoni, J. Nahring, N. Nakamura, H. Nakayama, T. A. Pakkanen, J. Pursiainen, A. K. Smith, *J. Chem. Soc., Dalton Trans.* **1996**, 625−630. [14c] T. Eguchi, B. T. Heaton, *J. Chem. Soc., Dalton Trans.* **1999**, 3523−3530.
[15] G. Ciani, M. Martinengo, V. G. Albano, F. Canziani, G. Giordano, S. Martinengo, P. Chini, *J. Organomet. Chem.* **1978**, *150*, C17−C19.
[16] [16a] G. F. Stuntz, J. R. Shapley, *J. Organomet. Chem.* **1981**, *213*, 389−403. [16b] D. C. Sonnenberger, J. D. Atwood, *Organometallics* **1982**, *1*, 694−698. [16c] D. Braga, R. Ros, R. Roulet, *J. Organomet. Chem.* **1985**, *286*, C8−C12. [16d] R. Della Pergola, L. Garlaschelli, S. Martinengo, F. Demartin, M. Manassero, M. Sansoni, *Gazz. Chim. Ital.* **1987**, *117*, 245−247. [16e] B. E. Mann, B. T. Pickup, A. K. Smith, *J. Chem. Soc., Dalton Trans.* **1989**, 889−893. [16f] M. P. Brown, D. Burns, M. M. Harding, S. Maginn, A. K. Smith, *Inorg. Chim. Acta* **1989**, *162*, 287−289. [16g] F. Ragaini, F. Porta, F. Demartin, *Organometallics* **1991**, *10*, 185−189. [16h] A. Strawczynski, C. Hall, G. Bondietti, R. Ros, R. Roulet, *Helv. Chim. Acta* **1994**, *77*, 754−770. [16i] R. Della Pergola, L. Garlaschelli, S. Martinengo, M. Manassero, M. Sansoni, *J. Organomet. Chem.* **2000**, *593−594*, 63−68.
[17] D. C. Sonnenberger, J. D. Atwood, *Inorg. Chem.* **1981**, *20*, 3243−3246.
[18] A. M. Argo, J. F. Odzak, F. S. Lai, B. C. Gates, *Nature* **2002**, *415*, 623−626.
[19] R. Della Pergola, L. Garlaschelli, M. Manassero, M. Sansoni, D. Strumolo, *J. Cluster Sci.* **2001**, *12*, 23−34.
[20] F. S. Livotto, P. R. Raithby, M. D. Vargas, *J. Chem. Soc., Dalton Trans.* **1993**, 1797−1803.
[21] B. J. Coe, S. J. Glenwright, *Coord. Chem. Rev.* **2000**, *203*, 5−80.
[22] See Figure 4s in the supporting information.
[23] S. Aime, W. Dastrù, R. Gobetto, A. Viale, in *Recent Advances in Hydride Chemistry*, ref.[1]
[24] [24a] A. Abragham, *The Principles of Nuclear Magnetic Resonance*, Oxford University Press, **1961**. [24b] A. E. Derome, *Modern NMR Techniques for Chemistry Research*, **1987**, Pergamon, Oxford. [24c] D. W. Claridge, *High-Resolution NMR Techniques in Organic Chemistry*, Tetrahedron Organic Chemistry Series Volume 19, **1999**, Pergamon, Oxford.
[25] D. F. Shriver; M. A. Dredzon, *The Manipulation of air-sensitive compounds*, 2nd ed. **1986**, Wiley New York.
[26] R. Della Pergola, L. Garlaschelli, S. Martinengo, *Inorg. Synth.* **1991**, *28*, 245−247.
[27] SAINT Reference manual, Siemens Energy and Automation, Madison, WI, **1994−1996**.
[28] G. M. Sheldrick, SADABS, Empirical Absorption Correction Program, University of Gottingen, 1997.
[29] B. A. Frenz, *Comput. Phys.* **1988**, *2*, 42.
[30] *Crystallographic Computing 5*, Oxford University Press: Oxford, U. K., **1991**; Chapter 11, p. 126.
[31] G. M. Sheldrick, (**1985**). SHELXS 86. Program for the solution of crystal structures. Univ. of Gottingen, Germany.

Received December 17, 2002

 © 2003 Wiley-VCH Verlag GmbH & Co. KGaA, Weinheim

Interaction of $V^{IV}O$, $V^{V}O_2$ and Cu^{II} with a Peptide Analogue SalGly-L-Ala

Tamás Jakusch,[a] Ágnes Dörnyei,[b] Isabel Correia,[c] Lígia M. Rodrigues,[d] Gábor K. Tóth,[e] Tamás Kiss,*[a] João Costa Pessoa,*[c] and Susana Marcão[c]

Keywords: Vanadium / Copper / Peptides / Speciation / Spectroscopy / Bioinorganic chemistry

The formation of complexes of a tripeptide analogue, salicylglycyl-L-alanine [$HOC_6H_4C(O)NHCH_2C(O)NHCH(CH_3)$-COOH, H_2SalGly-L-Ala], was studied with Cu^{II}, $V^{IV}O$ and $V^{V}O_2$ in aqueous solution using pH-potentiometric and spectroscopic (UV/Vis, CD, EPR and ^{51}V NMR) techniques. The results demonstrated the ambidentate character of the ligand. The metal ion-induced deprotonation and subsequent coordination of the two neighbouring amide groups was shown to occur in a cooperative way in the pH range 5–6. At pH ≈ 6.5 a complex with an (O^-, $2 \times CON^-$, COO^-) binding set becomes predominant for both Cu^{II} and $V^{IV}O$. The affinity of the phenolate-O^- for $V^{IV}O$ is high and the ligand is bound to this metal ion even at pH values greater than 10. Conversely, the affinity for $V^{V}O_2$ is significantly lower and no interaction between this metal oxo-ion and the ligand could be detected in the pH range 2–12. In contrast, with the dipeptide analogue H_2SalGly, chelation involving the deprotonated amide-N^- could be unambiguously detected.
(© Wiley-VCH Verlag GmbH & Co. KGaA, 69451 Weinheim, Germany, 2003)

Introduction

Vanadium is an important trace metal with a great variety of physiological effects, including its interference with various phosphate-metabolizing reactions.[1] This suggests interactions between vanadium ions and protein side-chain donors. Peptides are not the best molecules for modeling metal ion binding to proteins, since the specially arranged side-chain donor groups of the amino acid units, determined by the tertiary structure of the proteins, are usually the primary bindings sites of proteins, while in the oligopeptides the N- and C- terminal donors are the basic sites for metal ion coordination. However, peptides are the most closely related models for proteins, and in some cases proteins may have specific terminal metal ion bindings sites as in the case of albumin.[2] For $V^{IV}O$ one of the known biologically important interactions with peptides is that with the important cell constituent and natural tripeptide, glutathione (GSH). In fact it is believed that GSH may play a role in the redox transformations of vanadium in the cells.[3] The equilibria in the systems $V^{IV}O^{2+}$–GSH and $V^{IV}O^{2+}$–GSSG have been recently studied.[4–5]

In order that simple di- or tripeptides bind metal ions strongly enough, the amide-N^- should be involved in coordination, but in some cases suitable anchoring donors should be available to promote amide-NH deprotonation and subsequent coordination. Various metal ions were found to engage in this type of bonding, such as Pt^{II}, Pd^{II}, Cu^{II}, Ni^{II},[6] $V^{V}O_2$ [7] and $V^{IV}O$.[8] The usual anchoring donor for binding metal ions, including Cu^{II}, and inducing amide deprotonation is the terminal NH_2 group,[6] although in some cases the terminal COO^- or the side chain thiolate-S^- or imidazol-N also proved to be efficient at inducing this process.[6] For $V^{IV}O^{2+}$, the terminal NH_2 is not a suitable anchor,[9] but phenolate proved to be an efficient anchoring donor in cases such as H_2salGly (2-OH-hippuric acid) where the p*K* for the amide-NH deprotonation/coordination of 4.76 was found to be similar to values seen for $V^{IV}O$ and Cu^{II}.[8,10]

In this work the binding capability of the tripeptide analogue H_2SalGly-L-Ala (**1**) containing a phenolate anchoring donor has been studied, and the solution speciations and binding modes of $V^{IV}O$, $V^{V}O_2$ and Cu^{II} complexes of **1** are reported. In some cases complexes were obtained in the solid state and characterized.

Results and Discussion

The tripeptide analogue H_2SalGly-L-Ala (**1**) was synthesized by the procedure described in the Exp. Sect. Its for-

[a] Biocoordination Chemistry Research Group of the Hungarian Academy of Sciences,
P. O. Box 440, 6701 Szeged, Hungary
[b] University of Szeged, Department of Inorganic and Analytical Chemistry,
P. O. Box 440, 6701 Szeged, Hungary
[c] Centro Química Estrutural, Instituto Superior Técnico,
1049-001 Lisboa, Portugal
[d] Departamento de Química, Universidade do Minho,
Largo do Paço, 4709 Braga, Portugal
[e] University of Szeged, Department of Medical Chemistry,
Dóm tér 8, 6720 Szeged, Hungary
Supporting information for this article is available on the WWW under http://www.eurjic.org or from the author.

mula together with that of H_2SalGly are included in Scheme 1.

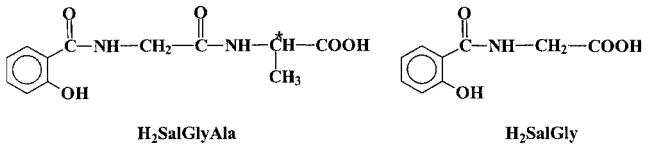

Scheme 1

Interactions of SalGly-L-Ala with Cu^{II} and $V^{IV}O$

The protonation and $V^{IV}O$ and Cu^{II} complex formation constants are in Table 1. H_2SalGly-L-Ala contains two dissociable protons: on the phenolic OH and the terminal COOH groups. The log K_{OH} value of 7.81 can be assigned to the less acidic phenolic OH and the log K value of 3.37 to the terminal COOH group. These data are similar to those of the corresponding dipeptide analogue, H_2SalGly (log K_{OH} = 8.16 and log K_{COOH} = 3.37).[8]

Table 1. Protonation (log K) and Cu^{II} and $V^{IV}O$ complex formation constants (log β with 3 S.D. values in parentheses) of the complexes of SalGly-L-Ala at T = 25 °C and I = 0.2 M (KCl)

Species	Cu^{II}	$V^{IV}O$
log K(phen-O^-)	7.81(1)	
log K(COO^-)	3.37(2)	
MLH	9.49(8)	9.98(11)
ML	4.45(5)	6.43(5)
MLH_{-1}	−0.49(6)	1.06(8)
MLH_{-2}	−6.64(5)	−4.31(6)
No. of points	297	245
Fitting[a] (mL)	0.0017	0.0032
pK(MLH)	5.03	3.55
pK(ML)	4.92	5.37
pK(MLH_{-1})	6.16	5.37

[a] Average difference between the experimental and calculated titration curves expressed in mL of the titrant.

Based on earlier speciation studies of the corresponding dipeptide H_2SalGly[8,10] and also Gly-like tripeptides,[6] the pH-metric titration curves measured for the Cu^{II}− and $V^{IV}O$−SalGly-L-Ala systems were evaluated by assuming 1:1 complex formation at the different states of protonation. Whenever 2:1 complexes were included in addition to the 1:1 complexes, they were always rejected by the PSEQUAD computer program. The best fit between the experimental and the calculated titration curves was obtained with the set of species listed in Table 1. The concentration distribution curves of the complexes formed in the Cu^{II}−SalGly-L-Ala and $V^{IV}O$−SalGly-L-Ala systems are depicted in Figures 1 and 2.

In agreement with the speciation curves the visible spectra of the metal-ligand systems (e.g. Figure 3 for the Cu^{II} system) start to deviate from that of the corresponding aqua ions $[Cu(H_2O)_6]^{2+}$ or $[VO(H_2O)_5]^{2+}$ only at pH > 3, where

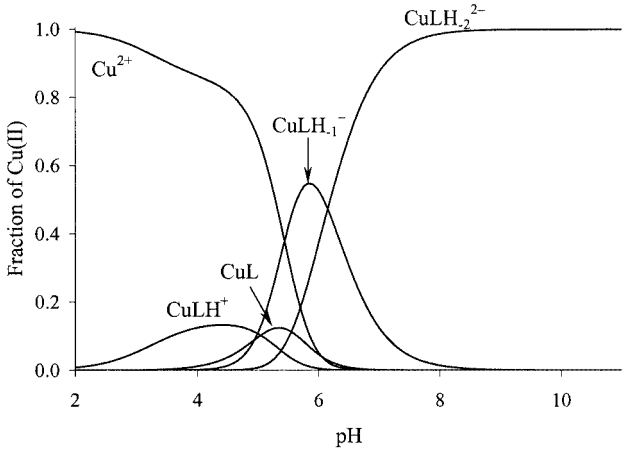

Figure 1. Species distribution curves as a function of pH for the Cu^{II}−SalGly-L-Ala system at a 1:2 ratio and c_{Cu} = 0.002 M

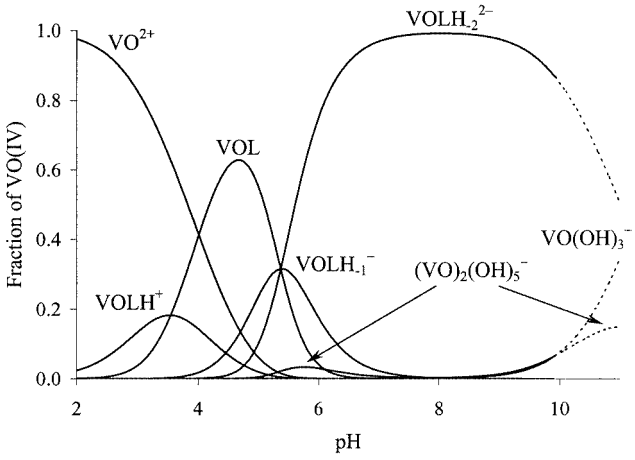

Figure 2. Species distribution curves as a function of pH for the $V^{IV}O$−SalGly-L-Ala system at a 1:2 ratio and c_{VO} = 0.002 M. Dashed lines indicate a higher uncertainty and thus only the tendency of the speciation as a result of slow pH equilibration (see Exp. Sect.)

the formation of the protonated species $[MLH]^+$ is indicated by the speciation curves. It can also be seen in Figure 3 that as complex formation proceeds, the d-d transition of the Cu^{II}-ligand system is shifted to higher energies and becomes constant at a pH of around 7.5, indicating the exclusive formation of a single species $[CuLH_{-2}]^{2-}$ (λ_{max} = 545 nm, ε = 240 $M^{-1}\cdot cm^{-1}$). At the same time in the corresponding $V^{IV}O$ system the visible spectra remain almost constant in the pH range 6.5−8.0 ($[VOLH_{-2}]^{2-}$: λ_{max} = 960 nm (ε = 120 $M^{-1}\cdot cm^{-1}$) and 690 nm (ε = 115 $M^{-1}\cdot cm^{-1}$). However, at higher pH the intensity of the absorption decreases as the ligand is displaced by OH^-. The CD spectra depicted in Figures 4 and 5 are in full agreement with these observations.

At pH < 5 the CD spectra of the $V^{IV}O$−SalGly-L-Ala system have relatively low intensities (species $[VOLH]^+$ and [VOL]). At pH > 5 their intensities increase (parallel with the increase in the visible absorption), and three peaks develop in the CD spectra at λ_{max} 760 nm (Δε < 0), 610 nm

 © 2003 Wiley-VCH Verlag GmbH & Co. KGaA, Weinheim

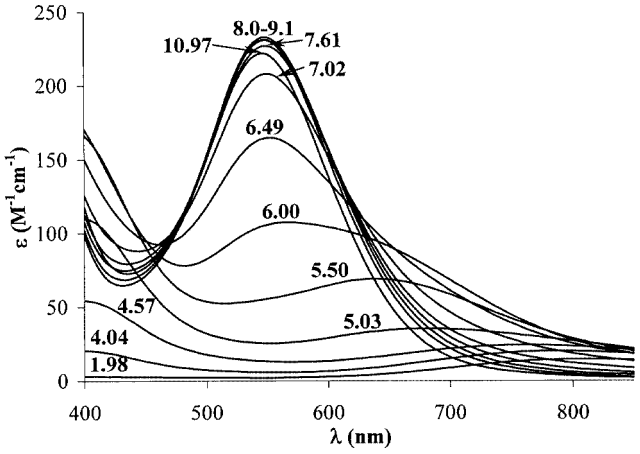

Figure 3. Visible absorption spectra of the Cu^{II}−SalGly-L-Ala system at a 1:2 metal ion to ligand ratio at several pH values and c_{Cu} = 0.006 M

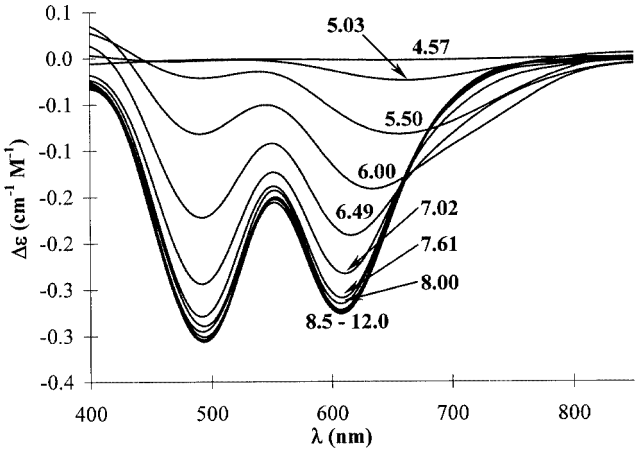

Figure 4. CD spectra of the Cu^{II}−SalGly-L-Ala system at a 1:2 metal ion to ligand ratio at several pH values and c_{Cu} = 0.006 M

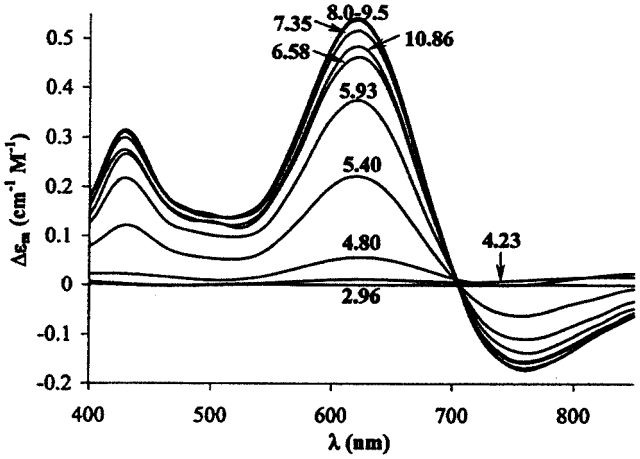

Figure 5. CD spectra of the $V^{IV}O$−SalGly-L-Ala system at a 1:2 metal ion to ligand ratio at several pH values and c_{VO} = 0.0045 M

($\Delta\varepsilon > 0$) and at 415 nm ($\Delta\varepsilon > 0$) (Figure 5), indicating coordination of the amide N^- group close to the chiral centre. Similarly, in the Cu^{II}−SalGly-L-Ala system the visible band at λ = 545 nm which is apparent by a pH of approximately 7 (see Figure 3), corresponds to two bands in the CD spectra at 490 nm ($\Delta\varepsilon = -0.3$ $M^{-1}\cdot cm^{-1}$) and at 610 nm ($\Delta\varepsilon = -0.28$ $M^{-1}\cdot cm^{-1}$). The significant blue shift in the absorption spectra and the intense CD bands indicate coordination of the amide N^- in the corresponding complex. In the CD spectrum of the GlyGly-L-Ala−Cu^{II} solutions, a band with λ_{max} at 475 nm ($\Delta\varepsilon = -0.8$ $M^{-1}\cdot cm^{-1}$) was observed.[11] The different CD spectra obtained here confirm that in the Cu^{II} complexes formed with **1**, which predominate at pH > 5, the phenolate O^- is bound to the metal ion.

The visible and CD spectra obtained at different pH values were used to calculate the spectrum of each individual species formed in the Cu^{II}− and $V^{IV}O$−SalGly-L-Ala systems, using the PSEQUAD computer program. Hydrolysis and observable increases in the absorbances of the very slightly cloudy solutions, especially in the case of the $V^{IV}O$−SalGly-L-Ala system, precluded the use of visible spectroscopic data to determine individual spectra precisely. CD data were more suitable for such a treatment. The fact that reasonable CD spectra could be simulated for each species (see Figure 6) confirms that the speciation models proposed and the stability constants calculated from the pH-metric measurements are correct.

It is worth noting here that significant changes and increases in the CD intensities can be observed only upon appearance of the $[MLH_{-2}]^{2-}$ species in both systems, and this is reflected in the calculated CD spectra of $[MLH_{-2}]^{2-}$. This indicates that coordination of the closest donor atom to the chiral centre (the first amide N^- from the C terminus) presumably occurs only in this species.

The EPR spectra help further to elucidate the binding modes of the complexes formed in the two systems. For the $V^{IV}O$ systems, Chasteen[12] introduced an additivity rule to estimate the hyperfine coupling constants $A_{\parallel}^{est}$ ($A_{\parallel}^{est} = \Sigma A_{\parallel,i}$), based on the contributions $A_{\parallel,i}$ of each of the four equatorial donor groups, its estimated uncertainty being $\pm$ 3 × 10^{-4} cm^{-1}. Most of the $A_{\parallel,i}$ parameters were presented by Chasteen[12] while the others were presented by Cornman et al. [$A_{\parallel}(N^-)$ = 34−35 × 10^{-4} cm^{-1}],[13] Tasiopoulous et al. [$A_{\parallel}(N^-)$ = 34−43 × 10^{-4} cm^{-1}],[14] Hamstra et al. [$A_{\parallel}(O_{amide})$ = 43−44 × 10^{-4} cm^{-1}],[15] and Costa Pessoa et al. [$A_{\parallel}(N^-)$ dipeptides = 34−36 × 10^{-4} cm^{-1} [16] and $A_{\parallel}(COO^-)$ = 42 × 10^{-4} cm^{-1}].[17] As can be seen, there is a rather high uncertainty in the reported $A_{\parallel}(N^-)$ values: 36±4 × 10^{-4} cm^{-1}. We chose the value 39 × 10^{-4} cm^{-1} for CON^-, which is within the uncertainty range. This was chosen without any theoretical precedent but because it gave a better agreement with the experimental coupling constants of the present system. Although a similar additivity rule has not been developed for Cu^{II} complexes, the large amount of EPR data available in the literature also allows us to make similar estimates for the coordinating donors in the corresponding Cu^{II} complexes. A rigorous comparison of the EPR spectra with the pH-metrically determined speciation curves may indicate some differences in the relative amount of some of the species at given pH values. This may be explained by the differences in the temperature, which was

 © 2003 Wiley-VCH Verlag GmbH & Co. KGaA, Weinheim

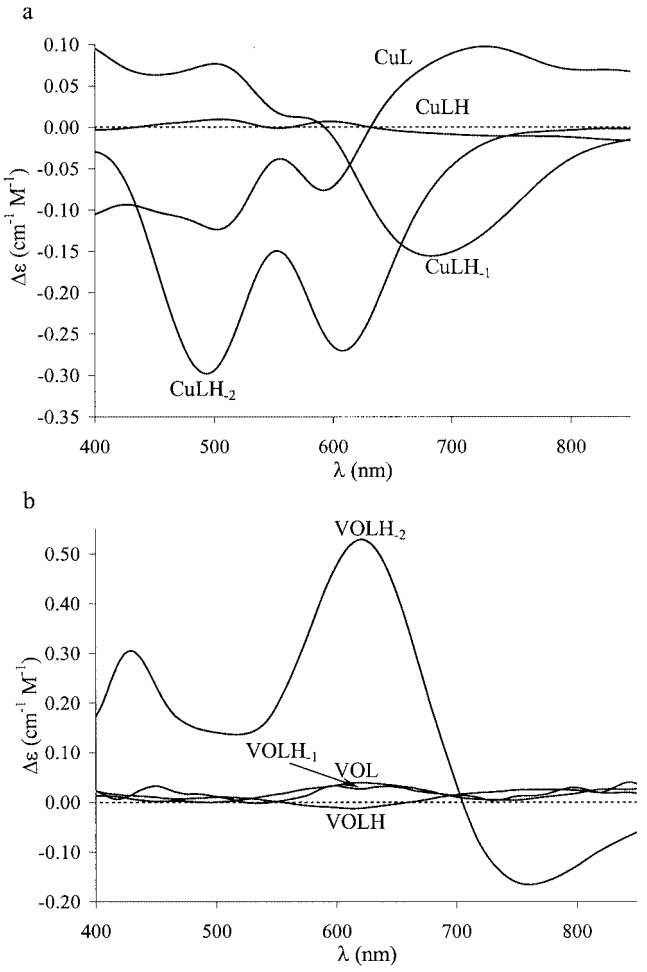

Figure 6. Simulated CD spectra for each individual species formed in (a) the Cu^{II}−SalGly-L-Ala system and (b) the $V^{IV}O$−SalGly-L-Ala system, using the program PSEQUAD

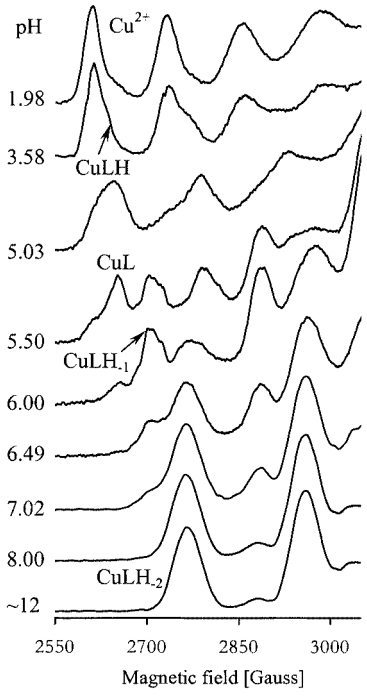

Figure 7. Low-field region of frozen EPR spectra (X-band) recorded at 77 K on the Cu^{II}−SalGly-L-Ala system at a 1:2 metal ion to ligand ratio at different pH values, c_{Cu} = 0.006 M

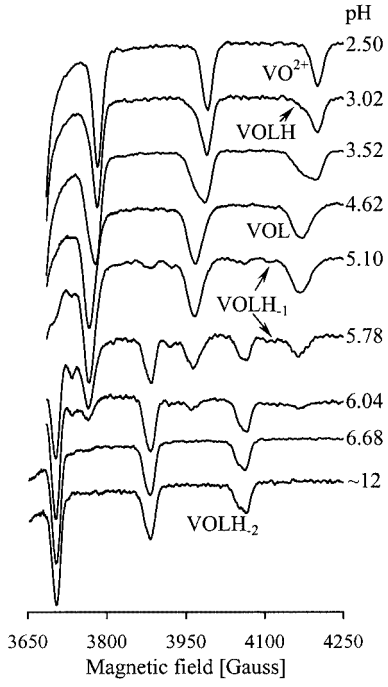

Figure 8. High-field region of frozen EPR spectra (X-band) recorded at 77 K on the $V^{IV}O$−SalGly-L-Ala system at a 1:2 metal ion to ligand ratio at different pH values, c_{VO} = 0.0045 M

25 °C for pH-metry and ca. −3 °C for EPR (the approximate freezing point of the sample), and also in the concentration of the metal ion. For this reason EPR is used only in a quantitative way to confirm the formation of each of the species assumed from the pH-metric speciation measurements. Figures 7 and 8 depict the low-field region (high-field in the case of $V^{IV}O$) of some of the frozen solution EPR spectra of the two systems at different pH values. Table 2 summarizes the EPR parameters obtained from simulation of the spectra by using the computer program of Rockenbauer,[18] and also the most likely binding modes of the complexes. For the $V^{IV}O$ system, CD and EPR spectra were also recorded at pH = 5.5 and c_L = 10 mM, with a variable c_{VO} concentration always confirming the presence of the MLH_{-1} species (see Figure S1, Supporting Information, see also the footnote on the first page of this article).

The pH-metric speciation curves (Figures 1 and 2) indicate that complex formation starts at a pH of about 3 in both systems with a protonated species $[MLH]^+$. In this species, like the corresponding complexes of the dipeptide analogue H_2SalGly, coordination at the terminal COO^- through (COO^-, CONH) chelation is most likely (see structure 1, Scheme 2). This binding mode explains why the observed EPR and visible spectra at pH around 3 show only minor differences from those of the aqua ions. In fact no significant differences are expected in the EPR and visible

 © 2003 Wiley-VCH Verlag GmbH & Co. KGaA, Weinheim

Table 2. Calculated EPR parameters ($g_{\|}$ and $A_{\|}$) for the complexes formed in the Cu^{II}– and $V^{IV}O$–SalGly-L-Ala systems

Species	Cu^{II}		$V^{IV}O$			Equatorial binding set
	$g_{\|}$	$A_{\|}$ 10^4 [cm^{-1}]	$g_{\|}$	$A_{\|}$ 10^4 [cm^{-1}]	$A_{\|}^{est}$	
MLH	2.380	147	1.934	180	178	(COO^-, CONH)
ML	2.358	148	1.937	176	171–174	(O^-, 2 × CONH) or (O^-, CONH, COO^-) or (O^-, CONH)
MLH_{-1}	2.270	178	1.945	165	164	(O^-, CON^-, CONH, COO^-)
MLH_{-2}	2.209	192	1.958	159	159	(O^-, 2 × CON^-, COO^-)

spectra for such binding modes when compared with the aqua ions.[16,19]

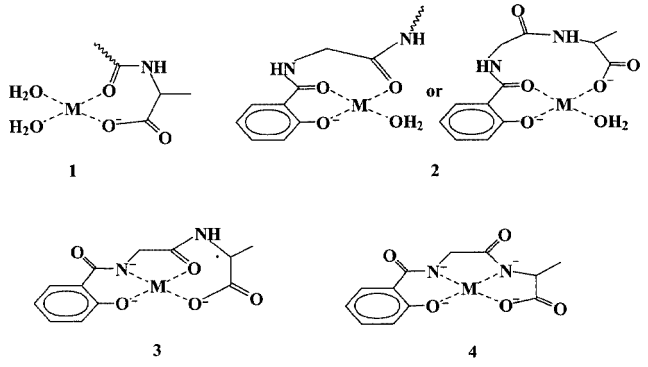

Scheme 2

Three protons are liberated from these complexes with stepwise p*K* values of 5.03, 4.92 and 6.16 for the Cu^{II} complexes, and 3.55, 5.37 and 5.37 for the $V^{IV}O$ complexes. The first deprotonation process, leading to the species [ML] in both systems, is attributable to the phenolic OH group of the metal-bound ligand. This indicates a rearrangement to (O^-, 2 × CONH) or (O^-, CONH, COO^-) binding modes (see structure 2, Scheme 2), as supported by the spectral changes. The EPR parameters (see Table 2) are characteristic of pure O-coordination, and agree well with those in the corresponding complex formed with H_2SalGly[8] and other aromatic hydroxycarboxylic acids.[20]

The next two p*K* values can be assigned to the deprotonation/coordination of the two amides, yielding (O^-, CON^-, CONH, COO^-) and (O^-, CON^-, CON^-, COO^-) joint chelate systems (structures 3 and 4, Scheme 2) respectively. As the simultaneous equatorial coordination of the second amide-O and the terminal COO^- may be sterically hindered, the tridentate (O^-, CON^-, COO^-) binding mode of the ligand (see Scheme 2) is also possible in species $VOLH_{-1}$. Due to the coordination of the two amide nitrogens, superhyperfine coupling (five lines with shf $A_{N\perp}$=15.5 G) can be observed in the perpendicular region of the EPR spectrum of the $CuLH_{-2}$ species. In the case of $V^{IV}O$, the EPR parameters estimated by the additivity rule are 164 ×10^{-4} cm^{-1} and 159 × 10^{-4} cm^{-1} which are in reasonable agreement with the experimental hyperfine coupling constants (Table 2). Since the species $[VOLH_{-1}]^-$, with one deprotonated amide N^-, could hardly be detected in the pH range 5–6 at a comparable metal ion to ligand ratio, EPR measurements in the wide L:M range of 20–1 were also carried out (see Exp. Sect.). Under such conditions the species was clearly detected by the appearance of a distinct signal (see Figure S1, Supporting Information). As mentioned above, the fact that significant increases in the $|\Delta\varepsilon|$ CD parameters are only observed for the fully deprotonated complex $[MLH_{-2}]^{2-}$ indicates the following sequence of amide deprotonation: first that is closer to the phenolate O^- then that is closer to the COO^-, the latter being closer to the chiral centre. Interestingly, the opposite sequence was observed for the organotin(IV)–peptide complexes,[16] which pointed to the C-terminal COO^- group being the primary anchor. With $V^{IV}O$ and Cu^{II}, the phenolate O^- seems to be the primary anchor. In the case of Gly-type tripeptides, the N-terminal site is the primary binder for Cu^{II}.[6] At pH > 10, a significant decrease in the intensities of the EPR signals was observed in the $V^{IV}O$–SalGly-L-Ala system (to compensate for this, the receiver gain and the modulation were increased) indicating the partial hydrolysis of the metal ion through formation of the EPR silent hydroxo-bridged species (represented by $[(VO)_2(OH)_5]^-$ in the speciation diagram).

Compounds in the Solid State

The tripeptide analogue H_2SalGly-L-Ala **1** was synthesized by the procedure described in the Exp. Sect. Complex **2**, formulated as VO(SalGly-L-Ala)·3.2H_2O·0.2EtOH, was prepared from solutions containing $V^{IV}O$ and H_2SalGly-L-Ala at a pH of around 5.5, i.e. where we expect the [VOL] stoichiometry to be predominant. Elemental analysis (see Exp. Sect.) indicates that the amide is not deprotonated, and the CD spectrum of **2** in a KBr disk shows a band pattern and a λ_{max} value similar to those of the VOL species shown in Figure 6b. The binding in the solid state presumably involves O^-, CONH, COO^- and H_2O, and eventually another amide O in the axial position. In frozen solution the experimental $A_{\|}$ is around 175–176 × 10^{-4} cm^{-1}, which corresponds either to (i) (O^-, CONH, COO^-, $H_2O)_{equatorial}$ coordination ($A_{\|}^{est}$ = 38.9 + 43.7 + 42.1 + 45.6 = 170 × 10^{-4} cm^{-1}) or to (O^-, CONH, 2 × $H_2O)_{equatorial}$ coordination ($A_{\|}^{est}$ = 38.9 + 43.7 + 45.6 + 45.6 = 174 × 10^{-4} cm^{-1}).

Complex **3**, formulated as K[Cu(SalGly-L-Ala)]·3.2H_2O, was also prepared from aqueous/ethanolic solutions at pH = 6. The elemental analysis agrees with the formulation of $CuLH_{-1}$ for this complex and the CD spectrum of **3** in a KBr disk shows a band pattern and a λ_{max} value close to those of the $CuLH_{-1}$ species (see Figure S2, Supporting

 © 2003 Wiley-VCH Verlag GmbH & Co. KGaA, Weinheim

Table 3. IR bands [cm^{-1}] and assignments of H_2SalGly-L-Ala and its VO and Cu complexes prepared in this work (vs: very strong, s: strong, m: medium, w: weak, vw: very weak; *: bands emerging from a broad band)

	Ligand **1**	Complex **2**	Complex **3**
Hydrogen bonded O−H and N−H	Broad band (2500−3500)	Broad band (2500−3600)	Broad band (2400−3700 with a few weak peaks emerging from it
ν(N−H)	3325 vs*	3346 m*	−
Aromatic C−H strech	3000 w*	3020 w*	≈3000 vw*
Aliphatic C−H strech	2932 w*	2990 w*	≈2950 vw*
Other amide bands	3072 vw* ,[23][24] 2613 vw*[a], 2499 vw*[a], 2411 vw*[a], 2290 vw*[a]	A few very weak bands	
$\nu(C{=}O)_{COOH}$	1730 s	−	−
Amide I (C=O)	1661 s, 1632 m (?)	1638 m-s* [22,p.72]	1605 s* [22]
Amide II	1547 s	1541 s	1534 s*
C=C Ring stretch	1593 s	1593 s*	≈1600 s*
$\nu_{as}(COO^-)$		1574 s* [22,p.72−73]	1572 s*
$\nu_s(COO^-)$		1370 m-s	1400 m-s (?)
$\nu(C{-}O_{Phe})$	1344 m-s (?)	1236 m-s	1256 s
ν(V=O)	−	966s	−
C−H Out-of-plane deformation	758 m-s	758 m-s	762 s

[a] These are multiple combination bands due to symmetrical, asymmetrical and overtone N−H bands.[21−24]

Information). The elemental analysis and spectra of this Cu^{II} complex are therefore consistent with a binding of the ligand through O^-, COO^- and CON^-. No individual ν(N−H) band could be detected emerging from the broad band in the 2400−3700 cm^{-1} range.

A comparison of the FTIR spectroscopic data for compounds **1**−**3** is summarised in Table 3. The data for **2** and **3** agree with the binding modes proposed. The assignments are based on Refs. 21−25, and by comparison with some $V^{IV}O$ and Cu^{II} complexes formed with the reduced Schiff base ligands derived from the reaction of salicylaldehyde and GlyGly or GlyGlyGly.[26] All compounds present broad bands in the wavenumber range corresponding to hydrogen-bonded O−H and N−H. In the case of **1** a strong ν(N−H) band emerges from this broad band as well as several other weak or very weak bands (Table 3). This is characteristic of compounds containing secondary amide groups.[23,24] The strong $\nu(C{=}O)_{COOH}$ band at 1730 cm^{-1} in the FTIR of **1** is absent in its $V^{IV}O$ and Cu^{II} complexes. For **2**, a narrow band emerges at 3346 cm^{-1} and a second weaker one at 3454 cm^{-1}, presumably also due to ν(N−H) of the amide groups.[21,23] All our efforts to characterise other solid compounds from these metal-ligand systems, particularly those of oxovanadium with a deprotonated amide, were unsuccessful. Either no solid could be isolated or when precipitation was achieved, no reasonable formulation could be found.

Interactions of H_2SalGly and H_2SalGly-L-Ala with V^VO_2

Vanadate(V)-promoted deprotonation of the amide NH and the formation of stable complexes with dipeptides through (NH_2, CON^-, COO^-) coordination was first detected by Rehder[7] using ^{51}V NMR spectroscopy (δ = −505−510 ppm). Pettersson et al.[27,28] gave complete speciation descriptions of V^VO_2 with dipeptides such as ProAla, AlaGly and AlaHis. A single complex species of moderate stability (at approx. tenfold excess of ligand ca. 50% of the vanadate was bound to the peptide) was formed with the above binding mode in fairly slow processes (completion of complex titration took several hours). The chemical shift values were as follows: δ = −495 ppm for ProAla, δ = −512 ppm for AlaGly and δ = −518 ppm for AlaHis.[27,28]

As phenolate proved to be a more efficient anchoring donor to promote amide deprotonation with $V^{IV}O$, we were also interested in studying this interaction with vanadate(V). The ^{51}V NMR spectrum of the vanadate(V)−SalGly system (c_VV= 0.003 M) displayed an extra peak (δ = −508.5 ppm) as well as the resonances of the V1 (δ = −561.8 ppm), V2 (δ = −574.8 ppm), V4 (δ = −579.2 ppm) and V5 (δ = −593.7 ppm) oxoanions. At a pH of around 7 the maximum amount of the complex was around 54 % with a tenfold excess of ligand (see Figure 9). The spectrum was identical after 24 h. This is in agreement with the earlier literature findings (vide supra), and an (O^-, CON^-,COO^-) binding mode has been suggested for the complex detected.[7,27−29] Interestingly, no new peaks were observed in the spectrum of the vanadate(V)−SalGly-L-Ala system which also had a tenfold excess of ligand (see Figure S3, Supporting Information), whether at pH 7 or 8. In both cases the polyoxoanions predominated in the system and the spectra were practically unchanged after 24 h.

In the case of tripeptides, amide deprotonation seems to occur at higher pH values when compared with dipeptides (e.g. for the corresponding Cu^{II} systems pK(CuA) = 4.40 for Cu^{II}−SalGly and pK(CuA) = 4.92 and pK($CuAH_{-1}$) = 6.16 for SalGly-L-Ala), where the likelihood of hydrolysis of the copper(II) is higher. This sensitive equilibrium between the metal-peptide complex and the binary (hydroxo)metal complex is finely shifted to the direction of peptide coordination with dipeptides, but to the direction of

 © 2003 Wiley-VCH Verlag GmbH & Co. KGaA, Weinheim

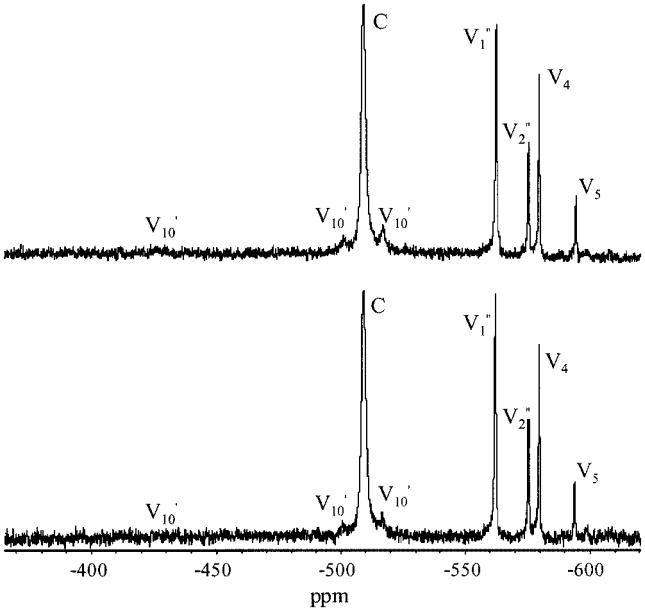

Figure 9. ^{51}V NMR spectra measured at pH ≈ 7 of a solution of the V^{V}−SalGly system at a 1:10 metal ion to ligand ratio. (a) in freshly prepared solution, (b) 24 h later, c_V = 0.003 M

oxoanion formation in the presence of tripeptides. Similar observations were made with organotin(IV)−di and tripeptide systems.[29]

Conclusions

The speciation and solution structural investigations discussed above strongly indicate that both the terminal COO^- and the phenolate O^- can behave as anchoring donors to chelate this tripeptide-analogue ligand. Coordination at a pH of around 3 starts at the terminal carboxylate through chelation with the neighbouring amide carbonyl. At a pH of approximately 4.5 the binding mode also involves the terminal phenolate and this induces deprotonation of the two amide-NH groups in a consecutive but rather cooperative way in the pH range 5−6. With the phenolate O^- anchor $V^{IV}O$ seems to be slightly more efficient in promoting deprotonation than Cu^{II} (the value of ΣpK_{amides} is 10.74 for $V^{IV}O$, and 11.08 for Cu^{II}), MLH_{-2} being the most important stoichiometry in the pH range 6−10, corresponding to an $(O^-, 2 \times CON^-, COO^-)_{equatorial}$ binding set. While Cu^{II} is able to promote amide deprotonation with normal tripeptides with about the same efficiency (ΣpK_{amides} is 11.82[8]), $V^{IV}O$ cannot induce deprotonation of the amide because of its low affinity for primary amine donors and the metal ion precipitates as $VO(OH)_2$. Interestingly, phenolate O^- did not prove to be such an efficient anchoring donor with vanadate(V) or $V^{V}O_2$ as with $V^{IV}O$. Amide deprotonation could not be detected by ^{51}V NMR spectroscopy in the case of the tripeptide analogue H_2SalGly-L-Ala. With the dipeptide analogue H_2SalGly, a species with an (O^-, N^-, COO^-) binding mode could be detected in the pH range 7−8. This is in full accordance with earlier literature reports concerning the interaction of vanadate^{V} with various dipeptides.[7,27−28] However, the moderate affinity of vanadate^{V} for amides, even with the more hard and probably more efficient phenolate O^- anchor, is reflected in the fact that even with a tenfold excess of ligand only around 50% of the metal ions are bound to SalGly, the rest being in the various oxoionic forms.

The considerably weaker ability of vanadium(V) to induce amide deprotonation, compared with vanadium(IV), can probably be explained by electrostatic ($V^{IV}O^{2+}$ vs. $V^{V}O_2^+$ towards LH_{-2}^{4-}) and steric arguments (there are 4 equatorial positions free around $V^{IV}O^{2+}$, while only 3 in the case of $V^{V}O_2^+$ because of the *cis* arrangement of the two oxo groups).

Experimental Section

Synthesis of H_2SalGly-L-Ala (1): The compound was synthesized by two different routes: (i) through the stepwise build up of the pseudopeptide from the individual components via the classical liquid phase method, (ii) through the Merrifield solid-phase approach.

Route 1

Z-GlyOH: To an ice-cold solution of glycine (7.5 g, 100 mmol) in 1 M NaOH (100 mL) was added benzyl chloroformate (16 mL, 100 mmol), dropwise with stirring. The pH of the solution was maintained at 10−10.5 by addition of 1 M NaOH. The mixture was stirred for 2 h and then extracted with diethyl ether. The aqueous layer was acidified to a pH ≈ 1 and the solid which precipitated was filtered, washed with water and dried. Yield (17.9 g, 86%), m.p. 119−120 °C (ref.[30] m.p. 120−121 °C). NMR ([D$_6$]DMSO): δ = 3.66 (d, J = 6 Hz, 2 H, CH_2Gly), 5.03 (s, 2 H, CH_2Ar), 7.34 (m, 5 H, Ar), 7.55 (t, J = 6 Hz, 1 H, NH), 12.25 (br. s, 1 H, COOH) ppm.

L-AlaOEt·HCl: Thionyl chloride (12.5 mL) was added dropwise to stirred and cooled (−10 °C) ethanol (50 mL), followed by the addition of L-Ala (4.46 g, 50 mmol). The temperature of the solution was increased and maintained at 40 °C for 4 h. The solvent was removed and crystallization from methanol/ethyl ether yielded 4.65 g (86%) of white crystals melting at 76 °C (ref.[31] m.p. 76 °C). NMR ([D$_6$]DMSO): δ = 1.22 (t, J = 7.2 Hz, 3 H, CH_2CH_3), 1.40 (d, J = 7 Hz, 3 H, CH_3 Ala), 4.00 (q, J = 7.2 Hz, 2 H, CH_2CH_3), 4.17 (apparent q, J = 7.2 Hz, 1 H, αCH Ala), 8.66 (br. s, 3 H, NH_3^+) ppm.

Z-Gly-L-AlaOEt: Z-GlyOH (4.2 g, 20 mmol) was dissolved in ethyl acetate (50 mL) and DCC (4.3 g, 21 mmol) was added after cooling to 0 °C. The mixture was stirred for 30 min whereupon L-AlaOEt·HCl (3.1 g, 20 mmol) and triethylamine (2.8 mL, 20 mmol) were added. The reaction mixture was stirred at room temperature overnight. The insoluble material was filtered off and the solution was washed successively with 1 M NaOH, 1 M HCl, and saturated NaCl. After drying with $MgSO_4$ the solvents were removed under reduced pressure. The oil obtained was crystallized from ethyl acetate/petroleum ether. The white crystals were filtered and dried (4.52 g, 73%), m.p. 60−64 °C; (ref.[31] m.p. 60−62 °C). NMR ($CDCl_3$): δ = 1.28 (t, J = 8 Hz, 3 H, CH_2CH_3), 1.40 (d, J = 7 Hz, 3 H, CH_3 Ala), 3.89−3.92 (m, 2 H, CH_2Gly), 4.19 (q, J = 7.2 Hz,

 © 2003 Wiley-VCH Verlag GmbH & Co. KGaA, Weinheim

2 H, CH_2CH_3), 4.52−4.60 (m, 1 H, αCH Ala), 5.13 (s, 2 H, CH_2Ar), 5.57 (br. s, 1 H, NH), 6.71 (br. s, 1 H, NH), 7.36−7.33 (m, 5 H, Ar) ppm.

HGly-L-AlaOEt·HBr: Z-Gly-L-AlaOEt (3.08 g, 10 mmol) was treated with 40% HBr/acetic acid (15 mL) at room temperature for 1 h with occasional stirring and protection from moisture. Diethyl ether was added and after cooling for a few hours the precipitated solid was filtered, washed with diethyl ether and dried. The chromatographically pure compound was used in the next step without further purification. Yield (2.42 g, 94%). NMR ([D_6]DMSO): δ = 1.20 (t, J = 7.2 Hz, 3 H, CH_2CH_3), 1.30 (d, J = 7.2 Hz, 3 H, CH_3 Ala), 3.57 (d, J = 3.3 Hz, 2 H, CH_2 Gly), 4.10 (q, J = 7.2 Hz, 2 H, CH_2CH_3), 4.23−4.32 (m, 1 H, αCH Ala), 8.01 (br. s, 3 H, NH_3^+), 8.70 (d, J = 7.2 Hz, 1 H, NH Ala) ppm.

HSalGly-L-AlaOEt: Salicylic acid (0.69 g, 5 mmol) was dissolved in ethyl acetate (20 mL) and the solution cooled to 0 °C. DCC (1.08 g, 5.2 mmol), HGlyAla·OEt·HBr (1.28 g, 5 mmol) and triethylamine (0.9 mL, 5 mmol) were then added successively. The reaction mixture was stirred at room temperature overnight. The insoluble material was filtered off and the solvents removed under reduced pressure. The residue was dissolved in a minimum amount of acetone and stored at 0 °C for 4 h. The precipitated solid was filtered off (dicyclohexylurea) and the solution concentrated. The oil obtained was crystallized from ethyl acetate/petroleum ether. (0.808 g, first crop, 55%, m.p. 104−106 °C). NMR ([D_6]DMSO): δ = 1.28 (d, J = 7.5 Hz, 3 H, CH_3 Ala), 1.17 (t, J = 7.2 Hz, 3 H, CH_2CH_3), 4.07 (q, J = 7.2 Hz, 2 H, CH_2CH_3), 3.94 (m, 2 H, CH_2 Gly), 4.20 (m, 1 H, αCH Ala), 6.91 (tap, J = 7.8 Hz, 2 H, 3-H and 5-H), 7.40 (tap, J = 8 Hz, 1 H, 4-H) 7.86 (dd, J = 1.2 Hz and 8 Hz,1 H, 6-H), 8.46,(d, J = 8.4 Hz, 1 H, NH Ala), 9.04 (t, J = 6 Hz, 1 H, NH Gly), 12.25 (br. s, 1 H, OH) ppm. $C_{14}H_{18}N_2O_5$ (294.3): calcd. C 57.14, H 6.16, N 9.52; found C 57.6, H 6.1, N 9.7.

H_2Sal-L-GlyAla (1): HSalGly-L-AlaOEt (0.734 g, 2.5 mmol) was dissolved in methanol (5 mL) and 1 M NaOH (5.5 mL, 5.5 mmol) was added. The mixture was stirred at room temperature for 4 h and 1 M HCl (2.5 mL, 2.5 mmol) was then added. The methanol was removed under reduced pressure and the solution thus obtained cooled in an ice bath and acidified with 1 M HCl (3 mL) with vigorous stirring. The white solid precipitated was filtered off, washed with water and dried (0.581 g, 87%), m.p. 197−199 °C. NMR ([D_6]DMSO): δ = 1.28 (d, J = 7.5 Hz, 3 H, CH_3 Ala), 3.94 (m, 2 H, CH_2 Gly), 4.20 (m, 1 H, αCH Ala), 6.91 (tap, J = 7.8 Hz, 2 H, 3-H and 5-H), 7.39 (tap, J = 7.8 Hz, 1 H, 4-H) 7.86 (dd, J = 1.2 Hz and 8 Hz, 1 H, 6-H), 8.34 (d, J = 7.5 Hz, 1 H, NH Ala), 9.03 (t, J = 6 Hz, 1 H, NH Gly), 12.20(s, 1 H, OH), 12.40 (br. s, 1 H, OH) ppm. $C_{12}H_{14}N_2O_5$ (266.3): calcd. C 54.13, H 5.30, N 10.52; found C 54.17, H 5.41, N 10.42.

Route 2

The dipeptide chain was elongated on an HMP resin (1.1 mmol/g). In the first step, Fmoc-Ala−OH (5.47, 17.6 mmol) was coupled to the resin (4 g, 4.4 mmol) in the presence of HOBt (2.38 g, 17.6 mmol), DCC (3.63 g, 17.6 mmol) and dimethylaminopyridine (1.07 g, 8.8 mmol). After removing the Fmoc protecting group by treatment with piperidine, the resultant free amino function was acylated with Fmoc−Gly−OH (2.97 g, 10 mmol). After completion of the dipeptide unit, the *N*-terminal Fmoc-protecting group was removed as previously described and the resultant primary amino group was acylated with salicylic acid (2.76 g, 20 mmol). The phenolic hydroxy group of the salicylic acid residue was unprotected. All the couplings were performed with *N*,*N*′-dicyclohexylcarbodiimide in the presence of 1-hydroxybenzotriazole. Amino acid or salicylic acid incorporation was monitored using the ninhydrin test. The completed peptide resins were treated with TFA/dichloromethane/water (35:60:5, vol/vol), at 0 °C for 1 h. The solvents were removed and the resultant free product was dissolved in 10% aqueous acetic acid, filtered and lyophilised (798 mg). The crude peptide derivative (100 mg) was purified by reverse-phase HPLC using a Nucleosil 7C-18 column (16 × 250 mm). The solvent system used was the following: 0.1% TFA in water, 0.1% TFA, 80% acetonitrile in water, gradient: 0% → 0% B over 10 min, then 10% → 30% over 50 min, flow 3.5 mL/min, detection at 226 nm. The appropriate fractions were combined and lyophilised. Peptide purity was above 97% (HPLC) and the measured Mw (227) value was in good agreement with the calculated one. NMR (D_2O): δ = 1.38 (d, J = 7.2 Hz, 9 Hz, 3 H, CH_3 Ala), 4.11 (s, 2 H, CH_2 Gly), 4.34 (m, 1 H, αCH Ala), 6.99 (tap, J = 7.8 Hz, 2 H, 3-H and 5-H), 7.46 (tap, J = 7.8 Hz, 1 H, 4-H) 7.50 (dd, J = 1.5 Hz, 2 and 9.46 Hz, 1 H, 6-H) ppm.

Synthesis of the Complexes

VO(SalGly-L-Ala)·3.2H_2O·0.2EtOH (2): To a solution of H_2SalGly-L-Ala (1 mmol) and sodium acetate−trihydrate (2 mmol) in ethanol/water (2.5:5 mL) was slowly added a solution of $VOSO_4$·5H_2O (1 mmol) in water (1 mL). The mixture was divided in two equal parts (**A** and **B**). The pH of solution **A** was adjusted to 5.5. A blue-green solid precipitated which was collected by filtration and washed with ethanol/water (1:2), diethyl ether and dried. Yield: 40% (80 mg). $C_{12}H_{12}N_2O_6V$·3.2H_2O·0.2EtOH: calcd. C 37.42, H 4.86, N 7.04; found C 37.4, H 5.3, N 7.00.

K[Cu(SalGly-L-Ala)]·3.2H_2O (3): To a solution of H_2SalGly-L-Ala (0.5 mmol) and KOH (0.5 mmol) in water (10 mL), was slowly added $Cu(CH_3COO)_2$·H_2O (0.5 mmol) in ethanol (5 mL). The pH was adjusted to 6 with 2 M KOH and kept at ≈ 45 °C for 1 h. A green precipitate was collected by filtration, washed with ethanol/water (1:2), ethanol and diethyl ether and dried. Yield: 42% (90 mg). $C_{12}H_{11}CuKN_2O_5$·3.2H_2O: calcd. C 34.03, H 4.14, N 6.61; found C 33.7, H 3.7, N 6.2.

Physical and Spectroscopic Studies

Melting points were recorded by using a Gallenkamp melting point apparatus and are uncorrected. NMR spectroscopic data were recorded either with a Varian Unity Plus 300 Spectrometer (for the several steps of the synthesis of **1**) in the solvent indicated, or with a Varian Unity-500 Spectrometer operating at frequencies of 131.404 MHz and 499.824 MHz, respectively, using a 5-mm broad-band probe at 25.0±0.5 °C. ^{51}V NMR chemical shifts were referenced to an external $VOCl_3$ solution at δ = 0 ppm. The ^{51}V NMR acquisition parameters were as follows: 33 kHz spectral width, 30-μs pulse width, 1 s acquisition time and 10 Hz line broadening. IR spectra were recorded with a BioRad FTS-3000 MX FTIR spectrometer. CD spectra were recorded with a JASCO-720 spectropolarimeter with a red-sensitive photomultiplier (EXWL-308). Visible spectra were recorded with a Hitachi U-2000 spectrophotometer. X-band (9.44 GHz) EPR spectra were usually recorded at 77 K (on glasses made by freezing solutions in liquid nitrogen) with a Bruker ESP 300E X-band spectrometer. Mass spectra were recorded with a Finnigan TSQ-7000 tandem quadrupole mass spectrometer equipped with an electrospray ion source. The HPLC apparatus was made by Knauer (Berlin, Germany).

All samples for the pH-potentiometric and spectrophotometric measurements were prepared under inert conditions (under high purity nitrogen or argon). For potentiometric measurements the

 © 2003 Wiley-VCH Verlag GmbH & Co. KGaA, Weinheim

ionic strength was adjusted to 0.2 M KCl and the temperature maintained at 25.0±0.1 °C. For the spectral measurements the temperature was maintained at 25.0±0.3 °C with circulating water.

pH Measurements for Spectroscopic Studies: For preparation of the solutions and pH calibrations a special double-walled glass vessel was used with entrances for the combined electrode (Radiometer ''Red Rod'' pHC2015−8), thermometer, nitrogen and reagents (e.g. base). A computerized system developed locally (IBM-PCXT 286 computer) was used to control the titration conditions for pH calibrations. The E.M.F measurements were made with a Denver Model 15 pH meter.

pH-Potentiometric Titrations: Stock solutions of $V^{IV}O$ and vanadate(V) for the pH-metric titrations were prepared and standardised as described earlier.[32] The purity of the ligand was checked and the exact concentration of its solutions was determined by the appropriate Gran plot.[33] The stability constants of the proton and metal complexes of the ligand were determined by pH-metric titration of 10.0 cm^3 samples. The ligand concentrations were in the range of 0.001 to 0.002 M and the metal ion to ligand molar ratio varied from 1:1 to 1:3. Titrations were performed from pH 2.0 up to pH 11 with KOH solution of known concentration (ca. 0.2 M) under purified argon unless very extensive hydrolysis or slow equilibration was observed. The reproducibility of titration points included in the evaluation was within 0.005 pH units in the whole pH range. The pH was measured with an Orion-710A precision digital pH meter equipped with an Orion Ross 8103BN type combined glass electrode, calibrated for hydrogen ion concentration as described earlier.[34] The ionic product of water, pK_w is 13.76. The concentration stability constants $\beta_{pqr} = [M_pL_qH_r] / [M]^p[L]^q[H]^r$ were calculated with the aid of the PSEQUAD computer program.[35] The formation of the hydroxo complexes of $V^{IV}O$ was taken into account. The following species were assumed: $[VO^{IV}(OH)]^+$ ($\log \beta_{10-1} = -5.94$), $[(V^{IV}O)_2(OH)_2]^{2+}$ ($\log \beta_{20-2} = -6.95$). Stability constants were calculated from the data of Henry et al.[36] and corrected for the different ionic strengths by using the Davies equation. $[(V^{IV}O)_2(OH)_5]^-$ ($\log \beta_{20-5} = -22.5$) and $[V^{IV}O(OH)_3]^-$ ($\log \beta_{10-3} = -18.0$).[37]

Spectroscopic Measurements: Unless otherwise stated, by visible (Vis) and circular dichroism (CD) spectra we mean a representation of ε_m or $\Delta\varepsilon_m$ values vs. λ [ε_m = absorption/(bc_M) and $\Delta\varepsilon_m$ = differential absorption/(bc_M) where b = optical path and c_M=total $V^{IV}O$ or Cu^{II} concentration]. The spectral range covered is normally 400−900 (Vis) and 400−1000 nm (CD). All measurements and operations of the spectropolarimeter were computer controlled. For the CD spectra a Fast Fourier-Transform noise-reduction routine (JASCO) was used without affecting peak shapes. For the $V^{IV}O$ system, the EPR, Vis and CD spectra were recorded by varying the pH with an approximately fixed total vanadium and ligand concentration, at L/M ratios of 1.76 ($c_{VO} \approx 0.003$ M) and 2.00 ($c_{VO} \approx 0.0045$ M), and at pH = 5.5 and $c_{ligand} \approx 0.010$ mM . L/M ratios were varied in the range of 20−1 by addition of $V^{IV}O$ stock solution. For the Cu^{II} system, the EPR, Vis and CD spectra were recorded varying the pH with $c_{Cu} \approx 0.006$ M and L/M = 2.

CD spectra of Solid Complexes: Samples of compounds **2** and **3** were prepared as described previously,[38] dispersed in KBr disks, and placed between two microscope slides. One or two such paired microscope slides were placed in the sample compartment. Each final spectrum is the average of 4 to 6 individual spectra, recorded as described above.

Supporting Information: Additional EPR, CD and ^{51}V NMR spectra for the $V^{IV}O$−SalGly-L-Ala and $V^{V}O_2$−SalGly-L-Ala systems are available (see also the footnote on the first page of this article).

Acknowledgments

The authors are grateful to Profs C. Geraldes and M. Castro (University of Coimbra, Portugal) for help in recording the NMR spectra. This work was carried out in as part of a COST D21 project, and was financially supported by the National Research Fund (OTKA T31896/2000), the Hungarian Academy of Sciences, the Fundo Europeu para o Desenvolvimento Regional, Fundação para a Ciência e Tecnologia, the POCTI Programme (project POCTI/35368/QUI/2000), and the Hungarian-Portuguese Intergovernmental S & T Co-operation Programme for 2000−2001.

[1] D. C. Crans, R. L. Bunch, L. A. Theisen, *J. Am. Chem. Soc.* **1989**, *111*, 7597−7607.
[2] G. Rakhit, B. Sarkar, *J. Inorg. Biochem.* **1981**, *15*, 233−241.
[3] H. Sakurai, S. Shimomura, F. Fukazawa, K. Ishizu, *Biochem. Biophys. Res. Commun.* **1980**, *90*, 293−298.
[4] J. Costa Pessoa, I. Tomaz, T. Kiss, E. Kiss, P. Buglyó, *J. Biol. Inorg. Chem.* **2002**, *7*, 225−240; T. Armas, A. Mederos, P. Gili, S. Dominguez, R. Hernandez-Molina, P. Lorenzo, E. J. Baran, M. L. Araujo, F. Brito, *Polyhedron* **2001**, *20*, 799−804.
[5] J. Costa Pessoa, I. Tomaz, T. Kiss, P. Buglyó, *J. Inorg. Biochem.* **2001**, *84*, 259−270.
[6] I. Sóvágó, in *Biocoordination Chemistry*, (Ed.: K. Burger), Ellis Horwood, New York **1990**, p. 135−184.
[7] D. Rehder, *Inorg. Chem.* **1988**, *27*, 4312−4316.
[8] T. Kiss, K. Petrohán, P. Buglyó, D. Sanna, G. Micera, J. Costa Pessoa, C. Madeira, *Inorg. Chem.* **1998**, *37*, 6389−6391.
[9] J. Costa Pessoa, S. M. Luz, R. Duarte, J. J. G. Moura, R. D. Gillard, *Polyhedron* **1993**, *23*, 2857−2867; J. Costa Pessoa, S. M. Luz, R. D. Gillard, *J. Chem. Soc., Dalton Trans.* **1997**, 569−576.
[10] E. B. Gonzalez, N. N. Daeid, K. B. Nolan, E. Farkas, *Polyhedron* **1994**, *13*, 1495−1499.
[11] R. B. Martin, *Met. Ions Biol. Syst.* **1974**, *1*, 129−157.
[12] N. D. Chasteen, in *Biological Magnetic Resonance*, (Eds.: J. Lawrence, L. J. Berliner, J. Reuben), Plenum Press, New York **1981**, vol. 3, p. 53−119.
[13] C. R. Cornman, E. P. Zovinka, Y. D. Boyajian, K. M. Geiser-Bush, P. D. Boyle, P. Singh, *Inorg. Chem.* **1995**, *34*, 4213−4219.
[14] A. J. Tasiopoulos, A. N. Troganis, A. Evangelou, C. P. Raptopoulou, A. Terzis, Y. G. Deligiannakis, T. A. Kabanos, *Chem. Eur. J.* **1999**, *5*, 910−921.
[15] B. J. Hamstra, A. L. P. Houseman, G. J. Colpas, J. W. Kampf, R. LoBrutto, W. D. Frasch, V. L. Pecoraro, *Inorg. Chem.* **1997**, *36*, 4866−4874.
[16] J. Costa Pessoa, S. M. Luz, R. D. Gillard, *J. Chem. Soc., Dalton Trans.* **1997**, 569−576.
[17] P. Buglyó, E. Kiss, I. Fábián, T. Kiss, D. Sanna, E. Garriba, G. Micera, *Inorg. Chim. Acta* **2000**, *306*, 174−183.
[18] A. Rockenbauer, L. Korecz, *Appl. Magn. Resonance* **1996**, *10*, 29−43.
[19] J. Costa Pessoa, L. F. Vilas Boas, R. D. Gillard, R. J. Lancashire, *Polyhedron* **1988**, *7*, 1245−1262.
[20] M. Jezowska-Bojczuk, H. Kozlowski, A. Zubor, T. Kiss, M. Branca, G. Micera, A. Dessi, *J. Chem. Soc., Dalton Trans.* **1990**, 2903−2907; G. Micera, A. Dessi, D. Sanna, T. Kiss, P. Buglyó, *Gazz. Chim. It.* **1993**, *123*, 573−577.
[21] D. H. Williams, I. Fleming, *Spectroscopic Methods in Organic Chemistry*, 5th ed., McGraw-Hill, London **1995**, p. 42, 49.
[22] K. Nakamoto, *Infrared and Raman Spectra of Inorganic and Coordination Compounds*, 5th ed., John Wiley & Sons, New York, **1997**, p. 62−73, 271.
[23] E. Silverstein, G. C. Bassler, T. C. Morril, *Spectrometric Identification of Organic Compounds*, 5th ed., John Wiley & Sons, New York **1991**, p. 122−125.
[24] G. Socrates, *Infrared and Raman Characteristic Group Fre-*

 © 2003 Wiley-VCH Verlag GmbH & Co. KGaA, Weinheim

quencies. Tables and Charts, 3rd ed., John Wiley & Sons, Chichester **2001**, p. 51, 107−113, 143−145.
[25] A. J. Tasiopoulos, E. J. Tolis, J. M. Tsangaris, A. Evangelou, J. D. Woollins, A. M. Slawin, J. Costa Pessoa, I. Correia, T. A. Kabanos, *J. Biol. Inorg. Chem.* **2002**, *7*, 363−374.
[26] T. Jakusch, I. Correia, J. Costa Pessoa, T. Kiss, *J. Inorg. Biochem.* **2001**, *86*, 278.
[27] K. Elvingson, M. Fritzsche, D. Rehder, L. Pettersson, *Acta Chem. Scand.* **1994**, *48*, 878−885.
[28] M. Fritzsche, K. Elvingson, D. Rehder, L. Pettersson, *Acta Chem. Scand.* **1997**, *51*, 483−491.
[29] T. Gajda, personal communication.
[30] George R. Pettit, *Synthetic Peptides*, Elsevier Scientific, Amsterdam **1980**, vol. 5.
[31] George R. Pettit, *Synthetic Peptides*, Academic Press, New York **1975**, vol. 3.
[32] I. Nagypál, I. Fábián, *Inorg. Chim. Acta* **1982**, *61*, 109−113.
[33] G. Gran, *Acta Chem. Scand.* **1950**, *4*, 559−575.
[34] H. M. Irving, M. G. Miles, L. D. Pettit, *Anal. Chim. Acta* **1967**, *38*, 575−481.
[35] L. Zékány, I. Nagypál, *PSEQUAD: A Comprehensive Program for the Evaluation of Potentiometric and/or Spectrophotometric Equilibrium Data Using Analytical Derivatives*'' in *Computational Methods for the Determination of Formation Constants*, (Ed.: D. J. Leggett), Plenum Press, New York, **1991**.
[36] R. P. Henry, P. C. H. Mitchell, J. E. Prue, *J. Chem. Soc., Dalton Trans.* **1973**, 1156−1159.
[37] A. Komura, M. Hayashi, H. Imanaga, *Bull. Chem. Soc. Jpn.* **1977**, *50*, 2927−2931; L. F. Vilas Boas, J. Costa Pessoa, in *Comprehensive Coordination Chemistry* (Eds.: G. Wilkinson, R. D. Gillard, J. A. McCleverty), Pergamon Press, Oxford **1987**, vol. 3, p. 453−583.
[38] I. Cavaco, J. Costa Pessoa, D. Costa, M. T. L. Duarte, P. M. Matias, R. D. Gillard, *J. Chem. Soc., Dalton Trans.* **1994**, 149−157.

Received September 16, 2002

 © 2003 Wiley-VCH Verlag GmbH & Co. KGaA, Weinheim

Coordination Modes in a (Thiosemicarbazone)copper(II)/Oxalato System − Structures of $[\{Cu(L)\}_2(ox)]\cdot 2H_2O$, $[Cu(HL)(ox)(H_2O)]$, $[\{Cu(HL)\}_2(ox)][Cu(ox)_2]\cdot 2H_2O$ and $[\{Cu(HL)\}_2(ox)](NO_3)_2$ − Ferro- vs. Antiferromagnetic Behavior in Dinuclear Compounds

Patricia Gómez-Saiz,[a] Javier García-Tojal,*[a] Miguel Maestro,[b] José Mahía,[b] Luis Lezama,[c] and Teófilo Rojo[c]

Keywords: Copper / Carboxylate ligands / Magnetic properties / Thiosemicarbazone complexes

Complexes with the formula $[\{Cu(L)\}_2(ox)]\cdot 2H_2O$ (**1**), $[Cu(HL)(ox)(H_2O)]$ (**2**), $[\{Cu(HL)\}_2(ox)][Cu(ox)_2]\cdot 2H_2O$ (**3**) and $[\{Cu(HL)\}_2(ox)](NO_3)_2$ (**4**) (HL = $C_7H_8N_4S$, pyridine-2-carbaldehyde thiosemicarbazone) have been synthesized from $Cu(L)(NO_3)$ and oxalic acid while modulating the stoichiometries and the pH of the media. Single crystal X-ray diffraction studies show that the structures of **1** and **4** contain dinuclear entities with distorted square pyramidal copper(II) ions. The dinuclear complexes are centrosymmetric in **1** and non-centrosymmetric in **4**. The metal centers are coordinated to the NNS atoms from the tridentate thiosemicarbazone ligand and to two oxygen atoms from the oxalato coligand. The latter ligand exhibits tetradentate behavior and acts as a bridge between the copper(II) ions. The thiosemicarbazone ligand is either present in the anionic (**1**) or the neutral (**4**) form. Compound **2** is composed of monomeric species containing square pyramidal copper(II) ions that are coordinated to the thiosemicarbazone ligand, one water molecule and one monodentate oxalato coligand. It is important to note that the oxalato is highly twisted in this complex, the O(1)–C(8)–C(9)–O(3) dihedral angle between the carboxylate groups is 79.9(4)°. Compound **3** contains both the dinuclear cationic species, analogous to those described for compound **4**, and square planar (bisoxalato)copper(II) anions. Strong hydrogen bonds and π-π stacking are present in these complexes. Structural and spectroscopic results suggest the presence of relevant ligand-to-metal charge transfers in these compounds. The EPR spectra of **1**, **2** and **4** exhibit rhombic symmetry. Magnetic measurements on **1** and **4** show antiferromagnetic and ferromagnetic coupling, respectively. The susceptibility data were fitted to the Bleaney–Bowers equation for copper(II) dinuclear complexes. The J/k values obtained are –6.20 and +7.73 K for compounds **1** and **4**, respectively.
(© Wiley-VCH Verlag GmbH & Co. KGaA, 69451 Weinheim, Germany, 2003)

Introduction

Numerous studies on the copper(II) derivatives of pyridine-2-carbaldehyde thiosemicarbazone (HL = $C_7H_8N_4S$, see Scheme 1) have been conducted during the last thirty years, mainly with regard to the biological properties of these compounds.[1] Spectroscopic results suggested the existence of a planar $[Cu(L)(H_2O)]^+$ species in aqueous solution (or, more correctly, tetragonally elongated $[Cu(L)(H_2O)_3]^+$ species), with a log K value (K = formation constant) of 16.90.[2] This species exhibits two acid−base equilibria with proton dissociation constants pK_{a1} = 2.40 (the equilibrium between $[Cu(HL)(H_2O)_3]^{2+}$ and $[Cu(L)(H_2O)_3]^+$) and pK_{a2} = 8.30 (the equilibrium between $[Cu(L)(H_2O)_3]^+$ and $[Cu(L)(OH)(H_2O)_n]$).[3] The coordination of the ligand by the copper(II) ion is maintained even at pH values below 1.4. The high stability of the metal-ligand system allowed for the isolation of several com-

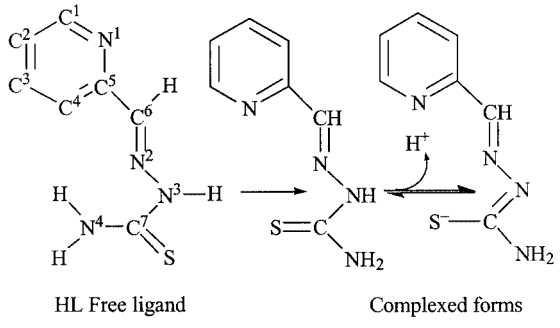

Scheme 1

[a] Departamento de Química, Universidad de Burgos, Plaza Misael Bañuelos s/n, 09001 Burgos, Spain
Fax: (internat.) +34-(0)47-258831
E-mail: qipgatoj@ubu.es
[b] Servicios Generales de Apoyo a la Investigación, Universidade da Coruña, Edificio Anexo a Facultade de Ciencias, Campus da Zapateira s/n, 15071 A Coruña, Spain
[c] Departamento de Química Inorgánica, Universidad del País Vasco, Aptdo. 644, 48080 Bilbao, Spain

Table 1. Summary of crystallographic data and parameters for **1**, **2**, **3** and **4**

	1	**2**	**3**	**4**
Formula	$C_{16}H_{18}Cu_2N_8O_6S_2$	$C_9H_{11}CuN_4O_5S$	$C_{20}H_{24}Cu_3N_8O_{16}S_2$	$C_{16}H_{16}Cu_2N_{10}O_{10}S_2$
M	609.58	350.82	887.22	699.59
System	Triclinic	Monoclinic	Triclinic	Orthorhombic
Space group	$P\bar{1}$	$P2_1/n$	$P\bar{1}$	*Ibca*
a/Å	6.1735(1)	11.068(2)	8.478(1)	13.053(2)
b/Å	9.6005(2)	10.148(2)	9.383(1)	12.998(2)
c/Å	10.4955(2)	12.020(2)	10.369(1)	28.835(4)
α/°	98.488(1)	90	68.543(2)	90
β/°	101.902(1)	112.303(3)	85.459(3)	90
γ/°	108.155(1)	90	80.115(3)	90
V/Å^3	563.16(2)	1248.9(3)	756.1(2)	4892.6(1)
Z	1	4	1	8
D_c/g cm^{-3}	1.797	1.866	1.949	1.900
μ/mm^{-1}	2.126	1.942	2.318	1.985
F(000)	616	712	894	1408
h,k,l range	±8, ±12, ±13	±13, (−10)−12, (−15)−14	(−7)−10, (−9)−11, ±12	(−16)−15, ±16, (−30)−36
θ range/°	2−28	2−26	2−26	2−26
GOF	1.035	1.021	0.996	0.996
R_1 (all data)	0.0383	0.0622	0.0599	0.1511
R_1 [$I > 2\sigma(I)$]	0.0336	0.0351	0.0366	0.0490
wR_2.(all data)	0.0926	0.0886	0.0898	0.1306
wR_2 [$I > 2\sigma(I)$]	0.0906	0.0780	0.0806	0.0919

pounds containing $[Cu(HL)]^{2+}$, as well as the $[Cu(L)]^+$, whose crystal structures have been characterized.[4] They exhibit a 1:1 metal/thiosemicarbazone stoichiometry, with the thiosemicarbazone acting as an NNS tridentate ligand. Magnetic studies on complexes with $[Cu(L)]^+$ fragments have also been carried out.[4f,4g,4j,4k] However, the magnetic behavior of derivatives containing the neutral ligand has not yet been studied. This is partly because monomeric compounds are formed with some of the ligands in an acidic medium. From this point of view, it would be important to find a ligand that is able to stabilize both the $[Cu(L)]^+$ and the acidic $[Cu(HL)]^{2+}$ species in dinuclear complexes. Therefore, the oxalato ligand, which is versatile and has a low pK_{a1} value and up to four chelating centers, could be used to study the influence of the neutral vs. anionic character of the ligand on the properties of these compounds.

Here we present the syntheses, crystal structures and spectroscopic features of the complexes $[\{Cu(L)\}_2(ox)]\cdot 2H_2O$ (**1**), $[Cu(HL)(ox)(H_2O)]$ (**2**), $[\{Cu(HL)\}_2(ox)][Cu(ox)_2]\cdot 2H_2O$ (**3**) and $[\{Cu(HL)\}_2(ox)](NO_3)_2$ (**4**). The magnetic behavior of compounds **1** and **4** is also discussed. Approximate molecular orbital calculations of the extended Hückel type have been carried out in order to understand the magnetic features in these systems.

Results and Discussion

Structural Analysis

The addition of potassium oxalate to an aqueous solution of $Cu(L)(NO_3)$ at pH = 4−8 yields compound **1**, which contains the anionic thiosemicarbazone ligand, irrespective of the ratio of the reactants. However, at very low pH values (close to 1), the amounts of the reactants play an important role. Thus, stoichiometric amounts of $Cu(L)(NO_3)$ and oxalic acid lead to the formation of compound **2**. In contrast, an excess of nitrate in the reaction medium yields **4**. A few crystals of **3** were isolated from an experiment designed to crystallize compound **2**. Unfortunately, we have not yet found a reproducible method of synthesizing this complex.

Single crystals suitable for X-ray data collection were obtained for the title complexes. Crystallographic details are given in Table 1.

The crystal structures of compounds **1** and **4** are formed by the $[Cu(L)]^+$ and $[Cu(HL)]^{2+}$ entities, respectively, linked through a bis-bidentate oxalato ligand, which leads to the dinuclear centrosymmetric $[\{Cu(L)\}_2(ox)]$ (**1**) and noncentrosymmetric $[\{Cu(HL)\}_2(ox)]^{2+}$ (**4**) species. Waters of crystallization are also present in the lattice of **1**. The nitrate counterions are also present in the lattice of **4**. The molecular structures of **1** and **4** are shown in Figure 1 and 2, respectively. Selected interatomic dimensions are given in Table 2. The copper(II) ions are five-coordinate with two nitrogen and one sulfur atoms from the thiosemicarbazone ligand [Cu−N(1), N(2), S: 2.044(2), 1.955(2), 2.2759(6) and 2.027(6), 1.956(5), 2.306(2) Å, for **1** and **4**, respectively] and one oxygen atom of the carboxylate [Cu−O(1): 1.966(2) and 1.943(4) Å, for **1** and **4**, respectively] in the basal position. The axial position is occupied by the oxygen atom belonging to the adjacent carboxylate group in the same oxalato ligand [Cu−O(2) 2.308(2) and 2.300(5) Å, for **1** and **4**, respectively]. The intramolecular Cu···Cu′ distances are 5.531(1) Å in **1**, and 5.320(2) Å in **4**. The distortions of the coordination polyhedra have been analyzed by means of the Addison's parameter from the limiting values correspond-

 © 2003 Wiley-VCH Verlag GmbH & Co. KGaA, Weinheim

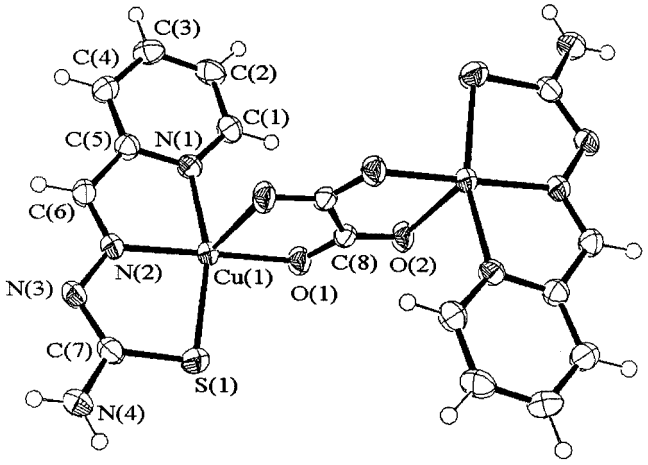

Figure 1. Molecular structure of **1** with thermal ellipsoids at the 50% probability level

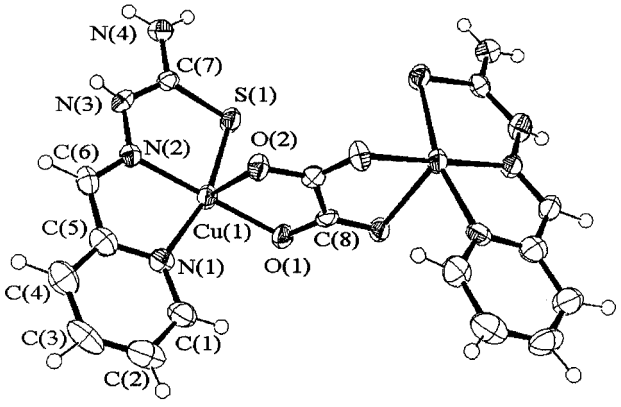

Figure 2. Molecular structure of **4** with thermal ellipsoids at the 50% probability level

ing to square pyramidal (SP, $\tau = 0$) and trigonal bipyramidal (TBP, $\tau = 1$) topologies.[5] The τ values obtained are 0.22 (**1**) and 0.26 (**4**), which indicate that the environment of the copper(II) ions is close to the SP topology. Note the different positions of the ligands in the dinuclear entities (*trans* and *cis* for **1** and **4**, respectively), which breaks the centrosymmetry in **4** and forms a C2 axis with respect to the oxalato ligand. The *cis* configuration of the dinuclear species is not usual in thiosemicarbazone derivatives.[6]

The crystal structure of complex **2** consists of $[Cu(HL)(ox)(H_2O)]$ monomers, as represented in Figure 3. Several distances and angles are shown in Table 2. Each copper(II) ion is five-coordinate, with one sulfur and two nitrogen atoms of the thiosemicarbazone ligand [Cu−N(1), N(2), S: 2.027(3), 1.967(3), 2.281(1) Å] and an oxygen O(1) atom of the oxalato ligand [Cu−O(1): 1.933(2) Å] in the basal plane. The axial position is occupied by the oxygen atom belonging to a water molecule [Cu−O(5) 2.285(3) Å]. The distortion of the coordination polyhedron gives a value of $\tau = 0.18$, characteristic of a geometry close to SP topologies.

The crystal structure of compound **3** is made up of centrosymmetric $[\{Cu(HL)(ox)\}_2]^{2+}$ cationic entities and $[Cu(ox)_2]^{2-}$ bis(oxalato)copper(II) anions. A perspective view of the structure is shown in Figure 4. Selected distances and angles are given in Table 2. The Cu(1) and Cu(2) copper(II) ions exhibit square-pyramidal ($\tau = 0.09$) and square-planar geometries, respectively. Cu(1) is coordinated to one sulfur and two nitrogen atoms of the thiosemicarbazone ligand [Cu−N(1), N(2), S: 2.026(3), 1.952(3), 2.275(1) Å] and an oxygen O(1) atom of the oxalato ligand (Cu−O(1): 1.943(2) Å) in the basal plane. The axial position is occupied by the oxygen atom belonging to the adjacent carboxylate group in the same oxalato ligand [Cu−O(2): 2.261(2) Å]. The intramolecular Cu···Cu′ distance is 5.439(1) Å. The Cu(2) atoms in the bis(oxalato)copper(II) anions are bonded to the O(1S) and O(3S) atoms of each oxalato ligand with bond lengths of 1.937(2) and 1.941(2) Å, respectively. It is interesting to note that the Cu(2)−O(2) distance is 2.756(2) Å, and so the possibility of pseudocoordination must not be ruled out. This could give rise to the presence of chains in the structure, in which the bis(oxalato)copper(II) anions would act as a bridge between the $[\{Cu(HL)(ox)\}_2]^{2+}$ entities.

The thiosemicarbazone ligand exhibits high planarity, except in the cationic entities of **3**. The maximum deviation from the pyridine plane in **1**, **2**, **3** and **4**, corresponds to the S (0.21 Å), N(4) (0.23 Å), S (−0.86 Å) and N(4) (0.34 Å) atoms respectively. The copper(II) ions are above the plane formed by the thiosemicarbazone N(1)N(2)S set (0.22, 0.18, 0.23 and 0.13 Å in **1**, **2**, **3** and **4**, respectively). Both thiosemicarbazone molecules in the dinuclear entity are coplanar on **1** and **3** (dihedral angle ca. 0.0°), but in **4**, the angle formed by the two planes is 10.3°.

The oxalato ligand is planar in **1** and in the cationic $[\{Cu(HL)(ox)\}_2]^{2+}$ species of **3**. However, the O(1S)−C(1S)−C(2S)−O(2S) dihedral angle in the bis(oxalato)copper(II) anions in **3** is 9.6(4)°. The value of the analogous O(1)−C(8)−C(9)−O(3) and O(1)−C(8)−C(8)^{i}−O(1)^{i} angles in **2** and **4** are 79.9(4) and 2.5°, respectively. The highly twisted oxalate molecules, as those reported in **2** (e.g., O−C−C−O angles greater than 50°), are not very usual.[7] There are several possible explanations for this phenomenon. i) The O(2) atom points in the direction of the out-of-plane d_x orbitals (d_{xz} or d_{yz}) of the copper(II) ion. However, the Cu−O(2) distance is too long (2.916 Å). An Extended Hückel molecular orbital (EHMO) analysis[8] on the crystallographic coordinates of compound **2** has been carried out following a published method.[9] It gives no evidence of any significant overlap population between the Cu and O(2) atoms. ii) The existence of tangential π-π stacking between the pyridine and uncoordinated carboxylato moieties can also be considered, with a minimum atom···atom distance of 3.47 Å [O(3)···N(1)^{v}]. The angle between the pyridine and carboxylato planes is 5.3°. However, these interactions are probably weak due to the substantially offset π-stacked geometry. iii) Finally, very strong hydrogen bonds involving the O(3) and O(4) atoms are present in the crystal (see Table 2). These atoms belong to the uncoordinated carboxylate group in the oxalato ligands. The strength of these hydrogen bonds influences the

 © 2003 Wiley-VCH Verlag GmbH & Co. KGaA, Weinheim

Table 2. Selected bond lengths (Å) and angles (°) for **1**, **2**, **3** and **4**; symmetry transformations used to generate equivalent atoms: **1**: *i*: $-x+1, -y+1, -z+1$; *ii*: $x-1, y, z$; *iii*: $x+1, y, z$; *iv*: $-x+3, -y+2, -z+2$; *v*: $-x+2, -y+1, -z+2$; *vi*: $-x+1, -y+2, -z+1$; **2**: *i*: $-x+1, -y+1, -z$; *ii*: $x+1/2, -y+3/2, z+1/2$; *iii*: $x, y-1, z$; *iv*: $-x+1/2, y-1/2, -z+1/2$; *v*: $-x+3/2, y+1/2, -z+1/2$; **3**: *i*: $-x, -y, -z+1$;; *ii*: $-x+1, -y, -z+2$; *iii*: $x, y, z+1$; *iv*: $-x, -y, -z+2$; **4**: *i*: $x, -y, -z+1/2$; *ii*: $-x, y, z-1/2$; *iii*: $x-1/2, y, -z+1/2$; *iv*: $x-1/2, -y, z$; *v*: $-x, -y+1/2, z$

	1[a]	**2**	**3**[b] [c] [d]	**4**[e]
Cu−N(1)	2.044(2)	2.027(3)	2.026(3)	2.027(6)
Cu−N(2)	1.955(2)	1.967(3)	1.952(3)	1.956(5)
Cu−O(1)	1.966(2)	1.933(2)	1.943(2)	1.943(4)
Cu−O(2)[a]/O(5)	2.308(2)	2.286(3)	2.261(2)	2.300(5)
Cu−S	2.2759(6)	2.281(1)	2.275(1)	2.306(2)
N(2)−C(6)	1.284(3)	1.278(4)	1.280(4)	1.279(8)
N(2)−N(3)	1.366(3)	1.360(4)	1.361(4)	1.365(7)
N(3)−C(7)	1.332(3)	1.352(4)	1.361(4)	1.355(8)
C(7)−S	1.743(2)	1.703(3)	1.704(4)	1.711(7)
N(4)−C(7)	1.336(3)	1.317(5)	1.310(5)	1.319(8)
N(1)−Cu−N(2)	80.79(8)	80.1(1)	80.2(1)	80.2(2)
S−Cu−N(1)	161.61(6)	162.71(8)	161.53(9)	163.8(2)
N(2)−Cu−O(1)	174.80(7)	173.7(1)	167.2(1)	179.5(2)
N(2)−Cu−O(2)[a]/O(5)	106.30(7)	85.9(1)	112.9(1)	100.9(2)
N(4)−C(7)−N(3)	116.1(2)	116.0(3)	116.9(3)	117.4(6)
N(4)−C(7)−S	119.2(2)	122.2(3)	122.1(3)	121.2(6)
Selected oxalate bonds				
O(1)[b]−C(8)/O(3)−C(9)	1.273(3)	1.273(4)/1.267(4)	1.266(4)	1.266(8)
O(2)[e]−C(8)/O(4)−C(9)	1.232(3)	1.238(4)/1.225(4)	1.244(4)	1.243(8)
C(8)−C(8)[a,b]/C(9)	1.565(4)	1.524(4)	1.559(7)	1.56(1)
Shortest Cu···Cu distances				
Intramolecular	5.531(1)[i]		5.438(1)[i]	5.320(2)[i]
Intermolecular	6.174(1)[ii,iii]	5.695(1)[i]	4.583(1)[c] 5.153(1)[d]	3.697(2)[v]

Hydrogen bonding contacts A−H···B

Compound	D−H···A	*d*(D−H)	*d*(H···A)	*d*(D···A)	<(DHA)
1	N(4)−H(4A)···N(3)[iv]	0.86(3)	2.19(3)	3.044(3)	172(4)
	N(4)−H(4B)···O(1S)[v]	0.86(3)	2.31(3)	2.983(3)	135(4)
2	O(5)−H(5A)···O(2)[ii]	0.84(4)	1.93(4)	2.757(4)	166(4)
	N(3)−H(3A)···O(3)[iii]	0.77(4)	1.90(4)	2.662(4)	173(4)
	N(4)−H(4A)···O(4)[iii]	0.70(4)	2.09(5)	2.790(5)	172(5)
	N(4)−H(4C)···O(2)[iv]	0.83(5)	2.35(5)	3.063(5)	145(4)
	O(5)−H(5B)···O(3)[v]	0.70(5)	2.02(5)	2.706(4)	166(6)
3	N(4)−H(4B)···O(2S)[ii]	0.78(4)	2.02(4)	2.798(5)	171(4)
	N(3)−H(3A)···O(4S)[iii]	0.85(4)	1.91(4)	2.727(4)	163(4)
4	N(3)−H(3B)···O(2X)[ii]	0.86	1.96	2.78(2)	159.0
	N(3)−H(3B)···O(2Y)[ii]	0.86	1.98	2.77(3)	151.4
	N(4)−H(4A)···O(1S)[iii]	0.86	2.08	2.797(8)	140.6
	N(4)−H(4B)···O(2)[iv]	0.86	2.07	2.890(7)	159.9

[a] In the case of compound **1**, O(2) and C(8) atoms related to the symmetry operation *i*. [b] In the case of compound **3**, O(1) and C(8) atoms related to the symmetry operation *i*. [c] In the case of compound **3**, Cu(1)···Cu(2) distance in the asymmetric unit. [d] In the case of compound **3**, Cu(1)···Cu(1)[iv]. [e] In the case of compound **4**, O(2) related to the symmetry operation *i*.

D···A intermolecular distances and the C(8)−O(2), C(9)−O(3), C(9)−O(4) bond lengths. This fact suggests that the hydrogen bonds are mostly responsible for the twisting of the oxalato ligand. On the other hand, for all these complexes, the longest C−O bonds in the coligands involve the oxygen atoms that are linked to the metal ions.

As in the case mentioned above, the lattice of these compounds contain several hydrogen bonds involving the N(3), N(4) and the oxygen atoms of the oxalato coligands (see Table 2).

The shortest distances between the planes of the pyridine and thiosemicarbazone fragments in different molecules are 3.28 [C(2)···N(2)[ii]], 3.32 [C(1)···N(3)[v]], 3.34 [C(5)···N(4)[iv]] and 3.32 Å [N(4)···C(5)[iv]] for **1**, **2**, **3** and **4**, respectively. This suggests the existence of π-π interactions of the slipped packing type,[10] as represented in Figure 5. Some structural parameters have been evaluated,[11,12] and the results are shown in Table 3. The coordination of a metal ion to the nitrogen heteroatom in heterocyclic molecules enhances the electron-withdrawing effect as a result of its positive charge, such that the stability of the π-π interaction increases.[13,14]

 © 2003 Wiley-VCH Verlag GmbH & Co. KGaA, Weinheim

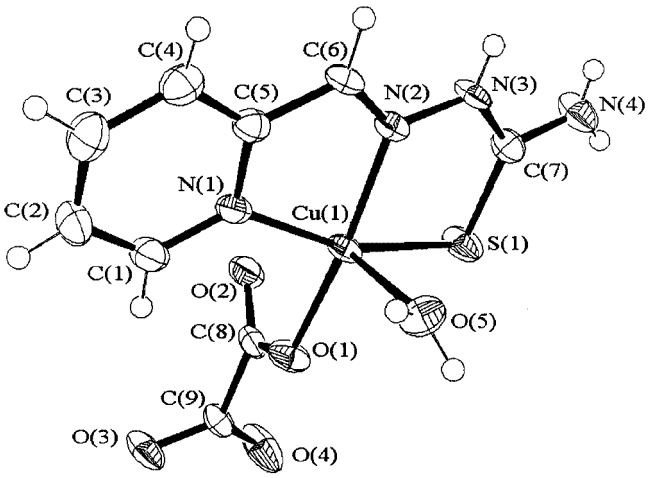

Figure 3. Molecular structure of **2** with thermal ellipsoids at the 50% probability level

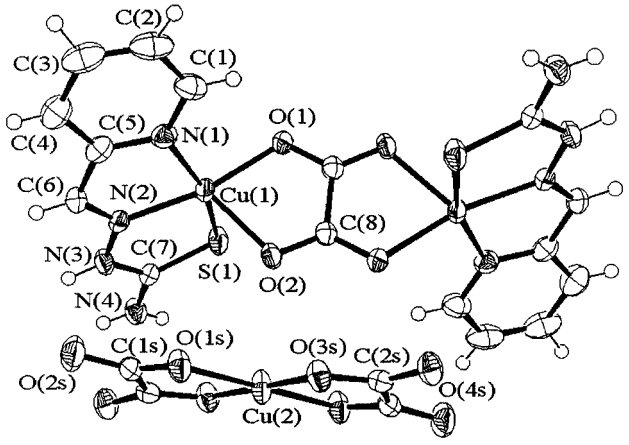

Figure 4. Molecular structure of **3** with thermal ellipsoids at the 50% probability level

These kinds of interactions have also been observed in other thiosemicarbazone systems.[15]

Complexation induces conformational changes in the ligand. Atoms N(1) and N(2) are *anti* with respect to the C(5)−C(6) bond in the free ligand,[16] however, they are *syn* after chelation. Furthermore, the N(2) and S atoms are *anti* with respect to the N(3)−C(7) bond in the neutral ligand[16] and the pyridinium $(H_2L)Cl{\cdot}H_2O$ cationic derivative.[17] However, in the metal complexes, they adopt a *syn* geometry. The C−C and C−N distances are similar to those found in the free ligand and its cationic form, with the exception of the N(3)−C(7) and C(7)−S bond lengths in compound **1**. These bond lengths are significantly different from those observed in the free ligand: 1.358(4) and 1.698(3) Å, respectively. This fact suggests that the double-bond character of the N(3)−C(7) bond in the thiosemicarbazone anionic ligand increases, and that of the C(7)−S bond decreases. However, the bond lengths in the complexed neutral thiosemicarbazone ligands are not different from those in the free ligand. These results are related to the thione vs. thiolate character of the ligand in the neutral or anionic forms, respectively, suggesting the presence of appreciable

Table 3. 1: N(1), C(1), C(2), C(3), C(4), C(5) ring in compound **1**; 2: C(6), N(2), N(3), C(7), S, N(4) set in compound **1**, N(3) is considered to be the "centroid"; 3: N(1), C(1), C(2), C(3), C(4), C(5) ring in compound **2**; 4: C(6), N(2), N(3), C(7), S, N(4) in compound **2**, N(3) is considered to be the "centroid"; 5: N(1), C(1), C(2), C(3), C(4), C(5) ring in compound **3**; 6: C(6), N(2), N(3), C(7), S, N(4) in compound **3**, N(4) is considered to be the "centroid"; 7: C(6), N(2), N(3), C(7), S, N(4) in compound **4**, N(4) is considered to be the "centroid"; 8: N(1), C(1), C(2), C(3), C(4), C(5) ring in compound **4**; DC: distance (Å) between the centroids of the sets *i* and *j*; ANG: angle (°) between the least-squares planes; DZ: distance (Å) between the "centroid" of *j* plane and the least-squares plane of *i* ring; DZ′: distance (Å) between the centroid of *i* ring and the least-squares plane of *j*; DXY: distance (Å) between the "centroids" of *i* and *j* projected onto the least-squares plane of *i*; DXY′: distance (Å) between the "centroids" of *i* and *j* projected onto the least-squares plane of *j*; DS: distance (Å) from the centroid of *i* to the nearest hydrogen atom of *j* plane

i	*j*	DC	ANG	DZ	DXY	DZ′	DXY′	DS
1	2[ii]	3.31	8.13	3.22	0.63	3.16	0.94	3.86
1	1[vi]	3.79	0.00	3.49	1.32	3.49	1.32	3.67
3	4[i]	3.34	3.97	3.32	0.45	3.25	0.45	3.34
3	4[v]	3.89	6.63	2.98	2.48	3.41	1.96	3.63
5	6[iv]	3.26	11.39	3.21	0.48	3.11	1.00	3.23
7	8[iv]	3.32	11.96	3.28	0.29	3.24	0.66	4.01
7	8[v]	3.37	8.35	3.33	0.63	3.27	0.90	3.92

metal-to-ligand π-back donation in the neutral thiosemicarbazone, due to an increase in the π-acceptor character of the sulfur atom of the ligand. The bond lengths are often in the range of experimental error. Other structural parameters, such as some bond angles and non-contact distances are more appropriate for the evaluation of the anionic vs. neutral character of the ligand on complexation.[18] The results summarized in Table 4 show that the distances and angles for the title complexes are in good agreement with those expected for compounds containing the pyridine-2-carbaldehyde thiosemicarbazone ligand in the anionic (**1**) and neutral (**2**, **3**, **4**) forms.

Spectroscopic Studies

The unambiguous assignment of the IR absorption bands in these compounds is made difficult by the highly delocalized thiosemicarbazone system and the oxalato coligands, which give rise to many infrared absorptions. One of the relevant features in some of the complexes is the presence of bands in the 2900−2300 cm^{-1} region which can be assigned to the ν(OH) and ν(NH) vibrations, which are shifted to lower energies as a result of the strong hydrogen bonds. This is in good agreement with the structural results.[19,20] The bands at 1646, 1347 and 800 cm^{-1} in **1** are assigned to the ν_{as}(COO), ν_s(COO) and ν(OCO) absorptions of the oxalato ligand, respectively.[21] Compound **2** shows absorptions at 1644, 1573, 1382, 1339, 830 and 805 cm^{-1} for both the coordinated and uncoordinated carboxylate groups. The complexity of the spectrum of compound **3** only allows for the identification of the bands at 1655, 1640, 1392 and 803 cm^{-1}, which correspond to the oxalato ligands. The same absorptions are found in **4** at

 © 2003 Wiley-VCH Verlag GmbH & Co. KGaA, Weinheim

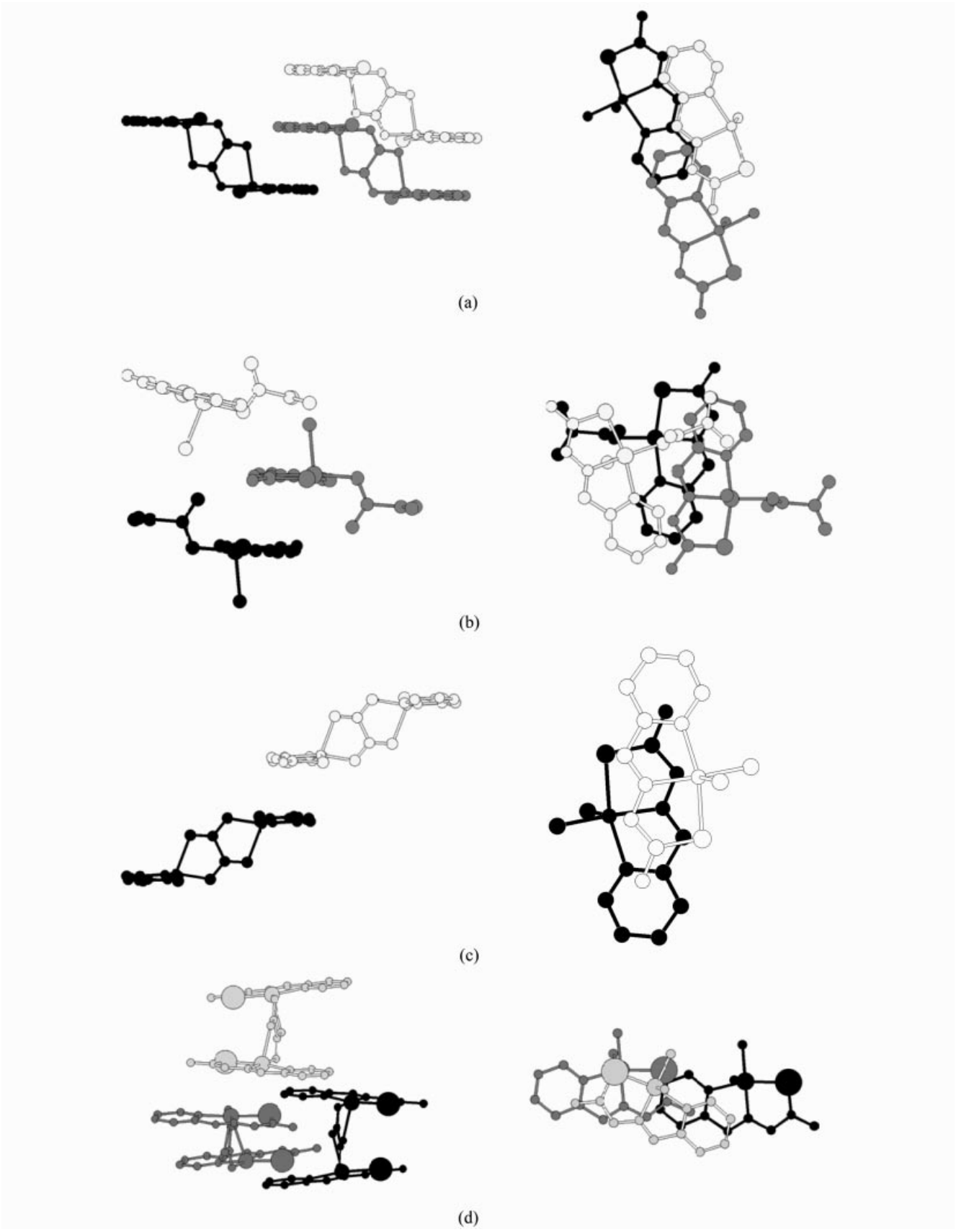

Figure 5. Details of π-π stacking for (a) **1**, (b) **2**, (c) **3** and (d) **4**; drawings (a) and (c) on the right represent monomeric fragments for clarity

 © 2003 Wiley-VCH Verlag GmbH & Co. KGaA, Weinheim

Table 4. Selected structural differences between copper(II) complexes containing neutral (HL) and anionic (L^-) pyridine-2-carbaldehyde thiosemicarbazone ligand (Å) and (°)

Compound	N(2)−N(3)−C(7)	S−C(7)−N(3)	S−C(7)−N(4)	Cu···N(3)	N(2)···C(7)
1	112.0(2)	124.7(2)	119.2(2)	2.94	2.24
2	117.0(3)	121.7(3)	122.4(3)	2.89	2.31
3	116.7(3)	121.0(3)	122.1(3)	2.89	2.32
4	117.6(6)	121.3(5)	121.2(6)	2.89	2.32
HL range	116−118	121−122	121−123	2.89−2.90	2.28−2.32
L^- range	109−114	123−127	117−119	2.94−3.00	2.22−2.23

1654, 1302 and 797 cm^{-1}. Furthermore, compound **4** shows bands at 1383 and 820 cm^{-1} that can be assigned to the ν_3 and ν_2 vibration modes of the nitrate counterion.

The reflectance spectra of the title compounds show bands in the 210−230, 275−290, 360−430 and 630−950 nm regions. These are assigned to ($\pi \rightarrow \pi^*$) pyridine, ($n \rightarrow \pi^*$) pyridine, ($n \rightarrow \pi^*$) thiosemicarbazone, LMCT N/O/S → d and d → d transitions, respectively.[22,23]

The absorption band observed in the 360−380 nm region is assigned to a S → Cu^{II} charge transfer transition. This band is shifted to lower energies in compound **1**. The decrease in energy for the complexes containing the ligand in the anionic form may be due to a decrease in the strength of the π-interactions between the copper and sulfur atoms, and hence results in a C−S bond with greater thiolate behavior.[4e,4h,4j] The absorptions between 420−430 nm can be assigned to LMCT O/N → Cu^{II} transitions, as was observed in other related compounds.[24]

The maxima observed in the 630−665 nm region are characteristic of d → d transitions for square pyramidal copper(II) complexes with a $d_{x^2-y^2}$ ground state. These bands show unresolved shoulders obscured by the tails above 700 nm, which can be due to the distortion of the coordination polyhedra in these compounds to trigonal-bipyramidal geometry. In this sense, the higher the distortion, the greater the wavelength. This is in accordance with the Addison's parameters calculated in the crystallographic section.

The X-band EPR spectra of complexes **1**, **2** and **4** at room temp. are shown in Figure 6. All the spectra exhibit rhombic signals. The obtained *g* values are given in Table 5. These values are similar to those observed for other pyridine-2-carbaldehyde thiosemicarbazone derivatives containing copper(II) ions with distorted square pyramidal topologies, with a $d_{x^2-y^2}$ ground state.[4b,4d−4k]

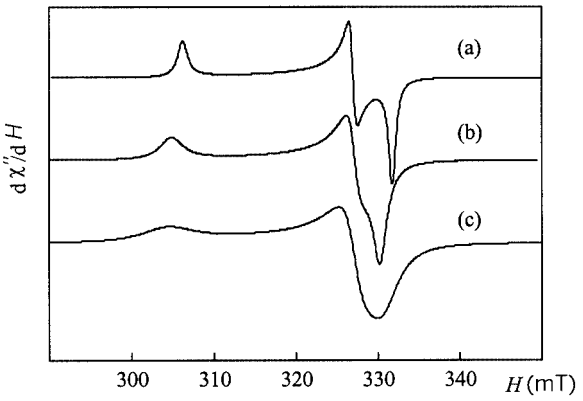

Figure 6. X-band EPR spectra of (a) **1**, (b) **2** and (c) **4** in the solid state at room temp.

Table 5. Experimental EPR parameters

Compound	Temperature	g_1	g_2	g_3
1	room temp.[a]	2.200	2.062	2.032
2	room temp.[a]	2.211	2.061	2.041
4	room temp.	2.212	2.062	2.044
	4 K	2.230	2.063	2.025

[a] No variation in the *g*-values from room temperature to 4 K.

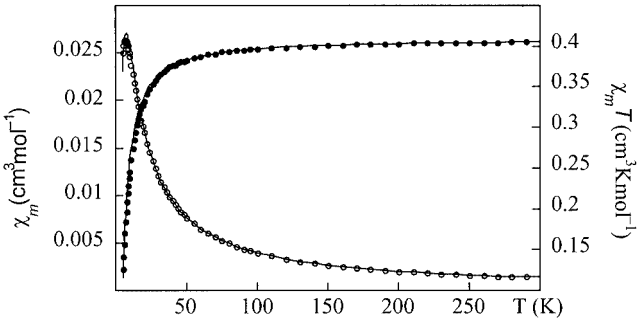

Figure 7. Thermal variation of the molar susceptibility (○○) and $\chi_m T$ (●●) for **1**; solid lines represent the best fit

Magnetic Behavior

The plots of the molar susceptibility (χ_m) vs. *T*, together with the $\chi_m T$ vs. *T* curves, for compounds **1** and **4** are given in Figure 7 and 8. In all the cases, the magnetic measurements obey the Curie−Weiss law at temperatures higher than 50 K. The Weiss temperatures are −3.47 (**1**) and +3.27 K (**4**). The C_m experimental values are 0.41 (**1**) and 0.42 $cm^3 \cdot K \cdot mol^{-1}$ (**4**), and the calculated μ_{eff} values at room temperature are 1.80 (**1**) and 1.84 BM (**4**). For compound **1**, the χ_m value increases with decreasing temperature, reaching a maximum at 7.0 K (0.026 $cm^3 \cdot K \cdot mol^{-1}$), and the $\chi_m T$ value continuously decreases when the temperature is lowered, indicating the presence of antiferromagnetic interactions. However, compound **4** does not exhibit a maximum in the plot of χ_m vs. *T*, and the $\chi_m T$ value increases on

 © 2003 Wiley-VCH Verlag GmbH & Co. KGaA, Weinheim

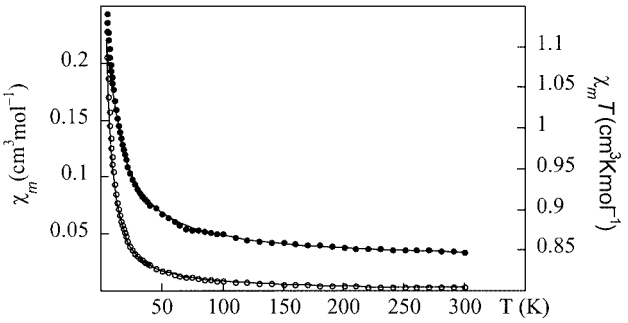

Figure 8. Thermal variation of the molar susceptibility (○○) and $\chi_m T$ (●●) for **4**. Solid lines represent the best fit

lowering the temperature, which is characteristic of ferromagnetic behavior.

Considering the dinuclear nature of these complexes, the susceptibility data was fitted to the expression derived from the Heisenberg isotropic spin Hamiltonian ($H = -2J\, S_1S_2$), for two coupled $S = 1/2$ ions, given by Bleaney−Bowers for copper(II) dinuclear compounds[25]:

$$\chi = \frac{Ng^2\beta^2}{kT}\left(\frac{2}{3+\exp(-2J/kT)}\right) + N\alpha$$

where $N\alpha$ = temperature independent contribution, N is Avogadro's number, β = Bohr magneton, and k = Boltzmann constant. The best least-squares fit (solid line in Figures 7 and 8) is obtained from the parameters $J/k = -6.20$ K (-4.30 cm^{-1}, taking into account 3% paramagnetic impurities) and $+7.73$ K ($+5.37$ cm^{-1}). The g values are 2.089 and 2.112 for complexes **1** and **4**, respectively. These g values are in good agreement with those obtained from EPR (2.098 (**1**) and 2.106 (**4**)). Taking into account the structural features, the existence of magnetic interactions between the different species was considered. However, an improvement in the fit was not observed.

The small values of the magnetic interactions suggest that the exchange propagation direction is in a different plane from that formed by the magnetic $d_{x^2-y^2}$ orbitals. These results agree with the presence of exchange coupling through the oxalato ligand. It must be pointed out that, in spite of the weak magnetic exchange in **4**, this is the strongest ferromagnetic interaction observed in oxalato-bridged copper(II) dinuclear complexes.[26]

It has been proposed[27] that the antiferromagnetic contribution to the magnetic exchange constant J for a dinuclear system with two unpaired electrons is proportional to the square of the energy difference (Δ^2) between the two molecular orbitals constructed from the $d_{x^2-y^2}$ magnetic orbitals. EHMO calculations using the crystallographic coordinates have been carried out to give a qualitative explanation for the magnetic behavior of these complexes. The Δ values are 0.016 and 0.021 eV for **1** and **4**, respectively. These results do not show a qualitative agreement between the gap of the two $d_{x^2-y^2}$ magnetic orbitals involved and the values of the exchange constant. There are at least three possibilities that can be proposed to explain such a disagreement. i) The limitations of the EHMO calculations do not allow us to give a perfect sequence for very similar J values in the pyridine-2-carbaldehyde (thiosemicarbazone)-copper(II) system.[4k] However, a good qualitative accordance is usually obtained for different J values, as those described here. ii) The crystal structure of **4** shows Cu···S^v distances of 3.184(2) Å, which relate copper(II) ions at 3.697(2) Å. The contraction of the cell at low temperatures decreases the Cu···S^v distance. However, as mentioned before, the fit of the curves when considering interactions between different species, was not improved. iii) The non-centrosymmetric nature exhibited by compound **4** could be responsible for the decrease in the antiferromagnetic contribution, which is not reflected in the magnitude of Δ^2, giving rise to the ferromagnetic behavior of this compound.[28]

Conclusion

The control of the experimental conditions in the pyridine-2-carbaldehyde (thiosemicarbazone)copper(II)/oxalato system results in the formation of a rich variety of compounds. In particular, both the amount of reagents and the pH of the medium play an important role in the syntheses of the complexes. As a result either monomeric (**2**) or dinuclear entities (**1** and **4**) can be obtained. The formation of one-dimensional systems is possible , as can be seen by the structure of compound **3**, but up to date, we have not been able to find a reproducible synthetic method to obtain this compound. These results can be used as structural models to predict the possible interactions between the $[Cu(L)(H_2O)_3]^+$ entities and carboxylate-containing biomolecules present in physiological medium.

Magnetic susceptibility data indicate the presence of weak antiferromagnetic and ferromagnetic interactions in **1** and **4**, respectively. The noncentrosymmetric structure of **4** seems to be responsible for the difference in sign of the magnetic properties observed, relative to compound **1** (centrosymmetric). These results demonstrate that the μ-oxalato (thiosemicarbazone)copper(II) systems are appropriate for tunable exchange interactions.

Experimental Section

Preparation of the Complexes: Thiosemicarbazide, pyridine-2-carbaldehyde, oxalic, nitric and trifluoroacetic acids, potassium oxalate, sodium nitrate and copper(II) nitrate were purchased from Fluka, Merck and Prolabo and used as received. Published methods with small modifications were used to synthesize HL[29] and $Cu(L)(NO_3)$.[4b,30]

$[\{Cu(L)\}_2(ox)]\cdot 2H_2O$ (1): An aqueous solution of potassium oxalate (0.092 g, 0.5 mmol) was added to a solution of $Cu(L)(NO_3)$ (0.30 g, 1 mmol) in water (40 mL). The pH was adjusted to 6 by adding NaOH (5 M). The reaction mixture was stirred for 3 h, then filtered, washed and dried. The yield was 0.21 g (70%). Dark-green crystals were obtained by the slow reaction of aqueous solutions of **1** and potassium oxalate in a diffusion device. $C_{16}H_{18}Cu_2N_8O_6S_2$ (609.58): calcd. C 31.5, H 3.0, N 18.4, S 10.5; found C 31.3, H

 © 2003 Wiley-VCH Verlag GmbH & Co. KGaA, Weinheim

3.0, N 18.0, S 10.3. Molar conductivity of $5\cdot10^{-4}$ M solutions in dimethylformamide at 25 °C: Λ_M = 5.2 $\Omega^{-1}\cdot cm^2\cdot mol^{-1}$. Selected IR bands (KBr): $\tilde{\nu}$ = 3568 m, 3438 m, 3385 m, 3104 m, 1646 br. vs, 1604 s, 1559 m, 1481 m, 1448 s, 1428 br. s, 1347 w, 1324 m, 1297 s,sh, 1229 m, 1172 s, 1155 s, 880 m, 800 m, 779 m, 626 m, 410 w cm^{-1}. UV-Vis: λ_{max} (reflectance spectrum on solid sample) λ = ca. 800 (vb,sh), 646 (b), 422 (sh), 378, 277, 227 nm.

[Cu(HL)(ox)(H$_2$O)] (2): Oxalic acid (0.63 g, 5 mmol) was dissolved in water (15 mL), and was allowed to react with an aqueous solution of Cu(L)(NO_3) (0.30 g, 1 mmol). The pH was adjusted to 1 by adding nitric acid. After 3 h of constant stirring, the blue solid was filtered, washed and dried. Yield 0.24 g (around 70%). This complex was also prepared from aqueous solutions of **1** and oxalic acid in a diffusion device, both solutions were acidified with several drops of trifluoroacetic acid. After two weeks, greenish-blue crystals suitable for X-ray studies were collected. $C_9H_{11}CuN_4O_5S$ (350.82): calcd. C 30.8, H 3.2, N 16.0, S 9.1; found C 30.5, H 2.8, N 16.2, S 8.8. Molar conductivity of $5\cdot10^{-4}$ M solutions in dimethylformamide at 25 °C: Λ_M = 69.0 $\Omega^{-1}\cdot cm^2\cdot mol^{-1}$. Selected IR bands (KBr): $\tilde{\nu}$ = 3354 m, 3231 w, 2864 w (br.), 2696 w, 1644 s, 1614 m, 1573 vs, 1473 s, 1448 m, 1382 w, 1339 m, 1298 vs (sh), 1273 s, 1226 m, 1182 m, 1109 m, 921 m (sh), 830 w, 804 w, 778 sh, 769 s, 653 m (sh), 623 w, 489 w, 414 w cm^{-1}. UV-Vis, λ_{max} (reflectance spectrum on solid sample) = ca. 720 (sh), 630 (b), 360, 287, ca. 220 nm. Deep-blue good quality crystals of [{Cu(HL)}$_2$(ox)][Cu(ox)$_2$]·2H$_2$O (**3**) co-crystallized, together with those of **2**. All the attempts to synthesize this compound separately were unsuccessful. Selected IR bands (KBr): $\tilde{\nu}$ = 3433 m, 3345 m, 3160 m, 1655 vs, 1638 vs, 1624 vs, 1613 vs,sh, 1582 s, 1392 m, 1299 m, 1254 m, 1226 m, 1178 s, 803 w, 778 s, 738 w, 694 w, 617 w, 490 w, 410 w cm^{-1}.

[{Cu(HL)}$_2$(ox$_{0.5}$)]·(NO$_3$)$_2$ (4): Aqueous solutions of oxalic acid (0.092 g, 0.5 mmol), sodium nitrate (0.42 g, 5 mmol) and Cu(L)(NO_3) (0.30 g, 1 mmol) were mixed with vigorous stirring. The pH of the resulting mixture was adjusted to about 1 by the addition of nitric acid. Four hours later, a turquoise-blue precipitate appeared. This was filtered, washed and dried. The yield was 0.24 g (around 70%). This complex can be also synthesized from an aqueous suspension of **1** by adding nitric acid (final pH ≈ 1). Finally, crystals of this compound were collected by slow evaporation of the mother liquors of **2**. $C_{16}H_{16}Cu_2N_{10}O_{10}S_2$ (699.59): calcd. C 27.5, H 2.3, N 20.0, S 9.2; found C 27.3, H 2.2, N 19.9, S 9.2. Molar conductivity of $5\cdot10^{-4}$ M solutions in dimethylformamide at 25 °C: Λ_M = 133.2 $\Omega^{-1}\cdot cm^2\cdot mol^{-1}$. Selected IR bands (KBr): $\tilde{\nu}$ = 3294 m, 3138 m, 1654 vs, 1624 s, 1616 s, 1586 s, 1474 m, 1434 s, 1383 s, 1339 s, 1302 s, 1280 s, 1224 s, 1178 m, 1163 m, 1019 w, 921 w, 879 w, 820 w, 797 w, 771 m, 742 m, 651 m, 623 w, 415 w cm^{-1}. UV-Vis, λ_{max} (reflectance spectrum on solid sample) = ca. 950 (vb, sh), 663 (vb), 428 (sh), 367 (sh), 283, ca. 214 nm.

Physical Measurements: Microanalyses were performed with a LECO CHNS−932 analyzer. Conductivity measurements were made by a CRISON 522 conductimeter. Infrared spectra were obtained with samples prepared as KBr pellets in the 400−4000 cm^{-1} region on a Nicolett Impact 410 FTIR spectrophotometer. Reflectance spectra were recorded on a Cary 2415 spectrometer in the range 200−2000 nm. For UV-visible solution measurements, a Varian UV-VIS-NIR spectrophotometer was employed in the range 200−900 nm. X-band EPR spectra were recorded on a Bruker EMX spectrometer, equipped with a standard Oxford continuous flow cryostat. Magnetic measurements of powdered samples were performed in the temperature range 5−300 K, using a Quantum Design MPMS−7 Squid magnetometer. Diamagnetic corrections were estimated from Pascal tables.

X-ray Crystallographic Studies: Crystal data collections were carried out on a Bruker Smart CCD area detector equipped with a single crystal diffractometer. Absorption corrections were made using the SADABS program.[31] Direct methods (SHELXS-97)[32] were employed to solve the structures and were then refined by full-matrix least-squares methods, using the SHELXL-97 computer program.[33] All non-hydrogen atoms were assigned anisotropic thermal parameters. Hydrogen positions were determined by difference Fourier syntheses and introduced in calculations with a riding model. The scattering factors and anomalous dispersion coefficients were taken from International Tables of X-ray Crystallography.[34] Refinements were made on F_o^2 for all reflections. The high thermal parameters in the nitrate ions of compound **4** are the cause of the disorder in some of the oxygen atom positions. CCDC−194996 (**1**), −194997 (**2**), −194998 (**3**) and −194999 (**4**) contain the supplementary crystallographic data for this paper. These data can be obtained free of charge at www.ccdc.cam.ac.uk/conts/retrieving.html [or from the Cambridge Crystallographic Data Centre, 12, Union Road, Cambridge CB2 1EZ, UK; fax: (internat.) +44−1223/336−033; E-mail: deposit@ccdc.cam.ac.uk].

Acknowledgments

We thank Dr. J. J. Delgado (SCAI, Universidad de Burgos, Spain) for the elemental analysis and Prof. R. Olazcuaga and Dr. F. Guillen (CNRS, Pessac, France) for the reflectance measurements. We also thank Dr. J. L. Pizarro for helpful discussions about the crystallographic data. This work has been carried out with the financial support of the Basque Government (PI99/53) and the Dirección General de Investigación del Ministerio de Ciencia y Tecnología (BQU2002-00435). P. G.-S. thanks the Universidad de Burgos for her Doctoral Fellowship.

[1] [1a] W. E. Antholine, J. M. Knight, H. Whelan, D. H. Petering, *Mol. Pharmacol.* **1977**, *13*, 89−98. [1b] L. A. Saryan, K. Mailer, C. Krishnamurti, W. E. Antholine, D. H. Petering, *Biochem. Pharmacol.* **1981**, *30*, 1595−1604. [1c] W. E. Antholine, F. Taketa, *J. Inorg. Biochem.* **1982**, *16*, 145−154. [1d] W. E. Antholine, F. Taketa, *J. Inorg. Biochem.* **1984**, *20*, 69−78. [1e] W. E. Antholine, J. M. Knight, D. H. Petering, *J. Med. Chem.* **1976**, *19*, 339−341. [1f] L. A. Saryan, E. Ankel, C. Krishnamurti, D. H. Petering, *J. Med. Chem.* **1979**, *22*, 1218−1221. [1g] S. B. Padhye, G. B. Kauffman, *Coord. Chem. Rev.* **1985**, *63*, 127−160. [1h] D. X. West, S. B. Padhye, P. B. Sonawane, *Struct. Bond.* **1991**, *76*, 1−50. [1i] D. X. West, A. E. Liberta, S. B. Padhye, R. C. Chikate, P. B. Sonawane, A. S. Kumbhar, R. G. Yerande, *Coord. Chem. Rev.* **1993**, *123*, 49−71. [1j] E. W. Ainscough, A. M. Brodie, W. A. Denny, G. J. Finlay, J. D. Ranford, *J. Inorg. Biochem.* **1998**, *70*, 175−185. [1k] J. García-Tojal, A. García-Orad, A. Alvarez Díaz, J. L. Serra, M. K. Urtiaga, M. I. Arriortua, T. Rojo, *J. Inorg. Biochem.* **2001**, *84*, 271−278.

[2] W. E. Antholine, J. M. Knight, D. H. Petering, *Inorg. Chem.* **1977**, *16*, 569−574.

[3] H. Beraldo, L. Tosi, *Inorg. Chim. Acta* **1986**, *125*, 173−182.

[4] [4a] C. F. Bell, C. R. Theocharis, *Acta Crystallogr., Sect. C* **1987**, *43*, 26−29. [4b] A. G. Bingham, H. Bögge, A. Müller, E. W. Ainscough, A. M. Brodie, *J. Chem. Soc., Dalton Trans.* **1987**, 493−499. [4c] E. W. Ainscough, E. N. Baker, A. M. Brodie, R. J. Cresswell, J. D. Ranford, J. M. Waters, *Inorg. Chim. Acta* **1990**, *172*, 185−190. [4d] E. W. Ainscough, A. M. Brodie, J. D. Ranford, J. M. Waters, *J. Chem. Soc., Dalton Trans.* **1991**, 1737−1742. [4e] E. W Ainscough, A. M. Brodie, J. D. Ranford, J. M. Waters, *J. Chem. Soc., Dalton Trans.* **1991**, 2125−2131.

 © 2003 Wiley-VCH Verlag GmbH & Co. KGaA, Weinheim

[4f] E. W. Ainscough, A. M. Brodie, J. D. Ranford, J. M. Waters, K. S. Murray, *Inorg. Chim. Acta* **1992**, *197*, 107−115. [4g] J. García-Tojal, M. K. Urtiaga, R. Cortés, L. Lezama, T. Rojo, M. I. Arriortua, *J. Chem. Soc., Dalton Trans.* **1994**, 2233−2238. [4h] J. García-Tojal, J. García-Jaca, R. Cortés, T. Rojo, M. K. Urtiaga, M. I. Arriortua, *Inorg. Chim. Acta* **1996**, *249*, 25−32. [4i] E. W. Ainscough, A. M. Brodie, J. D. Ranford, J. M. Waters, *J. Chem. Soc., Dalton Trans.* **1997**, 1251−1255. [4j] J. García-Tojal, L. Lezama, J. L. Pizarro, M. Insausti, M. I. Arriortua, T. Rojo, *Polyhedron* **1999**, *18*, 3703−3711. [4k] P. Gómez−Saiz, J. García-Tojal, A. Mendia, B. Donnadieu, L. Lezama, J. L. Pizarro, M. I. Arriortua, T. Rojo, *Eur. J. Inorg. Chem.* **2003**, 518−527.

[5] A. W. Addison, T. N. Rao, J. Reedijk, J. van Rijn, G. C. Verschoor, *J. Chem. Soc., Dalton Trans.* **1984**, 1349−1356.

[6] [6a] D. X. West, J. P. Jasinski, J. M. Jasinski, R. J. Butcher, *J. Chem. Cryst.* **1999**, *29*, 1089. [6b] E. Bermejo, A. Castiñeiras, R. Dominguez, R. Carballo, C. Maichle-Moessmer, J. Strehle, D. X. West, *Z. Anorg. Allg. Chem.* **1999**, *625*, 961. [6c] M. L. Duran, A. Sousa, J. Romero, A. Castiñeiras, E. Bermejo, D. X. West, *Inorg. Chim. Acta* **1999**, *294*, 79−82. [6d] J. M. Vila, M. T. Pereira, J. M. Ortigueira, M. Grana, D. Lata, A. Suarez, J. J. Fernandez, A. Fernandez, M. Lopez-Torres, H. Adams, *J. Chem. Soc., Dalton Trans.* **1999**, 4193−4201. [6e] M. B. Ferrari, G. G. Fava, C. Pelizzi, G. Pelosi, P. Tarasconi, *Inorg. Chim. Acta* **1998**, *269*, 297−301. [6f] X.-G. Cui, Q.-P. Hu, *Chinese J. Struct. Chem. (Jiegou Huaxue)* **1994**, *13*, 340.

[7] [7a] M. E. Kastner, D. A. Smith, A. G. Kuzmisssion, J. N. Cooper, T. Tyree, M. Yearick, *Inorg. Chim. Acta* **1989**, *158*, 185−199. [7b] S. W. Ng, V. G. K. Das, B.-S. Luo, T. C. W. Mak, *Z. Kristallogr.* **1994**, *209*, 882−884. [7c] J. C. Kim, J. Cho, A. J. Lough, *Inorg. Chim. Acta* **2001**, *317*, 252−258.

[8] C. Mealli, D. M. Proserpio, *CACAO Program, Computer Aided Composition of Atomic Orbitals, PC version*, July **1992**, *J. Chem. Ed.* **1990**, *67*, 399−402.

[9] J. García-Tojal, J. L. Pizarro, L. Lezama, M. I. Arriortua, T. Rojo, *Inorg. Chim. Acta* **1998**, *278*, 150−158.

[10] C. Janiak, *J. Chem. Soc., Dalton Trans.* **2000**, 3885−3896.

[11] A. Albert, F. H. Cano, *Cristalografia*, Publicaciones CSIC: Madrid, **1995**.

[12] I. Unamuno, J. M. Gutiérrez-Zorrilla, A. Luque, P. Román, L. Lezama, R. Calvo, T. Rojo, *Inorg. Chem.* **1998**, *37*, 6452−6460.

[13] C. A. Hunter, J. K. M. Sanders, *J. Am. Chem. Soc.* **1990**, *112*, 5525−5534.

[14] F. Cozzi, M. Cinquini, R. Annunziata, J. S. Siegel, *J. Am. Chem. Soc.* **1993**, *115*, 5330−5331.

[15] [15a] C.-Y. Duan, B.-M. Wu, T. C. W. Mak, *J. Chem. Soc., Dalton Trans.* **1996**, 3485−3490. [15b] Z.-H. Liu, C.-Y. Duan, J. Hu, X.-Z. You, *Inorg. Chem.* **1999**, *38*, 1719−1724. [15c] H. Cheng, D. Chun-ying, F. Chen-jie, L. Yong-jiang, M. Quing−jin, *J. Chem. Soc., Dalton Trans.* **2000**, 1207−1212. [15d] L. Ze-hua, D. Chun-ying, L. Ji-hui, L. Yong-jiang, M. Yu-hua, Y. Xiaozeng You, *New. J. Chem.* **2000**, *24*, 1057−1062.

[16] V. N. Byushkin, Y. M. Chumakov, N. M. Samus, I. O. Baka, *Zh. Strukt. Khim.* **1987**, *28*, 140−142.

[17] M. K. Urtiaga, M. I. Arriortua, J. García-Tojal, T. Rojo, *Acta Crystallogr., Sect. C* **1995**, *51*, 2172−2174.

[18] J. García-Tojal, T. Rojo, *Polyhedron* **1999**, *18*, 1123−1130.

[19] K. C. K. Swamy, S. Kumaraswamy, P. Kommana, *J. Am. Chem. Soc.* **2001**, *123*, 12642−12649.

[20] T. Steiner, *Angew. Chem. Int. Ed.* **2002**, *41*, 48−76, and references therein.

[21] K. Nakamoto, *Infrared and Raman Spectra of Inorganic and Coordination Compounds*, 5th edn., John Wiley & Sons, New York, **1997**.

[22] E. S. Stern, C. J. Timmons, *Electronic Absorption Spectroscopy in Organic Chemistry*, Edward Arnold, London, **1970**.

[23] D. X. West, M. A. Lockwood, J. N. Albert, A. E. Liberta, *Spectrochim. Acta, Ser. A* **1991**, *49*, 1809−1816.

[24] D. X. West, Y. Yang, T. L. Klein, K. I. Goldberg, A. E. Liberta, J. Valdés-Martínez, R. A. Toscano, *Polyhedron* **1995**, *14*, 1681−1693.

[25] B. Bleaney, K. D. Bowers, *Proc. R. Soc. London, Ser. A* **1952**, *214*, 451.

[26] [26a] O. Costisor, M. Brezeanu, Y. Journaux, K. Mereiter, P. Weinberger, W. Linert, *Eur. J. Inorg. Chem.* **2001**, 2061−2066. [26b] M. L. Calatayud, I. Castro, J. Sletten, F. Lloret, M. Julve, *Inorg. Chim. Acta* **2000**, *300*, 846−854. [26c] Z. Smekal, Z. Travnicek, F. Lloret, J. Marek, *Polyhedron* **1999**, *18*, 2787−2793. [26d] J. Cano, P. Alemany, S. Alvarez, M. Verdaguer, E. Ruiz, *Chem. Eur. J.* **1998**, *4*, 476−484.

[27] P. J. Hay, J. C. Thibeault, R. Hoffmann, *J. Am. Chem. Soc.* **1975**, *97*, 4884−4899.

[28] [28a] O. Kahn, M. F. Charlot, *Nouv. J. Chim.* **1980**, *4*, 567. [28b] M. Julve, M. Verdaguer, O. Kahn, A. Gleizes, M. Philoche-Levisalles, *Inorg. Chem.* **1983**, *22*, 368−370. [28c] Y. Akhriff, J. Server-Carrió, A. Sancho, J. García-Lozano, E. Escrivá, J. V. Folgado, L. Soto, *Inorg. Chem.* **1999**, *38*, 1174−1185, and references therein.

[29] F. E. Anderson, C. J. Duca, J. V. Scudi, *J. Am. Chem. Soc.* **1951**, *73*, 4967−4968.

[30] C. F. Bell, K. A. K. Lott, N. Hearn, *Polyhedron* **1987**, *6*, 39−44.

[31] R. H. Blessing, *Acta Crystallogr., Sect. A* **1995**, *51*, 33.

[32] G. M. Sheldrick, *SHELXS−97, A Program for Crystal Structure Solution*, Univ. of Göttingen, Göttingen, Germany, **1997**.

[33] G. M. Sheldrick, *SHELX97, Programs for Crystal Structure Analysis (Release 97−2)*, Institut für Anorganische Chemie der Universität, Tammannstraße 4, 3400 Göttingen, Germany, **1998**.

[34] *INTERNATIONAL Tables for X−Ray Crystallography*, Kluwer Academic Publishers, Dordrecht, The Netherlands, **1992**.

Received October 14, 2002

 © 2003 Wiley-VCH Verlag GmbH & Co. KGaA, Weinheim

Iron-Fragment-Substituted Heterosiloxanes of Gallium $[Cp(OC)_2Fe-SiR_2OGaR'_2]_2$ (R, R′ = Alkyl, Aryl) − Structures of $[Cp(OC)_2Fe-SiR_2OGaMe_2]_2$ (R = Me, Ph)[‡]

Wolfgang Malisch,*[a] Dirk Schumacher,[a] Bernd Schmiedeskamp,[a] Heinrich Jehle,[a] Dirk Eisner,[b] Wolfgang W. Schoeller,[b] and Martin Nieger[c]

Keywords: Gallium / Iron / Silanols / Silicon / Siloxanes

The trialkylgallanes GaR''_3 [R′ = Me, *i*Pr (**2a** and **2b**)] react with the ferrio-silanols $Cp(OC)_2Fe–Si(R)(R')OH$ [R = R′ = Me, *i*Pr, Ph (**1a**–**c**), R = Me, R′ = Ph (**1d**)] by alkane elimination to yield the iron-substituted siloxy-gallanes $[Cp(OC)_2Fe–Si(R)(R')OGaR''_2]_2$ (**3a**–**e**). According to molecular mass determination in benzene (**3a**, **3b**, **3d**), X-ray analyses (**3a**, **3d**) and NMR spectroscopy (**3e**), the novel hetero-siloxanes exist as dimers both in solution and in the solid state. The bonding situation and geometry of the ferrio-heterosiloxane $[Cp(OC)_2Fe–SiH_2OGaH_2]_2$ has been analyzed by density functional calculation.

(© Wiley-VCH Verlag GmbH & Co. KGaA, 69451 Weinheim, Germany, 2003)

Introduction

Heterosiloxanes, siloxanes containing Si−O−E moieties (E = heteroelement), represent a class of compounds in organometallic chemistry that has attracted widespread interest in material science and catalysis in recent decades. Due to the presence of the heteroelement, they may serve as models for heteroelement-doped silicates and silicones, which often exhibit special properties such as high thermal stability or catalytic activity. In this context, the preparation of group 13 heterosiloxanes (E = Al, Ga, In) has become a growing field of research concerning catalytically active zeolites, such as gallium-containing zeolites for the dehydrogenation and dehydrocyclization of alkanes.[3−8] Early studies by Schmidbaur[9−11] describe various heterosiloxanes represented by compounds such as $[R_3SiOEMe_2]_2$ (E = Ga, In; R = Me, Ph)[10] for group 13 elements. Recent work by Roesky has shown that the related reactions of organosilanetriols $RSi(OH)_3$ preferentially yield compounds such as $[RSiO_3E·D]_4$ (E = Al, Ga, In; D = THF, dioxane), characterized by three-dimensional polyhedral cage structures.[3−5] The access to transition metal-substituted silanols $L_nM-SiMe_{3-x}(OH)_x$ (x = 1−3) now offers the possibility of obtaining a novel kind of heterosiloxane in which the silicon atom bears a transition metal fragment. Metallo-silanols show reduced H acidity of the Si−OH function and remarkable stability towards self-condensation, a behavior contrasting with that of organosilanols $R_{4-x}Si(OH)_x$ (x = 1−3), which usually convert into siloxanes. This high stability, caused by the electron-rich metal fragment, predisposes metallo-silanols to act as excellent precursors for selective reactions with chlorosilanes, yielding metallo-siloxanes and -polysiloxanes $L_nM-SiMe_{3-x}(OSiR'_3)_x$ [x = 1−3; R'_3Si = Me_3Si, $Me_2(H)Si$].[12−20] Moreover, these properties should allow the preparation of metal fragment-substituted heterosiloxanes of gallium and indium by alkane elimination. These species could represent attractive models for silica- or zeolite-based catalysts, in which L_nM represents an catalytically active metal fragment.

In this paper we present the first examples of successful coupling reactions between metallo-silanols $Cp(OC)_2Fe-Si(R)(R')OH$ (R = R′ = Me, *i*Pr, Ph; R = Me, R′ = Ph)[13,14,21] and diverse trialkylgallanes. Moreover, we describe investigations concerning the influence of the transition metal fragment on the aggregation mode.

[‡] Synthesis and Reactivity of Silicon Transition Metal Complexes, 60. Part 59: Ref.[1], Metallo-Silanols and Metallo-Siloxanes, 31. Part 30: Ref.[2]

[a] Institut für Anorganische Chemie der Universität Würzburg, Am Hubland, 97074 Würzburg, Germany
Fax: (internat.) +49-(0)931-888-4618
E-mail: Wolfgang.Malisch@mail.uni-wuerzburg.de
[b] Fakultät für Chemie der Universität Bielefeld, Postfach 100131, 33501 Bielefeld, Germany
E-Mail: Wolfgang.schoeller@uni-bielefeld.de
[c] Institut für Anorganische Chemie der Universität Bonn, Gerhard-Domagk-Straße 1, 53121 Bonn, Germany

Supporting information for this article is available on the WWW under http://www.eurjic.org or from the author.

Results and Discussion

Synthesis of Iron Fragment-Substituted Heterosiloxanes of Gallium

Treatment of the trialkylgallanes **2a** and **2b** with stoichiometric amounts of the ferrio-silanols $Cp(OC)_2Fe-SiR_2OH$ [R = Me (**1a**), *i*Pr (**1b**), Ph (**1c**)] in *n*-pentane at room temperature yielded, by the elimination of alkane, after 2 h (**3a**, **3c**, **3d**) or 16 h (**3b**) the metal fragment-substituted heterosiloxanes **3a**−**d**. The trimethylgallane **2a** was preferably employed as an Et_2O adduct, which proved to be much easier to handle (Scheme 1).

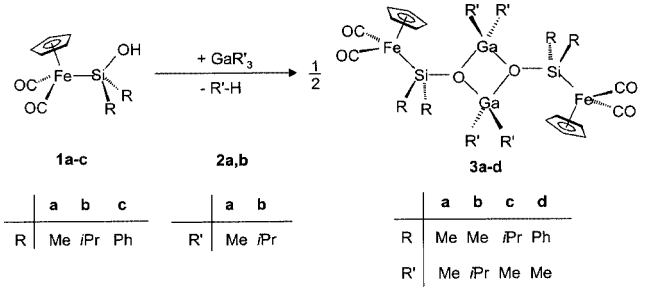

Scheme 1. Synthesis of iron fragment-substituted heterosiloxanes of gallium

Compounds **3a**−**d** are isolated after recrystallization from *n*-pentane at −78 °C as light yellow, microcrystalline powders in 73−86% yields. The compounds are slightly soluble in *n*-pentane or *n*-hexane and reasonably soluble in benzene or toluene. Unlike the starting materials, they may even be handled in air for short times without decomposition.

The ^{29}Si NMR resonances of **3a**−**d** show the typical downfield shifts of $Cp(OC)_2Fe$-substituted silicon atoms (**3a**: δ = 66.57 ppm, **3b**: δ = 64.10 ppm, **3c**: δ = 78.92 ppm, **3d**: 54.86 ppm). The observed range appears close to that for the corresponding ferrio-silanols (**2a**: δ = 66.05 ppm, **2b**: δ = 76.36 ppm, **2c**: 50.38 ppm).

Molecular mass determinations of **3a**, **3b**, and **3d** in benzene by freezing-point depression reveal the presence of dimers, originating from intermolecular interaction between the Lewis acidic group 13 element and the Lewis basic oxygen atoms of the Si−O units. This result is in good accordance with the findings for metal-free siloxy-gallanes.[9−11] The aggregation to dimers in the solid state was additionally confirmed by X-ray analyses of **3a** and **3d**. These results clearly indicate that the $Cp(OC)_2Fe$ fragment at the silicon does not induce O−Ga π-interaction sufficient to prevent dimerization.

Treatment of the ferrio-silanol $Cp(OC)_2FeSi(Me)(Ph)OH$ (**1d**), bearing a chiral silicon atom, with $GaMe_3{\cdot}Et_2O$ (**2a**) in *n*-pentane produces the heterosiloxane **3e** as a beige, microcrystalline solid in 82% yield.

The aggregation of **3e**, due to Ga−O interaction, results in the formation of *like* and *unlike* diastereomers (Figure 1), as can be directly confirmed in solution by ^1H NMR spectroscopy (C_6D_6, Figure 2). Since the two diastereomers differ in the topicities of their Ga-bonded methyl groups, the *like* diastereomer (*RR*/*SS*), which has a C_2 axis as symmetry element, provided free rotation around the O−Si axis, and has homotopic methyl groups, while the *unlike* diastereomer (*RS*/*SR*), characterized by a mirror plane, has diastereotopic methyl groups. This stereochemical situation gives rise to three signals for the Ga-bonded methyl groups in the ^1H NMR and the ^{13}C NMR spectra: two for the *unlike* form and one for the *like* form. The diastereomeric ratio can be determined as 50:50 by integration of these signals. Moreover, two signals, located very close to each other, are observed for all other NMR resonances, due to the existence of diastereomers.

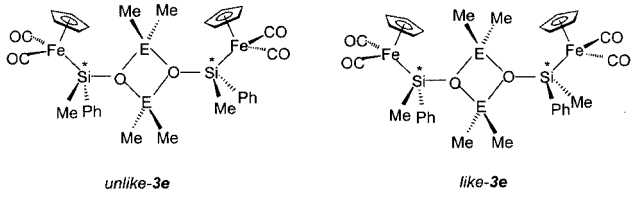

Figure 1. *unlike*- and *like*-**3e**

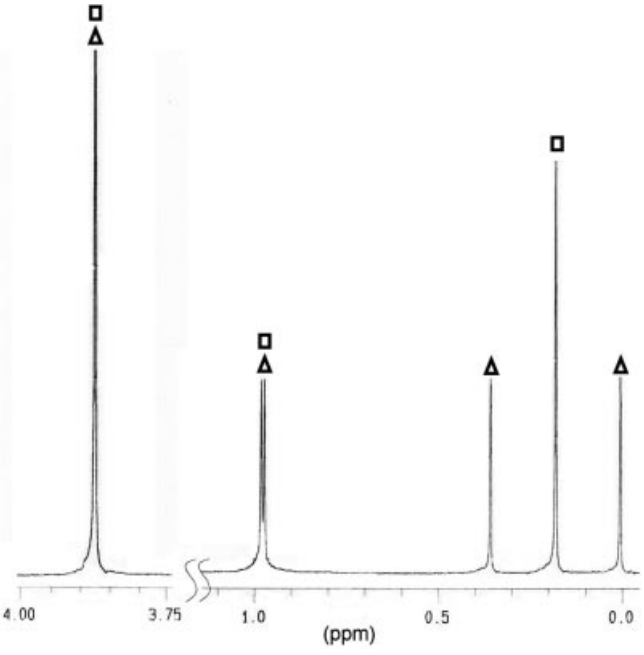

Figure 2. ^1H NMR([D_6]benzene, 300.4 MHz) of **3e** (aromatic region has been omitted for clarity); □ = *like*-**3e**, Δ = *unlike*-**3e**; *like*/*unlike* assignment of the SiMe and Cp signals is not possible

X-Ray Analyses of 3a and 3d

The results of the X-ray analyses of **3a** and **3d**, which to the best of our knowledge are the first structurally characterized siloxy-substituted diorgano compounds of gallium, are presented in Figure 3 and 4.

The structure-determining element is the rhombic, four-membered $[Ga-O]_2$ ring, a common feature of heteroatom-

 © 2003 Wiley-VCH Verlag GmbH & Co. KGaA, Weinheim

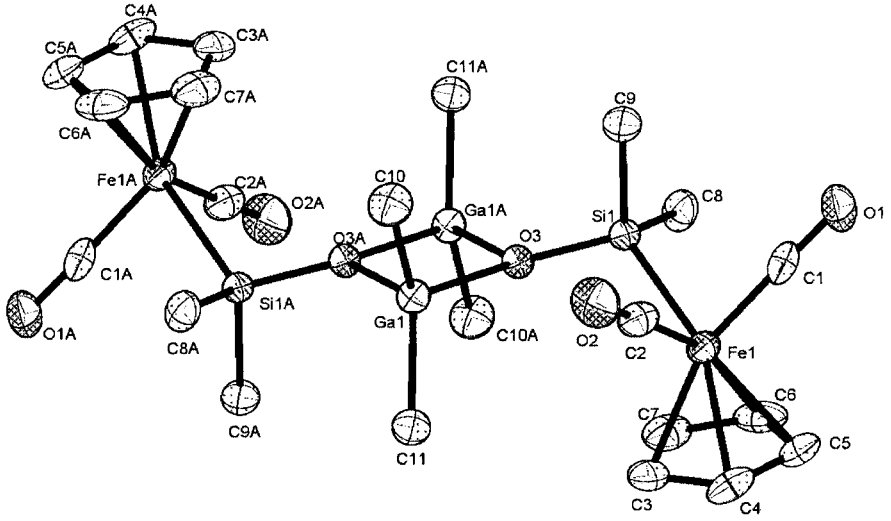

Figure 3. ORTEP plot of $[Cp(OC)_2FeSiMe_2-O-GaMe_2]_2$ (**3a**). Hydrogen atoms have been omitted for clarity; selected bond lengths [Å] and angles [°]: Ga1−O3 1.957(3), Ga1−O3A 1.977(3), Ga1−C10 1.965(5), Ga1−C11 1.942(5), Si1−O3 1.667(3), Fe1−Si1 2.3229(16), Fe1−C1 1.730(6), Fe1−C2 1.756(5), O1−C1 1.164(6), O2−C2 1.143(6); Ga1−O3−Ga1A 96.61(13), O3−Ga1−O3A 83.39(13), C10−Ga1−C11 130.7(2), O3−Ga1−C10 110.25(19), O3−Ga1−C11 107.62(18), Si1−O3−Ga1 134.63(18), Si1−O3−Ga1A 125.98(17), O3−Si1−Fe1 113.56(12), O3−Si1−C8 106.4(2), O3−Si1−C9 106.8(2), C8−Si1−C9 106.2(3)

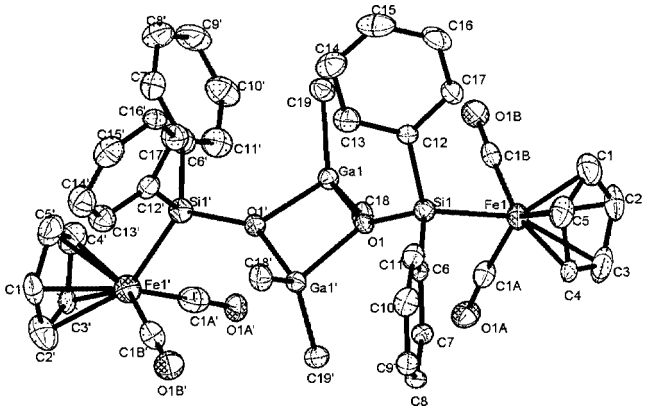

Figure 4. ORTEP plot of $[Cp(OC)_2FeSiPh_2-O-GaMe_2]_2$ (**3d**). Hydrogen atoms have been omitted for clarity; selected bond lengths [Å] and angles [°]: Fe1−C1a 1.7487(18), Fe1−C1b 1.7460(19), Fe1−Si1 2.3091(5), Si1−O1 1.6674(11), Si1′−O1′ 1.6703(11), O1−Ga1 1.9815(11), O1−Ga1′ 1.9754(11), O1′−Ga1′ 1.9792(19), O1′−Ga1 1.9748(11), Si1−C6 1.8914(17), Si1−C12 1.8909(16), Ga1−C19 1.9633(16), Ga1−C18 1.9615(16); C1a−Fe1−C1b 96.77(8), C1a−Fe1−Si1 86.86(6), C1b−Fe1−Si1 86.00(6), Fe1−Si1−C6 109.96(5), Fe1−Si1−C12 115.63, Fe1−Si1−O1 113.66(4), O1a−C1a−Fe1 175.59(16), O1b−C1b−Fe1 178.03(16), Ga1−O1−Ga1′ 96.78(5), Ga1−O1′−Ga1′ 96.87(5), O1−Ga1′−O1′ 82.10(4), O1−Ga1−O1′ 82.06(4), C18′−Ga1′−C19′ 127.04(7), C18−Ga1−C19 125.17(7); O1−Ga1−O1′−Ga1′ 11.24(4)

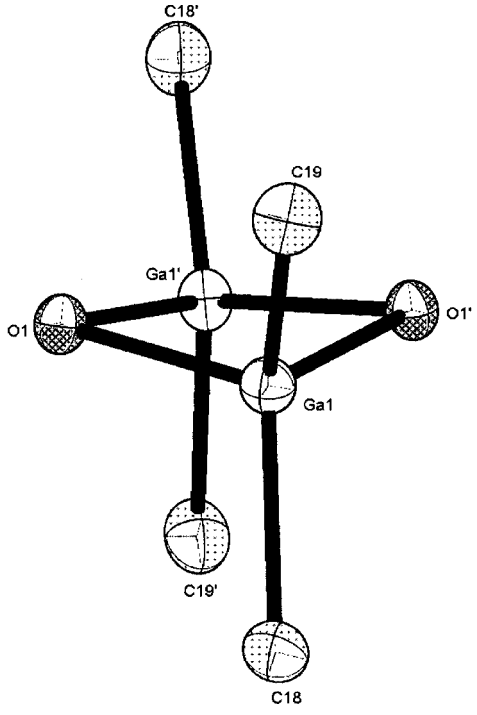

Figure 5. Butterfly geometry of the four-membered ring of **3d**

substituted group 13 dialkyl compounds, formed by the two oxygen atoms (O3/O3A in **3a**, O1/O1′ in **3d**) and the Lewis acidic gallium atoms (Ga1/Ga1A in **3a**, Ga1/Ga1′ in **3d**). In the case of **3a**, the four-membered ring, with a *trans* arrangement of the iron fragments, is planar (O3−Ga1A−O3A−Ga1 = 0°), while **3d**, with a *cis* position of the iron fragments, shows a butterfly geometry [O1−Ga1′−O1′−Ga1 = 11.24(4)°, Figure 5].

The group 13 element−oxygen bond lengths in **3a** [Ga1−O3 = 1.957(3) Å/Ga1−O3A = 1.977(3) Å] and **3d** [Ga1−O1 = 1.9815(11) Å/Ga1′−O1′ = 1.9792(19) Å] correspond to the bond lengths found for dimeric (alkoxy)-dialkylgallanes: {[(*t*Bu)$_2$Ga-μ-O(*t*Bu)]$_2$: 1.990 Å}[22] and lie in the range between a coordinative interaction and a sigma bond.[23] A distorted tetrahedral geometry at the group 13 element is indicated by the angles formed by the ligands of

 © 2003 Wiley-VCH Verlag GmbH & Co. KGaA, Weinheim

Ga1, with the smallest, endocyclic angle defined by the oxygen atoms [83.39(13)° (**3a**), 82.10(4)°/82.06(4)° (**3d**)] and the largest one formed by the two exocyclic methyl ligands [130.7(2)° (**3a**), 127.04.(7)°/125.17(7)° (**3d**)]. A nearly planar distorted trigonal coordination at the bridging oxygens is confirmed by the sum of angles, of 357°/358°, with individual angles between the ligands varying from 96.61(13)°/96.78(5)° to 134.63(18)°/132.47(6)° for **3a** and **3d**, respectively. The substituents at the silicon atoms in **3a** and **3d** show the expected tetrahedral arrangements, with small angles between the organic substituents and the oxygen [106.4(2)−106.8(2)° (**3a**); 103.37(6)°−108.72(7)° (**3d**)] and large angles including the metal fragment [110.05(16)°−113.56(12)° (**3a**); 109.96(5)°−115.63(6)° (**3d**)]. The iron-silicon distances of 2.3229(16) Å (**3a**) and 2.3091(5)/2.3086(5) Å (**3d**) and the silicon-oxygen distances of 1.667(3) (**3a**) and 1.6674(11)/1.6703(11) Å (**3d**) show no peculiarity compared to the Fe−Si distance in related complexes {$[Cp(OC)_2Fe\text{-}Si(F)(Me)O]_2$: 2.265(1) Å;[12] $Cp(OC)_2Fe\text{-}SiH_2\text{-}SiH_3$: 2.2980(9) Å,[24] $\{Cp(OC)_2Fe\text{-}Si(OMe)(Me)[2\text{-}(Me_2HNCH_2)C_6H_4]\}PF_6$: 2.305(2) Å[25]} or the Si−O distance in silanols and siloxanes {$(t$Bu$)(Me)_2SiOH$: 1.663 Å;[26] $[Cp(OC)_2Fe\text{-}Si(F)(Me)O]_2$: 1.603(1) Å[12]}.

DFT Calculations

Quantum chemical calculations[27] at a density functional level (B3LYP[28,29] with the 6−31 g(d) basis set[30−32]) were performed on parent **3**, omitting the alkyl groups at the gallium center. A *cis* (C_2 symmetry) and a *trans* (C_i symmetry) equilibrium structure are predicted. (Figure 6). Both structures relate to energy minima on the corresponding electronic hypersurface, as substantiated by corresponding vibrational analysis.

The two conformations are similar in energy, (ΔE = 3.0 kcal/mol, with ZPE correction), with the *trans* geometry being slightly more stable. The trigonal planar-coordinated oxygen atoms and the almost rectangular, planar arrangement of the four-membered gallium−oxygen ring are consistent with the experimentally obtained results. A fairly weak puckering effect is observed for the *cis* conformation ($< O-Ga-O'-Ga' = 2.4°$). Because of this small puckering, no further analysis of its energy potential was attempted. The resulting iron-silicon distances are somewhat shorter (2.28 Å) and the silicon−oxygen distances longer (1.69 Å) than those found experimentally.

The bonding situation in the heterosiloxanes is best described in terms of donor-acceptor bonds (see Figure 1). This view is also lent support by an analysis of the electron density distributions with the electron localization function (ELF). The electron density is shifted predominantly to the electronegative oxygen atoms, and no through-space interactions between the Ga atoms or the oxygen atoms could be found. A further analysis was also performed for substrates methyl-substituted at the gallium atoms. Again, the energy difference between *cis* and *trans* conformations is fairly small (ΔE = 0.4 kcal/mol, without ZPE correction).

Conclusion

This paper shows that the metallo-silanols $Cp(OC)_2Fe-SiR_2OH$ (R = Me, *i*Pr, Ph), although characterized by lower acidity than triorganosilanols, react with trialkylgallanes to yield the first transition metal fragment-substituted heterosiloxanes. The observed dimeric structures correspond with findings obtained for triorganosiloxy derivatives, which means that no sufficient influence on the

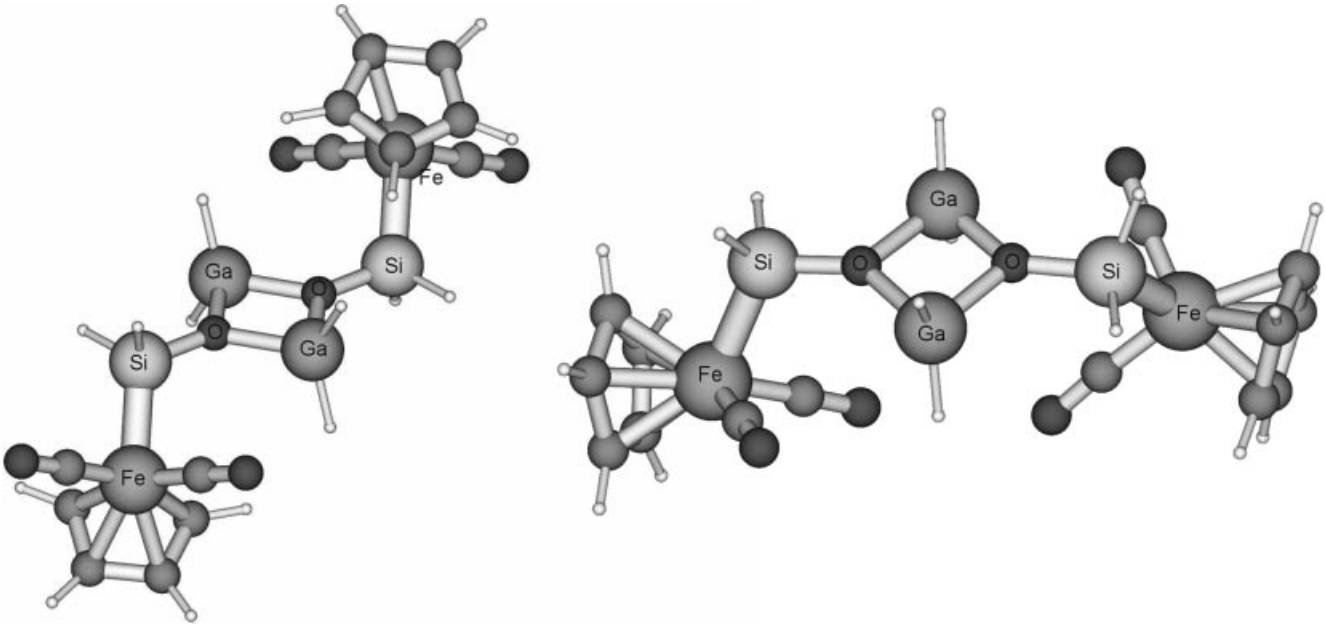

Figure 6. Plots of the equilibrium geometries of heterosiloxanes in *cis* and *trans* conformations, obtained at B3LYP/6−31 g(d) quantum chemical level of sophistication

 © 2003 Wiley-VCH Verlag GmbH & Co. KGaA, Weinheim

structure and aggregation is exerted by the presence of an $Cp(OC)_2Fe$ fragment. Because of this result, forthcoming papers will deal with siloxygallanes containing metal fragments with higher steric demand and increased electron density, such as $C_5Me_5(Me_3P)_2Fe$.

Experimental Section

General: All manipulations were performed under purified and dried nitrogen by standard Schlenk-type techniques. Solvents were rigorously dried with an appropriate drying agent, distilled, and saturated with nitrogen prior to use. IR: Perkin−Elmer 283 grating spectrometer. NMR: Jeol Lambda 300 (300.4 MHz, 75.6 MHz and 59.6 MHz, for ^1H, ^{13}C and ^{29}Si, respectively). ^1H and ^{13}C spectra are referenced to the residual proton signal or natural abundance carbon signal of [D$_6$]benzene at δ = 7.15 ppm (^1H) or δ = 128.0 ppm (^{13}C), respectively. ^{29}Si chemical shifts are referenced to external TMS. Molecular mass determinations by freezing point depression were performed in benzene solution with a Knauer 24.00 cryoscopic unit. Melting points: Du Pont-9000 thermal analysis system. Elemental analyses were performed in the laboratories of our institute. Starting materials were prepared by literature procedures: $Cp(OC)_2Fe$-$SiMe_2OH$ (**1a**),[13] $Cp(OC)_2Fe-Si(iPr)_2OH$ (**1b**),[21] $Cp(OC)_2Fe-SiPh_2OH$ (**1c**),[13] $Cp(OC)_2Fe-Si(Me)(Ph)OH$ (**1d**),[35] $GaMe_3{\cdot}OEt_2$ (**2a**)[33] and $Ga(iPr)_3$ (**2b**).[34]

1. Bis{{[dicarbonyl(η^5-cyclopentadienyl)ferrio]dimethylsiloxy}dimethylgallane} (3a): A solution of $Cp(OC)_2Fe-SiMe_2OH$ (**1a**, 235 mg, 0.93 mmol) in *n*-pentane (20 mL) was added dropwise at 0 °C to a stirred solution of $GaMe_3{\cdot}OEt_2$ (**2a**, 394 mg, 1.12 mmol) in *n*-pentane (10 mL). The reaction mixture was warmed to 25 °C over 15 min and stirred for an additional 2 h, resulting in the precipitation of **3a**. Compound **3a** was separated by filtration, washed with two portions of cold (0 °C) *n*-pentane (3 mL) and dried in vacuo. Yield 261 mg (80%), light yellow, microcrystalline powder, m.p. 101 °C (dec.). ^1H NMR ([D$_6$]benzene): δ = 4.19 (s, 5 H, C_5H_5), 0.69 [s, 6 H, $(H_3C)Si$], 0.19 ppm [s, 6 H, $(H_3C)Ga$]. $^{13}C\{^1H\}$ NMR ([D$_6$]benzene): δ = 215.7 (s, CO), 83.9 (s, C_5H_5), 12.5 [s, $(CH_3)Si$], −1.6 ppm [s, $(CH_3)Ga$]. $^{29}Si\{^1H\}$ NMR ([D$_6$]benzene): δ = 66.57 ppm (s). IR (*n*-pentane/toluene): $\tilde{\nu}$ = 1994 (w)/1989 (vs), 1943 (vs)/1930 (s) cm^{-1} (CO). $C_{22}H_{34}Fe_2Ga_2O_6Si_2$ (701.82, found 729.89): calcd. C 37.65, H 4.88; found C 37.78, H 4.56.

2. Bis{{[dicarbonyl(η^5-cyclopentadienyl)ferrio]dimethylsiloxy}di(1-methylethyl)gallane} (3b): This compound was prepared as described for **3a**, from $Cp(OC)_2Fe-SiMe_2OH$ (**1a**, 185 mg, 0.73 mmol), dissolved in *n*-pentane (10 mL), and $Ga(iPr)_3$ (**2b**, 219 mg, 1.10 mmol), dissolved in *n*-pentane (5 mL), at −78 °C and with stirring for 16 h after warming up to room temperature, resulting in partial precipitation of **3b**. Additional **3b** was crystallized at −78 °C. Compound **3b** was separated, washed with two portions of cold (−78 °C) *n*-pentane (3 mL), and dried in vacuo. Yield 248 mg (83%), light yellow, microcrystalline powder, m.p. 79 °C (dec.). ^1H NMR ([D$_6$]benzene): δ = 4.25 (s, 5 H, C_5H_5), 1.58 [d, $^3J_{HCCH}$ = 7.6 Hz, 12 H, $(H_3C)_2CH$], 1.20 [sept, $^3J_{HCCH}$ = 7.6 Hz, 2 H, $HC(CH_3)_2$], 0.84 ppm [s, 6 H, $(H_3C)Si$]. $^{13}C\{^1H\}$ NMR ([D$_6$]benzene): δ = 216.2 (s, CO), 84.0 (s, C_5H_5), 22.3 [s, $(CH_3)_2CH$], 21.2 [s, $CH(CH_3)_2$], 14.4 ppm [s, $(CH_3)Si$]. $^{29}Si\{^1H\}$ NMR ([D$_6$]benzene): δ = 64.10 ppm (s). IR (*n*-pentane/toluene): $\tilde{\nu}$ = 1998 (w)/1990 (vs), 1946 (vs)/1931 (s) cm^{-1} (CO). $C_{30}H_{50}Fe_2Ga_2O_6Si_2$ (814.02, found 858.79): calcd. C 44.26, H 6.19; found C 44.17, H 5.95.

3. Bis{{[dicarbonyl(η^5-cyclopentadienyl)ferrio]di(1-methylethyl)siloxy}-dimethylgallane} (3c): This compound was prepared as described for **3a**, from $Cp(OC)_2Fe-Si(iPr)_2OH$ (**1b**, 163 mg, 0.53 mmol), dissolved in *n*-pentane (10 mL), and $Me_3Ga{\cdot}Et_2O$ (**2b**, 104 mg, 0.55 mmol), dissolved in *n*-pentane (5 mL), at −78 °C, with stirring for 2 h after warming up to room temperature, resulting in partial precipitation of **3c**. Additional **3c** was crystallized at −78 °C. Compound **3c** was separated, washed with two portions of cold (−78 °C) *n*-pentane (3 mL), and dried in vacuo. Yield 186 mg (86%), light beige, microcrystalline powder, m.p. 94 °C (dec.). ^1H NMR ([D$_6$]benzene, 300.4 MHz): δ = 4.36 (s, 5 H, C_5H_5), 1.68 [sept, $^3J_{(HCCH)}$ = 7.1 Hz, 2 H, $HC(CH_3)_2$], 1.24 [d, $^3J_{(HCCH)}$ = 7.1 Hz, 6 H, $(H_3C)_2CH$], 1.24 [d, $^3J_{(HCCH)}$ = 7.1 Hz, 6 H, $(H_3C)_2CH$], 0.37 ppm (s, 6 H, H_3CGa). $^{13}C\{^1H\}$ NMR ([D$_6$]benzene, 75.45 MHz): δ = 216.7 (s, CO), 83.1 (s, C_5H_5), 24.8 [s, $CH(CH_3)_2$], 20.5 [s, $(CH_3)_2CH$], 19.6 [s, $(CH_3)_2CH$], 0.6 ppm (s, CH_3Ga). $^{29}Si\{^1H\}$ NMR ([D$_6$]benzene, 59.58 MHz): δ = 78.92 ppm (s). IR (Et_2O): $\tilde{\nu}$ = 1994 (vs), 1938 (vs) cm^{-1} (CO). $C_{30}H_{50}Fe_2Ga_2O_6Si_2$ (814.02, found 842.51): calcd. C 44.26, H 6.19; found C 43.98, H 6.01.

4. Bis{{[dicarbonyl(η^5-cyclopentadienyl)ferrio]diphenylsiloxy}-dimethylgallane} (3d): This compound was prepared as described for **3a**, from $Cp(OC)_2Fe-SiPh_2OH$ (**1c**, 180 mg, 0.48 mmol), dissolved in *n*-pentane (10 mL), and $Me_3Ga{\cdot}Et_2O$ (**2b**, 94 mg, 0.50 mmol), dissolved in *n*-pentane (5 mL), at −78 °C and with stirring for 2 h after warming up to room temperature, resulting in partial precipitation of **3d**. Additional **3d** was crystallized at −78 °C. Compound **3d** was separated, washed with two portions of cold (−78 °C) *n*-pentane (3 mL), and dried in vacuo. Yield 166 mg (73%), light beige, microcrystalline powder, m.p. 144 °C (dec.). ^1H NMR ([D$_6$]benzene, 300.4 MHz): δ = 7.80 [d, $^3J_{HCCH}$ = 6.8 Hz, 4 H, *o*-H], 7.30−7.18 (m, 6 H, *m*/*p*-H), 3.95 (s, 5 H, H_5C_5), −0.05 ppm (s, 6 H, H_3CGa). $^{13}C\{^1H\}$ NMR ([D$_6$]benzene, 75.45 MHz): δ = 215.8 (s, CO), 145.1 (s, *i*-C, C_6H_5Si), 134.9 (s, *o*-C, C_6H_5Si), 129.1 (s, *p*-C, C_6H_5Si), 127.8 (s, *m*-C, C_6H_5Si), 84.8 (s, C_5H_5), −1.4 ppm (s, CH_3Ga). $^{29}Si\{^1H\}$ NMR ([D$_6$]benzene, 59.58 MHz): δ = 54.86 ppm (s). IR (Et_2O): $\tilde{\nu}$ = 1999 (vs), 1945 (vs) cm^{-1} (CO). $C_{21}H_{21}FeGaO_3Si$ (475.05): calcd. C 53.10, H 4.46; found C 52.72, H 4.29.

5. (*RR*)-(*RS*)-Bis{{[dicarbonyl(η^5-cyclopentadienyl)ferrio](methyl)(phenyl)siloxy}-dimethylgallane} (3e): This compound was prepared as described for **3a**, from $Cp(OC)_2FeSi(Me)(Ph)OH$ (**1d**, 132 mg, 0.42 mmol), dissolved in *n*-pentane (25 mL), and $Me_3Ga{\cdot}Et_2O$ (**2b**, 85 mg, 0.45 mmol), dissolved in *n*-pentane (5 mL), at −78 °C and with stirring for 2 h after warming up to room temperature, resulting in partial precipitation of **3e**. Additional **3e** was crystallized at −78 °C. Compound **3e** was separated, washed with two portions of cold (−78 °C) *n*-pentane (3 mL) and dried in vacuo. Yield 142 mg (82%), light beige, microcrystalline powder, m.p. 92 °C (dec.). ^1H NMR ([D$_6$]benzene, 300.4 MHz): δ = 7.74−7.70 (m, 4 H, *o*-H), 7.23−7.11 (m, 6 H, *m*/*p*-H), 3.89/3.88 (s, 10 H, H_5C_5), 0.98/0.97 (s, 6 H, H_3CSi), 0.36 (s, 3 H, H_3CGa, *ul*), 0.18 (s, 6 H, H_3CIn, *lk*), 0.01 ppm (s, 3 H, H_3CIn, *ul*). $^{13}C\{^1H\}$ NMR ([D$_6$]benzene, 75.45 MHz): δ = 216.1/215.6 (s, CO), 146.8/146.6 (s, *i*-C, C_6H_5Si), 133.3/133.2 (s, *o*-C, C_6H_5Si), 128.9 (s, *p*-C, C_6H_5Si), 127.8/127.8 (s, *m*-C, C_6H_5Si), 84.3 (br. s, C_5H_5), 10.8/10.8 (s, CH_3Si), −0.7 (s, CH_3Ga, *ul*), −1.1 (s, CH_3Ga, *lk*), −1.5 ppm (CH_3Ga, *ul*). $^{29}Si\{^1H\}$ NMR ([D$_6$]benzene, 59.58 MHz): δ = 59.32/59.22 ppm (s). IR (Et_2O): $\tilde{\nu}$ = 1992 (vs), 1934 (vs) cm^{-1}. $C_{16}H_{19}FeGaO_3Si$ (412.98): calcd. C 46.53, H 4.64; found C 46.37, H 4.78.

6. X-ray Analyses of $[Cp(OC)_2Fe-SiMe_2O-GaMe_2]_2$ (3a) and $[Cp(OC)_2Fe-SiPh_2O-GaMe_2]_2$ (3d): Suitable crystals were obtained

 © 2003 Wiley-VCH Verlag GmbH & Co. KGaA, Weinheim

by slow evaporation of saturated solutions of **3a/3d** in *n*-pentane at room temperature. Data collection was performed on an Enraf−Nonius CAD4-diffractometer with use of graphite-monochromated Mo-K_α radiation (λ = 0.71073 Å) at 173(2) K. The positions of the hydrogen atoms were calculated by an idealized geometry.

Compound 3a: $C_{22}H_{34}Fe_2Ga_2O_6Si_2$, M = 701.82; triclinic; space group: $P\bar{1}$ (No. 2); a = 8.147(2) Å, b = 9.035(2) Å, c = 11.1026(19) Å; α = 80.259(19)°, β = 78.398(18)°, γ = 64.15(2)°; V = 717.3(3) Å^3; Z = 2; $D_{calcd.}$ = 1.625 g·cm^{-3}; crystal size: 0.55 × 0.50 × 0.50 mm^3; μ(Mo-K_α) = 2.965 mm^{-1}, semiempirical absorption correction ($T_{min.}/T_{max.}$: 0.9294/0.9993); scale range: 1.88° < θ < 22.92°; F(000): 356; total reflections: 2144; independent reflections: 1977; structure solution: SHELXS-96;[36] 1977 reflections used in structure refinement (158 parameters) with SHELXL-96;[37] GoF = 1.091, residual electron density: 0.414/−0.437 e·Å^{-3}, R_1 = 0.0319, wR_2 = 0.0810.

Compound 3d: $C_{42}H_{42}Fe_2Ga_2O_6Si_2$, M = 950.08; monoclinic; space group $P2_1/c$ (No. 14), a = 16.95554(3) Å, b = 13.5810(2) Å, c = 17.4890(3) Å, α = 90°, β = 91.691(1)°, γ = 90°, V = 4025.46(12) Å^3, Z = 4, $D_{calcd.}$ = 1.568 g·cm^{-3}; crystal size: 0.30 × 0.25 × 0.2 mm^3; μ(Mo-K_α) = 2.137 mm^{-1}; semi-empirical absorption correction ($T_{min.}/T_{max.}$: 0.7188/0.6165); scale range: 2.59° < θ < 28.30°; F(000): 1936, total reflections: 66887; independent reflections: 9935; structure solution: SHELXS-96;[36] 2059 reflections used in structure refinement (158 parameters) with SHELXL-96;[37] GoF = 1.056, residual electron density: 0.460/−0.480 e·Å^{-3}, R_1 = 0.0337, wR_2 = 0.0658.

CCDC-155725 (**3a**) and CCDC-184033 (**3d**) contain the supplementary crystallographic data for this paper. These data can be obtained free of charge at www.ccdc.cam.ac.uk/conts/retrieving.html [or from the Cambridge Crystallographic Data Centre, 12, Union Road, Cambridge CB2 1EZ, UK; Fax: (internat.) +44-1223/336-033; E-mail: deposit@ccdc.cam.ac.uk].

Acknowledgments

We gratefully acknowledge financial support from the Deutsche Forschungsgemeinschaft (Schwerpunktprogramm "Spezifische Phänomene in der Siliciumchemie") as well as from the Fonds der Chemischen Industrie. M. N. wishes to thank the DAAD for financial support.

[1] M. Vögler, M. Hofmann, I. Pavel, D. Moigno, M. Nieger, W. Kiefer, W. Malisch, *Inorg. Chem.*, in press.
[2] W. Malisch, H. Jehle, D. Schumacher, M. Binnewies, N. Söger, *J. Organomet. Chem.,* **2003**, *667*, 35−41.
[3] R. Murugavel, A. Voigt, M. G. Walawalkar, H. W. Roesky, *Chem. Rev.* **1996**, *96*, 2205−2236 and references therein.
[4] R. Murugavel, V. Chandrasekhar, H. W. Roesky, *Acc. Chem. Res.* **1996**, *29*, 183−189, and references therein.
[5] A. Voigt, R. Murugavel, E. Parisini, H. W. Roesky, *Angew. Chem. Int. Ed. Engl.* **1996**, *35*, 748−750.
[6] W. Hölderich, M. Hesse, F. Näumann, *Angew. Chem.* **1988**, *100*, 232−511; *Angew. Chem. Int. Ed. Engl.* **1988**, *27*, 226−245 .
[7] L. S. Marchenko, D. Z. Levin, V. A. Plakhotnik, E. S. Mortikov, *Izv. Akad. Nauk. SSSR Ser. Khim.* **1986**, 94−98.
[8] T. Inui, Y. Makino, F. Okazumi, A. Miyamoto, *J. Chem. Soc., Chem. Commun.* **1986**, 571−573.
[9] F. Schindler, H. Schmidbaur, *Angew. Chem.* **1965**, *77*, 206−216.
[10] H. Schmidbaur, F. Schindler, *Chem. Ber.* **1966**, *99*, 2178−2186.
[11] F. Schindler, H. Schmidbaur, *Angew. Chem.* **1967**, *79*, 697; *Angew. Chem. Int. Ed. Engl.* **1967**, *6*, 683−694.
[12] W. Ries, T. Albright, J. Silvestre, I. Bernal, W. Malisch, C. Burschka, *Inorg. Chim. Acta* **1986**, *111*, 119−128.
[13] W. Adam, U. Azzena, F. Prechtl, K. Hindahl, W. Malisch, *Chem. Ber.* **1992**, *125*, 1409−1411.
[14] W. Malisch, S. Schmitzer, G. Kaupp, K. Hindahl, H. Käb, U. Wachtler, in *Organosilicon Chemistry: From Molecules to Materials* (Eds.: N. Auner, J. Weis), Wiley-VCH, Weinheim, **1994**, 185−192.
[15] W. Malisch, K. Grün, N. Gunzelmann, S. Möller, R. Lankat, J. Reising, M. Neumayer, O. Fey, in *Selective Reactions of Metal-Activated Molecules* (Eds.: H. Werner, J. Sundermeyer), Vieweg, Braunschweig, **1995**, 183−190.
[16] W. Malisch, S. Möller, R. Lankat, J. Reising, S. Schmitzer, O. Fey, in *Organosilicon Chemistry II: From Molecules to Materials* (Eds.: N. Auner, J. Weis), Wiley-VCH, Weinheim, **1996**, 575−584.
[17] W. Malisch, S. Schmitzer, R. Lankat, M. Neumayer, F. Prechtl, W. Adam, *Chem. Ber.* **1995**, *128*, 1251−1255.
[18] W. Malisch, R. Lankat, O. Fey, J. Reising, S. Schmitzer, *J. Chem. Soc., Chem. Commun.* **1995**, 1917−1919.
[19] W. Malisch, M. Hofmann, G. Kaupp, H. Käb, J. Reising, *Eur. J. Inorg. Chem.,* in press.
[20] W. Malisch, M. Vögler, D. Schumacher, M. Nieger, *Organometallics* **2002**, *21*, 2891−2897.
[21] $Cp(OC)_2Fe-Si(iPr)_2OH$ was prepared analogously to **1a**, according to the literature.[13]
[22] M. B. Power, W. M. Cleaver, A. W. Apblett, A. R. Barron, J. W. Ziller, *Polyhedron* **1992**, *11*, 477−486.
[23] A. Haaland, *Angew. Chem.* **1989**, *101*, 1017−1032.
[24] W. Malisch, H. Jehle, S. Möller, G. Thum, J. Reising, A. Gburek, V. Nagel, C. Fickert, W. Kiefer, M. Nieger, *Eur. J. Inorg. Chem.* **1999**, *9*, 1597−1605.
[25] H. Kobayashi, K. Ueno, H. Ogino, *Organometallics* **1995**, *14*, 5490−5492.
[26] P. D. Lickiss, N. L. Clipston, D. W. H. Rankin, H. E. Robertson, *J. Mol. Struct.* **1995**, *344*, 111−116.
[27] Gaussian 98 (Revision A.1), M. J. Frisch, G. W. Trucks, H. B. Schlegel, G. E. Scuseria, M. A. Robb, J. R. Cheeseman, V. G. Zakrezewski, J. A. Montgomery, R. E. Stratmann, J. C. Burant, S. Dapprich, J. M. Millam, A. D. Daniels, K. N. Kudin, M. C. Strain, O. Farkas, J. Tomasi, V. Barone, M. Cossi, R. Cammi, B. Mennucci, C. Pomelli, C. Adamo, S. Clifford, J. Ochterski, G. A. Petersson, P. Y. Ayali, Q. Cui, K. Morokuma, D. K. Malick, A. D. Rabuck, K. Raghavachari, J. B. Foresman, J. Cioslowski, J. V. Ortiz, B. B. Stefanov, G. Liu, A. Liashenko, P. Piskorz, I. Komaromi, R. R. Gomperts, R. L. Martin, D. J. Fox, T. Keith, M. A. Al-Laham, C. Y. Peng, A. Nanyakkara, C. Gonzalez, M. Challacombe, P. M. W. Gill, B. G. Johnson, W. Chen, M. W. Wong, J. L. Andres, M. Head-Gordon, E. S. Replogle, J. A. Pople, Gaussian, Inc., Pittsburgh PA, **1998**.
[28] A. D. Becke, *J. Chem. Phys.* **1993**, *98*, 5648−5652.
[29] C. Lee, W. Yang, R. G. Parr, *Phys. Rev.* **1988**, *B37*, 785−789.
[30] W. J. Stevens, H. Basch, M. Krauss, *J. Chem. Phys.* **1984**, *81*, 6026−6033.
[31] W. J. Stevens, M. Krauss, H. Basch, P. G. Jasien, *Can. J. Chem.* **1992**, *70*, 612−630.
[32] T. R. Cundari, W. J. Stevens, *J. Chem. Phys.* **1993**, *98*, 5555−5565.
[33] G. Renwanz, *Ber. Dtsch. Chem. Ges.* **1932**, *65*, 1308−1309.
[34] J. P. Oliver, L. G. Stevens, *J. Inorg. Nucl. Chem.* **1962**, *24*, 953−960.
[35] $Cp(OC)_2Fe-Si(Me)(Ph)OH$ was prepared analogously to **1a**, according to the literature.[13]
[36] G. M. Sheldrick, SHELXS-96, *Program for Structure Solution*, Göttingen, **1996**.
[37] G. M. Sheldrick, SHELXL-96, *Program for Structure Refinement*, Göttingen, **1996**.

Received October 29, 2002

 © 2003 Wiley-VCH Verlag GmbH & Co. KGaA, Weinheim

Surface Organometallic Chemistry on Oxides: The First Well-Defined Selenium(IV) Derivative Grafted onto Silica

Hélène Provendier,[a] Catherine C. Santini,*[a] Jean-Marie Basset,[a] and Laurent Carmona[a]

Keywords: Acetaldehyde / Oxidation / Selenium / Supported catalysis / Surface chemistry

Treatment of $(EtO)_2SeO$ with Aerosil silica dehydroxylated at 500 °C results in the formation of a unique surface derivative [≡SiO–Se(O)OEt] (**1**), which has been fully characterized by elemental analysis, IR, labelling reaction and solid-state NMR spectroscopy. This is the first example of a silica-supported selenium(IV) derivative.
(© Wiley-VCH Verlag GmbH & Co. KGaA, 69451 Weinheim, Germany, 2003)

Introduction

Glyoxal and glyoxylic acid are important pharmaceutical intermediates (1.2×10^5 t·y^{-1}).[1−2] They are generally manufactured from ethylene glycol or from acetaldehyde, by use of different oxidizing agents such as air or nitric acid, respectively.[3] In both processes there is a high amount of residue, which causes waste disposal problems. Moreover, the separation of the products becomes expensive. A possible solution is the use of a highly selective oxidizing agent. For at least 80 years, selenium dioxide and seleneous and selenic acids have been known to oxidize acetaldehyde to glyoxal and glyoxylic acid.[4−6] However, they had to be used as stoichiometric oxidants, and precipitated as metallic selenium. Nevertheless, several studies confirm that all selenium derivatives can easily be reoxidized by any oxidant, such as tBuO$_2$H,[7] H_2O_2 [8] and O_2,[9] thus allowing selenium derivatives to be used in catalytic amounts, so their use as oxidizing agents attracted more interest. Moreover, one way to facilitate the separation of the reaction products and the oxidant, and also to reduce the risks due to the toxicity of selenium, is to link the oxidizing agent to a support.[10] Nicolaou's group has recently synthesized several natural products by means of a novel cycloaddition technique in which a prenylated phenol group is immobilized on a polystyrene-based selenyl bromide derivatized resin.[11] Another approach would be to graft selenium derivatives onto inorganic supports, such as silica.

In this work we report the synthesis, characterization and reactivity of the first silica-supported selenium oxide [≡SiOSe(O)OEt] (**1**). In order to determine the coordination sphere of Se in **1**, a systematic study on the oxidation of acetaldehyde with SeO_2, H_2SeO_3 and $PhSeO_2H$ was performed first.

[a] Laboratoire de Chimie Organométallique de Surface, UMR 9986 CNRS-CPE Lyon,
43 Bd du 11 Novembre 1918, 69616 Villeurbanne Cedex, France
E-mail: santini@cpe.fr
[b] Clariant,
B. P. 1, 60350 Brosly Breuil, France

Results and Discussion

The aim of this study was to develop a supported oxidant capable of replacing nitric acid for performing the oxidation reaction of acetaldehyde to glyoxal. It is known that several selenium derivatives can perform this oxidation. It was also important to determine which one of them could provide the best selectivity for glyoxal under stoichiometric reaction conditions. So several selenium derivatives were tested under homogeneous conditions in order to determine the influence of the coordination sphere around the selenium atom on this oxidation reaction and to reproduce a similar coordination sphere around Se grafted onto silica.

Molecular Homogeneous Oxidation of Acetaldehyde

We first reproduced Corey's results: the oxidation of acetaldehyde to glyoxal and glyoxylic acid in the presence of SeO_2, at 90 °C for 12 h, in acetic acid.[5]

The observed level of consumption of acetaldehyde reached 90%. As the yields of glyoxal (33%), glyoxylic acid (13%) and formic and oxalic acids (< 1%) did not account for the material balance, acetic acid had presumably also been formed. To confirm this hypothesis, the reaction was performed under the same experimental conditions, but now with propionic acid as solvent. In this case, the degree of conversion of acetaldehyde was the same (90%) and the yields of glyoxal (48−50%), glyoxylic acid (10−20%), formic acid (0−3%) and acetic acid (20%) gave the correct ma-

terial balance. Whatever the solvent, metallic selenium is formed and precipitates (Figure 1).

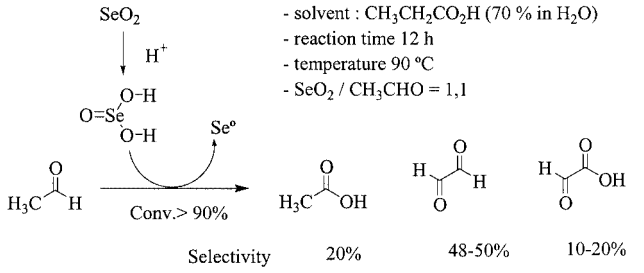

Figure 1. Distribution of oxidation products of acetaldehyde with SeO_2 in propionic acid

The degree of conversion of acetaldehyde and the selectivities for the products described are dependent on the reaction temperature, as depicted in Figure 2 (top). There is still formation of acetic acid, but whereas its selectivity decreases with temperature, its yield remains roughly constant (about 20%; Figure 2, bottom). From 25 up to 90 °C the total selectivity for glyoxal and glyoxylic acid together varies from 44 to 70%. However, the ratio of the selectivity for glyoxal to the selectivity for glyoxylic acid varies from 0.5 to 2.5, due to the fact that the yield of glyoxal increases from 8 to 45% whereas the yield of glyoxylic acid remains constant (Figure 2, bottom). As the level of conversion of acetaldehyde increases with temperature, this indicates that the limiting factor is the activation energy of the oxidation of acetaldehyde to glyoxal, and not the nature of the oxidant.

The oxidation of acetaldehyde was also performed with benzeneseleninic acid [PhSe(O)(OH)] and benzeneseleninic peracid [PhSe(O)(OOH)], generated in situ by addition of H_2O_2, both of which are known to be highly reactive oxidants.[8,12] Whatever the experimental conditions, mostly acetic acid is formed, in up to 50% yield, while less than 20% of glyoxal is obtained. No metallic selenium was observed and the reduced product PhSe−SePh was identified by ^{77}Se NMR [$\delta_{Se}(C_6D_6)$ = 460 ppm].[13]

The nature of the coordination sphere around the selenium atom seems to play a crucial role in the oxidation reaction studied. When the selenium atom is bonded to three oxygen atoms, there is increased formation of glyoxal than when it is bonded to two oxygen atoms and one carbon atom.

Surface Organometallic Chemistry

Reactions between organometallic complexes (MX_n: X = R, OR, NR_2, Cl, ...; M = transition metal or main group element) and a silica surface in most cases give organometallic fragments σ-bonded to the surface through one, two or three oxygen−metal bonds.[14−16] This kind of bonding can stabilize well-defined and highly electrophilic fragments capable of performing several kinds of catalytic reactions,[16] and in particular oxidation reactions.[17−25]

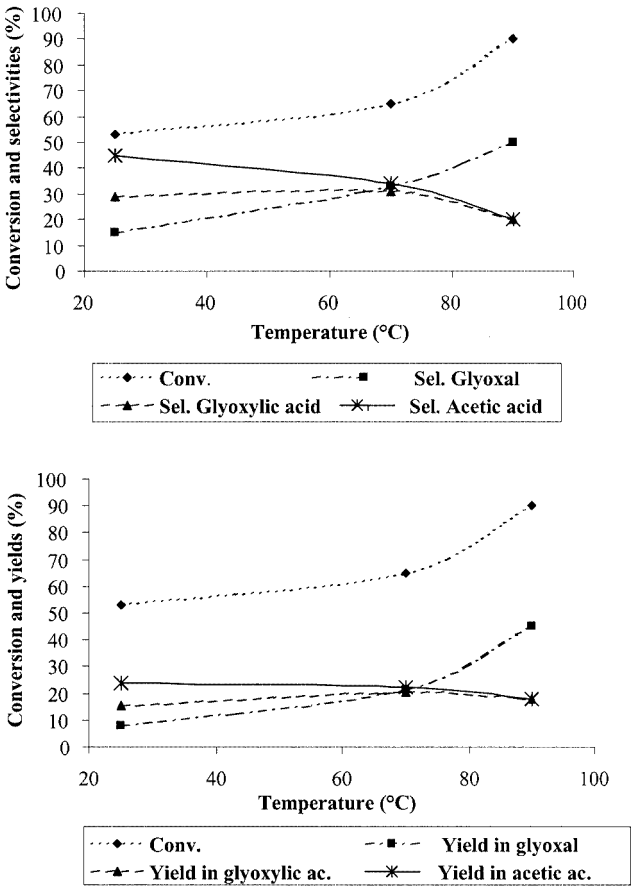

Figure 2. Variation of the conversion and selectivities (top) and conversion and yields (bottom) versus temperature in the oxidation reaction of acetaldehyde with SeO_2; reaction time 12 h

One possible route to the surface species M_1 or M_2 (Figure 3), presenting the required coordination sphere around the selenium atom for the oxidation of acetaldehyde to glyoxal, might be through reaction between Cl_2SeO or $(EtO)_2SeO$ and silica.

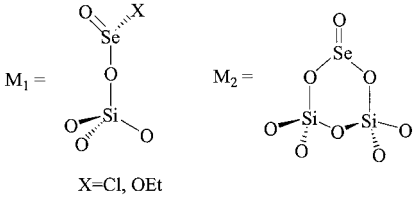

Figure 3. Target selenium species grafted on silica

Silica Surface

The support used is a Degussa flame Aerosil® silica, dehydroxylated at increasing temperatures (T [°C]), that we shall call $SiO_{2\text{-}(T)}$. The specific surface areas were 200 $m^2 \cdot g^{-1}$ for $SiO_{2\text{-}(500)}$. The silanol group content, determined by quantitative solid-state ^1H NMR and by treatment with CH_3Li, is 1.2 $OH \cdot nm^{-2}$ for $SiO_{2\text{-}(500)}$.[26−29]

 © 2003 Wiley-VCH Verlag GmbH & Co. KGaA, Weinheim

Surface Chemistry of Selenium on Silica

a) Reaction between Selenium Oxychloride $Cl_2Se{=}O$ and $SiO_{2\text{-}(500)}$

The reaction between $Cl_2Se{=}O$[30−31] and $SiO_{2\text{-}(500)}$ at room temperature was monitored by Fourier-Transform infrared (FTIR) spectroscopy and by quantitative analysis of the products. During the reaction the colour of the silica changed from white to yellow/orange. At first, the infrared spectra showed the nearly complete disappearance of the free silanol groups (≡Si−OH) as judged by the decrease in the intensity of the band at 3747 cm^{-1}. At the same time, a broad band attributable to hydrogen-bonded silanol appeared at 3300 cm^{-1}. After the pellet had been kept under dynamic vacuum at 25° for 36 h, however, the intensity of the band at 3747 cm^{-1} had mostly returned, and elemental analysis indicated selenium loading lower than 1% and a chlorine/selenium molar ratio of up to 10. These results indicated that the selenium oxychloride reacts, like thionyl chloride, with an ≡Si−OH group to form an ≡Si−Cl function, with no grafting reaction being observed.[32]

b) Reaction between Diethyl Selenite $(EtO)_2SeO$ and $SiO_{2\text{-}(500)}$

The reaction between $(EtO)_2SeO$ and $SiO_{2\text{-}(500)}$ was also monitored at room temperature by Fourier-Transform infrared (FTIR) spectroscopy and by quantitative analysis of the products. During the reaction the colour of the silica changed from white to deep yellow. After the addition of $(EtO)_2SeO$ (300 Torr) to $SiO_{2\text{-}(500)}$, the pellet was again kept under dynamic vacuum at 25° for 12 h in order to eliminate volatile materials. The infrared spectra showed the nearly complete disappearance of the free silanol groups (≡Si−OH), as judged by the decrease in the intensity of the band at 3747 cm^{-1}. At the same time, besides a broad band attributable to hydrogen-bonded silanol at 3300 cm^{-1}, new bands attributable to the ethoxy ligand vibrations appeared in the ν(C−H) stretching (2982, 2938, 2903 cm^{-1}) and deformation δ(C−H) (1488, 1447, 1389 and 1364 cm^{-1}) regions (Figure 4).

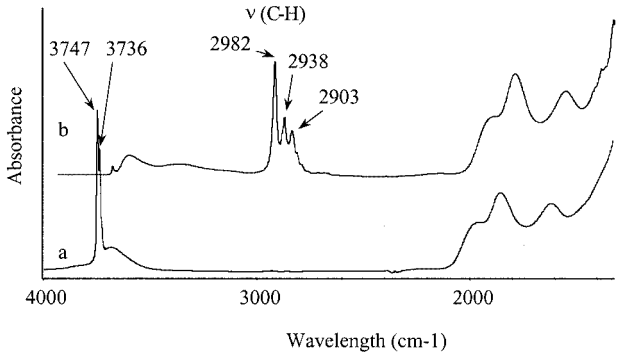

Figure 4. IR spectra of (a) partially labelled $Si^{18}O_{2\text{-}(500)}$, (b) after treatment with $(EtO)_2SeO$, (c) after 6 h under vacuum (10^{-5} Torr) at room temperature in the expanded 4000−2500-cm^{-1} region

The low-frequency region (1020−850 cm^{-1}) shows new bands at 934 (broad) and 874 (sharp) cm^{-1}. A reaction between $(EtO)_2SeO$ and partially ^{18}O-labelled surface hydroxy group (Figure 5) resulted in a shift of the 934-cm^{-1} band to 917 cm^{-1}. On this basis and by comparison with shifts of similar magnitude in the IR spectra of silica-supported ^{18}O-labelled molybdenum,[33] and titanium[34−35] species, the vibration at 934 cm^{-1} is attributed to ν(Si−OSe).

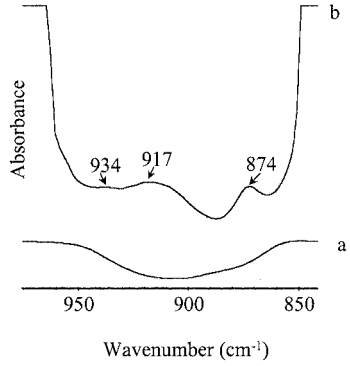

Figure 5. IR spectra of (a) partially labelled $Si^{18}O_{2\text{-}(500)}$, (b) after treatment with $(EtO)_2SeO$, (c) after 6 h under vacuum at room temperature (10^{-5} Torr) in the expanded 1000−850-cm^{-1} region

The band at 874 cm^{-1} could be attributed to the ν(Se=O) vibration.[30] From the literature,[13,36] it is known that the Se=O bond in $PhSeO_2H$ can be reduced in the presence of Ph_3P to form Ph_3PO by the following reaction.

$$PhSe(O)OH + Ph_3P \rightarrow PhSeOH + Ph_3PO$$

In order to confirm the presence of the Se=O bond in **1**, the reaction between **1** and a solution of triphenylphosphane in C_6D_6 was performed and monitored by ^{31}P NMR spectroscopy. After 2 h at 60 °C, the ^{31}P NMR spectrum presented, besides the resonance at δ = −5 ppm due to free Ph_3P, two new peaks, at δ = +24 ppm, due to Ph_3PO, and at δ = +35 ppm, attributed to Ph_3PSe (see below). The oxidation of Ph_3P to Ph_3PO was support for the continued presence of the Se=O bond in the grafted selenium species **1**.

The solid-state ^{13}C MAS NMR spectrum of **1** contained two resonances at δ = 17 and 57 ppm, attributed to the CH_3 and CH_2 of an ethoxy group, respectively.

Se elemental analysis of the solid sample indicated that for two different samples the loading in Se was 3.84 and 3.72%, corresponding to an Se/OH group ratio of ca. 1.2, and C elemental analysis (C 1.45%) gave a molar ratio of C/Se = 2.5.

In conclusion, these data are consistent with the formation of an Se-surface compound, the Se atom being linked to three different ligands: an ethoxy, an oxo and a siloxy group from the surface [≡SiOSe(O)OEt] (**1**).

Thermal Stability of 1

The excess of carbon in the elemental analysis and the presence in the infrared spectrum (Figure 4) of a broad band attributable to hydrogen-bonded silanol at 3300 cm^{-1}

 © 2003 Wiley-VCH Verlag GmbH & Co. KGaA, Weinheim

are probably due to physisorbed EtOH, which cannot be totally eliminated at room temperature even after 72 h under dynamic vacuum. On warming the sample at 60 °C or 100 °C, to eliminate the excess of ethanol, we observed a change in the colour of the pellet, which became orange (60 °C) to deep orange (100 °C) and the elemental analysis indicated a decrease in the % value of Se from 3.8 to 0.8. At the same time, small, red needles of metallic selenium appeared in the cold part of the glass equipment. Note that the formation of Ph_3PSe was observed during the reaction between **1** and PPh_3, suggesting that there was selenium leaching at 60 °C (see above).

An increase in the temperature caused changes of the species **1** towards metallic Se and traces of ≡SiOEt, characterized by solid-state ^{13}C MAS NMR (resonance at $\delta = 16$ and 60 ppm attributed to the CH_3 and CH_2, respectively, of an ethoxy group of $\equiv Si-OCH_2CH_3$).[25]

Reactivity of 1 towards Acetaldehyde

a) Surface Chemistry of Acetaldehyde on Silica

The reaction between acetaldehyde and silica $SiO_{2-(500)}$ was monitored in situ by infrared spectroscopy. It was observed that, as with $SiO_{2-(300)}$, there was formation of crotonaldehyde species by surface aldolization of adsorbed acetaldehyde.[37] In contrast, this reaction was not observed with $SiO_{2-(800)}$.[38]

$$2\ CH_3CHO \rightarrow CH_3CH{=}CHCHO + H_2O$$

b) Surface Chemistry of Acetaldehyde on 1

The reaction between acetaldehyde and silica modified with selenium derivative **1** was also monitored in situ by infrared spectroscopy (Figure 6, a and b). At first, comparison of the infrared spectra indicated that there was no more acetaldehyde (no band at 2804 and 1730 cm^{-1}), and no formation of crotonaldehyde species (no bands at 3042 and 1642 cm^{-1}) (Figure 6, b). No free silanol groups were generated, and a new, broad band at 3368 cm^{-1} could be attributed to a hydrogen-bonded OH group. The pattern due to the EtO group, at 2982, 2938 and 2903 cm^{-1}, was unchanged, suggesting that the ethoxy group was still present (Figure 6, a). The new weak band at 2881 cm^{-1} (versus 2804 cm^{-1} for free acetaldehyde) could be due to aldehydic C−H stretching for an aldehyde with an electronegative group in the α-position.[39] The vibration at 1725 cm^{-1} could be attributable to glyoxal, which shows only one carbonyl adsorption peak with no shift from the normal absorption position of monoaldehyde absorptions.[39]

At the same time, in the 950−850-cm^{-1} region, the band at 873 cm^{-1} attributed to ν(Se=O) had disappeared whereas the bands at 935 and 917 cm^{-1}, attributed to $\nu(Si-{}^{16}OSe)$ and $\nu(Si-{}^{18}OSe)$, respectively, were still present (Figure 7).

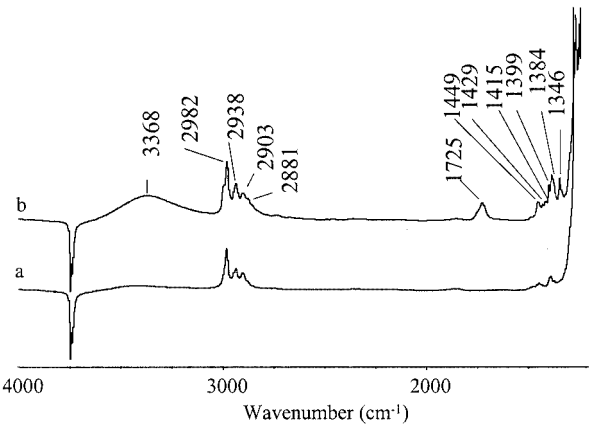

Figure 6. IR spectra of (a) difference spectrum of partially labelled $Si^{18}O_{2-(500)}$ after treatment with $(EtO)_2SeO$ and the spectrum of starting silica, (b) difference spectrum of **1** after treatment with acetaldehyde (at 25 °C and evacuation at 10^{-5} Torr) and the spectrum of starting silica in the expanded 4000−1200-cm^{-1} region

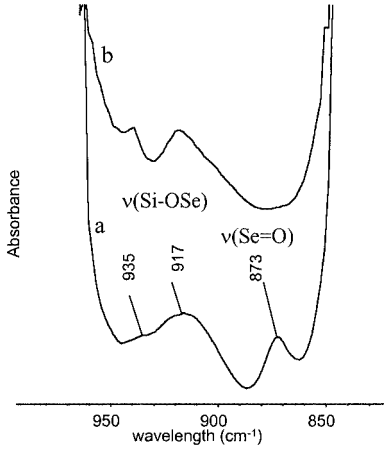

Figure 7. IR spectra of (a) difference spectrum of partially labelled $Si^{18}O_{2-(500)}$ after treatment with $(EtO)_2SeO$ and the spectrum of starting silica, (b) difference spectrum of **1** after reaction with acetaldehyde (at 25 °C and evacuation at 10^{-5} Torr) and the spectrum of starting silica in the expanded 1000−850-cm^{-1} region

All these data seemed to indicate that the stoichiometric reaction between acetaldehyde and surface species **1**, resulted firstly in the exchange of the ethoxy ligand by vinyl alcohol, with concomitant formation of ethanol, and secondly in the formation of the selenate(II) ester of the enol species **2**, stopping at this stage in the absence of protic solvent (Figure 8).

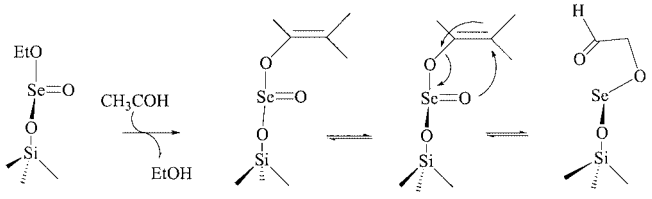

Figure 8. Proposed reaction between acetaldehyde and **1**

 © 2003 Wiley-VCH Verlag GmbH & Co. KGaA, Weinheim

Conclusion

The reaction between $(EtO)_2SeO$ and silica resulted in the formation of a unique surface species (≡SiO)Se(O)OEt (**1**), which has been fully characterized. Preliminary results from the reaction between acetaldehyde and **1** seemed to indicate that there was formation of ethanol and the selenate(II) ester of the enol derivative on the surface (**2**). However, the use of **1** as an oxidative reagent is limited, due to its low thermal stability and easy leaching of selenium in the presence of protic solvent.

Experimental Section

General: All chemicals were purchased from Aldrich. Cyclohexane was distilled under argon from Na/K alloy, degassed and stored under argon in the presence of Na. C_6D_6 (SDS, 99.6%) was degassed by three "freeze-pump-thaw" cycles and dried with freshly regenerated 3-Å molecular sieves. All operations were performed in the strict absence of oxygen and water, under purified argon with use of vacuum-line techniques. Elemental analyses were performed by the Central Analysis Service of the CNRS at Solaize. Solid-state NMR spectra were recorded with a Bruker DSX-300 machine equipped with a standard 4-mm double-bearing probe head and operating at 75.47 and 300.18 MHz for ^{13}C and ^{1}H, respectively. Chemical shifts are given with respect to TMS, with adamantane as an external reference (δ = 37.7 ppm for the highest chemical shift). Solution NMR spectra were recorded with Bruker AC 300 MHz (^{1}H, ^{13}C) and DRX 500 MHz (^{77}Se) spectrometers. Chemical shifts are reported in ppm and referenced to residual solvent resonances (C_6D_6: δ = 7.15 ppm for ^{1}H; δ = 128 ppm for ^{13}C), or external standards (^{77}Se, Me_2Se).[40] Infrared spectra were recorded under vacuum with a Nicolet 550 FT spectrometer in an infrared cell equipped with ZnSe windows. The conversion and selectivities were determined by HPLC. Two columns were necessary. For the detection of acetaldehyde, glyoxal and glyoxylic acid (as oxime derivatives),[41] an Interchim N7 column (symmetry C18, 5 μm; l = 25 cm, d = 4.6 mm; eluent: acetonitrile/water/sulfuric acid, 35:65:0.1 (v/v); flow rate: 1 mL/min; detection: UV 235 nm) thermostatted at 42 °C was used. *o*-Toluic acid was used as an internal reference. For the quantification of other acids (acetic, formic and oxalic ...) a Waters Phenomex column was used (l = 30 cm, d = 3/8″; eluent: 0.05 N sulfuric acid; flow rate: 0.5 mL/min; detection: UV 210 nm). Mass spectrometry was performed with an MAT 95 XL Thermoquest- Finnigan instrument (chemical ionization, NH_3). The mass was calculated by use of ^{80}Se (49.8%). The silica support (Aerosil® Degussa, 200 $m^2 \cdot g^{-1}$) was compacted into a disk (30 mg) for infrared studies or was hydrated, dried (80 °C) and crushed to prepare large quantities (1−2 g) for NMR studies and elemental analysis. Before the reaction, the silica was calcinated at 400 °C in air for 4 h to remove hydrocarbon impurities and dehydroxylated at the desired temperature (500 °C) under high vacuum (10^{-5} Torr) for 12 h (referred to as $SiO_{2\text{-}(500)}$). $Si^{18}O_2$ was prepared by calcination in air at 500 °C for 4 h, followed by partial dehydroxylation at 500 °C for 10 h. ^{18}O-enrichment of the surface hydroxy groups was achieved by exposing the silica to $H_2^{18}O$ vapour at room temperature for 12 h, followed by dehydroxylation under dynamic vacuum at 500 °C for 10 h.

General Procedure for the Oxidation of Acetaldehyde with SeO_2 or H_2SeO_3: A mixture of SeO_2 (39 mmol) and CH_3CHO (35 mmol) in propionic acid (70% in water, 10 mL) was stirred under argon at 90 °C for 12 h in a Schlenk tube fitted with a condenser. After filtration of metallic selenium, which had precipitated during the reaction, the reaction mixture was analysed by HPLC.

General Procedure for the Oxidation of Acetaldehyde with $PhSeO_2H$ or $PhSeO_2H$ + H_2O_2 (1:1, mol/mol): A mixture of $PhSeO_2H$ (39 mmol) and CH_3CHO (35 mmol) in propionic acid (70% in water, 10 mL) was stirred under argon at 90 °C for 12 h in a Schlenk tube fitted with a condenser [with $PhSeO_2H$ in the presence of H_2O_2 (1:1, mol/mol) the reaction time was 20 min]. A white precipitate was filtered off and identified as PhSe−SePh by ^{77}Se NMR [δ_{Se} (C_6D_6) = 460 ppm].[13] No metallic selenium was observed. The reaction mixture was then analysed by HPLC.

Synthesis of Diethoxy Selenite $(EtO)_2SeO$:[30−31] A mixture of SeO_2 (3.4 g, 31 mmol) and EtOH (20 mL, 348 mmol) in cyclohexane (35 mL) was stirred at reflux under argon for 16 h, in a Schlenk tube fitted with a Dean−Stark condenser. After filtration of metallic selenium and evaporation of the solvent, $(EtO)_2SeO$ was distilled (76 °C/15 mbar) as a pale yellow liquid (4.2 g, 74%). $C_4H_{10}O_3Se$ (185.1): calcd. C 25.8, H 5.4, Se 43.0; found C 24.6, H 5.4, Se 42.6. IR (vapour): $\tilde{\nu}$ = 874 ν(Se=O), 659 ν(Se−O) cm^{-1}. ^{1}H NMR (C_6D_6): δ = 3.85 (CH_2, ABX_3 system), 1.1 (CH_3, t, J^2_{HH} = 7 Hz) ppm. ^{13}C NMR (C_6D_6): δ = 57.4 (OCH_2), 16.8 (CH_3) ppm. ^{77}Se NMR (C_6D_6): δ = 1339.8 ppm. MS (CI): m/z (%) = 187 (50) [M + H (^{80}Se)]$^+$.

Reaction between Diethyl Selenite $(EtO)_2SeO$ and $SiO_{2\text{-}(500)}$: For in situ infrared experiments, silica (30 mg) was pressed into an 18-mm self-supporting disk, placed in a sealed glass high-vacuum reactor fitted with ZnSe windows, and partially dehydroxylated under vacuum (500 °C, 12 h). $(EtO)_2SeO$ (300 Torr) was then introduced at room temperature onto the silica disk, which was maintained at liquid nitrogen temperature. The infrared cell was isolated. The silica disk was warmed to room temperature and kept at this temperature for 1 h. The pellet turned from white to yellow/orange. The cell was attached to a high vacuum line and the excess of $(EtO)_2SeO$ was removed by reverse distillation in a liquid nitrogen cooled tube. The pellet was then kept under dynamic vacuum (10^{-5} Torr, 12 h at 25 °C) in order to eliminate volatile materials. For NMR and elemental analysis samples, the same procedure as above was used with 2 g of $SiO_{2\text{-}(500)}$ in a Schlenk tube attached to a high vacuum line. Elemental analysis: Se (3.84%) and C (1.45%). Solid-state ^{13}C MAS NMR: δ = 17 and 57 ppm.

Acknowledgments

We thank the CLARIANT Company for financial support (H. P.), Dr. M. Alarcon for fruitful discussion, Mr. J.-F. Viard for his help in the HPLC analyses, and Dr. B. Fenet (NMR services, ESCPE Lyon).

[1] G. Mattioda, B. Métivier, J.-P. Guetté, *Actual. Chim.* **1982**, *5−6*, 23−33.
[2] S. Mourey, *Info. Chim. Mag.* **1998**, *396*, 92−94.
[3] K. Weissermel, H.-J. Arpe, *Industrial Organic Chemistry*, 2nd ed., Wiley-VCH, Weinheim, **1993**.
[4] H. L. Riley, J. F. Morley, N. A. C. Friend, *J. Chem. Soc.* **1932**, 1875−1883.
[5] E. J. Corey, J.-P. Schaefer, *J. Am. Chem. Soc.* **1960**, *82*, 918−929.
[6] T. G. Back, *Organoselenium Chemistry*, Oxford University Press, Oxford, **1999**.
[7] K. B. Sharpless, K. M. Gordon, *J. Am. Chem. Soc.* **1976**, *98*, 1986−1987.
[8] G.-J. ten Brink, B. C. M. Fernandes, M. C. A. van Vliet, I. W.

 © 2003 Wiley-VCH Verlag GmbH & Co. KGaA, Weinheim

C. E. Arends, R. A. Sheldon, *J. Chem. Soc., Perkin Trans. 1* **2001**, 224−228.
[9] S. Mukhopadhyay, S. B. Chandalia, *Org. Process. Res. Dev.* **1999**, *3*, 455−459.
[10] R. T. Taylor, L. A. Flood, *J. Org. Chem.* **1983**, *48*, 5160−5164.
[11] K. C. Nicolaou, J. A. Pfefferkorn, H. J. Mitchell, A. J. Roecker, S. Barluenga, G.-Q. Cao, R. L. Affleck, J. E. Lillig, *J. Am. Chem. Soc.* **2000**, *122*, 9954−9976.
[12] G.-J. ten Brink, J.-M. Vis, I. W. C. E. Arends, R. A. Sheldon, *J. Org. Chem.* **2001**, *66*, 2429−2433.
[13] J. E. P. Davidson, E. A. Anderson, W. Buhr, J. R. Harrison, P. T. O′Sullivan, I. Collins, R. H. Green, A. B. Holmes, *Chem. Commun.* **2000**, 629−630.
[14] J.-M. Basset, F. Lefebvre, C. Santini, *Coord. Chem. Rev.* **1998**, *178*, 1703−1721.
[15] F. Lefebvre, J.-M. Basset, *J. Mol. Catal. A* **1999**, *146*, 3−12.
[16] C. Copéret, M. Chabanas, R. Petroff Saint-Arroman, J.-M. Basset, *Angew. Chem. Int. Ed.* **2003**, *42*, 152−181.
[17] H. C. L. Abbenhuis, S. Krijnen, R. A. van Santen, *Chem. Commun.* **1997**, 331−332.
[18] M. Crocker, R. H. M. Herold, A. Guy Orpen, *Chem. Commun.* **1997**, 2411−2412.
[19] T. Maschmeyer, M. C. Klunduk, C. M. Martin, D. S. Shephard, J. M. Thomas, B. F. G. Johnson, *Chem. Commun.* **1997**, 1847−1848.
[20] F. Quignard, A. Choplin, R. Teissier, *J. Mol. Cat. A:* **1997**, *120*, L27−L31.
[21] M. Crocker, R. H. M. Herold, A. G. Roosenbrand, C. A. Emeis, A. E. Wilson, *Colloids Surf. A* **1998**, *139*, 351.
[22] S. A. Holmes, F. Quignard, A. Choplin, R. Teissier, J. Kervennal, *J. Catal.* **1998**, *176*, 173−181.
[23] S. A. Holmes, F. Quignard, A. Choplin, R. Teissier, J. Kervennal, *J. Catal.* **1998**, *176*, 182−191.
[24] M. Crocker, R. H. M. Herold, A. Guy Orpen, M. T. A. Overgaag, *J. Chem. Soc., Dalton Trans.* **1999**, 3791−3804.
[25] D. Meunier, A. Piechaczyk, A. De Mallmann, J.-M. Basset, *Angew. Chem. Int. Ed.* **1999**, *38*, 3540−3542.
[26] G. Curthoys, V. Y. Davydov, A. V. Kiselev, S. A. Kiselev, B. V. Kuznetsav, *J. Colloid Interface Sci.* **1974**, *48*, 58−72.
[27] B. A. Morrow, A. J. McFarlan, *Langmuir* **1991**, *7*, 1695−1688.
[28] E. F. Vansant, P. Van Der Voort, K. C. Vrancken, *Stud. Surf. Sci. Catal.* **1995**, vol. 95.
[29] B. A. Morrow, *Stud. Surf. Sci. Catal.* **1990**, *5,* A161−A224.
[30] F. Ando, *Bull. Soc., Chem. Soc.* **1979**, *52*, 807−810.
[31] D. B. Denney, *J. Am. Chem. Soc.* **1981**, *103*, 2340−2347.
[32] T. Tao, G. E. Maciel, *J. Am. Chem. Soc.* **2000**, *122*, 3118−3126.
[33] M. Cornac, A. Janin, J. C. Lavalley, *Polyhedron* **1986**, *5*, 183−186.
[34] A. O. Bouh, G. L. Rice, S. L. Scott, *J. Am. Chem. Soc.* **1999**, *121*, 7201−7210.
[35] G. Ricchiardi, A. Damin, S. Bordiga, C. Lamberti, G. Spano, F. Rivetti, A. Zecchina, *J. Am. Chem. Soc.* **2001**, *123*, 11409−11419.
[36] L. G. Faehl, J. L. Kice, *J. Org. Chem.* **1979**, *44*, 2357−2361.
[37] M. I. Zaki, M. A. Hasan, F. A. Al-Sagheer, L. Pasupulety, *Langmuir* **2000**, *16*, 430−436.
[38] M. Allian, E. Borello, P. Ugliengo, G. Spano, E. Garrone, *Langmuir* **1995**, *11*, 4811−4817.
[39] R. M. Silverstein, G. C. Bassler, T. C. Morrill, *Spectrometric identification of organic compounds*, 5th ed., John Wiley & Sons, New York, **1991**.
[40] H. Duddeck, *Prog. Nucl. Magn. Reson. Spectrosc.* **1995**, *27*, 1−323.
[41] B. S. Furniss, A. J. Hannaford, V. Rogers, P. W. G. Smith, A. R. Tatchell, *Vogel's textbook of practical organic chemistry*, 4th ed., Longman, London, **1986**.

Received October 31, 2002

 © 2003 Wiley-VCH Verlag GmbH & Co. KGaA, Weinheim

Bridged Aminotroponiminate Complexes of Zinc

Michael T. Gamer[a] and Peter W. Roesky*[a]

Keywords: Aminotroponiminate / Coordination chemistry / N ligands / Zinc

Reactions of the *n*-propyl-bridged diaminotroponimine $H_2\{(i\text{Pr})\text{TP}\}$ with dialkylzinc compounds in toluene lead, depending on the stoichiometric ratio, either to dimetallic singly bridged products of composition $[(RZn)_2\{(i\text{Pr})\text{TP}\}]$ [R = Me (**1**), Et (**2**)] or to dimetallic doubly bridged helical products of composition $[Zn\{(i\text{Pr})\text{TP}\}]_2$ (**3**). Compound **3**, which was characterised by single-crystal diffraction methods, is the first bridged aminotroponiminate complex in which a helical structure is observed.

(© Wiley-VCH Verlag GmbH & Co. KGaA, 69451 Weinheim, Germany, 2003)

Introduction

Aminotroponiminates ($\{ATI\}^-$) are bidentate, monoanionic ligands containing a 10π-electron backbone. Like 1,4-diazabutadiene, $\{ATI\}^-$ forms five-membered metallacycles upon coordination to a metal atom. In contrast to 1,4-diazabutadiene, however, $\{ATI\}^-$ is believed to be much more resistant to electrophiles and nucleophiles. The ligand system was introduced into the coordination chemistry in the 1960s mostly by researchers at DuPont. Between 1961 and 1970 a large number of Mn^{II}, Fe^{II}, Co^{II}, and Ni^{II} complexes were prepared in order to study the magnetic moments and NMR contact shifts; only one Mn complex was characterised by single-crystal X-ray methods. This early work was reviewed by Holm in 1971.[1]

Recent reports from us and other research groups have described the preparation and characterisation of aminotroponiminates as cyclopentadienyl alternatives for main group and transition elements.[2] We have shown that bis(aminotroponiminate)yttrium amides are active as catalysts for hydroamination/cyclisation catalysis.[3] Recently we started to prepare singly bridged aminotroponiminates.[4] It was shown that the trimethylene-bridged ligand 1,3-bis[2-(isopropylamino)troponiminate]propane ($\{(i\text{Pr})\text{TP}\}^{2-}$) (**A**) ([$H_2\{(i\text{Pr})\text{TP}\}$ = trimethylenedinitrilobis[2-(isopropylamino)cyclohepta-2,4,6-triene]) is able to coordinate in a chelating or a metal-bridging mode to various metals of group 13 and the lanthanides.[4,5,6] Up to now $\{(i\text{Pr})\text{TP}\}^{2-}$ has only been treated with trivalent metals. In most cases a chelating coordination mode was observed with these metal centres. A metal−metal bridging mode has only been observed in those cases in which a chelating coordination mode is prevented due to steric reasons, for example $[(R_2Al)_2\{(i\text{Pr})\text{TP}\}]$ (R = Me, Et, *i*Bu).[6] We are interested in extending our research to the divalent metal zinc. To the best of our knowledge no zinc complexes of singly bridged aminotroponiminates are known. In contrast, two zinc complexes with non-bridged aminotroponiminate, which were structurally not characterised, have been reported by Holm[7] and Lippard;[8] some tropocoronand complexes are also known.[9]

Herein we report on the reaction of $H_2\{(i\text{Pr})\text{TP}\}$ with dialkylzinc compounds which lead exclusively to metal-bridging products. Depending on the stoichiometry either singly or doubly bridged helical products were obtained.

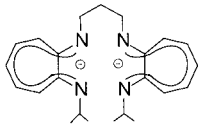

A

Results and Discussion

The dimetallic zinc complexes $[(RZn)_2\{(i\text{Pr})\text{TP}\}]$ [R = Me (**1**), Et (**2**)] were synthesised by reaction of the neutral ligand $H_2\{(i\text{Pr})\text{TP}\}$[4] with the corresponding dialkylzinc compounds R_2Zn in *n*-pentane [Equation (1)]. Upon cooling, **1**−**2** were obtained as yellow crystalline solids with a fairly high sensitivity towards air and moisture.

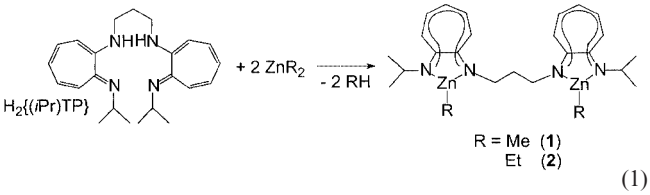

(1)

The reactivity of $ZnMe_2$ towards $H_2\{(i\text{Pr})\text{TP}\}$ is much higher than that of $ZnEt_2$. Compound **2** was synthesised by addition of $H_2\{(i\text{Pr})\text{TP}\}$ to a solution of $ZnEt_2$ in toluene

[a] Institut für Chemie, Freie Universität Berlin, Fabeckstraße 34−36, 14195 Berlin, Germany

at room temperature. In contrast, compound **1** was only obtained in high yields when performing the reaction at −50 °C. At room temperature the same reaction sequence leads to a mixture of **1** and higher substituted products such as $[Zn\{(i\text{Pr})TP\}]_2$ (**3**) (see below). The new complexes were characterised by standard analytical/spectroscopic techniques. The ^1H and ^{13}C NMR spectra also point to a symmetrical coordination of the $\{(i\text{Pr})TP\}^{2-}$ anion in solution. The signals of the isopropyl C*H* proton of **1** and **2** are well-resolved into a septuplet and show only a slight downfield shift [δ = 3.74 (**1**), 3.74 (**2**) ppm] compared to that of the free ligand $H_2\{(i\text{Pr})TP\}$ (δ = 3.55 ppm).[4] This is in agreement with comparable alkyllanthanide compounds of composition $[\{(i\text{Pr})TP\}LnR]$ [Ln = La, Lu; R = $CH(SiMe_3)_2$, CH_2SiMe_3] in which the isopropyl C*H* signal is also shifted downfield {δ = 3.67 ppm $[\{(i\text{Pr})TP\}_2LaCH(SiMe_3)_2]$,[4] δ = 3.93 ppm $[\{(i\text{Pr})TP\}_2LuCH_2SiMe_3]$}.[10] In contrast, the signals of the isopropyl C*H* in the comparable aluminium complexes $[(R_2Al)_2\{(i\text{Pr})TP\}]$ (R = Me, Et, *i*Bu) are shifted to higher field (δ = 3.50−3.54 ppm). For **1** and **2** sharp signals for the Zn−Me and Zn−Et groups, respectively, are observed in the ^1H NMR spectra (δ = −0.07 (**1**); 0.74, 1.58 (**2**) ppm] and in the $^{13}C\{^1H\}$ NMR spectra [δ = −10.8 (**1**); 3.0, 13.8 (**2**) ppm]. The signals of the $Zn-CH_3$ and $Zn-CH_2$ groups, respectively, are in general shifted to higher field than those of the starting material $ZnMe_2$ (^1H: δ = 0.51 ppm; $^{13}C\{^1H\}$: δ = −4.2 ppm)[11] and $ZnEt_2$ (^1H: δ = 0.08, 1.05 ppm;[12] $^{13}C\{^1H\}$: δ = 6.82, 10.35 ppm).[13]

The formation of **1** and **2** is in contrast to our previous observation of the coordination behaviour of the $\{(i\text{Pr})TP\}^{2-}$ anion. In group-3, group-13 and lanthanide chemistry the ligand always adopts a chelating coordination mode, if this is possible, for steric reasons. Since non-bridged diaminotroponiminate complexes of zinc are known,[7] we initially expected a chelating coordination of the ligand. To study the reactivity of the $\{(i\text{Pr})TP\}^{2-}$ ligand, $H_2\{(i\text{Pr})TP\}$ was treated in a 1:1 stoichiometric ratio with $ZnMe_2$ in toluene [Equation (2)]. After recrystallisation, the dimetallic zinc complex $[Zn\{(i\text{Pr})TP\}]_2$ (**3**) was obtained as yellow crystals. The new complex was characterised by standard spectroscopic techniques, and the solid-state structure was established by single-crystal X-ray diffraction.

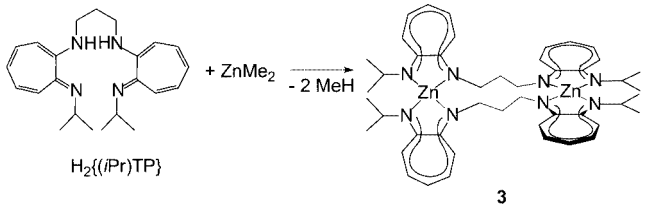

(2)

Compound **3** crystallises in the monoclinic space group *C*2/*c* having four molecules in the unit cell (Figure 1). The dimetallic complex adopts a helical structure with a crystallographic inversion centre. Both of these helical enantiomers are observed in the unit cell. The zinc atoms have a distorted tetrahedral coordination sphere. The N−Zn−N angles inside the aminotroponiminate moiety are 81.3(2) and 81.0(2)°. The other N−Zn−N angles range from 119.3(2) to 134.5(2)°. The Zn−N bond lengths are in the expected range of 198.3(5)−199.9(5) pm. In comparable tropocoronand complexes the Zn−N distances vary from 197.2(5) to 209.6(4) pm.[9b]

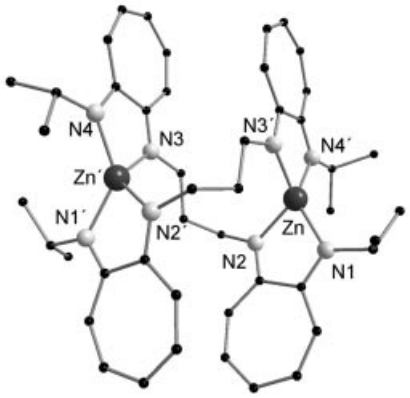

Figure 1. Perspective view of the molecular structure of **3**; selected distances [pm] and angles [°]: Zn−N1 198.5(5), Zn−N2 198.7(5), Zn−N3′ 199.9(5), Zn−N4′ 198.3(5); N1−Zn−N2 81.3(2), N1−Zn−N3′ 125.2(2), N1−Zn−N4′ 134.5(2), N2−Zn−N3′ 119.3(2), N2−Zn−N4′ 120.6(2), N3′−Zn−N4′ 81.0(2)

The ^1H and $^{13}C\{^1H\}$ NMR spectra of **3** show a diastereotopic splitting of the isopropyl CH_3 signals. Based on these observations we suggest that the helical structure observed in the solid state may be retained in solution. A similar diastereotopic splitting has been observed by other chiral (isopropylamino)troponiminate complexes such as $[\{(i\text{Pr})_2ATI\}_3Ln]$ (Ln = Y, La) [$\{(i\text{Pr})_2ATI\}$ = *N*-isopropyl-2-(isopropylamino)troponiminate]. The signal of the isopropyl C*H* proton of **3** is well resolved into a septuplet but shows a slight downfield shift (δ = 3.76 ppm) compared to that of the free ligand $H_2\{(i\text{Pr})TP\}$ (δ = 3.55 ppm).[4] This is in agreement with **1** and **2**. Compound **3** is the first bridged aminotroponiminate complex in which a helical structure is observed.

Conclusions

Reactions of $H_2\{(i\text{Pr})TP\}$ with dialkylzinc compounds in toluene led, in a 1:2 stoichiometric ratio, to the dimetallic singly bridged products of composition $[(RZn)_2\{(i\text{Pr})TP\}]$ [R = Me (**1**), Et (**2**)]. The reactivity of $ZnMe_2$ towards $H_2\{(i\text{Pr})TP\}$ is much higher than that of $ZnEt_2$. When $H_2\{(i\text{Pr})TP\}$ was treated in a 1:1 stoichiometric ratio with $ZnMe_2$ in toluene the dimetallic doubly bridged helical zinc complex $[Zn\{(i\text{Pr})TP\}]_2$ (**3**) was obtained. Due to the helical structure of **3** the ^1H and $^{13}C\{^1H\}$ NMR spectra of this compound show a diastereotopic splitting of the isopropyl CH_3 signals confirming that the helical structure observed in the solid state is retained in solution.

 © 2003 Wiley-VCH Verlag GmbH & Co. KGaA, Weinheim

Experimental Section

General: All manipulations of air-sensitive materials were performed with the rigorous exclusion of oxygen and moisture in flame-dried Schlenk-type glassware either on a dual manifold Schlenk line, interfaced to a high vacuum (10^{-4} Torr) line, or in an argon-filled M. Braun glove box. Ether solvents (tetrahydrofuran and diethyl ether) were predried with Na wire and distilled under nitrogen from Na/K alloy benzophenone ketyl prior to use. Hydrocarbon solvents (toluene and *n*-pentane) were distilled under nitrogen from $LiAlH_4$. All solvents for vacuum-line manipulations were stored in vacuo over $LiAlH_4$ in resealable flasks. Deuterated solvents were obtained from Aldrich Inc. (all 99 atom% D) and were degassed, dried, and stored in vacuo over Na/K alloy in resealable flasks. NMR spectra were recorded with a Jeol 400 MHz FT NMR spectrometer or with a Bruker AC 250. Chemical shifts are referenced to internal solvent resonances and are reported relative to tetramethylsilane. Elemental analyses were carried out with an Elementar vario EL. $ZnMe_2$ and $ZnEt_2$ were purchased from Aldrich Inc. H_2{(*i*Pr)TP} was prepared according to a literature procedure.[4]

[(MeZn)$_2${(*i*Pr)TP}] (1): A 2 M $ZnMe_2$ solution in toluene (5 mL, 10 mmol) was diluted with 25 mL of toluene. At −70 °C a solution of H_2{(*i*Pr)TP} (1.82 g, 5 mmol) in toluene (30 mL) was added. The reaction mixture was warmed up to −50 °C, followed by gas evolution. After the gas evolution had stopped (about 3 h), the mixture was warmed up to room temperature, filtered, and the solvent was removed. The resulting yellow solid was washed twice with *n*-pentane (5 mL) and dried in vacuo. Yield 2.17 g (83%). $C_{25}H_{36}N_4Zn_2$ (523.34): calcd. C 57.38, H 6.93, N 10.71; found C 56.94, H 6.80, N 10.32. ^{1}H NMR (C_6D_6, 400 MHz, 25 °C): δ = −0.07 (s, 6 H, ZnCH_3), 1.13 [d, 12 H, CH(CH_3)$_2$, $^3J_{H,H}$ = 6.2 Hz), 2.26 (quint, 2 H, $CH_2CH_2CH_2$, $^3J_{H,H}$ = 7.0 Hz), 3.33 (t, 4 H, NCH_2, $^3J_{H,H}$ = 7.0 Hz), 3.74 [sept, 2 H, CH(CH$_3$)$_2$, $^3J_{H,H}$ = 6.2 Hz], 6.36 (t, 2 H, H_{ring}, $^3J_{H,H}$ = 9.2 Hz), 6.52 (d, 2 H, H_{ring}, $^3J_{H,H}$ = 11.2 Hz), 6.52 (d, 2 H, H_{ring}, $^3J_{H,H}$ = 11.4 Hz), 6.92−7.01 (m, 4 H, H_{ring}) ppm. ^{13}C{^{1}H} NMR (C_6D_6, 100.40 MHz, 25 °C): δ = −10.8, 24.5, 33.5, 48.3, 48.7, 111.9, 112.0, 117.9, 134.6, 134.7, 160.2, 161.4 ppm.

[(EtZn)$_2${(*i*Pr)TP}] (2): A 1 M $ZnEt_2$ solution (4 mL, 4 mmol) in toluene was diluted with 25 mL of toluene. At ambient temperature a solution of H_2{(*i*Pr)TP} (0.73 g, 2 mmol) in toluene (30 mL) was added, immediately followed by gas evolution. The mixture was stirred for 6 h at room temperature, filtered, and the solvent was removed. The remaining yellow solid was washed twice with *n*-pentane (5 mL) and dried in vacuo. Yield 0.99 g (89%). $C_{27}H_{40}N_4Zn_2$ (551.37): calcd. C 58.81, H 7.31, N 10.16; found C 58.57, H 7.35, N 9.88. ^{1}H NMR (C_6D_6, 250 MHz, 25 °C): δ = 0.74 (q, 4 H, ZnCH_2CH$_3$, $^3J_{H,H}$ = 8.1 Hz), 1.15 [d, 12 H, CH(CH_3)$_2$, $^3J_{H,H}$ = 6.2 Hz], 1.58 (t, 6 H, ZnCH$_2$CH_3, $^3J_{H,H}$ = 8.1 Hz), 2.21 (quint, 2 H, $CH_2CH_2CH_2$, $^3J_{H,H}$ = 7.0 Hz), 3.38 (t, 4 H, NCH_2, $^3J_{H,H}$ = 7.0 Hz), 3.75 [sept, 2 H, CH(CH$_3$)$_2$, $^3J_{H,H}$ = 6.2 Hz], 6.36 (t, 2 H, H_{ring}, $^3J_{H,H}$ = 9.1 Hz), 6.55 (d, 2 H, H_{ring}, $^3J_{H,H}$ = 11.1 Hz), 6.59 (d, 2 H, H_{ring}, $^3J_{H,H}$ = 11.2 Hz), 6.91−7.05 (m, 4 H, H_{ring}) ppm. ^{13}C{^{1}H} NMR (C_6D_6, 62.9 MHz, 25 °C): δ = 3.0, 13.8, 25.3, 34.0, 48.8, 49.3, 112.7, 112.8, 118.7, 135.3, 135.5, 161.0, 162.1 ppm.

[Zn{(*i*Pr)TP}]$_2$ (3): At ambient temperature, 1 mL of a 2 M solution of $ZnMe_2$ in toluene (2 mmol) was added to a solution of H_2{(*i*Pr)TP} (0.79 g, 2 mmol) in 25 mL of toluene. The mixture was stirred for 3 h at room temperature. After the gas evolution had stopped, the solution was heated briefly under reflux. The mixture was then filtered, and the solvent was removed. The remaining yellow solid was washed twice with *n*-pentane (5 mL) and dried in vacuo. Single crystals were obtained from toluene at −40 °C. Yield 1.45 g (85%). $C_{40}H_{60}N_8Zn_2$ (855.80): calcd. C 64.56, H 7.07, N 13.09; found C 64.33, H 6.98, N 12.77. ^{1}H NMR (C_6D_6, 400 MHz, 25 °C): δ = 1.05 [d, 12 H, CH(CH_3)$_2$, $^3J_{H,H}$ = 6.2 Hz], 1.06 [d, 12 H, CH(CH_3)$_2$, $^3J_{H,H}$ = 6.2 Hz], 1.98 (quint, 4 H, $CH_2CH_2CH_2$, $^3J_{H,H}$ = 7.4 Hz), 3.24−3.31 (m, 4 H, NCH_2), 3.37−3.45 (m, 4 H, NCH_2), 3.76 [sept, 4 H, CH(CH$_3$)$_2$, $^3J_{H,H}$ = 6.2 Hz], 6.19 (t, 4 H, H_{ring}, $^3J_{H,H}$ = 9.1 Hz), 6.35 (d, 4 H, H_{ring}, $^3J_{H,H}$ = 11.5 Hz), 6.40 (d, 4 H, H_{ring}, $^3J_{H,H}$ = 11.7 Hz), 6.81−6.88 (m, 8 H, H_{ring}) ppm. ^{13}C{^{1}H} NMR (C_6D_6, 100.40 MHz, 25 °C): δ = 23.7, 24.0, 32.1, 47.4, 48.4, 111.3, 111.8, 115.8, 134.5, 134.7, 160.0, 161.3 ppm.

X-ray Crystallographic Studies of 3: Crystals of $C_{23}H_{30}N_4Zn$ were grown from a toluene solution. A suitable crystal was covered with mineral oil (Aldrich) and mounted on a glass fibre. The crystal was transferred directly to the −70 °C cold stream of an STOE IPDS diffractometer (Ag-K_α radiation). Subsequent computations were carried out with an Intel PIII PC. Data collection and refinement: SHELXS-97,[14] SHELXL-97;[15] monoclinic, space group *C*2/*c* (no. 15); lattice constants *a* = 1279.76(7), *b* = 1542.66(8), *c* = 2170.34(13) pm, β = 97.635(7)°, *V* = 4246.8(4) 10^6 pm^3, *Z* = 8; μ(Ag-K_α) = 0.623 mm^{-1}; $2\theta_{max.}$ = 38.00°; 3475 (R_{int} = 0.1560) independent reflections measured, 2660 of which were considered observed with $I > 2\sigma(I)$; max. residual electron density 1.718 and −0.721 e/A^{-3}; 262 parameters (all non-hydrogen atoms were calculated anisotropic; the positions of the H atoms were calculated for idealised positions) *R*1 = 0.0881; *wR*2 = 0.2182. CCDC-194178 contains the supplementary crystallographic data for this paper. These data can be obtained free of charge at www.ccdc.cam.ac.uk/conts/retrieving.html [or from the Cambridge Crystallographic Data Centre, 12 Union Road, Cambridge CB2 1EZ, UK; Fax: (internat.) + 44-1223/336-033; E-mail: deposit@ccdc.cam.ac.uk].

Acknowledgments

This work was supported by the Deutsche Forschungsgemeinschaft (Graduiertenkolleg: Synthetische, mechanistische und reaktionstechnische Aspekte von Metallkatalysatoren) and the Fonds der Chemischen Industrie.

[1] R. H. Holm, *Prog. Inorg. Chem.* **1971**, *14*, 241−401, and references therein.
[2] P. W. Roesky, *Chem. Soc., Rev.* **2000**, *29*, 335−345, and references therein.
[3] M. R. Bürgstein, H. Berberich, P. W. Roesky, *Organometallics* **1998**, *17*, 1452−1454.
[4] P. W. Roesky, *Inorg. Chem.* **1998**, *37*, 4507−4511.
[5] S. Schulz, M. Nieger, H. Hupfer, P. W. Roesky, *Eur. J. Inorg. Chem.* **2000**, 1623−1626.
[6] M. R. Bürgstein, N. P. Euringer, P. W. Roesky, *J. Chem. Soc., Dalton Trans.* **2000**, 1045−1048.
[7] C. E. Forbes, R. H. Holm, *J. Am. Chem. Soc.* **1970**, *92*, 2297−2303.
[8] K. J. Franz, N. Singh, B. Spingler, S. J. Lippard, *Inorg. Chem.* **2000**, *39*, 4081−4092.
[9] [9a] S. Imajo, K. Nakanishi, M. Roberts, S. J. Lippard, T. Nozoe, *J. Am. Chem. Soc.* **1983**, *105*, 2071−2073. [9b] L. H. Doerrer, S. J. Lippard, *Inorg. Chem.* **1997**, *36*, 2554−2563.
[10] P. W. Roesky, *J. Organomet. Chem.* **2000**, *603*, 161−166.
[11] L. A. Gayler, G. Wilkinson, *Inorg. Synth.* **1979**, *19*, 253−257.
[12] M. H. Abram, P. H. Rolfe, *J. Organomet. Chem.* **1967**, *7*, 35−43.

 © 2003 Wiley-VCH Verlag GmbH & Co. KGaA, Weinheim

[13] H. Müller, L. Rösch, W. Erb, R. Zeisberg, *J. Organomet. Chem.* **1977**, *140*, C17−C20.
[14] G. M. Sheldrick, *SHELXS-97, Program of Crystal Structure Solution*, University of Göttingen, Germany, **1997**.
[15] G. M. Sheldrick, *SHELXL-97, Program of Crystal Structure Solution*, University of Göttingen, Germany, **1997**.

Received January 7, 2003

 © 2003 Wiley-VCH Verlag GmbH & Co. KGaA, Weinheim

Structures and Thermodynamics of the Sulfuranes SF_3CN and $SF_2(CN)_2$ as well as of the Persulfurane $SF_4(CN)_2$ − An ab initio MO Study by the G3(MP2) Method[‡]

Yana Steudel[a] and Ralf Steudel*[a]

Keywords: Sulfuranes / Sulfur / Cyanides / Fluorides / Transition states / Reaction mechanisms

At the G3(MP2) level of theory the *trans* isomer **1a** of the hypothetical molecule $SF_4(CN)_2$ is more stable than the *cis* isomer **1b** by 8 kJ·mol^{-1}. The isomerization of **1a** to **1b** requires an activation enthalpy of 319 kJ·mol^{-1} at 298 K. The decomposition of *trans*-$SF_4(CN)_2$ to $SF_2(CN)_2$ and F_2 is endothermic (ΔH^o_{298} = 395 kJ·mol^{-1}) but the elimination of FCN from *trans*-$SF_4(CN)_2$ is exothermic by −7 kJ·mol^{-1}. The elimination of $(CN)_2$ from *cis*-$SF_4(CN)_2$ is exothermic by −137 kJ·mol^{-1}. The activation enthalpies for the latter two reactions were calculated as 251 and 311 kJ·mol^{-1}, respectively. Thus, $SF_4(CN)_2$ should be a thermally stable compound. In the sulfuranes SF_3CN and $SF_2(CN)_2$ the CN ligands prefer the equatorial positions; mutual exchange of an axial F atom by an equatorial CN group requires a reaction enthalpy of 51 kJ·mol^{-1} [SF_3CN] or 58 kJ·mol^{-1} [$SF_2(CN)_2$].
(© Wiley-VCH Verlag GmbH & Co. KGaA, 69451 Weinheim, Germany, 2003)

Introduction

The sulfur fluorides SF_4 and SF_6 are both important industrial products[1] and highly interesting molecules from a theoretical point of view. As so-called hypervalent or − better − hypercoordinate species they have attracted much attention.[2] In addition, numerous mixed derivatives of the types SF_3X and SF_5X have been prepared.[3] Fluorination of either dirhodane $(SCN)_2$ or SF_3CN by elemental fluorine produces SF_5CN, see Equations (1) and (2).[4−6]

$$(SCN)_2 + 5\,F_2 \rightarrow 2\,SF_5CN \quad (1)$$

$$SF_3CN + F_2 \rightarrow SF_5CN \quad (2)$$

Evidently, SF_3CN will be an intermediate in Equation (1). According to a combined electron diffraction and microwave spectroscopic investigation the molecule SF_5CN has C_{4v} symmetry in the gas phase.[5] While gaseous SF_5CN is stable up to 350 °C in a flow reactor at low pressures,[4] the related compound $SF_4(CN)_2$ has never been prepared. The same holds for the other members of the series $SF_{6-x}(CN)_x$ with $x > 2$.

To investigate the thermodynamic and the thermal stability of $SF_4(CN)_2$ we have studied for the first time the hypothetical decomposition reactions, presented in Equations (3) to (7) of this molecule using ab initio MO methods.

$$SF_4(CN)_2 \rightarrow SF_2(CN)_2 + F_2 \quad (3)$$

$$SF_4(CN)_2 \rightarrow SF_3CN + FCN \quad (4)$$

$$SF_4(CN)_2 \rightarrow SF_4 + (CN)_2 \quad (5)$$

All the expected decomposition products are experimentally known compounds. SF_3CN and $SF_2(CN)_2$ are accessible by metathesis reactions of SF_4 with Me_3SiCN at low temperatures [Equations (6) and (7)].[7]

$$SF_4 + Me_3SiCN \rightarrow SF_3CN + Me_3SiF \quad (6)$$

$$SF_3CN + Me_3SiCN \rightarrow SF_2(CN)_2 + Me_3SiF \quad (7)$$

An earlier report[8] on the synthesis of $SF_2(CN)_2$ according to Equations (6) and (7) was said to be partly in error.[7] SF_3CN is a colorless liquid which is stable at room temperature for a few days but slowly decomposes according to Equation (8).[7]

$$2\,SF_3CN \rightarrow SF_4 + SF_2(CN)_2 \quad (8)$$

The structure of SF_3CN has been determined by electron diffraction in the gas phase as well as by ab initio MO calculations at the MP2/6-31G* level of theory.[9] The molecule is of C_1 symmetry; its structure can be derived from

[‡] Sulfur Compounds, 227. Part 226: R. Steudel, *Chem. Rev.* **2002**, *102*, 3905.

[a] Institut für Chemie, Sekr. C2, Technische Universität Berlin, 10623 Berlin, Germany
Fax: (internat.) + 49-30/31426519
E-mail: steudel@schwefel.chem.tu-berlin.de

the structure of SF_4 by replacement of an equatorial fluorine atom by a cyano ligand. $SF_2(CN)_2$ is a colorless solid which rapidly decomposes at room temperature.[7] No structural analysis or theoretical treatment of this molecule has been published yet.

Calculations

Standard ab initio MO calculations were performed by using the Gaussian 98 series of programs.[10] The energies of various equilibrium structures and transition states were examined at the G3(MP2) level of theory.[11] In brief, the G3(MP2) method is a composite procedure which provides an accurate approximation to a high level of theory at QCISD(T)/GTMP2LARGE//MP2(full)/6-31G(d), with the incorporation of zero-point energy [calculated from HF/6-31G(d) vibrational wavenumbers, scaled by 0.8929] and higher level corrections. For small molecules this level of theory is usually within 6 kJ·mol^{-1} of accurate experimental values.[11] In the case of the hypervalent SF_6 molecule the related G2(MP2) method — using the same geometry calculation as in G3(MP2) — reproduced the very accurate experimental enthalpy of formation within 7.5 kJ·mol^{-1}.[12] A charge density analysis, at the MP2(full)/6-31G(d) level, was performed using the natural bond orbital (NBO) approach.[13] NBO atomic charges of small molecules have recently been demonstrated to agree well with experimental values obtained from X-ray diffraction data.[14] Unless otherwise noted, all relative energies reported in this publication are given as $\Delta H°_{298}$ and correspond to the G3(MP2) level, while structural parameters were obtained at the MP2(full)/6-31G(d) level.

The transition states obtained were characterized by one imaginary vibrational wavenumber (**TS1**: 693i; **TS2**: 264i; **TS3**: 694i; **TS4**: 890i) whereas the wavenumbers of the structures of minimal energy were all real. The intrinsic reaction coordinates were calculated at the HF/6-31G* level.[15]

Results and Discussion

Geometrical Structures

To check the accuracy of the G3(MP2) method for the treatment of hypervalent compounds the enthalpies of F_2, SF_4 and SF_6 were calculated and the reaction enthalpy for the formation of SF_6 from F_2 + SF_4 was obtained as

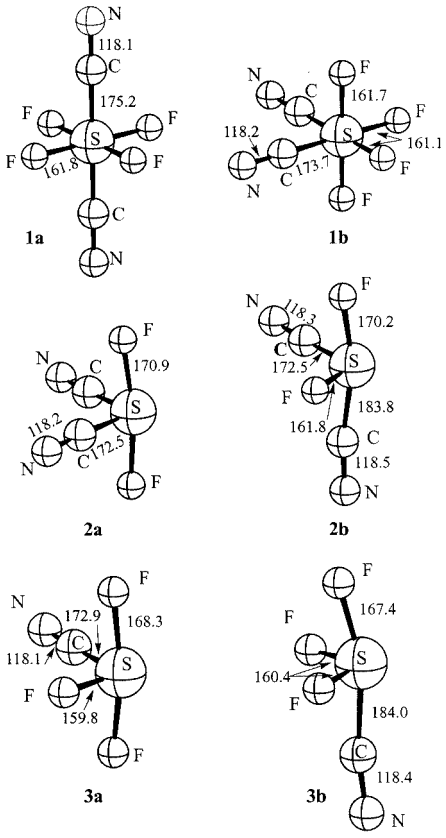

Figure 1. Molecular structures and bond lengths [pm] of two isomers each of the persulfurane $SF_4(CN)_2$ (**1a**, **1b**), the sulfurane $SF_2(CN)_2$ (**2a**, **2b**) and of the sulfurane $SF_3(CN)$ (**3a**, **3b**), calculated at the MP2(full)/6-31G(d) level of theory

−439.1 kJ·mol^{-1} at 0 K. From the best available experimental enthalpies of formation of these compounds[12] the reaction enthalpy is calculated as −450 ± 20 kJ·mol^{-1} at 0 K. This agreement is quite satisfactory.

The sulfuranes $SF_2(CN)_2$ and SF_3CN as well as the persulfurane $SF_4(CN)_2$ given in Equations (3) to (5) exist as several isomers depending on the axial/equatorial or *cis*/*trans* position of the cyano ligands. The molecular structures and internuclear distances of these six isomers are shown in Figure 1; additional geometrical parameters are listed in Table 1.

In the case of the two octahedral molecules $SF_4(CN)_2$ the isomer with the *trans* position of the two CN ligands (**1a**) is slightly more stable than the *cis* isomer **1b**, by 8 kJ·mol^{-1}. The NBO atomic charges [a.u.] on the fluorine atoms are −0.49 ± 0.01 in these isomers while the carbon atoms bear

Table 1. Selected bond angles of the sulfuranes $SF_2(CN)_2$ and SF_3CN [°], calculated at the MP2(full)/6-31G(d) level of theory

$SF_2(CN)_2$ (**2a**)	$SF_2(CN)_2$ (**2b**)	SF_3CN (**3a**)	SF_3CN (**3b**)
N1−C1−S 175.9	N1−C1−S 170.0	N−C−S 176.3	N−C−S 170.2
N2−C2−S 175.9	N2−C2−S 176.1	F1−S−C86.5	C−S−F1 163.0
F−S−F 170.7	F−S−F 84.7	F3−S−C 103.3	F2−S−F3 112.0
C−S−C 102.9	C−S−C 87.3	F1−S−F2 169.9	F1−S−F2 85.3
F2−S−C1 87.1	F2−S−C1 165.1	F1−S−F2 87.2	F3−S−C 85.3

 © 2003 Wiley-VCH Verlag GmbH & Co. KGaA, Weinheim

a small positive charge of 0.07 in **1a** and 0.03 in **1b**. Therefore, the nonbonding F···F interactions must be strongly repulsive while the nonbonding F···C interactions will be weak as far as Coulomb forces are concerned. The sulfur atoms are highly positively charged (+2.31 in both cases) and the nitrogen atoms are slightly negative (−0.22).

Isomer **1a** is of D_{4h} symmetry and **1b** is of C_{2v} symmetry. All bond angles in **1a** are exactly 90 or 180°, i.e. the SCN groups are strictly linear; in **1b** the SCN bond angle is 179.6°. The space requirement of the cyano ligands seems to be slightly larger than that of the fluorine atoms since the C−S−C angle in **1b** is 92.3° while the F−S−F angle in the same plane is only 87.5°. All other bond angles of this molecule are within 0.5° of either 90 or 180°.

The calculated bond lengths of *trans*-$SF_4(CN)_2$ are in fair agreement with the experimental data reported for the related molecule SF_5CN,[5] although ab initio MO calculations at the MP2(full)/6-31G(d) level slightly overestimate the internuclear distances. In addition, the bonds become progressively shorter as the fluorine content of the molecule increases. Thus, the S−F distances in SF_5CN are 155.8 and 156.6 pm compared to 161.8 pm in **1a**. Similarly, the C−N and S−C distances of 115.4 pm and 176.5 pm, respectively, in SF_5CN support our results for the corresponding bonds of **1a** which are 118.1 and 175.2 pm, respectively.

The sulfurane molecules of the type $SF_{4-x}(CN)_x$ can be derived from a trigonal bipyramid in which one corner is empty (or occupied by a lone pair of electrons). In this type of molecule the axial and equatorial positions are not equivalent. Since the electronegativity of the CN group is lower than that of the fluorine atoms the preferred position for the CN ligands in the two sulfuranes $SF_2(CN)_2$ and SF_3CN should be the equatorial plane, as observed in the case of other sulfuranes.[16] In fact, the symmetrical isomer of $SF_2(CN)_2$ (**2a**) with both CN ligands in the equatorial plane is by 58 kJ·mol^{-1} more stable than the less symmetrical form with one CN ligand equatorial and the other in an axial position (**2b**). When we tried to optimize a structure with both CN groups in axial positions (**2c**), the molecule rearranged to isomer **2a**. In the case of SF_3CN the CN ligand is in an equatorial position in the most stable isomer **3a**; the isomer **3b** with an axial CN ligand is by 51 kJ·mol^{-1} less stable than **3a**.

The geometrical parameters calculated for **3a** may be compared with the electron diffraction data of this molecule.[9] The bond lengths [pm] are as follows (calcd./exp. data): S−$F_{eq.}$ 159.8/155.2(4), S−F_{ax} 168.3/165.7(3), S−C 172.9/173.6(8), C−N 118.1/115.9(4). Given the systematic difference between the calculated r_e and the experimental r_a bond lengths the agreement is satisfactory. The NBO atomic charges of **3a** are as follows: $F_{eq.}$ −0.46, F_{ax} −0.59, S +1.85, C +0.01, N −0.21.

In all sulfurane isomers of the type SF_3CN and $SF_2(CN)_2$ the angles between the two axial S−X bonds are smaller than 180° and these axial bonds are bent away from the formally empty corner of the trigonal bipyramid, i.e. away from the position of the anticipated lone pair at the sulfur atom. The deviation from linearity is 10 ± 1° in the case of **2a** and **3a** but 18 ± 1° in the case of the less stable isomers **2b** and **3b** (see Table 1). This structural feature is well known from SF_4.[2]

The SCN groups are practically linear in the octahedral species **1a** and **1b** (179.8 ± 0.2°) but slightly bent in the various isomers of SF_3CN and $SF_2(CN)_2$: the equatorial SCN groups show bond angles of α = 176.1 ± 0.2° while the axial SCN groups are more strongly bent (α = 170.1 ± 0.1°).

Transition States and Thermodynamics

The reaction according to Equation (3) is strongly endothermic and therefore can be ruled out for any spontaneous decomposition of $SF_4(CN)_2$ at moderate temperatures. Using the most stable isomers of the reactants, the enthalpy change of reaction shown in Equation (3) is +395 kJ·mol^{-1} at 298 K. Under the same conditions reactions shown in Equations (4) and (5) are exothermic by −137 and −7 kJ·mol^{-1}, respectively. The Gibbs energies ($\Delta G°_{298}$) of the reactions according to Equations (3) to (5) are +341, −187 and −41 kJ·mol^{-1}, respectively, reflecting the increase in entropy during dissociation. From these data it follows that only the reverse reaction according to Equation (3) is a potential route for the synthesis of $SF_4(CN)_2$ at low temperatures.

The transition states for the decomposition reactions according to Equations (4) and (5) have been located on the potential energy hypersurface and their structures are shown in Figure 2. Starting from the most stable isomer **1a** only FCN can be eliminated directly. The corresponding transition state (**TS1**) is shown in Figure 2. The activation

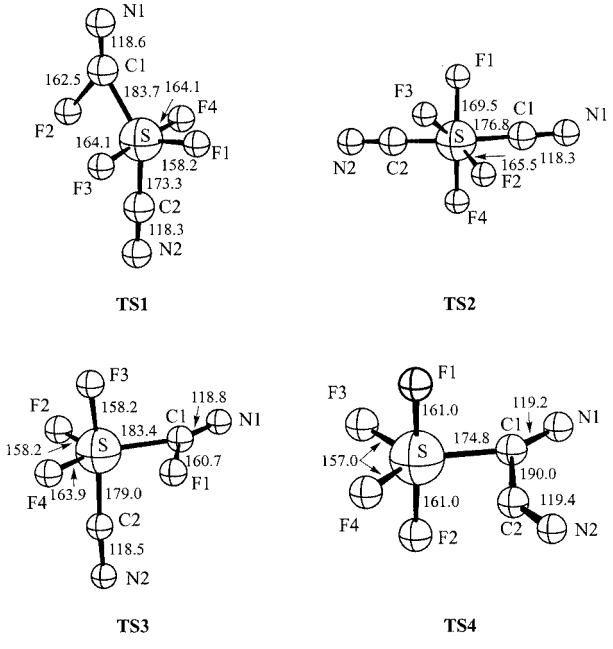

Figure 2. Molecular structures and bond lengths [pm] of the transition states for the elimination of FCN from *trans*-$SF_4(CN)_2$ **1a** (**TS1**), for the *cis* ⇄ *trans* isomerization between **1a** and **1b** (**TS2**), for the elimination of FCN from **1b** (**TS3**) and for the elimination of $(CN)_2$ from **1b**, calculated at the MP2(full)/6-31G(d) level of theory

 © 2003 Wiley-VCH Verlag GmbH & Co. KGaA, Weinheim

barriers are $\Delta H^{\neq}_{298} = 251\ kJ{\cdot}mol^{-1}$ and $\Delta G^{\neq}_{298} = 251\ kJ{\cdot}mol^{-1}$.

In the case of Equation (5) an intramolecular isomerization has to take place first to generate **1b** in which the two CN ligands are neighboring. Structure **1b** may then decompose with elimination of either FCN or $(CN)_2$. The transition state for the isomerization of **1a** to **1b** (**TS2**) is also shown in Figure 2. The activation enthalpy for this reaction is $319\ kJ{\cdot}mol^{-1}$ ($\Delta G^{\neq}_{298} = 317\ kJ{\cdot}mol^{-1}$). The subsequent decomposition of **1b** to SF_3CN + FCN requires an activation enthalpy of $271\ kJ{\cdot}mol^{-1}$ ($\Delta G^{\neq}_{298} = 271\ kJ{\cdot}mol^{-1}$) while the elimination of $(CN)_2$ from **1b** can be initiated by an activation enthalpy of $311\ kJ{\cdot}mol^{-1}$ ($\Delta G^{\neq}_{298} = 309\ kJ{\cdot}mol^{-1}$). The overall activation barriers starting from the most stable isomer **1a** are consequently $\Delta G^{\neq}_{298} = 317 + 271 = 588\ kJ{\cdot}mol^{-1}$ for the reaction according to Equation (4) and $\Delta G^{\neq}_{298} = 317 + 309 = 626\ kJ{\cdot}mol^{-1}$ for the reaction according to Equation (5). Evidently, these energies are unrealistically high since, for instance, the homolytic dissociation of SF_6 into SF_5 and an F atom requires a reaction enthalpy of only $453\ kJ{\cdot}mol^{-1}$.[17] Therefore, one would expect that *trans*-$SF_4(CN)_2$ (**1a**) also breaks down into two radicals rather than isomerizing intramolecularly with subsequent elimination of either FCN or $(CN)_2$ if a Gibbs activation energy of more than $600\ kJ{\cdot}mol^{-1}$ energy is provided.

The structures of the transition states for the elimination reactions according to Equations (4) and (5) (**TS3** and **TS4**) are shown in Figure 2. Their geometries (C_1 symmetry) are most interesting. In **TS3** a bent FCN unit is connected to the sulfur atom by both a weak S−F bond of length 208.3 pm and a C−S bond of length 183.4 pm; all four atoms are located essentially in one plane with an F−C−N angle of 139.4° (torsion angle N7−C−F2−S: −174°). The other two S−F bonds in that same plane have decreased in length from 161.4 ± 0.3 pm in **1b** to 158.2 and 159.9 pm, respectively, in **TS3**, while the fourth S−F bond has increased in length to 163.9 pm. The structure of **TS4** is characterized by a weak C−C bond of length 190.0 pm, much longer than calculated for isolated $(CN)_2$ (138.1 pm). The two CN units are exactly co-planar. The C−S−C angle is 81.6° but the two C−S bonds are very different with distances of 174.8 and 238.6 pm. In contrast, the two C−N bonds are almost identical with 119.2 and 119.4 pm, slightly longer than in **1b** (118.2 pm) and in $(CN)_2$ (118.5 pm). In other words, it is only *one* CN group which is moving away from the sulfur atom on transformation of **1b** into **TS4**. The other CN group is just bending; its S−C−N angle decreases from 179.6° in **1b** to 145.3° in **TS4**. The SF_4 unit of **TS4** is already very close in geometry to the isolated SF_4 molecule. Despite the low symmetry the S−F bond lengths of **TS4** are pairwise identical and the $F_{ax}-S-F_{ax}$ angle is 174.4°.

We did not succeed in localizing a transition state for the elimination of F_2 from either **1a** or **1b**. This strongly endothermic reaction may proceed without any additional activation energy.

Summarizing, it follows from the above thermodynamic data that the isomerization **1a**→**1b** is highly unfavorable and $SF_4(CN)_2$ is expected to decompose, if at all, with elimination of FCN from the ground state structure **1a**. However, the height of the barriers indicates that $SF_4(CN)_2$ molecules will be quite stable as far as unimolecular dissociation reactions are concerned.

Acknowledgments

We are grateful to Priv.-Doz. Dr. Dieter Lentz for suggesting this investigation to us. This work was supported by the Deutsche Forschungsgemeinschaft, the Verband der Chemischen Industrie and the Konrad-Zuse-Zentrum für Informationstechnik Berlin.

[1] *Ullmann's Encyclopedia of Industrial Chemistry*, VCH, Weinheim, **1988**, vol. A11, p. 337.
[2] Y. Drozdova, R. Steudel, W. Koch, K. Miaskiewicz, I. A. Topol, *Chem. Eur. J.* **1999**, *5*, 1936. A. E. Reed, F. Weinhold, *J. Am. Chem. Soc.* **1986**, *108*, 3586. A. E. Reed, P. von R. Schleyer, *J. Am. Chem. Soc.* **1990**, *112*, 1434. D. L. Cooper, T. P. Cunningham, J. Gerratt, P. B. Karadakov, M. Raimondi, *J. Am. Chem. Soc.* **1994**, *116*, 4414. R. Ponec, X. Gironés, *J. Phys. Chem. A* **2002**, *106*, 9506.
[3] R. D. Verma, R. L. Kirchmeier, J. M. Shreeve, *Adv. Inorg. Chem.* **1994**, *41*, 125. D. Lentz, K. Seppelt, in: *Chemistry of Hypervalent Compounds* (Ed.: K. Akiba), VCH-Wiley, New York, **1999**, p. 295.
[4] O. Loesking, H. Willner, *Angew. Chem.* **1989**, *101*, 1283.
[5] J. Jacobs, G. S. McGrady, H. Willner, D. Christen, H. Oberhammer, P. Zylka, *J. Mol. Struct.* **1991**, *245*, 275.
[6] J. Jacobs, S. E. Ulic, H. Willner, G. Schatte, J. Passmore, S. V. Sereda, C. T. Stanley, *J. Chem. Soc., Dalton Trans.* **1996**, 383.
[7] J. Jacobs, H. Willner, *Z. Anorg. Allg. Chem.* **1993**, *619*, 1221.
[8] R. C. Kumar, J. M. Shreeve, *Z. Naturforsch., Teil B* **1981**, *36*, 1407.
[9] H.-G. Mack, H. Oberhammer, J. Jacobs, M. Kronberg, H. Willner, *Inorg. Chem.* **1996**, *35*, 806.
[10] M. J. Frisch, G. W. Trucks, H. B. Schlegel, G. E. Scuseria, M. A. Robb, J. R. Cheeseman, V. G. Zakrzewski, J. A. Montgomery, R. E. Stratmann, J. C. Burant, S. Dapprich, J. M. Millam, A. D. Daniels, K. N. Kudin, M. C. Strain, O. Farkas, J. Tomasi, V. Barone, M. Cossi, R. Cammi, B. Mennucci, C. Pomelli, C. Adamo, S. Clifford, J. Ochterski, G. A. Petersson, P. Y. Ayala, Q. Cui, K. Morokuma, D. K. Malick, A. D. Rabuck, K. Raghavachari, J. B. Foresman, J. Cioslowski, J. V. Ortiz, B. B. Stefanov, G. Liu, A. Liashenko, P. Piskorz, I. Komaromi, R. Gomperts, R. L. Martin, D. J. Fox, T. Keith, M. A. Al-Laham, C. Y. Peng, A. Nanayakkara, C. Gonzalez, M. Challacombe, P. M. W. Gill, B. G. Johnson, W. Chen, M. W. Wong, J. L. Andres, M. Head-Gordon, E. S. Replogle, J. A. Pople, *Gaussian 98, Revision A.6*, Gaussian, Inc., Pittsburgh, PA, **1998**.
[11] L. A. Curtiss, P. C. Redfern, K. Raghavachari, V. Rassolov, J. A. Pople, *J. Chem. Phys.* **1999**, *110*, 4703.
[12] Y.-S. Cheung, Y.-J. Chen, C. Y. Ng, S.-W. Chiu, W.-K. Li, *J. Am. Chem. Soc.* **1995**, *117*, 9725 and references cited therein.
[13] A. E. Reed, L. A. Curtiss, F. Weinhold, *Chem. Rev.* **1988**, *88*, 899.
[14] M. Messerschmidt, A. Wagner, M. W. Wong, P. Luger, *J. Am. Chem. Soc.* **2002**, *124*, 732.
[15] K. Fukui, *Acc. Chem. Res.* **1981**, *14*, 363; C. Gonzales, H. B. Schlegel, *J. Phys. Chem.* **1989**, *90*, 2154.
[16] R. J. Gillespie, I. Hargittai, *The VSEPR Model of Molecular Geometry*, Allyn and Bacon, Boston, **1991**.
[17] C. W. Bauschlicher, A. Ricca, *J. Phys. Chem. A* **1998**, *102*, 4722.
Received January 13, 2003

 © 2003 Wiley-VCH Verlag GmbH & Co. KGaA, Weinheim

Calculated Enthalpies for Dimerisation of Binary, Unsaturated, Main-Group Element Hydrides as a Means to Analyse Their Potential for Multiple Bonding

Hans-Jörg Himmel[a]

Dedicated to Professor Hansgeorg Schnöckel

Keywords: Main-group element hydrides / Dimerization / Enthalpy / Multiple bonding / Calculations

Herein, the dimerisation of subvalent, binary, main-group element hydrides with the potential for multiple bonding is studied using both hybrid DFT (B3LYP) and ab initio [MP2 and CCSD(T)] methods. The [2+2] cycloaddition is an important and characteristic reaction of derivatives of ethylene. A comparison of dimerisation reactions for several compounds with the potential for multiple bonding should, therefore, shed light on the properties of these species. Our study includes the hydrides E_2H_2 (E = B, Al, Ga, N P or As), E_2H_4 (E = C, Si or Ge) and ENH_4 (E = B, Al or Ga) and their dimers. Several isomeric forms of the monomers and dimers have to be considered. The trends within a group and a period are established and the factors responsible for them are discussed. It turns out that, generally, the enthalpies for dimerisation increase for heavier homologues, reflecting that the most important factor is the reduced strength of the E–E bonds in the monomers prior to dimerisation and, to some degree, also the reduced ring strain in the cyclic dimers. The exceptions are the dimerisations of B_2H_2 and Al_2H_2, both of which lead to the tetrahedral E_4H_4 species (E = B or Al). Dimerisation of Al_2H_2 is associated with a smaller enthalpy than that for the dimerisation of B_2H_2. Comparisons and analyses are made complicated because of the changes in the structures of the isomeric global minima between homologues.

(© Wiley-VCH Verlag GmbH & Co. KGaA, 69451 Weinheim, Germany, 2003)

Introduction

There is an ongoing interest in the characterization of binary compounds of the heavier main-group elements with the potential for multiple bonding.[1−9] As early as 1976, for example, a first stable dialkylgermylene, $Dis_2GeGeDis_2$ [Dis = bis(trimethylsilyl)methyl] was synthesized and later characterized by X-ray diffraction to exhibit a nonplanar geometry with a Ge−Ge bond length of 2.347 Å and an angle sum of 348° at each of the Ge atoms.[10] At the same time, the first corresponding tin compound, $[Sn\{CH(SiMe_3)_2\}_2]_2$, was structurally characterized.[11] It took 26 more years, however, until the first compounds of Ge and Sn formally isoelectronic to an alkyne were discovered, both exhibiting bent *trans*-type structures with Ge−Ge and Sn−Sn bond lengths of 2.2850(5) and 2.6675(4) Å, respectively.[12,13] Only in the last two decades has more information about these species came to light, with the most-celebrated successes lying almost exclusively in the field of binary group-14 and group-15 element compounds and group-13/15 compounds with a direct bond between a group-13 and a group-15 element.[14]

B/N compounds with a direct bond between a boron and a nitrogen atom have been well known for a long time, and the isoelectronic and isolobal connections between alkenes and aminoboranes R_2NBR_2 (“inorganic ethylene”), cyclobutanes and dimeric aminoboranes $[(R_2NBR_2)_2]$, cyclobutenes and diazadiboretidines $[(RNBR)_2]$, and benzene and borazine $(RNBR)_3$ are well established.[15] Monomeric compounds, however, with tricoordinated Al or Ga atoms and the general formula $R_2AlNR'_2$ and $R_2GaNR'_2$ are stable under normal conditions only in the presence of bulky substituents at Al, Ga and/or N.[16−18] Otherwise, they are stable only as oligomers of the general formula $[R_2MNR'_2]_n$, with *n* being often 2 or 3. Recently, the monomers H_2AlNH_2, H_2GaNH_2 and H_2InNH_2 were generated and characterized in a matrix of solid Ar at 12 K.[19]

Despite considerable effort, binary group-13 element compounds with the potential for multiple bonding, RGaGaR (R being a sterically demanding organic group), have been synthesized and characterized only very recently. Species that are formally valence-isoelectronic with acetylene were discovered with the synthesis of compounds of the formula $Na_2[ArGaGaAr]$ (e.g., Ar = $Mes^*{}_2C_6H_3$ or 2,4,6-$i Pr_3C_6H_2$).[20] An adequate description of the Ga−Ga bond in related compounds is at present hotly debated.[21−24] Very recently, a neutral compound ArGaGaAr (Ar = 2,6-$Dipp_2C_6H_3$, Dipp = 2,6-$i Pr_2C_6H_3$) has been synthesized as

[a] Institut für Anorganische Chemie der Universität Karlsruhe, Engesserstr., Geb. 30.45, 76128 Karlsruhe, Germany

the first derivative of a compound that is formally valence-isoelectronic with ethylene.[25] Additionally, the hydride HGaGaH was generated in an Ar matrix at 12 K as one of the products of the reaction between Ga_2 and H_2, and it was characterized experimentally by its IR spectrum. The antisymmetric ν(Ga−H) stretching vibration of this species occurs at a wavenumber not far away from that of GaH (also isolated in a matrix of solid Ar).[26] This result indicates that the interaction between the Ga atoms in HGaGaH cannot be very strong. Finally, a molecule of the general formula ArInInAr (Ar again being 2,6-$Dipp_2C_6H_3$, Dipp = 2,6-*i*$Pr_2C_6H_3$) was characterized in the solid state.[27] The In−In interaction [bond length of 2.9786(5) Å] is weak, however, and therefore this compound cannot feature a strong In−In bond.

This work follows two others dealing with the differences in the chemistry of binary, main-group element compounds with the potential for multiple bonding. In the first of these two previous accounts, we have reported the trends of theoretically determined heats of hydrogenation for several binary, main-group element hydrides.[28] Heats of hydrogenation have been used extensively in the past to determine the degree of unsaturation of hydrocarbons and their derivatives. Our survey also included a comparison between the heats of hydrogenation of the model compounds Na_2[HGaGaH], $[HGaGaH]^{2-}$ and HGaGaH. The results indicate that the Na^+ ions in Na_2[HGaGaH] are deeply engaged in the bonding. Therefore, we and others[29] have suggested to describe this species and its derivatives as "Na_2Ga_2" cluster compounds. In the second report, we analyzed the energies for fragmentation.[30] To this end, dissociation was separated into two processes: the first one consists of fragmentation into fragments that still exhibit the same geometry as they had previously before fragmentation; in the second process, the fragments relax into their electronic ground state and their global energy-minimum structure. The separation in the two processes allows for a much more accurate determination of the bond energies, which can, at least principally, also be verified experimentally. Herein, we evaluate the standard enthalpies for dimerisation of several binary main-group element hydrides that are formally valence-isoelectronic to ethylene. Cycloaddition is a very well known and thoroughly investigated process for ethylene and its derivatives. Dimerisation reactions of some other corresponding binary main-group element compounds have been looked at earlier. To name just two of many examples, very recently the [2+2] cycloaddition reactions of a stiba(III)alkene and an arsa(III)imine were investigated experimentally,[31] and the [2+2] cycloaddition enthalpies for 1,3-disilacyclobutanes were determined by quantum chemical calculations.[32] In this paper, the calculated trends down the group and within a period will be discussed for the compounds under consideration. It should be noted that in this work we intend to accumulate information about the *chemistry* of subvalent, binary, main-group element hydrides. It is especially our aim to analyse theoretical aspects of the chemistry that can, at least in principle, be verified experimentally, although some species are too reactive to be investigated in experiments that rely on presently known techniques. A close inspection of the molecular orbitals or the electron density distribution is not the topic of this work.

Calculational Details

Calculations relied on the GAUSSIAN 98 programme package.[33] The B3LYP hybrid-DFT method, in combination with a 6-311+G(2df,p) basis set, was first used to pre-optimize the structures and to calculate their vibrational modes. In the second step, the structures were again fully optimized applying the MP2 method and a 6-311+G(2df,p) basis set. The calculated MP2 energies were corrected by their zero-point energies and thermally by their vibrational, rotational and translational energies at 298.2 K (all corrections were taken from the B3LYP calculations) to first give reaction energies at 298 K; then, *RT* (2.5 kJ·mol^{-1}) was subtracted, where necessary, to obtain the standard enthalpies for the reactions in the gas phase. Subsequently, the MP2 calculations were repeated, but this time using the TZVPP basis set and employing the TURBOMOLE programme package.[34] The reaction enthalpy values are quoted for all reactions and were derived from the calculations on the B3LYP and MP2 level of theory in combination with the 6-311+G(2df,p) and on the MP2 level of theory in combination with the TZVPP basis set. Tables 1−4 include the calculated dimensions of all the compounds addressed in this work and also first estimates of the enthalpies for dimerisation on the basis of the B3LYP and MP2 methods. Finally, the optimized geometries were used in "single-point" Coupled-Cluster Single Double Triple [CCSD(T)] calculations [again using the 6-311+G(2df,p) basis set and on the basis of the geometry optimized with B3LYP] to calculate the dimerisation energies once again, and (with the help of the zero-point energy and thermal corrections calculated with B3LYP) the dimerisation enthalpies. Table 5 contains all dimerisation energies and enthalpies calculated with the CCSD(T) method.

Results and Discussion

In the course of this discussion, we show that any attempt to connect the different reactivities of the species addressed in this work with the E−E bond character within the reactant is complicated, mainly because of the changes of the structures of the global energy minima between homologues. It is, therefore, crucial for this work to start with a detailed analysis of the global energy-minimum structures for all homologues. Most of these structures have been discussed in earlier works, but they generally have concentrated on only one compound and did not discuss the *differences* in the structures.

In some cases (e.g., for E_2H_2, where E = Al or Ga), the global minimum structures feature no significant E−E interaction [E_2H_2 exhibits a D_{2h}-symmetric ring structure E(μ-H)$_2$E in its lowest-energy isomer].[35,36] In these cases,

 © 2003 Wiley-VCH Verlag GmbH & Co. KGaA, Weinheim

we have considered both the global minimum structure and the isomer that has the best chance for a significant E−E interaction (e.g. the bent *trans* isomer HEEH in the case of E_2H_2).

Structures of the Monomers and Dimers

Group 13 (E = B, Al and Ga)

All E_4H_4 species exhibit a global energy-minimum structure with a tetrahedral E_4 unit. A ring structure defines a local minimum on the potential energy surface only in the case of calculations using the B3LYP method. Ab initio (MP2) methods failed to find a minimum for a cyclic structure. This cyclic structure found using the B3LYP method has an energy 190.5, 138.4 and 98.1 kJ·mol^{-1} (for E = B, Al and Ga, respectively) higher than the one of the tetrahedral global energy-minimum structure. The standard enthalpy differences between both isomers amount to 179.7, 136.9 and 98.7 kJ·mol^{-1}, respectively. For E = B and Al, the E−E distances are smaller for the tetrahedral isomer (1.6750 and 2.5902 Å vs. 1.6695 and 2.6387 Å for E = B and Al, respectively). In the case of Ga_4H_4, the ring structure has a slightly smaller Ga−Ga distance (2.5506 vs. 2.5615 Å). The E−H distances undergo only minuscule alterations (see Table 1). In the light of the calculations carried out using the MP2 method, however, it appears doubtful whether the ring-type structures really do define local minima on the potential energy surface.

For B_4H_4, T_d- and square-planar D_{4h}-symmetric structures have been reported previously.[37] The T_d-symmetric structure was found to be 349 kJ·mol^{-1} lower in energy than the D_{4h}-symmetric one. The B−B and B−H bond lengths for the T_d-symmetric form were calculated to be 1.7098 and 1.1875 Å, respectively. Thus, the B−B distance is very close to the one found experimentally in the known compound B_4Cl_4, which also exhibits a T_d-symmetric structure (1.71 Å).[38] The distances are in satisfying agreement with the results of our calculations (B−B and B−H bond lengths of 1.6695 and 1.1861 Å).

The derivatives $[Al(\eta^5\text{-}C_5Me_5)]_4$,[39] $[Al(SitBu_3)]_4$ [40] and $[AlSi(SiMe_3)_3]_4$,[41] have been synthesized and investigated structurally. They all consist of tetrahedral Al_4 units, in which the Al−Al distances are 2.77, 2.60 and 2.61 Å, respectively. These values are in good agreement with the Al−Al distance of 2.5902/2.6076 Å calculated herein for Al_4H_4. Previous calculations have led to Al−Al and Al−H distances of 2.617 and 1.589 Å.[42] A cyclic Al_4 unit can be stabilized in the presence of donors like NEt_3, resulting in a molecule $[Al_4Br_4(NEt_3)_4]$ in which the Al−Al separation is 2.64 Å.[43] The structures, as calculated for the tetrahedral Ga_4H_4 isomers, are in agreement with earlier accounts (see Figure 1). For example, the Ga−Ga bond

Table 1. Geometrical parameters (bond lengths [Å], bond angles [°]), energies and enthalpies [kJ·mol^{-1}] for isomerization and dimerisation of group-13 element hydrides studied in this work

E	Parameter	E_2H_2 Linear/bent *trans*[a] B3LYP/MP2/MP2TM	E_2H_2 Cyclic[b] B3LYP/MP2/MP2TM	E_2H_2 Cyclic[c] B3LYP	$(E_2H_2)_2$ Tetrahedral[d] B3LYP/MP2 /MP2TM
B	B−B	1.5051/1.5085/1.5099	−	1.6695	1.6750/1.6866/1.6885
	B−H	1.1714/1.1743/1.1715	−	1.1861	1.1813/1.1848/1.1818
	B−B−B		−	80.9	60.0/60.0/60.0
	H−B−B	180/180/180	−		
	ΔE [$(B_2H_2)_2$ cycl. T_d]			190.5	
	ΔH [$(B_2H_2)_2$ cycl. T_d]			179.7	
	ΔH for dim.			−244.3	−424.0/−481.5/−510.0
Al	Al−Al	2.6693/[e]/2.6399	2.9648/2.9274/2.9381	2.6387	2.5902/2.6076/2.6090
	Al−H	1.6213/[e]/1.6109	1.8267/1.8112/1.8148	1.5928	1.5932/1.5881/1.5903
	Al−Al−Al			87.6	60.0/60.0/60.0
	H−Al−Al	119.4/[e]/120.5	35.8/36.1/36.0		
	ΔE [Al_2H_2 D_{2h} − C_{2h}]		−59.7/[e]/−65.5		
	ΔH [Al_2H_2 D_{2h} − C_{2h}]				
	ΔE [$(Al_2H_2)_2$ cycl. T_d]			138.4	
	ΔH [$(Al_2H_2)_2$ cycl. T_d]			136.9	
	ΔH for dim. (D_{2h})			−74.1	−211.0/−185.5/−308.9
	ΔH for dim. (C_{2h})			−193.3	−330.2/[e]/−442.3
Ga	Ga−Ga	2.6090/2.5944/2.5121	3.0385/3.0148/2.9642	2.5506	2.5615/2.5961/2.5198
	Ga−H	1.6291/1.6226/1.5916	1.8758/1.8656/1.8377	1.5778	1.5809/1.5903/1.5560
	Ga−Ga−Ga			86.8	60.0/60.0/60.0
	H−Ga−Ga	120.7/121.7/122.7	35.9/36.1/36.3		
	ΔE [Ga_2H_2 D_{2h} − C_{2h}]		−56.9/−49.4/−48.8		
	ΔH [Ga_2H_2 D_{2h} − C_{2h}]		−58.9/−51.4/−50.8		
	ΔE [$(Ga_2H_2)_2$ cycl. T_d]			98.1	
	ΔH [$(Ga_2H_2)_2$ cycl. T_d]			98.7	
	ΔH for dim. (D_{2h})			−12.4	−111.1/−105.6/−277.7
	ΔH for dim. (C_{2h})			−130.3	−229.0/−208.6/−402.6

[a] Symmetry: $D_{\infty h}$ for B_2H_2, C_{2h} for Al_2H_2 and Ga_2H_2. [b] Symmetry: D_{2h}. [c] Symmetry used in the calculations: C_2. [d] Symmetry: T_d. [e] Calculation failed.

 © 2003 Wiley-VCH Verlag GmbH & Co. KGaA, Weinheim

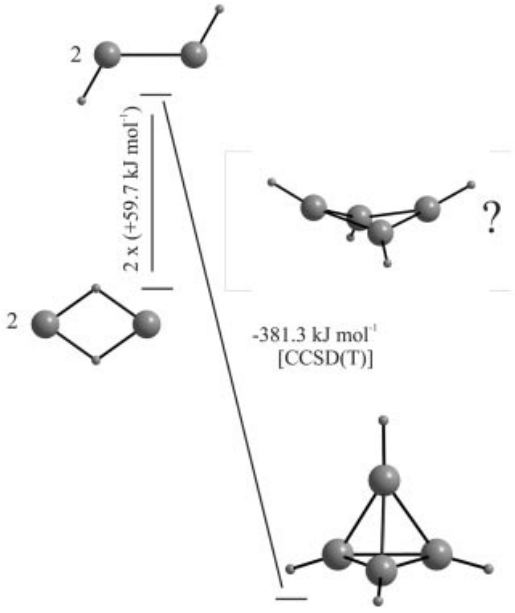

Figure 1. Geometries of cyclic Al(μ-H)$_2$Al, bent *trans*-HAlAlH and the dimerisation product Al_4H_4 with T_d symmetry and enthalpy for dimerisation (the cyclic structure that, according to B3LYP calculations, possibly defines a local energy minimum, is also visualized)

length in Ga_4H_4 was calculated previously to be 2.567 Å.[44] An example of a structurally characterized derivative is provided by the species [Ga{C(SiMe$_3$)$_3$}]$_4$,[45] for which Ga−Ga bond lengths of 2.680−2.702 Å were derived experimentally.

As to the monomers, B_2H_2 has a linear global energy-minimum structure with a triplet electronic ground state ($^3\Sigma_g^-$).[46] The B−B and B−H distances were calculated to be 1.516 and 1.177 Å, respectively. These values are in good agreement with the ones calculated herein (1.5051/1.5085 and 1.1714/1.1743 Å, respectively). Al_2H_2 and Ga_2H_2 both prefer a ring structure with two bridging H atoms, Al(μ-H)$_2$Al and Ga(μ-H)$_2$Ga.[35,36,47,48] According to the calculations presented herein, the bent *trans* structures, HAlAlH and HGaGaH (see Figure 1), have energies 59.7 and 57.0 kJ·mol^{-1} higher than the cyclic global energy-minimum form (the differences in standard enthalpy amount to 59.6 and 58.9 kJ·mol^{-1}, respectively). Previous calculations for bent *trans*-HAlAlH have yielded Al−Al and H−Al bond lengths of 2.782−2.602 Å (with more accurate methods tending to predict smaller values) and 1.608−1.602 Å, with the H−Al−Al bond angle being 119.3−120.0°.[49] These values compare with Al−Al and Al−H distances and H−Al−Al bond angles of 2.6693, 1.6213 Å and 119.4°, respectively, calculated herein. In the case of bent *trans*-HGaGaH, previous DFT calculations have resulted in Ga−Ga and Ga−H bond lengths of 2.5848 and 1.6261 Å and an H−Ga−Ga bond angle of 121.3°,[35] which are in good agreement with the values obtained herein (2.6090/2.5944 and 1.6291/1.6226 Å and 120.7/121.7°, respectively). As already mentioned, a derivative, ArGaGaAr (Ar = 2,6-Dipp$_2$C$_6$H$_3$, Dipp = 2,6-*i*Pr$_2$C$_6$H$_3$), was very recently synthesized and characterized by X-ray diffraction.[25] The Ga−Ga bond length of 2.6268(7) and the C−Ga−Ga bond angle of 123.16(7)° were obtained for this compound in the solid phase.

Group 14 (E = C, Si and Ge)

Cyclic structures define the global energy minima for all E_4H_8 species. The E−E and E−H distances were calculated to be 1.5509/1.5448 and 1.0920/1.0910 Å, 2.3724/2.3602 and 1.4865/1.4837 Å, and 2.4688/2.4653 and 1.5422/1.5427 Å for E = C, Si and Ge, respectively (see Table 2). The E−E−E angles are 88.5/87.8, 88.1/86.2 and 88.3/88.1° for E = C, Si and Ge, respectively. The values are in good agreement with the ones reported earlier. Thus, for cyclobutane, the C−C and C−H bond lengths have been determined to be 1.543 and 1.094 Å and the C−C−C and H−C−H bond angles have been determined to be 87.9 and 108.8°.[64] In the case of Si_4H_8, previous calculations have predicted a D_{2d}-symmetric global energy-minimum struc-

Table 2. Geometrical parameters (bond lengths [Å], bond angles [°]), energies and enthalpies [kJ·mol^{-1}] for isomerization and dimerisation of group-14 element hydrides studied in this work

E	Parameter	E_2H_4 [a] B3LYP/MP2/MP2TM	$(E_2H_4)_2$ [b] B3LYP/MP2/MP2TM
C	C−C	1.3244/1.3313/1.3323	1.5509/1.5448/1.5452
	C−H	1.0840/1.0835/1.0804	1.0920/1.0910/1.0873
	C−C−C		88.5/87.8/87.8
	H−C−H	116.5/117.1/117.3	108.4/109.0/109.3
	Δ*H* (dim.)		−49.8/−40.0/−100.2
Si	Si−Si	2.1624/2.1552/2.1532	2.3724/2.3602/2.3595
	Si−H	1.4787/1.4736/1.4733	1.4865/1.4837/1.4800
	Si−Si−Si		88.1/86.2/86.2
	H−Si−H	112.5/114.3/114.2	108.7/109.9/109.6
	Δ*H* (dim.)		−319.7/−358.7/−365.9
Ge	Ge−Ge	2.2945/2.2756/2.2427	2.4688/2.4653/2.4270
	Ge−H	1.5440/1.5374/1.5197	1.5422/1.5427/1.5218
	Ge−Ge−Ge		88.3/88.1/87.8
	H−Ge−H	108.0 /111.0/111.3	108.7/109.1/109.2
	Δ*H* (dim.)		−274.4/−328.3/−353.8

[a] Symmetry used in the calculations: D_{2h} for C_2H_4, C_{2h} for Si_2H_4 and Ge_2H_4. [b] Symmetry: D_{4h} for C_4H_8, D_{2d} for Si_4H_8 and Ge_4H_8.

 © 2003 Wiley-VCH Verlag GmbH & Co. KGaA, Weinheim

ture with a folded Si_4 ring, which is characterized by Si−Si and Si−H bond lengths of 2.368 and 1.470/1.472 Å and a H−Si−H bond angle of 109.4°.[50] The barrier leading to a D_{4h}-symmetric form with a planar Si_4 ring, however, apparently amounts to less than 10 kJ·mol^{-1},[51] which shows the high flexibility of the Si_4 ring. The derivatives with the general formula $[R_2Si]_4$, for which the structures in the solid crystalline phase were determined from experimental X-ray data, confirm this high flexibility. For example, folded Si_4 rings were found to be present, for R = *t*BuCH_2 or *i*Pr, in which the Si−Si bond lengths are 2.359−2.409 Å.[52] In the case where R = CH_3 or Me_3Si, however, the experimental data show that a planar Si_4 ring is formed (Si−Si bond length of 2.375 Å for R = CH_3).[53−55] It has been claimed that the Si−Si bond in Si_4H_8 is significantly weaker than the C−C bonds in corresponding alkanes, and the smaller contributions of the s valence orbitals to the formation of hybrid orbitals is one of the factors that have been proposed to be responsible for this trend.[56]

At 1.3244/1.3313 Å, the calculated C−C distance in H_2CCH_2 is close to the experimentally derived value of 1.339 Å. Previous calculations for H_2SiSiH_2 predict an Si−Si bond length of 2.116 or 2.217 Å (for calculations relying on the SCF or MCSCF method, respectively). Tetramesityldisilene is one derivative that had been already characterized experimentally by its X-ray diffraction pattern in 1983, yielding a value of 2.160 Å for the Si−Si bond length.[57] These experimental and calculated values are close to the one calculated herein (2.1624/2.1552 Å). For H_2GeGeH_2, previous calculations resulted in Ge−Ge and Ge−H bond lengths of 2.275−2.341 and 1.550 Å and an H−Ge−Ge bond angle of 109.0°.[58] As already mentioned, some stable dialkylgermylenes have been known for a long time to experimentalists[10] [including $(CH_3)_2GeGe(CH_3)_2$, which was investigated in Ar and N_2 matrices at 5 K by vibrational (IR and Raman) spectroscopy],[59] and in the ones that have been studied by X-ray diffraction, a typical Ge−Ge bond length of about 2.34 Å has been found, in satisfying agreement with the length predicted on the basis of quantum chemical calculations.[59,60] The values calculated herein (2.2945/2.2756 and 1.5440/1.5374 Å for the Ge−Ge and Ge−H bond lengths and 108.0/111.0° for the H−Ge−Ge bond angle) are in reasonable agreement with these numbers.

Group 15 (E = N, P and As)

In the gas phase, N_4H_4 prefers an open chain-like structure with two hydrogen atoms at both ends of the N_4 chain.[61,62] Crystals of this compound can be prepared, but they decompose at temperatures above −20 °C, with its isomer NH_4N_3 (exhibiting a high lattice energy) being among the detectable products.[63] According to our calculations, the N−N distances are 1.3770 Å for the separations of the terminal N atoms to their neighbouring ones and 1.2361 Å for the distance between the two inner N atoms of the chain. The cyclic structure defines a local minimum on the potential energy surface that exhibits an energy 242.4 kJ·mol^{-1} higher [222.3 kJ·mol^{-1} according to CCSD(T)] than the open chain-like isomer. Thus, the stand-

Table 3. Geometrical parameters (bond lengths [Å], bond angles [°]), energies and enthalpies [kJ·mol^{-1}] for isomerization and dimerisation of group-15 element hydrides studied in this work

E	Parameter	E_2H_2[a] B3LYP/MP2/MP2TM	$(E_2H_2)_2$ Cyclic[b] B3LYP/MP2/MP2TM	Chain[c] B3LYP/MP2/MP2TM
N	N−N	1.2354/1.2541/1.2544	1.4720/1.4711/1.4710	1.3770, 1.2361/1.3769,1.2538/1.3793, 1.2533
	N−H	1.0347/1.0320/1.0286	1.0208/1.0226/1.0186	1.0180, 1.0105/1.0189, 1.0116/1.0082, 1.0151
	N−N−N		89.8/89.6/89.6	113.1/111.8/111.6
	H−N−N	107.2/106.0/105.6	105.3/104.3/103.9	113.2, 109.5/112.3, 108.9/111.6, 108.4
	H−N−H			113.1/112.8/112.1
	ΔE [$(N_2H_2)_2$ cycl. chain]			−242.4/−229.0/−231.0
	ΔH [$(N_2H_2)_2$ cycl. chain]			−247.9/−234.5/−236.5
	ΔH (dim.)		+133.2/+149.0/+118.0	−114.7/−85.5/−118.5
P	P−P	2.0311/2.0372/2.0393	2.2618/2.2376/2.2407	2.2349, 2.0330/2.0413,2.2174, 2.0428/2.2192
	P−H	1.4259/1.4195/1.4193	1.4207/1.4164/1.4154	1.4184, 1.4193/1.4130,1.4142, 1.4130/1.4119
	P−P−P		90.0/89.6/89.6	101.6/99.3/99.4
	H−P−P	94.3/93.7/93.4	93.8/93.0/92.7	94.8, 99.9/94.9, 99.0/94.8, 98.7
	H−P−H			94.6/94.9/94.8
	ΔE [$(P_2H_2)_2$ cycl. chain]			47.2/69.2/59.5
	ΔH [$(P_2H_2)_2$ cycl. chain]			45.4/67.4/57.7
	ΔH (dim.)		−140.5/−161.8/−174.5	−95.1/−94.4/−116.8
As	As−As	2.2542/2.2601/2.2396	2.5017/2.4691/2.4415	2.4843, 2.2529/2.4530, 2.2652/2.4259, 2.2442
	As−H	1.5325/1.5248/1.5142	1.5291/1.5235/1.5118	1.5254, 1.5268 /1.5193, 1.5196/1.5080, 1.5083
	As−As−As		89.9/89.1/89.1	99.7/97.6/97.4
	H−As−As	92.6/92.2/91.8	91.6/91.0/90.5	97.0, 93.2/96.5, 93.5/96.2, 93.4
	H−As−H			92.7/93.3/93.2
	ΔE [$(As_2H_2)_2$ cycl. chain]			54.1/71.1/67.8
	ΔH [$(As_2H_2)_2$ cycl. chain]			52.8/69.8/66.5
	ΔH (dim.)		−142.5/−161.4/−187.0	−89.7/−91.6/−120.5

[a] Symmetry used in the calculations: C_{2h}. [b] Symmetry used in the calculations: D_{2d}. [c] Symmetry used in the calculations: C_i.

 © 2003 Wiley-VCH Verlag GmbH & Co. KGaA, Weinheim

ard enthalpy for conversion of the open chain-like isomer into the cyclic one amounts to 247.9 kJ·mol^{-1} according to B3LYP and 227.8 kJ·mol^{-1} according to CCSD(T). The tendency of N_4H_4 to form chains that feature a double bond between the inner N atoms, instead of a cyclic structure in which only single bonds are present, demonstrates the strength of the π bond relative to the σ bond. The cyclic isomer, tetrazetidine, is unstable and dissociates into two *trans*-diazene (N_2H_2) molecules, with the standard enthalpy for this dissociation calculated previously to be −121.5 kJ·mol^{-1}.[63] This value is in good agreement with our results (dissociation energy: −116.7 kJ·mol^{-1}; standard enthalpy: −133.2 kJ·mol^{-1}). Tetrazetidine exhibits a D_{2d}-symmetric global energy-minimum structure that is characterized by N−N and N−H bond lengths of 1.4720/1.4711 and 1.0208/1.0226 Å (cf. 1.479 and 1.025 Å)[64] and N−N−N and H−N−N bond angles of 89.8/89.6 and 105.3/104.3° (cf. 89.8° and 104.1°).[64] At 135.8 kJ·mol^{-1}, the strain energy of the cyclic tetrazetidine N_4H_4 isomer was previously calculated to be slightly higher than the one derived for cyclobutane (110.2 kJ·mol^{-1}).

In contrast to its lighter homologue, P_4H_4 prefers a cyclic structure, which has, according to our calculations, an energy that is 47.2 kJ·mol^{-1} lower [56.9 kJ·mol^{-1} using the CCSD(T) method] than the chain-like isomer (standard enthalpy difference of 45.4 kJ·mol^{-1} according to B3LYP, see Table 3). The cyclic P_4H_4 isomer exhibits D_{2d} symmetry. The calculated geometric parameters (2.2618/2.2376 and 1.4207/1.4164 Å for the P−P and P−H bond lengths and 90.0/89.6 and 93.8/93.0° for the P−P−P and H−P−P bond angles) are in good agreement with the results of earlier calculations (2.238 and 1.417 Å for the P−P and P−H bond lengths and 89.8° and 95.3° for the P−P−P and H−P−P bond angles).[64] As_4H_4 also exhibits a cyclic global energy-minimum structure, with the energy and the standard enthalpy differences relative to the open chain-like isomer amounting to 54.1 and 53.8 kJ·mol^{-1}, respectively, using the B3LYP method [90.4 and 90.1 kJ·mol^{-1} using the CCSD(T) method, see Figure 2]. In the cyclic form, the As−As and As−H bond lengths amount to 2.5017/2.4691 and 1.5291/1.5235 Å, respectively.

The value calculated herein for the N−N distance in HNNH (1.2354/1.2541 Å) is close to the experimentally determined value of 1.252 Å. In the case of HPPH, a P−P bond length of 2.099 was previously calculated,[64] with values for the P−H distance and the H−P−P bond angle of 1.420 Å and 94.9°, respectively. These numbers compare with the P−P bond lengths of 2.0311/2.0372 Å, the P−H bond lengths of 1.4259/1.4195 Å, and the H−P−P bond angles of 94.3°/93.7° calculated herein. Experimentally, a number of derivatives bearing the formula RPPR (R being a bulky organic group) were studied by X-ray diffraction, yielding typical P−P bond lengths of about 2.01 Å,[65] in good agreement with the theoretically derived value. Finally, for HAsAsH, a *trans* C_{2h} structure was predicted previously to be characterized by an As−As bond length of 2.227 Å and an H−As−As bond angle of 94.4°.[66] These values tally nicely with the ones calculated herein (2.2542/2.2601 Å and 92.6°/92.2°, respectively). One example of several derivatives characterized experimentally is the compound (2,4,6-tBu$_3$C$_6$H$_2$)AsAsCH(SiMe$_3$)$_2$, which was structurally characterized already in 1983 and exhibits an As−As bond length of 2.224(2) Å and C−As−As bond angles of 93.6(3) and 99.9(3)°.[67]

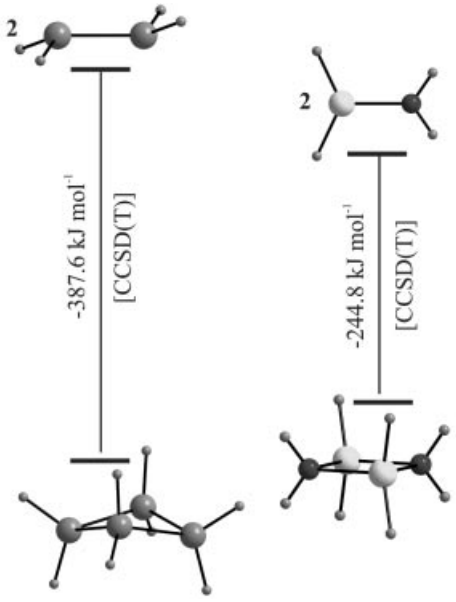

Figure 2. Comparison between the geometries of H_2GeGeH_2 and H_2GaNH_2 and their dimerisation products, the cyclic species Ge_4H_8 and $Ga_2N_2H_8$, and the standard enthalpies of their dimerisation

Group-13/Group-15 Compounds (H_2BNH_2, H_2AlNH_2 and H_2GaNH_2)

The dimers $(H_2ENH_2)_2$ are composed of planar E_2N_2 rings. Although there is a tendency, especially for E = Al or Ga, to form trimers instead of dimers, some derivatives of the dimers were synthesized and characterized either in the gas or crystal phase. Thus, for example, $(H_2GaNMe_2)_2$ has been characterized in the gas phase using electron diffraction,[68] and $[H_2GaN(H)NMe_2]_2$ has also been characterized experimentally.[69] In those studies, the Ga−N and Ga−H bond lengths and the Ga−N−Ga and H−Ga−H bond angles of $(H_2GaNMe_2)_2$ were determined to be 2.027 and 1.487 Å, and 90.6 and 109°. In the case of $[H_2GaN(H)NMe_2]_2$, values of 1.991−2.024 and 1.51 Å, and of 86.9/97.3 and 92.1/93.6° were obtained for the Ga−N and Ga−H bond lengths and the N−Ga−N and Ga−N−Ga bond angles, respectively. In both compounds, the Ga_2N_2 ring was shown to be planar. All experimental values are in excellent agreement with the results of our calculations for $(H_2GaNH_2)_2$ [D_{2h} symmetry, Ga−N and Ga−H bond lengths of 2.035 and 1.567 Å, respectively, and N−Ga−N and H−Ga−H bond angles of 86.0 and 125.5° (B3LYP values), see Figure 3] and previous calculations.[70] Very recently, the apparently air-stable derivative $[t$Bu(H)GaNEt$_2]_2$ was synthesized and structurally characterized.[71] The Ga−N and Ga−H bond lengths of this

 © 2003 Wiley-VCH Verlag GmbH & Co. KGaA, Weinheim

compound were reported to be 2.025(3) and 1.57(4) Å; the N−Ga−N bond angle is 88.8°. The trimer $[H_2GaNH_2]_3$ is also known and has been proved to be a valuable single-source precursor to solid GaN.[72] Another example, from Al chemistry, is provided by the compound $[Me_2AlN(H)NMe_2]_2$, for which an Al−N bond length and a N−Al−N bond angle were determined to be 1.958−1.953 Å and 87.2°, respectively.[73] These values compare with values of 1.9686 Å and 87.4° calculated herein for $(H_2AlNH_2)_2$.

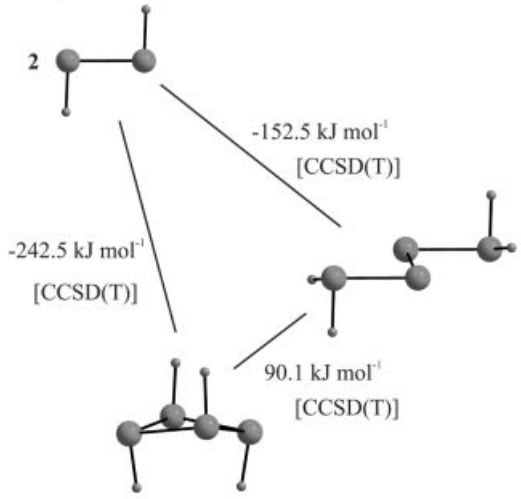

Figure 3. Geometries of HAsAsH and its dimerisation product As_4H_4 in its cyclic energy minimum and its chain-like forms, and enthalpies for dimerisation

Much effort has been put into the synthesis of monomeric compounds with the general formula $R^1R^2EE'R^3R^4$ (R^1−R^4 being bulky organic groups and E and E′ being group-13 and group-15 elements). The parent compounds $H_2EE'H_2$, however, are unstable and, therefore, special techniques, such as matrix isolation, are necessary to obtain access to them. The structure of H_2BNH_2 has been studied by microwave spectroscopy[74] and by matrix IR spectroscopy.[75] Recently, the heavier homologues H_2AlNH_2, H_2GaNH_2 and H_2InNH_2 were generated and characterized by matrix-isolation experiments.[19,76] All four of these monomers have been the subjects of several detailed theoretical works.[28,77−82] Experiments and calculations agree that they all are planar, C_{2v}-symmetric molecules. According to previous calculations using CCSD/TZ2P, H_2AlNH_2 is characterized by Al−N, Al−H and N−H bond lengths of 1.772, 1.576 and 1.004 Å, respectively, and H−Al−H and H−N−H bond angles of 124.1 and 110.0°, respectively.[83] Using DFT methods, the following parameters were calculated in a previous study of H_2GaNH_2: Ga−N 1.8211 Å, Ga−H 1.5621 Å, N−H 1.0086 Å, H−Ga−H 126.7° and H−N−H 111.7°.[19] All these values are in good agreement with the values calculated herein (see Table 4).

Standard Enthalpies for Dimerisation

The structures of the most relevant isomers of the monomers and dimers having now been established, we now turn our attention to a discussion of the dimerisation enthalpies. Tables 1−4 include the dimerisation enthalpies calculated using the B3LYP and MP2 methods, each in combination with the 6-311+G(2df,p) basis set, as well as the enthalpies derived from calculations with MP2, but this time with the TZVPP basis set. Finally, Table 5 lists the calculated values for the dimerisation enthalpies using the CCSD(T) method. The general trend is that the enthalpies as calculated with MP2/TZVPP are higher than the ones derived from MP2/6-311+G(2df,p) and B3LYP/6-311+G(2df,p) calculations. The differences are relatively small between the values calculated with CCSD(T)/6-311+G(2df,p) and MP2/TZVPP (see Table 5). This observation shows that expensive methods and/or large basis sets are necessary for calculating accurate enthalpies. The results give us confidence that the levels of calculations used herein are sufficient to establish, at least, the trends for the dimerisation enthalpies.

Figure 4 is presented to better visualize the observed trends of the enthalpies. We have calculated the enthalpies in several cases for two different isomeric forms of the monomers and dimers, and this process is necessary in some cases for a better comparison (if the global energy-minimum structures change for homologues). Nevertheless, Figure 4 shows only the trends for the global energy-minimum forms. The dimerisation of C_2H_4 to give cyclobutane can be used as a test system to judge the quality of the calculation methods, since reliable experimental enthalpy values exist for this reaction. With a standard enthalpy of $-75.3\ kJ{\cdot}mol^{-1}$, the value calculated with CCSD(T) comes very close to the experimental one of ca. $-72\ kJ{\cdot}mol^{-1}$.[84] With B3LYP and MP2 in combination with the 6-311+G(2df,p) method, this enthalpy comes out slightly lower than the experimental one.

The dimerisation enthalpies are all negative quantities (exothermic), with the only exception being the dimerisation of HNNH to give cyclic N_4H_4. The value of $+133.2\ kJ{\cdot}mol^{-1}$ calculated with B3LYP is in good agreement with the results of earlier calculations, which gave a value of $121.5\ kJ{\cdot}mol^{-1}$.[64] At $127.6\ kJ{\cdot}mol^{-1}$, the enthalpy as calculated using the CCSD(T) method is also in pleasing agreement with this previous report. As already mentioned, N_4H_4 prefers an open chain-like structure where the inner N atoms can establish significant π bonding. The dimerisation to give this chain like structure is exothermic [dimerisation enthalpy of $-115\ kJ{\cdot}mol^{-1}$ using the B3LYP and $-99.2\ kJ{\cdot}mol^{-1}$ using the CCSD(T) method]. Therefore the positive value calculated for the enthalpy of dimerisation to the N_4H_4 ring reflects the instability of the N_4H_4 ring. This instability is partially caused by the strain energy, which was estimated to be even slightly higher than the one of cyclobutane, C_4H_8 (135.8 vs. $110.4\ kJ{\cdot}mol^{-1}$).[64] The lone-pair repulsion is certainly one important factor to destabilize the cyclic form. Another factor is, in all certainty, the particularly strong N=N π bond, which can exist in the monomer and the dimer in its chain-like form, but not in the cyclic dimer. It has been pointed out that the π-bond increment (e.g., in N_2) is even higher than the σ-bond increment.[85]

 © 2003 Wiley-VCH Verlag GmbH & Co. KGaA, Weinheim

Table 4. Geometrical parameters (bond lengths [Å], bond angles [°]), energies and enthalpies [kJ·mol^{-1}] for isomerization and dimerisation for group-13/group-15 element hydrides with the general formulas H_2ENH_2 and $(H_2ENH_2)_2$ (E = B, Al or Ga)

E	Parameter	H_2ENH_2[a] B3LYP/MP2 /MP2TM	$(H_2ENH_2)_2$[b] B3LYP/MP2 /MP2TM
	B−N	1.3884/1.3923/1.3923	1.6080/1.6048/1.6066
	B−H	1.1920/1.1926/1.1903	1.2009/1.2022/1.1995
	N−H	1.0080/1.0077/1.0039	1.0123/1.0132/1.0092
B/N	H−N−H	113.3/113.8/113.8	107.9/108.2/108.1
	H−B−H	122.0/122.4 /122.4	115.2/115.7/115.7
	N−B−N		92.0/92.1/92.1
	Δ*H* (dim.)		−32.2/−5.4/−77.3
	Al−N	1.7744/1.7759/1.7795	1.9686/1.9674/1.9705
	Al−H	1.5772/1.5756/1.5769	1.5861/1.5849/1.5862
	N−H	1.0096/1.0104/1.0063	1.0163/1.0177/1.0134
Al/N	H−N−H	110.0/110.0 /109.9	106.1/106.2/106.1
	H−Al−H	124.3/124.1/124.1	122.9/123.1/123.5
	N−Al−N		87.4/87.3/87.3
	Δ*H* (dim.)		−202.9/−211.3/−240.4
	Ga−N	1.8235/1.8854/1.8119	2.0350/2.1359/2.0146
	Ga−H	1.5585/1.5718/1.5439	1.5670/1.5803/1.5537
	N−H	1.0085/1.0165/1.0051	1.0149/1.0354/1.0127
Ga/N	H−N−H	111.7/110.9/111.4	106.8/107.0/106.5
	H−Ga−H	127.0/129.2/126.4	125.5/131.2/125.5
	N−Ga−N		86.0/85.4/86.5
	Δ*H* (dim.)		−163.0/−152.6/−213.3

[a] Symmetry used in the calculations: D_{2h}. [b] Symmetry used in the calculations: D_{2h}.

Table 5. Energies $\Delta_R E$ and standard enthalpies $\Delta_R H^0$ [kJ·mol^{-1}] of dimerisation as calculated using the CCSD(T) method; for better comparison, the standard enthalpies derived from MP2/TZVPP calculations are also included

	$\Delta_R E$ [CCSD(T)]	$\Delta_R H^0$ [CCSD(T)]	$\Delta_R H^0$ [MP2/TZVPP]
2 B_2H_2 (linear) → $(B_2H_2)_2$ (T_d)	−493.7	−481.5	−510.0
2 Al_2H_2 (cyclic) → $(Al_2H_2)_2$ (T_d)	−284.5	−271.9	−308.9
2 Ga_2H_2 (cyclic) → $(Ga_2H_2)_2$ (T_d)	[a]	[a]	−277.7
2 C_2H_4 → $(C_2H_4)_2$	−90.3	−75.3	−100.2
2 Si_2H_4 → $(Si_2H_4)_2$	−364.0	−353.8	−365.9
2 Ge_2H_4 → $(Ge_2H_4)_2$	−398.6	−387.6	−353.8
2 N_2H_2 → $(N_2H_2)_2$ (chain)	−110.2	−99.2	−118.5
2 P_2H_2 → $(P_2H_2)_2$ (cyclic)	−167.2	−158.3	−174.5
2 As_2H_2 → $(As_2H_2)_2$ (cyclic)	−250.0	−242.5	−187.0
2 BNH_4 → $(BNH_4)_2$	−80.1	−67.2	−77.3
2 $AlNH_4$ → $(AlNH_4)_2$	−247.4	−236.5	−240.4
2 $GaNH_4$ → $(GaNH_4)_2$	−255.7	−244.8	−213.3

[a] The CCSD(T)/6-311+G(2df,p) calculation for Ga_4H_4 failed.

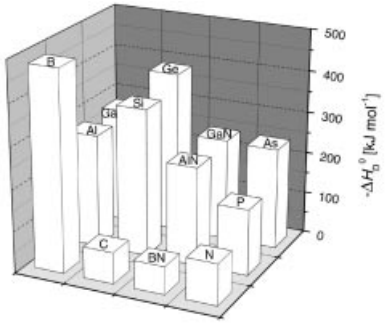

Figure 4. Standard enthalpies for dimerisation, ΔH^0_D, for the hydrides addressed in this work, as calculated using the CCSD(T) method (see Table 5); note that all species are considered in their global energy-minimum forms

It is clearly visible from Figure 4 that, while the compounds composed of group-14, -15 or -13/15 elements follow the same trend (increase of the dimerisation enthalpy down the group), the compounds composed of group-13 elements follow a different behaviour. The hydrides of the first long-period elements, H_2CCH_2, H_2BNH_2 and HNNH, have absolute dimerisation enthalpy values that are smaller than 100 kJ·mol^{-1}. The eye-catching exception is HBBH, which has the highest dimerisation enthalpy of all compounds addressed herein at −481.5 kJ·mol^{-1} [CCSDT(D) calculation]. Compound HBBH also is the only compound with a triplet electronic ground state. In total, the bond order in HBBH is two, as it is in H_2CCH_2 and HNNH. The two binding valence π orbitals, however, are each filled with *one* electron. In previous reports, we have probed the re-

 © 2003 Wiley-VCH Verlag GmbH & Co. KGaA, Weinheim

sponse of HBBH to hydrogenation (to give H_2BBH_2)[28] and fragmentation (to give two HB fragments).[30] Hydrogenation is accompanied by a gain in enthalpy of ca. -180 kJ·mol^{-1}. This value is only slightly higher than the one derived for hydrogenation of H_2CCH_2 (ca. -140 kJ·mol^{-1}). The fragmentation of HBBH to give two BH units in their singlet electronic state consumes ca. 450 kJ·mol^{-1}, a value close to the one computed for H_2SiSiH_2 (440 kJ·mol^{-1}). Thus, the bond in HBBH is not very weak and cannot be the only reason for the extremely high dimerisation enthalpy. The stability of the B_4H_4 tetrahedron certainly must be considered in this context.

Moving from the first to the second long period, the dimerisation enthalpies increase generally. The only exception can again be found in the compounds of group-13 elements. First we turn our attention, however, to compounds of group-15 elements. The dimerisation enthalpies calculated herein for P_2H_2 of -141 kJ·mol^{-1}, using the B3LYP method, and of -158.3 kJ·mol^{-1}, using the CCSD(T) method, compare nicely with a value of 149.5 kJ·mol^{-1} reported previously.[64] The smallest change is found for the compounds of group-15 elements. Note that the enthalpies as plotted in Figure 4 are for dimerisation to give the open chain-like structure for N_4H_4, but the ring-type ones for P_4H_4 and As_4H_4. As already mentioned, the global energy-minimum structure of the dimer changes from the chain-like geometry of N_4H_4 to the cyclic one of P_4H_4. As pointed out earlier, the strain energies drop dramatically from 134.8 kJ·mol^{-1} in N_4H_4 to no more than 24.1 kJ·mol^{-1} in P_4H_4.[64] This feature means that at least two factors have to be considered to explain the changes that are only moderate within the binary group-15 hydrides. The first, and maybe most important, factor certainly is that the capability to form significant π-bonding is still quite high for the phosphane and arsane compounds. This phenomenon implies that the stability of the monomers HEEH (E = group-15 element) does not decrease as much down the group as for the compounds composed of of group-14, -13 or -13/15 elements. The other factor is the stability of the dimer. As already mentioned, the lone-pair repulsion and the strain energy should decrease down the group, the latter because of the larger affordability of bond-angle deformations. It has been suggested that the strain energy in P_4H_4 is close to zero.[86] When considering dimerisation to give the *cyclic* isomers E_4H_4 in the case of E = N, P, and As (see Table 3), the enthalpies are only very small (at -118.5, -116.8, and -120.5 kJ·mol^{-1} for E = N, P, and As, respectively) according to the MP2/TZVPP method.

In the case of group-14 element compounds, the increase in the dimerisation enthalpy is larger than that for group-15 element compounds. Dimerisation of Si_2H_4 is accompanied by an enthalpy gain of 353.8 kJ·mol^{-1} according to the CCSD(T) estimate (and 365.9 kJ·mol^{-1} according to MP2/TZVPP). This means that the dimerisation enthalpy is 4.7 times higher than for the C analogue, while P_2H_2 dimerises with an enthalpy only 1.6 times higher than that of N_2H_2. One of the most important factors at work here is certainly the instability of the H_2SiSiH_2 reactant. In contrast to HPPH, which features a "classical" and comparably strong π bond, H_2SiSiH_2 features a different, weaker sort of π-interaction ("donor–acceptor" interactions). Another factor is again the strain energy in the cyclic dimer, which in both cases drops for the heavier homologues and increases the stability of the cyclic dimers. The experimental values for the strain energies of $(CH_2)_4$ and $(SiH_2)_4$ amount to ca. 118 and 96 kJ·mol^{-1}, respectively.[87][88] These values are in good agreement with the results of theoretical studies, which gave values of 119 and ca. 70 kJ·mol^{-1} using ab initio methods.[89,90] Apparently, the smaller ring strain in the silicon-containing rings is partially explained by efficient $\pi-\sigma^*$ interactions.[91] The decrease of the ring strain is certainly also of some importance for the smaller increase observed in the absolute values of the dimerisation enthalpy in moving from the second to the third long period (hydrides of Ge and As).

In the case of mixed group-13/15 element compounds, the trend, as well as the absolute values, of the dimerisation enthalpies are very similar to the ones calculated for binary group-15 element hydrides. Certainly it should be noted here that the bond properties change significantly from H_2BNH_2 to H_2AlNH_2 and again to H_2GaNH_2. In this series, the ionic contributions increase. In H_2GaNH_2 the charge separation is already substantial. These ionic contributions might be responsible for the differences between the group-13/15 element compounds and the binary group-14 element compounds. The dimerisation of H_2BNH_2 is only very weakly exothermic [dimerisation enthalpy of -67.2 kJ·mol^{-1} using the CCSD(T) method and -77.3 kJ·mol^{-1} using MP2/TZVPP]. Thus, H_2BNH_2 has the smallest dimerisation enthalpy of all compounds under investigation herein, even slightly smaller than the one calculated for C_2H_4 [-75.3 kJ·mol^{-1} according to CCSD(T)]. Nevertheless, H_2BNH_2 is much more reactive than H_2CCH_2 and is stabilized only in the form of adducts (e.g., $B_2H_4{\cdot}BH_3$) or by replacement of the H atoms by halogen and/or organic groups (e.g., Cl_2BNMe_2). Otherwise, this class of compounds oligomerises [e.g., to its trimer $(B_2H_4)_3$] or polymerises rapidly.

Finally, we now proceed to the discussion of the binary group-13 element hydrides. As indicated already, the situation here is much more complicated than that for the other groups. We have already mentioned and analysed the exceptionally high dimerisation enthalpy of HBBH. Moving to Al_2H_2 brings about a great change in the geometry of the global energy-minimum isomer. The large Al–Al separation in the global energy-minimum isomer, planar and cyclic Al(μ-H)$_2$Al (D_{2h} symmetry), does not permit any significant interaction between the two atoms. The bent *trans*-HAlAlH isomer with two terminal Al–H bonds has an energy that is about 60 kJ·mol^{-1} higher than the one of the cyclic Al(μ-H)$_2$Al form. The dimerisation of Al(μ-H)$_2$Al to give tetrahedral Al_4H_4 is associated with an enthalpy change of -271.9 kJ·mol^{-1} according to the CCSD(T) method (-308.9 kJ·mol^{-1} according to MP2/TZVPP). This change is only 56% of the standard enthalpy for the dimerisation of HBBH. This value is even significantly

 © 2003 Wiley-VCH Verlag GmbH & Co. KGaA, Weinheim

smaller than the one calculated for dimerisation of Si_2H_4 (-353.8 kJ·mol^{-1}), but larger than the one calculated for dimerisation of H_2AlNH_2 and P_2H_2 (-236.5 and -158.3 kJ·mol^{-1}). The standard enthalpy for dimerisation of Ga_2H_2 (for which the cyclic form has been shown again to be the lowest-energy isomer) is higher by a factor of 1.57 than the one calculated for dimerisation of Al_2H_2. In summary, the behaviour of the binary group-13 element hydrides differs significantly from the one found for the hydrides of group-14 and -15 elements and for mixed group-13/15 element compounds. If only the isomers with an intact E−E bond are considered for the E_2H_2 species, the dimerisation enthalpies are found to decrease down the group (-510.0, -442.3, and -402.6 kJ·mol^{-1} for E = B, Al and Ga, respectively, see Table 1).

Conclusions

This works attempts to shed light on the differences in reactivity between binary main-group element hydrides with the potential for multiple bonding. Although the chemical reactivity gives only indirect insight into the bond properties, it has the advantage that it can be verified, at least principally, by experiments. In two previous accounts we have studied the response of the compounds towards fragmentation and hydrogenation reactions. In this work, the standard enthalpies for dimerisation were calculated. The [2+2] cycloaddition is a characteristic and important reaction of derivatives of ethylene and, therefore, the comparison of the dimerisation enthalpies should shed light on the differences in the chemistry between compounds that formally are capable of forming a "double" bond. First, the structures of the monomers and dimers were analysed applying hybrid DFT (B3LYP) and ab initio (MP2) methods. In a second step, the MP2 and the CCSD(T) methods were used to determine the dimerisation enthalpies. The trends of the dimerisation enthalpies were established, and important factors responsible for these trends discussed. The results show that a general pattern is the increase of the dimerisation enthalpy for heavier homologues, with the largest changes occurring between the first and the second long period. Although structural differences in the energy-minimum structures of the monomers and dimers have to be considered (e.g., N_4H_4 exhibits a chain-like energy-minimum structure while P_4H_4 prefers a cyclic structure), the trend generally reflects the increasing weakness of the E−E bond in the monomers for the heavier homologues as the most-dominating effect. Other effects, such as the reduced ring strain in the cyclic dimers, play a significant, but most likely not the dominating, role. The eye-catching exception from this general pattern is found in group 13. Compound HBBH exhibits an unusually high dimerisation enthalpy; in fact, it is the highest value of all dimerisation processes studied herein. Possible reasons for this high enthalpy have been discussed.

The values derived herein for the dimerisation enthalpies give useful and reliable information about the differences in the chemistry of main-group element hydrides with the potential for multiple bonding. The results show that these differences are substantial and some trends are visible.

Acknowledgments

The author gratefully acknowledges the financial support by the Deutsche Forschungsgemeinschaft and the award of a Habilitanden-Stipendium.

[1] M. Driess, H. Grützmacher, *Angew. Chem.* **1996**, *108*, 900; *Angew. Chem. Int. Ed. Engl.* **1996**, *35*, 828.
[2] P. P. Power, *J. Chem. Soc., Dalton Trans.* **1998**, 2939.
[3] A. J. Downs, H.-J. Himmel, L. Manceron, *Polyhedron* **2002**, *21*, 473.
[4] T. Tsumuraya, S. A. Batcheller, S. Masamune, *Angew. Chem.* **1991**, *103*, 916.
[5] A. H. Cowley, *Acc. Chem. Res.* **1984**, *17*, 386.
[6] K. W. Klinkhammer, *Angew. Chem.* **1997**, *109*, 2414.
[7] A. H. Cowley, N. C. Nicholas, *Prog. Inorg. Chem.* **1986**, *34*, 1.
[8] F. G. A. Stone, R. West, (Eds.), *Advances in Organometallic Chemistry: Multiple Bonded Main Group Metals and Metalloids,* Academic, San Diego, CA, **1996**
[9] P. Jutzi, *Angew. Chem.* **2000**, *112*, 3953; *Angew. Chem. Int. Ed.* **2000**, *39*, 3797.
[10] D. E. Goldberg, D. H. Harris, M. F. Lappert, K. M. Thomas, *J. Chem. Soc., Chem. Commun.* **1976**, 261. P. J. Davidson, D. H. Harris, M. F. Lappert, *J. Chem. Soc., Dalton Trans.* **1976**, 2268. P. B. Hitchcock, M. F. Lappert, S. J. Miles, A. J. Thorne, *J. Chem. Soc., Chem. Commun.* **1984**, 480.
[11] D. E. Goldberg, D. H. Harris, M. F. Lappert, K. M. Thomas, *J. Chem. Soc., Chem. Commun.* **1976**, 261. D. E. Goldberg, P. B. Hitchcock, M. F. Lappert, K. M. Thomas, A. J. Thorne, T. Fjelberg, A. Haaland, B. E. R. Schilling, *J. Chem. Soc., Dalton Trans.* **1986**, 2387.
[12] M. Stender, A. D. Phillips, R. J. Wright, P. P. Power, *Angew. Chem. Int. Ed.* **2002**, *41*, 1785.
[13] A. D. Phillips, R. J. Wright, M. M. Olmstead, P. P. Power, *J. Am. Chem. Soc.* **2002**, *124*, 5930.
[14] R. T. Paine, H. Nöth, *Chem. Rev.* **1995**, *95*, 343.
[15] P. Paetzold, *Adv. Inorg. Chem.* **1987**, *31*, 123.
[16] A. J. Downs (Ed.), *Chemistry of Aluminium, Gallium, Indium and Thallium*, Blackie, Glasgow, U.K., **1993**.
[17] K. Knabel, I. Krossing, H. Nöth, H. Schwenk-Kirchner, M. Schmidt-Amelunxen, T. Seifert, *Eur. J. Inorg. Chem.* **1998**, 1095.
[18] P. P. Power, *Chem. Rev.* **1999**, *99*, 3463.
[19] [19a] H.-J. Himmel, A. J. Downs, T. M. Greene, *Chem. Commun.* **2000**, 871. [19b] H.-J. Himmel, A. J. Downs, T. M. Greene, *J. Am. Chem. Soc.* **2000**, *122*, 9793.
[20] J. Su, X. W. Li, R. C. Crittendon, G. H. Robinson, *J. Am. Chem. Soc.* **1997**, *119*, 5471.
[21] Y. Xie, H. F. Schaefer, III, G. H. Robinson, *Chem. Phys. Lett.* **2000**, *317*, 174.
[22] F. A. Cotton, A. H. Cowley, X. Feng, *J. Am. Chem. Soc.* **1998**, *120*, 1795. M. M. Olmstead, R. S. Simons, P. P. Power, *J. Am. Chem. Soc.* **1997**, *119*, 11705. T. L. Allen, W. H. Fink, P. P. Power, *J. Chem. Soc., Dalton Trans.* **2000**, 407.
[23] J. Grunenberg, N. Goldberg, *J. Am. Chem. Soc.* **2000**, *122*, 6045.
[24] A. J. Bridgeman, L. R. Ireland, *Polyhedron* **2001**, *20*, 2841.
[25] N. J. Hardman, R. J. Wright, A. D. Phillips, P. P. Power, *Angew. Chem.* **2002**, *114*, 2966.
[26] P. Pullumbi, C. Mijoule, L. Manceron, Y. Bouteiller, *Chem. Phys.* **1994**, *185*, 13.
[27] R. J. Wright, A. D. Phillips, N. J. Hardman, P. P. Power, *J. Am. Chem. Soc.* **2002**, *124*, 8538.
[28] H.-J. Himmel, H. Schnöckel, *Chem. Eur. J.* **2002**, *8*, 2397.
[29] N. Takagi, M. W. Schmidt, S. Nagase, *Organometallics* **2001**, *20*, 1646.
[30] H.-J. Himmel, H. Schnöckel, *Chem. Eur. J.*, **2003**, *9*, 748.

 © 2003 Wiley-VCH Verlag GmbH & Co. KGaA, Weinheim

[31] P. C. Andrews, C. L. Raston, B. W. Skelton, V.-A. Tolhurst, A. H. White, *Chem. Commun.* **1998**, 575.
[32] L. E. Gusel′nikov, V. G. Avakyan, S. L. Guselnikov, *J. Am. Chem. Soc.* **2002**, *124*, 662.
[33] M. J. Frisch, G. W. Trucks, H. B. Schlegel, G. E. Scuseria, M. A. Robb, J. R. Cheeseman, V. G. Zakrewski, J. A. Montgomery, R. E. Stratmann, J. C. Burant, S. Dapprich, J. M. Millam, A. D. Daniels, K. N. Kudin, M. C. Strain, O. Farkas, J. Tomasi, V. Barone, M. Cossi, R. Cammi, B. Mennucci, C. Pomelli, C. Adamo, S. Clifford, J. Ochterski, G. A. Petersson, P. Y. Ayala, Q. Cui, K. Morokuma, D. K. Malick, A. D. Rabuck, K. Raghavachari, J. B. Foresman, J. Cioslowski, J. V. Ortiz, B. B. Stefanov, G. Lui, A. Liashenko, P. Piskorz, I. Komaromi, R. Gomperts, R. L. Martin, D. J. Fox, T. Keith, M. A. Al-Laham, C. Y. Peng, A. Nanayakkara, C. Gonzalez, M. Challacombe, P. M. W. Gill, B. G. Johnson, W. Chen, M. W. Wong, J. L. Andres, M. Head-Gordon, E. S. Replogle and J. A. Pople, *Gaussian 98*, Revision A.3, Gaussian Inc., Pittsburgh PA, **1998**.
[34] R. Ahlrichs, M. Bär, M. Häser, H. Horn, C. Kölmel, *Chem. Phys. Lett.* **1989**, *162*, 165. K. Eichkorn, O. Treutler, H. Öhm, M. Häser, R. Ahlrichs, *Chem. Phys. Lett.* **1995**, *240*, 283. K. Eichkorn, O. Treutler, H. Öhm, M. Häser, R. Ahlrichs, *Chem. Phys. Lett.* **1995**, *242*, 652. K. Eichkorn, F. Weigend, O. Treutler, R. Ahlrichs, *Theor. Chem. Acc.* **1997**, *97*, 119. F. Weigend, M. Häser, *Theor. Chem. Acc.* **1997**, *97*, 331. F. Weigend, M. Häser, H. Patzelt, R. Ahlrichs, *Chem. Phys. Lett.* **1998**, *294*, 143.
[35] H.-J. Himmel, L. Manceron, A. J. Downs, P. Pullumbi, *Angew. Chem.* **2002**, *41*, 796; *Angew. Chem. Int. Ed.* **2002**, *114*, 829.
[36] H.-J. Himmel, L. Manceron, A. J. Downs, P. Pullumbi, *J. Am. Chem. Soc.* **2002**, *124*, 4448.
[37] R. Ahlrichs, P. Scharf, C. Ehrhardt, *J. Chem. Phys.* **1985**, *82*, 890. D. J. Swanton, R. Ahlrichs, *Theoret. Chim. Acta* **1989**, *75*, 163.
[38] M. Atoji, W. N. Lipscomb, *Acta Crystallogr.* **1953**, *6*, 547.
[39] C. Dohmeier, C. Robl, M. Tacke, H. Schnöckel, *Angew. Chem. Int. Ed. Engl.* **1991**, *30*, 564.
[40] A. Purath, C. Dohmeier, A. Ecker, H. Schnöckel, *Organometallics* **1998**, *17*, 1894.
[41] A. Purath, C. Dohmeier, A. Ecker, H. Schnöckel, *J. Organomet. Chem.* **1999**, *579*, 373.
[42] R. Ahlrichs, M. Ehrig, H. Horn, *Chem. Phys. Lett.* **1991**, *183*, 227.
[43] M. Mocker, C. Robl, H. Schnöckel, *Angew. Chem.* **1994**, *106*, 1860; *Angew. Chem. Int. Ed. Engl.* **1994**, *33*, 1754.
[44] A. Schnepf, R. Köppe, H. Schnöckel, *Angew. Chem. Int. Ed.* **2001**, *40*, 1241.
[45] W. Uhl, W. Hiller, M. Layh, W. Schwarz, *Angew. Chem.* **1992**, *104*, 1378.
[46] L. B. Knight, Jr., K. Kerr, P. K. Miller, C. A. Arrington, *J. Phys. Chem.* **1995**, *99*, 16842. T. Tague Jr., L. Andrews, *J. Am. Chem. Soc.* **1994**, *116*, 4970.
[47] G. V. Chertihin, L. Andrews, *J. Phys. Chem.* **1993**, *97*, 10295. J. C. Stephens, E. E. Bolton, H. F. Schaefer, III., L. Andrews, *J. Chem. Phys.* **1997**, *107*, 119.
[48] G. Treboux, J.-C. Barthelat, *J. Am. Chem. Soc.* **1993**, *116*, 11922.
[49] Z. Palágyi, R. S. Grev, H. F. Schaefer, III, *J. Am. Chem. Soc.* **1993**, *115*, 1936.
[50] See, for example: R. S. Grev, H. F. Schaefer, III, *J. Am. Chem. Soc.* **1987**, *109*, 6569.
[51] A. F. Sax, *Chem. Phys. Lett.* **1986**, *127*, 163.
[52] H. Matsumoto, M. Minemura, K. Takatsuma, Y. Nagai, M. Goto, *Chem. Lett.* **1985**, 1005.
[53] C. Kratky, H.-G. Schster, E. Hengge, *J. Organomet. Chem.* **1983**, *247*, 253.
[54] Y.-S. Chen, P. P. Gaspar, *Organometallics* **1982**, *1*, 1410.
[55] J. Rubio, F. Illas, *THEOCHEM* **1984**, *19*, 131.
[56] W. W. Schöller, T. Dabisch, *Inorg. Chem.* **1987**, *26*, 1081.
[57] M. W. Schmidt, P. N. Truong, M. S. Gordon, *J. Am. Chem. Soc.* **1987**, *109*, 5217.
[58] M. J. Fink, M. J. Michalczyk, K. J. Haller, R. West, J. Michl, *J. Chem. Soc., Chem. Commun.* **1983**, 1010.
[59] G. Trinquier, J.-P. Malrieu, P. Rivière, *J. Am. Chem. Soc.* **1982**, *104*, 4529. T. L. Windus, M. S. Gordon, *J. Am. Chem. Soc.* **1992**, *114*, 9559.
[60] P. Bleckmann, R. Minkwitz, W. P. Neumann, M. Schriewer, M. Thibud, B. Watta, *Tetrahedron Lett.* **1984**, *25*, 2467.
[61] A. Márquez, G. G. Gonzàlez, J. F. Sanz, *Chem. Phys.* **1989**, *138*, 99. G. Trinquier, *J. Am. Chem. Soc.* **1990**, *112*, 2130.
[62] N. Wiberg, H. Bayer, H. Bachhuber, *Angew. Chem.* **1975**, *87*, 202. J. Kroner, N. Wiberg, H. Bayer, *Angew. Chem.* **1975**, *87*, 203.
[63] M. Veith, G. Schlemmer, *Z. Anorg. Allg. Chem.* **1982**, *494*, 7.
[64] M. N. Glukhovtsev, R. D. Bach, S. Laiter, *Int. J. Quantum Chem.* **1997**, *62*, 373.
[65] W. W. Schoeller, C. Begemann, U. Tubbesing, J. Strutwolf, *J. Chem. Soc., Faraday Trans.* **1997**, *93*, 2957.
[66] A. H. Cowley, *Polyhedron* **1984**, *3*, 389.
[67] S. Nagase, S. Suzuki, T. Kurakake, *J. Chem. Soc., Chem. Commun.* **1990**, 1724.
[68] A. H. Cowley, J. G. Lasch, N. C. Norman, M. Pakulski, *J. Am. Chem. Soc.* **1983**, *103*, 5506.
[69] P. L. Baxter, A. J. Downs, D. W. H. Rankin, H. E. Robertson, *J. Chem. Soc., Dalton Trans.* **1985**, 807.
[70] B. Luo, W. L. Gladfelter, *Chem. Commun.* **2000**, 825.
[71] A. Y. Timoshkin, H. F. Bettinger, H. F. Schaefer, III, *J. Phys. Chem. A* **2001**, *105*, 3249.
[72] L. Grocholl, S. A. Cullison, J. Wang, D. C. Swenson, E. G. Gillan, *Inorg. Chem.* **2002**, *41*, 2920.
[73] See, for example: [73a] J. W. Hwang, S. A. Hanson, D. Britton, J. F. Evans, K. F. Jensen, W. L. Gladfelter, *Chem. Mat.* **1990**, *2*, 342. [73b] J. F. Janik, R. L. Wells, *Inorg. Chem.* **1997**, *36*, 4135. [73c] J. A. Jegier, S. McKernan, A. P. Purdy, W. L. Gladfelter, *Chem. Mat.* **2000**, *12*, 1003.
[74] Y. Kim, J. H. Kim, J. E. Park, H. Song, J. T. Park, *J. Organomet. Chem.* **1997**, *545–546*, 99.
[75] M. Sugie, H. Takeo, C. Matsumura, *J. Mol. Spectrosc.* **1987**, *123*, 286.
[76] J. D. Carpenter, B. S. Ault, *J. Phys. Chem.* **1991**, *95*, 3502.
[77] H.-J. Himmel, A. J. Downs, T. M. Greene, *J. Chem. Soc., Dalton Trans.* **2001**, *5*, 535.
[78] M. D. Allendorf, C. F. Melius, *J. Phys. Chem. A* **1997**, *101*, 2670.
[79] T. M. Gilbert, *Organometallics* **1998**, *17*, 5513.
[80] T. P. Hamilton, A. W. Shaikh, *Inorg. Chem.* **1997**, *36*, 754.
[81] R. D. Davy, K. L. Jaffrey, *J. Phys. Chem.* **1994**, *98*, 8930.
[82] R. D. Davy, H. F. Schaefer, III, *Inorg. Chem.* **1998**, *37*, 2291.
[83] A. Y. Timoshkin, H. F. Bettinger, H. F. Schaefer III, *J. Phys. Chem. A* **2001**, *105*, 3249.
[84] R. D. Davy, K. L. Jaffrey, *J. Phys. Chem.* **1994**, *98*, 8930.
[85] S. G. Lias, J. E. Bartmess, J. F. Liebman, J. L. Holmes, R. D. Levin, W. G. Mallard, *J. Phys. Chem. ref. Data (Suppl. 1)* **1988**, *17*.
[86] W. Kutzelnigg, *Angew. Chem.* **1984**, *96*, 262; *Angew. Chem. Int. Ed. Engl.* **1984**, *23*, 272.
[87] H. Schiffer, R. Ahlrichs, M. Häser, *Theor. Chim. Acta* **1989**, *75*, 1.
[88] P. George, M. Trachtman, A. M. Brett, C. W. Bock, *J. Chem. Soc., Perkin Trans. 2* **1977**, 1036. P. George, M. Trachtman, C. W. Bock, A. M. Brett, *Perkin Trans. 2* **1976**, 1222. P. George, M. Trachtman, C. W. Bock, A. M. Brett, *Tetrahedron* **1976**, *32*, 317.
[89] H. Watanabe, H. Shimoyama, T. Muraoka, T. Okawa, M. Kato, Y. Nagai, *Chem. Lett.* **1986**, 1057.
[90] See, for example: M. Zhao, B. M. Gimarc, *Inorg. Chem.* **1996**, *35*, 5378.
[91] R. S. Grev, H. F. Schaefer, III, *J. Am. Chem. Soc.* **1987**, *109*, 6569.
[92] Y. Naruse, J. Ma, S. Inagaki, *Tetrahedron Lett.* **2001**, *42*, 6553.

Received November 18, 2002

 © 2003 Wiley-VCH Verlag GmbH & Co. KGaA, Weinheim

Synthesis and Characterization of Pentaarylated [60]Fullerene Coordinated Complexes $[(\eta^2\text{-}Ar_5C_{60}H)M(PPh_3)_2]$ (M = Pt, Pd) and an ab initio Study on Their Isomerism

Li-Cheng Song,*[a] Peng-Chong Liu,[a] Qing-Mei Hu,[a] Zhenyang Lin,[b] and Yi-Bo Wang[b]

Keywords: Ab initio calculations / Fullerenes / Isomerism / Palladium / Platinum

This paper reports on the first examples of η^2-pentaarylated [60]fullerene organometallic complexes $[(\eta^2\text{-}Ar_5C_{60}H)M(PPh_3)_2]$ (**1**: Ar = Ph, M = Pt; **2**: Ar = *m*-MeC_6H_4, M = Pt; **3**: Ar = *p*-MeC_6H_4, M = Pt; **4**: Ar = Ph, M = Pd; **5**: Ar = *m*-MeC_6H_4, M = Pd; **6**: Ar = *p*-MeC_6H_4, M = Pd), which were synthesized by treatment of $[M(PPh_3)_4]$ with $Ar_5C_{60}H$ and fully characterized by elemental analyses and their ^1H NMR, ^{31}P NMR, IR, UV/Vis, and FAB-MS data. The ^1H NMR spectra displayed by the protons directly bonded to the C_{60} core and the ^{31}P NMR spectra caused by the PPh_3 ligands indicated that complexes **1**–**6** exist as mixtures of isomers. To gain insights into the isomerism of **1**–**6**, the regioselectivity of the pentaarylated derivatives $Ar_5C_{60}H$ as ligands coordinated to Pt^0 or Pd^0 has been studied by means of ab initio calculations. (© Wiley-VCH Verlag GmbH & Co. KGaA, 69451 Weinheim, Germany, 2003)

Introduction

It is known that the [60]fullerene derivatives $Ar_5C_{60}H$ were first synthesized by a three-pot method starting from C_{60}, involving chlorination of C_{60} to give $C_{60}Cl_6$, arylation of $C_{60}Cl_6$ with benzene or substituted benzene, and reduction of $Ar_5C_{60}Cl$ with an excess of PPh_3.[1,2] Later on, a more convenient one-pot method for preparation of $Ar_5C_{60}H$ was discovered, involving treatment of C_{60} with organocopper/magnesium reagents $Ar_2CuMgBr$, followed by treatment of the reaction mixture with aqueous NH_4Cl.[3,4] It is conceivable that the pentaarylated [60]fullerene derivatives $Ar_5C_{60}H$ might form organometallic complexes with single, double, triple, and even multiple metal centers through their pentaarylated cyclopentadienyl rings and other sites of the C_{60} core in a variety of coordination modes from η^1 to η^6. Up to now, however, except for the η^5-pentaarylated [60]fullerene organometallic compounds such as $\eta^5\text{-}Ph_5C_{60}M$ (M = Li, K, Tl, $CuPEt_3$),[3] there are no other reported organometallic complexes that contain pentaarylated [60]fullerene ligands coordinated to metal centers in a mode from η^1 to η^4 or in an η^6-fashion.

During recent years we have been interested in the synthesis, structural characterization, and properties of organotransition metal fullerene derivatives.[5] As part of this project, we recently carried out an investigation into the reactions between transition metal complexes $[M(PPh_3)_4]$ (M = Pt, Pd) and pentaarylated [60]fullerene derivatives $Ar_5C_{60}H$ to see which type of coordination mode might be adopted by $Ar_5C_{60}H$ in the products and whether the ligand-exchange reaction might be regioselective toward the reactive sites of pentaarylated [60]fullerene derivatives $Ar_5C_{60}H$. Here we report our results.

Results and Discussion

Synthesis and Characterization of Complexes $[(\eta^2\text{-}Ar_5C_{60}H)M(PPh_3)_2]$ (1–6)

An equivalent of each transition metal complex $[M(PPh_3)_4]$ (M = Pt, Pd) was treated with a pentaarylated [60]fullerene derivative $Ar_5C_{60}H$ (Ar = Ph, *m*-MeC_6H_4, *p*-MeC_6H_4) in THF at room temperature to give six products $[(\eta^2\text{-}Ar_5C_{60}H)M(PPh_3)_2]$ (**1**–**6**) in 51–63% yields, as shown in Scheme 1.

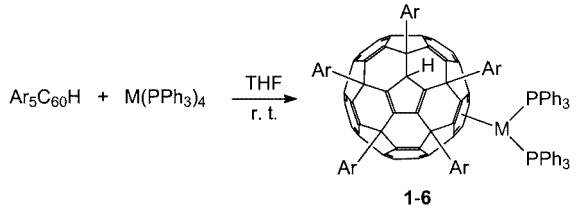

	1	2	3	4	5	6
Ar	Ph	*m*-MeC_6H_4	*p*-MeC_6H_4	Ph	*m*-MeC_6H_4	*p*-MeC_6H_4
M	Pt	Pt	Pt	Pd	Pd	Pd
%	53	63	55	58	51	58

Scheme 1

[a] Department of Chemistry, State Key Laboratory of Elemento-Organic Chemistry, Nankai University,
Tianjin 300071, China
Fax: (internat.) + 86-22/23504853
E-mail: lcsong@public.tpt.tj.cn
[b] Department of Chemistry, The Hong Kong University of Science and Technology
Clear Water Bay, Kowloon, Hong Kong, China

 © 2003 Wiley-VCH Verlag GmbH & Co. KGaA, Weinheim DOI: 10.1002/ejic.200200632

Apparently, products **1**−**6** can be formally regarded − similarly to the parent [60]fullerene metal complexes [(η^2-C_{60})M(PR_3)$_2$] (M = Pt,[6] Pd[7]) − as deriving from displacement of one PPh_3 ligand from M(PPh_3)$_3$ {generated in situ through dissociation of one PPh_3 ligand of starting material [M(PPh_3)$_4$]} by one equivalent of $Ar_5C_{60}H$. Interestingly, products **1**−**6** are, to the best of our knowledge, the first organometallic complexes containing pentaarylated [60]fullerene ligands $Ar_5C_{60}H$ coordinated to transition metals through their [6:6] bonds in an η^2-fashion.

Products **1**−**6** have been characterized by elemental (C,H,P) analysis and spectroscopic methods. In their FAB-MS spectra, while products **1**−**3**, **5**, and **6** show their molecular ions M^+ and their pentaarylated [60]fullerene ligand ions $Ar_5C_{60}H^+$ (Ar = Ph, *m*-MeC_6H_4, *p*-MeC_6H_4), product **4** displays the largest fragment ion [M^+ − Pd] and pentaarylated [60]fullerene ligand ion $Ph_5C_{60}H^+$. The UV/Vis spectra of **1**−**6** are all very similar to one another and each exhibits three absorption bands in the 239−489 nm range. In addition, the IR spectra of **1**−**6** each include four absorption bands, at 1431−1435, 1193−1190, 579−591, and 534−540 cm^{-1}, which resemble those of the free ligands C_{60}[8] and $Ar_5C_{60}H$ (Ar = Ph,[1] *m*-MeC_6H_4,[9] *p*-MeC_6H_4[2]).

For the ^{1}H NMR spectra, it should be noted that, while the hydrogen atom directly bonded to the C_{60} core in each of the free ligands $Ar_5C_{60}H$ (Ar = Ph,[3] *m*-MeC_6H_4,[9] *p*-MeC_6H_4[2]) displays only one singlet at δ = 5.2−5.3 ppm, the corresponding hydrogen atom in each of the compounds **1**−**6** exhibits two to four singlets at δ = 5.1−5.3 ppm. This implies that **1**−**6** might exist as mixtures of isomers. Similarly to the ^{1}H NMR spectra, the ^{31}P NMR spectra of **1**−**6** each show two to four singlets at δ = 29−33 ppm for the P atoms, which also suggests that compounds **1**−**6** exist as isomer mixtures. The ^{31}P NMR spectra of **1**−**3**, however, in contrast to those of **4**−**6**, have two groups of satellite peaks at both sides of the groups of singlets at δ ≈ 30 ppm, caused by ^{195}Pt-^{31}P coupling. It is worth noting that the chemical shifts (δ ≈ 30 pm) of **1**−**6** and the ^{195}Pt-^{31}P coupling constants (J ≈ 3960 Hz) of **1**−**3** are similar to those of [(η^2-C_{60})Pt(PPh_3)$_2$][6,10] and [(η^2-C_{60})Pd(PPh_3)$_2$],[7] apparently due to their similar structures. Figures 1 and 2 show the partial ^{1}H NMR and the whole ^{31}P NMR spectra of products **2** and **4**, respectively. The four singlets at δ ≈ 5.2 ppm in Figure 1(a) could each be assigned to the hydrogen atom directly bonded to C_{60} core in each of four isomers of product **2**, whereas the four singlets at δ ≈ 30 ppm in Figure 1(b) could each be attributed to the two P atoms in each of the four isomers. Similarly, the three singlets at δ ≈ 5.3 ppm in Figure 2(a) and the three singlets at δ ≈ 30 ppm in Figure 2(b) could be assigned to the hydrogen atoms directly bonded to the C_{60} cores and to the P atoms in three isomers of product **4**, respectively. In order to obtain some further details concerning the possible isomers of **1**−**6**, we carried out a computational study on the simplest ligand $Ph_5C_{60}H$ and its Pt complex [(η^2-$Ph_5C_{60}H$)Pt(PPh_3)$_2$] (**1**).

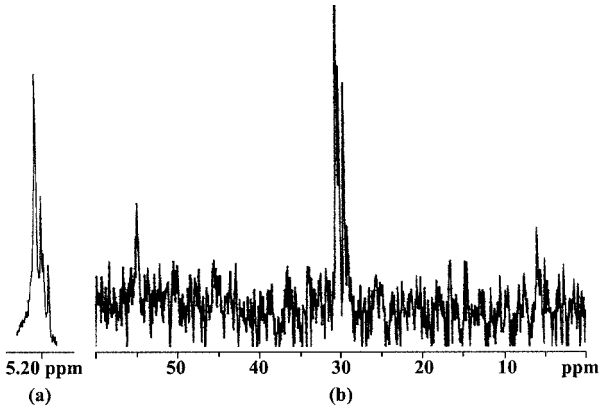

Figure 1. The partial ^{1}H NMR (a) and ^{31}P NMR (b) spectra of **2**

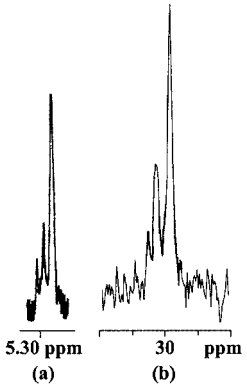

Figure 2. The partial ^{1}H NMR (a) and ^{31}P NMR (b) spectra of **4**

Computational Study on Possible Isomers of 1−6

As shown in Figure 3, the pentaarylated hydro[60]fullerenes $Ar_5C_{60}H$ (Ar = Ph, *m*-MeC_6H_4, *p*-MeC_6H_4), unlike the highly I_h-symmetric [60]fullerene, are C_s-symmetric molecules, each of which contains a series of carbon−carbon double bonds represented by **A**−**O**, **B**′, **C**′, **E**′−**K**′ and **M**′−**O**′. The double bonds represented by capital letters and those represented by the corresponding capital letters with primes are located symmetrically on the two sides of the symmetrical plane of $Ar_5C_{60}H$, which are actually the same in terms of their ability to coordinate with metal atoms M (M = Pt, Pd). Hence, each of the pentaarylated $Ar_5C_{60}H$ has 14 kinds of [6:6] double bonds formed between two six-membered rings represented by **A**−**N** or **A**, **B**′, **C**′, **D**, **E**′−**K**′, **L**, **M**′, **N**′ and one kind of [6:5] double bonds formed between six- and five-membered rings, represented by **O** and **O**′. However, since the **L**−**O** or **M**′−**O**′ double bonds could not coordinate with metal atoms M, due to the great steric hindrance between the two large PPh_3 ligands attached to M and the five aryl groups located around the double bonds **L**−**O** or **M**′−**O**′, products [(η^2-$Ar_5C_{60}H$)M(PPh_3)$_2$] (**1**−**6**) each have only 11 possible structural isomers **A**−**K** or **A**, **B**′, **C**′, **D**, **E**′−**K**′ generated through coordination of the remaining 11 kinds of the corresponding [6:6] double bonds. In fact, the isomers, which are derived from coordination of the [6:6] double bonds **B**′,

 © 2003 Wiley-VCH Verlag GmbH & Co. KGaA, Weinheim

C′, and **E′**−**K′** with M atoms, are the enantiomers of isomers **B**, **C**, and **E**−**K**.

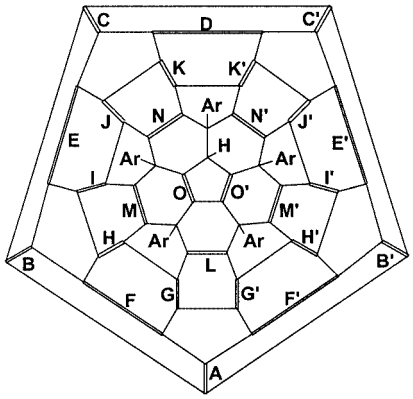

Figure 3. Possible η^2-coordinating sites of $Ar_5C_{60}H$ in a Schlegel diagram

Computational chemistry methods had previously been utilized to study [60]fullerene platinum and palladium complexes in the model complex $[(\eta^2\text{-}C_{60})Pt(PH_3)_2]$.[11−14] In order to further establish the actually existing isomers of **1**−**6** and the regioselectivity of the involved η^2-$Ar_5C_{60}H$ ligands in the products, we chose the platinum complex $[(\eta^2\text{-}Ph_5C_{60}H)Pt(PPh_3)_2]$ (**1**) as a representative with which to carry out ab initio DFT calculations on its 11 possible isomers. It is worth noting that we did not use $[(\eta^2\text{-}Me_5C_{60}H)Pt(PH_3)_2]$ as a model complex in calculations in this case, since it is oversimplified for the strong steric hindrance existing between the phenyl groups in **1**, which is very important for the isomer energies and the ^{1}H NMR calculations.

Density functional theory (DFT) calculations at the B3LYP level were performed in full structural optimizations. With the optimized structures, the ^{1}H magnetic shielding coefficients for the proton directly bonded to the C_{60} core were obtained by Hartree−Fock GIAO method. The energies and isotropic ^{1}H magnetic shielding coefficients are compiled in Table 1.

The reaction involved in the production of the 11 isomers is assumed to be thermodynamically controlled. Provided that a transformation equilibrium among all of the 11 isomers is present, the abundances of the isomers would be determinable only by their energy differences according to the Boltzmann distribution, as shown in Equation (1), where k, T, n_i, p_i, and E_i are the Boltzmann constant, absolute temperature, number of enantiomers of isomer i, and the abundance and energy of isomer i, respectively.

$$p_i = n_i e^{-E_i/kT} / \sum_j n_j e^{-E_j/kT} \quad (1)$$

As can be seen from Table 1, only six (namely **A**−**F**) of the 11 isomers have noticeable abundances at 298 K, the other isomers **G**−**K** derived from the corresponding double bonds **G**, **H**, **I**, **J**, and **K** having very low abundance.

The simulated partial ^{1}H NMR spectrum can be drawn from the isomer abundance data (peak areas) and the calculated ^{1}H shielding coefficients (chemical shifts). Figure 4(b) shows the calculated ^{1}H NMR spectrum of the isomer mixture of **1**, in which the peaks of isomers **F** and **A** or **B** and **D** are overlapped due to their very close values of the shielding coefficients. The similarity of Figure 4(b) with the actual spectrum Figure 4(a) suggests that the ab initio result is logical and acceptable. The four ^{1}H NMR signals of the proton directly bonded to the C_{60} core shown in Figure 4(a) can be assigned to isomers **F**+**A**, **B**+**D**, **C**, and **E**, respectively. It follows that this computational result is different from our initial assignment described above, in which each experimental singlet is related to one single isomer.

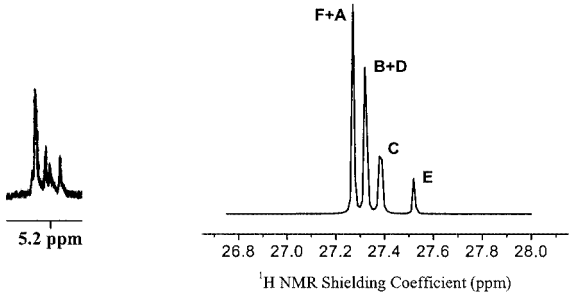

Figure 4. The partial ^{1}H NMR spectrum of the isomer mixture of **1**

Table 1. Calculated properties of the isomers of **1**

Coordination site of Pt	Number of enantiomer(s)	Energy [a. u.]	Estimated abundance at 298 K	^{1}H magnetic shielding coefficient [ppm]
B/B′	2	−4935.59686992	0.296691	27.3226
C/C′	2	−4935.59680000	0.275489	27.3849
A	1	−4935.59679828	0.137494	27.2744
F/F′	2	−4935.59637593	0.175715	27.2699
D	1	−4935.59572960	0.044272	27.3296
E/E′	2	−4935.59551091	0.070218	27.5225
H/H′	2	−4935.58867981	0.000050	27.4275
J/J′	2	−4935.58803199	0.000025	27.2833
G/G′	2	−4935.58764336	0.000017	27.2804
K/K′	2	−4935.58761027	0.000016	27.7785
I/I′	2	−4935.58735725	0.000012	27.8293

 © 2003 Wiley-VCH Verlag GmbH & Co. KGaA, Weinheim

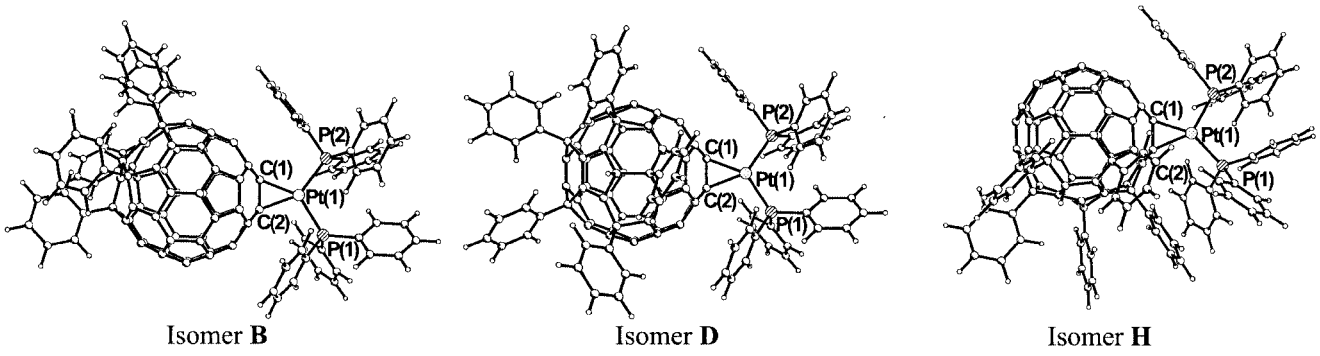

Figure 5. Optimized structures of isomers **B**, **D**, and **H**

Some of the structural parameters of the optimized structures for isomers **B**, **D**, and **H**, together with the corresponding values of the crystal structure of [(η^2-C_{60})Pt(PPh_3)$_2$],[10] are presented in Table 2, whereas Figure 5 shows the optimized structures of the three isomers.

As shown in Table 2, the calculated values for the optimized structures are similar to the crystal structural data of [(η^2-C_{60})Pt(PPh_3)$_2$], which indicates the accuracy of the calculation. That we chose the optimized structures of isomers **B**, **D**, and **H** is to illustrate that the stability and thus the abundance of each isomer is directly related to the steric effect. As can be seen intuitively in Figure 5, the phenyl groups in both $Ph_5C_{60}H$ and PPh_3 are most crowded in isomer **H**, then intermediate in isomer **D**, and least crowded in isomer **B**. This is consistent with the magnitudes of the abundances **B** > **D** > **H** shown in Table 1. In addition, the energy sequence **B** < **D** < **H** shown in Table 1 is also consistent with the magnitudes of the steric repulsion between the five C_{60}-bonded phenyl groups and the six phenyl groups of the two tertiary phosphane ligands in **B**, **D**, and **H**. In fact, isomers **A**, **B**/**B′**, and **C**/**C′** are the most stable ones, since the steric repulsions in these isomers are among the smallest. Finally, it can be concluded that the steric repulsion between the bulky phenyl substituents is most probably the key factor for the regioselectivity of $Ar_5C_{60}H$ ligands in coordinating with transition metals Pt and Pd in an η^2-fashion to form products **1**−**6**.

Table 2. Selected structural parameters of [(η^2-C_{60})Pt(PPh_3)$_2$] and isomers **B**, **D**, and **H**

Compound	(η^2-C_{60})Pt(PPh_3)$_2$	**B**	**D**	**H**
Bond lengths [Å]:				
C(1)−C(2)	1.502	1.515	1.509	1.511
Pt(1)−C(1)	2.145	2.137	2.133	2.117
Pt(1)−C(2)	2.115	2.142	2.147	2.187
Pt(1)−P(1)	2.304	2.362	2.362	2.366
Pt(1)−P(2)	2.254	2.348	2.348	2.357
Bond angles [°]:				
C(2)−C(1)−Pt(1)	68.3	69.4	69.9	72.0
C(1)−C(2)−Pt(1)	70.4	69.1	68.8	67.0
C(1)−Pt(1)−C(2)	41.3	41.5	41.3	41.1
C(2)−Pt(1)−P(1)	107.1	101.1	102.5	111.2
C(1)−Pt(1)−P(2)	109.2	105.3	104.7	101.3
P(1)−Pt(1)−P(2)	102.4	112.1	111.5	101.3

Experimental Section

General: All reactions were carried out under highly purified nitrogen by use of standard Schlenk or vacuum-line techniques. THF was distilled from Na/benzophenone ketyl. All solvents were bubbled with nitrogen for at least 15 min before use. [$Pt(PPh_3)_4$],[15] [$Pd(PPh_3)_4$],[16] $Ph_5C_{60}H$,[3] (m-$MeC_6H_4)_5C_{60}H$,[9] and (p-$MeC_6H_4)_5C_{60}H$[9] were prepared by literature methods. IR spectra were measured with a Bio-Rad FTS 135 spectrophotometer, whereas $^1H\{^{31}P\}$ NMR and UV/Vis spectra were recorded with a Bruker AC P200 and a Shimadzu UV 240 spectrometer, respectively. Elemental analysis of C and H was performed with an Elementar Vario EL analyzer, while P was determined by the vanadomolybdophosphoric acid colorimetric method. Melting points were determined with a Yanaco MP-500 apparatus.

Preparation of [(η^2-$Ph_5C_{60}H$)Pt(PPh_3)$_2$] (1): A 100-mL three-necked flask fitted with a stirrer bar, a serum cap, and an N_2 inlet tube was charged with $Ph_5C_{60}H$ (44 mg, 0.04 mmol) and THF (15 mL). $Pt(PPh_3)_4$ (50 mg, 0.04 mmol) was then added and the reaction mixture was stirred for 0.5 h at room temperature. After removal of the solvent under vacuum, the residue was chromatographed on an Al_2O_3 column with toluene/petroleum ether (3:2) as eluent, and the pink band was collected. After removal of the solvent, 42 mg (57%) of **1** was obtained as a red-brown solid. M.p. > 300°C. ^1H NMR (200 MHz, $CDCl_3$, TMS): δ = 5.13, 5.20, 5.22, 5.28 (4 s, 1 H, $C_{60}H$), 7.05−7.90 (m, 55 H, 11 Ph) ppm. ^{31}P NMR [81.0 MHz, toluene, $(CD_3)_2CO$ lock signal, H_3PO_4]: δ = 28.95, 29.35, 29.96, 30.24 (4 s surrounded with satellite peaks, $J_{Pt\text{-}P}$ = 3959 Hz, 2 P) ppm. IR (KBr): $\tilde{\nu}$ = 516.5 (s), 534.7 (m), 585.0 (w), 693.3 (vs), 742.4 (s), 1029.3 (w), 1094.6 (m), 1434.3 (s), 1491.9 (m), 1598.4 (w), 2863.8 (w), 2952.5 (w), 3056.7 (w) cm^{-1}. UV/Vis (THF): λ_{max} (log ε) = 239.7 (5.14), 288.7 (4.98), 488.9 (4.18) nm. FAB-MS: m/z = 1826 [$(Ph_5C_{60}H)Pt(PPh_3)_2^+$, ^{196}Pt], 1107 [$Ph_5C_{60}H^+$]. $C_{126}H_{56}P_2Pt$ (1826.86): calcd. C 82.84, H 3.09, P 3.39; found C 82.56, H 3.35, P 3.43.

Preparation of [{η^2-(m-$MeC_6H_4)_5C_{60}H$}Pt(PPh_3)$_2$] (2): Similarly, when (m-$MeC_6H_4)_5C_{60}H$ (47 mg, 0.04 mmol) was used in place of $Ph_5C_{60}H$, **2** (48 mg, 63%) was obtained as a red-brown solid. M. p. > 300°C. ^1H NMR (200 MHz, $CDCl_3$, TMS): δ = 2.03, 2.06, 2.17 (3 s, 15 H, CH_3 + 2 CH_3 + 2 CH_3), 5.13, 5.19, 5.21, 5.26 (4 s, 1 H, $C_{60}H$), 7.00−7.90 (m, 50 H, 6 Ph + 5 C_6H_4) ppm. ^{31}P NMR

 © 2003 Wiley-VCH Verlag GmbH & Co. KGaA, Weinheim

[81.0 MHz, toluene, $(CD_3)_2CO$ lock signal, H_3PO_4]: δ = 29.02, 29.43, 29.99, 30.28 (4 s surrounded with satellite peaks, J_{Pt-P} = 3962 Hz, 2 P) ppm. IR (KBr): $\tilde{\nu}$ = 516.9 (s), 534.1 (m), 580.0 (w), 693.2 (vs), 747.4 (s), 1094.5 (m), 1434.1 (m), 1480.2 (m), 1603.7 (w), 2856.0 (w), 2921.6 (w), 3052.9 (w) cm^{-1}. UV/Vis (THF): λ_{max} (log ε) 240.1 (5.16), 288.3 (5.01), 489.1 (4.20) nm. FAB-MS: *m/z* = 1895 [{$(MeC_6H_4)_5C_{60}H$}$Pt(PPh_3)_2^+$, ^{195}Pt], 1177 [$(MeC_6H_4)_5C_{60}H^+$]. $C_{131}H_{66}P_2Pt$ (1896.99): calcd. C 82.94, H 3.51, P 3.26; found C 82.79, H 3.74, P 2.91.

Preparation of [{η²-(*p*-$MeC_6H_4)_5C_{60}H$}$Pt(PPh_3)_2$] (3): Similarly, when (*p*-$MeC_6H_4)_5C_{60}H$ (47 mg, 0.04 mmol) was used in place of $Ph_5C_{60}H$, **3** (42 mg, 55%) was obtained as a red-brown solid. M. p. > 300°C. ^1H NMR (200 MHz, $CDCl_3$, TMS): δ = 2.26, 2.31, 2.36 (3 s, 15 H, CH_3 + 2 CH_3 + 2 CH_3), 5.06, 5.11, 5.13, 5.20 (4 s, 1 H, $C_{60}H$), 6.95−7.85 (m, 50 H, 6 Ph + 5 C_6H_4) ppm. ^{31}P NMR [81.0 MHz, toluene, $(CD_3)_2CO$ lock signal, H_3PO_4]: δ = 29.04, 29.44, 30.01, 30.33 (4 s surrounded with satellite peaks, J_{Pt-P} = 3959 Hz, 2 P) ppm. IR (KBr): $\tilde{\nu}$ = 517.0 (s), 534.9 (s), 583.0 (w), 692.8 (vs), 742.8 (s), 1095.6 (m), 1186.6 (m), 1434.6 (m), 1476.8 (m), 1509.2 (vs), 2848.3 (w), 2863.8 (w), 2952.5 (w), 3022.0 (w), 3052.9 (w) cm^{-1}. UV/Vis (THF): λ_{max} (log ε) 239.1 (5.16), 287.9 (5.00), 487.5 (4.13) nm. FAB-MS: *m/z* = 1895 [{$(MeC_6H_4)_5C_{60}H$}$Pt(PPh_3)_2^+$, ^{195}Pt], 1177 [$(MeC_6H_4)_5C_{60}H^+$], 720 [C_{60}^+]. $C_{131}H_{66}P_2Pt$ (1896.99): calcd. C 82.94, H 3.51, P 3.27; found C 83.17, H 3.63, P 3.18.

Preparation of [(η²-$Ph_5C_{60}H$)$Pd(PPh_3)_2$] (4): Similarly to the preparation of **1**, when $[Pd(PPh_3)_4]$ (46 mg, 0.04 mmol) was used in place of $[Pt(PPh_3)_4]$, **4** (40 mg, 58%) was obtained as a red-brown solid. M. p. > 300°C. ^1H NMR (200 MHz, $CDCl_3$, TMS): δ = 5.28, 5.30, 5.31 (3 s, 1 H, $C_{60}H$), 7.10−7.85 (m, 55 H, 11 Ph) ppm. ^{31}P NMR [81.0 MHz, toluene, $(CD_3)_2CO$ lock signal, H_3PO_4]: δ = 29.05, 31.22, 32.41 (3 s, 2 P) ppm. IR (KBr): $\tilde{\nu}$ = 486.0 (w), 513.0 (w), 540.0 (m), 692.0 (s), 739.0 (w), 1027.0 (w), 1093.0 (m), 1431.0 (m), 1490.0 (w), 1599.0 (w), 2863.0 (w), 2926.0 (w), 3058.0 (w) cm^{-1}. UV/Vis (THF): λ_{max} (log ε) 240.5 (5.04), 287.5 (4.83), 472.0 (3.99) nm. FAB-MS: *m/z* = 1630 [{$(Ph_5C_{60}H)Pd(PPh_3)_2$ − Pd}$^+$], 1107 [$Ph_5C_{60}H^+$]. $C_{126}H_{56}P_2Pd$ (1738.20): calcd. C 87.07, H 3.25, P 3.56; found C 87.14, H 3.51, P 3.74.

Preparation of [{η²-(*m*-$MeC_6H_4)_5C_{60}H$}$Pd(PPh_3)_2$] (5): Similarly to the preparation of **2**, when $[Pd(PPh_3)_4]$ (46 mg, 0.04 mmol) was used in place of $[Pt(PPh_3)_4]$, **5** (37 mg, 51%) was obtained as a red-brown solid. M. p. > 300°C. ^1H NMR (200 MHz, $CDCl_3$, TMS): δ = 2.01, 2.06, 2.17 (3 s, 15 H, CH_3 + 2 CH_3 + 2 CH_3), 5.25, 5.27 (2 s, 1 H, $C_{60}H$), 6.95−7.80 (m, 50 H, 6 Ph + 5 C_6H_4) ppm. ^{31}P NMR [81.0 MHz, toluene, $(CD_3)_2CO$ lock signal, H_3PO_4]: δ = 29.05, 31.27 (2 s, 2 P) ppm. IR (KBr): $\tilde{\nu}$ = 486.0 (w), 505.0 (w), 540.0 (s), 591.0 (w), 688.0 (s), 719.0 (s), 750.0 (m), 996.0 (w), 1027.0 (w), 1093.0 (w), 1120.0 (s), 1178.0 (m), 1435.0 (m), 1482.0 (w), 1597.0 (w), 1607.0 (m), 2856.0 (w), 2918.0 (w), 3043.0 (w) cm^{-1}. UV/Vis (THF): λ_{max} (log ε) 239.5 (5.09), 287.7 (4.93), 470.5 (4.00) nm. FAB-MS: *m/z* = 1806 [{$(MeC_6H_4)_5C_{60}H$}$Pd(PPh_3)_2^+$, ^{106}Pd], 1177 [$(MeC_6H_4)_5C_{60}H^+$]. $C_{131}H_{66}P_2Pd$ (1808.33): calcd. C 87.01, H 3.68, P 3.43; found C 87.06, H 3.75, P 3.48.

Preparation of [{η²-(*p*-$MeC_6H_4)_5C_{60}H$}$Pd(PPh_3)_2$] (6): Similarly to the preparation of **3**, when $[Pd(PPh_3)_4]$ (46 mg, 0.04 mmol) was used in place of $[Pt(PPh_3)_4]$, **6** (42 mg, 58%) was obtained as a red-brown solid. M. p. > 300°C. ^1H NMR (200 MHz, $CDCl_3$, TMS): δ = 2.26, 2.31, 2.36 (3 s, 15 H, CH_3 + 2 CH_3 + 2 CH_3), 5.20, 5.22 (2 s, 1 H, $C_{60}H$), 6.90−7.85 (m, 50 H, 6 Ph + 5 C_6H_4) ppm. ^{31}P NMR [81.0 MHz, toluene, $(CD_3)_2CO$ lock signal, H_3PO_4]: δ = 29.08, 31.08 (2 s, 2 P) ppm. IR (KBr): $\tilde{\nu}$ = 513.0 (s), 536.0 (m), 579.0 (w), 692.0 (s), 743.0 (m), 1019.0 (w), 1093.0 (w), 1190.0 (m), 1431.0 (m), 1509.0 (s), 2863.0 (w), 2926.0 (w), 2972.0 (w), 3027.0 (w), 3058.0 (w) cm^{-1}. UV/Vis (THF): λ_{max} (log ε) = 239.0 (4.85), 287.7 (4.70), 472.0 (3.89) nm. FAB-MS: *m/z* = 1808 [{$(MeC_6H_4)_5C_{60}H$}$Pd(PPh_3)_2^+$, ^{108}Pd], 1177 [$(MeC_6H_4)_5C_{60}H^+$]. $C_{131}H_{66}P_2Pd$ (1808.33): calcd. C 87.01, H 3.68, P 3.43; found C 86.98, H 3.70, P 3.65.

Computational Details: The geometry optimizations of the 11 isomers for [(η²-$Ph_5C_{60}H$)$Pt(PPh_3)_2$] were performed at the DFT B3LYP hybrid functional level by use of the effective core potential basis set LANL2DZ[17−19] for Pt and P. The standard 6-31G basis sets were chosen for C and H, except for those atoms in the phenyl rings, for which STO-3G was used. A polarization function [ξd(P)= 0.387] was added for P.[20] The ^1H NMR magnetic shielding tensors were calculated by the Gauge-Including Atomic Orbital (GIAO) method[21] at the Hartree−Fock level[22] by use of the LANL2DZ basis set for Pt, the 6-31G** basis set for P and for the H atoms directly bonded to C_{60}, and the 6-31G basis set for all other atoms. All calculations were performed with the parallel version of the GAUSSIAN 98 software package[23] on a multi-nodes Beowulf Linux cluster computer system.

Acknowledgments

We are grateful to the National Natural Science Foundation of China for financial support and to Prof. P. J. Fagan for providing the crystal data for [(η²-C_{60})$Pt(PPh_3)_2$].

[1] A. G. Avent, P. R. Birkett, J. D. Crane, A. D. Darwish, G. J. Langley, H. W. Kroto, R. Taylor, D. R. M. Walton, *J. Chem. Soc., Chem. Commun.* **1994**, 1463−1464.
[2] P. R. Birkett, A. G. Avent, A. D. Darwish, I. Hahn, H. W. Kroto, G. J. Langley, J. O'Loughlin, R. Taylor, D. R. M. Walton, *J. Chem. Soc., Perkin Trans. 2* **1997**, 1121−1126.
[3] M. Sawamura, H. Iikura, E. Nakamura, *J. Am. Chem. Soc.* **1996**, *118*, 12850−12851.
[4] M. Sawamura, H. Iikura, T. Ohama, U. E. Hackler, E. Nakamura, *J. Organomet. Chem.* **2000**, *599*, 32−36.
[5] [5a] L.-C. Song, J.-T. Liu, Q.-M. Hu, G.-F. Wang, P. Zanello, M. Fontani, *Organometallics* **2000**, *19*, 5342−5351. [5b] L.-C. Song, Y.-H. Zhu, Q.-M. Hu, *J. Chem. Res., Synop.* **2000**, 316−317. [5c] P. Zanello, F. Laschi, M. Fontani, L.-C. Song, Y.-H. Zhu, *J. Organomet. Chem.* **2000**, *593−594*, 7−11. [5d] Y.-H. Zhu, L.-C. Song, Q.-M. Hu, C.-M. Li, *Org. Lett.* **1999**, *1*, 1693−1695. [5e] L.-C. Song, Y.-H. Zhu, Q.-M. Hu, *Polyhedron* **1997**, *16*, 2141−2143. [5f] L.-C. Song, Y.-H. Zhu, Q.-M. Hu, *Polyhedron* **1998**, *17*, 469−473. [5g] Y.-L. Song, G.-Y. Fang, Y.-X. Wang, S.-T. Liu, C.-F. Li, L.-C. Song, Y.-H. Zhu, Q.-M. Hu, *Appl. Phys. Lett.* **1999**, *74*, 332−334. [5h] L.-C. Song, Y.-H. Zhu, Q.-M. Hu, *J. Chem. Res., Synop.* **1999**, 56−57. [5i] L.-C. Song, J.-T. Liu, Q.-M. Hu, L.-H. Weng, *Organometallics* **2000**, *19*, 1643−1647.
[6] P. J. Fagan, J. C. Calabrese, B. Malone, *Acc. Chem. Res.* **1992**, *25*, 134−142.
[7] V. V. Bashilov, P. V. Petrovshkii, V. I. Sokolov, S. V. Lindeman, I. A. Guzey, Y. T. Struchkov, *Organometallics* **1993**, *12*, 991−992.
[8] J. P. Hare, T. J. Dennis, H. W. Kroto, R. Taylor, A. W. Allaf, S. Balm, D. R. M. Walton, *J. Chem. Soc., Chem. Commun.* **1991**, 412−413.
[9] L.-C. Song, P.-C. Liu, Q.-M. Hu, P. Zanello, M. Fontani, *Chin. J. Chem.* **2000**, *18*, 395−401.
[10] P. J. Fagan, J. C. Calabrese, B. Malone, *Science* **1991**, *252*, 1160−1161.

 © 2003 Wiley-VCH Verlag GmbH & Co. KGaA, Weinheim

[11] N. Koga, K. Morokuma, *Chem. Phys. Lett.* **1993**, *202*, 330−334.
[12] J. A. López, C. Mealli, *J. Organomet. Chem.* **1994**, *478*, 161−171.
[13] D. L. Lichtenberger, L. L. Wright, N. E. Gruhn, M. E. Rempe, *J. Organomet. Chem.* **1994**, *478*, 213−221.
[14] F. Nunzi, A. Sgamellotti, N. Re, C. Floriani, *Organometallics* **2000**, *19*, 1628−1634.
[15] L. Malatesta, C. Cariello, *J. Chem. Soc.* **1958**, 2323−2328.
[16] L. Malatesta, M. Angoletta, *J. Chem. Soc.* **1957**, 1186−1188.
[17] P. J. Hay, W. R. Wadt, *J. Chem. Phys.* **1985**, *82*, 270−283.
[18] W. R. Wadt, P. J. Hay, *J. Chem. Phys.* **1985**, *82*, 284−298.
[19] P. J. Hay, W. R. Wadt, *J. Chem. Phys.* **1985**, *82*, 299−310.
[20] A. Hoellwarth, M. Boehme, S. Dapprich, A. W. Ehlers, A. Gobbi, V. Jonas, K. F. Koehler, R. Stegmann, A. Veldkamp, G. Frenking, *Chem. Phys. Lett.* **1993**, *208*, 237−240.
[21] K. Wolinski, J. F. Hilton, P. Pulay, *J. Am. Chem. Soc.* **1990**, *112*, 8251−8260.
[22] J. R. Cheeseman, G. W. Trucks, T. A. Keith, M. J. Frisch, *J. Chem. Phys.* **1996**, *104*, 5497−5509.
[23] M. J. Frisch,; G. W. Trucks, H. B. Schlegel, G. E. Scuseria, M. A. Robb, J. R. Cheeseman, V. G. Zakrzewski, J. A. Montgomery Jr., R. E. Stratmann, J. C. Burant, S. Dapprich, J. M. Millam, A. D. Daniels, K. N. Kudin, M. C. strain, O. Farkas, J. Tomasi, V. Barone, M. Cossi, R. Cammi, B. Mennucci, C. Pomelli, C. Adamo, S. Clifford, J. Ochterski, G. A. Petersson, P. Y. Ayala, Q. Cui, K. Morokuma, D. K. Malick, A. D. Rabuck, K. Raghavachari, J. B. Foresman, J. Cioslowski, J. V. Ortiz, A. G. Baboul, B. B. Stefanov, G. Liu, A. Liashenko, P. Piskorz, I. Komaromi, R. Gomperts, R. L. Martin, D. J. Fox, T. Keith, M. A. Al-Laham, C. Y. Peng, A. Nanayakkara, C. Gonzalez, M. Challacombe, P. M. W. Gill, B. G. Johnson, W. Chen, M. W. Wong, J. L. Andres, M. Head-Gordon, E. S. Replogle, J. A. Pople, *Gaussian 98* (Revision A.9), Gaussian, Inc., Pittsburgh PA, **1998**.

Received November 16, 2002

 © 2003 Wiley-VCH Verlag GmbH & Co. KGaA, Weinheim

Gold, Silver and Palladium Complexes with the 2,2′-Dipyridylamine Ligand

Mercedes Burgos,[a] Olga Crespo,[a] M. Concepción Gimeno,[a] Peter G. Jones,[b] and Antonio Laguna*[a]

Keywords: Gold / N Ligands / Palladium / Silver

Reaction of the 2,2′-dipyridylamine (Py_2NH) ligand with various gold and silver starting products leads to three- or four-coordinate complexes. The structure of compound $[Ag(NHPy_2)(PPh_3)]OTf$ shows weak interactions which produce bands of molecules parallel to the *z* axis. Other hydrogen bonds of the type C–H···O serve to link the ribbons. The derivative $PPN[Au(Py_2N)_2]$ has also been obtained using $PPN[Au(acac)_2]$ [PPN = bis(triphenylphosphanyl)iminio, acac = acetylacetonate] as starting product to deprotonate the ligand. The palladium complex $[PdCl_2(Py_2NH)_2]$ is also reported.

(© Wiley-VCH Verlag GmbH & Co. KGaA, 69451 Weinheim, Germany, 2003)

Introduction

A search of the CSD affords more than two hundred structures of coordination complexes containing the 2,2′-dipyridylamine ligand (dpa). In most of them, the ligand shows a bidentate coordination mode,[1] but coordination as a bridging ligand[2] is not unusual, and monodentate coordination has been found in $[M(dpa)_2(CO)_3]$[3] (M = Mo, W, one chelate and other monodentate dpa) and also in the more recently reported $[W(dpa)(CO)_5]$.[4] The copper complexes of this ligand have been the most widely studied, at first as models for copper-containing plant hormone binding sites,[1d,5] and also because of their interesting electrochemical behavior.[6] The blue-light emission of organoaluminium(III) and Zn^{II} complexes with dpa is well known. The chelating effect of dpa in these complexes seems to be the origin of the enhancement and shift from UV to blue of the intraligand $\pi \rightarrow \pi^*$ transition of dpa upon coordination.[7−10] Nevertheless, the thermal instability or the low emission quantum yields in the solid state make the use of these complexes for practical applications impossible. Recent investigations in this area have involved polymeric or polynuclear complexes.[1c] Interesting trinuclear complexes in which the dpa acts as a bridging ligand have been described. They show variable-temperature magnetic susceptibility, which ranges from strong antiferromagnetic coupling (tricopper, trinickel)[11−13] to spin crossover (tricobalt),[14,15] via Curie law behavior (trichromium).[2e,16] The coordination to coinage metals other than copper remains uninvestigated, as far as we know. The silver derivatives may be especially interesting due to the possibility of the formation of supramolecular structures. These structures may be derived from building blocks linked by coordinate covalent[17] or hydrogen bonds.[18] Such structures are an active field of research, and many of them are afforded by using *N*,*N*′-bidentate spacers.[19] Herein we report the synthesis of some gold and silver complexes with the dpa ligand, and also the palladium derivative $[PdCl_2(dpa)]$. The structure of compound $[Ag(NHPy_2)(PPh_3)]OTf$ shows weak interactions which produce bands of molecules parallel to the *z* axis. Other hydrogen bonds of the type C−H···O serve to link the ribbons.

Results and Discussion

The reaction of $[Py_2NH]$ with AgOTf in a 1:1 or 2:1 molar ratio affords the three coordinate $[Ag(OTf)(Py_2NH)]$ (**1**) or four coordinate $[Ag(Py_2NH)_2]OTf$ (**2**) species (Scheme 1). Their IR spectra show the vibrations corresponding to N−H deformation and C=N, C=C stretching modes of the pyridine rings at 1586, 1540 cm^{-1} (**1**) or 1601, 1524 cm^{-1} (**2**) and the band corresponding to the N−H stretching vibration at 3320 (**1**) or 3340 (**2**).[1c,20,21] Those bands corresponding to covalent (**1**, 1240 and 1119 cm^{-1}) or anionic (**2**, 1272 and 1154 cm^{-1}) trifluoromethanesulfonate anion are also present.[22] The conductivity of compound **1** in acetone solution shows a higher value than expected for a non-electrolyte. This can be explained by taking into account the lability of the trifluoromethanesulfonate anion, which, in solution, is probably highly dissociated. In the ^1H NMR spectra the pyridine protons appear as four signals in the range $\delta = 7.16-8.20$ (**1**) and 6.88−8.11 ppm (**2**). In **1**, one signal at $\delta = 11.30$ ppm (br. s)

[a] Departamento de Química Inorgánica, Instituto de Ciencia de Materiales de Aragón, Universidad de Zaragoza-CSIC, 50009 Zaragoza, Spain
[b] Institut für Anorganische und Analytische Chemie, Technische Universität Braunschweig, Postfach 3329, 38023 Braunschweig, Germany

 © 2003 Wiley-VCH Verlag GmbH & Co. KGaA, Weinheim **DOI: 10.1002/ejic.200200666**

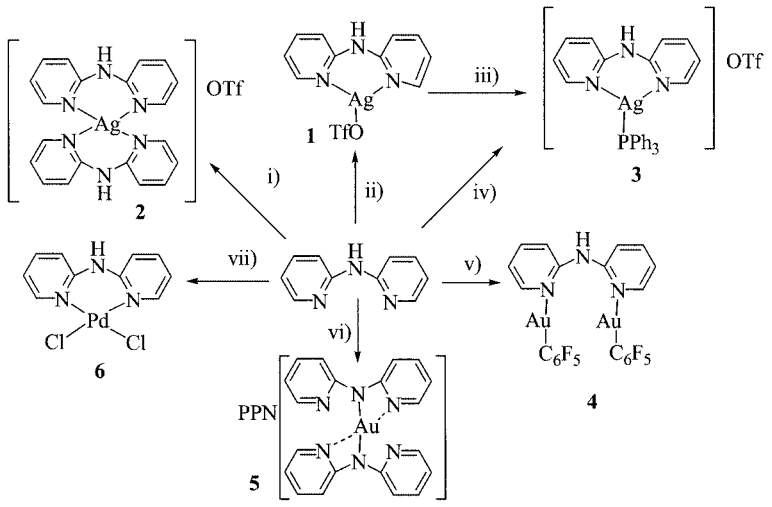

Scheme 1. i) 1/2 AgOTf, ii) AgOTf, iii) PPh_3, iv) [AgOTf(PPh_3)], v) 2 [Au(C_6F_5)(tht)], vi) PPN[Au(acac)$_2$], vii) [$PdCl_2$(PhCN)$_2$]

corresponds to the NH hydrogen atom, whereas in **2** it is overlapped with the resonances of the pyridinic protons. In the LSIMS (+) mass spectra the cationic molecular peaks appear at *m*/*z* = 428 (6%) for **1** and *m*/*z* = 450 (9%) for **2**. The displacement of the OTf ligand by PPh_3 in **1**, or the reaction of $NHPy_2$ with [Ag(OTf)(PPh_3)] in a 1:1 molar ratio, affords the derivative [Ag($NHPy_2$)(PPh_3)]OTf (**3**). The characteristic vibrations of the dpa ligand appear in the IR spectrum at 1640, 1581 and 3330 cm^{-1}; those corresponding to the OTf anion appear at 1283 and 1097 cm^{-1}. The ^1H NMR spectrum displays a broad resonance at δ = 9.64 ppm, which corresponds to the NH hydrogen atom. Three signals are observed in the δ = 5.5−8 ppm region, one of which involves the phenyl group and two the pyridinic protons. A broad signal at δ = 14.46 ppm is observed in the $^{31}P\{^1H\}$ NMR spectrum at room temperature. When the spectrum is recorded at −50 °C, the signal is split into two doublets, centered at δ = 17.6 ppm, due to the coupling of the phosphorus atom with the two silver isotopomers (J^{109}_{AgP} = 773.2, J^{107}_{AgP} = 678.4 Hz). The LSIMS (+) mass spectrum shows the cationic molecular peak at *m*/*z* = 541 (53%).

The molecular structure of **3** has been determined by X-ray diffraction studies. The geometry at the silver atom is distorted trigonal (Figure 1, Table 1). The major distortion comes from the restricted bite angle of the bidentate ligand [N11−Ag−N21 82.82(9)°], with concomitantly wide values for the other two angles [N11−Ag−P 139.80(7)°; N21−Ag−P 131.22(7)°]. The Ag−N distances [Ag−N11 2.264(2), Ag−N21 2.283(3) Å] are in the range of those observed in [Au_2Ag_2\{μ-(PPh_2)$_2$N\}($OClO_3$)(PPh_3)$_2$][23] [2.239(4) Å], in which the silver centers show trigonal geometries. Longer distances have been found in other silver complexes in which the silver atom is three-coordinate, such as [Ag\{1,2-(C_5H_4NS)$_2$-1,2-$C_2B_{10}H_{10}$\}(PPh_3)]OTf [2.345(2), 2.350(2) Å].[24] The Ag−P distance of 2.3414(8) Å is similar to that found in [Ag\{1,2-(C_5H_4NS)$_2$-1,2-$C_2B_{10}H_{10}$\}(PPh_3)]OTf (2.33832(7) Å] or to the shortest found in [Ag(dppf)(PPh_3)]OTf [dppf = 1,1′-bis(diphenylphosphanyl)ferrocene][25] [2.4244−2.4802(12) Å]. The silver center lies 0.30 Å out of the plane formed by the N11, N21 and P atoms, associated with a contact to a triflate oxygen, Ag−O3 2.725(3) Å. This value is somewhat longer than the 2.601(4) Å in [Ag_4\{μ-$SC_2B_{10}H_{10}$\}$_2$(μ-O_3SCF_3)$_2$(PPh_3)$_4$],[26] but both values can be considered to lie in a typical range for triflate-silver contacts. The same oxygen atom acts as an acceptor for a hydrogen bond from the NH group [N−O 3.021(4), H−O 2.20(2) Å] (Table 2). The overall effect of the two weaker interactions is to produce bands of molecules parallel to the *z* axis (Figure 2). Other "weak" hydrogen bonds of the type C−H···O play a role in the crystal packing; two H···O distances from *para*-H atoms of the phosphane phenyl rings are particularly short (2.31, 2.32 Å), and these H bonds serve to link the ribbons.

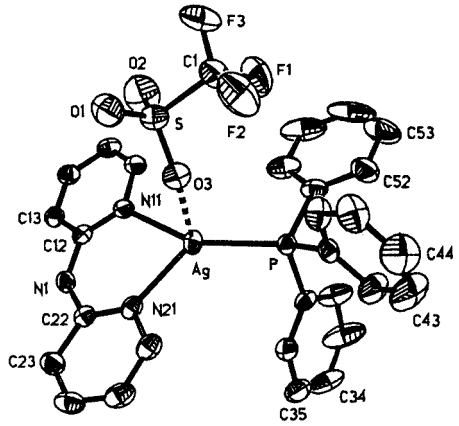

Figure 1. Structure of compound **3**; thermal ellipsoids are drawn with surfaces at the 50% probability level; hydrogens and solvent have been omitted for clarity

Gold(I) complexes have also been obtained by the reaction of Py_2NH with very different starting products (Scheme 1). Thus, the reaction of the ligand with

 © 2003 Wiley-VCH Verlag GmbH & Co. KGaA, Weinheim

Table 1. Selected bond lengths [Å] and angles [°] for **3**

Ag−N(11)	2.264(2)	N(1)−C(22)	1.377(4)
Ag−N(21)	2.283(3)	N(1)−C(12)	1.393(4)
Ag−P	2.3414(8)	N(11)−C(12)	1.335(4)
Ag−O(3)	2.725(3)	N(11)−C(16)	1.349(4)
P−C(51)	1.811(3)	N(21)−C(22)	1.333(4)
P−C(41)	1.820(3)	N(21)−C(26)	1.357(4)
P−C(31)	1.825(3)		
N(11)−Ag−N(21)	82.82(9)	C(41)−P−Ag	116.19(10)
N(11)−Ag−P	139.80(7)	C(31)−P−Ag	110.36(11)
N(21)−Ag−P	131.22(7)	C(22)−N(1)−C(12)	135.1(3)
N(11)−Ag−O(3)	94.01(8)	C(12)−N(11)−C(16)	117.2(3)
N(21)−Ag−O(3)	95.48(8)	C(12)−N(11)−Ag	126.8(2)
P−Ag−O(3)	101.64(6)	C(16)−N(11)−Ag	113.2(2)
C(51)−P−C(41)	104.46(16)	C(22)−N(21)−C(26)	117.4(3)
C(51)−P−C(31)	104.61(15)	C(22)−N(21)−Ag	127.3(2)
C(41)−P−C(31)	104.35(14)	C(26)−N(21)−Ag	114.8(2)
C(51)−P−Ag	115.66(12)	S−O(3)−Ag	130.65(1)

Table 2. Hydrogen bonds [Å and °] for **3**

D−H···A[a]	*d*(D−H)	*d*(H···A)	*d*(D···A)	<(DHA)
N(1)−H(01)···O(3)#1	0.841(18)	2.20(2)	3.021(4)	166(3)
C(34)−H(34)···O(1)#2	0.95	2.32	3.262(5)	169.9
C(54)−H(54)···O(2)#3	0.95	2.31	3.224(5)	162.1
C(46)−H(46)···O(3)	0.95	2.58	3.400(5)	144.5
C(99)−H(99A)···O(1)	0.99	2.65	3.554(8)	152.5
C(23)−H(23)···O(3)#1	0.95	2.68	3.446(4)	138.2

[a] Symmetry transformations used to generate equivalent atoms: #1 $x, -y + 1/2, z + 1/2$; #2 $x + 1, y, z + 1$; #3 $-x + 1, -y, -z + 1$.

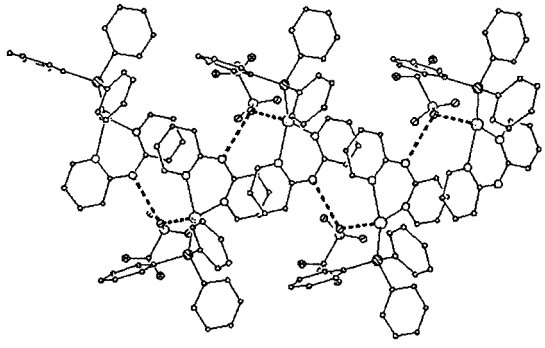

Figure 2. Crystal structure of **3**; hydrogens have been omitted for clarity; secondary interactions Ag···O and N···O are indicated by dashed lines

$[Au(C_6F_5)(tht)]$ in a 1:2 molar ratio affords the dinuclear complex $[Au_2(C_6F_5)_2(\mu\text{-}Py_2NH)]$ (**4**). Apart from the characteristic bands of dpa at 1610, 1532 and 3296 cm^{-1}, the IR spectrum of **4** shows the vibrations of the pentafluorophenyl ring bonded to gold(I) at 1507 and 961 cm^{-1}. In the ^1H NMR spectrum, three of the signals come from the pyridinic protons, one of which integrates for double the value of the others. The NH hydrogen atom resonance appears at $\delta = 8.57$ ppm. The ^{19}F NMR spectrum shows three signals, which correspond to the *ortho, metha* and *para* fluorine atoms. In the LSIMS (+) mass spectrum the molecular peak appears at $m/z = 899$ (68%).

When the reaction is carried out with $PPN[Au(acac)_2]$ in a 2:1 molar ratio, the ligand is deprotonated and the homoleptic derivative $PPN[Au(Py_2N)_2]$ (**5**) obtained. The IR and ^1H NMR spectra confirm the deprotonation of the coordinated ligands. In the ^1H NMR spectrum, once again, one of the signals belonging to the pyridinic protons is overlapped, in this particular case with the broad signal from the phenyl groups of the PPN cation. The anionic molecular peak at $m/z = 537$ (35%) is present in the LSIMS(−) mass spectrum. No crystal suitable for X-ray analyses has been obtained. Tentatively we propose three- or four-coordination at gold, involving coordination to the deprotonated nitrogen atoms and one or two of the pyridinic nitrogen atoms (see Scheme 1).

We have also obtained the palladium complex $[PdCl_2(Py_2NH)_2]$ by displacement of the PhCN ligands in $[PdCl_2(PhCN)_2]$ by Py_2NH. In the IR spectrum the characteristic vibrations of dpa appear at 3490, 1634 and 1587 cm^{-1}. Four resonances for the pyridinic hydrogen atoms, and the signal corresponding to the NH proton at $\delta = 9.50$ ppm, appear in the ^1H NMR spectrum. The LSIMS (+) mass spectrum shows the molecular peak at $m/z = 348$ (11%).

Experimental Section

General Remarks: AgOTf, Py_2NH, PPh_3 and $[PdCl_2(PhCN)_2]$ were purchased from Aldrich and used as received. The starting products $[Au(C_6F_5)(tht)]$,[27] $PPN[Au(acac)_2]$[28] and $[Ag(OTf)(PPh_3)]$[29] were synthesized according to literature methods.

Infrared spectra were recorded in the range 4000−200 cm^{-1} on a Perkin−Elmer FT-IR Spectrum 1000 spectrophotometer as Nujol mulls between polyethylene sheets. Conductivities were measured in ca. 5×10^{-4} M acetone solutions with a Jenway 4010 conductimeter. C, H, N, S analysis was carried out with a Perkin−Elmer 240C microanalyser. Mass spectra were recorded on a VG Autospec using the LSIMS techniques and nitrobenzyl alcohol as matrix and on a HP59987 A ELECTROSPRAY. ^1H, ^{19}F and ^{31}P NMR spectra were recorded on a Bruker ARX 300 in $CDCl_3$ solutions. Chemical shifts are quoted relative to $SiMe_4$ (^1H, external), $CFCl_3$ (^{19}F, external) and H_3PO_4 (85%) (^{31}P, external).

Synthesis of $[Ag(OTf)(Py_2NH)]$ (1): Py_2NH (0.1 mmol, 0.017 g) was added to a diethyl ether solution (20 mL) of Ag(OTf) (0.1 mmol, 0.025 g). The solution was stirred for 30 min. Upon concentration to ca. 5 mL compound **1** precipitated as a white solid (31 mg, yield 76%). $C_{11}H_9AgF_3N_3O_3S$ (428.1): calcd. C 30.85, H 2.10, N 9.8, S 7.45; found C 30.85, H 2.10, N 9.8, S 7.60. Λ_M 107 $\Omega^{-1}cm^2mol^{-1}$. ^1H NMR: $\delta = 7.16$ (dd, $J_{H,H} = 6.53$, 6.51 Hz, 2H-Py), 7.52 (d, $J_{H,H} = 8.74$ Hz, 2H-Py), 7.90 (dd, $J_{H,H} = 7.94$, 7.20 Hz, 2H-Py), 8.20 (br. m, 2H-Py), 11.30 (br. s, 1H-NH) ppm.

Synthesis of $[Ag(Py_2NH)_2]OTf$ (2): Py_2NH (0.2 mmol, 0.034 g) was added to a diethyl ether solution (20 mL) of Ag(OTf) (0.1 mmol, 0.025 g). The solution was stirred for 30 min. Upon concentration to ca. 5 mL compound **2** precipitated as a white solid (45 mg, yield

 © 2003 Wiley-VCH Verlag GmbH & Co. KGaA, Weinheim

76%). $C_{21}H_{18}AgF_3N_6O_3S$ (599.3): calcd. C 42.05, H 3.0, N 14.0, S 5.35; found C 41.65, H 2.7, N 14.1, S 5.15. Λ_M 119 $\Omega^{-1}cm^2mol^{-1}$. ^1H NMR: δ = 6.88 (br. m, 4H-Py), 7.3 (br. m, 4H-Py), 7.64 (br. m, 4H-Py), 8.11(br. m, 4H-Py) ppm.

Synthesis of [Ag(Py$_2$NH)(PPh$_3$)]·OTf (3). Method (a): Py_2NH (0.1 mmol, 0.017 g) was added to a dichloromethane solution (20 mL) of [Ag(OTf)(PPh_3)] (0.1 mmol, 0.052 g). After stirring for 30 min, the solution was concentrated to ca. 5 mL Addition of diethyl ether afforded **3** as a white solid. **Method (b):** PPh_3 (0.1 mmol, 0.026 g) was added to a dichloromethane solution (20 mL) of [Ag(OTf)(Py_2NH)] (0.1 mmol, 0.043 g). After stirring for 30 min, the solution was concentrated to ca. 5 mL. Addition of diethyl ether afforded **3** as a white solid (64 mg, yield 94%). $C_{29}H_{24}AgF_3N_3O_3PS$ (690.4): calcd. C 50.45, H 3.5, N 6.0, S 4.65; found C 50.2, H 3.2, N 6.25, S 4.7. Λ_M 102 $\Omega^{-1}cm^2mol^{-1}$. ^1H NMR: δ = 6.82 (br. m, 2H-Py), 7.38−7.54 (br. m, 2H-Py+ 15H-Ph), 7.63 (br. m, 2H-Py), 7.93 (br. m, 2H-Py), 9.64 (br. s, 1H-NH) ppm.

Synthesis of [Au$_2$(C$_6$F$_5$)$_2$(μ-Py$_2$NH)] (4): Py_2NH (0.1 mmol, 0.017 g) was added to a solution of [Au(C_6F_5)(tht)] (0.2 mmol, 0.091 g) in dichloromethane (20 mL). The solution was stirred for 30 min. Concentration to ca. 5 mL and addition of diethyl ether afforded **4** as a white solid (59 mg, yield 66%). $C_{22}H_9Au_2F_{10}N_3$ (899.2): calcd. C 29.35, H 1.0, N 4.65; found C 29.4, H 1.45, N 5.15. Λ_M 22 $\Omega^{-1}cm^2mol^{-1}$. ^1H NMR: δ = 7.0 (br. m, 2H-Py), 7.77 (br. m, 4H-Py), 8.29 (br. m, 2H-Py), 8.57 (br. s, 1H-NH) ppm. ^{19}F NMR: δ = −117 (m, 4F, *o-F*), −159.3 (t, 2F, *p-F*, ^3J(FF) 19.64 Hz), −163.1 (m, 4F, *m-F*) ppm.

Synthesis of PPN[Au(Py$_2$N)$_2$] (5): Py_2NH (0.1 mmol, 0.017 g) was added to a solution of PPN[Au(acac)$_2$] (0.05 mmol, 0.047 g) in dichloromethane (20 mL). The solution was stirred for 30 min and then concentrated to ca. 5 mL. Addition of hexane afforded **5** as a white solid (33 mg, yield 31%). $C_{56}H_{46}AuN_7P_2$ (1075.9): calcd. C 62.5, H 4.3, N 9.1; found C 62.7, H 4.1, N 9.45. Λ_M 73 $\Omega^{-1}cm^2mol^{-1}$. ^1H NMR: δ = 6.84 (br. m, 2H-Py), 7.41−7.6 (br. m, 2H-Py+ 30H-Ph), 7.67 (br. m, 2H-Py), 8.26 (br. m, 2H-Py) ppm.

Synthesis of [PdCl$_2$(Py$_2$NH)] (6): Py_2NH (0.1 mmol, 0.017 g) was added to a solution of [$PdCl_2(PhCN)_2$] (0.1 mmol, 0.035 g) in dichloromethane (20 mL). The solution was stirred for 30 min and then concentrated to ca. 5 mL Addition of diethyl ether afforded **5** as a yellow-orange solid (49 mg, yield 95%). $C_{10}H_9Cl_2N_3Pd$ (348.5): calcd. C 34.45, H 2.6, N 12.05; found C 34.15, H 2.65, N 11.80. ^1H NMR: δ = 6.92 (br. m, 2H-Py), 7.33 (br. m, 2H-Py), 7.62 (br. m, 2H-Py), 8.65 (br. m, 2H-Py), 9.50 (br. m, 1H-NH) ppm.

X-ray Crystallographic Study of Compound 3·CH$_2$Cl$_2$: Colorless prism; 0.23 × 0.11 × 0.09 mm. Crystal data: $C_{30}H_{26}AgCl_2F_3N_3O_3PS$, M = 775.34, monoclinic, space group $P2_1/c$, a = 12.0173(14), b = 28.699(3), c = 9.6308(9) Å, β = 102.311(3)°, V = 3245.1(6) Å ^{3}, T = −130 °C, Z = 4, μ = 0.953 mm^{-1}, 32407 reflections (Bruker SMART 1000-CCD, Mo-K_α radiation, $2\theta_{max}$ 56.6°, ω- and φ-scans), 7985 unique. The program SADABS, based on multiple scans, was used for the absorption correction (transmission max., min.: 0.928, 0.732). Solution by direct methods. Refinement on F^2; program system SHELXL-97[30]. Hydrogen atoms riding except for the aminic hydrogen, which was refined freely with an N−H distance restraint. Final $R1$ = 0.0428, $wR2$ = 0.1060, for 401 parameters; S(F^2) 0.930; max. Δρ 0.792 e·Å^{-3}.

CCDC-199151 contains the supplementary crystallographic data for this paper. These data can be obtained free of charge at www.ccdc.cam.ac.uk/conts/retrieving.html [or from the Cambridge Crystallographic Data Centre, 12, Union Road, Cambridge CB2 1EZ, UK; fax: (internat.) +44−1223/336−033; E-mail: deposit@ccdc.cam.ac.uk].

Acknowledgments

We thank the Dirección General de Investigación (D.G.I) (n° BQU2001-2409-C02-01), the Fonds der Chemischen Industrie, and the Caja de Ahorros de la Inmaculada for financial support.

[1] See for example: [1a] B. Yan, Y. Xu, X. Bu, N. K. Goh, L. S. Chia, G. D. Stucky, *J. Chem. Soc., Dalton Trans.* **2001**, 2009−2014. [1b] S. Youngme, W. Somjitsripunya, K. Chinnakali, S. Chantsraproma, H.-K. Fun, *Polyhedron* **1999**, *18*, 857−862. [1c] H. Zhu, M. Strobele, Z. Yu, Z. Wang, H. J. Meyer, X. You, *Inorg. Chem. Commun.* **2001**, *4*, 557−581. [1d] J. S. Thompson, J. F. Whitney, *Inorg. Chem.* **1984**, *23*, 2813−2819. [1e] K.-Y. Ho, W.-Y. Yu, K.-K. Cheung, C.-M. Che, *J. Chem. Soc., Dalton Trans.* **1999**, 1581−1586. [1f] M. Villanueva, J. L. Mesa, M. K. Urtiaga, R. Cortés, L. Lezama, M. J. Arriortua, T. Rojo, *Eur. J. Inorg. Chem.* **2001**, 1581−1586. [1g] P. Naumov, G. Jovanovski, M. G. B. Drew, S. W. Ng, *Inorg. Chim. Acta* **2001**, *314*, 154−162. [1h] C.-M. Liu, S. Gao, H.-M. Hu, Z.-M. Wang, *Chem. Commun.* **2001**, 1636−1637. [1i] J.-L. Zuo, H.-K. Fun, Z. Chinnakali, X.-Z. You, C.-M. Che, *New J. Chem.* **1998**, *22*, 923−925.

[2] See for example: [2a] G. B. Deacon, S. J. Faulks, B. M. Gatehouse, A. J. Jozsa, *Inorg. Chim. Acta* **1977**, *21*, L1. [2b] J. Ashenhurst, L. Brancaleon, S. Gao, W. Liu, H. Schmider, S. Wang, G. Wu, Q. G. Wu, *Organometallics* **1998**, *17*, 5334−5341. [2c] M. Tayebani, S. Gambarotta, G. Yap, *Organometallics* **1998**, *17*, 3639−3641. [2d] F. A. Cotton, L. M. Daniels, C. A. Murillo, I. Pascual, *Inorg. Chem. Commun.* **1998**, *1*, 1−3. [2e] R. Clerac, F. A. Cotton, L. M. Daniels, K. R. Dunbar, C. A. Murillo, I. Pascual, *Inorg. Chem.* **2000**, *39*, 752−756. [2f] F. A. Cotton, C. A. Murillo, X. Wang, *J. Chem. Soc., Dalton Trans.* **1999**, 3327−3328. [2g] R. Clerac, F. A. Cotton, L. M. Daniels, K. R. Dunbar, K. Kirschbaun, C. A. Murillo, A. A. Pinkerton, A. J. Schultz, X. Wang, *J. Am. Chem. Soc.* **2000**, *122*, 6226−6236. [2h] H. Gornitzka, D. Stalke, *Eur. J. Inorg. Chem.* **1998**, 311−317. [2i] F. A. Cotton, L. M. Daniels, C. A. Murillo, I. Pascual, *J. Am. Chem. Soc.* **1997**, *119*, 10223−10224. [2j] R. Clerac, F. A. Cotton, L. M. Daniels, K. R. Dunbar, C. A. Murillo, X. Wang, *Inorg. Chem.* **2001**, *40*, 1256−1264. [2k] R. Clerac, F. A. Cotton, L. M. Daniels, K. R. Dunbar, C. A. Murillo, X. Wang, *J. Chem. Soc., Dalton Trans.* **2001**, 386−391.

[3] R. A. Howie, G. P. Mcquillan, *J. Chem. Soc., Dalton Trans.* **1986**, 759−764.

[4] B. S. Creaven, R. A. Howie, C. Long, *Acta Crystallogr., Sect. C* **2000**, *56*, e181, IUC0000086.

[5] G. Pyrka, R. J. Seeney, A. A. Pinkerton, *Acta Crystallogr., Sect. C* **1991**, *47*, 510−512.

[6] A. Cinquantini, G. Opromolla, P. Zanello, *J. Chem. Soc., Dalton Trans.* **1991**, 3161−3163.

[7] W. Liu, A. Hassan, S. Wang, *Organometallics* **1997**, *16*, 4257−4259.

[8] J. Ashenhurst, L. Brancaleon, A. Hassan, W. Liu, H. Schmider, S. Wang, G. Wu, Q. G. Wu, *Organometallics* **1998**, *17*, 3186−3195.

[9] K. Y. Ho, W. Y. Yu, K. K. Cheung, C.-M. Che, *Chem. Commun.* **1998**, 2101−2102.

[10] Y. G. Ma, H.-Y. Chao, Y. Wu, S. T. Lee, W. Y. Yu, C.-M. Che, *Chem. Commun.* **1998**, 2491−2492.

[11] L. P. Wu, P. Field, T. Morrisey, C. Murphy, P. Nagle, B. Hathaway, C. Simmons, P. Thornton, *J. Chem. Soc., Dalton Trans.* **1990**, 3835−3840.

[12] S. Aduldecha, B. Hathaway, *J. Chem. Soc., Dalton Trans.* **1991**, 993−998.

 © 2003 Wiley-VCH Verlag GmbH & Co. KGaA, Weinheim

[13] R. Clérac, R. A. Cotton, K. R. Dunbar, C. A. Murillo, I. Pascual, *Inorg. Chem.* **1999**, *38*, 2655−2657.
[14] E. C. Yang, M. C. Cheng, M. S. Tsai, S. M. Peng, *J. Chem. Soc., Chem. Commun.* **1994**, 2377−2378.
[15] F. A. Cotton, K. R. Dunbar, T. Lu, C. A. Murillo, X. Wang, *Inorg. Chem.* **2000**, *39*, 3065−3070.
[16] R. Clérac, F. A. Cotton, L. M. Daniels, K. R. Dunbar, C. A: Murillo, I. Pascual, *Inorg. Chem.* **2000**, *39*, 748−751.
[17] J. M. Lehn, *Supramolecular Chemistry*, VCH, Weinheim. 1995, Chp. 9.
[18] C. B. Aakeroy, K. R. Seddon, *Chem. Soc. Rev.* **1993**, 397−407.
[19] [19a] S. R. Batten, R. Robson, *Ang. Chem. Int. Ed. Engl.* **1998**, *37*, 1461−1494. [19b] M. Munakata, L.-P. Wu, T. Kuroda-Sowa, *Adv. Inorg. Chem.* **1999**, *46*, 173−303. [19c] P. J. Hagrman, D. Hagrman, J. Zubieta, *Ang. Chem. Int. Ed. Engl.* **1999**, *38*, 2639−2684.
[20] W. R. McWhinnie, *J. Chem. Soc., Dalton Trans.* **1964**, 5165−5169.
[21] W. R. McWhinnie, *Coord. Chem. Rev.* **1970**, *5*, 293−311.
[22] [22a] D. H. Johnson, D. F. Shriver, *Inorg. Chem.* **1993**, *32*, 1045. [22b] G. A. Lawrence, *Chem. Rev.* **1986**, *86*, 17.
[23] R. Usón, A. Laguna, M. Laguna, M. C. Gimeno, P. G. Jones, C. Fittschen, G. M. Sheldrick, *J. Chem. Soc., Chem. Commun.* **1986**, 509−510.
[24] O. Crespo, M. C. Gimeno, A. Laguna, *J. Organomet. Chem.* **1998**, *561*, 13−18.
[25] M. C. Gimeno, P. G. Jones, A. Laguna, C. Sarroca, *J. Chem. Soc., Dalton Trans.* **1995**, 1473−1481.
[26] M. M. Artigas, O. Crespo, M. C. Gimeno, P. G. Jones, A. Laguna, M. D. Villacampa, *Inorg. Chem.* **1997**, *36*, 6454−6456.
[27] R. Usón, A. Laguna, M. Laguna, *Inorg. Synth.* **1989**, *26*, 85−91.
[28] E. J. Fernández, M. C. Gimeno, P. G. Jones, A. Laguna, M. Laguna, J. M. López-de-Luzuriaga, *J. Chem. Soc., Dalton Trans.* **1992**, 3365−3370.
[29] M. Bardají, O. Crespo, A. Laguna, A. K. Fisher, *Inorg. Chim. Acta* **2000**, *304*, 7−16.
[30] G. M. Sheldrick, SHELX-97, Program for Crystal Structure Determination, University of Göttingen, Göttingen, Germany, 1997.

Received December 5, 2002

 © 2003 Wiley-VCH Verlag GmbH & Co. KGaA, Weinheim

New Alkali Metal Boratabenzenes: Structures of K([18]-Crown-6)(C_5H_5BMe), of the Tetrahydropyran Solvate K(3,5-$Me_2C_5H_3B-NMe_2$)$(THP)_2$, and of Two THF Solvates of K[3,5-$Me_2C_5H_3B-N(SiMe_3)_2$][‡]

Xiaolai Zheng[a] and Gerhard E. Herberich*[a]

Keywords: Alkali metal salts / Borabenzene / Boratabenzene / Boron

The potassium salt K(C_5H_5BMe) (**8**) can be obtained from 2-(Me_3Sn)C_5H_5BMe (**7**)/KO*t*Bu in toluene in essentially quantitative yield. Metalation of 1-(dimethylamino)-3-methylene-1,2,3,6-tetrahydroborinine (**9**) with $MN(SiMe_3)_2$ (M = Na, K) in toluene afforded the unsolvated salts M(3,5-$Me_2C_5H_3B-NMe_2$) (M = Na: **11**; M = K: **12**). Morpholino derivatives M(3,5-$Me_2C_5H_3B-NC_4H_8O$) (M = Li: **17**; M = Na: **18**) and the potassium salt K[3,5-$Me_2C_5H_3B-N(SiMe_3)_2$] (**19**) were obtained similarly. The unsolvated salts are highly air- and water-sensitive, colorless powders. Crystallization with the help of auxiliary Lewis bases provided crystalline solvates K([18]-crown-6)(C_5H_5BMe) (**20**), K$(THP)_2$(3,5-$Me_2C_5H_3B-NMe_2$) (**21**), and the concomitant pseudopolymorphs K[3,5-$Me_2C_5H_3B-N(SiMe_3)_2$]$(THF)_{4/3}$ (α-**22**) and K[3,5-$Me_2C_5H_3B-N(SiMe_3)_2$]$(THF)_{3/2}$ (β-**22**), which were characterized structurally. The structures of α-**22** (space group *C*2/*c*) and β-**22** (space group 6_122) display novel chain forms, which have no precedents in boratabenzene and cyclopentadienide chemistry.

(© Wiley-VCH Verlag GmbH & Co. KGaA, 69451 Weinheim, Germany, 2003)

Introduction

The first boratabenzene salts (salts with anions of type **1**[2]) and the first transition metal complexes[3] with boratabenzene ligands were obtained in the very early 1970s. It soon became apparent that boratabenzene ions **1** are similar to the cyclopentadienide ion Cp^- (**2**).[4]

1 **2**

The structural characterization of boratabenzene salts was a relatively late achievement. The first structure determination was published in 1993, and characterized the TMPDA solvate of lithium 1-(dimethylamino)boratabenzene, Li(TMPDA)($C_5H_5B-NMe_2$) [TMPDA = $Me_2N(CH_2)_3NMe_2$] (**3**).[5a] The year 1995 saw the next two structure determinations, that of Li$(C_5H_5BH)(THF)_2$, which was found to possess an ionic structure [Li$(THF)_4$][Li$(C_5H_5BH)_2$] (**4**) with a sandwich-type anion,[5b] similar to the lithocenate ion,[6] and that of the ammonium salt $Me_3PhN(C_5H_5BMe)$ (**5**) with a naked boratabenzene ion.[5c]

More recently, the *B*-styryl derivative Na(OEt_2)[(*E*)-$C_5H_5BCH=CHPh$] (**6**) was found to be the first example of a zigzag chain structure in a boratabenzene salt.[5d] With the growing number of known structures it is becoming more and more evident that the structural chemistry of the ionic boratabenzenes is closely similar to that of the ionic cyclopentadienides.[7]

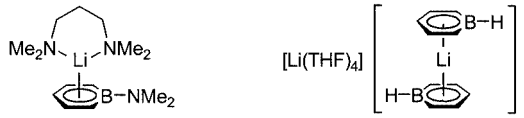

3 **4**

5 **6**, R = (*E*)-CH=CHPh

A variety of synthetic approaches to boratabenzene salts are now available. Deprotonation of dihydroborinines was the final step of the "tin route" to borabenzene derivatives in the very first generation of a boratabenzene salt, Li(C_5H_5BPh).[2a] Deprotonation of dihydroborinines has developed into the most versatile method, with a large variety of deprotonation reagents (including Li*t*Bu, LDA, NaH, and NaCp). Methods based on the "cobaltocene route" include the cyanide degradation of the cobalt sandwich

[‡] Borabenzene Derivatives, 40. Part 39: Ref.[1]

[a] Institut für Anorganische Chemie, Technische Hochschule Aachen
52056 Aachen, Germany
Fax: (internat.) + 49-241/8092288
E-mail: gerhard.herberich@ac.rwth-aachen.de

complexes $Co(C_5H_5BR)_2$ to give the first potassium salts $K(C_5H_5BR)$ (R = Me, Ph),[2b] and the reductive degradation of these complexes by elemental lithium, sodium amalgam, and Na/K alloy, which are now of only historical interest.[2d] From 1993 onwards, the renaissance of borabenzene and boratabenzene chemistry was very strongly stimulated by three new and efficient syntheses. The base-induced cyclization of pentadienylboranes,[5a,5c] and the related "dicarbanion route"[8] were based on classical lithiation and kaliation reactions, while a modification of the tin route provided the borabenzene adduct $C_5H_5B-PMe_3$ as a storage form of the borabenzene ring, and subsequent nucleophilic displacement of the Lewis base PMe_3 afforded a large variety of boratabenzene salts with Li, Na, and K counter ions.[5b,9]

In this paper we describe several new alkali metal boratabenzenes. We present four structure determinations, some of which display new structural motifs.

Results and Discussion

A New Synthesis of Potassium 1-Methylboratabenzene

While lithium 1-methylboratabenzene $Li(C_5H_5BMe)$ can readily be prepared in 10−40 g lots,[5c] the higher Na and K homologues have only been obtained in small quantities because of the practical limitations of the cobaltocene route.[2b−2d] In this work we used 2-$(Me_3Sn)C_5H_5BMe$ (**7**),[10] readily available by treatment of $Li(C_5H_5BMe)$ with Me_3SnCl,[10] as precursor for the preparation of the potassium salt $K(C_5H_5BMe)$ (**8**). Treatment of **7** with KO*t*Bu in toluene at ambient temperature slowly (24 h) produced **8** as a microcrystalline precipitate (Scheme 1). Workup by filtration and washing with hexane gave spectroscopically (NMR) pure samples of **8** in essentially quantitative yield. The reaction can by catalyzed by traces of pyridine, as evidenced by the much faster formation of the precipitate **8**. Earlier work had shown that the tin compound **7** displays a heterolytic equilibrium when traces of DMSO or pyridine are present;[10] the formation of $[Me_3Sn(py)_x]^+$ and $C_5H_5BMe^-$ ions is presumably the main cause of the observed catalytic effect.

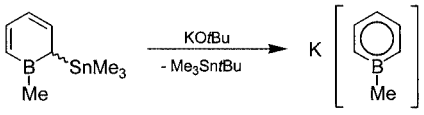

7 **8**

Scheme 1

Syntheses of Aminoboratabenzene Salts

The dicarbanion route provides a particularly efficient route to boratabenzene salts. With 2,4-dimethylpentadienes as starting materials, the dicarbanion route affords the 3-methylene-1,2,3,6-tetrahydroborinine **9** as primary product[8] and, after catalyzed isomerization, a mixture of the dihydroborinines **10a** and **10b**[8] in yields of up to 40%.[11] Metalation, with LDA/TMEDA in THF, for example, produces the lithium salt $Li(3,5\text{-}Me_2C_5H_3B-NMe_2)$ as a crystalline TMEDA solvate,[8] and with $LiN(SiMe_3)_2$ in hexane (or other hydrocarbon solvents) the unsolvated salt.[11] In this work we used the bases $NaN(SiMe_3)_2$ and $KN(SiMe_3)_2$ in toluene and obtained the homologous unsolvated salts $Na(3,5\text{-}Me_2C_5H_3B-NMe_2)$ (**11**) and $K(3,5\text{-}Me_2C_5H_3B-NMe_2)$ (**12**) as colorless powders.

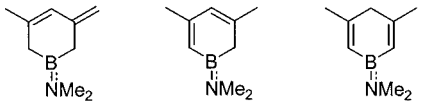

9 **10a** **10b**

11: $Na(3,5\text{-}Me_2C_5H_3B-NMe_2)$

12: $K(3,5\text{-}Me_2C_5H_3B-NMe_2)$

In many situations it is desirable to replace the *B*-(dimethylamino) substituent by other groups. This may be achieved by a two-step procedure (Scheme 2). Firstly, the dimethylamino compound mixture **10a/10b** is treated with BCl_3 to give the chloro derivatives **13a** and **13b**.[11] In a second step, the new substituent at the boron atom is introduced in many cases by treatment with a secondary amine/NEt_3. In this way we obtained the morpholino derivatives **14a** and **14b**, which after deprotonation by $LiN(SiMe_3)_2$ and $NaN(SiMe_3)_2$ gave the new salts $Li(3,5\text{-}Me_2C_5H_3B-NC_4H_8O)$ (**17**) and $Na(3,5\text{-}Me_2C_5H_3B-NC_4H_8O)$ (**18**) in high yields. Analogously, (*S*)-2-(methoxymethyl)pyrrolidine (SMPH) was used to produce the already published *B*-SMP compounds.[12] With bis(trimethylsilyl)amine, the lithium salt $Li[3,5\text{-}Me_2C_5H_3B-N(SiMe_3)_2]$ had previously been prepared.[11a] Use of $KN(SiMe_3)_2$ in toluene as the base afforded the homologous unsolvated potassium salt $K[3,5\text{-}Me_2C_5H_3B-N(SiMe_3)_2]$ (**19**) as a colorless powder.

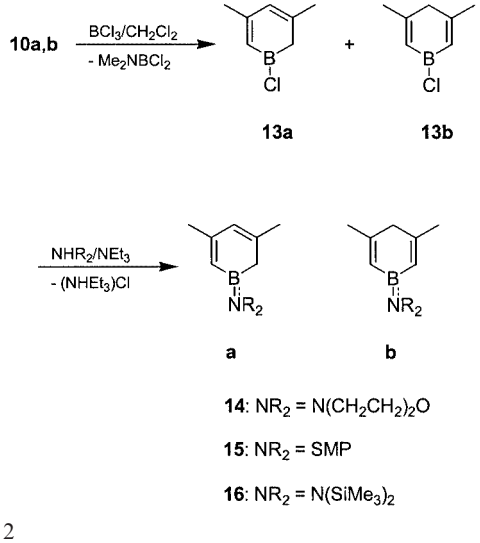

Scheme 2

17: $Li(3,5\text{-}Me_2C_5H_3B-NC_4H_8O)$

18: $Na(3,5\text{-}Me_2C_5H_3B-NC_4H_8O)$

19: $K(3,5\text{-}Me_2C_5H_3B-N(SiMe_3)_2$

 © 2003 Wiley-VCH Verlag GmbH & Co. KGaA, Weinheim

Crystalline Solvates

The new alkali metal boratabenzenes **8**, **11**, **12**, **17**, **18**, and **19** are all microcrystalline powders. Crystallization requires the use of donor solvents and generally produces solvates. Hence, the 1-methylboratabenzene **8** could be dissolved in a warm mixture of toluene/CH_2Cl_2 containing [18]-crown-6 and, when the system had cooled to ambient temperature, gave the solvate K([18]-crown-6)(C_5H_5BMe) (**20**) as crystalline blocks in high yield. Crystallization of the potassium compound **12** from toluene/tetrahydropyran gave the crystalline solvate $K(THP)_2$(3,5-$Me_2C_5H_3$-B−NMe_2) (**21**); the number of tetrahydropyran molecules in this compound was deduced from ^1H NMR spectroscopic data and later confirmed by a structure determination. The bis(trimethylsilyl)amino derivative K[3,5-$Me_2C_5H_3B-N(SiMe_3)_2$] (**19**) could be crystallized from THF and, unexpectedly, produced a mixture of two concomitant pseudopolymorphs[13] K[3,5-$Me_2C_5H_3B-N(SiMe_3)_2$]$(THF)_x$ with slightly different THF contents: α-**22** with 4/3 mol-equiv. of THF, and β-**22** with 3/2 mol-equiv. THF. The two compounds are not true polymorphs, because their compositions are not fully equal. Note also that two crystalline phases can only be formed in the same system as the result of kinetic control.

20: K([18]-crown-6)(C_5H_5BMe)

21: $K(THP)_2$(3,5-$Me_2C_5H_3B-NMe_2$)

α-**22**: K[3,5-$Me_2C_5H_3B-N(SiMe_3)_2$]$(THF)_{4/3}$ ≈ $[K(THF)]_2[K(THF)_2][3,5\text{-}Me_2C_5H_3B-N(SiMe_3)_2]_3$

β-**22**: K[3,5-$Me_2C_5H_3B-N(SiMe_3)_2$]$(THF)_{3/2}$ ≈ $[K(THF)]_2$[3,5-$Me_2C_5H_3B-N(SiMe_3)_2]_2(THF)$

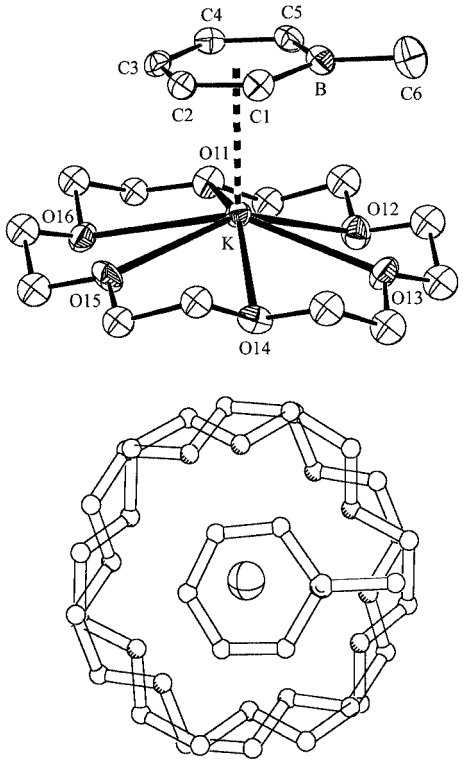

Figure 1. Molecular structure of **20** in the crystal; top: PLATON plot[14] at the 30% probability level; bottom:[15] top view, illustrating the disorder of the [18]-crown-6 ring with an occupancy ratio of 61(1):39(1); selected interatomic distances [Å]: K−C1 3.319(5), K−C2 3.207(5), K−C3 3.089(4), K−C4 3.083(5), K−C5 3.198(5), K−B 3.373(6), K−O11 2.915(5), K−O12 2.892(6), K−O13 2.788(6), K−O14 2.832(5), K−O15 2.848(6), K−O16 3.004(6), K−O21 2.850(8), K−O22 2.863(10), K−O23 2.856(10), K−O24 2.863(10), K−O25 2.794(9), K−O26 2.939(9), C1−B 1.513(7), C1−C2 1.371(7), C2−C3 1.378(7), C3−C4 1.378(7), C4−C5 1.398(7), C5−B 1.507(8)

Crystal Structures

The crown ether adduct **20** crystallizes in the orthorhombic space group $Pna2_1$ as a van der Waals crystal (Figure 1). The molecule is a contact ion pair of the cation $[K([18]\text{-crown-6})]^+$ and the anion $[C_5H_5BMe]^-$. The structural type is therefore the same as that of the known salts K([18]-crown-6)($C_5H_5B-NPh_2$) and K([18]-crown-6)($C_5H_5B-PPh_2$).[16] The observed rotational disorder of the crown ether ligand could readily be resolved.

The boratabenzene ring is essentially planar, with a maximum perpendicular deviation of 0.011(6) Å for the boron atom. The intra-ring geometry [C−B = 1.510(8) (av), C−C = 1.382(7) Å (av)] does not differ from that of $Me_3PhN(C_5H_5BMe)$ (**5**) [C−B = 1.500(3) (av), C−C = 1.390(3) Å (av)]. The K−C distances average 3.179(5) Å and are significantly shorter than those in K([18]-crown-6)($C_5H_5B-NPh_2$) [3.241(7) Å (av)] and K([18]-crown-6)($C_5H_5B-PPh_2$) [3.259(5) Å (av)],[16] presumably because of the much smaller *B*-exocyclic substituent in **20**.

The bis(tetrahydropyran) solvate **21** forms monoclinic crystals of space group *C*2/*c* with a zigzag chain structural motif (Figure 2). The potassium atom displays a pseudo-tetrahedral coordination sphere as previously observed in, for example, the structure of $K(py)_2Cp^*$.[17] The interplanar angle between two neighboring boratabenzene rings is 53.1(1)°, and the metal−boratabenzene distances amount to 2.818(3) and 2.834(3) Å. Since the boratabenzene ring interacts with two potassium cations almost symmetrically, the C_5B moiety is located in a perfect plane [maximum vertical deviation: 0.003(3) Å for C1]. In contrast with this situation, compounds with nonbridging boratabenzene ligands show a folding of the ring, with the boron atom always bending away from the central metal atom. This effect is particularly pronounced for 1-aminoboratabenzenes coordinated to highly charged centers. For instance, in ScCl(3,5-$Me_2C_5H_3B-NiPr_2)_2$ the folding angle of the C_5 plane against the C_2B plane amounts to 13°.[1]

The THF solvate K[3,5-$Me_2C_5H_3B-N(SiMe_3)_2$]$(THF)_{4/3}$ (α-**22**) crystallizes in the monoclinic space group *C*2/*c*; the asymmetric unit contains two independent THF molecules, 1.5 independent cations K^+, and 1.5 independent anions. The structure of α-**22** (Figures 3 and 4) displays two kinds of potassium atoms − K1 and K2, in a 2:1 ratio − with rather different coordination environments.

 © 2003 Wiley-VCH Verlag GmbH & Co. KGaA, Weinheim

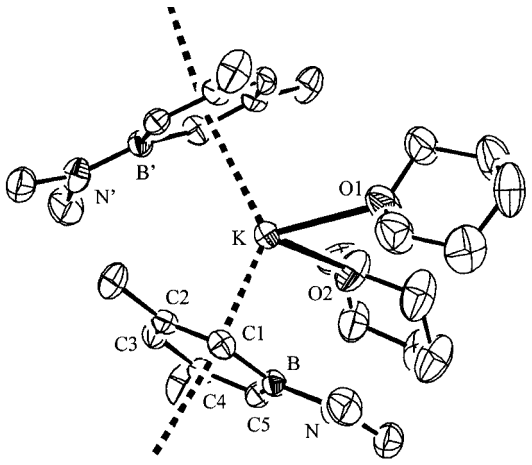

Figure 2. A representative fragment of the structure of **21** in the crystal (asymmetric unit and one anion in addition) (PLATON plot[14] at the 30% probability level); selected interatomic distances [A]: K−C1 3.282(4), K−C1′ 3.235(4), K−C2 3.139(4), K−C2′ 3.158(4), K−C3 3.021(4), K−C3′ 3.086(5), K−C4 3.055(4),K−C4′ 3.108(4), K−C5 3.188(5), K−C5′ 3.185(4), K−B 3.344(5), K−B′ 3.290(4), K−O1 2.719(3), K−O2 2.757(3), C1−C2 1.383(5), C2−C3, 1.396(4), C3−C4 1.395(4), C4−C5 1.365(5), C1−B,1.501(5), C5−B 1.502(5), N−B 1.468(5)

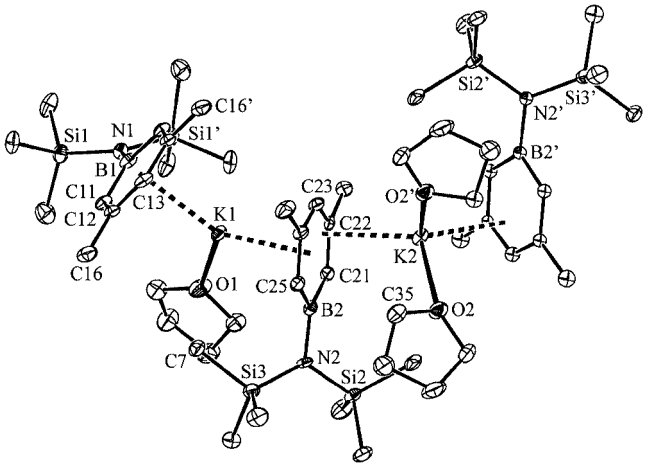

Figure 3. A representative fragment of the structure of α-**22** (PLATON plot[14] at the 30% probability level); the atoms K2, N1, C13, and B1 lie on twofold axes; selected interatomic distances [A]: K1−C11 3.243(5), K1−C11′ 3.250(4), K1−C12, 3.046(5), K1−C12′ 3.072(4), K1−C13 2.952(3), K1−B1 3.383(5); K1−C21 3.147(5), K2−C21 3.417(5), K1−C22 3.013(3), K2−C22 3.096(5), K1−C23 3.010(5), K2−C23 3.004(5), K1−C24 3.162(5), K2−C24 3.263(5), K1−C25 3.309(5), K2−C25 3.572(5), K1−B2 3.310(5), K2−B2 3.686(6); K1−O1 2.601(4), K2−O2 2.720(3); C11−C12 1.388(6), C12−C13 1.413(6), C11−B1 1.524(6), N1−B1 1.490(9); C21−C22 1.404(6), C22−C23 1.411(6), C23−C24 1.378(7), C24−C25 1.409(6), C25−B2 1.506(7), C21−B2 1.515(7), N2−B2 1.530(6); note also: K1···C7 3.422(5), K2···C35 3.451(6)

The atom K1 is surrounded, essentially in a trigonal mode, by an oxygen atom of a THF ligand and two bridging μ-boratabenzene ligands. Ligand **A** (B1, C11−C13, N1, etc.) occupies a special position, with the B1, C13, and N1 atoms lying on a crystallographic twofold axis, whereas ligand **B** (B2, C21−C25, N2, etc.) is in a general position. Both boratabenzene rings are planar [with vertical displacements of less than 0.007(5) Å] and are facially bonded to K1. The distances between the metal atom and the two C_5B planes are quite small [K1−**A** 2.781(3), K1−**B**: 2.794(3) Å], and the interplanar angle between the two rings is 44.6(2)°.

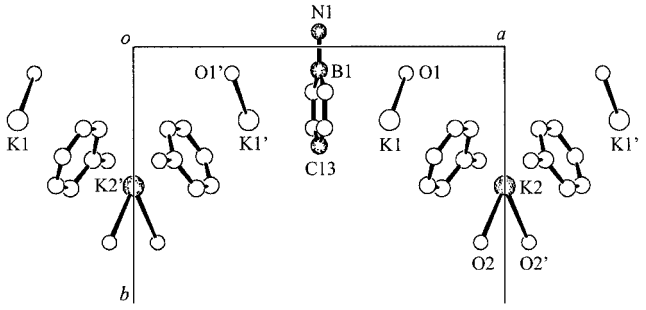

Figure 4. Simplified packing diagram (along *c* axis) of the structure of α-**22**;[15] only the K, O, and C_5B−N (boratabenzene) fragments are displayed; the atoms lying on twofold axes (K2, C13, B1, N1) are shown as dotted spheres

The potassium atom K2 is located on a twofold axis and exhibits a tetrahedral coordination sphere, being bonded to two THF oxygen atoms and to two boratabenzene ligands **B**. The more crowded geometry around the atom K2 causes the cation to slip away from the boratabenzene ring center, and the lengths K2−C25 [3.572(5) Å] and K2−B2 [3.686(6) Å] adopt rather large values. As expected, both the distance of the metal atom to the boratabenzene plane [2.924(3) Å] and the interplanar angle between the two boratabenzene planes [56.2(2)°] are much larger than the corresponding parameters involving the potassium atom K1. Obviously, the observed soft bonding situation is in line with the essentially electrostatic character of the potassium−boratabenzene interactions.

The packing of α-**22** can be explained with the help of a simplified diagram (Figure 4). It seems somewhat surprising that the one-dimensional polymer develops along the shortest lattice axis *a* [*a* = 14.924(5) Å; cf. *b* = 29.307(5) and *c* = 17.385(4) Å]. More unexpectedly, the polymer is not arranged in a zigzag chain, since the dihedral angle K2,K1,K1′,K2′ is less than 180°, even less than 90°. This novel structural motif has not previously been encountered in cyclopentadienyl chemistry.

Since K^+ is a rather large cation (ionic radius *r* = 1.51 Å for coordination number 8),[18] it tends to have short contacts, as observed in the present case [K1···C7 3.422(5), K2···C35 3.451(6) Å]. Besides packing forces, additional electrostatic interactions may favor the occurrence of short contacts. This is presumably the dominating cause for the short contact K1···C7, which places the negative charge of an *Si*-methyl group close to the cation.

The pseudo-polymorph K[3,5-$Me_2C_5H_3B$−$N(SiMe_3)_2$]-$(THF)_{3/2}$ (β-**22**) crystallizes in the hexagonal space group $P6_122$ with twelve boratabenzene moieties per unit cell (Figures 5 and 6). One molecule of THF per formula unit is coordinated to the cation, while 0.5 mol-equiv. of THF function solely as a space filling building block. The polymer chain extends along the lattice axis *c*, which is much

 © 2003 Wiley-VCH Verlag GmbH & Co. KGaA, Weinheim

longer than the others [c = 62.2944(17) Å; cf. a = b = 11.9545(2) Å].

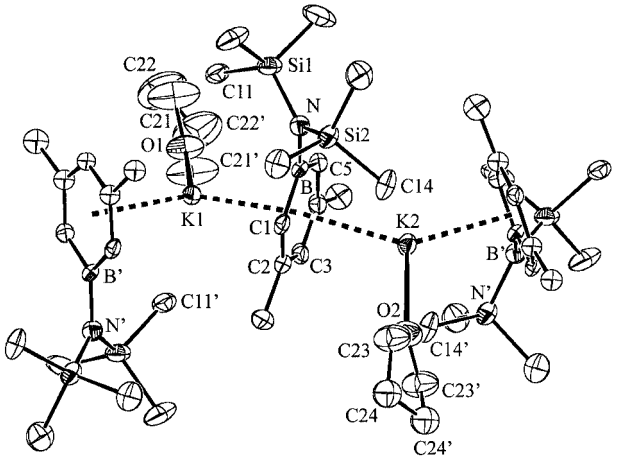

Figure 5. A representative fragment of the structure of β-**22** (PLATON plot[14] at the 30% probability level); the potassium atoms K1 and K2 lie on the twofold axes; selected interatomic distances [Å]: K1−C1 3.169(6), K2−C1 3.209(5), K1−C2 3.079(5), K2−C2 3.093(5), K1−C3 3.053(5), K2−C3 3.021(6), K1−C4 3.139(5), K2−C4 3.070(6), K1−C5 3.236(6), K2−C5 3.166(6), K1−B 3.278(6), K2−B 3.289(6); K1−O1 2.718(7), K2−O2 2.734(8); C1−C2 1.386(8), C2−C3 1.396(8), C3−C4 1.399(9), C4−C5 1.391(9), C1−B 1.508(8), C5−B 1.509(9), N−B 1.502(8); note also: K1···C11 3.328(6), K2···C14 3.311(6), K1···K2 5.599(2)

The K1−O1 and K2−O2 vectors coincide with twofold axes, and so the two potassium atoms possess trigonal coordination spheres. The distances from K1 and K2 to the best boratabenzene C_5B plane are 2.809(3) and 2.788(3) Å, respectively, and the bending angles of the sandwich units around K1 and K2 correspond to 133.3(2) and 140.5(2)°. The bridging boratabenzene ring is again planar [with a maximum vertical deviation of 0.007(6) Å for C5] and its intra-ring geometry is quite similar to that in α-**22**. We also again note the occurrence of short contacts between *Si*-methyl groups and the cations [K1···C11 3.328(6), K2···C14 3.311(6) Å].

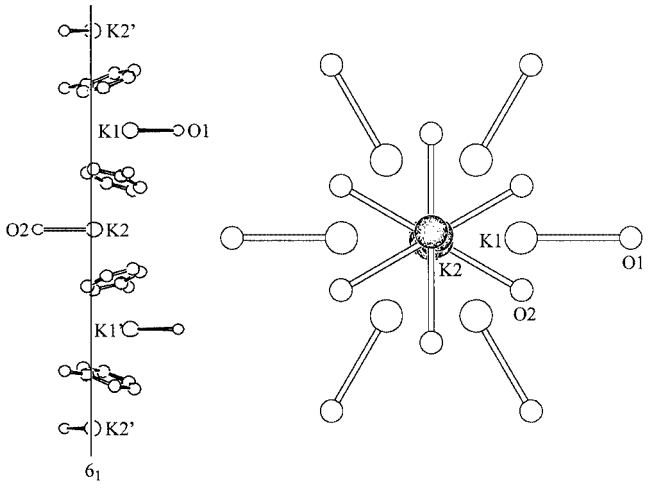

Figure 6. Simplified packing diagrams of the structure of β-**22**;[15] (a) left: view perpendicular to the sixfold screw axis 6_1 (direction [110]); only the K, O, and C_5B−N (boratabenzene) fragments are displayed; (b) right: view along the screw axis (direction [001]), showing only the K and O atoms

As shown in Figure 6 (a), the distance of K1 from the 6_1 axis (2.22 Å) is much larger than that of K2 (0.15 Å). As a consequence, the hexagonal helix of the symmetry-related cations K2 nearly coincide with the 6_1 axis whereas the cations K1 form an alternating outer hexagonal screw.

Conclusion

The structures of boratabenzene salts now known are collected in Table 1. They belong to one of four types: structures with naked anions (type A), contact ion pair structures (type B), structures with sandwich-type anions (type C), and chain structures with side-on-coordinated donor

Table 1. Crystal structures of boratabenzene salts

No.	Formula	Type	Ref.
1	$Me_3PhN(C_5H_5BMe)$ (**5**)	A	[5c]
2	$[Na(dibenzo\text{-}[18]\text{-}crown\text{-}6)(THF)_2](C_5H_5B{-}CH{=}CHPh)$[a]	A	[5d]
3	$[Na(dibenzo\text{-}[18]\text{-}crown\text{-}6)(THF)_2]_2(C_5H_5B{-}CH{=}CH\text{-}1,4\text{-}C_6H_4\text{-}CH{=}CH{-}BC_5H_5)$[a]	A	[19]
4	$Li(TMPDA)(C_5H_5B{-}NMe_2)$ (**3**)[b]	B	[5a]
5	$Li(TMEDA)(5\text{-}t\text{Bu-}3\text{-}MeC_5H_3B{-}NMe_2)$	B	[8]
6	$K([18]\text{-}crown\text{-}6)(C_5H_5B{-}NPh_2)$	B	[15]
7	$K([18]\text{-}crown\text{-}6)(C_5H_5B{-}PPh_2)(PhMe)_{0.5}$	B	[15]
8	$Li(TMEDA)(6\text{-}MePBb{-}NMe_2)$[c]	B	[20]
9	Li(TMEDA)(6-MePBbMe)[c]	B	[21]
10	$[Na(THF)_3]_2(C_5H_5B{-}CH{=}CH\text{-}1,4\text{-}C_6H_4\text{-}CH{=}CH{-}BC_5H_5)$[a]	B	[19]
11	$K([18]\text{-}crown\text{-}6)(C_5H_5BMe)$ (**20**)	B	this work
12	$[Li(THF)_4][Li(C_5H_5BH)_2]$ (**4**)	C	[5b,9]
13	$Li(3,5\text{-}Me_2C_5H_3B{-}SMP)$[d] [e]	C	[12]
14	$Na(OEt_2)(C_5H_5B{-}CH{=}CHPh)$ (**6**)[a]	D	[5d]
15	$K(THP)_2(3,5\text{-}Me_2C_5H_3B{-}NMe_2)$ (**21**)	D	this work
16	$[K(THF)]_2[K(THF)_2](3,5\text{-}Me_2C_5H_3B{-}N(SiMe_3)_2]_3$ (α-**22**)	D	this work
17	$[K(THF)]_2[3,5\text{-}Me_2C_5H_3B{-}N(SiMe_3)_2]_2(THF)$ (β-**22**)	D	this work

[a] With (*E*)-CH=CH units. [b] TMPDA = $Me_2N(CH_2)_3NMe_2$. [c] PBb = a pinene-fused, enantiomerically pure borabenzene moiety $C_{12}H_{15}B$. [d] SMP = (*S*)-2-(methoxymethyl)pyrrolidin-1-yl. [e] Polymer with alternating LiN_2O_2 and $Li(C_5H_5B)_2$ units.

 © 2003 Wiley-VCH Verlag GmbH & Co. KGaA, Weinheim

molecules (type D). We note that the disorder found in the structure of **20** may be understood as the consequence of the shape of the auxiliary base present. Simple crown ethers should be much more prone to disorder than the dibenzo crown ethers used in some of the previously studied compounds. Chain structures may be simple zigzag chains as in **6** and **21** but, as this work shows, may also be of much more complex types. Finally, we note that the structure elucidation of the simple, unsolvated alkali metal cyclopentadienides MCp (M = Li, Na, K) belongs to the milestones of cyclopentadienide chemistry.[22] The analogous structures of the most simple, unsolvated alkali metal boratabenzenes [M(C_5H_5BR), for instance with M = Li, K and R = H, Me, Ph] still wait to be resolved, however.

Experimental Section

General: All manipulations were carried out under nitrogen by use of standard Schlenk techniques. Et_2O, THF, and THP were distilled from sodium benzophenone ketyl. Hexane was distilled from Na/K alloy, toluene from sodium, and CH_2Cl_2 from CaH_2. Elemental analyses were performed at the Analytische Laboratorien, 51779 Lindlar, Germany. NMR spectra were recorded with a Varian Unity 500 (^{1}H, 500 MHz; ^{13}C, 125.7 MHz; ^{11}B, 160.4 MHz). Chemical shifts are given in ppm; they are referenced to TMS for ^{1}H and ^{13}C, and to $BF_3{\cdot}OEt_2$ for ^{11}B. Electron-impact mass spectra were recorded with a Finnigan MAT-95 at a nominal electron energy of 70 eV.

Potassium 1-Methylboratabenzene (8) and Its [18]-Crown-6 Solvate (20): 1-Methyl-2-(trimethylstannyl)-1,2-dihydroborinine (1.02 g, 4.00 mmol) was added to a solution of KO*t*Bu (0.44 g, 3.92 mmol) in toluene (20 mL). The reaction mixture was stirred at room temperature for 24 h, and a fine white precipitate formed during this time. The precipitate was collected by filtration through a frit, washed with hexane (3 × 10 mL), and dried under high vacuum to afford **8** (0.50 g, 98%) as a moisture- and air-sensitive, white powder. The potassium salt **8** (0.286 g, 2.20 mmol) and [18]-crown-6 (0.607 g, 2.30 mmol) were dissolved at 50 °C in a mixture of toluene and CH_2Cl_2 (8:1, 45 mL). The solution was stored overnight at ambient temperature to give the solvate **8**·([18]-crown-6) (≡ **20**) (0.711 g, 82%) as large, colorless, crystalline blocks.

Data for 8: ^{1}H NMR (500 MHz, [D$_8$]THF, 20 °C): δ = 0.44 (s, BMe), 5.91 (tt, *J* = 6.9, 0.9 Hz, 4-H), 6.23 (dd, *J* = 9.4, 0.9 Hz, 2-/6-H), 7.01 (dd, *J* = 9.4, 6.9 Hz, 2 H, 3-/5-H) ppm. ^{13}C{^{1}H} NMR (126 MHz, [D$_8$]THF, 20 °C): δ = 4.6 (br., BMe), 109.1 (C-4), 127.6 (br., C-2,6), 133.3 (C-3,5) ppm. ^{11}B{^{1}H} NMR (160 MHz, [D$_8$]THF, external $BF_3{\cdot}OEt_2$, 20 °C): δ = 35.4 ppm.

Data for 20: ^{1}H NMR (500 MHz, CD_2Cl_2, 20 °C): δ = 0.54 (s, BMe), 3.56 (s, 12 OCH_2), 5.32 (tt, *J* = 7.0, 1.2 Hz, 4-H), 6.29 (dd, *J* = 9.8, 1.2 Hz, 2-/6-H), 7.14 (dd, *J* = 9.8, 7.0 Hz, 2 H, 3-/5-H) ppm. ^{13}C{^{1}H} NMR (126 MHz, CD_2Cl_2, 20 °C): δ = 4.6 (br., BMe), 70.4 (OCH_2), 108.8 (C-4), 126.8 (br., C-2,6), 133.4 (C-3,5) ppm. ^{11}B{^{1}H} NMR (160 MHz, CD_2Cl_2, external $BF_3{\cdot}OEt_2$, 20 °C): δ = 35.3 ppm. $C_{18}H_{32}BKO_6$ (394.36): calcd. C 54.82, H 8.17; found C 54.95, H 7.80.

Sodium 1-(Dimethylamino)-3,5-dimethylboratabenzene (11): Sodium bis(trimethylsilyl)amide in toluene (0.6 M, 27.5 mL, 16.5 mmol) was added dropwise at −78 °C to a solution of 1-(dimethylamino)-5-methyl-3-methylene-1,2,3,6-tetrahydroborinine (**9**, 2.50 g, 16.5 mmol) in toluene (15 mL). The reaction mixture was kept at −78 °C for 1 h and was then warmed to ambient temperature. Stirring was continued for an additional 5 d, and a white precipitate gradually formed. The precipitate was collected by filtration through a frit, washed with toluene (3 × 10 mL), and dried under high vacuum to give **11** (1.75 g, 62%) as a moisture- and air-sensitive, white powder.

Data for 11: ^{1}H NMR (500 MHz, [D$_8$]THF, 20 °C): δ = 2.08 (s, 3-/5-Me), 2.66 (s, NMe_2), 5.16 (s, 4-H), 5.24 (s, 2-/6-H) ppm. ^{13}C{^{1}H} NMR (126 MHz, [D$_8$]THF, 20 °C): δ = 26.0 (3-/5-Me), 39.8 (NMe_2), 102.8 (C-4), 107.6 (br., C-2,6), 142.5 (C-3,5) ppm. ^{11}B{^{1}H} NMR (160 MHz, [D$_8$]THF, external $BF_3{\cdot}OEt_2$, 20 °C): δ = 32.0 ppm.

Potassium 1-(Dimethylamino)-3,5-dimethylboratabenzene (12) and Its THP Solvate 21: Potassium bis(trimethylsilyl)amide in toluene (0.5 M, 27 mL, 13.5 mmol) was added dropwise at −78 °C to a solution of 1-(dimethylamino)-5-methyl-3-methylene-1,2,3,6-tetrahydroborinine (**9**, 2.04 g, 13.7 mmol) in toluene (10 mL). The reaction mixture was kept at −78 °C for 1 h and was then warmed to ambient temperature. Stirring was continued for an additional 5 d and a white precipitate gradually formed. The precipitate was collected by filtration through a frit, washed with toluene (3 × 10 mL), and dried under high vacuum to give **12** (1.64 g, 64%) as a moisture- and air-sensitive, white powder. Crystallization of **12** (0.27 g) from a mixture of THP and toluene (1:1, 8 mL) at −30 °C overnight afforded **12**·$(THP)_2$ (≡ **21**) as colorless prisms. The ratio of THP to **12** in **21** was established by NMR spectroscopy and X-ray diffraction methods.

Data for 12: ^{1}H NMR (500 MHz, [D$_8$]THF, 20 °C): δ = 2.04 (s, 3-/5-Me), 2.64 (s, NMe_2), 5.13 (s, 4-H), 5.15 (s, 2-/6-H) ppm. ^{13}C{^{1}H} NMR (126 MHz, [D$_8$]THF, 20 °C): δ = 25.9 (3-/5-Me), 39.8 (NMe_2), 103.8 (C-4), 109.0 (br., C-2,6), 142.9 (C-3,5) ppm. ^{11}B{^{1}H} NMR (160 MHz, [D$_8$]THF, external $BF_3{\cdot}OEt_2$, 20 °C): δ = 33.0 ppm.

3,5-Dimethyl-1-morpholinodihydroborinines (14a, 14b): A mixture of morpholine (1.95 g, 22.4 mmol) and triethylamine (2.33 g, 23.0 mmol) in hexane (10 mL) was added dropwise at 0 °C to the 1-chloro-3,5-dimethyldihydroborines **13a** and **13b** (3.15 g, 22.4 mmol) in hexane (30 mL). A white precipitate of Et_3NHCl formed immediately. After the reaction mixture had been stirred at room temperature for 5 h, the solid was removed by filtration and washed with hexane (3 × 20 mL). The combined filtrates were concentrated to dryness under reduced pressure to afford **14a** and **14b** (3.87 g, 90%, **a/b** = 2:3) as a pale yellow solid, moderately sensitive to air and moisture.

Data for 14a and 14b: ^{1}H NMR (500 MHz, $CDCl_3$, 20 °C): **14a**: δ = 1.64 (s, 2 H, 2-CH_2), 1.98, 1.89 (s, 3-/5-Me), 2.89, 3.37 (t, *J* = 4.5 Hz, 4 H, 2 NCH_2), 3.60 (m, 4 H, 2 OCH_2), 5.66 (s, 1 H, 6-H), 5.76 (m, 1 H, 4-H); **14b**: δ = 1.96 (s, 6 H, 3-/5-Me), 2.81 (s, 2 H, 4-CH_2), 3.42 (t, *J* = 4.6 Hz, 4 H, 2 NCH_2), 3.63 (t, *J* = 4.6 Hz, 4 H, OCH_2), 5.90 (s, 2 H, 2-/6-H) ppm. ^{13}C{^{1}H} NMR (126 MHz, $CDCl_3$, 20 °C): **14a**: δ = 24.1 (br., C-2), 26.1, 26.6 (3-/5-Me), 42.6, 47.0 (2 NCH_2), 68.4 (2 OCH_2), 119.1 (br., C-6), 124.9 (C-4), 143.7 (C-3), 155.4 (C-5); **14b**: δ = 26.5 (3-/5-Me), 42.6 (C-4), 47.5 (2 NCH_2), 68.9 (2 OCH_2), 123.2 (br., C-2,6), 156.4 (C-3,5) ppm. ^{11}B{^{1}H} NMR (160 MHz, $CDCl_3$, external $BF_3{\cdot}OEt_2$, 20 °C): **14a**: δ = 39.8 ppm; **14b**: δ = 32.6 ppm. MS (EI): *m/z* (%) = 191 (100) [M$^+$], 176 (26) [M$^+$ − Me], 162 (5) [M$^+$ − 2 Me], 105 (14) [$Me_2C_5H_4B^+$], 91 (10) [$MeC_5H_4B^+$]. $C_{11}H_{18}B-NO$ (191.08): calcd. C 69.14, H 9.50, N 7.33; found C 69.05, H 9.57, N 7.45.

 © 2003 Wiley-VCH Verlag GmbH & Co. KGaA, Weinheim

Lithium 3,5-Dimethyl-1-morpholinoboratabenzene (17): Lithium bis(trimethylsilyl)amide in hexane (1.0 M, 5.4 mL, 5.4 mmol) was added dropwise at −78 °C to a solution 3,5-dimethyl-1-(morpholino)-dihydroborinines (**14a/14b**, 1.03 g, 5.4 mmol) in diethyl ether (10 mL). The reaction mixture was kept at −78 °C for 1 h and was then warmed to ambient temperature. Stirring was continued for an additional 24 h and a white precipitate formed. The precipitate was collected by filtration through a frit, washed with hexane (3 × 10 mL), and dried under high vacuum to give **17** (1.04 g, 98%) as a moisture- and air-sensitive, white powder.

Data for 17: ^{1}H NMR (500 MHz, [D$_8$]THF, 20 °C): δ = 1.99 (s, 3-/5-Me), 3.06 (t, J = 4.5 Hz, 2 NCH_2), 3.46 (t, J = 4.5 Hz, 2 OCH_2), 5.08 (s, 4-H), 5.09 (s, 2-/6-H) ppm. ^{13}C{^{1}H} NMR (126 MHz, [D$_8$]THF, 20 °C): δ = 25.7 (3-/5-Me), 48.0 (2 NCH_2), 69.3 (2 OCH_2), 103.0 (C-4), 107.1 (br., C-2,6), 142.7 (C-3,5) ppm. ^{11}B{^{1}H} NMR (160 MHz, [D$_8$]THF, external BF_3·OEt_2, 20 °C): δ = 31.2 ppm. $C_{11}H_{17}BLiNO$ (197.01): calcd. C 67.06, H 8.70, N 7.11; found C 66.90, H 8.74, N 6.89.

Sodium 3,5-Dimethyl-1-morpholinoboratabenzene (18): Sodium bis(trimethylsilyl)amide in toluene (0.6 M, 9.5 mL, 5.70 mmol) was added dropwise at −78 °C to a solution of 3,5-dimethyl-1-(morpholino)dihydroborinines (**14a/14b**, 1.09 g, 5.70 mmol) in toluene (10 mL). The reaction system was kept at −78 °C for 1 h and was then warmed to ambient temperature. The mixture was stirred for 24 h and a white precipitate formed. The precipitate was collected by filtration, washed with toluene (3 × 10 mL), and dried under high vacuum to afford **18** as a moisture- and air-sensitive, white powder (1.09 g, 90%).

Data for 18: ^{1}H NMR (500 MHz, [D$_8$]THF, 20 °C): δ = 2.08 (s, 3-/5-Me), 3.07 (t, J = 4.7 Hz, 2 NCH_2), 3.43 (t, J = 4.7 Hz, 2 OCH_2), 5.21 (s, 4-H), 5.24 (s, 2-/6-H) ppm. ^{13}C{^{1}H} NMR (126 MHz, [D$_8$]THF, 20 °C): δ = 26.0 (3-/5-Me), 48.2 (2 NCH_2), 69.3 (2 OCH_2), 103.7 (C-4), 107.6 (br., C-2,6), 142.7 (C-3,5) ppm. ^{11}B{^{1}H} NMR (160 MHz, [D$_8$]THF, external BF_3·OEt_2, 20 °C): δ = 32.0 ppm. $C_{11}H_{17}B$−NNaO (213.06): calcd. C 62.01, H 8.04, N 6.57; found C 61.76, H 7.87, N 6.68.

Potassium 1-[Bis(trimethylsilyl)amino]-3,5-dimethylboratabenzene (19) and Its THF Solvates (α- and β-22): Potassium bis(trimethylsilyl)amide in toluene (0.5 M, 9 mL, 4.5 mmol) was added dropwise at −78 °C to a solution of 1-bis(trimethylsilyl)amino-3,5-dimethyl-dihydroborinines (**16a/16b**, 1.2 g, 4.5 mmol) in toluene (10 mL). The system was kept at −78 °C for 1 h and was then warmed to ambient temperature. Stirring was continued for 24 h, and a fine white precipitate formed. The precipitate was collected by filtration through a frit, washed with toluene (3 × 10 mL), and dried under high vacuum to give **19** (1.25 g, 91%) as a moisture- and air-sensitive, white powder. Crystallization of **19** (0.25 g) from THF (5 mL) at −4 °C for a week afforded large, colorless crystals possessing ca. 1.4 equiv. of THF per unit **19** (^{1}H NMR). The concomitant presence of the two pseudo-polymorphs α-**22** and β-**22** was established by X-ray diffraction methods.

Data for 19: ^{1}H NMR (500 MHz, [D$_8$]THF, 20 °C): δ = 0.06 (s, 2 $SiMe_3$), 2.08 (s, 3-/5-Me), 5.43 (t, J = 1.5 Hz, 4-H), 5.52 (d, J = 1.5 Hz, 2-/6-H) ppm. ^{13}C{^{1}H} NMR (126 MHz, [D$_8$]THF, 20 °C): δ = 4.9 (2 $SiMe_3$), 25.7 (3-/5-Me), 107.9 (C-4), 121.9 (br., C-2,6), 141.5 (C-3,5) ppm. ^{11}B{^{1}H} NMR (160 MHz, [D$_8$]THF, external

Table 2. Crystal data, data collection parameters, and convergence results for **20**, **21**, α-**22**, and β-**22**

	20	**21**	α-**22**	β-**22**
Empirical formula	$C_{18}H_{32}BKO_6$	$C_{19}H_{35}BKNO_2$	$C_{13}H_{27}BKNSi_2$·$(C_4H_8O)_{4/3}$	$C_{13}H_{27}BKNSi_2$·$(C_4H_8O)_{3/2}$
Formula mass	394.37	359.41	399.60	411.60
Crystal system	orthorhombic	monoclinic	monoclinic	hexagonal
Space group	$Pna2_1$	$C2/c$	$C2/c$	$P6_122$
Radiation (λ [Å])	Cu-K_α (1.54184)	Mo-K_α (0.71073)	Cu-K_α (1.54184)	Mo-K_α (0.71073)
a [Å]	19.659(9)	18.062(7)	14.924(5)	11.9545(2)
b [Å]	9.921(4)	10.280(5)	29.307(5)	
c [Å]	11.114(3)	24.379(6)	17.385(4)	62.294(2)
β [°]		100.52(2)	106.07(3)	
V [Å^3]	2168(2)	4450(5)	7306(3)	7709.8(3)
Z	4	8	12	12
$d_{calcd.}$ [g/cm^3]	1.21	1.07	1.09	1.06
F(000)	848	1568	2608	2688
μ [cm^{-1}]	23.93	2.45	29.39	3.09
Absorption correction	empirical	not applied	empirical	not applied
Max./min. transmission	0.999/0.732		1.000/0.563	
θ range [°]	4.5−75.1	3.1−26.0	4.0−68.0	2.0−24.4
Temperature [K]	200	218	150	173
Scan mode	ω	ω−2θ	ω−2θ	ω
Crystal size [mm]	0.7 × 0.6 × 0.4	0.4 × 0.4 × 0.3	0.6 × 0.4 × 0.4	0.55 × 0.35 × 0.3
Reflections collected	9540	9581	13237	31996
Reflections unique	4466	4355	6655	4077
Reflections observed	3687	1370	3411	3512
Criterion for observation	$I > 2\,\sigma(I)$	$I > 2\,\sigma(I)$	$I > 2\,\sigma(I)$	$I > 2\,\sigma(I)$
Variables	299	363	346	216
R_1,[a] observed (all data)	0.074 (0.086)	0.056 (0.213)	0.070 (0.128)	0.080 (0.093)
wR_2,[b] observed (all data)	0.192 (0.201)	0.067 (0.087)	0.142 (0.160)	0.205 (0.213)
GOF[c]	1.103	0.702	0.839	1.172
Max. resd. density [e/Å^3]	0.48	0.18	0.56	0.53

[a] $R_1 = \|\|F_o\| - |F_c\|\|/|F_o|$. [b] $wR_2 = [w(F_o^2 - F_c^2)^2/w(F_o^2)^2]^{1/2}$, where $w = 1/[\sigma^2(F_o^2) + (aP)^2]$ and $P = [\max(F_o^2,0) + 2F_c^2]/3$. [c] GOF = $[w(F_o^2 - F_c^2)^2/(n - p)]^{1/2}$.

 © 2003 Wiley-VCH Verlag GmbH & Co. KGaA, Weinheim

BF_3·OEt_2, 20 °C): δ = 35.5 ppm. $C_{13}H_{27}BKNSi_2$ (303.45): calcd. C 51.46, H 8.97, N 4.62; found C 51.41, H 8.90, N 4.73.

X-ray Crystal Structure Determinations: Data collections for the compounds **20**, **21**, and α-**22** were performed with ENRAF-Nonius CAD4 diffractometers (Mo- or Cu-K_α radiation with graphite monochromators). The reflection data set for β-**22** was collected with a Bruker Apex X-ray diffractometer (Mo-K_α radiation with a graphite monochromator) equipped with a CCD area detector.[23] Crystal data, data collection parameters, and convergence results are listed in Table 2. Before symmetry-related reflections were merged, empirical absorption corrections on the basis of azimuthal scans[24] were applied to the data sets collected with the Cu-K_α radiation. All structures were solved by direct methods with the help of the SHELXS-97 program[25a] and refined on reflection intensities (F^2) by use of the SHELXL-97 program.[25b] The [18]-crown-6 ligand in the structure **20** suffers from rotational disorder. The two orientations, with an occupancy ratio of 61(1)/39(1), are related to each other by a rotational angle of ca. 20.5°. In the case of **21**, one of the two THP ligands displays flapping disorder (O2, C15−C19/C25−C29); the oxygen atom is well defined whereas all the other atoms split into two sites with an occupancy ratio of 64(1):36(1). Two types of THF are present in the structure of β-**22**; one serves as a ligand to the potassium atom, while the other acts solely as a space-filling molecule. The latter type of THF is disordered into two sites with the oxygen atom (O3) residing on a twofold crystallographic axis. Several restrains were applied in the disordered structural models to set the C−C and C−O distances, respectively, to be equal with a standard deviation of 0.03 Å. In the final structural refinements, non-hydrogen atoms other than disordered ones were assigned with anisotropic displacement parameters. Hydrogen atoms were either refined isotropically or included as riding with fixed displacement parameters [C−H = 0.98 Å, U_{iso}(H) = 1.3 U_{eq}(C)].[26]

Acknowledgments

This work was generously supported by the Deutsche Forschungsgemeinschaft and the Fonds der Chemischen Industrie.

[1] B. Wang, X. Zheng, G. E. Herberich, *Organometallics* **2002**, *21*, 1949−1954.
[2] [2a] A. J. Ashe, III, P. Shu, *J. Am. Chem. Soc.* **1971**, *93*, 1804−1805. [2b] G. E. Herberich, H. J. Becker, *Angew. Chem.* **1975**, *87*, 196−197; *Angew. Chem. Int. Ed. Engl.* **1975**, *14*, 184−185. [2c] G. E. Herberich, H. J. Becker, K. Carsten, C. Engelke, W. Koch, *Chem. Ber.* **1976**, *109*, 2382−2388. [2d] G. E. Herberich, W. Koch, H. Lueken, *J. Organomet. Chem.* **1978**, *160*, 17−23.
[3] [3a] G. E. Herberich, G. Greiss, H. F. Heil, *Angew. Chem.* **1970**, *82*, 838−839; *Angew. Chem. Int. Ed. Engl.* **1970**, *9*, 805−806. [3b] G. E. Herberich, G. Greiss, H. F. Heil, J. Müller, *J. Chem. Soc., Chem. Commun.* **1971**, 1328−1329.
[4] [4a] G. C. Fu, *Adv. Organomet. Chem.* **2001**, *47*, 101−119. [4b] A. J. Ashe, III, S. Al-Ahmad, X. Fang, *J. Organomet. Chem.* **1999**, *581*, 92−97. [4c] G. E. Herberich, "Boratabenzene Chemistry Revisited", in: *Advances in Boron Chemistry* (Ed.: W. Siebert), The Royal Society of Chemistry, Cambridge, U. K., **1997**, special publication no. 201, p. 211−223. [4d] G. E. Herberich, in *Comprehensive Organometallic Chemistry II* (Eds.: E. W. Abel, F. G. A. Stone, G. Wilkinson), Pergamon Press, Oxford, **1995**, vol. 1 (Ed.: C. E. Housecraft), p. 197−216. [4e]G. E. Herberich, H. Ohst, *Adv. Organomet. Chem.* **1986**, *25*, 199−216.
[5] [5a] G. E. Herberich, B. Schmidt, U. Englert, T. Wagner, *Organometallics* **1993**, *12*, 2891−2893. [5b] D. A. Hoic, W. M. Davis, G. C. Fu, *J. Am. Chem. Soc.* **1995**, *117*, 8480−8481. [5c] G. E. Herberich, B. Schmidt, U. Englert, *Organometallics* **1995**, *14*, 471−480. [5d] B. Y. Lee, S. Wang, M. Putzer, G. P. Bartholomew, X. Bu, G. C. Bazan, *J. Am. Chem. Soc.* **2000**, *122*, 3969−3970.
[6] [6a] S. Harder, M. H. Prosenc, *Angew. Chem.* **1994**, *106*, 1830−1832; *Angew. Chem. Int. Ed. Engl.* **1994**, *33*, 1744−1746. [6b] S. Harder, *Coord. Chem. Rev.* **1998**, *176*, 17−66.
[7] [7a] P. Jutzi, N. Burford, *Chem. Rev.* **1999**, *99*, 969−990. [7b] D. Stalke, *Angew. Chem.* **1994**, *106*, 2256−2259; *Angew. Chem. Int. Ed. Engl.* **1994**, *33*, 2168−2171. [7c] P. Jutzi, *J. Organomet. Chem.* **1990**, *400*, 1−17. [7d] P. Jutzi, *Adv. Organomet. Chem.* **1986**, *26*, 217−295.
[8] G. E. Herberich, U. Englert, M. U. Schmidt, R. Standt, *Organometallics* **1996**, *15*, 2707−2712.
[9] S. Qiao, D. A. Hoic, G. C. Fu, *J. Am. Chem. Soc.* **1996**, *118*, 6329−6330.
[10] G. E. Herberich, J. Rosenplänter, B. Schmidt, U. Englert, *Organometallics* **1997**, *16*, 926−931.
[11] [11a] G. E. Herberich, U. Englert, A. Fischer, J. Ni, A. Schmitz, *Organometallics* **1999**, *18*, 5496−5501. [11b] B. Wang, X. Zheng, G. E. Herberich, *Eur. J. Inorg. Chem.* **2002**, 31−41.
[12] X. Zheng, G. E. Herberich, *Organometallics* **2001**, *20*, 3097−3100.
[13] [13a] J. Bernstein, R. J. Davey, J.-O. Henck, *Angew. Chem.* **1999**, *111*, 3646−3669; *Angew. Chem. Int. Ed. Engl.* **1995**, *38*, 3440−3461. [13b] D. Braga, F. Grepioni, *Chem. Soc., Rev.* **2000**, *29*, 229−238.
[14] A. L. Spek, *Acta Crystallogr., Sect. A* **1990**, *46*, C34.
[15] E. Keller, *SCHAKAL88 − a FORTRAN Program for the Graphic Representation of Molecular and Crystallographic Models*, University of Freiburg, Freiburg, Germany, **1988**.
[16] D. A. Hoic, M. DiMare, G. C. Fu, *J. Am. Chem. Soc.* **1997**, *119*, 7155−7156.
[17] G. Rabe, H. W. Roesky, D. Stalke, F. Pauer, G. M. Sheldrick, *J. Organomet. Chem.* **1991**, *403*, 11−19.
[18] R. D. Shannon, *Acta Crystalogr., Sect. A* **1976**, *32*, 751−767.
[19] B. Y. Lee, G. C. Bazan, *J. Am. Chem. Soc.* **2000**, *122*, 8577−8578.
[20] G. E. Herberich, B. Ganter, M. Pons, *Organometallics* **1998**, *17*, 1254−1256.
[21] G. E. Herberich, U. Englert, B. Ganter, M. Pons, R. Wang, *Organometallics* **1999**, *18*, 3406−3413.
[22] R. E. Dinnebier, U. Behrends, F. Olbrich, *Organometallics* **1997**, *16*, 3855−3858.
[23] [23a] Bruker, *SMART v. 5.611, Program for Bruker CCD X-ray Diffractometer Control*, Bruker AXS Inc., Madison, Wisconson, USA, **1999**. [23b] Bruker, *SAINT+ v. 6.02, Program for Reduction of Data Collected on Bruker CCD Area Detector Diffractometer*, Bruker AXS Inc., Madison, Wisconson, USA, **1999**.
[24] A. C. T. North, D. C. Philips, F. S. Mathews, *Acta Crystallogr., Sect. A* **1968**, *24*, 351−359.
[25] [25a] G. M. Sheldrick, *SHELXS-97, Program for Structure Solution*, University of Göttingen, Göttingen, Germany, **1997**. [25b] G. M. Sheldrick, *SHELXL-97, Program for Structure Refinement*, University of Göttingen, Göttingen, Germany, **1997**.
[26] Crystallographic data (excluding structure factors) for the structures reported in this paper have been deposited with the Cambridge Crystallographic Data Centre as supplementary publications nos. CCDC-202182 (**20**), -202183 (**21**), -202184 (α-**22**), and -202185 (β-**22**). Copies of the data can be obtained free of charge on application to the CCDC, 12 Union Road, Cambridge CB2 1EZ, U. K. [Fax: (internat.) + 44-1223/336-033; E-mail: deposit@ccdc.cam.ac.uk].

Received January 27, 2003

 © 2003 Wiley-VCH Verlag GmbH & Co. KGaA, Weinheim

Synthesis of (η^3-Allyl)bromodicarbonylbis(pyrazole)molybdenum(II) and Reactivity towards [Au(acac)PPh_3]: Structure and Dynamic Behavior of the Monometallic Pyrazole and Heterometallic Pyrazolate Complexes

Paloma Paredes, Daniel Miguel, and Fernando Villafañe*

Keywords: Molybdenum / Gold / Heterometallic complexes / N ligands / Fluxionality

In our original article,[1] under the heading "Acac Complexes" (page 998) we inadvertently omitted that the use of acac complexes in synthesis has been reviewed.[2] Likewise, [Au(acac)PPh_3] has been used previously to synthesise a heterometallic complex.[3]

[1] P. Paredes, D. Miguel, F. Villafañe, *Eur. J. Inorg. Chem.* **2003**, 995.
[2] J. Vicente, M. T. Chicote, *Coord. Chem. Rev.* **1999**, *193–195*, 1143.
[3] J. Vicente, A. Arcas, D. Bautista, M. C. Ramírez de Arellano, *Organometallics* **1998**, *17*, 4544.

F. Villafañe

 © 2003 Wiley-VCH Verlag GmbH & Co. KGaA, Weinheim

EurJIC
European Journal of Inorganic Chemistry

June 2003
Issue 12
Pages 2185–2356

Papers available ahead of print in Early View at www.interscience.wiley.com

Earliest available Table of Contents:
Automatically, free of charge by e-mail through
www.interscience.wiley.com/alerts

COVER PICTURE

The cover picture shows the first example of an isolated organometallic compound containing two terminal alkynes undergoing an intramolecular oxidative coupling. Twenty-two- and twenty-six-membered rings or "metallamacrocycles" are obtained in 18–41% yields. The intramolecular oxidative coupling of organic compounds containing two terminal alkynes has played a critical role in the development of macrocycle chemistry, particularly with annulenes and dehydroannulenes, and macrocyclizations are playing an increasingly important role in organometallic chemistry, particularly as attention turns to architecturally novel types of target molecules that may have applications in materials chemistry or nanotechnology. Details are discussed in the article by J. A. Gladysz et al. on p. 2211 ff.

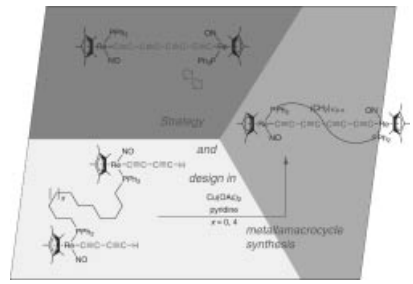

MICROREVIEW

Contents

2197 **S. D. Zarić**

Metal Ligand Aromatic Cation–π Interactions

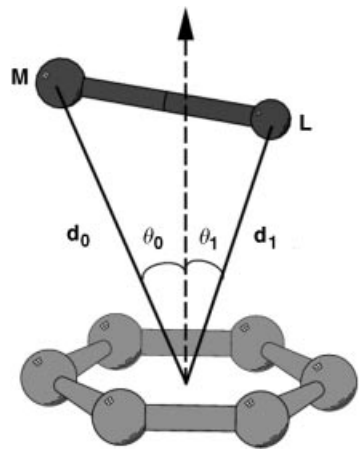

Keywords: Chelates / Density functional calculations / DNA / Hydrogen bonds / Metalloproteins / Pi interactions / RNA

 © 2003 Wiley-VCH Verlag GmbH & Co. KGaA, Weinheim

2211 **C. R. Horn, J. A. Gladysz***

Syntheses of Dimetallamacrocycles by Intramolecular Oxidative Couplings of Dinuclear Bis(1,3-butadiynyl) Complexes: A New Approach to Steric Shielding in (sp-Carbon chain)dirhenium Complexes [(η^5-C_5Me_5)Re(NO)(PR_3)-(C≡CC≡CC≡CC≡C)(R_3P)(ON)Re($\eta^5C_5Me_5$)]

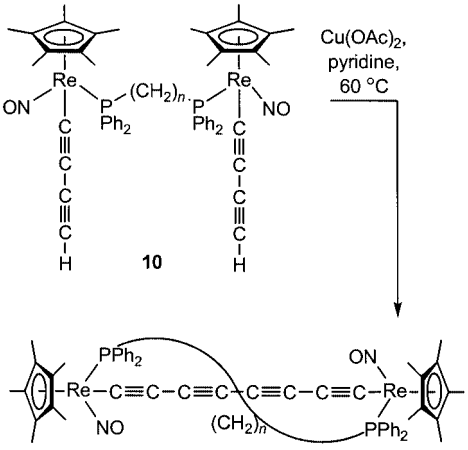

3
n = 10: **a** 18%
14: **b** 41%

Keywords: Rhenium / Alkynes / Oxidative coupling / Macrocycles / Cyclic voltammetry

2219 **R. Faissner, G. Huttner,* E. Kaifer, P. Kircher, P. Rutsch, L. Zsolnai**

Synthesis of *tripod* Ligands Containing Mixed Donor Sets with Phosphane and Pyrazole Donors − Bidentate Chelate Binding Modes and Dynamic Behaviour of tripod Ligands in d^8-Metal Complexes (Ni^{II}, Pd^{II}, Pt^{II})

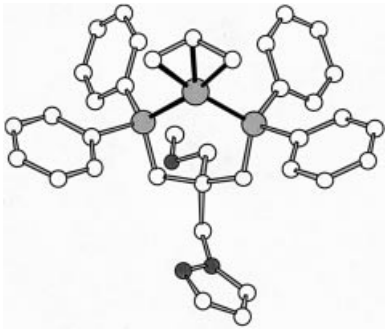

Keywords: Tripod ligands / Conformation / Nickel / Palladium / Platinum

2239 **R. Faissner, G. Huttner***

Nickel(II) Compounds Derived from *tripod* Ligands: Efficient Catalysts for the Stereoselective Heterodimerization of Styrene and Propene

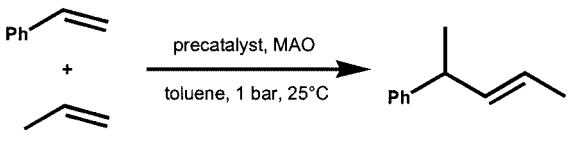

Keywords: Tripod ligands / Nickel / Catalysis / Heterodimerization

 © 2003 Wiley-VCH Verlag GmbH & Co. KGaA, Weinheim

2245 **H. Nöth,* D. Schlosser**

The Aminolysis of Beryllium Dichloride with Diisopropylamine and Reactions of Some Aminoberyllium Chlorides

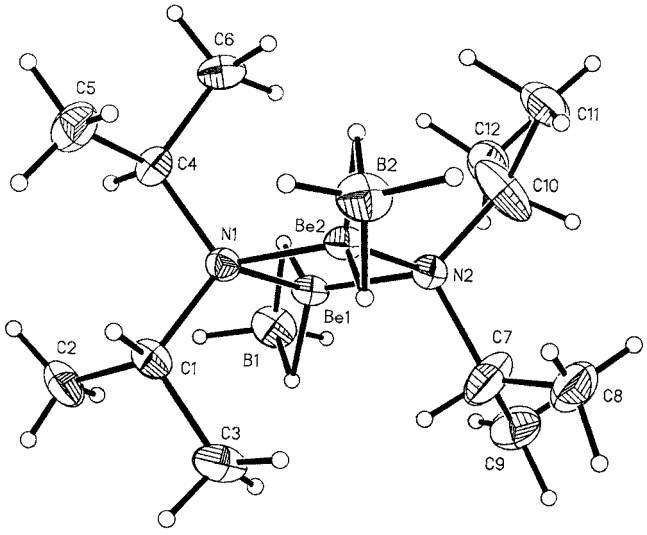

Keywords: Adduct formation / Amines / Beryllium / N ligands / NMR spectroscopy

2255 **A. Schmid, H. Piotrowski, T. Lindel***

One-Step Preparation of $[RuCp^*(\eta^6\text{-arene})]^+$ Sandwich Complexes

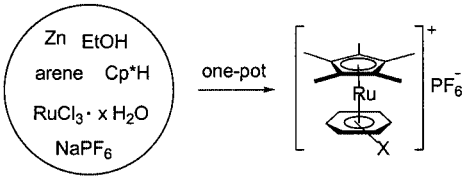

Keywords: Ruthenium / Sandwich complexes / NMR spectroscopy / Synthetic methods

2264 **J. Gun, A. Modestov, O. Lev, R. Poli***

Reduction of $[(C_5Me_5)_2Mo_2O_5]$ and $[(C_5Me_5)_2Mo_2O_4]$ in Methanol/Water/Trifluoroacetate Solutions Investigated by Combined On-Line Electrochemistry/Electrospray-Ionization Mass Spectrometry

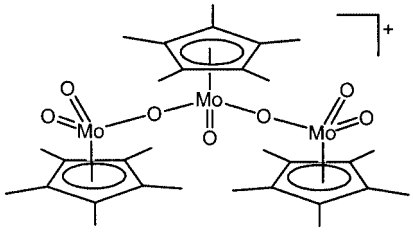

Keywords: Cyclopentadienyl ligands / Electrochemistry / Electrospray-ionization mass spectrometry / Molybdenum / Oxo ligands

2273 **A. F. Stassen, M. Grunert, E. Dova, M. Müller, P. Weinberger, G. Wiesinger, H. Schenk, W. Linert, J. G. Haasnoot,* J. Reedijk**

Magnetic, ^{57}Fe Mössbauer, and IR Monitoring of the Thermal Spin Transition in a New Family of Iron(II) Spin-Transition Complexes

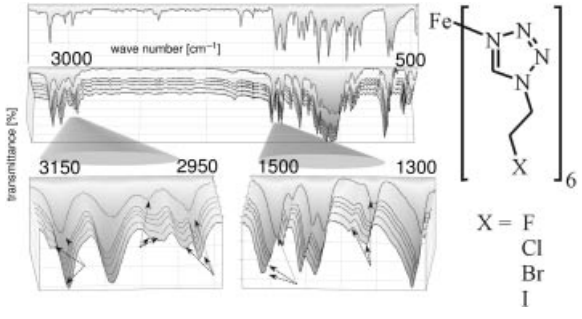

Keywords: Spin crossover / Iron / Tetrazole ligand / Mössbauer spectroscopy / Variable-temperature IR spectroscopy

 © 2003 Wiley-VCH Verlag GmbH & Co. KGaA, Weinheim

2283 **M. Viertelhaus, H. Henke, C. E. Anson, A. K. Powell***

Solvothermal Synthesis and Structure of Anhydrous Manganese(II) Formate, and Its Topotactic Dehydration from Manganese(II) Formate Dihydrate

Keywords: Manganese / Formates / Solvothermal synthesis / Solid-state reactions

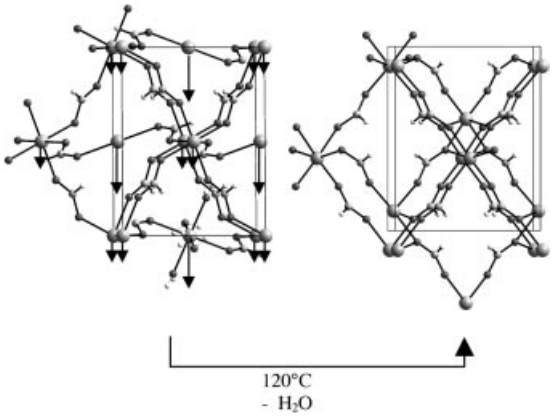

2290 **E. Coronado,* J. R. Galán-Mascarós, C. Giménez-Saiz, C. J. Gómez-García, C. Ruiz-Pérez**

Hybrid Organic/Inorganic Molecular Materials Formed by Tetrathiafulvalene Radicals and Magnetic Trimeric Clusters of Dimetallic Oxalate-Bridged Complexes: The Series $(TTF)_4\{M^{II}(H_2O)_2[M^{III}(ox)_3]_2\}\cdot nH_2O$ (M^{II} = Mn, Fe, Co, Ni, Cu and Zn; M^{III} = Cr and Fe; ox = $C_2O_4^{2-}$)

Keywords: Coordination chemistry / Hybrid materials / Magnetic properties / O ligands

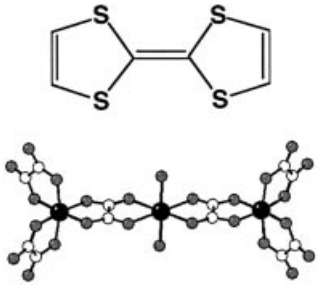

2299 **B. Baruah, V. O. Golub, C. J. O'Connor, A. Chakravorty***

Synthesis of Oxalato-Bridged (Oxo)vanadium(IV) Dimers Using L-Ascorbic Acid as Oxalate Precursor: Structure and Magnetism of Two Systems

Keywords: Vanadium / Bridging ligands / Magnetic properties

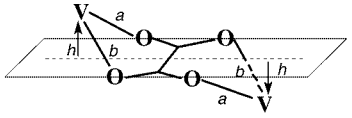

	a, b (Å)	h (Å)	J (cm^{-1})
$[(VO)_2(C_2O_4)_3(H_2O)_2]^{2-}$	2.023, 2.281	0.05	-6.50
$[(VO)_2(C_2O_4)(C_3H_2O_4)_2(H_2O)_2]^{2-}$	2.009, 2.218	0.17	-6.25

2304 **M. A. Cinellu,* G. Minghetti, M. V. Pinna, S. Stoccoro, A. Zucca, M. Manassero**

Synthesis and Characterization of Mononuclear Amidogold(III) Complexes − Crystal Structure of $[Au(N_2C_{10}H_7(CMe_2C_6H_4)\text{-}6](NHC_6H_3Me_2\text{-}2,6)][PF_6]$ − Oxidation of 4-Methylaniline to Azotoluene

Keywords: Gold / Nitrogen ligands / Metallacycles / Amido complexes / Amine oxidation

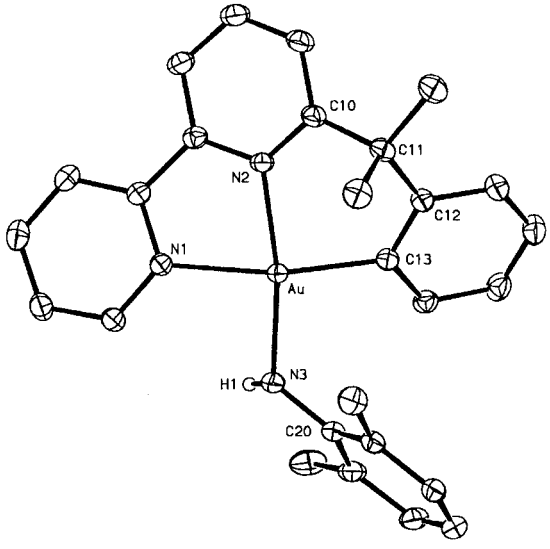

 © 2003 Wiley-VCH Verlag GmbH & Co. KGaA, Weinheim

2311 D. M. Shin, I. S. Lee,* Y. K. Chung*

Crystal Engineering with Structurally Flexible 1,1′-Substituted Ferrocenes for Nonlinear Optical Materials

Keywords: Crystal engineering / Hydrogen bonds / Nonlinear optics / π-Interactions

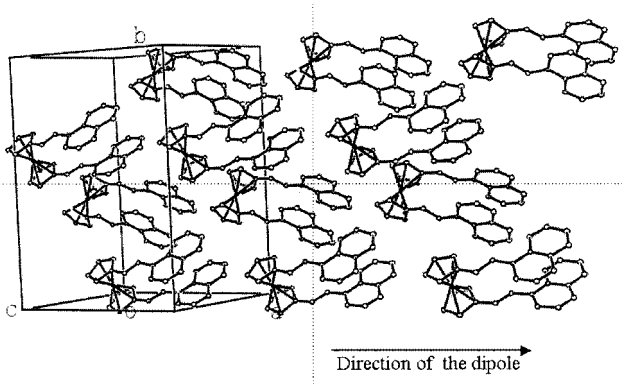

2318 P. A. N. Reddy, M. Nethaji, A. R. Chakravarty*

Ternary Mononuclear and Ferromagnetically Coupled Dinuclear Copper(II) Complexes of 1,10-Phenanthroline and *N*-Salicylidene-2-methoxyaniline that Show Supramolecular Self-Organization

Keywords: Copper / Magnetic properties / N ligands / Stacking interactions / Supramolecular chemistry

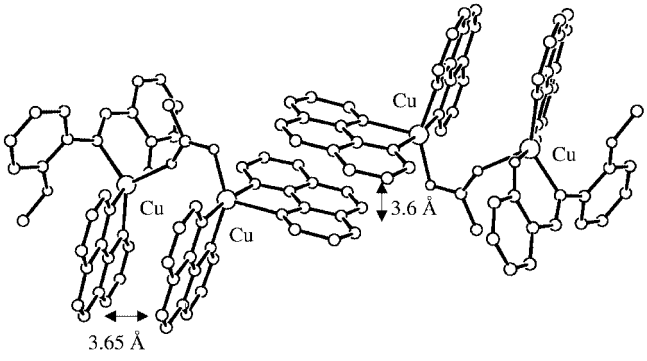

2325 H. Hou,* G. Li, Y. Song, Y. Fan, Y. Zhu, L. Zhu

Synthesis, Crystal Structures and Third-Order Nonlinear Optical Properties of Two Novel Ferrocenyl Schiff-Base Complexes $[Ag(L)_2](NO_3)\cdot(MeOH)\cdot(EtOH)$ and $[HgI_2(L)]$ {L = 1,2-Bis[(ferrocen-l-ylmethylene)amino]ethane}

Keywords: Schiff bases / Silver / Mercury / Nonlinear optics

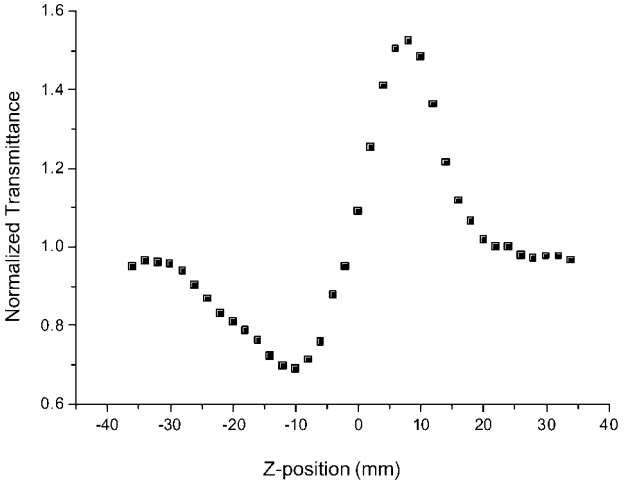

2333 K. Ueda,* T. Sugimoto, C. Faulmann, P. Cassoux

Synthesis, Crystal Structure, and Electrical Properties of Novel Radical Cation Salts of Iodine-Substituted TTF-Derived Donors with the Nitroprusside Anion Exhibiting Strong -I···NC- Interactions

Keywords: Cations / Radical ions / Fulvalenes / Conducting materials

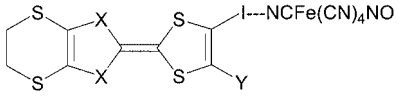

1: X = S, Y = I; **2**: X = Se, Y = I; **3**: X = S, Y = H

 © 2003 Wiley-VCH Verlag GmbH & Co. KGaA, Weinheim

2339 **M. C. Barral, R. González-Prieto, R. Jiménez-Aparicio,* J. L. Priego, M. R. Torres, F. A. Urbanos**

Polymeric, Molecular, and Cation/Anion Arrangements in Chloro-, Bromo-, and Iododiruthenium(II,III) Carboxylate Compounds

Keywords: Carboxylate / Diruthenium / Metal−metal bonds / Multiple bonds / Ruthenium

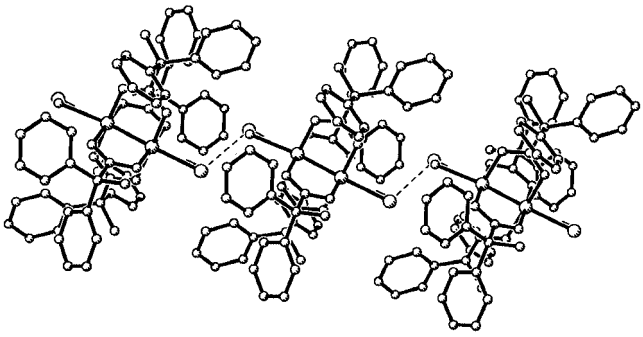

2348 **K. E. Splan, A. M. Massari, G. A. Morris, S.-S. Sun, E. Reina, S. B. T. Nguyen, J. T. Hupp***

Photophysical and Energy-Transfer Properties of (Salen)zinc Complexes and Supramolecular Assemblies

Keywords: Host-guest systems / Fluorescence / Supramolecular chemistry / Salen ligands

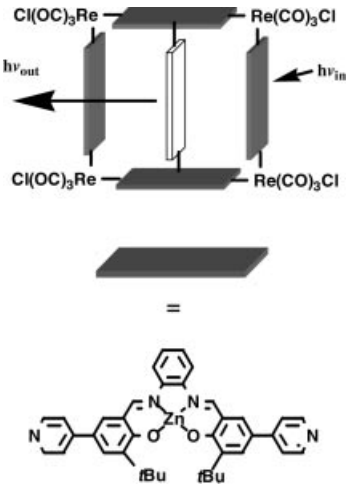

2352 **H. Paulsson,* M. Berggrund, A. Fischer, L. Kloo**

Iodoargentates and Cuprates Stabilized by Sulfonium Cations With Long Alkyl Chains

Keywords: Cations / Iodide / Copper / Silver / Crystal structure

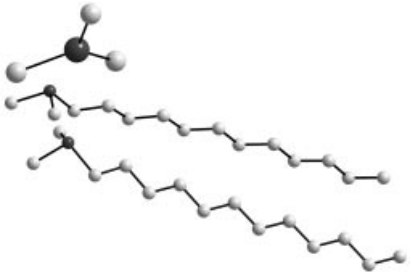

 © 2003 Wiley-VCH Verlag GmbH & Co. KGaA, Weinheim

Metal Ligand Aromatic Cation−π Interactions

Snežana D. Zarić[a,b]

Keywords: Chelates / Density functional calculations / DNA / Hydrogen bonds / Metalloproteins / Pi interactions / RNA

Cation–π interactions are important noncovalent bonding forces. This review covers a special type of cation–π interactions, the metal ligand aromatic cation–π (MLACπ) interaction, where ligands that are coordinated to a metal ion interact with aromatic groups. These interactions have been observed in metalloproteins, metal complexes, biomimetic metal complexes, and when DNA and RNA interact with metal cations. The energy of MLACπ interactions in different systems has been calculated by quantum chemical methods and was found to vary from 1 to 30 kcal/mol.
(© Wiley-VCH Verlag GmbH & Co. KGaA, 69451 Weinheim, Germany, 2003)

1. Introduction

Noncovalent interactions are very important for molecular systems ranging from molecular biology to material science.[1] Cation−π interactions are now recognized as important noncovalent binding forces.[2] In their review, Ma and Dougherty provided an overview of cation−π interactions that covered the nature of the interactions, and described cation−π interactions in artificial receptors and in biological structures.[2]

Since that review was published, a large number of papers have appeared that deal with cation−π interactions, especially in biological systems. Investigations on cation−π interactions in proteins and polypeptides have shown that cation−π interaction pairs contribute at least as much to protein stability and the structural motifs of a native protein as do more conventional noncovalent interactions.[3] In a few recent review articles, some theoretical and experimental aspects of cation−π interactions have been considered.[4]

In this review, a special type of cation−π interaction is considered, namely that in which the cation is part of a metal complex (Figure 1). In this type of cation−π interaction, the ligands that are coordinated to a metal ion interact with π systems. In the case of an aromatic π system, we called this interaction a metal ligand aromatic cation−π (MLACπ) interaction. Figure 1 depicts the NH_3 ligands of the $[Co(NH_3)_6]^{3+}$ cation interacting with benzene. Please note that we do not consider direct interactions of a π system with a transition metal atom, as exist in ferrocene and other sandwich compounds, where the π system interacts with the metal's d orbitals. A number of papers that deal with MLACπ interactions have appeared in the last few years.

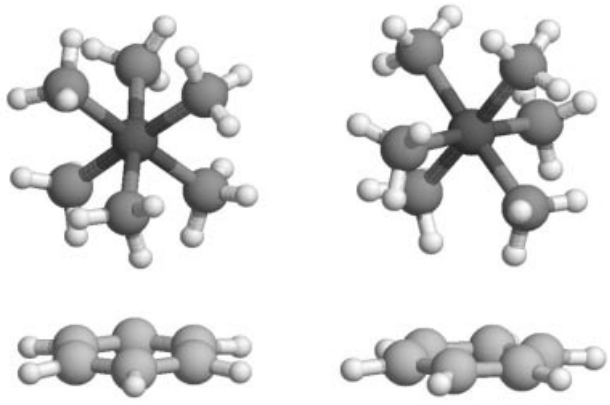

Figure 1. The η_3 and η_2 structures of $[Co(NH_3)_6]^{3+}-C_6H_6$ complexes

In all cases of MLACπ interactions that we report in this article, the ligand participating in the interaction possesses a hydrogen atom pointing towards the π system. By coordinating to a metal cation, ligands acquire partial positive charge that is located mainly on the hydrogen atoms of the ligand that interact with the π system.

Because hydrogen atoms of ligands are interacting with π systems (Figure 1), this interaction may be considered to be an X−H···π bond.[5,11] Because of the positive charge on

[a] Department of Chemistry, University of Belgrade,
Studentski trg 16, P. O. B. 158, 11001 Belgrade, Yugoslavia
E-mail: szaric@chem.bg.ac.yu
[b] Department of Biology, Chemistry and Pharmacy, Institute of Chemistry, Free University of Berlin,
Takustrasse 6, 14195 Berlin, Germany

MICROREVIEWS: This feature introduces the readers to the author's research through a concise overview of the selected topic. Reference to important work from others in the field is included.

the ligands in these MLACπ interactions, the X−H···π bonds are charge-assisted, which increases the strength of the X−H···π bonds and makes these bonds among the strongest of known X−H···π bonds.

Interactions of transition metal complexes with π systems have been predicted by quantum chemical calculations. It was anticipated that predicting the strengths of these interactions would be possible because theoretically calculated bonding energies for cation−π systems are in agreement with experimental data.[6] By using DFT (Density Functional Theory) calculations it has been shown that a cationic metal complex interacts strongly with the π system of benzene.[7] Based on these calculations, we proposed[7] that the cation−π interaction may exist when ligands coordinated to a metal ion can get in close contact with a π system. MLACπ interactions can occur in metalloproteins, metal complexes, supramolecular structures, and when DNA and RNA interact with metal cations.

These theoretical predictions have been supported by experimental evidence. Experimental findings of the interactions between nucleobases of DNA and RNA and cationic metal complexes[8] were published virtually simultaneously with the theoretical results.[7] MLACπ interactions in metalloproteins,[9] metal complexes,[10,11] and biomimetic metal complexes[5a] have been found also in crystal structures. MLACπ interactions in the gas phase[12] and in solution[11] have been investigated by spectroscopic methods in a few examples of metal complexes.

2. Calculations of MLACπ Interactions with Benzene

Calculations that predict a strong interaction of transition metal complexes with π systems have been performed for the interactions of the $[Co(NH_3)_6]^{3+}$ cation with benzene.[7,14] The DFT method was used for these calculations, as the most convenient form of quantum chemical methods, because it is suitable for transition metal complexes. In particular, DFT methods have given good results for all transition metal complexes, including transition metal complexes of the first row.[15] It has also been shown that the DFT method is suitable for studying cation−π interactions. Using the B3LYP method, calculations on the bonding energy of the $NH_4^+-C_6H_6$ complex were in agreement with experimental data.[7] In other calculations, reliable results with the DFT method were obtained also for cation−π systems.[16] Geometries were optimized with a the LANL2DZ basis set, while energies were calculated in a larger basis set (6-31G** basis set for all atoms, except for cobalt where LANL2DZ was used).[14]

The $[Co(NH_3)_6]^{3+}-C_6H_6$ cation−π complex has many possible conformers. Three conformers may exist by considering the number of NH_3 groups of the $[Co(NH_3)_6]^{3+}$ cation interacting with the benzene molecule, namely where the number of NH_3 groups involved in bonding is one (η_1), two (η_2) or three (η_3). The total number of possible conformers is larger, however, because for each of these structures, η_1, η_2 and η_3, the benzene molecule may adopt different orientations.

An η_1 conformer was not obtained as a stable structure in the calculations. Starting with this structure, geometry optimization terminated with a conformer of type η_3. The calculations showed that stationary points were obtained for several η_2 and η_3 structures. In all calculated η_2 and η_3 structures, only one hydrogen atom from each of the participating NH_3 groups interacts with the benzene unit. The geometries and energies of two η_2 structures are very similar; the only difference is in the orientation of the benzene ring. The four optimized η_3 structures are also similar to each other. The difference in energy between the η_3 and η_2 structures is approximately 2 kcal/mol. The most stable η_3 structure has a bonding energy of 32.18 kcal/mol, after basis-set-superposition error (BSSE) correction. Frequency calculations on all the optimized geometries showed that only this structure is an energy minimum. The most stable η_2 and η_3 structures are shown in Figure 1, and their bonding energies and geometric data are shown in Table 1.

Table 1. The bond lengths (in the case of the η_3 structures, the data are average bond lengths, except for H···centroid of the benzene ring) and bonding energies of η_2 and η_3 structures (the most stable conformers for η_2 and η_3 structures, shown in Figure 1) of $[Co(NH_3)_6]^{3+}-C_6H_6$ complex

	η_2 structure	η_3 structure
$N-H_{int}$ [Å]	1.040	1.037
$Co-N_{int}$ [Å]	2.023	2.015
$Co-N_{(cis)nonint}$ [Å]	2.025	
$Co-N_{(trans)nonint}$ [Å]	2.052	2.043
$C_{(benzene)}\cdots H_{int}$ [Å]	2.224	2.299
$H_{(1)int}$···centroid of benzene ring [Å]	2.513	2.676
$H_{(2)int}$···centroid of benzene ring [Å]	2.513	2.680
$H_{(3)int}$···centroid of benzene ring [Å]		2.727
ΔE_2 [a] [kcal/mol]	−31.37	−34.16
ΔE_{2B} [b] [kcal/mol]		−32.18

[a] Bonding energies without BSSE correction. [b] Bonding energies with BSSE correction.

In the calculated cation−π complexes there are changes caused by the cation−π interaction in the calculated geometries of the $[Co(NH_3)_6]^{3+}$ cation and of the benzene ring. The bond lengths change in the $[Co(NH_3)_6]^{3+}$ cation. Changes are largest for the Co−N bonds directed at the benzene ring (shortened by more than 0.01 Å) and the N−H bonds of hydrogen atoms that are directly involved in the interactions (lengthened by more than 0.01 Å). The hydrogen atoms in the benzene molecule are bent away from the cation. The cation−π interaction also causes some C−C bonds of the benzene ring to lengthen up to 0.008 Å.

Comparing the charges of a separate $[Co(NH_3)_6]^{3+}$ cation and a benzene molecule with the charges of the cation−π complex shows that there is an electron transfer from the π system to the cation. The average charge on the benzene unit in the η_2 structures of the $[Co(NH_3)_6]^{3+}-C_6H_6$ complex is +0.3077, and in the η_3 structures it is +0.3316.[14] The increase in charge transfer

 © 2003 Wiley-VCH Verlag GmbH & Co. KGaA, Weinheim

corresponds to an increase in the strength of the interaction.

The calculated strong interactions existing between the transition metal complex and the aromatic molecule indicate that these interactions can exist in all cases where ligands coordinated to a metal center can get in close contact with aromatic groups. The small difference in energy among different conformers indicates the large number of mutual orientations that can be adopted by the interacting ligands and benzene, and the large degree of variability in conformations that are possible in MLACπ interactions.

Interactions of the $[Co(NH_3)_6]^{3+}$ cation with ethylene and acetylene were also calculated and the bonding energies obtained were 17.02 and 18.30 kcal/mol, respectively.[17]

Calculations on the interactions of $[Mg(H_2O)_6]^{2+}$ with benzene were done using the Hartree−Fock (HF) method and 6-31G* basis set for geometry optimization.[18] Single-point energies at the optimized geometries were calculated by the MP2 method. The calculated bonding energies were corrected for BSSE. In the optimized geometry, three coordinated water molecules are oriented towards the benzene molecule. The hydrogen atoms of the water molecules point towards the C−C bonds of the benzene unit, with the H···C distance to the two closest carbon atoms being 2.56 and 2.79 Å. The elongation of the O−H bonds involved in the O−H···π contact is ca. 0.004 Å. The calculated bonding energy is 21.5 kcal/mol. Similar calculations with $[Zn(H_2O)_6]^{2+}$ gave almost the same geometry and bonding energy (21.3 kcal/mol). For the benzene−sodium hexahydrate complex, the bonding energy was reduced to 9.1 kcal/mol.[18]

It is interesting to compare calculations of the interactions of metal complexes with benzene with those of non-metal cations [$(CH_3)_4N^+$ and NH_4^+] with benzene. In calculated structures where metal complexes or $(CH_3)_4N^+$ interact with benzene, there are three NH_3 ligands or three CH_3 groups oriented towards benzene, while in the NH_4^+−benzene complex there are two hydrogen atoms that interact with benzene.[6h] The calculated bonding energy of benzene−sodium hexahydrate complex (9.1 kcal/mol) is similar to that of the $(CH_3)_4N^+$−benzene complex (ca. 10 kcal/mol),[6h] while the energy of interaction of the NH_4^+−benzene complex is large (ca. 18 kcal/mol).[6h,19a] The energy of interaction of the NH_4^+−benzene complex is relatively close to the bonding energy of metal complexes having a charge of +2, which shows that the positive charge is less dispersed in the NH_4^+ cation than it is in the metal complex cations and $(CH_3)_4N^+$.

In the NH_4^+−benzene complex the closest distance between an H atom (from the cation) and a C atom (from benzene) is 2.436 Å,[19b] and in the $[Co(NH_3)_6]^{3+}$−benzene complex that distance is 2.299 Å.[14] In both of these systems there is electron transfer; in the former, the charge of the benzene unit is 0.265,[19b] and in the latter, as was mentioned previously, it is 0.331.[14] Both features — the interacting distances and charges — are in agreement with the belief that the stronger interactions occur in the $[Co(NH_3)_6]^{3+}$−benzene system than in the NH_4^+−benzene complex.

3. MLACπ Interactions in Metal Complexes

Geometries in Crystal Structures

Intramolecular

Crystal structures of metal complexes containing a phenyl ring and coordinated nitrogen or oxygen atoms, obtained from the Cambridge Structural Database (CSD), were screened for intramolecular cation−π interactions between ligands coordinated to the metal center and the aromatic groups (MLACπ).[10] Geometric criteria were used for screening such that structures were chosen in which the distance between the metal ion and the centroid of the aromatic ring is less than d_0 = 5.5 Å (Figure 2). No restrictive criteria were used for the angle of the normal of the aromatic ring plane with the distance vector between the centroid of the aromatic ring and the metal ion, since intramolecular interactions were being investigated. It was found that the interaction is stronger if the hydrogen atom that interacts with the aromatic group is closer to the metal center,[9] and hence, structures were considered only in which there are two bonds between the hydrogen atom and the metal ion.

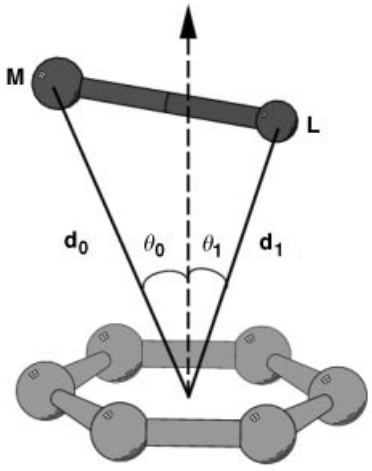

Figure 2. Distances (d_0, d_1), and angles (θ_0, θ_1) used to search for and characterize MLACπ interactions; M is a metal cation, L is a non-hydrogen atom ligand (L) closest to the ring centroid; the dashed line is the normal of the aromatic ring plane

It was found that intramolecular MLACπ interactions, between a coordinated ligand and the aromatic ring in the same complex, were observed in a number of crystal structures of transition metal complexes. Data concerning the MLACπ interactions in different crystal structures are compiled in Tables 2 and 3. The data show that there are numerous metal complexes in which there is close contact between an aromatic ring and a ligand and that different metal ions and ligands can be involved.

 © 2003 Wiley-VCH Verlag GmbH & Co. KGaA, Weinheim

Table 2. Intramolecular metal ligand aromatic cation−π (MLACπ) interactions in complexes with two bonds between the aromatic ring and the metal ion

RFCODE	Metal ion	X[a]	X···centroid of ring[b] [Å]	H···centroid of ring[c] [Å]	X···C[d] [Å]	H···C[e] [Å]	Y[f]	Ref.
BZSACS	Co^{3+}	N	3.98	3.82	3.27	3.16	S	[20]
				3.35		2.83		
CUBXAY	Co^{3+}	N	3.39	3.54	3.22	3.00	P	[21]
				3.64		2.94		
		N	4.11	3.49	3.37	3.44	P	
				4.17		2.89		
JORJAB	Co^{2+}	N	3.35	3.17	3.02	2.72	N	[22]
JUJPEJ	Cu^{2+}	N	3.92	3.22	3.36	2.82	N	[23]
TSACOP	Co^{3+}	N	3.79	3.45	3.12	2.96	S	[24]
				3.39		2.80		
TULBEH	Mn^{1+}	N	3.77	2.95	3.19	2.51	P	[25]
GAFKED10	Cd^{2+}	N	3.65	2.81	3.33	2.52	N	[26]
HELYUS	Ru^{2+}	N	3.83	3.06	3.18	2.61	S	[27]
PAXCAS	Mo^{4+}	N	3.89	3.13	3.07	2.43	S	[28]
PIRKAC	Ru^{1+}	N	3.55	3.39	3.14	2.92	P	[29]
				3.29		3.02		
TOJCIE	$Ru^{1/5+}$	O	3.94	3.00	3.27	2.37	P	[30]
VERGEE	Tc^{5+}	N	3.73	2.80	3.08	2.30	S	[31]
		N	3.72	2.80	3.04	2.25	S	
WEFLOI	Ru^{2+}	N	4.02	3.36	3.28	2.71	Si	[32]
AQTORU	Ru^{2+}	O	3.58		3.03		P	[33]
		O	2.74		3.09		P	
KAJROC	Rh^{2+}	N	4.48	3.59	3.46	2.67	Sb	[34]
		N	4.15	3.26	3.36	2.63	Sb	
BAXJOZ	Re^{4+}	O	3.98		3.34		P	[35]
CIRNUM	$Os^{2/3+}$	O	3.73		3.23		P	[36]
DIKMUF	Os^{2+}	O	3.64		3.14		P	[37]
		O	3.64		3.14		P	
PEDXAX	Ir^{3+}	N	3.63	2.76	3.01	2.25	P	[38]
		N	3.71	3.05	3.09	2.64	P	
				3.64		2.82		
PEWRUE	Re^{5+}	N	3.75		3.17		P	[39]
WAXGIL	Re^{3+}	N	3.53	2.69	3.14	2.48	P	[40]

[a] Heavy atom to which the interacting hydrogen atom is bound. [b] The distance between the heavy atom and the centroid of the aromatic ring. [c] The distance between the interacting hydrogen atom and the centroid of the aromatic ring. [d] The distance between the heavy atom and the closest carbon atom of the aromatic ring. [e] The distance between the interacting hydrogen atom and the closest carbon atom of the aromatic ring. [f] The atom between the metal ion and the aromatic ring.

In most of the complexes there are two or four bonds between the metal ion and the aromatic ring. The aromatic ring of an organic ligand can interact with a hydrogen atom of the other ligand, or with a hydrogen atom of the same ligand.

In complexes where there are only two bonds between the aromatic ring and the metal ion (Table 2) there is the possibility for the MLACπ interaction only with the ligand coordinated in the *cis* position and there is no possibility for an MLACπ interaction within the same ligand. In this group of complexes there is little freedom for the ligands to adjust their mutual orientations.

In structures with more than two bonds between the metal ion and the aromatic ring (Table 3) there is the possibility for MLACπ interactions with the hydrogen atom of the other ligand, but also with the hydrogen atom of the same ligand. There are fewer steric constraints in cases where there are interactions with hydrogen atoms of another ligand, and in these cases the distances of the interaction to the center of the ring are shorter.

These results show that steric constraints in the intramolecular MLACπ interactions in the complexes have an important influence on their geometry and, probably, the strength of these interactions.

Kumita et al. studied intramolecular interactions between a ligand and an aromatic ring using different experimental methods.[11] They observed these interactions in the crystal structures of K[Co(L)(aa)] [L = *N*,*N*-bis(methoxycarbonyl)-(*S*)-phenylalanine; aa = (*S*)-Phe, (*R*)-Phe, (*S*)-Trp] complexes. In these structures there are intraligand interactions with the distances between amino hydrogen atoms and the plane of the phenyl ring in the range 2.61−2.82 Å. Similar interactions were observed in the complex K[Co{*N*,*N*-bis(methoxycarbonyl)-(*S*)-leucine}-(*S*)-Phe].[61] Although there is the possibility, however, for intraligand interactions in complexes with aromatic amino acids as ligands, they do not always occur[62] since they depend very much on the interplay with other ligands in the complex; this feature shows that these interactions are in balance with other noncovalent interactions.

 © 2003 Wiley-VCH Verlag GmbH & Co. KGaA, Weinheim

Table 3. Intramolecular metal ligand aromatic cation−π (MLACπ) interactions in complexes with several bonds between the aromatic ring and the metal ion

RFCODE	Metal ion	X[a]	X···centroid of ring[b] [Å]	H···centroid of ring[c] [Å]	X···C[d] [Å]	H···C[e] [Å]	Ref.
CEBREG	Cu^{2+}	N	4.00	3.42	3.06	2.66	[41]
FUCSIF	Cu^{2+}	N	3.90	3.29	2.96	2.58	[42]
NEFRAR	Co^{3+}	N	3.90	3.22	2.99	2.54	[43]
POKAD02	Co^{3+}	N	3.75	3.08	2.90	2.56	[44]
		N	3.75	3.08	2.90	2.56	
TONPUH	Cu^{2+}	N	3.88	2.99	2.99	2.23	[45]
VAFSIE	Co^{3+}	N	3.85	3.03	2.92	2.33	[46]
RUFKUY	Rh^{3+}	N			2.93	2.46	[47]
NEGREW	Re^{1+}	N	3.81	3.16	2.82	2.38	[48]
			3.55	2.87	3.29	2.51	
DUSJIK	Ni^{3+}	N	3.27	2.21	3.46	2.54	[49]
DEMHAE	Ni^{2+}	N	3.55	2.87	3.29	2.62	[50]
			3.55	2.87	3.29	2.51	
DIXHAT	Cu^{2+}	N	4.48	3.79	3.84	3.18	[51]
		N	4.53	3.84	3.84	3.18	
GLTRCU01	Cu^{2+}	O	3.25	2.31	3.37	2.52	[52]
LETYCU10	Cu^{2+}	O	3.32	2.58	3.39	2.66	[53]
NALPIZ	Fe^{2+}	N	3.63	2.63	3.16	2.72	[54]
		N	3.63	2.63	3.16	2.29	
NOVBAB	Ni^{2+}	O	4.06	3.28	3.53	2.76	[55]
		O	3.93	3.23	3.27	2.49	
NUTKES	Mn^{2+}	O	3.24	2.36	3.32	2.74	[56]
		O	4.13	3.22	3.52	2.65	
TONPOB	Cu^{2+}	O	3.17		3.31		[45]
FOBTAR	Mo^{4+}	N	3.42	2.84	3.26	2.53	[57]
SIRCOL	Mo^{4+}	N	3.91	2.97	3.50	2.67	[58]
		N	3.91	2.97	3.50	2.67	
ZURREJ	Cd^{2+} Ni^{2+}	N	3.77	2.91	3.55	2.68	[59]
NOLQIO	Mo^{6+}	N	3.47	2.94	3.33	2.85	[60]

[a] Heavy atom to which the interacting hydrogen atom is bound. [b] The distance between the heavy atom and the centroid of the aromatic ring. [c] The distance between the interacting hydrogen atom and the centroid of the aromatic ring. [d] The distance between the heavy atom and the closest carbon atom of the aromatic ring. [e] The distance between the interacting hydrogen atom and the closest carbon atom of the aromatic ring.

Some C−H···π interactions, where the C−H unit is part of the ligand, have also been observed in metal complexes.[63] If the C−H groups are not very close to the metal ion there is no difference between these C−H···π interactions and those in organic molecules.[63a,64]

Intermolecular

Intermolecular interactions between hydrogen atoms and π systems have been observed in organometallic crystals.[5a] Investigation of these interactions show that they are common and appear to be typical hydrogen bonds. Many of these organometallic structures are ionic compounds. In most cases it has been shown that charge-assisted ($X-H^{\delta+}\cdots\pi^{\delta-}$) interactions possess shorter distances than neutral X−H···π bonds. It should be noted that in this study an X−H group was not always part of a ligand coordinated to a metal ion, but instead was part of any other molecule in the crystal structure.[5a]

Calculated Intramolecular MLACπ Interactions

DFT calculations were done on model systems with relatively small ligands to evaluate the energy of intramolecular MLACπ interactions.[10] The geometries and energies were calculated for structures with various conformations of the aromatic ring in the model systems. Based on the difference in energy for conformers with and without MLACπ interactions, the energy of the interactions was evaluated for model systems of cationic complexes of Co^{III} having a total charge of +1.

The calculations on complexes with two bonds between the aromatic ring and the metal ion were done on the model system $[CoCl_2(NH_3)_3(C_6H_5NH_2)]^+$. The coordinated aniline unit is in the *cis* position relative to the two NH_3 and two Cl^- ligands. The energy was calculated for the structure where the aromatic ring is positioned above either an NH_3 or Cl ligand. Based on the difference in energy between these two conformers, the energy of the MLACπ interaction was evaluated to be ca. 4 kcal/mol for this model system.

The $[CoCl(NH_3)_3Phe]^+$ complex was used as a model system to study the interactions in complexes having several bonds between the aromatic ring and the metal ion (Figure 3). There are three possible conformations of the phenyl ring in the coordinated phenylalaninato ligand. In one conformer there are no MLACπ interactions, in the second there is only an intraligand interaction, and in the third

 © 2003 Wiley-VCH Verlag GmbH & Co. KGaA, Weinheim

there are intraligand and interligand interactions. Based on the differences in the energy of these conformers, the energies of intraligand and interligand interactions were evaluated to be ca. 3.5 and 4 kcal/mol, respectively.[10]

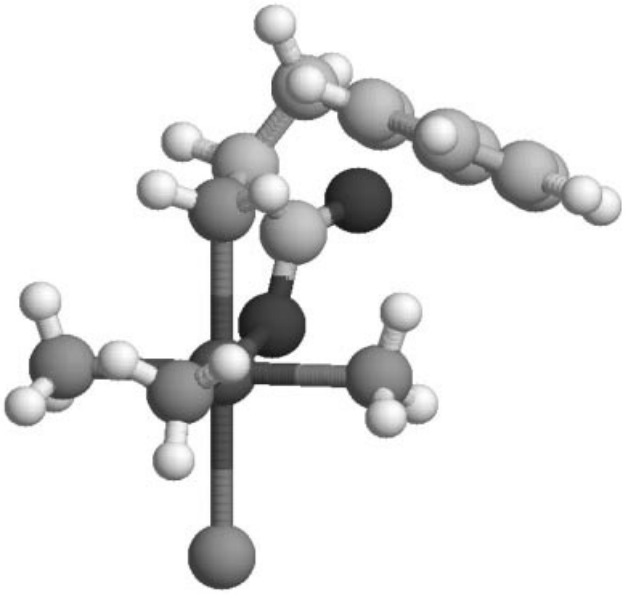

Figure 3. Model systems $[CoCl(NH_3)_3Phe]^+$ used for calculations of intramolecular metal ligand aromatic cation−π (MLACπ) interactions in metal complexes

Spectroscopic Evidence

IR Spectra

Interactions of a benzene unit with water molecules coordinated to K and Na ions were observed using infrared spectroscopy in gas-phase cluster ions of the form $M^+(C_6H_6)_n(H_2O)_m$, with M = Na or K.[12,13] Vibrational-predissociation spectroscopy indicates details of the structure because the OH stretching frequency of water is extremely sensitive to changes in its bonding environment. In the $K^+(C_6H_6)_3(H_2O)_1$ complex the stretching modes of water are very similar to that of free water. The introduction of a fourth benzene molecule significantly affects the OH spectrum, which is indicative of hydrogen bond formation.[12]

The O−H···π hydrogen bond was observed also in $K^+(C_6H_6)_5(H_2O)$, where a water molecule and three benzene molecules are bonded directly to the K^+ ion, and the fourth and fifth benzene molecules are bound to the coordinated water molecule. The interaction of the benzene molecules with the coordinated water molecule is observed by a shift in vibrational frequencies of the O−H stretching mode towards smaller wavenumbers by ca. 70 cm^{-1}. Vibrational spectra can also indicate differences in the strengths of hydrogen bonds in cases when there is a neutral benzene−water complex, and when water is bonded to a K^+ ion. The bonding of a water molecule to the ion enhances the π−hydrogen bond between the water and benzene molecules, leading to an additional shift in the OH stretching frequency.[12]

In the case of Na^+ ions, the most interesting complex is the self-assembled cluster ion, $Na^+(C_6H_6)_8(H_2O)_4$, which has a single structure of an inner shell of four water molecules and an outer layer of eight benzene molecules, each of the latter being fixed by a π−hydrogen atom bond to one of the eight interior O−H groups. The intense narrow bands observed in the vibrational spectra of $Na^+(C_6H_6)_8(H_2O)_4$ indicate a stable cluster ion configuration with eight H−π bonds.[13]

CD Spectra

The CD spectra of *trans*-(N)−K[Co(bcmpa)(aa)] (aa = amino acid) complexes were measured in a study of N−H···π interactions in Co^{III} complexes with amino acids.[11] The CD spectra of these complexes have four components in the d−d region. For one of these bands, there are indications that its origin can be attributed to a chiral amino acid, and the same band exhibited a solvent effect that is related to the vicinal effect of chiral amino acids. For complexes with aromatic amino acids [(*S*)-Trp, (*S*)-Phe, (*S*)-Tyr], there is a significant difference in the intensity of the band in aqueous and ethanol solutions, while the complexes with aliphatic amino acids [(*S*)-Ala, (*S*)−Leu, (*S*)-Pro] did not exhibit this solvent effect. The solvent effect in complexes with aromatic amino acids is a consequence of the N−H···π bond in solution, since the strength of the N−H···π bond varies in different solvents.[11]

^{1}H NMR Spectra

NMR spectroscopy is a powerful method for studying weak interactions in solution. ^{1}H NMR spectra of *trans*-(N)−K[Co(bcmpa)(aa)] (aa = amino acid) complexes were measured to obtain detailed structural information of the N−H···π interaction in solution.[11] If the N−H protons approach an aromatic system closely, they are expected to shift to higher field as a result of the ring-current effect. Indeed, in NMR spectra of metal complexes with aromatic amino acids, the peaks of NH protons at a higher field exhibited significant upfield shifts. Namely, for the Co^{III} complexes with aromatic amino acids, the two peaks of the amino protons at the higher and lower fields were observed in the ranges δ = 5.34−5.81 and 7.02−7.26 ppm, respectively, while those for the complexes with aliphatic amino acids were detected in the ranges δ = 6.01−6.29 and 7.22−7.40 ppm, respectively. In the crystal structure, one of the two coordinated amino protons is located exactly in the position expected for it to be affected by the shielding effect of an aromatic ring, but another one is slightly deviated from such a position. Since the geometry in solution is probably very similar to that observed in the crystal, the signals for these two protons are shifted differently because of their different shielding. Moreover, the values of chemical shift of the peaks at higher field for the Co^{III} complexes with *p*-X-substituted phenylalanines (X = OH, CH_3, H, Cl) demonstrate a significant substituent effect, which indicates that greater electron density on the aromatic ring results in a larger shielding effect. This observation suggests that the

 © 2003 Wiley-VCH Verlag GmbH & Co. KGaA, Weinheim

Table 4. Interactions of C−H groups of ligands with the π system of a chelate ring (data for normalized positions of the H atom)

CSD refcode	H···centroid of ring [Å]	C···centroid of ring [Å]	Chelate ring	Ref.
ACIPTI	2.43	3.51	TiOCCCO	[67]
BEPZOL	2.48	3.56	CuNCNCN	[68]
COTQAD	2.38	3.39	ZrNCCCN	[69]
COTQEH	2.36	3.38	HfNCCCN	[69]
FEBTAH	2.39	3.45	NiNCCCN	[70]
GORYER	2.46	3.54	MnOCCCN	[71]
GOXDAY	2.48	3.46	FeNCCCN	[72]
HALWAS	2.40	3.36	ZnNCCCN	[73]
HAMDAA	2.40	3.38	ZnNCCCN	[73]
HAMGUX	2.46	3.43	ZnNCCCN	[73]
JOXGIM	2.59	3.68	CuOCCCN	[74]
LICSEV	2.31	3.32	CuNCCCN	[75]
LOFZOV	2.36	3.35	NiOCCCN	[76]
MAMTOJ	2.46	3.52	CoOCCCN	[77]
MAMTUP	2.32	3.38	CuOCCCN	[77]
PIQZUK	2.45	3.53	ReOCCCN	[78]
SUMXIH	2.50	3.45	FeNCCCN	[79]
VAFQIC	2.30	3.38	ZnNCCCN	[80]
YINLUC	2.54	3.60	NiOCCCO	[81]
ZAXDOR	2.30	3.31	ZnOCCCN	[82]
ZONQOI	2.34	3.32	CoNCCCN	[83]
ZOPYUY	2.34	3.37	CuOCCCN	[84]

attractive interaction is maintained even in polar solvents such as DMSO.[11]

4. Interaction with a Chelate Ring

Geometries in the Crystal Structures

There is a special type of X−H···π interaction in which a hydrogen atom from a ligand coordinated to a metal ion interacts with a chelate ring that has delocalized π bonds.[65] It is considered that the metal atom is involved in π delocalization and that these rings can have aromatic character.[66] A search for crystal structures of transition metal complexes from the CSD showed that interactions between C−H groups and the π system of chelate rings are observed in many crystal structures. Geometrical parameters for some examples are shown in Table 4. All of these examples have a very short distance between the interacting hydrogen atom and the centroid of the chelate ring (< 2.6 Å), and the hydrogen atom is located in a position almost centered over the chelate ring's centroid. From a geometrical point of view, interactions in these structures are similar to strong C−H···π interactions in organic molecules.[63a,64]

These interactions occur in metal complexes of different metals and various chelate rings. In Table 4 most of these interactions listed are intermolecular ones, with only the compound ACIPTI presenting an intramolecular interaction.

It is very interesting to notice that in all cases shown in Table 4 the complexes are neutral and both the chelate ring and the C−H group belong to the same molecule. In cases of intermolecular interactions, the interaction occurs between two identical molecules: the C−H group of one molecule interacts with the chelate ring of the second molecule. It is assumed that the neutrality of the complexes is important for these types of interactions because it enables a chelate ring not to have a partial positive charge, which would be the case if the complex was positively charged. On the other hand, the π system of the chelate ring would not interact with a negatively charged complex. In the case of a neutral complex, the interacting H atom has a partial positive charge, which is enough charge for a weak C−H···π interaction to occur.

Calculation of the Energy of Interaction

DFT calculations were performed on model systems from crystal structures to evaluate the energy of these types of interactions. The calculated energies of these interactions are approximately 1 kcal/mol.[65] The calculated values for interacting energies are similar to the values calculated for C−H···π interactions in organic molecules.[63a,64] One of the model systems based on the crystal structure YINLUC in shown in Figure 4.

5. MLACπ Interactions in Biomimetic Metal Complexes

Interactions of the MLACπ type were found in the crystal structure of biomimetic zinc complexes that are related to the enzyme/substrate complexes in biological systems with mononuclear zinc species.[5b] In the structures of $[Zn(X_6Me_3ImMe_3)L]^{2+}$ (L = EtOH, NH_2CHO) the neutral ligand $X_6Me_3ImMe_3$ forms a cavity that mimics the enzyme pocket and stabilizes four coordinated zinc species N_3ZnL^{2+}. These complexes were the first obtained of four-coordinated zinc dicationic complexes involving either a terminal aliphatic alcohol or an amide ligand. In the X-ray

 © 2003 Wiley-VCH Verlag GmbH & Co. KGaA, Weinheim

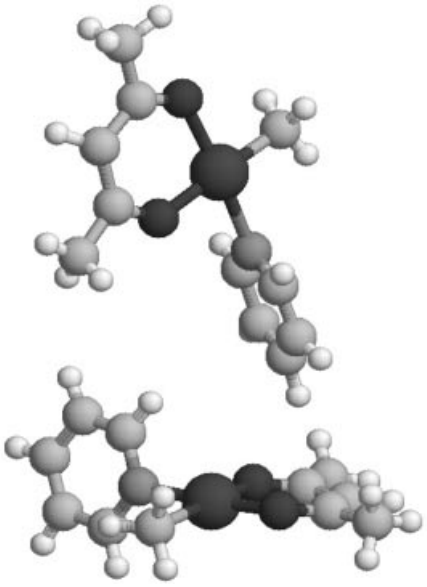

Figure 4. A model system, based on the crystal structure of YINLUC, used for calculations of the energy of C−H···π interactions with a chelate ring

structures of these complexes there are hydrogen bonds and CH···π interactions between the calix[6]arene hosts and the guests L. The CH groups that are directly connected to the oxygen atom have increased partial-positive charge because they are coordinated to an oxygen atom bonded to the metal ion. These CH groups interact with the aromatic group in the calixarene structure. The distance of the hydrogen atom closest to the centroid of the aromatic ring is 2.92 Å for $-CH_2OH$ (L = EtOH) and 2.70 Å for $-CH{=}O$ (L = NH_2CHO). These interactions, together with hydrogen bonds, play an important role in stabilizing the complex between the calix[6]arene host and the guest molecules L.[5b]

6. MLACπ Interactions in DNA and RNA Structures

Geometries in Crystal Structures

Cations play a very important role in the structure, stability, and reactivity of nucleic acids.[85] Among other noncovalent interactions, cation−π interactions between cations and nucleic acid bases have been observed in crystal structures of DNA and RNA.[8] Cation−π interactions with cationic metal complexes have been found by searching crystal structures of DNA and RNA using geometrical criteria.[8] These criteria was based on the geometries of a number of cation−π pairs in the human growth hormone/receptor complex (PDB entry 3HHR). These criteria requested that the distance between the metal ion and the centroid of the aromatic ring be smaller than 5.2 Å, and that the angle between the normal to the centroid and the centroid−metal ion bond be less than 52° (Figure 2).

It was assumed that cations interact favorably with π systems of nucleic acid bases, since cation−π interactions were detected in crystal structures of DNA and RNA. In the DNA structures of NDB entries BDL084[86] and BDJ025[87] a hydrated magnesium ion is located in the major grove and interacts with the π system of a cytosine unit (Figure 5). It was suggested that partial unstacking observed in the crystal structure was caused by cation−π interactions. The anticodon arm of yeast tRNA (NDB entry TRNA10[88]) contains one hydrated magnesium ion that is involved in MLACπ interactions. The water molecules coordinated to the magnesium ion form seven cation−π interactions, involving four tRNA bases. In the crystal structure of the tetrahymena group I intron P4−P6 domain (NDB entry URX053[89]), several magnesium ions are involved in cation−π interactions. In the same crystal structure it was also observed that the ligands of $[Co(NH_3)_6]^{3+}$ engage in MLACπ interactions with the RNA bases.

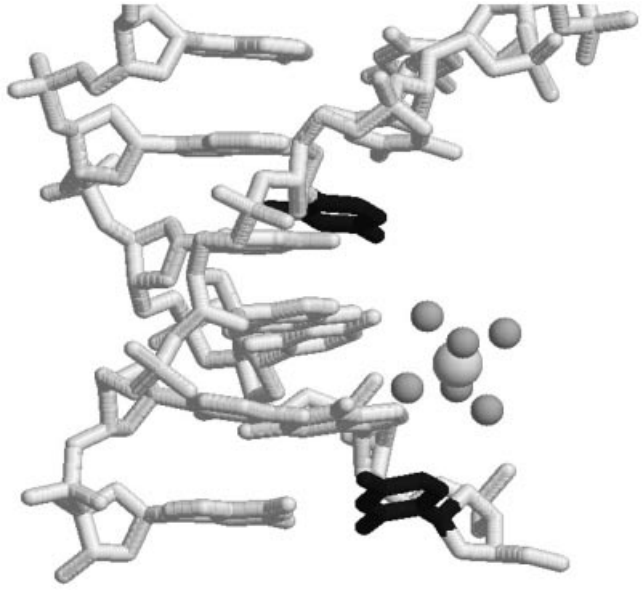

Figure 5. Part of the DNA crystal structure of BDL084[20] (NDB entries) showing the interaction of $[Mg(H_2O)_6]^{2+}$ with two cytosine units

The observation of cation−π interactions suggest a number of new mechanistic roles for cations in DNA bending, DNA−protein recognition, base flipping, RNA folding, and catalysis.[8]

Calculations

Ab initio (MP2) calculations were used to study local interactions between $[Mg(H_2O)_6]^{2+}$ and DNA bases observed in crystal structures.[18,90,91] The possibility of cation−π interactions was analyzed by assuming idealized[18] and crystal-structure geometries[18,90] of the interacting species.

The calculations on idealized geometries showed that hydrated metal cations can interact strongly with nucleobases in a cation−π manner.[18] Calculations on $[Mg(H_2O)_6]^{2+}$ with the cytosine π system were done with constraints that forced the magnesium hexahydrate unit to interact with the cytosine aromatic system and, at the same time, kept all of the cytosine atoms coplanar. The calculated interaction

 © 2003 Wiley-VCH Verlag GmbH & Co. KGaA, Weinheim

energy was 20.2 kcal/mol. This value is very close to the calculated interaction energy with a benzene molecule (see Section 2).[18] In the optimizations without any constrains, however, the complex undergoes a quick rearrangement to the conventional through-water, in-plane bonding pattern of magnesium ions, with strong hydrogen bonds to the N and O atoms of the cytosine unit. The interacting energy for this structure is much larger (68.2 kcal/mol) than that of the one above. Hence, in spite of relatively strong cation−π interaction between $[Mg(H_2O)_6]^{2+}$ and the cytosine π system, this configuration is very unstable because there is a much more stable alternative configuration in which the hydrated metal cation is in the plane of the nucelobases and forming conventional hydrogen bonds. To make cation−π interactions with nucleobases, the cation must be kept above the plane of the nucleobase by another strong interaction, which can be the case in certain biopolymers.

Calculations on the crystal-structure geometry were performed for the dodecamer BDL084[86] (NDB entry) to evaluate interacting energies in the crystal. Contacts of the magnesium hexahydrate unit with two cytosine molecules were observed in this structure, and it was suggested that both contacts can be considered as cation−π interactions.

Calculations were performed by two groups in two different ways. In the calculations of Šponer et al., the position of the Mg^{2+} ion was kept fixed with respect to the cytosine ring according to the geometry found in the crystal, while the cytosine ring and the positions of all six water molecules were fully relaxed.[18] In the optimized geometries for both contacts, the cytosine rings are substantially deformed with pyramidal amino groups. There is one water molecule interacting with the cytosine amino group, which can be considered to be an amino−acceptor interaction. The interaction energies are 13.5 and 8.1 kcal/mol. Crystal geometries were also optimized while the cytosine unit was kept planar. This constraint abolished the amino−acceptor interaction and the water molecules reoriented. The calculated interaction energies were very small (2.5 and 0.3 kcal/mol).[18]

In the second calculation, all atoms were kept at the same position as in the crystal structure and only the positions of the added hydrogen atoms were optimized.[90] The calculated bonding energies range from 1 to 3 kcal/mol. To see the effect of the magnesium ion on these interactions, the interacting energies between cytosine and loose water molecules were calculated in the presence and absence of the otherwise pentahydrated magnesium ion. The presence of the magnesium ion increased the interacting energy by ca. 1 kcal/mol.

The calculations on the interactions of $[Mg(H_2O)^6]^{2+}$ with DNA showed that the interaction energies in the crystal structures are very small. This energy is not sufficient to compensate for the decrease in energy resulting from the lack of alternative hydrogen bonding and the bending of the bond angle related to unstacking of the bases and, hence, this interaction cannot cause the bases to unstack. Further investigations[91] have shown that there are strong hydrogen bonding interactions between these cations and another base, and that these interactions are keeping the cation in its position, above the aromatic plane, observed in the crystal structure. This localization could have resulted in a favorable cation−π interaction.

7. MLACπ Interactions in Metalloproteins

Geometries in Crystal Structures

Using geometric criteria, crystal structures of metalloproteins from the PDB were screened for cation−π interactions between ligands coordinated to the metal ion and aromatic residues.[9] The criteria used were the same as those proposed by McFail-Isom et al.[8] for screening crystal structures of DNA and RNA for possible cation−π interactions, as was mentioned above. The screening was performed for the aromatic groups of phenylalanine, tyrosine, and tryptophan, but not for histidine. Histidine is very often directly coordinated to a metal ion and, therefore, a large number of structures would be obtained that do not contain the interactions of interest.

The MLACπ interactions with the aromatic rings of phenylalanine, tyrosine and tryptophan can be observed in a number of crystal structures of metalloproteins. Data concerning the interactions in different crystal structures are compiled in Table 5, which shows that this type of interaction exists in numerous metalloproteins. Practically all metals commonly occurring in enzymes can participate in such interactions. The ligands involved in the MLACπ interactions can be amino acids, water, substrates and inhibitors.

The positions of the hydrogen atoms are not available in the crystal structures of the protein structures listed in Table 5 and, hence, the geometry of the MLACπ interaction is characterized by the distance d_1 between the center of the aromatic ring and the non-hydrogen atom ligand closest to the ring centroid (Figure 2). In Table 5, the value of d_1 varies between 3.09 and 4.41 Å. The angle θ_1 is often smaller than 30°, but can be as large as 45°.

For the same protein, the data in Table 5 show that all crystal structures exhibit the same pattern of MLACπ interactions, although the redox state and coordination number may vary. In some metalloproteins, there are different ligands in different crystal structures, but they interact with the same aromatic group, as in the case of alcohol dehydrogenase (ADH). In other proteins there is more than one MLACπ interaction at one metal center. In some cases two ligands interact with the same aromatic group, while in other cases two ligands interact with two aromatic residues of amino acids. It was concluded from the atomic distances that, among the aromatic amino acids, it is tryptophan that forms the strongest MLACπ interaction, and that, among the ligands, water molecules form the strongest interactions.

This conclusion is in agreement with previous results that indicate that tryptophan is able to make relatively strong interactions.[2,3b,6c,6d] It demonstrates that the nature of the MLACπ interaction, of the ligands coordinated to a metal ion interacting with aromatic molecules, is related to other

 © 2003 Wiley-VCH Verlag GmbH & Co. KGaA, Weinheim

Table 5. Metalloproteins with metal ligand aromatic cation−π (MLACπ) interactions

Name/PDB code	Metal	Ligands/bond number	Aromatic residues	Distance d_1[a] [Å]	Angle θ_1 [a] [°]	Ref.
ADH/1adc	Zn^{2+}	Ethanol/2	Phe93	4.21	35.8	[92]
ADH/1ldy	Zn^{2+}	His67/2	Phe93	4.28	35.2	[93]
		CXF378/3		3.46	19.6	
ADH/1axe	Zn^{2+}	His67/2	Trp93	3.77	21.5	[94]
		ETF404/2	Trp93	3.65	40.9	
ADH/1axg	Zn^{2+}	His67/2	Phe93	3.94	16.6	[94]
		ETF404/2		3.94	44.6	
ADH/2ohx	Zn^{2+}	His67/2	Phe93	4.41	33.6	[95]
AO/1asp	Cu^{2+}	His62/3	Phe102	4.11	42.9	[96]
CBP/2cbp	Cu^{2+}	His39/2	Phe13	4.12	33.5	[97]
CheY/1chn	Mg^{2+}	H_2O300/1	Phe14	4.12	27.7	[98]
		H_2O301/1		3.50	24.9	
D9D/1afr	Fe^{2+}	Glu143/3	Trp139	3.93	26.0	[99]
EndN/1ak0	Zn^{2+}	His15/2	Tyr16	3.69	14.1	[100]
FBC/1hfc	Zn^{2+}	His168/2	Phe174	4.00	38.0	[101]
GLI1/2gli	Co^{2+}	His129/2	Trp108	3.09	17.9	[102]
HeC/1lla	Cu^{+}	His364/2	Phe360	3.50	16.9	[103]
MMP-8/1mmb	Zn^{2+}	His147/2	Phe153	3.82	34.9	[104]
NPR/1npc	Ca^{2+}	Thr195/3	Tyr194	3.58	16.0	[105]
SBA/1sbd	Ca^{2+}	Asn130/3	Trp132	3.37	27.7	[106]
SOD/1avm	Fe^{3+}	H_2O1/1	Trp163	3.35	16.3	[107]
		Asp161/3	Trp126	3.75	21.5	
SOD/1mmm	Fe^{2+}	H_2O207/1	Trp169	3.12	14.4	[108]
		Asp167/3	Trp128	3.53	16.0	
SOD/1ap5	$Mn^{2+(3+)}$	H_2O200/1	Trp161	3.52	25.4	[109]
		Asp159/3	Trp123	3.66	15.0	
SOD/1ar4	$Mn^{2+(3+)}$	H_2O1/1	Trp163	3.29	19.7	[110]
		Asp161/3	Trp126	3.75	21.7	
SOD/1mng(L)	Mn^{3+}	H_2O205/1	Trp168	3.57	19.7	[111]
		Asp166/3	Trp132	3.59	14.7	
SOD/1mng(U)	Mn^{3+}	H_2O205/1	Trp168	3.52	26.9	[111]
		Asp166/3	Trp132	3.54	15.4	
TNC/1tn4	Ca^{2+}	H_2O5/1	Tyr109	4.03	42.6	[112]

[a] Definitions of geometric parameters are given in Figure 2.

cation−π interactions that have already been observed and investigated.

The MLACπ interaction generally will be stronger when there are fewer bonds between the atom of the ligand coordinated to the metal ion and the interacting hydrogen atom. The water molecule, when acting as a ligand, has just a single bond between the H atom and the O atom attached to the metal ion and, thus, it is not surprising that the MLACπ interactions are the strongest when a water molecule is a ligand.

In the cases of SOD and AHD enzymes, there are indications that MLACπ interactions might be relevant for enzyme function.[9] The MLACπ interaction in the case of alcohol dehydrogenase is very interesting. In the crystal structure of the AHD−alcohol complex (PDB code 1adc/B),[92] the zinc(II) ion is tetracoordinated. Three of the ligands are amino acids, two cysteine units (Cys46 and Cys174) and one histidine unit (His67). The fourth ligand is the bound ethanol (Figure 6). Close to the metal ion is the aromatic ring of Phe93 that is in contact with the coordinated ethanol. The hydrogen atoms were modeled into this structure. For the CH_2 group of the ethanol unit, the shortest distance between a hydrogen atom and the centroid

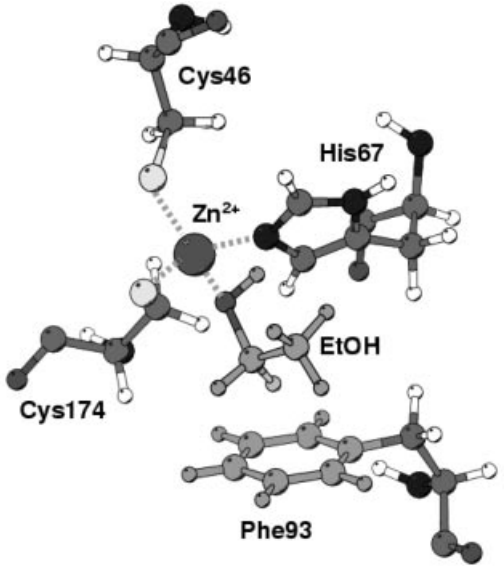

Figure 6. Part of the crystal structure of alcohol dehydrogenase (PDB code 1adc/B); all ligands are displayed that are coordinated to the metal ion and the aromatic residue (Phe93) displaying MLACπ interactions

 © 2003 Wiley-VCH Verlag GmbH & Co. KGaA, Weinheim

of the phenyl ring is 3.19 Å, and its distance to the closest carbon atom of the phenyl ring is 2.64 Å.

In other structures of alcohol dehydrogenases, which we have found by searching for MLACπ interaction, there are interactions of different ligands coordinated to the zinc atom that interacts with Phe93 (Table 5). These ligands are His, trifluoroethanol (ETF), and cyclohexylformamide (CXF), respectively. In the ADH structure 1axe/B,[94] there is a Phe93Trp mutation. Trp93 is involved in cation−π interactions with the coordinated ligands, His67 and ETF. The distance of the cation−π interactions with Trp93 are shorter, and probably are stronger than the interactions with Phe93. It was found experimentally that the mutation from Phe93 to Trp93 increases the tunneling of a hydrogen atom in the hydride transfer reaction from alcohol to NAD.[94] It could be that there is a connection between a stronger cation−π interaction and an increase of hydrogen atom tunneling. We assume that the cation−π interaction of the alcohol with Phe93 may play a role in the reaction mechanism of the enzyme ADH.

Calculations

The energy of the MLACπ interactions in metalloproteins was evaluated by DFT calculations on model systems built from the crystal structure of SOD. The calculated interacting energy of the metal ion complex (an iron ion with its coordinated ligands) with he indole ring of Trp163 was 10.09 kcal/mol.[9]

8. Concluding Remarks

This article has given an overview of MLACπ interactions that have been observed in different molecular systems, mainly in crystal structures, but also in solution and in the gas phase. The overview also includes calculations of MLACπ interactions that are primarily important for estimating interaction energies. MLACπ interactions play a role in the stability of metalloproteins, metal ion complexes, and biomimetic metal ion complexes. For some metalloenzymes these interactions are probably important for the mechanisms of enzymatic reactions.

MLACπ interactions are weaker than interactions of simple metal cations with the same charge, because the transition metal complexes are relatively large, and the charge is more dispersed. The calculated energies of MLACπ interactions vary from 1 to 30 kcal/mol. This range shows that, in some cases, these interactions are among the strongest noncovalent interactions, and can play an important stabilizing role.

The largest calculated energies were for the interactions in the optimized geometries of the $[Co(NH_3)_6]^{3+}$, $[Mg(H_2O)_6]^{2+}$, and $[Zn(H_2O)_6]^{2+}$ cations with benzene (32.2, 21.5, and 21.3 kcal/mol, respectively). A comparison of these three numbers indicates that the charge of the complex is a very important factor. Calculated energies of interactions in crystal structures are smaller, ranging from 1 to 10 kcal/mol. The main reason why these energies are smaller is that the geometries in the crystal structures do not optimize the MLACπ interactions because of constraints caused by other interactions. Also, most of the calculations were performed for metal complexes with a small charge. The weakest interactions, of ca. 1 kcal/mol, are calculated when a C−H group of the ligand interacts with a chelate ring. In these cases the charge of complexes is zero, and that is the reason why the calculated energy of the interaction are very small.

The range of energies of MLACπ interactions is similar to the range of energies of hydrogen bonds, and strong MLACπ interactions are among the strongest X−H···π bonds.

From the studies that are reviewed in this paper, the nature of MLACπ interactions is related to the other cation−π interactions, as is indicated by calculated values of charge transfer. Among the aromatic amino acids, tryptophan forms the strongest MLACπ interactions. To clarify these findings, more studies regarding the nature of MLACπ interactions are needed.

Acknowledgments

The author would like to thank Prof. E. W. Knapp for useful discussions, A. Galstyan for technical help, and the Alexander von Humboldt Foundation for a fellowship.

[1] [1a] G. A. Jeffrey, W. Saenger, *Hydrogen Bonding in Biological Structures*, Springer, Berlin, **1991**. [1b] *Comprehensive Supramolecular Chemistry* (Eds.: J.-M. Lehn, J. L. Atwood, J. E. D. Davies, D. D. MacNicol, F. Vögtle), Pergamon, Oxford, **1996**. [1c] S. Leininger, B. Olenyuk, P. J. Stang, *Chem. Rev.* **2000**, *100*, 853. [1d] M. M. Conn, J. Rebek, Jr, *Chem. Rev.* **1997**, *97*, 1647. [1e] K. Müller-Dethlefts, P. Hobza, *Chem. Rev.* **2000**, *100*, 143. [1f] G. R. Desiraju, *Acc. Chem. Res.* **2002**, *35*, 565.

[2] [2a] D. A. Dougherty, *Science* **1996**, *271*, 163. [2b] J. C. Ma, D. A. Dougherty, *Chem. Rev.* **1997**, *97*, 1303.

[3] [3a] J. P. Gallivan, D. A. Dougherty, *J. Am. Chem. Soc.* **2000**, *122*, 870. [3b] J. P. Gallivan, D. A. Dougherty, *Proc. Natl. Acad. Sci. USA* **1999**, *96*, 9459. [3c] Z. Shi, A. Olson, N. R. Kallenbach, *J. Am. Chem. Soc.* **2002**, *124*, 3284. [3d] E. V. Pletneva, A. T. Laederach, D. B. Fulton, N. M. Kostić, *J. Am. Chem. Soc.* **2001**, *123*, 6232. [3e] T. P. Burghardt, N. Juranic, S. Macura, K. Ajtai, *Biopolymers* **2002**, *63*, 261.

[4] [4a] G. W. Gokel, S. L. De Wall, E. S. Meadows, *Eur. J. Org. Chem.* **2000**, 2967. [4b] M. J. Calhorda, *Chem. Commun.* **2000**, 801. [4c] K. S. Kim, P. Tarakeshwar, J. Y. Lee, *Chem. Rev.* **2000**, *100*, 4145. [4d] O. Yamauchi, A. Odani, S. Hirota, *Bull. Chem. Soc. Jpn.* **2001**, *74*, 1525. [4e] T. Steiner, *Angew. Chem. Int. Ed.* **2002**, *41*, 48.

[5] [5a] D. Braga, F. Grepioni, E. Tedesco, *Organometallics* **1998**, *17*, 2669. [5b] O. Sénèque, M. Giorgi, O. Reinaud, *Chem. Commun.* **2001**, 984.

[6] [6a] J. W. Caldwell, P. A. Kollman, *J. Am. Chem. Soc.* **1995**, *117*, 4177. [6b] R. A. Krumpf, D. A. Dougherty, *Science* **1993**, *261*, 1708. [6c] S. Mecozzi, A. P. West, Jr., D. A. Dougherty, *Proc. Natl. Acad. Sci. USA* **1996**, *93*, 10566. [6d] S. Mecozzi, A. P. West, Jr., D. A. Dougherty, *J. Am. Chem. Soc.* **1996**, *118*, 2307. [6e] P. C. Kearney, L. S. Mizoue, R. A. Kumpf, J. E. Forman, A. McCurdy, D. A. Dougherty, *J. Am. Chem. Soc.* **1993**, *115*, 9907. [6f] R. C. Dunbar, S. J. Klippenstein, J. Hrusak, D. Stocking, H. Schwarz, *J. Am. Chem. Soc.* **1996**, *118*, 5277. [6g] K. S. Kim, J. Y. Lee, S. J. Lee, T.-K. Ha, D. H. Kim, *J. Am. Chem. Soc.* **1994**, *116*, 7399. [6h] J. Y. Lee, S. J. Lee, H. S. Choi, S. J. Cho, K. S. Kim, T.-K. Ha, *Chem. Phys. Lett.* **1995**, *232*, 67. [6i] E. Cubero, F. J. Luque, M. Orozco, *Proc. Natl. Acad. Sci. USA*

 © 2003 Wiley-VCH Verlag GmbH & Co. KGaA, Weinheim

1998, *95*, 5976. [6j] W. Zhong, J. P. Gallivan, Y. Zhang, L. Li, H. A. Lester, D. A. Dougherty, *Proc. Natl. Acad. Sci. USA* **1998**, *95*, 12088.
[7] S. D. Zaric, *Chem. Phys. Lett.* **1999**, *311*, 77.
[8] L. McFail-Isom, X. Shui, L. D. Williams, *Biochemistry* **1998**, *37*, 17105.
[9] S. D. Zaric, D. Popovic, E. W. Knapp, *Chem. Eur. J.* **2000**, *6*, 3935.
[10] M. Milcic, S. D. Zaric, *Eur. J. Inorg. Chem.* **2001**, 2143.
[11] H. Kumita, T. Kato, K. Jitsukawa, H. Einaga, H. Masuda, *Inorg. Chem.* **2001**, *40*, 3936.
[12] O. M. Cabarcos, C. J. Weinheimer, J. M. Lisy, *J. Chem. Phys.* **1998**, *108*, 5151.
[13] O. M. Cabarcos, C. J. Weinheimer, J. M. Lisy, *J. Chem. Phys.* **1999**, *110*, 8429.
[14] A. Zmiric, M. Milcic, S. D. Zaric, *Int. J. Quantum Chem.* **2002**, *87*, 354.
[15] [15a] S. Niu, M. B. Hall, *J. Am. Chem. Soc.* **1997**, *119*, 3077. [15b] J. L. C. Thomas, M. B. Hall, *Organometallics* **1997**, *16*, 2318. [15c] S. Zaric, M. B. Hall, *J. Phys. Chem.* **1998**, *102*, 1963. [15d] J. L. C. Thomas, C. W. Bauschlicher Jr., M. B. Hall, *J. Phys. Chem.* **1997**, *101*, 8530. [15e] D. L. Strout, S. Zaric, S. Niu, M. B. Hall, *J. Am. Chem. Soc.* **1996**, *118*, 6068. [15f] S. Niu, M. B. Hall, *J. Am. Chem. Soc.* **1998**, *120*, 6169. [15g] S. Niu, S. Zaric, D. L. Strout, C. A. Bayse, M. B. Hall, *Organometallics* **1998**, *17*, 5139. [15h] P. E. M. Siegbahn, R. H. Crabtree, *J. Am. Chem. Soc.* **1997**, *119*, 3103. [15i] T. Zigler, *Can. J. Chem.* **1995**, *73*, 743. [15j] C. Rovira, K. Kunc, J. Hutter, P. Ballone, M. Parrinelo, *J. Phys. Chem. A* **1997**, *101*, 8914.
[16] [16a] X. J. Tan, H. L. Jiang, W. L. Zhu, K. X. Chen, R. Y. Ji, *J. Chem. Soc., Perkin Trans.* **1999**, 107. [16b] P. C. Miklis, R. Ditchield, T. A. Spencer, *J. Am. Chem. Soc.* **1998**, *120*, 10482. [16c] J. B. Nickolas, B. P. Hay, D. A. Dixon, *J. Phys. Chem. A* **1999**, *103*, 1394. [16d] W. L. Zhu, H. L. Jiang, C. M. Puah, X. J. Tan, K. X. Chen, Y. Cao, R. Y. Ji, *J. Chem. Soc., Perkin Trans. 2* **1999**, 2615.
[17] S. D. Zaric, *Chem. Phys.* **2000**, *256*, 213.
[18] J. Sponer, J. E. Šponer, J. Leszczynski, *J. Biomol. Struct. Dyn.* **2000**, *17*, 1087.
[19] [19a] M. Aschi, F. Mazza, A. D. Nola, *J. Mol. Struc. Theochem.* **2002**, *587*, 177. [19b] W. L. Zhu, X. J. Tan, C. M. Puah, J. D. Gu, H. L. Jiang, K. X. Chen, C. E. Felder, I. Silman, J. L. Sussman, *J. Phys. Chem. A* **2000**, *104*, 9573.
[20] R. C. Elder, M. J. Heeg, E. Deutsch, *Inorg. Chem.* **1978**, *17*, 427.
[21] M. Atoh, K. Kashiwabara, H. Ito, T. Ito, J. Fujita, *Bull. Chem. Soc. Jpn.* **1984**, *57*, 3139.
[22] R. J. Butcher, H. H. Hayden, M. M. D. Deyrup, C. B. Storm, *Acta Crystallogr., Sect. C* **1992**, *48*, 1122.
[23] V. N. Biyushkin, V. I. Gerasimov, V. A. Neverov, K. F. Belyaeva, V. N. Shafranskii, I. A. Popa, *Koord. Khim.* **1991**, *17*, 1115.
[24] R. C. Elder, M. J. Heeg, M. D. Payne, M. Trkula, E. Deutsch, *Inorg. Chem.* **1978**, *17*, 431.
[25] G. Albertin, S. Antoniutti, A. Bacchi, E. Bordignon, F. Busatto, G. Pelizzi, *Inorg. Chem.* **1997**, *36*, 1296.
[26] T. Hasegawa, T. Iwamoto, *J. Inclusion Phenom. Macrocycl. Chem.* **1988**, *6*, 143.
[27] D. Sellmann, K. Engl, T. Gottschalk-Gaudig, F. W. Heinemann, *Eur. J. Inorg. Chem.* **1999**, 333.
[28] P. B. Hitchcock, D. L. Hughes, M. J. Maguire, K. Marjani, R. L. Richards, *J. Chem. Soc., Dalton Trans.* **1997**, 4747.
[29] D. Touchard, C. Morice, V. Cadierno, P. Haquette, L. Toupet, P. H. Dixneuf, *Chem. Commun.* **1994**, 859.
[30] C. J. Adams, M. I. Bruce, B. W. Skelton, A. H. White, *J. Organomet. Chem.* **1996**, *513*, 255.
[31] N. de Vries, C. E. Costello, A. G. Jones, A. Davison, *Inorg. Chem.* **1990**, *29*, 1348.
[32] B. J. Rappoli, K. J. McGrath, C. F. George, J. C. Cooper, *J. Organomet. Chem.* **1993**, *450*, 85.
[33] S. M. Boniface, G. R. Clark, T. J. Collins, W. R. Roper, *J. Organomet. Chem.* **1981**, *206*, 109.
[34] S. P. Best, P. Chandley, R. J. H. Clark, S. McCarthy, M. B. Hursthouse, P. A. Bates, *J. Chem. Soc., Dalton Trans.* **1989**, 581.
[35] M. Sacerdoti, V. Bertolasi, G. Gilli, A. Duatti, *Acta Crystallogr., Sect. B* **1982**, *38*, 96.
[36] A. J. Deeming, P. J. Manning, I. P. Rothwell, M. B. Hursthouse, N. P. C. Walker, *J. Chem. Soc., Dalton Trans.* **1984**, 2039.
[37] C. Conway, R. D. W. Kemmitt, A. W. G. Platt, D. R. Russell, L. J. S. Sherry, *J. Organomet. Chem.* **1985**, *292*, 419.
[38] A. J. Deeming, S. Doherty, J. E. Marshall, J. L. Powell, A. M. Senior, *J. Chem. Soc., Dalton Trans.* **1993**, 1093.
[39] U. Abram, S. Ritter, *Inorg. Chim. Acta* **1993**, *210*, 99.
[40] J. R. Dilworth, P. Jobanputra, J. R. Miller, S. J. Parrott, Qin Chen, J. Zubieta, *Polyhedron* **1993**, *12*, 513.
[41] H. Muhonen, R. Hamalainen, *Finn. Chem. Lett.* **1983**, 120.
[42] K. Yanagi, M. Minobe, *Acta Crystallogr., Sect. C* **1987**, *43*, 2060.
[43] P. Leverett, J. Petherick, P. A. Williams, R. S. Vagg, *J. Coord. Chem.* **1996**, *37*, 195.
[44] K. Jitsukawa, K. Iwai, H. Masuda, H. Ogoshi, H. Einaga, *J. Chem. Soc., Dalton Trans.* **1997**, 3691.
[45] G. Maccarrone, G. Nardin, L. Randaccio, G. Tabbi, M. Rosi, A. Sgamellotti, E. Rizzarelli, E. Zangrando, *J. Chem. Soc., Dalton Trans.* **1996**, 3449.
[46] Y. Fujii, H. Shinohara, M. Mikuriya, S. Kida, Y. Konishi, *Bull. Chem. Soc., Jpn.* **1988**, *61*, 3511.
[47] A. Fehn, S. Mihan, K. Polborn, W. Beck, *Z. Anorg. Allg. Chem.* **1997**, *623*, 665.
[48] L. Carlucci, G. Ciani, D. W. v. Gudenberg, G. D'Alfonso, *J. Organomet. Chem.* **1997**, *534*, 233.
[49] R. Machida, E. Kimura, Y. Kushi, *Inorg. Chem.* **1986**, *25*, 3461.
[50] L. R. Nassimbeni, M. L. Niven, K. J. Zemke, *J. Chem. Soc., Chem. Commun.* **1985**, 1788.
[51] H. Muhonen, W. E. Hatfield, *Acta Chem. Scand., Ser. A* **1986**, *40*, 41.
[52] I. Dey, B. P. Mukhopadhyay, B. N. Das, S. Chakraborty, A. Banerjee, *J. Crystallogr. Spectrosc. Res.* **1993**, *23*, 65.
[53] D. van der Helm, S. E. Ealick, J. E. Burks, *Acta Crystallogr., Sect. B* **1975**, *31*, 1013.
[54] I. Vernik, D. V. Stynes, *Inorg. Chem.* **1996**, *35*, 6210.
[55] S. Kanemasa, Y. Oderaotoshi, H. Yamamoto, J. Tanaka, E. Wada, D. P. Curran, *J. Org. Chem.* **1997**, *62*, 6454.
[56] T. S. Yaukey, O. W. Steward, Shih-Chi Chang, *Acta Crystallogr., Sect. C* **1998**, *54*, 1081.
[57] J. L. Kerschner, P. E. Fanwick, I. P. Rothwell, *J. Am. Chem. Soc.* **1987**, *109*, 5840.
[58] M. J. Bartos, C. E. Kriley, J. S. Yu, J. L. Kerschner, P. E. Fanwick, I. P. Rothwell, *Polyhedron* **1989**, *8*, 1971.
[59] H. Yuge, Y. Noda, T. Iwamoto, *Inorg. Chem.* **1996**, *35*, 1842.
[60] V. C. Gibson, C. Redshaw, W. Clegg, M. R. J. Elsegood, *J. Chem. Soc., Dalton Trans.* **1997**, 3207.
[61] H. Kumita, K. Jitsukawa, H. Masuda, H. Einaga, *Inorg. Chim. Acta* **1998**, *298*, 160.
[62] D. U. Miodragovic, G. A. G. A. Bogdanovic, S. M. Milosavljevic, M. J. Malinar, M. B. Celap, A. Spasojeciv-de Biré, S. Macura, N. Juranic, *Enantiomer* **2001**, *6*, 299.
[63] [63a] M. Nishio, M. Hirota, Y. Umezawa, *The CH/π Interaction, Evidence, Nature and Consequences*, John Wiley & Sons, Inc., New York, **1998**. [63b] L. Carlucci, G. Ciani, D. Proserpio, *Chem. Commun.* **1999**, 449. [63c] T. Steiner, M. Tamm, *J. Organomet. Chem.* **1998**, *570*, 235. [63d] K. S. B. Hancock, J. W. Steed, *Chem. Commun.* **1998**, 1409. [63e] C. B. C Colbert, J. Lewis, N. J. Long, [P. R. Raithby, A. J. P. White, D. J. Williams, *J. Chem. Soc., Dalton Trans.* **1997**, 99. [63f] A. Cavaglioni, R. Cini, *J. Chem. Soc., Dalton Trans.* **1997**, 1149. [63g] K. Jitsukawa, K. Iwai, H. Masuda, H. Ogoshi, H. Einaga, *J. Chem. Soc., Dalton Trans.* **1997**, 3691.
[64] G. R. Desiraju, T. Steiner, *The Weak Hydrogen Bonds in Structural Chemistry and Biology*, Oxford University Press, Oxford, **1999**.

 © 2003 Wiley-VCH Verlag GmbH & Co. KGaA, Weinheim

[65] G. A. Bogdanovic, A. Spasojevic-de Biré, S. D. Zaric, *Eur. J. Inorg. Chem.* **2002**, 1599.
[66] H. Masui, *Coord. Chem. Rev.* **2001**, *957*, 219.
[67] P. H. Bird, A. R. Fraser, C. F. Lau, *Inorg. Chem.* **1973**, *12*, 1322.
[68] A. Pajunen, S. Pajunen, *Acta Crystallogr., Sect. B* **1982**, *38*, 1586.
[69] J. L. Thorman, I. A. Guzei, V. G. Young, Jr, L. K. Woo, *Inorg. Chem.* **1999**, *38*, 3814.
[70] N. W. Alcock, W.-K. Lin, A. Jircitano, J. D. Mokren, P. W. R. Corfield, G. Johnson, G. Novotnak, C. Cairns, D. H. Busch, *Inorg. Chem.* **1987**, *26*, 440.
[71] N. Svenstrup, A. Bogevig, R. G. Hazell, K. A. Jorgensen, *J. Chem. Soc., Perkin Trans. 1* **1999**, 1559.
[72] N. Ueyama, N. Nishikawa, Y. Yamada, T. Okamura, A. Nakamura, *Inorg. Chim. Acta* **1998**, *283*, 91.
[73] M. P. Byrn, C. J. Curtis, Yu. Hsiou, S. I. Khan, P. A. Sawin, S. K. Tendick, A. Terzis, C. E. Strouse, *J. Am. Chem. Soc.* **1993**, *115*, 9480.
[74] W. S. Rees, Jr, C. R. Caballero, W. Hesse, *Angew. Chem. Int. Ed. Engl.* **1992**, *31*, 735.
[75] P. A. Liddell, K. R. Gerzevske, J. J. Lin, M. M. Olmstead, K. M. Smith, *J. Org. Chem.* **1993**, *58*, 6681.
[76] G. Scherhag, M. D. Spicer, *J. Chem. Soc., Dalton Trans.* **2000**, 1237.
[77] J. T. Pulkkinen, R. Laatikainen, M. J. Ahlgren, M. Perakyla, J. J. Vepsalainen, *J. Chem. Soc., Perkin Trans. 2* **2000**, 777.
[78] K. J. C. van Bommel, W. Verboom, H. Kooijman, A. L. Spek, D. N. Reinhoudt, *Inorg. Chem.* **1998**, *37*, 4197.
[79] E. Vogel, S. Will, A. S. Tilling, L. Neumann, J. Lex, E. Bill, A. X. Trautwein, K. Wieghardt, *Angew. Chem. Int. Ed. Engl.* **1994**, *33*, 731.
[80] X.-Z. Song, L. Jaquinod, W. Jentzen, D. J. Nurco, S.-L. Jia, R. G. Khoury, J.-G. Ma, C. J. Medforth, K. M. Smith, J. A. Shelnutt, *Inorg. Chem.* **1998**, *37*, 2009.
[81] M. Maekawa, M. Munakata, T. Kuroda-Sowa, *Inorg. Chim. Acta* **1994**, *227*, 149.
[82] R. Knoch, H. Elias, H. Paulus, *Inorg. Chem.* **1995**, *34*, 4032.
[83] A. K. -S. Tse, Ru-ji Wang, T. C. W. Mak, Kin Shing Chan, *Chem. Commun.* **1996**, 173.
[84] K. Bernardo, S. Leppard, A. Robert, G. Commenges, F. Dahan, B. Meunier, *Inorg. Chem.* **1996**, *35*, 387.
[85] [85a] M. Egli, G. Minasov, L. Su, A. Rich, *Proc. Natl. Acad. Sci. USA* **2002**, *99*, 4302. [85b] V. K. Misra, D. E. Draper, *Proc. Natl. Acad. Sci. USA* **2002**, *99*, 12456.
[86] X. Shui, L. McFail-Isom, G. G. Hu, L. D. Williams, *Biochemistry* **1998**, *37*, 8341.
[87] K. Grzeskowiak, K. Yanagi, G. G. Prive, R. E. Dickerson, *J. Biol. Chem.* **1991**, *266*, 8861.
[88] J. L. Sussman, S. R. Holbrook, R. W. Warrant, G. M. Church, S.-H Kim, *J. Mol. Biol.* **1978**, *123*, 607.
[89] J. H. Cate, A. R. Gooding, E. Podell, K. Zhou, B. L. Golden, A. A. Szewezak, C. E. Kundrot, T. R. Cech, J. A. Doudna, *Science* **1996**, *273*, 1696.
[90] E. C. Magnuson, J. Koehler, G. Lamm, G. R. Pack, *Inter. J. Quantum Chem.* **2002**, *88*, 236.
[91] A. S. Petrov, G. Lamm, G. R. Pack, *J. Phys. Chem. B* **2002**, *106*, 3294.
[92] H. Li, W. H. Hallows, J. S. Punzi, W. Pankiewicz, K. A. Watanabe, B. M. Goldstein, *Biochemistry* **1994**, *33*, 11734.
[93] H. Cho, S. Ramaswamy, V. Plapp, *Biochemistry* **1997**, *36*, 382.
[94] B. J. Banson, T. D. Colby, J. K. Chin, B. M. Goldstein, J. P. Klinman, *Proc. Natl. Acad. Sci. USA* **1997**, *94*, 12797.
[95] F. Colonna-Cesari, D. Perahia, N. Karplus, H. Eklund, C. I. Branden, O. Tapia, *J. Biol. Chem.* **1986**, *261*, 15273.
[96] A. Messerschmidt, R. Ladenstein, R. Huber, M. Bolognesi, L. Avigliano, R. Petruzzelli, A. Rossi, A. Finazzi-Agro, *J. Mol. Biol.* **1992**, *224*, 179.
[97] J. M. Guss, E. A. Merritt, R. P. Phizackerley, H. C. Freeman, *J. Mol. Biol.* **1996**, *262*, 686.
[98] L. Bellsolell, J. Prieto, L. Serrano, M. Coll, *J. Mol. Biol.* **1994**, *238*, 489.
[99] Y. Lindqvist, W. Huang, G. Schneider, J. Shanklin, *EMBO J.* **1996**, *15*, 4081.
[100] A. Volbeda, A. Lahm, F. Sakiyama, D. Suck, *EMBO J.* **1991**, *10*, 1607.
[101] J. C. Spurlino, A. M. Smallwood, D. D. Carlton, T. M. Banks, K. J. Vavra, J. S. Johnson, R. S. Cook, J. Falvo, R. C. Wahl, T. A. Pulvino, J. J. Wendloski, D. L. Smith, *Proteins: Struct., Funct., Genet.* **1994**, *19*, 98.
[102] N. P. Pavletich, C. O. Pabo, *Science* **1993**, *261*, 1701.
[103] B. Hazes, K. A. Magnus, C. Bonaventura, J. Bonaventura, Z. Dauter, K. H. Kalk, W. G. J. Hol, *Protein Sci.* **1993**, *2*, 597.
[104] F. Grams, M. Crimmin, L. Hinnes, P. Huxley, M. Pieper, H. Tschesche, W. Bode, *Biochemistry* **1995**, *34*, 14012.
[105] W. Stark, R. A. Pauptit, K. S. Wilson, J. N. Jansonius, *Eur. J. Biochem.* **1992**, *207*, 781.
[106] R. L. Olsen, A. Dessen, D. Gupta, S. Sabesan, J. C. Sacchettini, C. F. Brewer, *Biochemistry* **1997**, *36*, 15073.
[107] M. Schmidt, C. Scherk, O. Iakovleva, H. F. Nolting, B. Meier, F. Parak, *Inorg. Chim. Acta* **1998**, *275−276*, 65.
[108] R. A. Edwards, M. M. Whitteker, J. W. Whitteker, G. B. Jameson, E. N. Baker, *J. Am. Chem. Soc.* **1998**, *120*, 9684.
[109] Y. Guan, M. J. Hickey, G. E. O. Borgstahl, R. A. Hallewell, J. R. Lepock, D. O'Connor, Y. Hsien, H. S. Nick, D. N. Silverman, J. A. Tainer, *Biochemistry* **1998**, *37*, 4722.
[110] M. Schmidt, B. Meier, F. Parak, *J. Biol. Inorg. Chem.* **1996**, *1*, 532.
[111] M. S. Lah, M. M. Dixon, K. A. Pattridge, W. C. Stallings, J. A. Fee, M. L. Ludwig, *Biochemistry* **1995**, *34*, 1646.
[112] A. Houdusse, M. L. Love, M. N. Dominguez, Z. Grabarek, C. Cohen, *Structure* **1997**, *5*, 1695.

Received May 29, 2002

 © 2003 Wiley-VCH Verlag GmbH & Co. KGaA, Weinheim

Syntheses of Dimetallamacrocycles by Intramolecular Oxidative Couplings of Dinuclear Bis(1,3-butadiynyl) Complexes: A New Approach to Steric Shielding in (sp-Carbon chain)dirhenium Complexes $[(\eta^5\text{-}C_5Me_5)Re(NO)(PR_3)(C{\equiv}CC{\equiv}CC{\equiv}CC{\equiv}C)(R_3P)(ON)Re(\eta^5\text{-}C_5Me_5)]$

Clemens R. Horn[a] and John A. Gladysz*[a]

Keywords: Rhenium / Alkynes / Oxidative coupling / Macrocycles / Cyclic voltammetry

Reactions of the chiral racemic carbonyl complex $[(\eta^5\text{-}C_5Me_5)Re(NO)(NCCH_3)(CO)]^+\cdot BF_4^-$ and diphosphanes $Ph_2P(CH_2)_nPPh_2$ [2.4:1.0 mol ratio; n = 10 (**a**), 14 (**b**)] give the (bridging phosphane)dirhenium complexes $[(\eta^5\text{-}C_5Me_5)Re(NO)(CO)\{\mu\text{-}[PPh_2(CH_2)_nPh_2P]\text{-}P,P\}(OC)(ON)Re(\eta^5\text{-}C_5Me_5)]^{2+}\cdot 2BF_4^-$ (73–80%), which are reduced ($LiAlH_4$) to the dimethyl complexes $[(\eta^5\text{-}C_5Me_5)Re(NO)(CH_3)\{\mu\text{-}[PPh_2(CH_2)_nPh_2P]\text{-}P,P\}(ON)(H_3C)Re(\eta^5\text{-}C_5Me_5)]$ (92–96%). Reactions with $HBF_4\cdot OEt_2/C_6H_5Cl$, $HC{\equiv}CC{\equiv}CSiMe_3$, and *t*BuOK give, via π-HC≡C adducts (89–94%), the bis(trimethylsilylbutadiynyl) complexes $[(\eta^5\text{-}C_5Me_5)Re(NO)(C{\equiv}CC{\equiv}CSiMe_3)\{\mu\text{-}[PPh_2(CH_2)_nPh_2P]\text{-}P,P\}(Me_3SiC{\equiv}CC{\equiv}C)(ON)Re(\eta^5\text{-}C_5Me_5)]$ (**9a**,**b**; 95–66%). Desilylation (wet nBu$_4$NF) yields labile bis(butadiynyl) complexes, which are coupled [$Cu(OAc)_2$/pyridine] to the μ-octatetraynediyl complexes $[(\eta^5\text{-}C_5Me_5)Re(NO)\{\mu\text{-}[PPh_2(CH_2)_nPh_2P]\text{-}P,P\}\{\mu\text{-}(C^1{\equiv}CC{\equiv}CC{\equiv}CC{\equiv}C^8)\text{-}C^1,C^8\}(ON)Re(\eta^5\text{-}C_5Me_5)]$ (**3a**,**b**; 10–23% from **9a**,**b**). These represent some of the few cases of intramolecular oxidative homocouplings of terminal alkynes in metal coordination spheres. The electrochemical properties of **3a**,**b**, which undergo two one-electron oxidations, are compared to nonmacrocyclic analogs that lack the diphosphane bridge.

(© Wiley-VCH Verlag GmbH & Co. KGaA, 69451 Weinheim, Germany, 2003)

Introduction

Macrocyclization methodologies have played an important role in the development of synthetic organic chemistry.[1] A variety of general strategies are now established, with applications ranging from complex natural products to theoretically interesting unnatural substances such as annulenes. Many relevant physical organic studies have been conducted to define optimum substrate characteristics and conditions.[2] In contrast, macrocyclizations have attracted less focused or systematic attention to date in synthetic inorganic or organometallic chemistry.

Nonetheless, there has been a diverse range of activity. We have used olefin and alkyne metathesis reactions to effect macrocyclizations of a variety of transition-metal complexes, giving products in which metal atoms are part of the new ring (metall***a***macrocycle) or attached to the new ring (metall***o***macrocycle).[3−6] Sauvage has, in the pursuit of catenanes, molecular knots, and related novel species, investigated a number of macrocyclizations of coordination compounds.[7−9] Any complex in which *trans* positions are spanned by a chelate ligand is by definition macrocyclic, and Bessel and Takeuchi have recently reviewed this scattered literature.[10] There are also growing numbers of metallacrown species,[11] nearly all of which are macrocyclic. However, there are very few comparative evaluations of synthetic strategies.

The intramolecular oxidative coupling of organic compounds that contain two terminal alkynes has played a critical role in the development of macrocycle chemistry, particularly with annulenes and dehydroannulenes.[12,13] Many intermolecular oxidative couplings of transition-metal-containing terminal alkynes are also known. However, to the best of our knowledge there are few if any cases where an isolated inorganic or organometallic compound containing two terminal alkynes has undergone an intramolecular oxidative macrocyclization.[14] Oxidative cyclodimerizations and cyclooligomerizations can be effected with some such species, and representative examples are depicted in Scheme 1.[8,15] These entail the macrocyclization of an intermediate with two terminal alkynes.

We wondered whether such intramolecular oxidative couplings might prove applicable to a synthetic problem in our group. As detailed in the previous paper in this series,[5] we have sought (μ-octatetraynediyl)dirhenium or ReC≡CC≡CC≡CC≡CRe systems with sterically shielded sp-carbon chains. One motivation is the possibility of enhanced stabilities for the corresponding radical cations $[ReC{\equiv}CC{\equiv}CC{\equiv}CC{\equiv}CRe]^{+\cdot}\cdot X^-$ and dications [Re=C=

[a] Institut für Organische Chemie, Friedrich-Alexander-Universität Erlangen-Nürnberg,
Henkestraße 42, 91054 Erlangen, Germany
Fax: (internat.) + 49-9131/8526865
E-mail: gladysz@organik.uni-erlangen.de

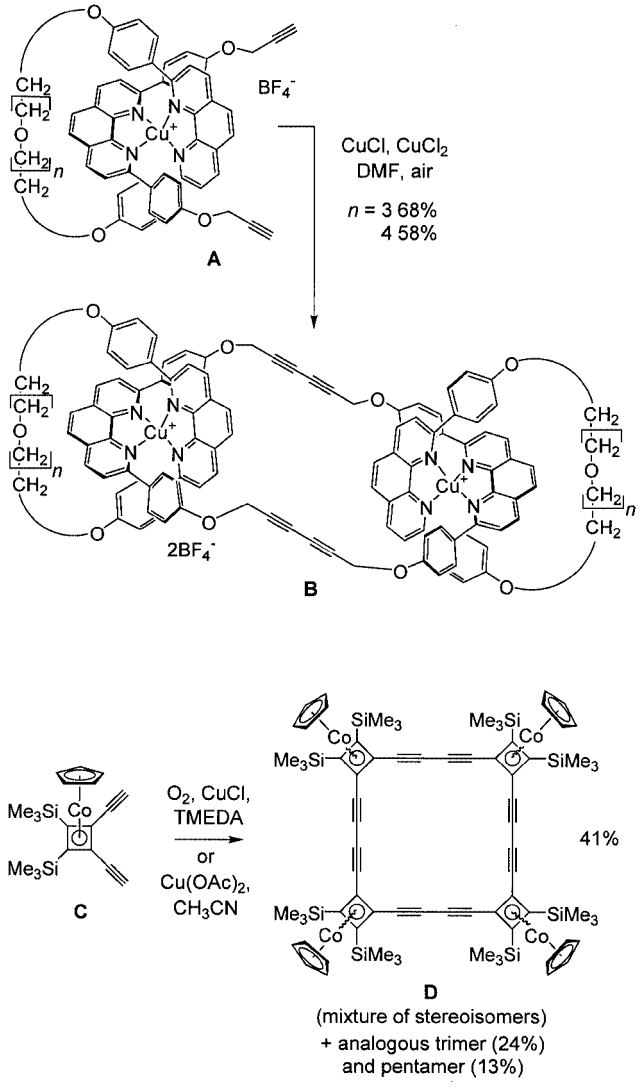

Scheme 1. Representative macrocycle syntheses involving oxidative dimerization or oligomerization of inorganic and organometallic compounds that contain two terminal alkynes[15]

C=C=C=C=C=C=C=Re]$^{2+}$·2X^{-}. Much evidence suggests that decomposition involves bimolecular chain/chain or chain/solvent reactions. As shown in Scheme 2, the complex **1**, which features an alkene-containing phosphane on each rhenium atom, undergoes olefin metathesis to give the macrocycle **2** in good yield. However, subsequent hydrogenations of the residual C=C bond, while sometimes giving the target molecule **3b**, were difficult to reproduce or scale up.[5]

We therefore considered alternative routes to **3b** by retrosynthetic analysis. One obvious possibility would be to generate the macrocycle by the intramolecular oxidative coupling of two butadiynylrhenium or ReC≡CC≡CH moieties.[13,16] This would in turn require linking two chiral rhenium fragments by an α,ω-diphosphane $Ph_2P(CH_2)_nPPh_2$. No hydrogenation step would be required, and intermolecular oxidative homocouplings of ReC≡CC≡CH complexes commonly proceed in high yield.[5,17] Accordingly, we set out to investigate this alternative route to **3b** and related

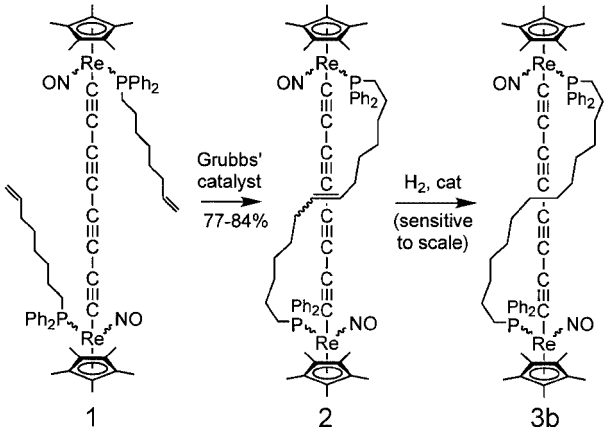

Scheme 2. Syntheses of macrocyclic dirhenium complexes by ring closing olefin metathesis

compounds, and describe its successful implementation below.

Results

The readily available chiral racemic cationic (acetonitrile)(carbonyl) complex [(η^5-C_5Me_5)Re(NO)(CO)(NCCH$_3$)]$^+$·BF$_4^-$ (**4**$^+$BF$_4^-$) reacts with a variety of phosphanes in refluxing 2-butanone to give the corresponding (carbonyl)(phosphane) complexes.[18] As shown in Scheme 3, similar reactions were conducted with the diphosphanes $Ph_2P(CH_2)_nPPh_2$ [**5**; *n* = 10 (**a**),[4,19] 14 (**b**)[4,19b]], but at 2.4:1.0 stoichiometries. Workups gave the target dicationic (bridging phosphane)dirhenium complexes [(η^5-C_5Me_5)Re(NO)(CO){μ-[PPh$_2$(CH$_2$)$_n$Ph$_2$P]-*P*,*P*}(OC)(ON)Re(η^5-C_5Me_5)]$^{2+}$·2BF$_4^-$ (**6a**,**b**$^{2+}$2BF$_4^-$) as yellow-

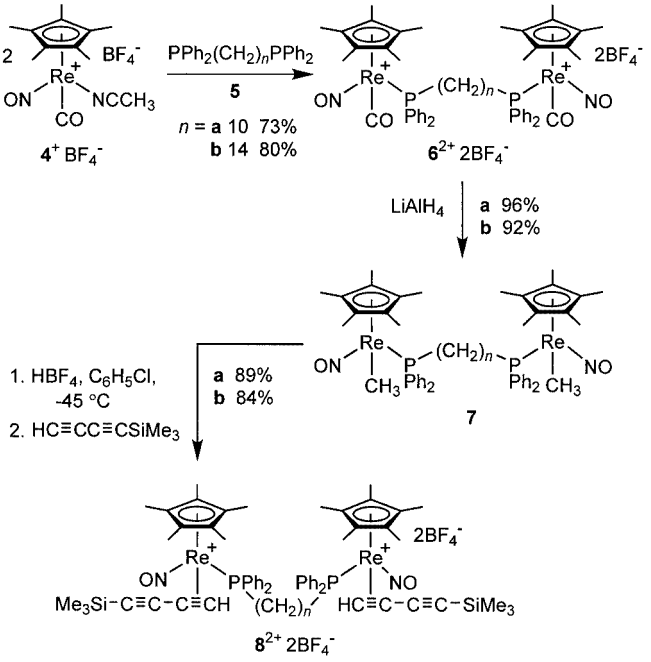

Scheme 3. Syntheses of nonmacrocyclic dirhenium complexes

 © 2003 Wiley-VCH Verlag GmbH & Co. KGaA, Weinheim

orange solids in 73−80% yields based on the limiting reactants **5a**,**b**. A third series of compounds derived from a diphosphane with a much longer methylene chain (**5c**; n = 32) were not as tractable and are detailed elsewhere.[20]

Complexes **6a**,**b**$^{2+}2BF_4^-$ and all new species below were characterized by IR, NMR (^1H, ^{13}C, ^{31}P), mass spectrometry, and microanalysis, as summarized in the Exp. Sect. Most features were very similar to those of triarylphosphane homologs reported previously.[17] However, the PPh_2 phenyl groups are diastereotopic, and the aryl ^{13}C NMR signals are therefore more complex. Although **6a**,**b**$^{2+}2BF_4^-$ must be mixtures of *rac* and *meso* diastereomers, only one set of ^{31}P and pentamethylcyclopentadienyl ^1H and ^{13}C NMR signals was observed. All of the nonmacrocyclic compounds below behaved similarly. The mass spectra of **6a**,**b**$^{2+}2BF_4^-$, and all other dications below, showed doubly charged ions corresponding to the (bridging phosphane)-dirhenium assemblies.

Complexes **6a**,**b**$^{2+}2BF_4^-$ were elaborated to butadiynyl complexes as described for many related species. As shown in Scheme 3, reductions with $LiAlH_4$ gave the dimethyldirhenium complexes [(η^5-C_5Me_5)Re(NO)(CH_3){μ-[$PPh_2(CH_2)_nPh_2P$]-*P*,*P*}(H_3C)(ON)Re(η^5-C_5Me_5)] (**7a**,**b**) as red powders in 92−96% yields. Reactions with HBF_4 in C_6H_5Cl generated substitution-labile chlorobenzene complexes,[21] which were treated with the diyne HC≡CC≡CSiMe$_3$.[22,23] Workups gave the π-bis(diyne) complexes [(η^5-C_5Me_5)Re(NO)(HC≡CC≡CCSiMe$_3$){μ-[$PPh_2(CH_2)_nPh_2P$]-*P*,*P*}(Me_3SiC≡CC≡CH)(ON)Re(η^5-C_5Me_5)]$^{2+}$·$2BF_4^-$ (**8a**,**b**$^{2+}2BF_4^-$), with each rhenium atom bound to an HC≡C moiety, as black powders in 89−84% yields. Such compounds can exist as mixtures of Re−(C≡C) rotamers, and NMR spectroscopic data indicated 67−76:33−24 ratios [(PPh_3)monorhenium analog: 67−79:33−21].[22,24]

As shown in Scheme 4, complexes **8a**,**b**$^{2+}2BF_4^-$ were deprotonated with *t*BuOK to give the σ-bis(trimethylsilylbutadiynyl) complexes [(η^5-C_5Me_5)Re(NO)(C≡CC≡CSiMe$_3$){μ-[$PPh_2(CH_2)_nPh_2P$]-*P*,*P*}(Me_3SiC≡CC≡C)(ON)Re(η^5-C_5Me_5)] (**9a**,**b**) as red powders in 95−66% yields. In previous studies, such compounds have been desilylated to the parent butadiynyl complexes using wet nBu_4NF.[5,17] However, the resulting ReC≡CC≡CH species are always much more labile. Indeed, all efforts to purify the bis(butadiynyl) complexes [(η^5-C_5Me_5)Re(NO)(C≡CC≡CH){μ-[$PPh_2(CH_2)_nPh_2P$]-*P*,*P*}(HC≡CC≡C)(ON)Re(η^5-C_5Me_5)] (**10a**,**b**) gave only impure, partially decomposed samples. Nonetheless, many NMR and IR signals could be assigned (Exp. Sect.).

In order to minimize this problem, combined deprotection/oxidation sequences were investigated. Eglinton conditions − stoichiometric $Cu(OAc)_2$ in pyridine − have proven to be most reliable for oxidative homocouplings of butadiynylmonorhenium complexes.[5,17] Thus, solutions of **9a**,**b** were first treated with wet nBu_4NF, and then filtered through alumina. Solvent removal gave crude **10a**,**b** (53−55%), which were taken up in pyridine and treated with $Cu(OAc)_2$. Substrate concentrations were ca. 0.0088 M.

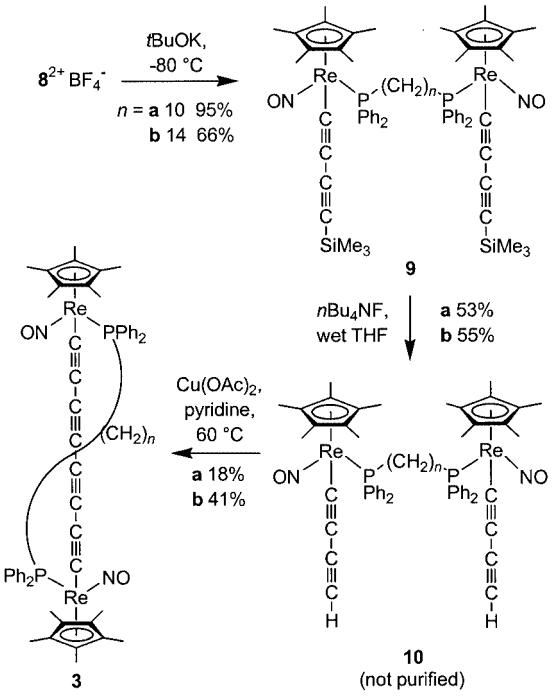

Scheme 4. Syntheses of macrocyclic dirhenium complexes by intramolecular oxidative coupling

Workups gave the target, macrocyclic (μ-octatetraynediyl)-dirhenium complexes [(η^5-C_5Me_5)Re(NO){μ-[PPh_2-$(CH_2)_nPh_2P$]-*P*,*P*}{μ-(C^1≡CC≡CC≡CC≡C^8)-C^1,C^8)}-(ON)Re(η^5-C_5Me_5)] (**3a**,**b**) in 18−41% yields from crude **10a**,**b** or 10−23% yields from **9a**,**b**.

Complexes **3a**,**b** were homogeneous by HPLC and TLC, and the latter gave a good microanalysis. Mass spectra showed intense molecular ion peaks (100%). In the case of **3a**, a small peak corresponding to a dimeric tetrarhenium by-product was also detected (8%). Dimeric and oligomeric by-products often form in couplings of organic compounds containing two terminal alkynes, and several cyclooligomers are obtained from **C** in Scheme 1. Thus, we believe that additional polyrhenium species likely form, but are perhaps not solubilized by the extractive workup employed. IR spectra of **3a**,**b** showed $\nu_{C\equiv C}$ and ν_{NO} bands (2104−2108 m, 1953 m, 1640−1637 s cm^{-1}) very close to those of the nonmacrocyclic triarylphosphane analogs **11** and **12**.[17]

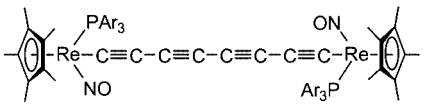

Ar = Ph: **11**
p-tol: **12**

The ^1H NMR spectrum of **3a** exhibited a doubled pentamethylcyclopentadienyl signal, and the ^{31}P NMR spectrum a doubled PAr_2 signal. Area ratios were ca. 50:50, and the latter is illustrated in Figure 1. Complex **3b** also showed two doubled signals, but the chemical shift differences were much smaller. For both compounds, these were assigned to

 © 2003 Wiley-VCH Verlag GmbH & Co. KGaA, Weinheim

the *rac* and *meso* diastereomers. Since none of the other dirhenium complexes show separate signals for the two diastereomers, steric communication between the chiral endgroups appears to be enhanced in the macrocycles **3a**,**b**. As would be intuitively expected, the shorter methylene tether in **3a** leads to more differentiated signals. The ^{13}C NMR chemical shifts of the sp-carbon atoms were within 1−2 ppm of those of **11** and **12**.[17] The ^{1}H and ^{31}P chemical shifts of **3a**,**b** were quite similar to those of the precursors **9a**,**b** and **10a**,**b**. The most pronounced differences were in the PCH_2 signals of **3a** ($\Delta\delta$ = 0.20−0.10).

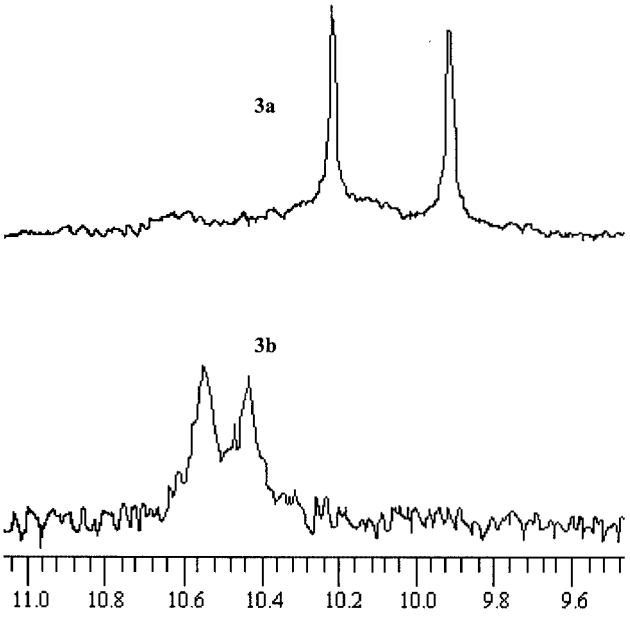

Figure 1. ^{31}P NMR spectra of macrocyclic dirhenium complexes

Finally, cyclic voltammograms of **3a**,**b** were recorded in CH_2Cl_2 under the standard conditions employed in earlier studies.[17] Two sequential oxidations were observed, and data are summarized in Table 1. Since comparisons to non-macrocyclic complexes were sought, **1** and **2** (Scheme 2) were also examined. Some previously reported data are included for reference, and analyzed in the discussion section. Preparative reactions of **3a**,**b** with the one-electron oxidant $(\eta^5\text{-}C_5H_5)_2Fe^{+\cdot}\cdot SbF_6^-$ in CH_2Cl_2 did not afford any tractable products.

Table 1. Summary of cyclic voltammetry data

Complex[a]	$E_{p,a}(1)$ $E_{p,a}(2)$ [V]	$E_{p,c}(1)$ $E_{p,c}(2)$ [V]	$E°(1)$ $E°(2)$ [V]	$\Delta E(1)$ $\Delta E(2)$ [mV]	$i_c/i_a(1)$ $i_c/i_a(2)$	K_c[b]
3a	0.23	0.16	0.20	70	0.2	$1.2\cdot10^4$
	0.50	0.38	0.44	120	0.5	
3b	0.24	0.16	0.20	80	0.8	$8.8\cdot10^4$
	0.53	0.45	0.49	80	1	
11	0.27	0.20	0.24	70	< 1	$5.9\cdot10^4$
	0.56	0.49	0.52	70	< 1	
12	0.20	0.12	0.16	80	1	$8.8\cdot10^4$
	0.49	0.41	0.45	80	1	
1	0.24	0.16	0.20	80	0.4	$5.9\cdot10^4$
	0.51	0.44	0.48	70	0.7	
2	0.24	0.16	0.20	80	0.7	$8.8\cdot10^4$
	0.52	0.45	0.49	70	0.9	

[a] CH_2Cl_2, 100 mV/s, $E°$ vs. SCE [E(ferrocene) = 0.46 V]. [b] Comproportionation constant; $\ln(K_c) = nF[E°(2) - E°(1)]/RT = 39.25[E°(2) - E°(1)]$ at 22.5 °C.

Discussion

The reactions in Scheme 4 establish that organometallic compounds containing two terminal alkynes or diynes can undergo intramolecular oxidative macrocyclization. The overall yields of **3a**,**b** from the protected diyne **9a**,**b** are only 10−23%, but rise to 18−44% when based upon the crude bis(butadiyne) complexes **10a**,**b**. The substrate concentrations are somewhat greater than those employed for the olefin metathesis of **1** in Scheme 2 (0.0088 vs. 0.0012−0.0007 M). Thus, there is some possibility that the yields in Scheme 4 could be improved at higher dilution. Nonetheless, we would still expect them to remain lower than that of the metathesis product **2** (77−84%). This is consistent with Sauvage's experience with systems such as **A** (Scheme 1). Although the oxidative coupling is successful,[7,8] olefin metatheses of related species proved superior.[9a,9b]

However, with respect to the target molecule **3b**, an additional hydrogenation step is needed after olefin metathesis (Scheme 2). This has proved very problematic, and without the new methodology in Scheme 4, it would not be possible to reliably access this molecule. Although this constitutes a strategic weakness of olefin metathesis, many alkene-containing metalla- and metallomacrocycles are readily hydrogenated.[3,4,9] Perhaps the triple bonds in **3b** are the origin of the problem. Nonetheless, it has proved possible to hydrogenate alkene moieties in macrocycles containing PtC≡CC≡CC≡CC≡CPt linkages.[4]

In **3a**, the linear ten-atom ReC≡CC≡CC≡CC≡CRe linkage must be spanned by a 12-atom P$(CH_2)_{10}$P linkage. Thus, **3a** should be considerably more strained than **3b**. Accordingly, the yield is lower, and a dimeric product can be detected by mass spectrometry. Nonetheless, the same phosphane is also capable of bridging a PtC≡CC≡CC≡CC≡CPt linkage.[4] In both cases, the methylene or sp^3-carbon chain must remain very close to the sp-carbon chain. However, there appears to be little effect on NMR or IR properties. In **3b**, there is the possibility of helical coiling of the sp^3-chain about the sp-chain, as recently demonstrated with similar diplatinum complexes.[4] Unfortunately, consistent with past experience with this series of compounds, all efforts to obtain single crystals have been unsuccessful. The presence of both diastereomers is believed to be a contributing factor.

These structural issues lead naturally to the effect of molecular architecture upon redox properties. The cyclic voltammogram of **3b** (Table 1) is qualitatively similar to those other ReC≡CC≡CC≡CC≡CRe species reported earlier. A cation radical and dication are readily generated. The oxi-

 © 2003 Wiley-VCH Verlag GmbH & Co. KGaA, Weinheim

dation potentials are intermediate between those of the PPh_3- and P(*p*-tol)$_3$-substituted analogs **11** and **12**, befitting a alkyldiphenylphosphane adduct [$E°(1)$ = 0.20 vs. 0.24 vs. 0.16 V; $E°(2)$ = 0.47 vs. 0.52 vs. 0.45 V]. The ΔE and i_c/i_a values indicate a high degree of reversibility. However, **12** gives a i_c/i_a ratio of 1 for both oxidations, whereas one value for **3b** is slightly less. Thus, there is no electrochemical indication of enhanced cation radical and dication stabilities, in agreement with our chemical data.

Complex **3a** exhibits similar oxidation potentials. However, the ΔE and i_c/i_a values indicate processes that are not electrochemically reversible, and only partially chemically reversible. This suggests that the more strained nature of this macrocycle somehow promotes decomposition of the cation radical and dication. The phosphane ligand in nonmacrocyclic **1** (Scheme 2) should electronically resemble a alkyldiphenylphosphane, and similar oxidation potentials are again observed. However, the alkene linkages can potentially react with the cation radical and/or dication. Accordingly, the reversibilities are between those of **3a** and **3b**. The metathesis product **2**, which is a mixture of C=C isomers, appears to give slightly more reversible oxidations.

There is only one example to date of an MC≡CC≡CC≡CC≡CM system that can be oxidized to spectroscopically detectable species, Lapinte's very electron-rich diiron complex [(η^5-C_5Me_5)Fe(dppe)(C≡C)$_4$-(dppe)Fe(η^5-C_5Me_5)].[25] Remarkably, the corresponding radical cation can be isolated in analytically pure form.[26] However, when the sp-carbon chains of dirhenium complexes **11** or **12** are shielded by an additional sp^3- or sp^3/sp^2-carbon chain, as in **2** and **3b**, no evidence for enhanced kinetic stabilities of oxidation products is found. In contrast, PtC≡CC≡CC≡CC≡CPt assemblies that are doubly bridged by the diphosphane **5b** exhibit significantly more reversible oxidations.[4] We therefore conclude that the sp-carbon chain of our first-generation system **3b** is sterically not shielded enough. Approaches to sterically more congested analogs are under investigation.[27]

Finally, **3a**,**b** are not the only metallamacrocycles that contain an M(C≡CC≡C)$_n$M linkage. Extremely interesting tetraplatinamacrocycles of the formula **13** have been previously reported by Tessier, Youngs, and Bruce.[28] All sixteen carbon atoms in these twenty-membered rings are sp-hybridized. However, the syntheses do not involve the oxidative homocoupling of alkynes. Rather, bis(butadiynyl)platinum complexes of the formula [*cis*-(L)$_2$Pt(C≡CC≡CH)$_2$] are condensed with platinum chloride or triflate complexes *cis*-(L)$_2$Pt(X)$_2$. Yields of **13** are routinely high (70−98%).

In conclusion, we have compared the applicability of two macrocyclization strategies for the synthesis of novel types of (μ-octatetraynediyl)dirhenium complexes. The new intramolecular oxidative coupling of bis(butadiynyl) complexes is successful, and increased application of such reactions in the synthesis of inorganic and organometallic macrocycles can be anticipated. However, olefin metathesis appears to constitute a generally superior macrocyclization method, and is problematic only in the few instances where subsequent alkene hydrogenation is unsuccessful. Future reports will describe the utility of alkyne metathesis for accessing similar types of targets.[6]

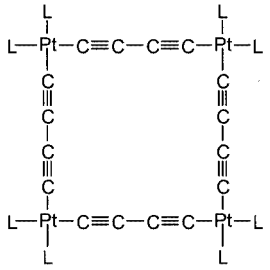

13
L = 1/2 diphosphane
or monophosphane

Experimental Section

General: General procedures, solvent and reagent purifications, and instrumentation were identical with those listed in recent full papers,[3c,17,18b] and are further detailed elsewhere.[20]

[(η^5-C_5Me_5)Re(NO)(CO){μ-[$PPh_2(CH_2)_nPh_2P$]-*P*,*P*}(OC)-(ON)Re(η^5-C_5Me_5)]$^{2+}$·2BF_4^- (6^{2+}2BF_4^-). a (*n* = 10): A Schlenk flask was charged with [(η^5-C_5Me_5)Re(NO)(CO)(NCCH$_3$)]$^+$·BF_4^- ($\mathbf{4}^+BF_4^-$;[18a] 2.430 g, 4.793 mmol), 1,2-dichloroethane (10 mL), and $Ph_2P(CH_2)_{10}PPh_2$ (**5a**;[4,19] 1.020 g, 2.000 mmol), and fitted with a reflux condenser. The solution was refluxed for 14 h. The solvent was removed by oil-pump vacuum. The residue was dissolved in a small amount of acetone and poured into rapidly stirred Et_2O. The precipitate was isolated by filtration and dried by oil-pump vacuum to give $\mathbf{6a}^{2+}2BF_4^-$ as a yellow orange solid (2.013 g, 1.457 mmol, 73%). M.p. 88 °C. ^{1}H NMR (400 MHz, $CDCl_3$, 32 °C, TMS): δ = 7.58−7.40 (m, 20 H, 4C$_6H_5$), 2.63 (m, 4 H, 2 PCH_2), 1.95 (s, 30 H, 2 C$_5$(CH_3)$_5$], 1.33−1.10 (m, 16 H, 8 CH_2) ppm. ^{13}C{^{1}H} NMR (100 MHz, $CDCl_3$, 32 °C, TMS): δ = 201.8 (d, $^2J_{C,P}$ = 9 Hz, *C*O), 132.4−129.5 (Ph signals), 105.9 [$C_5(CH_3)_5$], 32.1 (d, $^1J_{C,P}$ = 32 Hz, P*C*H$_2$),[29] 30.1 (d, $J_{C,P}$ = 12 Hz, *C*H$_2$), 29.9 (s, *C*H$_2$), 28.7 (s, *C*H$_2$), 23.9 (s, *C*H$_2$), 9.8 [s, C$_5$(*C*H$_3$)$_5$] ppm. ^{31}P{^{1}H} NMR (161 MHz, $CDCl_3$, 32 °C, H_3PO_4): δ = 9.1 (s) ppm. IR (solid film): $\tilde{\nu}$ = 1984 (s, CO), 1722 (s, NO) cm^{-1}. MS (FAB, 3-NBA/CH_2Cl_2):[30] *m*/*z* (%) = 1355 (72) [M + BF_4^-]$^+$, 890 (100) [M − {(η^5-C_5Me_5)Re(NO)(CO)}]$^+$, 634 (50) [M]$^{++}$. $C_{56}H_{70}B_2F_8N_2O_4P_2Re_2$ (1443.15): calcd. C 46.61, H 4.89, N 1.94; found C 46.74, H 4.99, N 1.90.

b (*n* = 14): Complex $\mathbf{4}^+$ BF_4^- (0.803 g, 1.584 mmol), 1,2-dichloroethane (10 mL), and $Ph_2P(CH_2)_{14}PPh_2$ (**5b**;[4,19b] 0.376 g, 0.664 mmol) were combined in a procedure analogous to that for $\mathbf{6b}^{2+}$ 2BF_4^-. An identical reaction and workup gave $\mathbf{6b}^{2+}$ 2BF_4^- as a yellow solid (0.792 g, 0.528 mmol, 80%). M.p. 84 °C. ^{1}H NMR (400 MHz, $CDCl_3$, 32 °C, TMS): δ = 7.60−7.26 (m, 20 H, 4 C$_6H_5$), 2.63 (m, 4 H, 2 PCH_2), 1.96 [s, 30 H, 2 C$_5$(CH_3)$_5$], 1.36−1.16 (m, 24 H, 12 CH_2) ppm. ^{13}C{^{1}H} NMR (100 MHz, $CDCl_3$, 32 °C, TMS): δ = 202.0 (d, $^2J_{C,P}$ = 8 Hz, *C*O), 132.4−129.6 (Ph signals), 106.0 [s, $C_5(CH_3)_5$], 32.2 (d, $^1J_{C,P}$ = 32 Hz, P*C*H$_2$),[29] 30.6 (d, $J_{C,P}$ = 15 Hz, *C*H$_2$), 30.2 (s, *C*H$_2$), 29.7 (s, *C*H$_2$), 29.6 (s, *C*H$_2$), 28.4 (s, *C*H$_2$), 24.0 (s, *C*H$_2$), 9.8 [s, C$_5$(*C*H$_3$)$_5$] ppm. ^{31}P{^{1}H} NMR (161 MHz, $CDCl_3$, 32 °C, H_3PO_4): δ = 9.3 (s) ppm. IR (solid film): $\tilde{\nu}$ = 1984 (s, CO), 1722 (s, NO) cm^{-1}. MS (FAB, 3-NBA/CH_2Cl_2):[30] *m*/*z* (%) = 1411 (10) [M + BF_4^-]$^+$, 962 (50) [(η^5-C_5Me_5)Re(NO)(CO)($PPh_2(CH_2)_{14}POPh_2$)]$^+$, 662 (40) [M]$^{++}$, 421

 © 2003 Wiley-VCH Verlag GmbH & Co. KGaA, Weinheim

(100) $[(\eta^5\text{-}C_5Me_5)Re(NO)(CO)]^+$. $C_{60}H_{78}B_2F_8N_2O_4P_2Re_2$ (1499.25): calcd. C 48.07, H 5.24, N 1.87; found C 48.67, H 5.36, N 1.75.

$[(\eta^5\text{-}C_5Me_5)Re(NO)(CH_3)\{\mu\text{-}[PPh_2(CH_2)_nPh_2P]\text{-}P,P\}(H_3C)(ON)Re(\eta^5\text{-}C_5Me_5)]$ (7). a (n = 10): A Schlenk flask was charged with $LiAlH_4$ (0.087 g, 2.272 mmol), **6a**$^{2+}$ $2BF_4^-$ (0.549 g, 0.380 mmol), and THF (20 mL). The suspension was stirred for 14 h. Small amounts of water were added until gas evolution ceased. The mixture was filtered through a 2-cm alumina pad. The solvent was removed from the filtrate by rotary evaporation and oil-pump vacuum to give **7a** as a red solid (0.453 g, 0.365 mmol, 96%). M.p. 54 °C. ^{1}H NMR (400 MHz, C_6D_6, 25 °C): δ = 7.88−7.05 (m, 20 H, 4 C_6H_5), 2.83, 2.45 (2 m, 4 H, 2 PCH_2), 1.63 [s, 30 H, 2 $C_5(CH_3)_5$], 1.43−1.15 (m, 16 H, 8 CH_2), 0.80 (apparent m, 6 H, 2 $ReCH_3$) ppm. ^{13}C{^{1}H} NMR (100 MHz, C_6D_6, 25 °C): δ = 136.6/136.3 (2 d, $^1J_{C,P}$ = 48/47 Hz, *i*-Ph), 134.1/132.8 (2 d, $^2J_{C,P}$ = 9/9 Hz, *o*-Ph), 131.2/131.0 (2 s, *p*-Ph), 129.8/128.6 (2 d, $^3J_{C,P}$ = 11/11 Hz, *m*-Ph), 97.4 [s, $C_5(CH_3)_5$], 33.5 (d, $^1J_{C,P}$ = 33 Hz, PCH_2),[29] 31.4 (d, $J_{C,P}$ = 15 Hz, CH_2), 29.4 (s, CH_2), 25.8 (s, CH_2), 23.9 (s, CH_2), 9.7 [s, $C_5(CH_3)_5$], −25.2 (d, $^2J_{C,P}$ = 7 Hz, $ReCH_3$) ppm. ^{31}P{^{1}H} NMR (161 MHz, C_6D_6, 25 °C, H_3PO_4): δ = 11.5 (s). IR (solid film): $\tilde{\nu}$ = 1633 (s, NO) cm^{-1}. MS (FAB, 3-NBA/CH_2Cl_2):[30] *m*/*z* (%) = 1242 (80) $[M]^+$, 877 (100) $[M - \{(\eta^5\text{-}C_5Me_5)Re(NO)(CH_3)\}]^+$. $C_{56}H_{76}N_2O_2P_2Re_2$ (1243.58): calcd. C 54.09, H 6.16, N 2.25; found C 53.57, H 6.12, N 2.10.

b (n = 14): Complex **6b**$^{2+}$$2BF_4^-$ (1.122 g, 0.748 mmol), $LiAlH_4$ (0.171 g, 4.502 mmol), and THF (20 mL) were combined in a procedure analogous to that for **7a**. An identical reaction and workup gave **7b** as a red solid (0.893 g, 0.687 mmol, 92%). M.p. 57 °C. ^{1}H NMR (400 MHz, C_6D_6, 32 °C): δ = 7.63−7.24 (m, 20 H, 4 C_6H_5), 3.08, 2.45 (2 m, 4 H, 2 PCH_2), 1.68 [s, 30 H, 2 $C_5(CH_3)_5$], 1.23−1.16 (m, 24 H, 12 CH_2), 0.82 (apparent m, 6 H, 2 $ReCH_3$) ppm. ^{13}C{^{1}H} NMR (100 MHz, C_6D_6, 32 °C): δ = 136.4/136.2 (2 d, $^1J_{C,P}$ = 42/42 Hz, *i*-Ph), 135.5/133.4 (2 d, $^2J_{C,P}$ = 9/9 Hz, *o*-Ph), 131.2/130.2 (2 s, *p*-Ph), 129.0/128.6 (2 d, $^3J_{C,P}$ = 11/11 Hz, *m*-Ph), 100.2 [s, $C_5(CH_3)_5$], 33.6 (d, $^1J_{C,P}$ = 33 Hz, PCH_2),[29] 31.5 (d, $J_{C,P}$ = 17 Hz, CH_2), 30.43 (s, CH_2), 30.39 (s, CH_2), 30.2 (s, CH_2), 29.9 (s, CH_2), 25.7 (s, CH_2), 9.8 [s, $C_5(CH_3)_5$], −25.3 (d, $^2J_{C,P}$ = 7 Hz, $ReCH_3$) ppm. ^{31}P{^{1}H} NMR (161 MHz, C_6D_6, 32 °C, H_3PO_4): δ = 11.6 (s) ppm. IR (solid film): $\tilde{\nu}$ = 1633 (s, NO) cm^{-1}. MS (FAB, 3-NBA/CH_2Cl_2):[30] *m*/*z* (%) = 1298 (30) $[M]^+$, 933 (100) $[M - \{(\eta^5\text{-}C_5Me_5)Re(NO)(CH_3)\}]^+$. $C_{60}H_{84}N_2O_2P_2Re_2$ (1299.69): calcd. C 55.45, H 6.51, N 2.16; found C 55.14, H 6.59, N 2.22.

$[(\eta^5\text{-}C_5Me_5)Re(NO)(HC{\equiv}CC{\equiv}CCSiMe_3)\{\mu\text{-}[PPh_2(CH_2)_n\text{-}Ph_2P]\text{-}P,P\}(Me_3SiC{\equiv}CC{\equiv}CH)(ON)Re(\eta^5\text{-}C_5Me_5)]^{2+}{\cdot}2BF_4^-$ (8^{2+} $2BF_4^-$). a (n = 10): A Schlenk flask was charged with **7a** (0.225 g, 0.181 mmol) and C_6H_5Cl (5 mL), and cooled to −45 °C (acetonitrile/CO_2). Then $HBF_4{\cdot}OEt_2$ (54% in Et_2O; 0.050 mL, 0.366 mmol) was added with stirring. After 10 min, $HC{\equiv}CC{\equiv}CSiMe_3$ (0.176 g, 1.443 mmol; mass of loaded/discharged syringe)[22,23] was added, and the cold bath was removed. After 2 h, the solvent was removed by rotary evaporation. The residue was extracted with CH_2Cl_2. The extract was poured into vigorously stirred pentane. The precipitate was collected by filtration and dried by oil-pump vacuum to give **8a**$^{2+}$$2BF_4^-$ as a black powder (0.263 g, 0.161 mmol, 89%, 69−75:31−25 mixture of Re−(C≡C) rotamers[22,24]). M.p. 90 °C. ^{1}H NMR (400 MHz, $CDCl_3$, 25 °C): δ = 7.56−7.24 (m, 20 H, 4 C_6H_5), 8.17/7.02 (2 br. s, 2 H, 2 $HC{\equiv}$),[32] 2.61 (m, 4 H, 2 PCH_2), 1.79/1.69 [2 s, 71:29, 30 H, 2 $C_5(CH_3)_5$],[32] 1.27−1.12 (m, 16 H, 8 CH_2), 0.30/−0.14 [2 s, 69:31, 18 H, 2 $Si(CH_3)_3$] ppm.[32] ^{13}C{^{1}H} NMR (100 MHz, $CDCl_3$, 25 °C):[31] δ (C≡*C*H not observed) = 133.0−127.4 (Ph signals), 114.2 (s, *C*≡CSi), 109.8/109.5 [s, $C_5(CH_3)_5$],[32] 95.0 (s, C≡*C*Si), 92.5 (br. s, *C*≡CH), 32.0−28.1 (CH_2 signals), 24.1 (br. s, CH_2), 9.1 [s, $C_5(CH_3)_5$], −0.5/−0.8 [2 s, 69:31, $Si(CH_3)_3$] ppm.[32] ^{31}P{^{1}H} NMR (161 MHz, $CDCl_3$, 25 °C, H_3PO_4): δ = 7.1/13.2 (2 s, 75:25) ppm.[32] IR (solid film): $\tilde{\nu}$ = 2138 (m, C≡C), 1683 (s, NO) cm^{-1} ppm. MS (FAB, 3-NBA/CH_2Cl_2):[30] *m*/*z* (%) = 1544 (30) $[M + BF_4^-]^+$, 1458 (70) $[M]^+$, 984 (100) $[M - \{(\eta^5\text{-}C_5Me_5)Re(NO)(HC{\equiv}CC{\equiv}CSiMe_3)\}]^+$, 729 (10) $[M]^{++}$. $C_{68}H_{90}B_2F_8N_2O_2P_2Re_2Si_2$ (1631.61): calcd. C 50.06, H 5.56, N 1.72; found C 49.80, H 5.47, N 1.52.

b (n = 14): Complex **7b** (0.824 g, 0.634 mmol), C_6H_5Cl (5 mL), $HBF_4{\cdot}OEt_2$ (54% in Et_2O; 0.172 mL, 1.262 mmol), and $HC{\equiv}CC{\equiv}CSiMe_3$ (0.615 g, 5.041 mmol) were combined in a procedure analogous to that for **8a**$^{2+}$$2BF_4^-$. An identical reaction and workup gave **8b**$^{2+}$$2BF_4^-$ as a black powder (0.901 g, 0.534 mmol, 84%, 67−76:33−24 mixture of Re−(C≡C) rotamers[22,24]). M.p. 92 °C. ^{1}H NMR (400 MHz, $CDCl_3$, 25 °C): δ = 7.56−7.24 (m, 20 H, 4 C_6H_5), 8.20/7.01 (2 br. s, 2 H, 2 $HC{\equiv}$),[32] 2.61 (m, 4 H, 2 PCH_2), 1.81/1.71 [2 s, 70:30, 30 H, 2 $C_5(CH_3)_5$],[32] 1.27−1.12 (m, 24 H, 12 CH_2), 0.30/−0.14 [2 s, 71:29, 18 H, 2 $Si(CH_3)_3$] ppm.[32] ^{13}C{^{1}H} NMR (100 MHz, $CDCl_3$, 25 °C):[31] δ (C≡*C*H not observed) = 133.9−128.4 (Ph signals), 114.3 (s, *C*≡CSi), 109.9/109.6 [2 s, $C_5(CH_3)_5$],[32] 94.9 (s, C≡*C*Si), 32.9−28.2 (CH_2 signals), 24.2 (br. s, CH_2), 9.2 [s, $C_5(CH_3)_5$], −0.5/−0.8 [2 s, 67:33, $Si(CH_3)_3$] ppm.[32] ^{31}P{^{1}H} NMR (161 MHz, $CDCl_3$, 32 °C, H_3PO_4): δ = 7.2/13.4 (2 s, 76:24) ppm.[32] IR (solid film): $\tilde{\nu}$ = 2140 (m, C≡C), 1683 (s, NO) cm^{-1}. MS (FAB, 3-NBA/CH_2Cl_2):[30] *m*/*z* (%) = 1602 (2) $[M + BF_4^-]^+$, 1041 (100) $[M - \{(\eta^5\text{-}C_5Me_5)Re(NO)(HC{\equiv}CC{\equiv}CSiMe_3)\}]^+$, 757 (10) $[M]^{++}$. $C_{72}H_{98}B_2F_8N_2O_2P_2Re_2Si_2$ (1687.71): calcd. C 51.24, H 5.85, N 1.66; found C 50.81, H 6.17, N 1.47.

$[(\eta^5\text{-}C_5Me_5)Re(NO)(C{\equiv}CC{\equiv}CSiMe_3)\{\mu\text{-}[PPh_2(CH_2)_nPh_2P]\text{-}P,P\}(Me_3SiC{\equiv}CC{\equiv}C)(ON)Re(\eta^5\text{-}C_5Me_5)]$ (9). a (n = 10): A Schlenk flask was charged with **8a**$^{2+}$$2BF_4^-$ (0.170 g, 0.104 mmol) and *t*BuOK (0.030 g, 0.273 mmol) and cooled to −75 °C (CO_2/acetone). Then pre-cooled THF (5 mL) was added. After 10 min, the cold bath was removed. The solution was stirred at room temperature for an additional 2 h, and then passed through an alumina pad (3 cm). The solvent was removed by oil-pump vacuum to give **9a** as a red solid (0.144 g, 0.099 mmol, 95%). M.p. 110−115 °C. ^{1}H NMR (400 MHz, C_6D_6, 32 °C): δ = 7.79−7.61 (m, 8 H of 4 C_6H_5), 7.18−6.93 (m, 12 H of 4 C_6H_5), 3.25, 2.49 (2 m, 4 H, 2 PCH_2), 1.53 [s, 30 H, 2 $C_5(CH_3)_5$], 1.42−1.04 (m, 16 H, 8 CH_2), 0.25 [s, 18 H, 2 $Si(CH_3)_3$] ppm. ^{13}C{^{1}H} NMR (100 MHz, C_6D_6, 32 °C): δ = 135.2/133.7 (2 d, $^1J_{C,P}$ = 46/49 Hz, *i*-Ph), 134.8/132.7 (2 d, $^2J_{C,P}$ = 11/11 Hz, *o*-Ph), 131.2/130.7 (2 s, *p*-Ph), 128.7/127.8 (2 d, $^3J_{C,P}$ = 11/11 Hz, *m*-Ph), 111.5 (s, ReC≡*C*),[31] 107.1 (d, $^2J_{C,P}$ = 15 Hz, Re*C*≡),[31] 100.3 [s, $C_5(CH_3)_5$], 93.6 (s, *C*≡CSi),[31] 80.6 (s, ≡*C*Si),[31] 34.1 (d, $^1J_{C,P}$ = 36 Hz, PCH_2),[29] 31.2 (d, $J_{C,P}$ = 15 Hz, CH_2), 29.6 (s, CH_2), 25.7 (s, CH_2), 24.0 (s, CH_2), 9.8 [s, $C_5(CH_3)_5$], 0.9 [s, $Si(CH_3)_3$] ppm. ^{31}P{^{1}H} NMR (161 MHz, C_6D_6, 32 °C, H_3PO_4): δ = 10.4 (s) ppm. IR (solid film): $\tilde{\nu}$ = 2118 (w, C≡C), 2096 (m, C≡C), 1640 (s, NO) cm^{-1}. MS (FAB, 3-NBA/CH_2Cl_2):[30] *m*/*z* (%) = 1456 (100) $[M]^+$, 983 (40) $[M - \{(\eta^5\text{-}C_5Me_5)Re(NO)(C{\equiv}CC{\equiv}CSiMe_3)\}]^+$. $C_{68}H_{88}N_2O_2P_2Re_2Si_2$ (1455.98): calcd. C 56.10, H 6.09, N 1.92; found C 55.99, H 6.11, N 2.01.

b (n = 14): Complex **8b**$^{2+}$$2BF_4^-$ (0.200 g, 0.118 mmol), *t*BuOK (0.027 g, 0.245 mmol), and THF (5 mL) were combined in a procedure analogous to that for **9a**. An identical reaction and workup gave **9b** as a red solid (0.118 g, 0.078 mmol, 66%). M.p. 111−120 °C. ^{1}H NMR (400 MHz, C_6D_6, 32 °C): δ = 7.64−7.60 (m, 8 H of

 © 2003 Wiley-VCH Verlag GmbH & Co. KGaA, Weinheim

4 C_6H_5), 7.15−6.93 (m, 12 H of 4 C_6H_5), 3.33, 2.53 (m, 4 H, 2 PCH_2), 1.52 [s, 30 H, 2 $C_5(CH_3)_5$], 1.42−1.04 (m, 24 H, 12 CH_2), 0.25 [s, 18 H, 2 $Si(CH_3)_3$] ppm. $^{13}C\{^1H\}$ NMR (100 MHz, C_6D_6, 32 °C): δ = 135.1/133.5 (2 d, $^1J_{C,P}$ = 47/49 Hz, *i*-Ph), 134.9/132.8 (2 d, $^2J_{C,P}$ = 10/11 Hz, *o*-Ph), 131.1/130.7 (2 s, *p*-Ph), 128.7/127.9 (2 d, $^3J_{C,P}$ = 10/10 Hz, *m*-Ph), 111.3 (s, ReC≡*C*),[31] 106.9 (d, $^2J_{C,P}$ = 14 Hz, Re*C*≡),[31] 100.1 [s, $C_5(CH_3)_5$], 93.5 (s, *C*≡CSi),[31] 80.9 (s, ≡*C*Si),[31] 33.9 (d, $^1J_{C,P}$ = 32 Hz, P*C*H$_2$),[29] 31.2 (d, $J_{C,P}$ = 8 Hz, *C*H$_2$), 29.8 (s, double intensity, *C*H$_2$), 29.6 (s, *C*H$_2$), 25.7 (s, *C*H$_2$), 24.0 (s, *C*H$_2$), 9.8 [s, $C_5(CH_3)_5$], 1.0 [s, $Si(CH_3)_3$] ppm. $^{31}P\{^1H\}$ NMR (161 MHz, C_6D_6, 32 °C, H_3PO_4): δ = 10.2 (s) ppm. IR (solid film): $\tilde{\nu}$ = 2173 (w, C≡C), 2096 (m, C≡C), 1640 (s, NO) cm^{-1}. MS (FAB, 3-NBA/CH_2Cl_2):[30] *m*/*z* (%) = 1513 (100) $[M]^+$, 1039 (50) $[M - \{(\eta^5\text{-}C_5Me_5)Re(NO)(C{\equiv}CC{\equiv}CSiMe_3)\}]^+$. $C_{72}H_{96}N_2O_2P_2Re_2Si_2$ (1512.10): calcd. C 57.19, H 6.40, N 1.85; found C 56.70, H 6.20, N 1.60.

[(η^5-C_5Me_5)Re(NO){μ-[$PPh_2(CH_2)_nPh_2P$]-*P*,*P*'}{μ-(C^1≡CC≡CC≡CC≡C^8)-*C*^{1},*C*^{8}'}(ON)Re(η^5-C_5Me_5)] (3). a (*n* = 10): A Schlenk flask was charged with **9a** (0.120 g, 0.082 mmol) and THF (10 mL), and wet nBu_4NF (1 M in THF; 0.032 mL, 0.032 mmol) was added with stirring. After 2 h, the solution was filtered through an alumina pad (1 cm) into a weighed Schlenk flask. The solvent was removed from the filtrate by oil-pump vacuum. To the red solid (**10a**; 0.060 g, 0.044 mmol, 53%) was added $Cu(OAc)_2$ (0.016 g, 0.090 mmol) and pyridine (5 mL). The suspension was stirred at 60 °C. After 24 h, the solvent was removed by oil-pump vacuum (the reaction can be monitored by TLC). The residue was extracted with CH_2Cl_2. The extract was filtered through a silica gel pad (2 cm). The solvent was removed by oil-pump vacuum to give **3a** as a red solid (0.010 g, 0.008 mmol, 10% from **9a** or 18% from **10a**).[33] **10a**: ^1H NMR (400 MHz, C_6D_6, 32 °C): δ = 7.72−7.05 (m, 20 H, 4 C_6H_5), 3.35, 2.47 (2 m, 4 H, 2 PCH_2), 2.14 (s, 2 H, ≡C*H*), 1.54 [s, 30 H, 2 $C_5(CH_3)_5$], 1.40−1.00 (m, 16 H, 8 CH_2) ppm. $^{31}P\{^1H\}$ NMR (161 MHz, C_6D_6, 32 °C, H_3PO_4): δ = 10.6 (s) ppm. IR (solid film): $\tilde{\nu}$ (≡CH not observed) = 2112 (w, C≡C), 1978 (m, C≡C), 1643 (s, NO) cm^{-1}. **3a**: ^1H NMR (400 MHz, C_6D_6, 25 °C): δ = 7.71−6.79 (m, 20 H, 4 C_6H_5), 3.19, 2.67 (2 m, 4 H, 2 PCH_2), 1.52, 1.51 [2 s, 30 H, 2 $C_5(CH_3)_5$], 1.47−1.20 (m, 16 H, 8 CH_2) ppm. $^{13}C\{^1H\}$ NMR (100 MHz, C_6D_6, 25 °C): δ = 136.3−127.9 (Ph signals), 113.3 (s, ReC≡*C*),[31] 110.6 (br. s, Re*C*≡*C*),[31] 100.5 [s, $C_5(CH_3)_5$], 66.2 (s, ReC≡C*C*≡C),[31] 63.5 (s, ReC≡CC≡*C*),[31] 33.2−28.2 (*C*H$_2$ signals), 24.3 (br. s, *C*H$_2$), 9.8 [s, $C_5(CH_3)_5$] ppm. $^{31}P\{^1H\}$ NMR (161 MHz, C_6D_6, 25 °C, H_3PO_4): δ = 10.2, 9.9 (2 s, 51:49) ppm. IR (solid film): $\tilde{\nu}$ = 2104 (m, C≡C), 1953 (m, C≡C), 1637 (s, NO) cm^{-1}. MS (FAB, 3-NBA/CH_2Cl_2):[30] *m*/*z* (%) = 1310 (100) $[M]^+$, 2619 (8) $[2\ M]^+$; no peak *m*/*z* (%) = 200 (> 5).

b (*n* = 14): Complex **9b** (0.136 g, 0.090 mmol), THF (10 mL), wet nBu_4NF (1 M in THF; 0.036 mL, 0.036 mmol), $Cu(OAc)_2$ (0.016 g, 0.090 mmol) and pyridine (5 mL) were combined in procedures analogous to those for **3a** (**10b**; 0.060 g, 0.044 mmol, 55%). Similar reactions (14 h, 65 °C) and workups gave **3b** as a red solid (0.024 g, 0.018 mmol; 23% from **9b** or 41% from **10b**). **10b**: ^1H NMR (400 MHz, C_6D_6, 32 °C): δ = 7.68−6.99 (m, 20 H, 4 C_6H_5), 3.31, 2.45 (2 m, 4 H, 2 PCH_2), 2.09 (s, 2 H, ≡C*H*), 1.52 [s, 30 H, 2 $C_5(CH_3)_5$], 1.49−1.07 (m, 16 H, 12 CH_2) ppm. $^{31}P\{^1H\}$ NMR (161 MHz, C_6D_6, 32 °C, H_3PO_4): δ = 10.4 (s) ppm. IR (solid film): $\tilde{\nu}$ = 3290 (w, ≡C*H*), 2112 (w, C≡C), 1978 (m, C≡C), 1643 (s, NO) cm^{-1}. **3b**: ^1H NMR (400 MHz, C_6D_6, 25 °C): δ = 7.63−6.95 (m, 20 H, 4 C_6H_5), 3.25, 2.58 (2 m, 4 H, 2 PCH_2), 1.60, 1.59 [2 s, 30 H, 2 $C_5(CH_3)_5$], 1.45−1.19 (m, 24 H, 12 CH_2) ppm. ^1H NMR (400 MHz, $CDCl_3$, 32 °C): δ = 7.63−7.59 (m, 4 H of 4 C_6H_5), 7.48−7.43 (m, 8 H of 4 C_6H_5), 7.35−7.28 (m, 8 H of 4 C_6H_5), 3.29, 2.48 (2 m, 4 H, 2 PCH_2), 1.68 [br. s, 30 H, 2 $C_5(CH_3)_5$], 1.36−1.23 (m, 24 H, 12 CH_2) ppm. $^{13}C\{^1H\}$ NMR (100 MHz, C_6D_6, 25 °C): δ (Re*C*≡ not observed) = 135.3−129.2 (Ph signals), 113.8 (s, ReC≡*C*),[31] 100.9 [s, $C_5(CH_3)_5$], 66.8 (s, ReC≡C*C*),[31] 64.3 (s, ReC≡CC≡*C*),[31] 33.6−28.1 (*C*H$_2$ signals), 24.2 (br. s, *C*H$_2$), 11.3 [s, $C_5(CH_3)_5$] ppm. $^{31}P\{^1H\}$ NMR (161 MHz, C_6D_6, 25 °C, H_3PO_4): δ = 10.6, 10.4 (2 s, 47:53) ppm. $^{31}P\{^1H\}$ NMR (161 MHz, $CDCl_3$, 32 °C, H_3PO_4): δ = 10.6, 10.3 (2 s, 48:52) ppm. IR (solid film): $\tilde{\nu}$ = 2108 (m, C≡C), 1953 (m, C≡C), 1640 (s, NO) cm^{-1}. MS (FAB, 3-NBA/CH_2Cl_2):[30] *m*/*z* (%) = 1366 (100) $[M]^+$; no peak *m*/*z* (%) = 200 (> 5). $C_{66}H_{78}N_2O_2P_2Re_2$ (1365.71): calcd. C 58.05, H 5.76, N 2.05; found C 57.95, H 5.70, N 1.80.

Acknowledgments

We thank the Deutsche Forschungsgemeinschaft (DFG; SFB 583) for support.

[1] P. R. Story, P. Busch, *Adv. Org. Chem.* **1972**, *6*, 67−97.
[2] See, for example: G. Illuminati, L. Mandolini, *Acc. Chem. Res.* **1981**, *14*, 95−109.
[3] [3a] J. M. Martín-Alvarez, F. A. Hampel, A. M. Arif, J. A. Gladysz, *Organometallics* **1999**, *18*, 955−957. [3b] E. B. Bauer, J. Ruwwe, J. M. Martín-Alvarez, T. B. Peters, J. C. Bohling, F. A. Hampel, S. Szafert, T. Lis, J. A. Gladysz, *Chem. Commun.* **2000**, 2261−2262. [3c] J. Ruwwe, J. M. Martín-Alvarez, C. R. Horn, E. B. Bauer, S. Szafert, T. Lis, F. Hampel, P. C. Cagle, J. A. Gladysz, *Chem. Eur. J.* **2001**, *7*, 3931−3950.
[4] J. Stahl, J. C. Bohling, E. B. Bauer, T. B. Peters, W. Mohr, J. M. Martín-Alvarez, F. Hampel, J. A. Gladysz, *Angew. Chem. Int. Ed.* **2002**, *41*, 1871−1876; *Angew. Chem.* **2002**, *114*, 1951−1957.
[5] C. R. Horn, J. M. Martín-Alvarez, J. A. Gladysz, *Organometallics* **2002**, *21*, 5386−5393.
[6] E. B. Bauer, S. Szafert, F. Hampel, J. A. Gladysz, *Organometallics*, in press.
[7] C. O. Dietrich-Buchecker, J.-P. Sauvage, *Chem. Rev.* **1987**, *87*, 795−810.
[8] C. O. Dietrich-Buchecker, C. Hemmert, A. K. Khémiss, J.-P. Sauvage, *J. Am. Chem. Soc.* **1990**, *112*, 8002−8008.
[9] [9a] B. Mohr, M. Weck, J.-P. Sauvage, R. H. Grubbs, *Angew. Chem. Int. Ed. Engl.* **1997**, *36*, 1308−1310; *Angew. Chem.* **1997**, *109*, 1365−1367. [9b] M. Weck, B. Mohr, J.-P. Sauvage, R. H. Grubbs, *J. Org. Chem.* **1999**, *64*, 5463−5471. [9c] G. Rapenne, C. Dietrich-Buchecker, J.-P. Sauvage, *J. Am. Chem. Soc.* **1999**, *121*, 994−1001. [9d] N. Belfrekh, C. Dietrich-Buchecker, J.-P. Sauvage, *Inorg. Chem.* **2000**, *39*, 5169−5172. [9e] A.-C. Laemmel, J.-P. Collin, J.-P. Sauvage, G. Accorsi, N. Armaroli, *Eur. J. Inorg. Chem.* **2003**, 467−474.
[10] C. A. Bessel, P. Aggarwal, A. C. Marschilok, K. J. Takeuchi, *Chem. Rev.* **2001**, *101*, 1031−1066.
[11] V. L. Pecoraro, A. J. Stemmler, B. R. Gibney, J. J. Bodwin, H. Wang, J. W. Kampf, A. Barwinski, *Prog. Inorg. Chem.* **1997**, *45*, 83−137.
[12] [12a] P. Siemsen, R. C. Livingston, F. Diederich, *Angew. Chem. Int. Ed.* **2000**, *39*, 2633−2657; *Angew. Chem.* **2000**, *112*, 2740−2767. [12b] M. L. Bell, R. C. Chiechi, C. A. Johnson, D. B. Kimball, A. J. Matzger, W. B. Wan, T. J. R. Weakley, M. M. Haley, *Tetrahedron* **2001**, *57*, 3507−3520.
[13] Macrocyclizations of organic compounds with two terminal 1,3-diynes are somewhat more germane to the new reactions presented herein. Although these are less common, there are many examples. For a recent report, see: M. A. Heuft, S. K. Collins, G. P. A. Yap, A. G. Fallis, *Org. Lett.* **2001**, *3*, 2883−2886.
[14] For fascinating template-mediated oxidative macrocyclizations

 © 2003 Wiley-VCH Verlag GmbH & Co. KGaA, Weinheim

of alkynylzinc porphyrins, see: D. W. J. McCallien, J. K. M. Sanders, *J. Am. Chem. Soc.* **1995**, *117*, 6611−6612. Although these macrocyclizations are clearly intramolecular, the templated assembly is not isolable.

[15] Selected lead references: [15a] F. Diederich, Y. Rubin, O. L. Chapman, N. S. Goroff, *Helv. Chim. Acta* **1994**, *77*, 1441−1457. [15b] U. H. F. Bunz, *Synlett* **1997**, 1117−1127. For yield data for the bottom reaction in Scheme 1, see: U. H. F. Bunz, G. Roidl, M. Altmann, V. Enkelmann, K. D. Shimizu, *J. Am. Chem. Soc.* **1999**, *121*, 10719−10726.

[16] For macrocyclizations in which a metal fragment is inserted between two terminal alkynes, see: [16a] J. J. Pak, T. J. R. Weakley, M. M. Haley, *Organometallics* **1997**, *16*, 4505−4507. [16b] E. Bosch, C. L. Barnes, *Organometallics* **2000**, *19*, 5522−5524. [16c] K. Campbell, R. McDonald, M. J. Ferguson, R. R. Tykwinski, *Organometallics* **2003**, *22*, 1353−1355.

[17] [17a] R. Dembinski, T. Bartik, B. Bartik, M. Jaeger, J. A. Gladysz, *J. Am. Chem. Soc.* **2000**, *122*, 810−822. [17b] W. E. Meyer, A. J. Amoroso, C. R. Horn, M. Jaeger, J. A. Gladysz, *Organometallics* **2001**, *20*, 1115−1127.

[18] [18a] A. T. Patton, C. E. Strouse, C. B. Knobler, J. A. Gladysz, *J. Am. Chem. Soc.* **1983**, *105*, 5804−5811. [18b] W. E. Meyer, A. J. Amoroso, M. Jaeger, J. Le Bras, W.-T. Wong, J. A. Gladysz, *J. Organomet. Chem.* **2000**, *616*, 44−53.

[19] [19a] W. E. Hill, C. A. McAuliffe, I. E. Niven, R. V. Parish, *Inorg. Chim. Acta* **1980**, *38*, 273−278. [19b] W. E. Hill, D. M. A. Minahan, J. G. Taylor, C. A. McAuliffe, *J. Chem. Soc., Perkin Trans. 2* **1982**, 327−330.

[20] C. R. Horn, Doctoral Dissertation, Universität Erlangen-Nürnberg, **2002**.

[21] T.-S. Peng, C. H. Winter, J. A. Gladysz, *Inorg. Chem.* **1994**, *33*, 2534−2542.

[22] W. Weng, T. Bartik, M. Brady, B. Bartik, J. A. Ramsden, A. M. Arif, J. A. Gladysz, *J. Am. Chem. Soc.* **1995**, *117*, 11922−11931.

[23] M. I. Bruce, P. J. Low, A. Werth, B. W. Skelton, A. H. White, *J. Chem. Soc., Dalton Trans.* **1996**, 1551−1566.

[24] [24a] J. J. Kowalczyk, A. M. Arif, J. A. Gladysz, *Organometallics* **1991**, *10*, 1079−1088. [24b] J. A. Ramsden, W. Weng, J. A. Gladysz, *Organometallics* **1992**, *11*, 3635−3645.

[25] F. Coat, C. Lapinte, *Organometallics* **1996**, *15*, 477−479.

[26] The oxidation of a novel $[Ru_2]C{\equiv}CC{\equiv}CC{\equiv}CC{\equiv}C[Ru_2]$ species has also been studied by cyclic voltammetry: K.-T. Wong, J.-M. Lehn, S-M. Peng, G.-H. Lee, *Chem. Commun.* **2000**, 2259−2260.

[27] R. Gröbl, Universität Erlangen-Nürnberg, work in progress.

[28] [28a] S. M. ALQaisi, K. J. Galat, M. Chai, D. G. Ray, III, P. L. Rinaldi, C. A. Tessier, W. J. Youngs, *J. Am. Chem. Soc.* **1998**, *120*, 12149−12150. [28b] M. I. Bruce, K. Costuas, J.-F. Halet, B. C. Hall, P. J. Low, B. K. Nicholson, B. W. Skelton, A. H. White, *J. Chem. Soc., Dalton Trans.* **2002**, 383−398.

[29] $^1H,^{13}C$ COSY experiments have established that the PCH_2 protons of monorhenium analogs of $\mathbf{6}^{2+}$ $2BF_4^-$ and **7** with $PPh_2(CH_2)_6CH{=}CH_2$ ligands reside on the carbon atom with the largest J(C,P) value.[5] These correlations were used to assign the PCH_2 ^{13}C NMR signals in this study.

[30] The $[M]^+$ ions represent the most intense peak in the isotope envelope.

[31] The assignments follow from coupling constant and chemical shift patterns established earlier.[22]

[32] These signals are for the major and minor rotamers, respectively.

[33] A correct microanalysis was not obtained for this compound.

Received January 16, 2003

 © 2003 Wiley-VCH Verlag GmbH & Co. KGaA, Weinheim

Synthesis of *tripod* Ligands Containing Mixed Donor Sets with Phosphane and Pyrazole Donors − Bidentate Chelate Binding Modes and Dynamic Behaviour of *tripod* Ligands in d^8-Metal Complexes (Ni^{II}, Pd^{II}, Pt^{II})

Ralf Faissner,[a] Gottfried Huttner,*[a] Elisabeth Kaifer,[a] Peter Kircher,[a] Peter Rutsch,[a] and Laszlo Zsolnai[a][†]

Dedicated to Professor Rolf Gleiter[‡]

Keywords: Tripod ligands / Conformation / Nickel / Palladium / Platinum

The synthesis of a series of *tripod* ligands $MeOCH_2C(CH_2X)(CH_2Y)(CH_2Z)$ (X = PR_2; Y, Z = PR'_2 or pz; pz = 1-pyrazolyl) based on the 3,3-difunctionalized oxetane $O^a[CH_2]_2C^a(CH_2OMs)(CH_2Br)$($O^a$–$C^a$) as the starting material is described. With their mixed donor sets these ligands coordinate to d^8-metal ions in a bidentate binding mode. One of the three donors remains uncoordinated in each case. Coordination of phosphane donors is generally preferred over coordination of pyrazole donors. With bulky phosphanes such as $–CH_2PMes_2$, however, pyrazole may compete with PR_2, depending on the kind of the d^8 fragment. Dynamic exchange between coordinated and noncoordinated pyrazole donors is observed. Tetracoordinate complexes of the general type L_2MR_2 are formed (L_2 symbolizes the *tripod* ligand in its bidentate chelate binding mode with two donors functions coordinating and the third one serving as a dangling arm; M = Ni^{II}, Pd^{II}, Pt^{II}). With nickel(II) as the d^8 species, tetrahedral or square-planar coordination geometries ensue, depending on the kind of donor functions and on the kind of co-ligands R. With palladium(II) and platinum(II) as the d^8 centres, square-planar coordination is observed throughout. The size of the chelate cycles varies from six to eight depending on the number of pyrazole entities within the cycle. The conformations and the conformational flexibility characterizing the chelate cycles have been analysed by X-ray analyses and by variable-temperature NMR. The classes of conformations observed may be formally reduced to chair, half-chair and twist-boat conformations. Dynamic exchange between these conformations is observed. In one case, the same compound forms two different types of crystals that differ by the conformation adopted by their chelate cycles. All compounds have been fully characterized by standard analytical techniques including X-ray structure analysis of 14 chelate compounds.
(© Wiley-VCH Verlag GmbH & Co. KGaA, 69451 Weinheim, Germany, 2003)

Introduction

The synthesis of neopentane-based *tripod* ligands $RCH_2C(CH_2X)(CH_2Y)(CH_2Z)$ that contain up to three different donor functions X, Y, Z, is generally well developed for different kinds of donor functions.[1−5] The selective introduction of nitrogen donor functions is, however, in most cases limited to special kinds of nitrogen donors[5] as well as to specific reaction schemes[5]. Pyrazole is a nitrogen-donor group of more general applicability in *tripod* synthesis[5e,5f] that may be especially easily incorporated in *tripod* ligands $HOCH_2C(CH_2pz)(CH_2PR_2)(CH_2X)$ by a series of nucleophilic substitutions and ring-opening reactions starting from the functionalized oxetane $O^a[CH_2]_2C^a(CH_2Br)(CH_2OMs)$($O^a-C^a$).[5e]

The scope of this type of reaction sequence was tested by applying different phosphorus nucleophiles as well as different nitrogen nucleophiles. The coordination properties of these ligands versus the d^8-metal ions nickel(II), palladium(II), and platinum(II) were tested to elucidate the competition between different types of donor groups. In such coordination compounds the potential *tripod* ligands will act as bidentate ligands with the third potential donor function uncoordinated.[5b,5f,6] The dynamic exchange between coordinated and uncoordinated ligand functions in *tripod* compounds as well as the conformation of the chelate cycles are also reported here.

Results

Ligand Synthesis

The *tripod* ligands **3** and **4** were obtained from oxetane precursors **2**, which were themselves synthesized from the functionally substituted oxetane **1** by standard procedures

[a] Anorganisch-Chemisches Institut der Universität Heidelberg, Im Neuenheimer Feld 270, 69120 Heidelberg, Germany
Fax: (internat.) + 496221/545707
E-mail: g.huttner@indi.aci.uni-heidelberg.de
[†] Deceased.
[‡] As a late contribution to his 65th birthday.

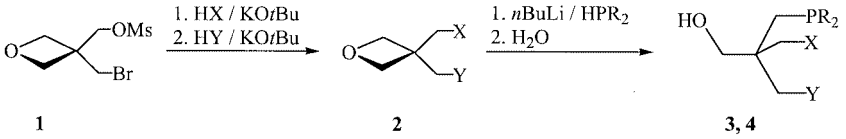

	X	Y
2a	PPh_2	pz
2b	PPh_2	py
2c	pz	pz

	PR_2	X	Y
3a	PPh_2	PPh_2	pz
3b	$P(m\text{-}Tol)_2$	PPh_2	pz
3c	$PMes_2$	PPh_2	pz
3d	PCy_2	PPh_2	pz
3e	PPh_2	PPh_2	py
4a	PPh_2	pz	pz
4b	$PMes_2$	pz	pz

pz = 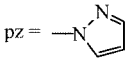

py = 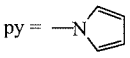

Scheme 1. Synthesis of OH-functionalized *tripod* compounds

(Scheme 1).[5e] Some compounds (**2a**, **2c**, **3a**, **4a**) have already been described.[5e] All the compounds **2**–**4** were fully characterized by the usual spectroscopic techniques as well as by elemental analyses (see Exp. Sect. and Tables 10, 12, and 14).

The transformation of the *tripod* ligands **3** and **4**, which bear a CH_2OH group at the backbone, into the corresponding methyl ethers **5** and **6** followed the standard protocol (Scheme 2).[3i,7] None of the difficulties often observed in the etherification of analogous *tripod* ligands containing either three different P donors or P donors and Cp derived donor functions were encountered.[3i,4d,8] Analytical data of **5** and **6** are given in the Exp. Sect. and Tables 10, 12, and 14.

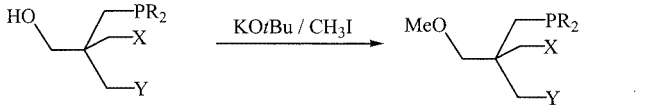

	PR_2	X	Y
5a	PPh_2	PPh_2	pz
5b	$P(m\text{-}Tol)_2$	PPh_2	pz
5c	$PMes_2$	PPh_2	pz
5d	PPh_2	PPh_2	py
6a	PPh_2	pz	pz
6b	$PMes_2$	pz	pz

Scheme 2. Synthesis of *tripod* ligands **5** and **6**

Coordination Chemistry

Coordination derivatives, in which compounds **5** and **6** bind to $MHal_2$ (M = Ni^{II}, Pd^{II}, Pt^{II}) as bidentate ligands, are obtained by standard procedures (see Exp. Sect.), in some cases as single crystals suitable for X-ray analysis (Scheme 3, Table 1).

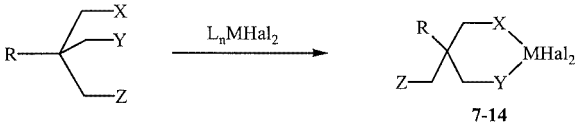

Scheme 3. Synthesis of coordination compounds **7**–**14**

Crystal structure analyses of metal complexes derived from the ligand **5a** were performed for compounds **7a**, **8**, and **9a** (Tables 2–4, 7, and Figures 1 and 2). All these compounds show a square-planar coordination around the metal centre. Ligand **5a** is observed to coordinate via its two PPh_2 donor groups exclusively while the pyrazole donor remains uncoordinated. The six-membered chelate cycle thus formed shows a half-chair conformation for **7a**, **8**, and **9a**. Figure 1 shows two examples. Within the chelate cycles showing a half-chair conformation (**7a/1**, **8**, **9a**) the CH_2OMe group occupies the axial position, with the more bulky CH_2pz group in the equatorial position throughout.

For **7a** two different crystal forms were obtained: one (**7a/1**·CH_2Cl_2) contains molecules with the chelate cycle in a half-chair conformation as well, and the other one (**7a/2**·0.5CH_2Cl_2) contains molecules in which the chelate cycle has a twist-boat conformation, showing that different conformations are accessible to the chelate cycles (Figure 2). These findings agree well with observations made on the chelate cycles in $[\{\kappa^2P\text{-}R_2PCH_2CH(OH)CH_2PR'_2\}Rh(\eta^4\text{-}cod)]^+PF_6^-$. For this type of diphosphane-containing chelate cycle a thorough analysis of the conformation hypersurface[9] as well as of the NMR dynamics[7,10] revealed a small energy difference between half-chair and twist-boat conformations of the chelate cycle. This agrees well with the fact that **7a** forms two different types of ring conformation in its crystals under standard crystallization conditions.

Ligands containing one phosphane and two pyrazole N donors are found to coordinate to nickel(II) by one phosphorus and one nitrogen donor (**11a**, **11c**, see Table 1) or by two pyrazole donors with the CH_2PR_2 group playing the

 © 2003 Wiley-VCH Verlag GmbH & Co. KGaA, Weinheim

Table 1. Coordination compounds **7**−**14**

Compd.	Ligand	Coord. groups X, Y		Noncoord. groups Z, R		$MHal_2$	Colour of compd.	Coord. geometry	Crystal structure
7a	**5a**	PPh_2	PPh_2	pz	CH_2OMe	$NiCl_2$	orange-coloured[a]	square-planar	yes
7b	**5b**	PPh_2	P(*m*-Tol)$_2$	pz	CH_2OMe	$NiCl_2$	orange-coloured	square-planar	no
7c	**5c**	PPh_2	$PMes_2$	pz	CH_2OMe	$NiCl_2$	ruby-coloured	square-planar	no
7d	**5d**	PPh_2	PPh_2	py	CH_2OMe	$NiCl_2$	orange-coloured	square-planar	no
8	**5a**	PPh_2	PPh_2	pz	CH_2OMe	$NiBr_2$	red	square-planar	yes
9a	**5a**	PPh_2	PPh_2	pz	CH_2OMe	$PdCl_2$	colourless	square-planar	yes
9b	**5b**	PPh_2	P(*m*-Tol)$_2$	pz	CH_2OMe	$PdCl_2$	pale yellow	square-planar	no
10	**5a**	PPh_2	PPh_2	pz	CH_2OMe	$PtCl_2$	colourless	square-planar	no
11a	**6a**	PPh_2	pz	pz	CH_2OMe	$NiBr_2$	violet	tetrahedral	yes
11b	**6a**	PPh_2	pz	pz	CH_2OMe	$NiCl_2$	violet	tetrahedral	no
11c	−[b]	PPh_2	pz	pz	CH_2OEt	$NiBr_2$	violet	tetrahedral	yes
12	**6a**	PPh_2	pz	pz	CH_2OMe	$PdCl_2$	yellow	square-planar	yes
13	**6b**	pz	pz	$PMes_2$	CH_2OMe	$NiCl_2$	blue−violet	tetrahedral	yes
14	−[c]	pz	pz	pz	Me	$NiBr_2$	blue	tetrahedral	yes

[a] In crystalline form: red. [b] Ligand $EtOCH_2C(CH_2PPh_2)(CH_2pz)_2$; synthesis see ref.[5e] [c] Ligand: $CH_3C(CH_2pz)_3$; synthesis see ref.[5e]

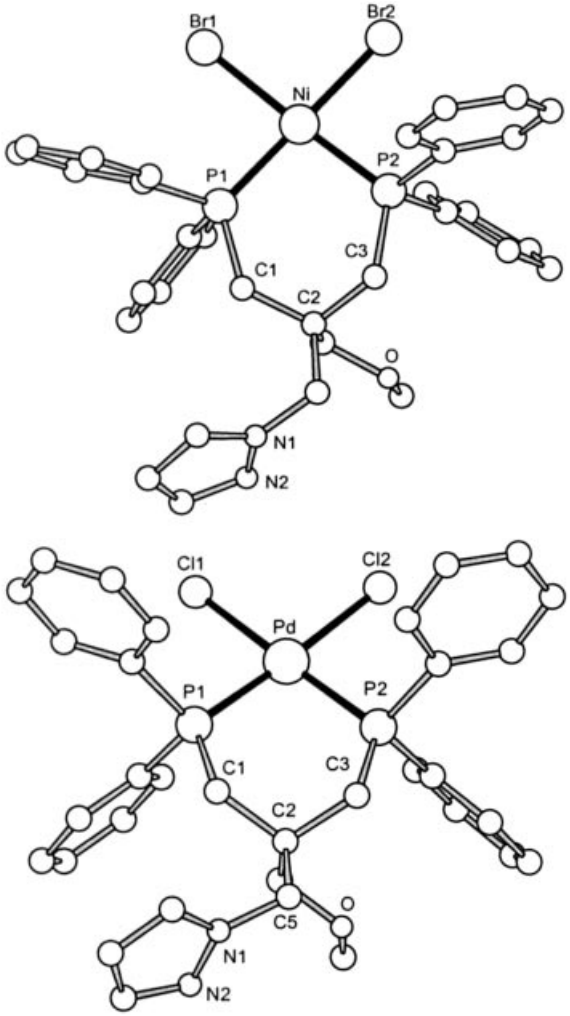

Figure 1. X-ray structure of compound **8** (top) and **9a** (bottom) derived from ligand **5a**

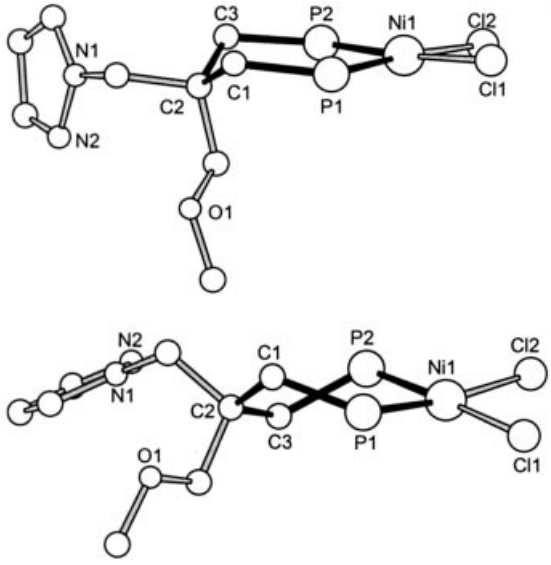

Figure 2. X-ray structure (without phenyl groups) of compound **7a/1** (top, half-chair conformation) and **7a/2** (bottom, twist-boat conformation)

role of a dangling arm (**13**, see Table 1). Figure 3 shows examples of the two coordination modes (*P*,*N* versus *N*,*N*). In addition to the ligands **6a** and **6b** two other *tripod* ligands containing a pz,pz donor set were used. Thus compounds **11c** and **14** (Table 1) are derived from ligands reported earlier.[5e] In each case the coordination geometry around nickel(II) is tetrahedral. Compounds **11a**−**c**, **13**, and **14** are paramagnetic − in contrast to compounds **7** and **8** with their square-planar nickel coordination.

Analytically pure **14** with its *tripod* ligand $CH_3C(CH_2pz)_3$[5e] crystallized as a conglomerate of different crystal forms, most of which were blue. Their structure corresponds to a tetrahedral coordination of the nickel atom as evidenced by crystallography (**14**, see Tables 1−4, 8). A few crystals were red-brown. Their quality was, however, insufficient for X-ray analysis. It is assumed that the difference in colour of these crystals is due to differing kinds of coordination, probably involving the formation of dinuclear entities with bromide acting as a bridging ligand. Thus, different chelate compounds containing $NiBr_2$ groups

 © 2003 Wiley-VCH Verlag GmbH & Co. KGaA, Weinheim

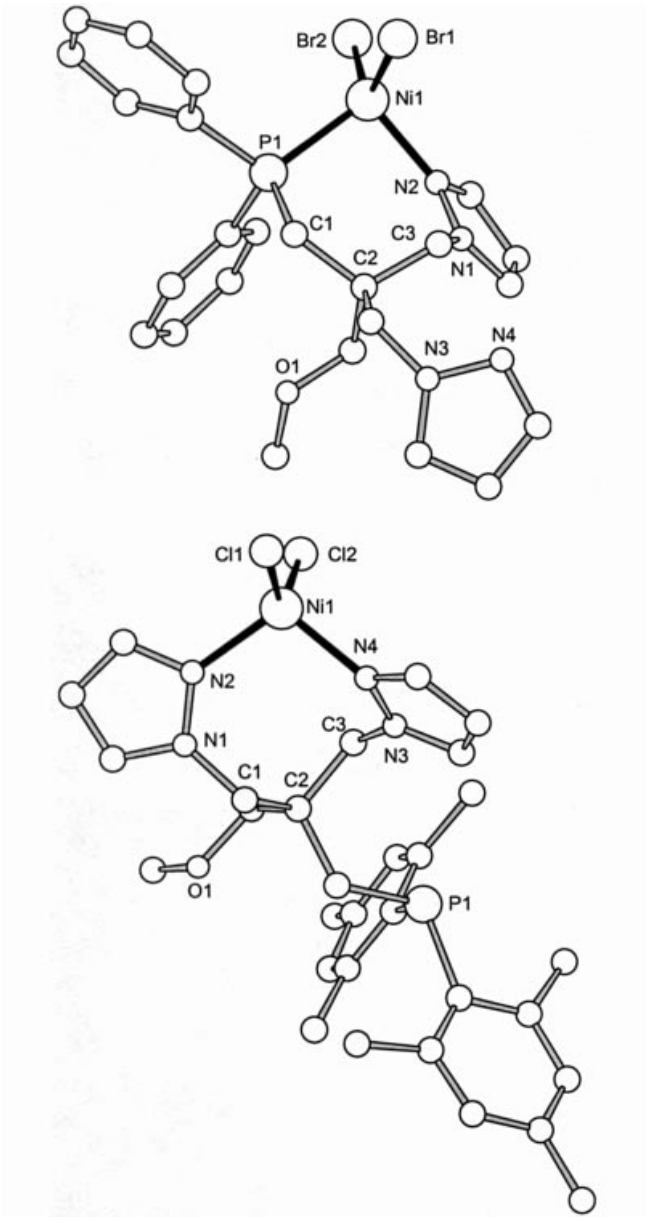

Figure 3. X-ray structure of compound **11a** (top) and **13** (bottom)

were prepared (**8**, **11a**, **11c**) in addition to **14**. The phenomenon could not be observed for **8** or **11a**. With **11c**, however, crystallization yielded violet crystals containing the tetrahedrally coordinated monomeric compound (analogous to **11a** depicted in Figure 3) and red-brown crystals containing the dinuclear species **15** (Figure 4). Both kinds of crystals were suitable for X-ray analysis. The nickel centres in **15** show idealized square-pyramidal coordination ($\tau = 0.16$, see Figure 4).[11]

With palladium(II) as the central metal ligand **6a** acts as a P,N ligand resulting in **12** (Table 1). However, the coordination around the palladium(II) atom is square-planar (Figure 5), in contrast to the tetrahedral coordination of nickel(II) (**11**) by the same ligand arrangement.

With each pyrazole group replacing a one-atom donor group (e.g. PR_2) of a six-membered chelate cycle, the number of atoms within the cycle increases by one, such that *P*,*N*-coordinated compounds (**11**, **12**) have seven-membered chelate cycles and *N*,*N*-coordinated compounds (**13**, **14**) contain eight-membered chelate cycles. Because the pyrazole ligands are coplanar with their substituents − with the carbon atom bonded to one of its nitrogen centres and the metal atom coordinated to the other − the conformation of the chelate cycles may be characterized by an idealized graph with a pseudo corner (Q) at the centre of the pyrazole N−N bond (Scheme 4).

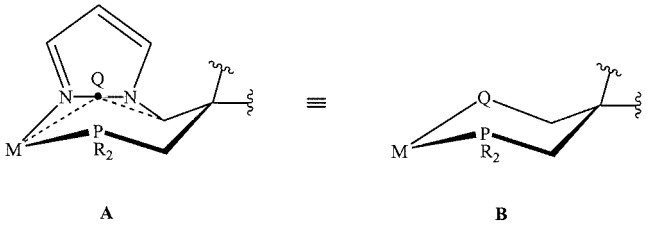

Scheme 4. Idealized graph for chelate cycles containing pyrazole donors: **A**: original; **B**: idealization

This kind of idealization reduces the pyrazole-containing chelate cycles to six-membered cycles (**B**, Scheme 4), even though they actually have seven or eight atoms within the cycle (**A**, Scheme 4) . The observed conformations may therefore be characterized in the same way as for six-membered cycles.

Table 2 indicates the conformation of the chelate cycles observed in each case. The difference between the two classes − (i) twist-boat and (ii) chair or half-chair − is most clearly evident from the pseudo torsion angle 3−2−6−5 (Table 2). Chair or half-chair conformations have 2−3 and 6−5 bonds that are almost parallel. The respective torsion angles are close to zero (deviation from −1.9 to +12.9°, see Table 2). For twist-boat conformations these bonds cannot be parallel, of course, and the corresponding torsion angles are between 44.3 and 67.0° (for absolute values, see Table 2). These two classes are, of course, also differentiated by the sequence of sign changes of the torsion angles around the cycles (columns M−2−3−4 to 6−M−2−3 in Table 2). The different types of conformation listed in Table 2 do obviously not reflect the either square-planar or tetrahedral coordination of the metal centre since the same types of conformations are found for both coordination modes.

Table 3 shows that the nickel−ligand distances respond significantly to the kind of coordination. Ni−P distances of ca. 217 pm are found for compounds showing a square-planar coordination of the nickel atom (Table 3) and of ca. 230 pm for tetrahedrally coordinated nickel compounds (Table 3). Ni−N distances have only been measured for compounds with tetrahedrally coordinated nickel atoms, and are 198 pm, within a few standard deviations, in each case (Table 3). As expected, all nickel compounds that contain at least one nitrogen donor in their chelate cycle show tetrahedral nickel coordination. The Ni−Cl and Ni−Br distances are around 221 and 236 pm, respectively (Table 3),

 © 2003 Wiley-VCH Verlag GmbH & Co. KGaA, Weinheim

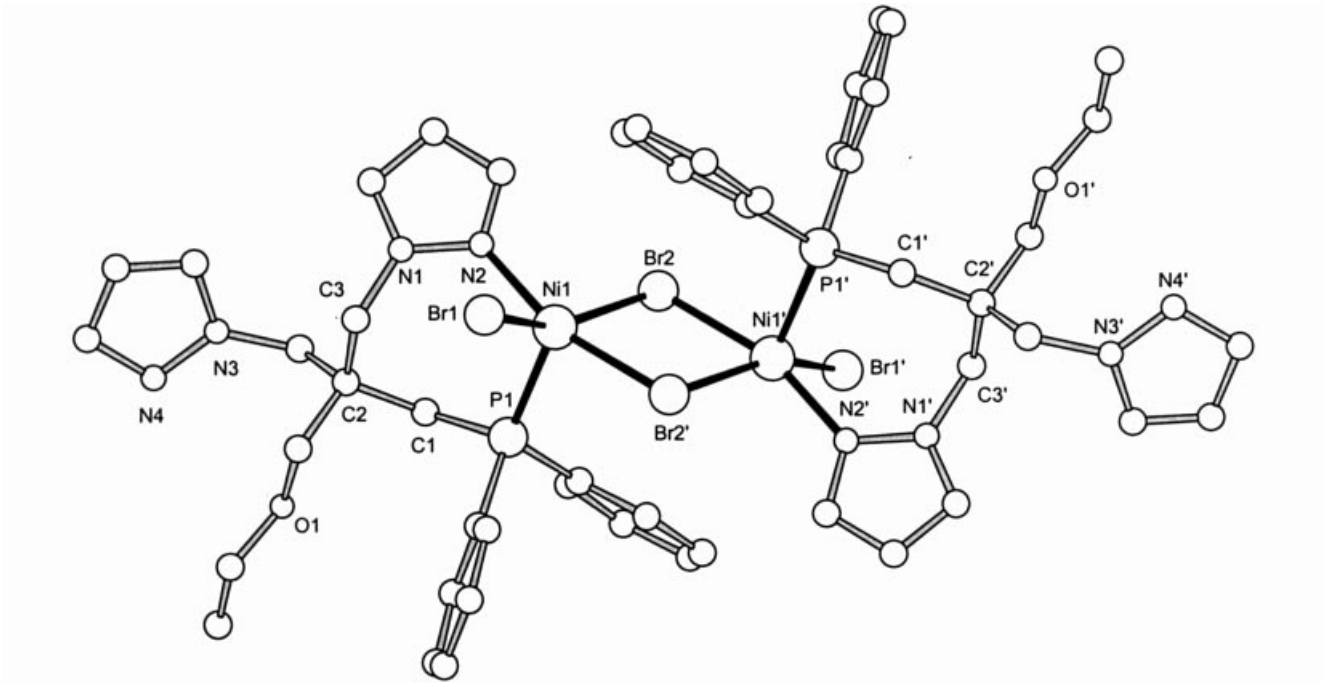

Figure 4. X-ray structure of the dinuclear nickel compound **15**; the compound is of crystallographic C_i symmetry

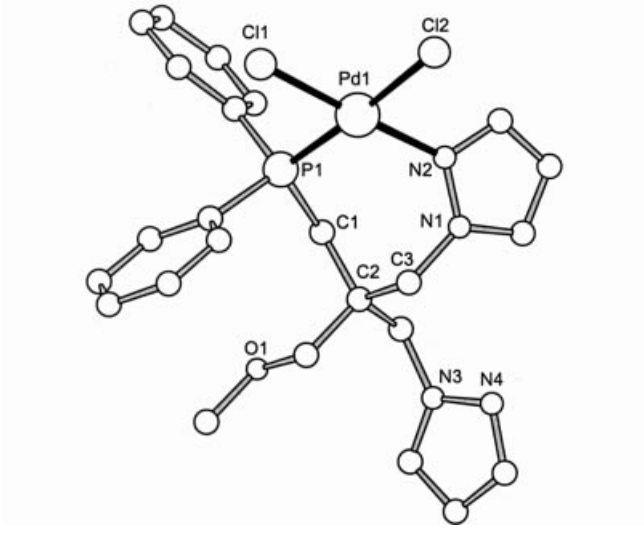

Figure 5. X-ray structure of compound **12**

with no detectable influence due to the kind of coordination geometry.

Compounds **9a** and **12** contain the palladium atom in a square-planar coordination with the chelate ligand coordinating via one N and one P donor (**12**). In **12** the Pd−Cl distances (Table 3) are influenced by their *trans* ligands, with the bond *trans* to the nitrogen donor [228.2(1) pm] being significantly shorter than that *trans* to the phosphorus donor [235.6(1) pm].

The Ni−P distance of the dinuclear compound **15** is 235.9 pm (Table 3, Figure 4), which is even longer than the Ni−P distances in compounds containing tetrahedrally coordinated nickel atoms. This corresponds to the apical position of the phosphorus donor in **15** (Figure 4). The Ni−Br distances are also longer than the Ni−Br distances observed in **8**, **11**, or **14** (Table 3). The shortest Ni−Br distance of **15** (245 pm) corresponds to the terminal Ni−Br bond. The bridging Ni−Br distances are still around 8 pm longer than this (Table 3). Consequently, all bonds are weakened by changing from tetra-coordination (**8**, **11**, and **14**) to penta-coordination (**15**). The fact that the monomeric arrangement in **11c** and the dimeric arrangement of the same compound in **15** are of almost equal energy is indicated by their co-crystallization as a conglomerate in the same experiment. The solubility of **11c** in CH_2Cl_2 is higher than that of **15**, such that attempts to dissolve red-brown **15** in CH_2Cl_2 led to violet solutions (Table 1) of **11c**.

The angles at the metal centre are in the ranges expected for square-planar and tetrahedral coordination (Table 4). In square-planar compounds the angles subtended by the coordinating atoms of the chelate ligands are somewhat larger than the ideal value of 90° (Table 4). For the tetrahedrally coordinated compounds these angles are smaller than expected for an ideal tetrahedron (109.4°, see Table 4). Deviation from this ideal value is greater for a P,N donor set (**11** and **12**, see Table 4) than for an N,N donor set (**13** and **14**, see Table 4).

NMR Dynamics

It is well known that L_2NiHal_2 (L = aryl phosphane) − even if square-planar in the solid state − may suffer distortions to tetrahedral arrangements at room temperature in solution such that no ^{31}P NMR signals are observed.[12]

When crystalline **7a**, which consists of crystals with the ligand in the chair conformation (**7a/1**) and crystals in twist-boat conformation (**7a/2**), is dissolved in CH_2Cl_2 no ^{31}P NMR signals are observed at room temperature. At −40°C a single sharp resonance is apparent, which broadens upon lowering the temperature further and gradually

 © 2003 Wiley-VCH Verlag GmbH & Co. KGaA, Weinheim

Table 2. Conformation and torsion angles [°] of the chelate cycles in **7a**, **8**, **9a**, **11**−**15**

Conformation of the chelate cycle[a]	Compound		M−2−3−4	2−3−4−5	3−4−5−6	4−5−6−M	5−6−M−2	6−M−2−3	3−2−6−5
Half-chair	**7a/1**	(2, 6 = P)	+40.6	−68.3	+66.3	−36.9	+7.6	−9.1	−1.4
Half-chair	**8**	(2, 6 = P)	+42.4	−65.7	+65.3	−42.3	+14.9	−14.7	+0.2
Half-chair	**9a**	(2, 6 = P)	+41.9	−70.7	+68.3	−37.1	+7.5	−9.6	−1.9
Chair	**11a**	(2 = P, 6 = Q)	+53.3	−58.8	+75.6	−78.4	+56.3	−49.0	+12.9
λ-twist	**7a/2**	(2, 6 = P)	+59.7	−44.4	−16.8	+62.7	−37.0	−11.2	−44.3
λ-twist	**11c**	(2 = P, 6 = Q)	+52.5	−54.2	−22.4	+82.8	−61.6	+11.1	−52.9
λ-twist	**12**	(2 = P, 6 = Q)	+64.5	−46.8	−33.6	+86.0	−51.6	−3.9	−57.7
λ-twist	**13**	(2, 6 = Q)	+70.0	−55.0	−32.5	+89.6	−51.0	−6.1	−61.7
λ-twist	**14**	(2, 6 = Q)	+78.3	−53.0	−37.1	+89.2	−44.3	−16.5	−67.0
λ-twist	**15**	(2 = P, 6 = Q)	+63.9	−45.1	−37.1	+84.5	−46.9	−6.7	−56.9

[a] A consistent numbering scheme for all the compounds as depicted below is used for the sake of easier comparison; the λ-enantiomer was considered throughout.

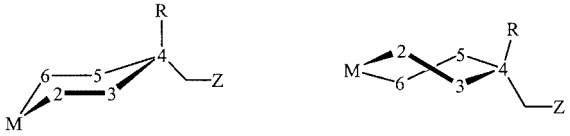

Table 3. Selected bond lengths [pm] in **7a**, **8**, **9a**, **11**−**15**

Coord. geometry[a]	Comp.	M, Hal	M−P	M−N	M−Hal
Square-planar	**7a/1**	Ni, Cl	216.8 (1), 217.4 (1)	−	221.1 (1), 221.3 (1)
Square-planar	**7a/2**	Ni, Cl	216.6 (1), 216.8 (1)	−	219.7 (1), 220.4 (1)
Square-planar	**8**	Ni, Br	217.8 (2), 217.8 (2)	−	234.5 (1), 236.0 (1)
Square-planar	**9a**	Pd, Cl	224.7 (2), 225.0 (2)	−	235.6 (1), 236.4 (1)
Square-planar	**12**	Pd, Cl	224.6 (1)	203.6 (2)	228.2 (1) (*trans* to N) 235.6 (1) (*trans* to P)
Tetrahedral	**11a**	Ni, Br	228.8 (1)	197.3 (1)	234.7 (1), 236.4 (1)
Tetrahedral	**11c**	Ni, Br	231.9 (2)	199.4 (5)	234.6 (1), 235.4 (1)
Tetrahedral	**13**	Ni, Cl	−	198.2 (3), 198.7 (3)	221.7 (1), 222.2 (1)
Tetrahedral	**14**	Ni, Br	−	197.7 (4), 198.4 (4)	234.8 (1), 237.9 (1)
Square-pyramidal	**15**	Ni, Br	235.9 (1)	207.0 (1)	252.6 (1) (bridged) 254.6 (1) (bridged) 245.2 (1) (terminal)

[a] Standard deviations in units of the least significant digit are given in each case.

Table 4. Selected bond angles [°] in **7a**, **8**, **9a**, **11**−**15**

Compd.	M, Hal	Hal−M−Hal[a]	Hal−M−P	Hal−M−N	P−M−P	P−M−N	N−M−N
7a/1	Ni, Cl	91.1(1)	86.2(1), 87.1(1), 175.2(1), 175.7(1)	−	96.0(1)	−	−
7a/2	Ni, Cl	93.0(1)	86.9(1), 88.3(1), 172.7(1), 178.0(1)	−	92.0(1)	−	−
8	Ni, Br	92.1(1)	86.1(1), 86.8(1), 174.0(1), 177.0(1)	−	95.2(1)	−	−
9a	Pd, Cl	90.0(1)	86.4(1), 88.4(1), 175.2(1), 175.8(1)	−	95.3(1)	−	−
11a	Ni, Br	124.8(1)	99.5(1), 116.7(1)	101.9(1), 113.9(1)	−	97.0(1)	−
11c	Ni, Br	124.3(1)	108.4(1), 109.4(1)	103.3(1), 112.9(1)	−	94.6(1)	−
12	Pd, Cl	90.6(1)	87.2(1), 176.9(1)	88.5(1), 178.3(1)	−	93.6(1)	−
13	Ni, Cl	125.9(1)	−	103.9(1), 105.8(1), 106.3(1), 108.3(1)	−	−	105.3(1)
14	Ni, Br	123.6(1)	−	98.7(1), 106.3(1), 108.0(1), 112.5(1)	−	−	106.8(1)
15	Ni, Br	84.4(1), 89.6(1), 154.9(3)	94.9(1), 98.1(1), 110.2(1)	88.0(1), 91.4(1), 164.0(1)	−	96.6(1)	−

[a] Standard deviations in units of the least significant digit are given in each case.

 © 2003 Wiley-VCH Verlag GmbH & Co. KGaA, Weinheim

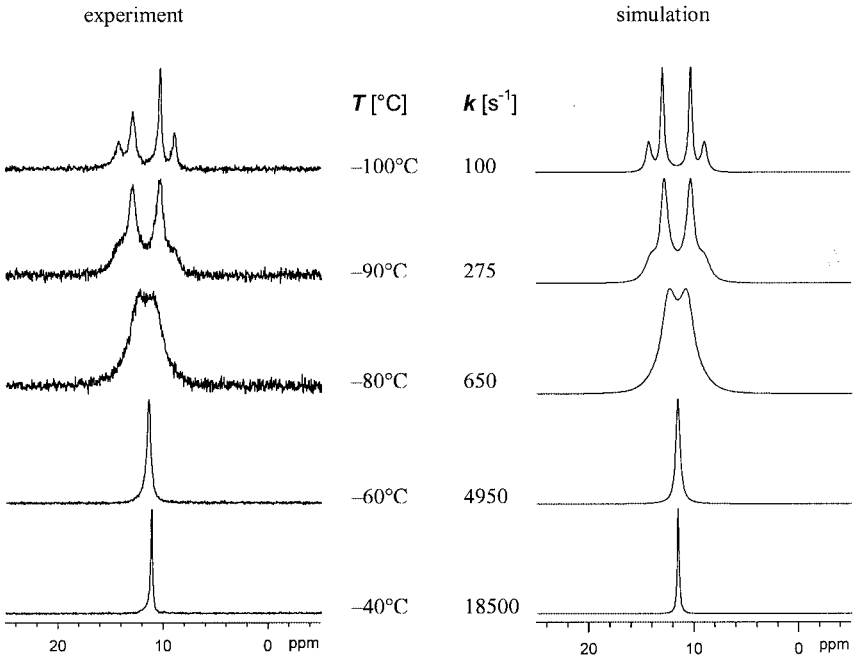

Figure 6. δ/λ isomerisation of **7a**; temperature dependence of the ^{31}P NMR spectra (81 MHz) of **7a** in CH_2Cl_2; experiment, simulation, and rate constants

evolves into a pattern corresponding to two doublets with a coupling constant of $^2J_{PP}$ = 108 Hz (Figure 6). The underlying process is interpreted in terms of a δ/λ isomerisation of the chelate cycle (Scheme 5).

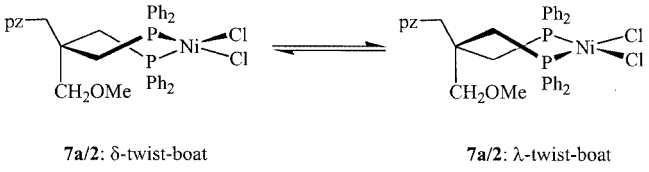

7a/2: δ-twist-boat **7a/2**: λ-twist-boat

Scheme 5. δ/λ isomerisation of the chelate cycle in **7a/2**

Due to the chiral conformation of the chelate cycle the two phosphorus nuclei within the cycle in a twist conformation are no longer equivalent. A pattern of two doublets is therefore expected for the ^{31}P NMR spectrum. The observed temperature dependence of the ^{31}P NMR spectra of **7a** can be neatly simulated[13] on the hypothesis of equilibrating δ- and λ-forms of the chelate cycle. Even though **7a** has also been obtained as crystals containing the chelate cycle in a chair conformation (**7a/1**) this conformation is not observed by NMR (temperature range below −40°C), which means that in solution the chair conformation has a higher energy than the twist-boat conformation. Figure 6 shows a comparison of the observed and the simulated ^{31}P NMR spectra of **7a**.

The rate constants for the δ/λ isomerisation of **7a** (Figure 6) give a linear Eyring plot with $\Delta G^{\neq}_{298}$ = 40.2±0.5 kJ/mol, $\Delta H^{\neq}$ = 28.1±0.9 kJ/mol and $\Delta S^{\neq}$ = −40.7±5.0 J/mol K. The coalescence temperature is 200 K (81.015 MHz), which results in $\Delta G^{\neq}_{200}$ = 37.0±0.8 kJ/mol, in fair agreement with the value taken from Eyring plot analysis ($\Delta G^{\neq}_{200}$ = 37.6±0.5 kJ/mol). The activation parameters for analogous processes, involving six-membered chelate cycles containing two phosphorus donors and a rhodium(I) centre, have recently been analysed in detail.[10] The activation enthalpies are somewhat higher (around 60 kJ/mol). The activation entropies are negative throughout, around −35 J/mol K. The ^{31}P NMR pattern observed for these rhodium chelate compounds is thus − mutatis mutandis − the same as the one observed for **7a**.[10] The main difference being that the ligands in the rhodium compounds are chiral while the ligand in **7a** is not.

Nickel compounds **7b** and **7c** contain two different PR_2 groups in the chelate cycle and their ligands are therefore chiral (Table 1). It was not possible to obtain crystals suitable for X-ray analysis of these compounds. With **7b** containing a PPh_2 donor and a P(*m*-Tol)$_2$ donor the limit of slow exchange could not be reached experimentally at the lowest achievable temperature in CH_2Cl_2 (−100°C for **7b**). With the more bulky $PMes_2$ donor group in the chelate cycle of **7c** (Table 1) a ^{31}P NMR spectrum close to the slow exchange limit was evident at −90°C. The solution could be undercooled to −110°C, at which point the slow exchange limit was reached. Above 0°C, where the high temperature limit is not yet reached, paramagnetic broadening starts to obscure individual resonances.

Throughout the temperature range −30 to −110°C a pattern with two doublets ($^2J_{PP}$ = 95 Hz) persists. A second structure, which appears as a broad singlet at −30°C, evolves into a pattern composed of a pair of two doublets with coupling constants of $^2J_{PP}$ = 98 and 101 Hz (Figure 7). This type of pattern is typical for the twist-boat conformation of a chiral chelate cycle.[10] The two doublets, which do not significantly change their appearance between

 © 2003 Wiley-VCH Verlag GmbH & Co. KGaA, Weinheim

−30°C and −110°C (signals at the left- and right-hand side of the spectrum depicted in Figure 7), are ascribed to the chair conformation of the chelate cycle, which is in only slow exchange with the twist-boat conformation, such that the appearance of the signals is not affected by exchange processes (Scheme 6). The thermodynamic stability of the chair and the twist-boat forms of the chelate cycle is different: the signals corresponding to the chair conformation have a 4:1 integral ratio to the signals corresponding to the twist-boat conformation at −30°C, while this ratio is only 3:2 at −110°C.

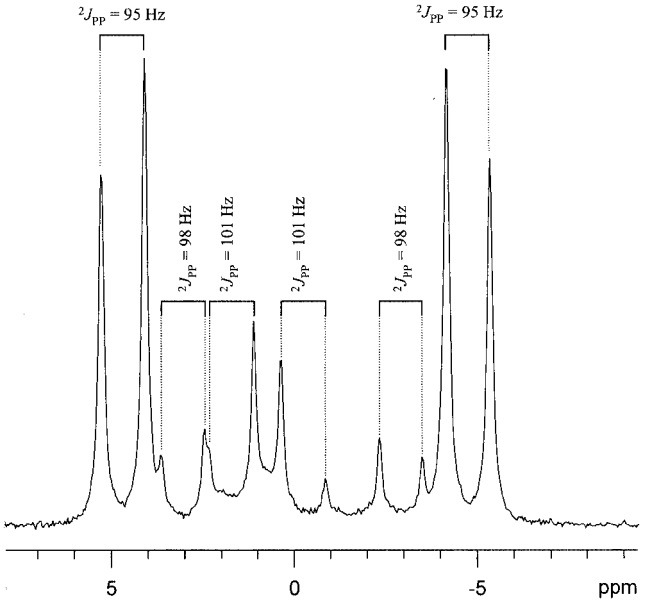

Figure 7. ^{31}P NMR spectrum of **7c** in CH_2Cl_2 at −110°C

The NMR data of **7b**−**7d** also clearly show that the ligands **5b**−**5d** bind by two phosphorus donors, with the CH_2pz group serving as a dangling arm. The structures of **7b**−**7d** are thus analogous to that of **7a** (Figure 2), which is known from crystallography (Tables 1−4). Interestingly, when the potential *tripod* ligands contain two pyrazole donors and one PR_2 donor (**6a**, **6b**) the preference for *P* coordination versus *N* coordination appears to depend on the bulkiness of the PR_2 ligand. While ligands containing one PPh_2 and two pyrazole donors show *P,N* coordination exclusively (**11a**, **11c**, **12**, **15**), ligand **6b** with a $PMes_2$,pz,pz donor set coordinates via the two pyrazole functions, with the CH_2PMes_2 group serving as a dangling arm in **13** (tetrahedral coordination). In **7c** where ligand **5c** offers a PPh_2, a $PMes_2$, and a pyrazole donor set the two phosphorus donors are bonded exclusively with the CH_2pz function playing the role of a dangling arm (square-planar coordination).

Temperature-dependent $^1H\{^{31}P\}$ NMR spectra of the palladium compound **12** (Figure 5) reveal a different type of dynamic exchange different to those already described. While the ^{31}P NMR signal of **12** is a singlet in the range −80 to 120°C the appearance of the proton spectrum changes drastically (Figure 8).

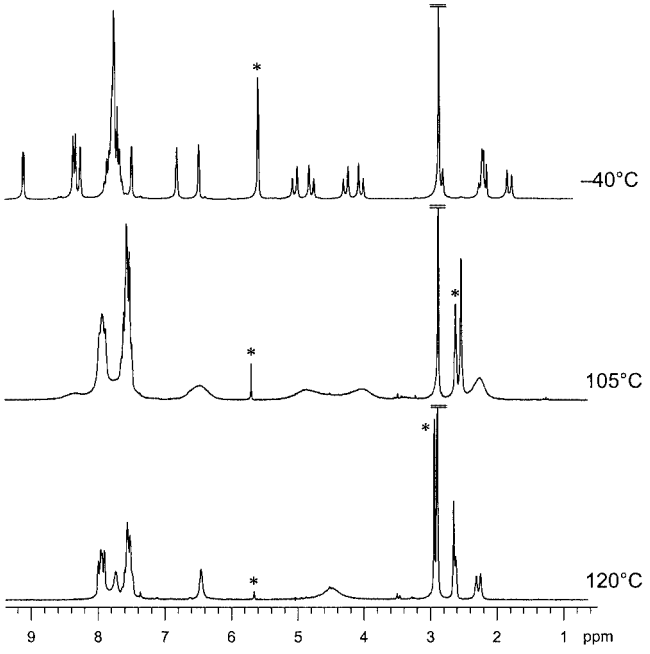

Figure 8. Variable-temperature $^1H\{^{31}P\}$ NMR spectra (200 MHz) of **12**; dynamic exchange is clearly apparent at δ ≈ 4.5 ppm and δ ≈ 6.5 ppm; spectra at 105 and 120°C were recorded in DMSO as solvent; at lower temperatures the solvent was CH_2Cl_2; asterisks designate solvent peaks

At −40°C a pattern of sharp signals is clearly evident, with all the resonances expected for **12** (Figure 8, Table 11). The signals corresponding to the coordinated CH_2pz arm and the noncoordinated one are clearly separated. The resonances of the coordinated pyrazole group are shifted downfield significantly (δ = 6.64, 8.98, 8.11), in contrast to the noncoordinated one (δ = 6.30, 7.33, 7.60). The methylene protons of the CH_2pz groups give rise to two doublets at δ = 3.79 and 4.02 ppm (noncoordinated) and 4.56 and 4.82 (coordinated), with similar coupling constants of about $^2J_{HH}$ = 14.5 Hz. At higher temperatures the corresponding signals coalesce. From the protons of the pyrazole groups (Table 11) only H4 (Scheme 13, Exp. Sect.) gives rise to a signal, which does not overlap with the signals of aromatic protons over the whole temperature range. Coalescence of signals of H4 for the coordinated and noncoordinated pro-

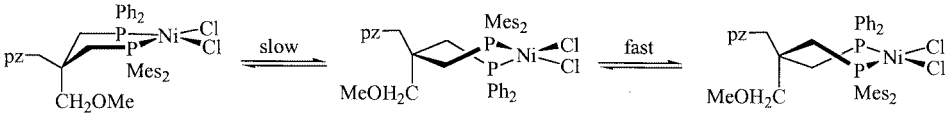

7c/1: half-chair **7c/2**: δ-twist-boat **7c/2**: λ-twist-boat

Scheme 6. Interconversion of the conformation of the chelate cycle in **7c**

 © 2003 Wiley-VCH Verlag GmbH & Co. KGaA, Weinheim

ton occurs at 105°C (k_c = 350 s^{-1}), corresponding to $\Delta G^{\neq}_{378}$ = 77.5±0.8 kJ/mol. The signals of the methylene group of the CH_2pz functions (coordinated and noncoordinated) are free from overlap with other signals over the whole temperature range. Coalescence is observed at 120°C (k_c = 150 s^{-1}), corresponding to $\Delta G^{\neq}_{403}$ = 80.0±0.8 kJ/mol. This kind of exchange phenomenon (Scheme 7) has not yet been observed for potential *tripod* ligands containing a P,N,N donor set.[5b]

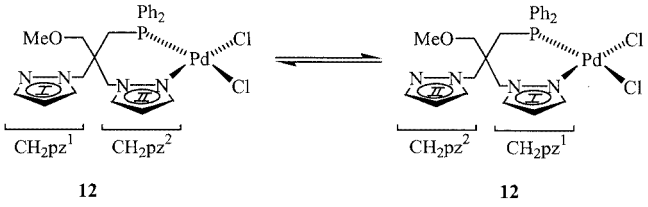

Scheme 7. Dynamic exchange of the coordinated and noncoordinated CH_2pz function of **12** at higher temperatures

Substitution Products

All compounds **7**−**14** (Table 1) contain the chelate ligands bonded to an $MHal_2$ entity. Even though the metal−halide bond lengths are independent of the type of chelate ligand within each set of compounds (square-planar, tetrahedral, see Table 3), exchange of the halide ligands by other functions might well influence the binding mode of the chelate ligand. To analyse this potential influence derivatives **16**−**19** (Scheme 8, Table 5) were synthesized in which one or both of the halide functions are replaced by organic substituents.

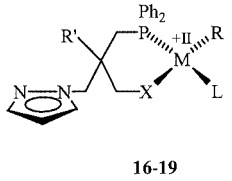

Scheme 8. General structure of **16**−**19**

Compound **7a**, after activation with $TlPF_6$, reacts with C_3H_5MgBr to produce **16a·PF$_6$** in which the phosphorus donors of the chelate cycle are *trans* to an η^3-coordinated allylic system (Scheme 9). The palladium compound **16b·PF$_6$** was obtained by treating $[Pd(\eta^3\text{-}C_3H_5)Cl]_2$ with the ligand $EtOCH_2C(CH_2PPh_2)(CH_2pz)_2$[5e] and with KPF_6 as the halide-abstracting reagent (Scheme 9).

Direct, selective substitution of just one halide function in compounds of the type $[(chelate)M^{II}Hal_2]$ was, however, not successful. Substitution products $[(chelate)M^{II}RHal]$ were synthesized by starting from $[L_2M^{II}RHal]$ [L_2 = cod, $(PPh_3)_2$] by reaction with the *tripod* ligands.

Compound **17** was obtained from [*trans*-$(PPh_3)_2$Ni(Mes)Br] using **5a** as the chelating agent (Scheme 10).

Similarly, the palladium compound **18** was obtained by the reaction of [(η^4-cod)PdClMe] with **5a** (Scheme 11).

The structures of compounds **16a·PF$_6$**, **16b·PF$_6$**, and **18** (Figure 9, Tables 6 and 9) were analysed by crystallography. Suitable single crystals could not be obtained for **17**.

When, instead of **5a**, ligand **6a** − with its two pyrazole functions − was treated with [*trans*-$(PPh_3)_2$Ni(Mes)Br] the formation of **6a·Ni(Br)Mes** as an analogue of **17** (Scheme 10) was indicated by its ^{31}P NMR spectrum (a sin-

Table 5. Substitution compounds **16**−**19**

Compd.	Ligand	Coord. group X	Noncoord. group R′	M(R)(L)	Colour of compd.	Coord. geometry	Crystal structure
16a·PF$_6$	**5a**	PPh_2	CH_2OMe	$Ni(allyl)^+$	yellow	square-planar	yes
16b·PF$_6$	−[a]	pz	CH_2OEt	$Pd(allyl)^+$	colourless	square-planar	yes
17	**5a**	PPh_2	CH_2OMe	Ni(Mes)Br	yellow	square-planar	no
18	**5a**	PPh_2	CH_2OMe	PdMeCl	pale grey	square-planar	yes
19·PF$_6$	**6a**	pz	CH_2OMe	$Ni(Mes)(PPh_3)^+$	yellow	square-planar	yes

[a] Ligand $EtOCH_2C(CH_2PPh_2)(CH_2pz)_2$; synthesis see ref.[5e]

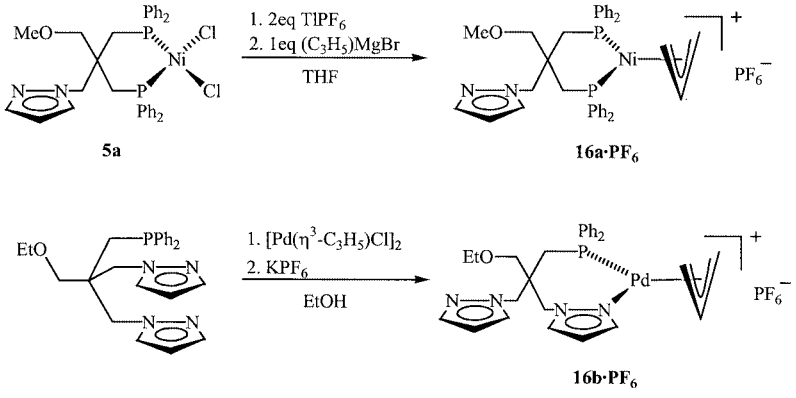

Scheme 9. Synthesis of cationic (η^3-allyl)metal complexes **16a·PF$_6$** and **16b·PF$_6$**

 © 2003 Wiley-VCH Verlag GmbH & Co. KGaA, Weinheim

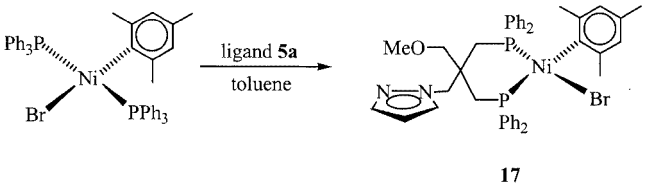

Scheme 10. Synthesis of compound **17**

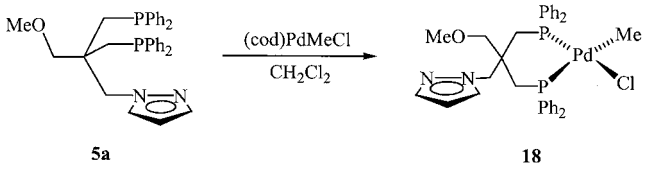

Scheme 11. Synthesis of compound **18**

glet at δ = 11.8 ppm). However, the compound could not be crystallized. Treatment of the reaction mixture with $TlPF_6$ resulted in the expected $Br^- \rightleftarrows PPh_3$ exchange to produce **19·PF$_6$** (Scheme 12), which could be characterized by X-ray analysis (Figure 10, Tables 6, 9).

The conformation of the chelate cycles (Table 6) in **16a**$^+$, **16b**$^+$, **18**, and **19**$^+$ is quantitatively similar to that described for [(chelate)$M^{II}Hal_2$] compounds (Table 2). In all four compounds the coordination around the metal atom is square-planar. The conformation of the chelate cycles (Table 6) corresponds to a chair (**16a**$^+$, **19**$^+$), a half-chair (**18**) and a twist-boat conformation (**16b**$^+$). The bond lengths between the chelate donor atoms and the metal atoms are very similar to the ones shown in Table 3. The M−C and M−Hal distances to the external ligands, as well as the valence angles at the metal centre, are all in the usual and normal range (Table 6). The only clear indication of a *trans* influence is observed for the M−P bonds in **18**. The N−P bond *trans* to the chloride ligand is not much different from the one observed in **12** (224.6 pm) with its P_2Cl_2 donor set (Table 3). The M−P distance *trans* to the methyl substituent in **18** is lengthened by the *trans* influence of the methyl group to 231.4 pm (Table 6). There is, however, some uncertainty with respect to the exact values of both distances, which may be larger than the calculated standard deviation (Table 6), due to the fact that crystals of **18** show some positional disorder between the chloride and the methyl substituents even though this disorder could be resolved by appropriate refinement (Table 9).

While the structure of the intermediate [**6a·Ni(Br)Mes**] formulated in the synthesis of **19·PF$_6$** may be − albeit indirectly − inferred from X-ray analysis of **19·PF$_6$** (see above) the structure of **17** [**5a·Ni(Br)Mes**] has to be inferred

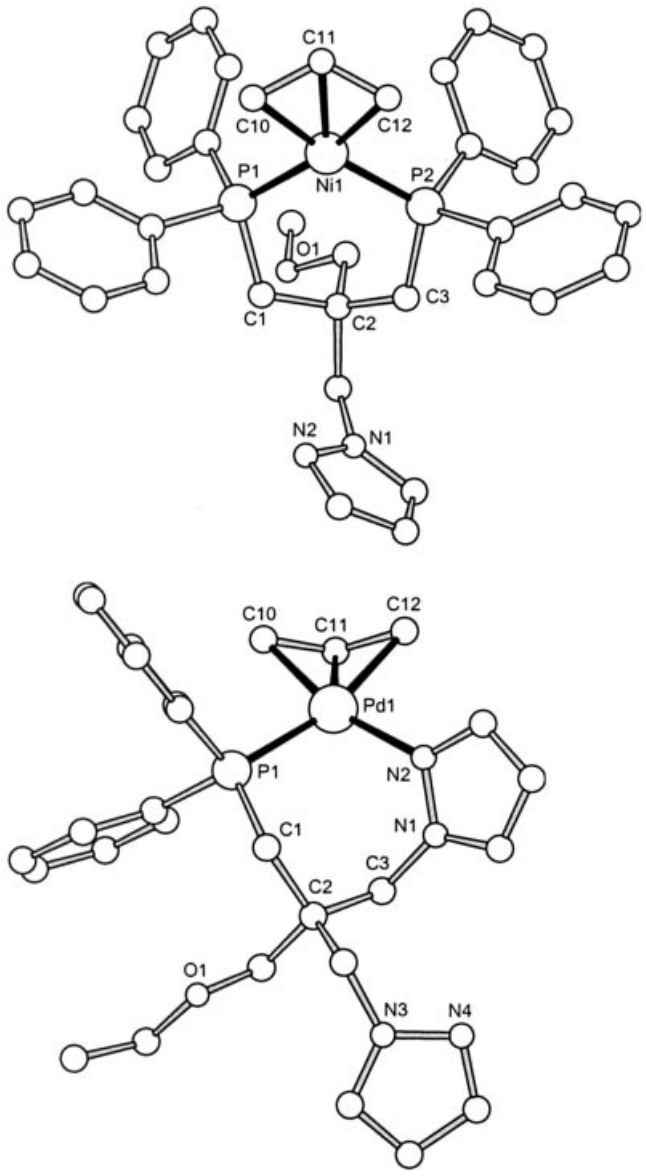

Figure 9. X-ray structure of the cation **16a**$^+$ (top) and **16b**$^+$ (bottom)

inter alia from NMR data. As expected for the diastereotopic phosphorus nuclei in **17** (the compound as a whole is chiral!) two doublets are observed in its ^{31}P NMR spectrum (see Exp. Sect. and remark therein). The diamagnetism of **17** proves the square-planar coordination of the nickel centre.

Even if the above results show that the conformation of the chelate cycles is not very much dependent on the kind

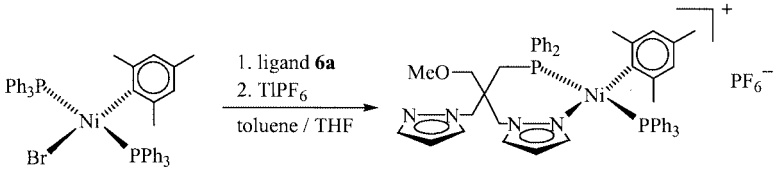

Scheme 12. Synthesis of **19·PF$_6$**

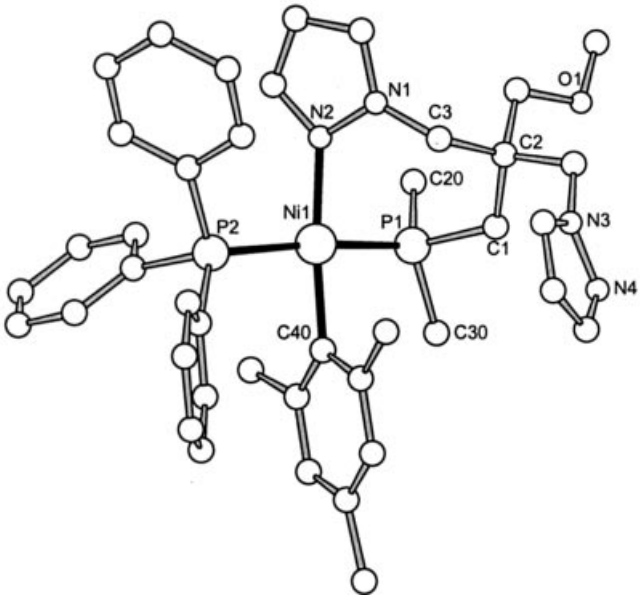

Figure 10. X-ray structure of the cation **19**$^+$ (for the sake of clarity, the phenyl groups of the *tripod* ligand are represented by their *ipso*-carbon atom only)

of co-ligands L in [(chelate)$M^{II}L_2$] there is a definite influence due to the kind of co-ligands on the type of coordination around a nickel(II) centre: ligand **6a** results in a tetrahedral coordination of the nickel atom with the $NiBr_2$ fragment (**11a**) while the same ligand coordinated to an $[Ni^{II}(PPh_3)(Mes)]^+$ fragment induces a square-planar coordination in **19**$^+$. The greater ligand field of PPh_3 and Mes (**19**$^+$) as compared with the two Br (**11a**) must be the reason for this.

Conclusion

1. The synthesis of *tripod* ligands $RCH_2C(CH_2PR_2)(CH_2pz)(CH_2X)$ with X being a phosphorus or a nitrogen donor has broad applicability.

2. These potential *tripod* ligands coordinate to d^8-metal ions (Ni^{II}, Pd^{II}, Pt^{II}) as bidentate chelate cycles, leaving the third group as a dangling arm. For ligands with a P,P,N donor set, coordination via the two phosphorus donors is generally observed. For ligands with a P,N,N donor set containing a bulky phosphorus donor (CH_2PMes_2), *N*,*N* coordination may be preferred over *P*,*N* coordination.

Table 6. Selected bond lengths [pm], bond angles [°], and torsion angles [°] of compounds **16a**, **16b**, **18**, and **19**

	16a·PF_6		**16b·PF_6**		**18**				**19·PF_6**			
	M	X	R, L	M	X	R, L	M	X	R	L	M	X	R	L
	Ni	PPh_2	η^3-$C_3H_5^-$	Pd	pz	η^3-$C_3H_5^-$	Pd	PPh_2	CH_3^-	Cl^-	Ni	pz	Mes^-	PPh_3
Chelate cycle[a][b]	Chair (2, 6 = P)			λ-twist (2 = P, 6 = Q)			Half-chair (2, 6 = P)				chair (2 = P, 6 = Q)			
M−2−3−4	+45.3			+60.2			+42.4				+58.6			
2−3−4−5	−62.4			−50.2			−67.3				−51.1			
3−4−5−6	+62.9			−32.1			+69.3				+65.5			
4−5−6−M	−46.7			+84.5			−45.2				−80.0			
5−6−M−2	+25.6			−53.7			+17.1				+66.8			
6−M−2−-3	−24.8			+0.9			−16.4				−61.0			
3−2−6−5	+0.7			−57.0			+0.7				+11.9			
M−C	200.8(1) (internal)			214.4(4) (internal)			218.0(3)				194.5(4) (*trans* to N)			
	202.3(1), 204.6(1) (terminal)			211.2(4) (*trans* to N)			–				–			
				220.7(3) (*trans* to P)										
M−Cl	–			–			236.3(1)				–			
M−P	217.0(2), 217.4(2)			230.0(1)			223.7(1) (*trans* to Cl^-)				222.4(3) (P = ligand)			
							231.4(1) (*trans* to CH_3^-)				225.8(3) (P = PPh_3)			
M−N	–			209.5(3)			–				196.1(7) (*trans* to Mes^-)			
P−M−R	93.5(1)			97.1(1)			88.1(1)				88.4(1)			
P−M−X	99.5(1)			96.5(1)			95.8(1)				91.0(1)			
L−M−X	94.8(1)			98.3(1)			90.1(1)				94.2(1)			
L−M−R	72.1(1)			67.8(1)			86.2(1)				87.3(1)			
L−M−P	166.4(1)			164.7(1)			173.6(1)				172.2(1)			
X−M−R	165.3(1)			165.7(1)			174.4(1)				171.6(1)			

[a] Standard deviations in units of the least significant digit are given in each case. [b] A consistent numbering scheme for all the compounds as depicted below is used for the sake of easier comparison.

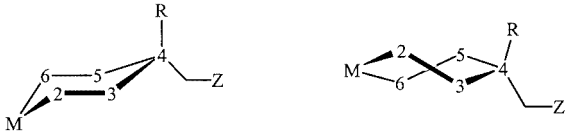

 © 2003 Wiley-VCH Verlag GmbH & Co. KGaA, Weinheim

3. For palladium(II) compounds derived from ligands containing a P,N,N donor set, dynamic exchange between coordinated and noncoordinated N donors is observed.

4. While palladium(II) and platinum(II) derivatives show a square-planar coordination throughout, the kind of coordination around the nickel atom (square-planar versus tetrahedral) depends on the donor set of the chelate ligand as well as on the kind of co-ligands.

Experimental Section

General Remarks: All manipulations involving phosphanes were carried out under argon by means of standard Schlenk techniques. All solvents were dried by standard methods[14] and distilled under argon. The solvents $CDCl_3$ and CD_2Cl_2 used for NMR spectroscopic measurements were degassed by three successive freeze-pump-thaw cycles and dried over molecular sieves (4 Å). NMR: Bruker Avance DPX 200 at 200.12 MHz (^{1}H); 50.323 MHz (^{13}C{^{1}H}); 81.015 MHz (^{31}P{^{1}H}); T = 303 K unless stated otherwise; chemical shifts (δ) in ppm with respect to $CDCl_3$ (^{1}H: δ = 7.27 ppm; ^{13}C: δ = 77.0 ppm) and CD_2Cl_2 (^{1}H: δ = 5.32 ppm; ^{13}C: δ = 53.5 ppm) as internal standards. ^{31}P chemical shifts (δ) in ppm with respect to 85% H_3PO_4 (^{31}P: δ = 0 ppm) as external standard. The NMR numbering scheme for the pyrazole cycle is shown in Scheme 13.[15] MS: Finnigan MAT 8230; EI (70 eV); FAB (xenon; matrix: 4-nitrobenzyl alcohol). UV/Vis: Perkin−Elmer Lambda 19. Elemental analyses: Microanalytical Laboratory of the Organisch-Chemisches Institut, University of Heidelberg.

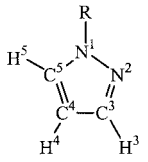

Scheme 13. Numbering scheme of pyrazole as used for NMR data

Crystallographic Structure Determinations: Suitable crystals were taken directly from the mother liquor, immersed in perfluorinated polyether oil, and fixed to a glass capillary at 200 K. The measurements were carried out with a Siemens P4 four-circle diffractometer or with an Enraf−Nonius Kappa CCD diffractometer, using graphite-monochromated Mo-K_α radiation throughout. For the Siemens P4 diffractometer measurements the intensities of three check reflections (measured every 100 reflections) remained constant throughout the data collection, thus indicating crystal and electronic stability. The data collected with the Siemens P4 diffractometer were corrected as usual, including an experimental ab-

Table 7. Crystallographic data of compounds **7a/1**, **7a/2**, **8**, **9a**, and **11a**

	7a/1	**7a/2**	**8**	**9a**	**11a**
Empirical formula (without solvate)	$C_{33}H_{34}Cl_2N_2NiOP_2$	$C_{33}H_{34}Cl_2N_2NiOP_2$	$C_{33}H_{34}Br_2N_2NiOP_2$	$C_{33}H_{34}Cl_2N_2OP_2Pd$	$C_{24}H_{27}Br_2N_4NiOP$
Formula mass [g/mol]	666.2	666.2	755.1	713.9	637.0
Solvate	1 CH_2Cl_2	0.5 CH_2Cl_2	−	1 CH_2Cl_2	−
Crystal size [mm]	0.20×0.30×0.40	0.20×0.30×0.40	0.30×0.30×0.40	0.20×0.20×0.30	0.30×0.20×0.05
Crystal system	monoclinic	triclinic	monoclinic	monoclinic	monoclinic
Space group	$P2_1/c$ (no. 14)	$P\bar{1}$ (no. 2)	$P2_1/n$ (no. 14)	$P2_1/c$ (no. 14)	$P2_1/n$ (no. 14)
Lattice constants:					
a [pm]	1136.6(3)	1140.2(3)	1110.1(3)	1144.0(2)	1082.5(2)
b [pm]	2283.6(5)	1118.0(3)	1304.6(2)	2300.8(4)	2004.4(4)
c [pm]	1359.7(6)	1609.3(3)	2211.3(4)	1367.4(2)	1168.4(2)
α [°]	90	81.27(2)	90	90	90
β [°]	93.68(2)	89.71(2)	93.41(1)	86.51(1)	92.75(3)
γ [°]	90	61.75(1)	90	90	90
V [10^6×pm^3]	3522(1)	1781(1)	3197(1)	3593(1)	2532(1)
Z	4	2	4	4	4
d_x [g×cm^{-3}]	1.417	1.320	1.569	1.473	1.671
T [K]	200	200	200	200	200
Measuring device	Siemens Nicolet-Syntex	Siemens Nicolet-Syntex	Siemens Nicolet-Syntex	Siemens Nicolet-Syntex	Nonius Kappa CCD
No. of reflect. for cell refinement	31	31	37	33	
Scan range [°]	3.5 ≤ 2Θ ≤ 54.0	4.1 ≤ 2Θ ≤ 48.0	3.6 ≤ 2Θ ≤ 51.0	3.5 ≤ 2Θ ≤ 51.0	4.0 ≤ 2Θ ≤ 55.0
Method	ω-scan, Δω = 0.54°	ω-scan, Δω =0.54°	ω-scan, Δω =0.54°	ω-scan, Δω =0.54°	ω-scan, Δω = 1.00°
Scan speed	10° min^{-1}	12° min^{-1}	12° min^{-1}	8° min^{-1}	5 s/frame
No. of measured reflections	8071	5826	6225	7030	10996
No. of unique reflections	7689	5510	5908	6681	5742
No. of observed reflections	5769	4543	3916	4626	4682
Observation criterion	$I \geq 2\sigma$	$I \geq 2\sigma$	$I \geq 2\sigma$	$I \geq 2\sigma$	$I \geq 2\sigma$
No. of param. refined	403	411	398	403	302
Resid. el. density [10^{-6}e·pm^{-3}]	0.61	0.95	0.61	0.79	0.45
R_1/R_w [%] (refinement on F^2)	4.3/13.5	4.9/15.4	4.5/12.2	5.0/11.0	3.2/7.6

 © 2003 Wiley-VCH Verlag GmbH & Co. KGaA, Weinheim

Table 8. Crystallographic data of compounds **11c**, and **12**−**15**

	11c	**12**	**13**	**14**	**15**
Empirical formula (without solvate)	$C_{25}H_{29}Br_2N_4NiOP$	$C_{24}H_{27}Cl_2N_4OPPd$	$C_{30}H_{39}Cl_2N_4NiOP$	$C_{14}H_{18}Br_2N_6Ni$	$C_{50}H_{58}Br_4N_8Ni_2O_2P_2$
Formula mass [g/mol]	651.0	595.8	632.2	488.8	1302.0
Solvate	0.5 CH_2Cl_2	−	−	−	−
Crystal size [mm]	0.30×0.30×0.30	0.20×0.10×0.05	0.08×0.15×0.40	0.30×0.20×0.20	0.30×0.30×0.30
Crystal system	monoclinic	triclinic	triclinic	orthorhombic	triclinic
Space group	$P2_1/c$ (no. 14)	$P\bar{1}$ (no. 2)	$P\bar{1}$ (no. 2)	*Pbca* (no. 61)	$P\bar{1}$ (no. 2)
Lattice constants:					
a [pm]	958.4(3)	792.1(2)	790.0(2)	1418.7(3)	943.3(2)
b [pm]	1345.0(3)	852.9(2)	1225.0(3)	1486.7(3)	982.3(2)
c [pm]	2266.8(5)	1860.4(4)	1577.2(3)	1694.3(3)	1574.2(2)
α [°]	90	94.76(3)	91.48(3)	90	80.15(1)
β [°]	80.63(2)	100.88(3)	90.15(3)	90	74.09(1)
γ [°]	90	91.97(3)	97.29(3)	90	70.04(1)
V [10^6×pm^3]	2883(1)	1228(1)	1514(1)	3574(1)	1314(1)
Z	4	2	2	8	1
d_x [g×cm^{-3}]	1.600	1.611	1.387	1.817	1.646
T [K]	200	200	200	200	200
Measuring device	Siemens Nicolet-Syntex	Nonius Kappa CCD	Nonius Kappa CCD	Nonius Kappa CCD	Siemens Nicolet-Syntex
No. of reflect. for cell refinement	31				32
Scan range [°]	4.3 ≤ 2Θ ≤ 52.0	4.5 ≤ 2Θ ≤ 55.0	3.4 ≤ 2Θ ≤ 55.1	4.6 ≤ 2Θ ≤ 52.0	4.4 ≤ 2Θ ≤ 51.0
Method	ω-scan, Δω =0.54°	ω-scan, Δω =1.00°	ω-scan, Δω =1.00°	ω-scan, Δω =1.00°	ω-scan, Δω =0.54°
Scan speed	8° min^{-1}	10 s/frame	2 s/frame	10 s/frame	8° min^{-1}
No. of measured reflections	5939	7896	13724	15731	5162
No. of unique reflections	5599	5538	6951	3525	4848
No. of observed reflections	3702	4670	4260	1544	3833
Observation criterion	$I \geq 2\sigma$	$I \geq 2\sigma$	$I \geq 2\sigma$	$I \geq 2\sigma$	$I \geq 2\sigma$
No. of param. refined	341	302	362	212	312
Resid. el. density [10^{-6}e·pm^{-3}]	0.87	0.43	0.83	0.78	0.76
R_1/R_w [%] (refinement on F^2)	5.5/15.3	3.1/6.8	5.2/12.7	4.9/6.5	3.6/9.9

sorption correction. Data from the Enraf−Nonius Kappa CCD device were processed using the standard Nonius software.[16] The calculations were performed using the SHELXT PLUS software package. Structures were solved by direct methods with the SHELXS-97 program and refined with the SHELXL-97 program.[17] Graphical handling of the structural data during solution and refinement was performed with XMPA.[18] Atomic coordinates and anisotropic thermal parameters of the non-hydrogen atoms were refined by full-matrix least-squares calculations. Data relating to the structure determinations are collected in Tables 7, 8, and 9. Figures 1−5, 9, and 10 were prepared using WinRay-32.[19] CCDC-194026 to -194039 contain the supplementary crystallographic data for this paper. These data can be obtained free of charge at www.ccdc.cam.ac.uk/conts/retrieving.html [or from the Cambridge Crystallographic Data Centre, 12 Union Road, Cambridge CB2 1EZ, UK; Fax: (internat.) + 44-1223/336-033; E-mail: deposit@ccdc.cam.ac.uk].

Materials: Silica gel (Kieselgel 32−63 μm, ICN Biomedicals GmbH) used for chromatography was degassed at 1 mbar for 24 h and saturated with argon. A solution of *n*BuLi in hexane (2.5 M) was used for deprotonations. **1**,[1c] **2a**,[5e] **2c**,[5e] **3a**,[5e] **4a**,[5e] $EtOCH_2C(CH_2PPh_2)(CH_2pz)_2$,[5e] $CH_3C(CH_2pz)_3$,[5e] $HPPh_2$,[20] $HPMes_2$,[21] [*trans*-$(PPh_3)_2$Ni(Mes)Br],[22] and [(cod)PdClMe][23] were prepared according to or by adaptation of literature procedures. All other chemicals were obtained from commercial suppliers and used without further purification. Boiling range of the light petroleum ether used: 40−60°C. NMR and analytical data are collected in Tables 10−15.

Ligand Synthesis

Synthesis of 2b: Pyrrole (0.81 g, 12 mmol) was dissolved in THF (50 mL) and deprotonated at 0°C with 1 equiv. of KO*t*Bu (1.35 g, 12 mmol). After warming to 25°C, the solution was stirred for 30 min and then added at 0°C to a solution of **1** (2.59 g, 10 mmol) in THF (50 mL). The reaction was completed by refluxing for 4 h. In another flask, $HPPh_2$ (2.23 g, 12 mmol) was dissolved in THF (50 mL) and deprotonated at 0°C with 1 equiv. of KO*t*Bu (1.35 g, 12 mmol). After warming to 25°C and stirring for 30 min, the red potassium phosphide solution was added dropwise to the first reaction mixture, which was maintained at 0°C. After warming to 25°C and stirring for 10 h (the phosphide substitution was monitored by TLC), the then yellow solution was quenched by the addition of deoxygenated water (20 mL). The aqueous phase was extracted with diethyl ether (30 mL, 2×). The combined organic phases were washed with deoxygenated brine, dried with $MgSO_4$, filtered, and concentrated in vacuo. The resulting viscous oil was purified by column chromatography on silica gel by using petroleum ether/diethyl ether (1:1; R_f = 0.47) as eluent to obtain 1.84 g (5.5 mmol, 55%) of **2b** as a colourless, microcrystalline powder. ^{31}P NMR ($CDCl_3$): δ = −26.9 (s, PPh_2) ppm. For further analytical data see Tables 10, 12, and 14.

General Procedure for the Synthesis of 3 and 4 The appropriately substituted oxetane **2** (1 equiv.) was dissolved in THF (50 mL). In a second flask, HPR_2 (1.2 equiv.) was dissolved in THF (50 mL) and deprotonated at 0°C with *n*BuLi (1.2 equiv.). After warming to 25°C and stirring for 30 min, the red lithium phosphide solution

 © 2003 Wiley-VCH Verlag GmbH & Co. KGaA, Weinheim

Table 9. Crystallographic data of compounds **16a**, **16b**, **18**, and **19**

	16a·PF_6	**16b·PF_6**	**18**	**19·PF_6**
Empirical formula (without solvate)	$C_{36}H_{39}F_6N_2NiOP_3$	$C_{28}H_{34}F_6N_4OP_2Pd$	$C_{34}H_{37}ClN_2OP_2Pd$	$C_{51}H_{53}F_6N_4NiOP_3$
Formula mass [g/mol]	781.3	725.0	693.5	1003.6
Solvate	0.75 CH_2Cl_2	–	–	0.35 CH_2Cl_2
Crystal size [mm]	0.30×0.30×0.40	0.05×0.05×0.30	0.20×0.10×0.05	0.10×0.05×0.05
Crystal system	monoclinic	orthorhombic	monoclinic	triclinic
Space group	*Cc* (no. 9)	$Pna2_1$ (no. 33)	$P2_1/n$ (no. 14)	$P\bar{1}$ (no. 2)
Lattice constants:				
a [pm]	1706.3(3)	1947.8(4)	1110.9(2)	1091.5(2)
b [pm]	1207.7(2)	1712.2(3)	1328.7(3)	1186.1(2)
c [pm]	1875.0(5)	898.3(2)	2174.2(4)	2098.4(4)
α [°]	90	90	90	91.25(3)
β [°]	95.80(1)	90	91.70(3)	105.04(3)
γ [°]	90	90	90	111.04(3)
V [10^6×pm^3]	3844(1)	2996(1)	3208(1)	2429(1)
Z	4	4	4	2
d_x [g×cm^{-3}]	1.460	1.607	1.430	1.412
T [K]	200	200	200	200
Measuring device	Siemens Nicolet-Syntex	Nonius Kappa CCD	Nonius Kappa CCD	Nonius Kappa CCD
No. of reflect. for cell refinement	25			
Scan range [°]	$4.1 \le 2\Theta \le 51.0$	$3.2 \le 2\Theta \le 52.0$	$3.7 \le 2\Theta \le 55.0$	$3.7 \le 2\Theta \le 50.0$
Method	ω-scan, Δω = 0.54°	ω-scan, Δω = 1.00°	ω-scan, Δω = 1.00°	ω-scan, Δω = 0.50°
Scan speed	12° min^{-1}	30 s/frame	30 s/frame	30 s/frame
No. of measured reflections	3430	43721	13378	16851
No. of unique reflections	3430	5882	7316	8526
No. of observed reflections	2772	5315	5458	5380
Observation criterion	$I \ge 2\sigma$	$I \ge 2\sigma$	$I \ge 2\sigma$	$I \ge 2\sigma$
No. of param. refined	477	399	375	548
Resid. el. density [10^{-6}e·pm^{-3}]	0.44	0.39	0.62	1.02
R_1/R_w [%] (refinement on F^2)	5.3/14.6	2.8/6.3	5.5/10.0	14.6/24.3

was added dropwise to the oxetane solution at 0°C. The mixture was allowed to warm to 25°C, while the reaction progress was monitored by TLC. Upon completion (10 h stirring at 25°C), the reaction was quenched by the addition of deoxygenated water (50 mL). The aqueous phase was extracted with diethyl ether (30 mL, 2×). The combined organic phases were washed with deoxygenated brine, dried with $MgSO_4$, filtered, and concentrated in vacuo yielding the crude products as pale yellow oils. The crude product was purified by column chromatography on silica gel. **3b**: Starting material **2a** (2.02 g, 6.0 mmol). Eluent petroleum ether/diethyl ether (2:1; R_f = 0.24). Yield 1.90 g (3.45 mmol, 58%) as a colourless, microcrystalline powder. ^{31}P NMR ($CDCl_3$): δ = −29.9 [d, $^4J_{PP}$ = 10 Hz, P(*m*-Tol)$_2$], −29.5 (d, $^4J_{PP}$ = 10 Hz, PPh$_2$) ppm. **3c**: Starting material **2a** (1.97 g, 5.85 mmol). Eluent petroleum ether/diethyl ether (1:1; R_f = 0.51). Yield 2.89 g (4.75 mmol, 81%) as a colourless, microcrystalline powder. ^{31}P NMR ($CDCl_3$): δ = −35.9 (d, $^4J_{PP}$ = 16 Hz, PMes$_2$), −28.3 (d, $^4J_{PP}$ = 16 Hz, PPh$_2$). **3d**: Starting material **2a** (2.02 g, 6.0 mmol). Eluent petroleum ether/diethyl ether (3:1; R_f = 0.35). Yield 1.35 g (2.5 mmol, 42%) as a colourless, microcrystalline powder. ^{31}P NMR ($CDCl_3$): δ = −29.9 (br. s, PPh$_2$), −18.5 [br. s, P(*c*-C_6H_{11})$_2$] ppm. **3e**: Starting material **2b** (670 mg, 2.0 mmol). Eluent petroleum ether/diethyl ether (2:1, R_f = 0.36). Yield 830 mg (1.6 mmol, 80%) as a colourless, microcrystalline powder. ^{31}P NMR ($CDCl_3$): δ = −29.5 (s, PPh$_2$) ppm. **4b**: Starting material **2c** (1.75 g, 8.0 mmol). Eluent petroleum ether/diethyl ether (2:3; R_f = 0.35). Yield 2.65 g (5.4 mmol, 68%) as a colourless, microcrystalline powder. ^{31}P NMR ($CDCl_3$): δ = −36.5 (s, PMes$_2$) ppm. For further analytical data see Tables 10, 12, and 14.

General Procedure for the Synthesis of 5 and 6: The substituted hydroxy compound **3** or **4** (1 equiv.), respectively, was dissolved in THF (50 mL) and the solution was cooled to 0°C. Addition of solid KO*t*Bu (2 equiv.) yielded a clear, pale yellow solution. After 5 min of stirring at 0°C, 2 equiv. of methyl iodide was added rapidly. Within a few minutes KI precipitated. The suspension was stirred for at 0°C 1 h (the methylation was monitored by TLC). The solvent was evaporated in vacuo at 0°C. The residue was dissolved in diethyl ether (30 mL) and the solution was filtered to remove potassium iodide. Removal of the solvent yielded the crude products as colourless oils. The crude product was purified by column chromatography on silica gel. **5a**: Starting material **3a** (1.77 g, 3.4 mmol). Eluent petroleum ether/diethyl ether (3:1; R_f = 0.36). Yield 1.41 g (2.6 mmol, 78%) as a colourless, microcrystalline powder. ^{31}P NMR ($CDCl_3$): δ = −28.7 (s, PPh$_2$) ppm. **5b**: Starting material **3b** (1.60 g, 2.9 mmol). Eluent petroleum ether/diethyl ether (3:1; R_f = 0.36). Yield 1.31 g (2.3 mmol, 80%) as a colourless, microcrystalline powder. ^{31}P NMR ($CDCl_3$): δ = −29.0 [d, $^4J_{PP}$ = 6 Hz, P(*m*-Tol)$_2$], −28.7 (d, $^4J_{PP}$ = 6 Hz, PPh$_2$) ppm. **5c**: Starting material **3c** (700 mg, 1.15 mmol). Eluent petroleum ether/diethyl ether (3:1; R_f = 0.43). Yield 615 mg (1.0 mmol, 87%) as a colourless, microcrystalline powder. ^{31}P NMR ($CDCl_3$): δ = −35.8 (d, $^4J_{PP}$ = 6 Hz, PMes$_2$), −28.3 (d, $^4J_{PP}$ = 6 Hz, PPh$_2$). **5d**: Starting material **3e** (625 mg, 1.2 mmol). Eluent petroleum ether/diethyl ether (2:1; R_f = 0.65). Yield 560 mg (1.05 mmol, 87%) as a colourless, microcrystalline powder. ^{31}P NMR ($CDCl_3$): δ = −29.2 (s, PPh$_2$) ppm. **6a**: Starting material **4a** (1.62 g, 4.0 mmol). Eluent petroleum ether/diethyl ether (2:1; R_f = 0.49). Yield 1.49 g (3.6 mmol, 89%) as a colourless, microcrystalline powder. ^{31}P

 © 2003 Wiley-VCH Verlag GmbH & Co. KGaA, Weinheim

Table 10. Chemical shifts (δ values), integrals [*x* H] and coupling constants *J* in the $^1H\{^{31}P\}$ NMR spectra of **2**−**6** in $CHCl_3$

Compd.[a][b]	CH_2N [2 H]	CH_2O [2 H]	CH_2P [4 H]	OH [1 H]	OCH_3 [3 H]	Pyrazole-H[c] H4[d] [1 H]	H5[d] [1 H]	H3[d] [1 H]	Aryl-H	Other
2b	4.48 s	4.30 d, 4.42 d [4 H] $^2J_{HH}$ = 6.2	2.44 s [2 H]	–	–	–	–	–	7.36−7.51 m [10 H]	6.19 pt, 6.72 pt [4 H] pyrrole-*H*[c]
3a	4.23 s	3.26 s	2.46 br. s	n. d.	–	6.18 t	7.09 d	7.49 d	7.33−7.46 m [20 H]	
3b	4.28 s	3.31 s	2.49 br. s	4.06 br. s	–	6.21 t	7.15 d	7.50 d	7.22−7.49 m [18 H]	2.35 br. s [6 H] *m*-CH_3
3c	4.13 d, 4.26 d $^2J_{HH}$ = 14.2	3.23 d, 3.36 d $^2J_{HH}$ = 12.0	2.49 m, 2.72 d, 2.86 d $^2J_{HH}$ = 14.3	3.92 br. s	–	6.16 t	6.90 d	(o)	6.78 m [4 H], 7.29−7.48 m [10 H]	2.24 s [6 H] *p*-CH_3 2.38 s, 2.40 s [12 H] *o*-CH_3
3d	4.29 br. s	3.30 d, 3.46 d $^2J_{HH}$ = 11.8	1.73 m, 2.33 d, 2.46 d $^2J_{HH}$ = 14.7	4.22 br. s	–	6.24 t	(o)	(o)	7.30−7.52 m [10 H]	1.21 m, 1.48 m, 1.73 m [22 H] cyclohexyl-*H*
3e	4.11 s	3.43 s	2.24 d, 2.39 d $^2J_{HH}$ = 14.3	n. d.	–	–	–	–	7.28−7.51 m [20 H]	6.12 pt, 6.69 pt [4 H] pyrrole-*H* [c]
4a	4.22 d, 4.46 d [4 H] $^2J_{HH}$ = 14.3	3.27 s	2.13 s [2 H]	4.37 br. s	–	6.26 t [2 H]	7.31 d [2 H]	7.60 d [2 H]	7.35−7.48 m [10 H]	
4b	4.24 d, 4.38 d [4 H] $^2J_{HH}$ = 14.3	3.33 s	2.55 s [2 H]	4.01 br. s	–	6.22 t [2 H]	7.38 d [2 H]	7.54 d [2 H]	6.83 m [4 H]	2.26 s [6 H] *p*-CH_3 2.40 br. s [12 H] *o*-CH_3
5a	4.44 s	3.03 s	2.51 br. s	–	2.80 s	6.24 t	(o)	7.56 d	7.32−7.48 m [20 H]	
5b	4.44 s	3.04 s	2.48 m	–	2.81 s	6.24 t	7.13 d	7.55 d	7.22−7.43 m [18 H]	2.33 s, 2.35 s [6 H] *m*-CH_3
5c	4.36 d, 4.45 d $^2J_{HH}$ = 14.0	3.00 d, 3.16 d $^2J_{HH}$ = 9.2	2.38 br. s, 2.54 d, 2.77 br. s $^2J_{HH}$ = 14.6	–	2.77 s	6.19 t	(o)	7.51 d	6.76 m [4 H], 7.28−7.50 m [10 H]	2.21 s [6 H] *p*-CH_3 2.34 s, 2.48 s [12 H] *o*-CH_3
5d	4.14 s	2.99 s	2.42 br. s	–	2.80 s	–	–	–	7.31−7.46 m [20 H]	6.12 pt, 6.62 pt [4 H] pyrrole-*H* [c]
6a	4.32 d, 4.43 d [4 H] $^2J_{HH}$ = 14.2	3.03 s	2.23 s [2 H]	–	2.92 s	6.28 t [2 H]	7.58 d [2 H]	7.71 d [2 H]	7.33−7.50 m [10 H]	
6b	4.34 d, 4.43 d [4 H] $^2J_{HH}$ = 14.2	3.11 s	2.66 s [2 H]	–	3.03 s	6.25 t [2 H]	7.55 br. s [2 H]	7.55 br. s [2 H]	6.82 m [4 H]	2.26 s [6 H] *p*-CH_3 2.42 br. s [12 H] *o*-CH_3

[a] s = singlet; d = doublet; t = triplet; m = multiplet; br. s = broad signal; pt = pseudo triplet; (o) = overlapped; n. d. = not detected. [b] Coupling constants in Hz. [c] Coupling constant $^3J_{HH}$ = 2.0 Hz. [d] See Scheme 13 for numbering scheme of the pyrazole.

NMR ($CDCl_3$): δ = −28.6 (s, *P*Ph_2) ppm. **6b**: Starting material **4b** (1.95 g, 4.0 mmol). Eluent petroleum ether/diethyl ether (2:1; R_f = 0.65). Yield 1.65 g (3.3 mmol, 82%) as a colourless, microcrystalline powder. ^{31}P NMR ($CDCl_3$): δ = −36.6 (s, *P*Mes_2) ppm. For further analytical data see Tables 10, 12, and 14.

Coordination Chemistry

General Procedure for the Synthesis of 7a−d: A solution of the respective *tripod* ligand **5** (1.05 mmol) in ethanol (10 mL) was added rapidly to a solution of $NiCl_2·6H_2O$ (240 mg, 1.0 mmol) in ethanol (10 mL). The colour of the reaction mixture changed immediately to red and within a few minutes the nickel complexes precipitated. After stirring at 25°C for 1 h, the precipitate was filtered off, washed with 10-mL portions of diethyl ether (3×), and dried in vacuo. **7a**: Starting material **5a** (565 mg). Yield 540 mg (0.85 mmol, 85%) as an orange-coloured microcrystalline solid. Recrystallization from CH_2Cl_2/Et_2O afforded two different kinds of red crystals (**7a/1**·CH_2Cl_2 and **7a/2**·0.5CH_2Cl_2), both suitable for X-ray structure analysis. ^{31}P NMR (CD_2Cl_2, −30°C): δ = 11.2 (s, *P*Ph_2) ppm. ^{31}P NMR (CD_2Cl_2, −100°C): δ = 9.6 (d, $^2J_{PP}$ = 108 Hz, *P*Ph_2), 13.6 (d, $^2J_{PP}$ = 108 Hz, *P*Ph_2) ppm. **7b**: Starting material **5b** (590 mg). Yield 500 mg (0.72 mmol, 72%) as an orange-coloured, microcrystalline solid. ^{31}P NMR (CD_2Cl_2, −30°C): δ = 11.3 [br. s, *P*Ph_2, *P*(*m*-Tol)$_2$] ppm. ^{31}P NMR (CD_2Cl_2, −100°C): δ = 9.4 (d, $^2J_{PP}$ = 110 Hz), 12.1−15.0 (m) ppm. **7c**: Starting material **5c** (650 mg). Yield 710 mg (0.95 mmol, 95%) as a ruby-coloured, microcrystalline solid. ^1H NMR and ^{13}C NMR: due to dynamic processes, no sharp signals could be detected. ^{31}P NMR (CD_2Cl_2, −30°C): δ = −6.6 (d, $^2J_{PP}$ = 95 Hz, chair-*P*Mes_2), −0.5 (br. s, twist-*P*Mes_2, twist-*P*Ph_2), 2.2 (d, $^2J_{PP}$ = 95 Hz, chair-*P*Ph_2) ppm. ^{31}P NMR (CD_2Cl_2, −100°C): δ = −4.8 (d, $^2J_{PP}$ = 95 Hz, chair-*P*Mes_2), −3.0 (d, $^2J_{PP}$ = 98 Hz, twist-*P*Mes_2), −0.2 (d,

 © 2003 Wiley-VCH Verlag GmbH & Co. KGaA, Weinheim

Table 11. Chemical shifts (δ values), integrals [*x* H] and coupling constants *J* in the $^1H\{^{31}P\}$ NMR spectra of **7**−**18** in CH_2Cl_2

Compd.[a][b]	CH_2N [2 H]	CH_2O [2 H]	CH_2P [4 H]	OCH_3 [3 H]	Pyrazole-H[c] H4[d] [1 H]	H5[d] [1 H]	H3[d] [1 H]	Aryl-H	Other
7a	3.82 s	1.98 s	2.26 d, 2.92 br. s $^2J_{HH}$ = 15.2	2.45 s	6.22 t	7.20 d	7.47 d	7.57−8.32 m [20 H]	
7b	3.82 s	1.96 d, 2.03 d $^2J_{HH}$ = 9.6	2.28 d, 2.30 d, 2.97 br. s $^2J_{HH}$ = 15.2	2.52 s	6.23 t	7.21 d	(o)	7.38−8.35 m [18 H]	2.51 br. s [6 H] *m*-C*H*$_3$
7d	3.66 s	2.24 s	2.08 d, 4.01 br. s $^2J_{HH}$ = 14.8	2.39 s	−	−	−	7.44−8.42 m [20 H]	6.09 pt, 6.43 pt [4 H] pyrrole-*H* [c]
8	3.74 s	1.88 s	2.50−2.60m	2.58 s	6.19 t	7.16 d	7.44 d	7.44−8.28 m [20 H]	
9a	4.07 s	2.09 s	2.33 d, 2.89 d $^2J_{HH}$ = 15.1	2.24 s	6.25 t	7.23 d	(o)	7.53−8.24 m [20 H]	
9b	4.02 s	1.99 d, 2.08 d $^2J_{HH}$ = 9.8	2.33 br. s, 2.81 d, 2.82 d $^2J_{HH}$ = 15.3	2.25 s	6.21 t	7.20 d	7.60 d	7.38−8.17 m [18 H]	2.43 br. s [6 H] *m*-C*H*$_3$
10	4.01 s	2.12 s	2.44 d, 2.94 d $^2J_{HH}$ = 15.3	2.25 s	6.24 t	7.23 d	(o)	7.52−8.21 m [20 H]	
12[c]	3.79 d[f], 4.02 d[f] [2 H] 4.56 d[g], 4.82 d[g] [2 H] $^2J_{HH}$ = 14.4[f], 14.8[g]	1.89 d, 1.96 d $^2J_{HH}$ = 9.6	1.51 d, 2.49−2.64 m [2 H] $^2J_{HH}$ = 14.4	2.59 s	6.30 t[f] [1 H] 6.64 t[g] [1 H]	7.33 d[f] [1 H] 8.98 d[g] [1 H]	7.60 d[f] [1 H] 8.11 d[g] [1 H]	7.51−8.25 m [10 H]	
16a·PF_6	4.19 s	2.32 s	2.52 d, 2.99 d $^2J_{HH}$ = 15.2	2.15 s	6.26 t	7.36 d	7.54 d	7.35−7.63 m [20 H]	2.15 br. s, 4.07 br. s [4 H] C*H*$_2$ 5.56 m [1 H] allyl-C*H*
17	3.84 s	2.30 d, 2.68 d $^2J_{HH}$ = 9.6	1.90−1.99 m, 2.36−2.47 m, 2.95 m	2.62 s	6.24 t	7.24 d	7.48 d	6.09−6.13 m [2 H], 7.09−8.22 m [20 H]	1.99 s [3 H] *p*-C*H*$_3$ 2.79 s, 2.83 s [6 H] *o*-C*H*$_3$
18[e]	4.06 pt $^2J_{HH}$ = 14.0	2.12 d, 2.46 d $^2J_{HH}$ = 9.6	2.00−2.31 m, 2.89 pt, 3.09 pt $^2J_{HH}$ = 14.2, 15.4	2.21 s	6.22 t	7.17 d	(o)	7.40−8.18 m [20 H]	0.67 s[h] [3 H] Pd-C*H*$_3$

[a] s = singlet; d = doublet; t = triplet; m = multiplet; br. s = broad signal; pt = pseudo triplet; (o) = overlapped. [b] Coupling constants in Hz. [c] Coupling constant $^3J_{HH}$ = 2.0 Hz. [d] See Scheme 13 for numbering scheme of the pyrazole. [e] Measuring temperature −40°C. [f] Noncoordinated CH_2pz group. [g] Coordinated CH_2pz group. [h] In ^1H NMR spectra: δ = 0.67 (dd, $^3J_{PH}$ = 3.8 and 7.8 Hz).

$^2J_{PP}$ = 101 Hz, twist-*P*Mes$_2$), 1.8 (d, $^2J_{PP}$ = 101 Hz, twist-*P*Ph$_2$), 3.1 (d, $^2J_{PP}$ = 98 Hz, twist-*P*Ph$_2$), 4.8 (d, $^2J_{PP}$ = 95 Hz, chair-*P*Ph$_2$) ppm, see Figure 7. **7d**: Starting material **5d** (560 mg). Yield 630 mg (0.95 mmol, 95%) as an orange-coloured, microcrystalline solid. ^{31}P NMR (CD_2Cl_2, −30°C): δ = 9.8 (s, *P*Ph$_2$) ppm. ^{31}P NMR (CD_2Cl_2, −100°C): δ = 10.4−10.8 (m, *P*Ph$_2$) ppm. For crystallographic data see Table 7; for further analytical data see Tables 11, 13, and 15.

General Procedure for the Synthesis of 8, 11a−c, 13, and 14: A solution of the respective *tripod* ligand **5** or **6** (1.05 mmol) in THF (20 mL) was added rapidly to a suspension of [(dme)$NiCl_2$] (220 mg, 1.0 mmol) or [(dme)$NiBr_2$] (310 mg, 1.0 mmol), respectively, in THF (20 mL). After stirring at 25°C for 12 h, all volatiles were removed in vacuo. The residual solid was washed with 10-mL portions of diethyl ether (3×) and dried in vacuo. **8**: Starting materials **5a** (565 mg) and [(dme)$NiBr_2$]. Yield 515 mg (0.68 mmol, 68%) as a red, microcrystalline solid. Recrystallization from CH_2Cl_2/Et_2O afforded red crystals suitable for X-ray structure analysis. ^{31}P NMR (CD_2Cl_2, −30°C): δ = 10.7 (s, *P*Ph$_2$) ppm. **11a**: Starting materials **6a** (440 mg) and [(dme)$NiBr_2$]. Yield 580 mg (0.91 mmol, 91%) as a blue-violet, microcrystalline solid. Recrystallization from CH_2Cl_2/Et_2O afforded blue-violet crystals suitable for X-ray structure analysis. UV/Vis (CH_2Cl_2): λ (ε) = 552 nm (200 $M^{-1}\cdot cm^{-1}$), 912 (110), 1007 (sh, 70). NMR: no NMR signals due to paramagnetism. **11b**: Starting materials **6a** (440 mg) and [(dme)$NiCl_2$]. Yield 485 mg (0.88 mmol, 88%) as a violet, microcrystalline solid. UV/Vis (CH_2Cl_2): λ (ε) = 527 nm (180 $M^{-1}\cdot cm^{-1}$), 890 (100), 997 (80). NMR: no NMR signals due to paramagnetism. **11c**: Starting materials $EtOCH_2C(CH_2PPh_2)(CH_2pz)_2$[5e] (455 mg) and [(dme)-$NiBr_2$]. Yield 525 mg (0.80 mmol, 80%) as a blue-violet, microcrystalline solid. Recrystallization from CH_2Cl_2/Et_2O afforded two different kinds of crystals, both suitable for X-ray structure analysis, which were identified as **11c**·0.5CH_2Cl_2 (blue-violet) and the dimer **15** (red-brown). UV/Vis (**11c**, CH_2Cl_2): λ (ε) = 550 nm (195 $M^{-1}\cdot cm^{-1}$), 913 (120), 1109 (sh, 50). NMR: no NMR signals due to paramagnetism. **13**: Starting materials **6b** (525 mg) and [(dme)$NiCl_2$]. Yield 495 mg (0.78 mmol, 78%) as a blue-violet, microcrystalline solid. Recrystallization from CH_2Cl_2/Et_2O afforded blue-violet crystals suitable for X-ray structure analysis. UV/Vis (CH_2Cl_2): λ (ε) = 520 nm (100 $M^{-1}\cdot cm^{-1}$), 579 (140), 974 (60). NMR: no NMR signals due to paramagnetism. **14**: Starting materials

 © 2003 Wiley-VCH Verlag GmbH & Co. KGaA, Weinheim

Table 12. Chemical shifts (δ values) and coupling constants *J* in the $^{13}C\{^1H\}$ NMR spectra of **2**−**6** in $CHCl_3$

Compd.[a][b]	CH_2N	CH_2O	CH_2P	OCH_3	C_q	Pyrazole-C C4[c]	C5[c]	C3[c]	Aryl-C	Other
2b	55.3 d $^3J_{CP}$ = 10.1	79.7 d $^3J_{CP}$ = 9.6	34.4 d $^1J_{CP}$ = 16.6	–	44.6 d $^2J_{CP}$ = 13.6	–	–	–	129.0−138.9 m	108.7, 121.9 pyrrole-*C*
3a	58.4 m	68.8 m	35.0 m	–	46.7 m	105.5	131.7	139.3	128.9−139.3 m	
3b	58.4 t $^3J_{CP}$ = 9.7	68.9 t $^3J_{CP}$ = 8.8	35.5 m	–	45.5 t $^2J_{CP}$ = 11.5	105.4	131.8	139.8	128.7−140.0 m	21.9 *m*-CH_3
3c	57.6 t $^3J_{CP}$ = 8.7	68.6 dd $^3J_{CP}$ = 8.3, 10.1	31.9 dd, 34.6 dd $^1J_{CP}$ = 17.5, 19.3 $^3J_{CP}$ = 9.2, 10.1	–	46.3 dd $^2J_{CP}$ = 12.0, 15.6	105.4	131.6	139.7	128.6−143.4 m	21.2 d *p*-CH_3 $^5J_{CP}$ = 1.8 23.7 d, 23.9 d *o*-CH_3 $^3J_{CP}$ = 13.8
3d	58.7 t $^3J_{CP}$ = 9.9	69.1 t $^3J_{CP}$ = 8.6	26.8−35.1 m	–	44.2 t $^2J_{CP}$ = 12.4	105.5	131.8	139.7	128.8−140.1 m	26.8−35.1 m cyclohexyl-*C*
3e	54.8 t $^3J_{CP}$ = 8.1	67.9 t $^3J_{CP}$ = 8.3	35.1 dd $^1J_{CP}$ = 18.1, $^3J_{CP}$ = 9.5	–	45.3 t $^2J_{CP}$ = 11.1	–	–	–	128.9−139.5 m	108.3, 123.0 pyrrole-*C*
4a	54.9 m	65.5 m	32.1 m	–	46.7 m	105.6	132.3	140.0	128.9−139.8 m	
4b	55.2 d $^3J_{CP}$ = 9.6	65.8 d $^3J_{CP}$ = 10.0	29.7 d $^1J_{CP}$ = 20.1	–	47.2 d $^2J_{CP}$ = 15.1	105.7	132.0	139.9	130.9−143.0 m	21.2 *p*-CH_3 23.8 d *o*-CH_3 $^3J_{CP}$ = 13.6
5a	57.6 t $^3J_{CP}$ = 9.3	76.8 t $^3J_{CP}$ = 8.6	35.4 dd $^1J_{CP}$ = 18.5, $^3J_{CP}$ = 9.5	58.3	44.3 t $^2J_{CP}$ = 12.0	105.5	131.5	139.4	128.7−140.0 m	
5b	57.6 t $^3J_{CP}$ = 9.2	76.8 t $^3J_{CP}$ = 8.5	35.2 m	58.3	44.3 t $^2J_{CP}$ = 12.0	105.4	131.5	139.3	128.5−140.0 m	21.8 *m*-CH_3
5c	57.6 t $^3J_{CP}$ = 9.2	77.1 m	32.6−34.7 m	58.5	45.2 dd $^2J_{CP}$ = 11.0, 15.6	105.4	131.4	139.3	128.5−143.1 m	21.2 *p*-CH_3 23.7 d, 23.9 d *o*-CH_3 $^3J_{CP}$ = 13.8
5d	55.3 t $^3J_{CP}$ = 8.7	76.6 t $^3J_{CP}$ = 8.3	35.0 dd $^1J_{CP}$ = 19.3, $^3J_{CP}$ = 11.0	58.2	44.4 t $^2J_{CP}$ = 12.0	–	–	–	128.7−140.0 m	108.1, 123.0 pyrrole-*C*
6a	54.8 d $^3J_{CP}$ = 8.6	74.1 d $^3J_{CP}$ = 8.1	32.0 d $^1J_{CP}$ = 18.1	58.6	45.6 d $^2J_{CP}$ = 12.1	105.5	132.2	139.8	128.8−139.9 m	
6b	55.0 d $^3J_{CP}$ = 10.6	74.2 d $^3J_{CP}$ = 9.6	28.9 d $^1J_{CP}$ = 19.1	58.8	46.1 d $^2J_{CP}$ = 15.6	105.5	132.0	139.6	130.7−143.1 m	21.2 *p*-CH_3 23.8 d *o*-CH_3 $^3J_{CP}$ = 14.0

[a] All signals are singlets unless otherwise stated; d = doublet; dd = doublet of doublet; t = triplet; m = multiplet. [b] Coupling constants in Hz. [c] See Scheme 13 for numbering scheme of the pyrazole.

$CH_3C(CH_2pz)_3$[5e] (285 mg) and [(dme)$NiBr_2$]. Yield 425 mg (0.87 mmol, 87%) as a blue, microcrystalline solid. Recrystallization from CH_2Cl_2/Et_2O afforded blue and red-brown crystals, but only the former were suitable for X-ray structure analysis. UV/Vis (CH_2Cl_2): λ (ε) = 550 nm (180 $M^{-1}\cdot cm^{-1}$), 600 (230), 1004 (90). NMR: no NMR signals due to paramagnetism. For crystallographic data see Tables 7 and 8; for further analytical data see Tables 11, 13, and 15.

General Procedure for the Synthesis of 9a, 9b, and 12: A solution of the respective *tripod* ligand **5** or **6** (0.5 mmol) in ethanol (15 mL) was added rapidly to a suspension of [(η^4-cod)$PdCl_2$] (145 mg, 0.5 mmol) in ethanol (10 mL). Within a few minutes the yellow reaction mixture was clearing up. After stirring at 25°C for 12 h, all volatiles were removed in vacuo. The residual solid was washed with portions of diethyl ether (10 mL, 3×) and dried in vacuo. **9a**: Starting material **5a** (270 mg). Yield 265 mg (0.37 mmol, 74%) as a colourless, microcrystalline solid. Recrystallization from CH_2Cl_2/Et_2O afforded colourless crystals suitable for X-ray structure analysis. ^{31}P NMR (CD_2Cl_2): δ = 15.8 (s, *P*Ph_2) ppm. ^{31}P NMR (CD_2Cl_2, −100°C): δ = 15.8 (d, $^2J_{PP}$ = 115 Hz, *P*Ph_2), 15.9 (d, $^2J_{PP}$ = 115 Hz, *P*Ph_2) ppm. **9b**: Starting material **5b** (280 mg). Yield 255 mg (0.34 mmol, 69%) as a pale yellow microcrystalline solid. ^{31}P NMR (CD_2Cl_2): δ = 15.8 [br. s, *P*Ph_2, *P*(*m*-Tol)$_2$] ppm. ^{31}P NMR (CD_2Cl_2, −100°C): δ = 14.9−15.8 (m), 16.6−17.1 (m) ppm. **12**: Starting material **6a** (210 mg). Yield 245 mg (0.41 mmol, 82%) as a yellow, microcrystalline solid. Recrystallization from CH_2Cl_2/Et_2O afforded yellow crystals suitable for X-ray structure analysis. ^{31}P NMR (CD_2Cl_2): δ = 9.8 (s, *P*Ph_2) ppm. For crystallographic data see Tables 7 and 8; for further analytical data see Tables 11, 13, and 15.

Synthesis of 10: A solution of the *tripod* ligand **5a** (135 mg, 0.25 mmol) in ethanol/THF (2:1; 15 mL) was added rapidly to a suspension of [*cis*-($CH_3CN)_2PtCl_2$] (85 mg, 0.25 mmol) in ethanol (10 mL). Within a few minutes the reaction mixture was clearing up and the platinum complex precipitated. After stirring at 25°C for 12 h, all volatiles were removed in vacuo. The residual solid was washed with portions of diethyl ether (10 mL, 3×) and dried in vacuo. Recrystallization from CH_2Cl_2/Et_2O afforded 150 mg (0.19 mmol, 75%) of **10** as colourless crystals. ^{31}P NMR (CD_2Cl_2): δ = −2.5 (s, with Pt satellites, $^1J_{PtP}$ = 1720 Hz, *P*Ph_2). ^{31}P NMR (CD_2Cl_2, −100°C): δ = −3.2 (d, $^2J_{PP}$ = 20 Hz, *P*Ph_2), −2.5 (d, $^2J_{PP}$ = 20 Hz, *P*Ph_2). For further analytical data, see Tables 11, 13, and 15.

Synthesis of 16a·PF_6: Solid $TlPF_6$ (2 equiv., 210 mg) was added, at 0°C, to a suspension of **7a** (200 mg, 0.3 mmol) in THF (50 mL) to

 © 2003 Wiley-VCH Verlag GmbH & Co. KGaA, Weinheim

Table 13. Chemical shifts (δ values) and coupling constants *J* in the $^{13}C\{^1H\}$ NMR spectra of **7**−**18** in CH_2Cl_2

Compd.[a][b]	CH_2N	CH_2O	CH_2P	OCH_3	C_q	Pyrazole-C C4[c]	Pyrazole-C C5[c]	Pyrazole-C C3[c]	Aryl-C	Others
7a	58.5	72.7	29.1	57.7	42.3	105.8 br. s	133.2 br. s	140.2 br. s	129.0−136.3 m	
7b	58.3	72.7	28.7 m	57.6	42.3	105.6	132.6	140.0	128.8−140.2 m	21.7, 21.8 *m*-CH_3
7d	58.0	73.1	30.3	57.6	43.4	–	–	–	128.8−138.8 m	108.9, 122.6 pyrrole-*C*
8	57.4	72.6	26.4	57.7	42.6	105.5	131.5	139.8	128.7−139.8 m	
9a	59.8 t $^3J_{CP}$ = 11.0	72.3 t $^3J_{CP}$ = 5.2	30.7−31.5 m	57.4	43.9	105.8	131.7	140.1	128.8−136.2 m	
9b	59.6 t $^3J_{CP}$ = 11.0	72.3 br. s	30.7−31.4 m	57.5	43.8	105.8	131.6	140.0	128.8−138.9 m	21.6, 21.7 *m*-CH_3
10	59.9 $^3J_{CP}$ = 11.6	72.1 t $^3J_{CP}$ = 5.1	29.9−30.8 m	57.5	43.9	105.8	131.7	140.1	128.8−136.1 m	
12	52.4 br. s[d], 54.0 br. s[e]	68.6 br. s	29.4 d $^1J_{CP}$ = 27.7	58.2	45.2	105.9[e], 108.5[d]	131.8[e], 136.2[d]	140.3[e], 145.5[d]	128.8−132.7 m	
16a·PF_6	60.3 br. s	74.0 br. s	30.6-31.3 m	57.5	43.6	105.9	132.2	140.2	129.8−134.5 m	72.6 allyl-CH_2, 117.6 allyl-*C*H
17	59.0 dd $^3J_{CP}$ = 6.0, 10.5	74.6 dd $^3J_{CP}$ = 5.5, 7.4	27.8 dd, 29.9 dd $^1J_{CP}$ = 18.0, $^3J_{CP}$ = 8.8	58.0	42.5 br. s	105.6	131.4	139.6	127.2−140.3 m	20.0 *p*-CH_3 26.8 *o*-CH_3
18	60.8 t $^3J_{CP}$ = 10.6	72.8 t $^3J_{CP}$ = 5.9	32.2 dd, 34.5 dd $^1J_{CP}$ = 27.6, $^3J_{CP}$ = 9.8	57.3	44.2 br. s	105.8	131.6	139.7	128.6−140.1 m	14.5 dd Pd-CH_3 $^2J_{CP}$ = 6.0, 103.0

[a] All signals are singlets unless otherwise stated; d = doublet; dd = doublet of doublet; t = triplet; m = multiplet; (o) = overlapped. [b] Coupling constants in Hz. [c] See Scheme 13 for numbering scheme of the pyrazole. [d] Coordinated CH_2pz group. [e] Noncoordinated CH_2pz group.

Table 14. Analytical data of ligands **2**−**6**

Compd.	Formula	*M* [g/mol]	EI-MS [*m*/*z* (%)]	$C_{calcd.}/C_{found}$	$H_{calcd.}/H_{found}$	$N_{calcd.}/N_{found}$	$P_{calcd.}/P_{found}$
2b	$C_{21}H_{22}NOP$	335.38	336 (100), 305 (39), 199 (57), 183 (66), 120 (97)	75.21/75.33	6.61/6.95	4.18/3.61	9.24/n. d.
3b	$C_{34}H_{36}N_2OP_2$	550.62	551 (28), 474 (100), 460 (76)	74.17/74.25	6.59/6.88	5.09/4.89	11.25/n. d.
3c	$C_{38}H_{44}N_2OP_2$	606.73	607 (15), 529 (5), 487 (100),369 (10), 337 (11)	75.23/75.46	7.31/7.98	4.62/4.40	10.21/n. d.
3d	$C_{32}H_{44}N_2OP_2$	534.66	534 (1), 452 (100), 183 (10)	71.89/71.67	8.29/8.15	5.24/5.10	11.59/11.47
3e	$C_{33}H_{33}NOP_2$	521.57	521 (10), 444 (100), 199 (14), 183 (24)	75.99/75.98	6.38/6.63	2.69/2.49	11.88/n. d.
4b	$C_{29}H_{37}N_4OP$	488.61	489 (49), 473 (67), 407 (22), 369 (45), 269 (100), 250 (39)	71.29/72.00	7.63/8.43	11.47/10.74	6.34/n. d.
5a	$C_{33}H_{34}N_2OP_2$	536.59	536 (11), 459 (100), 183 (10)	73.87/73.98	6.39/6.39	5.22/5.26	11.54/11.71
5b	$C_{35}H_{38}N_2OP_2$	564.64	564 (18), 487 (100), 473 (77), 183 (14)	74.45/74.71	6.78/7.07	4.96/4.84	10.97/n. d.
5c	$C_{39}H_{46}N_2OP_2$	620.75	620 (2), 543 (2), 501 (100), 269 (10)	75.46/75.50	7.47/7.65	4.51/4.49	9.98/n. d.
5d	$C_{34}H_{35}NOP_2$	535.60	535 (8), 458 (100), 199 (10), 183 (13)	76.24/76.11	6.59/6.58	2.62/2.54	11.57/11.50
6a	$C_{24}H_{27}N_4OP$	418.47	418 (100), 341 (82), 337 (52), 305 (37), 269 (59), 199 (52), 183 (44), 151 (36)	68.88/69.19	6.50/6.68	13.39/12.77	7.40/n. d.
6b	$C_{30}H_{39}N_4OP$	502.64	502 (100), 487 (41), 421 (34), 383 (59)	71.69/71.74	7.82/8.06	11.15/11.02	6.16/6.18

yield a white precipitate of TlCl. After stirring the reaction mixture at 0°C for 1 h, allylmagnesium bromide (0.35 mL of a 1 M solution in THF) was added dropwise. After stirring at 25°C for 10 h, the precipitate was filtered off through 2 cm of Kieselguhr and all volatiles were removed in vacuo. The orange-coloured residue was washed with portions of diethyl ether (10 mL, 2×) and then recrystallized from CH_2Cl_2/Et_2O to give 170 mg (0.22 mmol, 72%) of **16a·PF_6**·0.75CH_2Cl_2 as air-stable, yellow crystals suitable for X-ray structure analysis. ^{31}P NMR (CD_2Cl_2): δ = −144.0 (sept, $^1J_{PF}$ = 712 Hz, *P*F_6^-), 13.0 (s, *P*Ph_2) ppm. For crystallographic data see Table 9; for further analytical data see Tables 11, 13, and 15.

Synthesis of 16b·PF_6: A solution of the *tripod* ligand $EtOCH_2C(CH_2PPh_2)(CH_2pz)_2$[5e] (130 mg, 0.3 mmol) in EtOH (10 mL) was added rapidly to a suspension of $[Pd(\eta^3\text{-}C_3H_5)Cl]_2$ (55 mg, 0.15 mmol) in EtOH (10 mL). When a clear solution had formed (after about 30 min), solid KPF_6 (55 mg, 0.3 mmol) was added and within a few minutes the allyl complex precipitated. For complete precipitation the reaction mixture was cooled overnight to −30°C and afterwards filtered. The resultant grey residue was washed with portions of diethyl ether (10 mL, 2×), dried in vacuo, and recrystallized from CH_2Cl_2/Et_2O to give 140 mg (0.19 mmol, 64%) of **16b·PF_6** as air-stable, colourless crystals suitable for X-ray structure analysis. ^1H NMR and ^{13}C NMR: due to dynamic processes, no sharp signals could be detected. ^{31}P NMR (CD_2Cl_2): δ = −144.2 (sept, $^1J_{PF}$ = 710 Hz, *P*F_6^-), 11.5 (s, *P*Ph_2) ppm. For crystallographic data see Table 9; for further analytical data see Tables 11, 13, and 15.

Synthesis of 17: A solution of the *tripod* ligand **5a** (270 mg, 0.5 mmol) in toluene (15 mL) was added to a solution of [*trans*-$(PPh_3)_2Ni(Mes)Br$] (390 mg, 0.5 mmol) in toluene (15 mL). After stirring the orange-coloured reaction mixture at 25°C for 10 h, the solvent was removed in vacuo. The crude product was suspended in petroleum ether (20 mL). After filtration of the suspension, the residue was washed carefully with portions of petroleum ether

 © 2003 Wiley-VCH Verlag GmbH & Co. KGaA, Weinheim

Table 15. Analytical data of metal complexes **7**−**19**

Compd.	Formula	*M* [g/mol]	FAB-MS [*m*/*z* (%)]	$C_{calcd.}/C_{found}$	$H_{calcd.}/H_{found}$	$N_{calcd.}/N_{found}$	$P_{calcd.}/P_{found}$	$Cl_{calcd.}/Cl_{found}$
7a	$C_{33}H_{34}Cl_2N_2NiOP_2$	666.18	664 (4), 629 (100), 594 (18), 459 (36), 409 (24), 364 (31), 351 (28)	59.50/59.14	5.14/5.34	4.21/4.07	9.30/8.94	10.64/10.73
7b	$C_{35}H_{38}Cl_2N_2NiOP_2$	694.24	692 (4), 657 (100), 622 (10), 487 (19), 473 (16)	60.55/60.28	5.52/5.58	4.04/3.90	8.92/8.86	10.21/10.19
7c	$C_{39}H_{46}Cl_2N_2NiOP_2$	750.35	713 (50), 677 (100), 502 (59), 409 (85), 351 (42)	62.43/62.39	6.18/6.50	3.73/3.56	8.26/n. d.	9.45/n. d.
7d	$C_{34}H_{35}Cl_2NNiOP_2$	665.19	663 (4), 628 (100), 593 (18), 515 (35), 458 (34), 408 (15)	61.39/60.95	5.30/5.32	2.11/2.15	9.31/n. d.	10.66/n. d.
8	$C_{33}H_{34}Br_2N_2NiOP_2$	755.09	672 (69), 629 (54), 594 (17), 459 (25), 409 (15), 364 (18), 351 (15)	52.49/51.33	4.54/4.56	3.71/3.44	8.20/n. d.	21.16[a] /n. d.
9a	$C_{33}H_{34}Cl_2N_2OP_2Pd$	713.92	677 (100), 642 (17), 459 (77), 457 (50), 351 (59)	55.52/54.58	4.80/4.93	3.92/3.79	8.68/8.53	9.93/10.00
9b	$C_{35}H_{38}Cl_2N_2OP_2Pd$	741.97	705 (100), 670 (14), 487 (17)	56.66/56.32	5.16/5.13	3.78/3.64	8.35/8.44	9.56/9.52
10	$C_{33}H_{34}Cl_2N_2OP_2Pt$	802.58	801 (6), 766 (100), 731 (11), 634 (11), 459 (12)	49.39/49.50	4.27/4.55	3.49/3.35	7.72/7.35	8.83/9.20
11a	$C_{24}H_{27}Br_2N_4NiOP$	636.97	555 (28), 476 (100), 341 (10), 291 (28), 246 (64), 185 (38)	45.25/45.16	4.27/4.33	8.80/8.68	4.86/4.89	25.09[a]/24.85[b]
11b	$C_{24}H_{27}Cl_2N_4NiOP$	548.07	511 (88), 476 (76), 341 (26), 291 (49), 246 (100), 185 (47)	52.59/52.63	4.97/4.96	10.22/10.19	5.65/5.67	12.94/13.05
11c	$C_{25}H_{29}Br_2N_4NiOP$	651.00	569 (36), 490 (10), 431 (10), 355 (13), 327 (22), 305 (28), 281 (31), 246 (100)	46.12/45.56	4.49/4.55	8.61/8.44	4.76/4.72	24.55[a]/25.70[b]
12	$C_{24}H_{27}Cl_2N_4OPPd$	595.80	559 (100), 524 (28), 339 (81)	48.38/47.99	4.57/4.61	9.40/9.17	5.20/n. d.	11.90/n. d.
13	$C_{30}H_{39}Cl_2N_4NiOP$	632.23	595 (100), 559 (58), 502 (40), 488 (26), 435 (23), 383 (46)	56.99/56.88	6.22/6.27	8.86/8.94	4.90/4.89	11.22/11.21
14	$C_{14}H_{18}Br_2N_6Ni$	488.84	407 (100), 328 (29)	34.40/34.36	3.71/3.73	17.19/16.97		32.69[a]/32.43[b]
16a·PF$_6$	$C_{36}H_{39}F_6N_2NiOP_3$	781.32	635 (100), 594 (14), 409 (15), 364 (10)	52.24[c]/52.39	4.83[c]/4.88	3.32[c]/3.18	11.00[c]/n. d.	–
16b·PF$_6$	$C_{28}H_{34}F_6N_4OP_2Pd$	724.96	578 (100), 422 (35), 353 (30)	46.39/46.08	4.73/4.48	7.73/7.73	8.54/n. d.	–
17	$C_{42}H_{45}BrN_2NiOP_2$	794.37	792 (1), 673 (14), 594 (100), 409 (35), 364 (44)	63.50/63.32	5.71/5.73	3.53/3.52	7.80/7.67	10.06[a]/n. d.
18	$C_{34}H_{37}ClN_2OP_2Pd$	693.50	692 (3), 677 (93), 657 (41), 642 (15), 565 (10), 457 (100), 351 (39)	58.89/58.60	5.38/5.60	4.04/3.99	8.93/8.54	5.11/5.10
19·PF$_6$	$C_{51}H_{53}F_6N_4NiOP_3$	1003.60	857 (32), 595 (98), 476 (100), 381 (42)	59.69[d]/58.53	5.24[d]/5.25	5.42[d]/5.51	8.99[d]/n. d.	–

[a] $Br_{calcd.}$. [b] Br_{found}. [c] Calculated for **16a·PF$_6$**·0.75CH_2Cl_2. [d] Calculated for **19·PF$_6$**·0.35CH_2Cl_2.

(10 mL, 3×) to remove PPh_3, and dried in vacuo to give 285 mg (0.36 mmol, 72%) of **17** as a yellow, microcrystalline solid. ^{31}P NMR (CD_2Cl_2): δ = −8.0 (d, $^2J_{PP}$ = 41 Hz, *P*Ph_2 *trans* to Mes^-), 23.2 (d, $^2J_{PP}$ = 41 Hz, *P*Ph_2 *trans* to Br^-) ppm. For further analytical data see Tables 11, 13, and 15.

Synthesis of 18: A solution of the *tripod* ligand **5a** (270 mg, 0.5 mmol) in CH_2Cl_2 (15 mL) was added to a solution of [(η^4-cod)PdMeCl] (135 mg, 0.5 mmol) in CH_2Cl_2 (15 mL). After stirring the colourless reaction mixture at 25°C for 10 h, the solvent was removed in vacuo. The crude product was suspended in petroleum ether (20 mL). After filtration of the suspension, the resultant grey residue was washed with portions of petroleum ether (15 mL, 3×) and dried in vacuo. Recrystallization from CH_2Cl_2/Et_2O afforded 295 mg (0.43 mmol, 85%) of **18** as colourless crystals suitable for X-ray structure analysis. ^{31}P NMR (CD_2Cl_2): δ = −6.3 (d, $^2J_{PP}$ = 48 Hz, *P*Ph_2 *trans* to Me^-), 25.7 (d, $^2J_{PP}$ = 48 Hz, *P*Ph_2 *trans* to Cl^-) ppm. For crystallographic data see Table 9; for further analytical data see Tables 11, 13, and 15.

Synthesis of 19·PF$_6$: A solution of the *tripod* ligand **6a** (210 mg, 0.5 mmol) in toluene (15 mL) was added to a solution of [*trans*-(PPh_3)$_2$Ni(Mes)Br] (390 mg, 0.5 mmol) in toluene (15 mL). After stirring the orange-coloured reaction mixture at 25°C for 10 h, the solvent was removed in vacuo and the solid residue was dissolved in THF (30 mL). Solid $TlPF_6$ (175 mg, 0.5 mmol) was added and a precipitate of TlBr appeared immediately. The reaction mixture was stirred at 25°C for 3 h and then filtered through 2 cm of Kieselguhr to remove the $TlPF_6$. The solvent was removed in vacuo and the crude product was suspended in petroleum ether (20 mL). After filtration of the suspension, the residue was washed carefully with portions of petroleum ether (15 mL, 3×) to remove PPh_3, and dried in vacuo. Recrystallization from CH_2Cl_2/Et_2O afforded 250 mg (0.25 mmol, 50%) of **19·PF$_6$** as yellow crystals suitable for X-ray structure analysis. ^1H NMR and ^{13}C NMR: due to dynamic processes, no sharp signals could be detected. ^{31}P NMR (CD_2Cl_2): δ = −144.0 (sept, $^1J_{PF}$ = 712 Hz, *P*F_6^-), −5.8 (d, $^2J_{PP}$ = 272 Hz, *P*Ph_3), 7.9 (d, $^2J_{PP}$ = 280 Hz, *P*Ph_3), 19.4 (d, $^2J_{PP}$ = 280 Hz, *P*Ph_2), 21.7 (d, $^2J_{PP}$ = 272 Hz, *P*Ph_2) ppm. For this compound a ^{31}P NMR pattern of two doublets corresponding to the two P donors is expected. Instead, two such patterns are observed (δ = −5.8/21.7 and 7.9/19.4 ppm). The large coupling constants are in accord with a *trans* position of the two P donors in each case. There are obviously two isomers, and only the structure of the one characterized by X-ray crystallography is known. Attempts to isolate the other isomer have, so far, failed. For crystallographic data see Table 9; for further analytical data see Tables 11, 13, and 15.

Acknowledgments

We are indebted to the Deutsche Forschungsgemeinschaft and the Fonds der Chemischen Industrie for financial support. One of us

 © 2003 Wiley-VCH Verlag GmbH & Co. KGaA, Weinheim

(R. F.) is indebted to the local Graduiertenkolleg "Selektivität in der organischen und metallorganischen Synthese und Katalyse" for a scholarship. The technical support of T. Jannack (mass spectrometry) and the Microanalytical Laboratory of the Institute of Organic Chemistry is gratefully acknowledged.

[1] Phosphorus donors: [1a] H. Heidel, G. Huttner, G. Helmchen, *Z. Naturforsch., Teil B* **1993**, *48*, 1681. [1b] T. Seitz, A. Muth, G. Huttner, *Chem. Ber.* **1994**, *127*, 1837. [1c] T. Seitz, A. Muth, G. Huttner, *Z. Naturforsch., Teil B* **1995**, *50*, 1045. [1d] H. Heidel, G. Huttner, L. Zsolnai, *Z. Naturforsch., Teil B* **1995**, *50*, 729.

[2] Oxygen donors: [2a] J. Dale, S. B. Fredriksen, *Acta Chem. Scand.* **1992**, *46*, 271. [2b] T.-Y. Hsieh, M.-C. Cheng, S.-M. Peng, S.-T. Liu, *J. Chem. Soc., Dalton Trans.* **1994**, 3499. [2c] A. Muth, G. Reinhard, G. Huttner, T. Seitz, T. Klein, L. Zsolnai, *Z. Naturforsch., Teil B* **1994**, *49*, 889.

[3] Sulfur donors: [3a] S.-T. Liu, H.-E. Wang, M.-C. Cheng, S.-M. Peng, *J. Organomet. Chem.* **1989**, *376*, 333. [3b] S.-T. Liu, C.-H. Yieh, H.-J. Lu, *Phosphorus, Sulfur Silicon* **1989**, *44*, 261. [3c] S.-T. Liu, C.-L. Tsao, M. C. Cheng, S. M. Peng, *Polyhedron* **1990**, *21*, 2579. [3d] S.-T. Liu, K.-J. Liu, *Inorg. Chem.* **1990**, *29*, 4576. [3e] S.-C. Tsai, H.-E. Wang, C.-T. Huang, L.-M. Yiin, S.-T. Liu, *Chem. Ber.* **1995**, *128*, 151. [3f] G. Reinhard, R. Soltek, G. Huttner, A. Barth, O. Walter, L. Zsolnai, *Chem. Ber.* **1996**, *129*, 97. [3g] R. Soltek, G. Huttner, *Eur. J. Inorg. Chem.* **1998**, 1417. [3h] R. Soltek, G. Huttner, L. Zsolnai, A. Driess, *Inorg. Chim. Acta* **1998**, *269*, 143. [3i] P. Schober, R. Soltek, G. Huttner, L. Zsolnai, K. Heinze, *Eur. J. Inorg. Chem.* **1998**, 1407.

[4] Cp donors: [4a] B. Antelmann, U. Winterhalter, G. Huttner, B. C. Janssen, J. Vogelgesang, *J. Organomet. Chem.* **1997**, *545–546*, 407. [4b] B. Antelmann, G. Huttner, U. Winterhalter, *J. Organomet. Chem.* **1998**, *553*, 433. [4c] J. Vogelgesang, G. Huttner, E. Kaifer, P. Kircher, P. Rutsch, S. Cunskis, *Eur. J. Inorg. Chem.* **1999**, 2187. [4d] J. Vogelgesang, A. Frick, G. Huttner, P. Kircher, *Eur. J. Inorg. Chem.* **2001**, 949.

[5] Nitrogen donors: [5a] S.-T. Liu, C.-Y. Liu, *J. Org. Chem.* **1992**, *57*, 6079. [5b] H.-E. Wang, C.-Y. Liu, M.-C. Cheng, S.-M. Peng, S.-T. Liu, *Phosphorus, Sulfur Silicon* **1992**, *69*, 201. [5c] S.-T. Liu, C.-H. Yieh, H.-P. Dai, *Proc. Natl. Sci. Counc.* **1995**, *19*, 1. [5d] A. Jacobi, G. Huttner, U. Winterhalter, *Chem. Ber./Recueil* **1997**, *130*, 1279. [5e] A. Jacobi, G. Huttner, U. Winterhalter, S. Cunskis, *Eur. J. Inorg. Chem.* **1998**, 675. [5f] R. Faissner, G. Huttner, E. Kaifer, P. Rutsch, *Eur. J. Inorg. Chem.* **2003**, 1681–1693.

[6] A. Jacobi, G. Huttner, U. Winterhalter, *J. Organomet. Chem.* **1998**, *571*, 231.

[7] J. Karas, G. Huttner, K. Heinze, P. Rutsch, L. Zsolnai, *Eur. J. Inorg. Chem.* **1999**, 405.

[8] [8a] T. Seitz, G. Huttner, M. Büchner, *Z. Naturforsch., Teil B* **1994**, *49*, 1813. [8b] T. Seitz, A. Muth, G. Huttner, T. Klein, O. Walter, M. Fritz, L. Zsolnai, *J. Organomet. Chem.* **1994**, *469*, 155.

[9] V. Schulz, A. Frick, G. Huttner, *Eur. J. Inorg. Chem.* **2002**, 3111.

[10] A. Frick, V. Schulz, G. Huttner, *Eur. J. Inorg. Chem.* **2002**, 3129.

[11] A. W. Addison, T. N. Rao, J. Reedijk, J. van Rijn, G. C. Verschoor, *J. Chem. Soc., Dalton Trans.* **1984**, 1349.

[12] [12a] G. R. van Hecke, W. DeW. Horrocks Jr., *Inorg. Chem.* **1966**, *5*, 1968. [12b] L. H. Pignolet, W. DeW. Horrocks Jr., R. H. Holm, *J. Am. Chem. Soc.* **1970**, *92*, 1855. [12c] G. N. La Mar, E. O. Sherman, *J. Am. Chem. Soc.* **1970**, *92*, 2691.

[13] [13a] G. Binsch, H. Kessler, *Angew. Chem.* **1980**, *92*, 445; *Angew. Chem. Int. Ed. Engl.* **1980**, *19*, 411. [13b] K. Il'yasov, O. Nedopekin, *WIN-DYNAMICS 1.0 Release 951220, NMR Dynamic Spectra Simulation and Iteration*, Bruker-Franzen Analytik GmbH, Bremen, Germany (http://www.bruker.de).

[14] *Organikum*, Deutscher Verlag der Wissenschaften, Berlin, **1990**.

[15] P. Fresenius, K. Görlitzer, in: *Organisch-chemische Nomenklatur*, Wissenschaftliche Verlagsgesellschaft, Stuttgart, **1998**.

[16] *DENZO-SMN, Data Processing Software*, Nonius **1998** (http://www.nonius.com).

[17] [17a] G. M. Sheldrick, *SHELXS-97, Program for Crystal Structure Solution*, University of Göttingen, **1997**. [17b] G. M. Sheldrick, *SHELXL-97, Program for Crystal Structure Refinement*, University of Göttingen, **1997** (http://shelx.uni-ac.gwdg.de/shelx/index.html). [17c] *International Tables for X-ray Crystallography*, Kynoch Press, Birmingham, U.K., **1974**, vol. 4.

[18] L. Zsolnai, G. Huttner, *XPMA*, University of Heidelberg, **1994** (http://www.rzuser.uni-heidelberg.de/~il1/laszlo/xpm.html).

[19] R. Soltek, G. Huttner, *WinRay-32*, University of Heidelberg, **1998** (http://www.uni-heidelberg.de/institute/fak12/AC/huttner/html/winray.html).

[20] [20a] R. E. Ireland, D. M. Walba, *Org. Synth. Coll. Vol.* **1988**, *6*, 567. [20b] K. Issleib, H. O. Fröhlich, *Z. Naturforsch., Teil B* **1959**, *14*, 349.

[21] J. B. Lambert, J. H. So, *J. Org. Chem.* **1991**, *56*, 5960.

[22] R. M. Ceder, J. Cubillo, G. Muller, M. Rocamora, *J. Organomet. Chem.* **1992**, *429*, 391.

[23] R. E. Rülke, J. E. Ernsting, A. L. Spek, C. J. Elsevier, P. W. N. M. van Leeuwen, K. Vrieze, *Inorg. Chem.* **1993**, *32*, 5769.

Received September 23, 2002

 © 2003 Wiley-VCH Verlag GmbH & Co. KGaA, Weinheim

Nickel(II) Compounds Derived from *tripod* Ligands: Efficient Catalysts for the Stereoselective Heterodimerization of Styrene and Propene

Ralf Faissner[a] and Gottfried Huttner*[a]

Dedicated to Professor Günter Helmchen[‡]

Keywords: Tripod ligands / Nickel / Catalysis / Heterodimerization

The *tripod* ligands $RCH_2C(CH_2X)(CH_2Y)(CH_2Z)$ form tetracoordinate compounds with $NiHal_2$. If two of the donor functions X, Y, Z are phosphanes, square-planar coordination is observed. In contrast, donor sets X,Y,Z = P,N,N or N,N,N form tetrahedral compounds, by *P,N* or *N,N* coordination, that are active in the catalysis of olefin oligomerization with MAO as a co-catalyst. These catalyst systems are also active in the stereoselective heterodimerization of olefins. The co-dimerization of styrene and propene by these systems leads to 4-phenyl-2-pentene almost exclusively, with regioselectivities up to 98% and (*E*)/(*Z*) ratios of up to 95:5, surpassing other reported catalysts for this process. The products of these catalytic transformations have been fully characterized by GC/MS techniques as well by isolation, NMR and MS characterization of the pure compounds.

(© Wiley-VCH Verlag GmbH & Co. KGaA, 69451 Weinheim, Germany, 2003)

Introduction

Transition metal catalysed heterodimerization of olefins is a versatile method of carbon−carbon bond formation.[1,2] The co-dimerization of styrene and ethene has been much studied since its first report in 1965.[3] Many transition metals are active in this process[4,5] but catalysts containing nickel are the most active ones.[2,6,7] They could even be developed into systems that allow the enantioselective hydrovinylation of styrene.[7] Conversely, the long-standing problem of co-dimerizing styrene with propene[4a,5b,8] has only been partially solved.[7d,7e] The major prerequisite for an effective catalyst in this process appears to be a hemilabile co-ligand.[9]

Nickel(II) compounds containing P,N- or N,N-bonded chelate ligands are promising candidates as precatalysts in this type of reaction. The recent synthesis[10] of $(R'CH_2)(CH_2Z)C(CH_2\text{-}\kappa^1\text{-}X)(CH_2\text{-}\kappa^1\text{-}Y)NiHal_2$ compounds derived from potential *tripod* ligands $R'CH_2C(CH_2X)(CH_2Y)(CH_2Z)$ (R′ = H, OMe; X, Y, Z = PR_2, NR_2) has prompted the study of their catalytic properties as co-dimerization catalysts. The results of such a study are reported here.

[a] Anorganisch-Chemisches Institut der Universität Heidelberg, Im Neuenheimer Feld 270, 69120 Heidelberg, Germany
Fax: (internat.) + 49-6221/545707
E-mail: g.huttner@indi.aci.uni-heidelberg.de

[‡] As a late contribution to his 60th birthday.

Results and Discussion

The propensity of *tripod*-derived nickel(II) chelate compounds to act as precatalysts in styrene olefin co-dimerization was tested for compounds **1**−**5** (Scheme 1).

An initial check as to whether the compounds − when activated with MAO − lead to catalysts for ethene oligomerization[11] found that none of the compounds containing two phosphane donors in the chelate cycle (**5a**−**5d**) was active. However, compounds containing a P,N or an N,N donor set in the chelate cycle (**1**−**4**) are active as oligomerization catalysts. The ethene oligomers formed were soluble in toluene. GC/MS analysis of the toluene solution and of the gaseous phase revealed a broad distribution of oligomers up to an oligomerization degree around $n = 12$ with the expected decay of the respective yields with increasing degree of oligomerization (Scheme 2).

The oligomerization process is not stereoregular: instead of one single GC/MS peak at each oligomerization degree *n*, a pattern of overlapping peaks is observed, all of which correspond to the same mass number.

This first test with ethene as a substrate showed that compounds **1**−**4** − containing hemilabile P,N- and N,N-bonded chelates − are candidates as potential precatalysts of olefin co-dimerization. The next test therefore probed the activity of these compounds in the presence of MAO for propene dimerization.[12] The test was limited to **1a**, which was found to promote the dimerization of propene with more than 90% of the product being 2-methyl-1-pentene (Scheme 3). This product was isolated by distillation and

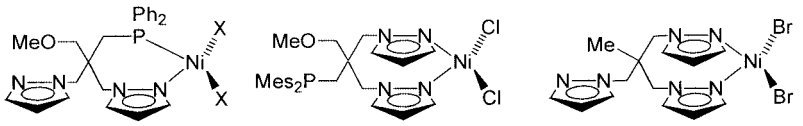

1 **2** **3**

1a: X = Cl
1b: X = Br

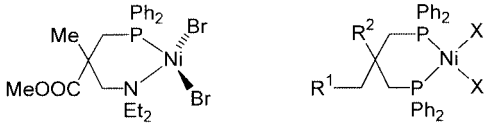

4 **5**

5a: R^1 = H R^2 = Me X = Cl
5b: R^1 = NEt_2 R^2 = Me X = Cl
5c: R^1 = pz R^2 = CH_2OMe X = Cl
5d: R^1 = pz R^2 = CH_2OMe X = Br

Scheme 1

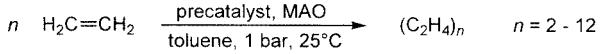

precatalyst = any of the compounds **1**-**4**

Scheme 2

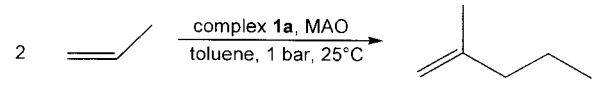

Scheme 3

identified unequivocally by 1D- and 2D-NMR spectroscopy (see Exp. Sect.).

This test shows that the catalytic process of dimerization is completely regioselective in this case.[13] Regioselectivity is an essential prerequisite for an effective heterodimerization catalyst. The next test was to analyse the potential catalytic dimerization of styrene and ethane with **1a** and **2** as precatalysts. The formation of heterodimers was observed in each case. From the many conceivable kinds of isomeric heterodimers only 3-phenyl-1-butene was formed (Scheme 4). The catalytic process was run until all styrene had been consumed (18 h, 0.1 mol % precatalyst). GC/MS analysis of the products showed that only around 30% of the products consisted of the dimer, while the rest were trimers or tetramers with all combinations of constituting olefins being present. However, no styrene dimer was observed.

These findings show that regioselective hydrovinylation of styrene is catalysed by the systems tested. They also demonstrate that the catalyst systems are too active since they activate the heterodimer for further C−C bond formation.

Consequently, the codimerization of *p*-chlorostyrene and ethene was analysed using **1a** and MAO as precatalyst system. This substituted styrene should be a less active olefin than styrene, such that the formation of oligomers containing more than one *p*-chlorostyrene moiety should be suppressed. It was observed that the catalyst system is still active with these components. The reaction is, however, much slower than with styrene, such that after 18 h (0.4 mol % precatalyst) only 45% of *p*-chlorostyrene had reacted. The almost exclusive product of this reaction is the heterodimeric compound 3-(*p*-chlorophenyl)-1-butene (Scheme 5). A very minor amount of a trimer composed of one *p*-chlorostyrene and two ethene moieties is formed. Thus, the

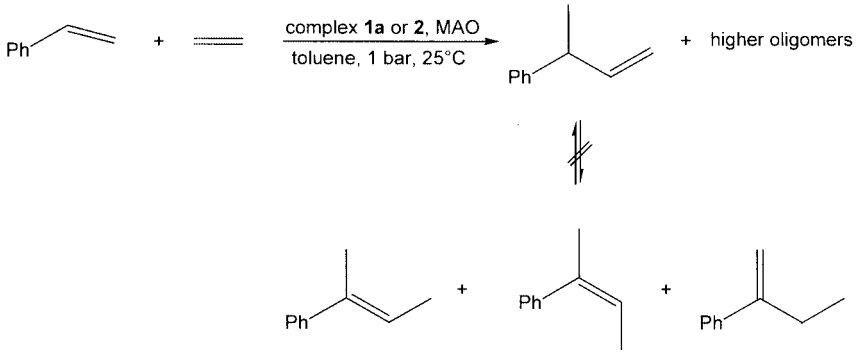

Scheme 4

 © 2003 Wiley-VCH Verlag GmbH & Co. KGaA, Weinheim

selectivity of the catalyst system for the formation of heterodimers increases with decreasing activity of the olefinic partners.

All the above tests give credit to the idea that styrene and propene might be the proper choice of olefins to be co-dimerized by the above catalyst systems.

As a precatalyst for the heterodimerization of styrene and propene the system $[(\eta^3\text{-allyl})NiBr]_2/PPh_3/AgOTf$ has been described recently.[7e] This reaction was run in CH_2Cl_2 at −20 °C to give the co-dimerization products in more than 90% yield based on styrene.

A catalyst system composed of P,N or N,N chelate compounds **1**−**4** and MAO in toluene gives good yields of the desired dimers even at room temperature (see Scheme 6). The identity of the heterodimers was proved beyond doubt by their isolation, by distillation, and a combination of mass spectra, 1D- and 2D-NMR experiments (see Exp. Sect.).

The regioselectivity of this process − depending on the reaction conditions − is up to 98%, corresponding to the almost exclusive formation of 4-phenyl-2-pentene[14] (**A**, **B**) as the dimerization products. The (*E*) isomer is the predominant compound in each case, with (*E*)/(*Z*) ratios (**A**/**B**) between 89:11 and 95:5 depending on the catalyst and the reaction conditions. The observed regioselectivity (up to 98%) and stereoselectivities (up to 95:5) are higher than those reported for the $[(\eta^3\text{-allyl})NiBr]_2$ system (regioselectivity: 80%; stereoselectivity: 88:12).[7e]

The results of this analysis (Table 1) show that compounds that contain at least one nitrogen donor in the chelate cycle (Runs 1−10) are active as precatalysts, while none of the compounds that contain two phosphorus donors in their chelate cycle (Runs 11−14) show any activity.

The selectivity of the systems containing hemilabile P,N and N,N chelates (**1**−**4**) with respect to the formation of 4-phenyl-2-pentene (**A**, **B**) depends on the catalyst/substrate ratio (see Table 1). With 1.5 mol % of the catalyst (relative to styrene) up to 80% dimeric products are obtained. With lower catalyst/styrene ratios the yield of dimeric products decreases and is only around 20% for a ratio of 0.1 mol % (Table 1). The activities of the individual catalyst systems based on **1**−**4** are not too different in this process (Table 1).

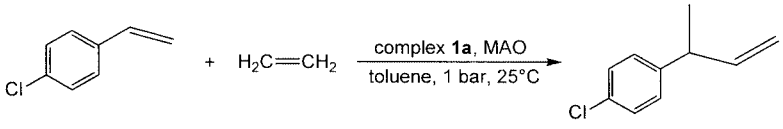

Scheme 5

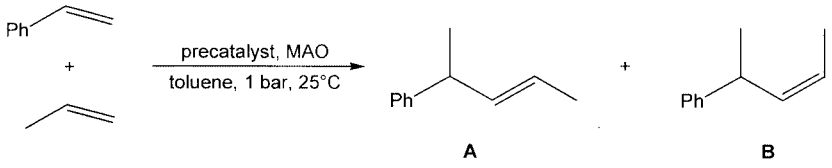

precatalyst = any of the compounds **1**-**4**

Scheme 6

Table 1. Catalytic activity of tripod compounds **1**−**5** in the heterodimerization of styrene and propene

Run[a]	Total yield[b] of dimers	Regioselectivity[c]	(*E*)/(Z) ratio of 3-phenyl-1-butene	Molar ratio catalyst/styrene	Coordinating donors of precatalyst		Precatalyst[d]
1	81%	85%	89:11	1.50 mol %	P,N	Br_2	**1b**
2	75%	88%	89:11	1.50 mol %	P,N	Cl_2	**1a**
3	56%	92%	90:10	0.75 mol %	P,N	Cl_2	**1a**
4	55%	97%	90:10	0.30 mol %	N,N	Cl_2	**2**
5	54%	89%	89:11	0.50 mol %	P,N	Br_2	**1b**
6	52%	95%	90:10	0.75 mol %	N,N	Br_2	**3**
7	29%	98%	95:5	0.10 mol %	N,N	Cl_2	**2**
8	22%	89%	89:11	0.10 mol %	P,N	Cl_2	**1**
9	21%	61%	90:10	0.75 mol %	P,N	Cl_2	**4**
10	19%	83%	89:11	0.10 mol %	P,N	Br_2	**1b**
11	−	−	−	0.75 mol %	P,P	Cl_2	**5a**
12	−	−	−	0.75 mol %	P,P	Cl_2	**5b**
13	−	−	−	0.75 mol %	P,P	Cl_2	**5c**
14	−	−	−	0.75 mol %	P,P	Br_2	**5d**

[a] Reaction time: 18 h; solvent: toluene; temperature: 25 °C; pressure: 1 bar. [b] Determined by GC/MS. [c] Regioselectivity towards 3-phenyl-1-butene (3-phenyl-1-butene/other dimers). [d] Co-catalyst: MAO.

 © 2003 Wiley-VCH Verlag GmbH & Co. KGaA, Weinheim

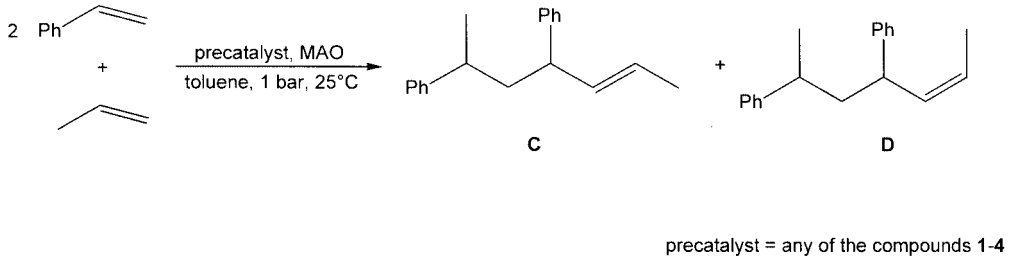

Scheme 7

Only **4**, which bears an Et_2N donor instead of a pyrazole donor (**1**−**3**), appears to be somewhat less reactive and less selective (Table 1). The reactivity of all systems is such that within 18 h styrene is quantitatively consumed, even if the molar ratio of catalyst/styrene is only 0.1 mol %.

In all experiments that lead to the catalytic formation of styrene/propene heterodimers (see Table 1), 4,6-diphenyl-2-heptene[15] is a by-product. This heterotrimer is composed of one propene and two styrene entities (**C**, **D**) (Scheme 7). The formation of **C** and **D** is completely regioselective. The (*E*)/(*Z*) ratio (**C**/**D**) is between 80:20 and 85:15 throughout, such that the reaction is also stereoselective in this respect. Both **C** and **D** were identified unequivocally by their isolation by distillation, and a combination of MS, 1D- and 2D-NMR experiments (see Exp. Sect.).

With "high" molar ratios of precatalyst/styrene (1.5 mol %), in addition to the trimer 4,6-diphenyl-2-heptene (**C**, **D**) other trimers composed of one styrene and two propene units are also formed, while with lower ratios (0.1−0.75 mol %) 4,6-diphenyl-2-heptene (**C**, **D**) is by far the predominant trimer (90−99%). The lowest percentage (65%) of **C** and **D** amongst these trimers was found with 1.5 mol % of **1b** as the precatalyst.

All the precatalysts **1**−**4** are paramagnetic nickel(II) compounds with a tetrahedral coordination around the metal atom. When the toluene solutions of these precatalysts are treated with MAO, these blue to violet tetrahedrally coordinated compounds turn red, which is characteristic of such diamagnetic square-planar nickel(II) compounds. This indicates that the substitution of the halide function by a methyl group occurs since the replacement of an Ni−Hal bond by an Ni−C bond in this type of compound leads to a transformation of tetrahedral into square-planar coordination due to the increased ligand field.[10b]

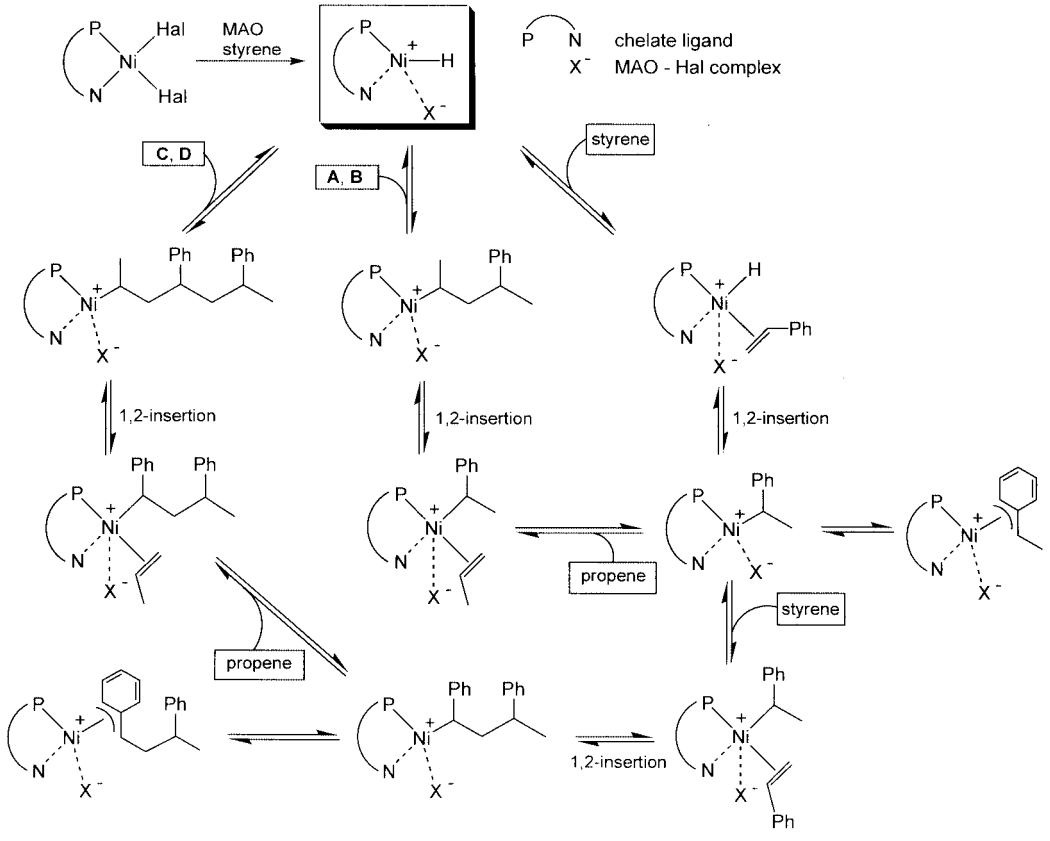

Scheme 8

 © 2003 Wiley-VCH Verlag GmbH & Co. KGaA, Weinheim

All of the above observations may be rationalized by the mechanistic scheme shown in Scheme 8. In principle the scheme is similar to the accepted hypothesis concerning olefin oligomerization by nickel catalysts.[7a,7e] Activation of the precatalyst by MAO and its reaction with styrene leads to a coordinatively unsaturated cationic Ni−H species, which is able to add styrene. (The individual steps, which result in the activated Ni−H species, are shown in refs.[2,7a,7e]) Coordinative reactivity results from X^- being trapped by MAO and by the hemilability of the Ni−N coordination (dashed lines in Scheme 8). The usual sequence of insertion steps leads to 4-phenyl-2-pentene (**A**, **B**) when propene is added as the second olefin (inner circle of Scheme 8). When styrene is also added as the second olefin the sequence shown in the outer circle of Scheme 8 leads to the formation of 4,6-diphenyl-2-heptene (**C**, **D**) provided that propene is the third olefinic constituent taken up by the catalyst. The observed regioselectivity is in complete agreement with this scheme. All routes incorporate 1,2-insertions as crucial steps, from which the observed regioselectivity follows as a natural consequence.

Conclusion

The *tripod* ligands $RC(CH_2X)(CH_2Y)(CH_2Z)$ (X,Y,Z = P,N,N or N,N,N) coordinate to $NiHal_2$ in a bidentate mode, resulting in tetrahedral nickel(II) compounds that are active as precatalysts (co-catalyst: MAO) in the heterodimerization of styrene and propene. The current results indicate that the yield of dimeric products and the selectivity of the catalysts may be further increased by optimising the reaction conditions (i.e. styrene/precatalyst ratio, reaction temperature, solvent). The yield of dimeric products reached so far is up to 80% with regioselectivities of up to 98% and stereoselectivities of up to 95%.

Pyrazole as a nitrogen donor in *tripod* ligands has been found to promote this selectivity, while the third non-coordinated donor function, serving as a dangling arm, has no major influence on the catalytic activities. This finding should stimulate further experiments in which different groups at the dangling arm are introduced to either change the solubility of the precatalysts or to fix them on a support.

Experimental Section

General Remarks: All (hetero)dimerization reactions were carried out under moisture- and oxygen-free conditions by means of standard Schlenk techniques. The Schlenk flasks were equipped with a gas balloon. All solvents were dried by standard methods[16] and distilled under argon. Complexes **1**−**5** were prepared according to literature procedures.[10] Ethene, propene, styrene, *p*-chlorostyrene, MAO (10% solution in toluene), and dodecane were purchased from Aldrich and were used without further purification. NMR: Bruker Avance DPX 200 at 200.12 MHz (^{1}H); 50.323 MHz ($^{13}C\{^1H\}$); T = 303 K; chemical shifts (δ) in ppm with respect to $CDCl_3$ (^{1}H: δ = 7.27 ppm; ^{13}C: δ = 77.0 ppm) as internal standard. GC/MS: Agilent 6890 (GC) interfaced to an Agilent 5973N (MS) equipped with an HP-5MS capillary column (30 m long, 0.25 mm inner diameter) with helium as carrier gas. Yields of the products (Table 1) refer to dodecane as internal standard.

Typical Procedure for the (Hetero)dimerization Reaction: Styrene (500−2000 mg), precatalyst **1**−**4** (5.0−20.0 mg; 0.1−1.5 mol %), and dodecane (200 mg) as internal standard were dissolved in toluene (25 mL) at 25 °C. MAO (3.0 mL of a 10% solution in toluene) was then added to the reaction mixture, and the solution immediately turned from violet to red. Ethene or propene (1 bar), respectively, was then introduced into the catalyst solution and the resultant reaction mixture was stirred at 25 °C for 18 h under ethene or propene (1 bar), respectively. For GC/MS analysis the reaction mixture (0.5 mL) was quenched with a solution of half-concentrated HCl (20 mL) and diethyl ether (20 mL). The aqueous phase was extracted with diethyl ether (20 mL). The combined organic layers were washed with brine and dried with $MgSO_4$. For preparative isolation of the oligomerization products the same type of workup procedure was applied in an appropriately scaled-up version. After removing the solvent, the following products were isolated by Kugelrohr distillation:

2-Methyl-1-pentene: ^{1}H NMR ($CDCl_3$): δ = 1.04 (t, $^3J_{H,H}$ = 7.2 Hz, 3 H, CH_2CH_3), 1.51−1.62 (m, 2 H, CH_2CH_3), 1.75 (s, 3 H, $=CCH_3$), 2.10 (t, $^3J_{H,H}$ = 7.5 Hz, 2 H, $=CCH_2$), 4.80 (br. s, 2 H, $=CH_2$) ppm. ^{13}C NMR ($CDCl_3$): δ = 14.2 (s, CH_2CH_3), 20.5 (s, CH_2CH_3), 23.1 (s, $=CCH_3$), 40.4 (s, $=CCH_2$), 110.2 (s, $=CH_2$), 137.8 (s, $=C_q$) ppm. MS (EI): *m*/*z* (%) = 84 (34) [M^+], 69 (100) [$M^+ - CH_3$], 55 (13) [$M^+ - CH_2CH_3$]. B.p. 60 °C (1013 mbar).

3-Phenyl-1-butene: ^{1}H NMR ($CDCl_3$): δ = 1.37 (d, $^3J_{H,H}$ = 6.9 Hz, 3 H, CH_3), 3.45−3.61 (m, 1 H, PhC*H*), 5.01−5.09 (m, 2 H, $=CH_2$), 5.98−6.07 (m, 1 H, $=CH$), 7.19−7.30 (m, 5 H, aromat. *H*) ppm. ^{13}C NMR ($CDCl_3$): δ = 21.1 (s, CH_3), 43.7 (s, Ph*C*H), 113.3 (s, $=CH_2$), 125.9−145.5 (m, aromat. *C*), 143.8 (s, $=CH$) ppm. MS (EI): *m*/*z* (%) = 132 (25) [M^+], 117 (100) [$M^+ - CH_3$], 91 (25) [$C_7H_7^+$], 77 (18) [$C_6H_5^+$], 65 (10) [$C_5H_5^+$], 51 (22) [$C_4H_3^+$]. B.p. 30 °C (0.1 mbar).

(*E*)-4-Phenyl-2-pentene (A): ^{1}H NMR ($CDCl_3$): δ = 1.46 (d, $^3J_{H,H}$ = 7.1 Hz, 3 H, PhCHC*H*$_3$), 1.80 (d, $^3J_{H,H}$ = 6.2 Hz, 3 H, $=CHCH_3$), 3.54 (quint, $^3J_{H,H}$ = 6.9 Hz, 1 H, PhC*H*), 5.51−5.68 (m, 1 H, $CH_3CH=$), 5.76 (dd, $^3J_{H,H}$ = 6.8, $^3J_{H,H}$ = 15.2 Hz, 1 H, CHC*H*=), 7.24−7.44 (m, 5 H, aromat. *H*) ppm. ^{13}C NMR ($CDCl_3$): δ = 18.1 (s, $=CHCH_3$), 21.8 (s, PhCH*C*H$_3$), 42.9 (s, Ph*C*H), 124.0 (s, $CH_3CH=$), 126.3−128.7 (m, aromat. *C*), 136.8 (s, CH*C*H=) ppm. MS (EI): *m*/*z* (%) = 146 (22) [M^+], 131 (100) [$M^+ - CH_3$], 116 (14) [$M^+ - 2CH_3$], 91 (31) [$C_7H_7^+$], 77 (10) [$C_6H_5^+$]. B.p. 35−40 °C (0.1 mbar).

(*E*)-4,6-Diphenyl-2-heptene (C): ^{1}H NMR ($CDCl_3$): δ = 1.39 (d, $^3J_{H,H}$ = 7.0 Hz, 3 H, PhCHC*H*$_3$), 1.83 (d, $^3J_{H,H}$ = 6.3 Hz, 3 H, $=CHCH_3$), 2.01−2.21 (m, 2 H, CH_2), 2.87 (sext, 1 H, $^3J_{H,H}$ = 7.2 Hz, PhC*H*CH$_3$), 3.25 (q, $^3J_{H,H}$ = 7.6 Hz, 1 H, PhC*H*CH=), 5.55−5.61 (m, 1 H, $CH_3CH=$), 5.76 (dd, $^3J_{H,H}$ = 7.9, $^3J_{H,H}$ = 15.0 Hz, 1 H, PhCHC*H*=), 7.25−7.47 (m, 10 H, aromat. *H*) ppm. ^{13}C NMR ($CDCl_3$): δ = 18.2 (s, $=CHCH_3$), 23.0 (s, PhCH*C*H$_3$), 37.8 (s, Ph*C*HCH$_3$), 45.1 (s, CH_2), 47.1 (s, Ph*C*HCH=), 125.6 (s, $CH_3CH=$), 126.4−146.0 (m, aromat. *C*), 135.4 (s, PhCH*C*H=) ppm. MS (EI): *m*/*z* (%) = 250 (12) [M^+], 145 (10) [M^+ − PhCHCH$_3$], 131 (100) [$M^+ - PhCH(CH_3)CH_2$], 105 (35) [PhCHCH$_3^+$], 91 (38) [$C_7H_7^+$], 77 (10) [$C_6H_5^+$]. B.p. 215−220 °C (0.1 mbar).

 © 2003 Wiley-VCH Verlag GmbH & Co. KGaA, Weinheim

Acknowledgments

We are indebted to the Deutsche Forschungsgemeinschaft and the Fonds der Chemischen Industrie for financial support. One of us (R. F.) is indebted to the local Graduiertenkolleg "Selektivität in der organischen und metallorganischen Synthese und Katalyse" for a scholarship.

[1] For recent reviews see: [1a] P. W. Jolly, G. Wilke, in: *Applied Homogenous Catalysis with Organometallic Compounds* (Eds.: B. Cornils, W. A. Herrmann), VCH, New York, **1996**, vol. 2, p. 1024. [1b] T. V. RajanBabu, in: *Comprehensive Asymmetric Catalysis* (Eds.: E. N. Jacobsen, A. Pfaltz, H. Yamamoto), Springer, New York, **1999**, vol. 1, p. 417.

[2] G. Wilke, *Angew. Chem.* **1988**, *100*, 189; *Angew. Chem. Int. Ed. Engl.* **1988**, *27*, 185.

[3] T. Alderson, E. L. Jenner, R. V. Lindsey, Jr., *J. Am. Chem. Soc.* **1965**, *87*, 5638.

[4] For Pd-catalysed reactions see: [4a] E. Drent (Shell Oil Company), US Patent 5227561, **1993** (*Chem. Abstr.* **1994**, *120*, 31520). [4b]G. J. P. Britovsek, W. Keim, S. Mecking, D. Sainz, T. Wagner, *J. Chem. Soc., Chem. Commun.* **1993**, 1632. [4c] G. J. P. Britovsek, K. J. Cavell, W. Keim, *J. Mol. Catal. A* **1996**, *110*, 7. [4d] R. Bayersdörfer, B. Ganter, U. Englert, W. Keim, D. Vogt, *J. Organomet. Chem.* **1998**, *552*, 187. [4e] N. J. Hovestad, E. B. Eggeling, H. J. Heidbüchel, J. T. B. H. Jastrzebski, U. Kragl, W. Keim, D. Vogt, G. van Koten, *Angew. Chem.* **1999**, *111*, 1763; *Angew. Chem. Int. Ed.* **1999**, *38*, 1655. [4f] E. B. Eggeling, N. J. Hovestad, J. T. B. H. Jastrzebski, D. Vogt, G. van Koten, *J. Org. Chem.* **2000**, *65*, 8857.

[5] For Co-catalysed reactions see: [5a] S. M. Pillai, G. L. Tembe, M. Ravindranathan, *J. Mol. Catal.* **1993**, *84*, 77. For Ru-catalysed reactions see: [5b] H. Umezaki, Y. Fujiwara, K. Sawara, S. Teranishi, *Bull. Chem. Soc. Jpn.* **1973**, *46*, 2230. [5c] C. S. Yi, Z. He, D. W. Lee, *Organometallics* **2001**, *20*, 802.

[6] [6a] N. Kawata, K. Maruya, T. Mizoroki, A. Ozaki, *Bull. Chem. Soc. Jpn.* **1974**, *47*, 413. [6b] B. Bogdanović, *Adv. Organomet. Chem.* **1979**, *17*, 105. [6c] R. Ceder, G. Muller, J. I. Ordinas, *J. Mol. Catal.* **1994**, *92*, 127. [6d] A. L. Monteiro, M. Seferin, J. Dupont, R. F. de Souza, *Tetrahedron Lett.* **1996**, *37*, 1157. [6e] G. Muller, J. I. Ordinas, *J. Mol. Catal. A* **1997**, *125*, 97. [6f] V. Fassina, C. Ramminger, M. Seferin, A. L. Monteiro, *Tetrahedron* **2000**, *56*, 7403.

[7] [7a] K. Angermund, A. Eckerle, F. Lutz, *Z. Naturforsch., Teil B* **1995**, *50*, 488. [7b] N. Nomura, J. Jin, H. Park, T. V. RajanBabu, *J. Am. Chem. Soc.* **1998**, *120*, 459. [7c] M. Nandi, J. Jin, T. V. RajanBabu, *J. Am. Chem. Soc.* **1999**, *121*, 9899. [7d] T. V. RajanBabu, N. Nomura, J. Jin, B. Radetich, H. Park, M. Nandi, *Chem. Eur. J.* **1999**, *5*, 1963. [7e] J. Jin, T. V. RajanBabu, *Tetrahedron* **2000**, *56*, 2145. [7f] A. Bösmann, G. Franciò, E. Janssen, M. Solinas, W. Leitner, P. Wasserscheid, *Angew. Chem.* **2001**, *113*, 2769; *Angew. Chem. Int. Ed.* **2001**, *40*, 2697. [7g] G. Franciò, F. Faraone, W. Leitner, *J. Am. Chem. Soc.* **2002**, *124*, 736. [7h] H. Park, T. V. RajanBabu, *J. Am. Chem. Soc.* **2002**, *124*, 734.

[8] [8a] T. Ito, K. Takahashi, Y. Takami, *Nippon Kagaku Kaishi* **1974**, 1097 (*Chem. Abstr.* **1974**, *81*, 77567). [8b] K. Kawakami, N. Kawata, K. Maruya, T. Mizoroki, A. Ozaki, *J. Catal.* **1975**, *39*, 134. [8c] A. G. Azizov, K. Z. Mamedov, S. M. Aliev, *Sb. Tr. Akad. Nauk Az. SSR, Inst. Neftekhim. Protsessov im. Akad. Yu. G. Mamedalieva* **1986**, *15*, 58 (*Chem. Abstr.* **1988**, *108*, 131117).

[9] [9a] C. Jeffrey, T. B. Rauchfuss, *Inorg. Chem.* **1979**, *18*, 2658. [9b] A. Bader, E. Lindner, *Coord. Chem. Rev.* **1991**, *108*, 27. [9c] C. S. Slone, D. A. Weinberger, C. A. Mirkin, *Prog. Inorg. Chem.* **1999**, *48*, 233.

[10] [10a] R. Faissner, G. Huttner, E. Kaifer, P. Rutsch, *Eur. J. Inorg. Chem.* **2003**, 1681−1693. [10b] R. Faissner, G. Huttner, E. Kaifer, P. Kircher, P. Rutsch, L. Zsolnai, *Eur. J. Inorg. Chem.* **2003**, 2219−2238, preceding paper.

[11] [11a] W. Keim, *Angew. Chem.* **1990**, *102*, 251; *Angew. Chem. Int. Ed. Engl.* **1990**, *29*, 235. [11b] D. Vogt, in: *Applied Homogenous Catalysis with Organic Compounds* (Eds.: B. Cornils, W. A. Herrmann), VCH, New York, **1996**, vol. 1, p. 245.

[12] [12a] G. Wilke, B. Bogdanović, P. Hardt, P. Heimbach, W. Keim, M. Kröner, W. Oberkirch, K. Tanaka, E. Steinrücke, D. Walter, H. Zimmermann, *Angew. Chem.* **1966**, *78*, 157; *Angew. Chem. Int. Ed. Engl.* **1966**, *5*, 151. [12b] Y. Chauvin, H. Olivier, in: *Applied Homogenous Catalysis with Organometallic Compounds* (Eds.: B. Cornils, W. A. Herrmann), VCH, New York, **1996**, vol. 1, p. 258.

[13] [13a] B. Bogdanović, *Adv. Organomet. Chem.* **1979**, *17*, 105. [13b] E. Balbolov, M. Mitkova, K. Kurtev, J.-P. Gehrke, R. Taube, *J. Organomet. Chem.* **1988**, *352*, 247. [13c] S. A. Svejda, M. Brookhart, *Organometallics* **1999**, *18*, 65.

[14] H. L. Goering, E. P. Seitz Jr., C. C. Tseng, *J. Org. Chem.* **1981**, *46*, 5304.

[15] M. F. Lipton, C. M. Sorensen, A. C. Sadler, *J. Organomet. Chem.* **1980**, *186*, 155.

[16] *Organikum*, Deutscher Verlag der Wissenschaften, Berlin, **1990**.

Received September 20, 2002

 © 2003 Wiley-VCH Verlag GmbH & Co. KGaA, Weinheim

The Aminolysis of Beryllium Dichloride with Diisopropylamine and Reactions of Some Aminoberyllium Chlorides[‡]

Heinrich Nöth*[a] and Dieter Schlosser[a]

Dedicated to Prof. Dr. D. Fenske on the occasion of his 60th birthday

Keywords: Adduct formation / Amines / Beryllium / N ligands / NMR spectroscopy

$BeCl_2$ is not aminolyzed by diisopropylamine. An excess of this amine reacts with $BeCl_2$ or $BeCl_2{\cdot}2OEt_2$ to give $BeCl_2{\cdot}HNiPr_2$ (**1**). This compound, on deprotonation with LiBu at low temperature, gives rise predominantly to dimers of $ClBe(NiPr_2)$ (**2**), together with $Be(NiPr_2)_2$ (**3**). Compound **2** adds diisopropylamine to give the adduct $ClBe(NiPr_2){\cdot}HNiPr_2$ (**4**), which provides **3** on treatment with LiBu. Compound **2** reacts with $LiBH_4$ to give dimeric iPr_2NBeBH_4 (**17**). The BH_4 group is μ^2-bonded to the Be centers, as shown by NMR spectroscopic data and an X-ray structure determination. Moreover, a number of dimeric organylberyllium diisopropylamides iPr_2NBeR have been prepared by treatment of **2** with LiR. In analogy, *tert*-butoxyberyllium diisopropylamide (**20**) has also been synthesized. Moreover, several 2,2,6,6-tetramethylpiperidinoberyllium and bis(trimethylsilyl)amino derivatives are reported. ^{9}Be NMR spectroscopic data of the new compounds are consistent with tricoordinated Be centers and dimeric units (MS, cryoscopy).

(© Wiley-VCH Verlag GmbH & Co. KGaA, 69451 Weinheim, Germany, 2003)

Introduction

The principles of the chemistry of beryllium−nitrogen compounds were explored particularly by Coates and coworkers, beginning in the 1950s.[2] Research focussed on dimethylamino derivatives, which in most cases proved to be dimeric (for $RBeNMe_2$; R = alkyl, aryl),[3] and the status of beryllium−nitrogen chemistry has been summarized by Lappert et al.[4] Unlike the trimeric $Be(NMe_2)_2$, and also $Be(NEt_2)_2$, which is dimeric, the silylamide $Be[N(SiMe_3)_2]_2$ proved to be monomeric.[5] Another monomeric beryllium bis(amide) is the 2,2,6,6-tetramethylpiperidino derivative $(tmp)_2Be$.[6] For $(iPr_2N)_2Be$, a monomer/dimer equilibrium in solution has been established.[6] Obviously, the steric requirements of the diisopropylamino group allow stabilization of both association states with a preference for the dimer in the solid, and it may therefore be expected that diisopropylamides of beryllium of type iPr_2NBeX should be monomeric for bulky groups X. In order to verify this we have been examining a number of beryllium amides of this kind.

Results

Reactions

So far, no systematic study of the aminolysis of beryllium dichloride has been performed.

Bis(dialkylamino)beryllium compounds are readily obtained from $BeCl_2{\cdot}2OEt_2$ and 2 equiv. of $LiNR_2$ as shown in Equation (1). This is the only known route to the sterically demanding monomeric bis(amides) $(tmp)_2Be$, $[t$Bu$(Me_3Si)N]_2Be$,[6] and $[(Me_3Si)_2N]_2Be$.[5] For sterically less bulky amine groups, one may also deprotonate adducts of secondary amines and beryllium dichloride with LiR [Equation (2)].[7] However, this route has not often been used. To date, most of the reported amine adducts of $BeCl_2$ have the composition $BeCl_2{\cdot}n$(amine) (n = 2−4).[8,9] In order to characterize the various steps from $BeCl_2$ to $(R_2N)_2Be$ we have studied the reaction between beryllium dichloride and diisopropylamine in more detail.

No adduct of $BeCl_2$ and $HNiPr_2$ has yet been described. The amine may not form a well-defined product, as has been found for the triethylamine adduct of $BeCl_2$.[9] We found that solid $BeCl_2$ does not react with an excess of $HNiPr_2$ at ambient temperature. Under reflux conditions, however, the crystals of $BeCl_2$ turned into a gray powder of composition $BeCl_2{\cdot}HNiPr_2$ (**1**) [Equation (3)]. This compound is more readily obtained by treatment of $BeCl_2{\cdot}2OEt_2$ with a large excess of diisopropylamine in diethyl ether solution. In this case the 1:1 adduct was formed

[‡] Chemistry of Beryllium Nitrogen Compounds, 4. Part 3: Ref.[1]

[a] Department of Chemistry, University of Munich, House D Butenandtstr. 5−13, 81377 München, Germany
E-mail: H.Noeth@lrz.uni-muenchen.de

$$BeCl_2{\cdot}2OEt_2 + 2\ LiNR_2 \rightarrow Be(NR_2)_2 + 2\ LiCl \quad (1)$$

3

$$BeCl_2{\cdot}2HNR_2 + 2\ LiR' \rightarrow Be(NR_2)_2 + 2\ LiCl + R'H \quad (2)$$

$$BeCl_2 + HNiPr_2 \rightarrow Cl_2Be{\cdot}HNiPr_2 \quad (3)$$

1

$$Cl_2Be{\cdot}HNiPr_2 + LiBu \rightarrow iPr_2NBeCl + LiCl + BuH \quad (4)$$

2

$$BeCl_2{\cdot}2OEt_2 + LiNiPr_2 \rightarrow iPr_2NBeCl + LiCl \quad (5)$$

$$iPr_2NBeCl + HNiPr_2 \rightarrow\!\leftarrow iPr_2NBeCl{\cdot}NHiPr_2 \quad (6)$$

4

$$iPr_2NBeCl{\cdot}HNiPr_2 + LiBu \rightarrow BuH + LiCl + (iPr_2N)_2Be \quad (7)$$

as an oily product, which became solid on removal of all volatile substances in vacuo. An excess of the amine is therefore not able to deprotonate **1**. This was to be expected, because it is unlikely that the amine would be able to remove a proton from $BeCl_2{\cdot}HNiPr_2$, as the beryllium amide should be more basic than diisopropylamine. A stronger base, such as LiR, is therefore needed for deprotonation.

Astonishingly, the reaction between LiBu and **1** at ambient temperature provided not only iPr_2NBeCl (**2**), but also by-products such as iPr_2NBeBu and $(iPr_2N)_2Be$ (**3**). This latter compound was actually the main product. Moreover, **2** could not be separated from the other products by sublimation in vacuo. Obviously, **2** reacted more rapidly than **1** with LiBu, to give iPr_2NBeBu, and, moreover, a $BeNiPr_2$/LiBu exchange, resulting in the formation of $Li(iNPr_2)$, competes favorably with other reactions and provides an opportunity to generate **3**.

At present, the 1:1 reaction between $LiNiPr_2$ and $BeCl_2{\cdot}2OEt_2$ in diethyl ether at 0 °C is the best choice for the preparation of **2** [Equation (5)]. Some $iPr_2NBeOEt$ and $(iPr_2N)_2Be$ is also formed in this reaction, but the chloride **2** can be separated by sublimation. In contrast, neither ligand exchange between $BeCl_2$ and $(iPr_2N)_2Be$ in boiling benzene nor the reaction between $(iPr_2N)_2Be$ and $BeCl_2{\cdot}2OEt_2$ in boiling THF or toluene afford **2**.

Molecular mass values and spectroscopic data for **2** indicate that the compound is dimeric in solution, containing tricoordinated Be atoms. These should be able to act as Lewis acidic centers. It was therefore expected that **2** might add a Lewis base. In the context of aminolysis, the addition of diisopropylamine to **2** was studied. The existence of a compound $iPr_2NBeCl{\cdot}HNiPr_2$ (**4**) was indicated in the reaction between $BeCl_2$ and 2 equiv. of the amine in diethyl ether after addition of 1 equiv. of LiBu. Needles separated from the resulting solution, their NMR spectroscopic data being consistent with compound **4** in admixture with iPr_2NBeBu and **3**.

Actually, after 10−20 min, the ^1H NMR spectrum of the 1:1 mixture of **2** and $HNiPr_2$ showed only the components, and about 24 h were required until the new signals attained maximum intensity. These signals can be interpreted in terms of the equilibrium according to Equation (6). Heating of this mixture to 75 °C restored the original situation (i.e., only the signals for diisopropylamine and **2** were visible), and it again took more than 24 h at ambient temperature to reform the equilibrium situation, which in solution lies

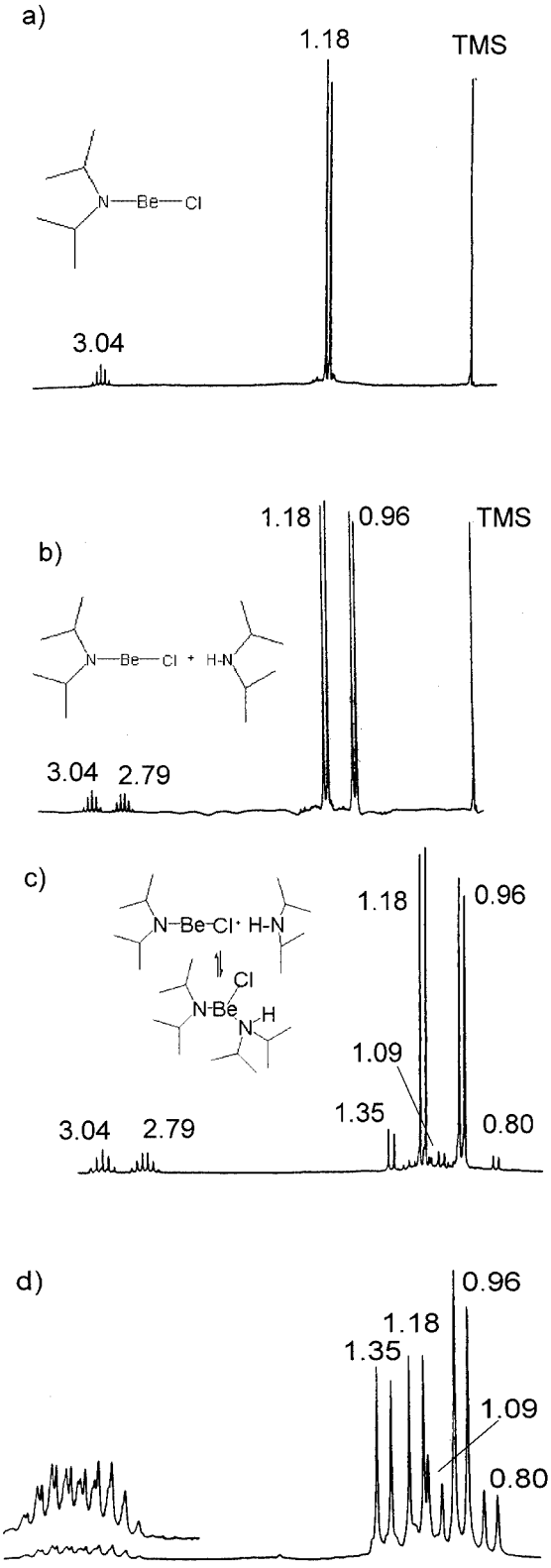

Figure 1. Time-dependent ^1H NMR spectra of the reaction mixture of diisopropylamine and (diisopropylamino)beryllium chloride; a) $(iPr_2NBeCl)_2$ at 200 MHz; b) $(iPr_2NBeCl)_2$ + iPr_2NH (1:2) at 200 MHz; 30 min after addition; c) as b) but 210 min after addition; d) equilibrium situation, 90 MHz spectrum after 68 h

 © 2003 Wiley-VCH Verlag GmbH & Co. KGaA, Weinheim

to 75% on the side of the adduct **4**. Figure 1 depicts some NMR spectra to illustrate this kind of interaction.

As was to be expected, the adduct $ClBe(NiPr_2)\cdot HNiPr_2$ did not react further with an excess of the amine. However, it was deprotonated by LiBu at low temperature, as shown in Equation (7), to produce bis(diisopropylamino)beryllium (**3**).[6] At ambient temperature, iPr_2NBeBu is a by-product. Thus, *direct aminolysis* of $BeCl_2$ by diisopropylamine is not possible, most probably because the *Be*-bonded amino group is more basic than the amine itself.[10]

Similarly, it was expected that $BeCl_2\cdot 2OEt_2$ should react with *N*-lithio-2,2,6,6-tetramethylpiperidine [Li(tmp)] in a 1:1 ratio to give (tmp)BeCl (**5**). In hexane solution, however, the main product (was $(tmp)_2Be$ (**6**). On the other hand, when the reaction was performed at −78 °C in the presence of diethyl ether, a viscous oil was obtained, and this was analyzed by NMR spectroscopy as a mixture of **6** (15%) and (tmp)BeOEt (**7**, 85%). These components could not be separated by fractional distillation. Analogously, the 1:1 reaction between $BeCl_2$ and tBu(Me_3Si)NLi in diethyl ether afforded a mixture of [tBu(Me_3Si)N]$_2$Be (**8**), tBu(Me_3Si)NBeCl (**9**), and tBu(Me_3Si)$_2$NBeOEt (**10**). From this mixture the bis(amide) **8** was separated by distillation. However, when the reaction was started at −100 °C, compound **8** was not present, and **9** and **10** were obtained in a 1:1.8 ratio. Compound **9** was separated by fractional sublimation. Similar behavior was observed for the 1:1 reaction between $BeCl_2$ and $LiN(SiMe_3)_2$ in diethyl ether. At room temperature, only [$(Me_3Si)_2N]_2$Be (**11**) was obtained besides $BeCl_2\cdot 2OEt_2$. At −78 °C, a 1:4:2 mixture of **11**, (Me_3Si)$_2$NBeCl (**12**), and (Me_3Si)$_2$NBeOEt (**13**) resulted. When the reaction was started at −100 °C, however, only **12** and **13** were detected by NMR, and these two compounds could be separated by fractional sublimation.

(tmp)BeCl **5** (tmp)$_2$Be **6** (tmp)BeOEt **7**

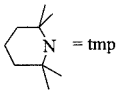

[(tBu)$Me_3SiN]_2$Be **8** (tBu)$Me_3SiNBeCl$ **9** (tBu)$Me_3SiNBeOEt$ **10**

[$(Me_3Si)_2N]_2$Be **11** (Me_3Si)$_2$NBeCl **12** (Me_3Si)$_2$NBeOEt **13**

Reactions of iPr_2NBeCl and other Aminoberyllium Chlorides

The aminoberyllium chlorides offer potential as reagents for the synthesis of other aminoberyllium compounds by nucleophilic substitution of the Cl atoms. $[iPr_2NBeCl]_2$ was used as a model compound for this kind of reaction. Treatment with LiBu in hexane gave a 68% yield of liquid iPr_2NBeBu (**14**), as shown in Equation (8).

$$[iPr_2NBeCl]_2 + 2\ LiBu \rightarrow [iPr_2NBeBu]_2 + 2\ LiCl \quad (8)$$

14

$$[iPr_2NBeCl]_2 + 2\ LitBu \rightarrow [iPr_2NBe(tBu)]_2 + 2\ LiCl \quad (9)$$

15

$$2\ tBuBeCl + 2\ LiNiPr_2 \rightarrow [iPr_2NBe(tBu)]_2 + 2\ LiCl \quad (10)$$

At 0 °C the reaction according to Equation (9) produced some gas, which may be due to elimination of isobutene and formation of the hydride $[iPr_2NBeH]_n$. However, workup by sublimation yielded compound **15** as a solid in 48% yield. The residue from the sublimation provided evidence for the formation of the hydride, because hydrogen was generated by hydrolysis with hydrochloric acid. When the reaction according to Equation (9) was performed at −78 °C the yield of **15** increased to 78%. This yield was also obtained in the reaction according to Equation (10).

In order to obtain information on the steric effect of the tmp group, $[tmpBeCl]_2$ was treated with LiBu and LitBu. The reaction between **5** and LiBu gave dimeric (tmp)BeBu (**16**) [Equation (11)]. This is a viscous oil, and its dimeric nature was determined by molecular mass measurement in cyclohexane. Temperature-dependent ^{9}Be NMR spectroscopy provided no evidence for a monomer/dimer equilibrium.

$$[(tmp)BeCl]_2 + 2\ LiBu \rightarrow [(tmp)BeBu]_2 + 2\ LiCl \quad (11)$$

16

$$[(tmp)BeCl]_2 + 2\ LitBu \rightarrow [(tmp)Be(tBu)]_2 + 2\ LiCl \quad (12)$$

17

$$[(tmp)BeCl]_2 + 2\ LitBu \rightarrow 2/n\ [(tmp)BeH]_n + LiCl + H_2C{=}CMe_2 \quad (13)$$

$$tBuBeCl\cdot OEt_2 + (tmp)Li \rightarrow (tmp)BeH + LiCl\cdot H_2C{=}CMe_2 \quad (14)$$

$$[iPr_2NBeCl]_2 + 2\ LiBH_4 \rightarrow [iPr_2NBeBH_4]_2 + 2\ LiCl \quad (15)$$

18

$$[iPr_2NBeCl]_2 + 2\ KOtBu \rightarrow [iPr_2NBeOtBu]_2 + 2\ KCl \quad (16)$$

19

$$[iPr_2NBeCl]_2 + 2\ py \rightarrow [iPr_2NBeCl\cdot py]_2 \quad (17)$$

20

$$[iPr_2NBeCl]_2 + 2\ EX_3 \rightarrow [iPr_2NBeCl\cdot EX_3]_2 \quad (18)$$

21 ($EX_3 = BCl_3$)

22 ($EX_3 = BBr_3$)

23 ($EX_3 = AlCl_3$)

When LitBu was allowed to react with $[(tmp)BeCl]_2$ in hexane according to Equation (12), gas evolution was noted. The ^{1}H and ^{13}C NMR spectra of the solution showed only very-low-intensity signals for a tBu group. When the reaction was performed at −78 °C, LiCl precipitated slowly [see Equation (13)]. On warming, gas evolution started at about 10 °C. When the reaction mixture obtained at −78 °C was subjected to NMR analysis, no signals for a *Be*-bonded tBu group could be observed. The ^{9}Be NMR signal found at $\delta = 11.9$ ppm ($h_{1/2} = 140$ Hz) shows the same shielding as for compound **16**, an indication of the formation of $[(tmp)Be(tBu)]_2$.

An attempt to prepare **17** by using monomeric tBuBeCl·OEt$_2$ as a starting material might have allowed a more straightforward substitution using (tmp)Li. Neither at 0 °C nor at −78 °C was this possible, however. Gas evolution was observed in both cases, and the filtrate from the

 © 2003 Wiley-VCH Verlag GmbH & Co. KGaA, Weinheim

suspension gave no evidence for the formation of **17** by NMR analysis. However, 1 equiv. of LiCl was formed, and the filtrate was virtually free of chloride. The yield of the crude material was 90% calculated for (tmp)BeH.[11] The reaction therefore has to be as shown in Equation (14).

Since ether cleavage has been observed in reactions between the aminoberyllium chlorides and $LiNR_2$ compounds in diethyl ether, resulting in ethoxy derivatives, we treated **2** with KO*t*Bu. The *tert*-butoxy derivative **19** was obtained in good yield, as shown in Equation (16) (see below for the structures of R_2NBeOR compounds).

Unlike the alkyl or alkoxy groups, which are usually unidentate substituents, the BH_4 group may be variously mono-, di-, or even tridentate. The reaction between **2** and $LiBH_4$ was therefore expected to give $iPr_2NBe(BH_4)$, which might be monomeric in the case of a structure such as $iPr_2NBe(\mu\text{-}H_3BH)$ but proved to be dimeric $[iPr_2NBeH_4]_2$ (**18**) as shown in Equation (15). However, analysis of the solution by ^{11}B NMR spectroscopy showed that the main product was iPr_2NBH_2, together with $(iPr_2N)_2BH$, $[iPr_2NB(H)Cl]_2$, and $Be(BH_4)_2$. Moreover, several ^9Be NMR signals were noted, but none could be reliably assigned. When the reaction according to Equation (15) was performed at −78 °C and the mixture was allowed to come to room temperature, however, crystals of **18** separated from a concentrated solution at −20 °C. The tetrahydroborate **18** is stable up to 85 °C, but very moisture-sensitive, although not spontaneously inflammable in contact with air. Its molecular structure was determined by X-ray crystallography.

While $[iPr_2NBeCl]_2$ should have Lewis-acidic properties, due to its tricoordinated Be atoms, only Lewis base behavior can be expected from its Cl atoms. Compound **2** reacts readily with pyridine (py) to form a deep red solution in hexane [Equation (17)]. The isolated product is $[iPr_2NBeCl{\cdot}py]_2$ (**20**), with tetracoordinate Be atoms as shown by ^9Be NMR spectroscopy ($\delta = 4.8$, $w_{1/2} = 1.5$ Hz). Triethylamine gave no stable adduct.[9] Surprisingly, **2** reacted with strong Lewis acids, provided they were strong chloride acceptors. Thus, 1:2 adducts $[iPr_2NBeCl]_2{\cdot}2ECl_3$ resulted from treatment of **2** with BCl_3, BBr_3, and $AlCl_3$ [Equation (18)]. One of the constitutions **A**−**C** would be expected for these adducts. Structure **A** can be ruled out, as the ^9Be NMR signal is typical of tetracoordinate Be. Structure **C** also does not have to be considered, primarily because two ^9Be NMR signals would be expected at low field for a tri- and a dicoordinated Be atom. The latter would have only an electron quadruplet, and the cation would certainly be a high-energy species. All NMR spectroscopic data, however, are in agreement with structure **B**, and we assume that the structure has C_{2v} symmetry.

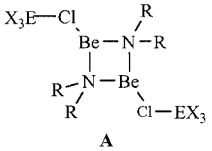

A

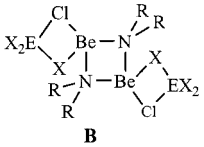

B

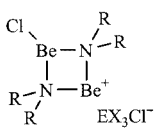

C

Spectroscopic Data

Beryllium is a single-isotope element. Its nuclear spin is 3/2, and it has a favorable longitudinal relaxation time. Although its nuclear quadrupole moment of $5.2{\cdot}10^{-2}$ ($e{\cdot}10^{-24}$ cm^2) is about 70% that of ^{11}B, the linewidths of the signals may become rather broad for Be atoms residing in asymmetric environments. On the other hand, the sensitivity of the ^9Be nucleus is smaller than that of ^{11}B only by a factor of 10. Nevertheless, the nuclear properties of ^9Be are very favorable for use of ^9Be NMR as a tool for obtaining structural information. As has been shown previously, chemical shifts and linewidths depend not only on the substituents but also, to a large extent, on the coordination number of Be.[12] Table 1 summarizes the ^9Be chemical shifts and ^1H, ^{13}C, and ^{14} N NMR spectroscopic data for the compounds reported in this study.

Because of the low solubility of $Cl_2Be{\cdot}HNiPr_2$ in most solvents, all of its NMR spectroscopic data were collected at 60 °C in C_6D_6 solutions. The ^9Be NMR signal at δ = 5.84 ppm, and particularly its linewidth (see Table 1), shows that the compound contains tricoordinated Be atoms. No ^{14}N resonance could be recorded. The ammonium-type character of the coordinated amine is represented by a ^1H NMR signal for the NH group at δ = 5.05 ppm, 4.5 ppm downfield from the free amine. The proton signal for the CH group is also shifted downfield (δ = 1.97 ppm).

While the ^9Be chemical shifts and the linewidths of the aminoberyllium chlorides **2**, **5**, **9**, and **13** (see Table 1) are consistent with a coordination number of three for the Be atoms, the ^1H and the ^{13}C NMR signals are less strongly influenced than in compound **2**. Tetracoordination at ^{14}N is confirmed by chemical shifts in the range from δ = −120 to −140 ppm.[13]

Unexpectedly, only two ^1H NMR signals were observed for the 36 protons of dimeric (tmp)BeCl. The eight methyl groups are represented by a single sharp signal at δ = 1.30 ppm, contrasting with a broad, unresolved multiplet for the CH_2 groups. Again in contrast, four ^{13}C NMR signals were found. Assignment to the four equivalent C atoms (atoms C1/C5, C2/C4, C3, and Me) of the tmp units was possible with the aid of $^{13}C(^1H\text{-NOE})$ experiments. Dimeric (tmp)BeOEt provided similar NMR spectra, the ^{13}C NMR spectrum showed clearly resolved signals for the two magnetically equivalent ethoxy groups. Those of the tmp groups are at higher field than in tmpH, except for the atoms C1/C5, which are bonded to a tetracoordinated N atom. Almost the same chemical shifts as for Et_2O were noted for the EtO groups. This is further evidence that the EtO group does not bridge the Be atoms (i.e., of the three possible dimeric aminoberyllium ethoxide structures **D**−**F** only the symmetrical amino-bridged species were formed).

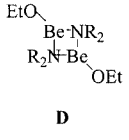

D

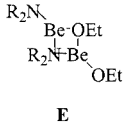

E

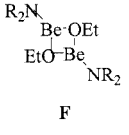

F

 © 2003 Wiley-VCH Verlag GmbH & Co. KGaA, Weinheim

Table 1. NMR spectroscopic data of the aminoberyllium compounds (in C_6D_6)

	δ^9Be [ppm]	$w_{1/2}$ [Hz]	δ^1H [ppm]	δ^{13}C [ppm]
iPr$_2$NH·BeCl$_2$	5.84	48	5.05 (NH)	
iPr$_2$NBeCl[a]	10.37	82	1.20 (d), 3.06 (sept)	23.77 (q, Me),
(iPr$_2$N)$_2$Be[b]	12.7	288	1.06 (d), 2.92 (sept)	26.10 (Me), 17.33 (CH)
(tmp)BeCl[c]	9.4	60	1.30 (s), 1.64 (m)	19.13 (d), 34.46 (q), 39.55 (d),50.38 (s)
(tmp)BeOEt[d]	7.7	40	1.08 (s), 1.16 (m), 1.36 (t),3.79 (q) (EtO)	17.63, 31.18, 36.81, 52.30 (tmp), 17.87, 61.15 (Et)
(tmp)$_2$Be	15.3	230	1.28 (s), 1.59(m)	19.07, 34.31, 39.85, 50.33
(tBu)Me$_3$SiNBeCl	11.6	90	0.25(s), 1.29(s)	4.40 (q, SiMe); 35.77, 51.52 (tBu)
(tBu)Me$_3$SiNBeOEt	9.12	85	0.16(s), 1.15(s), 1.23(Me), 2.78(CH$_2$)	3.27 (SiMe); 33.19, 50.42 (tBu), 18.89, 65.44 (Et)
[(tBu)Me$_3$SiN]$_2$Be	15.1	260	0.22(s), 1.32 (s)	4.30 (SiMe); 35.60, 51.67 (tBu)
[(Me$_3$Si)$_2$N]$_2$Be	12.5	195	0.19 (s)	3.98
(Me$_3$Si)$_2$NBeCl	6.93	60	0.25	4.08
(Me$_3$Si)$_2$NBeOEt	9.10	63	0.40 (s), 1.41 (Me),4.31 (CH$_2$)	4.96 (SiMe); 17.47, 63.15 (Et)
iPr$_2$NBeBu	16.6	180	1.14 (d), 3.04 (sept), 0.14, 0.88, 1.67 (Bu)	14.32, 30.68, 30.96 (Bu), 24.22, 45.74 (iPr)
iPr$_2$NBe(tBu)	19.1	190	0.92 (s), 1.26 (d), 3.31 (sept)	33.60 (tBu), 24.67, 46.27 (iPr)
iPr$_2$NBeBH$_4$	7.76	43	1.13(d), 3.04(sept)	23.53, 46.31

[a] $\delta^{14}N = -183$. [b] $\delta^{14}N = -280$. [c] $\delta^{14}N = -134$. [d] $\delta^{14}N = -112$.

The ^{9}Be nuclei of the alkylberyllium amides are strongly deshielded in relation to the aminoberyllium chlorides and ethoxides. This corresponds to similar shielding effects seen in aluminium chemistry.[14] Neither for (R$_2$NBeBu)$_2$ nor for [R$_2$NBe(tBu)]$_2$ were signals observed for the C atoms bound to Be. This phenomenon is due to short transversal relaxation times T_2, which result in line broadening, an effect well known in organoboron chemistry.[15] In the case of [iPr$_2$NBe(tBu)]$_2$, the NMR spectra show no change with temperature (20−80 °C). No partial monomerization is therefore observed up to 80 °C.

As indicated previously, compound (tmp)Be(tBu) is unstable and decomposes with gas evolution, most probably with formation of the hydride (tmp)BeH. Its ^{9}Be NMR spectrum should show a doublet due to $^1J(^9\text{Be}^1\text{H})$, but only a broad signal ($h_{1/2}$ = 140 Hz) at δ^9 Be = 11.9 ppm was observed. Both observations correspond to tricoordinated Be. Because a small coupling constant is to be expected for this compound, the linewidth may prevent detection of the coupling, as is the case with, for example, [(tmp)$_2$AlH]$_2$.[16] No $^1J(^9\text{Be}^1\text{H})$ coupling can be observed in the ^{1}H NMR spectrum of [iPr$_2$NBe(μ-H$_2$BH$_2$)]$_2$, while the ^{11}B resonance appears as a 1:4:6:4:1 quintuplet, showing that the four hydrogen atoms bonded to the B atoms are magnetically equivalent. This is typical for almost all metal tetrahydroborates and can be explained for covalent species by a rapid exchange between terminal and bridging positions.[17] In comparison with the shielding of the boron center in NaBH$_4$ [δ^{11}B = −41.7 ppm, $^1J(^{11}\text{B},^1\text{H})$ = 80.8 Hz[18]] or (Me$_3$Si)$_2$NMg(μ-H$_2$BH$_2$)·2THF [δ^{11}B = −39.1 ppm, $^1J(^{11}\text{B},^1\text{H})$ = 81.8 Hz][19] the boron nuclei in [iPr$_2$NBe(μ-H$_2$BH$_2$)]$_2$ are deshielded while the coupling constant remains the same.

IR spectroscopy, unlike NMR, did not prove to be very helpful for obtaining structural information. In case of the adduct BeCl$_2$·HNiPr$_2$, a sharp band at 3224 cm^{-1} corresponds to ν(NH), while the NH stretching band for the free amine is very broad, with a maximum at about 3250 cm^{-1}. A strong and sharp band at 555 cm^{-1} may be attributed to ν(BeCl$_2$). For the chlorides (R$_2$N−BeCl)$_2$ a strong band at 615±35 cm^{-1} is most likely due to ν(BeCl). We found no band characteristic for a Be−C stretching frequency, but the double-bridge bonding of the BH$_4$ group was readily noticeable by two bands for two bridging and two terminal hydrogen atoms (2500, 2430, 2120, 2090 cm^{-1}).

The NMR spectroscopic data of the Lewis acid adducts of **2** do not differ too much from the parent compound. Actually, there is also no pronounced difference in the ^{13}C chemical shifts for **2** and for diisopropylamine. The ammonium-type character of the diisopropylamino group is reflected in lowfield shifts for both the Me and the CH groups, while $^1J_{H,H}$ remains constant. The lowfield shifts observed for the BBr$_3$ adduct in relation to boron and aluminium trichloride adducts most probably reflects a paramagnetic downfield shift resulting from the bromine atoms. Moreover, one might have expected better shielding of the ^{9}Be nuclei in the EX$_3$ adducts of **3**. It is the smaller linewidth that points to the presence of tetracoordinated Be atoms. That the interaction between the halide atoms of the Lewis acids and the beryllium centers is weak can be seen from the ^{11}B and ^{27}Al chemical shifts. In case of the BCl$_3$ adduct the resonance is at higher field than that of BCl$_3$ but significantly deshielded with respect to free BCl$_4^-$ (δ^{11}B = 7 ppm)[20] while the ^{27}Al NMR signal of the AlCl$_3$ adduct is slightly better shielded than in the anion AlCl$_4^-$ (δ^{27}Al = 110 ppm).[21]

X-ray Structure of iPr$_2$NBeBH$_4$

Single crystals of iPr$_2$NBeBH$_4$ were obtained from a hexane solution at −20 °C. The compound crystallized in the monoclinic space group $P2_1/c$ with Z = 4 dimeric units. Figure 2 displays the molecular structure.

 © 2003 Wiley-VCH Verlag GmbH & Co. KGaA, Weinheim

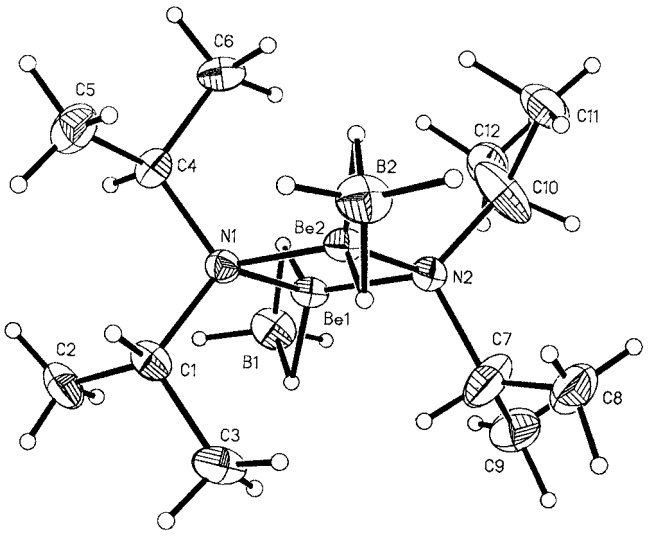

Figure 2. Molecular structure of $[i\mathrm{Pr_2NBeBH_4}]_2$; thermal ellipsoids are depicted on a 50% probability level; selected bonds lengths [A] and bond angles [°] (estimated standard deviations are represented in parentheses): Be1−N1 1.690(4), Be1−N2 1.703(4), Be2−N1 1.690(4), Be2−N2 1.697(4), Be1···B1 1.925(5), Be2···B2 1.950(5), Be1−H1a 1.50(3), Be1−H1b 1.53(3), B1−H1a 1.19(3), B1−H2a 1.23(3), B1−H3a 1.06(3), B1−H4a 1.11(3), B2−H1b 1.26(3), B2−H2b 1.25(3), B2−H3b 1.10(4), B1−H4b 1.06(4), N1−C1 1.513(4), N1−C4 1.504(4), N2−C7 1.520(5), N2−C10 1.486(4); N1−Be1−N2 99.9(2), N1−Be2−N2 100.1(2), Be1−N1−Be2 80.3(2), Be1−N2−Be2 79.7(2), H1a−Be1−H2a 78(2), H1b−Be2−H2b 80(2), H1a−B1−H2a 104(3), H1b−B2−H2b 100(2), H3a−B1−H4a 117(3), H3b−B2−H4b 112(3), C1−N1−C4 110.0(2), C7−N2−C10 110.9(2), Be1−N1−C1 117.7(2), Be1−N1−C4 113.3(2), Be2−N1−C1 116.0(2), Be2−N1−C4 117.0(2), Be2−N2−C7 111.2(3), Be2−N2−C10 120.1(3), Be1−N2 C10 121.2(3)

The central part of the molecule is an oblique four-membered Be_2N_2 ring with a comparatively short Be···Be distance of 2.179 Å, while the N···N distance is 2.697 Å. The Be−N bond lengths vary from 1.690(4) to 1.703(4) Å. Each Be atom is surrounded not only by two N atoms but also by two H atoms, with Be−H bond lengths of 1.46(3) and 1.53(3) Å. The Be−B distances are 1.938 and 1.942 Å, respectively.

As would be expected, the bridging hydrogen atoms show B−H bonds longer [av. 1.23(3) Å] than the terminal B−H bonds [1.17(3) Å]. The terminal H−B−H bond angles are more open [117(3)° at B1, 113(2)° at B2] than those of the bridging hydrogen atoms [104(2)° at B1, 100(2)° at B2]. The H−Be−H bond angles are more acute, with 78(2)° at Be1 and 80(2)° at Be2. It follows from the longer N···N distance in relation to the Be···Be distance that the bond angles at the N atoms are more acute [Be1−N1−Be2 80.3(3)°, Be1−N2−Be 2 79.7(2)°] than those at the Be atoms [N1−Be1−N2 99.9(2)°, N1−Be2−N2 100.1(2)°].

Discussion

Of the two possible routes to aminoberyllium chlorides considered, ligand exchange between $(R_2N)_2Be$ and $BeCl_2$ (or $BeCl_2{\cdot}2OEt_2$) was unsuccessful, unlike 1:1 reactions between $BeCl_2$ and $LiNR_2$ compounds [R_2N = N*i*Pr$_2$, tmp, N(SiMe$_3$*t*Bu)$_2$, N(SiMe$_3$)$_2$] in diethyl ether solution. Low temperatures are necessary to retard or suppress the formation of beryllium bis(amides), because the aminoberyllium chlorides formed react more rapidly than $BeCl_2$ with $LiNR_2$ at ambient temperature. However, the formation of ethoxyberyllium amides could not be prevented. This indicates that ether cleavage by $LiNR_2$ occurs to a considerable extent even at low temperature. All compounds of type R_2NBeX (X = R, Cl, EtO) are dimeric. Dimerization occurs through the N atoms, producing four-membered Be_2N_2 rings. No beryllates $Li[Be(NR_2)_nCl_mY_o]$ (Y = OEt; $n + m + o = 3$) could be detected in the diethyl ether solutions. Beryllates have been observed by Anderson and Coates[22] in reactions between $BeCl_2$ and $LiNMe_2$ in diethyl ether.

(tmp)Be(*t*Bu) could not be prepared, because it decomposes with gas evolution and presumably forms (tmp)BeH. This latter compound was, however, not obtained in a pure state. Isobutene elimination from *t*Bu−metal compounds is not unusual, as even Li*t*Bu itself decomposes into LiH and isobutene.[23]

Direct aminolysis of $BeCl_2$, either as the crystalline material or as $BeCl_2{\cdot}2OEt_2$, with diisopropylamine could not be achieved. The reactions stopped at the $BeCl_2{\cdot}HNiPr_2$ adduct stage. Obviously, the NH proton is not sufficiently acidic to react with additional amine to achieve aminolysis to either R_2NBeCl or $(R_2N)BeCl{\cdot}HNR_2$ (R = *i*Pr). This latter adduct is indeed formed, though only slowly, in the reaction between $(i\mathrm{Pr_2NBeCl})_2$ and diisopropylamine, but it readily disintegrates into the components in solution at higher temperatures. In this respect the aminolysis of $BeCl_2$ matches the aminolysis of $AlCl_3$ with secondary amines, which also stops at the adduct stage,[24] unlike the case of BCl_3, which is aminolyzed to give not only R_2NBCl_2 but also $(R_2N)_2BCl$ and even $B(NR_2)_3$ with many secondary amines.[25] The main reason for the lack of aminolysis of $BeCl_2$ and $AlCl_3$ is most probably that the amides formed have more strongly basic nitrogen centers than the amine itself, while in the boron case the basicity of the amino group is reduced due to B−N π-bonding. However, $BeCl_2{\cdot}HNiPr_2$ can be deprotonated with LiBu or $LiNR_2$ (i.e., with strong bases).

Experimental Section

General: All experiments were performed under anhydrous conditions with use of Schlenk techniques. Dinitrogen or argon were used as protecting gases. Anhydrous $BeCl_2$ was purchased from Aldrich and the amines from Fluka, while the LiR compounds were gifts from Chemetall GmbH (usually as 1.5 M solutions in hexane). The amines and the solvents used were dried in a conventional manner ($LiAlH_4$, CaH_2, P_2O_5). $BeCl_2$−diethyl ether was prepared from Be powder and HCl in diethyl ether.[26] All necessary safety measures were practiced in the experimental procedures, as Be compounds are toxic. After the experiments, the glassware was washed with conc. HCl and the solutions were collected in plastic flasks. These collected solutions were concentrated in vacuo using a rotary

 © 2003 Wiley-VCH Verlag GmbH & Co. KGaA, Weinheim

evaporator. The oily or pasty residues were properly labeled and disposed as special waste.

Physical Measurements: Molecular masses were determined by cryoscopy in cyclohexane solutions or by mass spectrometry. NMR: JEOL 90 or Bruker WP200 instruments. ^{1}H (int. TMS, int. CD_2Cl_2, int. C_6D_6), ^{9}Be (1 M solution of $BeCl_2$ in 1 M HCl/D_2O), ^{13}C (int. TMS, int. $CDCl_3$, or int. $C_6D_{6'}$), ^{14}N (ext. 1 M solution of NH_4NO_3 in D_2O). MS: Atlas CH7. IR: Perkin-Elmer 235 spectrometer. Elemental analysis: Automatic C/H/N analyzer, chloride titration with a Metroohm instrument. M.p.: Mel-Temp. in capillaries.

X-ray Analysis: Siemens P4 diffractometer, Mo-K_α radiation, graphite monochromator, LT2 device. Data collection at −80 °C, data reduction with the program SAINT,[27] structure solution with SHELX79,[28] data refinement with SHELXTL. Non-hydrogen atoms were refined with anisotropic thermal parameters. Hydrogen atom positions of the BH_4 group were taken from the difference Fourier map. These were freely refined with individual isotropic thermal parameters. H atoms of the isopropyl groups were placed in calculated positions and included in the final refinements as riding on their C atoms. Crystallographic data for **18** have been deposited with the Cambridge Crystallographic Data Center as supplementary publication CCDC-195196. Copies can be obtained free of charge on application to CCDC, 12 Union Road, Cambridge, CB2 1EZ, UK; E-mail: deposit@ccdc.ac.uk.

Beryllium Dichloride−Diisopropylamine (1). a) Anhydrous crystalline $BeCl_2$ (1.50 g, 19 mmol) was covered with diisopropylamine (13.5 mL, 100 mmol) in a two-necked flask, and the mixture was kept at reflux for 3 h. During this time the crystals disappeared and turned into a gray mass. The solid was isolated by filtration, washed with pentane, and dried in vacuo. Yield: 2.40 g (100%) of **1**, m.p. 65 °C. NMR recorded at 70 °C: see Table 1. $C_6H_{14}BeCl_2N$ (180.12): calcd. C 39.79, H 8.37, Cl 39.14, N 7.74; found C 39.22, H 8.41, Cl 39.20, N 7.83. **b)** Diisopropylamine (12.5 mL, 90 mmol) was dissolved in diethyl ether (25 mL). A solution of $BeCl_2$ in diethyl ether (4.5 M, 10 mL, 45 mmol) was added dropwise to the stirred solution over 15 min. An oily phase formed. The mixture was kept at reflux for 1 h (this is not actually necessary). No crystals formed from the oily phase in a refrigerator within 24 h. All volatile components were then removed in vacuo. A gray mass was left behind, and this, after drying in vacuo, gave 18.12 g (99.5%) of **1**, m.p. 65 °C. NMR spectroscopic and analytical data are the same within standard errors as for the compound obtained by procedure a).

Deprotonation of $BeCl_2$·HN*i*Pr$_2$ with LiBu: Diisopropylamine (14.1 mL, 100 mmol) was added to $BeCl_2$ (7.99 g, 100 mmol) and the mixture was heated at reflux for 3 h. The resulting gray solid mass was then suspended in hexane (50 mL) and the stirred suspension was treated with a solution of LiBu in hexane (1.58 M, 66.7 mL, 100 mmol) over 2 h. The resulting suspension was kept at reflux for 2 h, insoluble material (4.9 g) was removed by filtration, and the solvent was removed from the filtrate in vacuo. An oily residue (17.5 g) remained. Half of the material was distilled. This afforded two fractions: fraction 1 (0.8 g), b.p. up to 60 °C/0.1 Torr; fraction 2 (5.67 g), b.p. 60−63 °C/0.1 Torr, showing three ^{9}Be NMR signals at δ = 9.9 (main product), 15.9, and 3.2 ppm. Redistillation of fraction 2 yielded 3.25 g of product with b.p. 61−62 °C/0.1 Torr. It showed the following NMR signals: δ^{1}H = 0.1 ppm (m), 0.87 (d, $^3J_{H,H}$ = 6.69 Hz), 1.04 (d, $^3J_{H,H}$ = 6.75 Hz), 1.21 (d, $^3J_{H,H}$ = 5.86 Hz), 1.52 (m), 2.9 (m), 3.7 (m). δ^{9}Be = 10.2 ppm with a shoulder at δ = 16 ppm. On standing, this fraction became partly crystalline. The crystals (0.72 g) were separated and washed with pentane. They showed a ^{1}H NMR spectrum fairly similar to that described above, with the most intense signal at δ = 1.21 ppm (d). δ^{9}Be = 1.7 and 15.4 ppm (broad, $h_{1/2}$ = 170 Hz). The chloride content of all fractions was very low by qualitative analysis. From comparison of NMR spectroscopic data, all fractions contained **3**, **14**, and small amounts of **2**. Several attempts to produce crystals from various solvents with the second part of the crude product failed at −20 and −78 °C.

Ligand Exchange between $BeCl_2$ and (*i*Pr$_2$N)$_2$Be: (*i*Pr$_2$N)$_2$Be (10.0 g, 48 mmol) and hexane (50 mL) were added to $BeCl_2$ (3.83 g, 48 mmol). The mixture was kept at reflux for 48 h. Hexane was removed from a sample in vacuo. The oily residue showed ^{1}H NMR signals at δ = 1.09 (d) and 2.92 ppm (sept) typical of **3**. Irradiation of the mixture by an Hg lamp in the presence or absence of hexane also did not induce any reaction; 3.87 g of $BeCl_2$ was recovered. Similarly, a mixture of (*i*Pr$_2$N)$_2$Be (3.14 g, 15 mmol) and $BeCl_2$·2OEt$_2$ (6 mL of a 2.5 M solution in ether) showed no reaction after being kept at reflux for 24 h, as evidenced by ^{9}Be NMR resonance [signals at δ = 12.7 ppm (amide) and δ = 1.15 ppm for beryllium chloride−diethyl ether].

(Diisopropylamino)beryllium Chloride (2). a) $BeCl_2$·2OEt$_2$ (16.8 mL of a 2.59 M solution in diethyl ether, 50 mmol) was diluted with diethyl ether (20 mL). A suspension of LiN*i*Pr$_2$ (37 mmol) in hexane (50 mL) was added with stirring over 2 h. Insoluble material was removed by filtration after 16 h, and the solvent was stripped off from the filtrate in vacuo. The oily residue was distilled (b.p. ca. 85 °C/0.1 Torr), and the distillate afforded colorless crystals of **2**, m.p. 72 °C. NMR: see Table 1. $C_6H_{14}BeClN$ (144.65): calcd. C 49.82, H 9.76, Cl 24.51, N 9.68; found C 48.65, H 9.78, Cl 23.93, N 9.65. Molecular mass: 286. **b)** The reaction was performed similarly at 0 °C (16.8 mL of a 2.98 M $BeCl_2$ solution in diethyl ether, 50 mmol, diluted with 25 mL of ether) with freshly prepared LiN*i*Pr$_2$ (50 mmol) in hexane (75 mL). Stirring at 0 °C for 3 h, and then at ambient temperature overnight gave LiCl (2.05 g, 97%), which was isolated from the suspension by filtration. The filtrate contained 7.42 g of a solid crude product. Its sublimation at 95 °C/0.005 Torr provided waxy crystals of **2**, m.p. 72 °C; yield 6.62 g (86%). MS: Correct isotope pattern for [M$^{+\cdot}$] (288). All other data are as stated under a).

(Diisopropylamino)beryllium Chloride−Diisopropylamine Adduct 4: $BeCl_2$ (2.05 g, 26 mmol) was allowed to react at reflux with diisopropylamine (7.45 mL, 53 mmol) for 2 h. Hexane (50 mL) was then added to the cooled (0 °C) suspension, followed by LiBu (1.56 M in hexane, 16.9 mL, 26 mmol). This produced a white suspension. After the mixture had been heated at reflux for 2 h, some crystals had separated on the walls of the flask. Insoluble material was then rapidly removed by filtration (1.11 g) and the filtrate was reduced to 30 mL in vacuo. Crystal settled from the filtrate at −20 °C. Yield 4.18 g (68%) of **4**; m.p. 65 °C with decomp. NMR: see Table 1. $C_{12}H_{29}BeClN_2$ (245.84): calcd. C 58.63, H 11.89, Cl 14.42, N 11.39; found C 59.19, H 12.43, Cl 14.33, N 10.75.

(2,2,6,6-Tetramethylpiperidino)beryllium Chloride (5): A diethyl ether solution of $BeCl_2$ (3.5 M, 13.3 mL) was diluted with diethyl ether (50 mL) and cooled to −100 °C. A suspension of (tmp)Li (7.36 g, 50 mmol) in pentane/hexane (1:1) was added dropwise with vigorous stirring over a period of 3 h. Stirring was continued for another 3 h, and the suspension was then allowed to come to room temperature overnight with continuous stirring. Insoluble material (2.08 g) was removed by filtration, and the solvents were stripped off from the filtrate in vacuo. A brownish solid (10.4 g) was left. This crude product showed the following NMR spectroscopic data:

 © 2003 Wiley-VCH Verlag GmbH & Co. KGaA, Weinheim

δ^1H = 1.08 ppm (t), 1.16 (s), 3.9 [q, ^3J(H.H) = 7.08 Hz; (tmp)BeOEt, **7**], 1.30 (s), 1.64 [m, (tmp)BeCl, **5**], ratio of the singlets 2.2:1 (95% **5**, 5% **7**). δ^9Be = 9.4 ppm (**5**). Sublimation of the crude material at 110 °C/0.006 Torr yielded 6.84 g (74%) of **5**, m.p. 105−107 °C. NMR: see Table 1. $C_9H_{18}BeClN$ (184.74): calcd. C 58.31, H 9.84, Cl 19.19, N 7.89; found C 56.47, H 9.08, Cl 19.08, N 6.95. Molecular mass: 366. MS: 369 for [$M^{+\cdot}$] (correct isotopic pattern).

[*tert*-Butyl(trimethylsilyl)amino]beryllium Chloride (9): Analogously to the preparation of **5**, a diethyl ether solution of $BeCl_2$ (3.75 M, 13.3 mL, 50 mmol), diluted with diethyl ether (50 mL), was added at −100 °C to a suspension of $LiN(SiMe_3)CMe_3$ (6.66 g, 50 mmol) in pentane/hexane (1:1) (75 mL). Stirring was continued at −100 °C for 3 h and at −78 °Cfor 2 h. After the suspension had reached room temperature, the solid was filtered and the solvents were removed from the filtrate in vacuo. Residue: 8.43 g of a waxy solid. Sublimation at 125 °C/0.0049 Torr gave 3.4 g (36%) of **9**. NMR: see Table 1. $C_7H_{18}BeClNSi$ (188.81): cald. C 44.53, H 9.63, Cl 18.78, N 7.42; found C 43.92, H 9.05, Cl 18.54, N 6.86. Molecular mass: 375.

[Bis(trimethylsilyl)amino]beryllium Chloride (12) and Ethoxyberyllium Bis(trimethylsilyl)amide (13): This compound was prepared analogously to **9**, from $BeCl_2$ (25 mmol) in diethyl ether/pentane (1:1, 50 mL) and $LiN(SiMe_3)_2$ (4.18 g, 25 mmol) suspended in pentane/hexane (1:1, 50 mL) at −100 °C. After workup, 4.83 g of a slightly yellow, waxy solid was obtained, and this was shown by NMR analysis to be a 1:2.5 mixture of **12/13**. Fractional sublimation gave three fractions: a) at 110 °C/ 0.004 Torr, 1.24 g of compound **13**, m.p. 147−149 °C;NMR spectroscopic data see Table 1; b) at 110−117 °C/0.004 Torr, 2.18 g, this fraction was shown by NMR to be a mixture of **12** and **13**; c) 117 °C/0.004 Torr, 0.6 g of compound **12**, NMR: see Table 1. $C_6H_{18}BeClNSi_2$ (204.89): calcd. C 35.17, H 8.87, Cl 17.36, N 6.84; found C 34.23, H 8.25, Cl 17.21, N 6.23.

Butyl(diisopropylamino)beryllium (14): iPr$_2$NBeCl (3.18 g, 22 mmol) was dissolved in hexane (25 mL), and the solution was cooled to 0 °C. A solution of LiBu in hexane (1.56 M, 14.1 mL) was added dropwise, with stirring. The mixture was then kept at reflux for 1 h. After the solid material (LiCl) had been removed by filtration and the hexane had been distilled from the filtrate, the oily residue was distilled. Compound **14** had a b.p. of 78 °C/ 0.1 Torr. Yield 2.49 g (88%). NMR: see Table 1. $C_{10}H_{23}BeN$ (166.35): calcd. C 72.20, H 13.98, N 8.42; found C 71.08, H 12.41, N 7.95. Molecular mass: 426.

***tert*-Butyl(diisopropylamino)beryllium (15): a)** The compound was prepared as described for **14**, from iPr$_2$NBeCl(2.60 g, 18 mmol) in hexane (25 mL) and a solution of LitBu (1.50 M, 12 mL, 18 mmol), withstirring at ambient temperature for 3 h. Compound **15** showed a b.p. of 90 °C/0.005 Torr, Yield 1.44 g (48%), m.p. 84−86 °C. When the reaction was performed at −78 °C the yield rose to 78%. NMR spectroscopic data: see Table 1. $C_{10}H_{23}BeN$ (166.35): calcd. C 72.20, H 13.98, N 8.42; found C 69.58, H 13.05, N 7.93 (low C/H values due to insufficient protection against oxidation during the weighing process). Molecular mass: 331. **b)** tBuBeCl·OEt$_2$ (1.41 g, 8.0 mmol), dissolved in pentane (15 mL), was treated at −78 °C, with vigorous stirring, with a suspension of Li$N$$iPr_2$ (0.l86 g, 8 mmol) in pentane/hexane (1:1). After the mixture had been allowed to come to room temperature, the solid was removed by filtration and the solvents were removed in vacuo. The residue was distilled, b.p. 90 °C (oil bath)/0.005 Torr. Yield 1.01 g (76%) of **15**, m.p. 84−86 °C. NMR spectroscopic data are as found for compound **15** prepared by procedure a).

Butyl(2,2,6,6-tetramethylpiperidino)beryllium (16): (tmp)BeCl (2.03 g, 11 mmol) was dissolved in hexane (20 mL) and treated, whilst stirring, with LiBu (7.05 mL, 1.56 M solution in hexane diluted with 10 mL of hexane). The mixture was kept at reflux for 30 min. Insoluble material was removed by filtration and the solvents were removed in vacuo. The residue had a b.p. of 98−104 °C/ 0.006 Torr. Yield 1.32 g (58%) of **16**. NMR spectroscopic data: see Table 1. $C_{13}H_{27}BeN$ (206.42): calcd. C 75.67, H 13.21, N 6.79; found C 74.98, H 12.88, N 6.25. Molecular mass: 410.

Attempt to Prepare (tmp)Be(tBu) (17): a) (tmp)BeCl (2.77 g, 15 mmol) dissolved in pentane (40 mL) was cooled to −78 °C. A solution of LitBu (1.5 M, 10.0 mL, 15 mmol), diluted with pentane (15 mL), was then added with stirring over 3 h. After additional stirring for 2 h, the mixture was allowed to come to ambient temperature, whereupon vigorous gas evolution started at ca. 10 °C. Insoluble material was removed after stirring for additional 20 min, followed by stripping off of the solvents in vacuo. The residue (2.04 g), a yellowish, viscous oil, decomposed during attempted distillation. The residue was practically free of chloride. NMR (crude product): δ^1H = 1.01 ppm (s), 1.18 (s), 1.31 (s), 1.62 (m) in a ratio of 1.0:1.7:14.7:8.8. δ^{13}C = 18.55 ppm, 32.22, 32.76, 33.21, 34.37,

Table 2. NMR spectroscopic data of diisopropylamine, diisopropylaminoberyllium chloride, and its addition products with boron trihalides and aluminium trichloride (δ [ppm], linewidths $w_{1/2}$ [Hz])

	δ^9Be/δ^{11}B/δ^{27}Al ($w_{1/2}$)	δ^1H(Me, CH)	^1J(H,H)	δ^{13}C(Me, CH)
$HN(CHMe)_2$	−	0.96, 2.97	6.60	23.78, 45.50
$[ClBe[N(CHMe_2)_2]_2$	10.70/−/− (82)	1.20, 3.04	6.59	23.77, 45.84
$[ClBe[N(CHMe_2)_2]_2{\cdot}2BCl_3$	9.96/30.8/− (60)/(108)/−	1.19, 3.08	6.59	23.94, 45.66
$[ClBe[N(CHMe_2)_2]_2{\cdot}2BBr_3$	10.65/22.1/− (60)/(125)/−	1.37, 3.27	6.59	25.43, 47.12
$[ClBe[N(CHMe_2)_2]_2{\cdot}2AlCl_3$	10.04/−/104.5 (55)/−/(154)	1.18, 3.09	6.60	23.78, 45.30
$[ClBe[N(CHMe_2)_2py]_2$	4.82/−/− (1.5)	1.13 (d), 3.03 (sept), 6.72 (m), 7.08 (m), 8.89 (m)	6.45	24.22 (q), 45.71 (d), 124.62 (d), 138.70 (d), 148.29 (d)

 © 2003 Wiley-VCH Verlag GmbH & Co. KGaA, Weinheim

37.75. 39.87, 50.40, 52.21. δ^9Be = 11.9 ppm ($h_{1/2}$ = 145 Hz). **b)** *t*BuBeCl·OEt_2 (1.58 g, 9.00 mmol) was dissolved in pentane (20 mL) and the solution was cooled to −78 °C. A suspension of (tmp)Li (1.32 g, 9.00 mmol) in pentane/hexane (1:1) (20 mL) was added over 2 h. The solid that had formed was removed by filtration and the solvents were stripped off in vacuo. The NMR spectroscopic data are essentially the same as from experiment a), demonstrating that no single compound was produced [main product 90%; δ^1H = 1.31 ppm (s), 1.67 (m), by-products ca. 4 and 6%]. The product was essentially free of chloride.

(Diisopropylamino)beryllium Tetrahydroborate (18): A solution of $LiBH_4$ in diglyme (1.0 M, 5.8 mL, 5.8 mmol), to which diethyl ether (5 mL) had been added, was added to a solution of $(i\mathrm{Pr_2NBeCl})_2$ (0.83 g, 2.9 mmol) in diethyl ether (10 mL). After the addition, the mixture was kept at reflux for 1 h. Insoluble material was removed by filtration (G4), all solvents were stripped off in vacuo, and the residue was crystallized from pentane at −20 °C. Colorless, extremely moisture-sensitive crystals (0.54 g, 75%) were obtained, dec. at ca. 85 °C. NMR: see Table 1. IR: ν(BH): 2428, (st), 2405 (st), 2138 (st), 2068 (m) cm^{-1}. $C_{12}H_{36}B_2Be_2N_2$ (248.14): calcd. C 58.08, H 14.65, N 11.29; found C 56.46, H 9.53, N 10.59. The low H content seems to be due to insufficient protection of the compound during the weighing process. In addition, combustion occurred explosively. Molecular mass: 246.

***tert*-Butoxyberyllium Diisopropylamide (19):** $(i\mathrm{Pr_2NBeCl})_2$ (1.72 g, 5.94 mmol) was dissolved in hexane (30 mL) and treated with KO*t*Bu (1.47 g, 13.0 mmol) in hexane (15 mL). After the mixture had been heated at reflux for 30 min, the insoluble part was removed by filtration, the solvents were stripped off from the filtrate in vacuo, and the light brown residue was subjected to sublimation. Yield 1.70 g (78.5%) of **19** obtained at 150 °C/0.005 Torr, m.p. 138−139 °C. NMR: see Table 1. $C_{10}H_{23}BeNO$ (182.35): calcd. C 65.86, H 12.74, N 7.68; found C 63.47, H 11.65, N 7.08. Molecular mass: 359.

Adduct of (Diisopropylamino)beryllium Chloride and Boron Trichloride (21): $(i\mathrm{Pr_2NBeCl})_2$ (0.83 g, 2.9 mmol) was dissolved in dichloromethane (10 mL) and the solution was cooled to −78 °C. At this temperature, liquid BCl_3 (1 mL) was added and the mixture was stirred for 2 h. Excess BCl_3 and solvent were then removed in vacuo, and the dark brown solid residue was crystallized from pentane (3 mL). Yield 0.99 g (65%) of **22**, yellow solid, dec. at 132−140 °C. NMR: data see Table 2. $C_6H_{24}BBeCl_4N$ (261.83): calcd. C 27.52, H 4.89, Cl 54.16, N 5.35; found C 26.58, H 4.02, Cl 53.95, N 4.98.

Adduct of (Diisopropylamino)beryllium Chloride and Boron Tribromide (22): Analogously to the preparation of **22**, $(i\mathrm{Pr_2NBeCl})_2$ (0.62 g, 2.1 mmol) was treated with BBr_3 (0.47 mL, 5 mmol), dissolved in CH_2Cl_2. After removal of the dichloromethane from the solution, the dark brown residue was subjected to crystallization from pentane (9 mL) to give 0.98 g (58%) of dark brown **23**, dec. at 95−98 °C. NMR: see Table 2. $C_6H_{14}BBeBr_3ClN$ (395.18): calcd. C 18.23, H 3.58, N 3.55; found C 17.18, H 2.87, N 3.05; total halide contents: 0.41 mmol in 0.1 mol of compound **23**.

Adduct of (Diisopropylamino)beryllium Chloride and Aluminium Trichloride (23): Freshly sublimed $AlCl_3$ (0.69 g, 5.2 mmol) was added to a solution of $(i\mathrm{Pr_2NBeCl})_2$ (0.75 g, 2.6 mmol) in dichloromethane (10 mL). No reaction was observed after the mixture had been stirred for 1 h. After the mixture had been heated at reflux for 2 h, the $AlCl_3$ had dissolved. The solvent was then removed in vacuo and the yellow/brown solid was crystallized from pentane (8 mL). Yield: 0.89 g (62%) adduct as a light yellow solid, dec. at 115−117 °C. NMR: see Table 2. $C_6H_{14}AlBeCl_4N$ (278.04): calcd. C 25.92, H 5.09, N 5.04; found C 24.83, H 4.18, N 4.67.

Pyridine Adduct of (Diisopropylamino)beryllium Chloride (20): A solution of pyridine (0.70 mL, 6.6 mmol) in CH_2Cl_2 (5 mL) was added with stirring to a solution of $(i\mathrm{Pr_2NBeCl})_2$ (0.69 g, 3.3 mmol) in the same solvent (15 mL). A deep red solution formed. After 2 h, the solvent was removed in vacuo and the remaining brown solid was dissolved in pentane (5 mL). No crystals separated from this solution at −20 °C. On removal of the solvent a dark brown/red solid remained (1.48 g, 99%), dec. at 132−134 °C. NMR: see Table 2. $C_{11}H_{19}BeClN_2$ (223.78): calcd. C 59.04, H 8.58, Cl 15.84, N 12.52; found C 56.84, H 8.88, Cl 15.66, N 9.28.

Crystallographic Data and Structure Refinement Parameters for $(i\mathrm{Pr_2NBeBH_4})_2$: Empirical formula: $C_{12}H_{36}B_2Be_2N_2$, formula mass: 248.07, crystal color: colorless, crystal size: 0.32 × 0.30 × 0.42 mm, crystal system: monoclinic, space group: $P2_1/n$, unit cell dimensions: a = 7.813(2), b = 21.927(6), c = 10.437(4) Å, β = 93.60(3)°, V = 1784.5(9) $Å^3$, Z = 4, density (calcd.) = 0.923 g/cm^3, linear absorption coefficient: 0.46 cm^{-1}, F(000) = 559, wavelength: λ = 0.71073 Å, 2θ range for data collection: 3−46°, speed: 2.2−29.3 °/min, T = 18 °C, index ranges: h, k, $\pm l$, reflections collected: 2910, independent reflections: 2494, reflections observed (2.5σ): 1898, parameters refined: 273, R_i = 0.0281, structure solution: direct methods, R_1 = 0.0876, R_w = 0.080, largest residual electron density: 0.41 e/$Å^3$.

[1] H. Nöth, D. Schlosser, *Chem. Ber.* **1988**, *121*, 115−117.
[2] G. E. Coates, F. Glockling, *J. Chem. Soc.* **1954**, 22−27.
[3] G. E. Coates, A. H. Fishwick, *J. Chem. Soc. A* **1967**, 1199−1204.
[4] M. F. Lappert, P. P. Power, A. R. Sanger, R. C. Srivastava, *Metals and Metalloid Amides*, E. Horwood Ltd., Chichester, **1980**.
[5] H. Bürger, C. Forker, J. Goubeau, *Monatsh. Chem.* **1965**, *96*, 597−601.
[6] H. Nöth, D. Schlosser, *Inorg. Chem.* **1983**, *22*, 2700−2703.
[7] D. Schlosser, Diploma Thesis, University of Munich, **1983**.
[8] N. A. Bell, *Adv. Inorg. Radiochem.* **1972**, *14*, 255−332.
[9] R. Fricke, R. Röbke, *Z. Allg. Anorg. Chem.* **1928**, *170*, 25−34.
[10] It should be noted that the formation of the corresponding alkylammonium chlorides was observed when $BeCl_2$ was treated with tribenzylamine or trimethylamine: cited in ref.[9]
[11] No quantitative analysis of the hydride content was performed, but a qualitatively check gave hydrogen on hydrolysis.
[12] B. Lindmann, S. Forsen, in: *NMR and the Periodic Table* (Eds.: R. K. Harris, B. E. Mann), Academic Press, London, New York, San Francisco, **1978**, p. 183−194.
[13] M. Witanowski, G. A. Webb, *Annu. Rep. NMR Spectrosc.* **1972**, *5A*, 353−394; M. Witanowski, L. Stefaniak, G. A. Webb, *Ann. Rep. NMR Spectrosc.* **1977**, *7*, 118−245.
[14] J. Mason, *Multinuclear NMR*, Plenum Press, New York, London, **1987**, p. 259−278.
[15] H. Nöth, B. Wrackmeyer, "Nuclear Magnetic Resonance Spectroscopy of Boron Compounds" in: *NMR Basic Principles and Progress* (Eds.: P. Diehl, E. Fluck, R. Kosfeld), Springer Verlag, Berlin, Heidelberg, New York, **1978**.
[16] C. Klein, H. Nöth, G. Tacke, M. Thomann, *Angew. Chem.* **1993**, *105*, 924−926; *Angew. Chem. Int. Ed. Engl.* **1993**, *32*, 886−888.
[17] B. D. James, M. G. H. Wallbridge, *Prog. Inorg. Chem.* **1970**, *11*, 99.
[18] M. Ehemann, H. Nöth, G. Schmidt-Sudhoff, *Z. Anorg. Allg. Chem.* **1972**, *394*, 33−52.
[19] M. Bremer, Ph.D. Thesis, University of Munich, **1995**.

 © 2003 Wiley-VCH Verlag GmbH & Co. KGaA, Weinheim

[20] J. S. Hartmann, G. J. Schrobilgen, *Inorg. Chem.* **1972**, *11*, 940−951.
[21] J. F. Hinton, R. W. Briggs, in: *NMR and the Periodic Table* (Eds.: R. K. Harris, B. E. Mann), Academic Press, London, New York, San Francisco, **1978**, p. 183−194.
[22] R. A. Anderson, G. E. Coates, *J. Chem. Soc., Dalton Trans.* **1974**, 1171−1180.
[23] M. Weiner, G. Vogel, R. West, *Inorg. Chem.* **1962**, *1*, 654−658.
[24] D. G. Tuck, *Chemistry of Aluminium, Gallium, Indium and Thallium* (Ed.: A. J. Downs), Blackie Academic & Professionals, London, Glasgow, New York, Tokyo, Melbourne, Madras, **1993**, p. 430−473.
[25] H. Steinberg, R. J. Brotherton, *Organoboron Chemistry*, J. Wiley Sons, New York, London, Sydney, **1966**, chapters 2, 3.
[26] N. Y. Tutova, A. V. Kovoselova, K. N. Semenenko, *Zh. Neorgan. Khim.* **1959**, *4*, 550−552.
[27] *SMART, SAINT*, Siemens Analytical Instruments, Madison, vers. 4.1.
[28] W. G. Sheldrick, *SHELX79*, University of Göttingen, **1979.**
Received October 8, 2002

 © 2003 Wiley-VCH Verlag GmbH & Co. KGaA, Weinheim

One-Step Preparation of [RuCp*(η⁶-arene)]⁺ Sandwich Complexes

Alexander Schmid,[a] Holger Piotrowski,[a] and Thomas Lindel*[a]

Keywords: Ruthenium / Sandwich complexes / NMR spectroscopy / Synthetic methods

In a single step, several variously functionalized [RuCp*(η⁶-arene)]⁺ sandwich complexes have been prepared starting from $RuCl_3 \cdot xH_2O$ in yields ranging from 35 to 80%, referring to ruthenium. The protocol covers the preparation of valuable [RuCp*]⁺-complexed amino acids. In comparative experiments starting from the oligomer $[RuCp^*Cl_2]_n$ and using methanol/methanolate as the reducing agent, the formation of undesired side products was observed, resulting from nucleophilic substitution at the *o*-chloroanisole complex and from methoxylation of the Cp* ligand.
(© Wiley-VCH Verlag GmbH & Co. KGaA, 69451 Weinheim, Germany, 2003)

Introduction

Our program on the synthesis of oligomeric Ru-labelled diaryl ether peptoids[1] requires the availability of large quantities of various ruthenium sandwich complexes by a facile synthetic procedure. Radioactive labelling of peptoids[2] holds the promise to selectively bind and destroy tumour cells by combining the biological activity of biooligomers with the physical properties of metals. Ruthenium appears to be especially suitable because its radioactive isotopes cover half-lives ranging from three days to one year.[3] In this paper, we report a one-step procedure that provides large quantities of several [RuCp*]⁺ complexes, including some with amino acid ligands, to be used in bioorganometallic chemistry.

Pearson et al., Rich et al., and Matassa et al. have published pioneering work in the field of [RuCp]⁺-labelled peptoid diaryl ethers.[4] The [RuCp]⁺ complexation of the chloroarene precursors of the diaryl ethers follows a procedure based on the work of Gill and Mann.[5] Recently, the protocol was improved by Trost and Older,[6] but still needs four subsequent steps, starting from $RuCl_3 \cdot xH_2O$ (**1**). The situation may be simplified if [RuCp*]⁺ complexes are pursued instead (Cp* = pentamethylcyclopentadienyl). Kudinov et al. have obtained [RuCp*(η⁶-arene)]⁺ sandwich complexes from the reaction of $RuCl_3 \cdot xH_2O$ (**1**) with Cp*H and the three robust arenes benzene, toluene, and mesitylene in boiling alcohols as reducing agents.[7] The use of Zn — a milder reductant of the oligomer $[RuCp^*Cl_2]_n$ — in an overall two-step procedure was first reported by Chaudret et al.[8] In this paper we report a practically useful one-step procedure to [RuCp*(η⁶-arene)]⁺ sandwich complexes merging both approaches.

Results

Scheme 1 gives the reaction conditions we have developed. Upon addition of Zn (2 equiv.) to the ethanol solution of $RuCl_3 \cdot xH_2O$, a rapid colour change of the ethanolic solution from cherry red to dark blue occurred. Subsequently, the arene and Cp*H were added. The chosen stoichiometry gave the best yields. Table 1 gives 15 examples, 13 of which have been synthesised by the reported method. For comparison, only complexes **4**, **14** and **15** were obtained using methanol/methoxide as reducing agent, starting from the oligomer $[RuCp^*Cl_2]_n$.[14]

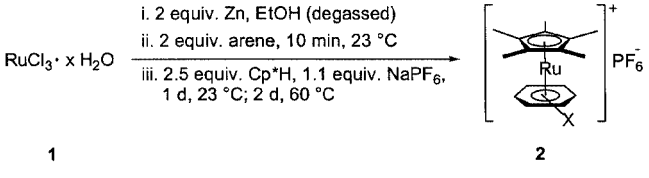

Scheme 1. One-step preparation of [RuCp*(η⁶-arene)]⁺ sandwich complexes

It was observed that the yield of the sandwich complexes **2** increased substantially with prolonged reaction times. While, for example, the reaction with acetophenone had proceeded to about 36% (referring to a Ru content of 37% in $RuCl_3 \cdot xH_2O$) after 10 minutes, a yield of 51% of the sandwich complex **11** was isolated after three days at 60 °C. Facile workup of the reaction mixture (Scheme 2) is very

[a] Department Chemie der Universität,
Butenandtstr. 5-13, 81377 München, Germany
Fax: (internat.) +49-89/2180-77734
E-mail: thomas.lindel@cup.uni-muenchen.de
Supporting information for this article is available on the WWW under http://www.eurjic.org or from the author.

important for practical applications and had to include the separation of non-polar by-products. The most convenient way was by partitioning of the column-filtered residue between water/methanol and *iso*-octane. Removal of inorganic salts was secured by exhaustive extraction of the crude product with dichloromethane. As reported by us for $[RuCp]^+$-complexed diaryl ether peptoids, aminopropyl-functionalised silica proved to be suitable for further purification of the cationic sandwich complexes by HPLC.[1]

Two new diastereomeric sandwich complexes (**13a**, **13b**) were obtained from (*E*)-ethyl cinnamate (entry 11), resulting from Diels–Alder cycloadditions of Cp*H to the olefinic double bond.[9] 2D NMR spectroscopic analysis (COSY, HSQC, HMBC) allowed the complete assignment of all chemical shifts to the diastereomers **13a** and **13b**. Since it was not possible to separate these diastereomers, even by HPLC, a NOESY spectrum of the mixture had to be the basis for the decision on which set of NMR signals belonged to which diastereomer. Complex **13a**, with the sandwich complex in the axial position of the norbornene system, shows a correlation between 7-H and 17-H while for the diastereomer **13b** a cross-peak between 8-H and 17-H is observed. For **13a** an X-ray analysis (Figure 1) confirmed its stereochemistry.

Figure 2 gives the crystal structure of the Cp*-monomethoxylated sandwich complex of ethyl benzene (**14**). Complex **14** was only formed by the oligomer route, and not in the direct preparation (entry 2).

We also prepared $[RuCp^*]^+$ complexes of amino acid esters (entries 14 and 15). The $[RuCp^*]^+$-complexed ethyl

Table 1. $[RuCp^*(\eta^6\text{-arene})]^+$ sandwich complexes obtained via the one-step procedure (Scheme 1, for entries 1–11, 14, 15) and via the oligomer route (entries 12, 13); the counterion is always hexafluorophosphate

Entry	Arene	Sandwich complex	Yield [%]
1		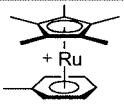 **3**	54
2	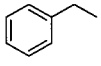	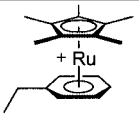 **4**	67
3		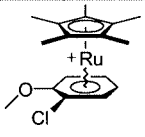 **5**	35
4	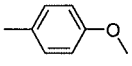	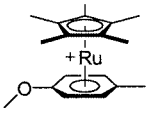 **6**	69
5		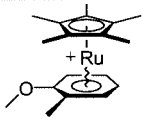 **7**	67
6	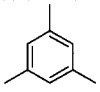	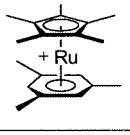 **8**	80
7	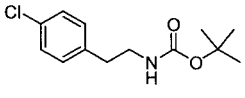	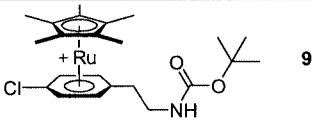 **9**	44
8	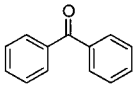	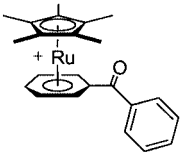 **10**	35

 © 2003 Wiley-VCH Verlag GmbH & Co. KGaA, Weinheim

Table 1. *(continued)*

9		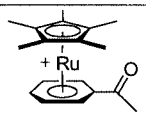 **11**	51
10	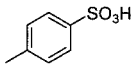	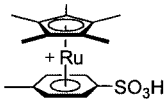 **12**	66
11	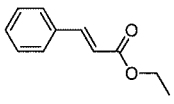	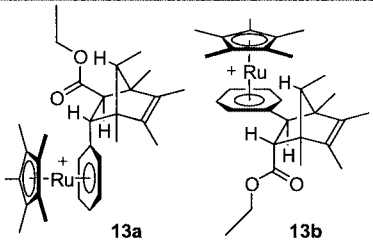 **13a** **13b**	51
12	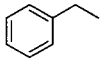	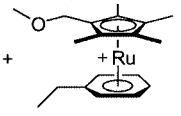 **4** + **14**	44 + 12
13		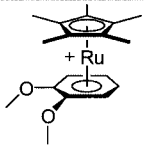 **15**	20
14	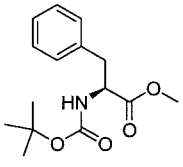	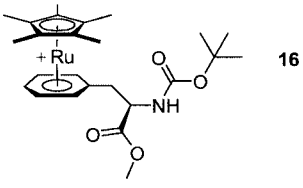 **16**	55
15	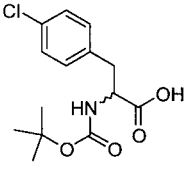	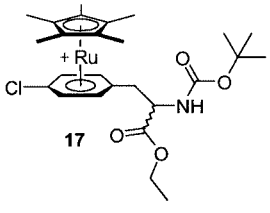 **17**	45

ester **17** was formed directly from the acid (entry 15) when the reaction was carried out in ethanol. The esterification can be prevented if *tert*-butanol is used as a solvent instead.

Discussion

There are several multi-step routes to [RuCp*(η⁶-arene)]⁺ sandwich complexes. For the Cp analogues, a popular approach uses the reaction of $[RuCp(CH_3CN)_3]^+$ half-sandwich complexes with various arenes. The tris-acetonitrile complexes are air-sensitive and should be freshly prepared before use.[10] The availability[11] of the oligomer $[RuCp^*Cl_2]_n$ has opened several synthetic routes to [RuCp*(η⁶-arene)]⁺ sandwich complexes using $LiBEt_3H$,[12] Zn,[8,13] methanol/methoxide,[14] or various alcohols/K_2CO_3 [15] as reducing agents. However, the purity of the oligomer $[RuCp^*Cl_2]_n$ may vary and therefore have an unpredictable influence on the yields (55 to 80%) of the desired [RuCp*(η⁶-arene)]⁺ sandwich complexes.[11,16] The only characterised complex was obtained for $n = 2$ in a benchmark procedure, but this complex should not be stored for long periods.[17] As a by-product of the synthesis of the oligomer, decamethylruthenocene is formed in about 10−30% yield.[18] In addition, it has been reported that on prolonged standing the oligomer may transform into an entity with lower solubility which is less available for further conversion.[16b] As a consequence, it is desirable to avoid

 © 2003 Wiley-VCH Verlag GmbH & Co. KGaA, Weinheim

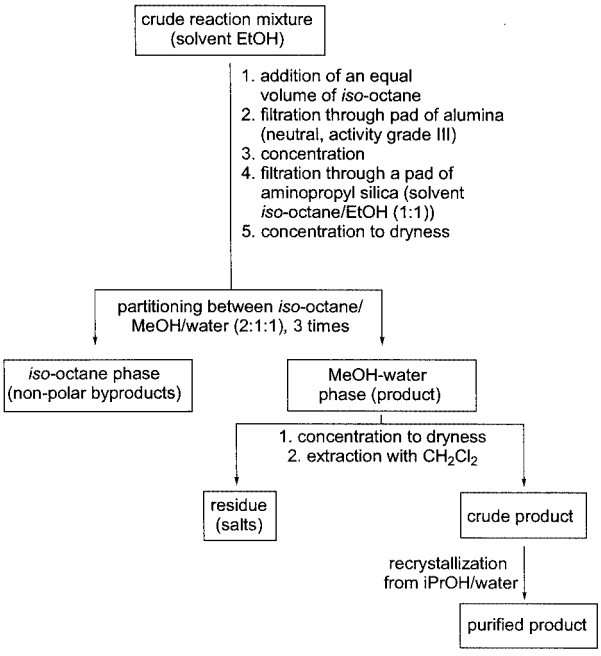

Scheme 2. Flow chart outlining the workup of the charged ruthenium complexes

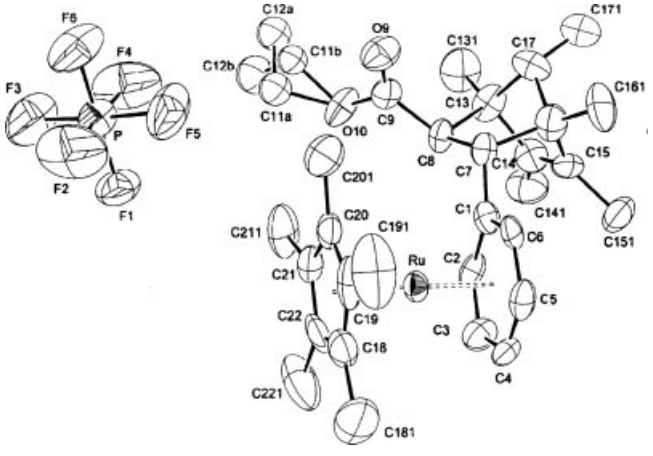

Figure 1. ORTEP plot of the Diels–Alder adduct **13a**; the atoms $C11_a$ and $C12_a$ (ethyl group) are disordered

the oligomer $[RuCp^*Cl_2]_n$ in the synthetic sequence. Koelle et al. circumvented that problem and synthesised alkoxoruthenium(II) complexes from the oligomer under mild conditions in quantitative yields. $[RuCp^*(Oalkyl)]_2$ is then reacted with two equivalents of arene to form the sandwich complex in yields ranging from 36% to 72%.[15,19] A pathway to $[RuCp^*(\eta^6\text{-arene})]^+$ sandwich complexes that does not begin with $RuCl_3 \cdot xH_2O$ (**1**) was pursued by Salzer and Ludi.[20] Ru^{II} triflate is reacted with a mixture of Cp*H and arene. The synthesis of $[Ru(H_2O)_6](OTf)_2$ is itself a three-step procedure including the distillation of the toxic RuO_4.[21]

The isolated yields obtained by our one-step procedure are similar to the more complicated protocols and vary from 35% (**5**, **10**) to 80% (**8**), relative to ruthenium (Table 1). At least partial reduction of $RuCl_3 \cdot xH_2O$ (**1**) prior to the addition of arene or Cp*H is indicated by the rapid colour change of the ethanolic solution from cherry red to dark blue. The excessive Zn may also act as a quencher of HCl after the subsequent reduction of the η^6-arene, Cp*H, and $NaPF_6$, as suggested by Salzer et al.[22] The $[RuCp^*]^+$ sandwich complexes of the electron-rich arenes **3**–**8** (entries 1–6) were prepared in order to establish the synthetic route. Compounds **3**, **6**, **8**, **10**, and **12** have been prepared before by other protocols.[23] The $[RuCp^*]^+$ sandwich complex **9** of *N*-Boc-protected *p*-chlorophenylethylamine (entry 7) is important for the synthesis of metal-complexed diaryl ether peptoids.[1] As for the correspondingly Boc-protected compounds **16** and **17**, the yield of compound **9** is very much improved if two equivalents of $NaHCO_3$ are added as a buffer before the addition of the arene. The Boc protecting groups would otherwise be cleaved off under the acidic conditions.

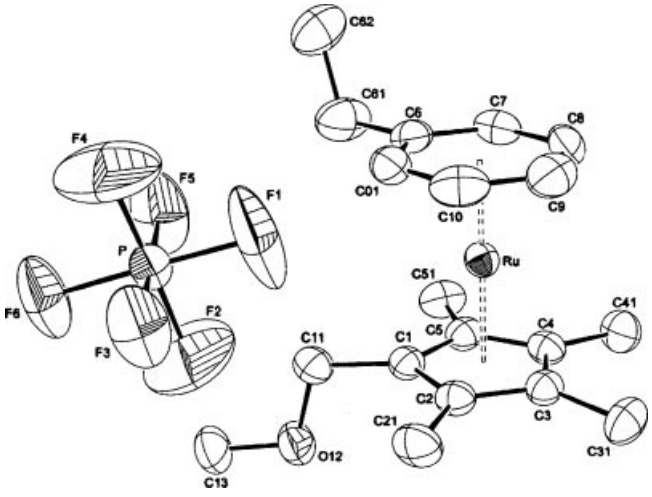

Figure 2. ORTEP plot of the methoxylated sandwich complex **14**

It was unclear if benzophenone (entry 8) would be complexed once or twice. Thus far, the doubly complexed sandwich complex of benzophenone has been obtained as by far the major product.[19] Our procedure provides the mono product **10** exclusively. The decrease in electron density in the uncomplexed phenyl group may prevent a second reaction. *p*-Toluenesulfonic acid (entry 10) cleanly gives the corresponding sandwich complex **12**.

Compared with our protocol (entries 2 and 3), difficulties were encountered when using methanol/methanolate as reducing agent of the oligomer $[RuCp^*Cl_2]_n$ ($n = 2$) (entries 12 and 13). Complexation of *o*-chloroanisole (entry 13) led to the dimethoxy sandwich complex **15** as the major product, with the desired chlorinated product formed in yields below 5%. Obviously, nucleophilic substitution is not suppressed under the reaction conditions. On the other hand, entry 3 demonstrates that the one-step procedure provides the desired *o*-chloroanisole complex **5**.

We discovered the monomethoxy sandwich **14** to be a side product (12%) when reacting ethylbenzene via the oligomer route (Scheme 3; Table 1, entry 12). An explanation could be the oxidation of the two Cp* ligands of the oligomer $[RuCp^*Cl_2]_n$ ($n = 2$) to two η^6-tetramethylfulvene li-

 © 2003 Wiley-VCH Verlag GmbH & Co. KGaA, Weinheim

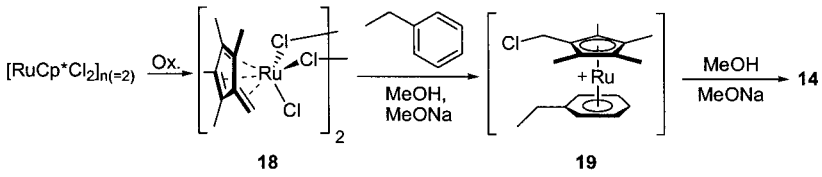

Scheme 3. Possible mechanism leading to the formation of the methoxylated sandwich complex **14** in methanol (explanation see text)

gands (Scheme 3). Upon treatment of **18** with carbon monoxide, Maitlis et al. have observed monochlorination of the Cp* ring.[24] In our case, ethylbenzene may take the role of carbon monoxide leading to the formation of the Cp*-chlorinated sandwich complex **19**. It has been reported that nucleophilic substitution by methoxide occurs readily.[24b]

In summary, this contribution presents, for the first time, a detailed study of the one-step preparation of [RuCp*(η⁶-arene)]⁺ sandwich complexes. Compounds **4**, **5**, **7**, **9**, **11**, **13a**, **13b**, **14**, **15**, **16**, and **17** have been prepared for the first time. The sandwich complexes **9**, **16** and **17** are used by us for applications in bioinorganic chemistry.[1] Very recently, Mann et al. used a similar protocol for the preparation of the trifluoromethylated complex [RuCp′(η⁶-benzene)]⁺PF_6^-, which was used as a starting point of the synthesis of other [RuCp′(η⁶-arene)]⁺ sandwich complexes.[25]

Experimental Section

General: All reactions were carried out under an argon atmosphere with distilled, non-anhydrous solvents. Yields refer to purified compounds. Reagents, of high commercial quality, were purchased from Aldrich, Acros, Merck and Fluka and were used without further purification. Reactions were controlled by thin-layer chromatography (0.25 mm E. Merck alumina plates NH_2 $F_{254}S$). TLCs were analysed under UV light (λ = 254 nm), followed by heating after treatment with 1,10-phenanthroline (2 M dipping solution in EtOH). E. Merck Al_2O_3 90 standardised (activity grade III, particle size 63−200 μm), E. Merck aminopropyl silica LiChroprep NH_2 (particle size 40−63 μm), and E. Merck silica 60 (particle size 40−63 μm) were used for preparative column chromatography. NMR spectra were recorded on a Varian VRX 400S spectrometer. The NMR shifts were calibrated using the solvent peak as internal reference and assigned on the basis of HSQC and HMBC experiments. All infrared spectra were recorded on an IFS 45 Bruker spectrometer. The UV/Vis spectra were recorded using a Omega 20 Bruins Instruments UV-spectrophotometer. High resolution fast atom bombardment (FAB) and electrospray ionization (ESI) mass spectra were recorded on a Finnigan MAT 95Q mass spectrometer. Only the three predominant isotopes are listed. Melting points were determined with a Electrothermal IA 9000 Series melting point microscope and are uncorrected.

General Procedure for the Preparation of the Ruthenium Sandwich Complexes: Zinc dust (2 equiv.) was added to a solution of $RuCl_3 \cdot xH_2O$ (35−40% Ru) in degassed EtOH (15 mL per mmol). After the solution had turned blue the arene (2 equiv.) was added and the mixture stirred for 10 min. In the case of the Boc-protected compounds **9**, **16**, and **17**, $NaHCO_3$ (2 equiv.) was added to the blue solution before the arene was added. 1,2,3,4,5-Pentamethylcyclopentadiene (2.5 equiv.) and $NaPF_6$ (1.1 equiv.) were added and the reaction mixture was stirred for 1 day at room temperature and for 2 days at 60 °C. *iso*-Octane (15 mL per mmol) was added and the mixture filtered through a pad of aluminium oxide. The filtrate was concentrated and filtered through a pad of aminopropyl silica [*iso*-octane/EtOH (1:1) as eluent]. After concentration of the filtrate to dryness, water (50 mL per mmol), *iso*-octane (100 mL per mmol) and MeOH (50 mL per mmol) were added. Further MeOH was added until the solution became clear. The *iso*-octane phase was separated and the polar phase was extracted with *iso*-octane (twice). The combined *iso*-octane phases were extracted with water/MeOH (1:1) and the polar phases were combined and concentrated to dryness. The product was extracted from the residue with dichloromethane (15 mL, three times) and recrystallised from water/isopropanol (addition of isopropanol to a boiling aqueous suspension).

(η⁶-Methylbenzene)(η⁵-pentamethylcyclopentadienyl)ruthenium Hexafluorophosphate (3): Yellowish powder (142 mg, 54%); m.p. 332 °C (decomp.). ^{1}H NMR (400 MHz [D$_4$]methanol): δ = 1.98 (s, 15 H, η⁵-CCH_3), 2.19 (s, 3 H, η⁶-$C_{ar}CH_3$), 5.82 (m, 5 H, η⁶-CH_{ar}) ppm. ^{13}C NMR (100 MHz, [D$_4$]methanol): δ = 10.52 (η⁵-CCH_3), 18.54 (η⁶-$C_{ar}CH_3$), 87.75 (η⁶-C_{ar}H), 88.44 (η⁶-C_{ar}H), 89.49 (η⁶-C_{ar}H), 97.42 (η⁵-CCH$_3$), 101.81 (η⁶-C_{ar}CH$_3$) ppm. IR (KBr): $\tilde{\nu}$ = 3435 cm^{-1} (m), 3095 (w), 2921 (m), 1637 (vw), 1528 (w), 1476 (m), 1457 (m), 1388 (s), 1075 (vw), 1036 (m), 836 (vs), 779 (vw), 585 (vs), 458 (vw), 409 (w). UV/Vis (MeOH): λ_{max} (ε) = 206 nm (46734 mol^{-1}dm^{3}cm^{-1}). MS (FAB+, NBA): *m*/*z* (%) = 328/329/331 (67/100/54) [M$^+$]. HRMS (ESI+): calcd. for $C_{17}H_{23}{}^{102}$Ru: 329.0837; found 329.0842.

(η⁶-Ethylbenzene)(η⁵-pentamethylcyclopentadienyl)ruthenium Hexafluorophosphate (4): Colourless powder (194 mg, 67%); m.p. 290 °C (decomp.). ^{1}H NMR (400 MHz, [D$_4$]methanol): δ = 1.17 (t, ^3J = 7.7 Hz, 3 H, η⁶-$C_{ar}CH_2CH_3$), 1.92 (s, 15 H, η⁵-CCH_3), 2.36 (q, ^3J = 7.7 Hz, 2 H, η⁶-$C_{ar}CH_2CH_3$), 5.91 (m, 5 H, η⁶-$C_{ar}H$) ppm. ^{13}C NMR (100 MHz, [D$_4$]methanol): δ = 10.57 (η⁵-CCH_3), 15.88 (η⁶-$C_{ar}CH_2CH_3$), 27.40 (η⁶-$C_{ar}CH_2CH_3$), 87.92 (η⁶-C_{ar}H), 88.49 (η⁶-C_{ar}H), 88.66 (η⁶-C_{ar}H), 97.48 (η⁵-CCH$_3$), 107.30 (η⁶-$C_{ar}CH_2CH_3$) ppm. IR (KBr): $\tilde{\nu}$ = 3435 cm^{-1} (s), 2975 (m), 2918 (m), 1629 (m), 1525 (w), 1477 (m), 1458 (m), 1417 (w), 1389 (m), 1074 (w), 1035 (m), 837 (vs), 767 (w), 558 (s), 493 (w), 461 (w). MS (ESI+): *m*/*z* (%) = 342/343/345 (57/100/55) [M$^+$]. HRMS (ESI+): calcd. for $C_{18}H_{25}{}^{102}$Ru: 343.0993; found 343.0997.

(η⁶-1-Chloro-2-methoxybenzene)(η⁵-pentamethylcyclopentadienyl)-ruthenium Hexafluorophosphate (5): Colourless powder (101 mg, 35%); m.p. 335 °C (decomp.). ^{1}H NMR (400 MHz, [D$_6$]acetone): δ = 2.02 (s, 15 H, η⁵-CCH_3), 4.02 (s, 3 H, η⁶-$C_{ar}OCH_3$), 5.96 (ddd, ^3J = 6.4, ^3J = 4.9, ^4J = 1.0 Hz, 1 H, η⁶-$C_{ar}H$), 6.12 (ddd, ^3J = 5.4, ^3J = 4.9, ^4J = 1.0 Hz, 1 H, η⁶-$C_{ar}H$), 6.38 (dd, ^3J = 5.4, ^4J = 1.0 Hz, 1 H, η⁶-$C_{ar}H$), 6.54 (dd, ^3J = 6.4, ^5J = 0.5 Hz, 1 H, η⁶-$C_{ar}H$) ppm. ^{13}C NMR (100 MHz, [D$_6$]acetone): δ = 10.13 (η⁵-CCH_3), 58.38 (η⁶-$C_{ar}OCH_3$), 74.95 (η⁶-C_{ar}H), 86.18 (η⁶-C_{ar}H), 87.21 (η⁶-C_{ar}H), 89.02 (η⁶-C_{ar}H), 95.67 (η⁶-C_{ar}Cl), 97.69 (η⁵-CCH$_3$), 130.93 (η⁶-C_{ar}OCH$_3$) ppm. IR (KBr): $\tilde{\nu}$ = 3436 cm^{-1} (m), 3104 (w), 2919 (vw), 1636 (w), 1514 (m), 1460 (m), 1429 (m), 1407

 © 2003 Wiley-VCH Verlag GmbH & Co. KGaA, Weinheim

(vw), 1391 (m), 1266 (s), 1224 (w), 1179 (vw), 1111 (vw), 1062 (w), 1029 (w), 1005 (m), 838 (vs), 794 (vw), 740 (vw), 685 (m), 660 (vw), 581 (vw), 559 (s), 514 (vw), 457 (vw), 424 (vw). UV/Vis (MeOH): λ_{max} (ε) = 214 nm (29363 $mol^{-1}dm^3cm^{-1}$). MS (ESI+): *m/z* (%) = 378/379/381 (43/100/76) [M^+]. HRMS (ESI+): calcd. for $C_{17}H_{22}{}^{35}ClO^{102}Ru$: 379.0396; found 379.0415.

(η⁶-1-Methoxy-4-methylbenzene)(η⁵-pentamethylcyclopentadienyl)-ruthenium Hexafluorophosphate (6): Colourless powder (195 mg, 69%); m.p. 324 °C (decomp.). ^{1}H NMR (400 MHz, [D$_4$]methanol): δ = 1.95/1.97 (2s, 15 H, η⁵-CCH_3), 2.13/2.14 (2s, 3 H, η⁶-C$_{ar}$CH_3), 3.77/3.78 (2s, 3 H, η⁶-C$_{ar}$OCH_3), 5.70/5.78 (2ddd, ^3J = 6.5, ^4J = 1.8, ^4J = 1.5 Hz, 2 H, η⁶-CH_{ar}), 5.84/5.91 (2ddd, ^3J = 6.5, ^4J = 1.8, ^4J = 1.5 Hz, 2 H, η⁶-CH_{ar}) ppm. ^{13}C NMR (100 MHz, [D$_4$]methanol): δ = 10.14/10.31/10.37 (η⁵-C*C*H$_3$), 17.64/17.84 (η⁶-C$_{ar}$*C*H$_3$), 57.32/57.35 (η⁶-C$_{ar}$O*C*H$_3$), 76. 75/76. 78 (η⁶-*C*$_{ar}$H), 88.20/88.32 (η⁶-*C*$_{ar}$H), 96.64/97.25/97.65 (η⁵-*C*CH$_3$), 99.05/99.72 (η⁶-*C*$_{ar}$CH$_3$), 133.36/133.92 (η⁶-*C*$_{ar}$OCH$_3$) ppm. IR (KBr): $\tilde{\nu}$ = 3435 cm^{-1} (vs), 2920 (w), 1632 (w), 1539 (m), 1486 (s), 1442 (w), 1390 (m), 1255 (s), 1183 (vw), 1102 (w), 1030 (w), 1010 (w), 840 (vs), 715 (w), 667 (w), 558 (s), 434 (w). UV/Vis (MeOH): λ_{max} (ε) = 211 nm (38686 $mol^{-1}dm^3cm^{-1}$). MS (ESI+): *m/z* (%) = 358/359/361 (57/100/55) [M^+]. HRMS (ESI+): calcd. for $C_{18}H_{25}O^{102}Ru$: 359.0943; found 359.0960.

(η⁶-1-Methoxy-2-methylbenzene)(η⁵-pentamethylcyclopentadienyl)-ruthenium Hexafluorophosphate (7): Colourless powder (188 mg, 67%); m.p. 323 °C (decomp.). ^{1}H NMR (400 MHz, [D$_4$]methanol): δ = 1.94/1.96 (2s, 15 H, η⁵-CCH_3), 2.08/2.10 (2s, 3 H, η⁶-C$_{ar}$CH_3), 3.82/3.83 (2s, 3 H, η⁶-C$_{ar}$OCH_3), 5.55/5.61 (2ddd, ^3J = 5.8, ^3J = 5.5, ^4J = 1.1 Hz, 1 H, η⁶-C$_{ar}$*H*), 5.73/5.79 (2ddd, ^3J = 6.2, ^3J = 5.5, ^4J = 1.1 Hz, 1 H, η⁶-C$_{ar}$*H*), 5.77/5.85 (2dd, ^3J = 5.8, ^5J = 0.4 Hz, 1 H, η⁶-C$_{ar}$*H*), 6.04/6.11 (2dd, ^3J = 6.2, ^5J = 0.4 Hz, 1 H, η⁶-C$_{ar}$*H*) ppm. ^{13}C NMR (100 MHz, [D$_4$]methanol): δ = 10.19/10.22/10.37 (η⁵-C*C*H$_3$), 13.89/14.12 (η⁶-C$_{ar}$*C*H$_3$), 57.37/57.41 (η⁶-C$_{ar}$O*C*H$_3$), 74.41/74.48 (η⁶-*C*$_{ar}$H), 85.85/85.92 (η⁶-*C*$_{ar}$H), 86.65/86.66 (η⁶-*C*$_{ar}$H), 89.63/89.79 (η⁶-*C*$_{ar}$H), 91.63/92.32 (η⁶-*C*$_{ar}$CH$_3$), 96.40/96.99/97.06/97.35 (η⁵-*C*CH$_3$), 132.54/133.20 (η⁶-*C*$_{ar}$OCH$_3$) ppm. IR (KBr): $\tilde{\nu}$ = 3435 cm^{-1} (s), 2919 (w), 1629 (w), 1530 (w), 1508 (w), 1473 (m), 1437 (w), 1412 (w), 1389 (w), 1260 (m), 1182 (w), 1104 (w), 1032 (w), 840 (vs), 742 (w), 673 (w), 558 (s). UV/Vis (MeOH): λ_{max} (ε) = 212 nm (37200 $mol^{-1}dm^3cm^{-1}$). MS (ESI+): *m/z* (%) = 358/359/361 (56/100/55) [M^+]. HRMS (ESI+): calcd. for $C_{18}H_{25}O^{102}Ru$: 359.0943; found 359.0935.

(η⁵-Pentamethylcyclopentadienyl)(η⁶-1,3,5-trimethylbenzene)-ruthenium Hexafluorophosphate (8): Colourless powder (224 mg, 80%); m.p. 325 °C (decomp.). ^{1}H NMR (400 MHz, [D$_6$]acetone): δ = 1.95 (s, 15 H, η⁵-CCH_3), 2.24 (s, 9 H, η⁶-C$_{ar}$CH_3), 5.84 (s, 3 H, η⁶-C$_{ar}$*H*) ppm. ^{13}C NMR (100 MHz, [D$_6$]acetone): δ = 9.96 (η⁵-C*C*H$_3$), 18.28 (η⁶-C$_{ar}$*C*H$_3$), 89.55 (η⁶-*C*$_{ar}$H), 95.47 (η⁵-*C*CH$_3$), 101.22 (η⁶-*C*$_{ar}$CH$_3$) ppm. IR (KBr): $\tilde{\nu}$ = 3435 cm^{-1} (s), 2969 (vw), 2921 (w), 1636 (m), 1534 (w), 1475 (vw), 1458 (w), 1389 (m), 1074 (vw), 1031 (m), 838 (vs), 558 (s), 455 (vw). UV/Vis (MeOH): λ_{max} (ε) = 210 nm (33051 $mol^{-1}dm^3cm^{-1}$). MS (ESI+): *m/z* (%) = 356/357/359 (57/100/55) [M^+]. HRMS (ESI+): calcd. for $C_{19}H_{27}{}^{102}Ru$: 357.1150; found 357.1146.

(η⁵-Pentamethylcyclopentadienyl)[η⁶-1-{2-(*tert*-butoxycarbonyl-amino)ethyl}-4-chlorobenzene]ruthenium Hexafluorophosphate (9): Yellowish powder (157 mg, 44%); m.p. 117 °C (decomp.). ^{1}H NMR (400 MHz, [D$_6$]acetone): δ = 1.35 [s, 9 H, (CH_3)$_3$CO], 2.01 (s, 15 H, η⁵-CCH_3), 2.63 (t, ^3J = 6.4 Hz, 2 H, η⁶-C$_{ar}$CH_2CH$_2$), 3.40 (td, ^3J = 6.7, ^3J = 6.4 Hz, 2 H, η⁶-C$_{ar}$CH$_2$CH_2), 6.10 (d, ^3J = 6.1 Hz, 2 H, η⁶-C$_{ar}$*H*C$_{ar}$HC$_{ar}$Cl), 6.18 (br. s, 1 H, CH$_2$CH$_2$N*H*), 6.36 (d, ^3J = 6.1 Hz, 2 H, η⁶-C$_{ar}$HC$_{ar}$*H*C$_{ar}$Cl) ppm. ^{13}C NMR (100 MHz, [D$_6$]acetone): δ = 11.02 (η⁵-C*C*H$_3$), 29.57 ((*C*H$_3$)$_3$CO], 34.71 (η⁶-C$_{ar}$*C*H$_2$CH$_2$), 42.88 (η⁶-C$_{ar}$CH$_2$*C*H$_2$), 79.99 [(CH$_3$)$_3$*C*O], 90.33 (η⁶-C$_{ar}$H*C*$_{ar}$HC$_{ar}$Cl), 90.60 (η⁶-*C*$_{ar}$HC$_{ar}$HC$_{ar}$Cl), 99.21 (η⁵-*C*CH$_3$), 104.10 (η⁶-*C*$_{ar}$CH$_2$), 105.50 (η⁶-*C*$_{ar}$Cl), 157.51 (NH*C*O) ppm. IR (KBr): $\tilde{\nu}$ = 3436 cm^{-1} (m), 3091 (w), 2980 (m), 2931 (w), 1706 (s), 1513 (m), 1477 (w), 1454 (m), 1390 (m), 1367 (m), 1339 (w), 1271 (m), 1251 (m), 1170 (s), 1088 (m), 1033 (m), 984 (w), 840 (vs), 780 (w), 739 (w), 623 (w), 558 (s), 454 (w), 412 (w). UV/Vis (MeOH): λ_{max} (ε) = 213 nm (37200 $mol^{-1}dm^3cm^{-1}$). MS (FAB+, NBA): *m/z* (%) = 491/492/494 (60/100/75) [M^+]. HRMS (ESI+): calcd. for $C_{23}H_{33}{}^{35}ClNO_2{}^{102}Ru$: 492.1243; found 492.1224.

(η⁶-Benzoylbenzene)(η⁵-pentamethylcyclopentadienyl)ruthenium Hexafluorophosphate (10): Yellowish powder (109 mg, 35%); m.p. 192 °C (decomp.). ^{1}H NMR (400 MHz, [D$_6$]acetone): δ = 1.95 (s, 15 H, η⁵-CCH_3), 6.31 (m, 3 H, η⁶-C$_{ar}$*H*), 6.49 (m, 2 H, η⁶-C$_{ar}$*H*CCO), 7.63 (dd, ^3J = 8.0, ^3J = 1.5 Hz, 2 H, C$_{ar}$*H*C$_{ar}$HCCO), 7.77 (m, 1 H, C$_{ar}$*H*C$_{ar}$HC$_{ar}$HCCO), 7.95 (dd, ^3J = 8.0, ^3J = 1.5 Hz, 2 H, C$_{ar}$*H*CCO) ppm. ^{13}C NMR (100 MHz, [D$_6$]acetone): δ = 11.31 (η⁵-C*C*H$_3$), 89.57 (η⁶-*C*$_{ar}$H), 89.92 (η⁶-*C*$_{ar}$H), 91.19 (η⁶-*C*$_{ar}$H), 97.74 (η⁶-*C*$_{ar}$CO), 99.82 (η⁵-*C*CH$_3$), 130.28 (*C*$_{ar}$H), 131.58 (*C*$_{ar}$H), 135.83 (*C*$_{ar}$H), 138.12 (*C*$_{ar}$CO), 194.73 (CO) ppm. IR (KBr): $\tilde{\nu}$ = 3429 cm^{-1} (s), 3094 (w), 2970 (s), 2925 (m), 1665 (s), 1598 (m), 1511 (w), 1477 (w), 1381 (m), 1294 (m), 1266 (m), 1161 (w), 1125 (m), 1083 (s), 1036 (w), 952 (m), 919 (w), 861 (m), 840 (vs), 738 (m), 717 (w), 697 (w), 637 (w), 558 (m), 447 (w), 409 (w). UV/Vis (MeOH): λ_{max} (ε) = 210 nm (10812 $mol^{-1}dm^3cm^{-1}$). MS (ESI+): *m/z* (%) = 418/419/421 (57/100/54) [M^+]. HRMS (ESI+): calcd. for $C_{23}H_{25}O^{102}Ru$: 419.0949; found 419.0939.

(η⁶-Acetylbenzene)(η⁵-pentamethylcyclopentadienyl)ruthenium Hexafluorophosphate (11): Yellowish powder (144 mg, 51%); m.p. 208 °C (decomp.). ^{1}H NMR (400 MHz, [D$_6$]acetone): δ = 2.00 (s, 15 H, η⁵-CCH_3), 2.62 (s, 3 H, CH_3CO), 6.29 (m, 2 H, η⁶-C$_{ar}$*H*CHCCO), 6.32 (m, 1 H, η⁶-C$_{ar}$*H*CHCHCCO), 6.61 (dd, ^3J = 6.1, ^3J = 1.2 Hz, 2 H, η⁶-C$_{ar}$*H*CCO) ppm. ^{13}C NMR (100 MHz, [D$_6$]acetone): δ = 11.33 (η⁵-C*C*H$_3$), 28.39 (*C*H$_3$CO), 88.35 (η⁶-*C*$_{ar}$H), 90.40 (η⁶-*C*$_{ar}$H), 91.23 (η⁶-*C*$_{ar}$H), 94.30 (η⁶-*C*$_{ar}$CO), 99.61 (η⁵-*C*CH$_3$), 198.07 (CO) ppm. IR (KBr): $\tilde{\nu}$ = 3435 cm^{-1} (s), 3098 (m), 2967 (m), 2926 (m), 1694 (s), 1636 (m), 1515 (w), 1497 (w), 1473 (m), 1455 (m), 1406 (w), 1390 (m), 1363 (w), 1292 (w), 1254 (s), 1079 (w), 1035 (m), 959 (w), 839 (vs), 741 (w), 584 (w), 559 (s), 465 (w), 416 (w). UV/Vis (MeOH): λ_{max} (ε) = 215 nm (27454 $mol^{-1}dm^3cm^{-1}$). MS (ESI+): *m/z* (%) = 356/357/359 (56/100/55) [M^+]. HRMS (ESI+): calcd. for $C_{18}H_{23}O^{102}Ru$: 357.0792; found 357.0776.

(η⁶-4-Methylbenzenesulfonic acid)(η⁵-pentamethylcyclopentadienyl)-ruthenium Hexafluorophosphate (12): Yellowish powder (203 mg, 66%); m.p. 258 °C (decomp.). ^{1}H NMR (400 MHz, [D$_6$]acetone): δ = 1.98 (s, 15 H, η⁵-CCH_3), 2.26 (s, 3 H, η⁶-C$_{ar}$CH_3), 5.82 (d, ^3J = 6.1 Hz, 2 H, η⁶-C*H*C$_{ar}$CH$_3$), 6.14 (d, ^3J = 6.1 Hz, 2 H, η⁶-C*H*C$_{ar}$SO$_3$H), 10.17 (br. s, 1 H, SO$_3$*H*) ppm. ^{13}C NMR (100 MHz, [D$_6$]acetone): δ = 11.13 (η⁵-C*C*H$_3$), 19.20 (η⁶-C$_{ar}$*C*H$_3$), 86.77 (η⁶-*C*$_{ar}$H), 89.21 (η⁶-*C*$_{ar}$H), 97. 85 (η⁵-*C*CH$_3$), 130.37 (η⁶-*C*$_{ar}$CH$_3$), 131.22 (η⁶-*C*$_{ar}$SO$_3$H) ppm. IR (KBr): $\tilde{\nu}$ = 3435 cm^{-1} (vs), 3060 (w), 2962 (w), 2919 (m), 2854 (w), 1631 (s), 1522 (w), 1476 (m), 1454 (m), 1388 (s), 1349 (w), 1234 (vs), 1223 (vs), 1107 (s), 1031 (vs), 1005 (vw), 875 (w), 797 (w), 671 (vs), 574 (s), 565 (s), 505 (w), 458 (w), 426 (s). UV/Vis (MeOH): λ_{max} (ε) = 212 nm (262744 $mol^{-1}dm^3cm^{-1}$). MS (ESI+): *m/z* (%) = 408/409/411 (57/100/59) [M^+]. HRMS (ESI+): calcd. for $C_{17}H_{23}O_3S^{102}Ru$: 409.0411; found 409.0437.

 © 2003 Wiley-VCH Verlag GmbH & Co. KGaA, Weinheim

Diels−Alder Adducts *rac*-13a and *rac*-13b: Yellowish powder (199 mg, 51%); m.p. 240 °C (decomp.). **13a:** ^{1}H NMR (400 MHz, [D$_6$]acetone): δ = 0.60 (d, ^3J = 6.7 Hz, 3 H, 171-H), 0.95 (dd, ^4J = 1.2, ^4J = 2.7 Hz, 3 H, 131-H), 1.05 (s, 3 H, 151-H), 1.11 (s, 3 H, 141-H), 1.34 (t, ^3J = 7.0 Hz, 3 H, C*H*$_3$CH$_2$O), 1.66 (d, ^4J = 1.2 Hz, 3 H, 161-H), 1.98 (s, 15 H, η⁵-CC*H*$_3$), 2.15 (q, ^3J = 6.7 Hz, 1 H, 17-H), 2.54 (d, ^3J = 4.6 Hz, 1 H, 8-H), 3.27 (d, ^3J = 4.6 Hz, 1 H, 7-H), 4.16−4.30 (q, ^3J = 7.0 Hz, 2 H, CH$_3$C*H*$_2$O), 5.60 (m, 1 H, η⁶-4-H), 5.89−6.03 (m, 4 H, η⁶-C$_{ar}$*H*) ppm; **13b:** δ = 0.55 [d, ^3J = 6.4 Hz, 3 H, C*H*$_3$C$_q$(C$_q$)(C$_q$)H], 0.65 [s, 3 H, (C=O)CH(C$_q$)C(C*H*$_3$)=C(CH$_3$)], 1.34 [s, 3 H, (C=O)CH(C$_q$)C(CH$_3$)=C(C*H*$_3$)], 1.34 (t, ^3J = 7.0 Hz, 3 H, C*H*$_3$CH$_2$O), 1.45 [dd, ^4J = 1.2, ^4J = 2.4 Hz, 3 H, (C=O)CHC$_q$(C*H*$_3$)], 1.59 [d, ^4J = 1.2 Hz, 3 H, (η⁶-C$_{ar}$)CHC$_q$(C*H*$_3$)], 1.82 [q, ^3J = 6.4 Hz, 1 H, CH$_3$C$_q$(C$_q$)(C$_q$)*H*], 2.04 (s, 15 H, η⁵-CC*H*$_3$), 2.94 [d, ^3J = 4.6 Hz, 1 H, (η⁶-C$_{ar}$)C*H*], 2.98 [d, ^3J = 4.6 Hz, 1 H, (C=O)C*H*], 4.16−4.30 (q, ^3J = 7.0 Hz, 2 H, CH$_3$C*H*$_2$O), 5.96−6.09 (m, 4 H, η⁶-C$_{ar}$*H*), 6.32 (m, 1 H, η⁶-C$_{ar}$*H*) ppm. ^{13}C NMR (100 MHz, [D$_6$]acetone): **13a:** δ = 9.60 (C-171), 10.80 (C-161), 11.68 (η⁵-C*C*H$_3$), 13.6 (C-131), 14.6 (C-141), 14.8 (C-151), 15.6 (*C*H$_3$CH$_2$O), 53.78 (C-8), 56.47 (C-7), 58.49 (C-17), 60.63 (C-16), 61.92 (C-13), 62.50 (O*C*H$_2$CH$_3$), 85.87 (C-4), 88.86 (C-2/6), 89.11 (C-3/5), 98.20 (η⁵-*C*CH$_3$), 108.34 (C-1), 136.55 (C-15), 137.74 (C-14), 175.87 (C=O) ppm; **13b:** δ = 9.20 [*C*H$_3$C$_q$(C$_q$)(C$_q$)H], 10.70 [(η⁶-C$_{ar}$)CHC$_q$(*C*H$_3$)], 11.48 (η⁵-C*C*H$_3$), 12.40 [(C=O)CHC$_q$(*C*H$_3$)], 14.90 [(C=O)CH(C$_q$)C(*C*H$_3$)=C(CH$_3$)], 15.50 [(C=O)CH(C$_q$)C(CH$_3$)=C(*C*H$_3$)], 15.60 (*C*H$_3$CH$_2$O), 52.11 [(η⁶-C$_{ar}$)*C*H], 56.56 [(C=O)*C*H], 57.90 [CH$_3$*C*$_q$(C$_q$)(C$_q$)H], 60.57 [(C=O)CH*C*$_q$(CH$_3$)], 60.75 [(η⁶-C$_{ar}$)CH*C*$_q$(CH$_3$)], 62.50 (O*C*H$_2$CH$_3$), 85.77 (η⁶-*C*$_{ar}$H), 88.92 (η⁶-*C*$_{ar}$H), 89.65 (η⁶-*C*$_{ar}$H), 98.23 (η⁵-*C*CH$_3$), 109.73 [(η⁶-*C*$_{ar}$)CH], 135.52 [(C=O)CH(C$_q$)C(CH$_3$)=*C*(CH$_3$)], 137.83 [(C=O)CH(C$_q$)*C*(CH$_3$)=C(CH$_3$)], 174.73 (C=O) ppm. IR (KBr): $\tilde{\nu}$ = 3435 cm^{-1} (m), 3101 (vw), 2963 (m), 2929 (m), 2873 (w), 1720 (vs), 1628 (vw), 1522 (vw), 1477 (m), 1455 (m), 1416 (vw), 1386 (m), 1312 (m), 1275 (w), 1239 (vw), 1183 (s), 1154 (w), 1138 (vw), 1079 (w), 1035 (m), 841 (vs), 739 (vw), 698 (vw), 558 (s), 460 (vw), 405 (m). MS (ESI+): *m*/*z* (%) = 548/549/551 (58/100/54) [M$^+$]. HRMS (ESI+): calcd. for C$_{31}$H$_{43}$O$_2$^{102}Ru: 549.2307; found 549.2299.

(η⁵-Pentamethylcyclopentadienyl)[η⁶-1-{2*S*-(*tert*-butoxycarbonylamino)-2*S*-(methoxycarbonyl)ethyl}benzene]ruthenium Hexafluorophosphate (16): Yellowish powder (195 mg, 55%); m.p. 90 °C (decomp.). ^{1}H NMR (400 MHz, [D$_6$]acetone): δ = 1.33 [s, 9 H, (C*H*$_3$)$_3$CO], 2.02 (s, 15 H, η⁵-CC*H*$_3$), 2.78 [dd, ^2J = 13.6 Hz, ^3J = 9.2 Hz, 1 H, η⁶-C$_{ar}$C*H*HCH(CO)NH], 2.96 [dd, ^2J = 13.6 Hz, ^3J = 5.2 Hz, 1 H, η⁶-C$_{ar}$CH*H*CH(CO)NH], 3.69 (s, 3 H, OC*H*$_3$), 4.42 [ddd, ^3J = 5.2, ^3J = 8.8, ^3J = 9.2 Hz, 1 H, CH$_2$C*H*(CO)NH], 5.96 (d, ^3J = 5.5 Hz, 1 H, η⁶-C$_{ar}$*H*), 6.02 (d, ^3J = 5.2 Hz, 2 H, η⁶-C$_{ar}$*H*), 6.04 (dd, ^3J = 5.2, ^3J = 5.5 Hz, 2 H, η⁶-C$_{ar}$*H*), 6.45 (d, ^3J = 8.8 Hz, 1 H, N*H*) ppm. ^{13}C NMR (100 MHz, [D$_6$]acetone): δ = 10.51 (η⁵-C*C*H$_3$), 28.45 [(*C*H$_3$)$_3$CO], 36.08 [η⁶-C$_{ar}$*C*H$_2$CH(CO)NH], 52.64 (O*C*H$_3$), 55.46 [CH$_2$*C*H(CO)NH], 79.84 [(CH$_3$)$_3$*C*O], 88.47 (η⁶-*C*$_{ar}$H), 89.18 (η⁶-*C*$_{ar}$H), 89.53 (η⁶-*C*$_{ar}$H), 97.29 (η⁵-*C*CH$_3$), 100.51 (η⁶-*C*$_{ar}$CH$_2$), 156.15 (NH*C*O), 172.03 (*C*OOCH$_3$) ppm. IR (KBr): $\tilde{\nu}$ = 3427 cm^{-1} (m), 2978 (m), 1743 (m), 1704 (s), 1514 (w), 1477 (w), 1455 (w), 1368 (m), 1254 (m), 1167 (m), 1033 (s), 984 (w), 843 (vs), 740 (vw), 558 (m). UV/Vis (MeOH): λ_{max} (ε) = 210 nm (206655 mol^{-1}dm^{3}cm^{-1}). MS (FAB+, NBA): *m*/*z* (%) = 515/516/518 (60/100/54) [M$^+$]. HRMS (FAB+): calcd. for C$_{25}$H$_{36}$NO$_4$^{102}Ru: 516.1688; found 516.1697.

(η⁵-Pentamethylcyclopentadienyl)[η⁶-1-{2-(*tert*-butoxycarbonylamino)-2-(ethoxycarbonyl)ethyl}-4-chlorobenzene]ruthenium Hexafluorophosphate (17): Yellowish powder (160 mg, 45%); m.p. 97 °C (decomp.). ^{1}H NMR (400 MHz, [D$_6$]acetone): δ = 1.21 (t, ^3J = 7.3 Hz, 3 H, CH$_2$C*H*$_3$), 1.34 [s, 9 H, (C*H*$_3$)$_3$CO], 2.00 (s, 15 H, η⁵-CC*H*$_3$), 2.80 [dd, ^2J = 13.6 Hz, ^3J = 9.5 Hz, 1 H, η⁶-C$_{ar}$C*H*HCH(-CO)NH], 2.98 [dd, ^2J = 13.6 Hz, ^3J = 5.1 Hz, 1 H, η⁶-C$_{ar}$CH*H*CH(CO)NH], 4.15 (q, ^3J = 7.3 Hz, 2 H, C*H*$_2$CH$_3$), 4.41 [ddd, ^3J = 5.1 Hz, ^3J = 8.8, ^3J = 9.5 Hz, 1 H, CH$_2$C*H*(CO)NH], 6.08 (d, ^3J = 5.9 Hz, 1 H, η⁶-C$_{ar}$*H*CCH), 6.19 (d, ^3J = 5.9 Hz, 1 H, η⁶-C$_{ar}$*H*CCH$_2$), 6.37 (d, ^3J = 5.9 Hz, 1 H, η⁶-C$_{ar}$*H*CCl) 6.39 (d, ^3J = 5.9 Hz, 1 H, η⁶-C$_{ar}$*H*CCl) 6.48 (d, ^3J = 8.8 Hz, 1 H, N*H*). ^{13}C NMR (100 MHz, [D$_6$]acetone): δ = 10.94 (η⁵-C*C*H$_3$), 15.40 (OCH$_2$*C*H$_3$), 29.41 [(*C*H$_3$)$_3$CO], 36.23 [η⁶-C$_{ar}$*C*H$_2$CH(CO)NH], 56.39 [CH$_2$*C*H(CO)NH], 63.00 (O*C*H$_2$CH$_3$), 80.83 [(CH$_3$)$_3$*C*O], 90.40 (η⁶-*C*$_{ar}$HCCH$_2$), 90.53 (η⁶-*C*$_{ar}$HCCl), 90.55 (η⁶-*C*$_{ar}$HCCl), 90.70 (η⁶-*C*$_{ar}$HCCH$_2$), 99.39 (η⁵-*C*CH$_3$), 101.84 (η⁶-*C*$_{ar}$CH$_2$), 105.64 (η⁶-*C*$_{ar}$Cl), 157.16 (NH*C*O), 172.30 (*C*OOCH$_2$) ppm. IR (KBr): $\tilde{\nu}$ = 3351 cm^{-1} (s), 3089 (w), 2983 (m), 2931 (s), 2852 (m), 2495 (w), 1740 (s), 1703 (vs), 1627 (m), 1609 (w), 1575 (w), 1527 (w), 1479 (m), 1453 (m), 1421 (w), 1392 (m), 1369 (m), 1344 (m), 1257 (m), 1218 (vw), 1164 (s), 1089 (m), 1032 (vs), 980 (w), 842 (vs), 558 (s), 442 (vw), 412 (m). UV/Vis (MeOH): λ_{max} (ε) = 213 nm (193339 mol^{-1}dm^{3}cm^{-1}). MS (FAB+, NBA): *m*/*z* (%) = 562/564/566 (43/100/41) [M$^+$]. HRMS (FAB+): calcd. for C$_{26}$H$_{37}$^{35}ClNO$_4$^{102}Ru: 564.1455; found 564.1459.

Procedure for the Preparation of the Ruthenium Sandwich Complexes 4, 14, and 15 via the Methanol/Methoxide Route: The arene (2 equiv.) was added to a solution of [Cp*RuCl$_2$]$_2$ (1 equiv.) in MeOH (6.5 mL per mmol) and NaOMe (1 equiv.). The solution was stirred for 3 h under reflux. After addition of $NaPF_6$ (1.1 equiv.) and MeOH (15 mL per mmol) the mixture was filtered through a pad of aluminium oxide. The filtrate was concentrated and filtered through a pad of aminopropyl silica [*iso*-octane/EtOH (1:1) as eluent]. After concentration of the filtrate to dryness, water (50 mL per mmol), *iso*-octane (100 mL per mmol) and MeOH (50 mL per mmol) were added. Further MeOH was added until the solution became clear. The *iso*-octane phase was separated and the polar phase extracted with *iso*-octane (twice). The combined *iso*-octane phases were extracted with water/MeOH (1:1) and the polar phases were combined and concentrated to dryness. The product was extracted from the residue with dichloromethane (15 mL, three times) and recrystallised from water/*iso*-propanol (addition of *iso*-propanol to a boiling aqueous suspension).

(η⁶-1,2-Dimethoxybenzene)(η⁵-pentamethylcyclopentadienyl)-ruthenium Hexafluorophosphate (15). Colourless powder (66 mg, 20%); m.p. 342 °C (decomp.). ^{1}H NMR (400 MHz, [D$_6$]acetone): δ = 2.01 (s, 15 H, η⁵-CC*H*$_3$), 3.93 (s, 6 H, η⁶-C$_{ar}$OC*H*$_3$), 5.75 (m, 2 H, η⁶-C$_{ar}$*H*), 6.33 (m, 2 H, η⁶-C$_{ar}$*H*) ppm. ^{13}C NMR (100 MHz, [D$_6$]acetone): δ = 10.52 (η⁵-C*C*H$_3$), 57.68 (η⁶-C$_{ar}$O*C*H$_3$), 75.36 (η⁶-*C*$_{ar}$H), 83.86 (η⁶-*C*$_{ar}$H), 95.86 (η⁵-*C*CH$_3$), 124.44 (η⁶-*C*$_{ar}$OCH$_3$) ppm. IR (KBr): $\tilde{\nu}$ = 3435 cm^{-1} (s), 3104 (w), 2920 (w), 1629 (w), 1526 (m), 1516 (m), 1485 (s), 1437 (m), 1417 (w), 1390 (m), 1267 (s), 1216 (m), 1177 (w), 1106 (m), 1031 (w), 1011 (s), 840 (vs), 748 (m), 584 (m), 558 (s), 524 (w), 458 (w). UV/Vis (MeOH): λ_{max} (ε) = 214 nm (32491 mol^{-1}dm^{3}cm^{-1}). MS (FAB+, NBA): *m*/*z* (%) = 374/375/377 (59/100/56) [M$^+$]. HRMS (ESI+): calcd. for C$_{18}$H$_{25}$O$_2$^{102}Ru: 375.0892; found 375.0905.

(η⁶-Ethylbenzene)[η⁵-(1-methoxymethyl-2,3,4,5-tetramethyl)cyclopentadienyl]ruthenium Hexafluorophosphate (14) and (η⁶-Ethylbenzene)(η⁵-pentamethylcyclopentadienyl)ruthenium Hexafluorophosphate (4): Colourless powder (1.62 g, 56%); m.p. 277 °C (decomp.). **14:** ^{1}H NMR (400 MHz, [D$_4$]methanol): δ = 1.17 (t, ^3J = 7.7 Hz, 3 H, η⁶-C$_{ar}$CH$_2$C*H*$_3$), 1.92 (s, 12 H, η⁵-CC*H*$_3$), 2.36 (q, ^3J = 7.7 Hz, 2 H, η⁶-C$_{ar}$C*H*$_2$CH$_3$), 3.40 (s, 3 H, η⁵-CCH$_2$OC*H*$_3$), 4.19

 © 2003 Wiley-VCH Verlag GmbH & Co. KGaA, Weinheim

(s, 2 H, η^5-CCH_2O), 5.91 (m, 5 H, η^6-C$_{ar}H$) ppm. ^{13}C NMR (100 MHz, [D$_4$]methanol): δ = 10.57 (η^5-CCH_3), 15.88 (η^6-C$_{ar}$CH_2CH_3), 27.40 (η^6-C$_{ar}$CH_2CH$_3$), 59.03 (η^5-CCH$_2$OCH_3), 66.04 (η^5-CCH_2O), 87.92 (η^6-C$_{ar}$H), 88.49 (η^6-C$_{ar}$H), 88.66 (η^6-C$_{ar}$H), 97.29 (η^5-CCH$_2$O), 97.48 (η^5-CCH$_3$), 107.30 (η^6-C$_{ar}$CH$_2$CH$_3$) ppm. IR (KBr): $\tilde{\nu}$ = 3435 cm^{-1} (s), 2975 (m), 2918 (m), 1629 (m), 1525 (w), 1477 (m), 1458 (m), 1417 (w), 1389 (m), 1074 (w), 1035 (m), 837 (vs), 767 (w), 558 (s), 493 (w), 461 (w). UV/Vis (MeOH): λ_{max} (ε) = 209 nm (36330 mol^{-1}dm^{3}cm^{-1}). MS (ESI+): *m*/*z* (%) = 372/373/375 (56/100/54) [M$^+$]. HRMS (ESI+): calcd. for $C_{19}H_{27}O^{102}Ru$: 373.1105; found 373.1117. For spectroscopic data of **4** see above.

Crystallographic Analysis: Single-crystal intensity data were collected from colourless crystals with a Stoe Imaging Plate Diffraction System **(13a)** or by use of an Enraf−Nonius Kappa CCD equipped with a rotating anode **(14)**. In both cases, graphite-monochromated Mo-K_α radiation (λ = 71.073 pm) was used and the measurement temperature was 200(2) K. A numerical absorption correction (XRed[26]) was applied to the data. All relevant information concerning the data collection are listed in Table 3. The structures were solved by direct methods (SIR97[27]) and refined using SHELXL-97 (full-matrix least-squares on F^2).[27,28] The hydrogen atoms were considered with a riding model. All other atoms were refined with anisotropic atomic displacement parameters, except a disordered ethyl group in **13a** which was refined isotropically.

Table 3. Data collection and structural refinement parameters for compounds **13a** and **14**

	13a	**14**
Formula	$C_{31}H_{42}F_6O_2PRu$	$C_{19}H_{27}F_6OPRu$
M_r	693.71	517.45
Crystal system	orthorhombic	monoclinic
Space group	$Pca2_1$	$P2_1/c$
Crystal size [mm^3]	0.02 × 0.30 × 0.32	0.02 × 0.08 × 0.10
a [pm]	2007.8(2)	1104.67(2)
b [pm]	914.78(4)	1237.41(2)
c [pm]	1739.88(9)	1597.03(2)
α [°]	90.0	90.0
β [°]	90.0	106.472(1)
γ [°]	90.0	90.0
V (Å^3)	3195.6(3)	2093.43(6)
Z	4	4
ρ calcd. [Mg·m^{-3}]	1.442	1.642
μ [mm^{-1}]	0.602	0.884
Transmission (min/max)	0.8619/0.9876	0.9360/0.9785
F(000)	1432	1048
Range in *hkl*	±22, ±10, ±19	±12, ±14, ±18
Reflections collected	17452	22699
Independent refl. ($R_{int.}$)	4886 (0.0631)	3269 (0.0872)
Data/restraints/parameters	4886/1/381	3269/0/259
Goodness-of-fit on F^2	0.885	1.033
*R*1 [$I > 2\sigma(I)$]	0.0412	0.0389
*R*1 (all data)	0.0715	0.0579
*wR*2 [$I > 2\sigma(I)$]	0.0761	0.0863
*wR*2 (all data)	0.0822	0.0919
Flack parameter	−0.05(4)	−
Largest diff. peak/hole	0.394/−0.338	0.548/−0.606

CCDC-189008 (**13a**) and CCDC-189009 (**14**) contain the supplementary crystallographic data for this publication. These data can be obtained free of charge via www.ccdc.cam.ac.uk/conts/retrieving.html (or from the Cambridge Crystallographic Data Centre, 12 Union Road, Cambridge, CB21EZ, UK; Fax: (internat.) +44-1223/336-033; E-mail: deposit@ccdc.cam.ac.uk).

Supporting Information Available: Spectra of selected compounds (see footnote on the first page of this article).

Acknowledgments

Petra Böhrer is thanked for technical assistance in the preparation of selected model compounds. Special thanks go to Degussa AG for a generous donation of $RuCl_3 \cdot xH_2O$.

[1] [1a] D. Leone-Stumpf, T. Lindel, *Chem. Eur. J.* **2001**, *7*, 3961−3965. [1b] D. Leone-Stumpf, T. Lindel, *Eur. J. Org. Chem.* **2003**, 1853−1858.
[2] The term "peptoid" is used to describe a "peptide-like compound" ("-oid" from the Old Greek ειδος "picture"). It was originally restricted to oligomers of *N*-substituted glycines: R. J. Simon, R. S. Kania, R. N. Zuckermann, V. D. Huebner, D. A. Jewell, S. Banville, S. Ng, L. Wang, S. Rosenberg, C. K. Marlowe, D. C. Spellmeyer, R. Tan, A. D. Frankel, D. V. Santi, F. E. Cohen, P. A. Bartlett, *Proc. Natl. Acad. Sci. USA* **1992**, *89*, 9367−9371.
[3] ^{97}Ru (half life 2.89 d, electron capture), ^{103}Ru (39.27 d, β$^-$), and ^{106}Ru (1.02 a, β$^-$); *Handbook of Chemistry and Physics*, 76th ed. (Ed.: D. R. Lide), CRC press, Boca Raton **1995**, p. 11−64.
[4] [4a] A. J. Pearson, J. G. Park, S. H. Yang, Y. H. Chuang, *J. Chem. Soc., Chem. Commun.* **1989**, 1363−1364. [4b] A. J. Pearson, J.-N. Heo, *Org. Lett.* **2000**, *2*, 2987−2990 and refs. cited therein. [4c] C. W. West, D. H. Rich, *Org. Lett.* **1999**, *1*, 1819−1822 and refs. cited therein. [4d] A. Marchetti, J. M. Ontoria, V. G. Matassa, *Synlett* **1999**, *S1*, 1000−1002.
[5] T. P. Gill, K. R. Mann, *Organometallics* **1982**, *1*, 485−488.
[6] B. M. Trost, C. M. Older, *Organometallics* **2002**, *21*, 2544−2546.
[7] [7a] V. S. Kaganovich, A. R. Kudinov, M. I. Rybinskaya, *Izv. Akad. Nauk SSSR, Ser. Khim.* **1986**, *2*, 492. [7b] A. R. Kudinov, M. I. Rybinskaya, Yu. T. Struchkov, A. I. Yanovskii, P. V. Petrovskii, *J. Organomet. Chem.* **1987**, *336*, 187−197.
[8] [8a] B. Chaudret, F. Jalón, *J. Chem. Soc., Chem. Commun.* **1988**, 711−713. [8b] B. Chaudret, F. Jalón, M. Pérez-Manrique, *New J. Chem.* **1990**, *14*, 331−338.
[9] J. E. Letourneau, M. A. Wellman, D. J. Burnell, *J. Org. Chem.* **1997**, *62*, 7272−7277.
[10] J. L. Schrenk, A. M. McNair, F. B. McCormick, K. R. Mann, *Inorg. Chem.* **1986**, *25*, 3501−3504.
[11] [11a] T. D. Tilley, R. H. Grubbs, J. E. Bercaw, *Organometallics* **1984**, *3*, 274−278. [11b] N. Oshima, H. Suzuki, Y. Moro-Oka, *Inorg. Chem.* **1986**, *25*, 3407−3412.
[12] P. J. Fagan, M. D. Ward, J. C. Calabrese, *J. Am. Chem. Soc.* **1989**, *111*, 1698−1719.
[13] B. Steinmetz, W. A. Schenk, *Organometallics* **1999**, *18*, 943−946.
[14] W. S. Sheldrick, A. Gleichmann, *J. Organomet. Chem.* **1994**, *470*, 183−187.
[15] [15a] U. Koelle, J. Kossakowski, R. Boese, *J. Organomet. Chem.* **1989**, *378*, 449−455. [15b] U. Koelle, M. H. Wang, *Organometallics* **1990**, *9*, 195−198.
[16] [16a] H. Lehmkuhl, M. Bellenbaum, J. Grundke, H. Mauermann, C. Krüger, *Chem. Ber.* **1988**, 1719−1728. [16b] U. Koelle, J. Kossakowski, *J. Organomet. Chem.* **1989**, *362*, 383.
[17] [17a] U. Koelle, J. Kossakowski, N. Klaff, L. Wesemann, U. Englert, G. E. Herberich, *Angew. Chem.* **1991**, *103*, 732−3; *Angew. Chem. Int. Ed. Engl.* **1991**, *30*, 690−1. [17b] U. Koelle, J. Kossakowski, D. Grumbine, T. D. Tilley, *Inorg. Synth.* **1992**, *29*, 225−228.
[18] [18a] A. N. Nesmeyanov, N. A. Vol′kenau, I. N. Bolesova, L. S. Shul′pina, *J. Organomet. Chem.* **1979**, *182*, C36−C38. [18b] E. Román, D. Astruc, *Inorg. Chim. Acta* **1979**, *37*, L465−L466.

 © 2003 Wiley-VCH Verlag GmbH & Co. KGaA, Weinheim

[19] X. D. He, B. Chaudret, F. Dahan, Y.-S. Huang, *Organometallics* **1991**, *10*, 970−979.
[20] M. Stebler-Roethlisberger, A. Salzer, H. B. Bürgi, A. Ludi, *Organometallics* **1986**, *5*, 298−302.
[21] P. Bernhard, H. B. Bürgi, J. Hauser, H. Lehmann, A. Ludi, *Inorg. Chem.* **1982**, *21*, 3936−3941.
[22] A. Bauer, U. Englert, S. Geyser, F. Podewils, A. Salzer, *Organometallics* **2000**, *19*, 5471−5476.
[23] [23a] **3, 6, 8**: ref. [7a]. [23b]**3**: M. E. Navarro Clemente, P. Juárez Saavedra, M. C. Vásquez, M. A. Paz-Sandoval, A. M. Arif, R. D. Ernst, *Organometallics* **2002**, *21*, 592−605. [23c] **10**: ref.[19]. [23d] **12**: ref.[20]
[24] [24a] L. Fan, C. Wei, F. I. Aigbirhio, M. L. Turner, O. V. Gusev, L. N. Morozova, D. R. T. Knowles, P. M. Maitlis, *Organometallics* **1996**, *15*, 98−104. [24b] L. Fan, M. L. Turner, H. Adams, N. A. Bailey, P. M. Maitlis, *Organometallics* **1995**, *14*, 676−684. [24c] D. R. T. Knowles, H. Adams, P. M. Maitlis, *Organometallics* **1998**, *17*, 1741−1749.
[25] J. K. Evju, K. R. Mann, *Organometallics* **2002**, *21*, 993−996.
[26] XRed, rev. 1.09, Stoe Data Reduction Program, Stoe, Darmstadt, Germany.
[27] A. Altomare, M. C. Burla, M. Camalli, G. L. Cascarano, C. Giacovazzo, A. Guagliardi, A. G. G. Moliterni, G. Polidori, R. Spagna: SIR97: a new tool for crystal structure determination and refinement; *J. Appl. Crystallogr.* **1999**, *32*, 115−119.
[28] G. M. Sheldrick, SHELXL-97, *Program for Crystal Structure Refinement*, University of Göttingen, Germany, 97−2 version.
Received October 20, 2002

 © 2003 Wiley-VCH Verlag GmbH & Co. KGaA, Weinheim

Reduction of $[(C_5Me_5)_2Mo_2O_5]$ and $[(C_5Me_5)_2Mo_2O_4]$ in Methanol/Water/Trifluoroacetate Solutions Investigated by Combined On-Line Electrochemistry/Electrospray-Ionization Mass Spectrometry

Jenny Gun,[a] Alexandre Modestov,[a] Ovadia Lev,[a] and Rinaldo Poli*[b]

Keywords: Cyclopentadienyl ligands / Electrochemistry / Electrospray-ionization mass spectrometry / Molybdenum / Oxo ligands

Complexes $[Cp^*_2Mo_2O_5]$ ($Cp^* = \eta^5$-C_5Me_5) and $[Cp^*_2Mo_2O_4]$ were investigated by combined on-line electrochemical (EC) reduction and electrospray-ionization mass spectrometry (ESI-MS) techniques in a trifluoroacetic acid buffered water/methanol solution. The reduction products at the larger negative potentials are identical for both compounds. The studies reveal the existence of a wide range of previously unknown di- and trinuclear Mo^V, Mo^{IV}, Mo^{III}, and mixed-valence complexes that were identified on the basis of their masses and characteristic isotope patterns. The structures of the initial compounds and the product of electroreduction with m/z = 713–729 were supported by in situ MS^n experiments that allowed the elucidation of the fragmentation pathway for the collision-induced dissociation.
(© Wiley-VCH Verlag GmbH & Co. KGaA, 69451 Weinheim, Germany, 2003)

Introduction

The development of the Electrospray-Ionization Mass Spectrometers (ESI-MS) by Yamashita and Fenn[1] has provided a very powerful technique for analyzing various charged inorganic,[2] organic[3] and organometallic species in solution.[4] Electrospray ionization at atmospheric pressure is a technique that makes use of an electrostatic sprayer to assist in the transfer of the ionic analytes that are initially present in solution into the gas phase.[5] In contrast to conventional ionization methods, which create undesirable fragment ions, the ESI technique usually gives simpler spectra.[6]

The on-line combination of electrochemistry with ESI-MS has been achieved in the last decade. Preparative electrochemistry, followed by ESI-MS analysis of the isolated products or products generated in situ, has been extensively explored by Bond et al.[7,8] Three other groups, those of Cole et al.,[9,10] Van Berkel et al.,[11,12] and Brajter-Toth et al.,[13] have used an electrochemical cell coupled on-line with mass spectrometry for the investigation of redox reactions.

[a] Lab Environmental Chemistry, The Casali Institute, The Institute of Chemistry, The Hebrew University of Jerusalem, Jerusalem 91904, Israel
Fax: (internat.) + 972-2/658-6155
E-mail: gunjen@pob.huji.ac.il
[b] Laboratoire de Synthèse et d'Electrosynthèse Organométalliques, Faculté des Sciences "Gabriel", Université de Bourgogne,
6 Boulevard Gabriel, 21000 Dijon, France
Fax: (internat.) + 33-3/80393720
E-mail: poli@u-bourgogne.fr

In our previous publication, which focused only on the reductive process of compound $[Cp^*_2Mo_2O_5]$,[14] we have shown how, from an analytical point of view, various operating conditions may be optimized to minimize spurious reactions in the electrospray chamber and obtain spectra that reflect compositions in solution. The previous study was carried out in an acetic acid buffered solution and most of the resulting reduction products were found to incorporate the acetate ligand. A subsequent chemical reduction study allowed the isolation and structural characterization of $[Cp^*MoO(O_2CCH_3)]_2$, which is closely related to one of the species observed by EC-ESI-MS.[15] With the goal of generating more reactive aqua species, and to reach the lower oxidation states of Mo, we have expanded the previous study to solutions containing the stronger trifluoroacetic acid, whose conjugate base has a poorer coordinating ability than does the acetate ion. To verify the electroreduction pathway of the compound $[(C_5Me_5)_2Mo_2O_5]$, we have expanded the electroreduction experiments to the previously described[16–18] Mo^V compound, $[(C_5Me_5)_2Mo_2O_4]$.

Experiments on sequential product-ion fragmentations (MS^n) by collision-induced dissociation (CID) were performed to elucidate the gas-phase degradation pathway for the starting and product compounds. In general, low-energy CID is a powerful technique because of the simplicity and reliability of performing sequential ion fragmentation MS^n experiments. Collisions between analyte ions and the helium gas, which serves as a damping buffer gas in the ion trap, are used for analyte ion fragmentations and excitations. Collision-induced decomposition produces ionic and neutral species simultaneously in the ion trap. Only the

charged species, however, can be directly identified using conventional multistage mass spectrometry. The chemical structure of the neutral species can only be hypothesized on the basis of the most-favored fragmentation mechanisms. Valuable information on the molecular structures of organic compounds has also been acquired by ESI-MS^n, but very few investigations have been conducted with organometallic compounds.[19,20]

Results and Discussion

Positive-Mode ESI-MS Spectra of the Starting Compounds

The positive-mode ESI-MS spectra of the starting compounds are shown in Figure 1, frames A and B. The inserts show the characteristic isotopic patterns of mono-, di-, and trinuclear Mo fragments. For mononuclear Mo species, the isotopic envelope consists of seven lines with two gaps located between the first and second and the sixth and seventh lines, respectively. The isotopic envelope of a dinuclear Mo ion consists of 14 peaks and has a width of 16 *m*/*z* units, while that of a trinuclear Mo species has a width of 23 *m*/*z* units. The width of the isotopic envelope is an important characteristic in our MS^n fragmentation experiments for the perfect isolation of the whole set of the molecules with the same structure. We shall refer to the various species by the value of *m*/*z* of the full isotopic pattern in the isotopic distribution and compare it to the calculated distributions[21] for the molecular assignment.

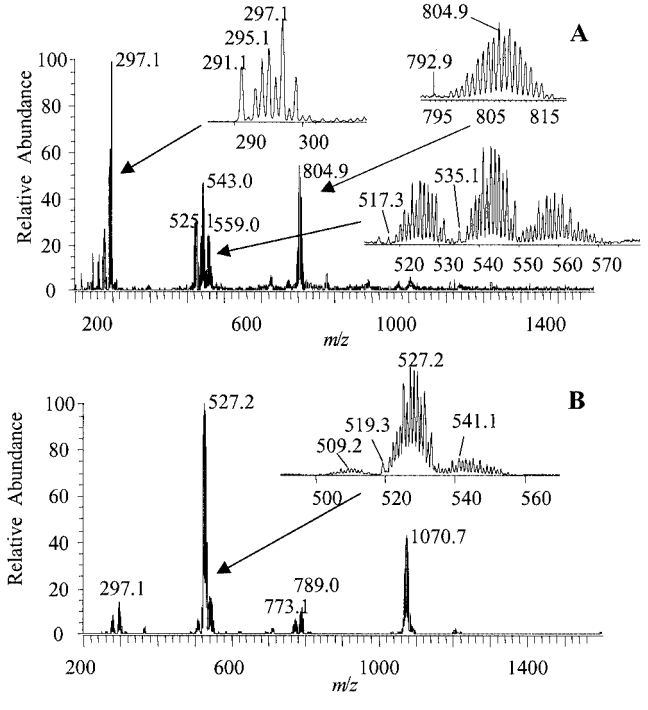

Figure 1. Positive-mode electrospray mass spectra in a mixture of 0.1 M CF_3COOH in H_2O/MeOH (1:1) (pH = 1.2) of (A) $[Cp^*_2Mo_2O_5]$ (0.1 mM) and (B) $[Cp^*_2Mo_2O_4]$ (0.1 mM)

Spectrum A was measured from a water/methanol solution of $[Cp^*_2Mo_2O_5]$ containing 0.1 M trifluoroacetic acid. It reveals three major regions of peaks, corresponding to mono-, di-, and trinuclear species, respectively. The ESI-MS spectrum of this compound in water/methanol containing 0.1 M ammonium acetate (pH = 4) has been described previously.[14] The lower pH (pH = 1.8) used in the present study changes the product distribution significantly in every region. The mononuclear region exhibits the $[Cp^*MoO_2]^+$ peak (*m*/*z* = 259−267) and the $[Cp^*MoO_3H_2]^+$ peak (*m*/*z* = 277−285) at approximately the same *relative* intensity as in the previous acetate buffer study. The strongest peak, however, corresponds to the methanol addition product, $[Cp^*MoO_2(MeOH)]^+$ (*m*/*z* = 291−299), which has only a very small intensity in the acetic buffer. The formation of adducts with solvent molecules in the ion trap is a well-known phenomenon.[22,23]

The main peak for dinuclear species corresponds to the protonated starting compound $[Cp^*_2Mo_2O_5H]^+$ (*m*/*z* = 535−551), as it was in the corresponding study in the acetic acid buffer.[14] The other most pronounced dinuclear peaks, corresponding to daughter ions formed in the ESI-MS chamber, had not been described previously, since their intensity was much lower when measured from the higher pH conditions. These dinuclear peaks increase in relative abundance with increasing temperatures of the heated capillary. The lighter set of peaks (*m*/*z* = 517−533) corresponds to the loss of one water molecule. This process must, of course, involve at least one of the Cp* methyl group's H atoms, leading to a tetramethylfulvene ligand. Therefore, the peak is assigned to complex $[Cp^*(C_4Me_4CH_2)Mo_2O_4]^+$. The methylene group of this ligand may be bonded to the molybdenum atom or to one of the oxygen atoms. The envelope at higher masses, on the other hand, results from the superposition of two envelopes, one (major) at *m*/*z* = 549−565 that is attributed to a MeOH adduct of the tetramethylfulvene complex just described, and one (minor) at *m*/*z* = 553−569 that probably results from the addition of water to the starting compound. The $[Cp^*_3Mo_3O_7]^+$ peak (*m*/*z* = 793−816) is the only relevant feature in the region of the trinuclear species.

The differences between Figure 1 and the corresponding spectrum from the experiment with the acetic acid buffer (see Figure 1 of ref.[14]) are consistent with our parallel speciation studies. We have shown that the complex $Cp^*MoO_2^+$ is the predominant species at pH < ca. 3, while a mixture of $[Cp^*MoO_2]^+$ and $[Cp^*MoO_3]^-$ {in equilibrium with $[Cp^*MoO_2(OH)]$ and $[Cp^*_2Mo_2O_5]$, depending on the H_2O/MeOH ratio} is present at a pH of ca. 4.[24] Indeed, the peaks corresponding to the dinuclear $[Cp^*_2Mo_2O_5]$ species are less abundant at the lower value of pH, while all those related to species $[Cp^*MoO_2]^+$ (mononuclear and trinuclear species) are comparatively more abundant. Indeed, the trinuclear species results from the addition of $[Cp^*MoO_2]^+$ to $[Cp^*_2Mo_2O_5]$ (vide infra).

The ESI-MS investigation of complex $[Cp^*_2Mo_2O_4]$, reported here for the first time, was carried out under the same conditions used for compound $[Cp^*_2Mo_2O_5]$, to allow comparisons to be made. The spectrum of the starting solution is shown in Frame B of Figure 1. The main peak corre-

 © 2003 Wiley-VCH Verlag GmbH & Co. KGaA, Weinheim

sponds to the protonated starting compound, $[(C_5Me_5)_2Mo_2O_4H]^+$ (m/z = 519−535), and the second-most important component (m/z = 1058−1085) is assigned to the tetranuclear $[Cp^*_4Mo_4O_6(OH)_3]^+$ complex. The latter is formally obtained by dimerization of the starting compound and addition of a water molecule and a proton. Evidence for the existence of a tetranuclear species has been provided for the corresponding Cp system.[25] The spectrum shows fewer peaks relative to that of the pentaoxo analogue. This situation can result from either a simpler composition in solution (the speciation of this compound in methanol/water is yet unknown) or from a greater gas-phase stability and, therefore, a less pronounced collision-induced decomposition. Both compounds adopt a neutral molecular structure in organic solvents.[16,26] To further explore this point, we proceeded with a detailed investigation of the gas-phase stability and MS^n fragmentation pathways of the starting compounds.

Gas-Phase Stability of the Starting Compounds

Figure 2 shows the relative abundances of the peaks of the starting compound (m/z = 535−551 for $[Cp^*_2Mo_2O_5H]^+$ and m/z = 519−535 for $[Cp^*_2Mo_2O_4H]^+$) as a function of the applied collision energy during the collision-activated decomposition events in the ion-trap mass spectrometer. Both dissociation profiles lead to S-shaped curves. The half-wave collision energy ($E_{1/2}$) corresponds to the energy (in the percentage of the maximum tickling voltage) at which the relative abundance as a fraction of the total ion current of the starting ion is 0.5.[27−30] For the same charge state (+1), the larger the value of $E_{1/2}$ the more stable is the compound in the gas phase. As it is evident from Figure 2, the value of $E_{1/2}$ of $[Cp^*_2Mo_2O_4]$ is almost twice that of $[Cp^*_2Mo_2O_5]$, which underscores the greater gas-phase stability of the former compound. This difference can be rationalized rather easily on the basis of the known structural and bonding differences between the two compounds. While the tetraoxo Mo^V complex contains a direct metal−metal bond and two oxo bridges, the pentaoxo compound contains one oxo bridge and no metal−metal interactions.

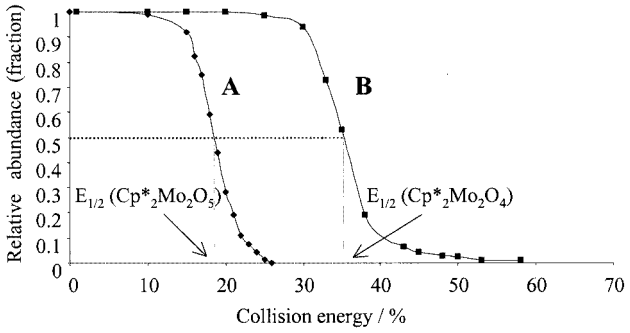

Figure 2. Dissociation profiles of the starting compounds {(A) $[Cp^*_2Mo_2O_5]$ and (B) $[Cp^*_2Mo_2O_4]$} in the same charge state as a function of increased collision energy in the ion trap; the solutions are as described in Figure 1

Fragmentation Pathways of the Starting Compounds

The dissociation profiles provided us with information about the stability of $[Cp^*_2Mo_2O_5]$ and $[Cp^*_2Mo_2O_4]$ complexes in the ion trap. An analysis of their degradation in the ion trap was carried out by their isolation therein, followed by the observation of their sequential multistep dissociations (MS^n experiments). The main results for $[Cp^*_2Mo_2O_5]$ and $[Cp^*_2Mo_2O_4]$ are shown in frames A and B of Figure 3, with the proposed fragmentation pathways in Schemes 1 and 2, respectively.

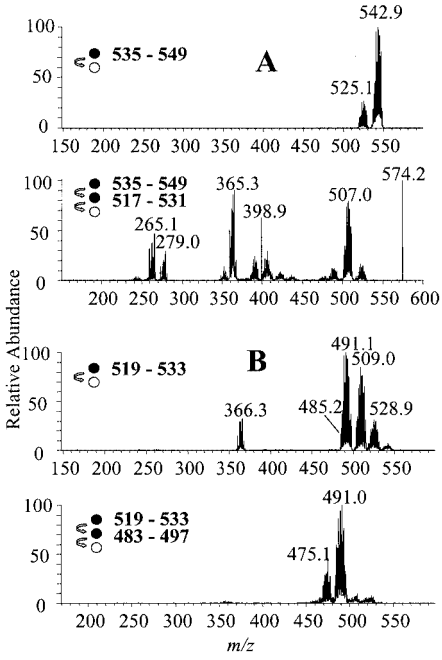

Figure 3. MS^n fragmentation pathways of compounds $[Cp^*_2Mo_2O_5]$ (A) and $[Cp^*_2Mo_2O_4]$ (B); the solutions are the same as those described in Figure 1

As concluded above from the dissociation profiles, $[Cp^*_2Mo_2O_5]$ is less stable than $[Cp^*_2Mo_2O_4]$ in the ion trap. The spectrum in Figure 3 (A) shows that the first CID step for the $[Cp^*_2Mo_2O_5H]^+$ ion generates only one daughter ion (m/z = 517−533) by loss of a water molecule. MS^3 fragmentation of this daughter ion leads to many products by further loss of water and of a neutral (fulvene)-dioxomolybdenum fragment. To the best of our knowledge, the C−H activation of a Cp* methyl group, that is associated to the elimination of a water molecule and to the transformation to a tetramethylfulvene ligand, has not been highlighted previously in an MS study. There is, however, at least one precedent in solution chemistry for compound $[\{Cp^*RuCl_2\}_2O]$.[31]

The main peaks are tentatively assigned in Scheme 1, although it is not possible to establish the particular methyl group that furnishes the hydrogen atoms. The m/z = 359−367 peak has the characteristic shape of a monomolybdenum species and is not observed at all in the regular ESI-MS. This compound would result from the elimination of a molybdic acid molecule with the abstraction of two H atoms from the Cp* methyl groups. This assignment is in

 © 2003 Wiley-VCH Verlag GmbH & Co. KGaA, Weinheim

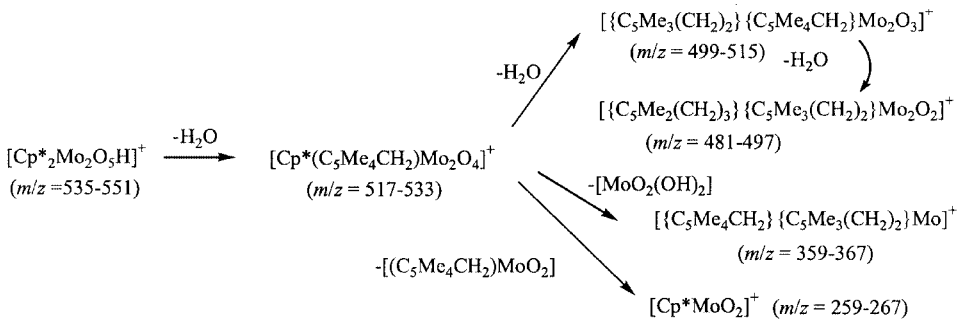

Scheme 1

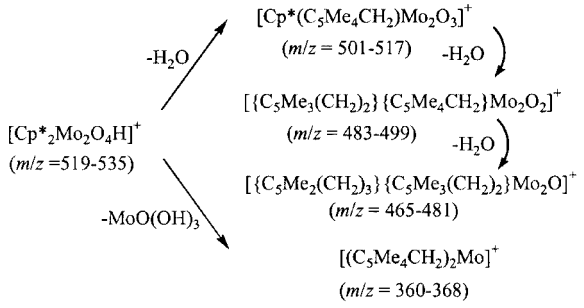

Scheme 2

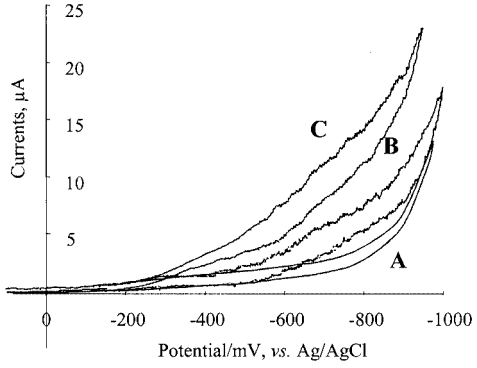

Figure 4. Cyclic voltammograms taken during the on-line combined EC/ESI-MS experiments. (a) blank solution; (b) 1.1 mM $[Cp^*_2Mo_2O_4]$; (c) 1.1 mM $[Cp^*_2Mo_2O_5]$, in H_2O/MeOH (1:1) containing CF_3COOH (0.1 M; pH = 1.2); scan rate: 0.5 mV/s

further agreement with related fragmentations of more reduced species, as will be shown later. We point out further that the exact structure of the proposed species containing two or more activated Me groups, e.g., $[(C_5Me_4CH_2)_2Mo]^+$ or $[\{C_5Me_2(CH_2)_3\}\{C_5Me_3(CH_2)_2\}Mo_2O]^+$, may implicate the formation of C−C or C−O bonds.

The CID of complex $[(C_5Me_5)_2Mo_2O_4]$ gives fewer peaks than its pentaoxo analogue. Most dinuclear peaks are related for the two compounds (16 fewer mass units corresponding to one oxygen atom). The main mononuclear peak (m/z = 360−369) is one mass unit higher than the main mononuclear peak derived from the pentaoxo solution, and, thus, the peak indicates that it is a one-electron-reduced form of it. The peak probably derives from the expulsion of a $MoO(OH)_3$ species from the parent dinuclear Mo^V complex, paralleling exactly the formation of the mononuclear species in Scheme 1.

Electrochemical Experiments

Figure 4 shows the voltammogram recorded in our flow-through electrochemical cell in parallel with the ESI-MS measurements. Curve A shows the background voltammogram, whereas curves B and C show the voltammograms of the $[Cp^*_2Mo_2O_4]$ and $[Cp^*_2Mo_2O_5]$ solutions, respectively. As the Mo concentration is identical for both solutions, any difference between curves B and C must be attributed to the difference in the oxidation state of the Mo atom in the starting compound. This assumption is supported by the volt-spectrogram of $[Cp^*_2Mo_2O_5]$ (vide infra), which clearly indicates that the electroreduction of $[Cp^*_2Mo_2O_5]$ proceeds through the formation of $[Cp^*_2Mo_2O_4]$.

The current−potential curves at the forward and backward scans are in parallel for both compounds and the heights are virtually independent of the scan rate over a rather wide range of scan rates (up to 100 $mV \cdot s^{-1}$). This observation means that the electrochemical reduction of both $[Cp^*_2Mo_2O_4]$ and $[Cp^*_2Mo_2O_5]$ is apparently controlled by an interfacial step rather than being limited by diffusion. In separate studies that are out of the scope of this paper, we have witnessed the formation of a polymer film on the electrode surface under the conditions of electroreduction. This phenomenon makes it impossible, solely on the basis of the voltammetric experiments, to elucidate the mechanisms of electroreduction of $[Cp^*_2Mo_2O_4]$ and $[Cp^*_2Mo_2O_5]$ and identify the electroreduction products.

Coupled Electrochemistry/ESI-MS Studies: Consumption of the Starting Species

The coupled EC/ESI-MS study was carried out with a slow (0.5 mV/s) linear potential sweep between 0 and −1 V, and then back again to 0 V, similar to the experiment described in our previous study.[14] Figure 5 shows the volt-spectrograms of the major mono-, di-, and trinuclear species. During the backward, anodic scan, the concentration profiles follow approximately the same pattern observed in

 © 2003 Wiley-VCH Verlag GmbH & Co. KGaA, Weinheim

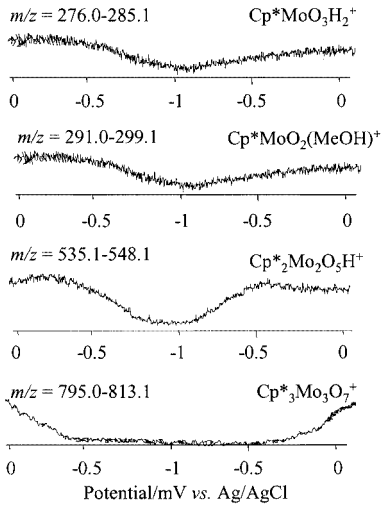

Figure 5. Dependence on potential of the relative abundance of the starting species during the coupled electrochemistry/ESI-MS of $[Cp^*_2Mo_2O_5]$; the experimental conditions are the same as those described in Figure 4

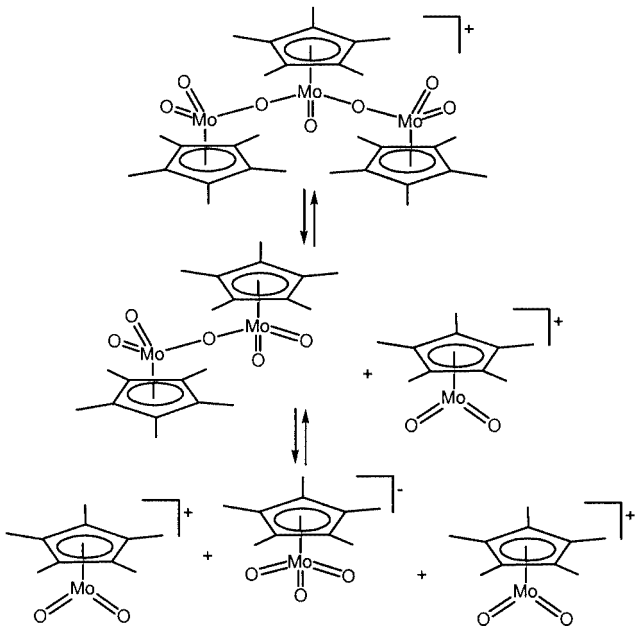

Scheme 8

the cathodic scan, indicating that the experiment is not polluted by film deposition processes.

The concentrations of both mononuclear species and of the dinuclear species start to decrease at a potential slightly less negative than $E = -0.5$ V. The trinuclear species, on the other hand, decreases in concentration much earlier, at $E \approx 0$ V, and reaches a minimum at $E = -0.5$ V. This result shows unambiguously that the trinuclear species must be present already in solution. If it had formed by a combination of $[Cp^*MoO_2^+]$ and $[Cp^*_2Mo_2O_5]$ in the spectrometer chamber only, its abundance would not decrease prior to that of either of the two other species. The reduction of the trinuclear species is thermodynamically easier than those of the mono- and dinuclear species, probably because of the metal−metal bond formation that is expected to accompany the process (vide infra). Since we have shown that a water-rich environment favors the spontaneous ionization of $[Cp^*_2Mo_2O_5]$ into $[Cp^*MoO_2]^+$ and $[Cp^*MoO_3]^-$, we propose equally that the trinuclear species is derived from the combination of $[Cp^*MoO_3^-]$ with two $[Cp^*MoO_2]^+$ ions, as shown in Scheme 3.

Electrochemical Formation of Reduced Dimer Compounds

Figure 6 shows the mass spectrum of the $[Cp^*_2Mo_2O_5]$ solution recorded at −1 V. Several new peaks, assigned to electroreduction products, are evident in this spectrum. Some of these peaks are associated with reduction products that are identical with, or related to, those observed previously under the same conditions in an acetic acid buffer (i.e., $[Cp^*_2Mo_2O_4H]^+$, $m/z = 519-535$). Other peaks, on the other hand, correspond to new species {i.e., $[Cp^*_2Mo_2(OH)(O_2CCF_3)_2]^+$, $m/z = 697-715$; $[Cp^*_2Mo_2O(OH)(O_2CF_3)_2]^+$, $m/z = 713-729$; $[Cp^*_2Mo_2O_3(O_2CCF_3)]^+$, $m/z = 615-633$}. The nature and the intensity/potential profiles of all electroreduction products obtained from the $[Cp^*_2Mo_2O_4]$ solution are identical with those derived from the pentaoxo solution. This observation indicates that all reduced products obtained from the pentaoxo solution are formed through the intermediacy of the tetraoxo complex.

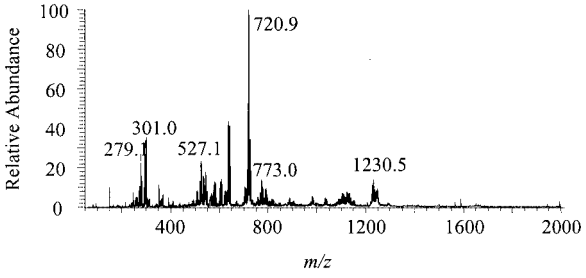

Figure 6. Positive-mode electrospray mass spectra in 0.28 mM CF_3COOH, H_2O/MeOH (1:1) (pH = 1.2) of $[Cp^*_2Mo_2O_5]$ (1.1 mM) after reduction ($E = -1$ V)

Figure 7 depicts volt-spectrograms of a few selected reduced dinuclear products, namely two $Mo^{V,V}_2$ species, $[Cp^*_2Mo_2O_4H]^+$ and $[Cp^*_2Mo_2O_3(O_2CCF_3)]^+$, a $Mo^{IV,IV}$ species, $[Cp^*_2Mo_2O(OH)(O_2CCF_3)_2]^+$, and a $Mo_2^{III,III}$ species, $[Cp^*_2Mo_2(OH)(O_2CCF_3)_2]^+$, together with their corresponding MS isotopic pattern and a tentatively assigned structure. Interestingly, the major electroreduction products observed in the current study are derived from subsequent two-electron addition processes, whereas the previous study in the acetic acid buffer also showed a dinuclear mixed-valence ($Mo^{IV,V}_2$) species. Mononuclear (acetato)Mo^V and -Mo^{IV} complexes were also evident in the previous study, but the corresponding trifluoroacetato species are not observed in the present investigation.

Another notable difference is that, whereas the observed $Mo^{V,V}_2$ products have the same stoichiometry under both

 © 2003 Wiley-VCH Verlag GmbH & Co. KGaA, Weinheim

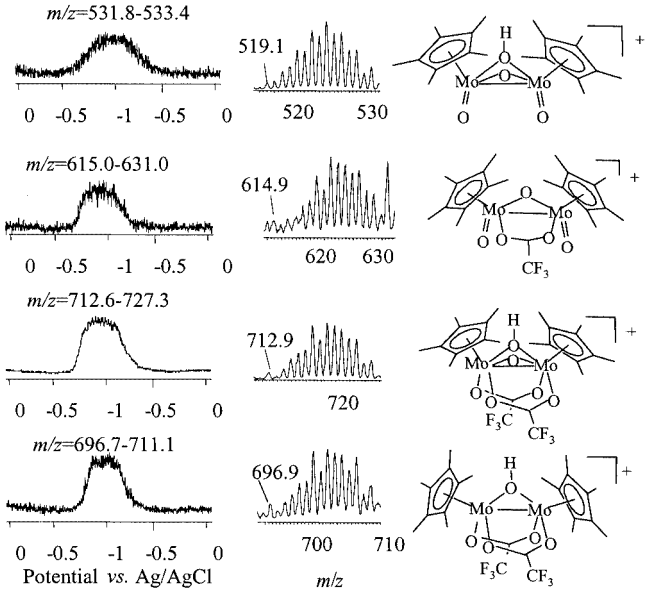

Figure 7. Dependence on potential of the relative abundance of the dinuclear species generated during the coupled electrochemistry/ESI-MS of $[Cp^*_2Mo_2O_5]$; left: volt-spectrograms with the range of *m/z* used for the integration. center: expanded isotopic pattern; right: tentative chemical structure; the experimental conditions are identical to those of Figure 5

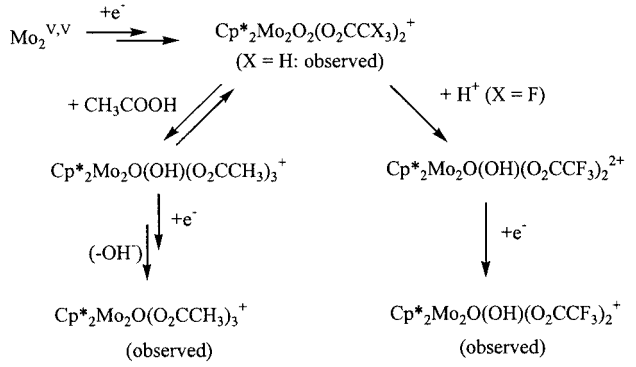

Scheme 4

conditions, the $Mo^{IV,IV}_2$ product is $[Cp^*_2Mo_2(O)(OH)(O_2CCF_3)_2]^+$ in the present study and $[Cp^*_2Mo_2O(O_2CCH_3)_3]^+$ in the previous acetate study. A peak for the corresponding $[Cp^*_2Mo_2O(O_2CCF_3)_3]^+$ ion is not observed in the present study. This result seems counterintuitive, because the stronger trifluoroacetic acid should be better suited to replace the hydroxo ligand. A possible, though somewhat speculative, interpretation relies on two fundamental differences between the two acids and the corresponding conjugate bases: while CF_3COOH is the stronger acid, CH_3COO^- is the better coordinating agent. Thus, reduction of the same $[Cp^*_2Mo_2O_3(O_2CCX_3)]^+$ ($Mo^{V,V}_2$; X = H, F) complex would lead to the same $[Cp^*_2Mo_2O_2(O_2CCX_3)_2]^+$ ($Mo^{IV,V}_2$) ion according to Scheme 4. This ion, however, would be observed only for the acetato system, because with the stronger acid (CF_3COOH) it would immediately be protonated. The CH_3COOH system could, on the other hand, lead to a triacetato species because of the stronger coordinating properties of the acetate ion. If this hypothesis holds true, each final $Mo^{IV,IV}_2$ product would be observed merely because the exchange process between hydroxide and (trifluoro)acetate, though thermodynamically favorable, is too slow under the present conditions. It is also worth mentioning that the neutral diacetato compound $[Cp^*_2Mo_2O_2(O_2CCH_3)_2]$ (i.e., a deprotonated version of the observed product for the trifluoroacetato system) has been isolated from a reductive chemical synthesis and characterized crystallographically.[15]

While electroreduction did not afford any dinuclear ions with oxidation states below IV when carried out in an acetic acid buffer, it also provides a $Mo^{III,III}_2$ complex in the presence of trifluoroacetic acid. This difference may again be attributed to the stronger acidity of CF_3COOH, which favors protonation of the oxo ligands and their elimination as water molecules.

The following approximate potential values for the appearance of every reduced dinuclear species may be measured on the volt-spectrograms in Figure 7: $[Cp^*_2Mo_2O_4H]^+$ ($Mo^{V,V}_2$), −0.55 V; $[Cp^*_2Mo_2O_3(O_2CCF_3)]^+$ ($Mo^{V,V}_2$), −0.60 V; $[Cp^*_2Mo_2(O)(OH)(O_2CCF_3)_2]^+$ ($Mo^{IV,IV}_2$), −0.68 V; $[Cp^*_2Mo_2O(O_2CCF_3)_2]^+$ ($Mo^{III,III}_2$), −0.76 V. A comparison of the onset reduction potentials with those observed in the previous acetate study is useful. The $[Cp^*_2Mo_2O_4H]^+$ product is not acid dependent. In both studies, the onset of this peak is at approximately the same potential as the onset for the $[Cp^*_2Mo_2O_5H]^+$ consumption and the two numerical values are quite similar (these numbers may be measured only with limited precision). The $[Cp^*_2Mo_2O_3(O_2CCF_3)]^+$ $Mo^{V,V}_2$ species starts to form at a more negative potential relative to the acetato analogue (−0.55 V). Further reduction to the $Mo^{IV,IV}_2$ species seems easier for the trifluoroacetato system, which is in agreement with expectations [cf. reduction at −0.74 and −0.78 V for the (acetato)$Mo^{IV,V}_2$ and -$Mo^{IV,IV}_2$ products, respectively]. Furthermore, reduction to the $Mo^{III,III}_2$ product starts at an even lower potential, while this process is not observed for the acetato system, as mentioned above.

Structural Elucidation of the Product at *m/z* = 713−729

The main product of the electroreductions of both $[Cp^*_2Mo_2O_5]$ and $[Cp^*_2Mo_2O_4]$, namely the $Mo^{IV,IV}_2$ ion interpreted as $[Cp^*_2Mo_2O(OH)(O_2CCF_3)_2]^+$, was the subject of more detailed MS^n studies. There are two reasons for choosing to study this product. First, we wanted to prove the general approach of our product identification. Second, we wanted to check whether any observed peaks are, in fact, attributable to daughter ions of this major peak, rather than to primary products of the electrochemical reduction.

Figure 8 shows the main results of the MS^n experiment. The spectrum shown in part A is produced from the isolation of the species at *m/z* = 713−729 and subsequent CID. There are four main daughter-ion products, the main

 © 2003 Wiley-VCH Verlag GmbH & Co. KGaA, Weinheim

one being that with m/z = 599−615. In fact, the lighter products increase in subsequent MS^n experiments, while the heavier one (32 mass units higher) is obviously the solvent (methanol) adduct formed by gas-phase reactions in the ion trap.[28] This assignment is further supported by the next MS^n step. The product ion at m/z = 599−615 was isolated and subjected consequently to further collision activation (MS^3), giving the spectrum shown in Figure 8 (B). The further generation of the peak at m/z = 634−650 can be understood easily in terms of the formation of the solvent adduct. Additional fragmentation by CID (MS^4) of the product ion with m/z = 502−518 results in one main product with m/z = 485−501 and a mononuclear peak with m/z = 361−369 [see Figure 8 (C)].

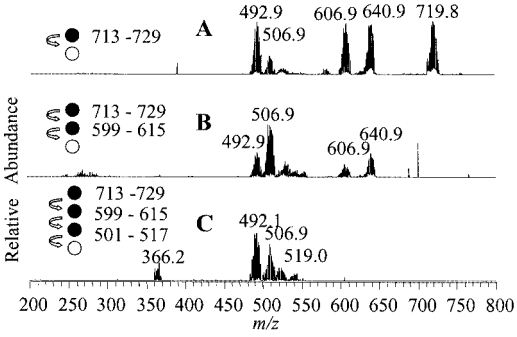

Figure 8. Structural elucidation by MS^n of the main product (m/z = 713−729) of the reduction of $[Cp^*_2Mo_2O_5]$ and $[Cp^*_2Mo_2O_4]$

The proposed product ion compositions and fragmentation pathways are shown in Scheme 5. The first fragment (m/z = 599−615) results from the loss of 114 units, which corresponds to the molecular weight of trifluoroacetic acid. Therefore, this fragment is still a dinuclear compound of Mo^{IV}. Under the conditions of the experiment (CID = 30% for every MS^n step), the next step of the fragmentation results in a prominent peak with the loss of 97 units, corresponding to a trifluoroacetyl group, and a minor peak with the loss of an additional 17 units (OH). The latter peak becomes the prominent one in the MS^4. Loss of the acetyl group results in a formal oxidation to a mixed-valence $Mo^{IV,V}_2$ ion that is not observed under the electroreduction conditions, whereas the subsequent loss of OH reforms a $Mo^{IV,IV}_2$ ion. The OH and MoO_2(OH) expulsion processes must involve one of the Cp* methyl group protons to yield a tetramethylfulvene ligand, as already observed above for the CID of the starting complexes. It is quite interesting to observe that, for the three fragmentation processes leading from dinuclear to mononuclear species with loss of a neutral inorganic Mo complex, the latter always corresponds to an oxide/hydroxide in the highest possible oxidation state; i.e., Mo^{VI} from $Mo^{VI,VI}_2$ (Scheme 1), Mo^{V} from $Mo^{V,V}_2$ (Scheme 2), and Mo^{V} from $Mo^{IV,V}_2$ (Scheme 5).

We conclude from Scheme 5 that the fragmentation pathway undertaken by the compound at m/z = 713−729 is similar to that of the starting compounds. It is noteworthy that the peaks at m/z = 485 and 361, generated by MS^4, are related to the fragments obtained from the Mo^{VI} precursor [m/z = 481 and 359, see Figure 3 (A)] and to those obtained from the Mo^{V} precursor [m/z = 483 and 360, see Figure 3 (B)]. Therefore, these mass values further support the notion that the ion at m/z = 713−729 corresponds to a $Mo^{IV,IV}_2$ complex.

Electrochemical Formation of Reduced Trinuclear Species

As can be seen by comparing Figures 1 and 6 there are prominent spectral changes in the trinuclear m/z region following the electrochemical reduction. Volt-spectrograms of the reduced trinuclear compounds are presented in Figure 9. Because of overlap between the isotopic envelopes of different trinuclear species, the volt-spectrogram integrations were carried out over limited ranges of m/z rather than over the entire envelope. The ranges used for the integrations are marked in the figure. As for the previous study with the acetic acid buffer, the envelope of the reduced trinuclear species is shifted by exactly 16 units to a lower value of m/z relative to its precursor complex $[Cp^*_3Mo_3O_7]^+$, suggesting its formulation is that of a proton-free hexaoxo species. In contrast to the previous study with the acetic acid buffer, on the other hand, further reduction occurs with successive steps of oxygen atom removal, resulting in the observation of $[Cp^*_3Mo_3O_6]^+$ ($Mo^{V,V,VI}_3$), $[Cp^*_3Mo_3O_5]^+$ ($Mo^{IV,V,V}_3$), and $[Cp^*_3Mo_3O_4]^+$ ($Mo^{IV,IV,IV}_3$). Once again, this behavior can be attributed to the stronger acidity of CF_3COOH. As for the dinuclear products discussed above, the formation of the trinuclear species in trifluoroacetic acid takes place through two-electron-transfer steps and the reduction potential becomes more negative as the oxidation state decreases. The onset potential values for the various reduced species, as measured from the volt-spectrograms in Figure 9 are, in order of decreasing number of oxygen atoms, −0.54, −0.61, and −0.75 V, repectively.

The structures assigned to various reduced species are only tentative and are drawn on the basis of the maximum symmetry principle. A $[(Cp^*Mo)_3(\mu\text{-}O)_6]$ core has been shown to exist in complex $[(Cp^*Mo)_3(\mu_2\text{-}OH)_n(\mu_2\text{-}O)_{6-n}]^{2+}$ (the value of n, probably 5, was not clearly established in the X-ray study)[32] and in related $[Cp^*_4Mo_5O_{11}]$ and $[Cp^*_6Mo_8O_{16}]$ clusters.[32,33] The oxidation state in these Mo_3O_6 cores, however, is lower ($Mo_3{}^{11+}-Mo_3{}^{14+}$). The dicapped $Mo_3(\mu_3\text{-}O)_2(\mu_2\text{-}O)_3$ unit is quite common in inorganic clusters, but has not been found as yet, to the best of our knowledge, for Cp*-substituted triangular clusters of any metal. Finally, the monocapped $Mo(\mu_3\text{-}O)(\mu_2\text{-}O)_3$ unit is also common for inorganic clusters. The first documented example containing half-sandwiched metal atoms comes from our own recent study of the chemical reduction of $[Cp^*_2Mo_2O_5]$ by zinc in methanol/water containing CF_3COOH.[34] The isolated compound contains the $[(Cp^*Mo)_3(\mu_3\text{-}O)(\mu_2\text{-}O)_3(\mu_2\text{-}O_2CCF_3)_3]^+$ ion, corresponding to a $Mo^{V,V,V}_3$ species.

No trinuclear species containing trifluoroacetate groups was detected in the present study, suggesting that this weakly coordinating anion has a high tendency to remain

 © 2003 Wiley-VCH Verlag GmbH & Co. KGaA, Weinheim

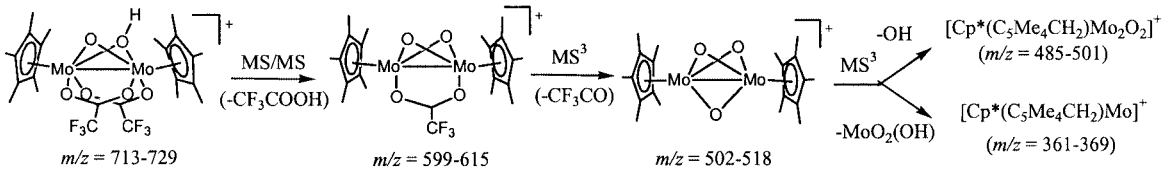

Scheme 5

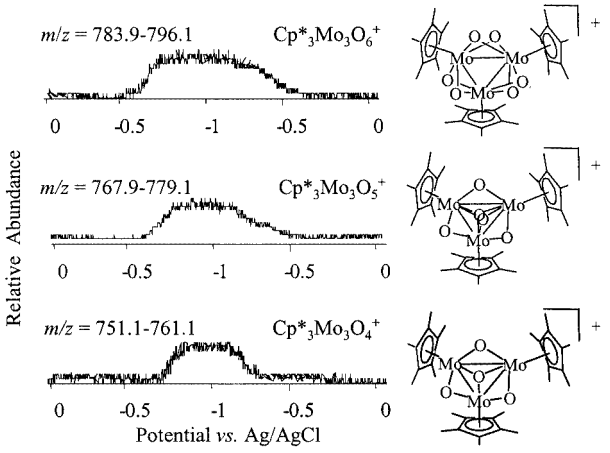

Figure 9. Volt-spectrograms of trimeric species generated during the coupled electrochemistry/ESI-MS of $[Cp^*_2Mo_2O_5]$, including the range of *m*/*z* used for the integration and the chemical formula; the experimental conditions are the same as those in Figure 4

dissociated in the highly dielectric aqueous medium. The isolation of the $[(Cp^*Mo)_3O_4(O_2CCF_3)_3]^+$ ion mentioned above, on the other hand, suggests the existence of a transient $[(Cp^*Mo)_3O_4]^{4+}$ species. Therefore, it is quite likely that a much wider variety of $[(Cp^*Mo)_3O_n]^{m+}$ derivatives may be isolated under different conditions of pH, solvent, and counterion. It is also likely that these complexes display very rich redox chemistry. Further synthetic studies are currently ongoing to test these hypotheses and to test the electrofunctionalization of organic substrates for possible catalytic applications.

Conclusion

The present study has provided new information on the nature of the $[Cp^*_2Mo_2O_5]$ in an aqueous medium and on electrochemical versatility of Cp*Mo species in water. Selected molecular structure assignments from values of *m*/*z* and isotopic distributions for Cp^*Mo^V and Cp^*Mo^{IV} reduction products where confirmed by MS^n fragmentation experiments in comparison with those of the Cp^*Mo^{VI} precursor. The study has shown that the lower pH conditions established by CF_3COOH provide access to a Cp^*Mo^{III} species, while reduction under acetic acid conditions went down as far as the oxidation state IV. The study has confirmed the robustness of the Cp*−Mo bond under aqueous conditions. Even at very low pH, there is no sign of the formation of species deriving from protonolysis of this bond. This feature, together with the proven rich redox chemistry of the system, holds promise for potential electrocatalytic applications in an aqueous environment.

Experimental Section

General Remarks: The starting compounds, $[(C_5Me_5)_2Mo_2O_5]$ and $[(C_5Me_5)_2Mo_2O_4]$, were prepared according to the literature procedure.[18] Unless otherwise stated, all solutions of test compounds were prepared in H_2O/MeOH mixture (1:1 by volume) containing 0.1 M CF_3COOH. CF_3COOH was purchased from Aldrich. HPLC-grade methanol was purchased from Baker. The water was triply distilled.

Electrospray Mass Spectrometry with an Ion Trap: A Finnigan (San Jose, USA) LCQ quadrupole ion-trap mass spectrometer equipped with an electrospray-ionization (ESI) interface was used for data acquisition. The ESI was operated in the positive-ion mode with a spray voltage of 4.5 kV, a capillary voltage of 3.5 V, and a source temperature of 120 °C. Mass spectra were obtained by scanning the mass analyzer from *m*/*z* = 100−2000 with a total of 5 microscans. The maximum injection time into the ion trap was 50 ms. The analyzer was operated at a background pressure of $2\cdot10^{-5}$ Torr. In all experiments, helium was introduced at an estimated pressure of 1 mTorr to improve the ion-trapping efficiency. The background helium also served as a collision gas during collision-activated decomposition events. The compounds were isolated in the ion trap with isolation width of 15 *m*/*z* units and were activated by using increased collision energy to obtain collision-energy-dissociation profiles.

Coupled Electrochemistry/Electrospray Mass Spectrometry: The electrochemical part of the experimental setup consisted of a PARC 273 potentiostat/galvanostat (Princeton, USA), connected to a specially designed flow-through electrochemical cell that has been described and characterized elsewhere.[35] The schematic of the electrochemical flow cell is shown in Figure 10. The working glassy-carbon-disk electrode (1) (Metrohm, Herisau, Switzerland), is placed on the bottom of the cell. Compartments of counter (2) and reference (3) electrodes were separated from the main flow of electrolyte by filters (Upchurch Scientific, Oak Harbor, WA, USA). Both electrodes were Ag/AgCl/1 M KCl. All reported potentials are given relative to the reference electrode. The analyte stream arrives on the working electrode surface through the outer tube (4) of the two coaxial system and the products of the electrode reaction are transferred to the mass spectrometer through the inner tube (5). The distance between the opening of the coaxial system and the working electrode was 50 μm. All tubes were from PEEK (Upchurch Scientific, Oak Harbor, WA, USA). The inner tube has an inner diameter of 125 μm, an outer diameter of 1.6 mm, and is 15 cm long. The flow of the solution was driven by a syringe pump.

 © 2003 Wiley-VCH Verlag GmbH & Co. KGaA, Weinheim

The product stream was diluted with excess methanol. After mixing with methanol, the sample stream was delivered to the ESI interface by tubing that is 30 cm long, and has an inner diameter of 125 μm. The flow rate of the product stream was ca. 35 $\mu L \cdot min^{-1}$. The methanol flow in the auxiliary tubing was 30 $\mu L \cdot min^{-1}$. The reagent flow rate was set to 5 $\mu L \cdot min^{-1}$. The current cell design permitted us to measure mass spectra and linear sweep voltammograms simultaneously.

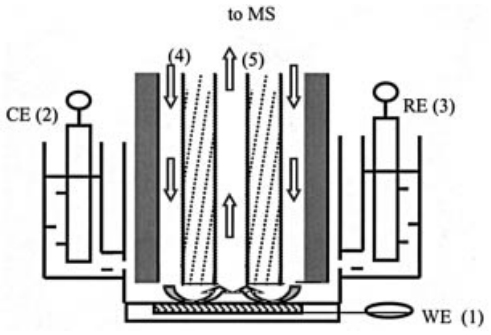

Figure 10. Scheme of the electrochemical cell used in this study: 1: working electrode (WE); 2: counter electrode (CE); 3: reference electrode (RE); 4: outer capillary (transfer line of reagents to working electrode); 5: inner capillary (transfer line of products to the ESI/MS)

Acknowledgments

R. P. thanks the CNRS and the Ministry of Research for funding. A. D. M. and O. L. acknowledge the financial support of the Israel Science Foundation. We are grateful to the French Embassy in Israel for an Arc-en-Ciel/Keshet travel grant and to Prof. M. Vorotyntsev for helpful discussion. We thank a reviewer for very useful comments.

[1] M. Yamashita, J. B. Fenn, *J. Phys. Chem.* **1984**, *88*, 4451−4459.
[2] I. I. Stewart, *Spectrochim. Acta, Part B* **1999**, *54*, 1649−1695.
[3] X. W. Wei, Z. Xu, *Chin, J. Org. Chem.* **1999**, *19*, 97−103.
[4] J. C. Traeger, *Int. J. Mass Spectr.* **2000**, *200*, 387−401.
[5] M. L. Vestal, *Mass Spectrom. Rev.* **1983**, *2*, 447−480.
[6] W. F. Smyth, *Trac-Trends Anal. Chem.* **1999**, *18*, 335−346.
[7] G. Wolfbauer, A. M. Bond, D. R. MacFarlane, *J. Chem. Soc., Dalton Trans.* **1999**, 4363−4372.
[8] A. M. Bond, R. Colton, D. G. Humphrey, P. J. Mahon, G. A. Snook, V. Tedesco, J. N. Walter, *Organometallics* **1998**, *17*, 2977−2985.
[9] X. Xu, W. Lu, R. B. Cole, *Anal. Chem.* **1996**, *68*, 4244−4253.
[10] W. Lu, X. Xu, R. B. Cole, *Anal. Chem.* **1997**, *69*, 2478−2484.
[11] F. Zhou, G. J. Van Berkel, *Anal. Chem.* **1995**, *67*, 3643−3649.
[12] H. Deng, G. J. Van Berkel, *Anal. Chem.* **1999**, *71*, 4284−4293.
[13] M. C. S. Regino, A. BrajterToth, *Electroanalysis* **1999**, *11*, 374−379.
[14] J. Gun, A. Modestov, O. Lev, D. Saurenz, M. A. Vorotyntsev, R. Poli, *Eur. J. Inorg. Chem.*, **2003**, 482−492.
[15] F. Demirhan, P. Richard, R. Poli, *Inorg. Chim. Acta*, in press.
[16] H. Arzoumanian, A. Baldy, M. Pierrot, M. Petrignani, *J. Organomet. Chem.* **1985**, *294*, 327−331.
[17] E. de Jesus, A. Vazquez de Miguel, P. Royo, A. M. M. Lanfredi, A. Tiripicchio, *J. Chem. Soc., Dalton Trans.* **1990**, 2779−2784.
[18] D. Saurenz, F. Demirhan, P. Richard, R. Poli, H. Sitzmann, *Eur. J. Inorg. Chem.* **2002**, 1415−1424.
[19] E. J. Alvarez, V. H. Vartanian, J. S. Brodbelt, *Anal. Chem.* **1997**, *69*, 1147−1155.
[20] M. J. Van Stipdonk, M. P. Ince, B. A. Perera, J. A. Martin, *Rapid Commun. Mass Spectr.* **2002**, *16*, 355−363.
[21] A. J. Gordon, R. A. Ford, *The Chemist's Companion. Handbook of Practical Data, Techniques and References*, J. Wiley and Sons, New York, **1983**.
[22] W. C. Byrdwell, W. E. Neff, *Rapid Commun. Mass Spectr.* **2002**, *16*, 300−319.
[23] A. K. Vrkic, R. A. J. O'Hair, *Int. J. Mass Spectr.* **2002**, *218*, 131−160.
[24] E. Collange, J. Garcia, R. Poli, *New J. Chem.* **2002**, *26*, 1249−1256.
[25] M. Cousins, M. L. H. Green, *J. Chem. Soc. A* **1969**, 16−19.
[26] A. L. Rheingold, J. R. Harper, *J. Organomet. Chem.* **1991**, *403*, 335−344.
[27] V. F. DeTuri, K. M. Ervin, *J. Phys. Chem. A* **1999**, *103*, 6911−6920.
[28] E. R. Talaty, B. A. Perera, A. L. Gallardo, J. M. Barr, M. J. Van Stipdonk, *J. Phys. Chem. A* **2001**, *105*, 8059−8068.
[29] K. X. Wan, M. L. Gross, T. Shibue, *J. Am. Soc., Mass Spec.* **2000**, *11*, 450−457.
[30] J. F. Gal, P. C. Maria, E. D. Raczynska, *J. Mass Spectrom.* **2001**, *36*, 699−716.
[31] L. Fan, M. L. Turner, M. B. Hursthouse, K. M. A. Malik, O. V. Gusev, P. M. Maitlis, *J. Am. Chem. Soc.* **1994**, *116*, 385−386.
[32] F. Bottomley, J. Chen, K. F. Preston, R. C. Thompson, *J. Am. Chem. Soc.* **1994**, *116*, 7989−7995.
[33] J. R. Harper, A. L. Rheingold, *J. Am. Chem. Soc.* **1990**, *112*, 4037−4038.
[34] F. Demirhan, J. Gun, O. Lev, A. Modestov, R. Poli, P. Richard, *J. Chem. Soc., Dalton Trans.* **2002**, 2109−2111.
[35] A. Modestov, J. Gun, O. Lev, manuscript in preparation.

Received November 16, 2002

 © 2003 Wiley-VCH Verlag GmbH & Co. KGaA, Weinheim

Magnetic, ^{57}Fe Mössbauer, and IR Monitoring of the Thermal Spin Transition in a New Family of Iron(II) Spin-Transition Complexes

Arno F. Stassen,[a] Matthias Grunert,[b] Eva Dova,[c] Martin Müller,[d] Peter Weinberger,[d] Günter Wiesinger,[d] Henk Schenk,[c] Wolfgang Linert,[b] Jaap G. Haasnoot,*[a] and Jan Reedijk[a]

Keywords: Spin crossover / Iron / Tetrazole ligand / Mössbauer spectroscopy / Variable-temperature IR spectroscopy

A new family of iron(II) tetrafluoroborate and perchlorate spin-crossover compounds has been synthesised and is discussed. The iron(II) ion is surrounded by six 1-ethyltetrazole ligands, which are halogen-substituted on the C2 atom of the ethyl group. The spin-crossover temperatures $T_{1/2}$ are high compared to the unsubstituted (1-alkyltetrazole)iron(II) complexes. The shape of the spin-transition curve (i.e. γ_{HS} vs. T) varies largely over the different complexes and appears to be influenced neither by the crystal packing, nor by the electronic effects. The temperature-dependent spin-transition behaviour has been studied by magnetic susceptibility and by ^{57}Fe-Mössbauer spectroscopy. These data have been supported by temperature-dependent mid-range infrared spectroscopy: the thermally induced spin transition has been observed by direct monitoring of the aromatic C–H stretching frequency.
(© Wiley-VCH Verlag GmbH & Co. KGaA, 69451 Weinheim, Germany, 2003)

Introduction

Among compounds featuring temperature-dependent spin transitions, the [Fe(1-alkyltetrazole)$_6$](anion)$_2$ compounds are probably the most studied complexes.[1−4] Methyl-, ethyl-, propyl- and isopropyltetrazole (*mtz*, *etz*, *ptz* and *iptz*) were used as ligands for iron(II) spin-crossover complexes[2] as early as 1982 by Franke et al. These complexes are special for several reasons, they were the first reported members of a family of spin-crossover complexes with monodentate ligands showing a strong cooperativity,[5] which led to the development of the model of the elastic interactions.[6] The synthesis of both the ligands and the complexes is straightforward and these iron(II) complexes are very stable compared to other iron(II) spin-crossover complexes. Finally, the spin-crossover behaviour among these four almost identical complexes differs strongly: the spin transition depends both on the ligand,[2] and the anion.[1,2,7]

Recently, the spin-crossover behaviour of a series of iron(II) complexes containing the new ligand 1-(2-chloroethyl)tetrazole (*teec*) was published.[8] These complexes show, depending on the anion and applied synthetic method, a wide variety of magnetic behaviour including transitions in two steps, residues of high-spin species at low temperature and a thermal hysteresis effect.

In order to study the influence of the size of the halogen atom in the 1-(2-haloethyl)tetrazole spin-crossover complexes, now also the fluorine- (*teef*), bromine- (*teeb*) and iodine-substituted (*teei*) ligands have also been synthesised. From donor-number calculations[9] and NMR spectroscopy[10] it is known that the electronic influence of the halogen atom on the electron density of the tetrazole ring is negligible. Therefore, the changes in ligand-field strength (and subsequently differences in spin-transition temperature $T_{1/2}$) should almost completely be caused by the crystal packing and not by electronic effects.

The ligands *teef*, *teeb* and *teei* have been used to synthesise iron(II) tetrafluoroborate and perchlorate complexes. The magnetic and spectral properties of these complexes have been studied to observe the influence of the ligand size on the thermal spin transition. Because of the potential explosive nature of perchlorate compounds, no Mössbauer or infrared measurements have been performed on the perchlorate complexes.

[a] Leiden Institute of Chemistry, Gorlaeus Laboratories, Leiden University,
P. O. Box 9502, 2300 RA Leiden, The Netherlands
Fax: (internat.) + 31-71/527-4671
E-mail: haasnoot@chem.leidenuniv.nl
[b] Institute of Applied Synthetic Chemistry, Vienna University of Technology,
Getreidemarkt 9/163-AC, 1060 Vienna, Austria
[c] Institute of Molecular Chemistry, Laboratory of Crystallography, Universiteit van Amsterdam,
Nieuwe Achtergracht 166, 1018WV Amsterdam, The Netherlands
[d] Institute of Solid State Physics, Vienna University of Technology,
Hauptstrasse 8-10/131, 1040 Vienna, Austria

Results and Discussion

IR Spectroscopy of the Ligands

Mid-range FT-IR spectra of the undiluted complexes, and the ligands as KBr pellets have been recorded within the range of 4400−450 cm^{-1} at room temperature. For the interpretation of the spectra the observed data were compared with general tables in the compilation of Hesse et al.,[11] several publications of analogous tetrazole compounds,[12−20] as well as with the spectra of the starting products. One of the most prominent absorption features for the tetrazole ring is detected around 3140 cm^{-1} (stretching vibration ν_{C-H} at the tetrazole ring[12−14]). At about 1485 cm^{-1} the $\nu_{N2=N3}$ stretching vibration[15,16] appears, which also influences the $\nu_{N1=C5}$ as well as the $\nu_{N1=Calkyl}$ stretching vibration. The shifts of most of the bands of the tetrazole ring, caused by substitution of different halogen atoms, are not significant. An exception is the band which shifts due to a heavier halogen substituent from 1107 to 1096 cm^{-1} and belongs to the ν_{C5-N1} stretching vibration,[14] as well as the in-plane deformation of the C5−H1 bond (δ_{C5-H1}). An in-plane ring vibration[13,14] (δ_{ring2}) shifts in the same manner from 963 to 900 cm^{-1}. In the aliphatic part this trend can only be observed for the $\nu_{N1-Calkyl}$[11] stretching band (shift between 1363 and 1353 cm^{-1}) and for the deformation of the C−H2 bonds[11] (δ_{C-H2}). Table 1 gives an overview of the changes upon coordination, and lists other important IR bands.

IR Spectroscopy of the Complexes

In the iron(II) tetrafluoroborate complexes, two deformation vibrations[21] (δ_{B-F}) belonging to the tetrafluoroborate are identified. The only clearly visible, non-overlapping, deformation vibrations are at 533 and 522 cm^{-1} in the case of *teef*, *teec* and *teeb*, whereas in the compound with *teei* as ligand, a band at 515 cm^{-1} with a shoulder at 522 cm^{-1} appears. The B−F stretching vibration (ν_{B-F}) is responsible for the broad background between 1600 and 800 cm^{-1}. The maximum is located at about 1060 cm^{-1}.

Vibrations in the spectra measured at room temperature for the pure ligands and the iron(II) tetrafluoroborate complexes show differences of about −3 and +70 cm^{-1}, respectively. Interestingly, these shifts show different sensitivity: shifts of the aromatic and aliphatic C−H stretching differ between pure ligand and complex, e.g. ν_{C5-H} (between +1 and +9 cm^{-1}), δ_{C-H2} (between 0 and +19 cm^{-1}) and the broad aromatic overtone band (+33 to +67cm^{-1}). No strong influence is observed on these bands due to the variation of the halogen substituent. However, the bands associated with the tetrazole ring vibrations are influenced by the halogen substituent. With increasing halogen mass, the difference in frequency between the bands observed in the pure ligand and the iron(II) complex containing this ligand increases. The stretching vibration $\nu_{N2=N3}$ shifts upon coordination by +16 cm^{-1} for the fluorine-substituted compound, +17 cm^{-1} for the chlorine-, +26 cm^{-1} for the bromine- and +27 cm^{-1} for the iodine-substituted com-

Table 1. Prominent mid IR bands of the (haloethyl)tetrazole ligands investigated; wavenumbers in cm^{-1}; ν = stretching, δ = deformation or in-plane vibration of the ring, γ out-of-plane

Compound	teef	teec	teeb	teei
ν(C−H)[12−14]	3138 s	3142 s	3136 s	3142 s
ν(C−H2)[11]	3003 w	3031 m	3040 m	3027 m
	2972 m	3009 w	3005 m	2999 w
	2909 w	2974 m	2976 m	2961 w
		2908 m	2952 w	
Aromatic overtone band	1750 w	1743 m	1739 m	1757 m
	1723 w			
ν(N2=N3)[13−16] {+ν(C5−N1) + ν(C_{alkyl}−N1)}	1487 s	1486 s	1481 s	1485 s
δ(C−H2)[11]	1429 m	1435 m	1432 m	1443 m
	1434 m	1423 m	1419 m	1425 m
ν(N1-C_{alkyl})[11]	1363 m	1358 m	1355 m	1353 m
ν(C−F)[11,17,18]	1263 m			
δ(ring1)[12−14]	1246 m	1255 m	1265 s	1263 m
ν(C=N4), ν(N1−N2)[14]	1174 vs	1176 vs	1174 vs	1172 vs
ν(C5−N1), δ(C5−H)[14]	1107 s	1101 s	1098 s	1096 s
ν(N3−N4)[12−14]	1041 s	1041 m	1033 m	1042 w
ν(N1−N2)[14]	973 sh	971 s	968 s	970 s
δ(ring2)[13,14] in-plane bending {δ(NCN)}	963 m	947 m	930 m	900 m
γ(H_2C-CH_2)	878 sh	914 s	892 s	887 sh
	858 s	875 s	872 s	881 s
γ(ring3)[13,14] out-of-plane	722 m	721 m	720 m	717 w
γ(ring4)[13,14] out-of-plane	679 s	677 s	673 vs	660 vs
		667 vs		
ν(C−Cl)[18]		461 s		

 © 2003 Wiley-VCH Verlag GmbH & Co. KGaA, Weinheim

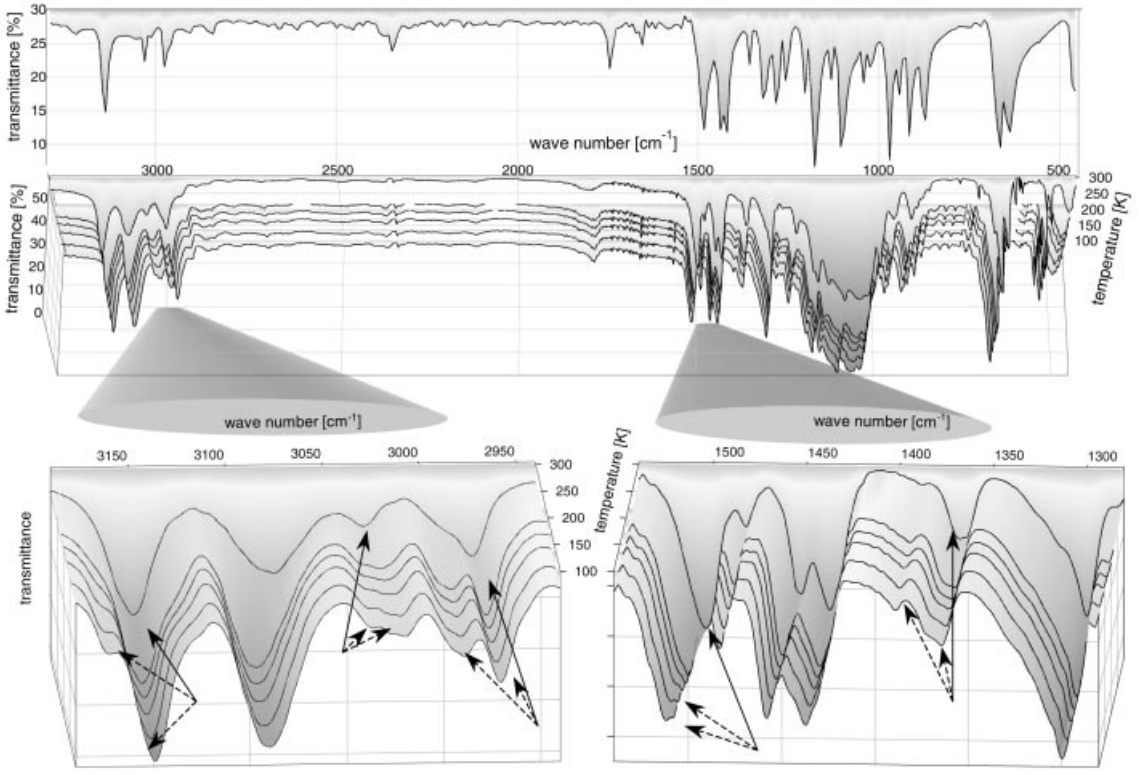

Figure 1. Comparison of the ligand (*teec*) top, with its iron(II) tetrafluoroborate complex, measured at different temperatures between 301 and 100 K (centre); the arrows mark changes of bands in the HS (solid) to a mixed HS−LS state (dashed)

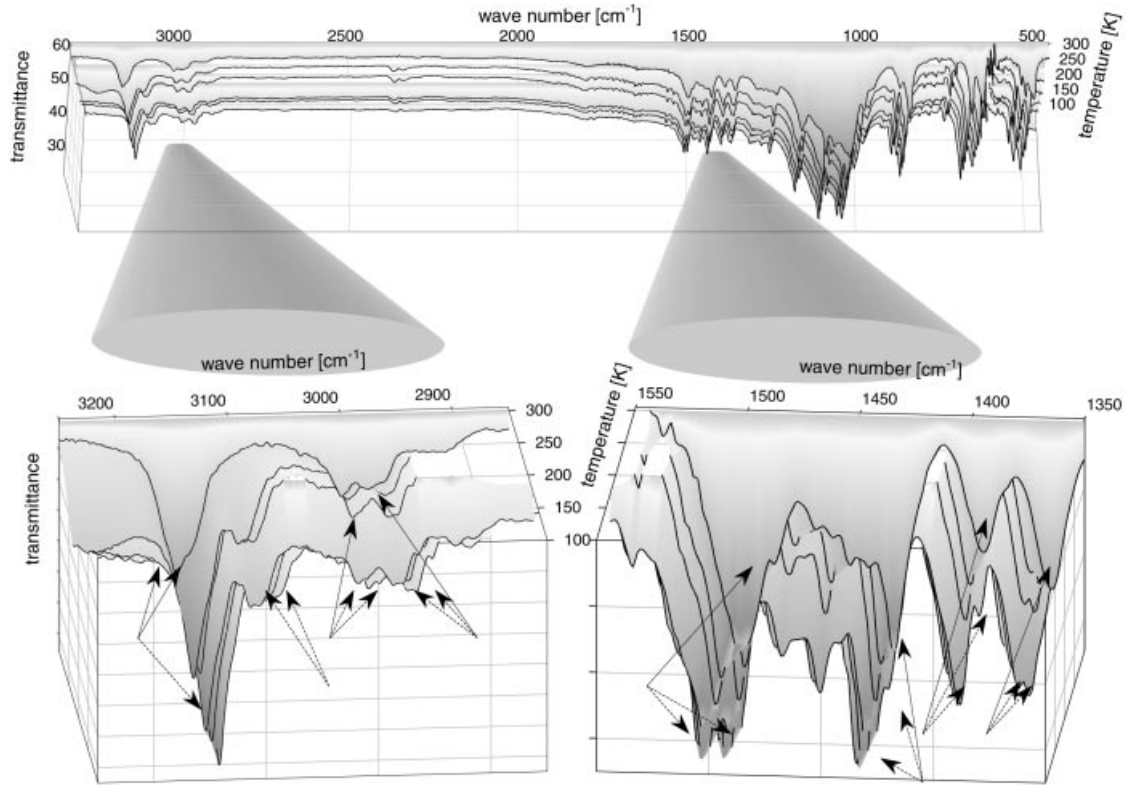

Figure 2. Temperature-dependent infrared spectroscopy of $[Fe(teef)_6](BF_4)_2$; the arrows mark changes of bands in the HS (solid) to a mixed HS−LS state (dashed)

 © 2003 Wiley-VCH Verlag GmbH & Co. KGaA, Weinheim

pound. The asymmetric out-of-plane ring vibrations around 650 cm^{-1} are not significantly influenced at all. Figure 1 provides an illustration of the changes in the mid-range IR spectrum of the *teec* ligand compared to its iron(II) tetrafluoroborate complex at room temperature in the high-spin state and at 100 K in the low-spin state.

Due to the change of the spin state of iron(II) from LS to HS, the anti-bonding e_g-orbitals are populated, thus weakening the Fe−N4 bond. This weakening results in a bond-length expansion[20] of about 5−10%. The expansion can be detected as a shift in the far-infrared region, as has been shown in a similar case.[19] The structural changes around the iron centre also influence bond strengths in the ligand. The stretching vibrations in the tetrazole ring ($\nu_{N2=N3}$) and the C5−H stretching vibration of the tetrazole hydrogen atom (which is located close to the metal centre) are mostly influenced, but the stretching vibrations of the alkyl chain are also slightly affected. The asymmetric ring vibration (γ_{ring2}, γ_{ring3}) and the C−H2 deformation of the chain (δ_{C-H2}) are not significantly influenced.

Figure 2 shows that upon cooling, a thermal iron(II) spin transition takes place yielding new small bands. These new bands are associated with the low-spin state. The new stretching vibration ν_{C5-H}, due to the LS species, shifts with larger substituents (F, Cl, Br and I) to higher energies (3101, 3172, 3175 and 3176 cm^{-1}). Bands known from the high-spin spectra are also shifted, mainly to higher energies (e.g. ν_{C5-H} and δ_{C-H2}). A splitting of one of the bands ($\nu_{N2=N3}$) is also observed. This effect has also been detected in the complexes of *teeb* and *teei*.

The vibrational spectrum of $[Fe(teef)_6](BF_4)_2$ shows the shoulder of the ν_{C-H}(HS) band vanishing upon cooling. The newly arising ν_{C-H}(LS) shows a band splitting, which is observed at about 3100 cm^{-1} (see Figure 2). Furthermore, strong band splittings in the low-spin case are observed for the $\nu_{N2=N3}$ vibration, whereas for most of the other stretching vibrations this splitting is not very well pronounced.

Table 2 lists the vibrational frequencies of the iron(II) tetrafluoroborate complexes with *teef*, *teec*, *teeb* and *teei* at room temperature in the high-spin state and at about 100 K. At this temperature, in all four complexes, the majority of the iron(II) ions that undergo a thermal spin transition will be in the low-spin state (Figure 9, A).

Table 2. Mid IR bands of iron(II) $[Fe(L)_6](BF_4)_2$ with L = *teef*, *teec*, *teeb*, *teei* at room temperature and at about 100 K; frequencies in cm^{-1}; ν = stretching, δ = deformation or in-plane of the ring, γ = out-of-plane, italic numbers = significant changes during the spin conversion, bold = bands which are only observed in HS or LS state

Compound	Fe−*teef* (HS)	Fe−*teef* (LS)	Fe−*teec* (HS)	Fe−*teec* (LS)	Fe−*teeb* (HS)	Fe−*teeb* (LS)	Fe−*teei* (HS)	Fe−*teei* (LS)
ν(C−H)[12−14]	*3145 s/3134 sh*	3141 s	3147 s	**3172 sh**/*3148 s*	3145 s	**3175 sh**/*3149 s*	3143s	**3176 m**/*3146 s*
		3101 m/3092						
ν(C−H)[11]	2999 m	*3008 m/2998 m*	3974 m	3089 s	3038 m	*3093 s/3075 sh*	*3026 m/3004 m*	*3021 m/3008 m*
	2975 m	*2974 m/2966 m*	3028 w	*3036 sh/3020 w*	3036 w	3035 w	2967 m	*2971 m/2963 sh*
			2972 m	*2989 m/2970 m*	2975 m	2984 m		
					2927 sh	2927 w		
Aromatic overtone band	1789 w	1794 w	1800 w	1786 m	1793 w	*1794 w/1781 w*	1790 m	*1796 m/1774 w*
ν(N2=N3)[13−16] {+ ν(C5−N1) + ν(C_{alkyl}−N1)}	1503 s	*1505 s/1495 s*	1503 s	*1512 s/1510 s*	*1507 s/1503 s*	*1511 s/1508 s*	1508 s	1514 s
δ(C−H2)[11]	1445 w	1434 w	1453 m	1458 m	1451 m	1455 m	1455 m	1461 m/1455 m
	1434w	1426vw	1437m	1437m	1429m	1431 m/1427 m	1428 m/1419 m	1443 m
								1427 m/1419 m
	1394 w	1394 w/1385 vw						
ν(N1−C_{alkyl})[11]	1364 w	1368 w/1363 w	1367 w	1389 vw/1364 w	1363 w	1363 w	1364 m	1368 m/1359 m
	1300 vw	1307 w	1299 m	1299 m	1285 m	1307 w/1288 m	1312 w	1313 w/1304 w
							1287 m/1276 m	1293 m/1281 m
ν(C−F)[11,17,18]	1265 vw	1273 w						
δ(ring1)[12−14]	1245 w	1248 w	1229 w	1235 w	1243 w	1247 w	1227 m	1235 m
ν(C=N4), ν(N1−N2)[14]	1174 vs/1164 sh	1176 m/1163 w	1172 vs	1170 vs	1170 vs	1170 vs	1194 s/1175 s	1198 s/1177 s
							1132 s	1135 s
ν(C5−N1) + δ(C5−H)[14] in-plane	1106 s	1108 vs	1101 vs	1102 vs	1097 vs	1097 vs	1094 s	1108 s/1095 s
ν(B−F)[21]	1051 vs	1052 vs	1062 vs	1062 vs	1059 vs	1061 vs	1056 vs	1055 vs
ν(N3−N4)[12−14]	1039 vs	1039 vs	1039 vs	1039vs	1040 vs	1038 vs	1040 sh	1046 vs/1040 sh
ν(N1−N2)[14]	994 w	997 w	1001 s		999 m		1019 s/1003 m	998 m
δ(ring2)[13,14] in-plane-banding {δ(NCN)}	970 vw	970 vw	959 w	961w	967 vw/946 w	970 w	939 m/930 m	932 m
γ(H_2C−CH_2)	886 w	884 w	910 m	913 m	880 m	887 m	893 w	897 w/869 w
δ(C−H2)[11]	861m	971 w/861 m	878 w	874 w	880 m	887 m	840 m	837 m
γ(ring3)[13−14] out-of-plane	721w	722 w	721 w	726 vw	720 w	725 vw	724 w	719 w
γ(ring4)[13−14] out-of-plane	679 s	681 s	666 s	668 vs	670 m	675 m/670 m	670 m/664 m	663 m
	648 s	645 s	645 m	653 m	650 m	654 m/648 m	653 m	647 m
					571 m	570 m		
δ(B−F)[21]	522 m	521 m	533 w	534 w	533 w	534 w	522 sh/515 m	524 m
	500 m	502 m	522 w	521 w	521 w	521 w		516 m
ν(C−Cl)[18]			473 m	480 w				

 © 2003 Wiley-VCH Verlag GmbH & Co. KGaA, Weinheim

Mössbauer Spectroscopy

teef

Representative spectra recorded at ambient and liquid helium temperatures and at a temperature within the spin transition regime are displayed in Figure 3. The substantial reduction of the absorption area due to the decreasing Lamb-Mössbauer factor upon increasing the temperature is obvious from this figure. This reduction indicates a significant weakening of the bond strength at higher temperatures and quite a low Debye temperature. On taking a closer look at the high-spin pattern (see Figure 4), a single doublet is insufficient to fit the data to a reasonable extent. This can only be performed successfully if the presence of two doublets with equal intensity is assumed. Due to the lack of resolution, however, a certain ambiguity remains concerning the exact absorption area, the error being estimated to lie around 10%. On cooling below ambient temperature the onset of the high-spin to low-spin transition can be detected at 160 K by the occurrence of a further subpattern exhibiting a significantly lower isomer shift and an almost collapsed quadrupole splitting (Table 3). Thus, the resolution of the low-spin state pattern is too poor to resolve the two species as observed in the high-spin case. The transition is found to be centred at about 140 K (Figure 5), which is in close agreement with the magnetic susceptibility results (vide infra). It is, however, an incomplete one, as at 4.2 K approximately 44% still remains in the high-spin state. The temperature dependence of the isomer shift (decreasing values on increasing the temperature) is mainly due to the second-order Doppler effect, with only a small contribution remaining from the change of the lattice dimensions depending on the temperature.

teeb

In the ^{57}Fe Mössbauer spectra of [Fe(*teeb*)$_6$](BF$_4$)$_2$ (see Figure 6 and Table 4), only one doublet is observed for the high-spin state. The transition to the low-spin state is gradual and complete, starting at about 210 K and being completed at about 110 K. The transition is centred at approximately 160 K, in agreement with the bulk magnetic data.

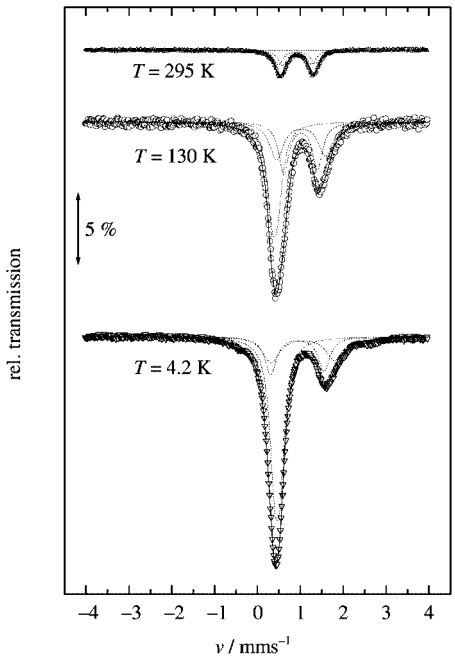

Figure 3. ^{57}Fe Mössbauer spectra recorded from [Fe(*teef*)$_6$](BF$_4$)$_2$ at different temperatures; triangles and circles are experimental points, solid (broken) lines computer fit described in the text

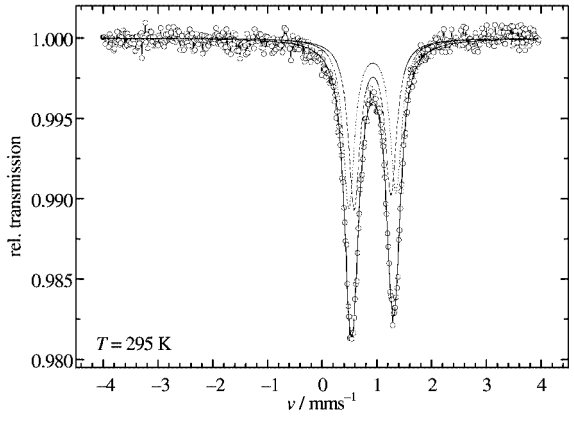

Figure 4. ^{57}Fe Mössbauer spectra recorded from [Fe(*teef*)$_6$](BF$_4$)$_2$ at room temperature; circles depict experimental points, solid (broken) lines are computer fits as described in the text

Table 3. Isomer shift (δ) and quadrupole splitting (Δ) obtained for [Fe(*teef*)$_6$](BF$_4$)$_2$

T [K]	A_{LS} [%]	δ_{LS} [mm·s^{-1}]	Δ_{LS} [mm·s^{-1}]	A_{HS1} [%]	δ_{HS1} [mm·s^{-1}]	Δ_{HS1} [mm·s^{-1}]	A_{HS2} [%]	δ_{HS2} [mm·s^{-1}]	Δ_{HS2} [mm·s^{-1}]
4.2	56	0.43	0.13	21	1.03	1.54	21	1.06	0.98
100	49	0.41	0.14	26	1.02	1.06	26	1.01	0.75
110	46	0.41	0.14	27	1.01	1.07	27	1.01	0.75
120	45	0.41	0.15	27	1.00	1.10	27	1.01	0.74
130	41	0.41	0.12	29	1.02	1.14	29	1.01	0.78
140	21	0.33	0.15	39	1.06	1.29	39	1.01	0.91
150	7	0.32	0.18	47	1.00	1.38	47	0.98	0.94
160	2	0.32	0.20	49	1.00	1.35	49	0.98	0.92
170	0	–	–	50	0.99	1.31	50	0.99	0.86
180	0	–	–	50	0.99	1.25	50	0.99	0.84
190	0	–	–	50	0.98	1.22	50	0.99	0.80
200	0	–	–	50	0.97	1.17	50	0.97	0.78
295	0	–	–	50	0.92	0.86	50	0.92	0.68

 © 2003 Wiley-VCH Verlag GmbH & Co. KGaA, Weinheim

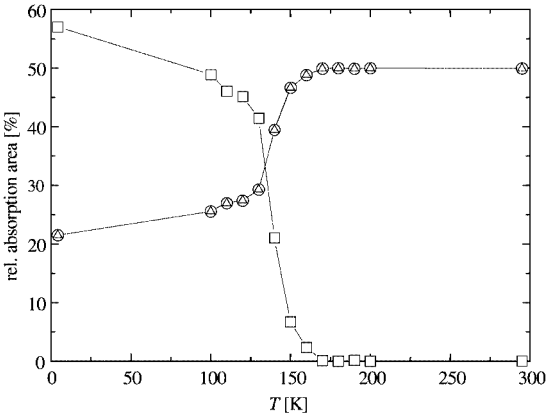

Figure 5. Relative absorption area vs. temperature derived from the ^{57}Fe Mössbauer spectra recorded from [Fe(*teef*)$_6$](BF$_4$)$_2$ with the low-spin component (squares) and the two high-spin components (circles and triangles); the lines are merely a guide to the eye

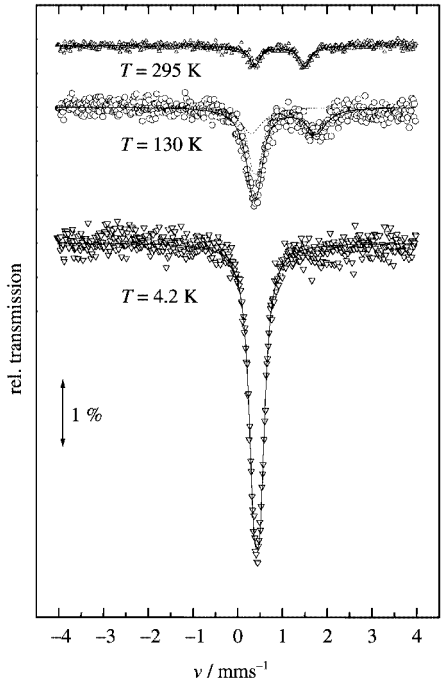

Figure 6. ^{57}Fe Mössbauer spectra recorded from [Fe(*teeb*)$_6$](BF$_4$)$_2$ at different temperatures; triangles and circles are experimental points, solid (broken) lines are computer fits as described in the text

teei

The spin transition observed from a ^{57}Fe Mössbauer spectrum of the compound [Fe(*teei*)$_6$](BF$_4$)$_2$ (see Figure 7, Table 5) is similar to the transition in [Fe(*teeb*)$_6$](BF$_4$)$_2$. The transition is gradual and complete and occurs between 160 and approximately 250 K. Again, only one doublet, associated with iron(II) high-spin species, is detected. The transition temperature as determined by Mössbauer spectroscopy is slightly below 200 K.

Figure 8 shows the spin-transition behaviour of all three compounds as obtained from ^{57}Fe Mössbauer spectroscopy; γ_{HS} can be directly calculated from the peak areas of the high-spin species (A_{HS}) and in the case of [Fe(*teef*)$_6$](BF$_4$)$_2$ from the combination of the peak areas A_{HS}' and A_{HS}''.

The isomer shift reflects the electron density at the Mössbauer nucleus. In the case of the high-spin state no significant influence of the individual ligand is observed. This is, however, not the case for the spectra arising from the low-spin state (Tables 3−5). The values obtained for [Fe(*teei*)$_6$](BF$_4$)$_2$ are considerably smaller than the others, indicating a larger (predominantly *s*-) electron density for this particular compound. For all three compounds under investigation the line width observed for both the high-spin and the low-spin pattern lies significantly beyond the value of the source (> 0.3 mm·s^{-1} compared to 0.22 mm·s^{-1}). This might be caused by slight inhomogeneities or defects in the sample disturbing the lattice periodicity.

Magnetic Susceptibility Measurements

In Figure 9, the fractions of the high-spin species vs. temperature (i.e. γ_{HS} vs. T) of all iron(II) spin-crossover complexes studied are shown. The compounds with tetrafluoroborate as the anion are plotted in graph A, the compounds with perchlorate as the anion are plotted in graph B.

teef

A significant difference is observed between the two magnetic susceptibility curves associated with the two complexes with *teef* as the ligand. The curve of the BF$_4$ complex shows a spin transition between 123 and 190 K with $T_{1/2}(1) = 137$ K and a second more gradual spin transition between 65 and 123 K with $T_{1/2}(2) = 108$ K. Each of these steps represent approximately one third of the iron(II) ions. One third of the ions do not undergo a temperature dependent spin transition, but remain in the high-spin state at all temperatures.

The curve of the magnetic susceptibility versus temperature for the perchlorate complex differs from the tetrafluoroborate complex, showing a one-step transition between 65 and 200 K with $T_{1/2} = 130$ K, thus featuring a higher spin-transition temperature than in the BF$_4$ complex. When the sample is cooled rapidly (cooling rate $>$ 50 K/min) a fraction of the iron(II) ions is trapped in the high-spin state. At approximately 55 K, this fraction transfers to the low-spin state, as depicted in Figure 9, B by a small decline of γ_{HS} between 55 and 65 K.

teeb

From magnetic susceptibility measurements of both the tetrafluoroborate and the perchlorate complexes the presence of only one magnetic site is concluded. Both compounds undergo an almost complete and gradual spin transition (over 90%) with transition temperatures of $T_{1/2} =$ 166 K for the tetrafluoroborate complex and $T_{1/2} = 150$ K for the perchlorate complex. In contrast to the *teec* com-

 © 2003 Wiley-VCH Verlag GmbH & Co. KGaA, Weinheim

Table 4. Isomer shift (δ) and quadrupole splitting (Δ) obtained for $[Fe(teeb)_6](BF_4)_2$

T [K]	A_{LS} [%]	δ_{LS} [mm·s^{-1}]	Δ_{LS} [mm·s^{-1}]	A_{HS} [%]	δ_{HS} [mm·s^{-1}]	Δ_{HS} [mm·s^{-1}]
4.2	100	0.43	0.14	0		
50	100	0.44	0.13	0		
100	100	0.43	0.13	0		
120	71.6	0.43	0.13	20.1	1.09	1.46
130	77.8	0.44	0.13	22.2	1.03	1.60
140	79	0.43	0.22	21.0	1.01	1.53
150	60.5	0.42	0.14	39.5	1.04	1.43
160	45.6	0.40	0.14	54.4	1.03	1.45
170	47.1	0.41	0.15	52.9	0.97	1.43
180	32	0.40	0.13	68	1.00	1.33
190	12.9	0.37	0.13	87.1	1.02	1.34
200	15	0.35	0.13	85	0.98	1.30
210	9.5	0.35	0.13	90.5	0.97	1.29
220	0			100	0.98	1.29
295	0			100	0.92	1.11

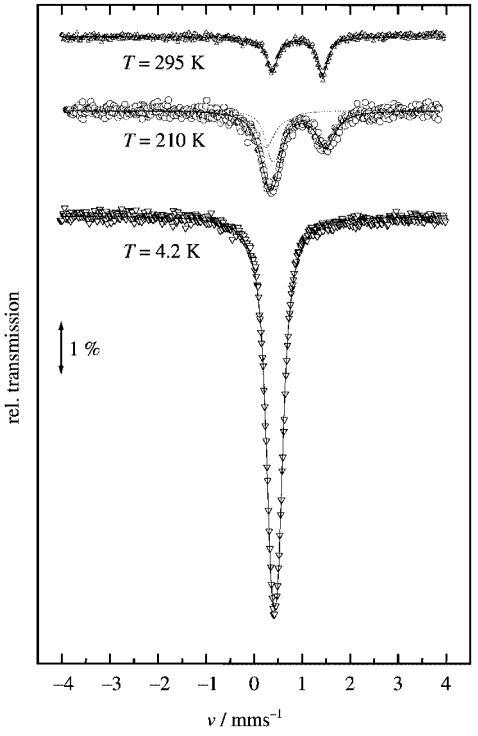

Figure 7. ^{57}Fe Mössbauer spectra recorded from $[Fe(teei)_6](BF_4)_2$ at different temperatures; triangles and circles are experimental points, solid (broken) lines are computer fits as described in the text

plexes[8] and to $[Fe(teef)_6](BF_4)_2$ the shape of the transition curves indicates that only one Fe site is present.

teei

In the magnetic susceptibility data of the *teei* compounds the transition curves of both the tetrafluoroborate and the perchlorate complex show a gradual transition. The transitions are 100% complete. The curves are steeper than those of the *teeb* complexes. It is also possible that in the $[Fe(teei)_6](ClO_4)_2$ compound two different magnetic sites are present, with an "inflection point" at 167.5 K. In the first derivative of the transition curve two maxima are visible at 150 and 195 K. The overall curve appears more gradual than the curve of the tetrafluoroborate compound.

Conclusion

In order to draw conclusions on the influence of the ligand, the results described in this paper are also compared with the equivalent *teec* complexes described previously.[8] The magnetic data of the crystallised *teec* compounds have been used for this purpose.

On summarising the two series of [(haloethyl)tetrazole]-iron(II) complexes, with BF_4^- and ClO_4^- as counterions several observations can be made (see Figure 9).

In both parts of Figure 9 (A and B) the sequence of the transition temperature of complexes with *teef*, *teeb* and *teei* as ligands corresponds with the size of the halogen atom. An increase in size correlates with an increase of the transition temperature. Because of the two-step transition in $[Fe(teec)_6](BF_4)_2$ and the partial transition in $[Fe(teec)_6](ClO_4)_2$ it is difficult to include these two in this order. What can be concluded is that the temperature range of the $[Fe(teec)_6](anion)_2$ samples is in the same range as that of the $[Fe(teeb)_6](anion)_2$ compounds, and between those of the *teef* and *teei* complexes.

In $[Fe(teef)_6](BF_4)_2$ a difference is observed between the spin transition obtained by Mössbauer spectroscopy and by magnetic susceptibility measurements. Both show a transition in approximately the same temperature range, but the fraction of iron(II) ions in the high-spin state at low temperature differs, with 44% high spin found by Mössbauer spectroscopy, and 35% by magnetic susceptibility. Ongoing structural measurements at low temperature will conclude whether a 1:2, or a 1:1, or no precise ratio at all, is found.[22]

Moreover, a splitting of the aromatic C−H bands in the $[Fe(teef)_6](BF_4)_2$ indicated the presence of different aromatic C−H vibrations, in other words in the same spin state, different tetrazole rings are present. Powder X-ray structure determination will have to be used to confirm whether the difference is caused by the presence of two

 © 2003 Wiley-VCH Verlag GmbH & Co. KGaA, Weinheim

Table 5. Isomer shift (δ) and quadrupole splitting (Δ) obtained for $[Fe(teei)_6](BF_4)_2$

T [K]	A_{LS} [%]	δ_{LS} [mm·s^{-1}]	Δ_{LS} [mm·s^{-1}]	A_{HS} [%]	δ_{HS} [mm·s^{-1}]	Δ_{HS} [mm·s^{-1}]
4.2	100	0.43	0.14	0		
50	100	0.43	0.25	0		
100	100	0.43	0.13	0		
150	100	0.42	0.17	0		
160	100	0.40	0.18	0		
170	92.5	0.40	0.28	7.5	0.87	1.57
180	87.7	0.41	0.40	12.3	0.86	1.67
190	61.2	0.37	0.31	38.8	0.88	1.30
200	48.6	0.42	0.21	51.4	0.89	1.35
210	38.4	0.41	0.14	61.6	0.87	1.26
220	38.0	0.34	0.21	62.0	0.92	1.13
230	25.6	0.31	0.20	74.4	0.97	1.14
240	9.7	0.33	0.21	90.3	0.95	1.13
295	0			100	1.05	1.20

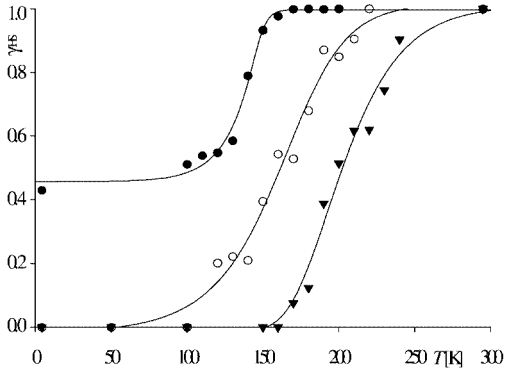

Figure 8. γ_{HS} (directly calculated from the relative absorption area of the high-spin species) vs. temperature derived from the ^{57}Fe Mössbauer spectra recorded from $[Fe(teef)_6](BF_4)$ (dots), $[Fe(teeb)_6](BF_4)$ (circles) and $[Fe(teei)_6](BF_4)_2$ (triangles); the sigmoidal lines are merely a guide to the eye

symmetrically non-equivalent tetrazole rings coordinated to the same iron(II) ion, or by two symmetrically non-equivalent iron(II) species. The last option is supported by the magnetic data and is proved independently by ^{57}Fe Mössbauer spectroscopy. In either case, the vibrational spectrum not only gives qualitative information about the spin-transition temperature $T_{1/2}$, but also about structural properties. This opens additional possibilities for the use of variable-temperature IR spectroscopy as a tool in the investigation of spin-crossover compounds.

The complexes with *teec* as ligand, $[Fe(teef)_6](BF_4)_2$ and $[Fe(teei)_6](ClO_4)_2$ all show a complicated spin-crossover behaviour, perhaps with the presence of two (or in the case of *teef* possibly even three) different sites. This spin-crossover behaviour is simpler in both the *teeb* compounds, perchlorate complex with *teef* ligands and the tetrafluoroborate complex with *teei* ligands, which all show gradual transitions without any steps.

Only in the complexes with *teeb* as the ligand is the influence of the counterion small (only a difference in transition temperature). In all other compounds the magnetic behaviour varies strongly from the tetrafluoroborate to the perchlorate complex. In the *teeb* complexes alone the transition curves shift to a slightly lower temperature when tetrafluoroborate is replaced by perchlorate. This behaviour has been observed before in mononuclear spin-crossover complexes.[23]

Structural analyses indicate that all compounds crystallise as iron(II) complexes with six (haloethyl)tetrazole ligands octahedrally surrounding each iron(II) centre.[22] At

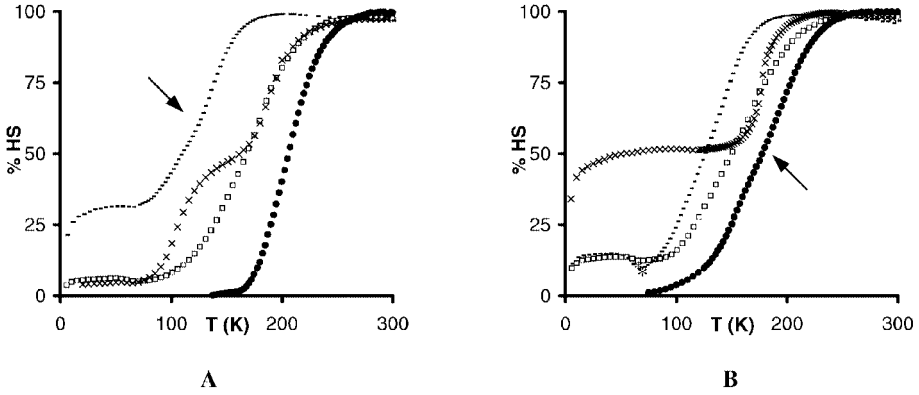

Figure 9. Transition curves of $[Fe(teex)_6](anion)_2$ with *teex* = *teef* (—), *teec* (×), *teeb* (squares), *teei* (dots); A) anion = BF_4^-, B) anion = ClO_4^- (for *teex* = *teec*, curves of the crystallised samples[8] are depicted); the arrows indicate the "bend" between two possible different transition curves, the * indicates the small step caused by thermal trapping in $[Fe(teef)_6](ClO_4)_2$

 © 2003 Wiley-VCH Verlag GmbH & Co. KGaA, Weinheim

room temperature, all compounds studied by powder XRD appear to be isostructural to $[Fe(teec)_6](BF_4)_2$, with space group $P2_1/c$,[22] except for $[Fe(teef)_6](BF_4)_2$, which is triclinic in structure instead of monoclinic. Further studies will indicate whether or not the complex spin transition is caused by structural or thermodynamic properties.[22]

Variable-temperature mid-range infrared spectroscopy has been applied to supplement data obtained by magnetic susceptibility measurements and Mössbauer spectroscopy. As shown by a comparison of the spectra of the free ligands and the respective complexes, band shifts are indeed seen to originate from the different substituents used. But the thermally induced spin transition of the iron(II) coordination centres definitely has the strongest impact on the vibrational spectra. The direct observation of the bond-strength changes of the Fe−N bonds upon spin transition in the far IR region turns out to be difficult, mainly because of the coupling of intra-ligand vibrational modes with the Fe−N stretching vibration. Nevertheless, an indirect monitoring of the Fe−N bond strength changes can be achieved by variable-temperature mid-range IR spectroscopy. The focus of interest is the stretching vibration of the single hydrogen atom on the tetrazole ring. This aromatic C−H vibration can easily be distinguished from the aliphatic C−H vibrations of the alkyl substituents. It does not couple with other vibrations and is reasonably sensitive to the bond-strength change of the neighbouring Fe−N bond. Thus, with variable-temperature IR as a tool, it is possible to monitor the spin transition (in this case qualitative, but in other cases quantitative). In the case of a reasonably large band shift of this C−H band, which depends on the packing of the complex, a quantification of the respective peak intensities allows an independent determination of $T_{1/2}$.[23]

The influence of the substituent of the ethyl tail on the electron density of the tetrazole is virtually nonexistent. Therefore, the differences in the spin-transition behaviour should be caused entirely by the crystal packing. The iron−iron distance, and thereby the strength of the elastic interaction (larger when the relative volume change is larger), as well as the relative size of the anion compared to the cationic centre, seem to be the most important causes for the differences in the spin-transition behaviour. But no correlation has been observed between spin transition (i.e. γ_{HS} vs. T) on the one hand, and space group, anion and ligand size on the other. Therefore, it is not yet possible to predict the magnetic properties of a new spin-crossover compound with 1-alkyltetrazoles as ligands.

Experimental Section

General Remarks: Vibrational spectra were recorded with a Perkin−Elmer 16 PC mid-range FT-IR spectrometer using a Graseby-Specac thermostattable sample holder with a Graseby-Specac automatic temperature controller within the temperature range of 100−300 K. To accomplish a reasonable signal-to-noise ratio 64 scans have been summed. Magnetic susceptibility measurements (5−300 K) were carried out using a Quantum Design MPMS-5 5T SQUID magnetometer (measurements carried out at 0.1 T). The data were corrected for the magnetisation of the sample holder and for diamagnetic contributions, which were estimated from the Pascal constants.[25] C,H,N determinations were performed with a Perkin−Elmer 2400 Series II analyser. The ^{57}Fe Mössbauer spectra were recorded between 4.2 and 295 K using a conventional constant acceleration drive system. The source used was ^{57}Co in an Rh matrix with an activity of about 50 mCi. The data were analysed using a least-squares fitting program package under the assumption of a discrete superposition of Lorentzian lines. Since the high-spin and the low-spin pattern overlap to a certain extent, the errors of the hyperfine parameters, determined from the computer fit, i.e. isomer shift and quadrupole splitting, increase with decreasing absorption area of the given sub-spectrum from ± 0.01 mm·s^{-1} above 20% area to 0.05 mm·s^{-1} for an area of the order of a few percent. The isomer-shift values displayed in the tables are given relative to the source. If the values are to be compared with shifts relative to α-Fe, 0.12 mm·s^{-1} have to be added.

2-(1-Fluoroethyl)tetrazole (*teef*): This compound was obtained by refluxing a mixture of (1-fluoroethyl)amine hydrochloride (0.05 mol, 5.0 g) and sodium azide (0.01 mol, 6.5 g) in acetic acid (30 mL) and triethyl orthoformate (60 mL) for 8 h. The excess solvents were removed by evaporation. The product was extracted by treating the residue with 2-propanol and removing the insoluble salts (sodium chloride and unchanged sodium azide) by filtration. After further evaporation of the solvent, a yellow oil remained. The pure ligand was obtained by placing the $[Cu(teef)_2Br_2]_n$ complex in ethanol, dissolving this complex in water and extracting the *teef* ligand with dichloromethane. The yield is approximately 1.2 g (20%). ^{1}H NMR (300 MHz, [D$_6$]DMSO): δ = 9.39 (s, CH), 4.88 (t, CH$_2$), 3.77 (t, CH$_2$) ppm. ^{13}C NMR (75 MHz, [D$_6$]DMSO): δ = 144.5 (CH), 48.7 (CH$_2$), 48.4 (CH$_2$) ppm.

2-(1-Bromoethyl)tetrazole (*teeb*): This compound was obtained by refluxing a mixture of (1-bromoethyl)amine hydrobromide (0.25 mol, 51 g) and sodium azide (0.3 mol, 22 g) in acetic acid (100 mL) and triethyl orthoformate (200 mL) for 6 h. After evaporation of the excess solvents and removal of the salts formed by filtration, the yellow oil obtained was dissolved in 2-propanol. After another subsequent filtration to remove the insoluble salts, *teeb* crystallised as a white solid after several weeks. The yield was approximately 0.9 g (20%). $C_3H_5BrN_4$ (177.0): calcd. C 20.4, H 3.0, N 31.7; found C 21.4, H 2.9, N 33.7. ^{1}H NMR (300 MHz, [D$_6$]DMSO): δ = 9.47 (s, CH), 4.92 (t, CH$_2$), 3.98 (t, CH$_2$) ppm. ^{13}C NMR (75 MHz, [D$_6$]DMSO): δ = 144.4 (CH), 49.2 (CH$_2$), 42.8 (CH$_2$) ppm.

2-(1-Iodoethyl)tetrazole (*teei*): This compound was synthesised according to the Finkelstein reaction,[26,27] which involves substitution, starting from 2-(1-bromoethyl)tetrazole (*teeb*) and sodium iodide (1.5 equiv.). A 10% solution of *teeb* and sodium iodide in acetone was stirred under reflux conditions for over 2 h. At this stage, the bromide was substituted for iodide and the insoluble sodium bromide precipitated. After cooling, the solution was filtered to remove the insoluble sodium bromide and after removal of the solvent, the remaining oil was dissolved in water; *teei* was obtained by extraction with chloroform after removal of the solvent. The oil obtained slowly crystallised from 2-propanol. The yield was approximately 1 g (60%). ^{1}H NMR (250 MHz, [D$_6$]DMSO): δ = 9.45 (s, CH), 4.82 (t, CH$_2$), 3.66 (t, CH$_2$) ppm. ^{13}C NMR (68 MHz, [D$_6$]DMSO): δ = 144.4 (CH), 49.9 (CH$_2$), 3.26 (CH$_2$) ppm.

***WARNING:** Perchlorate salts are potentially explosive and when used should be treated as such!*

$[Fe(teef)_6](BF_4)_2$: This complex was prepared by dissolving $Fe(BF_4)_2{\cdot}6H_2O$ (1.0 mmol, 0.30 g) and *teef* (6.0 mmol, 0.70 g) in

 © 2003 Wiley-VCH Verlag GmbH & Co. KGaA, Weinheim

ethanol (20 mL). The complex formed as white hexagonal-shaped crystallites, yield 90 mg (10%). $C_{18}H_{30}B_2F_{14}FeN_{24}$ (926.0): calcd. C 23.3, H 3.3, N 36.3; found: C 23.1, H 2.6, N 36.7.

[Fe(*teef*)$_6$](ClO$_4$)$_2$: This complex was formed by dissolving $Fe(ClO_4)\cdot 6H_2O$ (1.0 mmol, 0.36 g) and *teef* (6.0 mmol, 0.70 g) in ethanol (20 mL). The complex formed as white hexagonal-shaped crystallites, yield 140 mg (15%). $C_{18}H_{30}Cl_2F_6FeN_{24}O_8$ (951.3): calcd. C 22.7, H 3.2, N 35.3; found C 22.5, H 2.8, N 35.6.

[Fe(*teeb*)$_6$](BF$_4$)$_2$: This complex was formed by dissolving $Fe(BF_4)_2\cdot 6H_2O$ (1.0 mmol, 0.30 g) and *teeb* (0.6 mmol, 1.06 g) in ethanol (40 mL). The complex formed as white hexagonal-shaped crystallites, yield 240 mg (20%). $C_{18}H_{30}B_2Br_6F_8FeN_{24}$ (1291.5): calcd. C 16.7, H 2.3, N 26.0; found C 18.0, H 2.6, N 25.6.

[Fe(*teeb*)$_6$](ClO$_4$)$_2$: This complex was formed by dissolving $Fe(BF_4)_2\cdot 6H_2O$ (1.0 mmol, 0.30 g) and *teeb* (6.0 mmol, 1.06 g) in ethanol (40 mL). The complex formed as white hexagonal-shaped crystallites, yield 250 mg (20%). $C_{18}H_{30}Br_6Cl_2FeN_{24}O_8$ (1316.8): calcd. C 16.4, H 2.3, N 25.5; found C 17.5, H 2.7, N 24.9.

[Fe(*teei*)$_6$](BF$_4$)$_2$: This complex was formed by dissolving $Fe(BF_4)_2\cdot 6H_2O$ (1.0 mmol, 0.30 g) and *teei* (6.0 mmol, 1.34 g) in ethanol (40 mL). The complex formed as white hexagonal-shaped crystallites, yield 0.7 g (45%). $C_{18}H_{30}B_2F_8FeI_6N_{24}$ (1573.5): calcd. C 13.7, H 1.9, N 21.4; found C 13.8, H 1.9, N 21.5.

[Fe(*teei*)$_6$](ClO$_4$)$_2$: This complex was formed by dissolving $Fe(ClO_4)\cdot 6H_2O$ (1.0 mmol, 0.36 g) and *teei* (6.0 mmol, 1.34 g) in ethanol (40 mL). The complex formed as white hexagonal-shaped crystallites, yield 0.8 g (50%). $C_{18}H_{30}Cl_2FeI_6N_{24}O_8$ (1598.8): calcd. C 13.5, H 1.9, N 21.0; found for C 13.7, H 1.5, N 20.7.

Acknowledgments

Thanks for financial support go to the "Fonds zur Förderung der Wissenschaftlichen Forschung in Österreich" (Project 15874-N03), the Training and Mobility of Researchers Network (TMR) project "Thermal and Optical Spin State Switching" (TOSS) supported by the European Community under the Contract number ERB-FMRX-CT98-0199 and to the European Science Foundation under the project "Molecular Magnets". Jos van Brussel is acknowledged for the elemental analyses. The work described in this paper has been supported by the Leiden University Study group WFMO and has been performed under the auspices of the Graduate Research School HRSMC, a joint activity of Leiden University and the two Universities in Amsterdam.

[1] J. Jeftic, R. Hinek, S. C. Capelli, A. Hauser, *Inorg. Chem.* **1997**, 3080−3087.
[2] P. L. Franke, J. G. Haasnoot, A. P. Zuur, *Inorg. Chim. Acta* **1982**, 5−9.
[3] P. Gütlich, P. Poganiuch, *Angew. Chem. Int. Ed. Engl.* **1991**, 975−977.
[4] T. Buchen, P. Gütlich, *Chem. Phys. Lett.* **1994**, 262−266.
[5] A. Hauser, P. Gütlich, H. Spiering, *Inorg. Chem.* **1986**, 4245−4248.
[6] N. Willenbacher, H. Spiering, *J. Phys. Chem. Solid State Phys.* **1988**, *21*, 1423.
[7] P. Poganiuch, P. Gütlich, *Hyperfine Interact.* **1988**, 331−334.
[8] A. F. Stassen, E. Dova, J. Ensling, H. Schenk, P. Gütlich, J. G. Haasnoot, J. Reedijk, *Inorg. Chim. Acta* **2002**, 61−68.
[9] A. Camard, M. Grunert, W. Linert, unpublished results.
[10] A. F. Stassen, PhD Thesis, Leiden University, Leiden, The Netherlands, **2002**.
[11] M. Hesse, H. Meyer, B. Zeeh, *Spektroskopische Methoden in der Organischen Chemie*, 5th ed., Thieme Verlag, Stuttgart, **1995**.
[12] E. Lieber, D. R. Levering, L. J. Patterson, *Anal. Chem.* **1951**, *11*, 1594−1604.
[13] F. Billes, H. Endrédi, G. Keresztury, *THEOCHEM* **2000**, 183−200.
[14] S. C. S. Bugalho, E. M. S. Maçôas, M. L. S. Cristiano, R. Fausto, *Phys. Chem.* **2001**, 3541−3547.
[15] R. D. Holm, P. L. Donnelly, *J. Inorg. Nucl. Chem.* **1966**, *1887−1894*.
[16] E. O. J. John, R. D. Willet, B. Scott, R. L. Kirchmeier, J. M. Shreeve, *Inorg. Chem.* **1989**, 893−897.
[17] H. B. Jonassen, J. O. Terry, A. D. Harris, *J. Inorg. Nucl. Chem.* **1963**, 1239−1243.
[18] K. Nakamoto, *Infrared and Raman Spectra of Inorganic and Coordination Compounds*, 4th ed., ISBN 0-471-01066-9, John Wiley & Sons, New York, **1986**.
[19] J. Schweifer, P. Weinberger, K. Mereiter, M. Boca, C. Reichl, G. Wiesinger, G. Hilscher, P. J. v. Koningsbruggen, H. Kooijman, M. Grunert, W. Linert, *Inorg. Chim. Acta* **2002**, 297−306.
[20] P. Gütlich, A. Hauser, H. Spiering, *Angew. Chem. Int. Ed. Engl.* **1994**, 2024−2054.
[21] R. A. Nyquist, C. L. Putzig, M. A. Leuger, *Infrared and Raman Spectral Atlas of Inorganic Compounds and Organic Salts*, vols. 1, 3 and 4, Academic Press, **1996**.
[22] E. Dova, A. F. Stassen, M. Grunert, R. Peschar, J. G. Haasnoot, W. Linert, J. Reedijk, H. Schenk, manuscript to be submitted.
[23] L. Wiehl, *Acta Crystallogr., Sect. B* **1993**, 289−303.
[24] P. J. van Koningsbruggen, M. Grunert, P. Weinberger, *Monatsh. Chem.* **2003**, *134*, 183−198.
[25] I. M. Kolthoff, P. J. Elving, *Treatise on Analytical Chemistry*, vol. 4, New York, **1963**.
[26] A. Roedig, *Methoden Org. Chem (Houben-Weyl)* **1960**, vol. 4/5, pp. 595−605.
[27] J. A. Miller, M. J. Nunn, *J. Chem. Soc., Perkin Trans. 1* **1976**, 416.

Received November 27, 2002

 © 2003 Wiley-VCH Verlag GmbH & Co. KGaA, Weinheim

Solvothermal Synthesis and Structure of Anhydrous Manganese(II) Formate, and Its Topotactic Dehydration from Manganese(II) Formate Dihydrate

Martin Viertelhaus,[a] Henning Henke,[a] Christopher E. Anson,[a] and Annie K. Powell*[a]

Dedicated to Professor Hartmut Bärnighausen on the occasion of his 70th birthday

Keywords: Manganese / Formates / Solvothermal synthesis / Solid-state reactions

Recrystallization of manganese(II) formate dihydrate from formic acid under solvothermal conditions results in single crystals of anhydrous manganese(II) formate $Mn(O_2CH)_2$, and the structure of this phase has been determined by X-ray diffraction. The same product can be obtained by solid-state dehydration of single crystals of manganese formate dihydrate, giving crystals that, although of poor quality, still allow for a single crystal structure determination. The structural relationship between the hydrated and anhydrous phases and the nature of the transformation have been determined. Given the nature of the rearrangement involved in the solid-state reaction, it is remarkable that a crystalline product is obtained. Magnetic measurements of the anhydrous manganese(II) formate show it to be a three-dimensional antiferromagnet.

(© Wiley-VCH Verlag GmbH & Co. KGaA, 69451 Weinheim, Germany, 2003)

Introduction

Carboxylate-bridged polynuclear manganese complexes have been investigated for many years, particularly with regard to their magnetic properties. Examples include the oxo-centred trinuclear complexes[1] as well as $[Mn_{12}O_{12}(O_2CCH_3)_{16}(OH_2)_4]\cdot 4(H_2O)\cdot 2(CH_3CO_2H)$[2] and its related clusters synthesized with other carboxylic acids[3] which show the behaviour characteristic of "single molecule magnets". In addition to the interest in polynuclear clusters, much research on framework structures produced hydrothermally with carboxylates and related donors has been performed.[4] In this context and relevant to the work presented here the structures of anhydrous manganese acetate and manganese nitrate have only been determined relatively recently[5,6] whereas, for example, the structure of manganese carbonate[7] was determined in the early days of X-ray crystallography. In the course of our work on substitution of acetate ligands with formate, we have developed a new synthetic route to the preparation of crystalline anhydrous metal(II) formates.

With the exception of the strontium salt,[8] all the dihydrated metal(II) formates so far reported form an isomorphous series,[9] and isostructural mixed-metal formate dihydrates have also been described.[10] However, anhydrous diformates are only known for copper and cadmium formate.[11,12] These are synthesized at temperatures around 60−80 °C by slow evaporation of the solvent consisting of a mixture of water and formic acid. Other anhydrous formates are not available using this synthetic route.

Although scientific interest in metal(II) formate dihydrates has increased since they have been used as precursors for dehydrogenation catalysts,[13] very little is known about the structures of the anhydrous salts. With the knowledge of the synthesis and structures of the anhydrous formates, new types of metal oxide catalysts made from these formates are possible. With their increased density these anhydrous salts are more closely related to oxides than the dihydrates. The open framework structures of the precursors which are observed for other anhydrous formates (Mg, Fe, Co, Ni, Zn) are likely to influence the catalytic activity.

Even though metal formate dihydrates are model compounds for hydration/dehydration experiments and their decomposition properties have been well documented,[14] their dehydration products have only been characterized by X-ray powder diffraction (Mg,[15] Mn,[16] Fe,[17] Zn[18]), and their structures are not known. The dehydration of nickel and cobalt formate dihydrate only results in amorphous products.[19,20] However, the rehydration of the dehydrated product of manganese formate dihydrate has been reported and is reversible.[14a]

Using solvothermal conditions we have been able to synthesize a range of previously unreported anhydrous formates (Mg, Fe, Co, Ni, Mn, Zn) as crystalline products. We describe here the structure of anhydrous manganese(II) formate, as well as its formation by a remarkable solid-state dehydration reaction of the dihydrate.

[a] Institut für Anorganische Chemie, Universität Karlsruhe, Engesser Str. 15, Gebäude 30.45, 76128 Karlsruhe, Germany
Fax: (internat.) + 49-(0)721/608-8142
E-mail: powell@achpc50.chemie.uni-karlsruhe.de

Results and Discussion

Recrystallisation of manganese(II) formate dihydrate (MnFD) from formic acid under solvothermal conditions yields pale pink needle-shaped crystals of anhydrous manganese(II) formate (MnFA), suitable for X-ray diffraction (Scheme 1). The structure was determined at 200 K, and crystallographic details are summarised in Table 3. Under ambient conditions the same product in polycrystalline form can be obtained from concentrated formic acid.[21]

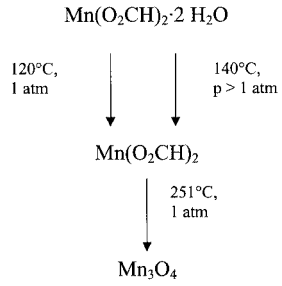

Scheme 1

Anhydrous manganese formate crystallizes in the orthorhombic space group *Pnca* (no. 60) with lattice parameters $a = 5.8127(8)$, $b = 7.509(2)$ and $c = 9.492(1)$ Å and $Z = 4$ (see Table 3). Although MnFA crystallises with an orthorhombic unit cell, while MnFD is monoclinic, inspection of the unit cell parameters shows that two of the three cell lengths are rather close to *b* and *c* for MnFD (Table 3). Since it was soon apparent that the two structures are indeed related (vide infra), and that MnFA can also be obtained via a solid-state dehydration of MnFD, the structure of MnFA was determined in the non-standard setting *Pnca* of the space group *Pbcn* (no. 60) in order to permit consistent labelling of the unit cell axes between the two structures. As the reported structure of MnFD was determined at ambient temperature,[22] we redetermined the structure of MnFD at 200 K, in order to make meaningful comparisons between the two structures.

The asymmetric unit of MnFA contains one independent manganese cation on the special position 4*c* on the twofold axis and one formate group $HCOO^-$ on the general position 8*d*. The coordinating oxygen atoms of the formate ligand differ with respect to their linkage. While O(1) forms μ_2-oxygen-bridges between neighbouring manganese centres, O(2) is monocoordinate. The Mn is coordinated by four O(1) atoms, with the remaining two *cis*-positions occupied by O(2) atoms. This results in the formation of infinite chains of Mn centres linked by pairs of μ_2-oxygen-bridges along **a**, as shown in Figure 1. The coordination spheres around the Mn cations can be described in terms of chains of edge-sharing octahedra. These chains are organized in a manner similar to $ZrCl_4$,[23] in particular with regard to local symmetry elements, with the metal atoms on twofold

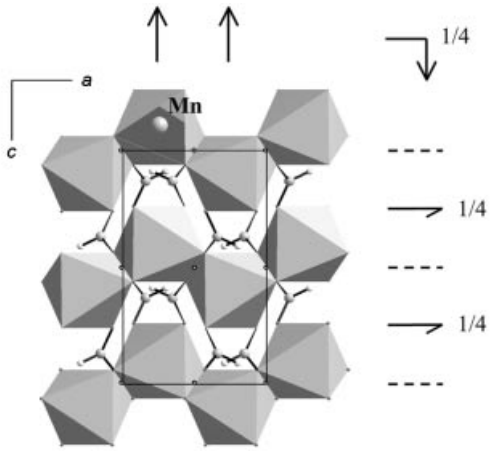

Figure 1. Projection of the structure of MnFA along *b* showing the edge-connected zig-zag chains of octahedrally coordinated Mn atoms; some of the symmetry elements of the space group *Pnca* (no. 60) are given as a help

axes and with inversion centres at the midpoint of the shared edges between octahedra. Similar chains are found in $TcCl_4$.[24] If the structure is viewed along the **a** axis, a rhomboidal network of Mn centres linked via *anti*,*anti*-bridging formate ligands is the characteristic motif (Figure 2). The Mn−O(1) distances in the μ_2-bridges are 2.231(2) and 2.210(2) Å, while the monocoordinate Mn−O(2^{II}) distance is 2.138(2) Å, shorter than in the bridges as might be expected. Bond lengths and angles are listed in Table 1.

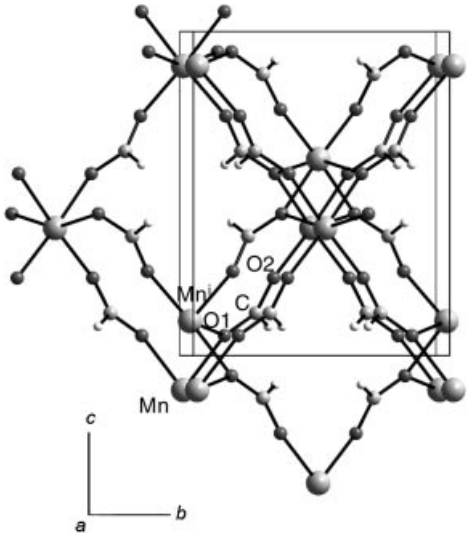

Figure 2. The network of formate groups connecting the manganese atoms of anhydrous MnFA. To aid the comparison with Figure 3 the drawing is slightly rotated with respect to *c*. Due to this rotation, all formate links at heights close to $x = 1/4$ and $x = 5/4$ appear doubled around the octahedrally coordinated manganese chain in the middle of the cell. With reference to Figure 3 the manganese atoms are shifted by 1/4 along *a* owing to the convention that a centre of inversion defines the origin. As a consequence Mn^i is related to Mn by $1 - x, -y, -z$.

 © 2003 Wiley-VCH Verlag GmbH & Co. KGaA, Weinheim

Table 1. Bond lengths and angles of MnFA
Symmetry codes: (i) $1 - x, -y, -z$; (ii) $x, 1/2 - y, -1/2 + z$; (iii) $1/2 - x, 1/2 + y, 1/2 + z$; (iv) $1/2 - x, -1/2 + y, -1/2 + z$; (v) $-1/2 + x, y, -z$; (vi) $1/2 - x, -y, z$

Bond lengths [Å]		Bond angles [°]	
Mn−O(1)	2.231(1)	O(2^{iv})−Mn−O(2^{ii})	93.86(10)
Mn−O(1^{i})	2.210(2)	O(2^{iv})−Mn−O(1^{v})	90.80(7)
Mn−O(2^{ii})	2.138(2)	O(2^{iv})−Mn−O(1^{i})	104.27(7)
O(1)−C	1.269(3)	O(1^{i})−Mn−O(1^{v})	158.01(9)
O(2)−C	1.236(3)	O(2^{iv})−Mn−O(1)	176.95(6)
C−H	1.00(3)	O(2^{iv})−Mn−O(1^{vi})	88.86(7)
Mn···Mn(i)	3.539(1)	O(1)−Mn−O(1^{i})	74.29(7)
Mn···Mn(iii)	6.052(1)	O(1)−Mn−O(1^{v})	89.85(5)
Mn(i)···Mn(iii)	5.475(1)	O(1)−Mn−O(1^{vi})	88.45(9)

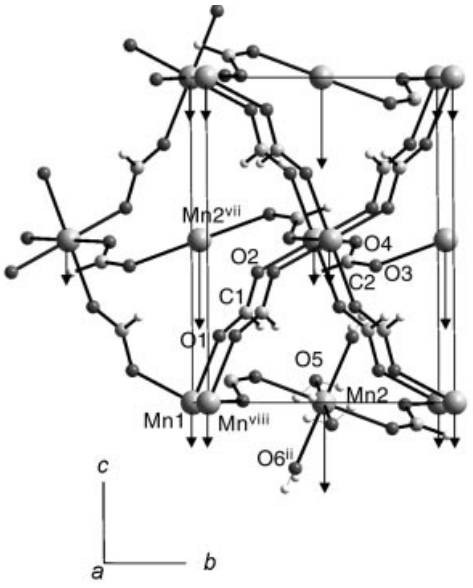

Figure 3. The structure of the dihydrate MnFD for comparison with Figure 2. Apart from the very similar formate-bridged network around atoms of type Mn(1) shown for layer heights close to $x = 0$ and additionally at $x = 1$ in most places, there are Mn(2)-centred loops linking the sheets at $x = 0$ and $x = 1$. Atom Mn(2) at $x = 1/2$ binds to four molecules of crystal water. Arrows indicate the relative moves necessary to reach the structure of MnFA. All equivalents of Mn(2) are shown with the water stripped off. Symmetry codes: (vii): $1 - x, -1/2 + y, 1/2 - z$, (viii): $1 + x, y, z$.

Differential thermal analysis (DTA) and thermogravimetry (TG) studies on MnFD in a nitrogen atmosphere show that the dehydration process takes place in the temperature range from 95 to 135 °C. A continuously decreasing sample mass is observed over this temperature range, with a mass loss of 19.3% (calculated value 19.9% for loss of two waters), and the appearance of an endothermic peak in the DTA curve. The decomposition of MnFA to Mn_3O_4 can be observed between 215 and 260 °C. During the mass loss of 37.4% (calcd. 38.0%) an exothermic peak can be seen in the DTA-curve (Scheme 1).

On dehydration of single crystals of MnFD at 120 °C, their plate-like habit is maintained, but they become off-white and opaque and are frequently cracked. This dehydration event clearly gives rise to a poorer quality sample with much larger spots on the image plate than for the solvothermal crystals. Thus, although the sample still appears to be a single crystal, it in fact consists of a collection of smaller crystallites which are, however, sufficiently aligned to allow for satisfactory structure determination and refinement. This showed that the dehydrated crystals had the identical structure to solvothermally-prepared MnFA, although as expected the final R-factors (Table 3) were higher than for the solvothermally prepared crystals.

A series of X-ray powder diffraction patterns measured during the course of dehydration shows the coexistence of both phases (MnFD and MnFA) (Figure 4). A similar heating experiment during which a sequence of orienting precession photographs was taken of a single crystal at 115 °C, also demonstrates the simultaneous presence of both phases within the same crystal specimen. The sharp diffraction spots of MnFD decrease in intensity while the more diffuse spots assigned to MnFA quickly become stronger. At 120 °C the slightly broadened (0*kl*) reflections of MnFA show clearly the systematic extinctions of the diagonal glide plane. Moreover, these observations give evidence that a fixed spatial relationship exists between the lattice of disappearing MnFD and freshly growing MnFA, indicating a topotactic transformation. Axes **b** and **c** retain their length approximately (see Table 3) and also their orientation within ±0.5°, whereas axis **a** undergoes changes both with regard to the angle of inclination (i.e. β of the monoclinic lattice decreases by over 7° to 90° in the orthorhombic phase) but also more drastically with regard to the shrinkage of the structure.

In contrast to MnFA, MnFD prepared under normal ambient conditions does not form needles, but plates with (100) as the dominant face. In accordance with the habit of the crystals the structure of MnFD consists of layers oriented parallel to the *bc*-plane. Figure 3, the corresponding section suitable for comparison with anhydrous MnFA (cf. Figure 2), shows that in MnFD nets of formate-bridged manganese atoms also exist in a variant similar to that of MnFA (see for instance O(1)−C(1)−O(2) coordinating Mn(1) plus all equivalent units at the same height of $x = 0$). Halfway along the x direction and exactly over the holes of the aforementioned network the other manganese species Mn(2) is surrounded by four water molecules in a planar arrangement. This coordination of Mn(2) is completed by two formate groups lying *trans* to each other (see the equivalent O(3)−C(2)−O(4) in Figure 3) forming crosslinks between the layers in $x = 0$ and $x = 1$. Thus the atom Mn(2) is part of a link extending from the upper left to the lower right of Figure 3.

Although the space group type of MnFD ($P12_1/c1$) is a subgroup of that of MnFA ($P2_1/n2_1/c2/a$), it is not possible that a simple displacive transition is taking place. Instead the mechanism has to be discontinuous due to the loss of the crystal water, causing a dramatic shrinkage of the unit cell along [100]. Whereas in the lower symmetry phase of the dihydrate Mn(1) and Mn(2) both lie on inversion centres, in *Pnca* they are grouped around the centres of inversion necessitating a rearrangement of the structure. The

 © 2003 Wiley-VCH Verlag GmbH & Co. KGaA, Weinheim

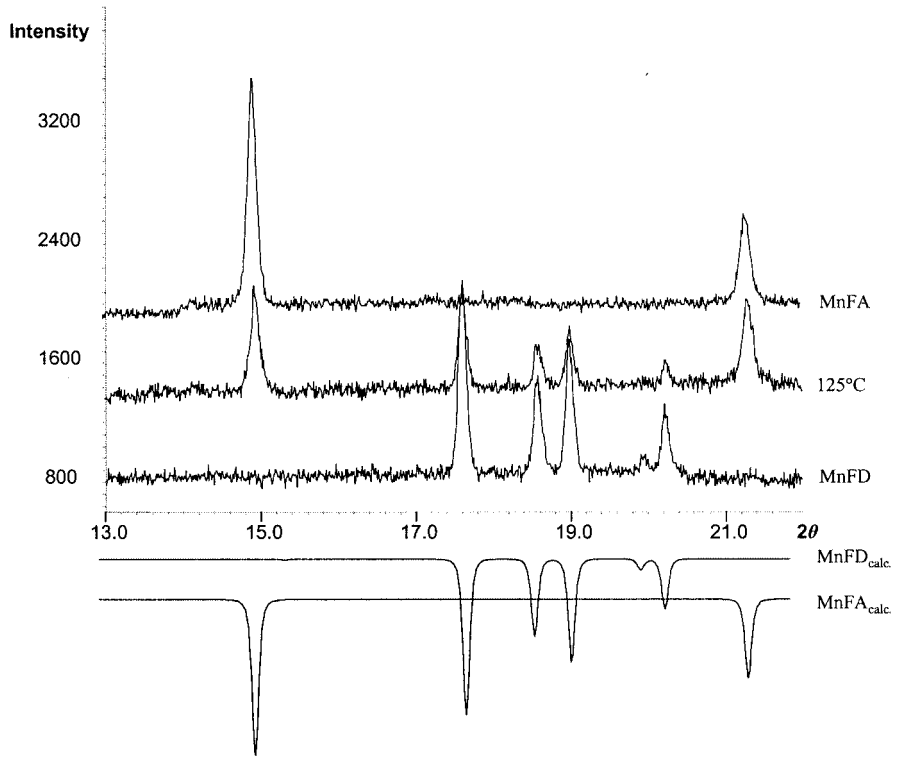

Figure 4. Heating powder diagrams with Cu-$K_{\alpha 1}$ radiation show the coexistence of MnFA and MnFD at an intermediate stage of the dehydration; for comparison the calculated patterns for MnFD and MnFA are given

shorter arrows of Figure 3 merely result from the convention that one of the centres of inversion in MnFA must be chosen to coincide with the origin of the unit cell. As indicated by the longer arrows of Figure 3 the topology of the anhydrous phase in Figure 2 is reproduced by virtue of a transverse move of Mn(2^{vii}) which brings it closer to Mn(1) and Mn(1^{viii}) in the upper and lower layer. The required relative shift in the **c**-direction amounts to ca. 2.77 Å. While in MnFD the distance between Mn(1) and Mn(2^{vii}) is 6.054(2) Å, and between Mn(1^{viii}) and Mn(2^{vii}) 6.917(2) Å, the distance between Mn and Mn^{i} in MnFA, is only 3.539(1) Å (see Table 1). These observations suggest an insertion mechanism on a local scale, which has the advantage that none of the existing bonds to formate groups need to be broken. With loss of the water ligands, the coordinatively-deficient Mn centres −OCHO−Mn(2)−OCHO− reorient themselves to gain additional coordination from formate oxygens O(1) and O(4), which as a consequence are now μ_2-bridging between Mn(1) and former Mn(2) centres, resulting in the zig-zag chains of crystallographically-equivalent Mn centres running along **a** in the structure of MnFA. This process requires a considerable contraction of the MnFD lattice in the **a**-direction amounting to ca. 2.98 Å.

It is remarkable that these large shifts are possible in a topotactical reaction without causing complete destruction of the crystal. As the broad reflections show the anhydrous phase consists of small domains. Their growth seems to start from numerous nucleation sites under the orienting influence of the parent phase MnFD. Similar observations have been reported for the dehydrations of brucite to periclase and of goethite to haematite and magnetite.[25]

Quite naturally nothing can be said by X-ray diffraction about the sequence of steps during the dehydration process. Here the topologies of MnFD and MnFA are simply compared leading to the conclusion that the reaction proceeds topotactically, such that the orientational relationship between both phases is preserved. Although the solid-state process is necessarily reconstructive, it seems to take place surprisingly smoothly.

The IR spectrum of MnFA is simpler than that of MnFD (Table 2); this is consistent with the two structures. Whereas in MnFD there are two inequivalent formate anions in the lattice, and several of the formate vibrational modes give rise to a pair of absorptions, there is only one independent anion in MnFA, and single bands are observed.

Full factor-group analyses for the two IR spectra predict three IR-active modes per formate "molecular" mode in the spectrum of MnFA, and four in the spectrum of MnFD. However, the numbers of observed bands is consistent with the simple molecular analysis.

In addition, there are no absorption bands from water in the MnFA spectrum. The IR spectrum for MnFA corresponds to the spectrum reported by Baraldi[26] for β-MnFA. Baraldi reported this β-MnFA as a metastable phase on the path towards α-MnFA which he identified only by IR spectroscopy. Since we do not observe this α-phase, we cannot say definitively which one is the thermodynamically more stable.

 © 2003 Wiley-VCH Verlag GmbH & Co. KGaA, Weinheim

Table 2. Wavenumbers (cm^{-1}) of the IR absorptions for solid MnFD and MnFA (s: strong, w: weak, sh: shoulder, vw: very weak, br.: broad, m: medium)

vibration[27]	MnFD[26]	MnFA
$\nu_{OH,aq}$	3360 s	
	3290 s	
	3220 sh	
$2\nu_4$	2995 vw	3002 w
$\nu_2 + \nu_4$	2940 vw	2935 sh
ν_1, CH stretch	2896 m	2906 m
	2890 vw	
$2\ \nu_5$	2760 w	2783 w
δ_{aq}	1666 w	
ν_4, OCO stretch, asym	1585 s	1602 s
ν_5, OCO deformation, asym	1397 s	1398 s
	1391 s	
	1370 w	
ν_2, OCO stretch, sym	1370 w	1342 s
	1362 s	
ν_6, out-of-plane deformation	1074 vw	1058 vw
ν_3, OCO-deformation, sym	830 w	793 s
	758 s	
γ_{aq}	695 w, br.	
	572 m	

The magnetic behaviour of MnFD has been thoroughly studied.[28] The magnetic susceptibility measurements on MnFA show all the characteristics of a three-dimensional antiferromagnet (Figure 5). The χ^{-1} vs. T plot for temperatures higher than 10 K leads to a Curie temperature Θ of -13.2 K and a Curie constant C of 4.24 emu mol^{-1} K^{-1} which corresponds to the g-factor of 1.97. Every manganese atom has two nearest manganese neighbours along the μ_2-oxygen-bridged chain [3.539(1) Å] and eight further manganese neighbours linked by four *syn-anti* formate bridges [5.475(1) Å] and four *anti-anti* formate bridges [6.052(1) Å]. With its ten direct neighbours the antiferromagnetic coupling of -3.12 cm^{-1} per manganese atom corresponds to an average coupling of -0.31 cm^{-1} $\Theta = 1/3\ S(S+1)\ \Sigma\ J$ with $S = 5/2$ and $\Sigma\ J$ is the sum over all interaction constants for each Mn).

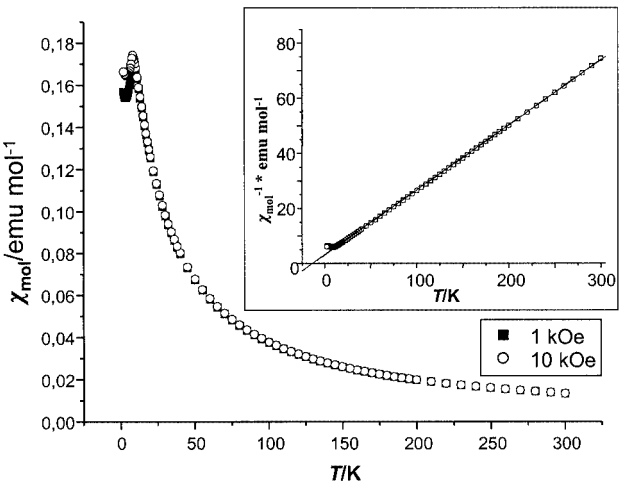

Figure 5. Plot of the magnetic susceptibility, χ_{mol}, of MnFA as a function of temperature in the range of 1.9 to 300 K; the inset shows a plot of χ_{mol}^{-1} versus T

Table 3. Crystal data and details of structure refinement

	MnFD	MnFA	MnFA[a]
Formula	$C_2H_6MnO_6$	$C_2H_2MnO_4$	$C_2H_2MnO_4$
Molecular weight	181.00	144.97	144.97
Crystal system	monoclinic	orthorhombic	orthorhombic
Space group	$P2_1/c$ (no. 14)	*Pnca* (no. 60)[b]	*Pnca* (no. 60)[b]
Temperature [K]	200±1	200±1	200±1
a [Å]	8.7882(18)	5.8127(8)	5.826(5)
b [Å]	7.2164(17)	7.5093(16)	7.549(7)
c [Å]	9.578(2)	9.4923(14)	9.565(10)
β [°]	97.64(3)	90[c]	90[c]
Volume [Å^3]	602.1(2)	414.33(12)	420.7(7)
Z	4	4	4
D_c [g cm^{-3}]	1.997	2.324	2.289
μ [Mo-K_α] [mm^{-1}]	2.154	3.064	3.018
Crystal size [mm]	0.10×0.20×0.20	0.25×0.20×0.20	0.10×0.20×0.20
Crystal shape	pale pink hexagonal plate with (100) dominant	pale pink block cut from needle along [100]	off-white, opaque plate
2θ range [°]	7.3−52.2	8.6−52.3	6.9−54.1
Reflection measured	2251	3897	632
Independent reflections	1038	402	382
R_{int}	0.0289	0.0506	0.0491
observed reflections [$I > 2\sigma(I)$]	856	341	262
wR_2 (all data)	0.0793	0.0833	0.1857
Goodness of fit	1.056	1.059	1.062
R_1 [$I > 2\sigma(I)$]	0.0273	0.0292	0.0568
parameters	109	37	28
max. diff. peak/hole [e·Å^{-3}]	+0.349/−0.303	+0.381/−0.373	+0.812/−0.723

[a] MnFA obtained by dehydration of a single crystal. [b] Non-standard setting of *Pbcn* (no. 60) (see text). [c] For symmetry reasons.

 © 2003 Wiley-VCH Verlag GmbH & Co. KGaA, Weinheim

With reference to *J*-values, which are reported for Mn−O(R)−Mn ($J = -1$ to $-5\ cm^{-1}$)[29] and Mn−O−C(R)−O−Mn interactions ($J = -0.2$ to $-0.3\ cm^{-1}$)[30] we can predict that the interactions between manganese atoms within the μ_2-oxygen-bridged chain should be stronger than between adjacent chains. Although the interchain interactions are probably an order of magnitude weaker than the intrachain ones there are four times as many such interactions between the chains as along them, and these may therefore be significant with regard to the three-dimensional antiferromagnetic behaviour. These would require three *J* values and fitting the data in this way would have led to overparametrisation. Antiferromagnetic ordering starts at 8 K, and the spinflop field is 1.2(1) Ts.

Conclusion

We have shown that the crystal structure of anhydrous manganese(II) formate is topotactically related to the structure of manganese(II) formate dihydrate. It can be obtained either by solvothermal reaction or, surprisingly, by the topotactical dehydration of MnFD. Although the μ_2-oxygen-bridges in MnFA lead to one-dimensional chains of oxygen-bridged manganese atoms the additional interchain interactions via formate bridges result in a three-dimensional antiferromagnetic behaviour.

Experimental Section

MnFD was synthesized as reported previously.[16]

Synthesis of $Mn(O_2CH)_2$ (1): $Mn(O_2CH)_2$ was obtained by solvothermal reaction in a steel autoclave with a Teflon-insert of internal volume 10 mL. In a typical experiment $Mn(O_2CH)_2{\cdot}2H_2O$ (0.2 g, 1.1 mmol) was heated in 3 mL of formic acid to 140 °C. During the experiment (88 h) the CO_2 produced as a result of the decomposition of formic acid raises the pressure to such an extent, that in the initial experiment the lid of the Teflon-insert is punctured resulting in the evaporation of the remaining solvent. Subsequently these conditions were reproduced by slightly loosening the autoclave lids to act as a vent in order to avoid damage of the insert. A quantitative yield of needle-like pink crystals of MnFA was obtained. X-ray powder diffraction and TG experiments showed that the product was pure and contained no dihydrate.

X-ray Crystallography: Single-crystal data were measured on a Stoe IPDS image plate area detector diffractometer using graphite-monochromatised Mo-K_α radiation ($\lambda = 0.71073$ Å). Structures were solved by direct methods and refined by full-matrix least-squares against F^2 (all data) using the SHELXTL software package.[31] Non-hydrogen atoms were assigned anisotropic thermal parameters; hydrogen atoms were fully refined with isotropic temperature factors. CCDC-200199 and -200200 contain the supplementary crystallographic data for this paper. These data can be obtained free of charge at www.ccdc.cam.ac.uk/conts/retrieving.html [or from the Cambridge Crystallographic Data Centre, 12, Union Road, Cambridge CB2 1EZ, UK; Fax: (internat.) +44−1223/336−033; E-mail: deposit@ccdc.cam.ac.uk].

Single-crystal photographs were taken on a Buerger precession camera from Huber (Mo radiation). The specimen was heated using a modified Enraf−Nonius FR 559 crystal heater,[32] with which the temperature of the crystal is maintained and controlled by a hot gas stream.

X-ray Powder Diffraction: The X-ray powder patterns were measured on a Stoe STADI P diffractometer using Cu-$K_{\alpha 1}$ radiation (Ge monochromator) and Debye−Scherrer geometry. The sample was placed in an open glass capillary and heated using a Stoe high-temperature attachment.

Thermal Analysis: The differential thermal analysis (DTA) and the thermogravimetry (TG) experiments were carried out using a Netzsch STA 409C system. Samples were heated in Al_2O_3 crucibles with a heating rate of $1\ K\ min^{-1}$ up to 600 °C under a nitrogen atmosphere with flow rate $30\ L\ h^{-1}$.

Susceptibility Measurement: Magnetic measurements were carried out with a Quantum-Design MPMS SQUID magnetometer. The powder sample was placed in a quartz tube and the susceptibility measured in the temperature range from 300 to 1.9 K.

IR Spectroscopy: FTIR spectra were measured using KBr pellets of the sample in the range from 4000 to $400\ cm^{-1}$ with a Perkin−Elmer Spectrum One spectrometer. For each spectrum four scans were measured at a resolution of $4\ cm^{-1}$.

Acknowledgments

We would like to thank PD Dr. Bernd Pilawa for help with the interpretation of the magnetic data.

[1] R. D. Cannon, R. P. White, *Prog. Inorg. Chem.* **1988**, *36*, 195−298.
[2] T. Lis, *Acta Crystallogr., Sect. B* **1980**, 2042−2046.
[3] [3a] H. J. Eppley, H.-L. Tsai, N. de Vires, K. Folting, G. Christou, D. N. Hendrikson, *J. Am. Chem. Soc.* **1995**, *117*, 301−317. [3b] S. M. J. Aubin, Z. Sun, I. A. Guzei, A. L. Rheingold, G. Christou, D. N. Hendrikson, *Chem. Commun.* **1997**, 2239−2240.
[4] [4a] Z. A. D. Lethbridge, A. D. Hiller, R. Cywinski, P. Lightfoot, *Dalton Trans.* **2000**, 1595−1599. [4b] P. A. Prasad, S. Neeraj, S. Natarajan, C. N. R. Rao, *Chem. Commun.* **2000**, 1251−1252. [4c] Z. A. D. Lethbridge, S. K. Tiwary, A. Harrison, P. Lightfoot, *Dalton Trans.* **2001**, 1904−1910.
[5] J. D. Martin, R. F. Hess, *Chem. Commun.* **1996**, 2419−2420.
[6] G. A. Tikhomirov, K. O. Znamenkov, I. V. Morozov, E. Kemnitz, S. I. Troyanov, *Zeitschr. Anorg. Allg. Chem.* **2002**, *28*, 296−273.
[7] R. W. G. Wyckoff, *American Journal of Science* **1920**, *50*, 317−360.
[8] J. L. Galigné, *Acta Crystallogr., Sect. B* **1971**, 2429−2431.
[9] K. Osaki, Y. Nakai, T. Watanabe, *J. Phys. Soc. Jap.* **1963**, *18*, 919.
[10] D. Stoilova, St. Peter, H. D. Lutz, *Zeitschr. Anorg. Allg. Chem.* **1994**, *620*, 1793−1798.
[11] F. Sapina, M. Burgos, E. Escrivá, J.-V. Folgado, D. Marcos, A. Beltrán, D. Beltrán, *Inorg. Chem.* **1993**, *32*, 4337−4344.
[12] G. Weber, *Actc Cryst. Sect. B* **1980**, 1947−1949.
[13] E. Kalalova, V. Ruzicka, *Coll. Czech. Chem. Commun.* **1962**, *27*, 424−429.
[14] [14a] R. C. Eckhardt, P. M. Fichte, T. B. Flanagan, *Trans. Faraday. Soc.* **1971**, *67*, 1143−1154. [14b] Y. Masuda, M. Hatakeyama, *Talanta* **1996**, *43*, 1705−1709. [14c] Y. Masuda, M. Hatakeyama, *Thermochim. Acta* **1998**, *308*, 165−170.
[15] D. Dollimore, J. P. Gupta, D. V. Nowell, *Thermochim. Acta* **1979**, *30*, 339−350.
[16] R. C. Eckhardt, T. B. Flanagan, *Trans. Faraday Soc.* **1964**, *60*, 1289−1298.

 © 2003 Wiley-VCH Verlag GmbH & Co. KGaA, Weinheim

[17] C. Malard, *C. R. Acad. Sc. Paris Ser. C* **1966**, 263, 480−483.
[18] T. Arii, A. Kishi, Y. Kobayashi, *Thermochim. Acta* **1999**, *325*, 151−156.
[19] G. Périnet, *Bull. Soc. franc. Minér. Crist.* **1966**, *89*, 325−328.
[20] T. Arii, A. Kishi, *Thermochim. Acta* **1999**, *325*, 157−165.
[21] V. Z. Vassileva, A. L. Karapetkova, *Bulg. Chem. Commun.* **1995**, *28*, 151−159.
[22] G. Weber, *Zeitschr. f. Krist.* **1982**, *158*, 315−318.
[23] B. Krebs, *Angew. Chem.* **1969**, *81*, 120; *Angew. Chem. Int. Ed. Engl.* **1969**, *8*, 146−147.
[24] M. Elder, B. R. Penfold, *Inorg. Chem.* **1966**, *5*, 1197−1200.
[25] [25a] U. Dahmen, M. G. Kim, A. W. Searcy, *Ultramicroscopy* **1987**, 23, 365−370. [25b] J. Lima-de-Faria, *Acta Crystallogr.* **1967**, 23, 733−736.
[26] P. Baraldi, *Spectrochim. Acta* **1979**, *35A*, 1003−1007.
[27] J. D. Donaldson, J. F. Knifton, S. D. Ross, *Spectrochim. Acta* **1964**, *20*, 847−51.
[28] [28a] P. Burlet, P. Burlet, J. Rossat-Mignod, A. de Combarieu, E. Bedin, *Phys. Stat. Sol.* **1975**, *71*, 675−685. [28b] P. Radhakrishna, B. Gillon, G. Chevier, *J. Phys.: Condens. Matter* **1993**, *5*, 6447−60.
[29] [29a] G. S. Papaefstathiou, R. Vicente, C. P. Raptopoulou, A. Terzis, A. Escuer, S. P. Perlepes, *Eur. J. Inorg. Chem.* **2002**, 2488−2493. [29b] G. Aromí, P. C. Berzal, P. Cames, O. Roubeau, H. Kooijman, A. L. Spek, W. L. Driessen, J. Reedijk, *Angew. Chem.* **2001**, *113*, 3552−3554; *Angew. Chem. Int. Ed.* **2001**, *40*, 3444−3446. [29c] M. D. Carducci, R. J. Doedens;, *Inorg. Chem.* **1989**, *28*, 2492−2494.
[30] V. Tangoulis, G. Psomas, C. Dendrinou-Samara, C. P. Raptopoulou, A. Terzis, D. P. Kessissoglou, *Inorg. Chem.* **1996**, *35*, 7655−7660.
[31] G. M. Sheldrick, *SHELXTL 5.1*, Bruker AXS Inc., Madison, WI, **1997.**
[32] B. Anselment, Dissertation, Universität Karlsruhe, **1986**.

Received December 20, 2002

 © 2003 Wiley-VCH Verlag GmbH & Co. KGaA, Weinheim

Hybrid Organic/Inorganic Molecular Materials Formed by Tetrathiafulvalene Radicals and Magnetic Trimeric Clusters of Dimetallic Oxalate-Bridged Complexes: The Series $(TTF)_4\{M^{II}(H_2O)_2[M^{III}(ox)_3]_2\}\cdot nH_2O$ (M^{II} = Mn, Fe, Co, Ni, Cu and Zn; M^{III} = Cr and Fe; ox = $C_2O_4^{2-}$)

Eugenio Coronado,*[a] José Ramón Galán-Mascarós,[a] Carlos Giménez-Saiz,[a] Carlos J. Gómez-García,[a] and Catalina Ruiz-Pérez[b]

Keywords: Coordination chemistry / Hybrid materials / Magnetic properties / O ligands

The first examples of trimeric, dimetallic, pure oxalate-bridged complexes [ox = $(C_2O_4)^{2-}$] have been synthesized and characterized structurally and magnetically for the two new series of crystalline molecular assemblies formulated as $(TTF)_4\{M^{II}(H_2O)_2[M^{III}(ox)_3]_2\}\cdot nH_2O$ [for M^{III} = Cr; M^{II} = Mn (**1**), Fe (**2**), Co (**3**), Ni (**4**), Cu (**5**) and Zn (**6**); for M^{III} = Fe; M^{II} = Mn (**7**), Fe (**8**), Co (**9**), Ni (**10**) and Zn (**11**)]. Both series (Cr_2M and Fe_2M) are isostructural. The crystal structure of $(TTF)_4\{Mn(H_2O)_2[Cr(ox)_3]_2\}14H_2O$ (**1**) [monoclinic, space group *C*2/*c* (no. 15), *a* = 13.240(5) Å, *b* = 19.450(5) Å, *c* = 27.690(5) Å, β = 97.63(5)°, *V* = 7068(3) Å^3 and *Z* = 4] shows alternating layers of the organic radical TTF, arranged in an unprecedented one-dimensional κ-type phase formed by parallel chains of orthogonal dimers along the *a* axis, and layers of centrosymmetrical Cr–Mn–Cr trimers with oxalate bridges. The magnetic measurements show ferromagnetic coupling within the trimers for the Cr_2M series and antiferromagnetic for the Fe_2M series, giving rise to high-spin molecules in both cases [*S* = 11/2, 10/2, 9/2, 8/2 and 7/2 in compounds (**1**–**5**), respectively, and *S* = 5/2, 6/2, 7/2 and 8/2 in compounds (**7**–**10**), respectively]. These high-spin ground states are confirmed by magnetization measurements at 2 K. The ESR spectra of all compounds confirm the presence of the metals and a small amount of isolated TTF radical in all the samples, which is typical for these kinds of radical salts.

(© Wiley-VCH Verlag GmbH & Co. KGaA, 69451 Weinheim, Germany, 2003)

Introduction

The discovery at the beginning of the 1990s of the ferromagnetic molecular material $\{NBu_4[CuCr(ox)_3]\}_x$ [ox = $(C_2O_4)^{2-}$], based on an oxalate-bridged two-dimensional dimetallic lattice,[1,2] has increased the interest in the oxalate ion as a bridging ligand to construct polynuclear complexes and extended lattices of transition metal ions of variable dimensionality in the search for new molecule-based magnets.[3,4] Thus, an extended family of two-dimensional dimetallic phases, formulated as $Bu_4N[M^{II}M^{III}(ox)_3]$ (M^{II} = Cr, Mn, Fe, Co, Ni and Cu; M^{III} = Cr, Fe and Ru),[5–11] has been obtained through the reaction of the chelate anions $[M^{III}(ox)_3]^{3-}$ with divalent first-row transition metal cations. These three series (M^{III} = Cr, Fe and Ru) behave as ferro- or ferrimagnets with critical temperatures ranging from 1.7 to 44 K, with the exception only of $Cr^{II}Cr^{III}$, which shows short-range antiferromagnetic interactions.[11]

Several attempts have been made to improve these transition temperatures. Substitution of the oxalate bridges by dithiooxalate (dto = $[C_2S_2O_2]^{2-}$) has led to the family of extended dimetallic assemblies of formula $Pr_4N[MCr(dto)_3]$ (M = Fe, Co, Ni and Zn).[12] Except for the Zn derivative, all the other members of this family behave as ferromagnets with T_c ranging from 8 to 23 K.

A more profound effect on the magnetic properties has been accomplished when mixtures of Cr^{III}, Fe^{III} and Ru^{III} were used for the construction of the anionic 2-D networks.[13] In this case, the competence of ferromagnetic $M^{II}-M^{III}$ (M^{III} = Cr and Ru) and antiferromagnetic $M^{II}-M^{III}$ (M^{III} = Fe) interactions within the magnetic layers increases the coercivity of these materials by at least one order of magnitude, and can be tuned depending on the metallic ratio in the solid. Thus, the series $[A][Fe^{II}Fe^{III}_xCr^{III}_{(1-x)}(ox)_3]$ presents a coercive field of 1.23 T for $x = 0.75 \pm 0.05$ with $A^+ = Bu_4N$ and 1.67 T for $x = 0.52 \pm 0.05$ with $A^+ = CoCp_2^*$.[14] This high coercive field can be increased up to 2.20 T in the series

[a] Instituto de Ciencia Molecular, Universidad de Valencia, Dr. Moliner 50, 46100 Burjasot, Spain
Fax:(internat.) + 34-96/354-4859
E-mail: eugenio.coronado@uv.es
[b] Laboratorio de Rayos X y Materiales Moleculares, Departamento de Física Fundamental II, Universidad de La Laguna, Avda. Astrofísico Francisco Sánchez s/n, 38204 La Laguna, Spain

Supporting information for this article is available on the WWW under http://www.eurjic.org or from the author.

$[A][Fe^{II}Ru^{III}_{x}Fe^{III}_{(1-x)}(ox)_3]$ for $x = 0.53$ with $A^+ = CoCp^*_2$.[15]

Another strategy consists of increasing the dimensionality of the lattice. Homo- and dimetallic chiral three-dimensional (3-D) oxalate-bridged networks ($[M^{II}_2(ox)_3]_n^{2n-}$ and $[M^{III}M^{I}(ox)_3]_n^{2n-}$) were prepared by using the triply chelated cations $[Z^{II}(bpy)_3]^{2+}$ and $[Z^{III}(bpy)_3]^{3+}$, where bpy is 2,2′-bipyridine.[3,16] Nevertheless, all these 3-D networks present antiferromagnetic exchange interactions, but no long-range order, except for two Co^{II} derivatives[17] (for the homometallic 3-D networks), or paramagnetic behaviors when M^{I} (alkali metal) isolates the magnetic M^{III} (Fe^{III} or Cr^{III}) metal ions in the network. More recently we have succeeded in preparing analogous dimetallic 3-D phases with a divalent (M^{II}) and a trivalent metal ion (Cr^{III}) connected through the oxalato bridges to give the anionic 3-D net of formula $[Cr^{III}M^{II}(ox)_3]_n^{n-}$.[18] These series contain the chiral $[Z^{II}(bpy)_3]^{2+}$ cation as counterion, which imposes the same overall chirality to the crystals. The series can be formulated as $[Z^{II}(bpy)_3](ClO_4)[Cr^{III}M^{II}(ox)_3]$ (Z^{II} = Ru, Fe, Co and Ni; M^{II} = Mn, Fe, Co, Ni, Cu and Zn). In this family of compounds we have also found, as in the related 2-D series, a ferromagnetic ordering, but at lower temperatures because of the weaker magnetic interactions between the metallic centers as a consequence of a loss of planarity in the oxalato bridge. It is noteworthy to mention that these series represent one of few examples of chiral magnets known to date.[19,20]

In addition to the possibility of modifying the magnetic polymeric structure, these magnetic systems allow us to use a novel approach to multiproperty materials. For instance, in all the cases where the 2-D oxalate-bridged networks are formed, the organic counterions (R_4X^+: X = N, P; R = *n*-alkyl or phenyl) are located between the anionic layers and determine the creation of the 2-D network and, at the same time, the interlayer separation. The idea of replacing these "inert" counterions by "electroactive" molecules, which could add a new property (magnetic, electrical or optical) to the material, can be used to prepare new multilayered materials presenting alternating layers and, thus, two alternating properties, resulting in coexistence or even synergy between them.

Our first attempt to construct magnetic-magnetic multilayered materials in this way was to prepare the series $[FeCp^*_2][M^{II}M^{III}(ox)_3]$ (M^{II} = Mn, Fe, Co, Ni and Cu; M^{III} = Cr and Fe), by using the paramagnetic ($S = 1/2$) decamethylferrocenium counterion.[21] The magnetic behavior of these series is roughly the same as that found for the tetrabutylammonium salts, indicating that the presence of paramagnetic units between the layers has no effect upon the magnetic ordering. The synthesis of optical-magnetic layered materials by using organic NLO-active cations, such as the $DAMS^+$ ion, has also been reported.[22] In this case, both properties are present in the material, but are completely independent from one another.

Maybe the most interesting possibility is that of preparing conducting-magnetic layered materials. In this direction, one of the most appealing possibilities is the radical cation of TTF derivatives, since TTF-type donors constitute the most widely used molecules in the synthesis of molecular conductors and superconductors.[23] In this context, the use of the organic donor bis(ethylenedithio)tetrathiafulvalene (BEDT-TTF or ET) has already led to two important discoveries in molecular materials science: the first superconductor with paramagnetic metal ions, the radical salt $(BEDT\text{-}TTF)_4(H_3O)[Fe(ox)_3]$;[24,25] and the first molecular metallic ferromagnet $(BEDT\text{-}TTF)_3[MnCr(ox)_3]$ where layers of the organic radical BEDT-TTF alternate with the ferromagnetic layers $[MnCr(ox)_3]^-$.[26] In the latter case, a cooperative magnetic property (ferromagnetism in the oxalato layer) coexists for the first time with another cooperative property (the metallic behavior of the ET layer) in a molecule-based material.

According to this approach, but using the organic donor tetrathiafulvalene (TTF), we have synthesized a new series of molecular assemblies that combine oxalate-bridged dimetallic complexes and TTF donors. Here we report the synthesis, structure and magnetic charaterization of this new series of compounds that can be formulated as $TTF_4\{M^{II}(H_2O)_2[M^{III}(ox)_3]_2\}\cdot nH_2O$ (M^{III} = Cr and Fe; M^{II} = Mn, Fe, Co, Ni, Cu and Zn) and that constitute the first hybrid compounds based on dimetallic $M^{II}M^{III}$ oxalate complexes and TTF molecules.[27]

Results and Discussion

Structure of $TTF_4\{Mn(H_2O)_2[Cr(ox)_3]_2\}\cdot 14H_2O$ (1)

Although all members of both the Cr_2M^{II} (M^{II} = Mn, Fe, Co, Ni, Cu and Zn) and Fe_2M^{II} (M^{II} = Mn, Fe, Co, Ni and Zn) series are crystalline, single crystals suitable for X-ray structure determination were obtained only for the Cr_2Mn (**1**) and Fe_2Fe (**8**) compounds. According to their unit cells, both compounds appeared to be isostructural. Thus, the crystal structure was determined only for the Cr_2Mn compound, because of the better quality of the single crystals. The isostructurality of all the other members of both series was checked by X-ray powder diffraction, which showed an isomorphous pattern for each, and similar unit cells (see Supporting information). In the case of the Cr_2Cu compound, small differences observed in the X-ray powder pattern suggest that, although it is a compound analogous to the others, some small crystallographic differences must be present, in agreement with its magnetic properties (see below).

The structure of **1** consists of alternating layers of the organic donor tetrathiafulvalene (TTF) and the trimeric linear complex $\{Mn(H_2O)_2[Cr(ox)_3]_2\}^{4-}$ laying in the *ab* plane (Figure 1). The asymmetric unit is formed by a complete TTF molecule, two half-TTF molecules and half a trimer. There are, therefore, four TTF molecules per trimer. The centrosymmetric linear $Cr^{III}-Mn^{II}-Cr^{III}$ trimers are formed by two octahedral $[Cr(ox)_3]^{3-}$ entities connected via an Mn^{2+} ion (Figure 2). The Mn atom, which is located at an inversion center, is surrounded by two bis(bidentate) oxalate anions, one from each $[Cr(ox)_3]^{3-}$ unit, and com-

 © 2003 Wiley-VCH Verlag GmbH & Co. KGaA, Weinheim

pletes its octahedral coordination with two water molecules in the axial positions. The $Mn-O_w$ distances for these two water molecules are shorter [Mn−O1 = 2.160(5) Å] than the $Mn-O_{ox}$ distances in the equatorial plane [Mn−O2 = 2.170(12) Å and Mn−O3 = 2.240(11) Å]. The long Mn−O3 distance produces a decrease in the chelate angle O2−Mn−O3, which is only 76.5(4)°. The two Cr^{III} atoms are made equivalent by the inversion center located on the Mn^{II} atom and they are surrounded by three bidentate oxalate groups, such as the $[Cr(ox)_3]^{3-}$ anion, sharing one of the oxalate groups with the central Mn atom. The Cr−O bond lengths [from 1.930(13) Å to 2.001(10) Å] are more homogeneous than those in the Mn^{II} environment. The average Cr−O distance (1.968Å) is very similar to those found for the free $[Cr(ox)_3]^{3-}$ anion in the K^+ and H_4N^+ salts (1.971 and 1.969, respectively),[28] indicating that the anion maintains its original geometry and size despite sharing one of the oxalate groups with the Mn^{2+} ion. In fact, the three O−Cr−O chelate angles between the two oxygen atoms of each oxalate group [81.4(4), 81.8(4) and 83.6(4)°] are very similar to those of the isolated anion [82.0(2), 82.1(2) and 82.4(2)°].[29]

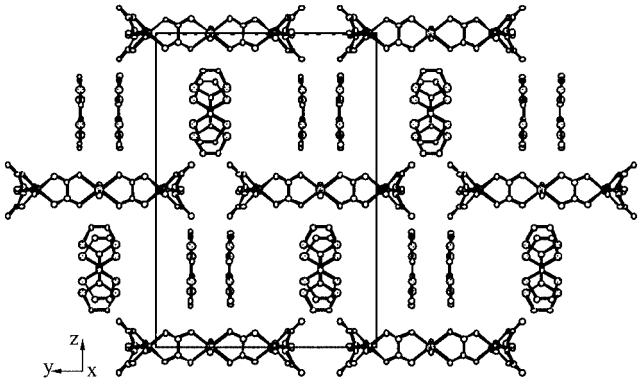

Figure 1. View of the unit cell of the salt $TTF_4\{Mn(H_2O)_2[Cr(C_2O_4)_3]_2\}$ (**1**) showing the alternating organic/inorganic layers in the *ab* plane

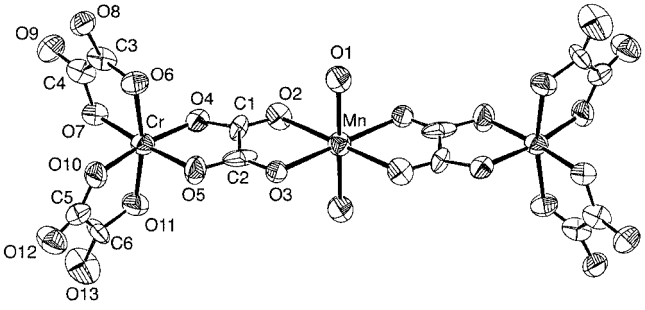

Figure 2. ORTEP representation (50% probability) of the $[Mn(H_2O)_2[Cr(C_2O_4)_3]_2]^{4-}$ anion showing the two $Cr(C_2O_4)_3$ units connected by the Mn ion

The dimetallic trimers form a 2-D framework wherein each trimer is connected by eight intermolecular hydrogen bonds [four O_w-O_{ox} distances of 2.740(11) Å and four of 2.760(12) Å] to its four nearest neighbors. These hydrogen bonds are formed between the water molecules coordinated to the Mn atom and one free oxygen atom from one of the terminal oxalate groups of the surrounding trimers (Figure 3). The dimetallic 2-D network can be described, therefore, as a pseudo-hexagonal lattice wherein each Mn^{II} atom is surrounded by six Cr^{III} atoms: two at 5.492(19) Å (the Mn−Cr intra-trimer distance) and four at 7.860(19) Å (the Mn−Cr inter-trimer distance) and each Cr^{III} atom is surrounded by three Cr^{III} ions [two at 6.740(19) Å and one at 8.480(19) Å] and three Mn^{II} ions [one at 5.490(19) Å and two at 7.860(19) Å].

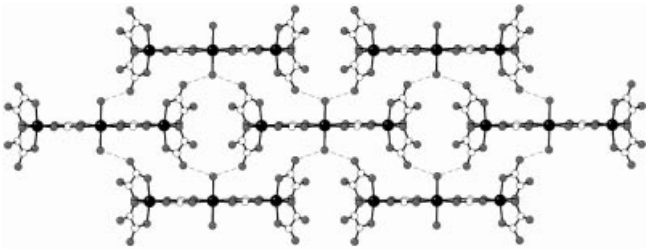

Figure 3. View of the anionic layer of the salt $TTF_4[Mn(H_2O)_2[Cr(C_2O_4)_3]_2]$ (**1**) showing the dimetallic trimers and the hydrogen bonds between them (dotted lines)

The organic layers are formed by three crystallographically independent TTF molecules, noted as **A**, **B** and **C**. These molecules form two types of eclipsed face-to-face dimers of TTF molecules (**A**−**A** and **B**−**C**) with short interplanar distances [3.410(14) and 3.370(14) Å, respectively]. The intradimer S−S distances are also very short [3.380(14) and 3.360(14) Å in the **A**−**A** and **B**−**C** dimers, respectively] and smaller than the sum of the van der Waals radii for two sulfur atoms (3.6 Å). There are two dimers (one **AA** and one **BC**) per anion. The dimers are disposed in an infinite chain formed by alternating orthogonal **AA** and **BC** dimers along the *a* axis (Figure 4). Inside the chain, both inter-dimer S−S distances also are short [3.540(13) and 3.560(14) Å for the **A**−**B** and **A**−**C** inter-dimer distances, respectively]. The neighboring chains are displaced in one dimer in such a way that the closest dimers of the neighboring chains are also orthogonal, giving rise to an infinite planar structure wherein each dimer is surrounded by four orthogonal dimers. This arrangement is similar to the so-called κ phase, which is the phase that has produced the highest number of organic superconductors in the TTF family, as well as those with the highest T_c.[23] Nevertheless, there are two features that make this κ phase original: one is that, to the best of our knowledge, this is the first time that such a phase has been observed for the donor TTF, and the other is that the intra- and inter-chain distances are not similar [the shortest inter-chain S···S distances are 6.560(19) and 6.580(19) Å, almost twice the shortest inter-dimer S···S distances inside the chains: 3.540(14) and 3.560(14) Å], whereas in the classical κ phases both distances are very close in value to one another. Thus, this

 © 2003 Wiley-VCH Verlag GmbH & Co. KGaA, Weinheim

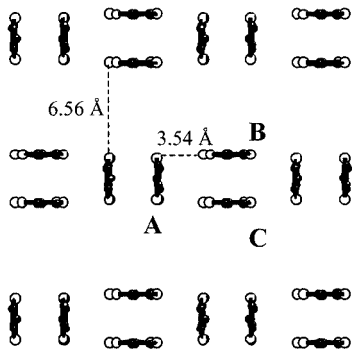

Figure 4. View of the organic layer showing the TTF dimers arranged in chains along the *a* axis and the two different intra- and inter-chain distances between dimers

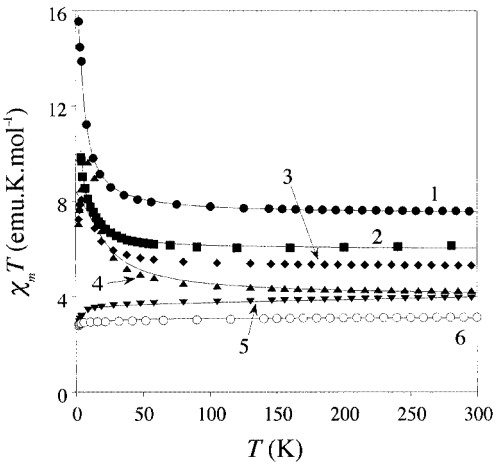

Figure 5. Plot of the value of the product $\chi_m T$ as a function of T for the Cr_2M series; M = Mn (**1**), Fe (**2**), Co (**3**), Ni (**4**), Cu (**5**) and Zn (**6**); the solid lines represent the best fit to the model (see text)

structure can be seen as a pseudo-κ or a one-dimensional-κ phase.

It is important to note that all the TTF molecules appear to be completely oxidized, according to the stoichiometry of the compound (4:1), and the charge of the anion (−4). Furthermore, the fact that these molecules are strongly dimerized, as discussed in this section, allows one to anticipate that the dimers will have no net spin from strong antiferromagnetic interactions between the unpaired electrons in each TTF molecule, and, therefore, all the magnetic contribution is expected to come from the inorganic lattice.

Magnetic Properties

(a) The Cr_2M Series

As can be seen in Figure 5, the product of the molar susceptibility and the temperature ($\chi_m T$, proportional to the square of μ_{eff}), plotted versus the temperature, shows a similar behavior for all the members of the Cr_2M family except for the Cu^{II} and Zn^{II} derivatives. Thus, compounds **1**−**4** exhibit, at room temperature, the Curie constant expected for magnetically diluted trimers Cr−M−Cr, with two independent Cr^{III} ions (S = 3/2) and an isolated M^{II} ion (with S = 5/2, 2, 3/2 and 1 for M^{II} = Mn, Fe, Co and Ni, respectively). Upon cooling, the value of the product $\chi_m T$ remains almost constant down to approx. 50 K. Below this temperature, the value of the product $\chi_m T$ increases with decreasing temperature, indicating the presence of ferromagnetic exchange interactions between the Cr^{III} and the M^{II} ions via the oxalate bridge. For the Fe^{II}, Co^{II} and Ni^{II} derivatives, the values of the products $\chi_m T$ reach maxima at approx. 3, 7 and 11 K, respectively and decrease below these temperatures. This feature is not observed in the Cr_2Mn derivative, with which no maximum is reached above 2 K. It is important to note that for the Ni^{II} derivative the increase in the value of $\chi_m T$ starts at higher temperatures and is more pronounced than for the other three derivatives, which suggests that the strongest ferromagnetic interaction occurs between the Cr^{III} and Ni^{II} ions. In all cases, the decrease in the value of the product $\chi_m T$ at very low temperature suggests the presence of a zero-field splitting of the metal ions and/or a predominant inter-trimer antiferromagnetic exchange interaction.

In the Cu^{II} and Zn^{II} derivatives of the Cr_2M series, the values of the products $\chi_m T$ at room temperature also show the Curie constants corresponding to magnetically diluted Cr−M−Cr trimers. In the Cu^{II} derivative, the value of the product $\chi_m T$, which is almost constant down to approx. 150 K, decreases smoothly below this temperature and then shows a sharper decrease below 40 K. The smooth decrease below 150 K suggests the presence of antiferromagnetic exchange interactions between the Cr^{III} and the Cu^{II} ions via the oxalate bridge, and the sharper decrease at lower temperatures indicates the presence of an extra contribution (zero-field splitting of the metal ions and/or inter-trimer antiferromagnetic exchange interactions). In the Cr_2Zn derivative, the value of the product $\chi_m T$ remains constant down to approx. 10 K, suggesting the typical paramagnetic behavior; below this temperature, a sharp decrease is observed.

The existence of antiferromagnetic exchange interactions between the Cr^{III} and the Cu^{II} ions via the oxalate bridge is surprising since a ferromagnetic coupling is expected for this pair. A possible reason is the existence of a different coordination geometry around the Cu^{II} ion, giving rise to a different structure, as indicated by the X-ray powder pattern (which is somewhat different to those of all the other members of both series). Thus, if we assume a quadrangular pyramidal structure, with the oxalate groups in the basal plane and a water molecule in the axial position, it is expected that the Cu^{II} ion should lie above the oxalate plane (as is usually found for this geometry), leading to a π-type interaction between the magnetic orbitals of the Cu^{II} ion and those of the oxalate group (see below) and, thus, to an antiferromagnetic coupling between both ions via the oxalate bridge. This idea is supported by EPR spectra (see below). It is also possible that there exists a 4 + 2 coordination, resulting from a shortening of the axial $Cu-O_w$ bond lengths and an elongation of two opposite equatorial $Cu-O_{ox}$ bonds, as a consequence of the pseudo-

 © 2003 Wiley-VCH Verlag GmbH & Co. KGaA, Weinheim

Jahn−Teller effect. This tetragonal distortion has already been observed in similar oxalate-bridged Cr−Cu−Cr trimers, which also present antiferromagnetic exchange interactions.[29] The Zn^{II} derivative behaves as a paramagnet because the diamagnetism of the Zn^{II} ion isolates the Cr^{III} ions, giving rise to a temperature-independent magnetic moment. The sharp decrease at very low temperatures indicates the antiferromagnetic inter-trimer exchange interactions that have already been mentioned, which, at least in this case, must be due to the coupling between Cr^{III} ions of neighboring trimers.

The isothermal magnetization of this series at 2 K confirms the ferromagnetic nature of the $Cr-M^{II}$ coupling and can be reproduced satisfactorily with the Brillouin function for the expected S values, although with g values smaller than those obtained from the susceptibility data. This fact is not surprising because of the presence of antiferromagnetic inter-trimer interactions and/or zero-field splitting of the ions, which are effective at low temperatures.

(b) The Fe_2M Series

The magnetic behavior of the Fe_2M series is similar to that of the Cu^{II} derivative of the Cr_2M family; all members show the Curie constant at room temperature corresponding to magnetically diluted Fe−M−Fe trimers (S = 5/2 for Fe^{III} and S = 5/2, 2, 3/2, 1 and 0 for M = Mn^{II}, Fe^{II}, Co^{II}, Ni^{II} and Zn^{II}, respectively), but when cooling each sample the value of the product $\chi_m T$ smoothly decreases below 200 K (Figure 6). The decrease becomes sharper with decreasing temperature, but at low temperatures they all present a smoothening of the slope and almost reach a plateau. Nevertheless, before the magnetic moment reaches a real plateau, a new and sharper decrease is observed at lower temperatures. This behavior is observed for all the members of the Fe_2M family, except, of course, for the Zn^{II} derivative, and indicates the presence of antiferromagnetic intra-trimer exchange interactions between the Fe^{III} and the M^{II} ions. As a result of this antiferromagnetic interaction, the resulting spin of the $Fe^{III}-M^{II}-Fe^{III}$ trimers must be $2S_{Fe} - S_M$, i.e., S = 5/2, 3, 7/2 and 4 for the Fe_2Mn, Fe_2Fe, Fe_2Co and Fe_2Ni derivatives, respectively. The tendency to reach a plateau at low temperatures confirms that the spin ground state is non-zero. Nevertheless, the presence of antiferromagnetic inter-trimer exchange interactions and/or zero-field splitting of the metal ions precludes the clear observation of the plateau and produces the observed sharp decrease in the value of the product $\chi_m T$ at low temperatures.

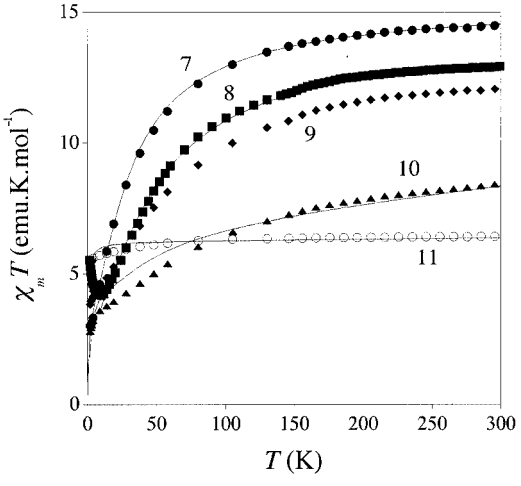

Figure 6. Plot of the value of the product $\chi_m T$ as a function of T for the Fe_2M series; M = Mn (**7**), Fe (**8**), Co (**9**), Ni (**10**) and Zn (**11**); solid lines represent the best fit to the model (see text)

As in the Cr_2M series, the isothermal magnetization of the Fe_2M series at 2 K confirms the antiferromagnetic nature of the $Fe-M^{II}$ coupling and it can be reproduced satisfactorily with the Brillouin function for the expected values of S. The values of g are also smaller than those obtained from the susceptibility data for the same reasons (vide supra).

According to the magnetic behaviors mentioned above, we have fitted the magnetic data of all compounds, except for M^{II} = Co and Zn, to a model of ferro- or antiferromagnetically coupled trimers with one exchange interaction (J) between the M^{III} and M^{II} ions (see Scheme 1).

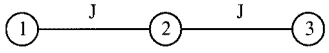

Scheme 1

The exchange Hamiltonian can be expressed as: $H_{ex} = -2J\ (S_1{*}S_2 + S_2{*}S_3)$, where S_1, S_2 and S_3 are the spin states of the metallic ions of the trimers (see Scheme 1). We have assumed that the exchange integral is the same for both interactions inside the trimer as they are equivalent by symmetry.

By using the Kambé method,[30] we obtained an analytical expression of the energy levels as a function of J for all the spin states of the trimers, where $S^* = S_1 + S_3$ and $S_T = S^* + S_2$.

$$E_i = -J\,[S_T(S_T + 1) - S^*(S^* + 1) - S_2(S_2 + 1)] \quad (1)$$

Finally, the susceptibility is obtained with the Van Vleck equation [Equation (2)].

$$\chi_m T = \left(\frac{N g^2 \mu_B^2}{k_B}\right) \frac{\sum_i a_i \exp\left(\frac{-E_i}{k_B T}\right)}{\sum_i b_i \exp\left(\frac{-E_i}{k_B T}\right)} \quad (2)$$

The values of the coefficients a_i and b_i, as well as the energy E_i, as a function of J, for all the spin states of the trimers Cr_2M (M^{II} = Mn, Fe, Ni and Cu) and Fe_2M (M^{II} = Mn, Fe, Ni and Cu) are listed in the Supporting information.

The applied model reproduces the magnetic behavior of all the studied compounds very well (solid lines in Figures 5 and 6). For the Zn derivatives, in both families the magnetic behaviors correspond to those of isolated Cr^{III} or Fe^{III} ions

 © 2003 Wiley-VCH Verlag GmbH & Co. KGaA, Weinheim

because of the isolating effect of the diamagnetic central Zn^{II} ion. Nevertheless, both compounds show a decrease in the value of the product $\chi_m T$ that can be reproduced well, modeled with the Curie−Weiss equation law [Equation (3)] using a weak antiferromagnetic inter-trimer interaction.

$$\chi_m = C/(T - \theta) \quad (3)$$

The magnetic parameters obtained with Equations (2) and (3) are displayed in Table 1. The ferromagnetic coupling found in the Cr_2M series is important for two reasons: first, because this ferromagnetic interaction leads to high-spin trimeric clusters comprising a large number of parallel unpaired electrons in the ground state (S = 11/2, 10/2, 9/2 and 8/2 for M^{II} = Mn, Fe, Co and Ni, respectively); second, because it confirms that the exchange interaction is ferromagnetic in oxalate-bridged $Cr^{III}-M^{II}$ systems. In fact, the exchange interactions obtained in our complexes (see Table 1) are in fair agreement with those reported in other oxalate-bridged dinuclear $Cr^{III}-M^{II}$ complexes where J values of 0.5 cm^{-1} (for M^{II} = Mn), 0.8 cm^{-1} (for M^{II} = Fe), 1.3 cm^{-1} (for M^{II} = Co), 2.7, 4.3 and 4.6 cm^{-1} (for M^{II} = Ni) and 2.2, 2.7 and 2.8 cm^{-1} (for M^{II} = Cu) have been reported.[1,31,32] Thus, our complexes provide additional experimental proof of the prediction of Okawa[3b] who suggested that Cr^{III} and M^{II} are ferromagnetically coupled in the 2-D lattice in the family of ferromagnets $Bu_4N[M^{II}Cr^{III}(ox)_3]$, and that the J value may be estimated assuming a linear relationship between the critical temperature and J (mean field approximation).[33] The J values estimated this way are 0.73, 1.76, 1.85, 3.55 and 2.90 cm^{-1} for M^{II} = Mn, Fe, Co, Ni and Cu, respectively, in relatively good agreement with the observed values for the exchange pair interactions in our Cr_2M trimers, except for the Cu derivative where a different structure must be considered.

Table 1. Magnetic parameters obtained with Equations (2) and (3) for the compounds of the series $(TTF)_4\{M^{II}(H_2O)_2[M^{III}(ox)_3]_2\}\cdot nH_2O$ (Cr_2M and Fe_2M series)

Compound	S	g	J [cm^{-1}]
Cr_2Mn (**1**)	11/2	1.917(2)	0.535(7)
Cr_2Fe (**2**)	10/2	1.885(6)	0.650(10)
Cr_2Co (**3**)	9/2	−	> 0
Cr_2Ni (**4**)	8/2	1.840(12)	3.40(3)
Cr_2Cu (**5**)	7/2	1.885(3)	−0.34(2)
Fe_2Mn (**7**)	5/2	2.208(2)	−1.49(7)
Fe_2Fe (**8**)	6/2	2.21(2)	−3.24(4)
Fe_2Co (**9**)	7/2	−	< 0
Fe_2Ni (**10**)	8/2	2.016(12)	−7.74(9)

Both the ferromagnetic coupling in the Cr_2M series and the antiferromagnetic one in the Fe_2M series can be explained easily by considering only the singly occupied molecular orbitals (SOMOs) of the interacting magnetic centers. Thus, the exchange interaction parameter $J_{MM'}$ can be expressed by the average of the individual interactions of the SOMOs (J_{ij}) as $J_{MM'} = (1/n_i n_j)\Sigma(J_{ij})$, where n_i and n_j are the number of unpaired electrons in the i and j SOMOs. Thus, in the Ni derivative of the Cr_2M series, all the possible exchange pathways are ferromagnetic because of orthogonality of the SOMOs of the Cr^{III} ion (of t_{2g} symmetry: d_{xy}, d_{xz} and d_{yx}) and those of the Ni^{II} ion ($d_{x^2-y^2}$ and d_{z^2}), which are all of e_g symmetry. In the other derivatives of the Cr_2M series (M = Co, Fe and Mn) there are SOMOs (of t_{2g} symmetry) that are not orthogonal to those of the Cr^{III} ion and contribute to the total value of $J_{MM'}$ with an antiferromagnetic term. As observed experimentally, this term is always smaller than the ferromagnetic one, since it decreases the value of $J_{MM'}$ for these three derivatives with respect to the Cr_2Ni derivative, maintaining the sign of the interaction.

Finally, in the Cr_2Cu derivative, the existence of the tetragonal distortion mentioned previously implies that the magnetic orbital of the Cu^{II} ion ($d_{x^2-y^2}$) is located in a plane perpendicular to the oxalate bridge and, consequently, it overlaps with the magnetic orbitals of the Cr^{III} ion, giving rise to the antiferromagnetic exchange interaction confirmed by the magnetic measurements. This distortion has been observed already in other oxalate-bridged complex of Cu^{II} and Cr^{III}.[29]

Unfortunately, the TTF entities must be completely ionized, as is deduced from the stoichiometry of four TTF units per $\{M^{II}(H_2O)_2[M^{III}(ox)_3]_2\}^{4-}$ anion, which precludes the existence of delocalized electrons in the organic sublattice, as confirmed by the EPR spectra of all the members of both series (see below) and by the very low electrical dc conductivity shown by the Cr_2Mn derivative ($\sigma = 2 \times 10^{-4}$ $S\cdot cm^{-1}$) and its high activation energy (approx. 200 meV).

The EPR spectra of both Zn derivatives are very similar to those of the precursor $[M^{III}(ox)_3]^{3-}$ anions; they show a single and large signal centered at $g \approx 3.7$ at any temperature from 300 to 4.5 K. The only difference between the Cr and Fe derivatives is the presence of a hyperfine structure in the spectrum of the Cr_2Zn compound because of the weak anisotropy of the Cr^{III} ion that gives rise to a zero-field splitting of the S = 3/2 ground spin state. We see in all the salts of both series a very weak signal at g = 2.0030−2.0060 with a linewidth of 18−22 G whose intensity increases with decreasing temperature. The weak intensity of this signal (two orders of magnitude weaker than the signal from the inorganic lattice) suggests that it corresponds to paramagnetic impurities coming from a small number of isolated TTF^+ radicals resulting from crystalline defects, and not to the localized electron of each TTF molecule, which confirms the results obtained from the static magnetic measurements that suggested that these entities must be strongly antiferromagnetically coupled, as expected from the strongly dimerized arrangement of the organic radicals, and do not contribute significantly to the total magnetic moment.

For the salts of the Cr_2M^{II} series, we can distinguish between those members containing an odd number of unpaired electrons in the inorganic sublattice (M^{II} = Mn, Co and Cu) and those containing an even number of unpaired electrons (M^{II} = Fe and Ni). In the first case, the EPR spectra at low temperatures show a strong signal for the three derivatives coming from the inorganic sublattice to-

 © 2003 Wiley-VCH Verlag GmbH & Co. KGaA, Weinheim

gether with the weak signal of the isolated TTF^+ impurities (Figure 7). This last signal is weaker in the case of the Mn derivative, a situation that agrees with the fact that this derivative is the one that gives crystals of better quality. In the second case (M = Fe and Ni), the inorganic sublattice is EPR-silent and only at very low temperatures it is possible to observe a signal very similar to that observed in the Cr_2Zn derivative, which suggests that it may be attributed to a small fraction of isolated $[Cr(ox)_3]^{3-}$ impurities, more abundant in the Fe derivative.

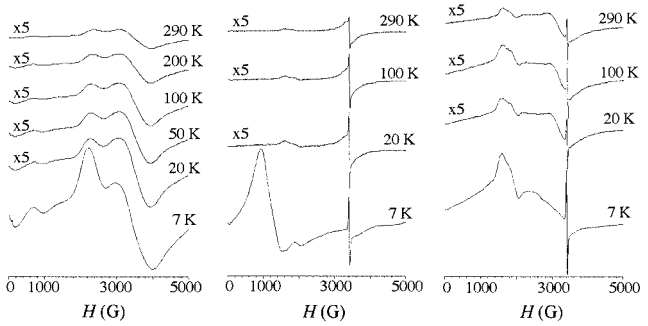

Figure 7. EPR spectra at different temperatures of the Cr_2Mn (**1**) (left), Cr_2Co (**3**) (center) and Cr_2Cu (**5**) (right) compounds

In the Fe_2M^{II} salts, we can also distinguish between the members containing an odd number of unpaired electrons in the trimer (M^{II} = Mn and Co) and those containing an even number of unpaired electrons (M^{II} = Fe and Ni). In this series, the behavior parallels that observed in the Cr_2M series; the Mn and Cu derivatives show, besides the TTF^+ signal, those signals of the anionic sublattice (Figure 8); the Fe and Ni derivatives are EPR-silent and only at very low temperatures do we observe a weak signal, very similar to that observed in the Fe_2Zn derivative, that may be attributed, as for the Cr_2M series, to a small fraction of isolated monomeric $[Fe(ox)_3]^{3-}$ impurities, which are also more abundant in the Fe derivative.

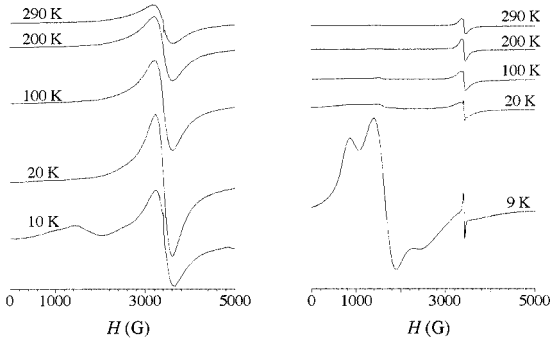

Figure 8. EPR spectra at different temperatures of the Fe_2Mn (**7**) (left) and Fe_2Co (**9**) (right) compounds

All these observations are in good agreement with the electronic structure proposed according to the magnetic measurements performed in these series.

Conclusion

In summary, we have presented a new family of organic/inorganic hybrids formed by trinuclear dimetallic oxalate complexes and TTF molecules that present different interesting properties. Indeed, these are the very first series of compounds that contain in their structure the organic donor TTF unit and dimetallic oxalate complexes.

From a structural point of view, both sublattices show unprecedented packing arrangements. It is the first time that a monodimensional pseudo-κ phase has been reported from orthogonal dimers of TTF molecules, while the inorganic layer is formed by dimetallic trimers formed exclusively by oxalate ligands without the presence of any other organic ligand blocking the possibility of polymerization. In this context, although no magnetic ordering is expected to occur in these kinds of lattices, they provide valuable information on the magnetic interactions between these metal ions, which should help us to understand the behavior of the extended magnetic lattices based on oxalate complexes. The predominant ferromagnetic interaction found in the $Cr^{III}-M^{II}-Cr^{III}$ trimeric clusters is especially remarkable since it stabilizes high-spin ground states (up to 11/2 for $FeCr_2$).

Experimental Section

General Remarks: All chemicals were of reagent grade and were used as purchased. Standard literature procedures were used to prepare the $K_3[M^{III}(ox)_3]\cdot 3H_2O$ (M^{III} = Cr and Fe) complexes.[34] The $(TTF)_3[BF_4]_2$ salt also was prepared according to a literature procedure.[35] Magnetic measurements were obtained using a Quantum Design MPMS-XL-5 SQUID magnetometer from polycrystalline samples held in gelatine capsules inside a plastic tube. The measured susceptibilities were corrected for core diamagnetism by using Pascal constants. All susceptibility measurements were performed at an applied field of 0.1 T on warming the samples from 2 to 300 K. The isothermal magnetization studies were performed at 2 K with applied magnetic fields up to 5 Tesla. EPR spectra for all the samples were performed on polycrystalline samples in quartz tubes from 300 to 4.2 K with a Bruker ER 200D spectrometer at 9.44 GHz equipped with a liquid Helium cryostat. For the Cr_2Mn compound, EPR spectra were recorded with a single crystal at different orientations and in a temperature range from 300 to 4.2 K with a Bruker ESP 300E spectrometer at 9.44 GHz equipped with a liquid helium cryostat. D.C. conductivity measurements were performed by the four-contacts method in two different crystals of the Cr_2Mn derivative because this salt produced the biggest single crystals. The contacts were pasted using silver paint and 10-μm diameter gold wires. The applied current (0.1−5 μA) was generated with a Keithley 224 current source and the potential was measured with a Keithley 199 microvoltimeter. The conductivity was measured on cooling and warming scans and no significant differences were observed. The cooling and warming rates were fixed at 1 K/

 © 2003 Wiley-VCH Verlag GmbH & Co. KGaA, Weinheim

min using the cryostat of the SQUID susceptometer (Quantum Design MPMS-XL-5).

$(TTF)_4\{Mn(H_2O)_2[Cr(ox)_3]_2\}\cdot 14H_2O$ (1): Single crystals of compound **1** suitable for X-ray diffraction analysis were obtained by slow diffusion of an aqueous solution (15 mL) of $K_3[Cr(ox)_3]\cdot 3H_2O$ (12 mg, 0.025 mmol) and $MnCl_2\cdot 4H_2O$ (5 mg, 0.025 mmol) into a degassed acetonitrile solution (15 mL) of $(TTF)_3[BF_4]_2$ (10 mg, 0.013 mmol). After 5 d, small shiny black crystals were isolated by filtration, washed with acetonitrile, and air-dried at room temperature. $C_{36}H_{48}Cr_2MnO_{40}S_{16}$ (1792.74): calcd. C 24.12, H 2.70, Cr 5.80, Mn 3.06, S 28.62; found C 24.30, H 2.62, Cr 6.03, Mn 2.78, S 29.21.

$(TTF)_4\{Fe(H_2O)_2[Cr(ox)_3]_2\}\cdot nH_2O$ ($n \approx 4$) (2): $K_3[Cr(ox)_3]\cdot 3H_2O$ (122 mg, 0.25 mmol) was dissolved in distilled water (10 mL). An aqueous solution (10 mL) of $FeSO_4\cdot 7H_2O$ (70 mg, 0.25 mmol) was added at room temperature under argon. A solution of $(TTF)_3[BF_4]_2$ (100 mg, 0.13 mmol) in degassed acetonitrile (30 mL) was added dropwise to this mixture. After a few minutes, shiny black microcrystals were filtered off from this solution, washed with acetonitrile and dried at room temperature. Yield: 102 mg (65%). $C_{36}H_{28}Cr_2FeO_{30}S_{16}$ (1613.50): calcd. C 26.80, H 1.75, Cr 6.45, Fe 3.46, S 31.80; found C 27.48, H 1.56, Cr 6.22, Fe 3.67, S 31.69.

$(TTF)_4\{Co(H_2O)_2[Cr(ox)_3]_2\}\cdot nH_2O$ ($n \approx 8$) (3): Shiny black microcrystals of this compound were prepared as was **2**, but using $Co(NO_3)_2\cdot 6H_2O$ instead of $FeSO_4\cdot 7H_2O$. Yield: 97 mg (59%). $C_{36}H_{36}CoCr_2O_{34}S_{16}$ (1685.64): calcd. C 25.65, H 2.15, Co 3.32, Cr 6.17, S 30.44; found C 25.51, H 2.29, Co 3.40, Cr 6.38, S 30.99.

$(TTF)_4\{Ni(H_2O)_2[Cr(ox)_3]_2\}\cdot nH_2O$ ($n \approx 6$) (4): Shiny black microcrystals of this compound were prepared as was **2**, but using $NiCl_2\cdot 6H_2O$ instead of $FeSO_4\cdot 7H_2O$. Yield: 63 mg (39%). $C_{36}H_{32}Cr_2NiO_{32}S_{16}$ (1652.37): calcd. C 26.17, H 1.95, Cr 6.29, Ni 3.55, S 31.05; found C 26.29, H 1.90, Cr 6.10, Ni 3.48, S 31.09.

$(TTF)_4\{Cu(H_2O)_2[Cr(ox)_3]_2\}\cdot nH_2O$ ($n \approx 3$) (5): Shiny black microcrystals of this compound were prepared as was **2**, but using $CuCl_2\cdot 2H_2O$ instead of $FeSO_4\cdot 7H_2O$. Yield: 59 mg (38%). $C_{36}H_{26}Cr_2CuO_{29}S_{16}$ (1603.18): calcd. C 26.97, H 1.63, Cu 3.96, Cr 6.49, S 32.00; found C 27.02, H 1.69, Cu 3.95, Cr 6.38, S 31.93.

$(TTF)_4\{Zn(H_2O)_2[Cr(ox)_3]_2\}\cdot nH_2O$ ($n \approx 6$) (6): Shiny black microcrystals of this compound were prepared as was **2**, but using $Zn(NO_3)_2\cdot 6H_2O$ instead of $FeSO_4\cdot 7H_2O$. Yield: 68 mg (42%). $C_{36}H_{32}Cr_2O_{32}S_{16}Zn$ (1659.07): calcd. C 26.06, H 1.94, Cr 6.27, S 30.92, Zn 3.94; found C 26.70, H 1.98, Cr 6.30, S 31.12, Zn 3.86.

$(TTF)_4\{Mn(H_2O)_2[Fe(ox)_3]_2\}\cdot nH_2O$ ($n \approx 9$) (7): $K_3[Fe(ox)_3]\cdot 3H_2O$ (124 mg, 0.25 mmol) was dissolved in distilled water (10 mL). An aqueous solution (10 mL) of $MnCl_2\cdot 4H_2O$ (50 mg, 0.25 mmol) was added at room temperature under argon. A solution of $(TTF)_3[BF_4]_2$ (100 mg, 0.13 mmol) in degassed acetonitrile (30 mL) was added dropwise to this mixture. After a few minutes, from this solution shiny black microcrystals were filtered off, washed with acetonitrile and dried at room temperature. Yield: 123 mg (74%). $C_{36}H_{38}Fe_2MnO_{35}S_{16}$ (1710.37): calcd. C 25.28, H 2.24, Fe 6.53, Mn 3.21, S 30.00; found C 25.48, H 2.08, Fe 6.62, Mn 3.12, S 30.45.

$(TTF)_4\{Fe(H_2O)_2[Fe(ox)_3]_2\}\cdot nH_2O$ ($n \approx 5$) (8): Shiny black microcrystals of this compound were prepared as was **7**, but using $FeSO_4\cdot 7H_2O$ instead of $MnCl_2\cdot 4H_2O$. Yield: 109 mg (68%). $C_{36}H_{30}Fe_3O_{31}S_{16}$ (1639.21): calcd. C 26.38, H 1.84, Fe 10.22, S 31.30; found C 26.47, H 1.73, Fe 10.28, S 32.31. Single crystals suitable for X-ray diffraction analysis of **8** were obtained by slow diffusion of an aqueous solution (15 mL) of $K_3[Fe(ox)_3]\cdot 3H_2O$ (12 mg, 0.025 mmol) and $FeSO_4\cdot 7H_2O$ (7 mg, 0.025 mmol) into a degassed acetonitrile solution (15 mL) of $(TTF)_3[BF_4]_2$ (10 mg, 0.013 mmol). After 5 d, small shiny black crystals were isolated by filtration, washed with acetonitrile, and air-dried at room temperature.

$(TTF)_4\{Co(H_2O)_2[Fe(ox)_3]_2\}\cdot nH_2O$ ($n \approx 7$) (9): Shiny black microcrystals of this compound were prepared as was **7**, but using $Co(NO_3)_2\cdot 6H_2O$ instead of $MnCl_2\cdot 4H_2O$. Yield: 87 mg (53%). $C_{36}H_{34}CoFe_2O_{33}S_{16}$ (1675.33): calcd. C 25.81, H 2.05, Co 3.34, Fe 6.67, S 30.62; found C 26.00, H 1.97, Co 3.29, Fe 6.58, S 31.01.

$(TTF)_4\{Ni(H_2O)_2[Fe(ox)_3]_2\}\cdot nH_2O$ ($n \approx 9$) (10): Shiny black microcrystals of this compound were prepared as was **7**, but using $NiCl_2\cdot 6H_2O$ instead of $MnCl_2\cdot 4H_2O$. Yield: 59 mg (35%). $C_{36}H_{38}Fe_2NiO_{35}S_{16}$ (1714.12): calcd. C 25.23, H 2.23, Fe 6.52, Ni 3.42, S 29.93; found C 25.28, H 2.15, Fe 6.56, Ni 3.19, S 30.22.

$(TTF)_4\{Zn(H_2O)_2[Fe(ox)_3]_2\}\cdot nH_2O$ ($n \approx 7$) (11): Black shiny microcrystals of this compound were prepared as was **7**, but using $Zn(NO_3)_2\cdot 6H_2O$ instead of $MnCl_2\cdot 4H_2O$. Yield: 62 mg (38%). $C_{36}H_{34}Fe_2O_{33}S_{16}Zn$: (1684.79): calcd. C 25.66, H 2.03, Fe 6.63, S 30.45, Zn 3.88; found C 26.02, H 1.93, Fe 6.63, S 30.64, Zn 3.69.

X-ray Crystallographic Study: The crystal structure analysis was performed on a shiny black prismatic single crystal of the Cr_2Mn compound of approximate dimensions 0.15 × 0.10 × 0.20 mm. Relevant crystallographic data and structure determination parameters for the Cr_2Mn compound are given in Table 2. Cell parameters were obtained by the least-squares refinement method with 25 reflections. Intensity data were measured at room temperature with an Enraf−Nonius CAD4 diffractometer with graphite-monochromated Mo-K_α radiation with the ω-2θ method. The structure was solved by direct methods using the SIR97 program,[36] followed by Fourier synthesis and refined on F^2, for all but 348 reflections with very negative F^2 or flagged for potential systematic errors, using the SHELXL-93 program (G. M. Sheldrick, University of Göttingen). The atoms of the TTF unit do not have two components with different occupation factors. Refinement of the TTF molecules was carried out with a constraint-restraint model, restraining displacement components along the bond directions and each TTF molecule in one different refinement cycle. All non-hydrogen atoms were refined anisotropically except for the oxygen atoms of three water molecules (O26, O27 and O28) that were disordered and assigned site-occupation factors of 0.68 and refined

Table 2. Crystallographic data for $(TTF)_4\{Mn(H_2O)_2[Cr(C_2O_4)_3]_2\}\cdot 14H_2O$ (**1**)

Empirical formula	$C_{36}H_{36}Cr_2MnO_{34}S_{16}$
Formula mass	1684.21
Space group	*C*2/*c*
a [Å]	13.240(5)
b [Å]	19.450(5)
c [Å]	27.690(5)
β [°]	97.63(5)
V [Å^3]	7067.5(3)
Z	4
$\rho_{calcd.}$ [g·cm^{-3}]	1.583
λ [Å]	0.71069
μ [cm^{-1}]	9.05
R[a]	0.076
R_ω[b]	0.212

[a] $R = \Sigma(|F_o| - |F_c|)/\Sigma|F_o|$. [b] $R_\omega = [\Sigma\omega(|F_o| - |F_c|)^2/\Sigma\omega|F_o|^2]^{1/2}$.

 © 2003 Wiley-VCH Verlag GmbH & Co. KGaA, Weinheim

isotropically, giving $R(F) = 0.076$ and $R^2(F) = 0.212$ by using 2187 observed reflections with $I \geq 3\sigma(I)$. CCDC-182551 contains the supplementary crystallographic data for this paper. These data can be obtained free of charge at www.ccdc.cam.ac.uk/conts/retrieving.html [or from the Cambridge Crystallographic Data Centre, 12 Union Road, Cambridge CB2 1EZ, UK; Fax: (internat.) + 44-1223/336-033; E-mail: deposit@ccdc.cam.ac.uk]. The X-ray powder diffraction patterns were recorded with a Siemens D-500 powder diffractometer (Cu-K_α) in the 2Θ range of 2−60° (with steps of 0.02°, and a measuring time of 15 s). Experimental unit cells were obtained by indexation of the reflections in a monoclinic space group with the CELSIZ program (Unit Cell Refinement v1.1, XRDUtilities). Unit cell parameters are summarized in the Supporting information, see also the footnote on the first page of this article.

Acknowledgments

This work was supported by the Spanish Ministerio de Ciencia y Tecnología (MCT) (Grants MAT2001-3507-C02-01 and BQU2002-01091) and the European Union (TMR ERB 4061 PL97-0197). J. R. G. M. and C. G. S. wish to thank the MCT for a research contract (Programa Ramón y Cajal).

[1] [1a] Z. J. Zhong, N. Matsumoto, H. Okawa, S. Kida, *Chem. Lett.* **1990**, 87−90.
[2] M. Ohba, H. Tamaki, N. Matsumoto, H. Okawa, S. Kida, *Chem. Lett.* **1991**, 1157−1160.
[3] S. Decurtins, H. W. Schmalle, P. Schneuwly, J. Ensling, P. Gütlich, *J. Am. Chem. Soc.* **1994**, *116*, 9521−9528 and references therein.
[4] S. Decurtins, H. W. Schmalle, R. Pellaux, P. Schneuwly, A. Hauser, *Inorg. Chem.* **1996**, *35*, 1451−1460.
[5] H. Tamaki, M. Mitsumi, K. Nakamura, N. Matsumoto, S. Kida, H. Okawa, S. Iijima, *Chem. Lett.* **1992**, 1975−1978.
[6] H. Tamaki, Z. J. Zhong, N. Matsumoto, S. Kida, M. Koikawa, N. Achiwa, Y. Hashimoto, H. Okawa, *J. Am. Chem. Soc.* **1992**, *114*, 6974−6979.
[7] S. Iijima, T. Katsura, H. Tamaki, N. Mitsumi, N. Matsumoto, H. Okawa, *Mol. Cryst. Liq. Cryst.* **1993**, *232*, 623−628.
[8] C. Mathoniere, S. G. Carling, P. Day, *J. Chem. Soc., Chem. Commun.* **1994**, 1551−1552.
[9] J. Larionova, B. Mombelli, J. Sanchiz, O. Kahn, *Inorg. Chem.* **1998**, *37*, 679−684.
[10] E. Coronado, J. R. Galán-Mascarós, C. J. Gómez-García, J. M. Martínez-Agudo, E. Martínez-Ferrero, J. C. Waerenborgh, M. Almeida, *J. Solid State Chem.* **2001**, *159*, 391−402.
[11] C. J. Nuttall, C. Bellitto, P. Day, *J. Chem. Soc., Chem. Commun.* **1995**, 1513−1514.
[12] H. Okawa, M. Mitsumi, M. Ohba, M. Kodera, N. Matsumoto, *Bull. Chem. Soc. Jpn.* **1994**, *67*, 2139−2144.
[13] A. Bhattacharjee, S. Iijima, *Phys. Stat. Sol. (a)* **1997**, *159*, 503−508.
[14] E. Coronado, J. R. Galán-Mascarós, C. J. Gómez-García, J. M. Martínez-Agudo, *Adv. Mater.* **1999**, *11*, 558−560.
[15] E. Coronado, J. R. Galán-Mascarós, C. J. Gómez-García, J. M. Martínez-Agudo, *Synth. Met.* **2001**, *122*, 501−507.
[16] S. Decurtins, H. W. Schmalle, P. Schneuwly, H. R. Oswald, *Inorg. Chem.* **1993**, *32*, 1888.
[17] M. Hernández-Molina, F. Lloret, C. Ruiz-Pérez, M. Julve, *Inorg. Chem.* **1998**, *37*, 4131−4135.
[18] E. Coronado, J. R. Galán-Mascarós, C. J. Gómez-García, J. M. Martínez-Agudo, *Inorg. Chem.* **2001**, *40*, 113−120.
[19] R. Andres, M. Brissard, M. Gruselle, C. Train, J. Vaisserman, B. Malezieux, J. P. Jamet, M. Verdaguer, *Inorg. Chem.* **2001**, *40*, 4633−4640.
[20] E. Coronado, C. J. Gómez-García, A. Nuez, F. M. Romero, E. Rusanov, H. Stoeckli-Evans, *Inorg. Chem.* **2002**, *41*, 4615−4620.
[21] M. Clemente-León, E. Coronado, J. R. Galán-Mascarós, C. J. Gómez-García, *Chem. Commun.* **1997**, 1727−1728.
[22] Z. Gu, O. Sato, T. Iyoda, K. Hashimoto, A. Fujishima, *Mol. Cryst. Liq. Cryst.* **1996**, *285*, 469−474.
[23] J. M. Williams, J. R. Ferraro, R. J. Thorn, K. D. Carlson, U. Geiser, H. H. Wang, A. M. Kini, M. H. Whangbo, in *Organic Superconductors. Synthesis, Structure, Properties and Theory* (Ed.: R. N. Grimes), Prentice Hall, Englewood Cliffs, New Jersey, USA, **1992**.
[24] M. Kurmoo, A. W. Graham, P. Day, S. J. Coles, M. B. Hursthouse, J. L. Caulfield, J. Singleton, F. L. Pratt, W. Hayes, L. Ducasse, P. Guionneau, *J. Am. Chem. Soc.* **1995**, *117*, 12209−12217.
[25] A. W. Graham, M. Kurmoo, P. Day, *J. Chem. Soc., Chem. Commun.* **1995**, 2061−2062.
[26] E. Coronado, J. R. Galán-Mascarós, C. J. Gómez-García, V. Laukhin, *Nature* **2000**, *408*, 447−449.
[27] A preliminary report of the structure and properties of these series has already been published: E. Coronado, J. R. Galán Mascarós, C. Gimenez-Saiz, C. J. Gómez-García, C. Ruiz-Perez, S. Triki, *Adv. Mater.* **1996**, *8*, 737−739.
[28] E. H. Merrachi, B. F. Mentzen, F. Chassugneux, *Rev. Chim. Miner.* **1986**, *23*, 329−342 and references therein.
[29] M. Andruh, R. Melanson, C. V. Stager, F. D. Rochon, *Inorg. Chim. Acta* **1996**, *251*, 309−317.
[30] K. Kambe, *J. Phys. Soc. Jpn.* **1950**, *5*, 48−51.
[31] M. Ohba, H. Tamaki, N. Matsumoto, H. Okawa, *Inorg. Chem.* **1993**, *32*, 5385−5390.
[32] Y. Pei, Y. Journaux, O. Kahn, *Inorg. Chem.* **1989**, *28*, 100−103.
[33] J. P. Renard, *Organic and Inorganic Low-Dimensional Crystalline Materials* (Eds: P. Delhaes, M. Drillon), NATO ASI Series 168, Plenum, New York, **1987**, p. 125.
[34] J. C. Baylar, E. M. Jones, *Inorganic Synthesis* (Ed.: H. S. Booth), McGraw-Hill, New York, USA, **1939**, vol.1, p 35.
[35] F. Wudl, *J. Am. Chem. Soc.* **1975**, *97*, 1962−1963.
[36] A. Altomare, M. C. Burla, M. Camalli, G. L. Cascarano, C. Giacovazo, A. Guagliardi, A. G. G. Moliterni, G. Polidori, R. Spagna, *J. Appl. Crystallogr.* **1999**, *32*, 115−119.

Received October 25, 2002

 © 2003 Wiley-VCH Verlag GmbH & Co. KGaA, Weinheim

Synthesis of Oxalato-Bridged (Oxo)vanadium(IV) Dimers Using L-Ascorbic Acid as Oxalate Precursor: Structure and Magnetism of Two Systems

Bharat Baruah,[a] Vladimir O. Golub,[b] Charles J. O'Connor,[b] and Animesh Chakravorty*[a,c]

Keywords: Vanadium / Bridging ligands / Magnetic properties

The reaction of an aqueous solution of NH_4VO_3 with L-ascorbic acid and Et_4NBr has afforded $[Et_4N]_2[(VO)_2(C_2O_4)_3(H_2O)_2]\cdot 4H_2O$ (**3**). A similar reaction, in which malonic acid is also added, has furnished $[Et_4N]_2[(VO)_2(C_2O_4)(C_3H_2O_4)_2(H_2O)_2]\cdot 2H_2O$ (**4**). In these syntheses the oxalate ion is derived from L-ascorbic acid. In both the complexes the dinuclear anion is centrosymmetric. In **3** the metal atoms are displaced from the plane of the bridging oxalate anion by 0.05 Å, the corresponding displacement in **4** being 0.17 Å. The terminal oxalato chelate ring in **3** is roughly planar but the malonato chelate ring in **4** has a distorted boat conformation. The V−O distances in **4** are systematically shorter than the corresponding distances in **3** by 0.02−0.06 Å. The V···V distance within the dimer is 5.616(2) Å in **3** and 5.529(2) Å in **4**. The two uncoordinated water molecules in the asymmetric unit of **3** constitute a hydrogen-bonded dimer and the lattice consists of a supramolecular anionic assembly held by five different types of O···O hydrogen bonds. The anionic assembly in **4** involves three types of O···O hydrogen bonds. The Et_4N^+ cations reside between the anionic layers. The magnetic susceptibility data of both **3** and **4** fit excellently with the Heisenberg dimer model in the temperature interval 2−300 K. The species are antiferromagnetic and the *J* values are $-6.50\ cm^{-1}$ for **3** and $-6.25\ cm^{-1}$ for **4**. The two opposing factors — V−O(bridge) bond length and the displacement of the metal atom from the oxalate plane — appear to have more or less balanced each other resulting in virtually equal *J* values for the two complexes.
(© Wiley-VCH Verlag GmbH & Co. KGaA, 69451 Weinheim, Germany, 2003)

Introduction

There is a long-standing chemical interest in the interaction of metal ions with L-ascorbic acid.[1] Very few authentic metal ascorbates have, however, been isolated and characterized.[1−4] Our familiarity[5−8] with vanadate esters of polyols prompted us to scrutinize the use of L-ascorbic acid as a possible diol ligand towards vanadium. We have not succeeded in isolating vanadate esters of L-ascorbic acid but the study has furnished a new route for the synthesis of oxalato-bridged (oxo)vanadium dimers incorporating the moiety **1**. The structure and magnetism of two representative species are reported in the present work.

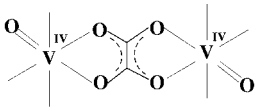

1

[a] Department of Inorganic Chemistry, Indian Association for the Cultivation of Science, Kolkata 700032, India
Fax: (internat.) + 91-33/2473-2805
E-mail: icac@mahendra.iacs.res.in
[b] Advanced Materials Research Institute, College of Sciences, University of New Orleans,
New Orleans, Louisiana 70148, USA
[c] Jawaharlal Nehru Centre for Advanced Scientific Research, Bangalore 560064, India

Results and Discussion

Synthesis

A rate study on the reaction of aqueous (oxo)vanadium(V) with L-ascorbic acid in strongly acidic media had suggested that a transient ascorbate complex is formed but it undergoes rapid redox transformation to (oxo)vanadium(IV) and dehydroascorbic acid.[9] In view of our diol work[5−8] the transient complex may have the bonding mode **2**.

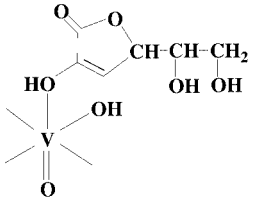

2

We have also failed to isolate a stable vanadium complex of L-ascorbic acid by the reaction of vanadium salts with L-ascorbic acid under different conditions of stoichiometry, pH and temperature. On the other hand, treatment of an aqueous solution of ammonium metavanadate with L-ascorbic acid and Et_4NBr in the ratio 1:1.5:1 at 70 °C gave a dark-green solution from which blue crystals of **3** slowly

deposited in excellent yields. The mixed oxalato-malonato complex **4** was obtained by a similar procedure from ammonium metavanadate, L-ascorbic acid, malonic acid and Et_4NBr in the ratio 1:0.5:1:1.

$[Et_4N]_2[(VO)_2(C_2O_4)_3(H_2O)_2]\cdot 4H_2O$ (**3**)

$[Et_4N]_2[(VO)_2(C_2O_4)(C_3H_2O_4)_2(H_2O)_2]\cdot 2H_2O$ (**4**)

In the above syntheses, the oxalate ion is derived by oxidative/hydrolytic degradation [10−12] of L-ascorbic acid. As an in situ precursor of oxalic acid, L-ascorbic acid has recently found a use in the synthesis of oxalate complexes of metal ions;[13−15] we report here the first examples in the case of vanadium. Both **3** and **4** reported here are new compounds, although a few analogues of **3** synthesized from oxalic acid/oxalate are known.[16−18] Mononuclear oxalato chelates of (oxo)vanadium(IV) have been known for a long time.[19]

Characterization data are given in the Exp. Sect. The complexes display a V=O stretch near 980 cm^{-1} and multiple carboxylate vibrations in the region 800−1720 cm^{-1}. In aqueous solutions three ligand-field transitions occur in the visible region. Details are given in the Exp. Sect.

Structure

In both the complexes the dinuclear anion is centrosymmetric, the centre of inversion lying on the C−C bond of the bridging oxalato moiety. The asymmetric unit in each case corresponds to half the molecular formula. In **3** the Et_4N^+ cations lie in general positions while in **4** they lie on twofold axes passing through the nitrogen atoms. Views of the anions of **3** and **4** are shown in Figures 1 and 2, respectively. Selected bond parameters are listed in Table 1.

In **3** the $OV(C_2O_4)VO$ fragment defines a good plane of mean deviation 0.01 Å. In **4** the fragment is not quite planar (mean deviation 0.04 Å), the vanadium atoms being displaced by 0.17 Å above and below the nearly perfect plane of the oxalate anion (the corresponding displacement in **3** is only 0.05 Å). In **3** the terminal oxalato chelate rings are roughly planar (mean deviation 0.05 Å), the dihedral angle between them being 106.7°. In the $V(C_3H_2O_4)$ fragment of

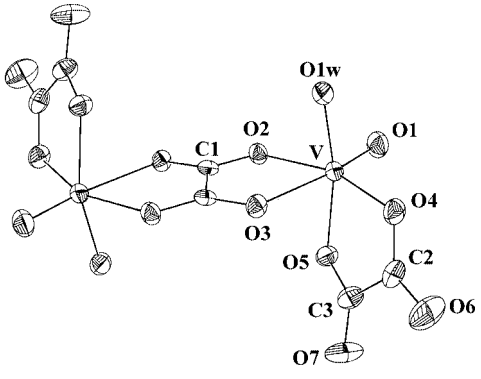

Figure 1. Perspective view and atom labeling scheme of $[(VO)_2(C_2O_4)_3(H_2O)_2]^{2-}$; all non-hydrogen atoms are represented by 30% thermal probability ellipsoids

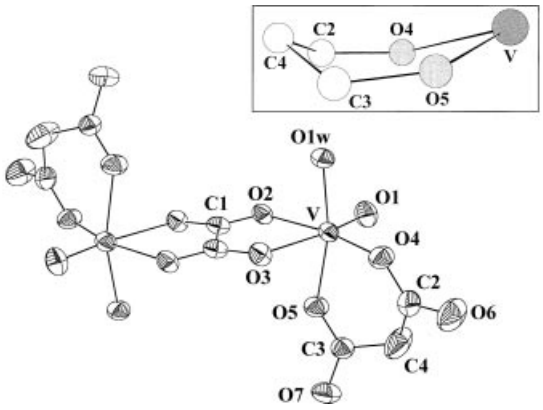

Figure 2. Perspective view and atom labeling scheme of $[(VO)_2(C_2O_4)(C_3H_2O_4)_2\ (H_2O)_2]^{2-}$; all non-hydrogen atoms are represented by 30% thermal probability ellipsoids

Table 1. Selected bond lengths [Å] and angles [°] for **3** and **4**

	3	**4**
Distances:		
V−O(1)	1.582(3)	1.561(6)
V−O(2)	2.023(3)	2.009(6)
V−O(3)	2.281(3)	2.218(6)
V−O(4)	1.993(3)	1.930(6)
V−O(5)	1.999(3)	1.953(6)
V−O(1w)	2.020(4)	2.013(7)
C(1)−O(2)	1.259(5)	1.248(10)
C(1A)−O(3)	1.235(5)	1.225(9)
C(2)−O(4)	1.295(6)	1.241(10)
C(3)−O(5)	1.263(6)	1.230(10)
C(2)−O(6)	1.214(6)	1.211(10)
C(3)−O(7)	1.210(6)	1.228(10)
Angles:		
O(1)−V−O(2)	97.2(2)	95.4(3)
O(1)−V−O(3)	172.8(2)	171.4(3)
O(1)−V−O(4)	103.7(2)	102.4(3)
O(1)−V−O(5)	102.6(2)	101.6(2)
O(1)−V−O(1w)	98.9(2)	98.2(3)
O(2)−V−O(3)	75.95(11)	76.1(2)
O(2)−V−O(4)	158.34(14)	162.1(3)
O(2)−V−O(5)	88.96(13)	88.1(2)
O(2)−V−O(1w)	90.5(2)	88.7(3)
O(3)−V−O(4)	83.37(13)	86.1(2)
O(3)−V−O(5)	79.63(12)	79.5(2)
O(3)−V−O(1w)	79.33(14)	80.8(3)
O(4)−V−O(5)	80.96(14)	89.1(3)
O(4)−V−O(1w)	92.0(2)	88.0(3)
O(5)−V−O(1w)	158.4(2)	160.2(3)

4 the malonato chelate ring has a distorted boat shape (inset in Figure 2) in which the V and C4 atoms are displaced by 0.4 Å in the same direction from the plane of the O4, O5, C2, C3 atoms.

In the distorted octahedral VO_6 coordination spheres, the V−O(1) (oxo) and V−O(3) (*trans* to oxo) distances are shorter and longer, respectively, than the other distances in both **3** and **4**. The V−O distances in **4** are systematically shorter than the corresponding distances in **3** by 0.02−0.06

 © 2003 Wiley-VCH Verlag GmbH & Co. KGaA, Weinheim

Å. The V···V distances within the dimer are 5.616(2) Å in **3** and 5.529(2) Å in **4**.

Hydrogen Bonding

The two uncoordinated water molecules (lattice water) in the asymmetric unit of **3** form a strongly hydrogen-bonded dimer, the O···O distance being 2.619(3) Å. The dimer is also involved in additional hydrogen bonding with coordinated and uncoordinated oxalato oxygen atoms and with the coordinated water molecule, which, in turn, is hydrogen-bonded to an uncoordinated oxalate oxygen atom. The lattice thus consists of a supramolecular anionic assembly held together by five different types of O···O hydrogen bonds (Table 2) as illustrated in Figure 3. The Et_4N^+ cations reside in between the anionic layers.

Table 2. Hydrogen bond lengths [Å] in **3** and **4**

3		**4**	
O4[a]···O2w[a]	2.822(5)	O6[c]···O2w	2.731(6)
O6···O2w	2.746(5)	O7[d]···O1w	2.591(5)
O7···O1w[b]	2.599(5)	O1w···O2w	2.678(5)
O1w[b]···O3w	2.701(5)		
O2w···O3w	2.619(5)		

[a] $1 - x, y, z$. [b] $1/2 - x, 1/2 + y, z$. [c] $-1/2 + x, 1 - y, 1/2 - z$. [d] $1/2 - x, y, 1/2 + z$.

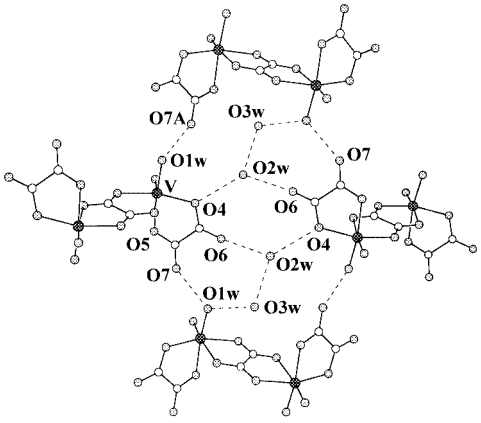

Figure 3. Hydrogen bonding in crystals of **3**

In the asymmetric unit of **4** there is only one lattice water, which is hydrogen-bonded to the coordinated water molecule and to an uncoordinated malonate oxygen atom. The coordinated water molecule is also hydrogen-bonded to an uncoordinated malonate oxygen atom. These three types of O···O hydrogen bonds generate the anionic assembly in the lattice of **4** (Figure 4, Table 2).

Magnetism

Magnetic data for **3** and **4** have been collected in the temperature range 2−300 K. Near perfect fits with the Heisenberg dimer model are attainable (Figures 5 and 6) using the parameters listed in Table 3. In both cases a susceptibility maximum occurs near 8 K and the compounds exhibit Curie−Weiss paramagnetism at high temperatures ($T >$ 50 K). The compounds are thus weakly antiferromagnetic and both the J values lie close to -6 cm^{-1}. The quality of

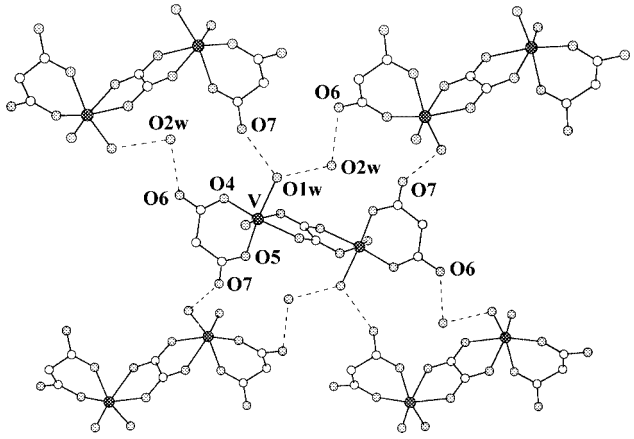

Figure 4. Hydrogen bonding in crystals of **4**

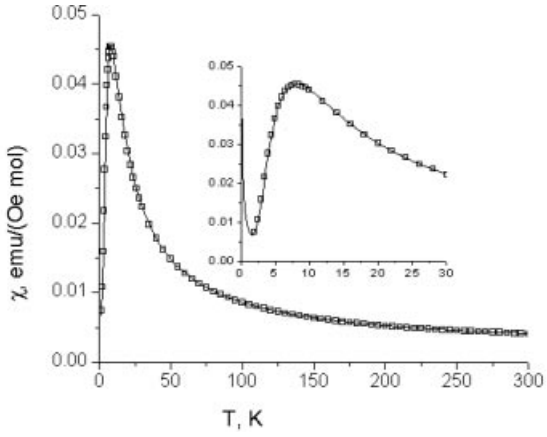

Figure 5. Variable-temperature magnetic susceptibility data of **3**; the solid line represents best fit to the dimer model

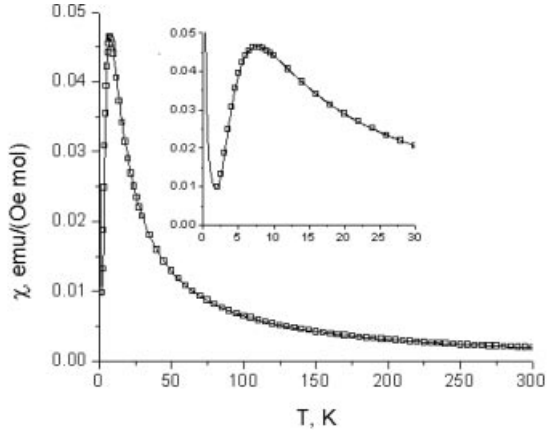

Figure 6. Variable-temperature magnetic susceptibility data of **4**; the solid line represents best fit to the dimer model

 © 2003 Wiley-VCH Verlag GmbH & Co. KGaA, Weinheim

Table 3. Best-fit magnetic parameters

Compound	*g*	*J*	ρ	*tip*
3	1.93 ± 0.01	−6.50 ± 0.05	0.01 ± 0.002	0.0018 ± 0.00005
4	1.95 ± 0.01	−6.25 ± 0.05	0.02 ± 0.002	−0.0004 ± 0.00005

the fit to the dimer model indicates that, in spite of the extensive hydrogen bonding in the lattice, the interdimer magnetic interactions, if any, are small. Consistent[20] with the weak antiferromagnetism, polycrystalline samples of each compound display a virtually isotropic EPR signal at 77 K (**3**: $g = 1.969$; **4**: $g = 1.963$). No zero-field splitting or half-field signals are observed.

The (oxo)vanadium(IV) (d^1) magnetic orbital overlaps with the bridging oxygen orbitals only in the π-fashion as idealized in **5**. The resulting magnetic coupling in the dimer is expected to be relatively weak.[20] Compounds **3** and **4** provide a unique opportunity for qualitatively scrutinizing the effect of certain bond parameters (*a*, *b* and *h* as shown in **6**) on the strength of magnetic coupling.

5

The shorter V−O (bridge) lengths ($a = 2.009$ Å, $b = 2.218$ Å) in **4** compared to those ($a = 2.023$ Å, $b = 2.281$ Å) in **3** may be expected to result in a stronger exchange coupling in **4**. On the other hand, the metal atom is much more displaced from the plane of the bridging oxalate in **4** (0.17 Å) than in **3** (0.05 Å) and this is expected to diminish the exchange interaction in **4**. The two opposing factors appear to have more or less balanced each other and the net bridge-mediated coupling of the magnetic orbitals in the two compounds are virtually equal.

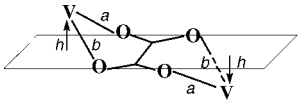

6

The present systems are somewhat stronger antiferromagnets than the two other structurally characterized compounds incorporating **1**: $[Ph_4P]_2[(VO)_2(C_2O_4)_3(H_2O)_2]\cdot 4H_2O$[17] ($J = -4.35$ cm^{-1}) and $[(VO)_2(C_2O_4)(H_2O)_6]Cl_2\cdot Bu_4NCl\cdot H_2O$[21] ($J = -3.85$ cm^{-1}). In $[(VO)_2(C_2O_4)(acac)_2(H_2O)_2]$[20] the value of J is -5.75 cm^{-1}, but its structure has not been determined.

Conclusion

Two oxalato-bridged (oxo)vanadium(IV) dimers **3** and **4** have been successfully assembled using L-ascorbic acid as an oxalate precursor. Structure determination has revealed significant differences in bond parameters of the $V(C_2O_4)V$ fragment in **3** and **4**. The V−O bond lengths follow the order **3** > **4** and the displacement of the metal atom from the bridging oxalate plane has the reverse order **4** > **3**. These inequalities act in opposite directions and the net antiferromagnetic coupling of the magnetic orbitals of the metal sites become virtually equal for **3** and **4** ($-J$ 6 cm^{-1}). Extensive hydrogen bonding is present in the lattice of both **3** and **4** but interdimer magnetic interactions are negligible.

Experimental Section

General: Ammonium metavanadate, L-ascorbic acid, malonic acid and tetraethylammonium bromide were obtained from S. D. Fine-Chem Ltd. All other chemicals and solvents were of analytical grade and were used as received. IR (KBr disk): Nicolet Magna IR 750 Series II spectrometer. UV/Vis: Shimadzu UVPC 1601 spectrometer. A Perkin−Elmer 2400 elemental analyzer was used for microanalysis (C,H,N).

$[Et_4N]_2[(VO)_2(C_2O_4)_3(H_2O)_2]\cdot 4H_2O$ (3): L-Ascorbic acid (0.113 g, 0.64 mmol) and tetraethylammonium bromide (0.09 g, 0.43 mmol) were added to a hot aqueous solution (20 mL) of NH_4VO_3 (0.05 g, 0.43 mmol). The solution was then stirred at 70 °C for 1 h. The dark-green solution thus obtained was further stirred at room temperature for 4 h and then left undisturbed exposed to air. After two weeks blue crystals were collected, washed with ethanol and air-dried. Yield: 0.28 g (84%). $C_{22}H_{52}N_2O_{20}V_2$ (766.5): calcd. C 34.47, H 6.84, N 3.66; found C 34.41, H 6.76, N 3.58. IR (KBr): $\tilde{\nu}$ = 984 (s, V=O), 1715, 1698 (s, C=O), 1658 (s, C=O), 1398, 1256 (s, C=O), 810 (m, O−C=O) cm^{-1}. UV/Vis (H_2O): λ_{max} (ε) = 595 sh (22), 783 (58), 960 sh nm (16 M^{-1}cm^{-1}).

$[Et_4N]_2[(VO)_2(C_2O_4)(C_3H_2O_4)_2(H_2O)_2]\cdot 2H_2O$ (4): L-Ascorbic acid (0.038 g, 0.22 mmol), malonic acid (0.045 g, 0.43 mmol) and tetraethylammonium bromide (0.09 g, 0.43 mmol) were added to a hot aqueous solution (20 mL) of NH_4VO_3 (0.05 g, 0.43 mmol). The blue solution thus obtained was treated as in the preparation of **3** furnishing blue crystals of **4**. Yield: 0.29 g (91%). $C_{24}H_{52}N_2O_{18}V_2$ (758.6): calcd. C 38.00, H 6.91, N 3.69; found C 37.91, H 6.96, N 3.56. IR (KBr): $\tilde{\nu}$: 975 (s, V=O), 1678, 1653 (s, C=O), 1589 (s, C=O), 1411, 1310 (s, C=O), 809 (m, O−C=O) cm^{-1}. UV/Vis (H_2O): λ_{max} (ε) =585 sh (19), 786 (65), 960 sh nm (13 M^{-1}cm^{-1}).

Crystal Structure Determination: Single crystals of complexes **3** and **4** were grown by slow evaporation of water from their aqueous solutions. Data were collected with a Nicolet R3m/V four-circle diffractometer with graphite-monochromated Mo-K_α radiation ($\lambda = 0.71073$Å) by the ω-scan technique in the range $3° \le 2\theta \le 47°$ for **3** and $3° \le 2\theta \le 50°$ for **4**. All data were corrected for Lorentz polarization, and an empirical absorption correction[22] was performed on each set of data on the basis of azimuthal scans

 © 2003 Wiley-VCH Verlag GmbH & Co. KGaA, Weinheim

Table 4. Crystallographic data for **3** and **4**

	3	**4**
Empirical formula	$C_{22}H_{52}N_2O_{20}V_2$	$C_{24}H_{52}N_2O_{18}V_2$
M_r [g mol^{-1}]	766.54	758.56
Crystal size [mm]	0.40 × 0.30 × 0.20	0.48 × 0.38 × 0.36
T [K]	293(2)	293(2)
Crystal system	orthorhombic	orthorhombic
Space group	*Pbca* (no. 61)	*Pccn* (no. 56)
a [Å]	13.950(4)	14.382(6)
b [Å]	14.679(5)	16.295(9)
c [Å]	17.663(4)	14.220(10)
V [Å^3]	3617(2)	3332(3)
Z	4	4
Calcd. density [g cm^{-3}]	1.408	1.512
μ [mm^{-1}]	0.594	0.640
R_{int}	0.0187	0.0307
Refls. measured	2716	2955
Independent refls.	2684	2923
R_1 [$I > 2\sigma(I)$]	0.0517	0.0760
WR_2 [$I > 2\sigma(I)$]	0.1387	0.1830
Goodness of fit on F^2	1.055	1.011

of six reflections. All calculations of data reduction, structure solution, and refinement were done with the programs of SHELXTL, Version 5.03.[23] The two structures were solved by direct methods and were refined by full-matrix least squares on F^2. All non-hydrogen atoms were refined anisotropically. All the hydrogen atoms in both the structures were included in calculated positions. Significant crystal data are listed in Table 4. CCDC-200295 (**3**) and -200296 (**4**) contain the supplementary crystallographic data for this paper. These data can be obtained free of charge at www.ccdc.cam.ac.uk/conts/retrieving.html [or from the Cambridge Crystallographic Data Centre, 12 Union Road, Cambridge CB2 1EZ, UK; Fax: (internat.) + 44-1223/336-033; E-mail: deposit@ccdc.cam.ac.uk].

Magnetic Measurements: Magnetic data of polycrystalline samples (H = 1000 Oe) were recorded on 23.64 mg of **3** and 39.50 mg of **4** in the 2−300 K temperature range using a Quantum Design MPMS-5S SQUID Spectrometer. Calibration and operation procedures have been reported elsewhere.[24] The data were fitted to the Heisenberg dimer model of two S = 1/2 spins [Equation (1)] taking into account the presence of monomeric paramagnetic impurities (second term) and temperature-independent magnetism (third term), where χ is the magnetic susceptibility, T the temperature, g the g factor, J the exchange constant, *tip* is the temperature-independent contribution. The best-fit parameters are given in Table 3.

$$\chi = (1-\rho)\frac{N_A g^2 \mu_B{}^2}{k_B T}\,\frac{2\exp(\frac{2J}{k_B T})}{1+3\exp(\frac{2J}{k_B T})} + \rho\frac{N_A g^2 \mu_B{}^2}{2k_B T} + tip \qquad (1)$$

The X-band EPR spectra of polycrystalline samples were measured with a Varian E-109C spectrometer fitted with a liquid nitrogen Dewar vessel using the following settings: sweep width 5000G, power 30dB, modulation 100 kHz, sweep center 3200 G, sweep time 240 s.

Acknowledgments

We thank the Department of Science and Technology and Council of Scientific and Industrial Research, New Delhi, for financial support.

[1] M. B. Davies, *Polyhedron* **1992**, *11*, 285−321.
[2] L. S. Hollis, A. R. Amundsen, A. W. Stern, *J. Am. Chem. Soc.* **1985**, *107*, 274−276.
[3] H. Yuge, T. K. Miyamoto, *Chem. Lett.* **1996**, 375−376.
[4] M. J. Arendse, G. K. Anderson, N. P. Rath, *Inorg. Chem.* **1999**, *38*, 5864−5869 (and references therein).
[5] S. Mondal, S. P. Rath, K. K. Rajak, A. Chakravorty, *Inorg. Chem.* **1998**, *37*, 1713−1719.
[6] S. P. Rath, K. K. Rajak, S. Mandal, A. Chakravorty, *Dalton Trans.* **1998**, 2097−2101.
[7] K. K. Rajak, S. P. Rath, S. Mondal, A. Chakravorty, *Inorg. Chem.* **1999**, *38*, 3283−3289.
[8] B. Baruah, S. Das, A. Chakravorty, *Inorg. Chem.* **2002**, *41*, 4502−4508.
[9] K. Kustin, D. L. Toppen, *Inorg. Chem.* **1973**, *12*, 1404 −1407.
[10] S. Lewin, *Vitamin C: Its Molecular Biology and Medicinal Potential*, Academic Press, London, **1976**, pp.11.
[11] M. B. Davis, J. Austin, D. A. Partridge, *Vitamin C: Its Chemistry and Biochemistry, Royal Society of Chemistry*, Cambridge, **1991**, pp.61.
[12] G. L. W. Simpson, B. J. Ortwerth, *Biochim. Biophy. Acta* **2000**, *1501*, 12−24.
[13] C. Ünaleroğlu, B. Zümreoğlu-Karan, Y. Zencir, T. Hökelek, *Polyhedron* **1997**, *16*, 2155−2161.
[14] A. M. Thomas, G. C. Mandal, S. K. Tiwary, R. K. Rath, A. R. Chakravarty, *J. Chem. Soc., Dalton Trans.* **2000**, 1395−1396.
[15] P. Orioli, B. Bruni, M. D. Vaira, L. Messori, F. Piccioli, *Inorg. Chem.* **2002**, *41*, 4312−4314.
[16] D. N. Sathyanarayana, C. C. Patil, *J. Inorg. Nucl. Chem.* **1966**, *28*, 2277−2283; B. B. Bhaumik, R. K. Chattopadhyay, *Indian J. Chem.* **1981**, *20A*, 417−419.
[17] J. Salta, C. J. O'Connor, S. Li, J. Zubieta, *Inorg. Chim. Acta* **1996**, *250*, 303−310.
[18] L. M. Zheng, H. W. Schmalle, S. Ferby, S. Decurtins, *Acta Crystallogr., Sect. C* **1998**, *54*, 1435−1438.
[19] P. M. Ehde, I. Anderson, L. Pettersson, *Acta Chim. Scand.* **1986**, *A40*, 489−499; W. R. Scheidt, C. Tsai, J. L. Hoard, *J. Am. Chem. Soc.* **1971**, *93*, 3867−3872; L. V. Boas, J. C. Pessoa, in *Comprehensive Coordination Chemistry* (Eds.: G. Wilkinson, R. D. Gillard, J. A. McCleverty), Pergamon Press, Oxford, **1987**, vol. 3, pp 515−522 (and references therein).
[20] M. Julve, M. Verdaguer, M. -F. Charlot, O. Kahn, *Inorg. Chim. Acta* **1984**, *82*, 5−12.
[21] S. Triki, F. Bérézovsky, J. S. Pala, M.-T. Garland, *Inorg. Chim. Acta* **2000**, *308*, 31−36.
[22] A. C. T. North, D. C. Phillips, F. S. Mathews, *Acta Crystallogr., Sect. A* **1968**, *24*, 351−359.
[23] G. M. Sheldrick, *SHELXTL*, version 5.03, Siemens Analytical Instruments, Inc., Madison, WI, **1994**.
[24] C. J. O'Connor, *Prog. Inorg. Chem.* **1979**, *29*, 203−283.

Received January 13, 2003

 © 2003 Wiley-VCH Verlag GmbH & Co. KGaA, Weinheim

Synthesis and Characterization of Mononuclear Amidogold(III) Complexes − Crystal Structure of $[Au(N_2C_{10}H_7(CMe_2C_6H_4)\text{-}6](NHC_6H_3Me_2\text{-}2,6)][PF_6]$ − Oxidation of 4-Methylaniline to Azotoluene

Maria Agostina Cinellu,*[a] Giovanni Minghetti,[a] Maria Vittoria Pinna,[a] Sergio Stoccoro,[a] Antonio Zucca,[a] and Mario Manassero[b]

Keywords: Gold / Nitrogen ligands / Metallacycles / Amido complexes / Amine oxidation

Mononuclear amidogold(III) complexes $[Au(C,N,N)(NRR')][PF_6]$ [C,N,N = $N_2C_{10}H_7(CMe_2C_6H_4)$-6, where $N_2C_{10}H_8$ = 2,2′-bipy; R = H, R′ = *p*-tolyl (**5**), *o*-xylyl (**6**), isobutyl (**7**), *sec*-butyl (**8**), R = R′ = Et (**9**)], $[Au(C,N)(AcO)(NHC_6H_4NO_2\text{-}4)]$ (**10**) [C,N = $NC_5H_4(CH_2C_6H_4)$-2, where NC_5H_5 = py] and $[Au(N,N)(NHC_6H_4NO_2\text{-}4)_2][PF_6]$ (**11**) (N,N = 2,2′-bipy), have been synthesized in fairly good yields by reaction of the hydroxo, methoxo, or acetato complexes **1**–**4** {$[Au(C,N,N)(OR)][PF_6]$ [R = H (**1**), Me (**2**)], $[Au(C,N)(AcO)_2]$ (**3**), $[Au(N,N)(OH)_2][PF_6]$ (**4**)} with amines. The structure of $[Au(C,N,N)(NHC_6H_3Me_2\text{-}2,6)][PF_6]$ (**6**) has been determined by X-ray diffraction. Reaction of the hydroxo complex **4** with $NH_2C_6H_4Me$-4 gives metallic gold, the protonated ligand $[N,NH][PF_6]$ and organic products, the main one being azotoluene.

(© Wiley-VCH Verlag GmbH & Co. KGaA, 69451 Weinheim, Germany, 2003)

Introduction

Amido complexes of late transition metals have attracted considerable interest[1] because of their involvement as intermediates in metal-catalyzed carbon−nitrogen bond-formation processes.[2] Isolation of such intermediates is often hampered by their high reactivity. Nevertheless several stable late transition metal amides have been synthesized and their structures in the solid state as well as their reactivity investigated.[3] While gold(III) (a d^8 metal ion) complexes with ammonia,[4] bidentate,[5] and terdentate[6] amines, and related amido complexes have been widely studied, mainly from a kinetic point of view, isolated complexes with simple amide ligands[7] are still scarcely represented.[8] This shortage of data[9] and a report on the intramolecular hydroamination of alkynes catalyzed by gold(III) salts[10] prompted us to investigate the reactivity of some gold(III) complexes with various amines.

Previously, we have described the synthesis, characterization, and reactivity of gold(III) cyclometallated derivatives $[Au(C,N,N)(Y)][PF_6]$ (C,N,N = 6-benzyl-2,2′-bipyridine) with various anionic ligands Y.[11] Among these, two stable amido complexes, $[Au(C,N,N)(NHC_6H_4NO_2\text{-}4)][PF_6]$ [C,N,N = $N_2C_{10}H_7(CHMeC_6H_4)$-6 and $N_2C_{10}H_7(CMe_2C_6H_4)$-6], could be obtained by σ-ligand metathesis of the corresponding methoxo complexes with *p*-nitroaniline.

Our study on amidogold(III) complexes has been extended to different amines and to different co-ligands to verify the effectiveness of the synthetic method and the influence of the ancillary ligand on the reactivity of the amidogold(III) complex. Here we show that a number of amidogold(III) complexes can be isolated with different co-ligands. The terdentate C,N,N ligand arising from 6-(1,1-dimethylbenzyl)-2,2′-bipyridine is the most effective in stabilizing different amido complexes, whereas the bidentate C,N and N,N ligands (deprotonated 2-benzylpyridine and 2,2′-bipyridine, respectively) could stabilize only the *p*-nitroanilide derivative. The gold complex $[Au(N,N)(OH)_2][PF_6]$[12] (**4**) can promote the oxidation of amines other than *p*-nitroaniline. With *p*-toluidine the main product is azotoluene.

The selective oxidation of aromatic amines under mild conditions is of current interest, as pointed out in a recent paper relevant to oxidation processes catalysed by an iron(III) complex.[13]

Results and Discussion

During previous studies on gold(III) chemistry we had found that several complexes, $[Au(C,N,N)Y]^+$, containing both gold−carbon and gold−heteroatom bonds are accessible by treatment of acetato, hydroxo, and methoxo com-

[a] Dipartimento di Chimica, Università di Sassari,
Via Vienna 2, 07100 Sassari, Italy
Fax: (internat.) + 39-079/229559
E-mail: cinellu@ssmain.uniss.it
[b] Dipartimento di Chimica Strutturale e Stereochimica Inorganica, Università di Milano, Centro CNR,
via Venezian 21, 20133 Milano, Italy
E-mail: m.manassero@csmtbo.mi.cnr.it

 © 2003 Wiley-VCH Verlag GmbH & Co. KGaA, Weinheim **DOI: 10.1002/ejic.200200377**

plexes with protic reagents at room temperature.[11] In particular, besides alkoxo, thiolato, and acetylide complexes, two stable gold amides have been synthesized by an exchange reaction of *p*-nitroaniline with [Au(C,N,N)(OMe)][PF_6] [C,N,N = $N_2C_{10}H_7(CHMeC_6H_4)$-6 and $N_2C_{10}H_7(CMe_2C_6H_4)$-6] in dichloromethane.[11]

New amidogold(III) complexes with three different ancillary ligands, all containing nitrogen donor atoms, have been obtained by the addition of different amines to hydroxo, methoxo, or acetato complexes under mild conditions that required excess amine to drive the equilibrium reaction to completion. The nature of the ancillary ligand dramatically affects the outcome of the reaction: with the terdentate cyclometallated ligand $N_2C_{10}H_7(CMe_2C_6H_4)$-6 both alkyl- and arylamides are obtained in fairly good yields (Scheme 1), whereas with the bidentate C,N ligand $NC_5H_4(CH_2C_6H_4)$-2 and the N,N ligand 2,2′-bipyridine only *p*-nitroanilide complexes have been isolated (Scheme 2). Addition of even large amounts of *p*-nitroaniline to complex **3** gives only substitution of one AcO group. Isolation of stable bis(amido) complexes other than the *p*-nitroaniline derivative, at least for complex **4**, is probably hampered by their high reactivity.

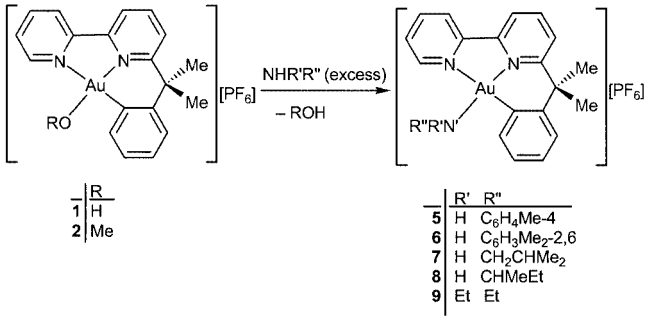

	R
1	H
2	Me

	R'	R"
5	H	C_6H_4Me-4
6	H	$C_6H_3Me_2$-2,6
7	H	CH_2CHMe_2
8	H	CHMeEt
9	Et	Et

Scheme 1

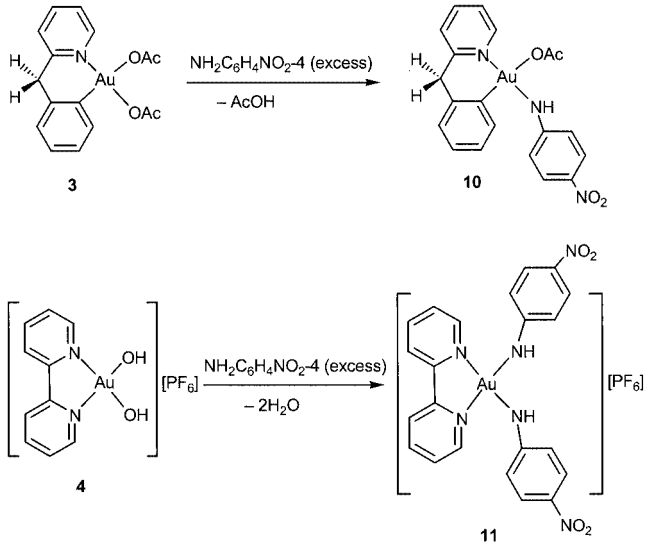

Scheme 2

Alkylamido complexes **7**–**9** were obtained simply in a one-pot reaction in high yields, whereas arylamido complexes **5** and **6** required either the use of molecular sieves to trap water or further treatment of the crude mixture with excess amine (see Exp. Sect.). With complex **2** the trend observed suggests that the exchange reaction proceeds, at least in this case, by nucleophilic attack of the amine at the gold centre followed by proton transfer to the coordinated methoxide ligand and elimination of methanol. Reaction of the more basic amine $NHEt_2$ goes to completion within a few hours. For complexes **3** and **4** other mechanisms could be operative: thus, for the neutral complex **3** dissociation of the acetato group *trans* to the carbon atom can be envisaged. Coordination of the amine and successive deprotonation should follow to give the amido species.

Complexes **5**–**11** are air-stable compounds with relatively high melting points and good stability in solution: no decomposition was observed even for amides having β-hydrogen atoms (**7**–**9**). In the FAB mass spectra (positive ions) of compounds **5**, **6**, **8**, **9**, and **11** the molecular ions [M^+] ([M − H], for **8**) have been observed. In the spectrum of the isobutylamido derivative **7** the major peak (100% intensity) corresponds to the species [Au(C,N,N)(NBA − H)], which is probably formed by an exchange reaction of the nitrobenzyl alcohol (NBA) with the amido complex. Peaks corresponding to this species are also found in the mass spectra of the alkylamido complexes **8** and **9**. The neutral complex [Au(C,N)(OAc)($NHC_6H_4NO_2$-4)] (**10**) gives a medium-intensity peak, corresponding to [M − AcO], as is also observed for the starting bis(acetato) complex. Of the two possible geometrical isomers, *trans*-N(am)–Au–N(py) or *trans*-N(am)–Au–C (am = amide; py = pyridine), the IR and NMR spectra, taken together, support a *trans*-N–Au–N arrangement. Indeed the acetato group stretching vibrations are observed at values consistent with an acetato group *trans* to a carbon atom (see Exp. Sect.) and the chemical shift of the H^6 proton at a value similar to that found for the bis(acetato) complex. The high *trans* influence of the deprotonated amine,[6e] with respect to that of the pyridine nitrogen atom, is probably responsible for making thermodynamically stable the isomer with high *trans*-influencing ligands in mutually *cis* positions. Analogous results were found for the reaction of the dichloro complexes [Au(C,N)Cl_2] with excess PPh_3, where only one chloride ion was replaced to give [Au(C,N)(PPh_3)Cl]$^+$, having a *trans*-P–Au–N arrangement [C,N = $C_6H_4CH_2NMe_2$-2,[14a] $NC_5H_4(CRR'C_6H_4)$-2[14b]].

In the IR spectra, weak to medium $\tilde{\nu}$(N–H) absorptions are observed in the range 3200–3336 cm^{-1}. In the ^1H NMR spectra the N*H* resonance could be assigned due to exchange with D_2O. In complexes **5**–**8** the NH resonance is shifted downfield with respect to the free ligand with $\Delta\delta$ = 1.5, 1.5, 2, and 1.6 ppm, respectively. In complexes **7** and **8** H–N–C–H spin–spin coupling, not present in the free amines, is observed. H–N–C–H spin–spin coupling has been reported in amine solutions when either the nitrogen atom is weakly basic or the nitrogen lone pair is coordinated with a Lewis acid.[15] Thus, it appears that substi-

 © 2003 Wiley-VCH Verlag GmbH & Co. KGaA, Weinheim

tution of a hydrogen ion with an [Au(C,N,N)] group lowers the basicity of the nitrogen atom of the amine.

Because the NHCHMeEt ligand in complex **8** has a stereogenic carbon atom β to the metal atom, the methylene protons are diastereotopic, giving rise to two sets of multiplets. Also, in complex **9** the two hydrogen atoms on each methylene group of the NEt_2 ligand are diastereotopic: the two signals are very broad at ambient temperature but a well-resolved ABX_3 pattern is observed at −20 °C. As reported previously for other N,N,C aurated derivatives,[11] the six-membered C,N ring is fluxional on the NMR time scale. Thus, one resonance alone is observed for the methyl protons on the benzylic carbon atom of complexes **5**−**9**: no significant variation is observed on lowering the temperature from 20 to −80 °C.

A diffraction study of suitable crystals of complex **6** revealed a structure that consists of $[Au(C,N,N)(NHC_6H_3Me_2\text{-}2,6)]^+$ cations and PF_6^- anions packed in a molar ratio 1:1 with normal van der Waals contacts. An ORTEP view of the cation with the atom labelling scheme is shown in Figure 1. Selected bond lengths and angles are reported in Table 1.

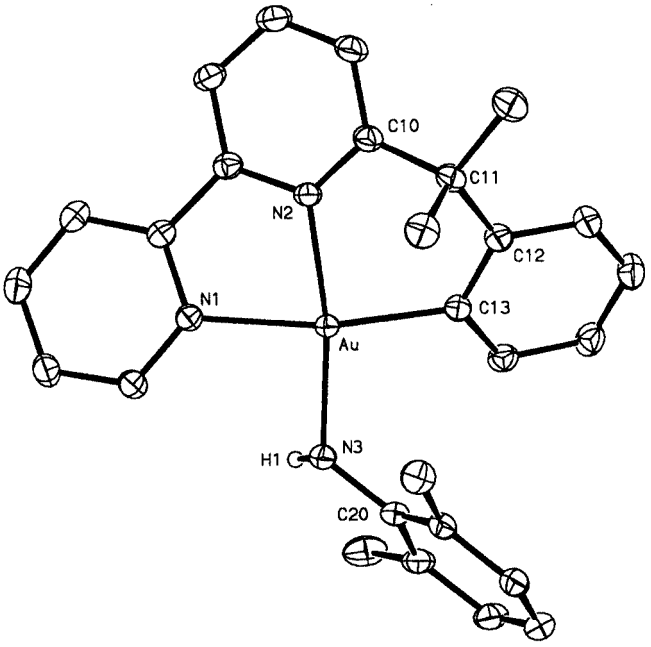

Figure 1. ORTEP view of the cation in compound **6**; ellipsoids are drawn at the 30% probability level

Table 1. Selected bond lengths [Å] and angles [°] with e.s.d.s in parentheses for the complex cation in compound **6**

Au−N(1)	2.128(2)	Au−N(2)	2.056(2)
Au−N(3)	2.015(2)	Au−C(13)	2.018(2)
N(3)−C(20)	1.401(3)	N(3)−H(1)	0.84(3)
N(1)−Au−N(2)	79.1(1)	N(1)−Au−N(3)	90.9(1)
N(1)−Au−C(13)	164.1(1)	N(2)−Au−N(3)	169.4(1)
N(2)−Au−C(13)	91.4(1)	N(3)−Au−C(13)	99.1(1)
Au−N(3)−C(20)	126.1(2)	Au−N(3)−H(1)	99(2)
C(20)−N(3)−H(1)	112(2)		

The gold atom in the cation displays a distorted square-planar coordination, with atoms Au(1), N(2), N(3), and C(13) essentially coplanar [maximum distances from their best plane being +0.005(2) Å for N(3) and −0.011(1) Å for Au], whereas atom N(1) is displaced by 0.484(2) Å out of the best plane. The distortion from the ideal square-planar geometry is probably due to the limited flexibility of the tridentate substituted bipyridine ligand. A similar distortion has been found in $[Au(C,N,N)Cl]^+$, which differs from the present one only in the substitution of the amido ligand with a chloride.[16] Bond lengths and angles in the present cation can be compared with those found in $[Au(C,N,N)Cl]^+$. Thus, the Au−N(1) and Au−C(13) bond lengths [2.128(2) and 2.018(2) Å, respectively] reported here are very similar to those in $[Au(C,N,N)Cl]^+$ [2.121(5) and 2.009(6) Å, respectively]. The slight elongation of the present Au−N(2) distance [2.056(2) Å] with respect to that of $[Au(C,N,N)Cl]^+$ [2.009(4) Å] indicates that the *trans* influence of the amide ligand is stronger than that of the chloride ligand. In the absence of suitable structural data[17] the Au(1)−N(3) bond length [2.015(2) Å] can be compared to the Pt−N distance found in *trans*-$[PtCl(NHC_6H_4I\text{-}4)(PEt_3)_2]$ [2.006(4) Å] and in a number of other (amido)Pt complexes (ref.[3l] and refs. therein). The six-membered metallacycle is in a boat conformation, with atoms N(2), C(10), C(12), and C(13) essentially coplanar, maximum deviations from their best plane being +0.025(2) and −0.025(2) Å for C(12) and C(10), respectively, whereas Au and C(11) lie 0.543(1) and 0.641(2) Å, respectively, above their best plane.

Reaction of complex **3** with amines other than *p*-nitroaniline led to mixtures of unidentified products and a small amount of gold. In contrast, complex **4** was quickly decomposed by the addition of amines and, with *p*-toluidine, it was possible to identify the main reaction products (Scheme 3). In addition to gold, which separated as a dark powder, 2,2′-bipyridine was recovered almost quantitatively (80%) as the salt $[N,NH][PF_6]$. Chromatography on silica gel of the organic fraction allowed us to isolate azotoluene (*trans* isomer) in 43% yield, based on the gold complex.

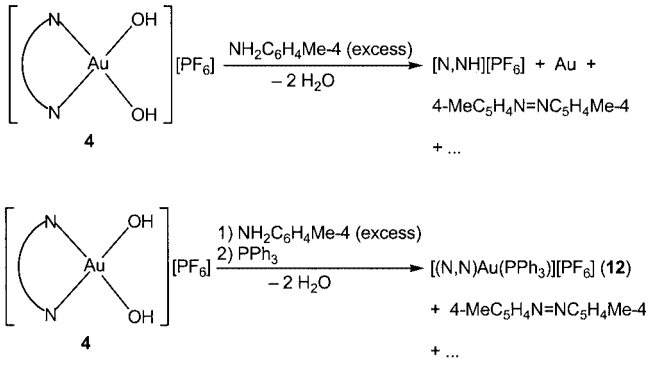

Scheme 3

The formation of azobenzene, as the main by-product, was observed in the oxidative carbonylation of amines cata-

lyzed by gold complexes, in particular when $HAuCl_4$ was employed in the reaction with aniline.[18] Azobenzene derivatives are also by-products in the $FeCl_2py_4^+$-catalyzed transformation of aromatic amines by H_2O_2,[13] as well as the main products of the ferrate oxidation of anilines, both in homogeneous[19] and in heterogeneous phases.[20] Different reaction mechanisms for the formation of azo compounds in the homogeneous phase have been claimed.[13,19]

In our case a bis(amido) intermediate can be envisaged for the formation of azotoluene. *N*,*N*′-Di-*p*-tolylhydrazine could form by N−N coupling of the bis(amido) complex $[Au(N,N)(NHC_6H_4Me_2\text{-}4)_2][PF_6]$, analogous to **11**, and then be oxidized to azotoluene.[21] This implies an unstable gold(I) intermediate $[Au(N,N)(solv)][PF_6]$ (solv = H_2O, MeCN). In an attempt to trap it, the reaction was carried out in the presence of PPh_3 (Scheme 3). Indeed, a gold(I) intermediate (**12**) was isolated, although not quantitatively, and identified as the known complex $[(N,N)Au(PPh_3)][PF_6]$.[22] The isolobal analogy between the cations $[(N,N)H]^+$ and $[(N,N)Au(PPh_3)]^+$ is notable.

Experimental Section

General: The gold complexes $[Au(C,N,N)Cl][PF_6]$ and $[Au(C,N)Cl_2]$ were obtained according to ref.[11] and ref.[14b], respectively. All the amines were used as received from commercial sources; the solvents were purified and dried according to standard methods. Celite (filter agent) and molecular sieves (4 Å) were purchased from Aldrich, and silica gel (70−230 mesh ASTM) from Merck. Elemental analyses were performed with a Perkin−Elmer Elemental Analyzer 240B by Mr. A. Canu (Dipartimento di Chimica, Università di Sassari). Conductivities were measured with a Philips PW 9505 conductimeter. Infrared spectra were recorded with a Perkin−Elmer 983 spectrophotometer; the values are given in cm^{-1}. ^1H and $^{31}P\{^1H\}$ NMR spectra were recorded with a Varian VXR 300 spectrometer operating at 299.9 and 121.4 MHz, respectively. Chemical shifts are given in ppm relative to internal TMS (^1H) or external H_3PO_4 (^{31}P). Mass spectra were obtained with a VG 7070 instrument operating under FAB conditions, with 3-nitrobenzyl alcohol (NBA) as supporting matrix or EI conditions. GC/MS analyses were conducted with a Hewlett-Packard G1800B Gas Chromatograph Electron Ionization Detector (GCD System).

[Au(C,N,N)(OH)][PF$_6$] (1): An aqueous solution of KOH (0.033 g, 0.59 mmol) was added to an aqueous suspension of $[Au(C,N,N)Cl][PF_6]$ (0.179 g, 0.27 mmol). The mixture was heated under reflux for 1 h whilst stirring and then filtered. The volume of the colourless filtrate was reduced in a rotary evaporator until crystallization was observed. The resultant white product was collected by filtration and dried in vacuo. Yield: 0.128 g (75%), m.p. 170 °C. $C_{19}H_{18}AuF_6N_2OP$ (632.32): calcd. C 36.09, H 2.87, N 4.43; found C 35.91, H 2.71, N 4.33. Λ_M ($5\cdot10^{-4}$ mol·dm^{-3}, Me_2CO) = 106 $\Omega^{-1}\cdot cm^2\cdot mol^{-1}$. IR (Nujol): $\tilde{\nu}$ = 3360 m (broad) (OH), 1599 s, 1561 m, 1082 m, 1025 s, 846 vs (broad) cm^{-1}. ^1H NMR ([D$_6$]acetone): δ = 9.21 (dd, ^3J = 5.4, ^4J = 1.9 Hz, 1 H, H$^{6'}$), 8.92−7.18 (m, 10 H, other aromatics), 4.58 (s, 1 H, OH), 2.11 (s, 6 H, CH_3) ppm. MS (FAB$^+$): *m*/*z* (%) = 487 (100) [M$^+$], 470 (30) [Au(C,N,N)], 393 (10) [M − OH − C_6H_5], 273 (50) [C,N,N].

[Au(C,N,N)(OMe)][PF$_6$] (2): This was prepared according to ref.[11]

[Au(C,N)(AcO)$_2$] (3): Solid AcOAg (0.339 g, 2.03 mmol) was added to a suspension of $[Au(C,N)Cl_2]$ (0.401 g, 0.92 mmol) in acetone (20 mL). The resulting suspension was stirred at room temperature for 8 h and then filtered through Celite. Addition of diethyl ether to the concentrated solution afforded a creamy solid product. Recrystallization from chloroform/diethyl ether gave an analytical sample. Yield: 0.300 g (67%), m.p. 152 °C (dec.). $C_{16}H_{16}AuNO_4$ (483.30): calcd. C 39.76, H 3.34, N 2.90; found C 39.23, H 3.14, N 2.92. IR (Nujol): $\tilde{\nu}$ = 1668 vs and 1627 vs (C=O), 1568 m, 1307 vs and 1278 vs (C−O), 1042 m, 1031 m, 1007 m, 762 s, 704 m, 679 s cm^{-1}. ^1H NMR ($CDCl_3$): δ = 9.02 (d, ^3J = 5.1 Hz, 1 H, H^6), 8.03−7.01 (m, 7 H, other aromatic H), 4.38 (s, 2 H, CH_2), 2.11 (s, 3 H, Me), 2.04 (s, 3 H, Me) ppm. MS (FAB$^+$): *m*/*z* (%) = 533 (20) $[Au(C,N)_2]$, 424 (100) [M − CH_3CO_2].

[Au(N,N)(OH)$_2$][PF$_6$] (4): This was prepared according to ref.[12]

[Au(C,N,N)(NH-*p*-tol)][PF$_6$] (5). Method (a): Solid *p*-toluidine (0.064 g, 0.6 mmol) was added to a solution of **1** (0.126 g, 0.2 mmol) in dichloromethane (20 mL). The resulting red−orange solution was stirred at room temperature for 15 h in the presence of activated molecular sieves. The filtered solution was then concentrated to a small volume and diethyl ether added to give a red−orange solid product. Yield: 0.118 g (82%). **Method (b):** Solid *p*-toluidine (0.042 g, 0.39 mmol) was added to a solution of **2** (0.082 g, 0.13 mmol) in dichloromethane (15 mL). The resulting red−orange solution was stirred for 23 h at room temperature and then concentrated to a small volume. Addition of diethyl ether gave a red−orange precipitate of the equilibrium mixture (^1H NMR criterion) which was treated with excess *p*-toluidine in dichloromethane solution for 24 h to give complete conversion of **2**. Yield: 0.072 g (76%), m.p. 193−194 °C. $C_{26}H_{25}AuF_6N_3P$ (721.46): calcd. C 43.28, H 3.49, N 5.83; found C 42.80, H 3.35, N 5.61. Λ_M ($5\cdot10^{-4}$ mol·dm^{-3}, Me_2CO) = 120 $\Omega^{-1}\cdot cm^2\cdot mol^{-1}$. IR (Nujol): $\tilde{\nu}$ = 3300 w (NH), 1600 s, 1560 m, 1500 s, 1250 s, 1160 m, 1100 m, 1070 m, 1040 m, 1025 vs, 846 vs (broad), 780 s, 640 w cm^{-1}. ^1H NMR (CD_2Cl_2): δ = 9.24 (dd, ^3J = 5.4, ^4J = 1.0 Hz, 1 H, H$^{6'}$), 8.66−7.06 (m, 10 H, other aromatic H), 6.97 (d, ^3J = 8.4 Hz, 2 H, H^{ortho}), 6.89 (d, ^3J = 8.4 Hz, 2 H, H^{meta}), 5.07 (s, 1 H, NH), 2.23 (s, 3 H, Me), 2.12 (s, 6 H, Me) ppm. MS (FAB$^+$): *m*/*z* (%) = 576 (100) [M$^+$], 470 (45) [Au(C,N,N)], 273 (40) [C,N,N].

[Au(C,N,N)(NH-*o*-xylyl)][PF$_6$] (6): Liquid *o*-xylidine (0.073 g, 0.6 mmol) was added to a solution of **1** (0.126 g, 0.2 mmol) in dichloromethane (20 mL). The resulting dark red solution was stirred at room temperature for 15 h in the presence of activated molecular sieves. The solution was then filtered and concentrated to a small volume and diethyl ether added to give a dark red solid product. Yield: 0.115 g (78%), m.p. 192 °C. $C_{27}H_{27}AuF_6N_3P$ (735.45): calcd. C 44.09, H 3.70, N 5.71%; found C 44.00, H 4.04, N 5.61. Λ_M ($5\cdot10^{-4}$ mol·dm^{-3}, Me_2CO) = 125 $\Omega^{-1}\cdot cm^2\cdot mol^{-1}$. IR (Nujol): $\tilde{\nu}$ = 3300 w (NH), 1590 s, 1220 s, 1080 m, 1038 s, 1020s, 840 vs (broad), 770 vs, 640 m cm^{-1}. ^1H NMR (CD_2Cl_2): δ = 9.12 (d, ^3J = 5.4 Hz, 1 H, H$^{6'}$), 8.61−6.84 (m, 10 H, other aromatic H), 7.03. (d, ^3J = 7.3 Hz, 2 H, H^{meta}), 6.92 (t, ^3J = 7.3 Hz, 1 H, H^{para}), 5.04 (s, 1 H, NH), 2.31 [s, 6 H, 2 Me (xylydine)], 2.12 [s, 6 H, 2 Me (bipy)] ppm. MS (FAB$^+$): *m*/*z* (%) = 590 (100) [M$^+$], 470 (65) [Au(C,N,N)], 273 (30) [C,N,N]. Crystals suitable for a diffraction study were obtained by slow diffusion of diethyl ether into a dichloromethane solution of **6**.

[Au(C,N,N)(NH-*i*Bu)][PF$_6$] (7): Liquid isobutylamine (0.102 g, 1.4 mmol) was added to a solution of **2** (0.092 g, 0.14 mmol) in dichloromethane (15 mL). The resulting greenish solution was stirred at room temperature for 6 h and then concentrated to a

 © 2003 Wiley-VCH Verlag GmbH & Co. KGaA, Weinheim

small volume. Addition of diethyl ether gave a greenish-yellow precipitate of the analytical sample. Yield: 0.095 g (97%), m.p. 153 °C. $C_{23}H_{27}AuF_6N_3P$ (687.45): calcd. C 40.18, H 3.96, N 6.11; found C 40.26, H 3.81, N 5.79. Λ_M ($5\cdot10^{-4}$ mol·dm^{-3}, Me_2CO) = 128 $\Omega^{-1}\cdot cm^2\cdot mol^{-1}$. IR (Nujol): $\tilde{\nu}$ = 3300 w (NH), 1596 s, 1562 m, 1064 m, 1042 s, 850 vs (broad) cm^{-1}. ^{1}H NMR (CD_2Cl_2): δ = 9.25 (dd, ^3J = 5.4, ^4J = 1.0 Hz, 1 H, H$^{6'}$), 8.62−7.32 (m, 10 H, other aromatic H), 3.30 (t, $^3J_{HN-CH}$ = 9.0 Hz, 1 H, NH), 2.98 (dd, $^3J_{H,C-CH}$ = 6.6, $^3J_{H,C-NH}$ = 9.0 Hz, 2 H, CH_2), 2.09 (s, 6 H, Me), 1.96 (m, 1 H, CH), 1.10 (d, ^3J = 6.8, 6 H, Me) ppm. FAB$^+$: *m*/*z* (%) = 622 (100) [Au(C,N,N)(NBA − H)], 470 (35) [Au(C,N,N)], 273 (40) [C,N,N].

[Au(C,N,N)(NH-*s*Bu)][PF$_6$] (8): Liquid *sec*-butylamine (0.102 g, 1.4 mmol) was added to a solution of **2** (0.092 g, 0.14 mmol) in dichloromethane (15 mL). The resulting orange solution was stirred at room temperature for 23 h and then concentrated to a small volume. Addition of diethyl ether gave an orange precipitate of the analytical sample. Yield: 0.086 g (89%), m.p. 150 °C (dec.). $C_{23}H_{27}AuF_6N_3P$ (687.45): calcd. C 40.18, H 3.96, N 6.11; found C 40.06, H 3.72, N 5.83. Λ_M ($5\cdot10^{-4}$ mol·dm^{-3}, Me_2CO) = 126 $\Omega^{-1}\cdot cm^2\cdot mol^{-1}$. IR (Nujol): $\tilde{\nu}$ = 3280 w (NH), 1590 s, 1520 m, 1080 s, 1040 s, 846 vs (broad) cm^{-1}. ^{1}H NMR (CD_2Cl_2): δ = 9.50 (dd, ^3J = 5.4, ^4J = 1.0 Hz, 1 H, H$^{6'}$), 8.58−7.27 (m, 10 H, other aromatics), 3.35 (d, $^3J_{HN-CH}$ = 4.0 Hz, 1 H, NH), 3.15 (m, 1 H, CH), 2.12 (s, 6 H, Me), 1.79 (m, 1 H, CH_AH$_B$), 1.64 (m, 1 H, CH$_A$$H_B$), 1.35 (d, ^3J = 6.3 Hz, 3 H, CH_3CH), 1.03 (t, ^3J = 7.3, 7.6 Hz, 3 H, CH_3CH$_2$) ppm. MS (FAB$^+$): *m*/*z* (%) = 622 (100) [Au(C,N,N)(NBA − H)], 541 (10) [M − H], 470 (40) [Au(C,N,N)], 273 (75) [C,N,N].

[Au(C,N,N)(NEt$_2$)][PF$_6$] (9): Liquid diethylamine (0.095 g, 1.3 mmol) was added to a solution of **2** (0.083 g, 0.13 mmol) in dichloromethane (15 mL). The resulting red solution was stirred at room temperature for 2 h then concentrated to a small volume. Addition of diethyl ether gave a dark orange precipitate of the analytical sample. Yield 0.086 g (96%), m.p. 160 °C. $C_{23}H_{27}AuF_6N_3P$ (687.45): calcd. C 40.18, H 3.96, N 6.11; found C 39.87, H 3.81, N 5.86. Λ_M ($5\cdot10^{-4}$ mol·dm^{-3}, Me_2CO) = 120 $\Omega^{-1}\cdot cm^2\cdot mol^{-1}$. IR (Nujol): $\tilde{\nu}$ = 1595 s, 1576 m, 1082 s, 1021 s, 846 vs (broad) cm^{-1}. ^{1}H NMR (CD_2Cl_2, −20 °C): δ = 9.37 (d, ^3J = 4.8 Hz, 1 H, H$^{6'}$), 8.57−7.29 (m, 10 H, other aromatics), 3.04 (m, ^2J = 14.3 Hz, ^3J = 7.0 Hz, 2 H, CH_AH$_B$), 2.62 (m, ^2J = 14.3 Hz, ^3J = 7.0 Hz, 2 H, CH$_A$$H_B$), 2.12 (s, 6 H, Me), 1.24 (t, ^3J = 7.0 Hz, 6 H, CH_3−CH$_2$) ppm. MS (FAB): *m*/*z* (%) = 622 (37) [Au(C,N,N)(NBA − H)], 542 (82) [M$^+$], 470 (90) [Au(C,N,N)], 273 (64) [C,N,N].

[Au(C,N)(OAc)(NHC$_6$H$_4$NO$_2$-4)] (10): Solid *p*-nitroaniline (0.138 g, 1 mmol) was added to a solution of complex **3** (0.120 g, 0.25 mmol) in dichloromethane (20 mL); the resulting yellow solution was then stirred for 24 h at room temperature. During this period the solution turned red−orange. Addition of diethyl ether to the concentrated solution caused precipitation of the equilibrium mixture (^{1}H NMR criterion). The mixture was then subjected to the procedure described above until complete conversion of **3** occurred. Yield: 0.085 g (60%), m.p. 157 °C (dec.). $C_{20}H_{18}AuN_3O_4$ (561.37): calcd. C 42.79, H 3.23, N 7.49; found C 42.68, H 3.15, N 7.27. IR (Nujol): $\tilde{\nu}$ = 3330 m (N−H), 1624 s (C=O), 1583 vs (NO_2), 1299 vs (broad) (C−O) + (NO_2), 1182 s, 1111 vs, 834 m, 753 m cm^{-1}. ^{1}H NMR ($CDCl_3$): δ = 8.94 (d, ^3J = 5.6 Hz,1 H, H^6), 8.02−7.01 (m, 7 H, other aromatic H), 7.89 (d, ^3J = 9.3 Hz, 2 H, H^{meta}), 6.65 (d, ^3J = 9.3 Hz, 2 H, H^{ortho}), 4.75 (s, 1 H, NH), 4.38 (s, 2 H, CH_2), 2.00 (s, 3 H, Me) ppm. MS (FAB$^+$): *m*/*z* (%) = 533 (100) [Au(C,N)$_2$], 502 (68) [M − $MeCO_2$], 366 (40) [Au(C,N)].

[Au(N,N)(NHC$_6$H$_4$NO$_2$-4)$_2$][PF$_6$] (11): Solid *p*-nitroaniline (0.341 g, 2.44 mmol) was added to a solution of **4** (0.130 g, 0.24 mmol) in acetone (20 mL); the resulting yellow solution was stirred at room temperature for 53 h. During this period the solution turned deep red. Addition of diethyl ether to the concentrated solution gave a red product, which was washed with methanol to give an analytical sample. Yield: 0.037 g (20%), m.p. 163 °C. $C_{22}H_{18}AuF_6N_6O_4P$ (772.39): calcd. C 34.20, H 2.35, N 10.88; found C 33.98, H 2.22, N 10.45. Λ_M ($5\cdot10^{-4}$ mol·dm^{-3}, Me_2CO) = 120 $\Omega^{-1}\cdot cm^2\cdot mol^{-1}$. IR (Nujol): $\tilde{\nu}$ = 3336 m (N−H), 1602 s, 1585 vs (NO_2), 1342 vs (broad) (NO_2), 1251 s, 1113 vs, 846 vs (broad) cm^{-1}. ^{1}H NMR ([D$_6$]acetone): δ = 9.35 (d, ^3J = 5.6 Hz, 2 H, H^6), 9.06 (d, ^3J = 7.6 Hz, 2 H, H^3), 8.79 (td, ^3J = 7.8, ^4J = 1.5 Hz, 2 H, H^4), 8.29 (t, ^3J = 7.1 Hz, 2 H, H^5), 7.78 (d, ^3J = 9.0 Hz, 4 H, H^{meta}), 7.10 (d, ^3J = 9.0 Hz, 4 H, H^{ortho}), 6.03 (s, 2 H, NH) ppm. MS (FAB$^+$): *m*/*z* (%) = 627 (20) [M$^+$], 490 (82) [M − NHC$_6$H$_4$NO$_2$-4], 353 [Au(N,N)].

Reaction of [Au(N,N)(OH)$_2$][PF$_6$] (4) with NH$_2$C$_6$H$_4$Me-4: Solid *p*-toluidine (0.098 g, 0.92 mmol) was added to a stirred solution of **4** (0.122 g, 0.23 mmol) in MeCN (20 mL); the resulting solution was stirred for 24 h at room temperature. During this period the solution turned dark red, and separation of a dark powder was observed. After filtration through Celite, the solution was concentrated to a small volume; subsequent addition of diethyl ether afforded a dirty white precipitate that was filtered off and identified as [N,NH][PF$_6$][23] (0.056 g, 80%). The mother liquor was concentrated to dryness to give a dark red solid, which was taken up with benzene and eluted through a column (15 × 1 cm) of silica gel. Removal of the solvent from the first eluate gave an orange crystalline product that was identified as *trans*-azotoluene. Yield: 0.021 g (43.4% with respect to complex **4**), m.p. 140 °C. MS (EI$^+$): *m*/*z* = 211 [MH$^+$], 119 [M − $C_6H_5CH_2$], 92 [C_6H_5Me]. ^{1}H NMR ($CDCl_3$): δ = 7.81 (d, ^3J = 8.1 Hz, 2 H), 7.30 (d, ^3J = 8.1 Hz, 2 H), 2.42 (s, 3 H, Me) ppm.

Reaction of [Au(N,N)(OH)$_2$][PF$_6$] (4) with NH$_2$C$_6$H$_4$Me-4 and PPh$_3$: A solution of PPh_3 (0.131 g, 0.5 mmol) in MeCN was added to a stirred solution of complex **4** (0.266 g, 0.5 mmol) and *p*-toluidine (0.214 g, 2 mmol) in MeCN (20 mL). The reaction mixture was stirred for 24 h at room temperature, filtered through Celite and concentrated to a small volume. Addition of diethyl ether afforded a dirty white product that was recrystallized from dichloromethane/diethyl ether to give an analytical sample, which was identified as [(N,N)Au(PPh_3)][PF$_6$] (**12**) (0.195 g, 51%), m.p. 195 °C (dec.). $C_{28}H_{23}AuF_6N_2P_2$ (760.39): calcd. C 44.22, H 3.05, N 3.68; found C 44.38, H 3.22, N 3.62. ^{1}H NMR (CD_2Cl_2): δ = 8.63 (d, ^3J = 4.1 Hz, 2 H, H^6), 8.33 (d, ^3J = 8.0 Hz, 2 H, H^3), 8.19 (t, ^3J = 7.3 Hz, 2 H, H^4), 7.72 (t, ^3J = 7.6 Hz, 2 H, H^5), 7.67−7.52 [m, 15 H, P(C$_6$$H_5$)$_3$] ppm. ^{31}P{^{1}H} NMR (CD_2Cl_2): δ = 31.3 (s, *P*Ph$_3$), −144.06 (sept, J_{P-F} = 711.1 Hz, *P*F$_6$) ppm. The mother liquor, containing organic products, was concentrated to dryness. The residue was then taken up with benzene and eluted through a column (20 × 1 cm) of silica gel. Removal of the solvent from the first eluate gave an orange crystalline product, which was identified as *trans*-azotoluene, yield 0.027 g (25.7%).

X-ray Data Collection and Structure Determination: Crystal data and other experimental details are summarized in Table 2. The diffraction experiment was carried out with a Bruker SMART CCD area-detector diffractometer at 223 K using Mo-K_α radiation (λ = 0.71073 Å) with a graphite crystal monochromator in the incident beam. Cell parameters and orientation matrix were obtained from the least-squares refinement of 141 reflections measured in three different sets of 15 frames each, in the range 3° < θ < 23°. At the

 © 2003 Wiley-VCH Verlag GmbH & Co. KGaA, Weinheim

end of data collection the first 50 frames, containing 325 reflections, were recollected to monitor crystal decay, which was not observed, so that no time-decay correction was needed. The collected frames were processed with the software SAINT,[24a] and an absorption correction was applied (SADABS)[24b] to the 19993 collected reflections, 7461 of which are unique, with R_{int} = 0.0307 ($R_{int} = \Sigma|F_o^2 - F_{mean}^2|/\Sigma F_o^2$). Calculations were performed with a Pentium III PC using the Personal Structure Determination Package,[25] and the physical constants tabulated therein. Scattering factors and anomalous dispersion corrections were taken from ref.[26] The structure was solved by direct methods (SHELXS 86)[27] and refined by full-matrix least squares using all reflections and minimizing the function $\Sigma w(F_o^2 - k|F_c|^2)^2$ (refinement on F^2). Anisotropic thermal factors were refined for all non-hydrogen atoms. The seven hydrogen atoms bonded to N(3) and to the two methyl groups of the 2,6-xylidine ligand were detected in the final Fourier maps and refined with fixed thermal parameters. The other hydrogen atoms were placed in their ideal positions (C−H = 0.97 Å, *B* 1.10 times that of the carbon atom to which they are attached) and not refined. In the final difference Fourier map the maximum residual was 0.96(13) e/Å^3 at 0.70 Å from Au. CCDC-189011 contains the atomic coordinates of the structure model, the supplementary crystallographic data for this paper. These data can be obtained free of charge at www.ccdc.cam.ac.uk/conts/retrieving.html [or from the Cambridge Crystallographic Data Centre, 12 Union Road, Cambridge CB2 1EZ, UK; Fax: (internat.) + 44-1223/336-033; E-mail: deposit@ccdc.cam.ac.uk].

Table 2. Crystallographic data

Compound	**6**
Empirical formula	$C_{27}H_{27}AuF_6N_3P$
Formula mass	735.47
Colour	orange
Crystal system	triclinic
Space group	$P\bar{1}$ (no.2)
a [Å]	9.772(1)
b [Å]	11.234(1)
c [Å]	12.429(1)
α [°]	107.44(1)
β [°]	95.64(1)
γ [°]	92.74(1)
V [Å^3]	1291.1(2)
Z	2
F(000)	716
D_c [g·cm^{-3}]	1.892
T [K]	223
Crystal dimensions [mm]	0.096 × 0.225 × 0.366
μ(Mo-K_α) [cm^{-1}]	58.11
Min./max. transmiss. factors	0.41/1.00
Scan mode	ω
Frame width [°]	0.30
Time per frame [s]	20
No. of frames	2650
Detector−sample distance [cm]	4.00
θ range[°]	3−26
Reciprocal space explored	full sphere
No. of reflections: total/independent	19993/7461
R_{int}	0.031
Final R_2/R_{2w} indices[a] (F^2, all reflections)	0.035/0.049
Conventional R_1 index [$I > 2\sigma(I)$]	0.019
Reflections with $I > 2\sigma(I)$	6839
No. of variables	364
Goodness of fit[b]	0.94

[a] $R_2 = [\Sigma(|F_o^2 - kF_c^2|)/\Sigma F_o^2]$, $R_2w = [\Sigma w(F_o^2 - kF_o^2)^2/\Sigma w(F_o^2)^2]^{1/2}$. [b] $[\Sigma w(F_o^2 - kF_c^2)^2/(N_o - N_v)]^{1/2}$, where $w = 4F_o^2/\sigma(F_o^2)^2$, $\sigma(F_o^2) = [\sigma^2(F_o^2) + (0.02F_o^2)^2]^{1/2}$, N_o is the number of observations and N_v the number of variables.

Acknowledgments

We are grateful to the University of Sassari for financial support (60%) and to the Regione Autonoma della Sardegna (RAS) for a grant to M. A. C. (L.R.9/8/1950, n. 43).

[1] [1a] H. E. Bryndza, W. Tam, *Chem. Rev.* **1988**, *88*, 1163−1188. [1b] M. D. Fryzuk, C. D. Montgomery, *Coord. Chem. Rev.* **1989**, *95*, 1−40. [1c] J. R. Fulton, A. W. Holland, D. J. Fox, R. G. Bergman, *Acc. Chem. Res.* **2002**, *35*, 44−56.

[2] [2a] D. M. Roundhill, *Chem. Rev.* **1992**, *92*, 1−27. [2b] J. F. Hartwig, *Angew. Chem. Int. Ed.* **1998**, *37*, 2046−2067. [2c] T. E. Müller, M. Beller, *Chem. Rev.* **1998**, *98*, 675−703. [2d] M. Beller, H. Trauthwein, M. Eichberger, C. Breindl, J. Herwig, T. E. Müller, O. R. Thiel, *Chem. Eur. J.* **1999**, *5*, 1306−1319. [2e] M. Beller, H. Trauthwein, M. Eichberger, C. Breindl, T. E. Müller, *Eur. J. Inorg. Chem.* **1999**, 1121−1132. [2f] J. P. Wolfe, S. L. Buchwald, *J. Org. Chem.* **2000**, *65*, 1144−1157. [2g] Y. Guari, G. P. F. van Strijdonck, M. D. K. Boele, J. N. H. Reek, P. C. J. Kamer, P. W. N. M. van Leeuwen, *Chem. Eur. J.* **2001**, *7*, 475−482.

[3] Recent examples of mononuclear late transition metal amido complexes. Nickel: [3a] K. Koo, G. L. Hillhouse, *Organometallics* **1995**, *14*, 4421−4423. [3b] D. D. VanderLender, K. A. Abboud, J. M. Boncella, *Inorg. Chem.* **1995**, *34*, 5319−5326. [3c] K. Koo, G. L. Hillhouse, *Organometallics* **1996**, *15*, 2669−2671. [3d] D. J. Mindiola, G. L. Hillhouse, *J. Am. Chem. Soc.* **2001**, *123*, 4623−4624. Palladium: [3e] Y.-J. Kim, J.-C. Choi, K. Osakada, *J. Organomet. Chem.* **1995**, *491*, 97−102. [3f] M. S. Drivers, J. F. Hartwig, *J. Am. Chem. Soc.* **1995**, *117*, 4708−4709. [3g] M. S. Driver, J. F. Hartwig, *J. Am. Chem. Soc.* **1996**, *118*, 7217−7218. [3h] M. S. Driver, J. F. Hartwig, *J. Am. Chem. Soc.* **1997**, *119*, 8232−8245. [3i] M. S. Driver, J. F. Hartwig, *Organometallics* **1997**, *16*, 5706−5715. [3j] G. García-Herbosa, N. G. Connelly, A. Muñoz, J. V. Cuevas, A. G. Orpen, S. D. Politzer, *Organometallics* **2001**, *20*, 3223−3229. [3k] S. Y. Ryu, H. Kim, H. S. Kim, S. Park, *J. Organomet. Chem.* **1999**, *592*, 194−197. Platinum: [3l] A. C. Albéniz, V. Calle, P. Espinet, S. Gómez, *Inorg. Chem.* **2001**, *40*, 4211−4216. Iridium: [3m] J. F. Hartwig, *J. Am. Chem. Soc.* **1996**, *118*, 7010−7011. Ruthenium: [3n] J. R. Fulton, M. W. Bouwkamp, R. G. Bergman, *J. Am. Chem. Soc.* **2000**, *122*, 8799−8800. Osmium: [3o] T. J. Crevier, B. K. Bennett, J. D. Soper, J. A. Bowman, A. Dehestani, D. A. Hrovat, S. Lovell, W. Kaminsky, J. M. Mayer, *J. Am. Chem. Soc.* **2001**, *123*, 1059−1071. Copper: [3p] J. Eriksson, P. I. Arvidsson, Ö. Davidsson, *J. Am. Chem. Soc.* **2000**, *122*, 9310−9311.

[4] [4a] B. Brønnum, H. S. Johansen, L. H. Skibsted, *Inorg. Chem.* **1988**, *27*, 1859−1862. [4b] L. H. Skibsted, J. Bjerrum, *Acta Chem. Scand., Ser. A* **1974**, *A28*, 740−746.

[5] B. P. Block, J. C. Bailar Jr., *J. Am. Chem. Soc.* **1951**, *73*, 4722−4725.

[6] [6a] F. Basolo, R. G. Pearson, *Mechanism of Inorganic Reactions*, 2nd ed., Wiley, New York, **1967**, pp. 410−414. [6b] W. H. Baddley, F. Basolo, H. B. Gray, C. Nölting, A. J. Poë, *Inorg. Chem.* **1963**, *2*, 921−928. [6c] C. F. Weick, F. Basolo, *Inorg. Chem.* **1966**, *5*, 576−582. [6d] D. L. Fant, C. F. Weick, *Inorg. Chem.* **1973**, *12*, 1864−1868. [6e] G. Nardin, L. Randaccio, G. Annibale, G. Natile, B. Pitteri, *J. Chem. Soc., Dalton Trans.* **1980**, 220−223.

[7] I.e. deprotonated primary or secondary amines: NHR^- or NRR'^- where R, R′ = alkyl, aryl, or silyl groups.

[8] [8a] H.-N. Adams, U. Grässle, W. Hiller, J. Strähle, *Z. Anorg. Allg. Chem.* **1983**, *504*, 7−12. [8b] U. Grässle, W. Hiller, J. Strähle, *Z. Anorg. Allg. Chem.* **1985**, *529*, 29−34.

 © 2003 Wiley-VCH Verlag GmbH & Co. KGaA, Weinheim

[9] See also: [9a] R. J. Puddephatt, *The Chemistry of Gold*, Elsevier, The Netherlands, **1978**, p. 77−83. [9b] J. Strahle, in: H. Schmidbaur, *Gold Progress in Chemistry, Biochemistry and Technology*, John Wiley and Sons, New York, **1999**, p. 339−342.
[10] [10a] Y. Fukuda, K. Utimoto, H. Nozaki, *Heterocycles* **1987**, *25*, 297−300. [10b] T. E. Müller, A.-K. Pleier, *J. Chem. Soc., Dalton Trans.* **1999**, 583−587.
[11] M. A. Cinellu, G. Minghetti, M. V. Pinna, S. Stoccoro, A. Zucca, M. Manassero, *J. Chem. Soc., Dalton Trans.* **1999**, 2823−2831.
[12] M. A. Cinellu, G. Minghetti, M. V. Pinna, S. Stoccoro, A. Zucca, M. Manassero, *J. Chem. Soc., Dalton Trans.* **2000**, 1261−1265.
[13] M. Costas, I. Romero, Ma. A. Martinez, A. Llobet, D. T. Sawyer, J. Caixach, *J. Mol. Cat. A: Chem.* **1999**, *148*, 49−58, and references therein.
[14] [14a] J. Vicente, M. T. Chicote, M. D. Bermudez, *J. Organomet. Chem.* **1984**, *268*, 191−195. [14b] M. A. Cinellu, A. Zucca, S. Stoccoro, G. Minghetti, M. Manassero, M. Sansoni, *J. Chem. Soc., Dalton Trans.* **1995**, 2865−2872.
[15] [15a] D. W. Meek, C. S. Springer Jr., *Inorg. Chem.* **1966**, *5*, 445−450. [15b] K. L. Henold, *J. Chem. Soc., Chem. Commun.* **1970**, 1340.
[16] M. A. Cinellu, A. Zucca, S. Stoccoro, G. Minghetti, M. Manassero, M. Sansoni, *J. Chem. Soc., Dalton Trans.* **1996**, 4217−4225.
[17] To the best of our knowledge, X-ray data relevant to Au−N bond lengths are available only for alkyl- not for arylamido species (refs.[6e,8]).
[18] F. Shi, Y. Deng, *Chem. Commun.* **2001**, 443−444.
[19] [19a] M. D. Johnson, B. J. Hornstein, *Chem. Commun.* **1996**, 965−966. [19b] H. Huang, D. Sommerfeld, B. C. Dunn, C. R. Lloyd, E. M. Eyring, *J. Chem. Soc., Dalton Trans.* **2001**, 1301−1305.
[20] L. Delaude, P. Laszlo, P. Lehance, *Tetrahedron Lett.* **1995**, *36*, 8505−8508.
[21] Autoxidation of 1,2-diphenylhydrazine to azotoluene has been reported: [21a] T. S. Calderwood, C. L. Johlman, J. L. Roberts Jr., C. L. Wilkins, D. T. Sawyer, *J. Am. Chem. Soc.* **1984**, *106*, 4683−4687. [21b] S. Jeon, D. T. Sawyer, *Inorg. Chem.* **1990**, *29*, 4612−4615.
[22] [22a] W. Clegg, *Acta Crystallogr., Sect. B* **1976**, *32*, 2712−2714. [22b] R. Uson, A. Laguna, J. L. Sanjoaquin, *J. Organomet. Chem.* **1974**, *80*, 147−154.
[23] The identity of this compound was confirmed by preparing it independently from bipy and an aqueous solution of HPF_6.
[24] [24a] *SAINT, Reference manual*, Siemens Energy and Automation, Madison, WI, **1994−1996**. [24b] G. M. Sheldrick, *SADABS, Empirical Absorption Correction* Program, University of Göttingen, **1997**.
[25] [25a] B. A. Frenz, *Comput. Phys.* **1988**, *2*, 42. [25b] B. A. Frenz, *Crystallographic Computing 5*, Oxford University Press, Oxford, U. K., **1991**, chapter 11, p. 12.
[26] *International Tables for X-ray Crystallography*, Kynoch Press, Birmingham, **1974**, vol.4.
[27] G. M. Sheldrick, *SHELXS-86, Program for the solution of crystal structures*, University of Göttingen, Germany, **1985**.

Received July, 2002

 © 2003 Wiley-VCH Verlag GmbH & Co. KGaA, Weinheim

Crystal Engineering with Structurally Flexible 1,1′-Substituted Ferrocenes for Nonlinear Optical Materials

Dong Mok Shin,[a] In Su Lee,*[b] and Young Keun Chung*[a]

Keywords: Crystal engineering / Hydrogen bonds / Nonlinear optics / π-Interactions

Cocrystals derived from 1,1′-bis(ethenyl-4-pyridyl)ferrocene (**1**) and resorcinol/phloroglucinol and a crystal of 1,1′-bis-(ethenyl-4-quinolinyl)ferrocene (**5**) have been studied with the aim of engineering crystalline NLO materials. X-ray structure analyses revealed a NLO active *syn*-type molecular conformation of **1** and **5** via hydrogen bonding with resorcinol/phloroglucinol and π-π interaction between quinoline rings, respectively. For **5**, all molecular dipoles are aligned in the same direction and the SHG efficiency is about 4 times that of urea.
(© Wiley-VCH Verlag GmbH & Co. KGaA, 69451 Weinheim, Germany, 2003)

Introduction

Crystal engineering, based on an understanding of physical phenomena such as charge transfer, electrostatic interaction, hydrogen bonding, van der Waals interaction, and π−π stacking, is a powerful technique for the production of functionalized solid materials with optimized properties.[1,2] It has been applied to various organometallic compounds.[3,4] Flexible π-bonds between metal and ligands produce highly variable organometallic structures (and packing modes), depending on the solid-state intra- and intermolecular nonbonding interactions.

Because of the significant electron-donating strength of the ferrocenyl group it is regarded as a good donor part of a donor−π-acceptor system for chromophores with high NLO responses.[5−10] Thus far, most efforts to synthesize NLO materials have concentrated on mono-acceptor conjugated ferrocenyl compounds, with little work on bis-substituted systems.[11] During an investigation into the preparation of chromophores with high NLO responses, we reported the crystal structures of 1,1′-bis(ethenyl-4-pyridyl)-ferrocene, **1**, and its cocrystals with 1,1′-binaphthol.[12] The two substituents on the cyclopentadienyl group of **1** adopt a typical 1,3′-orientation, i.e., in *anti*-fashion. Cocrystals of **1** with 1,1′-binaphthol in methanol and ethanol have the two substituents of the ferrocene at the 1- and 1′-positions, respectively. The use of optically pure 1,1′-binaphthol led to a noncentrosymmetric packing arrangement. Thus, the moiety **1** in cocrystals was quite flexible and its conformation appears to be sensitive to the hydrogen-bonding patterns with 1,1′-binaphthol molecules or incorporated solvent molecules. Consequently, we sought to establish a simple and transferable crystal engineering strategy for achieving the NLO active molecular conformation of the bis-substituted ferrocenyl molecule with readily available aromatic alcohols such as 1,3-dihydroxybenzene (resorcinol) and 1,3,5-trihydroxybenzene (phloroglucinol).[13,14] In addition, an analogue, 1,1′-bis(ethenyl-4-quinolyl)ferrocene, **5**, containing additional aromatic rings was synthesized to induce a π−π interaction between the aromatic rings, eventually leading to a *syn*-type molecular conformation. We report here the results of our investigation of the cocrystallization of **1** with resorcinol and phloroglucinol as well as the synthesis and crystal structure of **5**.

Results and Discussion

Cocrystallization of 1 with Resorcinol and Phloroglucinol: Crystal Structures of 2, 3, and 4

Resorcinol and phloroglucinol function as multifunctional hydrogen bond donors in the crystal engineering of one- or two-dimensional structures.[15,16]

When equimolar amounts of **1** and resorcinol were dissolved in THF and the resultant solution allowed to evaporate at room temperature, long block-shaped crystals of **2** were isolated in quantitative yield. X-ray crystallographic analysis reveals the formation of supramolecule **2** that contain **1** and resorcinol in the ratio 1:1 (Figure 1). A molecule of **1** and resorcinol are coupled via two hydrogen bonds between the pyridines of **1** and the hydroxy groups of **2**. The two cyclopentadienyl rings on **1** adopt an eclipsed con-

[a] School of Chemistry and Center for Molecular Catalysis, Seoul National University,
Seoul 151−747, Korea (South)
Fax: (internat.) + 82-2/889 0310
E-mail: ykchung@plaza.snu.ac.kr
[b] Advanced Materials Research Institute, LG Chemical Ltd., Research Park,
Taejon 305−380, Korea (South)
Supporting information for this article is available on the WWW under http://www.eurjic.org or from the author.

formation while the two substituents of **1** adopt a 1,1′ -orientation, i.e., a *syn*-fashion. For simultaneous hydrogen bonds with two widely separated oxygen atoms [O01−O02, 4.797(6) Å], the separation of the two pendant ligands smoothly increases from 3.398(7) (C11−C18) to 4.172(6) Å (N1−N2), which makes **1** appear to stretch its arms toward a resorcinol molecule. The two pyridine ring centers are 3.967 Å apart and the two ring planes make a torsion angle of 12.5(3)°. The phenyl ring of resorcinol in **2** is slightly inclined to make an angle of 64.1(2)°−83.8(2)° with the cyclopentadienyl rings and the pyridine rings of **1**. Compared with the symmetric molecular structure of free ligand **1**, the ferrocene fragment in **2** is largely deformed into an asymmetric structure, which is expected to have a nonzero molecular dipole moment. However, supramolecules **2** are packed in a centrosymmetric manner (space group: $P2_1/n$) and the net molecular dipole moments in the crystal should be zero.

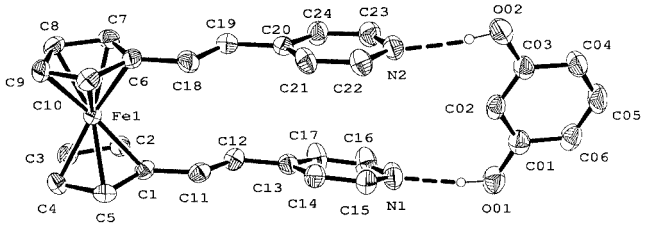

Figure 1. ORTEP drawing of **2** with 30% thermal ellipsoids

Cocrystallization of **1** with phloroglucinol was carried out in THF and EtOH, respectively. In THF at room temperature supramolecule **3** was formed, a unit of which consists of one molecule of **1**, one of phloroglucinol, and one solvent molecule of THF (Figure 2). The molecular structure of **1** (*syn*-type) and the hydrogen-bonding pattern are very similar to those in **2**. Of the three hydroxy groups of phloroglucinol, two make hydrogen bonds with pyridines of **1**, and the third is interconnected with a THF molecule. The conformation of phloroglucinol and the hydrogen bonds with the two pyridines are very similar to what is found in its cocrystal with 2,4-dimethylpyridine.[16] Supramolecules of **3** are packed in a centrosymmetric manner (Space group: $P2_1/n$) in the same way as **2**.

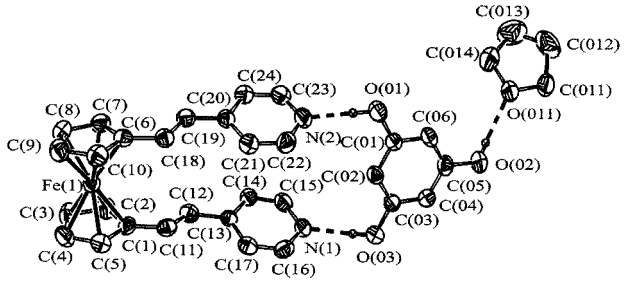

Figure 2. ORTEP drawing of **3** with 50% thermal ellipsoids

Cocrystallizion of **1** and phloroglucinol in EtOH at room temperature resulted in a supramolecule **4**, which consists of three components of **1**, phloroglucinol, and EtOH in the ratio 1:1:1. The crystal structure of **4** is a stair-like chain structure (Figure 3). A molecule of **1** in crystal **4** also makes double hydrogen bonds with a phloroglucinol molecule and shows a *syn*-type conformation, as it does in **2** and **3**. The incorporated EtOH molecule acts as a paste that connects components in the construction of a hydrogen-bonded supramolecular chain structure. It serves as a hydrogen donor to a phloroglucinol and also as a hydrogen acceptor to another phloroglucinol molecule. Every molecule of **1** within a supramolecular unit is fixed, facing the same direction, and their molecular dipole moments accumulate in a supramolecular unit. Crystal **4** belongs to the noncentrosymmetric space group, *Pc*. However, its asymmetric unit is composed of two triads of molecules with a pseudoinversion relation and two kinds of supramolecular chain face in opposite directions in a crystal (Figure 4). Therefore, the net dipole moment of the crystal **4** is expected to be close to zero.

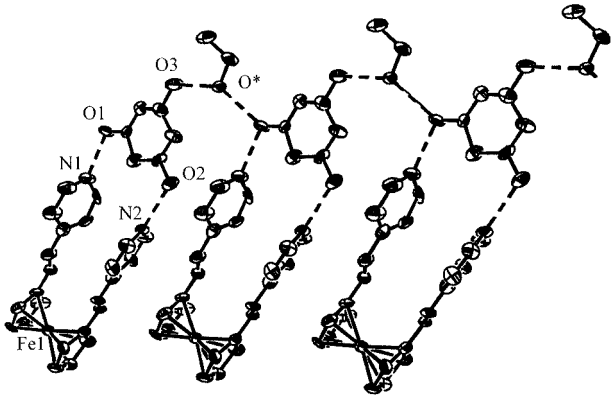

Figure 3. ORTEP drawing of **4** with 50% thermal ellipsoids

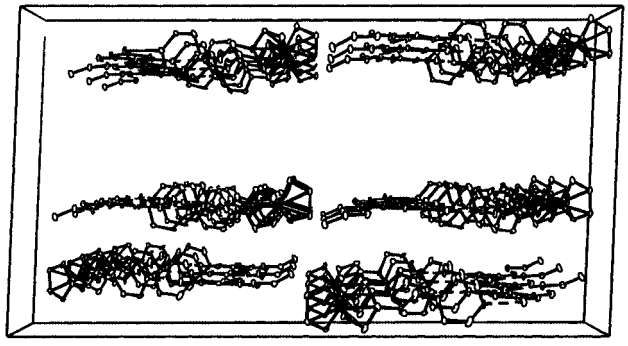

Figure 4. Cell packing diagram of **4**

Synthesis and Crystal Structure of 5

Compound **5**, an analogue of **1**, containing an additional aromatic ring for intramolecular stacking was prepared by treatment of 1,1′-ferrocenedicarboxaldehyde with the lithium carbanion of lepidine followed by protonation and dehydration (73% yield) (Scheme 1).

 © 2003 Wiley-VCH Verlag GmbH & Co. KGaA, Weinheim

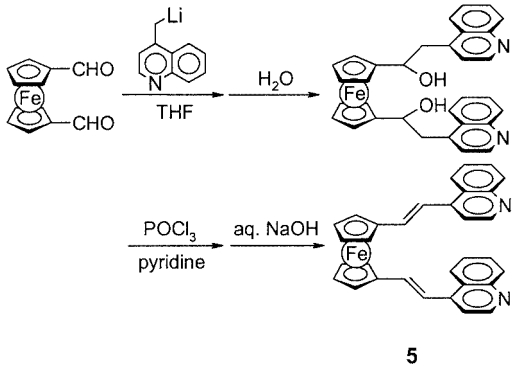

5

Scheme 1. Synthesis of **5**

Single crystals of **5** suitable for an X-ray study were grown by slow evaporation of an MeOH solution of **5**. Figure 5 shows a view of **5**, which belongs to the noncentrosymmetric space group, *Cc*.

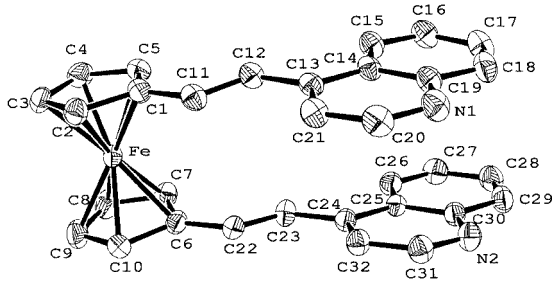

Figure 5. ORTEP drawing of **5** with 30% thermal ellipsoids

The molecular structure of **5** displays a polar conformation with a nonzero dipole moment. Two substituents of **5** adopt a 1,1′-orientation with an eclipsed conformation. The torsion angles of C(1)−C(11)−C(6)−C(22) and C(12)−C(13)−C(23)−C(24) are 8.6° and 8.0°, respectively, and the twist angle between two Cp rings is 7.5°. Two quinoline-bearing substituents lie on top of each other, indicating intramolecular stacking. The pyridine ring centers and the benzene ring centers are 3.657 and 3.876 Å apart, respectively. The tilt angle between two quinoline planes is 6.1(1)°, which quantitatively expresses the occurrence of π−π interactions between the two rings. Previously, Togni et al.[17] reported a similar eclipsed molecular structure for 1,1′-disubstituted ferrocene by virtue of the attractive interaction between two sulfur-containing fragments. However, in contrast to the highly tilted molecular structure in Togni's result, the Cp and quinoline rings of **5** are roughly coplanar with dihedral angles of 7.6(2)° and 11.2(2)°. A coplanar arrangement of Cp and substituents of **5** may allow maximum orbital mixing and effective electronic communication between an electron-donating ferrocene and electron-withdrawing quinoline groups, i.e., effective delocalization along the conjugated chains. Two N atoms of quinolines of **5** make contacts with quinoline and Cp rings in neighboring molecules (Figure 6). The CH···N distances of 2.59(4) and 2.78(4) Å and the C−H···N angles of 160(3)° and 167(3)° indicate weak C−H···N hydrogen-bonding interactions. The distances and angles fall in the range of reported interactions between $C(sp^2)$−H and N in a heterocyclic group.[18b−18d] Both intermolecular C−H···N interactions are arranged in almost the same direction and, eventually, cause all of the molecular dipoles in crystal **5** to align along the A axis (i.e., a polar crystal) (Figure 7). Such C−H···N interaction appears to be important in determining the crystal packing.[18]

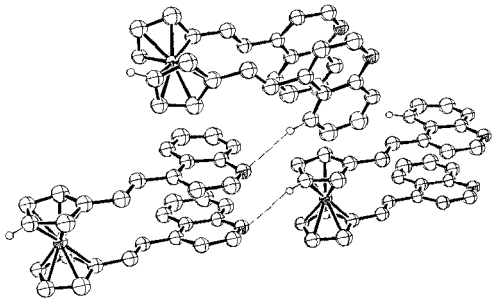

Figure 6. CH···N interactions of **5**

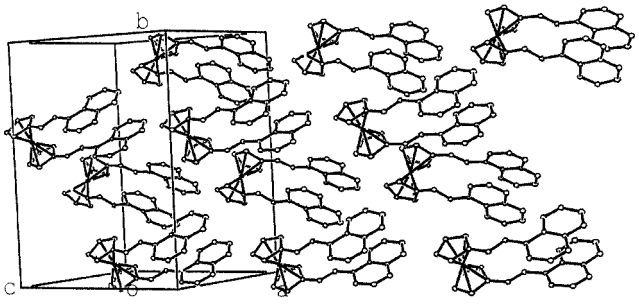

Figure 7. Cell packing diagram of **5**

Discussion

Ferrocenes adopt various conformations, depending on the magnitude of the rotational barrier, and are considered, in a sense, as nonrigid molecules that have a variable structure.[19] Free **1** crystallizes in the symmetric *anti*-conformation, which should possess a zero molecular dipole moment and hyperpolarizability.[12] However, in cocrystals of **2**, **3**, and **4**, the two substituents on the cyclopentadienyl groups of the ferrocene are situated at 1- and 1′-positions, and **1** shows a *syn*-type geometry. Resorcinol and phloroglucinol molecules act like molecular clips to create simultaneous double hydrogen bonds with a molecule of **1** and fix its conformation as a dipolar one − a prerequisite for a nonlinear optical molecule. Unlike the symmetric molecule of free **1**, asymmetric supramolecules of **2**, **3**, and **4** should possess nonzero molecular hyperpolarizabilities. However, the crystal arrangements of **2**, **3**, and **4** reveal an anti-parallel alignment of molecular dipoles, therefore no second-harmonic generations (SHG) are expected for the bulk materials. In the crystals **3** and **4**, solvent molecules of THF and EtOH are incorporated through hydrogen bonding with phloroglucinol. EtOH molecules of **4** serve as molecular

 © 2003 Wiley-VCH Verlag GmbH & Co. KGaA, Weinheim

pastes to construct a supramolecular chain and align all dipoles in a supramolecular unit in the same direction.

Compound **5** crystallizes in a dipolar *syn*-type conformation due to the significant π−π interaction between two pendent arms.[20] Moreover, an almost perfect dipole alignment is realized in crystal **5** through weak intermolecular C−H···N interactions. Thus, an effective SHG was expected. When Kurtz powder measurements were performed at 1.36 μm, **5** shows an SHG efficiency of about 4 times that of urea.[21] This is quite low compared with the highest bulk susceptibility (χ^2 up to 220 times the value for urea) reported for ferrocenyl derivatives,[10c] presumably due to the weak electron-accepting ability of the quinoline group.

Conclusion

We have demonstrated two crystal engineering approaches for achieving the NLO active molecular conformation of structurally flexible disubstituted ferrocenyl compounds. An X-ray crystal structure analysis of **5** shows that it crystallizes in a NLO active conformation. The efficiency of **5** in the second harmonic generation is 4 times that of urea. This is not a high value compared with the known bulk susceptibilities for ferrocenyl derivatives. We anticipate that the introduction of more electron-withdrawing groups into the skeleton of **5** will give more efficient NLO materials. Further related research will continue to be pursued.

Experimental Section

General Remarks: Resorcinol (Aldrich), phloroglucinol dihydrate (Aldrich), and lepidine (Lancaster) were used as received. The synthesis of **5** was carried out under nitrogen by using standard Schlenk techniques. Freshly distilled, dried, and oxygen-free solvents were used throughout. ^{1}H and ^{13}C NMR spectra were recorded with a Bruker 300 spectrometer. Elemental analysis was performed by the Analytical Center, College of Engineering, Seoul National University. High-resolution mass spectroscopy was carried out at the Korea Basic Science Institute (Daegu). 1,1′-Ferrocenedicarboxaldehyde and 1,1′-bis(ethenyl-4-pyridyl)ferrocene, **1**, were prepared according to published procedures.[22,23]

Cocrystallization of 1 with Resorcinol (Synthesis of 2): Compound **1** (20 mg, 0.051 mmol) and resorcinol (5.6 mg, 0.051 mmol) were dissolved in EtOH (5 mL). The resultant solution was allowed to evaporate at room temperature for 7 days. Long block-shaped crystals of **2** were isolated in quantitative yield. $C_{30}H_{26}FeN_2O_2$ (502.40): calcd. C 71.72, H 5.22, N 5.58; found C, 71.26, H 5.34, N 5.71.

Cocrystallization of 1 with Phloroglucinol (Syntheses of 3 and 4): Compound **1** (20 mg, 0.051 mmol) and phloroglucinol dihydrate (8.3 mg, 0.051 mmol) were dissolved in THF (5 mL). The resultant solution was allowed to evaporate at room temperature for about 7 days. Red needle-shaped crystals of **3** were then isolated in quantitative yield. $C_{34}H_{34}FeN_2O_4$ (590.50): calcd. C 69.16, H 5.80, N 4.74; found C, 68.99, H 5.46, N 4.83. Red cubic crystals of **4** were obtained quantitatively in the same way as **3**, using EtOH instead of THF as the reaction medium. $C_{32}H_{32}FeN_2O_4$ (564.46): calcd. C 69.16, H 5.80, N 4.74; found C, 68.99, H 5.46, N 4.83.

Synthesis of 5: Lepidine (1.2 mL, 9.1 mmol) was added at −78 °C to a solution of LDA (generated in situ by the reaction of diisopropylamine (1.3 mL, 9.3 mmol) in THF (30 mL) with *n*BuLi (4.0 mL, 10.0 mmol) at −78 °C). The resultant solution turned reddish during stirring at room temperature for 30 min. 1,1′-Ferrocenedicarboxaldehyde (0.66 g, 2.7 mmol) was then added at room temperature. This reaction mixture turned brownish as it was stirred at room temperature for 4 h, after which excess water (30 mL) and methylene dichloride (30 mL) were added. The methylene dichloride layer was collected, evaporated to dryness, and dissolved in pyridine (15 mL). The pyridine solution was cooled to 0 °C and excess $POCl_3$ (2 mL) was added dropwise. The resultant solution turned dark green during stirring at room temperature for 1 h, after

Table 1. Crystal data and structure refinement for **2**, **3**, **4**, and **5**

	2	**3**	**4**	**5**
Empirical formula	$C_{30}H_{26}FeN_2O_2$	$C_{34}H_{34}FeN_2O_4$	$C_{65}H_{64}Fe_2N_3O_8$	$C_{32}H_{24}FeN_2$
Molecular mass	502.38	590.48	1126.89	492.38
Crystal system	monoclinic	monoclinic	monoclinic	monoclinic
Space group	$P2_1/n$	$P2_1/n$	Pc	Cc
a, Å	9.199(4)	9.3745(7)	18.523(3)	13.031(1)
b, Å	23.122(4)	28.2106(12)	8.8577(14)	18.937(3)
c, Å	11.671(3)	11.0040(9)	33.919(5)	10.679(1)
α, deg.	90	90	90	90
β, deg.	98.868(2)	95.666(6)	92.354(12)	116.313(8)
γ, deg.	90	90	90	90
Volume, Å^3	2452.5(12)	2895.9(3)	5560.3(15)	2362.2(5)
Z	4	4	4	4
d(calcd.), Mg/m^3	1.361	1.354	1.349	1.385
θ range, deg	1.76-24.97	1.99-24.97	2.20-24.98	3.84−27.41
No. tot. Collection	4580	5398	5059	4484
No. unique data	4299	5075	5059	4484
No. params refined	420	474	711	412
$R1$	0.0480	0.0466	0.0439	0.0389
$wR2$	0.0913	0.0885	0.1165	0.0809
Gof	0.944	1.019	1.099	1.096

 © 2003 Wiley-VCH Verlag GmbH & Co. KGaA, Weinheim

Table 2. Selected intra- and intermolecular bond lengths (Å) and angles (°) for **1**,[12] **2**, **3**, **4**, and **5**

1					
C(1)−C(11)	1.46(2)	C(11)−C(12)	1.27(2)	C(12)−C(13)	1.49(2)
C(6)−C(18)	1.495(14)	C(18)−C(19)	1.32(2)	C(19)−C(20)	1.469(13)
2					
Fe(1)−C(7)	2.021(5)	Fe(1)−C(1)	2.053(4)	Fe(1)−C(6)	2.056(5)
C(1)−C(11)	1.455(6)	C(11)−C(12)	1.307(7)	C(12)−C(13)	1.458(7)
C(6)−C(18)	1.463(7)	C(18)−C(19)	1.307(7)	C(19)−C(20)	1.460(7)
C(16)−N(1)	1.321(8)	C(22)−N(2)	1.344(6)	C(01)−O(01)	1.346(6)
C(03)−O(02)	1.354(7)	N(1)−O(01)	2.733(6)	N(2)−O(02)	2.738(6)
C(1)−Fe(1)−C(6)	108.8(2)			O(01)−C(01)−C(02)	122.7(5)
O(02)−C(03)−C(02)	122.4(5)			N(1)−H(001)−O(01)	169(6)
N(2)−H(002)- O(02)	172(6)				
3					
Fe(1)−C(2)	2.032(4)	Fe(1)−C(6)	2.058(4)	C(01)−O(01)	1.361(4)
C(1)−C(11)	1.452(5)	C(11)−C(12)	1.304(6)	C(12)−C(13)	1.483(5)
C(6)−C(18)	1.453(5)	C(18)−C(19)	1.315(5)	C(19)−C(20)	1.458(5)
C(03)−O(03)	1.364(5)	C(05)−O(02)	1.371(5)	C(02)−C(03)	1.379(5)
N1−O03	2.795(5)	N2−O01	2.761(5)	O011−O02	2.772(5)
C(1)−Fe(1)−C(6)	109.14(16)			O(01)−C(01)−C(02)	122.1(4)
O(03)−C(03)−C(04)	118.0(4)			O(02)−C(05)−C(06)	122.7(4)
C(15)−N(1)−C(16)	114.1(4)			C(23)−N(2)−C(22)	114.6(4)
O011−H02−O02	172(6)			N2−H01−O01	173(4)
N1−H03−O03	176(6)				
4					
Fe(1)−C(8)	1.993(12)	Fe(1)−C(6)	2.074(10)	N(1)−C(16)	1.305(17)
C(1)−C(11)	1.488(12)	C(11)−C(12)	1.307(14)	C(12)−C(13)	1.477(12)
C(6)−C(18)	1.452(13)	C(18)−C(19)	1.215(14)	C(19)−C(20)	1.498(14)
C(22)−N(2)	1.312(19)	C(01)−O(1)	1.392(14)	C(03)−O(2)	1.256(13)
C(05)−O(3)	1.404(14)	Fe(2)−C(9′)	2.048(10)	Fe(2)−C(4′)	2.084(13)
C(01′)−O(1′)	1.358(15)	C(03′)−O(2′)	1.346.(13)	C(05′)−O(3′)	1.457(13)
C(1′)−C(11′)	1.478(14)	C(11′)−C(12′)	1.207(15)	C(12′)−C(13′)	1.459(11)
C(6′)−C(18′)	1.441(14)	C(18′)−C(19′)	1.313(13)	C(19′)−C(20′)	1.487(13)
N1−O2	2.779(13)	N2−O1	2.719(14)	N2′−O3′	2.748(13)
N1′−O1′	2.566(13)	O1*−O2′	2.769(11)	O1*−O1′	2.772(12)
O2*−O3	2.745(13)	O2*−O1	2.764(13)		
C(1)−Fe(1)−C(6)	109.4(4)			C(16)−N(1)−C(15)	114.9(10)
C(23)−N(2)−C(22)	118.4(12)			O(1)−C(01)−C(02)	117.0(9)
O(2)−C(03)−C(04)	118.4(10)			C(06)−C(05)−O(3)	118.3(11)
C(1′)−Fe(2)−C(6′)	110.3(4)			C(16′)−N(1′)−C(15′)	114.7(10)
C(23′)−N(2′)−C(22′)	116.8(11)			O(1′)−C(01′)−C(02′)	116.3(10)
O(2′)−C(03′)−C(04′)	125.8(9)			O(3′)−C(05′)−C(06′)	118.3(10)
5					
Fe−C(6)	2.055(3)	Fe−C(1)	2.060(3)	N(1)−C(20)	1.316(5)
C(1)−C(11)	1.452(4)	C(11)−C(12)	1.336(5)	C(12)−C(13)	1.466(4)
C(6)−C(22)	1.446(4)	C(22)−C(23)	1.328(4)	C(23)−C(24)	1.455(4)
N(1)−C(19)	1.375(4)	N(2)−C(31)	1.320(4)	N(2)−C(30)	1.373(4)
C(6)−Fe−C(1)	108.50(12)			C(20)−N(1)−C(19)	116.0(3)
C(31)−N(2)−C(30)	116.1(3)				

which ice was added to quench the excess $POCl_3$. After evaporation of pyridine, the residue was then dissolved in water (30 mL) and basified by aqueous 4 M NaOH. Extraction with methylene dichloride (100 mL) followed by chromatography on a silica gel column eluting with Et_2O/MeOH (v/v, 5:1) gave 1.70 g of **5** (73%). Single crystals suitable for X-ray study were grown by slow evaporation of a methanol solution of **5**. ^{1}H NMR (300 MHz, $CDCl_3$, 25 °C): δ = 4.42 (t, $^3J_{H,H}$ = 1.8 Hz, 4 H), 4.61 (t, $^3J_{H,H}$ = 1.8 Hz, 4 H), 7.03 (d, $^3J_{H,H}$ = 15.9 Hz, 2 H), 7.26~7.36 (m, 6 H), 7.61 (t, $^3J_{H,H}$ = 7.0 Hz, 2 H), 7.93 (d, $^3J_{H,H}$ = 8.5 Hz, 2 H), 8.01 (d, $^3J_{H,H}$ = 8.5 Hz, 2 H), 8.54 (d, $^3J_{H,H}$ = 4.7 Hz, 2 H) ppm. ^{13}C NMR (75 MHz, $CDCl_3$, 25 °C): δ = 68.98, 77.14, 83.58, 115.87, 120.58, 123.04, 126.08, 126.28, 129.25, 130.26, 133.06, 142.59, 148.87, 150.04, ppm. HRMS (EI) for $C_{32}H_{24}FeN_2$: calcd. 492.1289, obsd. 492.1284. $C_{32}H_{24}FeN_2$ (492.40): calcd. C 78.06, H 4.91, N 5.69; found C, 78.24, H 4.81, N 5.50.

Crystal Structure Determinations of 2, 3, 4, and 5: Diffractions for **2**, **3**, and **4** were measured by an Enraf−Nonius CAD4 automated diffractometer. Unit cells were determined by centering 25 reflections in the appropriate 2θ range. Other relevant experimental details are listed in Table 1. The structures for **2**, **3**, and **4** were solved by direct methods using SHELXS-86 and refined by full-matrix least-squares with SHELXL-93.[24] For **5**, the diffraction data were collected on an Enraf−Nonius CCD single crystal X-ray diffractometer and the structure solved by direct methods using SHELXS-97 and refined against all F^2 data (SHELXS-97).[25] All non-hydrogen atoms were refined anisotropically. All hydrogen

 © 2003 Wiley-VCH Verlag GmbH & Co. KGaA, Weinheim

atoms in **2**, **3**, and **5** and H(01*), H(02*), H(01), H(03), and H(01′) in **4** were found in the Fourier map and refined. The rest of the hydrogen atoms were located in ideal positions using a riding model with 1.2 times the equivalent isotropic temperature factors of the atoms to which they were attached. The absolute structures of **4** and **5** could not be defined as insufficient data were collected.

CCDC-196212 to -196215 contain the supplementary crystallographic data for this paper. These data can be obtained free of charge at www.ccdc.cam.ac.uk/conts/retrieving.html [or from the Cambridge Crystallographic Data Centre, 12, Union Road, Cambridge CB2 1EZ, UK; Fax: (internat.) +44-1223/336-033; E-mail: deposit@ccdc.cam.ac.uk].

SHG Measurements: The measurements of second harmonic generation (SHG) intensity were carried out by the Kurtz−Perry powder technique,[21] using a beam with $\lambda = 1.360$ μm and $I = 5$ MW/cm^2 generated by a BBO optical parametric oscillator pumped by a Nd:YAG laser. Samples were in the range 75−150 μm, and were 270 μm thick.

Acknowledgments

YKC expresses thanks for financial support from KOSEF (R01−1999−000−00041−012002) and KOSEF through the Center for Molecular Catalysis at Seoul National University, and DMS acknowledges receipt of the Brain Korea 21 fellowship.

[1] For general reviews on crystal engineering, see: [1a] G. R. Desiraju, *Crystal Engineering: The Design of Organic Solids*, Elsevier; Amsterdam, **1989**. [1b] J.-M. Lehn, *Supramolecular Chemistry*; VCH: Weinheim, **1995**. [1c] J. L. Atwood, J. E. D. Davies, D. D. MacNicol, F. Vögtle, Eds. *Comprehensive Supramolecular Chemistry*, Vol. 6, Pergamon: Oxford, **1996**. [1d] C. V. K. Sharma, G. R. Desiraju, In *Perspectives in Supramolecular Chemistry. The Crystal as a Supramolecular Entity*; G. R. Desiraju, Ed.; John Wiley & Sons: New York, **1996**. [1e] G. R. Desiraju, *Chem. Commun.* **1997**, 1475−1482. [1f] B. Moulton, M. J. Zaworotko, *Chem. Rev.* **2001**, *101*, 1629−1658.

[2] For recent works on crystal engineering, see: [2a] H. L. Eddaoudi, M. O'Keeffe, O. M. Yaghi, *Nature* **1999**, *402*, 276−279. [2b] K. Biradha, K. V. Domasevitch, B. Moulton, C. Seward, M. J. Zaworotko, *Chem. Commun.* **1999**, 1327−1328. [2c] M. D. Hollingsworth, U. Wermer-Zwanziger, J. D. Chaney, J. C. Huffman, K. D. M. Harris, S. P. Smart, *J. Am. Chem. Soc.* **1999**, *121*, 9732−9733. [2d] M. Eddaoudi, H. Li, O. M. Yaghi, *J. Am. Chem. Soc.* **2000**, *122*, 1391−1397. [2e] J. S. Miller, *Inorg. Chem.* **2000**, *39*, 4392−4408. [2f] J. S. Seo, D. Whang, H. Lee, S. I. Jun, J. Oh, Y. J. Jeon, K. Kim, *Nature* **2000**, *404*, 982−986. [2g] S. Noro, S. Kitagawa, M. Kondo, K. Seki, *Angew. Chem. Int. Ed.* **2000**, *39*, 2081−2084. [2h] J. R. Galan-Mascaros, K. R. Dunbar, *Chem. Commun.* **2001**, 217−218. [2i] Z. Xu, S. Lee, Y.-H. Kiang, A. B. Mallik, N. Tsomaia, K. T. Mueller, *Adv. Mater.* **2001**, *13*, 637−641. [2j] S. Ohba, H. Hosomi, Y. Ito, *J. Am. Chem. Soc.* **2001**, *123*, 6349−6352. [2k] C. Tabares, J. A. R. Navarro, J. M. Salas, *J. Am. Chem. Soc.* **2001**, *123*, 383−387.

[3] For reviews on organometallic crystal engineering, see: [3a] A. D. Burrows, C.-W. Chan, M. M. Chowdhry, J. E. McGrady, D. M. P. Mingos, *Chem. Soc. Rev.* **1995**, 329−340. [3b] D. Braga, F. Grepioni, *Chem. Commun.* **1996**, 571−578. [3c] D. Braga, F. Grepioni, *Acc. Chem. Res.* **1997**, *30*, 81−87. [3d] D. Braga, F. Grepioni, G. R. Desiraju, *Chem. Rev.* **1998**, *98*, 1375−1406. [3e] D. Braga, F. Grepioni, *Chem. Soc., Rev.* **2000**, 369−373. [3f] D. Braga, L. Maini, M. Polito, L. Scaccianoce, G. Cojazzi, F. Grepioni, *Coord. Chem. Rev.* **2001**, *216*, 225−248.

[4] For recent works on organometallic crystal engineering, see: [4a] C. L. Schauer, E. Matwey, F. W. Fowler, J. W. Lauher, *J. Am. Chem. Soc.* **1997**, *119*, 10245−10246. [4b] M. Munakata, L. P. Wu, T. Kuroda-Sowa, M. Maekawa, Y. Suenaga, G. L. Ning, T. Kojima, *J. Am. Chem. Soc.* **1998**, *120*, 8610−8618. [4c] Z.-N. Chen, H.-X. Zhang, K.-B. Yu, K.-C. Zheng, H. Cai, B.-S. Kang, *J. Chem. Soc., Dalton Trans.* **1998**, 1133−1136. [4d] C. B. Aakeröy, A. M. Beatty, D. S. Leinen, *J. Am. Chem. Soc.* **1998**, *120*, 7383−7384. [4e] C. B. Aakeröy, A. M. Beatty, B. A. Helfrich, *J. Chem. Soc., Dalton Trans.* **1998**, 1943−1946. [4f] D. Braga, L. Maini, F. Grepioni, *Angew. Chem. Int. Ed.* **1998**, *37*, 2240−2242. [4g] C. B. Aakeröy, A. M. Beatty, D. S. Leinen, *Angew. Chem. Int. Ed.* **1999**, *38*, 1815−1819. [4h] R. Atencio, K. V. Domasevitch, M. J. Zaworotko, *Cryst. Eng.* **2000**, *3*, 63−69. [4i] C. B. Aakeröy, A. M. Beatty, D. S. Leinen, K. R. Lorimer, *Chem. Commun.* **2000**, 935−936. [4j] C. Elschenbroich, F. Paganelli, O. Schiemann, *Organometallics* **2001**, *20*, 1875−1881.

[5] For general reviews on NLO materials, see: [5a] D. S. Chemla, J. Zyss, *Nonlinear Optical Properties of Organic Molecules and Crystals*, Academic Press, New York, **1987**. [5b] S. R. Marder, E. J. Sohn, G. D. Stucky *Materials for Nonlinear Optics: Chemical Perspectives*, American Chemical Society: Washington D. C., **1991**. [5c] J. Zyss, *Molecular Nonlinear Optics*, Academic Press, New York, **1994**. [5d] *Nonlinear Optical Properties of Organic Materials, Proceedings of SPIE*, **1988−1994**, *Vol. 971*. [5e] P. N. Prasad, D. J. Williams, *Introduction to Nonlinear Optical Effects in Molecules & Polymers*, John Wiley & Sons: New York, **1995**. [5f]T. Verbiest, S. Houbrechts, M. Kaurann, K. Clays, A. J. Persoons, *J. Mater. Chem.* **1997**, *7*, 2175−2189.

[6] For reviews on organometallic NLO materials, see: [6a] N. J. Long, *Angew. Chem. Int. Ed. Engl.* **1995**, *34*, 21−38. [6b] I. R. Whittall, A. M. McDonagh, M. G. Humphrey, M. Samoc, *Adv. Organomet. Chem.* **1998**, *42*, 291−362. [6c] I. R. Whittall, A. M. McDonagh, M. G. Humphrey, M. Samoc, *Adv. Organomet. Chem.* **1999**, *43*, 349−405.

[7] For reviews on ferrocenyl NLO materials see: S. Barlow, S. R. Marder, *Chem. Commun.* **2000**, 1555−1562.

[8] Among the influential studies on ferrocenyl NLO materials, see: [8a] L.-T. Cheng, W. Tam, G. R. Meredith, *Mol. Cryst. Liq. Cryst.* **1990**, *189*, 137−153. [8b] J. C. Calabrese, L.-T. Cheng, J. C. Green, S. R. Marder, W. Tam, *J. Am. Chem. Soc.* **1991**, *113*, 7227−7232. [8c] R. Loucif-Saïbi, J. A. Delaire, L. Bonazzola, G. Doisneau, G. Balavoine, T. Fillebeen-Khan, I. Ledoux, G. Puccetti, *Chem. Phys.* **1992**, *167*, 369−375. [8d] Z. Yuan, N. J. Taylor, Y. Sun, T. B. Marder, I. D. Williams, L.-T. Cheng, *J. Organomet. Chem.* **1993**, *449*, 27−37. [8e] D. R. Kanis, R. G. Lacroix, M. A. Ratner, T. J. Marks, *J. Am. Chem. Soc.* **1994**, *116*, 10089−10102. [8f] M. Blanchard-Desce, C. Runser, A. Fort, M. Barzoukas, J.-M. Lehn, V. Bloy, V. Alain, *Chem. Phys.* **1995**, *199*, 253−261.

[9] For recent examples on ferrecenyl NLO materials, see: [9a] U. Behrens, H. Brussaard, U. Hagenau, J. Heck, E. Hendrickx, J. Kornich, J. G. M. van-der-Linden, A. Persoons, A. L. Spek, N. Veldman, B. Voss, H. Wong, *Chem. Eur. J.* **1996**, *2*, 98−103. [9b] S. Barlow, H. E. Bunting, C. Ringham, J. C. Green, G. U. Bublitz, S. G. Boxer, J. W. Perry, S. R. Marder, *J. Am. Chem. Soc.* **1999**, *121*, 3715−3723. [9c] V. Cadierno, S. Conejero, M. P. Gamasa, J. Gimeno, I. Asselberghs, S. Houbrechts, K. Clays, A. Persoons, J. Borge, S. García-Granda, *Organometallics* **1999**, *18*, 582−597. [9d] I. S. Lee, H. Seo, Y. K. Chung, *Organometallics* **1999**, *18*, 1091−1096. [9e] K. N. Jayaprakash, P. C. Ray, I. Matsuoka, M. M. Bhadbhade, V. G. Puranik, P. K. Das, H. Nishihara, A. Sarkar, *Organometallics* **1999**, *18*, 3851−3858. [9f] T. Farrell, T. Meyer-Friedrichsen, M. Malessa, D. Haase, W. Saak, I. Asselberghs, K. Wostyn, K. Clays, A. Persoons, J. Heck, A. R. Manning, *J. Chem. Soc., Dalton Trans.* **2001**, 29−36. [9g] T. Farrell, A. Manning, T. C. Murphy, T. Meyer-Friedrichsen, J. Heck, I. Asselberghs, A. Persoons, *Eur. J. Inorg. Chem.* **2001**, 2365−2375.

 © 2003 Wiley-VCH Verlag GmbH & Co. KGaA, Weinheim

[10] Among examples of ferrocenes with large bulk NLO efficiency, see: [10a] M. L. H. Green, S. R. Marder, M. E. Thompson, J. A. Bandy, D. Bloor, P. V. Kolinsky, R. J. Jones, *Nature* **1987**, *330*, 360−362. [10b] B. J. Coe, C. J. Jones, J. A. McCleverty, D. Bloor, P. V. Kolinsky, R. J. Jones, *J. Chem. Soc., Chem. Commun.* **1989**, 1485−1487. [10c] S. R. Marder, J. W. Perry, W. P. Schaefer, B. G. Tiemann, *Organometallics* **1991**, *10*, 1896−1901. [10d] G. G. A. Balavoine, J.-C. Daran, G. Iftime, P. G. Lacroix, E. Manoury, J. A. Delaire, I. Maltey-Fanton, K. Nakatani, S. Di Bella, *Organometallics* **1999**, *18*, 21−29. [10e] J. A. Mata, E. Peris, I. Asselberghs, R. van Boxel, A. Persoons, *New J. Chem.* **2001**, *25*, 299−304. [10f] J. Chiffre, F. Averseng, G. G. A. Balavoine, J.-C. Daran, G. Iftime, P. G. Lacroix, E. Manoury, K. Nakatani, *Eur. J. Inorg. Chem.* **2001**, 2221−2236.

[11] J. A. Mata, E. Peris, R. Liusar, S. Uriel, M. P. Cifuentes, M. G. Humphrey, M. Samoc, B. Luther-Davies, *Eur. J. Inorg. Chem.* **2001**, 2113−2122.

[12] I. S. Lee, Y. K. Chung, J. Mun, C. S. Yoon, *Organometallics* **1999**, *18*, 5080−5085.

[13] For influent studies on NLO crystal design, see: [13a] J. L. Oudar, R. Hierle, *J. Appl. Phys.* **1977**, *48*, 2699−2704. [13b] J. Zyss, J. L. Oudar, *Phys. Rev. A* **1982**, *26*, 2028−2048. [13c] J. Zyss, G. Berthier, *J. Chem. Phys.* **1982**, *77*, 3635−3653. [13d] J. Zyss, J.-F. Nicoud, M. Coquillay, *J. Chem. Phys.* **1984**, *81*, 4160−4167. [13e] H. Tabei, T. Kurihara, T. Kaino, *Appl. Phys. Lett.* **1987**, *50*, 1855−1857. [13f] D. F. Eaton, A. G. Anderson, W. Tam, Y. Wang, *J. Am. Chem. Soc.* **1987**, *109*, 1886−1888. [13g] S. R. Marder, J. W. Perry, W. P. Schaefer, *Science* **1989**, *245*, 626−628. [13h] G. D. Stucky, M. L. F. Phillips, T. E. Gier, *Chem. Mater.* **1989**, *1*, 492−509. [13i] M. C. Etter, Z. Urbanczyk-Lipkowska, M. Zia-Ebrahimi, T. W. Punnunto, *J. Am. Chem. Soc.* **1990**, *112*, 8415−8426. [13j] J. K. Whitesell, R. E. Davis, L. L. Saunders, R. J. Wilson, J. P. Feagins, *J. Am. Chem. Soc.* **1991**, *113*, 3267−3270. [13k] M. C. Etter, K. S. Huang, *Chem. Mater.* **1992**, *4*, 824−827. [13l] Z. Kotler, R. Hierle, D. Josse, J. Zyss, R. Masse, *J. Opt. Soc., Am. B* **1992**, *9*, 534−547. [13m] J. Zyss, R. Masse, M. Bagieu-Beucher, J. P. Levy, *Adv. Mater.* **1993**, *5*, 120−124. [13n] V. Ramamurthy, D. F. Eaton, *Chem. Mater.* **1994**, *6*, 1128−1136.

[14] For recent crystal engineering works for NLO materials, see: [14a] Y. L. Fur, M. Bagieu-Beucher, R. Masse, J.-F. Nicoud, J.-P. Levy, *Chem. Mater.* **1996**, *8*, 68−75. [14b] V. R. Thalladi, S. Brasselet, H.-C. Weiss, D. Blaser, A. K. Katz, H. L. Carrell, R. Boese, J. Zyss, A. Nangia, G. R. Desiraju, *J. Am. Chem. Soc.* **1998**, *120*, 2563−2577. [14c] O. R. Evans, R.-G. Xiong, G. K. Wang, W. Lin, *Angew. Chem. Int. Ed.* **1999**, *38*, 536−538. [14d] V. R. Thalladi, R. Boese, S. Brasselet, I. Ledous, J. Zyss, R. K. R. Jetti, G. R. Desiraju, *Chem. Commun.* **1999**, 1639−1640. [14e] X.-L. Zhu, X.-Z. You, Y. Zhang, *Chem. Phys.* **2000**, *254*, 287−296. [14f] M. Muthuraman, R. Maase, J.-F. Nicoud, G. R. Desiraju, *Chem. Mater.* **2001**, *13*, 1473−1479. [14g] O. R. Evans, W. Lin, *Chem. Mater.* **2001**, *13*, 2705−2712. [14h] M. Ohkita, T. Suzuki, T. Tsuji, K. Nakatani, *Chem. Commun.* **2001**, 1454−1455.

[15] [15a] K. Kobayashi, K. Endo, Y. Aoyama, H. Masuda, *Tetrahedron Lett.* **1993**, *34*, 7929−7932. [15b] K. Endo, T. Sawaki, M. Koyanagi, K. Kobayashi, H. Masuda, Y. Aoyama, *J. Am. Chem. Soc.* **1995**, *117*, 8341−8352. [15c] Y. Aoyama, K. Endo, T. Anzai, Y. Yamaguchi, Y. Sawaki, K. Kobayashi, N. Kanehisa, H. Hashimoto, Y. Kai, H. Masuda, *J. Am. Chem. Soc.* **1996**, *118*, 5562−5571. [15d] L. R. MacGillivray, J. L. Atwood, *J. Am. Chem. Soc.* **1997**, *119*, 6931−6932. [15e] L. R. MacGillivray, K. T. Holman, J. L. Atwood, *Cryst. Eng.* **1998**, *1*, 87−96. [15f] L. R. MacGillivray, J. L. Reid, J. A. Ripmeester, *J. Am. Chem. Soc.* **2000**, *122*, 7817−7818.

[16] K. Biradha, M. J. Zaworotko, *J. Am. Chem. Soc.* **1998**, *120*, 6431−6432.

[17] A. Togni, M. Hobi, G. Rihs, G. Rist, A. Albinati, P. Zanello, Z. Damian, H. Kellwe, *Organometallics* **1994**, *13*, 1224−1234.

[18] [18a] R. Taylor, O. Kennard, *J. Am. Chem. Soc.* **1982**, *104*, 5063−5070. [18b] D. S. Reddy, D. C. Craig, G. R. Desiraju, *J. Am. Chem. Soc.* **1996**, *118*, 4090−4093. [18c] M. Mazik, D. Blaser, R. Boese, *Tetrahedron Lett.* **2000**, *41*, 5827−5831. [18d] M. Mazik, D. Blaser, R. Boese, *Tetrahedron* **2001**, *57*, 5791−5797. [18e] M. Ohkita, T. Suzuki, K. Nakatani, T. Tsuji, *Chem. Commun.* **2001**, 1454−1455.

[19] [19a] G. J. Palenik, *Inorg. Chem.* **1970**, *9*, 2424−2430. [19b] M. C. Grossel, M. R. Goldspink, J. A. Hrijac, S. C. Weston, *Organometallics* **1991**, *10*, 851−860. [19c] L. Lin, A. Berces, H.-B. Kraatz, *J. Organomet. Chem.* **1998**, *556*, 11−20.

[20] M. D. Blachard, R. P. Hughes, T. E. Concolino, A. L. Rheingold, *Chem. Mater.* **2000**, *12*, 1604−1610.

[21] [21a] S. K. Kurtz, T. T. Perry, *J. Appl. Phys.* **1968**, *39*, 3798−3813. [21b] J. P. Dougherty, S. K. Kurtz, *J. Appl. Crystallogr.* **1976**, *9*, 145−158.

[22] R. Sanders, U. T. Mueller-Westerhoff, *J. Organomet. Chem.* **1996**, *512*, 219−224.

[23] O Briel, K. Sunkel, I. Krossing, H. North, E. Schmalzlin, K. Meerholz, C. Brauchle, W. Beck, *Eur. J. Inorg. Chem.* **1999**, 483−490.

[24] [24a] G. M. Sheldrick, SHELXS-86, *Program for crystal structure solution*, *Acta Crystallogr. Sect. A* **1990**, *46*, 467. [24b] G. M. Sheldrick, SHELXL-93, *Program for crystal structure refinement*, University of Göttingen, Germany, **1993**.

[25] G. M. Sheldrick, SHELXL-97, *Program for the Refinement of Crystal Structures*, University of Göttingen, Germany, **1997**.

Received October 29, 2002

 © 2003 Wiley-VCH Verlag GmbH & Co. KGaA, Weinheim

Ternary Mononuclear and Ferromagnetically Coupled Dinuclear Copper(II) Complexes of 1,10-Phenanthroline and *N*-Salicylidene-2-methoxyaniline that Show Supramolecular Self-Organization

Pattubala A. N. Reddy,[a] Munirathinam Nethaji,[a] and Akhil R. Chakravarty*[a]

Keywords: Copper / Magnetic properties / N ligands / Stacking interactions / Supramolecular chemistry

The ternary copper(II) complex [Cu(phen)(L)](ClO_4) (**1**) and dinuclear copper(II) complex [Cu_2(phen)$_3$(L)(O_2CMe)](ClO_4)$_2$ (**2**) have been prepared and characterized structurally by X-ray crystallography (HL: *N*-salicylidene-2-methoxyaniline; phen: 1,10-phenanthroline). The crystal structure of **1** displays a square-pyramidal [4+1] coordination geometry in which the basal plane has three nitrogen donor atoms and the phenolate oxygen atom of the Schiff base. The methoxy oxygen atom exhibits axial coordination in the CuN_3O_2 chromophore. Complex **2** has a dinuclear copper(II) core in which the Cu(phen)$_2^{2+}$ and Cu(phen)(L)$^+$ units are linked by an acetate ion showing equatorial/axial modes of bonding. In the bis(phen) unit, the basal plane has three nitrogen atoms and the acetate oxygen atom with one phen nitrogen atom occupying the axial site. In the mono(phen) unit, the basal plane has three nitrogen atoms and one phenolate oxygen atom. The acetate oxygen atom occupies the axial site. The equatorial/axial bridging mode of the acetate ion makes the dicopper(II) unit weakly ferromagnetic ($2J$ = +22 cm^{-1}) and the complex in CH_2Cl_2 glass at 77 K shows an axial EPR spectrum [$g_{\|}$ = 2.23 ($A_{\|}$ = 150 × 10^{-4} cm^{-1}); $g_{\perp}$ = 2.03] corresponding to a ΔM_s = ±1 transition and a half-field signal due to a ΔM_s = ±2 transition. Complex **1** displays an axial EPR spectrum with $g_{\|} > g_{\perp}$ indicating a $\{d_{x^2-y^2}\}^1$ ground state. The complexes show a d–d band near 650 nm and a charge-transfer band at ca. 415 nm in methanol. The complexes are redox-active and exhibit a Cu^{II}/Cu^{I} couple near 0.0 V versus SCE in DMF and CH_2Cl_2/0.1 M TBAP. Complex **1** is catalytically active in the oxidation of ascorbic acid by dioxygen in aqueous methanol. Complex **2** also shows similar catalytic activity, but the core is susceptible to cleavage under the reaction conditions. The complexes show π–π stacking interactions. Complex **1** forms a one-dimensional chain through intermolecular π–π stacking interactions involving phen and the phenolate ring of the Schiff base. Complex **2** displays intramolecular and intermolecular π–π stacking interactions involving phen ligands leading to the formation of a supramolecular tetrameric structure.

(© Wiley-VCH Verlag GmbH & Co. KGaA, 69451 Weinheim, Germany, 2003)

Introduction

Ternary copper(II) complexes of the type [CuL^1L^2]$^{n+}$, where L^1 and L^2 together form a square-pyramidal [4+1] coordination geometry with labile binding sites, are of biological relevance.[1−6] Ternary complexes have been used to model the active site structures and catalytic properties of several type-2 copper proteins.[7−17] It has been observed that the biological activities of such copper proteins often are dependent on the noncovalent interactions between aromatic moieties.[1] The complexes are related to the formation of the tyrosine phenoxyl Tyr272 radical in a stacking interaction with Trp290 in galactose oxidase and the involvement of trihydroxyphenylalanine (topa) quinone in amine oxidase.[18,19] Such weak interactions play a crucial role in bioinorganic chemistry toward stabilizing the tertiary structure of proteins, reactivity of the metalloenzymes, in the molecular recognition process and in nucleic acids chemistry.[20,21]

Sigel et al. have studied the stacking interactions of the aromatic rings in ternary complexes.[22] Such weak interactions have profound influence on the structure and function of the complexes.[1,21,22] The present work stems from our interest to prepare ternary copper(II) complexes using an *N*,*N*-donor, 1,10-phenanthroline (phen), and an *O*,*N*,*O*-donor Schiff base, *N*-salicylidene-2-methoxyaniline (HL), to study such noncovalent interactions. We have been able to prepare a mononuclear ternary copper(II) complex [Cu(phen)(L)](ClO_4) (**1**) that forms a 1D chain by intermolecular π−π interactions involving the phen and Schiff-base ligands. We have also prepared a ferromagnetically coupled acetato-bridged dicopper(II) complex [Cu_2(phen)$_3$(L)(O_2CMe)](ClO_4)$_2$ (**2**) that is stabilized by novel intramolecular π−π interactions involving two phen ligands belonging to two copper centers. Interestingly, complex **2** undergoes self-organization through intermolecular π−π interactions of two phen ligands belonging to two dimeric species to form an unusual discrete supramolecular tetrameric species. Her-

[a] Department of Inorganic and Physical Chemistry, Indian Institute of Science,
Bangalore 560012, India
Fax: (internat.) + 91-80/3600683
E-mail: arc@ipc.iisc.ernet.in

Supporting information for this article is available on the WWW under http://www.eurjic.org or from the author.

 © 2003 Wiley-VCH Verlag GmbH & Co. KGaA, Weinheim **DOI: 10.1002/ejic.200200653**

Table 1. Spectral, magnetic and electrochemical data for complexes **1** and **2**

			1	**2**
(a)	IR[a]	ν(C=N)/cm^{-1}	1588	1614
		ν(ClO_4)/cm^{-1}	1096	1087
(b)	UV/Vis	λ_{max}/nm [ε/dm^3 mol^{-1} cm^{-1}][b]	641 [125],[c] 413 [2865],[d] 380 [2775],[d] 321 [2820][d]	650 [132],[c] 414 [2900],[d] 380 [2775],[d] 321 [2820][d]
(c)	EPR[e]	$g_{\parallel}$ ($10^4 \times A_{\parallel}$/cm^{-1})	2.28 [163]	2.23 [150]
		$g_{\perp}$	2.02	2.03
(d)		μ_{eff} (per Cu)[f]/μ_B	1.82	1.97[g]
(e)	CV	$E_{1/2}$/V [ΔE_P/mV][h] for Cu^{II}/Cu^{I} couple		
		in CH_2Cl_2/0.1 M TBAP	0.063 [546][i]	0.030 [640][j]
		in DMF/0.1 M TBAP	−0.070 [390][k]	

[a] KBr phase. [b] MeOH solvent. [c] d−d band. [d] Charge-transfer band. [e] In a DMF glass at 77 K for **1** and in a CH_2Cl_2 glass at 77 K for **2**. [f] In μ_B unit at 298 K. [g] $2J$ value of +22 cm^{-1}. [h] At 50 mV s^{-1}; $\Delta E_P = E_{pc} - E_{pa}$, where E_{pc} and E_{pa} are cathodic and anodic peak potentials; $E_{1/2} = (E_{pc} + E_{pa})/2$. [i] The i_{pc}/i_{pa} ratio of 3.5 (i_{pc} and i_{pa} are cathodic and anodic peak currents, respectively). [j] The i_{pc}/i_{pa} ratio of 14. [k] The i_{pc}/i_{pa} ratio of 4.1.

ein, we present the synthesis, crystal structure and properties of complexes **1** and **2**.

Results and Discussion

Synthesis and General Properties

The ternary monomeric complex **1** was prepared in high yield by a reaction of copper(II) perchlorate with 1,10-phenanthroline and the Schiff base (HL) in methanol. When the reaction of phen and HL is carried out with dimeric copper(II) acetate hydrate in methanol, followed by addition of sodium perchlorate, the major product is a dicopper(II) species of formulation $[Cu_2(phen)_3(L)(O_2CMe)](ClO_4)_2$ (**2**) along with **1** as a minor product. The complexes were characterized by analytical, spectral and single-crystal X-ray diffraction methods. The spectroscopic and magnetic data are given in Table 1.

The mononuclear complex **1** is one-electron paramagnetic. Magnetic susceptibility measurements in the range 30−302 K for the polycrystalline sample of **2** show weak ferromagnetic behavior of the complex. A theoretical fitting of the $\chi_M T$ vs. T plot gives a J value of +11 cm^{-1} with g = 2.17, $g1$ = 2.11 and ρ = 0.001 (Figure 1). Complexes **1** and **2** display axial X-band EPR spectra giving $g_{\parallel} > g_{\perp}$ indicating a $\{d_{x^2-y^2}\}^1$ ground state and a tetragonally distorted square-pyramidal geometry at the copper centers. Complex **2** in a CH_2Cl_2 glass at 77 K shows an additional signal at half-field corresponding to a $\Delta M_S = \pm 2$ transition indicating that it has dimeric nature and the triplet ground state (Figure 1).[23] This signal is, however, absent in a DMF glass at 77 K, possibly because of cleavage of the dimeric core. The complexes display a d−d band near 650 nm in methanol along with a charge-transfer band at ca. 415 nm.

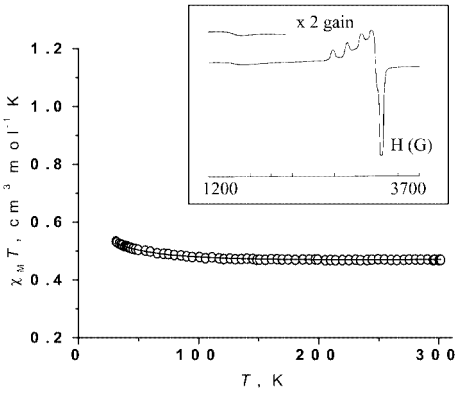

Figure 1. Plot of $\chi_M T$ vs. T for a polycrystalline sample of $[Cu_2(phen)_3(L)(O_2CMe)](ClO_4)_2$ (**2**) (circles); the solid line represents the best theoretical fit to the experimental data; an X-band EPR spectrum of **2** in a CH_2Cl_2 glass at 77 K is shown in the inset

Crystal Structures

Complexes **1** and **2** were characterized by single-crystal X-ray crystallography. Selected bond lengths and angles are given in Table 2. Perspective views of the molecules are shown in Figures 2 and 3. Complex **1** has a ternary structure consisting of a bidentate *N*,*N*-donor phen and tridentate *O*,*N*,*O*-donor Schiff base (L) bonded to the metal center in the cationic complex with a perchlorate counterion. While the basal plane is occupied by three nitrogen atoms and the phenolate oxygen atom, the methoxyl oxygen atom of the Schiff base shows axial bonding in the 4+1 coordination geometry with a CuN_3O_2 chromophore. The axial Cu−O bond length is 2.627(2) Å, which is similar to the metal-to-axial-tyrosinate-oxygen-atom distance of 2.69 Å in galactose oxidase.[18,24] The structure of **1** is distorted square-pyramidal, giving a trigonal distortion parameter (τ) value of 0.13.[25] In **1**, the torsion angle at the C=N (imine) moiety of the Schiff's base is 45.8°, which is similar to those angles observed in analogous complexes having axial sulfur ligation.[26] Complex **1** displays an intermolecular $\pi-\pi$ stacking interaction involving the phen and phenolate ring moieties with an interplanar distance of ca. 3.6 Å between the centroids of the rings that have essentially a parallel orientation (Figure 4).

The crystal structure of **2** displays a dicationic dicopper(II) complex crystallized with two perchlorate anions. The structure consists of two copper(II) centers, viz. $\{Cu(phen)_2^{2+}\}$ and $\{Cu(phen)(L)^{+}\}$, that are covalently

 © 2003 Wiley-VCH Verlag GmbH & Co. KGaA, Weinheim

Table 2. Selected bond lengths [Å] and angles [°] for [Cu(phen)(L)]ClO_4 (**1**) and [Cu_2(phen)$_3$(L)(O_2CMe)](ClO_4)$_2$ (**2**) with estimated standard deviations in parentheses

	1	**2**
Cu(1)···Cu(2)		4.342(2)
Cu(1)−O(1)	1.867(3)	1.857(5)
Cu(1)−O(2)	2.627(2)	
Cu(1)−O(3)		2.230(6)
Cu(1)−N(1)	1.930(3)	2.005(6)
Cu(1)−N(2)	2.039(3)	2.011(6)
Cu(1)−N(3)	1.999(3)	2.029(6)
Cu(2)−O(4)		1.966(5)
Cu(2)−N(4)		2.185(7)
Cu(2)−N(5)		1.983(6)
Cu(2)−N(6)		1.991(6)
Cu(2)−N(7)		2.069(6)
O(1)−Cu(1)−O(2)	134.06(11)	
O(1)−Cu(1)−O(3)		93.1(2)
O(1)−Cu(1)−N(1)	96.19(12)	93.0(2)
O(1)−Cu(1)−N(2)	146.32(13)	166.2(2)
O(1)−Cu(1)−N(3)	93.19(12)	89.2(2)
O(2)−Cu(1)−N(1)	68.98(11)	
O(2)−Cu(1)−N(2)	79.25(12)	
O(2)−Cu(1)−N(3)	87.10(12)	
O(3)−Cu(1)−N(1)		96.1(2)
O(3)−Cu(1)−N(2)		84.6(2)
O(3)−Cu(1)−N(3)		124.7(2)
N(1)−Cu(1)−N(2)	102.46(12)	100.7(2)
N(1)−Cu(1)−N(3)	153.94(13)	139.0(2)
N(2)−Cu(1)−N(3)	82.19(13)	81.0(2)
O(4)−Cu(2)−N(4)		112.2(2)
O(4)−Cu(2)−N(5)		93.5(2)
O(4)−Cu(2)−N(6)		92.8(2)
O(4)−Cu(2)−N(7)		148.2(2)
N(4)−Cu(2)−N(5)		79.6(3)
N(4)−Cu(2)−N(6)		94.6(2)
N(4)−Cu(2)−N(7)		99.4(2)
N(5)−Cu(2)−N(6)		172.7(3)
N(5)−Cu(2)−N(7)		95.5(3)
N(6)−Cu(2)−N(7)		81.0(2)

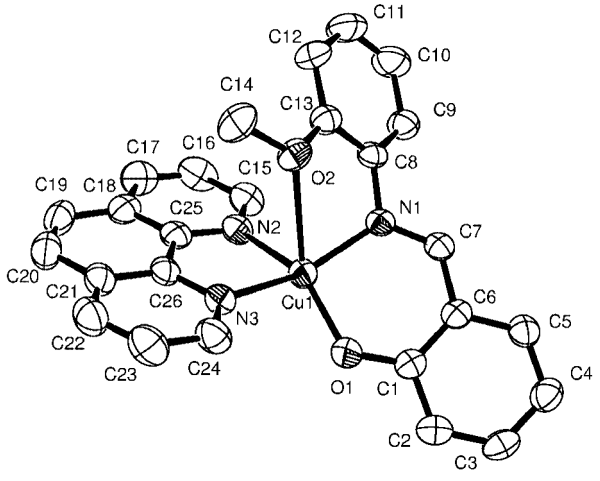

Figure 2. An ORTEP view of [Cu(phen)(L)](ClO_4) (**1**) showing thermal ellipsoids of 50% probability along with the atom numbering scheme.

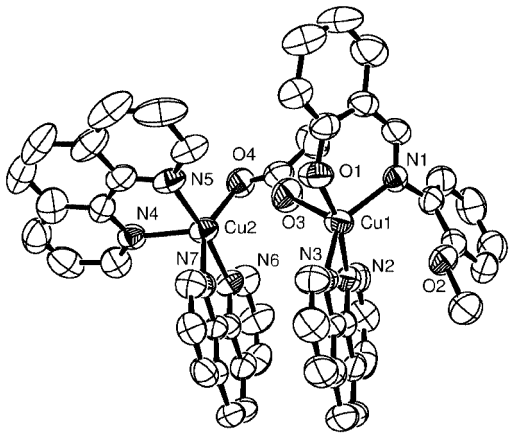

Figure 3. An ORTEP view of the cationic complex in [Cu_2(phen)$_3$(L)(O_2CMe)](ClO_4)$_2$ (**2**) showing thermal ellipsoids of 50% probability and the atom numbering scheme for the metal atom and the heteroatoms; for clarity, carbon atoms are not labeled

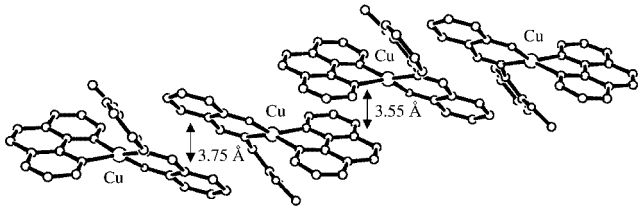

Figure 4. The intermolecular π−π stacking interaction in [Cu(phen)(L)](ClO_4) (**1**) involving phen ligands and phenolate rings to form a 1D chain

linked by an acetate ion showing a *syn*,*anti*-binding mode. The dimeric structure is stabilized by an intramolecular noncovalent π-stacking interaction involving two phen ligands belonging to two copper centers. An angle of 4.6° between the two phen planes indicates their near parallel orientation. A distance of 3.728 Å between the two centroids of the phen ligands suggests the significant stabilizing effect of the π−π interaction. Besides this interaction, two phen ligands belonging to two dimeric units are involved in an intermolecular π−π stacking interaction. This interaction leads to an association of two dimeric complexes into a discrete supramolecular tetrameric species (Figure 5). The Cu(1) center in **2** is bonded to one phen unit, the Schiff base and the bridging acetate ion. The Schiff base shows a bidentate chelating mode of bonding through the phenolate oxygen atom and the imine nitrogen atom. The methoxy oxygen atom essentially is nonbonded to the metal atom [Cu(1)···O(2), 2.966(6) Å]. The basal plane of Cu(1) comprises the phen unit and the Schiff-base ligand. The axial site is occupied by the acetate oxygen atom at a distance of 2.240(6) Å. The Cu(1) atom has a significantly distorted square-pyramidal [4+1] coordination geometry that gives a τ value of 0.45. The Cu(2) atom is bonded to one acetate and two phen ligands. The basal plane is occupied by three nitrogen atoms of the phen ligands and one oxygen atom of the acetate bridge. One nitrogen atom of a phen ligand occupies the axial site. The coordination geometry is axially

 © 2003 Wiley-VCH Verlag GmbH & Co. KGaA, Weinheim

elongated distorted square-pyramidal (4+1) with a CuN_4O chromophore ($\tau = 0.4$).

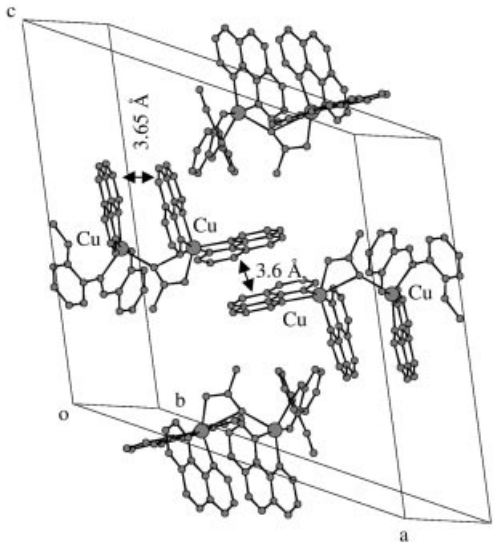

Figure 5. A unit-cell packing diagram showing the intra- and intermolecular π−π stacking interactions in $[Cu_2(phen)_3(L)(O_2CMe)](ClO_4)_2$ (**2**) to form the discrete supramolecular tetranuclear species; for clarity, the perchlorate anions are not shown

The Cu(1)−Cu(2) distance in **2** is 4.342(2) Å. The metal centers are linked by the acetate ion that shows an equatorial/axial mode of bonding. Such a binding mode involving the $d_{x^2-y^2}$ orbital of Cu(2) and the d_z^2 orbital of Cu(1) makes the metal centers essentially uncoupled because of the orthogonality of the orbitals. As a consequence, the magnetic exchange interaction in **2** becomes weakly ferromagnetic as is evidenced in the variable-temperature magnetic susceptibility studies and in the EPR spectrum in a CH_2Cl_2 glass at 77 K.[23,27] Complex **2** with two copper centers having different ligand environments and a weakly coupled dicopper(II) core has structural similarity to the dimeric sites of type-2 proteins, viz. dopamine β-hydroxylase and peptidylglycine α-hydroxylating monooxygenase.[3,28]

Redox and Catalytic Properties

The electron-transfer behavior of the complexes **1** and **2** was studied by cyclic voltammetry using a glassy-carbon working electrode. Selected data are given in Table 1 and voltammograms are shown in Figure 6. Complex **1** in CH_2Cl_2/0.1 M TBAP or DMF/0.1 M TBAP shows a cathodic peak near −0.25 V with an anodic counterpart at 0.34 V in CH_2Cl_2 and 0.13 V in DMF. The peaks are assignable to the Cu^{II}/Cu^{I} couple. The reduced ternary species [Cu(phen)(L)] is unstable as is evidenced from the i_{pc}/i_{pa} ratio of ca. 4.0.[29] The dimeric complex **2** displays a cathodic peak at −0.29 V with an anodic response at 0.35 V in CH_2Cl_2/0.1 M TBAP. Again, the i_{pc}/i_{pa} ratio of 14.0 indicates poor stability of the reduced species. The $E_{1/2}$ value of 0.03 V for the $Cu_2^{II}/Cu^{II}Cu^{I}$ couple compares well with that of **1**. The dimeric core was unstable in DMF/0.1 M TBAP solution. The DMF solution of **2** shows two cathodic peaks at −0.07 and −0.29 V with a broad anodic peak at 0.15 V. The cathodic peaks are assignable to the Cu^{II}/Cu^{I} couple of the $[Cu(phen)_2]^{2+}$ and $[Cu(phen)(L)]^{+}$ species.[30] It is likely that the weak axial bond of the acetate ion in **2** undergoes cleavage in a polar solvent such as DMF. Such a cleavage has been evidenced from the EPR spectrum of **2** showing no half-field signal in a DMF glass. Complex **2** also displays an irreversible cathodic peak at −0.89 V resulting from reduction of the Schiff's base.

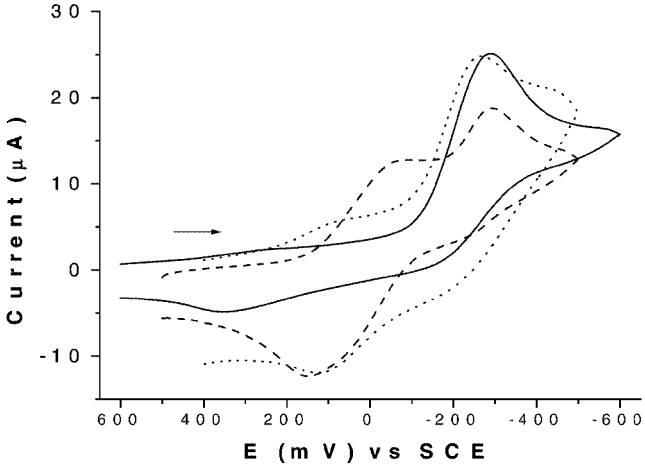

Figure 6. Cyclic voltammograms of $[Cu(phen)(L)](ClO_4)$ (**1**) in DMF/0.1 M TBAP (···), $[Cu_2(phen)_3(L)(O_2CMe)](ClO_4)_2$ (**2**) in DMF/0.1 M TBAP (---) and CH_2Cl_2/0.1 M TBAP (—) at 50 mV s^{-1}

Complex **1** reacts with ascorbic acid (H_2A) in aqueous methanol to form an unstable, brown copper(I) species, which on exposure to air converts to the parent complex. The catalytic cycle is effective at an H_2A/**1** molar ratio of 60:1. At higher concentrations of H_2A, a catalytically inactive oxalato species is formed. The formation of oxalic acid takes place from the oxidation of a dehydroascorbate species.[31] Complex **2** is also active in the oxidation of H_2A by dioxygen, but the complex is susceptible to cleavage in a polar reaction medium. The observed catalytic activity of **2** could be due to the formation of two catalytically active monomeric copper(II) species.

Conclusion

A ternary monomeric copper(II) complex having a tridentate *O*,*N*,*O*-donor Schiff base and bidentate *N*,*N*-donor phen unit was prepared and characterized structurally. The complex has a CuN_3O_2 square-pyramidal [4+1] coordination geometry with a methoxy oxygen atom as a weak axial ligand. A dicopper(II) complex was prepared and structurally characterized that has $Cu(phen)_2^{2+}$ and $Cu(phen)(L)^{+}$ units linked by an acetate ion showing equatorial/axial modes of bonding. Complex **2** has a ferromagnetically coupled dicopper(II) core. Crystal structures of the complexes **1** and **2** show intermolecular π−π stacking interactions. In addition, the dimeric complex **2** shows the presence of an intramolecular π−π stacking interaction involv-

 © 2003 Wiley-VCH Verlag GmbH & Co. KGaA, Weinheim

ing the phen ligands of two different metal centers having CuN_4O and CuN_3O_2 coordination environments. While complex **1** forms a 1D chain, the intermolecular interaction in **2** results in the aggregation of two dimeric units to form an unusual discrete supramolecular tetranuclear structure.

Experimental Section

Materials and Physical Measurements: Chemicals and reagents were obtained from commercial sources. Solvents were purified by standard procedures.[32] Salicylaldehyde was obtained from Aldrich. 2-Methoxyaniline and 1,10-phenanthroline were purchased from SD Fine Chemicals, Mumbai. Copper(II) acetate hydrate was from BDH (India). The Schiff-base ligand, *N*-salicylidene-2-methoxyaniline (HL) was prepared by a literature method.[33] The infrared, electronic and EPR spectra were recorded with Bruker Equinox 55, Hitachi U3000 and Varian E-109 X-band spectrometers, respectively. The elemental analysis was performed using a Heraeus CHN-O Rapid instrument. Magnetic susceptibility data of the polycrystalline samples were obtained from a George Associates Inc. Lewis-coil-force magnetometer system having Cahn balance and an APD closed-cycle cryostat. Diamagnetic corrections to the susceptibility data were made using Pascal's constants.[34] Variable-temperature magnetic susceptibility data for complex **2** in the 30−302 K range were corrected for temperature-independent paramagnetism ($N\alpha = 60 \times 10^{-6}$ cm^3 mol^{-1} per copper atom). The molar magnetic susceptibilities were fitted to the modified Bleaney−Bowers expression[35] based on the isotropic form of the Heisenberg−Dirac−van Vleck (HDvV) model with a spin Hamiltonian $H = -2JS_1S_2$ ($S_1 = S_2 = 1/2$ for d^9-d^9 configuration): $\chi_{Cu} = [Ng^2\beta^2/kT][3 + \exp(-2J/kT)]^{-1}(1 - \rho) + (Ng_1^2\beta^2/4kT)\rho + N\alpha$, where ρ is the fraction of monomeric impurity and $-2J$ is the singlet−triplet energy separation. The magnetic moments at various temperatures were calculated in μ_B units ($\mu_B \approx 9.274 \times 10^{-24}$ J T^{-1}). Electrochemical measurements were made at 25 °C with an EG&G PAR Model 253 Versastat Potentiostat/Galvanostat with electrochemical analysis software 270 for voltammetric work with a three-electrode setup comprising a glassy-carbon working electrode, a platinum-wire auxiliary electrode and a saturated calomel reference (SCE) electrode. The electrochemical data are uncorrected for junction potentials. Tetrabutylammonium perchlorate (TBAP) was used as a supporting electrolyte. Ferrocene was used as standard to monitor the reference electrode.

Syntheses

Preparation of [Cu(phen)(L)](ClO$_4$) (1) and [Cu$_2$(phen)$_3$(L)(O$_2$CMe)](ClO$_4$)$_2$ (2): The complexes were prepared as a mixture from a reaction of $Cu_2(O_2CMe)_4(H_2O)_2$ (0.2 g, 0.5 mmol) in methanol (5 mL) with phen (0.19 g, 1.0 mmol) whilst stirring for 0.5 h at 25 °C, followed by addition of the Schiff base (HL, 0.23 g, 1.0 mmol) in methanol (10 mL) and a methanolic solution of $NaClO_4$. On slow concentration, the reaction mixture gave large rhombohedral-shaped crystals of complex **2** (yield: ca. 60%) and thin plate-type

Table 3. Crystallographic data for $[Cu(phen)(L)]ClO_4$ (**1**) and $[Cu_2(phen)_3(L)(O_2CMe)](ClO_4)_2$ (**2**)

	1	**2**
Empirical formula	$C_{26}H_{20}ClCuN_3O_6$	$C_{52}H_{39}Cl_2Cu_2N_7O_{12}$
M_r	569.44	1151.88
Crystal system	triclinic	monoclinic
Space group	$P\bar{1}$ (no. 2)	$P2_1/n$ (no. 1014)
a [Å]	9.065(3)	20.845(8)
b [Å]	10.429(3)	12.727(5)
c [Å]	13.607(6)	21.520(8)
α [°]	99.86(3)	90.00
β [°]	103.42(3)	116.303(6)
γ [°]	100.14(3)	90.00
V [Å^3]	1201.0(8)	5118(3)
Z	2	4
T [K]	293(2)	293(2)
λ (Mo-K_α) [Å]	0.71073	0.71073
D_c [g cm^{-3}]	1.575	1.495
μ (Mo-K_α) [cm^{-1}]	10.70	10.06
F(000)	582	2352
Crystal colour and habit	dark green rectangular	dark green rhombohedral
Crystal size [mm]	0.55 × 0.40 × 0.09	0.36 × 0.28 × 0.12
$2\theta_{max}$ [°]	50	52
Reflns. collected	3918	10040
Independent reflns. [$I > 2\sigma(I)$]	3183	4353
Parameters refined	414	673
Goodness-of-fit on F^2	1.018	0.979
R_{int}	0.0379	0.0986
R (obsd. data)	0.0472	0.0826
wR (obsd. data)	0.1210	0.2080
R (all data)	0.0628	0.1844
wR (all data)	0.1314	0.2536
Maximum shift/e.s.d.	0.000	0.001
Largest diff. peak [e·Å^{-3}]	0.591	0.994

 © 2003 Wiley-VCH Verlag GmbH & Co. KGaA, Weinheim

crystals of **1** (yield: ca. 20%). The crystals were separated manually and dried under vacuum over P_4O_{10}. $C_{26}H_{20}ClCuN_3O_6$ (569.5) (**1**): calcd. C 54.72, H 3.51, N 7.37; found C 54.78, H 3.68, N 7.32. $C_{52}H_{39}Cl_2Cu_2N_7O_{12}$ (1151.9) (**2**): calcd. C 54.16, H 3.38, N 8.51; found C 54.01, H 3.52, N 8.40. IR (KBr phase): $\tilde{\nu}$ = 3065 br, 1588 s, 1522 s, 1430 m, 1320 m, 1186 m, 1096 vs, 842 m, 778 m, 721 m, 618 w cm^{-1} for **1**; $\tilde{\nu}$ = 3434 br, 3065 m, 1614 s, 1442 m, 1329 m, 1242 m, 1150 m, 1087 vs, 843 m, 748 m, 620 w cm^{-1} for **2** (vs, very strong; s, strong; m, medium, w, weak; br, broad). Complex **1**, formed as a single product, was prepared from the reaction of $Cu(ClO_4)_2 \cdot 6H_2O$ (0.37 g, 1.0 mmol) in methanol (10 mL) and phen (0.19 g, 1.0 mmol) in methanol (10 mL) followed by the addition of the Schiff base (HL, 0.23 g, 1.0 mmol) in methanol (5 mL). The mixture was stirred for 0.5 h at 25 °C. Removal of the solvent in a rotary evaporator gave **1** as a single product that was washed with water and diethyl ether before drying in vacuo over P_4O_{10} (yield: 70%). ***Caution!*** *Perchlorate salts are potentially explosive and should be handled in small quantities with suitable safety measures.*

X-ray Crystallographic Study: Intensity data for complex **1** in the triclinic crystal system were collected with an Enraf−Nonius CAD4 diffractometer fitted with a graphite-monochromated Mo-K_α radiation. The data were corrected for Lorentz, polarization and absorption effects.[36] The cell parameters and the intensity data for complex **2** were obtained from a Bruker SMART APEX CCD diffractometer, equipped with a fine-focus 1.75-kW sealed-tube Mo-K_α X-ray source, with increasing ω (width, 0.3° per frame) at a scan speed of 8 s/frame. The SMART software was used for data acquisition and the SAINT software for data extraction.[37] Absorption correction was done using SADABS.[38] The structures were solved and refined using SHELX programs.[39] The relations used for residuals are $R = \Sigma||F_o| - |F_c||/\Sigma|F_o|$; $R_w = \{\Sigma[w(F_o^2 - F_c^2)^2]/\Sigma[w(F_o)^2]\}^{1/2}$, $w = [\sigma^2(F_o)^2 + (AP)^2 + BP]^{-1}$, where $P = (F_o^2 + 2F_c^2)/3$ having A and B values of 0.0843 and 0.8796 for **1** and 0.1266 and 0.0000 for **2**. While complex **1** refined well without showing any significant disorder, the crystals of complex **2** diffracted poorly. The atoms belonging to the cationic complex of **2** and one perchlorate anion refined well. The other perchlorate anion in **2** showed positional disorders. This perchlorate anion was refined with two sets of five peaks having site occupancies of 0.7 and 0.3. The hydrogen atoms of **1** were located from the difference Fourier maps and were refined isotropically. The hydrogen atoms of **2** were generated and assigned isotropic thermal parameters, riding on their parent carbon atoms and used only for calculation of the F_o^2 structure factor. Selected crystal data for complexes **1** and **2** are given in Table 3. Perspective views of the complexes were obtained by ORTEP.[40] CCDC-192652 and -192653 contain the supplementary crystallographic data for this paper. These data can be obtained free of charge at www.ccdc.cam.ac.uk/conts/retrieving.html [or from the Cambridge Crystallographic Data Centre, 12 Union Road, Cambridge CB2 1EZ, UK; Fax: (internat.) + 44-1223/336-033; E-mail: deposit@ccdc.cam.ac.uk].

Acknowledgments

We thank the Department of Science and Technology, Government of India, for financial support (SP/S1/F01/2000) and for the CCD diffractometer facility. Thanks are due to the Alexander von Humboldt Foundation, Germany, for the donation of an electroanalytical system, and to the Bioinformatic Center of the Indian Institute of Science, Bangalore, for a database search. P. A. N. R. thanks CSIR, New Delhi, for a research fellowship.

[1] O. Yamauchi, A. Odani, M. Takani, *J. Chem. Soc., Dalton Trans.* **2002**, 3411−3421.
[2] B. Sarkar, *Chem. Rev.* **1999**, *99*, 2535−2544.
[3] J. P. Klinman, *Chem. Rev.* **1996**, *96*, 2541−2561.
[4] W. Kaim, J. Rall, *Angew. Chem. Int. Ed. Engl.* **1996**, *35*, 43−60.
[5] B. Abolmaali, H. V. Taylor, U. Weser, *Struct. Bonding* **1998**, *91*, 91−190.
[6] A. G. Blackman, W. B. Tolman, *Struct. Bonding* **2000**, *97*, 179−211.
[7] P. S. Subramanian, E. Suresh, P. Dastidar, S. Waghmode, D. Srinivas, *Inorg. Chem.* **2001**, *40*, 4291−4301.
[8] H. Masuda, T. Sugimori, A. Odani, O. Yamauchi, *Inorg. Chim. Acta* **1991**, *180*, 73−79.
[9] F. Zhang, A. Odani, H. Masuda, O. Yamauchi, *Inorg. Chem.* **1996**, *35*, 7148−7155.
[10] O. Yamauchi, A. Odani, T. Kohzuma, H. Masuda, K. Toriumi, K. Saito, *Inorg. Chem.* **1989**, *28*, 4066−4068.
[11] T. Sugimori, H. Masuda, O. Yamauchi, *Bull. Chem. Soc. Jpn.* **1994**, *67*, 131−137.
[12] K. Aoki, H. Yamazaki, *J. Chem. Soc., Dalton Trans.* **1987**, 2017−2021.
[13] M. A. Halcrow, L. M. LindyChia, X. Liu, E. J. L. McInnes, L. J. Yellowlees, F. E. Mabbs, I. J. Scowen, M. McPartlin, J. E. Davies, *J. Chem. Soc., Dalton Trans.* **1999**, 1753−1762.
[14] P. A. N. Reddy, M. Nethaji, A. R. Chakravarty, *Inorg. Chim. Acta* **2002**, *337*, 450−458.
[15] H. Sigel, R. Tribolet, O. Yamauchi, *Comments Inorg. Chem.* **1990**, *9*, 305−330.
[16] T. Sugimori, H. Masuda, N. Ohata, K. Koiwai, A. Odani, O. Yamauchi, *Inorg. Chem.* **1997**, *36*, 576−583.
[17] T. Yajima, M. Okajima, A. Odani, O. Yamauchi, *Inorg. Chim. Acta* **2002**, *339*, 445−454.
[18] N. Ito, S. E. V. Philips, C. Stevens, Z. B. Ogel, M. J. McPherson, J. N. Keen, K. D. S. Yadav, P. F. Knowles, *Nature* **1991**, *350*, 87−90.
[19] M. R. Parsons, M. A. Convery, C. M. Wilmot, K. D. S. Yadav, V. Blakely, A. S. Corner, S. E. V. Phillips, M. J. McPherson, P. F. Knowles, *Structure* **1995**, *3*, 1171−1184.
[20] [20a] J.-M. Lehn, *Angew. Chem. Int. Ed. Engl.* **1990**, *29*, 1304−1319. [20b] G. R. Desiraju, *Acc. Chem. Res.* **1996**, *29*, 441−449. [20c] P. J. Stang, B. Olenyuk, *Acc. Chem. Res.* **1997**, *30*, 502−518.
[21] [21a] C. A. Hunter, J. K. M. Sanders, *J. Am. Chem. Soc.* **1990**, *112*, 5525−5534. [21b] A. M. Pyle, J. K. Barton, *Prog. Inorg. Chem.* **1990**, *38*, 413−475. [21c] D. S. Sigman, T. W. Bruise, A. Mazumdar, C. L. Sutton, *Acc. Chem. Res.* **1993**, *26*, 98−104.
[22] [22a] H. Sigel, *Angew. Chem. Int. Ed. Engl.* **1975**, *14*, 394−402. [22b] H. Sigel, B. Song, *Met. Ions Biol. Syst.* **1996**, *32*, 135−205. [22c] H. Sigel, *Pure Appl. Chem.* **1989**, *61*, 923−932. [22d] H. Sigel, *Angew. Chem. Int. Ed. Engl.* **1982**, *21*, 389−400.
[23] K. Geetha, M. Nethaji, A. R. Chakravarty, N. Y. Vasanthacharya, *Inorg. Chem.* **1996**, *35*, 7666−7670.
[24] N. Ito, S. E. V. Philips, K. D. S. Yadav, P. F. Knowles, *J. Mol. Biol.* **1994**, *238*, 794−814.
[25] A. W. Addison, T. N. Rao, J. Reedijk, J. V. Rijn, G. C. Verschoor, *J. Chem. Soc., Dalton Trans.* **1984**, 1349−1356.
[26] B. K. Santra, P. A. N. Reddy, M. Nethaji, A. R. Chakravarty, *Inorg. Chem.* **2002**, *41*, 1328−1332,
[27] [27a] S. Meenakumari, S. K. Tiwary, A. R. Chakravarty, *Inorg. Chem.* **1994**, *33*, 2085−2089. [27b] M. Koman, D. Valigura, E. Durcanská, G. Ondrejovic, *J. Chem. Soc., Chem. Commun.* **1984**, 381−383. [27c] S. P. Perlepes, E. Libby, W. E. Streib, K. Folting, G. Christou, *Polyhedron* **1992**, *11*, 923−936. [27d] Y. Kani, M. Tsuchimoto, S. Ohba, H. Matsushima, T. Tokii, *Acta Crystallogr., Sect. C* **2000**, *56*, 923−925. [27e] C. T. Yang, B. Moubaraki, K. S. Murray, J. D. Ranford, J. J. Vittal, *Inorg. Chem.* **2001**, *40*, 5934−5941.
[28] S. T. Prigge, A. S. Kolhekar, B. A. Eipper, R. E. Mains, L. M. Amzel, *Science* **1997**, *278*, 1300−1305.

 © 2003 Wiley-VCH Verlag GmbH & Co. KGaA, Weinheim

[29] [29a] R. S. Nicholson, I. Shain, *Anal. Chem.* **1965**, *37*, 178−190. [29b] D. T. Sawyer, J. L. Ruberts, *Experimental Electrochemistry for Chemists*, John Wiley & Sons, New York, **1974**.
[30] C. Lee, F. C. Anson, *Inorg. Chem.* **1984**, *23*, 837−844.
[31] S. Lewin, *Vitamin C: Its Molecular Biology and Medical Potential*, Academic Press, London, **1976**.
[32] D. D. Perrin, W. L. F. Armarego, D. R. Perrin, *Purification of Laboratory Chemicals*, Pergamon Press, Oxford, **1980**.
[33] [33a] L. M. Shkol'nikova, A. E. Obodovskaya, E. A. Shugam, *Zh. Struct. Khim.* **1970**, *11*, 54−61. [33b] L. M. Shkol'nikova, A. E. Obodovskaya, E. A. Shugam, *Zh. Struct. Khim.* **1973**, *14*, 286−290.
[34] O. Kahn, *Molecular Magnetism,* VCH, New York, **1993**.
[35] B. Bleany, K. D. Bowers, *Proc. R. Soc., London, Sec. A* **1952**, *214*, 451−465.
[36] *DIFABS*, Program for applying empirical absorption corrections: N. Walker, D. Stuart, *Acta Crystallogr., Sect. A* **1983**, *39*, 158−166.
[37] Bruker *SMART and SAINT*, Versions 6.22a, Bruker AXS Inc., Madison, Wisconsin, USA, **1999**.
[38] R. H. Blessing, *Acta Crystallogr., Sect. A* **1995**, *51*, 33−38.
[39] G. M. Sheldrick, *SHELXL-97, Program for the Solution of Crystal Structures*, University of Göttingen, Göttingen, Germany, **1997**.
[40] C. K. Johnson, *ORTEP*, Report ORNL-3794, Oak Ridge National Laboratory, Oak Ridge, TN, **1976**.

Received November 27, 2002

 © 2003 Wiley-VCH Verlag GmbH & Co. KGaA, Weinheim

Synthesis, Crystal Structures and Third-Order Nonlinear Optical Properties of Two Novel Ferrocenyl Schiff-Base Complexes $[Ag(L)_2](NO_3)(MeOH)(EtOH)$ and $[HgI_2(L)]$ {L = 1,2-Bis[(ferrocen-l-ylmethylene)amino]ethane}

Hongwei Hou,*[a] Gang Li,[a] Yinglin Song,[b] Yaoting Fan,[a] Yu Zhu,[a] and Lu Zhu[a]

Keywords: Schiff bases / Silver / Mercury / Nonlinear optics

Two novel ferrocenyl complexes $[Ag(L)_2](NO_3)\cdot(MeOH)\cdot(EtOH)$ (**1**) and $[HgI_2(L)]$ (**2**) {L = 1,2-bis[(ferrocen-l-ylmethylene)amino]ethane} have been prepared and structurally characterized by means of X-ray single crystal diffraction. The central ion, silver(I) or mercury(II), has a distorted tetrahedral environment, the silver(I) ion coordinates with two L, and the mercury(II) ion binds one L and two iodine atoms. Their third-order nonlinear optical (NLO) properties were determined by Z-scan techniques in DMF solution. The results indicate that the two complexes exhibit very strong NLO absorption and strong self-focusing effects. The third-order NLO absorptive coefficients α_2 are 1.34×10^{-8} m W^{-1} for **1** and 3.1×10^{-9} m W^{-1} for **2**. The refractive indexes n_2 for the two complexes are 1.15×10^{-18} and 8.02×10^{-19} m^2 W^{-1}, respectively. The hyperpolarizability γ values are calculated to be 2.68×10^{-30} esu for **1** and 1.44×10^{-30} esu for **2**. The γ values are several orders of magnitude larger than those of the reported aryl and vinyl derivatives of ferrocene. (© Wiley-VCH Verlag GmbH & Co. KGaA, 69451 Weinheim, Germany, 2003)

Introduction

Ferrocene-containing compounds are currently receiving much attention due to their increasing role in the rapidly growing area of materials science. They have been used as homogeneous catalysts for various processes,[1] molecular sensors,[2] and molecular magnetic[3] and nonlinear optical materials.[4] In particular, several studies have been made on the nonlinear optical properties of ferrocene derivatives[4] since the first report that (*E*)-1-ferrocenyl-2-(*N*-methylpyridinium-4-yl)ethylene iodide and (*Z*)-1-ferrocenyl-2-(4-nitrophenyl)ethylene have large second harmonic generation efficiencies (220 and 62 times that of urea, respectively).[5]

Ferrocenyl Schiff bases as very important ferrocene derivatives have been studied in this context. Several groups have reported the NLO properties of various monoferrocenyl Schiff bases and bidentate diferrocenyl Schiff bases, but most have focused on second-order NLO properties of those compounds.[6−10] To the best of our knowledge, there are no reports on the third-order NLO properties of this type of compounds and the corresponding complexes.

Conversely, although the bidentate ferrocenyl Schiff base 1,2-bis[(ferrocen-l-ylmethylene)amino]ethane (L) has previously been prepared, its metal complexes are quite scarce due to its spontaneous hydrolytic degradation. However, a series of metal complexes with the parent amine of L, 1,2-bis[(ferrocenylmethyl)amino]ethane, have been obtained.[11−13] The only known complex containing L appears to be the $[ZnCl_2(L)]$ complex recently described by Li et al.[14] It is noteworthy that the syntheses of Ag- or Hg-containing ferrocenyl complexes are difficult, due mainly to the instability of Ag^I in solution and the poor solubility of Hg^{II} in ordinary solvents. To obtain Ag- or Hg-containing ferrocenyl compounds and find better third-order NLO materials, we utilized the reaction of L with Ag or Hg to synthesize two novel complexes, $[Ag(L)_2](NO_3)\cdot(MeOH)\cdot(EtOH)$ (**1**) and $[HgI_2(L)]$ (**2**), and further determined their third-order NLO properties using Z-scan techniques. The results reveal that both complexes have very strong third-order NLO absorptive and refractive properties in DMF solution. The hyperpolarizability γ values are calculated to be 2.68×10^{-30} esu and 1.44×10^{-30} esu for **1** and **2**, respectively.

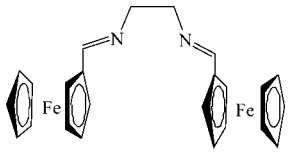

L

[a] Department of Chemistry, Zhengzhou University, Zhengzhou, 450052, P. R. China
Fax: (internat.) + 86-371/7761744
E-mail: houhongw@zzu.edu.cn
[b] Department of Physics, Harbin Institute of Technology, Harbin, 150001, P. R. China

Results and Discussion

Crystal Structure of $[Ag(L)_2](NO_3)(MeOH)(EtOH)$ (1)

The molecular structure of complex **1** was determined by single-crystal X-ray diffraction analysis. The asymmetric unit contains an $[Ag(L)_2]^+$ cation, one NO_3^- anion, and one crystallization molecule each of methanol and ethanol. The perspective view of the cation of **1** is illustrated in Figure 1.

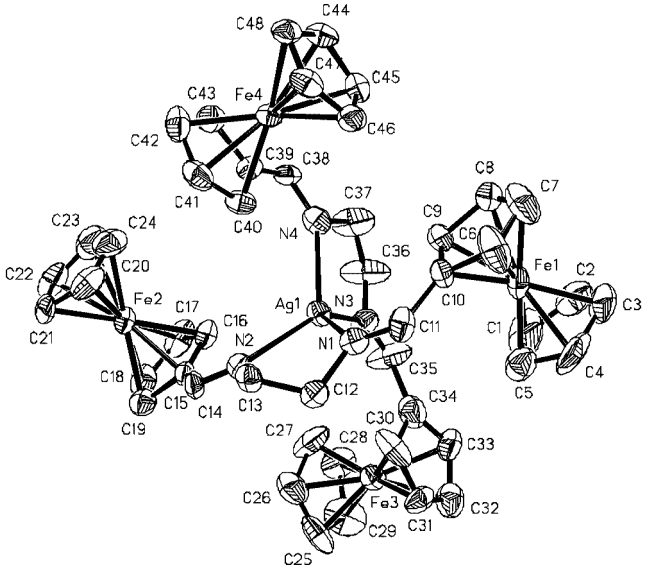

Figure 1. ORTEP drawing with atom-labeling scheme of the cation of $[Ag(L)_2](NO_3)\cdot(MeOH)\cdot(EtOH)$

The Ag^I ion is in a distorted tetrahedral environment with the four nitrogen atoms N1, N2, N3 and N4 of two L, which act as bidentate ligands. The Ag−N distances range from 2.277(8) to 2.397(8) Å. The angles N1−Ag1−N2 [77.7(3)°] and N3−Ag1−N4 [77.1(3)°] are acute, and are enforced by the ligand L. The other N−Ag1−N angles are in the range 125.2(3)−130.6(3)°. Hence, the average bond angle at Ag1 is 110.8°, while the dihedral angle between the planes [N1, Ag, N2] and [N3, Ag, N4] is 90.7°. Two five-membered rings, N1−C12−C13−N2−Ag1 and N3−C36−C37−N4−Ag1, adopt λ-conformations (the torsional angles of N1−C12−C13−N2 and N3−C36−C37−N4 are 63.7° and 26.0°, respectively). The geometry at the central Ag^I ion is, in fact, the same as that in the related compound $[Cu(L^1)_2]BF_4$ {L^1 = 1,2-bis[(ferrocen-1-ylmethylene)amino]benzene},[14] which is distorted by the bite of the ferrocenyl ligands.

The average $Fe-C_{ring}$ distance (2.014 Å) is close to that of the free ferrocene (2.04 Å). The average intra C−C bond length of cyclopentadienyl is 1.389 Å, which is shorter than that of the free ferrocene. The average C−C−C angle of 107.8(11)° is similar as those of reported compounds.[15] In each ferrocenyl moiety, the cyclopentadienyl rings are planar. The dihedral angle between the planes C15−C16−C17−C18−C19 and C20−C21−C22−C23−C24 at Fe2 is 3.5°, and is only 0.7° for the planes C39−C40−C41−C42−C43 and C44−C45−C46−C47−C48 at Fe4, but the other dihedral angles between the planes C6−C7−C8−C9−C10 and C1−C2−C3−C4−C5 at Fe1 and between the planes C30−C31−C32−C33−C34 and C25−C26−C27−C28−C29 at Fe3 are slightly larger at 6.6° and 7.6°, respectively. The ferrocenyl substituents on each ligand are *transoid*. The dihedral angles between the planes C6−C7−C8−C9−C10 and C10−C11−N1, C15−C16−C17−C18−C19 and C15−C14−N2, C39−C40−C41−C42−C43 and C39−C38−N4, and C30−C31−C32−C33−C34 and C34−C35−N3 are 4.2°, 14.6°, 26.3° and 10.6°, respectively, i.e., the ferrocenyl fragments are not coplanar with the L aldimine groups, unlike those in $[ZnCl_2(L)]$.[14] The intramolecular Ag1···Fe1, Ag1···Fe2, Ag1···Fe3, and Ag1···Fe4 distances are 4.772, 4.974, 4.813 and 5.011 Å, respectively, while the Fe1···Fe4, Fe1···Fe3, Fe2···Fe3, and Fe2···Fe4 distances are 6.634, 6.892, 7.153 and 6.977 Å, respectively.

The bond lengths and angles of the nitrate anion are as expected. The average N−O bond length is 1.132 Å, while the average intra-anion angle is 119.9°. The O2 and O3 atoms contribute to the packing by forming hydrogen bonds with crystallization molecules of methanol and ethanol, i.e. two hydrogen bonds arise from the interaction of the OH units in methanol and ethanol with O atoms of the nitrate anion (Figure 2).

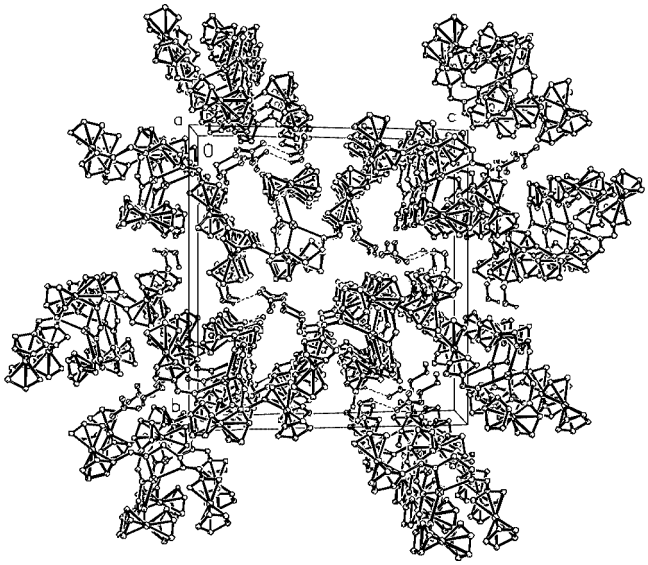

Figure 2. Crystal packing, viewed from the *a* axis, of $[Ag(L)_2](NO_3)\cdot(MeOH)\cdot(EtOH)$

Crystal Structure of $[HgI_2(L)]$ (2)

An X-ray diffraction analysis of **2** shows that a twofold axis exists in the molecular structure (Figure 3). The center Hg^{II} ion is coordinated by two nitrogen atoms of L and two iodine atoms, forming a distorted tetrahedral geometry, in contrast with the pseudo-tetrahedral zinc(II) center of $[ZnCl_2(L)]$.[14] The bond lengths of Hg−N and Hg−I are 2.392(6) and 2.6701(8) Å, respectively, which are close to

 © 2003 Wiley-VCH Verlag GmbH & Co. KGaA, Weinheim

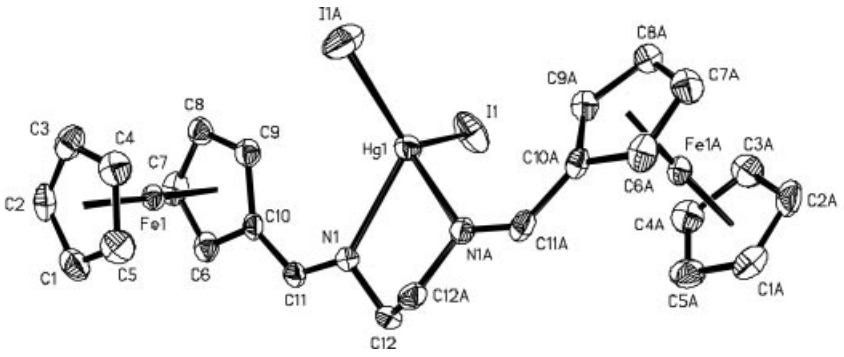

Figure 3. ORTEP drawing with atom-labeling scheme of $[HgI_2(L)]$

those of the reported coordination polymer $\{HgI_2[bpmp]_n\}$ [bpmp = *N*,*N*′-bis(4-pyridylmethyl)piperazine].[16] It is interesting that the acute N1−Hg1−N1A angle [74.5(3)°] was enforced by L as is the case for **1**. The widest bond angle around Hg1 is 128.29(4)°. Hence, the average bond angle at Hg^{II} is 107.5°, while the dihedral angle between the planes [Hg1, I1, I1A] and [Hg1, N1, N1A] is 76.7°. For $[ZnCl_2(L)]$ the reported N(1)−Zn(1)−N(2) bond angle is 84.3°, and the dihedral angle between [Zn(1), Cl(1), Cl(2)] and [Zn(1), N(1), N(2)] is 87.3°.

As with compound **1**, the ferrocenyl substituents are in a *transoid* arrangement and not coplanar with the L aldimine groups (the dihedral angle between the planes C6−C7−C8−C9−C10 and C10−C11−N1 is 11.0°). The cyclopentadienyl rings in each ferrocenyl fragment are planar and nearly parallel, with a dihedral angle of 2.2°. $Fe-C_{ring}$ distances range from 2.023(6) to 2.072(8) Å (average 2.04 Å) and intra-cyclopentadienyl C−C bond lengths lie in the range 1.400(12)−1.441(11) Å (average 1.42 Å); the C−C−C angles [average 108.0(5)°] of the ferrocenyl units are all similar to those reported in the literature.[15] The intermetallic distances Hg1···Fe1 and Fe1···Fe1A are 5.09 and 10.074 Å, respectively. The molecular packing is shown in Figure 4. The molecules are staggered, on viewing from the *c* axis, and the distance between neighboring Cp groups of different molecules is 3.622 Å, indicating π−π interactions. On the *ab* plane the molecules intercross.

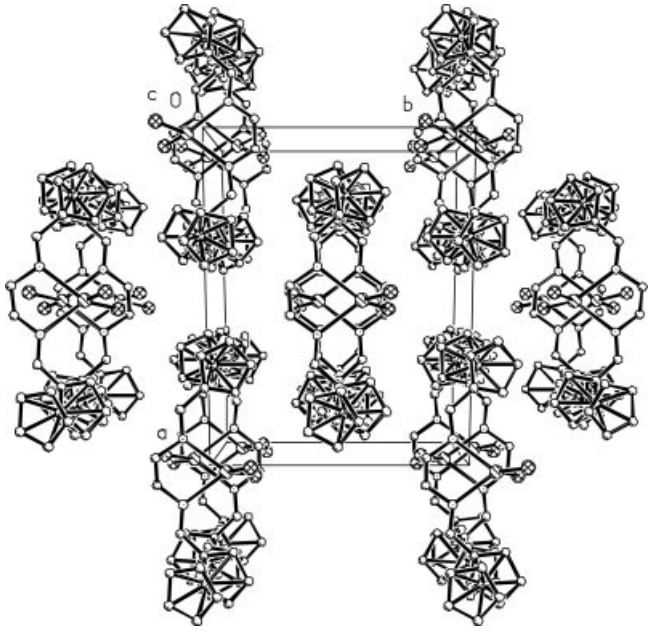

Figure 4. Crystal packing, viewed from the *c* axis, of $[HgI_2(L)]$

Spectroscopic Properties

The major IR peaks of the two compounds are consistent with the structural results. The characteristic IR bands of the ferrocenyl group at 3100 and 486 cm^{-1} due to ν(C−H) and ν(Fe−Cp) vibrations, respectively, are close to those of previously reported compounds.[11,15a] The imine stretching ν(C=N) shows a strong absorption at 1640 cm^{-1} in **1** and 1627 cm^{-1} in **2**. The strong absorption at 1384 cm^{-1} could be assigned to the N−O stretching mode of nitrate for **1**.

We found previously[17,18] that ferrocene exhibits two characteristic absorptions in the UV/Vis spectra at 440 nm (assigned to the $^1E_{1g}\leftarrow{}^1A_{1g}$ transition) and 325 nm (assigned to the $^1E_{2g}\leftarrow{}^1A_{1g}$ transition). Complexes **1** and **2** (in DMF) show three characteristic bands. The two absorptive peaks at 325 nm and 447 nm indicate a slight red-shift compared to free ferrocene. The effective bands at 275 nm of **1** and at 271 nm for **2** may be attributed to metal−ligand charge transfer (MLCT) transitions. Both compounds have a relatively low linear absorption, ranging from 500 to 1000 nm, promising low intensity loss and little temperature change due to photon absorption when light propagates in the materials.

The ^1H NMR spectra exhibit signals at δ = 8.49, 4.97, 4.53, 4.24−4.18, 3.72 ppm (for **1**) and 8.42, 4.83, 4.53, 4.30−4.27, 3.69 ppm (for **2**), which are similar to those of ligand L of δ = 8.19, 4.64, 4.36, 4.17, and 3.79 ppm.[12]

NLO Properties

The NLO determinations revealed that compounds **1** and **2** exhibit very strong nonlinear optical absorption and strong refractive effects.

 © 2003 Wiley-VCH Verlag GmbH & Co. KGaA, Weinheim

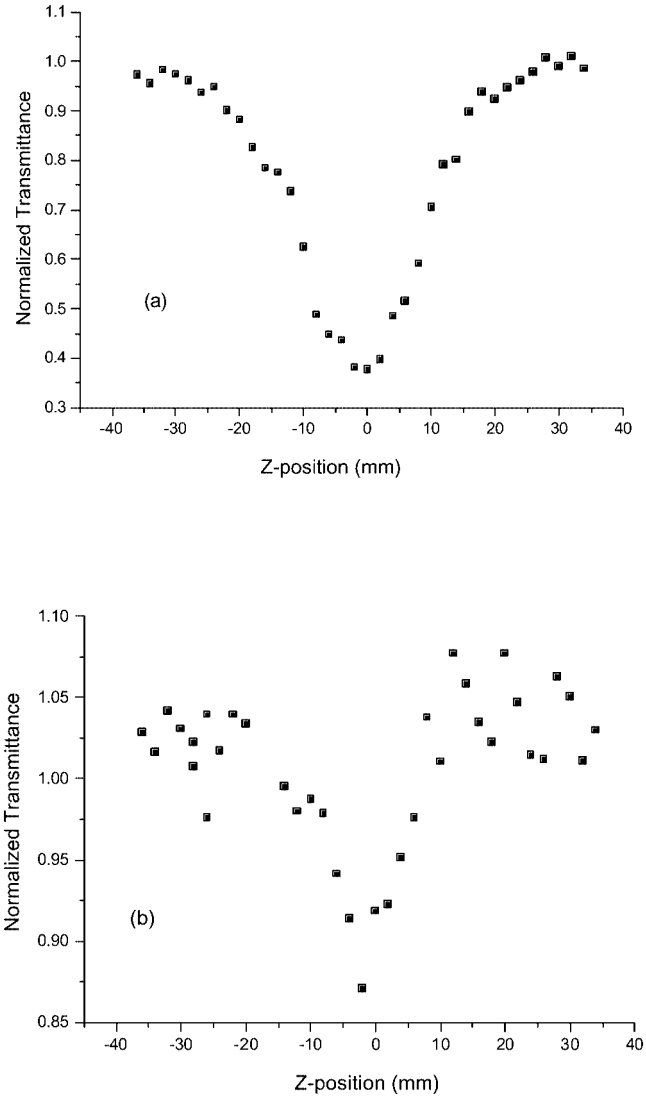

Figure 5. Data were collected under an open aperture configuration at 532 nm; (a; top) NLO absorptive behavior of $[Ag(L)_2](NO_3)\cdot(MeOH)\cdot(EtOH)$ in 8.5×10^{-4} mol·dm^{-3} DMF solution; (b; bottom) NLO absorptive behavior of $[HgI_2(L)]$ in 1.9×10^{-3} mol·dm^{-3} DMF solution

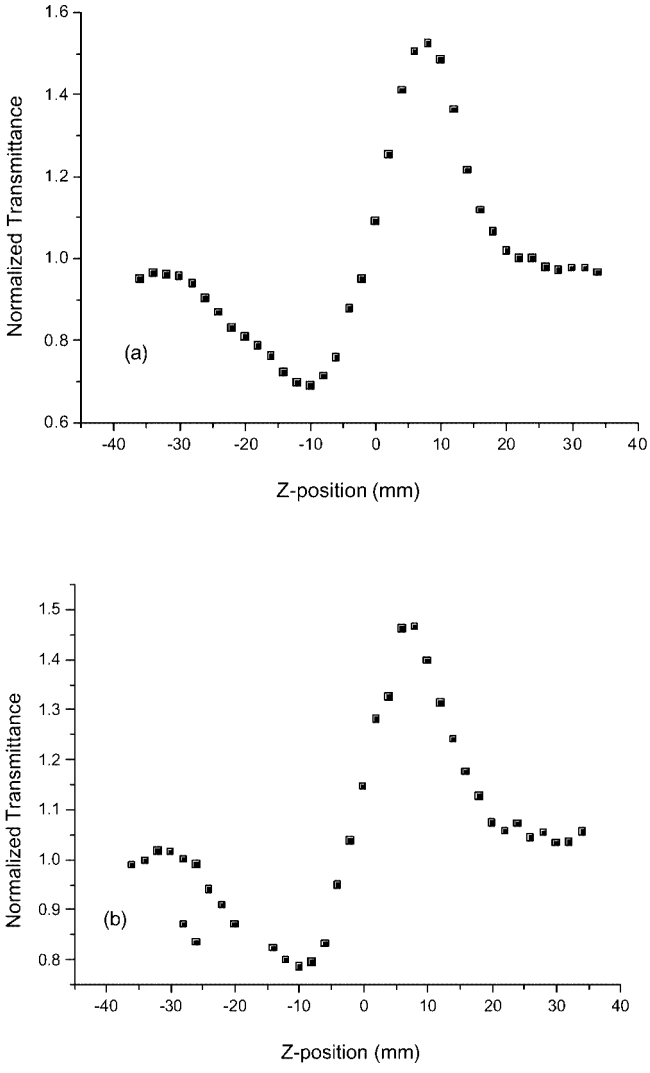

Figure 6. Data were assessed by dividing the normalized Z-scan data obtained under the closed aperture configuration by the normalized Z-scan data obtained under the open aperture configuration; self-focusing effects of (a; top) $[Ag(L)_2](NO_3)\cdot(MeOH)\cdot(EtOH)$ in 8.5×10^{-4} mol·dm^{-3} DMF solution at 532 nm and (b; bottom) $[HgI_2(L)]$ in 1.9×10^{-3}mol·dm^{-3} DMF solution at 532 nm

Figure 5(a and b) depict the NLO absorptive properties of complexes **1** and **2**, respectively. In Figure 5(a) the normalized transmittance drops to about 36% at the focus, showing that **1** has a strong NLO absorptive effect. The third-order NLO absorptive coefficient α_2 is 1.34×10^{-8} m W^{-1}. In Figure 5(b), the normalized transmittance of **2** drops to about 86% at the focus, and the corresponding α_2 value is 3.1×10^{-9} m W^{-1}. The NLO parameters of some known compounds are listed in Table 3, which shows that both **1** and **2** exhibit very strong NLO absorption, and that the α_2 values are larger than those of the reported compounds.[19−23]

Figure 6(a and b) give the NLO refractive effects of the two complexes; they have a similar positive sign for the refractive nonlinearity, which gives rise to self-focusing behavior. Figure 6(a) shows that the difference between valley-peak positions, $\Delta Z_{V\text{-}P}$, is 19 mm, and the difference between normalized transmittance values at valley and peak portions, $\Delta T_{V\text{-}P}$, is 0.86. The refractive index n_2 of **1** is calculated to be 1.15×10^{-18} m^2 W^{-1}. According to Figure 6(b), $\Delta Z_{V\text{-}P}$ and $\Delta T_{V\text{-}P}$ are 16 mm and 0.70, respectively, so that $n_2 = 8.02 \times 10^{-19}$ m^2 W^{-1} is obtained for **2**. Thus, both **1** and **2** have strong self-focusing behavior; similar refractive effects have been found for the clusters $MoCu_2OS_3(PPh_3)_3$, $WCu_2OS_3(PPh_3)_4$ and $W_2Ag_4S_8(AsPh_3)_4$.[20,23]

In accordance with the α_2 and n_2 values, the third-order susceptibility $\chi^{(3)}$ values can be calculated from $|\chi^{(3)}| = (|(9 \times 10^8 \varepsilon_0 n_0^2 c^2 \alpha_2)/2\nu|^2 + |c n_0^2 n_2/80\pi|^2)^{1/2}$. The $\chi^{(3)}$ values are 4.11×10^{-12} esu for **1** and 2.87×10^{-12} esu for **2**. From the discussions above, we can, reasonably, state that complexes **1** and **2** have similar NLO properties. Most high-performance NLO chromophores, organic polymers[24−30] and semiconductors[24−26] are neat materials. Impressive NLO values for ferrocenyl Schiff-base complexes are

 © 2003 Wiley-VCH Verlag GmbH & Co. KGaA, Weinheim

achieved with a much diluted solution, and much superior NLO performance can be expected if the solubilities can be improved significantly. We can use the hyperpolarizability γ to represent the NLO properties of neat materials; $\gamma = \chi^{(3)}/NF^4$, where N is the number density of a ferrocenyl complex in the sample (in cm^{-3}), and $F^4 = 3$ is the local field correction factor. Thus γ for compounds **1** and **2** are calculated to be 2.68×10^{-30} and 1.44×10^{-30} esu, respectively.

Molecules possessing extensively conjugated π-electron systems exhibit large optical nonlinearities, especially third-order as described by the second hyperpolarizability, γ.[31] The γ values of aryl and vinyl of ferrocene increase strongly with the length of the conjugated π-electron system (ranging from $1.61 \pm 0.18 \times 10^{-35}$ to $1.550 \pm 0.270 \times 10^{-33}$ esu).[31] Compared with the ferrocene derivatives, the γ values of ferrocenyl complexes **1** and **2** are several orders of magnitude larger. A reasonable explanation for this is that the ferrocenyl Schiff-base ligands in the title complexes bearing extended conjugated systems can influence the optical nonlinearity, and the heavy transition metals (Ag, Hg and Fe) may contribute to the optical nonlinearity due to the tailorability of the metal−ferrocenyl ligand interactions. The γ values of our complexes are also similar to those of the ferrocenyl complexes 1,8-bis(ferrocenyl)octatetrayne[32] and NiL^2_2 and PdL^2_2 [L^2 = $FcC(CH_3)=N_2HCS_2CH_2C_6H_5$].[33] To our knowledge, there have been no reports on third-order NLO properties of diferrocenyl Schiff-base complexes. We believe that our explorations may provide a useful channel to seek new third-order NLO materials.

Experimental Section

General: All chemicals were of reagent-grade quality obtained from commercial sources and used without further purification. 1,2-Bis[(ferrocen-l-ylmethylene)amino]ethane (L) was prepared according to the literature method.[12] IR data were recorded with a Nicolet NEXUS 470-FTIR spectrophotometer with KBr pellets in the 400−4000 cm^{-1} region. UV/Vis spectra were performed with an HP 8453 spectrophotometer. Elemental analyses (C, H and N) were carried out with a Carlo−Erba1106 Elemental Analyzer. ^{1}H NMR spectra were recorded at room temperature with a Bruker DPX 400 spectrometer.

Synthesis of $[Ag(L)_2](NO_3)\cdot(MeOH)\cdot(EtOH)$ (1): A solution of L (90.3 mg, 0.20 mmol) in ethanol (3 mL) was added dropwise to a solution of $AgNO_3$ (17.0 mg, 0.10 mmol) in methanol (2 mL). The resulting solution was allowed to stand at room temperature in the dark. Dark-red crystals suitable for X-ray single crystals analysis were obtained over 24 h. Yield: 66.1 mg (61%). Crystals of **1** are unstable in the air. IR: $\tilde{\nu}$ = 2830 m, 1640 s, 1384 s, 1247 m, 1104 m, 1013 m, 819 m, 518 m, 510 m, 486 m cm^{-1}. $C_{51}H_{58}AgFe_4N_5O_5$ (1152.3): calcd. C 53.11, H 5.03, N 6.07; found C 52.45, H 4.80, N 6.21. ^{1}H NMR (400 MHz, DMSO): δ = 8.49 (s, 4 H, N=CH), 4.97 (s, 8 H, C_5H_4), 4.53 (s, 8 H, C_5H_4), 4.24−4.18 (s, 20 H, C_5H_5), 3.72(s, 8 H, CH_2).

Synthesis of $[HgI_2(L)]$ (2): L (90.3 mg, 0.20 mmol) in ethanol (3 mL) was slowly added to a solution of HgI_2 (45.60 mg; 0.1 mmol) in DMSO (2 mL) at room temperature. After allowing the resulting mixture to stand in the dark for 2 d, dark-red crystals of **2** suitable for X-ray structure determination were formed. Yield 52.2 mg (57%). **2** is air-stable. IR: $\tilde{\nu}$ = 1627 s, 1437 m, 1371 m, 1254 m, 1105 m, 1030 m, 820 m, 510 m, 487 m cm^{-1}. $C_{24}H_{24}HgFe_2N_2I_2$ (906.6): calcd. C 31.77, H 2.65, N 3.09; found C 32.04, H 2.78, N 2.93. ^{1}H NMR (400 MHz, DMSO): δ = 8.42 (s, 2 H, N=CH), 4.83 (s, 4 H, C_5H_4), 4.53 (s, 4 H, C_5H_4), 4.30−4.27 (s, 10 H, C_5H_5), 3.69(s, 4 H, CH_2).

X-ray Crystallographic Study: Crystal data and experimental details for compounds **1** and **2** are contained in Table 1. All measurements were made with a Rigaku RAXIS-IV imaging plate area detector with graphite-monochromated Mo-K_α radiation (λ = 0.71073 Å). All data were collected at 291(2) K for **1** and 293(2) K for **2** using the ω-2θ scan technique and correction was applied for Lorenz polarization effects. A correction for secondary extinction was also applied. The two structures were solved by direct methods and ex-

Table 1. Crystal data and structure refinement for $[Ag(L)_2](NO_3)(MeOH)(EtOH)$ (**1**) and $[HgI_2(L)]$ (**2**)

	1	**2**
Empirical formula	$C_{51}H_{58}AgFe_4N_5O_5$	$C_{24}H_{24}Fe_2HgN_2I_2$
M	1152.29	906.54
Crystal system	monoclinic	monoclinic
Space group	$P2_1/n$	$C2/c$
a [Å]	12.382 (2)	15.726(3)
b [Å]	21.872(4)	11.809(2)
c [Å]	20.945(4)	14.326(3)
β [°]	102.64(3)	107.82(3)
V [Å^3]	5088.2(18)	2532.7(9)
$D_{calcd.}$ [mg m^{-3}]	1.504	2.377
T [K]	291(2)	293(2)
Z	4	4
μ(Mo-K_α) [mm^{-1}]	1.541	9.629
Reflections; unique; R(int)	8728; 5583; 0.0546	4371; 2447; 0.0498
Data; restraints; parameters	5583; 61; 597	2447; 0; 150
Goodness-of-fit on F^2	1.136	1.079
Final R,[a] Rw,[b] [$I > 2\sigma(I)$]	0.0891, 0.1999	0.0429, 0.0789
R (all data)	0.1674, 0.2313	0.0559, 0.0828

[a] $R = \Sigma||F_o| - |F_c||/\Sigma|F_o|$. [b] $Rw = [\Sigma(||F_o| - |F_c||)^2/\Sigma w|F_o|^2]^{1/2}$.

 © 2003 Wiley-VCH Verlag GmbH & Co. KGaA, Weinheim

Table 2. Selected bond lengths [Å] and bond angles [°] for **1** and **2**
Symmetry transformations used to generate equivalent atoms: #1 $-x+1$, y, $-z+/2$.

$[Ag(L)_2](NO_3)(MeOH)(EtOH)$ (**1**)			
Ag(1)−N(3)	2.277(8)	N(5)−O(2)	1.087(16)
Ag(1)−N(2)	2.330(7)	N(5)−O(1)	1.105(12)
Ag(1)−N(4)	2.357(7)	N(5)−O(3)	1.205(16)
Ag(1)−N(1)	2.397(8)	N(2)−C(14)	1.265(11)
N(1)−C(12)	1.478(10)	C(14)−C(15)	1.448(13)
N(2)−C(13)	1.519 (11)	N(1)−C(11)	1.294(12)
C(12)−C(13)	1.491 (13)	C(11)−C(10)	1.470(14)
N(3)−C(36)	1.408(12)	N(3)−C(35)	1.224(13)
C(36)−C(37)	1.400(12)	N(4)−C(38)	1.295(11)
N(4)−C(37)	1.481 (12)	C(38)−C(39)	1.422(13)
C(35)−C(34)	1.706(18)		
N(3)−Ag(1)−N(2)	130.6(3)	N(3)−Ag(1)−N(1)	128.0(3)
N(3)−Ag(1)−N(4)	77.1(3)	N(2)−Ag(1)−N(1)	77.7(3)
N(2)−Ag(1)−N(4)	126.1(3)	N(4)−Ag(1)−N(1)	125.22(3)
Ag(1)−N(1)−C(12)	104.2(6)	Ag(1)−N(2)−C(13)	106.5(5)
Ag(1)−N(3)−C(36)	111.9(6)	Ag(1)−N(4)−C(37)	106.9(6)
$[HgI_2(L)]$ (**2**)			
Hg(1)−N(1)	2.392(6)	Hg(1)−I(1)	2.6701(8)
N1−C11	1.285(8)	C12−C12#1	1.530(17)
N1−C12	1.459(9)	C10−C11	1.436(10)
N(1)−Hg(1)−N(1)#1	74.5(3)	N(1)−Hg(1)−I(1)#1	118.18(13)
N(1)−Hg(1)−I(1)	102.82(14)	N(1)#1−Hg(1)−I(1)#1	102.82(14)
N(1)#1−Hg(1)−I(1)	118.18(13)	I(1)−Hg(1)−I(1)#1	128.29(4)
C10−C11−N1	126.1(7)	N1−C12−C12#1	109.5(5)
C11−N1−Hg1	132.2(5)	C12−N1−Hg1	108.1(4)
C11−N1−C12	119.3(6)	C11−C10−C9	129.5(6)
C11−C10−C6	1236.6(7)		

Table 3. Optical parameters of selected NLO chromophores

Compounds	C [mol·dm^{-3}]	α_2 [m W^{-1}]	n_2 [m^2 W^{-1}]	$\chi^{(3)}$ [esu]	γ [esu]	Ref.
Cluster compounds:						
$WOS_3Cu_3(SCN)(Py)_5$	1.9×10^{-5}	6.0×10^{-11}	-1.2×10^{-17}	8.0×10^{-11}	2.2×10^{-27}	[19]
$MoOS_3Cu_3(SCN)(Py)_5$	2.0×10^{-5}	4.8×10^{-10}	-6.8×10^{-17}	2.0×10^{-10}	5.8×10^{-27}	[19]
$MoCu_2OS_3(PPh_3)_3$	7.4×10^{-5}	2.6×10^{-10}	5.0×10^{-17}	1.2×10^{-10}	9.8×10^{-28}	[20]
$WCu_2OS_3(PPh_3)_4$	1.2×10^{-4}		8.0×10^{-18}	2.0×10^{-11}	9×10^{-29}	[20]
$[Et_4N]_4[Mo_2O_2S_6Cu_6I_6]$	2.0×10^{-3}	4.0×10^{-10}	-6.0×10^{-17}			[21]
$[MoI(bPy)_2][MoOS_3Cu_3I_2(bPy)]$	3.4×10^{-5}	3.0×10^{-10}	-3.0×10^{-17}			[22]
$[WI(bPy)_2][MoOS_3Cu_3I_2(bPy)]$	4.8×10^{-5}	1.0×10^{-9}				[22]
$[MoOS_3Cu_3I(bMe\text{-}bPy)_2]$	2.4×10^{-5}	3.5×10^{-10}				[22]
$W_2Ag_4S_8(AsPh_3)_4$	1.3×10^{-4}	2.8×10^{-9}	5.9×10^{-17}	1.7×10^{-10}		[23]
Organic polymers:						
PA	neat			5.0×10^{-10}		[24−26]
PDA-PTS	neat			8.5×10^{-10}		[24−26]
PDA-4BCMU	neat			1.8×10^{-10}		[24−26]
Polyarylenes	neat			10^{-11} το 10^{-9}		[27]
σ-Conjugated polymers	neat			10^{-12} το 10^{-11}		[28,29]
Organic ladder polymers	neat			10^{-11} το 10^{-10}		[30]
Semiconductors:						
GaAs	neat			4.8×10^{-11}		[24−26]
Ge	neat			4.0×10^{-10}		[24−26]
Ferrocenyl complexes:						
1,8-Bis(ferrocenyl)octatetrayne					1.10×10^{-32}	[32]
NiL^2_2 (L^2=FcC(CH_3)=$N_2HCS_2CH_2C_6H_5$)				1.60×10^{-12}	2.71×10^{-33}	[33]
PdL^2_2				2.14×10^{-12}	3.06×10^{-33}	[33]
Ferrocene					$1.61 \pm 0.18 \times 10^{-35}$	[31]
Ferrocenecarboxaldehyde					$1.69 \pm 0.08 \times 10^{-35}$	[31]
$FcCH{=}CHC_6H_5$					$8.55 \pm 1.98 \times 10^{-35}$	[31]
1,1′−$Fc(CH{=}CHC_6H_5)_2$					$2.70 \pm 0.26 \times 10^{-34}$	[31]
$OHC(-FcCH{=}CHC_6H_5CH{=}CH-)_n$					$1.55 \pm 0.27 \times 10^{-33}$	[31]
$[Ag(L)_2](NO_3)$·(MeOH)·(EtOH) (**1**)	8.5×10^{-4}	1.34×10^{-8}	1.15×10^{-18}	4.11×10^{-12}	2.68×10^{-30}	this work
$[HgI_2(L)]$ (**2**)	1.1×10^{-3}	3.1×10^{-9}	8.02×10^{-19}	2.87×10^{-12}	1.44×10^{-30}	this work

 © 2003 Wiley-VCH Verlag GmbH & Co. KGaA, Weinheim

panded using the Fourier technique. The non-hydrogen atoms were found by successive full-matrix least-squares refinement on F^2 and refined with anisotropic thermal parameters. Hydrogen atoms were included but not refined. All calculations were performed using the SHELX-97 crystallographic software package.[34] Selected bond lengths and bond angles are listed in Table 2. CCDC-178522 (**1**) and -178521 (**2**) contain the supplementary crystallographic data for this paper. These data can be obtained free of charge at www.ccdc.cam.ac.uk/conts/retrieving.html [or from the Cambridge Crystallographic Data Centre, 12 Union Road, Cambridge CB2 1EZ, UK; Fax: (internat.) + 44-1223/336-033; E-mail: deposit@ccdc.cam.ac.uk].

NLO Measurements: The third-order NLO properties were measured by the Z-scan technique[35] with a 532-nm laser pulse of 8 ns duration in a solution of 8.5×10^{-4} mol·dm^{-3} (for **1**) and 1.1×10^{-3} mol·dm^{-3} (for **2**) (the different concentrations are due to the different solubilities of the two complexes in DMF). The NLO absorption components were evaluated by a Z-scan experiment under an open-aperture configuration. Light transmittance (T) is a function of incident light irradiance $I_i(Z)$, nonlinear absorption [$\alpha_2 = \alpha_2(I_i)$], and linear absorption (α_0) as illustrated in Equations (1) and (2).[35b] The NLO absorption data of the two complexes can be well represented by Equations (1) and (2), where Z is the distance of the sample from the focal point; α_0 and α_2 are the linear and nonlinear absorption coefficients, respectively; L is the sample thickness (1 mm in this study); I_0 is the peak irradiation intensity at focus; $Z_0 = \pi\omega_0^2/\lambda$ where ω_0 is the spot radius of the laser beam at focus, and λ is the wavelength of the laser; r is the radial coordinate; t is the time; and t_0 is the pulse width.

$$T(Z) = \frac{1}{\sqrt{\pi}q(Z)} \int_{-\infty}^{+\infty} In[1+q(Z)]e^{-\tau^2} d\tau \quad (1)$$

$$q(Z) = \int_0^{\infty}\int_0^{\infty} \alpha_2 \frac{I_0}{1+(Z/Z_0)^2} e^{[-2(r/\omega_0)^2-(t/t_0)^2]} \frac{1-e^{-\alpha_0 L}}{\alpha_0} rdrdt \quad (2)$$

The NLO refractive effects were assessed by dividing the normalized Z-scan data obtained under the closed-aperture configuration by the normalized Z-scan data obtained under the open aperture configuration. An effective third-order NLO refractive index n_2 can then be derived by Equation (3), where $\Delta T_{V\text{-}P}$ and is the difference between normalized transmittance values at valley and peak positions; I is the peak irradiation intensity at focus. Table 3 gives the γ values of some reported NLO materials.

$$n_2 = \frac{\lambda\alpha_0}{0.812\pi I(1-e^{-\alpha_0 L})} \Delta T_{V-P} \quad (3)$$

Acknowledgments

The authors thank the National Natural Science Foundation of China, Outstanding Young Teacher Foundation of Ministry of Education of China and the Outstanding Younger Foundation of Henan Province for financial support.

[1] A. Togni, T. Hayashi, *Ferrocenes. Homogenous Catalysis, Organic Synthesis, Materials Science*, VCH, Weinheim, Germany, **1995**.
[2] R. W. Wagner, P. A. Johnson, J. S. Lindsey, *J. Chem. Soc., Chem. Commun.* **1991**, 1463−1466.
[3] J. S. Miller, A. J. Epstein, *Angew. Chem. Int. Ed. Engl.* **1994**, *33*, 385−415.
[4] [4a] P. Nguyen, P. Gómez-Elipe, I. Manners, *Chem. Rev.* **1999**, *99*, 1515−1548. [4b] S. Barlow, D. O'Hare, *Chem. Rev.* **1997**, *97*, 637−669. [4c] D. R. Kanis, M. A. Ratner, T. J. Marks, *Chem. Rev.* **1994**, *94*, 195−242. [4d] N. J. Long, *Angew. Chem. Int. Ed. Engl.* **1995**, *34*, 21−38. [4e] T. Verbiest, S. Houbrechets, M. Kaurann, K. Clays, A. Persoons, *J. Mater Chem.* **1997**, *7*, 2175−2189. [4f] I. Cuadrado, M. Morán, C. M. Casado, B. Alonso, J. Losada, *Coord. Chem. Rev.* **1999**, *193−195*, 395−445. [4g] G. G. A. Balavione, J.-C. Daran, G. Iftime, P. G. Lacroix, E. Manoury, J. A. Delaire, I. Maltey-Fanton, K. Nakatani, S. D. Bella, *Organometallics* **1999**, *18*, 21−29. [4h] M. Blanchard-Desce, C. Runser, A. Fort, M. Barzoukas, J. M. Lehn, V. Alain, *Chem. Phys.* **1995**, *199*, 253−261.
[5] M. L. H. Green, S. R. Marder, M. E. Thompson, J. A. Bandy, D. Bloor, P. V. Kolinsky, R. J. Jones, *Nature* **1987**, *330*, 360−362.
[6] A. Houlton, N. Jassim, R. M. G. Roberts, J. Silver, P. McArdle, T. Higgins, *J. Chem. Soc., Dalton Trans.* **1992**, 2235−2241.
[7] I. Ratera, D. Ruiz-Molina, C. Sánchez, R. Alcalá, C. Rovira, J. Veciana, *Synth. Met.* **2001**, *121*, 1834−1835.
[8] J. Silver, J. R. Miler, A. Houlton, M. T. Ahmet, *J. Chem. Soc., Dalton Trans.* **1994**, 3355−3360.
[9] A. Houlton, J. R. Miler, J. Silver, N. Jassim, M. T. Ahmet, T. L. Axon, D. Bloor, G. H. Cross, *Inorg. Chim. Acta* **1993**, *205*, 67−70.
[10] S. K. Pal, A. Krishnan, P. K. Das, A. G. Samuelson, *J. Organomet. Chem.* **2000**, *604*, 248−259.
[11] E. W. Nause, M. G. Meirim, N. F. Blom, *Organometallics* **1988**, *7*, 2562−2565.
[12] A. Benito, J. Cano, R. Martínez-Máñez, J. Soto, J. Payá, F. Lloret, M. Julve, J. Faus, M. D. Marcos, *Inorg. Chem.* **1993**, *32*, 1197−1203.
[13] O. Knoesen, H. Görls, S. Lotz, *J. Organomet. Chem.* **2000**, *598*, 108−115.
[14] P. Li, I. J. Scowen, J. E. Davies, M. A. Halcrow, *J. Chem. Soc., Dalton Trans.* **1998**, 3791−3799.
[15] [15a] E. R. Lippincott, R. D. Nelson, *Spectrochim. Acta* **1958**, *10*, 307−309. [15b] F. Takusagawa, T. F. Koetzle, *Acta Crystallogr., Sect. B* **1979**, *35*, 2888−2896.
[16] Y. Y. Niu, H. W. Hou, Y. L. Wei, Y. T. Fan, Y. Zhu, C. X. Du, X. Q. Xin, *Inorg. Chem. Commun.* **2001**, *4*, 358−361.
[17] Y. S. Sohn, D. N. Hendrickson, H. B. Gray, *J. Am. Chem. Soc.* **1971**, *93*, 3603−3612.
[18] A. T. Armstrong, A. T. Smith, E. Elder, S. P. McGlynn, *J. Chem. Phys.* **1967**, *46*, 4321−4328.
[19] H. W. Hou, H. G. Ang, S. G. Ang, Y. T. Fan, M. K. M. Low, W. Ji, Y. W. Lee, *Phys. Chem. Chem. Phys.* **1999**, *1*, 3145−3149.
[20] S. Shi, H. W. Hou, X. Q. Xin, *J. Phys. Chem.* **1995**, *99*, 4050−4053.
[21] H. W. Hou, D. L. Long, X. Q. Xin, X. X. Huang, B. S. Kang, P. Ge, W. Ji, S. Shi, *Inorg. Chem.* **1996**, *35*, 5363−5367.
[22] H. W. Hou, H. G. Ang, S. G. Ang, Y. T. Fan, M. K. M. Low, W. Ji, Y. W. Lee, *Inorg. Chim. Acta* **2000**, *299*, 147−154.
[23] G. Sakane, T. Shibahare, H. W. Hou, X. Q. Xin, S. Shi, *Inorg. Chem.* **1995**, *34*, 4785−4789.
[24] J. L. Bredas, C. Adant, P. Tackx, A. Persoons, B. M. Pierce, *Chem. Rev.* **1994**, *94*, 243−278.
[25] H. Nakanishi, *Nonlinear Optics* **1991**, *1*, 223−226.
[26] T. Kobayashi, *IEICE Trans. Fundam.* **1992**, *E75-A*, 38−45.
[27] D. A. Halliday, P. L. Burn, D. D. C. Bradley, R. H. Friend, O. M. Gelsen, A. B. Holmes, A. Kraft, J. H. F. Martens, K. Pichler, *Adv. Mater.* **1993**, *5*, 40−44.
[28] F. Kajzar, J. Messier, C. Rosilio, *J. Appl. Phys.* **1986**, *60*, 3040−3044.
[29] F. Schellenberg, R. L. Byer, R. D. Miller, *Chem. Phys. Lett.* **1990**, *166*, 331−339.
[30] L. Yu, D. W. Polis, M. R. McLean, L. R. Dalton, *In Electroresponsive Molecular and Polymeric Systems* (Ed.: T. A. Skotheim), Marcel Dekker, New York, **1991**, vol. 2.

 © 2003 Wiley-VCH Verlag GmbH & Co. KGaA, Weinheim

[31] S. Ghosal, M. Samoc, P. N. Prasad, J. J. Tufariello, *J. Phys. Chem.* **1990**, *94*, 2847−2851.
[32] Z. Yuan, G. Stringer, I. R. Jobe, D. Kreller, K. Scott, L. Koch, N. J. Taylor, T. B. Marder, *J. Organomet. Chem.* **1993**, *452*, 115−120.
[33] Y. P. Tian, Z. L. Lu, X. Z. You, *Acta Chim. Sin. (Chin. Ed.)* **1999**, *57*, 1068−1074.
[34] [34a] G. M. Sheldrick, *SHELXS-97*, University of Göttingen, Germany, **1997**; G. M. Sheldrick, *Acta Crystallogr., Sect. A* **1990**, *46*, 467−473. [34b] G. M. Sheldrick, *SHELXL-97*, University of Göttingen, Germany, **1997**.
[35] [35a] H. W. Hou, X. Q. Xin, J. Liu, M. Q. Chen, S. Shi, *J. Chem. Soc., Dalton Trans.* **1994**, 3211−3214. [35b] M. Sheik-Bahae, A. A. Said, T. H. Wei, D. J. Hagan, E. W. Van Stryland, *IEEE J. Quant. Electron.* **1990**, *26*, 760−769.

Received November 12, 2003

 © 2003 Wiley-VCH Verlag GmbH & Co. KGaA, Weinheim

Synthesis, Crystal Structure, and Electrical Properties of Novel Radical Cation Salts of Iodine-Substituted TTF-Derived Donors with the Nitroprusside Anion Exhibiting Strong -I···NC- Interactions

Kazumasa Ueda,*[a] Toyonari Sugimoto,[b] Christophe Faulmann,[a] and Patrick Cassoux[a]

Keywords: Cations / Radical ions / Fulvalenes / Conducting materials

Radical-cation salts of iodine-substituted TTF derivatives [diiodoethylenedithiotetrathiafulvalene (**1**) diiodoethylenedithiodiselenadithiafulvalene (**2**), or iodoethylenedithiotetrathiafulvalene (**3**)] with the $[Fe(CN)_5NO]^{2-}$ nitroprusside anion, namely, $\mathbf{1}_4$·$[Fe(CN)_5NO]$, $\mathbf{2}_4$·$[Fe(CN)_5NO]$ and $\mathbf{3}_3$·$[Fe(CN)_5NO]$, were synthesized by electrocrystallization from solutions of the appropriate TTF derivative in CH_2Cl_2 with bis(tetraphenylphosphonium)nitroprusside $[(PPh_4)_2\{Fe(CN)_5NO\}]$ as electrolyte. An X-ray structure analysis indicates that the crystal structures of $\mathbf{1}_4$·$[Fe(CN)_5NO]$ and $\mathbf{2}_4$·$[Fe(CN)_5NO]$ are very similar. In both cases, molecules **1** and **2** are stacked along the *c* direction, with their long molecular axis parallel to each other. By contrast, in $\mathbf{3}_3$·$[Fe(CN)_5NO]$, molecules **3** are stacked in triad units in which two of the molecules are arranged in a face-to-face fashion and the remaining molecule is arranged in a head-to-tail fashion with respect to its neighboring molecules. In all cases, several effective iodine-nitrogen contacts between donor molecules and $[Fe(CN)_5NO]^{2-}$ anions are observed. The room temperature electrical conductivities of $\mathbf{1}_4$·$[Fe(CN)_5NO]$, $\mathbf{2}_4$·$[Fe(CN)_5NO]$ and $\mathbf{3}_3$·$[Fe(CN)_5NO]$ are $<10^{-6}$, 2.2×10^{-2} and 5 S cm^{-1}, respectively. The temperature dependence of the electrical conductivity of $\mathbf{3}_3$·$[Fe(CN)_5NO]$ reveals semiconducting behavior with a small activation energy of 30 meV. The temperature dependence of the electrical conductivity of $\mathbf{2}_4$·$[Fe(CN)_5NO]$ also reveals a semiconducting behavior, but with two regimes: above 200 K the activation energy is 60 meV and becomes much smaller — 0.2 meV — below this temperature.

(© Wiley-VCH Verlag GmbH & Co. KGaA, 69451 Weinheim, Germany, 2003)

Introduction

Much current research is directed toward the formation of new molecular materials in which electrical conductivity coexists with other physical phenomena. One of the recent trends in this area is the combination of conducting and optical properties. In this area, the $[Fe(CN)_5NO]^{2-}$ anion ($[NP]^{2-}$) is of highest interest because it possesses extremely long-lived metastable states at low temperature that can be generated by laser irradiation.[1−6] It has been proposed that this electronic transition might be accompanied by possible changes in the geometry of the complex anion.[5] These changes may, in turn, affect the conducting properties of derived radical salts of organic donor molecules. In this context, the use of the $[NP]^{2-}$ anion and related transition metal mononitrosyl counteranions in radical cation salts of TTF- and TSF-derived donors (TTF = tetrathiafulvalene; TSF = tetraselenafulvalene) has been contemplated.[7−10] The existence of metastable states has indeed been detected in $(BEDT\text{-}TTF)_4$·$K[NP]_2$ [BEDT-TTF = bis(ethylenedithio)tetrathiafulvalene] and $(TTF)_7[NP]_2$ by DSC measurements,[10] but no effect of the above-mentioned changes of the geometry of the $[NP]^{2-}$ anion on the conducting behavior of these radical-cation salts has yet been observed. One, possibly more effective, approach for constructing novel photochromic organic conductors might consist of introducing a strong interaction between the donor molecules and the counteranions. In such systems, the changes in geometry of the excited states of the counteranions could affect the conducting properties more efficiently through stronger intermolecular interactions.

On the other hand, promoting a stronger interaction between the organic donor and the inorganic counteranions of radical salts is being investigated more and more for ensuring a better control of the molecular arrangement of these salts.[11−17] For example, radical salts of iodine-substituted TTF-derived donors such as diiodoethylenedithiotetrathiafulvalene (**1**) diiodoethylenedithiodiselenadithiafulvalene (**2**), or iodoethylenedithiotetrathiafulvalene (**3**) with cyano-group-containing anions such as $Ag[(CN)_2]^-$, $Pd[(CN)_4]^{2-}$, or with the $[Pd(mnt)_2]^{2-}$ anion (mnt = maleonitriledithiolate), have been synthesized and their crystal structures examined.[15−17] A PM3 MO calculation of **3** indicates a HOMO extended to the iodine atom. The largest

[a] Equipe Précurseurs Moléculaires et Matériaux, LCC/CNRS
205 route de Narbonne, 31077 Toulouse Cedex 04, France
Fax: (internat.) + 33-5/61553003
[b] Research Institute for Advanced Science and Technology, Osaka Prefecture University
Sakai, Osaka 599-8570, Japan
Fax: (internat.) + 81-722/54-9935
E-mail: kazueda@riast.osakafu-u.ac.jp

coefficient of the lowest unoccupied molecular orbital (LUMO) on the iodine atom suggests that it would be the driving force of the strong interactions with the cyano group. Extremely short I···N distances in the crystal structure of $\mathbf{3}_3$·[$Ag(CN)_4$], which are almost 20% shorter than the sum of the van der Waals radii (3.53 Å), arise from an interaction between the lone pair on the nitrogen atom and the p_π LUMO on the iodine atom.[15] In the crystal structure of $\mathbf{2}_4$·[$Pd(CN)_4$], reticulated donor···anion contacts were constructed using the strong and directional -I···NC- interaction.[16]

Combining both strategies, it was hoped that radical-cation salts of iodine-substituted organic donors and the $[NP]^{2-}$ anion could be organic conductors in which the existence of metastable states in the $[NP]^{2-}$ anion could affect the electrical conducting properties via possibly strong -I···NC- interaction.

Herein we report the synthesis, crystal structure and electrical conducting properties of novel radical-cation salts formed from the iodine-substituted donor molecules **1**, **2** and **3**, and the $[NP]^{2-}$ anion.

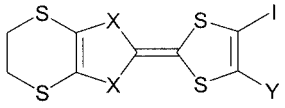

1: X = S, Y = I; **2**: X = Se, Y = I; **3**: X = S, Y = H

Results and Discussion

Synthesis

The iodine-substituted TTF-derived donors **1** and **3** were synthesized in accordance with the literature.[19] Compound **2** was synthesized by a modification of the method used for the preparation of **1** (see Exp. Sect.).

The salts $\mathbf{1}_4$·[$Fe(CN)_5NO$], $\mathbf{2}_4$·[$Fe(CN)_5NO$] and $\mathbf{3}_3$·[$Fe(CN)_5NO$], were synthesized by electro-crystallization from solutions of the appropriate iodine-substituted TTF-derived donors in CH_2Cl_2 with bis(tetraphenylphosphonium)nitroprusside [$(PPh_4)_2$·{$Fe(CN)_5NO$}] as electrolyte.

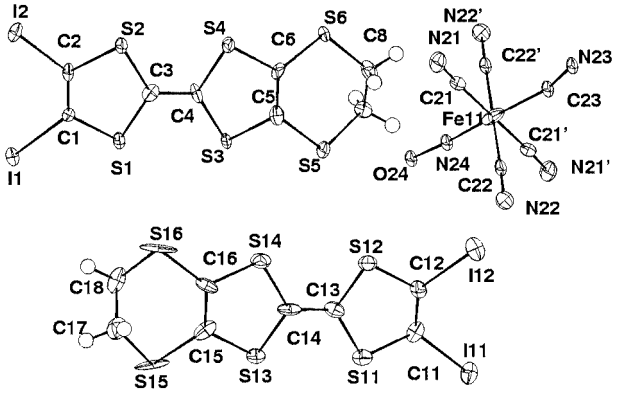

Figure 1. Atomic numbering scheme for $\mathbf{1}_4$·[NP]

Crystal Structures

1_4·[NP] and 2_4·[NP]

These two compounds are isostructural. The asymmetric unit (Figure 1 and 2) contains two donor molecules and half an [NP] entity, with the Fe atom lying on a center of inversion.

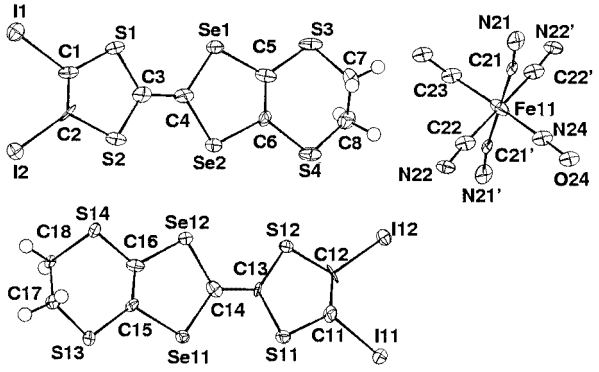

Figure 2. Atomic numbering scheme for $\mathbf{2}_4$·[NP]

Figure 3a and 3b show projections of the crystal structures of $\mathbf{1}_4$·[NP] and $\mathbf{2}_4$·[NP] down the *ab* plane. Their struc-

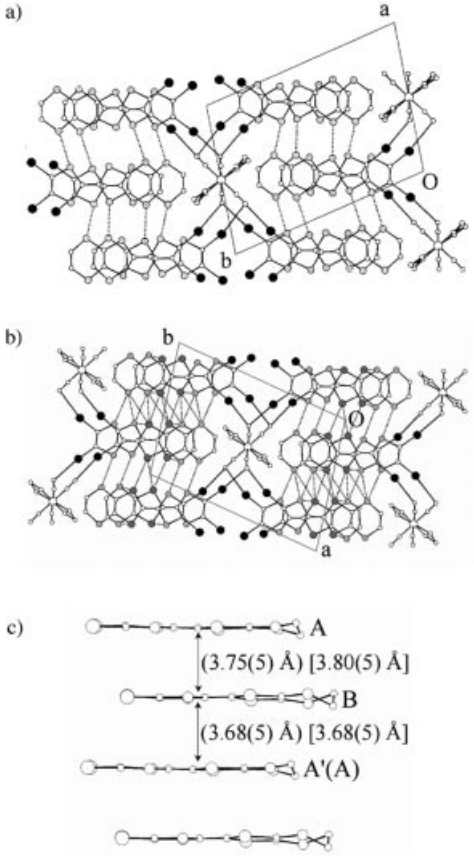

Figure 3. Projection down the *ab* plane for $\mathbf{1}_4$·[NP] (a) and $\mathbf{2}_4$·[NP] (b) and projection down the *bc* plane for both compounds (c). In Figure 3a and 3b, iodine, sulfur and selenium atoms are depicted with filled, light grey and dark grey circles, respectively. Thin dotted and solid lines show chalcogen-chalcogen and iodine-nitrogen intermolecular contacts, respectively

 © 2003 Wiley-VCH Verlag GmbH & Co. KGaA, Weinheim

tures consist of sheets of adjacent columns of donor molecules in the *ac* plane alternating with layer of anions along the *b* direction (Figure 3a and 3b). The donor molecules stack along the *c* direction, with their long molecular axis parallel to each other (Figure 3c). The inter-planar distances are 3.78(3) and 3.65(3) Å for $\mathbf{1}_4$·[NP], and 3.72(5) and 3.76(5) Å for $\mathbf{2}_4$·[NP] i.e., rather longer than the "π-cloud thickness".[18]

Since the $[NP]^{2-}$ ions are located at a center of symmetry, there is a positional disorder in the NO^+ and CN^- ligands. Two kinds of overlapping mode [**A/B** and **B/A′(A)**] are observed in $\mathbf{1}_4$·[NP], as shown in Figure 4, as well as in $\mathbf{2}_4$·[NP] (not shown).

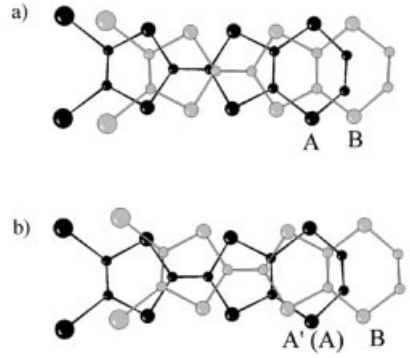

Figure 4. Modes of overlap of molecules **1** in $\mathbf{1}_4$·[NP]: (a) **A** and **B**, and (b) **B** and **A′(A)**

In both overlapping modes one molecule is stacked over the other molecule with a ring-over-bond type mode, since the molecules are slipped along their long axis.

Moreover, in $\mathbf{1}_4$·[NP], some effective side-by-side contacts are observed between donor molecules of adjacent columns. Indeed, interatomic distances rather shorter than the sum of the van der Waal's radii (3.70 Å) are observed between sulfur atoms of the ethylenedithio group and of the TTF moiety [S6···S11: 3.497(6); S2···S15: 3.536(6); S1···S16: 3.541(7); S14···S16: 3.601(8); S1···S5: 3.632(7) Å].

Even more importantly, several short contacts between the donor **1** and the $[NP]^{2-}$ anion through -I···NC- contacts are also observed, as indicated by several interatomic distances between iodine atoms of **1** and nitrogen atoms of the $[NP]^{2-}$ anion [I1···N22: 3.08(2); I2···N21: 3.11(1); I11···N22: 3.08(1); I12···N21: 3.25(2) Å], which are shorter than the sum (3.53 Å) of the van der Waals radii of the iodine and nitrogen atoms.

Due to the presence of Se atoms, $\mathbf{2}_4$·[NP] exhibits more contacts than $\mathbf{1}_4$·[NP]. The interaction between adjacent columns is accomplished through contacts between different sulfur atoms [S1···S1: 3.70(1); S2···S14: 3.59(1); S3···S11: 3.67(1); S4···S12: 3.55(1) and S11···S13: 3.66(1) Å], as well as between sulfur and selenium atoms [Se1···S3: 3.58(1) Å] and different selenium atoms [Se1···Se11: 3.67(1); Se2···Se2: 3.83(1); Se2···Se12: 3.67(1) and Se11···Se11: 3.77(1) Å], shorter than the sum of the corresponding van der Waals radii of the corresponding chalcogen atoms (3.70 Å for S···S, 3.80 Å for S···Se, and 3.90 for Se···Se). In addition, as for $\mathbf{1}_4$·[NP], several short interatomic distances [I1···N22: 3.25(3); I2···N21: 3.07(3); I11···N21: 3.07(3); I12···N22: 3.10(2) Å] are observed between the iodine atoms of **2** and nitrogen atoms of the $[NP]^{2-}$ anion.

$\mathbf{3}_3$·[NP]

The asymmetric unit (Figure 5) of $\mathbf{3}_3$·[NP] contains half an [NP] entity, with the Fe atom lying on a center of inversion, and two molecules of the donor **3**, among which one of the donor molecules (the one containing I11) has an occupancy of one half, since it is placed close to an inversion center.

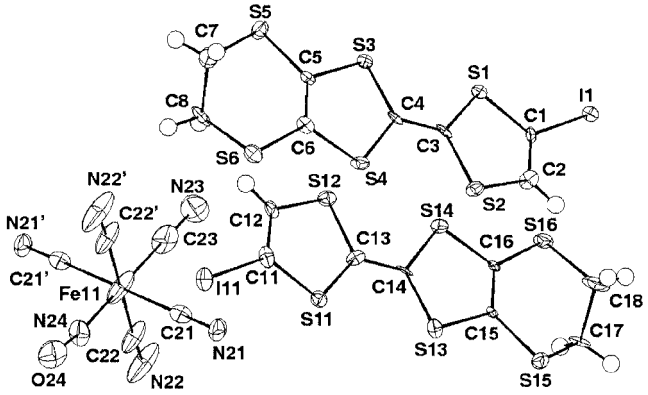

Figure 5. Atomic numbering scheme for $\mathbf{3}_3$·[NP]

Figure 6a and 6b shows the projections of the crystal structure down to the *bc* and *ab* planes. The structure consists of sheets of columns of **3** in the *ac* plane alternating with layers of $[NP]^{2-}$ anions along the *b* direction.

As shown in Figure 6b and 6c, the donor molecules **3** are stacked in a triad arrangement, ···**ABAABA**···. A **B** molecule is close to the center of symmetry, depicted as the gray circle, resulting in two orientations of the **B** molecule (**B** and **B′** generated by a symmetry operation of **B**) within a triad. Because of these two orientations of **B** molecules within the triad, there are two kinds of stacking mode: one of type **I** (shown at the top of Figure 6b and 6c), and the other of type **II** (shown at the bottom of Figure 6b and 6c). In the triad unit, two of the three molecules **3** (**A** and **B**) (type **I**), or **B′** and **A′′′** (type **II**) are arranged in a face-to-face fashion, whereas the remaining molecule (**A′** in type **I** and **A′′** in type **II**) is arranged in a head-to-tail fashion with respect to the **B** molecule (type **I**) or **B′** (type **II**). The inter-planar distances are 3.63(5) Å between the face-to-face molecules and 3.57(5) Å between the head-to-tail ones. The inter-planar distances are slightly longer than the "π-cloud thickness" (3.50 Å), but the [**A′/A"**] inter-planar distance between the triads is rather shorter [3.07(5) Å]. Figure 7a shows the overlap between the face-to-face molecules (**A** and **B** in mode **I**, or **B′** and **A′′′** in mode **II**). In this mode, **A** and **B** molecules are slipped transversally, resulting in a partial overlap of both molecules, but without any short S···S contacts.

In the head-to-tail mode (Figure 7b and **B/A′** or **A′′/B′** in Figure 6b and 6c), the molecules are slipped longitudinally,

 © 2003 Wiley-VCH Verlag GmbH & Co. KGaA, Weinheim

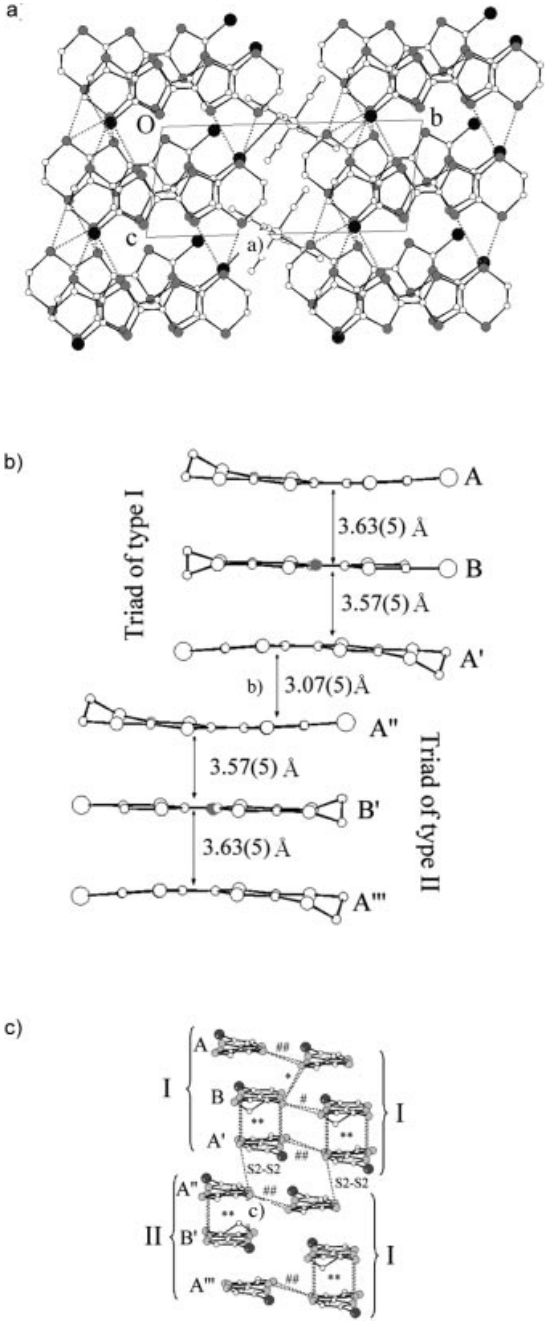

Figure 6. (a): Projection down the *bc* plane of $\mathbf{3}_3$·[NP]. Iodine and sulfur atoms are depicted with filled and grey circles, respectively. Dotted and solid lines show sulfur-sulfur and iodine-nitrogen contacts, respectively. (b): Projection down the *ab* plane showing the stacking modes of type **I** and **II** (the center of inversion is depicted as the grey circle). (c): Projection down the *ac* plane showing the S···S contacts between triads of type **I** and **II** (see text for the meaning of the symbols)

resulting in a ring-over-bond type overlap between these molecules. This configuration leads to several S···S contacts, depicted with the symbol ** in Figure 6c [S1···S14: 3.650(7); S2···S13: 3.43(3); S3···S12: 3.489(7) and S4···S11: 3.586(8) Å]. By contrast, the overlap between **A**′ and **A**′′ molecules belonging to different triads is minimal (one sulfur atom over a dithiacyclopentene ring; Figure 7c). **A**′ and **A**′′ are connected through one contact between the S2 atoms

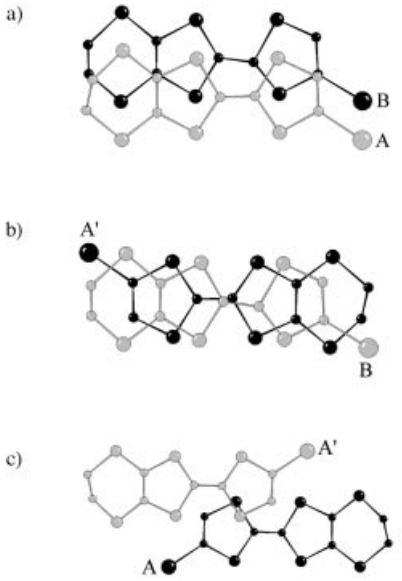

Figure 7. Modes of overlap in $\mathbf{3}_3$·[NP] between **A**/**B** (a), **B**/**A**′ (b), and **A**′/**A**′′ (c)

[3.502(4) Å]. Effective side-by-side contacts between sulfur atoms of adjacent triads are observed between **A** molecules [symbol ## in Figure 6c: S3···S6: 3.566(4); S5···S6: 3.427(5) Å], between **A** and **B** molecules [symbol * in Figure 6c: S3···S16: 3.551(7); S5···S16: 3.677(8) Å], and between **B** molecules when the adjacent triad is of the same nature [symbol # in Figure 6c: S13···S16: 3.49(1) and S15···S16: 3.37(1) Å]. Also, effective contacts between donor molecules and $[NP]^{2-}$ anions are observed, as indicated by short interatomic distances between the iodine atom of molecule **3** and nitrogen atoms of the $[NP]^{2-}$ anion [N21···I1: 2.93(1) and N22···I11: 3.51(2) Å].

In these three obtained salts, the I···N distances between the donor molecules and $[NP]^{2-}$ counterion are 8−18% shorter than the sum of the van der Waals radii of iodine and nitrogen atoms. These values indicate the existence of a strong interaction between the iodine atom of the donor molecules and a cyano group of the $[NP]^{2-}$ counterion. This strong interaction arises from an interaction between the lone pair on the nitrogen atom and the σ_p-LUMO on the iodine atom as is seen in the crystals of $\mathbf{3}_2$·$[Ag(CN)_2]$ and $\mathbf{2}_4$·$[Pd(CN)_4]$.[15,16]

Electrical Conductivity

The electrical conductivities of $\mathbf{1}_4$·[NP], $\mathbf{2}_4$·[NP] and $\mathbf{3}_3$·[NP] at room temperature are $<10^{-6}$, 2.2×10^{-2} and 5 S cm^{-1}, respectively. It should be noted that, although the structures of $\mathbf{2}_4$·[NP] and $\mathbf{1}_4$·[NP] are similar, the conductivity value determined for $\mathbf{2}_4$·[NP] is 10^4 times larger than that determined for $\mathbf{1}_4$·[NP]. This difference is likely to be due to the larger van der Waals radius of the selenium atom (2.00 Å), compared to that of the sulfur atom (1.85 Å), which induces interactions within the stack of $\mathbf{2}_4$·[NP] that are not observed in $\mathbf{1}_4$·[NP].

The temperature dependence of the resistivity was measured for $\mathbf{2}_4$·[NP] and $\mathbf{3}_3$·[NP] (Figure 8). In both cases the

 © 2003 Wiley-VCH Verlag GmbH & Co. KGaA, Weinheim

resistivity increases with decreasing temperatures, indicating a semiconducting behavior. In the case of $\mathbf{3}_3$·[NP], a small activation energy of 30 meV could be determined over the entire range (300−50 K) of temperatures. In contrast, two regimes are observed for $\mathbf{2}_4$·[NP]: from 293 K down to around 200 K the activation energy is 60 meV, and below 200 K a much smaller activation energy of 0.2 meV is found. The electrical conducting properties of these three salts can be readily understood by considering their crystal structures. The interplanar distances of **1** and **2** molecules in their columns are rather longer than the "π-cloud thickness". This means that the large interplanar distances between molecules suppress an effective overlap of the π-orbital of the donor molecules along the stacking direction. As a result of this unfavorable π-orbital interaction, these two salts have comparably low conducting behaviors. On the other hand, the semiconducting property of $\mathbf{3}_3$·[NP] can be reasonably understood by considering that the column structure is triadic and not uniform.

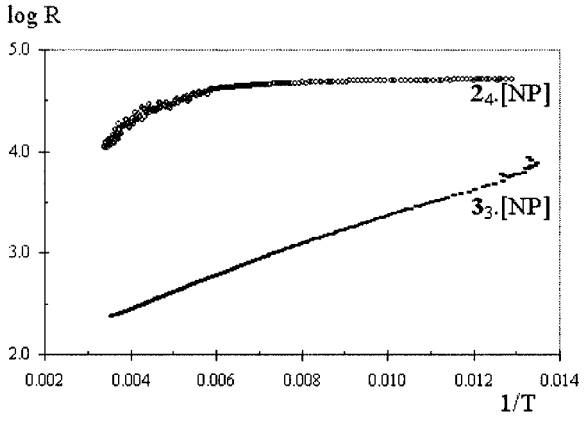

Figure 8. Temperature dependence of the resistance of single crystals of $\mathbf{2}_4$·[NP] (°) and $\mathbf{3}_3$·[NP] (−)

Conclusion

The synthesis, crystal structures and electrical conductivities of three new radical salts $\mathbf{1}_4$·[NP], $\mathbf{2}_4$·[NP] and $\mathbf{3}_3$·[NP] have been described. Both $\mathbf{2}_4$·[NP] and $\mathbf{3}_3$·[NP] are semiconductors, but two regimes, with a very low activation energy at low temperatures, are observed only for $\mathbf{2}_4$·[NP]. Although the structures of $\mathbf{2}_4$·[NP] and $\mathbf{1}_4$·[NP] are very similar, the only-sulfur containing $\mathbf{1}_4$·[NP] is an insulator with a room-temperature conductivity 10^4 times smaller than that of the sulfur-selenium containing $\mathbf{2}_4$·[NP].

The strategy of using iodine-substituted organic donors for promoting stronger donor-counteranion interaction actually led in the three salts studied here to effective contacts between the donor molecules and the $[NP]^{2-}$ anions. This is the first example in which donor molecules are connected with $[NP]^{2-}$ anions through strong and directional interactions of the -I···NC- type.

The detection of long-lived metastable states at low temperature generated by laser irradiation and conductivity measurements under irradiation remain to be carried out and are under progress.

Experimental Section

General Remarks: ^{1}H NMR spectra were recorded in $CDCl_3$ on a Bruker AC200 spectrometer. Chemical shifts are quoted relative to the residual solvent peak ($CDCl_3$: δ = 7.26 ppm). Mass spectra were recorded on a NERMAG R10-10 mass spectrometer operating in the DCI mode.

Synthesis of 2: Compound **2** was synthesized by a modification of the method used for the preparation of **1**.[19] A solution of 4,5-ethylenedithio-1,3-diselenol-2-one (217.9 mg, 0.7212 mmol) and 4,5-diiodo-2-thioxo-1,3-dithiole (556.8 mg) in toluene (20 mL) containing freshly distilled $P(OEt)_3$ (2.7 mL) was refluxed for 6 h. After removal of the solvent under reduced pressure a dark brown residue was obtained. This residue was purified by chromatography on silica gel using carbon disulfide (CS_2) as eluent to afford **2** (33.9 mg, 72% yield) which was recrystallized from CS_2/hexane. M.p. 173 °C. MS (DCI/NH_3): m/z = 643 [M^+] ^{1}H NMR ($CDCl_3/CS_2$): δ = 3.31 ppm.

Electrocrystallization of $\mathbf{1}_4$·[NP], $\mathbf{2}_4$·[NP] and $\mathbf{3}_3$·[NP]: Single crystals of $\mathbf{1}_4$·[NP], $\mathbf{2}_4$·[NP] and $\mathbf{3}_3$·[NP] were prepared by galvanostatic oxidation of the donor molecules (7.2 mg of **1** for $\mathbf{1}_4$·[NP], 9.1 mg of **2** for $\mathbf{2}_4$·[NP] and 3.8 mg of **3** for $\mathbf{3}_3$·[NP]) with $(Ph_4P)_2$[NP] (62 mg for $\mathbf{1}_4$·[NP] and $\mathbf{2}_4$·[NP], and 40 mg for $\mathbf{3}_3$·[NP]) as supporting electrolyte in CH_2Cl_2 (20 mL) under an argon atmosphere at 25 °C. A standard H-shaped cell and platinum-wire electrodes (1 mm diameter) were employed for the preparation of single crystals, applying constant currents (0.6 μA mg for $\mathbf{1}_4$·[NP] and $\mathbf{2}_4$·[NP], and 0.2 μA for $\mathbf{3}_3$·[NP]). Crystals were formed in the anode compartment, collected and washed with CH_2Cl_2: orange platelet-shaped crystals for $\mathbf{1}_4$·[NP], brown platelet-shaped crystals for $\mathbf{2}_4$·[NP], and black needle-shaped crystals for $\mathbf{3}_3$·[NP]. The composition of $\mathbf{1}_4$·[NP], $\mathbf{2}_4$·[NP] and $\mathbf{3}_3$·[NP] was determined by X-ray structure analyses.

X-ray Crystallographic Study: The X-ray diffraction data were collected at 180 K for $\mathbf{1}_4$·[NP] and $\mathbf{2}_4$·[NP], and 160 K for $\mathbf{3}_3$·[NP] on a STOE imaging plate diffractometer with graphite monochromated Mo-K_α radiation (λ= 0.71069 Å). Crystallographic data are gathered in Table 1.

The structures were solved by direct methods (SHELXS 97)[20] and refined on F_0^2 with full-matrix least-squares analysis. The calculations were carried out with the CRYSTALS[21] and WINGX[22] package programs running on a PC. For $\mathbf{1}_4$·[NP], the final cycle of least-squares refinement on F_0^2 for 5771 data and 367 parameters converged to $wR^2(F_0^2)$ = 0.231 for all data and to R = 0.075 for 3117 data with $I \geq 2\sigma(I)$. For $\mathbf{2}_4$·[NP], the final cycle of least-squares refinement on F_o^2 for 5888 data and 358 parameters converged to $wR^2(F_0^2)$ = 0.237 for all data and to R = 0.090 for 1915 data with $I \geq 2\sigma$ (I). For $\mathbf{3}_3$·[NP], the final cycle of least-squares refinement on F_o^2 for 3948 data and 349 parameters converged to $wR^2(F_0^2)$ = 0.181 for all data and to R = 0.072 for 3420 data with $I \geq 2\sigma(I)$. The drawings of the molecular structures were produced using CAMERON.[23] The atomic scattering factors were taken from International Tables for X-ray Crystallography.[24]

CCDC-193065−193067 ($\mathbf{1}_4$·[NP], $\mathbf{2}_4$·[NP]$\mathbf{3}_4$·[NP], respectively) contain the supplementary crystallographic data for this paper. These data can be obtained free of charge at www.ccdc.cam.ac.uk/conts/retrieving.html [or from the Cambridge Crystallographic Data Centre, 12, Union Road, Cambridge CB2 1EZ, UK; Fax: (internat.) +44-1223/336-033; E-mail: deposit@ccdc.cam.ac.uk].

 © 2003 Wiley-VCH Verlag GmbH & Co. KGaA, Weinheim

Table 1. Crystal data for $\mathbf{1}_4$·[NP], $\mathbf{2}_4$·[NP] and $\mathbf{3}_3$·[NP]

	$\mathbf{1}_4$·[NP]	$\mathbf{2}_4$·[NP]	$\mathbf{3}_3$·[NP]
Empirical formula	$C_{37}H_{16}FeI_8N_6OS\mathbf{2}_4$	$C_{37}H_{16}FeI_8N_6OS_{16}Se_8$	$C_{29}H_{15}I_3FeN_6OS_{18}$
M	2401.0	2766.2	1477.1
Crystal system	Triclinic	Triclinic	Triclinic
Space group	$P\bar{1}$	$P\bar{1}$	$P\bar{1}$
a [Å]	12.7200(13)	12.7630(19)	10.9690(15)
b [Å]	17.2380(20)	17.3930(30)	15.2250(21)
c [Å]	7.4400(8)	7.4840(12)	6.6320(9)
α [°]	97.111(13)	96.531(20)	99.468(16)
β [°]	92.968(12)	92.119(18)	96.697(17)
γ [°]	102.456(13)	102.264(19)	92.149(17)
V [Å ^{3}]	1575.5(6)	1609.7(8)	1091.0(4)
Z	1	1	1
$d_{calcd.}$ [g·cm^{-1}]	2.53	2.86	2.25
$F(000)$	1121.9	1265.8	711.9
μ(Mo-K_α) [cm^{-1}]	4.994	9.151	3.368
Data collection			
Temperature [K]	180	180	160
Diffractometer	Stoe IPDS	Stoe IPDS	Stoe IPDS
Scan mode	Φ	Φ	Φ
Scan range Φ [°]	$0 < \Phi < 250$	$0 < \Phi < 250$	$0 < \Phi < 250$
No. of collected reflns.	5771	5888	3948
No. of reflns. used	3117 [$I > 2\sigma(I)$]	1915 [$I > 2\ \sigma\ (I)$]	3420 [$I > 2\ \sigma\ (I)$]
R	0.075	0.090	0.072
wR_2	0.231	0.237	0.181
No. of parameters	367	358	349

Electrical Conductivity Measurement: The electrical conductivity measurements were carried out on single crystals of $\mathbf{1}_4$·[NP], $\mathbf{2}_4$·[NP] and $\mathbf{3}_3$·[NP] using the four-probe method in the temperature range of 50−300 K. Contacts to the electrode were ensured by gold paste.

Acknowledgments

We thank D. Berail from Motolorola Company for supplying printed circuits for conductivity measurements. K. U. thanks Osaka Prefecture University for a postdoctoral grant.

[1] H. T. Woike, W. Krasser, S. Haussühl, *Z. Kristallogr.* **1989**, *188*, 139−153.
[2] T. Woike, W. Krasser, P. Bechthold, S. Haussühl, *Phys. Rev. Lett.* **1984**, *53*, 1767−1770.
[3] H. Zöllner, W. Krasser, T. Woike, *Chem. Phys. Lett.* **1989**, *161*, 497−501.
[4] T. Woike, S. Haussühl, *Solid State Commun.* **1993**, *86*, 333−337.
[5] M. R. Pressprich, M. A. White, V. Vekhlter, P. Coppens, *J. Am. Chem. Soc.* **1994**, *116*, 5233−5238.
[6] M. D. Carducci, M. R. Pressprich, P. Coppens, *J. Am. Chem. Soc.* **1997**, *119*, 2669−2678.
[7] L. Kushch, L. Buravov, V. Tkacheva, E. Yagubskii, L. Zorina, S. Khasanov, R. Shibaeva, *Synth. Met.* **1999**, *102*, 1646−1649.
[8] M. Gener, E. Canadell, S. S. Khasanov, L. V. Zorina, R. P. Shibaeva, L. A. Kushch, E. B. Yagubskii, *Solid State Commun.* **1999**, *111*, 329−333.
[9] L. V. Zorina, S. S. Khasanov, R. P. Shibaeva, M. Gener, R. Rousseau, E. Canadell, L. A. Kushch, E. B. Yagubskii, O. O. Drozdova, K. Yakushi, *J. Mater. Chem.* **2000**, *10*, 2017−2023.
[10] M. Clemente-Leon, E. Coronado, J. R. Galan-Mascaros, C. J. Gomez-Garcia, E. Canadell, *Inorg. Chem.* **2000**, *39*, 5394−5397.
[11] A. Dolbecq, M. Fourmigué, P. Batail, *Chem. Mater.* **1994**, *6*, 1413−1418.
[12] K. Heuzé, M. Fourmigué, P. Batil, E. Canadell, P. Auban-Senzier, *Chem. Eur. J.* **1999**, *5*, 2971−2976.
[13] K. Heuzé, M. Fourmigué, P. Batail, *J. Mater. Chem.* **1999**, *9*, 2373−2379.
[14] A. S. Batsanov, A. J. Moore, N. Robertson, A. Green, M. R. Bryce, J. A. K. Howard, A. E. Underhill, *J. Mater. Chem.* **1997**, *7*, 387−389.
[15] T. Imakubo, H. Sawa, R. Kato, *Synth. Met.* **1995**, *73*, 117−122.
[16] T. Imakubo, H. Sawa, R. Kato, *J. Chem. Soc., Chem. Commun.* **1995**, 1667−1668.
[17] T. Imakubo, H. Sawa, R. Kato, *Synth. Met.* **1997**, *86*, 1883−1884.
[18] A. Bondi, *J. Phys. Chem.* **1964**, *68*, 441−451.
[19] B. Domercq, T. Devic, M. Fourmigué, P. Auban-Senzier, E. Canadell, *J. Mater. Chem.* **2001**, *11*, 1570−1575.
[20] G. M. Sheldrick, *SHELX97 − Programs for Crystal Structure Analysis* (release 97−2), Intitut für Anorganische Chemie der Universtät, Tammanstrasse 4, Göttingen, Germany **1998**.
[21] D. J. Watkin, C. K. Prout, J. R. Carruthers, P. W. Betteridge, R. I. Cooper, *CRYSTALS*, issue 11, Chemical Crystallography Laboratory, University of Oxford, Oxford, England, **2002**.
[22] WINGX, Main Reference; L. J. Farrugia, *J. Appl. Crystallogr.* **1999**, *32*, 837−838.
[23] D. J. Watkin, C. K. Prout, L. J. Pearce, *CAMERON*, Chemical Crystallography Laboratory, University of Oxford, Oxford, England, **1996**.
[24] D. T. Cromer, J. T. Waber, *International Table for X-ray Crystallography*, Kynoch Press, Birmingham, **1974**, vol. 4.

Received November 27, 2003

 © 2003 Wiley-VCH Verlag GmbH & Co. KGaA, Weinheim

Polymeric, Molecular, and Cation/Anion Arrangements in Chloro-, Bromo-, and Iododiruthenium(II,III) Carboxylate Compounds

M. Carmen Barral,[a] Rodrigo González-Prieto,[a] Reyes Jiménez-Aparicio,*[a] J. Luis Priego,[a] M. Rosario Torres,[b] and Francisco A. Urbanos[a]

Keywords: Carboxylate / Diruthenium / Metal−metal bonds / Multiple bonds / Ruthenium

The synthesis and characterization of the anhydrous compounds $[Ru_2X(\mu\text{-}O_2CR)_4]$ [R = CH_2CH_2OPh, X = Cl (**1a**), Br (**2a**), I (**3a**); R = $CMePh_2$, X = Br (**5a**), I (**6a**)] and of the solvated complexes $[Ru_2X(\mu\text{-}O_2CR)_4(H_2O)]$ [R = CH_2CH_2OPh, X = Cl (**1b**), I (**3b**); R = $CMePh_2$, X = Cl (**4b**), Br (**5b**), I (**6b**)] are described. Thermogravimetric analyses have been used to confirm the anhydrous or solvated natures of the complexes. The crystal structures of **1b·2MeOH**, **3b·0.5H$_2$O**, and **4b** have been investigated by X-ray diffraction and none of them shows the usual polymeric arrangement reported for tetracarboxylatodiruthenium(II,III) compounds. The structure of **3b·0.5H$_2$O** consists of cationic and anionic units, $[Ru_2(\mu\text{-}O_2CCH_2CH_2OPh)_4(H_2O)_2][Ru_2I_2(\mu\text{-}O_2CCH_2CH_2OPh)_4]$, and represents the first reported crystal structure of a tetracarboxylato(iodo)diruthenium(II,III) derivative. The structures **1b·2MeOH** and **4b** each show the presence of discrete dinuclear molecules. The crystal structure of $[Ru_2Cl(\mu\text{-}O_2CCMePh_2)_4(H_2O)]$ demonstrates that diruthenium compounds with the same halide and carboxylate ligands may adopt polymeric or discrete molecular dispositions. Magnetic susceptibility measurements of the complexes in the 2–300 K range have been carried out. Complex **2a** shows a strong antiferromagnetic coupling, consistent with the existence of linear chains in the solid state. The complexes $[Ru_2X(\mu\text{-}O_2CR)_4(H_2O)]$ show weak through-space antiferromagnetic coupling, in accordance with non-polymeric structures. The magnetic behaviour of **1a**, **3a**, **5a**, and **6a** suggests a mixture of arrangements.
(© Wiley-VCH Verlag GmbH & Co. KGaA, 69451 Weinheim, Germany, 2003)

Introduction

Since the synthesis of $[Ru_2Cl(\mu\text{-}O_2CMe)_4]$ was first published,[1] numerous diruthenium(II,III) complexes of the formula $[Ru_2Cl(\mu\text{-}O_2CR)_4]$ (R = alkyl, aryl) have been described.[2−4] These complexes have attracted much attention, mainly due to interest in their electronic and magnetic properties.[2−4] More recently, many efforts have been devoted to the use of carboxylate complexes with metal−metal bonds as building blocks in the formation of supramolecular metallospecies.[5−8] In the $[Ru_2Cl(\mu\text{-}O_2CR)_4]$ compounds, the diruthenium atoms are strongly bonded by four bridging carboxylate ligands, with one axial position occupied by one chlorine atom. In the solid state, most of them have polymeric structures with chloride ligands bridging the dinuclear units to give zigzag chains.[9−15] A similar structure with linear chains with four carboxylate ligands has been found.[16−19] Discrete dinuclear molecules in which a neutral ligand is coordinated to one of the axial positions have also been described,[20−22] as has a unique example showing zigzag chains made up jointly of cationic and anionic units.[13] The different arrangements observed in the diruthenium complexes are collected in Scheme 1.

The influence of the carboxylate ligand on the polymeric or molecular nature of the diruthenium complexes has been investigated and seems to be related to the presence of branched chains in the carboxylate ligand.[21,22] Few bromo and iodo derivatives have been reported,[23,24] and the influence of the halogen axial ligand on the structure has not been studied. $[Ru_2Br(\mu\text{-}O_2CH)_4]$ is the sole example of this kind of compounds whose crystal structure has been reported.[23]

In this paper we investigate the possibility of obtaining both discrete molecules and polymeric species with the same carboxylate ligand. The ligands 3-phenoxypropionate and 2,2-diphenylpropionate have been used. The preparation of new chloro, bromo, and iodo derivatives has been carried out and the influence of the halogen axial ligand on the arrangement of the complexes explored.

[a] Departamento de Química Inorgánica, Facultad de Ciencias Químicas, Universidad Complutense, Ciudad Universitaria, 28040 Madrid, Spain
Fax: (internat.) + 34-91/3944352
E-mail: qcmm@quim.ucm.es
[b] Centro de Asistencia a la Investigación de Rayos X, Facultad de Ciencias Químicas, Universidad Complutense, Ciudad Universitaria, 28040 Madrid, Spain

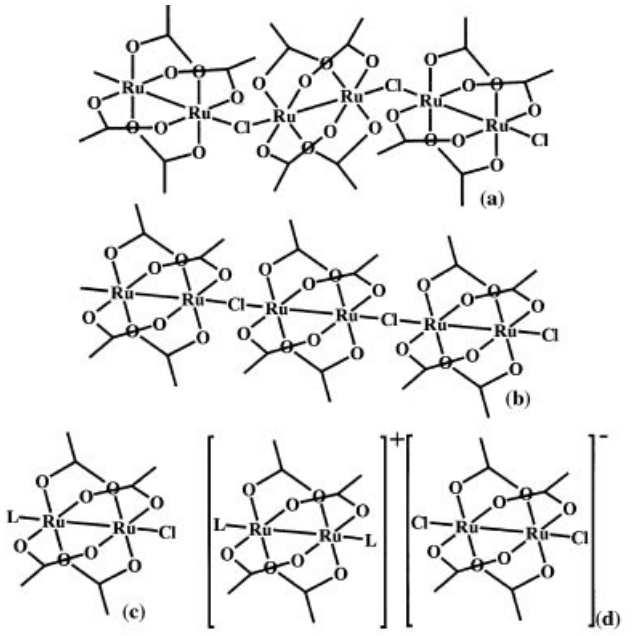

Scheme 1. Arrangement observed in diruthenium complexes: (a) zigzag chains, (b) linear chains, (c) discrete molecules, and (d) cation/anion species

Results and Discussion

Synthesis and Physicochemical Properties of the Compounds

The complex $[Ru_2Cl(\mu\text{-}O_2CCH_2CH_2OPh)_4]$ (**1a**) was prepared by treatment of $[Ru_2Cl(\mu\text{-}O_2CMe)_4]$ with 3-phenoxypropionic acid in methanol/water (1:1). Two metathesis cycles were carried out to ensure the complete replacement of the acetate ligands. $AgBF_4$ was added to a solution of **1a** in THF in order to obtain $[Ru_2(\mu\text{-}O_2CCH_2CH_2OPh)_4(THF)_2]BF_4$, which was treated in ethanol with an aqueous solution of KBr to produce the precipitation of $[Ru_2Br(\mu\text{-}O_2CCH_2CH_2OPh)_4]$ (**2a**). The synthesis of $[Ru_2I(\mu\text{-}O_2CCH_2CH_2OPh)_4(H_2O)]$ (**3b**) was carried out by using KI in place of KBr. The hydrate $[Ru_2Cl(\mu\text{-}O_2CCH_2CH_2OPh)_4(H_2O)]$ (**1b**) was obtained from a methanol solution of **1a**. The unsolvated $[Ru_2I(\mu\text{-}O_2CCH_2CH_2OPh)_4]$ (**3a**) was prepared by prolonged heating of **3b** under vacuum. Attempts to obtain the analogous hydrated $[Ru_2Br(\mu\text{-}O_2CCH_2CH_2OPh)_4(H_2O)]$ gave the polymeric **2a** in all cases.

Treatment of $[Ru_2Cl(\mu\text{-}O_2CMe)_4]$ with 2,2-diphenylpropionic acid in methanol/water (1:1) produced $[Ru_2Cl(\mu\text{-}O_2CCMePh_2)_4(H_2O)]$ (**4b**). The previously described compound $[Ru_2Cl(\mu\text{-}O_2CCMePh_2)_4]$[18] crystallized when petroleum ether was added to a solution of **4b** in CH_2Cl_2. The complexes $[Ru_2X(\mu\text{-}O_2CCMePh_2)_4(H_2O)]$ [X = Br (**5b**), I (**6b**)] were obtained from $[Ru_2(\mu\text{-}O_2CCMePh_2)_4(THF)_2]BF_4$ and KBr or KI. The unsolvated **5a** and **6a** were prepared by heating **5b** and **6b**, respectively, under vacuum.

The cleavage of the polymeric chains of **1a**−**6a** by donor solvent molecules occurs in all cases except for that of the complex **2a**. The presence of coordinated water molecules in the complexes was inferred from analytical, IR, and thermogravimetric data.

Crystals of **1b·2MeOH** were formed by cooling of (−18 °C) methanol solutions of **1a** or **1b**. After several unsuccessful attempts to obtain crystals of the bromo and iodo derivatives, single crystals of **3b·0.5H$_2$O** suitable for an X-ray crystal structure analysis grew from a methanol solution containing $[Ru_2(\mu\text{-}O_2CCH_2CH_2OPh)_4]^+$ and I^- over 48 h. Single crystals of **4b** were obtained by the same procedure from a solution containing $[Ru_2(\mu\text{-}O_2CCMePh_2)_4]^+$ and Cl^-.

The chloro complexes are quite soluble in polar organic solvents such as methanol or THF, but insoluble in petroleum ether or toluene. The solubilities of complexes **1**−**6** in polar organic solvents decrease along the series Cl, Br, and I, the iodo derivatives being only partially soluble in these solvents. The conductivities of these compounds in methanol (ca. 10^{-4} M) indicate that they are 1:1 electrolytes in this solvent.[25] The process of dissolution of the polymeric complexes **1a** and **3a**−**6a** in donor solvents results in the cleavage of the chains, giving discrete dinuclear units. Thus, from MeOH/H_2O solutions, molecular $[Ru_2Cl(\mu\text{-}O_2CR)_4(H_2O)]$ complexes have been obtained.

Spectroscopic Properties

The IR spectra of all compounds show the pattern typical of bridging carboxylate ligands in the COO stretching region.[4] Other bands corresponding to the carboxylate ligands and attributable to CH or phenyl groups are also observed. The IR spectra of **1b** and **3b**−**6b** clearly show absorption bands due to the presence of water molecules.

The electronic spectra of all compounds in methanol are similar to those of other diruthenium(II,III) complexes,[2] showing two bands in the UV/Vis range at ca. 430 and ca. 290 nm and attributable to $\pi(RuO, Ru_2)\rightarrow\pi^*(Ru_2)$ and π(axial ligand)$\rightarrow\pi^*(Ru_2)$ transitions, respectively, as proposed by Norman et al.[26] and by Miskowski and Gray.[27] All complexes also absorb in the near infrared region at ca. 1000 nm, due to a $\delta\rightarrow\delta^*$ transition.[28]

Thermogravimetric Studies

The thermogravimetric curves of the hydrated complexes **1b** and **3b**−**6b** each show weight loss between 145 and 210 °C, corresponding to one water molecule per complex. The assumption that this water molecule is bonded to one axial position of the diruthenium complexes was confirmed by the crystal structure determinations of **1b·2MeOH**, **3b·0.5H$_2$O** and **4b**. In a further experiment, the thermal decomposition of each compound was interrupted after the release of the water molecule, and their IR spectra were identical to those of the corresponding $[Ru_2X(\mu\text{-}O_2CR)_4]$ species. Moreover, the anhydrous complexes do not display any weight loss before 250 °C. The loss of the halide ligand for **1a**, **2a**, **3b**, and **6b** is clearly observed in the 250−290 °C range, followed by the loss of the carboxylate groups in two steps. The thermogravimetric curves for the other compounds show that the release of the halide and of the first

 © 2003 Wiley-VCH Verlag GmbH & Co. KGaA, Weinheim

two carboxylate ligands takes place at the same time. These data are in accordance with previous studies[29] on the thermal decomposition of pentakis(alkanoato)diruthenium(II,III) complexes.

Magnetic Properties

Magnetic measurements on compounds **1**−**6** at room temperature each show magnetic moments of 3.86−4.18 μ_B, corresponding to the presence of three unpaired electrons per dimer unit.[2] These magnetic moments are in accordance with the $\sigma^2\pi^4\delta^2(\pi^*\delta^*)^3$ ground-state configuration proposed by Norman et al.[26] In all complexes the molar susceptibility χ_M increases continuously with decreasing temperature (300−2 K), except for complexes **1a** and **2a**. The magnetic moment in all cases exhibits a pronounced decrease with temperature. This behaviour has been ascribed to a large zero-field splitting (ZFS) and some degree of antiferromagnetic coupling between the diruthenium units.[14,15,18,30−33] The model of Cukiernik et al.[14] was successfully used to fit the magnetic data of complexes **1b** and **3b**−**6b**. In this model, we used the isotropic *g* parameter instead of $g_\parallel$ and $g_\perp$ in order to reduce the number of parameters and to obtain more accurate values of *D* and *zJ*. Figure 1 shows the experimentally measured and calculated curves for complex **4b** by this model. Similar fits are obtained for the complexes **1b** and **3b**−**6b**.

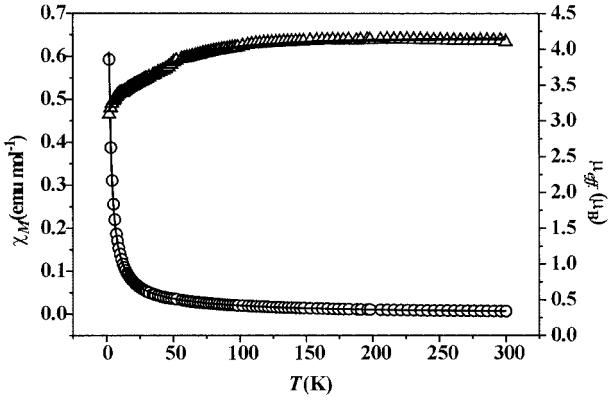

Figure 1. Temperature dependence of the molar susceptibility χ_M (circles) and $\mu_{eff.}$ (triangles) for complex **4b**; solid lines are the product of a least-squares fit to the model indicated in the text

Table 1 collects the calculated magnetic parameters (*g*, *D*, *zJ*, *TIP*, and *P*) for the complexes **1b**−**6b**, together with σ^2, which indicates the quality of the fits. All compounds show large zero-field splittings and low antiferromagnetic coupling values. The *D* values range from 50.60 to 64.72 cm^{-1}, similarly to those found previously for the analogous compounds.[8d,14,15,33−35] The molecular nature of the solvates **1b**−**6b** is in accordance with the low values (−0.04 to −1.33 cm^{-1}) of the antiferromagnetic coupling constants. Similar spin exchange by through-space pathways has recently observed in other molecular diruthenium complexes.[15]

Figure 2 displays the variation of the magnetic susceptibility with temperature for complex **2a**. A maximum is observed at 30 K. The paramagnetic tail and the turning point have been observed previously[18,33] in diruthenium(II,III) complexes with linear chain structures (Ru−Cl−Ru angle ca. 180°). In these cases strong antiferromagnetic coupling between the diruthenium(II,III) units through chlorine atoms gives rise to an inversion of the magnetic susceptibility curve and the approximation of the molecular field[14] cannot be used. Recently, we have developed a model[33] to fit this type of magnetic behaviour. A satisfactory agreement between experimentally measured and calculated curves of the molar susceptibility and the magnetic moment was obtained for complex **2a** (Figure 2) by use of this model.

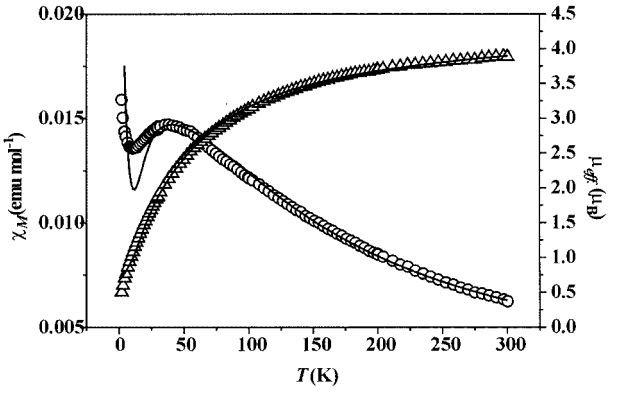

Figure 2. Temperature dependence of the molar susceptibility χ_M (circles) and $\mu_{eff.}$ (triangles) for complex **2a**; solid lines are the products of a least-squares fit to the model indicated in the text

The parameters obtained in the fit of the experimental data for complex **2a** are collected in Table 1. The *zJ* value calculated for complex **2a** is −9.08 cm^{-1}, analogous to those found[18,33] for $[Ru_2Cl(\mu\text{-}O_2CR)_4]$ [R = $CMePh_2$, CH_2CH_3, C(Me)=CHEt]. The high paramagnetic impurity value (3.3%), slightly higher than those observed

Table 1. Magnetic parameters obtained in the fits to the magnetic moment as a function of temperature

Compound	g	*D* [cm^{-1}]	*zJ* [cm^{-1}]	*TIP* [mL/mol]	*P* [%]	σ^2 [a]
1b	2.00	64.03	−1.33	1.49 10^{-3}	0.12	1.50 10^{-4}
2a	2.00	62.99	−9.08	8.31 10^{-4}	3.35	1.45 10^{-4}
3b	2.02	64.72	−0.04	7.90 10^{-4}	< 10^{-6}	6.85 10^{-6}
4b	2.15	50.60	−0.07	< 10^{-6}	0.01	3.00 10^{-5}
5b	2.09	62.80	−0.08	7.87 10^{-5}	< 10^{-4}	5.15 10^{-6}
6b	2.02	62.80	−0.20	6.41 10^{-4}	< 10^{-3}	3.33 10^{-5}

[a] $\sigma^2 = \Sigma(\mu_{eff.\,calcd.} - \mu_{eff.\,exp.})^2/\Sigma\mu_{eff.\,exp.}{}^2$.

 © 2003 Wiley-VCH Verlag GmbH & Co. KGaA, Weinheim

(1.7−2.7%) in the other linear chain compounds,[18,33] is probably due to the presence of the zigzag chain form in the solid.

In the variation of the magnetic susceptibility with temperature for complex **1a**, a maximum at 6 K and a shoulder at ca. 60 K are observed. These magnetic data cannot be fitted or the parameters obtained are anomalous. Since the elemental analysis and the spectroscopic and thermogravimetric data indicate that **1a** is a pure compound, the magnetic susceptibility data could indicate a mixture of two magnetically non-equivalent species. A similar mixture has been found previously[14] for the acetate complex.

As discussed above, the magnetic behaviour of complexes **3a**, **5a**, and **6a** cannot be fitted. These compounds were prepared by pumping the corresponding solvated complexes at 75 °C. If the anhydrous complexes have the usual polymeric structure through halogen bridging ligands, a rearrangement from the molecular to the polymeric structure must take place. In the solid state, however, this change could be difficult, and a mixture of arrays with different magnetic properties is possible. Complex **4b** may illustrate this behaviour. When this complex is heated to 75 °C under vacuum, the anhydrous $[Ru_2Cl(\mu\text{-}O_2CCMePh_2)_4]$ is obtained. The variation of the magnetic susceptibility of this solid shows a maximum at the same temperature (67 K) as the maximum observed in the crystalline polymeric[18,33] $[Ru_2Cl(\mu\text{-}O_2CCMePh_2)_4]$ (Figure 3), although the profile of the curves is different.

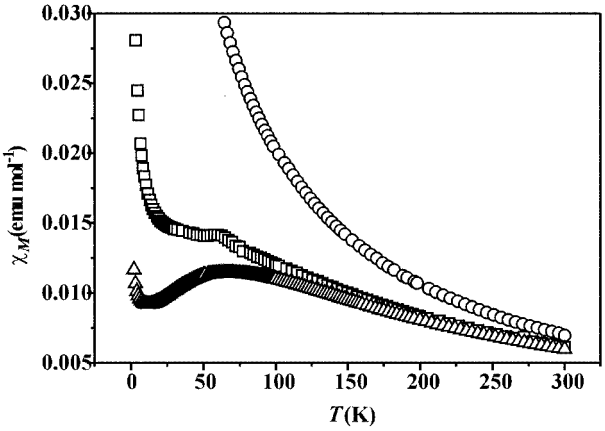

Figure 3. Temperature dependence of the molar susceptibility χ_M for complexes **4b** (circles), **4b** heated at 75 °C under vacuum (squares), and the polymeric $[Ru_2Cl(\mu\text{-}O_2CCMePh_2)_4]$ (triangles)

Crystal Structure of $[Ru_2Cl(\mu\text{-}O_2CCH_2CH_2OPh)_4(H_2O)]\cdot 2MeOH$ (1b·2MeOH)

In the structure of **1b·2MeOH**, the asymmetric unit is composed of halves of two different crystallographically independent centrosymmetric molecules (A and B) with the inversion centre in the middle of the Ru−Ru bonds. A PLUTO view of the molecule (A) is shown in Figure 4. Table 2 gives selected bond lengths and angles of the complex. Each dinuclear unit of **1b·2MeOH** has two ruthenium atoms linked by four bridging 3-phenoxypropionoate ligands. Each axial position is shared by the O_{water} and Cl atoms with a 50% occupancy. The same situation has been found[21] for the complex $[Ru_2Cl(\mu\text{-}O_2CCMe_3)_4(H_2O)]$. The ruthenium atoms have a distorted octahedral coordination geometry. The distortion arises essentially from the longer $Ru-L_{axial}$ and Ru−Ru distances with respect to $Ru-O_{eq}$.

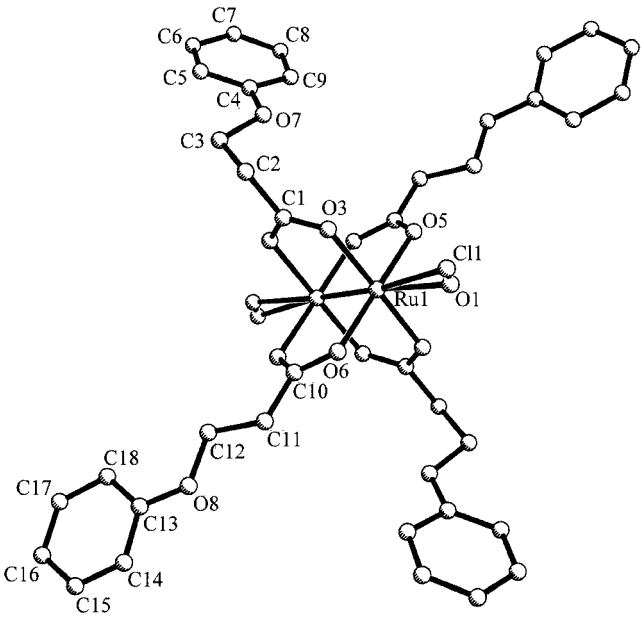

Figure 4. PLUTO view of the molecule (A) of the complex $[Ru_2Cl(\mu\text{-}O_2CCH_2CH_2OPh)_4(H_2O)]\cdot 2MeOH$ (**1b·2MeOH**); hydrogen atoms and MeOH molecules are omitted for clarity

The Ru−Ru distances in the two molecules are 2.278(2) and 2.280(2) Å. These distances are of the same order as those found in the other carboxylatodiruthenium(II,III) compounds.[2−4] The molecules are packed only by normal van der Waals forces.

The most important feature of these structures is their molecular nature. Only four crystal structures of molecular tetracarboxylato(chloro)diruthenium(II,III) complexes have been reported,[20−22] and their molecular natures have been attributed to the carboxylate bridges. The importance of the carboxylate ligands in the arrangement is illustrated by the structures of the compounds with O_2CCH_2OEt, O_2CCH_2OMe, and $O_2CCH_2CH_2OPh$. In the first case[13] a singular arrangement with formation of anionic, cationic, and polymeric units is formed. In the second case[15] a polymeric structure is observed, whereas in the last case a molecular arrangement is adopted.

Crystal Structure of $[Ru_2I(\mu\text{-}O_2CCH_2CH_2OPh)_4(H_2O)]\cdot 0.5H_2O$ (3b·0.5H$_2$O)

Crystals of **3b·0.5H$_2$O** were grown from a methanol solution containing $[Ru_2(\mu\text{-}O_2CCH_2CH_2OPh)_4]^+$ and I^-. The crystal structure determination shows packing of cationic $\{[Ru_2(\mu\text{-}O_2CCH_2CH_2OPh)_4(H_2O)_2]^+\}$ and anionic $\{[Ru_2I_2(\mu\text{-}O_2CCH_2CH_2OPh)_4]^-\}$ species, and water molecules. The asymmetric unit is composed of halves of the anion and the cation, with an inversion centre in the middle of the ruthenium−ruthenium bonds and half a molecule of

 © 2003 Wiley-VCH Verlag GmbH & Co. KGaA, Weinheim

Table 2. Selected bond lengths [Å] and angles [°] for $[Ru_2Cl(\mu\text{-}O_2CCH_2CH_2OPh)_4(H_2O)]\cdot 2MeOH$ (**1b·2MeOH**), $[Ru_2I(\mu\text{-}O_2CCH_2CH_2OPh)_4(H_2O)]\cdot 0.5H_2O$ (**3b·0.5H$_2$O**), and $[Ru_2Cl(\mu\text{-}O_2CCMePh_2)_4(H_2O)]$ (**4b**)

1b·2MeOH		**3b**·0.5H$_2$O		**4b**	
Ru(1)−Ru(1A)	2.278(2)	Ru(1)−Ru(1A)	2.310(2)	Ru(1)−Ru(1A)	2.2844(9)
Ru(1)−Cl(1)	2.468(6)	Ru(1)−I(1)	2.875(1)	Ru(1)−O(5)	2.37(1)
Ru(1)−O1	2.291(1)	Ru(1)−O(1)	2.038(7)	Ru(1)−Cl(1)	2.502(4)
Ru(1)−O(3)	2.030(6)	Ru(1)−O(2)	2.028(6)	Ru(1)−O(1)	2.026(4)
Ru(1)−O(4)	2.026(6)	Ru(1)−O(3)	2.026(7)	Ru(1)−O(2)	2.022(3)
Ru(1)−O(5)	2.032(6)	Ru(1)−O(4)	2.026(6)	Ru(1)−O(3)	2.029(4)
Ru(1)−O(6)	2.032(6)	Ru(2)−Ru(2A)	2.265(2)	Ru(1)−O(4)	2.029(3)
Ru(2)−Ru(2A)	2.280(2)	Ru(2)−O(9)	2.271(7)		
Ru(2)−Cl(2)	2.515(5)	Ru(2)−O(5)	2.026(8)		
Ru(2)−O2	2.290(1)	Ru(2)−O(6)	2.025(7)		
Ru(2)−O(9)	2.022(6)	Ru(2)−O(7)	2.002(8)		
Ru(2)−O(10)	2.021(6)	Ru(2)−O(8)	2.017(7)		
Ru(2)−O(11)	2.025(6)				
Ru(2)−O(12)	2.014(6)				
Ru(1A)−Ru(1)−Cl(1)	174.2(2)	Ru(1A)−Ru(1)−I(1)	177.56(6)	Ru(1A)−Ru(1)−Cl(1)	175.49(9)
Ru(1A)−Ru(1)−O(1)	173.2(4)	O(1)−Ru(1)−Ru(1A)	88.8(2)	Ru(1A)−Ru(1)−O(5)	174.9(3)
Ru(1A)−Ru(1)−O(3)	89.4(2)	O(2)−Ru(1)−Ru(1A)	88.7(2)	O(1)−Ru(1)−Ru(1A)	89.9(1)
Ru(1A)−Ru(1)−O(4)	89.3(2)	O(3)−Ru(1)−Ru(1A)	89.3(2)	O(2)−Ru(1)−Ru(1A)	88.8(1)
Ru(1A)−Ru(1)−O(5)	88.8(2)	O(4)−Ru(1)−Ru(1A)	89.0(2)	O(3)−Ru(1)−Ru(1A)	88.8(1)
Ru(1A)−Ru(1)−O(6)	90.1(2)	O(2)−Ru(1)−O(1)	88.5(3)	O(4)−Ru(1)−Ru(1A)	89.5(1)
O(3)−Ru(1)−O(4)	178.7(2)	O(3)−Ru(1)−O(1)	177.9(3)	O(2)−Ru(1)−O(1)	89.0(2)
O(3)−Ru(1)−O(5)	89.2(2)	O(4)−Ru(1)−O(1)	91.2(3)	O(1)−Ru(1)−O(3)	178.6(2)
O(3)−Ru(1)−O(6)	91.7(2)	Ru(2A)−Ru(2)−O(9)	176.4(2)	O(1)−Ru(1)−O(4)	89.4(2)
Ru(2A)−Ru(2)−Cl(2)	175.6(2)	O(5)−Ru(2)−Ru(2A)	89.6(2)		
Ru(2A)−Ru(2)−O(2)	173.1(5)	O(6)−Ru(2)−Ru(2A)	89.6(2)		
Ru(2A)−Ru(2)−O(9)	89.8(2)	O(7)−Ru(2)−Ru(2A)	89.5(2)		
Ru(2A)−Ru(2)−O(10)	89.3(2)	O(8)−Ru(2)−Ru(2A)	89.3(2)		
Ru(2A)−Ru(2)−O(11)	89.0(2)	O(5)−Ru(2)−O(6)	90.6(3)		
Ru(2A)−Ru(2)−O(12)	89.2(2)	O(7)−Ru(2)−O(5)	179.0(3)		
O(9)−Ru(2)−O(10)	90.9(2)	O(8)−Ru(2)−O(5)	89.3(3)		
O(9)−Ru(2)−O(11)	178.7(2)				
O(9)−Ru(2)−O(12)	89.0(2)				

water of crystallization. A PLUTO view of the compound is shown in Figure 5.

Both ions contain a diruthenium(II,III) unit with four 3-phenoxypropionate moieties as bridging ligands. The cationic complexes have two axially coordinated water molecules, and the anions two iodide ligands. Compound **3b·0.5H$_2$O** could thus be formulated as $[Ru_2(\mu\text{-}O_2CCH_2CH_2OPh)_4(H_2O)_2][Ru_2I_2(\mu\text{-}O_2CCH_2CH_2OPh)_4]\cdot H_2O$.

There are only two known complexes in which both cationic and anionic units possess diruthenium cores:[13,36] $[Ru_2Cl(\mu\text{-}O_2CCH_2OEt)_4(H_2O)]$ and $[Ru_2(\mu\text{-}O_2CPh)_4(HSO_4)(EtOH)]$. Complex **3b·0.5H$_2$O** is the first tetracarboxylato(iodo)diruthenium complex whose crystal structure has been determined.

The Ru−Ru bond length in the cation unit [2.265(2) Å] is analogous to that found in complex **1b·2MeOH**, which is typical of these types of compounds.[4,37] In the anionic unit, however, the Ru−Ru distance is 2.310(2) Å. This bond is longer than those observed in the analogous chloro derivatives[13,16,38] $[Ru_2Cl_2(\mu\text{-}O_2CR)_4]^-$ (R = CH_2OEt, Me, H, C_6H_4-*p*-OMe) but shorter than the longest Ru−Ru distance [2.427(1) Å] found in the cation[39] $[Ru_2(\mu\text{-}O_2CMe)_4(PCy_3)_2]^+$ which has the very strong axial donor ligand PCy_3. The Ru−I bond length in the anionic unit [2.875(1) Å] is longer than any other Ru−L_{axial} bond in diruthenium complexes, including the compound[23] $[Ru_2Br(\mu\text{-}O_2CH)_4]$ [2.7170(8)−2.7313(9) Å]. This large Ru−I bond length is in accordance with the large size of the iodide ligand. The Ru−O_{axial} bond length in the cationic unit [2.271(7) Å] is similar to that found in other $[Ru_2(\mu\text{-}O_2CR)_4(H_2O)_2]^+$ cations.[8c,13,16,40,41]

Crystal Structure of $[Ru_2Cl(\mu\text{-}O_2CCMePh_2)_4(H_2O)]$ (4b)

The molecular structure of **4b** is depicted in Figure 6, and selected bond lengths and angles are given in Table 2. This molecule has two Ru atoms linked by four 2,2-diphenylpropionate bridging ligands, with the axial positions occupied by one water molecule and one chloride ligand. Analogously to those described above for complex **1b·2MeOH**, the axial positions are shared by the O_{water} and Cl atoms with occupation factors of 50%. Although the hydrogen atoms of the axial water molecules were not located, the distances between the Cl and the O_{axial} atoms of the neighbouring molecule [3.04(1) Å] suggest hydrogen-bond interactions between them. Thus, the $[Ru_2Cl(\mu\text{-}O_2CCMePh_2)_4(H_2O)]$ molecules are packed, giving chains.

The molecular structure of complex **4b** contrasts with the polymeric structure reported[18] for $[Ru_2Cl(\mu\text{-}O_2CCMePh_2)_4]$. In spite of their different arrangements in

 © 2003 Wiley-VCH Verlag GmbH & Co. KGaA, Weinheim

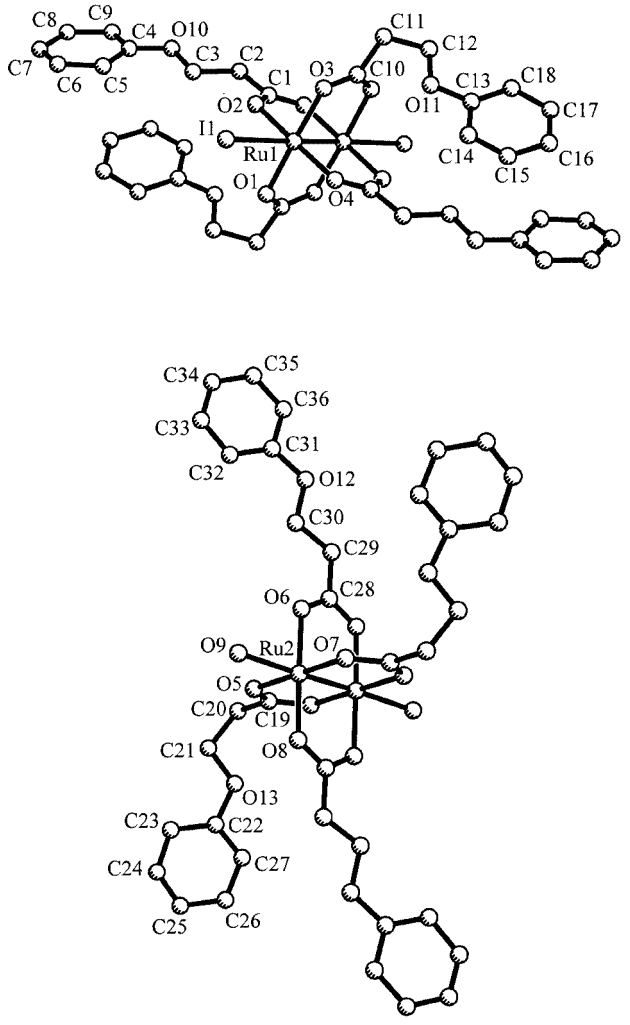

Figure 5. PLUTO view of $[Ru_2(\mu\text{-}O_2CCH_2CH_2OPh)_4(H_2O)_2][Ru_2I_2(\mu\text{-}O_2CCH_2CH_2OPh)_4]\cdot H_2O$ (**3b·0.5H$_2$O**); the water of hydration and hydrogen atoms have been omitted for clarity

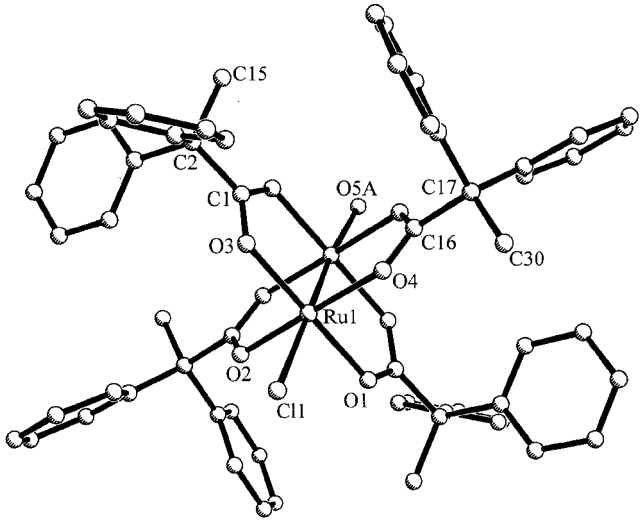

Figure 6. PLUTO view of $[Ru_2Cl(\mu\text{-}O_2CCMePh_2)_4(H_2O)]$ (**4b**); hydrogen atoms are omitted for clarity

the solid state, all distances, including the Ru−Cl bond length, are very similar in both complexes.

The synthesis and X-ray analysis of the molecular $[Ru_2Cl(\mu\text{-}O_2CCMePh_2)_4(H_2O)]$ demonstrates that different arrays are possible with the same carboxylate ligand.

Conclusion

The crystal structure determination of two new molecular diruthenium(II,III) compounds indicates that the usual polymeric structure of the tetracarboxylato(chloro)diruthenium(II,III) complexes can be broken by neutral molecules, giving discrete dinuclear species. These results also confirm that small differences in the electronic or steric requirements of the carboxylate ligand can have important consequences in the arrangement in the solid state, as illustrated by the different arrays found in the complexes with the ligands O_2CCH_2OEt, O_2CCH_2OMe, and $O_2CCH_2CH_2OPh$.

The synthesis of derivatives with different halide ligands reveals that the nature of the axial ligand has a great influence on the arrangement in the solid state. Thus, the chloro complex with 3-phenoxypropionate ligands displays a molecular structure, whereas the iodo derivative shows a less usual cation/anion array.

Nevertheless, compound $[Ru_2Cl(\mu\text{-}O_2CCMePh_2)_4]$ was known to have a polymeric structure while complex $[Ru_2Cl(\mu\text{-}O_2CCMePh_2)_4(H_2O)]$, with the same halide and carboxylate ligands, has a molecular structure. There must therefore be other factors that play a role in the arrangement of the diruthenium(II,III) compounds. Efforts to study these factors and their influence on diruthenium chemistry are currently underway.

Experimental Section

General Remarks: All reactions were carried out under inert gases, by use of standard Schlenk techniques. Ruthenium trichloride and carboxylic acids were obtained from commercial sources. Solvents were used without previous purification. The complexes $[Ru_2Cl(\mu\text{-}O_2CR)_4]$ (R = $CMePh_2$, Me) were prepared by literature procedures.[18,42] IR spectra were recorded as KBr discs with a Nicolet Magna-FTIR 550 spectrophotometer. Elemental analysis of C and H were performed by the Microanalytical Service of Complutense University, Madrid. Electronic spectra in the range 200−2500 nm were recorded with a Cary 5G spectrophotometer in methanol solutions (10^{-4} M). The thermogravimetric analyses were carried out with a Perkin−Elmer Pyris 1 TGA thermogravimetric analyzer. The samples were heated up to 600 °C in platinum crucibles, with a heating rate of 5 °C min^{-1}, and purged in a nitrogen stream. The variable-temperature magnetic susceptibility data were measured with a Quantum Design MPMSXL SQUID (Superconducting Quantum Interference Device) susceptometer over a temperature range of 2−300 K. Each raw data field was corrected for the diamagnetic contribution of both the sample holder and the compound to the susceptibility. The molar diamagnetic corrections for the complexes were calculated on the basis of Pascal's constants. The fit of experimental data was carried out using the commercial MATLAB V.5.1.0.421 program.

 © 2003 Wiley-VCH Verlag GmbH & Co. KGaA, Weinheim

Preparation of $[Ru_2Cl(\mu\text{-}O_2CCH_2CH_2OPh)_4]$ (1a) and $[Ru_2Cl(\mu\text{-}O_2CCH_2CH_2OPh)_4(H_2O)]$ (1b): An excess of 3-phenoxypropionic acid (0.50 g, 3.00 mmol) was added to a solution (30 mL) of $Ru_2Cl(\mu\text{-}O_2CMe)_4$ (0.24 g, 0.50 mmol) in methanol/water (1:1, 24 mL). The reaction mixture was heated at reflux for 4 h, giving a red-brown solid. The solution was filtered, and the solid was washed with diethyl ether (3 × 20 mL) and again treated with fresh carboxylic acid (3.00 mmol) under the same conditions to ensure the complete replacement of the acetate ligands. The red-brown solid was isolated by filtration, washed again with diethyl ether, and dried under vacuum to give **1a**. A solution of the above red-brown solid in hot methanol (20 mL) was allowed to stand at room temperature and later at −18 °C, yielding red-brown crystals of **1b·2MeOH**. These crystals were dried under vacuum at room temperature to give **1b**.

$[Ru_2Cl(\mu\text{-}O_2CCH_2CH_2OPh)_4]$ (1a): Yield: 0.34 g (75%). $C_{36}H_{36}ClO_{12}Ru_2$ (898.27): calcd. C 48.14, H 4.04; found C 48.32, H 4.04. IR (KBr): $\tilde{\nu}$ = 3061 w, 3040 w, 2933 w, 2892 w, 1599 m, 1587 m, 1529 m, 1497 s, 1460 vs, 1439 vs, 1418 s, 1317 m, 1244 s, 1225 s, 1039 m, 752 s, 703 m, 690 m cm^{-1}. UV/Vis (MeOH): $\lambda_{max.}$ (ε) = 297 (1653), 429 (786), 988 (18 $L{\cdot}mol^{-1}{\cdot}cm^{-1}$) nm. $\mu_{eff.}$ = 3.86 μ_B at room temperature.

$[Ru_2Cl(\mu\text{-}O_2CCH_2CH_2OPh)_4(H_2O)]$ (1b): Yield: 0.32 g (69%). $C_{36}H_{38}ClO_{13}Ru_2$ (916.29): calcd. C 47.19, H 4.18; found C 47.31, H 4.22. IR (KBr): $\tilde{\nu}$ = 3445 s, 3065 w, 3041 w, 2932 w, 1600 m, 1588 m, 1497 m, 1466 s, 1437 vs, 1243 s, 1041 m, 755 m, 693 m cm^{-1}. UV/Vis: identical to data of **1a**. $\mu_{eff.}$ = 3.98 μ_B at room temperature.

Preparation of $[Ru_2Br(\mu\text{-}O_2CCH_2CH_2OPh)_4]$ (2a): Silver tetrafluoroborate (0.07 g, 0.35 mmol) was added to a solution of $[Ru_2Cl(\mu\text{-}O_2CCH_2CH_2OPh)_4]$ (0.31 g, 0.35 mmol) in THF (30 mL). The reaction mixture was stirred for 24 h, giving a solid precipitate of AgCl and a brown solution. The precipitate was filtered through Celite and the solution was pumped to dryness. The solid was dissolved in ethanol (10 mL) and treated with an aqueous solution (10 mL) of KBr (0.42 g, 3.50 mmol), giving a dark brown precipitate, which was filtered, washed with water (3 × 20 mL) and dried under vacuum. Yield 0.24 g (72%). $C_{36}H_{36}BrO_{12}Ru_2$ (942.73): calcd. C 45.87, H 3.85; found C 45.77, H 3.86. IR (KBr): $\tilde{\nu}$ = 3060 w, 3041 w, 2930 w, 2888 w, 1599 s, 1587 s, 1470 vs, 1440 vs, 1419 s, 1243 vs, 1043 s, 753 s, 692 m cm^{-1}. UV/Vis (MeOH): $\lambda_{max.}$ (ε) = 291 (1857), 429 (829), 1004 (25 $L{\cdot}mol^{-1}{\cdot}cm^{-1}$) nm. $\mu_{eff.}$ = 3.88 μ_B at room temperature.

Preparation of $[Ru_2I(\mu\text{-}O_2CCH_2CH_2OPh)_4]$ (3a) and $[Ru_2I(\mu\text{-}O_2CCH_2CH_2OPh)_4(H_2O)]$ (3b): The preparation was carried out as described above for **2a**, but with KI (0.58 g, 3.50 mmol) in place of KBr. The solid isolated by this procedure was characterized as **3b**. Complex **3a** was obtained after **3b** had been heated under vacuum at 75 °C for 24 h. Single crystals of **3b·0.5H$_2$O** were obtained by the following procedure: $[Ru_2Cl(\mu\text{-}O_2CCH_2CH_2OPh)_4]$ (0.09 g, 0.10 mmol) was dissolved in methanol (15 mL) and treated with an aqueous solution of $AgNO_3$ (0.017 g, 0.10 mmol). The solution was filtered and treated with an excess of PPh_4I (0.26 g, 0.50 mmol). Crystals grew over 48 h.

$[Ru_2I(\mu\text{-}O_2CCH_2CH_2OPh)_4]$ (3a): Yield 0.24 g (70%). $C_{36}H_{36}IO_{12}Ru_2$ (989.73): calcd. C 43.69, H 3.67; found C 43.58, H 3.62. IR (KBr): $\tilde{\nu}$ = 3066 w, 3040 w, 2936 w, 2889 w, 1599 m, 1588 m, 1496 m, 1466 s, 1437 vs, 1318 m, 1243 s, 1040 m, 756 m, 692 m cm^{-1}. UV/Vis (MeOH): $\lambda_{max.}$ (ε) = 288 (1836), 427 (748), 976 (19 $L{\cdot}mol^{-1}{\cdot}cm^{-1}$) nm. $\mu_{eff.}$ = 3.96 μ_B at room temperature.

$[Ru_2I(\mu\text{-}O_2CCH_2CH_2OPh)_4(H_2O)]$ (3b): Yield 0.25 g (70%). $C_{36}H_{38}IO_{13}Ru_2$ (1007.74): calcd. C 42.91, H 3.80; found C 42.78, H 3.75. IR (KBr): $\tilde{\nu}$ = 3431 m, 3066 w, 3040 w, 2936 w, 2889 w, 1599 m, 1588 m, 1496 m, 1466 s, 1437 v s, 1318 m, 1243 s, 1040 m, 756 m, 692 m cm^{-1}. UV/Vis: identical to data of **3a**. $\mu_{eff.}$ = 4.18 μ_B at room temperature.

Preparation of $[Ru_2Cl(\mu\text{-}O_2CCMePh_2)_4(H_2O)]$ (4b): An excess of 2,2-diphenylpropionic acid (0.68 g, 3.00 mmol) was added to a solution (25 mL) of $Ru_2Cl(\mu\text{-}O_2CMe)_4$ (0.24 g, 0.50 mmol) in methanol/water (24 mL, 1:1). The reaction mixture was heated at reflux for 4 h, giving a red-brown solid. The solution was filtered, and the solid was washed with diethyl ether (2 × 10 mL) and dried under vacuum. Single crystals of **4b** were obtaining by the procedure described above for **3b·0.5H$_2$O**, with PPh_4Cl (0.19 g, 0.50 mmol) in place of PPh_4I.

$[Ru_2Cl(\mu\text{-}O_2CCMePh_2)_4(H_2O)]$ (4b): Yield 0.44 g (76%). $C_{60}H_{54}ClO_9Ru_2$ (1156.69): calcd. C 62.30, H 4.71; found C 62.20, H 4.69. IR (KBr): $\tilde{\nu}$ = 3446 w, 3141 w, 3057 w, 3021 w, 2994 w, 2941 w, 1598 w, 1494 m, 1464 s, 1436 s, 1394 vs, 1367 vs, 1029 m, 998 w, 760 m, 737 m, 731 m, 697 vs, 668 s cm^{-1}. UV/Vis (MeOH): $\lambda_{max.}$ (ε) = 287 (2962), 426 (818), 968 (21 $L{\cdot}mol^{-1}{\cdot}cm^{-1}$) nm. $\mu_{eff.}$ = 4.12 μ_B at room temperature.

Preparation of $[Ru_2Br(\mu\text{-}O_2CCMePh_2)_4]$ (5a) and $[Ru_2Br(\mu\text{-}O_2CCMePh_2)_4(H_2O)]$ (5b): The preparation was carried out similarly to that described for **2a**, with $[Ru_2Cl(\mu\text{-}O_2CCMePh_2)_4(H_2O)]$ (0.40 g, 0.35 mmol). The brown solid was characterized as **5b**. Complex **5a** was obtained after **5b** had been heated under vacuum at 75 °C for 24 h.

$[Ru_2Br(\mu\text{-}O_2CCMePh_2)_4]$ (5a): Yield 0.30 g (73%). $C_{60}H_{52}BrO_8Ru_2$ (1183.13): calcd. C 60.91, H 4.43; found C 60.80, H 4.39. IR (KBr): $\tilde{\nu}$ = 3088 w, 3058 w, 3031 w, 2984 w, 2940 w, 1599 w, 1494 m, 1466 m, 1440 m, 1392 vs, 1368 s, 1029 m, 751 m, 735 m, 698 s, 668 m cm^{-1}. UV/Vis (MeOH): $\lambda_{max.}$ (ε) = 330 (983), 425 (709), 944 (213 $L{\cdot}mol^{-1}{\cdot}cm^{-1}$) nm. $\mu_{eff.}$ = 4.13 μ_B at room temperature.

$[Ru_2Br(\mu\text{-}O_2CCMePh_2)_4(H_2O)]$ (5b): Yield 0.31 g (73%). $C_{60}H_{54}BrO_9Ru_2$ (1201.14): calcd. C 60.00, H 4.53; found C 59.92, H 4.50. IR (KBr): $\tilde{\nu}$ = 3435 m, 3088 w, 3058 w, 3031 w, 2984 w, 2940 w, 1599 w, 1494 m, 1466 m, 1440 m, 1392 vs, 1368 s, 1029 m, 751 m, 735 m, 698 s, 668 m cm^{-1}. UV/Vis: identical to data of **5a**. $\mu_{eff.}$ = 4.06 μ_B at room temperature.

Preparation of $[Ru_2I(\mu\text{-}O_2CCMePh_2)_4]$ (6a) and $[Ru_2I(\mu\text{-}O_2CCMePh_2)_4(H_2O)]$ (6b): The preparation was carried out as described previously for **3a** and **3b**, with $Ru_2Cl(\mu\text{-}O_2CCMePh_2)_4(H_2O)$ (0.40 g, 0.35 mmol).

$[Ru_2I(\mu\text{-}O_2CCMePh_2)_4]$ (6a): Yield 0.29 g (67%). $C_{60}H_{52}IO_8Ru_2$ (1230.12): calcd. C 58.59, H 4.26; found C 58.51, H 4.22. IR (KBr): $\tilde{\nu}$ = 3088 w, 3059 w, 3024 w, 2983 w, 2940 w, 1582 w, 1494 m, 1467 m, 1440 m, 1392 vs, 1368 s, 1030 m, 752 w, 733 w, 698 s, 668 m cm^{-1}. UV/Vis (MeOH): $\lambda_{max.}$ (ε) = 328 (1160), 426 (820), 968 (25 $L{\cdot}mol^{-1}{\cdot}cm^{-1}$) nm. $\mu_{eff.}$ = 4.09 μ_B at room temperature.

$[Ru_2I(\mu\text{-}O_2CCMePh_2)_4(H_2O)]$ (6b): Yield 0.29 g (67%). $C_{60}H_{54}IO_9Ru_2$ (1248.14): calcd. C 57.75, H 4.36; found C 57.65, H 4.32. IR (KBr): $\tilde{\nu}$ = 3436 m, 3088 w, 3059 w, 3024 w, 2983 w, 2940 w, 1582 w, 1494 m, 1467 m, 1440 m, 1392 vs, 1368 s, 1030 m, 752 w, 733 w, 698 s, 668 m cm^{-1}. UV/Vis: identical to data of **6a**. $\mu_{eff.}$ = 4.06 μ_B at room temperature.

X-ray Crystallographic Study: Details of the data collection and crystal structure refinement for **1b·2MeOH**, **3b·0.5H$_2$O** and **4b** are

 © 2003 Wiley-VCH Verlag GmbH & Co. KGaA, Weinheim

Table 3. Crystal data for $[Ru_2Cl(\mu\text{-}O_2CCH_2CH_2OPh)_4(H_2O)]\cdot 2MeOH$ (**1b·2MeOH**), $[Ru_2I(\mu\text{-}O_2CCH_2CH_2OPh)_4(H_2O)]\cdot 0.5H_2O$ (**3b·0.5H$_2$O**), and $[Ru_2Cl(\mu\text{-}O_2CCMePh_2)_4(H_2O)]$ (**4b**)

	1b·2MeOH	**3b**·0.5H_2O	**4b**
Empirical formula	$C_{38}H_{46}ClO_{15}Ru_2$	$C_{72}H_{78}I_2O_{27}Ru_4$	$C_{60}H_{54}ClO_9Ru_2$
Formula mass	980.37	2033.50	1156.69
Temperature [K]	293(2)	293(2)	293(2)
Wavelength [Å]	0.71073	0.71073	0.71073
Crystal system	triclinic	triclinic	triclinic
Space group	$P\bar{1}$	$P\bar{1}$	$P\bar{1}$
a [Å]	11.947(2)	13.128(2)	8.8056(7)
b [Å]	14.102(2)	13.357(2)	11.5292(9)
c [Å]	14.471(2)	14.601(2)	14.525(1)
α [°]	65.395(3)	91.861(3)	111.253(2)
β [°]	79.742(3)	115.779(3)	96.898(2)
γ [°]	79.961(3)	115.269(3)	95.949(1)
V [Å^3]	2167.5(6)	2008.7(6)	1347.0(2)
Z	2	2	1
$D_{calcd.}$ [g cm^{-3}]	1.499	1.689	1.423
μ [mm^{-1}]	0.822	1.583	0.666
F(000)	994	1010	589
Crystal size [mm]	0.07 × 0.10 × 0.6	0.06 × 0.22 × 0.40	0.16 × 0.18 × 0.60
Crystal colour	red-brown	red-brown	red-brown
θ range [°]	1.60−25.00	1.61−25.00	1.53−25.00
Index ranges	$-14 \le h \le 14$, $-16 \le k \le 8$, $-17 \le l \le 16$	$-15 \le h \le 15$, $-11 \le k \le 15$, $-17 \le l \le 14$	$-10 \le h \le 9$, $-10 \le k \le 13$, $-17 \le l \le 12$
Collected reflections	11355	10260	7064
Independent reflections	7539 [R(int) = 0.0815]	6981 [R(int) = 0.0528]	4706 [R(int) = 0.0328]
Completeness to θ = 25.00° [%]	98.7	98.6	98.9
Absorption correction	none	none	none
Refinement method	full-matrix least squares on F^2	full-matrix least squares on F^2	full-matrix least squares on F^2
Data/restraints/parameters	7539/2/463	6981/0/469	4706/0/326
Goodness-of-fit on F^2	0.907	1.000	1.115
Final R indices [$I > 2\sigma(I)$]	$R1$ = 0.0644, $wR2$ = 0.1539	$R1$ = 0.0582, $wR2$ = 0.1307	$R1$ = 0.0503, $wR2$ = 0.1354
R indices (all data)	$R1$ = 0.1423, $wR2$ = 0.1791	$R1$ = 0.1437, $wR2$ = 0.1759	$R1$ = 0.0664, $wR2$ = 0.1416
Largest diff. peak/hole [e·Å^{-3}]	1.311/−0.558	1.632/−0.909	2.242/−0.355

summarised in Table 3. Representative crystals were mounted on a Bruker Smart-CCD diffractometer with graphite-monochromated Mo-K_α (λ = 0.71073 Å) radiation. For **1b·2MeOH**, data were collected over a quadrant of the reciprocal space by combination of two exposure sets. For **3b·0.5H$_2$O** and **4b**, data were collected over a hemisphere of the reciprocal space by combination of three exposures sets. The cell parameters were determined and refined by least-squares fitting of all reflections collected. The structures of **1b·2MeOH** and **3b·0.5H$_2$O** were solved by Patterson (Ru atoms, SHELXS)[43] and conventional Fourier techniques and refined by full-matrix, least-squares on F^2 (SHELXL).[44] The structure of **4b** was solved by direct methods and all calculations were performed with the aid of the SHELXS and SHELXL.[43,44] Final mixed refinement was undertaken with anisotropic thermal parameters for the non-hydrogen atoms, except for the solvent molecules, which were refined only isotropically. The hydrogen atoms were included with fixed isotropic contributions at their geometrically calculated positions, except for **1b·2MeOH** (the hydrogen atoms of the OH group of the methanol molecules, which were located in a Fourier synthesis and refined together with the oxygen atom) and for **3b·0.5H$_2$O** (the hydrogen atoms of the coordination water molecules were not found by Fourier synthesis or geometrically). For **1b·2MeOH** the positional disorder of Cl and O_{water} was resolved by refining with geometric restraints and a variable $Ru-O_{water}$ distance.[45] For **3b·0.5H$_2$O**, one residual peak was found in the last cycles of refinement, and was assigned as a solvent water molecule and refined isotropically as oxygen atom. It was not possible to locate the hydrogen atoms of this molecule. For **4b**, the refinement was carried out in both the centric ($P\bar{1}$) and noncentric ($P1$) space groups. In spite of having more refinable parameters in the acentric model the thermal parameters of several atoms became negative. Thus, the centric space group ($P\bar{1}$) was chosen. CCDC-199023 to -199025 contain the supplementary crystallographic data for this paper. These data can be obtained free of charge at www.ccdc.cam.ac.uk/conts/retrieving.html [or from the Cambridge Crystallographic Data Centre, 12 Union Road, Cambridge CB2 1EZ, UK; Fax: (internat.) + 44-1223/336-033; E-mail: deposit@ccdc.cam.ac.uk].

Acknowledgments

We are grateful to the Ministerio de Ciencia y Tecnología (Dirección General de Investigación, project no. BQU 2000-0643) for financial support.

[1] T. A. Stephenson, G. Wilkinson, *J. Inorg. Nucl. Chem.* **1966**, *28*, 2285−2291.
[2] F. A. Cotton, R. A. Walton, *Multiple bonds between metal atoms*, 2nd ed., Oxford University Press, Oxford, U. K., **1993**.
[3] M. C. Barral, R. Jiménez-Aparicio, J. L. Priego, E. C. Royer, F. A. Urbanos, *An. Quim. Int. Ed.* **1997**, *93*, 277−283.

 © 2003 Wiley-VCH Verlag GmbH & Co. KGaA, Weinheim

[4] M. A. S. Aquino, *Coord. Chem. Rev.* **1998**, *170*, 141−202.
[5] [5a] F. A. Cotton, C. Lin, C. A. Murillo, *Inorg. Chem.* **2001**, *40*, 6413−6417. [5b] F. A. Cotton, C. Lin, C. A. Murillo, *J. Chem. Soc., Dalton Trans.* **2001**, 499−501. [5c] F. A. Cotton, J. P. Donahue, C. Lin, C. A. Murillo, *Inorg. Chem.* **2001**, *40*, 1234−1244.
[6] [6a] M. H. Chisholm, *Acc. Chem. Res.* **2000**, *33*, 53−61. [6b] J. L. Wesemann, M. H. Chisholm, *Inorg. Chem.* **1997**, *36*, 3258−3267. [6c] D. V. Baxter, R. H. Cayton, M. H. Chisholm, J. C. Huffman, E. F. Putilina, S. L. Tagg, J. L. Wesemann, J. W. Zwanziger, F. D. Darrington, *J. Am. Chem. Soc.* **1994**, *116*, 4551−4566.
[7] [7a] H. Miyasaka, R. Clérac, C. S. Campos-Fernández, K. R. Dunbar, *Inorg. Chem.* **2001**, *40*, 1663−1671. [7b] H. Miyasaka, C. S. Campos-Fernández, R. Clérac, K. R. Dunbar, *Angew. Chem. Int. Ed.* **2000**, *39*, 3831−3835. [7c] X. Ouyang, C. Campana, K. R. Dunbar, *Inorg. Chem.* **1996**, *35*, 7188−7189.
[8] [8a] Y. Sayama, M. Handa, M. Mikuriya, I. Hiromitsu, K. Kasuga, *Bull. Chem. Soc. Jpn.* **2000**, *73*, 2499−2504. [8b] M. Handa, D. Yoshioka, Y. Sayama, K. Shioni, M. Mikuriya, I. Hiromitsu, K. Kasuga, *Chem. Lett.* **1999**, 1033−1034. [8c] Y. Sayama, M. Handa, M. Mikuriya, I. Hiromitsu, K. Kasuga, *Chem. Lett.* **1999**, 453−454. [8d] M. Handa, Y. Sayama, M. Mikuriya, R. Nukada, I. Hiromitsu, K. Kasuga, *Bull. Chem. Soc. Jpn.* **1998**, *71*, 119−125.
[9] M. J. Bennett, K. G. Caulton, F. A. Cotton, *Inorg. Chem.* **1969**, *8*, 1−6.
[10] T. Togano, M. Mukaida, T. Nomura, *Bull. Chem. Soc. Jpn.* **1980**, *53*, 2085−2086.
[11] B. K. Das, A. R. Chakravarty, *Polyhedron* **1991**, *10*, 491−494.
[12] M. McCann, A. Carvill, P. Guinan, P. Higgings, J. Campbell, H. Ryan, M. Walsh, G. Ferguson, J. Gallagher, *Polyhedron* **1991**, *10*, 2273−2281.
[13] M. C. Barral, R. Jiménez-Aparicio, J. L. Priego, E. C. Royer, F. A. Urbanos, U. Amador, *Inorg. Chem.* **1998**, *37*, 1413−1416.
[14] F. D. Cukiernik, D. Luneau, J. C. Marchon, P. Maldivi, *Inorg. Chem.* **1998**, *37*, 3698−3704.
[15] M. C. Barral, R. Jiménez-Aparicio, D. Pérez-Quintanilla, J. L. Priego, E. C. Royer, M. R. Torres, F. A. Urbanos, *Inorg. Chem.* **2000**, *39*, 65−70.
[16] A. Bino, F. A. Cotton, T. R. Felthouse, *Inorg. Chem.* **1979**, *18*, 2599−2604.
[17] D. S. Martin, R. A. Newman, L. M. Vlasnik, *Inorg. Chem.* **1980**, *19*, 3404−3407.
[18] F. A. Cotton, Y. Kim, T. Ren, *Polyhedron* **1993**, *12*, 607−611.
[19] M. C. Barral, R. Jiménez-Aparicio, D. Pérez-Quintanilla, E. Pinilla, J. L. Priego, E. C. Royer, F. A. Urbanos, *Polyhedron* **1998**, *18*, 371−376.
[20] M. C. Barral, R. Jiménez-Aparicio, E. C. Royer, C. Ruiz-Valero, M. J. Saucedo, F. A. Urbanos, *Inorg. Chem.* **1994**, *33*, 2692−2694.
[21] M. C. Barral, R. Jiménez-Aparicio, J. L. Priego, E. C. Royer, M. J. Saucedo, F. A. Urbanos, U. Amador, *J. Chem. Soc., Dalton Trans.* **1995**, 2183−2187.
[22] M. C. Barral, R. Jiménez-Aparicio, J. L. Priego, E. C. Royer, F. A. Urbanos, U. Amador, *J. Chem. Soc., Dalton Trans.* **1997**, 863−868.
[23] T. Kimura, T. Sakurai, M. Shima, T. Togano, M. Mukaida, T. Nomura, *Bull. Chem. Soc. Jpn.* **1982**, *55*, 3927−3928.
[24] M. Mukaida, T. Nomura, T. Ishimori, *Bull. Chem. Soc. Jpn.* **1972**, *45*, 2143−2147.
[25] W. J. Geary, *Coord. Chem. Rew.* **1971**, *7*, 81−122.
[26] G. J. Norman, G. E. Renzoni, D. A. Case, *J. Am. Chem. Soc.* **1979**, *101*, 5256−67.
[27] V. M. Miskowski, H. B. Gray, *Inorg. Chem.* **1988**, *27*, 2501−2506.
[28] V. M. Miskowski, T. M. Loehr, H. B. Gray, *Inorg. Chem.* **1987**, *26*, 1098−1108.
[29] M. C. Rusjan, E. E. Sileo, F. D. Cukiernick, *Solid State Ionics* **1999**, *124*, 143−147.
[30] F. A. Cotton, E. Pedersen, *Inorg. Chem.* **1975**, *14*, 388−391.
[31] J. Telser, R. S. Drago, *Inorg. Chem.* **1984**, *23*, 3114−3120.
[32] G. Estiú, F. D. Cukiernik, P. Maldivi, O. Poizat, *Inorg. Chem.* **1999**, *38*, 3030−3039.
[33] R. Jiménez-Aparicio, F. A. Urbanos, J. M. Arrieta, *Inorg. Chem.* **2001**, *40*, 613−619.
[34] F. D. Cukiernik, A. M. Giroud-Godquin, P. Maldivi, J. C. Marchon, *Inorg. Chim. Acta* **1994**, *215*, 203−207.
[35] E. J. Beck, K. D. Drysdale, L. K. Thompson, L. Li, C. A. Murphy, M. A. S. Aquino, *Inorg. Chim. Acta* **1998**, *279*, 121−125.
[36] M. McCann, A. Carvill, C. Cardin, M. Convery, *Polyhedron* **1993**, *12*, 1163−1169.
[37] M. W. Cooke, C. A. Murphy, T. S. Cameron, E. J. Beck, G. Vamvounis, M. A. S. Aquino, *Polyhedron* **2002**, *21*, 1235−1244.
[38] B. K. Das, A. R. Chakravarty, *Inorg. Chem.* **1992**, *31*, 1395−1400.
[39] G. G. Briand, M. W. Cooke, T. S. Cameron, H. M. Farrel, T. J. Burchell, M. A. S. Aquino, *Inorg. Chem.* **2001**, *40*, 3267−3268.
[40] M. Handa, Y. Sayama, M. Mikuriya, R. Nukada, I. Hiromitsu, K. Kasuga, *J. Chem. Soc. Jpn.* **1995**, *68*, 1647−1653.
[41] K. D. Drysdale, E. J. Beck, T. S. Cameron, K. N. Roberston, M. A. S. Aquino, *Inorg. Chim. Acta* **1997**, *256*, 243−252.
[42] R. W. Mitchell, A. Spencer, G. Wilkinson, *J. Chem. Soc., Dalton Trans.* **1973**, 846−854.
[43] G. M. Sheldrick, *SHELXS 97, Program for the solution of crystal structures*, University of Göttingen, Germany, **1997**.
[44] G. M. Sheldrick, *SHELXL 97, Program for refinement of crystal structures*, University of Göttingen, Germany, **1997**.
[45] CSD, November **2002**.

Received January 8, 2003

 © 2003 Wiley-VCH Verlag GmbH & Co. KGaA, Weinheim

Photophysical and Energy-Transfer Properties of (Salen)zinc Complexes and Supramolecular Assemblies

Kathryn E. Splan,[a] Aaron M. Massari,[a] Gregory A. Morris,[a] Shih-Sheng Sun,[a] Eduardo Reina,[a] SonBinh T. Nguyen,[a] and Joseph T. Hupp*[a]

Keywords: Host-guest systems / Fluorescence / Supramolecular chemistry / Salen ligands

The absorption, emission, and energy-transfer properties of monomeric and supramolecular (salen)Zn complexes (square and rectangular assemblies) are reported. The monomeric complexes fluoresce in solution, displaying photophysical behavior similar to typical (porphyrin)zinc complexes. Rhenium coordination chemistry is used to assemble molecular rectangles and squares that largely retain the photophysical properties of the parent compounds. Host-guest assemblies obtained by binding a fifth (salen)Zn complex to a tetrakis-(salen) square are capable of efficient salen-to-salen electronic energy transfer. Energy transfer flow through these systems can be manipulated by modification of the salen building-block structure.

(© Wiley-VCH Verlag GmbH & Co. KGaA, 69451 Weinheim, Germany, 2003)

Introduction

(Salen)metal[1] complexes are most widely known for their ability to catalyze a broad range of chemical reactions, including the epoxidation of olefins, lactide polymerization, and the asymmetric ring-opening of epoxides.[2] While examining functionalized (salen)manganese complexes in the context of supramolecular assemblies for enantioselective epoxidation reactions we have found that the formation of supramolecular species, such as H-shaped trimeric assemblies and molecular squares featuring salen ligands as edges and transition metal ions as corners, can stabilize central or encapsulated (salen)metal complexes, substantially extending their lifetimes as functional catalysts.[3] In working with these complexes and assemblies, we were struck by their strong chromophoric character and wondered whether they might exhibit − by analogy to porphyrins and phthalocyanines − interesting, measurable photophysical properties. We report herein the properties and behavior of functionalized, photo-excited (salen)zinc species, both isolated complexes **1** and **2** and supramolecular assemblies **3**−**5**. We find that the (salen)zinc species are moderately fluorescent in solution at ambient temperature, exhibiting singlet excited-state lifetimes similar to those of common (porphyrin)zinc complexes[4] and displaying an ability in supramolecular assemblies to transfer energy between (salen)-metal subunits. While a few reports exist on the photophysical properties of flexible, metal-free salen ligands (primarily excited-state proton-transfer studies),[5] to the best of our knowledge no prior reports exist on the photophysical properties of (salen)metal complexes.

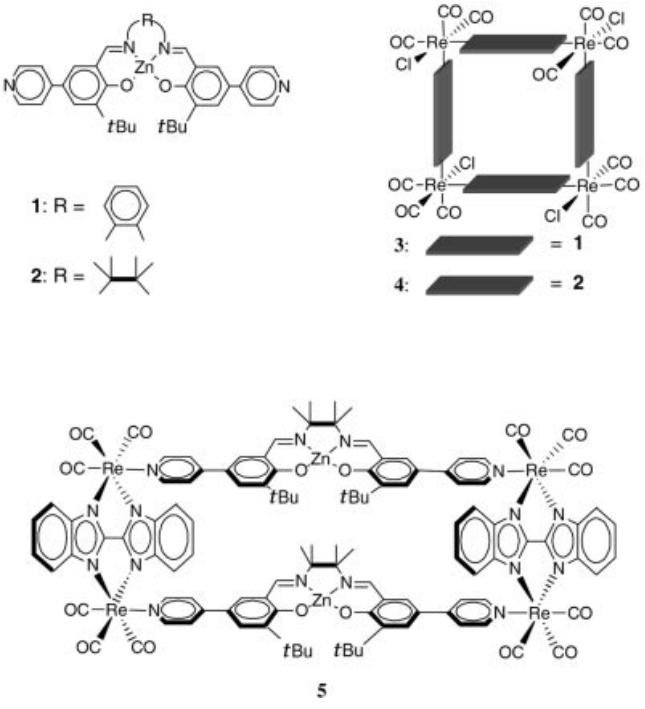

[a] Dept. of Chemistry and Institute for Environmental Catalysis
Northwestern University,
2145 Sheridan Rd., Evanston, IL 60208, USA
Fax: (internat.) + 1-847/491-7713
E-mail: jthupp@chem.nwu.edu

Results and Discussion

As indicated by the structures, pyridyl functionalities provide a basis for constructing supramolecular assemblies

 © 2003 Wiley-VCH Verlag GmbH & Co. KGaA, Weinheim **DOI: 10.1002/ejic.200200665**

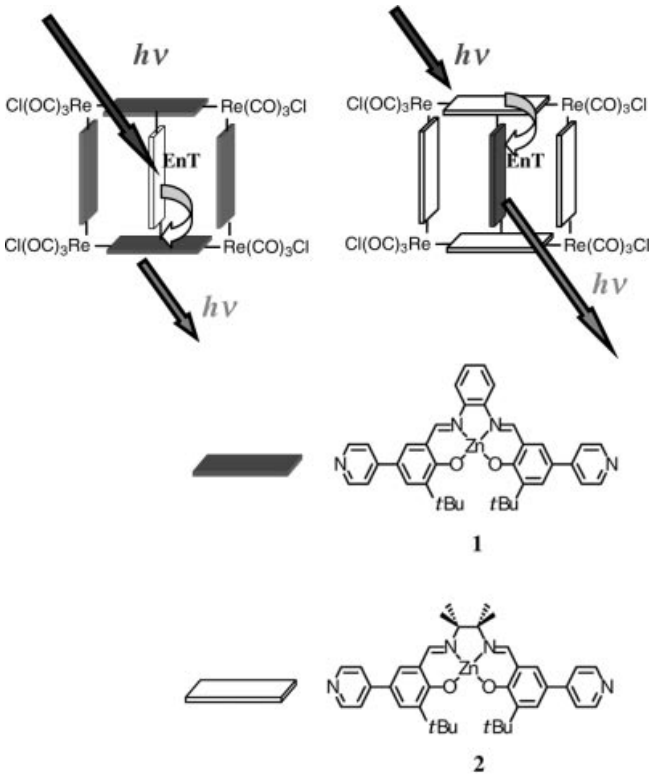

Scheme 1

using known rhenium(I) coordination chemistry.[6−8] The central zinc(II) ions rigidify the salen ligands, displace the hydroxylic protons whose transfer would otherwise dominate the photophysics,[9] and serve as axial ligation sites for reversible binding of Lewis basic groups, allowing for interior functionalization of **3** and **4**. In contrast to catalytically active metals such as manganese, chromium, and cobalt, however, the complexed zinc ions are electronically inactive in the compounds' ground and photo-excited states. Figure 1 shows the electronic absorption and emission spectra for **1** and **2** in tetrahydrofuran. The complexes are characterized by intense absorption in the near UV [ε(**1**) = 80000 $M^{-1}\cdot cm^{-1}$ and ε(**2**) = 52000 $M^{-1}cm^{-1}$] and in the blue region of the visible spectrum. These transitions increase in intensity and substantially red-shift upon zinc metallation when compared to the free-base derivatives of **1** and **2**, consistent with expanded conjugation over the entire ligand.[10] Semi-empirical electronic structure calculations (ZINDO-S, Hyperchem™ version 5.03) indicate predominantly $\pi\rightarrow\pi^*$ transitions for both compounds. The observed red shift for the phenyl-bridged complex **1** with respect to complex **2** is replicated qualitatively in the calculations and is consistent with expansion of the aromatic π-system in the emissive excited state of **1** versus **2**. Incorporation of **1** and **2** into molecular squares **3** and **4** results in only subtle changes in visible-region absorption characteristics (not shown), indicating little contribution from Re^I charge-transfer absorption.

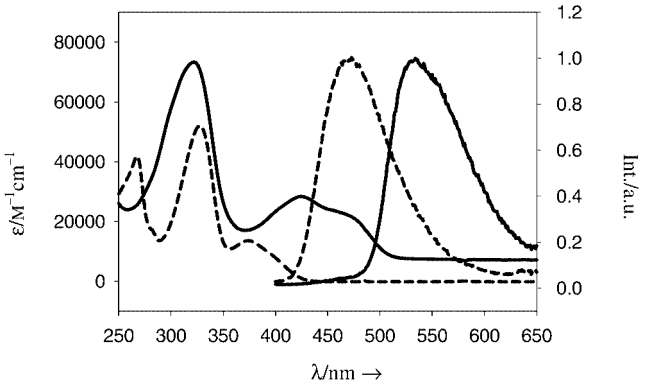

Figure 1. Absorption (left) and emission (right) spectra for **1** (—) and **2** (---) in THF

Table 1 summarizes the emission data collected for various (salen)zinc complexes. Briefly, the observed lifetimes and quantum yields of salen monomers **1** and **2** are similar to those typically seen for (porphyrin)zinc(II) complexes[4] and are consistent with singlet emission in competition with efficient singlet-to-triplet intersystem crossing. Extension of the study to supramolecular assemblies **3**−**5** (again see Table 1) shows that Re^I coordination induces slight emission blue shifts and causes a modest decrease in emission intensity and lifetime owing to enhanced intersystem crossing to non-emissive triplet states.[11] Interestingly, emission from **5** occurs from a singlet state that is about 3000 cm^{-1} *higher* in energy than the generally emissive metal-to-ligand charge-transfer (MLCT) excited states that characterizes most tricarbonylbis(imine)rhenium(I) complexes.[12] The MLCT states are typically long-lived and are nominally triplet states. That emission from these is not observed is likely indicative of an even lower energy for the salen-centered triplet state.

Table 1. Photophysical properties of salen complexes in THF

Compound	$\lambda_{em.\ max.}$ [nm]	φ_{fl}	τ_{fl} [ns]
1	532	0.11	0.63
2	471	0.19	1.15
3	526	0.073	0.62
4	460	0.039	0.50
5	454	0.031	0.36

Fluorescence titration of the salen square **3** with **2**, presumably to form a pentakis(salen) assembly,[13] yielded a binding constant of $9(\pm 3) \times 10^4$ M^{-1} in chloroform as solvent. As shown in Figure 2 (top), excitation at 400 nm, where both the square and the encapsulated salen absorb, results in fluorescence exclusively from the square. The increase in square emission intensity[14] and the absence of detectable emission from the encapsulated alkylsalen complex is indicative of efficient energy transfer (EnT) from the encapsulated salen to the surrounding square and is consistent with the good spectral overlap evidenced in Figure 1.[15] Based on the lifetimes of the component fluorophores the

 © 2003 Wiley-VCH Verlag GmbH & Co. KGaA, Weinheim

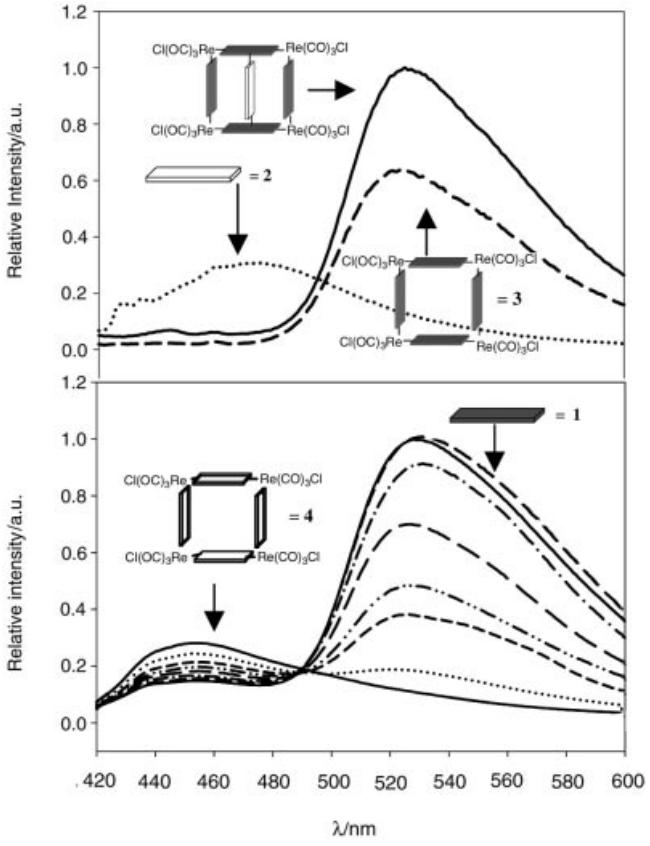

Figure 2. Top: emission spectra of 1 μM solutions of **2** (···), **3** (---), and an equimolar solution of **2** and **3** (—) in $CHCl_3$, based on 400 nm excitation; bottom: fluorescence titration of square **4** with **1**; sequential titrations show a quenching of square emission accompanied by an increase in guest salen emission

guest **2** to host **3** energy transfer rate constant is estimated as greater than 10^{-10} s^{-1}.

Based on the spectral overlap between compounds **1** and **2**, EnT should be observed from the alkylsalen complex (donor) to the phenyl complex (acceptor). Therefore, by reversing the back-bone functionalities of the salen building blocks the direction of energy transfer (EnT) can be controlled within the supramolecular assembly (Scheme 1). When **1** is added to square **4** (Figure 2, bottom) efficient energy transfer is observed. However, in contrast to the assembly described above in which the guest salen transfers energy to the host square, outside-to-inside EnT is observed, i.e. the salen walls act as antennae and transfer their energy to the encapsulated guest; see Scheme 1. A control experiment in which **4** was titrated with a derivative of **1** where the pyridyl moieties were replaced with non-binding *tert*-butyl groups underscores the importance of supramolecular assembly formation in facilitating rapid EnT. Neither quenching of the host square fluorescence nor sensitization of the candidate guest salen (*tert*-butylsalen) fluorescence was observed, consistent with the brevity of the host excited-state lifetime relative to diffusional encounter times.

To summarize, salen ligands, after complexation of Zn^{II}, display significant fluorescence and acquire roughly nanosecond singlet excited-state lifetimes. Substitution of alkyl groups by an arene on the salen backbone shifts the ligand's absorption spectrum well into the visible region. Square and rectangular supramolecular assemblies of salens, prepared by Re^{I} ligation of pendant pyridyl groups, also fluoresce at room temperature in solution, albeit with diminished quantum yields and lifetimes. Finally, electronic EnT is observed within pentakis(salen) assemblies. Modification of host and guest salen building blocks allows for manipulation of excitation energy flow through these systems.

Experimental Section

General: Monomeric salen complexes[16] **1** and **2** and dimetallic [{$(CO)_4Re$}$_2$BisBzIm] edges (BzIm = benzimidazolate)[7a,7b] were synthesized according to literature procedures. THF was dried with Na/benzophenone. All other chemicals and solvents were reagent grade and used as received. ^{1}H NMR spectra were recorded with a 400 MHz Varian Mercury spectrometer. FAB mass spectra were obtained in the Mass Spectrometry Laboratory, School of Chemical Sciences, University of Illinois or the Analytical Services Laboratory, Northwestern University.

3: Equimolar amounts of **1** (193 mg, 0.300 mmol) and $Re(CO)_5Cl$ (108 mg, 0.299 mmol) were refluxed in THF (100 mL) for 3 d under N_2. The reaction mixture was filtered and the initial dark precipitate was discarded. A yellow product (162 mg, 55%) was precipitated by concentrating the filtrate to 1/3 of its volume, adding hexanes, and cooling the solution to 0 °C. ^{1}H NMR (500 MHz, [D_6]DMSO): δ = 9.20 (br., 8 H), 8.59 (br., 8 H), 8.06 (br., 4 H), 7.94 (br., 4 H), 7.82 (br., 8 H), 7.71 (br., 4 H), 7.66 (br., 4 H), 7.43 (br., 8 H), 1.51 (s, 72 H) ppm. ^{13}C NMR (500 MHz, THF): δ = 197.7, 194.1, 175.4, 163.3, 154.3, 151.4, 144.6, 140.3, 135.1, 129.7, 128.4, 121.6, 121.0, 120.5, 116.7, 36.5, 30.1 ppm. FTIR (THF): ν_{CO} = 2024, 1913, 1885 cm^{-1}. $C_{164}H_{144}Cl_4N_{16}O_{20}Re_4Zn_4{\cdot}8H_2O$ (3951): calcd. C 49.85, H 4.08, N 5.67; found C, 50.22, H 4.29, N 5.30. FAB MS: calcd. *m*/*z* = 3807.2; found 3807.2.

4: A mixture of $Re(CO)_5Cl$ (50.0 mg, 0.138 mmol), **2** (90.0 mg, 0.138 mmol), and THF (50 mL) was heated to 60 °C for 40 h, during which time a yellow solid started to precipitate. The product was further precipitated by adding cold diethyl ether (excess) and was isolated by filtration to afford a yellowish powder. Yield 91% (120 mg). ^{1}H NMR (400 MHz, CD_3CN): δ = 8.55 (d, 16 H, *J* = 6.8 Hz), 8.49 (s, 8 H), 7.68 (s, 8 H), 7.66 (s, 8 H), 7.60 (d, 16 H, *J* = 6.8 Hz), 1.50 (s, 72 H), 1.27 (s, 48 H). LR FAB-MS: calcd. for $[M]^+$: *m*/*z* = 3839.5; found 3839.1. $C_{164}H_{176}Cl_4N_{16}O_{20}Re_4Zn_4{\cdot}4THF$ (4128): calcd. C 52.37, H 5.08, N 5.43; found C, 52.66, H 4.90, N 5.19.

5: Salen rectangle **5** was formed by allowing equimolar amounts of [{$(CO)_4Re$}$_2$BisBzIm] (103 mg, 0.125 mmol) and **2** (81.0 mg, 0.125 mmol) to react in refluxing THF (60 mL) under N_2 for2 d. The reaction mixture was cooled and concentrated to half of its volume. Upon addition of hexanes the desired product precipitated as a yellow powder in 69% yield (61.5 mg). ^{1}H NMR (500 MHz, 55 °C, [D_8]THF): δ = 8.42 (s, 4 H), 8.12 (br., 8 H), 7.81 (br., 8 H), 7.49 (s, 4 H), 7.43 (s, 4 H), 7.36 (br., 8 H), 7.31 (br., 8 H), 1.78 (s, 36 H), 1.41 (m, 24 H). FAB MS: calcd. for [M + H_2O]: *m*/*z* = 2855.6; found 2854.7.

Acknowledgments

We gratefully acknowledge the National Science Foundation (S. T. N.), the U. S. Department of Energy (J. T. H.), and the Nanoscale

 © 2003 Wiley-VCH Verlag GmbH & Co. KGaA, Weinheim

Science and Engineering Center at Northwestern University (REU/MIN undergraduate research fellowship for E. R.) for financial support. K. E. S. additionally thanks the Dow Foundation for a graduate fellowship. We also thank Wen Liu for assistance in lifetime measurements.

[1] For the remainder of this article, the term salen will be used to describe the general class of bis(salicylamide) ligands and complexes.

[2] [2a] L. Canali, D. C. Sherrington, *Chem. Soc. Rev.* **1999**, *28*, 85−93. [2b] E. N. Jacobsen, in *Comprehensive Organometallic Chemistry II* (Eds. E. W. Abel, F. G. A. Stone, and E. Willinson), Pergamon, New York, **1995**, vol. 12, pp. 1907−1135. [2c] T. M. Ovitt, G. W. Coates, *J. Am. Chem. Soc.* **1999**, *121*, 4072−4073. [2d] R. G. Konsler, J. Karl, E. N. Jacobsen, *J. Am. Chem. Soc.* **1998**, *120*, 10780−10781.

[3] [3a] G. A. Morris, S. T. Nguyen, J. T. Hupp, *J. Mol. Catal. A.* **2001**, *174*, 15−20. [3b] G. A. Morris, PhD Thesis, Department of Chemistry, Northwestern University, **2001**.

[4] K. Kalayasundarum, *Photochemistry of Polypyridine and Porphyrin Complexes*, Academic Press, Inc., San Diego, CA, **1992**, pp. 399−434.

[5] [5a] T. Kawasaki, T. Kamata, H. Ushijima, M. Kanakubo, S. Murata, F. Mizukami, Y. Fujii, Y. Usui, *J. Chem. Soc., Perkin Trans. 2* **1999**, 193−198. [5b] J. Zhao, B. Zhao, J. Liu, A. Ren, J. Feng, *Chem. Lett.* **2000**, 268−269.

[6] [6a] M. S. Wrighton, D. L. Morse, *J. Am. Chem. Soc.* **1974**, *96*, 998−1003. [6b] M. S. Wrighton, P. J. Giordano, *J. Am. Chem. Soc.* **1979**, *101*, 2888−2897. [6c] R. V. Slone, J. T. Hupp, *Inorg. Chem.* **1997**, *36*, 5422−5423.

[7] [7a] R. Uson, J. Gimeno, *J. Organomet. Chem.* **1981**, *220*, 173−179. [7b] K. D. Benkstein, J. T. Hupp, C. L. Stern, *Angew. Chem. Int. Ed.* **2000**, *39*, 2891−2893. [7c] K. D. Benkstein, C. L. Stern, K. E. Splan, R. C. Johnson, K. A. Walters, F. W. M. Vanhelmont, J. T. Hupp, *Eur. J. Inorg. Chem.* **2002**, *2002*, 2818−2822.

[8] The identity of the supramolecular complexes **3** and **4** has been confirmed by combustion analysis and mass spectroscopic data. Combustion analysis establishes an Re/ligand ratio of 1:1, disproving the presence of metal or ligand terminated oligomers. Predominant peaks in the mass spectroscopic data correspond to tetramers, while peaks of higher and lower weight species are not observed. Additionally, square **3** has been characterized by pulsed-field gradient NMR spectroscopy (PFG NMR), a technique recently employed to establish the identity of supramolecular squares (vs. ligands and oligomers) by determining the diffusion coeffiecent of the species present: W. H. Otto, M. H. Keefe, K. E. Splan, J. T. Hupp, C. K. Larive, *Inorg. Chem.* **2002**, *41*, 6172−6174.

[9] [9a] E. Hadjoudis, M. Vittorakis, I. Moustakali-Mavridis, *Tetrahedron* **1987**, *43*, 1345−1360. [9b] T. Sekikawa, T. Kobayashi, T. Inabe, *J. Phys. Chem. A* **1997**, *101*, 644−649.

[10] K. E. Splan, J. T. Hupp, unpublished results.

[11] In contrast, corresponding 5,15-dipyridylporphyrin assemblies exhibit slight red shifts upon coordination to Re^{I}, but also show diminished quantum yields and lifetimes relative to their respective monomers.[6c,7c]

[12] L. A. Wori, R. Duesing, P. Chen, L. Della Ciana, T. J. Meyer, *J. Chem. Soc., Dalton Trans.* **1991**, 849−858.

[13] Unfortunately, the low solubility of the assembly (< 10 μM) precluded corroborative characterization by NMR spectroscopy.

[14] Control experiments using large excesses of pyridine or 4-phenylpyridine in place of **2** had no effect upon the emission yield of the square.

[15] Replacement of **2** by a 5,15-bis(4-ethynylpyridyl)porphyrin, for which no spectral overlap with **4** is observed, yielded no detectable guest-to-host energy transfer.

[16] G. A. Morris, H. Zhou, C. L. Stern, S. T. Nguyen, *Inorg. Chem.* **2001**, *40*, 3222−3227.

Received December 3, 2002

 © 2003 Wiley-VCH Verlag GmbH & Co. KGaA, Weinheim

Iodoargentates and Cuprates Stabilized by Sulfonium Cations With Long Alkyl Chains

Heléne Paulsson,*[a] Malin Berggrund,[a] Andreas Fischer,[a] and Lars Kloo[a]

Keywords: Cations / Iodide / Copper / Silver / Crystal structure

$[DodMe_2S]_2AgI_3$ and $[DodMe_2S]Ag_2I_3$ were obtained from mixtures of dodecyldimethylsulfonium iodide and silver iodide in acetonitrile solution. $[DodMe_2S]_2AgI_3$ crystallizes in the orthorhombic crystal system, space group *Pbca* and contains trigonal planar anions AgI_3^{2-}, while $[DodMe_2S]Ag_2I_3$ crystallizes in the triclinic crystal system, space group $P\bar{1}$, and consists of polymeric anions $^1{}_\infty(Ag_2I_3)^-$. In both structures, the sulfonium cations form a layer of parallel and interpenetrating dodecyl chains with the sulfoniumdimethyl groups on both sides of the layer. $[DodMe_2S]_2CuI_3$ was obtained from dodecyldimethylsulfonium iodide and copper iodide mixtures and is isostructural with the corresponding silver compound.

(© Wiley-VCH Verlag GmbH & Co. KGaA, 69451 Weinheim, Germany, 2003)

Introduction

Metal iodides and polyiodides are interesting and important materials that are useful in various electrochemical applications.[1−4] In our laboratory, many alkyl iodide and polyiodide compounds have been synthesized in sulfonium-based reaction media, which have emerged as efficient electrolytes in dye-sensitised nanostructured solar cells of the Grätzel type.[5−7] While iodometallates with symmetric cations, such as trimethylsulfonium and triethylsulfonium ions, have been prepared previously, sulfonium cations with long-chain substituents, such as dodecyl and hexadecyl groups, have not been investigated so far. $[DodMe_2S]I$ is the only compound known in this field that has been structurally characterized.[5] This is rather surprising since these long chains would introduce new properties into the materials, yielding compounds that may combine the polarity of a halometallate and the nonpolar properties of the alkyl groups.

Low-dimensional compounds, such as hybrid organic-inorganic layered solids, have been shown to combine conductivity and magnetism or optics and magnetism.[8−11] Several inorganic host networks with structural flexibility of the interlayer separation have been investigated and large organic anions (amphiphiles) been successfully inserted. These amphiphiles may be formed from long-chain alkyl compounds with charged, polar endings consisting of ammonium-, phosphonium- or sulfate-based complexes. The long-chain alkyl groups form mono- or bilayers, which are favourably close-packed.[12−15] In amphiphiles with polar sulfonium groups, the structure of the packed alkyl layers is preferably tilted. This has been observed in both hydroxide double salts and highly conducting, so called Longmuir−Blodgett films.[13−14]

The main purpose of this work is to investigate metal-iodide-doped long-chain alkyl sulfonium iodides, with and without additional iodine. One experimental difficulty that is inherent in these systems is imposed by the physical properties, such as very high viscosities, which makes it difficult to obtain crystals with a sufficiently high quality for structure determinations. This problem may be diminished, though, by use of organic solvents such as acetone or acetonitrile. From using systems of metal-iodide-doped asymmetric trialkylsulfonium iodides, we have obtained the new compounds $[DodMe_2S]_2AgI_3$, $[DodMe_2]Ag_2I_3$ and $[DodMe_2S]_2CuI_3$, whose structures are presented here.

Results and Discussion

Crystal Structure of $[DodMe_2S]_2CuI_3$ and $[DodMe_2S]_2AgI_3$

Both compounds are isostructural and crystallise in the orthorhombic crystal system, space group *Pbca*. The structures consist of dimethyldodecylsulfonium cations and approximately trigonal planar MI_3^{2-} anions (M = Ag, Cu). Figure 1 shows the arrangement of both structures in the unit cell. The cations are arranged in such a way that all dodecyl chains are zigzag shaped and run parallel to each other, thus forming laminar layers with the SMe_2 groups sticking out on both sides of the surfaces;[5] the MI_3^{2-} anions are found between the layers. The geometry of the MI_3 groups is almost trigonal planar with bond lengths between 2.523(2) and 2.561(2) Å in CuI_3^{2-}. In AgI_3^{2-} the

[a] Dept. of Chemistry, Inorganic Chemistry, The Royal Institute of Technology (KTH),
Teknikringen 36, 10044 Stockholm, Sweden
Fax: (internat.) + 46-8/7909349
E-mail: Larsa@inorg.kth.se

 © 2003 Wiley-VCH Verlag GmbH & Co. KGaA, Weinheim DOI: 10.1002/ejic.200200667

range of interatomic distances is between 2.703(2) and 2.757(2) Å. The angles between the metal-iodine bonds are between 115.7(1) and 123.9(1)° (Cu) and 114.20(6) and 125.55(2)° (Ag). Thus, the arrangement around the central metal atoms deviates significantly from the ideal trigonal geometry.

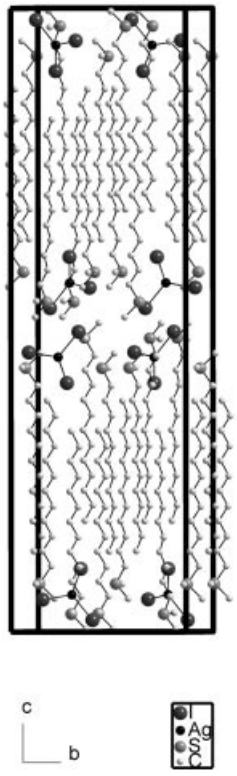

Figure 1. Structure of $[DodMe_2S]_2CuI_3$ and $[DodMe_2S]_2AgI_3$

While three-coordinate copper(I) appears frequently, this particular structural motif is not very common in the structural chemistry of discrete iodocuprates(I) and -argentates(I). So far, only one example of a compound containing AgI_3^{2-} anions has been published, namely in the structure of methyltriphenyl phosphonium triiodoargentate.[16] The geometry of the anion in this compound is in very good agreement with that in our study. In the case of iodocuprates, several examples of structures containing CuI_3 groups are known in compounds such as methyltriphenylphosphonium triiodocuprate[17] or cobaltocenium triiodocuprate.[18] Additionally, similar compounds for Cu^{II}, containing the CuX_3^- anion (X = Cl, Br), have been published recently.[19] The CuX_3^- conformation deviates from a perfect trigonal structure, as expected, due to potential Jahn-Teller instability. Also, due to the inherent instability of Cu^{II} in the presence of iodide, similar CuI_3^- ions are not known.

Crystal Structure of $[DodMe_2S]\ {}^1{}_\infty[Ag_2I_3]$

This compound crystallizes in the triclinic crystal system, space group $P\bar{1}$. It contains a polymeric structure consisting of one-dimensional, infinite Ag_2I_3 chains. These chains are made from two rows of edge-sharing AgI_4 tetrahedra, which are connected by common tetrahedron edges (Figure 2). The $Ag_2I_3^-$ anion is also present in the structures of $[NMe_4]Ag_2I_3$[20] and $CsAg_2I_3$.[21] Several iodocuprate(I) analogues are known, such as $CsCu_2I_3$ and RCu_2I_3 (R = *N*-methylpyridinium).[22–23]

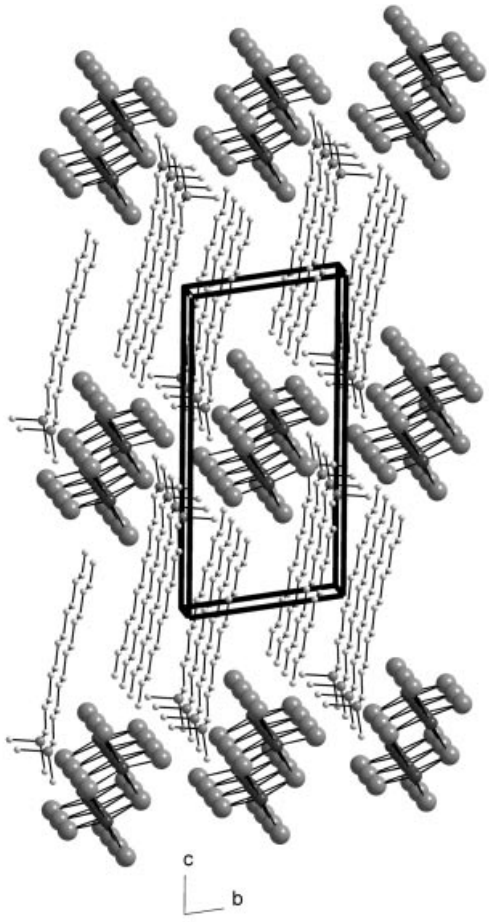

Figure 2. Structure of $[DodMe_2S]\ {}^1{}_\infty[Ag_2I_3]$

As in other polymeric anions of this type, the arrangement of the iodide ions around the silver ions is rather distorted. The I–Ag–I angles lie in a range of 100.0° to 119.7°, thus deviating significantly from the ideal tetrahedral coordination. The bond lengths illustrate the different nature of the two types of iodide ions that are present. Each I(1) connects four silver atoms and thus forms the corner of four common tetrahedra. The interatomic I(1)–Ag distances are therefore rather long (288.4–299.6 pm). I(2) and I(3) connect two silver ions and the distances between these iodide ions and the silver ions are in the range 279.7–283.0 pm.

Conclusions

Silver- and copper-iodide-containing dodecyldimethylsulfonium iodides are structurally stabilized by lamellar net-

 © 2003 Wiley-VCH Verlag GmbH & Co. KGaA, Weinheim

works formed by the long-chain dodecyl groups in $(DodMe_2S)^+$ cations, whereas the anionic building blocks may consist of either monomeric entities, such as AgI_3^{2-} and CuI_3^{2-}, or polymeric structures such as $Ag_2I_3^-$. The AgI_3^{2-} anions are preferably formed in the presence of elemental iodine. The structure of $[Ag^+(I^-)_3]^{2-}$ reveals that iodide ions obviously prefer silver ions to iodine molecules, since triiodide ions $(I_3)^-$ should otherwise be expected to form. Comparatively, thallium triiodide (TlI_3) has shown other properties since its crystal structure actually consists of Tl^+ and $(I_3)^-$ units.[5,24−25]

Experimental Section

General Remarks: The crystals for crystallographic analysis were grown as "hermits" in order to give maximum quality, and consequently the yield was not optimised. Bulk synthesis of the compounds typically produces a yield of about 70−80%. The purity of the products was checked by NMR and Raman spectroscopy as well as by a melting point determination.

Synthesis of $[DodMe_2S]_2CuI_3$ and $[DodMe_2S]_2AgI_3$: Crystals of $[DodMe_2S]_2CuI_3$ and $[DodMe_2S]_2AgI_3$ could be obtained by reacting dodecyldimethyl sulfonium iodide with the respective metal iodide in the sulfonium-to-metal-iodide proportion 1:0.3 and then dissolving the mixtures in an acetonitrile solution. The $[DodMe_2S]I$ used was synthesized by reacting equimolar amounts of dodecylmethyl sulfide and methyl iodide (see ref.[7]) Concerning the AgI_3-containing crystals, elemental iodine was also added in the sulfonium-to-iodine proportion 1:0.01. Upon slow evaporation of the solvent at room temperature, both compounds crystallized within a couple of days. In a typical synthesis, 10 mg of the respective mixture was dissolved in 0.1 mL acetonitrile and then left in an NMR tube for slow evaporation at room temperature yielding 6 mg (60%) of white or light yellow crystals.

Synthesis of $[DodMe_2S]Ag_2I_3$: White crystals of $[DodMe_2S]Ag_2I_3$ could be obtained from mixtures of $[DodMe_2S]I$ and silver iodide (AgI) in a similar way as mentioned above, though without any addition of iodine [yield: about 6 mg (60%)].

Crystal Structure Determination of $[DodMe_2S]_2CuI_3$ and $[DodMe_2S]_2AgI_3$: X-ray diffraction data for the crystals were collected using a Bruker Nonius KappaCCD diffractometer. Both compounds crystallise in the orthorhombic system. The space group *Pbca* could be unambiguously determined from the systematic absences. Numerical absorption corrections were applied[26] The positions of the Cu (Ag) and I atoms were determined by direct methods, and C and S atoms were localized in subsequent difference Fourier syntheses. Hydrogen atoms were placed at calculated positions and refined using a riding model. All parameters were refined against F^2. All non-hydrogen atoms were refined with anisotropic displacement parameters. Crystallographic details of the structure determinations are presented in Table 1.

Crystal Structure Determination of $[DodMe_2S]^1{}_\infty[Ag_2I_3]$: X-ray diffraction data were collected by using a Bruker Nonius KappaCCD diffractometer. The compound crystallises in the triclinic system; the space group $P\bar{1}$ could be confirmed during the structure determination. A numerical absorption correction was applied[26] The positions of Ag and I atoms were determined by direct methods,

Table 1. Crystallographic data, details of data collection and structure refinement calculations for $[DodMe_2S]_2CuI_3$ (**1**), $[DodMe_2S]_2AgI_3$ (**2**) and $[DodMe_2S]\ ^1{}_\infty[Ag_2I_3]$ (**3**)

Compound number	**1**	**2**	**3**
Empirical formula	$C_{28}H_{62}CuI_3S_2$	$C_{28}H_{62}AgI_3S_2$	$C_{14}H_{31}Ag_2I_3S$
Unit cell dimensions/pm	a = 971.66(3)	a = 974.93(3)	a = 683.53(6)
	b = 1504.91(3)	b = 1515.14(3)	b = 914.69(6)
	c = 5232.0(2) p	c = 5252.0(2)	c = 1937.6(2)
			α = 81.798(3)°
			β = 81.748(3)°
			γ = 88.568(4)°
Cell volume/10^6 pm^3	V = 7650.6(4)	V = 7758.0(4)	V = 1186.6(2)
Z	8		2
ρ(calcd.)/g·cm^{-3}	1.575	1.629	2.317
Crystal system, space group	orthorhombic, *Pbca* (No. 61)		triclinic, $P\bar{1}$ (No. 2)
Diffractometer	Bruker Nonius KappaCCD		
Temperature/K	297	297	297
Radiation	Mo-$K\alpha$, λ = 71.073 pm		
Absorption coefficient/ cm^{-1}	μ = 31.2	μ = 30.3	μ = 56.3
Absorption correction	numerical		
Theta range	8.16° < 2θ < 52.72°	10.22° < 2θ < 50.08°	10.24° < 2θ < 56.56°
Number of measured reflections	56315	58846	12942
Number of unique reflections	7757	6646	5662
R_{int}	0.0897	0.0577	0.0361
Number of refined parameters	307	307	182
Ratio reflections/parameters	25	21	31
Residuals R_1 (all reflections)[a]	0.112	0.0735	0.0870
R_1	0.0536 (4688 obsd. reflns.)	0.0459 (4887 obsd. reflns.)	0.0409 (3516 obsd. reflns.)
wR_2 (all reflections)[b]	0.0808	0.0852	0.101
Difference electron density	+0.75/−0.71	1.15/−0.73	+1.08/−1.32
CCDC number	198736	198737	198735

[a] $R1 = \Sigma||F_o| - |F_c||/\Sigma|F_o|$. [b] $wR2 = [\Sigma[w(F_o^2-F_c^2)^2]/\Sigma w(F_o^2)^2]^{0,5}$.

 © 2003 Wiley-VCH Verlag GmbH & Co. KGaA, Weinheim

and C and S atoms were localized in subsequent difference Fourier syntheses. Hydrogen atoms were placed at calculated positions and refined using a riding model. All parameters were refined against F^2. All non-hydrogen atoms were refined with anisotropic displacement parameters. Crystallographic details of the structure determinations are presented in Table 1.

CCDC-198735, -198736, and -198737 contain the supplementary crystallographic data for this paper. These data can be obtained free of charge at www.ccdc.cam.ac.uk/conts/retrieving.html [or from the Cambridge Crystallographic Data Centre, 12, Union Road, Cambridge CB2 1EZ, UK; Fax: (internat.) + 44-1223/336-033; E-mail: deposit@ccdc.cam.ac.uk].

Acknowledgments

The Swedish National Research Council is acknowledged for financial support and for the funding of the Bruker Nonius KappaCCD diffractometer.

[1] H. Stegemann, K.-F. Tebbe, L. A. Bengtsson, *Z. Anorg. Allg. Chem.* **1995**, *621*, 165−170.
[2] K.-F. Tebbe, R. Buchem, *Angew. Chem. Int. Ed. Engl.* **1997**, *36*, 1345−1346.
[3] P. H. Svensson, L. Kloo, J. Rosdahl, *Chem. A. Eur. J.* **1999**, *5*, 305−311.
[4] P. H. Svensson, L. Kloo, *Inorg. Chem.* **1999**, *38*, 3390−3393.
[5] P. H. Svensson, *PhD Thesis*, University of Lund **1998**.
[6] H. Paulsson, A. Hagfeldt, L. Kloo, paper to be published.
[7] H. Paulsson, M. Berggrund, A. Fischer, A. Hagfeldt, L. Kloo, paper to be published.
[8] J. F. Nicoud, *Science* **1994**, *263*, 636.
[9] P. Day, *Mol. Cryst. Liq. Cryst.* **1997**, *305*, 533−542.
[10] P. Gütlich, *Mol. Cryst. Liq. Cryst.* **1997**, *305*, 17−40.
[11] L. Ouahad, *Chem. Mater.* **1997**, *9*, 1909−1926.
[12] J. S. Miller, M. Drillon, *Magnetism: Molecules to Materials II*, Wiley-VCH, **2001**.
[13] T. Bjørnholm, T. Hassenkam, N. Reitzel, *J. Mater. Chem.* **1999**, *9*, 1975−1990.
[14] M. Meyn, K. Beneke, G. Lagaly, *Inorg. Chem.* **1993**, *32*, 1209−1215.
[15] V. Laget, C. Hornick, P. Rabu, M. Drillon, P. Turek, R. Ziessel, *Adv. Mater.* **1998**, *10*, 1024−1028.
[16] G. A. Bowmaker, A. Camus, B. W. Skelton, A. H. White, *J. Chem. Soc., Dalton Trans.* **1990**, *3*, 727−731.
[17] G. A. Bowmaker, G. R. Clark, D. A. Rogers, A. Camus, N. Marsich, *J. Chem. Soc., Dalton Trans.* **1984**, *1*, 37−45.
[18] H. Hartl, I. Bruedgam, *Z. Naturforsch., Teil B* **1989**, *44(8)*, 936−941.
[19] C. Hasselgren, S. Jagner, I. Dance, *Chem. A Eur. J.* **2002**, *8*, 1269−1278.
[20] J. K. Kildea, B. W. Skelton, A. H. White, *Austr. J. Chem.* **1986**, *39*, 171−175.
[21] C. Brink, N. F. Binnendijk, J. van de Linde, *Acta Crystallogr.* **1954**, *7*, 176−180.
[22] H. Hartl, F. Mahdjour-Hassan-Abadi, *Z. Naturforsch., Teil B* **1984**, *39*, 149−156.
[23] N. Jouini, L. Guen, M. Tournoux, *Rev. Chim. Miner.* **1980**, *17*, 486−491.
[24] P. H. Svensson, G. Raud, L. Kloo, *Eur. J. Inorg. Chem.* **2000**, *6*, 1275−1282.
[25] K. F. Tebbe, U. Georgy, *Acta Crystallogr., Sect. C* **1986**, *42*, 1675−1678.
[26] W. Herrendorf, H. Bärnighausen, HABITUS, a program for numerical absorption correction, Universities of Karlsruhe and Giessen, **1997**.

Received December 6, 2002

 © 2003 Wiley-VCH Verlag GmbH & Co. KGaA, Weinheim

EurJIC
European Journal of Inorganic Chemistry

Issue 13/2003

Pages 2357–2536

Papers available ahead of print in Early View at www.interscience.wiley.com

Earliest available Table of Contents:
Automatically, free of charge by e-mail through
www.interscience.wiley.com/alerts

COVER PICTURE

The cover picture shows the X-ray structure of an unprecedented supramolecular assembly comprising four porphyrins and six metal atoms (two Ru and four Zn); this very stable and symmetrical architecture was obtained by spontaneous self-assembly through four 4′-N(py)–Zn interactions of two equal bis(porphyrin)ruthenium self-complementary building blocks. The design of this and other robust and shape-persistent assemblies, obtained by coordination of *meso*-pyridylporphyrins to ruthenium, palladium and zinc centers, is comprehensively discussed in the microreview by E. Alessio et al. on p. 2371ff. NMR spectroscopy and X-ray crystallography were used jointly for the unambiguous characterization of the new species in solution and solid state, respectively. Very often the adducts of nanoscopic dimensions, in which the number, position, relative distance and orientation of the chromophores is well defined, were obtained through hierarchical supramolecular self-assembly: multi-porphyrin components were used as building blocks for the metal-mediated assembly of more elaborate architectures.

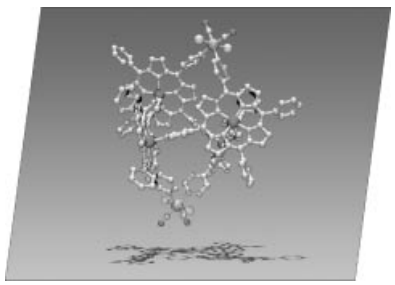

MICROREVIEW

Contents

2371 **E. Iengo, E. Zangrando, E. Alessio***

Discrete Supramolecular Assemblies of Porphyrins Mediated by Coordination Compounds

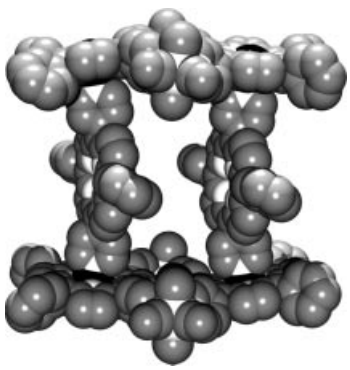

Keywords: Porphyrins / Supramolecular chemistry / Self-assembly / Ruthenium / Building blocks

 © 2003 Wiley-VCH Verlag GmbH & Co. KGaA, Weinheim

SHORT COMMUNICATIONS

2385 M.-L. Tong,* Y.-M. Wu, Y.-X. Tong, X.-M. Chen,* H.-C. Chang, S. Kitagawa*

Rational Design of a Ferromagnetic Trinuclear Copper(II) Complex with a Novel in-situ Synthesised Metalloligand

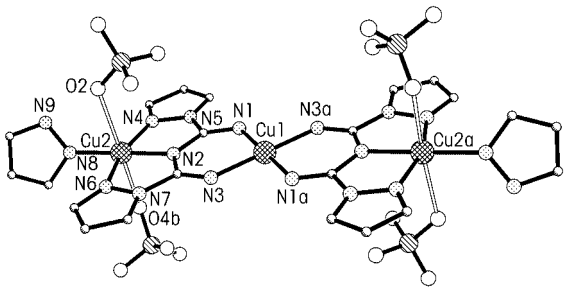

Keywords: Magnetic properties / Copper / N ligands / Nucleophilic addition

2389 A. Marin-Becerra, P. A. Stenson, J. McMaster, A. J. Blake, C. Wilson, M. Schröder*

Assembly of Dicobalt(III) Complexes Incorporating Di-μ-thiophenolate Moieties

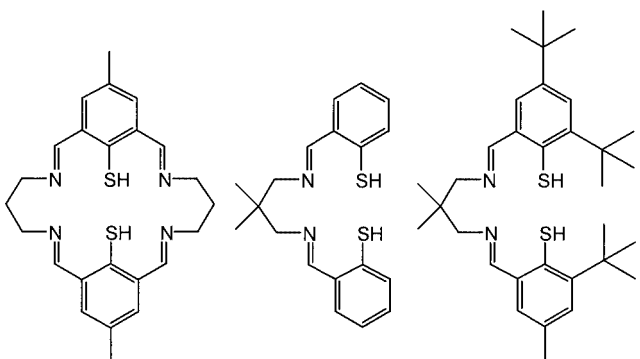

H_2L^1 H_2L^2 H_2L^3

Keywords: Cobalt / Schiff-base ligand / Thiolate

2393 J. Xie, X. Ren, S. Gao, W. Zhang, Y. Li, C. Lu, C. Ni, W. Liu, Q. Meng,* Y. Yao

The First One-Dimensional Molecular Material Featuring Maleonitriledithiolate as a Subunit Exhibiting Metamagnetic-Like Behavior

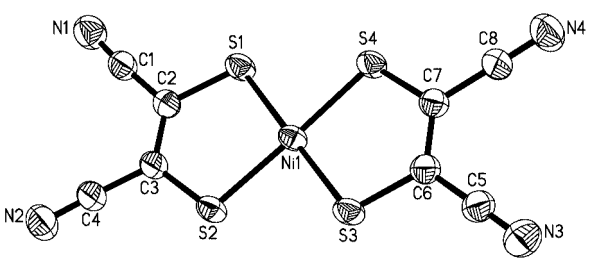

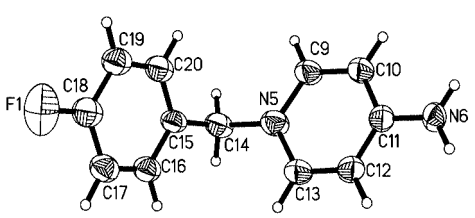

Keywords: Nickel / Maleonitriledithiolate / Crystal structure / Magnetic properties

 © 2003 Wiley-VCH Verlag GmbH & Co. KGaA, Weinheim

FULL PAPERS

2397 **M. A. Arillo, M. L. López, C. Pico, M. L. Veiga,* J. Campo, J. L. Martínez, A. Santrich-Badal**

Order−Disorder Transitions and Magnetic Behaviour in Lithium Ferrites $Li_{0.5+0.5x}Fe_{2.5-1.5x}Ti_xO_4$ (x = 1.28 and 1.50)

Keywords: Lithium ferrites / Order−disorder phenomena / Spinels / Spin-glass behaviour

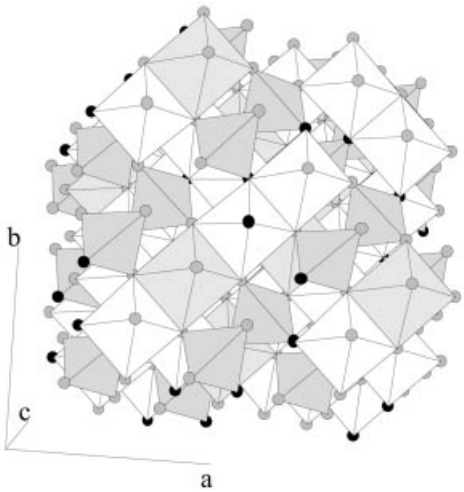

2406 **P. R. Marcoux, B. Hasenknopf,* J. Vaissermann, P. Gouzerh**

Developing Remote Metal Binding Sites in Heteropolymolybdates

Keywords: Polyoxometalates / Molybdenum / N ligands / Coordination chemistry

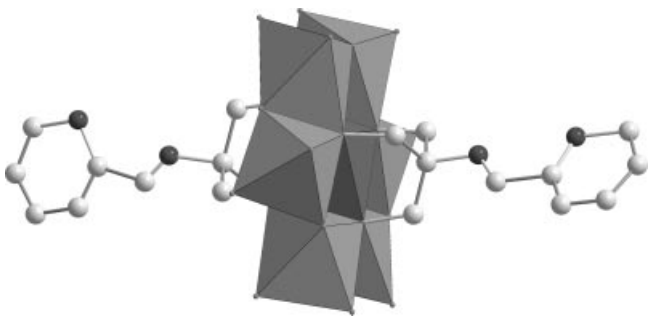

2413 **G. A. Carriedo, F. J. Garcia-Alonso, J. L. García-Alvarez, G. C. Pappalardo,* F. Punzo, P. Rossi**

Stereoisomer Discrimination Through π-Stacking Interactions in Spirocyclic Phosphazenes Bearing 2,2′-Dioxybiphenyl Units

Keywords: Phosphazenes / Pi interactions / Solid-state structure / Spiro compounds / Stereoisomer discrimination

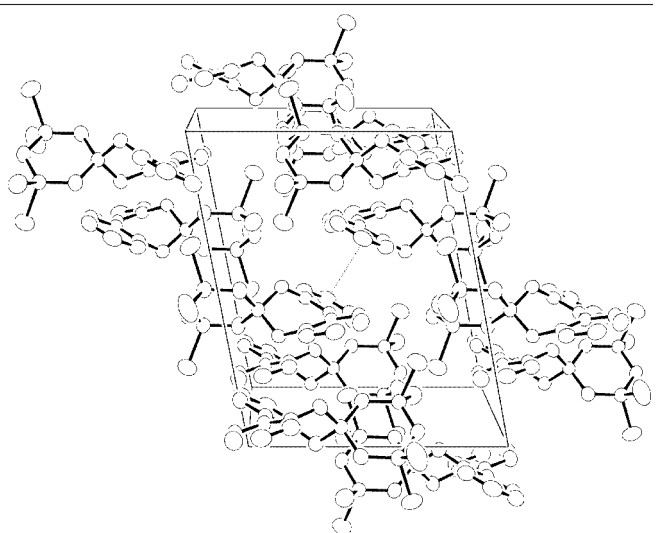

2419 **M. Hernando, K. Boulahya, M. Parras, J. M. González-Calbet,* U. Amador**

Synthesis and Microstructural Characterisation of Two New One-Dimensional Members of the $(A_3NiMnO_6)_\alpha(A_3Mn_3O_9)_\beta$ Homologous Series (A = Ba, Sr)

Keywords: Electron diffraction / High-resolution electron microscopy / One-dimensional oxides / Twinned microstructure

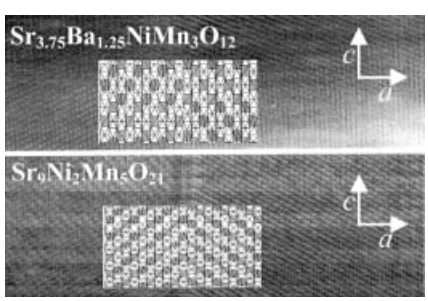

© 2003 Wiley-VCH Verlag GmbH & Co. KGaA, Weinheim

2426 Q. Zhang, G. Hua, P. Bhattacharyya, A. M. Z. Slawin, J. D. Woollins*

Syntheses and Coordination Chemistry of Aminomethylphosphine Derivatives of Adenine

Keywords: Adenine / P ligands / Chelate complexes / Heterometallic complexes

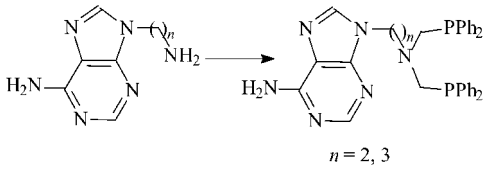

2438 I. del Hierro, R. Fernández-Galán, S. Prashar, A. Antiñolo, M. Fajardo, A. M. Rodríguez, A. Otero*

The Reactivity of Allyl and Olefin-Hydride Niobocene Derivatives Towards Isocyanides. X-ray Crystal Structure of [Nb(η^5-C_5H_4-$SiMe_3$)$_2$\{η^3-CH(R)CHCH(R)\}] (R = $SiMe_2tBu$)

Keywords: Niobium / Allyl ligands / Hydride ligands / Insertion reactions / Isocyanide

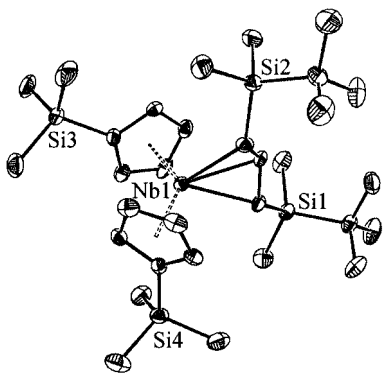

2446 R. J. Baker, H. Bettentrup, C. Jones*

The Reactivity of Primary and Secondary Amines, Secondary Phosphanes and N-Heterocyclic Carbenes towards Group-13 Metal(I) Halides

Keywords: Group-13 elements / Carbene ligands / Phosphanes / Sub-oxidation state

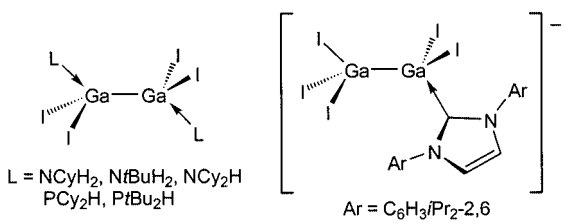

2452 S. Torelli, C. Belle,* C. Philouze, J.-L. Pierre, W. Rammal, E. Saint-Aman

A New Thioether-Based (N_2S_2)Copper(II/I) Complex Exhibiting a High Redox Potential

Keywords: S ligands / N ligands / Tripodal ligands / Copper / Redox chemistry

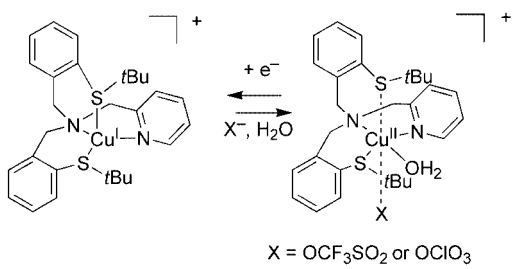

2458 M.-L. Martínez-Sarrión,* L. Mestres, M. Herráiz, O. Maqueda, N. Fernández, M.-F. García

Synthesis and Electrical Properties of the $Pr_{0.5+x-y}Bi_yLi_{0.5-3x}TiO_3$ System

Keywords: Phase diagrams / Perovskite phases / Conducting materials

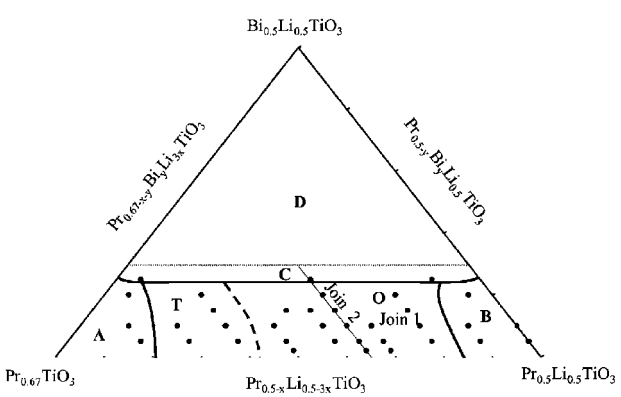

 © 2003 Wiley-VCH Verlag GmbH & Co. KGaA, Weinheim

2463 J. Cano, P. Royo,* H. Jacobsen, O. Blacque, H. Berke, E. Herdtweck

Neutral and Cationic [Bis(η^1-amidosilyl)-η^5-cyclopentadienyl]titanium and -zirconium Complexes: Synthesis, X-ray Molecular Structures and DFT Calculations

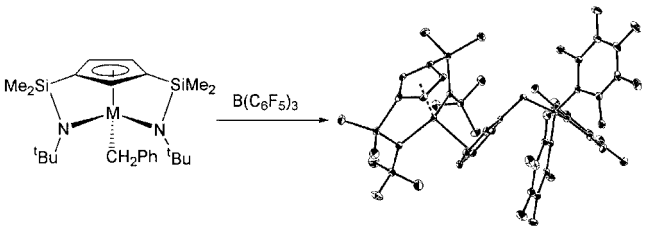

Keywords: Cations / Cyclopentadienyl ligands / Density functional calculations / Nitrogen ligands / Titanium / Zirconium

2475 T. Ruman, Z. Ciunik, S. Wołowiec*

Synthesis, X-ray Crystallographic and ^{1}H NMR Spectroscopic Structural Studies on Cobalt(II) Complexes of Homoscorpionate, Heteroscorpionates and Chiral Tris(pyrazolyl)borates Obtained from 5(3)-Isopropyl-3(5)-phenylpyrazole and 3,5-Dimethylpyrazole

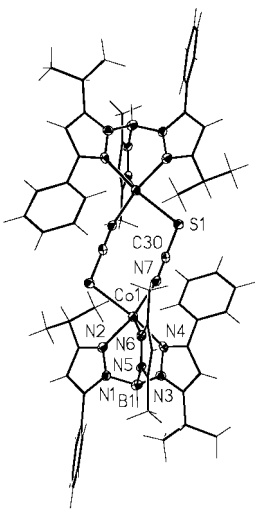

Keywords: Boron / Chirality / Cobalt / N ligands / NMR spectroscopy

2486 M. Yahia, H. Batis*

Properties of Undoped and Ca-Doped $LaMnO_3$ − Non-Stoichiometry and Defect Structure

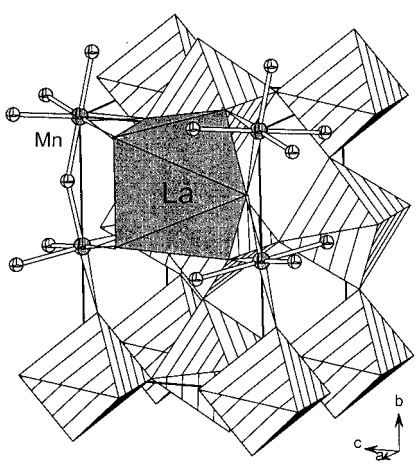

Keywords: Non-stoichiometry / Perovskites / Preparation

 © 2003 Wiley-VCH Verlag GmbH & Co. KGaA, Weinheim

2495 **L. Vander Elst, M. Port, I. Raynal, C. Simonot, R. N. Muller***

Physicochemical Characterization of P760, a New Macromolecular Contrast Agent with High Relaxivity

Keywords: Angiography / MRI contrast agents / NMRD / P760

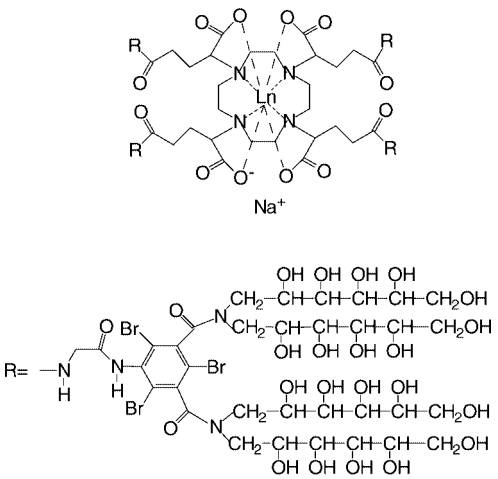

2502 **M. Shu, R. Walz, B. Wu, J. Seebacher, H. Vahrenkamp***

New Bis(mercaptoimidazolyl)(pyrazolyl)borate Ligands and Their Zinc Complex Chemistry

Keywords: Tripod ligands / Zinc / Bioinorganic chemistry

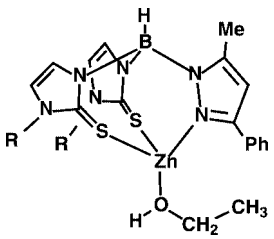

2512 **P. V. Bernhardt, F. Bozoglian, B. P. Macpherson, M. Martínez,* G. González, B. Sienra**

Discrete Cyanide-Bridged Mixed-Valence Co/Fe Complexes: Outer-Sphere Redox Behaviour

Keywords: Cobalt / Iron / Mixed-valence complexes / Redox processes

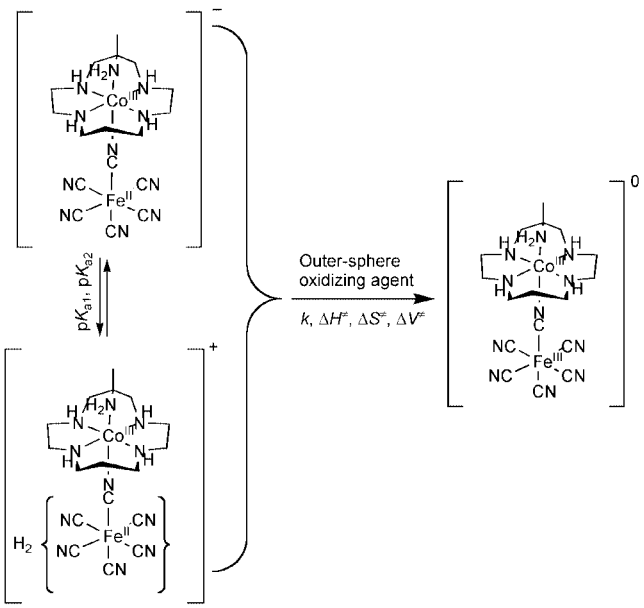

2519 **M. P. Bubnov,* I. A. Teplova, V. K. Cherkasov, G. A. Abakumov**

EPR Study of *o*-Semiquinone-Catecholate Cobalt Complexes with Bis(diphenylphosphanyl)-ethane

Keywords: Chelates / Cobalt / EPR spectroscopy / Quinones / Tautomerism

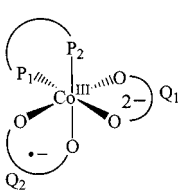

 © 2003 Wiley-VCH Verlag GmbH & Co. KGaA, Weinheim

2524 **B. Štíbr,* J. Holub, M. Bakardjiev, I. Pavlík, O. L. Tok, B. Wrackmeyer**

Phosphadicarbaborane Analogues of Ferrocene: New Isomers of [*closo*-(η^5-C_5H_5)$FePC_2B_8H_{10}$]

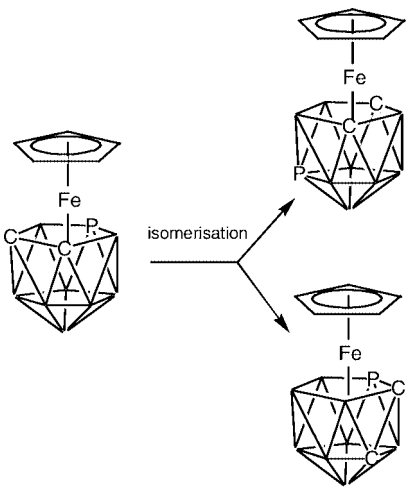

Keywords: Sandwich complexes / Boranes / Isomerisation / Carbaboranes / NMR spectroscopy

2529 **V. Balland, F. Banse,* E. Anxolabéhère-Mallart,* M. Nierlich, J.-J. Girerd***

Iron Complexes Containing the Ligand *N*,*N*′-Bis(6-methyl-2-pyridylmethyl)-*N*,*N*′-bis(2-pyridylmethyl)ethane-1,2-diamine: Structural, Spectroscopic, and Electrochemical Studies, Reactivity with Hydrogen Peroxide and the Formation of a Low-Spin Fe−OOH Complex

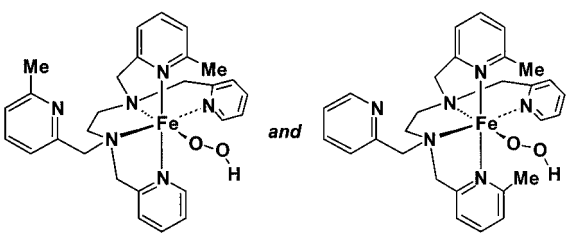

Keywords: Iron / N ligands / Peroxo ligands / Bioinorganic chemistry

 © 2003 Wiley-VCH Verlag GmbH & Co. KGaA, Weinheim

Discrete Supramolecular Assemblies of Porphyrins Mediated by Coordination Compounds

Elisabetta Iengo,[a][‡] Ennio Zangrando,[a] and Enzo Alessio*[a]

Keywords: Porphyrins / Supramolecular chemistry / Self-assembly / Ruthenium / Building blocks

Metal-driven self-assembly has emerged as a viable alternative to covalent synthesis in the construction of large and sophisticated multi-porphyrin architectures, whose complexity and function begin to approach the properties of naturally occurring systems. The design and preparation of robust and shape-persistent discrete assemblies, obtained by coordination of *meso*-pyridylporphyrins to ruthenium, palladium and zinc centers, is comprehensively discussed in this microreview, that covers research in this field carried out by the authors at the University of Trieste in the last few years. NMR spectroscopy and X-ray crystallography were used jointly for the unambiguous characterization of the new species in solution and solid state, respectively. Very often the adducts of nanoscopic dimensions, in which the number, position, relative distance and orientation of the chromophores is well defined, were obtained through hierarchical supramolecular self-assembly: multi-porphyrin components were used as building blocks for the metal-mediated assembly of more elaborate architectures.

(© Wiley-VCH Verlag GmbH & Co. KGaA, 69451 Weinheim, Germany, 2003)

Introduction

There is substantial interest in the construction of multiporphyrin assemblies which can mimic naturally occurring multichromophore aggregates,[1−4] thus generating potential electron- and/or energy-transfer molecular devices for advanced technological tasks.[5,6] Indeed, over the last few years, various molecular devices based on oligoporphyrins have been designed and prepared; these include photoinduced molecular switches, optoelectronic gates, fluorescence quenching sensors, photonic wires, and molecular elements for information storage essential for the miniaturization of electronic componentry and technology.[7]

[a] Dipartimento di Scienze Chimiche, Università di Trieste,
Via L. Giorgieri 1, 34127 Trieste, Italy
Fax: (internat.) + 39-040/5583903
E-mail: alessi@univ.trieste.it
[‡] Laboratoire de Chimie Organo-Minérale, UMR 7513 du CNRS, Université Louis Pasteur, Faculté de Chimie, 4, rue Blaise Pascal, 67070 Strasbourg Cedex, France

Elisabetta Iengo studied chemistry at the University of Trieste where she received her "Laurea" in 1998 and her PhD degree in 2002. In 1994 she spent a six-month period to the laboratories of Prof. P. J. Sadler, Birkbeck College, London (UK), within the Erasmus project. In 2002 she was awarded the prize for the best PhD thesis in Inorganic Chemistry by the Italian Chemical Society. She is currently a postdoctoral fellow in the laboratories of Dr. Jean-Pierre Sauvage, Université Louis Pasteur, Strasbourg (France). She is co-author of more than 25 publications in the fields of supramolecular chemistry and metal-based anticancer drugs.

Ennio Zangrando was born in Trieste (Italy). He received his degree in Chemistry at the University of Trieste in 1974 and some years later he joined the Department of Chemical Sciences at the same University as an Associate Researcher, prior to become Associate Professor of Inorganic Chemistry. In 1987−1988 he spent some months at the Laboratorium für chemisch-mineralogische Kristallographie of the Universität Bern with Professor H.-B. Bürgi. His research interest deal with X-ray crystallography, using conventional sources as well as synchrotron radiation. His work was dedicated to the structural properties of bio-inorganic complexes and has been extended in recent years to supramolecular chemistry.

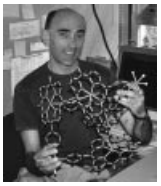

Enzo Alessio was born in 1958 and studied chemistry at the University of Trieste where he received his "Laurea" in 1982 and his PhD degree in 1989. In 2000 he was appointed Associate Professor of Inorganic Chemistry at the same University. He spent one year as NATO-CNR fellow in the research group of Professor Luigi G. Marzilli at Emory University (Atlanta). In 1996 he was awarded with the Nasini Prize to young researchers by the Italian Chemical Society. He is co-author of more than 100 publications in the fields of coordination chemistry, metal-based anticancer drugs and supramolecular chemistry.

MICROREVIEWS: This feature introduces the readers to the authors' research through a concise overview of the selected topic. Reference to important work from others in the field is included.

Three-dimensional macrocyclic oligomers of metalloporphyrins are also being actively investigated as host molecules for homogeneous catalysis and selective molecular recognition that can result from the specific geometry of cavities defined by porphyrin planes.[8] Interestingly, some oligomeric porphyrins have been tested for photodynamic therapy of tumors and DNA cleavage.[9] Design strategies to develop solid-state multichromophore arrays of defined rigidity, dimensionality, porosity, and selectivity are also a part of active research.[10]

Conventional linear synthetic strategies to porphyrin arrays have generally proved quite limiting; they frequently involve many sequential steps, separation of statistical mixtures and extensive chromatographic purification, always resulting in a low product yield.[11]

Self-assembly has emerged as a viable alternative to covalent synthesis in the construction of large multi-component porphyrin architectures. Both coordination and multiple hydrogen bonds,[12] or their combination,[13] have been used as the source of the noncovalent bonding interactions.

Metal-Mediated Self-Assembly of Porphyrins

The metal-mediated self-assembly approach has recently allowed the design and preparation, in reasonable yield, of increasingly sophisticated supramolecular assemblies of porphyrins whose complexity and function begin to approach the properties of naturally occurring systems.[14]

Within this approach, porphyrins and metalloporphyrins can be exploited essentially in two ways as modules in the construction of discrete or polymeric ordered architectures:

(i) Metalloporphyrins can be *acceptor building blocks* (Figure 1) provided that the metal atom inside the porphyrin core has at least one axial site available for coordination. Oligomers, polymers, and dendrimers of axially connected metalloporphyrins can be designed through selection of the coordination geometry of metal atoms (usually either five- or six-coordinate) and the geometry of the polydentate bridging ligands.

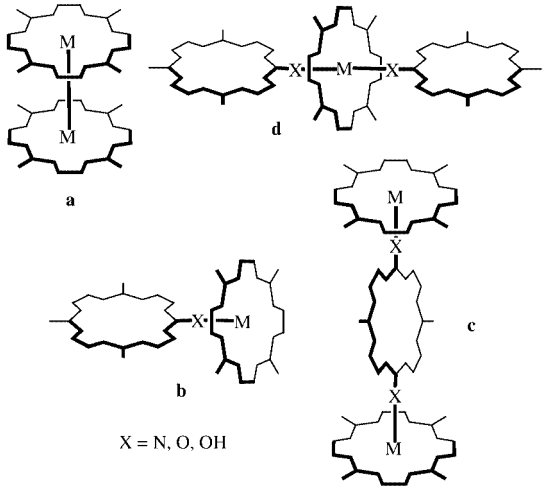

Figure 1. Some schematic examples of metalloporphyrins as acceptor building blocks in the construction of discrete supramolecular assemblies; the metal atom is five-coordinate in **a**−**c**, and six-coordinate in **d**; in **a** the thick line represents a generic bridging ligand; in **b**−**d** the axial ligands are porphyrins which bear X-donor substituents (X = N, O, OH) in peripheral (*meso*) positions

The number of coordination axial sites that can be exploited, their lability as well as the affinity toward different donor atoms can be fine-tuned by changing the nature and the oxidation state of the metal centers inserted into the porphyrin cores.[15] Metal−ligand bonds cover a range of energies depending on the nature of the metal and the ligand. The electronic structure (acidity of the metal center), and the access to the porphyrin core, can be designed by means of well-planned peripheral substitutions either at the β-pyrrole or *meso* position(s). For example, the zinc atom inside zinc−porphyrins prefers to adopt a five-coordinate square-pyramidal geometry and has a good affinity for nitrogen donor ligands. Many metalloporphyrin assemblies, obtained both in solution and as crystalline materials, are based on the zinc−porphyrin−N-heterocycle (pyridine, imidazole) interaction,[16] which is intrinsically weak (association constant, ca. 10^3 M^{-1}) and relatively labile.[14a] Stronger and more inert bonds to N-heterocycles are obtained with $Ru^{II}(CO)$−, $Os^{II}(CO)$−, or Rh^{III}-(halide)−porphyrins. Also in such cases, as with Zn−porphyrins, only one axial coordination site can be exploited for supramolecular construction because, even though the metal atom is six-coordinate, the carbonyl or halide ligands are very tightly bound and not easily displaced. On the other hand, Sn^{IV}−porphyrins adopt a six-coordinate geometry, prefer oxygen donor ligands, and exchange the axial ligands rather slowly.[15] Elegant examples of discrete self-assembled multi-metalloporphyrin arrays employing the mutually noninterfering coordination properties of Zn^{II}, Ru^{II}, and Sn^{IV} centers towards bifunctional ligands bearing pyridyl or carboxylic functionalities have been reported by the group of Sanders.[17]

Finally, the use of complexed ligands for axial coordination (i.e. metal-containing *donor* building blocks) allows for the introduction of further metal centers and thus leads to the construction of even more elaborate assemblies of porphyrins and metal functionalities.[18,19]

(ii) Porphyrins can behave as *donor building blocks*, provided that they have ligands appended to the periphery that can suitably coordinate to metal centers. Most of the examples reported in the literature take advantage of porphyrins elaborately decorated with covalently attached hydroxy or N-donor (imidazole, pyrazole, amine, pyridine) ligands usually at the *meso* positions. Within this framework, *meso*-pyridyl/phenylporphyrins (PyPs), or strictly related chromophores proved to be particularly versatile building blocks: PyPs can provide geometrically well-defined connections to as many as four metal centers by coordination of the pendant *meso*-pyridyl groups.

These two kinds of porphyrin modules, *acceptor* and *donor*, can be freely and rationally combined to build multiporphyrin self-assembling systems. When porphyrins bearing external coordination functionalities bind to other metalloporphyrins, assemblies of axially connected chromophores are generated (Figure 1).[20] Tailor-made

 © 2003 Wiley-VCH Verlag GmbH & Co. KGaA, Weinheim

metalloporphyrins bearing nitrogen and oxygen donor functionalities have been designed that spontaneously self-assemble in discrete arrays by virtue of the independent coordination properties of Zn^{II}, Ru^{II}, Rh^{III} and Sn^{IV} centers.[21]

A particular case of self-assembly is self-coordination, which may occur in metalloporphyrins with matching appended donor ligands (i.e. modules possessing *acceptor* and *donor* features with reciprocal affinity). Most of the examples reported to date concern the one-point self-coordination of metalloporphyrins bearing one peripheral N-donor site, usually a pyridyl or imidazolyl moiety; with few exceptions,[22] the metal atom inside the porphyrin has only one axial coordination site available [e.g. Zn^{II} or Ru^{II}(CO)]. The nature of the resulting architectures, either discrete polycyclic structures or linear oligomers/polymers, depends mainly on the relative geometry of the porphyrin plane (acceptor site) and of the donor site (Figure 2).[23] Also the concentration plays a crucial role in determining the nature of the resulting species; in some cases a polymeric structure was found in the solid state, while spectroscopic evidence suggested that closed cyclic structures (macrocyclic oligomers) prevailed in solution, at least at NMR concentrations.[23a,24]

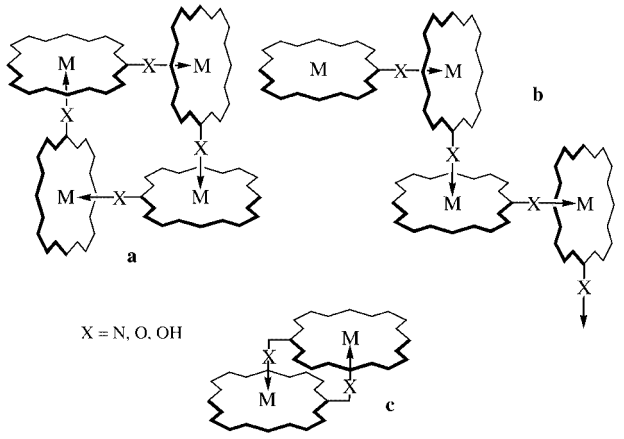

Figure 2. Schematic examples of supramolecular assemblies obtained by one-point self-coordination of metalloporphyrins which bear one X-donor substituent (X = N, O, OH) in the peripheral (*meso*) position; the nature of the resulting architectures, either discrete macrocyclic species (**a**, **c**) or linear stair-like oligomers/polymers (**b**), depends mainly on concentration and on the relative geometry of the metalloporphyrin plane (acceptor site) and of the donor site in the monomer

A convenient and extremely versatile synthetic strategy towards supramolecular assemblies of porphyrins exploits the formation of coordination bonds between donor sites on the porphyrins and external metal centers, that can either be naked ions or coordination compounds (Figure 3). In particular, when the design of three-dimensional structures or, in general, architectures containing cavities with precise size and shape is of interest, the use of coordination compounds as structural units has proved to be very efficient. A large and diverse number of transition-metal coordination geometries can be exploited in the construction of elaborate assemblies, giving access to different topologies rather difficult to obtain with the classical synthetic methods. Moreover, charge and polarity, as well as the introduction of additional functionalities, can be fine-tuned through the ancillary ligands.

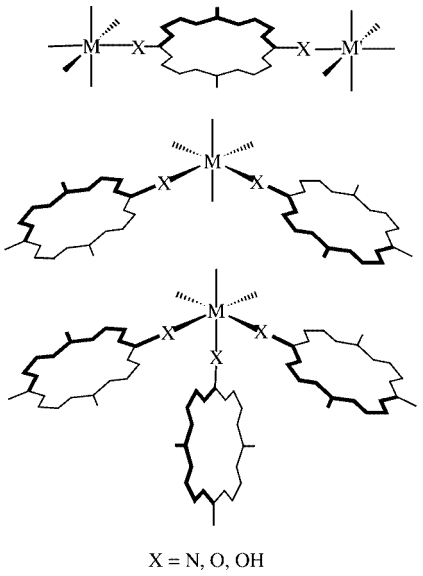

Figure 3. Some schematic examples of porphyrins connected through coordination compounds

Several polymeric structures of metal-coordinated porphyrins have been prepared as a result of exploring ways to construct three-dimensional channelled solids with different chemical architectures and potentially diverse catalytic activity.[10,25] However, as we are more interested in the construction of discrete assemblies endowed with particular properties and/or functions, as an example we describe here briefly the astonishing variety of 2D and 3D porphyrin assemblies obtained in less than a decade by the modular combination of PyPs (or related *meso*-substituted porphyrins) and square-planar Pt^{II} and Pd^{II} complexes with one or two available coordination sites.

Two-dimensional metallacycles of porphyrins, i.e. molecular squares, were obtained by treatment of *meso*-bis(4′-pyridyl)porphyrins (i.e. 4′-*cis*DPyP and 4′-*trans*DPyP) with the appropriate linear or angular metal fragments derived from *trans*-[$PdCl_2$(dmso)$_2$], *cis*-[$PtCl_2$(dmso)$_2$], and [Pt(dppp)$(OTf)_2$] or [Pd(dppp)$(OTf)_2$].[26] Depending on the geometries of the building blocks, the porphyrins can either sit on the corners (2+2 or 4+4 squares) or on the sides (4+4 squares) of the metallacycles; in this latter case the chromophores are actually oriented perpendicularly to the plane of the molecular square. With a similar synthetic approach, Drain and co-workers prepared more elaborate architectures, such as tessellated arrays of porphyrins.[27]

Three-dimensionality can be obtained by switching from 4′- to 3′-PyPs, in which the newly formed 3′-N(py)−M bond points out of the porphyrin plane. Reed, Boyd, and co-workers obtained a kinked bis(porphyrin)palladium complex by simple coordination of two 3′-MPyP units to

 © 2003 Wiley-VCH Verlag GmbH & Co. KGaA, Weinheim

the *trans*-$PdCl_2$ fragment.[28a] This jaw-like cleft has proved to be an efficient host for fullerene.[28b]

A more elaborate bis(porphyrin) host for fullerene, obtained by coordination of a covalent pyridylporphyrin dimer to [Pd(dppp)$(OTf)_2$], was recently reported by the group of Shinkai.[29] Interestingly, coordination to the bis(porphyrin) building block does not provide a receptor for C_{60}; coordination to the $Pd(dppp)^{2+}$ fragment interconverts the dimer from an *anti* to a *syn* conformation, thus creating a cavity for hosting fullerene.

The same group has described a molecular capsule self-assembled by coordination of two zinc−porphyrins to four $Pd(dppp)^{2+}$ fragments[30a] (and, more recently, also to chiral Pd fragments[30b]). Each porphyrin is substituted at *meso* positions with four rigid pyridylacetylene donor ligands oriented almost perpendicular to the plane of the chromophore; thus, coordination to the *cis* positions of the four bridging metal units leads to the two porphyrins being cofacial. The capsule was proved capable of selectively hosting a molecule of 4,4′-trimethylenebipyridine by two Zn−N interactions.

Fujita and co-workers, making use of a simple tetrapyridylporphyrin followed a similar approach. They reported a very elegant example of quantitative self-assembly of a porphyrin prism made up of three 3′-TPyP units and six $Pd(en)^{2+}$ fragments. The porphyrins behave as rigid molecular panels for the three-dimensional structure, while the six palladium complexes that clip them together sit at the apical positions, thus creating a large hydrophobic cavity, which should be capable of accommodating neutral organic molecules in aqueous solution.[31]

Finally, Reinhoudt and co-workers described the self-assembly of two porphyrin dendrimers, a pentamer and a nonamer. The central porphyrin is derivatized at the *meso* positions with four Pd centers; each of them can bind either one 4′-MPyP (pentamer) or a bis(4′-MPyP) building block (nonamer) by pyridyl coordination. These systems should be able to undergo energy transfer processes from the surface to the center of the assembly.[32]

It should be noted that most of the above examples employed the $Pd(chel)^{2+}$ fragment as a connecting unit. It can easily be anticipated that the use of other metal fragments, e.g. with different geometry and/or number of coordination sites, might lead to an even larger variety of architectures. In our work, summarized in the following pages, we exploited the coordination chemistry of octahedral Ru complexes.

Ruthenium-Mediated Discrete Assemblies of Porphyrins

At the beginning of our investigation in this field, we prepared a series of oligomers of perpendicularly linked porphyrins by axial coordination of the 4′-pyridyl groups of 4′-PyPs to [Ru(TPP)(CO)(EtOH)].[33] Later, by using *meso*-3′-pyridylporphyrins (3′-PyPs) as building blocks instead of 4′-PyPs, we synthesized the canted analogs of selected perpendicular assemblies.[34] The synthesis, characterization and photophysical behavior of these adducts have been the subject of a recent review and will not be discussed here.[35] Rather, we will focus on the coordination-driven construction of discrete supramolecular assemblies employing 4′-pyridylporphyrins and neutral, octahedral, ruthenium coordination compounds. Compared to most previous examples, which used doubly charged square-planar metal fragments as structural units, our approach is likely to lead to neutral assemblies, thus providing greater solubility in organic solvents. Moreover, the two additional coordinated "spectator" ligands in each octahedral complex, besides being, in principle, useful extra spectroscopic handles for the characterization, might prove advantageous for a better fine-tuning of the properties of the metal and for further functionalization of the assemblies as well.

Coordination of 4′-Pyridylporphyrins to Ruthenium Complexes

In the past we established that the Ru^{II}−dmso complexes, *trans*-[$RuCl_2$(dmso-*S*)$_4$] (**1**),[36,37] *trans*,*cis*,*cis*-[$RuCl_2$(dmso-*O*)$_2$(CO)$_2$] (**2**),[38] and *trans*,*cis*,*cis*-[$RuCl_2$(dmso)$_3$(CO)] (**3**),[38] are suitable precursors for neutral *90° angular acceptor* building blocks, as they easily replace two *cis*-dmso ligands with heterocyclic N-donor ligands L (Scheme 1). The newly formed Ru−N bonds on the *trans*,*cis*,*cis*-[$RuCl_2$(X)(Y)] fragment (X, Y = dmso-*S*, CO) are both stable and inert.

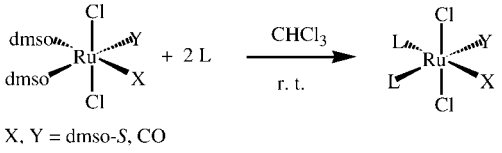

Scheme 1

For example, reaction of **1** or **2** with 2 equiv. of monopyridylporphyrin, 4′-MPyP, under mild conditions (chloroform, room temperature) gave the 1:2 complexes *trans*,*cis*,*cis*-[$RuCl_2$(dmso-*S*)$_2$(4′-MPyP)$_2$] (**4**) and *trans*,*cis*,*cis*-[$RuCl_2(CO)_2$(4′-MPyP)$_2$] (**5**), respectively.

^{1}H NMR spectroscopy proved particularly useful for characterizing the new Ru−4′-PyP complexes. Coordination to Ru mainly affected the resonances of the pyridyl ring(s) of 4′-PyPs, causing downfield shifts [Δδ(H2,6) from 0.3 to 0.9 ppm, Δδ(H3,5) from 0.03 to 0.18 ppm]. The resonances of the pyrrole protons are particularly informative about the geometry of the porphyrin, while the dmso-*S* signals, when present, give information about the coordination environment. IR and $^{13}C\{^1H\}$ NMR spectroscopic data concerning the chloride, dmso, and carbonyl ligands provided further evidence for the unambiguous assignment of the product geometry. In general, all the adducts show UV/Vis spectra similar to those of the corresponding 4′-PyPs, except for minor bathochromic shifts of the Soret (ca. 10 nm) and Q-bands (from 2 to 6 nm) and small changes in their relative absorption intensities; these are consistent with the removal of electron density from the porphyrin π-system upon ruthenium−pyridine bond formation, as reported in similar cases.[26b,39]

 © 2003 Wiley-VCH Verlag GmbH & Co. KGaA, Weinheim

In the ^{1}H NMR spectrum of the *cis*-disubstituted 4′-PyP species, such as *trans*,*cis*,*cis*-[$RuCl_2$(dmso-*S*)$_2$(4′-MPyP)$_2$] (**4**), we identified a signature that is quite characteristic of two mutually *cis*-coordinated pyridylporphyrins in free rotation about the metal−pyridyl axis: there are two sets of multiplets (1:2 ratio) for the phenyl protons (i.e. *o*H and *m*+*p*H) of the two *cis*-porphyrins (Figure 4). The signals of the major set, shifted upfield by about 0.2 ppm compared to those of the minor set, were assigned to the two phenyl rings *cis* to the pyridyl ring (positions 10 and 20). Such an upfield shift is caused by the rotation of the porphyrin about the Ru−pyridyl axis, which brings the phenyl rings at the 10 and 20 positions into the shielding cone of the adjacent porphyrin (Figure 5). The relatively small upfield shift suggests that the two porphyrins rotate freely and that the average time spent in the orientations inducing mutual shielding is rather short.

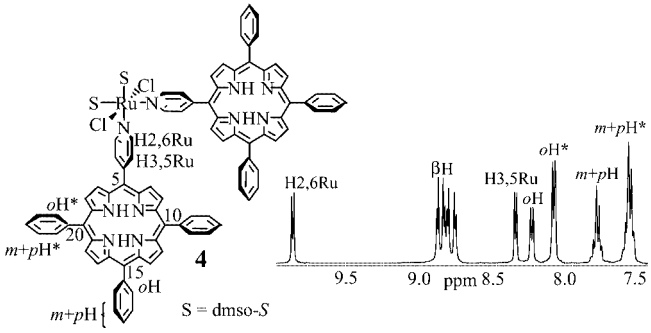

Figure 4. Downfield region of the ^{1}H NMR spectrum of *trans*,*cis*,*cis*-[$RuCl_2$(dmso-*S*)$_2$(4′-MPyP)$_2$] (**4**) in $CDCl_3$ (ppm); resonances of protons on phenyl rings at positions 10 and 20 are marked with an asterisk; see side drawing for detailed labeling scheme

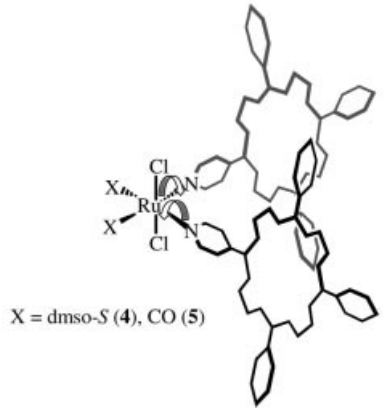

Figure 5. Schematic drawing of *trans*,*cis*,*cis*-[$RuCl_2$ (dmso-*S*)$_2$(4′-MPyP)$_2$] (**4**) and *trans*,*cis*,*cis*-[$RuCl_2(CO)_2$(4′-MPyP)$_2$] (**5**) showing that the phenyl rings at the *meso* positions 10 and 20 fall into the shielding cone of the *cis*-coordinated porphyrin

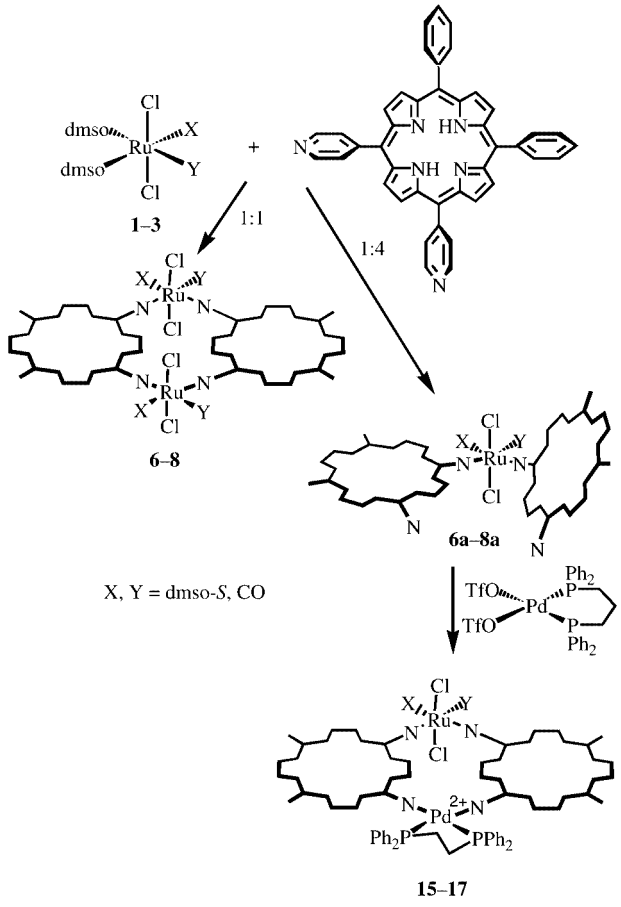

Scheme 2

As a logical extension of the synthetic results described above with 4′-MPyP, we then investigated the reaction of the *cis*-coordinating ruthenium precursors **1**−**3** with the angular porphyrin building block 4′-*cis*DPyP. We found that two different classes of products, namely molecular squares **6**−**8** and bis(pyridyl)porphyrin adducts **6a**−**8a**, are selectively formed depending on whether a stoichiometric amount (**6**−**8**) or an excess of 4′-*cis*DPyP (**6a**−**8a**) is used (Scheme 2). The two classes of products will be described separately.

Neutral Molecular Squares of Porphyrins Connected through Octahedral Ru^{II} Complexes[40]

Treatment of **1**−**3** with a stoichiometric amount of 4′-*cis*DPyP under mild conditions (chloroform, ambient temperature) led to the formation of the corresponding 2+2 homonuclear neutral squares of porphyrins of formula *trans*,*cis*,*cis*-[$RuCl_2$(X)(Y)(4′-*cis*DPyP)]$_2$ (X = Y = dmso-*S*: **6**; X = Y = CO: **7**; X = dmso-*S*, Y = CO: **8**) (Scheme 2).[40] These products were purified by column chromatography and fully characterized by means of NMR spectroscopy and FAB mass spectrometry. In general, the mobility of pyridylporphyrin adducts on silica gel is inversely related to the number of free 4′-N(py) sites. Thus, the most abundant and mobile product from each of the above reactions was

 © 2003 Wiley-VCH Verlag GmbH & Co. KGaA, Weinheim

attributed to a metallacyclic species and some minor bands with lower mobilities to open-chain oligomers with unbound 4′-N(py) sites.

The ^{1}H NMR spectrum of **6**, that unambiguously established the metallacyclic nature (no signals for unbound pyridyl rings are present) and high symmetry (D_{2h}) of this species is reported in Figure 6.

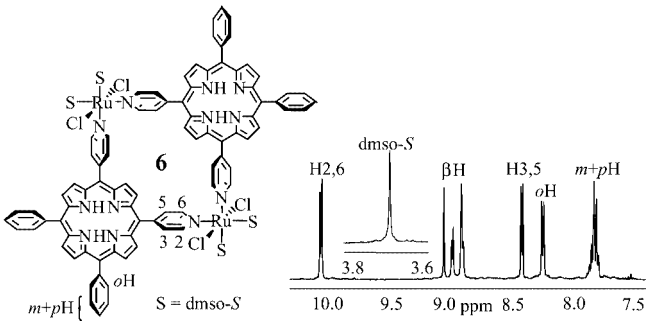

Figure 6. Schematic drawing of *trans,cis,cis*-[$RuCl_2$(dmso-*S*)$_2$(4′-*cis*DPyP)]$_2$ (**6**) with labeling scheme and its ^{1}H NMR spectrum (with the exception of the NH resonance) in $CDCl_3$ (ppm)

Contrary to what was found in the NMR spectra of **4** and **5**, the *o*H and the *m*+*p*H phenyl resonances of **6**−**8** are not each split into two multiplets, confirming that the chromophores are not free to rotate about the Ru−N bonds. The metallacycle *trans,cis,cis*-[$RuCl_2$(dmso-*S*)(CO)(4′-*cis*DPyP)]$_2$ (**8**) exists as an equimolar mixture of the two geometrical isomers **8′** and **8′′** (Figure 7); in one isomer (**8′**) the 4′-N(py) moieties of each porphyrin are *trans* to one CO and one dmso-*S* ligand, respectively, and the resulting metallacycle has a C_{2v} symmetry; in the other (**8"**), the two 4′-N(py) ligands of one 4′-*cis*DPyP are *trans* to CO, while those of the other are *trans* to dmso-*S* and the resulting molecular square has a C_{2h} symmetry. The two isomers could not be separated by column chromatography. Only the pyridyl protons of the two isomers have resolved resonances in the aromatic region of the NMR spectrum of the mixture of **8′** and **8′′**; all the other ^{1}H NMR resonances of **8′** and **8′′** overlap.

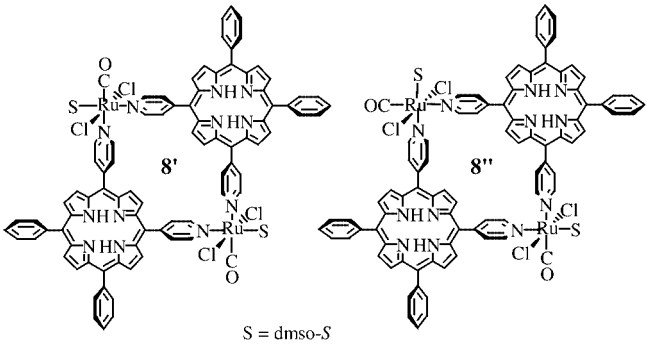

Figure 7. Schematic drawing of the two geometrical isomers of *trans,cis,cis*-[$RuCl_2$(dmso-*S*)(CO)(4′-*cis*DPyP)]$_2$, **8′** and **8′′**

The *trans,cis,cis*-[$RuCl_2$(dmso-*O*)$_2$(CO)$_2$] (**2**) precursor behaved somewhat differently from **1** and **3** and deserves further comment. The ^{1}H NMR spectrum of the crude reaction mixture between **2** and an equimolar amount of 4′-*cis*DPyP clearly indicated the presence of three major products with sharp and resolved resonances pertaining to cyclic symmetrical species, besides smaller amounts of open-chain oligomers with broad signals. The product with the largest mobility on silica gel, which is also the most abundant, was separated and purified by column chromatography and characterized as the molecular square *trans,cis,cis*-[$RuCl_2$(CO)$_2$(4′-*cis*DPyP)]$_2$ (**7**). A second product, namely **9**, which has an R_f value very similar to that of **7** on silica gel (0.67 versus 0.72 for **7**) was also obtained in its pure form after chromatography. The ^{1}H NMR spectrum of **9** has a pattern similar to that of **7**, thus establishing unambiguously its metallacyclic nature and high symmetry; it must be noted though that all signals of **9** are markedly upfield-shifted as compared to those of **7** (Figure 8).

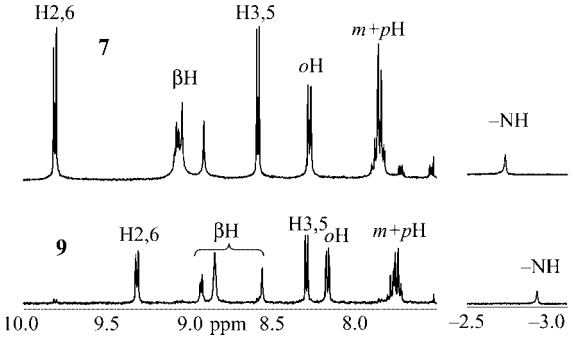

Figure 8. Comparison of the ^{1}H NMR spectra of the molecular square *trans,cis,cis*-[$RuCl_2$(CO)$_2$(4′-*cis*DPyP)]$_2$ (**7**, top) and of the "bowl-shaped" trinuclear metallacycle *trans,cis,cis*-[$RuCl_2$(CO)$_2$(4′-*cis*DPyP)]$_3$ (**9**, bottom)

According to FAB MS spectrometry compound **9** can be formulated as the trinuclear species [$RuCl_2$(CO)$_2$(4′-*cis*DPyP)]$_3$.[41] A triangular geometry in which three *cis*-coordinated 4′-*cis*DPyP units and three *trans,cis,cis*-[$RuCl_2$(CO)$_2$] fragments are coplanar would result in a very strained structure; more likely the two porphyrins coordinated to the same Ru fragment are not coplanar. A computer model showed that the result of the total energy minimization is a three-dimensional bowl-shaped architecture with a C_{3v} symmetry (Figure 9), with pairs of *cis*-porphyrins forming a ca. 90° dihedral angle to one another. Connection of each ruthenium atom to the center of the adjacent porphyrins yields a six-membered ring with a *chair*-like conformation. This model structure is in good agreement with the ^{1}H NMR spectroscopic data. The porphyrin units are mutually arranged so that each one lies partially in the shielding cone of the others, which may explain the upfield shifts observed for the porphyrin resonances in the ^{1}H NMR spectrum of **9** as compared to that of **7**.

The third product of the above reaction, **10**, has not been isolated in pure form thus far, having a mobility on silica very close to that of **9** (R_f = 0.65). From the ^{1}H NMR spectra of partially purified samples it is clear that **10** is a metallacycle, its pyridyl proton signals having chemical

 © 2003 Wiley-VCH Verlag GmbH & Co. KGaA, Weinheim

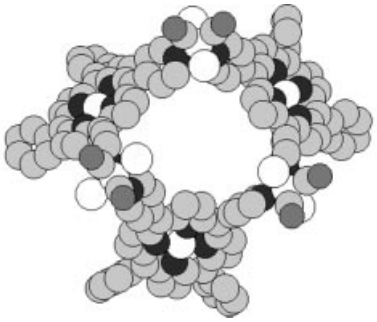

Figure 9. Computer-generated (Hyperchem) minimum energy model structure of the "bowl-shaped" trinuclear metallacycle *trans*,*cis*,*cis*-[$RuCl_2(CO)_2$(4′-*cis*DPyP)]$_3$ (**9**)

shifts in between those of **7** and **9**. Compound **10** could be either a conformational isomer of **9** or a porphyrin metallacycle with higher nuclearity (no mass spectrometric data are available for **10** as yet).

It must be stressed that no equilibration between these three products was observed; once isolated and redissolved they do not undergo any interconversion process and are indefinitely stable at ambient temperature. Therefore, the stoichiometric reaction between **2** and 4′-*cis*DPyP represents an example of a *combinatorial library* (Scheme 3). Most probably **7**, **9**, and **10** are kinetic products of the reaction. The fact that more than one cyclic geometry becomes accessible in this case is probably due to the presence of small ancillary ligands in the ruthenium fragments (X = Y = CO) which allow for the rotation of the *cis*-coordinated 4′-*cis*DPyP units around the $C_{meso}-C_{ring}$ bonds. This might not be the case for precursors **1** and **3**, in which rotation of the chromophores might be sterically disfavored by the bulkier dmso-*S* ligands.

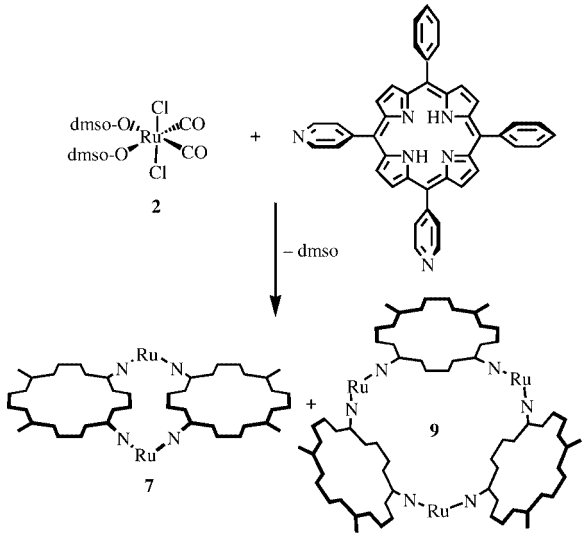

Scheme 3

The electronic absorption spectra of metallacycles **6**–**9** are very similar to those of 4′-*cis*DPyP, apart from a small bathochromic shift for the Soret band (ca. 8 nm); the molar extinction coefficient per porphyrin in each square (ε/porphyrin for the Soret band) is substantially the same as that found for 4′-*cis*DPyP ($\varepsilon = 29 \times 10^4$ cm^{-1} M^{-1}). A detailed investigation of the photophysical properties of molecular squares **6** and **7**, in comparison to some acyclic reference compounds, was performed by the group of Scandola.[42] In all the adducts investigated the emitting singlet excited state is shorter-lived than in the parent pyridylporphyrin molecule. A nice correlation between the lifetime shortening and the number of metal centers attached to each chromophore was found by keeping the nature of the Ru fragment, peripherally bound to the pyridylporphyrin, constant. A likely explanation for the pyridylporphyrin singlet quenching in the adducts can be identified in the "heavy-atom effect" of the metal.

As a general comment we might add that, compared to the other neutral molecular squares of porphyrins, described by Hupp and co-workers,[39a,43] that feature octahedral *fac*-[$Re(CO)_3Cl$] corner units, our compounds have the advantage of being more symmetrical: the two axial ligands of the Re^I corners are different (one Cl and one CO), thus generating mixtures of isomers when connected in a square.

Self-Assembling of Higher Order Architectures by Axial Ligation of Molecular Squares of Metalloporphyrins

Treatment of molecular square **7** with excess zinc acetate in chloroform/methanol mixtures led to the isolation of the corresponding zinc adduct *trans*,*cis*,*cis*-[$RuCl_2(CO)_2$(Zn·4′-*cis*DPyP)]$_2$ (**7**·Zn). The same reaction was not pursued on **6** and **8** because, as previously reported by us for other Zn·PyP–Ru–dmso-*S* complexes, a self-assembling process is expected to occur between the oxygen atom of the dmso-*S* ligand of one molecule and the zinc center of another molecule that leads to a broadening of some NMR resonances.[36] The ^{1}H NMR spectrum of **7**·Zn is very similar to that of **7**, except for the absence of the –NH signal; the resonances are always sharp and the spectrum is concentration independent in the range between 0.1 and 10 mM (as was the case also for **6**–**9**), indicating that no aggregation occurs in chloroform solution.[40]

Owing to the preference of zinc–porphyrins for five-coordinate square-pyramidal geometry, **7**·Zn is a rigid two-dimensional building block with two axial *acceptor* sites. Thus, it can be treated with appropriate multidentate donor ligands for the construction of more elaborate supramolecular adducts. This is made possible by the inertness of the Ru–pyridyl bond, which provides kinetic stability to the molecular square **7**·Zn.

Using ^{1}H NMR spectroscopy we investigated the reactivity of **7**·Zn towards a series of linear ditopic N-donor ligands (L), namely 4,4′-bipy, 4′-*trans*DPyP, and 4′-*trans*DPyP-npm. We found that treatment of **7**·Zn with 1 equiv. of L leads selectively to the quantitative assembling of sandwich-like 2:2 supramolecular adducts of formula [(**7**·Zn)$_2$(μ-L)$_2$] (**11**–**13**; L = 4,4′-bipy: **11**; L = 4′-*trans*DPyP: **12**; L = 4′-*trans*DPyP-npm: **13**), consisting of two molecular squares connected face-to-face by two bridg-

 © 2003 Wiley-VCH Verlag GmbH & Co. KGaA, Weinheim

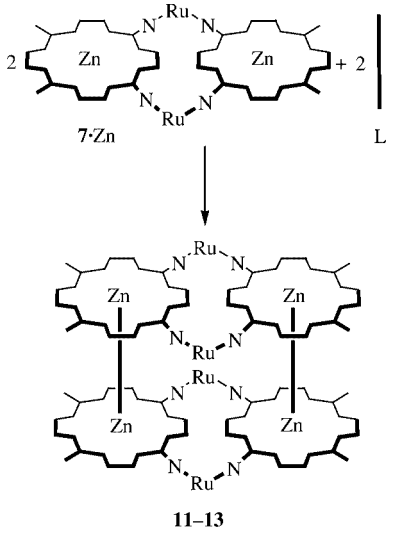

Scheme 4

ing ligands which are axially bound to the zinc−porphyrins (Scheme 4).

The rigid frame of the molecular squares ensures that the bridging ligands are arranged at a fixed distance and with a well-defined mutual orientation. Symmetrical axial coordination of the bridging ligands to the squares was unambiguously established by the large upfield shift of all their resonances due to the combined ring currents of both porphyrins (which decreases gradually as the proton distance from the zinc−porphyrins increases). Unequivocal determination of the solution structures of **11**−**13** and complete assignment of their NMR resonances was achieved by 2D H-H COSY and EXSY experiments.

NMR spectroscopic evidence also indicated that in compounds [(**7**·Zn)$_2$(μ-4′-*trans*DPyP)$_2$] (**12**) and [(**7**·Zn)$_2$(μ-4′-*trans*DPyP-npm)$_2$] (**13**) the two bridging pyridylporphyrins maintain the cofacial orientation found in the solid state for **12** (see below). Thus **12** and **13**, which feature six porphyrins each, might be better defined as molecular boxes of porphyrins (Figure 10).

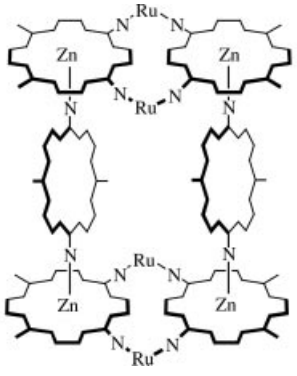

Figure 10. Schematic drawing of the molecular boxes of porphyrins **12** and **13**

Overall, the NMR spectroscopic features indicate that, at ambient temperature, the formation of [(**7**·Zn)$_2$(μ-L)$_2$] from **7**·Zn and L has an intermediate-to-slow rate on the NMR time-scale (relatively broad signals for L) and is a complete process (all-or-nothing process). Entropy considerations (no global conformational changes required owing to the rigidity of the building blocks) suggest that there must be considerable cooperativity between the addition of the first and of the second bridging ligand. Formation constants higher than 10^{18} M^{-2} were estimated in chloroform for compounds **11**−**13**. Accordingly, the NMR spectra of $CDCl_3$ solutions of both **11** and **12**, diluted to the limit of detection (ca 3×10^{-5} M), exclusively showed the resonances of the intact assemblies.

Single crystals of **11** and **12** suitable for X-ray investigations were obtained by slow diffusion of *n*-hexane into $CDCl_3$ solutions of each compound. The structural determination of compound **12** showed that the molecular sandwich architecture observed in solution is also found in the solid state (Figure 11). The distance between the two opposite molecular squares is ca. 19.5 Å. The two bridging 4′-*trans*DPyP ligands are slightly bowed inward and cofacial, at a distance of ca. 11.4 Å. The apical 4′-N(py) rings bound to the Zn ions are approximately perpendicular to the ZnN4 basal plane.

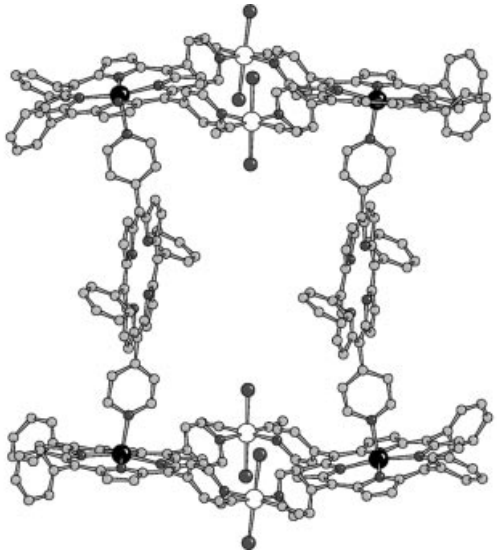

Figure 11. Perspective view of the solid-state structure of molecular box [(**7**·Zn)$_2$(μ-4′-*trans*DPyP)$_2$] (**12**); Ru atoms are represented by white spheres, Zn atoms by black spheres

To our surprise, the X-ray analysis of **11** showed that the solid-state architecture of this compound is different from that found in solution and consists of an infinite wire of **7**·Zn squares bridged by 4,4′-bipy ligands which are axially coordinated, alternatively, on the two opposite faces of each square, [(**7**·Zn)(μ-4,4′-bipy)]$_\infty$ (Figure 12). The polymeric chain structure found for **11** in the solid state is an unprecedented example of a molecular wire made of porphyrin metallacycles bridged by organic ligands. Two crystallographically different **7**·Zn macrocycles, *A* and *B*, alternate along the chain, forming a stair-like infinite structure featuring the (*ABA*)·(*ABA*) motive, with inversion centers lo-

 © 2003 Wiley-VCH Verlag GmbH & Co. KGaA, Weinheim

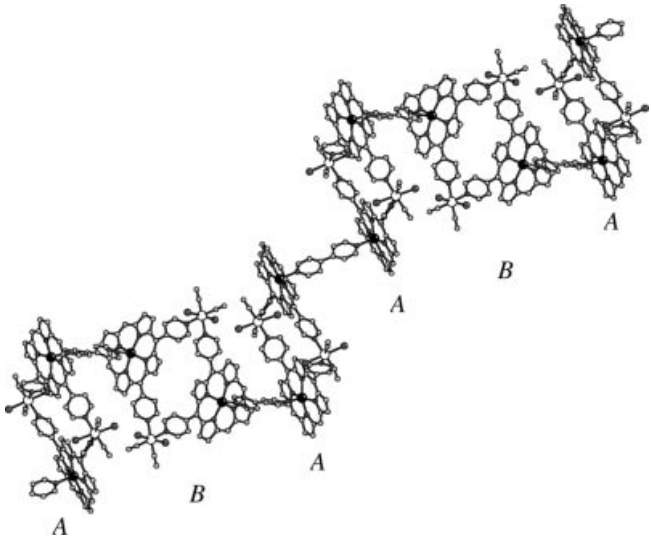

Figure 12. Solid-state structure of the one-dimensional polymeric compound $[(\mathbf{7}\cdot Zn)(\mu\text{-}4,4'\text{-bipy})]_\infty$ (**11**) composed of repeating *ABA* triplets (see text); Ru atoms are represented by white spheres, Zn atoms by black spheres

cated between two consecutive *ABA* triplets and in the center of units *B*.

In self-assembly processes, the equilibrium between discrete and polymeric species is dependent on concentration.[23a,24] The fact that in this case a polymer crystallizes out preferentially over sandwich **11**, even though this latter is the most favored assembly in solution in the range of concentrations examined (we had no spectroscopic evidence of polymeric or oligomeric material in solution), suggests that crystal packing forces must play a significant role in determining the solid-state structure.

In conclusion, we showed that molecular squares of porphyrins, after metallation, become suitable building blocks for the construction of more elaborate supramolecular arrays by axial coordination of bridging ligands. Although oligomers and polymers (molecular wires) of metalloporphyrins axially connected through bridging ligands have been described,[7a,23a,44] there are few examples concerning multiporphyrin systems. Anderson and co-workers extensively investigated the assembly of two flexible oligomers of covalently connected zinc−porphyrins through axial ligation of bridging N-donor ligands, thus obtaining 2D molecular ladder systems with increased inter-porphyrin conjugation.[45] To date, however, the stacking of 2D porphyrin macrocycles through axial ligation to yield 3D assemblies has been scarcely investigated; examples concerning the use of molecular squares of metalloporphyrins,[26a] and closely related systems such as molecular grids,[27] have been alluded to only briefly and are not well documented.

Compounds **12** and **13** are particularly stimulating for further investigation, as they can indeed be regarded as molecular boxes featuring two coplanar bridging pyridylporphyrins at a distance of about 11.4 Å. Even though cofacial bis(porphyrins) connected to one another by flexible or rigid organic bridges are well known,[46,47] systems in which the two porphyrins are not covalently linked are rather uncommon. A recent example of a porphyrin-based capsule constructed through Pd^{II}−pyridine bonds was reported by the group of Shinkai (see Introduction).[30] We are currently investigating the capability of **12** to behave as a host for the inclusion of guest molecules of appropriate shape and size through π-π interactions with the cofacial porphyrins.

Heterodimetallic Molecular Squares of Porphyrins

Treatment of **1**−**3** with excess 4′-*cis*DPyP under mild conditions led, after chromatographic purification, to the isolation of the bis(porphyrin) adducts *trans*,*cis*,*cis*-$[RuCl_2(X)(Y)(4'\text{-}cis\text{DPyP})_2]$ **6a**−**8a** in pure form (Scheme 2; X = Y = dmso-*S*: **6a**; X = Y = CO: **7a**; X = dmso-*S*, Y = CO: **8a**). Compounds **6a**−**8a** have one residual unbound 4′-N(py) ring on each of the two *cis*-coordinated 4′-*cis*DPyP units and are thus building blocks suited for two-point coordination.[48]

The nature and geometry of the products was established by ^1H and ^{13}C NMR spectroscopy. Signal integration (in **6a** and **8a**) revealed adduct stoichiometry, while H-H COSY spectra allowed unambiguous signal assignments.

Compounds **6a** and **7a** have C_{2v} symmetry, and thus the two porphyrins are equivalent. As observed before, coordination of 4′-*cis*DPyP to the ruthenium fragment induces downfield shifts for the H2,6 and H3,5 resonances of the 4′-N(py) ring involved in the new bond (position 5). Conversely, the resonances of the pyridyl and phenyl rings at positions 10 and 20, respectively, experience an upfield shift of ca. 0.2 ppm with respect to 4′-*cis*DPyP, which is characteristic of two mutually *cis*-pyridylporphyrins in free rotation about the metal−pyridyl axis, as already noted for monopyridylporphyrin derivatives **4** and **5** (see above). In **8a** the two 4′-*cis*DPyP units are inequivalent; the resonances of the two Ru−4′-N(py) rings are well resolved, whereas the other signals overlap.

Complexes **6a**−**8a** are indeed pre-programmed *donor* building blocks capable of chelating suitable 90° *acceptor* modules. As an example, we investigated their reactivity towards the bis(triflate) of $dpppPd^{II}$. ^1H NMR spectroscopy established that titration of $[Pd(dppp)(OTf)_2]$ into chloroform solutions of compounds **6a**−**8a** led readily to the quantitative formation of the corresponding heterodimetallic 2+2 molecular squares of formula $[Pd(dppp)\{trans,cis,cis\text{-}RuCl_2(X)(Y)(4'\text{-}cis\text{DPyP})_2\}](OTf)_2$ (**15**−**17**) (Scheme 2; X = Y = dmso-*S*: **15**; X = Y = CO: **16**; X = dmso-*S*, Y = CO: **17**). Chelation of the Pd−bis(phosphane) fragment by **6a**−**8a** induces characteristic shifts both in the ^1H NMR spectrum, which mainly concern the resonances of the previously unbound 4′-N(py) ring at position 10, and in the proton-decoupled ^{31}P NMR spectrum (upfield shift of ca. 10 ppm compared to $[Pd(dppp)(OTf)_2]$). The macrocycles were not affected by accidental excess of $[Pd(dppp)(OTf)_2]$ and no evidence of homometallic molecular squares was found. In solution squares **15** and **16** maintain the C_{2v} symmetry of the corresponding ruthenium precursor, and the two porphyrins at opposite corners are equivalent. The resonances of the

 © 2003 Wiley-VCH Verlag GmbH & Co. KGaA, Weinheim

Pd−4′-N(py) rings are well resolved from those of the Ru−4′-N(py) rings. Macrocycle **17** lacks the orthogonal mirror plane containing the two metal atoms; hence the two porphyrin units are inequivalent.

Treatment of **7a** with excess zinc acetate led to *trans*,*cis*,*cis*-[$RuCl_2(CO)_2$(Zn·4′-*cis*DPyP)$_2$] (**7a**·Zn), which self-assembles spontaneously in solution (see below). Titration of [Pd(dppp)$(OTf)_2$] into a $CDCl_3$ solution of **7a**·Zn quantitatively yielded the corresponding molecular square [Pd(dppp){*trans*,*cis*,*cis*-$RuCl_2(CO)_2$(Zn·4′-*cis*DPyP)$_2$}]$(OTf)_2$ (**16**·Zn), which represents the first example of a heterotrimetallic molecular square of porphyrins.

The structure of molecular square **16**, with two 4′-*cis*DPyP moieties alternating with the Pd^{II} and Ru^{II} angular units, was established by X-ray single crystal analysis (Figure 13). At the time we published this result it was the first case in which data on the solid-state structure of a molecular square of porphyrins became available.

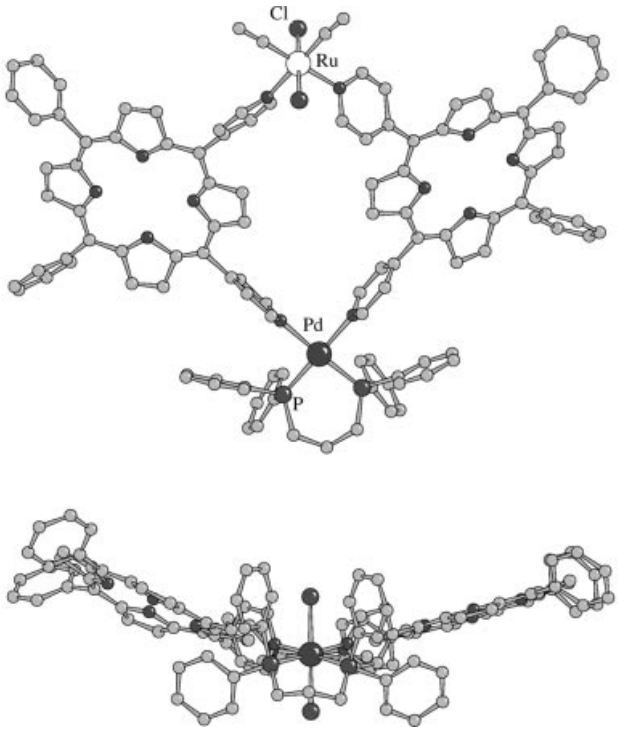

Figure 13. Two perspective views of the solid-state molecular structure of [Pd(dppp){*trans*,*cis*,*cis*-$RuCl_2(CO)_2$(4′-*cis*DPyP)$_2$}]$(OTf)_2$ (**16**); top: top-view; bottom: side-view along the Pd···Ru axis

In **16** the metal−porphyrin center distances are about 9.83 Å, and the diagonal Pd···Ru distance is ca. 14.0 Å; these dimensions are very similar to those found in ruthenium molecular square **7**·Zn (see above). Interestingly, the macrocycle exhibits in the solid state an arrangement with porphyrin least-squares planes that form a dihedral angle of 41.7(1)°, approximating a C_s symmetry (Figure 13).

In conclusion, we found that the reaction between 4′-*cis*DPyP and the ruthenium precursors **1**−**3** leads to different classes of products depending on the reagents ratio: either molecular squares **6**−**8** (1:1 ratio) or bis(pophyrin) complexes **6a**−**8a** (4:1 ratio). This experimental observation implies that the formation of such products is under kinetic control. This result might have been anticipated considering the inert nature of the Ru^{II}−4′-N(py) bond. It has been reported that when more labile metal centers are used as structural units, and thus the self-assembling reaction is under thermodynamic control, the most stable molecular square is the main reaction product regardless of the ratio of reagents being employed. Namely, when an excess of one of the two reagents is used, only the cyclometallated product (plus the unchanged building block) is obtained at the end of the reaction.[49]

In future, treatment of precursors **6a**−**8a** with other *angular* acceptor metal based units might be an efficient pathway to the construction of novel heterodimetallic 2+2 molecular squares of porphyrins, featuring metal ions of defined geometry and/or charge at opposite corners; specific reactions might be envisaged to derivatize these species selectively at either metal corner. Moreover, treatment of **6a**−**8a** with metal centers having different coordination numbers and geometries (for instance tetrahedral, or even octahedral naked ions) might lead to the formation of multiporphyrin−metal based assemblies in which the pairs of chromophores are locked with mutual orientations other than coplanar.

Two-Point Self-Coordination of the Dizinc(ii)−Bis(pyridylporphyrin)−Ruthenium Complex 7a·Zn

The bis(porphyrin)ruthenium complex *trans*,*cis*,*cis*-[$RuCl_2(CO)_2$(Zn·4′-*cis*DPyP)$_2$] (**7a**·Zn) described above is an unprecedented example of a metal-containing building block featuring two *donor* [the uncoordinated 4′-N(py) atoms] and two *acceptor* (the Zn atoms) sites, whose relative orientation depends on the torsion angles about the Ru−N bonds.[50]

^{1}H NMR spectroscopy indicates that **7a**·Zn self-assembles in $CDCl_3$ solution through 4′-N(py)−Zn interactions to yield selectively a single, highly symmetrical, discrete species (**7a**·Zn)$_n$, in which all donor and all acceptor sites of each **7a**·Zn unit are involved; accordingly (**7a**·Zn)$_n$ runs as a single spot on TLC plates and is significantly less polar than **7a**.

The single-crystal X-ray analysis of (**7a**·Zn)$_n$ established that the compound is actually a dinuclear species, (**7a**·Zn)$_2$, in which the four 4′-N(py) sites and the four Zn sites of the two **7a**·Zn units are mutually saturated (Figure 14).

The four porphyrins in (**7a**·Zn)$_2$ have a propeller-like arrangement, with a global S_4 symmetry (the improper rotation axis passes through the ruthenium atoms) and define a small internal cavity, partially occupied by two chloroform molecules. The adduct is a *meso* form derived from the combination of two **7a**·Zn units with opposite helical chirality. The Ru atoms, that display a distorted octahedral geometry, are ca. 19.6 Å apart; the four Zn ions, which have a square-pyramidal environment, occupy the vertices of a distorted tetrahedron (Figure 15). The distances between the carbonyl oxygen atoms of the two Ru ions (ca. 24.0 Å),

 © 2003 Wiley-VCH Verlag GmbH & Co. KGaA, Weinheim

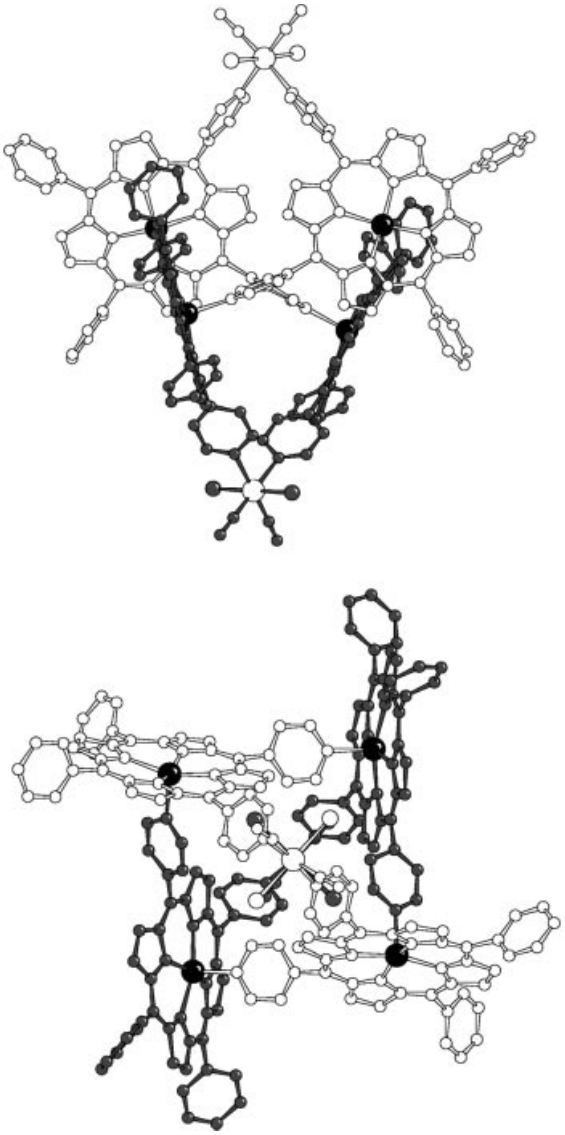

Figure 14. Two perspective views of the solid-state molecular structure of (**7a**·Zn)$_2$; the bottom view is along the S_4 axis; for clarity the two **7a**·Zn units have different shades; Ru atoms are represented by white spheres, Zn atoms by black spheres; adapted from ref.[50]

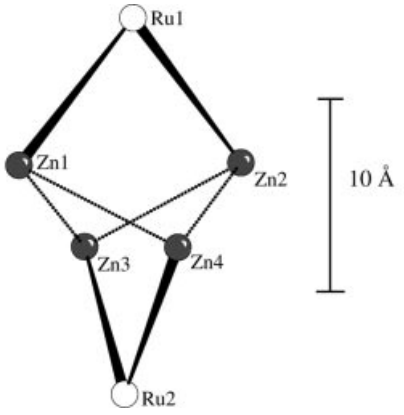

Figure 15. Disposition of the six metal ions in the solid-state molecular structure of (**7a**·Zn)$_2$; full lines represent each **7a**·Zn unit, while dotted lines represent the axial 4′-N(py)−Zn connections between porphyrins; the distorted tetrahedral arrangement of the four Zn ions is evident; the Zn···Zn distance in each **7a**·Zn unit averages to 12.463(4) Å, while the Zn···Zn distance between the two **7a**·Zn units is shorter [mean value of 9.830(4) Å]

are similar to those between the outermost phenyl carbon atoms and give a rough idea of the molecular size of (**7a**·Zn)$_2$.

The geometry of this highly symmetrical tetraporphyrin assembly in solution, determined by 1D and 2D H-H COSY and NOESY-EXSY NMR spectra, is essentially the same as that found in the solid state. The main NMR features of (**7a**·Zn)$_2$ (Figure 16) are the following: (i) All the porphyrins in (**7a**·Zn)$_2$ are equivalent to each other, because of C_2 and S_4 symmetry axes going through the two Ru atoms. (ii) All 4′-N(py) rings are bound either to Ru or to the Zn atom inside another porphyrin. Axial coordination to a Zn−porphyrin induces typical upfield shifts due to the anisotropic shielding cone of the porphyrin ring, in particular for the protons closest to Zn. All resonances are sharp at ambient temperature, with the exception of those of the pyridyl rings bound to Zn (because of the lability of Zn). (iii) Owing to the different coordination of the two 4′-N(py) rings on each 4′-*cis*DPyP unit of (**7a**·Zn)$_2$ (one bound to Ru and the other to Zn), each single porphyrin is in an asymmetric environment (Figure 16). In addition, each porphyrin has one side oriented towards the inside (*endo*) and the other towards the outside (*exo*) of the assembly; the *endo* protons (and those of the inner pyridyl rings in particular) are more shielded by the combined effects of the three porphyrins and therefore resonate more upfield than the corresponding *exo* protons. Thus, with the exception of the *meta*- and *para*-phenyl protons, each proton has its own well-resolved resonance. (iv) The two sides of each *meso* aromatic ring are exchanged by rotation around the $C_{meso}-C_{ring}$ bonds, which is slow on the NMR time-scale at room temperature. Finally, the ^{1}H NMR spectrum of a $CDCl_3$ solution of (**7a**·Zn)$_2$, diluted to the limit of detection (ca 3×10^{-5} M), exclusively showed the resonances of the intact adduct, indicating that the self-assembled structure is very stable. This finding agrees well with the high degree of cooperativity expected for the formation of (**7a**·Zn)$_2$.

Thus, **7a**·Zn is an unprecedented example of a metal-containing self-complementary building block that selectively recognizes itself through four 4′-N(py)−Zn interactions yielding a very stable and symmetrical dimeric species, (**7a**·Zn)$_2$, that features four porphyrins and six metal atoms (two Ru and four Zn).

To the best of our knowledge there are only two examples of systems assembled by two-point self-coordination. The group of Kobuke described that of a dizinc(II)−bis(imidazolyl)porphyrin dimer leading to a mixture of linear oligomers with potential application as optoelectronic materials.[51] Tsuda et al. have recently reported on the formation of a very stable cyclic supramolecular aggregate built as a result of many cooperative interactions from a *meso*−*meso*-linked Zn^{II}−bis(porphyrin) with pendant pyridyl groups.[52]

 © 2003 Wiley-VCH Verlag GmbH & Co. KGaA, Weinheim

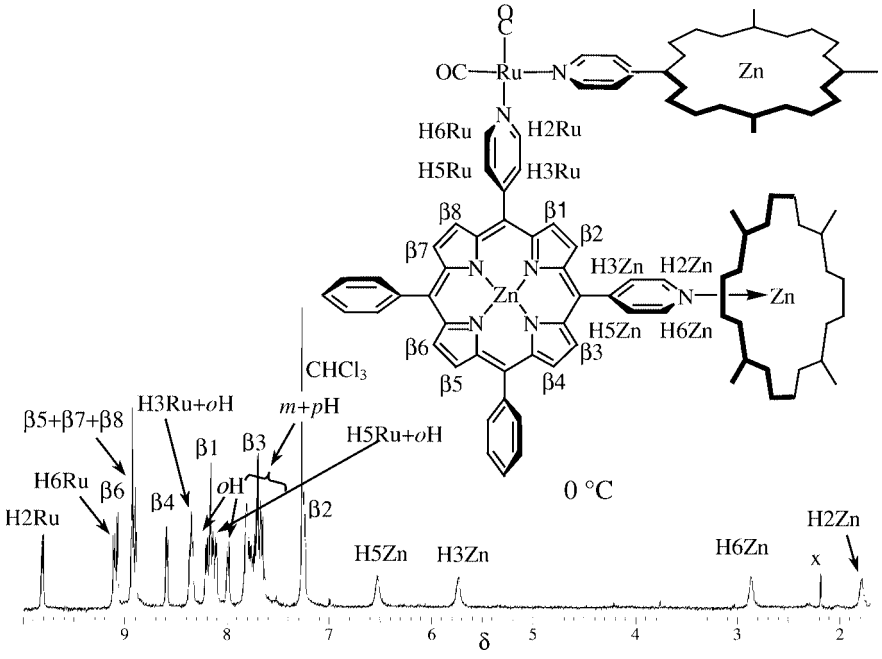

Figure 16. ^{1}H NMR spectra ($CDCl_3$) of (**7a**·Zn)$_2$ at 0 °C; an impurity is marked with x; for labeling scheme see the schematic drawing representing the coordination environment of each zincated porphyrin within (**7a**·Zn)$_2$ (top-view along the Cl−Ru−Cl bond system, Cl atoms omitted for clarity) reported on top of the spectrum

We are currently investigating the self-assembling properties of closely related building blocks featuring two donor and two acceptor binding sites. In particular, while maintaining the frame of the dizinc(II)−bis(pyridyl)porphyrin−ruthenium complex intact, we want to assess the effect of a change in the position of the N(py) atom (3′- instead of 4′-*cis*DPyP) or in the geometry of the bis(pyridyl)porphyrin (4′-*trans*DPyP instead of 4′-*cis*DPyP) on the nature of the self-assembled product. We also plan to assess the self-assembling behavior of complexes bearing three rather than two monocoordinated Zn−4′-*cis*DPyP ligands (that is three *donor* and three *acceptor* sites), either in *fac* or *mer* geometry.

Abbreviations: Tetraphenylporphyrin (TPP), 10,15,20-triphenyl-5-(4′-pyridyl)porphyrin (4′-MPyP), 15,20-diphenyl-5,10-bis(4′-pyridyl)porphyrin (4′-*cis*DPyP), 10,20-diphenyl-5,15-bis(4′-pyridyl)porphyrin (4′-*trans*DPyP), 5,10,15,20-tetrakis(4′-pyridyl)-porphyrin (4′-TPyP), 3,7,13,17-tetramethyl-2,8,12,18-tetra-*n*-propyl-5,15-bis(4′-pyridyl)porphyrin (4′-*trans*DPyP-npm), 10,15,20-triphenyl-5-(3′-pyridyl)porphyrin (3′-MPyP), 5,10,15,20-tetrakis(3′-pyridyl)porphyrin (3′-TPyP), 1,3-bis(diphenylphosphanyl)-propane (dppp), triflate (OTf).

Acknowledgments

We thank the Italian CNR (grants no. Agenzia2000 CNRC00B91D 004 and Agenzia2000 CNRC000951) and the University of Trieste (special grant for young researchers to E. I.) for financial support. Special thanks go to: Prof. Silvano Geremia (University of Trieste) for precious help in solving the X-ray structures, Prof. Mario Calligaris (University of Trieste) for the computer modelling, the group of Prof. Franco Scandola (University of Ferrara), and in particular Dr. Anna Prodi, for the photophysic investigations and for a long-standing and fruitful collaboration, Prof. Luigi G. Marzilli (Louisiana State University, USA) for useful suggestions and scientific advise, and for the FAB MS experiments.

[1] [1a] J. Deisenhofer, H. Michel, *Angew. Chem. Int. Ed. Engl.* **1989**, *28*, 829−847. [1b] R. Hubert, *Angew. Chem. Int. Ed. Engl.* **1989**, *28*, 848−869.

[2] [2a] T. Pullerits, V. Sundström, *Acc. Chem. Res.* **1996**, *29*, 381−389. [2b] G. McDermott, S. M. Prince, A. A. Freer, A. M. Hawthornwaite-Lawless, M. Z. Paziz, R. J. Codgell, N. W. Isaacs, *Nature* **1995**, *374*, 517−521. [2c] R. J. Codgell, N. W. Isaacs, A. A. Freer, J. Arrelano, T. D. Howard, M. Z. Paziz, A. M. Hawthornwaite-Lawless, S. M. Prince, *Prog. Biophys. Mol. Biol.* **1997**, *68*, 1−27.

[3] [3a] A. Zouni, H. T. Witt, J. Kern, P. Fromme, N. Krau, W. Saenger, P. Orth, *Nature* **2001**, *409*, 739−743. [3b] P. Jordan, P. Fromme, H. T. Witt, O. Klukas, W. Saenger, N. Krau, *Nature* **2001**, *411*, 909−917.

[4] G. T. Babcock, M. Wikström, *Nature* **1992**, *356*, 301−309.

[5] [5a] H. Kurreck, M. Huber, *Angew. Chem. Int. Ed. Engl.* **1995**, *34*, 849−866. [5b] A. Harriman, J.-P. Sauvage, *Chem. Soc. Rev.* **1996**, 41−48. [5c] M. D. Ward, *Chem. Soc. Rev.* **1997**, *26*, 365−375. [5d] R. W. Wagner, J. Seth, S. I. Yang, D. Kim, D. F. Bocian, D. Holten, J. S. Lindsey, *J. Org. Chem.* **1998**, *63*, 5042−5049, and references therein. [5e] A. Nakano, A. Osuka, I. Yamazaki, T. Yamazaki, Y. Nishimura, *Angew. Chem. Int. Ed.* **1998**, *37*, 3023−3027.

[6] [6a] M.-S. Choi, T. Aida, T. Yamazaky, I. Yamazaki, *Angew. Chem. Int. Ed.* **2001**, *40*, 3194−3198. [6b] M. Uyemura, T. Aida, *J. Am. Chem. Soc.* **2002**, *124*, 11392−11403. [6c] M.-S. Choi, T. Aida, T. Yamazaky, I. Yamazaki, *Chem. Eur. J.* **2002**, *8*, 2668−2678.

[7] [7a] V. Marvoud, J.-P. Launay, *Inorg. Chem.* **1993**, *32*, 1376−1382. [7b] H. L. Anderson, S. J. Martin, D. D. Bradley, *Angew. Chem. Int. Ed. Engl.* **1994**, *33*, 655−656. [7c] R. W.

 © 2003 Wiley-VCH Verlag GmbH & Co. KGaA, Weinheim

Wagner, J. S. Lindsey, J. Seth, D. F. Palaniappan, D. F. Bocian, *J. Am. Chem. Soc.* **1996**, *118*, 3996−3997. [7d] J. J. Hopfield, J. N. Onuchic, J. Beratan, *J. Phys. Chem.* **1989**, *93*, 6350−6357.

[8] [8a] T. Aida, S. Inoue, in *The Porphyrin Handbook* (Eds.: K. M. Kadish, K. M. Smith, R. Guillard), Academic Press, San Diego, CA, USA, **2000**, vol. 6, chapter 42. [8b] H. Ogoshi, T. Mizutani, T. Hayashi, Y. Kuroda, in *The Porphyrin Handbook* (Eds.: K. M. Kadish, K. M. Smith, R. Guillard), Academic Press, San Diego, CA, USA, **2000**, vol. 6, chapter 46.

[9] R. K. Pandey, G. Zheng, in *The Porphyrin Handbook* (Eds.: K. M. Kadish, K. M. Smith, R. Guillard), Academic Press, San Diego, CA, USA, **2000**, vol. 6, chapter 43.

[10] J. Chou, M. E. Kosal, H. S. Nalwa, N. A. Rakow, K. S. Suslick, in *The Porphyrin Handbook*, (Eds.: K. M. Kadish, K. M. Smith, R. Guillard), Academic Press, San Diego, CA, USA, **2000**, vol. 6, chapter 41.

[11] For a comprehensive recent review see: A. K. Burrel, D. L. Officer, P. G. Plieger, C. W. Reid, *Chem. Rev.* **2001**, *101*, 2751−2796.

[12] For examples of discrete multiporphyrin arrays formed by hydrogen bonding see: [12a] C. M. Drain, R. Fischer, E. G. Nolen, J.-M. Lehn, *J. Chem. Soc., Chem. Commun.* **1993**, 243−245. [12b] J. L. Sessler, B. Wang, A. Harriman, *J. Am. Chem. Soc.* **1995**, *117*, 704−714. [12c] Y. Kuroda, A. Kawashima, T. Urai, H. Ogoshi, *Tetrahedron Lett.* **1995**, *36*, 8449−8452. [12d] C. M. Drain, K. C. Russel, J.-M. Lehn, *Chem. Commun.* **1996**, 337−338. [12e] C. Ikeda, N. Nagahara, E. Motegi, N. Yoshioka, H. Inoue, *Chem. Commun.* **1999**, 1759−1760. [12f] R. A. Haycock, A. Yartsev, U. Michelsen, V. Sundström, C. A. Hunter, *Angew. Chem. Int. Ed.* **2000**, *39*, 3616−3619. [12g] T. S. Balaban, A. Eichhoffer, J.-M. Lehn, *Eur. J. Org. Chem.* **2000**, 4047−4057. [12h] C. M. Drain, X. Shi, T. Milic, F. Nifiatis, *Chem. Commun.* **2001**, 1416. [12i] G. Ercolani, *Chem. Commun.* **2001**, 1416−1417. [12j] X. Shi, K. M. Barkigia, J. Fajer, C. M. Drain, *J. Org. Chem.* **2001**, *66*, 6513−6522.

[13] [13a] C. Ikeda, Y. Tanaka, T. Fujihara, Y. Ishii, T. Ushiyama, K. Yamamoto, N. Yoshioka, H. Inoue, *Inorg. Chem.* **2001**, *40*, 3395−3405. [13b] C. A. Hunter, C. M. R. Low, M. J. Packer, S. E. Spey, J. G. Vinter, M. O. Vysotsky, C. Zonta, *Angew. Chem. Int. Ed.* **2001**, *40*, 2678−2682.

[14] For comprehensive recent reviews see: [14a] J.-C. Chambron, V. Heitz, J.-P. Sauvage in *The Porphyrin Handbook* (Eds.: K. M. Kadish, K. M. Smith, R. Guillard), Academic Press, San Diego, CA, USA, **2000**, vol. 6, chapter 40. [14b]J. Wojaczynski, L. Latos-Grazynsky, *Coord. Chem. Rev.* **2000**, *204*, 113−171. [14c] T. Imamura, K. Fukushima, *Coord. Chem. Rev.* **2000**, *198*, 133−156.

[15] J. K. M. Sanders, N. Bampos, Z. Clyde-Watson, S. L. Darling, J. C. Hawley, H.-J. Kim, C. C. Mak, S. J. Webb, in *The Porphyirin Handbook* (Eds.: K. M. Kadish, K. M. Smith, R. Guillard), Academic Press, San Diego, CA, USA, **2000**, vol. 3, chapter 1.

[16] For recent examples see: [16a] T. E. O. Screen, J. R. G. Thorne, R. G. Denning, D. G. Bucknall, H. L. Anderson, *J. Am. Chem. Soc.* **2002**, *122*, 9712−9713. [16b] L. J. Twyman, S. H. King, *Chem. Commun.* **2002**, 910−911. [16c] C. A. Hunter, R. Tregonning, *Tetrahedron* **2002**, *58*, 691−697. [16d] Y. d-P. Posner, G. K. Patra, I. Goldberg, *J. Chem. Soc., Dalton Trans.* **2001**, 2775−2782.

[17] [17a] H.-J. Kim, N. Bampos, J. K. M. Sanders, *J. Am. Chem. Soc.* **1999**, *121*, 8120−8121. [17b] M. J. Gunter, N. Bampos, K. D. Johnstone, J. K. M. Sanders, *New J. Chem.* **2001**, *25*, 166−173.

[18] [18a] K. Chichak, N. R. Branda, *Chem. Commun.* **1999**, 523−524. [18b] K. Chichak, N. R. Branda, *Chem. Commun.* **2000**, 1211−1212.

[19] [19a] E. Alessio, E. Ciani, E. Iengo, V. Yu. Kukushkin, L. G. Marzilli, *Inorg. Chem.* **2000**, *39*, 1434−1443. [19b] E. Iengo, R. Minatel, B. Milani, L. G. Marzilli, E. Alessio, *Eur. J. Inorg. Chem.* **2001**, 609−612. [19c] E. Iengo, E. Zangrando, S. Mestroni, G. Fronzoni, M. Stener, E. Alessio, *J. Chem. Soc., Dalton Tran.* **2001**, 1338−1346. [19d] B. Serli, E. Zangrando, E. Iengo, E. Alessio, *Inorg. Chim. Acta* **2002**, *339*, 265−272.

[20] [20a] A. Kimura, K. Funatsu, T. Imamura, H. Kido, Y. Sasaki, *Chem. Lett.* **1995**, 207−208. [20b] N. Kariya, T. Imamura, Y. Sasaki, *Inorg. Chem.* **1997**, *36*, 833−839. [20c] K. Funatsu, A. Kimura, T. Imamura, A. Ichimura, Y. Sasaki, *Inorg. Chem.* **1997**, *36*, 1625−1637. [20d] S. L. Darling, C. C. Mak, N. Bampos, N. Feeder, S. J. Teat, J. K. M. Sanders, *New J. Chem.* **1999**, *23*, 359−364.

[21] [21a] J. R. Redman, N. Feeder, S. J. Teat, J. K. M Sanders, *Inorg. Chem.* **2001**, *40*, 2486−2499. [21b] E. Stulz, Y.-F. Ng, S. M. Scott, J. K. M. Sanders, *Chem. Commun.* **2002**, 524−525.

[22] [22a] Y. Kobuke, H. Miyaji, *Bull. Chem. Soc., Jpn.* **1996**, *69*, 3563−3569. [22b] N. N. Gerasimchuk, A. A. Mokhir, K. R. Rodgers, *Inorg. Chem.* **1998**, *37*, 5641−5650. [22c] U. Michelsen, C. A. Hunter, *Angew. Chem. Int. Ed.* **2000**, *39*, 764−767.

[23] [23a] E. B. Fleischer, A. M. Shacter, *Inorg. Chem.* **1991**, *30*, 3763−3769. [23b] C. A. Hunter, L. D. Sarson, *Angew. Chem. Int. Ed. Engl.* **1994**, *33*, 2313−2316. [23c] Y. Kobuke, H. Miyaji, *J. Am. Chem. Soc.* **1994**, *116*, 4111−4112. [23d] X. Chi, A. J. Guerin, R. C. Haycock, C. A. Hunter, L. D. Sarson, *J. Chem. Soc., Chem. Commun.* **1995**, 2567−2569. [23e] T. Stibrany, J. Vasudevan, S. Knapp, J. A. Potenza, T. Emge, H. J. Sugar, *J. Am. Chem. Soc.* **1996**, *118*, 3980−3981. [23f] A. K. Burrell, D. L. Officer, D. C. W. Reid, K. Y. Wild, *Angew. Chem. Int. Ed.* **1998**, *37*, 114−117. [23g] K. Funatsu, T. Imamura, A. Ichimura, Y. Sasaki, *Inorg. Chem.* **1998**, *37*, 4986−4995. [23h] K. Funatsu, T. Imamura, A. Ichimura, Y. Sasaki, *Inorg. Chem.* **1998**, *37*, 1798−1804.

[24] [24a] X. Chi, A. J. Guerin, R. A. Haycock, C. A. Hunter, L. D. Sarson, *J. Chem. Soc., Chem. Commun.* **1995**, 2563−2565. [24b] G. Ercolani, *J. Phys. Chem. B* **1998**, 5699−5703. [24c] G. Ercolani, M. Ioele, D. Monti, *New J. Chem.* **2001**, *25*, 783−789.

[25] [25a] R. Krishna Kumar, I. Goldberg, *Angew. Chem. Int. Ed.* **1998**, *37*, 3027−3030. [25b] L. Pan, B. C. Noll, X. Wang, *Chem. Commun.* **1999**, 157−158. [25c] C. V. K. Sharma, G. A. Broker, J. G. Huddleston, J. W. Baldwin, R. M. Metzger, R. D. Rogers, *J. Am. Chem. Soc.* **1999**, *121*, 1137−1144. [25d] L. Pan, S. Kelly, X. Huang, J. Li, *Chem. Commun.* **2002**, 2334−2335. [25e] M. E. Kosal, J.-H. Chou, S. R. Wilson, K. S. Suslick, *Nat. Mater.* **2002**, *1*, 118−121.

[26] [26a] C. M. Drain, J.-M. Lehn, *J. Chem. Soc., Chem. Commun.* **1994**, 2313−2315. [26b] P. J. Stang, J. Fan, B. Olenyuk, *Chem. Commun.* **1997**, 1453−1454. [26c] J. Fan, J. A. Whiteford, B. Olenyuk, M. D. Levin, P. J. Stang, E. B. Fleischer, *J. Am. Chem. Soc.* **1999**, *121*, 2741−2752.

[27] C. M. Drain, F. Nifiatis, A. Vasenko, J. D. Batteas, *Angew. Chem. Int. Ed.* **1998**, *37*, 2344−2347.

[28] [28a] D. Sun, F. S. Tham, C. A. Reed, L. Chaker, M. Burgess, P. D. W. Boyd, *J. Am. Chem. Soc.* **2000**, *122*, 10704−10705. [28b] D. Sun, F. S. Tham, C. A. Reed, L. Chaker, P. D. W. Boyd, *J. Am. Chem. Soc.* **2002**, *124*, 6604−6612.

[29] M. Ayabe, A. Ikeda, S. Shinkai, S. Sakamoto, K. Yamaguchi, *Chem. Commun.* **2002**, 1032−1033.

[30] [30a] A. Ikeda, M. Ayabe, S. Shinkai, S. Sakamoto, K. Yamaguchi, *Org. Lett.* **2000**, 3707−3710. [30b] M. Ayabe, K. Yamashita, K. Sada, S. Shinkai, A. Ikeda, S. Sakamoto, K. Yamaguchi, *J. Org. Chem.* **2003**, *68*, 1059−1066.

[31] N. Fujita, K. Biradha, M. Fujita, S. Sakamoto, K. Yamaguchi, *Angew. Chem. Int. Ed.* **2001**, *40*, 1718−1721.

[32] W. T. S. Huck, A. Rohrer, A. T. Anilkumar, R. H. Fokkens, N. M. M. Nibbering, F. C. J. M. Van Veggel, D. N. Reinhoudt, *New J. Chem.* **1998**, 165−168.

[33] E. Alessio, M. Macchi, S. Heath, L. G. Marzilli, *Chem. Commun.* **1996**, 1411−1412.

[34] [34a] E. Alessio, S. Geremia, S. Mestroni, E. Iengo, I. Srnova, M. Slouf, *Inorg. Chem.* **1999**, *38*, 869−875. [34b] E. Alessio, S. Geremia, S. Mestroni, I. Srnova, M. Slouf, T. Gianferrara, A. Prodi, *Inorg. Chem.* **1999**, *38*, 2527−2529.

[35] E. Alessio, E. Iengo, L. G. Marzilli, *Supramol. Chem.* **2002**, *14*, 103−120.

 © 2003 Wiley-VCH Verlag GmbH & Co. KGaA, Weinheim

[36] E. Alessio, M. Macchi, S. L. Heath, L. G. Marzilli, *Inorg. Chem.* **1997**, *36*, 5614−5623.
[37] [37a] E. Alessio, G. Mestroni, G. Nardin, W. M. Attia, M. Calligaris, G. Sava, S. Zorzet, *Inorg. Chem.* **1988**, *27*, 4099−4106. [37b] M. Henn, E. Alessio, G. Mestroni, M. Calligaris, W. M. Attia, *Inorg. Chim. Acta* **1991**, *187*, 39−50.
[38] E. Alessio, B. Milani, M. Bolle, G. Mestroni, P. Faleschini, F. Todone, S. Geremia, M. Calligaris, *Inorg. Chem.* **1995**, *34*, 4722−4734.
[39] [39a] R. V. Slone, J. T. Hupp, *Inorg. Chem.* **1997**, *36*, 5422−5423. [39b] H. Yuan, L. Thomas, L. K. Woo, *Inorg. Chem.* **1996**, *35*, 2808−2817.
[40] E. Iengo, E. Zangrando, R. Minatel, E. Alessio, *J. Am. Chem. Soc.* **2002**, *124*, 1003−1013.
[41] E. Iengo, PhD dissertation, University of Trieste, **2002**.
[42] A. Prodi, C. J. Kleverlaan, M. T. Indelli, F. Scandola, E. Alessio, E. Iengo, *Inorg. Chem.* **2001**, *40*, 3498−3504.
[43] [43a] M. L. Merlau, M. del P. Mejia, S. T. Nguyen, J. T. Hupp, *Angew. Chem. Int. Ed.* **2001**, *40*, 4239−4242. [43b] K. E. Splan, M. H. Keefe, A. M. Massari, K. A. Walters, J. T. Hupp, *Inorg. Chem.* **2002**, *41*, 619−621.
[44] [44a] A. Endo, Y. Okamoto, K. Suzuki, J. Shimamura, K. Shimizu, G. P. Satô, *Chem. Lett.* **1994**, 1317−1320. [44b] A. Endo, U. Tagami, Y. Wada, M. Saito, K. Shimizu, G. P. Satô, *Chem. Lett.* **1996**, 243−244.
[45] [45a] H. L. Anderson, *Inorg. Chem.* **1994**, *33*, 972−981. [45b] G. S. Wilson, H. L. Anderson, *Chem. Commun.* **1999**, 1539−1540. [45c] P. N. Taylor, H. L Anderson, *J. Am. Chem. Soc.* **1999**, *121*, 11538−11545.
[46] [46a] H. L. Anderson, C. A. Hunter, M. N. Meah, J. K. M. Sanders, *J. Am. Chem. Soc.* **1990**, *112*, 5780−5789. [46b] H. L. Anderson, S. Anderson, J. K. M. Sanders, *J. Chem. Soc., Perkin Trans. 1* **1995**, 2231−2245 and references therein.
[47] For a recent review see: C. J. Chang, Y. Deng, A. F. Heyduk, C. K. Chang, D. G. Nocera, *Inorg. Chem.* **2000**, *39*, 959−966.
[48] E. Iengo, B. Milani, E. Zangrando, S. Geremia, E. Alessio, *Angew. Chem. Int. Ed.* **2000**, *39*, 1096−1099.
[49] B. Olenyuk, A. Fetchenkötter, P. J. Stang, *J. Chem. Soc., Dalton Trans.* **1998**, 1707−1728.
[50] E. Iengo, E. Zangrando, S. Geremia, R. Graff, B. Kieffer, E. Alessio, *Chem. Eur. J.* **2002**, *8*, 4670−4674.
[51] [51a] K. Ogawa, Y. Kobuke, *Angew. Chem. Int. Ed.* **2000**, *39*, 4070−4073. [51b] K. Ogawa, T. Zhang, K. Yoshihara, Y. Kobuke, *J. Am. Chem. Soc.* **2002**, *124*, 22−23.
[52] A. Tsuda, T. Nakamura, S. Sakamoto, K. Yamaguchi, A. Osuka, *Angew. Chem. Int. Ed.* **2002**, *41*, 2817−2820.

Received February 18, 2003

 © 2003 Wiley-VCH Verlag GmbH & Co. KGaA, Weinheim

Rational Design of a Ferromagnetic Trinuclear Copper(II) Complex with a Novel in-situ Synthesised Metalloligand

Ming-Liang Tong,*[a,b] Yin-Miao Wu,[a] Ye-Xiang Tong,[a] Xiao-Ming Chen,*[a] Ho-Chol Chang,[c] and Susumu Kitagawa*[c]

Keywords: Magnetic properties / Copper / N ligands / Nucleophilic addition

An interesting ferromagnetic linear trinuclear copper(II) compound containing an in-situ synthesised functional ligand has been rationally obtained and crystallographically characterised, confirming a new route to magnetic polynuclear clusters.

(© Wiley-VCH Verlag GmbH & Co. KGaA, 69451 Weinheim, Germany, 2003)

Introduction

Multi-metal-centred complexes or metal-complex assemblies with highly ordered solid-state structures have attracted much attention in the past few decades.[1,2] In homometallic systems, either ferromagnetic or antiferromagnetic behaviours can occur depending on the bridging ligand shape, bridging angles, and other factors.[3] Although high spin multiplicities of the ground state, along with ferromagnetic behaviour, have been achieved by applying the concept of strict orthogonality[4] between two magnetic orbitals in designing molecules, the rational design and synthesis of novel metal clusters with large ground spin-states is still a challenging and central topic in the field of molecular magnetism. The development of new metalloligands,[2,5] which have been found to play an important role not only in mediating magnetic interactions but also in introducing a catalytic site in metal assembled complexes, is undoubtedly one of best methods for meeting this challenge. Recently, in our attempt to synthesise coordination polymers with metal(II) salts and sodium dicyanamide [Na(dca)],[6] an unexpected product, namely [Cu(dcaOMe)$_2$] (**1**) [dcaOMe = di(methoxycarbimido)aminato], was formed by an interesting in situ nucleophilic addition reaction of the ligand (Scheme 1). We speculated that a series of functional polydentate ligands may be designed and generated by using other nucleophiles with potential ligation sites instead of MeOH, and that these ligands may be used in the synthesis of homo- and heterometallic clusters. We report here the successful use of pyrazole to furnish an interesting ferromagnetically coupled linear trinuclear copper(II) compound [Cu_3(dcadpz)$_2$(pz)$_2$(ClO_4)$_2$](ClO_4)$_2$·H_2O [**2**; dcadpz = di(pyrazolecarbimido)aminato; pz = pyrazole], which contains an interesting metalloligand as a ferromagnetic coupler.

Results and Discussion

Single-crystal X-ray analysis revealed that **1** is a neutral planar Cu^{II} complex (Figure 1, top). The Cu^{II} atom is coordinated in a planar-square geometry to four nitrogen atoms from two dcaOMe ligands. The Cu1−N bond lengths are 1.939(2) and 1.946(2) Å. The dcaOMe ligand is apparently formed by the addition reaction of dca and MeOH. Although this product was synthesised by the addition of methanol and dicyanimide in the presence of zinc chloride, followed by the replacement of zinc by copper(II) using an ammoniacal solution of copper(II) sulfate,[7,8] no X-ray structural analysis had been done prior to our work.

Complex **2** is a symmetrical linear trinuclear copper(II) complex. The crystallographically asymmetric unit consists of 1.5 Cu^{II} centres, one dcadpz ligand, one pz ligand, two ClO_4^- ions and 0.5 disordered lattice water molecules (Figure 1, bottom). The central Cu1 atom is located at an inver-

[a] State Key Laboratory of Optoelectronic Materials & Technologies and School of Chemistry and Chemical Engineering, Sun Yat-Sen University,
Guangzhou 510275, China
Fax: (internat.) +86-20/8411-2245
E-mail: cestml@zsu.edu.cn
cescxm@zsu.edu.cn
[b] State Key Laboratory of Structural Chemistry, Fujian Institute of Research on the Structure of Matter, Chinese Academy of Sciences,
Fuzhou 350002, China
[c] Department of Synthetic Chemistry and Biological Chemistry, Graduate School of Engineering, Kyoto University,
Yoshida, Sakyo-ku, Kyoto 606-8501, Japan
E-mail: kitagawa@sbchem.kyoto-u.ac.jp

Supporting information for this article is available on the WWW under http://www.eurjic.org or from the author.

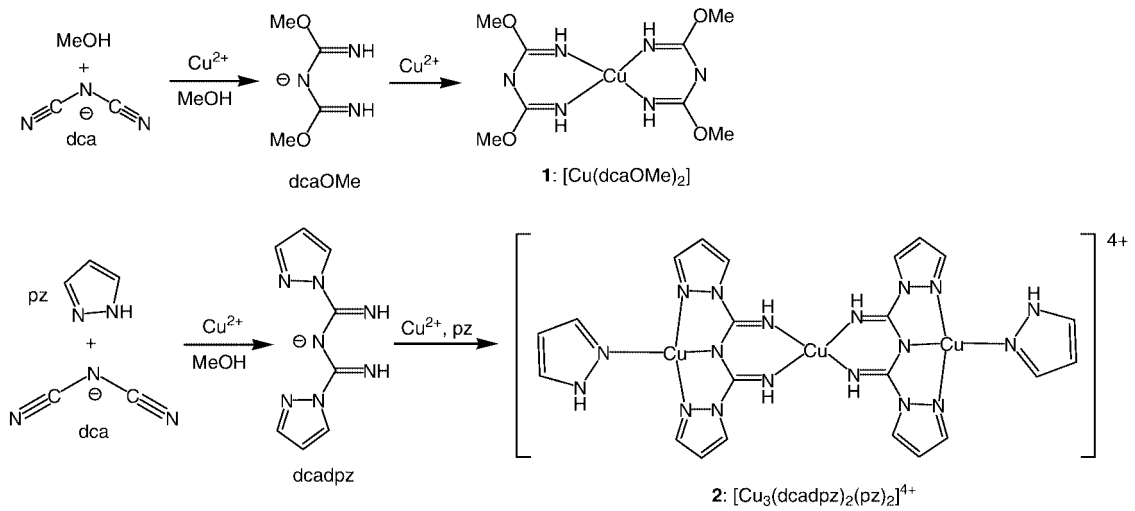

Scheme 1

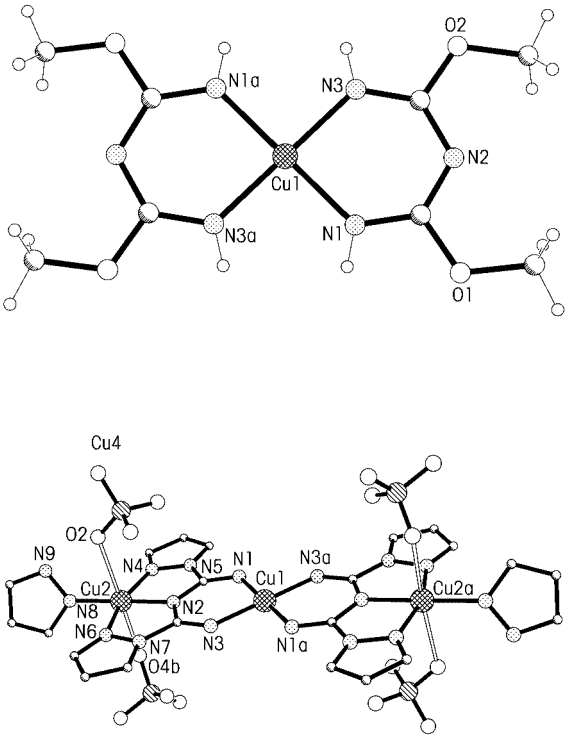

Figure 1. The coordination environment of the copper atoms in **1** (top) and **2** (bottom); selected bond lengths (Å): Cu(1)−N(1) 1.939(2), Cu(1)−N(3) 1.946(2) for **1**; Cu(1)−N(3) 1.949(4), Cu(1)−N(1) 1.955(4), Cu(2)−N(8) 1.957(4), Cu(2)−N(2) 1.958(4), Cu(2)−N(4) 1.976(4), Cu(2)−N(6) 1.980(4), Cu(2)−O(2) 2.518(5), Cu(2)−O(4b) 2.561(6) for **2**

sion centre and is coordinated in a perfectly square-planar geometry to four nitrogen atoms from two dcadpz ligands, with Cu1−N bond lengths of 1.949(4) and 1.955(4) Å, similar to those in **1**. Each of the terminal Cu2 atoms is coordinated in an elongated [4+2] distorted octahedral geometry with four nitrogen atoms in the equatorial positions [Cu2−N_{basal} bond lengths of 1.957(4)−1.980(4) Å], with three nitrogen atoms coming from a dcadpz ligand and the fourth from a monodendate pz ligand. The two oxygen atoms from two different perchlorate ions in the apical positions complete the octahedral geometry, with two long Cu2−O bond lengths of 2.518(5) and 2.561(6) Å. Each trinuclear Cu_3 unit is further connected to four adjacent Cu_3 units through quadruple μ-ClO_4^- bridges, resulting in a two-dimensional coordination layer (Figure 2). The uncoordinated ClO_4^- and the lattice water molecules are located between the layers and form hydrogen bonds with the imido groups, resulting in a three-dimensional network (Figure S1). It is interesting to note that the magnetic orbital of Cu1 is regarded as $d_{x^2-y^2}$ and is directed towards the four basal N atoms from the two dcadpz ligands, a situation similar to that found in the pioneering building block $[Cu(opba)]^{2-}$ [opba = *o*-phenylenebis(oxamato)].[2] The magnetic orbital of Cu2, mainly $d_{x^2-y^2}$, lies in the N_4(basal) plane and points towards the four basal donors.

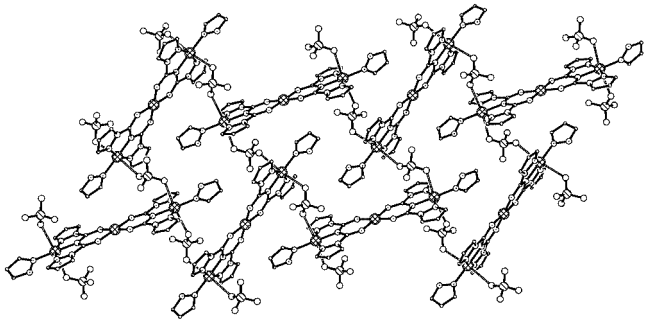

Figure 2. Perspective view of the 2D coordination layer along the *b* axis in **2**

The orientations of the magnetic orbits in **2** are verified by its magnetic behaviour. The value of the magnetic moment at room temperature is 3.25 μ_B per Cu_3 formula unit, consistent with three unpaired electrons per Cu_3 unit with $g = 2.17$. Upon lowering the temperature, the magnetic moment (μ_{eff}) gradually increases from 3.25 μ_B at 300 K to reach a maximum of 3.88 μ_B at 4.6 K (Figure 3), which is similar to the value (3.87 μ_B) of three ferromagnetically coupled Cu^{II} atoms. The plot of χ_M^{-1} versus T (50−300 K)

 © 2003 Wiley-VCH Verlag GmbH & Co. KGaA, Weinheim

obeys the Curie–Weiss Law [$\chi_M = C/(T - \theta)$] at 10 kOe with a Weiss constant, θ, of 1.74 K, and a Curie constant, C, of 1.30 $cm^3\ mol^{-1}$ K, indicating a significant ferromagnetic coupling between the three $S = 1/2$ spins within the Cu_3 unit through the dcadpz bridges. From the structural analysis, **2** is considered to consist of well-separated tri-copper(II) units connected by perchlorate ligands, with the closest Cu2···Cu2′ distance being 6.364 Å. The temperature dependence of μ_{eff} was analysed by an isolated three-spin model[1,9–11] ($H = -2J(S_{Cu2'}\cdot S_{Cu1} + S_{Cu1}\cdot S_{Cu2'})$] with MAGMUN4.0.[12] The best-fit parameters were $J = 7.18\ cm^{-1}$ with an averaged g value of 2.15. The three copper(II) ions are ferromagnetically coupled and each Cu_3 unit has a ground spin-multiplicity of 3/2, which is supported by the field dependence of the magnetization [Figure 3 (inset)], The $M(H)$ data show a linear behaviour from 0 to 20 kOe. The slope then starts to reduce and reaches a value of 2.92 Nβ at 50 kOe, which is very close to the saturated value of 3 Nβ per Cu_3 formula unit with $S = 3/2$. The existence of a ferromagnetic interaction in **2** apparently results from the spin orbital orthogonality: the central Cu atom is antisymmetric whereas the terminal Cu atom is symmetric, and hence the two $d_{x^2-y^2}$ orbitals are orthogonal to each other. This orthogonality is advantageous for ferromagnetic coupling. Magnetic susceptibility $\chi_M(T)$ and magnetization $M(H)$ measurements on single-phase polycrystalline samples of **1** were also performed to confirm the valence of the copper ion in **1**. The magnetic behaviour of **1** obeys the Curie–Weiss Law in the range 2–300 K with an effective magnetic moment of 1.81 μ_B at 300 K (Figure S2), consistent with the single unpaired electron of Cu^{II} in **1**.

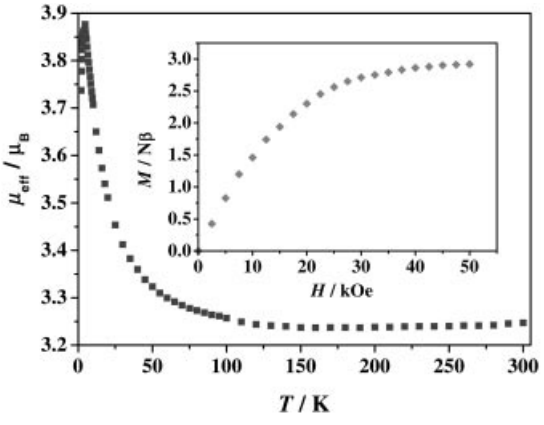

Figure 3. Temperature-dependent magnetic susceptibility plotted as μ_{eff} versus T and field-dependent magnetization plotted as M versus H (inset) at 2 K for a powdered sample of **2**

It is interesting to note that the neutral $Cu(dcadpz)_2$ metalloligand[13] features a planar structure and an intriguing functionality, possessing as it does three lone pairs on either side of the peripheral nitrogen atoms. Therefore, it may behave as a bis-bidentate ligand to connect two metal ions and may further act as a trinuclear building unit to generate low-dimensional coordination magnetic materials. In addition, it is characterised by its spin distribution. There is one unpaired electron arising from the central Cu^{2+} ion, and this electron occupies a $d_{x^2-y^2}$ orbital that is delocalised not only towards the nearest nitrogen atoms, but also towards the six peripheral donor atoms. Such a magnetic orbital interaction means that the $Cu(dcadpz)_2$ segment could be a very useful ferromagnetic coupler. Moreover, what interests us is that the metalloligand presented here can also be easily modified by adopting other starting materials instead of pyrazole. A new route for the synthesis of novel ferromagnetic couplers can therefore be anticipated that is quite different from another recently reported ferromagnetic coupler [$Cu(bptap)_2$], in which bptap was formed by the hydrolysis of tris(2-pyridyl)triazine in the presence of anhydrous $Cu(OAc)_2$ in absolute methanol.[11]

In summary, we provide here a rational strategy for the synthesis of an interesting polydentate ligand and its metal cluster by a simultaneous in-situ addition reaction of dicyanamide and pyrazole, followed by metal coordination. Investigation of this synthetic strategy towards other substituted pyrazole derivatives and the assembly of heteronuclear metal complexes constructed with this metalloligand is under way.

Experimental Section

Synthesis of 1 and 2: Purple crystals of **1** were synthesised by the reaction of $Cu(BF_4)_2\cdot 6H_2O$ (0.237 g, 1.0 mmol) and Na(dca) (0.089 g, 1.0 mmol) in MeOH at 50 °C in ca. 84% yield (0.136 g). The reaction of $Cu(ClO_4)_2\cdot 6H_2O$ (0.555 g, 1.5 mmol), Na(dca) (0.089 g, 1.0 mmol) and pyrazole (0.136 g, 2.0 mmol) in MeOH at 50 °C led to the formation of deep blue crystals of **2** in 78% yield (0.298 g).

1: $C_8H_{16}CuN_6O_4$ (323.8): calcd. C 29.72, H 4.99, N 26.01; found C 29.46, H 4.92, N 25.78

2: $C_{22}H_{26}Cl_4Cu_3N_{18}O_{17}$ (1147.0): calcd. C 23.10, H 2.29, N 22.06; found C 22.81, H 2.18, N 21.83. The IR spectra of **1** and **2** clearly indicate the absence of characteristic peaks for cyano groups, suggesting the transformation of cyano groups into carbimido groups during the reaction.

Crystal Structure Characterisation: X-ray diffraction data collection were carried out on a Bruker CCD diffractometer, using graphite-monochromated Mo-K_α radiation. All non-H atoms were refined anisotropically.

1: Purple crystals. $C_8H_{16}CuN_6O_4$, $M_r = 323.81$, monoclinic, space group $P2_1/n$ (no. 14), $a = 10.018(3)$, $b = 5.6635(14)$, $c = 11.632(3)$ Å, $\beta = 99.703(6)°$, $V = 650.6(3)$ Å^3, $Z = 2$, $D_c = 1.653\ g\ cm^{-3}$, $\mu = 17.00\ cm^{-1}$. Data collection ($4.01 \le 2\theta \le 26°$) was performed at 293 K on a Bruker CCD diffractometer (Mo-K_α, $\lambda = 0.71073$ Å). The structure was solved by direct methods and refined with full-matrix least-squares (SHELX-97),[14] giving a final R_1 value of 0.0400 for 98 parameters and 1032 unique reflections with $I \ge 2\sigma(I)$ and wR_2 of 0.1142 for all 1192 reflections.

2: Deep blue crystals, 293 K. $C_{22}H_{26}Cl_4Cu_3N_{18}O_{17}$, $M_r = 1147.03$, monoclinic, space group $P2_1/c$ (no. 14), $a = 9.362(6)$, $b = 12.469(7)$, $c = 17.570(8)$ Å, $b = 92.208(9)°$, $V = 2049.5(19)$ Å^3, $Z = 2$, $D_c = 1.859\ g\ cm^{-3}$, $\mu = 18.96\ cm^{-1}$. Final R_1 value of 0.0639 for 295 parameters and 3126 unique reflections with $I > 2\sigma(I)$ and wR_2 of 0.1895 for all 3991 reflections.

CCDC-204851 (**1**) and -204852 (**2**) contain the supplementary crystallographic data for this paper. These data can be obtained free of charge at www.ccdc.cam.ac.uk/conts/retrieving.html [or from the

 © 2003 Wiley-VCH Verlag GmbH & Co. KGaA, Weinheim

Cambridge Crystallographic Data Centre, 12, Union Road, Cambridge CB2 1EZ, UK; fax: (internat.) +44-1223/336-033; E-mail: deposit@ccdc.cam.ac.uk].

Acknowledgments

This work was supported by the NSFC (20001008 & 20131020), the Foundation for the Author of National Excellent Doctoral Dissertation of P. R. China (200122) and the Talent Training Program Foundation of the Higher Education Department of Guangdong Province (Q02017). M.-L. T. is grateful to JSPS for a postdoctoral fellowship.

[1] O. Kahn, *Molecular Magnetism*, VCH, Weinheim, 1993.
[2] O. Kahn, *Acc. Chem. Res.* **2000**, *33*, 647−657.
[3] Y. Rodríguez-Martín, M. Hernández-Molina, F. S. Delgado, J. Pasán, C. Ruiz-Pérez, J. Sanchiz, F. Lloret, M. Julve, *CrystEngCommun* **2002**, *4*, 522−535.
[4] O. Kahn, J. Galy, Y. Journaux, J. Jaid, I. Morgenstern-Badarau, *J. Am. Chem. Soc.* **1982**, *104*, 2165−2176.
[5] S.-I. Noro, S. Kitagawa, M. Yamashita, T. Wada, *Chem. Commun.* **2002**, 222−223.
[6] M.-L. Tong, J. Ru, Y.-M. Wu, X.-M. Chen, H.-C. Chang, K. Mochizuki, S. Kitagawa, *New J. Chem.* **2003**, *27*, 779−782.
[7] G. Rembarz, E. Fischer, K.-Ch. Röber, R. Ohff, H. Crahmer, *J. Prakt. Chem.* **1969**, *311*, 889−893.
[8] G. Götz, H. U. Kibbel, *Z. Chem.* **1975**, *15*, 278−281.
[9] X. Chen, S. Zhan, C. Hu, Q. Meng, Y. Liu, *J. Chem. Soc., Dalton Trans.* **1997**, 245−250.
[10] J. Tercero, C. Diaz, J. Ribas, J. Mahía, M. A. Maestro, *Inorg. Chem.* **2002**, *41*, 5373−5381.
[11] T. Kajiwara, A. Kamiyama, T. Ito, *Chem. Commun.* **2002**, 1256−1257.
[12] *MAGMUN4.0* was developed by Dr Zhiqiang Xu (zxu@hpower.com)and Kathy Minzhen He (heminzhen@yahoo.com) in collaboration with Prof. L. K. Thompson (lthomp@mun.ca) and Dr O. Waldmann (waldmann@physik.uni-erlangen.de).
[13] The neutral $Cu(dcadpz)_2$ metalloligand has been isolated and crystallographically characterised. Crystal data for $Cu(dcadpz)_2$: $C_{16}H_{16}CuN_{14}$, tetragonal, space group $P4_2/n$ (No. 86), $M_r = 467.97$, $a = b = 22.285(8)$, $c = 3.8905(15)$ Å, $V = 1932.2(12)$ Å^3, $Z = 4$. $R_1 = 0.0618$, $wR_2 = 0.0956$.
[14] G. M. Sheldrick, SHELXS-97, *Program for Crystal Structure Solution*, University of Göttingen, Germany, 1997.

Received April 8, 2003

 © 2003 Wiley-VCH Verlag GmbH & Co. KGaA, Weinheim

Assembly of Dicobalt(III) Complexes Incorporating Di-μ-thiophenolate Moieties

Armando Marin-Becerra,[a,b] Philip A. Stenson,[a] Jonathan McMaster,[a] Alexander J. Blake,[a] Claire Wilson,[a] and Martin Schröder*[a]

Keywords: Cobalt / Schiff-base ligand / Thiolate

The dinuclear $[Co^{III}Co^{III}]$ complexes $[Co_2(L^1)(\mu\text{-OAc})(OAc)(NH_3)](PF_6)_2$ and $[(Co_2(L^2)_2(\mu\text{-OAc})](PF_6)$, incorporating the rare $Co(\mu\text{-SR})_2Co$ moiety associated with Schiff-base co-ligands, are protected by bridging μ-OAc^- units situated within a domed cavity formed by the complexes; increasing the steric bulk of the ligand, as in $[L^3]^{2-}$, affords the mononuclear species $[Co(L^3)(OAc)]$.

(© Wiley-VCH Verlag GmbH & Co. KGaA, 69451 Weinheim, Germany, 2003)

Homo- and heterodimetallic complexes occur in a number of metalloenzymes, and increasing efforts have been directed towards the synthesis of compartmental macrocycles capable of mimicking their structural, spectroscopic and chemical properties.[1] Compartmental macrocyclic ligands derived from 2,6-dicarbonylphenols offer a stable framework for binding two metal cations in close proximity via a bridging phenolate, and may also be designed to incorporate unsymmetrical compartments and coordinating pendant groups.[1,2] We[3,4] and others[5,6] have developed synthetic strategies to thiophenolate macrocyclic analogues that stabilise the dinuclear dithiolate fragment within the macrocyclic core. The incorporation, however, of highly redox-active $Co^{II/III}$ centres into such coordination frameworks remains relatively rare.[7] We describe herein for the first time the synthesis and characterisation of two di-μ-thiolato dimetallic Co^{III} complexes, $[Co_2(L^1)(\mu\text{-OAc})(OAc)(NH_3)](PF_6)_2$ and $[Co_2(L^2)_2(\mu\text{-OAc})](PF_6)$, incorporating the macrocyclic ($[L^1]^{2-}$) and corresponding open-chain ($[L^2]^{2-}$) ligands, respectively. Interestingly and significantly, both complexes show novel coordination modes with very similar core structures at the metal centres. The complexes incorporate a pyramidal stereochemistry at the bridging thiolate donors, with the nonplanar, domed conformation of the ligand set affording a hydrophobic pocket for OAc^- binding.

Template reactions of Co^{II} and Co^{III} salts with 2,6-diformyl-4-methylthiophenol and 1,3-diaminopropane under a range of conditions generally do not afford the metal complexes in a pure, tractable form. Higher yields of up to 60% can be obtained, however, by transmetallation reactions of the analogous Zn^{II} complex. Thus, reaction of $[Zn_2(L^1)(OAc)](PF_6)$[3] with $Co(OAc)_2{\cdot}4H_2O$ in MeCN in the presence of NH_4PF_6 under aerobic conditions affords a red diamagnetic solid that precipitates from the reaction mixture. The IR spectrum of this product confirms the presence of both PF_6^- and OAc^- anions, with absorptions at 3353 and 3302 cm^{-1} indicating the presence of ammonia in the product. A broad signal (δ = 3.3−3.6 ppm), which exchanges with D_2O, in the ^1H NMR spectrum (CD_3CN) further supports the presence of coordinated NH_3. As the integral of this signal accounts for only one molecule of ammonia per macrocycle, the coordination at the two Co^{III} ions is, therefore, expected to be different. This hypothesis is supported by both ^1H and ^{13}C NMR spectroscopy, each of which shows two signals for the C(H)=N groups, at δ =

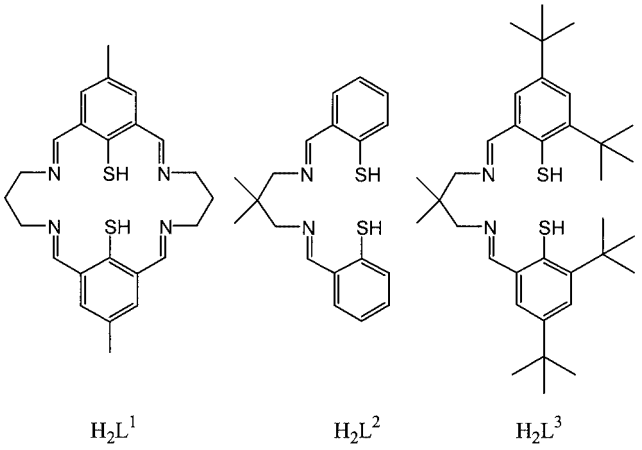

Scheme 1

[a] School of Chemistry, University of Nottingham, University Park,
Nottingham, NG7 2RD, UK
[b] Facultad de Química, Universidad Nacional Autónoma de México,
Mexico, D.F. 04105, México

Supporting information for this article is available on the WWW under http://www.eurjic.org or from the author.

8.22 and 8.28 ppm and at δ = 168 and 171 ppm, respectively. Asymmetry is also observed for the $N-CH_2$ groups of the macrocyclic ligand. The ^1H NMR spectrum also confirms the presence of two nonequivalent acetate anions, with signals at δ = 0.77 and 2.03 ppm. The chemical shift for the former appears rather low, but such upfield shielding can occur when an acetate ion is located close to an aromatic ring current, as in calixarenes that bind guest molecules within a hydrophobic pocket.[8] Therefore, we interpret the upfield shift for the OAc^- signal as a strong indication that it is located within the macrocyclic hydrophobic pocket.

The solid-state structure of $[Co_2(L^1)(\mu\text{-OAc})(OAc)(NH_3)](PF_6)_2$ is entirely consistent with the structure proposed in solution. The molecular structure (Figure 1) shows two octahedral Co^{III} centres, each bound to the N_2S_2 donor set provided by the macrocyclic ligand and to a bridging acetate ion. The coordination sphere of one Co^{III} centre is completed by a monodentate acetate ion while the remaining site on the other centre is occupied by an NH_3 molecule. The macrocyclic ligand adopts a folded conformation, with the bridging acetate ion located within the cleft of the macrocycle. Because of its domed shape, the cleft can be de-

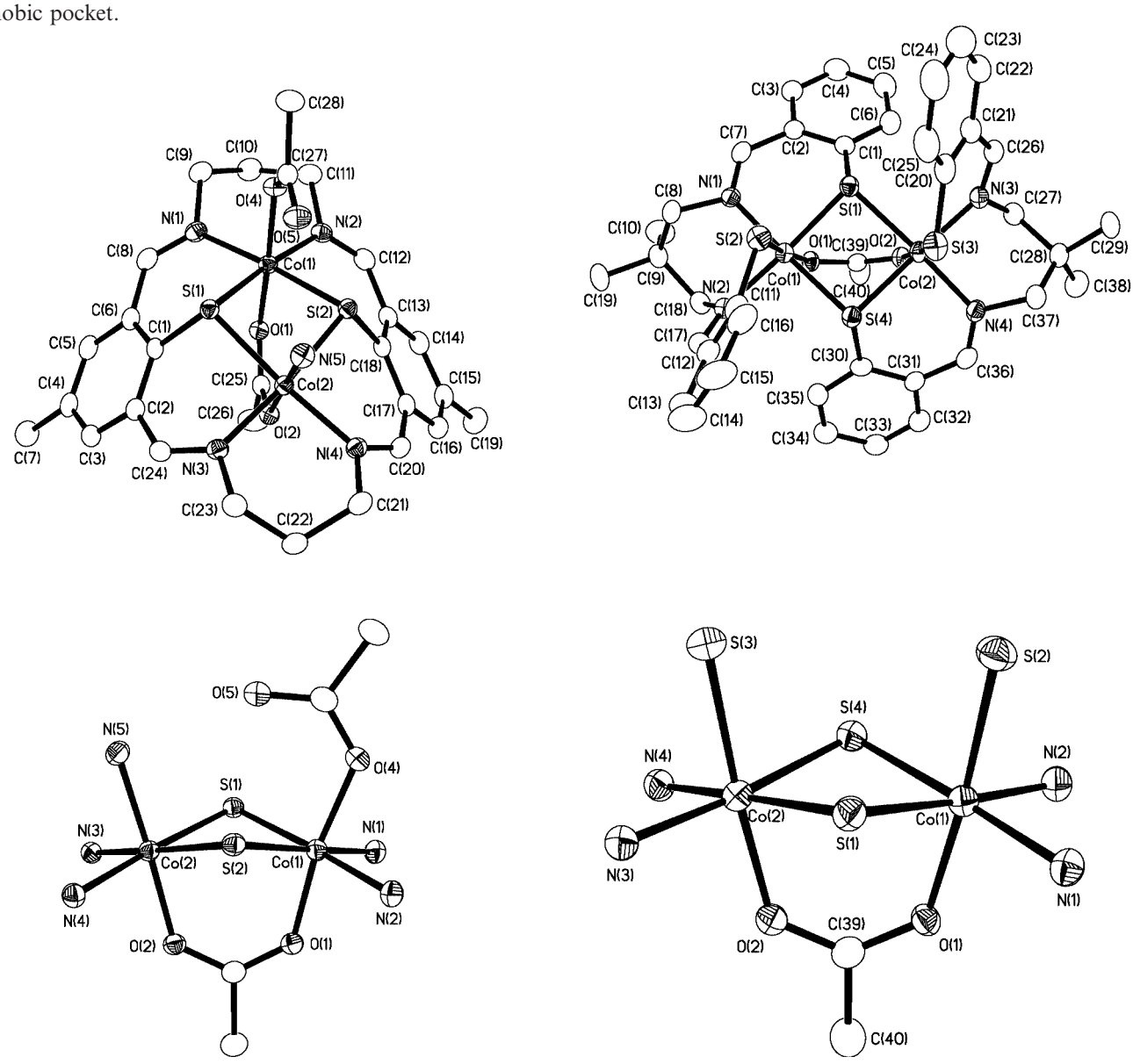

Figure 1. Two views of the structure of $[Co_2(L^1)(\mu\text{-OAc})(OAc)(NH_3)]^{2+}$ with displacement ellipsoids drawn at 50% probability: (top) a general view showing the atom numbering scheme; hydrogen atoms and PF_6^- anions are omitted for clarity; (bottom) a view of the metal coordination sphere; Co(1)···Co(2) 3.1750(5), Co(1)−O(1) 1.9181(16), Co(1)−O(4) 1.8968(17); Co(1)−N(1) 1.976(2), Co(1)−N(2) 1.975(2), Co(1)−S(1) 2.2239(6), Co(1)−S(2) 2.2216(6), Co(2)−O(2) 1.9202(16), Co(2)−N(5) 1.961(2), Co(2)−N(3) 1.975(2), Co(2)−N(4) 1.9792(19), Co(2)−S(1) 2.2399(6), Co(2)−S(2) 2.2416(6) Å

Figure 2. Two views of the structure of $[(Co_2(L^2)_2(\mu\text{-OAc})]^+$ cation with displacement ellipsoids drawn at 50% probability: (top) a general view showing the atom numbering scheme; hydrogen atoms and PF_6^- anions are omitted for clarity; (bottom) a view of the metal coordination sphere; Co(1)···Co(2) 3.2074(8), Co(1)−O(1) 1.967(3), Co(1)−N(1) 1.974(3), Co(1)−N(2) 1.974(3), Co(1)−S(1) 2.2306(11), Co(1)−S(2) 2.2284(12), Co(1)−S(4) 2.2806(11), Co(2)−N(3) 1.958(3), Co(2)−N(4) 1.969(3), Co(2)−O(2) 1.986(3), Co(2)−S(3) 2.2267(12), Co(2)−S(4) 2.2501(11), Co(2)−S(1) 2.2666(11) Å

 © 2003 Wiley-VCH Verlag GmbH & Co. KGaA, Weinheim

scribed by two dihedral angles, one between the two aromatic rings (97°), the other between the N_2S_2 planes (144)° (Figure 1). Cyclic voltammetry of $[Co_2L(\mu\text{-}OAc)(OAc)(NH_3)](PF_6)_2$ displays two reversible one-electron reductions (confirmed by coulometry) in MeCN (0.3 M $^nBu_4NPF_6$, C electrode, 293 K) at $E_{1/2} = -0.76$ and -0.96 V vs. Fc^+/Fc, assigned to the formation of $[Co^{III}Co^{II}]$ and $[Co^{II}Co^{II}]$ species, respectively.

Transmetallation of $[Zn(L^2)]$ with $Co(OAc)_2{\cdot}4H_2O$ in the presence of NH_4PF_6 affords a Co^{III} complex, the IR spectrum of which confirms the presence of both PF_6^- and OAc^- anions. ^1H NMR spectroscopy in CD_3CN indicates asymmetry in the complex and shows two signals for the C(H)=N groups at δ = 8.23 and 7.74 ppm, as well as two signals for the methyl groups at δ = 1.16 and 1.07 ppm. The signal belonging to the OAc^- anion can be observed at δ = 1.10 ppm and, as previously noted for $[Co_2L(\mu\text{-}OAc)(OAc)(NH_3)](PF_6)_2$, this upfield shift suggests the anion is exposed to an aromatic ring current.

The single-crystal X-ray structure of $[Co_2(L^2)_2(\mu\text{-}OAc)]PF_6$ (Figure 2) is in agreement with the spectroscopic data observed in solution, suggesting that the dinuclear structure is stable in solution, even in coordinating solvents such as MeCN. Although both metal ions exhibit the same coordination environment, the *cis* configuration adopted by the tetradentate ligand accounts for the various signals observed in the ^1H NMR spectrum. The overall structures of $[Co_2(L^2)_2(\mu\text{-}OAc)]PF_6$ and $[Co_2(L^1)(\mu\text{-}OAc)(OAc)(NH_3)](PF_6)_2$ are similar. The angle of the cleft defined by the aromatic rings is only 1° wider in the former and the N_2S_2 planes in $[Co_2(L^2)_2(\mu\text{-}OAc)]PF_6$ make an angle of 154°. As suggested by ^1H NMR spectroscopic data, an acetate anion is situated within this cleft. Cyclic voltammetry of $[Co_2(L^2)_2(\mu\text{-}OAc)]PF_6$ gives rise to only irreversible redox processes, reflecting the loss of redox stability on going from the macrocyclic chelate $[L^1]^{2-}$ to the polychelate $[L^2]^{2-}$, even though the resultant complexes have very similar coordination spheres.

Interestingly, reaction of $[Zn(L^3)]$ with $Co(AcO)_2{\cdot}4H_2O$ in $CHCl_3$ affords the corresponding *mononuclear* complex $[Co(L^3)(OAc)]$ (Figure 3), which shows octahedral coordination at Co^{III} with the OAc^- anion binding as a *cis*-chelate. The ligand $[L^3]^{2-}$ binds to the metal centre in a folded manner, the inherent steric hindrance of the ligand inhibiting the formation of dinuclear complex products. This observation is further confirmed by the formation of mononuclear complexes of $[L^3]^{2-}$ and related hindered ligands with square-planar Ni^{II}, Cu^{II} and Pd^{II}, and tetrahedral Zn^{II}.

Our current work seeks to examine the redox properties of these and related thiolate-bridged complexes and to develop new synthetic routes to heterodinuclear complexes.

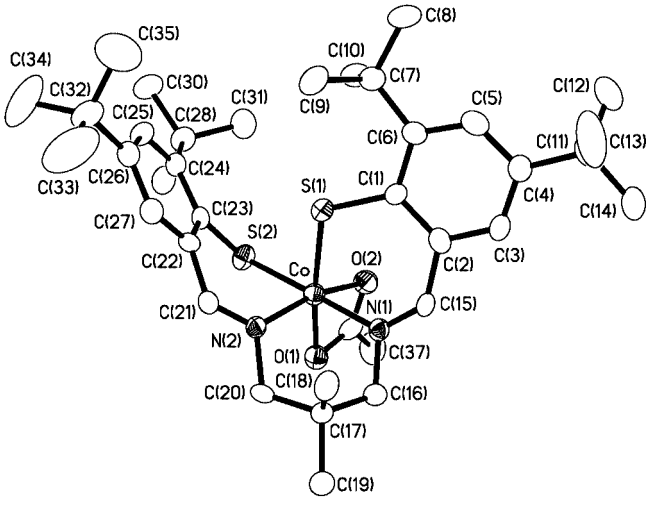

Figure 3. A view of the structure of $[Co(L^3)(OAc)]$ showing atom numbering, with displacement ellipsoids drawn at 50% probability; hydrogen atoms are omitted for clarity; Co−N(1) 1.953(5), Co−N(2) 1.886(5), Co−O(1) 2.023(4), Co−O(2) 1.992(4), Co−S(1) 2.201(2), Co−S(2) 2.231(2) Å

Experimental Section

X-ray Crystal Analysis: Crystal data for $[Co_2(L^1)(\mu\text{-}OAc)(OAc)(NH_3)](PF_6)_2{\cdot}3CH_3NO_2$: $C_{31}H_{44}Co_2F_{12}N_8O_{10}P_2S_2$ (M = 1160.66), triclinic, $P\bar{1}$, a = 11.7767(9), b = 14.8953(11), c = 15.1242(12) Å, α = 62.866(1), β = 82.093(1), γ = 74.901(1)°, V = 2279.0(3) Å^3, Z = 2, T = 150(2) K, $\rho_{calcd.}$ = 1.691 g cm^{-3}, $F(000)$ = 1180, μ(Mo-K_α) = 0.999 mm^{-1}, 10536 unique reflections measured, 621 variables, R_1 = 0.0380 [8575; $I > 2\sigma(I)$], $wR(F^2)$ = 0.107. Crystal data for $[(Co_2(L^2)_2(\mu\text{-}OAc)](PF_6)_2{\cdot}0.5CH_3CN$: $C_{41}H_{44.5}Co_2F_6N_{4.5}O_2PS_4$ (M = 1023.38), monoclinic, $P2_1/n$, a = 17.732(2), b = 10.5918(12), c = 23.506(2) Å, β = 97.187(2)°, V = 4380.0(14) Å^3, Z = 4, T = 150(2) K, $\rho_{calcd.}$ = 1.552 g cm^{-3}, $F(000)$ = 2100, μ(Mo-K_α) = 1.052 mm^{-1}, 10100 unique reflections measured, 561 variables, R_1 = 0.0523 [6840; $I > 2\sigma(I)$], $wR(F^2)$ = 0.1235. Crystal data for $[Co(L^3)(OAc)]{\cdot}0.5CHCl_3{\cdot}7/18(Et_2O)$: $C_{37}H_{55}CoN_2S_2{\cdot}0.5CHCl_3{\cdot}7/18(Et_2O)$ (M = 771.38), monoclinic, $C2/c$, a = 30.077(4), b = 12.519(2), c = 22.960(3) Å, β = 100.371(3)°, V = 8505(3) Å^3, Z = 8, T = 150(2) K, $\rho_{calcd.}$ = 1.205 g cm^{-3}, $F(000)$ = 3291, μ(Mo-K_α) = 0.630 mm^{-1}, 7937 unique reflections measured, 438 variables, R_1 = 0.0600 [2619; $I > 2\sigma(I)$], $wR(F^2)$ = 0.149. CCDC-200957, -200958 and -200959 contain the supplementary crystallographic data for this paper. These data can be obtained free of charge at www.ccdc.cam.ac.uk/conts/retrieving.html [or from the Cambridge Crystallographic Data Centre, 12 Union Road, Cambridge CB2 1EZ, UK; Fax: (internat.) + 44-1223/336-033; E-mail: deposit@ccdc.cam.ac.uk].

Synthesis of $[Co_2(L^1)(\mu\text{-}OAc)(OAc)(NH_3)](PF_6)_2$: $Co(OAc)_2{\cdot}4H_2O$ (0.05 g, 0.2 mmol) in MeOH (5 mL) was added to a solution of $[Zn_2(L^1)(OAc)]PF_6$ (0.077 g, 0.1 mmol) in MeOH (25 mL). The resulting red solution was heated under reflux for 1 h and then NH_4PF_6 (0.074 g, 0.4 mmol) was added. The resultant solution was heated under reflux for a further 1 h, after which time a red precipitate was observed. This precipitate was filtered and washed with cold MeOH and diethyl ether (0.059 g, 60% yield). $C_{28}H_{35}Co_2F_{12}N_5O_4P_2S_2$ (977.5): calcd. C 34.39, H 3.58, N 7.16; found C 34.60, H 3.52, N 7.13. MS (ES^+): m/z = 335 $[Co_2L(OAc)_2]^{2+}$. ^1H NMR (CD_3CN): δ = 8.28 (s, 2 H, CH=N), 8.22 (s, 2 H, CH=N), 4.57 (t, J = 13 Hz, 2 H, NCH_2) 4.22 (m, 4 H, NCH_2), 3.98 (d, J = 13 Hz, 2 H, NCH_2), 3.43 (br., 3 H, NH_3), 2.3−2.7 (m, 4 H, CCH_2C), 2.23 (s, 6 H, Ar-CH_3), 2.03 (s, 3 H, CH_3CO_2), 0.77 (s, 3 H, CH_3CO_2) ppm. ^{13}C NMR (CD_3CN): δ = 186.5 (CH_3CO_2), 180.0 (CH_3CO_2), 171.3 (C=N), 168.4 (C=N), 140.3 (ArC), 138.8 (ArC),

 © 2003 Wiley-VCH Verlag GmbH & Co. KGaA, Weinheim

138.7 (ArC), 134.4 (ArC), 134.0 (ArC), 125.9 (ArC), 62.7 (NCH_2), 60.8 (NCH_2), 28.2 (CCH_2C), 27.8 (CCH_2C), 23.0 (CH_3CO_2), 20.8 (CH_3CO_2), 19.6 (CH_3-Ar) ppm. IR (KBr): $\tilde{\nu}$ = 3353 m, 3302 m, 3132 w, 2939 w, 1628 s, 1606 m, 1567 w, 1529 w, 1434 s, 1378 m, 1320 s, 1299 m, 1127 w, 1074 m, 955 w, 934 w, 842 vs, 740 w, 585 w, 621 w, 558 s cm^{-1}. For $Co^{III}Co^{III}$ complex: λ_{max} = 540 nm (ε = 1822 M^{-1} cm^{-1}), 430 (2933). For $Co^{III}Co^{II}$ complex: λ_{max} = 534 nm (ε = 1822 M^{-1} cm^{-1}).

Synthesis of $[Co_2(L^2)_2(\mu\text{-AcO})]PF_6$: A solution of $Co(AcO)_2{\cdot}4H_2O$ (0.027 g, 0.11 mmol) in MeOH (5 mL) was added to a solution of $[Zn(L^2)]$ (0.040 g, 0.1 mmol) in $CHCl_3$ (20 mL) The yellow solution immediately changed colour to become deep red and then slowly became ill-defined red-brown. After heating the resulting solution under reflux for 20 min, NH_4PF_6 (0.163 g, 1.0 mmol) in MeOH (5 mL) was added. After a few minutes, a brownish precipitate was obtained, which was washed with MeOH and diethyl ether (0.039 g, 80% yield). This product can be recrystallised from MeCN/diethyl ether. Single crystals suitable for X-ray analysis were obtained by this procedure. $C_{40}H_{43}Co_2F_6N_4O_2PS_4$ (1002.9): calcd. C 47.90, H 4.32, N 5.59; found C 47.86, H 4.22, N 5.57. MS (FAB^+, 3-NOBA): *m/z* = 399, 858; (ES^+): *m/z* = 857 $[(C_{19}H_{20}N_2S_2Co)_2CH_3CO_2]^+$, 399 $[C_{19}H_{20}N_2S_2Co]^+$. IR (KBr): $\tilde{\nu}$ = 3053 w, 2934 w, 2873 w, 1636 m, 1615 s, 1583 m, 1515 m, 1470 m, 1410 s, 1371 w, 1342 w, 1303 m, 1255 w, 1225 m, 1186 w, 1080 w, 1087 w, 1027 m, 839 vs, 679 w, 755 s cm^{-1}. ^1H NMR (CD_3CN): δ = 8.23 (s, 1 H, CH=N), 7.93 (d, *J* = 7.7 Hz, 1 H, Ar), 7.75 (s, 1 H, CH=N), 7.25−7.48 (m, 6 H, Ar), 7.18 (t, *J* = 7.4 Hz, 1 H, Ar), 5.01 (d, *J* = 11.1 Hz, 1 H, NCH_2), 4.47 (d, *J* = 11.5 Hz, 1 H, NCH_2), 3.59 (d, *J* = 11.1 Hz, 1 H, NCH_2), 3.11 (d, *J* = 11.5 Hz, 1 H, NCH_2), 1.16 (s, 3 H, CCH_3), 1.10 (s, 3 H, CO_2CH_3), 1.07 (s, 3 H, CCH_3).

Synthesis of $[Co(L^3)(AcO)]$: A solution of $Co(AcO)_2{\cdot}4H_2O$ (0.0271 g, 0.11 mmol) in MeOH (3 mL) was added to a solution of $[Zn(L^3)]$ (0.063 g, 0.1 mmol) in $CHCl_3$ (20 mL). The solution was stirred at 40 °C for 10 min, the resulting red-brown solution was concentrated to dryness and then the green residue was washed with MeOH and recrystallised from $CHCl_3$/diethyl ether (0.27 g, 40% yield). Single crystals were obtained by diffusion of ether into a $CHCl_3$ solution. $C_{37}H_{57}CoN_2O_3S_2$ (700.92): calcd. C 63.40, H 8.20, N 4.00; found C 63.43, H 7.90, N 4.01. MS (ES^+): *m/z* = 623 ($C_{35}H_{52}N_2S_2Co$ = $[Co(L^3)]^+$ requires 623). IR (KBr): $\tilde{\nu}$ = 2955 s, 2904 w, 2868 w, 1623 s, 1516 s, 1470 s, 1393 m, 1357 m, 1265 m, 1198 w, 1152 m, 1060 w, 947 m, 760 m, 681 m cm^{-1}. This compound is unstable towards oxidation, as the ligand can be oxidised when the compound is heated under reflux for longer periods of time in solvents such as ethyl acetate or chloroform. Thus, increases in *m/z* by 16 or 32 units indicate the gain of one or two atoms of oxygen [MS (ES^+): *m/z* = 639 and 655]. A deep-red colour in solution is associated with oxidation of the ligand.

Acknowledgments

We thank EPSRC, CONACyT and DGAPA-UNAM (to A. M.-B.) for support, and the EPSRC National Mass Spectrometry Service at the University of Wales, Swansea for mass spectra. We also thank EPSRC for the award of a diffractometer.

[1] [1a] D. E. Fenton, *Chem. Soc. Rev.* **1999**, *28*, 159. [1b] A. Than, A. A. Feldman, B. Krebs, *Coord. Chem. Rev.* **1999**, *182*, 211.
[2] [2a] R. Robson, N. H. Pilkington, *Aust. J. Chem.* **1970**, *23*, 2225. [2b] S. Mohanta, K. K. Nanda, L. K. Thompson, U. Flörke, K. Nag, *Inorg. Chem.* **1998**, *37*, 1465. [2c] P. Zanello, S. Tamburini, P. A. Vigato, G. A. Mazzocchin, *Coord. Chem. Rev.* **1987**, *77*, 165. [2d] P. A. Vigato, S. Tamburini, D. E. Fenton, *Coord. Chem. Rev.* **1990**, *106*, 25. [2e] H. Okawa, H. Furutachi, D. E. Fenton, *Coord. Chem. Rev.* **1998**, *74*, 51. [2f] D. G. McCollum, G. P. A. Yap, L. Liable-Sands, A. L. Rheingold, B. Bosnich, *Inorg. Chem.* **1997**, *36*, 2230. [2g] L. M. Liable-Sands, C. Incarvito, A. L. Rheinghold, C. J. Qin, A. L. Gavrilova, B. Bosnich, *Inorg. Chem.* **2001**, *40*, 2147.
[3] A. J. Atkins, D. Black, A. J. Blake, A. Marin-Becerra, S. Parsons, L. Ruiz-Ramirez, M. Schröder, *Chem. Commun.* **1996**, 457.
[4] [4a] A. J. Atkins, A. J. Blake, M. Schröder, *J. Chem. Soc., Chem. Commun.* **1993**, 1662. [4b] N. D. J. Branscombe, A. J. Blake, A. Marin-Becerra, W.-S. Li, S. Parsons, L. Ruiz-Ramirez, M. Schröder, *Chem. Commun.* **1996**, 2573.
[5] [5a] S. Brooker, *Coord. Chem. Rev.* **2001**, *222*, 33. [5b] S. Brooker, P. D. Croucher, T. C. Davidson, G. S. Dunbar, C. U. Beck, S. Subramanian, *Eur. J. Inorg. Chem.* **2000**, 169. [5c] S. Brooker, G. B. Caygill, P. D. Croucher, T. C. Davidson, D. L. J. Clive, S. R. Magnuson, S. P. Cramer, C. Y. Ralston, *J. Chem. Soc., Dalton Trans.* **2000**, 3113. [5d] A. Christensen, H. S. Jensen, V. McKee, C. J. McKenzie, M. Munch, *Inorg. Chem.* **1997**, *36*, 6080. [5e] P. E. Kruger, V. McKee, *Chem. Commun.* **1997**, 1341.
[6] [6a] B. Kersting, G. Steinfeld, *Chem. Commun.* **2001**, 1376. [6b] B. Kersting, *Angew. Chem. Int. Ed.* **2001**, *40*, 3987; *Angew Chem.* **2001**, *113*, 4109. [6c] B. Kersting, G. Steinfeld, J. Hausmann, *Eur. J. Inorg. Chem.* **1999**, 179. [6d] B. Kersting, D. Siebert, *Eur. J. Inorg. Chem.* **1999**, 189.
[7] [7a] T. C. Higgs, D. Ji, R. S. Czernuszewicz, K. Spartalian, C. J. O′Connor, C. Seip, C. J. Carrano, *J. Chem. Soc., Dalton Trans.* **1999**, 807. [7b] J. C. Noveron, M. M. Olmstead, P. K. Mascharak, *J. Am. Chem. Soc.* **1999**, *121*, 3553. [7c] D. Bonnet, P. Leduc, E. Bill, G. Chottard, D. Mansuy, I. Artaud, *Eur. J. Inorg. Chem.* **2001**, 1449. [7d] B. Kersting, D. Siebert, D. Volkmer, M. J. Kolm, C. Janiak, *Inorg. Chem.* **1999**, *38*, 3871. [7e] B. Kersting, G. Steinfeld, *Inorg. Chem.* **2002**, *41*, 1140 and references therein.
[8] A. M. A van Wageningen, J. P. M. van Duynhoven, W. Verboom, D. N. Reinhoudt, *J. Chem. Soc., Chem. Commun.* **1995**, 1491.

Received January 11, 2003

 © 2003 Wiley-VCH Verlag GmbH & Co. KGaA, Weinheim

The First One-Dimensional Molecular Material Featuring Maleonitriledithiolate as a Subunit Exhibiting Metamagnetic-Like Behavior

Jingli Xie,[a] Xiaoming Ren,[a] Song Gao,[b] Wenwei Zhang,[a] Yizhi Li,[a] Changsheng Lu,[a] Chunlin Ni,[a] Wenlong Liu,[a] Qingjin Meng,*[a] and Yuangen Yao[c]

Keywords: Nickel / Maleonitriledithiolate / Crystal structure / Magnetic properties

An ion-pair complex $[FBzPyNH_2][Ni(mnt)_2]$ {$[FBzPyNH_2]^+$ = [1-(4′-fluorobenzyl)-4-amino]pyridinium and mnt^{2-} = maleonitriledithiolate} has been obtained by I_2 oxidation of the corresponding dianion complex. It forms a well-segregated stacking column structure in the solid state, and exhibits antiferromagnetic ordering below 2.5 K. It is the first complex in this series of complexes containing a maleonitriledithiolate dianion that exhibits metamagnetism.
(© Wiley-VCH Verlag GmbH & Co. KGaA, 69451 Weinheim, Germany, 2003)

Introduction

Much effort has been devoted to the study of square-planar M(dithiolene)$_2$ complexes in the areas of conducting and magnetic materials, dyes, non-linear optics and catalysis.[1,2] Recently, we have employed a strategy of constructing one-dimensional molecule-based magnets based on ion-pair complexes containing $[M(mnt)]^-$ (M = Ni^{III}, Pt^{III}; mnt^{2-} = maleonitriledithiolate) anions with benzylpyridinium derivatives as counterions. Interestingly, varying the counterions led to a broader palette of complexes with markedly different magnetic-exchange properties, although they all have extremely similar molecular and stacking structures. Versatile magnetic properties such as ferromagnetic ordering at 2 K, unusual magnetic transitions from ferromagnetic coupling to diamagnetism or from paramagnetic to diamagnetic, or spin-Peierls-like transitions have been witnessed.[3] In order to further understand the magnetic coupling mechanism in this series of complexes, we should explore the relationship between stacking structures and magnetic properties systematically. Within this framework, we report the synthesis and crystal structure of an ion-pair complex [1-(4′-fluorobenzyl)-4-aminopyridinium]-$[Ni(mnt)_2]$ (Scheme 1), which has well-segregated stacking columns. A study of its magnetic properties shows antiferromagnetic ordering below 2.5 K and metamagnetic-like behavior.

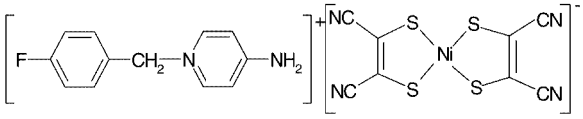

Scheme 1. Molecular structure of **2**

Results and Discussion

$[FBzPyNH_2]_2[Ni(mnt)_2]$ (**1**) was prepared by the direct combination of $NiCl_2{\cdot}6H_2O$, Na_2mnt and [1-(4′-fluorobenzyl)-4-amino]pyridinium chloride in H_2O in a 1:2:2 molar ratio. The title complex **2** was prepared by I_2 oxidation of **1**,[4] and well-shaped single crystals were obtained by allowing Et_2O to diffuse into an MeCN solution of **2** for about a week. Figure S1 depicts the molecular structure of **2**. The coordination geometry of Ni^{III} is square planar with four sulfur donor atoms; the Ni−S bond lengths and S−Ni−S bond angles are in agreement with reported values.[3] The CN groups of the mnt^{2-} ligand are bent away from the plane defined by the Ni atom and four sulfur atoms. The deviation of the four terminal N atoms from the plane are 0.2926 Å, 0.3666 Å, 0.0802 Å and 0.1736 Å, respectively. In the $[FBzPyNH_2]^+$ cation, the dihedral angles between the C(15)−C(14)−N(5) reference plane and the aryl rings are 80.5° for the phenyl ring and 106.6° for the pyridine ring; these values are in line with previous results.[3] It should be noted that **2** possesses well-segregated stacking column along the *c*-axis (Figure 1a). Within an anion column, there exists a slipped nickel-over-sulfur con-

[a] State Key Laboratory of Coordination Chemistry, Coordination Chemistry Institute, Nanjing University, 210093 Nanjing, P. R. China
Fax: (internat.) +86-25/331-4502
E-mail: njujlxie@yahoo.com
[b] State Key Laboratory of Rare Earths Materials Chemistry and Applications, College of Chemistry and Molecular Engineering, Peking University, Beijing 100871 P. R. China
[c] State Key Laboratory of Structural Chemistry, Fujian Institute of Research on the Structure of Matter, 350002 Fuzhou, P. R. China
Supporting information for this article is available on the WWW under http://www.eurjic.org or from the author.

figuration of $[Ni(mnt)_2]^-$ anions and the Ni···Ni distances between adjacent anions are identical (3.991 Å); the nearest S···S, S···Ni contacts are 3.797 Å and 3.663 Å, respectively. These distances are larger than the sum of the van der Waals radii of the corresponding atoms. The closest Ni···Ni separation between anion chains is 14.32 Å, which is significantly larger than the Ni···Ni separation within a chain. Therefore, each $[Ni(mnt)_2]^-$ anion column can be considered as a one-dimensional (1-D) magnetic chain from the viewpoint of the crystal structure (Figure 1b). The $[FBzPyNH_2]^+$ cations orient themselves in the solid state. The pyridine rings of the neighboring cations are essentially parallel to each other with an identical center-center distance of 3.893 Å (Figure S2).

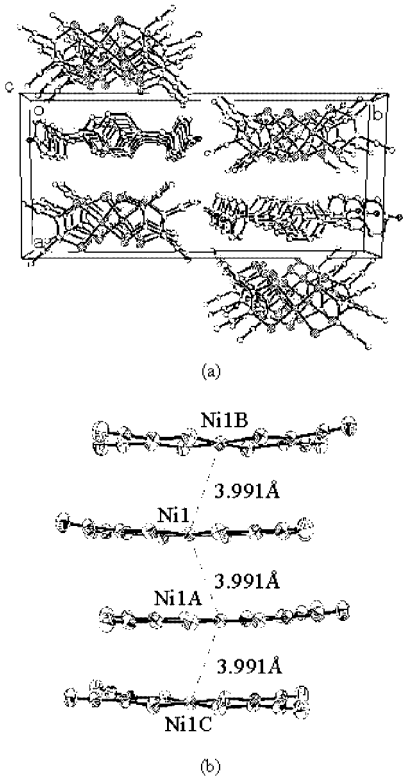

Figure 1. (a) Structure of anions and cations of **2** viewed along the *c*-axis; (b) side view of the 1-D anion chain of **2** (symmetry codes: A = x, 1.5 − y, 0.5 + z; B = x, 1.5 − y, −0.5 + z; C = x, y, z + 1)

The thermal variation of $\chi_m T$, measured at a field of 1 T, is shown in Figure 2. The observed $\chi_m T$ value at 308 K is 0.331 emu·K·mol^{-1}, slightly less than the theoretical value of 0.375 emu·K·mol^{-1} expected for a spin-only Ni^{III} ion with S = 1/2 and g = 2.0. Upon cooling down, the $\chi_m T$ values decreases smoothly and reaches a minimum of 0.223 emu·K·mol^{-1} at 24 K. This behaviour is characteristic of ferrimagnetic-like behavior. With a further decrease in temperature, the $\chi_m T$ values increase abruptly, reaching a maximum of 0.343 emu·K·mol^{-1} at 7.2 K, before decreasing again. The data above 24 K are best fit by the Bonner−Fisher model for a uniformly spaced chain of atoms with S = 1/2 spin.[5] Equation (1) for $H = -2JS_1 \cdot S_2$ [6] with $z = J/k_B T$.

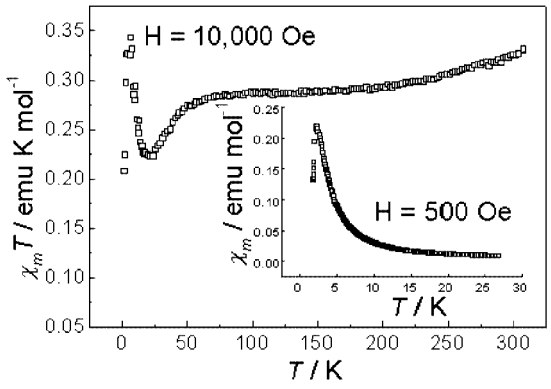

Figure 2. Temperature dependence of $\chi_m T$ for **2** measured at 10 KOe; inset: temperature dependence of χ_m for **2** measured at 500 Oe

$$\chi_m = \frac{Ng^2\mu_B^2}{k_B T} \frac{0.25 + 0.074975z + 0.075235z^2}{1.0 + 0.9931z + 0.172135z^2 + 0.757825z^3} \quad (1)$$

A fit of the data to Equation (1) gives $J = -6.8$ cm^{-1} and g = 2.0 (fixed), which suggests there exists weak antiferromagnetic coupling between adjacent S = 1/2 Ni^{III} spin carriers within the anion chain. The χ_m/T curve at 500 Oe field shows a sharp cusp at 2.5 K, suggesting a long-range antiferromagnetic (AF) ordering (inset of Figure 2). The M vs. H curve at 1.8 K exhibits a sigmoidal shape, indicating a metamagnetic-like behavior (Figure 3), which switches from an antiferromagnetic ground state to a ferrimagnetic-like state upon the application of a large enough field. At 1.8 K, the critical field is approximately 1000 Oe because the derivative dM/dH has an extremum (Figure S3). The saturation magnetization of **2** at 1.8 K (the higher applied magnetic field is 7 T) is 1310 emu·G·mol^{-1}, far from the theoretical saturation value of 5585 emu·G·mol^{-1}, which is usual in metamagnetic material if the temperature is not much lower than T_N.[7,8] The AF transition is further manifested by the in-phase signal (χ') of zero-field ac magnetic susceptibility, which has a maximum at about 2.5 K (T_N). No out-of-phase signal (χ'') could be detected and their is no frequency dependence, thus excluding any ferromagnetic

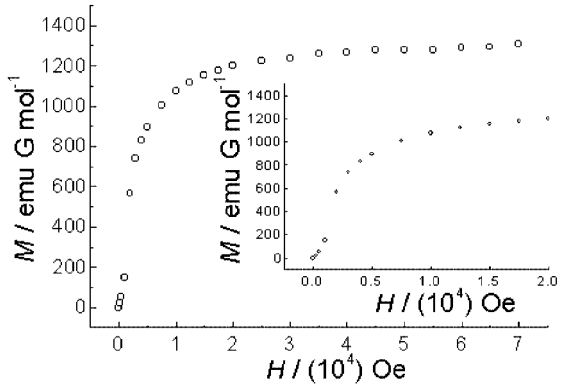

Figure 3. M-H curve of **2** measured at 1.8 K; inset: enlargement of the applied magnetic field range 0−20000 Oe

 © 2003 Wiley-VCH Verlag GmbH & Co. KGaA, Weinheim

phase or spin-glass behavior (Figure S4). The FCM curves of **2** measured at lower fields (200 Oe and 1000 Oe) both show a maximum in χ_m at about 2.5 K (Figure S5), suggesting long-range magnetic ordering, whereas a higher field (5000 Oe) leads to the absence of the peak down to 2.0 K (inset of Figure S5).

Of all the commonly studied dithiolate systems, metamagnetism has been observed in some charge-transfer salts such as $[Fe(Cp^*)_2][Ni(edt)_2]$ (edt = ethylenedithiolate), $[Mn(Cp^*)_2][M(tfd)_2]$ [M = Ni, Pd, Pt; tfd = bis(trifluoromethyl)ethylenedithiolate].[7–9] For complexes containing the $[Ni(mnt)_2]^-$ anion, previous studies have shown that the magnetic coupling between $[Ni(mnt)_2]^-$ anions is very sensitive not only to intermolecular separation,[2a] but also to the degree of overlap of neighboring $[Ni(mnt)_2]^-$ anions.[10–12] Several shorter contact distances, such as Ni···Ni, Ni···S, S···S, S···N, S···C and C···N, play important roles in the superexchange pathway due to extensive electron delocalization in the $[Ni(mnt)_2]^-$ unit.[13] At very low temperature, superexchange and/or through-space intrachain antiferromagnetic couplings must be considered in order to yield a three-dimensional AF ordering state below 2.5 K.

In summary, a metamagnetic-like behavior is observed in the title complex, which, to the best of our knowledge, is the first example of metamagnetism in this series of complexes containing the maleonitriledithiolate dianion.

Experimental Section

All manipulations were carried out in air unless otherwise noted. Starting materials were purchased from Aldrich (4-fluorobenzyl chloride, 4-aminopyridine), and were used without further purification. [1-(4′-Fluorobenzyl)-4-amino]pyridinium chloride ($[FBzPyNH_2]Cl$) and disodium maleonitriledithiolate (Na_2mnt) were synthesized following the published procedures.[4]

$[FBzPyNH_2]_2[Ni(mnt)_2]$ (1): This compound was prepared by the direct combination of $NiCl_2·6H_2O$, Na_2mnt and $[FBzPyNH_2]Cl$ in H_2O in a 1:2:2 molar ratio. The red precipitate that formed was filtered off, washed with water and dried under vacuum. Yield: 93%. $C_{32}H_{24}F_2N_8NiS_4$ (745.5): calcd. C 51.55, H 3.24, N 15.03; found C 51.81, H 3.22, N 15.11. IR (KBr): ν(NH_2) 3420.3 cm^{-1}, 1657.4 vs; ν(CN) 2196.4 vs; ν(C=C) of mnt^{2-} 1485.3 s.

$[FBzPyNH_2][Ni(mnt)_2]$ (2): An MeCN solution (10 mL) of I_2 (150 mg, 0.59 mmol) was slowly added to an MeCN solution (20 mL) of $[FBzPyNH_2]_2[Ni(mnt)_2]$ (746 mg, 1.0 mmol), and stirred for 15 min. MeOH (90 mL) was then added, and the mixture allowed to stand overnight. The microcrystals formed were filtered off, washed with MeOH and dried in vacuo. Yield: 87%. $C_{20}H_{12}FN_6NiS_4$ (542.3): calcd. C 44.30, H 2.23, N 15.50; found C 44.52, H 2.22, N 15.42. IR: ν(NH_2) 3347.9 cm^{-1}, 1654.4 vs; ν(CN) 2206.7 vs; ν(C=C) of mnt^{2-} 1453.3 m. Good-shaped single crystals suitable for X-ray analysis were obtained by allowing Et_2O to diffuse into an MeCN solution of **2** for about a week.

X-ray Crystallography Study: $C_{20}H_{12}FN_6NiS_4$, M_r = 542.31, black, needle-shaped crystal, monoclinic, space group $P2_1/c$, a = 12.0041(17) Å, b = 26.095(4) Å, c = 7.4809(11) Å, β = 101.448(3)°, V = 2296.7(6) Å^3, Z = 4, D_c = 1.568 g cm^{-3}, μ(Mo-K_α) = 1.237 mm^{-1}, λ = 0.71073 Å, $-14 \le h \le 14$, $-31 \le k \le 22$, $-8 \le l \le 8$. A crystal of dimensions 0.20 × 0.15 × 0.10 mm^3 was selected for indexing and intensity data collection at 298 K. Data collection: *SMART* (Bruker, 1997). ω-Scans covering reciprocal space up to θ_{max} 24.99° with 99.8% completeness, total of 11370 reflections (4031 unique) with R_{int} = 0.1139. Structure solution SHELXL-97, full-matrix least-squares based on F^2 using SHELXL-97, final R = 0.058, wR = 0.154, GOF = 1.006. Final residual density was in the range −0.497 to 0.923 e·Å^{-3}.

CCDC-201344 (**2**) contains the supplementary crystallographic data for this paper. These data can be obtained free of charge at www.ccdc.cam.ac.uk/conts/retrieving.html [or from the Cambridge Crystallographic Data Centre, 12, Union Road, Cambridge CB2 1EZ, UK; Fax: (internat.) +44-1223/336-033; E-mail: deposit@ccdc.cam.ac.uk].

Supporting Information: ORTEP view, side view of cation chain, dM/dH vs. H plot, in-phase signal (χ') and FCM curve for **2**) is available (see footnote on the first page of this article.

Acknowledgments

Financial support from the National Natural Science Foundation (No. 2017022, No. 29831010, No. 20125104), Jiangsu Science and Technology Department and The Center for Analysis and Determination of Nanjing University are gratefully acknowledged.

[1] [1a] N. Robertson, L. Cronin, *Coord. Chem. Rev.* **2002**, *227*, 93–127. [1b] P. Cassoux, L. Valade, H. Kobayashi, R. A. Clar, A. E. Underhill, *Coord. Chem. Rev.* **1991**, *110*, 115–160.
[2] [2a] A. T. Coomber, D. Beljonne, R. H. Friend, J. L. Brédas, A. Charlton, N. Robertson, A. E. Underhill, M. Kurmoo, P. Day, *Nature* **1996**, *380*, 144–146. [2b] A. E. Pullen, C. Faulmann, K. I. Pokhodnya, P. Cassoux, M. Tokumota, *Inorg. Chem.* **1998**, *37*, 6714–6720. [2c] M. Uruichi, K. Yakushi, Y. Yamashita, J. Qin, *J. Mater. Chem.* **1998**, *8*, 141–146. [2d] D. Arčon, A. Lappas, S. Margadonna, K. Prassides, E. Ribera, J. Veciana, C. Rovira, R. T. Henriques, M. Almeida, *Phys. Rev. B.* **1999**, *60*, 4191–4194.
[3] [3a] J. L. Xie, X. M. Ren, Y. Song, Y. Zou, Q. J. Meng, *J. Chem. Soc., Dalton Trans.* **2002**, 2868–2872. [3b] J. L. Xie, X. M. Ren, Y. Song, W. J. Tong, C. S. Lu, Y. G. Yao, Q. J. Meng, *Inorg. Chem. Commun.* **2002**, *5*, 395–398. [3c] J. L. Xie, X. M. Ren, Y. Song, W. W. Zhang, W. L. Liu, C. He, Q. J. Meng, *Chem. Commun.* **2002**, 2346–2347. [3d] X. M. Ren, Q. J. Meng, Y. Song, C. L. Lu, C. J. Hu, X. Y. Chen, Z. L. Xue, *Inorg. Chem.* **2002**, 5931–5933. [3e] J. L. Xie, X. M. Ren, C. He, Y. Song, Q. J. Meng, R. K. Kremer, Y. G. Yao, *Chem. Phys. Lett.* **2003**, *369*, 41–48.
[4] [4a] S. B. Bulgarevich, D. V. Bren, D. Y. Movshovic, P. Finocchiaro, S. Failla, *J. Mol. Struct.* **1994**, *317*, 147–155. [4b] A. Davison, H. R. Holm, *Inorg. Synth.* **1967**, *10*, 7–23.
[5] J. C. Bonner, M. E. Fisher, *Phys. Rev.* **1964**, *A135*, 640–658.
[6] W. E. Estes, D. P. Gavel, W. E. Hatfield, D. J. Hodgson, *Inorg. Chem.* **1978**, *17*, 1415–1421.
[7] V. Gama, D. Belo, S. Rabaça, I. C. Santos, H. Alves, J. C. Waerenborgh, M. T. Duarte, R. T. Henriques, *Eur. J. Inorg. Chem.* **2000**, 2101–2110.
[8] W. E. Broderick, J. A. Thompson, B. M. Hoffman, *Inorg. Chem.* **1991**, *30*, 2958–2960.
[9] V. Gama, D. Belo, I. C. Santos, R. T. Henriques, *Mol. Cryst. Liq. Cryst.* **1997**, *306*, 17–24.
[10] J. Nishijo, E. Ogura, J. Yamaura, A. Miyazaki, T. Enoki, T.

 © 2003 Wiley-VCH Verlag GmbH & Co. KGaA, Weinheim

Takano, Y. Kuwatani, M. Iyoda, *Solid State Commun.* **2000**, *116*, 661−664.
[11] S. Alvarez, R. Vicente, R. Hoffmann, *J. Am. Chem. Soc.* **1985**, *107*, 6253−6277.
[12] N. Robertson, C. Bergemann, H. Becker, P. Agarwal, S. R. Julian, R. H. Friend, N. J. Hatton, A. E. Underhill, A. Kobayashi, *J. Mater. Chem.* **1999**, *9*, 1713−1717.
[13] [13a] J. E. Huyett, S. B. Choudhury, D. M. Eichhorn, P. A. Bryngelson, M. J. Maroney, B. M. Hoffman, *Inorg. Chem.* **1998**, *37*, 1361−1367. [13b] B. L. Ramakrishna, *Inorg. Chim. Acta* **1986**, *114*, 31−34.

Received February 24, 2003

 © 2003 Wiley-VCH Verlag GmbH & Co. KGaA, Weinheim

Order−Disorder Transitions and Magnetic Behaviour in Lithium Ferrites $Li_{0.5+0.5x}Fe_{2.5-1.5x}Ti_xO_4$ (x = 1.28 and 1.50)

María Ángeles Arillo,[a] María Luisa López,[a] Carlos Pico,[a] María Luisa Veiga,*[a] Javier Campo,[b] José Luis Martínez,[c] and Alejandro Santrich-Badal[c]

Keywords: Lithium ferrites / Order−disorder phenomena / Spinels / Spin-glass behaviour

We report the structural characterization and magnetic behaviour of the spinels with general formula $Li_{0.5+0.5x}Fe_{2.5-1.5x}Ti_xO_4$, where x = 1.28 and 1.50. When the samples are cooled slowly, a 1:3 crystallographic order occurs, whereas a random disorder is observed when the samples are quenched. Neutron-powder-diffraction measurements were performed on the materials to characterize the structural transitions. Magnetic properties were studied by magnetic susceptibility (dc and ac), magnetisation and neutron-diffraction data and the results can be interpreted on the basis of a spin-glass behaviour.

(© Wiley-VCH Verlag GmbH & Co. KGaA, 69451 Weinheim, Germany, 2003)

Introduction

Lithium iron spinels, usually known as lithium ferrites, have been thoroughly studied materials because they are remarkably useful in many branches of technology.[1] The lithium ferrite $Li_{0.5}Fe_{2.5}O_4$ is known to occur in two crystalline forms.[2] Below 1008 K, there exists a 1:3 ordering of Li^+ and Fe^{3+} ions along the [110] directions of the unit cell, giving rise to the structural formula $(Fe)_T(Li_{0.5}Fe_{1.5})_OO_4$, in such a way that each lithium ion is followed by three iron cations that are all in octahedral coordination with oxygen ions. The remaining iron ions are located on the tetrahedral sites (space group $P4_332$).[3] Above 1000−1030 K, the 1:3 ordering is destroyed and the two types of cations are randomly distributed over the octahedral sites; the resulting phase is referred to as the disordered phase (space group $Fd3m$). By quenching rapidly from a high temperature, this latter phase can be retained indefinitely at room temperature or below.[4] The disordered $Li_{0.5}Fe_{2.5}O_4$ has an inverse spinel structure, with Fe^{3+} ions at tetrahedral 8*a* positions and Li^+ and Fe^{3+} ions distributed randomly over the 16*d* octahedral sites. The order−disorder transition in the lithium ferrite structure has been recorded by X-ray powder diffraction, and the relationship between the Wyckoff's positions of the $Fd3m$ and $P4_332$ states are as follows[5]:

$Fd3m \rightarrow P4_332$

$8a\ (8\ Fe^{3+}) \rightarrow 8c\ (8\ Fe^{3+})$

$16d\ (12\ Fe^{3+} + 4\ Li^+) \rightarrow 12d\ (12\ Fe^{3+}) + 4b\ (4Li^+)$

$32e\ (32\ O^{2-}) \rightarrow 24e\ (24\ O^{2-}) + 8c\ (8\ O^{2-})$

The magnetic properties of a spinel ferrite depend on their structural features, both of which are quite sensitive to the preparation conditions as well as to the amount and type of substitution. The most synthetically advantageous characteristic of spinel materials is that various ions can be placed at tetrahedral and octahedral sites within the structure, a situation that allows for control of their magnetic properties. In addition to ferromagnetism and antiferromagnetism (ferrimagnetism), another unique spin state − the so-called spin-glass (SG) state − can be assigned to spinel ferrites. The substitution of iron atoms by tetravalent titanium influences the above properties. Solid solutions of general formula $Li_{0.5+0.5x}Fe_{2.5-1.5x}Ti_xO_4$ ($0 \le x \le 1.67$) crystallise in the space groups $P4_332$ (in the ranges $0 \le x \le 0.4$ and $1.2 \le x \le 1.57$) and $Fd3m$ (in the ranges $0.4 \le x \le 1.2$ and $1.57 \le x \le 1.67$).[5,6] Several authors[6−9] have reported detailed studies using X-ray diffraction and Mössbauer spectroscopy for the structural resolution of this system in the range $1.1 \le x \le 1.67$, in agreement with the cation distribution proposed by Blasse[5] and White[10]. On the other hand, Dormann's group has proposed that this system shows local canted spin behaviour (LCS).[11−14] With increasing dilution of Fe atoms, the distribution of the canting angles enlarges and the average canting angle

[a] Departamento de Química Inorgánica I, Facultad de Ciencias Químicas, Universidad Complutense,
28040 Madrid, Spain
Fax: (internat.) +34-91-3944352
E-mail: mlveiga@quim.ucm.es
[b] Institut Max von Laue − Paul Langevin (ILL),
38042 Grenoble Cedex 9, France
[c] Instituto Ciencia de Materiales de Madrid, CSIC, Cantoblanco,
28049 Madrid, Spain

increases at each site. As a consequence, the average magnitude of the transverse component S_t increases. Moreover, S_t becomes more widely distributed. A discrepancy exists, however, between the results of the Mössbauer spectra and the magnetic studies. An explanation can be found by considering the Rosencwaig canting model.[7] Scharner et al.[6] proposed order−disorder transitions for $x = 1.2$ and 1.57, but they did not suggest the possibility of canting in both positions.

The aim of the present work is to establish by means of neutron diffraction studies the behaviour of the phases, where $x = 1.28$ and 1.50, that are obtained by slowly cooling (SC) and rapid quenching (Q). The Rietveld refinement was used to solve the problem of the cation ordering in these phases, and additional magnetic measurements (ac and dc magnetic susceptibility and magnetisation curves) were performed to study the simultaneous substitution with nonmagnetic atoms in this series $Li_{0.5+0.5x}Fe_{2.5-1.5x}Ti_xO_4$.

Results and Discussion

Structural Features

Structural characterization at room temperature of the lithium ferrites with compositions $x = 1.28$ and 1.50 formed by slow cooling (SC) was carried out by neutron diffraction. The reflections were characteristic of a spinel structure in which some additional superstructural lines appear, and all these reflections were indexed satisfactorily on the basis of a cubic unit cell (Figure 1). Therefore, the SC samples exhibited cation ordering on the octahedral sites, resulting in a superstructure that could be refined in the $P4_332$ space group. We found, however, that a slight improvement in the fit was achieved by using a multiphase refinement using both the ordered ($P4_332$) and disordered ($Fd3m$) structures.[15,16] Rietveld analysis indicated that these samples are comprised of 94.9% superstructure (or ordered structure) and 5.1% disordered structure (for $x = 1.28$), and 82.3% superstructural component and 17.7% disordered component (for $x = 1.50$). Crystallographic data for both compounds obtained by Rietveld refinements are reported in Table 1 and the R-factors indicate a reliable structural model. The atomic coordinates are given in Table 2 and the most representative bond lengths are given in Table 3. These results suggest that the ordered structures have not been isolated as single phases under the present experimental conditions, although they are clearly in the majority, and this fact will certainly influence the magnetic behaviour of the materials.

At higher temperatures (1073 K for $x = 1.28$ and 973 K for $x = 1.50$), all the Bragg reflections were indexed on the basis of a cubic symmetry and the patterns were refined in the space group $Fd3m$. A good agreement between the calculated and observed patterns is shown in Figure 1. Therefore, the SC samples must undergo an order−disorder phase transition from the space group $P4_332$ to the space group $Fd3m$. Moreover, the neutron-diffraction pattern at 1073 K for $x = 1.50$ revealed the presence of an impurity,

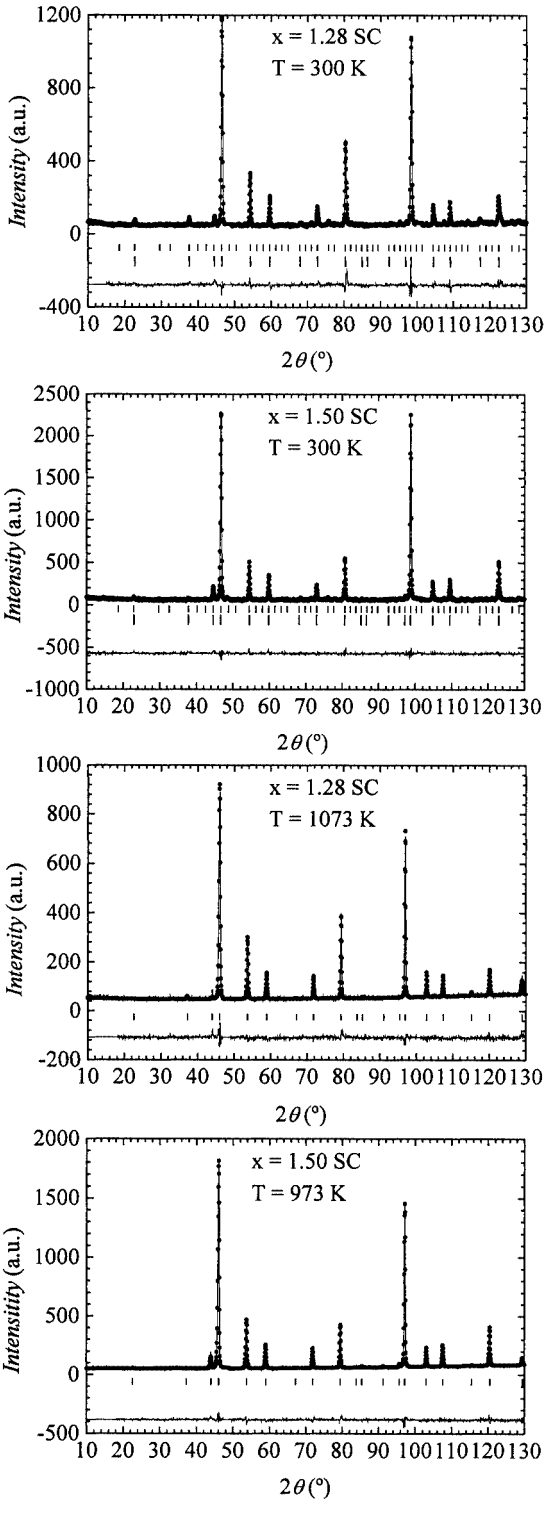

Figure 1. Observed, calculated and difference ND patterns of the slowly cooled (SC) samples at room temperature [peak positions of space group $P4_332$ (upper vertical marks) and $Fd3m$ (lower vertical marks) are indicated just below the patterns], and at different temperatures (space group $Fd3m$)

α-Fe_2O_3, whose amount increases with temperature, which suggests a decomposition process occurs for this spinel (pattern not shown). The most characteristic parameters obtained after the refinement are listed in Table 4 and a selec-

 © 2003 Wiley-VCH Verlag GmbH & Co. KGaA, Weinheim

Table 1. Lattice parameters, *a*, and *R*-factors for $Li_{0.5+0.5x}Fe_{2.5-1.5x}Ti_xO_4$ (slow cooling) obtained by neutron refinement at room temperature

	x = 1.28 (ordered)		x = 1.50 (ordered)	
a [Å]	8.3725(4)	8.3701(9)	8.3549(2)	8.3689(8)
Space group	$P4_332$	*Fd3m*	$P4_332$	*Fd3m*
Z	8		8	
R_B [%]	5.78	7.64	4.49	8.56
R_P [%]	6.96		6.68	
R_{WP} [%]	9.47		8.74	
%	94.9	5.1	82.3	17.7

Table 2. Structural parameters obtained from the Rietveld refinement of neutron powder-diffraction patterns of $Li_{0.5+0.5x}Fe_{2.5-1.5x}Ti_xO_4$ (slow cooling) at room temperature (N = occupation)

x = 1.28				
$P4_332$ (ordered)			*Fd3m* (at random)	
8*c*			8*a*	
$x = y = z$		−0.0026(7)	$x = y = z$	⅛
N (Li / Fe)		0.68 / 0.32	N (Li / Fe)	0.61 / 0.39
4*b*			16*d*	
$x = y = z$		⅝	$x = y = z$	½
N (Li / Fe)		0.46 / 0.04	N (Li /Fe / Ti)	0.53 / 0.19 / 1.28
	x	⅛	32*e*	
12*d*	y	0.3877(5)	$x = y = z$	0.2583(6)
	z	0.8623(4)	N (O)	1/6
N (Fe / Ti)		0.22 / 1.28		
8*c*				
$x = y = z$		0.3919(1)		
N (O1)		⅓		
	x	0.1077(3)		
24*e*	y	0.1096(4)		
	z	0.3741(1)		
N (O2)		1		
x = 1.50				
$P4_332$ (ordered)			*Fd3m* (at random)	
8*c*			8*a*	
$x = y = z$		−0.0002(4)	$x = y = z$	⅛
N (Li / Fe)		0.77 / 0.23	N (Li / Fe)	0.79 / 0.21
4*b*			16*d*	
$x = y = z$		⅝	$x = y = z$	½
N (Li / Fe)		0.48 / 0.02	N (Li / Fe / Ti)	0.46 / 0.04 / 1.50
	x	⅛	32*e*	
12*d*	y	0.3629(6)	$x = y = z$	0.2763(4)
	z	0.8871(2)	N (O)	1/6
N (Ti)		1.50		
8*c*				
$x = y = z$		0.3861(8)		
N (O1)		⅓		
	x	0.1093(1)		
24*e*	y	0.1221(4)		
	z	0.3874(6)		
N (O2)		1		

Table 3. Selected bond lengths [Å] for $Li_{0.5+0.5x}Fe_{2.5-1.5x}Ti_xO_4$ obtained by SC.

x = 1.28			
$P4_332$ (ordered)		*Fd3m*(at random)	
d M(8*c*)−O1	1.944(9)	d M(8*a*)−O	1.930(7)(x4)
d M(8*c*)−O2	1.980(1)(× 3)	mean Shannon	1.931(1)
average d M(8*c*)−O	1.971(2)	d M(16*d*)−O	2.024(1)(× 6)
mean Shannon	1.938(1)	mean Shannon	2.050(2)
d M(4*b*)−O2	2.034(7)(× 6)		
mean Shannon	2.150(8)		
d M(12*d*)−O1	1.956(4)(× 2)		
d M(12*d*)−O2	2.049(3)(× 2)		
	2.067(7)(× 2)		
average d M(12*d*)−O	2.024(5)		
mean Shannon	2.316(3)		
x = 1.50			
$P4_332$ (ordered)		*Fd3m* (at random)	
d M(8*c*)−O1	1.946(9)	d M(8*a*)−O	2.271(7)(× 4)
d M(8*c*)−O2	1.972(2)(× 3)	mean Shannon	1.949(2)
average d M(8*c*)−O	1.965(8)	d M(16*d*)−O	1.864(6)(× 6)
mean Shannon	1.947(2)	mean Shannon	2.041(4)
d M(4*b*)−O2	2.068(5)(× 6)		
mean Shannon	2.155(4)		
d M(12*d*)−O1	2.089(1)(× 2)		
d M(12*d*)−O2	1.874(2)(× 2)		
	1.996(9)(× 2)		
average d M(12*d*)−O	1.986(7)		
mean Shannon	2.307(5)		

Table 4. Crystallographic data and structural parameters obtained from the Rietveld refinement of neutron powder-diffraction pattern of $Li_{1.14}Fe_{0.58}Ti_{1.28}O_4$ (SC) at 1073 K and $Li_{1.25}Fe_{0.25}Ti_{1.5}O_4$ (SC) at 973 K.

	x = 1.28	x = 1.50
a (Å)	8.4508(3)	8.4521(3)
Space group	*Fd3m*	*Fd3m*
Z	8	8
R_B (%)	4.81	4.68
R_P (%)	5.75	8.03
R_{WP} (%)	7.41	12.0
8*a*		
$x = y = z$	1/8	1/8
N[a] (Li/Fe)	0.67/0.33	0.86/0.14
16*d*		
$x = y = z$	1/2	1/2
N[a] (Li/Fe/Ti)	0.47/0.25 /1.28	0.39/0.11/1.50
32*e*		
$x = y = z$	0.2614(5)	0.2626(5)
N[a] (O)	1/6	1/6

[a] N = occupation.

tion of the most important interatomic distances are included in Table 5. On the other hand, for the samples obtained by quenching (Q), all the reflections can be indexed using the extinction laws of the space group *Fd3m*.[17,18] The resulting fits are shown in Figure 2 at 2 K (Figure 2, a) and 300 K (Figure 2, b). A summary of the structural parameters obtained in these refinements is given in Table 6 and 7.

The structure of SC samples were first reported by Blasse,[5] who described them as cation-ordered for x = 1.20 and x = 1.50. The 1:3 order on the octahedral sublattice is given by the lithium (4*b*) and titanium ions (12*d*), although the titanium sublattice contains some iron ions. Nevertheless, the Rietveld refinement of the neutron-diffraction data for our samples $(Li_{0.5x}Fe_{1-0.5x})_T(Li_{0.5}Fe_{1.5-x}Ti_x)_OO_4$ ob-

 © 2003 Wiley-VCH Verlag GmbH & Co. KGaA, Weinheim

Table 5. Bond lengths [Å] for the samples $Li_{1.14}Fe_{0.58}Ti_{1.28}O_4$ (SC) at 1073 K and $Li_{1.25}Fe_{0.25}Ti_{1.5}O_4$ (SC) at 973 K.

d (M−O)	$x = 1.28$	$x = 1.50$
M(8*a*)−O	2.002(3) (× 4)	2.015(3) (× 4)
mean Shannon	1.937(2)	1.956(1)
M(16*d*)−O	2.025(2) (× 6)	2.011(9) (× 6)
mean Shannon	2.046(4)	2.037(4)

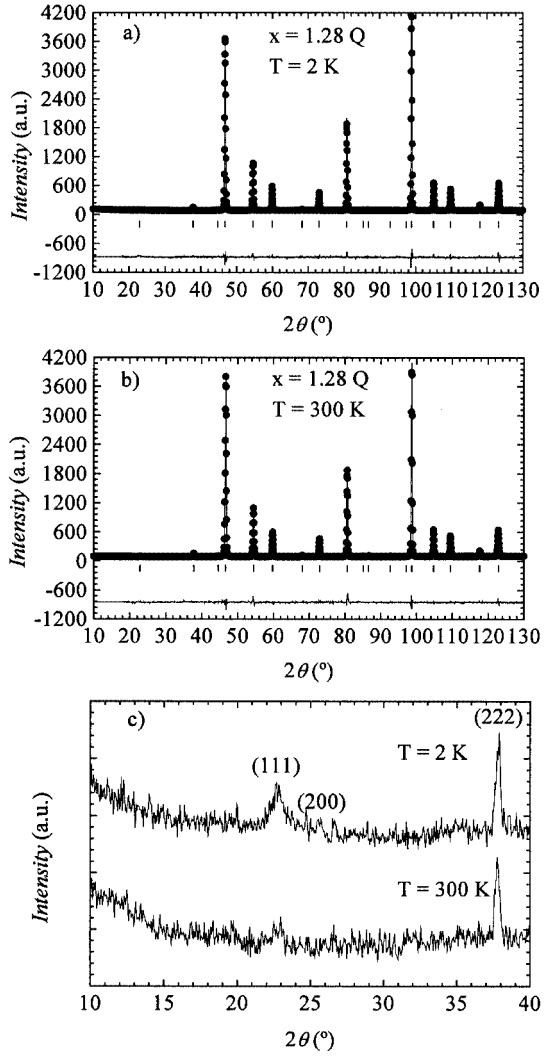

Figure 2. Neutron powder-diffraction pattern of the quenched (Q) compound with $x = 1.28$ at 2 K (a) and 300 K (b). Solid lines are the calculated profiles and dots are the experimental points. The difference profile is also shown. c) A comparison of the low-angle neutron diffraction patterns is shown at 2 and 300 K

tained by SC show that the cation distribution is slightly different from that suggested by Blasse in that the octahedral (4*b*) sites are occupied by Li^+/Fe^{3+} cations and the 12*d* sites are occupied by Fe^{3+}/Ti^{4+} cations. These samples show a cation-ordered superstructure with a minority disordered phase that also has been obtained for $Li_{0.5}Fe_{2.5-x}Cr_xO_4$.[16] The ordered form is close to an inverse spinel (space group $P4_332$) in which the 12*d* sites are

Table 6. Lattice parameter, *a*, *R*-factors and structural parameters for quenched (Q) $Li_{1.14}Fe_{0.58}Ti_{1.28}O_4$ at 2 K and at room temperature.

	$T = 2$ K	$T = 300$ K
a (Å)	8.3437(9)	8.3564(3)
Space group	*Fd*3*m*	*Fd*3*m*
Z	8	8
R_B (%)	3.43	3.34
R_P (%)	6.58	5.40
R_{WP} (%)	8.46	7.18
8*a*		
$x = y = z$	1/8	1/8
N[a] (Li/Fe)	0.65/0.35	0.66/0.34
16*d*		
$x = y = z$	1/2	1/2
N[a] (Li/Fe/Ti)	0.49/0.23 /1.28	0.48/0.24/1.28
32*e*		
$x = y = z$	0.2602(4)	0.2603(3)
N[a] (O)	1/6	1/6

[a] N = occupation.

Table 7. Bond lengths [Å] for $Li_{1.14}Fe_{0.58}Ti_{1.28}O_4$ Q at 2 K and at room temperature.

d (M−O)	$T = 2$ K	$T = 300$ K
M(8*a*)−O	1.955(1) (× 4)	1.958(7) (× 4)
mean Shannon	1.934(5)	1.936(2)
M(16*d*)−O	2.003(1) (× 6)	2.006(5) (× 6)
mean Shannon	2.047(5)	2.047(1)

occupied by iron and titanium ions giving rise to different M−O distances (Table 3, Table 5 and Table 7), whereas the Li^+/Fe^{3+} ions occupy the centre of regular octahedral 4*b* sites. The disordered form is an inverse spinel (space group *Fd*3*m*) in which the $Li^+/Fe^{3+}/Ti^{4+}$ atoms are distributed randomly over the regular octahedral sites, and the tetrahedral ones are occupied by Li^+/Fe^{3+} ions. Figure 3 illustrates these features in a fragment of the ordered (Figure 3, a) and disordered (Figure 3, b) structures. Finally, the values obtained in the refinement of the unit cell parameters for all samples reflect the abovementioned changes in the cationic site distribution resulting from an intracrystalline order−disorder process.[6]

Magnetic Behaviour

Figure 4 shows the dependence of the dc magnetic susceptibility of the title samples with temperature $\chi(T)$ in the range between 2 and 300 K measured at a field of 0.5 kOe. The $\chi(T)$ variation for the composition $x = 1.28$ (SC and Q) shows broad maxima at about 20 K and 17 K, respectively. The dc magnetic susceptibility decreases with temperature for the sample $x = 1.50$ (SC and Q). We observed that the magnetic susceptibility is remarkably smaller for the disordered samples than for the ordered ones, and this fact is consistent with a decrease of ordering. No Curie−Weiss behaviour was observed over the whole tem-

 © 2003 Wiley-VCH Verlag GmbH & Co. KGaA, Weinheim

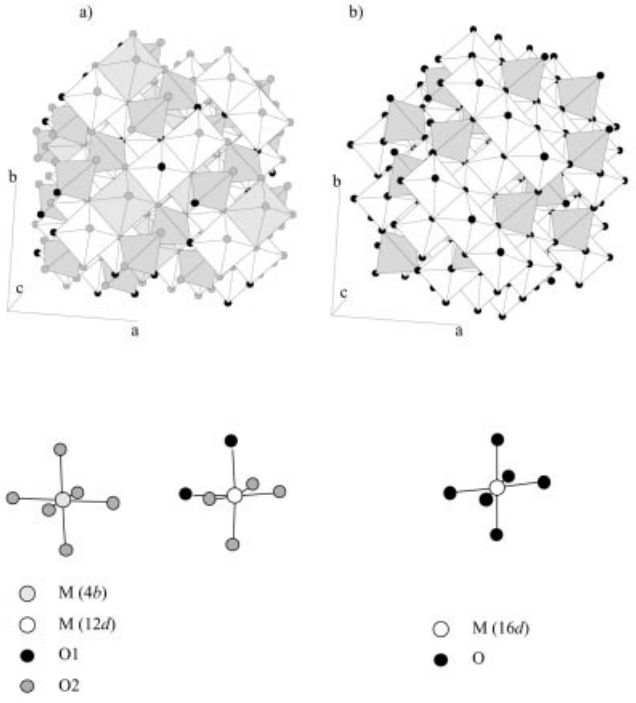

Figure 3. The structure of the $Li_{0.5+0.5x}Fe_{2.5-1.5x}Ti_xO_4$ spinels: a) ordered form (space group $P4_332$); b) disordered form (space group $Fd3m$)

perature range measured from the dc reciprocal susceptibility. The absence of a linear behaviour towards high temperature suggests that a ferrimagnetic transition is expected for a Curie temperature $T_C > 300$ K and, for example, these results are depicted in Figure 4 (part e) for the Q sample with $x = 1.28$ at $H = 1.5$ kOe.

Magnetisation measurements were performed in the temperature range $5 \leq T \leq 375$ K and some results are shown in Figure 5. We see that the magnetization increases with increasing applied field for each composition. In the present range of the magnetizing field, the magnetization does not show a saturation and it decreases slightly with increasing titanium content, in agreement with Néel's theorem of ferrimagnetism.[19] The individual magnetization in the A (tetrahedral) and B (octahedral) sites, M_A and M_B, of the two sublattices cannot be observed, but the net magnetization has been measured instead. Because the two magnetizations are oppositely directed, then $M = M_A - M_B$. The variation of magnetic moment with titanium content can be explained by assuming that, as the concentration of titanium ion increases, the relative number of Fe^{3+} ions decreases on both the A and B sites, but more on the B sites than on the A sites. This distribution is expected to disminish the A−B interactions, which in spinels, according to Néel's molecular field model, are stronger than A−A or B−B ones. Obviously, Ti^{4+} does not participate in any exchange interactions, but disminishes those resulting from the $Fe_A^{3+}-O-Fe_B^{3+}$ unit and the net effect is a decrease in the overall magnetization. Considering the spin-only moment for Fe^{3+} of 5 μ_B, the saturation moments have been estimated as being 0.3 μ_B and 1.05 μ_B for $x = 1.28$ and $x = 1.50$, respectively, but the values obtained at the highest fields (see Figure 5) are smaller than those expected from a collinear model. On the other hand, when the temperature is lowered, the magnetization curves below T_C show a clear ferromagnetic component with increasing importance. Such behaviour is evidence for a disordered spin-state (SG-like state) induced by disorder and frustration because of competing ferro- and antiferromagnetic exchange interactions.

As an example of the general behaviour, Figure 6 shows, for $x = 1.28$ (Q), the variation of the ac susceptibility with temperature ranging between 1.8 and 350 K at a magnetic field of 0.215 Oe for frequencies changing from 0.1 to 10 kHz. The susceptibility increases with increasing temperature, exhibiting a cusp, and then a marked decay. The cusp temperature is ca. 14−15 K, which is consistent with that observed in the dc measurement shown in Figure 4b. The inset of Figure 6 reflects that the cusp shows frequency dependence; it shifts to higher temperatures with increasing frequency and this feature is characteristic of the spin-glass behaviour stated above.

The spin-glass state occurs because of a combination of "randomness" and "frustration" in spin ordering, caused by the randomly mixed state of the ferromagnetic (spin-parallel) and antiferromagnetic (spin-antiparallel) spin interactions.[20] To obtain the spin-glass state in spinel ferrites, it is usual to substitute Fe^{3+} ions by nonmagnetic ions, such as Li^+ and Ti^{4+}, which results in the dilution of magnetic interactions (randomness) and the competition of exchange interactions (frustration). In this sense, Figure 7 shows a simplified model of the spin-glass phenomenon in a spinel ferrite AB_2O_4, in which the nearest neighbours of interacting metal ions bridged via the O^{2-} anion are shown. A denotes a tetrahedral site cation and B an octahedral one. In spinel oxides, the magnetic ions interact with each other through super-exchange antiferromagnetic interactions for which $|J_{AB}| >> |J_{BB}| > |J_{AA}|$ (J being the average value of the spin interactions). Thus, J_{AB} renders the undiluted spinel ferrimagnetism, with all A-site moments oriented antiparallel to all B-site moments, with BB and AA bonds remaining unsatisfied (left-hand side of Figure 7). After dilution of Fe^{3+} ions in the B sites by Li^+ and Ti^{4+} ions substitution, the magnetic order is broken and the frustration of certain moments occurs for BB and AA bonds (right-hand side of Figure 7).

To take into account the magnetic contribution to the Bragg diffraction peaks, the thermal evolution of the NPD patterns was acquired in the temperature ranges between 2−300 K, for $x = 1.28$ (SC) and 1.28 (Q), and 2−112 K, for $x = 1.50$ (Q), with $\lambda = 2.522$ Å and are shown in Figure 8a, 8b and 8c, respectively. Rietveld refinements in those temperature ranges were attempted, with and without a magnetic contribution, but the variation in intensity of the inner Bragg peaks — namely (111), (220), (311), (222), etc. — with the decrease in temperature was scarcely apparent, and this fact seems to indicate the absence of any magnetic long-range ordering (LRO) in these samples.[21]

 © 2003 Wiley-VCH Verlag GmbH & Co. KGaA, Weinheim

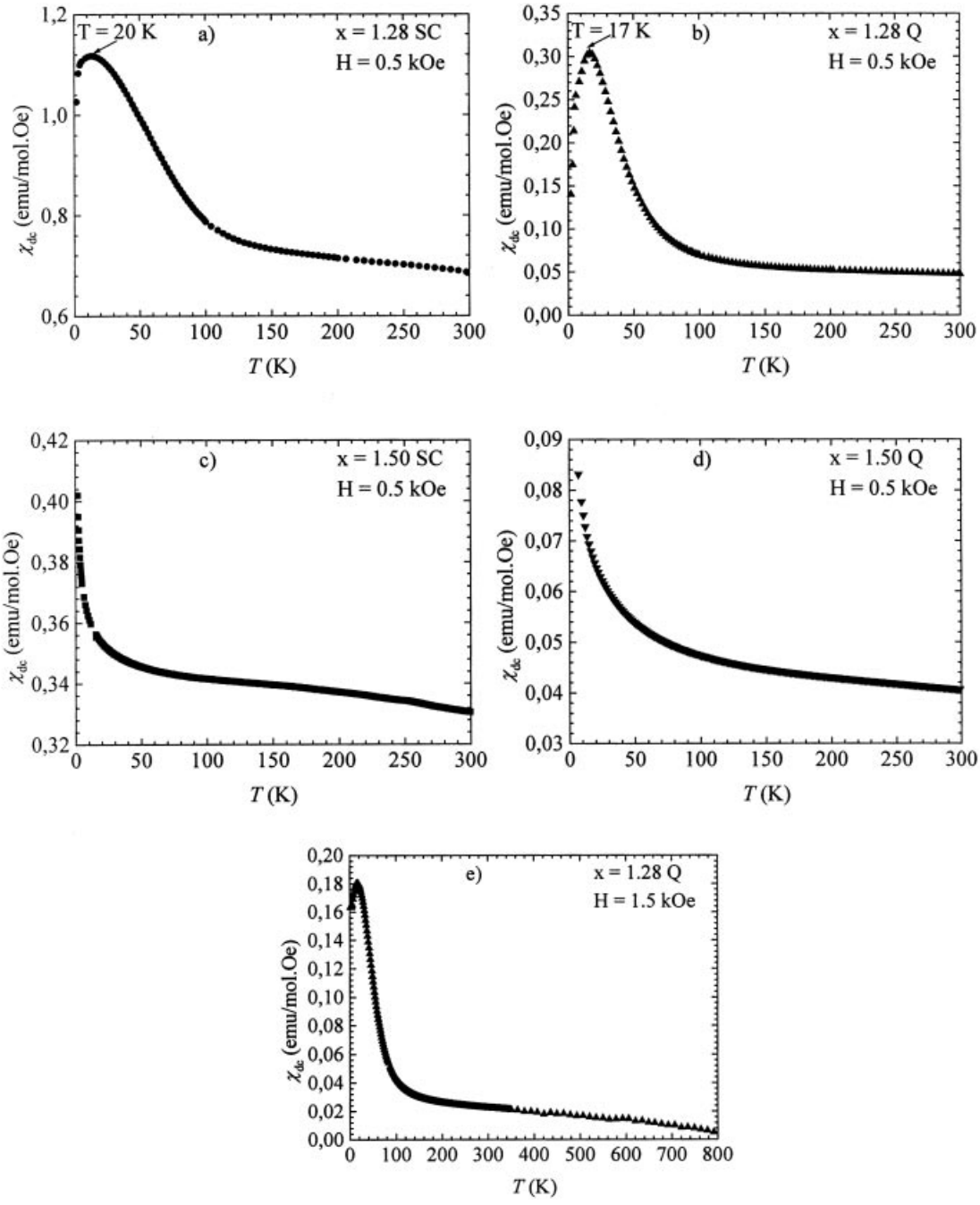

Figure 4. Variation of the dc magnetic susceptibility with temperature for $Li_{0.5+0.5x}Fe_{2.5-1.5x}Ti_xO_4$: $x = 1.28$ (SC and Q) and $x = 1.50$ (SC and Q). Applied field: 0.5kOe (a−d) and 1.5 kOe (e)

On the other hand, Figure 2 (part c) shows the variation of the (111) peak at 2 and 300 K for the sample $x = 1.28$ (Q), in which we see a slight increase in intensity at the lower temperature that seems to indicate a magnetic contribution. Moreover, it is noticeable that there is a considerable broadening of the (111) reflection, which suggests the presence of magnetic spin clusters.[22] Such a variation was not observed for our sample $x = 1.50$, from which the experimental data indicate a characteristic spin-glass behaviour.

Conclusions

Neutron-diffraction experiments were performed on lithium titanium ferrite $Li_{0.5+0.5x}Fe_{2.5-1.5x}Ti_xO_4$ ($x = 1.28$ and 1.50). The data show that the samples obtained by SC are ordered spinels of 1:3 type at octahedral sites, where Li^+ ions occupy octahedral (4*b*) and tetrahedral (8*c*) sites, Fe^{3+} cations are distributed over the octahedral (4*b* and 12*d*) and tetrahedral (8*c*) sites, and Ti^{4+} ions are exclusively located on octahedral (12*d*) sites. When the samples were quenched,

 © 2003 Wiley-VCH Verlag GmbH & Co. KGaA, Weinheim

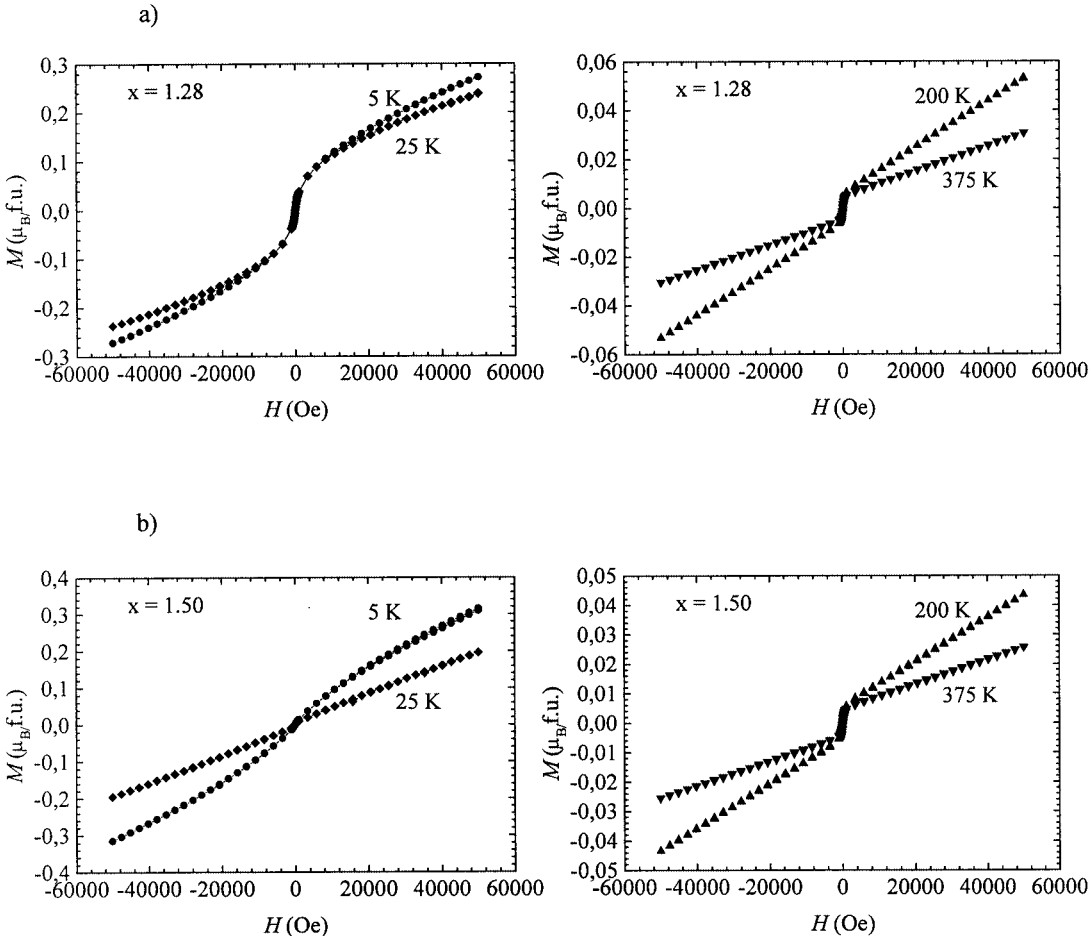

Figure 5. Isothermal magnetization vs. magnetic field at different temperatures for the samples obtained by quenching: a) $x = 1.28$; b) $x = 1.50$

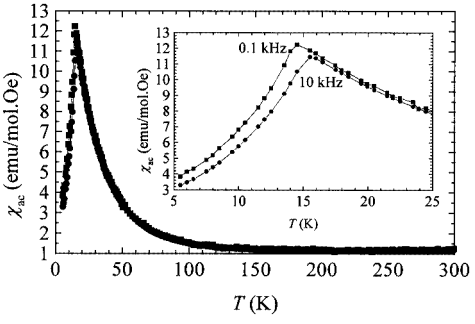

Figure 6. Real part of the ac magnetic susceptibility as a function of temperature from 1.8 to 350 K for $x = 1.28$ (Q) at $\nu = 0.1$ and 10 kHz, $H = 0.215$ Oe. Inset: temperature interval 5−25 K

the 1:3 ordering was destroyed and a change of symmetry occurred from $P4_332$ to $Fd3m$, so that the tetrahedral sites become occupied at random by Li^+/Fe^{3+} ions and the octahedral sites by $Li^+/Fe^{3+}/Ti^{4+}$ ions. Magnetic and neutron-diffraction measurements carried out on these samples confirm a spin-glass behaviour that is attributed to dilution of Fe^{3+} ions in the B sites by the substitution effect of Li^+ and Ti^{4+} ions. Therefore, magnetic order is broken and the

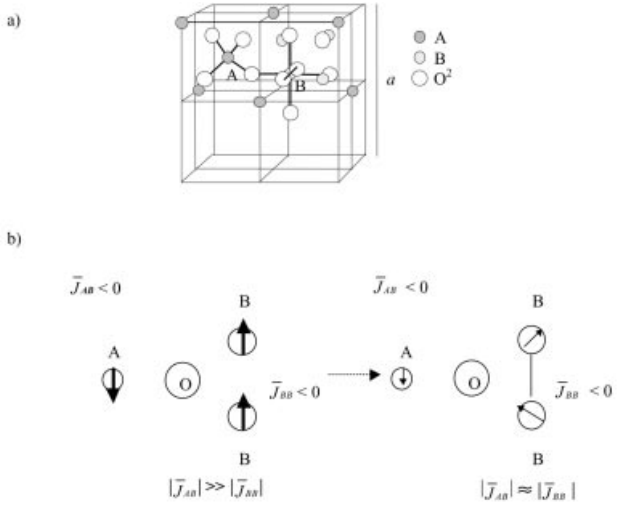

Figure 7. (a) Two octants in the unit cell of the spinel structure with lattice parameter a. The O^{2-} anions form a cubic close-packed structure, with A ions occupying the tetrahedral sites (A site), and B ions occupying the octahedral sites (B site). (b) Model of the spin-glass phenomenon in spinel ferrite. The nearest neighbours of the metal ions bridged via the O^{2-} anion in the spinel ferrite are shown: A (tetrahedral site cation), B (octahedral site cation). Arrows correspond to the spin of Fe ion

 © 2003 Wiley-VCH Verlag GmbH & Co. KGaA, Weinheim

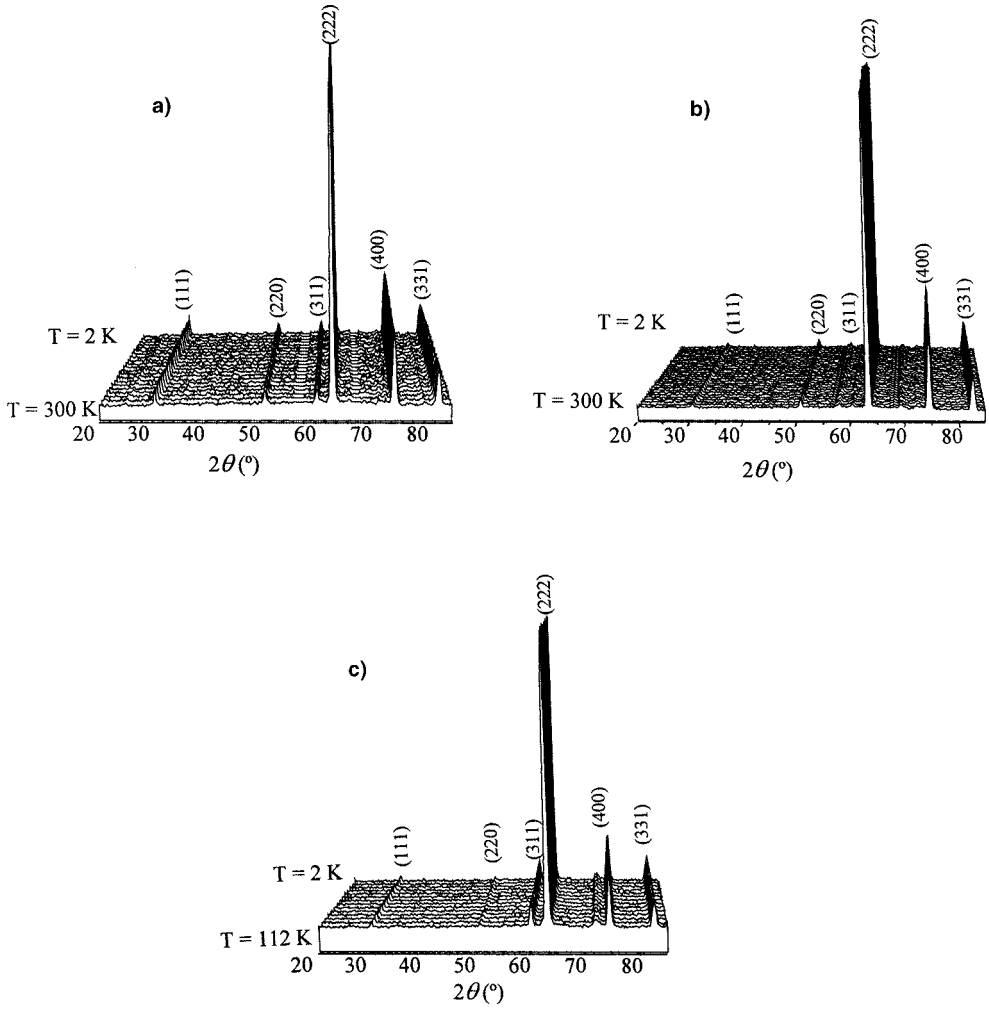

Figure 8. Thermal evolution of NDP collected at a wavelength λ = 2.522 Å in the following temperature ranges: a) 2−300 K (x = 1.28, SC), b) 2−300 K (x = 1.28, Q), c) 2−112 K (x = 1.50, Q)

frustration of certain moments occurs for BB and AA interactions.

Experimental Section

Polycrystalline samples of $Li_{0.5+0.5x}Fe_{2.5-1.5x}Ti_xO_4$ (where x = 1.28 and 1.50) were prepared by the "liquid mix" technique[23] from powdered mixtures of Li_2CO_3, Fe_2O_3 and TiO_2 (all reactants were supplied by Merck, Germany) in stoichiometric ratios. The samples were obtained by two methods: slow cooling (SC, at 1073 K for a day) or rapid quenching (Q) from temperatures above 1073 K for 12 h (x = 1.28) and 973 K for 12 h (x = 1.50) to room temperature.

Neutron powder-diffraction data were obtained at different temperatures for the samples x = 1.28 (ordered and disordered phases) and x = 1.50 (ordered phase) on the D1A high-resolution powder diffractometer (λ = 1.9110 Å) at the Institute Laue-Langevin (Grenoble, France). The multidetector D1B powder diffractometer with a wavelength of 2.522 Å was used to obtain the thermal patterns in the temperature ranges 2−300 K for x = 1.28 (ordered and disordered phases) and 2−112 K for x = 1.50 (disordered phase). Diffraction patterns were analysed by the Rietveld[24] method and the Fullprof programme.[25]

The magnetic-susceptibility measurements were performed using a commercial superconducting quantum-interference-device magnetometer, Quantum Design Magnetic Properties Measurement System 5S, on powder samples in a temperature range from 1.8 to 300 K under an applied magnetic field of 0.215 Oe. The magnetic field isothermal variations up to 60 kOe were obtained with the aid of a Quantum Design Physical Properties Magnetic System, which allowed the experimental setting of highly homogeneous magnetic fields at specific temperatures.

Acknowledgments

We are indebted to the CYCIT (MAT, 2002−01288) for financial support. We acknowledge the ILL and CR1G−D1B for collecting ND data. M.A.A. is grateful to the Comunidad de Madrid for a Postdoctoral Fellowship and A.S.B. thanks the Ministry of Education, Sports and Culture of Spain for financial support under a Postdoctoral Research Fellowship.

[1] M. Guillot, *Magnetic Properties of Ferrites* (Ed.: K. H. J. Buschow), *Electronic and Magnetic Properties of Metals and Ceramics*, Wiley-VCH, Weinheim, Germany, **1994**.
[2] P. B. Braun, *Nature* **1952**, *27*, 1123.
[3] S. J. Marin, M. O′Keeffe, D. E. Partin, *J. Solid State Chem.* **1994**, *113*, 413−419.
[4] J. L. Dormann, A. Tomas, M. Noguès, *Phys. Status Solidi* **1983**, *77*, 611−618.
[5] G. Blasse, *Philips Res. Repts. Suppl.* **1964**, *3*, 96−102.
[6] S. Scharner, W. Weppner, P. Schmid-Beurmann, *J. Solid State Chem.* **1997**, *134*, 170−181.
[7] J. L. Dormann, M. El Harfaoui, M. Nogues, J. Jové, *J. Phys. C* **1987**, *20*, L161−L166.
[8] J. L. Dormann, M. Noguès, *J. Phys.: Condens. Matter.* **1990**, *2*, 1223−1237.
[9] M. Seqqat, J. L. Dormann, M. Nogues, J. Jové, G. Nicoara, *Hyp. Inter.* **1994**, *94*, 2017−2021.
[10] G. O. White, C. E. Patton, *J. Magn. Magn. Mater.* **1978**, *9*, 299−317.
[11] M. El Harfaoui, J. L. Dormann, M. Noguès, G. Villers, V. Gaignaert, F. Bouree-Vigneron, *J. Physique Colloq.* **1988**, C8, *49*, 1147−1148.
[12] M. Noguès, M. Seqqat, F. Bouree-Vigneron, J. L. Dormann, G. Nicoara, *J. Magn. Magn. Mater.* **1992**, *104−107*, 1643−1644.
[13] M. Godinho, A. Carvalho, M. Noguès, J. L. Dormann, M. Seqqat, *J. Magn. Magn. Mater.* **1994**, *133*, 457−459.
[14] A. Belayachi, J. L. Dormann, M. Noguès, *J. Phys.: Condens. Matter.* **1998**, *10*, 1599−1619.
[15] W. Branford, M. A. Green, D. A. Neumann, *Chem. Mater.* **2002**, *14*, 1649−1656.
[16] L. Fernández-Barquín, M. V. Kuznetsov, Y. G. Morozov, Q. A. Pankhurst, I. P. Parkin, *Inter. J. Inorg. Mater.* **1999**, *1*, 311−316.
[17] M. A. Arillo, M. L. López, E. Perez-Cappe, C. Pico, M. L. Veiga, *Solid St. Ionics* **1998**, *107*, 307−312.
[18] M. A. Arillo, M. L. López, C. Pico, M. L. Veiga, J. Campo, J. L. Martínez, A. Santrich-Badal, *Phys. Rev. B*, in press.
[19] K. Standly, *Oxide Magnetic Materials*, Clarendon, Oxford, **1972**.
[20] S. F. Edwards, P. W. Anderson, *J. Phys. F: Met. Phys.* **1975**, *5*, 965−974.
[21] S. M. Yunus, H.-S. Shim, C.-H. Lee, M. A. Asgar, F. U. Hamed, A. K. M. Zakaria, *J. Magn. Magn. Mater.* **2001**, *232*, 121−132.
[22] S. M. Yunus, J. A. Fernández-Baca, M. A. Asgar, F. U. Ahmed, M. A. Hakim, *Physica B* **1999**, *262*, 112−124.
[23] M. Pechini, *U. S. Patent*, **1996**, 3 231/328.
[24] H. M. Rietveld, *J. Appl. Cryst.* **1969**, *2*, 65−71.
[25] J. Rodríguez Carvajal, FULLPROF, XV Congress of International Union of Crystallography, Toulouse **1990**, p. 127 (Revised version, **1994**).

Received December 20, 2002

 © 2003 Wiley-VCH Verlag GmbH & Co. KGaA, Weinheim

Developing Remote Metal Binding Sites in Heteropolymolybdates[‡]

Pierre R. Marcoux,[a] Bernold Hasenknopf,*[a] Jacqueline Vaissermann,[a] and Pierre Gouzerh[a]

Keywords: Polyoxometalates / Molybdenum / N ligands / Coordination chemistry

Anderson-type polyoxomolybdates $[MMo_6O_{18}\{(OCH_2)_3CNH_2\}_2]^{3-}$ (M = Mn^{III}, Fe^{III}) were prepared and structurally characterized. The tris(alkoxo) ligands are bound to the central heteroatom via their oxygen atoms. The corresponding compounds with M = Ni^{II} or Zn^{II} are not accessible since these cations have a preference for the amino functionality. The pendant amino groups of the manganese-containing derivative react with pyridinecarbaldehydes to give the corresponding imines. This provides new mono- and bidentate binding sites for metal cations.
(© Wiley-VCH Verlag GmbH & Co. KGaA, 69451 Weinheim, Germany, 2003)

Introduction

Organic moieties can be grafted onto polyoxometalates (POMs).[1] This provides an entry into the field of organic/inorganic hybrid compounds which combine the properties of the (oxo)metal cluster with those of the organic component.[2,3] Such functionalized POMs have been used in the preparation of polymers,[4−7] dendrimers,[8] and macroporous materials,[9] by covalently crosslinking the organic groups. Metallo-supramolecular chemistry can be used effectively for the construction of functional assemblies.[10−13] Both complete and lacunary POMs can act as ligands for a variety of metal cations,[14] and the resulting complexes have interesting electrical, optical, magnetic and catalytic properties.[15−21] The extra metal centers occasionally provide the way to the formation of 1-D[22,23] or 2-D[24] POM arrays. However, the complexation of metal ions at remote sites of organic ligands grafted on POMs is less common. Indeed the (ferrocenylimido)hexamolybdate reported by Maatta et al. was obtained by treating a ferrocenyl-substituted imido precursor with hexamolybdate.[25] More recently, Stein and co-workers obtained one-dimensional chains in the solid state by the coordination of Ag^I ions to $[Mo_{12}O_{46}(AsC_6H_4\text{-}4\text{-}NH_2)_4]^{4-}$.[26] To the best of our knowledge, complex formation in solution involving a ligand already bound to a polyoxometalate has not been reported in the literature.

Thus, our interest focused on the combination of POMs and other metals using organic ligands. This strategy is complementary to that involving the coordination of oxo ligands, in order to "bridge the gap between polyoxometalates and classic coordination compounds".[27] The organic molecules may display donor atoms other than oxygen, and their arrangement around the binding site may differ; thus, they provide the versatility to adjust to the chemical and geometrical preferences of the extra metal centers. Ideally, our approach would permit the selection of a specific ligand for a chosen metal ion, and to connect it to a chosen POM. The properties of the resulting assembly would be tuned by the individual optimization of the components.

The implementation of this concept requires the development of a flexible synthetic strategy. A key role is played by the organic linker between the POM and the remote coordination site. This molecule has to be bifunctional, with one side that can merge with a POM, and a reactive group on the other side to develop a coordination site. We chose tris(hydroxymethyl)aminomethane $[(HOCH_2)_3CNH_2$, TRIS] for this purpose since tris(alkoxo) moieties can be incorporated in Anderson,[28] Lindqvist,[29−31] Dawson[8,32] and other POMs,[32−34] while the free amino group can be used to create a new coordination site. The incorporation of TRIS into Anderson-type polyoxomolybdates was investigated first.

The Anderson structure $[H_x(M'O_6)M_6O_{18}]^{n-}$ (x = 0−6, n = 2−6) consists of a planar arrangement of six edge-sharing MO_6 (M = Mo, W) octahedra around a central heteroatom M′.[35−37] We have recently shown that two tris(hydroxymethyl)methane residues $RC(CH_2O)_3$ (R = CH_3, CH_2OH, CH_2NO_2) can cap both sides of the polyanion.[28] Two forms were found. In the first form − named δ for its approximate D_3 symmetry − the triol caps the central octahedron, while in the second form − named χ for its approximate C_{2v} symmetry − the triol caps a tetrahedral cavity. The central heteroatom can be a di- or trivalent transition metal cation, and we have prepared compounds with

[‡] Part 2. Part 1: Ref.[28]

[a] Laboratoire de Chimie Inorganique et Matériaux Moléculaires, UMR CNRS 7071, Université Pierre et Marie Curie,
Case Courrier 42, 4 place Jussieu, 75252 Paris cedex 05, France
Fax: (internat.) + 33-1/44273841
E-mail: hasen@ccr.jussieu.fr

 © 2003 Wiley-VCH Verlag GmbH & Co. KGaA, Weinheim **DOI: 10.1002/ejic.200200677**

Mn^{III}, Fe^{III}, Ni^{II} and Zn^{II} and the above-mentioned tris(hydroxymethyl)methane derivatives. Here, we present the results of the reactions with TRIS, and the derivatization of the pendant amino group. The protonated form of TRIS has been used as counterion for polyoxometalates.[38] It has been shown that amide and tertiary amine derivatives can be incorporated into the POM frameworks,[30,39] but to the best of our knowledge, TRIS itself has not been incorporated into the POMs yet. Difficulties with this compound have been linked to its role as a reductant.[39]

Results and Discussion

Grafting a Free Amino Group onto a POM

Treatment of $[N(C_4H_9)_4]_4[\alpha\text{-}Mo_8O_{26}]$ with manganese(III) acetate in the presence of TRIS gave $[N(C_4H_9)_4]_3[MnMo_6O_{18}\{(OCH_2)_3CNH_2\}_2]$ (**1**) which was isolated as orange crystals in an 80% yield. The compound was characterized by single-crystal X-ray diffraction. Crystal structure data are summarized in Table 1. The overall molecular structure of the anion (Figure 1) is very similar to the analogous compounds previously reported.[28] Six edge-sharing MoO_6 octahedra are arranged around a central MnO_6 unit, forming the Anderson structure. The two

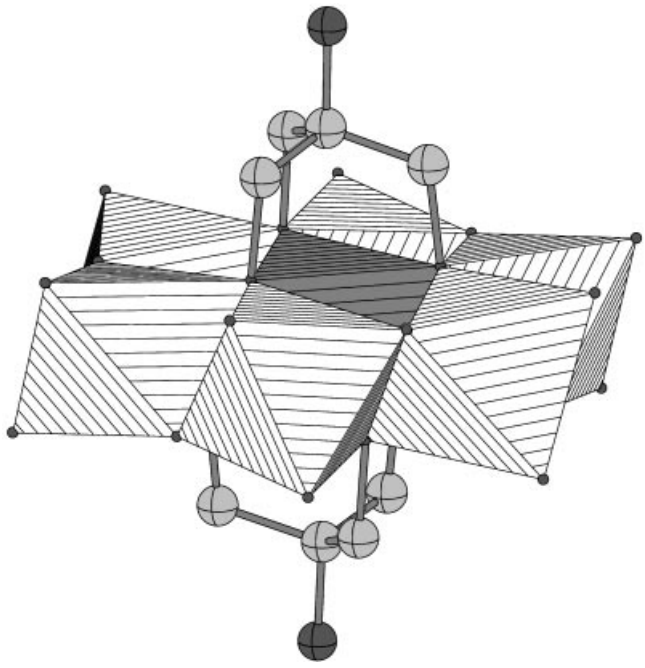

Figure 1. Structure of the anion of **1**: $[MnMo_6O_{18}\{(OCH_2)_3CNH_2\}_2]^{3-}$; the TRIS ligands cap both sides of the Anderson structure

Table 1. Crystal data and structure refinement for compounds **1**, **2**, **3** and **4**

Compound	**1**	**2**	**3**	**4**
Empirical formula	$C_{56}H_{124}MnMo_6N_5O_{26}$	$C_{56}H_{128}FeMo_6N_5O_{24}$	$C_{46}H_{99}Mo_2N_5O_{16}Zn_2$	$C_{68}H_{130}MnMo_6N_7O_{24}$
Formula mass	1914.2	1918.2	1301.0	2060.4
a [Å]	14.650(4)	25.845(11)	13.690(3)	23.243(4)
b [Å]	24.245(9)	24.518(13)	14.634(4)	14.298(3)
c [Å]	24.453(10)	14.649(12)	18.037(11)	27.595(4)
α [°]	90	90	75.31(4)	90
β [°]	90	101.55(6)	86.11(4)	99.28(1)
γ [°]	90	90	62.69(2)	90
V [Å^3]	8685(5)	9706(9)	3101(2)	9051(3)
Z	4	4	2	4
Crystal system	orthorhombic	monoclinic	triclinic	monoclinic
Space group	*Pcmn*	*C*2/*m*	$P\bar{1}$	*P*21/*c*
Crystal color	orange	yellow	none	orange
Linear abs. coeff. μ [cm^{-1}]	10.2	9.9	12.3	9.8
$D_{calcd.}$ [g·cm^{-3}]	1.46	1.38	1.39	1.51
Radiation	Mo-K_α (0.71069 Å)	Mo-K_α (0.71069 Å)	Mo-K_α (0.71069 Å)	Mo-K_α (0.71069 Å)
Scan mode	ω/2θ	ω/2θ	ω/2θ	ω/2θ
Scan range [°]	0.80 +0.345tan(θ)	0.80 +0.345tan(θ)	0.80 +0.345tan(θ)	0.80 +0.345tan(θ)
θ range [°]	1−25	1−26	1−28	1−25
T [K]	221	295	295	295
hkl range	0, 17; 0, 28; 0, 29	0, 31; 0, 30; −18, 17	0, 18; −17, 19; −23, 23	0, 27; 0, 16; −32, 32
No. of data collected	8355	9343	15540	17021
No. of unique data	7813	9132	14920	15879
R_{int}	none	0.03	0.04	0.05
No. of data in refinement	2998 $(F_o)^2 > 3\sigma(F_o)^2$	4048 $(F_o)^2 > 3\sigma(F_o)^2$	8070 $(F_o)^2 > 3\sigma(F_o)^2$	4248 $(F_o)^2 > 2\sigma(F_o)^2$
Absorption correction	ψ-scan	DIFABS	DIFABS	DIFABS
$T_{min.}$, $T_{max.}$	0.72, 1	0.71, 1	0.93, 1	0.94, 1
No. of variables	413	410	650	580
Final *R*	0.0620	0.0950	0.0458	0.0718
Final R_w	0.0713	0.116	0.0568	0.0791
Goodness of fit	1.04	1.00	1.03	1.10
Extinction coefficient	none	192	none	none
$\Delta\rho_{max}$ [e/Å^3]	−0.70, +1.13	−0.84, +1.29	−0.56, +0.79	−0.76, +0.97

 © 2003 Wiley-VCH Verlag GmbH & Co. KGaA, Weinheim

Table 2. Selected bond lengths and angles for the anions in **1**, **2** and **4**

	1	**2**	**4**
Distances:			
Mo−$O_{terminal}$	1.693(10)−1.718(10)	1.650(9)−1.720(14)	1.649(17)−1.703(13)
Mo−O_{bridge}	1.904(9)−1.925(9)	1.892(29)−1.925(11)	1.882(16)−1.952(13)
Mo−O_{alkoxo}	2.341(7)−2.403(7)	2.341(44)−2.360(8)	2.328(17)−2.415(13)
M−O[a]	1.943(8)−2.031(12)	1.971(8)−1.991(27)	1.948(16)−1.992(13)
Angles O−M−O:[a]			
Same TRIS	92.05(22)−92.88(30)	91.92(31)−92.84(22)	91.92(51)−93.40(50)
Opposite TRIS, *cis*	87.18(32)−88.10(22)	87.16(22)−88.08(31)	86.67(52)−88.02(53)
Opposite TRIS, *trans*	179.42(31)−179.78(49)	180.00(37)	178.99(56)−179.93(51)

[a] M = Mn (**1**, **4**); Fe (**2**).

organic moieties cap both sides of the planar hexagon. All the alkoxo ligands are bound to the Mn^{III} ion; thus, the structure corresponds to the δ type. Selected bond lengths and angles are compiled in Table 2. It should be noted that the rigidity of the POM framework prevents the Mn^{III} ion from undergoing marked Jahn−Teller distortions: the coordination octahedron is only very slightly elongated.

The reaction of $[N(C_4H_9)_4]_4[\alpha\text{-}Mo_8O_{26}]$ with iron(III) acetylacetonate in the presence of TRIS gave $[N(C_4H_9)_4]_3[FeMo_6O_{18}\{(OCH_2)_3CNH_2\}_2]$ (**2**) which was isolated as yellow crystals in a 50% yield. Structural analysis by X-ray diffraction of single crystals (Table 1) revealed the expected δ-type Anderson structure. Selected bond lengths and angles are compiled in Table 2.

IR spectra of compounds **1** and **2** (listed in the Exp. Sect.) are in agreement with the crystal structures.[28,40] It has to be pointed out that the IR spectra display a single, broad band at ca. 700 cm^{-1} which is assigned to the Mo−O−Mo bridges, in accordance with the δ structure. The IR spectra of the χ structure would present two bands in this region.[28]

The reactions of nickel(II) acetate or zinc(II) acetate with $[N(C_4H_9)_4]_4[\alpha\text{-}Mo_8O_{26}]$ and TRIS did not yield the expected Anderson-type compound. This result is in contrast to other tris(hydroxymethyl)methane derivatives that do form the functionalized Anderson-type POM with a central Ni^{II} or Zn^{II} metal ion.[28] Therefore, we decided to vary the reaction conditions and to use a different source of molybdate. From the reaction of zinc(II) acetate with $[N(C_4H_9)_4]_2[Mo_2O_7]$ in the presence of TRIS, we isolated a compound with the molecular formula $[N(C_4H_9)_4]_2[Mo_2Zn_2O_6\{(OCH_2)_2C(NH_2)CH_2OH\}_2(CH_3CO_2)_2]$ (**3**) in a moderate yield (36%). Structural analysis by single-crystal X-ray diffraction (Table 1) revealed the molecular structure. Figure 2 shows a ball-and-stick representation of the anion. It has no internal symmetry. One of the two molybdenum atoms (Mo1) has a distorted octahedral environment, whereas the other Mo atom (Mo2) displays distorted tetrahedral coordination. Both molybdenum centers have two terminal oxo ligands. Mo1 shares three bridging alkoxo ligands with the zinc atoms, two with Zn1 and one with Zn2. A terminal alkoxo ligand completes its coordination sphere. Mo2 shares one bridging oxo ligand with each zinc atom. The two zinc atoms also have different environments. Zn1 has a distorted trigonal bipyramidal environment, whereas Zn2 displays distorted tetrahedral coordination. Each of the Zn atoms is bound to the amino functional group of a TRIS molecule and to a monodentate acetate ligand, and is connected by a μ-oxo ligand to the Mo2 center. The μ-alkoxo bridges formed with the octahedral molybdenum complete the coordination spheres. Thus, the two TRIS molecules are complexed by two oxygen atoms and a nitrogen atom, leaving one OH group of each TRIS free.

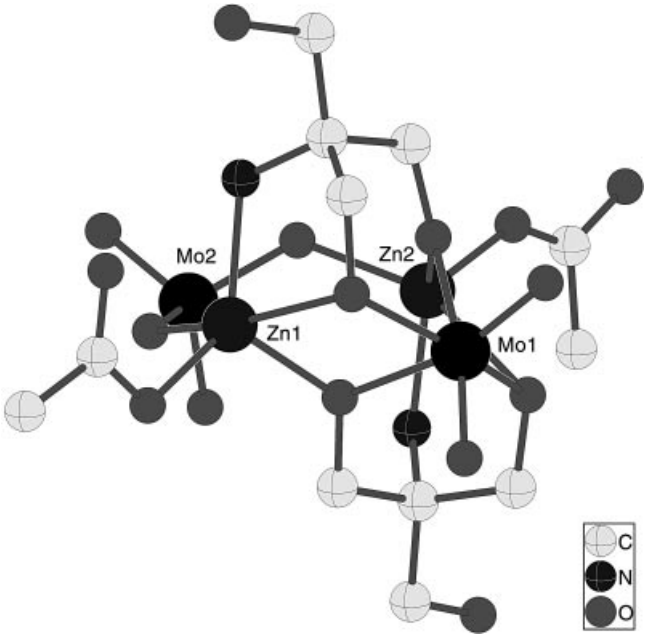

Figure 2. Ball-and-stick representation of the anion of **3**: $[Mo_2Zn_2O_6\{(OCH_2)C(NH_2)CH_2OH\}_2(CH_3CO_2)_2]^{2-}$; note the coordination of the amino groups to the zinc atoms

Compound **3** was also analyzed by solution NMR spectroscopy. In addition to the signals arising from the tetrabutylammonium cations and the acetate ligands, the ^1H NMR spectrum displays three broad signals of equal intensity which are assigned to the CH_2 groups of TRIS. In the ^{13}C NMR spectrum, the TRIS ligands give rise to four signals. This analysis does not exclude the fact that the structure of **3** is maintained in solution, with the overlap of some of the signals of the two TRIS molecules. Yet, it seems more likely

 © 2003 Wiley-VCH Verlag GmbH & Co. KGaA, Weinheim

that the spectra correspond to one or more compounds resulting from the fragmentation of **3**. The decomposition of **3** in solution is further supported by the appearance of some weak signals in the ^{13}C NMR spectrum.

Compound **3** is not suitable as a building block for hybrid molecular materials. However, it is important to point out that the amino group is coordinated to the zinc atom. Such a coordination mode may prohibit the formation of the Anderson structure, as it prevents the incorporation of the zinc atom into the (oxo)molybdenum framework. Based on the well-established HSAB concept,[41] it is not surprising that the soft Zn^{II} cation is bound to the nitrogen donor, whereas the hard Mo^{VI} center has a greater affinity towards the oxygen donors. The same factor is likely to play a role with the nickel(II) cation. Indeed, no Anderson-type compound was isolated from the reaction of nickel(II) acetate with $[N(C_4H_9)_4]_4[\alpha\text{-}Mo_8O_{26}]$ in the presence of TRIS, and only ill-defined mixtures of compounds were obtained.

Developing Remote Binding Sites

The free amino groups of compounds **1** and **2** could serve as ligands for transition metal ions, and we are currently exploring this possibility. Furthermore, they can react with suitable organic substrates, thus developing different binding sites. With this perspective, we decided to form imines by reaction with aldehydes. Imine formation is known to proceed under conditions under which the functionalized POMs are stable.

Reaction of **1** with 2-pyridinecarbaldehyde afforded $[N(C_4H_9)_4]_3[MnMo_6O_{18}\{(OCH_2)_3CN{=}C(2\text{-}C_5H_4N)\}_2]$ (**4**) which was isolated in a 77% yield. The complex was characterized by single-crystal X-ray diffraction. Crystallographic data are compiled in Table 1, and the molecular structure of the complex anion is displayed in Figure 3. The polyoxomolybdate retains the Anderson structure of the parent compound **1**. Bond lengths and angles (Table 2) are very similar in both compounds. The 1,2-diimine functional group provides a new bidentate chelating site for transition metal ions, on each side of the polyanion.

Reaction of **1** with 4-pyridinecarbaldehyde proceeded in the same manner giving the corresponding compound $[N(C_4H_9)_4]_3[MnMo_6O_{18}\{(OCH_2)_3CN{=}C(4\text{-}C_5H_4N)\}_2]$ (**5**), in a 70% yield. IR and NMR spectroscopic studies show that compounds **4** and **5** are very similar. Beside the typical vibrational bands for the Anderson-type core, the IR spectra present a band for the imine functionality at 1643 and 1641 cm^{-1}, respectively. In the ^1H NMR spectra, all signals are broadened by the presence of the paramagnetic Mn^{III} center. The chemical shifts for the pyridine rings are in the normal range between $\delta = 7$ and 9 ppm (for details see Exp. Sect.), whereas the CH_2O groups are highly deshielded since they are closer to the Mn^{III} center. Nevertheless, they also reflect imine formation. The signals for the CH_2O groups are displayed at $\delta = 52.5$ and 53.9 ppm in compounds **4** and **5**, respectively, relative to $\delta = 61.1$ ppm in the free amino compound **1**.

Compounds **4** and **5** differ only in the nature of the pendant binding sites. Complex **5** only has monodentate binding sites, whereas complex **4** has two bidentate binding sites. This opens the way to vary complex formation of transition metals with respect to the type of metal ions bound and the stability of the complex formed. We are currently exploring these possibilities. Our first attempts to coordinate Cu^{II} or Pd^{II} complexes to the grafted ligands on compounds **4** and **5** gave very insoluble compounds. As our long-term goal is developing defined structures in solution, we are now modifying the ligand, and the transition metal complex.

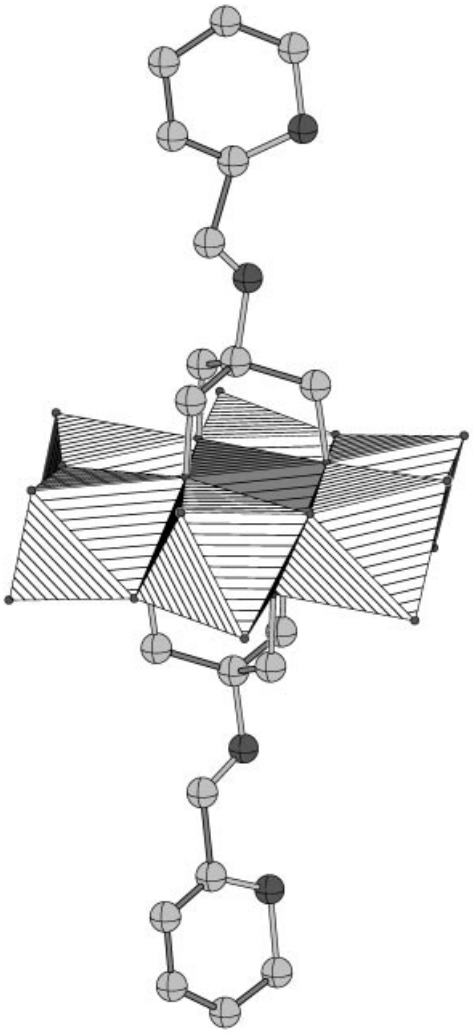

Figure 3. Structure of the anion of **4**: $[MnMo_6O_{18}\{(OCH_2)_3CN{=}C(2\text{-}C_5H_4N)\}_2]^{3-}$; a chelating binding site is displayed at both sides of the Anderson structure

Conclusion

We have shown the possibility of incorporating the TRIS ligand into a heteropolymolybdate. The self-assembly of such a functionalized POM arising from several metal ions (Mo^{VI}, Mn^{III}, Fe^{III}) and several ligands (oxo, alkoxo) is a highly complex process which relies on the molecular recognition of all the components. Their steric and electronic properties are complementary, thus allowing for the formation of the expected structure in high yields. The affinity of

 © 2003 Wiley-VCH Verlag GmbH & Co. KGaA, Weinheim

Zn^{II} and Ni^{II} metal ions for nitrogen donors the preference of Mo^{VI} for oxo and alkoxo ligands are antagonistic, therefore disrupting the formation of the Anderson structure. As a result, mixtures of compounds are present in solutions of molybdate, TRIS and Zn^{II} or Ni^{II} cations. It was possible to isolate one compound (**3**) of such a mixture in the solid state. This compound contains tetra- and hexacoordinate molybdenum atoms with only O donor atoms, and tetra- and pentacoordinate zinc atoms with N and O ligands.

The grafted ligands on the POM can be modified by organic reactions.[42] The development of the binding sites presented here is only one aspect of this chemistry, and it is clear that other functionalities can be introduced in the same way. The advantage of this flexible approach is that the synthesis of the POM core and the introduction of a specific function are two distinct steps. We are exploring this field by separately modifying the POM (molybdates, vanadates, ...) and the function (metal binding, hydrogen bonding, targeting biological substances, ...).

Experimental Section

General Remarks: $[N(C_4H_9)_4]_4[\alpha\text{-}Mo_8O_{26}]$[43] and $[N(C_4H_9)_4]_2[Mo_2O_7]$[44] were prepared by literature methods. All other chemicals, including solvents, were commercially available as reagent grade and used as received. Elemental analyses were performed by the "Service de microanalyse", Université Pierre et Marie Curie, Paris, France and by the "Service central d'analyse", CNRS, Vernaison, France.

Spectroscopy: NMR spectra (^1H, ^{13}C) were recorded with a Bruker AC300 spectrometer at 300 and 75.5 MHz, respectively, at 25 °C unless otherwise stated. Chemical shifts (δ) are expressed in ppm relative to Me_4Si, the high frequency direction being positive, with the residual solvent peak as standard. Assignment of signals is quoted with respect to numbering within the molecular fragments: "pyr" stands for the pyridine rings, "TBA" stands for the tetrabutylammonium cations. IR spectra were recorded using KBr pellets with a Bio-Rad FTS 165 spectrometer at 4 cm^{-1} resolution. Relative intensities are given after the wavenumber as vs = very strong, s = strong, m = medium, w = weak, sh = shoulder, br. = broad.

X-ray Crystal Structure Determination: Crystallographic data are summarized in Table 1. Data were recorded at room temperature with an Enraf−Nonius MACH3 diffractometer with graphite-monochromated Mo-K_α radiation. Unit cell dimensions with estimated standard deviations were obtained from least-squares refinements of the setting angles of 25 automatically centered reflections. Two standard reflections were monitored periodically. Some decay was observed (18, 38 and 22% for compounds **1**, **2** and **4**, respectively) and the data were scaled accordingly. Corrections were made for Lorentz and polarization effects and for absorption (based on Ψ scans for **1** and using DIFABS[45] for other compounds). Secondary extinction corrections were found necessary only for compound **2**. Computations were performed by using the PC version of CRYSTALS.[46] Atomic form factors for neutral atoms were taken from tabulated values.[47] Real and imaginary parts of anomalous dispersion were taken into account. The structures were solved by direct methods[48] and successive Fourier maps. For **1** and **2** non-hydrogen atoms were anisotropically refined except for the carbon atoms of the half cation contained in the asymmetric unit which presents some disorder, and for the oxygen atoms of the water molecules (compound **1**). Restraints were applied to the carbon−carbon distances in both cations and hydrogen atoms were not introduced. For **3** all non-hydrogen atoms were refined anisotropically. Application of restraints to one of the two acetate ligands was necessary. Hydrogen (C−H) atoms were introduced in calculated positions. For **4**, because of the few observed reflections only manganese, molybdenum and oxygen atoms were refined anisotropically. Restraints were applied to the carbon−carbon distances of the cations and no hydrogen atoms were introduced. In all cases least-squares refinements in full-matrix were carried out by minimizing the function $\Sigma w(|F_o| - |F_c|)^2$, where F_o and F_c are the observed and calculated structure factors. Models reached convergence with $R = \Sigma(||F_o| - |F_c||)/\Sigma wF_o$ and $R_w = [\Sigma w(|F_o| - |F_c|)^2/\Sigma w(F_o)^2]^{1/2}$, having values listed in Table 1. In the last stages of the refinement, each reflection was assigned a weight: $w = w'\{1 - [(|F_o| - |F_c|)/6\sigma|F_o|]^2\}^2$ with $w' = 1/\Sigma_r A_r T_r(X)$ with three coefficients for a Chebyshev series, for which $X = F_c/F_{c(max.)}$. In the final cycles, no parameter changed by more than 0.2σ (except for **2** where the value was 0.8σ due to the restraints applied to the acetate ligand) and the final difference Fourier maps were free of any significant residual density. CCDC-189392 (**1**), -189393 (**2**), -189394 (**3**) and -189395 (**4**) contain the supplementary crystallographic data for this paper. These data can be obtained free of charge at www.ccdc.cam.ac.uk/conts/retrieving.html [or from the Cambridge Crystallographic Data Centre, 12 Union Road, Cambridge CB2 1EZ, UK; Fax: (internat.) + 44-1223/336-033; E-mail: deposit@ccdc.cam.ac.uk].

Synthesis and Characterization

$[N(C_4H_9)_4]_3[MnMo_6O_{18}\{(OCH_2)_3CNH_2\}_2]$ (1): A mixture of $[N(C_4H_9)_4]_4[\alpha\text{-}Mo_8O_{26}]$ (8.00 g, 3.7 mmol), $Mn(CH_3COO)_3{\cdot}2H_2O$ (1.49 g, 5.6 mmol) and $(HOCH_2)_3CNH_2$ (1.56 g, 12.8 mmol) in 150 mL of acetonitrile was refluxed for 16 h. The orange solution was cooled to room temperature and filtered to remove a very fine black solid. The filtrate was exposed to ether vapor. After 2 h, a white precipitate was filtered off. The orange filtrate was again exposed to ether vapor for several days. Large orange crystals were obtained. They were isolated by filtration, washed with a small amount of acetonitrile and ether, and dried under vacuum. The crystal for X-ray analysis contained 2 H_2O. Yield: 7.42 g (80%). $C_{56}H_{124}MnMo_6N_5O_{24}$ (1882.21): calcd. C 35.74, H 6.64, Mo 30.58, Mn 2.92, N 3.72; found C 35.73, H 6.72, Mo 29.04, Mn 2.75, N 3.54. IR: $\tilde{\nu}_{max}$ = 3290 (ν_{as} NH, w), 2961 (ν CH, s), 2936 (ν CH, s), 2875 (ν CH, s), 1611 (w), 1480 (δ CH, s), 1384 (δ CH, m), 1348 (w), 1256 (w), 1151 (w), 1129 (w), 1108 (ν CO, m), 1040 (ν CO, s), 939 (ν Mo=O, s), 919 (ν Mo=O, s), 902 (ν Mo=O, s), 797 (w), 737 (w), 663 (ν Mo−O−Mo, vs), 563 (m), 520 (w), 461 (m), 413 (m), 368 (s), 321 (m), 282 (w) cm^{-1}. ^1H NMR ([D$_6$]DMSO): δ = 0.93 (t, ^3J = 7.3 Hz, 36 H, 4-H_{TBA}), 1.31 (m, 24 H, 3-H_{TBA}), 1.57 (m, 24 H, 2-H_{TBA}), 3.16 (m, 24 H, 1-H_{TBA}), 61.1 (s, 12 H, CH_2O) ppm.

$[N(C_4H_9)_4]_3[FeMo_6O_{18}\{(OCH_2)_3CNH_2\}_2]$ (2): A mixture of $[N(C_4H_9)_4]_4[\alpha\text{-}Mo_8O_{26}]$ (1.08 g, 0.5 mmol), $[Fe(acac)_3]$ (265 mg, 0.75 mmol, acac = acetylacetonate) and $(HOCH_2)_3CNH_2$ (182 mg, 1.5 mmol) in 20 mL of acetonitrile was refluxed for 16 h. The red suspension was cooled to room temperature, and a yellow-orange solid was removed by filtration. The red filtrate was exposed to ether vapor. After 3 d, a microcrystalline solid was isolated by filtration. The compound was recrystallized from DMF to obtain analytically pure **2** with 2 equiv. of DMF. Yield: 615 mg (49%). Crystals suitable for X-ray diffraction were grown by slow ether diffusion into an acetonitrile solution. $C_{62}H_{138}FeMo_6N_7O_{26}$

 © 2003 Wiley-VCH Verlag GmbH & Co. KGaA, Weinheim

(2029.31): calcd. C 36.70, H 6.85, Fe 2.75, Mo 28.37, N 4.83; found C 36.01, H 6.80, Fe 2.17, Mo 28.07, N 4.65. IR: $\tilde{\nu}_{max}$ = 2961 (ν CH, s), 2935 (ν CH, s), 2874 (ν CH, s), 1654 (w), 1482 (δ CH, m), 1382 (δ CH, w), 1153 (w), 1129 (w), 1041 (ν CO, s), 938 (ν Mo=O, vs), 920 (ν Mo=O, vs), 902 (ν Mo=O, vs), 802 (w), 665 (ν Mo−O−Mo, br., vs), 613 (w), 562 (m), 528 (w),487 (w), 450 (w), 410 (w), 367 (m), 324 (m), 278 (w) cm^{-1}. The paramagnetic nature of the compound prevents the recording of the NMR spectra.

$[N(C_4H_9)_4]_2[Mo_2Zn_2O_6\{(OCH_2)C(NH_2)CH_2OH\}_2(CH_3CO_2)_2]$ (3): A solution of $[N(C_4H_9)_4]_2[Mo_2O_7]$ (1.58 g, 2.0 mmol), $Zn(CH_3CO_2)_2$ (878 mg, 4.0 mmol) and $(HOCH_2)_3CNH_2$ (485 mg, 4.0 mmol) in 20 mL of acetonitrile was heated under reflux. After 20 min, the mixture became cloudy. After 16 h, the reaction mixture was filtered while hot. The filtrate was cooled to room temperature and exposed to ether vapor. Colorless crystals formed over a period of 2 months. They were isolated by filtration and dried under vacuum for analysis. Yield: 0.91 g (36%). The crystal used in the X-ray diffraction analysis was found to contain one equiv. of acetonitrile per polyanion. $C_{44}H_{96}Mo_2N_4O_{16}Zn_2$ (1259.91): calcd. C 41.95, H 7.68, N 4.45; found C 42.05, H 7.69, N 4.60. IR: $\tilde{\nu}_{max}$ = 2962 (ν CH, s), 2936 (ν CH, s), 2876 (ν CH, s), 2849 (s, sh), 2875 (w), 1615 (s), 1586 (s, sh), 1486 (δ CH, s), 1460 (δ CH, m), 1418 (m, sh), 1381 (δ CH, s), 1326 (m), 1278 (w), 1153 (m), 1104 (m, sh), 1088 (s, sh), 1075 (s), 1020 (ν CO, s), 972 (s), 939 (w, sh), 913 (ν Mo=O, vs), 890 (ν Mo=O, vs), 847 (ν Mo=O, vs), 825 (sh), 792 (sh), 739 (w), 671 (m), 662 (m), 615 (w), 561 (w), 525 (m), 449 (w), 421 (w), 336 (w), 330 (w), 292 (w) cm^{-1}. ^1H NMR ([D$_6$]DMSO, 80 °C): δ = 0.95 (t, ^3J = 7.0 Hz, 24 H, 4-H_{TBA}), 1.36 (m, 16 H, 3-H_{TBA}), 1.63 (m, 16 H, 2-H_{TBA}), 1.78 (s, 6 H, CH_3CO_2), 3.22 (m, 16 H, 1-H_{TBA}), 3.4−3.6 (br.), 3.9−4.05 (br.), 4.1−4.25 (br.), (ca. 4 H each) ppm. ^{13}C NMR ([D$_6$]DMSO, 80 °C): δ = 13.5 (C_{TBA}-4), 19.2 (C_{TBA}-3), 23.1 (C_{TBA}-2), 23.8 (CH_3COO), 56.7, 57.5 (C_{TBA}-1), 64.1, 70.8, 78.9, 176.1 (CH_3COO) ppm.

$[N(C_4H_9)_4]_3[MnMo_6O_{18}\{(OCH_2)_3CN{=}C(2\text{-}C_5H_4N)\}_2]$ (4): 2-Pyridinecarbaldehyde (330 μL, 3.5 mmol) and glacial acetic acid (10 μL, 0.17 mmol) were added to a boiling solution of **1** (3.00 g, 1.6 mmol) in 100 mL of methanol. After 10 min, an orange solid began to precipitate. The mixture was heated under reflux for further 3.5 h. After cooling to room temperature, a methanolic solution of $[N(C_4H_9)_4](OH)$ (c = 5.09·10^{-3} M, 34 mL, 0.17 mmol) was added and the orange precipitate was isolated by filtration, washed with methanol and dried under vacuum. Yield: 2.54 g (77%). Crystals suitable for X-ray diffraction were grown by slow ether diffusion into an acetonitrile solution. $C_{68}H_{130}MnMo_6N_7O_{24}$ (2060.40): calcd. C 39.64, H 6.36, N 4.76; found C 39.58, H 6.47, N 4.89. ^1H NMR ([D$_6$]DMSO, 80 °C): δ = 0.93 (t, ^3J = 7.6 Hz, 36 H, 4-H_{TBA}), 1.34 (m, 24 H, 3-H_{TBA}), 1.61 (m, 24 H, 2-H_{TBA}), 3.18 (m, 24 H, 1-H_{TBA}), 7.28 (2 H, 5-H_{pyr}), 7.84 (2 H, 4-H_{pyr}), 7.94 (2 H, 3-H_{pyr}), 8.24 (2 H, CH=N_{pyr}), 8.72 (2 H, 6-H_{pyr}), 52.5 (12 H, CH_2O) ppm. Heating is necessary for solubilization. The signals corresponding to protons on the anion are broadened due to the presence of Mn^{III}. ^{13}C NMR ([D$_6$]DMSO, 80 °C): δ = 12.82 (C_{TBA}-4), 18.79 (C_{TBA}-3), 22.78 (C_{TBA}-2), 57.71 (C_{TBA}-1), 121.6 (C_{pyr}-5), 125.7 (C_{pyr}-3), 135.8 (C_{pyr}-4), 148.0 (C_{pyr}-2), 151.6 (C_{pyr}-6), 198.0 (CH=N_{pyr}) ppm. IR: $\tilde{\nu}_{max}$ = 2961 (ν CH, s), 2936 (ν CH, s), 2875 (ν CH, s), 1643 (C=N, m), 1584 (Ar, w), 1567 (Ar, w), 1482 (δ CH, s), 1469 (δ CH, m), 1381 (δ CH, m), 1345 (w), 1262 (w), 1152 (w), 1095 (w), 1088 (w), 1026 (ν CO, s), 992 (w), 941 (ν Mo=O, s), 921 (ν Mo=O, s), 904 (ν Mo=O, s), 803 (w), 782 (w), 664 (ν Mo−O−Mo, vs), 592 (w), 562 (m), 463 (m), 410 (m), 366 (s), 321 (m), 260 (m) cm^{-1}.

$[N(C_4H_9)_4]_3[MnMo_6O_{18}\{(OCH_2)_3CN{=}C(4\text{-}C_5H_4N)\}_2]$ 5: The compound was obtained as an orange solid by the same procedure as for **4**. Compound **5** is more soluble than **4** in polar organic solvents. Yield: 2.23 g (70%). $C_{68}H_{130}MnMo_6N_7O_{24}$ (2060.40): calcd. C 39.64, H 6.36, N 4.76; found C 39.41, H 6.47, N 4.77. ^1H NMR (67 °C): δ = 0.98 (br., 36 H, 4-H_{TBA}), 1.41 (br., 24 H, 3-H_{TBA}), 1.66 (br., 24 H, 2-H_{TBA}), 3.17 (br., 24 H, 1-H_{TBA}), 7.56 (br., 4 H, 3-H_{pyr}, 6-H_{pyr}), 8.41 (br., 2 H, CH=N_{pyr}), 8.68 (br., 4 H, 4-H_{pyr}, 5-H_{pyr}), 53.9 (br., 12 H, CH_2O) ppm. ^{13}C NMR ([D$_6$]DMSO): δ = 13.60 (C_{TBA}-4), 19.33 (C_{TBA}-3), 23.07 (C_{TBA}-2), 57.50 (C_{TBA}-1), 123.6 (C_{pyr}-3, C_{pyr}-6), 136.1 (C_{pyr}-2), 149.4 (C_{pyr}-4, C_{pyr}-5), 197.6 (CH=N_{pyr}), 217.3 (CH_2O) ppm. IR: $\tilde{\nu}_{max}$ = 2961 (ν CH, s), 2935 (ν CH, s), 2874 (ν CH, s), 1641 (C=N, m), 1597 (Ar, m), 1559 (Ar, m), 1480 (δ CH, s), 1467 (δ CH, m), 1408 (m), 1381 (δ CH, m), 1348 (w), 1322 (w),1232 (w), 1170 (w), 1153 (w), 1094 (w), 1084 (w), 1026 (ν CO, s), 940 (ν Mo=O, s), 921 (ν Mo=O, s), 903 (ν Mo=O, s), 818 (w), 803 (w), 736 (w), 664 (ν Mo−O−Mo, vs), 563 (m), 521 (w), 465 (m), 410 (m), 367 (s), 322 (m) cm^{-1}.

Acknowledgments

We would like to acknowledge the support from the Pierre and Marie Curie University and the CNRS.

[1] P. Gouzerh, A. Proust, *Chem. Rev.* **1998**, *98*, 77−112.
[2] C. Sanchez, G. J. de Soler-Illia, F. Ribot, T. Lalot, C. R. Mayer, V. Cabuil, *Chem. Mater.* **2001**, *13*, 3061−3083.
[3] C. Hu, Y. Wang, Y. Li, E. Wang, *Chem. J. Internet* **2001**, *3*, 22.
[4] C. R. Mayer, R. Thouvenot, T. Lalot, *Chem. Mater.* **2000**, *12*, 257−260.
[5] C. R. Mayer, R. Thouvenot, T. Lalot, *Macromolecules* **2000**, *33*, 4433−4437.
[6] A. R. Moore, H. Kwen, A. M. Beatty, E. A. Maatta, *Chem. Commun.* **2000**, 1793−1794.
[7] C. G. Hamaker, A. M. Beatty, E. A. Maatta, in *Abstr. Pap. Am. Chem. Soc.* **2001**, vol. 221, pp. INOR-341.
[8] H. Zeng, G. R. Newkome, C. L. Hill, *Angew. Chem. Int. Ed.* **2000**, *39*, 1772−1774.
[9] R. C. Schroden, C. F. Blanford, B. J. Melde, B. J. S. Johnson, A. Stein, *Chem. Mater.* **2001**, *13*, 1074−1081.
[10] J.-P. Sauvage, *Transition Metals in Supramolecular Chemistry*, John Wiley & Sons, New York, **1999**.
[11] G. F. Swiegers, T. J. Malefetse, *Chem. Rev.* **2000**, *100*, 3483−3537.
[12] B. J. Holliday, C. A. Mirkin, *Angew. Chem. Int. Ed.* **2001**, *40*, 2022−2043.
[13] B. Hasenknopf, J.-M. Lehn, N. Boumediene, E. Leize, A. Van Dorsselaer, *Angew. Chem. Int. Ed.* **1998**, *37*, 3265−3268.
[14] M. T. Pope, *Heteropoly and Isopoly Oxometalates*, Springer Verlag, Berlin, **1983**.
[15] R. Villanneau, A. Proust, F. Robert, P. Gouzerh, *J. Chem. Soc., Dalton Trans.* **1999**, 421−426.
[16] M. Sadakane, M. H. Dickman, M. T. Pope, *Angew. Chem. Int. Ed.* **2000**, *39*, 2914−2916.
[17] Q.-H. Luo, R. C. Howell, M. Dankova, J. Bartis, C. W. Williams, W. D. Horrocks, Jr., V. G. Young, A. L. Rheingold, L. C. Francesconi, M. R. Antonio, *Inorg. Chem.* **2001**, *40*, 1894−1901.
[18] L. Ruhlmann, J. Canny, R. Contant, R. Thouvenot, *Inorg. Chem.* **2002**, *41*, 3811−3819.
[19] T. M. Anderson, X. Zhang, K. I. Hardcastle, C. L. Hill, *Inorg. Chem.* **2002**, *41*, 2477−2488.
[20] L. Xu, H. Zhang, E. Wang, D. G. Kurth, Z. Li, *J. Mater. Chem.* **2002**, *12*, 654−657.
[21] R. Neumann, *Prog. Inorg. Chem.* **1998**, *47*, 317−370.
[22] B. Yan, Y. Xu, X. Bu, N. K. Goh, L. S. Chia, G. D. Stucky, *J. Chem. Soc., Dalton Trans.* **2001**, 2009−20014.

 © 2003 Wiley-VCH Verlag GmbH & Co. KGaA, Weinheim

[23] J. R. Galan-Mascaros, C. Giménez-Saiz, S. Triki, C. J. Gomez-Garcia, E. Coronado, L. Ouahab, *Angew. Chem. Int. Ed. Engl.* **1995**, *34*, 1460−1462.
[24] A. Müller, E. Krickemeyer, S. K. Das, P. Kögerler, S. Sakar, H. Bögge, M. Schmidtmann, S. Sakar, *Angew. Chem. Int. Ed.* **2000**, *39*, 1612−1614.
[25] J. L. Stark, V. G. Young, Jr., E. A. Maatta, *Angew. Chem. Int. Ed. Engl.* **1995**, *34*, 2547−2548.
[26] B. J. S. Johnson, R. C. Schroden, C. Zhu, V. G. Young, Jr., A. Stein, *Inorg. Chem.* **2002**, *41*, 2213−2218.
[27] M. Piepenbrink, M. U. Triller, N. H. J. Gorman, B. Krebs, *Angew. Chem. Int. Ed.* **2002**, *41*, 2523−2525.
[28] B. Hasenknopf, R. Delmont, P. Herson, P. Gouzerh, *Eur. J. Inorg. Chem.* **2002**, 1081−1087.
[29] M. I. Khan, Q. Chen, J. Zubieta, D. P. Goshorn, *Inorg. Chem.* **1992**, *31*, 1556−1558.
[30] Q. Chen, D. P. Goshorn, C. P. Scholes, X. L. Tan, J. Zubieta, *J. Am. Chem. Soc.* **1992**, *114*, 4667−4681.
[31] A. Mueller, J. Meyer, H. Boegge, A. Stammler, A. Botar, *Z. Anorg. Allg. Chem.* **1995**, *621*, 1818−1831.
[32] Y. Hou, C. L. Hill, *J. Am. Chem. Soc.* **1993**, *115*, 11823−11830.
[33] M. I. Khan, Q. Chen, D. P. Goshorn, H. Hope, S. Parkin, J. Zubieta, *J. Am. Chem. Soc.* **1992**, *114*, 3341−3346.
[34] R. Delmont, A. Proust, F. Robert, P. Herson, P. Gouzerh, *C. R. Acad. Sci. Paris, Sér. IIc* **2000**, *3*, 147−155.
[35] M. T. Pope, in *Comprehensive Coordination Chemistry*, vol. 3, 1st ed. (Eds.: S. G. Wilkinson, R. D. Gillard, J. A. McCleverty), Pergamon Press, Oxford, **1987**, pp. 1023−1056.
[36] P. A. Lorenzo-Luis, P. Gili, *Recent Res. Dev. Inorg. Chem.* **2000**, *2*, 185−196.
[37] K. Nomiya, T. Takahashi, T. Shirai, M. Miwa, *Polyhedron* **1987**, *6*, 213−218.
[38] L. Bi, E. Wang, L. Xu, R. Huang, *Inorg. Chim. Acta* **2000**, *305*, 163−171.
[39] Q. Chen, J. Zubieta, *Inorg. Chim. Acta* **1992**, *198−200*, 95−110.
[40] I. L. Botto, A. C. Garcia, H. J. Thomas, *J. Phys. Chem. Solids* **1992**, *53*, 1075−1080.
[41] Pearson, *J. Am. Chem. Soc.* **1963**, *85*, 3533−3539.
[42] J. F. W. Keana, M. D. Ogan, Y. Lu, M. Beer, J. Varkey, *J. Am. Chem. Soc.* **1986**, *108*, 7957−7963.
[43] N. Hur, W. G. Klemperer, R.-C. Wang, in *Inorg. Synth.*, vol. 27 (Ed.: A. P. Ginsberg), John Wiley & Sons, New York, **1990**, p. 78.
[44] N. H. Hur, W. G. Klemperer, R.-C. Wang, in *Inorg. Synth.*, vol. 27 (Ed.: A. P. Ginsberg), John Wiley & Sons, New York, **1990**, pp. 79−80.
[45] N. Walker, D. Stuart, *Acta Crystallogr., Sect. A* **1983**, *39*, 158−166.
[46] D. J. Watkin, J. R. Carruthers, P. W. Betteridge, *CRYSTALS, An Advanced Crystallographic Computer Program*, Chemical Crystallography Laboratory, Oxford, **1989**.
[47] *International Tables for X-ray Crystallography*, Kynoch Press, Birmingham, **1974**, vol. IV.
[48] G. M. Sheldrick, *SHELXS86, Program for Crystal Structure Solution*, University of Göttingen Göttingen, **1986**.

Received December 11, 2002

 © 2003 Wiley-VCH Verlag GmbH & Co. KGaA, Weinheim

Stereoisomer Discrimination Through π-Stacking Interactions in Spirocyclic Phosphazenes Bearing 2,2′-Dioxybiphenyl Units

Gabino A. Carriedo ,[a] Francisco J. Garcia-Alonso,[a] Jose L. García-Alvarez,[a] Giuseppe C. Pappalardo,*[b] Francesco Punzo,[b] and Patrizia Rossi[c]

Keywords: Phosphazenes / Pi interactions / Solid-state structure / Spiro compounds / Stereoisomer discrimination

The molecular structure of the 2,2′-dioxybiphenyl spirocyclic tetrachlorocyclotriphosphazene $[N_3P_3Cl_4(O_2C_{12}H_8)]$ (**3**) was determined by X-ray crystallography. The structure and conformation of **3** in the crystal are compared and discussed with respect to those of its analogues trispiro and dispiro derivatives, $[N_3P_3(O_2C_{12}H_8)_3]$ (**1**) and $[N_3P_3Cl_2(O_2C_{12}H_8)_2]$ (**2**), respectively. Both the (*R*) and (*S*) stereoisomers are present in the lattice of **3** as arranged in pairs (*R*)···(*S*) held together through sandwich-type π-stacking interactions of the (C7–C12)/(C7–C12)′ phenyl rings of the 2,2′-dioxybiphenyl groups. The polymer-like assembly of **2** was formed by interactions between the (*R*) and (*S*) portions of two *meso* molecules [in the sequence ···(*R*)···(*S*)···(*R*)···(*S*)···(*R*)···(*S*)···]. In this case, the pertinent phenyl rings involved in the noncovalent π-interactions assume a parallel-displaced configuration. To the best of our knowledge, no chiral discrimination in cyclic phosphazenes has been hitherto described, and the present findings provide the first evidence for the discrimination of stereoisomers in spirophosphazenes and the noncovalent forces that govern the chiral recognition in these systems. The energy of the π-stacking interaction increases with increasing number of 2,2′-dioxybiphenyl groups; i.e., on passing from **3** to **2**. In the case of molecule **1**, the discrimination of enantiomers does not take place at all because the π-stacking interaction becomes impossible because of steric hindrance.
(© Wiley-VCH Verlag GmbH & Co. KGaA, 69451 Weinheim, Germany, 2003)

Introduction

Many outstanding properties in materials science are expected to arise from phosphazenic macromolecules and nanosized assemblies of hexa(aryloxy)cyclotriphosphazenes acting as chiral responders and host molecules.[1−3] The spirocyclotriphosphazenes, bearing one to three dioxyaryl or other nucleophilic groups that cyclize to form rings with the phosphorus atoms,[4,5] are optimal candidates for such applications. They represent a unique class of highly tailorable host molecules,[6,7] and they have received much attention for the synthesis of new, high-molecular-weight spiropolyphosphazenes containing functionalized and optically active groups.[8,9] The basic research interest in the structural characterization of spirocyclotriphosphazenes stems from their ability to form inclusion adducts with polymers,[6] their ability, in some cases, to induce polymerization of a guest,[7] and, especially, their potential for stereoisomer discriminaton. The discrimination of enantiomers, frequently called chiral recognition,[10] is a very important concept[11] with applications in, inter alia, Langmuir−Blodgett film technology,[12] chromatographic separation of enantiomers,[13] asymmetric catalysis, and new materials.[14]

The spirocyclophosphazenes **1**, **2** and **3**, referred to as trispiro, dispiro and monospiro derivatives, respectively, have pairs of conformations that are rapidly interconverting in solution. Scheme 1 gives a schematic drawing of **1**−**3** showing the labeling of the atoms.

The molecular assembly of nanometer-sized particles in the bulk has been reported recently[15] by us for the 2,2′-dioxybinaphthyl trispirocyclic cyclotriphosphazene (+)-$[N_3P_3(O_2C_{20}H_{12})_3]$ using a combined experimental (energy-dispersive X-ray diffraction) and theoretical (molecular dynamics) approach. Previously, we reported the stereochemistry of the spirocyclophosphazenes **1**−**3** in solution.[16] Although the discrimination of enantiomers in general cannot be performed in the gas phase or in dilute solutions, it can be revealed in the solid state. A complete investigation, however, of the enantiomeric composition, and the interactions between enantiomers, in the crystal structures of **1**−**3** has not yet been undertaken.

As is the discrimination of any other pair of enantiomers, the types of nonbonding intermolecular forces that can be exploited are based on van der Waals, electrostatic, hydro-

[a] Departamento de Química Orgánica e Inorganica, Facultad de Química, Universidad de Oviedo,
Oviedo 33071, Spain
[b] Dipartimento di Scienze Chimiche, Cattedra di Chimica Generale, Facoltà di Farmacia, Università di Catania,
Viale A. Doria 6, 95125 Catania, Italy
E-mail: gcpappalardo@dipchi.unict.it
[c] Dipartimento di Energetica "S. Stecco", Università di Firenze, Via di S. Marta, 3−1, 50139 Firenze, Italy

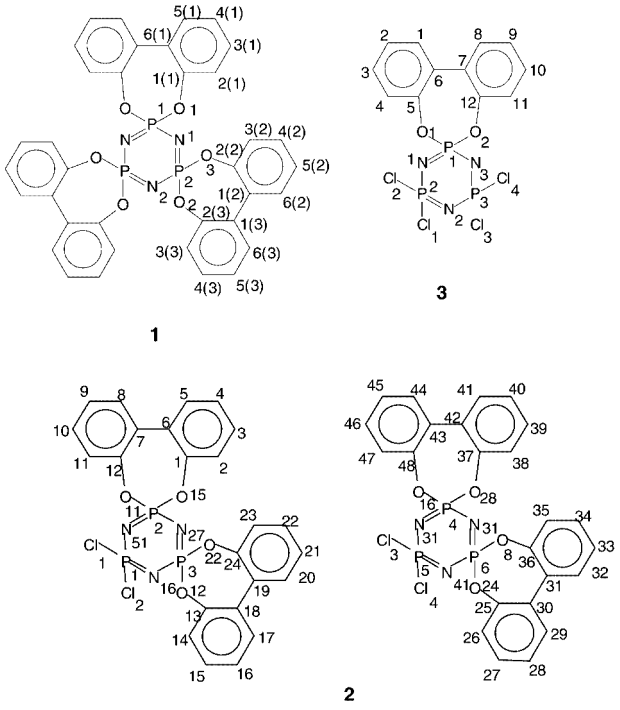

Scheme 1. Schematic drawings of **1**−**3** with atomic numbering schemes; labels of **1** are those given explicitly by Allcock in ref.[19]; labels of **2** were obtained from ref.[22], with separate labels referring to the two independent molecules

gen-bonding, and π-stacking interactions. The latter interactions are very important in systems containing aromatic rings.[17,18]

In this work, the unanswered questions concerning the occurrence, the origins, the configurations and the strengths of the interactions between the enantiomers of spirophosphazenes **1**−**3** is addressed using X-ray diffraction analyses.

Previously reported X-ray structural analyses of spirocyclophosphazenes bearing 2,2′-dioxybiphenyl groups have concerned the trispiro compound[19] $[N_3P_3(O_2C_{12}H_8)_3]$ (**1**), the transannular and spiro-substituted derivatives 1,3- and 1,1-$[N_3P_3(OCH_2CF_3)_4(O_2C_{12}H_8)]$,[20] and the tetra- and difluoro-substituted analogues[21] of **1** and **2**, $[N_3P_3F_4(O_2C_{12}H_8)]$ and $[N_3P_3F_2(O_2C_{12}H_8)_2]$. Accordingly, we have compared the solid-state structure of **3** with that of **2** (as reported[22] by Dez et al.) and that of the 2,2′-dioxybiphenyl trispirocyclic cyclotriphosphazene **1** as reported[19] by Allcock et al. The goals of this paper are thus twofold: First to provide experimental information about the structure of **3** in the crystal and to compare it with those of **1** and **2**, and, secondly, to detect in **1**−**3** the factors that discriminate between stereoisomers, the operating noncovalent interactions and their relative strengths, and the resulting configurations.

Results and Discussion

X-ray Structure

An ORTEP view of compound **3** is shown in Figure 1. Bond lengths and angles of **3** are reported in Table 1. To make comparisons between structures, we consider the following aspects of the compounds in the solid state: (i) the conformation of the P_3N_3 plane, (ii) the conformation of the 2,2′-dioxybiphenyl moieties, and (iii) the intermolecular interactions. The three phosphorus and three nitrogen atoms deviate significantly from the P_3N_3 mean plane [the maximum deviation is 0.135(4) Å (N2)]. An analysis of the summary of agreement between chemically equivalent bonds and angles for **3** (Table 2) shows that: (i) the P−N distances have a noteworthy value of χ^2 because the bonds P2−N1 and P3−N3 are significantly shorter than the other four P−N bonds; (ii) the P−N−P and N−P−N angles also attain a high value of χ^2, since the angles P2−N2−P3 and N1−P1−N3 are smaller that the remaining P−N−P and N−P−N angles, respectively, which thus indicates a loss of planarity inside the P_3N_3 ring; (iii) the C−C−C angles are quite different, as is seen from the value of χ^2 for the C−C−C angle. The high value found for the angle N−P−O is due to the manner in which the biphenyl moieties are disposed with respect to the P_3N_3 ring.

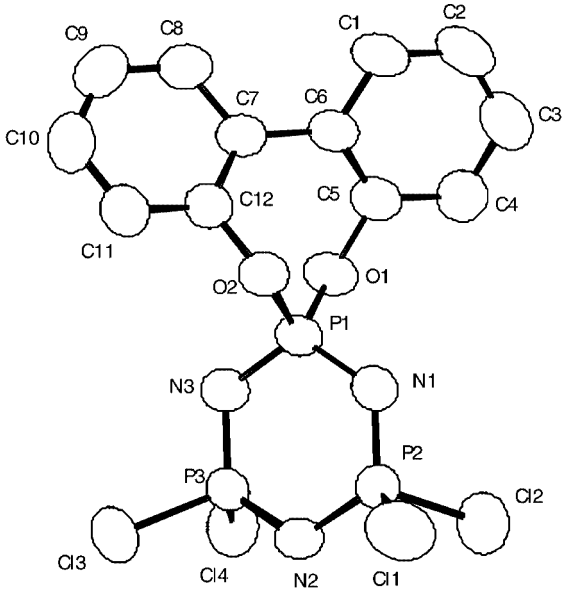

Figure 1. ORTEP view of **3**

For compound **2**, the reported[22] maximal deviations from the mean P_3N_3 planes are 0.007 and 0.054 Å for the two independent molecules **2(a)** and **2(b)**, respectively. In the case of compound **1**, the value of χ^2 found[19] for the P_3N_3 plane was 602.0, and a distortion of the P_3N_3 plane was also proposed. The analysis of the agreement between chemically equivalent bonds and angles for compound **2** attained a value of χ^2 for the C−C−C angle that is close to that found for **1** and **3**. Therefore, all the three compounds feature a significant distortion of the aromatic rings of the dioxybiphenyl moieties.

In compound **3** the dioxybiphenyl moiety is twisted by 48.19(4)° with respect to the P_3N_3 mean plane. This angle

 © 2003 Wiley-VCH Verlag GmbH & Co. KGaA, Weinheim

Table 1. Bond lengths [Å] and angles [°] for **3**

Bond lengths		Bond angles	
P(1)−O(2)	1.576(3)	O(2)−P(1)−O(1)	104.1(2)
P(1)−O(1)	1.568(3)	O(2)−P(1)−N(3)	112.1(2)
P(1)−N(3)	1.579(4)	O(1)−P(1)−N(3)	105.2(2)
P(1)−N(1)	1.604(4)	O(2)−P(1)−N(1)	105.2(2)
P(2)−N(1)	1.544(4)	O(1)−P(1)−N(1)	113.3(2)
P(2)−N(2)	1.584(4)	N(3)−P(1)−N(1)	116.5(2)
P(3)−N(3)	1.555(4)	N(1)−P(2)−N(2)	119.9(2)
P(3)−N(2)	1.579(4)	N(1)−P(2)−Cl(1)	108.8(2)
P(2)−Cl(1)	1.977(2)	N(2)−P(2)−Cl(1)	107.5(2)
P(2)−Cl(2)	1.995(2)	N(1)−P(2)−Cl(2)	109.3(2)
P(3)−Cl(3)	1.981(2)	N(2)−P(2)−Cl(2)	108.1(2)
P(3)−Cl(4)	2.004(2)	Cl(1)−P(2)−Cl(2)	101.9(1)
O(1)−C(5)	1.411(5)	N(3)−P(3)−N(2)	118.5(2)
O(2)−C(12)	1.419(5)	N(3)−P(3)−Cl(3)	109.0(2)
C(1)−C(2)	1.383(8)	N(2)−P(3)−Cl(3)	108.3(2)
C(1)−C(6)	1.401(6)	N(3)−P(3)−Cl(4)	110.1(2)
C(2)−C(3)	1.361(9)	N(2)−P(3)−Cl(4)	108.3(2)
C(3)−C(4)	1.374(8)	Cl(3)−P(3)−Cl(4)	101.41(8)
C(4)−C(5)	1.394(7)	C(5)−O(1)−P(1)	121.3(3)
C(5)−C(6)	1.371(6)	C(12)−O(2)−P(1)	120.0(3)
C(6)−C(7)	1.494(7)	P(2)−N(1)−P(1)	121.3(2)
C(7)−C(12)	1.378(6)	P(2)−N(2)−P(3)	119.4(2)
C(7)−C(8)	1.404(7)	P(3)−N(3)−P(1)	122.9(2)
C(8)−C(9)	1.381(8)	C(2)−C(1)−C(6)	120.0(6)
C(9)−C(10)	1.374(9)	C(3)−C(2)−C(1)	121.4(6)
C(10)−C(11)	1.375(8)	C(2)−C(3)−C(4)	120.2(6)
C(11)−C(12)	1.385(7)	C(3)−C(4)−C(5)	118.2(6)
		C(6)−C(5)−O(1)	119.8(4)
		C(6)−C(5)−C(4)	123.1(5)
		O(1)−C(5)−C(4)	117.0(4)
		C(5)−C(6)−C(1)	117.1(5)
		C(5)−C(6)−C(7)	122.3(4)
		C(1)−C(6)−C(7)	120.6(4)
		C(12)−C(7)−C(8)	116.9(4)
		C(12)−C(7)−C(6)	121.5(4)
		C(8)−C(7)−C(6)	121.6(4)
		C(9)−C(8)−C(7)	120.4(5)
		C(10)−C(9)−C(8)	120.8(5)
		C(9)−C(10)−C(11)	120.1(5)
		C(10)−C(11)−C(12)	118.6(5)
		C(11)−C(12)−C(7)	123.1(5)
		C(11)−C(12)−O(2)	116.9(4)
		C(7)−C(12)−O(2)	119.7(4)

is similar to those found for **1** and for the two independent molecules **2(a)** and **2(b)**.

According to the usual convention, a positive angle [(*R*) configuration] and a negative angle [(*S*) configuration] represent a clockwise and an anticlockwise twist, respectively, of the biphenyl axis from the mean ring plane when viewed from the phosphorus atom towards the biphenyl unit. For compound **2**, we found that the C1−C12 and C37−C48 biphenyl units have positive angles with the mean P_3N_3 plane, while the C13−C24 and C25−C36 planes have negative angles. In compound **1**, two of the three dioxybiphenyl moieties have a negative angle with the P_3N_3 plane while the other has a positive one. Allcock has suggested that such conformations of these groups are due to intermolecular repulsion interactions.[19]

Retrieving molecular structures deposited at the Cambridge Structural Database[23] that contain one or two (2,2′-dioxy-1,1′-biphenyl) groups bonded to a phosphorus atom shows that the angle between the aromatic rings of the 2,2′-dioxybiphenyl unit is in the range 35.6−58.5° with a mean value of 45.5°. This finding is in agreement with the value found in molecule **3** [40.8(1)°] as well as with those previously found[19,22] in **1** and **2**.

Table 2. Summary of agreement between chemically equivalent bonds [Å] and angles [°] for **3**

Bond or angle	No. of examples	Range [Å or °]	σ_{rms}	Mean	χ^2 [a]
P−N	6	1.544−1.604	0.004	1.574	144.44
P−O	2	1.568−1.576	0.003	1.572	3.56
P−Cl	4	1.977−2.004	0.002	1.989	117.25
O−C	2	1.411−1.419	0.005	1.415	1.28
C−C[b]	12	1.361−1.404	0.007	1.382	35.82
C−C[b]	1	1.494	0.007	1.494	−
N−P−N	3	116.5−119.9	0.2	118.3	146
P−N−P	3	119.4−122.9	0.2	121.2	153.5
O−P−O	1	104.1	0.2	104.1	−
N−P−O	4	105.2−113.3	0.2	108.9	1424.5
Cl−P−Cl	2	101.41−101.9	0.09	101.7	15.32
N−P−Cl	8	108.1−110.1	0.2	108.7	106.75
C−C−C	12	116.9−123.1	0.5	120.0	190

[a] The value of χ^2 is the common statistical quantity, calculated to test the significance of a deviation from the mean. It is the sum of the squares of the deviations from the mean divided by root-mean square σ^2. [b] Aromatic C−C bonds within phenyl groups. [c] Biphenoxy C−C bonds.

Crystal Packing and Discrimination of Stereoisomers

The unit cell of **3** contains four molecules assembled in two pairs, each pair being made up of the two stereoisomers [(*R*) and (*S*)] held together by π-stacking interactions between their aromatic rings (Figure 2).

The configuration attained by such a bimolecular assembly in the crystal packing of **3** evidences that the (*R*)···(*S*) discrimination from molecule to molecule features effectively eclipsed sandwich-type π-interactions between the aromatic ring (C7−C12) and the (C7−C12)′ ring of a centrosymmetrically related molecule ($' = -x + 1, -y + 1, -z + 1$) (Figures 2 and 4). In this dimer-like assembly of **3**, the distances between the carbon atoms range from 3.605(7) to 3.993(8) Å (Table 3) and the interacting phenyl planes are perfectly superimposed and parallel.

In the case of **2**, the selective crystallization of the *meso* form from a mixture of all the possible stereoisomers in solution[16] can be accounted for by the diminuation of entropy resulting from the more ordered arrangement attained in the solid (Figure 3), and thus to more effective packing forces for the polymer-like chain assembly of the molecules in the crystal. The structure of the lattice of **2** shows that such an intermolecular polymer-like assembly arises from π-stacking interactions between one enantiomeric portion of a *meso* molecule that discriminates the opposite enantiomeric portion of the adjacent *meso* molecule. In particular, two aromatic rings of **2(a)** interact through two aromatic rings of two different **2(b)** molecules: unit

 © 2003 Wiley-VCH Verlag GmbH & Co. KGaA, Weinheim

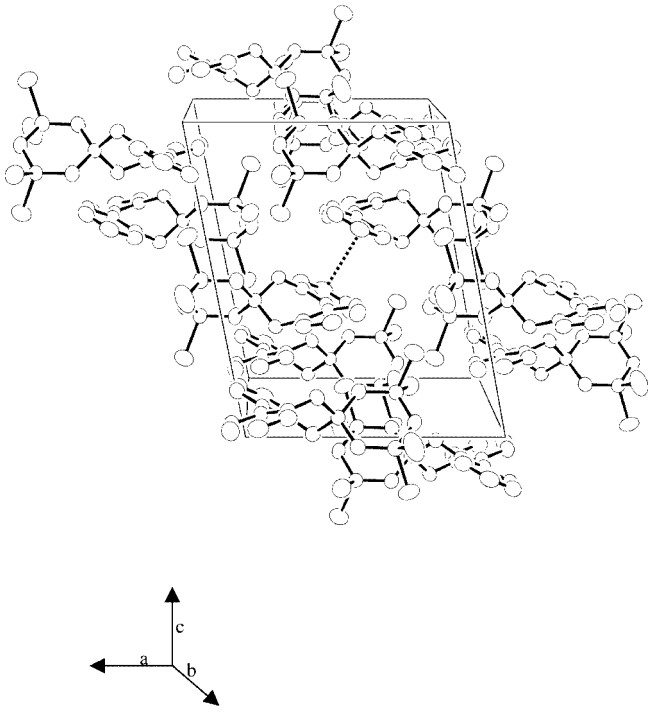

Figure 2. Crystal packing of **3**; the π-stacking interactions between the aromatic rings are denoted by dotted lines

Table 3. Selected intermolecular distances [Å] for molecules of **3** in the crystal

C7···C10′[a]	3.614(7)
C7···C11′	3.947(6)
C8···C10′	3.786(7)
C8···C11′	3.605(7)
C9···C11′	3.645(7)
C9···C12′	3.626(7)
C10···C11′	3.993(8)
C10···C12′	3.718(7)

[a] ′: $-x + 1, -y + 1, -z + 1$.

C7−C12 of **2(a)** interacts with unit C31−C36 of **2(b)**, and unit C13−C18 of **2(a)** interacts with unit C37′−C42′ of **2(b)** of a symmetry-related [$x + 0.5, y + 0.5, z$] molecule (Figure 3). The aromatic rings involved in these π-interactions assume a parallelly displaced configuration in which the (C7−C12)/(C31−C36), and (C13−C18)/(C37−C42)′ ring planes make angles of 4.6(3)° and 8.5(4)°, respectively (Figure 4). The distances of 3.78(2) and 3.85(3) Å between the planes (C7−C12)/(C31−C36) and (C13−C18)/(C37−C42)′, respectively, are similar to the value of 3.723(7) Å found for (C7−C12)/(C7−C12)′ in spirocyclophosphazene **3**.

In compound **3**, where only one 2,2′-dioxybiphenyl group is present, the sandwich-type π-stacking interaction between the rings responsible of the discrimination of enantiomers is stronger with respect to that in **2**. In compound **2**, the presence of two 2,2′-dioxybiphenyl moieties leads to the formation of a polymer-like structure through a parallelly displaced π-stacking interaction of the aromatic units of the dioxybiphenyl groups (Figure 4).

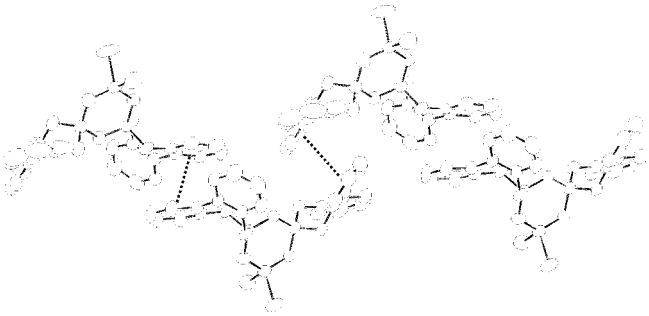

Figure 3. Molecular assembly of **2** (as obtained using the crystal coordinates available from ref.[22]); the chiral recognition (*R*)···(*S*) from molecule to molecule in the *meso* form is denoted by a dotted line

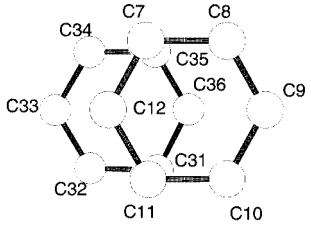

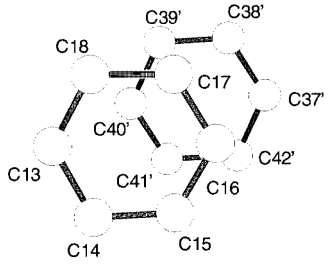

Figure 4. Sandwiched (**3**) and parallelly displaced (**2**) π-stacks of the aromatic units

In the case of compound **1**, in which the P_3N_3 ring bears three 2,2′-dioxybiphenyl groups, the intermolecular enantiomer discrimination does not operate. In fact, the molecules of **1** [(*SSR*) enantiomer] in the lattice[19] are not assembled with respect to each other in configurations that attain some π-stacking interactions, probably because of steric hindrance.

Conclusions

The 2,2′-dioxybiphenyl spirocyclic tetrachlorocyclotriphosphazene **3** was characterized crystallographically by X-ray analysis, and its structure is compared to that of the analogous derivatives **1** and **2**. Both the (*R*) and (*S*) stereoisomers are present in the unit cell of **3**. A twisting angle of ca. 48° between the dioxybiphenyl moiety and the P_3N_3 mean plane, and a significant distortion of the aromatic rings of the dioxybiphenyl moieties, are common features in the crystals of **1**−**3**.

 © 2003 Wiley-VCH Verlag GmbH & Co. KGaA, Weinheim

The molecules of **3** in the crystal are assembled in pairs. Each pair is self-assembled in stacks of (*R*) and (*S*) stereoisomers. This structure results from attractive noncovalent π-stacking interactions (eclipsed sandwich configurations of the interacting aromatic units) between the dioxybiphenyl groups of two centrosymmetrically related molecules. A noncovalent π-stacking interaction (parallelly displaced configuration of the interacting aromatic units) between dioxybiphenyl groups was found to be effective also for molecules of **2** in its crystal. The ordered polymer-like assembly (Figure 3) in the solid state is determined by enantiomeric discrimination between the (*R*) and (*S*) molecular portions of the *meso* molecules of **2** in a sequential fashion [···(*R*)···(*S*)···(*R*)···(*S*)···(*R*)···(*S*)···]. The binding energy between the enantiomers on passing from the eclipsed sandwich configuration of the π-stacks in **3** to the parallelly displaced configuration of the π-stacks in **2** should be the same, and have a value of ca. 3 kcal·mol^{-1} suggested by recent findings for the benzene dimmer.[17] An analogous recognition of the stereoisomers is not present in the case of **1** because the nonbonded π-interactions between the possible stereoisomers (*RRR*/*SRR*/*RSS*/*RSR*/*SSR*/*SSS*) cannot take place because of steric hindrance.

Experimental Section

Sample Preparation: Compound **3** (m.p. 193 °C) was prepared as reported in the literature.[24] Crystals of **3** were obtained by slow diffusion of hexane into a dichloromethane solution and successive recrystallization from dichloromethane.

Crystal Structure Determination: The cell parameters and intensity data for **3** were obtained with a Siemens P4 diffractometer, using graphite-monochromated Cu-K_α radiation (λ = 1.54184 Å). Cell parameters were determined by least-squares fitting of 25 centered reflections. The intensities of three standard reflections were measured every 60 min to check the stability of the diffractometer and the decay of the crystal. Intensity data were corrected for Lorentz and polarization effects, and an absorption correction was applied once the structure was solved by using the Walker and Stuart method.[25] The structure was solved using the SIR-97 program[26] and subsequently refined by the full-matrix least-squares SHELX-97 program.[27] The hydrogen atoms were found in difference syntheses and their positions were refined as well as their isotropic displacement parameters. All the non-hydrogen atoms were refined anisotropically. Atomic scattering factors and anomalous dispersion corrections for all the atoms were taken from literature data.[28] Geometrical calculations were performed by the PARST97 routine.[29] The molecular plot was produced by the ORTEP program.[30] Crystal and structure refinement data are reported in Table 4. CCDC-197311 contains the supplementary crystallographic data for this paper. These data can be obtained free of charge at www.ccdc.cam.ac.uk/conts/retrieving.html [or from the Cambridge Crystallographic Data Centre, 12 Union Road, Cambridge CB2 1EZ, UK; Fax: (internat.) + 44-1223/336-033; E-mail: deposit@ccdc.cam.ac.uk].

Table 4. Crystal data and structure refinement for **3**

Empirical formula	$C_{12}H_8Cl_4N_3O_2P_3$
Formula mass	460.92
Temperature [K]	293
λ [Å]	1.5418
Crystal system	monoclinic
Space group	$P2_1/n$
Unit cell dimensions [Å, °]	a = 11.085(5) b = 12.168(9), β = 100.92(4) c = 13.705(4)
V [Å]	1815(2)
Z	4
$D_{calcd.}$ [g/cm^3]	1.687
μ [mm^{-1}]	8.553
Crystal size [mm]	0.35 × 0.50 × 0.60
2θ range for data collection [°]	9 to 130
Reflections collected	2945
Data/restraints/parameters	2945/0/251
Final R indices [$I > 2\sigma(I)$]	$R1$ = 0.0545, $wR2$ = 0.1372
R indices (all data)	$R1$ = 0.0606, $wR2$ = 0.1495

Acknowledgments

This work was supported by MURST-PRIN 1999−2001 (Italy), and by DGICYT-Project 98-PB97-1276 (Spain). Thanks are due to Prof. Dr. Isabelle Dez (Inorganic Chemistry Laboratory, ETH-Zentrum, Zürich, Switzerland) for providing the atomic coordinates of molecule **2** in the crystal.

[1] R. De Jaeger, M. Gleria, *Prog. Polym. Sci.* **1998**, *23*, 179−276.
[2] C. W. Allen, *Coord. Chem. Rev.* **1994**, *130*, 137−173.
[3] T. Kobayashi, S. Isoda, K. Kubono, "Cyclophosphazenes: Structures and Molecular Selectivities," in *Comprehensive Supramolecular Chemistry* (Eds.: D. D. MacNicol, F. Toda, R. Bishop), Elsevier, Oxford, UK, **1996**, vol. 6, pp. 399−419.
[4] H. R. Allcock, U. Diefenbach, S. R. Pucher, *Inorg. Chem.* **1994**, *33*, 3091−3095.
[5] R. A. Pelc, K. Brandt, Z. Jedlinski, *Phosphorus, Sulfur Silicon Relat. Elem.* **1990**, *47*, 375−382.
[6] H. R. Allcock, A. P. Primrose, N. J. Sunderland, A. L. Rheingold, I. A. Guzei, M. Parvez, *Chem. Mater.* **1999**, *11*, 1243−1252.
[7] H. R. Allcock, E. N. Silverberg, G. K. Dudley, S. R. Pucher, *Macromolecules* **1994**, *27*, 7550−7555.
[8] G. A. Carriedo, F. J. Garcia Alonso, P. A. Gonzalez, J. L. Garcia-Alvarez, *Macromolecules* **1998**, *31*, 3189−3196.
[9] G. A. Carriedo, F. J. Garcia Alonso, P. Gómez Elipe, J. L. García Alvarez, M. P. Tarazona, M. T. Rodriguez, E. Saiz, J. T. Vazquez, J. I. Padrón, *Macromolecules* **2000**, *33*, 3671−3679.
[10] E. L. Eliel, S. H. Wilen, L. Mander, *Stereochemistry of Organic Compounds*, Wiley, New York, N. Y., **1994**, pp. 153−159.
[11] E. M. Arnett, N. G. Harvey, P. L. Rose, *Acc. Chem. Res.* **1989**, *22*, 131−138, and refs. [1−4] therein.
[12] P. Qian, M. Matsuda, T. Miyashita, *J. Am. Chem. Soc.* **1993**, *115*, 5624−5628.
[13] W. H. Pirkle, T. C. Pochapsky, *Chem. Rev.* **1989**, *89*, 347−362.
[14] L. Pu, *Chem. Rev.* **1998**, *98*, 2405−2494.
[15] M. E. Amato, R. Caminiti, G. A. Carriedo, F. J. Garcia-Alonso, J. L. García-Alvarez, G. M. Lombardo, G. C. Pappalardo, *Chem. Eur. J.* **2001**, *7*, 1486−1494.
[16] M. E. Amato, G. A. Carriedo, F. J. Garcia-Alonso, J. L. García-Alvarez, G. M. Lombardo, G. C. Pappalardo, *J. Chem. Soc., Dalton Trans.* **2002**, 3047−3053.

 © 2003 Wiley-VCH Verlag GmbH & Co. KGaA, Weinheim

[17] M. O. Sinnokrot, E. F. Valeev, C. D. Sherrill, *J. Am. Chem. Soc.* **2002**, *124*, 10887−10893, and refs. [1−13] therein.
[18] S. Tsuzuki, K. Honda, T. Uchimaru, M. Mikami, K. Tanabe, *J. Am. Chem. Soc.* **2002**, *124*, 104−112.
[19] H. R. Allcock, M. T. Stein, J. A. Stanko, *J. Am. Chem. Soc.* **1971**, *93*, 3173−3178.
[20] H. R. Allcock, M. L. Turner, K. B. Visscher, *Inorg. Chem.* **1992**, *31*, 4354−4364.
[21] A. Vij, S. J. Geib, R. L. Kirchmeier, J. M. Shreeve, *Inorg. Chem.* **1996**, *35*, 2915−2929.
[22] I. Dez, J. Levalois-Mitjaville, H. Grützmacher, V. Gramlich, R. De Jaeger, *Eur. J. Inorg. Chem.* **1999**, 1673−1684.
[23] F. H. Allen, O. Kennard, D. G. Watson, L. Brammer, A. G. Orten, R. Taylor, *J. Chem. Soc., Perkin Trans. 2* **1987**, 1972−1999.
[24] G. A. Carriedo, L. Fernandez-Catuxo, F. J. Garcia Alonso, P. Gomez-Elipe, P. A. Gonzalez, *Macromolecules* **1996**, *29*, 5320−5325.
[25] N. Walker, D. D. Stuart, *Acta Crystallogr., Sect. A* **1983**, *39*, 158−166.
[26] A. Altomare, M. C. Burla, M. Camalli, G. L. Cascarano, C. Giacovazzo, A. Guagliardi, A. G. Moliterni, G. Polidori, R. Spagna, *J. Appl. Crystallogr.* **1999**, *32*, 115−119.
[27] G. M. Sheldrick, *SHELX-97*, University of Göttingen, Germany, **1997**.
[28] *International Tables for X-ray Crystallography*, Kynoch Press, Birmingham, UK, **1974**, vol. 4**.**
[29] M. Nardelli, *Comput. Chem.* **1983**, *7*, 95−98**.**
[30] L. J. Farrugia, *J. Appl. Crystallogr.* **1997**, *30*, 565−570.

Received January 9, 2003

 © 2003 Wiley-VCH Verlag GmbH & Co. KGaA, Weinheim

Synthesis and Microstructural Characterisation of Two New One-Dimensional Members of the $(A_3NiMnO_6)_\alpha(A_3Mn_3O_9)_\beta$ Homologous Series (A = Ba, Sr)

María Hernando,[a] Khalid Boulahya,[a] Marina Parras,[a] Jose M. González-Calbet,*[a] and Ulises Amador[b]

Keywords: Electron diffraction / High-resolution electron microscopy / One-dimensional oxides / Twinned microstructure

Two new members of the one-dimensional $(A_3NiMnO_6)_\alpha(A_3Mn_3O_9)_\beta$ homologous series, with the compositions $(Sr_{0.75}Ba_{0.25})_5NiMn_3O_{12}$ and $Sr_9Ni_2Mn_5O_{21}$, have been synthesised. Their structures can each be described as a hexagonal array of infinite one-dimensional chains of face-sharing polyhedra, running parallel to the *c* axis and separated by the Sr/Ba cations. The structure of $(Sr_{0.75}Ba_{0.25})_5NiMn_3O_{12}$, which constitutes the ($\alpha = 3$, $\beta = 2$) member of the series, is made up of three face-sharing octahedra linked by one trigonal prism. For $Sr_9Ni_2Mn_5O_{21}$ ($\alpha = 2$, $\beta = 1$) the sequence of polyhedra along the chains corresponds to a motif consisting of two octahedra–one trigonal prism–three octahedra–one trigonal prism. The manganese atoms occupy the octahedral sites in both phases, while the Ni^{2+} cations are distributed in the trigonal-prismatic sites in a disordered way. Only a small fraction of these (close to 20%) is located at the centres of the trigonal prisms, 80% being displaced towards the rectangular faces of the polyhedra and giving rise to a square-planar-like coordination. Both oxides present twinned microstructures, as evidenced by SAED and HREM. (© Wiley-VCH Verlag GmbH & Co. KGaA, 69451 Weinheim, Germany, 2003)

Introduction

Growing interest has recently developed in a family of materials structurally related both to $A_3A'BO_6$ (K_4CdCl_6-type)[1] and to 2H-ABO_3 hexagonal perovskite.[2] In the former oxide, $A'O_6$ trigonal prisms (TP) and BO_6 octahedra (Oh) share triangular faces, in a 1:1 sequence, forming infinite polyhedra chains parallel to the *c* axis of a rhombohedral unit cell. The 2H-ABO_3 hexagonal perovskite is also composed of a hexagonal array of infinite chains, but the chains in this case are made up of face-sharing BO_6 octahedra. A large number of intermediate structures obtained by varying the number of octahedra between the trigonal prisms, maintaining the hexagonal array of the polyhedra one-dimensional chains have been described. In fact, all of these can be regarded as being formed by the ordered intergrowth of the structural units constituting the above structures. This building principle gives rise to the $(A_3A'BO_6)_\alpha(A_3B_3O_9)_\beta$ general formula, in which α and β denote the number of $A_3A'BO_6$ and 2H-ABO_3 structural blocks, respectively, in each term.[3]

A large number of oxides belonging to this family have been reported, due in part to the variety of elements that can be introduced into the oxygen framework. In this sense, the A cation usually corresponds to an alkaline earth metal, whilst the A′ and B sites can be occupied by many different metal atoms. In addition, the A′ and the B positions can be occupied by the same cation. Much of the work published on these materials has been performed on the A−(A′ = B)−O systems, in which A′ = B = Ni,[4,5] Co[6−8] and A = Ba, Sr, Ca. In the different stabilized members, Ni or Co seem to present both II and IV oxidation states.

When A′ = B = Mn, no one-dimensional hexagonal phases are known. In this sense it is worth noting that two-dimensional phases, also structurally related to 2H-$BaMnO_3$, have recently been reported. As an example, the compound $Ba_6Mn_5O_{16}$ [9] crystallizes in a laminar structure closely related to the 15-R polytype.[10] Note that Mn is only in the IV oxidation state. The same cationic relationship presents the one-dimensional $Ba_6Ni_5O_{15}$,[4] the ($\alpha = 3$, $\beta = 3$) member of the series, but Ni is now present both as Ni^{II} and as Ni^{IV}. According to this, one might think that one-dimensional oxides containing Mn as the sole metal in the polyhedra chains should be less stable, due to the low stability of Mn^{II} in a trigonal prism or in an octahedral environment. However, when A′ ≠ B = Mn, several one-dimensional phases in which Mn occupies the octahedral sites have been reported, whilst a metal of a different chemical nature, such as Zn,[11,12] Cu[13] or Ni,[14,16] is located in the TP. In the case of Ni, two phases have previously been reported: $Ca_3(Ni)_{TP}(Mn)_{Oh}O_6$ [14,15] and $Sr_4(Ni)_{TP}(Mn_2)_{Oh}O_9$,[16,17] corresponding to the ($\alpha = 3$, $\beta = 0$) and

[a] Departamento de Química Inorgánica, Facultad de Químicas, Universidad Complutense,
28040 Madrid, Spain
E-mail: jgcalbet@quim.ucm.es
[b] Departamento de Química, Facultad de Ciencias Experimentales y de la Salud, Universidad San Pablo-CEU,
28668 Madrid, Spain

($\alpha = 3$, $\beta = 1$) members of the series, respectively. In the former oxide, the polyhedra chains are made up of one octahedron and one trigonal prism sharing faces; in the latter, dimers of face-sharing octahedra are separated by one trigonal prism. In both cases, Mn ions, in the IV oxidation state, occupy the octahedral sites and Ni^{II} is situated in the TP positions. At this point it should be remarked that in some cases, such as in Ca_3NiMnO_6, the Ni atoms are located at the centres of the prisms, whereas in other cases, in $Sr_4Mn_2NiO_9$ for instance, approximately 80% of the Ni^{2+} ions are displaced towards one of the rectangular faces of the TP. This is fairly normal in Ni- or Cu-containing oxides such as Sr_3CuPtO_6,[18] $Sr_4Ni_3O_9$ [4] or $Sr_4CuIr_2O_9$.[19]

This paper reports the structural study of two new members, ($\alpha = 3$, $\beta = 2$) and ($\alpha = 2$, $\beta = 1$), of the $(A_3NiMnO_6)_\alpha(A_3Mn_3O_9)_\beta$ (A = Ba, Sr) series.

Results and Discussion

Chemical and Structural Characterization

Samples of nominal compositions $(Sr_{0.75}Ba_{0.25})_5NiMn_3O_{12}$ and $Sr_9Ni_2Mn_5O_{21}$ were confirmed to be single phases by X-ray diffraction (Figure 1). The average cationic ratios, determined by ICP, agree with the nominal compositions within experimental accuracy, the following metal

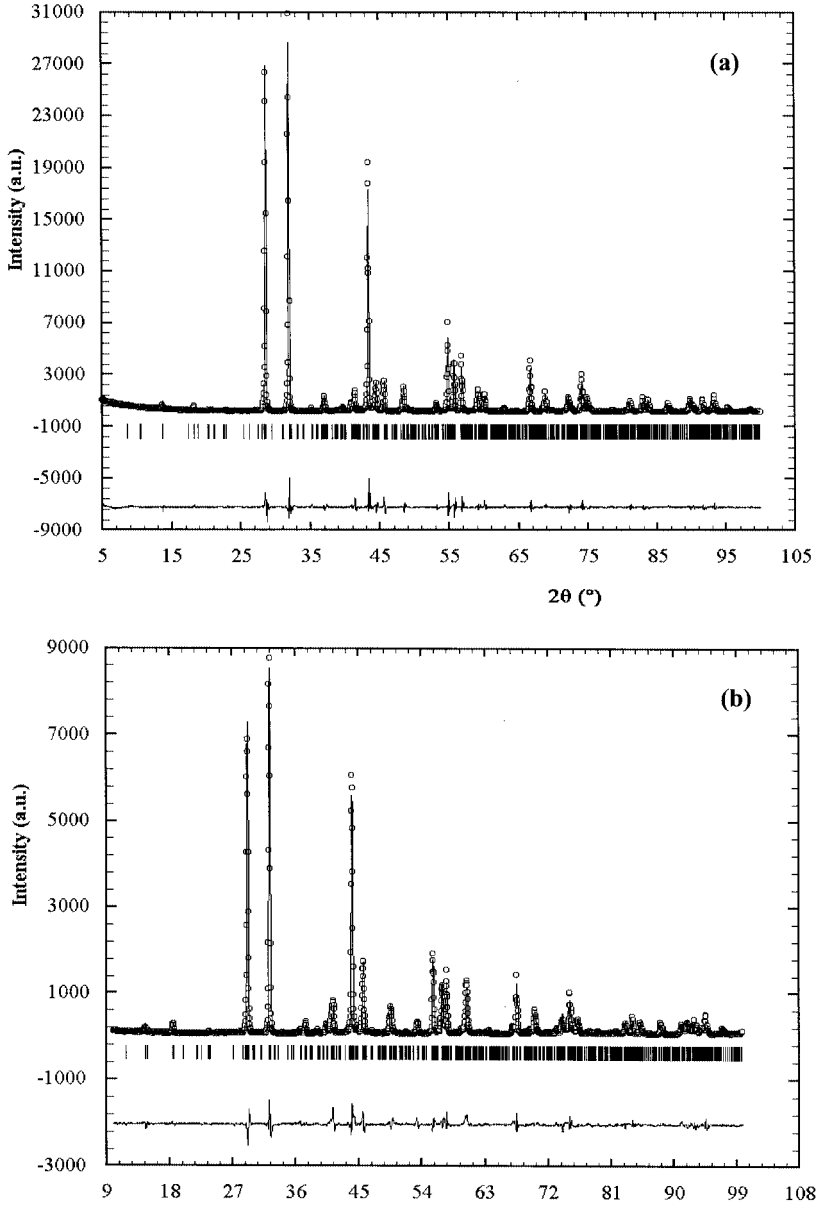

Figure 1. (a) Graphic results for the fitting of the X-ray powder diffraction data of $(Sr_{0.75}Ba_{0.25})_5NiMn_3O_{12}$: experimentally ascertained (points), calculated (solid line) and difference (bottom); (b) graphic results for the fitting of the X-ray powder diffraction data of $Sr_9Ni_2Mn_5O_{21}$: experimentally ascertained (points), calculated (solid line) and difference (bottom)

 © 2003 Wiley-VCH Verlag GmbH & Co. KGaA, Weinheim

contents being obtained: Sr 35.88±0.9% (35.8%), Ba 17.7±0.4% (18.7%), Mn 17.8±0.4% (17.99%) and Ni 7.0±0.2% (6.5%) − in agreement with the nominal $Sr_{3.75}Ba_{1.25}NiMn_3O_{12}$ composition − and Sr 50.8±1.3% (51.99%), Mn 17.4±0.4% (18.1%) and Ni 7.84±0.2% (7.7%) − consistent with the $Sr_9Ni_2Mn_5O_{21}$ nominal composition. EDS analyses, performed on numerous crystallites with use of $SrMnO_3$ and $BaMnO_3$ as standards, confirm the above compositions.

Figure 1 (a) shows the X-ray diffraction pattern of $Sr_{3.75}Ba_{1.25}NiMn_3O_{12}$. The whole pattern can be indexed within a hexagonal unit cell of parameters $a = 0.97114(2)$ nm and $c = 2.03649(6)$ nm as corresponding to the ($\alpha = 3$, $\beta = 2$) member of the $(A_3A'BO_6)_\alpha(A_3B_3O_9)_\beta$ series. On the other hand, the corresponding XRD pattern of $Sr_9Ni_2Mn_5O_{21}$ is depicted in Figure 1 (b), all the peaks being indexed in a rhombohedral unit cell with $a = 0.96065(5)$ nm and $c = 3.5836(2)$ nm, in agreement with the structural characteristics of the ($\alpha = 2$, $\beta = 1$) term of the above one-dimensional family.

SAED and HREM

$(Sr_{0.75}Ba_{0.25})_5NiMn_3O_{12}$ ($\alpha = 3$, $\beta = 2$)

Microstructural characterization by SAED and HREM confirms the XRD results; the most relevant SAED patterns are shown in Figure 2 (a and b). All the maxima can be indexed in the hexagonal unit cell described above. The condition reflections are compatible with the $P\bar{3}c1$ space group previously proposed for isostructural $Sr_5Co_4O_{12}$.[7] In addition, the intensity distribution of the spots on the SAED pattern of Figure 2 (b) seems to indicate the presence of twinning in the crystals. Actually, Figure 2 (c) shows the same [1$\bar{2}$10] reciprocal plane corresponding to the untwinned isostructural oxide $Sr_5Co_4O_{12}$.[6] The intensity distribution of the spots corresponding to the (*h*0*i*2*h*) reflections is modulated. This feature is a general one in all one-dimensional oxides belonging to the $(A_3A'BO_6)_\alpha(A_3B_3O_9)_\beta$ series, the direction of the modulation always being perpendicular to the planes containing the metal atoms in the TP sites. When this SAED pattern is compared to that shown in Figure 2 (b), it can be observed that the modulated distribution of the intensity of the spots is apparent not only along the [*h*0*i*2*h*]* direction but also along the [$\bar{h}$0*i*2*h*]* direction. This is due to twinning of the crystals, as confirmed by HREM. Indeed, in the image taken along the [1$\bar{2}$10] zone axis, shown in Figure 3, two large identical domains, inclined towards one another around the *c* axis, are clearly observed. In both domains, *d* spacings of 0.83 and 1.01 nm − along the *c* and the *a* axes, respectively − are observed, such interplanar distances corresponding to d_{001} and d_{100} of the hexagonal unit cell described above. The contrast variation observed in both domains is characteristic of the $\alpha = 3$, $\beta = 2$ structure. In the magnification of one domain (Figure 3, b), it can be seen that, along the *c* axis, two bright dots alternate with three less intense dots. Such contrast variation can be attributed to the (Oh−Oh−Oh−TP) polyhedra sequence since, in all these one-dimensional oxides, the metal columns in the trigonal sites and the Sr/Ba atoms are imaged as bright dots. The calculated image (inset in Figure 3, b) agrees with the experimentally ascertained one for $\Delta t = 7.5$ and $\Delta f = -90$ nm.

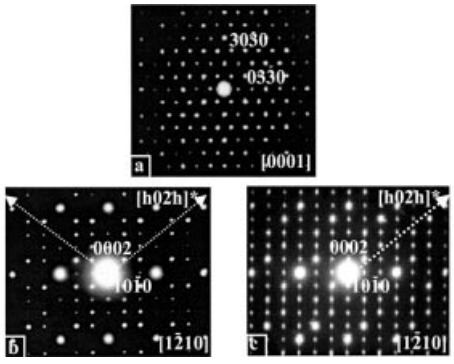

Figure 2. SAED patterns along the [0001] (a) and [1$\bar{2}$10] (b) zone axis corresponding to $(Sr_{0.75}Ba_{0.25})_5NiMn_3O_{12}$; (c) SAED pattern along the [1$\bar{2}$10] zone axis corresponding to $Sr_5Co_4O_{12}$

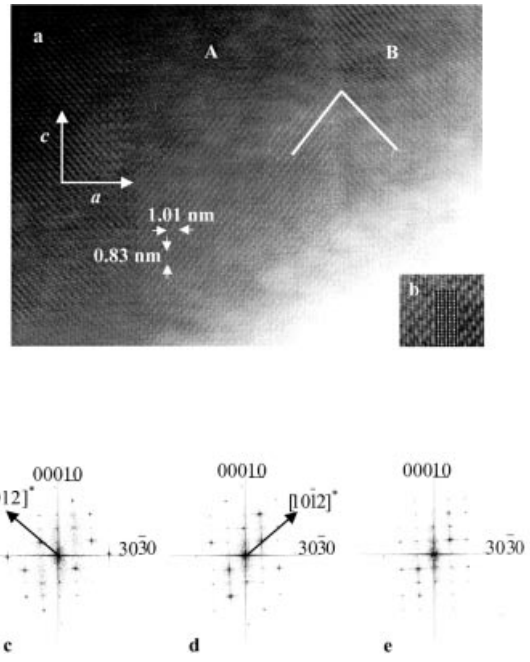

Figure 3. (a) HREM of $(Sr_{0.75}Ba_{0.25})_5NiMn_3O_{12}$ along [1$\bar{2}$10]; a twinned microstructure can clearly be seen; (b) magnification of one of the microdomains; calculated image is shown in the inset; optical Fourier transforms (FT) corresponding to domains marked with A (c) and B (d) in Figure 3a; (e) FT corresponding to the juxtaposition of both A and B domains

Optical Fourier Transforms of both domains, labelled A and B in Figure 3, are depicted in Figure 3 (c and d). Both patterns correspond to [1$\bar{2}$10]-oriented domains related to one another through a 90° rotation around *c**. Consequently, in the first domain, the intensity modulation is observed along the [*h*0*i*2*h*]* reciprocal direction whilst in the second domain the modulation is along the [$\bar{h}$0*i*2*h*]* one.

 © 2003 Wiley-VCH Verlag GmbH & Co. KGaA, Weinheim

Juxtaposition of the two patterns (Figure 3, e) fits with the experimental one of Figure 2 (b).

$Sr_9Ni_2Mn_5O_{21}$ ($\alpha = 2$, $\beta = 1$)

Figure 4 (a) corresponds to the SAED pattern of the title sample along the [1$\bar{2}$10] zone axis. Once again, the features of this SAED suggest the presence of twinning in the crystal. Actually, Figure 4 (b) shows a typical [1$\bar{2}$10] reciprocal plane of an untwinned crystal of $(Sr_{0.6}Ca_{0.4})_9Co_7O_{21}$,[3] an ($\alpha = 2$, $\beta = 1$) term of the $(A_3A'BO_6)_\alpha(A_3B_3O_9)_\beta$ homologous series. Only the *hkl* reflections with $-h + k + l = 3n$ are observed, according to the rhombohedral symmetry of this phase (space group *R*3*c*). Note that the intensity distribution of the (*h*0*i*4*h*)* peaks is modulated in a similar way as in $(Sr_{0.75}Ba_{0.25})_5NiMn_3O_{12}$. Comparison between the SAED patterns shown in Figure 4 (a and b) highlights the presence of reflections forbidden for a rhombohedral symmetry in the pattern corresponding to $Sr_9Ni_2Mn_5O_{21}$. Moreover, the ($\bar{h}$0*i*4*h*) peaks are also present, and so a pseudo-trigonal symmetry results. This can be associated with the presence of twinning in the crystals, as confirmed by HREM. Actually, in the corresponding micrograph along the same zone (Figure 5, a), the presence of several domains tilted by 90° to each other around the *c* axis, is apparent. Each domain shows the structural features corresponding to this member of the series (see the magnification of one domain depicted in Figure 3, b). The simulated image (inset in Figure 3, b) agrees with the experimentally ascertained one for $\Delta t = 8.5$ and $\Delta f = -90$ nm. The optical Fourier transforms at the two sides of the twin plane are depicted in Figure 5 (c and d). In each domain, the modulation appears either along the [*h*0*i*4*h*]* or along the [$\bar{h}$0*i*4*h*] directions. Juxtaposition of the patterns (Figure 5, e) results in the experimental SAED shown in Figure 4 (a).

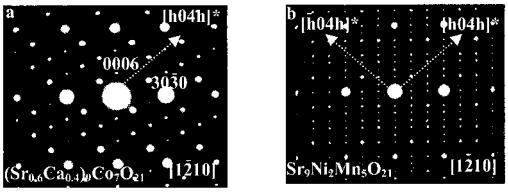

Figure 4. SAED patterns along the [1$\bar{2}$10] zone axis, corresponding to $Sr_9Ni_2Mn_5O_{21}$ (a) and $(Sr_{0.6}Ca_{0.4})_9Co_7O_{21}$ (b)

Structural Refinement

The fitting of experimental XRD patterns of the title compounds has been carried out by using as starting structural models those developed from SAED and HREM data. Thus, $Sr_{3.75}Ba_{1.25}Mn_3NiO_{12}$ consists of parallel chains made up of units of three face-sharing octahedra ($3O_h$) linked by a trigonal prism (TP), the sequence along a chain being: $-TP-3O_h-TP-3O_h-TP-3O_h-$. The structure of $Sr_9Mn_5Ni_2O_{21}$, on the other hand, is slightly more complex: the chains are made up of units of three face-sharing octahedra and units of two octahedra ($2O_h$) linked by trigonal prisms in a sequence: $-TP-3O_h-TP-2O_h-TP-3O_h-TP-2O_h-$.

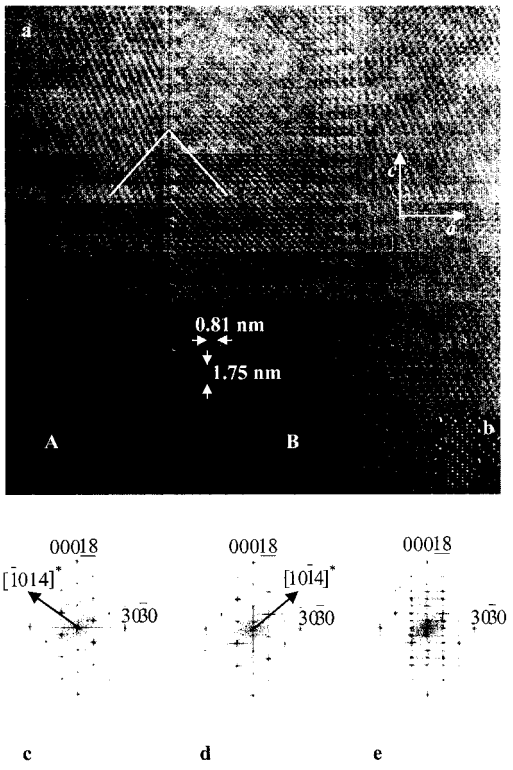

Figure 5. (a) HREM of $Sr_9Ni_2Mn_5O_{21}$ along [1$\bar{2}$10], a multitwinned microstructure can clearly be seen; (b) magnification of one of the microdomains shown in Figure 5 (a), calculated image is shown in the inset, optical Fourier transforms (FTs) corresponding to domains marked with A (c) and B (d) in Figure 5 (a); (e) FT corresponding to the juxtaposition of both A and B domains

On the basis of previous studies on similar systems,[14–17] we assume that the nickel ions are located in the prisms whereas the manganese atoms occupy the octahedra. It should be remarked that it is not possible to ascertain the actual occupation of both types of positions from XRD data. However, it was evident from the structural refinement that the atoms in the prisms are split into two positions. The atoms at the centre of the prisms are partially displaced towards the three square faces of the prisms, whereas the remaining atoms at the centres are displaced to one of the trigonal faces in some cases. This structural feature has very commonly been observed for nickel.[4,16,20]

Figure 1 (a and b) shows the result in graphic form of the fitting of the experimental X-ray diffraction pattern and the difference between observed and calculated data for $Sr_{3.75}Ba_{1.25}NiMn_3O_{12}$ and $Sr_9Ni_2Mn_5O_{21}$, respectively. The final structural parameters are collected in Tables 1 and 2, whereas Tables 3 and 4 show some selected interatomic distances. Figures 6 and 7 depict schematic representations of the structures of $Sr_{3.75}Ba_{1.25}NiMn_3O_{12}$ and $Sr_9Ni_2Mn_5O_{21}$, respectively.

As is well known, X-ray diffraction is not the best technique with which to study structural effects relating to light atoms such as oxygen in a "matrix" of metallic atoms, as is

Table 1. Final structural parameters of $(Sr_{0.75}Ba_{0.25})_5NiMn_3O_{12}$ [space group $P\bar{3}c$ (no. 165), a = 0.97114(2) nm, c = 2.03649(6) nm, V = 1.66334(7) nm^3, R_B = 0.070, R_{exp} = 0.058, R_{wp} = *0.18,* χ^2 = *10.1]*

Atom	*x/a*	*y/b*	*z/c*	*B* [Å^2]	Occupation
Sr(1)/Ba(1)	0.6786(9)	0.0064(8)	0.0500(9)	0.95(4)	0.75:0.25
Sr(2)/Ba(2)	0.3368(8)	0.0142(7)	0.1526(7)	0.95(4)	0.75:0.25
Sr(3)/Ba(3)	0.6547(7)	0	1/4	0.95(4)	0.75:0.25
Mn(1)	0	0	0	1.98(6)	1
Mn(2)	1/3	2/3	0.170(1)	1.98(6)	1
Mn(3)	1/3	2/3	0.297(2)	1.98(6)	1
Mn(4)	0	0	0.124(2)	1.98(6)	1
Mn(5)	1/3	2/3	0.420(1)	1.98(6)	1
Ni1Pc	0	0	1/4	1.44(5)	0.10(3)
Ni1Pd	−0.088(6)	−0.088(6)	1/4	1.44(5)	0.90(3)
Ni2Pc	1/3	2/3	0.059(2)	1.44(5)	0.28(4)
Ni2Pd	0.266(4)	0.600(4)	0.059(2)	1.44(5)	0.72(4)
O(1)	0.174(5)	−0.008(5)	0.054(4)	0.45(7)	1
O(2)	0.167(6)	0.666(5)	0.122(4)	0.45(7)	1
O(3)	0.516(6)	0.184(4)	0.020(3)	0.45(7)	1
O(4)	0.334(4)	0.815(6)	0.248(2)	0.45(7)	1
O(5)	0.147(5)	0.162(5)	0.178(3)	0.45(7)	1
O(6)	0.515(5)	0.346(6)	0.156(2)	0.45(7)	1

Table 2. Final structural parameters of $Sr_9Ni_2Mn_5O_{21}$ [space group $R\bar{3}c$ (no. 167), a = 0.96065(5) nm, c = 3.5836(2) nm, V = 2.8640(3) nm^3, R_B = 0.089, R_{exp} = 0.094, R_{wp} = *0.19,* χ^2 = *5.3]*

Atom	*x/a*	*y/b*	*z/c*	B (Å^2)	Occupation
Sr(1)	0.6507(7)	−0.0002(9)	0.1391(2)	0.93(6)	1
Sr(2)	0.325(1)	0	3/4	0.93(6)	1
Mn(1)	0	0	0	0.3(1)	1
Mn(2)	0	0	0.0688(4)	0.3(1)	1
Mn(3)	0	0	0.2140(5)	0.3(1)	1
Ni1Pc	0	0	0.367(4)	0.1(1)	0.22(6)
Ni1Pd	−0.064(5)	−0.064(5)	0.361(1)	0.1(1)	0.78(6)
O(1)	0.503(5)	0.165(4)	0.366(1)	0.21(7)	1
O(2)	0.828(4)	−0.015(5)	0.317(1)	0.21(7)	1
O(3)	−0.166(5)	0	3/4	0.21(7)	1
O(4)	0.504(3)	0.311(4)	0.4299(9)	0.21(7)	1

the case of our materials. However, the refinements were stable and it was possible to refine the positions of the oxygen atoms, provided that the number of refined parameters was kept not too large, which is why we used the same temperature factor for various atoms in some cases. The metal−oxygen distances in Tables 3 and 4 should therefore be regarded with some caution, although the metallic coordination (i.e., the polyhedra defined by the closest oxygen atoms around a given metal atom) is undoubtedly correct, as are the metal−metal distances.

The crystal structure of $(Sr_{0.75}Ba_{0.25})_5NiMn_3O_{12}$ is made up of one-dimensional $[Mn_{3/4}Ni_{1/4}O_3]$ chains. The space between chains is occupied by the Ba/Sr metal atoms, coordinated to oxygen atoms at distances ranging between 2.3 and 2.99 Å. There are two crystallographically different types of chains (see Figure 6), one involving −Mn(2)−Mn(3)−Mn(5)−Ni(2)− cations and the other one composed of an −Mn(4)−Mn(1)−Ni(1)− cationic sequence. The octahedral environments of Mn(1), (2) and (5) are quite regular, with average M−O distances corresponding to 2.05, 2.01 and 2.04 Å, respectively. The octahedra

Table 3. Selected interatomic distances less than 3.0 Å in $(Sr_{0.75}Ba_{0.25})_5NiMn_3O_{12}$; i and ii: generated by symmetry operations

Sr(1)/Ba(1)−O(1)	2.78(8)	Mn(1)−O(1)	2.05(2) × 6
Sr(1)/Ba(1)−O(1)^{i}	2.70(6)		
Sr(1)/Ba(1)−O(1)^{ii}	2.55(4)	Mn(2)−O(2)	1.88(2) × 3
Sr(1)/Ba(1)−O(2)	2.25(4)	Mn(2)−O(4)	2.14(2) × 3
Sr(1)/Ba(1)−O(3)	2.93(6)		
Sr(1)/Ba(1)−O(3)^{i}	2.82(6)	Mn(3)−O(4)	1.75(2) × 3
Sr(1)/Ba(1)−O(3)^{ii}	2.35(4)	Mn(3)−O(6)	1.80(2) × 3
Sr(1)/Ba(1)−O(6)	2.76(5)		
		Mn(4)−O(1)	2.25(2) × 3
Sr(2)/Ba(2)−O(1)	2.50(4)	Mn(4)−O(5)	1.87(2) × 3
Sr(2)/Ba(2)−O(2)	2.99(8)		
Sr(2)/Ba(2)−O(2)^{i}	2.96(7)	Mn(5)−O(3)	1.90(1) × 3
Sr(2)/Ba(2)−O(4)	2.73(6)	Mn(5)−O(6)	2.18(2) × 3
Sr(2)/Ba(2)−O(4)^{i}	2.66(5)		
Sr(2)/Ba(2)−O(5)	2.90(6)	Ni1Pc−O(5)	2.09(1) × 6
Sr(2)/Ba(2)−O(5)^{i}	2.75(7)		
Sr(2)/Ba(2)−O(6)	2.79(8)	Ni1Pd−O(5)	1.91(1) × 2
Sr(2)/Ba(2)−O(6)^{i}	2.67(5)	Ni1Pd−O(5)^{i}	2.00(1) × 2
		Ni1Pd−O(5)^{i,i}	2.77(2) × 2
Sr(3)/Ba(3)−O(4)	2.70(4) × 2		
Sr(3)/Ba(3)−O(4)^{i}	2.81(6) × 2	Ni2Pc−O(2)	2.06(2) × 3
Sr(3)/Ba(3)−O(5)	2.36(4) × 2	Ni2Pc−O(3)	2.17(3) × 3
Sr(3)/Ba(3)−O(6)	2.53(4) × 2		
		Ni2Pd−O(2)	1.90(4) × 2
		Ni2Pd−O(3)	2.05(1) × 2
		Ni2Pd−O(2)^{i}	2.60(3)
		Ni2Pd−O(3)^{i}	2.65(4)
Mn(1)−Mn(4)	2.53(4) × 2	Mn(3)−Mn(5)	2.50(4)
Mn(2)−Mn(3)	2.60(4)	Mn(4)−Ni1Pc	2.56(3)
Mn(2)−Ni2Pc	2.25(4)	Mn(4)−Ni2Pd	2.70(4)
Mn(2)−Ni2Pd	2.34(4)	Mn(5)−Ni2Pc	2.83(4)
		Mn(5)−Ni2Pd	2.91(4)

Table 4. Selected interatomic distances less than 3.0 Å in $Sr_9Ni_2Mn_5O_{21}$; i and ii: generated by symmetry operations

Sr(1)−O(1)	2.61(4)	Mn(1)−O(1)	1.97(4) × 6
Sr(1)−O(1)^{i}	2.82(4)		
Sr(1)−O(1)^{ii}	2.65(3)	Mn(2)−O(1)	2.05(3) × 3
Sr(1)−O(2)	2.38(4)	Mn(2)−O(4)	1.77(3) × 3
Sr(1)−O(2)^{i}	2.69(4)		
Sr(1)−O(2)^{ii}	2.80(5)	Mn(3)−O(2)	1.93(4) × 3
Sr(1)−O(3)	2.52(1)	Mn(3)−O(3)	2.05(3) × 3
Sr(1)−O(4)	3.00(3)		
Sr(1)−O(4)^{i}	2.44(4)	Ni1Pc−O(2)	2.40(5) × 3
		Ni1Pc−O(4)	1.96(5) × 3
Sr(2)−O(1)	2.46(4) × 2		
Sr(2)−O(2)	2.85(4) × 2	Ni1Pd−O(2)	2.06(6)
Sr(2)−O(3)	2.70(4) × 2	Ni1Pd−O(2)^{i}	2.13(6)
Sr(2)−O(4)	3.00(3) × 2	Ni1Pd−O(4)	1.94(5)
Sr(2)−O(4)^{i}	2.71(4) × 2	Ni1Pd−O(4)^{i}	2.04(4)
		Ni1Pd−O(2)^{i,i}	2.71(5)
		Ni1Pd−O(4)^{i,i}	2.58(5)
Mn(1)−Mn(2)	2.46(2) × 2	Mn(3)−Mn(3)	2.58(2)
Mn(2)−Ni1Pc	2.30(5)	Mn(3)−Ni1Pc	2.91(6)
Mn(2)−Ni1Pd	2.60(4)	Mn(3)−Ni1Pd	2.75(4)

 © 2003 Wiley-VCH Verlag GmbH & Co. KGaA, Weinheim

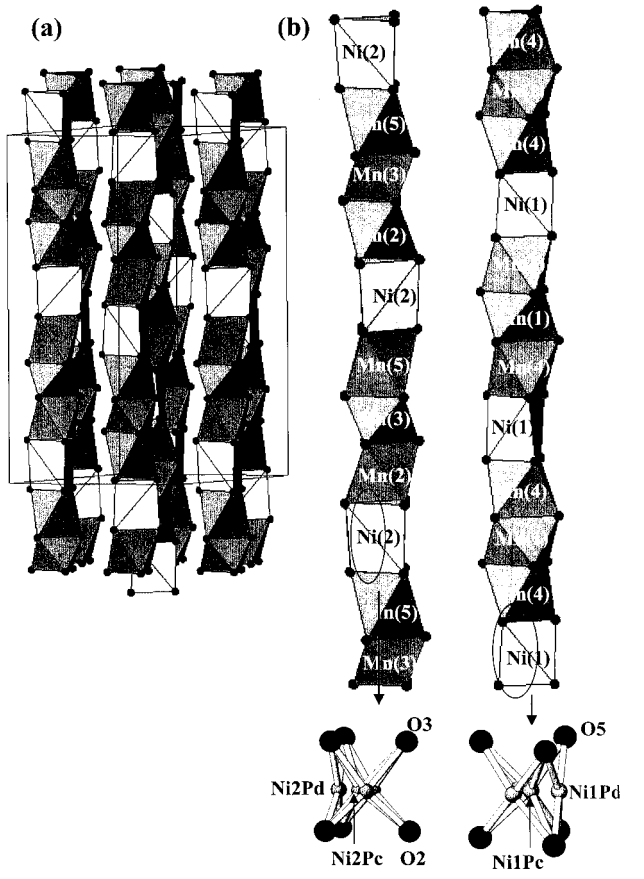

Figure 6. (a) Schematic representation of the structure of $(Sr_{0.75}Ba_{0.25})_5NiMn_3O_{12}$ (Ba/Sr atoms have been omitted for clarity); (b) the metallic sequence along the chains and the split of Ni ions in prismatic coordination are detailed

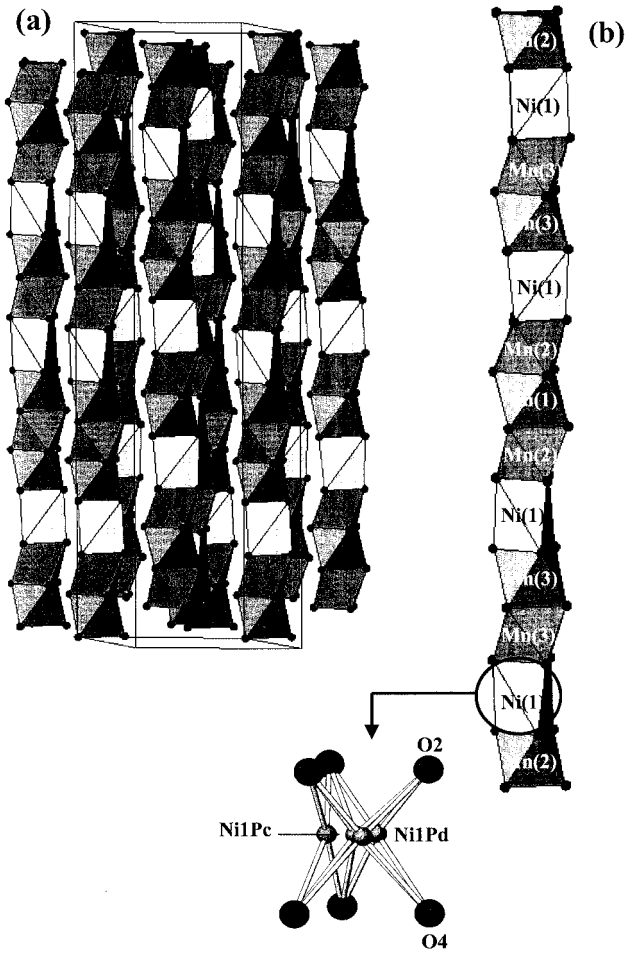

Figure 7. (a) Schematic representation of the structure of $Sr_9Ni_2Mn_5O_{21}$ (Sr atoms have been omitted for clarity); (b) the metallic sequence along the chains and the split of Ni ions in prismatic coordination are detailed

occupied by Mn(3) are less voluminous, with an average metal−oxygen distance of 1.80 Å. On the other hand, the Mn(4) atoms seem to be slightly displaced from the centres of the polyhedra, giving rise to distorted octahedra with average Mn(4)−O distance of 2.06 Å. A similar displacement of Mn has been reported in $Ba_6Mn_4ZnO_{15}$.[11] All the Mn−O distances in $(Sr_{0.75}Ba_{0.25})_5Mn_3NiO_{12}$ are similar to those previously reported in manganese-containing oxides. A particular feature of this structure is the Ni distribution in the TP sites. As can be seen in Table 1, most of the Ni cations (close to 80%) are displaced from the centres towards the square faces of the prisms. Only a small fraction (10%) of Ni(1), labelled as Ni1Pc in Tables 1 and 3, remains at the centres of the TP sites, with six equal Ni1Pc−O distances of 2.09 Å. The environments of the Ni2Pc atoms are less regular, since two different (but close) values of Ni2Pc−O distances are observed [$d_{average}$(Ni2Pc−O) = 2.11 Å]. These distances are very close to those found for Ni atoms in corresponding oxygen environments in Ca_3MnNiO_9 ($d_{average}$ = 2.145 Å)[14] and $Sr_4Ni_3O_9$ ($d_{average}$ = 2.09, 2.195 Å).[4] The remaining Ni1 and Ni2 (referred to as Ni1Pd and Ni2Pd in Table 1) are in square-planar coordination with average M−O distances of 1.95 and 1.97 Å, respectively; these values are also in agreement with Ni^{II}−O distances measured in comparable oxides with similar displacements of the Ni atoms, as in $Sr_4Ni_3O_9$ ($d_{average}$= 1.95, 2.07 Å) or $Sr_4NiMn_2O_9$ ($d_{average}$ = 2.02, 1.99 Å).[4,16] With regard to the M−M distances, the Mn−Mn ones range from 2.50 to 2.60 Å, characteristic of Mn^{IV}−Mn^{IV} in face-sharing octahedra. A similar value is obtained for the Ni1Pc−Mn distance (2.56 Å), but Ni2Pc is slightly displaced towards one of the triangular faces of the TP, giving rise to two very different distances to the neighbour Mn metal atoms. This feature has also been observed in $Sr_4NiMn_2O_9$.[16]

The structure of $Sr_9Ni_2Mn_5O_{21}$ also contains face-sharing [Mn/Ni]-polyhedra chains linked together by Sr−O bonds. The Sr cations are in nine- or tenfold coordination, at distances ranging from 2.38 to 3.00 Å. $Mn(1)O_6$ and $Mn(3)O_6$ define fairly regular octahedra, whereas Mn(2) is located in a distorted octahedron. All the Mn−O and all the Mn−Mn distances are consistent with previously reported bond lengths in comparable manganese oxides. With respect to the Ni environment, about 80% of the Ni atoms once again adopt square-like coordinations [$d_{average}$(NiPd−O) = 2.04 Å]. The remaining Ni atoms, lo-

 © 2003 Wiley-VCH Verlag GmbH & Co. KGaA, Weinheim

cated in trigonal-prismatic coordinations, are each displaced from the centre towards a triangular face of the TP, giving rise to three short (1.96 Å) and three long (2.4 Å) NiPc−O distances. This displacement gives rise to a short Mn(2)−NiPc distance (2.30 Å), close to that found in $Sr_4NiMn_2O_9$ (2.32 Å).[16]

Conclusions

The structural refinement shows that the two new one-dimensional Mn/Ni oxides present the general structural features corresponding to the ($\alpha = 3$, $\beta = 2$) and the ($\alpha = 2$, $\beta = 1$) members of the $(A_3A'BO_6)_\alpha(A_3B_3O_9)_\beta$ series for the $(Sr_{0.75}Ba_{0.25})_5NiMn_3O_{12}$ and $Sr_9Ni_2Mn_5O_{12}$ compositions, respectively. The particular characteristic of each structure is the displacement of most of the Ni atoms from the centres of the trigonal prisms toward the square faces. On the other hand, both materials present twinned microstructures. The presence of twinning in this type of oxides is usually observed when some cationic disorder exists through the polyhedra chains. In this sense, when metal cations of different chemical natures are randomly distributed in the Oh and the TP sites, twinned one-dimensional oxides result. In the samples studied, $Sr_9Mn_5Ni_2O_{21}$ and $Sr_{3.75}Ba_{1.25}NiO_{12}Mn_3$, there is no disorder relative to the cationic distribution in the two different oxygen environments since Mn is located in the octahedra whereas Ni is occupying the trigonal prisms. However, the particular arrangement of the Ni atoms in the TP sites could induces a certain disorder at the Ni positions, most probably the origin of the multi-twinning in the crystals.

Experimental Section

Polycrystalline $Sr_{3.75}Ba_{1.25}NiMn_3O_{12}$ and $Sr_9Ni_2Mn_5O_{21}$ were synthesised by the ceramic procedure by heating stoichiometric amounts of ACO_3 (A = Sr, Ba) (Aldrich, 99.9+%), $MnCO_3$ (Aldrich, 99.9+%) and NiO (Aldrich, 99.99%) in air. The former was treated at 1200 °C for 3 days and the latter at 1050 °C for 6 days with intermediate grinding. In both cases the products were quenched to room temperature.

The average cationic composition was determined by Inductive Coupled Plasma (ICP) while the local composition in every crystal was established by X-ray Energy Dispersive Spectroscopy (EDS). A JEOL 2000 FX electron microscope equipped with an OXFORD ISIS 300-analyser system was employed for this purpose.

Powder X-ray diffraction (XRD) patterns were collected by use of Cu-K_α radiation at room temperature with a PHILIPS X'PERT diffractometer equipped with a graphite monochromator. The diffraction data were analysed by the Rietveld[21] method, by use of the Fullproff program.[22]

Selected Area Electron Diffraction (SAED) was carried out with a JEOL 2000FX electron microscope fitted with a double-tilting goniometer stage (±45°). High-Resolution Electron Microscopy (HREM) was performed with a JEOL 4000EX electron microscope fitted with a double-tilting goniometer stage (±25°). Simulated HREM images were calculated by the multislice method with the aid of the MacTempas software package.

Acknowledgments

Financial support through research project MAT2001-1440 (CICYT, Spain) is acknowledged.

[1] J. J. Lander, *Acta Crystallogr.* **1951**, *4*, 148.
[2] G. Bergerhoff, O. Schmitz-Dumont, *Z. Anorg. Allg. Chem.* **1956**, *10*, 284.
[3] K. Boulahya, M. Parras, J. M. González-Calbet, *Chem. Mater.* **2000**, *12*, 25.
[4] F. Abraham, S. Minaud, C. Renard, *J. Mater. Chem.* **1994**, *4*, 1763.
[5] J. A. Campá, E. Gutiérrez-Puebla, M. A. Monge, I. Rasines, C. Rúiz-Valero, *J. Solid State Chem.* **1994**, *108*, 230.
[6] K. Boulahya, M. Parras, J. M. González-Calbet, *J. Solid State Chem.* **1999**, *145*, 116−127.
[7] W. T. A. Harrison, S. L. Hegwood, A. J. Jacobson, *J. Chem. Soc., Chem. Commun.* **1995**, 1953.
[8] K. Boulahya, M. Parras, J. M. González-Calbet, *J. Solid State Chem.* **1999**, *142*, 419−427.
[9] K. Boulahya, M. Parras, J. M. González-Calbet, J. L. Martínez, *Chem. Mater.* **2002**, *14*, 4006.
[10] L. Katz, R. Ward, *Inorg. Chem.* **1964**, *3*, 205−211.
[11] E. J. Cussen, J. F. Vente, P. D. Battle, *J. Am. Chem. Soc.* **1999**, *121*, 3958−3967.
[12] M. Hernando, K. Boulahya, M. Parras, J. M. González-Calbet, *Eur. J. Inorg. Chem.* **2002**, *12*, 3190−3196.
[13] V. G. Zubkov, G. V. Bazuev, A. P. Tyutyunnik, I. F. Berger, *J. Solid State Chem.* **2001**, *160*, 293−301.
[14] G. V. Bazuev, V. G. Zubkov, I. F. Berger, T. I. Arbuzova, *Solid State Science* **1999**, *1*, 365−372.
[15] S. Kawasaki, M. Takano, *J. Solid State Chem.* **1999**, *145*, 302−308.
[16] A. El Abed, E. Gaudin, S. Lemaux, J. Darriet, *Solid State Sciences* **2001**, *3*, 887−897.
[17] A. El Abed, E. Gaudin, J. Darriet, M.-H. Whangbo, *J. Solid State Chem.* **2002**, *163*, 513−518.
[18] J. L. Hodeau, H. Y. Tu, P. Bordet, T. Fournier, P. Strobel, M. Marezio, *Acta Crystallogr., Sect. B* **1992**, *48*, 1−11.
[19] P. D. Battle, G. R. Blake, J. Sloan, J. F. Vente, *J. Solid State Chem.* **1998**, *136*, 103−114.
[20] M. Evain, F. Boucher, O. Gourdon, V. Petricek, M. Dusek, P. Bezdicka, *Chem. Mater.* **1998**, *10*, 3068−3076.
[21] H. M. Rietveld, *J. Appl. Crystallogr.* **1969**, *2*, 65−71.
[22] J. Rodríguez-Carvajal, *Physica B.* **1993**, *192*, 55−69.

Received January 13, 2003

 © 2003 Wiley-VCH Verlag GmbH & Co. KGaA, Weinheim

Syntheses and Coordination Chemistry of Aminomethylphosphine Derivatives of Adenine

Qingzhi Zhang,[a] Guoxiong Hua,[a] Pravat Bhattacharyya,[a] Alexandra M. Z. Slawin,[a] and J. Derek Woollins*[a]

Keywords: Adenine / P ligands / Chelate complexes / Heterometallic complexes

Two aminomethylphosphane derivatives of adenine 9-(2-{bis[(diphenylphosphanyl)methyl]amino}ethyl)adenine (**La**) and 9-(3-{bis[(diphenylphosphanyl)methyl]amino}propyl)-adenine (**Lb**) were synthesised. Oxidation of **La** and **Lb** with H_2O_2, elemental sulfur or elemental selenium led to the corresponding oxidized products **4a/b**–**6a/b**. Both **La** and **Lb** behave as didentate ligands towards late transition metals. Reaction of **La** or **Lb** with [MX_2(cod)] (M = Pd, Pt; X = Cl, Me) gave chelate complexes **7a/b**–**10a/b**. Reaction of **La** or **Lb** with [AuCl(tht)] or [{RuCl(μ-Cl)(*p*-MeC_6H_4*i*Pr)}$_2$] gave the didentate bridging complexes **11a/b** and **12a**. All compounds have been fully characterised by microanalysis, IR, ^{1}H and ^{31}P{^{1}H} NMR spectroscopy, and EI/CI/FAB mass spectrometry. ^{1}H{^{31}P} NMR and ^{1}H-^{13}C correlation experiments were used to confirm the spectral assignments where necessary. Two compounds were structurally characterised by X-ray crystallographic analysis.

(© Wiley-VCH Verlag GmbH & Co. KGaA, 69451 Weinheim, Germany, 2003)

Introduction

Owing to their resemblance to the structure of adenosine and their broad-spectrum of antiviral or anticancer activity, adenine derivatives substituted at the 9-position constitute an important class of pharmacologically active compounds.[1] Among them 9-[2-(phosphonomethoxy)ethyl]adenine and its analogues have been extensively studied.[2,3] In bioinorganic chemistry, metal complexes capable of forming complementary hydrogen bonds occupy an increasingly important position in the development of biochemically active molecules. Houlton et al.[4] have prepared some interesting bifunctional complexes that combine the covalent bond-forming capabilities of the metal ion and a ligand surface capable of recognizing nucleotide bases by means of hydrogen bonding. The same group developed the concept of *directed metallation* and reported a series of nucleoside analogues in which the ribose group is replaced by a dimethylene/trimethylene tethered ethylenediamine [5−8] or 1,2-dithioethane.[9] Interaction of such chelate-tethered nucleoside analogues with metal ions gave interesting A−N^3-bound or A−C^8-bound mono- or polynuclear complexes. In an approach which combines the antitumour activities of diphosphanes and their gold complexes[10,11] and our experience in the synthesis coordination chemistry of P−C−N compounds,[12] we have incorporated the aminomethylphosphane unit into adenine through an aminodi/trimethylene linkage at the 9-position. The adenine analogues prepared in this way possess two functions: an excellent coordination tendency toward transition metals and the capacity for base-pair or complementary hydrogen-bonding interactions. Some enhanced biological activities are expected from the new combination of the bioactive adenine and aminophosphane as well as the corresponding complexes.

[a] Department of Chemistry, University of St Andrews, Fife, Scotland KY16 9ST, UK
Fax: (internat.) +44-1334/463-384
E-mail: jdw3@st-and.ac.uk

Results and Discussion

Preparation and Oxidation of La and Lb

Scheme 1 shows the synthesis of **La** and **Lb** and the corresponding oxidized compounds. Precursor **1a** was prepared using 1-bromo-2-chloroethane and the sodium salt of adenine, formed from adenine and sodium hydride in anhydrous DMF by a literature method,[13,14] while **1b** was prepared following a modified literature method using adenine and 1-bromo-3-chloropropane in the presence of anhydrous K_2CO_3 in anhydrous DMF, which proved to be milder than NaH and gave a higher yield of the target product.[15−17] Compounds **2**[18] and **3**[19] were also prepared according to the literature method, with slight modification.

Due to the low solubility of **3a** and **3b** in common organic solvents at room temperature, the condensation reactions with Ph_2PCH_2OH were carried out in refluxing acetonitrile. Monitoring by ^{31}P{^{1}H} NMR spectroscopy indicated that the reaction of **3a** or **3b** with a slight excess of Ph_2PCH_2OH (**3**: $Ph_2PCH_2OH \approx$ 1:2 molar ratio) gave **La**

 © 2003 Wiley-VCH Verlag GmbH & Co. KGaA, Weinheim **DOI: 10.1002/ejic.200300037**

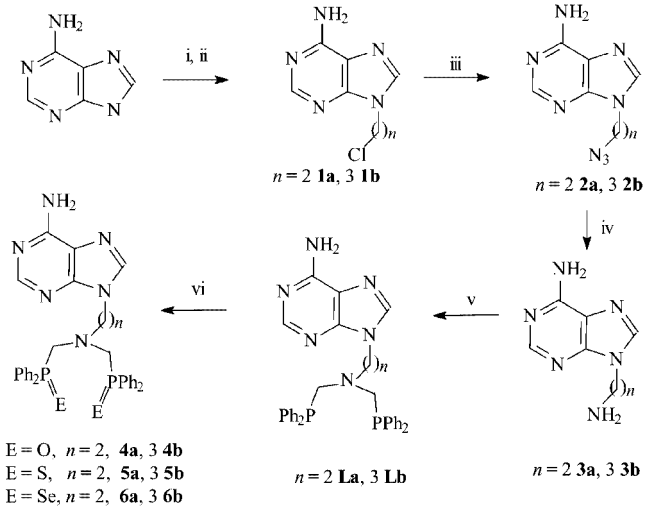

Scheme 1. Preparation and oxidation of **La** and **Lb**; i) NaH (60% in mineral oil) or K_2CO_3, anhydrous DMF, room temp.; ii) $ClCH_2CH_2Br$ or $ClCH_2CH_2CH_2Br$, room temp., 48 h; iii) NaN_3, DMF, 80 °C, 24 h; iv) H_2, 1 atm, Pd/C (10%), MeOH; v) Ph_2PCH_2OH, CH_3CN, reflux, overnight; vi) H_2O_2 (30%), 0 °C, THF, room temp., 2 h; or S_8/Se, THF, reflux, overnight

and **Lb** overnight. Workup by simple concentration and washing with Et_2O removes the excess Ph_2PCH_2OH, and recrystallisation from CH_3CN gave the air- and moisture-stable white solids **L** in good yields. The successful selectivity of N−C bond formation at the dangling alkylamino group rather than the aryl C^6-NH_2 at the purine ring can be attributed to the difference in basicities of the two primary amino groups. The alkylamino group at the 9-position is much more electron-rich than the amino group at the 6-position, whose lone pair is highly delocalised in the electron-withdrawing purine ring. Attempts to get 9-{2-[(diphenylphosphanyl)methylamino]ethyl}adenine and 9-{3-[(diphenylphosphanyl)methylamino]propyl}adenine by using a 1:1 molar ratio of reagents failed; double condensation always occurred under these conditions.

Oxidation of **La** and **Lb** with excess elemental sulfur or selenium in THF gave the corresponding sulfides and selenides. As shown by $^{31}P\{^1H\}$ NMR spectroscopy, however, there is always a trace of unidentified impurities ($\delta_P \approx 40.6$, 37.7 and 36.5 ppm for sulfides; $\delta_P \approx 27.0$ ppm for selenides) in the reaction mixture, implying that the P−C−N bond is not very robust under oxidation conditions. Attempts to get rid of the impurities were not successful by either chromatography or recrystallisation. Oxidation of **La** and **Lb** with aqueous H_2O_2 (30%) needs to be performed with caution. The oxidizing agent can only be used stoichiometrically or slightly in excess, otherwise oxidation at the N1 position of the purine ring occurs as described previously[20,21] and as observed in the mass spectrum. Even so, using our method there are still some unidentified impurities ($\delta_P \approx 30.9$, 27.0 and 26.0 ppm) in the reaction mixture that are very difficult to remove. Oxidation of **La** and **Lb** by air proved too slow to be useful as a preparative technique. Stirring a solution of **La** or **Lb** in THF in air at room temperature for four days only gives about 20% oxidation of the starting material.

Characterization of La, Lb and 1a/b−6a/b

La, **Lb** and compounds **1b, 2b, 3b, 4a/b−6a/b** were fully characterised by multinuclear NMR spectroscopy, EI/CI/FAB mass spectrometry, infrared spectrometry and microanalysis. All the compounds gave reasonable microanalysis results apart from **4a** and **4b**, which showed slightly lower carbon percentages than the calculated value due to the impurities described above. Their mass spectra show the molecular ions and the expected fragmentation pattern with appropriate isotope distributions. The sulfur and selenium species **5a/b−6a/b** show the $[M - S]^+$ and $[M - Se]^+$ fragment ions in their EIMS spectra. The corresponding $[M - O]^+$ ion was not observed for **4a/b**. In the IR spectra, all compounds display two broad medium intensity ν_{N-H} bands between 3349 and 3106 cm^{-1}. The strong N−H bending absorption of the NH_2 group and the stretching absorption of the C=N bond of the purine ring were observed at around 1655 cm^{-1} and 1598 cm^{-1}, respectively. Compounds **2a/b** show an $\nu_{N\equiv N}$ band at 2100 cm^{-1}. Compounds **4a** and **4b** display the $\nu_{P=O}$ absorption at ca. 1178 and 1176 cm^{-1}; the $\nu_{P=S}$ and $\nu_{P=Se}$ bands could not be assigned unambiguously for **5a/b** and **6a/b**.

The $^{31}P\{^1H\}$ NMR signals (Table 1 and 2) of **La/b** at around $\delta_P = -27$ ppm are similar to other bis[(diphenylphosphanyl)methyl]amine compounds.[22] The dichalcogenides **4a/b-6a/b** show signals shifted to higher frequency at ca. $\delta_P = 29$, 35 and 25 ppm compared with that of **La/b**. Interestingly, the $^{31}P\{^1H\}$ NMR spectra of the selenium species **6a/b** not only show a central singlet of 92% intensity with selenium satellites ($^1J_{P,Se} = 730$ Hz)[23] but also a small P−P coupling ($^4J_{P,P} = 9$ Hz) in the satellites. The latter is due to the inequivalence of the two phosphorus atoms arising from the $Ph_2P(Se)CH_2NCH_2P(^{77}Se)Ph_2$ isotopomer. Similar P−P couplings in the selenium satellites were also observed in $Ph_2P(Se)NHP(Se)Ph_2$ ($^2J_{P,P} = 29$ Hz)[24] and $Ph_2P(Se)OP(Se)Ph_2$ ($^2J_{P,P} = 44$ Hz).[25]

The ^1H NMR spectra of **1b**[14,26] and **3b**[27] in $[D_6]$DMSO or $[D_6]$DMSO + D_2O have been reported previously. In order to compare the NMR spectra of the precursors and the aminomethylphosphanes **La** and **Lb**, the same solvent should be employed. However, catalytic oxidation (with either catalyst or irradiation) of P^{III} compounds by DMSO has been reported[21,28−30] and we have also observed the gradual oxidation of some aminophosphane compounds in $[D_6]$DMSO during spectral acquisition, therefore the employment of $[D_6]$DMSO for **La** and **Lb** was precluded. For comparative purposes, in addition to the spectra in $[D_6]$DMSO, the ^1H NMR spectroscopic data of **1−3** in $CDCl_3$ containing a few drops of $[D_6]$DMSO were acquired. The data of **1a**, **2a** and **3a** will be reported elsewhere, and those of **1b**, **2b**, **3b** are listed in Table 3. In the ^1H NMR spectra the chemical shifts of the C^6-NH_2 group and one of the CH groups of the purine ring (C^2-H or C^8-H) vary with solvent ($[D_6]$DMSO, $CDCl_3$ or $CDCl_3$/$[D_6]$DMSO). On the other hand, in the $^{13}C\{^1H\}$ NMR

 © 2003 Wiley-VCH Verlag GmbH & Co. KGaA, Weinheim

Table 1. NMR spectroscopic data for compounds **La** and **4a−6a**

Entry	$^{31}P\{^1H\}$ NMR ($CDCl_3$) δ_P (ppm)	J (Hz)	^1H NMR ($CDCl_3$) δ_H (ppm)	J (Hz)	$^{13}C\{^1H\}$ NMR ($CDCl_3$) δ_C (ppm)	J (Hz)
					155.89 (C^6)	
					152.98 (C^2)	
			8.32 (s, 1 H, C^2-H)		150.10 (C^4)	
			7.10 (s, 1 H, C^8-H)		141.29 (C^8)	
			7.37−7.28 (m, 20 H, ArH)		137.65 (d, ArC^i)	$^1J_{P,C}$ = 13
L_a	−26.71 (s)		5.55 (br. s, 2 H, NH_2)		133.43 (d, ArC^o)	$^2J_{P,C}$ = 18
			4.05 (t, 2 H, AdeC$H_2$$CH_2$)	$^3J_{CH,CH}$ = 6	129.03 (d, ArC^m)	$^3J_{P,C}$ = 22
			3.61 (d, 4 H, PCH_2)	$^2J_{P,CH}$ or $^4J_{P,CH}$ = 5	128.81 (s, ArC^p)	
			3.27 (t, 2 H, C$H_2$$NPCH_2$)	$^3J_{CH,CH}$ = 6	119.54 (C^5)	
					59.71 (dd, PCH_2)	$^1J_{P,C}$ = 6, $^3J_{P,C}$ = 8
					56.00 (t, CH_2NPCH_2)	$^3J_{P,C}$ = 9
					42.16 (s, AdeCH_2CH_2)	
					154.20 (C^6)	
			8.24 (s, 1 H, C^2-H)		152.22 (C^2)	
			7.60 (s, 1 H, C^8-H)		150.19 (C^4)	
			7.70−7.31 (m, 20 H, ArH)		142.24 (C^8)	
4a	29.06 (s)		6.87 (v br. s, 2 H, NH_2)		132.47−128.20 (m, PhC)	
			4.19 (t, 2 H, AdeC$H_2$$CH_2$)	$^3J_{CH,CH}$ = 6	119.15 (C^5)	
			3.82 (d, 4 H, PCH_2)	$^2J_{P,CH}$ or $^4J_{P,CH}$ = 5	57.92 (t, CH_2NPCH_2)	$^3J_{P,C}$ = 6
			3.50 (t, 2H C$H_2$$NPCH_2$)	$^3J_{CH,CH}$ = 6	56.67 (dd, PCH_2)	$^1J_{P,C}$ = 82, $^3J_{P,C}$ = 7
					41.83 (s, AdeCH_2CH_2)	
					154.91 (C^6)	
			8.25 (s, 1 H, C^2-H)		151.98 (C^2)	
			7.85 (s, 1 H, C^8-H)		149.99 (C^4)	
			7.83−7.36 (m, 20 H, ArH)		142.03 (C^8)	
5a	35.37 (s)		5.93 (br. s, 2 H, NH_2)		132.48−128.65 (m, PhC)	
			4.19 (br. s, 4 H, PCH_2)		119.51 (C^5)	
			4.07 (t, 2 H, AdeC$H_2$$CH_2$)	$^3J_{CH,CH}$ = 6	59.34 (d, PCH_2)	$^1J_{P,C}$ = 58
			3.43 (t, 2 H, C$H_2$$NPCH_2$)	$^3J_{CH,CH}$ = 6	56.40 (br. s CH_2NPCH_2)	
					42.58 (s, AdeCH_2CH_2)	
					155.34 (C^6)	
			8.24 (s, 1 H, C^2-H)		152.41 (C^2)	
			7.88 (s, 1 H, C^8-H)		149.80 (C^4)	
			7.78−7.35 (m, 20 H, ArH)		141.61 (C^8)	
6a	25.26 (s)	$^1J_{P,Se}$ = 730	6.10 (br. s, 2 H, NH_2)		132.10−128.74 (m, PhC)	
		$^4J_{P,P'}$ = 9	4.41 (br. s, 4 H, PCH_2)		119.41 (C^5)	
			3.99 (t, 2 H, AdeC$H_2$$CH_2$)	$^3J_{CH,CH}$ = 6	59.34 (d, PCH_2)	$^1J_{P,C}$ = 51
			3.42 (t, 2 H, C$H_2$$NPCH_2$)	$^3J_{CH,CH}$ = 6	56.11 (br. s, CH_2NPCH_2)	
					42.72 (s, AdeCH_2CH_2)	

spectra, the resonance frequencies of the carbons (C^2, C^4, C^5, C^6 and C^8) of the purine ring of compounds **1−3** show little variation in different solvents. To assign the C^2−H and C^8−H protons unambiguously, ^1H-^{13}C heteronuclear correlation spectra (HMQC) were measured. It turned out that the C^8−H appears at lower frequency at around δ_H = 7.8 ppm in $CDCl_3$ or $CDCl_3$/[D_6]DMSO, while in [D_6]DMSO, it is close to the C^2−H resonance at around δ_H = 8.2 ppm. The C^6−NH_2 resonance in $CDCl_3$ or $CDCl_3$ + [D_6]DMSO is observed at around δ_H = 5.6 ppm, while in [D_6]DMSO it appears at around δ_H = 7.2 ppm.

Based on the above observation, we assign the higher frequency singlet at δ_H = 8.32−8.24 ppm to C^2−H and the lower one at δ_H = 7.10−7.88 ppm to C^8 in the ^1H NMR spectra of **La/b** and **4a/b−6a/b**. The ^1H-^{13}C heteronuclear correlation experiment confirmed the assignments. Like their precursors **1−3**, the broad singlet of C^6−NH_2 of **La**, **Lb** and **4−6** appears at around δ_H = 6 ppm. Among them, the resonance of C^6−NH_2 of the oxygen species **4a/b** appears at relatively higher frequency. The proton signals of the dangling chain of **La** and **4a/6a** are as easy to assign as their precursors **1a−3a**, which will be reported elsewhere, with the triplet of AdeC$H_2$$CH_2$ at higher frequency between δ_H = 4.48 and 4.05 ppm and the triplet of CH_2N(CH_2PPh_2) at lower frequency between δ_H = 3.61 and 3.42 ppm. For **Lb** and **4b/6b**, the triplet of AdeC$H_2$$CH_2$ between δ_H = 3.95 and 3.76 ppm and that of CH_2N(CH_2PPh_2) between δ_H = 3.09 and 2.79 ppm are at slightly lower frequency than in **La** and **4a/6a**, but still follow the tendency AdeC$H_2$$CH_2$ > CH_2N(CH_2PPh_2). The triplet of CH_2N(CH_2PPh_2) seems always less-well resolved and slightly broader than that of AdeC$H_2$$CH_2$, which may be attributed to the long-distance coupling of these methylene protons with phosphorus atoms. The AdeCH_2C$H_2$$CH_2$ signal in **Lb** and **4b−6b** appears as a well-resolved quintet at an even lower frequency, between δ_H = 1.87 and 1.69 ppm. The signal of C$H_2$$PPh_2$ of the above compounds appears between δ_H = 4.47 and 3.60 ppm as a doublet or

 © 2003 Wiley-VCH Verlag GmbH & Co. KGaA, Weinheim

Table 2. NMR spectroscopic data for compounds $\mathbf{L_b}$ and **4b−6b**

Entry	$^{31}P\{^1H\}$ NMR ($CDCl_3$) δ_P (ppm)	J (Hz)	^1H NMR ($CDCl_3$) δ_H (ppm)	J (Hz)	$^{13}C\{^1H\}$ NMR ($CDCl_3$) δ_C (ppm)	J (Hz)
					155.45 (C^6)	
			8.30 (s, 1 H, C^2-H)		152.82 (C^2)	
			7.25 (s, 1 H, C^8-H)		150.19 (C^4)	
			7.44−7.25 (m, 20 H, ArH)		141.33 (C^8)	
$\mathbf{L_b}$	−28.12 (s)		5.74 (br. s, 2 H, NH_2)		137.94 (d, ArC^i)	$^1J_{P,C} = 12$
			3.81 (t, 2 H, Ade$CH_2$$CH_2$)	$^3J_{CH,CH} = 6$	133.38 (d, ArC^o)	$^2J_{P,C} = 19$
			3.60 (d, 4 H, PCH_2)	$^2J_{P,CH}$ or $^4J_{P,CH} = 3$	128.80 (d, ArC^m)	$^3J_{P,C} = 21$
			2.79 (t, 2 H, $CH_2$$NCH_2P$)	$^3J_{CH,CH} = 6$	128.74 (s, ArC^p)	
			1.83 (quint, 2 H, AdeCH_2CH_2)		119.97(C^5)	
					59.01 (dd, PCH_2)	$^1J_{P,C} = 6$ or 9 $^3J_{P,C} = 6$ or 9
					53.18 (t, $CH_2$$NCH_2P$)	$^3J_{P,C} = 9$
					41.70 (s, Ade$CH_2$$CH_2$)	
					17.30 (s, Ade$CH_2$$CH_2$)	
					154.48 (C^6)	
			8.29 (s, 1 H, C^2-H)		150.31 (C^2)	
			7.58 (s, 1 H, C^8-H)		149.67 (C^4)	
			7.85−7.36 (m, 20 H, ArH)		141.80 (C^8)	
4b	29.43(s)		6.78 (v br. s, 2 H, NH_2)		132.79−128.19 (m, PhC)	
			3.76 (d + t, 6 H, PCH_2+ AdeCH_2)	$^2J_{P,CH}$ or $^4J_{P,CH} = 5$	119.65 (C^5)	
			3.09 (t, 2 H, $CH_2$$NCH_2P$)	$^3J_{CH,CH} = 6$	56.07 (dd, PCH_2)	$^1J_{P,C} = 83$, $^3J_{P,C} = 7$
			1.87 (quint, 2 H, AdeCH_2CH_2)	$^3J_{CH,CH} = 6$	55.75 (t, $CH_2$$NCH_2P$)	$^3J_{P,C} = 7$
					42.27 (s, Ade$CH_2$$CH_2$)	
					27.46 (s, Ade$CH_2$$CH_2$)	
					155.25 (C^6)	
			8.30 (s, 1 H, C^2-H)		152.38 (C^2)	
			7.70 (s, 1 H, C^8-H)		150.12 (C^4)	
			7.87−7.32 (m, 20 H, ArH)		141.36 (C^8)	
5b	35.27 (s)		5.84 (br. s, 2 H, NH_2)		132.76−128.74 (m, PhC)	
			4.29 (br. s, 4 H, PCH_2)		119.87 (C^5)	
			3.95 (t, 2 H, Ade$CH_2$$CH_2$)	$^3J_{CH,CH} = 7$	57.96 (d, PCH_2)	$^1J_{P,C} = 62$
			2.95 (t, 2 H, $CH_2$$NCH_2P$)	$^3J_{CH,CH} = 7$	53.56 (br. t, $CH_2$$NCH_2P$)	$^3J_{P,C} = 4$
			1.76 (quint, 2 H, AdeCH_2CH_2)	$^3J_{CH,CH} = 7$	41.74 (s, Ade$CH_2$$CH_2$)	
					27.02 (s, Ade$CH_2$$CH_2$)	
					155.22 (C^6)	
			8.29 (s, 1 H, C^2-H)		152.42 (C^2)	
			7.72 (s, 1 H, C^8-H)		150.15 (C^4)	
			7.88−7.30 (m, 20 H, ArH)		141.16 (C^8)	
6b	24.64 (s)	$^1J_{P,Se} = 730$	5.88 (br. s, 2 H, NH_2)		132.18−128.80 (m, PhC)	
		$^4J_{P,P'} = 9$	4.47 (br. s, 4 H, PCH_2)		119.99 (C^5)	
			3.95 (t, 2 H, Ade$CH_2$$CH_2$)	$^3J_{CH,CH} = 7$	57.67 (d, PCH_2)	$^1J_{P,C} = 52$
			2.92 (t, 2 H, $CH_2$$NCH_2P$)	$^3J_{CH,CH} = 7$	53.13 (t, $CH_2$$NCH_2P$)	$^3J_{P,C} = 4$
			1.69 (quint, 2 H, AdeCH_2CH_2)	$^3J_{CH,CH} = 7$	41.69 (s, Ade$CH_2$$CH_2$)	
					27.26 (s, Ade$CH_2$$CH_2$)	

broad singlet arising from the two-bond or four-bond couplings of CH and phosphorus. This resonance can appear at a higher or lower frequency than, and sometimes even overlapped with, that of Ade$CH_2$$CH_2$.

In the $^{13}C\{^1H\}$ NMR spectra, **La/Lb** and their oxidized compounds show very similar purine ring carbon signals (Table 1 and 2) to their precursors and other reported adenine analogues.[31] However, as revealed by a ^1H-^{13}C heteronuclear correlation experiment, the ^{13}C signal of $CH_2NCH_2PPh_2$ is shifted to higher frequency between $\delta_C = 57.92$ and 53.13 ppm and appears as a triplet or broad singlet due to coupling with the phosphorus atoms, while the signal of AdeCH_2CH_2 remains as a singlet between $\delta_C = 42.58$ and 41.69 ppm. The CH_2PPh_2 signal, which appears as a doublet of doublets, doublet or broad singlet due to the $^1J_{P,C}$ and/or $^3J_{P,C}$ couplings, appears at the highest frequency in the alkyl region. **La** and **Lb** exhibit neat signals in the aromatic carbon region and the coupling constants $^nJ_{P,C}$ (n = 1, 2, 3) are available in Table 1 and 2. The coupling constants $^nJ_{P,C}$ (n = 1, 2, 3) in **4a/b-6a/b**, however, are very difficult to observe due to the trace impurities that cause small overlapping signals in the aromatic carbon resonance region in **4a/b-6a/b**.

Compound **2b** was also characterised by X-ray crystallography (Figure 1 and Table 4). Two typical types of hydrogen bonding for the purine system are observed between adjacent molecules (Figure 1, bottom), they are the Watson−Crick type between N(6)−H of one molecule and N(1) of a second molecule, [N(6)−H(6A)···N(1A), d(D···A) 3.056(4) Å, d(H···A) 2.10 Å, ∠(DHA) 164(2)°], and the

 © 2003 Wiley-VCH Verlag GmbH & Co. KGaA, Weinheim

Table 3 NMR spectroscopic data for compounds **1b**−**3b**

Entry	^{1}H NMR ([D$_6$]DMSO)		^{1}H NMR ($CDCl_3$ for **1b**, **2b**; $CDCl_3$ + [D$_6$]DMSO for **3b**)		^{13}C{^{1}H} NMR ([D$_6$]DMSO)	^{13}C{^{1}H} NMR ($CDCl_3$ for **1b**, **2b**; $CDCl_3$ + [D$_6$]DMSO for **3b**)
	δ_H (ppm)	J (Hz)	δ_H (ppm)	J (Hz)	δ_C (ppm)	δ_C (ppm)
					155.96 (C^6)	155.30 (C^6)
	8.16 (s, 1 H, C^8-H)		8.38 (s, 1 H, C^2-H)		152.41 (C^2)	153.49 (C^2)
	8.15 (s, 1 H, C^2-H)		7.85 (s, 1 H, C^8-H)		149.52 (C^4)	150.08 (C^4)
	7.22 (br. s, 2 H, NH_2)		5.55 (br. s, 2 H, NH_2)		140.78 (C^8)	141.20 (C^8)
1b	4.30 (t, 2 H, AdeCH_2CH$_2$)	$^3J_{CH,CH}$ = 6	4.43 (t, 2 H, AdeCH_2CH$_2$)	$^3J_{CH,CH}$ = 6	118.76 (C^5)	119.82 (C^5)
	3.65 (t, 2 H, CH_2Cl)	$^3J_{CH,CH}$ = 6	3.53 (t, 2 H, CH_2Cl)	$^3J_{CH,CH}$ = 6	42.33 (AdeCH$_2$CH$_2$)	41.67 (AdeCH$_2$CH$_2$)
	2.31 (quint, 2 H, AdeCH$_2$CH_2)	$^3J_{CH,CH}$ = 6	2.40 (quint, 2 H, AdeCH$_2$CH_2)	$^3J_{CH,CH}$ = 6	40.58 (CH_2Cl)	41.33 (CH_2Cl)
					31.99 (AdeCH$_2$CH$_2$)	32.19 (AdeCH$_2$CH$_2$)
					155.91 (C^6)	155.73 (C^6)
			8.37 (s, 1 H, C^2-H)		152.92 (C^2)	153.35 (C^2)
	8.16 (s, 2 H, C^8-H + C^2-H)		7.81 (s, 1 H, C^8-H)		149.53 (C^4)	150.33 (C^4)
	7.21 (br. s, 2 H, NH_2)		5.91 (br. s, 2 H, NH_2)		140.73 (C^8)	140.77 (C^8)
2b	4.27 (t, 2 H, AdeCH_2CH$_2$)	$^3J_{CH,CH}$ = 7	4.32 (t, 2 H, AdeCH_2CH$_2$)	$^3J_{CH,CH}$ = 7	118.74 (C^5)	120.05 (C^5)
	3.39 (t, 2 H, CH_2Cl)	$^3J_{CH,CH}$ = 7	3.36 (t, 2 H, CH_2N_3)	$^3J_{CH,CH}$ = 7	48.12 (CH_2N_3)	48.38 (CH_2N_3)
	2.08 (quint, 2 H, AdeCH$_2$CH_2)	$^3J_{CH,CH}$ = 7	2.18 (quint, 2 H, AdeCH$_2$CH_2)	$^3J_{CH,CH}$ = 7	40.53 (AdeCH_2CH$_2$)	41.24 (AdeCH_2CH$_2$)
					28.63 (AdeCH$_2$CH$_2$)	29.26 (AdeCH$_2$CH$_2$)
					155.92 (C^6)	155.64 (C^6)
			8.21 (s, 1 H, C^2-H)		152.29 (C^2)	152.91 (C^2)
	8.14 (s, 2 H, C^2-H + C^8-H)		7.73 (s, 1 H, C^8-H)		149.54 (C^4)	150.14 (C^4)
3b	7.20 (br. s, 2 H, NH_2)		5.85 (br. s, 2 H, NH_2)		140.88 (C^8)	140.58 (C^8)
	4.21 (t, 2 H, AdeCH_2CH$_2$)	$^3J_{CH,CH}$ = 7	4.20 (t, 2 H, AdeCH_2CH$_2$)	$^3J_{CH,CH}$ = 7	118.70 (C^5)	119.60 (C^5)
	2.48 (t, 2 H, CH_2NH$_2$)	$^3J_{CH,CH}$ = 7	2.57 (t, 2 H, CH_2NH$_2$)	$^3J_{CH,CH}$ = 7	40.54 (AdeCH_2CH$_2$)	40.91 (AdeCH_2CH$_2$)
	1.86 (quint, AdeCH$_2$CH_2)	$^3J_{CH,CH}$ = 7	1.89 (quint, AdeCH$_2$CH_2)	$^3J_{CH,CH}$ = 7	38.43 (CH_2NH_2)	38.52 (CH_2NH_2)
	1.54 (br. s, 2 H, NH_2)		1.13 (br. s, NH_2)		33.27 (AdeCH$_2$CH$_2$)	33.48 (AdeCH$_2$CH$_2$)

Hoogsteen type between the other N(6)−H of this molecule and N(7) of a third molecule [N(6)−H(6B)···N(7B), d(D···A) 3..082(3) Å, d(H···A) 2.11 Å, ∠(DHA) 174(4)°].

Coordination Chemistry of La/b with Late Transition Metals

As shown in Scheme 2, **La/b** are excellent didentate ligands towards late transition metals. Reaction of **La/b** with [MX$_2$(cod)] gave a series of didentate complexes **7a/b**−**10a/b**. Interaction of **La/b** with two molar equivalents of [AuCl(tht)] gave the didentate bridging bimetallic complexes **11a/b**. The reaction of **La** and [{RuCl$_2$(η^6-*p*-MeC$_6$H$_4$*i*Pr)}$_2$] also gave the bimetallic compound **12a**. All the complexes gave reasonable microanalyses. Their FAB-MS or ES-MS spectra show the expected molecular ion and fragmentation ions, with appropriate isotope distribution. In the IR spectra the anticipated medium intensity ν_{N-H} stretching band at around 3395−3314 cm^{-1} and 3186−3144 cm^{-1}, and the very strong ν_{N-H} bending and $\nu_{C=N}$ stretching at around 1637 cm^{-1} and 1596 cm^{-1}, respectively, were observed as in the free ligands and oxidized compounds. In the complexes, medium intensity ν_{M-Cl} vibrations were also observed at 329−246 cm^{-1}; the two bands in this region for complexes **7a/b**, **8a/b** are in agreement with the *cis*-geometry of the chelate complexes.

The ^{31}P{^{1}H} NMR spectra of **7a/b**−**10a/b** (Table 5) show high-frequency shifts relative to the free ligands. The platinum species gave more information because of the platinum satellites. In complexes **8a/b** and **9a/b** the large $^1J_{Pt,P}$ coupling (3416 Hz) and the relatively small $^1J_{Pt,P}$ coupling (ca. 1782 Hz) are typical of a phosphorus *trans* to a chloride and a methyl group, respectively, and are thus in agreement with the *cis*-geometry. Complex **10a/b** displays two doublets ($^2J_{P,P} \approx 22$ Hz) corresponding to the two inequivalent phosphorus atoms. The doublet at ca. δ_P = 4.0 ppm with a large $^1J_{Pt,P}$ coupling of ca. 4200 Hz was assigned to the phosphorus *trans* to chloride and the signal with a small $^1J_{Pt,P}$ of about 1640 Hz at ca. δ_P = 0.8 ppm to the phosphorus atoms *trans* to the methyl group.

The ^{1}H NMR spectra of the complexes in CD_2Cl_2 or $CDCl_3$ (Table 5) are generally similar to that of the free ligand **La/b**, the chemical shifts of C^2−H ($\delta_H \approx 8.2$ ppm) > C^8−H ($\delta_H \approx 7.0$ ppm) and that of AdeCH_2 ($\delta_H \approx 3.7$ ppm) > CH_2NCH$_2$P ($\delta_H \approx 3.0$ ppm). Like **La/b**, the chelate complexes show a doublets of doublet, a doublet or a broad singlet for CH_2P, arising from $^2J_{P,CH}$ and/or $^4J_{P,CH}$ coupling, between the signals of AdeCH_2 and CH_2NCH$_2$P, except complex **9b**, while the CH_2P signal in the bridging complexes **11a/b** and **12a** appears at higher frequency than that of AdeCH_2. The platinum complexes display satellites for both CH_2P and the coordinated CH_3 groups. The coupling constants $^3J_{PtCH} \approx 38$ Hz for the dichloride compounds **8a/b**, $^3J_{PtCH} \approx 15$ Hz for **9a/b**, and $^3J_{PtCH}$ = 45 and 15 Hz for **10a/b** were obtained unambiguously from the ^{1}H{^{31}P} NMR spectra. The doublet of doublets for CH_3 at δ_H = 0.33 and 0.49 ppm with satellites ($^2J_{Pt,CH}$ = 54 Hz) in **10a/b** can be easily interpreted as being due to the coupling of this group with the two inequivalent phosphorus atoms.

 © 2003 Wiley-VCH Verlag GmbH & Co. KGaA, Weinheim

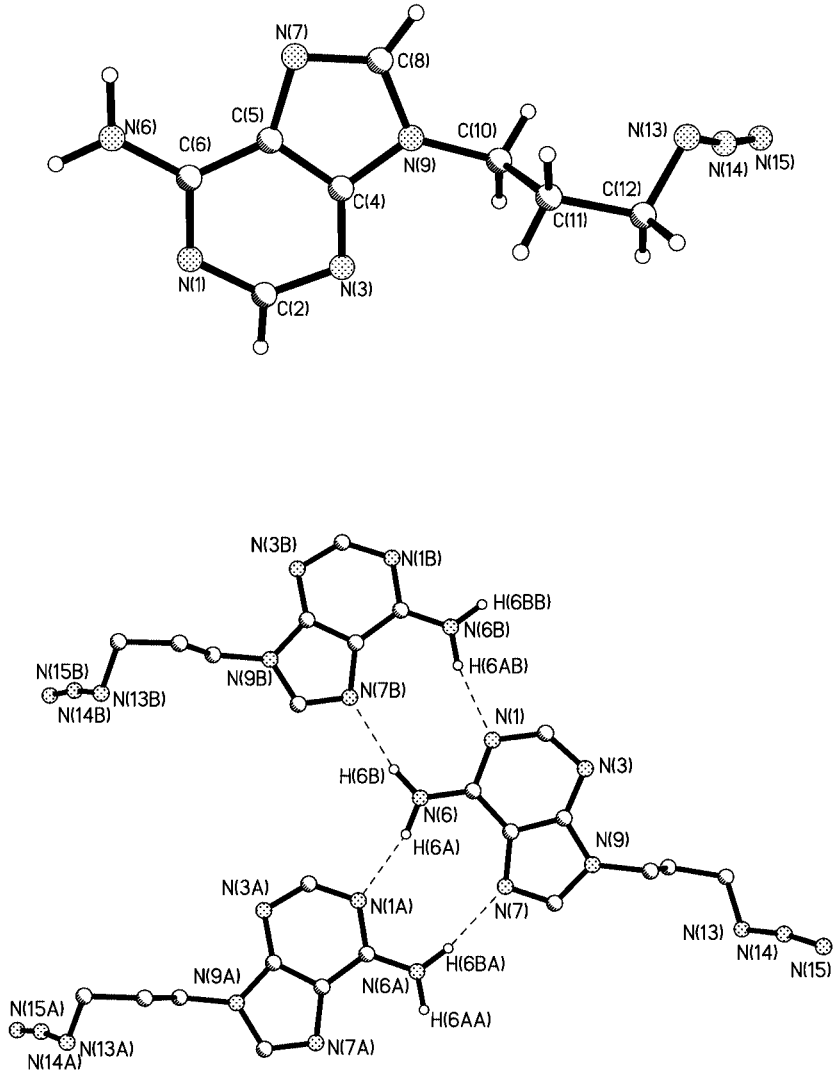

Figure 1. (top) The crystal structure of 9-(3-azidopropyl)adenine (**2b**); (bottom) the crystal structure of **2b** showing part of the hydrogen bonding

Table 4. Selected bond lengths (Å) and angles (°) in compound **2b**

C(2)−N(1)	1.340(3)	N(3)−C(2)	1.318(4)
C(4)−N(3)	1.348(3)	C(5)−C(4)	1.378(4)
C(6)−C(5)	1.395(4)	N(1)−C(6)	1.356(3)
C(6)−N(6)	1.340(3)	N(7)−C(5)	1.399(7)
C(8)−N(7)	1.306(3)	N(9)−C(8)	1.357(3)
N(9)−C(4)	1.373(3)	C(10)−N(9)	1.457(3)
C(11)−C(10)	1.492(4)	C(11)−C(12)	1.503(4)
C(12)−N(13)	1.450(5)	N(13)−N(14)	1.226(4)
N(14)−N(15)	1.117(4)		
C(2)−N(1)−C(6)	118.1(3)	N(3)−C(2)−N(1)	130.5(3)
C(4)−N(3)−C(2)	109.6(2)	N(3)−C(4)−C(5)	127.2(3)
C(6)−C(5)−C(4)	117.4(2)	N(1)−C(6)−C(5)	117.3(3)
N(7)−C(5)−C(4)	110.0(2)	C(8)−N(7)−C(5)	103.2(2)
N(9)−C(8)−N(7)	115.0(2)	C(4)−N(9)−C(8)	105.2(2)
C(5)−C(4)−N(9)	106.5(2)	N(9)−C(10)−C(11)	113.1(2)
C(12)−C(11)−C(10)	113.2(3)	N(13)−C(12)−C(11)	111.8(3)
N(14)−N(13)−C(12)	117.0(3)	N(15)−N(14)−N(13)	170.2(5)

However, the two peaks at δ_H = 0.39 ppm with satellites ($^2J_{Pt,CH} \approx 68$ Hz) in **9a/b** are somewhat confusing. The $^1H\{^{31}P\}$ NMR spectra reveal that the signals are not from the inequivalent CH_3 groups but are a doublet ($^3J_{P,CH} \approx 2$ Hz) due to the coupling of the equivalent methyl groups with either a *trans* or a *cis* phosphorus atom; it is not clear why only one coupling is observed.

Slow diffusion of petroleum ether (b.p. 60−80 °C) into a solution of **10b** in CH_2Cl_2 gave colourless crystals suitable for X-ray analysis (Figure 2 and Table 6). Figure 2 (top) reveals a platinum coordinated in a square plane with a maximum deviation of 0.04 Å for the P(14)−P(15)−C(40A)−Cl(1A)−Pt(1) mean plane. The six-membered chelate ring is chair-like, with the N(13)−C(14)−C(15) plane heavily folded above (72°) and the P(14)−Pt(1)−P(15) plane slightly below (15°) the mean plane P(14)−P(15)−C(14)−C15) (mean deviation 0.03 Å). As shown in Figure 2 (bottom), both the Watson−Crick [N(6)−H(6A)···N(1A); d(D···A) 3.069(10) Å, d(H···A)

 © 2003 Wiley-VCH Verlag GmbH & Co. KGaA, Weinheim

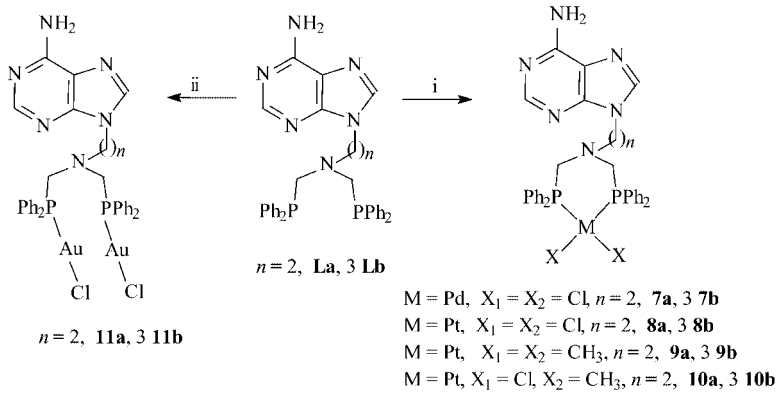

Scheme 2. Coordination of **La** and **Lb** to transition metals; i) $[MX_2(cod)]$ (M = Pd, Pt; X = Cl, CH_3), CH_2Cl_2, 2 h; ii) 2[AuCl(tht)], CH_2Cl_2, 2 h

2.12 Å, ∠(DHA) 164 (4)°] and Hoogsteen [N(6)−H(6B)···N(7B); d(D···A) 3.04(10) Å, d(H···A) 2.14 Å, νDHA 152(6)°] types of intermolecular hydrogen bonding between adjacent molecules are found in the crystal. A quarter molecule of solvate hexane was also observed. For clarity, the solvate molecule is omitted from the figure.

Conclusion

We report here two [(diphenylphosphanyl)methyl]amino analogues of adenosine **La/b** and their chalcogenide derivatives. **La** and **Lb** proved to be good didentate ligands towards late transition metals to give a series of didentate chelate complexes and didentate bridging complexes. All the compounds retain a free adenine moiety for complementary hydrogen bonding. Further studies on the interaction of these compounds with DNA and bioactivities are underway.

Experimental Section

General: All solvents and reagents were purchased from either Aldrich or Lancaster. Dichloromethane was heated to reflux over powdered calcium hydride and distilled under nitrogen. Diethyl ether and tetrahydrofuran were purified by reflux over sodium/benzophenone and distillation under nitrogen. Ligand preparations were performed under an oxygen-free nitrogen atmosphere using standard Schlenk techniques. Coordination reactions and workup were performed in dry solvents. Ph_2PCH_2OH,[32] $[MX_2(cod)]$ (M = Pd, Pt; X = Cl; cod = cycloocta-1,5-diene)[33] and [AuCl(tht)] (tht = tetrahydrothiophene)[34] were prepared following literature procedures.

Infrared spectra were recorded as KBr discs on a Perkin−Elmer system 2000 spectrometer. ^1H NMR spectra (300 MHz) were recorded on a Varian Gemini 2000 spectrometer, $^{31}P\{^1H\}$ NMR spectra at 121.4 MHz (referenced to external 85% H_3PO_4) and $^{13}C\{^1H\}$ NMR spectra at 67.9 MHz on a JEOL GSX 270 spectrometer, and $^1H\{^{31}P\}$ NMR and 2D NMR (^1H-^{13}C heteronuclear correlation experiment) on a Bruker Advance 300. Microanalyses were performed by the University Service within this Department and fast atom bombardment (FAB) or chemical ionization (CI) mass spectra by the EPSRC Mass Spectrometer Service (Swansea, UK). Precious metal salts were provided on loan by Johnson Matthey Plc.

9-(3-Chloropropyl)adenine (1b):[15−17] 1-Bromo-3-chloropropane was added to adenine (27 g, 199.8 mmol) and anhydrous K_2CO_3 in anhydrous DMF (300 mL). The mixture was stirred under an atmosphere of nitrogen for 4 days. The resultant suspension was filtered and the residue was washed with CH_2Cl_2 (3 × 30 cm^3). The combined filtrates were evaporated to dryness by rotary evaporation. The crude product was washed by water (600 cm^3) with sonication in an ultrasonic bath. Recrystallisation from ethanol (220 cm^3) gave 28.0 g of the white product. The mother liquor was concentrated and recrystallised three times to give three additional crops (5.92 g). Total yield: 33.92 g, 80.2%. $C_8H_{10}ClN_5$ (211.7): calcd. C 45.40, H 4.76, N 33.09; found C 45.79, H 4.54, N 33.34. IR (KBr disc): $\tilde{\nu}$ = 3289m cm^{-1}, 3114m, 1667vs, 1603vs. CIMS: *m/z* = 212 $[M + H]^+$, 176 $[M - Cl]^+$. EIMS: *m/z* = 211 $[M]^+$, 176 $[M - Cl]^+$, 148 $[M - CH_2CH_2Cl]^+$.

9-(3-Azidopropyl)adenine (2b):[18] Compound **1b** (20 g, 94.5 mmol) and sodium azide (18.4 g, 283 mmol) were mixed in DMF (150 cm^3). The mixture was stirred at 80 °C for 24 h, cooled to room temperature and then filtered. The solid was washed with CH_2Cl_2 (3 × 30 cm^3). The combined filtrates were vacuumed to almost dryness under rotary evaporation. The residue was taken up in H_2O (200 cm^3) with sonication. The crude product was filtered off and washed with water (3 × 30 cm^3). The combined aqueous layer was extracted with CH_2Cl_2 (3 × 600 cm^3). Removal of the solvent from the extracts led to another crop of crude product. The two crops of crude product were recrystallised from EtOH (300 cm^3) to gave 12.17 g of white solid. Further recrystallisation of the mother liquor gave another 3.90 g of product. Total yield: 16.07 g, 77.7%. $C_8H_{10}N_8$ (218.9): calcd. C 44.03, H 4.62, N 51.35; found C 44.13, H 4.44, N 52.06. IR (KBr disc): $\tilde{\nu}$ = 3302m cm^{-1}, 3140s, 2108vs, 1664vs, 1600vs. CIMS: *m/z* = 220 $[M + H]^+$, 219 $[M]^+$, 191 $[M - N_2]^+$, 163 $[M - CH_2N_3]^+$, 136 $[M - CH_2CH_2CH_2N_3]^+$.

9-(3-Aminopropyl)adenine (3b):[19] 9-(3-Azidoproyl)adenine (10 g, 5.76 mmol) was dissolved in methanol (700 cm^3). To this solution was added palladium on carbon (10%, 5.0 g) and hydrogen gas was bubbled in. Monitoring by TLC (SiO_2, CH_2Cl_2/ MeOH = 80:20) showed that the reaction was complete after about 22 h. The catalyst was removed by filtration through celite. Solvent removal from the filtrate by rotary evaporation gave the product as a white solid. Yield: 7.60 g, 83%. $C_8H_{12}N_6$ (192.2): calcd. C 49.99, H 6.29,

 © 2003 Wiley-VCH Verlag GmbH & Co. KGaA, Weinheim

Table 5. NMR spectroscopic data in CD_2Cl_2[a] or $CDCl_3$[b] for complexes of **La** and **Lb**

Entry	NMR δ_P (ppm) & J (Hz)	δ_H (ppm)	J (Hz)	Entry	NMR δ_P (ppm) & J (Hz)	δ_H (ppm)	δ_H (ppm)
		8.22 (br. s, 1 H, C^2-H)				8.20 (br. s, 1 H, C^2-H)	
		7.79−7.39 (m, 20 H, PhH)				7.89−7.46 (m, 20 H, PhH)	
		6.52 (br. s, 1 H, C^8-H				7.37 (br. s, 1 H, C^8-H)	
7a[a]	9.37 (s)	5.67 (br. s, 2 H, NH_2)		**7b**[a]	9.01 (s)	5.46 (br. s, 2 H, NH_2)	
		3.90 (t, 2 H, AdeCH_2CH_2)	$^3J_{CH,CH}$ = 6			3.79 (t, 2 H,AdeCH_2CH_2)	$^3J_{CH,CH}$ = 7
		3.46 (dd, 4 H, PCH_2)	$^2J_{P,CH}$ = 3 or 5 $^4J_{P,CH}$ = 3 or 5			3.42 (dd, 4 H, PCH_2)	$^2J_{P,CH}$ = 3 or 5 $^4J_{P,CH}$ = 3 or 5
		3.08 (t, 2 H, CH_2NCH_2P)	$^3J_{CH,CH}$ = 6			2.61 (t, 2 H, CH_2NCH_2P)	$^3J_{CH,CH}$ = 7
						1.85 (quint, 2 H, AdeCH_2CH_2)	$^3J_{CH,CH}$ = 7
						8.28 (br. s, 1 H, C^2-H)	
		8.02 (s, 1 H, C^2-H)				7.91−7.44 (m, 20 H, PhH)	
		7.81−7.33 (m, 20 H, PhH)				7.25 (br. s, 1 H, C^8-H)	
		6.37 (s, 1 H, C^8-H)				5.51 (br. s, 2 H, NH_2)	
8a[a]	−7.07 (s) $^1J_{Pt,P}$ = 3416	5.61 (br. s, 2 H, NH_2)		**8b**[b]	−7.13 (s) $^1J_{Pt,P}$ = 3416	3.74 (t, 2 H, AdeCH_2CH_2)	$^3J_{CH,CH}$ = 7
		3.90 (t, 2 H, AdeCH_2CH_2)	$^3J_{CH,CH}$ = 6			3.48 (d, 4 H, PCH_2)	$^2J_{P,CH}$ or $^4J_{P,CH}$ = 3, $^3J_{Pt,CH}$ = 37
		3.51 (d, 4 H, PCH_2)	$^2J_{P,CH}$ or $^4J_{P,CH}$ = 3			2.57 (t, 2 H, CH_2NCH_2P)	$^3J_{CH,CH}$ = 7
		3.01 (t, 2 H, CH_2NCH_2P)	$^3J_{Pt,PCH}$ = 38			1.86 (quint, 2 H, AdeCH_2CH_2)	$^3J_{CH,CH}$ = 7
						8.28 (s, 1 H, C^2-H)	
		8.02 (s, 1 H, C^2-H)				7.77−7.69 (m, 20 H, PhH)	
		7.62−7.33 (m, 20 H, PhH)				6.83 (s, 1 H, C^8-H)	
		5.90 (s, 1 H, C^8-H)				5.47 (br. s, 2 H, NH_2)	
9a[b]	2.21 (s) $^1J_{Pt,P}$ = 1782	5.68 (br. s, 2 H, NH_2)		**9b**[b]	1.70 (s) $^1J_{Pt,P}$ = 1784	3.57 (d, 2 H, PCH_2)	$^2J_{P,CH}$ or $^4J_{P,CH}$ = 3 $^3J_{Pt,CH}$ = 16
		3.83 (t, 2 H, AdeCH_2CH_2)	$^3J_{CH,CH}$ = 6			3.38 (t, 2 H, AdeCH_2CH_2)	$^3J_{CH,CH}$ = 7
		3.51 (br. s, 4 H, PCH_2)	$^3J_{Pt,CH}$ = 14			2.41 (t, 2 H, CH_2NCH_2P)	$^3J_{CH,CH}$ = 7
		2.88 (t, 2 H, CH_2NCH_2P)	$^3J_{P,H}$ = 2			1.68 (quint, 2 H, AdeCH_2CH_2)	$^3J_{CH,CH}$ = 7
		0.39 (d, 6 H, CH_3)	$^2J_{Pt,H}$ = 68			0.39 (d, 6 H, CH_3)	$^3J_{P,CH}$ = 2, $^2J_{Pt,CH}$ = 69
						8.19 (s, 1 H, C^2-H)	
		8.20 (s, 1 H, C^2-H)				7.82−7.38 (m, 20 H, PhH)	
		7.72−7.20 (m, 20 H, PhH)				7.11 (s, 1 H, C^8-H)	
		6.22 (s, 1 H, C^8-H)				5.42 (br. s, 2 H, NH_2)	
		5.86 (br. s, 2 H, NH_2)				3.57 (t, 2 H, AdeCH_2CH_2)	$^3J_{CH,CH}$ = 7
10a[a]	3.97 (d) $^1J_{Pt,P}$ = 4169	3.85 (t, 2 H, AdeCH_2CH_2)	$^3J_{CH,CH}$ = 6	**10b**[a]	4.47 (d) $^1J_{Pt,P}$ = 4211	3.52 (d, 2 H, PCH_2)	$^2J_{P,CH}$ or $^4J_{P,CH}$ = 3 $^3J_{Pt,PCH}$ = 45
	0.96 (d) $^1J_{Pt,P}$ = 1648, $^2J_{P,P}$ = 23	3.57 (d, 2 H, PCH_2)	$^2J_{P,CH}$ or $^4J_{P,CH}$ = 4, $^3J_{Pt,PCH}$ = 45		0.69(d) $^1J_{Pt,P}$ = 1637, $^2J_{P,P}$ = 21	3.49 (d, 2 H, PCH_2)	$^2J_{P,CH}$ or $^4J_{P,CH}$ = 3 $^3J_{Pt,PCH}$ = 16
		3.52 (d, 2 H, PCH_2)	$^2J_{P,CH}$ or $^4J_{P,CH}$ = 4, $^3J_{Pt,PCH}$ = 15			2.45 (t, 2 H, CH_2NCH_2P)	$^3J_{CH,CH}$ = 7
		2.57 (t, 2 H, CH_2NCH_2P)	$^3J_{CH,CH}$ = 6			1.71 (quint, 2 H, AdeCH_2CH_2)	$^3J_{CH,CH}$ = 7
		0.33 (dd, 3 H, CH_3)	$^3J_{P,CH}$ = 4, $^3J_{P'CH}$ = 7 $^2J_{Pt,CH}$ = 54			0.32 (dd, 3 H, CH_3)	$^3J_{P,CH}$ = 4, $^3J_{P'CH}$ = 7, $^2J_{PtCH}$ = 54
						8.25 (s, 1 H, C^2-H)	
		8.25 (s, 1 H, C^2-H)				7.76 (s, 1 H, C^8-H)	
		7.60 (s, 1 H, C^8-H)				7.71−7.41(m, 20 H, PhH)	
		7.56−7.43 (m, 20 H, PhH)				5.63 (br. s, 2 H, NH_2)	
11a[b]	17.41 (s)	5.76 (br. s, 2 H, NH_2)		**11b**[b]	17.34 (s)	4.29 (d, 4 H, PCH_2)	$^2J_{P,CH}$ or $^4J_{P,CH}$ = 1
		4.29 (d, 4 H, PCH_2)	$^2J_{P,CH}$ or $^4J_{P,CH}$ = 1			4.01 (t, 2 H, AdeCH_2CH_2)	$^3J_{CH,CH}$ = 7
		3.94 (t, 2 H, AdeCH_2CH_2)	$^3J_{CH,CH}$ = 6			2.90 (t, 2 H, CH_2NCH_2P)	$^3J_{CH,CH}$ = 7
		3.42 (t, 2 H, CH_2NCH_2P)	$^3J_{CH,CH}$ = 6			1.79 (quint, 2 H, AdeCH_2CH_2)	$^3J_{CH,CH}$ = 7
		8.11 (s, 1 H, C^2-H)					
		7.81−7.39 (m, 20 H, PhH + C^8-H)					
		5.47 (br. s, 2 H, NH_2)					
		5.03 (d, 4 H, ArH of Cy)	$^3J_{CH,CH}$ = 6				
		4.94 (d, 4 H, ArH of Cy)	$^3J_{CH,CH}$ = 6				
12a[a]	20.10 (s)	3.71 (br. s, 4 H, PCH_2)					
		3.59 (t, 2 H, AdeCH_2CH_2)	$^3J_{CH,CH}$ = 6				
		2.37 [sept, 2 H, $CH(CH_3)_2$]	$^3J_{CH,CH}$ = 6				
		2.07 (t, 2 H, CH_2NCH_2P)	$^3J_{CH,CH}$ = 6				
		1.67 (s, 6 H, CH_3)					
		0.85 [d, 12 H, $CH(CH_3)_2$]	$^3J_{CH,CH}$ = 6				

 © 2003 Wiley-VCH Verlag GmbH & Co. KGaA, Weinheim

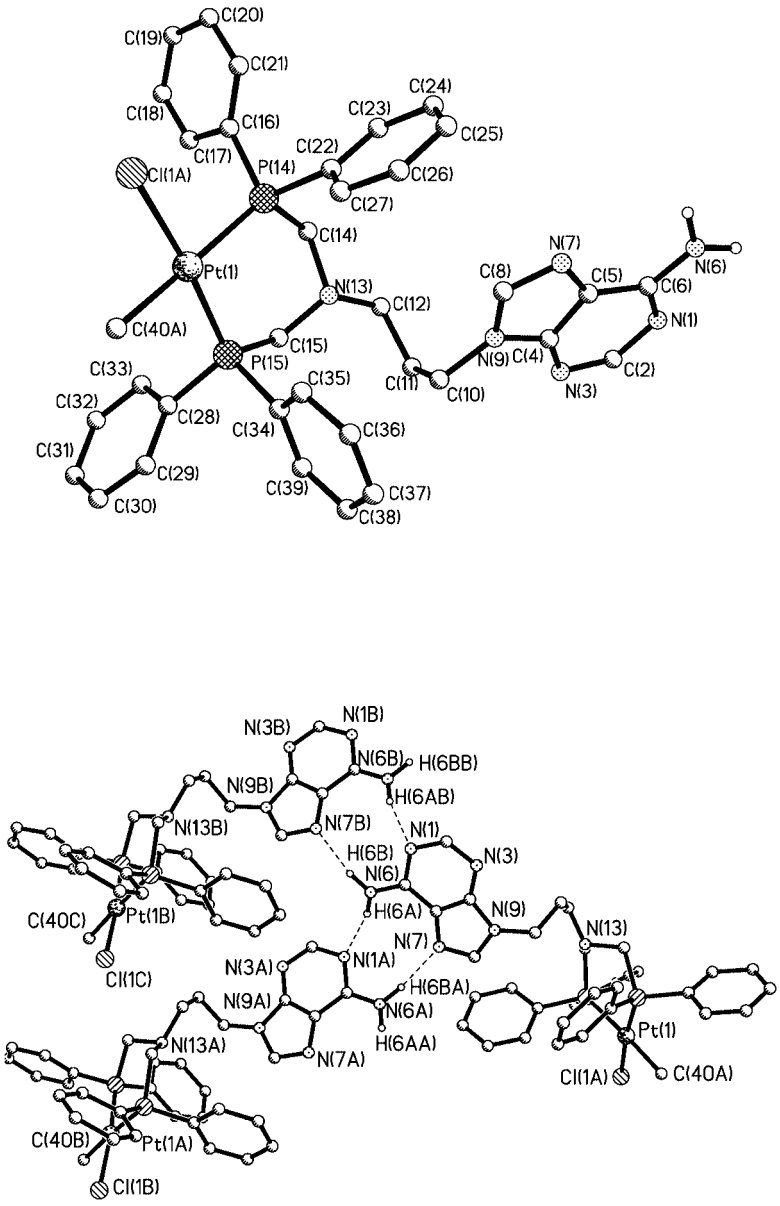

Figure 2. (top) Molecular structure of complex **10b**; (bottom) crystal structure of complex **10b** showing part of the hydrogen bonding

N 43.72; found C 49.37, H 6.28, N 42.73. IR (KBr disc): $\tilde{\nu}$ = 3349 m cm^{-1}, 3282s, 3112s, 1684vs, 1607vs. EIMS: *m*/*z* = 192 $[M]^+$.

9-(2-{Bis[(diphenylphosphanoyl)methyl]amino}ethyl)adenine (La): To a solution of 9-(2-aminoethyl)adenine (1.150 g, 6.45 mmol) in acetonitrile (150 cm^3) was added Ph_2PCH_2OH (2.79 g, 12.90 mmol). The mixture was refluxed overnight and then concentrated in vacuo until the solution became opaque (ca. 20 cm^3). Cooling in a fridge overnight led to the precipitation of the product. Subsequent filtration, and washing of the precipitate with cold acetonitrile (3 × 5 cm^3) and cold Et_2O (3 × 30 cm^3) gave the product as a white solid. Yield: 2.14 g, 57.9%. $C_{33}H_{32}N_6P_2$ (574.6): calcd. C 68.98, H 5.61, N 14.63; found C 67.54, H 5.47, N 13.90. IR (KBr disc): $\tilde{\nu}$ = 3315m cm^{-1}, 3136m, 1648vs, 1598vs, 742s, 696vs. ESMS$^+$: *m*/*z* = 613 $[M + K]^+$, 597 $[M + Na]^+$, 575 $[M + H]^+$.

9-(2-{Bis[(diphenylphosphanyl)methyl]amino}ethyl)adenine (4a): Aqueous hydrogen peroxide (92 μL, 811 μmol, 30%) was added to a solution of **La** (231 mg, 402 μmol) in THF (40 cm^3). The reaction mixture was stirred at 0−5 °C for 2 h, dried over molecular sieves and then passed through a short celite pad. The filtrate was concentrated to ca. 1 cm^3 by rotary evaporation. Et_2O (20 cm^3) was then added to precipitate the product, and filtration, washing with Et_2O (3 × 1 cm^3) and drying in vacuo gave a white solid. Yield: 222 mg, 92%. $C_{33}H_{32}N_6O_2P_2$ (606.6): calcd. C 65.34, H 5.32, N 13.85; found C 62.49, H 5.90, N 12.02. IR (KBr disc): $\tilde{\nu}$ = 3326m cm^{-1}, 3179m, 1648vs, 1599s, 1178vs, 718vs, 696vs. FABMS$^+$: *m*/*z* = 629 $[M + Na]^+$, 607 $[M + H]^+$.

9-(2-{Bis[(diphenylthiophosphanoyl)methyl]amino}ethyl)adenine (5a): Elemental sulfur (35 mg, 1.06 mmol) was added to a solution of **La** (300 mg, 522 μmol) in THF (20 cm^3). The reaction mixture was refluxed for 2 h and then concentrated to ca. 1 cm^3 by rotary evaporation. Et_2O (20 cm^3) was added to precipitate the product, and filtration, washing with Et_2O (3 × 1 cm^3) and drying in vacuo gave a white solid. Yield: 300 mg, 88%. $C_{33}H_{32}N_6P_2S_2$ (638.7): calcd. C 62.05, H 5.05, N 13.16; found C 59.76, H 5.09, N 14.41.

 © 2003 Wiley-VCH Verlag GmbH & Co. KGaA, Weinheim

Table 6. Selected bond lengths (Å) and angles (°) in compound **10b**

Pt(1)−Cl(1A)	2.337(4)	Pt(1)−C(40A)	2.017(5)
Pt(1)−P(14)	2.286(2)	Pt(1)−P(15)	2.219(2)
P(14)−C(14)	1.840(9)	P(15)−C(15)]	1.830(9)
C(14)−N(13)	1.470(10)	C(15)−N(13)	1.453(9)
C(12)−N(13)	1.468(10)	C(11)−C(12)	1.511(11)
C(11)−C(10)	1.496(11)	C(10)−N(9)	1.483(10)
N(9)−C(4)	1.376(10)	N(9)−C(8)	1.356(10)
C(8)−N(7)	1.317(10)	N(7)−C(5)	1.360(10)
C(6)−N(6)	1.333(11)	N(1)−C(6)	1.370(11)
C(6)−C(5)	1.431(12)	C(5)−C(4)	1.389(11)
C(4)−N(3)	1.310(10)	N(3)−C(2)	1.315(10)
C(2)−N(1)	1.363(10)		

C(40A)−Pt(1)−P(15)	86.9(8)	C(40A)−Pt(1)−Cl(1A)	88.0(8)
Cl(1A)−Pt(1)−P(14)	89.88(15)	P(14)−Pt(1)−P(15)	95.27(9)
Pt(1)−P(14)−C(14)	116.6(3)	P(14)−C(14)−N(13)	112.0(6)
C(14)−N(13)−C(15)	110.1(7)	N(13)−C(15)−P(15)	112.0(6)
C(15)−P(15)−Pt(1)	115.6(3)	N(13)−C(12)−C(11)	113.3(8)
N(13)−C(12)−C(11)	113.3(8)	N(9)−C(10)−C(11)	112.3(8)
C(4)−N(9)−C(8)	106.4(7)	N(9)−C(8)−N(7)	114.3(9)]
C(8)−N(7)−C(5)	102.6(8)	N(9)−C(4)−C(5)	103.7(8)
N(7)−C(5)−C(4)	112.9(8)	C(4)−N(3)−C(2)	112.7(8)
N(3)−C(4)−C(5)	127.5(8)	C(2)−N(1)−C(6)	117.2(8)
N(3)−C(2)−N(1)	128.8(9)	C(6)−C(5)−C(4)	115.8(8)
N(1)−C(6)−C(5)	117.9(8)		

IR (KBr disc): $\tilde{\nu}$ = 3320m cm^{-1}, 3170w, 1638vs, 1597s, 705s, 692s. FABMS$^+$: *m*/*z* = 661 [M + Na]$^+$, 639 [M + H]$^+$.

9-(2-{Bis[(diphenylselenophosphanoyl)methyl]amino}ethyl)adenine (6a): Elemental selenium (55 mg, 696 μmol) was added to a solution of **La** (200 mg, 340 μmol) in THF (20 cm^3). The reaction mixture was refluxed for 2 h. After cooling, the mixture was passed through celite. The filtrate was concentrated to ca. 1 cm^3 by rotary evaporation. Et_2O (20 cm^3) was added to precipitate the product, and filtration, washing with Et_2O (3 × 1 cm^3) and drying in vacuo gave a white solid. Yield: 190 mg, 74.5%. $C_{33}H_{32}N_6P_2Se_2$ (732.5): calcd. C 54.11, H 4.40, N 11.47; found C 53.87, H 3.82, N 12.50. IR (KBr disc): $\tilde{\nu}$ = 3333m cm^{-1}, 3188m, 1654vs, 1595vs, 746m, 690s. FABMS$^+$: *m*/*z* = 757 [M + Na]$^+$, 735 [M + H]$^+$.

9-(3-{Bis[(diphenylphosphanoyl)methyl]amino}propyl)adenine (Lb): Ph_2PCH_2OH (3.566 g, 16.5 mmol) was added to a solution of 9-(2-aminoethyl)adenine (1.46 g, 7.60 mmol) in acetonitrile (300 cm^3). The mixture was refluxed overnight and then concentrated in vacuo to ca. 20 cm^3 until a white solid precipitated. The solvent was then pipetted off. The solid was washed with CH_3CN (2 × 20 cm^3) and Et_2O (2 × 50 cm^3). Drying in vacuo gave the product as a white solid. Yield: 3.25 g, 55%. $C_{34}H_{34}N_6P_2$ (588.6): calcd. C 69.38, H 5.82, N 14.28; found C 67.96, H 5.83, N 15.01. IR (KBr disc): $\tilde{\nu}$ = 3297m cm^{-1}, 3134m, 1667vs, 1599vs, 743s, 697vs. ESMS$^+$: *m*/*z* = 611 [M + Na]$^+$, 589 [M + H]$^+$.

9-(3-{Bis[(diphenylphosphanoyl)methyl]amino}propyl)adenine (4b): Aqueous hydrogen peroxide (77 μL, 679 μmol, 30%) was added to a solution of **Lb** (200 mg, 340 μmol) in THF (40 cm^3). The reaction mixture was stirred at 0−5 °C for 2 h, dried over molecular sieves and then passed through a short celite pad. The filtrate was concentrated to ca. 1 cm^3 by rotary evaporation. Et_2O (20 cm^3) was added to precipitate the product, and filtration, washing with Et_2O (3 × 1 cm^3) and drying in vacuo gave a white solid. Yield: 182 mg, 86%. $C_{34}H_{34}N_6O_2P_2$ (620.6): calcd. C 65.80, H 5.52, N 13.54; found C 62.87, H 5.94, N 11.42. IR (KBr disc): $\tilde{\nu}$ = 3324m cm^{-1}, 3180m, 1648vs, 1599vs, 1573m, 1176s, 718s, 695s. FABMS$^+$: *m*/*z* = 643 [M + Na]$^+$, 621 [M + H]$^+$.

9-(3-{Bis[(diphenylthiophosphanoyl)methyl]amino}propyl)adenine (5b): Elemental sulfur (22 mg, 688 μmol) was added to a solution of **Lb** (200 mg, 340 μmol) in THF (20 cm^3). The reaction mixture was refluxed for 2 h and concentrated to ca. 1 cm^3 by rotary evaporation. Et_2O (20 cm^3) was added to precipitate the product, and filtration, washing with Et_2O (3 × 1 cm^3) and drying in vacuo gave a white solid. Yield: 191 mg, 86%. $C_{34}H_{34}N_6P_2S_2$ (652.8): calcd. C 62.56, H 5.25, N 12.87; found C 60.77, H 4.71, N 13.70. IR (KBr disc): $\tilde{\nu}$ = 3315m cm^{-1}, 3173w, 1638vs, 1597vs, 705, 692s. FABMS$^+$: *m*/*z* = 675 [M + Na]$^+$, 653 [M + H]$^+$.

9-(3-{Bis[(diphenylselenophosphanoyl)methyl]amino}propyl)adenine (6b): Elemental selenium (54 mg, 684 μmol) was added to a solution of ligand **2** (200 mg, 340 μmol) in THF (20 cm^3). The reaction mixture was refluxed for 2 h and passed through a short celite pad. The filtrate was concentrated to ca. 1 cm^3 by rotary evaporation. Et_2O (20 cm^3) was added to precipitate the product, and filtration, washing with Et_2O (3 × 1 cm^3) and drying in vacuo gave a white solid. Yield: 176 mg, 69%. $C_{34}H_{34}N_6P_2Se_2$ (746.6): calcd. C 54.70, H 4.59, N 11.26; found C 54.31, H 4.46, N 11.67. IR (KBr disc): $\tilde{\nu}$ = 3312m cm^{-1}, 3162m, 1638vs, 1597s, 746m, 691vs. FABMS$^+$: *m*/*z* = 769 [M + Na]$^+$, 747 [M + H]$^+$.

[PdCl$_2$(La)] (7a): [PdCl$_2$(cod)] (48 mg, 169 μmol) was added to a solution of **La** (100 mg, 169 μmol) in CH_2Cl_2. The reaction mixture was stirred at room temperature for 2 h and then concentrated to ca. 0.5 cm^3. Addition of Et_2O (10 cm^3), filtration and washing with light petroleum ether (3 × 1 cm^3) and Et_2O (3 × 1 cm^3) gave the product as a yellow solid. Yield: 102 mg, 80%. $C_{33}H_{32}Cl_2N_6P_2Pd$ (751.9): calcd. C 52.78, H 4.29, N 11.19; found C 54.71, H 5.00, N 9.81. IR (KBr disc): $\tilde{\nu}$ = 3387m cm^{-1}, 3203w, 1637vs, 1594s, 740s, 691s. ESMS$^+$: *m*/*z* = 790 [M + K]$^+$, 774 [M + Na]$^+$, 715 [M − HCl]$^+$, 697 [M − NH$_3$ − HCl]$^+$, 679 [M − HCl − Cl]$^+$.

[PdCl$_2$(Lb)] (7b): [PdCl$_2$(cod)] (69 mg, 242 μmol) was added to a solution of **Lb** (143 mg, 243 μmol) in CH_2Cl_2 (10 cm^3). A yellow precipitate appeared immediately. The reaction mixture was stirred at room temperature for 2 h and then concentrated to ca. 0.5 cm^3. Addition of Et_2O (10 cm^3), filtration and washing with light petroleum ether (3 × 1 cm^3) and Et_2O (3 × 1 cm^3) gave the product as a yellow solid. Yield: 177 mg, 95%. $C_{34}H_{34}Cl_2N_6P_2Pd$ (765.9): calcd. C 53.32, H 4.47, N 10.97; found C 49.74, H 4.03, N 10.81. IR (KBr disc): $\tilde{\nu}$ = 3314m cm^{-1}, 3144m, 1637vs, 1603s, 737s, 670s, 305w, 291m. ESMS$^+$: *m*/*z* = 789 [M + Na]$^+$, 767 [M + H]$^+$, 729 [M − Cl]$^+$, 694 [M − HCl − Cl]$^+$.

[PtCl$_2$(La)] (8a): [PtCl$_2$(cod)] (65 mg, 171 μmol) was added to a solution of **La** (102 mg, 177 μmol) in CH_2Cl_2 (20 cm^3). The reaction mixture was stirred for 2 h and then concentrated to ca. 0.5 cm^3. Addition of Et_2O (10 cm^3), filtration and washing with light petroleum ether (3 × 1 cm^3) and Et_2O (3 × 1 cm^3) gave the product as a white solid. Yield: 156 mg, 91%. $C_{33}H_{32}Cl_2N_6P_2Pt$ (840.6): calcd. C 47.15, H 3.84, N 10.00; found C 47.01, H 3.10, N 9.74. IR (KBr disc): $\tilde{\nu}$ = 3386m cm^{-1}, 3185w, 1637vs, 1596s, 741s, 692s, 313w, 286w. ESMS$^+$: *m*/*z* = 804 [M − HCl]$^+$.

[PtCl$_2$(Lb)] (8b): [PtCl$_2$(cod)] (78 mg, 208 μmol) was added to a solution of **Lb** (124 mg, 211 μmol) in CH_2Cl_2 (20 cm^3). A white precipitate appeared immediately. The reaction mixture was stirred for 2 h and then concentrated to ca. 0.5 cm^3. Addition of Et_2O (10 cm^3), filtration and washing with light petroleum ether (3 × 1 cm^3) and Et_2O (3 × 1 cm^3) gave the product as a white solid. Yield: 166 mg, 93%. $C_{34}H_{34}Cl_2N_6P_2Pt$ (854.6): calcd. C 47.34, H 3.46, N

 © 2003 Wiley-VCH Verlag GmbH & Co. KGaA, Weinheim

10.32; found C 47.78, H 4.01, N 9.83. IR (KBr disc): $\tilde{\nu}$ = 3338m cm^{-1}, 3163m, 1632vs, 1601s, 740s, 691vs, 314w, 292m. FABMS$^+$: m/z = 819 [M − Cl]$^+$, 783 [M − 2Cl]$^+$.

[Pt(CH$_3$)$_2$(La)] (9a): [Pt(CH$_3$)$_2$(cod)] (56 mg, 168 μmol) was added to a solution of **La** (100 mg, 174 μmol) in CH_2Cl_2 (10 cm^3). The reaction mixture was stirred for 2 h and then concentrated to ca. 0.5 cm^3. Addition of Et_2O (10 cm^3), filtration and washing with light petroleum ether (3 × 1 cm^3) and Et_2O (3 × 1 cm^3) gave the product as a white solid. Yield: 124 mg, 62%. $C_{35}H_{38}N_6P_2Pt$ (799.8): calcd. C 52.56, H 4.79, N 10.51; found C 51.64, H 4.24, N 10.19. IR (KBr disc): $\tilde{\nu}$ = 3323m cm^{-1}, 3179w, 1638vs, 1594s, 737m, 696s. ESMS$^+$: m/z = 825 [M + Na]$^+$, 800 [M]$^+$, 783 [M − CH_3]$^+$.

[Pt(CH$_3$)$_2$(Lb)] (9b): [Pt(CH$_3$)$_2$(cod)] (77 mg, 234 μmol) was added to a solution of **Lb** (138 mg, 234 μmol) in CH_2Cl_2 (10 cm^3). The reaction mixture was stirred for 2 h and then concentrated to ca. 0.5 cm^3. Addition of Et_2O (10 cm^3), filtration and washing with light petroleum ether (3 × 1 cm^3) and Et_2O (3 × 1 cm^3) gave the product as a white solid. Yield: 154 mg, 82%. $C_{36}H_{40}N_6P_2Pt$ (813.8): calcd. C 53.13, H 4.95, N 10.33; found C 52.41, H 4.52, N 10.66. IR (KBr disc): $\tilde{\nu}$ = 3328m cm^{-1}, 3163w, 1637vs, 1598s, 737m, 695vs. FABMS$^+$: m/z = 798 [M − CH_3]$^+$, 783 [M − H − 2CH_3]$^+$.

[PtCl(CH$_3$)(La)] (10a): [PtCl(CH$_3$)(cod)] (90 mg, 254 μmol) was added to a solution of **La** (147 mg, 254 μmol) in CH_2Cl_2 (20 cm^3). A white solid precipitated out gradually. The reaction mixture was stirred for 2 h and then concentrated to ca. 0.5 cm^3. Addition of Et_2O (10 cm^3), filtration and washing with light petroleum ether (3 × 1 cm^3) and Et_2O (3 × 1 cm^3) gave the product as an off-white solid. Yield: 190 mg, 91%. $C_{34}H_{35}ClN_6P_2Pt$ (820.2): calcd. C 49.79, H 4.30, N 10.25; found C 51.18, H 4.13, N 9.86. IR (KBr disc): $\tilde{\nu}$ = 3320w cm^{-1}, 3163w, 1638vs, 1595s, 739s, 694vs. FABMS$^+$: m/z = 804 [M − CH_3]$^+$, 785 [M − Cl]$^+$.

[PtCl(CH$_3$)(Lb)] (10b): [PtCl(CH$_3$)(cod)] (70 mg, 230 μmol) was added to a solution of **Lb** (117 mg, 230 μmol) in CH_2Cl_2 (10 cm^3). A white solid precipitated out gradually. The reaction mixture was stirred for 2 h and then concentrated to ca. 0.5 cm^3. Addition of Et_2O (10 cm^3), filtration and washing with light petroleum ether (3 × 1 cm^3) and Et_2O (3 × 1 cm^3) gave the product as an off-white solid. Yield: 149 mg, 91%. $C_{35}H_{37}ClN_6P_2Pt$ (834.2): calcd. C 50.39, H 4.47, N 10.07; found C 49.70, H 4.01, N 10.44. IR (KBr disc): $\tilde{\nu}$ = 3323m cm^{-1}, 3158m, 1636vs, 1600s, 738s, 694vs, 296m. FABMS$^+$: m/z = 798 [M − Cl]$^+$, 784 [M − Cl − CH_3]$^+$.

[(AuCl)$_2$(La)] (11a): [AuCl(tht)] (80 mg, 250 μmol) was added to a solution of **La** (74 mg, 129 μmol) in CH_2Cl_2 (10 cm^3). The reaction mixture was stirred for 2 h and a solid precipitated out after ca. 10 min. The resulting mixture was concentrated to ca. 0.5 cm^3. Addition of Et_2O (10 cm^3), filtration and washing with Et_2O (3 × 1 cm^3) gave the product as a white solid. Yield: 124 mg, 96%. $C_{33}H_{32}Au_2Cl_2N_6P_2$ (1039.4): calcd. C 38.13, H 3.10, N 8.09; found C 38.14, H 2.53, N 8.25. IR (KBr disc): $\tilde{\nu}$ = 3321m cm^{-1}, 3181w, 1639vs, 1596vs, 744s, 692s, 329m. FAB$^+$: m/z = 1003 [M − Cl]$^+$, 967 [M − 2Cl − H]$^+$.

[(AuCl)$_2$(Lb)] (11b): [AuCl(tht)] (80 mg, 250 μmol) was added to a solution of **Lb** (75 mg, 127 μmol) in CH_2Cl_2 (10 cm^3). The reaction mixture was stirred for 2 h and a solid precipitated out after ca.10 - min. The resulting mixture was concentrated to ca. 0.5 cm^3. Addition of Et_2O (10 cm^3), filtration and washing with Et_2O (3 × 1 cm^3) gave the product as a white solid. Yield: 120 mg, 92%. $C_{34}H_{34}Au_2Cl_2N_6P_2$ (1053.5): calcd. C 39.18, H 3.25, N 7.98; found C 38.76, H 3.08, N 7.98. IR (KBr disc): $\tilde{\nu}$ = 3317m cm^{-1}, 3161m, 1638vs, 1595s, 744s, 691vs, 326s. FABMS$^+$: m/z = 1017 [M − Cl]$^+$, 982 [M − 2 Cl − H]$^+$.

[RuCl$_2$(η^6-*p*-CH$_3$C$_6$H$_4$*i*Pr)(La)] (12a): [RuCl(μ-Cl)(*p*-CH$_3$-C$_6$H$_4$*i*Pr)]$_2$ (52 mg, 85 μmol) was added to a solution of **La** (50 mg, 87 μmol) in CH_2Cl_2 (20 cm^3). The reaction mixture was stirred for 2 h and then concentrated to ca. 0.5 cm^3. Addition of Et_2O (10 cm^3), filtration and washing with Et_2O (3 × 1 cm^3) gave the product as an orange solid. Yield: 85 mg, 83%. $C_{53}H_{60}Cl_4N_6P_2Ru_2$ (1187.0): calcd. C 53.63, H 5.09, N 7.08; found C 52.22, H 5.11, N 6.96. IR (KBr disc): $\tilde{\nu}$ = 3338m cm^{-1}, 3187w, 3054m, 1631vs, 1595s, 1474s, 1437s, 746s, 696vs. FABMS$^+$: m/z = 1188 [M + H]$^+$, 1212 [M + Na]$^+$.

Table 7. Details of the X-ray data collections and refinements for compounds **2b** and **10b**

Compound	**2b**	**10b**·1/4C_6H_{14}
Empirical formula	$C_8H_{10}N_8$	$C_{36.50}H_{40.50}ClN_6P_2Pt$
Crystal colour, habit	Colourless, block	Colourless, block
Crystal dimensions/mm	0.1 × 0.1 × 0.1	0.1 × 0.1 × 0.01
Crystal system	Orthorhombic	Orthorhombic
Space group	*Pbca*	*Pbca*
a/Å	15.2288(17)	7.9955(9)
b/Å	8.7153(10)	19.312(2)
c/Å	15.4248(16)	46.857(5)
U/Å^3	2047	7235
Z	8	8
M	218.24	855.73
Dc/g cm^{-3}	1.416	1.571
μ/mm^{-1}	0.100	4.076
F(000)	912	3412
Measured reflections	9475	29689
Independent reflections (R_{int})	1419(0.0876)	5187(0.1341)
Final *R*1, ω*R*2[$I > 2\sigma(I)$]	0.0456, 0.1036	0.0409, 0.0664

X-ray Crystallography: Table 7 lists details of data collections and refinements for **2b** and **10b**. Data were collected at room temperature using Mo-K_α radiation with a SMART system. Intensities were corrected for Lorentz-polarisation and for absorption. The structures were solved by the heavy-atom method or by direct methods. The positions of the hydrogen atoms were idealised. Refinements were by full-matrix least-squares based on F^2 using SHELXTL.[35] In complex **10b**, there is disorder of the chlorine and the methyl atoms attached to the platinum atom. The diagram in Figure 2 shows the major (70%) occupancy. CCDC-200672 (**2b**) and -200673 (**10b**) contain the supplementary crystallographic data for this paper. These data can be obtained free of charge at www.ccdc.cam.ac.uk/conts/retrieving.html [or from the Cambridge Crystallographic Data Centre, 12, Union Road, Cambridge CB2 1EZ, UK; Fax: (internat.) +44-1223/336-033; E-mail: deposit@ccdc.cam.ac.uk].

Acknowledgments

We wish to thank the JREI for equipment grants, Johnson Matthey plc for the loan of precious metals and Dr. Andrew Houlton for his inspiration of this work. Qingzhi Zhang is indebted to St Andrews University for financial support. We are also grateful to Dr. Stephen M. Aucott and Mrs. Joanna Wheatley in this lab for the kind donation of [PtMe$_2$(cod)], [PtMeCl(cod)] and [AuCl(tht)] (tht = tetrahydrothiophene).

 © 2003 Wiley-VCH Verlag GmbH & Co. KGaA, Weinheim

[1] J. Bourguignon, L. Desaubry, P. Raboisson, C-G. Wermuth, C. Lugnier, *J. Med. Chem.* **1997**, *40*, 1768−1770.
[2] L. M. Schultze, H. H. Chapman, N. J. P. Dubree, R. J. Jones, K. M. Kent, T. T. Lee, M. S. Louie, M. J. Postich, E. J. Prisbe, J. C. Rohloff, R. H. Yu, *Tetrahedron Lett.* **1998**, *39*, 1853−1856.
[3] A. Holy, J. Gunter, H. Dvorakova, M. Masojidkova, G. Andrei, T. Snoeck, J. Balzarini, E. D. Clercq, *J. Med. Chem.* **1999**, *42*, 2064−2086.
[4] A. Houlton, D. M. P. Mingos, D. J. Williams, *J. Chem. Soc., Chem. Commun.* **1994**, 503−504.
[5] C. Price, M. R. J. Elsegood, W. Clegg, N. H. Rees, A. Houlton, *Angew. Chem. Int. Ed. Engl.* **1997**, *36*, 1762−1764.
[6] M. A. Shipman, C. Price, A. E. Gibson, M. R. J. Elsegood, W. Clegg, A. Houlton, *Chem. Eur. J.* **2000**, *6*, 4371−4378.
[7] M. A. Shipman, C. Price, M. R. J. Elsegood, W. Clegg, A. Houlton, *Angew. Chem. Int. Ed.* **2000**, *39*, 2360−2362.
[8] C. Price, M. A. Shipman, N. H. Rees, M. R. J. Elsegood, A. J. Edwards, W. Clegg, A. Houlton, *Chem. Eur. J.* **2001**, *7*, 1194−1201.
[9] C. Price, B. R. Horrocks, A. Mayeux, M. R. J. Elsegood, W. Clegg, A. Houlton, *Angew. Chem. Int. Ed.* **2002**, *41*, 1047−1049.
[10] D. T. Hill, G. R. Girard, F. L. McCabe, R. K. Johnson, P. D. Stupik, J. H. Zhang, W. M. Reiff, D. S. Eggleston, *Inorg. Chem.* **1989**, *28*, 3529−3533.
[11] C. K. Mirabelli, D. T. Hill, L. F. Faucette, F. L. McCabe, G. R. Girard, D. B. Bryan, B. M. Sutton, J. O. Bartus, S. T. Crooke, R. K. Johnson, *J. Med. Chem.* **1987**, *30*, 2181−2190.
[12] Q. Zhang, S. M. Aucott, A. M. Z. Slawin, J. D. Woollins, *Eur. J. Inorg. Chem.* **2002**, 1635−1646.
[13] P. H. C. Mundill, R. W. Fries, W. Richard, C. Woenckhaus, B. V. Plapp, *J. Med. Chem.* **1981**, *24*, 474−479.
[14] O. F. Schall, G. W. Gokel, *J. Am. Chem. Soc.* **1994**, *116*, 6089−6100.
[15] A. Fkyerat, M. Demeunynck, J.-F. Constant, P. Michon, J. Lhomme, *J. Am. Chem. Soc.* **1993**, *115*, 9952−9959.
[16] P. Ciapetti, M. Taddei, *Tetrahedron* **1998**, *54*, 11305−11310.
[17] T. Itahara, *J. Chem. Soc., Perkin Trans. 2* **1996**, *12*, 2695−270.
[18] M. E. Masri, K. D. Berlin, *Org. Prep. Proc. Int.* **1995**, *27*, 161−169.
[19] M. Ho, B. A. Wilson, I. Katampe, *Bioorg. Med. Chem. Lett.* **1996**, *6*, 899−902.
[20] T. Saito, H. Hayashibara, Y. Kumazawa, T. Fujisawa, T. Fujii, *Heterocycles* **1990**, *31*, 1503−1596.
[21] T. Fujii, T. Saito, K. Kizu, Y. Hayashibara, S. Nakajuma, T. Fujisawa, *Chem. Pharm. Bull.* **1991**, *39*, 301−308.
[22] J. Fawcett, P. A. T. Hoye, P. D. W. Kemmitt, D. J. Law, D. R. Russell, *J. Chem. Soc., Dalton Trans.* **1993**, *17*, 2563−2568.
[23] S. W. Carr, R. Colton, *Aust. J. Chem.* **1981**, *34*, 35−44.
[24] P. Bhattacharyya, J. Novosad, J. Phillips, A. M. Z. Slawin, D. J. Williams, J. D. Woollins, *J. Chem. Soc., Dalton Trans.* **1995**, 1607−2495.
[25] M. J. Pilkington, A. M. Z. Slawin, D. J. Williams, J. D. Woollins, *Main Group Chem.* **1995**, *1*, 145−151.
[26] M. Kim, G. W. Gokel, *J. Chem. Soc., Chem. Commun.* **1987**, *22*, 1686−1688.
[27] N. J. Leonard, R. F. Lambert, *J. Org. Chem.* **1969**, *34*, 3240−3248.
[28] S. Bhattacharjee, R. Bhattacharyya, *J. Chem. Soc., Dalton Trans.* **1992**, 1357−1364.
[29] J. M. Berg, R. H. Holm, *J. Am. Chem. Soc.* **1985**, *107*, 925−932.
[30] A. Baceiredo, G. Bertrand, G. Sicard, *J. Am. Chem. Soc.* **1985**, *107*, 4781−4783.
[31] S. V. Calenbergh, J. K. von F. D. Kunzel, N. M. Blaton, O. M. Peeters, J. Rozenski, A. V. Aerschot, A. De Bruyn, D. De Keukeleire, A. P. Uzerman, P. Herdewijn, *J. Med. Chem.* **1997**, *40*, 3765−3772.
[32] H. Hellmann, J. Bader, H. Birkner, O. Schumacher, *Justus Liebigs Ann. Chem.* **1962**, *659*, 49.
[33] J. X. McDermott, J. F. White, G. M. Whitesides, *J. Am. Chem. Soc.* **1976**, *98*, 6521−6528.
[34] R. Uson, A. Laguna, M. Laguna, *Inorg. Synth.* **1989**, *26*, 85−91.
[35] G. M. Sheldrick, *SHELXTL*, Bruker AXS, Madison, WI, **1999**.

Received January 20, 2003

 © 2003 Wiley-VCH Verlag GmbH & Co. KGaA, Weinheim

The Reactivity of Allyl and Olefin-Hydride Niobocene Derivatives Towards Isocyanides. X-ray Crystal Structure of [Nb(η^5-$C_5H_4SiMe_3$)$_2$\{η^3-CH(R)CHCH(R)\}] (R = $SiMe_2tBu$)

Isabel del Hierro,[a] Rafael Fernández-Galán,[b] Sanjiv Prashar,[a] Antonio Antiñolo,[b] Mariano Fajardo,[a] Ana M. Rodríguez,[c] and Antonio Otero*[b]

Keywords: Niobium / Allyl ligands / Hydride ligands / Insertion reactions / Isocyanide

The new allylniobocene complexes [NbCp′$_2$(η^3-CHRCHCHR′)] [Cp′ = η^5-$C_5H_4SiMe_3$; R = R′ = $SiMe_2tBu$ (**1**); R = H, R′ = $SiPh_3$ (**2**)] have been prepared and characterised. The molecular structure of **1** has been determined by X-ray diffraction studies, which confirm that the allyl ligand is η^3-bonded to the metal centre. The reactivity of the niobocene complexes **1**, **2,** [NbCp′$_2$H(η^2-CH_2=CH_2)] (**3**), and [NbCp′$_2$(η^3-CH_2CHCH_2)] (**4**) towards aliphatic, *t*BuNC, *n*BuNC, and aromatic, $CNC_6H_3Me_2$-2,6, isocyanide compounds has been studied. From these reactions the new alkylniobocene [NbCp′$_2$(CH_2CH_3)(CNR)] [R = *t*Bu (**5**), $C_6H_3Me_2$-2,6 (**6**), *n*Bu (**7**)], η^1-allylniobocene derivatives [NbCp′$_2$(η^1-$CH_2CHCHSiPh_3$)($CNC_6H_3Me_2$-2,6)] (**8**), and a family of the first neutral η^1-iminoacylniobocene complexes [NbCp′$_2$\{η^1-C(=NR)R′\}(CNR)] (R = $C_6H_3Me_2$-2,6, R′ = Et (**9**); R = *n*Bu, R′ = Et (**10**); R = $C_6H_3Me_2$-2,6, R′ = CH_2CH=$CHSiPh_3$ (**11**); R = $C_6H_3Me_2$-2,6, R′ = CH_2CH=CH_2 (**12**)] were prepared.
(© Wiley-VCH Verlag GmbH & Co. KGaA, 69451 Weinheim, Germany, 2003)

Introduction

The chemistry of η^3-allyl complexes of transition metals is well documented.[1] However there are only a relatively small number of η^3-allyl complexes of niobium and tantalum despite the synthesis of [Nb(η^5-C_5H_5)$_2$(η^3-C_3H_5)] being first reported in 1970.[2] This was followed by the preparation of [M(η^5-C_5H_5)$_2$R] (M = Nb, Ta; R = 1-methylallyl, 2-methylallyl).[3] Several related systems such as the metallacyclic (η^3-allyl)metallocene cations have also been published.[4] Nakamura et al. have also synthesised a family of allylniobocene complexes,[5] and more recently the allyltantalum complexes [Ta(=NR)(η^5-C_5Me_5)(η^1-CH_2CHCH_2)(η^3-CH_2CHCH_2)] (R = Si*t*Bu$_3$, 2,6-*i*PrC_6H_3) were reported.[6]

Our research group's contribution in this field describes the synthesis and reactivity of η^3-allyl, [NbCp′$_2$(η^3-C_3H_5)], and chelate azaallyl [NbCp′$_2$\{N($SiMe_3$)C(*t*Bu)CH_2\}], niobocene derivatives[7] and forms part of our ongoing studies in the use of unsaturated molecules in the synthesis of new families of niobium organometallic compounds.[8]

The behaviour of isocyanide molecules towards alkyl or aryl transition-metal compounds is well documented and insertion reactions are usually observed.[9] Varying the alkyl or aryl substituent of the isocyanide compound allows fine tuning of the electronic and steric properties of the metal complex. Isocyanides are able to bind to the metal through either or both the carbon and nitrogen atom. η^2-Coordination normally occurs at electron deficient metal centres and is characteristic for high valence early transition metal complexes.

Our well documented studies of the first insertion reaction of CO into the niobium−carbon bond of alkylniobocene complexes which give the corresponding η^1-acyl derivatives,[10] have led us to consider the insertion reactions of isocyanide compounds. The isolobal relationship between carbon monoxide and isocyanide compounds suggests that similar types of reactivity can be expected although isocyanides are generally regarded as better σ donors and weaker π acceptors than carbon monoxide.[11]

We report here the synthesis and characterisation of new allylniobocene complexes and their reactivity as well as that of olefin-hydride species towards aliphatic and aromatic isocyanide reagents. We also present the molecular structure of an η^3-allylniobocene complex, which to the best of our knowledge is only the second reported example.

[a] Departamento de Tecnología Química, Ambiental y de los Materiales, E.S.C.E.T., Universidad Rey Juan Carlos, 28933 Móstoles (Madrid), Spain
[b] Departamento de Química Inorgánica, Orgánica y Bioquímica, Universidad de Castilla-La Mancha, Facultad de Químicas, Campus Universitario, 13071 Ciudad Real, Spain
Fax: (internat.) + 34-926/295-318
E-mail: Antonio.Otero@uclm.es
[c] ETS Ingenieros Industriales, Avd. Camilo José Cela, 3, 13071 Ciudad Real, Spain

 © 2003 Wiley-VCH Verlag GmbH & Co. KGaA, Weinheim **DOI: 10.1002/ejic.200300053**

Results and Discussion

The eighteen-electron allyl complexes [NbCp′$_2$(η^3-CHRCHCHR′)] [Cp′ = η^5-$C_5H_4SiMe_3$; R = R′ = $SiMe_2tBu$ (**1**); R = H, R′ = $SiPh_3$ (**2**)] were prepared by the metathesis reaction of [{NbCp′$_2$Cl}$_2$] and the corresponding potassium salt [K(η^3-CHRCHCHR′)] (Scheme 1).

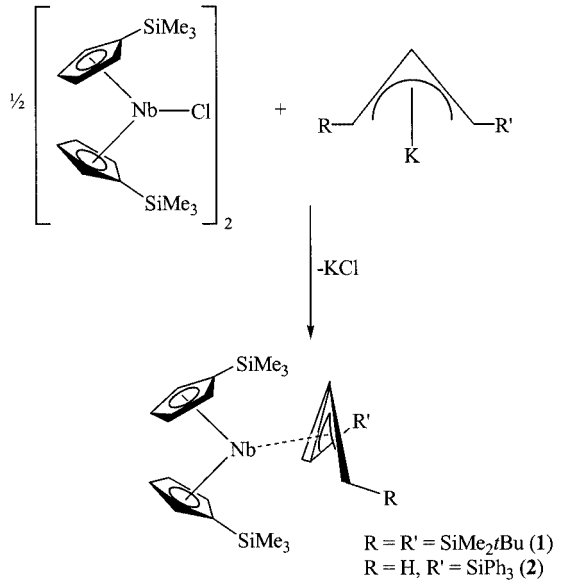

Scheme 1

Complexes **1** and **2** were characterised by NMR and mass spectroscopy (see Exp. Sect.). The ^{1}H NMR spectrum of **1** showed two sets of allylic proton signals, a doublet for the terminal allylic protons (two H_{anti}) and a triplet for the central allylic proton. Four signals were observed for the protons of the two cyclopentadienyl rings. The σ_v symmetry of **1** makes the protons 2-H, 5-H and 3-H, 4-H in each cyclopentadienyl ring equivalent (see Figure 1). The η^3-coordination of the allyl ligand results in the inequivalency of the two cyclopentadienyl rings and thus two sets of signals corresponding to the distinct cyclopentadienyl ligands were observed. In addition the two methyl groups of the allyl silyl substituents were found to be magnetically inequivalent and this was attributed to the greater restriction to rotation about the silicon−allyl−carbon bond of the allyl ligand.[12] The ^{13}C NMR spectrum observed was in accordance with the proposed structure (see Exp. Sect.).

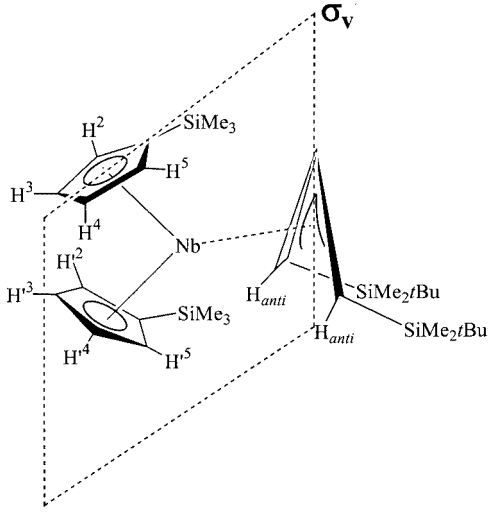

Figure 1. Proposed structure for [NbCp′$_2$(η^3-$tBuMe_2SiCHCHCH$-$SiMe_2tBu$)] (**1**)

The ^{1}H NMR spectrum of **2** showed eight signals for the protons of the cyclopentadienyl ligands and two singlets for the $SiMe_3$ ring substituents in accordance with an asymmetrical environment about the niobium centre. The inequivalence of the two cyclopentadienyl rings indicates an η^3 coordination of the allyl ligand (see Figure 2). Three sets of signals for the allylic group were observed, a doublet at $\delta = -0.09$ ppm assigned to the H_{anti} proton bonded to the silicon atom, a doublet of doublets at $\delta = 0.89$ ppm assigned to the H_{anti} of the unsubstituted terminal carbon and a multiplet at $\delta = 2.73$ ppm assigned to the central proton which overlaps with the signal assigned to the H_{syn} proton. The ^{13}C NMR spectrum observed was in accordance with the proposed structure (see Exp. Sect.).

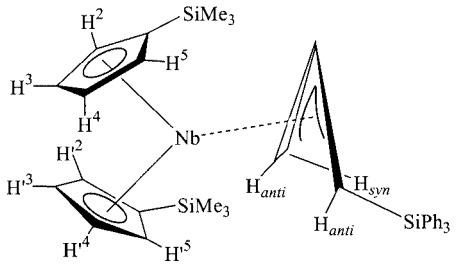

Figure 2. Proposed structure for [NbCp′$_2$(η^3-$CH_2CHCHSiPh_3$)] (**2**)

The molecular structure of **1** was established by single crystal X-ray diffraction and confirmed the η^3-coordination of the allyl ligand. The molecular structure and atom numbering scheme are shown in Figure 3. Selected bond lengths and angles for **1** are given in Table 1.

The structure of **1** shows the typical bent metallocene confirmation observed in niobocene complexes, with both cyclopentadienyl ligands bound to the metal in an η^5 mode. The environment of the niobium atom is completed by the η^3-allyl ligand. If the terminal carbon atoms of the allyl ligand are regarded as occupying two coordination sites, then the niobium metal centre can be considered as having a distorted tetrahedral geometry. The angle defined by Cent(1), Nb and Cent(2) is 131.48(1)°, by Cent(1), Nb and Cent(3) 113.13(2)°, and by Cent(2), Nb and Cent(3) 115.35(1)° [Cent(1) and Cent(2) are the centroids of the cyclopentadienyl ligands and Cent(3) is the centroid of the allyl ligand). The sum of these three angles is exactly 360° indicating that the vectors connecting the Nb atom with Cent(1), Cent(2) and Cent(3) are all in one plane.

 © 2003 Wiley-VCH Verlag GmbH & Co. KGaA, Weinheim

Table 1. Selected bond lengths [Å] and angles [°] for **1**

Bond lengths		Bond angles	
av Nb(1)−C[Cent(1)][a][b]	2.398	Cent(1)−Nb(1)−Cent(2)	131.48(1)
av Nb(1)−C[Cent(2)][a][b]	2.429	Cent(1)−Nb(1)−Cent(3)	113.13(2)
Nb(1)−C(1)	2.395(4)	Cent(2)−Nb(1)−Cent(3)	115.35(1)
Nb(1)−C(2)	2.366(4)	C(2)−Nb(1)−C(1)	34.4(1)
Nb(1)−C(3)	2.377(5)	C(3)−Nb(1)−C(1)	64.2(2)
Si(1)−C(1)	1.869(5)	C(2)−C(1)−Si(1)	118.9(3)
Si(1)−C(10)	1.914(5)	C(2)−C(1)−Nb(1)	71.6(2)
Si(2)−C(3)	1.839(5)	Si(1)−C(1)−Nb(1)	137.9(2)
Si(2)−C(4)	1.904(6)	C(1)−C(2)−C(3)	127.3(4)
C(1)−C(2)	1.408(6)	C(1)−C(2)−Nb(1)	74.0(3)
C(2)−C(3)	1.421(6)	C(3)−C(2)−Nb(1)	73.0(3)
		C(2)−C(3)−Si(2)	124.1(4)
		C(2)−C(3)−Nb(1)	72.1(2)
		Si(2)−C(3)−Nb(1)	133.7(2)

[a] Cent(1), Cent(2) and Cent(3) are the centroids of C(21)−C(25), C(31)−C(35) and C(1)−C(3), respectively. [b] Refers to the average bond length between Nb(1) and the carbon atoms of the C_5 ring of the corresponding cyclopentadienyl moiety.

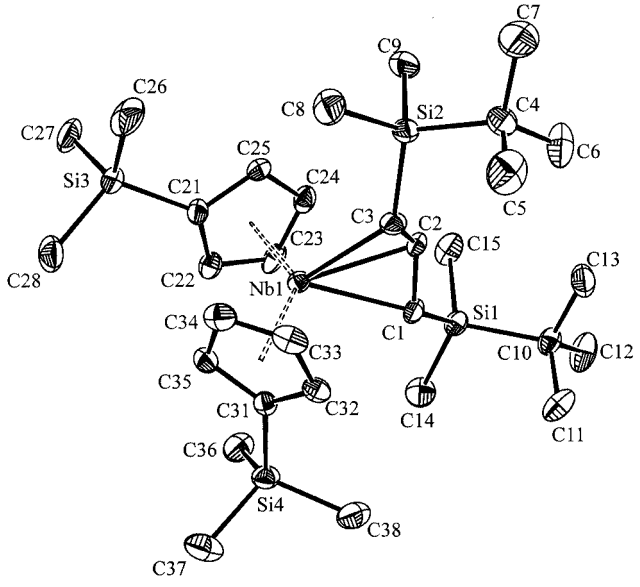

Figure 3. Molecular structure and atom-labelling scheme for [NbCp′$_2$(η^3-*t*BuMe$_2$SiCHCHCHSiMe$_2$*t*Bu)] (**1**), with thermal ellipsoids at 30% probability

The allyl ligand assumes a planar *cis-syn* geometry and shows η^3-coordination to the metal centre. The carbon atoms of the allyl ligand are nearly planar with C−C distances of 1.408(6) Å and 1.421(6) Å, which are similar to the only other X-ray characterised allylniobocene complex, namely [Nb(η^5-C_5H_5)$_2$(η^3-C_3H_5)].[13] The plane of the allyl group in **1** is not perpendicular to the plane defined by Nb(1), C(2) and C(3) but at an angle of 116.0(4)°, typically tilted away from perpendicular to maximize orbital overlap. These structural features are consistent with a strong bonding interaction between the allyl nonbonding orbital and the empty metal orbital, and little back-bonding from the metal to the allyl.[13] The close structural similarity between the niobium derivatives **1**, and [Nb(η^5-C_5H_5)$_2$(η^3-C_3H_5)] (d^2 metal centre) with [Ti(η^5-C_5H_5)$_2$(η^3-C_3H_3-1,3-Me$_2$)][14] (d^1 metal centre) is also an indication that the metal-to-ligand back donation is negligible. The effect of alkyl substitution at the terminal carbons of the allyl ligand is reflected in the elongated Nb−C(1) and Nb−C(3) distances 2.395(4) Å and 2.377(5) Å, respectively. These values are greater than the Nb−C(2) distance [2.366(4) Å] and longer that observed in the unsubstituted allyl compound.[13]

The reaction of the niobocene derivatives **1**, **2**, [NbCp′$_2$H(η^2-CH_2=CH_2)] (**3**)[10] and [NbCp′$_2$(η^3-CH_2CHCH_2)] (**4**)[7] with isocyanide compounds has been studied. The hydrido(ethylene)niobocene complex [NbCp′$_2$H(η^2-CH_2=CH_2)] (**3**) was found to react slowly at room temperature with *tert*-butyl isocyanide to give the ethyl isocyanide derivative [NbCp′$_2$(CH_2CH_3)(CN*t*Bu)] (**5**) in quantitative yield as a red oil (Scheme 2). The isocyanide ligand promotes the insertion of the olefin into the niobium−hydride bond and no further reaction was observed even when an excess of isocyanide was used or the reaction was carried out the at higher temperatures. Complex **5** was characterised spectroscopically. The most significant IR band for **5** corresponds to the isocyanide stretching mode ν(CN) at 2095 cm^{-1}. In the ^{13}C NMR spectrum of **5** the most interesting feature was the extremely low field resonance (δ = 270.0 ppm) which was observed for the metal-bonded isocyanide carbon. This resonance appears as a broad singlet due to the high relaxation time in the NMR time scale.[15]

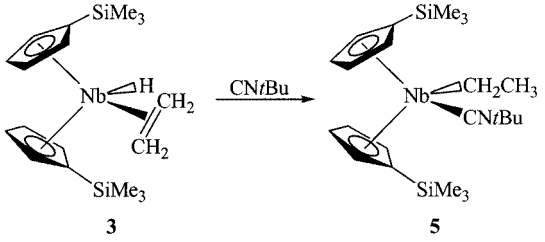

Scheme 2

 © 2003 Wiley-VCH Verlag GmbH & Co. KGaA, Weinheim

In contrast with the behaviour observed in the synthesis of **5**, an equimolar amount of 2,6-dimethylphenyl isocyanide reacts at room temperature with **3** to give, initially the ethyl isocyanide derivative [NbCp′$_2$(CH$_2$CH$_3$)(CNC$_6$H$_3$Me$_2$-2,6)] (**6**) which evolves rapidly at room temperature with the insertion of a second equivalent of the isocyanide ligand into the niobium-carbon bond to yield the neutral iminoacyl compound [NbCp′$_2${η^1-C(=N−C$_6$H$_3$Me$_2$-2,6)(CH$_2$CH$_3$)}(CNC$_6$H$_3$Me$_2$-2,6)] (**9**) (Scheme 3). Compound **6** could not be isolated as a pure sample, but as part of a mixture containing, in addition, **3** and **9**. However, **9** could be prepared and isolated as a pure sample by the reaction of **3** with two equivalents of the isocyanide reagent.

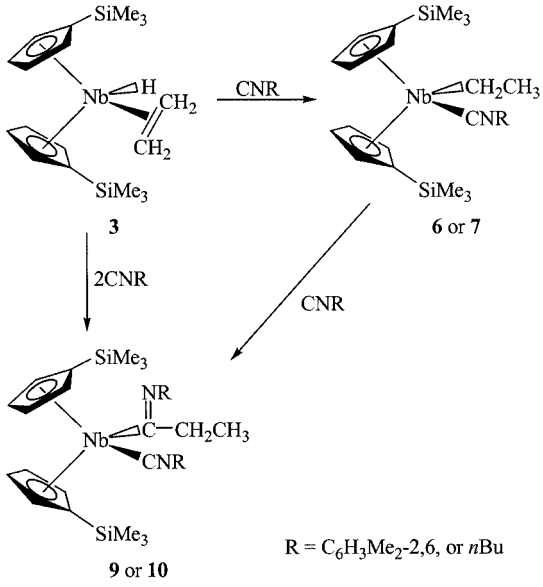

Scheme 3

Compound **6** was characterised by ^{1}H NMR spectroscopy where typical resonances corresponding to the cyclopentadienyl, ethyl and isocyanide ligands were observed (see Exp. Sect.). Complex **9** showed in the IR spectrum a band corresponding to the stretching mode ν(CN) at 2021 cm^{-1} of the linear isocyanide ligand. The ν(C=N) stretching frequency corresponding to the η^1-iminoacyl ligand was observed at 1657 cm^{-1}.[16] NMR evidence supports the proposal that the iminoacyl ligand in this compound is coordinated in an η^1 fashion. The ^{1}H NMR resonance of the inserted methylene group of the ethyl ligand observed is displaced to lower field, δ = 2.35 ppm, with respect to that observed in **6**, δ = 0.81 ppm. In the ^{13}C NMR spectrum a low field resonance, δ = 218.2 ppm, was observed for the carbon of the terminal isocyanide ligand bonded to niobium. A second signal shifted to higher field, δ = 153.6 ppm, was assigned to the carbon of the η^1-iminoacyl ligand. The previously reported cationic iminoacylniobium derivatives [NbCp′$_2$X(η^2-C(=NPh)CHCHRPh)][17] (X = Cl, H, CH$_3$) showed the signal attributed to the η^2-iminoacyl carbon in the range δ = 213−219 ppm which was in accordance with the data reported for complexes of other early transition metals.[18] Adams and co-workers have shown that the η^2-iminoacyl carbon in [Mo(η^5-C$_5$H$_5$)(CO)$_2$(η^2-MeCNMe)] resonates approximately δ = 40 ppm downfield of the corresponding resonance in [Mo(η^5-C$_5$H$_5$)(CO)$_2${P(OMe)$_3$}(η^1-MeCNPh)].[19] Royo and co-workers have proposed a related η^1 iminoacyltantalum system as an intermediate in the synthesis of compounds containing imido-η^2-iminoacyl ligands [Ta(η^5-C$_5$Me$_5$)(=N*t*Bu)Cl{η^2-C[C(Me)=NR]=NR}] (R = C$_6$H$_3$Me$_2$-2,6).[20]

Further evolution of **9** to give the coupling of the isocyanide and the η^1-iminoacyl groups to produce metallacyclic compounds was not observed.[21]

The reaction of *n*-butyl isocyanide with **3** also gave a mixture of products, namely the alkyl compound [NbCp′$_2$(CH$_2$CH$_3$)(CN*n*Bu)] (**7**) and the iminoacyl complex [NbCp′$_2${η^1-C(=N*n*Bu)(CH$_2$CH$_3$)}(CN*n*Bu)] (**10**) (Scheme 3). With an excess of isocyanide further reactions gave a mixture of products which we were unable to identify. **7** was characterised by ^{1}H NMR spectroscopy where typical resonances corresponding to the cyclopentadienyl, ethyl and isocyanide ligands were observed (see Exp. Sect.). In the ^{1}H NMR spectrum a second set of signals corresponding to the cyclopentadienyl, ethyl, isocyanide and iminoacyl ligands were assigned to compound **10** (see Exp. Sect.).

In the case of the allylniobocene derivatives, **1**, **2** and **4**, there was no reaction with *tert*-butyl isocyanide (even at 80 °C). Nevertheless the complexes rapidly reacted with *n*-butyl isocyanide although only to give mixtures of products which we were unable to identify.

Complex **1** did not react with 2,6-dimethylphenyl isocyanide at room temperature and at 80 °C the products from the reaction could not be identified. However, [NbCp′$_2$(η^3-CH$_2$CHCHSiPh$_3$)] (**2**) reacts with two equivalents of 2,6-dimethylphenyl isocyanide at room temperature to give initially the η^1-allyl isocyanide derivative [NbCp′$_2$(η^1-CH$_2$CH=CHSiPh$_3$)(CNC$_6$H$_3$Me$_2$-2,6)] (**8**) which undergoes an insertion reaction of further isocyanide to give the iminoacyl derivative [NbCp′$_2${η^1-C(=NC$_6$H$_3$Me$_2$-2,6)(CH$_2$CH=CHSiPh$_3$)}(CNC$_6$H$_3$Me$_2$-2,6)] (**11**) (Scheme 4).

In contrast [NbCp′$_2$(η^3-CH$_2$CHCH$_2$)] (**4**) did not react with the aryl isocyanide at room temperature, and the reaction had to be carried out at 80 °C in order to obtain the corresponding η^1-iminoacyl compound [NbCp′$_2${η^1-C(=NC$_6$H$_3$Me$_2$-2,6)(CH$_2$CH=CH$_2$)}(CNC$_6$H$_3$Me$_2$-2,6)] (**12**) [Scheme (5)]. Under these conditions the corresponding intermediate η^1-allyl derivative [NbCp′$_2$(η^1-CH$_2$CH=CH$_2$)(CNC$_6$H$_3$Me$_2$-2,6)] (**13**) was not detected. However, we have previously reported its preparation by a distinctive synthetic route.[7] The reaction of **13** with an equimolar amount of aryl isocyanide gave the iminoacyl complex **12** (Scheme 5).

The complexes **8**, **11** and **12** were characterised by IR and NMR spectroscopy (see Exp. Sect.). ^{1}H NMR spectroscopy for these compounds showed that the two cyclopentadienyl ligands are equivalent indicating a σ_h symmetry plane in

 © 2003 Wiley-VCH Verlag GmbH & Co. KGaA, Weinheim

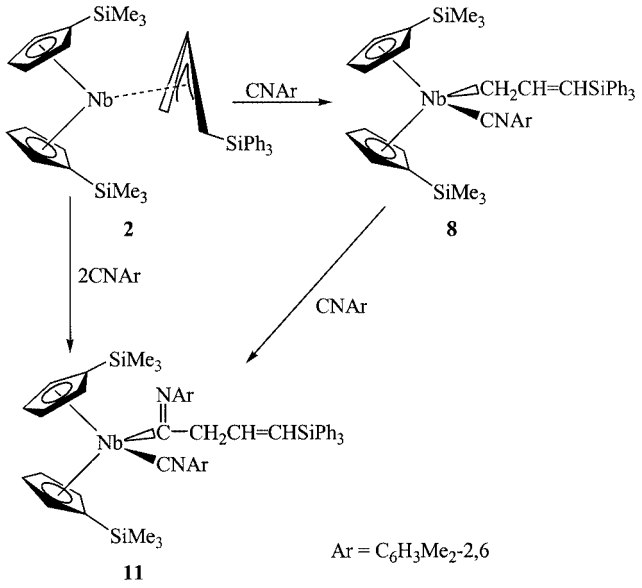

Scheme 4

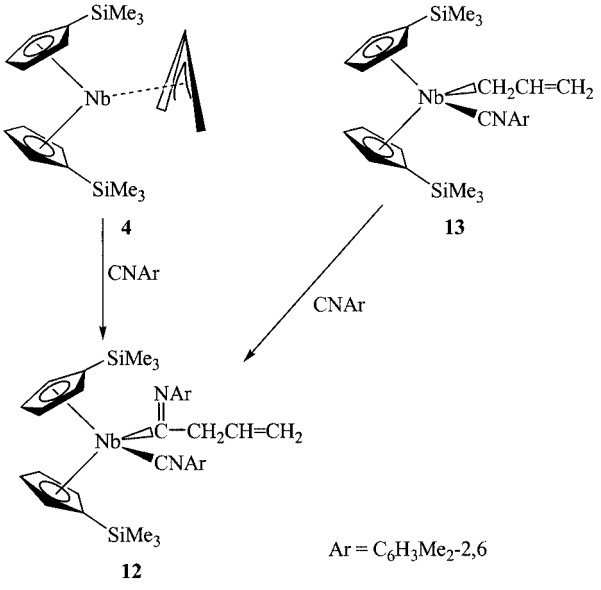

Scheme 5

the molecule. The disappearance of the *anti* and *syn* protons signals of the starting complexes clearly shows the change of bonding mode of the allyl ligand from η^3 to η^1 in the final product. The η^1-allyl complexes exhibited, in the ^{1}H NMR spectra, for this group, three sets of signals corresponding to a doublet for the CH_2 bonded to the niobium or iminoacyl carbon atom, a multiplet, at ca. $\delta = 5.7$ ppm, for the central group CH and a multiplet, at ca. $\delta = 4.6$ ppm, for the terminal olefinic protons. One the more important features of the ^{1}H NMR spectra was the position of the resonance of the methylene group of the η^1-allyl system which was found to resonate at $\delta = 1.65$ ppm for **8** and $\delta = 1.39$ ppm for **13**, when this group is directly bonded to niobium. However, for **11** and **12** where the methylene group is bonded to the iminoacyl carbon atom, the corresponding signal was shifted downfield to $\delta = 3.54$ ppm and 3.26 ppm, respectively.

The IR spectrum for compounds **11** and **12** showed a band corresponding to the stretching mode ν(CN) at 2019 and 2029 cm^{-1}, respectively, corresponding to the isocyanide ligand coordinated to the metal atom. The ν(C=N) stretching frequencies for **11** and **12**, corresponding to the η^1-iminoacyl ligands appeared at 1659 and 1677 cm^{-1}, respectively.

In conclusion, two new allylniobocene complexes have been prepared and the X-ray structure (only the second reported example) for one of these compounds has been determined. η^1-Iminoacylniobocene complexes have been synthesised and characterised by spectroscopic techniques. NMR spectroscopy studies have allowed us to establish the ease of the different isocyanide molecules insertion reactions in the different niobium systems, and corresponds to the following order CN*n*Bu > $CNC_6H_3Me_2$-2,6 > CN*t*Bu for the isocyanide molecules and [$NbCp'_2H(\eta^2$-$CH_2{=}CH_2)$] (**3**) > [$NbCp'_2(\eta^3$-$CH_2CHCHSiPh_3)$] (**2**) > [$NbCp'_2(\eta^3$-$CH_2CHCH_2)$] (**4**), for the organometallic substrates.

Experimental Section

General Remarks: All reactions were performed using standard Schlenk tube techniques under dry nitrogen. Solvents were distilled from appropriate drying agents and degassed before used.

The compounds [$NbCp'_2H(\eta^2$-$CH_2{=}CH_2)$] (**3**),[10] [$NbCp'_2(\eta^3$-$CH_2CHCH_2)$] (**4**),[7] [$K(\eta^3$-CHRCHCHR′)] (R = R′ = $SiMe_2t$Bu; R = H, R′ = $SiPh_3$)[12] and [$NbCp'_2(\eta^1$-$CH_2CH{=}CH_2)$-($CNC_6H_3Me_2$-2,6)] (**13**)[7] were prepared as described earlier. *t*BuNC, *n*BuNC, $CNC_6H_3Me_2$-2,6 were purchased from Aldrich and Fluka and used directly. IR spectra were recorded with a Perkin−Elmer PE 883 IR spectrophotometer. ^{1}H and ^{13}C spectra were recorded with Varian FT-300 and Varian Gemini FT-200 spectrometers and referenced to the residual deuterated solvent. Microanalyses were carried out with a Perkin−Elmer 2400 microanalyzer.

Preparation of [$NbCp'_2(\eta^3$-*t*$BuMe_2SiCHCHCHSiMe_2t$Bu) (1): [$K(\eta^3$-*t*$BuMe_2SiCHCHCHSiMe_2t$Bu)] (0.30 g, 1.47 mmol) in THF (50 mL) was added at 0 °C to a solution of [{$NbCp'_2Cl$}$_2$] (0.20 g, 0.50 mmol) in THF (10 mL). The resulting mixture was warmed to room temperature and stirred for 12 h. Solvent was removed in vacuo and hexane (50 mL) added to the green solid. After filtration, all volatiles were removed, from the filtrate, under reduced pressure to yield a dark green solid of the title complex (0.27 g, 87%). X-ray quality crystals were obtained by recrystallisation from cold hexane. ^{1}H NMR (200 MHz, C_6D_6, 25 °C): $\delta = -0.05$, 0.34 (2s, each 12 H, 2 × CHSi*Me*$_2t$Bu), 0.04 (d, $^3J_{H,H} = 11.1$ Hz, 2 H, 2 × C*H*$SiMe_2t$Bu), 0.23, 0.24 (2s, each 9 H, 2 × C_5H_4Si*Me*$_3$), 1.17 (s, 18 H, 2 × $CHSiMe_2t$Bu), 3.02 [t, 1 H, *H*C(CHSiMe_2tBu)$_2$], 4.28, 4.54, 4.78, 4.89 (4m, each 2 H, 2 × C_5H_4) ppm. ^{13}C{^{1}H} NMR (50 MHz, C_6D_6, 25 °C): $\delta = -6.1$, −2.4 (CHSi*Me*$_2t$Bu), 0.5, 0.8

 © 2003 Wiley-VCH Verlag GmbH & Co. KGaA, Weinheim

($C_5H_4SiMe_3$), 27.3, 33.7 ($CHSiMe_2tBu$), 39.9 [$CH(CHSiMe_2tBu)_2$], 96.0 [$CH(CHSiMe_2tBu)_2$], 85.6, 88.9, 94.3, 94.5, 101.6, 105.2 (C_5H_4) ppm. $C_{31}H_{59}NbSi_4$ (637.1): calcd. C 58.45, H 9.33; found C 58.29, H 9.25.

Preparation of [NbCp′$_2$(η^3-CH$_2$CHCHSiPh$_3$)] (2): The synthesis of **2** was carried out in an identical manner to that described for **1**. From [K(η^3-$CH_2CHCHSiPh_3$)] (0.31 g, 0.92 mmol) and [{NbCp′$_2$Cl}$_2$] (0.37 g, 0.46 mmol). Yield 0.47 g, 77%. ^{1}H NMR (200 MHz, C_6D_6, 25 °C): δ = −0.13 (d, 1 H, C*H*SiPh$_3$), 0.16, 0.32 (2s, each 9 H, 2 × $C_5H_4SiMe_3$), 1.15 (*anti*), 2.94 (*syn*) (2m, each 1 H, $CH_2CHCHSiPh_3$), 2.81, 3.39, 4.18, 4.38, 4.44, 4.59, 4.82, 5.51 (8m, each 1 H, 2 × C_5H_4), 7.27−8.10 (m, 15 H, Si*Ph*$_3$) ppm. ^{13}C{^{1}H} NMR (50 MHz, C_6D_6, 25 °C): δ = 0.1, 0.5 ($C_5H_4SiMe_3$) 21.8 ($CH_2CHCHSiPh_3$), 38.5 (*C*HSiPh$_3$), 88.1 ($CH_2CHCHSiPh_3$), 84.9, 87.0, 90.3, 93.2, 99.2, 100.1, 100.4, 100.7, 104.4, 105.3 (C_5H_4), 126.0−130.0 (Si*Ph*$_3$) ppm. $C_{37}H_{45}NbSi_3$ (666.9): calcd. C 66.63, H 6.80; found C 66.45, H 6.70.

Preparation of [NbCp′$_2$(CH$_2$CH$_3$)(CN*t*Bu)] (5): To a hexane solution (30 mL) of [NbCp′$_2$H(η^2-CH_2=CH_2)] (**3**) (0.28 g, 0.71 mmol) an equimolar amount of *tert*-butyl isocyanide (80 μL, 0.71 mmol) was added and the reaction mixture was stirred at room temperature for 16 h. The yellow solution gradually became red, and finally a red oily residue was obtained after removing the solvent. The red oily product was shown to be pure by NMR spectroscopy. At 60 °C the reaction takes place in 6 h. IR (KBr): ν_{CN} = 2095 cm^{-1}. ^{1}H NMR (200 MHz, C_6D_6, 25 °C): δ = 0.15 (s, 18 H, 2 × $C_5H_4SiMe_3$), 0.65 (q, $^3J_{H,H}$ = 7.6 Hz, 2 H, CH_2CH_3), 1.20 [s, 9 H, $CNC(CH_3)_3$], 1.33 (t, 3 H, CH_2CH_3), 4.63, 4.72, 5.04, 5.22 (4m, each 2 H, 2 × C_5H_4) ppm. ^{13}C{^{1}H} NMR (50 MHz, C_6D_6, 25 °C): δ = 0.6 ($C_5H_4SiMe_3$), 14.8 (CH_2CH_3), 23.6 (CH_2CH_3), 32.0 [$C(CH_3)_3$], 62.2 [$C(CH_3)_3$], 91.6, 95.6, 96.3, 102.5, 103.5 (C_5H_4), 270.0 (*C*N) ppm.

Preparation of [NbCp′$_2$(CH$_2$CH$_3$)(CNC$_6$H$_3$Me$_2$-2,6)] (6): To a deuterated benzene solution (1 mL) of [NbCp′$_2$H(η^2-CH_2=CH_2)] (**3**) (0.02 g, 0.05 mmol) in an NMR tube was added an excess of 2,6-dimethylphenyl isocyanide (0.01 g, 0.11 mmol). The reaction mixture was immediately monitored by ^{1}H NMR spectroscopy and a mixture of three compounds, the starting hydride-olefin compound **3** and the compounds **6** and **9**, in a 1:0.9:0.75 proportion, was identified. **6:** ^{1}H NMR (200 MHz, C_6D_6, 25 °C): δ = 0.16 (s, 18 H, 2 × $C_5H_4SiMe_3$), 0.81 (q, $^3J_{H,H}$ = 7.7 Hz, 2 H, CH_2CH_3), 1.45 (t, 3 H, CH_2CH_3), 1.64 (s, 6 H, $CNC_6H_3Me_2$), 3.71, 4.11, 5.13, 5.69 (4m, each 2 H, 2 × C_5H_4), 6.39−6.55 (m, 3 H, $CNC_6H_3Me_2$) ppm.

Preparation of [NbCp′$_2$(CH$_2$CH$_3$)(CN*n*Bu)] (7): The synthesis of **7** was carried out in an identical manner to that described for **6**. From [NbCp′$_2$H(η^2-CH_2=CH_2)] (**3**) (0.04 g, 0.10 mmol) and *n*-butyl isocyanide (11 μL, 0.10 mmol). A mixture of **3** and **7** in a 2:1 proportion was identified. **7:** ^{1}H NMR (200 MHz, C_6D_6, 25 °C): δ = 0.16 (s, 18 H, 2 × $C_5H_4SiMe_3$), 0.75 (m, 3 H, $CNCH_2CH_2CH_2CH_3$), 0.83 (q, $^3J_{H,H}$ = 7.7 Hz, 2 H, CH_2CH_3), 0.90 (m, 2 H, $CNCH_2CH_2CH_2CH_3$), 1.25 (m, 2 H, $CNCH_2CH_2CH_2CH_3$), 1.45 (t, 3 H, CH_2CH_3), 3.35 (m, 2 H, $CNCH_2CH_2CH_2CH_3$), 4.63, 4.69, 4.92, 5.17 (4m, each 2 H, 2 × C_5H_4) ppm.

Preparation of [NbCp′$_2$(η^1-CH$_2$CH=CHSiPh$_3$)(CNC$_6$H$_3$Me$_2$-2,6)] (8): The synthesis of **8** was carried out in an identical manner to that described for **6**. From [NbCp′$_2$(η^3-$CH_2CHCHSiPh_3$)] (**2**) (0.02 g, 0.03 mmol) and $CNC_6H_3Me_2$-2,6 (0.01 g, 0.09 mmol). ^{1}H NMR (300 MHz, C_6D_6, 25 °C): δ = 0.04 (s, 18 H, 2 × $C_5H_4SiMe_3$), 2.08 (s, 6 H, $CNC_6H_3Me_2$), 1.65 (d, 2 H, CH_2CH=$CHSiPh_3$), 4.70 (m, 2 H, CH_2CH=C*H*SiPh$_3$), 5.50 (m, 2 H, CH_2CH=$CHSiPh_3$), 4.60, 4.61, 4.89, 5.11, (4m, each 2 H, 2 × C_5H_4), 7.20−7.76 (m, 15 H, SiPh$_3$) ppm.

Preparation of [NbCp′$_2${η^1-C(=NC$_6$H$_3$Me$_2$-2,6)(CH$_2$CH$_3$)}(CNC$_6$H$_3$Me$_2$-2,6)] (9): The synthesis of **9** was carried out in an identical manner to that described for **5**. From [NbCp′$_2$H(η^2-CH_2=CH_2)] (**3**) (0.15 g, 0.39 mmol) and 2,6-dimethylphenyl isocyanide (0.10 g, 0.78 mmol). Yield 0.23 g, 90%. IR (KBr/Nujol): $\tilde{\nu}$ = 1657 ($\nu_{C=N}$, iminoacyl), 2021 (ν_{CN}, isocyanide) cm^{-1}. ^{1}H NMR (200 MHz, C_6D_6, 25 °C): δ = 0.09 (s, 18 H, 2 × $C_5H_4SiMe_3$), 0.90 (t, $^3J_{H,H}$ = 7.6 Hz, 3 H, CH_2CH_3), 2.15 (s, 6 H, $CNC_6H_3Me_2$), 2.17 (s, 6 H, η^1-C{$NC_6H_3Me_2$}), 2.35 (q, 2 H, CH_2CH_3), 4.93, 5.25, 5.28, 5.49 (4m, each 2 H, 2 × C_5H_4), 6.39−6.55 (m, 6 H, 2 × $CNC_6H_3Me_2$) ppm. ^{13}C{^{1}H} NMR (50 MHz, C_6D_6, 25 °C): δ = 0.4 ($SiMe_3$), 11.2 (CH_2CH_3), 19.1 ($CNC_6H_3Me_2$), 19.9 (η^1-C{$NC_6H_3Me_2$}), 44.7 (CH_2CH_3), 91.8, 96.0, 98.2, 98.5, 105.0 (C_5H_4), 120.5−128.9 (η^1-C{N$C_6H_3Me_2$} and CN$C_6H_3Me_2$), 153.6 (η^1-*C*{$NC_6H_3Me_2$}), 218.2 ($CNC_6H_3Me_2$) ppm. $C_{36}H_{49}N_2NbSi_2$ (658.9): calcd. C 65.63, H 7.50, N 4.25; found C 65.50, H 7.42, N 4.25.

Preparation of [NbCp′$_2${η^1-C(=N*n*Bu)(CH$_2$CH$_3$)}(CN*n*Bu)] (10): The synthesis of **10** was carried out in an identical manner to that described for **6**. From [NbCp′$_2$H(η^2-CH_2=CH_2)] (**3**) (0.04 g, 0.10 mmol) and *n*-butyl isocyanide (22 μL, 0.20 mmol). IR (KBr/Nujol): $\tilde{\nu}$ = 1690 ($\nu_{C=N}$, iminoacyl), 2046 (ν_{CN}, isocyanide) cm^{-1}. ^{1}H NMR (200 MHz, C_6D_6, 25 °C): δ = 0.26 (s, 18 H, 2 × $C_5H_4SiMe_3$), 0.96 (t, $^3J_{H,H}$ = 7.7 Hz, 3 H, CH_2CH_3), 0.81, 0.84 (2m, each 3 H, 2 × $CNCH_2CH_2CH_2CH_3$), 0.93, 0.97 (2m, each 2 H, 2 × $CNCH_2CH_2CH_2CH_3$), 1.30, 1.36 (2m, each 2 H, 2 × $CNCH_2CH_2CH_2CH_3$), 2.03 (q, 2 H, CH_2CH_3), 3.25, 3.30 (2m, each 2 H, 2 × $CNCH_2CH_2CH_2CH_3$), 3.38, 3.53, 5.06, 5.43 (4m, each 2 H, 2 × C_5H_4) ppm. ^{13}C{^{1}H} NMR (50 MHz, C_6D_6, 25 °C): δ = 1.3 ($C_5H_4SiMe_3$), 11.4 (CH_2CH_3), 13.5, 16.4, 25.3, 27.2, 34.2, 35.9, 60.4, 62.7 (*n*Bu), 49.5 (CH_2CH_3), 82.5, 93.6, 93.7, 94.7, 97.4 (C_5H_4), 162.6 (η^1-*C*{N*n*Bu}), 222.0 (*C*N*n*Bu) ppm. $C_{28}H_{49}N_2NbSi_2$ (562.8): calcd. C 59.76, H 8.78, N 4.98; found C 59.44, H 8.69, N 4.96.

Preparation of [NbCp′$_2${η^1-C(NC$_6$H$_3$Me$_2$-2,6)(CH$_2$CH=CHSiPh$_3$)}(CNC$_6$H$_3$Me$_2$-2,6)] (11): The synthesis of **11** was carried out in an identical manner to that described for **5**. From [NbCp′$_2$(η^3-$CH_2CHCHSiPh_3$)] (**2**) (0.11 g, 0.17 mmol) and 2,6-dimethylphenyl isocyanide (0.04 g, 0.34 mmol). Yield 0.13 g, 85%. IR (KBr/Nujol): $\tilde{\nu}$ = 1659 ($\nu_{C=N}$, iminoacyl), 2019 (ν_{CN}, isocyanide) cm^{-1}. ^{1}H NMR (200 MHz, C_6D_6, 25 °C): δ = 0.08 (s, 18 H, 2 × $C_5H_4SiMe_3$), 2.06, 2.07 (2s, each 6 H, 2 × $CNC_6H_3Me_2$), 3.54 (d, 2 H, CH_2CH=$CHSiPh_3$), 4.61 (m, 1 H, CH_2CH=C*H*SiPh$_3$), 5.70 (m, 1 H, CH_2CH=$CHSiPh_3$), 4.82, 5.22, 5.28, 5.52 (4m, each 2 H, 2 × C_5H_4), 6.50−7.00 (m, 15 H, SiPh$_3$), 7.20−7.90 (m, 6 H, 2 × $CNC_6H_3Me_2$) ppm. ^{13}C{^{1}H} NMR (50 MHz, C_6D_6, 25 °C): δ = 0.4 ($C_5H_4SiMe_3$), 19.1 ($CNC_6H_3Me_2$), 20.0 (η^1-C{$NC_6H_3Me_2$}), 61.9 (CH_2CH=$CHSiPh_3$), 91.8, 95.3, 97.7, 98.0, 105.6 (C_5H_4), 120.8 (CH_2CH=*C*HSiPh$_3$), 121.6−129.8 (η^1-C{N$C_6H_3Me_2$}, CN$C_6H_3Me_2$ and Si*Ph*$_3$), 150.1 (CH_2CH=$CHSiPh_3$), 171.1 (η^1-*C*{$NC_6H_3Me_2$}), 228.0 ($CNC_6H_3Me_2$) ppm. $C_{55}H_{63}N_2NbSi_3$ (929.3): calcd. C 71.09, H 6.83, N 3.01; found C 70.89, H 6.74, N 3.04.

Preparation of [NbCp′$_2${η^1-C(N-Me$_2$C$_6$H$_3$-2,6)(CH$_2$CH=CH$_2$)}(CNC$_6$H$_3$Me$_2$-2,6)] (12): The synthesis of **12** was carried out in an identical manner to that described for **5**. From [NbCp′$_2$(η^3-CH_2CHCH_2)] (**4**) (0.27 g, 0.66 mmol) and 2,6-dimethylphenyl isocyanide (0.17 g, 1.32 mmol). Yield 0.40 g, 90%. IR (KBr/Nujol): $\tilde{\nu}$ = 1677 ($\nu_{C=N}$, iminoacyl), 2029 (ν_{CN}, isocyanide) cm^{-1}. ^{1}H

 © 2003 Wiley-VCH Verlag GmbH & Co. KGaA, Weinheim

NMR (200 MHz, C_6D_6, 25 °C): δ = 0.09 (s, 18 H, 2 × $C_5H_4Si\mathit{Me}_3$), 2.15, 2.18 (2s, each 6 H, 2 × $CNC_6H_3\mathit{Me}_2$), 3.26 (d, 2 H, $C\mathit{H}_2CH{=}CH_2$), 4.73 (m, 2 H, $CH_2CH{=}C\mathit{H}_2$), 6.10 (m, 2 H, $CH_2C\mathit{H}{=}CH_2$), 4.95, 5.27, 5.29, 5.56 (4m, each 2 H, 2 × $C_5\mathit{H}_4$), 6.60−7.90 (m, 6 H, 2 × $CNC_6\mathit{H}_3Me_2$) ppm. $^{13}C\{^1H\}$ NMR (50 MHz, C_6D_6, 25 °C): δ = 0.4 ($C_5H_4Si\mathit{Me}_3$), 19.2, 19.3 ($CNC_6H_3\mathit{Me}_2$), 58.0 ($\mathit{C}H_2CH{=}CH_2$), 92.5, 96.4, 99.0, 99.3, 105.6 (C_5H_4), 110.6 ($CH_2CH{=}\mathit{C}H_2$), 153.6 ($CH_2\mathit{C}H{=}CH_2$), 115.3−129.9 (η^1-C{$N\mathit{C}_6H_3Me_2$} and $CN\mathit{C}_6H_3Me_2$), 170.0 (η^1-C{$NC_6H_3Me_2$}), 225.0 ($\mathit{C}NC_6H_3Me_2$) ppm. $C_{37}H_{49}N_2NbSi_2$ (670.9): calcd. C 66.24, H 7.36, N 4.18; found C 66.03, H 7.31, N 4.13.

X-ray Crystal Structure Determination of [NbCp′$_2$(η^3-*t*BuMe$_2$Si-CHCHCHSiMe$_2$*t*Bu)] (1): The crystallographic data and experimental details are given in Table 2. Crystallographic reflections were collected at 230 K on a Nonius-Mach3 diffractometer equipped with graphite-monochromated radiation (λ = 0.71073 Å). Unit cell dimensions were obtained by least-squares fit of the 2θ values of 25 high-order reflections by using the Mach3 centring routines. The intensities of 8372 reflections were collected ($2 < \theta < 28$); of these only 5489 reflections obeyed the condition $I > 2\sigma(I)$. Data were corrected in the usual fashion for Lorentz and polarisation effects and absorption correction was not necessary. The structure was solved by direct methods (SIR92)[22] and refinement on F^2 was carried out by full-matrix least-squares analysis (SHELXL-97).[23] A number of cycles of refinement with isotropic thermal parameters, followed by difference synthesis, enabled location of all the non-hydrogen atoms. For the final cycles of refinement all non-hydrogen atoms were refined anisotropically, while the hydrogen atoms were included in calculated positions but non refined. CCDC-201888 contains the supplementary crystallographic data for this paper. These data can be obtained free of charge at www.ccdc.cam.ac.uk/conts/retrieving.html [or from the Cambridge Crystallographic Data Centre, 12 Union Road, Cambridge CB2 1EZ, UK; fax:(internat.) +44−1223/336−033; Email: deposit@ccdc.cam.ac.uk].

Table 2. Crystal data and structure refinement for **1**

Empirical formula	$C_{31}H_{59}NbSi_4$
Molecular mass	637.05
Temperature	230(2) K
Wavelength	0.71073 Å
Crystal system, space group	Monoclinic, $P2_1/c$
Unit cell dimensions	a = 11.875(3) Å b = 25.236(3) Å, β = 107.57(2)° c = 12.701(2) Å
Volume	3628.6(12) Å^3
Z, calculated density	4, 1.166 g/cm^3
Absorption coefficient	4.81 cm^{-1}
F(000)	1368
Crystal size	0.3 × 0.2 × 0.2 mm
Limiting indices	$0 \le h \le 15$, $0 \le k \le 33$, $-14 \le l \le 14$
Reflections collected / unique	8372/8372 [R(int) = 0.0000]
Data/restraints/parameters	8372/0/337
Goodness-of-fit on F^2	1.014
Final R indices [$I > 2\sigma(I)$]	$R1$ = 0.0424, $wR2$ = 0.1039
R indices (all data)	$R1$ = 0.0828, $wR2$ = 0.1734
Largest diff. peak and hole	0.551 and −0.741 e·Å^{-3}

Acknowledgments

We gratefully acknowledge financial support from the Dirección General de Enseñanza Superior e Investigación Científica, Spain (Grants. No. BQU2002−04638-C02−01 and No. BQU2000−0463), the Junta de Comunidades de Castilla-La Mancha (PAC-02−003) and the Universidad Rey Juan Carlos (projects PIPR-02−09 and PIPR-02−02).

[1] K. R. Flower, *Adv. Organomet. Chem.* **2000**, *28*, 404−454.
[2] F. W. Sietger, H. J. de Liefde Meijer, *J. Organomet. Chem.* **1970**, *23*, 177−183.
[3] A. Van Baalen, C. J. Groenenboom, H. J. de Liefde Meijer, *J. Organomet. Chem.* **1974**, *74*, 245−253.
[4] H. C. Strauch, G. Erker, R. Fröhlich, *J. Organomet. Chem.* **2000**, *593/594*, 388−391.
[5] H. Yasuda, T. Arai, T. Okamoto, A. Nakamura, *J. Organomet. Chem.* **1989**, *361*, 161−171.
[6] D. M. Antonelli, A. Leins, J. M. Stryker, *Organometallics* **1997**, *16*, 2500−2502.
[7] A. Antiñolo, C. Huertas, I. del Hierro, M. F. Lappert, A. Otero, S. Prashar, A. M. Rodríguez, E. Villaseñor, *Organometallics* **1998**, *17*, 5874−5879.
[8] See for example: [8a] A. Antiñolo, F. Carrillo-Hermosilla, J. Fernández-Baeza, S. García-Yuste, A. Otero, J. Sánchez-Prada, E. Villaseñor, *J. Organomet. Chem.* **2000**, *609*, 123−129. [8b] A. Antiñolo, F. Carrillo-Hermosilla, J. Fernández-Baeza, S. García-Yuste, A. Otero, A. M. Rodríguez, J. Sánchez-Prada, E. Villaseñor, R. Gelabert, M. Moreno, J. M. Lluch, A. Lledós, *Organometallics* **2000**, *19*, 3654−3663. [8c] A. Antiñolo, F. Carrillo-Hermosilla, J. Fernández-Baeza, S. García-Yuste, A. Otero, J. Sánchez-Prada, E. Villaseñor, *Eur. J. Inorg. Chem.* **2000**, 1437−1443. [8d] A. Antiñolo, F. Carrillo-Hermosilla, J. Fernández-Baeza, A. M. Fernández de Toro, S. García-Yuste, A. Otero, J. C. Pérez-Flores, A. M. Rodríguez, *Inorg. Chim. Acta* **2000**, *300−302*, 131−137.
[9] E. Singleton, H. E. Oosthuizen, *Adv. Organomet. Chem.* **1983**, *22*, 209−310.
[10] A. Antiñolo, F. Carrillo-Hermosilla, I. del Hierro, A. Otero, M. Fajardo, Y. Mugnier, *Organometallics* **1997**, *16*, 4161−4166.
[11] [11a] F. A. Cotton, G. Wilkinson, C. A. Murillo, M. Bochmann, in *Advanced Inorganic Chemistry, 6th Ed.,* John Wiley & Sons, New York, **1999**; p. 246. [11b] L. D. Durfee, I. P. Rothwell, *Chem. Rev.* **1988**, *88*, 1059−1079.
[12] [12a] P. B. Hitchcock, M. F. Lappert, W.-P. Leung, D. Liu, T. C. M. Mak, Z.-X. Wang, *J. Chem. Soc., Dalton Trans.* **1999**, 1257−1262. [12b] R. Fernández-Galán, P. B. Hitchcock, M. F. Lappert, A. Antiñolo, A. M. Rodriguez, *J. Chem. Soc., Dalton Trans.* **2000**, 1743−1749.
[13] L. K. Cheatham, J. J. Graham, A. W. Apblett, A. R. Barrow, *Polyhedron* **1991**, *10*, 1075−1078.
[14] J. Chen, Y. Kai, N. Kasai, H. Yasuda, H. Yamamoto, A. Nakamura, *J. Organomet. Chem.* **1991**, *407*, 191−205.
[15] A. Antiñolo, F. Carrillo-Hermosilla, M. Fajardo, S. García-Yuste, A. Otero, S. Camanyes, F. Maseras, M. Moreno, A. Lledós, J. M. Lluch, *J. Am. Chem. Soc.* **1997**, *19*, 6107−6114.
[16] A. Castro, M. V. Galakhov, M. Gómez, P. Gómez−Sal, A. Martín, F. Sánchez, *J. Organomet. Chem.* **2000**, *595*, 36−53.
[17] A. Antiñolo, M. Fajardo, R. Gil-Sanz, C. López-Mardomingo, P. Martín-Villa, A. Otero, M. Kubicki, Y. Mugnier, S. El Krami, Y. Mourad, *Organometallics* **1993**, *12*, 381−388.
[18] E. Boring, M. Sabat, M. G. Finn, R. N. Grimes, *Organometallics* **1997**, *16*, 3993−4000.
[19] R. D. Adams, D. F. Chodosh, *Inorg. Chem.* **1978**, *17*, 41−48.
[20] J. Sánchez-Nieves, P. Royo, M. A. Pellinghelli, A. Tiripicchio, *Organometallics* **2000**, *19*, 3161−3169.
[21] [21a] A. Filippou, C. Volkl, P. Kiprof, *J. Organomet. Chem.* **1991**, *415*, 375−394. [21b] J. P. Daff, A. Monge, P. Palma, M.

 © 2003 Wiley-VCH Verlag GmbH & Co. KGaA, Weinheim

N. Poveda, C. Ruiz, P. Valerga, E. Carmona, *Organometallics* **1997**, *16*, 2263−2275.
[22] A. Altomare, G. Cascarano, C. Giacovazzo, A. Guagliardi, M. C. Burla, G. Polidori, M. Camalli, *J. Appl. Cryst.* **1994**, 435−435.
[23] G. M. Sheldrick, Program for the Refinement of Crystal Structures from Diffraction Data, University of Göttingen, Germany, **1997**.

Received January 27, 2003

 © 2003 Wiley-VCH Verlag GmbH & Co. KGaA, Weinheim

The Reactivity of Primary and Secondary Amines, Secondary Phosphanes and N-Heterocyclic Carbenes towards Group-13 Metal(I) Halides

Robert J. Baker,[a] Helga Bettentrup,[a] and Cameron Jones*[a]

Keywords: Group-13 elements / Carbene ligands / Phosphanes / Sub-oxidation state

The reactions of a variety of primary and secondary amines and secondary phosphanes with "GaI" have been examined. In all cases disproportionation reactions occurred which led to the gallium(II) iodide complexes $[Ga_2I_4(L)_2]$ [L = $NCyH_2$, N*t*BuH_2, NCy_2H, PCy_2H or P*t*Bu$_2$H (Cy = cyclohexyl)]. All complexes have been crystallographically characterised and have been shown to be dimers possessing Ga–Ga bonds. The reaction of the sterically hindered N-heterocyclic carbene IPr [:CN(Ar)C_2H_2N(Ar) (Ar = C_6H_3iPr$_2$-2,6)] with "GaI" was also carried out and the novel salt $[Ga_2I_5(IPr)][IPrH]$ was formed in good yield and crystallographically characterised. Finally, the related reaction of the less hindered cyclic carbene IMe [:CN(Me)C_2Me$_2$N(Me)] with InCl gave a low yield of the crystallographically characterised salt [{InCl(IMe)}$_2$(μ-Cl)(μ-O)][Cl] which presumably forms due to the presence of adventitious oxygen in the reaction mixture.
(© Wiley-VCH Verlag GmbH & Co. KGaA, 69451 Weinheim, Germany, 2003)

Introduction

Over the past five years there has been a rapidly increasing interest in the chemistry of metastable aluminium(I) and gallium(I) halide complexes $[\{MX(L)\}_n]$ (**1**: M = Al or Ga; X = halide; L = ether, amine or phosphane). These have been invariably prepared by the co-condensation of the metal(I) halide with the donor solvent using a specially designed reactor, and several have been crystallographically characterised, for example $[Al_4Br_4(NEt_3)_4]$.[1] Studies of the reactivity of group-13 metal(I) halide complexes have provided an array of remarkable results, not least of which come from their use in the formation of polyhedral halide, such as $[Al_{22}Br_{20}(THF)_{12}]$, amide, such as $[Ga_{84}\{N(SiMe_3)_2\}_{20}]^{4-}$, alkyl, such as $[Ga_{19}\{C(SiMe_3)_3\}_6]^-$, and silyl, such as $[Ga_{26}\{Si(SiMe_3)_3\}_8]^{2-}$, metalloid clusters.[2] Attempts have been made to prepare **1**, with M = Ga and L = PEt_3 or PPh_3, from the reaction of PEt_3 or PPh_3 with "GaI".[3] These reactions, however, led to partial disproportionation and the facile formation of the gallium(II) iodide complexes $[Ga_2I_4(PR_3)_2]$ (R = Et or Ph), and the mixed oxidation state complex $[Ga_3I_5(PEt_3)_3]$, all of which were crystallographically characterised. It is noteworthy that only two other neutral gallium(II) iodide adducts $[Ga_2I_4(L)_2]$ (L = NEt_3 [4] or $AsEt_3$ [5]), which were prepared by alternative routes, have been structurally authenticated.

Surprisingly there are no known structurally characterised indium analogues of **1**. Recently, we attempted the preparation of such a compound using an N-heterocyclic carbene (NHC) as the donor ligand in a reaction with InBr. As in the aforementioned reactions of phosphanes with "GaI" this led to partial disproportionation and the formation of the indium(II) bromide complex $[In_2Br_4(IMes)_2]$ with IMes being the cyclic carbene :CN(Mes)C(H)C(H)N(Mes) (Mes = mesityl).[6] In the present study we have extended this work by examining the reactivity of several NHCs towards indium(I) and gallium(I) halides. In addition, the reactions of a variety of primary and secondary amines and secondary phosphanes with "GaI" have been carried out and these have led to the formation of the first crystallographically characterised complexes of the type $[Ga_2I_4(L)_2]$ (L = NR_2H, NRH_2, PR_2H).

[a] Department of Chemistry, Cardiff University,
P. O. Box 912, Park Place, Cardiff, CF10 3TB, U.K.

Results and Discussion

Amine and Phosphane Reactions

In all reactions depicted in Scheme 1 "GaI" was prepared by sonicating gallium metal with 0.5 equiv. of I_2 in toluene at 50 °C according to the method of Green et al.[7] A toluene suspension of this material was treated with a variety of amines and phosphanes at −78 °C. Upon warming the reaction mixtures to room temperature gallium metal deposition was observed. The resulting suspensions were filtered and cooled to −30 °C affording moderate to high yields of the gallium(II) iodide adducts **2**−**6**. The mechanism of formation of these compounds presumably involves partial disproportionation of the "GaI" reagent upon treatment with the Lewis bases. All compounds are, however, quite stable at room temperature in both solution and the solid state and no further disproportionation to gallium(III) iodide complexes was observed.

 © 2003 Wiley-VCH Verlag GmbH & Co. KGaA, Weinheim **DOI: 10.1002/ejic.200300068**

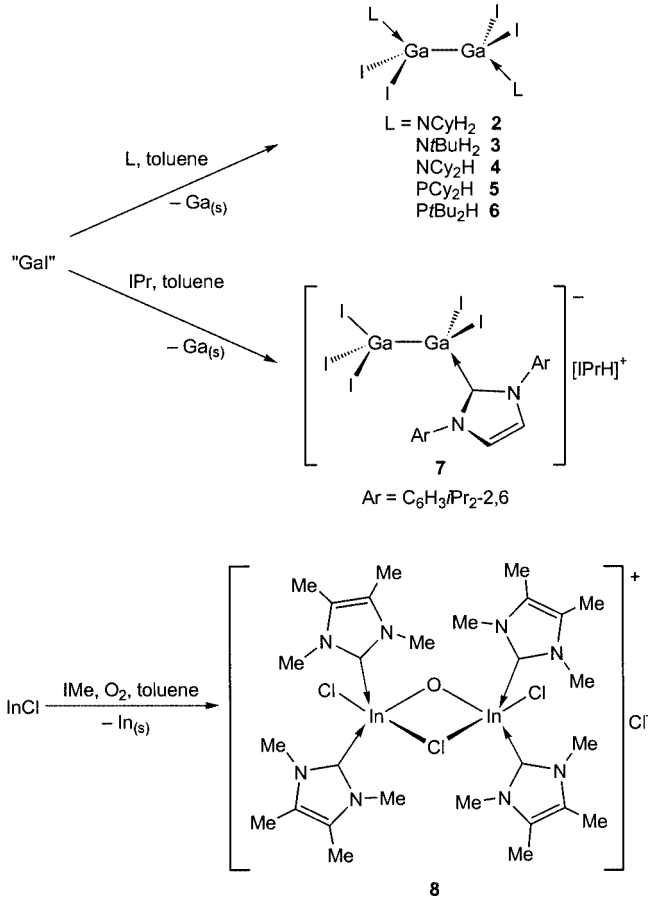

Scheme 1. Preparation of complexes **2**−**8**

The infrared spectra of all the amine complexes **2**−**4** display strong, broad N−H stretching absorptions in the expected region but the amine proton resonance was only observed in the ^{1}H NMR spectrum of **3**. The infrared spectra of **2**−**4** exhibit bands at 450, 453 and 409 cm^{-1} which have been assigned to Ga−N stretches from comparisons with related alkylgallium−amine adducts.[8] The infrared spectra of the secondary phosphane complexes **5** and **6** show P−H stretching bands at 2258 and 2353 cm^{-1}, respectively. In addition, their ^{31}P NMR spectra reveal doublet resonances with $^1J_{PH}$ coupling constants (**5**: 359 Hz; **6**: 351 Hz) of a significantly greater magnitude than those recorded for the free phosphanes (PCy_2H: 193 Hz; $PtBu_2H$: 198 Hz). A similar trend has been reported for secondary phosphane adducts of trialkylgallium compounds.[9] It should be noted that the reactions of several primary phosphanes, thiols and bulky alcohols with "GaI" were carried out but no tractable products could be obtained.

N-Heterocyclic Carbene Reactions

Due to the now well-known analogy between phosphanes and NHCs,[10] and given our previous preparation of [$In_2Br_4(IMes)_2$], it was thought worthwhile to examine the reactivity of a series of NHC ligands with "GaI". Unfortunately, success was only achieved with the reaction of the very hindered cyclic carbene IPr and "GaI" in toluene. Considerable gallium metal deposition was observed in this reaction and upon workup a good yield of the novel salt **7** resulted (Scheme 1). It is interesting that the nature of this product is different to that of the neutral complex [$In_2Br_4(IMes)_2$], but it seems likely that the imidazolium proton of the cation was abstracted from the solvent as this reaction is entirely reproducible in good yield, even when it is carried out under strictly anhydrous conditions. The fact that the anion of **7** contains only one coordinated carbene ligand, as opposed to the two cyclic carbene ligands in [$In_2Br_4(IMes)_2$], could be due to the greater bulk of the cylic carbene IPr and a lesser covalent radius of the metal atom in the former complex. It is also worth noting here that the formulation of "GaI" has been proposed to be $[Ga]_2[Ga_2I_6]$ based on Raman spectroscopic studies.[11] It is not inconceivable that the anion of **7** could be formed by displacement of one iodide ligand from the $[Ga_2I_6]^{2-}$ dianion of such a compound. The ^{1}H and ^{13}C NMR spectra of **7** show two sets of resonances which integrate in a 1:1 ratio and were assigned to the imidazolium cation and the cyclic carbene IPr coordinated to a gallium centre. The distinction between the two sets of resonances can be confidently made as the imidazolium cation has recently been structurally and spectroscopically characterised in the salt [IPrH][$InBr_4$].[12] The fact that sharp resonances were observed for both the imidazolium and carbene moieties over a range of temperatures suggests that the carbene ligand is strongly coordinated to the gallium centre and there is no carbene/imidazolium exchange occurring in this complex.

Reaction of the sterically less hindered cyclic carbene **:**CN(Me)C(Me)C(Me)N(Me) (IMe) with "GaI" also resulted in considerable gallium metal deposition, but only an inseparable mixture of unknown products formed. In contrast, the reaction of the same cyclic carbene with InCl afforded the unusual oxo-bridged dimer [{InCl(IMe)$_2$}$_2$(μ-Cl)(μ-O)][Cl] (**8**) in low yield (Scheme 1). This probably forms due to the presence of adventitious oxygen in the reaction mixture. Neither compound **8** nor any other product could be isolated or identified when the reaction was repeated under strictly anaerobic conditions. The spectroscopic data for **8** fully support its proposed structure; most notably an In−O stretch was observed at 335 cm^{-1} in its infrared spectrum. This is in good agreement with other examples in the literature.[13] No O−H stretching absorption could be seen in the same spectrum, which provides good evidence that there is no proton attached to the bridging oxygen centre.

Structural Studies

Crystals of **2**−**8** were grown from toluene solutions and the molecular structures of these compounds are depicted in Figures 1−7 (see also Tables 1 and 2). The five amine and phosphane complexes of Ga_2I_4, viz. **2**−**6**, display similar structural features in that their gallium centres all possess distorted tetrahedral environments and each

 © 2003 Wiley-VCH Verlag GmbH & Co. KGaA, Weinheim

$[Ga_2I_4(L)_2]$ molecule exhibits a staggered conformation with respect to the Ga−Ga bond. A previous report has suggested that some geometrical parameters of complexes of the type $[Ga_2I_4(L)_2]$ can be used to gauge the relative Lewis basicity of the donor ligands L with respect to the Ga^{II} centres in these complexes.[3] Specifically, differences in gallium−gallium bond lengths and trends towards more sp^2-like geometries at the gallium centres, as evidenced by an increase in the I−Ga−I angle, were employed for this task. The complexes in the present study do not, however, appear to follow any trends (see Table 1). For example, the Ga−Ga bond lengths in **2**−**6** are all very similar [2.4243(9)−2.459 Å (av.)] despite incorporating a range of amine and phosphane ligands of variable basicity. In addition, the I−Ga−I angles in all complexes do not vary to any great degree. We believe, however, that a better indication of the degree of sp^2 character at each gallium centre can be gained from the sum of the I−Ga−I and Ga−Ga−I angles around them. In the five complexes studied here, these values range from 332.1 to 336.4°. Again, this range is too narrow to draw any firm conclusions on the basicity of the ligands involved. The Ga−P bond lengths in complexes **5** and **6** are similar to those in $[Ga_2I_4(PEt_3)_2]$ (2.413 Å) and $[Ga_2I_4(PPh_3)_2]$ (2.445 Å),[3] whilst the Ga−N distances in compounds **2**−**4** are close to those in the only known tertiary amine complex of gallium(II) iodide, namely $[Ga_2I_4(NEt_3)_2]$ (2.094 Å av.).[4]

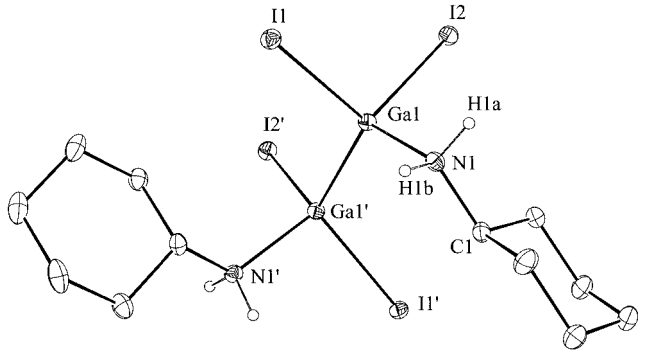

Figure 1. Molecular structure of **2**; symmetry operation: $' -x + 3/2, -y - 1/2, z$

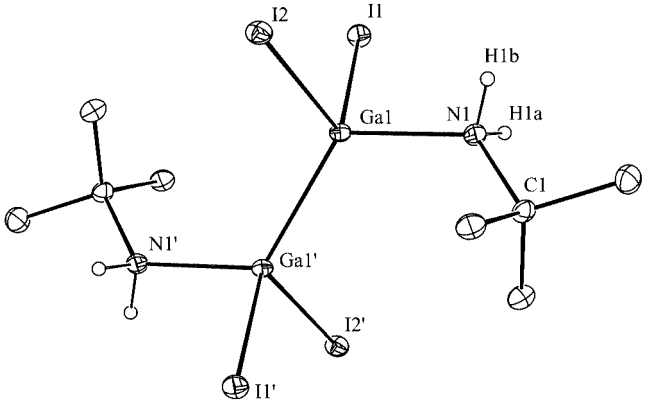

Figure 2. Molecular structure of **3**; symmetry operation: $' -x + 1, -y + 1, z$

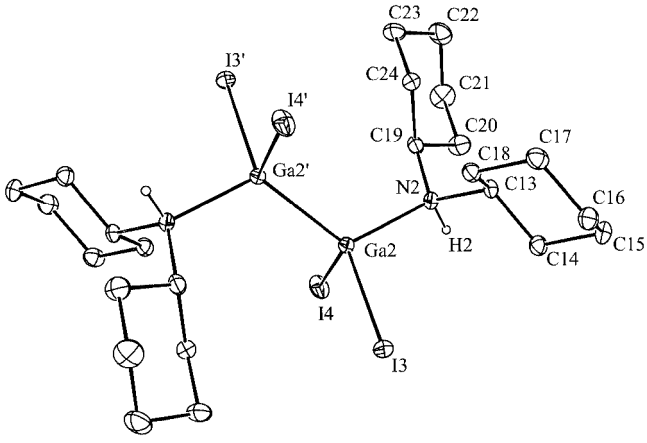

Figure 3. Molecular structure of **4**; symmetry operation: $' -x, -y + 1, -z$

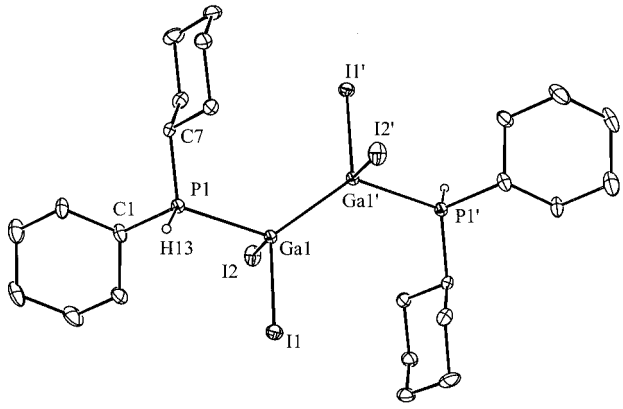

Figure 4. Molecular structure of **5**; symmetry operation: $' -x + 2, -y, -z + 2$

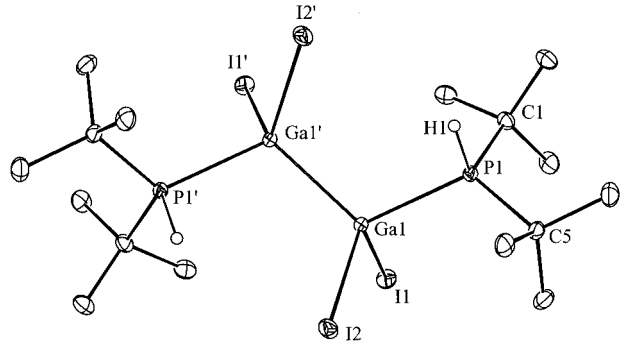

Figure 5. Molecular structure of **6**; symmetry operation: $' -x + 1, y, -z + 3/2$

The molecular structure of the anion of **7** is depicted in Figure 6. Both gallium centres have distorted tetrahedral coordination environments and the Ga−Ga distance [2.4739(12) Å] is slightly longer than any in **2**−**6**, and significantly longer than previously seen in the $[Ga_2I_6]^{2-}$ dianion, for example 2.413 Å in $[PPh_3H][Ga_2I_6]$.[14] All the Ga−I distances are similar to those in related systems, for example $[PPh_3H][Ga_2I_6]$, although the Ga−I bond lengths of the

 © 2003 Wiley-VCH Verlag GmbH & Co. KGaA, Weinheim

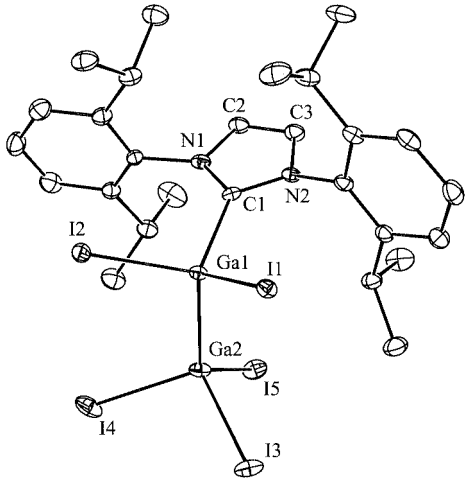

Figure 6. Structure of the anionic component of **7**; selected bond lengths [Å] and angles [°]: Ga(1)−Ga(2) 2.4739(12), Ga(1)−I(1) 2.5977(11), Ga(1)−I(2) 2.5819(10), Ga(2)−I(3) 2.6178(11), Ga(2)−I(4) 2.6153(12), Ga(2)−I(5) 2.6068(12), Ga(1)−C(1) 2.070(7), N(1)−C(1) 1.361(9), N(1)−C(2) 1.372(9), C(2)−C(3) 1.345(11), N(2)−C(3) 1.384(9), N(2)−C(1) 1.358(9); C(1)−Ga(1)−Ga(2) 117.54(18), C(1)−Ga(1)−I(2) 109.81(19), Ga(2)−Ga(1)−I(2) 108.64(4), C(1)−Ga(1)−I(1) 107.09(19), Ga(2)−Ga(1)−I(1) 109.57(4), I(2)−Ga(1)−I(1) 103.24(4), Ga(1)−Ga(2)−I(5) 120.13(4), Ga(1)−Ga(2)−I(4) 111.00(5), I(5)−Ga(2)−I(4) 105.40(4), Ga(1)−Ga(2)−I(3) 112.29(4), I(5)−Ga(2)−I(3) 103.80(4), I(4)−Ga(2)−I(3) 102.53(4), C(1)−N(1)−C(2) 111.1(6), C(1)−N(1)−C(4) 127.0(6), C(2)−N(1)−C(4) 121.0(6), C(1)−N(2)−C(3) 110.1(6), N(2)−C(1)−N(1) 104.7(6), C(3)−C(2)−N(1) 106.7(7), C(2)−C(3)−N(2) 107.4(7)

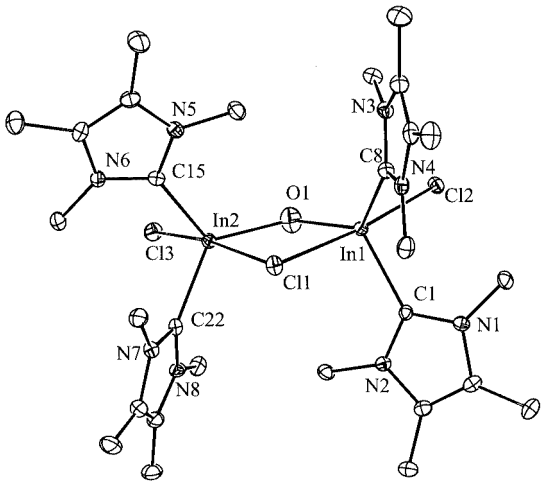

Figure 7. Structure of the cationic component of **8**; selected bond lengths [Å] and angles [°]: In(1)−Cl(1) 2.823(2), In(1)−Cl(2) 2.592(2), In(1)−O(1) 2.174(7), In(1)−C(1) 2.233(7), In(1)−C(8) 2.235(7), In(2)−Cl(1) 2.921(2), In(2)−Cl(3) 2.542(2), In(2)−O(1) 2.172(7), In(2)−C(15) 2.221(7), In(2)−C(22) 2.218(8); In(1)−O(1)−In(2) 113.6(3), In(1)−Cl(1)−In(2) 78.54(5), Cl(2)−In(1)−C(1) 94.64(18), Cl(2)−In(1)−C(8) 91.51(19), C(1)−In(1)−C(8) 109.2(3), Cl(1)−In(1)−Cl(2) 172.16(6), O(1)−In(1)−C(1) 120.0(3), O(1)−In(1)−C(8) 128.7(3), C(15)−In(2)−C(22) 107.9(3), C(15)−In(2)−Cl(3) 95.46(19), C(22)−In(2)−Cl(3) 92.6(2), C(15)−In(2)−O(1) 121.3(3), C(15)−In(2)−Cl(1) 87.00(19), C(22)−In(2)−O(1) 126.9(3), C(22)−In(2)−Cl(1) 81.1(2), Cl(1)−In(2)−Cl(3) 173.72(7), N(1)−C(1)−N(2) 105.5(6), N(3)−C(8)−N(4) 105.6(6), N(5)−C(15)−N(6) 103.9(6), N(7)−C(22)−N(8) 104.9(6)

Table 1. Selected bond lengths [Å] and angles [°] for compounds **2**−**6**

Compound	**2**	**3**	**4**	**5**	**6**
Ga−N/P	2.020(4)	2.036(3)	2.083 av.	2.424(2)	2.4459(10)
Ga−Ga	2.4287(10)	2.4243(9)	2.459 av.	2.4370(15)	2.4448(9)
Ga−I	2.5951(7)	2.5769(7)	2.586 av.	2.5924(10)	2.5935(6)
	2.5727(7)	2.5731(8)		2.5755(11)	2.5745(6)
I−Ga−I	108.17(2)	107.965(1)	104.8 av.	110.07(3)	104.91(2)
ΣI−Ga−I and Ga−Ga−I	335.8	334.8	334.8 av.	336.4	332.1

GaI_3 fragment are slightly longer than those associated with the carbene-coordinated gallium centre. The metric parameters of the coordinated NHC ligand are similar to those seen in other group-13 complexes, such as $[InBr_3(IPr)]$,[12] and the Ga−C interaction is similar to those in NHC−Ga(III) complexes, cf. 2.077 Å (av.) in $[GaH_3\{CN(i\text{Pr})C_2Me_2N(i\text{Pr})\}]$.[15]

The crystal structure of the cationic component of **8** is shown in Figure 7. The indium atoms both have distorted trigonal-bipyramidal coordination environments whilst the four-membered In_2ClO ring is essentially flat (In−Cl−In−O torsion angle 0.7°). The average In−C bond of 2.227 Å is similar to that found in the complex $[InH_3(IMes)]$ [2.250(10) Å].[16] Interestingly, both the terminal and bridging In−Cl bonds (2.567 Å av. and 2.872 Å av., respectively) are considerably longer than the norms for such bonds (2.45 and 2.59 Å)[17] and indeed, the bridging Cl^- ligand can be thought of as only having an interaction with the indium centres. The acuteness of the In−Cl−In angle [78.54(5)°] adds weight to this proposal. This situation most likely arises from the fact that each indium centre is coordinated by two highly nucleophilic NHC ligands, which weaken the bonds from the other ligands to these metal centres.

Conclusions

In conclusion, we have shown that "GaI" reacts with a range of primary and secondary amine and secondary phosphane ligands to give adducts of the type $[Ga_2I_4(L)_2]$ (L = Lewis base), which are formed by disproportionation reactions. A range of these complexes have been crystallographically characterised, as have the products from the related reactions of N-heterocyclic carbenes with either "GaI" or InCl. We believe that complexes of the type **2**−**6**

 © 2003 Wiley-VCH Verlag GmbH & Co. KGaA, Weinheim

Table 2. Crystallographic data for compounds **2**−**8**

	2	**3**	**4**	**5**	**6**·C_7H_8	**7**·$(C_7H_8)_4$	**8**·CH_2Cl_2
Empirical formula	$C_{12}H_{26}Ga_2I_4N_2$	$C_8H_{22}Ga_2I_4N_2$	$C_{24}H_{46}Ga_2I_4N_2$	$C_{24}H_{46}Ga_2I_4P_2$	$C_{23}H_{46}Ga_2I_4P_2$	$C_{82}H_{105}Ga_2I_5N_4$	$C_{29}H_{50}Cl_6In_2N_8O$
Formula mass	845.39	793.32	1009.67	1043.59	1031.58	1920.64	969.11
Temp. [K]	293(2)	150(2)	298(2)	150(2)	150(2)	150(2)	150(2)
Crystal system	orthorhombic	monoclinic	monoclinic	monoclinic	orthorhombic	monoclinic	monoclinic
Space group	*Pccn*	$P2_1/c$	$P2_1/c$	$P2_1/n$	*Pbcn*	$P2_1/c$	$P2_1/n$
a [Å]	20.992(4)	9.2720(19	19.688(4)	9.6600(19)	18.548(4)	17.216(3)	12.774(3)
b [Å]	8.0880(16)	10.325(2)	9.858(2)	14.478(3)	14.559(3)	27.028(5)	25.620(5)
c [Å]	13.222(3)	10.928(2)	17.111(3)	13.154(3)	13.125(3)	17.801(4)	13.118(3)
β [°]	90	94.22(3)	90.11(3)	107.98(3)	90	92.48(3)	92.49(3)
V [Å^3]	2244.9(8)	1043.3(4)	3321.0(11)	1749.8(6)	3544.3(12)	8275(3)	4289.1(15)
Z	4	2	4	2	4	4	4
$D_{calcd.}$ [g/cm^3]	2.501	2.525	2.019	1.981	1.933	1.542	1.501
μ [mm^{-1}]	7.896	8.484	5.356	5.171	5.105	2.559	1.481
Unique reflections	2567	2381	5837	3193	4061	14469	7503
Observed reflections [$I > 2\sigma(I)$]	2111	2093	4067	2784	3533	11598	6168
R (obsd. data)	0.0303	0.0300	0.0411	0.0452	0.0306	0.0598	0.0679
R_w (wR^2) (all data)	0.0636	0.0693	0.0906	0.1003	0.0720	0.1364	0.1522

have significant potential for use as precursors in the formation of heterocyclic and cage compounds containing low oxidation state Ga centres. To this end we are currently examining their reactivity towards a number of strong bases in the expectation that HI abstraction will occur. Our efforts in this area will be reported in a forthcoming publication.

Experimental Details

General Remarks: All manipulations were carried out using standard Schlenk and glove-box techniques under high-purity argon. Toluene was distilled from potassium whilst CH_2Cl_2 was distilled from CaH_2 then freeze/thaw-degassed prior to use. ^{1}H and ^{13}C NMR spectra were recorded with a Bruker DXP400 spectrometer and are referenced to the residual ^{1}H or ^{13}C resonances of the solvent used. ^{31}P NMR spectra were recorded with a Jeol Eclipse 300 spectrometer and are referenced to 85% H_3PO_4. APCI mass spectra were recorded using a VG Fisons Platform II instrument. FAB mass spectra were recorded by the EPSRC National Mass Spectrometric Service at Swansea University. IR spectra were recorded using a Nicolet 510 FT-IR spectrometer as Nujol mulls between CsI plates. Melting points were determined in sealed glass capillaries under argon and are uncorrected. Reproducible microanalyses were not obtained on any of the crystallographically characterised complexes because of the presence of solvent of crystallisation and/or the air-sensitive nature of these complexes. In all cases, however, the spectroscopic data pointed to the bulk materials having a purity of greater than 98%. "GaI'' was synthesised by a variation of the literature method[7] as were the cyclic carbenes IPr[18] and IMe.[19] All other chemicals were obtained commercially and used as received. Compounds **2**−**6** were prepared by the general procedure outlined below.

[$Ga_2I_4(NCyH_2)_2$] (2): GaI was synthesised by sonicating Ga (0.343 g, 4.92 mmol) and I_2 (0.62 g, 2.45 mmol) in toluene (10 mL) at 50 °C for approx. 2 h. The resulting green suspension was cooled to −78 °C and a solution of $NCyH_2$ (1.12 mL, 9.8 mmol) in toluene (5 mL) added to it over 5 min. The reaction mixture was warmed to room temperature and stirred for 12 h to give a brown solution and a precipitate of Ga metal. Filtration, concentration in vacuo and placement at −30 °C overnight yielded colourless crystals of **2** (0.38 g, 36%). M.p. 255−258 °C (dec). ^{1}H NMR (400 MHz, C_6D_6, 300 K): δ = 1.16 (m, 8 H, CH_2), 1.69 (m, 8 H, CH_2), 2.03 (m, 4 H, CH_2), 2.94 (m, 2 H, CH) ppm; NH_2 resonance not observed. ^{13}C NMR (100.6 MHz, C_6D_6, 300 K): δ = 35.6, 25.4, 24.9 (CH_2), 51.4 (CH) ppm. IR (Nujol): $\tilde{\nu}$ = 3427 (br.), 1940 (br.), 1463 (sh), 1377 (sh), 1260 (sh), 1087 (br.), 1017 (br.), 956 (m), 888 (w), 799 (s), 723 (m), 584 (w), 534 (w), 467 (m), 450 (m), 377 (br.), 331 (m). MS APCI: *m*/*z* (%) = 83 (100) [Cy^+], 100 (40) [$CyNH_3^+$], 268 (10) [Ga_2I^+].

[$Ga_2I_4(NtBuH_2)_2$] (3): Yield 48%. M.p. 161−164 °C (dec). ^{1}H NMR (400 MHz, C_6D_6, 300 K): δ = 1.17 (s, 18 H, *t*Bu), 8.52 (br., 4 H, NH_2) ppm. ^{13}C NMR (100.6 MHz, C_6D_6, 300 K): δ = 27.8 [$C(CH_3)_3$], 53.1 [$C(CH_3)_3$] ppm. IR (Nujol): $\tilde{\nu}$ = 3236 (sh), 3176 (sh), 1554 (sh), 1463 (s), 1374 (s), 1277 (m), 1257 (m), 1197 (w), 1163 (m), 1101 (br.), 1016 (w), 820 (m), 801 (m), 733 (m), 681 (m), 596 (br.), 453 (br.), 371 (w) cm^{-1}. MS FAB: *m*/*z* (%) = 57 (100) [tBu^+], 74 (24) [$tBuNH_3^+$].

[$Ga_2I_4(NCy_2H)_2$] (4): Yield 95%. M.p. 215−217 °C (dec). ^{1}H NMR (400 MHz, C_6D_6, 300 K): δ = 1.05 (m, 16 H, CH_2), 1.70 (m, 16 H, CH_2), 1.95 (m, 8 H, CH_2), 3.30 (m, 4 H, CH) ppm; NH resonance not observed. ^{13}C NMR (100.6 MHz, C_6D_6, 300 K): δ = 23.8, 23.9, 32.2 (CH_2), 57.7 (CH) ppm. IR (Nujol): $\tilde{\nu}$ = 3427 (w), 1453 (s), 1376 (s), 1260 (m), 1162 (w), 1122 (m), 1081 (s), 1028 (m), 960 (m), 916 (w), 895 (w), 800 (m), 715 (m), 409 (br.) cm^{-1} . MS FAB: *m*/*z* (%) = 182 (100) [Cy_2NH^+], 648 (8) [Ga_2I_2].

[$Ga_2I_4(PCy_2H)_2$] (5): Yield 41%. M.p. 78−81 °C (dec). ^{1}H NMR (400 MHz, C_6D_6, 300 K): δ = 1.10 (m, 16 H, CH_2), 1.62 (m, 16 H, CH_2), 2.09 (m, 8 H, CH_2), 2.59 (m, 4 H, CH), 4.45 (d, $^1J_{P-H}$ = 359 Hz, 2 H, PH) ppm. ^{13}C NMR (100.6 MHz, C_6D_6, 300 K): δ = 25.2 (d, $J_{P,C}$ = 13 Hz, CH_2), 27.1 (d, $^3J_{P,C}$ = 12 Hz, CH_2), 29.8 (d, $^4J_{P,C}$ = 8 Hz, CH_2), 32.2 (d, $^1J_{P,C}$ = 18 Hz, CH) ppm. ^{31}P{^{1}H} NMR (101.6 MHz, C_6D_6, 300 K): δ = −27.5 (s) ppm. IR (Nujol): $\tilde{\nu}$ = 2258 (m), 1448 (s), 1377 (s), 1349 (w), 1327 (w), 1295 (m), 1264 (m), 1202 (w), 1180 (w), 1117 (br.), 1002 (br.), 888 (m), 854 (w), 791 (m), 727 (w), 502 (br.), 381 (br.) cm^{-1} . MS FAB: *m*/*z* (%) = 197 (45) [$PCy_2H_2^+$]

[$Ga_2I_4(PtBu_2H)_2$] (6): Yield 54%. M.p. 137−140 °C (dec). ^{1}H NMR (400 MHz, C_6D_6, 300 K): δ = 1.26 (d, $^3J_{P-H}$ = 15 Hz, 36 H, *t*Bu);

 © 2003 Wiley-VCH Verlag GmbH & Co. KGaA, Weinheim

4.92 (d, $^1J_{P-H}$ = 351 Hz, 2 H, PH) ppm. ^{13}C NMR (100.6 MHz, C_6D_6, 300 K): δ = 21.2 [C(CH_3)$_3$], 53.1 (d, $^1J_{P,C}$ = 10 Hz C(CH_3)$_3$] ppm. ^{31}P{^{1}H} NMR (101.6 MHz, C_6D_6, 300 K): δ = −9.04 (s) ppm. IR (Nujol): $\tilde{\nu}$ = 2353 (w), 1459 (s), 1376 (s), 1260 (m), 1162 (w), 1086 (m), 1021 (m), 936 (w), 870 (w), 803 (m), 727 (s), 694 (m), 555 (w), 462 (br.), 383 (br.), 323 (m) cm^{-1}. MS FAB: *m*/*z* (%) = 57 (100) [*t*Bu], 793 (4) [M$^+$ − PH*t*Bu$_2$].

[Ga_2I_5(IPr)][IPrH] (7): GaI was synthesised by sonicating Ga (0.125 g, 1.79 mmol) and I_2 (0.22 g, 0.88 mmol) in toluene (10 mL) at 50 °C for approx. 2 h. The resulting green suspension was cooled to −78 °C and a solution of the cyclic carbene IPr (0.69 g, 1.79 mmol) in toluene (20 mL) added to it over 5 min. The reaction mixture was warmed to room temperature and stirred for 12 h to give a brown solution and a precipitate of Ga metal. Filtration, concentration in vacuo and placement at −30 °C overnight yielded colourless crystals of **7** (0.36 g, 42%). M.p. 238−242 °C (dec). ^{1}H NMR (400 MHz, CD_2Cl_2, 300 K): δ = 1.10 (d, $^3J_{HH}$ = 7 Hz, 12 H, CH_3, cation), 1.21 (d, $^3J_{H,H}$ = 7 Hz, 12 H, CH_3, cation), 2.33 [sept, $^3J_{H,H}$ = 7 Hz, 4 H, CH(CH_3)$_2$, cation], 7.31 (d, $^3J_{H,H}$ = 8 Hz, 4 H, *m*-CH, cation), 7.54 (t, $^3J_{H,H}$ = 8 Hz, 2 H, *p*-CH, cation), 7.99 (s, 2 H, NC_2H_2N, cation), 8.42 (s, 1 H, NCHN, cation), 1.00 (d, $^3J_{H,H}$ = 7 Hz, 12 H, CH_3, anion), 1.36 (d, $^3J_{H,H}$ = 7 Hz, 12 H, CH_3, anion), 2.68 [sept, $^3J_{H,H}$ = 7 Hz, 4 H, CH(CH_3)$_2$, anion], 7.26 (d, $^3J_{H,H}$ = 8 Hz, 4 H, *m*-CH, anion), 7.40 (t, $^3J_{H,H}$ = 8 Hz, 2 H, *p*-CH, anion), 7.99 (s, 2 H, NC_2H_2N, anion) ppm. ^{13}C NMR (100.6 MHz, CD_2Cl_2, 300 K): δ = 23.7, 25.7 (CH_3, cation), 29.1 [C(CH_3)$_2$, cation], 124.9 (*p*-Ar, cation), 125.2 (*m*-Ar, cation), 132.4 (*o*-Ar, cation), 134.7 (*ipso*-Ar, cation), 145.1 (NCHN, cation), 145.7 (NC_2H_2N, cation), 23.9, 24.5 (CH_3, anion), 28.8 [CH(CH_3)$_2$, anion], 125.0 (*p*-Ar, anion), 127.0 (*m*-Ar, anion), 131.1 (*o*-Ar, anion), 136.1 (*ipso*-Ar, anion), 146.1 (NC_2H_2N, anion) ppm. IR (Nujol): $\tilde{\nu}$ = 2853 (br.), 1526 (m), 1455 (s), 1372 (s), 1260 (m), 1096 (s), 1055 (s), 1014 (s), 799 (s), 748 (m), 722 (m), 686 (w), 625 (w), 507 (w), 461 (w), 392 (br.), 305 (w), 289 (w), 245 (w) cm^{-1}. MS FAB: *m*/*z* (%) = 389 (100) [IPrH$^+$], 909 (61) [Ga_2I_3(IPr)$^+$]

[{InCl(IMe)$_2$}$_2$(μ-Cl)(μ-O)][Cl] (8): A solution of the cyclic carbene IMe (0.66 g, 5.31 mmol) in toluene (10 mL) was added to a suspension of InCl (0.40 g, 2.66 mmol) in toluene (10 mL) held at −78 °C. The reaction mixture was stirred for 4 h during which time indium metal deposition was observed. The resulting suspension was filtered and volatiles removed from the filtrate in vacuo. The yellow residue was extracted with CH_2Cl_2 (2 × 5 mL). Concentration to ca. 5 mL and the addition of toluene (2 mL) followed by placement at −30 °C overnight yielded colourless crystals of **8** (0.37 g, 16%). M.p. 155−158 °C (dec). ^{1}H NMR (400 MHz, CD_2Cl_2, 300 K): δ = 2.11 (s, 24 H, CMe), 3.64 (s, 24 H, NMe) ppm. ^{13}C NMR (100.6 MHz, CD_2Cl_2, 300 K): δ = 8.14 (s, CMe), 34.62 (s, NMe) ppm. IR (Nujol): $\tilde{\nu}$ = 2919 (s), 2852 (s), 1634 (m), 1598 (m), 1588 (m), 1470 (sh), 1372 (s), 1250 (sh), 1081 (s), 1034 (s), 891 (w), 850 (w), 799 (m), 727 (sh), 688 (sh), 563 (m), 533 (m), 461 (sh), 392 (br.), 335 (s), 289 (w) cm^{-1}. MS FAB: *m*/*z* (%) = 125 (100) [IMeH$^+$].

Structure Determinations: Crystals of **2**−**8** suitable for X-ray structural determination were mounted in silicone oil. Crystallographic measurements were made using a Nonius Kappa CCD diffractometer. The structures were solved by direct methods and refined on F^2 by full-matrix least squares (SHELX97)[20] using all unique data. All non-hydrogen atoms are anisotropic with H atoms included in calculated positions (riding model). The structure of **4** contains two crystallographically independent monomeric moieties in the asymmetric unit. The geometries of the dimeric units generated from these are not significantly different and thus the ORTEP diagram of only one is shown in Figure 3. The geometrical parameters for **4** in Table 1 are, however, an average of those in the two molecules. Crystal data, details of data collections and refinement are given in Table 2. The molecular structures of the complexes are depicted in Figures 1−7 and show thermal ellipsoids set at the 30% probability level. CCDC-203134 (**2**), -203135 (**3**), -203136 (**4**), -203137 (**5**), -203138 (**6**), -203139 (**7**) and -203140 (**8**) contain the supplementary crystallographic data for this paper. These data can be obtained free of charge at www.ccdc.cam.ac.uk/conts/retrieving.html [or from the Cambridge Crystallographic Data Centre, 12 Union Road, Cambridge CB2 1EZ, UK; Fax: (internat.) + 44-1223/336-033; E-mail: deposit@ccdc.cam.ac.uk].

Acknowledgments

We gratefully acknowledge financial support from EPSRC (postdoctoral fellowship for R. J. B.). Thanks also go to the EPSRC Mass Spectrometry Service for the recording of FAB mass spectra.

[1] [1a] H. Schnöckel, A. Schnepf, *Adv. Organomet. Chem.* **2001**, *47*, 235−281. [1b] G. Linti, H. Schnöckel, *Coord. Chem. Rev.* **2000**, *206*−*207*, 285−319 and references therein.
[2] A. Schnepf, H. Schnöckel, *Angew. Chem. Int. Ed.* **2002**, *41*, 3533−3552, and references therein.
[3] A. Schnepf, C. U. Doriat, E. Möllhausen, H. Schnöckel, *Chem. Commun.* **1997**, 2111−2112.
[4] C. U. Doriat, M. Friesen, E. Baum, A. Ecker, H. Schnöckel, *Angew. Chem. Int. Ed. Engl.* **1997**, *36*, 1969−1971.
[5] B. Beagley, S. Godfrey, K. Kelly, S. Kungwankunakorn, C. McAuliffe, R. Pritchard, *Chem. Commun.* **1996**, 2179−2180.
[6] R. J. Baker, R. D. Farley, C. Jones, M. Kloth, D. M. Murphy, *Chem. Commun.* **2002**, 1196−1197.
[7] M. L. H. Green, P. Mountford, G. J. Smout, S. R. Speel, *Polyhedron* **1990**, *9*, 2763−2765.
[8] K. Aarset, C. E. Beer, K. Hagen, E. M. Page, D. A. Rice, *J. Phys. Chem. A* **2002**, *106*, 8762−8768.
[9] O. T. Beachley, Jr., J. D. Maloney, *Organometallics* **1997**, *16*, 4016−4019.
[10] R. E. Douthwaite, M. L. H. Green, P. J. Silcock, P. T. Gomes, *Organometallics* **2001**, *20*, 2611−2615, and references therein.
[11] M. Kehrwald, W. Köstler, G. Linti, T. Blank, N. Wilberg, *Organometallics* **2001**, *20*, 860−867.
[12] R. J. Baker, A. J. Davies, C. Jones, M. Kloth, *J. Organomet. Chem.* **2002**, *656*, 203−210.
[13] M. J. Zehe, D. A. Lynch, Jr, J. Benuel, D. K. Carlson, *J. Phys. Chem.* **1979**, *83*, 656−664.
[14] M. A. Khan, D. G. Tuck, M. J. Taylor, D. A. Rogers, *J. Crystallogr. Spectrosc. Res.* **1986**, *16*, 895.
[15] M. D. Francis, D. E. Hibbs, M. B. Hursthouse, C. Jones, N. A. Smithies, *J. Chem. Soc., Dalton Trans.* **1998**, 3249−3254.
[16] C. D. Abernethy, M. L. Cole, C. Jones, *Organometallics* **2000**, *19*, 4852−4857.
[17] As determined from a survey of the Cambridge Crystallographic Database.
[18] L. Jafarpour, E. D. Stevens, S. P. Nolan, *J. Organomet. Chem.* **2000**, *606*, 49−54.
[19] N. Kuhn, T. Kratz, *Synthesis* **1993**, 561−564.
[20] G. M. Sheldrick, *SHELX-97*, University of Göttingen, **1997**.

Received February 4, 2003

 © 2003 Wiley-VCH Verlag GmbH & Co. KGaA, Weinheim

A New Thioether-Based (N_2S_2)Copper(II/I) Complex Exhibiting a High Redox Potential

Stéphane Torelli,[a] Catherine Belle,*[a] Christian Philouze,[a] Jean-Louis Pierre,[a] Wassim Rammal,[a] and Eric Saint-Aman[b]

Keywords: S ligands / N ligands / Tripodal ligands / Copper / Redox chemistry

From the new ligand bis[2-(*tert*-butylthio)benzyl](2-pyridylmethyl)amine [$N_2(StBu)_2$], the corresponding complexes [$Cu^I\{N_2(StBu)_2\}$]CF_3SO_3 (**1**) and [$Cu^{II}\{N_2(StBu)_2\}$](H_2O)(CF_3SO_3)]CF_3SO_3 (**2**) were synthesized and characterized by X-ray crystallography. The Cu–S bonds are unusually shortened in **1** and elongated for the axial thioether in **2**. Redox studies show that **1** and **2** interconvert during the electron transfer with a high $Cu^{II/I}$ potential of 0.79 V vs. SCE in CH_2Cl_2.

(© Wiley-VCH Verlag GmbH & Co. KGaA, 69451 Weinheim, Germany, 2003)

Introduction

Blue (type 1) copper proteins involved in electron-transfer processes have, in their active site, a single Cu atom bound to two histidine nitrogen atoms and to one cysteine thiolate group.[1,2] One additional axial thioether ligand (of methionine) is usually found in the coordination sphere of the copper ion (e.g plastocyanin[3] or azurin[4,5]). The positive $Cu^{II/I}$ redox potential, found in the range of 0.2−0.8 V vs. NHE,[1] has long held the interest of bioinorganic chemists. Model complexes, described by Kitajima[6] and more recently by Tolman,[7] present structural and spectroscopic features close to those of the type 1 site, but significant differences in electrochemical properties are observed. Synthetic copper complexes, for which both Cu^{II} and Cu^{I} structures are available, could provide information about the structure/redox properties relationships.[8−10]

We present herein the preparation and characterization, in both the Cu^{I} and Cu^{II} oxidation states, of a copper complex from a new tripodal N_2S_2 donor ligand (Scheme 1). The $Cu^{II/I}$ redox potential is as high as that found in blue copper proteins. We focused our attention on the role of the thioether ligand; few structurally characterized Cu^{II} and Cu^{I} complexes involving a long axial Cu−S(thioether) bond have been studied electrochemically.[11,12]

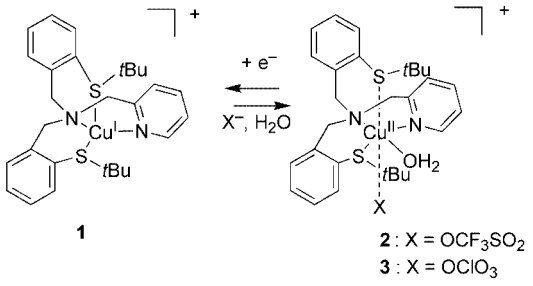

Scheme 1

Results and Discussion

By adding 1 equiv. of $Cu(CF_3SO_3)$, $Cu(CF_3SO_3)_2$ or $Cu(ClO_4)_2{\cdot}6H_2O$ to the ligand $N_2(StBu)_2$ {bis[2-(*tert*-butylthio)benzyl](2-pyridylmethyl)amine}, the Cu^{I} (**1**) and Cu^{II} (**2** and **3**) complexes were obtained (Scheme 1).

The X-ray structures of the cationic units are depicted in Figures 1 (for **1** and **2**) and 2 (for **3**). Selected bond lengths and angles are reported in Table 1.

The structure of **1** (Figure 1, A) shows a copper(I) center in a distorted tetrahedral geometry. The Cu−S distances in **1** are similar [Cu−S1 = 2.2421(7) Å and Cu−S2 = 2.2492(7) Å], although shorter than the usual $Cu^{I}-SR_2$ bond of 2.33(9) Å.[10]

The X-ray crystal structure of **2** reveals an elongated octahedral complex for the Cu^{II} redox state (Figure 1, B). Two nitrogen atoms, a thioether group and the water molecule are in the equatorial plane [a deviation of 0.007(3) Å from the mean plane for the copper atom is observed]. Two axial groups complete the octahedron: one S*t*Bu [Cu−S = 2.758(1) Å] and one oxygen atom of a CF_3SO_3 anion

[a] LEDSS, Chimie Biomimétique, UMR CNRS 5616, Université J. Fourier,
B. P. 53, 38041 Grenoble Cedex, France
Fax: (internat.) + 33-4/76514836
E-mail: Catherine.Belle@ujf-grenoble.fr
[b] LEOPR, Laboratoire d'Electrochimie Organique et de Photochimie Redox, UMR CNRS 5630, Université J. Fourier, B. P. 53, 38041 Grenoble, France

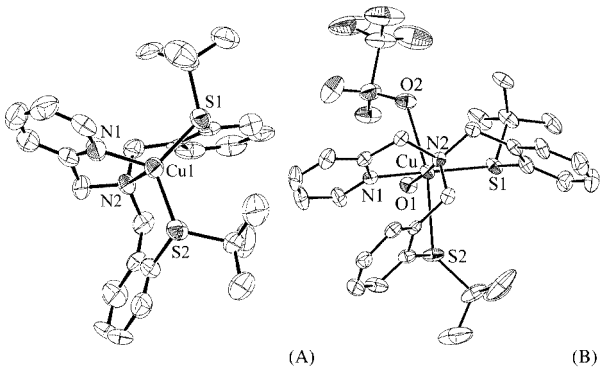

Figure 1. ORTEP view showing 50% displacement ellipsoids with partial atomic labeling for the cation (A) $[Cu^{I}(N_2(StBu)_2]^+$ of **1** and (B) $[Cu^{II}\{N_2(StBu)_2\}(H_2O)(CF_3SO_3)]^+$ of **2**; hydrogen atoms have been omitted for clarity

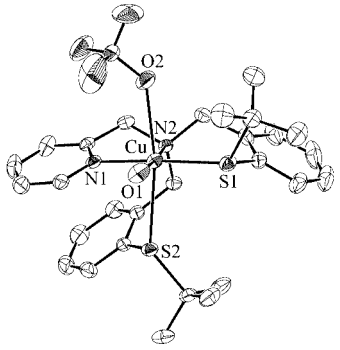

Figure 2. ORTEP view showing 50% displacement ellipsoid with partial atomic labeling for the cation $[Cu^{II}\{N_2(StBu)_2\}(H_2O)(ClO_4)]^+$ of **3**; hydrogen atoms have been omitted

[Cu−O = 2.457(3) Å] at semi-coordinating distances. Interestingly, **2** involves both an equatorial Cu−S(thioether) bond [2.354(1) Å], shorter than usual $Cu^{II}-SR_2$ bond lengths of 2.42 Å,[10] and one much longer axial Cu−S(thioether) bond [2.758(1) Å].

Complex **3** was obtained in a similar manner to complex **2** using $Cu(ClO_4)_2{\cdot}6H_2O$ as the metallic salt. The coordination sphere of the copper center in **3**, as in **2**, is described by an octahedral geometry (see Figure 2) with an oxygen atom of the perchlorate anion coordinated in an axial position. The structural data for the molecular entity **3** is close to that of **2** (see Table 1), except that the axial distances are longer in **3** [Cu−S*t*Bu = 2.822(1) Å and Cu−O = 2.546(3) Å] than in **2**.

Such an octahedral coordination with unequal Cu^{II}−S(thioether) bond lengths is unusual and has only been reported in complexes of non-tripodal ligands.[13,14]

The Cu−S distances in **2** (or **3**) can be compared to those found for the oxidized azurin,[4,5] characterized by two axial groups, an S(thioether) atom and a carbonyl oxygen atom of Gly45 in weak interaction with a copper(II) ion (near 3.1 Å). The equatorially bound S(thiolate) ligand (Cys) is 2.12 Å apart from the copper ion.

In CH_2Cl_2, the UV/Vis spectrum of **2** is characterized by a band at 345 nm ($\varepsilon \approx 2250\ M^{-1}{\cdot}cm^{-1}$) assigned to the S(thioether)→Cu^{II} LMCT band and a copper(II) d−d transition at 721 nm ($\varepsilon \approx 130\ M^{-1}{\cdot}cm^{-1}$).[15] In ethanolic solution, the LMCT band appears at 332 nm ($\varepsilon \approx 2180\ M^{-1}{\cdot}cm^{-1}$) and the d−d band is shifted up to 685 nm ($\varepsilon \approx 70\ M^{-1}{\cdot}cm^{-1}$). The changes observed in the UV/Vis spectra suggest the displacement of at least one ligand by a solvent molecule in the copper coordination sphere. In a frozen

Table 1. Selected bond lengths [Å] and angles [°] for **1**, **2** and **3**

1		**2**		**3**	
Cu−S1	2.2421(7)	Cu−S1	2.354(1)	Cu−S1	2.359(1)
Cu−S2	2.2492(7)	Cu−S2	2.758(1)	Cu−S2	2.822(1)
Cu−N1	2.023(2)	Cu−N1	2.007(4)	Cu−N1	1.987(4)
Cu−N2	2.123(2)	Cu−N2	2.037(4)	Cu−N2	2.026(3)
		Cu−O1	1.995(3)	Cu−O1	1.958(3)
		Cu−O2	2.457(3)	Cu−O2	2.546(3)
N1−Cu−N2	83.77(8)	N1−Cu−N2	82.7(1)	N1−Cu−N2	83.8(1)
N1−Cu−S1	118.16(7)	N1−Cu−S1	179.1(1)	N1−Cu−S1	176.87(8)
N1−Cu−S2	119.74(7)	N1−Cu−S2	85.9(1)	N1−Cu−S2	82.43(8)
N2−Cu−S1	104.13(6)	N1−Cu−O1	90.4(1)	N1−Cu−O1	91.4(1)
N2−Cu−S2	100.27(9)	N1−Cu−O2	82.6(1)	N1−Cu−O2	87.6(1)
S1−Cu−S2	118.71(2)	N2−Cu−O1	173.1(1)	N2−Cu−O1	174.8(1)
		N2−Cu−O2	90.8(1)	N2−Cu−O2	87.8(1)
		N2−Cu−S1	96.7(1)	N2−Cu−S1	95.6(1)
		N2−Cu−S2	92.9(1)	N2−Cu−S2	91.16(8)
		O1−Cu−O2	88.3(1)	O1−Cu−O2	90.0(1)
		O1−Cu−S1	90.23(9)	O1−Cu−S1	89.3(1)
		O1−Cu−S2	86.62(9)	O1−Cu−S2	90.27(9)
		O2−Cu−S1	98.06(9)	O2−Cu−S1	95.48(9)
		O2−Cu−S2)	167.34(9)	O2−Cu−S2	169.99(9)
		S1−Cu−S2	93.55(4)	S1−Cu−S2	94.53(4)

 © 2003 Wiley-VCH Verlag GmbH & Co. KGaA, Weinheim

solution of CH_2Cl_2/toluene (1:1) at 100 K, **2** displays a typical axial EPR spectrum (Figure 3, A), in agreement with the X-ray structure, with $g_{\|} = 2.19$, $g_{\perp} = 2.04$, $A_{\|} = 181 \times 10^{-4}$ cm^{-1}. In EtOH/toluene (1:1), two sets of overlapping signals centered at roughly $g_{1\|} = 2.17$, $A_{1\|} = 176 \times 10^{-4}$ cm^{-1} and $g_{2\|} = 2.29$, $A_{2\|} = 171 \times 10^{-4}$ cm^{-1} are observed (Figure 3, B). These features indicate that solvent molecules are involved in the coordination sphere of the metal center, giving rise to the formation of a mixture of complexes.

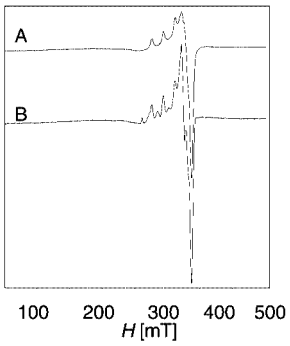

Figure 3. EPR spectrum at 100 K of **2**, at a microwave frequency of 9.419 GHz as a frozen solution, 3 mM in (A) CH_2Cl_2/toluene (1:1, v/v); (B) EtOH/toluene (1:1, v/v)

Thus, the electrochemical behaviors of **1** and **2** have been examined in coordinating solvents (MeOH or EtOH) and in a noncoordinating solvent (CH_2Cl_2) by CV and RDE experiments. In CH_2Cl_2 + TBAP (0.1 M) solution, the same CV features were found starting either from isolated **1** or from isolated **2**, i.e. compound **2** is the final product of the oxidation of **1** and vice versa (Scheme 1). The CV curve is characterized by a pair of peaks whose potentials depend strongly on the scan rate: their peak-to-peak separation increases from 0.21 V at 5 mVs^{-1} to 1.07 V at 5 Vs^{-1} (Figure 4). At low scan rates, E_{pa} and E_{pc} tend towards constant values of 0.41 V and 0.20 V vs. Fc/Fc$^+$. The RDE wave recorded in a CH_2Cl_2 solution of **1** is characterized by $E_{1/2} = 0.54$ V ($N = 600$ rpm).

Upon exhaustive potentiostatic electrolysis at 0.75 V (one exchanged electron), the RDE wave recorded in the resulting solution (Figure 4) matches well with that recorded in an electrolytic solution of **2**, $E_{1/2} = 0.14$ V ($N = 600$ rpm). Additionally, the UV/Vis features of both solutions are very close. The starting solution is fully restored upon further exhaustive reduction at −0.2 V. It can be seen that the anodic and cathodic $E_{1/2}$ values determined from RDE experiments performed in solution of **1** or **2** are different.

These results can be analyzed as the simple one-electron transfer depicted in Scheme 1. Simulations of the experimental CV curves allowed the determination of the apparent formal potential and the apparent heterogeneous electron-transfer rate constant of the overall mechanism: $E_{1/2} = 0.30 \pm 0.01$V and $k^0 = 2.0 \pm 0.9 \times 10^{-4}$ cm s^{-1}. The low value of k^0 suggests that the overall electrochemical mechanism involves coupled chemical reactions, i.e. the electron

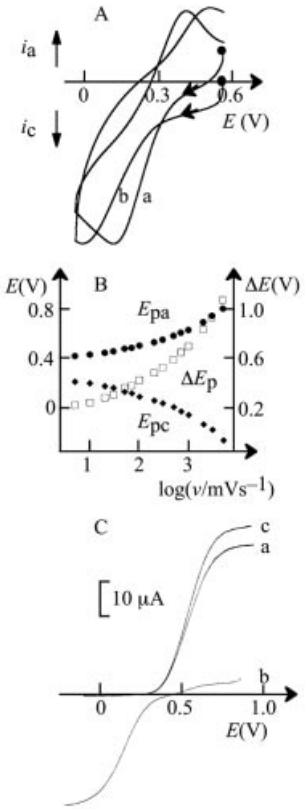

Figure 4. Voltammetric curves of **2** (A) and **1** (C), 1.2 mM, recorded in CH_2Cl_2 + TBAP (0.1 M), WE: glassy carbon ($\phi = 3$ mm), E vs. Fc/Fc$^+$; (A) CV at 0.03 (curve a) and 0.3 Vs^{-1} (curve b), normalized current vs. E; (B) anodic (E_{pa}), cathodic (E_{pc}) peak potential and peak-to-peak (ΔE_p) separation vs. scan rate; (C) RDE voltammetry, $N = 600$ rpm, initial (curve a), after oxidative electrolysis (0.8 exchanged electron, curve b), after re-reduction (curve c, the increase in the limiting current between curves a and c is due to a partial evaporation of CH_2Cl_2)

transfer implies changes in coordination and geometry during the redox cycle. The overall mechanism can thus be best described by the classic square scheme[2] in which the electron-transfer steps are followed by coordinate bond formations (or ruptures) accounting for the change in the coordination mode of the copper center according to its redox state, i.e. the electron transfer leads to an unstable intermediate which undergoes a fast rearrangement to yield the stable corresponding complex. Due to their very fast kinetics, the electroactivity of the intermediates could not be seen on the CV curves, the anodic and cathodic processes remaining electrochemically irreversible, even at high scan rate (10 Vs^{-1}). This precluded any precise determination of the kinetic constants by electrochemical simulations.

Intervention of a coupled chemical reaction is further confirmed by examining the electrochemical response of **1** or **2** in coordinating solvents. In an electrolytic EtOH solution of **2**, when scanning towards negative potentials (0.1 Vs^{-1}), the CV curve displays a main cathodic peak at $E_{pc} = 0.14$ V and a peak of low intensity at $E_{pc} = -0.15$ V. On the reverse scan, only one anodic peak is seen at $E_{pa} = 0.38$ V (Figure 5). After an exhaustive reduction/re-oxidation cy-

 © 2003 Wiley-VCH Verlag GmbH & Co. KGaA, Weinheim

cle, the final CV curve displays the same signals but with different intensities (Figure 5). This results in an ill-behaved RDE wave for **2** characterized by an apparent $E_{1/2}$ = 0.23 V (N = 600 rpm), while a more resolved RDE wave for **1** is seen at apparent $E_{1/2}$ = 0.35 V (N = 600 rpm). It can be assumed that in coordinating solvents, solvent molecules are involved in the coordination sphere of the metal center giving rise to the formation of different complexes in equilibrium [as previously observed in UV/Vis and EPR spectra measured in ethanol (see above)].

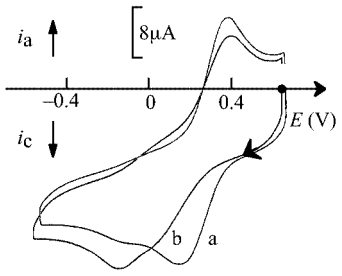

Figure 5. CV curves of **2**, 1.1 mM, recorded in EtOH + TBAP (0.1 M), WE: glassy carbon (ϕ = 3 mm), E vs. Fc/Fc^+, v = 0.1 Vs^{-1}; curve (a): initial; curve (b): after an oxidation/reduction cycle

Taking into account $E_{1/2}$ (Fc/Fc^+) = 0.49 V or 0.44 V vs. SCE, in CH_2Cl_2 or EtOH respectively, under our experimental conditions, the **1/2** electrochemical system presents a very high redox potential, similar to that of blue copper proteins (a value of 0.78 V vs. NHE is reported for fungal laccase).[16] As a consequence, whereas **1** is stable in CH_2Cl_2 or alcohol solution, **2** is partially reduced to the Cu^I state even in the presence of air (40% of Cu^{II} is reduced after 1 d in ethanol). High redox potential values have been reported for a few small $Cu^{II/I}$ molecular systems[17] but are rare for related copper systems involving tripodal ligands.[18,19] Compared to other redox couples involving tripodal N_2S_2 ligands, the **1/2** electrochemical system described herein displays a shift towards higher potentials by 0.2 V.[10]

Conclusion

The high redox potential of the **1/2** couple could result from a combination of: (i) the lower donating character of the aromatic thioether group compared to an aliphatic thioether group, (ii) the stabilization of the Cu^I redox state, as judged from the short Cu^I-SR_2 bonds, (iii) the long axial $Cu^{II}-SR_2$ bond leading to a weaker interaction, likely to be due to (iv) the geometric constraint afforded by the *t*Bu group. The present study may provide insights into the electron-transfer mechanism of the blue copper proteins. Further studies are in progress to understand the relationship between the subtle changes of the ligand and the deep changes induced in the redox properties of the related complexes.

Experimental Section

General: All chemicals were obtained from commercial sources and used as received. Solvents were purified by standard methods before use. ***Caution:*** Although no problems were encountered during the preparation of perchlorate salts, suitable care should be taken when handling such potentially hazardous compounds.

Spectrometry: Fast-atom bombardment (FAB) mass spectra in the positive mode were recorded with a Nermag R 1010C apparatus equipped with an M scan (Wallis) atom gun (8 kV, 20 mA). ESI mass spectra were obtained with a Bruker Esquire 3000 plus spectrometer with an ion trap. UV/Vis spectra were recorded using a Perkin−Elmer Lambda 2 spectrophotometer equipped with 1.0-cm matched quartz cells and operating in the range 200−900 nm; ε values are given in $M^{-1}\cdot cm^{-1}$. ^1H and ^{13}C NMR spectra were recorded with a Bruker Avance 300 spectrometer and a Bruker AC 200; chemical shifts (ppm) were referenced to residual solvent peaks. EPR spectra were recorded at 100 K with a Bruker ESP 300 spectrometer operating at 9.4 GHz (X-band), with 3 mM solutions.

Electrochemistry: Electrochemical experiments were carried out using a PAR model 273 potentiostat equipped with a Kipp-Zonen x-y recorder. All experiments were run at room temperature under argon. A standard three-electrode cell was used, with 0.1 M tetra-*n*-butylammonium perchlorate (TBAP) as supporting electrolyte. All potentials are referred to the regular Fc/Fc^+ redox couple used as internal reference. Vitreous carbon disc electrodes for cyclic voltammetry (CV) (5 mm diameter) and rotating disc electrode (RDE) (3 mm diameter) were polished with 1 μm diamond paste.

[2-(*tert*-Butylthio)benzyl](2-pyridylmethyl)amine: A solution of (2-pyridylmethyl)amine (477 μL, 4.54 mmol) in dry MeOH (10 mL) was added at room temperature to a solution of 2-(*tert*-butylthio)benzaldehyde (1 g, 5 mmol) in dry MeOH (100 mL) under Ar. After 3 h, $NaBH_4$ (455 mg, 11.5 mmol) was slowly added as a solid and the mixture stirred for an additional 2 h. After acidic treatment (HCl, 4 N), the solvent was removed under reduced pressure. The resulting product was dissolved in H_2O (50 mL) and extracted with CH_2Cl_2 to remove the excess of reduced aldehyde. The aqueous solution was then neutralized with saturated $NaHCO_3$ and extracted with CH_2Cl_2 (2 × 100 mL). The combined organic layers were washed with saturated NaCl, dried with Na_2SO_4 and concentrated under reduced pressure to give a brown oil. Yield: 1.2 g (91%). ^1H NMR (200 MHz, $CDCl_3$, TMS): δ = 8.51 (d, J = 4.8 Hz, 1 H, Py-*H*), 7.51−7.63 (m, 3 H, Py-*H*), 7.07−7.36 (m, 4 H, Ar-*H*), 4.11 (s, 2 H, NCH_2Ar), 3.92 (s, 2 H, NCH_2Py), 3.02 (s, 1 H, N*H*), 1.25 (s, 9 H, *t*Bu) ppm. ^{13}C NMR (50 MHz, $CDCl_3$, TMS): δ = 159.3, 148.9, 144.3, 138.5, 136.0, 131.8, 129.4, 128.8, 126.7, 122.0, 121.6, 54.0, 51.6, 46.9, 30.8 ppm. FAB+ MS: m/z = 286 [$M^+ + H^+$]. $C_{17}H_{21}N_2S$ (285): calcd. C 67.80, H 7.58, N 9.44, S 11.86; found C 68.00, H 7.74, N 9.78, S 11.19.

Bis[2-(*tert*-butylthio)benzyl](2-pyridylmethyl)amine [$N_2(StBu)_2$]: 2-(*tert*-Butylthio)benzaldehyde (847 mg, 4.23 mmol) and glacial acetic acid (878 μL, 15.36 mmol) were added to a solution of [2-(*tert*-butylthio)benzyl](2-pyridylmethyl)amine (1.1 g, 3.84 mmol) in dry MeOH (100 mL) under Ar. After 1 h, $NaBH_3CN$ (1.016 g, 15.36 mmol) was added and the mixture stirred overnight. Then, an acid treatment (HCl, 4 N) was performed and the solvent was removed under reduced pressure. The resulting product was dissolved in H_2O and extracted with CH_2Cl_2 to remove the excess of reduced aldehyde. The aqueous solution was neutralized with saturated $NaHCO_3$ and extracted with CH_2Cl_2 (2 × 100 mL). The combined organic layers were washed with saturated NaCl, dried

 © 2003 Wiley-VCH Verlag GmbH & Co. KGaA, Weinheim

Table 2. Crystallographic experimental details for **1**−**3**

	1·0.985CH_2Cl_2	**2**·C_4H_8O	**3**
Empirical formula	$C_{29}H_{36}CuF_3N_2O_3S_3$·0.985$CH_2Cl_2$	$C_{30}H_{38}CuF_6N_2O_7S_4$·$C_4H_8O$	$C_{28}H_{38}Cl_2CuN_2O_9S_2$
Formula mass	760.99	915.54	745.19
Symmetry	triclinic	orthorhombic	monoclinic
Morphology	pale brownish prism	turquoise prism	blue-green platelet
Crystal dimension [mm]	0.18 × 0.15 × 0.10	0.32 × 0.26 × 0.18	0.22 × 0.15 × 0.08
a [Å]	10.271(1)	12.0120(9)	32.86(1)
b [Å]	12.192(1)	16.2009(5)	11.906(4)
c [Å]	14.829(1)	21.616(2)	23.806(5)
α [°]	74.43(1)	90	90
β [°]	86.80(1)	90	129.55(3)
γ [°]	70.97(1)	90	90
V [Å^3]	1690(1)	4206.6(4)	7181(5)
T [K]	100.2	150	293
Space group	$P\bar{1}$	$P2_12_12_1$	*C*2/*c*
Z	2	4	8
Diffractometer	Enraf−Nonius Kappa CCD	Enraf−Nonius Kappa CCD	Enraf−Nonius CAD-4
Monochromator	graphite	graphite	graphite
Wavelength [Å]	0.7107 (Mo-K_α)	0.7107 (Mo-K_α)	0.7107 (Mo-K_α)
μ [mm^{-1}]	1.038	0.793	0.922
No. of reflections (measured)	11234	32320	6910
No. of reflections (unique)	4349	7043	6729
No. of reflections	3704 ($I > 1\sigma$)	4763 ($I > 2\sigma$)	4030 ($I > 2\sigma$)
$R_{int.}$	0.039	0.067	0.034
R	0.038	0.056	0.055
R(*w*)	0.059	0.057	0.065

with Na_2SO_4 and concentrated under reduced pressure. Addition of pentane afforded the product as a pale beige powder. Yield: 1.2 g (68%), m.p. 95 °C. ^{1}H NMR (200 MHz, $CDCl_3$, TMS): δ = 8. 53 (d, *J* = 4.8 Hz, 1 H, Py-*H*), 7.50−7.60 (m, 3 H, Py-*H*), 7.07−7.36 (m, 8 H, Ar-*H*), 4.15 (s, 4 H, NCH_2Ar), 3.92 (s, 2 H, NCH_2Py), 1.25 (s, 18 H, *t*Bu) ppm. ^{13}C NMR (50 MHz, $CDCl_3$, TMS): δ = 160.6, 148.9, 145.0, 139.0, 136.5, 132.7, 129.1, 129.6, 126.6, 122.9, 121.9, 60.7, 57.0, 47.3, 31.3 ppm. FAB+ MS: *m*/*z* = 465 [M^+ + H^+]. $C_{28}H_{36}N_2S_2$ (464): calcd. C 71.86, H 7.88, N 5.92, S 13.68; found C 72.37, H 7.81, N 6.03, S 13.80.

[Cu^{I}{N$_2$(S*t*Bu)$_2$}](CF$_3$SO$_3$) (1): Copper(I) trifluoromethanesulfonate (0.230 g, 0.43 mmol, toluene complex) was added to a solution of N$_2$(S*t*Bu)$_2$ (0.2 g, 0.43 mmol) in CH_2Cl_2 (20 mL). The solution was stirred for 10 min and diethyl ether added (10 mL). After 24 h, **1** was obtained as a polycrystalline pale powder. Yield: 65% (0.188 g). Crystals of **1** suitable for X-ray crystallography were obtained by layering hexane onto a CH_2Cl_2 solution of **1**. ESI MS: *m*/*z* = 527 [N$_2$(S*t*Bu)$_2$ + 1 Cu^+]. ^{1}H NMR (300 MHz, CD_3CN, TMS): δ = 8. 68 (d, *J* = 4.7 Hz, 1 H, Py-*H*), 7.79 (t, *J* = 7.0 Hz, 1 H, Py-*H*), 7.81−7.37 (m, 5 H, Ar-*H* + Py-*H*), 7.27 (d, 1 H, Ar-*H*), 3.89 (s, 4 H, NCH_2Ar), 3.78 (s, 2 H, NCH_2Py), 1.17 (s, 18 H, *t*Bu) ppm.

[Cu^{II}{N$_2$(S*t*Bu)$_2$}(H$_2$O)(CF$_3$SO$_3$)](CF$_3$SO$_3$) (2): Copper(II) trifluoromethanesulfonate (0.155 g, 0.43 mmol) was added to a solution of **N$_2$(S*t*Bu)$_2$** (0.2 g, 0.43 mmol) in EtOH (20 mL). The solution was stirred for 10 min and diethyl ether added (10 mL). After 24 h at −20 °C, **2** was obtained as a polycrystalline blue powder. Yield: 70% (0.250 g). Crystals of **2** suitable for X-ray crystallography were obtained vapor diffusion of diethyl ether into an ethanol solution of **2**. FAB MS (NBA matrix): *m*/*z* = 678 [N$_2$(S*t*Bu)$_2$ + 1 Cu^{2+} − H_2O + 1 CF_3SO_3 + 1 H^+]. $C_{30}H_{38}CuF_6N_2O_7S_4$ (844): calcd. C 42.67, H 4.54, Cu 7.53, F 13.5, N 3.32, S 15.19; found C 42.31, H 4.56, Cu 7.31, N 3.31, S 15.85.

[Cu^{II}{N$_2$(S*t*Bu)$_2$}(H$_2$O)(ClO$_4$)](ClO$_4$) (3): Copper(II) perchlorate hexahydrate (0.271 g, 0.715 mmol) was added to a solution of **N$_2$(S*t*Bu)$_2$** (0.3 g, 0.65 mmol) in EtOH (20 mL). The solution was stirred for 10 min and diethyl ether/THF added (10 mL). After 24 h at −20 °C, **3** was obtained as a polycrystalline green-blue powder. Yield: 45% (0.218 g). Crystals of **3** suitable for X-ray crystallography were obtained by vapor diffusion of diethyl ether into an acetonitrile solution of **3**. FAB MS (NBA matrix): *m*/*z* = 628 [N$_2$(S*t*Bu)$_2$ + 1 Cu^{2+} − H_2O + 1 ClO_4 + 1 H^+]. UV/Vis (CH_2Cl_2): λ (ε) = 357 (4146), 706 nm (392 M^{-1}·cm^{-1}); (EtOH): λ = 338 (3954), 655 nm (149 M^{-1}·cm^{-1}). EPR (9.6 GHz, 100 K, 3 mM, CH_2Cl_2/toluene, 1:1): $g_\parallel$ = 2.22, $g_\perp$ = 2.06, $A_\parallel$ = 175 × 10^{-4} cm^{-1}; (EtOH/toluene, 1:1) main features at: $g_\parallel$ = 2.22, $g_\perp$ = 2.02, $A_\parallel$ = 170 × 10^{-4} cm^{-1}.

X-ray Crystallographic Studies: Crystal data and crystallographic experimental data for complexes **1**−**3** are listed in Table 2. In both structures, collected reflections were corrected for Lorentz and polarization effects but not for absorption. The structures were solved by direct methods and refined using the TEXSAN software package.[20] All non-hydrogen atoms were refined with anisotropic thermal parameters. Hydrogen atoms were generated in idealized positions, riding on the carrier atoms, with isotropic thermal parameters. CCDC-203164 (**1**), -203165 (**2**) and -203166 (**3**) contain the supplementary crystallographic data for this paper. These data can be obtained free of charge at www.ccdc.cam.ac.uk/conts/retrieving.html [or from the Cambridge Crystallographic Data Centre, 12 Union Road, Cambridge CB2 1EZ, UK; Fax: (internat.) + 44-1223/336-033; E-mail: deposit@ccdc.cam.ac.uk].

 © 2003 Wiley-VCH Verlag GmbH & Co. KGaA, Weinheim

[1] R. H. Holm, P. Kennepohl, E. I. Solomon, *Chem. Rev.* **1996**, *96*, 2239−2314.
[2] M. C. Feiters, in *Metal ions in biological systems, Probing of proteins by metal ions and their low-molecular-weight complexes* (Eds.: A. Sigel, H. Sigel), New York, **2001**, vol. 38, pp. 522−534.
[3] J. M. Guss, H. C. Freeman, *J. Mol. Biol.* **1983**, *169*, 521−563.
[4] G. E. Norris, B. F. Anderson, E. N. Baker, *J. Am. Chem. Soc.* **1986**, *108*, 2782−2785.
[5] E. N. Baker, *J. Mol. Biol.* **1988**, *203*, 1071−1095.
[6] N. Kitajima, K. Fujisawa, Y. Moro-oka, *J. Am. Chem. Soc.* **1990**, *112*, 3210−3212.
[7] P. L. Holland, W. B. Tolman, *J. Am. Chem. Soc.* **2000**, *122*, 6331−6332.
[8] A. W. Addison, N. T. Rao, E. Sinn, *Inorg. Chem.* **1984**, *23*, 1957−1967.
[9] K. K. Nanda, A. W. Addison, R. J. Butcher, M. R. McDevitt, T. N. Rao, E. Sinn, *Inorg. Chem.* **1997**, *36*, 134−135.
[10] E. A. Ambundo, M. V. Deydier, A. J. Grall, N. Aguera-Vega, L. T. Dressel, T. H. Cooper, M. J. Heeg, L. A. Ochrymowycz, D. B. Rorabacher, *Inorg. Chem.* **1999**, *38*, 4233−4242.
[11] K. D. Karlin, P. L. Dahlstrom, J. Zubieta, *Transition Met. Chem.* **1981**, *6*, 314−315.
[12] K. D. Karlin, J. K. Yandell, *Inorg. Chem.* **1984**, *23*, 1184−1188.
[13] E. Bouwman, R. Day, W. L. Driessen, W. Tremel, B. Krebs, J. S. Wood, J. Reedijk, *Inorg. Chem.* **1988**, *27*, 4614−4618.
[14] H. Wu, C. R. Lucas, *Inorg. Chem.* **1993**, *32*, 526−531.
[15] E. I. Solomon, K. W. Penfield, D. E. Wilcox, *Struct. Bonding* **1983**, *53*, 1−57.
[16] V. T. Taniguchi, B. G. Malmström, F. C. Anson, H. B. Gray, *Proc. Natl. Acad. Sci. U. S. A.* **1982**, *79*, 3387−3389.
[17] S. Flanagan, J. Dong, K. Haller, S. Wang, W. R. Scheidt, R. A. Scott, T. R. Webb, D. M. Stanbury, L. J. Wilson, *J. Am. Chem. Soc.* **1997**, *119*, 8857−8868.
[18] K. D. Karlin, S. E. Sherman, *Inorg. Chim. Acta* **1982**, *65*, L39−L40.
[19] T. N. Sorrell, D. L. Jameson, *Inorg. Chem.* **1982**, *21*, 1014−1019.
[20] TEXSAN, *Single Crystal Structure Analysis Software*, Version 1.7, Molecular Structure Corporation, 3200 Research Forest Drive, The Woodlands, TX 77381, USA, **1995**.

Received February 6, 2003

 © 2003 Wiley-VCH Verlag GmbH & Co. KGaA, Weinheim

Synthesis and Electrical Properties of the $Pr_{0.5+x-y}Bi_yLi_{0.5-3x}TiO_3$ System

María-Luisa Martínez-Sarrión,*[a] Lourdes Mestres,[a] Marta Herráiz,[a] Oscar Maqueda,[a] Nestor Fernández,[b] and Mario-Fidel García[c]

Keywords: Phase diagrams / Perovskite phases / Conducting materials

The stoichiometry, polymorphism, and electrical behaviour of the solid solutions $Pr_{0.5+x-y}Bi_yLi_{0.5-3x}TiO_3$ with perovskite-like structure have been studied. Data are given as a solid solution triangle, XRD patterns for two polymorphs T and O, the composition dependence of their parameters, and ionic conductivity plots. A region of perovskite-like solid solutions was obtained when the bismuth content in the general formula $Pr_{0.5+x-y}Bi_yLi_{0.5-3x}TiO_3$ was $y \leq 0.10$ and the lithium content was $0.033 \leq x \leq 0.133$. The compounds are mixed conductors. With increasing amounts of lithium the ionic conductivity first increased, reached a maximum for $x = 0.20$, with a conductivity at 25 °C of $6.639 \cdot 10^{-3}$ S·cm^{-1}, and then decreased.

(© Wiley-VCH Verlag GmbH & Co. KGaA, 69451 Weinheim, Germany, 2003)

Introduction

There has been much recent interest in the development of novel ionic conductors as solid electrolytes in lithium batteries.[1−12] Fast ionic conductors with the general formula $RE_{0.5+x}Li_{0.5-3x}TiO_3$, where RE = La, Pr, Nd, and Sm have been reported,[7−12] for which the maximum conductivity was for the La series ($1.1 \cdot 10^{-3}$ S·cm^{-1} for $x = 0.07$ at room temperature).[7] More recently the phase diagram, crystal chemistry, and ionic conductivity of the system $La_{0.5+x-y}Bi_yLi_{0.5-3x}TiO_3$ have been reported.[13] The compounds of this system are ionic conductors whose conductivity increases as the amount of lithium increases, up to $x = 0.075$, but decreases when the amount of bismuth increases. The system with Bi needs less time in the thirst treatment at 1250 °C than a similar system without bismuth.[13]

We aimed to investigate the stoichiometry range, crystal chemistry, and electrical behaviour of materials of the general formula $Pr_{0.5+x-y}Bi_yLi_{0.5-3x}TiO_3$ and to establish the phase diagram at room temperature of the system $Pr_{0.67}TiO_3/Pr_{0.5}Li_{0.5}TiO_3/Bi_{0.5}Li_{0.5}TiO_3$. XRD patterns of perovskites with different Li and Bi contents have been analyzed and a study of the thermal treatment time with the content of Bi made. Finally, electrical conductivity data have been interpreted on the basis of the structural information deduced.

Results and Discussion

Phase Diagram

The triangle $Pr_{0.67}TiO_3/Pr_{0.5}Li_{0.5}TiO_3/Bi_{0.5}Li_{0.5}TiO_3$ in the system $Pr_6O_{11}/Li_2O/TiO_2/Bi_2O_3$ was chosen for detailed study since the $Pr_{0.67}TiO_3/Pr_{0.5}Li_{0.5}TiO_3$ join has been previously reported.[12] Thus, compositions of general formula $Pr_{0.5+x+y}Bi_yLi_{0.5-3x}TiO_3$ were synthesized as described in the Exp. Sect. The results of X-ray powder diffraction were then used to construct the composition diagram shown in Figure 1. ICP analysis confirmed the nominal composition, and these results were then used to construct the diagram.

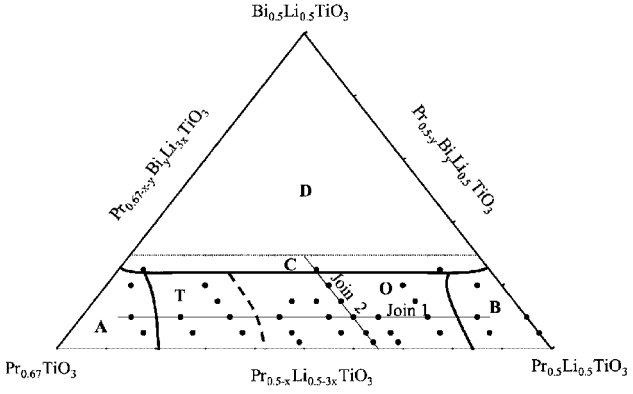

Figure 1. Composition triangle and joins studied for the system $Pr_{0.5+x-y}Bi_yLi_{0.5-3x}TiO_3$

[a] Departament de Química Inorgànica, Universitat de Barcelona, Martí i Franquès 1−11, 08028 Barcelona, Spain
Fax: (internat.) + 34-93/4907725
E-mail: marialuisa.martinez@qi.ub.es
[b] Departamento de Química Inorgánica, Universidad de La Habana,
Ciudad de la Habana, Cuba
[c] IMRE,
Ciudad de la Habana, Cuba

 © 2003 Wiley-VCH Verlag GmbH & Co. KGaA, Weinheim **DOI: 10.1002/ejic.200200657**

Five distinct areas were found on this triangle: a region of perovskite-like solid solutions and three mixed-phase regions. Almost all of the superior part of the triangle (region C) was a mixture of the perovskite-like phase, $Bi_4Ti_3O_{12}$ (identified from PDF 73-2181) and an unknown phase (Figure 2, a). The region that was within the vertex $Pr_{0.5}Li_{0.5}TiO_3$ (region B) was a mixture of perovskite-like compound and peaks belonging to Li_2TiO_3, (identified from PDF 33-0831) (Figure 2, b), while the region close to the vertex $Pr_{0.67}TiO_3$ (region A) was a mixture of a perovskite-like phase and $Pr_4Ti_9O_{24}$ (identified from PDF 45-0265) (Figure 2, e). However, a perovskite-like solid solutions area (regions O and T) was also found between these three regions (Figure 2, c and d). No use was made of the previous results for $La_{0.5+x-y}Bi_yLi_{0.5-3x}TiO_3$[13] to study higher bismuth contents here (area D) as melting occurs because of the greater content of bismuth as Bi_2O_3, which melts at about 830 °C.

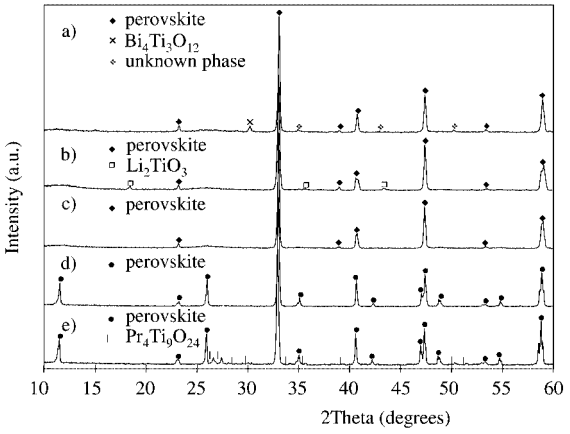

Figure 2. XRD patterns of the five regions on the composition triangle, showing both tetragonal (d) and orthorhombic (c) perovskite-like phases

Table 1 shows the X-ray powder diffraction data for $Pr_{0.57}Bi_{0.05}Li_{0.15}TiO_3$ (region T), which has a tetragonal perovskite-type structure. Table 2 shows the X-ray diffraction data for $Pr_{0.51}Bi_{0.05}Li_{0.325}TiO_3$ (region O), an orthorhombic perovskite-type structure. These two polymorphs are similar to those described in the $RE_{0.5+x}Li_{0.5-3x}TiO_3$ (RE = Pr, Nd) systems.[10,12]

Table 3 shows the X-ray diffraction data for $Pr_{0.58}Bi_{0.05}Li_{0.10}TiO_3$ (region A), containing reflections corresponding to a tetragonal perovskite-like structure and reflections corresponding to $Pr_4Ti_9O_{24}$. Table 4 shows the X-ray powder diffraction data for $Pr_{0.48}Bi_{0.025}Li_{0.5}TiO_3$ (region B) for which reflections corresponding to an orthorhombic perovskite-type structure and reflections corresponding to Li_2TiO_3 were observed. Finally, Table 5 shows X-ray powder diffraction data for $Pr_{0.43}Bi_{0.125}Li_{0.325}TiO_3$ (region C). In this region reflections corresponding to an orthorhombic perovskite-type structure, $Bi_4Ti_3O_{12}$, and an unknown phase were detected.

Perovskite-like phases mixed with titanium compounds are obtained in the areas A and B. In the area close to the

Table 1. Indexed powder pattern of the single-phase $Pr_{0.57}Bi_{0.05}Li_{0.15}TiO_3$ [tetragonal system: a = 3.833(8) Å, c = 7.721(2) Å, V = 113.48(6) Å^3, Z = 4]

hkl	$d_{obsd.}$ [Å]	$d_{calcd.}$ [Å]	I/I_o
001	7.671	7.721	21
100	3.843	3.834	4
011	3.427	3.434	24
102	2.718	2.720	100
111	2.556	2.558	8
112	2.219	2.219	23
013	2.138	2.137	3
004	1.931	1.930	12
020	1.917	1.917	28
113	1.869	1.866	4
202	1.722	1.717	2
121	1.673	1.674	4
114	1.573	1.572	14
122	1.569	1.567	29

Table 2. Indexed powder pattern of the single-phase $Pr_{0.51}Bi_{0.05}Li_{0.325}TiO_3$ [orthorhombic system: a = 5.434(3) Å, b = 7.674(4) Å, c = 5.415(1) Å, V = 225.83(7) Å^3, Z = 4]

hkl	$d_{obsd.}$ [Å]	$d_{calcd.}$ [Å]	I/I_o
101	3.835	3.836	5
121	2.714	2.713	100
112	2.312	2.311	2
220	2.219	2.218	13
022	2.214	2.212	14
040	1.919	1.918	37
222	1.717	1.716	3
123	1.565	1.564	24

Table 3. Indexed powder pattern of $Pr_{0.58}Bi_{0.05}Li_{0.10}TiO_3$

$d_{obsd.}$ [Å]	Perovskite d [Å]	*hkl*	$Pr_4Ti_9O_{24}$ d [Å]	*hkl*
7.705	7.671	001		
3.859	3.843	100		
3.434	3.427	011		
3.358			3.355	440
3.255			3.258	044
3.028			3.036	353
2.979			2.980	391
2.950			2.946	193
2.722	2.718	102		
2.625			2.629	115
2.560	2.556	111		
2.515			2.521	404
2.292			2.288	602
2.222	2.219	112		
2.141	2.138	013		
1.937	1.931	004		
1.919	1.917	020		
1.866	1.869	113		
1.812			1.814	800
1.775	1.720	202		
1.718			1.717	4106
1.677	1.673	121		
1.576	1.573	114		
1.570	1.569	122		

 © 2003 Wiley-VCH Verlag GmbH & Co. KGaA, Weinheim

Table 4. Indexed powder pattern of $Pr_{0.48}Bi_{0.025}Li_{0.5}TiO_3$

$d_{obsd.}$ [Å]	Perovskite		Li_2TiO_3	
	d [Å]	hkl	d [Å]	hkl
4.798			4.800	002
3.827	3.835	101		
2.706	2.714	121		
2.511			2.502	−131
2.309	2.312	112		
2.216	2.219	220		
2.209	2.214	022		
2.075			2.075	−133
1.915	1.919	040		
1.714	1.717	222		
1.566	1.565	123		

Table 5. Indexed powder pattern of $Pr_{0.43}Bi_{0.125}Li_{0.325}TiO_3$

d_{obs} [Å]	Perovskite		$Bi_4Ti_3O_{12}$	
	d [Å]	hkl	d [Å]	hkl
3.827	3.835	101		
2.954			2.970	117
2.710	2.714	121		
2.563[a]				
2.309	2.312	112		
2.214	2.214	022		
2.108[a]				
1.917	1.919	040		
1.815[a]				
1.714	1.717	222		
1.566	1.565	123		

[a] Unknown phase.

vertex $Pr_{0.67}TiO_3$ (region A), $Pr_4Ti_9O_{24}$ is segregated along with the perovskite-like phase. On progressing towards the join $Pr_{0.67}TiO_3/Pr_{0.5}Li_{0.5}TiO_3$ the lithium content increases and Li_2TiO_3 is segregated along with the perovskite-like phase near the $Pr_{0.5}Li_{0.5}TiO_3$ vertex (region B).

The cell volume was obtained for two joins on the composition triangle (Figure 1). Along join 1 [$Pr_{0.45+x}Bi_{0.05}Li_{0.5-3x}TiO_3$] the lithium and praseodymium composition and the number of vacancies changed and the composition of bismuth was constant, while along join 2 [$Pr_{0.558-y}Bi_yLi_{0.325}TiO_3$] the number of vacancies and the amount of lithium was constant.

The cell volume was plotted against the amount of bismuth or lithium (Figure 3, a and b, respectively) and was found to increase smoothly as the bismuth content increased; conversely, it decreased smoothly with increasing lithium content. The bismuth, praseodymium, and lithium should be in equivalent 12-coordinated sites. Substitution of praseodymium by bismuth does not affect considerably the cell parameters due to their similar ionic radius. Therefore, the substitution of praseodymium by lithium leads to a reduction of the cell volume because the lithium ionic radius is smaller.

Electrical Measurements (AC)

DC conductivity measurements were carried out, but electronic conductivity was not found in these compounds.

AC measurements were carried out from 25 to 300 °C for compounds on join 1, $Pr_{0.45+x}Bi_{0.05}Li_{0.5-3x}TiO_3$ ($0.033 \leq x \leq 0.133$), and join 2, $Pr_{0.558-y}Bi_yLi_{0.325}TiO_3$ ($y \leq 0.10$). Two semicircles and a spike were observed in the impedance complex plane plots (Figure 4). The centers of the semicircles were clearly depressed below the baseline, indicating the kind of non-Debye response that has been detected in other ionic conductors.[14−16]

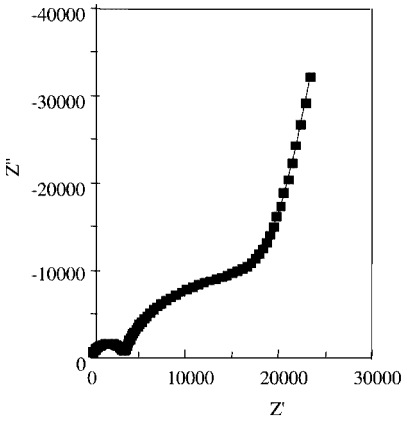

Figure 4. Impedance response at 155 °C for $Pr_{0.59}Bi_{0.01}Li_{0.325}TiO_3$

An equivalent circuit (Figure 5) with two RC elements and with CPE[16] (constant phase elements) for grain and

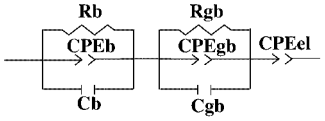

Figure 5. Equivalent circuit for fitting AC data and fitting results for $Pr_{0.59}Bi_{0.01}Li_{0.325}$ TiO_3 at 155 °C [Rb = 3535 Ω·cm, Cb = 9.12 10^{-12} F·cm^{-1}, Tb = 1.55 10^{-10} S·cm^{-1}, n = 0.88; Rgb = 15996 Ω·cm, Cgb = 2.41 10^{-9} F·cm^{-1}, Tgb = 5.37 10^{-10} S·cm^{-1}, n = 0.71; Tel = 9.37 10^{-10} S·cm^{-1}, n = 0.90; CPE equation: $Y = T\cdot\cos(n\pi/2)\cdot\omega^n + T\cdot\sin(n\pi/2)\cdot\omega^n$]

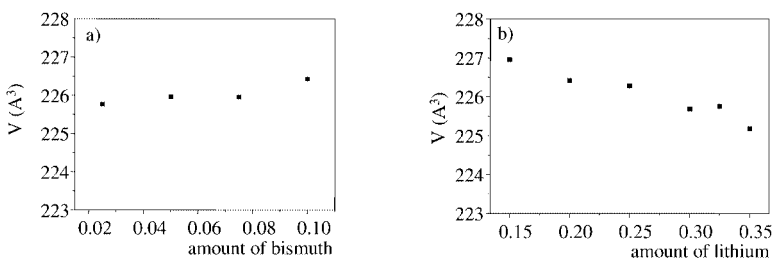

Figure 3. Cell volume with increasing concentration of a) bismuth and b) lithium

 © 2003 Wiley-VCH Verlag GmbH & Co. KGaA, Weinheim

grain boundary response and an additional CPE element to model a low conductivity surface layer lithium ions was used to model the experimental data. All fitting used the Zview software package.[17] The first and second semicircles showed capacities of around 0.4 pF and 3 nF respectively, and are, therefore, related to bulk and grain boundaries. The spike had a capacitance around 30−60 nF, which is probably too small to be related to an electrode/sample double layer, but is probably linked to a low-conductivity layer on the pellet surface. Such a result has been reported for high Na^+ or Li^+ ion conductors[12−14] and attributed to the presence of an Na^+ or Li^+ free layer on the crystal surface.

Bulk ionic conductivity data from the impedance complex plane plots for compounds on joins $Pr_{0.45+x}Bi_{0.05}Li_{0.5-3x}TiO_3$ ($0.033 \leq x \leq 0.133$) and $Pr_{0.558-y}Bi_yLi_{0.325}TiO_3$ ($y \leq 0.10$) are shown in Arrhenius format in Figure 6 (a and b, respectively).

The variation in ionic conductivity with the increase of lithium concentration is quite large (Figure 7, a), while the activation energy is between 0.45 and 0.46 eV. No change in the conductivity mechanism can be supposed, but the increasing lithium concentration initially increases the concentration of carriers, thereby increasing the conductivity to a maximum at $x = 0.2$ with a conductivity at 25 °C of $6.639 \cdot 10^{-6}$ S·cm^{-1}. Further increases in the lithium concentration decreases the number of vacancies and the conductivity paths, with a corresponding decrease in conductivity. These results agree with earlier results for the La system,[13] which report a conduction mechanism based on the A-site vacancies.

Along the join $Pr_{0.558-y}Bi_yLi_{0.325}TiO_3$, where the amount of lithium remains constant, the conductivity decreases slightly when the amount of bismuth increases (Figure 7, b). However, substitution of Pr by Bi is not accompanied by a significant change in the cell volume of the perovskite, and so this behavior does not seem to be related to any change in the "bottleneck" size. However, it could be related to the lone-electron pair of bismuth.[18−19] The activation energy in this case was 0.45−0.46 eV.

Conclusions

A large range of single-phase solid solutions have been synthesized in the triangle $Pr_{0.67}TiO_3/Pr_{0.5}Li_{0.5}TiO_3/Bi_{0.5}Li_{0.5}TiO_3$. The phase diagram in the single-phase region showed the existence of two polymorphs with perovskite-like structures, labeled O and T. Polymorph O is an orthorhombic distortion of the simple cubic perovskite, while polymorph T is a tetragonal perovskite. Region A is a mixture of a perovskite-like phase and $Pr_4Ti_9O_{24}$. Region B is a mixture of a perovskite-like compound and Li_2TiO_3, and region C is a mixture of the perovskite-like phase, $Bi_4Ti_3O_{12}$ and an unknown phase.

The increase of bismuth concentration reduced the time for the third treatment and when $y \geq 0.075$ it is not necessary.

The cell volume decreased with increasing lithium content, but remained almost constant with increasing amounts of bismuth. This is attributable to the effect of ionic radii, which are similar for praseodymium and bismuth but shorter for lithium.

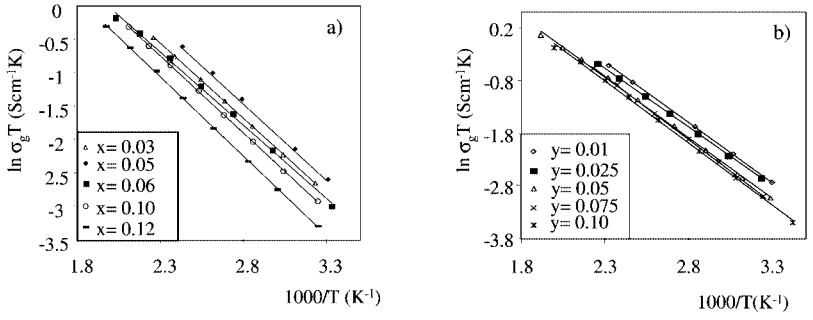

Figure 6. Arrhenius ionic conductivity plots for a) join 1 ($Pr_{0.45+x}Bi_{0.05}Li_{0.5-3x}TiO_3$) and b) join 2 ($Pr_{0.558-y}Bi_yLi_{0.325}TiO_3$)

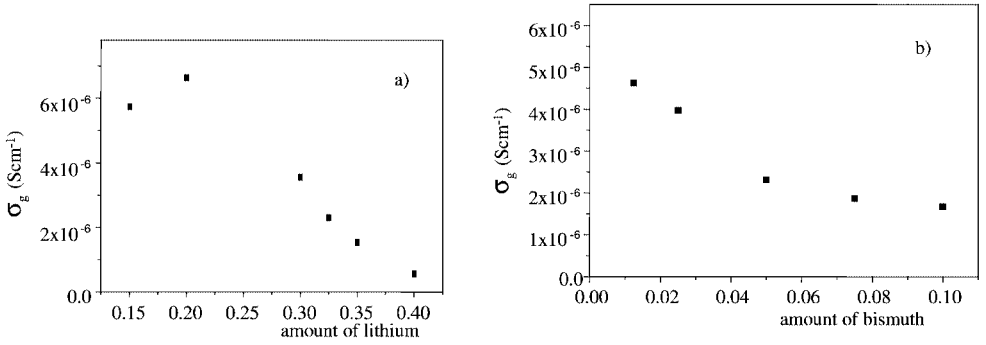

Figure 7. Plot of σ (bulk ionic conductivity) at room temperature vs. composition, a) in lithium along join 1 ($Pr_{0.45+x}Bi_{0.05}Li_{0.5-3x}TiO_3$) and b) in bismuth along join 2 ($Pr_{0.558-y}Bi_yLi_{0.325}TiO_3$)

 © 2003 Wiley-VCH Verlag GmbH & Co. KGaA, Weinheim

AC/DC measurements indicated that these compounds are ionic conductors. Li^+ ion conductivity increased with increasing lithium content up to $x = 0.2$ and subsequently decreased; the conductivity decreased slightly with increasing bismuth concentration.

The behaviour of the $Pr_{0.5+x-y}Bi_yLi_{0.5-3x}TiO_3$ system is similar to that of the $La_{0.5+x-y}Bi_yLi_{0.5-3x}TiO_3$ system,[13] but, analogously to other systems of praseodymium, its ionic conductivity is lower than that of the corresponding lanthanum system.[3,5,20]

Experimental Section

Synthesis: Pr_6O_{11} (99.9%, Fluka), TiO_2 (99.9%, Aldrich), Bi_2O_3 (> 99%, J. T. Baker), and Li_2CO_3 (> 99%, Merck) were used as starting materials. Pr_6O_{11} and TiO_2 were dried overnight at 900 °C prior to weighing. Pretreated and untreated oxides were mixed in the desired proportions in an agate mortar with acetone, dried, and heated at 650 °C for 2 h to drive off CO_2. After grinding, samples were pressed into pellets, put into platinum vessels and covered with a powder of the same composition to avoid lithium loss during thermal treatment. The pellets were fired at 1100 °C for 12 h, giving green products that were reground, repelleted, and fired at 1200 °C for a further 12 h. A third treatment was carried out at 1250 °C, the required time depending on the Bi composition. Samples rich in Bi were found to need less time for the third treatment. Finally, the last treatment involved 4 h for samples with $y \leq 0.01$, 2 h for samples for $0.01 < y \leq 0.025$ and 1 h for samples of $0.025 < y \leq 0.05$. In samples with concentrations of bismuth of $y \geq 0.75$ no third treatment was necessary. After the third treatment, the samples were quenched in air to room temperature to stabilize the high-temperature phase.

X-ray Diffraction: The solid solution range, crystalline phase identification, and lattice parameters were obtained by powder X-ray diffraction with a Siemens D-500 diffractometer, in reflection mode, with a detector sensitive to the position and a secondary monochromator of quartz, using Cu-K_α radiation. Lattice parameters were obtained using a silicon internal standard.

ICP: Chemical analysis was performed by inductively coupled plasma (ICP) spectroscopy (Thermo Jarrel ASH Corporation, model Spectrometer Polyscan TM 61E) to determine the Li, Bi and Ti contents. The results indicated that the loss of lithium during firing was within the error range of the instrument; thus, the nominal composition is used here.

Electrical Measurements: DC conductivity measurements were carried out using an HP-34401A multimeter. AC measurements were performed with an HP 4192A Impedance Analyzer over the range $100\ Hz < f < 13\ MHz$, only in the single-phase region. Samples were pressed into pellets and sintered at 1250 °C for 1 h. Pellet sides were then sanded and painted with gold paste (Engelhard-Clal T-10112), which was fixed in a tubular furnace with a maximum temperature of 900 °C.

Acknowledgments

This work was partially sponsored by financial support from Ministerio de Ciencia y Tecnologia, Proyecto BQU2002-00619 and Generalitat de Catalunya, Proyecto 2001SGR00052.

[1] C. Julien, G. A. Nazri, in: *Solid State Bateries: Materials Design and Optimization*, Kluwer Academic Publishers, Dordrecht, **1994**.
[2] R. M. Dell, *Solid State Ionics* **2000**, *134*, 139−158.
[3] M. L. Martínez Sarrión, L. Mestres, M. Morales, M. Herraiz, *J. Solid State Chem.* **2000**, *155*, 280−285.
[4] M. L. Martínez Sarrión, L. Mestres, R. Palacín, M. Herraiz, *Eur. J. Inorg. Chem.* **2001**, 1139−1144.
[5] M. Morales, M. L. Martínez Sarrión, *J. Mater. Chem.* **1998**, *8*, 1583−1587.
[6] M. Itoh, Y. Inaguma, W. H. Jung, L. Chen, T. Nakamura, *Solid State Ionics* **1994**, *70/71*, 203−207.
[7] Y. Inaguma, L. Chen, M. Itoh, T. Nakamura, *Solid State Ionics* **1994**, *70/71*, 196−202.
[8] Y. Inaguma, L. Chen, M. Itoh, T. Nakamura, *Solid State Communications* **1993**, *86*, 689−693.
[9] H. Kawai, J. Kuwano, *J. Electrochem. Soc.* **1994**, *141*, L78−L79.
[10] A. D. Robertson, S. García Martín, A. Coats, A. R. West, *J. Mater. Chem.* **1995**, *5*, 1405−1412.
[11] J. M. S. Skakle, G. C. Mather, M. Morales, R. I. Smith, A. R. West, *J. Mater. Chem.* **1995**, *5*, 1807−1808.
[12] M. Morales, A. R. West, *Solid State Ionics* **1996**, *91*, 33−43.
[13] M. L. Martínez-Sarrión, L. Mestres, M. Herráiz, O. Maqueda, A. Bakkali, N. Fernández, *Eur. J. Inorg. Chem.* **2002**, 1794−1800.
[14] P. G. Bruce, A. R. West, D. P. Almond, *Solid State Ionics* **1982**, *7*, 57−60.
[15] A. K. Jonscher, J. M. Reau, *J. Mater. Sci.* **1978**, *13*, 563−570.
[16] A. K. Jonscher, in: *Dielectric Relaxation in Solids*, Chelsea Dielectric Press, London, **1983**.
[17] *Zview for Windows* (version 1.4), Scribner Assoc. Inc., Charlotesville, Virginia, USA.
[18] Ph. Lacorre, *Solid State Sciences* **2000**, *2*, 755−758.
[19] F. Goutenoire, O. Isnard, E. Suard, O. Bohnke, Y. Laligant, R. Retoux, P. Lacorre, *J. Mater. Chem.* **2001**, *11*, 119−124.
[20] M. Itoh, Y. Inaguma, W. Jung, T. Nakamura, *Solid State Ionics* **1994**, *70/71*, 203−207.

Received November 21, 2002

 © 2003 Wiley-VCH Verlag GmbH & Co. KGaA, Weinheim

Neutral and Cationic [Bis(η¹-amidosilyl)-η⁵-cyclopentadienyl]titanium and -zirconium Complexes: Synthesis, X-ray Molecular Structures and DFT Calculations

Jesús Cano,[a] Pascual Royo,*[a] Heiko Jacobsen,[b][‡] Olivier Blacque,[b] Heinz Berke,[b] and Eberhardt Herdtweck[c]

Keywords: Cations / Cyclopentadienyl ligands / Density functional calculations / Nitrogen ligands / Titanium / Zirconium

Treatment of LiNH*t*Bu with THF solutions of $C_5H_4(SiMe_2Cl)_2$ gave $C_5H_4(SiMe_2NH$*t*$Bu)_2$ (**1**). Deprotonation of **1** with $M(NMe_2)_4$ (M = Ti, Zr) under different conditions provided the monocyclopentadienyl complexes $[M\{\eta^5\text{-}C_5H_3[SiMe_2(NH$*t*$Bu)]_2\}(NMe_2)_3]$ [M = Ti (**2**), Zr (**3**)] and the single (η-amidosilyl)cyclopentadienyl compounds $[M\{\eta^5\text{-}C_5H_3[SiMe_2(NH$*t*$Bu)][SiMe_2(\eta^1\text{-}N$*t*$Bu)]\}(NMe_2)_2]$ [M = Ti (**4**), Zr (**5**)]. The related dibenzyl compounds $[M\{\eta^5\text{-}C_5H_3[SiMe_2(NH$*t*$Bu)][SiMe_2(\eta^1\text{-}N$*t*$Bu)]\}(CH_2Ph)_2]$ [M = Ti (**6**), Zr (**7**)] resulted from treatment of **1** with $M(CH_2C_6H_5)_4$ (M = Ti, Zr). Further deprotonation of the amido complexes **4** and **5** and the benzyl complexes **6** and **7** by heating in toluene solution gave the bis(η-amidosilyl)cyclopentadienyl complexes $[M\{\eta^5\text{-}C_5H_3[SiMe_2(\eta^1\text{-}N$*t*$Bu)]_2\}(NMe_2)]$ [M = Ti (**8**), Zr (**9**)] and $[M\{\eta^5\text{-}C_5H_3[SiMe_2(\eta^1\text{-}N$*t*$Bu)]_2\}(CH_2Ph)]$ [M = Ti (**10**), Zr (**11**)], respectively. Treatment of the monobenzyl complexes **10** and **11** with $B(C_6F_5)_3$ yielded the cationic compounds $[M\{\eta^5\text{-}C_5H_3[SiMe_2(\eta^1\text{-}N$*t*$Bu)]_2\}]^+$ as $[(CH_2Ph)B(C_6F_5)_3]^-$ [M = Ti (**12**), Zr (**13**)] salts. All new compounds were characterized by NMR spectroscopy, and the crystal structures of **10** and **13** were studied by diffraction methods. DFT calculations for the neutral and cationic species are described and provide an explanation for the unusual η¹ coordination of a phenyl ring to a group-4 metal cation.
(© Wiley-VCH Verlag GmbH & Co. KGaA, 69451 Weinheim, Germany, 2003)

Introduction

The group-4 metallocenes $[MCp_2X_2]$[1] and cylopentadienylamido complexes $[M(\eta^5\text{-}C_5R_4\text{-}E\text{-}\eta^1\text{-}NR')X_2]$[2] are the two essential types of catalyst precursors for insertion polymerization of olefins based on the use of cyclopentadienyl ligands. After alkyl abstraction by a Lewis acid {MAO, $B(C_6F_5)_3$, $[CPh_3][B(C_6F_5)_4]$} the metallocene compounds generate the cationic, coordinatively unsaturated, 14-electron d^0 $[MCp_2R]^+$ species,[3] whereas the cyclopentadienylamido complexes provide the electronically more unsaturated 12-electron d^0 $[M(\eta^5\text{-}C_5R_4\text{-}E\text{-}\eta^1\text{-}NR')R']^+$ cations.[4] The technological applications[5] of these "constrained-geometry" catalysts are based not only on their electronic unsaturation, but also on their sterically open reactive sites, combined with rigidity of the molecular framework and thermal stability. These features facilitate the coordination of bulkier olefins, allowing the synthesis of various copolymers of ethylene with 1-hexene, 1-octene, styrene and other larger olefins.

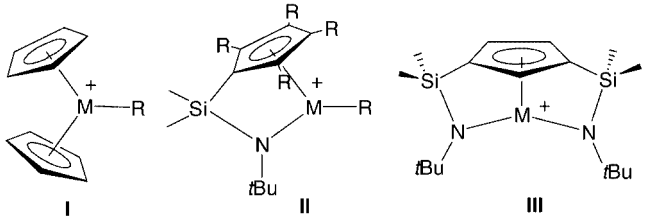

Scheme 1. Types of metallocene and (cyclopentadienylsilyl)amido cations

Amido ligands are π-donors and in this respect resemble Cp ligands. Even if π-electrons are included, however, the formal electron count of a single group never reaches that of the Cp moiety. Replacement of one Cp by an amido group, as demonstrated in structures **I** and **II**, establishes a 12-electron cyclopentadienylamido complex[6] on the basis

[a] Departamento de Química Inorgánica, Facultad de Química, Universidad de Alcalá, Campus Universitario, 28871 Alcalá de Henares, Spain
Fax: (internat.) + 34-91/8854683
E-mail: pascual.royo@uah.es
[b] Anorganisch-chemisches Institut der Universität Zürich Winterthurerstrasse 190, 8057 Zürich, Switzerland
Fax: (internat.) + 41-1/635-6802
E-mail: hberke@aci.unizh.ch
[c] Anorganisch-chemisches Institut der Technischen Universität München
Lichtenbergstrasse 4, 85747 Garching bei München, Germany
[‡] Present address: KemKom, 1864 Burfield Ave., Ottawa, Ontario K1J 6T1, Canada, E-mail: jacobsen@kemkom.com
Supporting information for this article is available on the WWW under http://www.eurjic.org or from the author.

of a 14-electron metallocene species **I**. Structures of type **III** with two amido ligands would indeed have the formal electron count of **I**. Despite this, complexes **III** are special, since they do not bear an alkyl group ready for Ziegler−Natta-type insertion polymerizations. Nevertheless, we have reported[7] that they still have potential for polarized metal−olefin binding similar to, for instance, the 18-electron Cp_3M^+ series (M = Ti, Zr).[8] For this reason we decided to study the synthesis and chemical behaviour of [bis(amidosilyl)cyclopentadienyl]titanium and -zirconium complexes of type **III**.

Here we report the syntheses of monocyclopentadienyl [M{η^5-C_5H_3[$SiMe_2$(NH*t*Bu)]$_2$}X_3], (amidosilyl)cyclopentadienyl [M{η^5-C_5H_3[$SiMe_2$(NH*t*Bu)][$SiMe_2$(η^1-N*t*Bu)]}X_2] and bis(amidosilyl)cyclopentadienyl [M{η^5-C_5H_3($SiMe_2$-η^1-N*t*Bu)$_2$}X] group-4 metal compounds and their cationic [M{η^5-C_5H_3($SiMe_2$-η^1-N*t*Bu)$_2$}]$^+$ derivatives. The X-ray molecular structures of the neutral [Ti{η^5-C_5H_3[$SiMe_2$(η^1-N*t*Bu)]$_2$}(CH_2Ph)] and the cationic [Zr{η^5-C_5H_3[$SiMe_2$(η^1-N*t*Bu)]$_2$}]$^+$[($CH_2C_6H_5$)B(C_6F_5)$_3$]$^-$ complexes were determined by diffraction methods and DFT calculations were carried out for the neutral and cationic species.

Results and Discussion

The cyclopentadiene C_5H_4($SiMe_2$NH*t*Bu)$_2$ (**1**) was isolated as a yellow liquid by treatment of the reported bis(chlorosilyl)cyclopentadiene[9] with 2 equiv. of LiNH*t*Bu in THF and was characterized by ^{1}H and ^{13}C NMR spectroscopy as a mixture of isomers (Scheme 2). The ^{1}H NMR spectrum of **1** recorded at 20 °C indicated a mixture of isomers **a**, **b**, **c** and **d** in a molar ratio of 8:4:1.3:1.

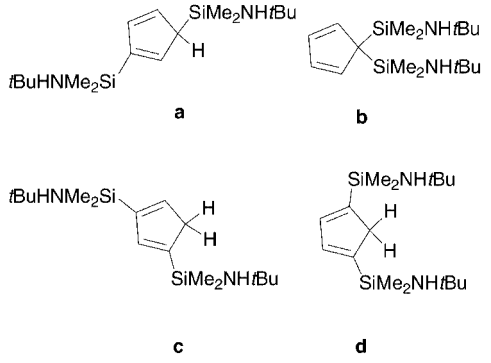

Scheme 2. Isomers of C_5H_4($SiMe_2$NH*t*Bu)$_2$ observed by NMR spectroscopy

In comparison with other previously reported disilyl-substituted compounds C_5H_4(SiR_3)$_2$,[10] in which the 1,1-isomer (**b**; R = Me, Cl) is by far the major component, the steric hindrance caused by the bulkier substituents (R = NH*t*Bu) means that the 1,3-isomer (**a**; two broad Si*Me*$_2$ singlets) is the major component in the isomeric mixture of **1**, being more favourable than the 1,1-isomer (**b**; one broad Si*Me*$_2$ singlet), as shown in Scheme 2. The other two isomers (2,4- and 2,5-), with both silyl groups bound to sp^2 carbon atoms, were less abundant components. All of these isomers interconvert, probably through successive 1,2-shifts of the silyl groups,[10] and increasing temperatures increase the **a**/**b** ratio to 4:1 at 50 °C, 8:1 at 70 °C and more than 10:1 at temperatures higher than 80 °C. The broad signals observed for **1a** at 20 °C appeared as four singlets when the ^{1}H NMR spectrum was recorded at −40 °C.

The tetraamide M(NMe_2)$_4$[11] and tetrabenzyl M(CH_2Ph)$_4$[12] compounds (M = Ti, Zr) were used to deprotonate the cyclopentadiene compound **1**, which possesses three acidic protons, to generate the metal-coordinated cyclopentadienyl ligand.

Monocyclopentadienyl Compounds

Immediate deprotonation of the most acidic cyclopentadiene proton took place when a toluene solution of **1** was treated at room temperature with 1 equiv. of Zr(NMe_2)$_4$ to give the monocyclopentadienyl compound **3** (Scheme 3) as the unique reaction product after 1 h (100% NMR yield). When Ti(NMe_2)$_4$ was used, heating at 50 °C was required to complete the reaction, the analogous titanium derivative **2** being isolated. Compound **2** was isolated as a dark red oil in quantitative yield after removal of the toluene and extraction into hexanes. The related tribenzyltitanium and -zirconium derivatives could not be isolated when M(CH_2Ph)$_4$ was used[13] because further deprotonation to give the mono- and bis(silylamido) benzyl derivatives took place very easily at room temperature.

The different thermal conditions required to deprotonate the tribasic diaminocyclopentadiene **1** show that the deprotonation with irreversible toluene elimination by the tetrabenzyl compounds M(CH_2Ph)$_4$ is much easier than the reversible elimination of amine by the amido derivatives M(NMe_2)$_4$, and that the zirconium compounds are more easily deprotonated than the more crowded titanium analogues, in spite of their weaker Ti−C and Ti−N bonds.[14] In all reactions the first deprotonation involves the most acidic cyclopentadiene proton.

The ^{1}H NMR spectra of **2** and **3** in C_6D_6 each show equivalent silylamido groups with NH (δ = 1.04, 1.08 ppm), *t*Bu (δ = 1.16, 1.15 ppm), and diastereotopic $SiMe_2$ (δ = 0.41, 0.43 ppm; δ = 0.42, 0.44 ppm) resonances close to those observed for **1**. Additionally, they each show an A_2B spin system for the ring protons and one singlet for all three equivalent NMe_2 groups. The expected spectral features were also observed in the ^{13}C NMR spectra, which each show one downfield shifted ring C_{ipso} resonance (δ = 127.8, 127.2 ppm) and Δδ (δ C_{tert} − δ C_{Me}) values[15] (15.3 ppm and 15.4 ppm) consistent with the presence of uncoordinated $SiMe_2$−NH*t*Bu groups.

Single (Amidosilyl)cyclopentadienyl Compounds

When toluene or THF solutions of complex **3**, prepared at room temperature, were heated at 65 °C, complete transformation of **3** into **5** was observed after 3 h. Compound **5** was the only NMR-detectable product under these conditions, and it could be isolated as a brown solid and characterized by elemental analysis and NMR spec-

 © 2003 Wiley-VCH Verlag GmbH & Co. KGaA, Weinheim

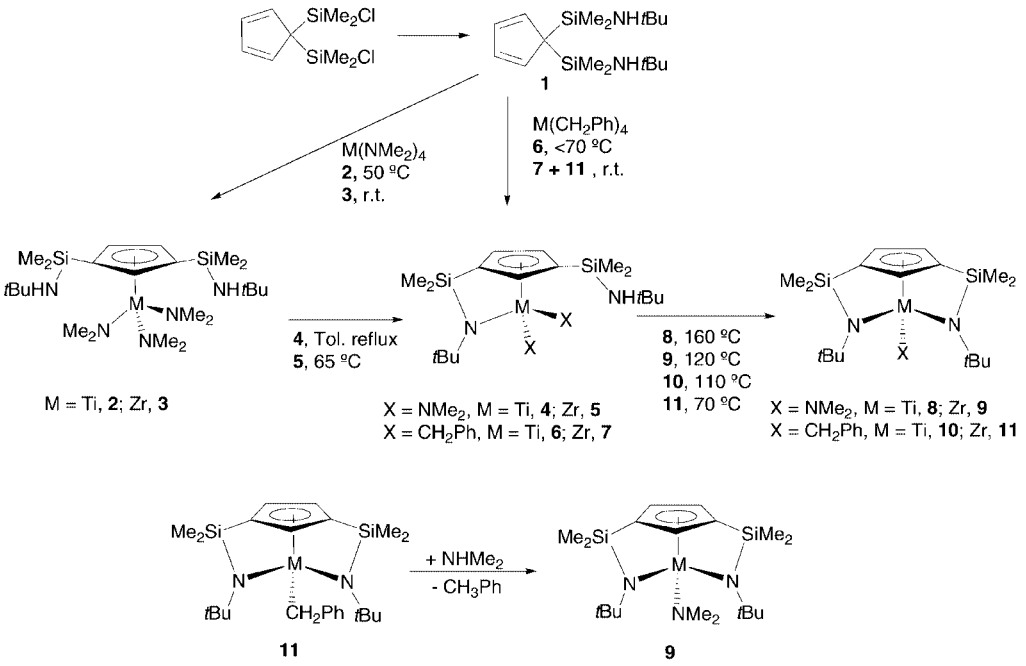

Scheme 3. Synthesis of cyclopentadienyl- and [(amidosilyl)- and bis(amidosilyl)cyclopentadienyl]titanium and -zirconium amide and benzyl complexes

troscopy. A similar transformation of **2** was achieved when a toluene solution of previously isolated **2** was heated at reflux for 5 h. The deprotonation of only one of the $SiMe_2NHtBu$ substituents with elimination of amine $NHMe_2$ occurred in a selective way to give pure **4**, which was isolated as a dark red oil and characterized by elemental analysis and NMR spectroscopy.

The related dibenzyl[*ansa*-(cyclopentadienylsilyl)amido]-titanium compound **6** was produced when a toluene solution of **1** and $Ti(CH_2Ph)_4$ was heated (below 70 °C) for 5 h. Higher temperatures could not be used, since further deprotonation would then occur, yielding small amounts of **8**. Under these conditions, **6** was the only reaction product that could be isolated, as a red-brown solid, and identified by elemental analysis and NMR spectroscopy. The third deprotonation could not be avoided when $Zr(CH_2Ph)_4$ was used, because deprotonation then occurs even at low temperature to give a mixture of **7** and other minor components. Because the products could not be separated, **7** was only characterized by NMR spectroscopy.

Coordination of the η⁵-cyclopentadienyl ligand increases the acidity of the NH*t*Bu amino protons [δ = 1.04 (**2**), 1.08 (**3**) ppm], and this is further increased after abstraction of the first amino hydrogen atom [δ = 0.86 (**4**), 0.85 (**5**) ppm]. For these reasons the reactions with the titanium reagents could be carried out selectively to give pure amido and benzyl compounds, whereas the tribenzyl compounds could not be isolated at room temperature.

The ^1H NMR spectra of the silylamido compounds **4**−**7** in C_6D_6 each show an ABC spin system for the three ring protons while the ^{13}C NMR spectra exhibit five resonances for the inequivalent ring carbon atoms, as expected for asymmetric molecules. Four resonances (^1H and ^{13}C) for the $SiMe_2$ moieties and two for the *t*Bu groups (^1H and ^{13}C), along with two ^{13}C resonances for their quaternary carbon atoms, are also observed for the two non-equivalent $SiMe_2NtBu$ and $SiMe_2NHtBu$ groups. Both can be easily distinguished by the different Δδ values[15] observed in the ^{13}C NMR spectra, which are smaller [15.5 (**4**), 15.7 (**5**), 16.0 (**6**, **7**) ppm] for uncoordinated NH*t*Bu groups than for bridging N*t*Bu groups [26.4 (**4**), 21.7 (**5**), 27.3 (**6**), 23.7 (**7**) ppm]. The amido complexes **4** and **5** also show two signals (^1H and ^{13}C) for non-equivalent NMe_2 ligands, whereas the benzyl derivatives **6** and **7** show four ^1H doublets and two ^{13}C resonances for diastereotopic methylene protons and carbon atoms of two non-equivalent benzyl ligands.

The chemical shifts observed in the ^1H and ^{13}C NMR spectra for all of the ring substituents of the analogous titanium and zirconium complexes show very slight differences, whereas resonances for the additional NMe_2 and CH_2Ph ligands appear at a lower field for the titanium than for the zirconium analogues. The *tert*-butyl ^1H and ^{13}C resonances of the coordinated amido ligand are shifted downfield with respect to a free NH*t*Bu group as a consequence of the π-donation to the metal centre, which is also consistent with a higher value of Δδ.

Bis(amidosilyl)cyclopentadienyl Compounds

Complete deprotonation of the uncoordinated $SiMe_2-NHtBu$ groups in the dibenzyl complexes **6** and **7** required heating of their toluene solutions under reflux or at 70 °C, respectively, to give the bis(silylamido) compounds **10**, isolated as orange crystals and **11**, isolated as a brown solid. Both complexes were identified by elemental analyses and NMR spectroscopy. Temperatures higher than reflux in toluene were required to achieve similar deprotonation

 © 2003 Wiley-VCH Verlag GmbH & Co. KGaA, Weinheim

of the amido complexes **4** and **5**. The reaction was monitored by ^{1}H NMR spectroscopy with a C_6D_6 solution of **5** in a Teflon-valved NMR tube. Complete deprotonation was observed after 12 h of heating at 120 °C, giving the bis(silylamido) compound **9** as the only reaction product. This reaction was reversible, however, and when the solution was cooled to room temperature, **9** reacted in solution with the eliminated amine $NHMe_2$ to give the starting product **5** quantitatively, and so could not be isolated in this way. Nevertheless, pure **9** could be obtained at a preparative level when the same thermal treatment of **5** was carried out in a Teflon-valved Schlenk tube after addition of 1 equiv. of the monobenzylzirconium compound **11**, which reacts with amine in an irreversible reaction to give **9** with elimination of toluene (see Scheme 3). Similar deprotonation of the titanium compound **4** required heating at temperatures higher than 160 °C to afford the bis(silylamido)titanium derivative **8**. This transformation was not quantitative, although pure **8** could be easily recovered because the reaction was not reversible on cooling to room temperature. Compounds **8** and **9** were isolated as brown and yellow solids, respectively, and identified by NMR spectroscopy.

Formation of the bis(silylamido) compounds is more selective, as it requires heating at temperatures above 100 °C, except in the case of the benzylzirconium compound **11** (70 °C). For the same reason the formation of the amidozirconium compound **9** is reversible in the presence of free amine.

The ^{1}H and ^{13}C NMR spectra of these diamido compounds **8**−**11** in C_6D_6 are consistent with the presence of a plane of symmetry, making the two silylamido groups equivalent. They show one singlet (^{1}H) and two resonances (^{13}C) for the *t*Bu groups and two signals (^{1}H and ^{13}C) for the non-equivalent methyl groups of the $SiMe_2$ moiety. Additionally, they show an A_2B spin system for the ring protons and three signals for the ring carbon atoms, along with one resonance for the methyl (**8**, **9**) and methylene (**10**, **11**) protons and carbon atoms of the NMe_2 and CH_2Ph ligands, respectively. The $\Delta\delta$[15] values are larger than those observed for non-coordinated $SiMe_2NH$*t*Bu groups in monocyclopentadienyl (**2**, **3**) and single silylamido (**4**−**7**) compounds, but lower than those observed for the metal-coordinated $SiMe_2$-η^1-N*t*Bu groups in silylamido compounds (**4**−**7**).

Orange crystals of **10** suitable for X-ray diffraction studies were isolated after extraction into hexane and slow cooling. The molecular structure of **10** is shown in Figure 1, and selected bond lengths and angles are listed in Table 1.

The titanium atom is in a pseudo-tetrahedral environment defined by the methylene carbon atom of the benzyl ligand, the centroid of the cyclopentadienyl ring, and the two coordinated nitrogen atoms of the silylamido groups. This is the first example of a neutral compound with a tridentate cyclopentadienyl ligand tethered by two silylamido groups.

Complex **10** shows Ti−N distances slightly longer than those reported for related $[Ti\{\eta^5\text{-}C_5R_4SiMe_2(\eta^1\text{-}NR')\}X_2]$ compounds with only one silylamido ligand (1.907−1.919

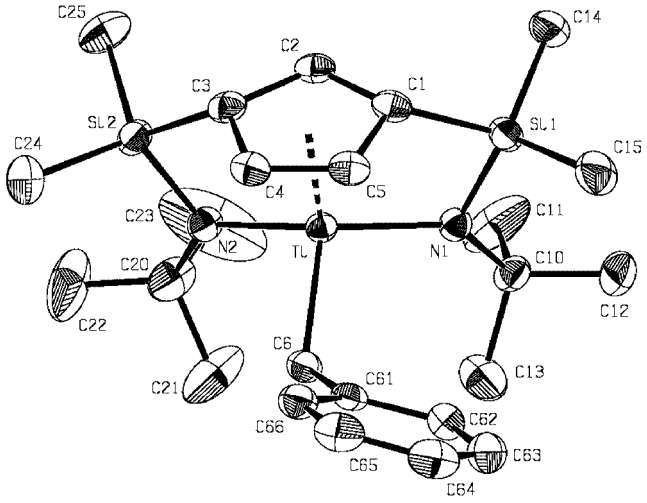

Figure 1. ORTEP drawing of the molecular structure of the major part of **10** in the solid state; thermal ellipsoids are drawn at the 50% probability level; the hydrogen atoms are omitted for clarity

Table 1. Selected interatomic distances [Å] and angles [°] for complexes [M = Ti (**10**), Zr (**13**)]; Cg denotes the centroid of the Cp ligand

	10	**13**
M−N1	1.9785(15)	2.0858(17)
M−N2	1.9808(15)	2.0812(17)
M−C1	2.3323(19)	2.4430(19)
M−C2	2.2915(18)	2.406(2)
M−C3	2.3432(18)	2.437(2)
M−C4	2.3885(18)	2.467(2)
M−C5	2.381(2)	2.466(2)
M−C6	2.1615(19)	
M···C32		3.019(2)
M−C33		2.571(3)
M···C34		3.057(3)
M−Cg	2.014	2.127
Si1−N1	1.7593(15)	1.7579(17)
Si1−C1	1.859(2)	1.865(2)
Si2−N2	1.7491(15)	1.7610(18)
Si2−C3	1.862(2)	1.870(2)
N1−M−N2	128.05(6)	126.89(7)
N1−M−C6	104.63(7)	
N1−M−C33		105.86(7)
N1−M−Cg	106.9	101.0
N2−M−C6	99.22(7)	
N2−M−C33		102.94(7)
N2−M−Cg	106.4	100.8
C6−M−Cg	111.0	
C33−M−Cg		121.1
Cg−C1−Si1	147.7	150.1
Cg−C3−Si2	146.9	150.5
C1−Si1−N1	93.70(8)	93.65(8)
C3−Si2−N2	93.92(8)	92.94(9)
M−N1−Si1	103.19(7)	105.56(8)
M−N2−Si2	103.53(8)	105.68(8)
M−C6−C61	124.25(13)	
M−C33−C32		94.56(15)
M−C33−C34		96.60(17)

 © 2003 Wiley-VCH Verlag GmbH & Co. KGaA, Weinheim

Å)[2h,4g,16,17,18] but similar to the distance (1.971Å)[19] reported for R = Me, R′ = *t*Bu, X_2 = 2 NMe_2 (see Table 2). This behaviour would be consistent with a weaker π-bonding contribution from the interaction between the nitrogen p_π orbital with the appropriate vacant metal d_π orbital due to the presence of a second amido group, which simultaneously increases the steric crowding and strain of the bicyclic structure. In contrast, the Si−N and Si−C distances observed for **10** are very close to those observed for all single silylamido compounds. The Ti−Cg distance is in the lower range found for singly bridged silylamido compounds. There is no deviation of the disilyl-substituted cyclopentadienyl ligand from η⁵-coordination, as deduced from the small differences in the Ti−C(ring) (2.347 Å average) and the C−C ring distances (1.419 Å average).

The amido nitrogen atom exhibits the expected planar disposition with sp^2 hybridization (the sum of bond angles around N is 360°) known for all structurally characterized silylamido complexes. The close Cg−C_{ring}−Si angles (147.3° average) account for the strain in these bicyclic compounds. In addition, the Cg−Ti−N angles are similar, whereas the Ti−N−Si angles are significantly narrower and the C1−Si1−N angles more open than those found in single silylamido compounds. This is also consistent with the differences observed in the bond lengths for a system in which the Si−N distances do not change whereas the Ti−N distances are longer. The N1−Ti−N2 angle is very open. The Ti−C6 distance is in the known range for benzyltitanium compounds.

The most significant structural feature of **10** is the orientation of the benzyl ligand, with its phenyl ring directed toward the cyclopentadienyl ring (see DFT calculations below). A similar orientation has also recently been observed for [Ti{1,3-[CH_2(2-C_4H_3N)]}$_2$(η⁵-C_5H_3)(NMe_2)].[20]

Cationic Compounds

Addition of C_6D_6 by vacuum transfer to a Teflon-valved NMR tube containing a mixture of $B(C_6F_5)_3$ and the benzyl compounds **10** or **11** in a 1:1 molar ratio immediately gave the partially soluble cationic species [M(η⁵-C_5H_3($SiMe_2$-η¹-N*t*Bu)$_2$]⁺, isolated as [$B(CH_2Ph)(C_6F_5)_3$]⁻ salts **12** and **13** as orange solids, which were identified by NMR spectroscopy and X-ray diffraction studies.

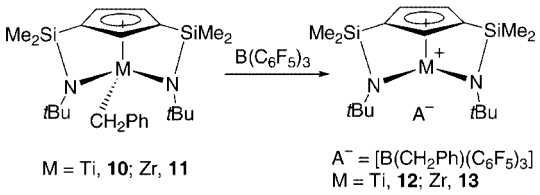

Scheme 4. Formation of cationic bis(amidosilyl)cyclopentadienyl complexes

The structures of the cations in C_6D_6 solutions were established by NMR studies. Their ^1H and ^{13}C NMR spectra are consistent with the C_s symmetry also observed for the neutral benzyl precursor compounds **10** and **11**. They each show one singlet (^1H) and two resonances (^{13}C) for the *t*Bu groups, two signals (^1H and ^{13}C) for non-equivalent methyl groups of the $SiMe_2$ groups, an A_2B spin system for the ring protons and three signals for the ring carbon atoms.

Table 2. Selected bond lengths [Å] and bond angles [°] for related complexes

Compound	M−N	M−Cg[a]	Cg−M−N	M−C	Si−N	Ref.
Ti[(C_5Me_4)$SiMe_2$(η¹-NBz)]Bz_2	1.919	2.045	107.4	2.131 2.158	1.731	[16]
Ti[(C_5Me_4)($SiMe_2${η¹-NCHMePh})] Cl(CH_2SiMe_3)	1.909(3)	2.030	107.2	2.106(5)		[17]
Ti[(C_5H_4)$SiMe_2$(η¹-NAr)]Cl_2	1.914(3)	2.016	105.1		1.755(3)	[2h]
Ti[(C_5H_4)$SiMe_2$(η¹-NAr){$CH_2B(C_6F_5)_2$} (C_6F_5)]	1.911(4)	2.033	105.3	2.169(5)	1.749(4)	[4g]
Ti[(C_5Me_4)$SiMe_2$(η¹-N*t*Bu)]Cl_2	1.907(4)	2.030	107.6			[19]
Ti[(C_5Me_4)$SiMe_2$(η¹-N*t*Bu)](NMe_2)$_2$	1.972(4) 1.924(5) 1.906(4)	2.083	105.5		1.722(4)	[19]
Ti(C_5Me_5)(NMe_2)$_3$	1.919(9)	2.132	119.4			[18]
Ti[C_5H_3{$SiMe_2$(η¹-N*t*Bu)}$_2$](CH_2Ph)	1.9785(15) 1.9808(15)	2.014	106.9 106.4	2.1615(19)	1.7593(15) 1.7491(15)	
[Ti{C_5H_3[$SiMe_2$(η¹-N*t*Bu)]$_2$}]⁺ [(CH_2Ph)B(C_6F_5)$_3$]⁻	1.959(4) 1.946(5)	1.997(5)	106.7 106.6	2.447(3)	1.773(5) 1.788(5)	[7]
Zr[(C_5Me_4)$SiMe_2$(η¹-N*t*Bu)](NMe_2)$_2$	2.108(4)[b] 2.060(5) 2.064(4)	2.233	100.2		1.730(4)	[19]
Zr[(C_5H_3){$SiMe_2$(η¹-N*t*Bu)}{$SiMe_2$(NMe_2)}]Cl(CH_3)	2.078	2.198	101.0	2.311	1.742	[21]
Zr[($C_{13}H_8$)$SiMe_2$(η¹-N*t*Bu)](CH_2SiMe_3)$_2$	2.061(2)			2.232(3) 2.248(3)	1.738	[22]
[Zr{C_5H_3[$SiMe_2$(η¹-N*t*Bu)]$_2$}]⁺ [(CH_2Ph)B(C_6F_5)$_3$]⁻	2.0858(17) 2.0812(17)	2.127	101.0 100.8	2.571(3)	1.7579(17) 1.7610(18)	

[a] Cg denotes the centroid of the cyclopentadienyl ring. [b] The M−N bond of the silylamido bridge.

 © 2003 Wiley-VCH Verlag GmbH & Co. KGaA, Weinheim

The $\Delta\delta$[15] values for the *t*Bu ^{13}C signals are slightly larger than those observed for corresponding neutral compounds. A surprising effect is observed when the ^{1}H and ^{13}C NMR spectra of the neutral benzyl precursor compounds **10**−**11** are compared with those of the corresponding cationic titanium and zirconium derivatives **12**−**13**: all of the NMR resonances for the cationic species are shifted upfield. It is also remarkable that this effect is particularly important for the ring CH proton located between the two silyl substituents. Furthermore, it is interesting to note that the ring C_{ipso} resonance is the signal at highest field for the neutral compounds whereas for the cationic derivatives it appears between the other two ring C resonances. This unexpected behaviour seems to be associated with the anisotropy of the benzyl ring exerted in the particular structure of these cationic species.

Orange crystals of **13**, appropriate for a single-crystal X-ray structure determination, were isolated from a C_6D_6 solution in the NMR tube. A perspective view of the molecular structure of **13** is shown in Figure 2, along with the non-hydrogen labelling scheme, and selected bond lengths and angles are listed in Table 1.

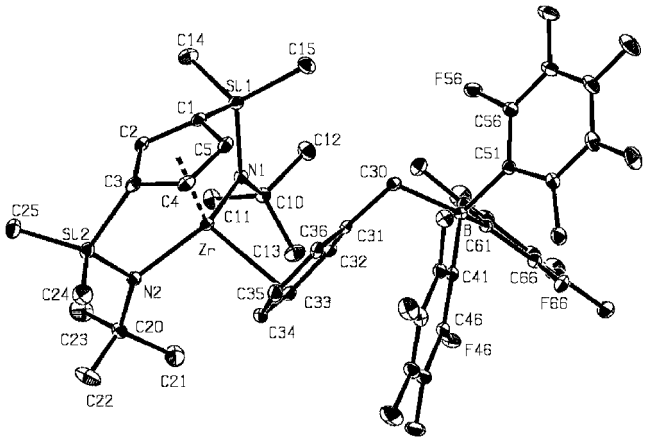

Figure 2. ORTEP drawing of the molecular structure of **13** in the solid state; thermal ellipsoids are drawn at the 10% probability level and hydrogen atoms are omitted for clarity

The pseudo-tetrahedral geometry about the Zr atom of **13** is defined by the centroid of the cyclopentadienyl ring and the two N-donors of the appended (dimethylsilyl)amido arms, with the remaining coordination site occupied by C(33) of the phenyl ring of the benzylborate anion. This disposition is very close to that observed for complex **12**[7] with the expected longer Zr−N and similar Si−N [1.773(5) Å; 1.788(5) Å for **12**] bonds. In comparison with those in the related neutral $[Zr\{(\eta^5\text{-}C_5R_4)SiMe_2(\eta^1\text{-}NR')\}X_2]$ compounds containing only one silylamido ligand, the Zr−N distances in **13** are similar,[21,22] but slightly shorter than the distances reported[19] for R = Me, R′ = *t*Bu, X_2 = 2 NMe_2. This behaviour is consistent with a similar π-bonding contribution from the two amido ligands to the more acidic zirconium cation. The Cg−Zr distance is significantly shorter than those observed in related single silylamido neutral complexes (see Table 2), indicating higher electron donation from the cyclopentadienyl ring.

The amido nitrogen atom exhibits the expected planar disposition with sp^2 hybridization (the sum of bond angles around N is 360°) known for all reported silylamido complexes. The constrained geometry of the $Cg-C_{ring}-Si-N-Zr$ cyclic systems is similar to that found for **12**. The ring C1 and C3 atoms, bearing the amidosilyl arms, are pyramidally distorted almost to the same extent, as shown by the sums of their bond angles (349.4° average) and by the $Cg-C_{ring}-Si$ angles (150.3° average). The angles at Si and N are in the range found for **12**, whereas the Cg−Zr−N angles (100.9° average) are significantly narrower than those observed in the related titanium cation **12** (106.65° average). This is consistent with the increased atomic radius of the Zr centre and is responsible for the slightly more constrained geometry shown by **13**.

The Zr−C33 bond [2.571(3) Å] is about 0.30 Å longer, whereas the distances to the neighbouring C32 and C34 atoms are about 0.8 Å longer than those observed for covalent Zr−C bonds, indicating an interaction of the empty hybrid metal orbital with the p_π orbital of the *meta*-C_{phenyl} atom of the borate anion.[23] The most significant feature of this structure is that the phenyl ring is oriented upward in the direction of the cyclopentadienyl ring, as also observed for the benzyl substituent in complex **10**.

Structure and Bonding of $[Ti\{\eta^5\text{-}C_5H_3(SiMe_2\text{-}\eta^1\text{-}N\mathit{t}Bu)_2\}]^+$ Cations

In this section we present density functional calculations performed on the model compound $[Ti\{\eta^5\text{-}C_5H_3(SiH_2\text{-}\eta^1\text{-}NH)_2\}]^+$ as well as on the real molecule $[Ti\{\eta^5\text{-}C_5H_3(SiMe_2\text{-}\eta^1\text{-}N\mathit{t}Bu)_2\}]^+$. The calculations for the model system serve to establish characteristic patterns in chemical bonding for bis(amidosilyl)cyclopentadienyl compounds of Ti and Zr. As mentioned above, these compounds can reasonably be regarded as 14-electron species, due to inclusion of the amido π-electrons. In the light of our previous analysis,[8c] we can expect that the bonding of $[Ti\{\eta^5\text{-}C_5H_3(SiR_2\text{-}\eta^1\text{-}NR)_2\}]^+$ cations should be governed by electrostatic interaction and ligand-to-metal donation, whereas back-bonding should play an only minor role.

Bonding of the Model System $[Ti\{\eta^5\text{-}C_5H_3(SiH_2\text{-}\eta^1\text{-}NH)_2\}]^+$

We first performed DFT calculations on the species with aryl ligands, $[Ti\{\eta^5\text{-}C_5H_3(SiH_2\text{-}\eta^1\text{-}NH)_2\}]^+[\eta^x\text{-}C_6H_5R]$ (R = H, CH_3, $CH_2BF_3^-$; x = 1, 2). For benzene, we considered different "up" and "down" coordination modes, as indicated in Scheme 5. For η^1-coordination, "up" and "down" coordination modes are characterized by dihedral angles (C4−C1−M−Cg) close to 0 and 180°, respectively, C1 being the benzene carbon atom coordinating to the metal centre, and C4 being the benzene carbon atom in the position *para* to C1. Similarly, for η^2-coordination, dihedral angles (X4−X1−M−Cg) close to 0 and 180° characterize "up" and "down" coordination modes, X1 being the mid-

 © 2003 Wiley-VCH Verlag GmbH & Co. KGaA, Weinheim

point between the two coordinating benzene carbon atoms, and X4 being the midpoint of the two corresponding benzene carbon atoms in the *para* position.

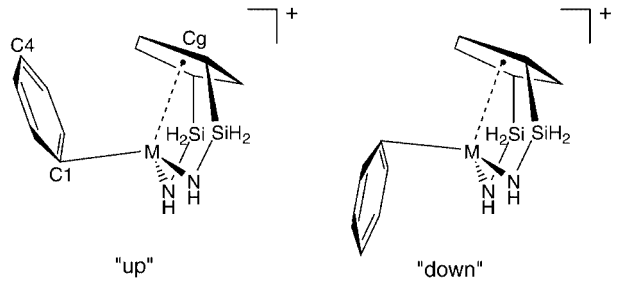

Scheme 5. The "up" and "down" coordination modes of the solvated model cation $[Ti\{C_5H_3(SiH_2NH)_2\}]^+$

The optimized geometry of the naked cation $[Ti\{\eta^5\text{-}C_5H_3(SiH_2\text{-}\eta^1\text{-}NH)_2\}]^+$ and its main empty frontier molecular orbital are displayed in Figure 3. The HOMO of the aryl ligand, dominates the orbital interaction through donation to the empty d_z^2 orbital at the metal centre.

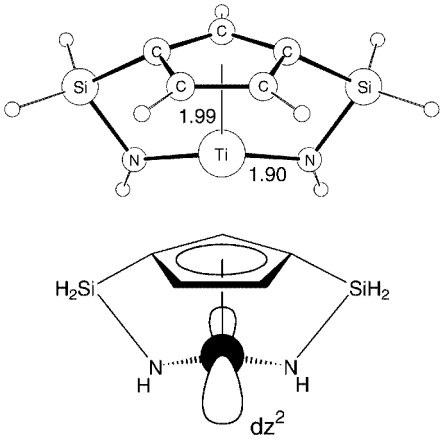

Figure 3. Optimized geometry for the model cation $[Ti\{C_5H_3(SiH_2NH)_2\}]^+$ and a main empty frontier MO

We recall from simple Hückel considerations that the HOMO of benzene consists of a set of degenerate e_{1g} orbitals, one of which is more likely to undergo η^1-type donation, whereas the other would induce a preference for η^2-coordination. For toluene, the degeneracy of the e_{1g} set is lifted, due to the antibonding hyperconjugation of the methyl group. In this case, the HOMO is most suited to η^1-coordination, having the largest orbital coefficient at the ring carbon atom in the position *para* to the methyl substituent.

The relative energies for various investigated complex geometries, together with optimized Ti−L bond lengths, are collected in Table 3. Relative energies are determined for groups of isomeric compounds, in which the energy of the isomer with the largest absolute value in total bonding energy is set to zero, and energies of isomers are reported with reference to the energy of the isomer at zero energy.

The energy differences are small, but significant. In particular, we note that η^1-coordination is favoured for the cationic complexes by about 10 kJ/mol. The small energy differences are accompanied by a fairly large change in the Ti−C bond length, of about 0.20 Å, indicating the subtle nature of this bonding interaction. The bond energies (*BE*s) of benzene and toluene amount to 89 kJ/mol and 100 kJ/mol, respectively.

Finally, complexes of the borate anion $C_6H_5CH_2BF_3^-$ are characterized by the Ti−C bonds, which are about 0.20 Å shorter than those in the related benzene or toluene complexes. Electrostatic interactions between the anionic ligand and the cationic metal fragment have a pronounced influence on the Ti−L bond strength. Again, η^1-coordination is favoured by 16 kJ/mol.

Complexes with the Cation $[Ti\{\eta^5\text{-}C_5H_3(SiMe_2\text{-}\eta^1\text{-}NtBu)_2\}]^+$

We begin with the molecular geometry of $[Ti\{\eta^5\text{-}C_5H_3(SiMe_2\text{-}\eta^1\text{-}N\mathit{t}Bu)_2\}\{\eta^1\text{-}C_6H_5CH_2B(C_6F_5)_3\}]$, which has also been established by crystal structure determination.[7] By our analysis, we can expect the following features for this compound. Firstly, the $[C_6H_5CH_2B(C_6F_5)_3]^-$ borate ligand should coordinate in η^1-fashion, being oriented upwards toward the site of the cyclopentadienyl ring. This structural feature is observed in the crystal structure of this compound. Furthermore, from simple Hückel orbital considerations, we expect that the coordinating ring carbon atom should be located *para* to the boron substituent. However, the solid-state structure reveals coordination through a *meta* carbon atom rather than one in the *para* position. We therefore optimized two representative geometries for both *meta* and *para* coordination, as shown in Figure 4.

For the *meta* coordination (Figure 4, a), inspection of the optimized geometries reveals the presence of short F···H distances ($d \approx 2.40$ Å), between the pentafluorophenyl rings and methyl groups of the metal fragment. For *para* coordi-

Table 3. Relative energies [kJ/mol] and metal-to-ligand bond lengths [Å] for coordination of the aryl double bond for various complexes of the type $[\{C_5H_3(SiH_2NH)_2\}Ti]^+[\eta^x\text{-}C_6H_5R]$ (R = H, CH_3, $CH_2BF_3^-$; x = 1, 2)

	R = H				R = Me		R = $CH_2BF_3^-$	
	η^1		η^2		η^1	η^2	η^1	η^2
	"up"[c]	"down"	"up"	"down"	"up"	"up"	"up"	"up"
E_{rel}[a]	0	6	9	8	0	12	0	16
d(Ti−C)[b]	2.46	2.54	2.69	2.66	2.43	2.67, 2.69	2.28	2.41, 2.66

[a] The most stable isomer is set to zero. [b] Bond lengths between the C_6H_5R ligand and the metal centre. [c] See Scheme 5 for a definition of "up" and "down" coordination.

 © 2003 Wiley-VCH Verlag GmbH & Co. KGaA, Weinheim

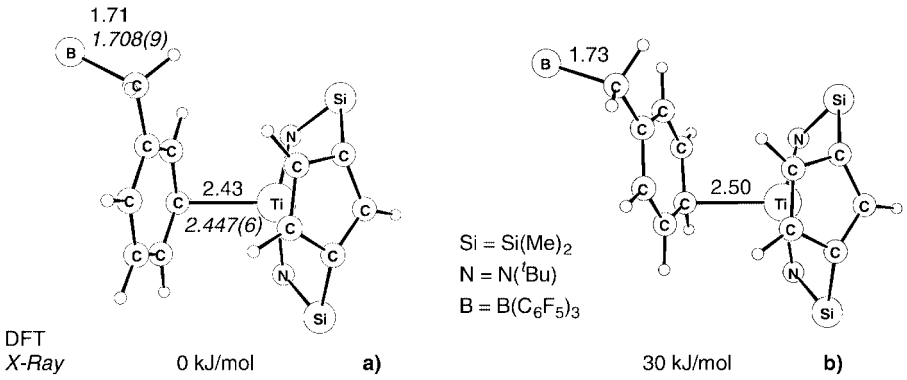

Figure 4. Relative energies and selected bond lengths for *meta* (a) and *para* coordination (b) of [Ti{η^5-C_5H_3($SiMe_2$N*t*Bu)$_2$}{η^1-$C_6H_5CH_2B(C_6F_5)_3$}]; comparison with X-ray analysis

nation (Figure 4, b), in contrast, no such short contacts can be found. The presence of such intramolecular hydrogen bonds might be the key point that explains why the *meta* geometry is energetically favoured by 30 kJ/mol. To produce further evidence for our argument, we also optimized *meta* and *para* geometries for [Ti{η^5-C_5H_3($SiMe_2$-η^1-N*t*Bu)$_2$}(η^1-$C_6H_5CH_2BF_3$)]. As was to be expected, since no short F···H contacts can be achieved in this case, orbital interactions now favour the latter coordination mode by 13 kJ/mol.

We then optimized the molecular geometry of [Ti{η^5-C_5H_3($SiMe_2$-η^1-N*t*Bu)$_2$}($CH_2C_6H_5$)], which is displayed in Figure 5. The geometry of the neutral benzyl complex again exhibits "up" coordination, with a typical Ti−C bond length of 2.19 Å. The optimized geometry is in good agreement with the crystal structure of this compound. The reaction energy (ΔE) for the formation of the benzyl complex from [Ti{η^5-C_5H_3($SiMe_2$-η^1-N*t*Bu)$_2$}{η^1-$C_6H_5CH_2B(C_6F_5)_3$}], which involves the cleavage of a C−B bond, followed by a reorientation of the benzyl fragment, amounts to −15 kJ/mol. The latter compound is therefore stable for kinetic, but not for thermodynamic, reasons. One factor lending kinetic stability to the unusual η^1-adduct is the energy of preparation of the $B(C_6F_5)_3$ fragment, associated with the pyramidalization of the trigonal-planar-coordinated boron atom, which substantially increases the value for the C−B bond strength by the order of 80 kJ/mol.[8c]

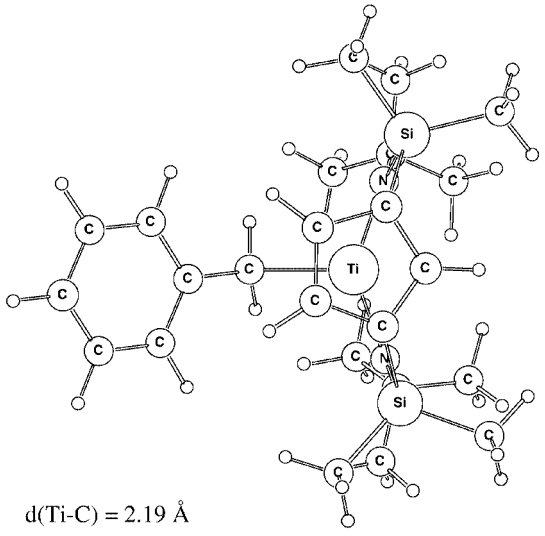

Figure 5. Optimized geometry of the benzyl complex [Ti{η^5-C_5H_3($SiMe_2$N*t*Bu)$_2$}($CH_2C_6H_5$)]

Conclusion

To conclude, we have synthesized a new type of [bis(η^1-amidosilyl)cyclopentadienyl]titanium and -zirconium complexes by direct deprotonation of the corresponding bis(aminosilyl)cyclopentadiene with metal tetraamide and tetrabenzyl derivatives under varying thermal conditions. The complexes obtained in this way may be classified into three categories: monocyclopentadienyl, *ansa*-(amidosilyl)cyclopentadienyl and bis[*ansa*-(amidosilyl)cyclopentadienyl] complexes. The first two categories show the structures and chemical behaviour expected for these well-known types of compounds. However, the bis[*ansa*-bis(amidosilyl)cyclopentadienyl] complexes are isolobal with previously reported tris(cyclopentadienyl) compounds and present reactivity pathways determined by the strong electrostatic character of the interactions, additionally facilitated by the unique accessible metal orbital. Treatment of the benzyl complexes with $B(C_6F_5)_3$ gave the cationic species, which were characterized by X-ray diffraction methods, indicating that the counter-ion is coordinated to the metal atom through a single interaction with the phenyl *m*-carbon atom of the benzyl borate anion.

Density functional calculations developed for the cationic complexes provide an explanation for their remarkable structural features, particularly the "up" (oriented toward the cyclopentadienyl ring) coordination of the benzyl group in the neutral benzyltitanium complex and of the ligand (solvent or counter-anion) bound in the cationic species.

Experimental Section

General Remarks: All experiments were carried out under argon by use either of a Vacuum Atmospheres glove box or of standard Schlenk techniques. Hydrocarbon solvents and THF were distilled from Na/benzophenone and stored under argon prior to use.

 © 2003 Wiley-VCH Verlag GmbH & Co. KGaA, Weinheim

1,1-Bis(chlorodimethylsilyl)cyclopentadiene, $Ti(NMe_2)_4$,[11] $Zr(NMe_2)_4$,[11] $Ti(CH_2Ph)_4$,[12] $Zr(CH_2Ph)_4$[12] and $B(C_6F_5)_3$,[24] were prepared by previously reported methods. NMR spectra were recorded with Varian Unity FT 300 and Varian FT 500 Unity Plus instruments in Teflon-valved tubes at probe temperature (20 °C). ^1H and ^{13}C NMR chemical shifts were measured relative to the residual resonances of C_6D_6 used as solvent, but the chemical shifts are reported with respect to TMS. ^{19}F NMR chemical shifts are referenced to external $CFCl_3$. Coupling constants are reported in Hz. C, H and N analyses were carried out with a Perkin−Elmer 240 C analyzer.

$C_5H_4(SiMe_2NHtBu)_2$ (1): A solution of LiNH*t*Bu (1.61 g, 20.5 mmol) in THF (40 mL) was added at 0 °C to a solution of C_5H_4-1,1-$(SiMe_2Cl)_2$ (2.51 g, 10 mmol) in THF and the mixture was stirred for 12 h. The volatiles were removed under vacuum and the residue was extracted into hexane to give a mixture of isomers of **1** as a yellow liquid after removal of the solvent (2.92 g, 9.0 mmol, 90%). ^1H NMR (C_6D_6, 20 °C) of the major component (**1a**): δ = −0.05 (br. s, 6 H, $SiMe_2$), 0.21 (br. s, 6 H, $SiMe_2$), 1.12 (s, 9 H, NH*t*Bu), 1.17 (s, 9 H, NH*t*Bu), 3, 57 (m, 1 H, CpH), 6.50 (m, 1 H, C_5H_3), 6.71 (m, 2 H, C_5H_3) ppm. Component **1b**: δ = 0.09 (s, 12 H, $SiMe_2$), 1.15 (s, 18 H, NH*t*Bu), 6.53 (m, 2 H, C_5H_4), 6.78 (m, 2 H, C_5H_4) ppm.

[Ti{η⁵-C_5H_3-1,3-[$SiMe_2(NHtBu)]_2$}$(NMe_2)_3$] (2): A solution of $Ti(NMe_2)_4$ (0.65 g, 2.9 mmol) in toluene (70 mL) was cooled to 0 °C, and **1** (0.94 g, 2.9 mmol) was added by syringe. The resulting red solution was stirred at 50 °C for 5 h. When the evolution of gas had stopped, the solvent was removed under vacuum and the residue was extracted into pentane (70 mL). After filtration and removal of the solvent, complex **2** was isolated as a deep red oil (1.45 g, 2.8 mmol, 97%). ^1H NMR (C_6D_6, 20 °C): δ = 0.41 (s, 6 H, $SiMe_2$), 0.43 (s, 6 H, $SiMe_2$), 1.04 (s, 2 H, NH*t*Bu), 1.16 (s, 18 H, N*t*Bu), 3.13 (s, 18 H, NMe_2), 6.31 (d, 2 H, C_5H_3), 6.60 (t, 1 H, C_5H_3) ppm. ^{13}C NMR (C_6D_6, 20 °C): δ = 2.9 ($SiMe_2$), 4.1 ($SiMe_2$), 34.0 (N*t*Bu), 49.3 ($NtBu_{tert}$), 50.3 (NMe_2), 119.9 (C_5H_3), 125.2 (C_5H_3), 127.8 (C_5H_{3ipso}) ppm. IR (Nujol): $\tilde{\nu}$ = 3383 (N−H) cm^{-1}. $C_{23}H_{53}N_5Si_2Ti$ (503.76): calcd. C 54.84, H 10.60, N 13.09; found C 54.17, H 10.23, N 12.82.

[Zr{η⁵-C_5H_3-1,3-[$SiMe_2(NHtBu)]_2$}$(NMe_2)_3$] (3): Compound **1** (0.05 g, 0.1 mmol) was added by syringe to a solution of $Zr(NMe_2)_4$ (0.041 g, 0.1 mmol) in C_6D_6 (0.6 mL). Complex **3** was immediately identified in the NMR spectrum as the unique product of the reaction. ^1H NMR (C_6D_6, 20 °C): δ = 0.42 (s, 6 H, $SiMe_2$), 0.44 (s, 6 H, $SiMe_2$), 1.08 (s, 2 H, NH*t*Bu), 1.15 (s, 18 H, N*t*Bu), 2.98 (s, 18 H, NMe_2), 6.50 (d, 2 H, C_5H_3), 6.78 (t, 1 H, C_5H_3) ppm. ^{13}C NMR (C_6D_6, 20 °C): δ = 2.8 ($SiMe_2$), 3.5 ($SiMe_2$), 33.9 (N*t*Bu), 45.6 (NMe_2), 49.3 ($NtBu_{tert}$), 120.5 (C_5H_3), 127.0 (C_5H_3), 127.2 (C_5H_{3ipso}) ppm. Pure **3** was only observed in NMR-tube experiments, while solid samples were always contaminated by small amounts of **5**.

[Ti{η⁵-C_5H_3-1-[$SiMe_2(NHtBu)$]-3-[$SiMe_2(η^1$-N*t*Bu)}$(NMe_2)_2$] (4): A solution of $Ti(NMe_2)_4$ (2.00 g, 8.9 mmol) in toluene (70 mL) was cooled to 0 °C, and **1** (2.91 g, 8.9 mmol) was added by syringe. The resulting red solution was heated at reflux for 5 h. When the evolution of gas had stopped, the solvent was removed under vacuum and the residue was extracted into pentane (70 mL). After filtration and removal of the solvent, complex **4** was isolated as a deep red oil (4.10 g, 8.8 mmol, 98%). ^1H NMR (C_6D_6, 20 °C): δ = 0.35 (s, 3 H, $SiMe_2NHtBu$), 0.43 (s, 3 H, $SiMe_2NHtBu$), 0.50 (s, 3 H, $SiMe_2NtBu$), 0.54 (s, 3 H, $SiMe_2NtBu$), 0.86 (s, 1 H, NH*t*Bu), 1.12 (s, 9 H, NH*t*Bu), 1.28 (s, 9 H, N*t*Bu), 2.87 (s, 6 H, NMe_2), 3.05 (s, 6 H, NMe_2), 6.12 (m, 1 H, C_5H_3), 6.31 (m, 1 H, C_5H_3), 6.50 (m, 1 H, C_5H_3) ppm. ^{13}C NMR (C_6D_6, 20 °C): δ = 2.1 ($SiMe_2$), 2.4 ($SiMe_2$), 2.4 ($SiMe_2$), 3.7 ($SiMe_2$), 34.1 (NH*t*Bu), 34.4 (N*t*Bu), 49.1 (NMe_2), 49.6 ($NHtBu_{tert}$), 50.4 (NMe_2), 60.8 ($NtBu_{tert}$), 109.1 (C_5H_{3ipso}), 121.2 (C_5H_3), 122.5 (C_5H_3), 123.7 (C_5H_3), 130.7 (C_5H_3) ppm. IR (Nujol): $\tilde{\nu}$ = 3385 (N−H) cm^{-1}. $C_{21}H_{46}N_4Si_2Ti$ (458.67): calcd. C 54.99, H 10.11, N 12.21; found C 54.67, H 9.97, N 12.04.

[Zr{η⁵-C_5H_3-1-[$SiMe_2(NHtBu)$]-3-[$SiMe_2(η^1$-N*t*Bu)]}$(NMe_2)_2$] (5): A solution of $Zr(NMe_2)_4$ (3.37 g, 12.6 mmol) in toluene (70 mL) was cooled to 0 °C, and **1** (4.09 g, 12.6 mmol) was added by syringe. The resulting yellow solution was warmed to 65 °C for 5 h. When the evolution of gas had stopped, the solvent was removed under vacuum and the residue was extracted into pentane (70 mL). After filtration and removal of the solvent, complex **5** was isolated as a light brown solid (6.19 g, 12.3 mmol, 98%). IR (Nujol): $\tilde{\nu}$ = 3384 (N−H) cm^{-1}. ^1H NMR (C_6D_6, 20 °C): δ = 0.35 (s, 3 H, $SiMe_2NHtBu$), 0.42 (s, 3 H, $SiMe_2NHtBu$), 0.57 (s, 3 H, $SiMe_2NtBu$), 0.59 (s, 3 H, $SiMe_2NtBu$), 0.85 (s, 1 H, NH*t*Bu), 1.11 (s, 9 H, NH*t*Bu), 1.27 (s, 9 H, N*t*Bu), 2.81 (s, 6 H, NMe_2), 2.82 (s, 6 H, NMe_2), 6.39 (m, 1 H, C_5H_3), 6.47 (m, 1 H, C_5H_3), 6.69 (m, 1 H, C_5H_3) ppm. ^{13}C NMR (C_6D_6, 20 °C): δ = 2.3 ($SiMe_2$), 2.7 ($SiMe_2$), 2.8 ($SiMe_2$), 3.0 ($SiMe_2$), 33.9 (NH*t*Bu), 34.9 (N*t*Bu), 44.2 (NMe_2), 44.5 (NMe_2), 49.6 ($NHtBu_{tert}$), 56.6 ($NtBu_{tert}$), 111.4 (C_5H_{3ipso}), 122.6 (C_5H_3), 122.9 (C_5H_3); 124.7 (C_5H_3), 126.7 (C_5H_3) ppm. $C_{21}H_{46}N_4Si_2Zr$ (502.01): calcd. C 50.24, H 9.24, N 11.16; found C 49.73, H 9.05, N 11.45.

[Ti{η⁵-C_5H_3-1-[$SiMe_2(NHtBu)$]-3-[$SiMe_2(η^1$-N*t*Bu)]}$(CH_2Ph)_2$] (6): A solution of $Ti(CH_2Ph)_4$ (2.14 g, 5.2 mmol) in toluene (70 mL) was cooled to 0 °C, and **1** (1.69 gr, 5.2 mmol) was added by syringe. The resulting yellow solution was warmed to 70 °C for 5 h. When the evolution of gas had stopped, the solvent was removed under vacuum and the residue was extracted into pentane (70 mL). After filtration and removal of the solvent, complex **6** was isolated as a red-brown solid (2.86 g, 5.1 mmol, 98%). ^1H NMR (C_6D_6, 20 °C): δ = 0.21 (s, 3 H, $SiMe_2NHtBu$), 0.27 (s, 3 H, $SiMe_2NHtBu$), 0.37 (s, 3 H, $SiMe_2NtBu$), 0.38 (s, 3 H, $SiMe_2NtBu$), 0.72 (s, 1 H, NH*t*Bu), 1.06 (s, 9 H, NH*t*Bu), 1.44 (s, 9 H, N*t*Bu), 2.46 (d, *J* = 10.5 Hz, 1 H, CH_2Ph), 2.55 (d, *J* = 10.5 Hz, 1 H, CH_2Ph), 2.81 (d, *J* = 10.5 Hz, 1 H, CH_2Ph), 2.97 (d, *J* = 10.5 Hz, 1 H, CH_2Ph), 5.83 (m, 1 H, C_5H_3), 6.14 (m, 1 H, C_5H_3), 6.83 (m, 1 H, C_5H_3), 6.87−7.20 (m, 10 H, CH_2Ph) ppm. ^{13}C NMR (C_6D_6, 20 °C): δ = 0.6 ($SiMe_2$), 1.5 ($SiMe_2$), 2.4 ($SiMe_2$), 2.9 ($SiMe_2$), 33.8 (NH*t*Bu), 34.2 (N*t*Bu), 49.8 ($NHtBu_{tert}$), 61.5 ($NtBu_{tert}$), 79.6 (CH_2Ph), 83.7 (CH_2Ph), 110.2 (C_5H_{3ipso}), 122.1 (C_5H_3), 122.5 (C_5H_3), 122.8 (C_5H_3), 123.0 (C_5H_3), 125.9 (C_6H_5), 126.8 (C_6H_5), 127.4 (C_6H_5), 128.5 (C_6H_5), 128.6 (C_6H_5), 128.7 (C_6H_5), 128.9 (C_6H_5), 129.8 (C_6H_5), 132.6 (C_6H_5), 149.6 (C_6H_{5ipso}), 150.1 (C_6H_{5ipso}) ppm. IR (nujol): $\tilde{\nu}$ = 3349 (N−H) cm^{-1}. $C_{31}H_{48}N_2Si_2Ti$ (552.78): calcd. C 67.36, H 8.75, N 5.07; found C 67.82, H 8.71, N 4.81.

[Zr{η⁵-C_5H_3-1-[$SiMe_2(NHtBu)$]-3-[$SiMe_2(η^1$-N*t*Bu)]}$(CH_2Ph)_2$] (7): A solution of $Zr(CH_2Ph)_4$ (2.93 g, 6.43 mmol) in toluene (70 mL) was cooled to 0 °C, and **1** (2.09 g, 6.43 mmol) was added by syringe. The resulting yellow solution was warmed to 40 °C for 5 h. The solvent was removed under vacuum and the residue was extracted into pentane (70 mL). After filtration and removal of the solvent, a mixture of complexes **7** and **11** was isolated. Formation of **7** was confirmed by IR and NMR spectroscopy, although pure **7** free of **11** could not be isolated. Data for **7**: IR (Nujol): $\tilde{\nu}$ = 3353 (N−H) cm^{-1}. ^1H NMR (C_6D_6, 20 °C): δ = 0.33 (s, 3 H, $SiMe_2NHtBu$), 0.34 (s, 3 H, $SiMe_2NHtBu$), 0.35 (s, 3 H, $SiMe_2NtBu$), 0.40 (s, 3 H, $SiMe_2NtBu$), 0.69 (s, 1 H, NH*t*Bu), 1.06

 © 2003 Wiley-VCH Verlag GmbH & Co. KGaA, Weinheim

(s, 9 H, NH*t*Bu), 1.13 (s, 9 H, N*t*Bu), 1.66 (s, 1 H, CH_2Ph), 1.72 (s, 1 H, CH_2Ph), 2.12 (s, 1 H, CH_2Ph), 2.17 (s, 1 H, CH_2Ph), 6.21 (m, 1 H, C_5H_3), 6.35 (m, 1 H, C_5H_3), 6.60 (m, 1 H, C_5H_3), 6.90−7.30 (m, 10 H, C_6H_5) ppm. ^{13}C NMR (C_6D_6, 20 °C): δ = 1.3 ($SiMe_2$), 2.0 ($SiMe_2$), 2.4 ($SiMe_2$), 2.5 ($SiMe_2$), 33.7 (NH*t*Bu), 33.8 (N*t*Bu), 49.7 (NH*t*Bu_{tert}), 54.9 (CH_2Ph), 57.5 (N*t*Bu_{tert}), 57.9 (CH_2Ph), 109.6 (C_5H_{3ipso}), 122.2 (C_5H_3), 122.5 (C_5H_3), 124.8 (C_5H_3), 125.6 (C_5H_3), 125.9 (C_6H_5), 126.4 (C_6H_5), 126.6 (C_6H_5), 127.8 (C_6H_5), 129.3 (C_6H_5), 129.6 (C_6H_5), 129.6 (C_6H_5), 129.8 (C_6H_5), 131.9 (C_6H_5), 145.8 (C_6H_{5ipso}), 146.2 (C_6H_{5ipso}) ppm.

[Ti{η⁵-C_5H_3-1,3-[$SiMe_2$(η¹-N*t*Bu)]$_2$}(NMe_2)] (8): When a C_6D_6 solution of the diamido complex **4** was heated at 160 °C for 12 h in a sealed NMR tube, a slow reaction took place with elimination of $NHMe_2$ to give **8**, identified by its ^1H and ^{13}C NMR spectra, together with the starting complex **4**. When the reaction mixture was cooled to room temperature, the reaction proved to be irreversible. ^1H NMR (C_6D_6, 20 °C): δ = 0.50 (s, 6 H, $SiMe_2$), 0.52 (s, 6 H, $SiMe_2$), 1.38 (s, 18 H, N*t*Bu), 2.83 (s, 6 H, NMe_2), 6.17 (d, 2 H, C_5H_3), 6.71 (t, 1 H, C_5H_3) ppm. ^{13}C NMR (C_6D_6, 20 °C): δ = 2.7 ($SiMe_2$), 2.8 ($SiMe_2$), 35.2 (N*t*Bu), 51.3 (NMe_2), 59.3 (N*t*Bu_{tert}), 117.7 (C_5H_{3ipso}), 121.3 (C_5H_3), 131.9 (C_5H_3) ppm.

[Zr{η⁵-C_5H_3-1,3-[$SiMe_2$(η¹-N*t*Bu)]$_2$}(NMe_2)] (9). Method A: When a C_6D_6 solution of the diamido complex **5** was heated at 120 °C for 12 h in a sealed NMR tube, a slow reaction took place with elimination of $NHMe_2$ to give **9**, identified by its ^1H and ^{13}C NMR spectra. However, when the reaction mixture was cooled to room temperature, a reversible reaction with the free $NHMe_2$ present in solution once more yielded the starting complex **5**. **Method B:** A 1:1 molar ratio of the benzyl derivative **11** (1.46 g, 3.1 mmol) and the diamido derivative **5** (1.45 g, 3.1 mmol) in toluene was heated at 120 °C in a Teflon-valved Schlenk tube for 12 h. The solvent was removed under vacuum and the residue was extracted into pentane (50 mL). After filtration and removal of the solvent, complex **9** (1.32 g, 2.9 mmol, 94%) was isolated as a yellow solid. ^1H NMR (C_6D_6, 20 °C): δ = 0.51 (s, 6 H, $SiMe_2$), 0.55 (s, 6 H, $SiMe_2$), 1.31 (s, 18 H, N*t*Bu), 2.77 (s, 6 H, NMe_2), 6.34 (d, 2 H, C_5H_3), 6.78 (t, 1 H, C_5H_3) ppm. ^{13}C NMR (C_6D_6, 20 °C): δ = 2.9 ($SiMe_2$), 3.0 ($SiMe_2$), 35.6 (N*t*Bu), 45.1 (NMe_2), 55.8 (N*t*Bu_{tert}), 117.7 (C_5H_{3ipso}) 119.8 (C_5H_3), 133.2 (C_5H_3) ppm. $C_{19}H_{39}N_3Si_2Zr$ (456.93): calcd. C 49.94, H 8.60, N 9.20; found C 50.28, H 8.31, N 8.86.

[Ti{η⁵-C_5H_3-1,3-[$SiMe_2$(η¹-N*t*Bu)]$_2$}(CH_2Ph)] (10): A solution of $Ti(CH_2Ph)_4$ (5.34 g, 12.9 mmol) in toluene (70 mL) was cooled to 0 °C, and **1** (4.21 g, 12.9 mmol) was added by syringe. The resulting deep red solution was warmed at 70 °C for 5 h. The solvent was removed under vacuum and the residue was extracted into pentane (70 mL). After filtration and removal of the solvent, complex **10** was isolated as a waxy, red solid, which was recrystallized from hexane to give orange crystals (5.88 g, 12.7 mmol, 98%). ^1H NMR (C_6D_6, 20 °C): δ = 0.39 (s, 6 H, $SiMe_2$), 0.40 (s, 6 H, $SiMe_2$), 1.42 (s, 18 H, N*t*Bu), 2.59 (s, 2 H, CH_2Ph), 6.12 (d, 2 H, C_5H_3), 6.39 (t, 1 H, C_5H_3), 6.89 (m, 1 H, C_6H_5), 6.95 (m, 2 H, C_6H_5), 7.22 (m, 2 H, C_6H_5) ppm. ^{13}C NMR (C_6D_6, 20 °C): δ = 2.1 ($SiMe_2$), 2.2 ($SiMe_2$), 35.6 (N*t*Bu), 59.3 (N*t*Bu_{tert}), 69.6 (CH_2Ph), 117.7 (C_5H_{3ipso}), 121.5 (C_5H_3), 126.3 (C_5H_3), 128.5 (C_6H_5), 130.3 (C_6H_5), 132.6 (C_6H_5), 152.4 (C_6H_{5ipso}) ppm. $C_{24}H_{40}N_2Si_2Ti$ (460.63): calcd. C 62.58, H 8.75, N 6.08; found C 62.68, H 8.68, N 5.76.

[Zr{η⁵-C_5H_3-1,3-[$SiMe_2$(η¹-N*t*Bu)]$_2$}(CH_2Ph)] (11): A solution of $Zr(CH_2Ph)_4$ (2.93 g, 6.43 mmol) in toluene (70 mL) was cooled to 0 °C, and **1** (2.09 g, 6.43 mmol) was added by syringe. The resulting yellow solution was heated at reflux for 5 h. The solvent was removed under vacuum and the residue was extracted into pentane (70 mL). After filtration and removal of the solvent, complex **11** was isolated as a brown solid. (3.20 g, 6.34 mmol, 99%). ^1H NMR (C_6D_6, 20 °C): δ = 0.40 (s, 6 H, $SiMe_2$), 0.42 (s, 6 H, $SiMe_2$), 1.27 (s, 18 H, N*t*Bu), 2.12 (s, 2 H, CH_2Ph), 6.14 (d, 2 H, C_5H_3), 6.53 (t, 1 H, C_5H_3) 6.9−7.23 (m, 5 H, C_6H_5) ppm. ^{13}C NMR (C_6D_6, 20 °C): δ = 2.4 ($SiMe_2$), δ = 2.4 ($SiMe_2$), 35.8 (N*t*Bu), 55.8 (CH_2Ph), 57.1 (N*t*Bu_{tert}), 116.5 (C_5H_{3ipso}), 120.7 (C_5H_3), 126.4 (C_5H_3), 128.5 (C_6H_5), 129.8 (C_6H_5), 132.7 (C_6H_5), 150.6 (C_6H_{5ipso}) ppm. $C_{24}H_{40}N_2Si_2Zr$ (503.97): calcd. C 57.20, H 8.00, N 5.56; found C 57.01, H 7.65, N 5.48.

[Ti{η⁵-C_5H_3-1,3-[$SiMe_2$(η¹-N*t*Bu)]$_2$}]⁺ [(CH_2Ph)B(C_6F_5)$_3$]⁻ (12): A toluene (20 mL) solution of the monobenzyl complex **10** (0.125 g, 0.25 mmol) was treated at room temperature with $B(C_6F_5)_3$ (0.126 g, 0.25 mmol), and the mixture was stirred for 30 min and cooled to −35 °C. The solvent was filtered off from the resulting insoluble residue, which was then dried under vacuum to give **12** (0.13 g, 60% yield) as an orange, crystalline solid. ^1H NMR (C_6D_6, 20 °C): δ = 0.19 (s, 6 H, $SiMe_2$), 0.38 (s, 6 H, $SiMe_2$), 1.12 (s, 18 H, N*t*Bu), 3.49 (s, 2 H, BCH_2), 5.03 (d, 2 H, C_5H_3), 5.86 (t, 1 H, C_5H_3), 6.21−7.10 (m, 5 H, C_6H_5) ppm. ^{13}C NMR (C_6D_6, 20 °C): δ = 0.6 ($SiMe_2$), 1.4 ($SiMe_2$), 34.6 (N*t*Bu), 59.3 (N*t*Bu_{tert}), 122.1 (C_5H_{3ipso}) 126.1 (C_5H_3), 126.2 (C_5H_3), 128.3 (C_6H_5), 128.7 (C_6H_5), 132.9 (C_6H_5), 135.1 (C_6F_5), 140.1 (C_6F_5), 145.8 (C_6F_5), 150.9 (C_6F_5) ppm. ^{19}F NMR (300 MHz, C_6D_6, 20 °C, CCl_3F): δ = 132.1 (m, 2 F, *o*-C_6F_5), 163.7 (m, 1 F, *p*-C_6F_5), 167.3 (m, 2 F, *m*-C_6F_5) ppm. $C_{42}H_{40}BF_{15}N_2Si_2Ti$ (972.63): calcd. C 51.87, H 4.15, N 2.88; found C 51.98, H 4.04, N 3.08.

[Zr{η⁵-C_5H_3-1,3-[$SiMe_2$(η¹-N*t*Bu)]$_2$}]⁺ [(CH_2Ph)B(C_6F_5)$_3$]⁻ (13): A toluene (20 mL) solution of the monobenzyl complex **11** (0.116 g, 0.25 mmol) was treated with $B(C_6F_5)_3$ (0.126 g, 0.25 mmol) at room temperature and the mixture was stirred for 30 min and cooled to −35 °C. The solvent was filtered off from the resulting insoluble residue, which was then dried under vacuum to give **13** (0.21 g, 83% yield) as a dark brown oil. After recrystallization, a suitable orange monocrystal of **13** was separated for X-ray diffraction studies. ^1H NMR (C_6D_6, 20 °C): δ = 0.17 (s, 6 H, Si*Me*$_2$), 0.36 (s, 6 H, Si*Me*$_2$), 0.99 (s, 18 H, N*t*Bu), 3.42 (s, 2 H, BC*H*$_2$), 5.20 (d, 2 H, C_5H_3), 6.01 (t, 1 H, C_5H_3), 6.10 (m, 1 H, *p*-C_6H_5), 6.34 (m, 2 H, *m*-C_6H_5), 6.87 (m, 2 H, *o*-C_6H_5) ppm. ^{13}C NMR (C_6D_6, 20 °C): δ = 1.5 (Si*Me*$_2$), 1.6 (Si*Me*$_2$), 34.8 (N*t*Bu), 58.6 (N*t*Bu_{tert}), 121.4 (C_5H_3), 123.5 (C_5H_{3ipso}), 127.4 (C_5H_3), 127.9 (C_6H_5), 128.1 (C_6H_5), 128.3 (C_6H_5), 136.5 (C_6F_5), 138.3 (C_6F_5), 147.8 (C_6F_5), 149.8 (C_6F_5), 162.0 (C_6H_{5ipso}) ppm. ^{19}F NMR (300 MHz, C_6D_6, 20 °C, CCl_3F): δ = 132.1 (m, 2 F, *o*-C_6F_5), 163.6 (m, 1 F, *p*-C_6F_5), 167.2 (m, 2 F, *m*-C_6F_5) ppm. $C_{42}H_{40}BF_{15}N_2Si_2Zr$ (1015.97): calcd. C 49.65, H 3.97, N 2.76; found C 50.51, H 3.71, N 3.35.

Crystal Structure Determination for Compound 10: Crystals of **10** were grown from a hexane solution. An orange fragment in perfluorinated ether was selected and transferred to a glass capillary, which was mounted in a cold N_2 stream. Preliminary examination and data collection were carried out with a Nonius KappaCCD device at the window of a rotating anode X-ray generator with use of graphite-monochromated Mo-K_α radiation (λ = 0.71073 Å), controlled by the Collect software package.[25] Collected images were processed by use of Denzo. The unit cell parameters were obtained by full-matrix, least-squares refinements of 4895 reflections.[26] A total number of 41477 reflections were integrated. After merging, 4739 reflections remained, and these were used for all further calculations. Absorption effects were corrected during the scaling procedure. The structure was solved by direct methods[27] and refined by standard difference Fourier techniques.[28] All non-hydrogen atoms of the asymmetric unit were refined with aniso-

 © 2003 Wiley-VCH Verlag GmbH & Co. KGaA, Weinheim

tropic thermal displacement parameters. All hydrogen atoms were found in the difference Fourier map and refined freely with individual isotropic thermal displacement parameters, except for those located at a disordered *tert*-butyl group, which were placed in calculated positions (riding model). Full-matrix, least-squares refinements were carried out by minimization of $\Sigma w(F_o^2-F_c^2)^2$ by use of the SHELXL-97 weighting scheme and stopped at a maximum shift/err < 0.001.[28,29,30] One *tert*-butyl group in **10** appears to be disordered over two positions (73:27).

Crystal Structure Determination for Compound 13: Crystals of **13** were grown from a C_6D_6 solution. An orange plate in perfluorinated ether was selected and transferred to a glass capillary. Preliminary examination and data collection were carried out with a Nonius KappaCCD device at the window of a rotating anode X-ray generator by use of graphite-monochromated Mo-K_α radiation ($\lambda = 0.71073$ Å), controlled by the Collect software package.[26] Collected images were processed by use of Denzo. The unit cell parameters were obtained by full-matrix, least-squares refinements of 8080 reflections.[27] A total number of 44162 reflections were integrated. After merging, 8099 reflections remained and were used for all further calculations. Absorption effects were corrected during the scaling procedure. The structure was solved by direct methods[27] and refined by standard difference Fourier techniques.[28] All non-hydrogen atoms of the asymmetric unit were refined with anisotropic thermal displacement parameters. All hydrogen atoms were found in the difference Fourier map and refined freely with individual isotropic thermal displacement parameters. Full-matrix, least-squares refinements were carried out by minimization of $\Sigma w(F_o^2-F_c^2)^2$ by use of the SHELXL-97 weighting scheme and stopped at a maximum shift/err < 0.001. A correction for extinction effects was applied.[28–30]

CCDC-200139 (**10**) and -200140 (**13**) contain the supplementary crystallographic data for this paper. These data can be obtained free of charge at www.ccdc.cam.ac.uk/conts/retrieving.html [or from the Cambridge Crystallographic Data Centre, 12 Union Road, Cambridge CB2 1EZ, UK; Fax: (internat.) + 44-1223/336-033; E-mail: deposit@ccdc.cam.ac.uk].

Computational Details: Gradient corrected density functional calculations were carried out, with corrections for exchange and correlation according to Becke[31] and Perdew,[32] respectively (BP86). Geometries were optimized by use of the TURBOMOLE[33] program system within the framework of the RI-*J* approximation.[34] For the model systems, a triple-ζ valence basis plus polarization TZVP[35] was employed. For the geometry optimization of the real molecules, the main group elements were described by a split-valence basis set[36] with one set of polarization functions for the non-H atoms, and Ti was treated with the TZVP basis. For the determination of bond energies, final energies were obtained in a single-point calculation using the TZVP basis set for all atoms.

Table 4. Crystallographic data for complexes **10** and **13**

	10	**13**
Empirical formula	$C_{24}H_{40}N_2Si_2Ti$	$C_{42}H_{40}BF_{15}N_2Si_2Zr$
Formula mass	460.63	1015.97
Colour/shape	orange/fragment	orange/plate
Crystal size [mm]	0.36 × 0.23 × 0.20	0.56 × 0.30 × 0.10
Crystal system	monoclinic	triclinic
Space group	$P2_1/c$ (No. 14)	$P\bar{1}$ (No. 2)
a [Å]	10.6962(1)	11.7349(1)
b [Å]	16.0412(2)	13.4253(1)
c [Å]	15.3339(2)	14.4024(1)
α [°]	90	77.4374(3)
β [°]	99.6928(7)	88.2620(4)
γ [°]	90	86.9316(5)
V [Å³]	2593.43(5)	2211.12(3)
Z	4	2
T [K]	123	293
$\rho_{calcd.}$ [g cm^{-3}]	1.180	1.526
μ [mm^{-1}]	0.435	0.399
F_{000}	992	1028
θ range [°]	1.85–25.34	1.45–25.38
Data collected (*h*,*k*,*l*)	±12, ±19, ±18	±14, ±16, ±17
No. of reflns. collected	41477	44162
No. of independent reflns./R_{int}	4739 (all)/0.033	8099 (all)/0.033
No. of obsd. reflns. ($I > 2\sigma(I)$)	4193 (obsd.)	7177 (obsd.)
No. of params. refined	414	729
*R*1 (obsd./all)	0.0333/0.0394	0.0306/0.0370
*wR*2 (obsd./all)	0.0855/0.0895	0.0752/0.0788
GOF (obsd./all)	1.045/1.045	1.040/1.040
max./min. Δρ [e·Å^{-3}]	+0.32/−0.27	+0.30/−0.27

Acknowledgments

The authors acknowledge the MCyT (project MAT2001-1309) for financial support and the EC (project COST-D12/0016/98). J. C. acknowledges CAM for a fellowship.

[1] [1a] P. C. Möhring, N. J. Coville, *J. Organomet. Chem.* **1994**, *479*, 1–29. [1b] H. H. Brintzinger, D. Fischer, R. Mülhaupt, B. Rieger, R. M. Waymouth, *Angew. Chem. Int. Ed. Engl.* **1995**, *34*, 1143–1170. [1c] G. G. Hlatky, *Coord. Chem. Rev.* **1999**, *181*, 243–296. [1d] H. G. Alt, A. Köppl, *Chem. Rev.* **2000**, *100*, 1205–1222. [1e] L. Resconi, L. Cavallo, A. Fait, F. Piemontesi, *Chem. Rev.* **2000**, *100*, 1253–1345.

[2] [2a] P. J. Shapiro, E. E. Bunel, W. E. Piers, J. E. Bercaw, *Synlett* **1990**, *2*, 74–84. [2b] P. J. Shapiro, E. Bunel, W. P. Schäfer, J. E. Bercaw, *Organometallics* **1990**, *9*, 867–869. [2c] P. J. Shapiro, W. E. Cotter, W. P. Schäfer, J. A. Labinger, J. E. Bercaw, *J. Am. Chem. Soc.* **1994**, *116*, 4623–4640. [2d] J. Okuda, *Chem. Ber.* **1990**, *123*, 1649–1651. [2e] A. K. Hughes, A. Meetsma, J. H. Teuben, *Organometallics* **1993**, *12*, 1936–1945. [2f] W. A. Herrmann, M. J. A. Morawietz, *J. Organomet. Chem.* **1994**, *482*, 169–181. [2g] S. Ciruelos, T. Cuenca, R. Gómez, P. Gómez-Sal, A. Manzanero, P. Royo, *Organometallics* **1996**, *15*, 5577–5585. [2h] R. Gómez, P. Gómez-Sal, A. Martín, A. Núñez, P. A. del Real, P. Royo, *J. Organomet. Chem.* **1998**, *564*, 93–100. [2i] A. L. Mcknight, R. M. Waymouth, *Chem. Rev.* **1998**, *98*, 2587–2598. [2j] J. Klosin, W. J. Kruper, Jr., P. N. Nickias, G. R. Roof, P. DeWaele, K. A. Abboud, *Organometallics* **2001**, *20*, 2663–2665. [2k] K. Kunz, G. Erker, S. Döring, R. Fröhlich, G. Kehr, *J. Am. Chem. Soc.* **2001**, *123*, 6181–6182.

[3] [3a] M. Bochmann, *J. Chem. Soc., Dalton Trans.* **1996**, 255–270. [3b] C. P. Casey, D. W. Carpenetti II, H. Sakurai, *Organometallics* **2001**, *20*, 4262–4265. [3c] C. G. Brandow, A. Mendiratta, J. E. Bercaw, *Organometallics* **2001**, *20*, 42534261.

[4] [4a] Y.-X. Chen, P.-F. Fu, C. L. Stern, T. J. Marks, *Organometallics* **1997**, *16*, 5958–5963. [4b] B. E. Bosch, G. Erker, R. Fröhlich, O. Meyer, *Organometallics* **1997**, *16*, 5449–5456. [4c] Y.-X. Chen, T. J. Marks, *Organometallics* **1997**, *16*, 3649–3657. [4d] A. Bertuleit, C. Fritze, G. Erker, R. Fröhlich, *Organometallics* **1997**, *16*, 2891–2899. [4e] G. Lanza, I. L. Fragalà, T. J. Marks, *J. Am. Chem. Soc.* **1998**, *120*, 8257–8258. [4f] F. Amor, A. Butt, K. E. Du Plooy, T. B. Spaniol, J. Okuda, *Organometallics* **1998**, *17*, 5836–5849. [4g] R. Gómez, P. Gómez-Sal, P. A. del Real, P. Royo, *J. Organomet. Chem.* **1999**, *588*, 22–27. [4h] R. J. Keaton, K. C. Jayaratne, J. C. Fettinger, L. R. Sita, *J. Am. Chem. Soc.* **2000**, *122*, 12909–12910. [4i] J.-F. Carpentier, V. P.

 © 2003 Wiley-VCH Verlag GmbH & Co. KGaA, Weinheim

Maryin, J. Luci, R. F. Jordan, *J. Am. Chem. Soc.* **2001**, *123*, 898−909.
[5] [5a] J. C. Stevens, F. J. Timmers, D. R. Wilson, G. F. Schmidt, P. N. Nickias, R. K. Rosen, G. W. Knight, S. Y. Lai, *Eur. Patent Appl.* EP **1991**, 416815 (Dow Chemical Co.) (*Chem. Abstr.* **1991**, *115*, 93163). [5b] J. M. Canich, *Eur. Patent Appl*. EP **1991**, 420436 (Exxon Chemical Co) (*Chem. Abstr.* **1991**, *115*, 184145).
[6] V. C. Gibson, *J. Chem. Soc., Dalton Trans.* **1994**, 1607−1618.
[7] [7a] J. Cano, P. Royo, A. Tiripicchio, M. A. Pellinghelli, M. Lanfranchi, *Angew. Chem. Int. Ed.* **2001**, *40*, 2495−2497. [7b] P. Royo, J. Cano, M. A. Flores, B. Peña, EP **2001**, 1225179 A1; US **2002**, 0115560 A1.
[8] [8a] B. E. Bursten, L. F. Rhodes, J. Strittmatter, *J. Am. Chem. Soc.* **1989**, *111*, 2758−2766. [8b] T. Brackemeyer, G. Erker, R. Fröhlich, *Organometallics* **1997**, *16*, 531−536. [8c] H. Jacobsen, H. Berke, S. Doring, G. Kehr, G. Erker, R. Fröhlich, O. Meyer, *Organometallics* **1999**, *18*, 1724−1735. [8d] N. Kliegrewe, T. Brakemeyer, R. Fröhlich, G. Erker, *Organometallics* **2001**, *20*, 1952−1955.
[9] J. M. Rozell, P. R. Jones, *Organometallics* **1985**, *4*, 2206−2210.
[10] [10a] Y. A. Ustynyuk, A. V. Kisin, J. M. Pribytkova, A. A. Zarkin, N. D. Antonova, *J. Organomet. Chem.* **1972**, *42*, 47−63. [10b] P. Jutzi, *Chem. Rev.* **1986**, *86*, 983−996.
[11] G. M. Diamond, R. F. Jordan, J. L. Petersen, *J. Am. Chem. Soc.* **1996**, *118*, 8024−8033.
[12] U. Zucchini, E. Albizzati, U. Giannini, *J. Organomet. Chem.* **1971**, *26*, 357−372.
[13] Y. Mu, W. E. Piers, L. R. MacQuarrie, M. Zaworotko, J. Young, *Organometallics* **1996**, *15*, 2720−2726.
[14] D. M. P. Mingos, *Essential Trends in Inorganic Chemistry*, Oxford Univ. Press, Oxford, **1998**, p. 368.
[15] [15a] W. A. Nugent, B. L. Haymore, *Coord. Chem. Rev.* **1980**, *31*, 123−175. [15b] D. E. Wigley, *Prog. Inorg. Chem.* **1994**, *42*, 239−482. [15c] M. J. Humphries, M. L. H. Green, M. A. Leech, V. C. Gibson, M. Jolly, D. N. Williams, M. R. J. Elsegood, W. Clegg, *J. Chem. Soc., Dalton Trans.* **2000**, 4044−4051.
[16] J. Okuda, T. Eberle, T. P. Spaniol, *Chem. Ber./Recueil* **1997**, *130*, 209−215.
[17] J. Okuda, S. Verch, R. Sturmer, T. P. Spaniol, *J. Organomet. Chem.* **2000**, *605*, 55−67.
[18] A. Martín, M. Mena, C. Yelamos, R. Serrano, P. R. Raithby, *J. Organomet. Chem.* **1994**, *467*, 79−84.
[19] D. W. Carpenetti, L. Kloppenburg, J. T. Kupec, J. L. Petersen, *Organometallics* **1996**, *15*, 1572−1581.
[20] W. S. Seo, Y. J. Cho, S. C. Yoon, J. T. Park, Y. Park, *J. Organomet. Chem.* **2001**, *640*, 79−84.
[21] Y. Mu, W. E. Piers, L. R. MacQuarrie, M. Zaworotko, *Can. J. Chem.* **1996**, *74*, 1696−1703.
[22] J. Okuda, F. J. Schattenmann, S. Wocadlo, W. Massa, *Organometallics* **1995**, *14*, 789−795.
[23] [23a] K. Shelly, D. C. Finster, Y. J. Lee, W. R. Scheidt, C. A. Reed, *J. Am. Chem. Soc.* **1985**, *107*, 5955−5959. [23b] M. Laguna, M. D. Villacampa, M. Contel, J. Garrido, *Inorg. Chem.* **1998**, *37*, 133−135. [23c] A. S. Batsanov, S. P. Crabtree, J. A. K. Howard, C. W. Lehmann, M. Kilner, *J. Organomet. Chem.* **1998**, *550*, 59−61.
[24] A. G. Massey, A. J. Park, *J. Organomet. Chem.* **1964**, *2*, 245−250.
[25] *COLLECT*, *Data Collection Software for Nonius Kappa CCD Devices*, Hooft, R.Nonius B. V., Delft, The Netherlands, **1998**.
[26] Z. Otwinowski, W. Minor, *Processing of X-ray Diffraction Data Collected in Oscillation Mode*, *Methods in Enzymology*, vol. 276: *Macromolecular Crystallography*, part A (Eds.: C. W. Carter, Jr., R. M. Sweet), Academic Press, New York, **1997**, p. 307−326.
[27] A. Altomare, G. Cascarano, C. Giacovazzo, A. Guagliardi, M. C. Burla, G. Polidori, M. Camalli, *J. Appl. Crystallogr.* **1994**, *27*, 435−436.
[28] G. M. Sheldrick, *SHELXL-97*, Universität Göttingen, Germany **1998**.
[29] *International Tables for Crystallography*, vol. C, Tables 6.1.1.4 (pp. 500−502), 4.2.6.8 (pp. 219−222), and 4.2.4.2 (pp. 193−199) (Ed.: A. J. C. Wilson), Kluwer Academic Publishers, Dordrecht, **1992**.
[30] A. L. Spek, *Acta Crystallogr., Sect. A* **1990**, *46*, C34.
[31] A. D. Becke, *Phys. Rev.* **1988**, *A38*, 3098−3100.
[32] J. P. Perdew, *Phys. Rev.* **1986**, *B33*, 8822−8824.
[33] [33a] R. Ahlrichs, M. Bär, M. Häser, H. Horn, C. Kölmel, *Chem. Phys. Lett.* **1989**, *162*, 165−169. [33b] O. Treutler, R. Ahlrichs, *J. Chem. Phys.* **1995**, *102*, 346−354. [33c] R. Ahlrichs, M. von Arnim, *Methods and Techniques in Computational Chemistry: METECC-95* (Eds.: E. Clementi, G. Corongiu), STEF, Cagliari, **1995**, chapter 13.[33d]R. Ahlrichs, M. von Arnim, *J. Comput. Chem.* **1998**, *19*, 1746−1757.
[34] [34a] K. Eichkorn, O. Treutler, H. Öhm, M. Häser, R. Ahlrichs, *Chem. Phys. Lett.* **1995**, *242*, 652−660. [34b] K. Eichkorn, F. Weigand, O. Treutler, R. Ahlrichs, *Theor. Chem. Acc.* **1997**, *97*, 119−124.
[35] A. Schäfer, C. Huber, R. Ahlrichs, *J. Chem. Phys.* **1994**, *100*, 5829−5835.
[36] A. Schäfer, H. Horn, R. Ahlrichs, *J. Chem. Phys.* **1992**, *97*, 2571−2577.

Received December 20, 2002

 © 2003 Wiley-VCH Verlag GmbH & Co. KGaA, Weinheim

Synthesis, X-ray Crystallographic and ^{1}H NMR Spectroscopic Structural Studies on Cobalt(II) Complexes of Homoscorpionate, Heteroscorpionates and Chiral Tris(pyrazolyl)borates Obtained from 5(3)-*Iso*propyl-3(5)-phenylpyrazole and 3,5-Dimethylpyrazole[‡]

Tomasz Ruman,[a] Zbigniew Ciunik,[b] and Stanislaw Wołowiec*[a]

Keywords: Boron / Chirality / Cobalt / N ligands / NMR spectroscopy

Condensation of 5(3)-isopropyl-3(5)-phenylpyrazole with sodium borohydride led to a mixture of tris(pyrazolyl)borate ligands (Tp^x) – the homoscorpionate hydrotris(5-isopropyl-3-phenylpyrazolyl)borate and the heteroscorpionates hydro(3-isopropyl-5-phenylpyrazolyl)bis(5-isopropyl-3-phenylpyrazolyl)borate and hydrobis(3-isopropyl-5-phenylpyrazolyl)(5-isopropyl-3-phenylpyrazolyl)borate – that were converted into Tp^{x}Co(NCS) complexes. The molecular structures of pentacoordinate[hydrotris(5-isopropyl-3-phenylpyrazolyl)-borato](tetrahydrofuran)(thiocyanato)cobalt(II) (**1-THF**) and [hydrobis(3-isopropyl-5-phenylpyrazolyl)(5-isopropyl-3-phenylpyrazolyl)borato](tetrahydrofuran)(thiocyanato)-cobalt(II) (**3-THF**) were elucidated crystallographically. Hydro(3,5-dimethylpyrazolyl)bis(5-isopropyl-3-phenylpyrazolyl)borate was also obtained by condensation of 2.1 equiv. of 5(3)-isopropyl-3(5)-phenylpyrazole and 0.9 equiv. of 3,5-dimethylpyrazole with sodium borohydride, and it was converted into [hydro(3,5-dimethylpyrazolyl)bis(5-isopropyl-3-phenylpyrazolyl)borato](thiocyanato)cobalt(II) (**4**), which was characterized by X-ray crystallography. The latter was converted thermally under mild conditions (358 K in toluene) into [hydro(3,5-dimethylpyrazolyl)(3-isopropyl-5-phenylpyrazolyl)(5-isopropyl-3-phenylpyrazolyl)borato](thiocyanato)cobalt(II) (**9**) in 45% yield, as was concluded from the ^{1}H NMR spectrum of the post-reaction mixture. The dimer of **9** was obtained as single crystals from toluene/hexane and its structure was determined crystallographically. Two chiral Tp^x ligands of opposite boron-centered configurations are coordinated to cobalt(II) ions in a κ^3 fashion. The pentacoordinate metal ions are bridged head-to-tail by the thiocyanate anions. This chiral Tp^x ligand is the first example of a borate with fixed boron-centered chirality.
(© Wiley-VCH Verlag GmbH & Co. KGaA, 69451 Weinheim, Germany, 2003)

Introduction

Some 3(5)-R^1,5(3)-R^2-substituted pyrazoles (3-R^1,5-R^{2}pzH) form spontaneously both homo- and heteroscorpionate tris(pyrazolyl)borate anions when condensed with borohydride (BH_4^-).[1−10] The phenomenon was noticed originally by Trofimenko, who found that 3-isopropylpyrazole gave homoscorpionate tris(3-isopropylpyrazolyl)borate (Tp$^{i\mathrm{Pr}}$), which underwent thermal conversion in the Tp$^{i\mathrm{Pr}2}$Co complex into bis[hydrobis(3-isopropylpyrazolyl)-(5-isopropylpyrazolyl)borato]cobalt(II).[1] Metal-ion complexes of homoscorpionate Tp^x ligands have potentially C_{3v} symmetry when coordinated in a κ^3 manner, while the same type of coordination in case of heteroscorpionate Tp^x results in the formation of C_s local symmetry around the metal ion. Tp^x ligands of C_s symmetry form spontaneously from one pyrazole or by the use of two different pyrazoles. Hereafter, the latter species are named synthetic heteroscorpionates. Many synthetic heteroscorpionates have been prepared to date.[10−17] Recently, [hydro(3,5-dimethylpyrazolyl)bis(5-methyl-3-phenylpyrazolyl)borato](thiocyanato)-cobalt(II) was converted thermally into [hydro(3,5-dimethylpyrazolyl)(3-methyl-5-phenylpyrazolyl)(5-methyl-3-phenylpyrazolyl)borato](thiocyanato)cobalt(II) in ca. 30% yield upon heating the starting heteroscorpionate complex at 428 K in propylbenzene under reflux.[10] Encouraged by that result, we have replaced 5(3)-methyl-3(5)-phenylpyrazole with 5(3)-isopropyl-3(5)-phenylpyrazole to synthesize heteroscorpionates bearing 3- and 5-substituents of comparable size on the two pyrazolyl residues of Tp^x. We observed the ready formation of homo- and two heteroscorpionates when sodium borohydride was condensed with 3 equiv. of 5(3)-isopropyl-3(5)-phenylpyrazole. Three Tp^{x}Co(NCS) complexes were obtained and separated from this synthetic mixture, and two of them were characterized crystallographically. The ambivalent binding of 5(3)-isopro-

[‡] Complexes of Heteroscorpionate Trispyrazolylborate Ligands, VIII. Part VII: Ref.[17]

[a] Faculty of Chemistry, Rzeszów University of Technology, 6 Powstanców Warszawy Ave., 35-959 Rzeszów, Poland
[b] Faculty of Chemistry, University of Wroclaw, 14 Joliot-Curie Str., 50-383 Wroclaw, Poland

pyl-3(5)-phenylpyrazole was then used for the thermal conversion in good yield under mild conditions of the synthetic heteroscorpionate in [hydro(3,5-dimethylpyrazolyl)bis(5-isopropyl-3-phenylpyrazolyl)borato](thiocyanato)cobalt(II) into its counterpart bearing a chiral Tp^x ligand.

Results and Discussion

Heteroscorpionate tris(pyrazolyl)borates formed spontaneously when the pyrazoles used to construct Tp^x were 3(5)-isopropylpyrazole,[1] 4-bromo-3(5)-isopropylpyrazole,[1,2] 3(5)-neopentylpyrazole,[3] 3(5)-mesitylpyrazole,[4] 5-methyl-3,4-diphenylpyrazole,[5] 3(5)-methylpyrazole,[6] 3(5)-phenylpyrazole,[7] 3(5)-cyclohexylpyrazole,[8] 4-bromo-3(5)-cyclohexylpyrazole,[8] (4*R*,7*R*)-7-isopropyl-4-methyl-4,5,6,7-tetrahydroindazole,[9] and 5(3)-methyl-3(5)-phenylpyrazole.[10] In the latter case, the sodium salt of heteroscorpionate Na[HB(3-Ph,5-Mepz)$_2$(3-Me,5-Phpz)] was separated from the homoscorpionate $NaTp^{Ph,Me}$ counterpart because of the good solubility of $NaTp^{Ph,Me}$ in hot heptane. Moreover, prolonged heating of sodium homoscorpionate in heptane under reflux caused considerable conversion of $NaTp^{Ph,Me}$ into sodium heteroscorpionate.[10,11] On the other hand, the heteroscorpionate Tp^x ligands were obtained by deliberate synthesis with the use of two different pyrazoles.[10−17]

Previously, we demonstrated that heating of [hydro(3,5-dimethylpyrazolyl)bis(5-methyl-3-phenylpyrazolyl)borato](thiocyanato)cobalt(II) {[HB(3-Ph,5-Mepz)$_2$(3,5-diMepz)]Co(NCS)} in propylbenzene at 428 K led to the formation of [hydro(3,5-dimethylpyrazolyl)(3-methyl-5-phenylpyrazolyl)(5-methyl-3-phenylpyrazolyl)borato](thiocyanato)cobalt(II) complex, containing a chiral Tp^x ligand, in ca. 30% yield.[14] The reaction was accompanied by formation of other products, namely [hydro(3,5-dimethylpyrazolyl)bis(3-methyl-5-phenylpyrazolyl)borato](thiocyanato)cobalt(II) and complexes later identified as $Tp^xCo(NCS)$ species containing Tp^x ligands of different composition resulting from cross-exchange of pyrazole units between the two Tp^x ligands.[11] These products form readily when thiocyanate in [HB(3-Ph,5-Mepz)$_2$(3,5-diMepz)]Co(NCS) is replaced with carboxylates, such as lactate, pyruvate, or 2-hydroxybutyrate.[11] This instability of Tp^x ligands containing the 3,5-dimethylpyrazolyl residue led to the formation of hydrobis(3,5-dimethylpyrazolyl)[5(3)-methyl-3(5)-phenylpyrazolyl]borate and even hydrotris(3,5-dimethylpyrazolyl)borate anions that are able to form bis(ligand) homo- and heteroleptic $Tp^xCoTp^{x\prime}$ complexes because of the low steric hindrance of the Tp^x ligands. Consequently, the dismutation of $Tp^xCo(OOCR)$ into $Tp^xCoTp^{x\prime}$ and $Co(OOCR)_2$ took place. To avoid the dismutation of $Tp^xCo(X)$ complexes, we have synthesized the Tp^x ligand composed of the 3(5)-isopropyl-5(3)-phenylpyrazole unit, with medium-sized substituents placed at both the 3- and 5-positions of the pyrazole unit. Thus, we have produced homo- and heteroscorpionate anionic ligands that are sterically more crowded in comparison with hydro(3,5-dimethylpyrazolyl)bis(5-methyl-3-phenylpyrazolyl)borate and have performed thermal conversion of the corresponding $Tp^xCo(NCS)$ complex into chiral Tp^x at lower temperature.

Spontaneously Formed Tp^x Heteroscorpionates Constructed of 5(3)-Isopropyl-3(5)-phenylpyrazole

Condensation of sodium borohydride with 5(3)-isopropyl-3(5)-phenylpyrazole and prolonged heating of the reaction mixture in heptane under reflux led to the formation of three Tp^x anions. These anions were bound into isolated $Tp^xCo(NCS)$ complexes − namely, [hydrotris(5-isopropyl-3-phenylpyrazolyl)borato](tetrahydrofuran)(thiocyanato)-cobalt(II) [$Tp^{Ph,iPr}$Co(NCS)(THF), **1-THF**], [hydro(3-isopropyl-5-phenylpyrazolyl)bis(5-isopropyl-3-phenylpyrazolyl)borato](thiocyanato)cobalt(II) {[HB(3-Ph,5-*i*Prpz)$_2$(3-*i*Pr,5-Phpz)]Co(NCS), **2**}, and [hydrobis(3-isopropyl-5-phenylpyrazolyl)(5-isopropyl-3-phenylpyrazolyl)-borato](tetrahydrofuran)(thiocyanato)cobalt(II) {[HB(3-*i*Pr,5-Phpz)$_2$(3-Ph,5-*i*Prpz)]Co(NCS)(THF), **3-THF**} − and two of them (**1-THF** and **3-THF**) were characterized by X-ray crystallography. Views of the molecules of **1-THF** and **3-THF** are presented in Figures 1 and 2, respectively.

Both Tp^x ligands are coordinated in a κ^3 manner to the central metal ion. The complexes are pentacoordinate, with a nitrogen atom donor of a thiocyanate unit and an oxygen atom of THF completing the coordination sphere. The cobalt-centered (β) and boron-centered (α) bite angles (measured disregarding the hydrogen atoms) in **1-THF** and **3-THF** are β = 75.6 and 86.4°, respectively, and α = 140.7 and 159.1°, respectively. We see that the Tp^x ligand in **3-THF** is much more relaxed. The release of the steric hindrance in the Tp^x ligand in **3-THF**, relative to that in **1-THF**, is probably the reason for the spontaneous transformation, even in the case of the sodium salt. On the other

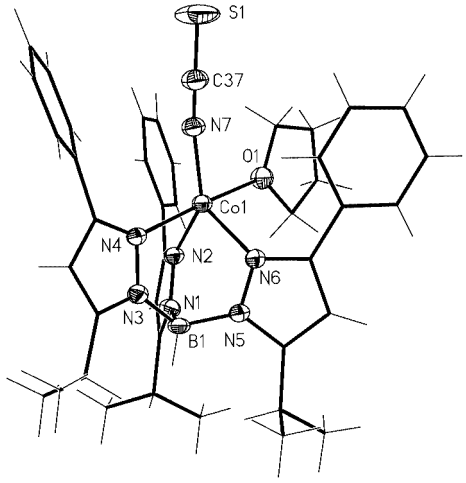

Figure 1. View of **1-THF**; selected bond lengths [Å] and angles [°]: Co(1)−N(7) 1.946(3), Co(1)−N(2) 2.053(3), Co(1)−N(4) 2.154(3), Co(1)−N(6) 2.048(3), Co(1)−O(1) 2.189(3); N(2)−Co(1)−N(4) 84.65(11), N(2)−Co(1)−N(6) 95.02(12), N(4)−Co(1)−N(6) 88.56(12), N(7)−Co(1)−N(2) 139.30(14), N(7)−Co(1)−N(4) 96.96(12), N(7)−Co(1)−N(6) 125.64(14), N(2)−Co(1)−O(1) 89.88(11), N(4)−Co(1)−O(1) 174.52(11), N(6)−Co(1)−O(1) 91.58(11), N(7)−Co(1)−O(1) 87.41(12)

 © 2003 Wiley-VCH Verlag GmbH & Co. KGaA, Weinheim

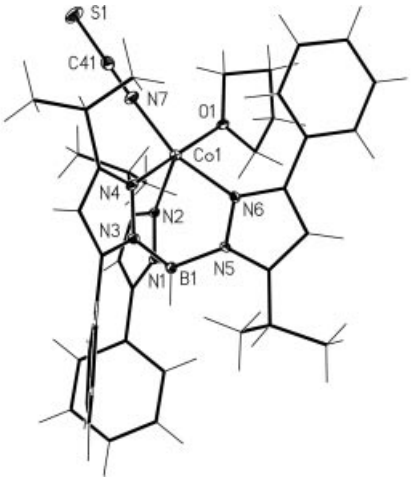

Figure 2. View of **3-THF**; selected bond lengths [Å] and angles [°]: Co(1)−N(7) 1.980(3), Co(1)−N(2) 2.056(3), Co(1)−N(4) 2.125(3), Co(1)−N(6) 2.067(2); Co(1)−O(1) 2.133(2), N(7)−Co(1)−N(2) 110.06(10), N(7)−Co(1)−N(4) 95.42(10), N(7)−Co(1)−N(6) 159.12(11), N(2)−Co(1)−N(4) 90.12(10), N(2)−Co(1)−N(6) 90.78(10), N(4)−Co(1)−N(6) 85.61(9), N(7)−Co(1)−O(1) 86.71(9), N(2)−Co(1)−O(1) 95.61(9), N(4)−Co(1)−O(1) 172.82(9), N(6)−Co(1)−O(1) 89.96(9)

hand, the boron−cobalt distance in **1-THF** is considerably shorter (3.07 Å) than that in **3-THF** (3.11 Å). The chemical shifts observed in the ^{1}H NMR spectra of **1**−**3** taken in [D$_4$]methanol corroborate strictly with those structural features (Figure 3).

The spectrum of **1-CD$_3$OD** is simple because of the effective C_{3v} symmetry of the complex and is composed of an upfield-shifted *o*-H(3-Ph) resonance at δ = −57.4 ppm, and a single downfield-shifted resonance at δ = 18.3 ppm for all of the 18 methyl group protons of the 5-*i*Pr substituent (Figure 3, trace A). The resonance of the methyl group protons of the 3-*i*Pr unit, which integrates to six protons at δ = −24.8 ppm in spectrum B, is diagnostic of **2-CD$_3$OD**. The methyl group protons of two 5-*i*Pr substituents show two separate signals at δ = 19.1 and 26.1 ppm because of diastereotopicity at the boron side of Tp^x in **2-CD$_3$OD**. The local chirality is caused by the fact that the 5-*i*Prpz residues are flanked by two different pyrazolyl moieties, i.e., the units 3-Ph,5-*i*Prpz and 3-*i*Pr,5-Phpz. The resonance of C*H*(3-*i*Prpz) is shifted upfield, as is that of *o*-H(3-Ph), which was anticipated on the basis of previous studies.[1,3,4,9−11,13−18] All other resonances − i.e., B-*H*, 4-H, and those of the 5-substituents − are shifted downfield (Figure 3, trace B). This feature is also observed for **3-CD$_3$OD** (Figure 3, trace C). In this case, the resonance of the methyl group protons of two 3-*i*Pr substituents are split into a doublet because of diastereotopicity at the cobalt side of Tp^x in **3-CD$_3$OD**. The chemical shift of C*H*$_3$(3-*i*Pr) is similar in both **2-CD$_3$OD** and **3-CD$_3$OD**.

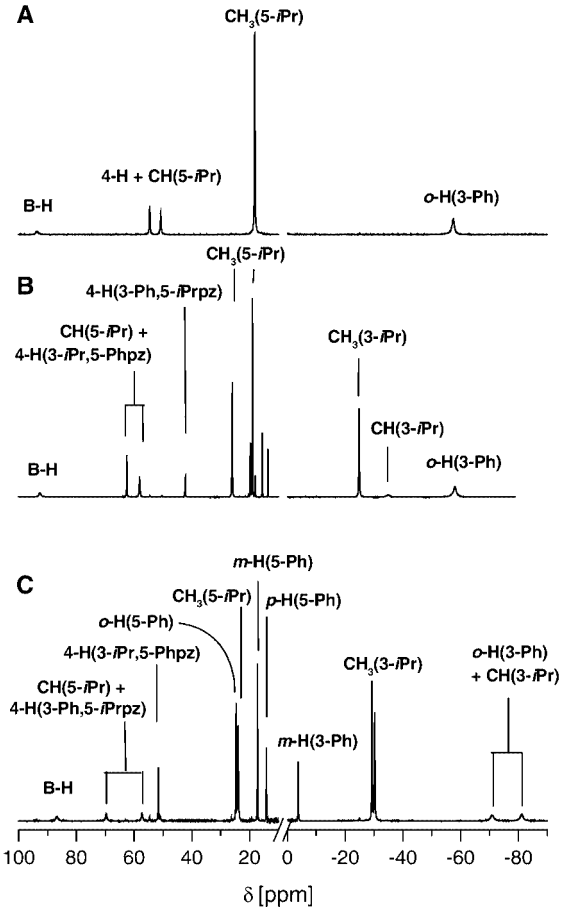

Figure 3. ^{1}H NMR spectra of **1-CD$_3$OD** (A), **2-CD$_3$OD** (B), and **3-CD$_3$OD** (C) in [D$_4$]methanol at 298 K; the 10−0-ppm region has been omitted for the sake of clarity.

Although the relationship between the solid-state structures of pentacoordinate ***n*-THF** complexes and ***n*-CD$_3$OD** counterparts (where ***n*** = **1** or **3**) is not straightforward, the correlation demonstrated by the data in Table 1 is remarkable.

Table 1. Relationship between structures and their ^{1}H NMR chemical shifts

Compound	Geometric factors[a]			Chemical shifts[b]			
	β [°]	α [°]	B···Co [Å]	δ(B-*H*) [ppm]	δ(C*H*,3-*i*Pr) [ppm]	δ(C*H*$_3$,3-*i*Pr) [ppm]	δ(*o*-H,3-Ph) [ppm]
1-CD$_3$OD	140.6	75.5	3.07	93.7	−	−	−57.4
2-CD$_3$OD[c]	−	−	−	92.7	−34.8	−24.8	−57.9
3-CD$_3$OD	159.0	86.4	3.11	86.7	−71.1	−29.8[d]	−81.2
4-CD$_3$OD[e]	141.3	77.6	2.97	95.6	−	−	−69.6
9-CD$_3$OD[e]	152.5	83.0	3.11	85.0	−70.2	−29.1[d]	−78.2

[a] Data from X-ray crystallographic measurements for Tp^{x}Co(NCS)(THF) complexes, unless otherwise stated. [b] Measured in [D$_4$]methanol. [c] No X-ray crystallographic data available. [d] Averaged value for two separate resonances. [e] Geometric factors measured for tetracoordinate Tp^{x}Co(NCS) and pentacoordinate [Tp^{x}Co(NCS)]$_2$, respectively.

 © 2003 Wiley-VCH Verlag GmbH & Co. KGaA, Weinheim

The correlation between the chemical shift of the B-*H* proton and the cobalt−boron distance is obvious; the longer the distance between the cobalt atom and the boron-attached hydrogen atom in an ***n*-THF** complex, the lower is the value of the chemical shift of the B-*H* proton in ***n*-CD_3OD**. A similar trend is found on the cobalt side of the Tp^x ligands; the mean distances between the C(*ortho*) atom of the 3-phenyl substituents and the cobalt ion in **1-THF** and **3-THF** are 3.52 and 3.46 Å, respectively, and, consequently, the chemical shifts of *o*-H(3-Ph) are δ = −57.4 and −81.2 ppm in **1-CD_3OD** and **3-CD_3OD**, respectively. A comparison of the bite angles in **1-THF** and **3-THF** indicates that steric crowding imposed by three 3-phenyl substituents around the cobalt ion in **1-CD_3OD** keeps the *o*-H(3-Ph) protons remote from the paramagnetic center, while the more relaxed surrounding of cobalt(II) in **3-CD_3OD** allows for the closer contact between the *o*-H(3-Ph) protons and the metal ion. Thus, the intermediate position of the resonances of the B-*H* and *o*-H(3-Ph) protons of **2-CD_3OD** is a rather expected result. The unexpected feature in the spectrum of **2-CD_3OD** is the considerably smaller chemical shift of the C-*H*(3-*i*Pr) proton in comparison with that in **3-CD_3OD**. This feature may be caused by the 3-*i*Pr substituent being pushed away by the two flanking 3-Ph substituents in the former complex. The ^1H NMR spectroscopic results obtained for the other two complexes described here will be discussed later.

Synthesis, Structure and Properties of [HB(3-Ph,5-*i*Prpz)$_2$-(3,5-diMepz)]Co(NCS) (4)

The ambivalent bonding of 3(5)-isopropyl-5(3)-phenylpyrazole to boron resulted in spontaneous formation of heteroscorpionates, which was demonstrated above. We did not intend to optimize the yield of the synthesis of the Tp^x ligands described. Instead, we have constructed the synthetic heteroscorpionate composed of two pyrazole units, i.e., two 3-Ph,5-*i*Prpz units and one 3,5-diMepz unit. The sodium salt of the Tp^x ligand was obtained as a pure product in good yield. We have assumed that the ligand remained unchanged during the synthesis of the [HB(3-Ph,5-*i*Prpz)$_2$(3,5-diMepz)]Co(NCS) complex, which was obtained by a standard procedure under mild conditions. During workup, we found that prolonged heating (12 h) of the complex in methanol was accompanied by formation of bis(ligand) complexes, similar to that found in the case of [HB(3-Ph,5-Mepz)$_2$(3,5-diMepz)]Co(NCS).[10,11] Examination by mass spectrometry of the white precipitate of side-products isolated from hot methanol indicated that a series of the following complexes were formed by cross-exchange of the pyrazolyl moieties: [HB(Ph,*i*Prpz)$_2$(3,5-diMepz)]$_2$Co [*m*/*z* (%) = 1014 (80)], [HB(Ph,*i*Prpz)$_2$(3,5-diMepz)]-[HB(Ph,*i*Prpz)(3,5-diMepz)$_2$]Co [*m*/*z* (%)= 923 (100)], [HB(Ph,*i*Prpz)(3,5-diMepz)$_2$]$_2$Co [*m*/*z* (%) = 832 (40)], [HB(Ph,*i*Prpz)(3,5-diMepz)$_2$][HB(3,5-diMepz)$_3$]Co [*m*/*z* (%) = 742 (10)], and [HB(3,5-diMepz)$_3$]$_2$Co [*m*/*z* (%) = 651 (40)]. The [HB(3-Ph,5-*i*Prpz)$_2$(3,5-diMepz)]Co(NCS) complex was much less prone, however, to undergo this conversion than was the [HB(3-Ph,5-Mepz)$_2$(3,5-diMepz)]Co(NCS) one.[11] Thus, we were able to isolate and grow crystals of **4** from the polar solvent THF. The molecular structure of **4** is presented in Figure 4. The cobalt is tetracoordinate in **4** despite the replacement of one pyrazolyl residue of medium steric demand (3-Ph,5-*i*Prpz in **1-THF**) by a sterically rather nondemanding one (3,5-diMepz). The cobalt-centered and boron-centered bite angles of the latter ligand in tetracoordinate **4** are slightly larger (141.3 and 77.6°, respectively) in comparison with those in **1-THF** (see Table 1). Nevertheless, the ligand is bound more tightly than are homo- and heteroscorpionate in **1-THF** and **3-THF**, respectively, which can be concluded from the relatively short cobalt−boron distance and the largest chemical shift of the B-*H* proton in **4-CD_3OD** (Table 1).

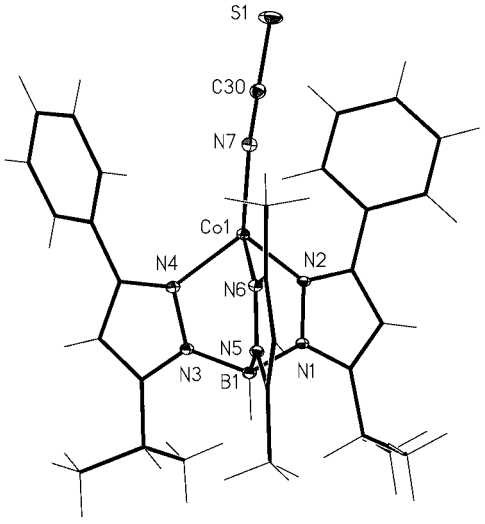

Figure 4. View of **4**; selected bond lengths [Å] and angles [°]: Co(1)−N(7) 1.9178(15), Co(1)−N(2) 2.0154(14), Co(1)−N(4) 2.0124(15), Co(1)−N(6) 2.0020(15); N(7)−Co(1)−N(2) 120.60(6), N(7)−Co(1)−N(4) 130.29(6), N(7)−Co(1)−N(6) 116.50(6), N(4)−Co(1)−N(2) 92.42(6), N(6)−Co(1)−N(2) 95.74(6), N(6)−Co(1)−N(4) 93.28(6)

Steric Demands of Tp^x Ligands in [HB(3-Ph,5-*i*Prpz)$_2$(3,5-diMepz)]CoTp (5), [HB(3-*i*Pr,5-Phpz)$_2$(3-Ph,5-*i*Prpz)]CoTp (6), [HB(3-Ph,5-*i*Prpz)$_2$(3-*i*Pr,5-Phpz)]CoTp (7), and $Tp^{Ph,iPr}$CoTp (8); Tp = Tris(pyrazolyl)borate

The presence of small- or medium-sized substituents at positions 3 and 5 of pyrazole units renders the $Tp^xCo(X)$ complexes able to coordinate Tp as the X unit in all of the compounds studied. Previously, it has been noted that the presence of merely one sterically demanding 3-*tert*-butyl or 3,5-di-*tert*-butylpyrazolyl residue precluded such a conversion.[13,10]

The comparison of the steric demands of Tp^x ligands has been made for their Tp^xCoTp complexes, which were generated in situ. The ^1H NMR spectra of pentacoordinate $Tp^xCo(NCS)(CD_3OD)$ complexes are shown in Figures 3 and 5 (A). The metathesis of the thiocyanate ion and the Tp unit occurred quantitatively without formation of Tp_2Co except in the case of $Tp^{Ph,iPr}Co(NCS)$. The Tp^x ligands of intermediate steric hindrance described here were expected to form stable hexacoordinate Tp^xCoTp com-

 © 2003 Wiley-VCH Verlag GmbH & Co. KGaA, Weinheim

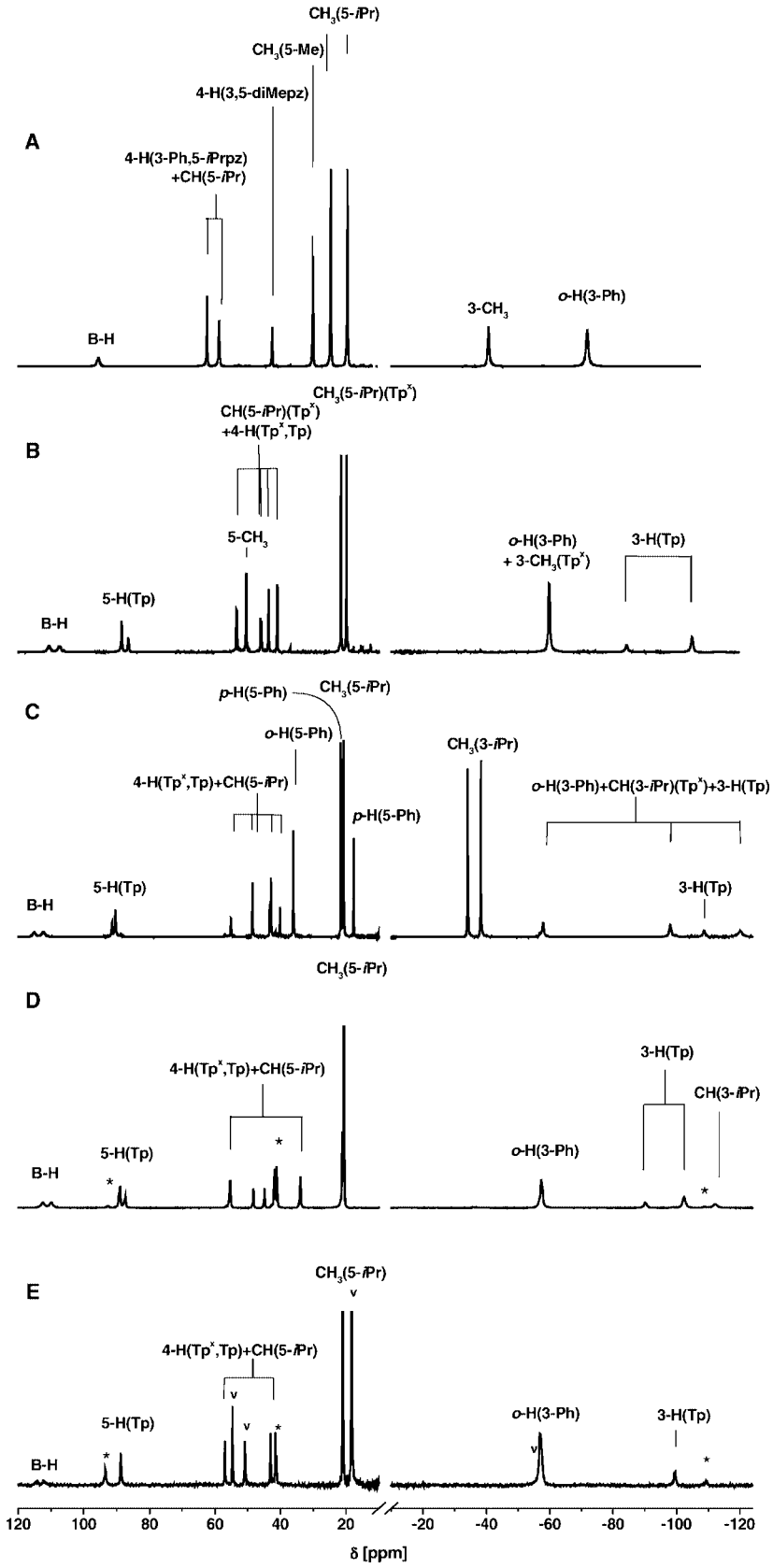

Figure 5. ^{1}H NMR spectra of [HB(3-Ph,5-*i*Prpz)$_2$(3,5-diMepz)]Co(NCS)(CD$_3$OD) (**4-CD$_3$OD**) (A), [HB(3-Ph,5-*i*Prpz)$_2$(3,5-diMepz)]CoTp (**5**) (B), [HB(3-*i*Pr,5-Phpz)$_2$(3-Ph,5-*i*Prpz)]CoTp (**6**) (C), [HB(3-*i*Pr,5-Phpz)(3-Ph,5-*i*Prpz)$_2$]CoTp (**7**) (D), and Tp^{Ph,iPr}CoTp (**8**) (E) in [D$_4$]methanol at 298 K; the resonances of Tp$_2$Co are labeled with asterisks (traces D and E), the resonances of starting Tp^{Ph,iPr}Co(NCS)(CD$_3$OD) complex (**1-CD$_3$OD**) are labeled with a "v"

 © 2003 Wiley-VCH Verlag GmbH & Co. KGaA, Weinheim

plexes, as was found in other cases.[1,3,5,9−11,13−17,20−25] The reactions between the thiocyanate-bearing starting complexes and KTp were monitored by ^{1}H NMR spectroscopy of [D$_4$]methanol solutions. The resulting spectra are presented in Figure 5 (B−E).

The ^{1}H NMR spectra of [HB(3-Ph,5-*i*Prpz)$_2$(3,5-diMepz)]CoTp, (**5**, trace B), [HB(3-Ph,5-*i*Prpz)(3-*i*Pr,5-Phpz)$_2$]CoTp (**6**, trace C), and [HB(3-*i*Pr,5-Phpz)(3-Ph,5-*i*Prpz)$_2$]CoTp (**7**, trace D) reveal that mutual rotation of the Tp and heteroscorpionate Tp^x ligands around the central metal ion at 298 K is slow on the timescale of the method; the resonances of the 3-H, 4-H, and 5-H protons of the Tp ligand appear as two signals with a ratio of intensities of 2:1. Other Tp^{x}CoTp complexes bearing Tp^x heteroscorpionates − [HB(3-Ph,5-Mepz)$_2$(3-Me,5-Phpz)]$^-$,[10] [HB(3-Ph,5-Mepz)$_2$(3,5-diMepz)]$^-$,[14] and [HB(3-Ph,5-Mepz)$_2$-(3,5-diEtpz)]$^-$,[24] − behave similarly.

Considering the chemical shifts of the 3-H and/or 5-H signals of the Tp ligand as a measure of the strength of the Co−N(Tp) bonds, we find that shorter Co−N(Tp) bonds are observed for those pyrazolyl(Tp) units that are flanked by the sterically less demanding pyrazolyl residues of Tp^x.

Thus, in the antiperiplanar isomer −

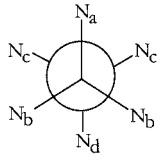

in which N$_a$ and N$_b$ stand for nitrogen donor atoms of the pz$_a$ and pz$_b$ units, respectively, of Tp and N$_c$ and N$_d$ are the nitrogen donor atoms of the pz$_c$ and pz$_d$ units, respectively, of heteroscorpionate Tp^x − the chemical shifts of the 3-H(pz$_a$,Tp) signals are higher in comparison with those of the 3-H(pz$_b$,Tp) signals when the 3-R substituents at pz$_c$ are smaller than the 3-R substituents at pz$_d$. This situation was found for **6**, in which pz$_c$ is 3-*i*Pr,5-Phpz, whereas pz$_d$ is 3-Ph,5-*i*Prpz (Table 2). In all other cases of Tp^{x}CoTp complexes (where Tp^x is the heteroscorpionate ligand), the pz$_c$ units are sterically more demanding, resulting in the 2:1 pattern observed for the resonances of the 3-H(Tp) and, 5-H(Tp) protons of pz$_b$ and pz$_a$, respectively, and the peaks with intensity of two hydrogen atoms are shifted more paramagnetically. For example, in **5** the two 3-Ph(pz$_c$,Tp^x) substituents are in a *synclinal* position with respect to the pz$_a$(Tp) unit. Thus, the pz$_a$(Tp) unit is bound more weakly in comparison to the two pz$_b$(Tp) units, which are flanked by *synclinal* 3-Ph,5-*i*Prpz and 3,5-diMepz units. Consistently, the isotropic shifts of 3-H(pz$_a$,Tp) and 5-H(pz$_a$,Tp) are smaller in comparison to those of 3-H(pz$_b$,Tp) and 5-H(pz$_b$,Tp) (Table 2).

Tp^x ligands with intermediate-sized 3- and 5-substituents weaken the bonding of Tp at the cobalt(II) center in Tp^{x}CoTp complexes, as is demonstrated by the hyperfine shift of the B-*H* signal being lower by 1.3−13.6 ppm (the average values of chemical shifts for Tp^x and Tp units are listed in column 5 of Table 2) in comparison with that in Tp$_2$Co. A more precise parameter is the shift of the 3-H and 5-H(Tp) signals (Δ_3 and Δ_5 in column 6). For Tp^{x}CoTp complexes with homoscorpionate Tp^x ligands, this weakening, composed of both steric and electronic effects (*trans*

Table 2. Characteristic features of ^{1}H NMR spectra of Tp^{x}CoTp complexes

Entry	Formula of complex	Chemical shift (intensity) [mean]of 3-H(Tp)	5-H(Tp)	B-*H*[c]	Δ[a] Δ_3; Δ_5	SD[b] SD$_3$; SD$_5$
1	Tp$_2$Co[d]	−109.1	93.1	120.4	−	−
2	Tp^{Ph,Me}CoTp[10]	−100.3	89.3	113.9	8.8; 3.8	−
3	Tp^{Ph,iPr}CoTp[d]	−99.3	88.7	113.1	9.8; 4.4	−
4	Tp^{iPr,4Br}CoTp[25]	−96.3	86.2	107.6	15.5; 6.9	−
5	Tp^{Cy}CoTp[9]	−103.8	91.8	116.7	5.3; 1.3	−
6	Tp^{Cy,4Br}CoTp[9]	−102.7	90.4	113.5	6.4; 2.7	−
7	[HB(3-Me,5-Phpz)(3-Ph,5-Mepz)$_2$]CoTp[10]	−86.9(1H); −101.4(2H); [−96.6]	88.1(1H); 91.1(2H); [90.1]	112.6	12.5; 3.0	14.5; 3.0
8	[HB(3,5-diMepz)(3-Ph,5-Mepz)$_2$]CoTp[14]	−81.1(1H); −100.1(2H); [−93.8]	85.6(1H); 88.2(2H); [87.3]	107.8	15.3; 5.8	19.0; 2.6
9	[HB(3,5-diEtpz)(3-Ph,5-Mepz)$_2$]CoTp[24]	−82.5(1H); −101.3(2H); [−95.0]	86.2(1H); 88.5(2H); [87.7]	108.6	14.1; 5.4	18.8; 2.3
10	[HB(3-*i*Pr,5-Phpz)(3-Ph,5-*i*Prpz)$_2$]CoTp[d]	−90.3(1H); −102.5(2H); [−98.4]	87.7(1H); 89.3(2H); [88.8]	111.5	10.7; 4.3	12.2; 1.6
11	[HB(3-Ph,5-*i*Prpz)(3-*i*Pr,5-Phpz)$_2$]CoTp[d]	−98.1(2H); −108.8(1H); [−101.7]	90.4(2H); 91.4(1H); [90.7]	113.7	7.4; 2.4	10.7; 1.0
12	[HB(3,5-diMepz)(3-Ph,5-*i*Prpz)$_2$]CoTp[d]	−81.8(1H); −101.7(2H); [95.1]	86.4(1H); 88.5(2H); [87.8]	109.0	14.0; 5.3	19.9; 2.1
13	[HB(5-*i*Prpz)(3-Ph,5-Mepz)$_2$]CoTp[17]	−84.2(1H); −97.2(2H); [−92.9]	79.5(1H); 91.1(2H); [87.2]	109.1	16.2; 5.9	13.0; 11.6
14	[HB(3,5-diMepz)(3-Ph,5-*i*Prpz)(3-*i*Pr,5-Phpz)]-CoTp[d]	−89.0; −96.8; −108.3; [98.0]	89.0; 96.9; 108.3; [98.1]	110.6	11.1; 5.0	

[a] Calculated as chemical shifts [ppm] of 3-H(Tp) and 5-H(Tp) in the Tp^{x}CoTp complex minus those in Tp$_2$Co (Entry 1, columns 3 and 4). [b] Calculated as the absolute value of the chemical shift difference [ppm] between 3-H(Tp) [or 5-H(Tp)] in Tp^{x}CoTp complexes. [c] Averaged for B-*H* resonances of Tp and Tp^x. [d] This paper.

 © 2003 Wiley-VCH Verlag GmbH & Co. KGaA, Weinheim

effect) imposed by the 3−5-substituents, of the Tp^x ligands can be put into order: $Tp^{i\mathrm{Pr},4\mathrm{Br}} > Tp^{\mathrm{Ph},i\mathrm{Pr}} > Tp^{\mathrm{Ph,Me}} > Tp^{\mathrm{Cy},4\mathrm{Br}} > Tp^{\mathrm{Cy}}$.

Unfortunately, the crystallographic data are not available for those compounds, with one exception,[24] therefore a strict relationship between chemical shift observed in the ^{1}H NMR spectra and distances cannot be made. The difference between the effective size of the 3- and/or 5-substituents can be precisely derived, however, from the data of the heteroscorpionate Tp^xCoTp complexes based upon the differences between the chemical shifts of pairs of resonances of the 3-H proton and those of the 5-H(Tp) proton (SD_3 and SD_5, respectively, column 7 in Table 2). These resonances were assigned (Entries 7−14, Table 2) according to the symmetry of the studied species. Thus, the pairs of pyrazolyl residues resulting in differentiation of steric hindrance can be put in order: 3-Ph,5-*i*Prpz/3,5-diMepz > 3-Ph,5-Mepz/3,5-diMepz > 3-Ph,5-Mepz/3,5-diEtpz > 3-Ph,5-Mepz/3-Me,5-Phpz > 3-H,5-*i*Prpz/3-Me,5-Phpz > 3-H,5-*i*Prpz/3-Ph,5-*i*Prpz.

This comparison seems to be reliable. It shows, for instance, even a subtle difference in steric hindrance between 3,5-diMepz and 3,5-diEtpz (Entries 8 and 9), and the influence of steric hindrance imposed by 5-substituents, 5-Me vs. 5-*i*Pr (Entries 8 and 12) or 5-Me vs. 5-Ph (Entries 7 and 8).

Thermal Conversion of 4 into [HB(3-Ph,5-*i*Prpz)(3-*i*Pr,5-Phpz)(3,5-diMepz)]Co(NCS) (9)

Previously, we have demonstrated that [HB(3-Ph,5-Mepz)$_2$(3,5-diMepz)]Co(NCS) underwent conversion into chiral [HB(3-Me,5-Phpz)(3-Ph,5-Mepz)(3,5-diMepz)]-Co(NCS) in 30% yield when heated in propylbenzene for a prolonged time. That reaction was accompanied by the formation of [HB(3-Me,5-Phpz)$_2$(3,5-diMepz)]Co(NCS) and some other products − including bis(ligand) complexes $Tp^xCoTp^{x\prime}$ which were formed with Tp^x ligands of lower steric hindrance − obtained as a mixture.[10] These complexes also form as a result of scrambling of the pyrazolyl residues when the attempt was made to exchange the thiocyanate anion of [HB(3-Ph,5-Mepz)$_2$(3,5-diMepz)]Co(NCS) for carboxylate anions.[11] To avoid this kind of reactivity and to construct a ligand of higher steric demand, with the hope of leading to the thermal conversion under less dramatic conditions, we have replaced the 5-methyl-3-phenylpyrazolyl residue with the 5-isopropyl-3-phenylpyrazolyl one and converted the synthesized [HB(3-Ph,5-*i*Prpz)$_2$(3,5-diMepz)]Co(NCS) complex thermally. The reaction was monitored by ^{1}H NMR spectroscopy. Figure 6 presents the series of spectra taken for the [D$_8$]toluene solutions containing the starting complex and the species formed upon heating them. The ^{1}H NMR spectra of the Tp^xCo(NCS) complexes in this solvent are particularly easy to interpret because the low-field region of the spectra show exclusively the resonances of the 4-H protons of the 3,5-disubstituted Tp^x ligands. Thus, at 357 K the starting compound is represented by two resonances at δ = 60.7 and 53.1 ppm of 2:1 intensity ratio (Figure 6). Upon heating the starting complex at this temperature, three resonances for the 4-H protons, of 1:1:1 intensity ratio, appeared at δ = 62.3, 57.4, and 56.7 ppm, which were attributed to [HB(3-Ph,5-*i*Prpz)(3-*i*Pr,5-Ph)(3,5-diMepz)]Co(NCS) (**9**). The chiral complex was formed in 45% yield within 450 min (Figure 7). The formation of the chiral product was accompanied by formation of [HB(3-*i*Pr,5-Phpz)$_2$(3,5-diMepz)]Co(NCS) (see the resonances labeled as 10 in Figure 6) resulting from double borotropic shift in [HB(3-Ph,5-*i*Prpz)$_2$(3,5-diMepz)]Co(NCS). Although yet another product was formed under those condition, the yield of chiral product was much improved in comparison with the conversion performed for [HB(3-Ph,5-Mepz)$_2$(3,5-diMepz)]Co(NCS).[10]

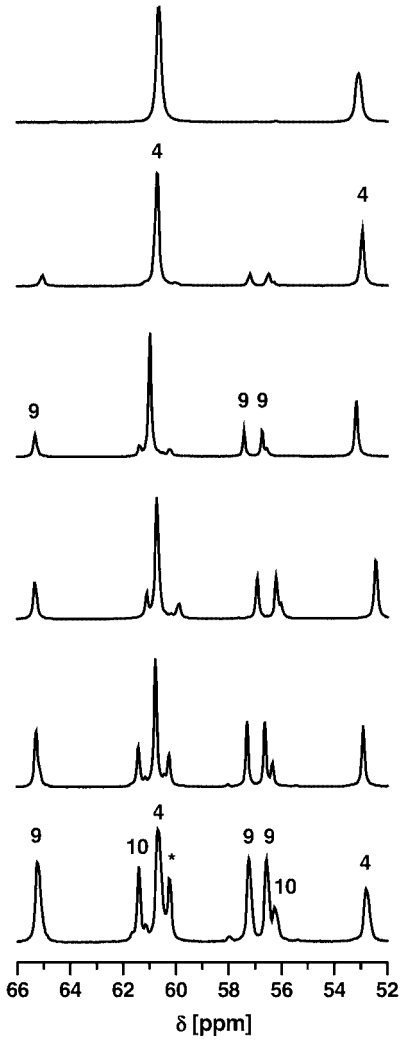

Figure 6. Selected fragments of the ^{1}H NMR spectra of the complexes formed during thermal conversion of [HB(3-Ph,5-*i*Prpz)$_2$(3,5-diMepz)]Co(NCS) (**4**) in [D$_8$]toluene; the resonances of the 4-H protons of the starting compound (trace A), [HB(3-Ph,5-*i*Prpz)(3-*i*Pr,5-Phpz)(3,5-diMepz)]Co(NCS) (**9**), [HB(3-*i*Pr,5-Phpz)$_2$(3,5-diMepz)]Co(NCS) (**10**), and unidentified side-product, are denoted by the arabic numerals 4, 9, and 10, and an asterisk, respectively

 © 2003 Wiley-VCH Verlag GmbH & Co. KGaA, Weinheim

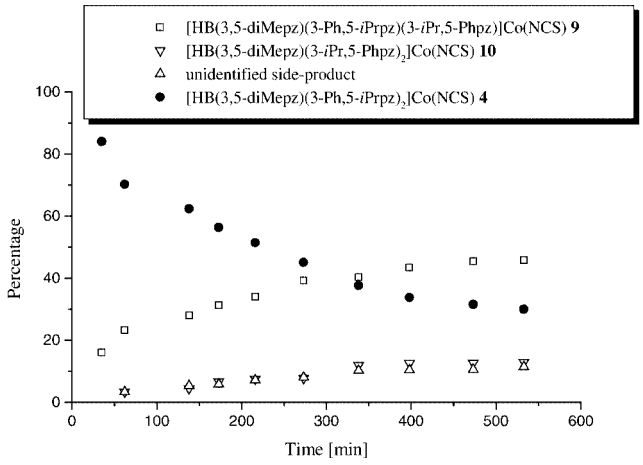

Figure 7. Percentage of the complexes formed during thermal conversion of **4** at 357 K in [D_8]toluene over the course of time

A large-scale procedure eventually gave pure **9**, which was obtained from the post-reaction mixture by fractional crystallization from toluene/heptane as a second crop of crystals. The structure of isolated dimeric compound $\mathbf{9_2}$ was determined crystallographically (Figure 8). Tp^x ligands impose intermediate steric hindrance and, therefore, the central cobalt(II) ion in **9** is pentacoordinate. Typically, the three coordination sites are occupied by the pyrazolyl nitrogen atoms, the thiocyanate nitrogen atom and, additionally, by the sulfur atom of a second thiocyanate anion that bridges to another cobalt(II) center in the dimeric complex. Two Tp^x ligands have opposite configuration at the chiral boron atom. Thus, the *meso* form of dimer of $\mathbf{9_2}$ was obtained in the solid state. The ^{1}H NMR spectrum of **9-CD_3OD** in [D_4]methanol is presented in Figure 9 (trace A). The upfield-shifted resonances belong to protons of the C-3 substituents − *o*-H(3-Ph) (δ = − 78.2 ppm), C*H*(3-*i*Pr) (δ = −70.2 ppm), 3-CH_3 (δ = −57.1 ppm), and diastereoisotopic CH_3(3-*i*Pr) (δ = −30.1, −28.1 ppm) − whereas the three resonances of the 4-H protons, and those belonging to the protons of the 5-substituent and the B-*H* unit, are shifted downfield. The conversion in situ of **9-CD_3OD** into Tp^xCoTp by simple titration of **9-CD_3OD** with KTp in [D_4]methanol produced the heteroleptic complex, which showed seven resonances, with intensity corresponding to one proton, of six 4-H (Tp^x and Tp) protons and one C*H*(5-*i*Pr) proton in the region of the spectrum between δ = 38 and 53 ppm (see inset in trace B). The diastereoisomers of Tp^xCo[OOCC(*S*)H(OH)CH_3] generated in situ by titration of **9-CD_3OD** with sodium (*S*)-lactate are present in solution in equal concentrations, as is concluded from the 1:1 intensity pattern of all the resonances of the two diastereoisomers in the ^{1}H NMR spectrum of

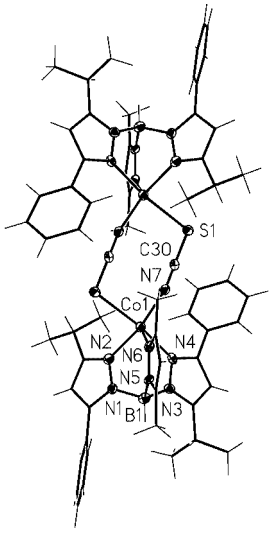

Figure 8. View of the dimer of **9**; selected bond lengths [Å] and angles [°]: Co(1)−N(7) 1.976(7), Co(1)−N(6) 2.031(6), Co(1)−N(2) 2.053(7), Co(1)−N(4) 2.142(7), Co(1)−S(1) 2.581(3); N(7)−Co(1)−N(6) 113.6(3), N(7)−Co(1)−N(2) 150.8(3), N(6)−Co(1)−N(2) 95.6(3), N(7)−Co(1)−N(4) 95.8(3), N(6)−Co(1)−N(4) 88.8(2), N(2)−Co(1)−N(4) 83.7(3), N(7)−Co(1)−S(1) 89.69(19), N(6)−Co(1)−S(1) 95.90(19), N(2)−Co(1)−S(1) 87.81(19), N(4)−Co(1)−S(1) 170.64(19)

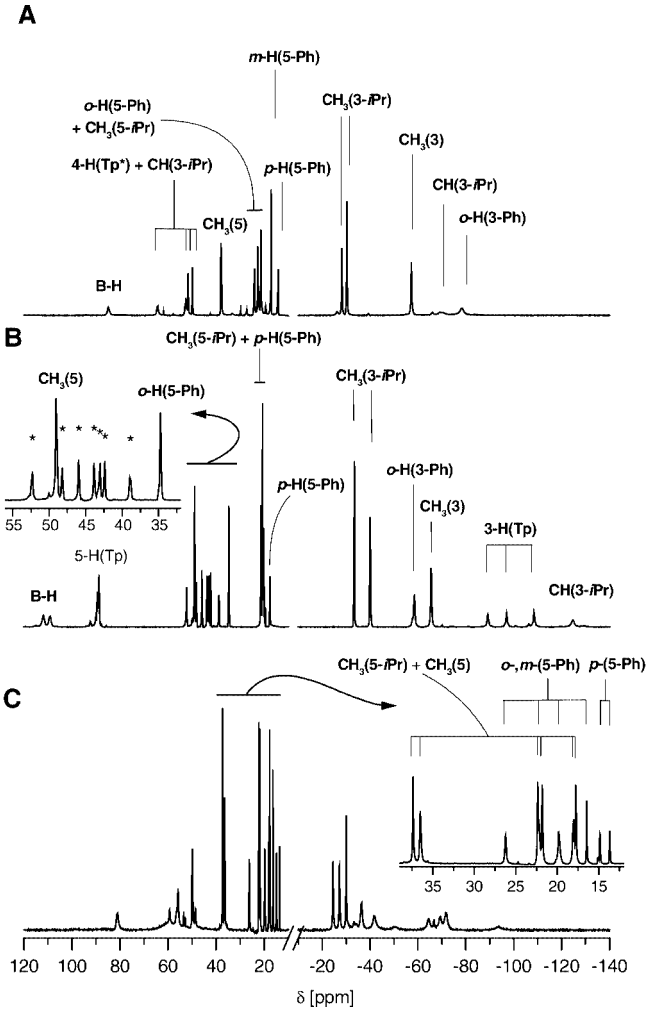

Figure 9. ^{1}H NMR spectra of [HB(3-Ph,5-*i*Prpz)(3-*i*Pr,5-Phpz)(3,5-diMepz)]Co(NCS)(CD_3OD) (A), [HB(3-Ph,5-*i*Prpz)(3-*i*Pr,5-Phpz)(3,5-diMepz)]CoTp (B), and [HB(3-Ph,5-*i*Prpz)(3-*i*Pr,5-Phpz)(3,5-diMepz)]Co(OOCCH(OH)CH_3] (C) in [D_4]methanol at 298 K; seven resonances of intensity corresponding to one hydrogen atom are labeled with asterisks in the inset of trace B and are attributed to the 4-H(Tp,Tp^x) and C*H*(5-*i*Pr) protons

 © 2003 Wiley-VCH Verlag GmbH & Co. KGaA, Weinheim

$Tp^xCo[OOCC(S)H(OH)CH_3]$ presented as trace C. The bottom inset in Figure 9 shows the details of the 13−37-ppm region of the spectrum, in which we observe six methyl group resonances of the 3-CH_3 and CH_3(5-*i*Pr) groups and six *o*-, *m*-, and *p*-(5-Ph) resonances. The two diastereoisomers differ in energy and consequently have considerably different spectra. The spectrum remains unchanged over the course of time (24 h) indicating that rather little inversion of configuration at the boron atom takes place.

No tetracoordinate anionic borates with boron-centered chirality have been obtained to date. Tetrahedral (or nearly tetrahedral) neutral boron compounds with boron-centered chirality have been reported.[26−31] Several compounds of this type, with boron-centered chirality imposed by peripheral chiral substituents, have been structurally characterized.[28−31] Generally, separable enantiomers (diastereoisomers) of opposite boron-centered chirality interconvert rapidly at ambient temperatures ($\Delta G^{\ddagger}_{25}$ = 60−90 kJ/mol).[28−33] The chiral tripodal Tp^x ligand described in this report was designed as a chiral ancillary for facial Tp^xML_n complexes with catalytic activity. Currently, we are working on the isolation of the enantiomerically pure sodium salts of the chiral ligands and their thallium(I) complexes and the preparation of the catalytically active complexes of those ligands.

Experimental Section

Syntheses

5(3)-Isopropyl-3(5)-phenylpyrazole (3-Ph,5-*i*PrpzH): The 3(5)-Ph,5(3)-*i*PrpzH unit was synthesized from the corresponding diketone obtained by the general procedure of Swamer and Hauser.[19] Sodium hydride (19.2 g, 0.80 mol) was suspended in diethyl ether (100 mL) containing ethyl isobutyrate (106.8 mL, 92.6 g, 0.80 mol) under nitrogen in a 2-L three-neck round-bottom flask. The flask was later connected to a wet test-meter, condenser and a dropping funnel. The glass device was flushed with nitrogen. Acetophenone (46.6 mL, 47.86 g, 0.4 mol), dissolved in diethyl ether (100 mL), was added dropwise to the mixture. The reaction was initiated by gentle heating of the mixture. The progress of the reaction was monitored by measuring the volume of hydrogen gas evolved. The reaction was stopped after the evolution of hydrogen had ceased (8 L of gas was collected). Ice-cold water (300 mL) and hydrochloric acid were added to the reaction mixture. The diethyl ether phase was extracted with water (2 × 0.8 L) and the combined water extracts, which contained diketone, were left overnight to react with hydrazine monohydrate (20 mL 20.2 g, 0.4 mol). The solution turned orange and turbid. The pyrazole was extracted three times with diethyl ether (2 L). The solvent was evaporated in a rotary evaporator and the oily product was kept under reduced pressure overnight. Hexane (100 mL) was added to the crude product and the mixture was stirred at room temperature for 24 h. The light-yellow powder of 3(5)-Ph,5(3)-*i*PrpzH was collected and dried under high vacuum (8.8 g, 11.8%). ^{1}H NMR ($CDCl_3$): δ = 1.31 [d, J^3 = 6.7 Hz, 6 H,CH_3(*i*Pr)], 3.01 [sept, 1 H, CH(*i*Pr)], 6.36 (s, 1 H, 4-H), 7.3−7.8 (m, 5 H, *o*-, *m*-, *p*-phenyl), 8.5 (br. s, 1 H, NH) ppm. MS (ESI, positive polarization): *m*/*z* (%) = 186.3 (100) $[C_{12}H_{14}N_2]^+$.

Synthesis of Sodium Tris(pyrazolyl)borates

Sodium Hydrotris(5-isopropyl-3-phenylpyrazolyl)borate {Na[HB(3-Ph,5-*i*Prpz)$_3$]}, Sodium Hydro(3-isopropyl-5-methylpyrazolyl)bis(5-isopropyl-3-phenylpyrazolyl)borate, and Sodium Hydrobis(3-isopropyl-5-phenylpyrazolyl)(5-isopropyl-3-phenylpyrazolyl)borate: $NaBH_4$ (0.1389 g, 3.67 mmol) and 3-Ph,5-*i*PrpzH (2.0033 g, 10.77 mmol) in octadecane (40 mL) were heated with vigorous stirring in a 250-mL three-neck round-bottom flask equipped to a wet test-meter and condenser. The mixture was heated until 400 mL of hydrogen gas was evolved and then heating was continued for 40 min. Heptane (100 mL) was added to the solution after it had cooled to ca. 100 °C and then left overnight at room temperature. The solid was separated by filtration, washed with petroleum ether and dried under high vacuum. Yield 0.305 g (0.60 mmol, 16.3%). The mixture of sodium salts of Tp^x ligands was converted into $Tp^xCo(NCS)$ complexes as reported earlier[10] and was quantified as a mixture based upon the intensity of the integrals of the resonances in the ^{1}H NMR spectrum. The mixture comprised [HB(3-*i*Pr,5-Phpz)(3-Ph,5-*i*Prpz)$_2$]Co(NCS) (80.4%), [HB(3-*i*Pr,5-Phpz)$_2$(3-Ph,5-*i*Prpz)]Co(NCS) (10.8%), and [HB(3-Ph,5-*i*Prpz)$_3$]Co(NCS) (8.8%). The complexes were separated and identified by their ^{1}H NMR spectra (see below).

Synthesis and Separation of and [Hydrotris(5-isopropyl-3-phenylpyrazolyl)borato](thiocyanato)cobalt(II) [$Tp^{Ph,iPr}$Co(NCS)(THF), 1-THF], [Hydro(3-isopropyl-5-phenylpyrazolyl)bis(5-isopropyl-3-phenylpyrazolyl)borato](thiocyanato)cobalt(II) {[HB(3-Ph,5-*i*Prpz)$_2$(3-*i*Pr,5-Phpz)]Co(NCS), 2}, and [Hydrobis(3-isopropyl-5-phenylpyrazolyl)(5-isopropyl-3-phenylpyrazolyl)borato](thiocyanato)cobalt(II) {[HB(3-*i*Pr,5-Phpz)$_2$(3-Ph,5-*i*Prpz)]Co(NCS)(THF), 3-THF}: The complexes were synthesized as described previously[10] starting from $NaTp^x$ mixture (0.305 g, 0.52 mmol) and separated by fractional crystallization from THF/heptane at 4 °C. The blue, cube-shaped crystals of **1-THF** were collected as the first product (30 mg, 0.040 mmol, 7.7% yield), dark-blue needle-shaped crystals of **2-THF** (150 mg, 0.20 mmol, 38.5% yield) were obtained as the second crop and, finally, violet-blue crystals of analytically pure **3-THF** (38 mg, 0.050 mmol, 9.6% yield) were obtained. The crystals of **1-THF** and **3-THF** were examined by X-ray crystallography (Table 3), whereas all attempts to grow the crystals of **2-THF** gave crystalline material that was very sensitive to change of temperature, which precluded good-quality X-ray crystallographic measurement.

1-THF: $C_{41}H_{48}BCoN_7OS$ (756.66): calcd. C 65.08, H 6.39, N 12.96; found C 65.21, H 6.41, N 12.62. ^{1}H NMR (CD_3OD, 298 K): δ = −57.4 [6 H, *o*-H(3-Ph)], 3.7 [3 H, *p*-H(3-Ph)], 4.5 [6 H, *m*-H(3-Ph)], 18.3 [18 H, CH_3(5-*i*Pr)], 50.8 and 54.7 [3 H, CH(5-*i*Pr) and 3 H, 4-H(3-Ph,5-*i*Prpz)], 93.7 (B-H) ppm. IR (KBr): $\tilde{\nu}$ = 2588 (ν_{BH}), 2059 (ν_{NCS}) cm^{-1}.

2-THF: $C_{41}H_{48}N_7BCoOS$ (756.66): calcd. C 65.08, H 6.39, N 12.96; found C 65.12, H 6.23, N 12.48. ^{1}H NMR (CD_3OD, 298 K): δ = −57.9 [4 H, *o*-H(3-Ph)], −34.8 [1 H, CH(3-*i*Pr)], −24.8 [6 H, CH_3(3-*i*Pr)], 0.9 [2 H, *p*-H(3-Ph)], 1.2 [4 H, *m*-H(3-Ph)], 13.7 [1 H, *p*-H(5-Ph)], 15.8 [2 H, *m*-H(5-Ph)], 19.1 [6 H, CH_3(5-*i*Pr)], 19.8 [2 H, *o*-H(5-Ph)], 26.1 [6 H, CH_3(5-*i*Pr)], 42.4 [1 H, 4-H(3-*i*Pr,5-Phpz)], 58.2 and 62.6 [2 H, CH(5-*i*Pr) and 2 H, 4-H(3-Ph,5-*i*Prpz)], 92.7 (B-H) ppm. IR (KBr): $\tilde{\nu}$ = 2557 (ν_{BH}), 2062 (ν_{NCS}) cm^{-1}.

3-THF: $C_{41}H_{48}N_7BCoOS$ (756.66): calcd. C 65.08, H 6.39, N 12.96; found C 65.40, H 6.61, N 13.02. ^{1}H NMR (CD_3OD, 298 K): δ = −80.8, −70.8 [2 H, *o*-H(3-Ph) and 2 H, CH(3-*i*Pr)], −30.3, −29.4 [6 H, two diastereoisotopic CH_3(3-*i*Pr)], −3.8 [2 H, *m*-H(3-Ph)], 0.4 [1 H, *p*-H(3-Ph)], 14.2 [2 H, *p*-H(5-Ph)], 17.3 [4 H, *m*-H(5-Ph)], 23.9

 © 2003 Wiley-VCH Verlag GmbH & Co. KGaA, Weinheim

Table 3. Crystal data and structure refinement

Compound	**1-THF**	**3-THF**	**4**	**9_2**
Empirical formula	$C_{41}H_{48}BCoN_7OS$	$C_{41}H_{48}BCoN_7OS$	$C_{30}H_{34}BCoN_7S$	$C_{30}H_{34}BCoN_7S$
Formula mass	756.66	756.66	594.44	594.44
T [K]	293(2)	100(2)	100(2)	100(2)
λ [Å]	0.71073	0.71073	0.71073	0.71073
Crystal system	monoclinic	monoclinic	triclinic	triclinic
Space group	$P2_1/c$	$P2_1/c$	$P\bar{1}$	$P\bar{1}$
a [Å]	11.960(2)	9.860(2)	8.5970(17)	10.618(4
b [Å]	14.731(3)	19.415(3)	12.048(2)	11.717(4)
c [Å]	23.516(3)	20.782(3)	15.011(3)	13.128(4)
α [°]	90	90	89.59(3)	111.95(3)
β [°]	90.858(12)	91.762(15)	88.05(3)	99.83(3)
γ [°]	90	90	75.07(3)	93.96(3)
V [Å^3]	4142.8(12)	3976.5(12)	1501.4(5)	1476.8(9)
Z	4	4	2	2
$D_{calcd.}$ [Mg·m^{-3}]	1.213	1.264	1.315	1.337
μ [mm^{-1}]	0.504	0.525	0.673	0.684
F(000)	1596	1596	622	622
Crystal size [mm]	0.24 × 0.20 × 0.16	0.20 × 0.13 × 0.13	0.18 × 0.16 × 0.14	0.33 × 0.07 × 0.05
θ range for data collection [°]	3.36−28.54	3.50−26.00	3.59−28.34	3.42−28.40
Ranges of h, k, l	−15/15, −19/15, −30/31	−8/12, −23/23, −25/24	−11/11, −10/16, −19/19	−14/9, −15/15, −16/17
Reflections collected	28281	22893	10451	10255
Independent reflections/R_{int}	9651/0.0891	7672/0.0741	6606/0.0197	6500/0.1089
Data/parameters	9651/476	7672/476	6606/367	6500/367
GOF(F^2)	1.102	1.072	1.075	0.959
Final R_1/wR_2 indices ($I > 2\sigma_I$)	0.0852/0.1300	0.0671/0.0741	0.0330/0.0790	0.0867/0.1433
Extinction coefficient	0.0002(3)	0.00095(15)		
Min./max. Transmission				0.8670/0.9695
Largest diff. peak/hole [e·Å^{-3}]	0.323/−0.304	0.289/−0.303	0.319/-0.386	0.365/-0.432

[6 H, CH_3(5-*i*Pr)], 24.7 [4 H, *o*-H(5-Ph)], 51.6 [2 H, 4-H(3-*i*Pr,5-Phpz)], 57.2, 69.7 [1 H, CH(5-*i*Pr) and 1 H, 4-H(3-Ph,5-*i*Prpz)], 86.8 (B-H) ppm. IR (KBr): $\tilde{\nu}$ = 2597 (ν_{BH}), 2083 (ν_{NCS}) cm^{-1}.

Sodium Hydro(3,5-dimethylpyrazolyl)bis(5-isopropyl-3-phenylpyrazolyl)borate {Na[HB(3-Ph,5-*i*Prpz)$_2$(3,5-diMepz)]}: A mixture of $NaBH_4$ (0.2848 g, 7.53 mmol), 3-Ph,5-*i*PrpzH (2.9401 g, 15.81 mmol) and 3,5-diMepzH (0.6517 g, 6.78 mmol) in octadecane (40 mL) was heated with vigorous stirring in a 250-mL three-neck round-bottom flask equipped with a wet test-meter and condenser. The device was flushed with nitrogen before heating began. The temperature was increased gradually to the boiling point of octadecane (317 °C). Heating was continued until 630 mL of hydrogen gas was collected. Heptane (100 mL) was added to the solution after it had been cooled to ca. 100 °C and then the mixture was left overnight at 4 °C. The solid (0.6150 g, 16.4%) was separated by filtration at room temperature, washed with petroleum ether and then dried under high vacuum. From the heptane filtrate another sodium salt was recovered, i.e., sodium hydrotris(5-isopropyl-3-phenylpyrazolyl)borate (12%), which was synthesized also by a separate procedure (vide supra). ^{1}H NMR (CD_3OD, 298 K): δ = 1.53 [d, 12 H, CH_3(*i*Pr)], 2.19 [s, 6 H, 3- and 5-CH_3], 3.02 [sept, 2 H, CH(3-*i*Pr)], 5.91 [s, 1 H, 4-H(3,5-diMepz)], 6.43 [s, 2 H, 4-H(3-*i*Pr,5-Phpz)], 7.8−7.2 [10 H, m, *o*-, *m*-, and *p*-H(3-*i*Pr,5-Phpz)] ppm.

[Hydro(3,5-dimethylpyrazolyl)bis(5-isopropyl-3-phenylpyrazolyl)-borato](thiocyanato)cobalt(II) {[HB(3-Ph,5-*i*Prpz)$_2$(3,5-diMepz)]-Co(NCS), 4}: This complex was synthesized by adding Na[HB(3-Ph,5-*i*Prpz)$_2$(3,5-diMepz)] (110 mg, 0.22 mmol) in THF (5 mL) into an aqueous solution (50 mL) of 0.1 M $Co(NO_3)_2$ and 0.5 M KNCS. The resulting blue product was extracted into CH_2Cl_2 (100 mL), the organic layer was washed with water (2 × 100 mL), the CH_2Cl_2 was evaporated in a rotary evaporator. The solid residue was dissolved in THF (5 mL) and recrystallized by the co-diffusion of hexane (ca. 80 mL) at 4 °C. After two weeks, the product was collected as blue crystals (123 mg, 0.18 mmol, 82% yield). One of the crystals was analyzed crystallographically (Table 3).

4: $C_{30}H_{34}N_7BCoS$ (594.44): calcd. C 60.61, H 5.76, N 16.49; found C 60.42, H 5.61, N 16.40. ^{1}H NMR (CD_3OD, 298 K): δ = −69.6 [4 H, *o*-H(3-Ph)], −39.5 (3 H, 3-CH_3), 1.6 [4 H, *m*-H(3-Ph)], 2.8 [2 H, *p*-H(3-Ph)], 19.7 [6 H, CH_3(5-*i*Pr)], 24.7 [6 H, CH_3(5-*i*Pr)], 30.1 (3 H, 5-CH_3), 42.5 [1 H, 4-H(3,5-diMepz)], 58.7 [2 H, CH(5-*i*Pr)], 62.4 [2 H, 4-H(3-Ph,5-*i*Prpz)], 95.6 (1 H, BH) ppm. IR (KBr): $\tilde{\nu}$ = 2557 (ν_{BH}), 2064 (ν_{NCS}) cm^{-1}.

In Situ Conversions of Tp^{x}Co(NCS) into Tp^{x}CoTp Complexes: The complexes were converted into their Tp^{x}CoTp counterparts in [D_4]methanol on a micromolar scale by the stepwise addition of 1 M KTp in [D_4]methanol into the starting thiocyanate complex (ca. 6 mg), dissolved in [D_4]methanol (400 μL). The progress of reaction was monitored by ^{1}H NMR spectroscopy.

Thermal Conversion of 4 into [Hydro(3,5-dimethylpyrazolyl)(3-isopropyl-5-phenylpyrazolyl)(5-isopropyl-3-phenylpyrazolyl)borato]-(thiocyanato)cobalt(II) (9): Heteroscorpionate complex **4** (6.3 mg, 9.5 μmol) was dissolved in [D_8]toluene (450 μL) in an NMR tube, which was placed in the cavity of the NMR instrument and heated at 357 K for 23 h or at 377 K for 14 h. The progress of reaction was monitored by ^{1}H NMR spectroscopy. Large-scale conversion was performed with **4** (300 mg) in toluene (30 mL) at 357 K for 500 min. The resulting solution was layered with heptane and left to crystallize at room temperature. The first crop of crystals was identified as **4** by its ^{1}H NMR spectrum, while violet needles of **9_2** were obtained as the second crop (67 mg, 22% yield). The structure of **9_2** was determined crystallographically (Table 3).

 © 2003 Wiley-VCH Verlag GmbH & Co. KGaA, Weinheim

9: $C_{30}H_{34}BCoN_7S$ (594.44): calcd. C 60.61, H 5.76, N 16.49; found C 60.63, H 5.80, N 16.59. ^{1}H NMR (CD_3OD, 298 K): δ = −78.2 [2 H, *o*-H(3-Ph)], −70.2 [1 H, CH(3-*i*Pr)], −57.2 (1 H, 3-CH_3), −30.1, −28.1 [3 H, 3 H, CH_3(3-*i*Pr)], −4.2 [2 H, *m*-H(3-Ph)], 0.8 [1 H, *p*-H(3-Ph)], 14.4 [1 H, *p*-H(5-Ph)], 17.4, [2 H, *m*-H(3-Ph)], 21.5, 22.8 [3 H, 3 H, CH_3(5-*i*Pr)], 24.3 [2 H, *o*-H(3-Ph)], 33.1 (3 H, 5-CH_3), 50.0, 51.9, 52.9 [1 H, 1 H, 1 H, 4-H(pz)], 64.7 [1 H, CH(5-*i*Pr)], 85.0 (1 H, BH) ppm. IR (KBr): $\tilde{\nu}$ = 2557 (ν_{BH}), 2121, 2058 (ν_{NCS}) cm^{-1}.

Methods: ^{1}H NMR spectra were obtained with a Bruker AMX300 spectrometer operating in the quadrature mode at 300 MHz. The residual peaks of deuterated solvents were used as internal standards. IR spectra were recorded with a Perkin−Elmer 1725X spectrophotometer. Elemental analyses were performed with an EA 1108 apparatus (Carbo Erba) at the Department of Organic Chemistry, Faculty of Chemistry, Rzeszów University of Technology. Mass spectra were obtained using a Finnigan MAT TSQ 700 spectrometer by the ESI method from chloroform with a 4.5-kV ionization potential and a capillary temperature of 250 °C. Crystal data are given in Table 1 together with refinement details. Measurements were performed at 293 K for **1-THF** and at 100 K for **3-THF**, **4** and $\mathbf{9_2}$ using an Oxford Cryosystem device with a Kuma KM4CCD κ-axis diffractometer with graphite-monochromated Mo-K_α radiation. The crystals were positioned at 65 mm from the CCD camera. 612 frames were measured at 0.75° intervals with a counting time of 10−15 s. Accurate cell parameters were determined and refined by least-squares fit of 2500−3800 of the strongest reflections. The data were corrected for Lorentz and polarization effects. No absorption correction was applied for **1-THF**, **3-THF** and **3**, and analytical absorption correction was applied for $\mathbf{9_2}$. Data reduction and analysis were carried out with the Oxford Diffraction (Poland) Sp. z o.o (formerly Kuma Diffraction Wroclaw, Poland) programs. Structures were solved by direct methods (program SHELXS-97)[34] and refined by the full-matrix least-squares method on all F^2 data using the SHELXL-97 programs.[35] Non-hydrogen atoms were refined with anisotropic displacement parameters; hydrogen atoms were included from geometry of molecules and Δρ maps but were not refined. CCDC-200532 (**1-THF**), -200533 (**3-THF**), -200534 (**4**) and -189010 ($\mathbf{9_2}$) contain the supplementary crystallographic data for this paper. These data can be obtained free of charge at www.ccdc.cam.ac.uk/conts/retrieving.html [or from the Cambridge Crystallographic Data Centre, 12 Union Road, Cambridge CB2 1EZ, UK; Fax: (internat.) + 44-1223/336-033; E-mail: deposit@ccdc.cam.ac.uk].

Acknowledgments

We thank KBN (Poland) for a Grant (no. 3 T09A 05219).

[1] S. Trofimenko, J. C. Calabrese, P. J. Domaille, G. S. Thompson, *Inorg. Chem.* **1989**, *28*, 1091−1101.
[2] U. E. Bucher, A. Currao, R. Nesper, H. Rüegger, M. L. Venanzi, E. Younger, *Inorg. Chem.* **1995**, *34*, 66−74.
[3] J. C. Calabrese, S. Trofimenko, *Inorg. Chem.* **1992**, *31*, 4810−4814.
[4] A. L. Rheingold, C. B. White, S. Trofimenko, *Inorg. Chem.* **1993**, *32*, 3437−3477.
[5] J. Juang, L. Lee, B. S. Haggerty, A. L. Rheingold, M. A. Waters, *Inorg. Chem.* **1995**, *34*, 4268−4270.
[6] D. D. LeCloux, M. C. Keyes, M. Osawa, V. Reynolds, W. B. Tolman, *J. Am. Chem. Soc.* **1994**, *33*, 6361−6368.
[7] A.. Albinati, M. Bovens, H. Rüegger, M. L. Venanzi, *Inorg. Chem.* **1997**, *36*, 5991−5999.
[8] D. J. Darensbourg, E. L. Maynard, M. W. Holtcamp, K. K. Klausmeyer, J. H. Reibenspies, *Inorg. Chem.* **1996**, *35*, 2682−2684.
[9] S. Trofimenko, A. L. Rheingold, L. M. Liable-Sands, *Inorg. Chem.* **2002**, *41*, 1889−1896.
[10] M. Łukasiewicz, Z. Ciunik, T. Ruman, M. Skóra, S. Wołowiec, *Polyhedron* **2001**, *20*, 237−244.
[11] T. Ruman, Z. Ciunik, E. Szklanny, S. Wołowiec, *Polyhedron* **2003**, *22*, 2743−2753.
[12] P. Ghosh, D. D. Churchill, M. Rubinstein, G. Parkin, *New J. Chem.* **1999**, *23*, 961−963.
[13] M. Łukasiewicz, Z. Ciunik, S. Wołowiec, *Polyhedron* **2000**, *19*, 2119−2125.
[14] T. Ruman, M. Łukasiewicz, Z. Ciunik, S. Wołowiec, *Polyhedron* **2001**, *20*, 2551−2558.
[15] T. Ruman, Z. Ciunik, J. Mazurek, S. Wołowiec, *Eur. J. Inorg. Chem.* **2002**, 754−760.
[16] T. Ruman, Z. Ciunik, A. Goclan, M. Łukasiewicz, S. Wolowiec, *Polyhedron* **2001**, *20*, 2965−2970.
[17] T. Ruman, Z. Ciunik, S. Wołowiec, *Eur. J. Inorg. Chem.* **2003**, 89−93.
[18] G. N. LaMar, J. P. Jesson, P. J. Meakin, *J. Am. Chem. Soc.* **1971**, *93*, 1286−1288.
[19] F. W. Swamer, C. R. Hauser, *J. Am. Chem. Soc.* **1950**, *72*, 1352−1356.
[20] J. C. Calabrese, P. J. Domaille, S. Trofimenko, G. J. Long, *Inorg. Chem.* **1991**, *30*, 2795−2801.
[21] A. Kremer-Aach, W. Kläui, R. Bell, A. Strerath, H. Wunderlich, D. Mootz, *Inorg. Chem.* **1997**, *36*, 1552−1563.
[22] A. L. Rheingold, G. P. A. Yap, L. M. Liable-Sands, I. A. Guzei, S. Trofimenko, *Inorg. Chem.* **1997**, *36*, 6261−6265.
[23] C. Janiak, S. Temizdemir, S. Dechert, W. Deck, F. Girgsdies, M. J. Kolm, T. G. Scharmann, O. M. Zipffel, *Eur. J. Inorg. Chem.* **2000**, 1229−1241.
[24] T. Ruman, Z. Ciunik, S. Wołowiec, *Polyhedron*, in press.
[25] J. C. Calabrese, P. J. Domaille, J. S. Thompson, S. Trofimenko, *Inorg. Chem.* **1990**, *29*, 4429−4437.
[26] L. Deloux, M. Srebnik, *Chem. Rev.* **1993**, *93*, 763−784. In this review on asymmetric boron-catalyzed reactions, the oxazaborolidines with chiral boron centers and other catalytically active putative transient tetracoordinate boron species are described.
[27] E. Vedejs, S. C. Fields, M. R. Schrimpf, *J. Am. Chem. Soc.* **1993**, *115*, 11612−11613.
[28] E. Vedejs, S. C. Fields, M. R. Schrimpf, *J. Org. Chem.* **1995**, *60*, 3028−3034.
[29] J. Mortler, M. Vaultier, B. Plunian, L. Touper, *Heterocycles* **1999**, *50*, 703−713.
[30] S. Toyota, M. Oki, *Bull. Chem. Soc. Jpn.* **1992**, *65*, 1832−1840.
[31] W. Kliegel, U. Schumacher, S. J. Rettig, J. Trotter, *Can. J. Chem.* **1992**, *70*, 1188−1194.
[32] M. S. Korobov, L. E. Nivorozhkin, L. E. Konstantinovski, V. I. Minkin, *J. Chem. Soc., Chem. Commun.* **1982**, 169−170.
[33] A. J. Boulton, C. S. Prado, *J. Chem. Soc., Chem. Commun.* **1982**, 1008−1009.
[34] G. M. Sheldrick, *SHELXS-97, Program for solution of crystal structures*, University of Göttingen, **1997**.
[35] G. M. Sheldrick, *SHELXL-97, Program for crystal structure refinement*, University of Göttingen, **1997**.

Received January 13, 2003

 © 2003 Wiley-VCH Verlag GmbH & Co. KGaA, Weinheim

Properties of Undoped and Ca-Doped $LaMnO_3$ − Non-Stoichiometry and Defect Structure

Mondher Yahia[a] and Habib Batis*[a]

Keywords: Non-stoichiometry / Perovskites / Preparation

Oxygen-excessive $LaMnO_{3+y}$ samples with $0.02 \leq y \leq 0.26$ have been prepared by thermal decomposition in air at 450 °C of a precursor obtained from an aqueous solution of lanthanum nitrate and manganese acetate (atomic ratio La/Mn = 1). The obtained solid is annealed at different temperatures from 700 to 1000 °C and under three oxygen pressures: 1.00, 0.21, and 10^{-4} atm. Samples with $0.14 \leq y \leq 0.26$ are simple-phased rhombohedral perovskites, the distortion of which decreases as the oxygen content (and Mn^{4+} content) increases. Samples with $0.02 \leq y \leq 0.09$, obtained under low oxygen pressure (10^{-4} atm), have orthorhombic symmetry. In this case, the order of lattice parameters $c/\sqrt{2} < a < b$, characteristic of O′-perovskites, is a consequence of the Jahn–Teller distortion of the oxide octahedron around the d^4 Mn^{4+} cation. The volume (V_f) per $LaMnO_{3+y}$ formula unit decreases regularly with increasing oxygen content (i.e., oxidation). Study has shown that the oxygen content is best described in terms of La and Mn vacancies, rather than of interstitial anions. Density measurements confirm the cation vacancy model involving equal amounts in La and Mn sublattices. The infrared spectra of $LaMnO_{3+y}$ samples have been interpreted in connection with the structures of these solids. Correlations have been established between the spectral evolution and the crystal distortion of these compounds. $La_{1-x}Ca_xMnO_{3\pm y}$ oxides with $0 < x \leq 1$ have been synthesised by the same route, at 700 °C and under an oxygen pressure of 0.21 atm. It is shown that a negative correlation exists between the calcium content *x* and the degree of non-stoichiometry: at low Ca content, the oxygen content is higher. The ability to form over-stoichiometric compounds in air decreases with increasing Ca content and mostly disappears at $x \geq 0.7$. Samples with $0.1 \leq x \leq 0.4$ are simple-phased rhombohedral perovskites with constant Mn^{3+}/Mn^{4+} ratios. Samples with $0.5 \leq x \leq 1$ have orthorhombic symmetry. In this case, a linear variation of the Mn^{4+} content as a function of the Ca content is observed. The defect structure of these compounds is described in terms of La and Mn vacancies when $0 < x \leq 0.7$ ($0 \leq y \leq 0.19$) and anion vacancies when $0.8 \leq x \leq 1$ ($-0.04 \leq y < 0$).

(© Wiley-VCH Verlag GmbH & Co. KGaA, 69451 Weinheim, Germany, 2003)

Introduction

Perovskite-type oxides can be represented as ABO_3, where B is a transition cation of the 3d, 4d, or 5d group and A is either a lanthanide (generally La, but sometimes Ce, Pr, or Nd) or an alkaline earth metal (Ca, Sr, or Ba). In the crystal structure, the A ion is coordinated by twelve oxygen ions, which in turn belong to eight BO_6 octahedrons sharing corners. The stability, derived primarily from the Madelung energy of the stacking of rigid BO_6 octahedrons, requires that B be a cation with a preference for octahedral coordination. The A ion occupying the large dodecahedral interstice has to have an appropriate size.[1−3]

They have been studied for their physical characteristics, such as ferroelectricity, piezoelectricity, magnetism, superconductivity at high temperature etc. During the last two decades they have been consistently proposed as alternative catalysts for reactions involving hydrogen, such as hydrogenolysis of hydrocarbons[4] as well as for reaction combustion of carbon monoxide and light hydrocarbons.[5−11]

The great variety of A and B ions able to take part in the structure, the possibility of changing the valence of the B ion by proper selection of A and also the partial substitution of cations to form compounds of formula $(AA')(BB')O_3$ make feasible the preparation of perovskites with very specific properties.

Lanthanum manganite oxides of formula $LaMnO_{3+y}$, exhibit non-stoichiometry on one or more sub-lattices.[12] The opinion is widely shared that the oxygen excess is partially compensated by the oxidation of Mn^{3+} (d^4) to Mn^{4+} (d^3) in the B sub-lattice. Consequently, it can be seen that the Jahn−Teller effect of Mn^{3+} ions, and hence the structure distortion, will decrease with increasing number of Mn^{4+} ions. In fact, there are two characteristic distortions that influence the perovskite structure of manganites. One consists of co-operative tilting of MnO_6 octahedrons. This kind of distortion is a consequence of the ionic radii and is common in perovskites with small central cations (Goldschmidt factor $t < 1$). The other kind of structure distortion is associated with the Jahn−Teller effect of Mn^{3+} ions, resulting

[a] Laboratoire d'Études de Solides Catalyseurs, Département de Chimie, Faculté des Sciences de Tunis,
1060 Tunis, Tunisie

 © 2003 Wiley-VCH Verlag GmbH & Co. KGaA, Weinheim **DOI: 10.1002/ejic.200300025**

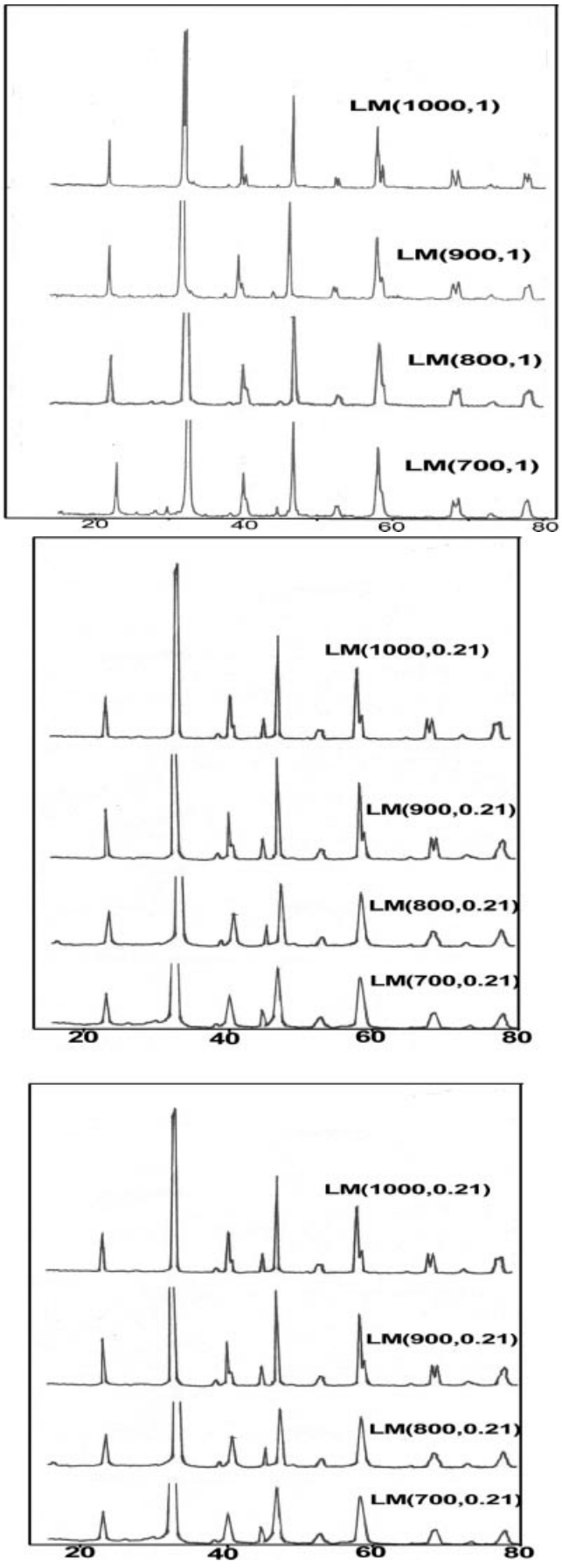

Figure 1. XRD diagrams of LM(*T*,*P*) samples

in the distortion of $Mn^{3+}O_6$ octahedrons and their co-operative ordering below a certain critical temperature. Despite the extensive literature on non-stoichiometric manganite perovskites, a detailed and systematic investigation over a wide range of y values to delineate the stability region of the homogeneous phase in the $LaMnO_{3+y}$ system is still lacking. As well as the non-stoichiometric $LaMnO_{3+y}$ family, Mn^{4+} ions can also be introduced into compounds of general formula $La_{1-x}C_xMnO_{3+y}$ by substitution of La^{3+} by a divalent ion (C = divalent cation, usually an alkaline earth). Such compounds have been extensively studied,[13−18] due to their potential for application as air electrodes in high-temperature solid oxide fuel cells. In the case of Sr-doped $LaMnO_3$, the range of concentration x is limited by the larger size of Sr^{2+} in relation to that of the La^{3+} ion. Given the importance of C content on the Mn^{3+}/Mn^{4+} ratio and therefore on the defect structure, it seems appropriate to consider the related system $La_{1-x}Ca_xMnO_{3\pm y}$ and to acquire knowledge of its defect structure over the whole range of concentrations ($0 \leq x \leq 1$).

The objectives of this study are:

(i) to prepare, by a simple and reproducible route, $LaMnO_{3+y}$ and $La_{1-x}Ca_xMnO_{3\pm y}$ compounds over a wide range of y and x values,

(ii) to determine their phase stabilities and oxygen non-stoichiometries,

(iii) to determine the best model for their defect chemistry,

(iiii) to study the effect of Mn^{4+} content on the frequency of Mn−O characteristic infrared absorption bands in undoped and in Ca-doped lanthanum manganites.

Results

1-LM(*T*,*P*) Oxides

The diffraction patterns of the LM(*T*,*P*) compounds were closely related to the patterns that would be expected of simple perovskite structures. Differences between the ideal

Table 1. Crystallographic parameters of LM(*T*,*P*) oxides

T [°C]	Symmetry	*a* [Å]	*b* [Å]	*c* [Å]	V_f [Å^3]	y
$P = 10^{-4}$ atm						
700	ortho. *Pbnm*	5.55(2)	5.63(2)	7.75(3)	60.55	0.09
800	ortho. *Pbnm*	5.54(2)	5.65(1)	7.78(3)	60.83	0.06
900	ortho. *Pbnm*	5.57(2)	5.69(1)	7.74(2)	61.33	0.03
1000	ortho. *Pbnm*	5.57(2)	5.72(1)	7.72(3)	61.50	0.02
$P = 0.21$ atm						
700	hex. $R\bar{3}c$	5.508(5)	−	13.39(3)	58.63	0.24
800	hex. $R\bar{3}c$	5.512(5)	−	13.38(3)	58.67	0.21
900	hex. $R\bar{3}c$	5.519(4)	−	13.35(2)	58.73	0.16
1000	hex. $R\bar{3}c$	5.525(3)	−	13.37(1)	58.92	0.14
$P = 1$ atm						
700	hex. $R\bar{3}c$	5.516(3)	−	13.33(1)	58.57	0.26
800	hex. $R\bar{3}c$	5.520(3)	−	13.32(1)	58.58	0.23
900	hex. $R\bar{3}c$	5.524(3)	−	13.33(1)	58.72	0.17
1000	hex. $R\bar{3}c$	5.528(5)	−	13.39(3)	59.07	0.16

 © 2003 Wiley-VCH Verlag GmbH & Co. KGaA, Weinheim

and observed patterns were the split reflections, implying distortions of the lattice from cubic symmetry (Figure 1). The XRD patterns of LM(T,0.21) and LM(T,1) oxides were refined in the space group $R\bar{3}c$, hexagonal description (Z = 6). Those of LM(T,10^{-4}) were refined in the *Pbnm* space group, orthorhombic description (Z = 4). The unit cell parameters determined after the refinement as well as the volume per unit formula (V_f) and oxygen contents (y) of the samples are listed in Table 1.

Mn−O distances were determined, taking those perovskites $LaNiO_3$[19] and $GdFeO_3$[20] exhibiting $R\bar{3}c$ and *Pbnm* space groups, respectively, as starting models. For $LaNiO_3$, La atoms are at 6a (0,0,$^1/_4$); Mn at 6b (0,0,0); and O at 18e (x,0,$^1/_4$) with $x \approx 0.547$. For $GdFeO_3$, La atoms are at 4c (x,y,$^1/_4$) with $x \approx 0.984$, $y \approx 0.063$; Mn at 4b (0,$^1/_2$,0); O1 at 4c with $x \approx 0.1005$, $y \approx 0.4672$ and O2 at 8d (x,y,z) with $x \approx 0.6957$, $y \approx 0.3016$, $z \approx 0.0506$.

Figure 2 shows the plot of unit formula volume (V_f) vs. y. A net decrease in the volume is observed as the oxygen content increases. This effect can be correlated with the increasing content of Mn^{4+} (= $2y$), which is smaller than Mn^{3+} [21] The presence of smaller cations in the B sublattice of the ABO_3 perovskite is responsible both for the reduction in unit cell volume and for the increase in the Goldschmidt tolerance factor[22] ($t = d_{A-O}/\sqrt{2}d_{B-O}$), hence the decrease of the rhombohedral distortion of the lattice. In contrast, for small y values (hence low Mn^{4+} concentrations), a more distorted structure is favoured, as observed for LM(T,10^{-4}) oxides, which show orthorhombic symmetry. In this case, the order of lattice parameters $c/\sqrt{2} < a < b$, characteristic of O′-perovskites,[3] is a consequence of the Jahn−Teller distortion of the oxide octahedron around the d^4 Mn^{3+} cation. A region of non-stoichiometry $0 < y < 0.15$ for $LaMnO_{3+y}$ was reported by Wold and Arnott,[23] with a change in symmetry (at room temperature) from orthorhombic to rhombohedral for an Mn^{4+} concentration greater than 21% ($LaMnO_{3.105}$), which closely agrees with our observation. The rhombohedral symmetry was observed even for the samples with the highest Mn^{4+} contents, as clearly shown by the characteristic splitting of the diffraction peaks (Figure 1). Moreover the rhombohedral angles of these samples are still considerably larger than 60° (which corresponds to cubic symmetry): α_r = 60.6°, for instance, for sample LM(700,1), with 52% Mn^{4+}. A sample of composition $LaMnO_{3.2}$ reported by Tofield and Scott[24] also showed a rhombohedral symmetry with an angle α_r = 60.3°.

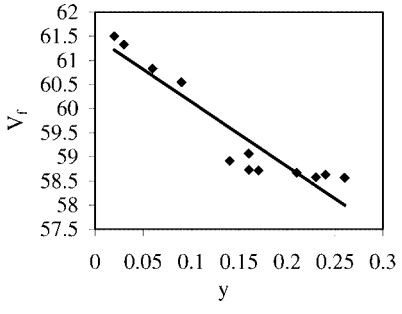

Figure 2. Variation of unit formula volume V_f with excess oxygen content y

To evaluate the nature of defects in LM(T,P) oxides, experimental density values were compared to those of five models of defect distribution in the lattice previously reported by Van Roosmalen et al.[25] For each of these models, the calculated density is defined by $d = M/N \cdot V_f$, where M is the molar mass of the formula unit, V_f is the formula unit volume, and N is the Avogadro constant. The variation of V_f as a function of y was derived from Figure 2. $V_f = (61.53 - 13.88 \cdot y)$ Å^3. The density calculated as a function of y for the five models, together with the experimentally determined densities obtained for LM(T,P) samples are reported in Table 2.

Table 2. Theoretical and experimentally determined density values [g·cm^{-3}] as a function of y

y	O_i[a]	V_{Mn}[b]	V_{La} and V_{Mn}[c]	V_{La}[d]	V_{La} and V_O[e]	ρ_{exp}
0.26	7.05	6.66	6.49	6.24	6.12	6.55(2)
0.24	7.01	6.65	6.49	6.26	6.08	6.54(2)
0.23	6.99	6.64	6.49	6.28	6.06	6.56(2)
0.21	6.94	6.64	6.49	6.30	6.02	6.54(2)
0.17	6.86	6.61	6.49	6.34	5.95	6.55(2)
0.16	6.84	6.60	6.49	6.35	5.93	6.55(2)
0.14	6.80	6.59	6.50	6.38	5.89	6.53(2)
0.09	6.70	6.57	6.50	6.43	5.80	6.53(2)
0.06	6.64	6.55	6.51	6.46	5.75	6.52(2)
0.03	6.58	6.54	6.52	6.49	5.70	6.53(2)
0.02	6.56	6.53	6.52	6.50	5.68	6.51(2)

[a] $LaMnO_3O_{i,y}$ (O interstitial). [b] $LaMn_{(3-2y/3)}O_3$ (Mn vacancies). [c] $La_{3/3+y}V_{La,y/3+y}Mn_{3/3+y}V_{Mn,y/3+y}O_3$ (La and Mn vacancies). [d] $La_{1-2y/3}V_{La,2y/3}MnO_3$ (La vacancies). [e] $La_{0.8}MnO_{2.7+y}$ (La and O vacancies).

From the agreement between the observed and calculated densities, it is obvious that an equal distribution of concentrations of Mn and La vacancies in cationic sub-lattices is the predominant defect model. The analysis results, which show an atomic ratio La/Mn = 1, are in good agreement with this proposed model.

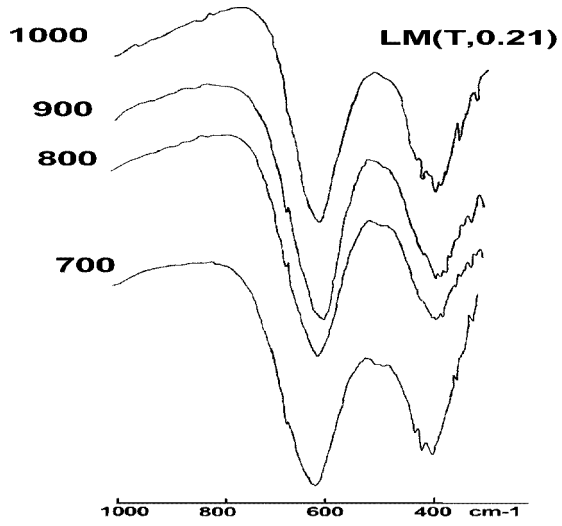

Figure 3. IR spectra of LM(T,0.21) samples

 © 2003 Wiley-VCH Verlag GmbH & Co. KGaA, Weinheim

Table 3. Higher frequency band as a function of y

y	0.24	0.21	0.16	0.14	0.09	0.06	0.03	0.02
ν_1 [cm^{-1}]	618	612	610	604	597	594	589	577
d_{MnO} [Å]	1.959	1.961	1.963	1.966	2.010[a]	2.012[a]	2.016[a]	2.018[a]
$r_{Mn_x}+ r_O$ [Å][b]	1.995	2.001	2.011	2.015	2.025	2.031	2.038	2.040
Δ [Å]	−0.036	−0.040	−0.048	−0.049	−0.015	−0.019	−0.022	−0.022

[a] Average value of three Mn−O distances due to Jahn−Teller deformation. [b] r_{Mn} is the Mn site radius defined by: $r_{Mn} = [3\cdot(1 - y)]/(3 + y)\cdot r_{Mn^{3+}} + 6y/(3 + y)\cdot r_{Mn^{4+}} + y/(3 + y)\cdot r_V$, where r_V is the radius of a vacancy, taken equal to 0.60 Å[24] and $r_{Mn^{3+}} = 0.65$ Å; $r_{Mn^{4+}} = 0.54$ Å.

All samples showed similar types of IR spectra. As an example, Figure 3 shows the IR spectra of LM(T,0.21) samples. Two absorption bands, at 800−550 and 450−300 cm^{-1}, were observed in each spectrum. The higher frequency band extends from about 800 to 500 cm^{-1}. Its absorption maximum decreases progressively with increasing y values (Table 3). The lower frequency band extends from about 475 cm^{-1} to the limit of the available experimental range at about 300 cm^{-1}, with a centre at 380 cm^{-1}.

IR spectra of ABO_3 perovskite oxides have been studied by several workers.[26−29] In general, the ABO_3 perovskites show two prominent bands in the 1000−300 cm^{-1} spectral region. The assignment of absorption bands by factor group analysis in these oxides has not been as successful as in fluorides[29−32]; in an ABO_3 perovskite of cubic symmetry there should be three sets of triply degenerate infrared-active modes of symmetry F_{1u} and one inactive mode of symmetry F_{2u}. This F_{2u} mode, however, can become active through distortion of the crystal lattice from the ideal cubic structure. The perturbation needs only be slight and would of course split the degeneracies in all modes. Fair success has been obtained by considering the internal modes of the BO_3 octahedron and the external ones of the A−(BO_3) groups. In the discussion of the vibration nature of the BO_3 group, it is considered to be arranged as central B atom octahedrally surrounded by six O half-atoms. Nakagawa et al.[30] therefore assigned the ν_1 mode to the B−O stretching normal vibration where the motion is primarily that of a change in the length of the B−O bond. Two modes − ν_2 and ν_4 − were assigned to the B−O bending normal vibration, where the motion is that of a change in the O−B−O bond angle. Both the relative magnitude and the sign of the displacements will depend on the bond-force constants and relative masses of the atoms. Moreover, the frequency of these bands has been related to the strength of the metal−oxygen covalency.[26] A fourth mode − ν_3 − was assigned to the A−(BO_3) vibration. The stretching vibration would be expected to occur at frequencies higher than the bending vibration, from comparison of the change in potential energy due to repulsive forces between ions in the two normal vibrations.

Infrared absorption bands in the vicinities of 600 and 400 cm^{-1} were observed for the various manganites investigated. The higher frequency band ν_1 was assigned to the Mn−O stretching normal vibration and the lower band ν_2 to the Mn−O bending vibration. Detailed analysis of distorted $LaMnO_{3+y}$ spectra showed additional bands, probably due to systematic distortion from ideal cubic symmetry to the orthorhombic structure for LM(T,10^{-4}) and to the rhombohedral structure for LM(T,0.21) and LM(T,1), which would split degenerate modes to give additional distinct frequencies. Spectra are given in Figure 4 to illustrate the importance of cell deformation for the number, shape, and position of IR bands.

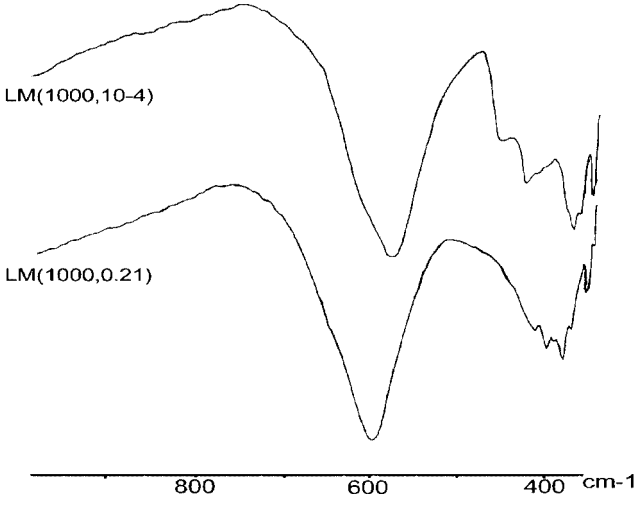

Figure 4. IR spectra of LM(1000,0.21) and LM(1000,10^{-4}) samples

Table 3 gives the vibrational frequencies of the M−O (ν_1) bond together with d_{Mn-O} distances as a function of non-stoichiometry y, which measures Mn^{4+} concentration in the MnO_3 sub-lattice. It can be seen that ν_1 decreases with decreasing y and increasing d_{Mn-O} distances.

2-LCMx(*T*,*P*) Oxides

All samples ($0 \leq x \leq 1$) were obtained after treatment under air at 700 °C. The diffraction patterns are given in Figure 5. X-ray powder diffraction patterns of all samples were completely indexed as the perovskite-type structure and showed the absence of simple oxides such as La_2O_3, Mn_2O_3, MnO_2, and CaO over the whole range of x values. The maximum incorporation rate seems to be influenced by the ionic radius of the substituted cation. Indeed, in the $LaMnO_3$ type of perovskite structure, the coordination number of La^{3+} ions is 12 with an ionic radius of 1.36 Å, and that of Ca^{2+} in the same site is 1.34 Å,[23] smaller than that of other alkaline metal ions such as Sr^{2+}. Thus, it is to

 © 2003 Wiley-VCH Verlag GmbH & Co. KGaA, Weinheim

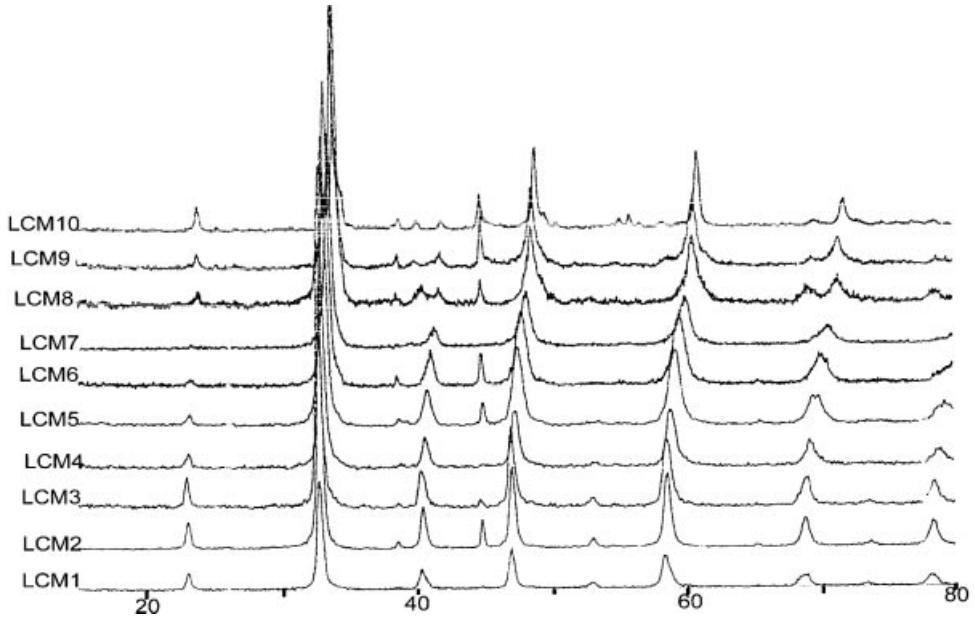

Figure 5. XRD diagrams of LCMx samples

Table 4. Crystallographic parameters of LCMx oxides

LCMx	Symmetry	a [Å]	b [Å]	c [Å]	V_f [Å^3]	Ca/Mn	O/Mn	Mn^{4+} (%)	d [g·cm^{-3}]
LCM1	hexag. $R\bar{3}c$	5.492(6)	–	13.34(6)	58.08	0.11(2)	3.19(2)	49	6.29
LCM2	hexag. $R\bar{3}c$	5.488(5)	–	13.27(5)	57.70	0.21(2)	3.14(2)	49	–
LCM3	hexag. $R\bar{3}c$	5.483(7)	–	13.28(7)	57.58	0.30(2)	3.10(2)	50	5.94
LCM4	hexag. $R\bar{3}c$	5.450(3)	–	13.43(5)	57.57	0.39(2)	3.06(2)	51	–
LCM5	ortho. *Pbnm*	5.36(4)	7.69(1)	5.46(1)	56.26	0.50(2)	3.05(2)	60	5.55
LCM6	ortho. *Pbnm*	5.36(2)	7.65(1)	5.40(2)	55.35	0.60(2)	3.03(2)	66	–
LCM7	ortho. *Pbnm*	5.33(2)	7.57(1)	5.37(2)	54.16	0.70(2)	3.00(2)	70	5.25
LCM8	ortho. *Pbnm*	5.36(6)	7.39(3)	5.40(5)	53.47	0.79(2)	2.99(2)	77	–
LCM9	ortho. *Pbnm*	5.31(3)	7.37(3)	5.39(4)	52.73	0.90(2)	2.97(2)	84	4.82
LCM10	ortho. *Pbnm*	5.34(3)	7.33(3)	5.30(3)	51.86	1.00(2)	2.96(2)	92	4.52

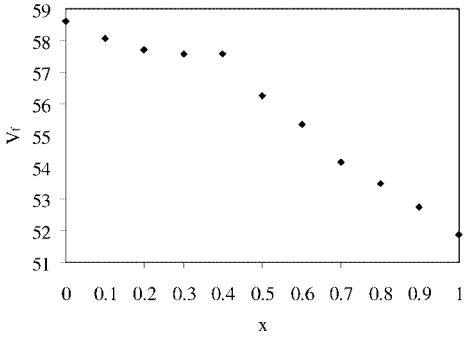

Figure 6. Variation of unit formula volume V_f with substitution level x

be expected that the limit of substitution of Ca^{2+} in $LaMnO_3$ should be much higher than that reported for Sr^{2+} ($x = 0.6$).

The influence of the calcium content on the perovskite-type structure is clearly shown by the evolution of the number and the profile of XRD peaks (Figure 5). For $0 \leq x < 0.5$, the XR diffraction diagrams are similar to those of LM(T,0.21) samples and so are indexed in the same space group (i.e., $R\bar{3}c$). For higher x values the splitting and broadening of XRD are indicative of lower symmetry. Therefore, for $0.5 \leq x \leq 1$, the diffraction patterns are indexed in space group *Pbnm*, orthorhombic description. The lattice parameter determined from XRD patterns of LCMx samples together with unit formula volume V_f, density, and atomic ratios are listed in Table 4.

Ca incorporation induces a cell contraction, as shown by the decrease in V_f when the substitution rate increases (Figure 6). Analysis results show that the atomic Ca/Mn ratio is almost equal to the theoretical value x while the O/Mn ratio decreases from 3.19 (for $x = 0.1$) to 2.96 (for $x = 1$). As in the case of $LaMnO_{3+y}$, experimental densities were determined for (La,Ca)$MnO_{3\pm y}$ and listed in Table 4.

The experimentally ascertained density value for each sample was compared to those of the previously discussed five models of defect distribution in the lattice. Two models were retained to describe the defect chemistry in

 © 2003 Wiley-VCH Verlag GmbH & Co. KGaA, Weinheim

(La,Ca)$MnO_{3\pm y}$. The first, Mn and La vacancies in equal concentrations, described the observed results well for $x \leq 0.7$. The second, with anion vacancies, described experimental results well for $x > 0.7$. Theoretical and experimental values are reported in Figure 7.

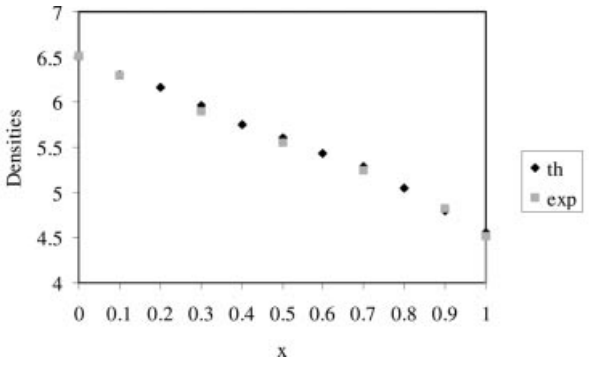

Figure 7. Theoretical (th) and experimentally determined (exp) densities of LCMx as a function of x

The oxygen non-stoichiometry y and the Mn^{4+} content are reported in Figure 8 as a function of Ca content x. The oxygen content y decreases with increasing x from $y = 0.24$ (for $x = 0$) to $y = -0.04$ (for $x = 1$). The Mn^{4+} concentration is constant for $0 \leq x \leq 0.4$ and increases almost linearly with increasing x for $0.5 \leq x \leq 1$.The maximum value, 0.92, for $x = 1$ shows that $CaMnO_{2.92}$ sample is in a reduced state. IR spectra of LCMx oxides (Figure 9) showed two absorption bands.

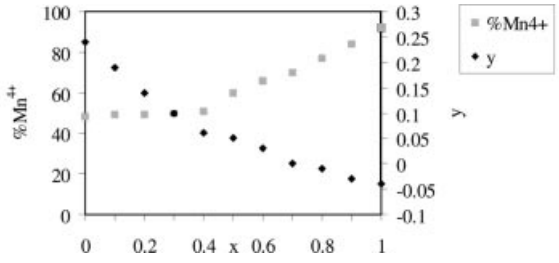

Figure 8. Variation of Mn^{4+} concentration and oxygen excess y with substitution level x in LCMx samples

The profiles of these bands changed with the substitution rate x. The higher frequency band, ν_1, was observed in the vicinity of 605 cm^{-1} for $x \leq 0.4$. For $0.5 \leq x \leq 1$, this band became asymmetric, with a high-frequency tail and extended from about 800 to 500 cm^{-1}. Its half-width increased from 90 to 180 cm^{-1}.The second band, of lower frequency, was initially centred at 380 cm^{-1} with shoulders at 392, 384, and 368 cm^{-1}. As x increased, this band broadened, shifted to somewhat higher frequencies and exhibited additional fine structure in the spectral range 350−520 cm^{-1}. For $x = 1$, the spectrum showed absorption bands in the 700−350 cm^{-1} region. In the spectral range of the ν_1 absorption mode, two bands were observed at 700 and 605 cm^{-1}. The lower frequency bands − at 514, 458, 421, 378, and 372 cm^{-1} − were in the spectral range of the ν_2 and

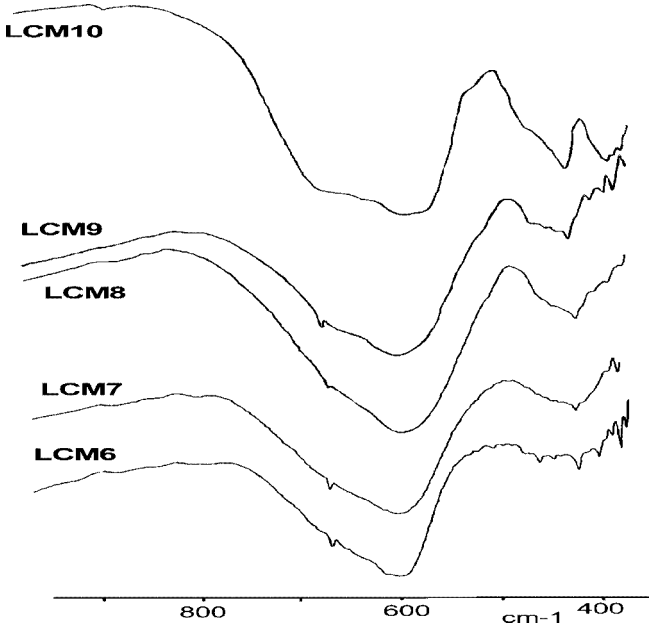

Figure 9. IR spectra of LCMx samples

ν_4 absorption modes of MnO_3 groups. Their splitting, in comparison to absorption bands in LCMx ($x \leq 0.4$) spectra, was indicative of an additional distortion of LCMx ($x \geq 0.5$) perovskite structures.

Discussion

$LaMnO_{3+y}$ oxides have been prepared as monophased perovskite structures from aqueous solutions of lanthanum nitrate $La(NO_3)_3{\cdot}6H_2O$ and manganese acetate $Mn(CH_3COO)_3$. The excess oxygen content y varied in a large range between 0.02 and 0.26. This was dependent of treatment, temperature and oxygen pressure. The y values thus decreased with increasing temperature and decreasing oxygen pressure. This tendency seemed to be confirmed under high oxygen pressures (200 atm) with a limiting y value of 0.31[33] Values comparable to $y = 0.26$ have been obtained by other preparation routes such as the sol-gel[34,35] and citrate methods[33] and calcination under an oxygen stream (1 atm).

XRD patterns showed a deviation from that of an ideal cubic structure. The splitting of peaks increased as the oxygen pressure of final treatment decreased. XRD patters were performed in the space group *Pbnm* ($Z = 4$), orthorhombic description for $y \leq 0.09$ ($[Mn^{4+}] \leq 18\%$), and in the space group $R\bar{3}c$ ($Z = 6$), rhombohedral description for $y \geq 0.14$ ($[Mn^{4+}] \geq 28\%$). The order, $c/\sqrt{2} < a < b$, of LM(T,10^{-4}) solids (orthorhombic structure), characteristic of O′-perovskites, is a consequence of the Jahn−Teller distortion of the oxide octahedron around the d^4 Mn^{3+} cation.[36] Long-range Jahn−Teller distortion is reduced when oxidation of some Mn^{3+} to Mn^{4+} occurs in $LaMnO_{3+y}$ with $y > 0.09$. There is a difference with the results ob-

 © 2003 Wiley-VCH Verlag GmbH & Co. KGaA, Weinheim

tained by Hervieu et al.[37] and Verelest et al.,[34] who observed the formation of a cubic phase for $LaMnO_{3.165}$ oxide ($[Mn^{4+}] = 33\%$). In our case we observe rhombohedral symmetry even for the samples with higher Mn^{4+} contents, as clearly shown by the characteristic splitting of the diffraction peaks. Such splitting could be masked by a lack of crystallinity in the samples.

From the quoted cell parameters, we find the volume per unit formula V_f to decrease with increasing oxidation from 61.50 Å^3 for $y = 0.02$ ($[Mn^{4+}] = 4\%$) to 58.92 Å^3 for $y = 0.26$ ($[Mn^{4+}] = 52\%$). This tendency is also observed when oxidation to Mn^{4+} is partially compensated by the substitution of La^{3+} cations by Ca^{2+} in $La_{1-x}Ca_xMnO_{3\pm y}$ (Figure 10). In this case, V_f decreases to 51.86 Å^3 for $x = 1$. There is a good agreement between our V_f values and those reported in the literature for different oxygen stoichiometries, such as $LaMnO_{3.12}$[24] and $LaMnO_{3.158}$,[25] which interpolate well in Figure 10.

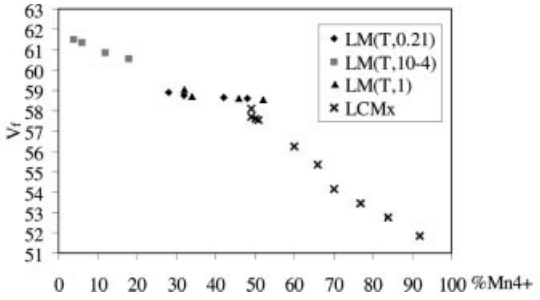

Figure 10. Variation of unit formula volume of LM and LCMx with Mn^{4+} content

The continuity in V_f vs. y variation between undoped and Ca-doped $LaMnO_3$ samples suggests that the symmetry of the manganite structure is largely determined by the concentration of Mn^{4+} ions. This is probably related to the mechanism of incorporation of the excess oxygen. The models involving vacancies either in cation or anion sublattices rather than oxygen interstitials were proposed as the predominant defects. This defect distribution in LM and LCMx solids, may be expressed by Kröger−Vink notations:[38]

LM samples:

$$LaMnO_3 + {}^{y}/_{2}\cdot O_2 \rightleftarrows LaV_{y/3}'''Mn_{1-2y}Mn_{2y}^{\circ}V_{y/3}'''O_{3+y};\quad [Mn^{4+}] = 2\cdot y$$

LCMx ($x \leq 0.7$) samples:

$$La_{1-x}Ca_x'Mn_{1-x}Mn_x^{\circ}O_3 + {}^{y}/_{2}\cdot O_2 \rightleftarrows La_{1-x}Ca_x'V_{y/3}'''Mn_{1-x-2y}Mn_{x+2y}^{\circ}V_{y/3}'''O_{3+y};\ [Mn^{4+}] = x + 2\cdot y$$

LCMx ($x \geq 0.7$) samples:

$$La_{1-x}Ca_x'Mn_{1-x}Mn_x^{\circ}O_3 \rightleftarrows La_{1-x}Ca_x'Mn_{1-x+2y}Mn_{x-2y}^{\circ}O_{3-y}V_y^{\circ\circ} + {}^{y}/_{2}\cdot O_2;\ [Mn^{4+}] = x - 2\cdot y$$

For LCMx samples, the Mn^{4+} content depends on the synthesis conditions as well as on the substitution level. As the temperature, oxygen pressure, and time of calcination were the same for all these samples, the $[Mn^{4+}]$ concentration plotted as a function of the Ca content should show a linear variation. This behaviour was observed for $x > 0.4$ (Figure 8). Fairly similar results for Sr-substituted manganite have been reported in the literature by many authors.[14−39] These authors showed that the concentration of Mn^{4+} was mostly determined by the substitution level of La^{3+} by Sr^{2+} rather than the synthesis conditions. For $0 \leq x \leq 0.4$, the Mn^{4+} content calculated from the substitution of lanthanum by calcium is different from that determined by chemical analysis, which indicated a deviation from the stoichiometry of lowly substituted LCMx compounds. Indeed, both the substitution level and the creation of cationic vacancies contribute to the determination of the Mn^{4+} concentration (see equations above). The results given in Figure 8 show that the ability to form over-stoichiometric compounds in air at 700 °C decreases with increasing calcium content and mostly disappears at $x = 0.7$. For $x > 0.7$, substoichiometric LCMx compounds were formed, their defect structures explained by the presence of anionic vacancies.

The structural modifications studied by XRD as a function of excess oxygen y and substitution level x were corroborated to IR investigations on the number and position of characteristic absorption bands. The observed band locations were explained in terms of an inverse relationship between atomic separation and vibrational frequency, and the band widths and splitting by the degree of degeneracy of the absorption mode and the resulting departure from cubic symmetry. $LaMnO_{3+y}$ ($y \geq 0.14$) and LCMx ($x \leq 0.4$) are rhombohedral, and the ν_1 band is narrower than this band in the orthorhombic materials [i.e., $LaMnO_{3+y}$ ($y \leq 0.09$) and LCMx ($x \geq 0.5$)].

The displacement of the ν_1 band to lower frequencies (Table 3) could be explained by consideration of the Mn−O bond order concept. Indeed, in the schematic energy level diagram of ABO_3 perovskites[40] the e_g electrons are in antibonding orbitals and so the bond order would decrease with an increase in the number of e_g electrons. This accounts for the observed decrease in the stretching frequency with increasing Mn^{3+} ($t_{2g}^3e_g^{*1}$) concentration (i.e. with decreasing y values). These results are in agreement with those reported for $LaBO_3$ oxides [B = Cr (d^3); Mn (d^4); Fe (d^5)] for which vibrational frequencies were in the order $\nu_{Cr-O} > \nu_{Mn-O} > \nu_{Fe-O}$.[41]

From the d_{Mn-O} values (Table 3) it can be seen that the increase in d_{Mn-O} together with the decrease in y induces a decrease in the vibrational frequency of the Mn−O bonds. This would be in agreement with a decrease in the bond force constant. Since the vibration ν_1 is primarily motion of oxygen ions, it is reasonable to expect that there should be little difference between Mn^{3+}−O and Mn^{4+}−O spectra. The Mn^{4+}−O frequency is slightly higher than that of Mn^{3+}−O because of the smaller lattice size and the fact that Mn^{4+} has a higher charge, thus increasing the Mn−O force constant. Moreover, the observed distances d_{Mn-O} were compared to the ionic radius sums $r_{Mn} + r_O$, where r_O is the ionic radius of the oxide ion (1.40 Å)[23] and r_{Mn} is the average ionic radius of the manganese site in the deficient structure [(c) in Table 1]. The differences between theoretical and observed distances (Δ) are included in

 © 2003 Wiley-VCH Verlag GmbH & Co. KGaA, Weinheim

Table 3. The negative Δ values probably reflect partial covalent bond character and this covalent character would be weaker for LM(T,10^{-4}) oxides.

The spectra of lowly substituted LCMx ($x \leq 0.4$) perovskites are similar to those of rhombohedral LM solids. The fair constancy of ν_1 band frequency in the vicinity of 605 cm^{-1} is in agreement with the constancy of the Mn^{3+}/Mn^{4+} ratio (Figure 8). These observations also show that a change in the cations in perovskite A sites from La, with a mass of 139, to Ca, with a mass of 40, has no effect on the internal stretching mode frequency of B−O bond. Consequently, it is reasonable that the spectral components associated with common structural elements, namely MnO_3 octahedra, of LM and LCMx with rhombohedral symmetry should be similar. However, the A−MnO_3 lattice vibration frequency, ν_3, which is beyond the range of the spectrometer, should necessarily be different. With increasing substitution level x, the deviation from ideal cubic symmetry increases together with the Mn^{4+} content in the Mn sub-lattice, resulting in a lattice shrinkage due to the smaller size of the tetravalent ion. Consequently, the degeneracy seems to be completely removed and the infrared absorption bands are split in some components.

Conclusion

$LaMnO_{3+y}$ and $La_{1-x}Ca_xMnO_{3\pm y}$ perovskites with wide ranges of y ($0.02 \leq y \leq 0.26$) and x values ($0 \leq x \leq 1$) have been obtained by thermal treatment of aqueous-decomposed precursors at different temperatures and under different oxygen pressures. The influence of oxygen excess content y and the substitution level x in lanthanum manganites over a wide range of concentrations on the Mn^{4+} content, the symmetry of the perovskite structure, the defect chemistry and the infrared absorption bands of the stretching and bending Mn−O bond has been studied. All samples showed a deviation from ideal cubic symmetry even for the highest Mn^{4+} contents. Their symmetries were described as rhombohedral for $LaMnO_{3+y}$ ($y \geq 0.14$) and $La_{1-x}Ca_xMnO_{3\pm y}$ ($x \leq 0.4$) and orthorhombic for $LaMnO_{3+y}$ ($y \leq 0.09$) and $La_{1-x}Ca_xMnO_{3\pm y}$ ($x \geq 0.5$). Through consideration of five limiting defect structure models, the situation with equal vacancies on both La and Mn sites was proposed for $LaMnO_{3+y}$ and $La_{1-x}Ca_xMnO_{3\pm y}$ ($x \leq 0.7$), while oxygen vacancies were favoured as the predominant defect in the oxygen deficient region [i.e. $La_{1-x}Ca_xMnO_{3\pm y}$ ($x > 0.7$)]. The linear decrease in the volume per unit formula of the Ca-doped and undoped lanthanum manganites as well as the absorption frequencies and profiles of infrared bands characteristic of Mn−O bond were correlated with the change in Mn^{4+} content.

The next question to be solved with these compounds is to evaluate the change in surface composition and its behaviour toward probe molecule adsorptions and catalytic activity in combustion reactions.

Experimental Section

$LaMnO_{3+y}$ and $La_{1-x}Ca_xMnO_{3\pm y}$ samples, with x ranging from 0.00 to 1.00, were prepared in polycrystalline form from aqueous solutions of lanthanum nitrate, manganese acetate (for $LaMnO_{3+y}$) and calcium nitrate (for $La_{1-x}Ca_xMnO_{3\pm y}$). The obtained solution, with La/Mn and La+Ca/Mn atomic ratios equal to 1, was stirred constantly for2 h. Upon removal of the excess solvent by heating at 70 °C in vacuo (17 Torr), a gel containing the metal in solid solution was formed. The gel was dried at 110 °C for 24 h and was then decomposed at 450 °C in air. This treatment enabled total elimination of organic and nitrate materials. The resulting black powder was heated at different temperatures ranging from 700 to 1000 °C and at three different partial oxygen pressures for $LaMnO_{3+y}$ and in air (P_{O_2} = 0.21 atm) at 700 °C for (La,Ca)$MnO_{3\pm y}$. Each solid was maintained at the desired temperature for 24 h. The sample was then rapidly cooled to room temperature.

Throughout this article, the formal notations of LM(T,P) and LCMx, respectively, are used. LM(T,P) corresponds to $LaMnO_{3+y}$ obtained at a temperature T (700, 800, 900, or 1000 °C) and oxygen pressure (10^{-4}, 0.21, or 1 atm) and LCMx corresponds to $La_{1-x}Ca_xMnO_{3\pm y}$ obtained at T = 700 °C and P = 0.21 atm.

X-ray powder diffraction (XRD) patterns were obtained with Cu-K_α radiation in a Kigaku goniometer. For unit cell determinations, the patterns were collected by step-scanning from 10 to 80° in 2θ, in increments of 0.05° and a counting of 4 s each step. Lattice constants were refined by the least-squares method with the aid of the SILEX program.

Infrared spectra were recorded with a Perkin−Elmer FT-IR Paragon 1000PC in the 2000−300 cm^{-1} spectral range. The substance (ca. 0.3 wt%) was mixed thoroughly with dry KBr and pressed into discs of 0.5 mm thickness and 10 mm in diameter.

The lanthanum, manganese, and calcium contents in the solids were determined by atomic absorption spectroscopy. The concentrations of Mn^{3+} and Mn^{4+} ions were determined by redox titration.[42,43]

The densities of the samples were obtained by determining the volume of a known amount of powder in a pycnometer by use of bromobenzene. The experiments were performed in a climate room with a temperature of 19−20 °C. About 4−5 g of powder was used for each measure.

Acknowledgments

We would like to thank Professor A. Belhadj Amara, Faculté des Sciences de Bizerte, for helpful discussion and experimental support. We are deeply indebted to Dr. F. B. Amor, Faculté des Sciences de Tunis, for performing the refinements of XRD patterns.

[1] F. S. Galasso, *Structure, properties and preparation of perovskite-type compounds*, Pergamon, Oxford, **1969**.
[2] J. B. Goodenough, *Progress in solid state chemistry* (Ed.: H. Reiss), Pergamon, Oxford, **1971**, vol. 5.
[3] B. Goodenough, J. M. Longo, in: *Landolt-Bodenstein, Numerical Data and Functional Data in Science and Technology, New series* (Ed.: K. H. Hellwege), **1970**, vol. 4a, p. 131.
[4] N. Gunasekaran, J. J. Carberry, R. Doshi, C. B. Alcock, *J. Catal.* **1994**, *146*, 583.
[5] R. J. H. Voorhoeve, J. P. Remeika, L. E. Trimble, A. S. Cooper, F. J. Disalvo, P. K. Gallager, *J. Solid State Chem.* **1975**, *14*, 395.

 © 2003 Wiley-VCH Verlag GmbH & Co. KGaA, Weinheim

[6] J. G. McCarty, H. Wise, *Catal. Today* **1990**, *8*, 231.
[7] N. Yamazoe, Y. Teraoka, *Catal. Today* **1990**, *8*, 175.
[8] G. Kremnic, J. M. L. Nieto, J. M. D. Tascon, L. G. Tejuka, *J. Chem. Soc., Faraday Trans.* **1985**, *81*, 939.
[9] P. D. Petrolekas, I. S. Metcalfe, *J. Catal.* **1995**, *152*, 147.
[10] T. Nitadori, S. Kurihara, M. Misono, *J. Catal.* **1986**, *98*, 221.
[11] Y. Yao, *J. Catal.* **1975**, *36*, 266.
[12] R. J. H. Voorhoeve, *Adv. Mat. Catal.* **1977**, 129.
[13] H. Taguchi, M. Shimada, *J. Solid State Chem.* **1987**, *67*, 37.
[14] M. Gaudon, C. Laberty, F. Ansart, P. Stevens, A. Rousset, *Solid State Sc.* **2002**, *4*, 125.
[15] J. W. Stevenson, M. M. Nasrallah, H. U. Anderson, D. M. Sparlin, *J. Solid State Chem.* **1993**, *102*, 175.
[16] J. H. Kuo, H. U. Anderson, D. M. Sparlin, *J. Solid State Chem.* **1989**, *83*, 52.
[17] K. Knizek, Z. Jirak, E. Pollert, F. Zounova, S. Sratislav, *J. Solid State Chem.* **1992**, *100*, 292.
[18] H. Taguchi, N. Nigao, M. Shimada, *J. Solid State Chem.* **1992**, *97*, 476.
[19] J. L. Garcia-Munoz, J. Rodriguez-Carvayal, P. Lacorre, J. B. Torrance, *Phys. Rev. B* **1992**, *46*, 4414.
[20] M. Marezio, J. P. Remeika, P. D. Dernier, *Acta Crystallogr., Sect. B* **1982**, *24*, 1986−38.
[21] R. D. Shannon, *Acta Crystallogr., Sect. A* **1976**, *32*, 751.
[22] V. M. Goldschmidt, *Skr. Norske Vidensk. Akad.* **1926a**, no. 2, **1926b**, no. 8.
[23] A. Wold, R. J. Arnott, *J. Phys. Chem. Solids* **1959**, *9*, 176.
[24] B. C. Tofield, W. R. Scott, *J. Solid State Chem.* **1974**, *10*, 183.
[25] J. A. M. Van Roosmalen, E. H. P. Cordfunke, *J. Solid State Chem.* **1994**, *110*, 106.
[26] G. V. Subba Rao, C. N. R. Rao, J. R. Ferraro, *Appl. Spectrosc.* **1970**, *24*, 436.
[27] J. T. Last, *Phys. Rev.* **1957**, *105*, 1740.
[28] G. Blasse, *J. Inorg. Nucl. Chem.* **1975**, *37*, 1347.
[29] S. D. Ross, *Inorganic Infrared and Raman Spectra*, Mc Graw-Hill, London, **1972**, p. 108.
[30] J. Nakagawa, A. Tsushida and Tshimanouchi, *J. Chem. Pys.* **1976**, *47*, 982.
[31] C. H. Perry, E. F. Young, *J. Appl. Phys.* **1967**, *38*, 4616.
[32] A. S. Barker, J. A. Ditzenberger, H. Guggenheim, *Phys. Rev.* **1968**, *175*, 1180.
[33] J. A. Alonso, M. J. Martinez-Lope, M. T. Casais, *Eur. J. Solid State Inorg. Chem.* **1996**, *33*, 331.
[34] M. Verelst, N. Rangavittal, C. N. Rao, A. Rousset, *J. Solid State Chem.* **1993**, *104*, 74.
[35] H. Tagichi, S. Matsu-ura, M. Nagao, T. Choso, K. Tabata, *J. Solid State Chem.* **1997**, *129*, 60.
[36] J. B. A. Elemans, B. Van Laar, K. R. Van Der Veen, B. O. Loostra, *J. Solid State Chem.* **1971**, *3*, 238.
[37] M. Hervieu, R. Mahesh, N. Ragavittal, C. N. R. Rao, *Eur. J. Solid Stae Chem.* **1995**, *32*, 79.
[38] F. A. Kröger, *The chemistry of imperfect crystals*, North Holland, Amsterdam, **1964**.
[39] A. Chakraborty, S. P. Devi, S. Roy, H. S. Maiti, *Mater. Lett.* **1994**, *20*, 63.
[40] J. B. Goodenough, *Les Oxydes des métaux de transition*, Gauthier-Villars Paris, Bruxelles, Lausannes, Montréal, **1973**, p. 253.
[41] P. Ganguly, N. Y. Vasanthacharya, *J. Solid State Chem.* **1986**, *61*, 164.
[42] Y. Takeda, S. Nakai, N. Imanishi, C. Q. Shen, O. Yamamoto, *Mat. Res. Bull.* **1991**, *26*, 153.
[43] K. S. Chan, J. Ma, S. Jaenicke, G. K. Chuah, J. L. Lee, *Appl. Catal. A* **1994**, *107*, 201.

Received January 14, 2003

 © 2003 Wiley-VCH Verlag GmbH & Co. KGaA, Weinheim

Physicochemical Characterization of P760, a New Macromolecular Contrast Agent with High Relaxivity[‡]

Luce Vander Elst,[a] Marc Port,[b] Isabelle Raynal,[b] Christian Simonot,[b] and Robert N. Muller*[a]

Keywords: Angiography / MRI contrast agents / NMRD / P760

P760-Gd, a hydrophilic derivative of DOTA-Gd with a molecular mass of 5.6 kDa, has been characterized in various media: aqueous solution, protein-containing solution, and Zn^{2+}-containing solution. Several investigations have been carried out, including the determination of the number of inner-sphere water molecules by laser-induced luminescence of the europium complex, water ^1H nuclear magnetic relaxation rates as a function of field strength, and ^{17}O relaxometry of water of the gadolinium complex, pulsed magnetic field gradient spin echo of proton, and ^2H transverse relaxation rates of the labeled lanthanum analogue. The large proton relaxivity of P760-Gd in water results from the long rotational correlation time of the hydrated complex ($\tau_R \approx 2$ ns at 310 K). As with DOTA-Gd, no significant Zn^{2+} transmetallation process was observed by proton relaxometry. Finally, analysis of the non-covalent binding of P760-Gd to serum proteins by proton relaxometry showed that P760-Gd does not interact with human serum albumin.
(© Wiley-VCH Verlag GmbH & Co. KGaA, 69451 Weinheim, Germany, 2003)

Introduction

Intensive research into the development of MR Blood Pool Agents (BPAs) has now been in progress for more than 10 years. Depending on their pharmacokinetic properties, these BPAs may be divided into three different classes: Low Diffusion Agents (LDAs), Rapid Clearance Blood Pool Agents (RCBPAs), and Slow Clearance Blood Pool Agents (SCBPAs).[1−3]

P760-Gd (Guerbet, Roissy − France) (Figure 1) is an original MR Contrast Agent belonging to the Low Diffusion Agent pharmacokinetic category. Indeed, because of its intermediate molecular size, P760-Gd can diffuse through the vascular endothelium, but at a much lower rate than a non-specific agent such as DOTA-Gd, whereas its renal excretion remains totally free.[1,3−5]

Very little concerning the physicochemical properties of this DOTA-Gd derivative has been reported. Its proton relaxivity at 20 MHz and 37 °C is quite large (24.7 s^{-1} mM^{-1}),[5] in good agreement with its large molecular size. In this work, an extensive in vitro physicochemical characterization of P760-Gd was performed. The number of inner-sphere water molecules q was evaluated by laser-induced luminescence of P760-Eu. The residence time τ_M of the coordinated water molecule was estimated by analysis of the temperature dependence of the water ^{17}O transverse relaxation of P760-Gd solution, whereas the rotational correlation time τ_R was calculated from the ^2H transverse relaxation rate of deuterated P760-La. The translational diffusion coefficient D, useful for calculation of the outer-sphere contribution to the relaxation rate and for the estimation of the molecular volume, was obtained by proton NMR on P760-La. The rate and magnitude of transmetallation by Zn^{2+} ions in aqueous phosphate solutions at pH = 7.0 was evaluated by proton relaxometry.

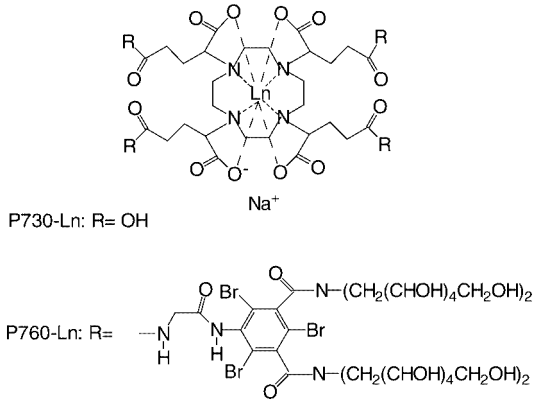

Figure 1. Chemical structures of P730 and P760

[‡] Part of this work has been presented at the 7th Meeting of the International Society of Magnetic Resonance in Medicine, Glasgow, UK, **2001**.

[a] NMR Laboratory, Department of Organic Chemistry, University of Mons-Hainaut,
7000 Mons, Belgium
Fax: (internat.) + 32/65373520
E-mail: robert.muller@umh.ac.be
[b] Research Department, Guerbet,
B. P. 50400, 95943 Roissy CdG, France

Finally, the proton T_1 Nuclear Magnetic Relaxation Dispersion (NMRD) curve of P760-Gd in water and its longitudinal proton relaxation rate in a 4% HSA solution were analyzed. In view of the clinical context of this kind of study, most of the data are reported at 310 K, physiological body temperature.

Results and Discussion

q Determination

Horrocks and Sudnick have shown that the differences in the decay rates of Eu^{3+} or Tb^{3+} luminescence in H_2O ($1/\tau_{H_2O(ms)}$) and D_2O ($1/\tau_{D_2O(ms)}$) solutions are related to the number of water molecules in the first coordination sphere [Equation (1)].[6] Recently, Beeby et al.[7] have refined the method, by consideration of the contributions from water molecules diffusing close to the Ln^{3+} complex and of other protons, exchangeable oscillators [Equation (2)]. The measured luminescence lifetimes of P760-Eu in H_2O and D_2O were 0.63 ms and 2.32 ms, respectively. The corresponding calculated *q* values are 1.16 by use of Horrock's equation or 1.03 according to Beeby et al., in good agreement with the expected value of 1.

$$q = 1.05\left(\frac{1}{\tau_{H_2O}} - \frac{1}{\tau_{D_2O}}\right) \quad (1)$$

$$q_{corr} = 1.2\left(\frac{1}{\tau_{H_2O}} - \frac{1}{\tau_{D_2O}} - 0.25\right) \quad (2)$$

τ_R Determination

The ^2H relaxation rates of diamagnetic compounds are predominantly functions of the interaction between the quadrupolar moment (Q) and the electric field gradient at the nucleus (q), and hence depend on the rotational correlation time τ_R. For small molecules, the extreme narrowing condition ($\omega_I^2\tau_R^2 << 1$) is fulfilled and R_1 and R_2 are equal. For larger molecules characterized by larger values of τ_R, $\omega_I^2\tau_R^2 \geq 1$ and consequently, $R_2 >> R_1$. At the magnetic field used for the ^2H NMR measurements (B_0 = 7.05 T), this situation occurs when $\tau_R \geq 1$ ns. At 310 K, the spectrum of the monodeuterated P760-La analogue shows a broad resonance ($\Delta\nu_{1/2}$ = 218 Hz) arising from the slowly rotating deuterium nuclei. The linewidth can thus be used to measure R_2 ($R_2 = \pi\,\Delta\nu_{1/2}$) and its dependence on the temperature. Values of τ_R calculated from R_2 by use of Equation (3) and a quadrupolar coupling constant e^2qQ/h equal to 170 kHz are 2.2 ns at 310 K and 3.3 ns at 298 K. In Equation (3), I is the nuclear spin and η is the asymmetry parameter of the field gradient. This latter parameter is negligible for deuterium nuclei involved in carbon−deuterium bonds.[8]

$$\frac{1}{T_2} = \frac{3}{400}\frac{2I+3}{I^2(2I-1)}\left(1+\frac{\eta^2}{3}\right)\left(\frac{e^2Qq}{\hbar}\right)^2\left[3\tau_R + \frac{5\tau_R}{1+\omega_I{}^2\tau_R{}^2} + \frac{2\tau_R}{1+4\omega_I{}^2\tau_R{}^2}\right] \quad (3)$$

A rough estimation of the τ_R value of P760-Gd has been made on the basis of the τ_R value of DOTA-Gd at 310 K (τ_R = 59 ps)[9] and the two molecular volumes [V^m(DOTA-Gd) = 0.38 nm^3 and V^m(P760-Gd) = 11.5 nm^3 obtained from photon correlation spectroscopy data[5]] from the relationship: $\tau_R^{P760\text{-}Gd} = \tau_R^{DOTA\text{-}Gd}$. V^m(P760-Gd)/V^m(DOTA-Gd) derived from the Stokes−Einstein equation [see Equation (4)] and by the assumption that the microviscosity factor f_R can be set to 1 either for DOTA-Gd or for P760-Gd. Such an estimation gives a value of 1.79 ns for P760-Gd, for a viscosity (η) of 0.69 mPa·s corresponding to a 1 mM solution.

$$\tau_R = \frac{\eta f_R V_m}{kT} \quad (4)$$

As the actual viscosity of the deuterated P760-La solution (28 mM) is equal to 1.32 mPa·s at 310 K, this value can be corrected by the viscosity factor, giving a τ_R value of 3.4 ns.

These calculations are somewhere imprecise, because the above molecular volumes calculated from the diffusion constant by the Stokes−Einstein−Debye model did not take the microviscosity factor (f_T) for the translational diffusion[10] into account [Equations (5) and (6), where r and r_s are the radius of the solute and solvent molecules, respectively]. If the microviscosity factors are included in the calculations, the calculated molecular volumes of DOTA-Gd and P760-Gd are 0.78 nm^3 and 14.4 nm^3, respectively

$$D = \frac{kT}{6\pi\eta f_T r} \quad (5)$$

$$f_T{}^{-1} = \frac{3r_s}{2r} + \frac{1}{\left(1+\frac{r_s}{r}\right)} \quad (6)$$

$$f_R{}^{-1} = 6\frac{r_s}{r} + \frac{1}{\left(1+\frac{r_s}{r}\right)^3} \quad (7)$$

By including the microviscosity factor for the rotational correlation time f_R [≈ 0.4 for DOTA-Gd and ≈ 0.68 for P760-Gd calculated by Equation (7)[10]], the estimated τ_R^{310} of P760-Gd by Equations (4) and (7) are 2 ns for a viscosity of 0.69 mPa·s (corresponding to a 1 mM solution) and 3.9 ns for a viscosity of 1.32 mPa·s (corresponding to a 28 mM solution), a value somewhat larger than that obtained from deuterium relaxation measurement. The activation energy for the rotation (E_R) was derived from the temperature dependence [Equation (8)] and was found to be equal to 32.3 kJ/mol, a value larger than those already reported for smaller complexes (Figure 2).[11−13]

 © 2003 Wiley-VCH Verlag GmbH & Co. KGaA, Weinheim

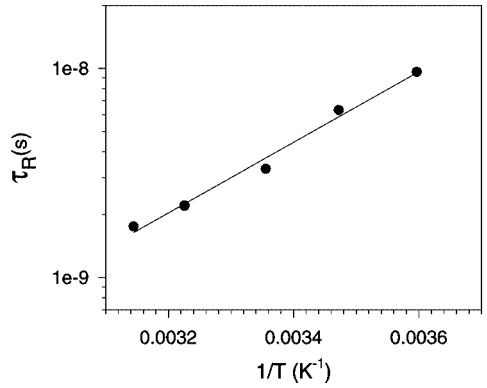

Figure 2. Temperature dependence of τ_R values obtained by deuterium NMR

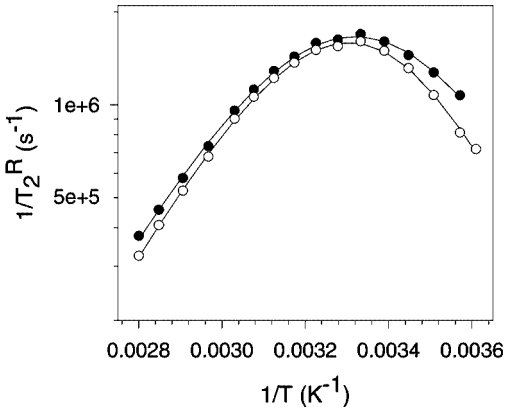

Figure 3. ^{17}O reduced transverse relaxation rate of water in P760-Gd solution (concentration: 19 mM) versus the reciprocal of the temperature; the closed circles correspond to the reduced relaxation rate calculated with the diamagnetic contribution of water, and the open circles correspond to the reduced relaxation rate calculated with the diamagnetic relaxation rate of a solution of P760-La

$$\tau_R = \tau_R^{298}\, exp\left(\frac{E_R}{R}\left(\frac{1}{T} - \frac{1}{298.15}\right)\right) \quad (8)$$

τ_M Determination

The rate of exchange of the water molecule in the first coordination sphere of Gd^{3+} can be determined by analysis of the temperature dependence of the paramagnetic transverse relaxation rate ($R_2 = 1/T_2$) of the ^{17}O NMR signal of water in the gadolinium complex solution.[11−13] The temperature dependence of ^{17}O R_2 from 288 to 357 K was studied.

Analysis of the experimental data may be performed by use of two different hypotheses concerning the diamagnetic contribution, and theoretical fittings were performed for both, with or without quadrupolar contribution, providing four different solutions (Table 1). In the first approach, the reduced relaxation rate $\{1/T_2^R = 55.55\cdot(T_2\cdot q\cdot[\text{P760-Gd}])^{-1}\}$ was calculated by assuming that the diamagnetic contribution was that of pure water (closed circles, Figure 3). The fitting of the experimental data was then performed either with a model in which the transverse relaxation rate of the bound nuclei of ^{17}O ($1/T_2^M$) results mainly from scalar interaction with the gadolinium ion, as described in ref.[11] (2nd column of Table 1), or with a second model in which the quadrupolar contribution to $1/T_2^M$ was taken into account (3rd column of Table 1).

Both types of fittings allow for the determination of the following parameters:

(i) the hyperfine coupling constant between the oxygen-17 nucleus and the electronic spin of Gd^{3+} ($A/\hbar$),

(ii) the parameters related to the electronic relaxation times τ_{S1} and τ_{S2} (i.e., the correlation time for the modulation of the zero field splitting τ_V), the activation energy E_V for this process, and B which depends on the trace of the square of the zero field splitting tensor (Δ^2) and on the electron spin S $\{B = \Delta^2[4S(S + 1) - 3]/25\}$,

(iii) the parameters of the water exchange rate [i.e., the enthalpy ($\Delta H^{\neq}$) and the entropy ($\Delta S^{\neq}$) of activation],

(iv) when the quadrupolar contribution is taken into account, additional parameters describing this contribution are included [see Equation (3)]: the rotational correlation time τ_R and the activation energy for the rotation, which were fixed to the value estimated from the data obtained by ^{2}H NMR ($\tau_R^{298} = 3$ ns, $E_R = 32.3$ kJ/mol), as well as a term related to the quadrupolar coupling constant and the asymmetry parameter of ^{17}O set to the value of water $[(1 + \eta^2/3)^{1/2}(e^2qQ/h) = 7.58$ MHz].[13]

Table 1. Parameters obtained by the fittings of the ^{17}O NMR spectroscopic data

	Without quadrupolar contribution and with water diamagnetic contribution	With quadrupolar contribution and water diamagnetic contribution	Without quadrupolar contribution and with P760-La diamagnetic contribution	With quadrupolar contribution and P760-La diamagnetic contribution[a]
τ_V^{298} [ps]	7.5±1.0	7.7±0.4	0.7±1.6	10.1±0.4 (18.2±1.6)
B [10^{20} s^{-2}]	0.77±0.06	0.84±0.04	0.69±0.10	1.02±0.08 (1.26±0.20)
E_v [kJ/mol]	5.6±12.8	5.2±4.4	12.6±7.7	11.2±5.6 (11.9±7.5)
$A/\hbar$ [10^6 rad s^{-1}]	−2.91±0.12	−2.91±0.10	−2.50±1.3	−2.82±0.02 (−2.50±0.02)
$\Delta H^{\neq}$ [kJ/mol]	42.9±0.26	43.4±0.06	44.8±0.32	47.8±0.12 (45.4±0.88)
$\Delta S^{\neq}$ [J/mol·K]	27.2±0.74	28.9±0.27	30.9±0.48	41.6±0.34 (33.1±3.42)
τ_M^{310} [ns]	101±19	98±6	137±25	118±10 (133±59)

[a] Two sets of fitted parameters giving similarly good fits are reported.

 © 2003 Wiley-VCH Verlag GmbH & Co. KGaA, Weinheim

In the second approach, the change in viscosity and the possible contribution of the oxygen atoms of water molecules interacting with the hydrophilic arms of P760-Gd were included in the diamagnetic contribution by measurement of the oxygen-17 transverse relaxation rate of water in a 19 mM solution of P760-La. From these data, a second set of reduced relaxation rates $1/T_2^R$ was obtained (open circles, Figure 3). On comparing the two $1/T_2^R$ sets, we observed a decrease in the reduced transverse relaxation rate over the whole temperature range, with a more pronounced effect at low temperature (Figure 3) when the P760-La diamagnetic contribution was taken into account. The fitting parameters with P760-La diamagnetic contribution, with or without quadrupolar contribution, are listed in Table 1 (4th and 5th columns). With the first approach, the results of the fitting show that the water residence time is short (about 100 ns at 310 K) and close to that reported for the parent compound DOTA-Gd at the same temperature.[13] The use of the appropriate diamagnetic contribution (2nd approach) gives slightly larger values of τ_M (average value of 128 ns).

It should be pointed out that the fitted values of the hyperfine coupling constant τ_V and B are interrelated and that similarly good fits can be obtained with two different sets of parameters, as shown in the last column of Table 1.

Determination of the Self-Diffusion Coefficient (D) by ^{1}H NMR

The aim of the measurement of D was twofold. Firstly, it is useful for estimation of the molecular radius [see Equation (5)], and secondly, the value of the relative diffusion coefficient ($D_{water} + D_{complex}$) is one of the parameters describing the outer-sphere contribution to the relaxation rate. The measurements were performed at four temperatures (293, 298, 303, and 310 K) and 4.7 T by the gradient spin echo method with selective saturation of the water resonance on a 3.3 mM P760-La solution in water; D was calculated from the variation in the intensity of the resonance at $\delta = 3.8$ ppm as a function of the applied gradient. To avoid interference between the signal arising from residual water, the intensities were measured with gradient strengths larger than 170 Gauss/cm. The obtained values are shown in Table 2. The value obtained at 293 K is in good agreement with the previously reported value of 1.5 10^{-10} m^2s^{-1} obtained by photon correlation spectroscopy.[5] Consequently, the radius calculated from the Debye−Stokes theory [Equation (5)] with f_T equal to 1 is 1.53 nm, a value slightly larger than that obtained by PCS ($r = 1.4$ nm). Refinement of the calculation by use of the translational microviscosity theory gives a value of 1.64 nm [Equation (6)]. This value corresponds to a τ_R^{310} of 2.1 ns ($\eta = 0.69$ mPa·s), consistent with the previous value of 2 ns found by deuterium transverse relaxation rates experiments.

Table 2. Diffusion coefficients measured on P760-La and water in a 3.3 mM solution at different temperatures

Temperature [K]	D of P760-La [10^{-10} m^2s^{-1}]	D of H_2O [10^{-10} m^2s^{-1}] in the P760-La solution
293	1.40	18.52
298	1.62	21.01
303	1.81	23.93
310	1.98	27.28

Transmetallation by Zn^{2+} Ions

Transmetallation of gadolinium complexes by Zn^{2+} ions induces a release of Gd^{3+} ions, which form insoluble phosphate complexes in the presence of phosphate ions; these released lanthanide ions no longer contribute to the proton paramagnetic relaxation rate of the solution. Subsequently, the water proton relaxation rate decreases during the transmetallation process and its evolution can be used to monitor the phenomenon quantitatively.[14] Under identical experimental conditions ($B_0 = 0.47$ T, $T = 310$ K, 2.5 mM of gadolinium complex, 2.5 mM of Zn^{2+} ions, and phosphate buffer pH = 7), no significant change in the paramagnetic relaxation rate was reported for the macrocyclic gadolinium complexes DOTA-Gd and HPDO3A-Gd {[10-(2-hydroxypropyl)-1,4,7-tris(methoxycarbonyl)-1,4,7,10-tetraazacyclododecane]gadolinium(III)} whereas R_1^p was about 57% of its initial value for DTPA-Gd and 22% for DTPA BMA-Gd after 1400 min, showing that significant transmetallation takes place for these open-chain gadolinium complexes. A similar experiment was performed with P760-Gd, but because of the large relaxivity of this complex at 20 MHz and to the limitations of the instrument, the concentrations of the gadolinium complex and of Zn^{2+} ions had to be reduced to 0.5 mM. As would be expected for a macrocyclic complex, the results show no significant evolution of the proton paramagnetic relaxation rate over a period of 1400 min and agree with the absence of transmetallation by Zn^{2+} ions (Figure 4).

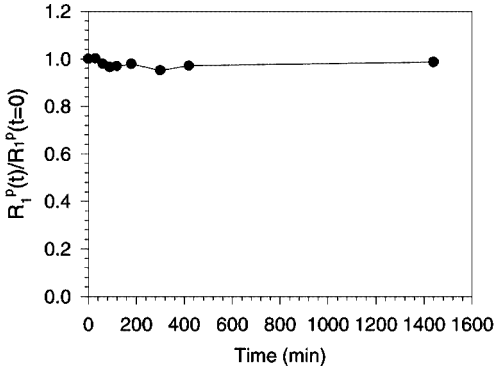

Figure 4. Evolution of the ratio $R_1^p(t)/R_1^p(t = 0)$ with time for a solution containing 0.5 mM of P760-Gd and $ZnCl_2$ at pH = 7.0 and 37 °C ($B_0 = 0.47$ T)

NMRD Fitting

The proton longitudinal relaxation rates were measured between 0.01 and 300 MHz on a 0.19 mM P760-Gd solution; the transverse relaxation rates were measured between 20 and 300 MHz. The calculated relaxivities (the relaxation rate enhancement afforded by 1 mmol/L of the gadolinium

 © 2003 Wiley-VCH Verlag GmbH & Co. KGaA, Weinheim

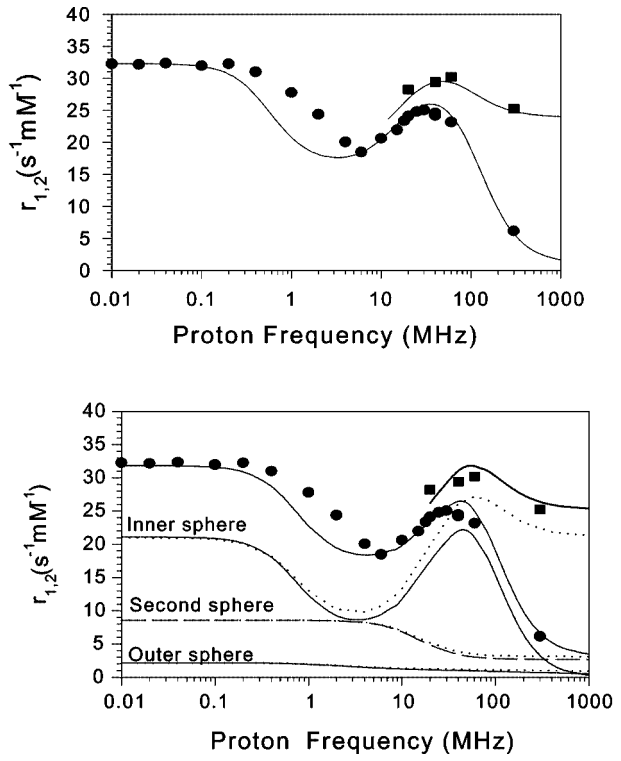

Figure 5. Proton NMRD data obtained at 310 K on a 0.19 mM solution (circles: r_1; squares: r_2; best fit); the top graph was obtained by use of the classical inner-sphere and outer-sphere theories with d = 0.36 nm, r = 0.31 nm, τ_{SO} = 740 ps, τ_V = 14 ps, τ_R = 1.8 ns, and τ_M = 320 ns; the bottom graph was obtained by use of the inner-sphere, outer-sphere, and second-sphere theory with d = 0.6 nm, r = 0.325 nm, τ_{SO} = 410 ps, τ_V = 13 ps, τ_R = 1.7 ns, τ_M = 170 ns, 25 water molecules in the second sphere at a distance of 0.4 nm and τ_{SS} = 15.6 ps

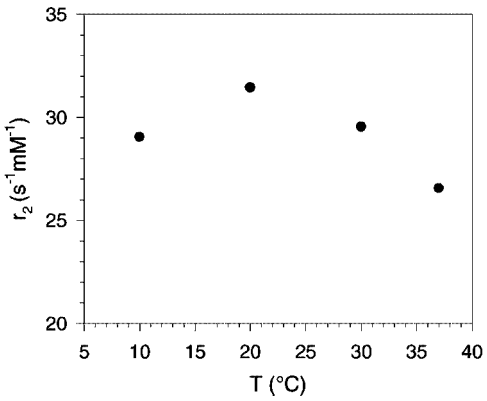

Figure 6. Proton transverse relaxivity of P760-Gd versus temperature at 7.05 T

complex) versus proton Larmor frequencies (proton NMRD curve) are shown on Figure 5.

In a first approach, ^{1}H NMRD curves were fitted according to the classical inner-sphere model described by Solomon[15] and Bloembergen[16] and to the outer-sphere model described by Freed.[17] In these fittings, q (the number of water molecules coordinated to the Gd^{3+} ion) was fixed to 1, r (the distance between the proton nuclei of the inner-sphere water molecule and the Gd^{3+}) was set to 0.31 nm, the relative diffusion constant D was set to the values obtained above by ^{1}H NMR spectroscopy (2.93 10^{-9} m^2s^{-1}), d (the distance of closest approach for the outer-sphere contribution) was set at 0.36 nm,[18,19] and the parameters describing the electronic relaxation times, τ_V and τ_{SO} (the electronic relaxation time at zero field), were optimized for the outer-sphere and the inner-sphere contributions simultaneously. Parameters τ_R and τ_M were allowed to fluctuate around the values obtained by ^{2}H and ^{17}O NMR spectroscopy. Satisfactory fits of the data could be obtained at low fields and at high fields with a τ_R value of 1.8 ns and a τ_M value of 320 ns (Figure 5, top graph). This latter value is significantly larger than that determined by ^{17}O NMR spectroscopy. The τ_{SO} and τ_V values are slightly larger than those reported for the parent compound DOTA-Gd (τ_{SO}^{310} = 480 ps and τ_V^{310} = 11 ps[13]). These discrepancies could be related to the fact that the simple model used to fit the ^{1}H NMRD curve is not appropriate to describe the behavior of slowly tumbling paramagnetic molecules[20] or to the presence of a second sphere of water molecules due to the hydrophilic nature of the P760-Gd complex. Such a second sphere, not included in this fitting of the proton NMRD data, can be taken into account (see below).

Data for r_2 were also obtained at 310 K and at magnetic fields ranging from 0.47 to 7.05 T (Figure 5). In addition, the temperature dependence of r_2 at 7.05 T was also studied (Figure 6). At this field, r_2 is predominantly determined by the inner-sphere interaction and so depends mainly on τ_R and τ_M [Equation (9)]. The data (Figure 6) suggest a situation of intermediate water exchange in the temperature range investigated with a limitation of r_2 by the water exchange.

$$r_2 \cong \frac{0.001}{55.55}\frac{1}{T_{2M} + \tau_M} \quad (9)$$

Values of (T_{2M} + τ_M) calculated from the experimental data [Equation (9)] range between 570 and 670 ns. Consequently, values of τ_M of the order of hundreds of nanoseconds and τ_R values greater than 1.3 ns would be expected. The theoretical fitting of r_2 NMRD data by the classical inner- and outer-sphere models[15–17] and the parameters obtained by the fitting of r_1 data agree very well with the experimental data.

In a second approach, the interactions between the gadolinium ion and water molecules in its second sphere were considered.[21] The hydrogen atoms of these water molecules are assumed to be at a distance of 0.4 nm, and the distance of closest approach was set to 0.6 nm because of the size of the complex. To obtain reasonable r_1 and r_2 fittings, the distance r had to be increased to 0.325 nm. With these settings, the experimental data could be fitted as shown in Figure 5 (bottom graph). The τ_R value (1.7 ns) is similar to that obtained above, but the value of τ_M (170 ns) is closer to that obtained by ^{17}O NMR spectroscopy. The τ_{SO} (410 ps) and τ_V (13 ps) values are similar to those reported for the parent compound DOTA-Gd. In this fitting, 25 water molecules

 © 2003 Wiley-VCH Verlag GmbH & Co. KGaA, Weinheim

are found in the second sphere and their interaction with the paramagnetic center is modulated by a correlation time (τ_{SS}) equal to 15.6 ps.

Interaction of P760-Gd with HSA and Blood Proteins

Proton relaxation measurements were performed at 20 MHz and at 37 °C on P760-Gd solutions (0.05−1.9 mM) in 4% non-defatted HSA. No significant change in the longitudinal proton relaxation rate was observed [R_1^p(water)/R_2^p(HSA, 4%) = 1.08 for a 1mM solution of P760-Gd], showing either that P760-Gd does not interact with HSA or that there is an interaction between P760-Gd and HSA but that the rotational correlation time of the paramagnetic center is not significantly modified by the binding. Similarly, longitudinal and transverse paramagnetic relaxation rates of 0.2 mM of P760-Gd in serum were only slightly increased (increase of 6% for R_1^p and 27% for R_2^p) at 310 K and 7.05 T, confirming the results discussed above.

Conclusion

The large longitudinal and transverse proton relaxivities ($r_1 \approx 25$ $s^{-1}mM^{-1}$ and $r_2 \approx 29.5$ $s^{-1}mM^{-1}$ at 310 K and 0.94 T) of P760-Gd are related to its large molecular weight (5.6 kDa), and consequently to its quite large rotational correlation time ($\tau_R \approx 2$ ns at 310 K). Like its parent complex DOTA-Gd, this original complex does not undergo transmetallation by zinc(II) ions and the residence time of its coordinated water molecule is of the order of a few hundred nanoseconds at 310 K. The r_1 relaxivity of P760-Gd is one of the highest reported in the literature for a gadolinium complex without any protein binding.[20] The proton relaxivity data clearly show that the expected benefits from the τ_R increase are not completely achieved because of the too slow water-exchange rate. For such types of complex, maximum r_1 and r_2 values of the order of 35 $s^{-1}mM^{-1}$ and 45 $s^{-1}mM^{-1}$, respectively, should be achievable at magnetic fields of 1.1−1.5 T, assuming a water residence time of about 20 ns.

Experimental Section

Chemical Synthesis

Synthesis of Ligand L (P730): Alkylation of cyclen with racemic dimethyl 2-bromoglutarate (K_2CO_3/CH_3CN/reflux) resulted in the formation of expected octamethyl ester. Base hydrolysis (6 M NaOH, 80 °C) afforded octacarboxylic acid ligand L (P730).[22]

Synthesis of L-Ln Complexes (Gd, Eu, La). P730-Ln: Lanthanide complexes were formed by heating of ligand L and Ln_2O_3 (Gd_2O_3, Eu_2O_3, La_2O_3) at pH = 5−6 in deionized water (80−100 °C, 1−24 h).

Synthesis of the Deuterated La Complex: Dry P730-La was heated at reflux in D_2O at pD = 3 (DCl) for 4 d. The solution was filtered and concentrated. After crystallization, the complex was isolated by filtration. Isotopic exchange assessed by mass spectrometry showed that the compound was monodeuterated on the α-carbon atom of the arm.

Synthesis of P760-Ln (Gd, Eu, La): A solution of L-Ln complex and polyhydroxylated aminotribromoisophthalic derivative R (4 equiv.) was mixed with 1-[3-(dimethylamino)propyl]-3-ethylcarbodiimide (EDCI). The reaction mixture was stirred at pH = 7 for 2 d (room temperature). The solution was ultrafiltered through a 3KDa membrane (FILTRON®). After removal of water by evaporation, the white solid was dried at reduced pressure.[5]

Chemicals: All commercial chemicals [$ZnCl_2$ (Merck) and Titrisol buffer pH 7.0 (Merck)] were used without further purification. Non-defatted human albumin (fraction V) was purchased from Sigma (Bornem, Belgium).

Viscosity: The viscosity of P760 Gd was measured with a Visco-Clock viscosimeter (SCHOTT − Germany) at 37 °C by the capillary standard procedure described in the European Pharmacopoeia, 3rd ed., **2001**, method number 2.2.9.

Luminescence Studies on the Eu Complexes: The Eu^{III} phosphorescence emission spectra were acquired with an LS-50B Perkin−Elmer spectrofluorimeter equipped with a pulsed Xenon lamp and a Hamamatsu R928 photomultiplier tube operating in time-resolved mode. Solutions of the Eu^{III} complex ($9.7\cdot10^{-3}$ M and $5.7\cdot10^{-3}$ M in H_2O and D_2O, respectively) were used in these experiments. Lifetimes (τ) were obtained by monitoring of the emission intensity at 616 nm resulting from pulsed excitation at 395 nm and 140 (H_2O) or 240 (D_2O) different delay times. Excitation and emission slit widths of 5 and 20 nm, respectively, were used and the gate time was 0.4 ms. The decays of the europium emitting state were fitted by use of an equation of the form $I(t) = I(0)\exp(-t/\tau)$, with the aid of a current software fitting procedure (Microsoft Excel®). High correlation coefficients were observed in each case (typically 0.9999). The number of water molecules (q) bound to the inner coordination sphere of the europium ion was quantified by use either of the relation proposed by Horrocks and Sudnick[6] [Equation (1)], in which τ is the lifetime (in ms) of the complex in H_2O and D_2O, or of the equation reported by Beeby et al.[7] [Equation (2)].

NMR: Proton Nuclear Magnetic Relaxation Dispersion (NMRD) profiles were recorded with a Field Cycling Relaxometer (Field Cycling Systems, Oradell, New Jersey, USA) working between 0.24 mT and 1.2 T on 0.6 mL solutions contained in 10 mm o.d. tubes. Proton relaxation rates were also measured at 0.235, 0.47, 0.94, and 1.5 T with Minispec PC-110, PC-120, PC-140, and mq-60 (Bruker, Karlsruhe, Germany). The additional relaxation rates at 7.05 T were obtained with a Bruker AMX 300 (Bruker, Karlsruhe, Germany) spectrometer. ^1H NMRD data were fitted according to the theoretical inner-sphere model described by Solomon[15] and Bloembergen[16] and to the outer-sphere contribution described by Freed.[17] Calculations were performed with previously described software.[23,24] Transmetallation by Zn^{II} ions was evaluated from the decrease in the water proton longitudinal relaxation rate at 310 K and 20 MHz (Bruker Minispec PC 120) of buffered solutions (pH = 7, phosphate buffer) containing 0.5 mM of the gadolinium complex and 0.5 mM of Zn^{II} according to the procedure described previously.[14] ^{17}O and ^2H NMR spectra were recorded on 2 mL samples (10 mm o.d. tubes) with a Bruker AMX 300 spectrometer (Bruker, Karlsruhe, Germany) with a broadband probe and a Bruker BVT 2000 unit for temperature control. ^{17}O transverse relaxation times of distilled water (pH = 6.5) were measured by use of a CPMG sequence and a subsequent two-parameter fit of the data points. The 90° and 180° pulse lengths were 25 μs and

 © 2003 Wiley-VCH Verlag GmbH & Co. KGaA, Weinheim

50 μs, respectively. The value for the ^{17}O T_2 of water in P760-Gd ([P760-Gd] = 19 mM, pH = 6.0−7.0) was obtained from linewidth measurement. All ^{17}O NMR spectra were proton-decoupled. The analyses of the ^{17}O data and of the transverse relaxation rates of deuterium were described elsewhere.[11] All T_1 measurements at 7.05 T (^1H, ^2H) were performed with the inversion recovery or fast inversion recovery Fourier transform technique and a subsequent three-parameter fit of the peak heights. Diffusion coefficients were measured with an Avance 200 spectrometer fitted with a thermostatted diffusion probe and the gradient spin echo sequence (25−30 gradient strengths ranging from 10 to 250 G/cm for water diffusion measurement or from 170 to 750 G/cm for P760-La diffusion measurement; gradient pulse duration: 1 ms, diffusion time: 6.05 ms, NA:1 for water or 8−32 for P760-La, TR: 8−10 s depending on the temperature). The sample (260 μL) was contained in a 5 mm o.d. tube. Thermostatting was guaranteed by the water flow inside the probe.

Acknowledgments

The authors thank Mrs. Patricia de Francisco for her help in preparing the manuscript and Mrs. Corinne Piérart for her help in recording the relaxometric data. This work was supported by the ARC Programs 95/00-194 and 00-05-258 of the French Community of Belgium, and the Fonds National de la Recherche Scientifique (FNRS) of Belgium.

[1] M. Port, D. Meyer, B. Bonnemain, C. Corot, M. Schaefer, O. Rousseaux, C. Simonot, Ph. Bourrinet, S. Benderbous, A. Dencausse, L. Devoldere, *Mag. Res. Mat. Phys. Biol. Med.* **1999**, *8*, 172−176.
[2] M. Port, C. Corot, O. Rousseaux, I. Raynal, L. Devoldere, J.-M. Idée, A. Dencausse, S. Le Greneur, C. Simonot, D. Meyer, *Mag. Res. Mat. Phys. Biol. Med.* **2001**, *12*, 121−127.
[3] F. Bourasset, A. Dencausse, Ph. Bourrinet, M. Ducret, C. Corot, *Mag. Res. Mat. in Phys. Biol. Med.* **2001**, *12*, 82−87.
[4] C. Corot, X. Violas, Ph. Robert, M. Port, *Invest. Radiol.* **2000**, *35*, 213−218.
[5] C. Corot, M. Port, I. Raynal, A. Dencausse, M. Schaefer, O. Rousseaux, C. Simonot, L. Devoldere, J. Lin, M. Foulon, Ph. Bourrinet, B. Bonnemain, D. Meyer, *J. Magn. Reson. Imag.* **2000**, *11*, 182−191.
[6] W. De W. Horrocks, Jr., D. R. Sudnick, *J. Am. Chem. Soc.* **1979**, *101*, 334−340.
[7] A. Beeby, I. M. Clarkson, R. S. Dickins, S. Faulkner, D. Parker, L. Boyle, A. S. de Sousa, J. A. G. Williams, M. Woods, *J. Chem. Soc., Perkin Trans. 2* **1999**, *2*, 493−503.
[8] H. H. Mantsch, H. Saito, I. C. P. Smith, *Prog. Nucl. Magn. Reson. Spectrosc.* **1977**, *11*, 211−272.
[9] L. Vander Elst, S. Laurent, R. N. Muller, *Invest. Radiol.* **1998**, *33*, 828−83.
[10] A. Gierer, K. Wirtz, *Z. Naturforsch., Teil A* **1953**, *8*, 532−38.
[11] L. Vander Elst, F. Maton, S. Laurent, F. Seghi, F. Chapelle, R. N. Muller, *Magn. Reson. Med.* **1997**, *38*, 604−614.
[12] K. Micskei, L. Helm, E. Brücher, A. E. Merbach, *Inorg. Chem.* **1993**, *32*, 3844−3850.
[13] D. H. Powell, O. M. Ni Dhubhghaill, D. Pubanz, L. Helm, Y. S. Lebedev, W. Schlaepfer, A. E. Merbach, *J. Am. Chem. Soc.* **1996**, *118*, 9333−9346.
[14] S. Laurent, L. Vander Elst, F. Copoix, R. N. Muller, *Invest. Radiol.* **2001**, *36*, 115−122.
[15] I. Solomon, *Phys. Rev.* **1955**, *99*, 559−565.
[16] N. Bloembergen, *J. Chem. Phys.* **1957**, *27*, 572−573.
[17] J. H. Freed, *J. Chem. Phys.* **1978**, *68*, 4034−4037.
[18] S. Aime, M. Botta, M. Fasano, S. Paoletti, P. L. Anelli, F. Uggeri, M. Virtuani, *Inorg. Chem.* **1994**, *33*, 4707−4711.
[19] F. Uggeri, S. Aime, P. L. Anelli, M. Botta, M. Brocchetta, C. de Haën, G. Ermondi, M. Grandi, P. Paoli, *Inorg. Chem.* **1995**, *34*, 633−642.
[20] I. Bertini, O. Galas, C. Luchinat, G. Parigi, *J. Magn. Reson. A* **1995**, *113*, 151−158.
[21] S. Aime, M. Botta, F. Fedeli, E. Gianolio, E. Terreno, P. Anelli, *Chem. Eur. J.* **2001**, *7*, 5262−5269.
[22] M. Woods, S. Aime, M. Botta, J. A. K. Howard, J. M. Moloney, M. Navet, D. Parker, M. Port, O. Rousseaux, *J. Am. Chem. Soc.* **2000**, *122*, 9781−9792.
[23] R. N. Muller, D. Declercq, P. Vallet, F. Giberto, B. Daminet, H. W. Fischer, F. Maton, Y. Van Haverbeke, in *Proc., ESMRMB, 7th Annual Congress, Strasbourg, France*, **1990**, p. 394.
[24] P. Vallet, Ph.D. Dissertation, Univ. of Mons-Hainaut, Belgium, **1992**.

Received January 18, 2003

 © 2003 Wiley-VCH Verlag GmbH & Co. KGaA, Weinheim

New Bis(mercaptoimidazolyl)(pyrazolyl)borate Ligands and Their Zinc Complex Chemistry

Mouhai Shu,[a] Rainer Walz,[a] Biao Wu,[a] Jan Seebacher,[a] and Heinrich Vahrenkamp*[a]

Keywords: Tripodal ligands / Zinc / Bioinorganic chemistry

Nine new tripodal NS_2 ligands of the bis(mercaptoimidazolyl)(pyrazolyl)borate type with varying 3-R-mercaptoimidazolyl moieties were prepared as their potassium salts. Treatment with zinc salts yielded the complex types L·Zn–Cl, L·Zn–I, L·Zn–ONO_2, L·Zn–$OClO_3$ and [L·Zn(imidazole)]ClO_4. Attempts at the formation of L·Zn–OH or cationic L·Zn complexes resulted in dismutation and formation of ZnL_2 complexes. Hydrolytic destruction yielded one [OZn_4(thiooimidazolate)$_6$] complex. The ZnS_2NO coordination which is present in the enzyme-substrate complex of alcohol dehydrogenase could be successfully modelled by an [L·Zn(C_2H_5OH)]$^+$ complex. The L·Zn–X complexes showed very low catalytic activity in the dehydrogenation of 2-propanol or the hydrogenation of *p*-nitrobenzaldehyde. The new compounds were identified by a total of 12 structure determinations.
(© Wiley-VCH Verlag GmbH & Co. KGaA, 69451 Weinheim, Germany, 2003)

Introduction

The importance of tris(pyrazolyl)borate ligands for coordination chemistry can only be compared with that of cyclopentadienyl ligands in organometallic chemistry. This holds specifically for the classical or bioinorganic coordination chemistry of zinc[1,2] to which we have made contributions.[3] The advantage of these tripodal ligands is that they quite reliably support an N_3ZnX coordination motif which has given them then name "tetrahedral enforcers" and which has made them so valuable for the bioinorganic chemistry of zinc.[3,4]

The N_3Zn motif represents the attachment of a zinc ion to three histidine residues in a protein. Considering that cysteine is equally important for zinc binding in enzymes, one would like to have sulfur-containing tripodal ligands with qualities similar to those of the pyrazolylborates for a model complex chemistry. The accumulated experience with tripodal ligands containing thiolate functions has shown, however, that these are not suitable because the bridging tendency of the thiolates cannot be suppressed. In this context Reglinski's discovery of the tris(mercaptoimidazolyl)-borates[5] must be considered a breakthrough. As shown since by Reglinski himself[6,7] and his competitors,[8,9] including ourselves,[10] these tripods are very good "tetrahedral enforcers" and allow a fruitful biomimetic zinc model complex chemistry. The reason for this is the fact that their sulfur donors are "tame" thiolates with a low bridging tendency due to their thiol-thione tautomerism as depicted below.

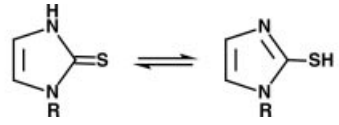

Having the easily accessible tris(pyrazolyl)- and tris(mercaptoimidazolyl)borates available as N_3 and S_3 donors, we decided to aim at their combination in the form of N_2S and NS_2 donors. Specifically, the NS_2 tripods should be valuable as they allow us to mimic the $(NS_2)ZnX$ coordination in alcohol dehydrogenase. With this in mind both the research group of Parkin and ourselves set out to study the chemistry of the bis(mercaptoimidazolyl)(pyrazolyl)borates. Parkin has published the synthesis of one such ligand and some basic metal complex chemistry of it.[11–13] We have communicated the first correct structural model of the enzyme-substrate complex of alcohol dehydrogenase in the form of a $(NS_2)Zn(C_2H_5OH)$ complex.[14]

This paper summarises our recent work on bis(mercaptoimidazolyl)(pyrazolyl)borate ligands, their basic zinc complex chemistry and attempts to apply them for the modelling of the zinc enzyme alcohol dehydrogenase. Nine new ligands **L** were prepared and their zinc complexes identified by a total of twelve structure determinations.

[a] Institut für Anorganische und Analytische Chemie der Universität Freiburg
Albertstr. 21, 79104 Freiburg, Germany
Fax: (internat.) + 49-761/203-6001
E-mail: vahrenka@uni-freiburg.de

 © 2003 Wiley-VCH Verlag GmbH & Co. KGaA, Weinheim **DOI: 10.1002/ejic.200300079**

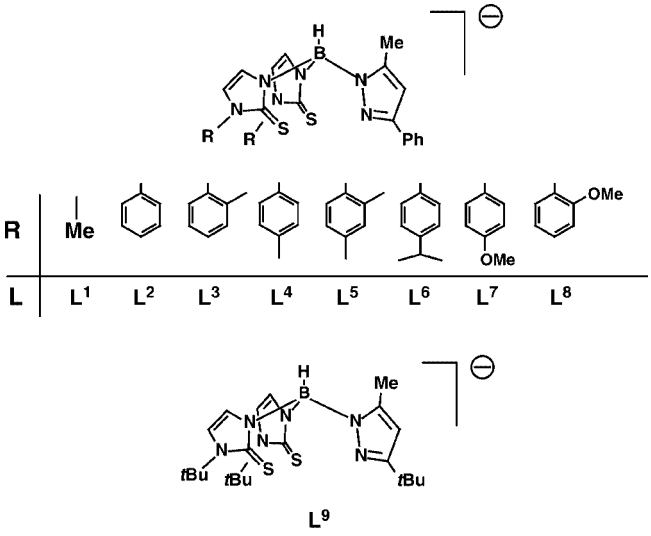

Results and Discussion

Ligand Synthesis

From our work with tris(pyrazolyl)borates we have the experience that their biomimetic zinc complex chemistry requires a good encapsulation of the metal ion. This is achieved by bulky substituents at the 3-positions of the pyrazole rings. We applied this for the new NS_2 ligands **L** by incorporating 5-methyl-3-phenylpyrazole units in $\mathbf{L^1}$ to $\mathbf{L^8}$ and 3-*tert*-butyl-5-methylpyrazole in $\mathbf{L^9}$. Likewise, the thioimidazole units were made bulky with substituents at the outer nitrogen atoms, mostly with aromatic groups ($\mathbf{L^2}$ to $\mathbf{L^8}$), but also with methyl ($\mathbf{L^1}$) and *tert*-butyl ($\mathbf{L^9}$). Thus, all our NS_2 ligands are more bulky than the one with *N*-methylthioimidazole and unsubstituted pyrazole groups reported previously.[13]

The synthesis of the tripodal ligands **L** from KBH_4 and the nitrogen heterocycles is favoured by the fact that the thioimidazoles react more readily with KBH_4 than the pyrazoles. Thus, lower reaction temperatures are possible which ensures better yields and which allows us to run the preparations in a one-pot procedure. Mixtures of KBH_4, pyrazole and thioimidazole (1:1:2) were allowed to react in a melt at ca. 160 °C to form $\mathbf{L^1}$, $\mathbf{L^2}$, $\mathbf{L^5}$ and $\mathbf{L^9}$. Later it turned out that the preparations in boiling toluene gave better yields and cleaner products. Furthermore, a 10% excess of the pyrazole was found to improve the yield of ligand **L** considerably. Ligands $\mathbf{L^3}$, $\mathbf{L^4}$, $\mathbf{L^6}$, $\mathbf{L^7}$ and $\mathbf{L^8}$ were prepared this way. The isolated compounds K[**L**] are colourless powders which are somewhat air- and light-sensitive, sparingly soluble in aromatic hydrocarbons, and which decompose upon melting between 160 and 200 °C.

Simple Zinc Complexes

Like the tris(pyrazolyl)- and tris(mercaptoimidazolyl)-borates, the mixed ligands **L** easily form stable zinc halide complexes. This was applied for the products **1a**−**1f** by treating the corresponding ligands with the zinc halides.

$\mathbf{L^1}$•ZnCl	$\mathbf{L^2}$•ZnCl	$\mathbf{L^3}$•ZnCl
1a	**1b**	**1c**
$\mathbf{L^5}$•ZnCl	$\mathbf{L^6}$•ZnCl	$\mathbf{L^8}$•ZnCl
1d	**1e**	**1f**

The structures of **1c** and **1d** were determined, of which the one of **1c** is displayed here (Figure 1). There is very close agreement in terms of bond lengths and angles between **1c** and **1d**, and the coordination environment of the zinc ion also resembles that in the previously reported complex L·ZnI of a related NS_2 ligand.[11] The deviations from tetrahedral symmetry at the zinc ion are small. The largest bond angle is N−Zn−Cl, reflecting the steric hindrance between the phenyl substituent on the pyrazole and the Zn−Cl unit.

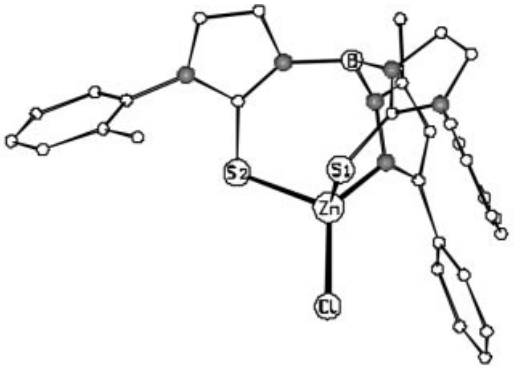

Figure 1. Molecular structure of complex **1c**; selected bond lengths [A] and angles [°]: Zn−Cl 2.201(1), Zn−S1 2.335(1), Zn−S2 2.329(1), Zn−N 2.041(2); Cl−Zn−S1 110.91(3), Cl−Zn−S2 109.11(3), Cl−Zn−N 120.09(6), S1−Zn−S2 107.60(3), S1−Zn−N 108.24(6), S2−Zn−N 99.82(6)

Other than the zinc halide and the zinc thiolate species,[15] the simple **L**·Zn complexes with anions of oxo acids turned out to be quite labile. Attempts to prepare acetates invariably led to the formation of ZnL_2 complexes (see below). The same was observed when trying to prepare nitrates. Only those ligands **L** with sterically demanding substituents, typically in the *ortho* positions of the aromatic rings, yielded nitrate complexes, of which **2a**−**2c** were isolated.

$\mathbf{L^3}$•$ZnONO_2$	$\mathbf{L^6}$•$ZnONO_2$	$\mathbf{L^8}$•$ZnONO_2$
2a	**2b**	**2c**

The structure determination of **2a** (Figure 2) proved the composition of the nitrate complexes and the semibidentate nature of the nitrate ligand. Again, the tetrahedral ligand environment is not seriously distorted, and again the N−Zn−O angle is unusually large due to steric hindrance. The semibidentate attachment of the nitrate coupled with its orientation with respect to the two sulfur donors makes the S1−Zn−O1 angle rather large and the S2−Zn−O1 angle rather small. In all these respects **2a** resembles the Zn−NO_3 complex of a related tris(mercaptoimidazolyl)borate ligand.[10]

 © 2003 Wiley-VCH Verlag GmbH & Co. KGaA, Weinheim

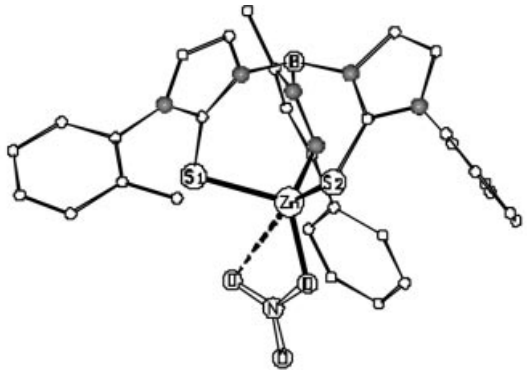

Figure 2. Molecular structure of complex **2a**; selected bond lengths [Å] and angles [°]: Zn−O1 1.965(5), Zn−O2 2.782(6), Zn−S1 2.307(2). Zn−S2 2.315(2), Zn−N 2.017(6); O1−Zn−S1 117.8(2), O1−Zn−S2 105.0(2), O1−Zn−N 115.3(2), S1−Zn−S2 108.6(1), S1−Zn−N 99.8(2), S2−Zn−N 110.2(2)

ZnL_2 Complexes

It has already been observed that the **L**·ZnX complexes of these NS_2 ligands are amenable to dismutation, with formation of the corresponding ZnL_2 complexes.[13] Our investigations were also plagued frequently by this tendency. Many attempts to prepare **L**·Zn complexes with hard coligands did not yield the desired **L**·ZnX species, but instead ZnL_2 and, presumably, ZnX_2. The reason for this is the highly preferred ZnS_4 coordination in the uncharged ZnL_2 molecules. In the following we describe those reactions that led to ZnL_2 species, even though we performed no designed (viz. trivial) synthesis of a ZnL_2 complex.

According to one of the goals of this work, namely the modelling of zinc enzymes, we intended to prepare $[L{\cdot}Zn{-}OH_2]^+$ or **L**·Zn−OH complexes. The most straightforward way to do this[3] is the reaction between a tripodal ligand **L** and hydrated zinc perchlorate, either directly or in combination with KOH. This was done here with L^1, L^5 and L^9. Although some evidence could be gathered for the formation of **L**·Zn−OH species (see below), they could not be isolated in a pure form, and the final products of the reactions were the ZnL_2 complexes **3a**, **3d** and **3f**. Also, as mentioned above, the **L**·Zn−OAc complexes were not stable enough to be isolated, and in the case of L^3 a clean dismutation yielded **3b**. Furthermore, the **L**·Zn−NO_3 complexes of those ligands **L** that are sterically less hindered, evaded their isolation by dismutation. In case of L^4 and L^7 this resulted in the isolation of pure **3c** and **3e**.

ZnL^1_2 **3a**	ZnL^3_2 **3b**	ZnL^4_2 **3c**
ZnL^5_2 **3d**	ZnL^7_2 **3e**	ZnL^9_2 **3f**

Structure determinations of **3a**, **3b**, **3c**, **3d** and **3f** revealed that in all cases the ligands **L** act as bidentate sulfur donors, i.e. the pyrazolyl arm of the tripod is uncoordinated. This corresponds to the observations made previously for similar ZnL_2 complexes[13] and for those derived from the tris(mercaptoimidazolyl)borates.[10] The molecular structures of **3a** and **3f** are shown as representative examples in Figures 3 and 4, respectively. In all complexes **3** the Zn−S bond lengths are in the range 2.33−2.40 Å, which is rather long but typical for this kind of ZnS_4 species.[10,13] The bond angles at the zinc ion show quite a range around the tetrahedral angle, the extremes being 89° in **3a** and 125° in **3c**.

Hydrolysis Products

During our attempts to prepare **L**·Zn−OH or $[L{\cdot}Zn]^+$ species by treating **L** with $Zn(ClO_4)_2$ it also became obvious that the (mercaptoimidazolyl)borates are not only more easily formed than the pyrazolylborates but also more easily hydrolysed. Thus, the acidic conditions brought about by dissolving hydrated zinc perchlorate in alcohols frequently led to the partial destruction of the ligands **L**, and free mercaptoimidazoles were found in the solutions. In three cases zinc complexes of the mercaptoimidazoles were the result of such hydrolytic cleavages.

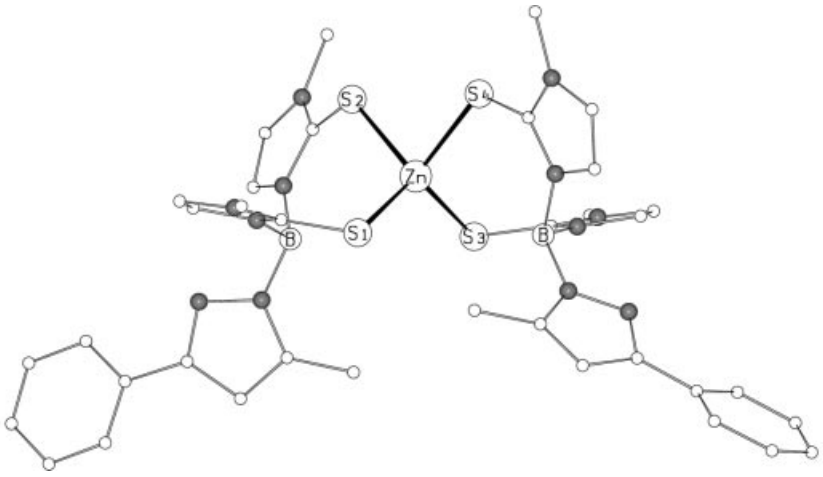

Figure 3. Molecular structure of **3a**; selected bond lengths [Å] and angles [°]: Zn−S1 2.336(2), Zn−S2 2.382(2), Zn−S3 2.346(2), Zn−S4 2.401(2); S1−Zn−S2 110.77(8), S1−Zn−S3 115.68(8), S1−Zn−S4 114.64(8), S2−Zn−S3 112.93(7), S2−Zn−S4 89.28(6), S3−Zn−S4 110.70(7)

 © 2003 Wiley-VCH Verlag GmbH & Co. KGaA, Weinheim

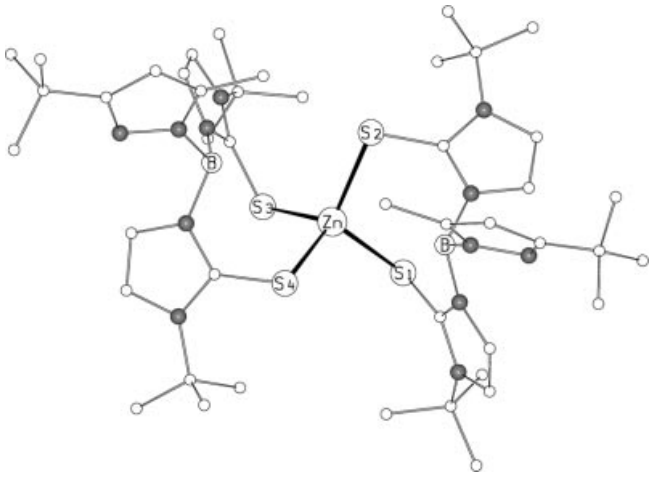

Figure 4. Molecular structure of **3f**; selected bond lengths [Å] and angles [°]: Zn−S1 2.359(2), Zn−S2 2.371(2), Zn−S3 2.368(2), Zn−S4 2.403(2); S1−Zn−S2 109.35(6), S1−Zn−S3 100.35(5), S1−Zn−S4 111.09(5), S2−Zn−S3 110.72(5), S2−Zn−S4 118.99(5), S3−Zn−S4 104.65(5)

In two of these cases the free mercaptoimidazole was incorporated as a coligand in the intended **L**·Zn complexes: $Zn(ClO_4)_2{\cdot}6H_2O$ and $\mathbf{L^3}$ yielded complex **4a**, and with $\mathbf{L^6}$ complex **4b** was formed. Both **4a** and **4b** were characterised by structure determinations. The structure of **4a** is shown in Figure 5. In **4a** and **4b** the tripod ligand is bound to the zinc ion in the normal fashion; the mercaptoimidazole is attached as a neutral molecule. Its bonding situation is that of a thioimidazoline, i.e. of a thiourea derivative. This is a very common situation in zinc complex chemistry, and the Zn−S bond length (2.33 Å in **4a**, 2.31 Å in **4b**) corresponds to expectation.[16] The deviations from tetrahedral symmetry at the zinc ion (smallest angle 99°, largest angle 123°) are in the same range as observed above.

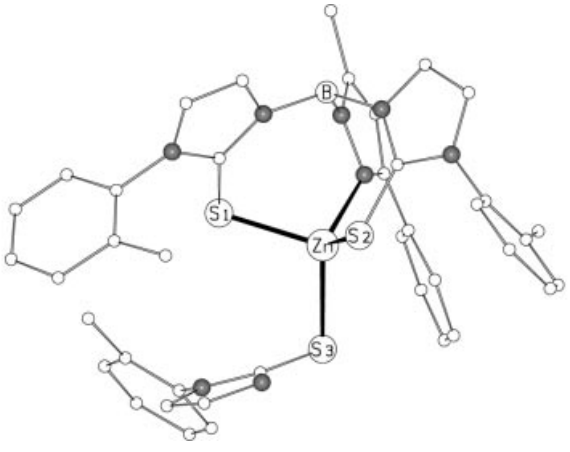

Figure 5. Molecular structure of **4a**; selected bond lengths [Å] and angles [°]: Zn−S1 2.323(2), Zn−S2 2.332(2), Zn−S3 2.326(2), Zn−N 2.027(5); N−Zn−S1 98.6(1), N−Zn−S2 105.6(1), N−Zn−S3 122.6(1), S1−Zn−S2 112.9(1), S1−Zn−S3 104.0(1), S2−Zn−S3 112.5(1)

$[\mathbf{L^3}{\cdot}Zn(N\text{-tolylthioimidazoline})]ClO_4$ **4a**

$[\mathbf{L^6}{\cdot}Zn(N\text{-cumylthioimidazoline})]ClO_4$ **4b**

In the case of $\mathbf{L^1}$ the hydrolytic destruction resulted in a zinc complex that bears only mercaptoimidazolate ligands. After addition of KOH to the reaction mixture, $[OZn_4(methimazolate)_6]$ (**5**) was obtained, another crystalline form of which has already been described.[17] Complex **5** is an analogue of $OZn_4(OAc)_6$,[18] i.e. a variant of the classical basic beryllium acetate structure with the six chelating N,S ligands spanning the edges of the Zn_4 tetrahedron. Figure 6 shows the structure of **5**, all details of which have already been discussed.[17]

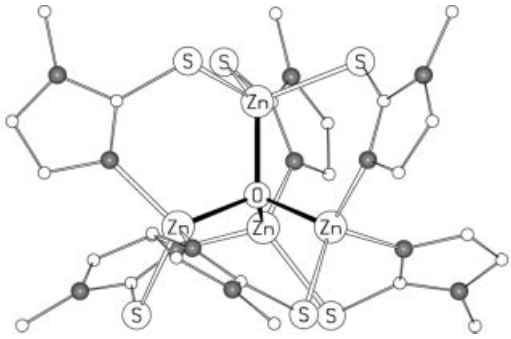

Figure 6. Molecular structure of **5**.; selected bond lengths [Å]: Zn−O 1.955(2), Zn−N 2.000(4), Zn−S 2.325(1) and 2.340(1)

Attempts at Enzyme Modelling

With the intention to prepare **L**·Zn−OH, **L**·Zn(H_2O) or $[\mathbf{L}{\cdot}Zn]^+$ complexes, i.e. functional models for the resting state of zinc enzymes, we performed a number of reactions between the ligands **L** and zinc salts of noncoordinating anions under varying pH conditions. So far, however, none of the intended species, which would be the starting point for modelling alcohol dehydrogenase chemistry, could be obtained in a pure form. However, in two cases evidence for the existence of a **L**·Zn−OH species could be gathered. Treatment of zinc perchlorate with $\mathbf{L^1}$ and KOH allowed the precipitation of a compound whose elemental analyses and spectra may be in agreement with its formulation as **6a**. Likewise, a species which may be formulated as **6b** was obtained with $\mathbf{L^2}$. Both compounds, however, show considerable amounts of impurities in their NMR spectra, and both could not be purified due to their lability toward hydrolysis or dismutation as described above.

$\mathbf{L^1}{\cdot}ZnOH$ **6a**

$\mathbf{L^2}{\cdot}ZnOH$ **6b**

Only with one ligand **L**, namely the *o*-methoxy-substituted $\mathbf{L^8}$, could stable complexes be prepared, which come close to containing naked $[\mathbf{L}{\cdot}Zn]^+$. Treatment with zinc perchlorate in methanol yielded **7**, and under the same conditions in ethanol **8** was obtained. The identification of **7** rests on its spectra. The presence of zinc-bound perchlorate is evident from the sharp and intense IR band at 1093

 © 2003 Wiley-VCH Verlag GmbH & Co. KGaA, Weinheim

cm^{-1}, in analogy to the structurally characterised [tris(mercaptoimidazolyl)borate]zinc perchlorate complex.[10] The ethanol complex **8** is a relative of two [tris(mercaptoimidazolyl)borate]zinc−alcohol complexes.[10,19]

$\mathbf{L^8}$•$ZnOClO_3$ $[\mathbf{L^8}$•$Zn(C_2H_5OH)]ClO_4$

7 **8**

The structure of **8** is shown in Figure 7. The ethanol ligand occupies the fourth coordination site of the zinc ion, the coordination geometry of which is tetrahedral to a good approximation. The Zn−O bond length is very similar to that in the nitrate complexes (see above), indicating a strong Zn−O(ethanol) bond. The ethanol ligand in the crystalline compound is connected by a hydrogen bond to a second ethanol molecule, which explains the absence of characteristic OH bands in the 3300−3700 cm^{-1} region in the IR spectrum. The molecular shape of **8** does not offer a convincing clue why it is just ligand $\mathbf{L^8}$ that makes complexes like **7** and **8** stable. Yet it is evident that the *o*-methoxy substituents enforce an orientation of the three phenyl groups that creates a bowl-like shape of the whole ligand, which may provide just enough stabilization of the Zn−EtOH unit in its interior.

Complex **8** is the first zinc complex in which an alcohol molecule is bound to a zinc ion with NS_2 ligation, creating a tetrahedral $ZnONS_2$ system. This bonding pattern reproduces the attachment of ethanol to the active centre of alcohol dehydrogenase.[20] In our preliminary communication on **8**[14] we have elaborated the close geometrical relation between the $ZnONS_2$ cores of **8** and of the enzyme structure of highest resolution. Hence, in terms of bioinorganic chemistry, the formation and structure of **8** are the most relevant result of this paper (Figure 7).

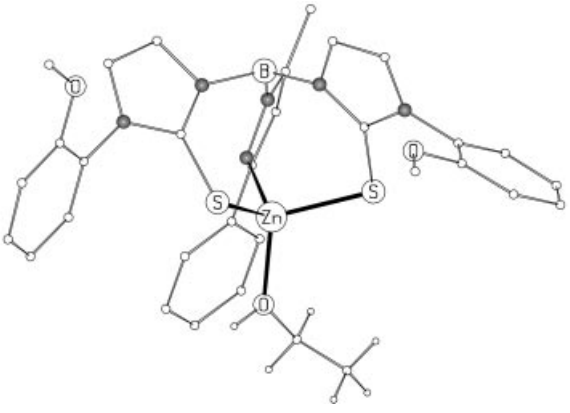

Figure 7. Molecular structure of **8**; selected bond lengths [Å] and angles [°]: Zn−O 1.970(3), Zn−S1 2.282(1), Zn−S2 2.314(1), Zn−N 2.012(3); O−Zn−S1 105.4(1), O−Zn−S2 109.8(1), O−Zn−N 116.9(1), S1−Zn−S2 113.2(1), S1−Zn−N 111.7(1), S2−Zn−N 100.2(1)

Having achieved structural modelling of alcohol dehydrogenase we also attempted functional modelling. As done before,[10,21,22] we used (benzyl)nicotinamide chloride ([BNA]Cl) as a mimic of NAD^+ and (dihydrobenzyl)nicotinamide (BNAH) as a mimic of NADH. For attempts at oxidation we used 2-propanol as an electron-rich alcohol and for attempts at reduction *p*-nitrobenzaldehyde as an electron-poor aldehyde. Thus, the model reactions were:

$$(CH_3)_2CHOH + BNA^+ \rightarrow (CH_3)_2CO + BNAH \quad (1)$$

$$p\text{-}O_2N\text{-}C_6H_4CHO + BNAH \rightarrow p\text{-}O_2N\text{-}C_6H_4CH_2OH + BNA^+ \quad (2)$$

It is known that reaction (1) does not proceed in the absence of a catalyst, but reaction (2) proceeds very slowly. Trying some of the **L**·Zn−X complexes described here we found that they show no or very low catalytic efficiency for both processes. The best results, obtained with complex **2a**, consisted in a 2−3% yield of acetone and traces of *p*-nitrobenzyl alcohol after 24 h of heating. These are the poorest results in our studies on the functional modelling of alcohol dehydrogenase, although the applied "catalysts" are the closest structural models of the enzyme. Conversely, the best catalytic results were obtained by us with zinc complexes whose structure has no resemblance at all with that of the enzyme.[22]

Conclusions

This work has shown that the tripodal NS_2 ligands **L** are easily accessible. They fill half of the gap between the analogous N_3 (i.e. pyrazolylborate) and S_3 (i.e. mercaptoimidazolylborate) ligands. Provided that the as-yet-unknown tripodal N_2S ligands of this type are also accessible, the door would be open for a complete set of comparative investigations of metal complexes with homologous tripodal N_3, N_2S, NS_2, and S_3 ligands. We intend to undertake this investigation with **L**·ZnX complexes, putting emphasis on enzyme model compounds.

The preliminary **L**·ZnX chemistry in this paper has revealed that the resulting complexes are not as inert as their tris(pyrazolylborate)·ZnX counterparts. One reason for this seems to be the high stability of the dismutation products ZnL_2 which comes from their ZnS_4 coordination in an uncharged complex. The other reason seems to be the geometrical disposition of the mercaptoimidazolyl moieties, which provides less encapsulation for the ZnX units than that of the pyrazolyl moieties, because their aromatic substituents point away from rather than enclosing the centre of the complexes. The relative stabilities of the **L**·ZnX complexes, however, give a clue on how to improve this situation: it seems that *ortho* substituents on the phenyl groups induce an orientation of them that creates a bowl-shaped environment around the ZnX units and hence the desired encapsulation.

The perchlorate complex **7** and the ethanol complex **8** are the best examples for this kind of stabilization. Complex **7** is as close as possible to being "naked" $[\mathbf{L}\cdot Zn]^+$, and **8** is the best model so far for the enzyme-substrate complex of alcohol dehydrogenase. Both **7** and **8** also demonstrate the subtle stability differences in these complexes of weakly bound ligands: perchlorate is a better ligand than methanol (**7** crystallises from methanol) but a weaker ligand than

 © 2003 Wiley-VCH Verlag GmbH & Co. KGaA, Weinheim

ethanol (**8** crystallises from ethanol). Thus **7** and **8** on one side show the way to improve the ligand design for making more stable **L**·Zn complexes of this type, on the other side they offer themselves as starting materials for a functional and possibly catalytic **L**·Zn chemistry.

Experimental Section

General: For general working and measuring procedures, see ref.[23] All procedures for the ligand syntheses were performed under an inert gas. 5-Methy-3-phenylpyrazole[24] and 3-*tert*-butyl-5-methylpyrazole[25] were prepared according to the published procedures. All *N*-substituted mercaptoimidazoles were prepared from the corresponding amino acetals $RNHCH_2CH(OEt)_2$ and HSCN according to an established procedure.[26,27] They were characterised by ^1H NMR spectroscopy in $CDCl_3$ as follows:

R = methyl: ^1H NMR ($CHCl_3$): δ = 3.66 ppm (s, 3 H, NMe), 6.59 (d, *J* = 2.0 Hz, 1 H, 4-H), 6.78 (d, *J* = 2.2 Hz, 1 H, 5-H). R = phenyl: ^1H NMR ($CHCl_3$): δ = 6.75 ppm (m, 2 H, 4-H, 5-H), 7.31−7.56 (m, 5 H, Ph). R = *o*-tolyl: ^1H NMR ($CHCl_3$): δ = 2.19 ppm (s, 3 H, Me), 6.66 (d, *J* = 2.4 Hz, 1 H, 4-H), 6.86 (d, *J* = 2.4 Hz, 1 H, 5-H), 7.00−7.43 (m, Ar). R = *p*-tolyl: ^1H NMR ($CHCl_3$): δ = 2.41 ppm (s, 3 H, Me), 6.80 (d, *J* = 1.6 Hz, 1 H, 4-H), 6.84 (d, *J* = 1.6 Hz, 1 H, 5-H), 7.28 (m, 2 H, Ar), 7.45 (m, 2 H, Ar). R = 2,4-xylyl: ^1H NMR ($CHCl_3$): δ = 2.16 ppm (s, 3 H, Me), 2.38 (s, 3 H, Me), 6.69 (d, *J* = 2.4 Hz, 1 H, 4-H), 6.81 (d, *J* = 2.4 Hz, 1 H, 5-H), 7.15 (m, 3 H, Ar), 7.26 (s, 1 H, Ar). R = *p*-cumyl: ^1H NMR ($CHCl_3$): δ = 1.28 ppm (d, *J* = 6.8 Hz, 6 H, Me), 2.97 (sept, *J* = 6.8 Hz, 1 H, CH), 6.80 (d, *J* = 2.4 Hz, 1 H, 4-H), 6.84 (d, *J* = 2.4 Hz, 1 H, 5-H), 7.34 (d, *J* = 6.6 Hz, 2 H, Ar), 7.50 (d, *J* = 6.6 Hz, 2 H, Ar). R = *p*-anisyl: ^1H NMR ($CHCl_3$): δ = 3.85 ppm (s, 3 H, OMe), 6.80 (d, *J* = 2.4 Hz, 1 H, 4-H), 6.98 (d, *J* = 2.2 Hz, 1 H, 5-H), 7.00 (d, *J* = 6.8 Hz, 2 H, Ar), 7.47 (d, *J* = 6.8 Hz, 2 H, Ar). R = *o*-anisyl: ^1H NMR ($CHCl_3$): δ = 3.74 ppm (s, 3 H, OMe), 6.81 (d, *J* = 2.1 Hz, 1 H, 4-H), 6.88 (d, *J* = 2.1 Hz, 1 H, 5-H), 6.98 (m, 2 H, Ar), 7.39 (m, 2 H, Ar). R = *tert*-butyl: ^1H NMR ($CHCl_3$): δ = 1.81 ppm (s, 9 H, *t*Bu), 6.67 (d, *J* = 2.4 Hz, 1 H, 4-H), 6.84 (d, *J* = 2.4 Hz, 1 H, 5-H).

Ligand Synthesis: All ligands **L** were prepared by thermal reaction between KBH_4, the pyrazole and the imidazole. Initially, the reactions were performed by melting the reagents (procedure A) which resulted in low yields and unsatisfactory purity of the products. Then it was found that the ligands **L** also form in boiling toluene (procedure B) which is the preferred procedure.

Procedure A: A 1:1 mixture of KBH_4 and the pyrazole was heated to 120 °C (thermometer immersed into the melt). The melt was stirred for 30 min. Then, 2 mol-equiv. of the mercaptoimidazole was added and the temperature raised slowly to 140 °C and kept at this temperature (30−60 min) until hydrogen evolution stopped. After cooling to room temp., the resulting solid was powdered and the raw product crystallised from ethanol at −30 °C.

Procedure B: A 1:1.1:2 mixture of KBH_4, the pyrazole and the imidazole was dried in vacuo at 60 °C for 2 h. 125 mL of dry toluene was added and the mixture refluxed for 4 days by heating with an oil bath (150 °C). Then, the volume of the solution was reduced in vacuo to 50 mL, and the mixture was poured into 200 mL of petroleum ether (boiling range 60−70 °C). The resulting precipitate was washed with a small amount of benzene and then with petroleum ether and dried in vacuo.

L^1: By procedure A from KBH_4 (1.70 g, 31.6 mmol), pyrazole (5.00 g, 31.6 mmol) and the imidazole (7.21 g, 63.2 mmol). Yield 4.10 g (30%); m.p. 200 °C (dec.). $C_{18}H_{20}BKN_6S_2$ (434.44): calcd. C 49.77, H 4.64, N 19.34; found C 48.59, H 4.90, N 17.60. ^1H NMR ($CDCl_3$): δ = 2.33 [s, 3 H, Me (pz)], 3.58 (s, 6 H, NMe), 6.30 [s, 1 H, H (pz)], 6.45 [d, *J* = 2.0 Hz, 2 H, H (im)], 6.63 [d, *J* = 2.0 Hz, 2 H, H (im)], 7.31 (m, 3 H, Ph), 7.51 (d, *J* = 7.4 Hz, 2 H, Ph) ppm. IR (KBr): $\tilde{\nu}$ = 2392 m (BH) cm^{-1}.

L^2: By procedure A from KBH_4 (920 mg, 17.1 mmol), the pyrazole (2.70 g, 17.1 mmol) and the imidazole (6.03 g, 34.2 mmol). Yield 4.9 g (50%); m.p. 180 °C (dec.). $C_{28}H_{24}BKN_6S_2$ (558.58): calcd. C 60.21, H 4.33, N 15.05; found C 56.50, H 4.83, N 13.69. ^1H NMR ($CDCl_3$): δ = 2.29 [s, 3 H, Me (pz)], 6.29 [s, 2 H, H (pz)], 6.72 (d, *J* = 2.4 Hz, 2 H, H (im)], 6.75 [d, *J* = 2.4 Hz, 2 H, H (im)], 7.30−7.51 (m, 13 H, Ar), 7.53 (d, *J* = 7.4 Hz, 2 H, Ph) ppm. IR (KBr): $\tilde{\nu}$ = 2483 m (BH) cm^{-1}.

L^3: By procedure B from KBH_4 (1.08 g, 20.0 mmol), the pyrazole (3.47 g, 22.0 mmol) and the imidazole (7.60 g, 40.0 mmol). Yield 10.1 g (86%); m.p. 205 °C (dec.). $C_{30}H_{28}BKN_6S_2$ (586.63): calcd. C 61.42, H 4.81, N 14.33, S 10.93; found C 61.36, H 5.12, N 14.23, S 10.47. ^1H NMR (CD_3OD): δ = 2.16 [s, 6 H, Me (tol)], 2.43 [s, 3 H, Me (pz)], 6.31 [s, 1 H, H (pz)], 6.59 [d, *J* = 2.2 Hz, 2 H, H (im)], 6.79 [d, *J* = 2.2 Hz, 2 H, H (im)], 7.27 (m, 8 H, Ar), 7.75 (d, *J* = 7.0 Hz, 2 H, Ph) ppm. IR (KBr): $\tilde{\nu}$ = 2451 m (BH) cm^{-1}.

L^4: By procedure B from KBH_4 (1.08 g, 20.0 mmol), the pyrazole (3.47 g, 22.0 mmol) and the imidazole (7.60 g, 40.0 mmol). Yield 9.86 g (84%); m.p. 165 °C (dec.). $C_{30}H_{28}BKN_6S_2$ (586.63): calcd. C 61.42, H 4.81, N 14.33, S 10.93; found C 61.29, H 5.25, N 14.25, S 9.91. ^1H NMR (CD_3OD): δ = 2.37 [s, 6 H, Me (tol)], 2.42 [s, 3 H, Me (pz)], 6.30 [s, 1 H, H (pz)], 6.57 [d, *J* = 2.2 Hz, 2 H, H (im)], 6.92 [d, *J* = 2.2 Hz, 2 H, H (im)], 7.28 (m, 8 H, Ar), 7.45 [d, *J* = 8.2 Hz, 4 H, H (tol)], 7.74 (d, *J* = 7.0 Hz, 2 H, Ph) ppm. IR (KBr): $\tilde{\nu}$ = 2482 m (BH) cm^{-1}.

L^5: By procedure A from KBH_4 (0.54 g, 10.0 mmol), the pyrazole (3.16 g, 20.0 mmol) and the imidazole (8.16 g, 40.0 mmol). Yield 0.74 g (12%); m.p. 185 °C (dec.). $C_{32}H_{32}BKN_6S_2$ (614.69): calcd. C 62.53, H 5.25, N 13.67; found C 58.72, H 5.31, N 12.33. ^1H NMR ($CDCl_3$): δ = 2.12 [s, 6 H, Me (xyl)], 2.34 [s, 6 H, Me (xyl)], 2.75 [s, 3 H, Me (pz)], 6.36 [s, 1 H, H (pz)], 6.54 [d, *J* = 2.0 Hz, 2 H, H (im)], 6.68 [d, *J* = 2.0 Hz, 2 H, H (im)], 7.04−7.15 (m, 6 H, xyl), 7.40−7.43 (m, 3 H, Ph), 7.69−7.75 (m, 2 H, Ph) ppm. IR (KBr): $\tilde{\nu}$ = 2487 m (BH) cm^{-1}.

L^6: By procedure B from KBH_4 (1.08 g, 20.0 mmol), the pyrazole (3.47 g, 22.0 mmol) and the imidazole (8.72 g, 40.0 mmol). Yield 4.63 g (36%); m.p. 165 °C (dec.). $C_{34}H_{36}BKN_6S_2$ (642.74): calcd. C 63.54, H 5.65, N 13.08, S 9.98; found C 63.21, H 5.91, N 13.07, S 10.08. ^1H NMR (CD_3OD): δ = 1.22 [d, *J* = 6.8 Hz, 18 H, Me (*i*Pr)], 2.08 [s, 3 H, Me (pz)], 2.89 [sept, *J* = 6.8 Hz, 2 H, CH (*i*Pr)], 6.26 [s, 1 H, H (pz)], 6.37 [d, *J* = 2.2 Hz, 2 H, H (im)], 6.75 [d, *J* = 2.2 Hz, 2 H, H (im)], 7.24 (m, 8 H, Ar), 7.42 (d, *J* = 8.3 Hz, 4 H, Cum), 7.68 (d, *J* = 7.0 Hz, 2 H, Ph) ppm. IR (KBr): $\tilde{\nu}$ = 2476 m (BH) cm^{-1}.

L^7: By procedure B from KBH_4 (0.54 g, 10.0 mmol), the pyrazole (1.74 g, 11.0 mmol) and the imidazole (4.12 g, 20.0 mmol). Yield 5.57 g (90%); m.p. 175 °C (dec.). $C_{30}H_{28}BKN_6O_2S_2$ (618.63): calcd. C 58.25, H 4.56, N 13.58, S 10.37; found C 57.68, H 4.42, N 13.20, S 10.13. ^1H NMR (CD_3OD): δ = 2.44 [s, 3 H, Me (pz)], 3.82 (s, 6 H, OMe), 6.29 [s, 1 H, H (pz)], 6.57 [d, *J* = 2.2 Hz, 2 H, H (im)], 6.90 [d, *J* = 2.2 Hz, 2 H, H (im)], 7.00 (d, *J* = 8.4 Hz, 4 H, C_6H_4),

 © 2003 Wiley-VCH Verlag GmbH & Co. KGaA, Weinheim

7.31 (m, 3 H, Ph), 7.44 (d, J = 8.3 Hz, 4 H, C_6H_4), 7.72 (d, J = 7.0 Hz, 2 H, Ph) ppm. IR (KBr): $\tilde{\nu}$ = 2486 m (BH) cm^{-1}.

L^8: By procedure B from KBH_4 (0.70 g, 13.0 mmol), the pyrazole (2.26 g, 14.3 mmol) and the imidazole (5.35 g, 26.0 mmol). Yield 6.79 g (85%); m.p. 185 °C (dec.). $C_{30}H_{28}BKN_6O_2S_2$ (618.63): calcd. C 58.25, H 4.56, N 13.58, S 10.37; found C 57.99, H 4.60, N 13.54, S 10.43. ^1H NMR ([D$_6$]DMSO): δ = 2.43 [s, 3 H, Me (pz)], 3.73 (s, 6 H, OMe), 6.24 [s, 1 H, H (pz)], 6.76 [d, J = 2.1 Hz, 2 H, H (im)], 6.82 [d, J = 2.1 Hz, 2 H, H (im)], 6.85−7.49 (m, 1 H, Ar), 7.74 (d, J = 7.1 Hz, 2 H, Ph) ppm. IR (KBr): $\tilde{\nu}$ = 2441 w (BH) cm^{-1}.

L^9: By procedure A from (0.54 g, 10.0 mmol) of KBH_4, (3.00 g, 20.0 mmol) of the pyrazole and (6.24 g, 40.0 mmol) of the imidazole. Yield 0.51 g (10%), m.p. 160 °C (dec.). The product contained considerable amounts of impurities. ^1H NMR ([D$_6$]DMSO): δ = 1.18 [s, 9 H, *t*Bu (pz)], 1.73 [s, 18 H, *t*Bu (im)], 2.15 [s, 3 H, Me (pz)], 5.59 [s, 1 H, H (pz)], 6.26 [d, J = 2.0 Hz, 2 H, H (im)], 6.79 [d, J = 2.0 Hz, 2 H, H (im)] ppm. IR (KBr): $\tilde{\nu}$ = 2496m (BH) cm^{-1}.

Zinc Halide Complexes. General Procedure: A solution of the zinc halide in 10 mL of methanol was added dropwise, with stirring, to a solution of the ligand in 50 mL of dichloromethane. After 2 h of stirring, the solution was filtered, the filtrate reduced to half of its volume in vacuo and then cooled to −30 °C overnight. The resulting precipitate of the raw product was filtered off, washed with 1−2 mL of methanol and dried in vacuo. If necessary it was recrystallised from CH_2Cl_2/CH_3OH or CH_2Cl_2/CH_3CN. All **L**·ZnHal complexes were obtained as colourless powders.

1a: From **L^1** (200 mg, 0.46 mmol) and $ZnCl_2$ (63 mg, 0.46 mmol). Yield 57 mg (25%); m.p. 225 °C (dec.). $C_{18}H_{20}BClN_6S_2Zn$ (496.20): calcd. C 43.57, H 4.06, N 16.94; found C 42.86, H 4.13, N 16.32. ^1H NMR ($CDCl_3$): δ = 2.42 [s, 3 H, Me (pz)], 3.57 [s, 6 H, Me (im)], 6.22 [s, 1 H, H (pz)], 6.60 [d, J = 2.0 Hz, 2 H, H (im)], 7.15 [d, J = 2.0 Hz, 2 H, H (im)], 7.28 (m, 3 H, Ph), 7.74 (d, J = 7.4 Hz, 2 H, Ph) ppm. IR (KBr): $\tilde{\nu}$ = 2503 m (BH) cm^{-1}.

1b: From **L^2** (300 mg, 0.52 mmol) and $ZnCl_2$ (71 mg, 0.52 mmol). Yield 156 mg (48%); m.p. 215 °C (dec.). $C_{28}H_{24}BClN_6S_2Zn$ (620.33): calcd. C 54.21, H 3.90, N 13.55; found C 54.68, H 4.05, N 13.57. ^1H NMR ($CDCl_3$): δ = 2.29 [s, 3 H, Me (pz)], 6.29 [s, 1 H, H (pz)], 6.75 [d, J = 2.4 Hz, 2 H, H (im)], 6.81 [d, J = 2.4 Hz, 2 H, H (im)], 7.30−7.51 (m, 13 H, Ar), 7.53 (d, J = 7.4 Hz, 2 H, Ph) ppm. IR (KBr): $\tilde{\nu}$ = 2507 m (BH) cm^{-1}.

1c: From **L^3** (196 mg, 0.33 mmol) and $ZnCl_2$ (46 mg, 0.34 mmol). Yield 180 mg (84%); m.p. 270 °C (dec.). $C_{30}H_{28}BClN_6S_2Zn$ (648.38): calcd. C 55.57, H 4.35, N 12.96, S 9.89; found C 55.23, H 4.58, N 13.33, S 9.34. ^1H NMR ($CDCl_3$): δ = 2.06 [s, 3 H, Me^1 (tol)], 2.28 [s, 3 H, Me^2 (tol)], 2.49 [s, 3 H, Me (pz)], 6.39 [s, 1 H, H (pz)], 6.88 [s, 2 H, H (im)], 7.05 [s, 2 H, H (im)], 7.25−7.37 (m, 11 H, Ar), 7.53 (d, J = 7.2 Hz, 2 H, Ph) ppm. IR (KBr): $\tilde{\nu}$ = 2559 w (BH) cm^{-1}.

1d: From **L^5** (614 mg, 1.00 mmol) and $ZnCl_2$ (136 mg, 1.00 mmol). Yield 0.25 mg (37%), m.p. 220 °C (dec.). $C_{32}H_{32}BClN_6S_2Zn$ (676.43): calcd. C 56.82, H 4.77, N 12.42; found C 56.99, H 4.70, N 12.36. ^1H NMR ($CDCl_3$): δ = 2.14 [s, 6 H, Me (xyl)], 2.37 [s, 6 H, Me (xyl)], 2.48 [s, 3 H, Me (pz)], 6.38 [s, 1 H, H (pz)], 6.83 [d, J = 2.0 Hz, 2 H, H (im)], 6.99 [d, J = 2.0 Hz, 2 H, H (im)], 7.00−7.17 (m, 6 H, xyl), 7.31−7.37 (m, 3 H, Ph), 7.53−7.58 (m, 2 H, Ph) ppm. IR (KBr): $\tilde{\nu}$ = 2505 m (BH) cm^{-1}.

1e: From **L^6** (206 mg, 0.33 mmol) and $ZnCl_2$ (46 mg, 0.34 mmol). Yield 169 mg (67%), m.p. 240 °C (dec.). $C_{36}H_{40}BClN_6S_3Zn$ (764.60): calcd. C 56.55, H 5.27, N 10.99, S 12.58; found C 56.31, H 5.60, N 11.02, S 12.25. ^1H NMR ($CDCl_3$): δ = 1.26 [d, J = 7.0 Hz, 12 H, Me (*i*Pr)], 2.93 [sept, J = 7.0 Hz, 2 H, CH (*i*Pr)], 6.38 [s, 1 H, H (pz)], 7.01 [d, J = 2.0 Hz, 2 H, H (im)], 7.07 [d, J = 2.0 Hz, 2 H, H (im)], 7.28 (m, 8 H, Ar), 7.45 (m, 3 H, Ar), 7.62 (d, J = 7.4 Hz, 2 H, Ph) ppm. IR (KBr): $\tilde{\nu}$ = 2512 w (BH) cm^{-1}.

1f: From **L^8** (301 mg, 0.49 mmol) and ZnI_2 (155 mg, 0.49 mmol). Yield 257 mg (69%), m.p. 230 °C (dec.). $C_{30}H_{28}BIN_6O_2S_2Zn·0.5(CH_2Cl_2)$ (771.83 +42.47): calcd. C 44.99, H 3.59, N 10.32, S 7.88; found C 45.79, H 3.95, N 10.75, S 8.25. ^1H NMR ($CDCl_3$): δ = 2.49 [s, 3 H, Me (pz)], 3.85 (s, 6 H, OMe), 5.32 (s, 1 H, CH_2Cl_2), 6.15 [s, 1 H, H (pz)], 6.91−7.95 [m, 15 H, H (im) + Ar] ppm. IR (KBr): $\tilde{\nu}$ = 2511 w (BH) cm^{-1}.

Zinc Nitrate Complexes

2a: A solution of **L_3** (196 mg, 0.33 mmol) in 5 mL of dichloromethane was added dropwise with stirring to a solution of $Zn(NO_3)_2·6H_2O$ (95 mg, 0.34 mmol) in 10 mL of methanol. After 4 h of stirring, the precipitate was filtered off. Recrystallisation from dichloromethane/acetonitrile yielded 158 mg (71%) of **2a**, m.p. 220 °C (dec.). $C_{30}H_{28}BN_7O_3S_2Zn$ (674.93): calcd. C 53.39, H 4.18, N 14.53, S 9.50; found C 53.29, H 4.29, N 14.42, S 9.30. ^1H NMR (CD_2Cl_2): δ = 1.96 [s, 3 H, Me^1 (tol)], 2.25 [s, 3 H, Me^2 (tol)], 2.53 [s, 3 H, Me (pz)], 6.46 [s, 1 H, H (pz)], 6.96 [d, J = 2.2 Hz, 2 H, H (im)], 7.08 [d, J = 2.2 Hz, 2 H, H (im)], 7.37 (m, 11 H, Ar), 7.52 (d, J = 6.0 Hz, 2 H, Ph) ppm. IR (KBr): $\tilde{\nu}$ = 2479 w (BH), 1382 vs (NO_3), 1294 vs (NO_3) cm^{-1}.

2b: Like **2a** from **L^6** (214 mg, 0.33 mmol) and $Zn(NO_3)_2·6H_2O$ (95 mg, 0.34 mmol). Yield 169 mg (73%); m.p. 180 °C (dec.). $C_{34}H_{36}BN_7O_3S_2Zn$ (731.04): calcd. C 55.86, H 4.96, N 13.41, S 8.77; found C 56.26, H 5.46, N 12.87, S 8.01. ^1H NMR ($CDCl_3$): δ = 1.27 [d, J = 6.9 Hz, 12 H, Me (*i*Pr)], 2.96 [sept, J = 6.9 Hz, 2 H, CH (*i*Pr)], 6.40 [s, 1 H, H (pz)], 7.00 [s, 4 H, H (im)], 7.36 (s, 8 H, Cum), 7.38 (m, 3 H, Ph), 7.56 (d, J = 5.4 Hz, 2 H, Ph) ppm. IR (KBr): $\tilde{\nu}$ = 2486 w (BH), 1373 s (NO_3), 1292 s (NO_3) cm^{-1}.

2c: Like **2a** from **L^8** (307 mg, 0.52 mmol) and $Zn(NO_3)_2·4H_2O$ (137 mg, 0.52 mmol). Yield 115 mg (31%), m.p. 215 °C (dec.). $C_{30}H_{28}BN_7O_5S_2Zn$ (706.93): calcd. C 50.97, H 3.99, N 13.87, S 9.07; found C 50.43, H 4.28, N 13.51, S 8.93. ^1H NMR ($CDCl_3$): δ = 2.44 [s, 3 H, Me (pz)], 3.75 (s, 6 H, OMe), 6.32 [s, 1 H, H (pz)], 6.86 [d, J = 2.2 Hz, 2 H, H (im)], 6.96 [d, J = 2.2 Hz, 2 H, H (im)], 7.10−7.48 (m, 11 H, Ar), 7.54−7.60 (m, 2 H, Ph) ppm. IR (KBr): $\tilde{\nu}$ = 2489 w (BH), 1384 vs (NO_3), 1294 vs (NO_3) cm^{-1}.

ZnL_2 Complexes

3a: A solution of (171 mg, 0.46 mmol) of $Zn(ClO_4)_2·6H_2O$ in 20 mL of methanol was added with stirring to a solution of (200 mg, 0.46 mmol) of **L^1** in 50 mL of dichloromethane. After 30 min, powdered KOH (29 mg, 0.50 mmol) was added. After 20 h of stirring and filtration, the volume of the solution was reduced to one half in vacuo. Cooling to −4 °C overnight produced a colourless precipitate of **6a** (characterisation see below). Attempts to purify this product by dissolution in dichloromethane and slow concentration yielded, after 4 weeks, 18 mg (4%) of colourless crystalline **3a**; m.p. 230 °C (dec.). $C_{36}H_{40}B_2N_{12}S_4Zn·3H_2O$ (856.14 +54.02): calcd. C 47.51, H 5.09, N 18.47; found C 46.40, H 5.03, N 19.25. ^1H NMR ($CDCl_3$): δ = 1.49 (s, 6 H, H_2O), 2.38 [s, 6 H, Me (pz)], 3.43 [s, 12 H, Me (im)], 6.22 [s, 2 H, H (pz)], 6.67 [d, J = 2.0 Hz, 4 H, H (im)], 7.17 [d, J = 2.0 Hz, 4 H, H (im)], 7.31 (m, 6 H, Ph), 7.75 (d, J = 7.4 Hz, 4 H, Ph) ppm. IR (KBr): $\tilde{\nu}$ = 2500 m (BH) cm^{-1}.

 © 2003 Wiley-VCH Verlag GmbH & Co. KGaA, Weinheim

3b: A solution of **L³** (196 mg, 0.33 mmol) in methanol (5 mL) was added dropwise with stirring to a solution of $Zn(CH_3COO)_2$ (62 mg, 0.34 mmol) in methanol (10 mL). After 4 h of stirring, the precipitate of raw **3b** was filtered off. Crystallisation from methanol/dichloromethane by slow concentration yielded 146 mg (76%) of **3b** as colourless crystals; m.p. 250 °C (dec.). $C_{60}H_{56}B_2N_{12}S_4Zn$ (1160.46): calcd. C 62.10, H 4.86, N 14.48, S 11.05; found C 61.90, H 4.90, N 14.56, S 11.27. ^{1}H NMR ($CDCl_3$): δ = 1.97 [s, 3 H, Me (tol)], 2.04 [s, 3 H, Me (tol)], 2.53 [s, 3 H, Me (pz)], 6.33 [s, 1 H, H (pz)], 6.59 [d, *J* = 2.0 Hz, 2 H, H (im)], 6.68 [d, *J* = 2.0 Hz, 2 H, H (im)], 7.18−7.41 (m, 11 H, Ar), 7.89 (d, *J* = 7.2 Hz, 2 H, Ph) ppm. IR (KBr): ṽ = 2521 m (BH) cm^{-1}.

3c: Like **3b** from **L⁴** (196 mg, 0.33 mmol) and $Zn(NO_3)_2{\cdot}6H_2O$ (95 mg, 0.34 mmol). Yield 159 mg (83%) of **3c** as colourless crystals; m.p. 240 °C (dec.). $C_{60}H_{56}B_2N_{12}S_4Zn$ (1160.46): calcd. C 62.10, H 4.86, N 14.48, S 11.05; found C 61.10, H 4.74, N 14.24, S 10.56. ^{1}H NMR ($CDCl_3$): δ = 2.43 [s, 6 H, Me (tol)], 2.75 [s, 3 H, Me (pz)], 6.38 [s, 1 H, H (pz)], 6.84 [d, *J* = 2.2 Hz, 2 H, H (im)], 6.94 [d, *J* = 2.2 Hz, 2 H, H (im)], 7.10−7.45 (m, 11 H, Ar), 7.74 (d, *J* = 7.2 Hz, 2 H, Ph) ppm. IR (KBr): ṽ = 2477 w (BH) cm^{-1}.

3d: A solution of $Zn(ClO_4)_2{\cdot}6H_2O$ (372 mg, 1.00 mmol) in methanol (10 mL) was slowly added dropwise with stirring to a solution of **L⁵** (614 mg, 1.00 mmol) in dichloromethane (10 mL). After 2 h of stirring, all volatiles were removed in vacuo. The residue was extracted with four 5-mL portions of dichloromethane. The combined extracts were concentrated to dryness and the residue dissolved in a minimum amount of benzene. Slow concentration produced a precipitate of crystalline solvated **3d**. Filtration and drying for 3 h in vacuo yielded 200 mg (32%) of **3d** as a colourless powder; m.p. 230 °C (dec.). $C_{64}H_{64}B_2N_{12}S_4Zn$ (1216.58): calcd. C 63.19, H 5.30, N 13.82; found C 63.26, H 5.66, N 12.80. ^{1}H NMR ($CDCl_3$): δ = 2.00 [s, 6 H, Me (xyl)], 2.21 [s, 6 H, Me (xyl)], 2.94 [s, 3 H, Me (pz)], 6.15 [s, 1 H, H (pz)], 6.25 [d, *J* = 2.0 Hz, 2 H, H (im)], 6.55 [d, *J* = 2.0 Hz, 2 H, H (im)], 6.79−7.00 (m, 6 H, xyl), 7.45−7.53 (m, 3 H, Ph), 8.32−8.35 (m, 2 H, Ph) ppm. IR (KBr): ṽ = 2513 m (BH) cm^{-1}.

3e: Like **3b** from **L⁷** (206 mg, 0.33 mmol) and $Zn(NO_3)_2{\cdot}6H_2O$ (95 mg, 0.34 mmol). Yield 127 mg (63%) of **3e** as colourless crystals; m.p. 245 °C (dec.). $C_{60}H_{56}B_2N_{12}O_4S_4Zn$ (1224.46): calcd. C 58.86, H 4.61, N 13.73, S 10.48; found C 58.54, H 4.83, N 13.52, S 10.12. ^{1}H NMR (CD_2Cl_2): δ = 2.75 [s, 3 H, Me (pz)], 3.83 (s, 6 H, OMe), 6.38 [s, 1 H, H (pz)], 6.83 [s, 2 H, H (im)], 6.96 (d, *J* = 8.4 Hz, 4 H, anisyl), 7.44 (d, *J* = 8.4 Hz, 4 H, anisyl), 7.46 (m, 3 H, Ph), 7.74 (d, *J* = 7.4 Hz, 2 H, Ph) ppm. IR (KBr): ṽ = 2488 m (BH) cm^{-1}.

3f: Like **3d** from $Zn(ClO_4)_2{\cdot}6H_2O$ (372 mg, 1.00 mmol) and **L⁹** (500 mg, 1.00 mmol). Recrystallisation from acetonitrile yielded 120 mg (24%) of **3f** as colourless crystals; m.p. 180 °C (dec.). $C_{44}H_{72}B_2N_{12}S_4Zn$ (984.40): calcd. C 53.69, H 7.37, N 17.07, S 13.03; found C 52.61, H 6.84, N 16.98, S 12.56. ^{1}H NMR (CD_2Cl_2): δ = 1.28 [s, 9 H, *t*Bu (pz)], 1.70 [s, 18 H, *t*Bu (im)], 2.44 [s, 3 H, Me (pz)], 5.78 [s, 1 H, H (pz)], 6.82 [d, *J* = 2.0 Hz, 2 H, H (im)], 6.87 [d, *J* = 2.2 Hz, 2 H, H (im)] ppm. IR (KBr): ṽ = 2520 m (BH) cm^{-1}.

Hydrolysis Products

4a: A solution of **L³** (196 mg, 0.33 mmol) in dichloromethane (5 mL) was added dropwise, with stirring, to a solution of $Zn(ClO_4)_2{\cdot}6H_2O$ (124 mg, 0.34 mmol) in ethanol (10 mL). After stirring for 24 h, all volatiles were removed in vacuo, the residue extracted with dichloromethane, filtered and the filtrate concentrated to dryness again. Recrystallisation from dichloromethane/ethanol yielded 110 mg (35%) of **4a** as colourless crystals; m.p. 210 °C (dec.). $C_{40}H_{38}BClN_8O_4S_3Zn$ (902.64): calcd. C 53.23, H 4.24, N 12.41, S 10.66; found C 51.94, H 4.36, N 11.95, S 10.02. ^{1}H NMR (CD_2Cl_2): δ = 1.78 [s, 3 H, Me (tol)], 1.96 [s, 3 H, Me (tol)], 2.12 [s, 3 H, Me (tol)], 2.49 [s, 3 H, Me (pz)], 6.40 [s, 1 H, H (pz)], 6.72 [s, 1 H, H (im)], 6.73 [d, *J* = 2.2 Hz, 1 H, H (im)], 6.80 [s, 1 H, H (im)], 6.84 [s, 1 H, H (im)], 7.00 [s, 2 H, H (im)], 7.10−7.39 (m, 17 H, Ar), 10.64 (s, 1 H, NH) ppm. IR (KBr): ṽ = 2463 w (BH) cm^{-1}.

4b: Like **4a** from **L⁶** (214 mg, 0.33 mmol) and $Zn(ClO_4)_2{\cdot}6H_2O$ (124 mg, 0.34 mmol). Yield 88 mg (27%) of **4b** as colourless crystals, m.p. 180 °C (dec.). $C_{46}H_{50}BClN_8O_4S_3Zn$ (986.80): calcd. C 55.99, H 5.11, N 11.36, S 9.75; found C 55.27, H 5.52, N 11.10, S 9.07. ^{1}H NMR ($CDCl_3$): δ = 1.28 [d, *J* = 7.0 Hz, 18 H, Me(*i*Pr)], 2.52 [s, 3 H, Me (pz)], 2.97 [sept, *J* = 7.0 Hz, 3 H, CH(*i*Pr)], 6.39 [s, 1 H, H (pz)], 6.83 [s, 1 H, H (im)], 6.94 [s, 1 H, H (im)], 6.99 [s, 2 H, H (im)], 7.14 [s, 2 H, H (im)], 7.29 (d, *J* = 8.0 Hz, 6 H, C_6H_4), 7.39 (m, 3 H, Ph), 7.43 (d, *J* = 8.0 Hz, 6 H, C_6H_4), 7.47 (d, *J* = 7.8 Hz, 2 H, Ph), 10.92 (s, 1 H, NH) ppm. IR (KBr): ṽ = 2468 w (BH) cm^{-1}.

5: A solution of **L¹** (350 mg, 0.80 mmol) in dichloromethane (50 mL) was added dropwise, with stirring, to a solution of $Zn(ClO_4)_2{\cdot}6H_2O$ (300 mg, 0.18 mmol) in methanol (100 mL). After 2 h of stirring, powdered KOH (46 mg, 0.80 mmol) was added and the mixture stirred for another 20 h. After filtration, the filtrate was concentrated to half its volume. Within a few weeks 74 mg (9%) of colourless crystalline **5**, m.p. 167 °C, was obtained. $C_{24}H_{30}N_{12}OS_6Zn_4{\cdot}6H_2O$ (956.50 + 108.06): calcd. C 27.08, H 3.98, N 15.79; found C 27.03, H 3.26, N 16.59. ^{1}H NMR ($CDCl_3$): δ = 1.51 (s, 2 H, H_2O), 3.49−3.69 (m, 3 H, Me), 6.78−7.10 (m, 2 H, H (im) ppm.

Enzyme Models

6a: The precipitate of **6a**, which is an intermediate in the formation of **3a** (see above), was dried in vacuo. 46 mg (21%) of raw **6a** remained as a colourless powder; m.p. 220 °C (dec.). $C_{18}H_{21}BN_6OS_2Zn$ (477.74): calcd. C 45.25, H 4.43, N 17.59, S 13.42; found C 43.44, H 4.16, N 17.56, S 12.66. ^{1}H NMR ($CDCl_3$): δ = 2.36 [s, 3 H, Me (pz)], 3.50 [s, 6 H, Me (im)], 6.22 [s, 1 H, H (pz)], 6.61 [d, *J* = 2.0 Hz, 2 H, H (im)], 7.14 [d, *J* = 2.0 Hz, 2 H, H (im)], 7.28 (m, 3 H, Ph), 7.77 (d, *J* = 7.4 Hz, 2 H, Ph) ppm. IR (KBr): ṽ = 3630 vw (OH), 2503 m (BH) cm^{-1}.

6b: A solution of $Zn(ClO_4)_2{\cdot}6H_2O$ (130 mg, 0.35 mmol) in methanol (20 mL) was added with stirring to a solution of **L²** (200 mg, 0.35 mmol) in dichloromethane (100 mL). After 30 min, powdered KOH (22 mg, 0.39 mmol) was added. After stirring for 20 h, the mixture was filtered and the filtrate reduced in vacuo to half its volume. Cooling to −30 °C for 3 days precipitated 96 mg (44%) of raw **6b** as colourless powder, m.p. 220 °C (dec.) which started decomposing upon attempts of further purification. $C_{28}H_{25}BN_6OS_2Zn$ (601.88): calcd. C 55.88, H 4.19, N 13.96, Zn 10.86; found C 54.68, H 4.05, N 13.57, Zn 10.71. ^{1}H NMR ($CDCl_3$): δ = 2.29 [s, 3 H, Me (pz)], 6.29 [s, 2 H, H (pz)], 6.73 [d, *J* = 2.4 Hz, 2 H, H (im)], 6.80 [d, *J* = 2.4 Hz, 2 H, H (im)], 7.30−7.51 (m, 13 H, Ar), 7.53 (d, *J* = 7.3 Hz, 2 H, Ph) ppm. IR (KBr): ṽ = 3650 w (OH), 2499 m (BH) cm^{-1}.

7: A solution of **L⁵** (665 mg, 1.08 mmol) and anhydrous methanol (60 mL) was slowly added dropwise, with stirring, to a solution of $Zn(ClO_4)_2{\cdot}6H_2O$ (400 mg, 1.08 mmol) in anhydrous methanol (60 mL). After stirring for 1 h, the precipitate was filtered off and the filtrate reduced to 80 mL in vacuo. The resulting precipitate

 © 2003 Wiley-VCH Verlag GmbH & Co. KGaA, Weinheim

was also filtered off and the filtrate concentrated to dryness. The residue was extracted with dichloromethane (14 mL). After filtration, the extract was concentrated to dryness and the residue dried in vacuo. 438 mg (55%) of **7** remained as a colourless powder; m.p. 230 °C (dec.). $C_{30}H_{28}BClN_6O_6S_2Zn$ (744.37): calcd. C 48.41, H 3.79, N 11.29, S 8.62; found C 48.57, H 4.30, N 11.28, S 8.43. ^{1}H NMR ($CDCl_3$): δ = 2.28 [s, 3 H, Me (pz)], 3.68 (s, 6 H, OMe), 6.49 [s, 1 H, H (pz)], 6.94−7.70 [m, 15 H, H (im), Ar], 7.93 [d, J = 7.2 Hz, 2 H, Ph] ppm. IR (KBr): $\tilde{\nu}$ = 2476 w (BH), 1179 vs, 1093 vs (ClO_4) cm^{-1}.

8: A solution of $\mathbf{L}^8$ (309 mg, 0.50 mmol) in anhydrous ethanol (25 mL) was slowly added dropwise, with stirring, to a solution of $Zn(ClO_4)_2{\cdot}6H_2O$ (186 mg, 0.50 mmol) in anhydrous ethanol (25 mL) and the mixture stirred for 15 h. After filtration, the volume was reduced to one half in vacuo and the resulting precipitate filtered off. Recrystallisation from anhydrous ethanol yielded 313 mg (71%) of **8** as colourless crystals, m.p. 200 °C (dec.). $C_{32}H_{34}BClN_6O_7S_2Zn{\cdot}C_2H_5OH$ (790.44 + 46.07): calcd. C 48.82, H 4.82, N 10.05, S 7.67; found C 47.75, H 4.87, N 9.74, S 7.33. ^{1}H NMR ($CDCl_3$): δ = 1.18 [t, J = 7.0 Hz, 6 H, CH_3 (Et)], 2.50 [s, 3

Table 1. Crystallogaphic details

	1c	**1d**	**2a**	**3a**	**3b**	**3c**
Empirical formula	$C_{30}H_{28}BClN_6S_2Zn$	$C_{32}H_{32}BClN_6S_2Zn \cdot 2CH_3CN$	$C_{30}H_{28}BN_7O_3S_2Zn$	$C_{36}H_{40}B_2N_{12}S_4Zn \cdot 3H_2O$	$C_{60}H_{56}B_2N_{12}S_4Zn \cdot CH_3CN{\cdot}2H_2O$	$C_{60}H_{56}B_2N_6S_4Zn \cdot H_2O$
Molecular mass	648.33	758.49	674.89	910.11	1237.54	1178.47
Crystal size [mm]	0.15 × 0.2 × 0.35	0.4 × 0.3 × 0.3	0.1 × 0.1 × 0.2	0.4 × 0.3 × 0.2	0.05 × 0.1 × 0.2	0.1 × 0.1 × 0.3
Space group	$P2_1/c$	$P\bar{1}$	$P2_1/n$	$P\bar{1}$	$P\bar{1}$	$P\bar{1}$
Z	4	2	4	2	2	2
a [Å]	11.322(2)	10.087(2)	10.243(1)	8.98(2)	11.234(2)	10.788(1)
b [Å]	14.625(2)	11.908(2)	29.169(3)	15.07(3)	17.060(2)	15.874(1)
c [Å]	18.481(2)	17.035(3)	11.475(1)	17.55(4)	17.377(2)	19.024(2)
α [°]	90	102.41(3)	90	77.35(3)	75.297(3)	106.094(2)
β [°]	95.549(3)	95.34(3)	113.356(3)	80.10.(3)	81.242(3)	104.962(2)
γ [°]	90	110.13(3)	90	78.80(3)	87.280(3)	105.176(2)
V [Å^3]	3045.9(7)	1845.0(6)	3147.8(6)	2252.4(8)	3183.7(8)	2822.5(4)
d(calcd.) [g·cm^{-3}]	1.41	1.37	1.42	1.34	1.55	1.37
μ(Mo-K_α) [mm^{-1}]	1.06	0.89	0.96	0.78	1.14	0.64
hkl range	h: −15 to 9 k: −19 to 19 l: −24 to 24	h: −12 to 0 k: − 13 to 14 l: −20 to 20	h: −13 to 5 k: −38 to 38 l: −15 to 14	h: −11 to 0 k: −18 to 18 l: −21 to 21	h: −14 to 14 k: −22 to 22 l: −23 to 23	h: −13 to 14 k: −20 to 21 l: −25 to 24
Measured reflections	19180	7657	20120	9427	29078	25673
Independent reflections	7362	7230	7680	8831	14881	13177
Observed refl. [$I > 2\sigma(I)$]	5294	5589	2749	5204	5199	6271
Parameters	370	448	398	523	746	712
Refined reflections	7362	7230	7680	8831	14881	13177
R_1 (obsd. refl.)	0.035	0.046	0.072	0.066	0.079	0.056
wR_2 (all refl.)	0.113	0.132	0.256	0.238	0.282	0.145
Residual electron density [e/Å^3]	+0.5/−0.4	+1.3/−0.6	+0.8/−0.8	+1.3/−0.9	+1.1/−0.6	+0.7/−0.7

	3d	**3f**	**4a**	**4b**	**5**	**8**
Empirical formula	$C_{64}H_{64}B_2N_{12}S_4Zn{\cdot}8C_6H_6$	$C_{44}H_{72}B_2N_{12}S_4Zn$	$C_{40}H_{38}BClN_8O_4S_3Zn{\cdot}CH_2Cl_2$	$C_{46}H_{50}BClN_8O_4S_3Zn{\cdot}CH_2Cl_2$	$C_{24}H_{30}N_{12}OS_6Zn_4{\cdot}6H_2O$	$C_{32}H_{34}BClN_6O_7S_2Zn{\cdot}2C_2H_5OH$
Molecular mass	1841.47	984.37	987.52	1071.68	1064.56	882.58
Crystal size [mm]	0.2 × 0.25 × 0.35	0.5 × 0.4 × 0.4	0.15 × 0.15 × 0.25	0.1 × 0.05 × 0.05	0.2 × 0.1 × 0.1	0.25 × 0.15 × 0.1
Space group	$C2/c$	$P\bar{1}$	$P2_1/c$	$P\bar{1}$	$R\bar{3}$	$P\bar{1}$
Z	4	2	4	2	6	2
a [Å]	26.507(3)	10.576(1)	11.399(1)	10.897(1)	15.993(2)	10.962(1)
b [Å]	20.022(2)	16.243(1)	11.133(1)	15.635(2)	15.993(2)	14.131(2)
c [Å]	20.914(3)	16.809(1)	35.651(3)	17.131(2)	33.715(5)	14.834(2)
α [°]	90	105.253(2)	90	66.431(2)	90	101.011(2)
β [°]	112.828(2)	101.468(2)	97.978(2)	74.600(2)	90	109.568(2)
γ [°]	90	104.034(2)	90	80.263(3)	120	94.234(2)
V [Å^3]	10229.9(18)	2594.2(4)	4480.6(6)	2572.6(5)	7468.0(15)	2101.6(4)
d(calcd.) [gcm^{-3}]	1.20	1.26	1.46	1.38	1.40	1.40
μ(Mo-K_α) [mm^{-1}]	0.38	0.68	0.92	0.81	2.20	0.81
hkl range	h: −35 to 33 k: −26 to 19 l: −27 to 27	h: −12 to 13 k: −21 to 21 l: −22 to 22	h: −15 to 6 k: −14 to 13 l: −47 to 44	h: −14 to 14 k: −20 to 20 l: −22 to 22	h: −19 to 19 k: −19 to 19 l: −41 to 41	h: −14 to 14 k: −18 to 18 l: −19 to 19
Measured reflections	32298	23401	27857	23909	19601	19203
Independent reflections	12428	11738	10752	12173	3219	9895
Observed refl. [$I > 2\sigma(I)$]	4317	6604	5145	2730	2134	5057
Parameters	596	576	578	605	106	509
Refined reflections	12428	11738	10752	12173	3219	9895
R_1 (obsd. refl.)	0.069	0.078	0.077	0.105	0.043	0.061
wR_2 (all refl.)	0.204	0.230	0.264	0.387	0.132	0.187
Residual electron density [e/Å^3]	+1.2/−0.5	+1.2/−0.8	+1.3/−1.1	+1.1/−0.8	+1.3/−0.4	+0.8/−0.8

 © 2003 Wiley-VCH Verlag GmbH & Co. KGaA, Weinheim

H, Me (pz)], 3.62 [dq, J = 7.0/5.2 Hz, 4 H, CH_2 (Et)], 3.82 (s, 6 H, OMe), 6.40 [s, 1 H, H (pz)], 6.94 [d, J = 2.1 Hz, 2 H, H (im)], 7.02 [d, J = 2.1 Hz, 2 H, H (im)], 7.03−7.48 (m, 11 H, Ar), 7.54−7.60 (m, 2 H, Ph) ppm. IR (KBr): $\tilde{\nu}$ = 2499 w (BH), 1180 s, 1096 s, br. (ClO_4) cm^{-1}.

Catalytic Studies. Oxidation of 2-Propanol: 2a (33.8 mg, 0.05 mmol) and [BNA]Cl (12.5 mg, 0.05 mmol) were dissolved in [D_6]DMSO (2 mL). 2-Propanol (0.2 mL, 2.6 mmol) was added and the mixture stirred for 24 h at 100 °C in the dark. The oxidation reaction was monitored by recording the ^{1}H NMR signals of acetone at δ = 2.08 ppm and of the benzyl group of BNAH at δ = 4.30 ppm.

Reduction of *p*-Nitrobenzaldehyde: 2a (20.3 mg, 0.03 mmol), *p*-nitrobenzaldehyde (4.5 mg, 0.03 mmol) and BNAH (6.5 mg, 0.03 mmol) were dissolved in [D_6]DMSO (2 mL) and the mixture was stirred at 100 °C for 24 h. The reduction was monitored by recording the ^{1}H NMR signals of *p*-nitrobenzyl alcohol at δ = 4.25 ppm and of the benzyl group of BNA^+ at δ = 5.91 ppm.

Structure Determinations:[28] Crystals were obtained as described above. Diffraction data were recorded at 200 K (**2a**, **3c**, **3d**, **3f**, **4a**, **4b**, **5**, **8**) and at room temp. (**1c**, **1d**, **3a**, **3b**) with a Nonius CAD4 (**1d**, **3a**, **3d**, **5**) or a Bruker Smart CCD diffractometer (**1c**, **2a**, **3b**, **3c**, **3f**, **4a**, **4b**, **8**). Empirical absorption corrections were applied for **3b**, **3c**, **4a**, **4b** and **8**. The structures were solved with direct methods and refined anisotropically with the SHELX program suite.[29] Hydrogen atoms were included with fixed distances and isotropic temperature factors 1.5-times those of their attached atoms. Parameters were refined against F^2. The R values are defined as $R_1 = \Sigma|F_o - F_c|/\Sigma F_o$ and $wR_2 = \{\Sigma[w(F_o^2 - F_c^2)^2]\Sigma[w(F_o^2)^2]\}^{1/2}$. Drawings were produced with SCHAKAL.[30] Table 1 lists the crystallographic data.

Acknowledgments

This work was supported by the Deutsche Forschungsgemeinschaft (Graduiertenkolleg "Ungepaarte Elektronen") and the Fonds der Chemischen Industrie. We are indebted to Drs. W. Deck, M Tesmer and H. Brombacher for assistance during the crystal structure determinations.

[1] G. Parkin, *Adv. Inorg. Chem.* **1995**, *42*, 291−393.
[2] N. Kitajima, W. B. Tolman, *Prog. Inorg. Chem.* **1995**, *43*, 419−531.
[3] H. Vahrenkamp, *Acc. Chem. Res.* **1999**, *32*, 589−596.
[4] G. Parkin, *Chem. Commun.* **2000**, 1971−1985.
[5] M. Garner, J. Reglinski, I. Cassidy, M. D. Spicer, A. R. Kennedy, *Chem. Commun.* **1996**, 1975−1976.
[6] J. Reglinski, M. D. Spicer, M. Garner, A. R. Kennedy, *J. Am. Chem. Soc.* **2000**, *121*, 2317−2318.
[7] I. Cassidy, M. Garner, A. R. Kennedy, G. B. S. Potts, J. Reglinski, P. A. Slavin, M. D. Spicer, *Eur. J. Inorg. Chem.* **2002**, 1235−1239.
[8] J. L. White, J. M. Tanski, D. Rabinovich, *J. Chem. Soc., Dalton Trans.* **2002**, 2987−2991, and references cited therein.
[9] B. M. Bridgewater, G. Parkin, *Inorg. Chem. Commun.* **2001**, *4*, 126−129.
[10] M. Tesmer, M. Shu, H. Vahrenkamp, *Inorg. Chem.* **2001**, *40*, 4022−4029.
[11] C. Kimblin, T. Hascall, G. Parkin, *Inorg. Chem.* **1997**, *36*, 5680−5681.
[12] C. Kimblin, B. M. Bridgewater, T. Hascall, G. Parkin, *J. Chem. Soc., Dalton Trans.* **2000**, 1267−1274.
[13] C. Kimblin, B. M. Bridgewater, D. G. Churchill, T. Hascall, G. Parkin, *Inorg. Chem.* **2000**, *39*, 4240−4243.
[14] J. Seebacher, M. Shu, H. Vahrenkamp, *Chem. Commun.* **2001**, 1026−1027.
[15] J. Seebacher, H. Vahrenkamp, unpublished.
[16] In 2002 the Cambridge Crystallographic Data File had 76 entries for zinc complexes of thiourea-derived ligands.
[17] R. Castro, J. A. Garcia-Vazquez, J. Romero, A. Sousa, Y. D. Chang, J. Zubieta, *Inorg. Chim. Acta* **1995**, *237*, 143−146.
[18] H. Kayama, Y. Saito, *Bull. Chem. Soc. Jpn.* **1954**, *27*, 12−16.
[19] C. Kimblin, B. M. Bridgewater, D. G. Churchill, G. Parkin, *Chem. Commun.* **1999**, 2301−2302.
[20] S. Ramaswamy, H. Eklund, B. V. Plapp, *Biochemistry* **1994**, *33*, 5230−5237.
[21] R. Walz, H. Vahrenkamp, *Inorg. Chim. Acta* **2000**, *314*, 58−62.
[22] Y. Zhang, H. Vahrenkamp, *Inorg. Chim. Acta*, in print.
[23] M. Förster, R. Burth, A. K. Powell, T. Eiche, H. Vahrenkamp, *Chem. Ber.* **1993**, *126*, 2643−2648.
[24] R. Alsfasser, M. Ruf, S. Trofimenko, H. Vahrenkamp, *Chem. Ber.* **1993**, *126*, 703−710.
[25] J. Elguero, R. Jaquier, *Bull. Soc. Chim. Fr.* **1966**, 2832−2845.
[26] R. G. Jones, E. C. Kornfeld, K. C. McLaughlin, R. C. Anderson, *J. Am. Chem. Soc.* **1949**, *71*, 4000−4002.
[27] J. Kister, G. Assef, G. Mille, J. Metzger, *Can. J. Chem.* **1979**, *57*, 813−821.
[28] CCDC-203392 (**1c**), -203393 (**1d**), -203394 (**2a**), -203395 (**3a**), -203396 (**3b**), -203397 (**3c**), -203398 (**3d**), -203399 (**3f**), -203400 (**4a**), -203401 (**4b**), -203402 (**5**) and -156428 (**8**) contain the supplementary crystallographic data for this paper. These data can be obtained free of charge at www.ccdc.cam.ac.uk/conts/retrieving.html [or from the Cambridge Crystallographic Data Centre, 12 Union Road, Cambridge CB2 1EZ, UK; Fax: (internat.) + 44-1223/336-033; E-mail: deposit@ccdc.cam.ac.uk].
[29] *SHELXTL*, program package of the Bruker Smart CCD diffractometer, version 5.1, **2002**.
[30] E. Keller, *SCHAKAL for Windows*, Universität Freiburg, **1999**.
Received February 12, 2003

 © 2003 Wiley-VCH Verlag GmbH & Co. KGaA, Weinheim

Discrete Cyanide-Bridged Mixed-Valence Co/Fe Complexes: Outer-Sphere Redox Behaviour

Paul V. Bernhardt,[a] Fernando Bozoglian,[b] Brendan P. Macpherson,[a] Manuel Martínez,*[c] Gabriel González,[c] and Beatriz Sienra[b]

Keywords: Cobalt / Iron / Mixed-valence complexes / Redox processes

The outer-sphere redox behaviour of a series of $[L_nCo^{III}NCFe^{II}(CN)_5]^-$ (L_n = *n*-membered pentadentate aza-macrocycle) complexes have been studied as a function of pH and oxidising agent. All the dinuclear complexes show a double protonation process at pH ≈ 2 that produces a shift in their UV/Vis spectra. Oxidation of the different non-protonated and diprotonated complexes has been carried out with peroxodisulfate, and of the non-protonated complexes also with trisoxalatocobaltate(III). The results are in agreement with predictions from the Marcus theory. The oxidation of $[Fe(phen)_3]^{3+}$ and $[IrCl_6]^{2-}$ is too fast to be measured, although for the latter the transient observation of the process has been achieved at pH = 0. The study of the kinetics of the outer-sphere redox process, with the $S_2O_8^{2-}$ and $[Co(ox)_3]^{3-}$ oxidants, has been carried out as a function of pH, temperature, and pressure. As a whole, the values found for the activation volumes, entropies, and enthalpies are in the following margins, for the diprotonated and non-protonated dinuclear complexes, respectively: $\Delta V^{\neq}$ from 11 to 13 and 15 to 20 $cm^3\ mol^{-1}$; $\Delta S^{\neq}$ from 110 to 30 and –60 to –90 $J\ K^{-1}\ mol^{-1}$; $\Delta H^{\neq}$ from 115 to 80 and 50 to 65 $kJ{\cdot}mol^{-1}$. The thermal activation parameters are clearly dominated by the electrostriction occurring on outer-sphere precursor formation, while the trends found for the values of the volume of activation indicate an important degree of tuning due to the charge distribution during the electron transfer process. The special arrangement on the amine ligands in the isomer *trans*-$[L_{14}Co^{III}NCFe^{II}(CN)_5]^-$ accounts for important differences in solvent-assisted hydrogen bonding occurring within the outer-sphere redox process, as has been established in redox reactions of similar compounds.

(© Wiley-VCH Verlag GmbH & Co. KGaA, 69451 Weinheim, Germany, 2003)

Introduction

Mixed-valence compounds have been of interest for a long time,[1] given the variable nature of valence localisation (or delocalisation) and the nature and tunability of their MMCT bands.[2] Their potential use as possible electrochromic materials for a variety of situations has already been established.[3,4] As a whole, their redox properties are of great importance, both for their applications and for an understanding of their electronic structure.[5] Despite all these facts, few redox studies on these types of complexes are available in the literature,[6] due primarily to the typically limited stability of the oxidized or reduced species involved in the process. Indeed, few well-characterised discrete (non-polymeric) mixed-valence complexes are known that exhibit redox bistability. In this respect the preparation of a family of well-characterised cyanide-bridged compounds has provided an ideal entry into this field.[7–9]

We have been involved in the study of a number of outer-sphere redox reactions of Co^{III} macrocyclic complexes with $[Fe(CN)_6]^{4-}$, where the importance of solvent reorganisation, in the process, proved to be crucial to differences in the derived thermal and baric activation parameters.[10] Furthermore, the existence of a tight outer-sphere complexation, prior to the rate-determining electron transfer, has been found to be a dominant factor, even in situations where ion-pairing seems very unlikely.[11,12] From these studies, the formation of a discrete Co^{III}/Fe^{II} species, produced by an inner-sphere redox process starting from the reduced Co^{II} macrocyclic complexes and the corresponding $[Fe(CN)_6]^{3-}$ ligand, similar to those detected for the classical CoEDTA/$Fe(CN)_6$ systems has been envisaged.[13] Further studies on these compounds have led us to the full characterisation of a series of molecular mixed-valence $Fe^{II}CNCo^{III}$ complexes with different macrocycles and geometries surrounding the Co^{III} centre.[7–9] During this period, a few redox studies on discrete dinuclear Fe/Ru mixed-valence compounds have appeared,[14,15] but neither the pH

[a] Department of Chemistry, University of Queensland, Brisbane 4072, Australia
[b] Cátedra de Química Inorgánica, Facultad de Química, Universidad de la República
Avenida General Flores 2124, 11800 Montevideo, Uruguay
[c] Departament de Química Inorgànica, Universitat de Barcelona
Martí i Franquès 1–11, 08028 Barcelona, Spain
Supporting information for this article is available on the WWW under http://www.eurjic.org or from the author.

 © 2003 Wiley-VCH Verlag GmbH & Co. KGaA, Weinheim **DOI: 10.1002/ejic.200200626**

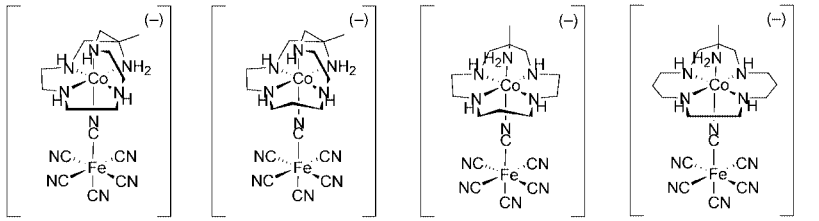

cis-$[L_{13}CoNCFe(CN)_5]^-$ *cis*-$[L_{14}CoNCFe(CN)_5]^-$ *trans*-$[L_{14}CoNCFe(CN)_5]^-$ *trans*-$[L_{15}CoNCFe(CN)_5]^-$

Scheme 1

dependence of such reactions nor the use of transition metal complexes as redox partners has been examined. Furthermore, the stability and full characterisation of the complexes involved was not achieved in some cases.

In this paper we present a mechanistic study of the outer-sphere oxidation processes of the complexes indicated in Scheme 1 with a variety of oxidants such as $S_2O_8^{2-}$, $[Co(ox)_3]^{3-}$, $[IrCl_6]^{2-}$, and $[Fe(phen)_3]^{3+}$. In this case the full characterisation of the reduced and oxidised species has already been carried out; the temperature, pressure, and pH dependence of these reactions has also been investigated.

The differences in macrocycle size and its geometrical wrapping arrangement, are bound to produce important differences in both the electron transfer process and the encounter complex formation equilibrium. The reduction potential of the iron centre being affected by the nature of the wrapped cobalt ion, and the encounter complex affected by the external shape of the macrocycle attached to the cobalt atom.

Results and Discussion

Products

All the complexes have been prepared and characterised according to published procedures[7–9] and there are no aspects that merit special mention. The new *cis*-$[L_{13}Co^{III}NCFe^{II}(CN)_5]^-$ complex behaves as the already known derivatives with macrocycles of different sizes. Given the fact that the outer-sphere redox behaviour of these dinuclear complexes was to be studied under different acidity conditions, and that the $[Fe(CN)_6]^{4-}$ moiety of the molecule is likely to undergo protonation at low pH,[16] speciation of the dinuclear complexes as a function of pH has been carried out. Figure 1 (top) shows typical electronic spectral shifts obtained when the solution of the mixed valence complex is taken from a high to low pH. Despite the two sets of different shifts observed in the spectra, for all the complexes studied, the potentiometric titration indicated a double protonation process at pH $\approx$ 2 that could not be resolved in two different steps. The SPECFIT analysis[17] of the changes shown in Figure 1 (top), indicated the effective presence of two protonation steps with distinct electronic spectra (Figure 1, bottom). The estimated values of pK_{a1} and pK_{a2} are, however, too close for a reliable differentiation, and selecting a pH value that ensured the presence

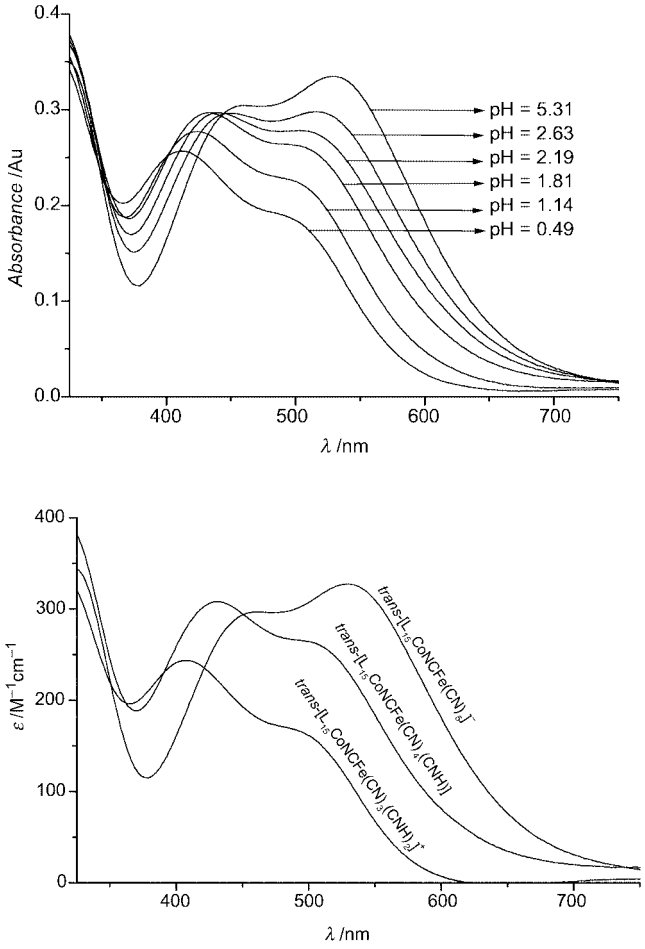

Figure 1. Top: UV/Vis spectral changes obtained for a solution 1×10^{-3} M of complex *trans*-$[L_{15}Co^{III}NCFe^{II}(CN)_5]^-$ on changing the acidity conditions; bottom: SPECFIT estimation of the UV/Vis spectra of the *trans*-$[L_{15}Co^{III}NCFe^{II}(CN)_5]^-$, *trans*-$[L_{15}Co^{III}NCFe^{II}(CN)_4(CNH)]$, and *trans*-$[L_{15}Co^{III}NCFe^{II}(CN)_3(CNH)_2]^+$ complexes for the same experiment (T = 298 K, I = 1.0 M $LiClO_4$)

of the monoprotonated complex, $[L_nCo^{III}NCFe^{II}(CN)_4(CNH)]$, as the main species in solution proved impossible.

As a result of this, the study has only been carried out on the complexes $[L_nCo^{III}NCFe^{II}(CN)_5]^-$ and $[L_nCo^{III}NCFe^{II}(CN)_3(CNH)_2]^+$. Table 1 includes all the spectroscopic data and $p\beta_{12}$ values determined spectrophotometrically for the series of dinuclear complexes included in this study. The diprotonated species are less stable than the corresponding non-protonated ones, with respect to de-

 © 2003 Wiley-VCH Verlag GmbH & Co. KGaA, Weinheim

Table 1. UV/Vis spectral and pβ_{12} data determined for the $[L_nCo^{III}NCFe^{II}(CN)_5]^-$ systems included in this study (T = 298 K, I = 1.0 M $LiClO_4$)

Species	λ_{max} [nm] (ε [$M^{-1}cm^{-1}$])	λ_{max} [nm] (ε [$M^{-1}cm^{-1}$])	λ_{max} [nm] (ε [$M^{-1}cm^{-1}$])	pβ_{12}
cis-$[L_{13}Co^{III}NCFe^{II}(CN)_5]^-$	325(367)	448(390)	498(380)	2.1
cis-$[L_{13}Co^{III}NCFe^{II}(CN)_4(CNH)_2]^+$	319(513)	390(377)	478(256)	
cis-$[L_{14}Co^{III}NCFe^{II}(CN)_5]^-$	328(480)	462(490)	504(500)	2.1
cis-$[L_{14}Co^{III}NCFe^{II}(CN)_4(CNH)_2]^+$	317(555)	392(375)	482(270)	
trans-$[L_{14}Co^{III}NCFe^{II}(CN)_5]^-$	324(410)	440(430)	513(490)	2.1
trans-$[L_{14}Co^{III}NCFe^{II}(CN)_4(CNH)_2]^+$	316(457)	388(352)	485(207)	
trans-$[L_{15}Co^{III}NCFe^{II}(CN)_5]^-$	328(410)	462(370)	530(420)	2.2
trans-$[L_{15}Co^{III}NCFe^{II}(CN)_4(CNH)_2]^+$	314(320)	392(211)	485(135)	

composition into their Co^{III} and Fe^{II} parents; nevertheless, on neutralization of the resulting solution, a recombination of the two metal centres takes place to form the mixed-valence dinuclear complex.[10] This lesser stability is not surprising, taking into account the increase of positive charge density introduced onto the dinuclear complexes by the double protonation. We have investigated the Fe-centered oxidation processes of these complexes by cyclic voltammetry at pH = 0, where all the compounds are doubly protonated (Table 2).

Table 2. Electrochemical Fe^{III}/Fe^{II} reduction data for the dinuclear complexes studied, protonated species in 1.0 M $HClO_4$, non-protonated in 1.0 M aqueous solution of $LiClO_4$

Species	$E^0(Fe^{III}/Fe^{II})$ [mV][a]
cis-$[L_{13}Co^{III}NCFe^{II}(CN)_5]$	626
cis-$[L_{13}Co^{III}NCFe^{II}(CN)_3(CNH)_2]^+$	775
cis-$[L_{14}Co^{III}NCFe^{II}(CN)_5]$	614
cis-$[L_{14}Co^{III}NCFe^{II}(CN)_3(CNH)_2]^+$	778
trans-$[L_{14}Co^{III}NCFe^{II}(CN)_5]$	644
trans-$[L_{14}Co^{III}NCFe^{II}(CN)_3(CNH)_2]^+$	775
trans-$[L_{15}Co^{III}NCFe^{II}(CN)_5]$	612
trans-$[L_{15}Co^{III}NCFe^{II}(CN)_3(CNH)_2]^+$	773

[a] Versus NHE, average value for the anodic and cathodic cyclic voltammogram peaks.

A positive shift of ca. 130−165 mV is observed for all the systems when two of the terminal cyanide ions are protonated on the reduced dinuclear complexes, which is in line with the general rule of increasing reduction potential on increasing the positive charge of the reduced species.[18] The same sort of changes have been observed for the reduction potential of hexacyanoferrates measured at 1.0 M HCl,[19] or when the $\{L_nCo^{III}\}$ moiety is attached to one of the cyanide ligands.[7,8] As for the possible protonation sites of the $[L_nCo^{III}NCFe^{II}(CN)_5]^-$ complexes, it is clear that they have to be at the axial and one of the equatorial positions of the $\{Fe(CN)_5\}$ fragment of the molecule. The protonation of two consecutive equatorial positions cannot be expected to have such similar pK_a values. In this respect the IR spectrum of protonated *cis*-$[L_{13}Co^{III}NCFe^{II}(CN)_3(CNH)_2]^+$ only shows the peak at 2120 cm^{-1} corresponding to the μ-CN and a rather broad band at 2055 cm^{-1}, which indicates the shifting to higher energies, as well as the loss in symmetry, due to protonation (Figure S1, Supporting Information, see also the footnote on the first page of this article).[20,21] In order for the integrity of the complex to be held, which prevents the formation of $Co_3[Fe^{III}(CN)_6]_2$, protonation of the amine groups of the macrocycle must not occur. The amine protons of the macrocycle are structurally (for any of the two possible conformations, *cis* or *trans*) too far away to prevent protonation of any of the equatorial cyanide groups on the iron centre. Furthermore the ^{13}C NMR spectrum of a sample of *trans*-$[L_{15}Co^{III}NCFe^{II}(CN)_5]^-$ in 1.0 M $HClO_4$ (Figure S2, Supporting Information) agrees with the integrity of the Co^{III} moiety of the complex.

Redox Kinetics

It has already been qualitatively established that a well-behaved redox process is observed for the oxidation of the *trans*-$[L_{15}Co^{III}NCFe^{II}(CN)_5]^-$ complex with the $S_2O_8^{2-}$ ion.[7] Despite its high standard potential (2010 mV), the electron transfer mechanism of the peroxodisulfate ion prevents the very fast reaction rate that would be expected,[22] producing a k_{ex} of ca. 10^{-18} M^{-1} s^{-1} by the direct application of the Marcus relationship.[23] Furthermore, no dependence on the pH is expected for the reduction potential in the acidity region used for this study. Given that some redox kinetics on dinuclear Ru/Fe mixed-valence compounds had already been studied with this oxidising agent,[24] the kinetics of the redox process between the $S_2O_8^{2-}$ ion and all the $[L_nCo^{III}NCFe^{II}(CN)_5]^-$ systems have also been studied. Figure 2 shows the general kinetic behaviour found for these systems at varying $[S_2O_8^{2-}]$, temperature and pH; second-order rate constants extrapolated at 298 K, and thermal and pressure activation parameters are collected in Table 3.

The reaction of the four dinuclear complexes prepared with $[Fe(phen)_3]^{3+}$ has also been probed, in this case the high reduction potential at pH = 0 (1050 mV)[25,26] produces a redox reaction rate so fast that it cannot be measured even with a stopped-flow system. That is, the spectra measured at 1:1 concentration ratios and at 0.8 ms after mixing correspond exactly to the 1:1 mixture of $[Fe(phen)_3]^{2+}$ and $[L_nCo^{III}NCFe^{II}(CN)_5]^-$. In this case it seems clear that the reaction rate is extremely fast, as ex-

 © 2003 Wiley-VCH Verlag GmbH & Co. KGaA, Weinheim

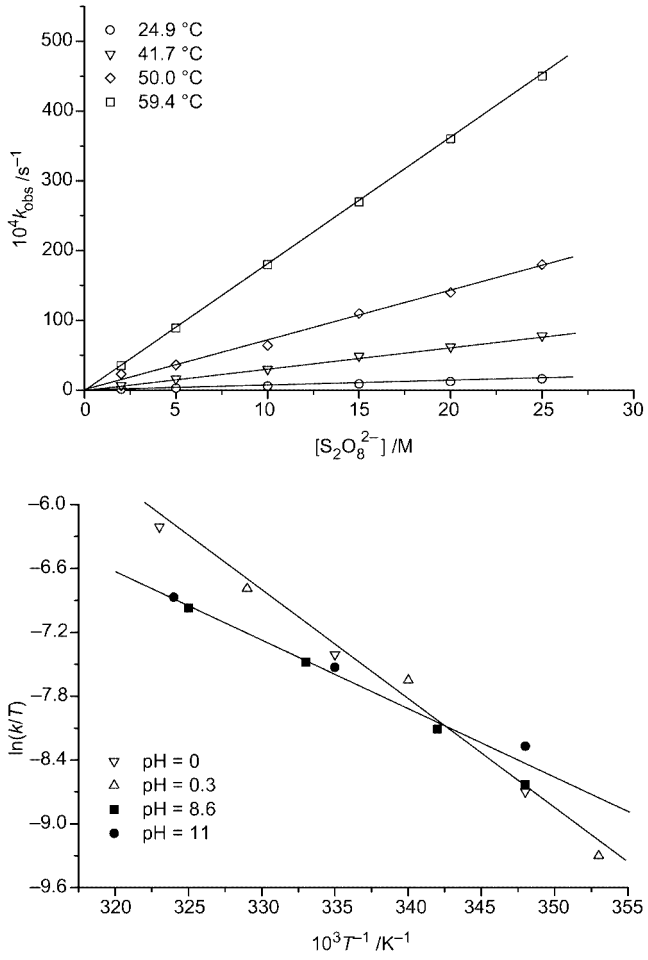

Figure 2. Top: plot of the values of the first-order rate constant, k_{obs}, for the $S_2O_8^{2-}$ oxidation of the *trans*-$[L_{14}Co^{III}NCFe^{II}(CN)_3(CNH)_2]^+$ complex at different temperatures; bottom: Eyring plot derived from the value of the second-order rate constant, k, for the *trans*-$[L_{15}Co^{III}NCFe^{II}(CN)_5]^-$ (pH = 8.6 and 11) and *trans*-$[L_{15}Co^{III}NCFe^{II}(CN)_3(CNH)_2]^+$ (pH = 0.0 and 0.3) plus $S_2O_8^{2-}$ systems (I = 1.0 M $LiClO_4$)

pected from the calculated value of E^0 = 275 mV and the validity of the Marcus relationship for these systems ($k_{ex}\{[Fe(phen)_3]^{3+/2+}\}$ = 1.3 × 10^7 M^{-1} s^{-1} and $k_{ex}\{[Fe(CN)_6]^{3-/4-}\}$ = 2.4 × 10^2 to 2 × 10^4 M^{-1} s^{-1}),[26,27] which produces an estimated cross reaction rate constant of 7.1 × 10^6 to 10 × 10^7 M^{-1} s^{-1} for the adiabatic redox process occurring on the iron moiety of the dinuclear complex.[28] The instability of $[Fe(phen)_3]^{3+}$ in solutions at higher pH prevented oxidation measurements on the non-protonated $[L_nCo^{III}NCFe^{II}(CN)_5]^-$ complexes.

The reaction with $[IrCl_6]^{2-}$ was also tried, given the lower potential (892 mV),[29] as well as its independence of pH in the range used for this study. At pH = 0, the transient spectrum measured at 0.8 ms after mixing $[IrCl_6]^{2-}$ and $[L_nCo^{III}NCFe^{II}(CN)_5]^-$ in a 1:1 ratio, effectively shows the presence of an Ir^{IV} oxidising agent which disappears in less than 0.05 s under these second-order conditions. This process could not be observed at pH = 5, where the initial spectrum after mixing corresponds exactly to a 1:1 mixture of the oxidised $[L_nCo^{III}NCFe^{III}(CN)_5]$ complexes and the Ir^{III} species. Taking into account that the redox reaction of $[Fe(CN)_6]^{4-}$ with $[IrCl_6]^{2-}$ has already been measured, and that the values found fit very well with the Marcus relationship,[30] the estimated values of $k_{ex}\{[L_nCoNCFe(CN)_5]^{0/-}\}$ for the different dinuclear systems cannot be smaller than that for the $[Fe(CN)_6]^{3-/4-}$ simple system. Taking into account that the reduction potential of $[Fe(CN)_6]^{3-/4-}$ at 1.0 M HCl is 688 mV;[19] if a nitrogen atom of one of the cyanide ligands of the hexacyanoferrate(II) has a proton, or an electron-withdrawing Co^{III} centre of the dinuclear complex attached, both the value of k_{ex} and that of E^0 seem to increase significantly.

Further inspection of the available oxidants with the appropriate potentials[26] indicated that $[Co(ox)_3]^{3-}$ should be an excellent partner for the process (570 mV[31] and $k_{ex}\{[Co(ox)_3]^{3-/4-}\}$ = 3 × 10^{-7} to 1.4 × 10^{-12} M^{-1} s^{-1}).[32,33] Consequently, the oxidation of the $[L_nCo^{III}NCFe^{II}(CN)_5]^-$ species with tris(oxalato)cobaltate-

Table 3. Kinetic (extrapolated at 298 K) and thermal and baric activation parameters for the oxidation processes studied (I = 1.0 M $LiClO_4$)

Species	Oxidant	k^{298} [M^{-1} s^{-1}]	$\Delta H^{\neq}$ [kJ mol^{-1}]	$\Delta S^{\neq}$ [J K^{-1} mol^{-1}]	$\Delta V^{\neq}$ [cm^3 mol^{-1}]
cis-$[L_{13}Co^{III}NCFe^{II}(CN)_3(CNH)_2]^+$	$S_2O_8^{2-}$	6.98	114±9	114±29	12.7±0.8
cis-$[L_{13}Co^{III}NCFe^{II}(CN)_5]^-$	$S_2O_8^{2-}$	6.24	63±3	58±10	19.6±2.0
	$[Co(ox)_3]^{3-}$	0.121[a]	65±3	86±10	14.6±1.1
cis-$[L_{14}Co^{III}NCFe^{II}(CN)_3(CNH)_2]^+$	$S_2O_8^{2-}$	7.40	109±7	98±22	10.6±1.2
cis-$[L_{14}Co^{III}NCFe^{II}(CN)_5]^-$	$S_2O_8^{2-}$	6.80	58±6	72±20	19.7±0.6
	$[Co(ox)_3]^{3-}$	0.128[a]	68±5	73±17	16.9±2.2
trans-$[L_{14}Co^{III}NCFe^{II}(CN)_3(CNH)_2]^+$	$S_2O_8^{2-}$	5.61	80±2	2±7	1.5±0.1
trans-$[L_{14}Co^{III}NCFe^{II}(CN)_5]^-$	$S_2O_8^{2-}$	4.95	61±1	65±3	4.1±0.1
	$[Co(ox)_3]^{3-}$	0.103[a]	51±2	131±8	11.5±1.4
trans-$[L_{15}Co^{III}NCFe^{II}(CN)_3(CNH)_2]^+$	$S_2O_8^{2-}$	17.6	85±4	23±15	11.4±0.7
trans-$[L_{15}Co^{III}NCFe^{II}(CN)_5]^-$	$S_2O_8^{2-}$	16.2	55±5	76±16	19.1±1.7
	$[Co(ox)_3]^{3-}$	0.113[a]	63±6	90±19	17.9±1.9

[a] In s^{-1}, K_{OS} in the 50−200 M^{-1} range for all the systems studied.

 © 2003 Wiley-VCH Verlag GmbH & Co. KGaA, Weinheim

(III) at pH = 9 was carried out at different temperatures, concentrations, and pressures. Unfortunately, the stability of this complex is not very high and, although it could be used at pH = 9 by adding some EDTA to the solution medium to avoid precipitation of Co^{2+} salts, no studies could be carried out at pH = 0, where the decomposition of the tris(oxalato) complex was too fast when compared with the redox process studied. Figure 3 shows the general kinetic behaviour of the observed reaction rate constants under pseudo-first-order conditions. In this case, as seen in Figure 3, the kinetic behaviour is a bit more complex than with the $S_2O_8^{2-}$ oxidant, and a limiting outer-sphere (OS) precursor formation is observed according to $k_{obs} = (k_{et} \times K_{OS} \times [oxidant])/(1 + K_{OS} \times [oxidant])$. The value of k_{et} can be derived from the asymptotic limit of the plots. The temperature and pressure dependence of the derived rate constants produced the thermal and pressure activation parameters are shown in Table 3, together with the corresponding kinetic parameters extrapolated to 298 K.

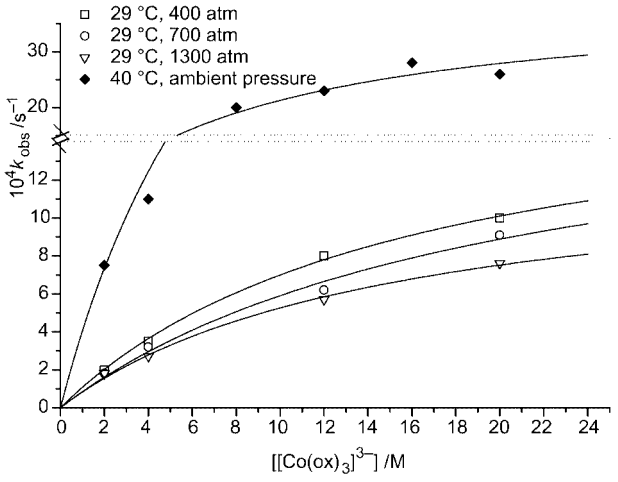

Figure 3. Plot of the values of the first-order rate constant, k_{obs}, for the $[Co(ox)_3]^{3-}$ oxidation of the *cis*-$[L_{13}Co^{III}NCFe^{II}(CN)_5]^-$ system at different temperatures and pressures and at pH = 9.0 (I = 1.0 M $LiClO_4$)

From a general point of view, the redox reaction with peroxodisulfate as oxidant seems to provide more information about the process studied, because it can be carried out at acidic, alkaline, or neutral pH (i.e. with the doubly protonated and non-protonated dinuclear complexes). A detailed observation of the activation parameters results in a clear differentiation between the non-protonated or diprotonated form of the dinuclear species, despite the minor differences found in k^{298}. Activation enthalpies are much higher for the diprotonated complexes and activation entropies are also more positive. These much more positive values for $\Delta S^{\neq}$ found for the $[L_nCo^{III}NCFe^{II}(CN)_3(CNH)_2]^+$ series of complexes, are indicative of the large differences in electrostriction on going from the reactants to the precursor outer-sphere complex involving the $SO_4^{(\cdot)}$ radical ({[1+] + [1−]} at low pH versus {[1−] + [1−]} for the non-protonated complex). These differences are compensated by larger values of $\Delta H^{\neq}$, producing the compensation plot shown in Figure 4, which is a clear indication of the constant reaction mechanism operating for these processes.

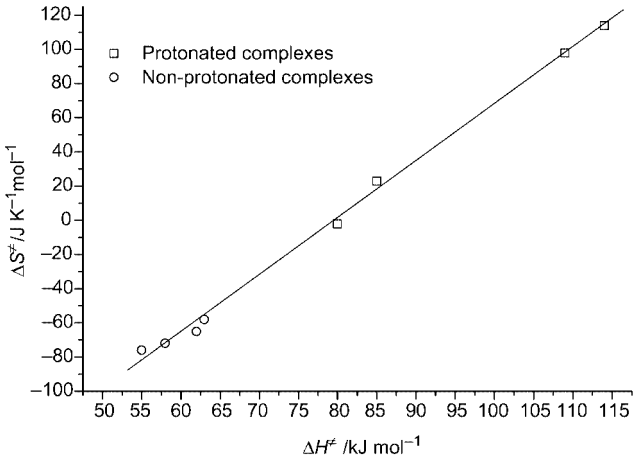

Figure 4. Compensation $\Delta H^{\neq}/\Delta S^{\neq}$ plot for the $S_2O_8^{2-}$ oxidation reactions studied for the *trans*-$[L_{15}Co^{III}NCFe^{II}(CN)_5]^-$/*trans*-$[L_{15}Co^{III}NCFe^{II}(CN)_3(CNH)_2]^+$ dinuclear complexes

Another surprising fact is that for the *trans*-arranged dinuclear complexes of the L_{14} and L_{15} macrocycles, the above-mentioned differences in the activation enthalpies and entropies decrease severely. Some ordering, relating to the geometrical arrangement of the macrocyclic ligand, in the transition state, or the precursor complex, must be responsible for the dramatic decrease of the $\Delta S^{\neq}$ values for the reaction with the protonated complex. The relative positions of a protonated equatorial CN group and the facing secondary amine protons of the macrocycle,[7−9] easily allow for a much more ordered positioning of the $SO_4^{(\cdot)-}$ radical in the outer sphere for the $[L_nCo^{III}NCFe^{II}(CN)_5]^-$ complex, producing an important decrease in the $\Delta S^{\neq}$ values. If that is so, the general enthalpic demands for the transition state for the electron transfer on such a precursor are bound to be smaller as seen in the data for all the $[L_nCo^{III}NCFe^{II}(CN)_3(CNH)_2]^+$ complexes in reactions with the $S_2O_8^{2-}$ ion (Table 3).

As for the activation volumes, when the oxidation takes place on the non-protonated species the values determined for $\Delta V^{\neq}$ are more positive. Given that the electrostriction on going to the precursor outer-sphere complex would produce the opposite trend, as explained before, the sequence of values found for $\Delta V^{\neq}$ has to be dominated by the proper electrostriction effect occurring during the electron transfer process on the dinuclear species. At low pH the charge of the complex increases from [1+] to [2+] on electron transfer, while it decreases from [1−] to [0] for the non-protonated complex; consequently, the actual electron transfer process at low pH implies an increase on electrostriction with respect to a decrease at high pH. Nevertheless, the general important expansion observed, for all but the $[L_nCo^{III}NCFe^{II}(CN)_5]^-$ complex, must originate in solvent-assisted hydrogen bonding within the precursor complex,

 © 2003 Wiley-VCH Verlag GmbH & Co. KGaA, Weinheim

producing an important ordered expansion.[34] This fact also explains the inherent ordering derived from the values of $\Delta S^{\neq}$ that were obtained for the $[L_nCo^{III}NCFe^{II}(CN)_5]^-$ complex in reactions with the $S_2O_8^{2-}$ ion. This expansion/ordering combination must be much smaller for the protonated systems where solvent-assisted hydrogen bonding becomes less important.[10−12] For the $[L_n$-$Co^{III}NCFe^{II}(CN)_5]^-$ system, the values found for the activation entropy at low pH already indicated a unique behaviour of the system. If the possible explanation cited above, derived from the facing secondary amine protons of the macrocycle, is so, solvent assistance for the positioning of the $SO_4^{(\cdot)-}$ radical in the outer sphere of the protonated species should be even less important. As a consequence, the values of $\Delta V^{\neq}$ for those complexes with much less solvent-assisted hydrogen bonding takes place, would tend to the expected contraction values, both from electron transfer electrostriction (specially for the oxidation of the diprotonated species) and inner-sphere contributions.

With respect to the $[Co(ox)_3]^{3-}$ oxidation data in Table 3, the thermal activation parameters are similar to those obtained for the $S_2O_8^{2-}$ oxidation process, with the non-protonated $[L_nCo^{III}NCFe^{II}(CN)_5]^-$ complexes. The fact that, in this case, the values determined for k^{298} correspond to the first-order rate constant (see Figure 3), only relates the activation parameters to the electron transfer process, the outer-sphere equilibrium constant being in the range 50−200 M^{-1}, which is similar to that found for similar systems.[10−12,27,35,36] The values determined for $\Delta H^{\neq}$ are practically the same as those found for the $S_2O_8^{2-}$ reaction, as expected given the small values associated with ΔH^0_{OS}, while those for $\Delta S^{\neq}$ are definitively more negative. Given the fact that no electrostriction related to the outer-sphere precursor complex formation is accounted for, and that no protonated species are present at this pH, the high degree of ordering approaching the transition state has to be related with the above-mentioned formation of solvent-assisted interactions during the electron transfer process. These types of interactions have also been held responsible for the behaviour of other systems,[37] and have explained the ordering/expansion effect detected in the previously discussed $[L_nCo^{III}NCFe^{II}(CN)_5]^-/S_2O_8^{2-}$ redox processes, where outer-sphere electrostriction is held to a minimum. In this respect, the values determined for the activation volumes are positive in all cases and are very similar to those determined for the reaction with the peroxodisulfate anion. Again, the value determined for the *trans*-$[L_{14}Co^{III}NCFe^{II}(CN)_5]^-$ complex is smaller than the rest, although it does not reach the extremely low values found for the peroxodisulfate reaction. Solvent assistance in outer-sphere complexation during electron transfer, can again be held responsible for the this decrease.

In conclusion, we have been able to completely characterise the solution redox behaviour of a complete family of discrete cyano-bridged mixed-valence Co^{III}/Fe^{II} complexes. Further studies are being carried out in order to increase the stabilisation of the Co^{II}/Fe^{II} oxidation state of the complex by tuning of the donor atoms in the macrocycle, which should allow for a wider accessibility of the redox systems.

Experimental Section

Products: All the dinuclear Co^{III}/Fe^{II} complexes have been prepared according to published procedures. The synthesis of *trans*- and *cis*-$[L_{14}Co^{III}NCFe^{II}(CN)_5]^-$ and *trans*-$[L_{15}Co^{III}NCFe^{II}(CN)_5]^-$ (isolated as their Na^+ salts) have been reported.[7−9] The analogue *cis*-$[L_{13}Co^{III}NCFe^{II}(CN)_5]^-$ has been prepared by the same procedure starting from *cis*-$[CoL_{13}Cl]^{2+}$.[38] Characterisation data for $Na[L_{13}$-$Co^{III}NCFe^{II}(CN)_5]$: $C_{16}H_{25}CoFeN_{11}Na\cdot 11H_2O$ (707.39): calcd. C 27.17, H 6.70, N 21.78; found C 27.2, H 8.6, N 22.2. ^{13}C NMR (62.9 MHz, D_2O): δ = 19.6, 49.0, 51.1, 51.9 (× 2), 53.5, 55.8, 56.4, 66.6, 175.0 (× 5), 191.0 ppm. IR (KBr disk): $\tilde{\nu}$ = 2040 (equatorial CN), 2072 (axial CN), 2115 (μ-CN) cm^{-1}. UV/Vis (H_2O): λ_{max} (ε) = 325 (367), 448 (390), 498 nm (380 $M^{-1}cm^{-1}$). Cyclic voltammogram $E_{1/2}$ (versus NHE; 1.0 M $LiClO_4$) = −543, 626 mV. The oxidants $[Co(ox)_3]^{3-}$ and $[Fe(phen)_3]^{3+}$ were prepared according to published procedures.[39−41] Other chemicals used were analytical grade, commercially available, and were used without further purification. All buffers were prepared according to well-established procedures.[42] The buffer concentration was set to 0.01 M, and final pH values were such that only one of the acid-base equilibrium species of each system was present in solution. Ionic strength was achieved by the addition of $LiClO_4$.

Acidity Constants: Potentiometric titrations (1.0 M, $HClO_4$) of the different dinuclear $[L_nCo^{III}NCFe^{II}(CN)_5]^-$ complexes were carried out in order to determine their acidity constants. The solutions were transferred to a 50 mL cell and thermostatted at 25 °C; addition of small amounts of standard 0.1 M NaOH produced successive e.m.f. readings on a Metrohm 713 pH meter (glass and Ag/AgCl reference electrodes). Argon was bubbled through the solution during the experiment to avoid the presence of CO_2. The general technique was the same as that described in the literature;[43] even though only one step was detected, the stoichiometry indicated a double deprotonation. Spectrophotometric titrations[44] of the complexes carried out with a Cary 50 instrument produced changes in the UV/Vis spectrum with pH (Figure 1, top) which indicated the presence of two distinct processes. Nevertheless, the pK_a values were too close to allow the selective formation of the monoprotonated complex,[18] and consequently only studies on the non-protonated and diprotonated species were carried out.

Electrochemistry: Electrochemical experiments were carried out with an EG&G PAR 263A instrument with a glassy carbon working electrode, a platinum wire secondary electrode and an Ag/AgCl reference electrode; solutions were degassed prior to the cyclic voltammetry experiment. Voltammograms of the complexes were carried out at 1×10^{-3} M complex concentration in water (1.0 M $LiClO_4$) and in 1.0 M $HClO_4$ in order to account for differences due to the protonation of the cyanide ligands.

Kinetics: The reactions were monitored by UV/Vis spectroscopy in the 800−300 nm range; runs with $t > 170$ s were recorded with an HP8452A instrument equipped with a thermostatted multicell transport; runs within the 7−170 s margin were recorded with an HP8452A or a J&M TIDAS instrument and using a High-Tech SFA-11 Rapid Kinetics Accessory. For the kinetic runs at elevated pressure, a previously described pressurizing system, and cylindrical or pillbox cell were used.[45,46] Observed rate constants were derived from absorbance/time traces at the wavelengths where a maximum increase or decrease of absorbance was observed; Table

 © 2003 Wiley-VCH Verlag GmbH & Co. KGaA, Weinheim

S1 (Supporting Information) indicates all the obtained k_{obs} values for all the complexes studied as a function of the reducing and oxidising species, their concentration, pH, temperature, and pressure. No dependence of the observed rate constants on the selected wavelengths was detected, as generally expected for reactions where a good retention of isosbestic points is observed. The general kinetic technique was that previously described; in all cases pseudo-first-order conditions were maintained.[11,12] For reactions involving $[Co(ox)_3]^{3-}$, EDTA was added to the reaction medium to prevent the precipitation of the Co^{2+} reaction product.[10,47]

Acknowledgments

We acknowledge financial support for the BQU2001-3205 project from the Ministerio de Ciencia y Tecnología and the Australian Research Council (Grant 00/ARCL073G). Financial support from AECI (ICI) is also acknowledged. Helpful comments from Dr. Julia Torres are gratefully acknowledged.

[1] J. H. Buser, A. Ludi, *J. Chem. Soc., Chem. Commun.* **1972**, 1299.
[2] M. B. Robin, P. Day, *Adv. Inorg. Chem. Radiochem.* **1967**, *10*, 247.
[3] K. R. Dunbar, R. A. Heintz, *Prog. Inorg. Chem.* **1997**, *45*, 283.
[4] R. J. Mortimer, *Chem. Soc., Rev.* **1997**, *26*, 147.
[5] N. S. Hush, *Prog. Inorg. Chem.* **1967**, *8*, 391.
[6] D. E. Khoshtariya, H. C. Bajaj, P. Tregloan, R. van Eldik, *J. Phys. Chem. A* **2000**, *104*, 5535.
[7] P. V. Bernhardt, M. Martínez, *Inorg. Chem.* **1999**, *38*, 424.
[8] P. V. Bernhardt, B. P. Macpherson, M. Martínez, *Inorg. Chem.* **2000**, *39*, 5203.
[9] P. V. Bernhardt, B. P. Macpherson, M. Martínez, *J. Chem. Soc., Dalton Trans.* **2002**, 1435.
[10] M. Martínez, M. A. Pitarque, R. van Eldik, *Inorg. Chim. Acta* **1997**, *256*, 51.
[11] M. Martínez, M. A. Pitarque, *J. Chem. Soc., Dalton Trans.* **1995**, 4107.
[12] M. Martínez, M. A. Pitarque, R. van Eldik, *J. Chem. Soc., Dalton Trans.* **1994**, 3159.
[13] D. H. Huchital, R. G. Wilkins, *Inorg. Chem.* **1967**, *6*, 1022.
[14] A. R. Parise, L. M. Baraldo, J. A. Olabe, *Inorg. Chem.* **1996**, *35*, 5080.
[15] P. Pereztejeda, P. Neto-Ponce, F. Sánchez, *J. Chem. Soc., Dalton Trans.* **2001**, 1686.
[16] J. Jordan, G. J. Ewing, *Inorg. Chem.* **1962**, *1*, 587.
[17] R. A. Binstead, A. D. Zuberbühler, *SPECFIT version 2.10*, Spectrum Software Associates, Malborough, **1996**.
[18] G. Charlot, *Les Reactions Chimiques en Solution − L'Analyse Quantitative Minerale*, Masson, Paris, **1969**.
[19] J. M. Leal, P. L. Domingo, B. García, S. Ibeas, *J. Chem. Soc., Faraday Trans.* **1993**, *89*, 3571.
[20] B. I. Swanson, J. J. Rafalko, *Inorg. Chem.* **1976**, *15*, 253.
[21] K. Nakamoto, *Infrared and Raman Spectra of Inorganic and Coordination Compounds*, Wiley, New York, **1997**.
[22] D. House, *Chem. Rev.* **1962**, 185.
[23] U. Fürholz, A. Haim, *Inorg. Chem.* **1987**, *26*, 3243.
[24] A. E. Almaraz, L. A. Gentil, L. M. Baraldo, J. A. Olabe, *Inorg. Chem.* **1996**, *35*, 7718.
[25] H. Doine, T. W. Swaddle, *Can. J. Chem.* **1988**, *66*, 2763.
[26] A. G. Lappin, *Redox Mechanisms in Inorganic Chemistry*, Ellis Horwood, New York, **1994**.
[27] A. Zahl, R. van Edlik, T. W. Swaddle, *Inorg. Chem.* **2002**, *41*, 757.
[28] R. A. Marcus, *Angew. Chem. Int. Ed. Engl.* **1993**, *32*, 1111.
[29] D. W. Margerum, K. L. Chellappa, F. P. Bossu, G. L. Burce, *J. Am. Chem. Soc.* **1975**, *97*, 6894.
[30] R. J. Campion, N. Purdie, N. Sutin, *Inorg. Chem.* **1964**, *3*, 1091.
[31] R. A. Marusak, P. Osvath, M. Kemper, A. G. Lappin, *Inorg. Chem.* **1989**, *28*, 1542.
[32] J. O. Ehighaokhuo, J. F. Ojo, O. J. Olubuyide, *J. Chem. Soc., Dalton Trans.* **1985**, 1665.
[33] R. A. Holwerda, D. B. Knaff, H. B. Gray, J. D. Clemmer, R. Crowley, J. M. Smith, A. G. Mauk, *J. Am. Chem. Soc.* **1980**, *102*, 1142.
[34] G. González, M. Martínez, E. Rodríguez, *J. Chem. Soc., Dalton Trans.* **1995**, 891.
[35] R. M. L. Warren, A. G. Lappin, A. Tatehata, *Inorg. Chem.* **1992**, *31*, 1566.
[36] M. Martínez, M. A. Pitarque, R. van Eldik, *J. Chem. Soc., Dalton Trans.* **1996**, 2665.
[37] D. A. Geselowitz, A. Hammershoi, H. Taube, *Inorg. Chem.* **1987**, *26*, 1842.
[38] G. A. Lawrance, T. M. Manning, M. Maeder, M. Martínez, M. A. O'Leary, W. C. Patalinghug, B. W. Skelton, A. H. White, *J. Chem. Soc., Dalton Trans.* **1992**, 1635.
[39] A. A. Schilt, R. C. Taylor, *J. Inorg. Nucl. Chem.* **1959**, *9*, 211.
[40] J. C. Bailar, J. E. M. Jones, *Inorg. Synth.* **1939**, *1*, 550.
[41] J. Macyk, R. van Eldik, *J. Chem. Soc., Dalton Trans.* **2001**, 2288.
[42] D. D. Perrin, *Aust. J. Chem.* **1963**, *16*, 572.
[43] J. Torres, C. Kremer, E. Kremer, H. Pardo, L. Suescun, A. Mombru, S. Domingo, A. Mederos, *J. Alloy Comp.* **2001**, *323−324*, 119.
[44] H. H. Perkampus, *UV-Vis Spectroscopy and its Applications*, Springer, Berlin, **1992**.
[45] M. G. Basallote, J. Durán, M. J. Fernández-Trujillo, G. González, M. A. Máñez, M. Martínez, *Inorg. Chem.* **1998**, *37*, 1623.
[46] M. G. Basallote, J. Durán, M. J. Fernández-Trujillo, G. González, M. A. Máñez, M. Martínez, *J. Chem. Soc., Dalton Trans.* **1999**, 3379.
[47] D. Gaswick, A. Haim, *J. Am. Chem. Soc.* **1971**, *93*, 7347.

Received November 15, 2002

 © 2003 Wiley-VCH Verlag GmbH & Co. KGaA, Weinheim

EPR Study of *o*-Semiquinone-Catecholate Cobalt Complexes with Bis(diphenylphosphanyl)ethane

Michael P. Bubnov,*[a] Irina A. Teplova,[a] Vladimir K. Cherkasov,[a] and Gleb A. Abakumov[a]

Keywords: Chelates / Cobalt / EPR spectroscopy / Quinones / Tautomerism

Three novel cobalt compounds with bis(diphenylphosphanyl)-ethane (dppe) and semiquinone and catecholate ligands were synthesized and investigated by EPR spectroscopy in solution. They are: [(dppe)Co(3,6-DBSQ)(Cat_{ox}^{Cl})] (**1**), [(dppe)Co(3,6-DBCat)(phen-SQ)] (**2**), and [(dppe)Co(3,6-DBSQ)$_2$] (**3**), where 3,6-DBSQ and 3,6-DBCat are the radical anion and dianion of 3,6-di-*tert*-butyl-*o*-benzoquinone, respectively, Cat_{ox}^{Cl} is the dianion of perchloroxanthrenequinone-2,3, and phen-SQ is the radical anion of phenanthrenequinone. According to the ratio of the redox potentials of the *o*-quinone fragments, **1** and **2** are mixed semiquinone-catecholate complexes, and the 3,6-di-*tert*-butyl-*o*-quinone fragment appears as a semiquinone in **1** and as a catecholate in **2**. Compound **3** exists as a mixture of redox isomers, namely semiquinone-catecholate and bis-semiquinone species.

(© Wiley-VCH Verlag GmbH & Co. KGaA, 69451 Weinheim, Germany, 2003)

Introduction

In 1980, Pierpont first observed a reversible intramolecular metal−ligand electron transfer of a cobalt bis-semiquinone complex in solution.[1]

$$[\alpha,\alpha'\text{-bpyCo}^{III}(3,5\text{-Cat})(3,5\text{-SQ})] \rightleftarrows [\alpha,\alpha'\text{-bpyCo}^{II}(3,5\text{-SQ})_2]$$

3,5-SQ and 3,5-Cat are the anion-radical and dianion of 3,5-di-*tert*-butyl-*o*-benzoquinone.

A similar equilibrium involving a two-electron transfer was described later[2] for the manganese complex [(py)$_2$Mn(3,5-DBCat)$_2$].

$$[(py)_2Mn(3,5\text{-DBCat})_2] \rightleftarrows [(py)_2Mn(3,5\text{-DBSQ})_2]$$

Reversible electron transfer, taking place in the solid state, was first observed by our group[3,4] in 1990 and by Hendrickson[5] in 1993. Further development of the understanding of reversible metal−ligand electron transfer in semiquinone metal complexes was dedicated to investigation of solid-phase transformations.[6−14]

Number of mono-semiquinone complexes of Rh,[15−18] Ir,[19] Cu,[20] and Ni[21] of general formula [L_nMSQ] demonstrate reversible electron transfer in solution (L_n is a neutral ligand for Rh, Ir, and Cu, or monovalent one for Ni). It has been shown that complexes exist in solution as an equilibrium mixture of redox isomers that interconvert rapidly (according to the EPR time scale) between one another. The equilibrium position and the rate of isomerization depend on the nature of the *o*-semiquinone, the neutral ligands, and the solvent. In all cases, decreasing the temperature shifts the equilibrium position towards the catecholate isomer.

All of the complexes [L_nM("Q")$_2$] that were investigated to date contain "Q" fragments that are derivatives of the same quinone and so their initial electronic ground state a priori is degenerate. The aim of this work was to obtain six-coordinate cobalt complexes containing different *o*-quinone fragments.

Most of publications listed above are dedicated to complexes containing nitrogen atom donors. We have not found in the literature any bis-quinone complexes with dppe. Moreover dppe contains two phosphorous atoms (^{31}P, I = 1/2, 100%), the hyperfine splitting of which in the EPR spectrum provides information regarding the spin distribution in complex molecules.

Results and Discussion

Cobalt compounds of types **1**−**3** can be obtained through oxidative addition reactions of the corresponding *o*-quinones to four-coordinate [(dppe)(3,6-di-*tert*-butylcatecholato)cobalt] [Equation (1)].

$$[L_nCo^{II}(Cat')] + Q'' \rightarrow [L_nCo^{III}(Cat')(SQ'')] \quad (1)$$

Stable paramagnetic adducts were studied by EPR spectroscopy in solution. The appearance of the EPR spectrum

[a] G. A. Razuvaev Institute of Organometallic Chemistry of RAS, 49 Tropinina str., Nizhny Novgorod, GSP-445, Russia 603950
Fax: (internat.) + 7-8312/661-497
E-mail: bmp@imoc.sinn.ru

of a particular product depends on the redox potential ratio of the quinone fragments. We have observed three situations.

The first takes place when additional quinone is quite a stronger acceptor than is 3,6-DBQ, which has formed the initial catecholate. We have used perchlorooxanthrenequinone-2,3 [Equation (2)].

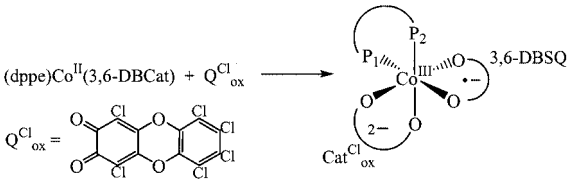

(2)

The presented EPR spectrum (Figure 1) displays one unpaired electron localized on the 3,6-DBSQ fragment: $a_{H1(SQ)} = a_{H2(SQ)} = 0.30$ mT, $g_i = 2.0016 \pm 0.0005$. Perchloroxanthrenequinone receives two electrons and becomes a catecholate dianion. The cobalt atom is oxidized from the oxidation state +2 to +3. The different hyperfine coupling constants on the ^{31}P nuclei ($a_{P2} = 1.30$ mT, $a_{P1} = 0.30$ mT) reflect planar and apical positions of the corresponding nuclei with respect to the plane of the *o*-semiquinone.[22,23] The coupling constant on ^{59}Co ($a_{Co} = 1.00$ mT) are typical for octahedral *o*-semiquinone-catecholate complexes of cobalt(III) with one unpaired electron localized primarily (> 99% according to ref.[15]) on the semiquinone unit.[1] Thus, the result is a six-coordinate semiquinone-catecholate complex of low-spin cobalt(III).

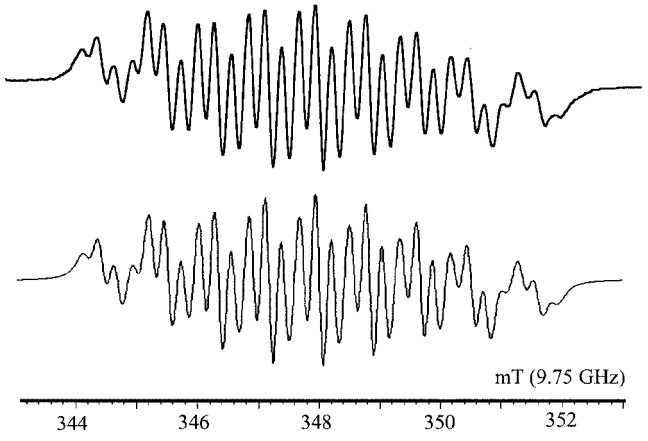

Figure 1. Room temperature x-band EPR spectrum (top) of [(dppe)Co(3,6-DBSQ)(Cat$^{Cl}_{ox}$)] (**1**) (toluene, 290 K) and (bottom) its simulation (EPR line width = 0.2 mT)

The second situation occurs when the additional quinone is a quite-weaker acceptor than is quinone, which has formed the initial catecholate; e.g., when it is phenanthrenequinone [Equation (3)].

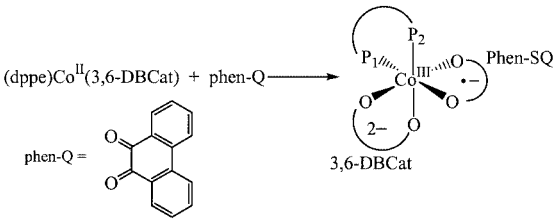

(3)

The hyperfine coupling with protons of 3,6-DBSQ is absent ($g_{iso} = 2.0016 \pm 0.0005$, Figure 2). Only hyperfine coupling is observed with ^{59}Co and one $^{31}P_2$ ($a_{Co} \approx a_{P2} \approx 0.85$ mT). The interaction with the protons of phen-SQ and P_1 is unresolved because of a relatively large line width. The spectrum view changes slightly with temperature. Optimal resolution was achieved at 250 K. An acceptable simulation indicates an essentially larger line width than was observed in the case **1** (0.20 mT for **1** and 0.73 mT for **2**). Diminution of the ^{59}Co and ^{31}P coupling constants is expected. This feature is explained by lower acceptor properties of phen-Q relative to 3,6-DBQ.[24,25]

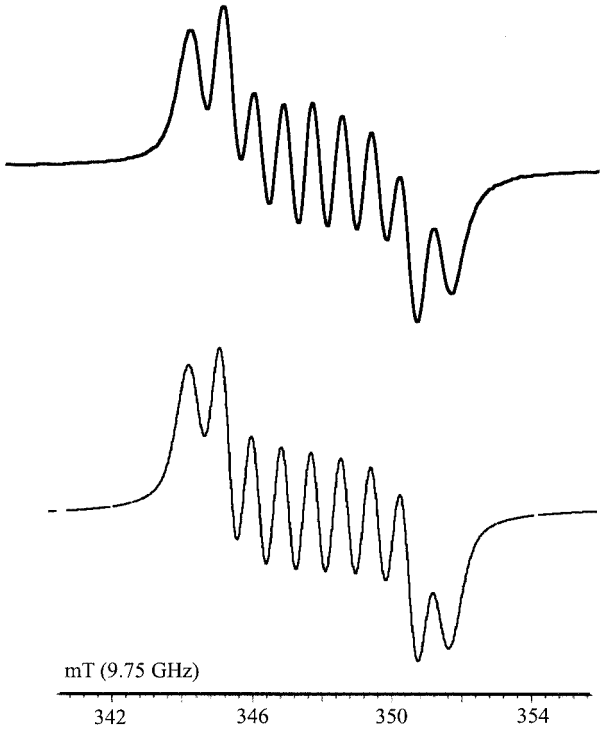

Figure 2. X-Band EPR spectrum (top) of [(dppe)Co(3,6-DBCat)(phen-SQ)] (**2**) (toluene, 250 K) and (bottom) its simulation (EPR line width = 0.73 mT)

Thus, additional phenanthrenequinone accepts one electron and becomes a semiquinone, the cobalt(II) ion loses one electron and becomes a cobalt(III) ion, and the 3,6-DBSQ unit remains a catecholate. The resulting six-coordinate complex of cobalt(III) contains one unpaired electron localized on the phenanthrenesemiquinone and the 3,6-DBQ fragment in the catecholate form.

The third situation takes place when both the quinone fragments are the same [Equation (4)].

 © 2003 Wiley-VCH Verlag GmbH & Co. KGaA, Weinheim

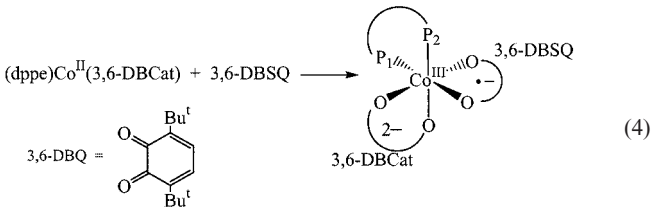

(4)

The EPR spectrum consists of one broad, unresolved line, the form and intensity of which depends on the temperature (g_{iso} = 2.0020±0.0005, Figure 3). No hyperfine structure is observed. A bearable simulation of the spectrum at 210 K indicates a line width of 5.0 mT. Based on literature data,[1,26] we propose that line broadening takes place because of the following equilibrium [Equation (5)]:

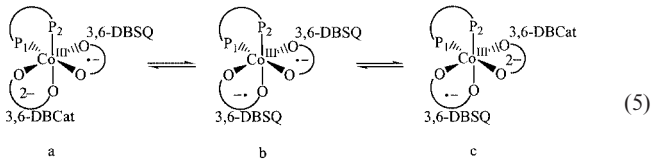

(5)

This equilibrium is a tautomeric interconversion of isomers **a** and **c** followed by a reversible electron transfer. It can occur though the intermediacy of a bis-semiquinone adduct of cobalt(II) (**b**). The presence of this intermediate containing at least three unpaired electrons could be the reason for the broadening and temperature dependence of the EPR spectrum.

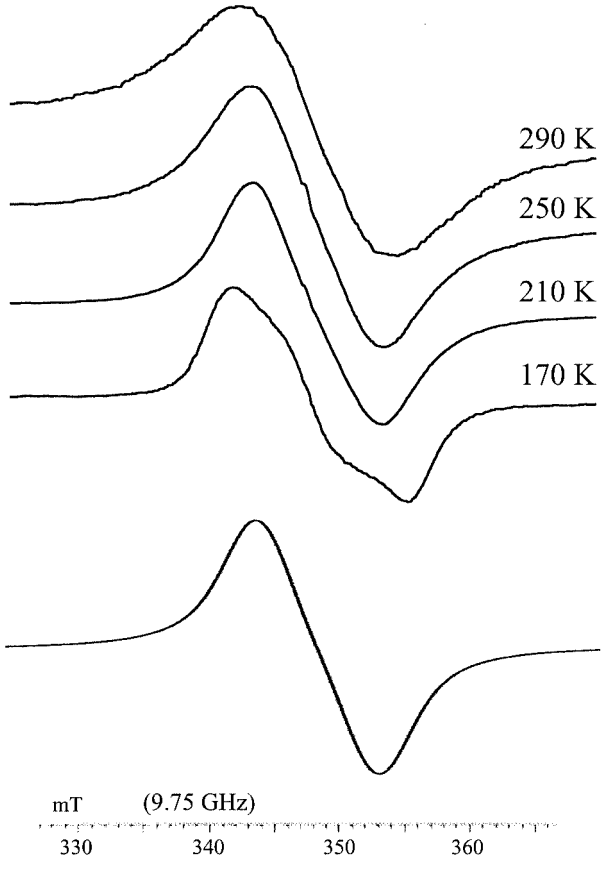

Figure 3. Temperature dependence of the x-band EPR spectrum (top) of [(dppe)Co(3,6-DBCat)(3,6-DBSQ)] (**3**) (g = 2.002±0.0005) and (bottom) its simulation at T = 210 K (a_{Co} = a_{P2} = 1.3 mT; line width = 5.0 mT).

One can imagine the EPR spectrum in the absence of this intermediate. In the case of slow interconversion (relative to the timescale of EPR spectroscopy) of **a** and **c**, the EPR spectrum should reflect, as was observed for 1, a hyperfine interaction with the cobalt nucleus of two different phosphorus atoms (one planar and one apical with respect to the plane of the semiquinone unit) and two protons of one semiquinone ring.

In the case of fast exchange, the EPR spectrum would show an interaction of the unpaired electron with the cobalt nucleus, the two different phosphorus atoms with equal constants, and the four protons of 3,6-DBSQ with one half-constant (≈ 0.15 mT).[27]

In the case of a medium rate of interconversion, i.e., when the lifetime of this intermediate is close to the characteristic time of EPR spectroscopy, an EPR spectrum presenting slow exchange phenomena will transform to depict fast exchange with an increase in temperature, according to known rules.[28] Only some components of the spectrum can undergo broadening.

Total EPR spectroscopic line broadening can take place in the case where one of the exchanging particles has a very broad (maybe infinite) line width and/or a very short lifetime. The particles **a** and **c** presented above have equal lifetimes because of their total identity; the EPR spectra corresponding to fast and slow exchange between them have already been described. A complex of cobalt(II) with two semiquinone units (particle **b**) having at least three unpaired electrons should display a very broad line. Interconversion of **a** to **c** passing through form **b** leads to lines broadening. However, the molar fraction of this cobalt(II) adduct appears to be relatively low because it is possible to observe the spectrum of **3** and its g factor is the same as it is in the cases of **1** and **2**.

In a publication describing a similar situation for complex [(α,α′-bpy)Rh(3,6-DBCat)(3,6-DBSQ)], EPR spectroscopic line broadening occurs upon warming it in solution as well as in the solid state at a very small high-spin fraction that cannot be detected by magnetic susceptibility.[26]

A very small impurity of a Co^{II} species seems to be present in the cases of the complexes **1** and **2**. This impurity might be the reason for the relatively large line widths. By comparing the EPR spectroscopic line widths of complexes **1** and **2** with the values of $E_{1/2}$ of the corresponding quinones [$E_{1/2}$(phen-Q) = −0.66 V, $E_{1/2}$(3,6-DBQ) = −0.39 V, $E_{1/2}(Q_{ox}^{Cl})$ = −0.03 V] it becomes clear why the EPR spectrum of **2** is poorly resolved in comparison with **1**. The difference between the values of $E_{1/2}$ of Q_{ox}^{Cl} and 3,6-DBQ (Δ ≈ 0.36 V) is larger than between 3,6-DBQ and phen-Q (Δ ≈ 0.27 V). Based on these general considerations it becomes clear that the energy separation between the Co^{III}(Cat′)(SQ′′) and Co^{II}(SQ′)(SQ′′) states is larger in the Q_{ox}^{Cl}−3,6-DBQ pair than in the 3,6-DBQ−phen-Q pair, and

 © 2003 Wiley-VCH Verlag GmbH & Co. KGaA, Weinheim

so the amount of an impurity of a Co^{II} species is, respectively, smaller. As a consequence, the line widths in the EPR spectrum of **1** are smaller than they are in the case of **2**. Of course, these comments are qualitative and approximate because they are based on the assumption that the first values of $E_{1/2}$ of quinones correlate with the second ones.

Complex **3** was isolated and characterized in the solid state. Moreover, it was obtained in another way [Equation (6)].

$$[Co(3,6\text{-DBSQ})_3] + dppe \rightarrow [(dppe)Co(3,6\text{-DBCat})(3,6\text{-DBSQ})] + 3,6\text{-DBQ} \quad (6)$$

A magnetic susceptibility investigation indicates a magnetic moment of ca. 1.76 μ_B, which corresponds to one unpaired electron per complex. The magnetic moment as a function of temperature remains constant down to ca. 10 K.

The EPR spectrum of **3** (powder), which displays one broad, unresolved line, is quite similar to those reported[26] to have been observed for [(α,α′-bpy)Rh(3,6-DBCat)(3,6-DBSQ)], and no temperature changes were detected. Thus, complex **3** appears to be a "Co^{III}(SQ)(Cat)" species in the solid state that lacks the "$Co^{II}(SQ)_2$" impurity.

Conclusion

Naturally, the charge on the quinone fragment − "3,6-DBQ" in complex [(dppe)Co("3,6-DBQ")("Q")] − depends on the redox potential of the neighboring quinone fragment "Q". If "Q" is a stronger acceptor, such as "Q^{Cl}_{ox}", then "3,6-DBQ" becomes a semiquinone unit, but if "Q" is a weaker acceptor ("phen-Q") then it remains a catecholate unit. When "Q" ligands are identical, the complex remains in the Co^{III}(Cat)(SQ) state, in general, but a very small impurity of a Co^{II} species essentially causes lines to broaden in the EPR spectrum. Complex [(dppe)Co(3,6-DBCat)(3,6-DBSQ)] in the solid state exists as a "Co^{III}-(Cat)(SQ)" species without any "$Co^{II}(SQ)_2$" impurity.

Experimental Section

General Remarks: EPR spectra were recorded on a Bruker ER 200D-SRC (X-band) spectrometer with an ER 4111 VT variable temperature unit. Coupling constants were determined with the help of a simulator (WINEPR SimFonia 1.25). All the operations with semiquinone and catecholate compounds were carried out under vacuum. Solvents were dried by standard procedures and degassed before use.

Phenanthrenequinone, dppe, $CoCl_2$, and solvents were obtained commercially. 3,6-DBQ,[29,30] perchloroxanthrenequinone-2,3[31] and $[Co(3,6\text{-DBSQ})_3]$[32] were obtained according to known procedures.

[Bis(diphenylphosphanyl)ethane](3,6-di-*tert*-butylcatecholato)cobalt: An evacuated ampoule containing 3,6-di-*tert*-butyl-*o*-quinone (0.22 g, 1.0 mmol) in THF (30 mL) and a large excess of thallium amalgam was shaken until the color of the suspension became bright yellow. The light suspension of thallium catecholate was carefully decanted to another evacuated ampoule. Thallium amalgam was carefully washed several times with THF (5 × 10 mL) until the solvent became colorless. (*Attention!* Thallium catecholate is extremely air sensitive.) Thallium catecholate was added to a mixture of dppe (0.4 g, 1 mmol) and $CoCl_2$ (0.13 g, 1.0 mmol) in THF (70 mL). The reaction mixture was heated under reflux for 1 h, and then the solvent was changed to toluene. The brown solution was filtered, partly evaporated, diluted with *n*-hexane, and then kept at −10 °C overnight. The resulting air-stable, brown, crystalline solid was filtered, washed with cold light petroleum, and then dried under vacuum. Yield 0.2 g (33%). IR (Nujol): $\tilde{\nu}$ = 515 s, 525 (C_3P skeleton vibrations); 735, 695 v.s. $\delta_\perp$ C−H (Ph); 1105 (ν_{P-C}); 1260, 1250 (ν_{C-O}, Cat); 940, 980, 1395, 1375, 1440 (3,6-DBCat) cm^{-1}. $C_{40}H_{44}CoO_2P_2$ (677.67) calcd. C 70.90, H 6.50, Co 8.71; found C 70.95, H 6.49, Co 8.75.

Sample Preparation: Equimolar amounts of [(dppe)Co(3,6-DBCat)] and the corresponding quinone were placed into a special ampoule for EPR spectroscopic investigations. The ampoule was evacuated and purified toluene was condensed inside.

[Bis(diphenylphosphanyl)ethane)(3,6-di-*tert*-butyl-*o*-benzosemiquinono)(3,6-di-*tert*-butylcatecholato)cobalt (3): Dppe (0.4 g, 1 mmol) in THF (50 mL) was added to $[Co(3,6\text{-DBSQ})_3]$ (0.716 g, 1.0 mmol) in THF (80 mL) and then the mixture was carefully warmed. The solvent was evaporated and the residue was washed with *n*-hexane (3 × 50 mL). The solid was dissolved in CH_2Cl_2, and then diluted with *n*-hexane. Slow evaporation led to a dark-blue microcrystalline solid, which was filtered, washed by cold light petroleum, and dried under vacuum. Yield: 0.5 g (ca. 50%). An additional crop of crystals was obtained after cooling the mother solution. IR (Nujol): $\tilde{\nu}$ = 480, 495, 535 (C_3P skeleton vibrations); 695 v.s., 740 m $\delta_\perp$ C−H (Ph); 1105 (ν_{P-C}); 1270, 1280 (ν_{C-O}, Cat); 1410 s (ν_{C-O}, SQ) cm^{-1}. $C_{54}H_{64}CoO_4P_2$ (897.98) calcd. C 72.24, H 7.13, Co 6.58; found C 72.32, H 7.18, Co 6.60.

Acknowledgments

The authors are thankful to Dr. V. N. Ikorskii and Prof. V. I. Ovcharenko who have made the magnetochemical measurements. This work was supported by the Russian Foundation of Basic Research, Grants No. 00-15-97336 and 01-03-33065. EPR spectroscopic investigations were carried out in the Analytical Center of the G. A. Razuvaev Institute of Organometallic Chemistry of RAS, which is supported by the Russian Foundation of Basic Research (grant No. 00-03-40116).

[1] R. M. Buchanan, C. G. Pierpont, *J. Am. Chem. Soc.* **1980**, *102*, 4951−4957.
[2] M. W. Lynch, D. N. Hendrickson, B. J. Fitzgerald, C. G. Pierpont, *J. Am. Chem. Soc.* **1984**, *106*, 2041−2049.
[3] G. A. Abakumov, V. K. Cherkasov, V. I. Nevodchikov, M. P. Bubnov, *Abstracts of the XIVth International Conference on Organometallic Chem.,* Detroit, Michigan, USA, **1990**, p. 278.
[4] G. A. Abakumov, V. K. Cherkasov, M. P. Bubnov, O. G. Ellert, Zh. V. Dobrokhotova, L. N. Zakharov, Yu. T. Struchkov, *Dokl. RAN* **1993**, *328*, 332.
[5] D. M. Adams, A. Dei, A. L. Rheingold, D. N. Hendrickson, *J. Am. Chem. Soc.* **1993**, *115*, 8221.
[6] A. S. Attia, C. G. Pierpont, *Inorg. Chem.* **1997**, *36*, 6184.
[7] O. S. Jung, C. G. Pierpont, *Inorg. Chem.* **1994**, *33*, 2227.
[8] O. S. Jung, C. G. Pierpont, *J. Am. Chem. Soc.* **1994**, *116*, 2229.
[9] S. Attia, O. S. Jung, C. G. Pierpont, *Inorg. Chim. Acta* **1994**, *226*, 91.

 © 2003 Wiley-VCH Verlag GmbH & Co. KGaA, Weinheim

[10] O. S. Jung, D. H. Jo, Y. A. Lee, B. J. Conclin, C. G. Pierpont, *Inorg. Chem.* **1997**, *36*, 19.
[11] Roux, D. M. Adams, J. P. Itie, A. Polian, D. N. Hendrickson, M. Verdaguer, *Inorg. Chem.* **1996**, *35*, 2846.
[12] S. Attia, C. G. Pierpont, *Inorg. Chem.* **1998**, *37*, 3051−3056.
[13] D. M. Adams, B. Li, J. D. Simon, D. N. Hendrickson, *Angew. Chem.* **1995**, *107*, 1580; *Angew. Chem. Int. Ed. Engl.* **1995**, *34*, 1481.
[14] G. Pierpont, O. S. Jung, *Inorg. Chem.* **1995**, *34*, 4281.
[15] G. A. Abakumov, V. I. Nevodchikov, V. K. Cherkasov, *Dokl. RAN* **1984**, *278*, 641−645.
[16] G. A. Abakumov, V. I. Nevodchikov, V. K. Cherkasov, *Izv. Akad. Nauk SSSR, Ser. Khim.* **1985**, *12*, 2709−2716.
[17] G. A. Abakumov, V. I. Nevodchikov, V. K. Cherkasov, *Izv. Akad. Nauk SSSR, Ser. Khim.* **1986**, *1*, 65−71.
[18] G. A. Abakumov, G. A. Razuvaev, V. I. Nevodchikov, V. K. Cherkasov, *J. Organomet. Chem.* **1988**, *341*, 485−494.
[19] G. A. Abakumov, V. K. Cherkasov, V. I. Nevodchikov, M. P. Bubnov, *Izv. Akad. Nauk SSSR, Ser. Khim.* **1987**, *8*, 1861−1864.
[20] G. A. Abakumov, V. A. Garnov, V. I. Nevodchikov, V. K. Cherkasov, *Dokl. RAN* **1989**, *304*, 107−111.
[21] R. R. Rakitin, P. M. Solozhenkin, N. I. Kopitsya, V. S. Pupkov, A. I. Prokof'ev, *Dokl. Akad. Nauk.* **1988**, *300*, 1177.
[22] V. I. Nevodchikov, G.A. Abakumov, V. K. Cherkasov, G. A. Razuvaev, *J. Organomet. Chem.* **1981**, *214*, 119−124.
[23] G. A. Abakumov, V. I. Nevodchikov, V. K. Cherkasov, G. A. Razuvaev, *Dokl. Akad. Nauk SSSR* **1981**, *258*, 924−927.
[24] V. A. Muraev, V. K. Cherkasov, G. A. Abakumov, G. A. Razuvaev, *Dokl. Acad. Nauk SSSR* **1977**, *236*, 620−623.
[25] G. A. Razuvaev, I. A. Teplova, K. G. Shalnova, G. A. Abakumov, *J. Organomet. Chem.* **1978**, *157*, 353−358.
[26] G. A. Abakumov, V. K. Cherkasov, M. P. Bubnov, L. N. Zakharov, G. K. Fukin, *Russ. Chem. Bull.* **1999**, *48*, 1762−1766.
[27] M. I. Kabachnik, N. N. Bubnov, A. I. Prokof'ev, S. P. Solodovnikov, *Science Rev., Ser. B* **1981**, V.3, XXIV, N22, 197−297.
[28] J. E. Wertz, J. R. Bolton, *Electron spin resonance, elementary theory and practical applications*, McGraw-Hill, New York, **1972**.
[29] I. S. Belostotska'a, N. L. Komisarova, E. V. Dghuaran, V. V. Ershov, *Izv. Akad. Nauk SSSR, Ser. Khim.* **1972**, 1594−1596.
[30] N. L. Komisarova, I. S. Belostotska'a, E. V. Dghuaran, V. V. Ershov, *Izv. Akad. Nauk USSR, Ser. Khim.* **1973**, 1380−1382.
[31] L. G. Abakumova, A. V. Lobanov, G. A. Abakumov, *Izv. Akad. Nauk. SSSR, Ser. Khim.* **1978**, 204.
[32] C. W. Lange, B. J. Conklin, C. G. Pierpont, *Inorg. Chem.* **1994**, *33*, 347−353.

Received November 28, 2002

 © 2003 Wiley-VCH Verlag GmbH & Co. KGaA, Weinheim

Phosphadicarbaborane Analogues of Ferrocene: New Isomers of [*closo*-(η^5-C_5H_5)$FePC_2B_8H_{10}$]

Bohumil Štíbr,*[a] Josef Holub,[a] Mario Bakardjiev,[a] Ivan Pavlík,[b] Oleg L. Tok,[c] and Bernd Wrackmeyer[c]

Keywords: Sandwich complexes / Boranes / Isomerisation / Carbaboranes / NMR spectroscopy

Thermal isomerisation of the ferraphosphadicarbaborane [1-Cp-*closo*-1,2,4,5-$FePC_2B_8H_{10}$] (**1a**; Cp = η^5-$C_5H_5^-$) at elevated temperatures (180–350 °C) leads to the formation of three new isomeric complexes. These were characterized by multinuclear (^1H, ^{11}B, ^{31}P, and ^{13}C) NMR spectroscopy and mass spectrometry as [1-Cp-*closo*-1,2,3,8-$FePC_2B_8H_{10}$] (**1b**), [1-Cp-*closo*-1,10,2,4-$FePC_2B_8H_{10}$] (**1c**), and *closo*-[1,2,4,10-$FePC_2B_8H_{10}$] (**1d**). The formation of **1b** is accompanied by an unusual agglomeration of the P and C heteroatoms. Complexes **1b** and **1c** have also been isolated as side products from the direct reaction between *nido*-[7,8,9-$PC_2B_8H_{11}$] (**2**) and $[CpFe(CO)_2]_2$ in refluxing mesitylene, and **1a** and **1b** from the pyrolysis of [7-Fp-(η^1-*nido*-7,9,10-$PC_2B_8H_{10}$)] [**3**; Fp = $CpFe(CO)_2$] at 350 °C. NMR intercomparisons of all five [1-Cp-*closo*-$FePC_2B_8H_{10}$] isomers thus far isolated have been made.
(© Wiley-VCH Verlag GmbH & Co. KGaA, 69451 Weinheim, Germany, 2003)

Introduction

We have recently been interested in the synthesis and chemistry of the eleven-vertex *nido* phoshadicarbaboranes (phosphadicarbollides), which are analogues of tricarbollides.[1] In this field of boron cluster chemistry we have reported the synthesis of the two isomeric neutral compounds 7,8,11-$PC_2B_8H_{11}$ and 7,8,9-$PC_2B_8H_{11}$.[2,3] Deprotonation of these compounds gave the corresponding anions [7,8,11-$PC_2B_8H_{10}]^-$ and [7,8,9-$PC_2B_8H_{10}]^-$.[2,3] These anions can be regarded as Cp analogues as they are monoanionic and contain an open pentagonal face[1] capable of donating five electrons in an η^5-type coordination to metal fragments. This analogy was demonstrated just recently by the complexation of *nido*-7,8,9-$PC_2B_8H_{11}$ with $[CpFe(CO)_2]_2$ resulting ultimately in the synthesis of the first two representatives of the [1-Cp-*closo*-$FePC_2B_8H_{10}$] series (compounds **1a** and **1e**). These compounds are the first phosphadicarbaborane analogues of ferrocene. It was demonstrated that their formation proceeds via two isolable η^1-bonded, P-substituted complexes of general formula [Fp-*nido*-(η^1-$PC_2B_8H_{10}$)].[4] By analogy with dicarbollide[5] and tricarbollide complexes,[6] the complexes **1a** and **1e** were expected to undergo cluster rearrangement by migration of the heteroatomic CH and P cage units at higher temperatures to form further [1-Cp-*closo*-$FePC_2B_8H_{10}$] isomers. We report in this paper several variations of reactions from which we have isolated another three isomers of this constitution. The numbering system for the eleven-vertex *nido* and twelve-vertex *closo* skeletons used in this work is shown in structures **I** and **II**. These structures are presented in a simplified manner; unmarked vertices in the schemes stand for cluster BH units, while C and P denote CH and bare phosphorus vertices, respectively. For convenience, the Fe atom in structures of type **1** is numbered first, followed by P and C vertexes.

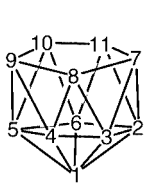

I

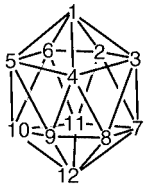

II

[a] Institute of Inorganic Chemistry, Academy of Sciences of the Czech Republic (Research Center for New Inorganic Compounds and Advanced Materials, University of Pardubice), 25068 Rez, Czech Republic
Fax: (internat.) + 420-220/941-502
E-mail: stibr@iic.cas.cz
[b] University of Pardubice, Department of General and Inorganic Chemistry (Research Center for New Inorganic Compounds and Advanced Materials),
53210 Pardubice, Czech Republic
Fax: (internat.) + 420-4/603-7068
E-mail: koanch.fcht@upce.cz
[c] Laboratorium für Anorganische Chemie der Universität Bayreuth,
Postfach 101251, 95440 Bayreuth
Fax: (internat.) + 49-921/552-157
E-mail: B.Wrack@uni-bayreuth.de

 © 2003 Wiley-VCH Verlag GmbH & Co. KGaA, Weinheim **DOI: 10.1002/ejic.200300002**

Results and Discussion

Syntheses

As shown in path i) of Scheme 1, prolonged heating of **1a** in mesitylene at reflux temperature produces the complexes [1-Cp-*closo*-1,2,3,8-$FePC_2B_8H_{10}$] (**1b**) and [1-Cp-*closo*-1,10,2,4-$FePC_2B_8H_{10}$] (**1c**) in yields of 15 and 13%, respectively. The conversion is, however, very slow and incomplete, and compound **1a** was recovered in 60% yield. The formation of **1b** from **1a** is very unusual as it is associated with the migration of one of the cage carbon atoms from the original *m*-position to the *o*-position with respect to the P center. Moreover, the second carbon atom is moved into the lower structural belt, to form a contiguous P−C−C string with a P−C bond in the pentagonal belt adjacent to the Fe center. The formation of **1c** from **1a** is associated with a migration of the P-vertex into an *m*-position with respect to the Fe center and *m*-separation of the C-vertices within the pentagon adjacent to the Fe atom to achieve a maximum space separation of the P and C vertices, a feature encountered in the isoelectronic [1-Cp-*closo*-1,2,4,10-$FeC_3B_8H_{11}$] tricarbollide series.[7] A different type of maximum separation of the C and P heteroatoms is encountered in the isomer [1-Cp-*closo*-1,2,4,10-$FePC_2B_8H_{10}$] (**1d**). As shown in path ii) of Scheme 1, this complex was isolated in a yield of 23%, together with the isomer **1b** (yield 52%), from thermal rearrangement of **1a** at 350 °C. The result of the **1a** → **1d** rearrangement is a movement of the one of the C vertexes into an *m*-position with respect to both C and P atoms in the lower belt near B(12). Moreover, isomer **1d** was additionally obtained in a yield of 51% by the thermolysis of **1e**[4] at 350 °C (see path iii of Scheme 1), the rearrangement being associated with a migration of one carbon vertex into or within the pentagonal belt connected to the B(12) atom.

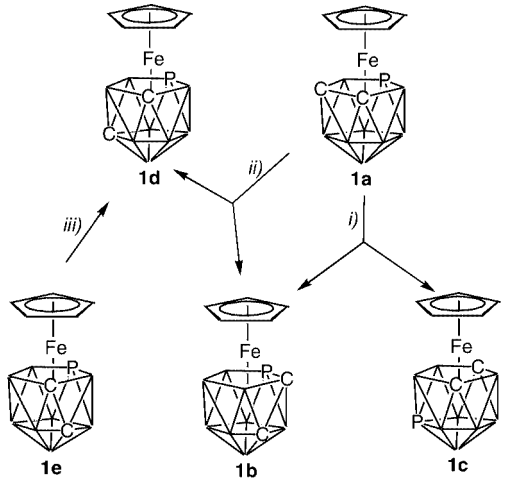

Scheme 1. i) mesitylene, reflux, 3 hours. ii), iii) 350 °C, 2 hours

Complexes **1b** and **1c** can also be obtained directly from the phosphadicarbaborane **2** by treatment with $[CpFe(CO)_2]_2$ in refluxing mesitylene (two days). The main products isolated from this reaction were, however, the previously reported[4] compounds **1a** (yield 33%) and **3** (yield 28%); nevertheless, the reaction is accompanied by the formation of the isomeric complexes **1b** and **1c** (yields 10 and 7%, respectively). Alternatively, complex **1b** was also generated (yield 23%), together with compound **1a**[4] (yield 52%), by heating the *nido* compound **3**[4] at 350 °C in vacuo. It is obvious that complexes **1b** and **1c** in these experiments have been formed by rearrangement of **1a** as in path i) of Scheme 1. All the new isomeric complexes **1b**−**1d** are orange or dark orange compounds that are remarkably stable in air.

Structural Studies

Even though we were able to grow crystals of almost all new complexes of type **1**, the structural determinations of these species were unsuccessful owing to disorder problems encountered during structure solution. Nevertheless, the constitution of all new isomers **1b**−**1d** could be easily derived from multinuclear NMR (^1H, ^{11}B, ^{31}P, and ^{13}C) and two-dimensional [^{11}B-^{11}B]-COSY NMR measurements[8] combined with $^1H\{^{11}B(selective)\}$ experiments,[9] and the interpretation of the data led to complete assignments of all resonances to individual BH, CH, and P vertices. The mass spectra of compounds **1b**−**1d** exhibit the same molecular cut-off at $m/z = 275$, as expected for the identical molecular formulation. Some absorption bands in the IR spectra have been assigned to BH and CH vibrations.

The ^{11}B NMR spectra of all five isomers of general constitution **1** thus far isolated are depicted graphically in Figure 1 as simplified stick diagrams indicating the ^{11}B chemical shifts and relative intensities. The ^{11}B resonances fall within a relatively narrow span (ca. 20 ppm), which corresponds well to that of the isostructural [1-Cp-*closo*-$FeC_3B_8H_{11}$] compounds and their amino derivatives (also ca. 20 ppm).[1,7] The ^{11}B resonances of the BH units adjacent to the P vertex are generally either split into a doublet or at least broadened owing to unresolved ^{31}P-^{11}B scalar coupling. As shown in Figure 2, the ^{31}P resonances are very sensitive to structural changes among individual isomers of general formula **1**. The ^{31}P resonances of the isomers containing the Fe−P bond (**1a**, **1b**, **1d**, and **1e**) fall within a range of ca. $\delta = +20$ to -45 ppm, while the $^{31}P(10)$ resonance in **1c** is shifted to low frequency ($\delta^{31}_P = -166$ ppm), to a range typical of phosphorus in polyhedral boranes with a *closo* structure.[10] Therefore, the ^{31}P NMR signals at higher frequencies in the range of $\delta = +20$ to -55 ppm are a consequence of Fe−P bonding. As expected, the ^1H and $^{13}C\{^1H\}$ NMR chemical shifts associated with the Cp ring are not significantly affected by structural changes in the phosphadicarbaborane cage.

As shown in Figure 1, the ^{11}B NMR spectra of the C_s-symmetric isomers **1a**[4] and **1c** consist of 1:2:1:2:2 patterns of doublets, which is consistent with a plane of symmetry intersecting the Fe(1), B(or P)(10), and B(12) vertices. The spectra of **1a**[4] and **1c** are very similar to those of their tricarbollide congeners [1-Cp-*closo*-1,2,4,5-$FeC_3B_8H_{11}$] (**4a**)[11] and [1-Cp-*closo*-1,2,4,10-$FeC_3B_8H_{11}$] (**4b**),[7] except that the spectra of the ferraphosphadicarbollides are shifted

 © 2003 Wiley-VCH Verlag GmbH & Co. KGaA, Weinheim

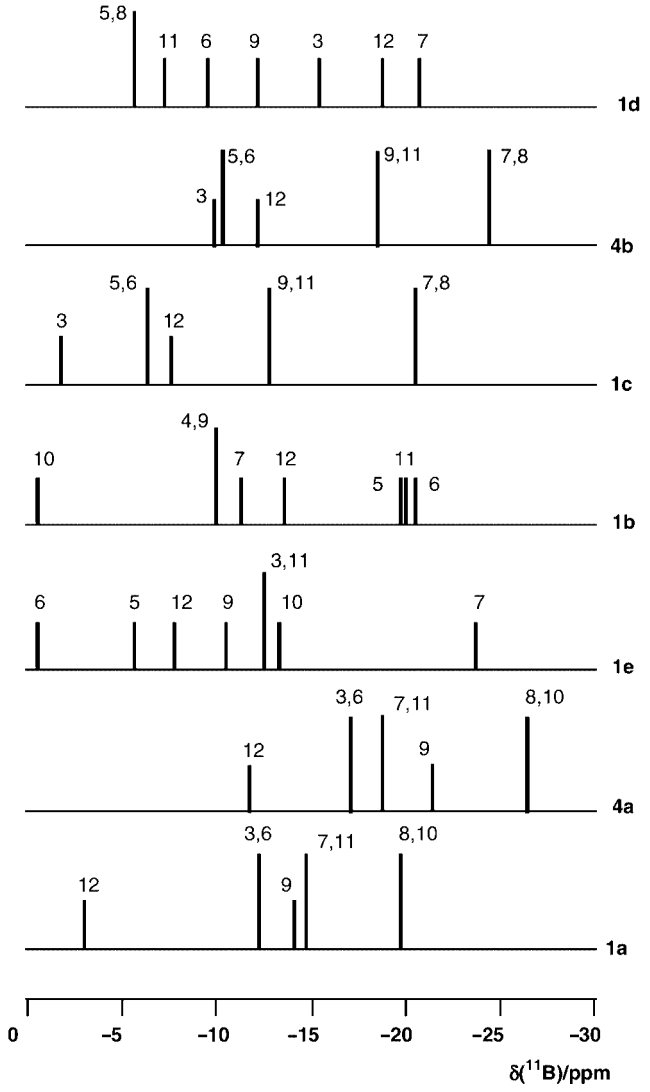

Figure 1. Simplified stick diagrams showing intercomparison of the ^{11}B NMR chemical shifts and relative intensities for all known ferraphosphadicarbollide [1-Cp-*closo*-$FePC_2B_8H_{10}$] (**1**) isomers with those for selected isostructural ferratricarbollides [1-Cp-*closo*-$FeC_3B_8H_{11}$] (**4**); data for **1a** and **1e** from ref.[4] and data for **4a** and **4b** from refs.[7,11]

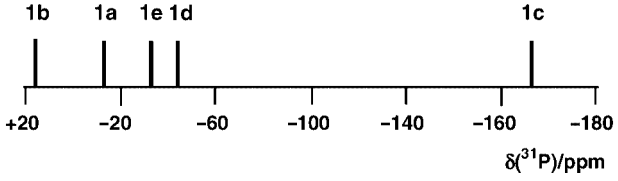

Figure 2. Stick representation of the ^{31}P NMR chemical shifts for all known ferraphosphadicarbollide [1-Cp-*closo*-$FePC_2B_8H_{10}$] (**1**) isomers; data for **1a** and **1e** from ref.[4]

downfield ($\Delta\delta$ = ca. 5 ppm). In agreement with the existence of the symmetry plane, the ^1H and $^{13}C\{^1H\}$ NMR spectra of **1c** show two singlet resonances of integral intensities 5:2, assigned to Cp and two equivalent CH(2,4) units, respectively. As expected for the asymmetric derivatives **1b**, **1d**, and **1e**,[4] their ^{11}B NMR spectra are characterized by eight different resonances some of which overlap. The ^1H and $^{13}C\{^1H\}$ NMR spectra of these asymmetrical isomers contain three resonances of relative areas 5:1:1 attributed to Cp and two different cage CH units. In the case of **1b**, which is a single isomer containing a P−C bond, one of the CH resonances shows distinct $^2J_{P,H}$ and $^1J_{P,C}$ doublet splittings.

Conclusions

We have demonstrated that another three structurally diverse isomers of general *closo* ferraphosphadicarbollide structure **1** can be isolated from various high-temperature reactions involving − directly or indirectly − the previously reported isomer **1a**.[4] There is no doubt that the separation of carbon atoms is not the only driving force responsible for the observed rearrangements, as the isomer **1b**, containing a contiguous P-C-C string, is formed as the main kinetic product. This fact is in sharp contrast to the rearrangements of the structurally related ferratricarbollide complexes[6,7] and to those of the [$CpCoC_2B_9H_{11}$] cobaltadicarbollides as well.[5] The isomerisations leading to **1b−1d** can be explained by the triangular-face rotation mechanism,[12] although the participation of other mechanisms (diamond-square-diamond,[13] pyramidal rotation,[14] and Lipscomb's hybrid[15]), cannot be excluded. It should also be noted that all the complexes isolated contain at least one heteroatom on the coordinating face and, in comparison with complexes of the [$CpCoC_2B_9H_{11}$] series,[5] no [$CpFePC_2B_8H_{10}$] isomer containing P or C heteroatoms in position 12 (*para* with respect to the Fe center) has been formed. These will probably be formed at temperatures higher than 400−500 °C; application of such severe conditions led to complete decomposition. The isomeric complexes of structure **1** are expected to undergo various substitution reactions either on the cluster atoms or the Cp ring, which might generate interesting substitution derivatives. Also, application of boron or carbon degradation reactions is expected to lead to other structurally interesting smaller-cage ferraphoshacarborane systems. These and related reactions aimed at establishing reactivity systemization within a series of phosphacarborane analogues of ferrocene are in progress.

Experimental Section

General Procedures: All reactions were carried out with use of standard vacuum or inert-atmosphere techniques as described by Shriver,[16] although some operations, such as column LC, were carried out in air. The starting compounds **1a**, **1e**, **2,** and **3** were prepared according to the literature.[3,4] Dichloromethane, hexane, and mesitylene (Fluka) were dried over CaH_2 and freshly distilled before use. Other chemicals were reagent or analytical grade and were used as purchased. Column chromatography was carried out using silica gel (Aldrich, 130−270 mesh) as the stationary phase. The purity of individual chromatographic fractions was checked by analytical TLC on Silufol (silica gel on aluminum foil; detection by iodine vapor, followed by 2% aqueous $AgNO_3$ spray). Melting points were measured in sealed capillaries under argon and are un-

 © 2003 Wiley-VCH Verlag GmbH & Co. KGaA, Weinheim

corrected. Multinuclear (^{1}H, ^{11}B, ^{31}P, and ^{13}C) NMR and IR spectroscopy, and mass spectrometry have been performed essentially with the instrumentation described in other related papers from our laboratories.[4,17]

[1-Cp-1,2,3,8-FePC$_2$B$_8$H$_{10}$] (1b) and [1-Cp-1,10,2,4-FePC$_2$B$_8$H$_{10}$] (1c): a) A solution of compound **1a** (100 mg, 0.36 mmol) in mesitylene (20 mL) was heated under reflux for three days. Most of the mesitylene was removed by evaporation and the mixture was then worked up by repeated chromatography on a silica gel column (40 × 1.5 cm) using hexane as a mobile phase to collect three main fractions of R_f (hexane) 0.60, 0.50, and 0.43, from which complexes **1c** (13 mg, 13%), **1b** (15 mg, 15%), and the starting compound **1a** (60 mg, 60%) were isolated, respectively, by evaporation of the solvent and identified by ^{11}B NMR spectroscopy.

1c: R_f (hexane) 0.60. M.p. 80 °C. ^{1}H{^{11}B } NMR ($CDCl_3$): δ = 4.81 (s, 5 H, Cp), 3.14 (d, $^2J_{P,H}$ = 24 Hz, 2 H, $H_{5,6}$), 2.82 (d, $^2J_{P,H}$ = 23 Hz, 1 H, H_{12}), 2.50 (s, 2 H, $H_{2,4}$), 1.72 (s, 2 H, $H_{7,8}$), 1.70 (d, $^2J_{P,H}$ = 23 Hz, 2 H, $H_{9,11}$) ppm. ^{11}B NMR ($CDCl_3$): δ = −2.0 (d, $^1J_{B,H}$ = 166 Hz, 1 B, B_3), −6.4 (d, $^1J_{B,H}$ ≈ 160, $^1J_{B,P}$ = 35 Hz, 2 B, $B_{5,6}$), −7.5 (d, $^1J_{B,H}$ ≈ 160 Hz, 1 B, B_{12}), −15.4 (d, $^1J_{B,H}$ = 165 Hz, 2 B, $B_{9,11}$), −21.1 (d, $^1J_{B,H}$ = 161 Hz, 2 B, $B_{7,8}$) ppm. ^{31}P{^{1}H } NMR ($CDCl_3$): δ = −166.2 (s, 1 P, P_{10}) ppm. IR (KBr): $\tilde{\nu}$ = 2924 (CH), 2580 (BH) cm^{-1}. MS (70 eV, EI), *m/z* (%) = 275 (5) $[M]^+$, 273 (85) $[M - 2H]^+$. $C_7H_{15}B_8FeP$ (272.54): calcd. C 30.85, H 5.55; found C 30.98, H 5.70.

1b: R_f (hexane) 0.50. M.p. 180 °C. ^{1}H{^{11}B} NMR ($CDCl_3$): δ = 4.99 (s, 5 H, Cp), 4.21 (s, 1 H, $H_{4\ or\ 9}$), 3.46 (s, 1 H, H_8), 3.41 (s, 1 H, H_{10}), 2.29 (s, 1 H, $H_{4\ or\ 9}$), 2.23 (d, $^2J_{P,H}$ = 26 Hz, 1 H, H_7), 1.76 (s, 1 H, H_{12}), 1.52 (s, 1 H, H_5), 1.44 (d, $^2J_{P,H}$ = 26 Hz, 1 H, H_{11}), 1.94 (d, $^2J_{P,H}$ = 18 Hz, 1 H, H_3), 1.35 (d, $^2J_{P,H}$ = 15 Hz, 1 H, H_6) ppm. ^{11}B NMR ($CDCl_3$): δ = −0.9 (d, $^1J_{B,H}$ = 150 Hz, 1 B, B_{10}), −9.9 (d, $^1J_{B,H}$ ≈ 160 Hz, 2 B, $B_{4,9}$), −12.0 (d, $^1J_{B,H}$ = 162, $^1J_{B,P}$ = 36 Hz, 1 B, B_7), −13.7 (d, $^1J_{B,H}$ = 162 Hz, 1 B, B_{12}), −19.7 (d, $^1J_{B,H}$ = 162 Hz, 1 B, B_5), −20.0 (d, $^1J_{B,H}$ ≈ 160 Hz, 1 B, B_{11}), −21.6 (d, $^1J_{B,H}$ ≈ 160 Hz, 1 B, B_6) ppm. ^{13}C{^{1}H,^{11}B} NMR ($CDCl_3$): δ = 80.4 (s, 5 C, Cp), 58.6 (s, 1 C, C_8), 45.8 (s, $^1J_{C,P}$ = 74 Hz, 1 C, C_3) ppm. ^{31}P{^{1}H } NMR ($CDCl_3$): δ = 17.7 (s, 1 P, P_2) ppm. IR (KBr): $\tilde{\nu}$ = 2925 (CH), 2548 (BH) cm^{-1}. MS (70 eV, EI), *m/z* (%) = 275 (5) $[M]^+$, 273 (85) $[M - 2H]^+$. $C_7H_{15}B_8FeP$ (272.54): calcd. C 30.85, H 5.55; found C 31.20, H 5.73.

b) A solution of compound **2** (500 mg, 3.25 mmol) in mesitylene (20 mL) was treated with $[CpFe(CO)_2]_2$ (1500 mg, 4.23 mmol) and the mixture was heated under reflux for 24 h. Most of the mesitylene was removed by evaporation and the mixture was then worked up by repeated chromatography on a silica gel column (40 × 2.5 cm) using hexane as a mobile phase to isolate (ordered by decreasing R_f values) compounds **1c** (58 mg, 7%), **1b** (82 mg, 10%), **1a** (294 mg, 33%), and **3** (318 mg, 28%), which were identified by ^{11}B NMR spectroscopy.

c) Compound **3** (0.063 g, 0.19 mmol) was heated at 350 °C in an evacuated ampoule for 2 h. The melt was then cooled to ambient temperature and extracted with CH_2Cl_2 (2 × 10 mL). The extract was filtered, the solvents evaporated to dryness and the solid residue was separated by chromatography on silica gel in hexane. Two orange fractions of R_f = 0.50 and 0.43 were collected from which compounds **1b** (12 mg, 23%) and **1a**[4] (27 mg, 52%) were isolated, respectively, after evaporation of the solvents and drying in vacuo at ambient temperature and identified by ^{11}B NMR spectroscopy.

[1-Cp-1,2,4,10-FePC$_2$B$_8$H$_{10}$] 1d: a) Compound **1a** (100 mg, 0.36 mmol) was heated at 350 °C in an evacuated ampoule for 2 h. The melt was then cooled to ambient temperature and extracted with CH_2Cl_2 (2 × 10 mL). The extract was filtered, the solvents evaporated to dryness and the solid residue was separated by chromatography on silica gel in hexane. Two orange fractions of R_f = 0.60 and 0.50 were collected, from which compounds **1d** (12 mg, 23%) and **1b** (27 mg, 52%) were isolated, respectively, on evaporation of the solvents and drying in vacuo at ambient temperature.

1d: R_f (hexane) 0.60. M.p. 80 °C.^{1}H{^{11}B} NMR ($CDCl_3$): δ = 4.84 (s, 5 H, Cp), 3.53 (s, 1 H, $H_{5\ or\ 8}$), 3.27 (s, 1 H, $H_{5\ or\ 8}$), 2.99 (s, 1 H, $H_{4\ or\ 10}$), 2.81 (d, $^2J_{P,H}$ = 23 Hz, 1 H, H_{11}), 2.73 (s, 1 H, H_9), 2.36 (s, 1 H, $H_{4\ or\ 10}$), 1.91 (d, $^2J_{P,H}$ = 18 Hz, 1 H, H_3), 1.85 (s, 1 H, H_{12}), 1.84 (d, $^2J_{P,H}$ = 16 Hz, 1 H, H_6), 1.58 (d, $^2J_{P,H}$ = 22 Hz, 1 H, H_7) ppm. ^{11}B NMR ($CDCl_3$): δ = −6.4 (d, $^1J_{B,H}$ ≈ 160 Hz, 2 B, $B_{5,8}$), −7.3 (d, $^1J_{B,H}$ ≈ 160 Hz, 1 B, B_{11}), −8.6 (d, 1 B, B_6), −12.1 (d, $^1J_{B,H}$ = 169 Hz, 1 B, B_9), −15.7 (d, $^1J_{B,H}$ = 166, $^1J_{B,P}$ = 31 Hz, 1 B, B_3), −18.2 (d, $^1J_{B,H}$ = 161 Hz, 1 B, B_{12}), −21.1 (d, $^1J_{B,H}$ = 158 Hz, 1 B, B_7) ppm. ^{13}C{^{1}H } NMR ($CDCl_3$): δ = 79.8 (s, 5 C, Cp), 49.5 (s, 1 C, C_{10}), 46.5 (s, 1 C, C_4). ^{31}P{^{1}H } NMR ($CDCl_3$): δ = −41.3 (s, 1 P, P_2) ppm. IR (KBr): $\tilde{\nu}$ = 2924 (CH), 2580 (BH) cm^{-1}. MS (70 eV, EI), *m/z* (%) = 275 (5) $[M]^+$, 273 (100) $[M - 2H]^+$. $C_7H_{15}B_8FeP$ (272.54): calcd. C 30.85, H 5.55; found C 31.25, H 5.69.

b) Compound **1e** (20 mg, 0.07 mmol) was heated at 350 °C in an evacuated ampoule for 2 h. The melt was then cooled to ambient temperature and extracted with CH_2Cl_2 (2 × 5 mL). The extract was filtered, the solvents evaporated to dryness and the solid residue was separated by chromatography on silica gel in hexane to isolate the main orange band of R_f = 0.60, from which compound **1d** (10.2 mg, 51%) was isolated after evaporation of the solvents and drying in vacuo at ambient temperature; it was identified by NMR spectroscopy.

Acknowledgments

This work was supported by the Alexander von Humboldt Stiftung (FRG) (B. Š.), the Deutsche Forschungsgemeinschaft (B. W., O. L. T.), the Fonds der Chemischen Industrie (B. W.) and the Ministry of Education of the Czech Republic (project no. LN00A028). We also thank Drs J. Fusek, Z. Plzák, and E. Večerníková for some NMR measurements, and mass and IR spectra.

[1] B. Štíbr, J. Holub, F. Teixidor, in *Advances in Boron Chemistry* (Ed.: W. Siebert), Royal Society of Chemistry, Cambridge, **1997**, pp. 333−340.
[2] J. Holub, D. L. Ormsby, J. D. Kennedy, R. Greatrex, B. Štíbr, *Inorg. Chem. Commun.* **2000**, *3*, 178−181.
[3] B. Štíbr, J. Holub, M. Bakardjiev, D. Hnyk, O. L. Tok, W. Milius, B. Wrackmeyer, *Eur. J. Inorg. Chem.* **2002**, 2320−2326.
[4] B. Štíbr, J. Holub, M. Bakardjiev, I. Pavlík, O. L. Tok, B. Wrackmeyer, M. Herberhold, *Chem. Eur. J.* **2003**, *9*, 2239−2244.
[5] M. K. Kaloustian, R. J. Wiersema, M. F. Hawthorne, *J. Am. Chem. Soc.* **1972**, *94*, 6679−6686.
[6] B. Grüner, A. Lehtonen, R. Kivekäs, R. Sillanpää, J. Holub, F. Teixidor, C. Viñas, B. Štíbr, *Inorg. Chem.* **2000**, *39*, 2577−2580.
[7] B. Štíbr, J. Holub, F. Teixidor, C. Viñas, *Collect. Czech. Chem. Commun.* **1995**, *60*, 2023−2027.
[8] [8a] J. D. Kennedy, in *Multinuclear NMR* (Ed.: J. Mason), Plenum Press, New York, **1987**, p. 221. [8b] W. C. Hutton, T. L. Venable, R. N. Grimes, *J. Am. Chem. Soc.* **1984**, *106*, 29−37. [8c] J. Schraml, J. M. Bellama, *Two-Dimensional NMR Spectroscopy*, Wiley, New York, **1982**.
[9] X. L. R. Fontaine, J. D. Kennedy, *J. Chem. Soc., Dalton Trans.* **1987**, 1573.
[10] W. Keller, W. Haubold, B. Wrackmeyer, *Magn. Reson. Chem.* **1999**, *37*, 545−550.

 © 2003 Wiley-VCH Verlag GmbH & Co. KGaA, Weinheim

[11] B. Štíbr, unpublished results.
[12] E. L. Muetterties, W. H. Knoth, *Polyhedral Boranes*, Marcel Dekker, New York, N. Y., **1968**, pp. 55−72.
[13] W. N. Lipscomb, *Science* **1966**, *153*, 373−376.
[14] [14a] D. Grafstein, J. Dvorak, *Inorg. Chem.* **1963**, *2*, 1128−1133. [14b] L. I. Zakharkin, V. Kalinin, *Dokl. Akad. Nauk SSSR* **1966**, *169*, 590−591.
[15] H. D. Kaesz, R. Bau, H. A. Beall, W. N. Lipscomb, *J. Am. Chem. Soc.* **1967**, *89*, 4218−4220.
[16] D. F, Shriver, M. A. Drezdon, *Manipulation of Air Sensitive Compounds*, 2nd ed., Wiley, New York, **1986**.
[17] J. Plešek, B. Štíbr, X. L. R. Fontaine, J. D. Kennedy, S. Heřmánek, T. Jelínek, *Collect. Czech. Chem. Commun.* **1991**, *56*, 1618−1635.

Received January 2, 2003

 © 2003 Wiley-VCH Verlag GmbH & Co. KGaA, Weinheim

Iron Complexes Containing the Ligand *N*,*N*′-Bis(6-methyl-2-pyridylmethyl)-*N*,*N*′-bis(2-pyridylmethyl)ethane-1,2-diamine: Structural, Spectroscopic, and Electrochemical Studies, Reactivity with Hydrogen Peroxide and the Formation of a Low-Spin Fe−OOH Complex

Véronique Balland,[a] Frédéric Banse,*[a] Elodie Anxolabéhère-Mallart,*[a] Martine Nierlich,[b] and Jean-Jacques Girerd*[a]

Keywords: Iron / N ligands / Peroxo ligands / Bioinorganic chemistry

The ligand *N*,*N*′-bis(6-methyl-2-pyridylmethyl)-*N*,*N*′-bis(2-pyridylmethyl)ethane-1,2-diamine ($L_6^2$2M) has allowed to prepare the new Fe^{II} complex [($L_6^2$2M)$FeCl_2$] (**1**), and to compare its structural and spectroscopic characteristics with [($L_6^2$2M)FeCl]PF_6 (**2**). The molecular structure of **1**, resolved by X-ray diffraction, exhibits the ligand tetracoordinated with the two non-methylated pyridine rings coordinated. As shown by UV/Vis spectroscopy and cyclic voltammetry, upon dissolution in methanol or acetonitrile, one chloride ion is released and replaced by a pyridine group. Therefore, complexes **1** and **2** adopt identical structures in solution, i.e. [($L_6^2$2M)$FeCl^+$. However, upon oxidation complex **1** gives several ferric complexes with the ligand $L_6^2$2M pentacoordinated, or tetracoordinated with two chloride ions. This peculiar behaviour is due to the presence of chloride ions in solution in the case of **1**. Upon reaction with H_2O_2 in methanol, complex **2** leads to the formation of low-spin [($L_6^2$2M)$Fe^{III}(OOH)^{2+}$, whereas it is not observed in the case of **1**. Based on the presence or not of chloride ions in solution, a mechanism is proposed for the reactivity of complexes **1** and **2** toward H_2O_2.

(© Wiley-VCH Verlag GmbH & Co. KGaA, 69451 Weinheim, Germany, 2003)

Introduction

Dioxygen activation by biological iron-containing systems performing monooxygenation reactions is an attractive sequence since it has considerable scientific and commercial interests. Whatever the system considered, the intermediate responsible for the target reaction, i.e. oxidation of the substrate, is proposed to be a high-valent iron-oxygen species. For mononuclear as well as for dinuclear systems, the events can be schematically described by the same universal sequence: dioxygen reacts with the metal centre(s) in the ferrous state leading to a hydroperoxo ferric complex which then evolves to the high valent entity after O−O bond cleavage. Only in the case of methane monooxygenase (MMO), which contains a non-heme dinuclear active site, has a high valent entity (compound Q), formulated as $Fe^{IV}-(\mu\text{-}O)_2-Fe^{IV}$, been characterised.[1,2] In the case of mononuclear systems with either heme or non-heme active sites, the high valent Fe-oxygen species has not been directly observed, but rather proposed by analogy with compounds I and II of peroxidases which have been identified as Fe^{IV}=O entities.[3]

Evidence has been obtained for the existence of hydroperoxo species, which are the precursors of the fleeting high valent entities, in natural systems such as MMO(dinuclear)[4] and bleomycin (mononuclear),[5] and several synthetic models have also been prepared.[6] To date, no evidence for conversion of a hydroperoxo species to a high valent iron-oxo species in synthetic models has been obtained spectroscopically. However, the recent synthesis of a dinuclear $Fe^{IV}-(\mu\text{-}O)_2-Fe^{IV}$ complex from a mononuclear Fe^{III}-alkylperoxo species[7] shows that such a process may be viable.

In this paper we report the structure and characterisation of a new Fe^{II} complex [($L_6^2$2M)$FeCl_2$] containing the ligand *N*,*N*′-bis(6-methyl-2-pyridylmethyl)-*N*,*N*′-bis(2-pyridylmethyl)ethane-1,2-diamine ($L_6^2$2M). This ligand is a bulkier analogue of the ligand TPEN, which has been shown to give access to a low-spin Fe−OOH intermediate.[8] The behaviour of the new complex [($L_6^2$2M)$FeCl_2$] in solution is considered in detail and its reactivity with H_2O_2 is also presented. We have also investigated the reactivity of the complex [($L_6^2$2M)FeCl]PF_6, previously reported by Bernal et al.,[9] with H_2O_2, and report evidence for the formation of a low-spin Fe−OOH complex from this reaction.

[a] Laboratoire de Chimie Inorganique, UMR CNRS 8613, Université Paris-Sud,
91405 Orsay, France
[b] DRECAM/SCM bat 125, CEA Saclay,
91191 Gif-sur-Yvette, France

Supporting information for this article is available on the WWW under http://www.eurjic.org or from the author.

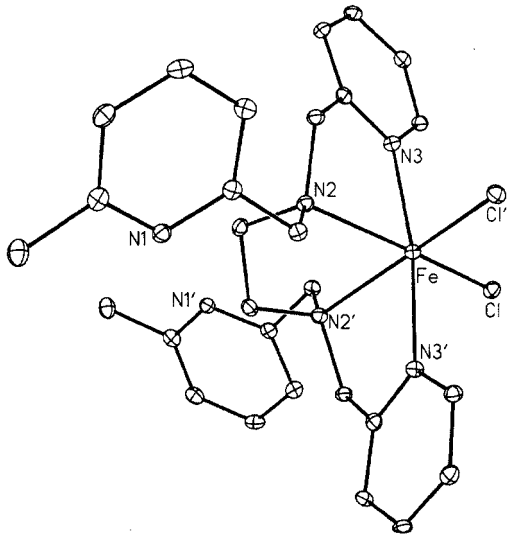

Figure 1. X-ray structure of the molecular complex $[(L_6^2 2M)FeCl_2]$ (**1**)

Results and Discussion

X-ray Crystal Structure

The structure of $[(L_6^2 2M)FeCl_2]$ (**1**) is presented in Figure 1. The Fe^{II} ion has a distorted octahedral geometry with two pyridine nitrogen atoms (N_3) in axial positions and two amino nitrogen atoms (N_2) in equatorial positions. The coordination sphere is completed by two chloride ligands in the equatorial plane.

The potentially hexadentate ligand $L_6^2 2M$ behaves here as a tetradentate ligand with the sterically hindered 6-methylpyridine groups not coordinating to the metal centre. This structure is analogous to those obtained for Fe complexes with tetradentate ligands derived from *N*,*N*′-bis(2-pyridylmethyl)ethane-1,2-diamine.[10−12]

A selection of structural data is reported in Table 1. The Fe−ligand bond lengths are characteristic of a high spin ferrous ion,[12] with the average bond length being 2.256 Å. As expected, the pyridine nitrogen atoms are closer to the Fe than the amino nitrogen atoms (cf. Table 1). The value of ca. 78° for the N_2-Fe-N_2 angle is typical of a five membered metallacycle.[13] Other angles between atoms in the Fe^{II} coordination sphere are also consistent with a strongly distorted octahedral geometry (cf. Table 1).

Table 1. Selected bond lengths and angles for $[(L_6^2 2M)FeCl_2]$ (**1**)

Bond lengths [Å]		Bond angles [°]	
Fe−N_2	2.320 (3)	N_2-Fe-N_2	78.18 (15)
Fe−N_3	2.192 (3)	N_3-Fe-N_3	170.90 (16)
Fe−Cl	2.4276 (10)	Cl−Fe−Cl	106.24 (5)

Table 2. UV/Vis data for $[(L_6^2 2M)FeCl_2]$ (**1**), $[(L_6^2 2M)FeCl]^+$(**2**), and some similar complexes in acetonitrile and methanol; abbreviations used for the ligands: L_5^2 = *N*-methyl-*N*,*N*′,*N*′-tris(2-pyridylmethyl)ethane-1,2-diamine; L_5^+ = *N*,*N*′,*N*′-tris(2-pyridylmethyl)-*N*′-trimethylammoniopentyl-ethane-1,2-diamine; trispicen = *N*,*N*′,*N*′-tris(2-pyridylmethyl)ethane-1,2-diamine; $LBzl_2$ = *N*,*N*′-dibenzyl-*N*,*N*′-bis(2-pyridylmethyl)ethane-1,2-diamine; L_4^2 = *N*,*N*′-dimethyl-*N*,*N*′-bis(2-pyridylmethyl)ethane-1,2-diamine

Complexes	λ_{max} [nm], ε [$M^{-1}cm^{-1}$]	
	CH_3CN	CH_3OH
$[(L_6^2 2M)FeCl_2]$	388, 1700	381, 1700
$[(L_6^2 2M)FeCl]PF_6$	378, 1700	376, 1700
$[(L_5^2)FeCl]PF_6$ [9]	399, 1840	
$[(L_5^+)FeCl](ClO_4)_2$ [14]	398, 1600	
$[(L_5^2)FeCl]Cl$[15]		385, 1750
[(trispicen)FeCl]PF_6 [8]		395, 1900
$[(LBzl_2)FeCl_2]$[12]	411, 1180	
$[(L_4^2)FeCl_2]$[16]	415, 770	

UV/Vis Spectroscopy

The electronic spectra of complexes $[(L_6^2 2M)FeCl_2]$ (**1**) and $[(L_6^2 2M)FeCl]PF_6$ (**2**) have been recorded in both acetonitrile and methanol, and the data are summarised in Table 2. The spectroscopic characteristics of both **1** and **2** are very similar in both solvents. In each case, the spectrum is dominated by an intense band in the UV corresponding to a pyridine π−π* transition (not reported in Table 2) and another at ca. 400 nm that is attributed to a Fe^{II}-to-pyridine MLCT transition. The ε values for the latter are characteristic of high-spin Fe^{II} systems.[14]

The fact that both $[(L_6^2 2M)FeCl_2]$ and $[(L_6^2 2M)FeCl]^+$ display similar spectra in solution suggests that they adopt a similar structure. Moreover, it is very likely that no solvent molecule is involved in the coordination sphere since the spectra obtained are identical in CH_3OH and CH_3CN.

The spectrum of $[(L_6^2 2M)FeCl_2]$ is different to that of $[(LBzl_2)FeCl_2]$ (cf. Table 2) and related complexes with a $[LFeCl_2]$ structure (L designates a tetradentate aminopyridine ligand).[12,16] These usually display a MLCT band at ca. 410 nm in acetonitrile. In contrast, $[(L_6^2 2M)FeCl_2]$ displays a MLCT band whose position and intensity are very similar to those observed for $[(L_6^2 2M)FeCl]PF_6$ (cf. Table 2) and similar complexes with three pyridines and an ethanediamine fragment.[8,9,14,15,17] The data reported for high spin Fe^{II} complexes with ethane-1,2-diamine/pyridine ligands show that the ε value of the MLCT band appears to correlate with the number of coordinated pyridines; for example, $\varepsilon \approx 1000\ M^{-1}cm^{-1}$ for complexes with two pyridines bound to Fe^{II} [12,16] while those with three pyridines bound to Fe^{II} [8,9,14,15,17] have $\varepsilon \approx 1600-2000\ M^{-1}cm^{-1}$.

It is also possible to compare the λ_{max} of the MLCT for *bis*-chloro complexes containing a tetradentate ligand ($\lambda_{max} \approx 410$ nm) with *mono*-chloro complexes containing a pentadentate ligand ($\lambda_{max} \approx 380$ nm). Substituting a π donor Cl^-, which destabilises the t_{2g} set of d orbitals, with a π accepting pyridine, which stabilises the t_{2g} set, will increase the gap between the t_{2g} metal orbitals and the pyri-

 © 2003 Wiley-VCH Verlag GmbH & Co. KGaA, Weinheim

dine π* orbitals thus resulting in a shift of the λ_{max} of the MLCT to shorter wavelength.

Both the λ_{max} of ca. 380 nm and the ε value of 1700 $M^{-1}cm^{-1}$ obtained for $[(L_6^2 2M)FeCl_2]$ are thus consistent with a structure where three pyridines are coordinated to the metal. The neutral structure observed in the solid state by X-ray diffraction is therefore not maintained in CH_3CN or CH_3OH solution since a chloride ligand is displaced by one of the pendant pyridines.

Cyclic Voltammetry

The cyclic voltammograms of $[(L_6^2 2M)FeCl]PF_6$ and $[(L_6^2 2M)FeCl_2]$ recorded at 20 °C in acetonitrile are presented in Figure 2.

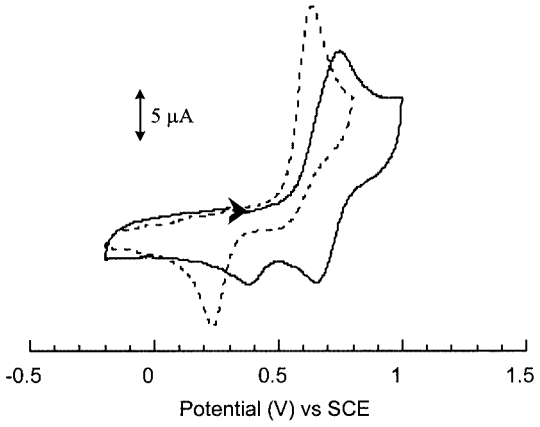

Figure 2. Cyclic voltammograms of $[(L_6^2 2M)Fe^{II}Cl]PF_6$ (**2**) (−) and $[(L_6^2 2M)Fe^{II}Cl_2]$ (**1**) (- - -) in acetonitrile at 20 °C

The cyclic voltammogram of $[(L_6^2 2M)FeCl]PF_6$ is analogous to the one previously reported by Bernal et al. for the same complex.[9] It exhibits one broad quasi-reversible wave with $E_{1/2}$ = 0.70 V (ΔE_p = 100 mV) and an extra cathodic wave at 0.38 V on the reverse scan. The broad quasi-reversible response corresponds to oxidation of $[(L_6^2 2M)Fe^{II}Cl]^+ \rightarrow [(L_6^2 2M)Fe^{III}Cl]^{2+}$. The second cathodic peak can be attributed to the reduction of a species obtained after rapid transformation of $[(L_6^2 2M)Fe^{III}Cl]^{2+}$ generated at the electrode. Indeed, the intensity of this last wave is decreased when the scan rate is increased. By analogy with the electrochemical behaviour of $[(L_5^3)Fe^{II}Cl]^+$ (L_5^3 = *N*-Methyl-*N*,*N*′,*N*′-tris(2-pyridylmethyl)propane-1,3-diamine) in CH_3OH[13] we propose that this transient complex can be formulated as $[(L_6^2 2M)Fe^{III}(OH)]^{2+}$, with the OH^- coming from residual water in the supporting electrolyte (see Exp. Sect.).

As depicted in Figure 2, $[(L_6^2 2M)FeCl_2]$ displays completely irreversible electrochemistry, with the anodic wave at E_{ox} = 0.63 V and a cathodic wave at 0.23 V. The oxidation potential of 0.63 V is close to that of $[(L_6^2 2M)Fe^{II}Cl]PF_6$ (E_{ox} = 0.75V; cf. Figure 2). This observation is in agreement with the conclusions drawn from the UV/Vis spectra (see above), i.e. formation of $[(L_6^2 2M)Fe^{II}Cl]^+$ from $[(L_6^2 2M)Fe^{II}Cl_2]$ in solution. Moreover, the one electron $Fe^{II} \rightarrow Fe^{III}$ oxidation observed for neutral $[LFeCl_2]$ complexes {L = *N*,*N*′-di-R-*N*,*N*′-bis(2-pyridylmethyl)ethane-1,2-diamine (R = H, Me, benzyl)} is usually reversible in acetonitrile, with $E_{1/2}$ values in the range 0.045−0.232 V vs. SCE,[10,12,18,19] significantly lower than the value of 0.63 V observed here. For example, the neutral complex $[L_4^2 Fe^{II}Cl_2]$ {L_4^2 = *N*,*N*′-dimethyl-*N*,*N*′-bis(2-pyridylmethyl)-ethane-1,2-diamine} has $E_{1/2}$ = 0.18 V.[19] The value of 0.63 V indicates that neutral $[(L_6^2 2M)Fe^{II}Cl_2]$ rearranges to $[(L_6^2 2M)Fe^{II}Cl]Cl$ in acetonitrile, in agreement with UV/Vis spectroscopy studies. In contrast, the wave at 0.23 V on the reverse scan is characteristic of the reduction of the bis chloro complex $[(L_6^2 2M)Fe^{III}Cl_2]^+$.

The lower E_{ox} potential value for complex **1** (0.63 V) compared to complex **2** (0.75 V) suggests the existence of a rapid chemical reaction subsequent to the electron transfer (EC mechanism).[20] Variation of the scan rate between 50 and 500 mV/s had no influence on the shape of the voltammogram, indicating that even the fastest scan rate was in-

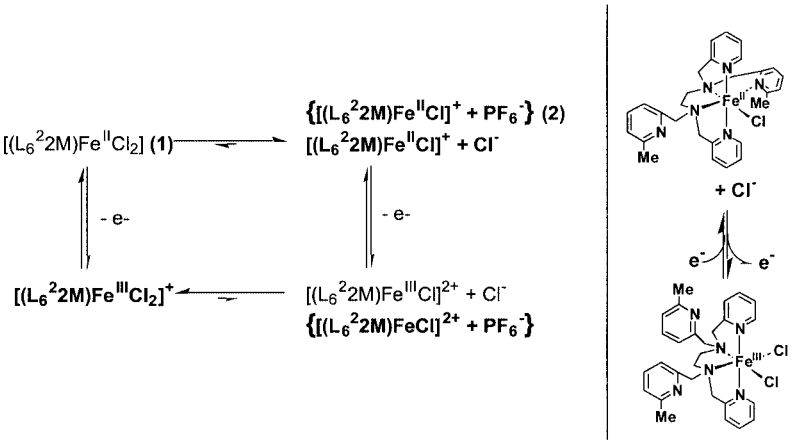

Scheme 1. Summary of electrochemical results for $[(L_6^2 2M)FeCl_2]$ (**1**) and $[(L_6^2 2M)FeCl]PF_6$ (**2**) in acetonitrile; species detected appear in bold characters; the second ferric complex detected in the cyclic voltammogram of **2** (see text) has been neglected here; the right part illustrates the EC mechanism observed for **1**

 © 2003 Wiley-VCH Verlag GmbH & Co. KGaA, Weinheim

sufficiently rapid to allow observation of the fast chemical reaction following the electron transfer. From the above observations, we propose that this chemical reaction is the rapid complexation of the Fe^{III} species by free Cl^- ions, thus generating the $[(L_6^22M)Fe^{III}Cl_2]^+$ complex, in which the ligand is tetradentate with two pendant pyridines. Indeed the oxidation wave of free Cl^- is not observed even at 500 mV/s.

The results obtained from the electrochemical studies are summarised in Scheme 1. Dissolution of $[(L_6^22M)Fe^{II}Cl_2]$ (**1**) in acetonitrile immediately gives $[(L_6^22M)Fe^{II}Cl]^+$. When oxidised, this complex gives the unstable ferric analog which then interacts immediately with the free Cl^- to give $[(L_6^22M)Fe^{III}Cl_2]^+$ in which the ligand L_6^22M is tetradentate. This latter complex is reduced at 0.23V.

In the case of $[(L_6^22M)FeCl]PF_6$ (**2**), no extra Cl^- is available in solution to react with $[(L_6^22M)FeCl]^{2+}$ in which the L_6^22M ligand coordinates in a pentadentate fashion. As a matter of fact, this latter ferric complex is stable and can be easily detected. These electrochemical studies suggest that, although both complexes adopt the same structure at the ferrous level, they give different species on oxidation.

The electrochemical behaviour of these two complexes was also investigated in CH_3OH, and in both cases, the Fe^{II}/Fe^{III} system is completely irreversible. The complex $[(L_6^22M)Fe^{II}Cl]PF_6$ (**2**) reacts rapidly to form $[(L_6^22M)Fe^{III}(OCH_3)]^{2+}$ and $[(L_6^22M)Fe^{III}(OH)]^{2+}$. Such behaviour has already been observed for complexes with similar pentadentate ligands.[13,21] This indicates that the chloride ion is easily substituted in CH_3OH when the complex is in its ferric state. Following oxidation of $[(L_6^22M)Fe^{II}Cl_2]$ (**1**), the complexes $[(L_6^22M)Fe^{III}(OCH_3)]^{2+}$ and $[(L_6^22M)Fe^{III}(OH)]^{2+}$ are observed as for **2**. However, a third cathodic wave is detected at a lower potential (ca. 12 mV, see Supporting Information). By analogy with the study in CH_3CN, this latter wave is attributed to the reduction of $[(L_6^22M)Fe^{III}Cl_2]^+$. The chloride ions have such a high affinity for Fe^{III} even in CH_3OH that for $Cl^-/Fe = 2$, the bis-chloro-Fe^{III} complex is obtained.

Reactivity with H_2O_2

The reactivities of the complexes $[(L_6^22M)FeCl_2]$ and $[(L_6^22M)FeCl]PF_6$ with an excess of H_2O_2 was studied in CH_3OH by using a variety of techniques.

The reaction of H_2O_2 with $[(L_6^22M)FeCl]PF_6$ has previously been studied by Bernal et al. but no intermediate was clearly identified.[9] We present here a reinvestigation of this reaction. Addition of 100 equivalents of H_2O_2 to $[(L_6^22M)FeCl]PF_6$ in methanol at −40 °C resulted in the appearance of a low intensity band at 530 nm in the UV/Vis spectrum. This is attributed to a hydroperoxo-to-Fe^{III} charge transfer transition, with an energy similar to other low-spin $Fe^{III}-OOH$ species involving a ligand containing three pyridines coordinated to the metal.[6] The low intensity of the band indicates either a low conversion to Fe−OOH or a high instability of the hydroperoxo product. The maximum intensity is observed after ca. one hour (at −40 °C), which reflects a steady state for this intermediate, due to the large excess of H_2O_2. Similar behaviour was observed for $[(TPEN)FeCl]^+$ {TPEN = *N*,*N*,*N*′,*N*′-tetrakis(2-pyridylmethyl)ethane-1,2-diamine}, but a much more stable $Fe^{III}-OOH$ intermediate was obtained at room temperature.[8]

The EPR spectrum of the solution was recorded at 4 K. It exhibits several resonances that arise from more than one species (cf. Figure 3). A $g = 4.2$ signal is attributed to a high spin Fe^{III} degradation species (not shown in Figure 3).[22] Other resonances around $g = 2$ are characteristic of low-spin Fe^{III} complexes. Two sets of very close g values can be distinguished with $g_{max} = 2.2$ or 2.18; $g_{inter} = 2.12$ and 2.12; $g_{min} = 1.97$ or 1.96. Starting with the complex $[(L_6^22M)Fe(OH_2)](PF_6)_2$, Bernal et al. have observed identical values.[9] These sets of g values are characteristic of low-spin Fe^{III} in nearly axial symmetry, and are consistent with EPR data reported for low-spin $Fe^{III}-OOH$ entities.[6] For example, the Fe^{III} complex of the TPEN ligand exhibits g values of 2.22, 2.15, and 2.00.[8]

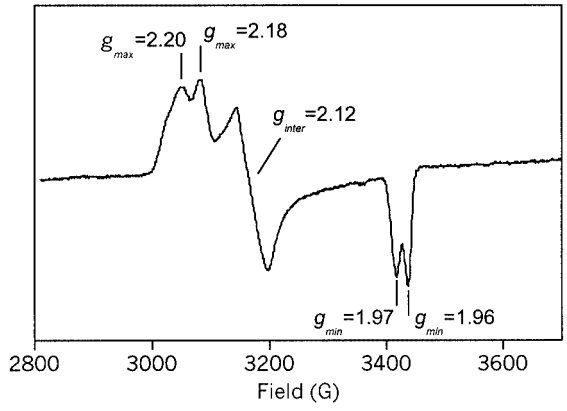

Figure 3. EPR spectrum of a mixture of $[(L_6^22M)Fe^{II}Cl]PF_6$ (**2**) and 100 equivalents of H_2O_2 in CH_3OH at 4 K

The simplest way to rationalise the presence of two close but different sets of g values is to propose two different coordination modes for the ligand L_6^22M. Indeed, the ratio of coordinated pyridines to coordinated methylated pyridines can be 1:2 or 2:1 when this ligand coordinates in a pentadentate fashion, as represented in Scheme 2.

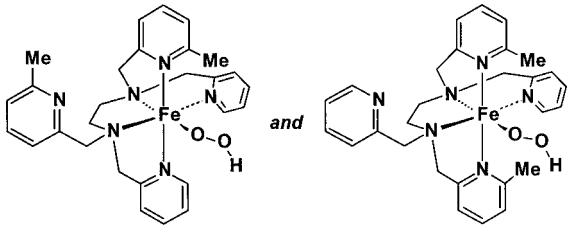

Scheme 2. Proposed structures for the two low-spin intermediates of formula $[(L_6^22M)Fe(OOH)]^{2+}$

Starting with the complex $[(L_6^22M)FeCl_2]$ (**1**), no reaction intermediate was observed by UV/Vis spectroscopy at −40 °C even though it adopts a structure in solution ident-

 © 2003 Wiley-VCH Verlag GmbH & Co. KGaA, Weinheim

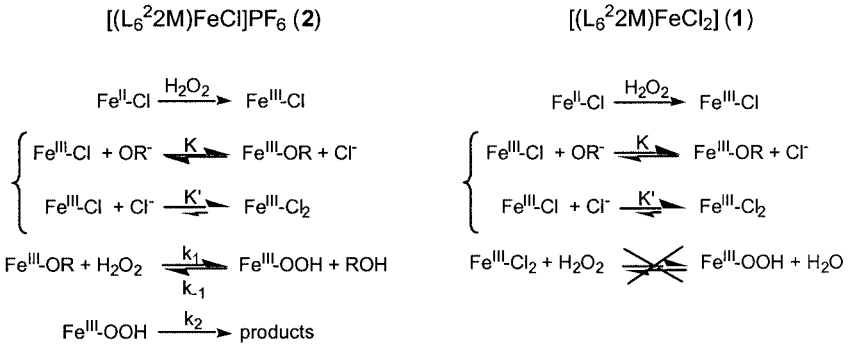

Scheme 3. Mechanism proposed for the reactivity toward H_2O_2 of complexes **1** and **2** (R=H or CH_3)

ical to that of complex **2** i.e. $[(L_6^22M)Fe^{II}Cl]^+$ (see above). The only difference between **1** and **2** is the presence of chloride ions in solution in the case of **1**. As shown by electrochemistry, oxidation of complex **1** leads to the formation of $[(L_6^22M)Fe^{III}Cl_2]^+$, in which the ligand coordinates in a tetradentate fashion. To the best of our knowledge, no reaction intermediate has ever been reported upon addition of H_2O_2 to a complex containing a linear tetracoordinate ligand.

The fact that $[(L_6^22M)FeCl]PF_6$ (**2**) but not $[(L_6^22M)FeCl_2]$ (**1**) has allowed to observe a low-spin mononuclear Fe−OOH intermediate, substantiates the mechanism we proposed for the formation of Fe−OOH intermediates.[13] In this paper, adjustment of kinetic data was made by considering very fast pre-equilibria to give a mononuclear Fe^{III} complex upon oxidation of the Fe^{II} precursor.[13] Here we propose that $[(L_6^22M)FeCl_2]$ is not able to give a mononuclear Fe−OOH complex since the ferric complex obtained contains the ligand L_6^22M bound in a tetradentate fashion following substitution of a pyridyl arm by a free chloride ion (cf. Scheme 3).

The statement that a mononuclear Fe−OOH is not obtained from complex **1** may not be rigorously true. Indeed, when complex **1** is oxidised in CH_3OH, it also gives the Fe^{III}−OH and Fe^{III}−OCH_3 complexes as in the case of **2**. These species are precursors of the Fe−OOH complex (cf. Scheme 3). However, since the conversion of **2** into the Fe−OOH is low as noted above, it will be even lower starting from complex **1**, and not observable under these experimental conditions.

Conclusion

We have synthesised two Fe^{II} complexes of the ligand L_6^22M. The crystal structure of neutral $[(L_6^22M)FeCl_2]$ (**1**) shows two chloride ions coordinated to the metal centre in *cis* positions and the potential hexadentate ligand coordinated in a tetradentate fashion. The complex $[(L_6^22M)FeCl]PF_6$ (**2**) contains the ligand bound in a pentacoordinate fashion, as revealed by UV/Vis and cyclic voltammetry. However, it probably exhibits two different coordination modes, with one pendant pyridine which may be either methylated or not methylated. Upon dissolution in acetonitrile or methanol, one chloride ion of $[(L_6^22M)FeCl_2]$ (**1**) is replaced by a nitrogen atom of a methylated pyridine group. Therefore, the two Fe^{II} complexes adopt similar structures in solution. Upon electrochemical oxidation in acetonitrile, $[(L_6^22M)FeCl]PF_6$ (**2**) gives its ferric analog whereas $[(L_6^22M)FeCl_2]$ (**1**) is subject to a fast EC mechanism to give $[(L_6^22M)Fe^{III}Cl_2]^+$ in which the ligand is tetracoordinate. When oxidised in MeOH, both **1** and **2** give $[(L_6^22M)Fe^{III}(OR)]^{2+}$ (R = H or CH_3), but a third complex, $[(L_6^22M)Fe^{III}Cl_2]^+$, is also observed for **1** with the ligand bound tetradentate.

These different structures at the Fe^{III} oxidation state are probably responsible for the different reactivities in the presence of H_2O_2. Two similar low-spin Fe^{III}−OOH intermediates have been characterised for $[(L_6^22M)FeCl]PF_6$ (**2**) upon reaction with H_2O_2 at −40 °C. These two Fe^{III}−OOH species very likely differ only in the number of coordinated methylated pyridines. The complexes reported here are unstable when compared to Fe^{III}−OOH complexes obtained with similar ligands. Compared to the parent ligand TPEN[8] the instability observed here may be related to the bulkiness of the L_6^22M ligand. Indeed it is likely that this ligand is not well adapted to the small Fe^{III} ion, due to steric congestion provided by the pyridine rings.

Starting from $[(L_6^22M)FeCl_2]$ (**1**) in MeOH, no intermediate could be detected under the same experimental conditions.

Although both Fe^{II} complexes have analogous structures in solution, their reactivities in the presence of H_2O_2 are different. This clearly establishes that the $Fe^{II} \rightarrow Fe^{III}$ oxidation is the first process occurring during the reaction between a ferrous complex and H_2O_2. The HOO^- ligand then reacts with the ferric complex obtained. The observations reported in this paper confirm the mechanism proposed to analyse the kinetic data of a similar low-spin Fe^{III}−OOH complex.[13]

Experimental Section

Materials: Starting materials were purchased from Acros. Solvents were purchased from Merck and used without further purification.

 © 2003 Wiley-VCH Verlag GmbH & Co. KGaA, Weinheim

Synthesis of *N,N′*-bis(6-methyl-2-pyridylmethyl)-*N,N′*-bis(2-pyridylmethyl)ethane-1,2-diamine ($L_6^2$2M): This ligand was prepared following the method reported by Toftlund and Yde-Andersen.[23]

Synthesis of [($L_6^2$2M)$FeCl_2$] (1): This synthesis was performed by using Schlenk tubes and a vacuum-argon line. A solution of $L_6^2$2M (140 mg) in THF was added to a solution of $FeCl_2{\cdot}2H_2O$ (50 mg, 1.01 equiv.) in THF (10 mL) and a yellow powder rapidly precipitated. The reaction mixture was stirred for 30 minutes, the solvent was partially removed and the powder was isolated by filtration. Yield 86 mg (48%). Crystals suitable for structural determination were obtained by slow diffusion of *tert*-butyl methyl ether into an acetonitrile solution of the complex. Elemental analysis, found: C 58.43, H 5.30, Cl 12.47, N 14.15; calculated for $C_{28}H_{32}Cl_2FeN_6$ (579.4): C 58.12, H 5.58, Cl 12.1, N 14.53.

Synthesis of [($L_6^2$2M)FeCl]PF_6 (2): This synthesis was performed under an argon atmosphere as for complex **1** following the method reported by Bernal et al.[9] A methanol solution of $L_6^2$2M (515 mg) was added to a solution of $FeCl_2{\cdot}2H_2O$ (185 mg, 1 equiv.) in methanol (5 mL). The yellow solution was stirred for 15 minutes and $NaPF_6$ (200 mg, 2 equiv.) in methanol was then added. The majority of the solvent was removed and of to give a yellow powder. Yield 470 mg (50%). Elemental analysis, found: C 38.44, H 4.07, N 9.67; calculated for $C_{28}H_{32}N_6FeClPF_6{\cdot}NaPF_6{\cdot}H_2O$ (874.8): C 38.44, H 3.92, N 9.61.

Physical Measurements: Elemental analyses were performed by the Service Central d'Analyses du CNRS (Vernaison-France). UV/Vis spectra were recorded on a Varian Cary 300 Bio spectrophotometer at 20 °C with 1 cm quartz cuvettes. Stopped-flow experiments were performed with a Biologic SFM-300 equipped with a Julabo F 30C cryostat. Spectra were recorded in the range 200−1022 nm with a 0.5 cm optical path and a 50 μL cuvette. The delay after mixing is 3 ms. Cyclic Voltammograms were measured using an EGG PAR model M270 scanning potentiostat operating at scan rates of 10−1000 $mV{\cdot}s^{-1}$. Studies were carried out under an argon atmosphere in acetonitrile or methanol solutions using 0.2 M tBu_4NClO_4 (puriss grade, Fluka) as the supporting electrolyte, and 10^{-3} M of the complex. In order to minimise the amount of water contained in the system, the supporting electrolyte solution was dried over Al_2O_3 prior to use. The working electrode was a glassy carbon disk (0.32 cm^2) polished with 1 μm diamond paste. The reference electrode was Ag-$AgClO_4$ (0.3 V vs. SCE electrode) separated from the test solution by a salt bridge containing the solvent/supporting electrolyte, with a gold auxiliary electrode. All potentials are given vs. SCE electrode (0.241 V vs. NHE electrode).

Crystallographic Data Collection: The data were collected on a Nonius−Kappa-CCD area detector diffractometer by using graphite-monochromated Mo-K_α radiation. The lattice parameters were determined from ten images recorded with 2° -scans and later refined on all data. The data were recorded at 123 K. A 180° -range was scanned with 2° steps with a crystal to detector distance fixed at 30 mm. Data were corrected for Lorentz polarisation. The structure was solved by direct methods by using SHELXS[24] and refined by full-matrix least-squares on F^2 with anisotropic thermal parameters for all non H atoms using SHELXL-97.[25] H atoms were introduced at calculated positions as riding atoms with an isotropic displacement parameter equal to 1.2 (CH and CH_2) times that of the parent atom. The molecular plots were drawn by using SHELXTL.[26] All calculations were performed on a Silicon Graphics R10000 workstation. The crystal data and parameters for data collection are summarised in Table 3.

CCDC-199948 contains the supplementary crystallographic data for this paper. These data can be obtained free of charge at www.ccdc.cam.ac.uk/conts/retrieving.html [or from the Cambridge Crystallographic Data Centre, 12, Union Road, Cambridge CB2 1EZ, UK; Fax: (internat.) +44−1223/336-033; E-mail: deposit@ccdc.cam.ac.uk].

Supporting Information (see footnote on the first page of this article): Voltammograms of complexes (**1**) (- - -) and (**2**) (−) in CH_3OH at 20 °C.

Table 3. Summary of X-ray crystallographic data for [($L_6^2$2M)$FeCl_2$] (**1**)

Empirical formula	$C_{28}H_{32}Cl_2FeN_6$
Formula mass	579.35
Crystal system	orthorhombic
space group	Pbcn
a [Å]	12.548(3)
b [Å]	10.046(2)
c [Å]	21.009(4)
V [Å^3]	2648.3(9)
Z	4
D(calcd.) [g/cm^3]	1.453
μ [cm^{-1}]	0.801
Crystal size [mm]	0.15 × 0.10 × 0.10
Radiation type	Mo-*K*α
Temperature [K]	123(2)
θ range [deg]	2.53−24.67
No. of reflns. collected	16004
No. of reflns. merged	2107
No. of reflns. obsd.	1648
Observation criterion	$I > 2\sigma(I)$
no of params refined	168
R[a]	0.0458
R_w[b]	0.0968
Goodness of fit	0.932

[a] $R = \Sigma(||F_o| - |F_c||)/\Sigma|F_o|$. [b] $R_w = [\Sigma w(||F_o| - |F_c||)^2/\Sigma w(|F_o|)^2]^{1/2}$.

[1] M. Merkx, D. A. Kopp, M. H. Sazinsky, J. L. Blazyk, J. Müller, S. J. Lippard, *Angew. Chem. Int. Ed.* **2001**, *40*, 2782.
[2] B. J. Wallar, J. D. Lipscomb, *Chem. Rev.* **1996**, *96*, 2625.
[3] B. Meunier, J. Bernadou, in: *Structure and Bonding, Vol. 97* (Ed.: B. Meunier), **2000**, pp. 1.
[4] J. DuBois, T. J. Mizoguchi, S. J. Lippard, *Coord. Chem. Rev.* **2000**, *200−202*, 443.
[5] R. M. Burger, in: *Structure and Bonding, Vol. 97* (Ed.: B. Meunier), **2000**, pp. 287.
[6] J. J. Girerd, F. Banse, A. J. Simaan, in: *Structure and Bonding, Vol. 97* (Ed.: B. Meunier), **2000**, pp. 146.
[7] M. Costas, J.-U. Rohde, A. Stubna, R. Y. N. Ho, L. Quaroni, E. Münck, L. Que, *J. Am. Chem. Soc.* **2001**, *123*, 12931.
[8] A. J. Simaan, S. Döpner, F. Banse, S. Bourcier, G. Bouchoux, A. Boussac, P. Hildebrandt, J. J. Girerd, **2000**, *Eur. J. Inorg. Chem.* 1627.
[9] I. Bernal, I. M. Jensen, K. B. Jensen, C. J. McKenzie, H. Toftlund, J. P. Tuchagues, *J. Chem. Soc., Dalton Trans.* **1995**, 3667.
[10] N. Arulsamy, D. J. Hodgson, J. Glerup, *Inorg. Chim. Acta* **1993**, *209*, 61.
[11] K. Chen, L. Que, *Chem. Commun.* **1999**, 1375.
[12] A. J. Simaan, S. Poussereau, G. Blondin, J. J. Girerd, D. Defaye, C. Philouze, J. Guilhem, L. Tchertanov, *Inorg. Chim. Acta* **2000**, *299*, 221.
[13] V. Balland, F. Banse, E. Anxolabéhère-Mallart, M. Ghiladi, T. Mattioli, C. Philouze, G. Blondin, J.-J. Girerd, *Inorg. Chem.*, in press.

 © 2003 Wiley-VCH Verlag GmbH & Co. KGaA, Weinheim

[14] P. Mialane, A. Novorojkine, G. Pratviel, L. Azéma, M. Slany, F. Godde, A. Simaan, F. Banse, T. Kargar-Grisel, G. Bouchoux, J. Sainton, O. Horner, J. Guilhem, L. Tchertanova, B. Meunier, J. J. Girerd, *Inorg. Chem.* **1999**, *38*, 1085.
[15] A. J. Simaan, F. Banse, P. Mialane, A. Boussac, S. Un, T. Kargar-Grisel, G. Bouchoux, J. J. Girerd, *Eur. J. Inorg. Chem.* **1999**, 993.
[16] N. Raffard, PhD thesis, Université Paris XI (Orsay), **2002**.
[17] A. Hazell, C. J. McKenzie, L. P. Nielsen, S. Schindler, M. Weitzer, *J. Chem. Soc., Dalton Trans.* **2002**, 310.
[18] A. Nivorozhkin, E. Anxolabéhère-Mallart, P. Mialane, R. Davydov, J. Guilhem, M. Cesario, J.-P. Audière, J.-J. Girerd, S. Styring, L. Schussler, J.-L. Seris, *Inorg. Chem.* **1997**, *36*, 846.
[19] N. Raffard, V. Balland, J. Simaan, S. Létard, M. Nierlich, K. Miki, F. Banse, E. Anxolabéhère-Mallart, J.-J. Girerd, *C. R. Chimie* **2002**, *5*, 99.
[20] A. J. Bard, L. R. Faulkner, *Electrochimie; principes, méthodes et applications*, Masson, Paris - New York - Barcelona - Milano - Mexico - Sao Paulo, **1983**.
[21] L. Duelund, R. Hazell, C. J. McKenzie, L. P. Nielsen, H. Toftlund, *J. Chem. Soc., Dalton Trans.* **2001**, 152.
[22] A. J. Simaan, F. Banse, J. J. Girerd, K. Wieghardt, E. Bill, *Inorg. Chem.* **2001**, *40*, 6538.
[23] H. Toftlund, S. Yde-Andersen, *Acta Chem. Scand., Ser. A* **1981**, *35*, 575.
[24] G. M. Sheldrick, *Acta Crystallogr., Sect. A* **1990**, *46*, 467.
[25] G. M. Sheldrick, *SHELXL-97: Program for the Refinement of Crystal Structures*, University of Göttingen, Germany, **1997**.
[26] G. M. Sheldrick, *SHELXTL*, version 5.1, University of Göttingen, Germany, **1999**.

Received December 19, 2002

 © 2003 Wiley-VCH Verlag GmbH & Co. KGaA, Weinheim

EurJIC
European Journal of Inorganic Chemistry

Issue 14/2003

Pages 2537–2718

Papers available ahead of print in Early View at www.interscience.wiley.com

Earliest available Table of Contents:
Automatically, free of charge by e-mail through
www.interscience.wiley.com/alerts

COVER PICTURE

The cover picture shows the X-ray crystal structures of ruthenium and rhodium complexes of chiral 1,1′-bis(phosphetano)ferrocenes. These diphosphanes rank among the ligands inducing excellent enantioselectivities in rhodium-promoted hydrogenations of prochiral olefins. X-ray crystal structures of their metal complexes afford information about their coordinating behaviour and preferred conformations in catalytically active species. Details are discussed in the article by A. Marinetti et al. on p. 2583 ff.

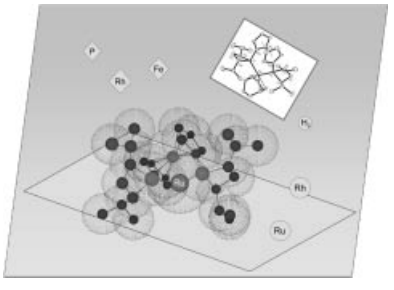

MICROREVIEW

Contents

2551 **G. Jia,* Z. Lin, C. P. Lau**

Reactions of Dihydrogen(norbornadiene) Complexes

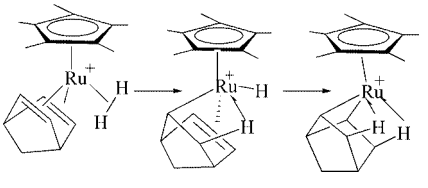

Keywords: Transition metals / Hydride ligands / Hydrogenations / Norbornadiene / Dihydrogen ligands

 © 2003 Wiley-VCH Verlag GmbH & Co. KGaA, Weinheim

SHORT COMMUNICATIONS

2563 **J. Kim,* J. M. Lim, Y. Do***

A Novel One-Dimensional Chain Complex Composed of Oxo-Centered Trinuclear Manganese Clusters

Keywords: Magnetic properties / Manganese / Oxo ligands / Clusters

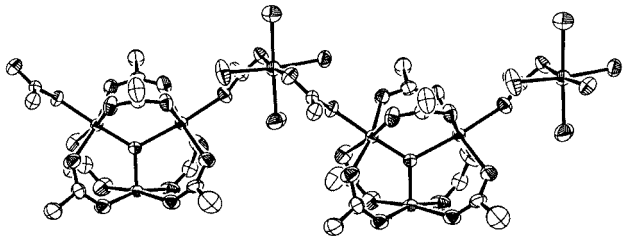

2567 **Y.-G. Li, N. Hao, E.-B. Wang,* Y. Lu, C.-W. Hu, L. Xu**

A Novel Three-Dimensional Metal-Organic Framework Constructed from Two-Dimensional Interpenetrating Layers Based on Trinuclear Cobalt Clusters: $[Co_3(btec)(C_2O_4)(H_2O)_2]_n$

Keywords: Hydrothermal synthesis / Carboxylate ligands / Cobalt / Coordination polymers / Magnetic properties

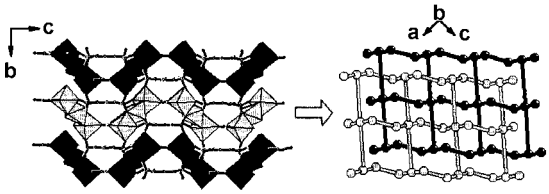

2572 **J. Zhang, Y.-R. Xie, Q. Ye, R.-G. Xiong,* Z. Xue, X.-Z. You***

Blue to Red Fluorescent Emission Tuning of a Cadmium Coordination Polymer by Conjugated Ligands

Keywords: Cadmium / Fluorescence / Coordination polymers / Crystal Engineering / Hydrothermal synthesis

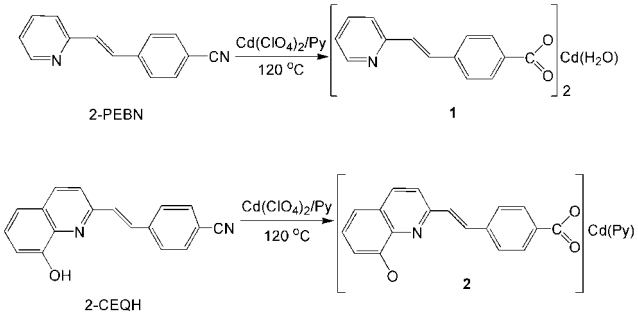

2578 **L.-M. Duan, C.-L. Pan, J.-Q. Xu,* X.-B. Cui, F.-T. Xie, T.-G. Wang**

Two- and Three-dimensional Frameworks Constructed From Bicapped Keggin Clusters

Keywords: Polyoxometalates / Hydrothermal synthesis / Cluster compounds / Crystal structure

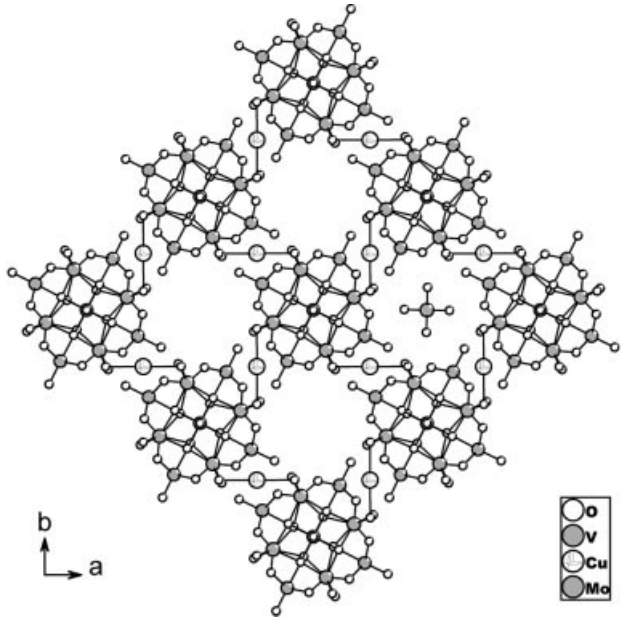

 © 2003 Wiley-VCH Verlag GmbH & Co. KGaA, Weinheim

FULL PAPERS

2583 **A. Marinetti,* F. Labrue, B. Pons, S. Jus, L. Ricard, J.-P. Genêt**

Rhodium and Ruthenium Complexes of 1,1′-Bis(phosphetano)ferrocenes: Structural Characterisation and Catalytic Behaviour

Keywords: Asymmetric catalysis / Hydrogenations / P ligands / Phosphetane / Rhodium / Ruthenium

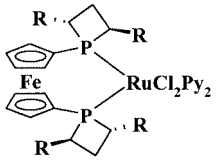

2591 **Y. V. Mironov, O. A. Efremova, D. Y. Naumov, W. S. Sheldrick, V. E. Fedorov***

Synthesis and Structures of Compounds Based on Chalcocyanide Tetranuclear Rhenium Clusters: Bonding Cluster Complexes by diene-Bridged Cu^{II} Units

Keywords: Rhenium / Clusters / Chalcogen / Copper / Solid-state structures

2596 **A.-M. Albrecht-Gary,* S. Blanc, F. Biaso, F. Thomas, P. Baret, G. Gellon, J.-L. Pierre, G. Serratrice***

Iron(III) Chelation: Tuning of the pH Dependence by Mixed Ligands

Keywords: Tripodal ligands / Iron / Thermodynamics / UV/Vis spectroscopy / Siderophores

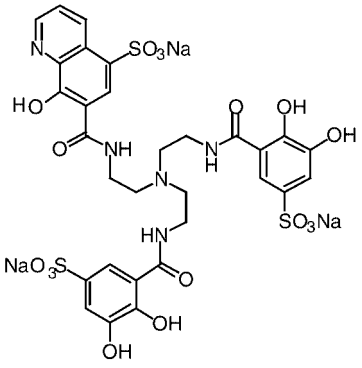

pFe^{III} = 32.3 (pH = 7.4; [L]/[Fe] = 10)

2606 **S. Di Bella,* I. Fragalà**

Second-Order Nonlinear Optical Properties of Tetraaza-Coordinated Nickel(II) Complexes

Keywords: Nickel / Nonlinear optics / Semiempirical calculations

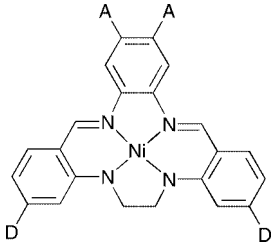

2612 **E. Rotondo,* G. Bruschetta, G. Bruno, A. Rotondo, M. L. Di Pietro, M. Cusumano**

NMR Investigation and Dynamic Behaviour of $[2,2'$-Bipyridylbis(pyridine)platinum(II)$]^{2+}$ and Related Cationic Complexes − Crystal Structure of $[Pt(bipy)(py)_2](PF_6)_2$

Keywords: Intercalations / N ligands / NMR spectroscopy / Platinum

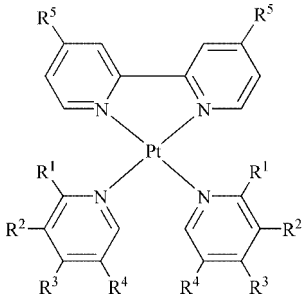

1 ($R^1 = R^2 = R^3 = R^4 = R^5 = H$)
2 ($R^1 = Me$, $R^2 = R^3 = R^4 = R^5 = H$)
3 ($R^2 = Me$, $R^1 = R^3 = R^4 = R^5 = H$)
4 ($R^2 = CN$, $R^1 = R^3 = R^4 = R^5 = H$)
5 ($R^2 = Ph$, $R^1 = R^3 = R^4 = R^5 = H$)
6 ($R^3 = Ph$, $R^1 = R^3 = R^4 = R^5 = H$)
7 ($R^2 = R^4 = Me$, $R^1 = R^3 = R^5 = H$)
8 ($R^5 = Ph$, $R^1 = R^2 = R^3 = R^4 = H$)
9 ($R^5 = Ph$, $R^3 = CN$, $R^1 = R^2 = R^4 = H$)

 © 2003 Wiley-VCH Verlag GmbH & Co. KGaA, Weinheim

2619 **M. Galanski,* C. Baumgartner, V. Arion, B. K. Keppler**

Bis(2-aminobutanol)dichloroplatinum(II) Complexes and Their Singly and Doubly Ring-Closed Butanolato Species − Novel Prodrugs for Platinum-Based Antitumour Chemotherapy?

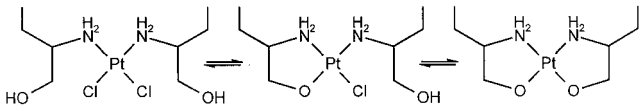

Keywords: Antitumour agents / Bioinorganic chemistry / N,O ligands / Platinum

2626 **A. Antiñolo, R. Fernández-Galán, B. Gallego, A. Otero,* S. Prashar, A. M. Rodríguez**

Synthesis and Reactivity of Alkylzirconium Complexes Incorporating Asymmetrically Substituted *ansa* Ligands − X-ray Crystal Structure of [Zr{$Me_2Si(\eta^5\text{-}C_5Me_4)(\eta^5\text{-}C_5H_3Me)$}$(CH_2Ph)Cl$]

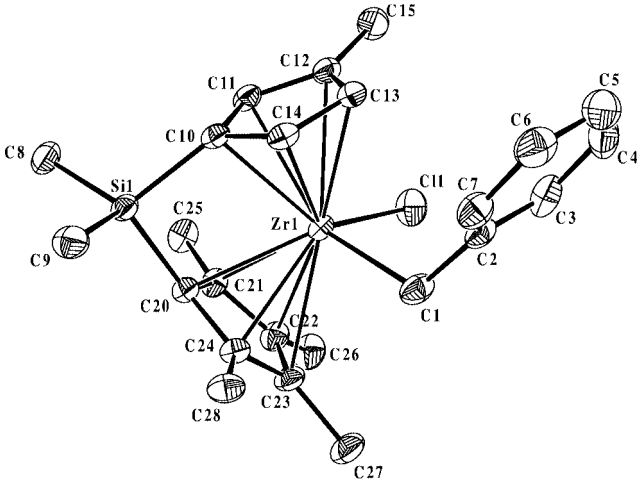

Keywords: Metallocenes / Zirconium / Insertion reactions / Isocyanides

2633 **H. Sugimoto,* K. Siren, H. Tsukube, K. Tanaka**

Mono-Dithiolene Molybdenum(IV) Complexes of *cis*-1,2-Dicyano-1,2-ethylenedithiolate (mnt^{2-}): New Models for Molybdenum Enzymes

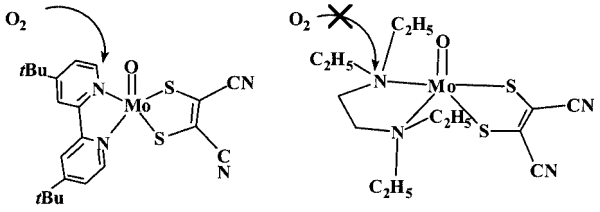

Keywords: Molybdenum / Bioinorganic chemistry / Oxo ligands / S ligands / Oxidation

2639 **P. Gómez-Saiz, J. García-Tojal,* M. A. Maestro, J. Mahía, F. J. Arnaiz, L. Lezama, T. Rojo**

New 1,3,4-Oxadiazolecopper(II) Derivatives Obtained from Thiosemicarbazone Complexes

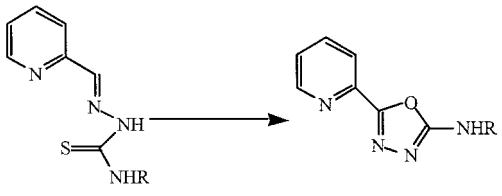

Keywords: Copper / Magnetic properties / Thiosemicarbazone complexes / Oxadiazole complexes / X-ray diffraction

 © 2003 Wiley-VCH Verlag GmbH & Co. KGaA, Weinheim

2651 **Y. Li, W.-T. Wong***

Syntheses, Reactivity Studies and the Catalytic Properties of a Series of Tetraosmium−Gold Mixed-Metal Clusters

Keywords: Osmium / Gold / Clusters / Electrochemistry / Carbonylations

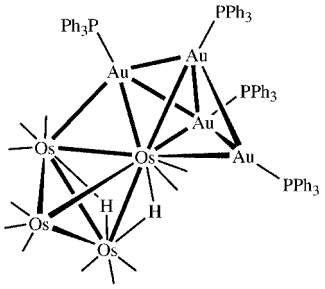

2663 **M.-H. Chiang, C. W. Williams, L. Soderholm,* M. R. Antonio***

Coordination of Actinide Ions in Wells−Dawson Heteropolyoxoanion Complexes

Keywords: Actinides / Electrostatic interactions / Lanthanides / Polyoxometalates / X-ray absorption spectroscopy

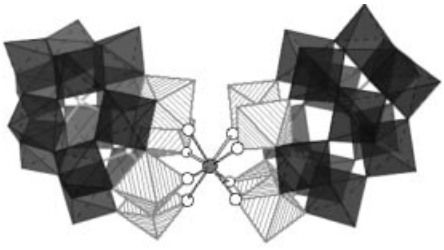

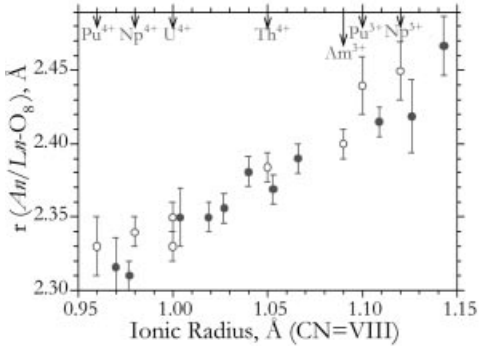

2670 **Z.-Y. Fu, S.-M. Hu, J.-C. Dai, J.-J. Zhang, X.-T. Wu***

Three Novel Polymeric Frameworks Assembled from Cd^{II}, Co^{II}, and Mn^{II} with the Mixed Organic Ligands 3,4-Pyridinedicarboxylate, 1,3-Bis(4-pyridyl)propane, or 1,2-Bis(4-pyridyl)-ethane

Keywords: Coordination polymer / Crystal engineering / Mixed ligands / Structural topology

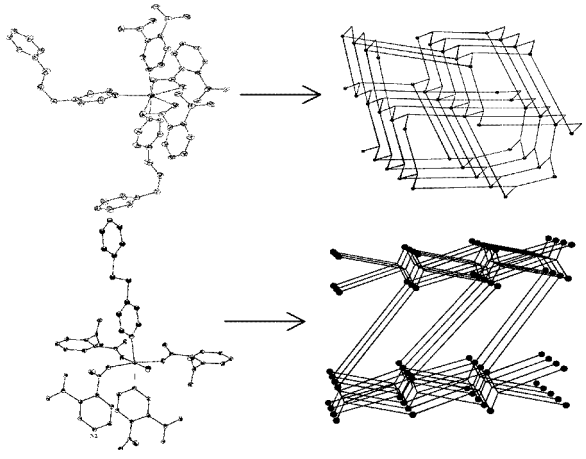

2678 **J. Tao,* X. Yin, Y.-B. Jiang, L.-F. Yang, R.-B. Huang, L.-S. Zheng***

Syntheses and Crystal Structures of Two Novel Zinc(II) Coordination Polymers

Keywords: Coordination polymers / Zinc / N ligands / Hydrogen bonds / Photoluminescence

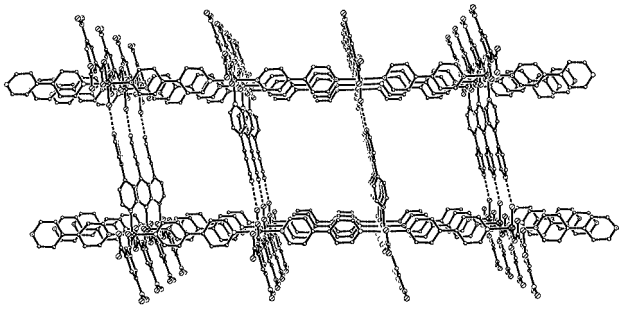

 © 2003 Wiley-VCH Verlag GmbH & Co. KGaA, Weinheim

2683 **E. Zangrando,* M. Trani, E. Stabon, C. Carfagna, B. Milani, G. Mestroni**

Synthesis and Molecular Structures of Nickel(II) and Cobalt(III) Complexes with 2-(Arylimino)-3-(hydroxyimino)butane

Keywords: Cobalt / Crystal structures / N-donor ligands / Nickel / Stacking interactions

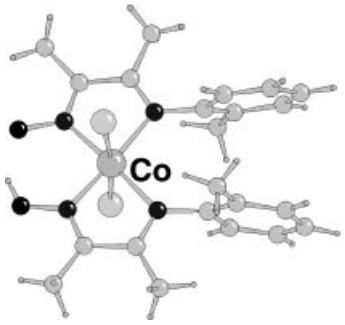

2693 **R. M. Claramunt, P. Cornago, M. Cano,* J. V. Heras, M. L. Gallego, E. Pinilla, M. R. Torres**

New Tris(pyrazolyl)triazine and Pyrazolylpyridine Gold(I) and Palladium(II) Derivatives Based on the 3,5-Bis(4-butoxyphenyl)pyrazole Group − Architectures with Different Types of Bonding Interactions

Keywords: Gold / Hydrogen bonds / Palladium / Supramolecular Chemistry / Triazine

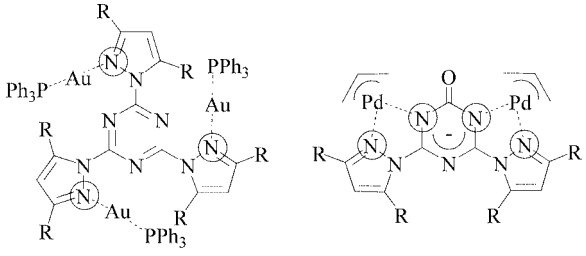

2705 **J. Luo, M. Hong,* R. Wang, R. Cao, L. Han, Z. Lin**

Synthesis, Crystal Structure and Fluorescence of Two Novel Mixed-Ligand Cadmium Coordination Polymers with Different Structural Motifs

Keywords: Cadmium / Coordination polymers / Fluorescence / N ligands

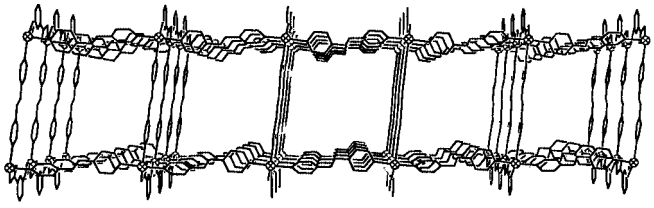

2711 **E. López-Torres, M. A. Mendiola,* C. J. Pastor, J. R. Procopio**

Diorganotin(IV) Complexes of a Cyclic Thiosemicarbazone Ligand: Crystal Structures of $[SnPh_2(C_{15}H_{10}N_3S)Cl]$ and $[SnMe_2(C_{15}H_{10}N_3S)_2]$

Keywords: Nitrogen heterocycles / S ligands / Tin

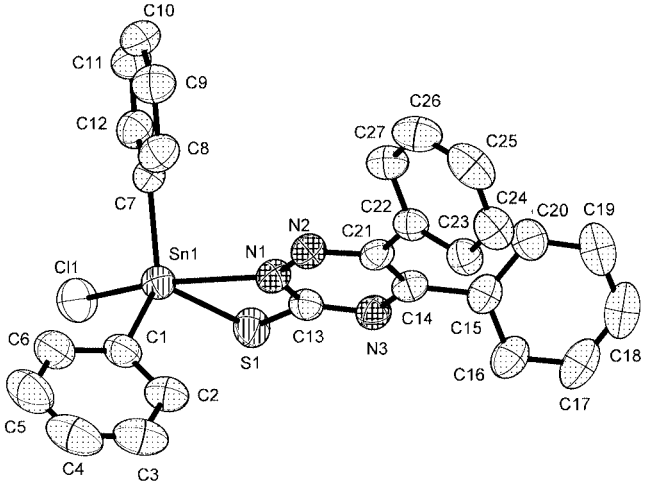

 © 2003 Wiley-VCH Verlag GmbH & Co. KGaA, Weinheim

Reactions of Dihydrogen(norbornadiene) Complexes

Guochen Jia,*[a] Zhenyang Lin,[a] and Chak Po Lau[b]

Keywords: Transition metals / Hydride ligands / Hydrogenations / Norbornadiene / Dihydrogen ligands

Dihydrogen(olefin) complexes have been proposed as active species in catalytic hydrogenation reactions. We have studied the hydrogen-transfer reactions of dihydrogen(olefin) complexes, especially those containing the norbornadiene (NBD) ligand, in order to address the following questions: (i) how the alignment of a H_2 ligand relative to an olefin ligand may affect their reactivity; (ii) in general, what is the detailed pathway for intramolecular hydrogen transfer from an H_2 ligand to an olefin ligand; and (iii) how will the hydrogen transfer reactions proceed in the presence of both an H_2 and a hydride ligand.

(© Wiley-VCH Verlag GmbH & Co. KGaA, 69451 Weinheim, Germany, 2003)

Introduction

Over the last two decades, extensive studies have been carried out on dihydrogen transition metal complexes, especially on their syntheses and structural characterizations.[1,2] There has also been an interest in their reactivities and roles in catalysis.[3] Dihydrogen complexes of the types $[M(R)(H_2)L_n]$ and $[M(olefin)(H_2)L_n]$ have been proposed as intermediates in catalytic hydrogenation reactions.[4−7] As model complexes for reactions involving intramolecular hydrogen transfer from a coordinated dihydrogen ligand to the α-carbon atom of a σ-bonded carbon ligand, several dihydrogen complexes containing σ-bonded carbon ligands (e.g. alkynyl,[8] alkenyl,[9] and aryl[10]) have been synthesized in recent years. Intramolecular hydrogen transfer from a coordinated dihydrogen ligand to the α-carbon atom of the R

[a] Department of Chemistry and Open Laboratory of Chirotechnology of the Institute of Molecular Technology for Drug Discovery and Synthesis, The Hong Kong University of Science and Technology,
Clear Water Bay, Kowloon, Hong Kong
[b] Department of Applied Biology & Chemical Technology, The Hong Kong Polytechnic University,
Hung Hom, Kowloon, Hong Kong

Guochen Jia (right) was born in China in 1962. He received his BSc degree in chemistry from the Wuhan University in 1983 and his PhD degree in 1989 from The Ohio State University in 1989 under the guidance of Professors Devon W. Meek and Andrew Wojcicki. After his postdoctoral stays with Professor Robert H. Morris at the University of Toronto and Professor Richard J. Puddephatt at the University of Western Ontario, he joined the Hong Kong University of Science and Technology as an assistant professor in 1992 and he is now an associate professor. His research interest includes transition-metal hydrides, vinylidenes, carbynes, metallabenzynes, carbon-rich organometallics, and homogeneous catalysis.

Zhenyang Lin (left) is now an associate professor at the chemistry department of the Hong Kong University of Science and Technology (HKUST). He received his BSc degree in chemistry from the Wuhan University of Geology in 1982 and his MPhil degree in 1985 from the Fujian Institute of Research on the Structure of Matter, Chinese Academy of Sciences. His doctoral research was carried out from October 1986 to August 1989 in the Inorganic Chemistry Laboratory of the University of Oxford under the supervision of Professor D. Michael P. Mingos. After his postdoctoral work with Professor Michael B. Hall at the Texas A&M University, he was appointed to an assistant professorship at HKUST in 1994. His research interest is in the area of theoretical/computational inorganic and organometallic chemistry.

Chak Po Lau (center) was born in Hong Kong and he received his undergraduate and graduate training in the United States. He earned his PhD under the guidance of the late Professor Carl H. Brubaker, Jr. at the Michigan State University in 1977. After his postdoctoral stay with the late Professor William E. Hatfield and Professor Maurice Brookhart at the UNC at Chapel Hill, he joined the Beijing Institute of Chemistry in China as an associated scientist. He returned to Hong Kong and became a lecturer at the then Hong Kong Polytechnic in 1983, and he is now Professor at the Department of Applied Biology & Chemical Technology of the Hong Kong Polytechnic University. His research interest includes homogeneous catalysis, transition-metal hydride chemistry, and hydrogen bond (dihydrogen bond) mediated chemical reactions.

MICROREVIEWS: This feature introduces the readers to the authors' research through a concise overview of the selected topic. Reference to important work from others in the field is included.

group in $[M(R)(H_2)L_n]$ has been demonstrated with well-defined dihydrogen complexes.[8–9]

The current review is related to intramolecular hydrogen transfer reactions involving complexes of the type $[M(olefin)(H_2)L_n]$. The reactions are interesting because they are relevant to catalytic hydrogenation reactions. In addition, a detailed study on intramolecular hydrogen transfer from H_2 to olefin ligands may help to develop a field of chemistry based on the coupling of σ-bonds and unsaturated substrates.

In the past few years, we have tried to generate reactive dihydrogen(olefin) complexes in order to study the intramolecular hydrogen transfer from an H_2 ligand to olefin ligands. In particular, we wish to address the following questions.

(i) Structures **1** and **2** show two possible ways of arranging an H_2 ligand and an olefin ligand around a metal center if rotation of the olefin about the metal−olefin bond can effectively be restricted. With the restriction, the M−H_2 bond could be perpendicular to the olefin double bond (**1**) or parallel to the olefin double bond (**2**). The different arrangements of the H_2 ligand relative to the olefin ligand may affect the reactivity. This has been suggested by M. Poliakoff et al. when explaining the formation of norbornene (NBE) and nortricyclene in the photocatalytic hydrogenation of norbornadiene (NBD) using $[M(CO)_6]$.[11] We wish to see if similar reactions can also occur with other systems.

(ii) There are several possible pathways to transfer a dihydrogen ligand to an olefin ligand. For example, the dihydrogen ligand may undergo oxidative addition to give a dihydride intermediate before the hydrogen transfer; the hydrogen transfer reactions could proceed through a concerted mechanism (simultaneous transfer of the two hydrogen atoms to a double bond); or through a stepwise mechanism in which one of the hydrogen atoms from the coordinated H_2 is transferred to the olefin to give an alkyl(hydrido) complex, followed by reductive elimination. It is of interest to see which of the possible pathways is operative.

(iii) The presence of a hydride ligand in dihydrogen(olefin) complexes may affect the reactivity of the dihydrogen(olefin) complexes. It would be interesting to see how the hydrogen transfer reactions will proceed in the presence of both an H_2 and a hydrido ligand.

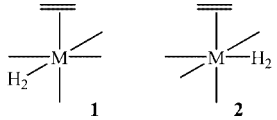

1 **2**

In this review, we will summarize the catalytic hydrogenation reactions involving dihydrogen(olefin) complexes and our recent work, aiming at addressing the above-mentioned questions.

Discussion

Dihydrogen(olefin) Complexes in Catalytic Hydrogenation

Catalytic hydrogenation reactions involving dihydrogen(olefin) complexes have been suggested for several systems. In some cases, the dihydrogen(olefin) intermediates have been detected. Complexes $[M(CO)_6]$ (M = Cr, Mo, and W)[11] are photocatalytically active for the hydrogenation of olefins. When norbornadiene is used as the substrate, the hydrogenation reactions give a mixture of norbornene and nortricyclene. After a detailed investigation by UV laser photolysis of $[M(CO)_6]$ and $[M(\eta^4\text{-NBD})(CO)_4]$ in the presence of H_2 and D_2, it was suggested that nortricyclene (**4**) is produced through the intermediates *fac*-$[M(H_2)(\eta^4\text{-NBD})(CO)_3]$ (**3**), while norbornene (**6**) is generated through the intermediates *mer*-$[M(H_2)(\eta^4\text{-NBD})(CO)_3]$ (**5**) (Scheme 1). Intramolecular hydrogen transfer within $[Cr(H_2)(\eta^4\text{-NBD})(CO)_3]$ is supported by the fact that the decay of the IR signals does not depend on the hydrogen pressure. Involvement of the dihydrogen intermediates in the hydrogenation reactions is also supported by an in situ NMR spectroscopic investigation of hydrogenation with parahydrogen.[12] A number of dihydrogen(olefin) complexes related to the catalytic system have been characterized by IR spectroscopy, e.g. *cis*-$[M(H_2)(\eta^2\text{-}C_2H_4)(CO)_4]$ (M = Cr, Mo, W), *mer*-$[M(H_2)(\eta^2\text{-}C_2H_4)_2(CO)_3]$ (M = Mo, W), *fac*-$[M(H_2)(\eta^4\text{-NBD})(CO)_3]$ (M = Cr, Mo, W), *mer*-$[M(H_2)(\eta^4\text{-NBD})(CO)_3]$ (M = Cr, Mo, W), and $[M(H_2)(\eta^2\text{-NBD})(CO)_4]$ (M = Mo, W).

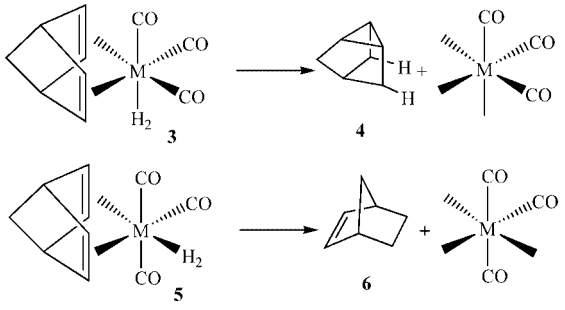

Scheme 1

In a related study,[13] Poliakoff et al. studied the hydrogenation of dimethyl fumarate (DF) using $[Fe(CO)_4(\eta^2\text{-DF})]$ (**7**). When irradiated, **7** (in a polyethylene matrix) reacts with H_2 to give dimethyl succinate (**11**) and $[Fe(CO)_5]$ (**10**). The reaction sequence is shown in Scheme 2. The intermediates $[Fe(CO)_3(\eta^4\text{-DF})]$ (**8**) and $[Fe(CO)_3(H_2)(\eta^2\text{-DF})]$ (**9**) have been detected by FT-IR spectroscopy.

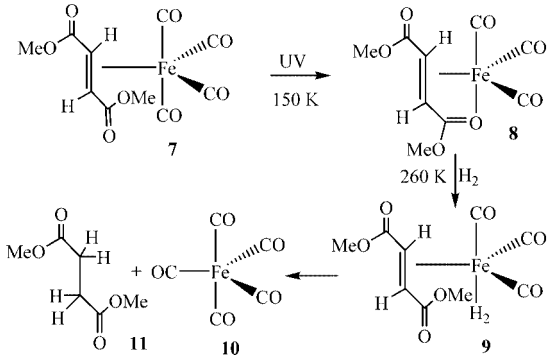

Scheme 2

 © 2003 Wiley-VCH Verlag GmbH & Co. KGaA, Weinheim

Budzelaar et al. recently reported catalytic hydrogenation reactions using rhodium complexes, such as [L_{Me}Rh(CH_2=CH_2)$_2$], [L_{Me}Rh(COE)], and [L_{Me}Rh(COE)(CH_3CN)] [L_{Me} = (2,6-$C_6H_3Me_2$)NCMeCHCMeN(2,6-$C_6H_3Me_2$)].[14] The dihydrogen(olefin) complexes [Rh{(2,6-$C_6H_3Me_2$)-NCMeCHCMeN(2,6-$C_6H_3Me_2$)}(H_2)(olefin)] (**13**), which undergo oxidative addition reactions to give the dihydrido species **14**, were suggested as intermediates in the catalytic cycle, as shown in Scheme 3. The dihydrogen complex [Rh{(2,6-$C_6H_3Me_2$)NCMeCHCMeN(2,6-$C_6H_3Me_2$)}(H_2)-(COE)] (**16**) has been detected at low temperatures by NMR spectroscopy.

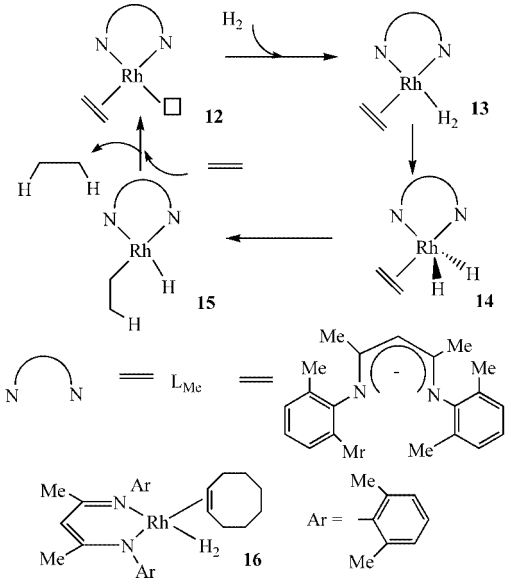

Scheme 3

We have reported the catalytic hydrogenation of olefins using [Ru(Tp)(PPh_3)(L)(CH_3CN)]$^+$ (**17**) [Tp = hydrotris(1-pyrazolyl)borate; L = PPh_3, CH_3CN].[7] It was proposed that [Ru(Tp)(L)(H_2)(olefin)]$^+$ (**20**) is involved in the hydrogenation (Scheme 4), although the intermediate was not detected. It was suggested that the first hydrogen transfer might proceed through reactions analogous to the oxidative coupling of olefins.

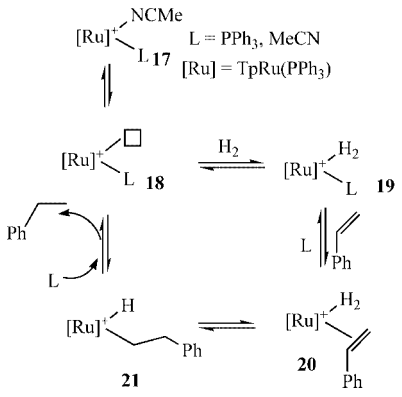

Scheme 4

Modeling Reactions of Dihydrogen(olefin) Complexes

One of the main purposes of our work is to address how the relative arrangements of the H_2 and olefin ligands affect the hydrogen-transfer reactions. Structures **1** and **2** mentioned in the Introduction represent two ideal situations in which the olefin ligand has a specific orientational preference. However, monoolefin ligands do not necessarily show this kind of structural preference because the barriers of rotation about the metal-olefin bond are not prohibitively high.[15] Therefore, in our studies we have used diolefin ligands, such as NBD and COD, to restrict the rotation. Structures **A** and **B** show two possible structural isomers in which a diolefin ligand and an H_2 ligand are arranged in a *mer* and *fac* manner, respectively. Structure **A** models the structure of **1**, while structure **B** is closely related to structure **2**.

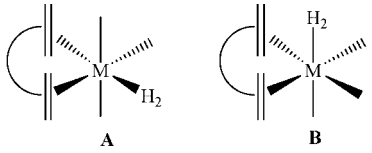

Complexes with a mer Arrangement of the H_2 and Diolefin Ligands

The protonation reactions of [RuH(NBD)(PCP)] (**22**) [PCP = 2,6-(PPh_2CH_2)$_2$$C_6H_3$] provide examples of studying the reactions of dihydrogen(olefin) complexes with a structural feature related to structure **1** (or **A**).[16] It was shown that protonation of complex **22** with excess CD_3CO_2D in the presence of PPh_3 gives [Ru(O_2CCD_3)(PPh_3)(PCP)] (**23d$_3$**) and partially deuterated (ca. 75% D in the *endo* positions) norbornene (see Scheme 5). The deuterium is only incorporated at the *endo* position of norbornene. In-situ NMR spectroscopic experiments revealed that Ru−H in **22** readily undergoes H/D exchange with CD_3CO_2D to give [RuD(NBD)(PCP)] (**22d$_1$**), and that the H/D exchange reaction is faster than the hydrogenation reaction.

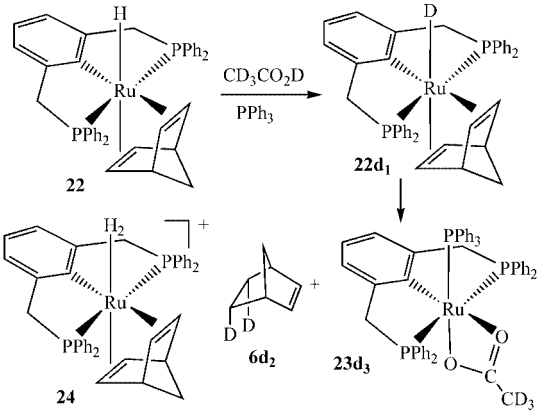

Scheme 5

Considering the fact that [RuH(H_2)(dppe)$_2$]$^+$ contains a dihydrogen ligand[17] and that norbornadiene (NBD) is less

 © 2003 Wiley-VCH Verlag GmbH & Co. KGaA, Weinheim

electron-donating than dppe, it was proposed that protonation of [RuH(NBD)(PCP)] (**22**) initially produces the dihydrogen complex $[Ru(H_2)(NBD)(PCP)]^+$ (**24**), which mediates the formation of norbornene and the H/D exchange reaction. A computational study[16] confirms that complex $[Ru(H_2)(NBD)\{2,6\text{-}(PH_2CH_2)_2C_6H_3\}]^+$ (**30**), a model complex of **24**, is indeed a typical octahedral dihydrogen complex, with a short H−H bond (0.868 Å). Scheme 6 shows the proposed mechanism for the H/D exchange reaction of **22** with CD_3CO_2D, and the formation of NBE in the protonation reactions with acetic acid. Reaction of **22** with CD_3CO_2D could produce the η^2-H−D complex $[Ru(HD)(NBD)(PCP)]^+$ (**24d$_1$**), which can then be deprotonated by $CD_3CO_2^-$ to give **22d$_1$**. The mechanism is similar to those proposed for the H/D exchange of $[W(D_2)(CO)_3(P\textit{i}Pr_3)_2]$ with H_2O,[18] and for the H/D exchange of $[Ru(Tp)(H_2)(PPh_3)_2]^+$ with D_2O.[7] Hydrogen transfer within $[Ru(H_2)(NBD)(PCP)]^+$ or its isotopomers would give NBE. For example, $[D_2]$NBE could be formed from $[Ru(D_2)(NBD)(PCP)]^+$ (**24d$_2$**) (Scheme 6). Such a proposition is consistent with the fact that protonation of **22** with CD_3CO_2D gave deuterated NBE in which the deuterium is at the *endo* positions of NBE.

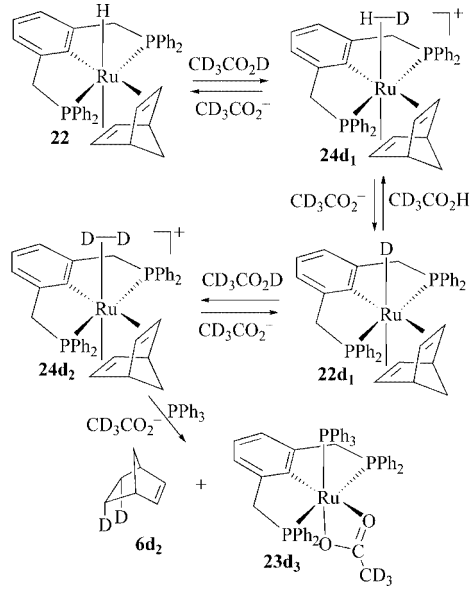

Scheme 6

Protonation of **22** with HOTf in the presence of acetonitrile produces [Ru(MeCN)(NBD)(PCP)]OTf (**25**) and $[Ru(MeCN)_3(PCP)]$OTf (**26**), along with NBE (Scheme 7). Formation of [Ru(MeCN)(NBD)(PCP)]OTf (**25**) supports the proposition that protonation of **22** initially produces the dihydrogen complex **24**, as [Ru(MeCN)(NBD)(PCP)]OTf could be easily formed by displacement of the H_2 ligand in $[Ru(H_2)(NBD)(PCP)]$OTf using MeCN. Apparently, $[Ru(H_2)(NBD)(PCP)]$OTf also undergoes a hydrogen-transfer reaction in the presence of MeCN to give norbornene and $[Ru(MeCN)_3(PCP)]$OTf.

There are several possible reaction pathways for the hydrogenation of the NBD ligand in $[Ru(H_2)(NBD)$-

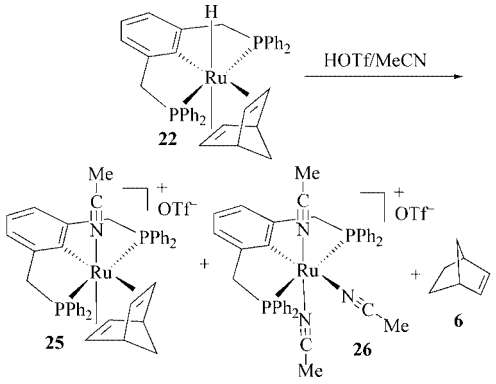

Scheme 7

$(PCP)]^+$. As shown in Scheme 8, the hydrogen transfer reactions could proceed by a concerted mechanism (simultaneous transfer of the two hydrogen atoms of the H_2 ligand to the double bond) (path 1); or through a stepwise mechanism in which one of the hydrogen atoms of coordinated H_2 is transferred to NBD to give the alkyl(hydrido) complex $[RuH(C_7H_9)(PCP)]^+$ (**28**), followed by reductive elimination (path 2); or via a dihydrido intermediate **29**, prior to hydrogen transfer (path 3).

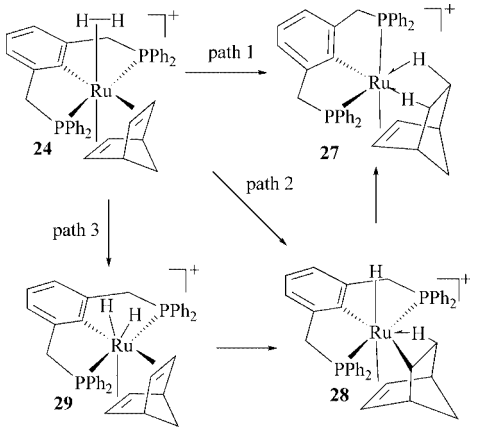

Scheme 8

Density functional calculations at the B3LYP level of theory were performed to examine the favorable reaction pathway for the conversion of the model complex $[Ru(H_2)(NBD)\{2,6\text{-}(H_2PCH_2)_2C_6H_3\}]^+$ (**30**) to the assumed product $[Ru(NBE)\{2,6\text{-}(H_2PCH_2)_2C_6H_3\}]^+$ (**31**).[16] Here, **30** and **31** are the model complexes of **24** and **27** proposed in Scheme 8, respectively.

The results from the calculation[16] eliminate the oxidative addition product, the dihydrido complex **29**, as an intermediate. The dihydrido species was found to correspond to a transition state (see below). The results are understandable, since it is unlikely that a complex can have both a stable dihydrogen and a stable dihydrido form, without changing the geometry significantly (i.e. both forms correspond to a minimum on the potential energy surface). The calculations also eliminate the concerted pathway.

 © 2003 Wiley-VCH Verlag GmbH & Co. KGaA, Weinheim

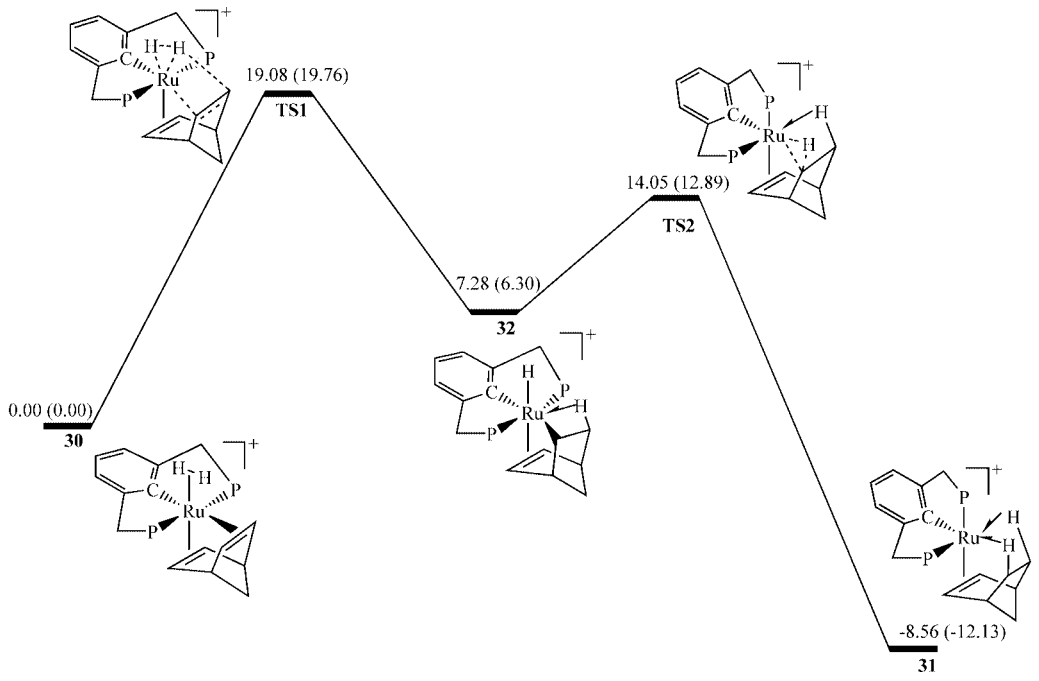

Figure 1. Schematic illustration of the reaction pathways of $[Ru(H_2)(NBD)(2,6\text{-}(PH_2CH_2)_2C_6H_3)]^+$, with calculated relative free energies [kcal/mol] and reaction energies [kcal/mol] (in parentheses), modified from ref.[16]

On the other hand, it was found that conversion of **24** to **27** through a stepwise process is feasible. Figure 1 shows the reaction steps for the conversion of **30** to **31** via **32** (the model complex of **28** proposed in Scheme 8), together with the relative free energies and reaction energies (in parentheses) calculated for all the species. The favorable stepwise mechanism involves two steps: one hydrogen atom of the coordinated H_2 ligand is transferred to NBD to form the pentagonal-bipyramidal intermediate **32** via the transition state **TS1**, with an energy barrier of 19.08 kcal/mol; the second hydrogen transfer then completes the hydrogenation of one of the two double bonds of NBD to form the NBE complex **31**, with a lower energy barrier of only 6.77 kcal/mol. As mentioned above, the first transition state (**TS1**) corresponds to a dihydrido species.

In another study on the reactivity of dihydrogen(olefin) complexes with a structural feature of **1** (or **A**), the protonation reaction of $[OsClH(PPh_3)\{Ph_2P(CH_2)_2CH{=}CH(CH_2)_2PPh_2\}]$ (**33**) has been investigated.[19] Protonation of **33** with HOTf produces the dihydrogen(olefin) complex $[OsCl(H_2)(PPh_3)\{Ph_2P(CH_2)_2CH{=}CH(CH_2)_2PPh_2\}]OTf$ (**34**), which has been characterized by NMR spectroscopy (Scheme 9).

Interestingly, the coordinated olefin double bond in **34** could not be hydrogenated, even when a solution of **34** in CD_2Cl_2 was stored under a H_2 (1 atm) for 1 d. Instead, the fluxional hydrido(dihydrogen) complex $[OsH(H_2)(PPh_3)\{Ph_2P(CH_2)_2CH{=}CH(CH_2)_2PPh_2\}]OTf$ (**35**) is slowly produced when **34** is exposed to H_2. Protonation of $[OsH_2(PPh_3)\{Ph_2P(CH_2)_2CH{=}CH(CH_2)_2PPh_2\}]$ (**36**) with HOTf also produces **35**. The coordinated olefin double bond in **35** could not be hydrogenated either.

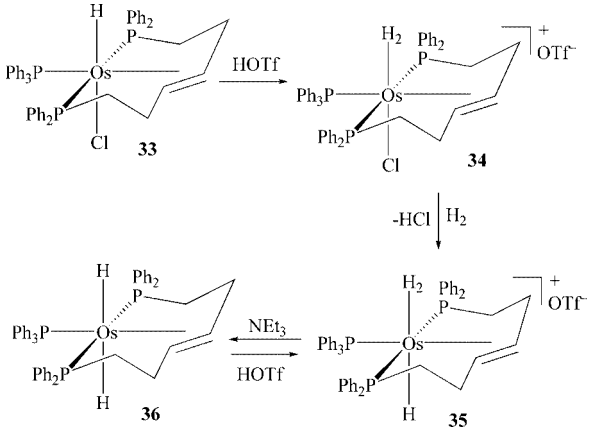

Scheme 9

These unexpected results were also examined by a computational study.[19] The calculated free energy change ($\Delta G°$) for the process, **37** + H_2 → $[OsCl(H_2)(PH_3)\{H_2P(CH_2)_6PH_2\}]^+$ (a model complex for the hydrogenated product of complex **34**), is ca. −1.0 kcal/mol, suggesting that the hydrogenation is thermodynamically feasible.

The computational study[19] found that the reaction was kinetically unfavorable, due to the constraint imposed by the $Ph_2P(CH_2)CH{=}CH(CH_2)_2PPh_2$ ligand. The reasons for the kinetically unfavorable reaction have been explained as follows. The optimized model complex $[OsCl(H_2)(PH_3)\{H_2P(CH_2)_2CH{=}CH(CH_2)_2PH_2\}]^+$ (**37**) contains an H_2 ligand with an H−H distance of 1.011 Å. The coordinated −HC=CH− unit is orientated in such a way that one olefinic carbon atom is closer to the η^2-H_2 ligand, while the

 © 2003 Wiley-VCH Verlag GmbH & Co. KGaA, Weinheim

other is further away. The possible intermediates (Scheme 10), which can lead to the hydrogenation product by a reductive elimination step, are all inaccessible due to the conformational constraint imposed by the $Ph_2P(CH_2)_3CH(CH_2)_2PPh_2$ ligand. **38** does not correspond to a minimum on the potential energy surface. In addition, the separation of the hydrido and the bonded alkyl ligands prevents the reductive elimination, which leads to a hydrogenated product. The activation energy leading to **39** is calculated to be as high as 50 kcal/mol since the hydrogen-receiving carbon atom is further away from the η^2-H_2 ligand in the starting dihydrogen complex (**37**). Once again, **40** is not a local minimum as the five ligands in the pseudo-pentagonal-bipyramidal structure are all sterically bulky. The situation is different from the PCP system. The PCP ligand is more flexible in terms of its coordination arrangement, and can stabilize an intermediate (see Figure 1) in which both the agostic H−C and the bonded alkyl group are *cis* to the hydrido ligand, allowing further reductive elimination.

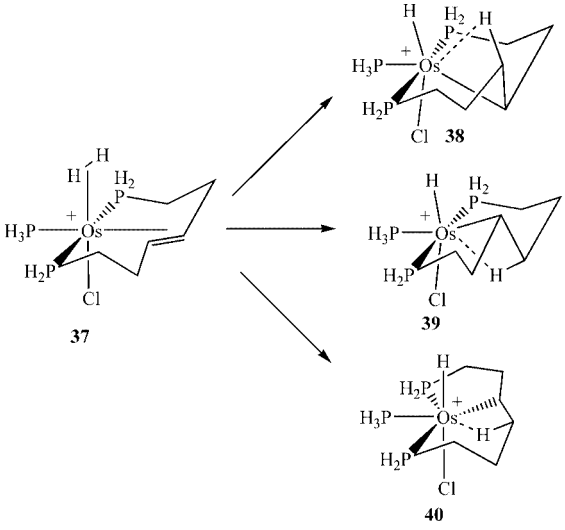

Scheme 10

The results discussed above suggest that whether an dihydrogen(olefin) complex in which an H_2 ligand is *cis* to both carbon atoms of an olefinic group (structure **1** or **A**) would undergo hydrogen transfer or not, depends on the structures of the intermediates formed after the first hydrogen transfer. If a relatively stable intermediate, in which the hydrido and the bonded alkyl ligands are *cis* to each other, is formed, reductive elimination, which forms a bond between the hydrido and bonded alkyl ligands, becomes feasible. However, when the ligand environment does not allow such an intermediate to form, reductive elimination is not possible, therefore no hydrogenation reactions will proceed.

In a related study, Esteruelas et al. reported the protonation reactions of $[OsH_2(diolefin)(P\mathit{i}Pr_3)_2]$ (diolefin = NBD: **41**; tetrafluorobenzobarrelene: **42**; and 1,3-hexadiene: **43**).[20] Protonation of **41** and **42** with HBF_4 does not lead to hydrogen-transfer products, but gives the trihydrido complexes **44** and **45**, respectively. Protonation of **43** with HBF_4 gives the cyclohexenyl complex **46** (Scheme 11).

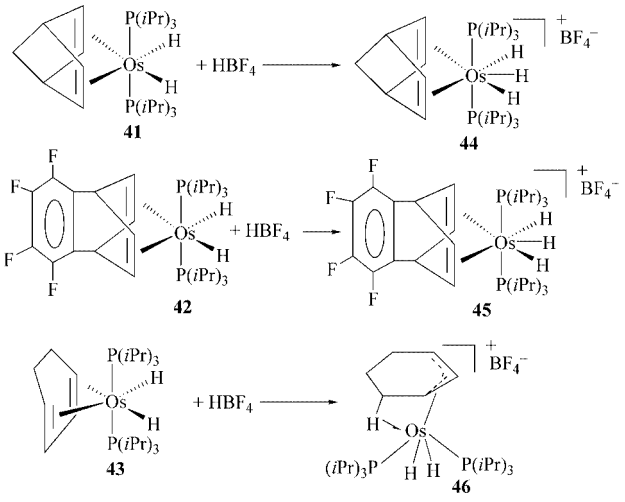

Scheme 11

Complexes with a fac Arrangement of the H_2 and Diolefin Ligands

The reactions of dihydrogen(olefin) complexes with a structural feature related to structure **2** (or **B**) have previously been suggested for *fac*-$[M(H_2)(\eta^4\text{-NBD})(CO)_3]$ (M = Cr, Mo, W).[11]

The protonation reactions of [Cp*RuH(diolefin)] have been studied in order to further model reactions of dihydrogen(olefin) complexes with a structural feature related to structure **2** (or **B**).[21] Protonation of [Cp*RuH(COD)] (**47**) at −76 °C with HBF_4 produces the thermally unstable dihydrogen(olefin) complex $[Cp^*Ru(H_2)(COD)]BF_4$ (**48**), which was characterized by NMR spectroscopy at low temperature.[21] On warming up to room temperature, complex **48** undergoes a dehydrogenation reaction to give [Cp*Ru(η^6-cyclooctatriene)]BF_4 (**49**), rather than a hydrogenation reaction (Scheme 12). The successful characterization of **48** suggests that a dihydrogen complex can be obtained through protonation of [Cp*RuH(diolefin)].

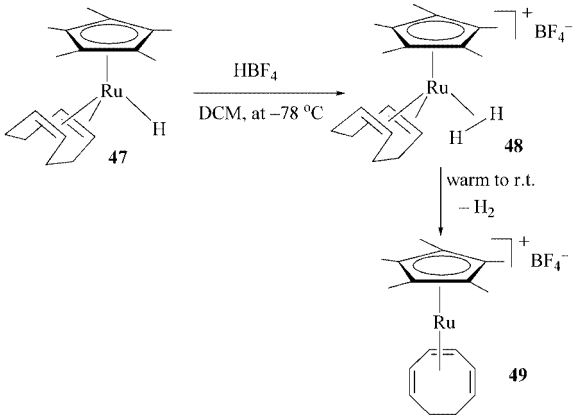

Scheme 12

 © 2003 Wiley-VCH Verlag GmbH & Co. KGaA, Weinheim

Protonation of [Cp*RuH(NBD)] (**50**) in dichloromethane produces nortricyclene (**4**) and the dimetallic complex **51**.[21] Nortricyclene is also formed, along with the η^6-benzene complex **53**, when a benzene solution of [Cp*Ru(H_2O)(NBD)]BF_4 (**52**) is exposed to H_2 (Scheme 13).[22] Since the complex [Cp*Ru(H_2)(COD)]$^+$ contains a dihydrogen ligand, it was proposed that the reaction of [Cp*Ru(H_2O)(NBD)]BF_4 with H_2, or protonation of [Cp* RuH(NBD)], initially gives the dihydrogen complex [Cp* Ru(H_2)(NBD)]BF_4 (**54**), which undergoes a hydrogen-transfer reaction to give nortricyclene (**4**) and a [Cp*Ru]$^+$ fragment (Scheme 14). In dichloromethane, the [Cp*Ru]$^+$ fragment reacts with **50** to give the dimetallic complex **51**. In benzene solution, the [Cp*Ru]$^+$ fragment is trapped with benzene producing complex **53**.

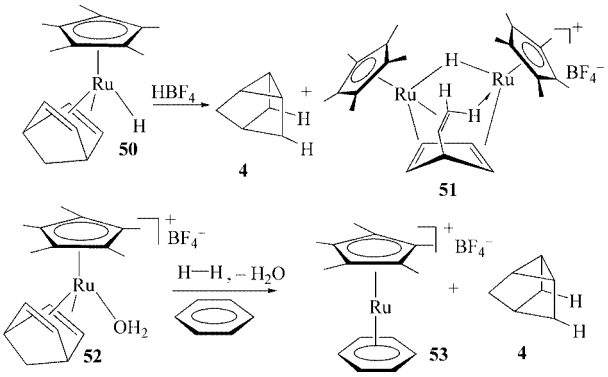

Scheme 13

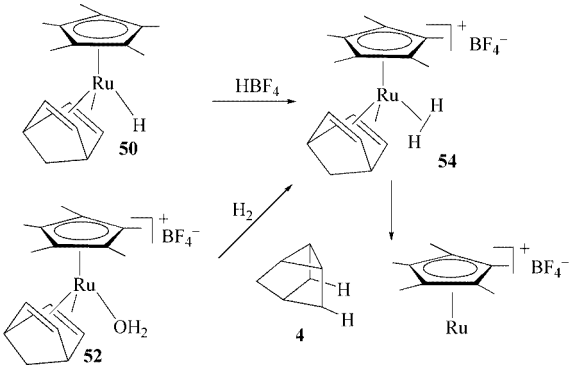

Scheme 14

The detailed reaction steps were examined by a computational study.[22] Complex [CpRu(H_2)(NBD)]$^+$ (**55**), a model complex of **54**, was calculated to be a typical dihydrogen complex with an H−H distance of 0.854 Å. Once again, a stepwise mechanism was found to be responsible for the hydrogen-transfer reaction of the model complex **55**, to give **57**. The computed energy profiles for the reactions are illustrated in Figure 2. In the hydrogen transfer reaction, the first hydrogen atom is transferred from the η^2-H_2 ligand to one of the olefinic carbon atoms, leading to the formation of the hydrido intermediate **56**, which contains an agostic interaction. The hydrogen transfer reaction occurs with an energy barrier of 5.5 kcal/mol. The first transition state **TS3** corresponds to a dihydrido species. The energy barrier for the first hydrogen-transfer step is much less than that of the PCP system described above. It is understandable that reductive elimination to give NBE could not proceed from intermediate **56** as the hydrido ligand and the alkyl carbon atom are separated by a C−H agostic ligand. On the other hand, the hydrido ligand can transfer to the other olefinic functionality with a very small energy barrier. The reactions of H_2 with NBD, to give nortricyclene, are both kinetically and energetically very favorable.

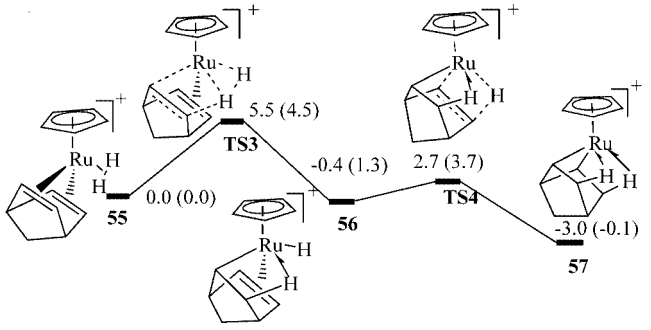

Figure 2. Schematic illustration of the reaction pathways of [CpRu(H_2)(NBD)]$^+$, with calculated relative free energies [kcal/mol] and reaction energies [kcal/mol] (in parentheses), modified from ref.[22]

Reactions of dihydrogen(olefin) complexes with a structural feature related to **2** (or **B**) have also been studied through the protonation reactions of [RuH(Cl)(NBD)(PPh_3)$_2$].[23] Protonation of ruthenium complexes [RuH(X)L_4] {L_4 = (dppe)$_2$, X = Cl, Br;[24a,24b] L_4 = (dppp)$_2$, X = Cl;[24c] L_4 = (dcpe)$_2$, X = Cl;[24d] L_4 = (PPh_3)[2,6-(Ph_2PCH_2)$_2$$C_5H_3N$], X = Cl[25]} are known to give dihydrogen complexes of the type [M(X)(H_2)L_4]$^+$. Thus, it was expected that protonation of [MH(Cl)(NBD)(PPh_3)$_2$] could also produce the dihydrogen complex [MCl(H_2)(NBD)(PPh_3)$_2$]$^+$, which may undergo hydrogenation to produce nortricyclene, as in the case of *fac*-[M(H_2)(η^4-NBD)(CO)$_3$] (M = Cr, Mo, W)[11] and [Cp* Ru(H_2)(NBD)]$^+$.[21,22]

Interestingly, the expected hydrogenation product nortricyclene is not produced when [RuH(Cl)(NBD)(PPh_3)$_2$] (**58**) is protonated. Instead, protonation of **58** in C_6D_6 with a limiting amount of HOTf gives [RuH(OTf)(NBD)(PPh_3)$_2$] (**59**), norbornene (**6**) and [$RuCl_2$(PPh_3)$_2$]$_2$ (**60**) (Scheme 15). Protonation of **58** in dichloromethane with a limiting amount of HOTf gives [RuH(OTf)(NBD)(PPh_3)$_2$] (**59**), norbornene (**6**) and the unusual trimetallic complex [Ru_3Cl_5(PPh_3)$_6$]OTf (**61**). In these protonation reactions, the hydrido complex [RuH(OTf)(NBD)(PPh_3)$_2$] is presumably formed by protonation of the Cl ligand. The dimetallic complex [$RuCl_2$(PPh_3)$_2$]$_2$ (**60**) and the trimetallic complex [Ru_3Cl_5(PPh_3)$_6$]OTf (**61**) are presumably formed from the reaction of [RuCl(PPh_3)$_2$]$^+$ (generated whilst forming norbornene) with HCl {generated by protolysis of the chloride ligand of **58** to give [RuH(OTf)(NBD)(PPh_3)$_2$]}.

 © 2003 Wiley-VCH Verlag GmbH & Co. KGaA, Weinheim

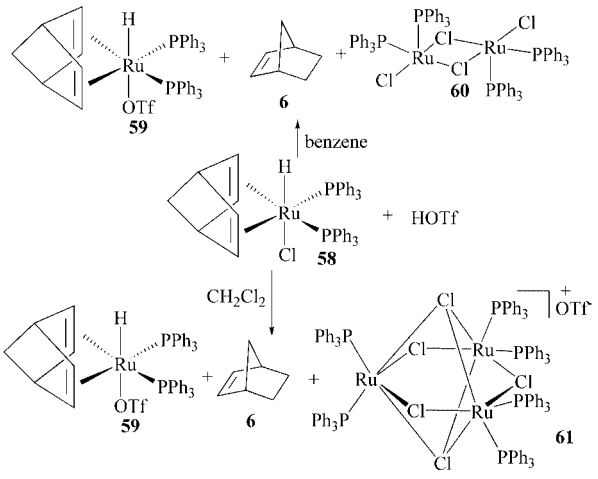

Scheme 15

In view of the fact that *fac*-[$M(H_2)(\eta^4$-NBD)$(CO)_3$] (M = Cr, Mo, W)[11] and [Cp*Ru(H_2)(NBD)]$^+$ [21,22] undergo hydrogen-transfer reactions to give nortricyclene, it was proposed that NBE may not be produced via the intermediate [RuCl(H_2)(NBD)$(PPh_3)_2]^+$. Instead, the formation of norbornene in the protonation reaction was thought to be related to the protonation of the chloro ligand (Scheme 16). Protonation of the chloro ligand could give the hydrogen chloride complex [RuH(HCl)(NBD)$(PPh_3)_2]^+$ (**62**), which can then undergo a hydrogen-transfer reaction to give NBE. A substitution reaction involving **62** would give [RuH(OTf)(NBD)$(PPh_3)_2$] (**59**). Protonation of halogeno ligands[26] has been observed during the protonation reactions of chloro(hydrido) complexes such as [PtHCl[P(tBu)$_2$Me]$_2$],[26] [$OsH_2Cl_2(P$*i*Pr$_3)_2$],[27a] and [OsH_2Cl(NO)(P*i*Pr$_3)_2$].[27b] Although well-characterized hydrogen halide complexes are still rare,[28] many alkyl halide complexes [M(XR)L_n][29] and halogeno complexes with an intra- or intermolecular MX···H interaction[30] have been reported.

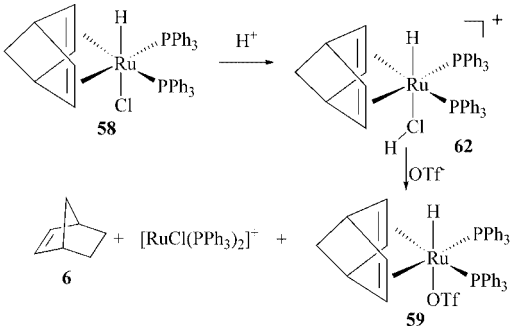

Scheme 16

Protonation of the chloro ligand is supported by the following observations. [RuH(OTf)(NBD)$(PPh_3)_2$] was produced as one of the protonation products. In the presence of CH_3CN in C_6D_6 or CD_2Cl_2, [RuH(Cl)(NBD)$(PPh_3)_2$] (**58**) reacts rapidly with HOTf to give [RuH(CH_3CN)-(NBD)$(PPh_3)_2$]OTf (**63**) as the only product [Equation (1)].

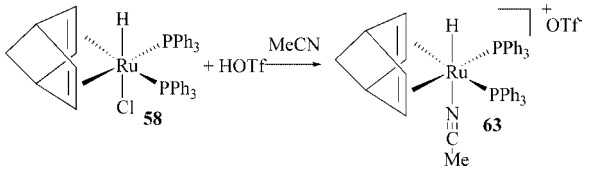

(1)

Involvement of the hydrogen chloride complex **62** in the formation of norbornene is consistent with the deuterium-labeling experiment, where protonation of [RuH(Cl)(NBD)$(PPh_3)_2$] with DOTf produced deuterated norbornene, in which the deuterium atom is at the *endo* position. This suggests that the deuterium atom is transferred to the olefin from the same side of the ruthenium center.

The feasibility of hydrogenation through the intermediate [RuH(HCl)(NBD)$(PPh_3)_2]^+$ was further supported by a computational study.[23] Calculations reveal that the model complex [RuH(HCl)(NBD)$(PH_3)_2]^+$ (**64**) is a reasonable species with a long Ru−Cl distance (2.838 Å) and that hydrogenation from the intermediate is both thermodynamically and kinetically favorable.

Figure 3 presents the energy profiles for the detailed reaction pathways starting from the hydrogen chloride complex **64** and the dihydrogen complex **64′**. The two starting complexes have comparable stability. The results from the calculation indicate that the reaction pathway starting from the hydrogen chloride complex **64** is both kinetically and thermodynamically more favorable than the pathway starting from the dihydrogen complex **64′**. The reaction pathway starting from the dihydrogen complex **64′** has to overcome two consecutive energy barriers, and gives the less stable precursor complex **66′** which leads to the formation of nortricyclene. One can conclude that the chloro ligand is indeed assisting the hydrogenation process by placing a hydrogen atom at a position proximal to the olefin ligand, through the HCl ligand. Clearly, the presence of the chloro ligand suppresses the formation of nortricyclene by the reaction starting from the dihydrogen complex.

In contrast to [RuH(Cl)(NBD)$(PPh_3)_2$], protonation of [OsH(Cl)(NBD)$(PPh_3)_2$] (**67**) with a limiting amount of HOTf in benzene or dichloromethane only produces [OsH-(OTf)(NBD)$(PPh_3)_2$] (**68**) [Equation (2)]. Neither norbornene, nor nortricyclene, were observed in the protonation reactions. The different reactivities of the Os and Ru complexes has been attributed to the stronger metal−olefin interaction in the osmium complex and therefore, the Os−NBD bonds remain intact in the reactions.

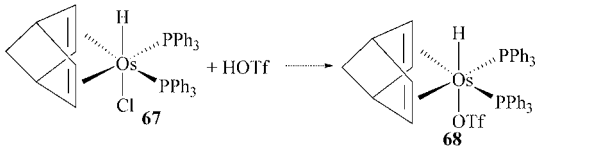

(2)

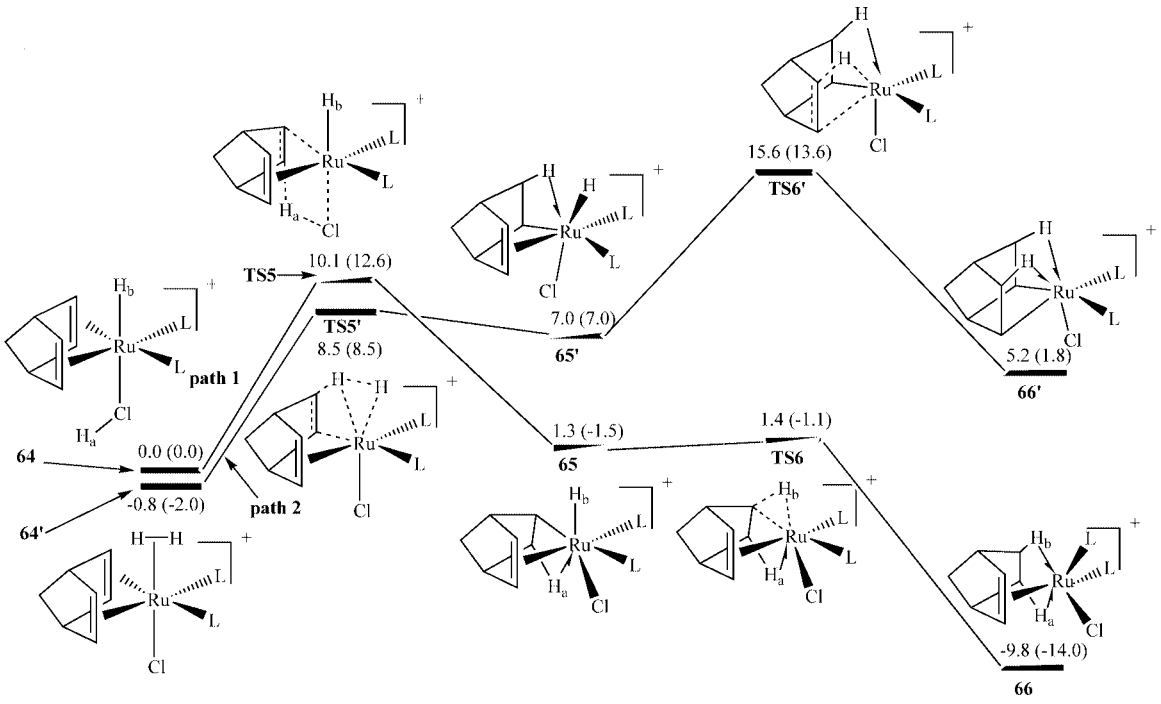

Figure 3. Schematic illustration of the reaction pathways of $[RuCl(H_2)(NBD)(PH_3)_2]^+$ and $[RuH(HCl)(NBD)(PH_3)_2]^+$, with calculated relative free energies [kcal/mol] and reaction energies [kcal/mol] (in parentheses), modified from ref.[23]

Dihydrogen(olefin) Complexes with an Additional Hydrido Functionality

One might ask how the hydrogen transfer reaction will proceed in the presence of both H_2 and a hydrido ligand. Thus, the reactions of H_2 with $[MH(OTf)(NBD)(PPh_3)_2]$ (M = Ru, Os) have been carried out in order to answer the question.[31]

In benzene, complex $[RuH(OTf)(NBD)(PPh_3)_2]$ (**59**) reacts with H_2 to give norbornene (**6**) and the hydrido complex $[(\eta^6\text{-}C_6H_6)RuH(PPh_3)_2]OTf$ (**69**). In the presence of added PPh_3, complex **59** reacts with H_2 to give norbornane (**70**) and $[RuH(PPh_3)_4]OTf$ (**71**) (Scheme 17).

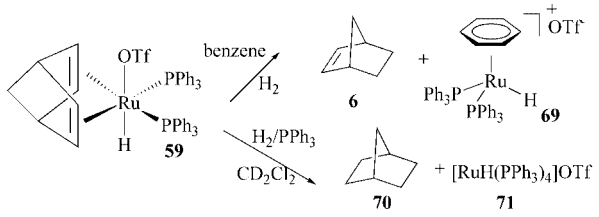

Scheme 17

The complex $[OsH(OTf)(NBD)(PPh_3)_2]$ (**68**) also reacts with H_2 in benzene to give norbornane (**70**) and the hydrido complex $[(\eta^6\text{-}C_6H_6)OsH(PPh_3)_2]OTf$ (**72**) (Scheme 18). In CD_2Cl_2 at room temperature, complex **68** reacts with H_2 in the presence of added PPh_3 to give norbornane and $[OsH_3(PPh_3)_4]^+$ (**73**).

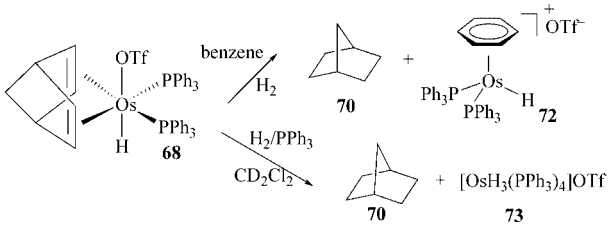

Scheme 18

Since triflate is a weakly coordinating ligand that can readily be displaced under mild conditions,[32] and since a number of dihydrogen complexes of the type $[MH(H_2)(L_4)]^+$ (M = Ru, Os; L = phosphorus ligands) have previously been well characterized,[33] it was suggested that the first step of the reactions of $[MH(OTf)(NBD)(PPh_3)_2]$ with H_2 is to displace the triflate anion in $[MH(OTf)(NBD)(PPh_3)_2]$ with an H_2 molecule. This gives the dihydrogen complexes $[MH(H_2)(NBD)(PPh_3)_2]^+$ (M = Ru, Os), which lead to the hydrogenation of the NBD ligand. The norbornane is presumably formed by further hydrogenation of norbornene.

Density functional theory calculations[31] on the model complexes $[MH(H_2)(NBD)(PH_3)_2]^+$ (M = Ru, Os) confirm that complexes $[RuH(H_2)(NBD)(PH_3)_2]^+$ (**74**) and $[OsH(H_2)(NBD)(PH_3)_2]^+$ (**75**) are all typical dihydrogen complexes in which the nonclassical η^2-H_2 ligand is *trans* to the hydrido ligand and have short H−H distances of 0.793 and 0.831 Å, respectively. The related complex

 © 2003 Wiley-VCH Verlag GmbH & Co. KGaA, Weinheim

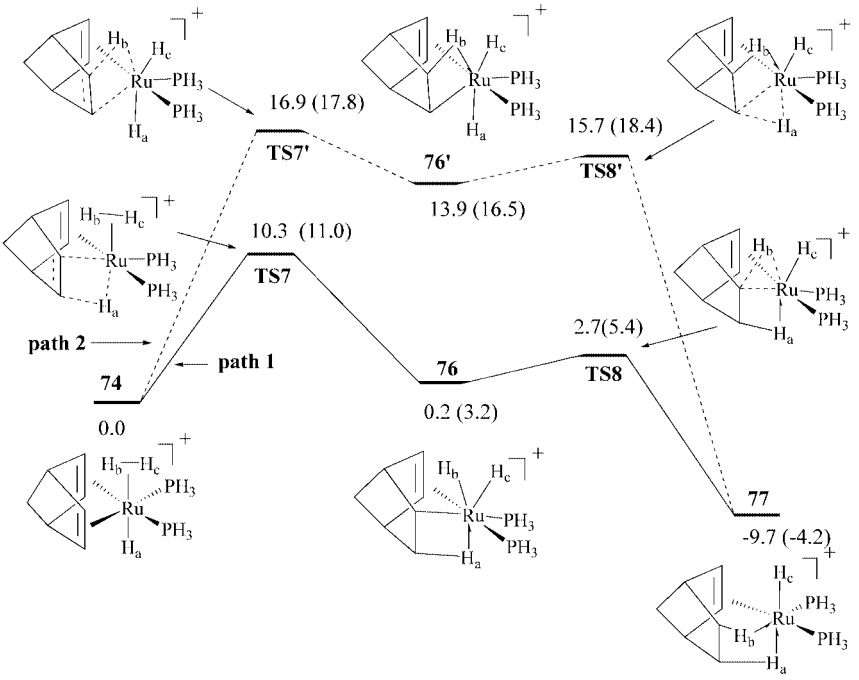

Figure 4. Schematic illustration of the reaction pathways of $[RuH(H_2)(NBD)(PH_3)_2]^+$, with calculated relative free energies [kcal/mol] and reaction energies [kcal/mol] (in parentheses), modified from ref.[31]

$[OsH_3(NBD)(P\mathit{i}Pr_3)_2]^+$, where the two phosphane groups are *trans* to each other, is known to adopt a trihydrido structure.[20]

There are two possible routes for the hydrogenation of the NBD ligands in the dihydrogen complexes $[MH(H_2)(NBD)(PPh_3)_2]^+$ (M = Ru, Os): the NBD ligand can be hydrogenated by transfer of the first hydrogen atom either from the hydrido or the dihydrogen ligand to the olefin ligand, followed by transfer of the second hydrogen atom to give norbornene.

The computational study[31] shows that the hydrogen transfer reactions of $[MH(H_2)(NBD)(PPh_3)_2]^+$, i.e. the conversion of the model complex $[RuH(H_2)(NBD)(PH_3)_2]^+$ (**74**) to $[RuH(NBE)(PH_3)_2]^+$ (NBE = norbornene) (**77**), favors a pathway (Path 1 in Figure 4) starting with the hydrogen transfer from the hydrido ligand (H_a), followed by the cleavage of the dihydrogen ligand to form a *cis*-dihydrido intermediate **76**. The second hydrogen atom is then transferred from one (H_b) of the two hydrido ligands to complete the hydrogenation, giving the coordinated NBE complex **77**.

The overall lower activation energies of Path 1 compared with those of Path 2 have been related to the structures of the transition states **TS7** and **TS7′**.[31] The first transition state **TS7** of Path 1 is a nonclassical complex with a slightly longer H_b-H_c distance (0.841 Å). However, the first transition state **TS7′** of Path 2 has a much longer H_b-H_c distance (1.387 Å), and typical Ru−hydrido distances, notably $Ru-H_a$ and $Ru-H_c$. The short Ru−H distances suggest that **TS7′** could be considered as a trihydrido species, with two hydrido ligands (H_a and H_c) *trans* (or nearly *trans*) to each other. This trihydrido structure, compared with that of **TS7**, has a relatively high energy because of the strong *trans* influence between H_a and H_c. The *trans* influence of a hydrido ligand weakens the metal−ligand interaction at the position *trans* to it, and thus destabilizes the system.[34]

Conclusion

Dihydrogen(olefin) complexes have been proposed as active species in catalytic hydrogenation reactions. Hydrogen-transfer reactions of dihydrogen(olefin) complexes have been modeled with reactive dihydrogen(NBD) complexes, with different orientations of the olefin ligands relative to the H_2 ligand. They have also been studied by computational methods.

In the modeling reactions, the hydrogen transfer does not proceed through simultaneous transfer of the H_2 ligand to the olefin ligands, but through a stepwise pathway. Dihydrogen complexes in which the $M-(H_2)$ bond is perpendicular to the olefin double bond (**1**) can transfer the first hydrogen atom of an H_2 ligand to an olefin ligand, to give an alkyl(hydrido) intermediate (**78**) in which the hydrido ligand is *cis* to an alkyl bond (Scheme 19). The intermediate can then transfer the second hydrogen atom to the substrate by reductive elimination, to form a bond between the hydrido and the bonded alkyl ligands, thus giving the normal hydrogenated products. Dihydrogen complexes in which the $M-(H_2)$ bond is parallel to the olefin double bond (**2**) can transfer the first hydrogen atom of an H_2 ligand to an olefin ligand to give a alkyl(hydrido) intermediate (**79**) in which the hydrido ligand is separated from the alkyl bond by an agostic C−H bond. Reductive elimination from this inter-

 © 2003 Wiley-VCH Verlag GmbH & Co. KGaA, Weinheim

mediate is difficult as the hydrido ligand and the alkyl carbon atom are separated by the C−H agostic ligand. Instead, the hydrido ligand can transfer to other olefin ligands, if present, and lead to other products. The reaction energy barrier for the first hydrogen transfer for complexes with a structural feature related to **2** is found to be smaller than that for complexes with a feature of structure **1**. The situation is similar to the insertion reactions of **80** and **81**, where **80** undergoes insertion reactions 40 times faster.[35]

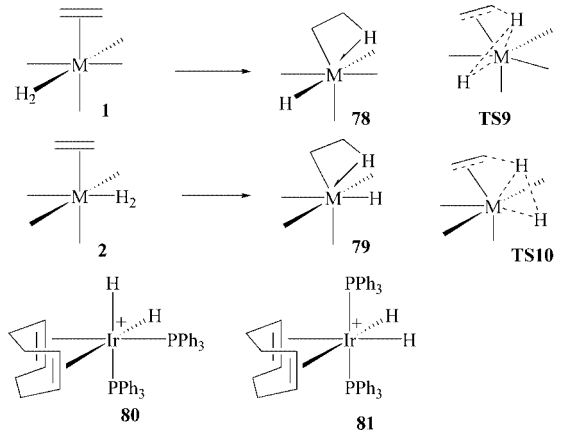

Scheme 19

In the first proton-transfer step, the dihydrido species in most cases of our studies were found to be transition states (rather than intermediates) in which one of the hydrido ligands has a weak interaction with the receiving carbon atom. In the transition state, the olefinic double bond is also lengthened relative to that in the starting complex. These transition states are denoted **TS9** and **TS10**. The first step of the hydrogen transfer reaction is similar to the oxidative coupling of olefins or acetylenes, as illustrated by Equation (3), for the conversion of **82** to **83**.[36] An interesting question can be asked as to whether other σ-ligands (e.g. C−H, Si−H, B−H) can undergo similar reactions with unsaturated substrates, such as olefins, acetylenes and ketones.

(3)

The presence of other ligands may affect the hydrogen-transfer reactions. For example, in the hydrogen-transfer reactions of $[MH(H_2)(NBD)(PPh_3)_2]^+$ (M = Ru, Os), the first hydrogen transfer from the hydrido ligand is preferred over that from the dihydrogen ligand; in the protonation of $[RuHCl(NBD)(PPh_3)_2]$, the dihydrogen complex $[MCl(H_2)(NBD)(PPh_3)_2]^+$ is not involved in the hydrogenation.

This article discussed the hydrogen-transfer reactions of dihydrogen(olefin) complexes in which the olefin ligands have a specific orientational preference. The study showed that intramolecular hydrogen transfer from dihydrogen to olefin ligands is feasible for dihydrogen(olefin) complexes in which the $M-H_2$ bond is perpendicular to the olefin double bond or parallel to the olefin double bond. It is expected that hydrogen-transfer reactions should also occur for complexes in which the olefin can rotate "freely", although further work is needed to confirm this.

Acknowledgments

The authors acknowledge financial support from the Hong Kong Research Grants Council. This work was also partially supported by the University Grant Committee Area of Excellence Scheme (Aoe).

[1] [1a] R. H. Crabtree, *Angew. Chem. Int. Ed. Engl.* **1993**, *32*, 789−805. [1b] D. M. Heinekey, W. J. Oldham Jr., *Chem. Rev.* **1993**, *93*, 913−926. [1c] P. G. Jessop, R. H. Morris, *Coord. Chem. Rev.* **1992**, *121*, 155−284.

[2] [2a] G. J. Kubas, *Dihydrogen and σ-Bond Complexes*, Kluwer Academic/Plenum Press, New York, **2001**. [2b] *Recent Advances in Hydride Chemistry* (Eds: M. Peruzzini, R. Poli), Elsevier, Amsterdam, The Netherlands, **2001**.

[3] [3a] M. A. Esteruelas, L. A. Oro, *Chem. Rev.* **1998**, *98*, 577−588. [3b] G. Jia, C. P. Lau, *Coord. Chem. Rev.* **1999**, *190*, 83−108. [3c] *Recent Advances in Hydride Chemistry* (Eds: M. Peruzzini, R. Poli), Elsevier, Amsterdam, The Netherlands, **2001**, chapter 9.

[4] R. H. Crabtree, *The Organometallic Chemistry of the Transition Metals*, 3rd ed., John Wiley & Sons, New York, **2001**, pp. 237−238.

[5] [5a] C. Bianchini, A. Meli, M. Peruzzini, P. Frediani, C. Bohanna, M. A. Esteruelas, L. A. Oro, *Organometallics* **1992**, *11*, 138−145. [5b] C. Bianchini, C. Bohanna, M. A. Esteruelas, P. Frediani, A. Meli, L. A. Oro, M. Peruzzini, *Organometallics* **1992**, *11*, 3837−3844.

[6] [6a] A. Andriollo, M. A. Esteruelas, U. Meyer, L. A. Oro, R. A. Sánchez-Delgado, E. Sola, C. Valero, H. Werner, *J. Am. Chem. Soc.* **1989**, *111*, 7431−7437. [6b] M. A. Esteruelas, L. A. Oro, C. Valero, *Organometallics* **1992**, *11*, 3362−3369.

[7] W. C. Chan, C. P. Lau, Y. Z. Chen, Y. Q. Fang, S. M. Ng, G. Jia, *Organometallics* **1997**, *16*, 34−44.

[8] [8a] M. J. Tenorio, M. C. Puerta, P. Valerga, *J. Chem. Soc., Chem. Commun.* **1993**, 1750−1751. [8b] J. Espuelas, M. A. Esteruelas, F. J. Lahoz, L. A. Oro, C. Valero, *Organometallics* **1993**, *12*, 663−670.

[9] S. H. Liu, S. T. Lo, T. B. Wen, Z. Y. Zhou, C. P. Lau, G. Jia, *Organometallics* **2001**, *20*, 667−672.

[10] [10a] G. Barea, M. A. Esteruelas, A. Lledós, A. M. López, E. Oñate, J. I. Tolosa, *Organometallics* **1998**, *17*, 4065−4076. [10b] R. H. Crabtree, M. Lavin, L. Bonneviot, *J. Am. Chem. Soc.* **1986**, *108*, 4032−4037. [10c] A. C. Albeniz, M. Heinekey, R. H. Crabtree, *Inorg. Chem.* **1991**, *30*, 3632−3635. [10d] A. C. Albeniz, G. Schulte, R. H. Crabtree, *Organometallics* **1992**, *11*, 242−249. [10e] D. G. Gusev, F. M. Dolgushin, M. Y. Antipin, *Organometallics* **2001**, *20*, 1001−1007. [10f] J. N. Coalter III, J. C. Huffman, K. G. Caulton, *Organometallics* **2000**, *19*, 3569−3578. [10g] S. H. Liu, S. T. Lo, T. B. Wen, I. D. Williams, Z. Y. Zhou, C. P. Lau, G. Jia, *Inorg. Chim. Acta* **2002**, *334*, 122−130.

[11] [11a] S. A. Jackson, P. M. Hodges, M. Poliakoff, J. J. Turner, F. W. Grevels, *J. Am. Chem. Soc.* **1990**, *112*, 1221−1233. [11b] P. M. Hodges, S. A. Jackson, J. Jacke, M. Poliakoff, J. J. Turner, F. W. Grevels, *J. Am. Chem. Soc.* **1990**, *112*, 1234−1244.

[12] A. Thomas, M. Haake, F. W. Grevels, J. Bargon, *Angew. Chem. Int. Ed. Engl.* **1994**, *33*, 755−757.

[13] G. I. Childs, A. I. Cooper, T. F. Nolan, M. J. Carrott, M. W. George, M. Poliakoff, *J. Am. Chem. Soc.* **2001**, *123*, 6857−6866.

 © 2003 Wiley-VCH Verlag GmbH & Co. KGaA, Weinheim

[14] P. H. N. Budzelaar, N. N. P. Moonen, R. de Gelder, J. M. M. Smits, A. W. Gal, *Eur. J. Inorg. Chem.* **2000**, 753−769.
[15] W. H. Lam, Z. Lin, *J. Organomet. Chem.* **2001**, *635*, 84−91.
[16] S. H. Liu, S. M. Ng, T. B. Wen, Z. Y. Zhou, Z. Lin, C. P. Lau, G. Jia, *Organometallics* **2002**, *21*, 4281−4292.
[17] E. P. Cappellani, S. D. Drouin, G. Jia, P. A. Maltby, R. H. Morris, C. T. Schweitzer, *J. Am. Chem. Soc.* **1994**, *116*, 3375−3388.
[18] G. J. Kubas, C. J. Burns, G. R. K. Khalsa, L. S. Van der Sluys, G. Kiss, C. D. Hoff, *Organometallics* **1992**, *11*, 3390−3404.
[19] S. H. Liu, X. Huang, Z. Lin, C. P. Lau, G. Jia, *Eur. J. Inorg. Chem.* **2002**, 1697−1702.
[20] A. Castillo, M. A. Esteruelas, E. Oñate, N. Ruiz, *J. Am. Chem. Soc.* **1997**, *119*, 9691−9698.
[21] G. Jia, W. S. Ng, C. P. Lau, *Organometallics* **1998**, *17*, 4538−4540.
[22] S. H. Liu, X. Huang, W. S. Ng, T. B. Wen, M. F. Lo, Z. Y. Zhou, I. D. Williams, Z. Lin, G. Jia, *Organometallics* **2003**, *22*, 904−906.
[23] S. H. Liu, S. Y. Yang, S. T. Lo, Z. Xu, W. S. Ng, T. B. Ng, Z. Y. Zhou, Z. Lin, C. P. Lau, G. Jia, *Organometallics* **2001**, *20*, 4161−4169.
[24] [24a] P. A. Maltby, M. Schlaf, M. Steinbeck, A. J. Lough, R. H. Morris, W. T. Klooster, T. F. Koetzle, R. C. Srivastava, *J. Am. Chem. Soc.* **1996**, *118*, 5396−5407. [24b] B. Chin, A. J. Lough, R. H. Morris, C. T. Schweitzer, C. D'Agostino, *Inorg. Chem.* **1994**, *33*, 6278−6288. [24c] E. Rocchini, A. Mezzetti, H. Rüegger, U. Burckhardt, V. Gramlich, A. Del Zotto, P. Martinuzzi, P. Rigo, *Inorg. Chem.* **1997**, *36*, 711−720. [24d] A. Mezzetti, A. Del Zotto, P. Rigo, E. Farnetti, *J. Chem. Soc., Dalton Trans.* **1991**, 1525−1530.
[25] G. Jia, H. M. Lee, I. D. Williams, C. P. Lau, Y. Z. Chen, *Organometallics* **1997**, *16*, 3941−3949.
[26] R. Kuhlman, *Coord. Chem. Rev.* **1997**, *167*, 205−232.
[27] [27a] R. Kuhlman, W. E. Streib, K. G. Caulton, *Inorg. Chem.* **1995**, *34*, 1788−1792. [27b] D. V. Yandulov, W. E. Streib, K. G. Caulton, *Inorg. Chim. Acta* **1998**, *280*, 125−137.
[28] [28a] F. O. Fischer, S. Walz, G. Kreis, F. R. Kreibl, *Chem. Ber.* **1977**, *110*, 1651−1658. [28b] Z. Mazej, H. Borrmann, K. Lutar, B. Zemva, *Inorg. Chem.* **1998**, *37*, 5912−5914.
[29] See for example, [29a] J. Huhmann-Vincent, B. L. Scott, G. J. Kubas, *Inorg. Chem.* **1999**, *38*, 115−124. [29b] D. Huang, J. C. Huffman, J. C. Bollinger, O. Eisenstein, K. G. Caulton, *J. Am. Chem. Soc.* **1997**, *119*, 7398−7399. [29c] M. D. Butts, B. L. Scott, G. J. Kubas, *J. Am. Chem. Soc.* **1996**, *118*, 11831−11843 and references therein. [29d] R. J. Kulawiec, R. H. Crabtree, *Coord. Chem. Rev.* **1990**, *99*, 89−115 and references therein.
[30] See for example, [30a] D. C. Roe, W. J. Marshall, F. Davidson, P. D. Soper, V. V. Grushin, *Organometallics* **2000**, *19*, 4575−4582 and references therein. [30b] N. A. Jasim, R. N. Perutz, *J. Am. Chem. Soc.* **2000**, *122*, 8685−8693. [30c] D. H. Lee, H. J. Kwon, B. P. Patel, L. M. Liable-Sands, A. L. Rheingold, R. H. Crabtree, *Organometallics* **1999**, *18*, 1615−1621. [30d] M. A. Esteruelas, M. Oliván, E. Oñate, N. Ruiz, M. Tajada, *Organometallics* **1999**, *18*, 2953−2960. [30e] C. R. S. M. Hampton, I. R. Butler, W. R. Cullen, B. R. James, J. P. Charland, J. Simpson, *Inorg. Chem.* **1992**, *31*, 5509−5520. [30f] D. Sellmann, I. Barth, M. Moll, *Inorg. Chem.* **1990**, *29*, 176−181. [30g] T. G. Richmond, *Coord. Chem. Rev.* **1990**, *105*, 221−250.
[31] S. T. Lo, X. Xu, T. B. Wen, W. S. Ng, S. H. Liu, Z. Y. Zhou, Z. Lin, C. P. Lau, G. Jia, *Organometallics* **2000**, *19*, 4523−4530.
[32] W. Beck, K. Sünkel, *Chem. Rev.* **1988**, *88*, 1405−1421.
[33] See for example, [33a] M. Schlaf, A. J. Lough, R. H. Morris, *Organometallics* **1997**, *16*, 1253−1259. [33b] C. Bianchini, D. Masi, M. Peruzzini, M. Casarin, C. Maccato, G. A. Rizzi, *Inorg. Chem.* **1997**, *36*, 1061−1069. [33c] J. A. Ayllón, C. Gervaux, S. Sabo-Etienne, B. Chaudret, *Organometallics* **1997**, *16*, 2000−2002. [33d] E. Rocchini, A. Mezzetti, H. Rüegger, U. Burckhardt, V. Gramlich, A. Del Zotto, P. Martinuzzi, P. Rigo, *Inorg. Chem.* **1997**, *36*, 711−720. [33e] D. G. Gusev, R. Hübener, O. Orama, H. Berke, *J. Am. Chem. Soc.* **1997**, *117*, 3716−3731 and references therein.
[34] [34a] Z. Lin, M. B. Hall, *J. Am. Chem. Soc.* **1992**, *114*, 6102−6108. [34b] Z. Xu, I. Bytheway, G. Jia, Z. Lin, *Organometallics* **1999**, *18*, 1761−1766.
[35] R. H. Crabtree, *Acc. Chem. Res.* **1979**, *12*, 331−338.
[36] R. H. Crabtree, *The Organometallic Chemistry of the Transition Metals*, 3rd ed., John Wiley & Sons, New York, **2001**, p. 168.

Received January 28, 2003

 © 2003 Wiley-VCH Verlag GmbH & Co. KGaA, Weinheim

A Novel One-Dimensional Chain Complex Composed of Oxo-Centered Trinuclear Manganese Clusters

Jinkwon Kim,*[a] Jin Mook Lim,[b] and Youngkyu Do*[b]

Keywords: Magnetic properties / Manganese / Oxo ligands / Clusters

A new linear chain complex of oxo-centered trinuclear manganese clusters, $[\{Mn^{III}_2Mn^{II}O(O_2CCHCl_2)_6(H_2O)\}\{Mn(O_2CCHCl_2)_2(H_2O)_4\}]_n$ (**1**), has been synthesized by treatment of a mixture of $Mn(OAc)_2{\cdot}4H_2O$ and dichloroacetic acid in dichloromethane with $KMnO_4$. In this complex chains are formed by hydrogen bonding between carboxylate oxygens and coordinated water molecules, forming a two-dimensional structure. Antiferromagnetic coupling was observed by variable-temperature magnetic measurements.

(© Wiley-VCH Verlag GmbH & Co. KGaA, 69451 Weinheim, Germany, 2003)

Introduction

In the past few decades manganese chemistry has attracted much attention for the design of a new class of clusters for two reasons: first, to develop polynuclear manganese clusters as models for the water oxidation center of photosynthetic electron-transport chains in plants,[1] and second, to design new single-molecule magnets.[2] The first single-molecule magnetic behavior was observed in $[Mn_{12}O_{12}(OAc)_{16}(H_2O)_4]$ in 1993.[3] Single-molecule magnets (SMMs), as a prototype of nanomagnets, display an intramolecular magnetic hysteresis loop: each independent molecule in these materials possesses the ability to function as a magnetizable magnet owing to its intrinsic intramolecular properties rather than intermolecular interactions and long-range ordering.[4]

In the course of recent exploration of new manganese cluster complexes,[5] many oxo-centered trinuclear manganese carboxylate clusters with the common composition $[Mn_3O(O_2CR)_6L_3]$ have been synthesized and their physical properties studied extensively as model complexes for elucidating intramolecular electronic and magnetic interactions in clusters.[6−11] Furthermore, they have been used as a rich source of polynuclear complexes with a variety of interesting structural and physical properties.[12−14] Recently, we have focused our efforts on finding various synthetic routes to develop polynuclear manganese carboxylate clusters and were successful in synthesizing new Mn_6, Mn_8 and Mn_{18} clusters.[15,16] As part of our continuing interests to prepare new manganese clusters, we have studied the reaction of $Mn(OAc)_2{\cdot}4H_2O$ with $KMnO_4$ in the presence of an excess amount of dichloroacetic acid in dichloromethane. Herein, we report the synthesis and magnetic properties of an unprecedented linear-chain complex of oxo-centered trinuclear Mn clusters $[\{Mn^{III}_2Mn^{II}O(O_2CCHCl_2)_6(H_2O)\}\{Mn(O_2CCHCl_2)_2(H_2O)_4\}]_n$ (**1**).

Results and Discussion

The reaction mixture of $Mn(O_2CMe)_2{\cdot}4H_2O$ and dichloroacetic acid in dichloromethane solvent was treated with a fine powder of $KMnO_4$ with vigorous stirring to afford a dark brown solution. It is interesting to note that the same reaction in aqueous media gives $[Mn_{12}O_{12}(O_2CHCl_2)_{16}(H_2O)_4]$,[15] meaning that an aqueous medium provides a more acidic environment suitable for stabilizing higher oxidation state of manganese. Crystals suitable for X-ray crystallography were obtained by slow diffusion of *n*-pentane into a dichloromethane solution of **1**.

Complex **1** crystallizes in the monoclinic space group $P2_1/n$. The asymmetric unit of **1**, as depicted in Figure 1, consists of an oxo-centered trinuclear $[Mn_3(\mu_3\text{-}O)]^{6+}$ core and an $[Mn(H_2O)_4]^{2+}$ moiety. The manganese ions of the mixed-valent $[Mn^{II}Mn^{III}_2(\mu\text{-}O)]^{6+}$ core are bridged by six dichloroacetate ligands. The $[Mn(H_2O)_4]^{2+}$ moiety is bridged by Mn3 and the neighboring Mn1′ through dichloroacetates with a *syn-anti* conformation. One terminal water molecule is coordinated to Mn2 to give an octahedral geometry. On the basis of Jahn−Teller distortions and bond-valence sum calculations,[17,18] two manganese ions (Mn1 and Mn2) were assigned to Mn^{III}. The axial Mn1−O17 and Mn1−O13 bonds [1.830(5) and 1.951(5) Å, respectively] are shorter than the other equatorial bonds

[a] Department of Chemistry, Kongju National University, 182 Shinkwan, Kongju, Chungnam 314-701, Korea
Fax: (internat.) +82-41/850-8479
E-mail: jkim@kongju.ac.kr
[b] Department of Chemistry, School of Molecular Science BK21 and Center for Molecular Design and Synthesis, Daejeon 305-701, Korea

[2.034(5)−2.096(5) Å] due to Jahn−Teller contraction, while the axial Mn2−O4 and Mn2−O7 bonds [2.124(6) and 2.244(6) Å, respectively] are rather longer than the other equatorial bonds [1.818(5)−1.989(5) Å] due to a Jahn−Teller elongation effect. The Mn^{II} ions (Mn3 and Mn4) have uniform Mn−O bond lengths [Mn3−O: 2.119(6)−2.179(5) Å; Mn4−O: 2.149(7)−2.220(6) Å]. The μ_3-O atom is essentially coplanar with the Mn_3 plane, with an O17−Mn_3 plane separation of only 0.002 Å. The oxo-bridged $Mn^{III}\cdots Mn^{III}$ distance of 3.224(2) Å is shorter than the oxo-bridged $Mn^{II}\cdots Mn^{III}$ distances of 3.401(2) and 3.467(2) Å, which are similar to a known $[Mn^{II}Mn^{III}_2(\mu\text{-}O)]^{6+}$ core.[8] The carboxylate-only bridged $Mn^{II}\cdots Mn^{II}$ distances are 4.893(2) Å and 4.899(2) Å. The adjacent chains are significantly associated via hydrogen bonding between the coordinated water molecule and the carboxylate oxygen atoms, as illustrated in Figure 2. The O···O distances of these hydrogen bonds are within the range 2.631(9)−3.067(9) Å. The interchain Mn···Mn distances of adjacent chains are 5.116 Å for Mn2···Mn2# ($-x$, $1-y$, $-z$) and 5.117 Å for Mn4···Mn4# ($1-x$, $-y$, $-z$), indicating significant magnetic interactions between the chains.

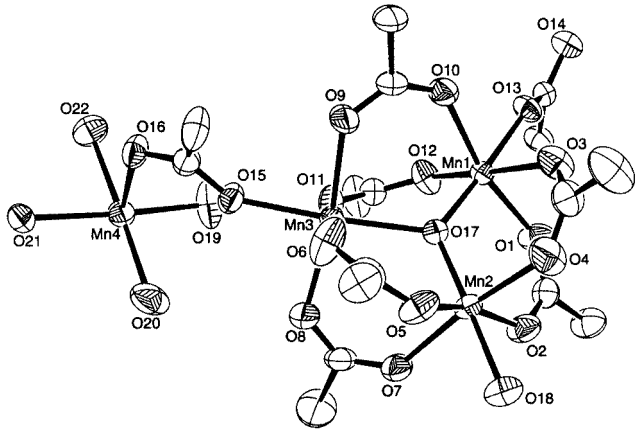

Figure 1. ORTEP diagram of **1** with atom numbering scheme; chlorine and hydrogen atoms are omitted for clarity; selected distances (A): Mn1···Mn2 3.224(2), Mn1···Mn3 3.467(2), Mn2···Mn3 3.401(2), Mn3···Mn4 4.899(2), Mn1··· Mn4# (x, $y-1$, z) 4.893(2)

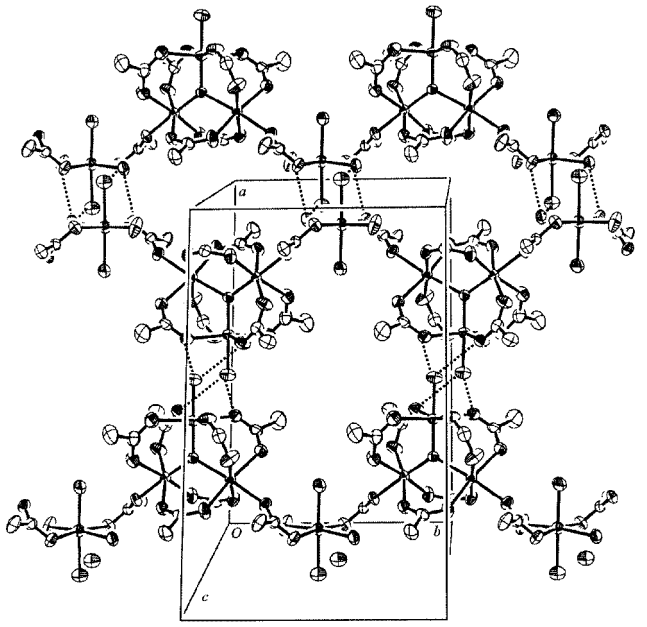

Figure 2. View down the *c*-axis showing the two-dimensional structure via interchain hydrogen bonding; chlorine atoms are omitted for clarity

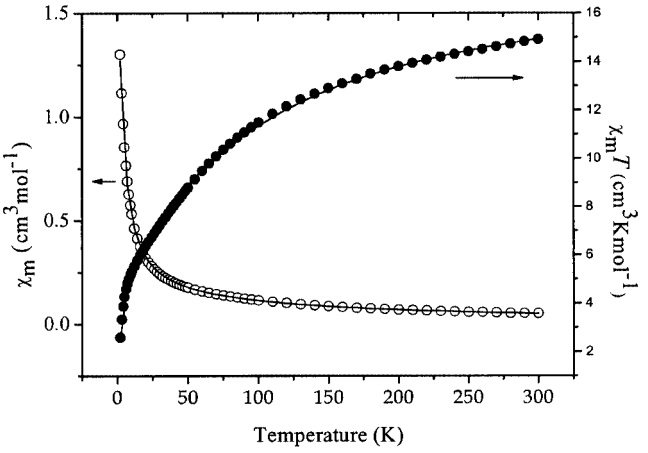

Figure 3. Temperature dependence of χ_{mol} (○) and χ_mT (·) at 500 Oe; the solid line represents the best fit of the data according to Equation (4)

Variable-temperature magnetic susceptibility data were measured for compound **1** from 2.0 to 300 K at 500 Oe. The resulting plot of χ_mT versus T for **1** is given in Figure 3. The χ_mT value is 14.9 $cm^3\cdot K\cdot mol^{-1}$ at 300 K, which is in good agreement with the spin-only value expected for high-spin, non-interacting $Mn^{II}_2Mn^{III}_2$ ions.

The spin Hamiltonian for the isotropic magnetic exchange interaction in a trinuclear Mn_3O unit is given in Equation (1).

$$\hat{H} = -2[J_{12}(\hat{S}_1\cdot\hat{S}_2) + J_{23}(\hat{S}_2\cdot\hat{S}_3) + J_{31}(\hat{S}_3\cdot\hat{S}_1)] \quad (1)$$

In complex **1**, there are two exchange parameters, $J = J_{12} = J_{31}$ for Mn^{II}-Mn^{III} interactions and $J' = J_{23}$ for the Mn^{III}-Mn^{III} interactions. The molar susceptibility is given by Equation (2) for the ground-state total spin of 1/2.[10] In this expression, the Weiss constant, θ, is introduced to roughly simulate interactions of paramagnetic species. Equation (3) represents the theoretical model for an $[Mn(H_2O)_4]^{2+}$ site. The intrachain exchange interaction of Mn^{II}-Mn^{II} might be quite weak, considering that the coupling constant has been estimated as only -0.20 cm^{-1} in a linear chain Mn^{II} complex bridged by a carboxylate ligand with a *syn-anti* bonding mode.[19] Furthermore, hydrogen-bond-mediated magnetic interactions between manganese ions are also weak.[20] Thus, based on these facts, the expected χ_mT value of **1** can be modeled with Equation (4).

 © 2003 Wiley-VCH Verlag GmbH & Co. KGaA, Weinheim

$$\chi_{Mn_3O} = \frac{N\mu_B^2 g^2}{3k(T-\theta)} F(T;J,J') \quad (2)$$

$$\chi_{Mn} = \frac{N\mu_B^2 g^2}{3k(T-\theta)} S(S+1) \quad (3)$$

$$\chi_m = \chi_{Mn_3O} + \chi_{Mn} \quad (4)$$

The susceptibility data are fitted reasonably well by Equation (4), as shown in Figure 3. The fitting parameters are $J = -5.95$ cm^{-1}, $J' = -9.52$ cm^{-1}, $g = 2.16$, $\theta = -2.4$ K. The J, J', and g values are similar to the values for other mixed-valent $Mn^{II}Mn^{III}{}_2O$ complexes.[8] The θ value of −2.4 K implies that paramagnetic centers such as the $[Mn(H_2O)_4]^{2+}$ moiety and the Mn_3O units interact antiferromagnetically through intrachain bridging carboxylate bonds as well as interchain hydrogen bonds.

Experimental Section

General Remarks: All reagents and solvents were purchased from commercial sources and used as received. Elemental analysis was carried out by the Analytical Laboratory of the Korea Basic Science Institute, Seoul. Infrared spectra were recorded on a Perkin−Elmer 16 PC spectrophotometer. Variable-temperature magnetic susceptibility measurements were carried out on a crystalline sample of **1** in the 2−300 K temperature range using a Quantum Design MPMS*XL* susceptometer equipped with a 50 kG magnet at magnetic fields of 500 Oe. The correction for the diamagnetism of the complex was estimated from Pascal's constants, and the magnetic data were corrected for diamagnetic contributions of the sample holder.

Preparation of 1: $Mn(O_2CMe)_2{\cdot}4H_2O$ (2.02 g, 8.16 mmol) and dichloroacetic acid (12 mL) were dissolved in 8 mL of dichloromethane and treated with a fine powder of $KMnO_4$ (0.51 g, 3.2 mmol) with vigorous stirring to afford a dark brown solution. After filtration to remove insoluble impurities a large amount of pentane was added to give a dark brown solid. Dark brown single crystals for X-ray analysis were obtained by slow diffusion of pentane into a dichloromethane solution of **1** at room temperature. $C_{16}H_{18}Cl_{16}Mn_4O_{22}$ (1349.3): calcd. C 14.24, H 1.34; found C 14.18, H 1.35. IR (KBr): $\tilde{\nu}$ = 1677(vs), 1663(vs), 1623(vs), 1599(vs), 1396(vs), 1227(m), 956(w), 926(s), 781(m), 714(s), 676(s), 550(w) cm^{-1}.

X-ray Crystallographic Study: A dark brown crystal (0.30 × 0.30 × 0.20 mm^3) was selected and mounted on a glass fiber. Intensity data were collected on an Enraf−Nonius CAD4 Diffractometer equipped with monochromated Mo-K_α radiation (λ = 0.71073 Å). Unit-cell parameters were determined from a least-squares fit of 25 accurately centered reflections. These dimensions and other parameters, including conditions of data collection, are summarized in Table 1. Data were collected at 293 K in the ω/2θ scan mode. The absorption correction was performed by a semi-empirical psi-scan. The structure was solved by direct methods using the SHELXS-97 and refined with SHELXL-97 by full-matrix least-squares methods on F^2.[21] All non-hydrogen atoms were refined anisotropically, while the hydrogen atoms were included in their calculated positions. The C−H bond lengths were fixed and the U values were assigned based approximately on the U value of the attached atom. CCDC-207185 contains the supplementary crystallographic data for this paper. These data can be obtained free of charge at www.ccdc.cam.ac.uk/conts/retrieving.html [or from the Cambridge Crystallographic Data Center, 12, Union Road, Cambridge CB2 1EZ, UK; Fax: (internat.) +44-1223/336-033; E-mail: deposit@ccdc.cam.ac.uk].

Table 1. Crystallographic data for complex **1**

Empirical formula	$C_{16}H_{18}Cl_{16}Mn_4O_{22}$
Molecular weight	1349.26
Crystal system	monoclinic
Space group	$P2_1/n$
a (Å)	18.966(2)
b (Å)	11.552(1)
c (Å)	22.626(4)
β [°]	113.78(1)
V (Å^3)	4536(1)
Z	4
ρ_{calc} (mg m^{-3})	1.976
$F(000)$	2648
μ (mm^{-1})	2.102
Temperature (K)	293(2)
$2\theta_{max}$ (°)	50
Transmission factor	0.7515−0.9999
Reflections collected	8214
Independent reflections	7998 [R_{int} = 0.0424]
Observed reflections [$I > 2\sigma(I)$]	6203
Data/restraints/parameters	7998/0/524
Goodness-of-fit on F^2	1.074
Final R indices [$I > 2\sigma(I)$]	R_1 = 0.0692, wR_2 = 0.1789
R indices for all data	R_1 = 0.0969, wR_2 = 0.2180

Acknowledgments

This work was supported by the NRL program of the Ministry of Science and Technology, Korea.

[1] *Manganese Redox Enzymes* (Ed.; V. L. Pecoraro), VCH Publishers, New York, **1992**.
[2] D. Gatteschi, R. Sessoli, *Angew. Chem. Int. Ed.* **2003**, *42*, 268−297.
[3] R. Sessoli, D. Gatteschi, A. Caneschi, M. A. Novak, *Science* **1993**, *365*, 141−143.
[4] L. Thomas, F. Lionti, R. Ballou, D. Gatteschi, R. Sessoli, B. Barbara, *Nature* **1996**, *383*, 145−147.
[5] A. Caneschi, D. Gatteschi, R. Sossoli, *J. Chem. Soc., Dalton Trans.* **1997**, 3963−3970.
[6] D. Cannon, R. P. White, *Prog. Inorg. Chem.* **1988**, *36*, 195−298.
[7] R. Wu, M. Poyraz, F. E. Sowrey, C. E. Anson, S. Wocaldo, A. K. Powell, U. A. Jayasooriya, R. D. Cannon, T. Nakanoto, M. Katada, H. Sano, *Inorg. Chem.* **1998**, *37*, 1913−1921.
[8] J. An, Z.-D. Chen, J. Bian, X.-L. Jin, S.-X. Wang, G.-X. Xu, *Inorg. Chim. Acta* **1999**, *287*, 82−88.
[9] J. Ribas, B. Albela, H. Stoeckli-Evans, G. Christou, *Inorg. Chem.* **1997**, *36*, 2352−2360.
[10] J. K. McCusker, H. G. Jang, S. Wang, G. Christou, D. N. Hendrickson, *Inorg. Chem.* **1992**, *31*, 1874−1880.
[11] J. B. Vincent, H.-R. Chang, K. Folting, J. C. Huffman, G. Christou, D. N. Hendrickson, *J. Am. Chem. Soc.* **1987**, *109*, 5703−5711.
[12] K. Brechin, C. Boskovic, W. Wernsdorfer, J. Yoo, A. Yamagu-

 © 2003 Wiley-VCH Verlag GmbH & Co. KGaA, Weinheim

chi, E. C. Sanudo, T. R. Concolino, A. L. Rheingold, H. Ishimoto, D. N. Hendrickson, G. Christou, *J. Am. Chem. Soc.* **2002**, *124*, 9710−9711.
[13] E. K. Brechin, R. A. Coxall, A. Parkin, A. Parsons, P. A. Tasker, R. E. P. Winpenny, *Angew. Chem. Int. Ed.* **2001**, *40*, 2700−2703.
[14] S. Wang, M. S. Wemple, J. Yoo, K. Folting, J. C. Huffman, K. S. Hagen, D. N. Hendrickson, G. Christou, *Inorg. Chem.* **2000**, *39*, 1501−1513.
[15] J. Kim, H. Cho, A. K. Gupta, J. M. Lim, Y. Do, *Int. J. Nanoscience* **2002**, *1*, 1−5.
[16] J. Kim, J. Hong, unpublished results.
[17] D. Brown, D. Altermatt, *Acta Crsytallogr.* **1985**, *B41*, 244−247.
[18] N. E. Brese O'Keeffe, *Acta Crystallogr., Sect. B* **1991**, *47*, 192−197.
[19] J. Kim, J. M. Lim, M. C. Suh, H. Yun, *Polyhedron* **2002**, *20*, 1947−1951.
[20] Y. Rodríguez-Martín, C. Ruiz-Pérez, J. González-Platas, J. Sanchiz, F. Lloret, M. Julve, *Inorg. Chim. Acta* **2001**, *315*, 120−125.
[21] G. M. Sheldrick, SHELX-97 User Guides, Crystallographic Department, University of Göttingen, Germany, 1997.

Received April 14, 2003

 © 2003 Wiley-VCH Verlag GmbH & Co. KGaA, Weinheim

A Novel Three-Dimensional Metal-Organic Framework Constructed from Two-Dimensional Interpenetrating Layers Based on Trinuclear Cobalt Clusters: $[Co_3(btec)(C_2O_4)(H_2O)_2]_n$

Yang-Guang Li,[a] Na Hao,[a] En-Bo Wang,*[a,b] Ying Lu,[a] Chang-Wen Hu,[a] and Lin Xu[a]

Keywords: Hydrothermal synthesis / Carboxylate ligands / Cobalt / Coordination polymers / Magnetic properties

A novel coordination polymer $[Co_3(btec)(C_2O_4)(H_2O)_2]_n$ (**1**; btec = 1,2,4,5-benzenetetracarboxylate) has been hydrothermally synthesized and characterized by IR, XPS, XRPD, TG analysis and single-crystal X-ray diffraction. The structural analysis reveals that **1** exhibits a new three-dimensional metal-organic framework constructed from two-dimensional parallel interpenetrating networks based on trinuclear cobalt cluster building blocks. Such interpenetrating composite networks in **1** represent the first example in the {M-btec} (M = transition metal) system. Variable-temperature magnetic susceptibility measurements indicate an antiferromagnetic behavior in **1**.
(© Wiley-VCH Verlag GmbH & Co. KGaA, 69451 Weinheim, Germany, 2003)

Introduction

The design and synthesis of infinite high-dimensional (especially two- and three-dimensional) metal-organic frameworks has attracted extensive interest in recent years, not only due to their intriguing structural motifs but also their potential applications in catalysis, molecular adsorption, and optical, electronic and magnetic materials.[1−2] Although it is not yet possible to prepare fully predictable metal-organic frameworks on the basis of rational design, recent exciting developments in coordination and organic chemistry provide great possibilities for the creative synthesis of desired novel frameworks.[3−5]

Among various metal-organic frameworks, the entangled structure, in which two or more infinite networks interpenetrate each other, is an attractive structural feature and has been widely researched.[6] In general there are two important factors for the formation of interpenetrating structures: one is that infinite networks contain large pores or cavities for interpenetration, and the other is that the individual 2-D networks should possess some appropriate elements of corrugation or undulation.[5] The use of long organic bridging ligands is often regarded as an effective strategy for the construction of such compounds.[7] In this aspect, organic aromatic polycarboxylate ligands, such as 1,4-benzenedicarboxylate and 1,3,5-benzenetricarboxylate, have been widely used in the construction of high-dimensional structures with large pores and/or undulated layers;[8] some interpenetrating frameworks have also been successfully prepared.[9] More recently, 1,2,4,5-benzenetetracarboxylate (btec) has proved to be a good candidate for assembling high dimensional metal-organic architectures owing to its two interesting structural features. In the first place, it contains multiple bridging moieties, which leads to a variety of connection modes with transitional metal centers and provides abundant structural motifs. Secondly, it can act both as a hydrogen-bond donor and as a hydrogen-bond acceptor due to the existence of protonated and/or deprotonated carboxyl groups.[10a] To date, a series of 2-D and 3-D metal-organic compounds in the {M-btec} (M = transition metal) system with large pores or undulated networks have been reported,[10] however, no interpenetrating structural feature in this system has hitherto been observed.

During our research on the hydrothermal synthesis of metal-organic frameworks in {M-btec} systems, another kind of organic bis-chelating oxalate ligand ($C_2O_4^{2-}$) has been introduced and a new coordination polymer, $[Co_3(btec)(C_2O_4)(H_2O)_2]_n$ (**1**), has been synthesized. Compound **1** exhibits a 3-D metal-organic framework consisting of 2-D interpenetrating networks on the basis of trinuclear cobalt cluster building blocks. To the best of our knowledge, compound **1** represents the first example in the {M-btec} system that possesses the interpenetrating structural feature. Furthermore, the btec ligand shows an unusual coordination mode linked with ten metal centers.

Results and Discussion

The hydrothermal reaction of an alkaline aqueous solution of $Co(C_2O_4)\cdot 2H_2O$, H_4btec and NaOH gives rise to

[a] Institute of Polyoxometalate Chemistry, Department of Chemistry, Northeast Normal University,
Changchun, 130024, P. R. China
Fax: (internat.) +86-431/568-4009
E-mail: wangenbo@public.cc.jl.cn
[b] State Key Laboratory of Structural Chemistry, Fujian Institute of Research on the Structure of Matter, Chinese Academy of Sciences,
Fuzhou, 350002, P. R. China
Supporting information for this article is available on the WWW under http://www.eurjic.org or from the author.

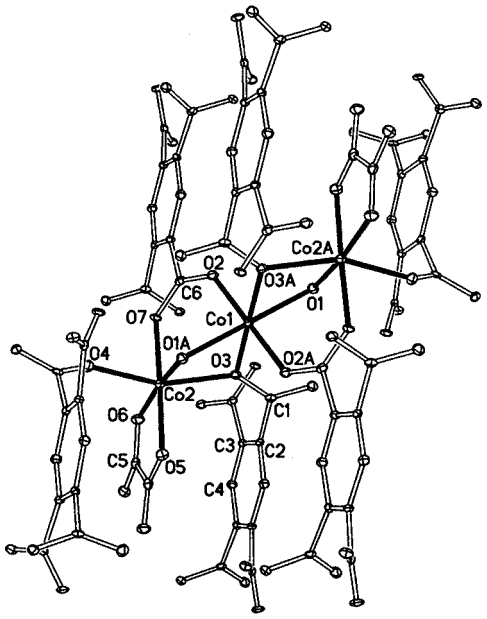

Figure 1. ORTEP drawing of **1** showing the local coordination environment of Co^{II} (thermal ellipsoids at 50% probability)

1 as purple block crystals. Single-crystal X-ray diffraction analysis revealed that **1** exhibits a novel 3-D metal-organic framework based on trinuclear cobalt cluster building blocks. The fundamental unit is shown in Figure 1. There are two crystallographically unique Co centers in the asymmetric unit, both displaying a distorted octahedral coordination geometry. The Co(1) center coordinates to four oxygen atoms of four different carboxylate groups, with $Co(1)-O_{(carboxyl)}$ distances in the range 1.9966(18)−2.0639(19) Å, and to two oxygen atoms of water molecules, with $Co(1)-O_{(water)}$ distances of 2.1991(19) Å. The O−Co(1)−O bond angles vary from 78.43(7)° to 180.00(14)°. The Co(2) center coordinates to three oxygen atoms of three different carboxylate groups [$Co(2)-O_{(carboxyl)}$ 2.0765(18)−2.1607(19) Å], two oxygen atoms of the oxalate ligand [$Co(2)-O_{(oxalate)}$ 2.0638(19)−2.131(2) Å] and one oxygen atom of a water molecule [$Co(2)-O_{(water)}$ 2.234(2) Å]. The O−Co(2)−O bond angles range from 75.71(7)° to 174.70(8)°. The three $\{CoO_6\}$ octahedra are connected together to form a linear trinuclear Co cluster in an edge-sharing mode. In addition, four carboxylate groups of the btec ligand exhibit two kinds of coordination modes with Co centers, as shown in Scheme 1. Two carboxylate groups act as a bidentate ligand, bridging two Co centers, while the other two exhibit an unusual bidentate bridging mode, linking three Co centers. Thus, one btec ligand is connected to ten Co centers, which has rarely been observed in previous reports.[10h] Furthermore, the oxalate groups ($C_2O_4^{2-}$) act as a bidentate bridging ligand to link trinuclear Co clusters into an interesting 1-D undulated chain. All these undulated chains are further connected by the btec ligands to form a 2-D grid-like network with large pores, as shown in Figure 2. The pore size is ca. 9.16 × 10.03 Å. The most important structural feature of **1** is that two such individual 2-D grid-like networks are self-entangled to form an interesting 2-D parallel interpenetrating layer (see Scheme 2 and Figure S1). To the best of our knowledge, no interpenetrating composite

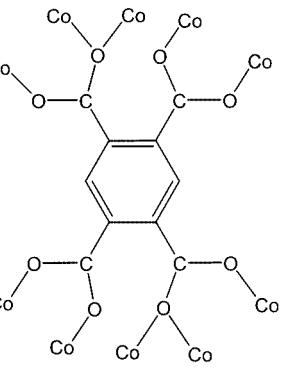

Scheme 1. The coordination mode of the btec ligand in compound **1**

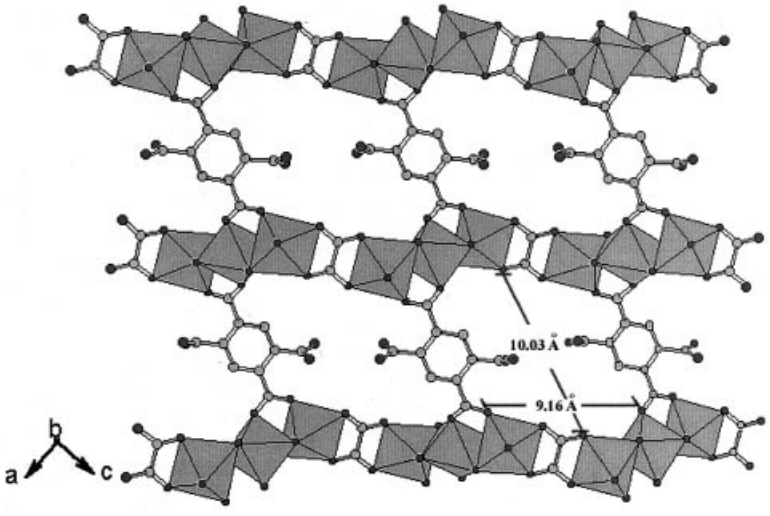

Figure 2. Polyhedral representation of the individual 2-D gridlike network of **1** viewed along the *b* axis; the polyhedra represent $\{CoO_6\}$ octahedra

 © 2003 Wiley-VCH Verlag GmbH & Co. KGaA, Weinheim

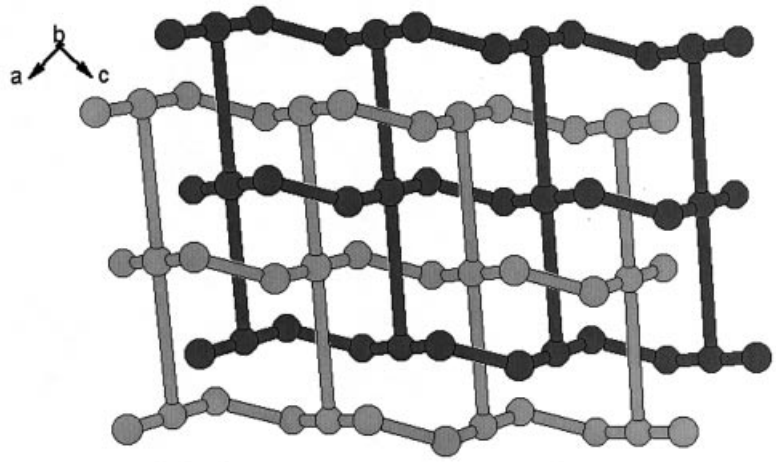

Scheme 2. Simplified schematic representation of the 2-D parallel interpenetrating network of **1** along the *b* axis

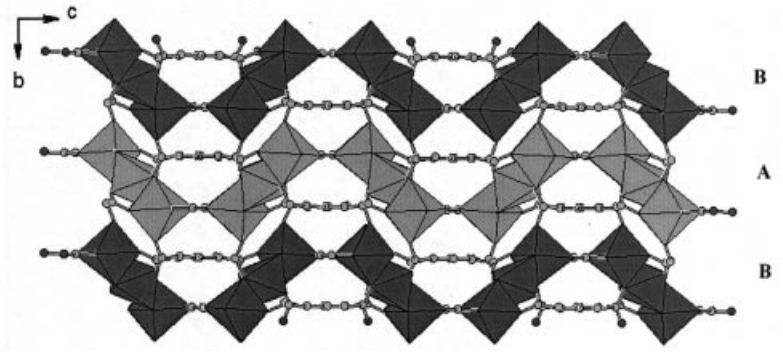

Figure 3. Polyhedral representation of the 3-D metal-organic framework of compound **1** viewed along the *a* axis; the light and dark colors represent two 2-D interpenetrating layers with different extending directions, respectively

network has hitherto been observed in the {M-btec} system. It is noteworthy that the presence of both large pores and an undulated element in the individual 2-D grid-like network provides the possibility of assembling interpenetrating architectures.

It is also interesting that these 2-D interpenetrating networks exhibit a wavelike layered structure along the *a* axis with each arched unit supported by the btec bridging ligand (see Figure 3). The adjacent 2-D interpenetrating layers extend perpendicular to each other in the *ac* plane and are alternately arranged in an ABAB mode along the *b* axis as shown in Figure 3. Thus, a 3-D metal-organic framework is formed by the connection of btec ligands (see Figure 3 and Figure S2).

The valence sum calculations of Co and O atoms are listed in Table S1. The bond-valence calculations (Co, 2.00) suggest all Co atoms are in the +2 oxidation state.[11] This result is also supported by an XPS measurement of the compound in the energy region of $Co2p^{1/2}$ and $Co2p^{3/2}$. The XPS spectrum (shown in Figure S3) gives one peak at 780.8 eV, attributable to Co^{2+}.[12] The O(1) atom has a bond-valence sum of 0.48, suggesting that it belongs to a coordinated water molecule. The O(2)−O(7) atoms have bond-valence sums of 1.90, 1.80, 1.92, 1.86, 1.85 and 1.81, respectively. These results indicate that all the oxygen atoms of the btec ligand and oxalate groups are deprotonated.[13] These results are consistent with the charge-balance considerations and alkaline synthetic conditions of compound **1**.

The variable-temperature magnetic susceptibility was measured from 2 K to 300 K at 5000 Oe for **1**. The magnetic data of **1** are displayed in Figure 4, plotted as the thermal variation of $\chi_m T$ and $1/\chi_m$. The $\chi_m T$ vs. T plot has a value of 9.32 emu·K·mol^{-1} at 300 K, and decreases continuously on cooling to a value of 0.54 emu·K·mol^{-1} at 2 K. The inverse susceptibility ($1/\chi_m$) plot as a function of temperature (T) is linear, closely following the Curie−Weiss law with C = 10.17 emu·K·mol^{-1}, corresponding to about one S = 3/2 spin per formula unit with g = 2.31 for Co^{II} centers. The effective magnetic moment per metal atom at 300 K, 4.47 μ_B, is in the range of experimentally observed values for high spin Co^{II} ions. The Weiss temperature, θ = −25.59 K, indicates that predominantly antiferromagnetic interactions exist between metallic Co^{II} centers. According to the structure of compound **1**, it could be presumed that the main magnetic interactions between the metal centers might happen in 1-D $\{Co_3(H_2O)_2(C_2O_4)\}$ chains, while the superexchange interactions between Co ions through the btec bridge can be ignored owing to the length of the btec ligands.[14]

The simulated and experimental XRPD patterns of compound **1** are shown in Figure S4. Their peak positions are

 © 2003 Wiley-VCH Verlag GmbH & Co. KGaA, Weinheim

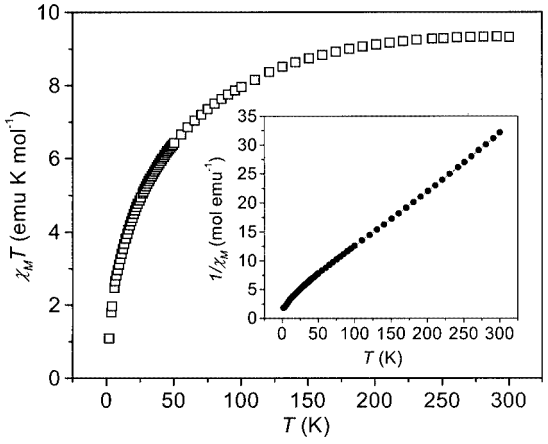

Figure 4. Thermal variation of $\chi_m T$ and $1/\chi_m$ for compound **1**

in good agreement with each other, indicating the phase purity of the products. The differences in intensity may be due to the preferred orientation of the powder samples. In the TG curve of compound **1** (see Figure S5), there is only one weight loss of 58.6% in the temperature range 200−450 °C, corresponding to the successive release of coordinated water, oxalate and btec ligands. Elemental analysis found that the brown residue might be CoO. The whole weight loss (58.6%) is in good agreement with the calculated value (59.2%).

Conclusion

In this work, a novel 3-D metal-organic framework $[Co_3(btec)(C_2O_4)(H_2O)_2]_n$ with 2-D parallel interpenetrating networks has been reported. Compound **1** is the first example in the {M-btec} system that possesses this interpenetrating structural feature. Both the large porous network and the undulated structural features are realized in the individual 2-D network (Figure 2) of **1** by the self-assembly of btec, $C_2O_4^{2-}$ and the linear trinuclear Co cluster building blocks, which provide great feasibility for the construction of interpenetrating network. The successful preparation of **1** indicates that metal-organic frameworks might be designed and synthesized according to specific structural features and inherent stereochemical and interactive information stored in the metal ions and organic ligands.[10a]

Experimental Section

Synthesis of 1: Compound **1** was synthesized from the reaction of $Co(C_2O_4)\cdot 2H_2O$ (0.091 g, 0.5 mmol), H_4btec (0.13 g, 0.5 mmol), NaOH (0.04 g, 1 mmol) and H_2O (8 mL, 444 mmol) in an 18 mL Teflon-lined autoclave under autogenous pressure at 160 °C for two days, followed by slow cooling (10 °C/h) to room temperature. The pH value of the reaction solution was ca. 8 and the final pH value was ca. 8.5. The product was washed with distilled water and air-dried at 50 °C. The product was of high quality in the form of purple block crystals (Yield: 0.079 g, 86% based on Co). $C_{12}H_6Co_3O_{14}$ (551.0): calcd. C 26.2, H 1.1, Co 32.1; found C 26.9, H 0.9, Co 31.9. Selected FT-IR data (KBr pellet): $\tilde{\nu}$ = 1638(s) cm^{-1}, 1589(s), 1509 (s), 1457(s), 1396(s), 1352(w), 1309(s), 1209(w), 1155(w), 1105(m), 915(s), 887(s), 836(s), 827(w), 808(w), 794(s), 763(w), 736(w), 698(w), 684(w), 635(w), 587(s), 535(s), 485 (s), 460 (w).

X-ray Crystallography: A purple crystal of **1** with dimensions of 0.578 ×0.378 × 0.258 mm^3 was glued onto a glass fiber. Data were collected on a Rigaku R-AXIS RAPID IP diffractometer with Mo-K_α monochromated radiation (λ = 0.71073 Å) at 93 K in the range of $2.12 < \theta < 27.12°$. An empirical absorption correction was applied.[15] The structure was solved by direct methods and refined by full-matrix least-squares methods on F^2 with the SHELXL-97 software package.[16] All non-hydrogen atoms were refined anisotropically. The hydrogen atoms on C atoms were located from difference electron-density maps. Crystal data: $C_{12}H_6Co_3O_{14}$, M_r = 550.96, orthorhombic, *Pbcn*, a = 7.0821(14), b = 12.557(3), c = 15.997(3) Å, $\alpha = \beta = \gamma = 90°$, U = 1422.6(5) Å^3, Z = 4, D_c = 2.572 gcm^{-3}, μ = 3.550 mm^{-1}, $F(000)$ = 1084, $R1$ = 0.0263, $wR2$ = 0.0831 and S = 1.065 for 1625 reflections with $I > 2\sigma(I)$ and 133 parameters ($R1$ = 0.0309, $wR2$ = 0.0845 for all 2988 data). CCDC-205531 contains the supplementary crystallographic data for this paper. These data can be obtained free of charge at www.ccdc.cam.ac.uk/conts/retrieving.html [or from the Cambridge Crystallographic Data Centre, 12, Union Road, Cambridge CB2 1EZ, UK; fax: (internat.) +44-1223/336-033; E-mail: deposit@ccdc.cam.ac.uk].

Acknowledgments

This work was financially supported by the National Natural Science Foundation of China (20171010).

[1] [1a] S. Leininger, B. Olenyuk, P. J. Stang, *Chem. Rev.* **2000**, *100*, 853−908. [1b] G. F. Swiegers, T. J. Malefetse, *Chem. Rev.* **2000**, *100*, 3483−3538. [1c] P. J. Hagrman, D. Hagrman, J. Zubieta, *Angew. Chem. Int. Ed.* **1999**, *38*, 2638−2684.

[2] [2a] R. Kitaura, S. Kitagawa, Y. Kubota, T. C. Kobayashi, K. Kindo, Y. Mita, A. Matsuo, M. Kobayashi, H.-C. Chang, T. C. Ozawa, M. Suzuki, M. Sakata, M. Takata, *Science* **2002**, *298*, 2358−2361. [2b] J. S. Seo, D. Whang, H. Lee, S. I. Jun, J. Oh, Y. J. Jeon, K. Kim, *Nature* **2000**, *404*, 982−986. [2c] V. V. Pavlishchuk, I. A. Koval, E. Goreshnik, A. W. Addison, G. A. Albada, J. Reedijk, *Eur. J. Inorg. Chem.* **2001**, *1*, 297−301.

[3] [3a] M. Eddaoudi, J. Kim, N. Rosi, D. Vodak, J. Wachter, M. O'Keeffe, O. M. Yaghi, *Science* **2002**, *295*, 469−472. [3b] N. Takeda, K. Umemoto, K. Yamaguchi, M. Fujita, *Nature* **1999**, *398*, 794−796. [3c] R. Kitaura, K. Seki, G. Akiyama, S. Kitagawa, *Angew. Chem. Int. Ed.* **2003**, *42*, 428−431. [3d] X.-H. Bu, W. Chen, S.-L. Lu, R.-H. Zhang, D.-Z. Liao, W.-M. Bu, M. Shionoya, F. Brisse, J. Ribas, *Angew. Chem. Int. Ed.* **2001**, *40*, 3201−3203.

[4] [4a] Y.-G. Li, G.-J.-H. De, M. Yuan, E.-B. Wang, R.-D. Huang, C.-W. Hu, N.-H. Hu, H.-Q. Jia, *Dalton Trans.* **2003**, 331−334. [4b] G.-Y. Luan, Y.-G. Li, S.-T. Wang, E.-B. Wang, Z.-B. Han, C.-W. Hu, N.-H. Hu, H.-Q. Jia, *Dalton Trans.* **2003**, 233−235. [4c] Y. Lu, E.-B. Wang, M. Yuan, G.-Y. Luan, Y.-G. Li, *J. Chem. Soc., Dalton Trans.* **2002**, 3029−3031.

[5] S. R. Batten, R. Robson, *Angew. Chem. Int. Ed.* **1998**, *37*, 1460−1494.

[6] A web site has been set up by Prof. S. R. Batten containing known examples of interpenetrating nets: http://web.chem.-monash.edu.au/Department/Staff/Batten/intptn.htm.

[7] [7a] G.-F. Liu, B.-H. Ye, Y.-H. Ling, X.-M. Chen, *Chem. Commun.* **2002**, 1442−1443 and references cited therein. [7b] N. L. Rosi, M. Eddaoudi, J. Kim, M. O'Keeffe, O. M. Yaghi, *Angew. Chem. Int. Ed.* **2002**, *41*, 284−287.

 © 2003 Wiley-VCH Verlag GmbH & Co. KGaA, Weinheim

[8] [8a] H. Li, M. Eddaoudi, M. O'keeffe, O. M. Yaghi, *Nature* **1999**, *402*, 276−279. [8b] H. K. Fun, S. S. S. Raj, R. G. Xiong, J. L. Zuo, Z. Yu, X. Z. You, *J. Chem. Soc., Dalton Trans.* **1999**, 1915−1916. [8c] S. S.-Y. Chui, S. M.-F. Lo, J. P. H. Charmant, A. G. Orpen, I. D. Williams, *Science* **1999**, *283*, 1148−1150. [8d] J.-C. Dai, X.-T. Wu, Z.-Y. Fu, C.-P. Cui, S.-M. Hu, W.-X. Du, L.-M. Wu, H.-H. Zhang, R.-Q. Sun, *Inorg. Chem.* **2002**, *41*, 1391−1396.

[9] [9a] J. Tao, M. L. Tong, X. M. Chen, *J. Chem. Soc., Dalton Trans.* **2000**, 3669−3674. [9b] C. J. Kepert, M. J. Rosseinsky, *Chem. Commun.* **1998**, 31−32.

[10] [10a] R. Cao, D. F. Sun, Y. C. Liang, M. C. Hong, K. Tatsumi, Q. Shi, *Inorg. Chem.* **2002**, *41*, 2087−2814. [10b] Y. G. Li, H. Zhang, E. B. Wang, N. Hao, C. W. Hu, Y. Yu, D. Hall, *New. J. Chem.* **2002**, *26*, 1619−1623. [10c] Y. G. Li, N. Hao, Y. Lu, E. B. Wang, Z. H. Kang, C. W. Hu, *Inorg. Chem.* **2003**, ASAP article. [10d]C.-D. Wu, C.-Z. Lu, W.-B. Yang, S.-F. Lu, H.-H. Zhuang, J.-S. Huang, *Eur. J. Inorg. Chem.* **2002**, 797−800. [10e] R. Murugavel, D. Krishnamurthy, M. Sathiyendiran, *J. Chem. Soc., Dalton Trans.* **2002**, 34−39. [10f] D. P. Cheng, M. A. Khan, R. P. Houser, *Crystal Growth & Design* **2002**, *2*, 415−420. [10g] L.-J. Zhang, J.-Q. Xu, Z. Shi, W. Xu, T.-G. Wang, *Dalton Trans.* **2003**, 1148−1152. [10h] H. Kumagai, C. J. Kepert, M. Kurmoo, *Inorg. Chem.* **2002**, *41*, 3410−3422. [10i] J.-Z. Zou, Q. Liu, Z. Xu, X.-Z. You, X.-Y. Huang, *Polyhedron* **1998**, *17*, 1863−1869 and references there in. [10j] D. Q. Chu, J. Q. Xu; L. M. Duan, T. G. Wang, A. Q. Tang, L. Ye, *Eur. J. Inorg. Chem.* **2001**, 1135−1137.

[11] I. D. Brown, D. Altermatt, *Acta Crystallogr., Sect. B* **1985**, *41*, 244−247.

[12] T. J. Chuang, C. R. Brundle, D. W. Rice, *Surf. Sci.* **1976**, *59*, 413.

[13] R. K. Chiang, C. C. Huang, C. S. Wur, *Inorg. Chem.* **2001**, *40*, 3237−3239.

[14] [14a] N. Guillou, S. Pastre, C. Livage, G. Férey, *Chem. Commun.* **2002**, 2358−2359. [14b] R. Cao, Q. Shi, D. Sun, M. C. Hong, W. H. Bi, Y. J. Zhao, *Inorg. Chem.* **2002**, *41*, 6161−6168.

[15] T. Higashi, *Program for Absorption Correction*, Rigaku Corporation, Tokyo, Japan, **1995**.

[16] [16a] G. M. Sheldrick, SHELXL-97, *Program for Crystal Structure Refinement*, University of Göttingen, Germany, **1997**. [16b] G. M. Sheldrick, SHELXS-97, *Program for Crystal Structure Solution*, University of Göttingen, Germany, **1997**.

Received April 17, 2003

 © 2003 Wiley-VCH Verlag GmbH & Co. KGaA, Weinheim

Blue to Red Fluorescent Emission Tuning of a Cadmium Coordination Polymer by Conjugated Ligands

Jing Zhang,[a] Yong-Rong Xie,[a] Qiong Ye,[a] Ren-Gen Xiong,*[a] Ziling Xue,[b] and Xiao-Zeng You*[a]

Keywords: Cadmium / Fluorescence / Coordination polymers / Crystal Engineering / Hydrothermal synthesis

The hydrothermal hydrolysis reactions of $Cd(ClO_4)_2 \cdot (6H_2O)$ with 4-[2-(2-pyridyl)ethenyl]benzonitrile (2-PEBN) and 2-[2-(4-cyanophenyl)ethenyl]-8-quinolinol (2-CEQH) afforded two coordination polymers aquabis{4-[2-(2-pyridyl)-ethenyl]benzoate}cadmium(II) (**1**) and 2-[2-(4-carboxylatophenyl)ethenyl]-8-quinolinolate(pyridine)cadmium(II) (**2**), respectively. Complexes **1** and **2** display strong blue and red fluorescent emission, respectively. Both **1** and **2** have a 2-D grid framework containing a dimer as the corner unit. Crystal data for **1**: monoclinic, $P2_1/c$, a = 15.2411(2), b = 19.8651(2), c = 15.6929(1) Å, α = β = 90, γ = 96.961(1)°; for **2**: monoclinic, $P2_1/c$, a = 11.9219(1), b = 8.9515(1), c = 18.8204(1)Å, α = γ = 90.00, β = 104.372(1)°.

(© Wiley-VCH Verlag GmbH & Co. KGaA, 69451 Weinheim, Germany, 2003)

Introduction

Full-color electroluminescent displays require three color components — green, blue and red. Stable blue or red metal-organic coordination polymers useful in electroluminescent devices are still rare and challenging to prepare. However, organic polymers, such as poly(*p*-phenylene vinylene) and polythiophenes etc., permit color tuning through changes in their length, substitution, regioregularity, and degree of conjugation.[1] A common approach to control the emitted color of organic materials is to append fluorescent chromophores to a polymeric backbone or to blend dyes into inert polymeric matrices.[2] Similarly, the emission wavelength of most metal-organic complexes can be tuned or changed by adjusting the length or conjugation of ligand since fluorescent emission is mostly dominated by the coordinated ligand transition.[3,4] In addition, metal-organic fluorescent coordination polymers have many more advantages — such as high thermal stability, good mechanical properties and relatively high emitting intensity — over pure organic materials. These coordination polymers have thus attracted much attention recently.[5] The synthesis and rational design of suitable organic ligands is still a great challenge since the introduction of special physical properties can be achieved through conjugation of the ligand, combined with the crystal engineering strategy and hydro(solvo)thermal synthesis method.[6] Furthermore, 8-quinolinolate complexes of, for example, Al^{3+} and Be^{2+} and their derivatives have also attracted much attention due to their potential application for full-color, flat-panel displays.[7] To this end, the hydrolysis reactions of $Cd(ClO_4)_2 \cdot (6H_2O)$ with 4-[2-(2-pyridyl)ethenyl]benzonitrile (2-PEBN) and 2-[2-(4-cyanophenyl)ethenyl]-8-quinolinol (2-CEQH) under hydrothermal reaction conditions afford two different emitting color fluorescent coordination polymers, aquabis{4-[2-(2-pyridyl)ethenyl]benzoate}cadmium(II) (**1**) and 2-[2-(4-carboxylatophenyl)ethenyl]-8-quinolinolate(pyridine)cadmium(II) (**2**) (Scheme 1), respectively. Complexes **1** and **2** display strong blue and red fluorescent emission, respectively. Interestingly, both **1** and **2** have a 2-D grid framework containing a dimer as corner unit. To the best of our knowledge, **1** is the first example of a double-square grid while **2** also has an unusual herringbone-type network with a dimer as the connecting node. Herein we report their synthesis, solid-state structures and fluorescent properties.

[a] Coordination Chemistry Institute, The State Key Laboratory of Coordination Chemistry, Nanjing University, 210093 Nanjing, P. R. China
Fax: (internat.) +86-25/331-4502
or (internat.) +86-25/331-7761
E-mail: xiongrg@netra.nju.edu.cn
[b] Department of Chemistry, University of Tennessee, Knoxville, Tennessee, 37996

Results and Discussion

The coordination polymers **1** and **2** were prepared under hydrothermal reaction conditions from $Cd(ClO_4)_2 \cdot 6H_2O$

 © 2003 Wiley-VCH Verlag GmbH & Co. KGaA, Weinheim **DOI: 10.1002/ejic.200300230**

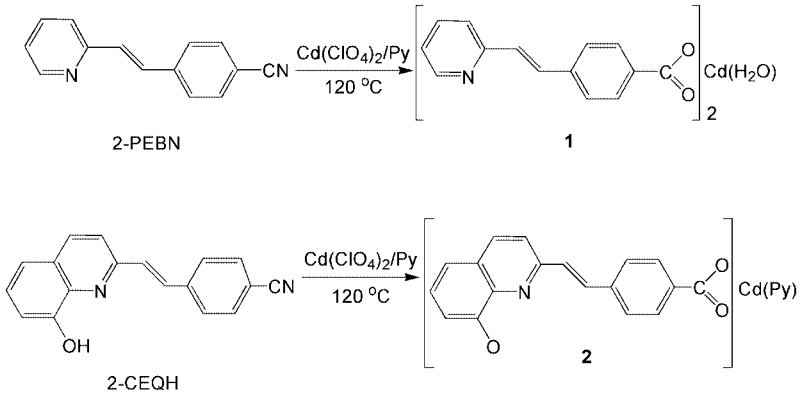

Scheme 1

and 2-PEBN or 2-CEQH respectively. In these two reactions, the cyano groups were hydrolyzed into carboxylates to give 4-[2-(2-pyridyl)ethenyl]benzoate (2-PEBA) in **1** and 2-[2-(4-carboxylatephenyl)ethenyl]-8-quinolinolate (2-CEQA) in **2**. The presence of the carboxylates was confirmed by the presence of two very strong peaks at 1600 and 1380 cm^{-1} for **1** and 1582 and 1405 cm^{-1} for **2** in the IR spectra. No peak around 2100 cm^{-1} was found, suggesting that the cyano groups are no longer present in **1** and **2**. TGA analysis showed an onset temperature for **1** at 300 °C with a weight loss of 1.77%; **1** decomposes beyond 350 °C. This weight loss at 300 °C corresponds to the removal of one water molecule per formula unit (calcd. 1.58%) in **1**. An onset temperature of 280 °C was observed for **2**.

The two-dimensional polymeric structures of **1** and **2** were revealed by X-ray single-crystal diffraction. The local coordination environment around the Cd center in **1** can best be described as a slightly distorted octahedron (Figure 1) in which each Cd center coordinates to two N atoms, one O atom from the bridging water and three O atoms from three different 2-PEBA ligands. Thus there are two kinds of 2-PEBA ligands, with one acting as a tridentate spacer to link three Cd centers and the other as a bidentate spacer to bridge two Cd centers, resulting in the formation of a 2-D rectangular grid network (Figure 2a). A simplified network representation (Figure 2b) clearly shows that each net shares eight 2-PEBA ligands as a rhombic side and four dimers as a connecting node. Thus, **1** can be considered as a double-rectangular grid network with a dimer as connecting node. To the best of our knowledge, **1** is the first such network example in supramolecular motifs.[8,9]

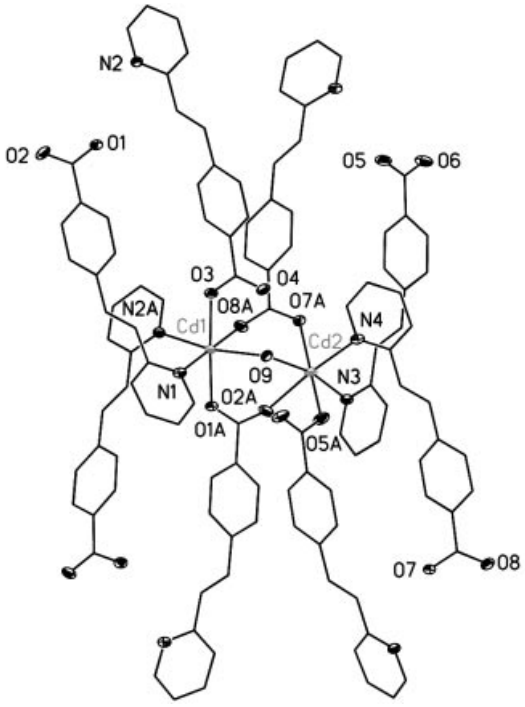

Figure 1. The asymmetric unit representation of **1** showing the local geometry around the Cd center; key bond lengths (Å): Cd1−O1A 2.213(2), Cd1−O3 2.253(2), Cd1−O8A 2.356(2), Cd1−O9 2.420(2), Cd1−N1 2.465(3), Cd1−N2A, 2.375(3), Cd2−O2A 2.389(3), Cd1−O5A 2.226(3), Cd1−O7A 2.211(2), Cd1−O9 2.413(2), Cd1−N3 2.374(3), Cd2−N4 2.461(3)

Like **1**, the local coordination geometry around each Cd center in **2** can also be described as a slightly distorted octahedron (Figure 3), in which each Cd center coordinates to two O atoms from a chelating, bridging 2-CEQA ligand and to two O atoms from the chelating carboxylate group of a different 2-CEQA ligand; the coordination sphere is completed by two N atoms, one from the chelating, bridging quinolinolate and one from pyridine. Thus, each 2-CEQA ligand acts as a pentadentate spacer to bridge three Cd centers, resulting in the formation of a 2-D rectangular grid network (Figure 4a). A simplified network representation of **2** (Figure 4b) clearly demonstrates that each rectangular grid shares four 2-CEQA ligands as a rhombic side and four dimers as connecting node resulting in the formation of a 2-D herringbone-type network. The structural feature in **2** is unusual as most supramolecular motifs with a herringbone net contain only one metal center as the connecting node.[8,9]

 © 2003 Wiley-VCH Verlag GmbH & Co. KGaA, Weinheim

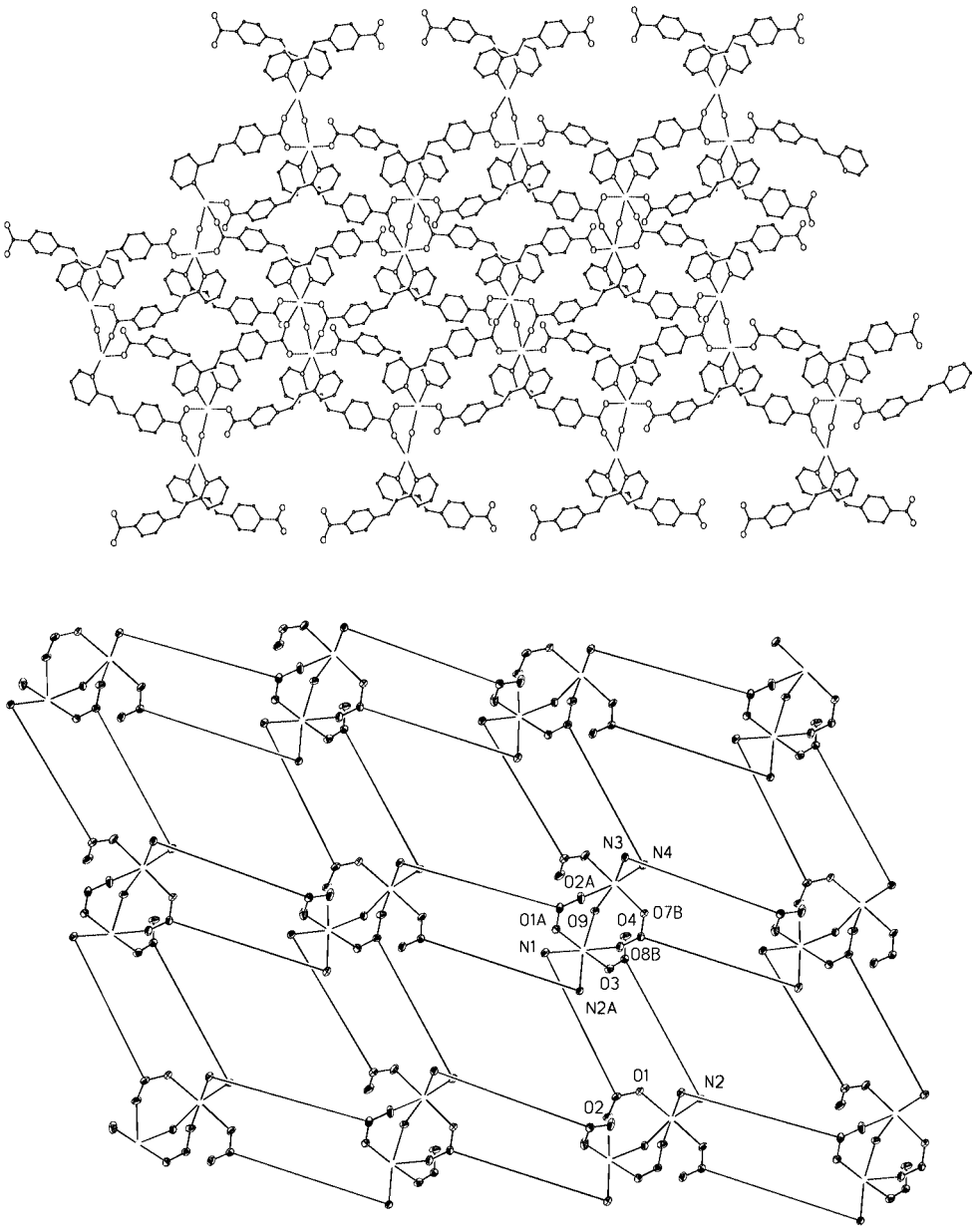

Figure 2. (a) 2-D grid network representation of **1**; (b) a simplified network representation of **1** in which the straight line is the 4-[2-(2-pyridyl)ethenyl]benzene group

The most important feature in the structures of **1** and **2** is that both have a 2-D condensed polymeric structure; this unique structure perhaps leads to significant enhancement of the fluorescent intensities, which are approximately two to three times larger than those of free 2-PEBA and 2-CEQA. These enhancements are perhaps a result of coordination of those ligands to Cd^{II}, which increases the ligands' conformational rigidity, thereby reducing the non-radiative decay of the intraligand $^1(\pi\text{-}\pi^*)$ excited state. Similar enhancement of the intraligand fluorescence has also been reported for $[Zn(terpyridine)_2]^{2+}$ and $[Zn(L)_2(OAc)_2]$ (L = *N*,*N*′-bisbenzyl-2,7-diamino-1,8-naphthyridine) [10] as well as $Zn(Norf)_2{\cdot}4(H_2O)$ (Norf = norfloxacin).[3] The solid-state diffuse reflectance UV/Vis spectra of **1** and **2** show two intense bands at 381 and 239 nm for **1** and 337 and 220 nm for **2**, which are assigned to intraligand π-π* transitions of 2-PEBA (388 and 246 nm) and 2-CEQA (338 and 215 nm). These bands match well with those in the excitation spectra of **1**, **2** and the free ligands (λ_{max} = 391 nm for 2-PEBA and λ_{max} = 348 nm for 2-CEQA). The emissions of **1** [λ_{max} = 418 nm, τ (lifetime) = 1.8 ns, Φ_{em} (quantum efficiency) ≈ 0.34; the short lifetime suggests that luminescence should be assigned to fluorescence] and **2** (λ_{max} = 600 nm, τ = 1.9 ns, Φ_{em} ≈ 0.46; Figure 5), are

 © 2003 Wiley-VCH Verlag GmbH & Co. KGaA, Weinheim

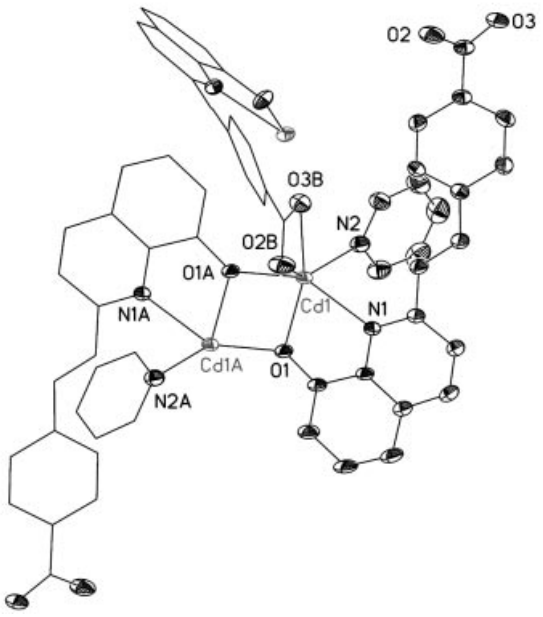

Figure 3. The asymmetric unit representation of **2** showing the local geometry around the Cd center; key bond lengths (Å): Cd1−O1 2.253(2), Cd1−O2B 2.369(3), Cd1−O3B 2.356(3), Cd1−N1 2.317(3), Cd1−N2 2.367(3)

Table 1. Crystal data and structure refinement for **1** and **2**

	1	**2**
Empirical formula	$C_{56}H_{40}N_4O_9Cd_2$	$C_{23}H_{16}N_2O_3Cd$
Mol. wt.	1137.72	480.78
T (K)	293(2)	293(2)
Crystal system	monoclinic	monoclinic
Space group	*P*21/*c*	*P*21/*c*
a, Å	15.2411(2)	11.9219(1)
b, Å	19.865(2)	8.9515(1)
c, Å	15.6929(1)	18.8204(1)
α, Deg	90.00	90.00
β, Deg	96.961(1)	104.372(1)
γ, Deg	90.00	90.00
V, Å^3	4716.25(8)	1945.64(3)
Z	4	4
ρ (cald), g/cm^3	1.602	1.641
μ (Mo-K_α), cm^{-1}	9.67	11.490
F(000)	2288	960
GOF	0.946	0.944
*R*1, *wR*2 [$I > 2\sigma(I)$][a]	0.0449, 0.0970	0.0426, 0.1004
(all data)	0.0790, 0.1062	0.0566, 0.1058

[a] $R1 = \Sigma||F_o| - |F_c||/\Sigma|F_o|$. $wR2 = [\Sigma w(F_o^2 - F_c^2)^2/\Sigma w(F_o^2)^2]^{1/2}$.

neither MLCT (metal-to-ligand charge transfer) nor LMCT (ligand-to-metal charge transfer) in nature, and can be tentatively assigned to the intraligand fluorescent emission since a similar weak emission (2-PEBA for $\lambda_{max} = 420$ nm, $\tau = 1.0$ ns, $\Phi_{em} \approx 0.11$) and (2-CEQA for $\lambda_{max} = 604$ nm, $\tau = 1.0$ ns, $\Phi_{em} \approx 0.16$) is also observed for the free ligands. Thus, the emitting color of a Cd coordination polymer can be tuned by ligand conjugation. Due to the low solubility of compounds **1** and **2** in common solvents such as water, ethanol, benzene, chloroform, ethyl acetate, acetone and acetonitrile, a film can be prepared by the spin-coating method.

In conclusion, through tuning of ligand length and conjugation, complexes **1** and **2** display a strong fluorescent emission at different wavelengths, and may be used as excellent advanced materials for blue- or red-light-emitting diode devices. These polymeric structures show high thermal stability and their low solubility in most common solvents means that they could be used in LED devices.

Experimental Section

Synthesis of Cd(2-PEB)$_2$·(H$_2$O) (1): Hydrothermal treatment of $Cd(ClO_4)_2 \cdot 6H_2O$ (1.0 mmol), PEBN (2.0 mmol), pyridine (0.6 mL) and water (0.6 mL) for 2 days at 120 °C yielded pale-yellow, crystalline blocks of **1** with only one pure phase. The yield of **1** was about (0.313 g) 55% based on PEBN. $C_{56}H_{40}Cd_2N_4O_9$ (1137.8): calcd. C 59.07, H 3.52, N 4.92; found C, 59.07, H 3.45, N 5.03. IR (KBr): $\tilde{\nu} = 3400$ cm^{-1} (br., w), 3008 (w), 1600 (s), 1551 (m), 1480 (m), 1420 (w), 1380 (s), 1180 (w), 1160 (m), 1010 (w), 960 (m), 850 (w), 793 (m), 742 (w), 700 (w), 681 (w), 640 (w), 532 (w), 434 (w).

Synthesis of Cd(2-CEQA)(Py) (2): The procedure with 2-CEQB was similar to that for **1**. Yellow block crystals (one phase) of **2** were harvested in 0.312 g (65%) yield based on 2-CEQB. $C_{23}H_{16}CdN_2O_3$ (480.8): calcd. C 57.41, H 3.33, N 5.82; found C, 57.60, H 3.42, N 5.90. IR (KBr): $\tilde{\nu} = 3424$ cm^{-1} (br., w), 1583 (s), 1532 (s), 1504 (w), 1445 (s), 1405 (s), 1371 (sh, w), 1278 (w), 1101 (m), 1035 (w), 1010 (w), 958(w), 833 (w), 779 (w), 739 (w), 703 (w), 616 (w), 417 (w).

X-ray Crystallographic Determinations of 1 and 2: Data were collected at room temperature from epoxy-coated crystals mounted on a glass fiber. All measurements were made on a CCD Smart diffractometer with graphite-monochromated Mo-K_α radiation ($\lambda = 0.71073$ Å). Empirical absorption corrections were applied in each case. The relevant crystallographic data are presented in Table 1. The structure was solved by direct methods using the program SHELXTL (Sheldrick, 1997).[11] All the non-hydrogen atoms were located from the trial structure and then refined anisotropically with SHELXTL using full-matrix least-squares procedure. The hydrogen atom positions were fixed geometrically at calculated distances and allowed to ride on the parent carbon atoms. The final difference Fourier map was found to be featureless. CCDC-167840 (**1**) and CCDC-167841 (**2**) contain the supplementary crystallographic data for this paper. These data can be obtained free of charge at www.ccdc.cam.ac.uk/conts/retrieving.html [or from the Cambridge Crystallographic Data Centre, 12, Union Road, Cambridge CB2 1EZ, UK; Fax: (internat.) +44-1223/336-033; E-mail: deposit@ccdc.cam.ac.uk].

Acknowledgments

This work was funded by The Major State Basic Research Development Program (Grant No. G2000077500), the National Natural Science Foundation of China, and National Science Foundation of the U.S.A.

 © 2003 Wiley-VCH Verlag GmbH & Co. KGaA, Weinheim

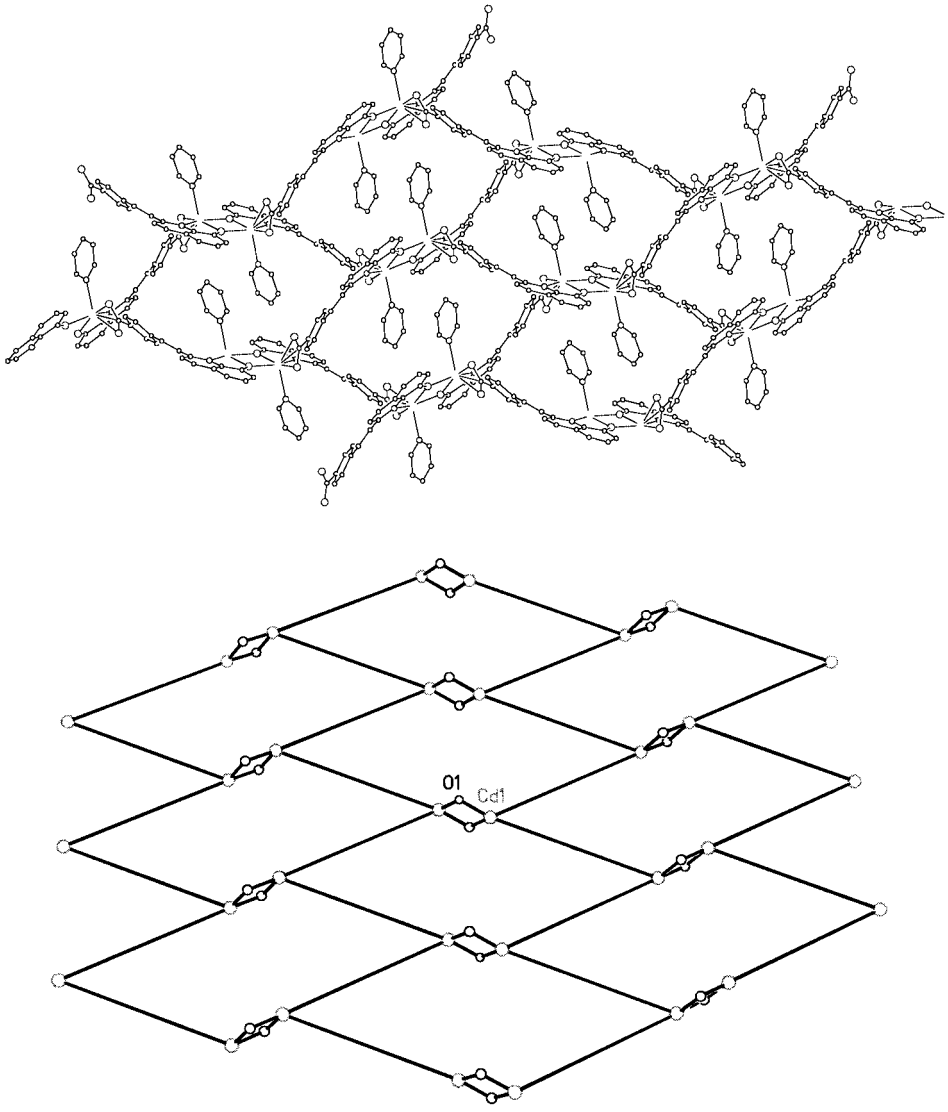

Figure 4. (a) 2-D grid network representation of **2**; (b) a simplified network representation of **1** in which the straight line is the 2-[2-(4-carboxylatephenyl)ethenyl]quinoline group

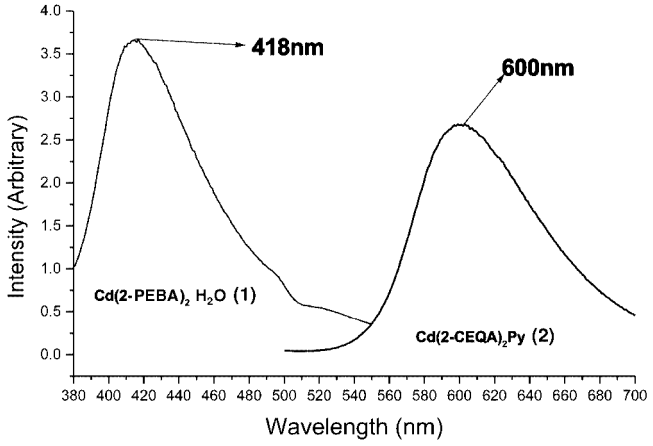

Figure 5. Fluorescence spectra of **1** and **2** in the solid state at room temperature

[1] [1a] H. S. Joshi, R. Jamshidi, Y. Tor, *Angew. Chem. Int. Ed.* **1999**, *38*, 2722. [1b] S. A. Jenekhe, *Adv. Mater.* **1995**, *7*, 309. [1c] F. Hide, M. A. B. Diaz-Garcia, J. Schartz, A. J. Heeger, *Acc. Chem. Res.* **1997**, *30*, 430. [1d] A. Kraf, A. C. Grimsdale, A. B. Holmes, *Angew. Chem. Int. Ed.* **1998**, *37*, 402. [1e] R. D. McCullough, *Adv. Mater.* **1998**, *10*, 93. [1f] T. Noda, H. Ogawa, N. Noma, Y. Shirota, *Adv. Mater.* **1997**, *9*, 720.

[2] [2a] M. Berggren, O. Inganas, G. Gustafsson, J. Rasmusson, M. R. Andersson, T. Hjertberg, O. Wennerstrom, *Nature* **1994**, *372*, 444. [2b] M. Aguiar, F. E. Karasz, L. Akcelrud, *Macromolecules* **1995**, *28*, 4598. [2c] S.-J. Chung, J.-I. Jin, K.-K. Kim, *Adv. Mater.* **1997**, *9*, 551. [2d] T. Christ, A. Greiner, R. V. Sander, J. Stumpflen, H. Wendorff, *Adv. Mater.* **1997**, *9*, 219. [2e] S. E. Dottinger, M. Hohloch, J. L. Segura, E. Steinhuber, M. Hanack, A. Tompert, D. Oelkrug, *Adv. Mater.* **1997**, *9*, 233. [2f] E. M. Girotto, M.-A. De Paoli, *Adv. Mater.* **1998**, *10*, 790. [2g] D. E. Biller, H. Baumgartel, *Angew. Chem. Int. Ed.* **1998**, *37*, 646.

[3] [3a] R.-G. Xiong, J.-L. Zuo, X.-Z. You, B. F. Abrahams, Z.-P. Bai, C.-M. Che, H.-K. Fun, *Chem. Commun.* **2000**, 2061. [3b] R.-G. Xiong, J.-L. Zuo, X.-Z. You, H.-K. Fun, S. S. S. Raj, *Organometallics* **2000**, *19*, 4183. [3c] H.-K. Fun, S. S. S. Raj, R.-

 © 2003 Wiley-VCH Verlag GmbH & Co. KGaA, Weinheim

G. Xiong, J.-L. Zuo, Z. Yu, X.-Z. You, *J. Chem. Soc., Dalton Trans.* **1998**, 1915. [3d] J. Zhang, W. Lin, Z.-F. Chen, R.-G. Xiong, B. F. Abrahams, H.-K. Fun, *J. Chem. Soc., Dalton Trans.* **2001**, 1804. [3e] Z.-F. Chen, R.-G. Xiong, J. Zhang, X.-T. Chen, Z.-L. Xue, X.-Z. You, *Inorg. Chem.* **2001**, *40*, 4075. [3f] R.-X. Yuan, R.-G. Xiong, Z.-F. Chen, X.-Z. You, S.-M. Peng, G.-H. Lee, *Inorg. Chem. Commun.* **2001**, *4*, 430.

[4] [4a] D. M. Ciurtin, N. G. Pschirer, M. D. Smith, U. H. F. Bunz, H.-C. zur Loye, *Chem. Mater.* **2001**, *13*, 2743 and references therein. [4b] J. E. Fiscus, S. Shotwell, R. C. Layland, M. D. Smith, H.-C. zur Loye, U. H. F. Bunz, *Chem. Commun.* **2001**, *24*, 2674. [4c] O. Teichert, W. S. Sheldrick, *Z. Anorg. Allg. Chem.* **1999**, *625*, 1860.

[5] [5a] K. Y. Ho, W. Y Yu, K. K. Cheung, C. M. Che, *Chem. Commun.* **1998**, 2101. [5b] K. Y. Ho, W. Y. Yu, K. K. Cheung, C. M. Che, *J. Chem. Soc., Dalton Trans.* **1999**, 1581. [5c] Y. G. Ma, H. Y. Chao, Y. Wu, S. T. Lee, W. Y. Yu, C. M. Che, *Chem. Commun.* **1998**, 2491.

[6] [6a] O. R. Evans, R.-G. Xiong, Z. Wang, G. K. Wong, W. Lin, *Angew. Chem. Int. Ed.* **1999**, *38*, 536. [6b] W. Lin, O. R. Evans, R.-G. Xiong, Z. Wang, *J. Am. Chem. Soc.* **1998**, *120*, 13272. [6c] W. Lin, Z. Wang, L. Ma, *J. Am. Chem. Soc.* **1999**, *121*, 11249.

[7] [7a] C. W. Tang, S. A. Van Slyke, *Appl. Phys. Lett.* **1987**, *51*, 913. [7b] Y. Hamada, T. Sano, M. Fujita, T. Fujii, Y. Nishino, K. Shibata, *Chem. Lett.* **1993**, 905.

[8] [8a] J.-M. Lehn, *Supramolecular Chemistry*; VCH Publishers: New York, **1995**. [8b] S. R. Batten, R. Robson, *Angew. Chem. Int. Ed.* **1998**, *37*, 1460 and references therein. [8c] S. Leininger, B. Olenyuk, P. J. Stang, *Chem. Rev.* **2000**, *100*, 853 and references therein. [8d] M. Fujita, *Chem. Soc. Rev.* **1998**, *27*, 417 and references therein. [8e] M. Kondo, M. Shimamura, S.-I. Noro, S. Minakoshi, A. Asami, K. Seki, S. Kitagawa, *Chem. Mater.* **2000**, *12*, 1288. [8f] J. K. Bera, K. R. Dunbar, *Angew. Chem. Int. Ed.* **2002**, *41*, 4453. [8g] Y. H. Kiang, G. B. Gardner, S. Lee, Z.-T. Xu, *J. Am. Chem. Soc.* **2000**, *122*, 6871. [8h] C. Janiak, *Angew. Chem. Int. Ed. Engl.* **1997**, *36*, 1431.

[9] [9a] M. J. Zaworotko, *Chem. Soc. Rev.* **1994**, *23*, 284 and references therein. [9b] L. R. MacGillivrary, J. L. Atwood, *Angew. Chem. Int. Ed.* **1999**, *38*, 1018 and references therein. [9c] F. A. Cotton, L. M. Daniels, C. Lin, C. A. Murillo, *J. Am. Chem. Soc.* **1999**, *121*, 4538. [9d] O. M. Yaghi, H. Li, C. Davis, D. Richardson, T. L. Groy, *Acc. Chem. Res.* **1998**, *31*, 474 and references therein. [9e] D. Hagrman, C. Zubieta, D. J. Rose, J. Zubieta, R. C. Haushalter, *Angew. Chem. Int. Ed. Engl.* **1997**, *36*, 873. [9f] G. B. Gardner, D. Venkataraman, J. S. Moore, S. Lee, *Nature* **1995**, *374*, 792. [9g] J. Lu, C. Yu, T. Niu, T. Paliwala, G. Gisci, F. Somosa, A. J. Jacobson, *Inorg. Chem.* **1998**, *37*, 4637. [9h] H. Miyasaka, C. S. Campos-Fernandez, R. Clerac, K. R. Dunbar, *Angew. Chem. Int. Ed.* **2000**, *39*, 3831. [9i] R. W. Saalfrank, H. Maid, N. Mooren, F. Hampel, *Angew. Chem. Int. Ed.* **2001**, *41*, 304.

[10] [10a] N. W. Alcock, P. R. Barker, J. M. Haider, M. J. Hannon, C. L. Painting, Z. Pikramenou, E. A. Plummer, K. Rissanen, P. Saarenketo, *J. Chem. Soc., Dalton Trans.* **2000**, 1447. [10b] C.-M. Che, C.-W. Wan, K.-Y. Ho, Z.-Y. Zhou, *New J. Chem.* **2001**, *25*, 62. [10c] X. Xue, X.-S. Wang, L.-Z. Wang, R.-G. Xiong, B. F. Abrahams, X.-Z. You, Z. Xue, C.-M. Che, *Inorg. Chem.* **2002**, *41*, 6544. [10d] R. G. Xiong, X. Xue, H. Zhao, X.-Z. You, B. F. Abrahams, Z. Xue, *Angew. Chem. Int. Ed.* **2002**, *41*, 3800.

[11] G. M. Sheldrick, (1997). SHELXTL V5.1 Software Reference Manual, Bruker AXS, Inc., Madison, Wisconsin, USA.

Received April 22, 2003

 © 2003 Wiley-VCH Verlag GmbH & Co. KGaA, Weinheim

Two- and Three-Dimensional Frameworks Constructed From Bicapped Keggin Clusters

Li-Mei Duan,[a,b] Cheng-Ling Pan,[a] Ji-Qing Xu,*[a] Xiao-Bing Cui,[a] Feng-Tong Xie,[a] and Tie-Gang Wang[a]

Keywords: Polyoxometalates / Hydrothermal synthesis / Cluster compounds / Crystal structure

The novel two- and three-dimensional solid materials $[Cu(en)_2(H_2O)]\{PMo^{VI}_8V^{IV}_6O_{42}[Cu(en)_2][Cu_{0.5}(en)]_3\}\cdot 5.5H_2O$ and $H_3\{V^{V}Mo^{VI}_8V^{IV}_6O_{42}[Cu(en)_2]_4\}[MoO_4]_2\cdot 14H_2O$ (en = ethylenediamine) have been hydrothermally assembled and structurally characterized. Both networks are based on mixed Mo/V bicapped Keggin clusters interconnected through the transition metal complex moieties.
(© Wiley-VCH Verlag GmbH & Co. KGaA, 69451 Weinheim, Germany, 2003)

The design and synthesis of framework materials linked by well-defined building blocks is still a challenge for the solid-state inorganic and material chemist. Polyoxometalates (POMs) have received considerable attention due to their diverse structures and unusual properties, with potential applications in fields such as catalysis, magnetism, optics and medicine.[1] Some POMs of the bicapped Keggin structure have been synthesized, such as discrete clusters $[V_{15}O_{42}]^{9-}$, $[PMo_{12}V_2O_{42}]^{5-}$ and $[PMo_8V_6O_{42}]^{5-}$,[2] the dimer cluster anions $[Mo_{16}V_{14}O_{84}]^{14-}$ [3] and one-dimensional chains connected through V−O−V bonds.[4] Our group has recently reported the first transition metal coordination compound supported on a metal-oxygen cluster with a bicapped Keggin structure.[5] There has recently been increasing interest in the assembly of higher-dimensional networks comprised of POM clusters and various bridging groups, either inorganic or organometallic. Typical compounds connected by metal cations include $[(CH_3)_4]_4Na_2H[\alpha\text{-}PW_{11}O_{39}]\cdot 8H_2O$,[6a] $[Gd(H_2O)_3]_3[GdMo_{12}O_{42}]\cdot 3H_2O$[6b] and a series of mixed-metal framework materials based on spherical $[V_{18}O_{42}(XO_4)]$ cages linked through $[M(H_2O)_4]$ groups (X: V, S; M: Fe, Co, Mn, Zn).[6c,6d] By introducing organic groups, some two-dimensional solid materials consisting of POMs and transition metal complexes have been assembled, such as $[\{Cu_3(4,7\text{-phen})_3\}_2\{Mo_{14}O_{45}\}]$, $[\{Cu(en)_2\}_2Mo_8O_{26}]$, $[Co(2,2'\text{-bpy})Mo_3O_{10}]$ and $[Co(en)_2][Co(bpy)_2]_2[PMo_8V_8O_{44}]\cdot 4.5H_2O$,[7] however, only a few three-dimensional compounds like $[\{Cu_2(triazolate)_2(H_2O)_2\}Mo_4O_{13}]$, $[Cu_2Mo_2O_8(4,4'\text{-bpy})]_n\cdot 4H_2O$ and $[\{Cu(1,2\text{-pn})_2\}_7\{V_{16}O_{38}(H_2O)\}_2]\cdot 4H_2O$[8] are known.

As a continuation of the hydrothermal synthesis of various polyoxometalates, we are trying to construct higher-dimensional frameworks from POM clusters through different bridging groups, especially transition metal complexes, and several compounds such as the two-dimensional $[\{Co(en)_2\}_2Sb_8V_{14}O_{42}(H_2O)]\cdot 6H_2O$ and $K\{V_{12}{}^{IV}V_6{}^{V}O_{42}Cl\text{-}[Ni(en)_2]_3\}\cdot 8H_2O$ have been assembled.[9] Here, we report the hydrothermal synthesis and structural characterization of two- and three-dimensional framework materials $[Cu(en)_2(H_2O)]\{PMo^{VI}_8V^{IV}_6O_{42}[Cu(en)_2][Cu_{0.5}(en)]_3\}\cdot 5.5H_2O$ (**1**) and $H_3\{V^{V}Mo^{VI}_8V^{IV}_6O_{42}[Cu(en)_2]_4\}[MoO_4]_2\cdot 14H_2O$ (**2**), both of which are based on the further condensation of the bicapped Keggin clusters $[XMo_8V_6O_{42}]^{7-}$ (X = P, V) through the linkage of $[Cu(en)_2]^{2+}$ bridging groups. To the best of our knowledge, no higher-dimensional networks constructed from bicapped Keggin clusters connected by transition metal coordination complexes have been reported until now.

The extended structure of compound **2** consists of $[(VO_4)Mo_8V_4O_{36}(VO)_2]^{7-}$ clusters, each of which is interconnected through eight $[Cu(en)_2]^{2+}$ bridging groups to eight other neighboring clusters via μ_2-O-Cu interactions, generating a three-dimensional network. The MoO_4^{2-} anions and water molecules occupy the cavities of the network solid. The structure of the cluster anion $[(VO_4)Mo_8V_4O_{36}(VO)_2]^{7-}$ in compound **2** is shown in Figure 1. The polyoxomolybdovanadate $[(VO_4)Mo_8V_4O_{36}(VO)_2]^{7-}$ has a reduced bicapped Keggin structure, which can be described as one Keggin core of $[VMo_8V_4O_{40}]^{11-}$ capped by two additional $\{VO\}^{2+}$ units. The vanadium atoms in compound **2** display three different coordination environments, including a disordered VO_4 tetrahedron at the center, distorted VO_6 octahedra as the sphere shell com-

[a] College of Chemistry and State Key Laboratory of Inorganic Synthesis and Preparative Chemistry, Jilin University, Changchun, 130023, China
E-mail: xjq@mail.jlu.edu.cn
[b] College of Chemistry, Inner Mongolia University for Nationalities, Tongliao, 028000, China

 © 2003 Wiley-VCH Verlag GmbH & Co. KGaA, Weinheim **DOI: 10.1002/ejic.200300070**

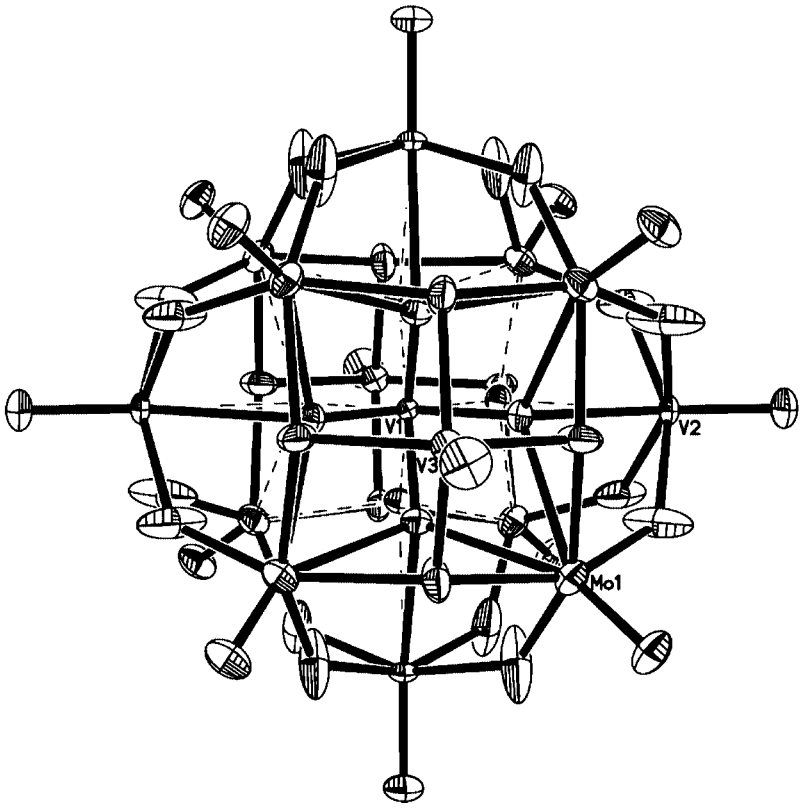

Figure 1. View of the $[V^{V}Mo^{VI}{}_{8}V_{6}{}^{IV}O_{42}]^{7-}$ cluster in compound **2**

position and VO_5 square pyramids at the capping positions. The central V(1) atom is located at the inversion center (0, 0, 0), which indicates that the central V(1) atom is surrounded by a cube of eight oxygen atoms with each oxygen site half-occupied. All the central V(1)−O distances are 1.689(10) Å, while the O−V(1)−O angles vary from 109.1(3)° to 110.2(7)°. The V(2)−O bond lengths in each VO_6 distorted octahedron vary as follows: 1.607(8) Å for terminal oxygens, 1.942(8)−1.945(7) Å for double or triply bridging oxygens and 2.418(10) Å for the oxygens of the central VO_4 tetrahedron. The V(3)−O distances in the VO_5 square pyramid are 1.633(12) Å for the capping terminal oxygens and 1.938(6) Å for the bridging oxygens. The Mo(1) atoms in the cluster have a distorted octahedral environment with the following Mo(1)−O distances: Mo(1)−$O_{terminal}$ 1.676(6) Å; Mo(1)−O_{bridge} 1.797(7)−2.065(10) Å and Mo(1)−O_{center} 2.412(10)−2.465(10) Å. The $MoO_4{}^{2-}$ ions contained in the cavities are slightly distorted tetrahedra with Mo(2)−O bond lengths 1.757(6) Å and O−Mo(2)−O angles of 107.3(4)° or 110.6(2)°.

As shown in Figure 2, all eight terminal oxo groups of the distorted MoO_6 octahedra in every $[(VO_4)Mo_8V_4O_{36}(VO)_2]^{7-}$ cluster are connected to a copper center, which, in turn, is coordinated to four nitrogen donors from two ethylenediamine molecules. The CuN_4 moiety of each $[Cu(en)_2]^{2+}$ group is rectangular, with Cu−N bond lengths of 2.007 and 2.008 Å, and N−Cu−N angles of 94.7(3)° and 85.3 (3)°. We may therefore describe the CuN_4O_2 unit as a highly distorted octahedron, with two axial Cu−O bonds being obviously elongated. Thus, each $[(VO_4)Mo_8V_4O_{36}(VO)_2]^{7-}$ cluster is connected to all of the adjacent ones through $[Cu(en)_2]^{2+}$ bridging groups in different directions via weak μ_2-O-Cu interactions, forming a

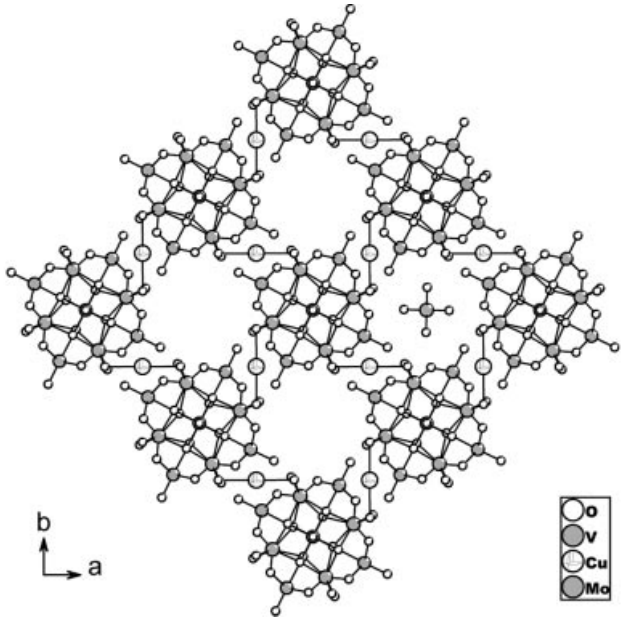

Figure 2. View of the three-dimensional framework structure of **2**, showing the clusters of $[V^{V}Mo^{VI}{}_{8}V_{6}{}^{IV}O_{42}]^{7-}$ interconnected through $[Cu(en)]^{2+}$ bridging groups; H_2O and en have been omitted for clarity

 © 2003 Wiley-VCH Verlag GmbH & Co. KGaA, Weinheim

three-dimensional network. Usually, the lattice waters and/or some cations reside in the cavities, while in compound **2** the MoO_4^{2-} anions occupy the cavities of the three-dimensional network along with water molecules. Furthermore, this is the first example where MoO_4^{2-} ions are found together with bicapped Keggin $[(VO_4)Mo_8V_4O_{36}(VO)_2]^{7-}$ cluster anions.

The X-ray structure analysis of compound **1** reveals that the $[PMo^{VI}{}_8V^{IV}{}_6O_{42}]^{7-}$ cluster anion is similar to the polyoxoanion $[VMo^{VI}{}_8V^{IV}{}_6O_{42}]^{7-}$ of compound **2**. In comparison with other bicapped Keggin polyoxoanions, the unusual feature[5] of **1** is that the $[Cu(en)_2]^{2+}$ units along the *b* axis supported on the bicapped Keggin structure unit $[PMo_8V_6O_{42}]^{7-}$ are not bridging groups. The two-dimensional network structure of **1** (Figure 3) consists of $\{PMo_8V_6O_{42}\ [Cu(en)_2]\}$ cages, each of which is connected to three other neighboring cluster units via $[Cu(en)_2]^{2+}$ bridging groups with Cu−O distances of 2.498−2.880 Å. This generates a two-dimensional network composed of $[\{PMo_8V_6O_{42}[Cu(en)_2]\}\{Cu(en)_2\}\{PMo_8V_6O_{42}[Cu(en)_2]\}]_n$, which is wave-like along the crystallographic *a* axis. To the best of our knowledge, this is the first example of such a compound possessing an extended structure constructed from bicapped Keggin structure clusters.

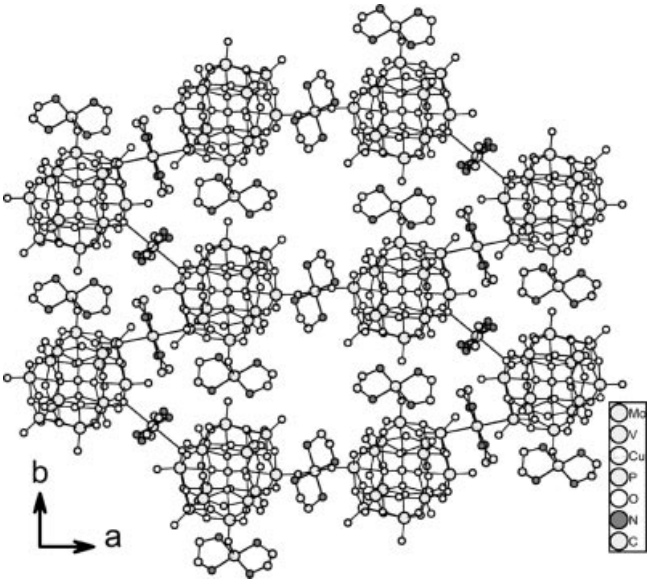

Figure 3. View of the two-dimensional network structure of **1**, showing the framework of $\{PMo_8V_6O_{42}[Cu(en)_2]\}$ clusters interconnected through $[Cu(en)_2]^{2+}$ bridging groups along the [001] direction

The assignments of oxidation states for the vanadium and molybdenum are consistent with their coordination geometries and are confirmed by valence sum calculations.[10] In compound **1**, the valence sums for the eight Mo atoms are 5.72, 5.74, 5.79, 5.85, 5.87, 5.83, 5.78 and 5.82, respectively, with an average value of 5.80; for the six V atoms the values are 3.96, 4.04, 4.12, 4.05, 4.12 and 4.07, respectively, with an average value of 4.06. The calculated values are 5.96 for Mo1, 6.04 for Mo2, 5.10 for the central V1 atom, 4.29 for V2 and 4.02 for the capping V3 atom in compound **2**. The room temperature ESR spectra of crystalline samples of compounds **1** and **2** display signals with $g = 1.976$ and $g = 2.055$, respectively, indicating the existence of V^{IV}. According to these ESR results, bond valence sum calculations, charge balance and elemental analyses, compounds **1** and **2** are formulated as $[Cu(en)_2(H_2O)]\{PMo^{VI}{}_8V^{IV}{}_6O_{42}[Cu(en)_2][Cu_{0.5}(en)]_3\}\cdot 5.5H_2O$ and $H_3\{V^{V}Mo^{VI}{}_8\ V^{IV}{}_6O_{42}[Cu(en)_2]_4\}[MoO_4]_2\cdot 14H_2O$, respectively.

In summary, we have synthesized the first two- and three-dimensional solid materials constructed from bicapped Keggin structure clusters and $[Cu(en)_2]^{2+}$ bridging groups. The successful design and synthesis of compounds **1** and **2** confirms once more that the further condensation of various POM clusters into higher-dimensional extended networks through the linkage of the transition metal complexes is feasible by controlling the synthesis conditions of the hydrothermal system. The formation of a particular product is usually restricted by various factors, and the rational synthesis of many kinds of compounds, including POMs and their polymers, is still difficult even under hydrothermal conditions. However, certain conditions are important for the assembly of higher-dimensional networks, such as the pH value of the reaction system, the species and metal-to-organic ligand ratio. For example, both compounds **1** and **2** were prepared with an en:Cu^{2+} molar ratio of less than 2, with the pH value ranging from 7 to 8. We have found that the formation of the $[Cu(en)_2]^{2+}$ complex supported on the polyoxomolybdovanadate or its polymer is very difficult when the en:Cu^{2+} molar ratio is greater than 3. Under particular synthetic conditions, certain types of targeted POMs or their polymers are reproducible and their structural type are roughly predictable, although the mechanism of the assembly remains elusive. Further systematic research is currently under way.

Experimental Section

Synthesis of 1: Compound **1** was synthesized as black block-shaped crystals by a hydrothermal method. A mixture of $CuCl_2\cdot 2H_2O$ (1.20 g), $Na_2MoO_4\cdot 2H_2O$ (1.6 g), NH_4VO_3 (0.8 g), en (0.6 mL), H_3PO_4 (0.5 mL, 50%) and distilled water (12 mL) at pH 7.0 was placed in a Teflon-lined reactor and heated at 170 °C for three days. After cooling to room temperature crystals of the title compound were isolated. $C_{14}H_{69}Cu_{3.5}Mo_8N_{14}O_{48.5}PV_6$ (2536.3): calcd. C 6.63, H 2.74, N 7.73; found C 6.74, H 2.65, N 7.58. The IR spectrum of **1** exhibits an intense band at 725 cm^{-1} attributed to ν(Mo-O, V-O), other bands at 1596, 1455, 1397, 1283, 1125 cm^{-1} that are characteristic of en, and bands at 1106, 1049 cm^{-1} attributed to ν(P-O).

Synthesis of 2: This compound was also synthesized by a hydrothermal method. A mixture of $CuAc_2\cdot H_2O$ (0.8 g), $(NH_4)_6Mo_7O_{24}\cdot 4H_2O$ (1.2 g), V_2O_5 (0.6 g), KOH (0.2 g), en (0.3 mL) and water (20 mL) was sealed in a 30 cm^3 Teflon-lined reactor and kept at 180 °C for four days at a pH of about 7.0. The autoclave was then cooled to room temperature. Black block-shaped crystals of **2** suitable for an X-ray diffraction analysis were isolated and washed

 © 2003 Wiley-VCH Verlag GmbH & Co. KGaA, Weinheim

with water, then dried at ambient temperature. Compound **2** is stable in air and insoluble in water and common organic solvents. $C_{16}H_{92}Cu_4Mo_{10}N_{16}O_{64}V_7$ (3103.1): calcd. C 6.16, H 3.08, N 7.22; found C 6.28, H 3.21, N 7.09. The infrared spectrum of **2** exhibits strong absorption peaks at 954, 929 and 853, 760 cm^{-1} attributed to the ν(M=O) or ν(M-O-M) (M = Mo or V) bands. A series of bands at 1591, 1457, 1281, 1197, 1113 and 1055 cm^{-1} is attributed to the en groups.

X-ray Crystallography: *Crystal data for* ***1****:* $C_{14}H_{69}Cu_{3.5}Mo_8N_{14}O_{48.5}PV_6$, dimensions 0.39 × 0.28 × 0.12 mm^3, orthorhombic, space group *Pccn*, a = 47.8809 (13), b = 13.3322 (4), c = 20.2559 (6) Å, V = 12930.5(6) $Å^3$, Z = 8, D_c = 2.606 g/cm^3, μ(Mo-K_α) = 3.576 mm^{-1}. The data were collected at 293 K using a Rigaku R-AXIS RAPID diffractometer (graphite monochromated Mo-K_α radiation; λ = 0.71073 Å, 1.88 ≤ θ ≤ 23.33°). Unique reflections were used to solve the structure by direct methods (SHLXTL 97). The structure was refined on F^2 by full-matrix least-squares techniques, converging at R = 0.0579 [$I \geq 2\sigma(I)$] with a goodness-of-fit on F^2 of 1.188 for 872 parameters and 58933 reflections, 9314 unique [R(int) = 0.0563]. The Cu(1), Cu(3) and Cu(4) atoms have an occupancy of 0.5 because of their special position. All non-hydrogen atoms were refined anisotropically.

Crystal data for ***2****:* $C_{16}H_{92}Cu_4Mo_{10}N_{16}O_{64}V_7$, dimensions 0.45 × 0.38 × 0.23 mm^3, tetragonal, space group *I*4/*m*, a = 14.1958 (5), c = 20.1604 (11) Å, V = 4062.7(3) $Å^3$, Z = 2, D_c = 2.537 g/cm^3, μ(Mo-K_α) = 3.385 mm^{-1}**.** The data were collected at 293 K using a Rigaku R-AXIS RAPID diffractometer (graphite monochromated Mo-K_α radiation; λ = 0.71073 Å, 1.75 ≤ θ ≤ 23.25°). Unique reflections were used to solve the structure by direct methods (SHLXTL 97). The structure was refined on F^2 by full-matrix least-squares techniques, converging at R = 0.0508 [$I \geq 2\sigma(I)$] with a goodness-of-fit on F^2 of 1.113 for 152 parameters and 9820 reflections, 1509 unique [R(int) = 0.0895]. The Mo(2), Cu(1), V(1), V(2), O(1), O(5) and O(6) have an occupancy of 0.25, 0.5, 0.125, 0.5, 0.5, 0.5 and 0.25, respectively, because of their special position. All non-hydrogen atoms were refined anisotropically.

CCDC-198448 (**1**) and -203045 (**2**) contain the supplementary crystallographic data for this paper. These data can be obtained free of charge at www.ccdc.cam.ac.uk/conts/retrieving.html [or from the Cambridge Crystallographic Data Center, 12, Union Road, Cambridge CB2 1EZ, UK; Fax: (internat) +44-1223/336-033; E-mail: deposit@ccdc.cam.ac.uk].

Acknowledgments

This work was supported by the National Natural Science Foundation of China (No. 20271021).

[1] [1a] M. T. Pope, *Heteropoly and Isopoly Oxometalates*, Springer, NewYork, **1983**. [1b] M. T. Pope, A. Müller, *Angew. Chem. Int. Ed. Engl.* **1991**, *30*, 34−38. [1c] A. Müller, F. Peters, M. T. Pope, D. Gatteschi, *Chem. Rev.* **1998**, *98*, 239−272. [1d] D. E. Katsoulis, *Chem. Rev.* **1998**, *98*, 359−388. [1e] V. Day, W. Klemperer, *Science* **1985**, *228*, 533−541. [1f] P. J. Hagrman, J. Zubieta, *Angew. Chem. Int. Ed.* **1999**, *38*, 2638−2684.

[2] [2a] D. Hou, K. S. Hagen, C. L. Hill, *J. Chem. Soc., Chem. Commun.* **1993**, 426−428. [2b] Q. Chen, C. L. Hill, *Inorg. Chem.* **1996**, *35*, 2403−2405. [2c] Y. Xu, J. Q. Xu, G. Y. Yang, T. G. Wang, Y. Xing, Y. H. Ling, H. Q. Jia, *Polyhedron* **1998**, *17*, 2441−2445.

[3] Y. P. Zhang, R. C. Haushalter, A. ClearField, *J. Chem. Soc., Dalton Trans.* **1995**, 1149−1150.

[4] [4a] G. Y. Luan, E. B. Wang, Z. B. Han, Y. G. Li, *Inorg. Chem. Commun.* **2001**, *4*, 541−543. [4b] V. Shivaiah, S. Hajeebu, S. K. Das, *Inorg. Chem. Commun.* **2002**, *5*, 996−999. [4c] A. Müller, M. Koop, P. Schiffels, H. Bögge, *Chem. Commun.* **1997**, 1715−1716.

[5] C. L. Pan, J. Q. Xu, Y. Sun, D. Q. Chu, L. Ye, Z. L. Lü, T. G. Wang, *Inorg. Chem. Commun.* **2003**, *6*, 233−237.

[6] [6a] N. Honma, K. Kusaka, T. Ozeki, *Chem. Commun.* **2002**, 2896−2897. [6b] C. D. Wu, C. Z. Zhuang, J. S. Huang, *J. Am. Chem. Soc.* **2002**, *124*, 3836−3837. [6c] M. I. Khan, *J. Solid State Chem.* **2000**, 105−112. [6d] M. I. Khan, E. Yohannes, D. Powell, *Chem. Commun.* **1999**, 23−24.

[7] [7a] D. Hagrman, P. J. Zapf, J. Zubieta, *Chem. Commun.* **1998**, 1283−1284. [7b] J. R. D. DeBord, R. C. Haushalter, L. M. Meyer, D. J. Rose, P. J. Zapf, J. Zubieta, *Inorg. Chim. Acta* **1997**, *256*, 165−168. [7c] P. J. Zapf, C. J. Warren, R.C. Haushalter, J. Zubieta, *Chem. Commun.* **1997**, 1543−1544. [7d] C. M. Liu, D. Q. Zhang, M. Xiong, D. B. Zhu, *Chem. Commun.* **2002**, 1416−1417.

[8] [8a] D. Hagrman, J. Zubieta, *Chem. Commun.* **1998**, 2005−2006. [8b] C. Z. Lu, C. D. Wu, S. F. Lu, J. C. Liu, Q. J. Wu, H. H. Zhuang, J. S. Huang, *Chem. Commun.* **2002**, 152−153. [8c] B. Z. Lin, S. X. Liu, *Chem. Commun.* **2002**, 2126−2127.

[9] [9a] L. J. Zhang, X. L. Zhao, J. Q. Xu, T. G. Wang, *J. Chem. Soc., Dalton Trans.* **2002**, 3275−3276. [9b] C. L. Pan, J. Q. Xu, G. H. Li, X. B. Cui, L. Ye, G. D. Yang, *Dalton Trans.* **2003**, 517−518.

[10] M. O'Keeffe, A. Navrotsky, *Structure and Bonding in Crystals*, Vol. II, Academic Press, New York, 1981, P.18−29.

Received February 4, 2003

 © 2003 Wiley-VCH Verlag GmbH & Co. KGaA, Weinheim

Rhodium and Ruthenium Complexes of 1,1′-Bis(phosphetano)ferrocenes: Structural Characterisation and Catalytic Behaviour

Angela Marinetti,*[a] Francis Labrue,[a] Bénédicte Pons,[a] Sébastien Jus,[a] Louis Ricard,[b] and Jean-Pierre Genêt[a]

Keywords: Asymmetric catalysis / Hydrogenations / P ligands / Phosphetane / Rhodium / Ruthenium

The first structural characterisation of ruthenium and rhodium complexes of the 1,1′-bis(phosphetano)ferrocenes **1** (FerroTANEs) – namely [{(*S*,*S*)-*i*Pr-**1**}$RuCl_2Py_2$] and [{(*S*,*S*)-*i*Pr-**1**}Rh(COD)OTf] – is reported. X-ray data show that the ruthenium complex and the rhodium chelate complex both adopt δ conformations, as a result of the (*S*,*S*) configuration of the phosphetane moiety. The ruthenium complexes promote the catalytic hydrogenation of β-keto esters with moderate to high enantioselectivities. The behaviour of the rhodium complexes of **1** is compared with that of other phosphetane-based catalysts in the hydrogenation of methyl *N*-acetamidocinnamate.
(© Wiley-VCH Verlag GmbH & Co. KGaA, 69451 Weinheim, Germany, 2003)

Introduction

The 1,1′-bis(phosphetano)ferrocenes **1** (FerroTANEs) rank among those ligands that induce excellent enantioselectivities in rhodium-promoted hydrogenations.[1] In particular, their practical utility has been demonstrated in the synthesis of amido succinates by asymmetric hydrogenation of itaconate derivatives.[2] In these reactions, ligands **1** perform better, in terms of efficiency and enantioselectivity, than other well known diphosphanes such as DuPHOS, DIPAMP or PHANEPHOS. Recently, their high efficiency in the catalytic hydrogenation of (*E*)-β-amino acid derivatives has also been established.[3] It thus seems that the combination of a conformationally constrained phosphetane ring with the relatively flexible ferrocene backbone represents a favourable structural feature for high catalytic efficiency. For comparison, the structurally analogous 1,1′-bis(phospholanyl)ferrocenes give only moderate to low enantioselectivities in hydrogenation reactions.[4]

Besides their good catalytic properties, the potential utility of diphosphanes **1** is also founded on their easy availability: diphosphanes **1** are easily accessible from fairly inexpensive chiral 1,3-diols and their structures and catalytic properties are easily and finely tuned by variation of the R groups at the α-positions of the phosphetane rings.

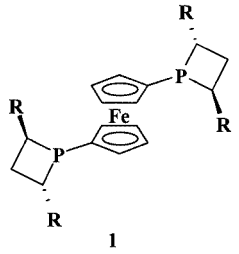

1

Following our initial report on the synthesis and preliminary catalytic screening of these ligands, we wish to disclose here the preparation and first structural characterisation of ruthenium and rhodium complexes of **1**, which are efficient catalyst precursors for hydrogenation reactions. Additional data on their catalytic properties is also reported.

Results and Discussion

Crystal Structures of the [(*S*,*S*-1c)$RuCl_2(Py)_2$] and [(COD)Rh(*S*,*S*-1c)OTf] Complexes

With regard to the excellent catalytic properties of the 1,1′-bis(phosphetano)ferrocenes **1**, it is highly interesting to investigate the coordinating behaviour of these new ligands towards catalytically active transition metals, as well as the structural features of their complexes. With this aim, we prepared the [{(*S*,*S*)-*i*Pr-**1**}$RuCl_2(Py)_2$] complex **2**, which is a potential precursor for hydrogenation catalysts. The synthesis of **2** was performed according to the Bergens procedure:[5] the reaction between **1** and the [(NBD)$RuCl_2Py_2$] complex (NBD = norbornadiene, Py = pyridine) at room temperature. Facile and quantitative displacement of the

[a] Laboratoire de Synthèse Sélective Organique et Produits Naturels – ENSCP,
11, rue Pierre et Marie Curie, 75231 Paris Cedex 05, France
Fax: (internat.) + 33-1/4407 1062
E-mail: marinet@ext.jussieu.fr
[b] Laboratoire Hétéroéléments et Coordination – Ecole Polytechnique,
91128 Palaiseau Cedex, France

unsaturated ligand by the chelating diphosphane is observed, as shown in Equation (1).

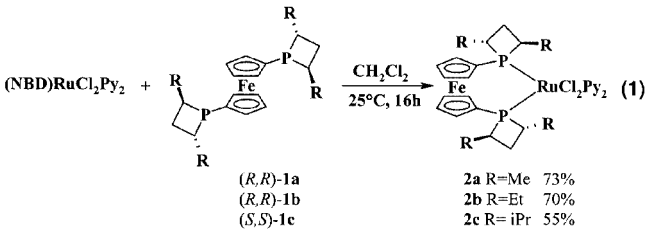

The ruthenium complexes **2** are obtained in moderate to high yields after crystallisation from dichloromethane/pentane mixtures, as air-stable, orange, crystalline solids. NMR spectroscopy shows that complexes **2** have C_2-symmetrical structures, with equivalent phosphetane and also pyridine moieties. The ^{31}P NMR resonance of complexes **2** is shifted downfield with $\Delta\delta$ of 60−70 ppm relative to **1**, the less hindered complex **1a** undergoing the larger shift upon coordination.

The first structural characterisation of any 1,1′-bis(phosphetano)ferrocene−transition metal derivative has been performed on complex **2c**. An ORTEP drawing is shown in Figure 1, and selected bond lengths and angles are reported in Table 1.

Complex **2c** crystallises in the orthorhombic system, with one dichloromethane molecule per molecular unit. The ruthenium atom is approximately octahedral. The bis-equatorially coordinated diphosphane gives a P−Ru−P bite angle of 98.57(3)°, in good agreement with the expected value, as large deflections from the ideal 90° (metal natural bite angle) up to about 100° are usually observed in square-planar and octahedral complexes of dppf[6] and other 1,1′-bis(phosphanyl)ferrocenes.[7] The conformation of the Cp rings is staggered, with a torsion angle of 45.7°. The rotation of the cyclopentadienyl rings against each other, together with their tilt, produces a fairly large P−P distance of 3.51 Å (as compared with the Cp−Cp′ distances of 3.28 Å).

Table 1. Selected interatomic distances [Å] and angles [deg] for complex **2c**

Ru(1)−P(1)	2.321(1)	Ru(1)−Cl(2)	2.437(1)
Ru(1)−P(2)	2.319(1)	P(1)−C(1)	1.892(3)
Ru(1)−N(1)	2.231(3)	P(1)−C(3)	1.887(3)
Ru(1)−N(2)	2.170(3)	P(2)−C(11)	1.908(3)
Ru(1)−Cl(1)	2.425(1)	P(2)−C(9)	1.884(3)
P(1)−Ru(1)−P(2)	98.57(3)	C(1)−P(1)−C(3)	76.3(1)
N(1)−Ru(1)−N(2)	81.7(1)	C(4)−P(1)−Ru(1)	119.9(1)
P(1)−Ru(1)−N(1)	90.20(7)	C(11)−P(2)−C(12)	77.3(2)

The structural parameters of the phosphetane rings show standard values, with small intracyclic C−P−C angles of 76.3(1) and 77.3(2)°, respectively, and ring bending angles of 25.5 and 17.6°, respectively.

A significant structural feature of the complex is the δ conformation[8] adopted by the ferrocene backbone, which enforces a dissymmetric coordination of the phosphetane rings (see Figure 2): the C(3) and C(9) ring atoms, and the corresponding isopropyl substituents, are shifted away from the ruthenium coordination plane, in pseudoaxial positions, while the C(1) and C(11) atoms occupy pseudoequatorial positions. The corresponding dihedral angles between the P(1)−Ru−P(2) plane and the P−C axis are −93°

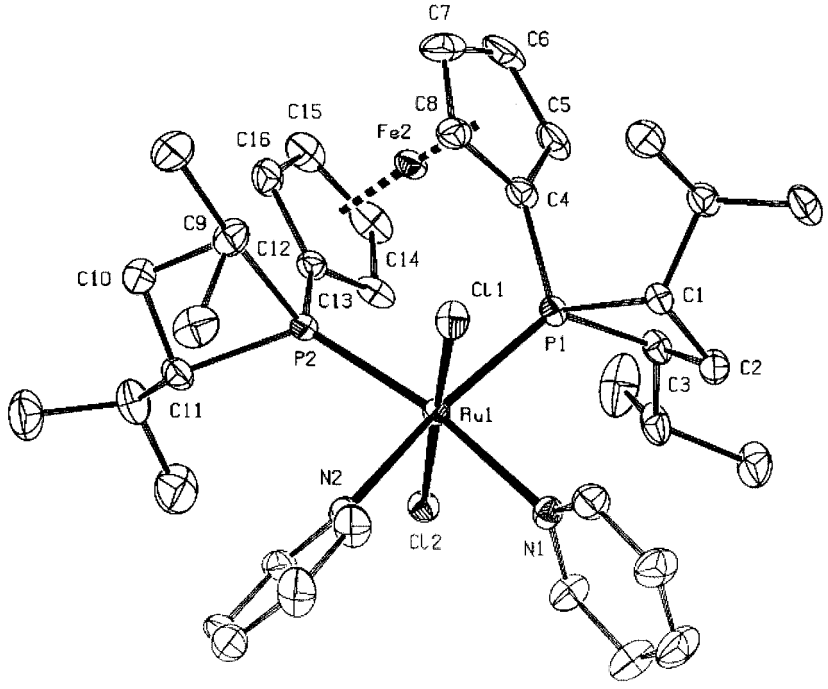

Figure 1. ORTEP drawing for the ruthenium complex **2c**

 © 2003 Wiley-VCH Verlag GmbH & Co. KGaA, Weinheim

[P(1)−C(3)], 163° [P(1)−C(1)], −128° [P(2)−C(9)] and 141° [P(2)−C(11)]. The δ conformation of the ferrocene backbone therefore tends to minimise the steric hindrance between the isopropyl groups, which are oriented toward the metal, and the other ligands in the equatorial coordination plane of ruthenium. In a sense, this also balances the dissymmetry of the ruthenium environment created by the chiral phosphetane units and could decrease the asymmetric discrimination from these ligands somewhat.

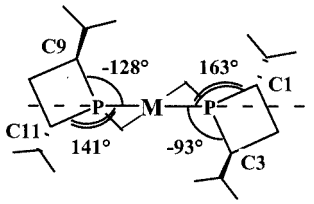

Figure 2. Coordination mode of the bis(phosphetano)ferrocene moiety in the ruthenium complex **2c**

A similar coordination mode is observed in the rhodium complex **3c**, containing the same ligand **1c**. An ORTEP drawing and selected bond angles and distances for complex **3c** are shown in Figure 3 and Table 2, respectively.

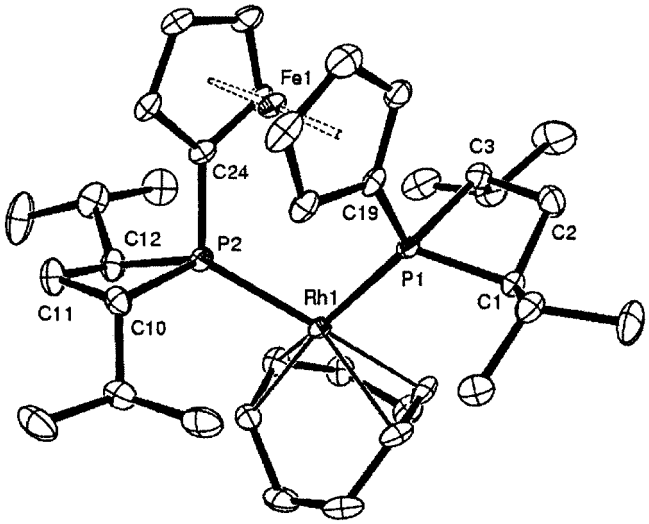

Figure 3. ORTEP drawing of the [(COD)Rh(**1c**)OTf] complex **3c**

Table 2. Selected interatomic distances [A°] and angles [deg] for complex **3c**

Rh(1)−P(1)	2.324(1)	C(1)−C(2)	1.570(5)
Rh(1)−P(2)	2.317(1)	C(2)−C(3)	1.554(6)
P(1)−C(1)	1.877(4)	P(2)−C(10)	1.885(3)
P(1)−C(3)	1.884(4)	P(2)−C(12)	1.869(4)
P(1)−C(19)	1.810(3)	P(2)−C(24)	1.813(3)
P(1)−Rh(1)−P(2)	96.90(3)	C(1)−P(1)−C(3)	78.1(2)
C(19)−P(1)−Rh(1)	121.5(1)	C(10)−P(2)−C(12)	77.9(2)

Phosphetane **1c** thus generally seems to favour δ conformations in its transition metal complexes, as a result of its (*S*,*S*) stereochemistry.

Ruthenium-Promoted Hydrogenations of β-Keto Esters

As shown by Bergens, many [(diphosphane)$RuCl_2Py_2$] complexes afford efficient hydrogenation catalysts after treatment with acids. This is also the case for complexes **2**: when activated by addition of four equivalents of HBr, these complexes catalyse the asymmetric hydrogenation of carbonyl derivatives. Methyl acetoacetate and ethyl isobutyrylacetate were selected as model substrates for the hydrogenation reactions (Table 3).

Under the conditions given (see Table 3), ligands **1a**−**c** display moderate to high enantioselectivities as a function of the phosphetane α-substituents: the enantiomeric excesses of the final β-hydroxy esters increase significantly with increasing steric hindrance of the ligand. Thus, for instance, *ee*s of 44%, 56%, and 80% were obtained in the hydrogenation of methyl acetoacetate with use of ligands **1a**, **1b**, and **1c**, respectively. The observed trend contrasts with the behaviour of the same ligands in rhodium-promoted hydrogenations of olefinic substrates, where the best enantioselectivities are attained with the 2,4-diethyl-substituted ligand.[2] This once again confirms the need for highly specific tuning of the ligand substituents for any given reaction.

Two other ruthenium catalyst precursors were evaluated under the above hydrogenation reactions: catalysts were formed in situ from **1a**−**c** and $[(C_6H_6)RuCl_2]_2$ or [(COD)-Ru(2-methylallyle)$_2$],[9] by known procedures. Selected results are given in Table 3. Both catalytic systems give activities and enantioselectivities either comparable to or somewhat lower than those obtained with complexes **2**. Thus, in our hands, complexes **2** were the most suitable catalyst precursors, being well defined, bench-stable and easy to handle.

The few catalytic tests above show that the 1,1′-bis(phosphetano)ferrocenes **1** afford moderate catalytic activities and quite high, albeit not magnificent, enantioselectivities in ruthenium-promoted hydrogenations of carbonyl derivatives. At first sight it seems that, in these reactions, ligands **1** will be not very competitive with other chiral ligands,[10] and especially with atropisomeric diphosphanes.[11] Of course, this cannot be regarded as a final settlement, as very few substrates, catalytic systems, and conditions have been evaluated. Fine tuning of the phosphetane substituents and/or of the reaction conditions could allow better achievements.

Rhodium-promoted Hydrogenations of Functionalised Olefins

The catalytic efficiency of 1,1′-bis(phosphetano)ferrocenes **1** in rhodium(I)-promoted hydrogenations of functionalised olefins has already been established.[1−3] The main purpose of this study was to gain insight into their behaviour in these reactions, in comparison with that of other phosphetane-based ligands, namely CnrPHOS[12] and BPE-4.[13]

 © 2003 Wiley-VCH Verlag GmbH & Co. KGaA, Weinheim

Table 3. Asymmetric hydrogenation of β-keto esters

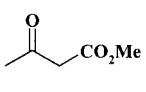

4

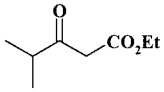

5

Substrate	Ligand	Ru precatalyst	Conditions[a]	Conv. (%)	*ee* (config.)
4	**1a**	(**1a**)$RuCl_2Py_2$ + HBr	(a)	100	44 (*R*)
	1a	$(COD)Ru(C_4H_7)_2$ + HBr	(b)	100	11 (*R*)
	1b	(**1b**)$RuCl_2Py_2$ + HBr	(a)	100	56 (*R*)
	1c	(**1c**)$RuCl_2Py_2$ + HBr	(a)	100	**80 (*R*)**
5	**1a**	(**1a**)$RuCl_2Py_2$ + HBr	(a)	31	53 (*S*)
	1a	$(COD)Ru(C_4H_7)_2$ + HBr	(b)	36	58 (*S*)
	1b	(**1b**)$RuCl_2Py_2$ + HBr	(b)	50	80 (*S*)
	1c	(**1c**)$RuCl_2Py_2$ + HBr	(a)	40	**84 (*S*)**
	1c	$[(C_6H_6)RuCl_2]_2$	(a)	40	64 (*S*)
	1c	$[(C_6H_6)RuCl_2]_2$	(c)	100	63 (*S*)

[a] Reaction conditions: 1 mmol substrate, S/C = 100, MeOH (1 mL) as solvent, reaction time 24 h−48 h; (a) 50 °C; 10 bar H_2, (b) 50 °C; 80 bar H_2, (c) 80 °C, 10 bar.

More precisely, we examine here the enantioselectivity of the catalytic hydrogenation of dehydro amino acid derivatives, as a function of several experimental parameters. An analogous study on the CnrPHOS and BPE ligands highlighted, among other things, an unusually strong effect of the hydrogen pressure on the enantioselectivity, with higher *ee*s being obtained at higher pressures.[14] The preliminary data on this phenomenon were confirmed by the additional experiments shown in Table 4 and Figure 4. Methyl α-acetamidocinnamate **6** was hydrogenated, at various hydrogen pressures, in the presence of a rhodium catalyst generated in situ from $[Rh(COD)_2OTf]$ and (*S*,*S*)-CyBPE-4. Mechanical stirring was applied to ensure efficient adsorption of H_2 into the solution. For comparison, the *ee*s obtained with magnetic stirring are reported in entry 1 (from ref.[14]): mechanical stirring improves the enantioselectivity of reactions performed under otherwise identical conditions. This is probably related to more efficient and homogeneous dihydrogen exchange between gas and liquid phases.

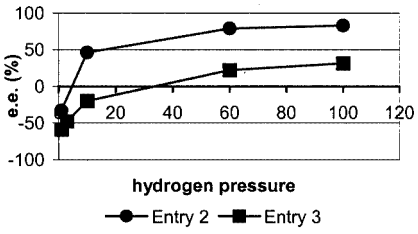

Figure 4. Plotting of data from Entries 2 and 3 in Table 4

Table 4. Enantiomeric excesses of the *N*-acetylphenylalanine methyl ester obtained from **6** by Rh/(*S*,*S*)-CyBPE-4-promoted hydrogenations

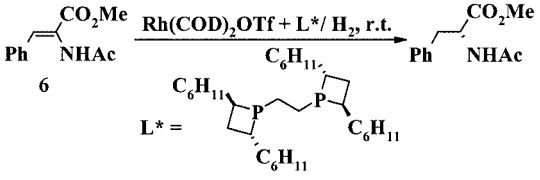

		P(H_2) - bar				
Entry	Solvent	1	3	10	60	100
1[a]	C_6H_6/CH_2Cl_2 : 4/1			15 (*R*)		70 (*R*)
2	C_6H_6/CH_2Cl_2 : 4/1	33 (*S*)	-	46 (*R*)	79 (*R*)	**83** (*R*)
3	CH_2Cl_2	**59** (*S*)	48 (*S*)	20 (*S*)	22 (*R*)	31 (*R*)

[a] From ref.[14] 1% catalyst, substrate concentration: 0.1 M, room temperature.

Two series of experiments were performed, in CH_2Cl_2 and in a C_6H_6/CH_2Cl_2 mixture (4:1). The expected significant effect of hydrogen pressure on stereoselectivity was observed in each case: increased hydrogen pressure clearly favours formation of the *R* enantiomer, while the *S* enantiomer predominates at low pressures. The enantioselectivity levels depend on the solvent used, higher *ee*s being attained in the benzene/dichloromethane mixtures. Mechanistic implications of analogous results have already been discussed in our preliminary communication. Most probably, the reversal of stereoselectivity should be related to some form of "tilting" over to a new reaction pathway which operates at

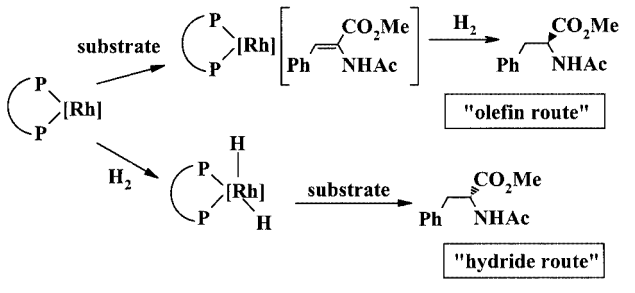

higher pressures. According to the most recent studies on rhodium-promoted enamide hydrogenation with electron-rich phosphanes,[15] competition between the "olefin" and the "hydride" mechanisms, operating at high pressure, seems to be a reasonable hypothesis.

After the above studies, we wondered whether the ferrocenyl-substituted phosphetanes **1** would or would not display analogous behaviour in rhodium-promoted hydrogenations. We therefore examined the pressure effect in the hydrogenation of the dehydroamino esters **6** with the preformed complexes **3** as the catalyst precursors.

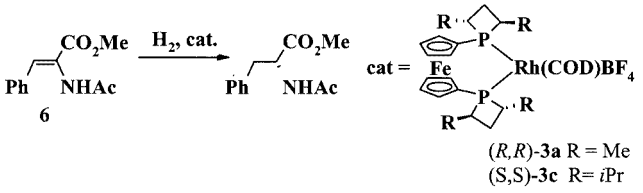

From the data in Table 4 it appears that the pressure/enantioselectivity relationship for phosphetanes **1a** and **1c** does not follow the same trend as for Cy-BPE-4 and CnrPHOS: a slight decrease in the enantioselectivity is observed at higher pressure, both in dichloromethane/benzene mixtures and in methanol as solvents (see entries 1, 2, 5, and 6). This suggests that the pressure effect observed with Cy-BPE-4 and CnrPHOS cannot be assigned specifically to their phosphetane-type structures; their catalytic behaviour should be influenced by their whole structures. In particular, their electronic properties should be crucial, as it has been demonstrated that the stereochemical issue of the hydrogenation of dehydroamino acid derivatives is mainly governed by the electron-donating power of the diphosphane ligands.[14]

FerroTANEs **1** simply behave like other electron-rich diphosphanes such as DuPHOS[16] or BisP,[17] the (*S*,*S*)-configured ligand **1c** giving the expected (*R*)-configured product in good enantiomeric excesses. The enantiomeric excesses are then slightly modulated by hydrogen pressure, as well as by any other experimental conditions, in the usual manner.

Thus far, the best conditions for the hydrogenation of **6** are the following: phosphetane **1a** as the ligand, 1 bar of H_2 pressure, MeOH as the solvent, and a reaction temperature of about 50 °C. An enantiomeric excess of 96% is obtained.

The results in Table 5 also suggest that hydrogenation reactions with ligands **1a** and **1c** require slightly different optimal conditions. Fine tuning of the reaction conditions is thus required for each ligand-substrate couple in order to attain the highest selectivities, even within a single series of ligands.

When a different substrate is considered, optimisation is once again necessary, as variation of the experimental parameters has unpredictable effects on enantiomeric excesses. In the hydrogenation of methyl acetamidoacrylate with complex **3c**, for instance, we have observed that an increased H_2 pressure improves the enantioselectivity from 87%, under 1 bar pressure, to 94% under 5 bar (at room temperature, in MeOH; *R* enantiomer).

Table 5. Enantiomeric excesses of the catalytic hydrogenations promoted by complexes **3a** and **3c**; all experiments give the *R*-configured β-amino ester

				P(H_2)				
Entry	Solvent	Catalyst	T °C	1	5	10	30	50
1	C_6H_6/CH_2Cl_2 : 4/1	**3c**	23	87	86	85	78	75
2	C_6H_6/CH_2Cl_2 : 4/1		50	75	74			
3	MeOH		23		83			
4	C_6H_6/CH_2Cl_2 : 4/1	**3a**	23		83			
5	MeOH		23	94	90		86	
6	MeOH		50	**96**	91			

The electron-rich character of P-ferrocenyl-substituted phosphetanes was ascertained by IR spectroscopy of the [Cl(CO)Rh{(*R*,*R*)-1-ferrocenyl-2,4-dimethylphosphetane}] complex **7a**.

The ν(CO) value for the ferrocenyl-substituted phosphetane complex **7a** appears at lower frequency than in the analogous *P*-phenylphosphetane complex **7c**, within the range expected for electron-rich phosphanes. For comparison, the ν(CO) values for analogous rhodium complexes of cyclic and acyclic phosphanes are reported in Table 6. The data in Table 6 also suggest that phosphetanes are poorer donating ligands than the corresponding phospholanes, as an effect of ring size.

Table 6. ν(CO) values for the [Cl(CO)RhL_2] complexes **7**

Complex		**7a**		**7b**	**7c**
L	PEt_3		$PhPEt_2$		
ν(CO) cm^{-1} (CH_2Cl_2)	1955[18]	1956	1962[18]	1963	1969

In summary, the hydrogenation reactions of dehydro amino acid derivatives promoted by rhodium complexes of the 1,1′-bis(phosphetano)ferrocenes **1** do not display the unusual pressure/enantioselectivity relationship shown by other C_2-symmetric bis(phosphetane) ligands. Ligands **1** behave like electron-rich diphosphanes and afford significantly high enantioselectivities under optimised experimental conditions.

Experimental Section

All reactions were performed under inert atmosphere (Ar) by use of Schlenk techniques. Solvents were purified according to standard

 © 2003 Wiley-VCH Verlag GmbH & Co. KGaA, Weinheim

procedures. ^{1}H, ^{13}C, and ^{31}P NMR spectra were recorded on a Bruker AM 400 at 400.13 Hz, 100.6 Hz, and 162 Hz, respectively. HPLC was performed on a Waters 600 chromatograph equipped with a variable wavelength detector and Daicel Chiracel OD-H column. Optical rotations were measured on a Perkin−Elmer 241 polarimeter, with a 1 dm cell. IR spectra were recorded on a Bruker IFS 48 instrument.

General Procedure for the Synthesis of *trans*-[RuCl$_2${1,1′-Bis(dialkylphosphetanyl)ferrocene}Py$_2$] (2): A solution of *trans*-[RuCl$_2$(NBD)Py$_2$][5] (100 mg, 0.23 mmol) and ligand **1** (0.23 mmol) in CH_2Cl_2 (13 mL) was stirred overnight at room temperature. The solvent was removed under vacuum and the residue was recrystallized from a dichloromethane/pentane mixture to afford complexes **2** as yellow, crystalline solids.

***trans*-[RuCl$_2${1,1′-Bis[(*R*,*R*)-2,4-dimethyl-1-phosphetanyl]ferrocene}Py$_2$] (2a):** Yield 120 mg, 73%. ^{31}P NMR ($CDCl_3$): δ = 87. ^{1}H NMR ($CDCl_3$): δ = 9.6 (br., 4 H), 7.60 (m, 2 H), 7.3 (br., 4 H), 5.14 (br. s, 2 H, CH_{cp}), 4.50 (m, $J \approx 1$ Hz, 4 H, CH_{cp}), 4.34 (m, $J \approx 1$ Hz, 2 H, CH_{cp}), 2.66 (m, 2 H), 2.40 (m, 4 H), 1.79 (m, 2 H), 1.28 (dd, $^3J_{H,H}$ = 7.7, $^3J_{P\text{-}H}$ = 16.4 Hz, 6 H, CH_3), 0.92 (dd, $^3J_{H,H}$ = 6.3, $^3J_{P\text{-}H}$ = 14.4 Hz, 6 H, CH_3) ppm. ^{13}C NMR ($CDCl_3$, 100 MHz): δ = 152.6 (br., CH_{Py}), 152.1 (br., CH_{Py}), 136.0 (CH_{Py}), 123.6 (br., CH_{Py}), 123.4 (br., CH_{Py}), 77.6 (t, J = 7.8 Hz, CH_{Cp}), 74.0 (t, J = 3.4 Hz, CH_{Cp}),73.0 (m, AXX′, C_{Cp}P), 72.0 (CH_{Cp}), 71.0 (t, J = 1.8 Hz, CH_{Cp}), 40.1 (t, J = 7.6 Hz, CH_2), 32.0 (m, AXX′, PCH), 30.2 (m, AXX′, PCH), 18.8 (CH_3), 17.5 (t, J = 2.3 Hz, CH_3) ppm. $[\alpha]_D = -782$ (c = 0.2, $CHCl_3$). $C_{30}H_{38}Cl_2FeN_2P_2Ru$ (716.028): calcd. C 50.30, H 5.35, N 3.91; found C 50.66, H 5.96, N 3.82.

***trans*-[RuCl$_2${1,1′-Bis[(*R*,*R*)-2,4-diethyl-1-phosphetanyl]ferrocene}Py$_2$] (2b):** Yield 124 mg, 70%. ^{31}P NMR ($CDCl_3$): δ = 82 ppm. ^{1}H NMR ($CDCl_3$): δ = 9.6 (br., 4 H), 7.60 (t, $J_{H,H}$ = 7.4 Hz, 2 H,CH), 7.3−7.0 (br., 4 H, CH), 5.10 (s, 2 H, CH_{cp}), 4.50 (s br, 4 H, CH_{cp}), 4.32 (m, 2 H, CH_{cp}), 2.77 (br., 2 H), 2.40 (br., 2 H), 2.22 (m, 2 H), 2.04−1.95 (m, 4 H), 1.70 (m, 2 H), 0.87 (m, 4 H), 0.79 (t, $^3J_{H,H}$ = 6.9 Hz, 6 H, CH_3), 0.57 (t, $^3J_{H,H}$ = 7.4 Hz, 6 H, CH_3) ppm. ^{13}C NMR ($CDCl_3$, 100 MHz): δ = 152.4 (br., CH_{Py}), 136.0 (CH_{Py}), 123.4 (br., CH_{Py}), 77.5 (t, J = 7.8 Hz, CH_{Cp}), 74.0 (t, J = 3.4 Hz, CH_{Cp}), 73.5 (m, AXX′, C_{Cp}P), 72.0 (CH_{Cp}), 70.8 (CH_{Cp}), 39.2 (m, AXX′, PCH), 37.6 (m, AXX′, PCH), 34.0 (t, J = 7.3 Hz, CH_2), 25.7 (CH_2CH_3), 23.8 (CH_2CH_3), 13.0 (t, J = 7.5 Hz, CH_3), 12.0 (t, $J_{P,C}$ = 5.9 Hz, CH_3) ppm. $[\alpha]_D = -907$ (c = 0.5, $CHCl_3$). $C_{34}H_{46}Cl_2FeN_2P_2Ru$ (772.091): calcd. C 52.86, H 6.00, N 3.63; found C 52.41, H 6.32, N 3.76.

***trans*-[RuCl$_2${1,1′-Bis[(*S*,*S*)-2,4-diisopropyl-1-phosphetanyl]ferrocene}Py$_2$] (2c):** Yield 105 mg (55%). ^{31}P NMR ($CDCl_3$): δ = 71. ^{1}H NMR ($CDCl_3$): δ = 9.68 (br., 2 H, CH_{Py}), 9.61 (br., 2 H, CH_{Py}), 7.57 (t, $J_{H,H}$ = 7.2 Hz, 2 H, CH_{Py}), 7.19 (br., 2 H, CH_{Py}), 7.09 (br., 2 H, CH_{Py}), 5.29 (s, 2 H, CH_{Cp}), 4.51 (s, 2 H, CH_{Cp}), 4.45 (s, 2 H, CH_{Cp}), 4.28 (m, J≈2 Hz, 2 H, CH_{Cp}), 3.10 (m, 2 H), 2.77 (m, 2 H), 2.0 (m, 4 H), 1.75 (m, 2 H), 1.44 (m, 2 H), 1.05 (d, $^3J_{H,H}$ = 6.5 Hz, 6 H, CH_3), 0.79 (d, $^3J_{H,H}$ = 6.6 Hz, 6 H, CH_3), 0.59 (d, $^3J_{H,H}$ = 6.7 Hz, 6 H, CH_3), 0.56 (d, $^3J_{H,H}$ = 6.6 Hz, 6 H, CH_3). ^{13}C NMR ($CDCl_3$, 100 MHz): δ = 153.7 (CH_{Py}), 153.0 (CH_{Py}), 135.9 (CH_{Py}), 123.8 (CH_{Py}), 123.1 (CH_{Py}), 77.9 (CH_{Cp}), 73.7 (CH_{Cp}), 73.2 (C_{Cp}P), 72.4 (CH_{Cp}), 70.3 (CH_{Cp}), 46.4 (m, PCH), 44.0 (m, PCH), 29.2 (CH), 27.8 (CH_2), 24.5 (CH_3), 23.5 (CH_3), 19.8 (CH_3), 19.2 (CH_3) ppm. For crystal data see Table 7.

Table 7. Crystal structure determination for compound **2c**

Empirical formula	$C_{39}H_{56}Cl_4FeN_2P_2Ru$
Formula mass	913.52
Crystal habit	tan needles
Crystal dimensions [mm]	0.20 × 0.14 × 0.14
Crystal system	orthorhombic
Space group	*P*212121
a [Å]	9.651(5)
b [Å]	19.366(5)
c [Å]	22.000(5)
α [°]	90.000(5)
β [°]	90.000(5)
γ [°]	90.000(5)
V [Å^3]	4112(3)
Z	4
d [g·cm^{-3}]	1.476
*F*000	1888
μ [cm^{-1}]	1.088
Absorption corrections	0.8118 min
0.8626	max
Diffractometer	KappaCCD
X-ray source	Mo-*K*α
λ [Å]	0.71069
Monochromator	graphite
T [K]	150.0(10)
Scan mode	phi
Maximum *q*	30.02
hkl ranges	−13 13; −27 27; −30 30
Reflections measured	11960
Independent reflections	11960
R_{int}	0.0000
Reflections used	11161
Criterion	> 2σ(*I*)
Refinement type	Fsqd
Hydrogen atoms	mixed
Parameters refined	450
Reflections / parameter	24
wR	20.0965
*R*1	0.0353
Flack's parameter	0.006(17)
Weighs *a*, *b*1	0.0380; 5.3251
GoF	1.072
difference peak / hole [e Å^{-3}]	0.767(0.090) / −0.944(0.090)

General Procedure for Hydrogenations Carried out with Complexes 2 as Catalyst Precursors: Hydrogenation experiments were carried out at a 1 mmol scale. The ruthenium complex **2** ($1\cdot10^{-2}$ mmol) was weighed into a small glass reactor fitted with a rubber septum and flushed with argon. Degassed MeOH (1 mL) and then a solution of HBr_{aq} in MeOH (0.16 M, 0.25 mL, 4 equivalents) were added with stirring at room temperature. After a few minutes, the substrate was introduced by syringe. The reaction vessel was placed in a stainless steel autoclave under argon. The argon atmosphere was replaced by hydrogen at the given pressure. The reaction was allowed to proceed for 24−48 h at the temperature given in Table 3. Conversion rates were determined by ^{1}H NMR spectroscopy. The enantiomeric excesses of the final alcohols were determined by chiral CG and the absolute configurations were assigned from the GC retention times by comparison with known samples. **Methyl 3-hydroxybutyrate**: Lipodex A, flow 1 mL·min^{-1}, initial temperature 35 °C (30 min), rate 1 °C·min^{-1}, final temperature 70 °C; retention times 45 (*S*) and 48 (*R*) min. **Ethyl 4-methyl-3-hydroxypentanoate**: Lipodex A, flow 1 mL·min^{-1}, initial temperature 50 °C (5 min),

 © 2003 Wiley-VCH Verlag GmbH & Co. KGaA, Weinheim

rate 0.5 °C·min^{-1}, final temperature 70 °C; retention times 48.6 (*S*) and 49.2 (*R*) min.

Preparation of other Catalyst Precursors: (a) According to ref.[9] [(cod)Ru(2-methylallyl)$_2$] (3.2 mg, 1·10^{-2} mmol) and FerroTANE **1** (1.1·10^{-2} mmol) were dissolved in acetone (1 mL) under argon. An HBr_{aq} solution (0.16 M in MeOH, 137 μL, 2.2 equivalents) was then added at room temperature, and the mixture was stirred for 30 min. The solvent was evaporated and the crude residue was taken up in degassed MeOH and used as the catalyst for the hydrogenation reactions (see Table 3). (b) The catalyst precursor was prepared at room temperature by mixing the [(benzene)$RuCl_2$]$_2$ complex (2.5 mg) with **1** in a 1:2 ratio, in CH_2Cl_2 at room temperature. After evaporation of the solvent, the crude residue was used as the catalyst precursor.

General Procedure for the Synthesis of the [(COD)Rh(1)OTf] Complexes 3: A dichloromethane solution of diphosphane **1** (0.2 mmol, 1 mL CH_2Cl_2) was added dropwise, at room temperature, to a solution of $(COD)_2RhOTf$ (93 mg, 0.2 mmol) in the same solvent (1 mL). After the mixture had been stirred for about 15 min, the solvent was removed and the residue was recrystallised either from a dichloromethane/ether mixture (for **3c**) or from a dichloromethane/pentane mixture (for **3a**) to afford a yellow-orange solid.

[(COD)Rh{1,1′-Bis[(*R*,*R*)-2,4-dimethyl-1-phosphetanyl]ferrocene}OTf] (3a): Yield 97 mg, 65%. ^{31}P NMR ($CDCl_3$): δ = 65 (d, $J_{P\text{-}Rh}$ = 147 Hz) ppm. ^{1}H NMR ($CDCl_3$): δ = 5.8 (br. m, 2 H, CH_{COD}), 5.15 (br. m, 2 H, CH_{COD}), 4.70 (s, 2 H, CH_{Cp}), 4.66 (s, 2 H, CH_{Cp}), 4.62 (s, 2 H, CH_{Cp}), 4.37 (s, 2 H, CH_{Cp}), 1.65 (dd, $^3J_{H\text{-}P}$ = 19.7, $^3J_{H,H}$ = 7.6 Hz, 6 H, CH_3), 0.99 (dd, $^3J_{H\text{-}P}$ = 16.3, $^3J_{H,H}$ = 7.0 Hz, 6 H, CH_3) ppm.

[(COD)Rh{1,1′-Bis[(*S*,*S*)-2,4-diisopropyl-1-phosphetanyl]ferroceneOTf} (3c): Yield 120 mg, 70%. ^{31}P NMR ($CDCl_3$): δ = 47 (d, $J_{P\text{-}Rh}$ = 146 Hz). ^{1}H NMR ($CDCl_3$): δ = 5.56 (br. m, 2 H, CH_{COD}), 4.90 (br. m, 2 H, CH_{COD}), 4.80 (s, 2 H, CH_{Cp}), 4.60 (s, 4 H, CH_{Cp}), 4.37 (s, 2 H, CH_{Cp}), 2.2−2.8 (18H), 2.05 (q, *J* = 10.1 Hz, 2 H), 1.84 (d, $^3J_{H,H}$ = 6.5 Hz, 6 H, CH_3), 1.15 (d, $^3J_{H,H}$ = 6.1 Hz, 6 H, CH_3), 0.70 (d, $^3J_{H,H}$ = 6.3 Hz, 6 H, CH_3), 0.69 (d, $^3J_{H,H}$ = 5.5 Hz, 6 H, CH_3) ppm. $C_{37}H_{56}F_3FeO_3P_2RhS{\cdot}CH_2Cl_2$ (942.132): calcd. C 48.37, H 6.20; found C 49.80, H 6.56. For crystal data see Table 8.

The triflate anion (near −0.37, 0.10, 0.31) was highly disordered. Attempts to generate disorder (Shelxl FRAG and PART) all resulted in some non-positive thermal displacement parameters. Consequently, it was decided to account for its electron density by use of the Platon SQUEEZE function.

Rhodium-Promoted Hydrogenations of Methyl α-Acetamidocinnamate: The hydrogenation experiments described in Table 4 were performed in a Teflon-coated autoclave, with mechanical stirring. The rhodium catalyst was prepared at room temperature by mixing [$(COD)_2RhOTf$] (11.2 mg, 2.4·10^{-2} mmol) and (*S*,*S*)-Cy-BPE-4 (14.4 mg, 2.8·10^{-2} mmol) in CH_2Cl_2 (2 mL) for about 10 min. A degassed solution of the substrate (525 mg, 2.4 mmol) in 18 mL of solvent (CH_2Cl_2 or CH_2Cl_2/C_6H_6, 1:4 mixture) was then added and the system was pressurised with dihydrogen. The reaction time was about 24 h. The catalyst was removed by filtration through a short alumina column, with a cyclohexane/ethyl acetate mixture (1:1) as the eluent. Enantiomeric excesses were determined either by chiral HPLC or by chiral GC. The absolute configuration was assigned from the retention times by comparison with known samples. HPLC: Chiracel OD-H column, hexane/2-propanol (90:10), retention times: 11.5 min (*R*) and 14.8 min (*S*). GC: Chirasil-L-Val column, flow = 1 mL/min, *T* = 140 °C, retention times: 37 min (*R*), 39 min (*S*).

Table 8. Crystal structure determination for compound **3c**

Molecular formula	$C_{37}H_{56}F_3FeO_3P_2RhS$
Molecular weight	858.58
Crystal habit	orange plate
Crystal dimensions [mm]	0.22 × 0.08 × 0.06
Crystal system	orthorhombic
Space group	*P*212121
a [Å]	11.9840(10)
b [Å]	17.1000(10)
c [Å]	18.8990(10)
α [°]	90.00
β [°]	90.00
γ [°]	90.00
V [Å^3]	3872.9(4)
Z	4
d [g-cm^{-3}]	1.472
*F*000	1784
μ [cm^{-1}]	0.986
Absorption corrections	multiple scans; 0.8123 min, 0.9432 max
Diffractometer	KappaCCD
X-ray source	Mo-K_α
λ [Å]	0.71069
Monochromator	graphite
T [K]	150.0(10)
Scan mode	phi and omega scans
Maximum θ	30.03
hkl ranges	−16 16; −23 23; −26 26
Reflections measured	11222
Unique data	11222
Rint	0.0000
Reflections used	10128
Criterion	> 2σ(*I*)
Refinement type	Fsqd
Hydrogen atoms	mixed
Parameters refined	382
Reflections/parameter	26
wR	20.1184
*R*1	0.0416
Flack's parameter	0.050(18)
Weights *a*, *b*	0.0702; 1.9976
GoF	1.040
difference peak/hole [e·Å^{-3}]	0.825(0.104)/−0.546(0.104)

The same experimental procedure was applied to the hydrogenation reactions reported in Table 5. The preformed rhodium complexes **3a** and **3c** were used as the catalysts. Experiments were carried out at a 1 mmol scale, with a catalyst:substrate ratio of 5·10^{-3}.

Synthesis of the [Cl(CO)RhL_2] Complexes 7: 2,4-Dimethyl-1-ferrocenylphosphetane,[18] 2,4-dimethyl-1-phenylphosphetane,[19] and 2,5-dimethyl-1-phenylphospholane[20] were prepared as described previously. The rhodium complex [$ClRh(CO)_2]_2$ (20 mg, 5·10^{-2} mmol) and the phosphetane (or phospholane) ligand (20·10^{-2} mmol) were allowed to react in CH_2Cl_2 (2 mL) at room temperature for 15 min. ^{31}P NMR analysis of the crude reaction mixture in C_6D_6 showed quantitative formation of a single rhodium-phosphane complex. Complexes **7a**−**c** were characterised by NMR spectroscopy, without further purification. IR spectra of the crude complexes were recorded in CH_2Cl_2.

[ClRh(CO)(2,4-Dimethyl-1-ferrocenylphosphetane)] (7a): ^{31}P NMR (C_6D_6): δ = 63.6 (d, $J_{P\text{-}Rh}$ = 117 Hz). ^{1}H NMR (C_6D_6): δ = 5.32 (m, 1 H, CH_{Cp}), 4.38 (s, 5 H, $CH_{Cp'}$), 4.26 (m, 2 H, CH_{Cp}), 4.19 (m, 1 H, CH_{Cp}), 3.32 (m, 1 H), 2.52 (m, 1 H), 2.3−2.0 (m, 2 H), 1.69 (dt, *J* = 10.0, *J* = 7.7 Hz, CH_3), 1.15 (q, *J* = 7.8 Hz, CH_3).

 © 2003 Wiley-VCH Verlag GmbH & Co. KGaA, Weinheim

^{13}C NMR (C_6D_6): δ = 188.7 (dt, J_{CRh} = 75, $J_{C,P}$ = 17 Hz, CO), 78.6 (t, J = 8.9 Hz, CH_{Cp}), 71.8 (CH_{Cp}), 71.6 (t, J = 14.1 Hz, C_{Cp}), 71.0 (C_{Cp}), 70.8 (CH_{Cp}), 69.6 ($CH_{Cp'}$), 39.5 (t, J = 5.3 Hz, CH_2), 31.3 (t, J = 18.4 Hz, PCH), 30.0 (t, J = 18.9 Hz, PCH), 20.1 (CH_3), 17.5 (CH_3) ppm.

[ClRh(CO)(2,5-Dimethyl-1-phenylphospholane)] (7b): ^{31}P NMR (C_6D_6): δ = 49.5 (d, $J_{P\text{-}Rh}$ = 123 Hz). ^1H NMR (C_6D_6): δ = 7.7 (m, 2 H), 7.2 (m, 3 H), 1.28 (dd, $^3J_{H\text{-}P}$ = 14.6, $^3J_{H,H}$ = 7.0 Hz, 3 H, CH_3), 0.75 (dd, $^3J_{H\text{-}P}$ = 16.0, $^3J_{H,H}$ = 7.2 Hz, 3 H, CH_3) ppm.

[ClRh(CO)(2,4-Dimethyl-1-phenylphosphetane)] (7c): ^{31}P NMR (C_6D_6): δ = 66.1 (d, $J_{P\text{-}Rh}$ = 116 Hz). ^1H NMR (C_6D_6): δ = 7.7 (m, 2 H), 7.1−7.2 (m, 3 H), 3.6 (m, J = 7.5 Hz, 1 H), 2.7 (m, 1 H), 2.2 (m, 1 H), 2.0 (m, 1 H), 1.61 (dt, J = 10.1, J = 7.5 Hz, CH_3), 0.88 (q, J = 7.4 Hz, CH_3) ppm.

CCDC-211829 (**2c**) and -211830 (**3c**) contain the supplementary crystallographic data for this paper. These data can be obtained free of charge at www.ccdc.cam.ac.uk/conts/retrieving.html [or from the Cambridge Crystallographic Data Centre, 12, Union Road, Cambridge CB2 1EZ, UK; Fax: (internat.) +44-1223/336-033; E-mail: deposit@ccdc.cam.ac.uk].

[1] A. Marinetti, F. Labrue, J.-P. Genêt, *Synlett* **1999**, 1975−1977.
[2] U. Berens, M. J. Burk, A. Gerlach, W. Hems, *Angew. Chem. Int. Ed.* **2000**, *39*, 1981−1984.
[3] D. Heller, H. J. Drexler, J. You, W. Baumann, K. Drauz, H.-P. Krimmer, A. Börner, *Chem. Eur. J.* **2002**, *8*, 5196−5203.
[4] M. J. Burk, M. F. Gross, *Tetrahedron Lett.* **1994**, *35*, 9363−9366.
[5] O. M. Akotsi, K. Metera, R. D. Reid, R. McDonald, S. H. Bergens, *Chirality* **2000**, *12*, 514−521.
[6] An average value of 95.60° for the bite angle of dppf complexes has been calculated: P. Dierkes, P. W. N. M. van Leeuwen, *J. Chem. Soc., Dalton Trans.* **1999**, 1519−1529.
[7] F. Maienza, M. Wörle, P. Steffanut, A. Mezzetti, *Organometallics* **1999**, *18*, 1041−1049. U. Nettekoven, M. Widhalm, P. C. J. Kamer, P. W. N. M. van Leeuwen, K. Mereiter, M. Lutz, A. L. Spek, *Organometallics* **2000**, *19*, 2299−2309. A. R. Elasgir, F. Gassner, H. Görls, E. Dinjus, *J. Organomet. Chem.* **2000**, *597*, 139−145.
[8] *Inorg. Chem.* **1970**, *9*, 1−5.
[9] J.-P. Genêt, C. Pinel, V. Ratovelomanana-Vidal, S. Mallart, X. Pfister, L. Bischoff, M. C. Cano De Andrade, S. Darses, C. Galopin, A. Laffitte, J. A, *Tetrahedron: Asymmetry* **1994**, *5*, 675−690.
[10] M. J. Burk, T. G. P. Harper, C. S. Kalberg, *J. Am. Chem. Soc.* **1995**, *117*, 4423−4424.
[11] For recent reviews see: H. Kumobayashi, T. Miura, N. Sayo, T. Saito, X. Zhang, *Synlett* **2001**, 1055−1064. M. McCarthy, P. J. Guiry, *Tetrahedron* **2001**, *57*, 3809−3844.
[12] A. Marinetti, J.-P. Genêt, S. Jus, D. Blanc, V. Ratovelomanana-Vidal, *Chem. Eur. J.* **1999**, *5*, 1160−1165.
[13] A. Marinetti, S. Jus, J.-P. Genêt, L. Ricard, *J. Organomet. Chem.* **2001**, *624*, 162−166.
[14] A. Marinetti, S. Jus, J.-P. Genêt, *Tetrahedron Lett.* **1999**, *40*, 8365−8368.
[15] I. D. Gridnev, N. Higashi, K. Asakura, T. Imamoto, *J. Am. Chem. Soc.* **2000**, *122*, 7183−7194. I. D. Gridnev, M. Yasutake, N. Higashi, T. Imamoto, *J. Am. Chem. Soc.* **2001**, *123*, 5268−5276. S. Feldgus, C. R. Landis, *Organometallics* **2001**, *20*, 2374−2386.
[16] M. J. Burk, J. E. Feaster, W. A. Nugent, R. L. Harlow, *J. Am. Chem. Soc.* **1993**, *115*, 10125−10138.
[17] T. Imamoto, J. Watanabe, Y. Wada, H. Masuda, H. Yamada, H. Tsuruta, S. Matsukawa, K. Yamaguchi, *J. Am. Chem. Soc.* **1998**, *120*, 1635−1636.
[18] A. Marinetti, S. Jus, F. Labrue, A. Lemarchand, J.-P. Genêt, L. Ricard, *Synthesis* **2001**, 2095−2104.
[19] A. Marinetti, V. Kruger, F.-X. Buzin, *Tetrahedron Lett.* **1997**, *38*, 2947−2950.
[20] M. J. Burk, J. E. Feaster, R. L. Harlow, *Tetrahedron: Asymmetry* **1991**, *2*, 569−592.

Received January 24, 2003

 © 2003 Wiley-VCH Verlag GmbH & Co. KGaA, Weinheim

Synthesis and Structures of Compounds Based on Chalcocyanide Tetranuclear Rhenium Clusters: Bonding Cluster Complexes by diene-Bridged Cu^{II} Units

Yuri V. Mironov,[a,b] Olga A. Efremova,[b] Dmitry Yu. Naumov,[b] William S. Sheldrick,[a] and Vladimir E. Fedorov*[b]

Keywords: Rhenium / Clusters / Chalcogen / Copper / Solid-state structures

Six new tetrahedral chalcocyanide cluster compounds, $[\{Cu_2(dien)_3\}Re_4S_4(CN)_{12}]$ (**1**), $[\{Cu(dien)(NH_3)\}_2Re_4Se_4(CN)_{12}]\cdot 2.5H_2O$ (**2**), $[\{Cu_2(dien)_3\}Re_4Q_4(CN)_{12}]\cdot nH_2O$ (Q = Se (**3**), Te (**4**)] and $[K(H_2O)_2]_2[\{Cu_3(dien)_4\}\{Re_4Q_4(CN)_{12}\}_2]\cdot 8H_2O$ where Q = Se (**5**), Te (**6**) (dien = diethylenetriamine), have been synthesized by treating aqueous solutions of the salt-like cluster compounds $K_4Re_4Q_4(CN)_{12}\cdot nH_2O$ with solutions of copper(II) chloride in aqueous ammonia containing diethylenetriamine. All six compounds have been characterized by single-crystal X-ray diffraction analysis. Compound **1** has a chain-like polymeric structure; orthorhombic, space group $Pmn2_1$. Compound **2** has a molecular structure; triclinic, space group $P\bar{1}$. Compounds **3** and **4** are isostructural and also exhibit molecular structures; monoclinic, space group $P2_1/n$. Compounds **5** and **6** are isostructural and display a cross-bridged chain-like polymeric structure; triclinic, space group $P\bar{1}$.

(© Wiley-VCH Verlag GmbH & Co. KGaA, 69451 Weinheim, Germany, 2003)

Introduction

Considerable recent research has been devoted to designing new polymeric compounds with extended structures based on rhenium cluster compounds.[1−4] Such compounds may have interesting catalytic, magnetic or zeolitic properties. The directional choice of cluster/ligand and cluster/cation combinations helps to control both the topology and the dimensionality of solids. A useful approach for this purpose consists of assembling two building blocks, which are often cluster complexes with terminal ligands that can act as bridges and transition metal complexes with vacant or readily substituted coordination sites. Typical examples are Re cluster chalcocyanide complexes with terminal CN ligands and aqua or amine transition metal complexes.[5−13] The next logical step in such investigations is to use polydentate ligands to block some of the available positions around the transition metal atom, so as to control the positions available for coordination with the CN ligands. The first examples of such complexes were published recently.[14] Here we present six complexes containing $[Re_4Q_4(CN)_{12}]^{4-}$ cluster anions and Cu^{II} cations, coordinated by dien ligands and bridging CN ligands of the cluster units. Our data demonstrate the significant dependence of the stoichiometry and structure of the product on the reaction conditions and internal ligands of the cluster unit. We have prepared one chain-like coordination polymer $[\{Cu_2(dien)_3\}_2Re_4S_4(CN)_{12}]$ (**1**) (dien = diethylenetriamine), three molecular complexes $[\{Cu(dien)(NH_3)\}_2Re_4Se_4(CN)_{12}]$ (**2**) and $[\{Cu_2(dien)_3\}Re_4Q_4(CN)_{12}]\cdot 8H_2O$ [Q = Se (**3**), Q = Te (**4**)], and two polymeric complexes $[K(H_2O)_2]_2[\{Cu_3(dien)_4\}\{Re_4Q_4(CN)_{12}\}_2]\cdot 8H_2O$ [Q = Se (**5**), Q = Te (**6**)]. One of the most interesting features of the polymeric complexes is their construction by dien-bridging of Cu^{II} atoms.

Results

Syntheses

The chain-like one-dimensional compound **1** was synthesized by treating an aqueous solution of the Re_4 thiocyanide cluster $K_4[Re_4S_4(CN)_{12}]$ with an ammonia solution of $CuCl_2$ and dien. Two molecular complexes, **2** and **3**, and the polymeric compound **5** were obtained in a similar manner using $K_4[Re_4Se_4(CN)_{12}]$ as a starting material. Analogously, the molecular complex **4** and the polymeric compound **6** were prepared using $K_4[Re_4Te_4(CN)_{12}]$ as a starting material. Thus, by performing the reactions with different ratios of the starting components, complexes with differing compositions and structures were obtained for cluster anions $[Re_4Q_4(CN)_{12}]^{4-}$ with the Q = Se and Te.

These investigations extend our earlier studies on the reactions of $K_4Re_4Te_4(CN)_{12}$ with aqua or ammine complexes of the transition metals, which yield cyano-bridged cluster complexes with differing dimensionalities. Transition

[a] Lehrstuhl für Analytische Chemie, Ruhr-Universität Bochum, 44780 Bochum, Germany
[b] Institute of Inorganic Chemistry of Russian Academy of Sciences, 3, Acad. Lavrentiev prospect, 630090 Novosibirsk, Russia

metal atoms in such complexes are coordinated by the N atoms of the cyanide ligands and by the N or O atoms, respectively, of ammonia and water molecules. Recent work[14] has shown that some of the coordination sites around the transition metal atom may effectively be blocked by bidentate ligands such as ethylenediamine.

Structures

All six compounds have been characterized by single-crystal X-ray diffraction. Compound **1** is polymeric, with the cluster anions $[Re_4S_4(CN)_{12}]^{4-}$ bridged by the cationic chains $[(dien)Cu-dien-Cu(dien)]^{4+}$ (Figure 1). The structure of the $[Re_4S_4(CN)_{12}]^{4-}$ anion is similar to that in the starting material and related compounds. It contains an Re_4S_4 cubane-like cluster core formed from a nearly regular Re_4 tetrahedron, with Re−Re and Re−(μ_3-S) distances in the ranges 2.739(2)−2.767(1) and 2.337(7)−2.434(7) Å, respectively. Each Re atom is further ligated by three cyano ligands. Each Cu atom in the cationic chain-like building blocks is coordinated in a square-pyramidal manner (*CN* = 5) by three N atoms of the tridentate dien, with Cu−N distances of 1.94(2)−2.03(2) Å, one N atom of the bridging dien, with a Cu−N length of 1.97(2) Å, and by one N atom of a CN^- ligand of the cluster anion with a Cu−N length of 2.20(2) Å.

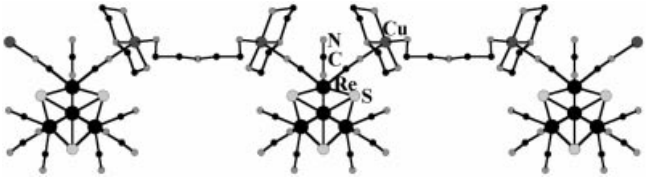

Figure 1. Chain fragment of the structure of compound **1**

In compound **2**, two $[Cu(dien)(NH_3)]^{2+}$ cations are coordinated to the N atoms of CN^- ligands of the $[Re_4Se_4(CN)_{12}]^{4-}$ anion (Figure 2). Each Cu atom is coordinated by the three N atoms of the dien ligand, with Cu−N distances of 2.01(1)−2.05(1) Å, one atom of an NH_3 ligand, with Cu−N distances of 1.99(1) and 2.03(1) Å, and by one N atom of a bridging CN^- ligand of the cluster anion with Cu−N distances of 2.38(1) and 2.19(1) Å. Once again the coordination number of each Cu is 5, and the copper atoms exhibit square-pyramidal coordination spheres with an axial cyanide nitrogen atom. Both $\{Cu(dien)(NH_3)\}^{2+}$ cations are coordinated to the same Re_4 cluster anion $[Re_4Se_4(CN)_{12}]^{4-}$. In the cluster anion the Re−Re and Re−(μ_3-S) distances are 2.792(1)−2.811(1) and 2.448(2)−2.470(2) Å, respectively, and are similar to that in the starting compound.

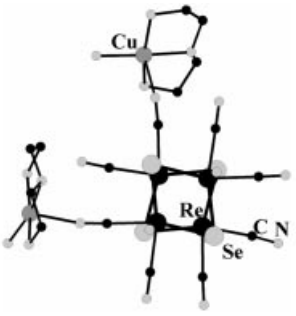

Figure 2. View of the $[\{Cu(dien)(NH_3)\}_2Re_4Se_4(CN)_{12}]$ molecule in compound **2**

Compounds $[\{Cu_2(dien)_3\}Re_4Q_4(CN)_{12}]\cdot nH_2O$ [Q = Se (**3**) and Te (**4**)] are isostructural. Their compositions are similar to that of **1**, but their structures are slightly different. Whereas compound **1** has a chain-like polymeric structure (Figure 1), **3** and **4** are molecular (Figure 3) and contain cluster anions $[Re_4Q_4(CN)_{12}]^{4-}$ (Q = Se, Te) and non-bridging cationic $[Cu_2(dien)_3]^{4+}$ units. In **1** both Cu atoms are crystallographically equivalent and coordinated to N atoms of CN^- ligands of different clusters. In **3** and **4** the Cu atoms exhibit different coordination environments. One Cu atom has a similar arrangement to the Cu atom in compound **1**; the second Cu atom is coordinated by three N atoms of one dien ligand and by two N atoms of another dien ligand, which bridges the two Cu atoms of the cationic unit through its third N atom. Thus, both Cu atoms in $[Cu_2(dien)_3]^{4+}$ cation are five-coordinate and, once again, have square-pyramidal coordination spheres.

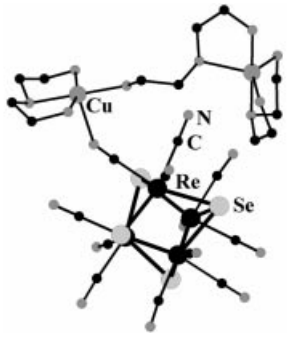

Figure 3. View of the $[\{Cu_2(dien)_3\}Re_4Se_4(CN)_{12}]$ molecule in compound **3**

$[K(H_2O)_2]_2[\{Cu_3(dien)_4\}\{Re_4Q_4(CN)_{12}\}_2]\cdot 8H_2O$ [Q = Se (**5**) and Te (**6**)] are also isostructural. The structures of the anionic components $[Re_4Q_4(CN)_{12}]^{4-}$ are similar to those in the starting materials and related compounds. The Re−Re distances are 2.8624(9)−2.8821(11) Å (**5**) and 2.798(1)−2.809(1) Å (**6**), and the Re−(μ_3-Q) distances are 2.624(1)−2.649(1) Å (**5**) and 2.457(2)−2.484(2) Å (**6**). The secondary building unit of this structure is provided by the molecular complex $[\{Cu_3(dien)_4\}\{Re_4Te_4(CN)_{12}\}_2]$ (Figure 4), in which two cluster anions $[Re_4Te_4(CN)_{12}]^{4-}$ are bridged by the cation $[Cu_3(dien)_4]^{6+}$, which can be described as [(dien)Cu−(dien)Cu(dien)−Cu(dien)]. There are two symmetry-equivalent Cu atoms, each coordinated by three N atoms of one dien ligand, one N atom of the bridging dien ligand, and by one N atom of a CN^- ligand of the $[Re_4Q_4(CN)_{12}]^{4-}$ anion [Cu−N distances are 2.009(9)−2.03(1), 2.011(9) and 2.376(9) Å for compound **5** and 2.03(1)−2.04(1), 2.04(1) and 2.38(1) Å for compound **6**]. The third Cu atom lies at the centre of this cation and is symmetrically coordinated by four N atoms of two bridg-

 © 2003 Wiley-VCH Verlag GmbH & Co. KGaA, Weinheim

ing dien ligands with Cu−N distances of 1.999(9)−2.086(8) Å (**5**) and 2.02(1)−2.099(9) Å (**6**) and at the same time by two additional *trans*-situated N atoms of CN^- ligands of two different anions (Figure 4). The opposite Cu−N distances are 2.579 Å for **5** and 2.581 Å for **6** and are slightly longer than the corresponding distances of five-coordinate Cu atoms. Thus, this Cu atom is octahedrally ($CN = 6$) coordinated and bridges the molecular units $[\{Cu_3(dien)_4\}\{Re_4Q_4(CN)_{12}\}_2]$ to construct the polymeric structure. The negative charge of this one-dimensional network is compensated by K^+ cations. N atoms of CN^- ligands coordinate to these cations as shown in Figure 5.

Figure 4. Anionic connectivity pattern in the crystal structure of compound **5**

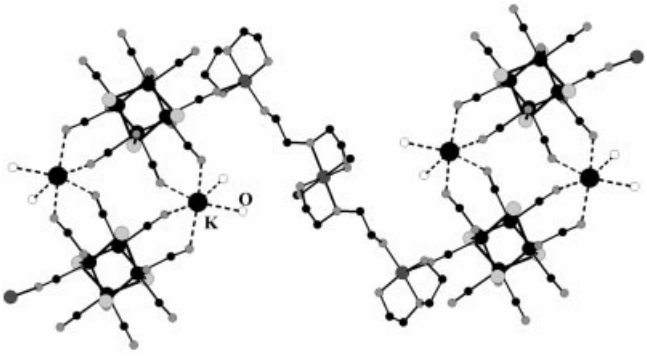

Figure 5. $[\{Cu_3(dien)_4\}\{Re_4Se_4(CN)_{12}\}_2]^{2-}$ secondary building unit in the crystal structure of compound **5** with associated potassium cations

In compounds **1**, **5** and **6** Cu atoms bridged by dien ligands are bonded to cluster anions, whereas in **3** and **4** the complex cation $\{Cu_2(dien)_3\}$ is coordinated to one cluster anion only (Figure 6). Such coordinations have not previously been observed in Cu complexes; in all known similar complexes three N atoms of the dien ligand are always coordinated to one Cu atom as, for example, in $[Cu(dien)]_3[Fe(CN)_6]_2 \cdot 6H_2O$.[15] There are only two known examples of metal compounds (both Ag-containing complexes) with bridging dien ligands.[16]

From the structure analyses we conclude that the coordination of copper atoms is very important: it determines not only the stoichiometry but also the main features of the crystal structure. Evidently, in solutions of these systems, which contain two competitive N-donor ligands, NH_3 and dien, some cationic complexes − monomeric $[Cu(NH_3)(dien)]^{2+}$, and oligomeric [(dien)Cu−(μ-dien)−Cu(dien)]$^{4+}$ and [(dien)Cu−(μ-dien)−Cu−(μ-dien)−Cu(dien)]$^{6+}$ are formed. The formation of oligomers can be explained by a deficiency of ligands in the coordination sphere of Cu^{2+} of simple complexes with stoichiometry [Cu(dien)] (dien has three N-donor atoms only). Copper atoms of similar complexes are unsaturated in their coordination and therefore tend to complete their environment by means of bond formation with other dien ligands. In the complexes **1**, **3**, **4** such interaction leads to oligomeric cations [(dien)Cu−(μ-dien)−Cu(dien)]$^{4+}$ where an additional μ-dien ligand becomes a bridged one. If the concentration of Cu^{2+} ions is decreased (as in the syntheses of **5** and **6**), oligomeric cations with two bridged μ-dien ligands, [(dien)Cu−(μ-dien)−Cu−(μ-dien)−Cu(dien)]$^{6+}$, are formed. However, the copper atoms in such oligomers are again unsaturated − a reason for further interaction with CN ligands of the cluster anions.

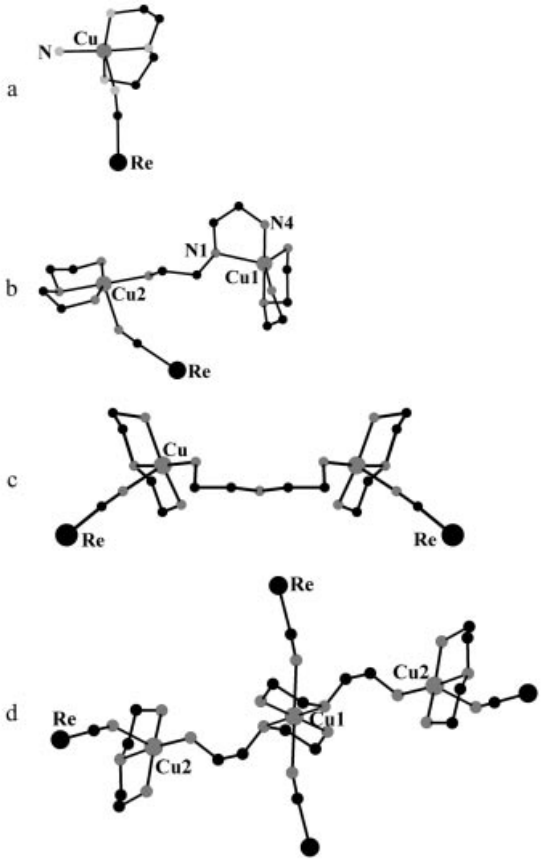

Figure 6. Ligand environment of Cu atoms: a (in **2**), b (in **3**, **4**), c (in **1**) and d (in **5**, **6**)

As expected, the ratio of reagents is an important experimental factor that affects the composition of the resultant compounds. For example, for a Cu/dien ratio near 1:1, complex **2** is formed. If the concentration of dien is increased, complexes **1**, **3**−**6** with higher dien contents are realized. It is of interest that, although in all these reactions the concentration of Cu^{2+} ions was sufficient to form complexes

 © 2003 Wiley-VCH Verlag GmbH & Co. KGaA, Weinheim

containing only Cu^{2+} cations {the ratio $Cu^{2+}/[Re_4Q_4(CN)_{12}]^{4-} > 2$}, two compounds (**5** and **6**) were obtained that are crystallized with additional K^+ cations. This may be due to structural factors: these compounds contain longer oligomeric cations [(dien)Cu−(μ-dien)−Cu−(μ-dien)−Cu(dien)]$^{6+}$.

Comparison of complex **1** (Figure 6, c) with **3** and **4** (Figure 6, b) shows that the latter can be transformed into the structure of **1** by breaking the Cu1−N1(μ-dien) bond and then joining the CN group of the cluster complex to a vacated coordination site of the copper atom.

Experimental Section

Materials and Syntheses: All reagents were used as purchased. $[K_4Re_4Te_4(CN)_{12}]\cdot 5H_2O$ was synthesized by the reaction of $[Re_4Te_4(TeCl_2)_4Cl_8]$ with KCN in water.[17] Se and S analogues were synthesized by the reactions of $[Re_4Se_4(TeCl_2)_4Cl_8]$ and $[Re_4S_4(TeCl_2)_4Cl_8]$, respectively, with KCN as described for $[K_4Re_4Se_4(CN)_{12}]\cdot 6H_2O$.[12] $[Re_4Q_4(TeCl_2)_4Cl_8]$ (Q = Te, Se, S) were synthesized by the reaction of $ReCl_5$ with elemental Te or with a mixture of elemental Se or S with elemental Te.[18] FT-IR: Bruker IFS-85, Perkin−Elmer 1760X. Elemental analyses: Vario EL of Elementar Analysensysteme GmbH.

$[\{Cu_2(dien)_3\}Re_4S_4(CN)_{12}]$ (1): A solution of $CuCl_2$ (0.04 g) in concentrated aqueous ammonia (5 mL) was mixed with a solution of $[K_4Re_4S_4(CN)_{12}]\cdot 5H_2O$ (0.02 g) in water (5 mL). Diethylenetriamine (dien) (0.04 mL) was added to the reaction mixture and the resultant solution was kept for two weeks in a vessel covered by a watch glass. Dark red crystals that formed during this time were filtered off and dried on filter paper. Yield: 0.02 g (67%). $C_{24}H_{55}Cu_2N_{21}O_8Re_4S_4$ (2148.17): calcd. C 17.8, H 2.4, N 18.1, S 7.9; found C 17.5, H 2.9, N 17.9, S 7.6. IR (KBr): $\tilde{\nu}$ = 2180 (w), 2153 (s) [ν(CN)] cm^{-1}.

$[\{Cu(dien)(NH_3)\}_2Re_4Se_4(CN)_{12}]\cdot 2.5H_2O$ (2): A solution of $CuCl_2$ (0.030 g) in concentrated aqueous ammonia (2 mL) was mixed with a solution of $[K_4Re_4Se_4(CN)_{12}]\cdot 5H_2O$ (0.015 g) in water (2 mL); dien (0.02 mL) was added to the reaction mixture and the resultant solution was kept for two weeks in a vessel covered by a watch glass. Black crystals that formed during this time were filtered off and dried on filter paper. Yield: 0.014 g (82%). $C_{20}H_{37}Cu_2N_{20}O_{2.5}Re_4Se_4$ (1785.42): calcd. C 13.5, H 2.1, N 15.7; found C 13.4, H 2.0, N 15.7. IR (KBr): $\tilde{\nu}$ = 2145 cm^{-1}.

$[\{Cu_2(dien)_3\}Re_4Se_4(CN)_{12}]\cdot 8.25H_2O$ (3): A solution of $CuCl_2$ (0.020 g) in concentrated aqueous ammonia (2 mL) was mixed with a solution of $[K_4Re_4Se_4(CN)_{12}]\cdot 5H_2O$ (0.015 g) in water (2 mL); dien (0.04 mL) was added to the reaction mixture and the resultant solution was kept for one week in a vessel covered by a watch glass. Black needle-like crystals that formed during this time were filtered off and dried on filter paper. Yield: 0.012 g (67%). $C_{24}H_{55.5}Cu_2N_{21}O_{8.25}Re_4Se_4$ (1958.11): calcd. C 14.7, H 2.7, N 15.0; found C 15.0, H 2.5, N 15.2. IR (KBr): $\tilde{\nu}$ = 2142 [ν(CN)] cm^{-1}.

$[\{Cu_2(dien)_3\}Re_4Te_4(CN)_{12}]\cdot 8H_2O$ (4): A solution of $CuCl_2$ (0.015 g) in concentrated aqueous ammonia (2 mL) was mixed with a solution of $[K_4Re_4Te_4(CN)_{12}]\cdot 5H_2O$ (0.007 g) in water (2 mL); dien (0.04 mL) was added to the reaction mixture. The resultant solution was kept for two weeks in a vessel covered by a watch glass. Black needle-like crystals formed during this time were filtered off and dried on filter paper. Yield: 0.008 g (95%). $C_{24}H_{55}Cu_2N_{21}O_8Re_4Te_4$ (2148.17): calcd. C 13.4, H 2.6, N 13.7; found C 13.6, H 2.5, N 14.0. IR (KBr): $\tilde{\nu}$ = 2134 [ν(CN)] cm^{-1}.

$[K(H_2O)_2]_2[\{Cu_3(dien)_4\}\{Re_4Se_4(CN)_{12}\}_2]\cdot 8H_2O$ (5): A solution of $CuCl_2$ (0.005 g) and dien (0.04 mL) in concentrated aqueous ammonia (2 mL) was mixed with a solution of $[K_4Re_4Se_4(CN)_{12}]\cdot 5H_2O$ (0.015 g) in water (2 mL). The resultant solution was kept for two weeks in a vessel covered by a watch glass. Black crystals that formed during this time were filtered off and dried on filter paper. Yield: 0.013 g (76%). $C_{40}H_{76}Cu_3K_2N_{36}O_{12}Re_8Se_8$ (3643.47): calcd. C 13.2, H 2.1, N 13.8; found C 13.3, H 2.5, N 14.0. IR (KBr): $\tilde{\nu}$ = 2145 [ν(CN)] cm^{-1}.

$[K(H_2O)_2]_2[\{Cu_3(dien)_4\}\{Re_4Te_4(CN)_{12}\}_2]\cdot 8H_2O$ (6): A solution of $CuCl_2$ (0.005 g) in concentrated aqueous ammonia (2 mL) was mixed with a solution of $[K_4Re_4Te_4(CN)_{12}]\cdot 5H_2O$ (0.015 g) in water (2 mL); dien (0.04 mL) was added to the reaction mixture. The resultant solution was then kept for two weeks in a vessel covered by a watch glass. Black prismatic crystals that formed during this time were filtered off and dried on filter paper. Yield: 0.016 g (96%). $C_{40}H_{76}Cu_3K_2N_{36}O_{12}Re_8Te_8$ (4032.58): calcd. C 11.9, H 1.9, N 12.5; found C 12.0, H 1.9, N 13.6. IR (KBr): $\tilde{\nu}$ = 2136 [ν(CN)] cm^{-1}.

Crystallography: Single-crystal X-ray diffraction data were collected by standard techniques [Mo-K_α radiation (λ = 0.71073 Å), ω-scan mode] with Enraf-Nonius CAD4 (compound **1**) and Siemens P4 (compounds **2**−**6**) diffractometers under ambient conditions. Data were corrected for absorption with azimuthal scans. The structures were solved by direct methods and refined by least-squares methods against F^2. All non-hydrogen atoms were refined anisotropically taking into account all independent reflections. The positions of the hydrogen atoms of the dien groups were idealized; those of water molecules were not located. All calculations were carried out with an IBM PC using the SHELX-97 program package.[19,20]

1: Dark red prism, crystal dimensions 0.24 × 0.20 × 0.18 mm, orthorhombic, space group $Pmn2_1$, Z = 2, a = 15.272(2), b = 8.8743(9), c = 17.946(3) Å, V = 2432.2(6) Å^3, $\rho_{calcd.}$ = 2.215 g cm^{-1}, μ = 10.986 mm^{-1}, 4887 measured reflections, 4402 independent (R_{int} = 0.0387), $R(F)$ = 0.0392 for 2673 reflection with $F_{hkl} \geq 4\sigma(F_{hkl})$ and $R_w(F^2)$ = 0.0963 for all independent reflections. The absolute structure was established by use of the Flack parameter.

2: Black block, crystal dimension 0.22 × 0.22 × 0.65 mm, triclinic, space group $P\bar{1}$, Z = 2, a = 12.242(3), b = 12.969(4), c = 15.439(6) Å, α = 95.12(3), β = 110.38(3), γ = 114.02(2)°, V = 2020.8(11) Å^3, $\rho_{calcd.}$ = 2.934 g cm^{-1}, μ = 16.620 mm^{-1}, 7487 measured reflections, 7143 independent (R_{int} = 0.0503), $R(F)$ = 0.0465 for 5824 reflections with $F_{hkl} \geq 4\sigma(F_{hkl})$ and $R_w(F^2)$ = 0.1243 for all independent reflections.

3: Black needles, crystal dimensions 0.08 × 0.10 × 0.65 mm, monoclinic, space group $P2_1/n$, Z = 4, a = 13.839(3), b = 15.181(3), c = 24.015(4) Å, β = 95.78(2)°, V = 5019.7(17) Å^3, $\rho_{calcd.}$ = 2.798 g cm^{-1}, μ = 12.581 mm^{-1}, 10444 measured reflections, 8941 independent (R_{int} = 0.0589), $R(F)$ = 0.0613 for 5209 reflections with $F_{hkl} \geq 4\sigma(F_{hkl})$ and $R_w(F^2)$ = 0.1488 for all independent reflections.

4: Black needle, crystal dimensions 0.14 × 0.14 × 0.4 mm, monoclinic, space group $P2_1/n$, Z = 4, a = 13.844(3), b = 15.288(6), c = 24.194(6) Å, β = 95.287(13)°, V = 5099(2) Å^3, $\rho_{calcd.}$ = 2.591 g cm^{-1}, μ = 13.403 mm^{-1}, 9221 measured reflections, 8828 independent (R_{int} = 0.0463), $R(F)$ = 0.0499 for 5601 reflections with $F_{hkl} \geq 4\sigma(F_{hk})$ and $R_w(F^2)$ = 0.0952 for all independent reflections.

 © 2003 Wiley-VCH Verlag GmbH & Co. KGaA, Weinheim

5: Black plate, crystal dimensions 0.10 × 0.14 × 0.18 mm, triclinic, space group $P\bar{1}$, $Z = 1$, $a = 13.547(3)$, $b = 13.622(3)$, $c = 14.126(3)$ Å, $\alpha = 68.55(3)$, $\beta = 64.58(3)$, $\gamma = 87.69(3)°$, $Z = 1$, $V = 2170.2(7)$ Å^3, $\rho_{calcd.} = 2.788$ g cm^{-1}, $\mu = 15.340$ mm^{-1}, 7980 measured reflections, 7641 independent ($R_{int} = 0.0691$), $R(F) = 0.0552$ for 5413 reflections with $F_{hkl} \geq 4\sigma(F_{hkl})$ and $R_w(F^2) = 0.1311$ for all independent reflections.

6: Black plate, crystal dimensions 0.04 × 0.10 × 0.30 mm, triclinic, space group $P\bar{1}$, $Z = 2$, $a = 13.619(3)$, $b = 13.660(3)$, $c = 14.166(3)$ Å, $\alpha = 68.33(2)$, $\beta = 64.94(1)$, $\gamma = 87.42(2)°$, $V = 2199.1(8)$ Å^3, $\rho_{calcd.} = 3.045$ g cm^{-1}, $\mu = 14.430$ mm^{-1}, 8090 measured reflections, 7748 independent ($R_{int} = 0.0244$), $R(F) = 0.0374$ for 6081 reflections with $F_{hkl} \geq 4\sigma(F_{hkl})$ and $R_w(F^2) = 0.0739$ for all independent reflections.

Acknowledgments

This work was supported by the Russian Foundation for Basic Research, grant 02-03-32264 and INTAS 00-00689. Also, Y. V. M. is grateful to the Alexander von Humboldt foundation for a fellowship.

[1] Y. V. Mironov, V. E. Fedorov, *Rus. Chem. Bull., Int. Ed.* **2002**, *51*, 569−580.
[2] J-C. P. Gabriel, K. Boubekeur, S. Uriel, P. Batail, *Chem. Rev.* **2001**, *101*, 2037−2066.
[3] Y. V. Mironov, V. E. Fedorov, C. C. McLauchlan, J. A. Ibers, *Inorg. Chem.* **2000**, *39*, 1809−1811.
[4] Z. Zheng, T. G. Gray, R. H. Holm, *Inorg. Chem.* **1999**, *38*, 4888−4895.
[5] N. G. Naumov, A. V. Virovets, V. E. Fedorov, *J. Struct. Chem. Engl. Transl.* **2000**, *41*, 499−520.
[6] N. G. Naumov, D. V. Soldatov, J. A. Ripmeester, S. B. Artemkina, V. E. Fedorov, *Chem. Commun.* **2001**, 571−572.
[7] S. B. Artemkina, N. G. Naumov, A. V. Virovets, S. A. Gromilov, D. Fenske, V. E. Fedorov, *Inorg. Chem. Commun.* **2001**, *4*, 423−426.
[8] M. V. Bennett, L. G. Beauvais, M. P. Shores, J. R. Long, *J. Am. Chem. Soc.* **2001**, *123*, 8022−8032.
[9] M. V. Bennett, M. P. Shores, L. G. Beauvais, J. R. Long, *J. Am. Chem. Soc.* **2000**, *122*, 6664−6668.
[10] L. G. Beauvais, M. P. Shores, J. R. Long, *J. Am. Chem. Soc.* **2000**, *122*, 2763−2772.
[11] Y. V. Mironov, A. V. Virovets, S. B. Artemkina, V. E. Fedorov, *Angew. Chem. Int. Ed.* **1998**, *37*, 2507−2509.
[12] Y. V. Mironov, A. V. Virovets, W. S. Sheldrick, V. E. Fedorov, *Polyhedron* **2001**, *20*, 969−974.
[13] Y. V. Mironov, O. Oeckler, A. Simon, V. E. Fedorov, *Eur. J. Inorg. Chem.* **2001**, 2751−2753.
[14] Y. V. Mironov, V. E. Fedorov, I. Ijjaali, J. A. Ibers, *Inorg. Chem.* **2001**, *40*, 6320−6323.
[15] H-Z. Kou, d-Z. Liao, P. Cheng, Z-H. Jiang, S-P. Yan, G-L. Wang, X-K. Yao, H-G. Wang, *J. Chem. Soc., Dalton Trans.* **1997**, 1503−1506.
[16] E. C. Plappert, D. M. P. Mingos, S. E. Lawrence, D. J. Williams, *J. Chem. Soc., Dalton Trans.* **1997**, 2119−2123.
[17] Y. V. Mironov, A. V. Virovets, S. B. Artemkina, V. E. Fedorov, *J. Struct. Chem. Engl. Transl.* **1999**, *40*, 313−315.
[18] Y. V. Mironov, T. E. Albrecht-Schmitt, J. A. Ibers, *Inorg. Chem.* **1997**, *36*, 944−946.
[19] G. M. Sheldrick, *SHELXTL DOS/Windows/NT*, version 5.10; Bruker Analytical X-ray Instruments, Inc., Madison, WI, **1997**.
[20] CCDC-193908 to -193913 contain the supplementary crystallographic data for this paper. These data can be obtained free of charge at www.ccdc.cam.ac.uk/conts/retrieving.html [or from the Cambridge Crystallographic Data Centre, 12 Union Road, Cambridge CB2 1EZ, UK; Fax: (internat.) + 44-1223/336-033; E-mail: deposit@ccdc.cam.ac.uk].

Received October 22, 2002

 © 2003 Wiley-VCH Verlag GmbH & Co. KGaA, Weinheim

Iron(III) Chelation: Tuning of the pH Dependence by Mixed Ligands

Anne-Marie Albrecht-Gary,*[a] Sylvie Blanc,[a] Frederic Biaso,[b] Fabrice Thomas,[b] Paul Baret,[b] Gisele Gellon,[b] Jean-Louis Pierre,[b] and Guy Serratrice*[b]

Keywords: Tripodal ligands / Iron / Thermodynamics / UV/Vis spectroscopy / Siderophores

The iron(III) chelating properties of two heteropodands with 8-hydroxyquinoline and catechol binding groups were examined and compared to those of the corresponding homopodal analogues, O-TRENSOX and TRENCAMS. Like the parent homopodands, the two heteropodands are based on the TREN scaffold and the chelating units are connected by amide groups, TRENSOX2CAMS having two 8-hydroxyquinoline and one catechol arms and TRENSOXCAMS2 one 8-hydroxyquinoline and two catechol moieties. The aqueous coordination chemistry of these ligands was examined by potentiometric and spectrophotometric methods in combination with ^{1}H NMR spectroscopy. The respective pFe^{III} values showed a cooperative effect of the mixed chelating units. Moreover, the pFe^{III} dependence on pH showed that the mixed ligands exhibit a higher complexing ability than the parent ligands over the pH range 5–9 which is of biological relevance. This result could be of great interest for medical applications.
(© Wiley-VCH Verlag GmbH & Co. KGaA, 69451 Weinheim, Germany, 2003)

Introduction

Siderophores are iron chelating agents that are excreted by microorganisms to render iron soluble in the environment and favour the uptake of this metal. Iron chelation by some natural or synthetic chelators can be applied to human diseases characterised by iron overload. Although the coordination chemistry of a great number of water-soluble synthetic iron chelators has been described,[1] the pH dependence of the coordination abilities has not been thoroughly investigated. Most of the comparative data in the literature are allowed by the use of the pFe^{III} values (calculated for $[Fe^{III}]_{tot}$ = 1 μM, $[L]_{tot}$ = 10 μM at pH = 7.4) and, of course, pFe^{III} reflects only the complexing ability of a given ligand at physiological pH. Owing to the fact that pH can vary in a relatively large range between the different biological compartments, an understanding of the pH dependence of the pFe^{III} value may be a decisive criterion for the understanding of the in vivo behaviour of a given iron chelator. On the other hand, the design and the synthesis of iron chelators with high pFe^{III} values in a large range of pH, constitutes an interesting challenge for chemists. We previously reported the dependence of pFe^{III} on pH for two homopodands based on catechol and on 8-hydroxyquinoline bidentate units.[2,3] We showed that the tris(catechol) ligand TRENCAMS is a stronger ferric chelator than the tris(hydroxyquinolinate) analogue O-TRENSOX at pH values greater than 7 and that the opposite sequence is observed at pH values lower than 7. In order to obtain an efficient chelator of iron(III) over a large range of pH, we have synthesised mixed tripodal siderophores with both catechol and 8-hydroxyquinoline moieties. Recently, the synthesis of mixed tripodal ligands based on (i) two hydroxypiridinone and one catechol moieties, and (ii) two hydroxypiridinone and one 2-hydroxyisophtalamide groups has been published.[4] We report in this paper the synthesis, acid-base properties, and ferric complexation of two monotopic tripodal mixed ligands TRENSOX2CAMS (**L^1**) and TRENSOXCAMS2 (**L^2**; Figure 1). These molecules belong to a family of tripods with a tris(2-aminoethyl)amine group anchoring arms that bear bidentate coordination subunits (namely either a 5-sulfo-8-hydroxyquinoline-7-carbamoyl group or 5-sulfo-2,3-dihydroxybenzoyl unit). The ligands differ by the number of catecholylamide groups, none for ligand **L^0** (O-TRENSOX), one for ligand **L^1**, two for ligand **L^2** and three for ligand **L^3** (TRENCAMS; Figure 1). Combining potentiometric and absorption spectrophotometric titrations with ^{1}H NMR spectroscopy we were able to characterise in water the protonated and ferric species formed with ligands **L^1** and **L^2** over a large pH range.

[a] Laboratoire de Physico-Chimie Bioinorganique, UMR CNRS 7509, European School of Chemistry, 25 rue Becquerel, 67200 Strasbourg, France,
Fax: (internat.) +33-(0)3/90 24 26 39
E-mail: amalbre@chimie.u-strasbg.fr
[b] Laboratoire de Chimie Biomimétique, LEDSS, UMR CNRS 5616, Université Joseph Fourier,
BP 53, 38041 Grenoble Cedex 9, France
Fax: (internat.) +33-(0)4/76 51 48 36
E-mail: guy.serratrice@ujf-grenoble.fr
Supporting information for this article is available on the WWW under http://www.eurjic.org or from the author.

 © 2003 Wiley-VCH Verlag GmbH & Co. KGaA, Weinheim **DOI: 10.1002/ejic.200200643**

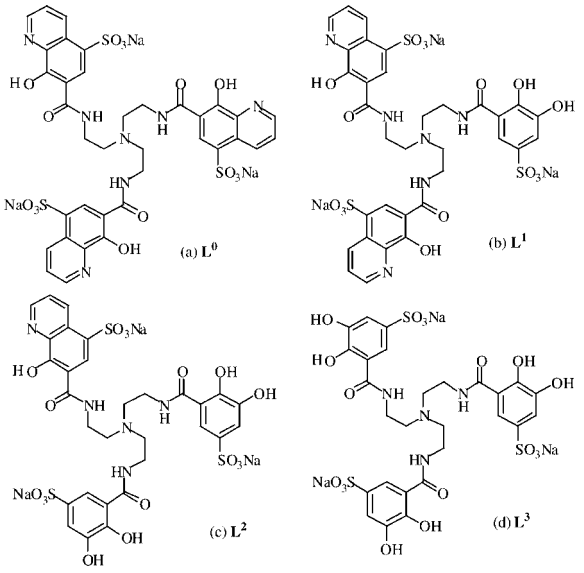

Figure 1. Chemical formulae of the tripodal ligands: (a) **L⁰** (O-TRENSOX), (b) **L¹** (TRENSOX2CAMS), (c) **L²** (TRENSOX-CAMS2), (d) **L³** (TRENCAMS)

Results and Discussion

Synthesis

The synthesis of the heterotripodal hexadentate ligands **L¹** and **L²** is presented in Figure 2. The two catecholate subunits of ligand **L²** were connected to the tripodal scaffold by direct condensation[5] of two equivalents of 2,3-dimethoxybenzoic chloride with one equivalent of tris(2-aminoethyl)amine (TREN) [path (a′)], then the oxinate subunit was grafted onto the free primary amine group by coupling with activated (CDI) 7-carboxy-8-hydroxyquinoline. The synthesis of **L¹** required protection of one arm of TREN with a trityl group [paths (a, b, c)]. Phenol groups were protected with benzyl groups (oxine) and methyl groups (catechol), respectively; deprotections were performed with BBr_3. Finally, regiospecific sulfonation in position 5 of both oxinate and catecholate subunits afforded the hydrosoluble ligands **L¹** and **L²**.

Acid-Base Properties of Ligands

The protonation constants of **L¹** and **L²** were determined by combination of potentiometric and spectrophotometric

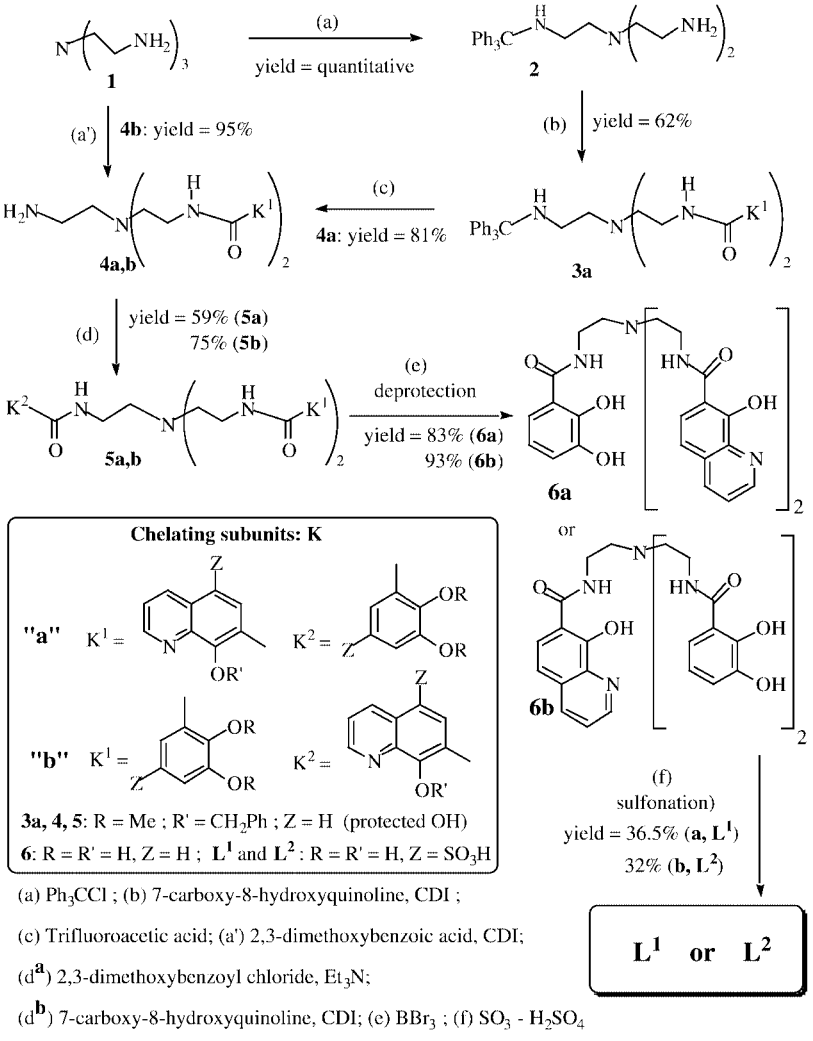

Figure 2. Synthesis of the heterotripodal ligands **L¹** and **L²**

 © 2003 Wiley-VCH Verlag GmbH & Co. KGaA, Weinheim

titrations (see details in Exp. Sect.). Both ligands possess a total of ten protonable functions. However, protonation of the three sulfo groups that are moderately strong acids (log $K^H < 2$)[6] was not considered likely under our conditions. Seven stepwise protonation constants were determined for each ligand. The corresponding values and statistical errors are given in Table 1. Speciation diagrams are presented in Figures S1 and S2 of the supporting information.

Table 1. Assignment of the successive protonation constants of various heterotripodal ligands with 8-hydroxyquinoline and/or catechol subunits; solvent: water, $I = 0.10$ M ($NaClO_4$), $T = (25.0 \pm 0.2)$ °C; numbers in parentheses correspond to statistical errors (3σ) on the last digit

Function	L^0 [a]	L^1	L^2	L^3[b]
NH pyridinium	1.8(1) 2.55(8) 3.01(4)	1.8(2) 2.89(15)	2.34(6)	
OH quinoline	7.44(4) 8.18(5) 8.62(4)	7.85(9) 8.78(3)	7.93(2)	
OH catechol (*ortho*)		5.62(6)	5.55(4) 7.35(2)	5.57(5) 6.32(4) 7.05(4)
OH catechol (*meta*)		11.5(2)	11.41(8)[c] 12.5(3)[c]	12.05(10)[d]
NH ammonium	6.36(3)	6.96(6)	6.56(3)	8.01(2)

[a] Ref.[2] [b] Ref.[3] [c] Spectrophotometric determinations under basic conditions. [d] Average value for the three *meta* catechol OH groups.

The protonation constants of $\mathbf{L^1}$ were determined by potentiometry except for log $K_1^H = 11.5$ and log $K_7^H = 1.8$, which were determined spectrophotometrically. As for $\mathbf{L^2}$, the values in Table 1 represent averages of values determined by both methods, except for log $K_5^H = 6.56$ (determined by potentiometry) and log $K_1^H = 12.5$ (determined by spectrophotometry).

The protonation constants were attributed to $\mathbf{L^1}$ and $\mathbf{L^2}$ by comparison with the log K^H values of the ligand $\mathbf{L^0}$, bearing three hydroxyquinoline groups,[2] and with those of the tris(catecholate) ligand $\mathbf{L^3}$ [3] (Table 1). The highest protonation constants (11.5 for $\mathbf{L^1}$; 12.5 and 11.41 for $\mathbf{L^2}$) can be assigned to the *meta* hydroxyl groups of the sulfocatecholyl moieties. These values are in agreement with those reported under similar conditions for some sulfocatechol derivatives such as 1,2-dihydroxybenzene-4-sulfonic acid (log $K^H = 12.16$),[7] 1,2-dihydroxybenzene-3,5-disulfonic acid (Tiron; log $K^H = 12.5$)[8] or *N*,*N*-dimethyl-2,3-dihydroxy-5-sulfonatobenzamide (DMBS; log $K^H = 11.5$).[9] The values of the lowest protonation constants (1.8 and 2.89 for $\mathbf{L^1}$; 2.34 for $\mathbf{L^2}$) correspond to the pyridine nitrogen of the sulfohydroxyquinoline moieties. Compared to 8-hydroxyquinoline-5-sulfonic acid (log $K^H = 3.93$),[10] the protonation constants determined for $\mathbf{L^1}$ and $\mathbf{L^2}$ are two orders of magnitude lower. This could be explained by the electron-withdrawing effect of the carbonyl linker in position 7, which is similar to that of the nitro group in 7-nitro-8-hydroxyquinoline-5-sulfonic acid (log $K^H = 2.01$).[11] The hydroxyl protonation constant of 8-hydroxyquinoline-5-sulfonic acid[10] is equal to 8.42 and those of $\mathbf{L^0}$ vary between 7.44 and 8.62.[2] We attribute the values 8.78 and 7.85 for $\mathbf{L^1}$ and 7.93 for $\mathbf{L^2}$ to the protonation of the 8-hydroxyquinoline OH groups.

Based on the fact that the species $\mathbf{L^2}H_3$ and $\mathbf{L^2}H_4$ have the same absorption spectra, suggesting that protonation does not occur on a chromophore, the protonation constant log $K_5^H = 6.56$ was attributed to the tertiary amine nitrogen of $\mathbf{L^2}$ anchor. This was confirmed by the ^{1}H NMR titration of $\mathbf{L^2}$ which showed an inflection point at pD ≈ 6 and a significant upfield shift of the methylene protons, characteristic of the protonation of its closest acid-base site, i.e. the tertiary amine (Figure 3). Similarly for $\mathbf{L^1}$, the protonation constant log $K_4^H = 6.96$ was attributed to the tertiary amine.

The values of log K^H of the tertiary amine anchor determined for $\mathbf{L^1}$ and $\mathbf{L^2}$ are close to that of $\mathbf{L^0}$ (log $K^H = 6.36$).[2] They are, however, much lower than that of the tris(catechol) ligand $\mathbf{L^3}$ (log $K^H = 8.01$).[3] It has already been reported[12] that the protonation of this site is sensitive to the ability of the tertiary amine to form hydrogen bonds with substituents in the β-position of the TREN scaffold. Formation of a hydrogen bond between the lone electron pair of the tertiary amine nitrogen and the amide hydrogen

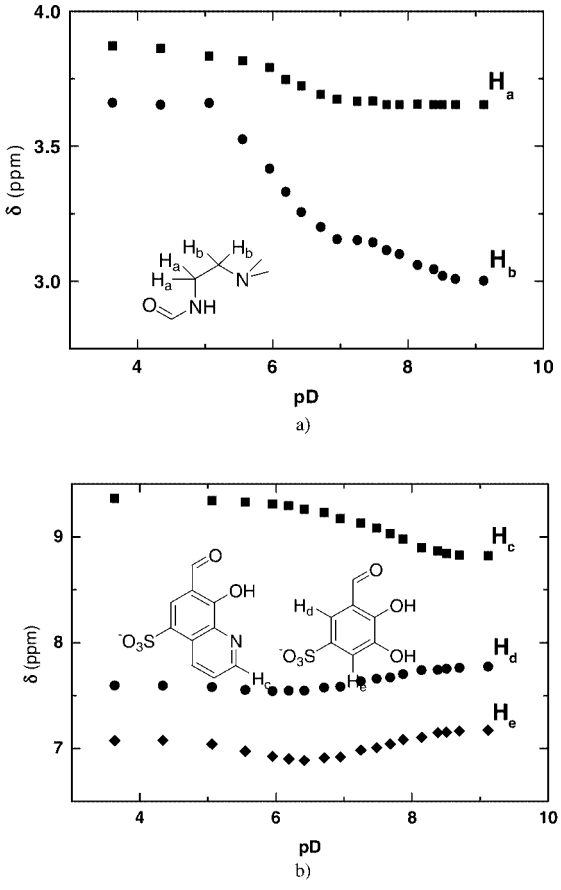

Figure 3. ^{1}H NMR chemical shift variation as a function of pD for the methylene (a) and aromatic (b) protons of $\mathbf{L^2}$; solvent: D_2O, $[\mathbf{L^2}] = 5$ mM

 © 2003 Wiley-VCH Verlag GmbH & Co. KGaA, Weinheim

decreases strongly its basicity, providing a sufficient stabilisation of the deprotonated form of the amine, as observed with the tripodal ligands bearing 8-hydroxyquinoline groups.

The interactions of the amide linkers with the tertiary amine nitrogen can be further affected by the protonation state of the *ortho*-hydroxyl groups either of the 8-hydroxyquinoline or the catechol subunits. Indeed, the protonation of these sites could induce a different geometry around the TREN anchor, as suggested by the shoulder at pD = 7−8.5 in the curve H_b during the ^{1}H NMR titration of ligand **L²** (Figure 3). The isomer shift of the H_c as well as H_d and H_e (Figure 3) observed for **L²** increases from pD = 6.5 to 9 with an inflection point at pD = 7.5−8 in relation to the protonation of hydroxyl groups (log K^H = 7.35 and 7.93). This indicates that such a protonation is responsible for a conformational change around the amide-catechol axis, which induces a shift of the proton resonance.

The remaining protonation constants (7.35 and 5.55 for **L²** and 5.62 for **L¹**) are attributed to the catechol hydroxyl groups *ortho* with respect to the amide linker. These values are in agreement with those of other tripodal catecholylamide-type ligands.[13]

The calculated electronic spectra of protonated species of **L¹** and **L²** are given in Figure 4. The spectral properties of **L¹** and **L²** are qualitatively in agreement with those of other 8-hydroxyquinoline and/or catechol based ligands. Catechol derivatives show a $\pi \rightarrow \pi^*$ transitions in the UV region (300−400 nm) with the maximum of the absorption band shifting to longer wavelengths and the molar absorption coefficient increasing as the hydroxyl groups are deprotonated.[14] Similarly, 8-hydroxyquinoline-5-sulfonic acid displays spectral variations in this region upon protonation.[15] It should be noted that molar absorption coefficients of the heterotripodal ligands (≈2 × 10^4 M^{-1}·cm^{-1} at around 340 nm and ≈5−6 × 10^4 M^{-1}·cm^{-1} at around 270 nm for totally deprotonated **L¹** and **L²**) are higher than the value obtained by addition of molar absorption coefficients of simple 8-hydroxyquinolinate or catecholate ligands.[15,16]

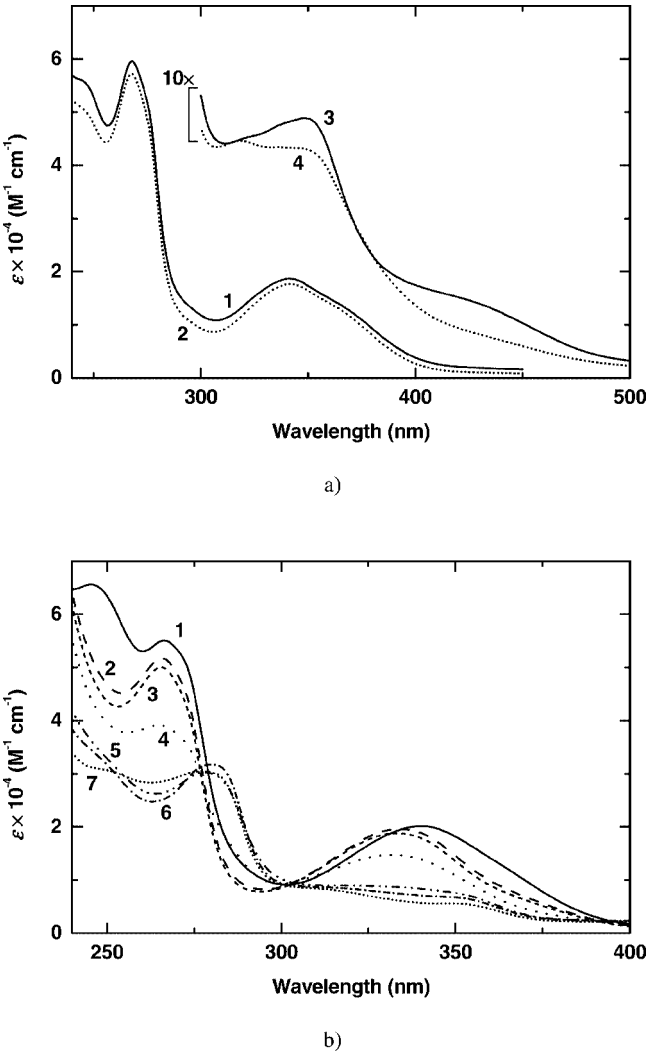

Figure 4. Calculated electronic spectra of the protonated species of heterotripodal ligands; solvent: water, I = 0.10 M ($NaClO_4$), T = (25.0 ± 0.2) °C: (a) ligand **L¹**: (1) $\mathbf{L^1H_7}$, (2) $\mathbf{L^1H_6}$, (3) $\mathbf{L^1H}$, (4) **L¹**; (b) ligand **L²**: (1) **L²**, (2) $\mathbf{L^2}$ H, (3) $\mathbf{L^2H_2}$, (4) $\mathbf{L^2H_3} \equiv \mathbf{L^2H_4}$, (5) $\mathbf{L^2H_5}$, (6) $\mathbf{L^2H_6}$, (7) $\mathbf{L^2H_7}$; charges are omitted for the sake of clarity

Characterisation of the Ferric Complexes

Both ligands are hexadentate and form only 1:1 ferric complexes. The potentiometric titration curves recorded for a 1:1 metal-to-ligand ratio (Figure 5) show a large pH jump at a = 7, indicating that all the ligand protons are released when the ferric ion is bound. Since both **L¹** and **L²** form ferric complexes totally at pH values less than 3 the global stability constant log β_{FeL} could not be determined from the potentiometric data.

The spectra obtained during the spectrophotometric titrations of ferric complexes of **L¹** and **L²** are shown in Figures S3 and S4. The absorbance data were refined with the Letagrop-Spefo[17,18] and Specfit[19−22] programs and provided values of global stability constants of ferric complexes of both **L¹** and **L²**. The spectrophotometric data obtained from the competition for ferric ion between **L²** and EDTA were treated with the Specfit program allowing the determination of the stability constant log β_{FeL}. All the results are summarised in Table 2.

The electronic spectra of de-, mono- and polyprotonated ferric complexes of **L¹** and **L²** calculated from the refinement of absorbance data are shown in Figure 6; speciation diagrams are presented in Figure 7.

The ferric complexes of catechol derivatives generally show a strong ligand-to-metal charge transfer (LMCT) band with a maximum at about 700 nm for mono(catecholate) species, at about 560 nm for bis(catecholate) species and finally at about 480 nm for tris(catecholate) complexes. The charge-transfer bands observed are due to electronic transitions from the highest valence orbitals of the ligand to the 3d orbitals of iron(III).[23] As the maximum moves to shorter wavelengths with increasing number of coordinating ligands the molar absorption coefficient increases. Electron-withdrawing substituents on the aromatic rings of the catechol moieties increase the molar absorption coefficient but have little effect on the wavelength of the maximum. Ferric

 © 2003 Wiley-VCH Verlag GmbH & Co. KGaA, Weinheim

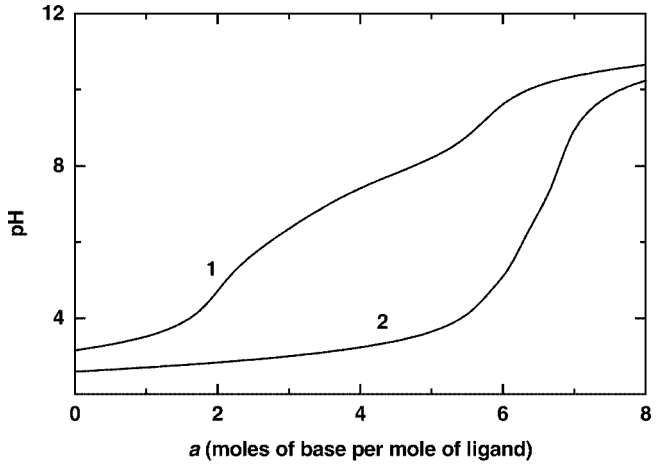

a)

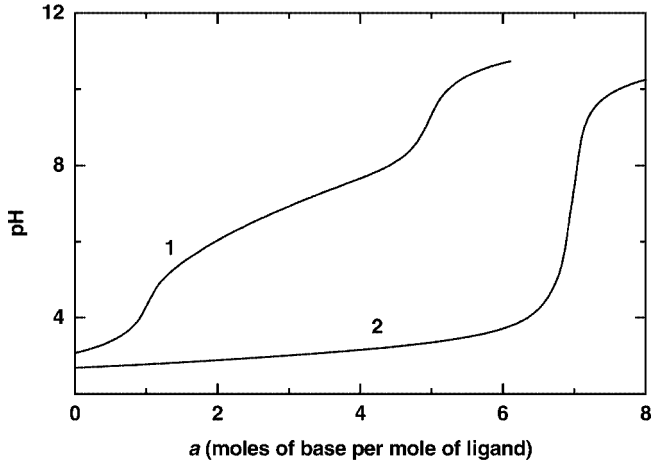

b)

Figure 5. Potentiometric titration curves for the heterotripodal ligands and their ferric complexes; solvent: water, I = 0.10 M ($NaClO_4$), T = (25.0 ± 0.2) °C: (a) titration of $\mathbf{L^1}$ (1 mM): (1) free ligand, (2) 1:1 ferric complex; (b) titration of $\mathbf{L^2}$ (1 mM): (1) free ligand, (2) 1:1 ferric complex

complexes of 8-hydroxyquinoline-5-sulfonic acid are characterised by two absorption maxima in the visible region. The maximum at 443 nm is assigned to an LMCT band belonging to the phenolic oxygen, while the band at 595 nm is due to charge transfer from the pyridine nitrogen to the metal cation.[2] It should be noted that in common with $\mathbf{L^0}$ and $\mathbf{L^3}$, both $\mathbf{L^1}$ and $\mathbf{L^2}$ form protonated ferric complexes, indicating that the coordination sites of the complexes can be protonated without losing the ferric ion. This behaviour can be attributed to a change of catecholate or oxinate bonding mode to the salicylate mode (coordination with carbonyl and *o*-hydroxyl oxygens).

It is of interest to consider the different multiprotonated ferric complexes of $\mathbf{L^1}$ and $\mathbf{L^2}$ by examining their electronic spectra (Table 2) as this can provide information on the coordination modes and their successive deprotonation constants pK_{FeLH_n} (defined in Table 3). These values are calculated from the difference between the values of log β_{FeLH_n}

Table 2. Cumulative stability constants β_{FeLHn}, pFe^{III} values and UV/Vis spectral characteristics of ferric complexes formed with the tripodal ligands; solvent: water, I = 0.10 M ($NaClO_4$), T = (25.0 ± 0.2) °C; numbers in parentheses correspond to statistical errors (3σ) on the last digit; an incertitude of 5% is estimated for the molar absorption coefficients

Ligand	Species	log β_{FeLH_n}[a]	pFe^{III}[b]	λ_{max} (nm)[c]	ε_{max} ($M^{-1}\cdot cm^{-1}$)
$\mathbf{L^0}$ [2]	$Fe\mathbf{L^0}H_5$	42.2(1)	29.5	435	8200
				525*	3500
	$Fe\mathbf{L^0}H$	36.5(2)		443	5200
				595	5200
	$Fe\mathbf{L^0}$	30.9(1)		443	5400
				595	5400
$\mathbf{L^1}$	$Fe\mathbf{L^1}H_5$	48.6(2)	31.6	440*	6900
				540*	3700
	$Fe\mathbf{L^1}H_3$	46.2(4)		560	4000
	$Fe\mathbf{L^1}H_2$	44.3(3)		580	3900
	$Fe\mathbf{L^1}H$	41.6(2)		560	4500
	$Fe\mathbf{L^1}$	36.8(4)		550	4500
$\mathbf{L^2}$	$Fe\mathbf{L^2}H_5$	55.91(3)	32.3	409	4700
				520*	3300
	$Fe\mathbf{L^2}H_4$	53.7(1)		573	3500
	$Fe\mathbf{L^2}H_2$	47.7(3)		542	4500
	$Fe\mathbf{L^2}H$[d]	44.7(6)		525	4800
	$Fe\mathbf{L^2}$ [d]	41.3(6)		525	4800
$\mathbf{L^3}$ [3]	$Fe\mathbf{L^3}H_5$	64.05(7)	29.6	495	4300
	$Fe\mathbf{L^3}H_3$	57.4(1)		520	4800
	$Fe\mathbf{L^3}H$	49.1(1)		500	5000
	$Fe\mathbf{L^3}$	43.6(1)		488	5300

[a] $\beta_{FeLHn} = [FeLH_n]/([Fe^{III}] \times [L] \times [H^+]n)$. [b] Calculated for $[Fe^{III}]_{tot} = 10^{-6}$ M, $[L]_{tot} = 10^{-5}$ M, pH = 7.4. [c] * = shoulder. [d] Species have identical electronic spectra.

and are reported in Table 3 together with the values from tris(catecholate) and tris(8-hydroxyquinolinate) complexes for comparison. The deprotonation constants of ferric $\mathbf{L^1}$ and $\mathbf{L^2}$ complexes have been attributed by considering that the deprotonation of an 8-hydroxyquinoline group involved in the ferric coordination occurs at a pH much lower than that of the deprotonation of the catechol group. This is supported by the pK_{FeLH_n} values recently determined for tripodal ferric complexes containing a C-pivot scaffold with either an 8-hydroxyquinoline (ligand COX)[24] or a catechol subunit (ligand CacCAM).[25] In particular, the values of pK_{FeLH} (2.12 for Fe-COX and 6.59 for Fe-CacCAM) have been unambiguously attributed to the coordination of the third chelating arm.

The electronic spectrum of $Fe\mathbf{L^1}H_5$, which exhibits two shoulders at 440 nm (ε = 6940 $M^{-1}\cdot cm^{-1}$) and 540 nm (ε = 3680 $M^{-1}\cdot cm^{-1}$), is similar to that of the bis(salicylate) complex of $\mathbf{L^0}$ [2] involving a coordination with two 8-hydroxyquinoline arms of the ligand through the oxygen atoms of the carbonyl and hydroxyl groups. The spectrum of the $Fe\mathbf{L^1}H_3$ complex exhibits an absorption band at λ_{max} = 560 nm (ε = 3970 $M^{-1}\cdot cm^{-1}$), in agreement with the bis(oxinate) coordination. The oxygen and pyridine nitrogen atoms of two 8-hydroxyquinoline arms are involved in the coordination. The value $pK_{FeL^1H_5}$ = 2.4 ($Fe\mathbf{L^1}H_5/Fe\mathbf{L^1}H_3$ equilibrium) corresponds to the deprotonation of both 8-hydroxyquinoline nitrogens in a two-proton step. The small

 © 2003 Wiley-VCH Verlag GmbH & Co. KGaA, Weinheim

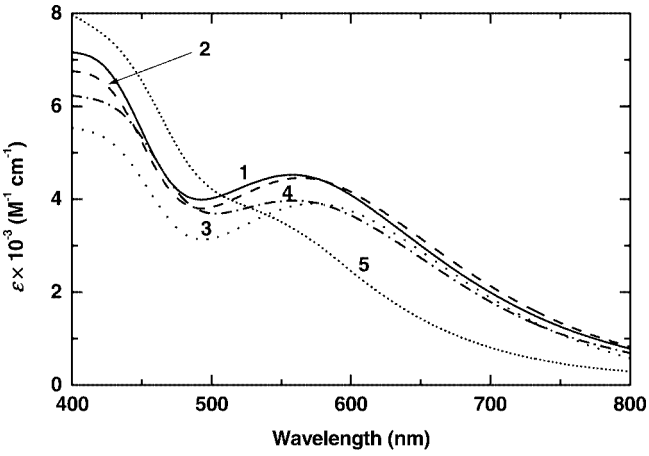

a)

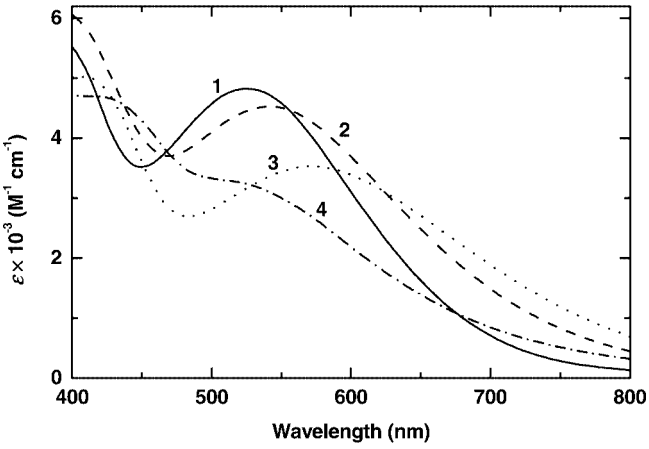

b)

Figure 6. Calculated electronic spectra of the ferric complexes formed with the heterotripodal ligands; solvent: water, I = 0.10 M ($NaClO_4$), T = (25.0 ± 0.2) °C: (a) ferric $\mathbf{L^1}$ species: (1) Fe$\mathbf{L^1}$, (2) Fe$\mathbf{L^1}$H, (3) Fe$\mathbf{L^1}H_2$, (4) Fe$\mathbf{L^1}H_3$, (5) Fe$\mathbf{L^1}H_5$; (b) ferric $\mathbf{L^2}$ species: (1) Fe$\mathbf{L^2}$ ≡ Fe$\mathbf{L^2}$ H, (2) Fe$\mathbf{L^2}H_2$, (3) Fe$\mathbf{L^2}H_4$, (4) Fe$\mathbf{L^2}H_5$; charges are omitted for the sake of clarity

red-shift of λ_{max} to 580 nm for the formation of Fe$\mathbf{L^1}H_2$ without significant change of ε (3930 $M^{-1}\cdot cm^{-1}$) might be attributed to the deprotonation of the ammonium nitrogen. The value $pK_{FeL^1H_3}$ = 1.9 shows a strong stabilisation of the deprotonated tertiary amine nitrogen by intramolecular hydrogen bonds. The increase of ε to 4490 $M^{-1}\cdot cm^{-1}$ with the concomitant blue shift of λ_{max} to 560 nm for the formation of Fe$\mathbf{L^1}$H is in agreement with the coordination of the catechol arm in a salicylate mode. The last deprotonation equilibrium is accompanied with a spectral change (λ_{max} = 550 nm, ε = 4560 $M^{-1}\cdot cm^{-1}$) that is indicative of a shift to a catecholate coordination and formation of the Fe$\mathbf{L^1}$ species. It should be pointed out that the values of pK_{FeLH_2} and pK_{FeLH} (2.7 and 4.8) are significantly lower than those observed for tris(catecholate) complexes: 8.34 (two-proton step) and 5.5 for $\mathbf{L^3}$, and 4.1 and 5.74 for MECAMS[9] (Table 3), while the pK_a's of the free ligand are of the same order of magnitude.

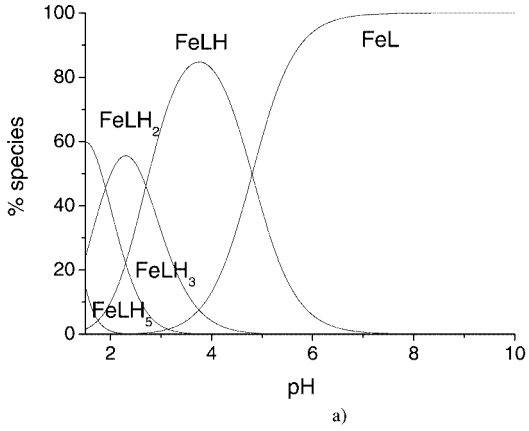

a)

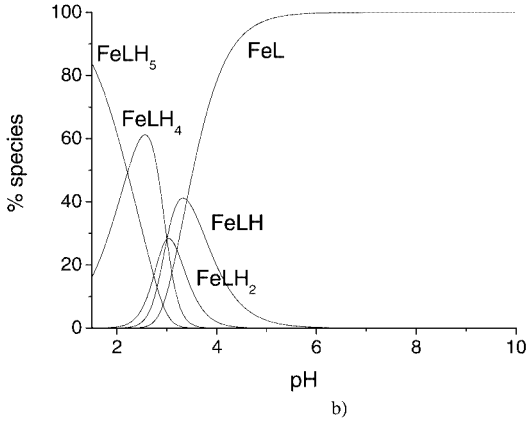

b)

Figure 7. Speciation diagrams for (a) ferric-$\mathbf{L^1}$ complexes, (b) ferric-$\mathbf{L^2}$ complexes

Table 3. Successive deprotonation constants of ferric complexes;[a] solvent: water, I = 0.10 M ($NaClO_4$), T = (25.0 ± 0.2) °C

Ligand[a][b]	pK_{FeLH_5}	pK_{FeLH_4}	pK_{FeLH_3}	pK_{FeLH_2}	pK_{FeLH}
$\mathbf{L^0}$ [2]	5.7[c]				5.6
$\mathbf{L^1}$	2.4[d]		1.9	2.7	4.8
$\mathbf{L^2}$	2.2	6.0[d]		3.0	3.4
$\mathbf{L^3}$ [3]	3.1	3.5	8.34[d]		5.5
Enterobactin[26]			2.5	3.52	4.95
MECAMS [9]			3.46	4.10	5.74
COX [24]		4.8[e]			2.12
CacCAM [25]				5.15	6.59

[a] K_{FeLHn} = ([$FeLH_{n-1}$] × [H])/[$FeLH_n$]. [b] MECAMS: 1,3,5-tris{[(2,3-dihydroxy-5-sulfobenzoyl)amino]methyl}benzene; COX: 1,1,1-tris[3-(8-hydroxyquinoline-7-carboxamido)propyl]-(polyethylene glycol$_{<43>}$methyl ether]; CacCAM: 2,2,2-tris[3-(2,3-dihydroxybenzamido)propyl]acetic acid. [c] K_{FeLHn} = ([FeLH] × $[H]^4$)/[$FeLH_5$]. [d] K_{FeLHn} = ([$FeLH_{n-2}$] × $[H]^2$)/[$FeLH_n$]. [e] K_{FeLHn} = ([FeLH] × $[H]^3$)/[$FeLH_4$].

The spectral properties of the Fe$\mathbf{L^2}H_5$ species (ε = 4700 $M^{-1}\cdot cm^{-1}$ at λ_{max} = 409 nm and a shoulder at 520 nm with ε = 3260 $M^{-1}\cdot cm^{-1}$) are intermediate between the bis(salicylate) coordination of ferric $\mathbf{L^3}$ (two catechols)[3] and ferric $\mathbf{L^0}$ (two 8-hydroxyquinolines).[2] This confirms that $\mathbf{L^2}$ forms a bis(salicylate) complex with one catechol and one

 © 2003 Wiley-VCH Verlag GmbH & Co. KGaA, Weinheim

8-hydroxyquinoline coordinated to the ferric ion. For the formation of Fe$\mathbf{L^2}H_4$ the λ_{max} is red-shifted to 573 nm, consistent with the change of coordination from a salicylate to an oxinate mode for the 8-hydroxyquinoline arm. There is only a slight change in ε (3530 $M^{-1}\cdot cm^{-1}$), indicating that iron is still coordinated by two arms. The value $pK_{FeL^2H_5}$ = 2.2 of the Fe$\mathbf{L^2}H_5$/ Fe$\mathbf{L^2}H_4$ equilibrium corresponds well to the pyridinium nitrogen deprotonation. The formation of the Fe$\mathbf{L^2}H_2$ and Fe$\mathbf{L^2}H$ species is accompanied by spectral shifts of λ_{max} from 573 nm to 542 nm and 525 nm, respectively, and an increase of ε to 4530 $M^{-1}\cdot cm^{-1}$ and 4820 $M^{-1}\cdot cm^{-1}$ is observed. The equilibrium between Fe$\mathbf{L^2}H_4$ and Fe$\mathbf{L^2}H_2$ ($pK_{FeL^2H_4}$ = 6.0) is attributed to the coordination of the third arm (catechol) in a salicylate mode and the change of coordination from salicylate to catecholate for the coordinated catechol arm. The equilibrium between Fe$\mathbf{L^2}H_2$ and Fe$\mathbf{L^2}H$ corresponds to the shift of bonding mode from salicylate to catecholate of the third catechol arm ($pK_{FeL^2H_2}$ = 3.0). As for Fe$\mathbf{L^1}$ complexes, the deprotonation of the catechol groups upon complexation occurs at lower pH than for tris(catechol) ligands cited above. The last equilibrium leading to Fe$\mathbf{L^2}$ species does not induce any spectral changes. It is likely that the deprotonation of the tertiary amine nitrogen is involved. The value of pK_{FeL^2H} = 3.4 is higher than the corresponding constant for ferric $\mathbf{L^1}$ complex ($pK_{FeL^1H_3}$ = 1.9).

pFe^{III} Values

Since the ligands are weak acids, proton competition occurs depending on their protonation constants and the pH. The pFe^{III} value (−log [Fe^{III}]) is thus a better measure of the relative efficiency of the ligands under given conditions of pH, $[Fe^{III}]_{tot}$ and $[L]_{tot}$. The pFe^{III} values have been calculated for pH values over the range 2−10 and are reported as the plot of pFe^{III} vs. pH presented in Figure 8, together with the plots calculated for $\mathbf{L^0}$ and $\mathbf{L^3}$.

The important result, as seen from Figure 8, is that the mixed ligands $\mathbf{L^1}$ and $\mathbf{L^2}$ are stronger iron chelating agents than $\mathbf{L^0}$ and $\mathbf{L^3}$ over the pH range 5−9. This shows that mixed ligands lead to enhanced affinity for the ferric ion at pH above 5 ($\mathbf{L^1}$) or 6 ($\mathbf{L^2}$) relative to ligands with three identical arms. This is related to the different basicities of the binding subunits. Catechol is more basic than 8-hydroxyquinoline, which leads to a stronger competition of protons with ferric ions for catechol ligands at low pH. Hence, 8-hydroxyquinoline is a better chelating agent at low pH, while catechol is a stronger chelator at high pH as observed for $\mathbf{L^0}$ [tris(8-hydroxyquinoline) ligand] and $\mathbf{L^3}$ [tris-(catechol) ligand]. Our results with $\mathbf{L^1}$ (one catechol group) and $\mathbf{L^2}$ (two catechol groups) show that a greater pK_a difference between the proton dissociation of the catechol in the free ligand and that of the same group in the complex is observed in comparison to other tripodal ligands containing only catechol groups (see Table 3). This suggests that the initial coordination of the 8-hydroxyquinoline arm with Fe^{III} favours proton loss of the free catechol and thus increases the affinity of this group for Fe^{III}. This can explain that the highest values for pFe^{III} are obtained with $\mathbf{L^1}$ and $\mathbf{L^2}$ over the pH range 5−9, which is biologically relevant, as shown by the plot in Figure 8. We have also reported in Table 2 the pFe^{III} values calculated under standard conditions (pH = 7.4, $[L]_{tot} = 10^{-5}$ M, $[Fe^{III}]_{tot} = 10^{-6}$ M) for $\mathbf{L^1}$ (31.6) and for $\mathbf{L^2}$ (32.3). These values are higher than those determined for $\mathbf{L^0}$ (29.5) and for $\mathbf{L^3}$ (29.6) and among the highest values determined for an iron sequestering agent.

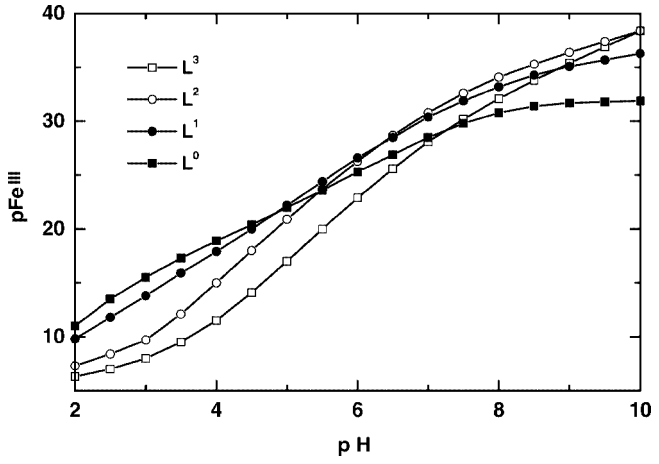

Figure 8. Plot of pFe versus pH for the tripodal ligands; calculated for $[L]_{tot} = 10^{-5}$ M and $[Fe^{III}]_{tot} = 10^{-6}$ M

Conclusion

Iron(III) complexation by two heterotripodal ligands $\mathbf{L^1}$ and $\mathbf{L^2}$ has been characterised. The results are compared to the parent homotripodal ligands allowing the study of the variation of the ligand properties from tris(8-hydroxyquinoline) to tris(catechol) ligand. The thermodynamic and spectroscopic study reveals that in the acidic medium the complex formation starts with two arms coordinating the ferric ion in the salicylate coordination mode. Both 8-hydroxyquinoline subunits are involved in the case of $\mathbf{L^1}$, and one 8-hydroxyquinoline and one catecholate subunit in the case of $\mathbf{L^2}$. This indicates that 8-hydroxyquinoline is a better ligand than catechol at low pH values. Despite the fact that catechol oxygens are better donors than the oxygen and nitrogen atoms of 8-hydroxyquinoline, the competition between H^+ and the metal cation "balances" the complexation efficiency. The striking feature of the mixed ligands is their higher complexing ability than that of the parent ligands over a range of biologically relevant pH values, and especially at neutral pH. This can be explained by the finely tuned complexation power of 8-hydroxyquinoline and catechol groups. It should be noted that the complexation efficiency of the tris(8-hydroxyquinoline) ligand $\mathbf{L^0}$ is less sensitive to pH than the tris(catechol) ligand $\mathbf{L^3}$ over the pH range 2−10. The results described in this work illustrate the great interest of the mixed ligands approach, which, via a synergistic action, leads to a more efficient iron complexing agent than the homopodate ligands.

 © 2003 Wiley-VCH Verlag GmbH & Co. KGaA, Weinheim

Experimental Section

Materials and Equipment: Solvents were purified by standard techniques. The amine TREN was distilled from over CaH_2. All other compounds were of reagent grade and were used without further purification. Mass spectra were obtained on NERMAG R 10 10C or Thermo Finnigan Polaris Q or Bruker Esquire-LC 1.6n (electrospray) mass spectrometers. ^1H and ^{13}C NMR spectra were recorded in 5 mm tubes at 25 °C with Bruker AC 200 or WM 250 or Avance 300 spectrometers (δ ppm, TMS reference). Microanalyses were performed by the Central Service of CNRS, Solaise (France). Melting points were determined with a Büchi apparatus and are not corrected.

***N*¹,*N*¹-bis(2-aminoethyl)-*N*²-(trityl)-1,2-ethanediamine (2):** Under argon at room temperature, triphenylchloromethane (2.65 g, 9.5 mmol) in dry CH_2Cl_2 (150 mL) was added dropwise to a solution of tris(2-aminoethyl)amine (1; 5.56 g, 38 mmol) in CH_2Cl_2 (100 mL). The mixture was stirred overnight and then successively washed with 10% NaOH (ca. 100 mL) and brine. The organic phase was dried over sodium sulfate and concentrated under vacuum to give **2** as a yellowish solid (3.7 g, yield: 9.5 mmol, 100%). M.p. 63−65 °C. ^1H NMR (200 MHz, $CDCl_3$): δ = 7.5 (m, 6 H, ArH), 7.3−7.1 (m, 9 H, ArH), 2.9 (br. s, 5 H, NH), 2.7 (t, $^3J_{H,H}$ = 6 Hz, 4 H, CH_2), 2.6 (t, $^3J_{H,H}$ = 6 Hz, 2 H, CH_2), 2.4 (t, $^3J_{H,H}$ = 6 Hz, 4 H, CH_2), 2.2 (t, $^3J_{H,H}$ = 6 Hz, 2 H, CH_2) ppm. ^{13}C NMR (250 MHz, $CDCl_3$): δ = 146.1 (Cq), 128.5 (CH), 127.7 (CH), 126.1 (CH), 70.6 (Cq), 57.4 (CH_2), 55.0 (CH_2), 40.8 (CH_2), 39.9 (CH_2) ppm. MS (DCI, NH_3/isobutane): *m*/*z* = 389 $[M + H]^+$, 243 $[C_{19}H_{15}]^+$.

Compound 3a: Under a stream of argon in order to remove CO_2 as and when it is produced, a solution of 8-benzyloxy-7-carboxyquinoline (3.65 g, 13 mmol) in dry THF (150 mL) was treated with a solution of carbonyldiimidazole (CDI; 2.2 g, 13.6 mmol) in THF (40 mL), under reflux for 2 h. Tripod **2** (2.535 g, 6.5 mmol) in THF (50 mL) was then added dropwise and the mixture was stirred overnight under reflux. The solvent was evaporated off and CH_2Cl_2 was added to the residue. The solution was washed successively with saturated NH_4Cl and brine and then dried. Concentration afforded a dark oil which was chromatographed (silica, cyclohexane/CH_2Cl_2 gradient, then CH_2Cl_2/methanol 1 → 2%) to give **3a** as a yellow foam (3.7 g, 4 mmol, 62%). ^1H NMR (250 MHz, $CDCl_3$): δ = 8.95 (dd, $^3J_{H,H}$ = 1.6, 4.0 Hz, 2 H, ArH), 8.14 (m, 4 H, ArH), 8.07 (br. t, $^3J_{H,H}$ = 4.8 Hz, 2 H, NH amide), 7.6−7.0 (m, 29 H, ArH), 5.5 (s, 4 H, CH_2 benzyl), 3.2 (dt, $^3J_{H,H}$ = 6.3, 4.8 Hz, 4 H, CH_2), 2.47 (t, $^3J_{H,H}$ = 5.5 Hz, 2 H, CH_2), 2.21 (t, $^3J_{H,H}$ = 6.3, 4.8 Hz, 4 H, CH_2), 2.13 (t, $^3J_{H,H}$ = 5.3 Hz, 2 H, CH_2), 2.0 (br. s, 1 H, NH) ppm. ^{13}C NMR (250 MHz, $CDCl_3$): δ = 165.1 (CO), 153.8 (Cq), 149.5 (CH), 146.1 (Cq), 142.6 (Cq), 136.7 (Cq), 136.0 (CH), 131.3 (Cq), 128.8−128.5 (unresolved CH's), 127.6 (unresolved CH's), 126.0 (CH), 125.3 (Cq), 123.1 (CH), 122.3 (CH), 78.3 (CH_2), 70.7 (Cq), 53.9 (CH_2), 52.5 (CH_2), 40.5.(CH_2) ppm. MS (DCI, NH_3/isobutane): *m*/*z* = 911 $[MH]^+$, 243 $[C_{19}H_{15}]^+$; 91 $[C_7H_7]^+$. $C_{59}H_{54}N_6O_4$ (911.1): calcd. C 77.78, H 5.97, N 9.22; found C 77.40, H 5.92, N 9.31.

Compound 4a: Under argon at room temperature, a solution of **3a** (3.61 g, 4 mmol) in CH_2Cl_2 (100 mL) was stirred with CF_3CO_2H (3.7 g, 32 mmol) for 12 h. The mixture was treated with 10% NaOH, then washed with brine, dried and concentrated. Column chromatography (silica, CH_2Cl_2 then CH_2Cl_2/methanol 5%/isopropylamine 1%) afforded **4a** as a beige foam (2.15 g, 81%). ^1H NMR (300 MHz, $CDCl_3$, 22 °C, TMS): δ = 8.95 (dd, $^3J_{H,H}$ = 1.7, 4.1 Hz, 2 H, Hquin), 8.22 (br. t, $^3J_{H,H}$ = 5.6 Hz, 2 H, NH amide), 8.11 (dd, $^3J_{AB}$(H-H) = 1.7, 4.1 Hz, 2 H, Hquin), 7.97 (d, $^3J_{H,H}$ = 8.6 Hz, 2 H, Hquin), 7.5−7.3 (m, 14 H, ArH and Hquin), 5.5 (s, 4 H, CH_2 benzyl), 3.25 (dt, $^3J_{H,H}$ = 5.6, 6.4 Hz, 4 H, CH_2), 3.2 (br. t, 2 H, NH_2), 2.59 (m, 2 H, CH_2), 2.50 (m, 2 H, CH_2), 2.36 (t, ^{3}(H-H) = 6.4 Hz, 4 H, CH_2) ppm. ^{13}C NMR (300 MHz, $CDCl_3$): δ = 165.5 (CO), 153.7 (Cq), 149.6 (CH), 142.4 (Cq), 136.7 (Cq), 136.1 (CH), 131.3 (Cq), 128.9 (CH), 128.8 (CH), 128.7 (CH), 127.3 (CH), 125.3 (Cq), 123.2 (CH), 122.3 (CH), 78.5 (CH_2), 55.1 (CH_2), 53.5 (CH_2), 38.9(CH_2), 37.9(CH_2) ppm. MS (DCI, NH_3/isobutane): *m*/*z* = 669 $[M + H]^+$.

Compound 5a: 2,3-Dimethoxybenzoic acid (0.62 g, 3.4 mmol) was dissolved in $SOCl_2$ (15 mL) and the mixture was stirred overnight under argon. The solution was then evaporated to dryness to give 2,3-dimethoxybenzoic chloride (0.685 g). Compound **4a** (2.27 g, 3.4 mmol), triethylamine (0.35 g, 3.5 mmol) and dry CH_2Cl_2 (150 mL) were added and the mixture was stirred at room temperature under argon. The mixture was treated successively with 25% NaOH and brine and then dried and the solvent was evaporated off. Column chromatography (silica, CH_2Cl_2 then CH_2Cl_2/methanol 1 → 5%) gave **5a** as a white foam (1.665 g, 2 mmol, yield = 59%). ^1H NMR (250 MHz, CD Cl_3): δ = 8.94 (dd, $^3J_{H,H}$ = 1.6, 4.0 Hz, 2 H, Hquin), 8.2−8.1 (m, 7 H, Hquin + NH amide), 7.6−7.3 (m, 15 H, ArH), 7.01 (t, $^3J_{H,H}$ = 7.9 Hz, 1 H, H catech.), 6.89 (dd, $^3J_{H,H}$ = 1.6, 6.4 Hz, 1 H, H catech.), 5.55 (s, 4 H, CH_2 benzyl), 3.80 (s, 3 H, OCH_3), 3.75 (s, 3 H, OCH_3), 3.41−3.25 (m, 6 H, CH_2), 2.6 (m, 2 H, CH_2), 2.4 (m, 4 H, CH_2) ppm. ^{13}C NMR (250 MHz, $CDCl_3$): δ = 165.2 (CO), 165.0 (CO), 153.8(Cq), 152.3 (Cq), 149.5 (CH), 147.4 (Cq), 142.4 (Cq), 136.7 (Cq), 135.9 (CH), 131.2 (Cq), 128.6 (unresolved CH's), 127.4 (CH), 126.8 (Cq), 125.0 (Cq), 123.9 (CH), 123.0 (CH), 122.4 (CH), 122.2 (CH), 114.9 CH), 78.3 (CH_2), 61.1 (CH_3), 55.7 (CH_3), 52.7 (CH_2), 52.4 (CH_2), 37.5 (CH_2), 37.2 (CH_2) ppm. MS (FAB, NBA matrix): *m*/*z* = 833 $[M + H]^+$, 541, 305 $[C_{19}H_{17}N_2O_2]^+$. $C_{49}H_{48}N_6O_7$ (832.9): calcd. C 70.66, H 5.81, N 10.09; found C 70.21, H 5.83, N 9.96.

Compound 6a: Under argon at 0 °C, BBr_3 (5.3 g, 21 mmol) in CH_2Cl_2 (30 mL) was added dropwise to a solution of **5a** (1.52 g, 1.8 mmol) in CH_2Cl_2 (250 mL). After stirring overnight at room temperature, the mixture was cooled to 0 °C and treated with methanol (50 mL). After 4 h the solution was concentrated and then repeatedly evaporated with methanol to remove the borate. The residue was treated with 4 N NaOH and extracted with CH_2Cl_2 to remove the impurities. The aqueous solution was acidified with 4 N HCl to give a beige precipitate which was washed with water and then dried under vacuum to give pure 6a (0.937 g, 1.5 mmol, 83%). ^1H NMR (300 MHz, DMSO): δ = 9.0−8.7 (m, 5 H, NH + ArH),8.3−8.1 (m, 2 H, ArH), 8.0 −7.8 (m, 2 H, ArH), 7.6−7.5 (m, 2 H, ArH), 7.3−7.1 (m, 4 H, ArH), 6.9−6.8 (m, 1 H, ArH), 3.5−3.3 (m, 6 H, CH_2), 2.8−2.7 (m, 6 H, CH_2) ppm. ^{13}C NMR (250 MHz, $CDCl_3$): δ = 169.6 (CO), 167.7 (CO), 156.7 (Cq), 151.2 (Cq), 149.4(Cq), 148.7 (CH), 146.2 (Cq), 139.1 (Cq), 135.9 (CH), 130.4 (Cq), 125.2 (CH), 118.5 (CH), 117.7 (CH), 117.6 (CH), 116.6 (CH), 112.8 (Cq), 52.9 (CH_2), 52.8 (CH_2), 37.3 (CH_2), 37.2 (CH_2) ppm. MS (DCI, NH_3/isobutane): *m*/*z* = 625 $[M + H]^+$.

Compound L¹: In portions, **6a** (0.7 g, 1.1 mmol) was added to oleum (SO_3/H_2SO_4; 15 mL) while stirring vigorously. After stirring overnight at room temperature, the mixture was carefully poured onto ice to give a beige precipitate. Filtration and washing with cold water gave the product, which was recrystallised from a minimum amount of water. The pure product (acidic form) was thoroughly dried under vacuum at 30 °C. A yellow powder was obtained (0.347 g, 0.4 mmol, 36.5%). ^1H NMR (300 MHz, D_2O/NaOD): δ = 8.65 (dd, $^3J_{H,H}$ = 1.6, 8.6 Hz, 2 H, Hquin), 8.56 (dd,

 © 2003 Wiley-VCH Verlag GmbH & Co. KGaA, Weinheim

$^3J_{H,H}$ = 1.5, 4.1 Hz, 2 H, Hquin), 8.40 (s, 2 H, Hquin), 7.63 (d, $^3J_{H,H}$ = 2.5 Hz, 1 H, Hcatech.), 7.47 (dd, $^3J_{H,H}$ = 4.1, 8.6 Hz, 2 H, Hquin), 7.03 (d, $^3J_{H,H}$ = 2.6 Hz, 1 H, Hcatech.), 3.54 (m, 6 H, CH_2), 2.85 (m, 6 H, CH_2) ppm. ^{13}C NMR (300 MHz, D_2O-NaOD): δ = 171.3 (Cq), 170.7 (Cq), 170.2 (Cq), 161.3 (Cq), 148.9 (Cq), 147.4 (CH), 145.1 (Cq), 134.6 (CH), 129.1 (CH), 127.8 (Cq), 125.9 (Cq), 123.9 (CH), 119.6 (Cq), 119.0 (CH), 116.1 (Cq), 111.4 (Cq), 111.0 (CH), 53.2 (CH_2), 36.9 (CH_2) ppm. MS (Electrospray, methanol/water, +ve mode): *m/z* = 865 $[M + H]^+$. $C_{33}H_{32}N_6O_{16}S_3 \cdot 3.5H_2O$: calcd. C 42.72, H 4.24, N 9.06, S 10.37; found C 42.51, H 3.85, N 8.49, S 9.62.

Compound 4b: Under argon, a mixture of 2,3-dimethoxybenzoic acid (5.28 g, 29 mmol) and CDI (5.16 g, 31.9 mmol) in dry CH_2Cl_2 (350 mL) was refluxed for 1.5 h. A solution of TREN (2.11 g, 14.5 mmol) in CH_2Cl_2 (40 mL) was added dropwise and reflux was maintained overnight. The solution was filtered and washed with 4 N NaOH then brine. After drying over anhydrous Na_2SO_4, the solvent was eliminated to afford an oil. Chromatography (silica, CH_2Cl_2/methanol 1 → 8% and $iPrNH_2$ 1%) gave **4b** as a pale yellow oil (6.53 g, 13.7 mmol, 95%) pure enough for the following steps. ^{1}H NMR (200 MHz, $CDCl_3$): δ = 8.22 (br. t, $^3J_{H,H}$ = 5 Hz, 2 H, NH), 7.61 (dd, $^3J_{H,H}$ = 1.6, 8 Hz, 2 H, ArH), 7.11 (t, $^3J_{H,H}$ = 8 Hz, 2 H, ArH), 7.01 (dd, $^3J_{H,H}$ = 1.6, 8 Hz, 4 H, ArH), 3.88 (s, 6 H, OCH_3), 3.87 (s, 6 H, OCH_3), 3.60 (dt, $^3J_{H,H}$ = 5.8, 6.2 Hz, 4 H, CH_2), 2.75 (m, 8 H, CH_2), 2.64 (m, 2 H, CH_2), 2.2 (br. s, 2 H, NH_2) ppm. ^{13}C NMR (200 MHz, $CDCl_3$): δ = 165.3 (CO), 152.3 (Cq), 147.2 (CH), 126.7 (Cq), 124.1 (CH), 122.3 (CH), 115.1 (CH), 61.1 (OCH_3), 57.0 (CH_2), 55.87 (OCH_3), 53.5 (CH_2), 39.7 (CH_2), 37.6 (CH_2) ppm. MS (DCI, NH_3/isobutane): *m/z* = 475 [M + H], 432, 280, 208, 182.

Compound 5b: Under argon a solution of 7-carboxy-8-hydroxyquinoline (2.30 g, 12 mmol) and CDI (2.27 g, 14 mmol) in dry THF (200 mL) was refluxed for 3 h. Compound **4b** (6 g, 12 mmol) in THF (80 mL) was added dropwise and the reflux was maintained during 12 h. The THF was evaporated off and the residue was dissolved CH_2Cl_2 and treated with NH_4Cl and brine. Drying and evaporation of the solvent afforded an orange foam which was chromatographed (silica, $iPrNH_2$ 1%, CH_2Cl_2, MeOH 1 → 5%) to give **4b** (5.8 g, 9 mmol, 75%) pure enough for the following step. ^{1}H NMR (20 MHz, CD Cl_3): δ = 8.82 (dd, $^3J_{H,H}$ = 1.6, 4.2 Hz, 1 H, Hquin), 8.19 (br. t, 3 H, NH), 8.11−8.02 (m, 1 H, Hquin),7.56−7.44 (m, 3 H, ArH + Hquin),7.27−6.86 (m, 6 H, ArH + Hquin), 3.83 (s, 6 H, 0 CH_3), 3.76 (s, 6 H, 0 CH_3), 3.65−3.56 (m, 6 H, CH_2), 2.94−2.82 (m, 6 H, CH_2) ppm. ^{13}C NMR (250 MHz, $CDCl_3$): δ = 167.2 (CO), 165.5 (CO), 154.4 (Cq), 152.2 (Cq), 148.1 (CH), 147.1 (Cq), 138.9 (Cq), 135.6 (Cq), 130.1 (Cq), 126.7 (Cq), 126.1 (CH), 124.0 (CH),122.8 (CH), 122.2 (CH), 116.7 (CH), 114.9 (CH), 112.8 (Cq), 61.1 ($COCH_3$), 55.7 ($COCH_3$), 53.7 (COH_2), 53.2 (CH_2), 37.8 (CH_2), 37.7 (CH_2) ppm.

Compound 6b: Under argon at 0 °C, BBr_3 (9.04 g, 36 mmol) in CH_2Cl_2 (30 mL) was added dropwise to a solution of **5b** (1.94 g, 3 mmol) in CH_2Cl_2 (300 mL). After stirring overnight at room temperature, the mixture was treated with methanol (50 mL) at 0 °C. The solution was concentrated and then repeatedly evaporated with methanol. The residue was treated with 4 N NaOH and extracted with CH_2Cl_2. The aqueous solution was then acidified to pH 7.6 with 4 N HCl to give a beige precipitate which was washed with water and dried under vacuum to give **6b** pure enough for the following step (1.65 g, 2.8 mmol, 93%). ^{1}H NMR (200 MHz, DMSO): δ = 8.9 (m, 1 H, Hquin), 8.7 (m, 3 H, NH), 8.32 (d, $^3J_{H,H}$ = 8.2 Hz, 1 H, Hquin), 7.94 (d, $^3J_{H,H}$ = 8.0 Hz, 1 H, Hquin), 7−6.3 (dd, $^3J_{H,H}$ = 4.80, 4 Hz, 1 H, Hquin), 7.37 (d, $^3J_{H,H}$ = 28.2 Hz, 1 H, Hquin.), 7.20 (d, $^3J_{H,H}$ = 7.4 Hz, 2 H, Hcat.), 6.84 (d, $^3J_{H,H}$ = 7.4 Hz, 2 H, Hcat.), 6.54 (t, $^3J_{H,H}$ = 7.4 Hz, 2 H, Hcat.), 3.42 (m, 6 H, CH_2), 2.77 (m, 6 H, CH_2) ppm. ^{13}C NMR (250 MHz, DMSO): δ = 169.7 (CO), 167.9 (CO), 156.4 (Cq), 149.4 (Cq), 149.0 (CH), 146.1 (Cq), 139.0 (Cq), 136.1 (CH), 130.5 (Cq), 125.3 (CH), 123.4 (CH), 118.8 (CH), 117.9 (CH), 117.3 (CH), 116.8 (CH), 115.1 (Cq), 112.7 (Cq), 52.6 (CH_2), 36.8 (CH_2) ppm. MS (DCI, NH_3/isobutane): *m/z* = 590 [M + H].

Compound L^2: In portions, **6b** (1.49 g, 2.5 mmol) was added to oleum (SO_3/H_2SO_4) (20 mL) while stirring vigorously. After stirring at room temperature for 12 h, the mixture was carefully poured onto ice to give a brown precipitate. Filtration and washing with cold water afforded the product, which was recrystallised from a minimum amount of water. The pure product (acidic form) was dried under vacuum at 30 °C. A yellowish powder was obtained (0.672 g, 0.8 mmol, 32%). ^{1}H NMR (250 MHz, D_2O/NaOD): δ = 8.48 (m, 1 H, Hquin), 8.48 (m, 1 H, Hquin), 8.23 (s, 1 H, Hquin), 7.30 (m, 1 H, Hquin), 7.14 (m, 2 H, Hcatech), 6.49 (m, 2 H, Hcatech), 3.30 (m, 6 H, CH_2), 2.62 (m, 6 H, CH_2) ppm. ^{13}C NMR (250 MHz, D_2O-NaOD): δ = 174.3 (Cq), 174.0 (Cq), 173.1 (Cq), 170.2 (Cq), 163.2 (Cq), 150.1 (CH), 147.8 (Cq), 137.0 (CH), 131.6 (CH), 130.3 (Cq), 128.6 (CH), 126.5 (Cq), 122.1 (Cq), 117.6 (Cq), 115.5 (CH), 115.4 (CH), 113.8 (Cq), 55.9 (CH_2), 39.3 (CH_2), 39.2 (CH_2) ppm. MS (Electrospray, methanol/water, +ve mode): *m/z* = 830 $[M + H]^+$, 750 $[M - SO_3]$. $C_{30}H_{31}N_5O_{17}S_3$ $5H_2O$: calcd. C 39.17, H 4.49; N 7.61; S 10.46; found C 39.29, H 4.59, N 7.64, S 9.65.

Potentiometric and Spectrophotometric Measurements: The solutions were prepared with boiled deionised water, de-oxygenated and flushed continuously with argon (purified by a Sigma Oxiclear cartridge) in order to exclude CO_2 and O_2. The ionic strength was maintained at 0.1 M with sodium perchlorate (Prolabo, Puriss or Merck, p.a.) and all measurements were carried out at (25.0 ± 0.2) °C. Perchloric acid (70%, Fluka; approx. 0.1 M) and sodium hydroxide (Normex, Carlo Erba; approx. 0.1 M) concentrations were determined respectively by titration of sodium tetraborate solution (purris. p. a., ACS, Fluka, approx. 0.1 M) in the presence of methyl red as indicator (Pointet Girard, France) and potassium hydrogenphthalate (purris. p. a., Fluka, approx. 0.1 M), with phenolphthalein as indicator (Prolabo, France). The ligands L^1 and L^2 were dissolved in aqueous 0.1 M $NaClO_4$ medium and their concentrations were calculated by weight. Stock iron(III) solutions [$Fe(ClO_4)_3 \cdot 9H_2O$, pract., Fluka or Aldrich; approx. 0.01 M], prepared under acidic conditions (0.1 M $HClO_4$), were back titrated with $Th(NO_3)_4 \cdot 5H_2O$ (Merck, approx. 0.1 M) in the presence of excess EDTA (Titrisol, Merck, approx. 0.1 M) and xylenol orange (Merck) as end-point indicator.[27] The concentration was also controlled spectrophotometrically by using the molar extinction coefficient[28] of 4160 $M^{-1} \cdot cm^{-1}$ at 240 nm in 0.1 M $HClO_4$. The acid in excess was evaluated by a potentiometric titration with standardised 0.1 M NaOH solution using quantitative formation of a complex with maltol (99%, Aldrich).[29] L^1 and L^2 ferric complexes were prepared by mixing adequate volumes of stock ferric perchlorate and stock ligand solutions. The free hydrogen concentrations were measured with a glass-Ag/AgCl combined electrode (Metrohm or Tacussel High Alkalinity, filled with 0.1 M NaCl and saturated with AgCl). The electrode was calibrated in order to read the pH according to the classical method (neutralisation of 0.1 M $HClO_4$ by 0.1 M NaOH).[30]

The potentiometric titrations were performed into a jacketed cell, thermostatted by the water flow of a Haake thermostat, using either a digital millivoltmeter (Tacussel Isis 20,000) with a piston-

 © 2003 Wiley-VCH Verlag GmbH & Co. KGaA, Weinheim

fitted microburette (Gilmont) or an automatic titrator system (Metrohm, DMS Titrino 716) connected to an IBM Aptiva microcomputer. The titrations of the ligands ($[\mathbf{L}] \approx 10^{-3}$ M, $2.5 < pH < 10.5$ for $\mathbf{L^1}$ and $3.9 < pH < 9.8$ for $\mathbf{L^2}$) and of their iron(III) complexes ($[Fe^{III}]_{tot} = [\mathbf{L}]_{tot} \approx 10^{-3}$ M, $2.2 < pH < 11.0$ for $\mathbf{L^1}$ and $2.3 < pH < 8.9$ for $\mathbf{L^2}$) were carried out by addition of known volumes of standardised sodium hydroxide. The data obtained during the potentiometric titrations were fitted with the Superquad[31] or Hyperquad[32] software packages.

Spectrophotometric measurements were carried out on double-beam UV/Vis spectrophotometers, either Uvikon 941 (Kontron) or Perkin–Elmer (Lambda 2), equipped with a thermostatting cell holder (Perkin–Elmer PTP-1) and connected to an IBM PC 340 microcomputer for data acquisition (UV Winlab software, Perkin–Elmer). Absorption spectra of the free ligands ($[\mathbf{L}]_{tot} \approx 10^{-4}$ M, 240 nm $< \lambda <$ 400 nm, $2.5 < pH < 10.5$ for $\mathbf{L^1}$ and $2.6 < pH < 12.5$ for $\mathbf{L^2}$) and of their iron(III) species ($[\mathbf{L}]_{tot} = [Fe^{III}]_{tot} \approx 10^{-4}$ M, 400 nm $< \lambda <$ 800 nm, for $\mathbf{L^1}$ $2.5 < pH < 10.5$ and $1.0 < pH < 9.0$ for $\mathbf{L^2}$) were measured at different pH values using quartz spectrophotometric cells of 0.2 or 1 cm optical path length (Hellma) against 0.1 M aqueous $NaClO_4$ solution as a reference. Absorption spectra recorded as a function of pH for ferric complexes of $\mathbf{L^1}$ and $\mathbf{L^2}$ are given in the supporting information (Figures S3 and S4).

A batch competition titration between the ferric $\mathbf{L^2}$ complex and EDTA (99.5%, A.C.S. reagent, Aldrich) was carried out under conditions of $[\mathbf{L^2}]_{tot} = 5.4 \times 10^{-5}$ M, $[Fe^{III}]_{tot} = 4.5 \times 10^{-5}$ M, $[EDTA]_{tot} = 9.21 \times 10^{-4}$ M and the pH values adjusted with perchloric acid over the range 3.9 to 5.5 (in steps of 0.1 pH unit). The solution was equilibrated for two days and then the absorption spectra were recorded (400–800 nm).

The spectrophotometric data using absorbance values from 20 wavelengths (between 400 and 800 nm) were processed with both the Specfit[19–22] and Letagrop-Spefo[17,18] programs in order to calculate the thermodynamic constants of the absorbing species and their corresponding electronic spectra. The range of values for the residual-squares sum $[\Sigma(A_{exp} - A_{calcd.})^2]$ of the fits was over the range 10^{-2} to 10^{-3}. The calculated electronic spectra are presented in Figure 6.

NMR Titration: The proton NMR titration was carried out for $\mathbf{L^2}$ over the pD range 3.5–9.2 in order to attribute protonation constants to different protonable sites of the ligand. The ligand was dissolved in D_2O. The pD was adjusted with DCl or NaOD solutions. pH measurements were performed with a Tacussel PHN 850 apparatus equipped with a microelectrode Radiometer XC61. pD values were calculated according to $pD = pH_{meas} + 0.4$.[33]

Acknowledgments

This work has been supported by the Centre National de la Recherche Scientifique (UMR, 7509 and 5616, PCV program), the Faculty of Chemistry, University Louis Pasteur, Strasbourg (France) and the University Joseph Fourier, Grenoble (France). The authors thank Professor C. Béguin (LEDSS) for his interest in these studies.

[1] A. M. Albrecht-Gary, A. L. Crumbliss, *Iron Transport and Storage in Microorganisms, Plants and Animals*, in Metal Ions in Biological Systems (Eds.: A. Sigel and H. Sigel), M. Dekker **1998**; vol. 35, pp. 239–327.
[2] G. Serratrice, H. Boukhalfa, C. Béguin, P. Baret, C. Caris, J. L. Pierre, *Inorg. Chem.* **1997**, *36*, 3898–3910.
[3] F. Thomas, C. Béguin, J. L. Pierre, G. Serratrice, *Inorg. Chim. Acta* **1999**, *291*, 148–157.
[4] S. M. Cohen, B. O'Sullivan, K. N. Raymond, *Inorg. Chem.* **2000**, *39*, 4339–4346.
[5] S. M. Cohen, K. N. Raymond, *Inorg. Chem.* **2000**, *39*, 3624–3631.
[6] L. E. Maley, D. P. Mellor, *Austr. J. Sci. Res.* **1949**, 579–594.
[7] Y. Murakami, K. Nakamura, M. Tokunaga, *Bull. Chem. Soc. Jpn.* **1963**, *36*, 669–675.
[8] D. H. Zhu, M. J. Kappel, K. N. Raymond, *Inorg. Chim. Acta* **1988**, *147*, 115–121.
[9] W. R. Harris, K. N. Raymond, F. L. Weitl, *J. Am. Chem. Soc.* **1981**, *103*, 2667–2675.
[10] P. Letkeman, A. E. Martell, R. J. Motekaitis, *J. Coord. Chem.* **1980**, *10*, 47–52.
[11] S. A. Abbasi, *Pol. J. Chem.* **1983**, *57*, 355–361.
[12] S. M. Cohen, M. Meyer, K. N. Raymond, *J. Am. Chem. Soc.* **1998**, *120*, 6277–6286.
[13] S. J. Rodgers, L. Chi-Woo, Y. N. Chiu, K. N. Raymond, *Inorg. Chem.* **1987**, *26*, 1622–1625.
[14] T. M. Garrett, P. W. Miller, K. N. Raymond, *Inorg. Chem.* **1989**, *28*, 128–133.
[15] R. Näsänen, A. Ekman, *Acta Chem. Scand.* **1952**, *6*, 1384–1390.
[16] V. L. Pecoraro, F. L. Weitl, K. N. Raymond, *J. Am. Chem. Soc.* **1981**, *103*, 5133–5140.
[17] L. G. Sillen, *Acta Chem. Scand.* **1964**, *18*, 1085–1098.
[18] L. G. Sillen, B. Warnqvist, *Ark. Kemi.* **1968**, *31*, 377–390.
[19] H. Gampp, M. Maeder, C. J. Meyer, A. D. Zuberbühler, *Talanta* **1985**, *32*, 95–101.
[20] F. J. C. Rossoti, H. S. Rossoti, R. J. Whewell, *J. Inorg. Nucl. Chem.* **1971**, *33*, 2051–2065.
[21] H. Gampp, M. Maeder, C. J. Meyer, A. D. Zuberbühler, *Talanta* **1985**, *32*, 257–264.
[22] H. Gampp, M. Maeder, C. J. Meyer, A. D. Zuberbühler, *Talanta* **1986**, *33*, 943–951.
[23] T. B. Karpishin, M. S. Gebhard, E. I. Solomon, K. N. Raymond, *J. Am. Chem. Soc.* **1991**, *113*, 2977–2984.
[24] D. Imbert, P. Baret, D. Gaude, I. Gautier-Luneau, G. Gellon, F. Thomas, G. Serratrice, J. L. Pierre, *Chem. Eur. J.* **2002**, *8*, 1091–1100.
[25] D. Imbert, F. Thomas, P. Baret, G. Serratrice, D. Gaude, J. L. Pierre, J. P. Laulhère, *New J. Chem.* **2000**, *24*, 281–288.
[26] L. D. Loomis, K. N. Raymond, *Inorg. Chem.* **1991**, *30*, 906–911.
[27] *Méthodes d'analyses complexométriques avec les Titriplex*, Merck, Darmstadt, 1990.
[28] R. Bastian, R. Weberling, F. Palilla, *Anal. Chem.* **1956**, *28*, 459–462.
[29] C. Gerard, R. P. Hugel, *J. Chem. Research (M)* **1980**, 3927–3957.
[30] A. E. Martell, R. J. Motekaitis, in *Determination and Use of Stability Constants*, VCH Weinheim, 1988, Chapter 1, pp. 7–19.
[31] P. Gans, A. Sabatini, A. Vacca, *J. Chem. Soc., Dalton Trans.* **1985**, 1195–1200.
[32] P. Gans, A. Sabatini, A. Vacca, *Talanta* **1996**, *43*, 1739–1753.
[33] P. K. Glasoe, A. Long, *J. Phys. Chem.* **1960**, *64*, 188–190.

Received November 25, 2002

 © 2003 Wiley-VCH Verlag GmbH & Co. KGaA, Weinheim

Second-Order Nonlinear Optical Properties of Tetraaza-Coordinated Nickel(II) Complexes

Santo Di Bella*[a] and Ignazio Fragalà[a]

Keywords: Nickel / Nonlinear optics / Semiempirical calculations

In this contribution, we report the design and theoretical analysis, using the INDO/SCI-SOS quantum chemical formalism, of novel molecular architectures based on planar $[N_4]$-, (2-aminobenzylideneiminato)- and tetraazamacrocycle-coordinated nickel(II) complexes, having second-order nonlinear optical (NLO) properties. Calculations indicate that these molecules possess comparable, or even larger, second-order nonlinearity to the bis(salicylaldiminato)Ni^{II} Schiff-base analogues. The nonlinearity of substituted complexes is dominated by the nature and position of substituents on the tribenzo[*b*,*f*,*l*] and/or cyclotetradecine rings, and is determined by the relative directions of the ground- and excited-state dipole moments. Moreover, substitution with acceptor groups in the dibenzo[*b*,*l*] rings involves a significant octupolar contribution to optical nonlinearity.

(© Wiley-VCH Verlag GmbH & Co. KGaA, 69451 Weinheim, Germany, 2003)

Introduction

An intense research activity is currently associated with the synthesis and development of molecule-based second-order nonlinear optical (NLO) materials,[1] involving organic chromophores[2] and metal complexes.[3] The latter represent an emerging and growing class of materials by virtue of unique properties associated with the metal center. Various classes of transition metal complexes have been explored systematically, including organometallic and coordination complexes.[3]

Most second-order NLO metal complexes, as organic NLO chromophores, can be envisaged within a simple molecular scheme constituted by a donor−π-conjugate-bridge−acceptor (D−π−A) structure, in which an organometallic group selectively replaces the donor and/or the acceptor, or the bridge moieties.[3a] This requirement is because metal complexes possess intense, low-energy metal-to-ligand charge transfer (MLCT), ligand-to-metal charge transfer (LMCT), or intraligand charge transfer (ILCT) excitations. Therefore, they can behave effectively as donor and/or acceptor groups of the D−π−A system, or to be a constituent of the polarizable bridge.

Bis(salicylaldiminato)M^{II} (M = Co, Ni, Cu, Zn) Schiff-base complexes are prototypical examples of the latter case.[4,5] Complexation is accompanied by formation of geometrically constrained acentric, generally planar, structures. It always involves an enhancement of optical nonlinearity, compared to that of related free ligands and, in some cases, a "switching on" of the NLO response with resulting tunable hyperpolarizabilities, ranging from negative to positive β values.[6] Moreover, the nature of the metal deeply influences the nonlinearity.[7] The role of the metal centre in determining the NLO response in such structures is twofold, since it can act both as the donor and as the bridging moiety of the D−π−A system. Finally, the appropriate donor/acceptor substitution pattern results in an "in-plane" two-dimensional second-order nonlinearity.[8] Thus, bis(salicylaldiminato)M^{II} Schiff-base complexes represent suitable templates for second-order NLO molecular materials. Actually, starting from unsubstituted bis(salicylaldiminato)M^{II} Schiff-base complexes it is possible to design other molecular structures in which, instead of changing the donor or the acceptor substituents on the benzene rings, the donor atoms are changed.

In this paper, we report the design and a theoretical analysis, using the INDO/S-SOS quantum chemical formalism,[7a,9] of novel molecular architectures based on planar $[N_4]Ni^{II}$ complexes, having second-order NLO properties (Scheme 1). We demonstrate that these (2-aminobenzylideneiminato)- and tetraazamacrocycle-coordinated nickel(II) complexes represent suitable candidates for second-order NLO molecular materials.

Results and Discussion

Theoretical Method

Within the framework of the Sum-Over-excited-particle-hole-States (SOS) perturbation theory, the molecular quadratic hyperpolarizability, for instance the second harmonic

[a] Dipartimento di Scienze Chimiche, Università di Catania and INSTM UdR di Catania,
V.le A. Doria 8, 95125 Catania, Italy
Fax: (internat.) + 39-095/580138
E-mail: sdibella@dipchi.unict.it

Supporting information for this article is available on the WWW under http://www.eurjoc.org or from the author.

 © 2003 Wiley-VCH Verlag GmbH & Co. KGaA, Weinheim **DOI: 10.1002/ejic.200300023**

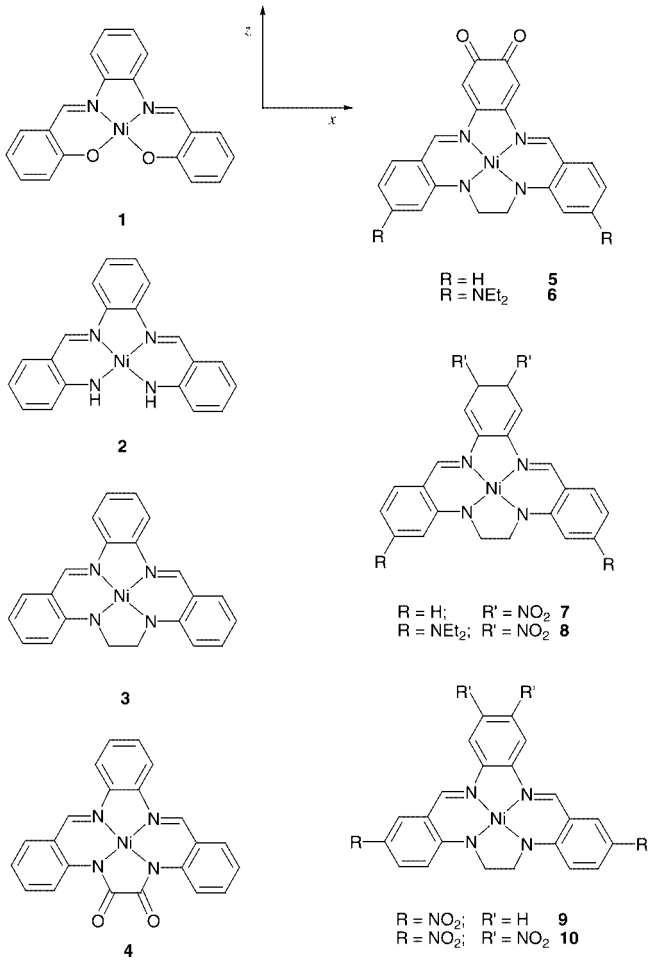

Scheme 1

generation, $\beta_{ijk}(2\omega; \omega, \omega)$, can be related exactly to all the excited states of the molecule in terms of energy, $\hbar\omega_{ge}$, transition dipole moment, r^{i}_{ge}, and dipole moment variation, $\Delta\mu^{i}_{ge} = r^{i}_{ee} - r^{i}_{gg}$, between ground ($g$) and excited ($n$) states.[10] The hyperpolarizability determined by a sum-over-states expression can be partitioned into two contributions,[9] the so-called two-level ($\beta_{ijk,2}$) terms and three-level ($\beta_{ijk,3}$) terms, such that: $\beta_{ijk}(2\omega; \omega, \omega) = \beta_{ijk,2} + \beta_{ijk,3}$. Each two-level component in the sum for $\beta_{ijk,2}$ contains only two states, the ground and one excited state, and is related to the product $r^{j}_{ge}r^{k}_{ge}\Delta\mu^{i}_{ge}$ (generic two-level term); the three-level contributions involve the ground state and two excited states, e, e', and are related to the product $r^{j}_{ge'}r^{i}_{e'e}r^{k}_{ge}$ (generic three-level term). For dipolar molecules, the molecular hyperpolarizability is generally related to the β_{μ} value, i.e., the vector component of the β_{ijk} tensor along the dipole moment direction, given by

$$\beta_{\mu} = \sum_{i=1}^{3} \frac{\mu_i \beta_i}{|\mu|}$$

where μ is the ground state dipole moment and $\beta_i = \beta_{iii} + 1/3\Sigma_{j\neq i}(\beta_{ijj} + \beta_{jij} + \beta_{jji})$. For most dipolar molecules, in which $\Delta\mu^{i}_{ge}$ and r^{i}_{ge} matrix elements are parallel to the dipolar i axis, the $\beta_{ijk,2}$ sum generally dominates the NLO response, resulting in 1D dipolar species with a single hyperpolarizability diagonal tensor component β_{iii}, so that $\beta_{\mu} \approx \beta_{iii}$. A further simplification of this approach can be made by restricting the "summation" to one excited state, the so-called "two-state" model,[11] in which: $\beta_{iii} \propto (r_{ge})^2\Delta\mu_{ge}/\hbar\omega_{ge}$. On the other hand, only nonzero, off-the-i-diagonal, dipole moment ($\Delta\mu^{j}_{ge}$, $j \neq i$) or transition dipole moment (r^{j}_{ge}, $j \neq i$) matrix elements, contribute to off-diagonal β_{ijk} hyperpolarizability tensor components. For dipolar molecules of C_{2v} symmetry, β has seven nonvanishing tensor components, five of which are independent. The nonzero components are β_{zzz}, $\beta_{xzx} = \beta_{xxz}$, β_{zxx}, $\beta_{yzy} = \beta_{yyz}$, β_{zyy}, where z is the C_2 axis. Since transition dipole moments perpendicular to the zx molecular plane are generally small, the components $\beta_{yzy} = \beta_{yyz}$, β_{zyy} are usually negligible. Thus, the parameter $u = \beta_{\text{off-diagonal}}/\beta_{zzz}$, where $\beta_{\text{off-diagonal}} = 1/3(\beta_{xzx} + \beta_{xxz} + \beta_{zxx})$, reflects the anisotropy of the in-plane optical nonlinearity.[12]

Computational Details and Results

Table 1. Computed ground-state dipole moment and second-order NLO response for (2-aminobenzylideneiminato)- and tetraazamacrocycle-coordinated nickel(II) complexes **1**−**10**, and for representative free ligands **3a**, **6a**, **8a** and **10a**

Compd.[a][b]	μ_g [D]	$\hbar\omega$ [eV]	β_{zzz}	$\beta_{xzx} = \beta_{xxz}$	β_{zxx}	u	β_{μ}
1[c]	7.4	0.0	−8.4	0.4	0.4	−0.05	−8.1
		0.92	−13.3	1.2	2.7	−0.13	−12.0
2	2.7	0.0	−10.4	2.1	2.1	−0.20	−8.2
		0.92	−20.5	4.1	5.4	−0.23	−15.7
3	2.4	0.0	−12.9	1.9	1.9	−0.15	−11.0
		0.92	−26.2	4.1	5.5	−0.17	−21.7
3a	2.2	0.0	−5.2	0.8	0.8	−0.15	−4.3
		0.92	−7.8	1.7	2.5	−0.25	−5.8
4	13.6	0.0	−7.4	1.1	1.1	−0.15	−6.4
		0.92	−14.1	0.0	3.9	−0.09	−12.2
5	10.2	0.0	39.0	−0.4	−0.4	−0.01	38.7
		0.92	75.0	−0.7	−4.1	−0.02	74.3
6	14.6	0.0	49.7	11.8	11.8	0.24	61.5
		0.92	89.6	24.9	15.6	0.24	111.4
6a	14.0	0.0	38.2	13.2	13.3	0.35	50.1
		0.92	67.1	24.2	21.7	0.35	88.4
7	7.8	0.0	43.0	−9.4	−9.4	−0.22	33.3
		0.92	94.4	−20.7	−24.5	−0.23	72.3
8	12.3	0.0	57.7	−0.3	−0.3	−0.01	57.2
		0.92	126.2	−9.2	−13.5	−0.08	115.1
8a	13.0	0.0	49.2	−2.5	−2.5	−0.05	45.9
		0.92	99.8	−9.9	−12.3	−0.11	87.7
9	3.7	0.0	−10.9	5.2	5.2	−0.48	−5.7
		0.92	−21.5	10.2	17.5	−0.59	−8.8
10	5.5	0.0	28.1	−12.3	−12.3	−0.44	15.5
		0.92	54.9	−24.4	−35.5	−0.51	26.4
10a	6.2	0.0	14.9	−6.5	−6.5	−0.44	6.1
		0.92	25.2	−12.1	−15.1	−0.52	7.6

[a] In units of 10^{-30} cm^5 esu^{-1}. Values of nonresonant hyperpolarizability are given in the phenomenological convention, where β_{ijk} is by a factor of $^1/_4$ smaller than in the Taylor series convention (see ref.[14]). [b] For definition of parameters, see text. [c] Computed μg and β_{μ} data for compound **1** differ slightly from those previously reported,[6a] because of the presently adopted optimized geometrical parameters and the different number of CIS configurations.

 © 2003 Wiley-VCH Verlag GmbH & Co. KGaA, Weinheim

The all-valence INDO/S (Intermediate Neglect of Differential Overlap) model,[13] in connection with the SOS formalism,[10] was employed. Details of the computationally efficient ZINDO-SOS-based method for describing second-order molecular optical nonlinearities have been reported elsewhere.[7a,9] Standard parameters and basis functions were used.[13] In particular, the resonance integrals for the nickel atom were chosen to be $\beta_{sp} = -1$ eV and $\beta_d = -45$ eV.[13b] In the present approach, the closed-shell-restricted Hartree−Fock (RHF) formalism was adopted. The monoexcited configuration interaction (CIS) approximation was employed to describe the excited states. In all calculations, the lowest 250 energy transitions between SCF and CIS electronic configurations were chosen to undergo CI

Table 2. Computed linear optical spectroscopic data of relevant, low-energy CT transitions and relative contributions of the two-level and three-level terms to the static second-order NLO response (10^{-30} cm^5 esu^{-1}) for complexes **1**−**10** and representative free ligands **3a**, **6a**, **8a** and **10a**[a]

Compd.[a]	State	Polarization	$\hbar\omega_{ge}$ [eV]	r_{ge}^z [D]	r_{ge}^x [D]	$\Delta\mu_{ge}^z$ [D]	$\beta_{zzz,2}$	$\beta_{zzz,3}$	$\beta_{zxx,2}$	$\beta_{zxx,3}$	$\lvert\beta_\mu\rvert$
1	S1	*x*	2.85	0.00	1.86	–1.8					
	S2	*z*	3.14	5.99	0.00	–4.64					
	$\sum_n S_n$						–11.7	3.3	–3.7	3.3	8.1
2	S1	*x*	2.70	0.00	2.11	–2.74					
	S2	*z*	2.78	5.97	0.00	–4.40					
	$\sum_n S_n$						–14.3	3.9	–3.8	5.9	8.2
3	S1	*x*	2.62	0.00	–1.77	–3.12					
	S2	*z*	2.71	6.07	0.00	–4.79					
	$\sum_n S_n$						–20.1	7.2	–4.2	6.1	11.0
3a	S1	*x*	3.08	0.00	2.41	–1.68					
	S2	*z*	3.31	–4.12	0.00	–1.68					
	$\sum_n S_n$						–6.6	1.4	–0.9	1.7	4.3
4	S3	*x*	2.76	0.00	–1.19	–2.14					
	S4	*z*	3.05	6.41	0.00	–6.00					
	$\sum_n S_n$						–16.5	9.1	0.6	0.5	6.4
5	S2	*x*	2.03	0.00	–0.21	12.72					
	S4	*z*	2.73	–8.04	0.00	4.65					
	$\sum_n S_n$						53.0	–14.0	6.7	–7.1	38.7
6	S1	*x*	2.06	0.00	–0.80	12.14					
	S2	*z*	2.80	8.27	0.00	4.08					
	$\sum_n S_n$						88.0	–38.3	14.5	–2.7	61.5
6a	S1	*x*	2.57	0.00	–1.42	6.99					
	S2	*z*	3.11	9.59	0.00	10.66					
	$\sum_n S_n$						74.8	–36.6	12.2	1.1	50.1
7	S1	*x*	2.12	0.00	–1.74	14.69					
	S2	*x*	2.58	0.00	–5.10	1.83					
	S3	*z*	2.66	–9.43	0.00	4.59					
	$\sum_n S_n$						40.0	3.0	13.7	–23.1	33.3
8	S1	*x*	2.12	0.00	–1.54	14.22					
	S2	*x*	2.60	0.00	5.23	3.00					
	S3	*z*	2.72	11.07	0.00	6.27					
	$\sum_n S_n$						86.4	–28.7	23.0	–23.3	57.2
8a	S1	*x*	2.41	0.00	4.57	3.92					
	S2	*z*	2.86	9.03	0.00	13.26					
	S4	*x*	2.98	0.00	–5.07	6.17					
	$\sum_n S_n$						102.8	–53.6	18.7	–21.2	45.9
9	S3	*x*	2.72	0.00	4.14	–3.35					
	S4	*z*	2.80	–5.73	0.00	–5.33					
	S5	*x*	3.20	0.00	–9.53	0.75					
	$\sum_n S_n$						–12.6	1.7	–3.7	8.9	5.7
10	S1	*x*	2.33	0.00	–2.30	7.71					
	S2	*x*	2.64	0.00	5.54	2.88					
	S3	*z*	2.70	8.80	0.00	2.84					
	$\sum_n S_n$						6.0	22.1	8.4	–20.7	15.5
10a	S1	*x*	2.49	0.00	–4.35	0.67					
	S6	*z*	3.12	–4.88	0.00	5.90					
	S7	*z*	3.18	7.86	0.00	–5.31					
	$\sum_n S_n$						–6.9	21.8	–0.3	–6.1	6.1

[a] For definition of parameters, see text.

 © 2003 Wiley-VCH Verlag GmbH & Co. KGaA, Weinheim

mixing and were included in the SOS. This SOS truncation was found to be sufficient for complete convergence of the second-order response in all cases considered. Non-resonant hyperpolarizabilities were calculated within a perturbation series expansion employing the Ward definition,[10] the so-called phenomenological convention.[14] All calculations were performed using the ZINDO Version 3.5 program of the Cerius^2 package from Accelrys Inc.[15] on an SGI Origin3800 system. Metrical parameters of **1**−**10** used for INDO/S calculations were taken from fully optimized structures (at ZINDO/1 level) using the HyperChem package.[16] A C_{2v} planar structure of the bis(2-aminobenzylideneiminato) or the tetraazamacrocycle frameworks was always found in all cases presently considered.[17] Present optimised planar structures are consistent with available crystallographically derived planar structures of related complexes (vide infra). Moreover, optimized geometrical parameters (Supporting Information, see also the footnote on the first page of this article) are in favorable agreement with available experimental data (vide infra). In addition, INDO/S calculations were performed for representative free ligands **3a**, **6a**, **8a**, and **10a**, on the basis of their optimized structures (at ZINDO/1 level). Optimized structures of ligands **3a**−**10a** indicate a nonplanar structure of the tetraazamacrocycle framework, with C_2 symmetry. The computed ground state dipole moment and second-order NLO response for **1**−**10** and representative free ligands are collected in Table 1, while calculated low-energy CT transitions and analysis of relative two-level and three-level contributions to the static hyperpolarizability[18] are reported in Table 2.

Discussion

Bis(salicylaldiminato)M^{II} Schiff-base complexes have recently been developed as a new and versatile class of efficient second-order NLO materials.[4−8] The optical nonlinearity of the unsubstituted [Ni(salophen)] (**1**), has been related to a low-energy charge transfer (CT) transition, characterized as being principally $\pi \rightarrow \pi^*$ (HOMO → LUMO) in character, essentially involving the metal $3d_{xz}$,oxygen $2p_z$ and C=N orbitals.[6a] Therefore, the optical nonlinearity of M(salophen) complexes strongly depends on the nature of the (MN_2O_2) chelate and is tuned by the D/A substitution on the benzo rings.[6a,7,8] On this basis, it is expected that alternative chelate NLO structures could be envisaged on changing the donor atoms of the (salophen) template.

Substitution of the oxygen donor atoms of [M(salophen)] by NH groups results in the isoelectronic MN_4, bis(2-aminobenzylideneiminato) [M(abphen)] planar chelate. Some physicochemical properties of [M^{II}(abphen)] (M = Co, Ni, Cu) complexes have been previously reported.[19] These complexes presumably possess a planar structure,[19a] according to the present optimized planar structure of [Ni(abphen)] (**2**). On switching from **1** to **2**, theoretical data indicate a decrease of the ground state dipole moment, μ_g, which, analogously to **1**, is directed between the imino groups. Thus, the calculated smaller value of μ_g of **2** can be related to the less electron-withdrawing effect of NH groups compared to oxygen donor atoms. The calculated nonlinearity of **2** is similar to that of **1**, and can be related essentially to a single low-energy excited state, having a polarization parallel with respect to the molecular dipolar (*z*) axis. In fact, although the lowest state consists of an *x*-polarized transition, the associated low intensity (r^x_{ge} = 2.11 D) and CT character ($\Delta\mu_{ge}$ = −2.74 D) imply a negligible contribution to off-diagonal β_{ijk} tensors and, hence, to optical nonlinearity (Table 2). Thus, analogously to **1**, a single diagonal hyperpolarizability tensor component, β_{zzz}, parallel to the dipolar *z* axis of the molecule, mainly contributes to the NLO response (Table 1). Moreover, the slightly larger β_μ value of **2** can be related essentially to the calculated red-shift of the low-energy, *z*-polarized CT transition. A red-shift of the lowest electronic transitions also can be observed experimentally on comparing optical absorption spectra of **1**[6a] and **2**.[19a] Finally, calculated negative β values are a consequence of the negative dipole moment change between the ground and excited states, $\Delta\mu_{ge}$, associated with the β-determining CT transition (Table 2). While in the ground state the dipole moment is directed between the imine groups, in the excited state it has an opposite orientation, i.e., between the nitrogen donor atoms. Thus, [M(abphen)] complexes represent a new family of second-order NLO chromophores having an analogous nonlinearity to that of [M(salophen)] complexes.

A closely related structure to [M(abphen)] is offered by the macrocyclic M[14]N_4 complexes of the tribenzo[*b*,*f*,*l*][1,4,8,11]tetrazacyclotetradecine (TAD) ligand, which represents a versatile system readily accessible to a variety of substitutions, both in the tribenzo[*b*,*f*,*l*] as well as the cyclotetradecine rings.[20] First, we consider the prototypical unsubstituted planar Ni(TAD) complex **3**.[21] As expected, on passing from **2** to **3** we observe only minor changes as far as calculated linear and nonlinear optical features (Tables 1 and 2). In fact, analogously to **2**, μ_g is directed between the imino groups and negative values of $\Delta\mu_{ge}$ and β are predicted. The larger β values of **3** are a consequence of the red-shift of its lowest electronic transitions, as have also been observed experimentally.[20d] Again, these results indicate that M(TAD) complexes possess NLO characteristics like those of [M(salophen)] and [M(abphen)]. In view of their versatility to achieve substituted donor−acceptor derivatives, they represent attractive candidates for further theoretical investigations.

As the first example of an Ni(TAD)-substituted species, we consider the 12,13-dione complex **4**. Its 2,3,6,19-tetramethyl derivative,[22a] as well as a variety of substituted species,[22b,22c] has been synthesized and characterized previously. The calculated dipole moment of **4** is larger than the unsubstituted derivative **3**, because of the electron-withdrawing effect of the dioxo groups. However, its calculated nonlinearity is smaller than that of the unsubstituted complex **3** (Table 1). The presence of the 12,13-dioxo groups results in a blue-shift of the lowest electronic transitions,

 © 2003 Wiley-VCH Verlag GmbH & Co. KGaA, Weinheim

with a consequent lower two-level contribution to optical nonlinearity (Table 2). Note that the calculated blue-shift of the lowest CT transitions on passing from **3** to **4** is in favorable agreement with that observed experimentally.[20d,22a,22c]

These results suggest that enhancement of nonlinearity in **3** necessarily implies that the acceptor substituents be on the benzo[*b*,*f*,*l*] rings. For this purpose we consider the 16,17-dione derivative **5**, whose related planar semiquinone has been synthesized and characterized previously.[20b] On switching from **3** to **5**, we observed a dramatic increase of the ground state dipole moment, which now has an opposite orientation, i.e., it is directed between the [1,4] nitrogen donor atoms of the TAD ring, thus involving positive values of $\Delta\mu_{ge}$, β_{ijk} and β_{μ} (Tables 1 and 2). Moreover, we predicted a significant larger optical nonlinearity, in terms of both static and dynamic hyperpolarizabilities. In a two-state picture, this situation is consistent with the calculated stronger (**3** vs. **5**) low-energy, *z*-polarized CT transition, strengthened by the larger charge delocalization over the benzo[*f*] ring in the excited state involved, because of the 16,17-dioxo substituents.

The optical nonlinearity of **5** is further enhanced by considering the donor 3,10-diethylamino substitution on the benzo[*b*,*l*] rings (**6**). This feature is due to the further strengthening of both the *z*- and *x*-polarized, lowest CT transitions. Moreover, the latter transition involves a very large $\Delta\mu_{ge}$ and is responsible for the appreciable calculated off-diagonal β_{ijk} tensors, thus resulting in a sizeable two-dimensional (2D) NLO character of **6** ($u = 0.24$) (Tables 1 and 2). Clearly, the two-state model is inadequate to describe the optical nonlinearity of such a system, since at least two states mainly contribute to the molecular hyperpolarizability.

Replacement of dioxo groups in **5** by two strong electron acceptors, such as nitro groups (**7**), does not result in an appreciable improvement in β_{μ}. Unlike **5**, however, the nitro derivative **7** possesses some 2D character, owing to the strengthening of the lowest-energy, *x*-polarized CT transition, as in **6**, and to the presence of an additional low-energy, *x*-polarized CT transition. Moreover, the off-diagonal β_{ijk} tensors have an opposite sign with respect the diagonal β_{zzz} one, with a resulting negative nonlinear anisotropy ($u = -0.22$). Negative off-diagonal β_{ijk} values for **7** are consequence of the larger negative contribution of three-level terms compared with two-level terms (Table 2).

The further donor substitution in **7** with two 9,16-diethylamino groups (**8**), leads to a one-dimensional character of the calculated optical nonlinearity, in spite of the existence, analogously to **7**, of two lowest-energy *x*-polarized CT transitions. In this case, however, both two-level and three-level contributions cancel each other, thus resulting in a single diagonal hyperpolarizability tensor component, β_{zzz}, and β_{μ} values similar to those of **6** (Table 2).

The 8,17-nitro substitution on the benzo[*b*,*l*] rings (**9**) offers the possibility to obtain an enhanced in-plane 2D character of the optical nonlinearity (Table 1). Actually, the calculated in-plane anisotropy for the dipolar complex **9** ($u = -0.5$) involves a significant octupolar contribution[12] to the optical nonlinearity. The negative in-plane anisotropy of **9** depends on off-diagonal β_{ijk} tensors, which have an opposite (positive) sign with respect to the diagonal (negative) β_{zzz} tensor (Table 2). Again, as in **7** and **8**, the presence of two low-energy *x*-polarized CT transitions leads to off-diagonal tensors dominated by the contribution of the three-level terms. In this case, however, the presence of 8,17-dinitro substituents on the benzo[*b*,*l*] rings implies that values of $\Delta\mu_{ge}$ associated with the two mentioned *x*-polarized CT transitions have opposite signs, resulting in a low two-level sum contribution. Thus, the calculated positive off-diagonal β_{ijk} values of **9** are a consequence of the larger positive contribution of three-level vs. two-level sums (Table 2). Note that, the 8,17-dinitrobenzo[*b*,*l*] ring substitution involves a blue-shift of the lowest calculated electronic transitions on passing from **3** to **9** (Table 2), according to observed changes in optical absorption maxima.[20c,20d]

The combination of **7** and **9** in the tetrasubstituted nitro derivative **10** is expected to involve an enhanced nonlinearity with negative in-plane anisotropy. Actually, compound **10** is characterized by the two lowest *x*-polarized CT transitions, in addition to the *z*-polarized CT transition, and results in an increased nonlinearity, relative to **9**, again with a significant octupolar contribution. Both diagonal and off-diagonal tensors are dominated by the three-level terms (Table 2).

The evaluation of NLO properties of related free ligands **3a**−**10a** allows a useful comparison to be made with complexes **3**−**10** (Tables 1 and 2). Their calculated optical nonlinearity is generally lower (ca. 60% for **3a**, **10a**; 20% for **6a**, **8a**) and parallels the two-dimensional character of related Ni^{II} complexes. The enhancement of the hyperpolarizability on switching from free ligands to Ni^{II} complexes, which is less evident for D/A-substituted species **6a** and **8a**, can be related to the involvement of metal 3d orbitals that leads to a larger charge delocalization over the planar macrocycle and, hence, to red-shifted, and sometimes stronger, CT transitions (Table 2). Therefore, the optical nonlinearity of the present donor−acceptor TAD derivatives is dominated by substituents on the tribenzo[*b*,*f*,*l*] rings. In these cases, the metal ion mostly acts as a bridge of the D−π−A system, as previously observed for donor−acceptor bis(salicylaldiminato)Ni^{II} complexes.[3a,4]

Conclusions

In this paper, we have demonstrated that starting from bis(salicylaldiminato)Ni^{II} Schiff'-base complexes it is possible to design alternative molecular NLO structures by changing the donor atoms of the (salophen) template. Thus, calculations on a series of novel molecular architectures, based on planar $[N_4]Ni^{II}$ complexes, indicate that these molecules possess comparable, or even larger, second-order nonlinearity to those of bis(salicylaldiminato)Ni^{II} Schiff-base analogues. The nonlinearity of substituted Ni(TAD)

 © 2003 Wiley-VCH Verlag GmbH & Co. KGaA, Weinheim

complexes is dominated by the nature and position of substituents on the tribenzo[*b*,*f*,*l*] and/or cyclotetradecine rings, and is dictated by the relative magnitude and direction of the ground- and excited-state dipole moments. In particular, analogously to [Ni(salophen)] complexes, the donor substituents on the dibenzo[*b*,*l*] rings and the acceptors on the benzo[*f*] ring, involve larger nonlinearity. However, substitution with acceptor groups in the dibenzo[*b*,*l*] rings of the [Ni(TAD)] complex involves an enhanced octupolar β contribution with respect the dipolar one. This feature is a very interesting one with the perspective of designing polarization-independent materials for electro-optical applications.

Acknowledgments

This research was supported by the MIUR (Cofinaziamento per programmi di ricerca di interesse nazionale 2001).

[1] [1a] *Nonlinear Optics of Organic Molecules and Polymers* (Eds.: H. S. Nalwa, S. Miyata), CRC Press, Boca Raton, FL, **1997**. [1b] *Molecular Nonlinear Optics* (Ed.: J. Zyss), Academic Press, New York, **1994**. [1c] N. P. Prasad, D. J. Williams, *Introduction to Nonlinear Optical Effects in Molecules and Polymers*, John Wiley & Sons, New York, **1991**.

[2] For recent, general reviews on NLO studies involving organic chromophores, see, for example: [2a] J. J. Wolff, R. Wortmann, *Adv. Phys. Org. Chem.* **1999**, *32*, 121−217. [2b] T. Verbiest, S. Houbrechts, M. Kaurann, K. Clays, A. Persoons, *J. Mater. Chem.* **1997**, *7*, 2175−2189.

[3] For recent, general reviews on NLO studies involving metal complexes, see, for example: [3a] S. Di Bella, *Chem. Soc. Rev.* **2001**, *30*, 355−366. [3b] I. R. Whittall, A. M. McDonagh, M. G. Humphrey, *Adv. Organomet. Chem.* **1998**, *42*, 291−362.

[4] S. Di Bella, I. Fragalà, *Synth. Met.* **2000**, *115*, 191−196.

[5] P. G. Lacroix, *Eur. J. Inorg. Chem.* **2001**, 339−348.

[6] [6a] S. Di Bella, I. Fragalà, I. Ledoux, M. A. Diaz-Garcia, T. J. Marks, *J. Am. Chem. Soc.* **1997**, *119*, 9550−9557. [6b] P. G. Lacroix, S. Di Bella, I. Ledoux, *Chem. Mater.* **1996**, *8*, 541−545.

[7] [7a] S. Di Bella, I. Fragalà, T. J. Marks, M. A. Ratner, *J. Am. Chem. Soc.* **1996**, *118*, 12747−12751. [7b] S. Di Bella, I. Fragalà, I. Ledoux, T. J. Marks, *J. Am. Chem. Soc.* **1995**, *117*, 9481−9485.

[8] [8a] S. Di Bella, I. Fragalà, *New J. Chem.* **2002**, *26*, 285−290. [8b] S. Di Bella, I. Fragalà, I. Ledoux, J. Zyss, *Chem. Eur. J.* **2001**, *7*, 3738−3743.

[9] D. R. Kanis, M. A. Ratner, T. J. Marks, *Chem. Rev.* **1994**, *94*, 195−242.

[10] J. F. Ward, *Rev. Mod. Phys.* **1965**, *37*, 1−18.

[11] J. L. Oudar, D. S. Chemla, *J. Chem. Phys.* **1977**, *66*, 2664−2668.

[12] S. Brasselet, J. Zyss, *J. Opt. Soc. Am. B* **1998**, *15*, 257.

[13] [13a] M. C. Zerner, G. Loew, R. Kirchner, U. Mueller-Westerhoff, *J. Am. Chem. Soc.* **1980**, *102*, 589−599. [13b] W. P. Anderson, D. Edwards, M. C. Zerner, *Inorg. Chem.* **1986**, *25*, 2728−2732. [13c] A. D. Bacon, M. C. Zerner, *Theor. Chim. Acta* **1979**, *53*, 21−54. [13d] J. Ridley, M. C. Zerner, *Theor. Chim. Acta* **1973**, *32*, 111−134.

[14] A. Willetts, J. E. Rice, D. M. Burland, D. P. Shelton, *J. Chem. Phys.* **1992**, *97*, 7590−7599.

[15] Accelrys Inc., *Cerius*^{2} *Modeling Environment, Release 3.5* Accelrys Inc., San Diego, **1998**.

[16] *HyperCube HYPERCHEM*, Release 5 for Windows, HyperCube, **1997**.

[17] Of course, in all these cases the presence of the 2,3-methylene groups in the [1,4,8,11]tetrazacyclotetradecine (TAA) ring of TAA complexes, as well as diethylamino and/or nitro substituents in TAA complexes, does not result in C_{2v} symmetry of the whole molecule.

[18] S. Di Bella, *New J. Chem.* **2002**, *26*, 495−497.

[19] [19a] B. M. Higson, E. D. McKenzie, *J. Chem. Soc., Dalton Trans.* **1972**, 269−280. [19b] E. D. McKenzie, R. D. Moore, J. M. Worthington, *Inorg. Chim. Acta* **1975**, *14*, 37−44.

[20] See, for example: [20a] S. Jonasdottir, C.-G. Kim, J. Kampf, D. Coucouvanis, *Inorg. Chim. Acta* **1996**, *243*, 255−270. [20b] D. Coucouvanis, S. G. Jonasdottir, D. Christodoulou, C. G. Kim, J. W. Kampf, *Inorg. Chem.* **1993**, *32*, 2987−2988. [20c] D. St. C. Black, C. H. Bos Vanderzalm, L. C. H. Wong, *Aust. J. Chem.* **1979**, *32*, 2303−2311. [20d] M. Green, P. A. Tasker, *Inorg. Chim. Acta* **1971**, *5*, 65−69.

[21] Actually, a planar structure is expected for Ni(TAA) on the basis of their physicochemical properties.[20d] Moreover, the structure of the 16,17-diolato derivative is planar, as indicated by single-crystal X-ray diffraction studies.[20a] In addition, geometrical parameters of the present optimized structure of **3** are in favorable agreement with those found experimentally for the 16,17-diolato derivative.[20a] For example, selected bond lengths [Å]: M−N 1.860(4) (exp.); 1.861, 1.908 (calcd.); C=N 1.317(8) (exp.); 1.329 (calcd.); selected bond angles [°]: N−Ni−N 178.8(1), 94.2(1), 85.9(1) (exp.); 177.6, 93.2, 85.8 (calcd.).

[22] [22a] D. Christodoulou, M. G. Kanatzidis, D. Coucouvanis, *Inorg. Chem.* **1990**, *29*, 191−201. [22b] D. St. C. Black, G. I. Moss, *Aust. J. Chem.* **1987**, *40*, 129−142. [22c] D. St. C. Black, C. H. Bos Vanderzalm, L. C. H. Wong, *Aust. J. Chem.* **1982**, *35*, 2435−2443.

Received January 14, 2003

 © 2003 Wiley-VCH Verlag GmbH & Co. KGaA, Weinheim

NMR Investigation and Dynamic Behaviour of [2,2′-Bipyridylbis(pyridine)platinum(II)]$^{2+}$ and Related Cationic Complexes − Crystal Structure of $[Pt(bipy)(py)_2](PF_6)_2$

Enrico Rotondo,*[a] Giuseppe Bruschetta,[a] Giuseppe Bruno,[a] Archimede Rotondo,[a] Maria Letizia Di Pietro,[a] and Matteo Cusumano[a]

Keywords: Intercalations / N ligands / NMR spectroscopy / Platinum

Detailed ^{1}H and ^{13}C{^{1}H} NMR analysis has been carried out on complexes with the general formulae $[Pt(bipy)(n\text{-}Rpy)_2](PF_6)_2$ and $[Pt(4\text{-}Phbipy)(n\text{-}Rpy)_2](PF_6)_2$ [bipy = 2,2′-bipyridyl; 4-Phbipy = 4,4′-diphenyl-2,2′-dipyridyl; *n*-Rpy = pyridine or substituted pyridines]. The resonance assignments and X-ray structures of these complexes are important steps on our route to: (i) interpretation of the intercalative geometry on the basis of the magnetic changes produced on interaction with DNA, (ii) rational design of new intercalators. The X-ray structure of the parent complex $[Pt(bipy)(py)_2](PF_6)_2$ (py = pyridine) shows pyridine rings quasiperpendicular to the coordination plane. In solution, because of the hindered rotation about Pt–N bonds of *ortho*- and *meta*-monosubstituted pyridines, this arrangement leads to "head-to-head" *s-cis* C_s and "head-to-tail" *s-trans* C_2 rotamers in equilibrium. NMR line shape and ^{13}C relaxation time constant measurements were carried out in order to evaluate activation energies and anisotropic rotational motion of *n*-Rpy. In some of these complexes a second dynamic process could be frozen on the ^{13}C NMR timescale below 265 K. This lower activation energy process can reasonably be attributed to minimal bipyridyl torsion angle flipping driving a concerted molecular motion about the core of the four N-donors. Indeed, the X-ray structure of **1** proves distortion with a slight alternate up and down shift of the four nitrogen atoms about the coordination plane. Significantly, the fast rotation of unhindered pyridine rings does not allow NMR detection of this molecular distortion.
(© Wiley-VCH Verlag GmbH & Co. KGaA, 69451 Weinheim, Germany, 2003)

Introduction

Energy barriers for rotation about Pt−N bonds and the fluxional behaviour of rotational isomers of Pt^{II} square-planar complexes have attracted renewed interest in the last decade. These barriers are, in fact, important factors in stereocontrolled transition metal mediated self-assembly.[1] On the other hand, Pt−N(guanine) (or -adenine) rotational barriers can play key roles in inhibition of DNA duplication ensuing Pt^{II}−purine base inter- and intra-strand bond formation.[2] In the course of studies concerning the interactions of square-planar complexes and DNA[3] we have reported the intercalating properties of **7**.[4] Our attention was then attracted by complexes of general formulae $[Pt(bipy)(n\text{-}Rpy)_2](PF_6)_2$ and $[Pt(4\text{-}Phbipy)(n\text{-}Rpy)_2](PF_6)_2$ (**1**−**9**, Scheme 1).

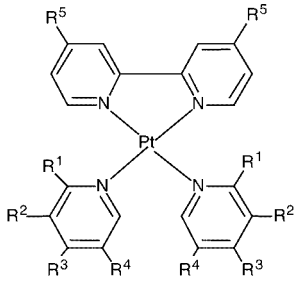

	1	2	3	4	5	6	7	8	9
R^1	H	CH_3	H	H	H	H	H	H	H
R^2	H	H	CH_3CN	Ph	H	CH_3	H	H	
R^3	H	H	H	H	H	Ph	H	H	CN
R^4	H	H	H	H	H	H	CH_3	H	
R^5	H	H	H	H	H	H	H	Ph	Ph

Scheme 1

Indeed, the flat Pt(bipy) moiety is particularly well suited to intercalate DNA, whereas the rotational barriers of coordinated *n*-Rpy and phenyl substituents might either prevent or allow more extended intercalation, depending on the energy necessary to induce other aromatic rings to lay in the coordination plane.

Despite the popularity of such $[Pt(bipy)(n\text{-}Rpy)_2](PF_6)_2$ complexes, there are only a few NMR spectroscopic data concerning them. The aim of this paper is to provide NMR resonance assignments, together with dynamic and struc-

[a] Dipartimento di Chimica Inorganica, Analitica, e Chimica Fisica, Facotà di Scienze, Università di Messina,
Salita Sperone 31, 98166 Messina, Italia
E-mail: rotondo@chem.unime.it

 © 2003 Wiley-VCH Verlag GmbH & Co. KGaA, Weinheim **DOI: 10.1002/ejic.200300032**

tural features of these molecules, in particular highlighting pyridine rotation about the Pt−N bond. These properties are fundamental for mapping of the complexes' intercalative geometries and for rational design of new intercalator families.

Results and Discussion

NMR Analysis

Tables 1 and 2 report selected ^{1}H and ^{13}C{^{1}H} NMR resonance frequencies of **1**−**9**. Peak assignments are supported by conventional 1D and 2D homo- and heteronuclear experiments. Unambiguous resonance assignments, as well as structural feature determinations, are obligatory steps in any NMR attempt to shed light on the DNA double helix intercalative geometries of these complexes.[5] All reported crystal structures of [Pt(bipy)(*n*-Rpy)$_2$]$^{2+}$ cations concordely showed orientations of the heteroaromatic pyridine rings quasiperpendicular to the coordination plane.[4,6] The X-ray structure of [Pt(bipy)(*n*-Rpy)$_2$](PF$_6$)$_2$ shown here confirms this arrangement, which forces the 6,6′-bipy protons to point toward the centre of the pyridine's ring current. NMR spectra consistently show a shift of the 6,6′-H(bipy) signals by about 1 ppm to lower frequency with respect to the analogous [Pt(bipy)(am)$_2$](PF$_6$)$_2$ (am = mono- and bidentate aliphatic amines) resonances.[7] The anisotropic diamagnetic shifts of 6,6′-bipy proton signals, monitored both for substituted and for unsubstituted pyridines, suggest that, in solution, the heteroaromatic rings preserve the quasiperpendicular orientation shown in the crystal structure. This preferred orientation does not, however, rule out the possibility of rotation. In order to obtain more clues relating to the capabilities of the aromatic rings in these molecules to rotate about the Pt−N bond, we measured and compared spin lattice relaxation time constants of selected ^{13}C atoms in **1**, **2**, **5** and **8**. Under decoupling conditions and for purely dipolar relaxations of aromatic C−H in the extreme narrowing limit, the Equation below applies.[8]

$$1/T_{1-DD} = \rho_{C\text{-}DD} = \tau_C [\gamma_H^2\gamma_C^2\eta^2/r^6]$$

If contributions of not directly attached protons are neglected and the C−H distance considered constant, relaxation time constants can be taken as a measure of the aromatic ring anisotropic spin diffusion. For aromatic ring carbon atoms bonded to fragments sufficiently large to be regarded as fixed matrices, diffusion preferentially occurs by rotation about the connection axis. This relatively fast motion slows down the relaxation rates of *ortho*- and *meta*-carbon atoms without altering the *para*-carbon atoms, the proton-attached dependent local fields of which are not affected by the rotation.[8,9] On this basis, the time constants (T_1) at room temperature are consistent with rotation of pyridine, *para*-substituted pyridine and phenyl rings, and hindered rotation of *meta*- and *ortho*-substituted pyridine rings (Table 3).

Table 1. ^{1}H NMR chemical shifts [ppm] of **1**−**9** in [D$_6$]acetone at 298 K

	bipy fragment				Pyridine fragment					
	3	4	5	6	2	3	4	5	6	Me
1	8.78	8.59	7.81	8.01	9.34	7.89	8.30	7.89	9.34	
trans-**2**	8.80	8.60	7.83	7.95		7.91	8.19	7.63	9.21	3.34
cis-**2**	8.80	8.60	7.83	7.95		7.91	8.19	7.70	9.46	3.49
3[a]	8.68	8.58	7.74	7.96	9.22		8.11	7.72	9.12	2.45
trans-**4**	8.79	8.60	7.79	8.09	9.96		8.73	8.13	9.68	
cis-**4**	8.79	8.60	7.79	8.09	9.92		8.73	8.13	9.73	
trans-**5**	8.79	8.59	7.81	8.17	9.77		8.56	7.96	9.41	
cis-**5**	8.79	8.59	7.81	8.17	9.75		8.56	7.93	9.37	
6	8.78	8.58	7.82	8.12	9.37	8.19		8.19	9.37	
7	8.84	8.64	7.81	7.96	9.08		7.96		9.08	2.38
8	9.29		8.09	8.03	9.39	7.91	8.33	7.91	9.39	
9	9.32		8.07	8.07	9.78	8.38		8.38	9.78	

[a] *cis* and *trans* rotamer resonances overlapped within 0.01 ppm throughout.

Table 2. Selected ^{13}C{^{1}H} NMR chemical shifts [ppm] of **1**−**9** in [D$_6$]acetone at 298 K

	bipy fragment					Pyridine fragment				
	2	3	4	5	6	2	3	4	5	6
1	157.6	125.6	143.7	129.7	151.0	153.4	129.6	142.9	129.6	153.4
trans-**2**	161.9	125.6	143.8	129.9	150.6	158.0	130.1	142.2	126.2	153.8
cis-**2**	161.9	125.6	143.8	129.9	150.8	157.9	130.3	142.3	126.2	152.7
trans-**3**[a]	157.6	125.7	143.8	129.7	151.1	153.2	140.5	143.4	128.8	150.6
cis-**3**[a]	157.6	125.7	143.8	129.7	151.1	153.0	140.5	143.4	128.8	150.5
trans-**4**[a]	157.2	125.5	143.9	129.5	151.4	156.9	114.7	145.8	130.0	156.6
cis-**4**[a]	157.2	125.5	143.9	129.5	151.4	156.7	114.7	145.8	129.9	156.3
trans-**5**[a]	157.5	125.7	143.8	129.7	151.3	151.1	142.1	140.5	129.5	151.8
cis-**5**[a]	157.5	125.7	143.8	129.7	151.3	151.3	142.0	140.5	129.5	151.7
6	157.6	125.7	143.8	129.7	151.1	153.3	126.4	153.6	126.4	153.3
7	157.4	125.6	143.6	129.7	151.1	150.2	139.5	143.9	139.5	150.2
8	158.0	123.4	154.9	126.4	151.1	153.6	129.7	143.0	129.7	153.6
9	157.8	123.6	155.2	126.3	151.3	155.0	131.9	126.0	131.9	155.0

[a] Assignments for the two rotamers could be inverted.

Table 3. ^{13}C relaxation time constants [s] of selected aromatic C−H carbon atoms in [D$_6$]acetone at 298 K; standard deviations are less than 5%

	bipy				Pyridine			Phenyl		
	C-3	C-4	C-5	C-6	C-*ortho*	C-*meta*	C-*para*	C-*ortho*	C-*meta*	C-*para*
1	1.4	1.4	1.4	1.5	1.9	1.8	1.3			
2[a]	1.3	1.2	1.1	1.3	1.2	1.1	1.2			
5[a]	1.1	nd	0.9	1.0	1.4	1.3	1.2	1.9	1.7	1.2
8	0.9		1.0	1.1	1.7	1.7	1.0	1.8	1.8	1.1

[a] No appreciable time constant differences found for the two rotamers.

For *ortho*- and *meta*-monosubstituted bis(pyridine) complexes the quasiperpendicular orientation implies the existence of "head-to-tail" *s-trans* and "head-to-head" *s-cis* rotamers of C_2 and C_s symmetry, respectively (two enantiomers can be envisaged for the C_2 molecules, owing to the chirality axes). The rates of these stereoisomer interconvertions depend on the lower activation energy path either

 © 2003 Wiley-VCH Verlag GmbH & Co. KGaA, Weinheim

of a dissociative step involving Pt−N bond breaking, or of a single pyridine asynchronous rotation about the Pt−N bond. The NMR spectra of the monosubstituted pyridine complexes at 298 K show the resonances of the two rotamers in slow exchange on the NMR timescale. Signal integration showed approximately equal thermodynamic stability between rotamer couples. Resonance assignments (which rotamer is which) were made, when feasible, through positive NOEs between methyl (or aryl) groups and the opposite proton of the adjacent *cis*-pyridine (6-H for 2- and 5-H for 3-monosubstituted pyridines, respectively) observed for the C_s but not for the C_2 configurations (Scheme 2).

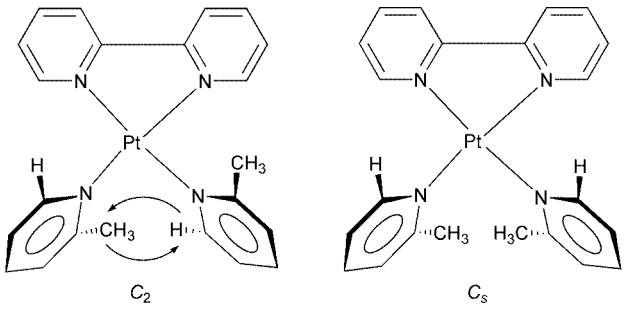

Scheme 2. Two-dimensional representation, symmetry and NOE contacts of the two rotamers of **2**

Pyridine-nitrogen, *ortho*-carbon and -proton resonances were used as probes for the conformational line shape analysis. The activation energy for rotamer interchange, calculated at coalescence, strongly differs as a function of the substituent position. We could not detect coalescence for 2-Mepy rotamers **2** even at 430 K in [D_6]DMSO ($\Delta G^{\neq} >$ 130 kJ), while 3-substituted pyridines **3**, **4** and **5**, in acetone, showed an activation energy of about 70 kJ (Table 4). The difference can be attributed to steric interactions between ligands differently hindering the pyridine crossing of coordination planes. The displacement of solvent molecules required by rotation, electronic effect of substituents on the Pt−N bond and, perhaps, stacking interactions between *cis*-pyridines may make contributions to these activation energies. These results are not consistent with a dissociative mechanism, which can also be ruled out on the basis of the permanence, above the coalescence temperatures, of ^{195}Pt satellites in the 2/6-py ^{1}H resonances.

Table 4. Activation energies for asynchronous rotation about the Pt−N bonds of monosubstituted bis(pyridine) complexes ($\Delta G^{\neq}_{(1)}$) and for molecular concerted distortion ($\Delta G^{\neq}_{(2)}$)

	$\Delta G^{\neq}_{(1)}$ [kJ·mol^{-1}]	$\Delta G^{\neq}_{(2)}$ [kJ·mol^{-1}]
2 (2-Me-py)	> 130	57 ± 2 (265 K)
4 (3-CN-py)	71.9 ± 1 (326 K)	57 ± 2 (265 K)
5 (3-Ph-py)	71.6 ± 1 (323 K)	57 ± 2 (265 K)
3 (3-Me-py)	68.5 ± 1 (320 K)	57 ± 2 (265 K)

At 240 K, the ^{13}C{^{1}H} NMR spectrum of **3** showed the doubling of the C-2 and C-6 resonances as a consequence of a second dynamic process (Figure 1). At the same temperature, analogous carbon resonance splitting was observed for the other *ortho*- and *meta*-monosubstituted pyridine complexes. We suggest these splittings are due to freezing of square-planar-distorted conformations. As a matter of fact, the solid-state structure of **1** shows a small, propeller-like torsion of the bipyridyl rings about the C2−C2′ axis, displacing the N donors slightly out of the coordination plane. The X-ray structure also shows a "bumping" of bipy, constraining the pyridine's N3−Pt−N4 angle (about 80°). The 6,6′-H of slightly distorted bipy pushes the two opposite pyridines up and down the ring centre, respectively, causing a distortion of the ring planes by about 10° with respect to the perpendicular alignment. Steric crowding also forces the nitrogen donors of the Pt−N4 core alternatively up and down the mean coordination plane. Concerted bipy torsion angle flipping, pyridine ring windscreen-wiper rocking and up and down N-donors twisting about the mean coordination plane create a time-averaged planar symmetry for the bis(pyridine) complex. At low temperatures, freezing of the concerted flipping destroys the bipy averaged planarity, doubling the number of *ortho*- and *meta*-monosubstituted *s-trans* conformers. Indeed, the "frozen" C_2 propeller-like torsion of bipy generates two pairs of diastereomers from the two monosubstituted *s-trans* Δ and Λ enantiorotamers: namely ΔΔ′ and ΔΛ′ arising from the original Δ rotamer, and the corresponding enantiomers ΛΔ′ and ΛΛ′ from the original Λ rotamer (Scheme 3). On the other side, the *s-cis* rotamer is split into an enantiomer couple of C_1 symmetry, whose *cis*-pyridine nuclei resonate, in principle, at different frequencies. Significantly, only the C-2 and the C-6 pyridine nuclei, because of their preferential observation positions just on the top of the bipy moiety, double their resonances, indicating the molecular distortion freezing at low temperature.

In conclusion, variable-temperature spectra of rotamers show two different fluxional processes. We attribute the lower activation energy barrier to overall concerted flipping. The higher barrier must be due to asynchronous rotation of a single pyridine moiety about the Pt−N bond. In principle, simultaneous 180° rotation of the two heteroaromatic rings can physically not be distinguished from bipy flipping driving the concerted molecular motion. It is known, however,[10] that simultaneous rotation of both pyridines has a larger activation energy than the asynchronous single-ring rotation, so it seems reasonable to attribute the low fluxional activation energy to concerted flipping and the higher to the asynchronous rotation. No splitting of the resonances at low temperatures was observed for pyridine and *para*-substituted pyridine complexes **1**, **6**, **8** and **9**. This is consistent with low rotational barriers of these unhindered pyridines, which do not allow detection, at low temperatures, of bipy torsion freezing.

Discussion of Structure 1

Although **1** is the parent complex of an interesting class of metal species, the crystal structure, reported here with the PF_6^- counter ion, was not previously available. The

 © 2003 Wiley-VCH Verlag GmbH & Co. KGaA, Weinheim

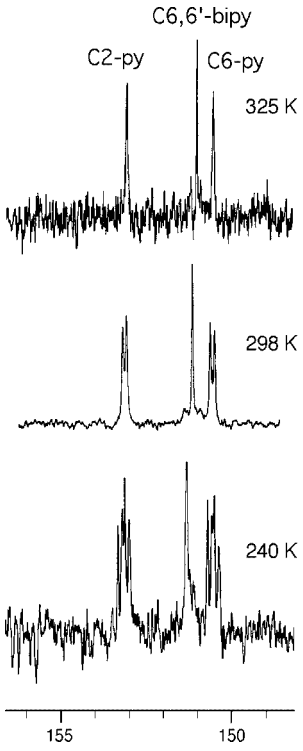

Figure 1. $^{13}C\{^1H\}$ spectra of **3** run at different temperatures

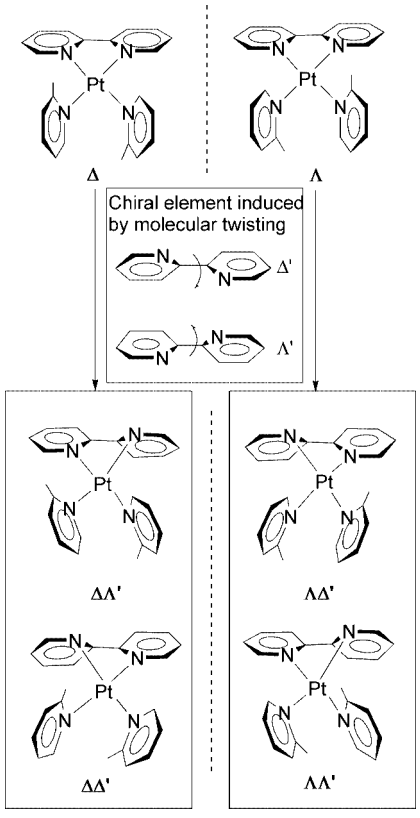

Scheme 3. Splitting due to the freezing of the C_2 twisting

complex crystallizes in the $P\bar{1}$ space group with one molecule in the asymmetric unit. The expected square-planar geometry is evident for the Pt coordination, whereas the anions show the usual octahedral conformation with just slight distortions (Figure 2 and Tables 5−7).

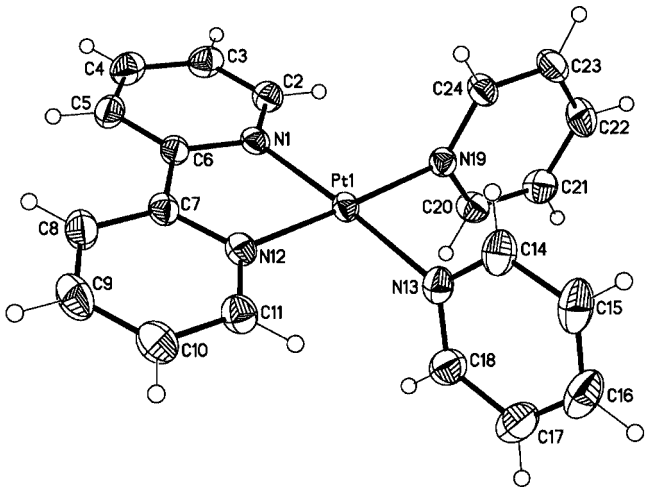

Figure 2. ORTEP view for the positively charged part of **1** with thermal ellipsoids to 30% of probability

Table 5. Crystal data and structure refinement for **1**

Empirical formula	$C_{20}H_{18}F_{12}N_4P_2Pt$
Formula mass	799.41
Temperature	298(2) K
Wavelength	0.71073 Å
Crystal system	triclinic
Space group	$P\bar{1}$
Unit cell dimensions	a = 8.5573(13) Å; α = 79.661(12)°
	b = 10.9811(19) Å; β = 77.035(12)°
	c = 14.671(2) Å; γ = 71.971(12)°
Volume	1268.4(4) Å^3
Z	2
Density (calcd.)	2.093 Mg/m^3
Absorption coefficient	5.764 mm^{-1}
F(000)	764
Crystal size	0.58 × 0.46 × 0.32 mm
Θ range for data collection	1.96−27.50°
Index ranges	$-10 \le h \le 1$, $-14 \le k \le 13$,
	$-19 \le l \le 18$
Reflections collected	6822
Independent reflections	5657 [R(int) = 0.0214]
Completeness to Θ = 27.50°	97.1%
Absorption correction	empirical
Max. and min. transmission	0.2458 and 0.0801
Refinement method	full-matrix least-squares on F^2
Data/restraints/parameters	5657/72/353
Goodness-of-fit on F^2	1.068
Final R indices [$I > 2\sigma(I)$]	R_1 = 0.0255, wR_2 = 0.0605
R indices (all data)	R_1 = 0.0325, wR_2 = 0.0646
Extinction coefficient	0.0112(5)
Largest diff. peak and hole	1.558 and −1.396 e·Å^{-3}

This square coordination plane is almost planar [max. deviation from the mean plane: N13 −0.0585(2) Å], though the bipyridyl short-bite strains the coordination angles and although the molecular symmetry is C_{2v}, the platinum atom is not able to occupy a special crystallographic position. The Pt−N distances are consistent with previously reported analogous crystal structures (Table 6).[3b,11,12]

 © 2003 Wiley-VCH Verlag GmbH & Co. KGaA, Weinheim

Table 6. Selected bond lengths [Å] and angles [°] for **1**

Pt1−N1	2.002(3)	Pt1−N12	2.002(3)
Pt1−N13	2.019(3)	Pt1−N19	2.024(3)
N1−C6	1.361(5)	C6−C7	1.467(6)
C7−N12	1.356(5)	C11−N12	1.338(5)
N1−Pt1−N12	81.01(13)	N1−Pt1−N13	176.38(13)
N12−Pt1−N13	96.85(14)	N1−Pt1−N19	97.69(13)
N12−Pt1−N19	177.27(12)	N13−Pt1−N19	84.57(13)
C2−N1−Pt1	125.7(3)	C6−N1−Pt1	114.7(3)
C7−C8−C9	119.5(5)	C10−C9−C8	119.1(4)
C11−N12−Pt1	126.1(3)	C7−N12−Pt1	114.9(3)

Table 7. Hydrogen bonds for **1** [Å and °]; symmetry transformations used to generate equivalent atoms: #1: $-x+1, -y+1, -z+2$; #2: $-x+1, -y+2, -z+1$; #3: $-x+2, -y+1, -z+1$

D−H···A	*d*(D−H)	*d*(H···A)	*d*(D···A)	<(DHA)
C(11)H(11)···F(2)#1	0.93	2.49	3.237(6)	137.4
C(23)H(23)···F(11)#2	0.93	2.51	3.390(6)	157.1
C(3)H(3)···F(7)#3	0.93	2.51	3.261(6)	138.4

The bipy plane almost overlaps the coordination plane [angle between mean planes: 3.69(8)°], while, as already observed in the cited papers,[3b,11,12] the pyridine aromatic rings are almost perpendicular to the coordination plane [angles between mean planes: 80.2(2)° and 80.8(1)°].

These moieties are not pointing directly toward the metal atom, which is slightly out from the pyridine averaged planes [0.196(1) and −0.323(1) Å]. This "clamp-like" closure may reasonably be due to the steric bumping of the pyridines against the bipy "wings", which is also consistent with the slightly greater corresponding strain detected for the palladium analogues.[13]

Other than the usual intermolecular hydrogen bonds, in which three fluorine atoms play the acceptor roles (see Tables), remarkable dipolar interactions take place between the fluorine and the metal atoms along the apical positions

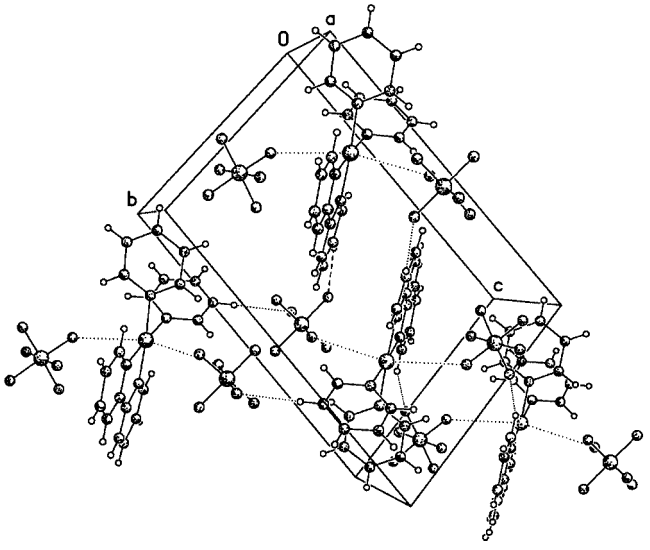

Figure 3. ORTEP view of the cell crystal packing for **1**

[Pt1···F5 3.298(5), Pt1···F8 3.338(5) Å]. These distances are shorter than those measured when pyridine is branched, probably because of steric hindrance.[3] Moreover, an intermolecular stacking interaction is present between the same ring of two bipyridyl moieties related by a symmetry inversion centre [distance between the two perfectly parallel planes: 3.339(1) Å].

All these attracting interactions produce three different types of dimeric aggregates in which the two units are related by an inversion centre and at least two pairs of interactions (see Figure 3).

Experimental Section

General: ^{1}H and $^{13}C\{^1H\}$ NMR spectra were recorded with a Bruker ARX 300 spectrometer, at 300.13 and 75.47 MHz, respectively. The ^{1}H NMR spectra were calibrated against the residual proton signals of the solvent as internal reference ([D$_6$]acetone: δ = 2.04 ppm), the $^{13}C\{^1H\}$ spectra were calibrated against the septuplet of the solvent ([D$_6$]acetone: δ = 29.80 ppm); $^{13}C\{^1H\}$ spin-lattice relaxation time constants were measured under N_2 by the "inversion recovery"[14] sequence.

Synthesis: The complexes were prepared by a previously described general procedure,[3,4] by heating of an aqueous suspension of [Pt(bipy)Cl$_2$] with an excess of the appropriate pyridine derivative at reflux. After dissolution of the solid, NH_4PF_6 was added and the resulting complexes [Pt(bipy)(*n*-Rpy)$_2$](PF$_6$)$_2$ precipitated as white or pale yellow substances, which were recrystallized from water/acetone. Elemental analyses were performed at the Microanalytical Laboratory of Redox snc (Milano).

[Pt(bipy)(py)$_2$](PF$_6$)$_2$ (1): ^{1}H NMR (300 MHz, [D$_6$]acetone): δ = 9.34 (dd, ^3J = 5.1, ^4J = 1.5 Hz, 4 H, 2-py, 6-py), 8.78 (d, ^3J = 8.2 Hz, 2 H, 3,3′-bipy), 8.59 (td, ^3J = 7.9, ^4J = 1.4 Hz, 2 H, 4,4′-bipy), 8.30 (tt, ^3J = 7.7, ^4J = 1.5 Hz, 2 H, 4-py), 8.01 (m, 2 H, 6,6′-bipy), 7.89 (m, 4 H, 3-py, 5-py), 7.81 (m, 2 H, 5,5′-bipy) ppm. $^{13}C\{^1H\}$ NMR (75 MHz, [D$_6$]acetone): δ = 157.6 (2 C, 2,2′-bipy), 153.4 (4 CH, 2-py, 6-py), 151.0 (2 CH, 6,6′-bipy), 143.7 (2 CH, 4,4′-bipy), 142.9 (2 CH, 4-py), 129.7 (2 CH, 5,5′-bipy), 129.6 (4 CH, 3-py, 5-py), 125.6 (2 CH, 3,3′-bipy) ppm. $C_{20}H_{18}F_{12}N_4P_2Pt$ (799): calcd. C 30.03, H 2.25, N 7.01; found C 30.11, H 2.38, N 7.09.

(*s-cis*/*s-trans*)-[Pt(bipy)(2-Mepy)$_2$](PF$_6$)$_2$ (2): ^{1}H NMR (300 MHz, [D$_6$]acetone): δ = 9.46, 9.21 (dd, ^{3} = 5.6, ^4J = 1.5 Hz, 2 H/2 H, 6-py), 8.80 (d, ^3J = 7.7 Hz, 4 H, 3,3′-bipy), 8.60 (td, ^3J = 7.9, ^4J = 1.4 Hz, 4 H, 4,4′-bipy), 8.19 (m, 4 H, 4-py), 7.95 (m, 4 H, 6,6′-bipy), 7.91 (m, 4 H, 3-py), 7.83 (m, 4 H, 5,5′-bipy), 7.70, 7.63 (td, ^3J = 7.7, ^4J = 1.4 Hz, 2 H/2 H, 5-py), 3.49, 3.34 (s, 6 H/6 H, CH$_3$) ppm. $^{13}C\{^1H\}$ NMR (75 MHz, [D$_6$]acetone): δ = 161.9 (4 C, 2,2′-bipy), 158.0, 157.9 (2 C/2 C, 2-py), 153.8, 152.7 (2 CH/2 CH, 6-py), 150.8, 150.6 (2 CH/2 CH, 6,6′-bipy), 143.8 (4 CH, 4,4′-bipy), 142.2, 142.3 (2 CH/2 CH, 4-py), 130.3, 130.1 (2 CH/2 CH, 3-py), 129.9 (4 CH, 5,5′-bipy), 126.2 (4 CH, 5-py), 125.6 (4 CH, 3,3′-bipy), 27.1, 26.5 (2 CH$_3$/2 CH$_3$) ppm. $C_{22}H_{22}F_{12}N_4P_2Pt$ (827): calcd. C 31.92, H 2.66, N 6.77; found C 32.20, H 2.78, N 6.88.

(*s-cis*/*s-trans*)-[Pt(bipy)(3-Mepy)$_2$](PF$_6$)$_2$ (3): ^{1}H NMR (300 MHz, [D$_6$]acetone): δ = 9.22 (s, 4 H, 2-py), 9.12 (s, 4 H, 6-py), 8.68 (d, ^3J = 7.7 Hz, 4 H, 3,3′-bipy), 8.58 (td, ^3J = 7.7, ^4J = 1.4 Hz, 4 H, 4,4′-bipy), 8.11 (d, ^3J = 7.6 Hz, 4 H, 4-py), 7.96 (d, ^3J = 5.6 Hz, 4 H, 6,6′-bipy), 7.74 (m, 4 H, 5,5′-bipy), 7.72 (m, 4 H, 5-py), 2.45

 © 2003 Wiley-VCH Verlag GmbH & Co. KGaA, Weinheim

(s, 12 H, CH_3) ppm. $^{13}C\{^1H\}$ NMR (75 MHz, [D_6]acetone): δ = 157.6 (4 C, 2,2′-bipy), 153.2, 153.0 (2 CH:2 CH, 2-py), 151.1 (4 CH, 6,6′-bipy), 150.6, 150.5 (2 CH:2 CH, 6-py), 143.8 (4 CH, 4,4′-bipy), 143.4 (4 CH, 4-py), 140.5 (4 C, 3-py), 129.7 (4 CH, 5,5′-bipy), 128.8 (4 CH, 5-py), 125.7 (4 CH, 3,3′-bipy), 18.4 (4 CH_3) ppm. $C_{22}H_{22}F_{12}N_4P_2Pt$ (827): calcd. C 31.92, H 2.66, N 6.77; found C 32.17, H 2.76, N 6.88.

(*s-cis*/*s-trans*)-[Pt(bipy)(3-CNpy)$_2$](PF$_6$)$_2$ (4): ^1H NMR (300 MHz, [D_6]acetone): δ = 9.96, 9.92 (s, 2 H:2 H, 2-py), 9.73, 9.68 (d, ^3J = 7.8 Hz, 2 H:2 H, 6-py), 8.79 (d, ^3J = 7.9 Hz, 4 H, 3,3′-bipy), 8.73 (m, 4 H, 4-py), 8.60 (td, ^3J = 7.9, ^4J = 1.4 Hz, 4 H, 4,4′-bipy), 8.13 (m, 4 H, 5-py), 8.09 (m, 4 H, 6,6′-bipy), 7.79 (td, ^3J = 7.9, ^4J = 1.5 Hz, 4 H, 5,5′-bipy) ppm. $^{13}C\{^1H\}$ NMR (75 MHz, [D_6]acetone): δ = 157.2, (4 C, 2,2′-bipy), 156.9, 156.7 (2 CH:2 CH, 2-py), 156.6, 156.3 (2 CH:2 CH, 6-py), 151.4 (4 CH, 6,6′-bipy), 145.8 (4 CH, 4-py), 143.9 (4 CH, 4,4′-bipy), 130.0, 129.9 (4 CH, 5-py), 129.5 (4 CH, 5,5′-bipy), 125.5 (4 CH, 3,3′-bipy), 115.5 (4 CN), 114.7 (4 C, 3-py) ppm. $C_{22}H_{16}F_{12}N_6P_2Pt$ (849): calcd. C 31.09, H 1.88, N 9.89; found C 30.65, H 2.01, N 10.01.

(*s-cis*/*s-trans*)-[Pt(bipy)(3-Phpy)$_2$](PF$_6$)$_2$ (5): ^1H NMR (300 MHz, [D_6]acetone): δ = 9.77, 9.75 (s, 2 H:2 H, 2-py), 9.41, 9.37 (dd, ^3J = 5.6, ^4J = 1.5 Hz, 2 H:2 H, 6-py), 8.79 (d, ^3J = 7.7 Hz, 4 H, 3,3′-bipy), 8.59 (m, 4 H, 4,4′-bipy), 8.56 (m, 4 H, 4-py), 8.17 (m, 4 H, 6,6′-bipy), 7.96, 7.93 (td, ^3J = 7.7, ^5J = 1.3 Hz, 2 H:2 H, 5-py), 7.81 (m, 4 H, 5,5′-bipy), 7.75 (m, 8 H, *o*-Ph), 7.54 (m, 8 H, *m*-Ph), 7.47 (m, 4 H, *p*-Ph) ppm. $^{13}C\{^1H\}$ NMR (75 MHz, [D_6]acetone): δ = 157.5 (4 C, 2,2′-bipy), 151.8, 151.7 (2 CH/2 CH, 6-py), 151.3 (4 CH, 6,6′-bipy), 151.3, 151.1 (2 CH/2 CH, 2-py), 143.8 (4 CH, 4,4′-bipy), 142.1, 142.0 (2 C/2 C, 3-py), 140.5 (4 CH, 4-py), 135.2 (4 C, C_{ipso}), 130.6, 130.5 (2 CH/2 CH, *p*-Ph), 130.2 (8 CH, *m*-Ph), 129.7 (4 CH, 5,5′-bipy), 129.5 (4 CH, 5-py), 128.2 (8 CH, *o*-Ph), 125.7 (4 CH, 3,3′-bipy) ppm. $C_{32}H_{26}F_{12}N_4P_2Pt$ (951): calcd. C 40.37, H 2.73, N 5.89; found C 40.11, H 2.98, N 6.05.

[Pt(bipy)(4-Phpy)$_2$](PF$_6$)$_2$ (6): ^1H NMR (300 MHz, [D_6]acetone): δ = 9.37 (dd, ^3J = 5.1, ^5J = 1.3 Hz, 4 H, 2-py, 6-py), 8.78 (d, ^3J = 8.2 Hz, 2 H, 3,3′-bipy), 8.58 (td, ^3J = 8.2, ^4J = 1.4 Hz, 2 H, 4,4′-bipy), 8.19 (dd, ^3J = 5.1, ^5J = 1.3 Hz, 4 H, 3-py, 5-py), 8.12 (m, 2 H, 6,6′-bipy), 7.93 (m, 4 H, *o*-Ph), 7.82 (td, ^3J = 7.9, ^4J = 1.4 Hz, 2 H, 5,5′-bipy), 7.58 (overlapped m, 6 H, *m*-Ph, *p*-Ph) ppm. $^{13}C\{^1H\}$ NMR (75 MHz, [D_6]acetone): δ = 157.6 (2 C, 2,2′-bipy), 153.6 (2 C, 4-py), 153.3 (4 CH, 2-py, 6-py), 151.1 (2 CH, 6,6′-bipy), 143.8 (2 CH, 4,4′-bipy), 135.5 (2 C, C_{ipso}), 132.1 (2 CH, *p*-Ph), 130.4 (4 CH, *m*-Ph), 129.7 (2 CH, 5,5′-bipy), 128.3 (4 CH, *o*-Ph), 126.4 (4 CH, 3-py, 5-py), 125.7 (2 CH, 3,3′-bipy) ppm. $C_{32}H_{26}F_{12}N_4PPt_2$ (951): calcd. C 40.37, H 2.73, N 5.89; found C 40.13, H 2.95, N 6.06.

[Pt(bipy)(3,5-Me$_2$py)$_2$](PF$_6$)$_2$ (7): ^1H NMR (300 MHz, [D_6]acetone): δ = 9.08 (s, 4 H, 2-py, 6-py), 8.84 (d, ^3J = 8.6 Hz, 2 H, 3,3′-bipy), 8.64 (td, ^3J = 8.6, ^4J = 1.5 Hz, 2 H, 4,4′-bipy), 7.96 (overlapped m, 4 H, 6,6′-bipy, 4-py), 7.82 (m, 2 H, 5,5′ bipy), 2.38 (s, 12 H, CH_3) ppm. $^{13}C\{^1H\}$ NMR (75 MHz, [D_6]acetone): δ = 157.4 (2 C, 2,2′-bipy), 151.1 (2 CH, 6,6′-bipy), 150.2 (4 CH, 2-py, 6-py), 143.9 (2 CH, 4-py), 143.6 (2 CH, 4,4′-bipy), 139.5 (4 C, 3-py, 5-py), 129.7 (2 CH, 5,5′-bipy), 125.6 (2 CH, 3,3′-bipy), 18.1 (4 CH_3) ppm. $C_{24}H_{26}F_{12}N_4P_2Pt$ (855): calcd. C 33.68, H 3.04, N 6.55; found C 33.07, H 2.91, N 6.87.

[Pt(4-Phbipy)(py)$_2$](PF$_6$)$_2$ (8): ^1H NMR (300 MHz, [D_6]acetone): δ = 9.39 (dd, ^3J = 5.1, ^4J = 1.5 Hz, 4 H, 2-py, 6-py), 9.29 (d, ^4J = 1.7 Hz, 2 H, 3,3′-bipy), 8.33 (tt, ^3J = 7.7, ^4J = 1.5 Hz, 2 H, 4-py), 8.09 (m, 2 H, 5,5′-bipy), 8.06 (m, 4 H, *o*-Ph), 8.03 (m, 2 H, 6,6′-bipy), 7.91 (m, 4 H, 3-py, 5-py), 7.65 (overlapped m, 6 H, *m*-Ph, *p*-Ph) ppm. $^{13}C\{^1H\}$ NMR (75 MHz, [D_6]acetone): δ = 158.0 (2 C, 2,2′-bipy), 154.9 (2 C, 4,4′-bipy), 153.6 (4 CH, 2-py, 6-py), 151.1 (2 CH, 6,6′-bipy), 143.0 (2 CH, 4-py), 135.7 (2 C, C_{ipso}), 132.4 (2 CH, *p*-Ph), 130.5 (4 CH, *m*-Ph), 129.7 (4 CH, 3-py, 5-py), 128.7 (4 CH, *o*-Ph), 126.4 (2 CH, 5,5′-bipy), 123.4 (2 CH, 3,3′-bipy) ppm. $C_{32}H_{26}F_{12}N_4P_2Pt$ (951): calcd. C 40.37, H 2.73, N 5.89; found C 40.16, H 2.99, N 6.04.

[Pt(4-Phbipy)(4-CNpy)$_2$](PF$_6$)$_2$ (9): ^1H NMR (300 MHz, [D_6]acetone): δ = 9.78 (dd, ^3J = 5.1, ^5J = 1.2 Hz, 4 H, 2-py, 6-py), 9.32 (d, ^4J = 1.7 Hz, 2 H, 3,3′-bipy), 8.38 (dd, ^3J = 5.1, ^5J = 1.2 Hz, 4 H, 3-py, 5-py), 8.07 (overlapped m, 8 H, 5,5′-bipy, 6,6′-bipy, *o*-Ph), 7.67 (overlapped m, 6 H, *m*-Ph, *p*-Ph) ppm. $^{13}C\{^1H\}$ NMR (75 MHz, [D_6]acetone): δ = 157.8 (2 C, 2,2′-bipy), 155.2 (2 C, 4,4′-bipy), 155.0 (4 CH, 2-py, 6-py), 151.3 (2 CH, 6,6′-bipy), 135.6 (2 C, C_{ipso}), 132.6 (2 CH, *p*-Ph), 131.9 (4 CH, 3-py, 5-py), 130.5 (4 CH, *m*-Ph), 128.7 (4 CH, *o*-Ph), 126.3 (2 CH, 5,5′-bipy), 126.0 (2 C, 4-py), 123.6 (2 CH, 3,3′-bipy), 115.5 (2 CN) ppm. $C_{34}H_{24}F_{12}N_6P_2Pt$ (1001): calcd. C 40.76, H 2.40, N 8.39; found C 40.60, H 2.45, N 8.41.

Crystal Structure Determination of 1: Crystals suitable for X-ray analysis were obtained by recrystallization from methanol solution. Diffraction data were collected from a colourless 0.58 × 0.46 × 0.32 mm irregular specimen at room temperature by use of a Siemens P4 automated four-circle single-crystal diffractometer with graphite-monochromated Mo-K_α radiation (λ = 0.71073 Å). Lattice parameters were obtained from least-squares refinement of the setting angles of 42 and 39 reflections within 5.34° ≤ θ ≤ 17.50° range. 6822 reflections were measured by the fixed speed θ-2θ scan technique up to 2θ ≤ 55°. No crystal decay was evidenced by reference reflections monitored each 197 measurements. Intensities were evaluated by profile fitting of a 96-step peak scan among 2θ shells procedure[15] and then corrected for Lorentz polarization effects. Absorption correction was applied by Gaussian integration of the indexed crystal shape. Data collection, reduction and face-indexed absorption correction were performed with the aid of the XSCANS[16] and SHELXTL packages.[17] The structure was solved by the Patterson standard method in the SHELXS package,[18] and refined by minimization of the function $\Sigma w(F_o^2 - F_c^2)^2$ by the full-matrix, least-squares technique based on all independent F^2, by use of SHELXL-97.[19] All non-hydrogen atoms were treated as anisotropic. Hydrogen atoms were placed in idealized positions and all the isotropic thermal parameters were fixed to the best fitting value. An empirical extinction parameter was included in the last refinement cycles. The last difference map showed expected electron density residuals close to the metal atoms (max. and min. values: 1.558 and −1.396 e·Å^{-3}). The final geometrical calculations and drawings were carried out with the aid of the PARST program[20] and the XPW[21] utility of the Siemens package, respectively. CCDC-201345 (**1**) contains the supplementary crystallographic data for this paper. These data can be obtained free of charge at www.ccdc.cam.ac.uk/conts/retrieving.html [or from the Cambridge Crystallographic Data Centre, 12 Union Road, Cambridge CB2 1EZ, UK; Fax: (internat.) + 44-1223/336-033; E-mail: deposit@ccdc.cam.ac.uk].

[1] R. Robson, B. F. Abrahams, S. R. Batten, R. W. Gable, B. F. Hoskins, J. Liu, *Supramolecular Architecture*, ACS Symposium Series 499 (Ed.: T. Bein), American Chemical Society, Washington D.C., **1992**, chapter 19. J.-C. Chambron, C. Dietrich-Buchecker, J.-P. Sauvage, "Transition Metals as Assembling and Templating Species", in: *Comprehensive Supramolecular Chemistry* (Ed.: J.-M. Lehn, Chair), Pergamon Press, Oxford, U.K., **1996**, vol. 9, chapter 2, p. 43.

 © 2003 Wiley-VCH Verlag GmbH & Co. KGaA, Weinheim

[2] N. Margiotta, F. P. Fanizzi, J. Kobe, G. Natile, *Eur. J. Inorg. Chem.* **2001**, *5*, 1303−1310.
[3] [3a] M. Cusumano, A. Giannetto, *J. Inorg. Biochem.* **1997**, *65*, 137. [3b] M. Cusumano, M. L Di Pietro, A. Giannetto, *Inorg. Chem.* **1999**, *38*, 1754.
[4] M. Cusumano, M. L. Di Pietro, A. Giannetto, F. Nicolò, E. Rotondo, *Inorg. Chem.* **1998**, *37*, 563−568.
[5] C. M. Dupureur, J. K. Barton, *Inorg. Chem.* **1997**, *36*, 33−43; P. J. Dandliker, M. E. Núñez, J. K. Barton, *Biochemistry* **1998**, *37*, 6491−6502.
[6] F. H. Allen, J. E. Davies, J. J. Galloy, O. Johnson, O. Kennard, C. F. Macrae, E. M. Mitchell, G. F. Mitchell, J. M. Smith, D. G. Watson, *J. Chem. Info. Comp. Sci.* **1991**, *31*, 187.
[7] E. Rotondo, unpublished results.
[8] H.-O. Kalinowski, S. Berger, S. Braun, *Carbon-13 NMR Spectroscopy*, John Wiley & Sons, New York, **1988**.
[9] G. C. Levy, *J. Chem. Soc., Chem. Commun.* **1972**, 47.
[10] M. Fuss, H.-U. Siehl, B. Olenyuk, P. J. Stang, *Organometallics* **1999**, *18*, 758−769.
[11] Z. Qin, M. C. Jennings, R. J. Puddephatt, *Chem. Commun.* **2001**, 2676−2677.
[12] H.-Q. Liu, S.-M. Peng, C. M. Che, *Chem. Commun.* **1995**, 509−510.
[13] G. Bruno, to be published.
[14] D. J. Craik, G. C. Levy, *Top. Carbon-13 NMR Spectrosc.* **1984**, *4*, 239.
[15] R. Diamond, *Acta Crystallogr., Sect. A* **1969**, *25*, 43−55.
[16] Bruker, *XSCANS*, release 2.31, Bruker AXS Inc., Madison, Wisconsin, **1999**.
[17] G. M. Sheldrick, *SHELXTL*, VMS version 5.05, Siemens Analytical X-ray Instruments Inc., Madison, Wisconsin, **1991**.
[18] A. Altomare, O. Cascarano, C. Giacovazzo, A. Guagliardi, M. C. Burla, G. Polidori, M. Camalli, *J. Appl. Crystallogr.* **1994**, *27*, 435−436.
[19] G. M. Sheldrick, *SHELXL-97, Program for Crystal Structure Refinement*, Univ. of Göttingen, Germany, **1997**.
[20] M. Nardelli, *J. Appl. Crystallogr.* **1985**, *28*, 659; release November **1999**.
[21] G. M. Sheldrick, *Acta Crystallogr., Sect. A* **1990**, *46*, 467.
Received January 16, 2003

 © 2003 Wiley-VCH Verlag GmbH & Co. KGaA, Weinheim

Bis(2-aminobutanol)dichloroplatinum(II) Complexes and Their Singly and Doubly Ring-Closed Butanolato Species − Novel Prodrugs for Platinum-Based Antitumour Chemotherapy?

Markus Galanski,*[a] Christian Baumgartner,[a] Vladimir Arion,[a] and Bernhard K. Keppler[a]

Keywords: Antitumour agents / Bioinorganic chemistry / N,O ligands / Platinum

Cytotoxic hydroxyethyl-substituted (amine)platinum(II) and -(IV) complexes have recently attracted attention because of the ability of their hydroxyethyl groups to coordinate through the oxygen atom to the platinum centre during oxidation with hydrogen peroxide or through intramolecular ligand exchange reactions in dichloroplatinum(II) complexes. The last point in particular is of great interest, because the intramolecular attack of the hydroxy group dramatically influences the mode of action of platinum(II) compounds. On the other hand, there is also the chance to use such reactions specifically for the synthesis of novel anticancer platinum-based drugs for chemotherapy. We have therefore focused our chemistry program on the synthesis of dichloroplatinum(II) complexes that are in a position to form singly and, especially, doubly ring-closed alcoholato species and on investigation of their structures by X-ray crystallography. It was possible to determine the crystal structures of [Pt{(*R*)-(−)-HL}$_2$Cl$_2$], [Pt{(*S*)-(+)-HL}$_2$Cl$_2$], [Pt{(*R*)-(−)-HL}{(*S*)-(+)-HL}Cl$_2$], [Pt{(*S*)-(+)-HL}{(*S*)-(+)-L}Cl], [Pt{(*R*)-(−)-L}$_2$] and [Pt{(*S*)-(+)-L}$_2$] (HL = 2-aminobutanol-κ*N*, L = 2-aminobutanolato-κ^2*N*,*O*). The results obtained may represent the first step towards novel prodrugs for platinum-based antitumour chemotherapy.

(© Wiley-VCH Verlag GmbH & Co. KGaA, 69451 Weinheim, Germany, 2003)

Introduction

Alongside the worldwide success of cisplatin [= *cis*-diamminedichloroplatinum(II)] and carboplatin [= *cis*-diammine(1,1-cyclobutanedicarboxylato)platinum(II)] which are routinely used in clinics against certain types of cancer,[1−5] the so-called third-generation platinum drug oxaliplatin {= [*trans*-(1*R*,2*R*)-cyclohexane-1,2-diamine]oxalatoplatinum(II) (Figure 1)} is also today in clinical use.[6]

In order to overcome the severe side-effects of platinum-based chemotherapy, to improve clinical effectiveness and to broaden the spectrum of activity, there is still a need for other platinum antitumour agents. During recent years, part of the research in this field has focused on platinum(II) and -(IV) complexes with peripheral functional groups. OH- and COOH-substituted ligands were especially of interest because of their potential to act as donors or acceptors for hydrogen bonds, which could play an important role in the binding of platinum compounds to DNA, the major target of platinum-based chemotherapy.[7] Moreover, these compounds were also used as starting materials for further derivatization,[8,9] with the aim of attaching suitable carrier molecules for drug targeting.[10,11]

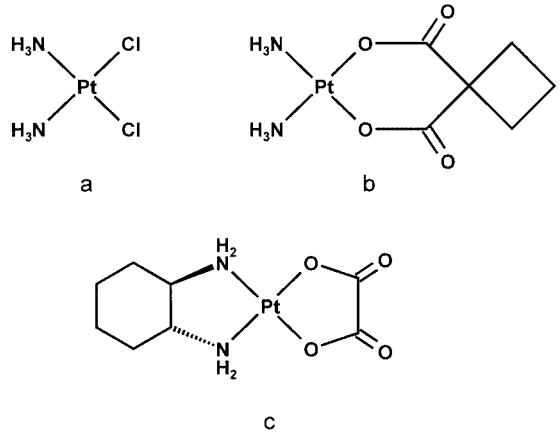

Figure 1. Platinum(II) complexes in clinical use: cisplatin (a), carboplatin (b) and oxaliplatin (c)

Hydroxyethyl residues have recently attracted attention because of their ability to coordinate to the platinum centre through the oxygen atom: (i) during oxidation with hydrogen peroxide[12] or (ii) through an intramolecular ligand exchange reaction in dichloroplatinum(II) complexes.[13]

In investigation of the binding of potentially cytotoxic platinum coordination compounds to nucleotides, the above intramolecular ligand exchange reaction might at first sight

[a] Institute of Inorganic Chemistry, Vienna University, Waehringer Strasse 42, 1090 Vienna, Austria
Fax: (internat.) + 43-1/4277-52680
E-mail: galanski@ap.univie.ac.at
Supporting information for this article is available on the WWW under http://www.eurjic.org or from the author.

be regarded as an undesirable side reaction of a competitive character, complicating the mechanism of action.[14−16] On the other hand, though, such reactions have also been used specifically for the synthesis of novel tumour-inhibiting platinum(IV) drugs.[17]

CZE-CE-MS studies have shown[18] that the binding behaviour of dichlorobis[(2-hydroxyethyl)amine]platinum(II) towards 5′-GMP is dramatically increased by a decrease in the pH from 7.4 to 6.0. This is of great interest in view of the lower pH values encountered in solid tumours and fits with a pH-dependent ring-closing/opening reaction of *N*-(hydroxyethyl)-substituted diaminedichloroplatinum(II) complexes.

The intramolecular ligand exchange reactions described above have been investigated by NMR spectroscopy but there was still a lack of structural information from X-ray crystallography. To fill this gap, and to develop new platinum-based antitumour drugs, we have focused on the synthesis and crystallisation of substituted dichlorobis[(2-hydroxyethyl)amine]platinum(II) complexes and especially their singly and doubly ring-closed species.

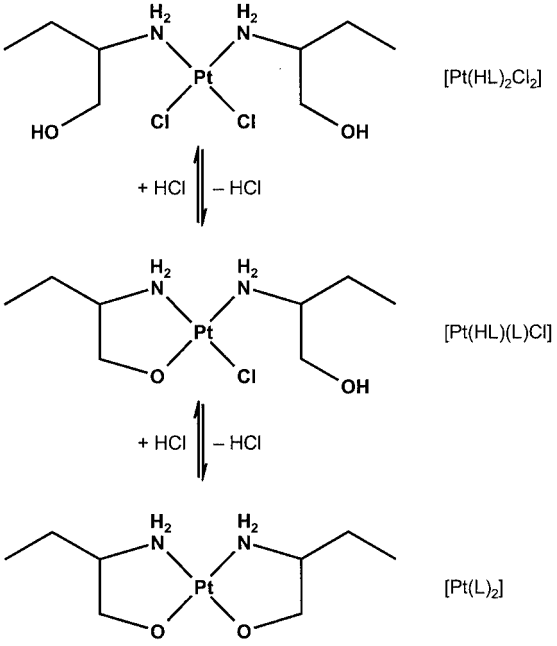

Figure 2. Intramolecular ligand exchange reactions resulting in singly ([Pt(HL)(L)Cl]) and doubly ([Pt(L)$_2$]) ring-closed species

Results and Discussion

Synthesis of the bis(2-aminobutanol)dichloroplatinum(II) complexes starts from potassium tetrachloroplatinate(II), K_2PtCl_4, which is converted in situ to the corresponding tetraiodoplatinate(II) by treatment with KI. After addition either of enantiomerically pure 2-aminobutanol or of the racemic mixture, the (2-aminobutanol)diidoplatinum(II) compounds are formed. Conversion of the diiodo to the dichloro complexes was performed by treatment of the diiodo compounds with silver nitrate, which afforded the diaminediaquaplatinum(II) species, and subsequent addition of KCl or HCl to provide the bis(2-aminobutanol)dichloroplatinum(II) complexes. Depending on pH, chloride ion concentration and crystallisation, either pure dichloroplatinum(II) complexes, [Pt(HL)$_2$Cl$_2$], or a mixture of [Pt(HL)$_2$Cl$_2$] and the singly ring-closed species [Pt(HL)(L)Cl] can be isolated (Figure 2). The doubly ring-closed coordination compound could not be detected during this synthetic pathway. The tailor-made synthesis of [Pt(L)$_2$] was achieved by (i) abstraction of the chloro ligands and (ii) by shifting the pH to values above 7 with a basic ion exchanger.

The purities of the synthesized complexes can best be judged by ^{1}H and ^{13}C NMR spectroscopy. In the case of the enantiomerically pure [Pt{(*S*)-(+)-HL}$_2$Cl$_2$] complex, six proton resonances are detected [δ = 0.86 (CH_3), 1.49 (CH$_3$CH_2), 1.70 (CH$_3$CH_2), 2.74 (C*H*), 3.60 (CH_2OH), 4.07 (CH_2OH) ppm]. Because of the asymmetrically substituted methine carbon atom, the two methylene groups show two sets of multiplets, in agreement with their diastereotopic character. Four different ^{13}C signals were found: atδ = 10.0 (*C*H$_3$), 24.6 (CH$_3$*C*H$_2$), 59.4 (*C*H) and 62.5 (*C*H$_2$OH) ppm. The corresponding resonances of the doubly ring-closed species were found to be atδ = 0.80 (CH_3), 1.34 (CH$_3$CH_2), 1.53 (CH$_3$CH_2), 2.48 (C*H*), 2.88 (CH_2O), 3.01 (CH_2O), 10.76 (*C*H$_3$), 22.90 (CH$_3$*C*H$_2$), 64.07 (*C*H) and 73.02 (*C*H$_2$O) ppm. Most indicative of the ring-closing reaction are the ^{1}H and ^{13}C chemical shifts of the methylene group next to the oxygen atom. In the chelating (*S*)-(+)-2-aminobutanolato ligands both of the singly and of the doubly ring-closed species, marked shifts of the ^{1}H resonances to higher field and downfield shifts of the ^{13}C signals in relation to the monodentate-coordinated (*S*)-(+)-2-aminobutanol can be seen.

During the synthesis it was possible to isolate crystals suitable for X-ray crystallographic studies. In the presence of hydrochloric acid, compound **1**, [Pt{(*R*)-(−)-HL}$_2$Cl$_2$], could be isolated as the dichloroplatinum(II) complex, whereas the structure of **2** {solution of [Pt{(*S*)-(+)-HL}$_2$Cl$_2$] in water and KCl} is made up of two different compounds − the dichloroplatinum(II) complex [Pt{(*S*)-(+)-HL}$_2$Cl$_2$] and the singly ring-closed species [Pt{(*S*)-(+)-HL}{(*S*)-(+)-L}Cl] − in a 1:1 ratio.

It was also possible to determine the structures of the corresponding doubly ring-closed enantiomerically pure bis(2-aminobutanolato)platinum(II) complexes **3** ([Pt{(*R*)-(−)-L}$_2$]) and **4** ([Pt{(*S*)-(+)-L}$_2$]) in the crystal.

Furthermore, the structure of **S1**, a 1:1 mixture of [Pt{(*R*)-(−)-HL}{(*S*)-(+)-HL}Cl$_2$] and [Pt{(*S*)-(+)-HL}$_2$Cl$_2$] isolated from the synthesis with a racemic mixture of 2-aminobutanol ligands, could also be resolved. Crystal data, data collection parameters and structure refinement details for **S1** are given in Table S4 of the Supporting Information, while the structure is shown in Figure S4.

Figure 3 summarises the results of the single-crystal X-ray structure of one of the two independent molecules of **1**, [Pt{(*R*)-(−)-HL}$_2$Cl$_2$]. The second independent molecule is shown in Figure S1 in the Supporting Information. The

 © 2003 Wiley-VCH Verlag GmbH & Co. KGaA, Weinheim

platinum(II) atom has a square-planar coordination geometry. Two 2-aminobutanol ligands act as neutral monodentate ligands and bind to Pt^{II} through the terminal nitrogen atoms [Pt1−N1 2.057(5), Pt1−N2 2.035(6) Å]. These bond lengths are similar to Pt−N [2.042(4) Å] in $Pt^{II}Cl_2(EA)_2$ and shorter than Pt−N [2.070(3) Å] in $Pt^{IV}Cl_4(EA)_2\cdots H_2O$ (EA = ethanolamine).[19] In addition to two *cis*-disposed organic ligands, two chloride anions Cl1 and Cl2 are bound to Pt^{II} at 2.327(2) and 2.3139(19) Å, respectively. The bond lengths in the coordinated 2-aminobutanol ligands are in a normal range [O1−C1 1.402(10), O2−C5 1.435(9); C1−C2 1.550(13), C5−C6 1.516(10); C2−N1 1.489(9), C6−N2 1.512(9); C2−C3 1.516(9), C6−C7 1.490(9); C3−C4 1.533(13), C7−C8 1.548(11) Å]. Both coordinated NH_2 groups are involved in intramolecular hydrogen bonding (Figure 3) (N1-H1A···O2 with N1-H1A 0.90, H1A···O2 2.121, N1···O2 2.956 Å and N1-H1A···O2 153.77°; and N2-H2A···O1 with N2-H2A 0.90, H2A···O1 2.319, N2···O1 3.049 Å and N2-H2A···O1 138.21°). Both molecules are involved in a three-dimensional hydrogen-bonding network, the packing being dominated by O−H···O, N−H···O and N−H···Cl interactions. Detailed geometrical parameters for the intramolecular contacts in the second independent molecule of **1**, together with intermolecular contacts in **1**, are given in Table S1.

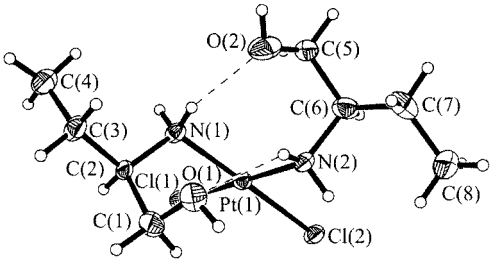

Figure 3. ORTEP diagram of one of the independent molecules of **1** with thermal ellipsoids at 50% probability

The structure of **2** is made up of two different molecules: [Pt{(*S*)-(+)-HL}$_2$Cl$_2$] (**I**) and [Pt{(*S*)-(+)-HL}{(*S*)-(+)-L}Cl] (**II**). There are four crystallographically independent molecules in the asymmetric unit: two (A and C) of composition I and two other ones (B and D) of composition II. In addition, molecule C was found to exist in the crystal as two conformers in ca. 0.4:0.6 ratio, differing slightly in the positions of the terminal ethyl groups (Figure S2). The molecular structures of **2-IA** and **2-IIB** are shown in Figures 4 and 5, respectively.

Two neutral 2-aminobutanol ligands act in monodentate fashion and coordinate to Pt^{II} through the terminal amino groups' N1 and N2 atoms in both molecules A and C. They each exhibit a square-planar coordination geometry around Pt, with two nitrogen atoms and two chloride ligands in a *cis* arrangement with average r.m.s. deviations of 0.03 and 0.02 Å, respectively. As in **2-IA** and **2-IC**, the coordination geometry around Pt^{II} in **2-IIB** and **2-IID** can be described as square-planar. The deviation of the coordinated atoms from their mean planes does not exceed 0.04 Å. One neutral 2-aminobutanol ligand acts in monodentate fashion and coordinates to Pt^{II} through N3 in **2-IIB** (Figure 5) and through N7 in **2-IID** (Figure S3), whereas another one, deprotonated at the OH group, chelates to the Pt atom through the N4/O4 (**2-IIB**) and N8/O8 (**2-IID**) atoms, giving a *cis* arrangement of amino groups. The fourth coordination place around Pt^{II} in molecules B and D is occupied by chloride anions Cl3 and Cl6, respectively. The chelate ring Pt2O4C13C14N4 in B has an envelope conformation.

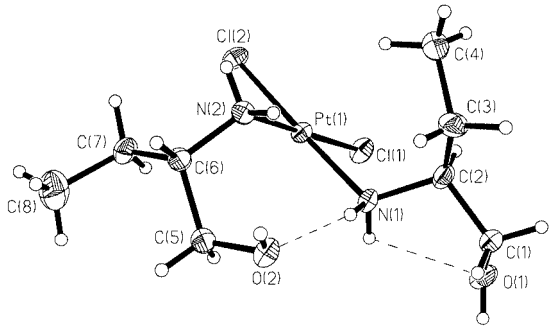

Figure 4. ORTEP diagram of **2-IA** with thermal ellipsoids at 50% probability

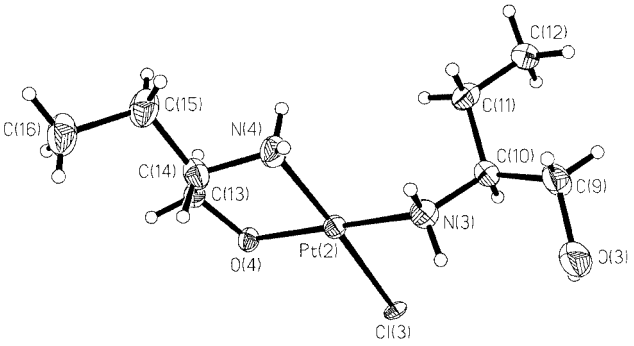

Figure 5. ORTEP diagram of **2-IIB** with thermal ellipsoids at 50% probability

The flap[20] atom protrudes from the plane of the coordinated atoms by 0.63 Å. In contrast, the Pt4O8C29C30N8 chelate ring has a distorted envelope conformation with a weak tendency towards a zigzag arrangement of C29 (+0.09 Å) and C30 (−0.54 Å) (Figure S3). The dihedral angles O4−C13−C14−N4 and O8−C29−C30−N8 compare well, at 48.1(7)° (B) and 50.7° (D). The bite angles, at 82.83(19) and 83.33(19)°, are also similar. The N3−C10 and N7−C26 bonds in the non-chelated ligands in B and D orient almost vertically to the planes of bound platinum atoms with corresponding angles Pt2−N3−C10 and Pt4−N7−C26 at 119.2(4) and 118.6(4)°. All asymmetric carbon atoms in **2** are (*S*)-chiral centres. The corresponding Pt−N, Pt−O and Pt−Cl bond lengths in molecules A, B, C and D as well as the bond lengths in the ligands are quoted in Tables 1 and 2.

 © 2003 Wiley-VCH Verlag GmbH & Co. KGaA, Weinheim

Table 1. Bond lengths [Å] in the platinum(II) coordination polyhedron of **2**

Atom1−Atom2	Molecule A	Atom1−Atom2	Molecule C
Pt1−N1	2.057(4)	Pt3−N5	2.065(5)
Pt1−N2	2.061(5)	Pt3−N6	2.060(5)
Pt1−Cl1	2.3080(15)	Pt3−Cl4	2.3102(16)
Pt1−Cl2	2.3264(16)	Pt3−Cl5	2.3283(14)
Atom1−Atom2	Molecule B	Atom1−Atom2	Molecule D
Pt2−O4	2.041(4)	Pt4−O8	2.012(4)
Pt2−N3	2.052(5)	Pt4−N8	2.024(5)
Pt2−N4	2.026(5)	Pt4−N7	2.044(5)
Pt2−Cl3	2.3740(14)	Pt4−Cl6	2.3477(15)

Table 2. Bond lengths [Å] in the chelated and non-chelated ligands of **2**

Atom1−Atom2	Molecule B	Atom1−Atom2	Molecule D
O4−C13	1.413(7)	O8−C29	1.413(8)
C13−C14	1.508(9)	C29−C30	1.520(9)
C14−C15	1.561(10)	C30−C31	1.542(9)
C15−C16	1.534(10)	C31−C32	1.487(11)
N4−C14	1.502(8)	N8−C30	1.495(8)
Atom1−Atom2	Molecule A	Atom1−Atom2	Molecule C
O1−C1	1.437(8)	O5−C17	1.435(8)
C1−C2	1.507(8)	C17−C18	1.509(9)
C2−C3	1.519(9)	C18−C19	1.47(3)
C3−C4	1.519(9)	C18−C19X	1.52(2)
N1−C2	1.509(8)	C19−C20	1.548(19)
O2−C5	1.408(7)	C19X−C20X	1.546(18)
C5−C6	1.553(9)	N5−C8	1.483(8)
C6−C7	1.509(9)	O6−C21	1.415(8)
C7−C8	1.539(9)	C21−C22	1.496(9)
N2−C6	1.487(8)	C22−C23	1.516(9)
		C23−C24	1.532(10)
		N6−C22	1.476(8)
Atom1−Atom2	Molecule B	Atom1−Atom2	Molecule D
O3−C9	1.432(9)	O7−C25	1.397(8)
C9−C10	1.524(9)	C25−C26	1.512(9)
C10−C11	1.528(9)	C26−C27	1.491(9)
C11−C12	1.543(9)	C27−C28	1.537(9)
N3−C10	1.488(8)	N7−C26	1.490(8)

Two intramolecular hydrogen bonds are observed between the amino group of one coordinated 2-aminobutanol ligand as donor and the hydroxy groups of both coordinated HL ligands as acceptors in A and C (Figures 4 and S1) (N1-H1A···O2 with N1−H1A 0.90, H1A···O2 2.070 Å and N1−H1A···O2 155.34°, and N1-H1B···O1 with N1−H1B 0.90, H1A···O2 2.390 Å and N1−H1A···O2 111.82° in A; and N5-H5A···O6 with N5−H5A 0.90, H5A···O6 1.958 Å and N5−H5A···O6 157.72°, and N5-H5B···O5 with N5−H5B 0.90, H5A···O6 2.382 Å and N5−H5A···O6 110.83° in C). All four molecules A, B, C and D are involved in a three-dimensional hydrogen-bonding network, the packing is dominated by O-H···O, N-H···O and N-H···Cl hydrogen-bonding interactions. Detailed geometrical parameters for the intermolecular contacts in **2** are listed in Table S2.

Both **3** {[Pt{(*R*)-(−)-L}$_2$]} and **4** {[Pt{(*S*)-(+)-L}$_2$]} crystallize in a non-centrosymmetric orthorhombic space group $P2_12_12$. The asymmetric units in **3** and **4** consist of one half of the complex molecule, related to the other by a twofold rotation axis lying in the molecule mean plane across the platinum atom. The results of X-ray crystal structure analyses of **3** and **4** are summarized in Figures 6 and 7.

In both enantiomers [C2 is an (*R*)-chiral centre in **3** and an (*S*)-chiral one in **4**] Pt^{II} has square-planar coordination with two mutually *cis*-arranged 2-aminobutanol ligands deprotonated at the OH group and chelated through NH_2 and O^-. None of the coordinated atoms protrudes from the corresponding least-squares mean plane by more than 0.002 Å for **3** and 0.004 Å for **4**. Two five-membered chelate rings, with bite angles of 83.31(13) and 83.32(9)° for **3** and **4**, respectively, are formed. A zigzag arrangement of the ligand atoms in the five-membered chelate rings alternately above and below the mean least-squares plane through PtN_2O_2 is observed in both complexes. Unlike in the case of $Pt^{IV}(Eta)_2Cl_2$,[21] the two chelate rings PtO1C1C2N1 and the symmetry-related one in the molecules of **3** and **4** are twisted in the opposite sense and their configurations can be described as δλ or λδ. The dihedral angles O1−C1−C2−N1 in **3** and **4**, which serve as measures of the deviation of the corresponding chelate rings from planarity, are −47.1(4) and 46.6(3)°, respectively. These values are similar to those in $Pt^{IV}(Eta)_2Cl_2$. The Pt−O1 and Pt−N1 bond lengths in **3** and **4** compare well, at 2.031(2) and 2.024(2) Å, and 2.029(4) and 2.018(3) Å, respectively. The distributions of electron density over the chelate rings are very similar for

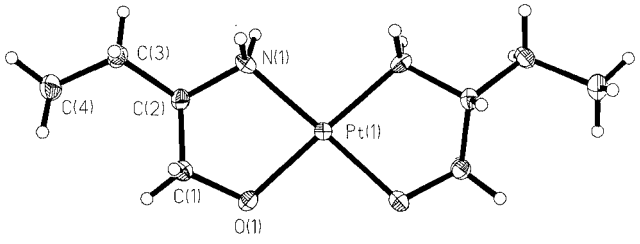

Figure 6. ORTEP diagram of **3** with thermal ellipsoids at 50% probability

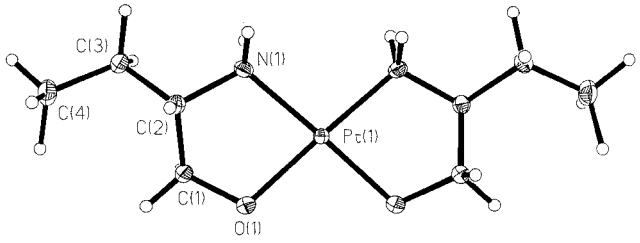

Figure 7. ORTEP diagram of **4** with thermal ellipsoids at 50% probability

 © 2003 Wiley-VCH Verlag GmbH & Co. KGaA, Weinheim

the two enantiomers [O1−C1 at 1.433(5) and 1.434(3), C2−C3 at 1.523(6) and 1.527(4), C3−C4 at 1.524(6) and 1.520(4), N1−C2 at 1.509(5) and 1.500(4) Å for **3** and **4**, respectively].

The NH_2 and the deprotonated OH groups, together with the water molecules, are involved in intermolecular hydrogen bonding, forming a chain of tail-to-head-arranged $Pt^{II}L_2$ molecules (where HL = 2-aminobutanol), bridged by layers of hydrogen-bonded water molecules and running along the *c* axis, as shown for **3** in Figure 8.

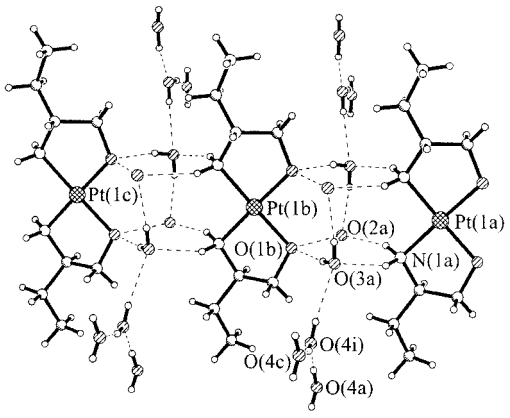

Figure 8. A portion of the crystal structure of **3** projected on the *ac* plane

Detailed geometrical parameters for the hydrogen bonds in **3** are quoted in Table S3. Another interesting feature is the stacked arrangement of $Pt^{II}L_2$ molecules, with a 4.2 Å intermolecular separation along the *b* axis (Figure 9). Very weak C−H···Pt intermolecular contacts with the C−H vector directed to the platinum atom (< C−H···Pt 176.5°) at ca. 3.1 Å are worth mentioning. At ca. 2.6 Å, they are significantly longer than the intramolecular contacts observed in other platinum(II) compounds with square-planar geometries.[22,23]

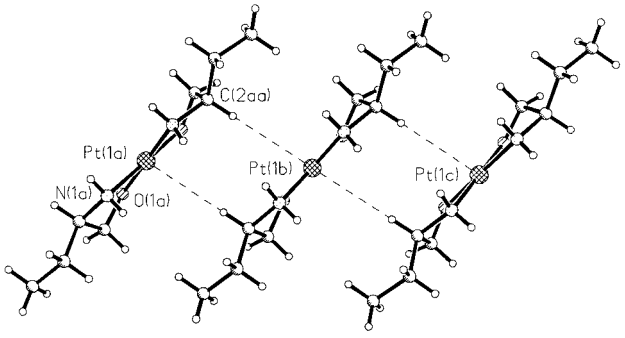

Figure 9. Portion of the crystal structure of **3**, showing stacking arrangement of $Pt^{II}L_2$ along the *b* axis

Conclusion

Cytotoxic hydroxyethyl-substituted amineplatinum(II) and -(IV) complexes have recently attracted attention because of: (i) the potential of their hydroxy groups to act as donors or acceptors of hydrogen bonds, thus influencing the mode of action, (ii) their use as starting materials for further derivatisation, and (iii) the ability of their hydroxyethyl groups to coordinate to the platinum centre through the oxygen atom during oxidation with hydrogen peroxide or through intramolecular ligand exchange reactions in dichloroplatinum(II) complexes.

The last point in particular is of great interest, because the intramolecular attack of the hydroxy group dramatically influences the mode of action of platinum(II) compounds, as was shown recently. Moreover, there is the chance to use such reactions specifically for the synthesis of novel anticancer platinum-based drugs for chemotherapy. We have therefore focused our chemistry program on the synthesis of dichloroplatinum(II) complexes that are in a position to form singly or − especially − doubly ring-closed alcoholato species and on investigation of their structures by X-ray crystallography.

The results obtained may represent the first step towards novel prodrugs for platinum-based antitumour chemotherapy.

Experimental Section

General Remarks: All chemicals were obtained from commercial suppliers and used as received. The ^1H and ^{13}C NMR spectra were recorded with a Bruker DPX 400 Ultrashield™ Magnet at 400.13 and 100.62 MHz. The elemental analyses were performed with a Perkin−Elmer 2400 CHN Elemental Analyser by the microlaboratory of the Institute of Physical Chemistry, University of Vienna.

(*SP*-4−2)-[Bis{(*R*)-(−)-2-aminobutanol}]diiodoplatinum(II): K_2PtCl_4 (3.621 g, 8.72 mmol) was dissolved in doubly distilled water (35 mL) and treated with KI (7.5 g, 45.18 mmol). The solution was stirred for 20 min at room temperature. A solution of (*R*)-(−)-2-aminobutanol (1.45 g, 16.27 mmol) in doubly distilled water (10 mL) was added dropwise to the brown suspension of tetraiodoplatinate. After the mixture had been stirred at room temperature for 5 h, $[Pt\{(R)\text{-}(-)\text{-}HL\}_2I_2]$ was obtained as a precipitate. After filtration, the yellow solid was washed twice with ice-cold water (10 mL). The product was dried over P_4O_{10}. $C_8H_{22}I_2N_2O_2Pt$ (627.18): calcd. C 15.32, H 3.54, N 4.47; found C 15.36, H 3.27 N 4.29. Yield: 2.722 g (50%).

(*SP*-4−2)-[Bis{(*S*)-(+)-2-aminobutanol}]diiodoplatinum(II): The synthetic procedure was the same as that used for $[Pt((R)\text{-}(-)\text{-}HL)_2I_2]$. $C_8H_{22}I_2N_2O_2Pt$ (627.18): calcd. C 15.32, H 3.54, N 4.47; found C 15.29, H 3.36, N 4.92. Yield: 3.4362 g (76%).

[Bis(2-aminobutanol)]diiodoplatinum(II): The synthetic procedure was the same as that used for $[Pt\{(R)\text{-}(-)\text{-}HL\}_2I_2]$. $C_8H_{22}I_2N_2O_2Pt$ (627.18): calcd. C 15.32, H 3.54, N 4.47; found C 15.02, H 3.30, N 4.25. Yield: 6.848 g (91%).

(*SP*-4−2)-[Bis{(*R*)-(−)-2-aminobutanol}]dichloroplatinum(II) (1): $[Pt\{(R)\text{-}(-)\text{-}HL\}_2I_2]$ (1.5 g, 2.39 mmol) was suspended in doubly distilled water (20 mL). $AgNO_3$ (0.772 g, 4.54 mmol) was added, and the mixture was stirred for 12 h at room temperature. AgI was removed by filtration. The slightly yellow filtrate was reduced to a volume of 10 mL, and concentrated HCl (1.4 mL, 16.38 mmol) was added. After 5 min, the dichloro complex began to crystallise as yellow needles. ^1H NMR (H_2O/D_2O, 9:1; 1 drop of $DCl_{conc.}$): δ = 0.74 (t, $^3J_{H,H}$ = 7.6 Hz, 6 H, CH_3), 1.28−1.67 (m, 4 H, CH_3CH_2),

 © 2003 Wiley-VCH Verlag GmbH & Co. KGaA, Weinheim

2.62 (m, 2 H, C*H*), 3.51 (m, 2 H, CH_2OH), 3.93 (m, 2 H, CH_2OH) ppm. ^{13}C NMR (H_2O/D_2O, 9:1; 1 drop of $DCl_{conc.}$): δ = 10.06 (2 C, *C*H_3), 24.66 (2 C, CH_3CH_2), 59.34 (2 C, *C*H), 62.49 (2 C, *C*H_2OH). $C_8H_{22}Cl_2N_2O_2Pt$ (444.27): calcd. C 21.63, H 4.99, N 6.31; found C 21.56, H 4.87, N 6.17. Yield: 0.55 g (41%).

(SP-4-2)-[Bis{(*S*)-(+)-2-aminobutanol}]dichloroplatinum(II) and (SP-4-3)-{(*S*)-(+)-2-aminobutanol}[{(*S*)-(+)-2-aminobutanolato}-κ*N*,*O*]chloroplatinum(II) (2): [Pt{(*S*)-(+)-HL}$_2$I$_2$] (1.8 g, 2.87 mmol) was suspended in doubly distilled water (20 mL). $AgNO_3$ (0.936 g, 5.51 mmol) was added to the mixture, which was stirred at room temperature for 12 h. AgI was filtered off, and KCl (0.53 g 7.11 mmol) was added to the slightly yellow filtrate. The colour of the filtrate turned to dark yellow; after 10 min, yellow needles began to crystallise. The mixture was stored at 4 °C for 3 h; 550 mg of a crystalline product could be collected. [Pt{(*S*)-(+)-HL}$_2$Cl$_2$]: ^{1}H,^{13}C-COSY NMR (H_2O/D_2O, 9:1): δ = 0.86/10.0 (*CH*$_3$), 1.49/24.6 (CH_3CH_2), 1.70/24.6 (CH_3CH_2), 2.74/59.4 (*CH*), 3.60/62.5 (CH_2OH), 4.07/62.5 (CH_2OH). [Pt{(*S*)-(+)-HL}{(*S*)-(+)-L}Cl], monodentate ligand: ^{1}H,^{13}C-COSY NMR (H_2O/D_2O, 9:1): δ = 0.86/10.0 (*CH*$_3$), 1.54/22.2 (CH_3CH_2), 1.67/22.2 (CH_3CH_2), 2.78/61.5 (*CH*), 3.60/62.4 (CH_2OH), 3.95/62.4 (CH_2OH). [Pt{(*S*)-(+)-HL}{(*S*)-(±)-L}Cl], bidentate ligand: ^{1}H,^{13}C-COSY NMR (H_2O/D_2O, 9:1): δ = 0.86/10.0 (*CH*$_3$), 1.54/22.2 (CH_3CH_2), 1.67/22.2 (CH_3CH_2), 2.56/60.4 (*CH*), 3.35/72.6 (CH_2OPt), 3.58/72.6 (CH_2OPt). $C_8H_{22}Cl_2N_2O_2Pt{\cdot}0.1C_8H_{20}ClN_2O_2Pt$ (485.05): calcd. C 21.79, Cl 15.35, H 5.01, N 6.35; Pt, 43.91; found C 21.50, Cl 15.35, H 4.84, N 6.84; Pt 43.96.

[Bis(2-aminobutanol)]dichloroplatinum(II) (S1): The synthetic procedure was the same as that used for [Pt{(*S*)-(+)-HL}$_2$Cl$_2$]. ^{1}H NMR (H_2O/D_2O, 9:1; [Pt(HL)$_2$Cl$_2$] and [Pt(HL)(L)Cl]): δ = 0.90 (t, $^3J_{H,H}$ = 7.5 Hz, CH_3), 1.42−1.81 (m, CH_3CH_2), 2.48−2.88 (m, C*H*), 3.32−4.14 (m, CH_2O) ppm. ^{13}C NMR (H_2O/D_2O, 9:1; [Pt(HL)$_2$Cl$_2$] and [Pt(HL)(L)Cl]): δ = 9.91, 9.95, 10.13, 10.15, 10.30 (*C*H_3), 22.37, 22.41, 24.49, 24.51, 24.70, 24.77 (CH_3CH_2), 59.51, 60.44, 60.48, 61.47, 61.54 (*C*H), 65.51, 62.58, 62.75 (*C*H_2OH), 72.64 (*C*H_2OPt). $C_8H_{22}Cl_2N_2O_2Pt$ (444.27): calcd. C 21.63, H 4.99, N 6.31; found C 21.72, H 4.79, N 6.25. Yield: 1.390 g (47%).

(*SP*-4-2)-[Bis{(*R*)-(−)-2-aminobutanolato}-κ^2*N*,*O*]platinum(II) (3): [Pt{(*R*)-(−)-HL}$_2$Cl$_2$] (0.3 g) was dissolved in doubly distilled water (10 mL) and treated with rinsed Amberlite IRA-400 (Cl^-) basic ion exchanger (20 mL). The suspension was stirred at room temperature for 24 h. The ion exchanger was filtered off and the colourless filtrate was concentrated to 1 mL under reduced pressure. The solution was stored over P_4O_{10} until colourless crystals had formed. ^{1}H NMR (H_2O/D_2O, 9:1): δ = 0.86 (t, $^3J_{H,H}$ = 7.6 Hz, 4 H, CH_3), 1.42 (m, 2 H, CH_3CH_2), 1.59 (m, 2 H, CH_3CH_2), 2.54 (m, 2 H, C*H*), 2.94 (m, 2 H, CH_2O), 3.06 (m, 2 H, CH_2O) ppm. ^{13}C NMR (H_2O/D_2O, 9:1): δ = 10.78 (2 C, *C*H_3), 22.89 (2 C, CH_3CH_2), 64.09 (2 C, *C*H), 73.01 (2 C, *C*H_2O).

(*SP*-4-2)-[Bis{(*S*)-(+)-2-aminobutanolato}-κ^2*N*,*O*]platinum(II) (4): The synthetic procedure was the same as that used for [Pt{(*R*)-(−)-L}$_2$]. ^{1}H NMR (H_2O/D_2O, 9:1): δ = 0.80 (t, $^3J_{H,H}$ = 7.3 Hz, 6 H, CH_3), 1.34 (m, 2 H, CH_3CH_2), 1.53 (m, 2 H, CH_3CH_2), 2.48 (m, 2 H, C*H*), 2.88 (m, 2 H, CH_2O), 3.01 (m, 2 H, CH_2O) ppm. ^{13}C NMR (H_2O/D_2O, 9:1): δ = 10.76 (s, 2 C, *C*H_3), 22.90 (s, 2 C, CH_3CH_2), 64.07 (s, 2 C, *C*H), 73.02 (s, 2 C, *C*H_2O).

[Bis(2-aminobutanolato)-κ^2*N*,*O*]platinum(II): The synthetic procedure was the same as that used for [Pt{(*R*)-(−)-L}$_2$]. ^{1}H NMR (H_2O/D_2O, 9:1): δ = 0.79 (t, $^3J_{H,H}$ = 7.3 Hz, 6 H, CH_3), 1.34 (m, 2 H, CH_3CH_2), 1.51 (m, 2 H, CH_3CH_2), 2.46 (m, 2 H, C*H*), 2.86 (m, 2 H, CH_2O), 3.00 (m, 2 H, CH_2O) ppm. ^{13}C NMR (H_2O/D_2O, 9:1): δ = 10.76 (2 C, *C*H_3), 22.90 (2 C, CH_3CH_2), 64.08 (2 C, *C*H), 72.90 (2 C, *C*H_2O). $C_8H_{20}N_2O_2Pt{\cdot}2H_2O$ (407.38): calcd. C 23.59, H 5.94, N 6.88; found C 23.86, H 5.54, N 6.60. Yield: 0.178 g (71%).

X-ray Crystallographic Study: X-ray diffraction measurements were performed with a Nonius Kappa CCD diffractometer at 120 K. Single crystals were positioned at 35, 40, 35, 35 and 30 mm from the detector and 496, 636, 597, 597 and 414 frames were measured, each for 25, 90, 50, 50 and 65 s over a 2, 1.5, 1.5, 1.5 and 2° scan for **1**−**4** and **S1**, respectively. The data were processed by use of Denzo-SMN software. Crystal data, data collection parameters, and structure refinement details for **1**−**4** are given in Table 3. Crystal data, data collection parameters, and structure refinement de-

Table 3. Crystallographic data for **1**−**4**

Complex	**1**	**2**	**3**	**4**
Empirical formula	$C_8H_{22}Cl_2N_2O_2Pt$	$C_{32}H_{86}Cl_6N_8O_8Pt_4$	$C_4H_{15}NO_{3.5}Pt_{0.5}$	$C_4H_{15}NO_{3.5}Pt_{0.5}$
Formula mass	444.27	1704.15	230.71	230.71
Space group	monoclinic, $P2_1$ (no. 4)	monoclinic, $P2_1$ (no. 4)	orthorhombic, $P2_12_12$ (no. 18)	orthorhombic, $P2_12_12$ (no.18)
a [Å]	9.9598(3)	10.763(2)	21.527(4)	21.514(4)
b [Å]	9.1516(3)	20.795(4)	5.482(1)	5.481(1)
c [Å]	15.5623(5)	12.072(2)	6.618(1)	6.616(1)
β [°]	107.7389(19)	91.24		
V [Å^3]	1351.03(7)	2701.3(8)	781.0(2)	780.1(2)
Z	4	2	4	4
λ [Å]	0.71073	0.71073	0.71073	0.71073
$\rho_{calcd.}$ [g cm^{-3}]	2.184	2.095	1.962	1.964
Crystal size [mm]	0.11 × 0.10 × 0.10	0.11 × 0.11 × 0.09	0.29 × 0.29 × 0.06	0.23 × 0.22 × 0.04
T [K]	120	120	120	120
μ [cm^{-1}]	107.67	106.69	90.08	90.18
Flack parameter	0.031(10)	0.012(5)	0.058(15)	0.009(10)
*R*1[a]	0.0411	0.0465	0.0307	0.0235
*wR*2[b]	0.0755	0.0728	0.0820	0.0561
GOF[c]	1.008	0.989	1.108	1.072

[a] $R1 = \Sigma(F_o - F_c)/\Sigma F_o$. [b] $wR2 = \{\Sigma[w(F_o^2 - F_c^2)^2]/\Sigma[w(F_o^2)^2]\}^{1/2}$. [c] GOF = $\{\Sigma[w(F_o^2 - F_c^2)^2]/(n - p)\}^{1/2}$, where *n* is the number of reflections and *p* is the total number of parameters refined.

 © 2003 Wiley-VCH Verlag GmbH & Co. KGaA, Weinheim

tails for **S1** are given in Table S4 of the Supporting Information. The structures were solved by direct methods and refined by full-matrix, least-squares techniques. Non-hydrogen atoms were refined with anisotropic displacement parameters. H atoms were calculated and allowed to ride (**1**−**3** and **S1**) or located on difference Fourier maps (**4**) and isotropically refined, except for those attached to solvate O2 atoms in **3** and **4**, which were not included in the refinements. One of the 2-aminobutanol ligands in **S1** was found to be severely disordered, producing a very short C6−C7 bond and trigonal-planar geometry at C6. Splitting of the atoms C6, C7, C8 and O2 and refinement with a free variable, such that the combined S.O.F. summed to 1.0, resulted in two components with chemically reasonable geometries in a ca. 0.5:0.5 ratio. Both components were modelled by using appropriate SADI restraints to optimize the positions of C6X, C7X, C8X and O2X with respect to C6, C7, C8 and O2. Split atoms were also restrained to have similar anisotropic displacement parameters (ADPs). Redetermination of the structure in the chiral space group $P2_1$ resulted in a distorted geometry and large ADPs. Disorder modelling in one of the independent molecules in **2** required similar SADI restraints and equivalent anisotropic displacement parameters to be applied to the peripheral ethyl group. Two conformers in ca. 0.4:0.6 ratio resulted. Refinement of Flack parameters was useful in assigning the absolute configuration of **2**−**4**. In all these structures the contribution of the inverted enantiomer is negligible. Computer programs: SHELXS-97[24] (structure solution), SHELXL-97[25] (refinement), ORTEP[26] (molecular diagrams), Pentium II computer, scattering factors.[27] CCDC-201452 (**1**), -201455 (**2**), -201453 (**3**), -201454 (**4**) and -201456 (**S1**) contain the supplementary crystallographic data for this paper. These data can be obtained free of charge at www.ccdc.cam.ac.uk/conts/retrieving.html [or from the Cambridge Crystallographic Data Centre, 12 Union Road, Cambridge CB2 1EZ, UK; Fax: (internat.) + 44-1223/336-033; E-mail: deposit@ccdc.cam.ac.uk].

Acknowledgments

The support of the FWF (Fonds zur Förderung der wissenschaftlichen Forschung) and COST is gratefully acknowledged. We are thankful to Dr. T. Weyhermüller for the discussion of X-ray data and his suggestions concerning the static disorder in S1 and to Dr. G. Giester for the collection of X-ray data.

[1] B. Rosenberg, L. VanCamp, T. Krigas, *Nature* **1965**, *205*, 698−699.
[2] B. Rosenberg, L. VanCamp, J. E. Trosko, V. H. Mansour, *Nature* **1969**, *222*, 385−386.
[3] B. Rosenberg, *Interdiscip. Sci. Rev.* **1978**, *3*, 134−147.
[4] B. Lippert (Ed.), *Cisplatin: Chemistry and Biochemistry of a Leading Anticancer Drug*, Verlag Helvetica Chimica Acta Zürich (Switzerland) and Wiley-VCH, Weinheim (Germany), **1999**.
[5] P. J. O'Dwyer, J. P. Stevenson, S. W. Johnson, *Drugs* **2000**, *59* (Suppl. 4), 19−27.
[6] E. Cvitkovic, M. Bekradda, *Semin. Oncol.* **1999**, *26*, 647−662.
[7] J. Reedijk, *Inorg. Chim. Acta* **1992**, *198*−*200*, 873.
[8] M. S. Robillard, A. Valentijn, P. M. Rob, N. J. Meeuwenoord, G. A. Van der Marel, J. H. Van Boom, J. Reedijk, *Angew. Chem. Int. Ed.* **2000**, *39*, 3096−3099.
[9] J. N. Jolley, A. I. Yanovsky, L.-R. Kelland, K. B. Nolan, *J. Inorg. Biochem.* **2001**, *83*, 91−100.
[10] L. Cai, K. Lim, S. Ren, R. S. Cadena, W. T. Beck, *J. Med. Chem.* **2001**, *44*, 2959−2965.
[11] M. Galanski, W. Zimmermann, M. Berger, Ch. Baumgartner, G. Giester, B. K. Keppler, *Eur. J. Inorg. Chem.* **2002**, 417−421.
[12] R. Kuroda, S. Neidle, I. M. Ismail, P. J. Sadler, *J. Chem. Soc., Dalton Trans.* **1983**, *4*, 823−825.
[13] M. Galanski, W. Zimmermann, Ch. Baumgartner, B. K. Keppler, *Eur. J. Inorg. Chem.* **2001**, *5*, 1145−1149.
[14] A. Zenker, M. Galanski, T. L. Bereuter, B. K. Keppler, W. Lindner, *J. Biol. Inorg. Chem.* **2000**, *5*, 498−504.
[15] A. C. G. Hotze, Y. Chen, T. W. Hambley, S. Parsons, N. A. Kratochwil, J. A. Parkinson, V. P. Munk, P. J. Sadler, *Eur. J. Inorg. Chem.* **2002**, *5*, 1035−1039.
[16] M. S. Robillard, M. Galanski, W. Zimmermann, B. K. Keppler, J. Reedijk, *J. Inorg. Biochem.* **2002**, *88*, 254−259.
[17] M. S. Davies, P. N. Wong, A. R. Battle, G. Haddad, M. J. McKeage, T. W. Hambley, *J. Inorg. Biochem.* **2002**, *91*, 205−211.
[18] A. Küng, M. Galanski, Ch. Baumgartner, B. K. Keppler, *Inorg. Chim. Acta* **2002**, *339*, 9−13.
[19] W. Zimmerman, M. Galanski, B. K. Keppler, G. Giester, *Inorg. Chim. Acta* **1999**, *292*, 127−130.
[20] Basic Terminology of stereochemistry (IUPAC Recommendations 1996), *Pure Appl. Chem.* **1996**, *68*, 2195−2222.
[21] R. Kuroda, S. Neidle, I. M. Ismail, P. J. Sadler, *J. Chem. Soc., Dalton Trans.* **1983**, 823−825.
[22] A. Albinati, C. G. Anklin, F. Ganazzoli, H. Rüegg, P. S. Pregosin, *Inorg. Chem.* **1987**, *26*, 503−508.
[23] A. Albinati, C. Arz, P. S. Pregosin, *Inorg. Chem.* **1987**, *26*, 508−513.
[24] G. M. Sheldrick, SHELXS-97, *Program for Crystal Structure Solution*, University of Göttingen, Germany, **1997**.
[25] G. M. Sheldrick, SHELXL-97, *Program for Crystal Structure Refinement*, University of Göttingen, Germany, **1997**.
[26] C. K. Johnson, Rep. ORNL-5138, OAK Ridge National Laboratory, OAK Ridge, TN, **1976**.
[27] *International Tables for X-ray Crystallography*, Kluwer Academic Press, Dordrecht, The Netherlands, **1992**, vol. C, Tables 4.2.6.8 and 6.1.1.4.

Received January 24, 2003

 © 2003 Wiley-VCH Verlag GmbH & Co. KGaA, Weinheim

Synthesis and Reactivity of Alkylzirconium Complexes Incorporating Asymmetrically Substituted *ansa* Ligands − X-ray Crystal Structure of [Zr{$Me_2Si(\eta^5$-$C_5Me_4)(\eta^5$-$C_5H_3Me)$}$(CH_2Ph)Cl$]

Antonio Antiñolo,[a] Rafael Fernández-Galán,[a] Beatriz Gallego,[a] Antonio Otero,*[a] Sanjiv Prashar,[b] and Ana M. Rodríguez[c]

Keywords: Metallocenes / Zirconium / Insertion reactions / Isocyanides

The monoalkyl complexes [Zr{$Me_2Si(\eta^5$-$C_5Me_4)(\eta^5$-$C_5H_3R)$}$(R')Cl$] [R = Me, R′ = CH_2Ph (**1**); R = Me, R′ = CH_2SiMe_3 (**2**); R = *i*Pr, R′ = CH_2Ph (**3**); R = *i*Pr, R′ = CH_2SiMe_3 (**4**); R = $SiMe_3$, R′ = CH_2Ph (**5**); R = $SiMe_3$, R′ = CH_2SiMe_3 (**6**)] have been synthesized by the reaction of the corresponding *ansa*-metallocene dichloride complex and 1 equiv of the alkyl Grignard reagent. Dialkyl complexes with large alkyl groups only formed for the zirconocene complex containing the *ansa* ligand $Me_2Si(\eta^5$-$C_5Me_4)(\eta^5$-$C_5H_4)$ and with the benzyl substituent giving [Zr{$Me_2Si(\eta^5$-$C_5Me_4)(\eta^5$-$C_5H_4)$}$(CH_2Ph)_2$] (**7**). When the alkyl substituent is CH_2SiMe_3 only the monoalkyl derivative, [Zr{$Me_2Si(\eta^5$-$C_5Me_4)(\eta^5$-$C_5H_4)$}$(CH_2SiMe_3)Cl$] (**8**), was formed. The insertion reaction of the isocyanide reagent $CNC_6H_3Me_2$-2,6 into the zirconium–carbon σ-bond of complexes **1**–**8** gave the corresponding η^2-iminoacyl compound [Zr{$Me_2Si(\eta^5$-$C_5Me_4)(\eta^5$-$C_5H_3R)$}{η^2-R′C=$NC_6H_3Me_2$-2,6}Cl] [R = Me, R′ = CH_2Ph (**9**); R = Me, R′ = CH_2SiMe_3 (**10**); R = *i*Pr, R′ = CH_2Ph (**11**); R = *i*Pr, R′ = CH_2SiMe_3 (**12**); R = $SiMe_3$, R′ = CH_2Ph (**13**); R = $SiMe_3$, R′ = CH_2SiMe_3 (**14**); R = H, R′ = CH_2SiMe_3 (**16**)] and [Zr{$Me_2Si(\eta^5$-$C_5Me_4)(\eta^5$-$C_5H_4)$}{η^2-$PhCH_2C$=$NC_6H_3Me_2$-2,6}(CH_2Ph)] (**15**). The molecular structure of **1** has been determined by single-crystal X-ray diffraction studies.

(© Wiley-VCH Verlag GmbH & Co. KGaA, 69451 Weinheim, Germany, 2003)

Introduction

Zirconocene complexes are of considerable interest due to their synthetic and catalytic applications.[1] The relationship between the properties of different zirconocene catalysts and their molecular structures has been the subject of in-depth studies. The main emphasis of these studies has centred on the steric effects of various ring substituents and bridging units on the properties of the catalysts and their polymer products.[2] However, considerably less work has been carried out into the electronic effects that different ligands exert on the relative electron densities at the zirconium centre,[3] even though they will influence the reactivity of the catalysts.[4]

Although modifications of cyclopentadienyl ligands simultaneously change both the steric and electronic effects, a rational design of new olefin polymerization catalysts requires an approach in which the electron density at the metal atom and the shape of a coordination site can be predicted.[5] Recent studies have demonstrated that the incorporation of an *ansa* bridge may have a profound influence on the chemistry of metallocene systems.[6] The electrochemical properties of group-4 *ansa*-metallocene complexes have previously been reported[7] and indicate that a positive shift of E° occurs versus their non-*ansa* analogues. For example, the complex [Zr{$Me_2Si(\eta^5$-$C_5H_4)_2$}Cl_2] is reduced at a lesser negative potential than [$Zr(\eta^5$-$C_5H_5)_2Cl_2$] (by 0.1 V).[7a] Therefore it is well established that the electron density at the metal atom is modified by the alkyl group substituents of the cyclopentadienyl ligand. In methyl-substituted zirconocene dihalide complexes [$Zr(\eta^5$-$C_5H_{5-n}Me_n)_2Cl_2$] (n = 0−5) such trends were observed in shifts of electrochemical reduction potentials.[8] We have observed the same effect in our recently presented study on the electrochemistry of niobium(IV) dichloride complexes which contain the same *ansa* ligands as those discussed presently in this paper.[9]

Alkylzirconocene cations are currently of interest due to their role as single-site Ziegler−Natta olefin polymerization catalysis.[10] Common precursors to these cationic catalysts include dimethyl- and dibenzylzirconocenes which are stable species.[10,11]

[a] Departamento de Química Inorgánica, Orgánica y Bioquímica, Universidad de Castilla-La Mancha, Facultad de Químicas, Campus Universitario, 13071 Ciudad Real, Spain
Fax: (internat.) + 34-926/295-318
E-mail: Antonio.Otero@uclm.es
[b] Departamento de Tecnología Química, Ambiental y de los Materiales, E.S.C.E.T., Universidad Rey Juan Carlos, 28933 Móstoles (Madrid), Spain
[c] ETS Ingenieros Industriales, Avd. Camilo José Cela, 3, 13071 Ciudad Real, Spain

 © 2003 Wiley-VCH Verlag GmbH & Co. KGaA, Weinheim **DOI: 10.1002/ejic.200300150**

We recently developed a general synthesis of some $SiMe_2$-bridged asymmetric *ansa*-zirconocene complexes[12] and this series of highly active C_1-symmetric catalysts polymerize propylene with a high level of stereospecificity.[12b] Our research in this area is now focused on the elucidation of the mechanism of olefin polymerization as well as on the use of new types of metallocene complexes in stereoselective catalysis.[13]

In this paper we report our studies on the synthesis, characterization, and reactivity of new benzyl- and [(trimethylsilyl)methyl]zirconium derivatives containing asymmetric *ansa* ligands. Special attention is paid to the steric factors that govern the alkylation reactions due to the implication that this may have on the stereoselective mechanism in α-olefin polymerization.

Results and Discussion

The synthesis of the monoalkyl complexes, [Zr{$Me_2Si(\eta^5$-$C_5Me_4)(\eta^5$-$C_5H_3R)$}(R′)Cl] [R = Me, R′ = CH_2Ph (**1**); R = Me, R′ = CH_2SiMe_3 (**2**); R = *i*Pr, R′ = CH_2Ph (**3**); R = *i*Pr, R′ = CH_2SiMe_3 (**4**); R = $SiMe_3$, R′ = CH_2Ph (**5**); R = $SiMe_3$, R′ = CH_2SiMe_3 (**6**)], was carried out by the reaction of 1 equiv. of the alkyl Grignard reagent with the corresponding *ansa*-metallocene dichloride derivative (Scheme 1).

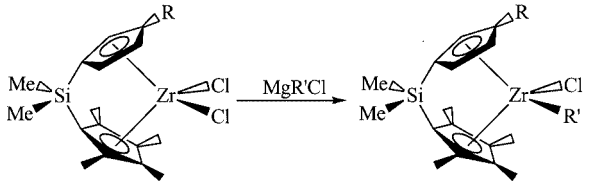

R = Me, R' = CH_2Ph (**1**);
R = Me, R' = CH_2SiMe_3 (**2**);
R = *i*Pr, R' = CH_2Ph (**3**);
R = *i*Pr, R' = CH_2SiMe_3 (**4**);
R = $SiMe_3$, R' = CH_2Ph (**5**);
R = $SiMe_3$, R' = CH_2SiMe_3 (**6**)

Scheme 1

The planar chirality exhibited by the *ansa*-zirconocene dichloride complexes, [Zr{$Me_2Si(\eta^5$-$C_5Me_4)(\eta^5$-$C_5H_3R)$}Cl_2] (R = Me, *i*Pr, $SiMe_3$),[12] means that the two chloride positions are not equivalent. Thus, in the monoalkyl substitution reaction there exists the possibility of the formation of two stereoisomers. In all cases ^{1}H NMR spectroscopy revealed that only one of these isomers was present. In addition signals were observed for the nonequivalent methyl groups of the permethylated cyclopentadienyl moiety (4 singlets), the methyl groups of the $SiMe_2$ bridge (2 singlets), and the three protons of the monosubstituted cyclopentadienyl fragment (3 multiplets) (see Exp. Sect.). The methylene protons of the alkyl group (CH_2SiMe_3 or CH_2Ph) are diastereotopic due to the chiral nature of the metal centre and thus two doublets were observed in the ^{1}H NMR spectra of **1**−**6**. The signals corresponding to the differing alkyl groups (cyclopentadienyl- and metal-substituted) were also observed.

The corresponding dialkyl complexes were not obtained even when an excess of the alkylating reagent was used. This fact may be due to the bulky nature of the metal-bonded alkyl substituent or the presence of the β-alkyl substituent of the monosubstituted cyclopentadienyl moiety or indeed attributed to a combination of the two factors.

In the previously reported dimethyl complexes [Zr{$Me_2Si(\eta^5$-$C_5Me_4)(\eta^5$-$C_5H_3R)$}Me_2] (R = H, Me, *i*Pr, $SiMe_3$), dialkyl substitution was shown to readily occur.[12b] The obvious reason for this reactivity can be attributed to the small size of the methyl group which allows the easy entry to the metal centre of two alkyl ligands which in addition also seem to be unaffected by the absence or presence of the β-cyclopentadienyl substituent.

For the *ansa*-zirconocene dichloride complex [Zr{$Me_2Si(\eta^5$-$C_5Me_4)(\eta^5$-$C_5H_4)$}Cl_2] (i.e. no β-substituent present) the alkylation reaction with the benzyl group gave the disubstituted derivative, [Zr{$Me_2Si(\eta^5$-$C_5Me_4)(\eta^5$-$C_5H_4)$}$(CH_2Ph)_2$] (**7**) (Scheme 2). This indicates that in the case of benzylation that the conditioning factor leading to mono- or disubstitution corresponds to the nature of β-substitution in the *ansa*-cyclopentadienyl ligand.

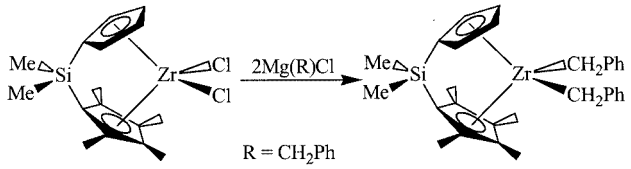

Scheme 2

When the same reaction was carried out but using $Mg(CH_2SiMe_3)Cl$ as the alkylating agent only the monoalkyl derivative, [Zr{$Me_2Si(\eta^5$-$C_5Me_4)(\eta^5$-$C_5H_4)$}(CH_2SiMe_3)Cl] (**8**), was isolated (Scheme 3). Therefore we can infer that for the bulkier CH_2SiMe_3 ligand, its voluminous nature (and not the substituent present in the cyclopentadienyl moiety) is the primary factor in the steric demands imposed on the final product.

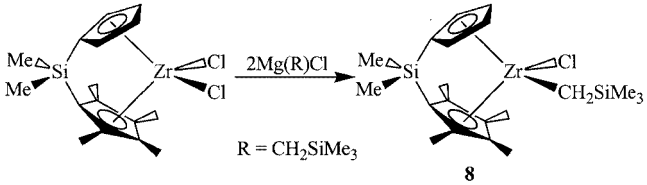

Scheme 3

The syntheses of bis(CH_2SiMe_3) derivatives of non-*ansa*-zirconocene complexes, [Zr(η^5-$C_5H_4R)_2(CH_2SiMe_3)_2$] (R = H, Me, Et, *i*Pr, *t*Bu), have been reported.[14] However, the attempted preparation of the hafnium analogue with R = *t*Bu proved unsuccessful and gave only the monosubstituted derivative [Hf(η^5-C_5H_4tBu)$_2(CH_2SiMe_3)$Cl].[14a] In addition, when the size of the alkyl ligand was increased to $CH(SiMe_3)_2$, only the synthesis of the monoalkyl deriva-

 © 2003 Wiley-VCH Verlag GmbH & Co. KGaA, Weinheim

tives, $[Zr(\eta^5\text{-}C_5H_4R)_2\{CH(SiMe_3)_2\}Cl]$ (R = H, Me, Et, *i*Pr, *t*Bu, $SiMe_3$), was possible.[15] It seems obvious therefore that steric constraints and not electronic effects are responsible for the substitution reaction behaviour. In the *ansa* complexes where there is no free rotation of the C_5 rings, their substituents are located in fixed positions and thus those located in the β-positions will always influence sterically the reactions at the metal centre. In addition, one can imagine that the flexibility of the cyclopentadienyl rings in non-*ansa* derivatives makes them less sensitive to steric factors than their more rigid *ansa*-metallocene analogues and this may explain why we only obtained the monoalkyl compound $[Zr\{Me_2Si(\eta^5\text{-}C_5Me_4)(\eta^5\text{-}C_5H_4)\}(CH_2SiMe_3)Cl]$ (**8**) and that dialkyl derivatives $[Zr(\eta^5\text{-}C_5H_4R)_2(CH_2SiMe_3)_2]$ (R = H, Me, Et, *i*Pr, *t*Bu)[15] could be readily formed for the non-*ansa* analogues.

For **7** and **8** ^{1}H NMR spectroscopy confirms the di- and monoalkyl substitution, respectively. The difference in symmetry of **7** (bis, C_s) and **8** (mono, C_1) is reflected in the ^{1}H NMR spectra. For the C_s symmetry in **7** only two signals were observed for the four protons of the unsubstituted cyclopentadienyl ring, two signals for the four methyl groups of the tetramethylcyclopentadienyl ring, one singlet for the two methyl groups of the *ansa*-$SiMe_2$ bridge, and one singlet for the methylene protons corresponding to the two benzyl ligands. For the C_1 symmetry in **8** four signals were observed for the four protons of the unsubstituted cyclopentadienyl ring, four signals for the four methyl groups of the tetramethylcyclopentadienyl ring, two singlets for the two methyl groups of the *ansa*-$SiMe_2$ bridge and two multiplets for the diastereoscopic methylene protons corresponding to the CH_2SiMe_3 ligand.

The molecular structure of **1** was established by single-crystal X-ray diffraction studies. The molecular structure and atomic numbering scheme are shown in Figure 1. Selected bond lengths and angles for **1** are given in Table 1.

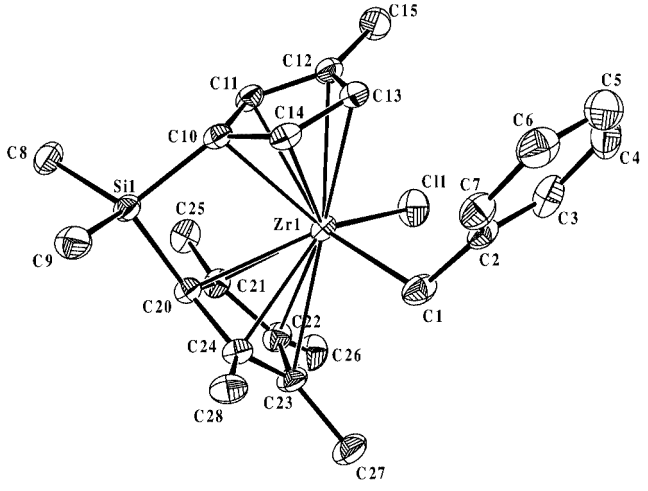

Figure 1. Molecular structure and atom-labeling scheme for $[Zr\{Me_2Si(\eta^5\text{-}C_5Me_4)(\eta^5\text{-}C_5H_3Me)\}(CH_2Ph)Cl]$ (**1**) with thermal ellipsoids at 30% probability

The structure of **1** shows the typical bent metallocene conformation observed in zirconocene dichloride complexes. The *ansa* ligand chelates the zirconium atom and both C_5 rings are bound to the metal atom in an η^5-mode. The environment of the zirconium atom is completed by a chlorine atom and the α-carbon atom of the benzyl group. The structure also reveals that the methyl substituent of the monosubstituted C_5 ring is orientated away from the benzyl group in a manner similar to that recently reported for imido *ansa*-niobocene complexes.[12a] The structural parameters of **1** are directly similar to those of its parent zirconocene dichloride complex $[Zr\{Me_2Si(\eta^5\text{-}C_5Me_4)(\eta^5\text{-}C_5H_3Me)\}Cl_2]$.[12a]

Table 1. Selected bond lengths [Å] and angles [°] for **1**; Cent(1) and Cent(2) are the centroids of C(10)−C(14) and C(20)−C(24), respectively; * refers to the average bond length between Zr(1) and the carbon atoms of the C_5 ring of the corresponding cyclopentadienyl moiety

Zr(1)−Cent(1)	2.221
Zr(1)−Cent(2)	2.226
av Zr(1)−C[Cent(1)]*	2.525
av Zr(1)−C[Cent(2)]*	2.533
Zr(1)−Cl(1)	2.4261(9)
Zr(1)−C(1)	2.327(3)
C(1)−C(2)	1.475(4)
Cent(1)−Zr(1)−Cent(2)	126.50
Si(1)−C(10)−Cent(1)	162.02
Si(1)−C(20)−Cent(2)	162.23
C(10)−Si(1)−C(20)	94.72(11)
Cl(1)−Zr(1)−Cent(1)	109.43
Cl(1)−Zr(1)−Cent(2)	109.96
C(1)−Zr(1)−Cent(1)	106.94
C(1)−Zr(1)−Cent(2)	103.47
Cl(1)−Zr(1)−C(1)	95.90(9)
Zr(1)−C(1)−C(2)	118.3(2)

The reaction of the isocyanide reagent $CNC_6H_3Me_2$-2,6 with **1**−**8** has been studied (Scheme 4). The products of the insertion reactions $[Zr\{Me_2Si(\eta^5\text{-}C_5Me_4)(\eta^5\text{-}C_5H_3R)\}\{\eta^2\text{-}R'C{=}NC_6H_3Me_2\text{-}2,6\}Cl]$ [R = Me, R′ = CH_2Ph (**9**); R = Me, R′ = CH_2SiMe_3 (**10**); R = *i*Pr, R′ = CH_2Ph (**11**); R = *i*Pr, R′ = CH_2SiMe_3 (**12**); R = $SiMe_3$, R′ = CH_2Ph (**13**); R = $SiMe_3$, R′ = CH_2SiMe_3 (**14**); R = H, R′ = CH_2SiMe_3 (**16**)] and $[Zr\{Me_2Si(\eta^5\text{-}C_5Me_4)(\eta^5\text{-}C_5H_4)\}\{\eta^2\text{-}PhCH_2C{=}NC_6H_3Me_2\text{-}2,6\}(CH_2Ph)]$ (**15**) were characterized by ^{1}H and ^{13}C NMR spectroscopy.

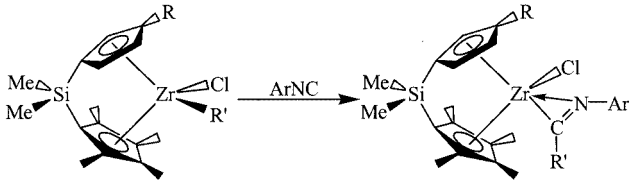

Ar = $C_6H_3Me_2$-2,6

R = Me, R' = CH_2Ph (**9**);
R = Me, R' = CH_2SiMe_3 (**10**);
R = *i*Pr, R' = CH_2Ph (**11**);
R = *i*Pr, R' = CH_2SiMe_3 (**12**);
R = $SiMe_3$, R' = CH_2Ph (**13**);
R = $SiMe_3$, R' = CH_2SiMe_3 (**14**)

Scheme 4

 © 2003 Wiley-VCH Verlag GmbH & Co. KGaA, Weinheim

The migratory insertion of alkyl groups towards isocyanide ligands allows the introduction of iminoacyl groups which are present in different coordination modes. In fact, for high-valent oxophilic early transition metals, the iminoacyl group typically adopts an η^2-coordination mode through both the nitrogen and carbon atoms.[16] Similarly, an η^2-coordination mode is proposed for the iminoacyl ligand in **9**−**16** on the basis of IR and ^{13}C NMR spectroscopy which show the characteristic stretching vibration $\nu(C{=}N)$ at ca. 1600 cm^{-1} and iminoacyl quaternary carbon atom signal at $\delta \approx 250$ ppm, respectively. The ^1H NMR spectra of **9**−**16** in addition to the expected signals for the *ansa*-metallocene protons, gave signals corresponding to the iminoacyl alkyl group (see Exp. Sect.).

The iminoacyl group can position itself in two distinct conformations, the "proximal" or "N-outside" and the "distal" or "N-inside" configurations (see Figure 2). ^1H and ^{13}C NMR spectroscopic data indicate the presence of only one of the two possible conformations. Although it has been demonstrated that the N-outside isomer is the resulting initial kinetic iminoacyl product of the insertion reaction, most group-4 metal derivatives show the structure of the N-inside isomer which results from thermodynamic control.[17] For **9**−**16** the isolated product was observed not to evolve over time and therefore we tentatively propose that they are the products resulting from thermodynamic control and adopt the N-inside conformation.

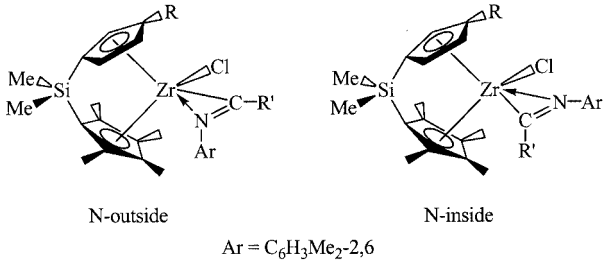

Figure 2. Two possible conformations for the (iminoacyl)metal complexes **9**−**16**

A second insertion was not observed even when stoichiometries other than 1:1 were tested.

Conclusions

In this paper we report our studies of the steric factors involved in the synthesis of alkylzirconocene complexes containing asymmetric *ansa* ligands. The preparation and characterization of mono- and dialkyl derivatives is described. The structural characterization of the monoalkyl complexes show the disposition of the β-alkyl substituent of the monosubstituted cyclopentadienyl moiety is such to orientate it away from the metal-bonded alkyl ligand. Insertion reactions with a bulky isocyanide, to give η^2-iminoacyl complexes, are also described.

Experimental Section

General Remarks: All reactions were performed using standard Schlenk tube techniques under dry nitrogen. Solvents were distilled from appropriate drying agents and degassed before use. Compounds [Zr{$Me_2Si(\eta^5$-$C_5Me_4)(\eta^5$-$C_5H_3R)$}Cl_2] (R = H, Me, *i*Pr, $SiMe_3$) were prepared as described earlier.[12a] $Mg(CH_2Ph)Cl$, $Mg(CH_2SiMe_3)Cl$, and $CNC_6H_3Me_2$-2,6 were purchased from Aldrich and used directly. IR spectra were recorded with a Perkin−Elmer PE 883 IR spectrophotometer. ^1H and ^{13}C spectra were recorded with a Varian FT-300 spectrometer and referenced to the residual deuterated solvent. Microanalyses were carried out with a Perkin−Elmer 2400 microanalyzer.

Preparation of [Zr{$Me_2Si(\eta^5$-$C_5Me_4)(\eta^5$-$C_5H_3Me)$}$(CH_2Ph)Cl$] (1): A 2 M solution of $Mg(CH_2Ph)Cl$ in THF (0.60 mL, 1.19 mmol) was added at −78 °C to a stirred solution of [Zr{$Me_2Si(\eta^5$-$C_5Me_4)(\eta^5$-$C_5H_3Me)$}Cl_2] (0.50 g, 1.19 mmol) in THF (50 mL). The solution was allowed to warm to room temperature and stirred for 6 h. The solvent was removed in vacuo and the remaining solid extracted in hexane. A orange crystalline solid was obtained by concentrating and cooling (−30 °C) the solution (0.45 g, 79%). ^1H NMR (300 MHz, C_6D_6, 25 °C): δ = 0.19 and 0.28 (2 s, each 3 H, $SiMe_2$), 1.52, 1.58, 1.66, and 1.95 (4 s, each 3 H, C_5Me_4), 2.07 (s, 3 H, C_5H_3Me), 1.70 and 1.86 (2 d, $^2J_{H,H}$ = 18.9 Hz, each 1 H, CH_2Ph), 4.91, 5.06, and 5.47 (3 m, each 1 H, C_5H_3), 6.75−7.25 (m, 5 H, CH_2Ph) ppm. $^{13}C\{^1H\}$ NMR (75 MHz, C_6D_6, 25 °C): δ = −0.5, −0.6 ($SiMe_2$), 11.2, 12.3, 14.6, 14.7 (C_5Me_4), 15.3 (C_5H_3Me), 38.2 (CH_2Ph), 102.1, 112.1, 113.9, 121.4, 134.9 (C_5H_3), 93.7, 121.9, 126.2, 131.1, 131.5 (C_5Me_4), 124.0, 126.9, 127.0, 128.5, 128.7, 153.6 (CH_2Ph) ppm. $C_{24}H_{31}ClSiZr$ (474.3): calcd. C 60.78, H 6.59; found C 60.59, H 6.54.

Preparation of [Zr{$Me_2Si(\eta^5$-$C_5Me_4)(\eta^5$-$C_5H_3Me)$}$(CH_2SiMe_3)Cl$] (2): A 1 M solution of $Mg(CH_2SiMe_3)Cl$ in Et_2O (0.96 mL, 0.96 mmol) was added at −78 °C to a stirred solution of [Zr{$Me_2Si(\eta^5$-$C_5Me_4)(\eta^5$-$C_5H_3Me)$}Cl_2] (0.40 g, 0.96 mmol) in THF (50 mL). The solution was allowed to warm to room temperature and stirred for 16 h. The resulting yellow solution was stirred under reflux for 2 h. The solvent was removed in vacuo and hexane added to the resulting solid. The mixture was filtered and the filtrate concentrated and cooled to −30 °C. The yellow solid that precipitated from the solution was isolated by filtration (0.37 g, 81%). ^1H NMR (300 MHz, C_6D_6, 25 °C): δ = 0.23 (s, 9 H, CH_2SiMe_3), 0.29 and 0.34 (2 s, each 3 H, $SiMe_2$), 1.48, 1.65, 1.92, and 2.00 (4 s, each 3 H, C_5Me_4), 2.30 (s, 3 H, C_5H_3Me), 1.77 and 1.91 (2 d, $^2J_{H,H}$ = 21.6 Hz, each 1 H, CH_2SiMe_3), 5.02, 5.09, and 6.60 (3 m, each 1 H, C_5H_3) ppm. $^{13}C\{^1H\}$ NMR (75 MHz, C_6D_6, 25 °C): δ = −0.4, −0.7 ($SiMe_2$), 2.9 (CH_2SiMe_3), 12.2, 12.3, 14.5, 14.6 (C_5Me_4), 15.5 (C_5H_3Me), 42.1 (CH_2SiMe_3), 103.4, 111.4, 112.5, 122.8, 134.6 (C_5H_3), 93.7, 122.2, 122.5, 130.1, 131.6 (C_5Me_4) ppm. $C_{21}H_{35}ClSi_2Zr$ (470.4): calcd. C 53.62, H 7.50; found C 53.36, H 7.43.

Preparation of [Zr{$Me_2Si(\eta^5$-$C_5Me_4)(\eta^5$-C_5H_3*i*Pr)$}$(CH_2Ph)Cl$] (3): The synthesis of **3** was carried out in an identical manner to that of **1**: 2 M solution of $Mg(CH_2Ph)Cl$ in THF (0.38 mL, 0.76 mmol) and [Zr{$Me_2Si(\eta^5$-$C_5Me_4)(\eta^5$-C_5H_3*i*Pr)$}$Cl_2$] (0.34 g, 0.76 mmol). Yield 0.26 g, 69%. ^1H NMR (300 MHz, C_6D_6, 25 °C): δ = 0.32 and 0.34 (2 s, each 3 H, $SiMe_2$), 1.03 and 1.07 (2 d, $^3J_{H,H}$ = 7.1 Hz, each 3 H, $HCMe_2$), 1.61, 1.67, 1.74, and 2.00 (4 s, each 3 H, C_5Me_4), 1.72 and 1.84 (2 d, $^2J_{H,H}$ = 17.2 Hz, each 1 H, CH_2Ph) 3.13 (sept, 1 H, $HCMe_2$), 5.05, 5.32, and 5.65 (3 m, each 1 H, C_5H_3), 6.88−7.33 (m, 5 H, CH_2Ph) ppm. $^{13}C\{^1H\}$ NMR (75 MHz, C_6D_6, 25 °C): δ = −0.8, −0.3 ($SiMe_2$), 11.2, 12.4, 14.4, 14.8

 © 2003 Wiley-VCH Verlag GmbH & Co. KGaA, Weinheim

(C_5Me_4), 22.1, 24.1 ($HCMe_2$), 28.0 ($HCMe_2$), 38.1 (CH_2Ph), 102.5, 110.9, 112.2, 121.4, 122.7 (C_5H_3), 94.1, 125.7, 126.1, 131.1, 131.8 (C_5Me_4), 122.6, 126.9, 127.0, 128.7, 128.8, 153.2 (CH_2Ph) ppm. $C_{26}H_{35}ClSiZr$ (502.3): calcd. C 62.17, H 7.02; found C 61.89, H 6.99.

Preparation of [Zr{Me$_2$Si(η^5-C$_5$Me$_4$)(η^5-C$_5$H$_3$*i*Pr)}(CH$_2$SiMe$_3$)Cl] (4): The synthesis of **4** was carried out in an identical manner to that of **2**: 1 M solution of $Mg(CH_2SiMe_3)Cl$ in Et_2O (0.85 mL, 0.85 mmol) and [Zr{$Me_2Si(\eta^5\text{-}C_5Me_4)(\eta^5\text{-}C_5H_3iPr)$}$Cl_2$] (0.38 g, 0.85 mmol). Yield 0.28 g, 65%. ^{1}H NMR (300 MHz, C_6D_6, 25 °C): δ = 0.23 (s, 9 H, CH_2SiMe_3), 0.44 and 0.55 (2 s, each 3 H, $SiMe_2$), 1.17 and 1.36 (2 d, $^3J_{H,H}$ = 6.8 Hz, each 3 H, $HCMe_2$), 1.72, 1.76, 1.86, and 1.90 (4 s, each 3 H, C_5Me_4), 1.80 and 1.94 (2 d, $^2J_{H,H}$ = 21.6 Hz, each 1 H, CH_2SiMe_3), 3.85 (sept, 1 H, $HCMe_2$), 5.30, 5.50, and 6.31 (3 m, each 1 H, C_5H_3) ppm. $^{13}C\{^1H\}$ NMR (75 MHz, C_6D_6, 25 °C): δ = −1.0, −0.4 ($SiMe_2$), 3.2 ($SiMe_3$), 12.4, 12.5, 15.1, 15.4 (C_5Me_4), 22.0, 24.4 ($HCMe_2$), 28.5 ($HCMe_2$), 44.0 (CH_2SiMe_3), 100.2, 112.4, 113.9, 120.6, 122.6 (C_5H_3), 98.4, 125.6, 126.8, 132.3, 132.4 (C_5Me_4) ppm. $C_{23}H_{39}ClSi_2Zr$ (498.4): calcd. C 55.43, H 7.89; found C 55.09, H 7.78.

Preparation of [Zr{Me$_2$Si(η^5-C$_5$Me$_4$)(η^5-C$_5$H$_3$SiMe$_3$)}(CH$_2$Ph)Cl] (5): The synthesis of **5** was carried out in an identical manner to that of **1**: 2 M solution of $Mg(CH_2Ph)Cl$ in THF (0.32 mL, 0.64 mmol) and [Zr{$Me_2Si(\eta^5\text{-}C_5Me_4)(\eta^5\text{-}C_5H_3SiMe_3)$}$Cl_2$] (0.30 g, 0.64 mmol). Yield 0.26 g, 76%. ^{1}H NMR (300 MHz, C_6D_6, 25 °C): δ = 0.27 (s, 9 H, $SiMe_3$), 0.32 and 0.39 (2 s, each 3 H, $SiMe_2$), 1.62, 1.73, 1.74, and 1.94 (4 s, each 3 H, C_5Me_4), 1.96 and 2.00 (2 d, $^2J_{H,H}$ = 18.5 Hz, each 1 H, CH_2Ph), 5.36, 5.71, and 5.90 (3 m, each 1 H, C_5H_3), 6.91−7.30 (m, 5 H, CH_2Ph) ppm. $^{13}C\{^1H\}$ NMR (75 MHz, C_6D_6, 25 °C): δ = −0.9, −0.6 ($SiMe_2$), −0.5 ($SiMe_3$) 11.1, 12.6, 14.3, 14.9 (C_5Me_4), 38.15 (CH_2Ph), 108.0, 116.3, 117.2, 121.5, 123.4 (C_5H_3), 95.7, 129.3, 130.6, 133.1, 136.4 (C_5Me_4), 126.1, 127.4, 127.5, 128.8, 129.5, 152.8 (CH_2Ph) ppm. $C_{26}H_{37}ClSi_2Zr$ (532.4): calcd. C 58.65, H 7.00; found C 58.46, H 6.96.

Preparation of [Zr{Me$_2$Si(η^5-C$_5$Me$_4$)(η^5-C$_5$H$_3$SiMe$_3$)}(CH$_2$SiMe$_3$)Cl] (6): The synthesis of **6** was carried out in an identical manner to that of **2**: 1 M solution of $Mg(CH_2SiMe_3)Cl$ in Et_2O (0.63 mL, 0.63 mmol) and [Zr{$Me_2Si(\eta^5\text{-}C_5Me_4)(\eta^5\text{-}C_5H_3SiMe_3)$}$Cl_2$] (0.30 g, 0.63 mmol). Yield 0.28 g, 85%. ^{1}H NMR (300 MHz, C_6D_6, 25 °C): δ = 0.21 (s, 9 H, CH_2SiMe_3), −0.05 and 0.24 (2 s, each 3 H, $SiMe_2$), 0.41 (s, 9 H, $C_5H_3SiMe_3$), 1.60, 1.78, 1.85, and 1.92 (4 s, each 3 H, C_5Me_4), 1.81 and 1.98 (2 d, $^2J_{H,H}$ = 19.4 Hz, each 1 H, CH_2SiMe_3), 5.43, 5.91, and 7.30 (3 m, each 1 H, C_5H_3) ppm. $^{13}C\{^1H\}$ NMR (75 MHz, C_6D_6, 25 °C): δ = −0.9, −0.6 ($SiMe_2$), 0.0 (CH_2SiMe_3), 1.4 ($C_5H_3SiMe_3$), 12.2, 12.4, 15.1, 15.2 (C_5Me_4), 48.9 (CH_2SiMe_3), 107.9, 115.9, 118.9, 122.5, 126.5 (C_5H_3), 95.8, 124.3, 124.9, 130.7, 131.3 (C_5Me_4) ppm. $C_{23}H_{41}ClSi_3Zr$ (528.5): calcd. C 52.27, H 7.82; found C 52.00, H 7.74.

Preparation of [Zr{Me$_2$Si(η^5-C$_5$Me$_4$)(η^5-C$_5$H$_4$)}(CH$_2$Ph)$_2$] (7): The synthesis of **7** was carried out in an identical manner to that of **1**: 2 M solution of $Mg(CH_2Ph)Cl$ in THF (0.74 mL, 1.48 mmol) and [Zr{$Me_2Si(\eta^5\text{-}C_5Me_4)(\eta^5\text{-}C_5H_4)$}$Cl_2$] (0.30 g, 0.74 mmol). Yield 0.30 g, 79%. ^{1}H NMR (300 MHz, C_6D_6, 25 °C): δ = 0.26 (s, 6 H, $SiMe_2$), 1.58 and 1.80 (2 s, each 6 H, C_5Me_4), 2.69 (s, 4 H, 2 × CH_2Ph), 5.06 and 6.14 (2 m, each 2 H, C_5H_4), 6.82−7.25 (m, 10 H, 2 × CH_2Ph) ppm. $^{13}C\{^1H\}$ NMR (75 MHz, C_6D_6, 25 °C): δ = −0.6 ($SiMe_2$), 11.6, 14.6 (C_5Me_4), 38.1 (CH_2Ph), 100.5, 113.0, 121.1, (C_5H_4), 98.2, 124.4, 135.7 (C_5Me_4), 125.9, 126.8, 129.2, 153.7 (CH_2Ph) ppm. $C_{30}H_{36}SiZr$ (515.9): calcd. C 69.84, H 7.03; found C 69.66, H 6.91.

Preparation of [Zr{Me$_2$Si(η^5-C$_5$Me$_4$)(η^5-C$_5$H$_4$)}(CH$_2$SiMe$_3$)Cl] (8): The synthesis of **8** was carried out in an identical manner to that of **2**: 1 M solution of $Mg(CH_2SiMe_3)Cl$ in Et_2O (0.74 mL, 0.74 mmol) and [Zr{$Me_2Si(\eta^5\text{-}C_5Me_4)(\eta^5\text{-}C_5H_4)$}$Cl_2$] (0.30 g, 0.74 mmol). Yield 0.25 g, 75%. ^{1}H NMR (300 MHz, C_6D_6, 25 °C): δ = 0.25 (s, 9 H, CH_2SiMe_3), 0.23 and 0.28 (2 s, each 3 H, $SiMe_2$), 1.43, 1.70, 1.86, and 1.95 (4 s, each 3 H, C_5Me_4), 1.79 and 1.95 (2 d, $^2J_{H,H}$ = 18.3 Hz, each 1 H, CH_2SiMe_3), 5.01, 5.48, 6.71, and 6.95 (4 m, each 1 H, C_5H_4) ppm. $^{13}C\{^1H\}$ NMR (75 MHz, C_6D_6, 25 °C): δ = −0.6, −0.5 ($SiMe_2$), 2.8 (CH_2SiMe_3), 12.1, 12.2, 14.5, 14.8 (C_5Me_4), 42.9 (CH_2SiMe_3), 104.4, 110.8, 111.5, 123.0, 123.7 (C_5H_4), 94.9, 123.9, 125.6, 130.8, 131.4 (C_5Me_4) ppm. $C_{20}H_{33}ClSi_2Zr$ (456.3): calcd. C 52.64, H 7.29; found C 52.29, H 7.23.

Preparation of [Zr{Me$_2$Si(η^5-C$_5$Me$_4$)(η^5-C$_5$H$_3$Me)}{η^2-PhCH$_2$C=N(C$_6$H$_3$Me$_2$-2,6)}Cl] (9): 2,6-Dimethylphenyl isocyanide (0.14 g, 1.05 mmol) and **1** (0.50 g, 1.05 mmol) were dissolved in THF (100 mL). The resulting orange solution was stirred at room temperature for 18 h. The solvent was removed in vacuo and the remaining solid extracted with toluene (30 mL). An orange solid was obtained by concentrating (5 mL) and cooling (−30 °C) the solution (0.54 g, 84%). IR (Nujol): $\tilde{\nu}$ = 1590 ($\nu_{C=N}$) cm^{-1}. ^{1}H NMR (300 MHz, C_6D_6, 25 °C): δ = 0.43 and 0.45 (2 s, each 3 H, $SiMe_2$), 1.46, 1.71, 1.88, and 1.97 (4 s, each 3 H, C_5Me_4), 2.03 (s, 3 H, C_5H_3Me), 2.17 and 2.20 (2 s, each 3 H, $C_6H_3Me_2$), 3.22 and 3.59 (2 d, $^2J_{H,H}$ = 18.0 Hz, each 1 H, CH_2Ph), 5.50, 5.62, and 5.73 (3 m, each 1 H, C_5H_3), 6.55 (2 H), 6.69 (1 H) (2 m, $C_6H_3Me_2$), 6.83−7.15 (m, 5 H, CH_2Ph) ppm. $^{13}C\{^1H\}$ NMR (75 MHz, C_6D_6, 25 °C): δ = −0.7, −0.2 ($SiMe_2$), 12.4, 12.5, 15.1, 15.3, 15.5 (C_5Me_4, C_5H_3Me), 20.0, 20.1 ($C_6H_3Me_2$), 38.2 (CH_2Ph), 104.1, 104.4, 114.4, 119.4, 137.3 (C_5H_3), 108.0, 115.1, 120.9, 131.1, 134.9 (C_5Me_4), 125.6, 127.6, 127.7, 128.8, 128.9, 144.2 (CH_2Ph), 126.2, 126.3, 126.9, 127.0, 128.4, 128.7, 171.0 ($C_6H_3Me_2$), 246.7 (CCH_2Ph) ppm. $C_{33}H_{40}ClNSiZr$ (605.4): calcd. C 65.47, H 6.66, N 2.31; found C 65.21, H 6.58, N 2.29.

Preparation of [Zr{Me$_2$Si(η^5-C$_5$Me$_4$)(η^5-C$_5$H$_3$Me)}{η^2-Me$_3$Si-CH$_2$C=N(C$_6$H$_3$Me$_2$-2,6)}Cl] (10): The synthesis of **10** was carried out in an identical manner to that of **9**: **2** (0.50 g, 1.06 mmol) and 2,6-dimethylphenyl isocyanide (0.14 g, 1.06 mmol). Yield 0.49 g, 77%. IR (Nujol): $\tilde{\nu}$ = 1620 ($\nu_{C=N}$) cm^{-1}. ^{1}H NMR (300 MHz, C_6D_6, 25 °C): δ = −0.05 (s, 9 H, CH_2SiMe_3), 0.50 and 0.54 (2 s, each 3 H, $SiMe_2$), 1.50, 1.89, 1.95, and 1.99 (4 s, each 3 H, C_5Me_4), 2.28 (s, 3 H, C_5H_3Me), 2.16 and 2.17 (2 s, each 3 H, $C_6H_3Me_2$), 1.95 and 2.41 (2 d, $^2J_{H,H}$ = 18.5 Hz, each 1 H, CH_2SiMe_3), 5.50, 5.62, and 5.73 (3 m, each 1 H, C_5H_3), 6.86 (s, 3 H, $C_6H_3Me_2$) ppm. $^{13}C\{^1H\}$ NMR (75 MHz, C_6D_6, 25 °C): δ = −0.4, 0.3 ($SiMe_2$), 0.8 (CH_2SiMe_3), 12.5, 12.7, 14.8, 15.6, 15.8 (C_5Me_4, C_5H_3Me), 19.8, 20.7 ($C_6H_3Me_2$), 32.2 (CH_2SiMe_3), 100.2, 103.8, 113.5, 118.8, 130.7 (C_5H_3), 108.5, 114.7, 118.3, 130.2, 130.3 (C_5Me_4) 125.6, 127.3, 127.4, 128.3, 128.4, 144.2 ($C_6H_3Me_2$), 245.4 (CCH_2SiMe_3) ppm. $C_{30}H_{44}ClNSi_2Zr$ (601.5): calcd. C 59.90, H 7.37, N 2.33; found C 59.63, H 7.32, N 2.28.

Preparation of [Zr{Me$_2$Si(η^5-C$_5$Me$_4$)(η^5-C$_5$H$_3$*i*Pr)}{η^2-PhCH$_2$C=N(C$_6$H$_3$Me$_2$-2,6)}Cl] (11): The synthesis of **11** was carried out in an identical manner to that of **9**: **3** (0.40 g, 0.80 mmol) and 2,6-dimethylphenyl isocyanide (0.10 g, 0.80 mmol). Yield 0.39 g, 78%. IR (Nujol): $\tilde{\nu}$ = 1605 ($\nu_{C=N}$) cm^{-1}. ^{1}H NMR (300 MHz, C_6D_6, 25 °C): δ = 0.39 and 0.44 (2 s, each 3 H, $SiMe_2$), 0.99 and 1.25 (2 d, $^3J_{H,H}$ = 7.1 Hz, each 3 H, $HCMe_2$), 1.42, 1.69, 1.93, and 1.97 (4 s, each 3 H, C_5Me_4), 2.12 and 2.14 (2 s, each 3 H, $C_6H_3Me_2$), 3.12 and 3.76 (2 d, $^2J_{H,H}$ = 17.1 Hz, each 1 H, CH_2Ph), 3.35 (sept, 1 H, $HCMe_2$), 5.67 (2 H), 5.92 (1 H) (2 m, C_5H_3), 6.52 (2 H), 6.69

 © 2003 Wiley-VCH Verlag GmbH & Co. KGaA, Weinheim

(1 H) (2 m, $C_6H_3Me_2$), 6.88−7.26 (m, 5 H, CH_2Ph) ppm. $^{13}C\{^1H\}$ NMR (75 MHz, C_6D_6, 25 °C): δ = −0.6, −0.2 ($SiMe_2$), 12.4, 12.8, 15.0, 15.2 (C_5Me_4), 22.5, 24.6 ($HCMe_2$), 29.1 ($HCMe_2$), 39.3 (CH_2Ph), 19.5, 20.4 ($C_6H_3Me_2$), 100.7, 112.6, 114.1, 122.6, 123.4 (C_5H_3), 105.3, 126.7, 127.2, 133.4, 134.4 (C_5Me_4), 125.3, 127.4, 127.6, 128.8, 128.9, 152.2 (CH_2Ph), 126.1, 126.9, 127.0, 128.9, 129.0, 165.3 ($C_6H_3Me_2$), 246.3 (CCH_2Ph) ppm. $C_{35}H_{44}ClNSiZr$ (633.5): calcd. C 66.36, H 7.00, N 2.21; found C 66.01, H 6.91, N 2.18.

Preparation of [Zr{Me$_2$Si(η^5-C$_5$Me$_4$)(η^5-C$_5$H$_3$*i*Pr)}{η^2-Me$_3$SiCH$_2$C=N(C$_6$H$_3$Me$_2$-2,6)}Cl] (12): The synthesis of **12** was carried out in an identical manner to that of **9**: **4** (0.45 g, 0.90 mmol) and 2,6-dimethylphenyl isocyanide (0.12 g, 0.90 mmol). Yield 0.43 g, 75% IR (Nujol): $\tilde{\nu}$ = 1570 ($\nu_{C=N}$) cm^{-1}. ^1H NMR (300 MHz, C_6D_6, 25 °C): δ = 0.35 and 0.39 (2s, each 3 H, $SiMe_2$), 0.25 (s, 9 H, CH_2SiMe_3), 1.05 and 1.33 (2 d, $^3J_{H,H}$ = 7.1 Hz, each 1 H, $HCMe_2$), 1.48, 1.72, 1.95, and 2.00 (4 s, each 3 H, C_5Me_4), 2.15 and 2.16 (2 s, each 3 H, $C_6H_3Me_2$), 3.01 and 3.54 (2 d, $^2J_{H,H}$ = 18.0 Hz, each 1 H, CH_2SiMe_3), 3.42 (sept, 1 H, $HCMe_2$), 5.60, 5.63, and 5.92 (3 m, each 1 H, C_5H_3), 6.60 (2 H), 6.84 (1 H) (2 m, $C_6H_3Me_2$) ppm. $^{13}C\{^1H\}$ NMR (75 MHz, C_6D_6, 25 °C): δ = −1.0, −0.7 ($SiMe_2$), 2.6 ($SiMe_3$), 12.9, 13.0, 16.5, 16.6 (C_5Me_4), 22.7, 25.3 ($HCMe_2$), 30.0 ($HCMe_2$), 35.1 (CH_2SiMe_3), 19.3, 20.3 ($C_6H_3Me_2$), 98.7, 112.7, 114.9, 124.2, 125.6 (C_5H_3), 104.9, 125.8, 126.4, 133.8, 133.9 (C_5Me_4), 126.9, 127.8, 128.1, 131.4, 131.6, 160.7 ($C_6H_3Me_2$), 248.1 (CCH_2SiMe_3) ppm. $C_{32}H_{48}ClNSi_2Zr$ (629.6): calcd. C 61.05, H 7.68, N 2.22; found C 60.72, H 7.62, N 2.23.

Preparation of [Zr{Me$_2$Si(η^5-C$_5$Me$_4$)(η^5-C$_5$H$_3$SiMe$_3$)}{η^2-PhCH$_2$C=N(C$_6$H$_3$Me$_2$-2,6)}Cl] (13): The synthesis of **13** was carried out in an identical manner to that of **9**: **5** (0.45 g, 0.85 mmol) and 2,6-dimethylphenyl isocyanide (0.11 g, 0.85 mmol). Yield 0.45 g, 81%. IR (Nujol): $\tilde{\nu}$ = 1590 ($\nu_{C=N}$) cm^{-1}. ^1H NMR (300 MHz, C_6D_6, 25 °C): δ = 0.31 (s, 9 H, $SiMe_3$), 0.37 and 0.41 (2 s, each 3 H, $SiMe_2$), 1.39, 1.59, 1.88, and 1.96 (4 s, each 3 H, C_5Me_4), 2.11 and 2.13 (2 s, each 3 H, $C_6H_3Me_2$), 3.03 and 3.85 (2 d, $^2J_{H,H}$ = 18.0 Hz, each 1 H, CH_2Ph), 5.81, 6.10, and 6.45 (3 m, each 1 H, C_5H_3), 6.56 (2 H), 6.70 (1 H) (m, $C_6H_3Me_2$), 6.88−7.26 (m, 5 H, CH_2Ph) ppm. $^{13}C\{^1H\}$ NMR (75 MHz, C_6D_6, 25 °C): δ = −0.6, −0.3 ($SiMe_2$), 0.7 ($SiMe_3$), 11.9, 12.4, 15.0, 15.2 (C_5Me_4), 19.9, 20.5 ($C_6H_3Me_2$), 38.1 (CH_2Ph), 104.2, 108.0, 110.9, 118.3, 125.8 (C_5H_3), 107.2, 118.7, 119.6, 134.8, 135.7 (C_5Me_4), 125.6, 127.0, 127.1, 128.6, 128.7, 144.1 (CH_2Ph), 126.1, 126.9, 127.7, 129.2, 129.9, 171.0 ($C_6H_3Me_2$), 247.8 (CCH_2Ph) ppm. $C_{35}H_{46}ClNSi_2Zr$ (663.6): calcd. C 63.35, H 6.99, N 2.11; found C 63.17, H 6.94, N 2.10.

Preparation of [Zr{Me$_2$Si(η^5-C$_5$Me$_4$)(η^5-C$_5$H$_3$SiMe$_3$)}{η^2-Me$_3$SiCH$_2$C=N(C$_6$H$_3$Me$_2$-2,6)}Cl] (14): The synthesis of **14** was carried out in an identical manner to that of **9**: **6** (0.40 g, 0.76 mmol) and 2,6-dimethylphenyl isocyanide (0.10 g, 0.76 mmol). Yield 0.40 g, 80%. IR (Nujol): $\tilde{\nu}$ = 1605 ($\nu_{C=N}$) cm^{-1}. ^1H NMR (300 MHz, C_6D_6, 25 °C): δ = 0.00 (s, 9 H, CH_2SiMe_3), 0.31 (s, 9 H, $SiMe_3$), 0.53 and 0.54 (2 s, each 3 H, $SiMe_2$), 1.39, 1.89, 1.96, and 2.04 (4 s, each 3 H, C_5Me_4), 2.14 and 2.16 (2 s, each 3 H, $C_6H_3Me_2$), 2.13 and 2.41 (2 d, $^2J_{H,H}$ = 12.5 Hz, each 1 H, CH_2SiMe_3), 5.85, 6.05, and 6.24 (3 m, each 1 H, C_5H_3), 6.85 (2 H), 7.11 (1 H) (m, $C_6H_3Me_2$) ppm. $^{13}C\{^1H\}$ NMR (75 MHz, C_6D_6, 25 °C): δ = −0.0, 0.1 ($SiMe_2$), 0.6 (CH_2SiMe_3), 1.4 ($C_5H_3SiMe_3$), 12.1, 12.5, 14.8, 15.9 (C_5Me_4), 19.8, 21.0 ($C_6H_3Me_2$), 31.5 (CH_2SiMe_3), 103.9, 107.5, 109.8, 111.1, 115.3, 116.9 (C_5H_3), 103.9, 124.2, 125.0, 131.6, 132.4 (C_5Me_4), 125.5, 127.1, 127.5, 129.1, 129.8, 171.0 ($C_6H_3Me_2$), 246.4 (CCH_2SiMe_3) ppm. $C_{32}H_{50}ClNSi_3Zr$ (659.7): calcd. C 58.26, H 7.64, N 2.12; found C 57.97, H 7.57, N 2.08.

Preparation of [Zr{Me$_2$Si(η^5-C$_5$Me$_4$)(η^5-C$_5$H$_4$)}{η^2-PhCH$_2$C=N(C$_6$H$_3$Me$_2$-2,6)}(CH$_2$Ph)] (15): The synthesis of **15** was carried out in an identical manner to that of **9**: **7** (0.30 g, 0.58 mmol) and 2,6-dimethylphenyl isocyanide (0.08 g, 0.58 mmol). Yield 0.30 g, 80%. IR (Nujol): $\tilde{\nu}$ = 1590 ($\nu_{C=N}$) cm^{-1}. ^1H NMR (300 MHz, C_6D_6, 25 °C): δ = 0.47 and 0.49 (2 s, each 3 H, $SiMe_2$), 1.39, 1.47, 1.83, and 1.77 (4 s, each 3 H, C_5Me_4), 2.06 and 2.07 (2 s, each 3 H, $C_6H_3Me_2$), 1.62 and 2.12 (2 d, $^2J_{H,H}$ = 16.5 Hz, each 1 H, CH_2Ph), 3.05 and 3.40 (2 d, $^2J_{H,H}$ = 18.4 Hz, each 1 H, $NCCH_2Ph$), 5.13, 5.46, 5.63, and 5.92 (4 m, each 1 H, C_5H_4), 6.78 (2 H), 6.87 (1 H) (m, $C_6H_3Me_2$), 6.90−7.26 (m, 10 H, 2 × CH_2Ph) ppm. $^{13}C\{^1H\}$ NMR (75 MHz, C_6D_6, 25 °C): δ = −0.9, 0.3 ($SiMe_2$), 12.3, 12.4, 15.1, 15.4 (C_5Me_4), 19.5, 19.6 ($C_6H_3Me_2$), 38.2, 44.8 (CH_2Ph), 100.9, 112.4, 114.9, 118.4, 119.4 (C_5H_4), 106.0, 125.4, 125.6, 131.2, 134.8 (C_5Me_4), 125.0, 125.7, 127.0, 127.1, 128.6, 128.7, 141.9, 146.2 (CH_2Ph), 126.4, 126.7, 127.7, 128.9, 129.0, 156.6 ($C_6H_3Me_2$), 247.8 (CCH_2Ph) ppm. $C_{39}H_{45}NSiZr$ (647.1): calcd. C 72.39, H 7.01, N 2.16; found C 72.11, H 6.92, N 2.15.

Preparation of [Zr{Me$_2$Si(η^5-C$_5$Me$_4$)(η^5-C$_5$H$_4$)}{η^2-Me$_3$SiCH$_2$C=N(C$_6$H$_3$Me$_2$-2,6)}ZrCl] (16): The synthesis of **16** was carried out in an identical manner to that of **9**: **8** (0.25 g, 0.55 mmol) and 2,6-dimethylphenyl isocyanide (0.07 g, 0.55 mmol). Yield 0.25 g, 77%. IR (Nujol): $\tilde{\nu}$ = 1600 ($\nu_{C=N}$) cm^{-1}. ^1H NMR (300 MHz, C_6D_6, 25 °C): δ = −0.09 (s, 9 H, CH_2SiMe_3), 0.51 and 0.54 (2 s, each 3 H, $SiMe_2$), 1.58, 1.81, 1.85, and 2.14 (4 s, each 3 H, C_5Me_4), 2.21 and 2.26 (2 s, each 3 H, $C_6H_3Me_2$), 3.79 and 3.96 (2 d, $^2J_{H,H}$ = 15.5 Hz, each 1 H, CH_2SiMe_3), 5.65, 5.97, 6.23, and 6.47 (3 m, each 1 H, C_5H_3), 6.86 (m, 3 H, $C_6H_3Me_2$) ppm. $^{13}C\{^1H\}$ NMR (75 MHz, C_6D_6, 25 °C): δ = −0.6, −0.2 ($SiMe_2$), 15.5 (CH_2SiMe_3), 12.4, 12.5, 15.1, 15.3 (C_5Me_4), 20.0, 20.1 ($C_6H_3Me_2$), 38.2 (CH_2SiMe_3), 101.9, 104.4, 114.4, 119.3, 125.6 (C_5H_3), 104.0, 131.0, 134.8, 137.2, 144.1 (C_5Me_4), 126.2, 126.9, 127.0, 128.8, 128.9, 171.2 ($C_6H_3Me_2$), 246.7 (CCH_2SiMe_3) ppm. $C_{29}H_{42}ClNSi_2Zr$ (587.50): calcd. C 59.29, H 7.21, N 2.38; found C 59.00, H 7.15, N 2.35.

Table 2. Crystal data and structure refinement for **1**

Empirical formula	$C_{24}H_{31}ClSiZr$
Formula mass	474.25
Temperature [K]	250(2)
Wavelength [Å]	0.71073
Crystal system, space group	triclinic, $P\bar{1}$
a [Å]	8.853(8)
b [Å]	11.134(3)
c [Å]	11.998(2)
α [°]	102.55(2)
β [°]	100.09(3)
γ [°]	90.23(4)
Volume [Å^3]	1135(1)
Z, calculated density [g/cm^3]	1, 1.387
Absorption coefficient [cm^{-1}]	6.61
F(000)	492
Crystal size [mm]	0.3 × 0.2 × 0.2
Limiting indices	$-11 \le h \le 11$ $-14 \le k \le 14$ $0 \le l \le 12$
Reflections collected/unique	5313/5057 [*R*(int) = 0.0366]
Data/restraints/parameters	5057/0/248
Goodness-of-fit on F^2	1.058
Final *R* indices [$I > 2\sigma(I)$]	*R*1 = 0.0338, *wR*2 = 0.0879
R indices (all data)	*R*1 = 0.0468, *wR*2 = 0.0975
Largest diff. peak and hole [e·Å^{-3}]	0.444 and −0.798

 © 2003 Wiley-VCH Verlag GmbH & Co. KGaA, Weinheim

X-ray Crystal-Structure Determination of [Zr{$Me_2Si(\eta^5$-$C_5Me_4)(\eta^5$-$C_5H_3Me)$}$(CH_2Ph)Cl$] (1): Intensity data were collected with a NONIUS-MACH3 diffractometer equipped with a graphite monochromator and Mo-K_α radiation source (λ = 0.71073 Å) using an $\omega/2\theta$-scan technique. The final unit cell parameters were determined from 25 well-centered reflections and refined by least-squares methods. Data were corrected for Lorentz and polarization effects but not for absorption. The structure was solved by direct methods using the SHELXS computer program[18] and refined on F^2 by full-matrix least squares (SHELXL-97).[19] All non-hydrogen atoms were refined with anisotropic thermal parameters. The hydrogen atoms were included in calculated positions and were refined with an overall isotropic temperature factor using a riding model. Weights were optimized in the final cycles. Crystallographic data are given in Table 2. CCDC-205931 contains the supplementary crystallographic data for this paper. These data can be obtained free of charge at www.ccdc.cam.ac.uk/conts/retrieving.html [or from the Cambridge Crystallographic Data Centre, 12 Union Road, Cambridge CB2 1EZ, UK; Fax: (internat.) + 44-1223/336-033; E-mail: deposit@ccdc.cam.ac.uk].

Acknowledgments

We gratefully acknowledge financial support from the Dirección General de Enseñanza Superior e Investigación Científica, Spain (Grants no. BQU2002-04638-C02-01 and no. BQU2000-0463), the Junta de Comunidades de Castilla-La Mancha (PAC-02-003) and the Universidad Rey Juan Carlos (PIPR-02-09).

[1] *Comprehensive Organometallic Chemistry II* (Eds.: E. W. Abel, F. G. A. Stone, G. Wilkinson), Pergamon Press, Oxford, **1995**, vol. 4.

[2] [2a] L. Resconi, L. Cavallo, A. Fait, F. Piemontesi, *Chem. Rev.* **2000**, *100*, 1253−1346. [2b] H. H. Brintzinger, D. Fischer, R. Mülhaupt, B. Reiger, R. M. Waymouth, *Angew. Chem.* **1995**, *107*, 1255−1283; *Angew. Chem. Int. Ed. Engl.* **1995**, *36*, 1143−1170.

[3] M. Bühl, G. Hopp, W. von Philipsborn, S. Beck, M. H. Prosenc, U. Rief, H. H. Brintzinger, *Organometallics* **1996**, *15*, 778−785.

[4] [4a] P. C. Möhring, N. J. Coville, *J. Organomet. Chem.* **1994**, *479*, 1−29. [4b] N. Piccolrovazzi, P. Pino, G. Consiglio, A. Sironi, M. Moret, *Organometallics* **1990**, *9*, 3098−3105. [4c] J. Okuda, R. W. Albach, E. Herdtweck, *Polyhedron* **1991**, *10*, 1741−1748. [4d] W. Kaminsky, R. Engehausen, K. Zoumis, W. Spaleck, J. Rohrmann, *Makromol. Chem.* **1992**, *193*, 1643−1651. [4e] I. M. Lee, W. J. Gauthier, J. M. Ball, B. Iyengar, S. Collins, *Organometallics* **1992**, *11*, 2115−2122. [4f] C. Janiak, U. Versteeg, K. C. H. Lange, R. Weimann, E. Hahn, *J. Organomet. Chem.* **1995**, *501*, 219−234.

[5] *Ziegler Catalysts* (Eds.: G. Fink, R. Mülhaupt, H. H. Brintzinger), Springer-Verlag, Berlin, **1995**.

[6] [6a] S. L. J. Conway, T. Dijkstra, L. H. Doerrer, J. C. Green, M. L. H. Green, A. H. H. Stephens, *J. Chem. Soc., Dalton Trans.* **1998**, 2689−2695. [6b] J. H. Shin, G. Parkin, *Chem. Commun.* **1999**, 887−888. [6c] H. Lee, B. M. Bridgewater, G. Parkin, *J. Chem. Soc., Dalton Trans.* **2000**, 4490−4493. [6d] P. J. Shapiro, *Coord. Chem. Rev.* **2002**, *231*, 67−81.

[7] [7a] J. Langmaier, Z. Samec, V. Varga, M. Horacek, R. Choukroun, K. Mach, *J. Organomet. Chem.* **1999**, *584*, 323−328. [7b] J. Langmaier, Z. Samec, V. Varga, M. Horacek, K. Mach, *J. Organomet. Chem.* **1999**, *579*, 348−355. [7c] U. Wieser, D. Babushkin, H.-H. Brintzinger, *Organometallics* **2002**, *21*, 920−923.

[8] P. G. Gassman, D. W. Macomber, J. W. Hershberger, *Organometallics* **1983**, *2*, 1470−1472.

[9] A. Antiñolo, T. Expósito, I. del Hierro, D. Lucas, Y. Mugnier, I. Orive, A. Otero, S. Prashar, *J. Organomet. Chem.* **2002**, *655*, 63−69.

[10] R. F. Jordan, *Adv. Organomet. Chem.* **1991**, *32*, 325−387.

[11] [11a] M. Bochmann, *J. Chem. Soc., Dalton Trans.* **1996**, 255−270. [11b] X. Yang, C. L. Stern, T. J. Marks, *J. Am. Chem. Soc.* **1994**, *116*, 10015−10031. [11c] D. Veghini, M. W. Day, J. E. Bercaw, *Inorg. Chim. Acta* **1998**, *280*, 226−232.

[12] [12a] A. Antiñolo, I. López-Solera, I. Orive, A. Otero, S. Prashar, A. M. Rodríguez, E. Villaseñor, *Organometallics* **2001**, *20*, 71−78. [12b] A. Antiñolo, I. López-Solera, A. Otero, S. Prashar, A. M. Rodríguez, E. Villaseñor, *Organometallics* **2002**, *21*, 2460−2467.

[13] [13a] C. Alonso-Moreno, A. Antiñolo, I. López-Solera, A. Otero, S. Prashar, A. M. Rodríguez, E. Villaseñor, *J. Organomet. Chem.* **2002**, *656*, 129−138. [13b] A. Antiñolo, R. Fernández-Galán, I. Orive, A. Otero, S. Prashar, *Eur. J. Inorg. Chem.* **2002**, 2470−2476.

[14] [14a] M. R. Collier, M. F. Lappert, R. Pearce, *J. Chem. Soc., Dalton Trans.* **1973**, 445−451. [14b] M. F. Lappert, C. J. Pickett, P. I. Riley, P. I. W. Yarrow, *J. Chem. Soc., Dalton Trans.* **1981**, 805−813.

[15] [15a] J. L. Atwood, G. K. Barker, J. Holton, W. E. Hunter, M. F. Lappert, R. Pearce, *J. Am. Chem. Soc.* **1977**, *99*, 6645−6652. [15b] M. F. Lappert, P. I. Riley, P. I. W. Yarrow, J. L. Atwood, W. E. Hunter, M. J. Zaworotko, *J. Chem. Soc., Dalton Trans.* **1981**, 814−821.

[16] L. D. Durfee, I. P. Rothwell, *Chem. Rev.* **1988**, *88*, 1059−1079.

[17] G. Erker, *Acc. Chem. Res.* **1984**, *17*, 103−109.

[18] G. M. Sheldrick, *Acta Crystallogr., Sect. A* **1990**, *46*, 467−473.

[19] G. M. Sheldrick, *Program for the Refinement of Crystal Structures from Diffraction Data*, University of Göttingen, Göttingen, Germany, **1997**.

Received March 20, 2003

 © 2003 Wiley-VCH Verlag GmbH & Co. KGaA, Weinheim

Mono-Dithiolene Molybdenum(IV) Complexes of *cis*-1,2-Dicyano-1,2-ethylenedithiolate (mnt^{2-}): New Models for Molybdenum Enzymes

Hideki Sugimoto,*[a] Kazushi Siren,[b] Hiroshi Tsukube,[a] and Koji Tanaka[b]

Keywords: Molybdenum / Bioinorganic chemistry / Oxo ligands / S ligands / Oxidation

New mono-dithiolene molybdenum(IV) complexes of *cis*-1,2-dicyano-1,2-ethylenedithiolato [$(mnt)^{2-}$] have been synthesized as models for molybdenum enzymes, with 4,4′-di-*tert*-butyl-2,2′-bipyridine (Bu_2bpy) and, *N*,*N*′-tetraethylethylenediamine (Et_4en) as ancillary ligands, and characterized by IR, UV/Vis, elemental analysis, ESI-mass and electrochemical techniques. The temperature-dependent ^1H NMR spectra, recorded in CD_3CN solution, indicated that [MoO(mnt)(Bu_2bpy)] (**1**) has a rigid structure but [MoO(mnt)(Et_4en)] (**2**) showed dynamic conformational inversion processes involving the chelating ethylenediamine unit. The complexes exhibited different reactivities toward molecular oxygen: **1** gave a single oxo-bridged dimolybdenum dimer complex [$Mo_2O_3(mnt)_2(Bu_2bpy)_2$] (**3**), while **2** did not react with O_2 and kept its mononuclear structure. Both complexes have almost the same redox potential for $Mo^{IV/V}$, and so the steric bulkiness and conformational dynamics were thought to cause this marked contrast. The obtained dimolybdenum complex **3** was also structurally characterized and investigated, and found to be a new dimolybdenum complex with one dithiolene per molybdenum. The crystal structure of the starting complex **4** was also reported. (© Wiley-VCH Verlag GmbH & Co. KGaA, 69451 Weinheim, Germany, 2003)

Introduction

Molybdenum enzymes are widely distributed in nature and participate in catalytic cycles in biological reactions of the earth's carbon, nitrogen, and sulfur.[1] Crystallographic and X-ray absorption spectroscopic studies have revealed that most of these enzymes have active sites containing mononuclear molybdenum(IV) or -(VI) complexes coordinated by pterin-dithiolene cofactor ligands:[2] Formate dehydrogenase and dimethyl sulfoxide reductase have two dithiolene ligands, while sulfite oxidase, xanthin oxidase and nitrate reductase have one dithiolene per molybdenum center. Holm and co-workers and Ueyama and co-workers have presented mono- and des-oxo molybdenum(IV), and di- and mono-oxo molybdenum(VI) complexes with bis-dithiolene and -dithiolate ligands, which can be regarded as model complexes of the former enzymes.[3] Although other molybdenum complexes with two dithiolene ligands have been characterized,[4] only a few molybdenum complexes that contain one dithiolene ligand. Nicholas et al. isolated the mono-oxo complex of [$Mo^{IV}O(mnt)(Ph_2PCH_2CH_2PPh_2)$]·$(CH_3)_2CO$ (mnt = *cis*-1,2-dicyano-1,2-ethylenedithiolate),[5] the first example of a structurally characterized molybdenum(IV) complex with mono-dithiolene ligands; however, its oxygen transfer properties were not elucidated. Enemark et al. reported several mono-dithiolene mono-oxo molybdenum complexes, [$Mo^{V}O(L)(3,5\text{-}Me_2Tp)$] (L = $C_6H_4S_2$, $C_7H_6S_2$, $C_2H_2S_2$, Me_2Tp = hydrotris(3,5-dimethylpyrazol-2-yl-borato),[6] in which the molybdenum centers were in a +5 oxidation state and their hexacoordinate structures provided no open site for substrate binding. More recently, Holm et al. have presented a series of mono-dithiolene molybdenum(V), -(VI) complexes, mono-oxo derivatives $[MoOCl_2(L)]^-$, $[MoO(2\text{-}Ads)_2(L)]^-$ [L: dithiolene = $S_2C_2Me_2$ (1,2-dimethyl-1,2-ethylenedithiolate), bdt (1,2-benzenedithiolate)], $[MoO(SC_6H_2\text{-}2,4,6\text{-}i Pr_3)_2(bdt)]^-$, $[MoOCl(SC_6H_2\text{-}2,4,6\text{-}i Pr_3)_2(bdt)]^-$, and di-oxo derivatives $[MoO_2(L1)(bdt)]^-$ (L1 = $OSiPh_3$, $SC_6H_2\text{-}2,4,6\text{-}i Pr_3$), as structural analogues for active sites of the sulfite oxidase enzyme family.[7] The mono-oxo molybdenum centers of these complexes also have an oxidation number of +5, as found in a resting form of native enzymes.

Here, we describe the synthesis and characterization of mono-dithiolene molybdenum(IV) complexes as new synthetic models for the active sites of sulfite oxidase, xanthin oxidase, and nitrate reductase. In addition to the mnt ligand, the ancillary ligands 4,4′-di-*tert*-butyl-2,2′-bipyridine (Bu_2bpy) provide σ-/π-bonding, and *N*,*N*′-tetraethylethylenediamine (Et_4en) give σ-donation character. Because most substrates in molybdenum enzyme reactions are neutral or negatively charged, the use of neutral Bu_2bpy and Et_4en

[a] Department of Chemistry, Graduate School of Science, Osaka City University,
Sumiyoshi-ku, Osaka 558−8585, Japan
Fax: (internat.) +81-6-6605-2522
E-mail: sugimoto@sci.osaka-cu.ac.jp
[b] Institute for Molecular Science,
Myodaiji, Okazaki 444−8585, Japan
Supporting information for this article is available on the WWW under http://www.eurjic.org or from the author.

 DOI: 10.1002/ejic.200200638 © 2003 Wiley-VCH Verlag GmbH & Co. KGaA, Weinheim

ligands offers different reactivities from those of previously reported model complexes having anionic ligands. Therefore, the present study offers new molybdenum models and also new insights into the reactivity of molybdenum enzymes.

Results and Discussion

Synthesis of Complexes

[MoO(mnt)(Bu_2bpy)] (**1**) was prepared by reacting [MoO_2Cl_2(Bu_2bpy)] (**4**) with Na_2mnt in CH_3OH. The IR spectrum of complex **1** shows strong absorptions at 2195 and 939 cm^{-1} assignable to ν(CN) of mnt and ν(Mo=O). Its ESI-mass signals centered at m/z = 561 in the presence of small amount of K^+ are consistent with the characteristic isotopic pattern of {[M] + K}$^+$. [MoO(mnt)(Et_4en)] (**2**) was obtained from the in situ reaction of MoO_2Cl_2 with Et_4en, and Na_2mnt in CH_3OH. The structure was similarly confirmed: IR: $\tilde{\nu}$ = 2194 and 906 cm^{-1}, ESI-mass m/z = 465 [M + K]$^+$. Elemental analysis data indicated that each complex had one oxo, one dithiolene, and one ancillary ligand (Figure 1). With Mo^{VI}, Na_2mnt, and ligands (1:1:1) the two complexes were obtained in 36 and 38% yield, respectively, suggesting that molybdenum(IV) formation is based on the reduction of molybdenum(VI) by the dithiolate of mnt^{2-}. In fact, the two-electron oxidized form of mnt^{2-}, $[(mnt)_2]^{2-}$ {$[C_2(CN)_2SS-SSC_2(CN)_2]^{2-}$}, was isolated from the filtrate (Figure S1 in the Supporting Information; see also the footnote on the first page of this article). Thus, we changed the ratio Mo^{VI}:Na_2mnt:ligands to 1:2:1, and improved the yield of [**1**] (56%). However, that of [**2**] was not improved under similar conditions and only a blue−green solution that was identical with $[Mo(mnt)_3]^{2-}$ was obtained.

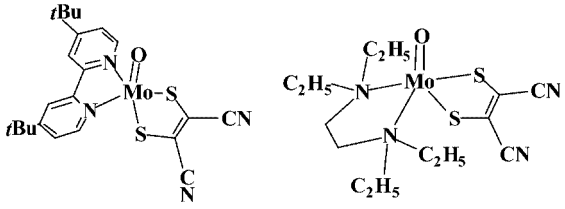

Figure 1. Structures of complexes **1** and **2**

Solution Structures of [MoO(Bu_2bpy)(mnt)] (1) and [MoO(Et_4en)(mnt)] (2): ^{1}H NMR Studies

Sharp ^{1}H NMR signals of [MoO(Bu_2bpy)(mnt)] (**1**) appeared in the region characteristic of diamagnetic molybdenum(IV)-d^2 complexes in CD_3CN: The signals for bipyridyl and butyl protons were observed at δ = 8.61, 8.44 and 7.68, and 1.42 ppm, respectively. Similarly, for [MoO(Et_4en)(mnt)] (**2**) the ^{1}H NMR spectrum supported a diamagnetic molybdenum(IV) complex structure, and showed temperature-dependent ^{1}H NMR behavior in CD_3CN (Figure 2).

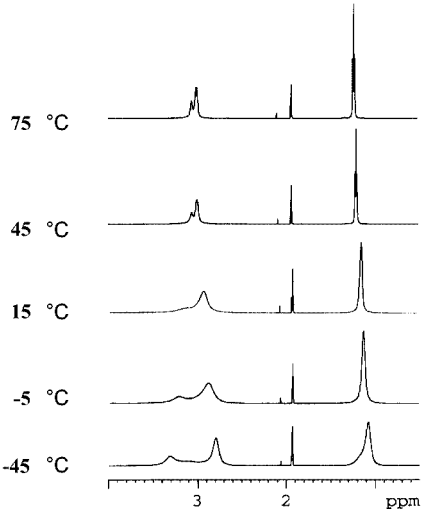

Figure 2. ^{1}H NMR spectra of [MoO(mnt)(Et_4en)] (**2**) in CD_3CN at various temperatures

At 75 °C, three signals appeared that were classified into two groups: Et and the C_2H_4 unit of ethylenediamine, based on their integration ratio. Methyl and methylene protons of the Et groups appeared at δ = 1.22 ppm (triplet) and δ = 3.00 ppm (broad doublet), while the C_2H_4 protons of ethylenediamine appeared as a broad singlet signal at δ = 3.05 ppm. These observations indicate that the four Et groups and two methylenes of C_2H_4 are equivalent within the ^{1}H NMR time scale. All the signals broadened as the temperature decreased from 75 to 15 °C. At lower temperatures, the broad signals for $CH_3-CH_2-$and for $-CH_2-CH_2-$ protons appeared at δ = 1.08, 2.79, and δ = 3.20 ppm, respectively, though the signals for methyl and ethylene protons were still observed as broad signals. Such temperature-dependent spectral changes could be as due to a conformational inversion between pseudo-gauche and -steric strain conformations of the chelating ethylenediamine unit (Scheme 1), since each chemical shift (ppm) also moved. Similar conformational inversion has been reported in dimolybdenum and ditungsten complexes with ethylenediamine, [$M_2(O)_2(\mu\text{-}O)_2(\mu\text{-}L)$] (M = Mo, W; L = edta (ethylenediaminetetraacetato), tpen (*N,N,N′,N′*-tetrakis(2-pyridylmethyl)ethylenediamine)).[8]

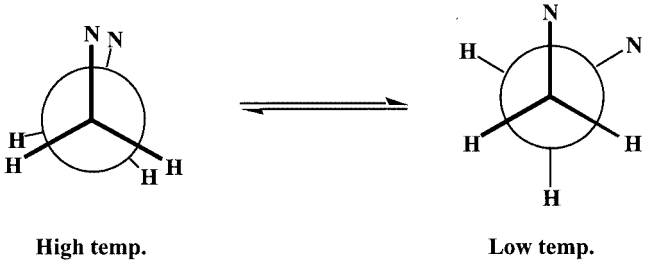

Scheme 1. Proposed conformational change of **2** in CD_3CN (molybdenum center; [MoO(mnt)], is omitted for clarity

 © 2003 Wiley-VCH Verlag GmbH & Co. KGaA, Weinheim

Reactivity of [MoO(Bu$_2$bpy)(mnt)] (1) and [MoO(Et$_4$en)(mnt)] (2)

Complex **1** shows interesting reactivity towards molecular oxygen in acetonitrile and acetone, giving the oxo-bridged dimolybdenum(V) complex $[Mo_2O_3(Bu_2bpy)_2(mnt)_2]$ (**3**), the structure of which was confirmed by X-ray crystallography (Figure 5). Although the molecular oxygen is not a substrate in native molybdenum enzymes, it is a good oxygen donor. The reaction showed a color change, from yellow to deep blue-gray (Figure 3, a). The peaks centered at 492 and 590 nm intensified and the final spectrum exhibited a similar shape to that of mono-oxo bridged $[Mo_2O_3(Bu_2bpy)_2(mnt)_2]$ (**3**) in CH_3CN, which was isolated independently as a crystalline powder. The ESI-MS spectrum recorded with the reaction solution is consistent with m/z = 1060 and the isotope pattern of dinuclear $[Mo_2O_3(Bu_2bpy)_2(mnt)_2]$ (**3**). Since comproportionation, $Mo^{IV} + Mo^{VI} \rightarrow 2\ Mo^{V}$, is common in molybdenum chemistry,[9] the air oxidation process of **1** leading to **3** can be noted as Equation (1), in which the di-oxo molybdenum(VI) complex is a transient species.

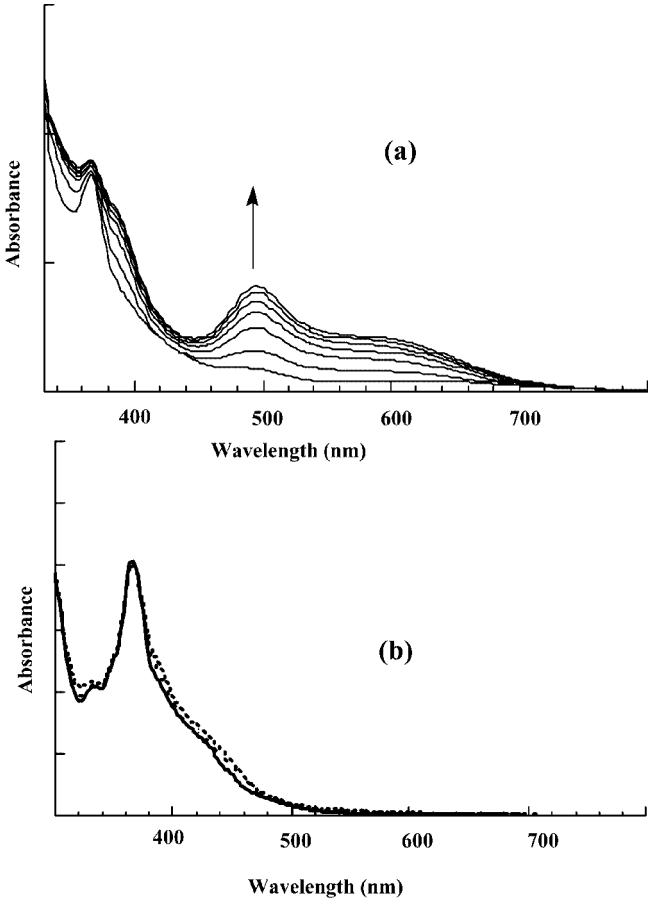

Figure 3. Spectral changes (every 5 h) of complexes **1** (a, 0.25 mM) and **2** (b, 0.25 mM) in acetonitrile (with exposure to air)

$$[MoO(Bubpy)(mnt)] + O_2 \rightarrow [MoO_2(Bubpy)(mnt)],$$
$$[MoO(Bubpy)(mnt)] + [MoO_2(Bubpy)(mnt)] \rightarrow [Mo_2O_3(Bu_2bpy)_2(mnt)_2] \quad (1)$$

In contrast, complex **2** did not react with molecular oxygen in CH_3CN (Figure 3, b). Although the redox potentials assigned to $Mo^{IV/V}$ for **1** and **2** were almost the same, 0.20 and 0.22 V vs. Ag/Ag^+, respectively, both complexes showed largely different reactivities toward molecular oxygen. The rigid molybdenum(IV)-porphyrin complex $[Mo^{IV}O(oep)]$ (oep = 2,3,7,8,12,13,17,18-octaethylporphyrinato) forms the dimerized $[\{Mo^{V}O(oep)\}_2(\mu\text{-}O)]$ via intermediate $[Mo^{VI}O(O_2)(oep)]$ upon treatment with O_2.[10] ^1H NMR studies indicate that complex **2** has a flexible ethylenediamine ligand, although complex **1** has a rigid bipyridyl ligand. Therefore, for the dimerization, an outer-sphere oxidation process is excluded but an inner-sphere oxidation process by O_2 may occur. Both the steric bulkiness of the four ethyl groups in **2**, and its dynamic behavior, prevent interaction of the molybdenum center in **2** with O_2 and so its reactivity differs from that of **1**. Xanthin oxidase, which has one dithiolane, prevents dimerization and retains a mononuclear molybdenum structure when exposed to molecular oxygen.[11] Thus, judging from the above described results, **2** rather than **1** may serve as an effective xanthine oxidase model. We have further demonstrated that the reactivity of the molybdenum-mono-dithiolene complexes, [MoO(mnt)], could be changed by varying the ancillary ligands.

Some of molybdenum(IV) mono-oxo bis(dithiolene) complexes react with trimethylamine N-oxide (Me_3NO) to give the corresponding molybdenum(VI) di-oxo complexes of $[MoO_2(dithiolene)_2]^{2-}$.[3f] When complexes **1** and **2** were treated with Me_3NO, electronic spectral changes were observed, but the corresponding molybdenum(VI) di-oxo complexes could not be isolated and their reaction could not be followed precisely (Figure 4).

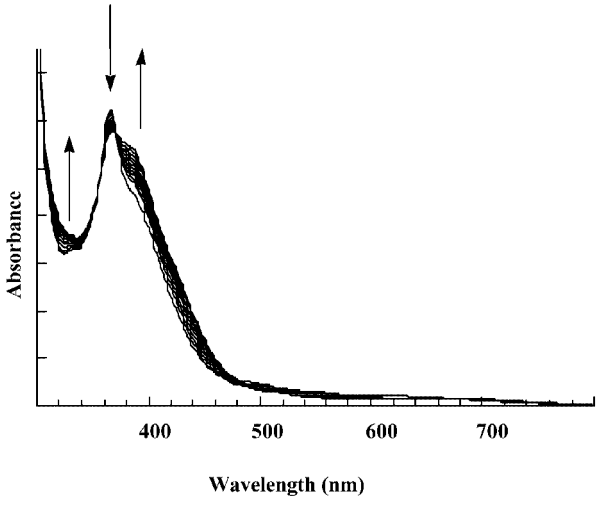

Figure 4. Spectral change (every 1 h) of the complex formed (0.25 mM) after addition of $(CH_3)_3NO$ (5.0 mM) in CH_3CN to **1**

 © 2003 Wiley-VCH Verlag GmbH & Co. KGaA, Weinheim

Crystal Structure of $[Mo_2O_3(Bu_2bpy)_2(mnt)_2]$

The molecular structure of complex **3** is shown in Figure 5 and the selected bond lengths [Å] and angles [°] are summarized in Table 1.

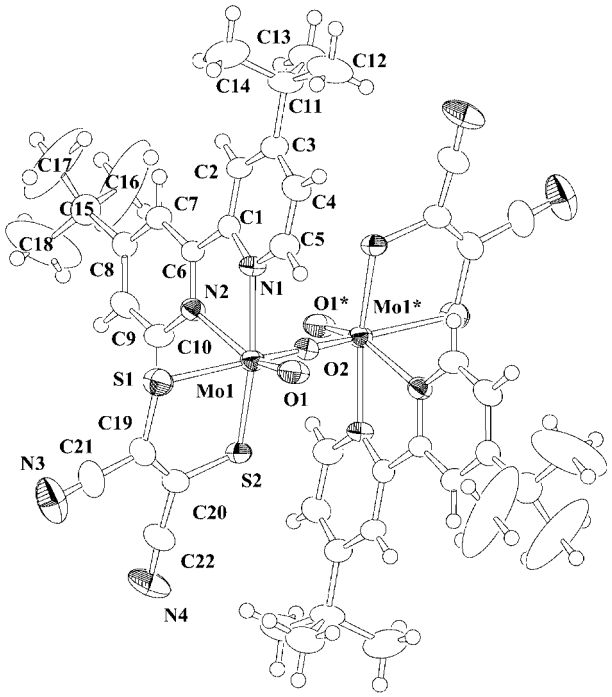

Figure 5. Molecular structure of complex $[Mo_2O_3(Bu_2bpy)_2(mnt)_2]$ (**3**) with the atomic numbering scheme showing 50% probability thermal ellipsoids

Table 1. Selected bond lengths [Å] and angles [°] for **3**·$2CH_3C(O)CH_3$

Mo1−S1	2.464(1)	Mo1−S2	2.394(1)
Mo1−O1	1.680(4)	Mo1−O2	1.8694(4)
Mo1−N1	2.238(4)	Mo1−N2	2.327(4)
S1−C19	1.738(6)	S2−C20	1.735(6)
C19−C20	1.359(8)		
S1−Mo1−S2	84.38(5)	S1−Mo1−O1	96.7(2)
S1−Mo1−O2	158.60(4)	S1−Mo1−N1	95.7(1)
S1−Mo1−N2	81.7(1)	S2−Mo1−O1	107.7(1)
S2−Mo1−O2	83.60(3)	S2−Mo1−N1	164.3(1)
S2−Mo1−N2	95.0(1)	O1−Mo1−O2	103.8(1)
O1−Mo1−N1	88.0(2)	O1−Mo1−N2	157.0(2)
O2−Mo1−N1	91.2(1)	O2−Mo1−N2	81.81(10)
N1−Mo1−N2	69.5(1)	Mo1−S1−C19	103.1(2)
Mo1−S2−C20	105.7(2)		

Complex **3** has a $[Mo_2O_3]$ neutral core, with each molybdenum center in a distorted octahedral geometry provided by two nitrogens of one Bu_2bpy, two sulfurs of one mnt, a terminal oxo group, and the bridging oxo group which occupies a crystallographic inversion center. Its $[Mo_2O_3]$ core is strictly *anti* planar, in which one molybdenum has an O2N2S2 donor set. The S1 atom is *trans* to the bridging oxygen O2; S2 is *trans* to N1; and N2 is *trans* to a terminal oxygen O1. Similar structures have been reported for $[Mo_2O_3(2\text{-}SC_5H_3N)_4]$,[12] $[Mo_2O_3(2\text{-}SC_5H_3N\text{-}3\text{-}SiNe_3)_4]$ (2-$SC_5H_3N_4$ = pyridine-2-thiolato),[13] $[Mo_2O_3(N,N'$-dimethyl-N,N'-bis(2-mercaptophenyl)ethylenediamine$)_2]$,[14] and $[Mo_2O_3(N,N'$-dimethyl-N,N'-bis(2-mercaptoethyl)ethylenediamine$)_2]$.[15] In these complexes, all nitrogen donors occupied *trans* positions to the oxygen donors, while the sulfur donors were *cis* to each other. In complex **3**, a somewhat longer Mo1−N2 bond length [2.327(4) Å] than that of Mo1−N1 [2.238(4) Å] was observed due to the *trans* influence of a strong Mo-dπ and terminal O−pπ interaction. A similar trend is found for Mo−S1 [2.464(1) Å] and Mo-S2 [2.394(1) Å] bond lengths. The $Mo-O_{terminal}$ [1.680(4) Å] and $Mo-O_{bridging}$ [1.8694(4) Å] distances are in the range found in the above example $[Mo_2O_3]$ complexes. Although some dinuclear molybdenum(v) complexes with one dithiolene per molybdenum center have been reported by Holm et al., their dimers have a di-oxo bridged Mo_2O_4 core of $[Mo_2O_2(\mu\text{-}O)_2(bdt)_2]^{2-}$.[7] Moreover, mono-dithiolene molybdenum(VI) $(Et_4N)_2\{Mo^{VI}O_2(Ph_3Si\text{-}bdt)\}_2(\mu\text{-}O)]$, having a dinuclear core bridged by one oxo group, has also been reported.[16] Since complex **3** has a mono-oxo bridged dimolybdenum(V) core, it is a new kind of mono-dithiolene dimolybdenum complex.

Experimental Section

Materials: The ligands Bu_2bpy and Na_2mnt were prepared as described in the literature.[17,18] Acetonitrile was dried with calcium hydride and distilled under dinitrogen. Methanol was dried over molecular sieves and also distilled under dinitrogen. THF was distilled from sodium/benzophenone. Tetrabutylammonium hexafluorophosphate ($TBAPF_6$) was recrystallized twice from hot ethanol. All other commercially available reagents were used as purchased. The preparation of complexes **1**−**3** was carried out under dinitrogen or argon.

Preparation of Complexes

[MoO(mnt)(Bu_2bpy)] (1): Na_2mnt (47 mg, 0.26 mmol) was added to a methanolic solution (10 mL) of $[MoO_2Cl_2(Bu_2bpy)]$ (**4**, see below) (60 mg, 0.13 mmol) and the solution was stirred for 1 day. After concentration of the solution to 3 mL, a yellow−brown microcrystalline powder, deposited upon addition of H_2O (1 mL), was collected by filtration and dried in vacuo. Yield 38 mg (56%). $C_{22}H_{24}MoN_4OS_2$ (520.53): calcd. C 50.76, H 4.65, N 10.76; found C 51.05, H 4.73, N 10.58. ESI-MS (acetonitrile): m/z = 561 $[M + K]^+$. IR (KBr): $\tilde{\nu}$ = 2195 [ν(C−N)], 939 cm^{-1} [ν(Mo=O)]. UV/Vis (acetonitrile): λ (ε, mol dm^3 cm^{-1}) = 607 (110), 492 (261), 369 (4090), 335 nm (2466). ^1H NMR ([D_3]acetonitrile, 25 °C): δ = 8.61 (d, 2 H), 8.44 (s, 2 H), 7.68 (d, 2 H), and 1.42 (s, 18 H) ppm. Redox potential (acetonitrile): $Mo^{V/IV}$, 0.20 V (reversible) vs. Ag/Ag^+.

[MoO(mnt)(Et_4en)] (2): MoO_2Cl_2 (99 mg, 0.5 mmol) was added to CH_3OH (10 mL) and then N,N'-tetraethylethylenediamine (102 μL, 0.5 mmol) was injected. After 15 min stirring, Na_2mnt (93 mg, 0.5 mmol) was gradually added to the solution. A yellow−orange microcrystalline powder then precipitated from the resulting red−brown solution, and was collected by filtration and dried in vacuo. Yield 81 mg (38%). $C_{14}H_{24}MoN_4OS_2$ (424.04): calcd. C 39.62, H 5.70, N 13.20; found C 39.91, H 5.56, N 12.98. ESI-MS (acetonitrile): m/z = 465 $[M + K]^+$. IR (KBr): $\tilde{\nu}$ = 2194 [ν(C−N)], 906 cm^{-1} [ν(Mo=O)]. UV/Vis (acetonitrile): λ (ε, mol dm^3 cm^{-1}) = 512 (512), 365 (7771), 331 nm (4167). ^1H NMR ([D_3]ace-

 © 2003 Wiley-VCH Verlag GmbH & Co. KGaA, Weinheim

tonitrile, 25 °C.): δ = 3.05 (br., 4 H), 3.00 (d, 8 H), and 1.22 (t, 12 H) ppm. Redox potential (acetonitrile): $Mo^{V/IV}$, 0.20 V (reversible) vs. Ag/Ag^+.

$[Mo_2O_3(mnt)_2(Bu_2bpy)_2]$ (3). Method a: Na_2mnt (93 mg, 0.5 mmol) was added to a colorless acetone solution (10 mL) containing MoO_2Cl_2 (99 mg, 0.5 mmol) and Bu_2bpy (134 mg, 0.5 mmol). The resulting orange suspension was then stirred until a clear orange solution was obtained, which on exposure to air for 1 day gave black crystals of **3**. The crystals were collected by filtration and dried in air. Yield 115 mg (44%, based on two molybdenums).

Method b: Complex **1** (30 mg, 0.058 mmol) was dissolved in CH_3CN (10 mL) under argon to give a solution that upon exposure to air changed from yellow to blue-gray. Overnight, black−purple crystals then precipitated out of the solution, and were collected by filtration and dried in air. Yield 24 mg (78%). Precipitates obtained by methods a and b have the same IR and UV/Vis spectra.

$C_{44}H_{48}Mo_2N_8O_3S_4$ (1057.04): calcd. C 49.99, H 4.58, N 10.60; found C 50.21, H 4.54, N 10.55. ESI-MS (dimethylformamide): m/z = 1060 $[M]^-$. IR (KBr): $\tilde{\nu}$ = 2205 [ν(C−N)], 947 cm^{-1} [ν(Mo=O)]. Redox potential (dimethylformamide): $Mo^VMo^V/Mo^{IV}Mo^V$, −0.93 V (reversible) and −1.64 V (E_{pc}, irreversible) vs. Ag/Ag^+. UV/Vis (acetonitrile): λ (ε, mol dm^3 cm^{-1}) = 604 (sh) (663), 498 (1390), 342 nm (1060).

$[MoO_2Cl_2(Bu_2bpy)]$ (4): Bu_2bpy (134 mg, 0.5 mmol) was added to a freshly distilled THF solution (10 mL) containing MoO_2Cl_2 (99 mg, 0.5 mmol). The resulting colorless solution was evaporated to 2 mL to give a white microcrystalline powder, which was collected by filtration and dried in air. Yield 203 mg (87%). IR (KBr): $\tilde{\nu}$ = 939, 908 cm^{-1} [ν(Mo=O)]. ^1H NMR ([D_3]acetonitrile, 25 °C): δ = 9.46 (d, 2 H), 9.00 (s, 2 H), 8.07 (d, 2 H), 1.50 (s, 18 H) ppm.

X-ray Crystallographic Study: A single crystal of $[Mo_2O_3(Bu_2bpy)_2(mnt)_2]$ (**3**) was obtained upon standing for one day from the acetone solution, and a single crystal of $[MoO_2Cl_2(Bu_2bpy)]$ (**4**) was obtained by recrystallization from acetone solution. Each crystal was attached to the top of a glass fiber. X-ray data of complex **3** and **4** were then collected with graphitec-monochromated Mo-*Kα* radiation on a Rigaku/MSC Mercury CCD diffractometer at −100 °C and on a Rigaku AFC7R diffractometer at −50 °C, respectively. The structures were solved by direct methods (SIR, 92)[19] and expanded using Fourier techniques.[20] The non-hydrogen atoms of all complexes were refined anisotropically by the full-matrix least-squares method. All calculations were performed using TEXSAN.[21] Further crystallographic data are summarized in Table 2.

Complex **4** (see Supporting Information, Figure S2 and Table S1) has a distorted octahedral arrangement about the molybdenum atom, with two oxygen atoms in *cis* positions and the two chlorine atoms in *trans* positions. The bond lengths and angles around the molybdenum center are very similar to those of $[MoO_2Cl_2(4,4'$-dimethyl-2,2′-bipyridine)][22] and $[Mo_2O_2Cl_2(1,10$-phenanthroline)];[23] the structural arrangements are also the same in these complexes and **4**. It is noteworthy that **4** crystallized in a chiral space group $P2_12_12_1$, indicating that spontaneous resolution of complex occurred. Conversely, $[MoO_2Cl_2(4,4'$-dimethyl-2,2′-bipyridine)] crystallized in an achiral space group $P2_1/n$.

CCDC-198986 and -198987 contain the supplementary crystallographic data for this paper. These data can be obtained free of charge at www.ccdc.cam.ac.uk/conts/retrieving.html [or from the Cambridge Crystallographic Data Centre, 12 Union Road, Cambridge CB2 1EZ, UK; Fax: (internat.) +44-1223/336-033; E-mail: deposit@ccdc.cam.ac.uk].

Table 2. Crystallographic data for $[Mo_2O_3(Bu_2bpy)_2(mnt)_2]\cdot 2CH_3C(O)CH_3$ [**3**·$2CH_3C(O)CH_3$] and $[MoO_2Cl_2(Bu_2bpy)]$ (**4**)

	3·$2CH_3C(O)CH_3$	**4**
Empirical formula	$C_{50}H_{60}Mo_2N_8O_5S_4$	$C_{18}H_{24}Cl_2MoN_2O_2$
Formula mass	1173.19	467.25
T [°C]	−100	−50.0
a [Å]	11.331(1)	13.451(4)
b [Å]	21.412(2)	18.221(6)
c [Å]	11.636(1)	8.405(3)
β [°]	91.392(6)	
V [Å^3]	2822.4(5)	2060(1)
Z	2	4
Space group	$P2_1/a$ (no. 14)	$P2_12_12_1$ (no. 19)
$d_{calcd.}$ [g/cm^3]	1.380	1.506
Crystal size [mm]	0.20 × 0.20 × 0.20	0.33 × 0.26 × 0.26
μ(Mo-$K\alpha$) [cm^{-1}]	6.41	9.08
No. of unique reflns.	6635	2639
No. obsd. reflns.	5800, all	1905, $I > 2.0\sigma(I_o)$
R (%)	8.3[a]	4.1[b]
Rw (%)	22.2[c]	5.1[d]

[a] $R = \Sigma(F_o^2 - F_c^2)/\Sigma F_o^2$. [b] $R = \Sigma||F_o| - |F_c||/\Sigma|F_o|$. [c] $Rw = [(\Sigma w(F_o^2 - F_c^2)^2/\Sigma w(F_o^2)^2]]^{1/2}$. [d] $Rw = [(\Sigma w(F_o - F_c)^2/\Sigma w(Fo^2)^2]]^{1/2}$.

Other Measurements: Cyclic voltammetry was performed with a Hokuto HA-501 potentiostat and a Hokuto HB-105 function generator, equipped with a Graphtec WX2400 X-Y recorder, or a Hokuto HZ-3000. The working and counter electrodes were a glassy-carbon disk and a platinum wire, respectively. Cyclic voltammograms were recorded at 50 mV·s^{-1}. The sample solutions (ca. 1.0 mM) in 0.1 M $TBAPF_6$/acetonitrile were deoxygenated with a stream of dinitrogen gas. The reference electrode was Ag/Ag^+ and the half-wave potential of Fc^+/Fc [$E_{1/2}(Fc^{+/o})$] vs. Ag/Ag^+ was 0.015 V in CH_3CN. Electronic spectra were recorded with a Shimazu 2550 or HP 5254A spectrophotometer at 20 °C. IR spectra were recorded with a Perkin−Elmer Spectrum GX infrared spectrophotometer. ^1H NMR spectra were measured with a JEOL-Lambda 300 (300 MHz) or Bruker AVANCE 600 (600 MHz) spectrometer. ESI-MS was obtained with a PE SCIEX API300.

Supporting Information Available (see the footnote on the first page of this article): ORTEP drawings $(mnt)_2^{2-}$, the oxidized form of mnt^{2-}, (Figure S1) and complex **4** (Figure S2). Selected bond lengths and angles of complex **4** (Table S1).

Acknowledgments

This work was partly supported by the Joint Studies Program (2001−2002) of the Institute for Molecular Science, Japan and by CREST of the Japan Science and Technology Corporation.

[1] [1a] R. Hille, *Chem. Rev.* **1996**, *96*, 2757. [1b] W. R. Hagen, A. F. Arendsen, *Struct. Bonding* **1998**, *90*, 161.
[2] A. Messerschmidt, R. Huber, T. Poulos, K. Wieghardt, "*Handbook of Metalloproteins*", John Wiley & Sons, New York, **2000**, *2*, 1024.
[3] [3a] B. S. Lim, R. H. Holm, *J. Am. Chem. Soc.* **2001**, *123*, 1920. [3b] B. S. Lim, J. P. Donahue, *Inorg. Chem.* **2000**, *39*, 263. [3c] J. P. Donahue, C. R. Goldsmith, U. Nadiminti, R. H. Holm, *J. Am. Chem. Soc.* **1998**, *120*, 12869. [3d] H. Oku, N. Ueyama, A.

 © 2003 Wiley-VCH Verlag GmbH & Co. KGaA, Weinheim

Nakamura, *Inorg. Chem.* **1997**, *36*, 1504. [3e] N. Ueyama, H. Oku, M. Kondo, T. Okamura, N. Yoshinaga, A. Nakamura, *Inorg. Chem.* **1996**, *35*, 643. [3f] H. Oku, N. Ueyama, M. Kondo, A. Nakamura, *Inorg. Chem.* **1994**, *33*, 209.
[4] [4a] E. S. Davies, R. L. Beddoes, D. Collison, A. Dinsmore, A. Docrat, J. A. Joule, C. R. Wilson, C. D. Garner, *J. Chem. Soc., Dalton Trans.* **1997**, 3985. [4b] S. K. Das, P. K. Chaudhury, D. Biswas, S. Sarkar, *J. Am. Chem. Soc.* **1994**, *116*, 9061. [4c] D. Coucouvanis, A. Hadjikyriacou, A. Toupadakis, S-M. Koo, O. Ileperuma, M. Draganjac, A. Salifoglou, *Inorg. Chem.* **1991**, *30*, 754. [4d] K. Nagarajan, P. K. Chaudhury, B. R. Srinivasan, S. Sarkar, *Chem. Commun.* **2001**, 1786.
[5] K. M. Nicholas, M. A. Khan, *Inorg. Chem.* **1987**, *26*, 1633.
[6] I. K. Dhawan, J. H. Enemark, *Inorg. Chem.* **1996**, *35*, 4873.
[7] B. S. Lim, M. W. Willer, M. Miao, R. H. Holm, *J. Am. Chem. Soc.* **2001**, *123*, 8343.
[8] R. Hazama, K. Umakoshi, A. Ichimura, S. Ikari, Y. Sasaki, T. Ito, *Bull. Chem. Soc., Jpn.* **1995**, *68*, 456.
[9] R. H. Holm, *Coord. Chem. Rev.* **1990**, *101*, 183.
[10] J. W. Bucher, "*The Porphyrins*", (Ed.: D. Dolphin), Academic, New York, **1978**, *1*, 389.
[11] C. Enroth, B. T. Eger, K. Okamoto, T. Nishino, T. Nishino, E. F. Pai, *Proc. Natl. Acad. Sci.* **2000**, *20*, 10723.
[12] F. A. Cotton, P. E. Fanwick, J. W. Fitch, *Inorg. Chem.* **1978**, *17*, 3254.
[13] E. Block, M. Gernon, H. Kang, G. Ofori-Okai, J. Zubieta, *Inorg. Chem.* **1991**, *30*, 1736.
[14] K. R. Barnard, M. Bruck, S. Huber, C. Grittini, J. H. Enemark, R. W. Gable, A. G. Wedd, *Inorg. Chem.* **1997**, *36*, 637.
[15] P. L. Dahlstrom, J. R. Hyder, P. A. Vella, J. Zubieta, *Inorg. Chem.* **1982**, *21*, 927.
[16] H. Oku, N. Ueyama, A. Nakamura, *Bull. Chem. Soc., Jpn.* **1999**, *72*, 2261.
[17] T. B. Hadda, H. L. Bozec, *Inorg. Chim. Acta* **1993**, *204*, 103.
[18] A. Davison, R. H. Holm, *Inorg. Synth.* **1967**, *10*, 8.
[19] A. Altomare, M. C. Burla, M. Camalli, C. Giacovazzo, A. Guagliardi, G. Polidori, *J. Appl. Crystallogr.* **1994**, *27*, 435.
[20] P. T. Beurskens, G. Admiraal, G. Beurskens, W. P. Bosmanm, S. Garcia-Granda, R. O. Gould, J. M. M. Smits, C. Smykalla, The DIRDIF Program System. Technical Report: Crystallography Laboratory, University of Nijmegen, The Netherlands, **1994**.
[21] TEXSAN. Single Crystal Structure Analysis Pakage. Molecular Structure Corporation: The Woodlands, TX 77382, **1992**, USA.
[22] D. M. Baird, F. L. Yang, D. J. Kavanaugh, G. Finness, K. R. Dunber, *Polyhedron* **1996**, *15*, 2597.
[23] P. B. Viossat, N. Rodier, *Acta Crystallogr., Sect. B* **1979**, *35*, 2715.

Received November 22, 2002

 © 2003 Wiley-VCH Verlag GmbH & Co. KGaA, Weinheim

New 1,3,4-Oxadiazolecopper(II) Derivatives Obtained from Thiosemicarbazone Complexes

Patricia Gómez-Saiz,[a] Javier García-Tojal,*[a] Miguel A. Maestro,[b] José Mahía,[b] Francisco J. Arnaiz,[a] Luis Lezama,[c] and Teófilo Rojo[c]

Keywords: Copper / Magnetic properties / Thiosemicarbazone complexes / Oxadiazole complexes / X-ray diffraction

Pyridine-2-carbaldehyde thiosemicarbazone and pyridine-2-carbaldehyde 4*N*-methyl thiosemicarbazone ligands (HL_I and HL_Imm respectively) undergo an oxidative cyclization when treated with bromate or iodate, leading to 2-amino-5-pyridin-2-yl-1,3,4-oxadiazole and 2-methylamino-5-pyridin-2-yl-1,3,4-oxadiazole (HL_{II} and HL_{II}mm). This reaction occurs either with free ligands or when coordinated to copper(II). Some of the starting ($[\{Cu(L_I mm)(NO_3)\}_2]$ (**3**), intermediate $Cu(L_I)(IO_3)\cdot(H_2O)$ (**1**), $[\{Cu(L_I)I\}_2]$ (**2**), $[\{Cu(L_I mm)Br\}_2]$ (**4**), and final compounds $[\{Cu(HL_{II})(H_2O)_3\}_2](SO_4)_2$ (**5**), $[\{Cu(HL_{II}mm)(H_2O)_2(SO_4)\}_2]\cdot 2H_2O$ (**6**), (HL_{II}) (**7**), $[HL_{II}mm]\cdot 3H_2O$ (**8**) have been isolated and characterized by elemental analyses, IR, UV-visible, NMR, and EPR spectroscopy. The structures of **2**, **3**, **4**, **5**, **6**, and **8**, solved by X-ray diffraction methods, contain dinuclear entities with either square-pyramidal (**2**, **3**, **4**) or octahedral (**5**, **6**) copper(II) ions. Structural and spectroscopic results suggest that ligand-to-metal charge transfer occurs in these compounds. The EPR spectra at 120 K exhibit rhombic (**1**, **3**, **4**), isotropic (**2**), and axial (**5**, **6**) signals. Magnetic measurements show antiferromagnetic couplings for **2**, **4**, **5**, and **6**. The susceptibility data were fitted by the Bleaney–Bowers equation for copper(II) dimers. The obtained J/k values are –20.20, –8.85, –2.75, and –2.78 K for **2**, **4**, **5**, and **6**, respectively. However, ferromagnetic intradimeric interactions are present in **3** (J/k = +9.90 K) together with antiferromagnetic interdimer coupling ($z'J'/k$ = –1.70 K). Magneto-structural studies show the influence of the non-thiosemicarbazone coligand in the magnetic behaviour of these complexes.

(© Wiley-VCH Verlag GmbH & Co. KGaA, 69451 Weinheim, Germany, 2003)

Introduction

Several copper(II) complexes of N-heterocyclic carbaldehyde thiosemicarbazones are of interest because they show a greater carcinostatic activity than the free thiosemicarbazone.[1–3] However, despite several proposals, the mechanism of their action in cells[4–13] is unclear. A deeper knowledge of their reactivity is essential to understand their interactions with biological molecules.

Among the reactions involving thiosemicarbazones, some published mechanisms of the oxidative cyclization give rise to thiadiazoles, thiadiazolines, pyrazolones, 1,2,4-triazoline-5-thiones, and other compounds.[14–16] Recently, we reported the oxidation of pyridine-2-carbaldehyde 4*N*-methyl-thiosemicarbazonatocopper(II) entities that led to the attainment of a copper(II) complex with the 2-methylamino-5-pyridin-2-yl-1,3,4-oxadiazole ligand, using potassium bromate as oxidant (see Scheme 1).[17] The singularity of this reaction lies not only in the fact that 1,3,4-oxadiazoles are obtained from a non−acylated substrate for the first time, but in the novel process of desulfurization of thiosemicarbazones that implies this oxidative cyclization. The usual methods of preparing oxadiazoles consist of the cyclization of substrates such as acyl thiosemicarbazides[18] or acyl thioureas[19,20] with a variety of oxidants.

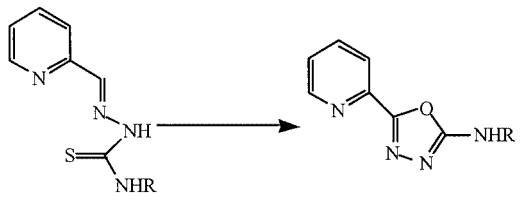

Scheme 1

We present here the synthesis and spectroscopic studies of 8 new compounds, $[Cu(L_I)(IO_3)]\cdot(H_2O)$ (**1**), $[\{Cu(L_I)I\}_2]$ (**2**), $[\{Cu(L_I mm)(NO_3)\}_2]$ (**3**), $[\{Cu(L_I mm)Br\}_2]$ (**4**), $[\{Cu(HL_{II})(H_2O)_3\}_2](SO_4)_2$ (**5**), $[\{Cu(HL_{II}mm)(H_2O)_2$-

[a] Departamento de Química, Universidad de Burgos,
Plaza Misael Bañuelos s/n, 09001 Burgos, Spain
Fax: (internat.) +34-47-258831
E-mail: qipgatoj@ubu.es
[b] Servicios Generales de Apoyo a la Investigación, Universidade da Coruña,
Edificio Anexo a Facultade de Ciencias, Campus da Zapateira s/n, 15071 A Coruña, Spain
[c] Departamento de Química Inorgánica, Universidad del País Vasco,
Aptdo. 644, 48080 Bilbao, Spain
Supporting information for this article is available on the WWW under http://www.eurjic.org or from the author.

$(SO_4)\}_2]\cdot 2H_2O$ (**6**), (HL_{II}) (**7**), and (HL_{II}mm)$\cdot 3H_2O$ (**8**) (HL_I = pyridine-2-carbaldehyde thiosemicarbazone, HL_Imm = pyridine-2-carbaldehyde 4*N*-methylthiosemicarbazone, HL_{II} = 2-amino-5-pyridin-2-yl-1,3,4-oxadiazole and HL_{II}mm = 2-methylamino-5-pyridin-2-yl-1,3,4-oxadiazole), together with the structural characterization of six of them and the magnetic properties of **2**, **3**, **4**, **5**, and **6**. These compounds are reactants, products or intermediates in the oxidative cyclization process. A mechanism is proposed for the reaction.

Results and Discussion

The Oxidation Process

The reactions involved in the oxidative attack of bromate on HL_Imm derivatives are summarized in Scheme 2.

The oxidative cyclization proceeds smoothly with the addition of bromate to a dark green aqueous solution of complex **3** adjusted to pH ≈ 6. After filtering off compound **4** the colour of the solution gradually becomes lighter. At the same time, the pH decreases to 3−4 and an irritant gas evolves from the reaction mixture, and single crystals of **6** are obtained after two days. The reaction is faster when small amounts of acid are added with slight heating. Excess acid and too much heat have led to brown solutions from which crystals of bis(pyridinecarboxylate)copper(II) were isolated.[17] Ligand **8** can be removed from **6** by the addition of $K_4[Fe(CN)_6]\cdot 3H_2O$ in ethanol. Furthermore, it can also be synthesized by direct oxidative cyclization of HL_Imm.

The oxidation of HL_I was developed in exactly the same way as for HL_Imm, and analogous compounds were identified. This procedure was also applied to a new ligand, HL_Idm (pyridine-2-carbaldehyde 4*N*,4′*N*-dimethylthiosemicarbazone), prepared following a published method.[21] However, no oxidation compounds could be isolated with either the thiosemicarbazone free ligand or the respective copper(II) complex as starting material, suggesting that steric effects can influence the oxidative cyclization.

The cyclization of the free ligands takes place either with bromate or iodate, requires pH ≈ 0−1 and yields similar results. For copper(II) complexes, oxidation with bromate occurs even at pH≈6, but no evidence of oxidative cyclization of thiosemicarbazone−copper(II) compounds was detected using iodate at pH≈6. This seems to accord with the reduction potentials: $E°$ (BrO_3^-/Br^-) = 1.15 V, $E°$ (IO_3^-/I^-) = 1.09 V. The reaction of a thiosemicarbazonatocopper(II) complex with bromate yields different products from those obtained with iodate. In fact, bromato thiosemicarbazonecopper(II) derivatives cannot be isolated. The use of acidic media gives rise to mixtures of compounds in both cases. Several attempts using chlorate as oxidant did not produce evidence of oxidative cyclization. This is surprising given its reduction potential [$E°$ (ClO_3^-/Cl^-) = 1.45 V at pH ≈ 0]; kinetic factors could account for this result.

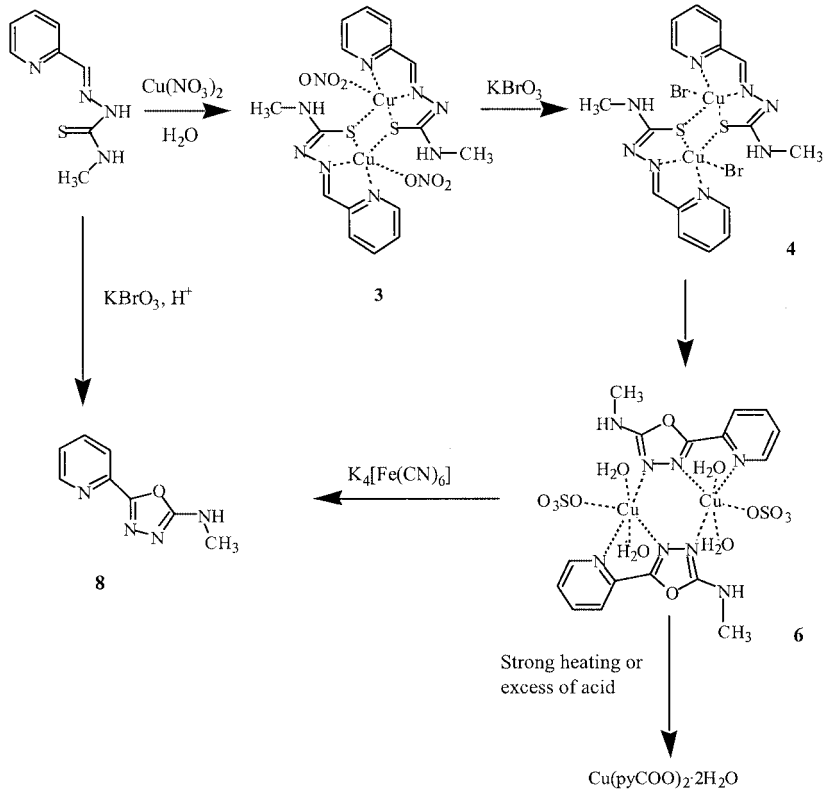

Scheme 2

 © 2003 Wiley-VCH Verlag GmbH & Co. KGaA, Weinheim

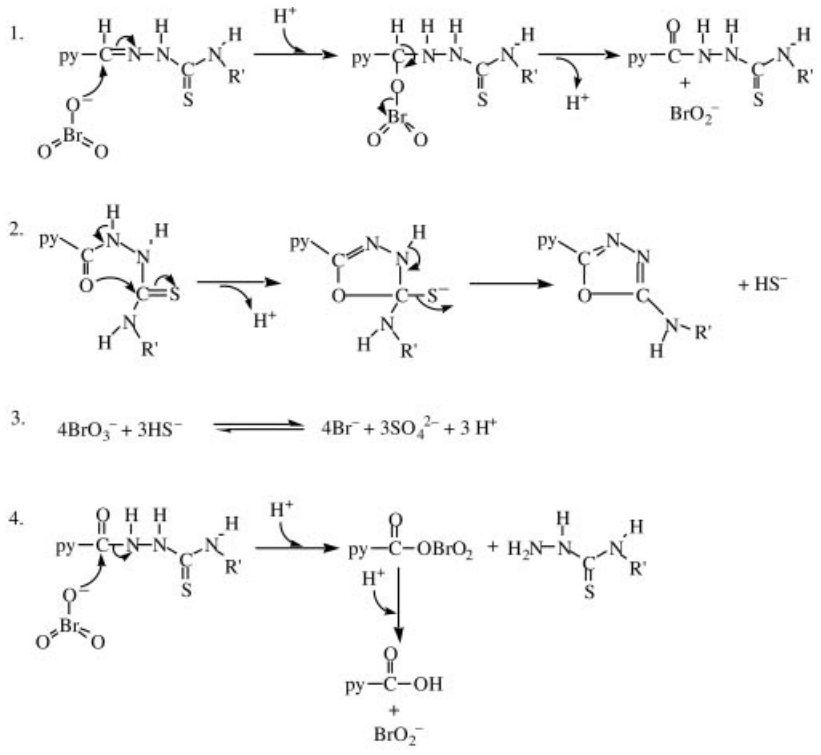

Scheme 3

From the experimental results we propose the two-step mechanism shown in Scheme 3 for the free ligand, and an analogous mechanism is proposed for the copper(II) complexes:

i) Formation of the Acylthiosemicarbazide

An initial nucleophilic attack of the bromate anion on the azomethinic carbon of the thiosemicarbazone ligand yields a new carbonyl group and bromite is released. The bromite can act as an oxidizing agent on other thiosemicarbazone ligands, giving rise to hypobromite ions. The successively reduced bromo derivatives from each oxidation step thus act as oxidants until the complete conversion of bromate into bromide.

Consequently, an acidic media should favor the beginning of the reaction, which is in good agreement with our experimental observations.

ii) Cyclization to 2-Amino-5-pyridin-2-yl-1,3,4-oxadiazole

In a second step, the acylthiosemicarbazide cyclizes to 2-amino-5-pyridin-2-yl-1,3,4-oxadiazole and, as a result, is desulfurized. This reorganization leads to a decrease in pH (in good agreement with experimental observations). The removal of the sulfur atom from the ligand, to give sulfate, could be due to concomitant inorganic processes such as those represented in reaction 3. Furthermore, the coupled reaction 3 shifts, to the right, reaction 2.

Further bromate attack on the acylic carbon would cleave the acylthiosemicarbazide, in competition with step ii). As a result, pyridine-2-carboxylic acid and other secondary products would be obtained (Scheme 3, reaction 4), which is in good agreement with the experimental results.

Since most published oxidation reactions leading to oxadiazoles take acylated compounds as reactants,[18−20] it seems highly probable that this intermediate is formed in a first step. Oxidative attacks similar to reaction 1 have been reported for the conversion of carbodiimide into urea using dimethyl sulfoxide as oxidant.[22,23] Furthermore, bromate derivatives oxidize primary alcohols to esters,[24] synthesize benzoxiodol-3-one starting from 2-iodobenzoic acid[25] and oxidize a keto group in the preparation of benzilic acid from benzoin.[26]

Conversely, cyclizations of open-chain compounds such as thioureas, thiosemicarbazides, semicarbazones or even thiosemicarbazones have been employed[19,27,28] to prepare ring-type molecules. These processes are an alternative to conventional organic synthesis, usually proceeding quickly and in only one step. The method we present here, starting from easily prepared thiosemicarbazonecopper(II) complexes, allows the preparation of 2-amino-1,3,4-oxadiazoles as the only product and requires, in some cases, less than an hour.

Structural Analysis

Crystal Structures of the Thiosemicarbazone Derivatives

The molecular structure of compound **2** is shown in Figure 1. Selected distances and angles are given in Table 1. The crystal contains $[Cu(L_I)I]$ entities, which stack through the sulfur atom of the thiosemicarbazone ligand to give the

 © 2003 Wiley-VCH Verlag GmbH & Co. KGaA, Weinheim

centrosymmetric [{Cu(L_I)I}$_2$] dimer. Each copper(II) ion has a distorted square-pyramidal topology ($\tau = 0.17$)[29] and is surrounded by one sulfur and two nitrogen atoms of one thiosemicarbazone ligand and the iodo ligand in the basal plane. The axial position is occupied by the sulfur atom of the symmetric [Cu(L_I)I] entity inside the dimer.

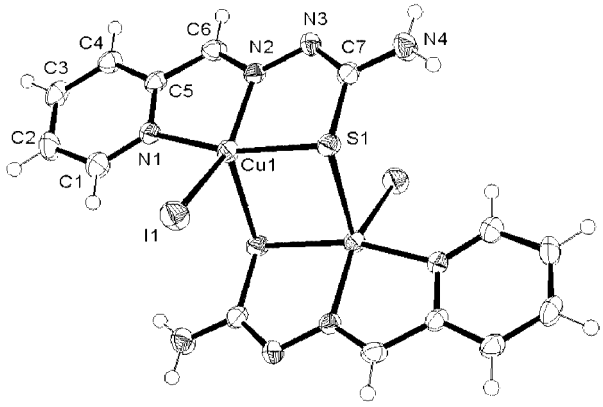

Figure 1. Molecular structure of **2** with thermal ellipsoids at 50% probability level

Table 1. Selected bond lengths [Å] and angles [°] for **2** and **4**

	2	**4**
Cu−N(1)	2.033(4)	2.034(4)
Cu−N(2)	1.997(4)	1.980(5)
Cu−S	2.271(1)	2.269(2)
Cu−X	2.6009(7)	2.3710(9)
Cu−S^i	2.775(1)	2.833(2)
Cu···Cu^i [a]	3.455(1)	3.577(2)
Cu···Cu^{ii}	5.319(1)	4.932(2)
N(3)−C(7)	1.335(6)	1.331(7)
C(7)−S	1.749(5)	1.739(6)
S−Cu−N(1)	163.4(1)	163.8(2)
X−Cu−N(2)	152.9(1)	162.7(1)
Cu−S−Cu^i	85.80(4)	88.3(1)
S−Cu−S^i	94.20(4)	91.7(1)

[a] Symmetry transformations used to generate equivalent atoms: **2**: i = $-x+1, -y+1, -z+1$; ii = $-x+1, -y+2, -z+1$; **4**: i = $-x+1, -y+1, -z+2$; ii = $-x+1, -y, -z+2$.

The molecular structure of complex **3** has been described elsewhere[17] (see Figure 2).

Compound **4** consists of [Cu($L_I$mm)Br] entities linked through the sulfur atom of the thiosemicarbazone ligand, leading to dinuclear centrosymmetric [{Cu($L_I$mm)Br}$_2$] species. A perspective view of the dimer is shown in Figure 3, and selected bond lengths and angles are given in Table 1. Each copper(II) ion is 5-coordinate, with two nitrogens and the sulfur atom of the ligand and the bromo ligand at the basal positions, while the axial position is occupied by the sulfur atom of the symmetric thiosemicarbazonatocopper(II) entity. The calculated τ factor[29] is 0.02, which indicates that the copper(II) ions have close to the square-pyramidal topology.

Both thiosemicarbazones (HL_I and HL_Imm) can be considered as rigid and quasi-planar in these compounds. Considering the basal plane as that defined by the N(1)N(2)S donor set, the Cu and S^i atoms lie at 0.012 and 2.689 Å above it for **2**, 0.090 and 2.832 Å in complex **3**, and at 0.051 and 2.870 Å in complex **4**. The coligands [I, O(1), and Br for **2**, **3**, and **4** respectively] sit 1.158, 0.162, and 0.598 Å below the mentioned plane.

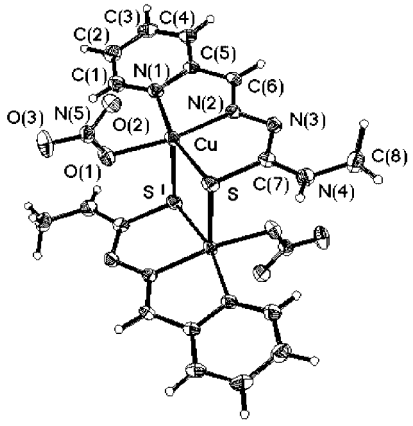

Figure 2. Molecular structure of **3** with thermal ellipsoids at 50% probability level

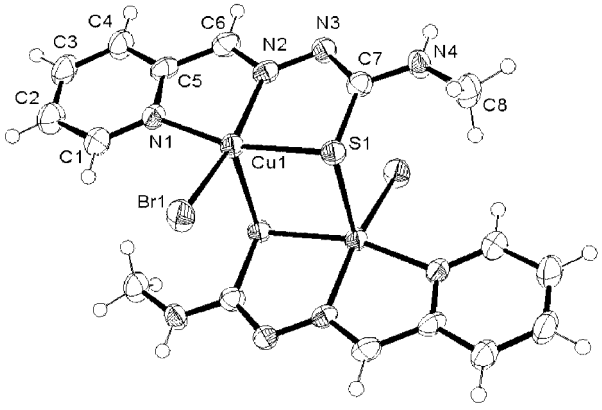

Figure 3. Molecular structure of **4** with thermal ellipsoids at 50% probability level

It is worth mentioning the presence of chains of dimers that stack along the *y* axis at distances that suggest the occurrence of π−π interactions. Thus, the minimum distances found are 3.32 Å [C(7)···C(3)^{ii}) in **2**, 3.38 Å [N(2)···C(5)^{ii}] in **3**, and 3.44 Å [N(3)···C(1)^{ii}] in complex **4**. In addition, π−π interactions occur along the *z* axis in compound **3**, with a minimum distance of 3.35 Å [C(3)···C(6)^{iv}, iv = $-x, -y+1, -z$]. The dimers are also interconnected by intermolecular hydrogen contacts (see Supporting Information, and also the footnote on the first page of this article).

Both thiosemicarbazones undergo conformational changes upon coordination. N(1) and N(2) are *anti* with respect to the C(5)−C(6) bond and atoms N(2) and S are *anti* with respect to the N(3)−C(7) linkage in the free ligands.[30,31] In both cases, they become *syn* after chelation. Furthermore, C(8) and S are *syn* in the free ligand as in **4**; but they are *anti* in complex **3**. This could be due to the steric hindrance induced by the size of the nitrato ligand.

 © 2003 Wiley-VCH Verlag GmbH & Co. KGaA, Weinheim

Table 2. Selected structural differences between copper(II) complexes containing neutral and anionic HL_I or HL_Imm (Å, °) for **2**, **3**, and **4**

Compound	N(2)−N(3)−C(7)	S−C(7)−N(3)	S−C(7)−N(4)	Cu···N(3)	N(2)···C(7)
2	111.2(4)	124.9(4)	118.4(4)	2.99	2.23
3	111.5(2)	124.9(2)	116.8(2)	2.96	2.22
4	112.1(5)	124.6(5)	119.0(4)	2.96	2.22
HL range	116−118	121−122	121−123	2.89−2.90	2.28−2.32
L^- range	109−114	123−127	117−119	2.94−3.00	2.22−2.23

All C−C and C−N lengths are similar in the free and coordinated ligands except for those corresponding to the N(3)−C(7) and C(7)−S bonds, which are 1.358(4) and 1.698(3) Å and 1.369(2) and 1.649(2) Å for HL_I and HL_Imm, respectively.[30,31] The N(3)−C(7) and C(7)−S bond lengths decrease and increase, respectively, upon coordination, which has been related to the respective gain and loss in double-bond character upon complexation. The results summarized in Table 2 show that the selected parameters for **2**, **3**, and **4** are in good agreement with those expected for compounds containing HL_I or HL_Imm in anionic form.[32]

As can be seen, complexes **2**, **3** and **4** are made up of [Cu(L)X] units connected through the thioamide sulfur atom, giving rise to $\{Cu_2(\mu\text{-}SL)_2\}$ dimeric entities similar to other copper(II) derivatives of pyridine-2-carbaldehyde thiosemicarbazone.[33,34] A significant difference between compound **2** and the analogous chloro and bromo derivatives[34] is the short deviation of the copper(II) ion with respect to the basal plane in **2** (0.012 Å) compared with those for $[\{Cu(L_I)Cl\}_2]$ and $[\{Cu(L_I)Br\}_2]$ (around 0.2 Å).

Crystal Structures of the Oxadiazole Derivatives

A perspective view of the structure of complex **5** is shown in Figure 4. Selected interatomic dimensions are given in Table 3. The crystal structure consists of cationic dimeric $[\{Cu(HL_{II})(H_2O)_3\}_2]^{4+}$ entities and sulfate groups as counterions. Each copper(II) ion adopts a tetragonally distorted octahedral "4+2" geometry, being bonded to the oxygen atoms of three water molecules and to three nitrogen atoms: two belonging to one of the oxadiazoles and one to the ligand of the symmetric entity inside the dimer, which acts as a bridge between the two metal ions. The high thermal parameters in the sulfate ions cause disorder in some of the oxygen atom positions.

The molecular structure of **6** has been described previously;[17] the dimeric structure is shown in Figure 5.

In relation to the plane formed by the N(1)N(2)N(3) chelating set in **5** and **6**, the copper(II) atoms lie at 0.172 and 0.351 Å, respectively. In addition, the O(2S) and O(4) atoms are displaced by 0.159 and 0.866 Å, respectively, above the NNN plane.

The structure of **8**[17] consists of (HL_{II}mm) neutral units and three water molecules of crystallization which stabilizes the crystal lattice through a network of hydrogen bonds.

The oxadiazole ligands in these compounds contain two aromatic rings (pyridinic and oxadiazolic) whose planes are at 7.1, 6.3, and 7.4° with respect to each other (for, **5**, **6**, and **8**, respectively), indicating that complexation induces a higher planarity in the oxadiazole ligands. These values are in good agreement with those observed for [Cu(HL_{II}-

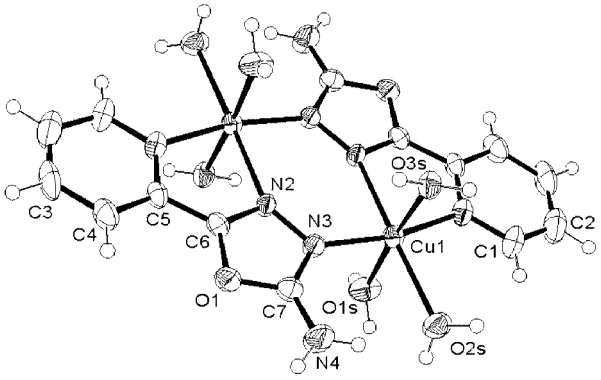

Figure 4. Molecular structure of the dimeric cationic entity of **5** with thermal ellipsoids at 50% probability level

Table 3. Selected bond lengths [Å] and angles [°] for **5**

Cu−N(1)	2.053(3)	C(5)−C(6)−N(2)	125.8(3)
Cu−N(2)^i	2.377(3)	N(1)−Cu−N(2)^i	76.7(1)
Cu−N(3)	2.009(3)	N(1)−Cu−N(3)	167.6(1)
Cu−O(1S)	1.967(3)	N(1)−Cu−O(1S)	90.1(1)
Cu−O(2S)	2.357(3)	N(1)−Cu−O(2S)	99.0(1)
Cu−O(3S)	1.980(2)	N(1)−Cu−O(3S)	88.8(1)
Cu···Cu^i [a]	4.481(2)	N(3)−Cu−O(1S)	90.3(1)
Cu···Cu^{ii}	7.460(1)		

[a] Symmetry transformations used to generate equivalent atoms: i = $-x+1, -y, -z+1$; ii = $-x+1, -y, -z$.

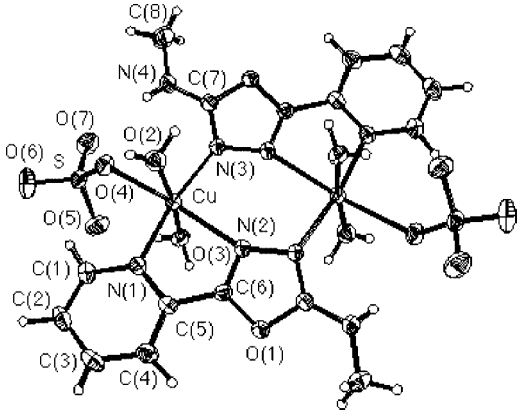

Figure 5. Molecular structure of the dimeric complex **6** with thermal ellipsoids at 50% probability level

 © 2003 Wiley-VCH Verlag GmbH & Co. KGaA, Weinheim

$mm)_2(H_2O)_2](NO_3)_2$ and $[Cu(HL_{II}mm)(oxalate)(H_2O)]\cdot H_2O$ (1.8 and 0.3°, respectively).[35]

The bond lengths in these complexes are quite similar to those of the free ligand. However, the C(5)−C(6)−N(2) angle decreases upon coordination[17] (see Table 3). The N(3) and C(8) atoms are *syn* with respect to the C(7)−N(4) bond in the structure of $HL_{II}mm$ whereas in complex **6** they show an *anti* conformation. Taking into account that the above-mentioned $[Cu(HL_{II}mm)_2(H_2O)_2](NO_3)_2$ and $[Cu(HL_{II}mm)(oxalate)(H_2O)]\cdot H_2O$ complexes also display the *syn* conformation, this conformational change could be attributed to steric hindrance induced by the sulfato group.[35]

Several hydrogen bonds involving the water molecules and sulfate anions help stabilize the lattice in complexes **5** and **6**, leading to a sheet-like structure (see Supporting Information). The sheets are connected by π−π stacking interactions with a shortest interplanar atom···atom separation of C(4)···C(6)^{v} (3.45 Å, $v = -x + 2, -y, -z + 1$) and N(3)···C(3)^{vii} (3.378 Å, vii = $x-1, y, z$) for **5** and **6**, respectively. A peculiar view of the packing in complex **6** with alternating layers of dimers parallel to the (−1, 3, 0) and (−3, −9, 1) planes is shown in Figure 6.

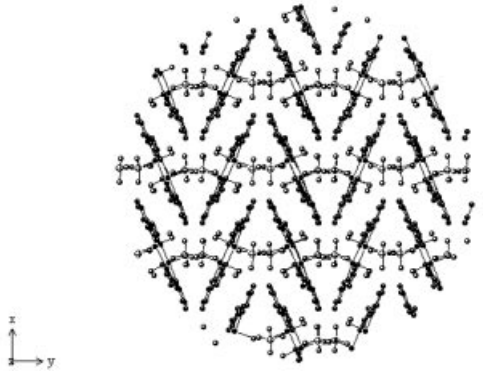

Figure 6. Arrow-like perspective of complex **6**

Analysis of the molecular packing of **8** suggests the lattice is stabilized by several hydrogen bonds, involving mainly the N(1), N(3) and N(4) atoms of the ligand and the lattice water (see Supporting Information). Pseudo-chains of coplanar molecules parallel to the (2, 6, −4) plane alternate with other chains of molecules parallel to the (−2, 6, 4) plane along the *y* axis (Figure 7). Each column is made up of sets of three molecules interconnected by π−π interactions (minimum distances 3.330 and 3.269 Å for C(6)···C(7)^{v} and C(7)···N(1)^{iii}, respectively). In addition, the molecules belonging to each column are linked through another hydrogen bond, which involves the N(4) and N(1) atoms.

Spectroscopic Studies

The IR spectrum of complex **1** exhibits absorptions at 808 and 735 cm^{-1} which can be assigned to the ν_1 and ν_3 vibrations of the halato group. Complex **3** shows strong bands at 1517, 1234, and 1023 cm^{-1} assignable to the ν_5, ν_1, and ν_2 modes of the monodentate nitrato ligand,[36] in good agreement with the structural results.

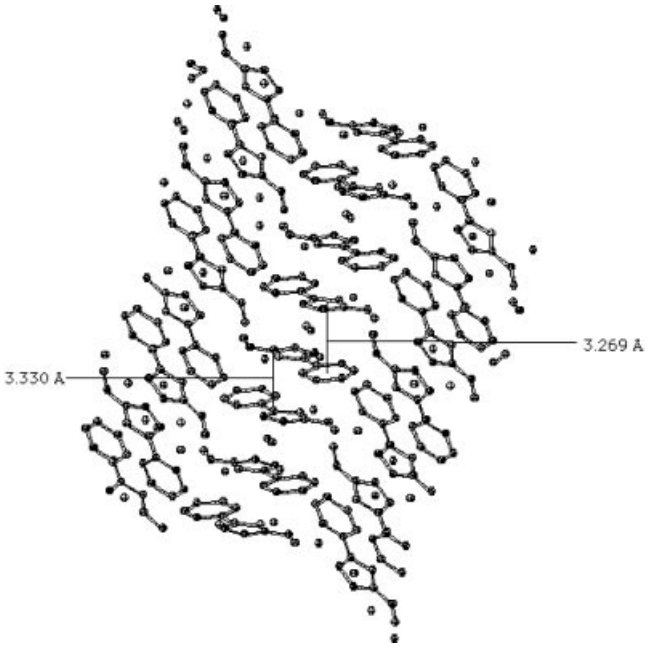

Figure 7. Pseudo-chains formed by the stackings of molecules in **8**

For **5** and **6** the 1300−900 cm^{-1} region displays many absorptions due to the coexistence of the oxadiazole and sulfate ligands, hampering definitive assignments. Nevertheless, the bands at 1095, 1065, and 640 cm^{-1} for complex **5** could be assigned to the ν_3 and ν_4 modes of the T_d sulfate. Conversely, **6** shows absorptions at: 1108(ν_3), 1050 (ν_3), 968 (ν_1), 645 (ν_4), 617 (ν_4), and 455 (ν_2) cm^{-1} that can be attributed to a monodentate-coordinated sulfate with C_{3v} symmetry.

The diffuse reflectance spectra of the thiosemicarbazone complexes are characterized by bands in the 210−245, 260−295, 380−415, and 460−500 nm regions, corresponding to intraligand (π→π*), (n→π*), LMCT $S\rightarrow Cu^{II}$, and $X\rightarrow Cu^{II}$ (X = N, O, Br, I), respectively[37−39] (see Table 4). The bands observed in solid samples in the 575−740 nm region are characteristic of d→d transitions for compounds exhibiting a square-pyramidal geometry with a $d_{x^2-y^2}$ ground state. A shoulder observed at 895 and 979 nm in the spectra of the nitrato and iodo derivatives is attributed to the distortion towards trigonal bipyramidal topology.

The UV−visible spectra of complexes **3** and **4** in aqueous solution are very similar (see Table 4) and differ significantly from their respective solid spectra, especially in the LMTC region, as also occurs with the spectra of complexes **1** and **2** in solution. This strongly suggests that $[Cu(L_Imm)(H_2O)_3]^+$ and $[Cu(L_I)(H_2O)_3]^+$, respectively, are present in aqueous solution. The band at 225 nm in the spectrum of complex **2** [and the analogous $Cu(L_Imm)I$] is also present in aqueous solutions of KI, being attributed to charge-transfer bands between the iodide ion and the solvent molecules.

The UV−visible spectra of the oxadiazole complexes **5** and **6** show absorptions in the 220−230, 260−285, and

 © 2003 Wiley-VCH Verlag GmbH & Co. KGaA, Weinheim

Table 4. UV-visible spectroscopic data [λ (nm), ε ($M^{-1}\cdot cm^{-1}$)]

1[a]	224, 277, 380(sh), ≈409(sh), 600(sh), 742(sh)
1[b]	280(14600), 315(10750), 382(9600), 629(170)
2[a]	230, 267, 407, 467(sh), 650, 979(sh)
2[b]	225(27600), 281(16600), 317(12500), 383(11250), 628(190)
3[a]	237, 274, 412, 468(sh), 597, 895(sh)
3[b]	244(sh,8100), 287(11600), 328(11900), 384(10800), 624(160)
4[a]	277(sh), 405, 473(sh), 595, 717(sh,b)
4[b]	244(sh, 8300), 287(11700), 330(11900), 385(10700), 624(160)
5[a]	223, 285, 339(sh), 368(sh), 705(b), 1118(b)
5[b]	252(sh, 5300), 291(11700), 749(20)
6[a]	225, 269, 339(sh), 401(sh), 482(sh), 698, 1166
6[b]	297(13600), 765(20)
7[c]	296 (21300)
7[d]	203(18000), 293(31100)
8[c]	300 (11100)
8[d]	204 (23500), 298 (40800)

[a] In solid. [b] In water solution ($6\cdot10^{-5}$ M). [c] In ethanolic solution ($6\cdot10^{-5}$ M). [d] In methanolic solution ($6\cdot10^{-5}$ M).

330−500 nm regions which can be attributed to intraligand π→π*, n→π* and LMCT N/O→Cu^{II} transitions, respectively.[35] A very broad absorption at around 700 nm and a less intense shoulder in the 1100−1170 nm range are also observed, which are consistent with a copper(II) chromophore with a tetragonally distorted octahedral geometry.[40] These bands could be assigned to the $^2E_g \leftarrow {}^2B_{1g}$ and $^2A_{1g} \leftarrow {}^2B_{1g}$ transitions, respectively − in good agreement with the results reported for analogous triazole systems.[41] The solution spectra of complexes **5** and **6** are similar to those of the $[Cu(HL_{II}mm)_2(H_2O)_2](NO_3)_2$ complex. Furthermore, a study involving the latter has shown that some LMTC bands shift to higher energies in solution, overlapping with the intraligand absorptions.[35]

The *g* tensors for the powder X-band EPR spectra of the title complexes are shown in Table 5. The spectra of compounds **1**, **3**, and **4** are characteristic of a $d_{x^2-y^2}$ ground state for square-pyramidal copper(II) chromophores,[42] similar to those reported for other copper(II) thiosemicarbazone complexes.[33,34,43] Compound **2** exhibits a broad (≈ 200 G peak-to-peak) isotropic signal at room temperature in the $g = 2.074$ region. Upon lowering the temperature to 120 K the signal intensity increases but its shape does not change. The X-band EPR spectra of complexes **5** and **6** consist of an axial signal whose *g* values accord with a copper(II) ion in an elongated octahedral geometry.

Table 5. Experimental EPR parameters

Complex	g_1	g_2	g_3
1[a]	2.178	2.047	2.032
2[a]	$g_{iso} = 2.074$		
3[b]	$g_{\parallel} = 2.181$	$g_{\perp} = 2.043$	
3[c]	2.186	2.049	2.025
4[b]	$g_{\parallel} = 2.149$	$g_{\perp} = 2.038$	
4[c]	2.152	2.043	2.031
5[a]	$g_{\parallel} = 2.363$	$g_{\perp} = 2.077$	
6[a]	$g_{\parallel} = 2.294$	$g_{\perp} = 2.082$	

[a] No variation in the *g* values from room temperature to 120 K. [b] At room temperature. [c] At 120 K.

Magnetic Behaviour

Plots of the molar susceptibility (χ_m), together with the $\chi_m T$ vs. *T* curves for compounds **2**, **3**, **4**, **5**, and **6** are given in Figures 8, 9, 10, 11, and 12, some of which show a shoulder around 60 K that is characteristic of O_2. The magnetic measurements all obey the Curie−Weiss law above 50 K. The Weiss temperatures are −9.46 (**2**), +2.87 (**3**), −5.75 (**4**), −1.76 (**5**), and −1.26 K (**6**). The C_m experimental values range from 0.40 to 0.44 $cm^3\cdot K\cdot mol^{-1}$ and the calculated μ_{eff} values at room temperature are 1.8 BM for

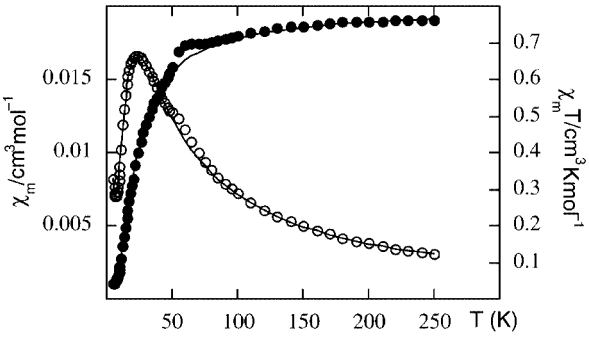

Figure 8. Thermal variation of the molar susceptibility (open circles) and $\chi_m T$ (black circles) for **2**. Solid lines represent the best fit

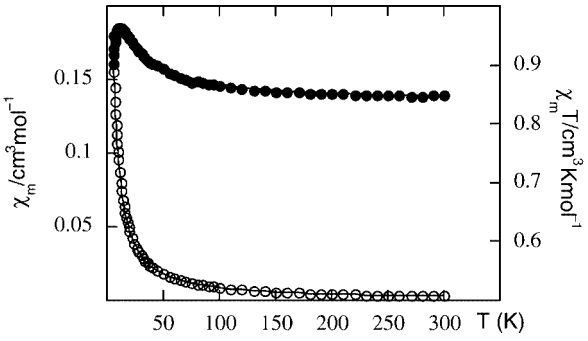

Figure 9. Thermal variation of the molar susceptibility (open circles) and $\chi_m T$ (black circles) for **3**. Solid lines represent the best fit

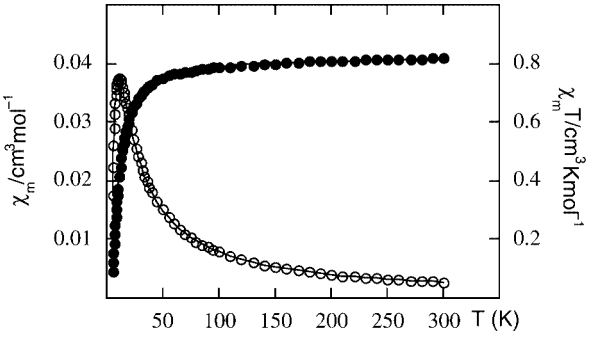

Figure 10. Thermal variation of the molar susceptibility (open circles) and $\chi_m T$ (black circles) for **4**. Solid lines represent the best fit

 © 2003 Wiley-VCH Verlag GmbH & Co. KGaA, Weinheim

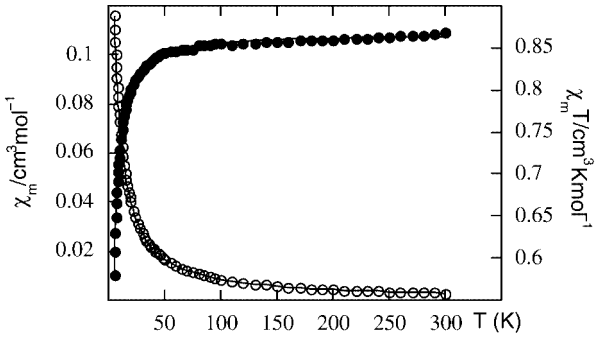

Figure 11. Thermal variation of the molar susceptibility (open circles) and $\chi_m T$ (black circles) for **5**. Solid lines represent the best fit

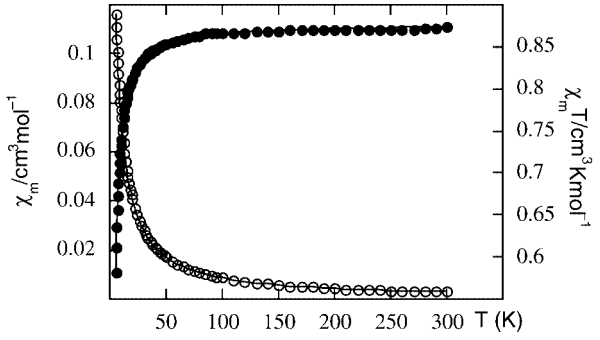

Figure 12. Thermal variation of the molar susceptibility (open circles) and $\chi_m T$ (black circles) for **6**. Solid lines represent the best fit

all compounds. The χ_m values increase with decreasing temperature for most complexes, reaching a maximum at 22.0 (0.008 cm^3·mol^{-1}, **2**), 11.0 (0.019 cm^3·mol^{-1}, **4**), 3.3 K (0.058 cm^3·mol^{-1}, theoretical values arising from the fit in **5**) and 3.4 K (0.058 cm^3·mol^{-1}, theoretical values arising from the fit in **6**). The $\chi_m T$ value continuously decreases on lowering the temperature, indicating the presence of antiferromagnetic interactions. However, compound **3** does not exhibit a maximum in the χ_m vs. T plot and $\chi_m T$ increases on lowering the temperature, which is characteristic of ferromagnetic behaviour.

Taking into account the dimeric nature of these complexes, we fitted the susceptibility data with the Bleaney−Bowers expression for copper(II) dinuclear compounds,[44] derived from the Heisenberg isotropic spin Hamiltonian ($H = -2J \cdot S1S2$), for two coupled $S = 1/2$ ions:

$$\chi = \frac{Ng^2\beta^2}{kT}\left(\frac{2}{3 + \exp(-2J/kT)}\right) + N\alpha \quad (1)$$

where $N\alpha$ = a temperature independent contribution, N is the Avogadro constant, β = Bohr magneton, and k = the Boltzmann constant. The best least-squares fit (solid line in Figures 8−12) is obtained with $J/k = -20.20$ K (-14.03 cm^{-1}, taking into account 5% paramagnetic impurities in **2**), -8.85 K (-6.14 cm^{-1}, **4**), -2.75 K (-1.91 cm^{-1}, **5**), and -2.78 K (-1.93 cm^{-1}, **6**). For **3**, the influence of intermolecular interactions must be considered in the fit treated in the molecular field approximation, and the values obtained are $J/k = +9.90$ K and $z'J' = -1.70$ K ($+6.88$ and -1.18 cm^{-1}, respectively). The g-values of 2.06, 2.11, 2.10, 2.15, and 2.16 for **2**, **3**, **4**, **5**, and **6**, respectively, are in good agreement with those obtained from EPR, 2.07 (**2**), 2.09 (**3**), 2.08 (**4**), 2.17 (**5**), and 2.15 (**6**). Taking into account the structural features, the existence of interdimeric magnetic interactions in these compounds should be considered. However, the fit was improved only for **3**, due to the opposite sign of the ferromagnetic intradimer vs. antiferromagnetic interdimer interactions. The data are given in Table 6 together with a summary of the J values for all copper(II) dinuclear derivatives of HL_I and HL_Imm described to date.

The strength of the magnetic interactions in the **2**, **3**, and **4** thiosemicarbazone derivatives suggests that the exchange propagation direction is in a different plane to that formed by the magnetic $d_{x^2-y^2}$ orbitals. These results agree well with the existence of an intradimer exchange coupling in the Cu_2S_2 units. However, the relatively intense antiferromagnetic coupling in **2** and the ferromagnetic interactions in **3** have not been observed before in the pyridine-2-carbaldehyde thiosemicarbazone−copper(II) system. Ferromagnetic interactions in other thiosemicarbazone−copper(II) systems have been referenced,[45] but, as far as we are aware, no magneto-structural studies have been carried out.

The results suggest that the nature of the coligands in the basal plane influences in the magnetic behaviour. Here, O-donor coligands show the smallest antiferromagnetic contributions to the J values. It has been established that the less electronegative is the donor atom in the basal plane the stronger the induced antiferromagnetic coupling is, due to a greater hybridization of the $d_{x^2-y^2}$ metal orbital towards the bridge.[46,47] Figure 13 shows a good accordance between the average J values and Pauling's electronegativity of the compounds in Table 6.

Conversely, the relationship between J and other structural parameters is not evident even for a given X-donor set. Several concomitant factors could be involved in the values of the exchange coupling constants for these compounds, such as the Cu···Cu intradimer distance, SP vs. BPT distortions around the copper(II) ion, deviation of the metal ion from the basal plane, deviation of the coligand from the basal plane, Cu−X apical distances, N(2)−Cu−S−Cu′/N(1)−Cu−O(1)−Cu′ dihedral angles which give a measurement of the shift of the [Cu(L)X] entities constituting the dimer, the influence of the thiosemicarbazone and coligands.

A qualitative study of the relationship between the magnetic exchange constant J and the square of the energy difference (Δ^2) between the two magnetic orbitals involved[48] required an extended Hückel molecular orbitals (EHMO) analysis.[49] Such EHMO calculations, using the crystallographic coordinates of the compounds following a procedure previously described,[50] gave a Δ^2 for **3** that is at least ten times smaller than those obtained for antiferro-

 © 2003 Wiley-VCH Verlag GmbH & Co. KGaA, Weinheim

Table 6. Comparison of the J, Δ^2, and selected structural parameters for pyridine-2-carbaldehyde thiosemicarbazonecopper(II) dinuclear complexes

Compounds, [donor atom of the basal coligand]	Bridging atom (X′)	Cu···Cu′ / Cu−X′ (Å)	Cu−X···Cu′ angle (°)	J (cm^{-1})	Δ^2 $(eV)^2 \cdot 10^3$
[{Cu($L_I$mm)(NO_3)}$_2$], [O]	S	3.4482(2) / 2.7659(6)	85.83(2)	+6.88	0.12
[{Cu(L_I)(NO_2}$_2$],[71] [O]	S	3.554(1) / 2.918(2)	85.5(1)	−3.40	1.09
[{Cu(L_I)Cl}$_2$],[34] [Cl]	S	3.486(2) / 2.760(2)	87.01(4)	−4.70	11.45
[{Cu(L_I)Br}$_2$],[34] [Br]	S	3.474(1) / 2.743(2)	87.12(5)	−4.70	17.42
[{Cu($L_I$mm)Br)}$_2$], [Br]	S	3.577(2) / 2.832(2)	88.31	−6.14	3.72
[{Cu(L_I)I}$_2$], [I]	S	3.455(1) / 2.775(1)	85.80(4)	−14.03	15.62
[{Cu(L_I)(NCS)}$_2$],[33] [N]	S	3.450(3) / 2.754(5)[a]	85.9(1)[a]	−5.09	45.80
[{Cu(L_I)(NCO)}$_2$],[33] [N]	S[b]	[b]	[b]	−4.24	[b]
[{Cu(L_I)(N_3)}$_2$],[33] [N]	S[b]	[b]	[b]	−2.93	[b]
[{Cu(L_I)(HCOO)}$_2$],[71] [O]	S	3.503(2) / 2.820(2)	86.34(5)	−2.80	1.68
[{Cu(L_I)(CH_3COO)}$_2$],[61,72]	O	3.442(1) / 2.427(2)	103.5(1)	−3.10	1.60
[{Cu(L_I)(CH_3CH_2COO)}$_2$],[71] [O]	O	3.460(2) / 2.387(2)	105.35(9)	−3.30	1.85

[a] Average value. [b] Crystal data not available.

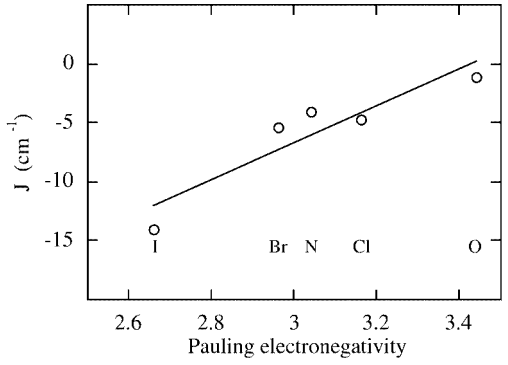

Figure 13. Plot of the average values of J (cm^{-1}) vs. the Pauling's electronegativities. The electronegativities are 3.44, 3.16, 3.04, 2.96, and 2.66 for O^-, Cl^-, N^-, Br^-, and I^- donors, respectively

magnetic derivatives in good accordance with its ferromagnetic behaviour. Unfortunately, the limitations of the EHMO calculations did not allow us to determine a perfect sequence for the J values. The most important disagreement involves Δ^2 for [{Cu(L_I)(NCS)}$_2$] and [{Cu(L_I)I}$_2$], but can be explained by taking into account that [{Cu(L_I)(NCS)}$_2$] is the only noncentrosymmetric compound in Table 6. Thus, it has been proposed that lowering the symmetry gives rise to a decrease in the antiferromagnetic contribution which is not reflected in the magnitude of Δ^2.[51,52]

The small values obtained for the magnetic exchange constant in **5** and **6** contrast with those reported for similar dimeric compounds containing copper(II) ions bridged through analogous diazole and triazole ligands.[41,53−56] This is consistent with the value of Δ gap in the EHMO analysis (0.099 eV for **5**), which is smaller than those reported for pyrazolate bridged compounds.[57,58] Such behaviour can be explained considering that the d_{z^2} orbitals lie in the O(4)−Cu−N(2) direction for compounds **5** and **6**, which involves the longest bond lengths and points to the oxadiazole bridges. The magnetic $d_{x^2-y^2}$ orbitals, however, are perpendicular to the exchange propagation direction.

Conclusion

HL_I and HL_Imm react with potassium bromate or iodate in an oxidative cyclization process that involves the elimination of sulfur and the attainment of the respective HL_{II} and HL_{II}mm ligands. This reaction also occurs when the copper(II) derivatives of these thiosemicarbazone ligands are used as reactants. The oxadiazole−copper(II) complexes so-formed maintain the dimeric nature of their thiosemicarbazonecopper(II) precursors. The planarity of the ligands gives rise to π−π stacking interactions that, along with the hydrogen bonding, stabilize the crystal packing. Weak antiferromagnetic intradimeric interactions are present in both thiosemicarbazone and oxadiazole−copper(II) systems. However, the nitrato derivative **3** shows ferromagnetic behaviour. The relative scarcity of pyridine-2-carbaldehyde thiosemicarbazone−copper(II) compounds, as well as the limitations of the semiempirical calculations developed, prevents good quantitative results. However, the influence of the electronegativity of the non-thiosemicarbazone basal donor atom seems to be clear.

Experimental Section

Materials: Thiosemicarbazides, pyridine-2-carbaldehyde, copper(II) sulfate pentahydrate, copper(II) nitrate trihydrate, potassium bromate and iodate, sodium bromide, potassium iodide, and potassium ferrocyanide trihydrate were purchased from commercial sources and used as received. Published methods with small modifications were used to synthesize HL_I,[59] HL_Imm,[31,60] Cu(L_I)(NO_3,[61] and [{Cu($L_I$mm)(NO_3)}$_2$].[17] All operations should be carried out in a fume cupboard.

Preparation of the Complexes

Synthesis of 1, 2, 5, and 7: Compound **1** was synthesized by the addition of solid potassium iodate (0.85 g, 4 mmol) to an aqueous solution of Cu(L_I)(NO_3) (0.30 g, 1 mmol) with continuous stirring. The pH of the reaction mixture was adjusted to 6.0 by addition of aqueous NaOH. A few minutes later, an abundant green precipitate appeared which was filtered off and dried (yield 0.30 g, 70%).

 © 2003 Wiley-VCH Verlag GmbH & Co. KGaA, Weinheim

$C_7H_9CuIN_4O_4S$ (435.69): calcd. C 19.3, H 2.1, N 13.2, S 7.8; found C 19.3, H 2.1, N 12.9, S 7.4. The molar conductivity of $5\cdot10^{-4}$ M solutions in water (dimethylformamide) at 25 °C is Λ_M = 97.4 (immediate reaction to give **2**) $\Omega^{-1}\cdot cm^2\cdot mol^{-1}$. Selected IR bands ($cm^{-1}$, KBr): 3498 m, 3438 m, 3365 m, 3296 m, 3170 m, 1640 s, 1606 s, 1484 m, 1448 m, 1436 m, 1383 w, 1322 m, 1222 m, 1162 s,sh, 708 m, 781 s, 735 s.

Attempts to recrystallize **1** in water furnished good-quality crystals of a new thiosemicarbazonatocopper(II) derivative that was identified as **2** (0.05 g, 16% yield). $C_7H_7CuIN_4S$ (369.67): calcd. C 22.7, H 1.9, N 15.2, S 8.1; found. C 22.3, H 1.9, N 15.3, S 7.6. The molar conductivity of $5\cdot10^{-4}$ M solutions in water (dimethylformamide) at 25 °C is Λ_M = 123 (31.3) $\Omega^{-1}\cdot cm^2\cdot mol^{-1}$. Selected IR bands ($cm^{-1}$, KBr): 3423 s, 3279 m, 3135 m, 1625 s, 1600 s, 1480 s, 1446 vs, 1436 vs, 1226 m, 1166 s, 1155 m,sh, 909 m, 875 w, 778 m, 622 m, 469 m,b, 420 m.[62]

Aqueous solutions of $Cu(L_I)(NO_3)$ (0.30 g, 1 mmol) and potassium bromate (0.17 g, 1 mmol) were mixed with stirring. The pH of the reaction mixture was adjusted to 6 by addition of aqueous 5 M NaOH and maintained with stirring overnight at room temperature. A small amount of precipitate appeared, which was filtered off and washed with water and acetone. The product was identified as the $[\{Cu(L_I)(Br)\}_2]$ complex.[34] Bright green crystals of **5** were then obtained from the mother liquor after one week at room temperature (0.22 g, 58% yield). $C_{24}H_{24}Cu_2N_8O_{16}S_2$ (751.6): calcd. C 24.6, H 3.6, N 14.4, S 8.2; found. C 24.6, H 3.6, N 14.3, S 8.2. The molar conductivity of $5\cdot10^{-4}$ M solutions in water (dimethylformamide) at 25 °C is Λ_M = 227 (32.6) $\Omega^{-1}\cdot cm^2\cdot mol^{-1}$. Selected IR bands ($cm^{-1}$, KBr): 3381 m,b, 3077 m,b, 1684 s, 1577 m, 1518 m, 1493 m, 1441 m, 1350 m,sh, 1143 s,b, 1133 s, 1100−1000 s, 789 m, 751 m, 734 m, 619 m,b.

The HL_{II} ligand (**7**) was removed from complex **5** by the addition of $K_4[Fe(CN)_6]\cdot3H_2O$[17] (yield: 0.06 g, 45%). $C_8H_{14}N_4O_4$ (230.23): calcd. C 51.8, H 3.7, N 34.5; found. C 51.9, H 3.8, N 34.1. Selected IR bands (cm^{-1}, KBr): 3288 s, 3115 s, 1649 vs, 1588 vs,sh, 1562 s, 1460 vs, 1448 m, 1321 m, 1285 m, 1251 w, 1092 s, 1052 s, 1042 s, 786 m, 773 m, 742 s, 686 s, 620 m, 410 m. ^1H NMR (400 MHz; $[D_6]$DMSO, ppm): δ = 8.63 (dt, ^3J = 5 and 1.4 Hz, 1 H, H^1), 7.95 (d, ^3J 2 Hz, 1 H, H^4), 7.92 (m, 1 H, H^3), 7.47 (m, 1 H, H^2), 7.38 (s, 2 H, NH_2).

Ligand **7** can also be prepared by oxidative cyclization of HL_I in the absence of copper(II) as follows: solid potassium bromate (0.5 g, 3 mmol) was added to a suspension of the thiosemicarbazone in water (0.54 g, 3 mmol) acidified with H_2SO_4 to pH = 0−1. After a few minutes, the reaction mixture turned orange and a brown solid appeared. The suspension was filtered off and a solution of NaOH (5 M) was slowly added to the resulting clear solution to reach a pH ≈ 5 at 0 °C. After a further few minutes ligand **7** appeared as a white product which was washed with water and recrystallized from ethanol (yield 0.31 g, 45%).

Synthesis of 3, 4, 6, and 8: The oxidative cyclization procedure for HL_Imm is analogous to that described above for HL_I. The synthesis and characterization of complex **3** has been reported in the literature.[17]

Aqueous solutions of **3** (0.32 g, 0.5 mmol) and potassium bromate (0.17 g, 1 mmol) were allowed to react at pH 6 overnight. A green precipitate appeared that was filtered off, washed with water and acetone and dried. The product was identified as complex **4** (yield 0.03 g, 10%). $C_{16}H_{18}Br_2Cu_2N_8S_2$ (673.4): calcd. C 28.6, H 2.7, N 16.6, S 9.5; found. C 29.0, H 3.0, N 16.9, S 9.1. The molar conductivity of $5\cdot10^{-4}$ M solutions in water (dimethylformamide) at 25 °C is Λ_M = 118.2 (10) $\Omega^{-1}\cdot cm^2\cdot mol^{-1}$. Selected IR bands ($cm^{-1}$, KBr): 3219 m, 1593 s, 1570 m, 1534 s, 1472 s, 1357 vs,b, 1304 s, 1281 s, 1227 s, 1183 m, 1119 m, 1042 s, 898 w, 883 w, 862 w, 777 w, 607 m.[63]

After filtering complex **4**, the mother liquor was allowed to stand at room temperature, and after two days crystals of the complex **6** were obtained.[17]

The $HL_{II}mm$ ligand (**8**) can be obtained by analogous procedures to those described for **7**.[17,64−66]

Physical Measurements: Microanalyses were performed with a LECO CHNS-932 analyser. Conductivity measurements were made by a CRISON 522 conductimeter. Infrared spectra were obtained in the 400−4000 cm^{-1} region on a Nicolett Impact 410 FTIR spectrophotometer with samples prepared as KBr pellets. Reflectance spectra were carried out on a Cary 2415 spectrometer in the 200−2000 nm range. For UV-visible solution measurements, a Varian UV-VIS-NIR spectrophotometer was employed (200−900 nm). X-band EPR spectra were recorded on a Bruker EMX spectrometer, equipped with a standard Oxford continuous flow cryostat. Magnetic measurements of powdered samples were carried out in the range 5−300 K using a Quantum Design MPMS-7 Squid magnetometer. Diamagnetic corrections were estimated from Pascal tables.

X-ray Crystallographic Studies: Crystal data collections were carried out on a Bruker Smart CCD area detector equipped with a single crystal diffractometer. Absorption corrections were made using the SADABS program.[67] Direct methods (SHELXS-97)[68] were employed to solve the structures and then were refined by full-matrix least-squares method, using SHELXL-97.[69] All non-hydrogen atoms were assigned anisotropic thermal parameters. Hydrogen positions were determined by difference Fourier syntheses and introduced in calculations with a riding model. The scattering factors and anomalous dispersion coefficients were taken from International Tables of X-ray Crystallography.[70] Refinements were made on F_0^2 for all reflections. Crystallographic data (excluding structure factors) for the structures reported in this paper have been deposited with the Cambridge Crystallographic Data Centre. The deposition numbers are CCDC−199599, −199600, and −199601 for compounds **2**, **4**, and **5**, respectively. Copies of the data can be obtained free of charge on application to The Director, CCDC, 12 Union Road, Cambridge CB2 1EZ, UK [Fax: (internat.) +44−1223/336033; E-mail: deposit@ccdc.cam.ac.uk]. Crystallographic details for the crystal structures of compounds **2**, **4**, and **5** are shown in Table 7.

Supporting Information

Supporting information for this article (Hydrogen bond parameters (Å, °) for the six crystal structures) is available from the WWW under http://www.wiley-vch.de/home/eurjic or from the author.

Acknowledgments

We thank Dr. J. J. Delgado (SCAI, Universidad de Burgos, Spain) for the elemental analysis and Professor R. Olazcuaga and Dr. F. Guillen (CNRS, Pessac, France) for the reflectance measurements. This work has been carried out with the financial support of the Ministerio de Ciencia y Tecnología (BQU, 2002-00435) and the Junta de Castilla y León (BU15/03). P. G.-S. thanks the Universidad de Burgos for her Doctoral Fellowship.

 © 2003 Wiley-VCH Verlag GmbH & Co. KGaA, Weinheim

Table 7. Summary of crystallographic data and parameters for the **2**, **4**, and **5**

	2	**4**	**5**
Formula	$C_7H_7CuIN_4S$	$C_{16}H_{18}Br_2Cu_2N_8S_2$	$C_{14}H_{24}Cu_2N_8O_{16}S_2$
M	369.67	673.4	751.6
System	Triclinic	Triclinic	Monoclinic
Space group	$P\bar{1}$	$P\bar{1}$	$P2_1/n$
a/Å	7.7994(2)	8.1165(6)	8.6438(4)
b/Å	8.5440(2)	8.2597(7)	16.9146(7)
c/Å	9.1997(2)	9.4001(8)	8.9918(4)
α/°	111.977(1)	66.291(1)	–
β/°	98.218(1)	80.284(2)	92.999(1)
γ/°	107.940(1)	71.364(2)	–
U/Å^3	517.17(2)	546.15(8)	1312.9(1)
Z	2	1	2
D_c/g cm^{-3}	2.374	2.047	1.901
μ/mm^{-1}	5.261	5.818	1.870
F(000)	350	330	764
2θ Range (°)	2–28	2–28	2–28
GOF	1.050	1.012	1.048
R_1(all data)	0.0475	0.0726	0.0621
$R_1[I > 2\sigma(I)]$	0.0393	0.0522	0.0397
wR_2(all data)	0.1101	0.1749	0.0904
$wR_2[I > 2\sigma(I)]$	0.1053	0.1483	0.0802

[1] E. J. Blanz, F. A. French, *Cancer Res.* **1968**, *28*, 2419.
[2] [2a] G. R. Gale, in: *Antineoplastic and Immunosuppressive Agents Part II* (Eds.: A. C. Sartorelli, D. G. Johns); Springer: Berlin, **1975**; pp. 829–840. [2b] D. H. Petering, H. G. Petering, in: *Antineoplastic and Immunosuppressive Agents Part II* (Eds.: A. C. Sartorelli, D. G. Johns); Springer: Berlin, **1975**; pp. 841–849.
[3] S. Padhye, R. Chikate, A. Kumbhar, J. M. Sahllon, M. P. Chitnis, *Biometals* **1992**, *5*, 67–71.
[4] [4a] E. C. Moore, M. S. Zedeck, K. C. Agrawal, A. C. Sartorelli, *Biochemistry* **1970**, *9*, 4492–4498. [4b] L. Thelander, A. Gräslund, *J. Biol. Chem.* **1983**, *258*, 4063–4066.
[5] R. W. Byrnes, M. Mohan, W. E. Antholine, R. X. Xu, D. H. Petering, *Biochemistry* **1990**, *29*, 7046–7053.
[6] W. E. Antholine, F. Taketa, *J. Inorg. Biochem.* **1984**, *20*, 69–78.
[7] L. A. Saryan, K. Mailer, C. Krishnamurti, W. Antholine, D. Petering, *Biochem. Pharmacol.* **1981**, *30*, 1595–1604.
[8] I. H. Hall, C. B. Lackey, T. D. Kistler, J. S. Ives, H. Beraldo, L. J. Ackerman, D. X. West, *Arch. Pharm. Pharm. Med. Chem.* **2000**, *333*, 217–225.
[9] K. H. Reddy, P. S. Reddy, P. R. Babu, *J. Inorg. Biochem.* **1999**, *77*, 169–176.
[10] M. C. Miller III, C. N. Stineman, J. R. Vance, D. X. West, I. H. Hall, *Appl. Organomet. Chem.* **1999**, *13*, 9–19.
[11] J. García-Tojal, A. García-Orad, J. L. Serra, J. L. Pizarro, L. Lezama, M. I. Arriortua, T. Rojo, *J. Inorg. Biochem.* **1999**, *75*, 45–54.
[12] J. García-Tojal, J. L. Pizarro, A. García-Orad, A. R. Pérez-Sanz, M. Ugalde, A. Alvarez Díaz, J. L. Serra, M. I. Arriortua, T. Rojo, *J. Inorg. Biochem.* **2001**, *86*, 627–633.
[13] J. García-Tojal, A. García-Orad, A. Alvarez Díaz, J. L. Serra, M. K. Urtiaga, M. I. Arriortua, T. Rojo, *J. Inorg. Biochem.* **2001**, *84*, 271–278.
[14] L. Somogyi, *Liebigs Ann. Chem.* **1991**, 1267–1271.
[15] R. Milcent, T. -H. Nguyen, *J. Heterocycl. Chem.* **1986**, *23*, 881–883.
[16] J. S. Casas, M. V. Castaño, E. E. Castellano, J. Ellena, M. S. García-Tasende, A. Gato, A. Sánchez, L. M. Sanjuán, J. Sordo, *Inorg. Chem.* **2002**, *41*, 1150–1557.
[17] P. Gómez-Saiz, J. García-Tojal, M. A. Maestro, F. J. Arnaiz, T. Rojo, *Inorg. Chem.* **2002**, *41*, 1345–1347.
[18] [18a] F. A. Omar, N. M. Mahfouz, M. A. Rahman, *Eur. J. Med. Chem.* **1996**, *31*, 819–825. [18b] B. S. Vashi, D. S. Mehta, V. H. Shah, *Indian J. Chem. Sect. B* **1996**, *35*, 111–115. [18c] G. Rama Rao, K. Mogilaiah, B. Sreenivasulu, *Indian J. Chem. Sect. B* **1996**, *35*, 339–344. [18d] H. A. Albar, M. S. I. Makki, H. M. Faidallah, *Indian J. Chem. Sect. B* **1996**, *35*, 23–29. [18e] V. I. Kelarev, R. A. Karakhanov, S. S. Gasanov, G. V. Morozova, K. P. Kuatbekova, *Russ. J. Org. Chem.* **1993**, *29*, 323–329. [18f] K. Raman, H. K. Singh, S. K. Salzman, S. S. Parmar, *J. Pharm. Sci.* **1993**, *82*, 167–169. [18g] P. S. Fernandes, T. M. Sonar, *Indian J. Chem. Soc.* **1986**, *63*, 427–429. [18h] S. P. Hiremath, N. N. Goudar, M. G. Purohit, *Indian J. Chem. Sect. B* **1981**, *20*, 388–390.
[19] S. P. Hiremath, J. S. Biradar, S. M. Kudari, *J. Indian Chem. Soc.* **1984**, *61*, 74–76.
[20] S. P. Hiremath, V. N. Sonar, K. R. Sekhar, M. G. Purohit, *Indian J. Chem. Sect. B* **1989**, *28B*, 626–630.
[21] M. A. Malik, D. J. Phillips, *J. Inorg. Nucl. Chem.* **1974**, *36*, 2229.
[22] K. E. Pfitzner, J. G. Moffatt, *J. Am. Chem. Soc.* **1965**, *87*, 5661.
[23] J. G. Moffatt, *J. Org. Chem.* **1971**, *36*, 1909.
[24] L. Farkas, O. Schächter, *J. Am. Chem. Soc.* **1949**, *71*, 2827.
[25] D. B. Dess, J. C. Martin, *J. Org. Chem.* **1983**, *48*, 4155–4156.
[26] D. A. Ballard, W. M. Dehn, *Organic Synthesis*, Collective Volume; **1932**; pp. 1, 89.
[27] H. Ulrich, A. A. R. Sayigh, *Angew. Chem.* **1966**, *5*, 704–712.
[28] R. Noto, P. Lo Meo, M. Gruttaduria, G. Werber, *J. Heterocycl. Chem.* **1999**, *36*, 667–674.
[29] A. W. Addison, T. N. Rao, J. Reedijk, J. van Rijn, G. C. Verschoor, *J. Chem. Soc., Dalton Trans.* **1984**, 1349–1356.
[30] V. N. Byushkin, Y. M. Chumakov, N. M. Samus, I. O. Baka, *Zh. Strukt. Khim.* **1987**, *28*, 140–142.
[31] D. X. West, G. A. Bain, R. J. Butcher, J. P. Jasinski, R. Y. Pozdniakiv, J. Valdés-Martínez, R. A. Toscano, S. Hernández-Ortega, *Polyhedron* **1996**, *15*, 665–674.
[32] J. García-Tojal, T. Rojo, *Polyhedron* **1999**, *18*, 1123–1130.
[33] J. García-Tojal, L. Lezama, J. L. Pizarro, M. Insausti, M. I. Arriortua, T. Rojo, *Polyhedron* **1999**, *18*, 3703–3711.
[34] J. García-Tojal, M. K. Urtiaga, R. Cortés, L. Lezama, T. Rojo, M. I. Arriortua, *J. Chem. Soc., Dalton Trans.* **1994**, 2233–2238.
[35] P. Gómez-Saiz, J. García-Tojal, M. A. Maestro, J. Mahía, F. J. Arnáiz, T. Rojo, *Polyhedron* **2002**, *21*, 2257–2263.
[36] K. Nakamoto, *Infrared and Raman Spectra of Inorganic and Coordination Compounds*, 5th edn., Wiley, New York, **1997**.
[37] E. S. Stern, C. J. Timmons, *Electronic Absorption Spectroscopy in Organic Chemistry*, Edward Arnold, London, **1970**.
[38] D. X. West, M. A. Lockwood, J. N. Albert, A. E. Liberta, *Spectrochim. Acta* **1991**, *49A*, 1809–1816.
[39] A. G. Bingham, H. Bögge, A. Müller, E. W. Ainscough, A. M. Brodie, *J. Chem. Soc., Dalton Trans.* **1987**, 493–499.
[40] A. B. P. Lever, *Inorganic Electronic Spectroscopy*, 2nd ed.; Elsevier: Amsterdam, **1986**.
[41] W. M. E. Koomen-van Oudenniel, R. A. G. de Graaf, J. G. Haasnoot, R. Prins, J. Reedijk, *Inorg. Chem.* **1989**, *28*, 1128–1133.
[42] B. J. Hathaway, *Coord. Chem. Rev.* **1970**, *5*, 143.
[43] E. W. Ainscough, A. M. Brodie, J. D. Ranford, J. M. Waters, *J. Chem. Soc., Dalton Trans.* **1991**, 1737–1742.
[44] B. Bleaney, K. D. Bowers, Pr oc. *R. Soc., London, Ser. A* **1952**, *214*, 451.
[45] M. Zentková, J. Kovác, A. Zentko, A. Kosturiak, A. Hudák, *J. Magn. Magn. Mater.* **1991**, *102*, L1.
[46] P. Román, C. Guzmán-Miralles, A. Luque, J. I. Beitia, J. Cano, F. Lloret, M. Julve, S. Alvarez, *Inorg. Chem.* **1996**, *35*, 3741–3751.
[47] J. Cano, P. Alemany, S. Alvarez, M. Verdaguer, E. Ruiz, *Chem. Eur. J.* **1998**, *4*, 476–484.
[48] P. J. Hay, J. C. Thibeault, R. Hoffmann, *J. Am. Chem. Soc.* **1975**, *97*, 4884–4899.

 © 2003 Wiley-VCH Verlag GmbH & Co. KGaA, Weinheim

[49] C. Mealli, D. M. Proserpio, *CACAO Program, Computer Aided Composition of Atomic Orbitals, PC version*, July **1992**, *J. Chem. Ed.* **1990**, *67*, 399−402.
[50] J. García-Tojal, J. L. Pizarro, L. Lezama, M. I. Arriortua, T. Rojo, *Inorg. Chim. Acta* **1998**, *278*, 150−158.
[51] O. Kahn, M. F. Charlot, *Nouv. J. Chim.* **1980**, *4*, 567.
[52] Y. Akhriff, J. Server-Carrió, A. Sancho, J. García-Lozano, E. Escrivá, J. V. Folgado, L. Soto, *Inorg. Chem.* **1999**, *38*, 1174−1185 and references therein.
[53] R. Prins, P. J. M. W. L. Birker, J. G. Haasnoot, G. C. Verschoor, J. Reedijk, *Inorg. Chem.* **1985**, *24*, 4128−4133.
[54] P. M. Slangen, P. J. van Koningsbruggen, J. G. Haasnoot, J. Jansen, S. Gorter, J. Reedijk, H. Kooijman, W. J. J. Smeets, A. L. Spek, *Inorg. Chim. Acta* **1993**, *212*, 289−301.
[55] P. M. Slangen, P. J. van Koningsbruggen, K. Goubitz, J. G. Haasnoot, J. Reedijk, *Inorg. Chem.* **1994**, *33*, 1121−1126.
[56] S. Ferrer, P. J. van Koningsbruggen, J. G. Haasnoot, J. Reedijk, H. Kooijman, A. L. Spek, L. Lezama, A. M. Arif, J. S. Miller, *J. Chem. Soc., Dalton Trans.* **1999**, 4269−4276.
[57] D. Ajo, A. Bencini, F. Mani, *Inorg. Chem.* **1988**, *27*, 2437−2444.
[58] E. Spodine, A. M. Atria, J. Valenzuela, J. Jalocha, J. Manzur, A. M. García, M. T. Garland, O. Peña, J.-Y. Saillard, *J. Chem. Soc., Dalton Trans.* **1999**, 3029−3034.
[59] F. E. Anderson, C. J. Duca, J. V. Scudi, *J. Am. Chem. Soc.* **1951**, *73*, 4967−4968.
[60] D. X. West, D. L. Huffman, J. S. Saleda, A. E. Liberta, *Transition Met. Chem.* **1991**, *16*, 565.
[61] A. G. Bingham, H. Bögge, A. Müller, E. W. Ainscough, A. M. Brodie, *J. Chem. Soc., Dalton Trans.* **1987**, 493−499.
[62] Compound **2** can be also obtained by addition of potassium iodide (0.166 g, 1 mmol) to an aqueous solution of $Cu(L_I)(NO_3)$ (0.30 g, 1 mmol) (yield 0.34 g, 93%).
[63] Compound **4** can be also prepared by mixing aqueous solutions of **3** (0.32 g, 0.5 mmol) and sodium bromide (0.1 g, 1 mmol) (yield 0.30 g, around 90%). Dark green crystals of **4** were obtained by slow reaction of **3** and sodium bromide in a diffusion device.
[64] The use of iodate as oxidizing agent in the cyclization of HL_Imm and HL_I gave the same results. However, the formation of iodine in the reaction forced us to make more separations to obtain the pure compounds and as a result the yield decreased.
[65] An analogous procedure carried out on complex **3** with iodate as oxidant yielded the $[Cu(L_I mm)(IO_3)]$ complex (yield 0.39 g, 90%) $C_8H_9CuIN_4O_3S$ (431.7): calcd. C 22.2, H 2.3, N 12.9, S 7.4; found C, 22.2, H 2.3, N 12.9, S 7.2. The molar conductivity of $5\cdot10^{-4}$ M solutions in water (dimethylformamide) at 25 °C is Λ_M = 73 (50) $\Omega^{-1}\cdot cm^2\cdot mol^{-1}$. Selected IR bands ($cm^{-1}$, KBr): 3220 m, 2979 w, 1597 s, 1572 s, 1538 vs, 1477 vs, 1355 vs, 1308 m, 1288 vs, 1225 s, 1180 s, 1178 m, 1116 s, 1097 m, 1038 m, 811 vs, 779 s, 751 vs, 732 vs, 720 vs, 608 m, 489 m. UV-visible bands in water, λ_{max} [nm] (ε, $M^{-1}\cdot cm^{-1}$): 287 (13000), 328 (13200), 385 (12000), 622 (170). EPR in the room temp.-to-120 K range (X-band, solid sample): g_1 = 2.195, g_2 = 2.054 and g_3 = 2.030. Likewise, the complex analogous to **2** was also synthesized and identified as $[Cu(L_I mm)I]$ (yield 0.33 g, 85%). $C_8H_9CuIN_4S$ (383.7): calcd. calcd. C 25.0, H 2.4, N 14.6, S 8.3; found C 25.0, H 2.4, N 14.8, S 7.8. The molar conductivity of $5\cdot10^{-4}$ M solutions in water (dimethylformamide) at 25 °C is Λ_M = 110 (41) $\Omega^{-1}cm^2mol^{-1}$. Selected IR bands (cm^{-1}, KBr): 3216 m, 3021 w, 2973 w, 1593 s, 1568 s, 1534 vs, 1472 s, 1354 vs, 1307 s, 1283 vs, 1225 s, 1178 s, 1118 s, 1099 m, 1039 s, 770 s, 603 w. UV-visible bands in water, λ_{max} [nm] (ε, $M^{-1}\cdot cm^{-1}$): 224 (25200), 287 (12300), 329 (12400), 386 (11250), 622 (150). EPR in the room temp.-to-120 K range (X-band, solid sample): $g_{\|}$ = 2.121 and $g_{\perp}$ = 2.038.
[66] Furthermore, complexes **5** and **6** were also prepared by adding $CuSO_4\cdot5H_2O$ to the acid, orange oxidizing solution of bromate and **7** or **8**, respectively, before the addition of NaOH.
[67] R. H. Blessing, *Acta Crystallogr., Sect. A* **1995**, *51*, 33−38.
[68] G. M. Sheldrick, *SHELXS−97, A Program for Crystal Structure Solution*, Univ. of Göttingen, Göttingen, Germany, **1997**.
[69] G. M. Sheldrick, *SHELXL-97*, P*rogram for the Refinement of Crystal Structures from Diffraction Data*; University of Göttingen: Göttingen, Germany, **1997**.
[70] *INTERNATIONAL Tables for X-Ray Crystallography*, Kluwer Academic Publishers, Dordrecht, The Netherlands, **1992**.
[71] P. Gómez-Saiz, J. García-Tojal, B. Donnadieu, L. Lezama, J. L. Pizarro, M. I. Arriortua, T. Rojo, *Eur. J. Inorg. Chem.* **2003**, 518−527.
[72] C. F. Bell, C. R. Theocharis, *Acta Crystallogr., Sect. C* **1987**, *43*, 26−29.

Received December 13, 2004

 © 2003 Wiley-VCH Verlag GmbH & Co. KGaA, Weinheim

Syntheses, Reactivity Studies and the Catalytic Properties of a Series of Tetraosmium−Gold Mixed-Metal Clusters

Yat Li[a] and Wing-Tak Wong*[a]

Keywords: Osmium / Gold / Clusters / Electrochemistry / Carbonylations

Treatment of the mixture of $[Os_4(\mu\text{-}H)_4(CO)_{12}]$ and $[AuPPh_3Cl]$ with excess triethylamine afforded three novel tetraosmium–gold mixed-metal clusters, $[Os_4Au_2(\mu\text{-}H)_2(CO)_{11}(PPh_3)_3]$ (**4**), $[Os_4Au_3(\mu\text{-}H)_3(CO)_{11}(PPh_3)_3]$ (**5**), and $[Os_4Au_4(\mu\text{-}H)_2(CO)_{11}(PPh_3)_4]$ (**6**) in moderate yields. Cluster $[Os_4Au(\mu\text{-}H)_3(CO)_{11}(NMe_3)(PPh_3)]$ (**2**) was also obtained in a similar reaction in the presence of trimethylamine *N*-oxide. They were fully characterized by different spectroscopic techniques, and the solid-state structures were established by X-ray analysis. These dimetallic clusters exhibit an osmium/gold ratio ranging from 1 to 4. Their electronic absorption properties, electrochemistry, and catalytic properties, as a result of the oxidative carbonylation of aniline, were investigated in terms of the Os/Au ratio.
(© Wiley-VCH Verlag GmbH & Co. KGaA, 69451 Weinheim, Germany, 2003)

Introduction

The chemistry of transition mixed-metal clusters containing (phosphane)gold units has been well established in the past decade.[1−14] The initial interest in these clusters stemmed from the perceived isolobal analogy between a hydride and a (phosphane)gold group.[15] This interest has continued to develop since they were found to be potential homogeneous dimetallic catalysts. The introduction of heterometallic metal−metal bonding into these clusters leads to an increase in the polarity of the molecule, which probably results in the enhancement of the catalytic activity. Examples of catalysis by mixed-metal clusters that contain (phosphane)gold groupings have been reported.[16−24] Previously, we reported that $[Os_4Au(\mu\text{-}H)_3(CO)_{12}(PPh_3)]$ (**1**) catalyzes the oxidative carbonylation of aniline to give methyl phenylcarbamate in methanol with good conversion and selectivity.[25] This paper reports in detail the syntheses and characterization of a series of novel tetraosmium−gold mixed-metal clusters with Os/Au ratios ranging from 1 to 4. A better understanding of the role of gold atoms in the dimetallic system has been developed through the study of their electronic absorption properties, electrochemistry, and catalytic properties.

[a] Department of Chemistry, The University of Hong Kong, Pokfulam Road, Hong Kong, P. R. China
Fax: (internat.) + 852/25472933
E-mail: wtwong@hkucc.hku.hk

Results and Discussion

The preparation of **1**−**6** is summarized in Scheme 1. In fact, the synthesis and characterization of **1** and **3** were reported by Lewis in the 1980s,[26] and it is surprising that the high-nuclearity tetraosmium−gold mixed-metal clusters can also be isolated in a similar reaction with an excess amount of triethylamine. It appears that the protons in $[Os_4(\mu\text{-}H)_4(CO)_{12}]$ were successively eliminated by Et_3N as $[Et_3NH]^+$, the vacant sites formed were then simultaneously filled up by $[AuPPh_3]^+$ to afford a series of osmium−gold mixed-metal clusters. The formation of gold clusters is also favorable in a reducing environment; as a result, the Au−Au bonds are formed in **3**−**6**. Nevertheless, further elimination of protons in **3**−**6** is improbable due to the limited reducing power of Et_3N. Recently, Raithby et al. have reported on the deprotonation of the cluster $[Os_4H(CO)_{12}(AuPR_3)_3]$ in the presence of $[AuPR_3]^+$ in an attempt to produce tetragold clusters, but met with little success. They alternatively used the chelated gold salt $[Au_2(Ph_2PCH_2PPh_2)Cl_2]$ to treat with the anion $[Os_4H_4(CO)_{11}]^{2-}$ and give $[Os_4(\mu\text{-}H)_2(CO)_{11}\{Au_2(dppm)\}_2]$.[27] The successful isolation of **5** and **6** proves that the deprotonation of (hydrido)osmium clusters in the presence of $[Au(PPh_3)]^+$ could be an efficient method for preparing the high-nuclearity osmium−gold mixed-metal clusters in a systematic manner.

These osmium−gold mixed-metal clusters were isolated with relatively small yields, even in the presence of excess $[AuPPh_3Cl]$, where the equilibrium between formation and decomposition of these mixed-metal clusters was established. Changing in stoichiometry of $[AuPPh_3Cl]$ has no significant effect on the product yields. This deprotonation reaction is also thought to be successive. Independent depro-

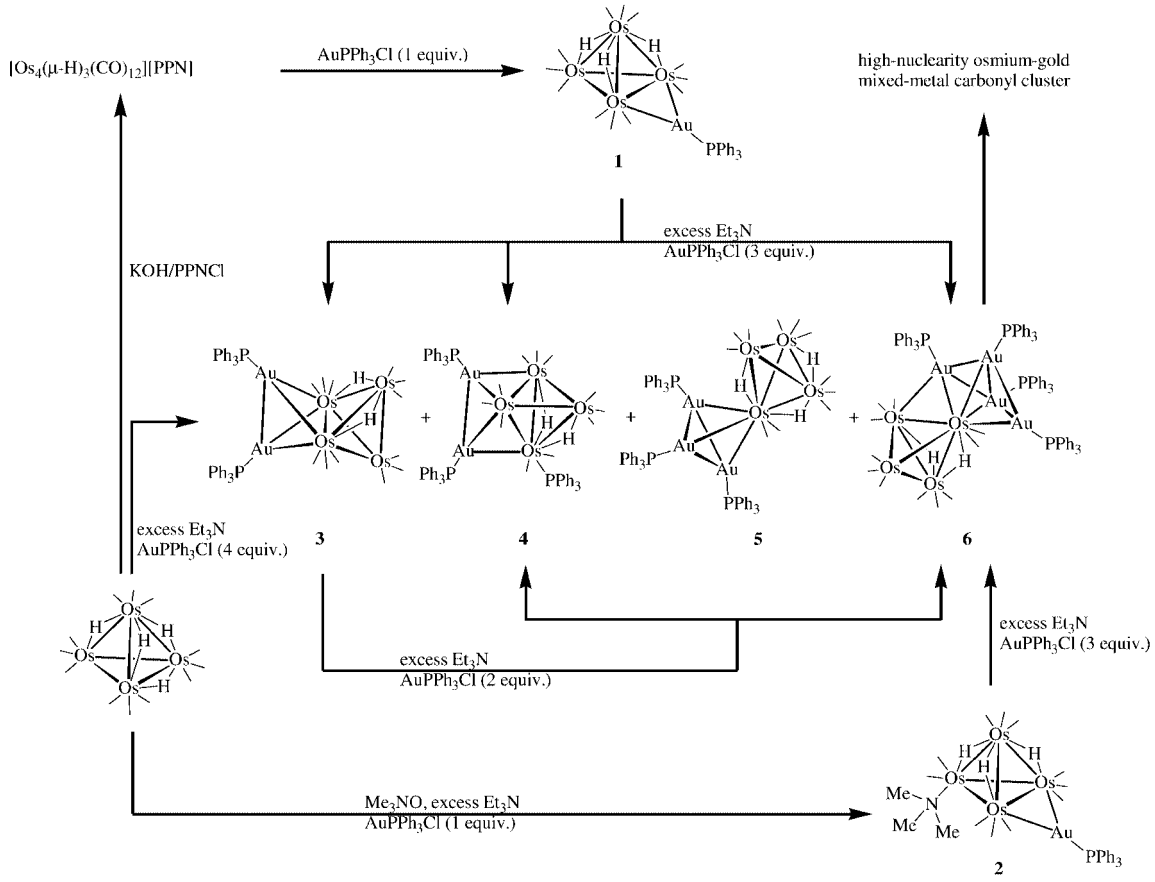

Scheme 1

tonation of all isolated compounds with an excess of the [$AuPPh_3Cl$] compound were studied (Scheme 1). This showed that **1**−**3** can be further converted into **4** or **6** in moderate yields. In addition, the deprotonation of **6** with an excess of [$AuPPh_3Cl$] gives an insoluble microcrystalline solid, which is believed to be a high-nuclearity osmium−gold mixed-metal carbonyl cluster with an Os/Au ratio of 3:2. The nature of this compound is still under active investigation.

Structural Characterization

The molecular structure of **2** is depicted in Figure 1. Four osmium atoms define a distorted tetrahedron. The Os(1)−Os(2) bond is symmetrically bridged by Au(1), with a bite angle Os(1)−Au(1)−Os(2) of 64.47(4)° and Os−Au bond lengths of 2.768(2) and 2.753(2) Å. The dihedral angle between the planes of Os(1)−Os(2)−Os(3) and Os(1)−Au(1)−Os(2) is 120.2° which is slightly larger than the corresponding value 109.5° that is observed in **1**.[25] The trimethylamine is terminally bonded to Os(3) with an Os(3)−N(1) distance of 2.24(2) Å which is similar to the value of 2.25(1) Å in $[Os_4(\mu\text{-}H)_4(CO)_{10}(NMe_3)\{\eta^1\text{-}NC_5H_4(N{=}N)C_6H_5\}]$.[28] The Os−Os bond lengths are observed in the range of 2.803(2)−3.009(2) Å, where the hydrido- or ligand-bridged Os−Os bonds are significantly elongated. The hydride ions bridging the Os(1)−Os(3) and Os(2)−Os(3) edges are chemically equivalent, which corresponds to the double integral hydride signal that is observed in the ^1H NMR spectrum of **2**.

The molecular structure of **4** is depicted in Figure 2, where the tetraosmium tetrahedron is terminally coordinated with eleven carbonyl ligands. Two {$AuPPh_3$} ligands bridge two adjacent Os−Os edges to form a distorted square pyramid [Au(1), Au(2), Os(1), Os(2), and Os(4)] which shares the plane Os(1)−Os(2)−Os(4) with the tetraosmium tetrahedron. A similar metal framework was observed in $[Os_4(CO)_{13}(AuPEt_3)_2]$.[29] The Au(1)−Au(2) bond [3.055(1) Å] is slightly shorter than the corresponding one in $[Os_4(CO)_{13}(AuPEt_3)_2]$ [3.128(1) Å], but is significantly longer than that in **3** [2.793(4) Å] where the two $AuPR_3$ groups bridge the same Os−Os edge.[26] An extra triphenylphosphane ligand is terminally bonded to Os(4), having an Os(4)−P(1) bond length of 2.362(6) Å. The gold− and osmium−triphenylphosphane protons give two multiplets with an integral ratio of 2:1 in the ^1H NMR spectrum of **4**. However, the P atoms of three different chemical environments in **4** give only one ^{31}P NMR signal. This is probably due to the fluxional behavior of the {$AuPPh_3$} ligand at room temperature on the NMR timescale which is frequently found in homo- and heteronuclear clusters.[30−32] Low-temperature ^{31}P NMR spectroscopy was carried out for **4** at 223 K and the signal resolved into two singlets with an intensity ratio of 2:1 (Figure 3). The formation of

 © 2003 Wiley-VCH Verlag GmbH & Co. KGaA, Weinheim

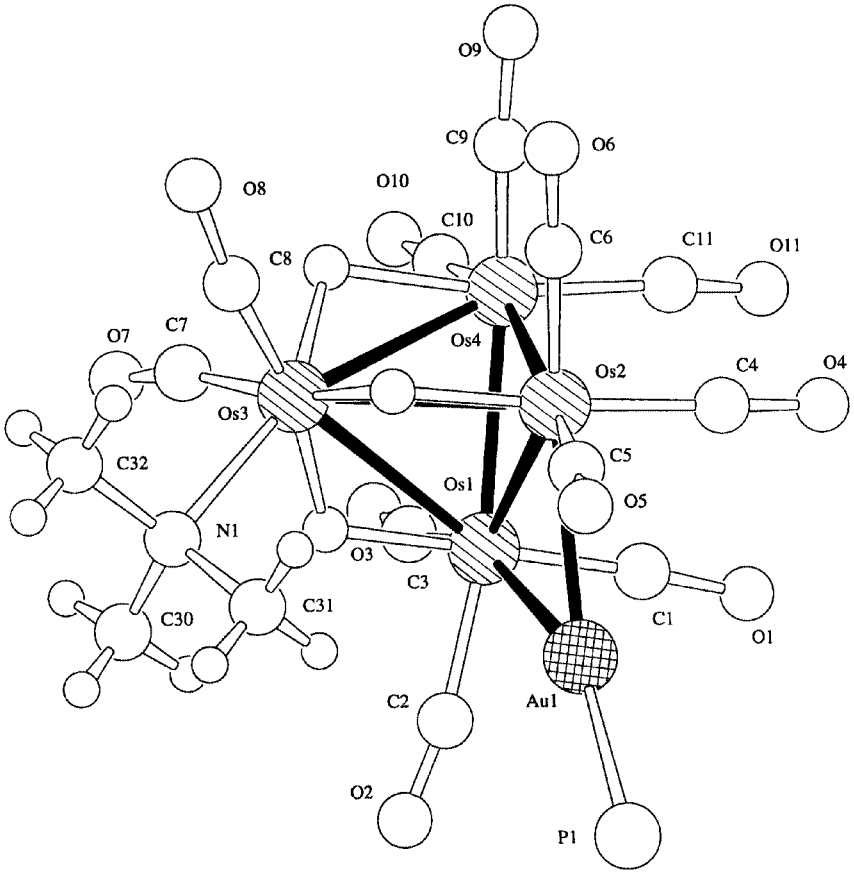

Figure 1. Simplified molecular structure of $[Os_4Au(\mu\text{-}H)_3(CO)_{11}(NMe_3)(PPh_3)]$ (**2**) with the atom numbering scheme (phenyl groups are omitted for clarity)

osmium−triphenylphosphane may be due to a triphenylphosphane impurity in the starting material, a similar observation has been reported in the case of $[Os_3(CO)_8(PPh_3)\{Au(PPh_3)\}(2\text{-}NHC_5H_4N)]$.[33] However, the moderate yield of **4** implies that the Au−P bond cleavage probably occurs in the reaction, giving free triphenylphosphane ligands.

The ^1H NMR spectrum of **5** shows that one double doublet and two triplet peaks with an integral ratio of 2:1:2, which corresponds to the 45 phenyl protons, are observed in the aromatic region. The protons are differentiated into *ortho*-, *meta*-, and *para*-phenyl protons according to their coupling patterns and integral values. A broad signal is found in the hydride region; therefore, variable-temperature ^1H NMR spectroscopic studies were carried out for **5**. At 223 K, the broad signal was resolved into three sharp singlet peaks with equal integral values. The ^{31}P NMR spectrum of **5** exhibits a singlet peak attributable to the three equivalent $\{AuPPh_3\}$ ligands.

To the best of our knowledge, cluster **5** is the first example of a cluster with an Os_4Au_3 metal core. The X-ray analysis shows that the gold atoms are terminally coordinated to one of the vertices of the tetraosmium tetrahedron and bonded with each other by Au−Au bonds to form another tetrahedron [Au(1), Au(2), Au(3), and Os(1)] (Figure 4). The Au−Au bond lengths lie in the range of 2.796(3)−2.860(2) Å, which is significantly shorter than the values that were observed in **4**. The two tetrahedrons are fused together by sharing the central Os(1) atom, which has the highest metal−metal connectivity, with three Os−Os contacts and three Os−Au contacts. This kind of coordination mode is rare and significantly different from the metal core arrangement observed in $[Ru_4Au_3(\mu_3\text{-}H)(CO)_{12}(PPh_3)_3]$.[34] The dihedral angle between the planes Os(1)−Os(2)−Os(4) and Os(1)−Au(1)−Au(2) is 79.3°, while the angle of Au(3)−Os(1)−Os(3) is 148.0°. It seems that the tetrahedrons bend towards each other. In terms of electron counting, each Au atom is simply considered as a one-electron donor, and the tangential gold−gold interactions are ignored. Overall, the molecule of **5** has 60 cluster valence electrons, and is isoelectronic with $[Os_4(\mu\text{-}H)_4(CO)_{12}]$ in the neutral oxidation state. It is surprising that **5** was not observed in the deprotonation reactions of **1**−**4**. It is reasonable to believe that the presence of the

 © 2003 Wiley-VCH Verlag GmbH & Co. KGaA, Weinheim

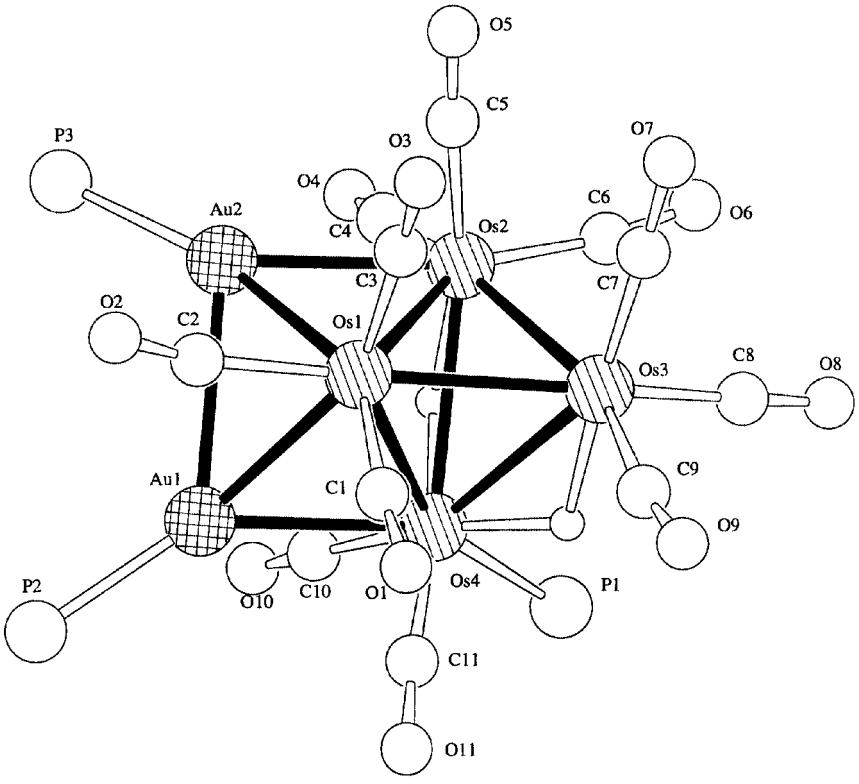

Figure 2. Simplified molecular structure of $[Os_4Au_2(\mu\text{-}H)_2(CO)_{11}(PPh_3)_3]$ (**4**) with the atom numbering scheme (phenyl groups are omitted for clarity)

bridging $\{AuPPh_3\}$ ligand in **1**−**4** probably makes the reaction unfavorable; an extra amount of energy is required to break the Os−Au bonds before the formation of **5**.

Cluster **6** exhibits aromatic ^1H NMR signals that are similar to those of **5**. Variable-temperature ^1H NMR studies were conducted for **6** at 223 K, the broad hydride peak was resolved into two sets of two sharp singlets, which correspond to the isomers of **6** in solution, named **6a** and **6b**, due to the disposition of hydrides. Three possible isomers of **6** are shown in Figure 5. It suggests that the ^1H NMR signal of the hydrido bridge on the Os*−Os bond is slightly different from the bridge on the Os−Os bond, where Os* is more electron-rich. The hydride ions of **6a** are most likely arranged in type C which gives relatively separated ^1H NMR signals at $\delta = -18.97$ and -14.52 ppm. Since the hydride signals of **6b** are relatively downfield and have a similar chemical shift, it is probably attributed to a type A isomer. Similarly, the fluxional behavior of $\{AuPPh_3\}$ ligands was also identified in the ^{31}P NMR spectrum of **6** at room temperature. The broad signal was resolved into eight singlet signals of equal intensity in the low-temperature ^{31}P NMR spectrum at 233 K, which is consistent with the existence of **6a** and **6b**.

The molecular structure of **6** is depicted in Figure 6. Similarly, the metal framework consists of a tetraosmium tetrahedron, and the Au(3) atom asymmetrically bridges the Os(1)−Os(2) edge. The other three gold atoms are terminally bonded to Os(1), and bonded with each other by Au−Au bonds to give a trigonal bipyramid that is defined by the atoms [Os(1), Au(1), Au(2), Au(3), and Au(4)]. The Au−Au bond lengths are observed in the range of 2.804(2)−3.069(2) Å, and are similar to the equivalent values observed in $[Os_4(\mu\text{-}H)_2(CO)_{11}\{Au_2(dppm)\}_2]$. As a result, the metal framework may be viewed as a tetrahedron fused with a trigonal bipyramid by sharing the Os(1) atom and connected by the Os(1)−Au(3) bond. The novel metal core geometry of **6** is significantly different from the arrangement observed in $[Os_4(\mu\text{-}H)_2(CO)_{11}Au_2(dppm)_2]$. The Os(1) atom has the highest metal−metal connectivity, with three Os−Os contacts and four Os−Au contacts. An overall of 60 cluster valence electrons is also observed in **6**.

Electrochemistry

The electrochemistry of **1**−**6** and the starting materials $[Os_4(\mu\text{-}H)_4(CO)_{12}]$ and $[N(PPh_3)_2][Os_4(\mu\text{-}H)_3(CO)_{12}]$ were investigated in acetonitrile using cyclic voltammetry and controlled potential coulometry with tetrabutylammonium hexafluorophosphate (TBAHFP) as the supporting electrolyte. The results of the voltammetric and controlled potential coulometry experiments are summarized in Table 1.

The cyclic voltammogram of **1** contains two irreversible anodic waves with a large potential difference between the

 © 2003 Wiley-VCH Verlag GmbH & Co. KGaA, Weinheim

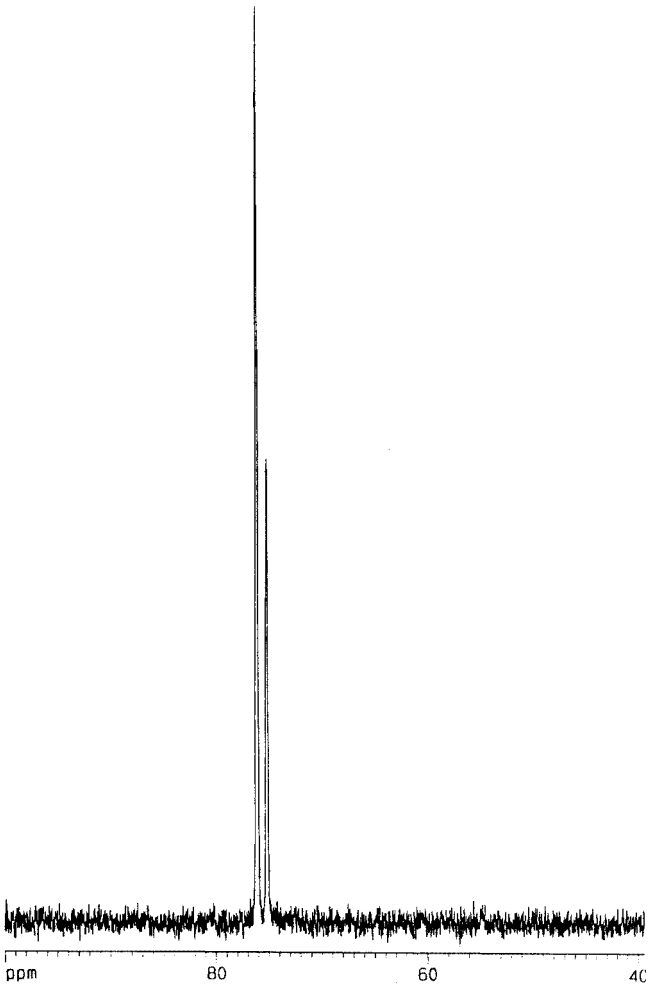

Figure 3. Low-temperature (223 K) ^{31}P NMR spectrum of $[Os_4Au_2(\mu\text{-}H)_2(CO)_{11}(PPh_3)_3]$ (**4**)

first and second oxidation peaks (around 1 V) (Figure 7, a) Reduction of **1** is believed to be difficult, as no cathodic wave is located within the solvent limit. The electrochemical behavior of **1** and $[PPN][Os_4(\mu\text{-}H)_3(CO)_{12}]$ is similar. The incorporation of the $\{AuPPh_3\}$ ligand seems to have no significant effect on the energy level of the HOMO of $[PPN][Os_4(\mu\text{-}H)_3(CO)_{12}]$.

The isolobal parent cluster $[Os_4(\mu\text{-}H)_4(CO)_{12}]$ unexpectedly has a different redox behavior to **1**. The cyclic voltammogram of $[Os_4(\mu\text{-}H)_4(CO)_{12}]$ contains an irreversible cathodic wave and an irreversible anodic wave. Accurate data of the controlled potential coulometry cannot be obtained because of the limited solubility of $[Os_4(\mu\text{-}H)_4(CO)_{12}]$ in organic solvents. Compared to **1** and $[PPN][Os_4(\mu\text{-}H)_3(CO)_{12}]$, the reduction of $[Os_4(\mu\text{-}H)_4(CO)_{12}]$ is believed to be more feasible but the oxidation is more difficult. The large positive shift (600 mV) in the oxidation potential implies that the substitution of the isolobal $\{AuPPh_3\}$ for hydrogen in $[Os_4(\mu\text{-}H)_4(CO)_{12}]$ seems to be able to activate the tetraosmium cluster towards the oxidation reaction by raising the HOMO.

Although the metal frameworks of **1** and **2** are exactly the same, the substitution of the carbonyl ligand by a trimethylamine ligand leads to different electrochemical behavior. The cyclic voltammogram of **1** exhibits both irreversible cathodic and anodic peaks (Figure 7, b). There is a positive shift in both the cathodic and anodic peaks with reference to those with equivalent values of **1**. This suggests that the coordination of the trimethylamine ligand lowers both the HOMO and the LUMO, which makes the oxidation more difficult while the reduction becomes easier.

The redox properties of the known compound **3** were also studied as a reference. The electrochemical behavior of **3** is similar to that of **1**. There are two irreversible anodic peaks, but no cathodic peak was located within the solvent limit. Controlled potential coulometry revealed that each oxidation peak involves 1 F/mol of **3**, which is different from the double-electron oxidation process observed in **1**. The first oxidation potential of **3** is similar to the value of **1**; however, it displays a 520 mV positive shift in the second oxidation potential. This shows that the monoanion of **3** undergoes a second oxidation, which is much easier since the oxidation process involves only one electron. The difference in the redox properties of **3** from **1** might be attributed to the presence of the Au−Au bond, which might alter the relative positions of the HOMO and LUMO.

As expected, the redox behavior of **4** is significantly different from that of **3**. This is probably due to the different arrangement in the metal core and the ligand effect of an extra osmium−triphenylphosphane ligand, which is similar to the case of the trimethylamine ligand observed in **2**. In fact, the cyclic voltammogram of **4** closely resembles that of **2**. The less negative reduction potential of **4** suggests that the osmium−triphenylphosphane ligand significantly lowers the LUMO of the cluster and makes the reduction easier. However, the oxidation potential of **4** is similar to the value obtained in **3** and **1**. The HOMO and LUMO of these kinds of mixed-metal clusters are believed to be metal- and ligand-based, respectively.

The cyclic voltammograms of **5** and **6** are similar, and also similar to that of **3**. Both exhibit two irreversible anodic waves. Comparing the oxidation potentials of $[Os_4(\mu\text{-}H)_4(CO)_{12}]$, **1**, **3**, **5**, and **6** (Os/Au range from 0 to 4), they display a slightly negative shift in the first oxidation potential as the number of gold atoms increase. This is probably because the delocalization of electrons in the high-nuclearity cluster is more significant, and the effect of losing an electron can be shared by more metal centers, making the oxidation easier. The energy level of the metal-based HOMO is believed to be raised, corresponding to the decrease in the oxidation potential. The second oxidation potential of **6** is similar to the equivalent value of **3**. However, **5** exhibits a significantly lowered second oxidation potential, with a negative shift of ca. 300 mV as compared with **6**. This suggests that the novel metal core arrangement of **5** might interrupt the arrangement of the HOMO and LUMO, making the cluster more reactive towards oxidation. It is difficult to correlate the reduction potential with the change in gold atom numbers, since the cathodic

 © 2003 Wiley-VCH Verlag GmbH & Co. KGaA, Weinheim

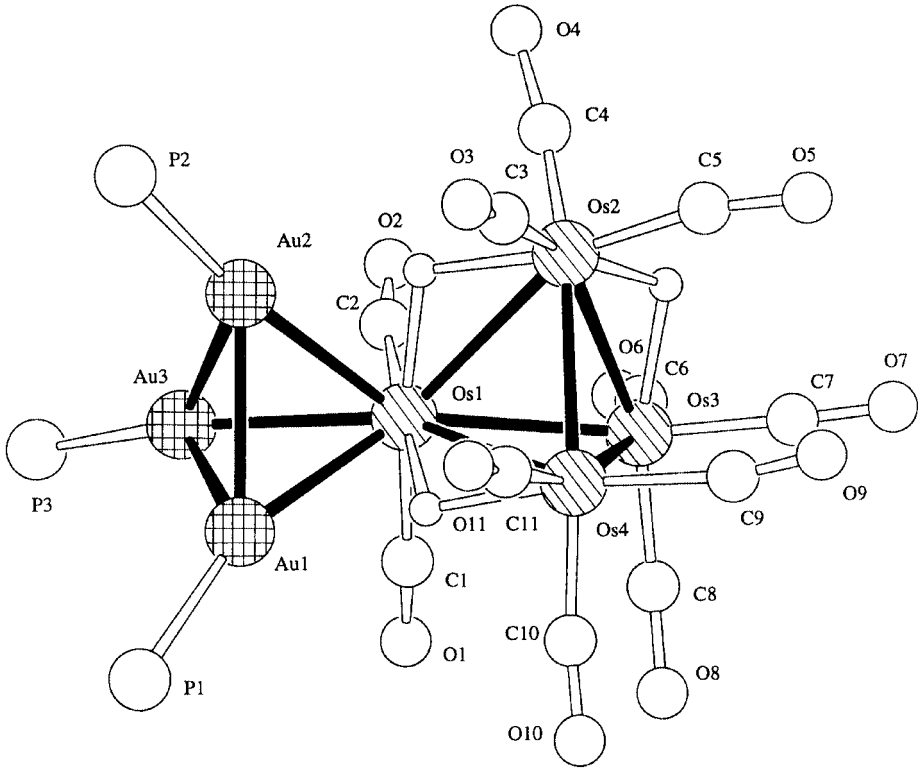

Figure 4. Simplified molecular structure of $[Os_4Au_3(\mu\text{-}H)_3(CO)_{11}(PPh_3)_3]$ (**5**) with the atom numbering scheme (phenyl groups are omitted for clarity)

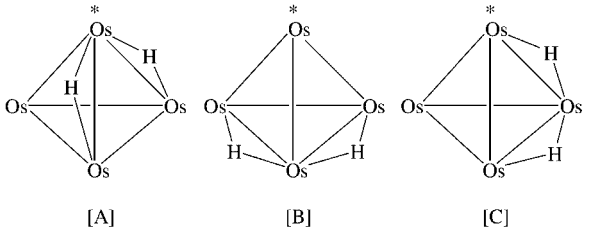

Figure 5. Three possible isomers of **6** (*: Os extensively connected with tetragold cluster)

wave of **1**, **3**, and **5** are not observed within the solvent limit.

Electronic Absorption Properties

Clusters **1**−**6** displayed a trend of color changes from yellow to red in the solid state, prompting us to examine them by optical spectroscopy. Table 2 presents the electronic absorption spectroscopic data for **1**−**6** together with the cluster $[PPN][Os_4(\mu\text{-}H)_3(CO)_{12}]$ in dichloromethane at ambient temperature.

The energy absorption bands of these osmium−gold mixed-metal clusters are within the range of 320 to 401 nm. Cluster **2** exhibits the highest energy absorption band at 320 nm. This implies that the energy gap between the HOMO and LUMO is the largest and is consistent with the large peak-to-peak separation (ca. 2.5 V) of the redox potentials observed in its cyclic voltammogram. On the other hand, both of the clusters **4** and **6** have the lowest energy absorption band at 401 nm, which corresponds to the small HOMO−LUMO energy gap. Consequently, the peak-to-peak separation of the redox waves (ca. 1.9 V) observed in their cyclic voltammograms is significantly small in comparison to the value of **2**. The similar separations in **4** (1.91 V) and **6** (1.96 V) suggest that the energy gap between HOMO and LUMO might be directly proportional to the separation of redox potentials in the cyclic voltammogram, in cases where the HOMO−LUMO involved in the electronic transition is assumed to have the same orbitals where the redox reaction occurs. According to this assumption, it might be possible to estimate the redox potential out of the solvent limit by using the electronic absorption spectroscopic data as a reference. As the electronic energy absorption bands of **1**, **3**, and **5** are observed in the range of 320 to 401 nm, the separation of their first anodic peak and first cathodic peak is believed to be within the range of 1.9 to 2.5 V. The transition energy gap between the HOMO−LUMO seems to decrease slightly as the HOMO is raised due to the increasing number of gold atoms in the cluster (Figure 8). This is fully consistent with their electrochemical behavior. Cluster **5** is an exceptional case, having a high-energy electronic absorption band that is attributable to the large separation of HOMO and LUMO. The reason might be related to the novel coordination mode of the gold atoms.

Catalytic Properties of 1 and 6 towards the Oxidative Carbonylation of Aniline

The catalytic performance of **1** and **6** towards the oxidative carbonylation of aniline in methanol was investigated

 © 2003 Wiley-VCH Verlag GmbH & Co. KGaA, Weinheim

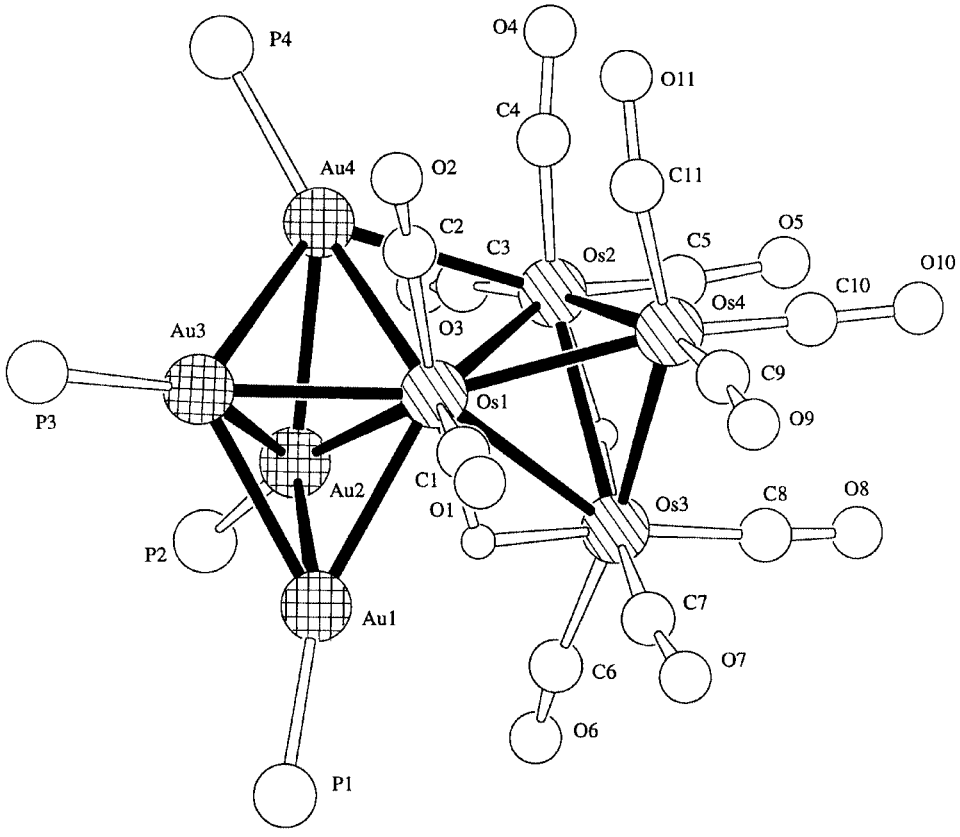

Figure 6. Simplified molecular structure of $[Os_4Au_4(\mu\text{-}H)_2(CO)_{11}(PPh_3)_4]$ (**6**) with the atom numbering scheme (phenyl groups are omitted for clarity)

Table 1. Electrochemical data of **1**−**6** and some starting materials

Cluster[a]	Oxidation		Reduction
	E_{pa2} [V][b]	E_{pa1} [V][b]	E_{pc1} [V][b]
$[Os_4(\mu\text{-}H)_4(CO)_{12}]$[c]	−	0.71	−1.99
$[PPN][Os_4(\mu\text{-}H)_3(CO)_{12}]$	1.01(2)	0.13(2)	−
1	1.11(2)	0.12(2)	−
2	−	0.51(2)	−2.00(2)
3	0.59(1)	0.18(1)	−
4	−	0.13(2)	−1.78(2)
5	0.37(1)	0.14(1)	−
6	0.56(1)	−0.08(1)	−2.02(2)

[a] About 10^{-3} M cluster in 0.1 M TBAHFP in acetonitrile at 298 K, the working electrode was a glassy carbon electrode, the auxiliary electrode and the reference electrode were a platinum wire and $Ag/AgNO_3$ (0 V) under the same conditions, calibrated with ferrocene. Scan rate was 100 $mV \cdot s^{-1}$. [b] E_{pa} and E_{pc} are the anodic and cathodic potentials, respectively, Values in parentheses are Faraday per mol of cluster. [c] Limited solubility in acetonitrile.

[Equation (1)]. The effect of reaction time, temperature, concentration of methanol, pressure (P_{CO} and P_{O_2}) and promoters (sulfuric acid and triphenylphosphane) were studied and optimized. Some selected catalytic results are presented in Table 3. The catalytic properties of the polynuclear and mononuclear homometallic starting materials, including $[Au(PPh_3)Cl]$, $[Os(CO)_3(DEAAB)Cl]$, $[Os(CO)_2(PAN)Cl]$, and $[N(PPh_3)_2][Os_4(\mu\text{-}H)_3(CO)_{12}]$ were also studied under the same conditions as a reference.

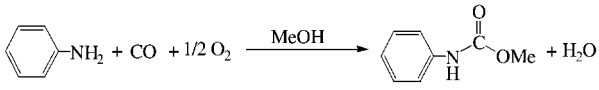

(1)

The catalysts **1** and **6** are active towards the oxidative carbonylation of aniline even without the promoters (Entries 2 and 3). However, the selectivity to carbamate is relatively low. The presence of promoters (triphenylphosphane and sulfuric acid) seems extremely important in achieving a reasonable selectivity in carbamate (Entries 5 and 6). Although catalysts **1** and **6** display slightly different interactions with the promoters, the overall catalytic performance towards the oxidative carbonylation of aniline in yielding carbamate is similar. This suggests that the effect of the osmium/gold ratio on this catalytic reaction is not significant. Consequently, a similar catalytic performance is believed to be found in the catalytic systems involving **2**−**5.**

The catalytic properties of catalysts $[Au(PPh_3)Cl]$ and $[PPN][Os_4(\mu\text{-}H)_3(CO)_{12}]$ are similar (Entries 4 and 7), but much less selective than the dimetallic systems. The synergism of dimetallic catalyst systems is believed to be significant in enhancing the selectivity towards carbamate. Two mononuclear osmium systems $[Os(CO)_2Cl(PAN)]$ and $[Os(CO)_3Cl(DEAAB)]$ were also studied, and exhibited a much lower TOF as compared with the cluster systems. In ad-

 © 2003 Wiley-VCH Verlag GmbH & Co. KGaA, Weinheim

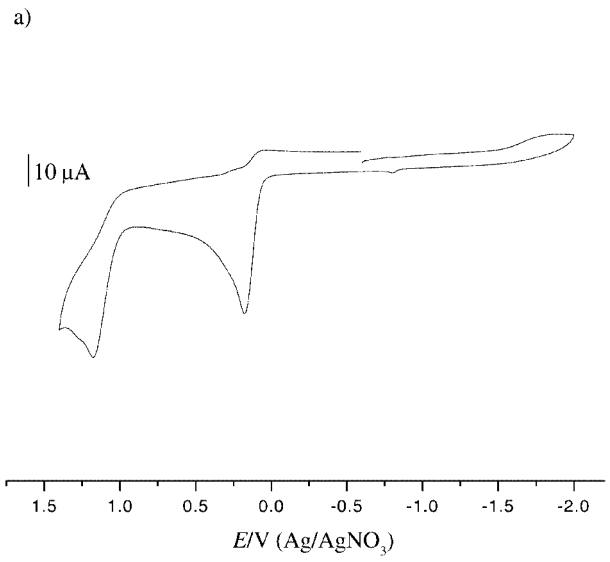

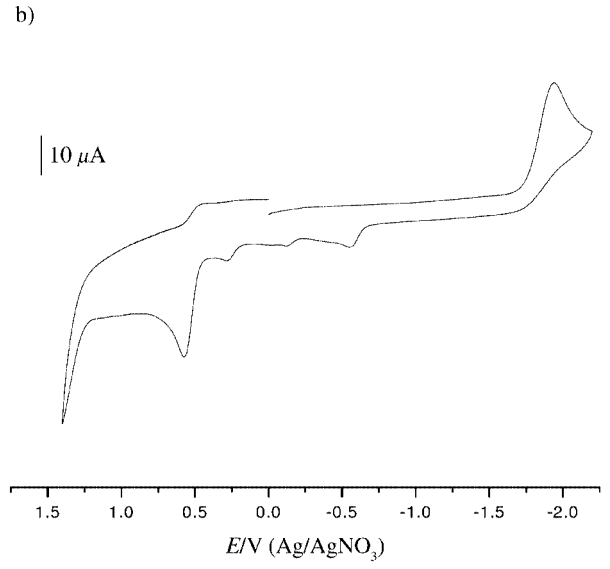

Figure 7. Cyclic voltammogram of a) **1** and b) **2** in acetonitrile, with 0.1 M TBAHFP as the supporting electrolyte, using a glassy carbon working electrode at 298 K; the voltammogram is recorded against an $Ag/AgNO_3$ reference electrode

Table 2. The electronic absorption spectroscopic data for **1**−**6** together with the cluster $[PPN][Os_4(\mu\text{-}H)_3(CO)_{12}]$

Cluster	λ_{max} [nm] (ε [dm^3 mol^{-1} cm^{-1}])[a]	Color
$[PPN][Os_4(\mu\text{-}H)_3(CO)_{12}]$	327 (11000)	yellow
1	330 (14000)	yellow
2	320 (12000)	yellow
3	366 (10000)	red
4	401 (12000)	red
5	334 (8000)[b]	yellow
6	401(11000)[b]	red

[a] In dichloromethane. [b] Shoulder.

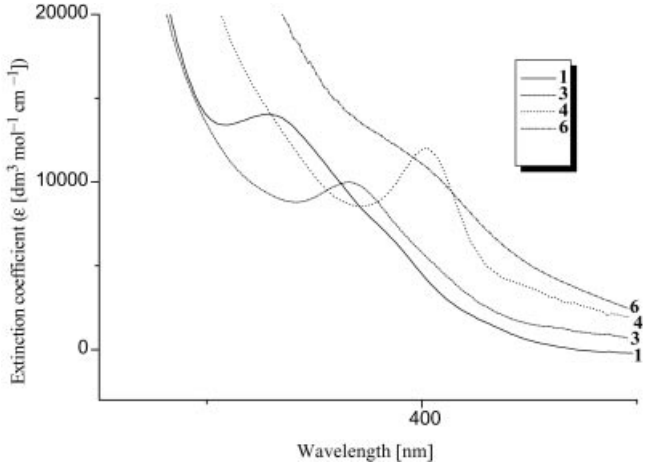

Figure 8. Electronic absorption bands of **1**, **3**, **4**, and **6**

dition, it is interesting to note that the distribution of by-products observed in polynuclear and mononuclear systems is different. Formaniline is the major by-product of mononuclear osmium systems, while the cluster systems favor the formation of azobenzene. This implies that the two systems might follow different catalytic pathways, which supports the proposition that the cluster is the active catalytic species in solution.

Conclusion

A series of novel osmium−gold mixed-metal clusters, exhibiting an osmium/gold ratio range from 1 to 4, were prepared in a systematic manner. The electrochemical studies show that the incorporation of an $\{AuPPh_3\}$ unit may activate the tetraosmium−carbonyl cluster toward oxidation by lowering the oxidation potential. A slightly negative shift of oxidation potential was observed as the number of gold atoms increased. This was further confirmed by the electronic absorption studies. The correlation between the redox behavior and the electronic absorption properties was established. Clusters **1** and **6** catalyze oxidative carbonylation of aniline yielding carbamate with a good activity and selectivity in the presence of promoters. The dimetallic synergism is proved, and the effect of the Os/Au ratio on catalytic performance does not seem to be significant. The dimetallic cluster is believed to be the active catalyst in the solution.

Experimental Section

General Remarks: All reactions and manipulations were carried out under argon using standard Schlenk techniques, except for the chromatographic separations. Solvents were purified by standard procedures and distilled prior to use.[35] Reactions were monitored by analytical thin-layer chromatography (Merck Kieselgel 60 F_{254}), and the products were separated by thin-layer chromatography on plates coated with silica (Merck Kieselgel 60 F_{254}). All chemicals, unless otherwise stated, were purchased commercially and used as

 © 2003 Wiley-VCH Verlag GmbH & Co. KGaA, Weinheim

Table 3. Catalytic results of **1**, **6**, and the starting materials towards the oxidative carbonylation of aniline

Entry	Catalyst[a]	Conversion(%)	Selectivity (%)					TOF[b]
			Methyl phenylcarbamate	*N*-Methyl-aniline	Quinazoline	Formaniline	Azobenzene	
1	[PPN][$Os_4(\mu\text{-}H)_3(CO)_{12}$]	35	0	22	0	0	78	210
2	**1**	97	8	0	4	4	46	582
3	**6**	97	9	4	8	4	18	582
4[c]	[PPN][$Os_4(\mu\text{-}H)_3(CO)_{12}$]	99	8	0	5	3	46	594
5[c]	**1**	63	65	10	15	0	0	378
6[c]	**6**	92	41	5	8	0	23	552
7[c]	[$Au(PPh_3)Cl$]	97	13	0	5	1	32	582
8[d]	[$Os(CO)_2Cl$(PAN)]	24	15	16	5	16	8	48
9[d]	[$Os(CO)_3Cl$(DEAAB)]	25	21	10	2	14	6	50

[a] Catalytic conditions: 155 °C, 4 MPa of CO, 2 MPa of O_2, 2 h, 20 mL of methanol. [b] Mol of aniline converted per mol of cluster per hour, catalyst/substrate ≈ 1200. [c] Promoters present (PPh_3/catalyst ≈ 10 and catalyst/H_2SO_4 ≈ 10). [d] PAN: 1-(2-pyridylazo)-2-naphthol; DEAAB: 4-(diethylamino)azobenzene; catalyst/substrate ≈ 600.

received. [$Os_4(\mu\text{-}H)_4(CO)_{12}$] and [$N(PPh_3)_2$][$Os_4(\mu\text{-}H)_3(CO)_{12}$] were prepared by the literature methods.[36−38] Infrared spectra were recorded with a Bio-Rad FTS-135 IR spectrometer, using 0.5 mm calcium fluoride solution cells, ^1H and ^{31}P NMR spectra with a Bruker DPX400 spectrometer using CD_2Cl_2, and referenced to $SiMe_4$ and 85% H_3PO_4, respectively. Variable-temperature ^1H and ^{31}P NMR spectra were obtained with a Bruker DPX500 spectrometer. Positive ionization fast atom bombardment (FAB) mass spectra were recorded with a Finnigan MAT 95 mass spectrometer, using *m*-nitrobenzyl alcohol as the matrix solvent. Electronic absorption spectra were obtained with a Hewlett−Packard 8453 diode array UV/Vis spectrophotometer using quartz cells, with a 1-cm path length at room temperature. Butterworth Laboratories, UK performed the microanalyses. The Energy Dispersive X-ray Analysis measurements were performed with a Scanning Electron Microscope (Leica Cambridge Stereo 360, 20KV).

Synthesis of [$Os_4Au(\mu\text{-}H)_3(CO)_{11}(NMe_3)(PPh_3)$] (2): Solid samples of [$Os_4(\mu\text{-}H)_4(CO)_{12}$] (110 mg, 0.1 mmol) and 1 equiv. of [$AuPPh_3Cl$] (49 mg, 0.1 mmol) were dissolved in 30 mL of dichloromethane; 1 equiv. of Me_3NO was then added dropwise to the solution mixture, followed by several drops of Et_3N at ambient temperature. The solution became yellow after stirring for 15 min, and the solvent was removed under reduced pressure. The residue was chromatographed by TLC using a mixture of *n*-hexane/dichloromethane (1:1, v/v) as eluent. The yellow band of [$Os_4Au(\mu\text{-}H)_3(CO)_{11}(NMe_3)(PPh_3)$] (**2**) was isolated. Yield: ca. 24 mg (15%). ^1H NMR (400 MHz, CD_2Cl_2, 298 K): δ = −25.32 (s, 2 H, hydride), −18.98 (s, 1 H, hydride), 2.95 (s, 9 H, methyl), 7.42 (m, 15 H, phenyl) ppm. ^{31}P NMR (400 MHz, CD_2Cl_2, 298 K): δ = 85.09 (s, PPh_3) ppm. IR [ν(CO)/cm^{-1}; CH_2Cl_2]: $\tilde{\nu}$ = 1933 m, 1975 w, 1983 w, 1989 w, 2024 s, 2028 s, 2039 s, 2074 m. FAB-MS [M^+]: *m*/*z* = 1590. $C_{32}H_{27}AuNO_{11}Os_4P$ (1590.31): calcd. C 24.17, H 1.71, N 0.88; found C 24.3, H 1.7, N 0.9.

Reaction of [$Os_4(\mu\text{-}H)_4(CO)_{12}$] with [$AuPPh_3Cl$] in Excess Et_3N: A solid sample of [$Os_4(\mu\text{-}H)_4(CO)_{12}$] (110 mg, 0.1 mmol) and excess [$AuPPh_3Cl$] (196 mg, 0.4 mmol) were dissolved in 30 mL of dichloromethane under argon. Excess Et_3N was added dropwise to this pale yellow solution, giving a dark brownish red clear solution after stirring for an additional 3 h. The decomposition of products was observed and then the solvent was reduced in vacuo. The residue was filtered, some unchanged [$Os_4(\mu\text{-}H)_4(CO)_{12}$] (32 mg, 0.029 mmol) was recovered. The filtrate was then subjected to preparative TLC using a solution mixture of *n*-hexane/dichloromethane (2:3, v/v) as eluent. The four consecutive orange bands were characterized as [$Os_4Au_2(\mu\text{-}H)_2(CO)_{12}(PPh_3)_2$] (**3**) (10 mg, 5%), [$Os_4Au_2(\mu\text{-}H)_2(CO)_{11}(PPh_3)_3$] (**4**) (9 mg, 4%), [$Os_4Au_3(\mu\text{-}H)_3(CO)_{11}(PPh_3)_3$] (**5**) (7 mg, 3%), and [$Os_4Au_4(\mu\text{-}H)_2(CO)_{11}(PPh_3)_4$] (**6**) (20 mg, 7%). **4**: ^1H NMR (400 MHz, CD_2Cl_2, 298 K): δ = −19.69 (s, 1 H, hydride), −19.66 (s, 1 H, hydride), 7.21 (m, 15 H, $OsPPh_3$), 7.38 (m, 30 H, $AuPPh_3$) ppm. ^{31}P NMR (400 MHz, CD_2Cl_2) 298 K: δ = 76.09 (s, PPh_3); 223 K: 76.10 (s, PPh_3), 75.17 (s, PPh_3) ppm. IR [ν(CO)/cm^{-1}; CH_2Cl_2]: $\tilde{\nu}$ = 1997 m, 2018 s, 2060 m. FAB-MS [M^+]: *m*/*z* = 2251. $C_{65}H_{47}Au_2O_{11}Os_4P_3$ (2251.90): calcd. C 34.67, H 2.10; found C 34.8, H 2.2. **5**: ^1H NMR (400 MHz, CD_2Cl_2) 298 K: δ = −16.52 (br., 3 H, hydride), 6.98 (t, $J_{H,H}$ = 7.35, 18 H, *meta*-PPh_3), 7.22 (t, $J_{H,H}$ = 7.50, 9 H, *para*-PPh_3), 7.30 (dd, $J_{H,H}$ = 7.90, 18 H, *ortho*-PPh_3); 223 K: δ = −17.87 (s, 1 H, hydride), −16.68 (s, 1 H, hydride), −14.13 (s, 1 H, hydride) ppm. ^{31}P NMR (400 MHz, CD_2Cl_2, 298 K): δ = 56.97 (s, PPh_3) ppm. IR [ν(CO)/cm^{-1}; CH_2Cl_2]: $\tilde{\nu}$ = 1985 m, 2003 s, 2032 s, 2062 s. FAB-MS [M^+]: *m*/*z* = 2449. $C_{65}H_{48}Au_3O_{11}Os_4P_3$ (2449.71): calcd. C 31.87, H 1.97; found C 31.9, H 1.9. **6**: ^1H NMR (400 MHz, CD_2Cl_2): 298 K: δ = −16.46 (br., 2 H, hydride), 6.98 (t, $J_{H,H}$ = 7, 24 H, *meta*-PPh_3), 7.22 (t, $J_{H,H}$ = 7, 12 H, *para*-PPh_3), 7.32 (dd, $J_{H,H}$ = 13, 24 H, *ortho*-PPh_3); 223 K: **6a**: δ = −18.97 (s, 1 H, hydride), −14.52 (s, 1 H, hydride); **6b**: δ = −18.59 (s, 1 H, hydride), −18.24 (s, 1 H, hydride) ppm. ^{31}P NMR (400 MHz, CD_2Cl_2): 298 K: δ = 64.27 (s, PPh_3); 223 K: δ = 50.45 (s, PPh_3), 53.90 (s, PPh_3), 66.76 (s, PPh_3), 68.82 (s, PPh_3), 73.79 (s, PPh_3), 79.73 (s, PPh_3), 82.50 (s, PPh_3), 83.58 (s, PPh_3) ppm. IR [ν(CO)/cm^{-1}; CH_2Cl_2]: $\tilde{\nu}$ = 1972 w, 1993 s, 2015 m, 2051 s. FAB-MS [M^+]: *m*/*z* = 2907. $C_{83}H_{62}Au_4O_{11}Os_4P_4$ (2908.12): calcd. C 34.28, H 2.15; found C 34.2, H 2.1.

Reaction of 1 with [$AuPPh_3Cl$] in Excess Et_3N: A solution of **1** (96 mg, 0.06 mmol) and excess [$AuPPh_3Cl$] in dichloromethane was stirred at room temperature. To this yellow solution, excess Et_3N was added dropwise to give a dark orange red solution. After stirring for 3 h, decomposition of products was observed. The solvent was then removed in vacuo. The residue was then subjected to TLC separation using *n*-hexane/dichloromethane (1:1, v/v) as the eluent. Three bands were obtained in the order of elution as **3** (17 mg, 14%), **4** (33 mg, 24%), and **6** (24 mg, 14%).

Reaction of 2 with [$AuPPh_3Cl$] in Excess Et_3N: To a yellow solution of **2** (32 mg, 0.02 mmol) and excess [$AuPPh_3Cl$] in dichloromethane, excess Et_3N was added. The yellow solution changed to orange after stirring for 3 h, accompanied by some decomposition prod-

 © 2003 Wiley-VCH Verlag GmbH & Co. KGaA, Weinheim

ucts. The solvent was reduced under reduced pressure and the residue was chromatographed on silica with *n*-hexane/dichloromethane (1:1, v/v) as the eluent. Cluster **6** (7 mg, 12%) was isolated in moderate yield together with some unchanged **2** (12 mg, 0.008 mmol).

Reaction of 3 with [AuPPh$_3$Cl] in Excess Et$_3$N: An orange sample of **3** (40 mg, 0.02 mmol) and excess [AuPPh$_3$Cl] were mixed in dichloromethane. Excess Et$_3$N was added and the resultant orange solution was stirred at ambient temperature for 4 h. The solvent was reduced under reduced pressure and the residue was subjected to preparative TLC with *n*-hexane/dichloromethane (1:1, v/v) as the eluent. Two consecutive orange bands were identified as **4** (14 mg, 31%) and **6** (10 mg, 17%).

Reaction of 4 with [AuPPh$_3$Cl] in Excess Et$_3$N: An orange solution of **4** (47 mg, 0.02 mmol) and excess [AuPPh$_3$Cl] in dichloromethane were stirred with excess Et$_3$N for 6 h. No observable change could be detected, but a slight decomposition of starting material occurred.

Reaction of 5 with [AuPPh$_3$Cl] in Excess Et$_3$N: The reactivity of **5** cannot be thoroughly studied due to the limited availability of sample.

Reaction of 6 with [AuPPh$_3$Cl] in Excess Et$_3$N: A red solution of **6** (32 mg, 0.01 mmol) and excess [AuPPh$_3$Cl] were mixed in dichloromethane. Excess Et$_3$N was added and the resulting solution was stirred for an additional 6 h; purple insoluble microcrystalline precipitates appeared. These solids were confirmed as mixed-metal clusters with an Os/Au ratio of 3:2 by Energy Dispersive X-ray Analysis with SEM. IR [ν(CO)/cm^{-1}; KBr]: $\tilde{\nu}$ = 1952 m, 1979 s.

Catalytic Reactions: The catalytic reactions were performed inside a Parr high-pressure stainless steel reactor (100 mL) with internal magnetic stirring. The methanol, aniline, catalysts and promoters were charged into the reaction vessel. The reactor was sealed with six cap screws in a split-ring cover clamp. The air in the vessel was replaced with dinitrogen by 3 freeze-pump-thaw cycles. It was ensured that there was no leakage of gas. The reaction gas (CO and O_2) was then introduced into the reactor inside the fumehood. The reactor was heated to the preset temperature with a thermoregulated heater for a preset time period. At the end of the reaction, the reactor was cooled with an ice bath in order to quench the reaction immediately and the reaction gas was evacuated in the fumehood. The resulting liquid mixture was analyzed by GC and GC-MS with an HP 5890A and G1800C GCD Series II, respectively.

Electrochemical Studies: Electrochemical measurements were performed with an EG&G Princeton Applied Research (PAR) Model 273A potentiostat, connected to an interfaced computer employing PAR 270 electrochemical software. Cyclic volatmmograms and bulk electrolyses were carried out in a gas-tight cell consisting of three chambers that were separated at the bottom by fine frits equipped with a glassy carbon (Bioanalytical) or a carbon cloth (80 mm^2) working electrode, a platinum gauze auxiliary electrode (Aldrich), and an Ag/AgNO$_3$ reference electrode (Bioanalytical) at room temperature; 0.1 M *n*-tetrabutylammonium hexafluorophosphate (TBAHFP) in anhydrous deoxygenated acetonitrile was used as a supporting electrolyte. Ferrocene was added at the end of each experiment as an internal standard. The working potential (E_w) for redox processes was ca. 0.15 V more positive/negative than the corresponding electrode potential (E_p); the coulometric experiment was performed in duplicate.

X-ray Crystallographic Study: Single crystals were grown from their appropriate solvent systems under favorable conditions. Intensity data were collected at ambient temperature using a Bruker SMART 1K CCD diffractometer with graphite-monochromated Mo-K_α radiation using ω scans. Details of the intensity data collection and crystal data are given in Table 4, and selected bond lengths and angles are listed in Table 5. The data were corrected for Lorentz and polarization effects. The structures were solved by direct methods (SIR92[39] or SHELXS-86[40]), and expanded using Fourier techniques (DIRDIF94).[41] Some non-hydrogen atoms were refined anisotropically, while the rest were refined isotropically. Hydrogen atoms were included but not refined. All calculations were

Table 4. Crystal data and data collection parameters for **2** and **4**−**6**

	2	**4**	**5**	**6**
Empirical formula	$C_{32}H_{27}NO_{11}PAuOs_4$	$[C_{65}H_{47}O_{11}P_3Au_2Os_4]\cdot CHCl_3$	$C_{65}H_{48}O_{11}P_3Au_3Os_4$	$[C_{83}H_{62}O_{11}P_4Au_4Os_4]\cdot 2CHCl_3$
Formula mass	1590.31	2371.11	2449.71	3146.71
Crystal color, habit	Red, block	Red, plate	Red, block	Red, plate
Crystal dimensions [mm]	0.24 × 0.21 × 0.10	0.33 × 0.22 × 0.05	0.19 × 0.17 × 0.11	0.35 × 0.39 × 0.05
Crystal system	orthorhombic	triclinic	monoclinic	monoclinic
Space group	*Pbca* (no. 61)	$P\bar{1}$ (no. 2)	$P2_1/n$ (no. 14)	$P2_1/c$ (no. 14)
a [Å]	10.359(1)	12.157(1)	20.094(3)	14.789(2)
b [Å]	18.232(2)	14.377(1)	14.974(2)	24.768(3)
c [Å]	41.268(3)	23.463(2)	23.129(4)	24.760(3)
α [Å]	90	94.63(2)	90	90
β [Å]	90	93.04(2)	103.16(1)	96.10(1)
γ [Å]	90	90.14(2)	90	90
V [Å^3]	7793(1)	4081.7(6)	6776(1)	9018(1)
Z	8	2	4	4
D_c [g cm^{-3}]	2.710	1.929	2.401	2.317
μ(Mo-K_α) [cm^{-1}]	168.46	99.95	140.82	124.16
Reflections collected	49414	25597	42348	56388
Unique reflections	9763	17728	15893	18512
Observed reflections [$I > 1.5\sigma(I)$]	1471	9071	2149	2564
R	0.0323	0.0615	0.0443	0.0432
R_w	0.0305	0.0754	0.0529	0.0449
Goodness of fit *S*	1.143	1.735	1.556	1.437

 © 2003 Wiley-VCH Verlag GmbH & Co. KGaA, Weinheim

Table 5. Selected bond lengths [Å] and angles [°] for **2** and **4**−**6**

	2	**4**	**5**	**6**
Os(1)−Os(2)	2.944(2)	2.897(1)	2.978(3)	3.002(2)
Os(1)−Os(3)	3.009(2)	2.832(1)	2.814(3)	2.992(2)
Os(1)−Os(4)	2.803(2)	2.973(1)	2.974(2)	2.798(2)
Os(2)−Os(3)	3.012(2)	2.796(1)	2.888(3)	2.929(2)
Os(2)−Os(4)	2.816(2)	3.006(1)	2.802(3)	2.806(3)
Os(3)−Os(4)	2.965(2)	3.017(1)	2.778(3)	2.775(2)
Au(1)−Os(1)	2.768(2)	2.742(1)	2.749(2)	2.783(2)
Au(1)−Os(2)	2.753(2)			
Au(1)−Os(2)		2.883(1)		
Au(2)−Os(1)		2.751(1)	2.744(3)	2.745(2)
Au(2)−Os(2)		2.789(1)		
Au(3)−Os(1)			2.759(2)	2.726(2)
Au(4)−Os(1)				2.820(2)
Au(1)−Au(2)		3.055(1)	2.796(3)	2.898(2)
Au(2)−Au(3)			2.860(2)	2.874(2)
Au(1)−Au(3)			2.804(2)	2.810(2)
Au(2)−Au(4)				2.804(2)
Au(3)−Au(4)				3.069(2)
Au(1)−P(1)	2.281(8)		2.25(1)	2.265(10)
Au(1)−P(2)		2.300(6)		
Au(2)−P(2)			2.26(1)	2.283(10)
Au(2)−P(3)		2.309(6)		
Au(3)−P(3)			2.26(1)	2.24(1)
Au(4)−P(4)				2.33(1)
Os(4)−P(1)		2.362(6)		
Os(3)−N(1)	2.24(2)			
Os(1)−Au(1)−Os(2)	64.47(4)			
Os(1)−Au(1)−Os(4)		63.76(3)		
Os(1)−Au(2)−Os(2)		63.05(3)		
Os(1)−Au(4)−Os(2)				62.80(5)
Au(2)−Au(1)−Os(1)		56.36(3)		
Au(2)−Au(1)−Os(4)		82.54(3)		
Au(1)−Os(1)−Au(2)		67.57(3)	61.20(6)	
Au(1)−Os(1)−Au(3)			61.21(6)	
Au(2)−Os(1)−Au(3)			62.62(6)	

performed using the teXsan[42] crystallographic software package of Molecular Structure Corporation. CCDC-194826 to -194829 contain the supplementary crystallographic data for this paper. These data can be obtained free of charge at www.ccdc.cam.ac.uk/conts/retrieving.html [or from the Cambridge Crystallographic Data Centre, 12 Union Road, Cambridge CB2 1EZ, UK; Fax: (internat.) + 44-1223/336-033; E-mail: deposit@ccdc.cam.ac.uk].

Acknowledgments

We gratefully acknowledge financial support from the Hong Kong Research Grants Council and the University of Hong Kong. Y. L. acknowledges the receipt of a postgraduate studentship (1999−2002) and the Li Po Chun Scholarship (2001−2002) administered by the University of Hong Kong and the Sir Edward Youde Memorial Fellowship (2001−2002) awarded by the Sir Edward Youde Memorial Trustees.

[1] J. Lewis, P. R. Raithby, in: *Metal Clusters In Chemistry* (Eds.: P. Braunstein, L. A. Oro, P. R. Raithby), Wiley-VCH, Weinheim, **1999**, pp. 348−380.
[2] I. Salter, in: *Comprehensive Organometallic Chemistry II* (Eds.: E. W. Abel, F. G. A. Stone, G. Wilkinson), Pergamon Press, Oxford, **1995**, vol. 10, pp. 255−322.
[3] A. J. Amoroso, J. Lewis, P. R. Raithby, W. T. Wong, in: *The Chemistry of the Copper and Zinc Triads* (Eds.: A. J. Welch, S. K. Chapman), The Royal Society of Chemistry, Cambridge, **1993**, pp. 202−206.
[4] Z. Ahkter, A. J. Edwards, S. L. Ingham, J. Lewis, A. M. Martin Castro, P. R. Raithby, G. P. Shields, *J. Clust. Sci.* **2000**, *11*, 217−226.
[5] Z. Ahkter, J. F. Gallagher, J. Lewis, P. R. Raithby, G. P. Shields, *J. Organomet. Chem.* **2000**, *614*−*615*, 231−237.
[6] A. J. Amoroso, M. A. Beswick, C. K. Li, J. Lewis, P. R. Raithby, M. C. Ramirez de Arellano, *J. Organomet. Chem.* **1999**, *573*, 247−253.
[7] Z. Ahkter, S. L. Ingham, J. Lewis, P. R. Raithby, *J. Organomet. Chem.* **1998**, *550*, 131−139.
[8] C. M. Hay, N. E. Leadbeater, J. Lewis, P. R. Raithby, K. Burgess, *New J. Chem.* **1998**, *22*, 787−788.
[9] Z. Akhter, S. L. Ingham, J. Lewis, P. R. Raithby, *Angew. Chem. Int. Ed. Engl.* **1996**, *35*, 992−993.
[10] C. Cathey, J. Lewis, P. R. Raithby, M. C. Ramirez de Arellano, *J. Chem. Soc., Dalton Trans.* **1994**, 3331−3332.
[11] Z. Akhter, S. L. Ingham, J. Lewis, P. R. Raithby, *J. Organomet. Chem.* **1994**, *474*, 165−171.
[12] M. M. Harding, B. Kariuki, A. J. Mathews, A. K. Smith, P. Braunstein, *J. Chem. Soc., Dalton Trans.* **1994**, 33−36.
[13] B. F. G. Johnson, F. J. Lahoz, J. Lewis, N. D. Prior, P. R. Raithby, W.-T. Wong, *J. Chem. Soc., Dalton Trans.* **1992**, 1701−1708.
[14] C. M. Hay, B. F. G. Johnson, J. Lewis, N. D. Prior, P. R. Raithby, W. T. Wong, *J. Organomet. Chem.* **1991**, *401*, C20−C22.
[15] R. Hoffmann, *Angew. Chem. Int. Ed. Engl.* **1982**, *21*, 711−724.
[16] L. Pignolet, in: *Catalysis by Di- and Polynuclear Metal Cluster Complexes* (Eds.: R. D. Adams, F. A. Cotton), Wiley-VCH, New York, **1998**, pp. 95−126.
[17] P. Braunstein, J. Rose, in: *Metal Clusters in Chemistry* (Eds.: P. Braunstein, L. A. Oro, P. R. Raithby), Wiley-VCH, Weinheim, Germany, **1999**, vol. 2, pp. 616−677.
[18] R. Pierantozzi, K. J. McQuade, B. C. Gates, M. Wolf, H. Knozinger, W. Ruhmann, *J. Am. Chem. Soc.* **1979**, *101*, 5436−5438.
[19] J. Evans, J. X. Gao, *J. Chem. Soc., Chem. Commun.* **1985**, 39−40.
[20] M. A. Aubart, B. D. Chandler, R. A. T. Gould, D. A. Krogstad, M. F. J. Schoondergang, L. H. Pignolet, *Inorg. Chem.* **1994**, *33*, 3724−3734.
[21] M. A. Aubart, L. H. Pignolet, *J. Am. Chem. Soc.* **1992**, *114*, 7901−7903.
[22] L. H. Pignolet, M. A. Aubart, K. L. Criaghead, R. A. T. Gould, D. A. Krogstad, J. S. Wiley, *Coord. Chem. Rev.* **1995**, *143*, 219−263.
[23] L. I. Rubinstein, L. H. Pignolet, *Inorg. Chem.* **1996**, *35*, 6755−6762.
[24] M. A. Aubart, J. F. D. Koch, L. H. Pignolet, *Inorg. Chem.* **1994**, *33*, 3852−3854.
[25] Y. Li, W. X. Pan, W. T. Wong, *J. Cluster Sci.* **2002**, *13*, 223−233.
[26] B. F. G. Johnson, D. A. Kaner, J. Lewis, P. R. Raithby, M. J. Taylor, *Polyhedron* **1982**, *1*, 105−107.
[27] M. R. A. Al-Mandhary, J. Lewis, P. R. Raithby, *J. Organomet. Chem.* **1997**, *536*, 549−551.
[28] Y. Li, W. T. Wong, *J. Cluster Sci.* **2001**, *12*, 595−617.
[29] C. M. Hay, B. F. G. Johnson, J. Lewis, R. C. S. Mcqueen, P. R. Raithby, R. M. Sorrell, M. J. Taylor, *Organometallics* **1985**, *4*, 202−205.
[30] K. P. Hall, B. R. C. Theobald, D. I. Guilmour, D. M. P. Mingos, A. J. Welsh, *J. Chem. Soc., Chem. Commum.* **1982**, 528−530.
[31] L. J. Farrugia, M. J. Freeman, M. Green, A. G. Orpen, F. G. A. Stone, I. D. Salter, *J. Organomet. Chem.* **1983**, *249*, 273−288.

 © 2003 Wiley-VCH Verlag GmbH & Co. KGaA, Weinheim

[32] S. R. Bunkall, H. D. Holden, B. F. G. Johnson, J. Lewis, G. N. Pain, P. R. Raithby, M. J. Taylor, *J. Chem. Soc., Chem. Commum.* **1984**, 25−27.
[33] K. Burgess, B. F. G. Johnson, J. Lewis, P. R. Raithby, *J. Chem. Soc., Dalton Trans.* **1983**, 1661−1665.
[34] J. A. K. Howard, I. D. Slater, F. G. A. Stone, *Polyhedron* **1984**, *3*, 567−573.
[35] D. D. Perrin, W. L. F. Armarego, *Purification of Laboratory Chemicals*, 4th ed., Butterworth-Heinemann, Oxford, **1996**.
[36] H. D. Kaesz, S. A. R. Knox, J. W. Koepke, R. B. Saillant, *J. Chem. Soc., Chem. Commun.* **1971**, 477.
[37] B. F. G. Johnson, J. Lewis, P. R. Raithby, G. M. Scheldrick, K. Wong, *J. Chem. Soc., Dalton Trans.* **1978**, 673−676.
[38] C. Zuccaro, G. Pampaloni, F. Calderazzo, *Inorg. Synth.* **1989**, *26*, 293−295.
[39] SIR92: A. Altomare, G. Cascarano, C. Giacovazzo, A. Guagliardi, *J. Appl. Crystallogr.* **1993**, *26*, 343−350.
[40] SHELXS 86, Program for Crystal Structure Solution: G. M. Sheldrick, *Acta Crystallgr., Sect. A* **1990**, *46*, 467−473.
[41] DIRDIF94: P. T. Beurskens, G. Admiraal, G. Beurskens, W. P. Bosman, R. de Gelder, R. Israel, J. M. M. Smits, *The DIRDIF-94 program system*, Technical Report of the Crystallography Laboratory, University of Nijmegen, The Netherlands, **1994**.
[42] TeXsan: Crystal Structure Analysis Package, Molecular Structure Corporation, The Woodlands, TX, USA, **1985** and **1992**.

Received December 27, 2002

 © 2003 Wiley-VCH Verlag GmbH & Co. KGaA, Weinheim

Coordination of Actinide Ions in Wells−Dawson Heteropolyoxoanion Complexes

Ming-Hsi Chiang,[a] Clayton W. Williams,[a] L. Soderholm,*[a] and Mark R. Antonio*[a]

Keywords: Actinides / Electrostatic interactions / Lanthanides / Polyoxometalates / X-ray absorption spectroscopy

Although many low-valent (III, IV) actinide (An) ions are known to form coordination complexes with the α-2 isomer of the lacunary Wells–Dawson polyoxoanion, $[P_2W_{17}O_{61}]^{10-}$, there is little structural information about the An–O interactions, particularly in solution. We have probed the An–O coordination environment for the series of clusters $[An(\alpha\text{-}2\text{-}P_2W_{17}O_{61})_2]^{n-}$ with An^{4+} (Th^{4+}, U^{4+}, Np^{4+}, Pu^{4+}) and An^{3+} (Np^{3+}, Pu^{3+}, Am^{3+}) in both solution and solid phases using X-ray absorption fine structure (XAFS). Comparisons are made with the lanthanide (Ln) coordination environments in the series of 4*f*-ion clusters, $[Ln^{n+}(\alpha\text{-}2\text{-}P_2W_{17}O_{61})_2]^{n-20}$, and with the related monovacant Lindqvist anions, $[Ln^{n+}(W_5O_{18})_2]^{n-12}$, for $n = 3, 4$. The average An–O_8 and Ln–O_8 distances correlate with their cationic VIII-coordinate ionic radii, indicating that the An and Ln ions have indistinguishable coordination behavior. Metrical details are consistent with simple charge and size considerations for both trivalent and tetravalent An ions as well as Ln ions coordinated with α-2-$[P_2W_{17}O_{61}]^{10-}$ and $[W_5O_{18}]^{6-}$. This result is contrasted to trends established for these *f*-ions coordinated to the Preyssler anion $[Ln^{n+}P_5W_{30}O_{110}]^{n-15}$.

(© Wiley-VCH Verlag GmbH & Co. KGaA, 69451 Weinheim, Germany, 2003)

Introduction

A significant body of international work demonstrates that polyoxometalates like the lacunary monovacant Wells−Dawson anion $[P_2W_{17}O_{61}]^{10-}$ act as stabilizing chelators of tetravalent actinide (An) ions.[1] The stabilization of these otherwise-reactive cations of uranium and the *trans*-U elements provides the basis for the application of polyoxoanions to selected aspects of An separations science in nuclear waste processing.[2] One recent practical application conceived at the CEA (Commissariat à l'Energie Atomique − France) concerns the use of α-2-$[P_2W_{17}O_{61}]^{10-}$ as a reagent for the confinement and off-line analysis of U^{4+} as part of the plutonium recovery process known as PUREX.[3,4] Another application advanced by the CEA to separate Am^{3+} from Cm^{3+} and trivalent lanthanide (Ln) elements involves its selective oxidation to Am^{4+} in the presence of α-2-$[P_2W_{17}O_{61}]^{10-}$ followed by solvent extraction. In this process, known as SESAME,[5,6] neither Cm^{3+} nor Ln^{3+} (except Ce) are oxidized thereby facilitating their separation from Am^{4+} as a valence-stabilized complex of α-2-$[P_2W_{17}O_{61}]^{10-}$. In research at JAERI (Japan Atomic Energy Research Institute), the process known as PARC is similarly planned to exploit the chemistry of α-2-$[P_2W_{17}O_{61}]^{10-}$ for separation of Am.[7] These applications are driven by the oxidizing power of α-2-$[P_2W_{17}O_{61}]^{10-}$ and its coordination chemistry, specifically its service as a valence-controlling complexant.

Despite current practice and future promise, there are few metrical details about the coordination of An^{4+} ions in complexes with α-2-$[P_2W_{17}O_{61}]^{10-}$. Such information would provide insights about the strength and nature of the An-ligand interactions. A large collection of previous work has shown that An^{4+} ions are strongly chelated by the α-2-$[P_2W_{17}O_{61}]^{10-}$ anion in butterfly-like complexes with 1:2 stoichiometry wherein one An cation is coordinated between two α-2-$[P_2W_{17}O_{61}]^{10-}$ anions. Although there is considerable physical and spectroscopic evidence for clusters of the general form $[An(\alpha\text{-}2\text{-}P_2W_{17}O_{61})_2]^{n-}$ ($n = 16$ for An^{4+}, and $n = 17$ for An^{3+}),[1,4,8] no complete crystal structures are available.[9] The combination of results from exhaustive studies of the coordination chemistry of U^{4+} in $[U(\alpha\text{-}2\text{-}P_2W_{17}O_{61})_2]^{16-}$ both in the solid state and in aqueous solution indicates a square antiprismatic environment of 8 O about U.[4] The oxophilic *trans*-uranium elements are assumed to maintain this same coordination environment throughout the 5*f* series of $[An(\alpha\text{-}2\text{-}P_2W_{17}O_{61})_2]^{n-}$ complexes. Similar, albeit weaker, complexation with the trivalent actinides is also known.[10] The crystal structures of the lanthanide clusters $[Lu(\alpha\text{-}2\text{-}P_2W_{17}O_{61})_2]^{17-}$ and $[Ce(\alpha\text{-}2\text{-}P_2W_{17}O_{61})_2]^{16-}$ reveal eight-coordinate square antiprism geometries for both Lu^{3+} and Ce^{4+}.[11,12] The common structure is illustrated in Figure 1(a). It shows that the central 4*f*-ion is coordinated to 2 α-2-$[P_2W_{17}O_{61}]^{10-}$ anions in a *syn* conformation through 4 O atoms on each.

[a] Chemistry Division, Argonne National Laboratory,
9700 South Cass Avenue, Argonne, IL 60439-4831, USA
Fax: (internat.) + 1-630/252-4225
E-mail: ls@anl.gov
mantonio@anl.gov

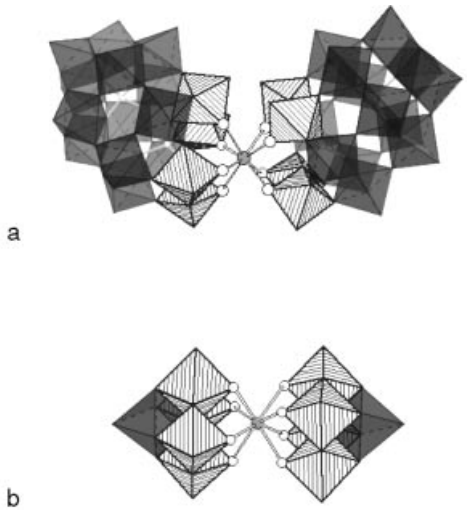

Figure 1. Molecular structures of (a) $[Lu(\alpha\text{-}2\text{-}P_2W_{17}O_{61})_2]^{17-}$ [11] and (b) $[Np(W_5O_{18})_2]^{8-}$ [13] that emphasize the square antiprism oxygen coordination environments of the Lu^{3+} (IR = 0.977 Å) and Np^{4+} (IR = 0.98 Å) ions, depicted as the central solid circles. The striped WO_6 octahedra contain the O atoms, depicted as open circles, that bind the Ln and An ions. The shaded WO_6 polygons complete the ligand structures

Insights about the structural aspects of An−O coordination and its influence on the stability of the An^{4+} complexes are what interest us for both fundamental and practical reasons. In order to probe An^{4+}−O bonding and stabilization throughout the 5*f*-series of complexes $[An(\alpha\text{-}2\text{-}P_2W_{17}O_{61})_2]^{16-}$ for An ≡ Th, U, Np, Pu we report the An L_3-edge XANES (X-ray absorption near edge structure) and EXAFS (extended X-ray absorption fine structure). These techniques provide access to a quantitative understanding of the An−O coordination for the solution specimens generated under electrochemical control and for the poorly-crystalline solids examined herein, for which conventional molecular level measurements like X-ray diffraction can be problematic. The results are compared with those for the An^{3+} complexes of $[An(\alpha\text{-}2\text{-}P_2W_{17}O_{61})_2]^{17-}$ for An ≡ Np, Pu, Am, and discussed in light of available metrical information for Ln^{3+} polyoxoanion complexes of $\alpha\text{-}2\text{-}[P_2W_{17}O_{61}]^{10-}$ and $[W_5O_{18}]^{6-}$. This latter tungsten oxide is known as the monovacant Lindqvist isopolyoxoanion. It binds tetravalent An as well as trivalent and tetravalent Ln ions to form complexes of 1:2 stoichiometry, $[An(W_5O_{18})_2]^{8-}$ and $[Ln^{n+}(W_5O_{18})_2]^{n-12}$. Many crystal structures have been determined of the actinide[13−15] and lanthanide[16−24] decatungstate clusters, as typified by the illustration in Figure 1(b). The direct comparisons of the An^{4+}−O and An^{3+}−O bonding in terms of interatomic distances provides an atomic-level perspective of the An coordination environments in polyoxometalates.

Results and Discussion

The An L_3 XANES data for the solid salts and aqueous solutions of the $[An(\alpha\text{-}2\text{-}P_2W_{17}O_{61})_2]^{n-}$ anions are shown in Figure 2. All spectra reveal a steeply rising edge peak whose position is diagnostic of the An oxidation state. The U, Np, and Pu solution XANES collected at rest potential all have edge energies consistent with An^{4+}. After obtaining these spectra, the Np and Pu samples were electrochemically reduced in situ, and the XANES spectra were recorded of the blue solutions held at reducing potentials. These data, shown as the dashed lines in Figure 2, have edge energies shifted with respect to the data obtained at rest potential. Analyses of the edge positions indicate that both Np^{4+} and Pu^{4+} have been reduced to An^{3+}. The 4.6 and 4.3 eV differences between the $Np^{4+} - Np^{3+}$ and $Pu^{4+} - Pu^{3+}$ edge peak positions of Table 1 attest to the An^{4+}/An^{3+} redox activity in the clusters, which is an independent subject of interest.[1] The edge resonances and their shifts with oxidation state are consistent with previous work on the trivalent and tetravalent An ions.[25,26] The results from the fits to the XANES spectra, including peak positions, line widths, and intensities, are detailed in Table 1.

The L_3-edge $k^3\chi(k)$ EXAFS for the heteropolyoxoanion complexes with An^{3+} and An^{4+} is shown in the left panels of Figure 3 as solid lines. These data were Fourier trans-

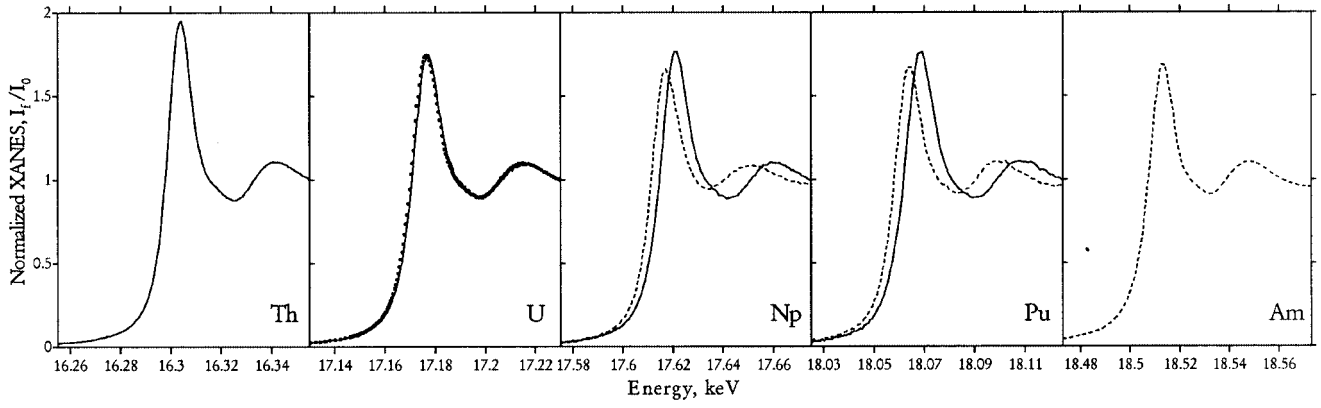

Figure 2. Normalized fluorescence L_3-edge XANES for the series of clusters $[An(\alpha\text{-}2\text{-}P_2W_{17}O_{61})_2]^{n-}$ with An of, in left to right panel order, Th; U; Np; Pu; Am. The An^{4+} and An^{3+} spectra are shown as solid and dashed lines, respectively. All Np and Pu XANES spectra were obtained as solution samples. Th and Am XANES were obtained as solid samples, and the U spectra were obtained as both solution and solid samples, shown here with open circles and a solid line, respectively

 © 2003 Wiley-VCH Verlag GmbH & Co. KGaA, Weinheim

Table 1. Ionic radii (IR) and physical forms of the $[An(\alpha\text{-}2\text{-}P_2W_{17}O_{61})_2]^{n-}$ complexes with An^{4+} (Th, U, Np, Pu) and An^{3+} (Np, Pu, Am). Inflection points from the first differential L_3-edge Th, U, Np, Pu, and Am XANES and results − positions (eV), widths (eV), and heights − from curve fitting to the normalized XANES of Figure 2 with one Gaussian peak shape and one arctangent function. Estimated error for positions and widths, ±0.5 eV; all arctangent heights, 1.00±0.01

An	Th^{4+}	U^{4+}		Np^{4+}	Np^{3+} [b]	Pu^{4+}	Pu^{3+} [b]	Am^{3+}
IR, CN=VIII[a]	1.05	1.00		0.98	1.12	0.96	1.10	1.09
Color/Phase	white/solid	violet/solution	violet/solid	yellow/solution	blue/solution	pink/solution	blue/solution	orange/solid
Inflection Point	16299.7	17171.5	17171.7	17616.1	17611.5	18063.1	18058.8	18508.4
Gaussian Position	16303.9	17175.9	17176.5	17620.3	17616.1	18067.6	18063.1	18513.2
Gaussian FWHM	12.3	15.5	15.5	16.1	15.7	16.9	15.2	11.9
Gaussian Height	1.10	0.98	0.97	1.04	0.84	1.08	0.93	0.83
Arctan energy	16296.0	17171.1	17171.4	17616.5	17611.5	18065.4	18059.7	18503.8
Arctan FWHM	15.9	19.3	18.9	20.1	16.0	20.5	17.9	15.6

[a] Obtained from Shannon[27] for coordination number (CN) 8. [b] XAFS data for the heteropoly blues of $[An^{3+}(\alpha\text{-}2\text{-}P_2W_{17}O_{61})_2]^{n-}$ with Np and Pu collected in situ following exhaustive electrolysis at −1.00 V and −0.30 V, respectively, vs. Ag/AgCl.

Table 2. Metrical results − oxygen coordination number, An−O interatomic distance and Debye−Waller (DW) factor, and energy shift − obtained from curve fitting the Th, U, Np, Pu, Am L_3-edge $k^3\chi(k)$ EXAFS of Figure 3 for $[An(\alpha\text{-}2\text{-}P_2W_{17}O_{61})_2]^{n-}$ with An^{4+} (Th, U, Np, Pu) and An^{3+} (Np, Pu, Am) in solution and solid forms

An	Th^{4+}	soln −U^{4+}− solid		Np^{4+}	Np^{3+}	Pu^{4+}	Pu^{3+}	Am^{3+}
CN, N_O	8.5(10)	8.4(10)	8.2(10)	8[a]	8[a]	8[a]	8[a]	7.6(10)
Dist., r_{An-O} Å	2.38(1)	2.35(1)	2.33(1)	2.34(2)	2.45(2)	2.33(2)	2.44(2)	2.40(1)
DW, σ^2, Å^2	0.006(1)	0.007(1)	0.008(2)	0.007(1)	0.019(8)	0.006(1)	0.011(2)	0.008(1)
E_0 Shift, eV	3.1(5)	3.0(8)	2.5(8)	5.5(9)	5.5(9)	5.0(9)	4.1(9)	1.7(9)

[a] Fixed parameter.

formed without phase-shift corrections to reveal a single strong peak, due to An−O coordination, as shown in the right panels of Figure 3 (solid lines). There are no other features of physical significance, despite the presence of the distant P and W atoms in the framework structure. The An−O interatomic distances obtained from the curve fitting of the $k^3\chi(k)$ EXAFS are presented in Table 2. The fits to the experimental $k^3\chi(k)$ EXAFS are shown as dashed lines in the left panels of Figure 3. The FTs representing the best fits (dashed lines) exhibit good correspondence with the primary data (solid lines), thereby confirming that the one-shell fits of 8 oxygen atoms adequately describe the An−O coordination in $[An(\alpha\text{-}2\text{-}P_2W_{17}O_{61})_2]^{n-}$ for both An^{3+} and An^{4+} in solution as well as in the solid phase. These results are consistent with the previous EXAFS model for Ln bonding with the monovacant Wells−Dawson anion $[\alpha\text{-}2\text{-}P_2W_{17}O_{61}]^{10-}$,[11] and with the independent work of Bion et al.[4] who have shown that the 8 O environment of U^{4+} is the same for the solid and the solution. The average An−O_8 and Ln−O_8 bond lengths for the $[An(\alpha\text{-}2\text{-}P_2W_{17}O_{61})_2]^{n-}$ and $[Ln(\alpha\text{-}2\text{-}P_2W_{17}O_{61})_2]^{n-}$ series of clusters are presented in Figure 4 as a function of 5*f*- and 4*f*-ionic radii (IR) of Shannon[27] for coordination number (CN) VIII.

The 8 data points for the An-coordinated complexes [Pu^{4+}, Np^{4+}, U^{4+} (solid and solution), Th^{4+}, Am^{3+}, Pu^{3+}, and Np^{3+}] are shown as solid squares in Figure 4(a). There is a linear dependence of the bond lengths from the smallest (Pu^{4+}, IR = 0.960 Å) and highest charge cations to the largest (Np^{3+}, IR = 1.12 Å) and lowest charge ones. The overall increase of the An−O distances with increasing ionic radii is evident from the linear least-squares fit (R^2 = 0.929), which is shown as the solid line in the figure. The slope and intercept are 0.77(9) and 1.58(9) Å, respectively.

The Ln−O distances in the isostructural $[Ln^{3+}(\alpha\text{-}2\text{-}P_2W_{17}O_{61})_2]^{17-}$ and $[Ce^{4+}(\alpha\text{-}2\text{-}P_2W_{17}O_{61})_2]^{16-}$ complexes are plotted against their published eight-coordinate ionic radii[27] in Figure 4(b). The 11 open squares illustrate the systematic increase of the Ln−O distances with the increasing ionic radii of Ce^{4+}, Lu^{3+}, Er^{3+}, Y^{3+}, Dy^{3+}, Tb^{3+}, Gd^{3+}, Eu^{3+}, Nd^{3+}, Pr^{3+}, and Ce^{3+}. The linear least-squares fit (R^2 = 0.949) is shown as the solid line in the figure. The slope, 0.78(6), and intercept, 1.56(6), of this fit are statistically equivalent to those obtained from the fit to the An−O distances of Figure 4(a), suggesting that the An and Ln ions have similar coordination behavior as a function of ionic size.

As with the An and Ln Wells−Dawson butterfly complexes of Figure 1(a), the Lindqvist decatungstate complexes provide an 8 O square antiprism coordination environment, illustrated in Figure 1(b), for both An and Ln cations. In view of the resemblance of the innermost O coordination environments provided by these two polyoxoanions, evaluation of the Lindqvist Ln−O bond length dependence on IR as shown in Figure 4(c) is informative. For the six $[Ln^{3+}(W_5O_{18})_2]^{9-}$ (Ln^{3+} ≡ Dy, Tb, Gd, Sm, Nd, Pr) previously published[18] crystal structures with the same countercations−$K_3Na_4H_2$−there is a linear dependence of bond length with IR. The least-squares fit (R^2 = 0.846) to the 6 distances − open squares in Fig-

 © 2003 Wiley-VCH Verlag GmbH & Co. KGaA, Weinheim

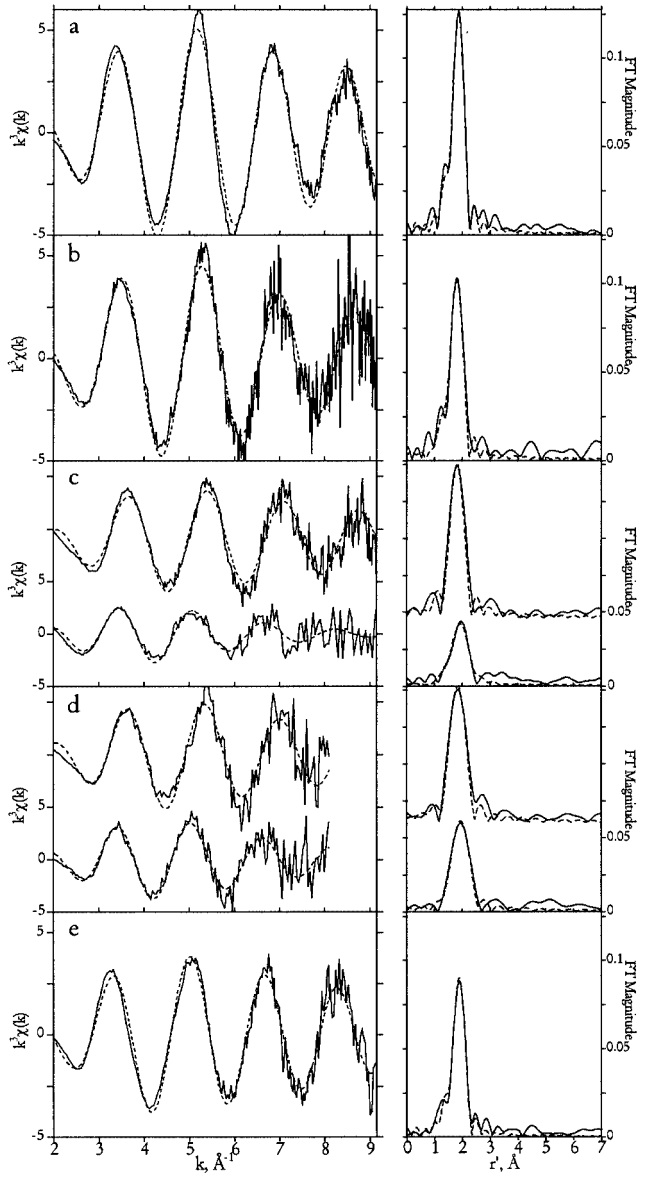

Figure 3. (Left panel) The experimental $k^3\chi(k)$ EXAFS data (solid lines) for $[An(\alpha\text{-}2\text{-}P_2W_{17}O_{61})_2]^{n-}$ with An of (a) Th^{4+}, (b) U^{4+}; (c) Np^{4+} (top) and Np^{3+} (bottom); (d) Pu^{4+} (top) and Pu^{3+} (bottom); (e) Am^{3+}. (Right panel) Fourier transform data (solid lines) of the $k^3\chi(k)$ EXAFS to the immediate left. The best fits are shown as dashed lines in both the Left and Right panels

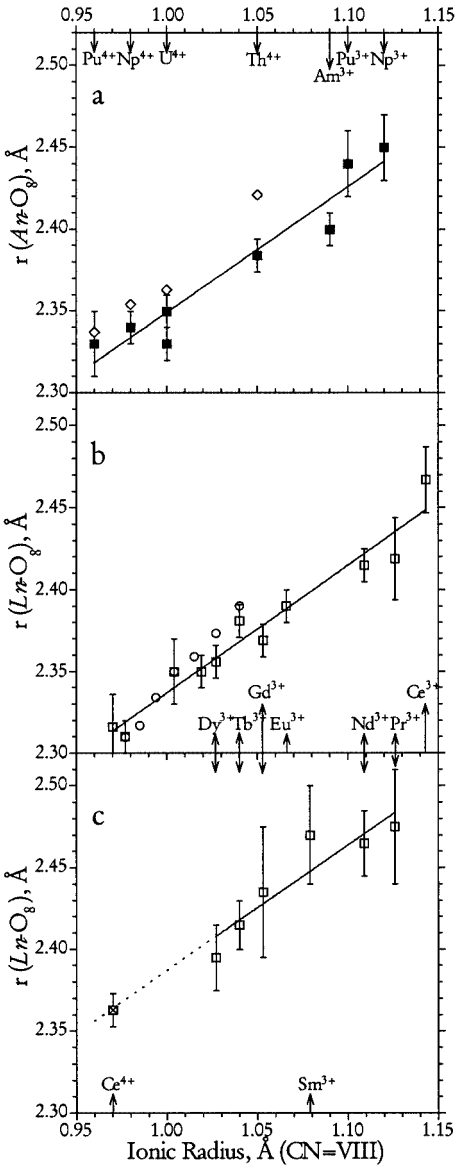

Figure 4. Variation of the $An-O_8$ and $Ln-O_8$ interatomic distances with the appropriate ionic radii of Shannon[27] for CN= VIII. (a) The EXAFS results for the solid K^+ salts and solutions of $[An(\alpha\text{-}2\text{-}P_2W_{17}O_{61})_2]^{n-}$ with An^{3+} and An^{4+} ions (solid squares) and the least-squares fit (solid line). Open diamonds are the $An-O_8$ distances for the AnO_2 solids of Th^{4+}, 2.421(1) Å;[43] U^{4+}, 2.363(1) Å;[44] Np^{4+}, 2.354(1) Å;[45] Pu^{4+}, 2.337(1)[45] Å. (b) The EXAFS-determined $Ln^{n+}-O_8$ distances (open squares) for the solid K^+ salts of $[Ln^{n+}(\alpha\text{-}2\text{-}P_2W_{17}O_{61})_2]^{n-20}$ and the least-squares fit (solid line) with 11 ions (Ce^{4+}, Lu^{3+}, Er^{3+}, Y^{3+}, Dy^{3+}, Tb^{3+}, Gd^{3+}, Eu^{3+}, Nd^{3+}, Pr^{3+}, and Ce^{3+}, in order of increasing IR). The EXAFS-determined distances of Ishiguro et al.[32] for the trivalent aquo ions of Lu−Tb are shown as open circles. (c) The crystallographically-determined average distances of Ozeki et al.[18] for 6 $Na_4K_3H_2[Ln^{3+}(W_5O_{18})_2]$ salts (open squares) and the least-squares fit (solid line), which is extrapolated to the IR for Ce^{4+} (0.97 Å) for comparison with the average crystallographic $Ce^{4+}-O_8$ distance determined for $Na_8[Ce^{4+}(W_5O_{18})_2]$[24]

ure 4(c) − is shown as the solid line, which was extrapolated (dashed line) to the IR minimum (0.96 Å) of Figure 4(a). The soundness of the extrapolation is evident from the coincidence of the crystallographically determined $Ce^{4+}-O$ interatomic distance (square at 0.97 Å) for $[Ce^{4+}(W_5O_{18})_2]^{8-}$.[24] The slope, 0.77(16), and intercept, 1.62(18), of the Ln−O distance vs. IR correlation for the Lindqvist complexes are statistically equivalent with those for the Ln and An Wells−Dawson complexes, thus providing quantitative evidence for the similarity of coordination environments in these two tetradentate polyoxometalate ligands.

Having viewed the Ln- and An−O distances in the context of polyoxometalate structural chemistry, it is informative to gauge the distances of Figure 4(a) and (b) (solid and open squares, respectively) with those for other systems in which Ln and An ions are known to be 8 coordinate with

 © 2003 Wiley-VCH Verlag GmbH & Co. KGaA, Weinheim

O atoms. For example, the solid dioxides, AnO_2, are prototypical materials in which all An^{4+} are 8 coordinate. The An−O bond lengths for Pu^{4+}, Np^{4+}, U^{4+}, and Th^{4+} in the AnO_2 fluorite structures are presented in Figure 4(a) as open diamonds. Although these are generally longer than the An−O distances [Figure 4(a), solid squares] for the Wells−Dawson complexes of An^{4+}, they are within agreement in view of the experimental uncertainties, including the 0.04 Å difference between the $[Th(\alpha\text{-}2\text{-}P_2W_{17}O_{61})_2]^{16-}$ and ThO_2 distances.

Comprehensive studies of the $Ln^{3+}\cdot nH_2O$ aquo species indicate that the hydration number (n) is 8 for the small, heavy ions at the end of the 4*f* series, $Tb^{3+}-Lu^{3+}$.[28−31] The Ln−O bond lengths, from the work of Ishiguro et al.,[32] for these 8 coordinate Ln aquo ions is shown in Figure 4(b) (open circles). The bond lengths for the $[Ln(\alpha\text{-}2\text{-}P_2W_{17}O_{61})_2]^{17-}$ complexes [Figure 4(b), open squares] with Tb−Lu ($0.977 \leq IR \leq 1.04$ Å) generally agree with those for the corresponding aquo ion species. In view of the differences in nuclearity and charge between the tetradentate anionic (10−) heteropolyoxometalate and the monodentate neutral water molecule, it is surprising that the bond lengths are so much alike.

Because the large, light Ln^{3+} and An^{3+} ions can assume hydration numbers of 9 or more, there is a dearth of metrical detail for additional systematic comparisons. In fact, the fixed eightfold O coordination for all An/Ln ions in the Wells−Dawson butterfly series of Figure 1(a) may not result in the formation of especially robust complexes with the large Ln^{3+} and An^{3+} compared with the smaller ones, including the tetravalent ions. This view is borne out in the data of Figure 5, which is a plot of the formation constants, $\log\beta_2$, available from the work of Bion et al.[10] versus 1/IR for CN = VIII of Ce^{3+}, Am^{3+}, Eu^{3+}, U^{4+}, Ce^{4+}, and Pu^{4+}. Based upon interpretations of similar plots for other Ln^{3+} complexes,[29,31] the overall direct dependence of $\log\beta_2$ with 1/IR is evidence that the coordination does not change.

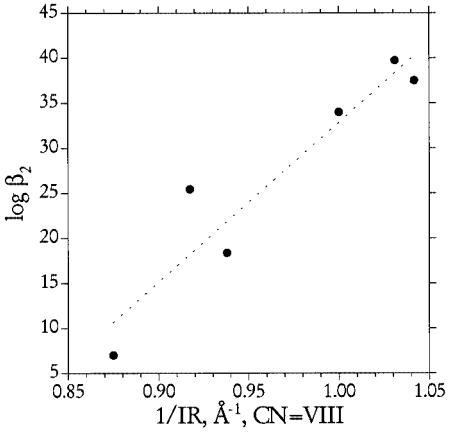

Figure 5. The absolute formation constants, log β_2, of Bion et al.[10] versus 1/IR of Shannon[27] for CN = VIII of the Ce^{3+}, Am^{3+}, Eu^{3+}, U^{4+}, Ce^{4+}, and Pu^{4+} ions (in order of increasing 1/IR) for the Wells−Dawson butterfly complexes of Figure 1(a). The least-squares fit (dashed line, $R^2 = 0.889$) with slope = 177±31 and intercept = −145±30.

Moreover, the regular variation of $\log\beta_2$ with 1/IR indicates similar cation-anion interactions throughout the 4*f*- and 5*f*-series of Wells−Dawson complexes. Although detailed insights are not available with the limited data (six points) of Figure 5, the approximately linear correlation ($R^2 = 0.889$) is consistent with our EXAFS data. The fairly large formation constants of Figure 5 for U^{4+}, Ce^{4+}, and Pu^{4+} are consistent with their short bond lengths and, hence, strong complexation. As expected, the largest ion, Ce^{3+}, of the series in Figure 5, has the smallest formation constant and the longest distance.

The variation of interatomic distances and formation constants with IR, depicted in Figures 4 and 5, show no indication of precipitous changes in An−anion interactions that would account for the stability of the An^{4+} complexes. Instead, a simple electrostatic explanation, arising from ionic charge and size changes, is consistent with all the data in hand. Although the Wells−Dawson and Lindqvist anions stabilize the small An^{4+} ions, this is not general behavior in An and Ln polyoxometalate chemistry. For example, we have found that the Preyssler anion, $[P_5W_{30}O_{110}]^{15-}$, stabilizes Ce^{3+} over Ce^{4+},[33,34] despite the large negative charge on the anion. Tetravalent Ce forms one of the strongest complexes of the Wells−Dawson series, $[Ce(\alpha\text{-}2\text{-}P_2W_{17}O_{61})_2]^{16-}$, but has yet to form a complex with the Preyssler anion.[33,34] Similarly, although Pu^{4+} is stabilized in $[Pu(\alpha\text{-}2\text{-}P_2W_{17}O_{61})_2]^{16-}$, it is Pu^{3+} that is stabilized in $[PuP_5W_{30}O_{110}]^{12-}$.[35] Whereas the present results support the use of the monovacant α-2-$[P_2W_{17}O_{61}]^{10-}$ isomer in the PUREX and SESAME processes for U^{4+} analyses and Am^{4+} valence control, respectively, a predictive understanding of the effects of different polyoxometalates on An redox speciation is not yet available.

Conclusion

The technological prospects of polyoxometalates, in general, and of α-2-$[P_2W_{17}O_{61}]^{10-}$, in particular, for use in radioactive waste processing operations are due to, in part, the strength of their chemical interactions with *f*-elements, particularly the tetravalent 5*f* (actinide) ions. By comparisons with published structures of An dioxides with 8 O coordination environments, we have shown that the $An^{4+}-O$ interactions in complexes of $[An(\alpha\text{-}2\text{-}P_2W_{17}O_{61})_2]^{16-}$ are of the expected magnitude. The variations of An−O interatomic distances and formation constants with An ionic radii are consistent with behavior expected from simple electrostatic considerations of charge and size. Identical behavior was found for $Ln^{3+}-O$ and $Ce^{4+}-O$ coordination in $[Ln(\alpha\text{-}2\text{-}P_2W_{17}O_{61})_2]^{17-}$ and $[Ce(\alpha\text{-}2\text{-}P_2W_{17}O_{61})_2]^{16-}$ as well as for the Lindqvist complex anions, $[Ln^{3+}(W_5O_{18})_2]^{9-}$ and $[Ce(W_5O_{18})_2]^{8-}$. The stability of U^{4+}, Np^{4+}, and Pu^{4+} in complexes $[An(\alpha\text{-}2\text{-}P_2W_{17}O_{61})_2]^{16-}$ and $[An(W_5O_{18})_2]^{8-}$ is understood in terms of strong electrostatic interactions between the spherical An^{4+} cations and the anionic polyoxometalate ligands.

 © 2003 Wiley-VCH Verlag GmbH & Co. KGaA, Weinheim

Experimental Section

CAUTION. Th, U, Np, Pu, and Am are radioactive elements. All experiments with these isotopes were performed in specialized laboratories using procedures designed and approved to minimize radiological and chemical hazards. For the transuranic elements, i.e., Np, Pu, and Am, their limited availability, together with radiation exposure concerns, require the use of only mg quantities and thereby limit studies to small sample sizes.

Syntheses: The lacunary, monovacant isomer, $K_{10}[\alpha\text{-}2\text{-}P_2W_{17}O_{61}]\cdot 20H_2O$, was isolated as described elsewhere.[36] The 1:2 $[An(\alpha\text{-}2\text{-}P_2W_{17}O_{61})_2]^{n-}$ complexes with natural Th and U, ^{237}Np, ^{242}Pu, and ^{243}Am were prepared in milligram-scale quantities, by methods adapted from larger-scale syntheses of the lanthanide complexes,[37] through the dropwise addition of one equivalent of Th^{4+}, U^{4+}, Np^{4+}, Pu^{4+}, and Am^{3+} in 1 M $HClO_4$ to warm (60 °C) stirred solutions containing two equivalents of $K_{10}[\alpha\text{-}2\text{-}P_2W_{17}O_{61}]\cdot 20H_2O$ in 0.5 M CH_3CO_2Li buffers of pH = 4.7. The resulting white, violet, yellow, pink, and orange colored solid potassium salts, respectively, were obtained by cooling and slow evaporation of the mother liquor. The An sources were $Th(NO_3)_4\cdot nH_2O$ (Alfa−Aesar); UCl_4 (Strem); purified ^{237}Np stock solution of $[Np(V)O_2]ClO_4$ that was electrochemically reduced to Np^{4+} according to previous procedures;[26,38] purified ^{242}Pu stock solution of $[Pu^{4+}(ClO_4)_4]$ in which the tetravalent oxidation state of Pu was maintained by vigorous sparging with NO; column-purified $^{243}AmCl_3$. The series of 1:2 $[Ln^{3+}(\alpha\text{-}2\text{-}P_2W_{17}O_{61})_2]^{17-}$ complexes for Ce, Pr, Nd, Eu, Gd, Tb, Dy, Y, Er, and Lu as well as $[Ce^{4+}(\alpha\text{-}2\text{-}P_2W_{17}O_{61})_2]^{16-}$ were synthesized and isolated as solid potassium salts in the same manner from $K_{10}[\alpha\text{-}2\text{-}P_2W_{17}O_{61}]\cdot 20H_2O$ and commercial Ln nitrates and Ln chlorides.

Measurements: Aqueous electrolytes consisting of 2:1 v/v mixtures of 0.5 M CH_3CO_2Li buffer at pH = 4.7 and 1 M $HClO_4$ were used for the solution XAFS experiments and in situ bulk electrolyses, which were performed with a BAS 100B/W electrochemical workstation and a purpose-built cell of previous design.[26,39] Carbon rod (Alfa) working and auxiliary electrodes and a Ag/AgCl reference electrode (BAS) were used as described elsewhere.[34] We first collected data for dilute (ca. 1 mM) solutions of $[An^{4+}(\alpha\text{-}2\text{-}P_2W_{17}O_{61})_2]^{16-}$ for An ≡ U, Np, and Pu in the spectroelectrochemical cell with the electrodes at rest potential. This was followed by exhaustive (99−99.9%) electrolysis at −1.00 V and −0.30 V to produce the reduced heteropoly blue species with Np^{3+} and Pu^{3+}, $[An^{3+}(\alpha\text{-}2\text{-}P_2W_{17}O_{61})_2]^{n-}$, that were maintained throughout the data acquisition with the electrode polarized at these potentials. Subsequent oxidation of the heteropoly blues provided X-ray and electrochemical signals that were the same as those for the starting materials, indicating reversibility of the redox chemistry. All XAFS data were obtained at the 7 GeV APS BESSRC CAT station 12 BM-B with a Si<111> monochromator and focusing optics.[40] The An L_3-edge X-ray data were acquired with a multi-element fluorescence detector (Canberra) and the Ln L_3-edge data were acquired with a Lytle-type ion chamber (The EXAFS Co.) in the conventional 45/45° configuration without slits and filters. Energy calibration was maintained with respect to Y metal powder (Th and U L_3-XAFS), Zr foil (Np and Pu L_3-XAFS), and Nb foil (Am L_3-edge XAFS) by setting the inflection points in the first differential transmission XANES data to 17.038, 17.998, and 18.986 eV, respectively. Between four and twelve scans were summed for the solution species and solid samples. XANES and EXAFS data analyses were performed with WinXAS.[41] All EXAFS data were truncated at $k_{max} \approx 9$ Å^{-1} to reduce noise in the FT data and to keep the inner-sphere An−O structural information clear. In view of the range of data available here ($\Delta k \approx 7$ Å^{-1}, $\Delta r \approx 2$ Å^{-1}) and the maximum number of independent parameters ($N_{idp} \approx 8$), we were careful to use conservative models in the curve fitting with single-scattering phase and backscattering amplitude calculations from FEFF8.01.[42] Three or, at most, 4 parameters (O coordination number, N_O; An−O interatomic distance, r; Debye−Waller factor, σ^2; energy shift, ΔE_0) were refined in the single-shell curve fitting with $S_0^2 = 1$.[38]

Acknowledgments

We thank S. Skanthakumar of the Chemistry Division Actinide Facility and the staff of the BESSRC CAT at the Advanced Photon Source for assistance. This work is supported by the U.S. DOE, BES−Chemical Sciences and Material Sciences and, during the initial stages, by sponsorship of the Environmental Management Science Program, Office of Science and Technology, Office of Environmental Management, all under contract No. W-31-109-ENG-38.

[1] A. B. Yusov, V. P. Shilov, *Radiochem., Engl. Transl.* **1999**, *41*, 1−23.
[2] D. E. Katsoulis, *Chem. Rev.* **1998**, *98*, 359−388.
[3] L. Bion, P. Moisy, C. Madic, *Radiochim. Acta* **1995**, *69*, 251−257.
[4] L. Bion, P. Moisy, F. Vaufrey, S. Meot-Reymond, E. Simoni, C. Madic, *Radiochim. Acta* **1997**, *78*, 73−82.
[5] C. Madic, J. Bourges, J.-F. Dozol, *AIP Conf. Proc.* **1995**, *346*, 628−638.
[6] M. Kamoshida, T. Fukasawa, F. Kawamura, *J. Nucl. Sci. Technol.* **1998**, *35*, 185−189.
[7] T. Asakura, L. Donnet, S. Picart, J. M. Adnet, *J. Radioanal. Nucl. Chem.* **2000**, *246*, 651−656.
[8] D. Chartier, L. Donnet, J. M. Adnet, *Radiochim. Acta* **1999**, *85*, 25−31.
[9] An illustration of the structure of $[U^{4+}(\alpha\text{-}2\text{-}P_2W_{17}O_{61})_2]^{16-}$ is provided by A. Müller, F. Peters, M. T. Pope, D. Gatteschi, *Chem. Rev.* **1998**, *98*, 239−271 without presentation of metrical information.
[10] L. Bion, F. Mercier, P. Decambox, P. Moisy, *Radiochim. Acta* **1999**, *87*, 161−166.
[11] Q.-H. Luo, R. C. Howell, M. Dankova, J. Bartis, C. W. Williams, W. D. Horrocks Jr., V. G. Young, A. L. Rheingold, L. C. Francesconi, M. R. Antonio, *Inorg. Chem.* **2001**, *40*, 1894−1901.
[12] V. N. Molchanov, L. P. Kazanskii, E. A. Torchenkova, V. I. Simonov, *Sov. Phys. Crystallogr., Engl. Transl.* **1979**, *24*, 96−97.
[13] I. A. Charushnikova, A. Y. Garnov, N. N. Krot, S. B. Katser, *Radiochem., Engl. Transl.* **1997**, *39*, 424−429.
[14] A. M. Golubev, L. A. Muradyan, L. P. Kazanskii, E. A. Torchenkova, V. I. Simonov, V. I. Spitsyn, *Soviet J. Coord. Chem. Engl. Transl.* **1977**, 715−720.
[15] W. P. Griffith, N. Morley-Smith, H. I. S. Nogueira, A. G. F. Shoair, M. Suriaatmaja, A. J. P. White, D. J. Williams, *J. Organomet. Chem.* **2000**, *607*, 146−155.
[16] T. Ozeki, M. Takahashi, T. Yamase, *Acta Crystallogr., Sect. C: Cryst. Struct. Commun.* **1992**, *C48*, 1370−1374.
[17] T. Ozeki, T. Yamase, *Acta Crystallogr., Sect. C: Cryst. Struct. Commun.* **1993**, *C49*, 1574−1577.
[18] T. Ozeki, T. Yamase, *Acta Crystallogr., Sect. B: Struct. Sci.* **1994**, *B50*, 128−134.
[19] T. Ozeki, T. Yamase, *Acta Crystallogr., Sect. C: Cryst. Struct. Commun.* **1994**, *C50*, 327−330.
[20] M. Sugeta, T. Yamase, *Bull. Chem. Soc., Jpn.* **1993**, *66*, 444−449.

 © 2003 Wiley-VCH Verlag GmbH & Co. KGaA, Weinheim

[21] T. Yamase, T. Ozeki, *Acta Crystallogr., Sect. C: Cryst. Struct. Commun.* **1993**, *C49*, 1577−1580.
[22] T. Yamase, T. Ozeki, K. Ueda, *Acta Crystallogr., Sect. C: Cryst. Struct. Commun.* **1993**, *C49*, 1572−1574.
[23] T. Yamase, T. Ozeki, M. Tosaka, *Acta Crystallogr., Sect. C: Cryst. Struct. Commun.* **1994**, *C50*, 1849−1852.
[24] C. Rosu, T. J. R. Weakley, *Acta Crystallogr., Sect. C: Cryst. Struct. Commun.* **1998**, *54*, CIF-access paper IUC9800047.
[25] S. D. Conradson, I. Al Mahamid, D. L. Clark, N. J. Hess, E. A. Hudson, M. P. Neu, P. D. Palmer, W. H. Runde, C. D. Tait, *Polyhedron* **1998**, *17*, 599−602.
[26] L. Soderholm, M. R. Antonio, C. Williams, S. R. Wasserman, *Anal. Chem.* **1999**, *71*, 4622−4628.
[27] R. D. Shannon, *Acta Crystallogr., Sect. A* **1976**, *32*, 751−767.
[28] A. Habenschuss, F. H. Spedding, *J. Chem. Phys.* **1980**, *73*, 442−450.
[29] E. N. Rizkalla, G. R. Choppin, in: *Handbook on the Physics and Chemistry of Rare Earths, Vol. 15* (Eds.: K. A. Gschneidner, Jr, L. Eyring), Elsevier Science, New York, **1991**, pp. 393−442.
[30] C. Cossy, L. Helm, D. H. Powell, A. E. Merbach, *New J. Chem.* **1995**, *19*, 27−35.
[31] H. Kanno, *Mater. Sci. Forum* **1999**, *315−317*, 477−483.
[32] S. Ishiguro, Y. Umebayashi, M. Komiya, *Coord. Chem. Rev.* **2002**, *226*, 103−111.
[33] M. R. Antonio, L. Soderholm, *Inorg. Chem.* **1994**, *33*, 5988−5993.
[34] M. R. Antonio, L. Soderholm, C. W. Williams, N. Ullah, L. C. Francesconi, *J. Chem. Soc., Dalton Trans.* **1999**, 3825−3830.
[35] M. R. Antonio, M.-H. Chiang, C. W. Williams, L. Soderholm, unpublished results **2003**.
[36] R. Contant, *Inorg. Synth.* **1990**, *27*, 104−111.
[37] J. Bartis, S. Sukal, M. Dankova, E. Kraft, R. Kronzon, M. Blumenstein, L. C. Francesconi, *J. Chem. Soc., Dalton Trans.* **1997**, 1937−1944.
[38] M. R. Antonio, L. Soderholm, C. W. Williams, J.-P. Blaudeau, B. E. Bursten, *Radiochim. Acta* **2001**, *89*, 17−25.
[39] M. R. Antonio, L. Soderholm, I. Song, *J. Appl. Electrochem.* **1997**, *27*, 784−792.
[40] M. A. Beno, M. Engbretson, G. Jennings, G. S. Knapp, J. Linton, C. Kurtz, U. Rütt, P. A. Montano, *Nucl. Instrum. Methods Phys. Res. A* **2001**, *467−468*, 699−702.
[41] T. Ressler, *J. Synchrotron Radiat.* **1998**, *5*, 118−122.
[42] J. J. Rehr, R. C. Albers, *Rev. Mod. Phys.* **2000**, *72*, 621−654.
[43] F. Hund, W. Durrwachter, *Z. Anorg. Allg. Chem.* **1951**, *265*, 67−72.
[44] R. E. Rundle, N. C. Baenziger, A. S. Wilson, R. A. McDonald, *J. Am. Chem. Soc.* **1948**, *70*, 99−105.
[45] W. H. Zachariasen, *Acta Crystallogr.* **1949**, *2*, 388−390.

Received January 9, 2003

 © 2003 Wiley-VCH Verlag GmbH & Co. KGaA, Weinheim

Three Novel Polymeric Frameworks Assembled from Cd^{II}, Co^{II}, and Mn^{II} with the Mixed Organic Ligands 3,4-Pyridinedicarboxylate, 1,3-Bis(4-pyridyl)propane, or 1,2-Bis(4-pyridyl)ethane

Zhi-Yong Fu,[a] Sheng-Min Hu,[a] Jing-Cao Dai,[a] Jian-Jun Zhang,[a] and Xin-Tao Wu*[a]

Keywords: Coordination polymer / Crystal engineering / Mixed ligands / Structural topology

Hydrothermal reactions of Cd^{II}, Co^{II}, and Mn^{II} with the mixed ligands 3,4-pyridinedicarboxylate (pydc), 1,3-bis(4-pyridyl)-propane (bpp), or 1,2-bis(4-pyridyl)ethane (bpe) gave crystals of $\{[Cd(pydc)(bpp)]\cdot 0.5H_2O\}_n$ (**1**), $\{[Co(pydc)(H_2O)(bpe)_{0.5}]\cdot 0.5H_2O\}_n$ (**2**), and $\{[Mn(pydc)(H_2O)(bpe)_{0.5}]\cdot 0.5H_2O\}_n$ (**3**), respectively. Single-crystal X-ray analyses reveal that these are all three-dimensional non-interpenetrating coordination polymers. Their structures alter markedly with the conformation and the function of the ligands. In **1**, the 3,4-pyridinedicarboxylate acted as a three-connector, a coordination topology of the type (3,5) [containing 3 and 5 connected centers] being generated through self-assembly, while in **2** and **3**, with the help of the four-connector 3,4-pyridinedicarboxylate and the terminal ligand water molecule, another three-dimensional framework with a coordination topology of the type (**4**, **5**) was obtained.
(© Wiley-VCH Verlag GmbH & Co. KGaA, 69451 Weinheim, Germany, 2003)

Introduction

The design and construction of coordination polymers are of great interest due to their intriguing new structural topologies and potential applications as functional materials.[1−6] Many attractive networks with various structural motifs, including honeycomb,[7−8] brick wall,[9] rectangular grid,[10−11] bilayer,[12−15] ladder,[16−17] herringbone,[18] diamondoid,[19−21] and octahedral[22−23] geometries, have been constructed in the past decade by use of single bridging organic ligands such as 4,4′-bipyridine, pyrazine, and related species. Recently, in order to fabricate more novel complicated supramolecular networks, the employment of metal ions with different kinds of organic ligands has gradually become established as a useful strategy.[24−25] This method may provide new structural motifs not accessible by the application of metal ions with a single ligand. The structural and functional features of the whole self-assembled entities contain the information of their components.[26] To date, however, there has been only one reported polymer with pydc as ligand,[27] and no frameworks constructed by it together with other organic ligands have been observed. This paper reports the synthesis and characterization of three new coordination polymers assembled from metal ions and the mixed ligands 3,4-pyridinedicarboxylate, 1,3-bis(4-pyridyl)propane, or 1,2-bis(4-pyridyl)ethane: namely $\{[Cd(pydc)(bpp)]\cdot 0.5H_2O\}_n$ (**1**), $\{[Co(pydc)(H_2O)(bpe)_{0.5}]\cdot 0.5H_2O\}_n$ (**2**), and $\{[Mn(pydc)(H_2O)(bpe)_{0.5}]\cdot 0.5H_2O\}_n$ (**3**) [pydc = 3,4-pyridinedicarboxylate, bpp = 1,3-bis(4-pyridyl)propane, bpe = 1,2-bis(4-pyridyl)ethane]. Single-crystal X-ray analyses show that the conformations and the functions of the ligands play an important role in affecting the final structural motifs of the polymers. In **1,** with 3,4-pyridinedicarboxylic acid acting as a tritopic subunit and 1,3-bis(4-pyridyl)propane acting as a ditopic subunit, the self-assembly results in an interesting three-dimensional framework with a coordination topology of the (3,5) type, while in **2** and **3**, with 3,4-pyridinedicarboxylic acid acting as a tetratopic subunit, 1,2-bis(4-pyridyl)ethane acting as a ditopic subunit, and a water molecule acting as terminal ligand, another appealing three-dimensional framework with a coordination topology of the (4,5) type is obtained. To the best of our knowledge, these are two new, previously unreported types of structural motifs.

Results and Discussion

Syntheses

In the synthesis of **1**, a molar ratio of 2:2:1 (Cd/pydc/bpp) was used in the preparation, but a framework with a stoichiometric ratio of 1:1:1 was obtained. In order to investigate what would happen if the latter ratio was applied, more experiments were done, but unfortunately no single crystal was obtained. When Co^{II} and Mn^{II} were used to repeat the above experimental procedure, complexes **2**

[a] State Key Laboratory of Structural Chemistry, Fujian Institute of Research on the Structure of Matter, Chinese Academy of Sciences,
Fuzhou, Fujian 350002, China
Fax: (internat.) + 86-591/3714946
E-mail: wxt@ms.fjirsm.ac.cn

 © 2003 Wiley-VCH Verlag GmbH & Co. KGaA, Weinheim **DOI: 10.1002/ejic.200300018**

and **3**, with 2:2:1 stoichiometric ratios exactly the same as those of the original reactants, were generated.

Crystal Structures

Single-crystal X-ray analysis reveals that **1** has a three-dimensional, non-interpenetrating coordination network. Each Cd^{II} center has a slightly distorted $\{CdN_3O_4\}$ pentagonal bipyramid coordination sphere, with one 1,3-bis(4-pyridyl)propane nitrogen donor and four oxygen donors of two chelating bidentate carboxylate groups of the 3,4-pyridinedicarboxylate in the equatorial plane. The coordination sphere is completed by one nitrogen donor of 1,3-bis(4-pyridyl)propane and one nitrogen donor of 3,4-pyridinedicarboxylate in the axial direction (Figure 1). The metal centers provide the penta-connecting trigonal bipyramid nodes, while the ligands act as di-connectors and tri-connectors, respectively. The spontaneous association of these subunits results in a new kind of 3D framework (Figure 2, a). In a side view of the network (Figure 2, b), it is interesting to observe that two kinds of rings exist. One is a cyclohexane-like ring, made up of three Cd^{II} ions and three centers of 3,4-pyridinedicarboxylate, displaying a chair conformation, while the other is also a six-membered ring, formed by four Cd^{II} ions and two centers of the 3,4-pyridinedicarboxylate, exhibiting a boat conformation. Viewed onto the *ac* plane, the whole feature of the framework looks like the bellows of an accordion, showing folds. The metal centers, which are distributed in the sheets, are not all coplanar. Rather, half fall in one plane, and half in an adjacent plane, displaying a helical conformation. Two rods of the 1,3-bis(4-pyridyl)propane two-connectors form two edges of the sheet and two rods of the 3,4-pyridinedicarboxylate tri-connectors make up the other edges (connections between nodes within the structure are referred to in general as rods). The third rod of 3,4-pyridinedicarboxylate links to the adjacent layer, producing a remarkable three-dimensional framework. Infinite narrow channels exist in the framework and their arrangement fits the symmetry of the space group *C*2/*c*. The height of one channel is exactly the width of another and each pair of diagonal channels displays a centrosymmetric configuration. Close examination of the channels revealed that water molecules acting as guests were embedded in the cavities and formed hydrogen bonds with the framework (O2···O5 2.776 Å).

Compounds **2** and **3** have the same structural motif, except for the difference in the metal center (Co for **2**, Mn for **3**). The local coordination geometry around the centrosymmetric metal center can be described as a slightly distorted octahedron configuration (Figure 3). One nitrogen atom of the 3,4-pyridinedicarboxylate and one nitrogen atom of 1,2-bis(4-pyridyl)ethane occupy the axial positions of the coordination sphere. Three oxygen atoms of 3,4-pyridinedicarboxylate and one oxygen atom of a water molecule coordinate the metal center in the equatorial plane. What is different from **1** is that two kinds of coordination modes exist in the carboxylate groups of the 3,4-pyridinedicarboxylate in **2** and **3** (Scheme 1). One is bidentate and the other is monodentate, which makes the 3,4-pyridinedicarboxylate ligands act as tetra-connectors. While the water molecule acting as a terminal ligand occupies one reaction site of the octahedral coordination sphere, this makes the six-coordinate metal center also provide a penta-connecting node. Nevertheless, it has a tetragonal pyramid configuration, different from the penta-connecting trigonal bipyramid conformation existing in **1**. The self-assembly of the tetra-connectors and the penta-connecting nodes creates a two-dimensional layer (Figure 4, a). Viewed down the *b* axis, the metal centers of the dinuclear units, located in the layer, are distributed in two different planes (Figure 4, b). The di-connector 1,2-bis(4-pyridyl)ethane occupies the other two reaction sites of the penta-connecting nodes and links the adjacent metal double layers from top and bottom, extending the structural motif into three dimensions (Figure 5). Just as in **1**, the water molecule is also enclathrated in the small cavity of the framework and it also forms a hydrogen bond with its host (O4···O6 2.743Å for **2** and O4···O6 2.819Å for **3**).

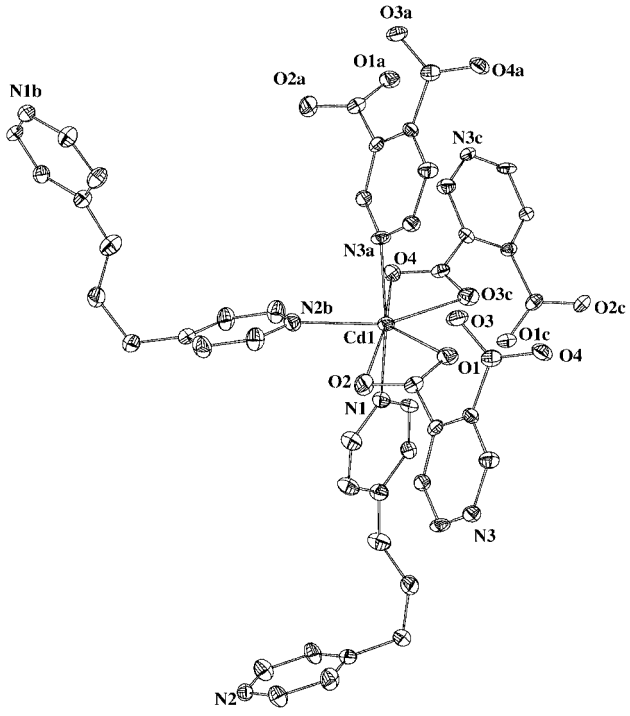

Figure 1. ORTEP drawing (at 30% probability) of **1** around the Cd center; the hydrogen atoms are omitted for clarity; symmetry code: a = x, $-1 + y$, z; b = $3/2 - x$, $-1 + y$, $1/2 + z$; c = $1 - x$, $2 - y$, $-1/2 + z$

Carboxylate ligands (such as trimesate, terephthalate, pydc etc.) have a great ability to construct coordination architectures with metal ions, adopting several different coordination fashions, ranging from unidentate to bidentate, sometimes in more than one way in the coordination architecture[28] Their bridging modes are highly dependent on the coordination modes of the carboxy groups, which can affect the final structural motifs of the polymers.[29] In compound **1**, in which the carboxy groups have a chelating bidentate coordination mode, the pydc ligands act as tri-connectors and connect the Cd centers, forming parts of the

 © 2003 Wiley-VCH Verlag GmbH & Co. KGaA, Weinheim

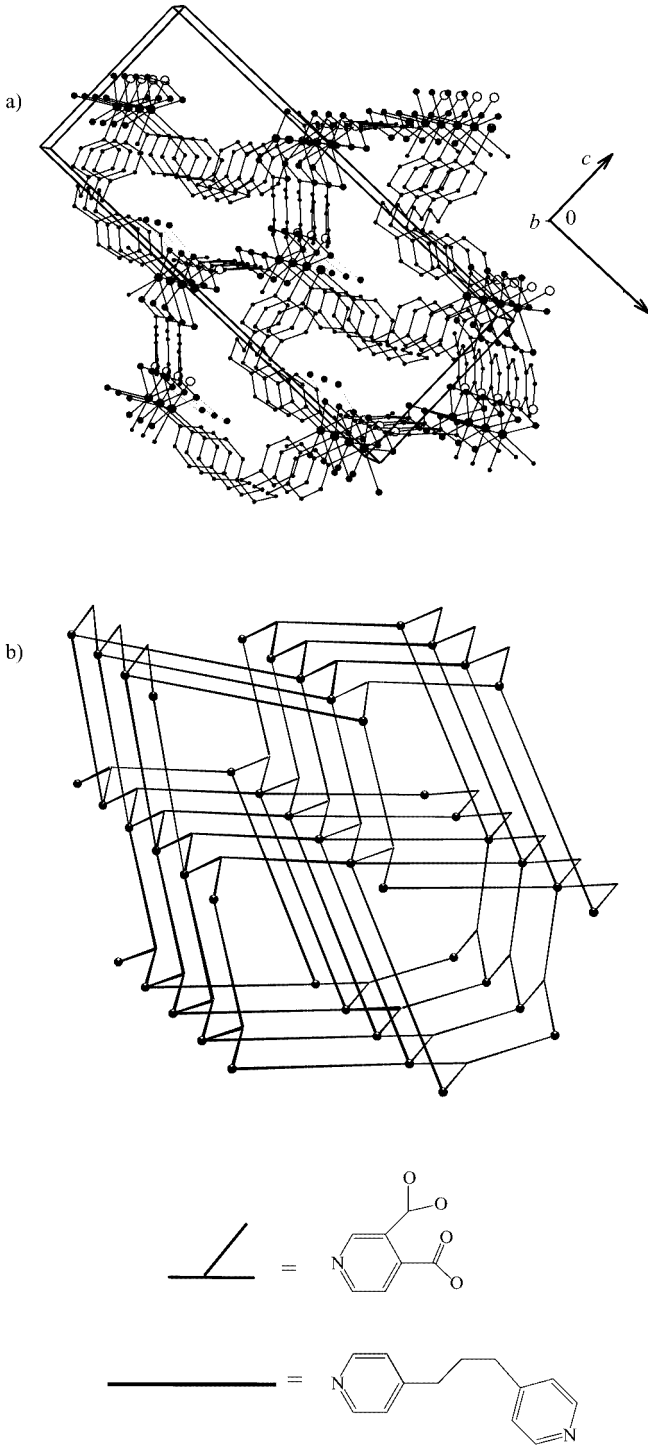

Figure 2. (a) View of the extended structure of **1**, showing the building blocks aggregated to a three-dimensional framework with a coordination topology of the type (3,5); (b) view of the topology of ring linkage in the framework; the close circles symbolize the Cd^{II} ions

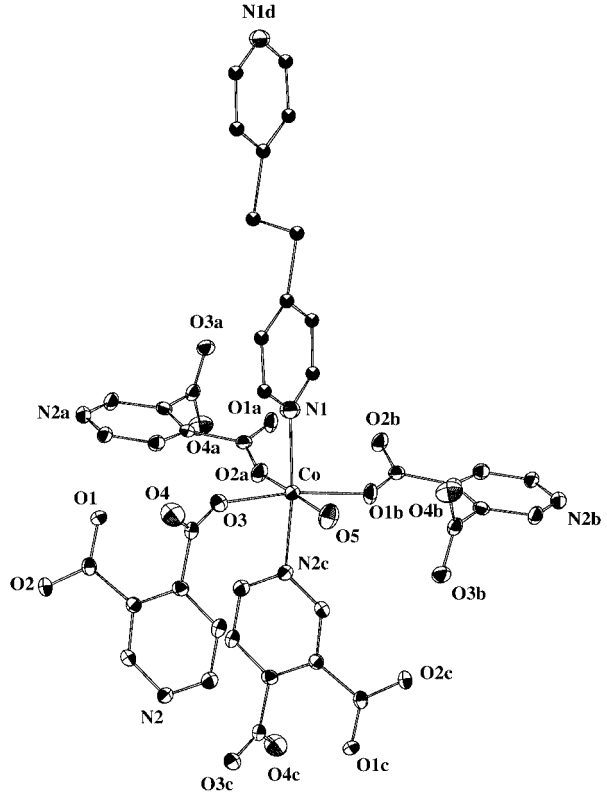

Figure 3. ORTEP drawing (at 30% probability) of **2** around the Co center; the hydrogen atoms are omitted for clarity; the structure of compound **3** is analogous; symmetry code: a = $-x + 1/2$, $y + 1/2$, $-z + 1/2$; b = x, $-y$, $z + 1/2$; c = $-x + 1/2$, $-y - 1/2$, $-z + 1$

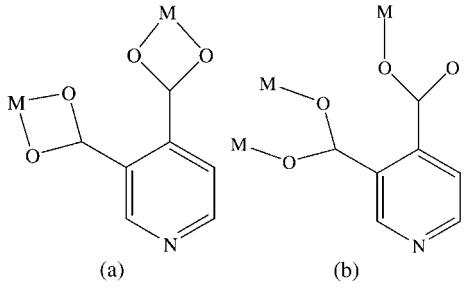

Scheme 1. The coordination fashions of the carboxylate group: (a) compound **1**: chelating bidentate; (b) compounds **2** and **3**: bi- and monodentate

rings, while in compounds **2** and **3** the bi- and monodentate coordination modes make the pydc act as tetra-connectors, which interlock the M (Co, Mn) centers, resulting in M(pydc) layers. The water molecule in **2** and **3** acting as an end-capping unit, also plays an important role affecting the structural feature of the polymers, which making the hexa-coordinate metal center provide a penta-connecting node. The whole structural feature of a coordination architecture results from the conformation of ligand and the coordination mode of metal center.[30−31] Different metal coordination geometries and different orientations of the interaction sites in a given ligand cause the framework to display various structural motifs.

Thermal Stability

To study the stability of these materials, thermogravimetric analyses (TGA) were performed on polycrystalline samples of these three compounds. The data for **1** showed

 © 2003 Wiley-VCH Verlag GmbH & Co. KGaA, Weinheim

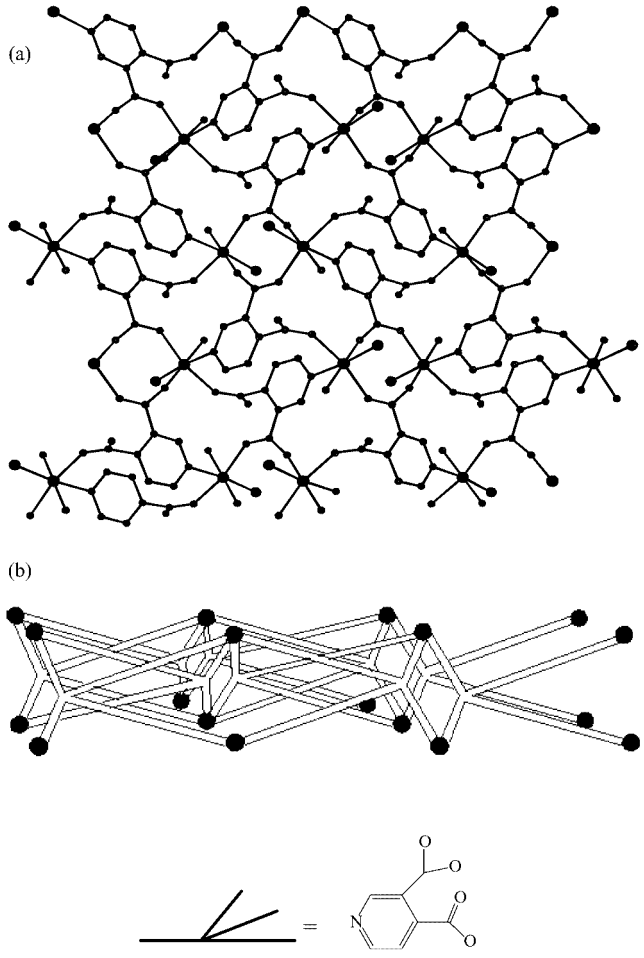

Figure 4. (a) View of the two-dimensional layer connected by the 3,4-pyridinedicarboxylate ligands in **2** from the *a* direction; (b) a schematic view of the two-dimensional layer from the *b* direction

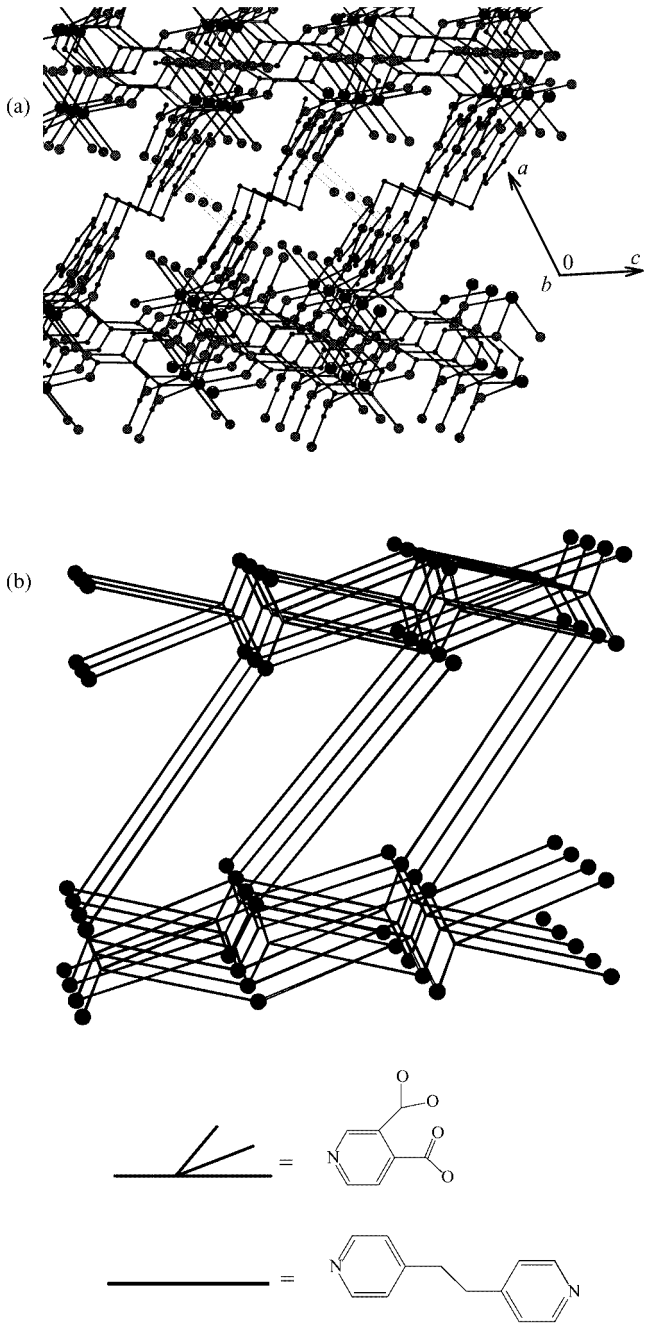

Figure 5. (a) View of the extended structures of **2**, showing the building blocks aggregated into a three-dimensional framework with a coordination topology of the (4,5) type; (b) view of the topology of ring linkage in the framework; the close circles symbolize the metal centers (M = Co and Mn for **2** and **3**, respectively)

the two following, strikingly clean and well-separated, weight loss steps. In the first region (100−130 °C), it lost all guest water molecules (2% observed, 1.86% calculated). On further heating, the material lost weight continuously, corresponding to the preliminary decomposition of the whole framework, and an obvious decomposition was observed at 300 °C, corresponding to the final decomposition of the whole framework (Figure 6, a). The thermal decomposition behavior of compounds **2** and **3** was similar. The first weight loss in **2** started at ca. 105 °C up to 150 °C to give a weight loss of ca. 3%, corresponding to the loss of the solvated water molecule (2.62% calculated). On further heating, it lost one coordinated water molecule per formula unit between 150 °C and 250 °C (5.4% observed, 5.25% calculated). Immediately above 250 °C, an obvious weight loss continuing to 290 °C was observed, corresponding to the loss of half a bpe molecule per formula unit (27.4% observed, 26.84% calculated). The decomposition of **2** was complete at ca. 500 °C (Figure 6, b). In compound **3**, an initial weight loss of 2.7% at 150 °C, corresponding to the removal of the solvated water molecule (2.65% calculated), was followed by further weight loss of 5.92% (5.31% calculated) at 305 °C for evacuation of the coordinated water molecule. From 305 to 350 °C, the TGA trace of **3** showed a sharp decline to give a total weight loss of ca. 28.3% (27.16% calculated), corresponding to the loss of half a bpe molecule per formula unit. Finally, compound **3** decomposed completely at about 510 °C (Figure 6, c). All TGA data indicate that the guest water molecules play an important role in stabilizing these coordination networks. When these are liberated from the cavities, the frameworks im-

 © 2003 Wiley-VCH Verlag GmbH & Co. KGaA, Weinheim

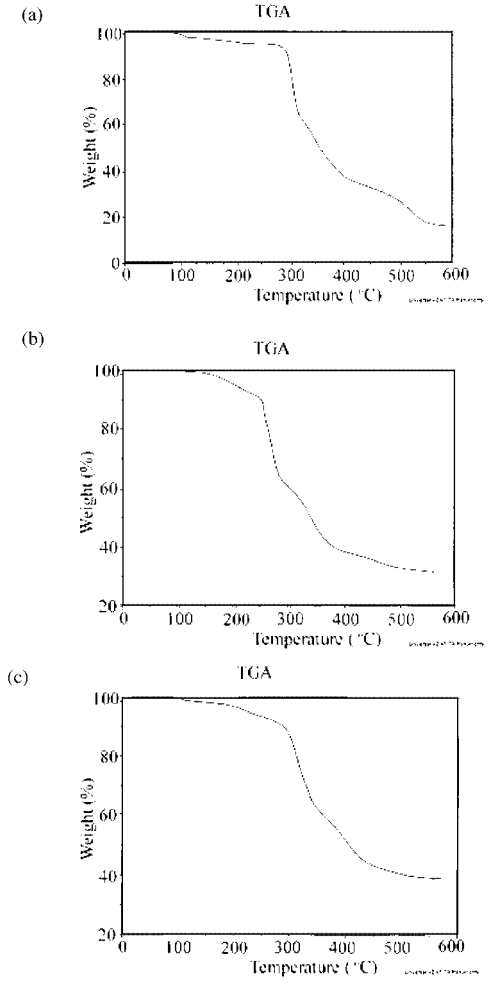

Figure 6. TGA diagram for the coordination polymers: (*a*) compound **1**; (*b*) compound **2**; (c) compound **3**

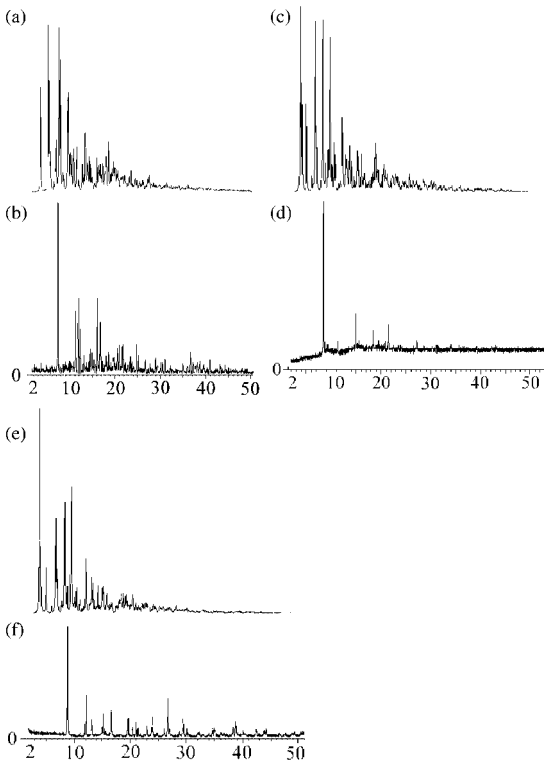

Figure 7. X-ray diffraction pattern for: (a) **1**, as synthesized; (b) solid of **1** heated at 130 °C for 2 h; (c) **2**, as synthesized; (d) solid of **2** heated at 150 °C for 2 h; (e) **3**, as synthesized; (f) solid of **3** heated at 150 °C for 2 h

mediately begin to collapse. The corresponding X-ray powder diffraction (XRPD) data also confirm these changes (Figure 7).

Fluorescent Properties

The emission spectra of complexes **1**−**3** in the solid state at room temperature are shown in Figure 8. It can be observed that the intense emissions occurring in the same range for the three different metals can be assigned to ligand-metal charge-transfer (LMCT) bands, similar to those observed for dipyridinocrown ether ligands[32] (Figure 8, a: λ_{ex} = 210 nm, λ_{em} = 326 nm for **1**; Figure 8, b: λ_{ex} = 300 nm, λ_{em} = 398 nm for **2**; Figure 8, c: λ_{ex} = 220 nm, λ_{em} = 350 nm for **3**). Interestingly, a weak emission occurring at 486 nm for **2** (Figure 8, b: λ_{ex} = 300 nm), assigned as metal-ligand charge-transfer (MLCT) band, can be also observed. The reason for the MLCT phenomenon only occurring in compound **2** and not in compounds **1** and **3** may be that compound **2** contains the d^7 Co^{2+} metal center, in which d-electronic transition is easier than in the d^{10} Cd^{2+} metal center and in the d^5 Mn^{2+} metal center in the other two compounds.

Conclusion

Three new coordination polymers have been obtained by self-assembly of Cd^{II}, Co^{II}, and Mn^{II} with the mixed ligands 3,4-pyridinedicarboxylate (pydc), 1,3-bis(4-pyridyl)-propane (bpp), or 1,2-bis(4-pyridyl)ethane (bpe). The stabilities of these compounds are dependent on the existence of their guest molecules; when these guest molecules are liberated, the frameworks collapse. The structural figures of these whole frameworks contain the information of their components. In **1**, the penta-connecting trigonal bipyramid nodes combining with the di- and tri-connectors result in a (3,5) connected framework, while in **2** and **3**, with the penta-connecting tetragonal pyramid nodes cooperating with the di- and tetra-connectors, another interesting (4,5) connected framework was obtained.

This work shows that the conformations and the functions of the ligands play an important role in affecting the final structural motifs of the polymers. Investigation of the different coordination modes of the ligands may also help in the design of novel structural frameworks and fabrication of new functional materials.

Experimental Section

Materials and Methods: All chemicals were purchased and used without further purification. The C, H and N microanalyses were carried out with a Vario EL III elemental analyzer. Infrared spectra

 © 2003 Wiley-VCH Verlag GmbH & Co. KGaA, Weinheim

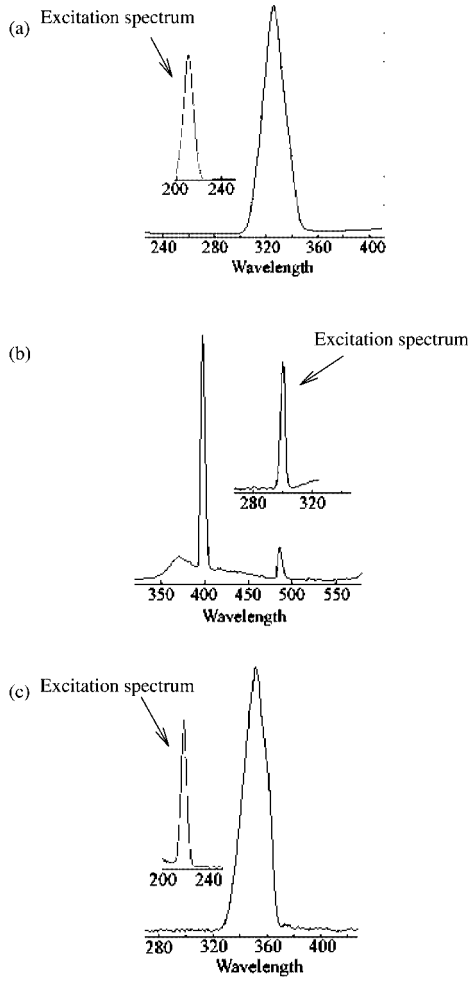

Figure 8. Solid-state emission spectra of the complexes at room temperature: (a) **1**; (b) **2**; (c) **3**

(KBr pellets) were recorded in the 4000−400 cm^{-1} range with a Nicolet Magna 750 FT-IR spectrometer. Thermogravimetric analysis (TGA) was performed under nitrogen with a heating rate of 10 °C·min^{-1} using a TA5200/MDSC2910 system (TA Instruments, Inc.). Fluorescent spectra were measured with an Edinburgh FL-FS90 TCSPC system. X-ray powder diffraction were recorded with a Bruker AXS D8 advanced automated diffractometer with Cu-K_α radiation; the sample was heated in air and the measurement was performed after the sample had cooled down to room temperature.

Synthesis of $C_{20}H_{19}CdN_3O_{4.5}$ (1): An aqueous mixture (10 mL) containing 3,4-pyridinedicarboxylic acid (1 mmol), $Cd(NO_3)_2{\cdot}4H_2O$ (1 mmol), 1,3-bis(4-pyridyl)propane (0.5 mmol), and NaOMe (2 mmol) was placed in a Parr Teflon-lined stainless steel vessel (25 mL), and the vessel was sealed and heated to 150 °C for 168 h, then cooled at 2.5 °C h^{-1} to room temperature. Colorless needle-like crystals (0.14 g) were obtained in 56% yield. $C_{20}H_{19}CdN_3O_{4.5}$ (484.77): calcd. C 49.28, H 3.93, N 8.63; found C 48.29, H 3.67, N 8.62. IR (KBr pellet): $\tilde{\nu}$ = 3361 m, 3221 w, 3053 w, 2945 m, 1614 s, 1606 s, 1585 s, 1570 s, 1547 m, 1406 s, 1417 s, 1385 s, 1227 m, 1061 w, 1011 m, 847 s, 814 m, 785 m, 721 m, 683 m, 525 w cm^{-1}.

Synthesis of $C_{13}H_{12}CoN_2O_{5.50}$ (2): An aqueous mixture (10 mL) containing 3,4-pyridinedicarboxylic acid (1 mmol), $Co(NO_3)_2{\cdot}6H_2O$ (1 mmol), 1,2-bis(4-pyridyl)ethane (0.5 mmol), and NaOMe (2 mmol) was placed in a Parr Teflon-lined stainless steel vessel (25 mL), and the vessel was sealed and heated to 150 °C for 168 h, then cooled at 2.5 °C h^{-1} to room temperature. Red block crystals (0.15 g) were obtained in 43% yield. $C_{13}H_{12}CoN_2O_{5.50}$ (343.18): calcd. C 45.50, H 3.52, N 8.16; found C 45.11, H 3.46, N 8.13. IR (KBr pellet): $\tilde{\nu}$ = 3350 m, 3084 w, 2945 w, 1641 s, 1616 m, 1572 s, 1547 s, 1412 s, 1398 s, 1230 w, 1171 w, 1016 w, 816 w, 677 w cm^{-1}.

Synthesis of $C_{13}H_{12}MnN_2O_{5.50}$ (3): An aqueous mixture (10 mL) containing 3,4-pyridinedicarboxylic acid (1 mmol), $MnCl_2{\cdot}4H_2O$ (1 mmol), 1,2-bis(4-pyridyl)ethane (0.5 mmol), and NaOMe(2 mmol) was placed in a Parr Teflon-lined stainless steel vessel (25 mL), and the vessel was sealed and heated to 150 °C for 168 h, then

Table 1. Crystal data and refinement details for the structures of **1**, **2**, and **3**

Complex	**1**	**2**	**3**
Empirical formula	$C_{20}H_{18}CdN_3O_{4.5}$	$C_{13}H_{12}CoN_2O_{5.50}$	$C_{13}H_{12}MnN_2O_{5.50}$
Formula mass	484.77	343.18	339.19
Space group	Pca2(1)	*C*2/*c*	*C*2/*c*
a [Å]	24.5356(10)	23.2508(1)	23.001(2)
b [Å]	7.6283(2)	10.9695(3)	11.2151(11)
c [Å]	10.5098(4)	11.5021(2)	11.6851(12)
α	90	90	90
β	90	113.609(1)	112.971(2)
γ	90	90	90
V [Å^3]	1967.07(12)	2688.06(9)	2775.3(5)
Z	4	8	8
μ(Mo-K_α) [mm^{-1}]	1.144	1.305	0.979
θ range [°]	1.66−25.06	1.91−25.04	1.92−25.04
$d_{calcd.}$ [g/cm^3]	1.637	1.696	1.624
Final *R* indices [$I > 2\sigma(I)$][a]	$R1$ = 0.0405	$R1$ = 0.0476	$R1$ = 0.0608
	$wR2$ = 0.0712	$wR2$ = 0.1110	$wR2$ = 0.1342
Max/mean shift in final cycle	0.000/0.000	0.000/0.000	0.000/0.000
Maximum/minimum ρ [e×Å^{-3}]	0.657/−0.636	0.617/−0.675	0.631/−0.475

[a] $R = \Sigma(||F_o| - |F_c||)/\Sigma|F_o|$; $wR = \{\Sigma w[(F^2_o - F^2_c)]/\Sigma w[(F^2_o)^2]\}^{0.5}$; $w = [\sigma^2(F^2_o) + (0.0283P)^2 + 0.0000P]^{-1}$ for compound **1**, $w = [\sigma^2(F^2_o) + (0.0523P)^2 + 13.5832P]^{-1}$ for compound **2**, and $w = [\sigma^2(F^2_o) + (0.0546P)^2 + 21.5163P]^{-1}$ for compound **3**, where $P = (F^2_o + 2F^2_c)/3$.

 © 2003 Wiley-VCH Verlag GmbH & Co. KGaA, Weinheim

Table 2. Selected bond lengths [Å] and bond angles [°] for **1**, **2**, and **3**; symmetry codes: a = $-x + 3/2$, $y - 1$, $z + 1/2$; b = x, $y - 1$, z; c = $-x + 1$, $-y + 2$, $z - 1/2$ for **1**; a = $-x + 1/2$, $y + 1/2$, $-z + 1/2$; (b) x, $-y$, $z + 1/2$; c = $-x + 1/2$, $-y - 1/2$, $-z + 1$ for **2** and **3**

$\{[Cd(pydc)(bpp)]\cdot 0.5H_2O\}_n$ (**1**):			
Cd(1)−N(1)	2.347(6)	Cd(1)−O(4c)	2.390(6)
Cd(1)−O(1)	2.351(5)	Cd(1)−O(3c)	2.496(5)
Cd(1)−N(2a)	2.381(4)	Cd(1)−O(2)	2.524(6)
Cd(1)−N(3b)	2.382(7)		
N(1)−Cd(1)−O(1)	98.47(19)	N(2a)−Cd(1)−O(3c)	139.2(2)
N(1)−Cd(1)−N(2a)	83.3(3)	N(3b)−Cd(1)−O(3c)	90.5(2)
O(1)−Cd(1)−N(2a)	138.2(2)	O(4c)−Cd(1)−O(3c)	53.47(18)
N(1)−Cd(1)−N(3b)	169.4(2)	N(1)−Cd(1)−O(2)	87.2(2)
O(1)−Cd(1)−N(3b)	92.1(2)	O(1)−Cd(1)−O(2)	53.85(17)
N(2a)−Cd(1)−N(3b)	89.6(3)	N(2a)−Cd(1)−O(2)	84.7(2)
N(1)−Cd(1)−O(4c)	88.3(2)	N(3b)−Cd(1)−O(2)	100.1(2)
O(1)−Cd(1)−O(4c)	135.6(2)	O(4c)−Cd(1)−O(2)	170.2(2)
N(2a)−Cd(1)−O(4c)	86.1(2)	O(3c)−Cd(1)−O(2)	135.12(17)
N(3b)−Cd(1)−O(4c)	83.4(2)	O(1)−Cd(1)−O(3c)	82.53(16)
N(1)−Cd(1)−O(3c)	89.73(19)		
$\{[Co(pydc)(H_2O)(bpe)_{0.5}]\cdot 0.5H_2O\}_n$ (**2**):			
Co(1)−O(2a)	2.037(3)	Co(1)−O(5)	2.157(3)
Co(1)−O(1b)	2.077(3)	Co(1)−N(1)	2.166(3)
Co(1)−O(3)	2.108(3)	Co(1)−N(2c)	2.168(3)
O(2a)−Co(1)−O(1b)	98.46(11)	O(3)−Co(1)−N(1)	87.95(12)
O(2a)−Co(1)−O(3)	95.29(11)	O(5)−Co(1)−N(1)	92.08(13)
O(1b)−Co(1)−O(3)	165.53(11)	O(2a)−Co(1)−N(2c)	85.06(12)
O(2a)−Co(1)−O(5)	178.63(12)	O(1b)−Co(1)−N(2c)	88.25(12)
O(1b)−Co(1)−O(5)	81.13(11)	O(3)−Co(1)−N(2c)	88.50(12)
O(3)−Co(1)−O(5)	85.02(12)	O(5)−Co(1)−N(2c)	93.62(12)
O(2a)−Co(1)−N(1)	89.26(13)	N(1)−Co(1)−N(2c)	173.00(13)
O(1b)−Co(1)−N(1)	96.65(12)		
Co(1)−O(2a)	2.037(3)	Co(1)−O(5)	2.157(3)
Co(1)−O(1b)	2.077(3)	Co(1)−N(1)	2.166(3)
Co(1)−O(3)	2.108(3)	Co(1)−N(2c)	2.168(3)
$\{[Mn(pydc)(H_2O)(bpe)_{0.5}]\cdot 0.5H_2O\}_n$ (**3**):			
Mn(1)−O(2a)	2.117(4)	Mn(1)−O(3)	2.161(3)
Mn(1)−O(1b)	2.144(3)	Mn(1)−N(2c)	2.301(4)
Mn(1)−O(5)	2.225(4)	Mn(1)−N(1)	2.290(4)
O(2a)−Mn(1)−O(1b)	99.52(14)	O(5)−Mn(1)−N(2c)	96.86(15)
O(2a)−Mn(1)−O(5)	179.49(14)	O(3)−Mn(1)−N(2c)	86.56(14)
O(1b)−Mn(1)−O(5)	79.97(14)	O(2a)−Mn(1)−N(1)	88.27(15)
O(2a)−Mn(1)−O(3)	95.39(14)	O(1b)−Mn(1)−N(1)	99.22(15)
O(1b)−Mn(1)−O(3)	163.24(14)	O(5)−Mn(1)−N(1)	91.76(16)
O(5)−Mn(1)−O(3)	85.12(14)	O(3)−Mn(1)−N(1)	88.79(14)
O(2a)−Mn(1)−N(2c)	83.16(14)	N(2c)−Mn(1)−N(1)	169.81(16)
O(1b)−Mn(1)−N(2c)	87.65(14)		

cooled at 2.5 °C h^{-1} to room temperature. Yellow block crystals (0.14 g) were obtained in 41% yield. $C_{13}H_{12}MnN_2O_{5.50}$ (339.19): calcd. C 46.03, H 3.57, N 8.26; found C 46.21, H 3.33, N 8.22. IR (KBr pellet): $\tilde{\nu}$ = 3358 s, 3055 m, 2945 w, 1637 s, 1614 s, 1576 s, 1547 s, 1414 s, 1398 s, 1228 m, 1012 m, 818 m, 675 m cm^{-1}.

X-ray Crystallographic Study: Crystallographic data for compounds **1**, **2**, and **3** are listed in Table 1. Data for **1**, **2**, and **3** were collected at room temperature with a Siemens SMART-CCD area-detector diffractometer with Mo-K_α radiation (λ = 0.71073 Å) and graphite monochromator using the ω-scan mode. Data reductions and absorption corrections were performed with SMART and SADABS software, respectively. The structures were solved by direct methods by use of SHELXS-97[33] and refined on F^2 by full-matrix, least squares.[34] All non-hydrogen atoms were treated anisotropically. The positions of hydrogen atoms were generated geometrically. The selected bond lengths and bond angles for the cluster cores of **1**, **2**, and **3** are listed in Table 2. CCDC-196855 to -196857 contain the supplementary crystallographic data for this paper. These data can be obtained free of charge at www.ccdc.cam.ac.uk/conts/retrieving.html [or from the Cambridge Crystallographic Data Centre, 12 Union Road, Cambridge CB2 1EZ, UK; Fax: (internat.) + 44-1223/336-033; E-mail: deposit@ccdc.cam.ac.uk].

Acknowledgments

This work is supported by grants from the State Key Laboratory of Structural Chemistry, Fujian Institute of Research on the Structure of Matter, the Chinese Academy of Sciences (CAS), and also the Ministry of Science and Technology of China (001CB1089), the National Science Foundation of China (20273073, 90206040), and the Science Foundation of CAS and Fujian Province, for research funding support (2002F014). Z.-Y. F. and J.-C. D. wish to thank Dr. J.-M. Lin for the PRXD determination and Prof. W.-D. Cheng for useful discussions on fluorescent properties.

[1] S. R. Batten, R. Robson, *Angew. Chem. Int. Ed.* **1998**, *37*, 1460−1494.
[2] M. J. Zaworotko, *Chem. Soc. Rev.* **1994**, 283−288.

 © 2003 Wiley-VCH Verlag GmbH & Co. KGaA, Weinheim

[3] P. J. Hagrman, D. Hagrman, J. Zubieta, *Angew. Chem. Int. Ed.* **1999**, *38*, 2639−2684.
[4] S. Noro, S. Kitagawa, M. Kondo, K. Seki, *Angew. Chem. Int. Ed.* **2000**, *39*, 2081−2084.
[5] M. Kondo, T. Yoshitomi, K. Seki, H. Matsuzaka, S. Kitagawa, *Angew. Chem. Int. Ed. Engl.* **1997**, *36*, 1725−1727.
[6] R. Robson, *Comprehensive Supramolecular Chemistry*, Pergamon, England, **1996**, chapter 22, pp. 733−755.
[7] M. Hayashi, Y. Miyamoto, T. Inoue, N. Oguni, *J. Chem. Soc., Chem. Commun.* **1991**, 1752−1753.
[8] G. B. Gardner, D. Venkataraman, J. S. Moore, S. Lee, *Nature* **1995**, *374*, 792−795.
[9] R. W. Gable, B. F. Hoskins, R. Robson, *J. Chem. Soc., Chem. Commun.* **1990**, 1677−1678.
[10] M. Fujita, Y. J. Kwon, S. Washizu, K. Ogura, *J. Am. Chem. Soc.* **1994**, *116*, 1151−1152.
[11] L. R. MacGillivray, R. H. Groeneman, J. L. Atwood, *J. Am. Chem. Soc.* **1998**, *120*, 2676−2677.
[12] M. Kondo, T. Yoshitomi, K. Seki, H. Matsuzaka, S. Kitagawa, *Angew. Chem. Int. Ed. Engl.* **1997**, *36*, 1725−1727.
[13] K. N. Power, T. L. Hennigar, M. J. Zaworotko, *New J. Chem.* **1998**, 177−181.
[14] C. J. Kepert, M. J. Rosseinsky, *Chem. Commun.* **1999**, 375−376.
[15] Z. Y. Fu, X. T. Wu, J. C. Dai, L. M. Wu, C. P. Cui, S. M. Hu, *Chem. Commun.* **2001**: 1856−1857.
[16] P. Losier, M. J. Zaworotko, *Angew. Chem. Int. Ed. Engl.* **1996**, *35*, 2779−2782.
[17] T. L. Hennigar, D. C. MacQuarrie, P. Losier, R. D. Rogers, M. J. Zaworotko, *Angew. Chem. Int. Ed. Engl.* **1997**, *36*, 972−973.
[18] M. A. Withersby, A. J. Blake, N. R. Champness, P. A. Cooke, P. Hubberstey, M. Schroder, *New J. Chem.* **1999**, *23*, 573−575.
[19] L. R. MacGillivray, S. Subramanion, M. J. Zaworotko, *Chem. Commun.* **1994**, 1325−1326.
[20] L. Carlucci, G. Ciani, D. M. Proserpio, A. Sironi, *J. Chem. Soc., Chem. Commun.* **1994**, 2755−2756.
[21] O. M. Yaghi, H. Li, *J. Am. Chem. Soc.* **1995**, *117*, 10401−10402.
[22] T. Soma, H. Yuge, T. lwamoto, *Angew. Chem. Int. Ed. Engl.* **1994**, *33*, 1665−1666.
[23] S. Subramanian, M. J. Zaworotko, *Angew. Chem. Int. Ed. Engl.* **1995**, *34*, 2127−2129.
[24] F. A. Cotton, C. Lin, C. A. Murillo, *Chem. Commun.* **2001**, 11−12.
[25] S. M. Lo, S. Y. Chui, L. Y. Shek, Z. Lin, X. X. Zhang, G. Wen, I. D. Williams, *J. Am. Chem. Soc.* **2000**, *122*, 6293−6294.
[26] S. Leininger, B. Olenyuk, P. J. Stang, *Chem. Rev.* **2000**, *100*, 853−908.
[27] E. E. Sileo, D. Vega, R. Baggio, M. T. Garland, M. A. Blesa, *Aust. J. Chem.* **1999**, *52*, 205−212.
[28] M. Eddaoudi, D. B. Moler, H. Li, B. Chen, T. M. Reineke, M. O'keeffe, O. M. Yaghi, *Acc. Chem. Res.* **2001**, *34*, 319−330.
[29] J. C. Dai, X. T. Wu, Z. Y. Fu, C. P. Cui, S. M. Hu, W. X. Du, L. M. Wu, H. H. Zhang, R. Q. Sun, *Inorg. Chem.* **2002**, *41*, 1391−1396.
[30] S. Leininger, B. Olenyuk, P. J. Stang, *Chem. Rev.* **2000**, *100*, 853−908.
[31] K. N. Power, T. L. Hennigar, M. J. Zaworotko, *New J. Chem.* **1998**, 177−181.
[32] A. Tahri, E. Cielen, K. J. V. Aken, G. J. Hoornaert, F. C. D. Schryver, N. Boens, *J. Chem. Soc., Perkin Trans. 2* **1999**, 1739−1748.
[33] G. M. Sheldrick, *Acta Crystallogr., Sect. A* **1990**, *46*, 467.
[34] G. M. Sheldrick, *SHELXL-97*, *Program for X-ray Crystal Structure Refinement*, University of Göttingen, Göttingen, Germany, **1997**.

Received January 12, 2003

 © 2003 Wiley-VCH Verlag GmbH & Co. KGaA, Weinheim

Syntheses and Crystal Structures of Two Novel Zinc(II) Coordination Polymers

Jun Tao,*[a] Xin Yin,[a] Yun-Bao Jiang,[a] Le-Fu Yang,[a] Rong-Bin Huang,[a] and Lan-Sun Zheng*[a]

Keywords: Coordination polymers / Zinc / N ligands / Hydrogen bonds / Photoluminescence

Two novel zinc(II) coordination polymers, $[Zn_3(\mu_3\text{-}OH)_2(nip)_2]$ (**1**) and $[Zn_2(nip)_2(4,4'\text{-bpy})_3\cdot(OH_2)]$ (**2**) (H_2nip = 5-nitroisophthalic acid, 4,4′-bpy = 4,4′-bipyridyl), were obtained by the hydrothermal reactions of zinc nitrate, 5-nitroisophthalate (nip) (for **1**) and zinc nitrate, 5-nitroisophthalate and 4,4′-bipyridyl (for **2**). Complex **1** displays a two-dimensional structure that is built from $[Zn_3(\mu_3\text{-}OH)_2]_n$ chains, while complex **2** is a three-dimensional structure formed by the interpenetration of two-dimensional hydrogen-bonded bilayers. The photoluminescent properties of complex **1** have also been investigated.

(© Wiley-VCH Verlag GmbH & Co. KGaA, 69451 Weinheim, Germany, 2003)

Introduction

Recently, coordination polymer frameworks have attracted great attention not only owing to their fascinating applications in the areas of magnetism, optics, electronics, catalysis and sorption,[1−5] but also to their interesting topologies.[6] Among the frameworks reported so far, two types of interactions — coordinate covalent bonds and non-covalent intermolecular forces such as hydrogen bonding and π-π stacking — play major roles in constructing and stabilizing these polymers. Currently, the direct mixing of metal ions and a single organic ligand by means of coordinative covalent and/or hydrogen-bonding interactions has produced a great variety of such frameworks. One of our research interests has focused on a systematic study of the construction of coordination polymers by using mixed organic ligands under hydrothermal conditions,[7] and recently we have been investigating the influences of substituted isophthalate derivatives, such as 5-nitroisophthalate (nip), in which the two carboxylate groups can form covalent bonds with metal centers while the nitro group acts as a hydrogen-bond acceptor and can form strong hydrogen bonds, on the assembly process of coordination polymers.[8] Here we report the syntheses and crystal structures of two novel zinc(II) coordination polymers with the 5-nitroisophthalate ligand (nip), namely $[Zn_3(\mu_3\text{-}OH)_2(nip)_2]$ (**1**) and $[Zn_2(nip)_2(4,4'\text{-bpy})_3\cdot(OH_2)]$ (**2**). Interestingly, the nitro groups in complex **1** play important roles in the formation of the hydrogen bonds, while in complex **2** the 4,4′-bpy ligands act as hydrogen-bond acceptors.

[a] Department of Chemistry and State Key Laboratory of Physical Chemistry of Solid Surfaces, Xiamen University, Xiamen 361005, China
Fax: (internat.) +86-592/218-3047
E-mail: taojun@jingxian.xmu.edu.cn

Results and Discussion

The structures of $[Zn_3(\mu_3\text{-}OH)_2(nip)_2]$ (**1**) and $[Zn_2(nip)_2(4,4'\text{-bpy})_3\cdot H_2O]$ (**2**) were determined by single-crystal X-ray crystallography. Selected bond lengths and angles for **1** and **2** are listed in Table 1 and 2, respectively,

Table 1. Selected bond lengths [Å] and angles [deg] for **1**[a]

Zn1−O1	1.997(1)	Zn1−O2	1.920(1)
Zn2−O1	2.086(1)	Zn2−O3	2.135(1)
O1−Zn1−O1A	85.25(7)	O1−Zn1−O2	110.65(7)
O2−Zn1−O1A	129.14(2)	O2−Zn1−O2B	96.08(6)
O1−Zn2−O3	97.18(5)	O1−Zn2−O1D	180.00(10)
O1−Zn2−O3D	82.82(5)	O3−Zn2−O3E	88.46(6)

[a] Symmetry codes: A x, $-y$, $z+1$; B $-x$, $-y$, $-z+1$; C $-x$, y, z; D $-x$, $-y$, $-z$; E $-x$, y, $-z$.

Table 2. Selected bond lengths [Å] and angles [deg] for **2**[a]

Zn1−O1	2.245(6)	Zn1−O2	2.386(6)
Zn1−O4A	2.076(4)	Zn1−N1	2.164(5)
Zn1−N3	2.179(5)	Zn1−N5	2.208(4)
Zn2−O7	2.280(4)	Zn2−O8	2.140(4)
Zn2−O1W	2.058(5)	Zn2−O10B	2.033(4)
Zn2−N2	2.181(5)	Zn2−N4C	2.177(5)
O4A−Zn(1)−O1	86.52(19)	O4A−Zn1−O2	142.33(18)
N1−Zn1−N5	91.07(17)	N1−Zn1−N3	175.41(19)
O4A−Zn1−N1	89.59(18)	N1−Zn1−O1	88.93(18)
O8−Zn2−O7	60.23(15)	O1W−Zn2−O7	164.30(18)
O10B−Zn2−O1W	102.0(2)	O10B−Zn2−O8	153.66(17)
O1W−Zn2−N4C	90.3(2)	O8−Zn2−N4C	88.27(18)
O1W−Zn2−N2	91.7(2)	N4C−Zn2−N2	178.01(19)

[a] Symmetry codes: A $x+1$, y, z; B $x-1$, y, z; C x, y, $z+1$.

 © 2003 Wiley-VCH Verlag GmbH & Co. KGaA, Weinheim **DOI: 10.1002/ejic.200300021**

Table 3. Crystallographic data for complex **1** and **2**

	1	2
Chemical formula	$C_{16}H_8N_2O_{14}Zn_3$	$C_{46}H_{32}N_8O_{13}Zn_2$
Mol. wt.	648.35	1035.54
Space group	*C*2/*m*	$P\bar{1}$
a (Å)	14.7847(16)	10.1001(8)
b (Å)	10.2014(11)	11.0760(8)
c (Å)	6.2298(7)	22.919(2)
α (°)	90	99.774(4)
β (°)	91.797(6)	91.441(4)
γ (°)	90	115.304(4)
V (Å^3)	939.15(18)	2270.5(3)
Z	2	2
D_c (g·cm^{-3})	2.293	1.515
μ (mm^{-1})	3.889	1.132
R_1, wR_2 (all data)	0.0512, 0.0971	0.0665, 0.1787

with crystallographic and refinement data in Table 3. As shown in Figure 1, compound **1** contains two-dimensional sheets constructed from $[Zn_3(\mu_3\text{-}OH)_2]_n$ chains and nip ligands, in which the crystallographically equivalent unit is one half of a nip ligand, one half of a Zn1 center, one quarter of a Zn2 center and one half of a μ_3-hydroxy group. The Zn1 center has pseudo-tetrahedral coordination symmetry, and is ligated by two oxygen atoms from two crystallographically equivalent μ_3-hydroxy groups [Zn1−O1 = 1.997(1) Å] and two oxygen atoms from two carboxylate groups [Zn1−O2 = 1.902(1) Å] of two symmetry-related nip ligands. The Zn2 atom is bound to four oxygen atoms from four different nip ligands in the equatorial plane and two oxygen atoms from two μ_3-hydroxy groups to give a pseudo-octahedral center [Zn2−O1 = 2.086(1) Å and Zn2−O3 = 2.135(1) Å]. The average Zn−O(H)−Zn angle (108.26°) in **1** is close to those found in typical tetrahedral Zn complexes containing μ_3-hydroxy groups, rather than the trigonal-planar one generally observed for μ_3-hydroxy groups.[9] The infinite $[Zn_3(\mu_3\text{-}OH)_2]_n$ chain-like structural motif shown in Figure 2 is also observed in the structures of three-dimensional basic zinc 4,4′-biphenyldicarboxylate and discrete basic zinc crotonate.[9a,10]

The infinite $[Zn_3(\mu_3\text{-}OH)_2]_n$ chains are stacked in parallel and connected by the nip ligands to give a two-dimensional undulating sheet. Viewed along the crystallographic *a* axis (Figure 3), the resulting two-dimensional framework is reminiscent of the shape of a compressed square, and obviously contains the C_{2h} point group. The nitro groups are found on the wave crest of both sides of the sheet, and the μ_3-hydroxy groups point away from the $[Zn_3(\mu_3\text{-}OH)_2]_n$ chains and into the trough. These undulating two-dimensional sheets are stacked in a parallel fashion with the wave crests coinciding with the troughs of adjacent sheets, and vice versa. The whole three-dimensional structure is then stabilized by inter-layer moderate hydrogen bonds (O1···O4 = 3.109 Å) between the μ_3-hydroxy groups in one

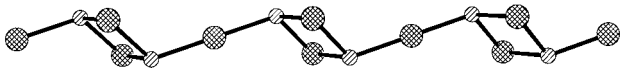

Figure 2. Perspective view of the one-dimensional $[Zn_3(\mu_3\text{-}OH)_2]_n$ structural motif

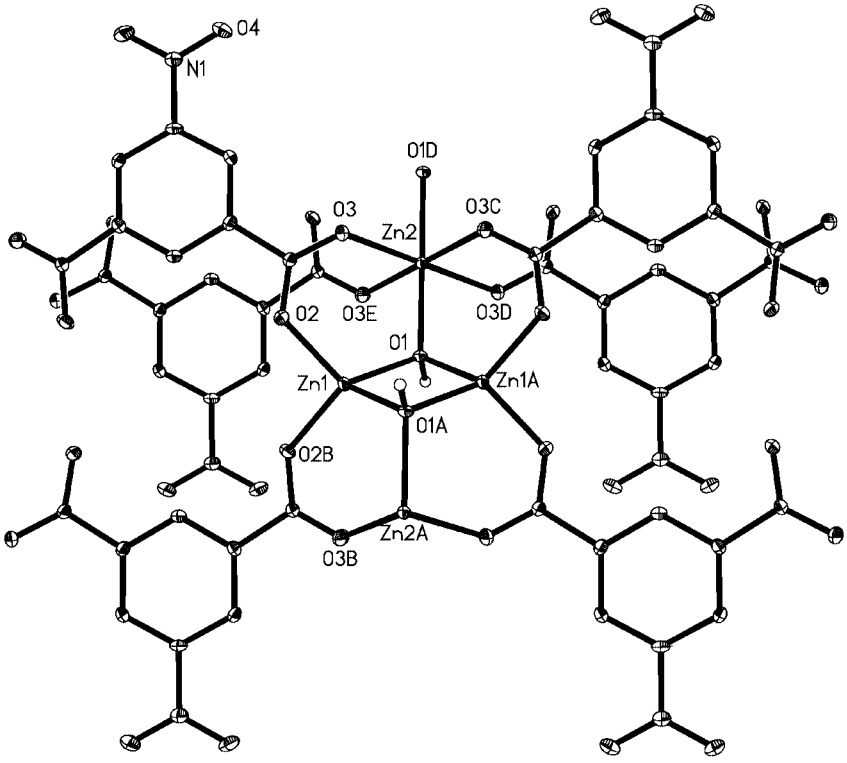

Figure 1. The coordination environments of zinc atoms in **1** with the atomic labeling scheme (30% probability)

 © 2003 Wiley-VCH Verlag GmbH & Co. KGaA, Weinheim

sheet and the nitro oxygen atoms in the adjacent sheet (Figure 4); they are bifurcated hydrogen bonds with $d_1 = d_2$.[11]

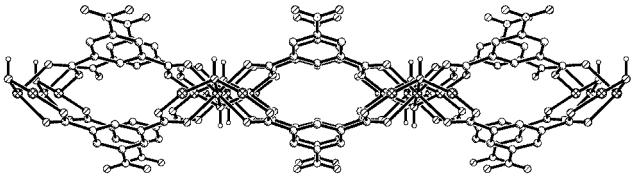

Figure 3. The two-dimensional structure of **1** viewed along the *a* axis

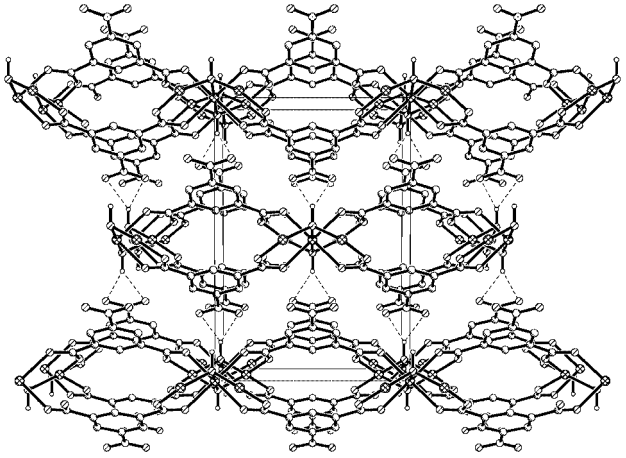

Figure 4. The hydrogen-bonded three-dimensional structure of **1** packed along the *a* axis

The crystal structure of **2** consists of hydrogen-bonded two-dimensional bilayered cuboids as the fundamental building unit. In the asymmetric unit there are two crystallographically unique Zn atoms, three 4,4′-bpy ligands, two nip ligands and one water molecule. The immediate coordination arrangement around the zinc centers in **2** is shown in Figure 5. The Zn1 atom lies in a slightly distorted octahedral environment, consisting of three nitrogen atoms from three different 4,4′-bpy ligands and three oxygen atoms from two symmetry-related nip carboxylate groups. The Zn2 atom, slightly different from Zn1 in its coordination environment, is ligated by two nitrogen atoms from two different 4,4′-bpy ligands, three oxygen atoms from two symmetry-related nip carboxylate groups and one water molecule, completing an octahedral coordination at Zn2. It is interesting to note that the 4,4′-bpy ligand containing the N5 and N6 atoms is linked to the Zn1 atom through only one of the nitrogen ends (N5), while the other end (N6) is hydrogen bonded to the coordinated water molecule in the adjacent layer [O1W···N6D = 2.758(7) Å], the water molecule is also hydrogen-bonded to the oxygen atom [O1W···O9B 2.653(7) Å] of a nip carboxylate group. Even more interesting is the fact that the three crystallographically unique 4,4′-bpy ligands are all non-coplanar, as can be seen from their different dihedral angles (N1−N2 = 36.4°, N3−N4 = 20.6° and N5−N6 = 29.6°).

The distinctive feature of **2** is that the alternating $[Zn(nip)(4,4'\text{-bpy})]_n$ and $[Zn(nip)(H_2O)]_n$ chains are covalently linked by μ_2-4,4′-bpy bridges, resulting in an interesting two-dimensional (4,4) coordination sheet with 4,4′-bpy ligands (N5−N6) suspended on one side (Figure 6). Two such sheets, located at an inversion center, are linked into a

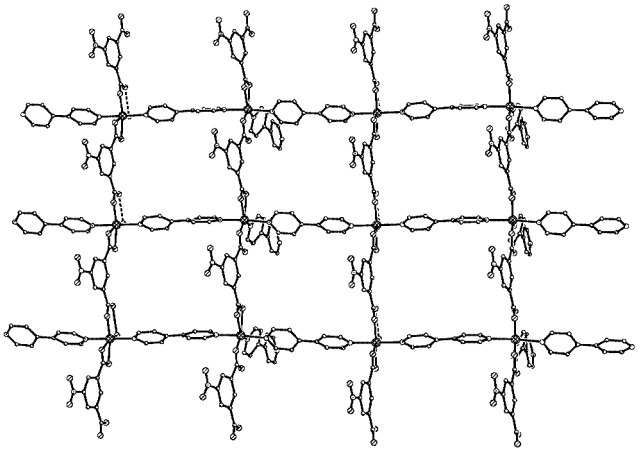

Figure 6. Perspective view of the two-dimensional (4,4) sheet of **2**

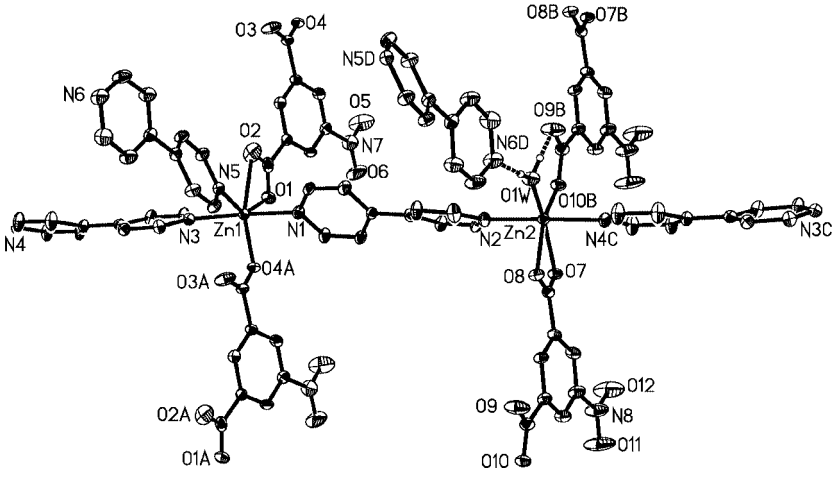

Figure 5. The coordination environments of zinc atoms in **2** with the atomic labeling scheme (30% probability)

 © 2003 Wiley-VCH Verlag GmbH & Co. KGaA, Weinheim

two-dimensional bilayer by inter-layer hydrogen bonds [O1W···N6 = 2.758(7) Å] in a face-to-face fashion, whereas the nitro groups adopt an orientation that can be regarded as being *trans* to one another on either side of the bilayer, as shown in Figure 7. To the best of our knowledge, although several coordination bilayers having been reported,[7c,12] this is the first example of a bilayer connected through hydrogen bonds in coordination polymers. The cuboidal $[Zn_8(nip)_8(4,4'\text{-bpy})_8]$ building block with dimensions of ca. $10.100 \times 11.456 \times 13.971$ Å^3 in the bilayer is significantly different from those in other bilayer structures or three-dimensional structures.[7b,7c,12]

Although large void spaces exist within a single bilayer, there are no encapsulated guest molecules because of interpenetration. As shown in Figure 8, each bilayer is interpenetrated by two adjacent identical ones in a parallel fashion, the resulting extended array is therefore an infinite catenane of 2D architecture, as reported previously.[7c,12a] This is consistent with the fact that crystal structures with large cavities are inclined to self-interpenetrate.

As we previously reported, zinc oxide or hydroxide coordination polymers exhibit photoluminescent properties,[7a,7d] and we have also investigated the photoluminescent properties of **1** (Figure 9). In the solid state, **1** exhibits intense photoluminescence upon photoexcitation at 308 nm, the emission of **1** (λ_{max} = 354 nm) might be attributable to the formation of $[Zn_3(\mu_3\text{-}OH)_2]_n$ chains and/or ligand-to-metal charge transfer (LMCT).[7a,7d,13]

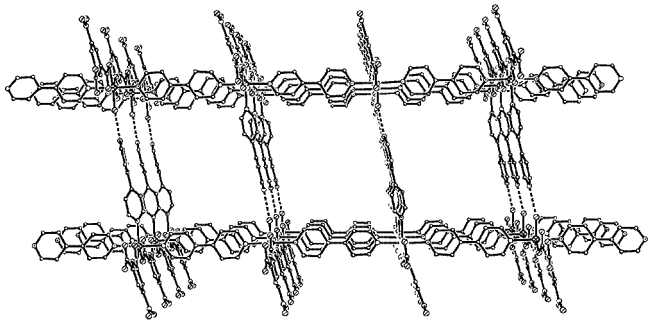

Figure 7. Perspective view of the two-dimensional bilayer of **2**

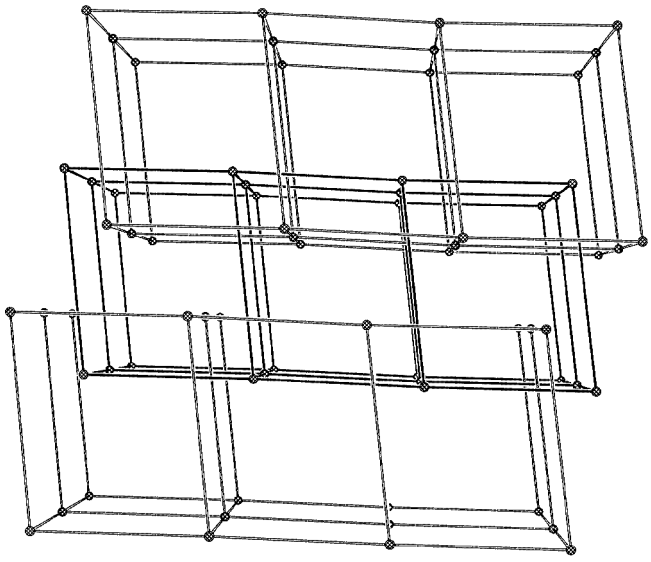

Figure 8. Perspective view of the twofold interpenetrated framework of **2**

Thermogravimetric analyses (TGA) of complexes **1** and **2** performed on polycrystalline samples reveal that **1** and **2** are thermally stable up to ca. 295 and 300 °C, respectively, indicating that even hydrogen-bonded frameworks can also be thermally stable at high temperatures.

In summary, two novel zinc(II) coordination polymers $[Zn_3(\mu_3\text{-}OH)_2(nip)_2]$ (**1**) and $[Zn_2(nip)_2(4,4'\text{-bpy})_3\cdot(OH_2)]$ (**2**) have been hydrothermally synthesized. Their structures are both two-dimensional with inter-layer hydrogen bonds, and **2** is the first hydrogen-bonded bilayer in coordination polymers.

Experimental Section

General Remarks: All starting materials were reagent grade and used as purchased. The elemental analyses were performed on a

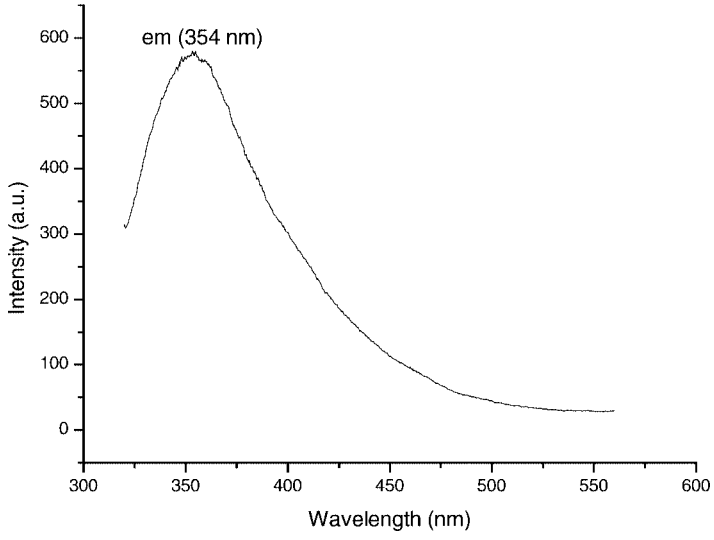

Figure 9. The solid-state photoluminescent spectrum of **1** at room temperature

 © 2003 Wiley-VCH Verlag GmbH & Co. KGaA, Weinheim

Perkin−Elmer 240 elemental analyzer. The infrared spectra were recorded on a Nicolet 5DX spectrometer with KBr pellets. Thermal gravimetric analyses were performed in dinitrogen on a Perkin−Elmer 7 thermogravimetric analyzer with a heating rate of 10 °C/min.

Synthesis of 1: An aqueous mixture of $Zn(NO_3)_2{\cdot}6H_2O$ (0.158 g, 0.5 mmol), H_2nip (0.106 g, 0.5 mmol) and NaOH (0.04 g, 1 mmol) in a molar ratio of 1:1:2 was placed in a Teflon-lined stainless vessel, then the mixture was heated at 180 °C for 80 h. Colorless plate-like crystals were obtained in 50% yield based on zinc after the mixture was cooled to room temperature. $C_{16}H_8N_2O_{14}Zn_3$ (648.35): calcd. C 29.64, H 1.24, N 4.32; found C 30.01, H 1.40, N 4.22. IR (KBr): $\tilde{\nu}$ = 3538(m), 3084(w), 2925(w), 1636(s), 1614(vs), 1571(s), 1522(m), 1425(m), 1385(s), 1352(vs), 1206(w), 1127(s), 1065(w), 1027(w), 835(w), 785(m), 556(w) cm^{-1}.

Synthesis of 2: This compound was prepared as colorless plate-like crystals by the procedure described above for **1** except for the addition of 4,4′-bpy (H_2nip:4,4′-bpy = 1:2). Yield: 65% based on zinc. $C_{46}H_{32}N_8O_{13}Zn_2$ (1035.54): calcd. C 53.35, H 3.11, N 10.82; found C 53.10, H 2.83, N 11.01. IR (KBr): $\tilde{\nu}$ = 3427(s), 3090(w), 2924(w), 1610(vs), 1566(m), 1531(s), 1414(s), 1368(vs), 1345(s), 1219(m), 1073(m), 1064(w), 821(m), 789(w), 542(w) cm^{-1}.

Crystallographic Analysis: Data collection (single crystal with dimensions of 0.37 × 0.12 × 0.05 mm^3 for **1** and 0.40 × 0.20 × 0.05 mm^3 for **2**) was performed at 296(2) K on a Bruker APEX CCD-based diffractometer equipped with Mo-K_α radiation (λ = 0.71073 Å). The structures were solved by direct methods using SHELXS-97[14] and refined with full-matrix least-squares technique using SHELXL-97.[15] All non-hydrogen atoms were refined anisotropically and the hydrogen atoms of the organic ligands were placed geometrically. The H atom of the hydroxyl group in **1** was located in the calculated position, and the H atoms of the coordinated water in **2** were found by Fourier syntheses. Selected crystallographic data and structure determination parameters for complexes **1** and **2** are presented in Table 3.

CCDC-201058 (**1**) and -201059 (**2**) contain the supplementary crystallographic data for this paper. The structure of **2** was re-refined after the data were deposited to CCDC. These data can be obtained free of charge at www.ccdc.cam.ac.uk/conts/retrieving.html [or from the Cambridge Crystallographic Data Center, 12 Union Road, Cambridge CB2 1EZ, UK; Fax: (internat.) +44-1223/336-033; E-mail: deposit@ccdc.cam.ac.uk].

Acknowledgments

This work was supported by the Innovation Foundation for Young Scientific Talents of Fujian Province (NO. 2002J004), NNSF of China (NO. 20021002), Department of Science and Technology of China (NO. 2002CCA01600) and the Research Program of Xiamen University (NO. Y07015).

[1] [1a] X. X. Zhang, S. S.-Y. Cui, I. D. Williams, *J. Appl. Phys.* **2000**, *87*, 6007. [1b] L.-S. Long, X.-M. Chen, M.-L. Tong, Z.-G. Sun, Y.-P. Ren, R.-B. Huang, L.-S. Zheng, *J. Chem. Soc., Dalton Trans.* **2001**, 2888. [1c] S. Konar, P. S. Mukherjee, E. Zangrando, F. Lloret, N. R. Chaudhuri, *Angew. Chem. Int. Ed.* **2002**, *41*, 1561. [1d] P. Kapoor, A. Pathak, R. Kapoor, P. Venugopalan, *Inorg. Chem.* **2002**, *23*, 6153. [1e] G. J. Halder, C. J. Kepert, B. Moubaraki, K. S. Murray, J. D. Cashion, *Science* **2002**, *298*, 1762.

[2] [2a] Z.-F. Chen, R.-G. Xiong, B. F. Abrahams, X.-Z. You, C.-M. Che, *J. Chem. Soc., Dalton Trans.* **2001**, 2453. [2b] M.-L. Tong, J.-X. Shi, X.-M. Chen, *New J. Chem.* **2002**, *26*, 814. [2c] C.-G. Zheng, Y.-L. Xie, R.-G. Xiong, X.-Z. You, *Inorg. Chem. Commun.* **2001**, *4*, 405.

[3] [3a] J. Y. Lu, K. A. Runnels, C. Norman, *Inorg. Chem.* **2001**, *40*, 4516. [3b] S. S. Zhu, P. J. Carroll, T. M. Swager, *J. Am. Chem. Soc.* **1996**, *118*, 8713.

[4] [4a] B. G. Lor, E. G. Puebla, M. Lglesaias, M. A. Monge, C. R. Valero, N. Snejko, *Inorg. Chem.* **2002**, *41*, 2429. [4b] N. Snejko, S. Cascales, B. G. Lor, E. G. Puabla, M. Iglesias, C. R. Vannels, M. A. Morge, *Chem. Commun.* **2002**, 1366. [4c] L. Pan, H. Liu, X. Lei, X. Huang, D. H. Olson, N. J. Turro, J. Li, *Angew. Chem. Int. Ed.* **2003**, *42*, 542.

[5] [5a] M. Eddaoudi, J. Kim, N. Rosi, D. Vodak, J. Wachter, M. O'Keeffe, O. M. Yaghi, *Science* **2002**, *295*, 469. [5b] S. Noro, S. Kitagawa, M. Kondo, K. Seki, *Angew. Chem. Int. Ed.* **2000**, *39*, 2082. [5c] B. Chen, M. Eddaoudi, S. T. Hyde, M. O'Keeffe, O. M. Yaghi, *Science* **2001**, *291*, 1021. [5d] J. Y. Lu, A. M. Babb, *Chem. Commun.* **2002**, 1340.

[6] [6a] S. R. Batten, R. Robson, *Angew. Chem. Int. Ed.* **1998**, *37*, 1460. [6b] M. J. Zaworotko, *J. Am. Chem. Soc.* **2002**, *124*, 9990.

[7] [7a] J. Tao, M.-L. Tong, J.-X. Shi, X.-M. Chen, S. W. Ng, *Chem. Commun.* **2000**, 2043. [7b] J. Tao, M.-L. Tong, X.-M. Chen, *J. Chem. Soc., Dalton Trans.* **2000**, 3669. [7c] J. Tao, X.-M. Zhang, M.-L. Tong, X.-M. Chen, *J. Chem. Soc., Dalton Trans.* **2001**, 770. [7d] J. Tao, J.-X. Shi, M.-L. Tong, X.-X. Zhang, X.-M. Chen, *Inorg. Chem.* **2001**, *40*, 6328. [7e] J. Tao, Y. Zhang, M.-L. Tong, X.-M. Chen, Y. Tan, C.-L. Lin, X. Huang, J. Li, *Chem. Commun.* **2002**, 1342. [7f] J. Tao, X. Yin, R.-B. Huang, L.-S. Zheng, *Inorg. Chem. Commun.* **2002**, *5*, 1000.

[8] [8a] X. Yin, J. Tao, R.-B. Huang, L.-S. Zheng, *Main Group Metal Chem.* **2002**, 691. [8b] J. Tao, X. Yin, S.-Y. Yang, R.-B. Huang, L.-S. Zheng, *Main Group Metal Chem.* **2002**, 707.

[9] [9a] W. Clegg, D. R. Harbron, C. D. Homan, P. A. Hunt, I. R. Little, B. P. Straughan, *Inorg. Chim. Acta* **1991**, *186*, 51. [9b] J. Hermann, A. Erxleben, *Inorg. Chim. Acta* **2000**, *304*, 125. [9c] J. S. Seo, D. Whang, H. Lee, S. I. Jun, J. Oh, Y. J. Jeon, K. Kim, *Nature* **2000**, *404*, 982.

[10] N. L. Rosi, M. Eddaoudi, J. Kim, M. O'Keeffe, O. M. Yaghi, *Angew. Chem. Int. Ed.* **2002**, *41*, 284.

[11] T. Steiner, *Angew. Chem. Int. Ed.* **2002**, *41*, 48.

[12] [12a] Z.-Y. Fu, X.-T. Wu, J.-C. Dai, L.-M. Wu, C.-P. Cui, S.-M. Hu, *Chem. Commun.* **2001**, 1856. [12b] M. J. Zaworotko, *Chem. Commun.* **2001**, 1.

[13] [13a] A. Meijerink, G. Blasse, M. Glasbeek, *J. Phys. Condens. Matter.* **1990**, *2*, 6303. [13b] R. Bertoncello, M. Bettinelli, M. Vassrin, A. Gulino, E. Tondello, A. Vittadini, *Inorg. Chem.* **1992**, *31*, 1558.

[14] G. M. Sheldrick, SHELXS-97, *Program for Crystal Structure Solution*, University of Göttingen, Germany, 1997.

[15] G. M. Sheldrick, SHELXL-97, *Program for Crystal Structure Refinement*, University of Göttingen, Germany, 1997.

Received January 14, 2003

 © 2003 Wiley-VCH Verlag GmbH & Co. KGaA, Weinheim

Synthesis and Molecular Structures of Nickel(II) and Cobalt(III) Complexes with 2-(Arylimino)-3-(hydroxyimino)butane

Ennio Zangrando,*[a] Manuela Trani,[b] Elisa Stabon,[a] Carla Carfagna,[c] Barbara Milani,[a] and Giovanni Mestroni[a]

Keywords: Cobalt / Crystal structures / N-donor ligands / Nickel / Stacking interactions

We report new series of Ni^{II} and Co^{III} complexes with nitrogen-donor chelating ligands of the (*E*,*E*)-2-(arylimino)-3-(hydroxyimino)butane type (Ar–N⌒N–OH). These ligands are characterized by a hydrophilic (OH group) and a hydrophobic region (aryl group). Ni^{II} derivatives were obtained either as trimers of formula $[Ni_3(Ar–N⌒N–OH)_3Br_4(OH)][Br]$, with the hydrophobic groups oriented on the same side, or as bis(chelated) derivatives with *cis* geometry, depending on the steric hindrance of the aryl groups. Co^{III} complexes were obtained only as bis(chelated) derivatives, with the two ligands coplanar. The "*iso*-oriented" arrangement of ligands in bis(chelated) Co^{III} complexes is favored by weak interactions between the two ligands, namely O–H···O hydrogen bond and stacking interactions between the aryl groups. Co^{III} complexes might find application as catalysts for *living* or *controlled* radical polymerization of polar olefins, and preliminary results are reported.

(© Wiley-VCH Verlag GmbH & Co. KGaA, 69451 Weinheim, Germany, 2003)

Introduction

Recent studies report that the molecular weights of polymers synthesized from olefin monomers with the aid of transition-metal catalysts or promoters can be tuned by the steric hindrance of the ancillary ligands.[1–6] In particular, the steric properties can be modulated by the introduction of 2- or 2,6-substituted aryl groups in planar bi-, tri- and tetradentate nitrogen-donor chelates. Some notable examples are reported in Figure 1.

When the substituted aryl groups are arranged perpendicular to the plane of the chelate, they create a particular steric hindrance above and below the plane of the chelate itself (Figure 1). Bi- and tridentate ligands of variable steric hindrance are easily accessible thanks to the synthetic procedure based on the condensation reaction between biacetyl (or 2,6-diacetylpyridine) and an appropriate aromatic amine.[1,2] On the other hand, convenient modulation of the steric hindrance is more difficult to achieve for tetradentate N-donor chelating ligands such as porphyrins or bis(dimethylglyoximate) derivatives.

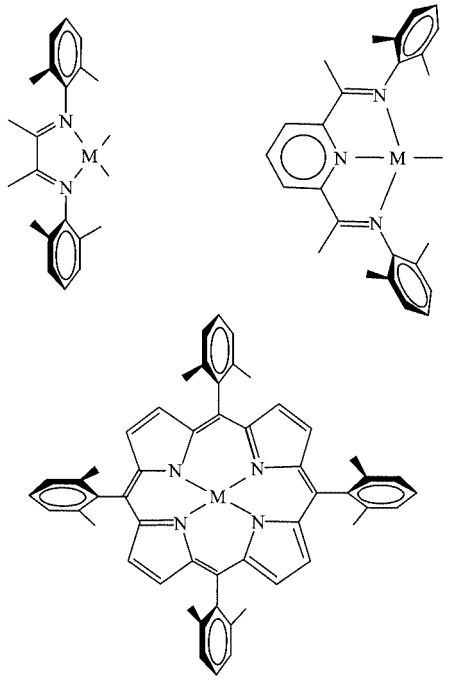

Figure 1. Examples of bi-, tri-, and tetradentate nitrogen-donor ligands and of the corresponding complexes

Such nitrogen-donor chelating ligands are of particular interest in the field of homogeneous catalysis. Depending on the nature of the metal, the olefin, and the experimental conditions, different reactions can be performed: nickel

[a] Dipartimento di Scienze Chimiche, Università di Trieste,
Via L. Giorgeri 1, 34127 Trieste, Italy
Fax: (internat.) + 39-040/5583903
E-mail: zangrando@univ.trieste.it
[b] Department of Chemistry, Sanford S. Atwood Chemistry Center,
1515 Pierce Dr, Atlanta, GA 30322, USA
[c] Istituto di Scienze Chimiche, Università di Urbino,
Piazza Rinascimento 6, 61029 Urbino, Italy

complexes with bidentate chelating ligands or cobalt and iron complexes with tridentate chelating ligands, in the presence of MAO, promote the oligomerization or polymerization of ethylene or propylene by a coordinative mechanism.[1−5] Moreover, cobalt complexes with planar tetradentate chelating ligands have successfully been used in oligomerization and polymerization of polar olefins by a radical mechanism in the presence of AIBN [2,2′-azobis(isobutyronitrile)].[6−10] In particular, organometallic Co^{III} complexes with planar sterically hindered N-donor tetradentate chelating ligands polymerize polar olefins by a *living* radical mechanism.[6] In the absence of steric bulk, these complexes promote the oligomerization of the same substrates, yielding oligomers characterized by terminal C=C double bonds.[7] Cobalt derivatives with dimethylglyoxime (cobaloximes)[9] and analogous complexes, in which the bridging H atom is replaced by a BF_2 group,[10] turned out to be very efficient and cheap oligomerization catalysts. The presence of two OH···O bridging moieties in cobaloxime derivatives ensures coplanarity of the two molecules of ligand, which is necessary for these complexes to show catalytic activity.[7]

Interestingly, the effect of steric hindrance induced by chelating ligands is the same regardless of the type of polymerization mechanism. In both cases the chain termination step, a β-H elimination process, proceeding either through a coordinative[1] or a radical mechanism,[9,11,12] is slowed down with increasing bulkiness of the aryl moiety.

Very recently we reported that complexes of type *cis*-$[Co(CH_2Ph)_2(N-N)_2][PF_6]$ (N−N = bipy, phen) promote acrylonitrile polymerization by a *controlled* radical mechanism,[13] with behavior intermediate between that exhibited by cobalt complexes with sterically hindered and nonhindered planar tetradentate N-donor chelating ligands.

In this study we report the synthesis and characterization of nickel and cobalt complexes with a series of bidentate N-donor chelating ligands: namely, (*E*,*E*)-2-(arylimino)-3-(hydroxyimino)butanes (Ar−N∩N−OH) (Figure 2, a). The ligands in which the aryl group is phenyl or *o*-tolyl, are known[14,15] and the series has now been extended to other substituted amines.

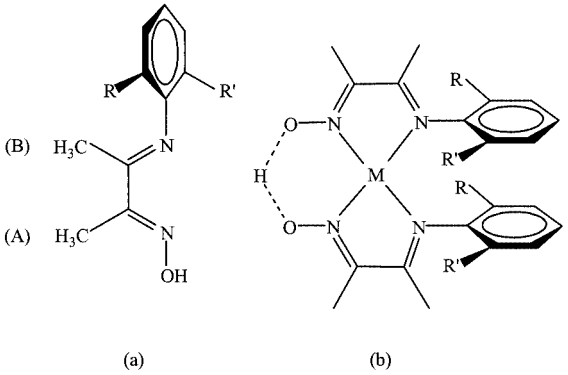

Figure 2. (a) Generic 2-(arylimino)-3-(hydroxyimino)butane ligand (Ar−N∩N−OH);(b) corresponding bis(chelated) planar complex

These ligands are characterized by a hydrophilic (OH) and a hydrophobic region (Ar). Therefore, with a ligand/metal ratio of 2:1, the formation of planar bis(chelated) species can be predicted, thanks to the possibility of establishing weak interactions between the two molecules of Ar-N∩N−OH, such as the hydrogen bond between the oxygen atoms and/or the stacking interaction between the aromatic rings (Figure 2, b). Unlike that in the planar bis(dimethylglyoxime) derivatives, the steric bulk in these complexes is directed normally to the equatorial plane and can be modulated by varying the nature of substituents in the 2- and the 6-positions of the aromatic ring.

Some results on the catalytic activity of the cobalt derivatives in the polymerization of methyl methacrylate (MMA) are also presented.

Results and Discussion

Synthesis and Characterization of 2-(Arylimino)-3-(hydroxyimino)butane Ligands 1a−1i

The chelating ligands (*E*,*E*)-2-(arylimino)-3-(hydroxyimino)butane are obtained by condensation of biacetyl monoxime with a series of different substituted aromatic amines (Scheme 1).

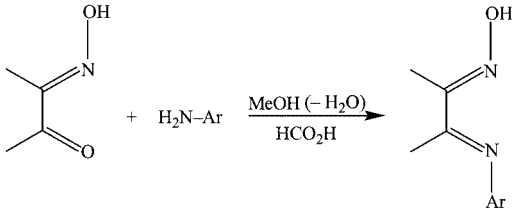

Ar = Ph **1a** 2-MeC_6H_4 **1b** 4-MeC_6H_4 **1c**
2-*i*PrC_6H_4 **1d** 2-*t*BuC_6H_4 **1e** 2,6-$Me_2C_6H_3$ **1f**
3,5-$Me_2C_6H_3$ **1g** 2,4,6-$Me_3C_6H_2$ **1h** 2,6-*i*PrC_6H_3 **1i**

Scheme 1. Synthesis of Ar−N∩N−OH ligands **1a−1i**

Syntheses were conducted in methanol at reflux for 5 h, starting from stoichiometric amounts of reagents, and in the presence of formic acid in catalytic amount. All ligands were obtained in high yields as white, crystalline solids. Crystals of **1h** suitable for X-ray diffraction analysis were obtained upon slow cooling of the reaction mixture.

Its structural characterization, with regard to the two N=C double bonds, shows a *syn*-methyl,*syn*-methyl conformation (Figure 3) that would require a rotation about the C(2)−C(3) bond in order to behave as a chelating ligand. The planarity of the O−N=C−C=N fragment, with a torsion angle of 162.7(5)°, is indicative of π-electron delocalization in the heterodiene fragment, as confirmed by the C(2)−C(3) bond length of 1.462(6) Å. This in fact appears to be slightly shorter than the accepted value of 1.48 Å for a $C(sp^2)-C(sp^2)$ single bond.[16] It may be of interest to point out the difference between the C=N−C angles at the N(2) imino and the N(1) oxime nitrogen atoms [120.1(5) and 111.8(4)°, respectively]. The mesitylene ring is roughly

 © 2003 Wiley-VCH Verlag GmbH & Co. KGaA, Weinheim

perpendicular to the planar residue of the molecule, making a dihedral angle of 73°, an arrangement induced by steric hindrance between the groups. The crystal packing consists of chains with a zigzag motif, running along the crystallographic *c* axis, where O(1)−H ··N(2) hydrogen bonds [O···N = 2.749(5) Å] connect adjacent molecules. The molecular geometry and the packing resemble those found in the *p*-tolyl analogue.[15]

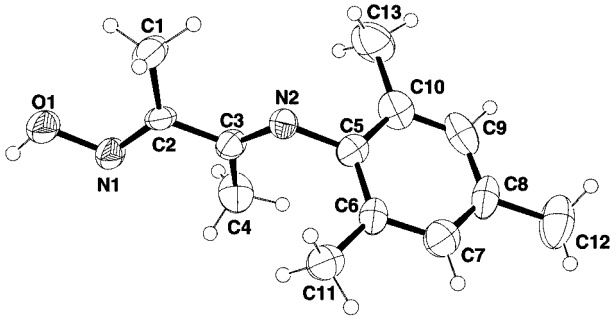

Figure 3. Molecular structure of ligand **1h** (ORTEP drawing, thermal ellipsoids 40% probability); selected bond lengths [A] and angles [°]: O(1)−N(1) 1.395(4), N(1)−C(2) 1.283(5), N(2)−C(3) 1.269(5), N(2)−C(5) 1.434(6), C(1)−C(2) 1.487(5), C(2)−C(3) 1.462(6), C(3)−C(4) 1.493(5); C(2)−N(1)−O(1) 111.8(4), C(3)−N(2)−C(5) 120.1(5)

The ligands have been characterized by ^{1}H NMR spectroscopy in $CDCl_3$ (Table 1). ^{1}H NMR spectra exhibit two characteristic regions: aromatic (protons of the aryl groups at δ ≈ 6−7.5 ppm) and aliphatic (methyl groups of the biacetyl monoxime backbone and aromatic ring substituents at δ ≈ 2−3 ppm). A broad peak belonging to the OH group is also visible between δ ≈ 7.80 and 8.40 ppm. The assignment of signals to protons was based on NOE and COSY experiments. The signal of methyl group (A) in all the ligands was further downfield than that of the methyl group (B) (Figure 2, a); for the aryl protons, a downfield shift is observed on going from the β to the γ and to the α protons. The latter trend was also observed for alkyl substituents on the aromatic ring. These chelating ligands were used for the synthesis of both Ni^{II} and Co^{III} complexes.

Synthesis and Characterization of the Ni^{II} Complexes 2a, 2b, 2d, 2e, 2h, 2i; 3h

Synthesis of complexes was carried out in CH_2Cl_2, at room temperature, for 3 h, starting from $[NiBr_2(C_4H_{10}O_2)]$ ($C_4H_{10}O_2$ = ethylene glycol dimethyl ether) and using a ligand/nickel ratio of 1:1 or 2:1 (Scheme 2, a). The products were isolated as brown solids upon addition of diethyl ether or *n*-pentane to the reaction mixture.

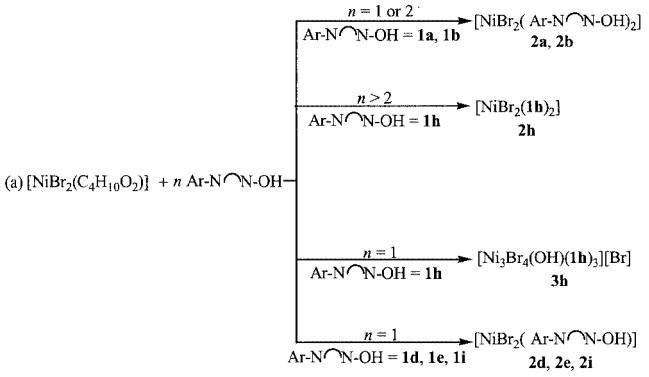

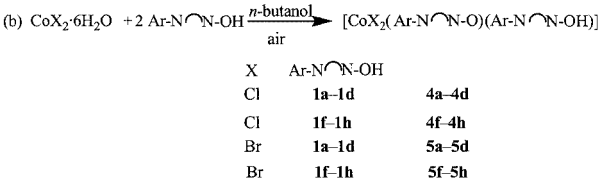

Scheme 2. Synthesis of (a) nickel and (b) cobalt complexes

The products of the reaction were characterized by elemental analyses (Table 2) and, depending on the nature of the ligand, complexes of different stoichiometry were obtained. In particular, when ligands of low steric hindrance, such as **1a** and **1b**, were used, the products were bis(chelated) complexes of formula $[NiBr_2(Ar-N^{\cap}N-OH)_2]$ (**2a**, **2b**), regardless of the ligand/nickel ratio used in the synthesis. With the more hindered ligands **1d**, **1e**, and **1i**, a monochelated species was obtained when the synthesis was carried out with a ligand/nickel ratio of 1:1 (**2d**, **2e**, **2i**). No

Table 1. ^{1}H NMR spectroscopic data for ligands **1a**−**1i**

Ligand[a]	CH_3 (A)	CH_3 (B)	OH	H^{α}	$H^{\alpha'}$	H^{β}	$H^{\beta'}$	H^{γ}
1a	2.20 (s)	2.01 (s)	8.25 (t)	6.72 (d)	6.72 (d)	7.30	7.30	7.09 (t)
1b	2.23 (s)	2.05 (s)	8.19 (s)	1.94 (s)	6.56 (d)	7.16−7.20 (m)	7.16−7.20 (m)	7.00 (t)
1c	2.18 (s)	2.00 (s)	n.d.	6.62 (d)	6.62 (d)	7.12 (d)	7.12 (d)	2.33 (s)
1d	2.24 (s)	1.99 (s)	7.85 (s)	1.15 (d), 2.88 (m)	6.51 (d)	7.29 (d)	7.05−7.17 (m)	7.05−7.17 (m)
1e	2.26 (s)	2.01 (s)	8.39 (s)	1.30 (s)	6.40 (d)	7.39 (d)	7.15 (t)	7.05 (t)
1f	2.25 (s)	1.84 (s)	7.90 (s)	1.96 (s)	7.03 (d)	7.03 (d)	6.91 (t)	
1g	2.18 (s)	2.00 (s)	7.90 (s)	6.34 (s)	6.34 (s)	2.30 (s)	2.30 (s)	6.72 (s)
1h	2.25 (s)	1.83 (s)	8.14 (s)	1.93 (s)	1.93 (s)	6.85 (s)	6.85 (s)	2.22 (s)
1i	2.27 (s)	1.87 (s)	8.34 (s)	1.13 (d), 2.58−2.65 (m)	1.13 (d), 2.58−2.65 (m)	7.05−7.15 (m)	7.05−7.15 (m)	

[a] Spectra recorded in $CDCl_3$, at room temperature; δ, ppm; s = singlet, d = doublet, t = triplet, m = multiplet; n.d. = not determined; the signals of the protons of the alkyl substituents on the aryl group are reported in the place of the corresponding protons.

 © 2003 Wiley-VCH Verlag GmbH & Co. KGaA, Weinheim

Table 2. Elemental analyses for the nickel complexes **2a**, **2b**, **2d**, **2e**, **2h**, **2i** and **3h** and the cobalt complexes **4a**−**4d**, **4f**−**4h**, **5a**−**5d**, **5f**−**5h**

Ni complexes (yield)	C[a]	H[a]	N[a]
2a (53%)	41.30 (42.10)	4.13 (4.10)	9.66 (9.81)
2b (51%)	42.90 (44.11)	4.63 (4.71)	9.23 (9.35)
2d[b] (57%)	35.20 (37.54)	4.39 (4.44)	6.34 (6.74)
2e[b] (44%)	36.80 (37.29)	4.49 (4.47)	6.01 (6.34)
2h (60%)	48.80 (47.67)	5.87 (5.53)	8.83 (8.55)
2i[b] (53%)	40.80 (40.13)	5.26 (5.05)	5.60 (5.84)
3h (52%)	38.80 (40.10)	4.65 (4.70)	6.87 (7.20)
Co complexes (yield)	C[a]	H[a]	N[a]
4a (71%)	49.20 (49.91)	4.71 (4.81)	11.50 (11.64)
5a (83%)	42.10 (42.13)	4.00 (4.06)	9.84 (9.82)
4b (75%)	51.10 (51.88)	5.28 (5.34)	11.00 (11.00)
5b (76%)	44.20 (44.10)	4.58 (4.71)	9.39 (9.35)
4c (80%)	51.70 (51.88)	5.35 (5.34)	11.00 (11.00)
5c (78%)	44.10 (44.10)	4.51 (4.71)	9.41 (9.35)
4d (82%)	54.90 (55.23)	6.25 (6.24)	9.81 (9.91)
5d (80%)	47.72 (47.72)	5.39 (5.39)	8.59 (8.56)
4f (72%)	53.30 (53.64)	5.78 (5.81)	10.20 (10.24)
5f (74%)	45.50 (45.95)	4.90 (5.14)	8.77 (8.93)
4g (74%)	53.60 (53.64)	5.80 (5.81)	10.40 (10.42)
5g (80%)	46.30 (45.95)	5.03 (5.14)	9.01 (8.93)
4h (73%)	55.40 (55.23)	6.29 (6.24)	9.93 (9.91)
5h (73%)	46.80 (47.72)	5.36 (5.39)	8.36 (8.56)

[a] Calculated values in parentheses. [b] The yield was calculated by formulating the complex as [$NiBr_2$(Ar−N∩N−OH)].

bis(chelated) species was isolated when a ligand/nickel ratio > 1:1 was used. For the ligand with the mesityl group, **1h**, the bis(chelated) derivative [$NiBr_2$(**1h**)$_2$] (**2h**) was the product when the synthesis was performed with an excess of ligand. On the other hand, a monochelated species was obtained when a ligand/nickel ratio of 1:1 was used.

Single crystals suitable for X-ray analysis were obtained for the complexes with ligands **1a** (Figure 4) and **1h** (Figure 5), by slow precipitation from a dichloromethane solution with diethyl ether.

The structural determination of complex **2a** confirms its formulation as a bis(chelated) species with the nickel atom in a distorted octahedral coordination geometry. The two bromide ions are in a *cis* arrangement and the two *cis* chelating ligands **1a** are bound to the metal atom in a *head-to-tail* configuration with a dihedral angle of 85.8(4)° (Figure 4). The Ni−N coordination bond lengths involving oxime nitrogen donors *trans* to bromide are longer than the Ni−N(1) and Ni−N(3) bonds *trans* to each other by about 0.08 Å. The Ni−Br bond lengths of 2.561(2) Å are between the values found for the bridging Br^- in **3h** (see below). The N(2)−Ni−Br(1) and N(4)−Ni−Br(2) bond angles of about 165.5° deviate significantly from those expected for a regular octahedron. Nevertheless, each oxime hydrogen atom is pointing, at about 2.5 Å, toward the halide ion and the values for the bond angles could give support to an OH···Br interaction.

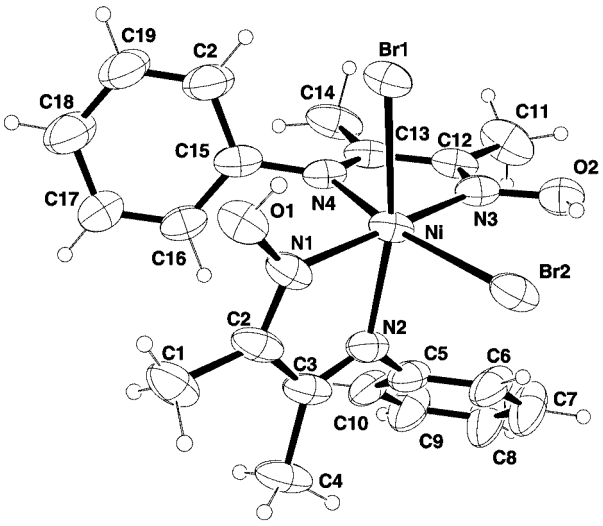

Figure 4. Molecular structure of compound **2a** (ORTEP drawing, thermal ellipsoids 40% probability); selected bond lengths [Å] and angles [°]: Ni−N(1) 2.026(8), Ni−N(2) 2.109(7), Ni−N(3) 2.018(8), Ni−N(4) 2.094(8), Ni−Br(1) 2.561(1), Ni−Br(2) 2.561(2); N(1)−Ni−N(2) 76.4(3), N(3)−Ni−N(4) 75.8(3), N(1)−Ni−N(3) 172.5(3), N(2)−Ni−Br(1) 166.1(3), N(4)−Ni−Br(2) 165.0(2), Br(1)−Ni−Br(2) 93.38(5)

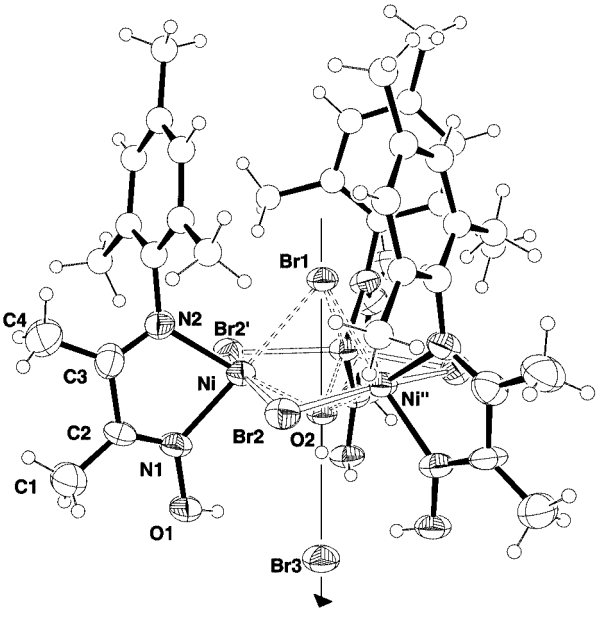

Figure 5. Molecular structure of compound **3h**; for sake of clarity aryl C atoms are indicated as spheres of fixed radius; selected bond lengths [Å] and angles [°]: Ni−Ni′′ 3.026(2), Ni−Br(1) 2.598(2), Ni−Br(2′) 2.551(2), Ni−Br(2) 2.578(2), Ni−O(2) 1.999(5), Ni−N(1) 2.024(8), Ni−N(2) 2.051(8); N(1)−Ni−N(2) 78.6(4), O(2)−Ni−N(1) 105.9(4), O(2)−Ni−N(2) 175.5(4), O(2)−Ni−Br(1) 76.8(3), O(2)−Ni−Br(2) 82.02(5), O(2)−Ni−Br(2′) 82.73(5), N(1)−Ni−Br(1) 175.4(3), N(2)−Ni−Br(1) 98.8(2), Br(2)−Ni−Br(2′) 164.67(7), Ni−Br(1)−Ni′′ 71.24(6), Ni−Br(2)−Ni′′ 72.32(6), Ni−O(2)−Ni′′ 98.4(3); symmetry codes: (′) $-x + y + 1, -x + 1, z$; (′′) $-y + 1, x - y, z$

The X-ray analysis of the complex with ligand **1h** reveals that it is a trinuclear species, corresponding to the formulation [Ni_3Br_4(OH)(**1h**)$_3$][Br] (**3h**).

 © 2003 Wiley-VCH Verlag GmbH & Co. KGaA, Weinheim

The unique and unexpected structure of complex **3h** is shown in Figure 5, together with selected bond lengths and angles. Its C_3 symmetry is illustrated by the view along the symmetry axis (Figure 6). The metal ions of three monochelated Ni(**1h**) fragments form an equilateral triangle. On each edge, the pair of nickel atoms, separated by 3.026(2) Å, is μ_2-bridged by a bromide ligand, slightly displaced by 0.2 Å from the Ni_3 plane, with Ni−Br(2) bond lengths of 2.551(2) and 2.578(2) Å. Another bromide ion and a hydroxy oxygen atom μ_3-bridge all the nickel ions with coordination distances of 2.578(2) and 1.999(5) Å, respectively. These capping species lie on the threefold axis, above [Br(1) +1.923(2) Å] and below [O(2) −0.97(1) Å] the metal plane. The coordination geometry around each nickel atom thus involves the nitrogen-donor atoms of a chelating ligand **1h**, three bromide ions, and a hydroxy group with bond angles that considerably deviate from the ideal octahedral values.

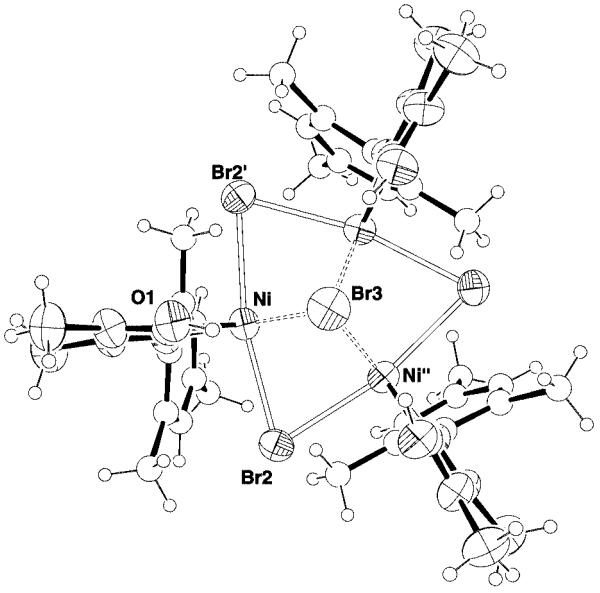

Figure 6. Projection down the threefold axis of the molecular structure of **3h**

In the ligand, the C(2)−C(3) bond length of 1.522(14) Å, although of low accuracy, agrees with a single bond character indicating that, upon coordination, the delocalization inside the O−N=C−C=N moiety of the ligand seems to be removed.

To the best of our knowledge, two structures containing a strictly analogous Ni_3X_3 core (X = halide)[17,18] and with metal atoms capped by an oxygen atom and another halide ion have been reported; their Ni−Ni distances, averaged to 3.05 Å, are closely similar to those here. One of these, with tetramethylethylenediamine as chelating ligand (L) and with chloride replacing the bromide anions, has the same stoichiometry $[Ni_3X_4(OH)L_3][X]$.[17a] A trimeric copper species $[Cu_3(ClO_4)(OH)L'_3]^+$ containing the deprotonated ligand **1a** (L′) has also been reported.[17b] However, the crystal structure shows that L′ behaves as a tridentate species: it chelates a metal ion with the N atoms and simultaneously binds a close copper unit through the O donor, becoming almost coplanar with the metal triangle.

It is worth noting that in the current compound the electronic structural features of ligand **1h** give rise to an assembly possessing well-defined hydrophobic and hydrophilic domains. The former is delimited by the mesitylene groups. The aromatic rings, inclined to form an angle of 80.7(3)° with the Ni_3 plane, enclose the μ_3-bridging Br(1). The hydrophilic area is confined at the oxime groups side, where a bromide ion is displaced by an hydroxy oxygen μ_3-bridge. The bromide ion, Br(3), is settled on the threefold axis and accounts for the neutral charge of the whole compound. The latter anion is located at 3.236(10) Å from the oxime oxygen atoms O(1) and at 3.322(7) Å from O(2), probably interacting with the hydrogen atoms of the hydroxy groups (Figure 5).

On the basis of these results, a reaction mechanism is proposed for the formation of the different synthetic products (Scheme 3).

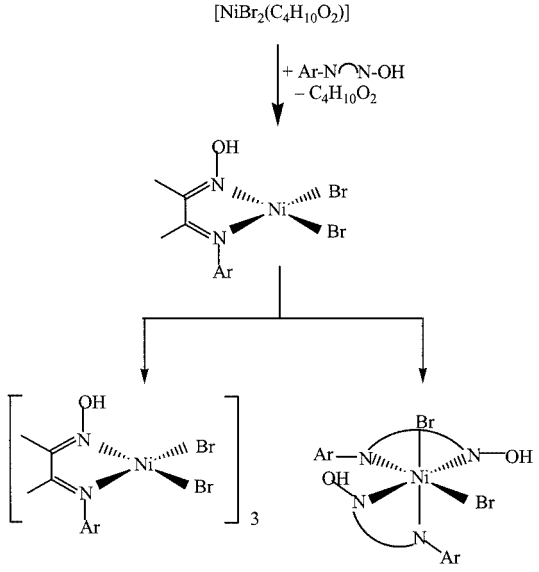

Scheme 3. Proposed mechanism for the synthesis of nickel complexes

The reaction proceeds by initial formation of the monochelated monomeric species, which, depending on the steric hindrance of the ligand, can then evolve along different pathways. For ligands of low steric hindrance (**1a**, **1b**), the reaction moves rapidly towards the formation of bis(chelated) complexes, even at low ligand/Ni ratios. For the mesityl derivative, with ligand/Ni = 1:1, the monochelated derivative is isolated as the trimer **3h**, while with an excess of ligand the bis(chelated) species **2h** is the product. With the sterically more hindered ligands **1d**, **1e** and **1i**, only the formation of monochelated species of unknown nuclearity is observed.

Synthesis and Characterization of Co^{III} Complexes 4a−4d, 4f−4h, 5a−5d, 5f−5h

Synthesis was carried out in the presence of air, in *n*-butanol, at room temperature, for 3 h, starting from

 © 2003 Wiley-VCH Verlag GmbH & Co. KGaA, Weinheim

$CoX_2 \cdot nH_2O$ salts (X = Cl, Br) and using a ligand/cobalt ratio of 1:1 or 2:1 (Scheme 2, b). In all cases, the formation of a red solid is observed immediately after addition of the ligands, followed by its transformation in the final product into a green microcrystalline solid. A total of 14 complexes (chloro and bromo derivatives) have been synthesized. However, the synthesis of **4a** and **5a** derivatives was reported several years ago.[14]

On the basis of elemental analyses (Table 2), all the complexes were formulated as $[CoX_2(Ar-N^{\cap}N-O)(Ar-N^{\cap}N-OH)]$ [X = Cl (**4**), Br (**5**)]. Therefore, in contrast to the nickel derivatives, only octahedral bis(chelated) species are obtained with all the ligands tested, regardless of the ligand/cobalt ratio used.

Single crystals suitable for X-ray analysis were obtained for **5b** and **5h** by crystallization from CH_2Cl_2/*n*-pentane. Figures 7 and 8 (ORTEP drawings, thermal ellipsoids at 50% probability) give perspective views of the molecular structures of compounds **5b** and **5h**, the latter being located on a crystallographic twofold axis passing through the metal atom and in the middle between the oxime oxygen atoms. Unlike in the nickel derivatives, the two bromide ions are in a *trans* arrangement, so the chelating ligands define the equatorial plane of the molecule. Moreover, they are bound to the cobalt atom in a *head-to-head* configuration, in contrast to the *head-to-tail* arrangement proposed for **4a** and **5a** on the basis of steric considerations.[14] The Co−Br and Co−N coordination bond lengths have comparable values in the two complexes. In contrast, the values of the Br−Co−Br bond angles, probably affected by steric hindrance between the bromide ions and the proximal

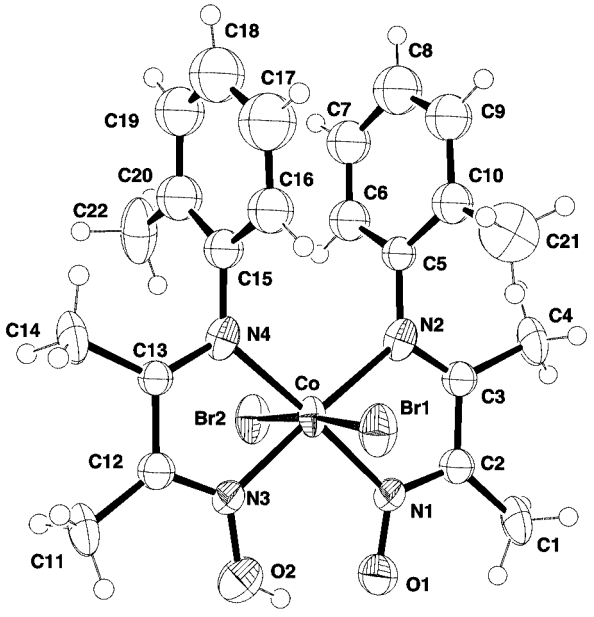

Figure 7. Molecular structure of compound **5b**; selected coordination bond lengths [Å] and angles [°]: Co−Br(1) 2.389(2), Co−Br(2) 2.385(2), Co−N(1) 1.895(11), Co−N(2) 2.006(11), Co−N(3) 1.906(11), Co−N(4) 1.997(11); N(1)−Co−N(2) 80.6(3), N(1)−Co−N(3) 96.2(5), N(1)−Co−N(4) 176.3(5), N(2)−Co−N(3) 176.7(5), N(2)−Co−N(4) 103.1(5), N(3)−Co−N(4) 80.1(3), Br(1)−Co−Br(2) 174.12(13)

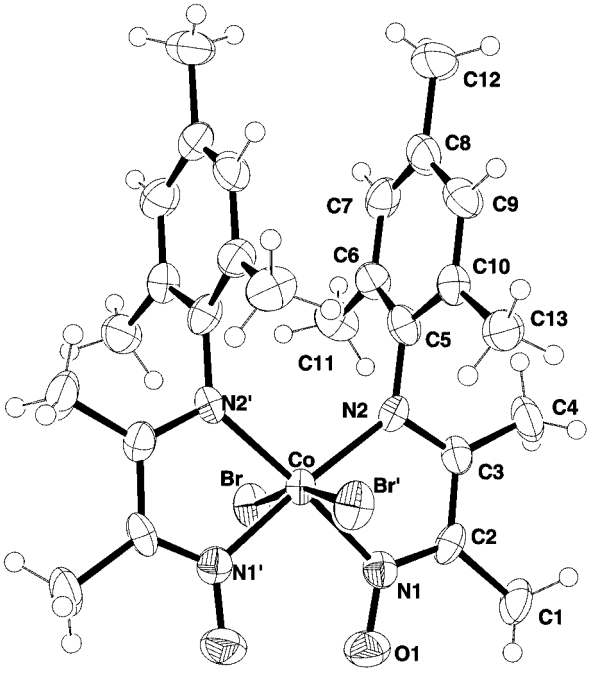

Figure 8. Molecular structure of compound **5h** with atom labelling scheme of the crystallographically independent moiety; selected bond lengths [Å] and angles [°]: Co−Br 2.386(1), Co−N(1) 1.912(6), Co−N(2) 2.006(6); N(1′)−Co−N(1) 95.2(3), N(1)−Co−N(2) 80.7(2), N(1)−Co−N(2′) 175.9(2), N(2)−Co−N(2′) 103.5(3), N(1′)−Co−Br 85.1(2), N(1)−Co−Br 85.3(2), N(2)−Co−Br 94.4(2), N(2′)−Co−Br 94.4(2), Br−Co−Br′ 165.64(7); primed atoms at $-x+1, -y+1, z$

methyl groups on the phenyl rings, are 174.1(1) and 165.64(7)° in the *o*-tolyl and in the mesityl derivative, respectively. The atoms of the five-membered rings are close to coplanar and the calculated angles of 1.6 (**5b**) and 5.4° (**5h**) represent a slight tilting between the chelating ligand moieties.

The *head-to-head* arrangement of the mixed Schiff-base/oxime ligands favors the formation of an OH···O bridge. The mean O···O distance for the two structures of 2.42(1) Å is shorter than those found in the widely studied $[Co(DH)_2]$ and [Co(DO)(DOH)(pn)] complexes[19] [mean values of 2.487(2) and 2.45(1) Å,[20] respectively]. It was suggested that the O···O distance should parallel the ease of deprotonation, as indicated by the slower exchange of the proton in (DO)(DOH)pn than in $(DH)_2$ complexes of similar axial ligands.[21,22] The formation of the H-bridge in **5h** causes a remarkable shortening of the N−O [1.288(7) Å] and of the N(oxime)=C [1.292(9) Å] bonds with respect to those detected in the free ligand, and the same trend is also observed for **5b**, although the values found here are less accurate.

Moreover, the aromatic rings, with an orientation similar to that found in the uncoordinated ligand, ensure intramolecular π-stacking. In fact, the interplanar angle formed by the facing *o*-tolyl rings in **5b** is 15.0(3)° and the C···C distances between the *ipso*-carbon atoms and the carbon atoms in *para* positions are 3.35 and 3.84 Å, respectively. It is worth noting that the dihedral angle between the aryl

 © 2003 Wiley-VCH Verlag GmbH & Co. KGaA, Weinheim

groups in **5h** is reduced to 5.5(3)°, and that the C···C separations are correspondingly somewhat shorter (3.18 and 3.76 Å, respectively), indicating a closer approach and hence a more efficient π-interaction between the bulky mesitylene groups.

Therefore, the *head-to-head* arrangement of the chelating ligands gives rise to an H-bridge and to an aryl π-stacking that act as a double clamp providing additional stability to the complexes. The geometrical data for the cobalt compounds reported here are quite comparable, but a detailed analysis shows that the steric effects around the metal center can be modulated by changing the nature of the aryl substituents.

These complexes were characterized in solution by recording NMR spectra in $CDCl_3$ at room temperature (Table 3). The signal of the methyl group (A) bound to the carbon atom closest to the oxime nitrogen atom is the most shifted (almost 0.40 ppm downfield shift) with respect to the signals of the free ligand. No signal due to the hydroxy group is visible in the spectra of the complexes. It can be seen that the spectrum of complexes with the *o*-tolyl-substituted ligand presents two sets of signals of different intensity both for the alkyl and aryl protons, thus indicating the presence of two species in solution. At room temperature the signals are quite broad. An NOE was observed between the methyl group of *o*-tolyl and $H^{\alpha'}$ and H^{β}. On the other hand, when the signals of the methyl groups (A and B) of the skeleton were irradiated in different NOE experiments, no NOE was seen, other than that expected between the two signals themselves. These results suggest that the two species in solution correspond to two rotamers, differing in the relative orientations of the methyl group of the *o*-tolyl substituents: namely *syn* and *anti* isomers. The broadness of the signals suggests that the two rotamers are in equilibrium and the rate of this equilibrium is slow on the NMR timescale.

The Co^{III} complex with ligand **1g**, [Co(Cl)$_2${**1g**-(H)}(**1g**)], was treated with $NaBH_4$ in methanol in the presence of CH_3I, to yield a red, microcrystalline solid. The elemental analysis confirms the ratio Co/**1g** = 1:2 and is in agreement with the formation of the organometallic derivative [Co(CH_3)(I){**1g**-(H)}(**1g**)] (**6g**). The ^{1}H NMR spectrum, recorded in $CDCl_3$ at room temperature, shows three singlets of the same intensity in the region of the aromatic protons, and five singlets for the methyl groups, one of which is of half intensity with respect to the other four peaks. This last is therefore attributed to the methyl group bound to the cobalt atom. The other assignments of signals to protons were based on comparison with the spectrum of the starting complex **4g**. In particular, the groups in the α- and β-positions of the aromatic rings generate two different signals, thus indicating the lack of the equatorial plane of the complex as a plane of symmetry. The Co−CH_3 and Co−I bonds are therefore in a *trans* configuration. Finally, it is reasonable to assume that the two N$^\frown$N ligands are bound to the cobalt atom in the *head-to-head* arrangement, as in the starting complex. This behavior is analogous to that typical of the dimethylglyoxime and (DO)(DOH)pn derivatives.[23]

Polymerization of Methyl Methacrylate

Some preliminary test polymerizations of methyl methacrylate were performed with complex **5b** by carrying out the reaction in the presence of AIBN as initiator, in THF as solvent. The result is compared with the activity of the system based on AIBN itself (Table 4).

Table 4. Polymerization of methyl methacrylate

Promoter[a]	Yield [g]	Mw	*Mw*/*Mn*
AIBN	2.34	420 000	1.7
AIBN + **5b**[b]	5.59	83 300	1.4

[a] Reaction conditions: $n_{AIBN} = 2.9 \cdot 10^{-2}$ mmol; solvent THF V = 11 mL; MMA V = 12 mL; T = 60 °C; t = 5 h. [b] [AIBN]/[Co] = 15.

Table 3. ^{1}H NMR spectroscopic data for cobalt complexes **4a**−**4d**, **4f**−**4h**, **5a**−**5d**, **5f**−**5h**

Complexes[a]	CH_3 (A)	CH_3 (B)	H^{α}	$H^{\alpha'}$	H^{β}	$H^{\beta'}$	H^{γ}
4a	2.67 (s)	2.05 (s)	6.77 (d)	6.77 (d)	6.91 (t)	6.91 (t)	7.10 (t)
5a	2.66 (s)	2.07 (s)	6.85−6.92 (m)	6.85−6.92 (m)	6.85−6.92 (m)	6.85−6.92 (m)	7.08 (t)
4b	2.67 (s)	2.04 (s)	1.96 (s)	6.64 (d)	6.90−7.00 (m)	7.28 (dd)	6.90−7.00 (m)
5b	2.68 (s)	2.06 (s)	2.04 (s)	6.65 (d)	6.85−7.00 (m)	7.48 (d)	6.85−7.00 (m)
4c	2.65 (s)	2.06 (s)	6.64−6.71 (m)	6.64−6.71 (m)	6.64−6.71 (m)	6.64−6.71 (m)	2.30 (s)
5c	2.65 (s)	2.08 (s)	6.70−6.74 (m)	6.70−6.74 (m)	6.70−6.74 (m)	6.70−6.74 (m)	2.30 (s)
4d	2.67 (s)	2.10 (s)	1.10 (d), 1.28 (d) 2.90 (m)	6.75 (dd)	6.42 (t)	7.13 (dd)	7.04 (t)
5d	2.69 (s)	2.12 (s)	1.12 (d), 1.32 (d) 2.97 (m)	6.97 (dd)	6.41 (t)	7.13 (d)	7.02 (t)
4f	2.70 (s)	2.06 (s)	2.03 (s)	2.03 (s)	6.64 (d)	6.64 (d)	6.86 (t)
5f	2.72 (s)	2.08 (s)	2.10 (s)	2.10 (s)	6.64 (d)	6.64 (d)	6.86 (t)
4g	2.65 (s)	2.05 (s)	6.44 (s)	6.44 (s)	2.16 (s)	2.16 (s)	6.71 (s)
5g	2.64 (s)	2.07 (s)	6.53 (s)	6.53 (s)	2.16 (s)	2.16 (s)	6.70 (s)
4h	2.69 (s)	2.07 (s)	1.99 (s)	1.99 (s)	6.47 (s)	6.47 (s)	2.21 (s)
5h	2.71 (s)	2.09 (s)	2.06 (s)	2.06 (s)	6.48 (s)	6.48 (s)	2.23 (s)

[a] Spectra recorded in $CDCl_3$, at room temperature; δ [ppm]; s = singlet, d = doublet, dd = double doublet, t = triplet, m = multiplet; n.d. = not determined; the signals of the protons of the alkyl substituents on the aryl group are reported in the place of the corresponding protons.

 © 2003 Wiley-VCH Verlag GmbH & Co. KGaA, Weinheim

The addition of the complex, even if in low amount with respect to AIBN, resulted in a doubling of the yield of polymerization and, at the same time, in a fivefold decrease in the molecular weight together with a decrease in polydispersity. These complexes therefore show a behavior typical of chain-transfer catalysts (CCTCs).[7]

Conclusion

The coordination chemistry of the new N-ligands towards Ni^{II} and Co^{III} has been studied, different behavior being observed depending both on the ligand and on the metal. In the case of Ni^{II}, when unhindered ligands were used, octahedral bis(chelated) species were obtained, while the product with more hindered ligands was a monochelated trimer. In this last compound the three molecules of chelating ligands are "*iso*-oriented", producing one hydrophilic and one hydrophobic hole. In the case of Co^{III}, octahedral bis(chelated) species are obtained with all the ligands used. Their main structural feature is the presence of weak interactions between the two coplanar N-ligands, namely O−H···O hydrogen bond and stacking interactions between the aryl groups.

These bis(chelated) Co^{III} complexes have several similarities to the well-known cobaloximes[7] and to (DO)-(DOH)pn derivatives,[24] previously studied by us and further investigated by Finke.[25,26] As reported in the introduction, these complexes are efficient chain transfer catalysts, and give oligomers in high yield for methyl methacrylate and styrene. The new complexes reported here could behave very similarly but, thanks to the variable steric hindrance, could give polymers instead of oligomers. The molecular mass of the polymers should increase on increasing the steric bulk of the N-ligands. The study of their catalytic behavior and the characterization of polymers is currently under investigation.

Experimental Section

Materials and Instrumentation: Chemicals and solvents were obtained from commercial sources (Aldrich, Carlo−Erba) and were used as received. NMR spectra were recorded with a Jeol EX 400 spectrometer operating at 400.0 MHz for ^1H. ^1H chemical shifts were measured relative to the residual solvent peak versus TMS ($CDCl_3$ at $\delta = 7.26$ ppm and CD_2Cl_2 at $\delta = 5.33$ ppm for ^1H). Two-dimensional correlation spectra (COSY) were obtained with the automatic program of the instrument. NOE experiments were run with a ^1H pulse of 90° and 12.5 μs. THF was dried with metallic sodium. MMA used in the polymerization reactions was purified by extraction with a water solution of NaOH and distilled.

Synthesis of Ligands: (*E*,*E*)-2-(Hydroxyimino)-3-(phenylimino)butane (**1a**), (*E*,*E*)-2-(hydroxyimino)-3-(*o*-tolylimino)butane (**1b**), (*E*,*E*)-2-(hydroxyimino)-3-(*p*-tolylimino)butane (**1c**), (*E*,*E*)-2-(hydroxyimino)-3-[(2-isopropylphenyl)imino]butane (**1d**), (*E*,*E*)-2-[(2-*tert*-butylphenyl)imino]-3-(hydroxyimino)butane (**1e**), (*E*,*E*)-2-[(2,6-dimethylphenyl)imino]-3-(hydroxyimino)butane (**1f**), (*E*,*E*)-2-[(3,5-dimethylphenyl)imino]-3-(hydroxyimino)butane (**1g**), (*E*,*E*)-2-(hydroxyimino)-3-[(2,4,6-trimethylphenyl)imino]butane (**1h**), (*E*,*E*)-2-[(2,6-diisopropylphenyl)imino]-3-(hydroxyimino)butane (**1i**)]. These ligands were synthesized by heating a solution of biacetyl monoxime (0.02 mol) and the stoichiometric amount of amine at reflux in methanol (5 mL) in the presence of formic acid (3 drops) as catalyst for 4−5 h. Ligands **1a**, **1b**, **1c**, and **1d** were obtained by cooling the solutions at 4 °C for 2−3 h after reflux. White crystals were filtered off, washed with ether, and dried in vacuo. Ligand **1d** was recrystallized from *n*-pentane. Ligands **1e**, **1f**, **1g**, **1h**, and **1i** were obtained by cooling the solutions at room temp after reflux. Ligand **1i** precipitated from the heated solution after 1.5 h reaction time. Crystalline precipitates were filtered, washed with ether, and dried in vacuo. All ligands are colorless, with the exception of **1e**, which precipitated as a yellow solid. The values of elemental analyses are reported in Table 5.

Table 5. Elemental analyses for ligands **1a**−**1i** (calculated values in parentheses)

Ligands	C	H	N
1a	67.30 (68.15)	6.78 (6.86)	15.70 (15.89)
1b	68.70 (69.45)	7.40 (7.42)	14.80 (14.72)
1c	67.90 (69.45)	7.43 (7.42)	14.90 (14.72)
1d	71.30 (71.52)	8.37 (8.31)	12.90 (12.83)
1e	71.40 (72.38)	8.55 (8.67)	12.00 (12.05)
1f	70.60 (70.56)	7.92 (7.89)	13.80 (13.71)
1g	69.60 (70.56)	7.85 (7.89)	13.70 (13.71)
1h	71.50 (71.52)	8.28 (8.31)	12.83 (12.83)
1i	74.60 (74.38)	9.45 (8.58)	10.90 (10.84)

Synthesis of Bis(chelated) Ni^{II} Complexes 2a, 2b, and 2h: Bis(chelated) Ni^{II} complexes were synthesized by addition of [$NiBr_2$-($C_4H_{10}O_2$)] ($9.7\cdot10^{-4}$ mol) to a stirred solution of ligand ($1.94\cdot10^{-3}$ mol) in CH_2Cl_2 (7 mL). Solutions were stirred for 3 h. Complexes **2a**, **2b**, and **2h** were isolated upon concentration of the solution and addition of diethyl ether or *n*-pentane. The products precipitated as brown solids, which were filtered and dried under vacuum.

Synthesis of Monochelated Ni^{II} Complexes 2d, 2e, 2i, and 3h: Monochelated Ni^{II} complexes were prepared by addition of [$NiBr_2$-($C_4H_{10}O_2$)] ($C_4H_{10}O_2$ = ethylene glycol dimethyl ether) ($9.7\cdot10^{-4}$ mol) to a stirred solution of ligand ($1.56\cdot10^{-3}$ mol) in CH_2Cl_2 (7 mL). Solutions were stirred for 3 h. For **3h**, **2d**, and **2e**, insoluble impurities were filtered off. Solutions were concentrated under vacuum to 1−2 mL, and then treated with ether. Light brown powders were filtered, washed with ether or *n*-pentane, and dried in vacuo. Insoluble **2i** precipitated as a light brown powder, which was filtered, washed with ether, and dried in vacuo.

Synthesis of Bis(chelated) Co^{III} Complexes 4a−4d, 4f−4h, 5a−5d, and 5f−5h: Syntheses of bis(chelated) Co^{III} complexes were performed by addition of the ligand ($2.9\cdot10^{-3}$ mol) to a stirred solution of the Co^{II} salt hexahydrate ($CoCl_2\cdot6H_2O$, $CoBr_2\cdot6H_2O$) ($1.4\cdot10^{-3}$ mol) in *n*-butanol (10 mL). Solutions were stirred for 3 h. Solids were filtered off, washed with *n*-butanol, and dried in vacuo. Crystalline precipitates were obtained by recrystallization from CH_2Cl_2/pentane or CH_2Cl_2/ether (**4a** and **5a** only). Complexes **5f**, **5h**, and **5d** are brown, while all other complexes are green.

Synthesis of Bis(chelated) Organometallic Co^{III} Complex 6g: Complex **6g** was prepared by addition of CH_3I (0.5 mL) and an excess of $NaBH_4$, in that order, to a stirred solution of the chloride derivative **4g** (0.16 g) in methanol (10 mL) under an inert gas. The solution was stirred at room temperature for 1 h, and the red crystalline

 © 2003 Wiley-VCH Verlag GmbH & Co. KGaA, Weinheim

Table 6. Crystallographic data for compounds **1h**, **2a**, **3h**, **5b**, and **5h**

	1h	**2a**·0.5CH_2Cl_2	**3h**·H_2O	**5b**	**5h**
Empirical formula	$C_{13}H_{18}N_2O$	$C_{20.5}H_{25}Br_2ClN_4NiO_2$	$C_{39}H_{56}Br_5N_6Ni_3O_5$	$C_{22}H_{27}Br_2CoN_4O_2$	$C_{26}H_{35}Br_2CoN_4O_2$
Formula mass	218.29	613.43	1264.58	598.23	654.33
Crystal system	monoclinic	monoclinic	trigonal	orthorhombic	tetragonal
Space group	$P2_1/c$ (no. 14)	$C2/c$ (no. 15)	$R\bar{3}$ (no. 148)	$Pna2_1$ (no. 33)	$I4_1cd$ (no. 110)
a [Å]	7.379(5)	21.737(5)	13.945(4)	15.176(7)	13.623(2)
b [Å]	15.635(6)	15.002(4)		8.273(3)	
c [Å]	11.167(5)	16.382(4)	50.665(16)	18.738(7)	29.901(8)
β [°]	93.74(5)	110.46(3)			
V [Å^3]	1285.6(12)	5005(2)	8532.5(44)	2352.6(16)	5549.2(19)
Z	4	8	6	4	8
$\rho_{calcd.}$ [g cm^{-3}]	1.128	1.628	1.477	1.689	1.566
F(000)	472	2456	3786	1200	2656
μ (Mo-K_α) [mm^{-1}]	0.072	4.099	4.534	4.153	3.528
θ range [°]	2.24−25.02	1.69−24.41	2.33−26.98	2.68−27.95	2.52−29.95
T [K]	293(2)	130(2)	293(2)	293(2)	293(2)
Reflns. collected	2394	7621	17970	3992	4153
Reflns. unique/R(int)	2271/0.0730	3965/0.0509	4005/0.1358	2898/0.0580	1932/0.0690
Reflns. obsd. [$I > 2\sigma(I)$]	1592	2781	1495	1408	1246
Variables	151	296	182	179	164
$R1$[a]	0.0692	0.0596	0.0646	0.0586	0.0423
$wR2$[a]	0.0849	0.1276	0.1541	0.0997	0.0712
GOF (F^2)[b]	0.901	1.066	1.160	1.083	1.044
Residuals [e/Å^3]	0.168, −0.181	0.675, −0.770	0.981, −0.734	0.688, −0.777	0.470, −0.354

[a] $R1 = \Sigma||F_o| - |F_c||/\Sigma|F_o|$; $wR2 = \{\Sigma w(F_o^2 - F_c^2)^2/\Sigma w(F_o^2)^2\}^{1/2}$ for observed reflections. [b] GOF = $\{\Sigma w(F_o^2 - F_c^2)^2/\Sigma w\,(n - p)\}^{1/2}$.

solid was then filtered off and dried in vacuo. $C_{25}H_{34}CoIN_4O_2$ (608.40): calcd. C 49.35, H 5.63, N 9.21; found C, 50.00, H 5.73, N 9.26. ^{1}H NMR ($CDCl_3$) δ = 1.68 (s, 3 H), 1.73 (s, 6 H), 2.12 (s, 6 H), 2.15 (s, 6 H), 2.30 (s, 6 H), 5.96 (s, 2 H), 6.60 (s, 2 H), 6.89 (s, 2 H) ppm.

X-ray Crystallographic Study: Crystal data, data collections, and refinement parameters for the structures reported are summarized in Table 6. Data sets of **1h**, **2a**, **3h**, **5b**, and **5h** were collected at room temperature by the ω/2θ scan technique with a CAD4 Enraf−Nonius diffractometer, equipped with graphite monochromator using Mo-K_α radiation (λ = 0.71073 Å). Intensities of three standard reflections, monitored during data collections, showed no noticeable variation in intensity for any of the crystals. Intensities were corrected for Lorentz polarization effects and data sets of **3h**, **5b**, and **5h** also for absorption, based on an empirical ψ-scan method. Diffraction data of **2a** were obtained with a Nonius DIP-1030H system with Mo-K_α radiation (graphite-monochromated). A total of 30 frames were collected, each with an exposure time of 20 min, over a half of reciprocal space with a rotation of 6° about the detector being located at 100 mm from the crystal. Cell refinement and data reduction were carried out with the aid of the programs Mosflm[27] and Scala.[27] The structures were solved by Patterson or direct methods and successive Fourier analyses (SHELXS-97)[28] and refined by the full-matrix least-squares method based on F^2, with the aid of SHELXL-97.[28] A difference Fourier map allowed a disordered molecule of CH_2Cl_2 to be detected (half occupancy) in **2a**, while a residual in **3h** was assigned to a water oxygen atom. All the calculations were performed with the aid of the WinGX System, version 1.64.03.[29] CCDC-199885, -199886, -199887, -199888, and -199889 contain the supplementary crystallographic data for this paper. These data can be obtained free of charge at www.ccdc.cam.ac.uk/conts/retrieving.html [or from the Cambridge Crystallographic Data Centre, 12 Union Road, Cambridge CB2 1EZ, UK; Fax: (internat.) + 44-1223/336-033; E-mail: deposit@ccdc.cam.ac.uk].

Polymerization Reactions: The polymerization reactions were carried out by use of Schlenk techniques, under an inert gas. The AIBN and the cobalt complex were added to the dry THF solution containing MMA at 60 °C for 5 h. The amounts are reported in Table 4. The polymer was obtained as a white powder after the addition of ethanol. The powder was filtered and vacuum-dried.

Molecular Mass Measurements: The analyses were recorded with a Knauer HPLC (pump K-501, UV detector K-2501) with a PLgel 5 μm 10^4 Å column and THF as solvent (flow rate 0.6 mL/min). Polystyrene standards were used. The polyMMA samples were dissolved as follows: 3 mg of each sample in 120 μL of 1,1,1,3,3,3-hexafluoro-2-propanol, and THF was then added up to 10 mL. The statistical calculations were performed by use of the Bruker Chromstar software program.

Acknowledgments

This work was supported by the Ministero dell'Università e della Ricerca Scientifica (MURST-Rome) Grant no. 9903153427.

[1] D. J. Tempel, M. Brookhart, *Organometallics* **1998**, *17*, 2290−2296.
[2] [2a] L. Johnson, M. Brookhart, C. M. Killian, S. D. Arthur, J. Feldman, E. F. McCord, S. J. McLain, K. A. Kreutzer, M. A. Bennett, E. B. Coughlin, S. D. Ittel, A. Parthasarathy, D. J. Tempel, Wo 96/23010, **1996**. [2b] S. D. Ittel, L. K. Johnson, M. Brookhart, *Chem. Rev.* **2000**, *100*, 1169−1203.
[3] G. J. P. Britovsek, V. C. Gibson, B. S. Kimberley, P. J. Maddox, S. J. McTavish, G. A. Solan, A. J. P. White, D. J. William, *Chem. Commun.* **1998**, 849−850.
[4] T. R. Younkin, E. F. Connor, J. I. Henderson, S. K. Friedrich, R. H. Grubbs, D. A. Bansleben, *Science* **2000**, *287*, 460−462.
[5] B. L. Small, M. Brookhart, *Macromolecules* **1999**, *32*, 2120−2130.
[6] B. B. Wayland, G. Poszmik, S. L. Mukerjee, *J. Am. Chem. Soc.* **1994**, *116*, 7943−7944.
[7] A. A. Gridnev, S. D. Ittel, *Chem. Rev.* **2001**, *101*, 3611−3659.

 © 2003 Wiley-VCH Verlag GmbH & Co. KGaA, Weinheim

[8] N. S. Enikopolopyan, B. R. Smirnov, G. V. Ponomarev, I. M. Belgovskii, *J. Poly. Sci. Polym. Chem. Ed.* **1981**, *19*, 879−889.
[9] A. F. Burczyk, K. F. O'Driscoll, G. L. Rempel, *J. Polym. Sci.* **1984**, *22*, 3255−3262.
[10] D. Kukulj, J. P. A. Heuts, T. P. Davis, *Macromolecules* **1998**, *31*, 6034−6041.
[11] J. Halpern, F. T. T. Ng, G. L. Rempel, *J. Am. Chem. Soc.* **1979**, *101*, 7124−7126.
[12] F. T. T. Ng, G. L. Rempel, J. Halpern, *J. Am. Chem. Soc.* **1982**, *104*, 621−623.
[13] B. Milani, E. Stabon, E. Zangrando, G. Mestroni, *Inorg. Chim. Acta*, in press.
[14] E. Uhlig, E. Dinjus, M. Helbig, *Z. Anorg. Allg. Chem.* **1970**, *373*, 279−284.
[15] V. Bertolasi, G. Gilli, A. C. Veronese, *Acta Crystallogr., Sect. B* **1982**, *38*, 502−511.
[16] F. H. Allen, O. Kennard, D. G. Watson, L. Brammer, A. G. Orpen, R. Taylor, "Typical interatomic distances: organic compounds", in *International Tables for Crystallography*, vol. C (Ed.: A. J. C. Wilson), Kluwer Academic Publishers, Dordrecht, The Netherlands, **1995**.
[17] [17a] U. Turpeinen, A. Pajunen, *Finn. Chem. Lett.* **1976**, 6−11. [17b] R. J. Butchers, C. J. O′Connor, E. Sinn, *Inorg. Chem.* **1981**, *20*, 537−545.
[18] E. Bouwman, P. Evans, H. Kooijman, J. Reedijk, A. L. Spek, *J. Chem. Soc., Chem. Commun.* **1993**, 1746−1748.
[19] $(DH)_2$ = bis(dimethylglyoximato); tetradentate ligand (DO)-(DOH)pn = N^2,$N^{2\prime}$-propanediylbis(2-imino-3-butanone oxime).
[20] L. Randaccio, N. Bresciani Pahor, E. Zangrando, L. G. Marzilli, *Chem. Soc., Rev.* **1989**, *18*, 225−250.
[21] N. Bresciani Pahor, M. Forcolin, L. G. Marzilli, L. Randaccio, M. F. Summers, P. J. Toscano, *Coord. Chem. Rew* **1985**, *63*, 1−125.
[22] R. J. Gulshl, T. L. Brown, *Inorg. Chem.* **1974**, *13*, 959−965.
[23] G. Costa, G. Mestroni, *Tetrahedron Lett.* **1967**, *41*, 4005−4007.
[24] B. E. Daikh, R. G. Finke, *J. Am. Chem. Soc.* **1991**, *113*, 4160−4172.
[25] B. E. Daikh, R. G. Finke, *J. Am. Chem. Soc.* **1992**, *114*, 2938−2943.
[26] B. E. Daikh, T. J. R. Weakely, R. G. Finke, *Inorg. Chem.* **1992**, *31*, 137−139.
[27] Collaborative Computational Project, Number 4, *Acta Crystallogr., Sect. D* **1994**, *50*, 760−763.
[28] G. M. Sheldrick, *SHELX97, Programs for Crystal Structure Analysis*, release 97-2, University of Göttingen, Germany, **1998**.
[29] L. J. Farrugia, *J. Appl. Crystallogr.* **1999**, *32*, 837−838.

Received January 7, 2003

 © 2003 Wiley-VCH Verlag GmbH & Co. KGaA, Weinheim

New Tris(pyrazolyl)triazine and Pyrazolylpyridine Gold(I) and Palladium(II) Derivatives Based on the 3,5-Bis(4-butoxyphenyl)pyrazole Group – Architectures with Different Types of Bonding Interactions

Rosa M. Claramunt,[a] Pilar Cornago,[a] Mercedes Cano,*[b] José V. Heras,[b] M. Luz Gallego,[b] Elena Pinilla,[b,c] and M. Rosario Torres[c]

Keywords: Gold / Hydrogen bonds / Palladium / Supramolecular Chemistry / Triazine

The 3,5-bis(4-butoxyphenyl)pyrazolyl group (Pz^{bp2}) has been used as a building block for mono- and polymetallic derivatives of 2,4,6-tris[3,5-bis(4-butoxyphenyl)pyrazol-1-yl]-1,3,5-triazine ($TPz^{bp2}Tz$, **1**), 2-[3,5-bis(4-butoxyphenyl)pyrazol-1-yl]pyridine ($Pz^{bp2}Py$, **2**), and 3,5-bis(4-butoxyphenyl)pyrazole (HPz^{bp2}, **3**) ligands. The synthesis and characterisation of the new hexadentate ligand **1** are described, together with the chemistry of its metal complexes containing $[Pd(\eta^3\text{-}C_3H_5)]^+$ and $[Au(PPh_3)]^+$ fragments. The related complexes containing $Pz^{bp2}Py$ (**2**) were also studied and their structural characteristics were compared to those of the $TPz^{bp2}Tz$ species. The role of the counter-ion on the supramolecular assembly of complexes containing the HPz^{bp2} ligand **3** was made clear by the X-ray structures of $[Pd(\eta^3\text{-}C_3H_5)(HPz^{bp2})_2](BF_4)$ and $[Au(HPz^{bp2})(PPh_3)](NO_3)$. Hydrogen bonds and/or bonding interactions are responsible for pseudohelical one-dimensional polymers or supramolecular columnar arrays, respectively.
(© Wiley-VCH Verlag GmbH & Co. KGaA, 69451 Weinheim, Germany, 2003)

Introduction

Research into the self-assembly of transition metal complexes is of increasing interest for the design of supramolecular structures.[1–7] Of the strategies currently in use to control molecular aggregates, non-covalent interactions such as metal coordination and hydrogen bonding have been of much use in recent years.[8,9]

Our group has acquired some expertise in studying metal complexes containing long chain-substituted pyrazole groups. The coordinative ability of 3,5-bis(4-butoxyphenyl)-pyrazolate towards gold(I) derivatives, for example, yielded complexes such as $[Au(Pz^{bp2})(PPh_3)]$, with supramolecular aurophilic Au···Au interactions,[10a,11,12] and $[(PPh_3)Au(\mu\text{-}Pz^{bp2})Au(PPh_3)]^+$, presenting intramolecular Au···Au contacts and molecular entities controlled by interactions through the corresponding counter-ions.[10b] Similar effects have also been described for related silver(I) derivatives.[5] On the other hand, π-allyl palladium(II) fragments are useful to provide stable complexes containing *N*,*N*′-bidentate ligands,[13] making these metal groups suitable for our coordinative purposes.

In addition, 1,3,5-triazine ligands have also been shown to be versatile for the preparation of metal complexes with a large variety of structural architectures.[14]

To extend these results, we decided to study new metal derivatives of a polydentate ligand, 2,4,6-tris[3,5-bis(4-butoxyphenyl)pyrazol-1-yl]-1,3,5-triazine ($TPz^{bp2}Tz$, **1**), containing three pyrazole groups in addition to the three nitrogen atoms of the triazine core (Scheme 1). Their coordination capability towards $[Pd(\eta^3\text{-}C_3H_5)]^+$ and $[Au(PPh_3)]^+$ fragments is analysed in a search for polymetallic complexes. The nature of the counter-ion and the effect of the

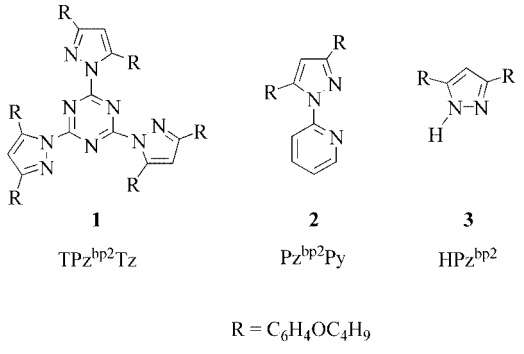

1 $TPz^{bp2}Tz$ **2** $Pz^{bp2}Py$ **3** HPz^{bp2}

Scheme 1

[a] Departamento de Química Orgánica y Biología, Facultad de Ciencias, Universidad de Educación a Distancia, Senda del Rey, 28040 Madrid, Spain
[b] Departamento de Química Inorgánica I, Facultad de Ciencias Químicas, Universidad Complutense, 28040 Madrid, Spain
Fax: (internat.) +34–91/3944352
E-mail: mmcano@quim.ucm.es
[c] Laboratorio de Difracción de Rayos-X, Facultad de Ciencias Químicas, Universidad Complutense, 28040 Madrid, Spain

OR substituents on the pyrazole groups are also considered as elements for potential supramolecular architectures.

The chemistry of the new complexes is described and compared to that observed on treatment of the same metal fragments with bidentate 2-[3,5-bis(4-butoxyphenyl)pyrazol-1-yl]pyridine (**2**) and monodentate 3,5-bis(4-butoxyphenyl)pyrazole (**3**) ligands, regarded as building blocks presenting coordinative positions related to those of the new ligand $TPz^{bp2}Tz$ (**1**) (Scheme 1).

Results and Discussion

Synthesis and Structural Characterisation of the 2,4,6-Tris[3,5-bis(4-butoxyphenyl)pyrazol-1-yl]-1,3,5-triazine Ligand ($TPz^{bp2}Tz$, 1)

We treated 3,5-bis(4-butoxyphenyl)pyrazole (**3**) with 2,4,6-trichlorotriazine (stoichiometry 3:1) in dry THF under argon atmosphere, by the procedure that we have already described for several 2,4,6-tris(pyrazol-1-yl)-2,4,6-triazines,[15] to obtain the 2,4,6-tris[3,5-bis(4-butoxyphenyl)-pyrazol-1-yl]-1,3,5-triazine ligand (**1**, $TPz^{bp2}Tz$) in a 30% yield.

This ligand was fully characterized by spectroscopic techniques and its main properties in relation to the gold(I) and palladium(II) complexes are commented on in the following sections.

Treatment of $[Pd(\eta^3\text{-}C_3H_5)]^+$ and $[Au(PPh_3)]^+$ with 3,5-Bis(4-butoxyphenyl)pyrazole. Formation of $[Pd(\eta^3\text{-}C_3H_5)(HPz^{bp2})_2](BF_4)$ (4) and $[Au(HPz^{bp2})(PPh_3)](NO_3)$ (5)

Both pyrazole derivatives **4** and **5** (Scheme 2) were isolated as stable, white solids, soluble in dichloromethane and acetone. Elemental analysis, IR and ^1H NMR spectroscopy data agree with the proposed formulations.

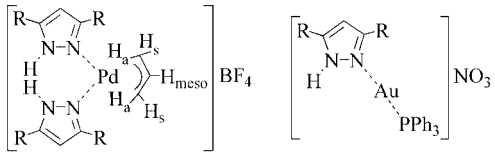

4 **5**

R = $C_6H_4OC_4H_9$

Scheme 2

Compound **4** was synthesised by treatment of the cationic complex $[Pd(\eta^3\text{-}C_3H_5)(S)_2]^+$ (S = solvent), prepared in situ, with **3** in the same solvent in a 1:2 molar ratio. The IR spectrum of **4** displays characteristic bands of the pyrazole ligand. Between them, a ν(NH) absorption band at 3307 cm^{-1} was observed. This band was slightly shifted to higher frequencies in relation to that of the free ligand (3229 cm^{-1}), which has been shown to have a strong hydrogen bond.[16] Related, but weaker, hydrogen bond interactions are therefore suggested for **4** (it has been reported that HPz-type ligands with free NH bonds present a ν(NH) absorption band at 3400 cm^{-1}).[17] Two ν(BF) absorption bands at 1067 and 1039 cm^{-1}, from the BF_4^- group, were also observed and support the presence of interactions towards that counter-ion (two bands agree with a distorted tetrahedral geometry in contrast to the broad single band at 1070 cm^{-1} for the tetrahedral free anion).[18]

On the other hand, the ^1H NMR results indicate the presence of an η^3-allyl group, together with two equivalent coordinated pyrazole ligands, each of these showing non-equivalence in the two butoxyphenyl substituents. The allylic part of the spectrum can be interpreted in terms of a symmetrical η^3-allyl group, so there are three different proton environments: H_{meso} in the central carbon, H_s (*syn*) and H_a (*anti*). The signal at highest field (δ = 3.18 ppm), and with the largest coupling constant (J = 12.7), is assigned to the H_a protons nearest to the metal, with the other doublet signal at δ = 3.92 ppm (J = 6.8) being assigned to the H_s protons. The H_{meso} signal appears a as multiplet at lower field (δ = 5.70 ppm).

Compound **5** was prepared by addition of one equivalent of **3** to a dichloromethane solution of $[Au(NO_3)(PPh_3)]$, previously obtained by treatment of $[AuCl(PPh_3)]$ with $AgNO_3$.[19] A ν(NH) absorption band at 3250 cm^{-1} in the IR spectrum of **5** suggests the presence of hydrogen bond interactions, analogously to what was observed in **4**. A band for the ionic NO_3^- group at 1384 cm^{-1} [18,19] agrees with the formation of a cationic complex $[Au(HPz^{bp2})(PPh_3)]^+$.

On the other hand, a 1:1 PPh_3/HPz ratio is established from the ^1H NMR spectrum (clearly observed from the 15:1

Table 1. Selected bond lengths [Å] and angles [°] for **4** with e.s.d.s. in parentheses, including the hydrogen bond geometries

	A	B	C	
Pd–N1	2.10(2)	2.12(1)	2.12(1)	
Pd–N3	2.11(1)	2.12(1)	2.10(1)	
Pd–C9	2.10(1)	2.10(1)	2.10(1)	
Pd–C10	2.13(2)	2.10(1)	2.10(1)	
Pd–C11	2.15(2)	2.12(2)	2.12(2)	
C9–C10	1.382(5)	1.384(5)	1.384(5)	
C10–C11	1.377(5)	1.384(5)	1.386(5)	
N1–Pd–N3	91.1(3)	93.4(4)	93.3(4)	
N1–Pd–C9	98.8(6)	97.9(4)	100.0(4)	
N1–Pd–C10	132.8(6)	130.3(4)	131.1(4)	
N1–Pd–C11	167.1(6)	167.2(4)	169.3(4)	
N3–Pd–C11	100.8(6)	99.3(4)	97.1(4)	
N3–Pd–C9	170.0(6)	168.3(3)	166.1(4)	
N3–Pd–C10	132.9(6)	132.7(4)	131.2(4)	
C9–Pd–C10	38.2(3)	38.3(2)	38.7(2)	
C9–Pd–C11	69.3(5)	69.3(3)	69.8(3)	
C10–Pd–C11	37.6(3)	38.3(2)	38.4(2)	
Hydrogen bond geometries				
D–H···A	D···A	D–H	H···A	D–H···A
N2A–H2A···F9′ [a]	2.81(2)	0.86	1.97	167.9
N4A–H4A···F2	2.89(1)	0.86	2.06	162.9
N2B–H2B···F7	3.02(1)	0.86	2.19	161.7
N4B–H4B···F1	2.81(1)	0.86	1.99	174.0
N2C–H2C···F11	2.81(1)	0.86	1.91	163.8
N4C–H4C···F5	2.81(1)	0.86	2.01	175.1

[a] The atomic numbering as in Scheme 5.

 © 2003 Wiley-VCH Verlag GmbH & Co. KGaA, Weinheim

ratio between the integrated signals of aromatic PPh_3 and H4 pyrazole protons). In contrast to the behaviour observed for palladium derivative **4**, complex **5** features two equivalent butoxyphenyl substituents, suggesting the presence of a metallotropic equilibrium as previously found for related complexes.[20]

Crystal and Molecular Structures of 4 and 5

Single crystals of **4** and **5** suitable for single-crystal X-ray analysis were obtained after recrystallisation from dichloromethane/diethyl ether and dichloromethane/hexane, respectively. Selected bond lengths and angles with their estimated standard deviations are listed in Tables 1 and 2.

Table 2. Selected bond lengths [Å] and angles [°] for **5** with e.s.d.s. in parentheses, including the hydrogen bond geometries

N3−O5	1.236(9)			
N3−O3	1.245(8)			
N3−O4	1.213(8)			
Au1−N1	2.077(5)			
Au1−P1	2.239(2)			
P1−C32	1.800(8)			
P1−C26	1.826(8)			
P1−C38	1.822(7)			
Au1···O1′ [a]	3.540(6)			
N1−Au1−P1	178.1(2)			
O5−N3−O3	117.9(8)			
O5−N3−O4	121.0(8)			
O3−N3−O4	121.2(7)			
Hydrogen bond geometries				
D−H···A	D···A	D−H	H···A	D−H···A
N2−H2···O3	2.764(9)	0.95(6)	1.82(7)	171(6)
C4−H4A···O4′′	3.382(9)	0.93	2.63	137.3
C40−H40A···O5′′′	3.31(1)	0.93	2.88	115.1

[a] $R_1 = \Sigma(|F_o| - |F_c|)/\Sigma|F_o|$.

The palladium derivative **4** crystallises in the monoclinic system, space group $P2_1/n$, as three $[Pd(\eta^3\text{-}C_3H_5)(HPz^{bp2})_2]^+$ species (A, B, and C, showing different dihedral angles between phenyl and pyrazole groups) associated through BF_4^- groups in the asymmetric unit (Figure 1, top). Each BF_4^- group was bonded through strong N−H···F hydrogen bonds (Table 1) with two N−H pyrazole groups bridging two neighbouring complexes. The geometry of each palladium(II) atom in A, B, and C can be described as approximately square-planar. Two pyrazole ligands coordinate to each palladium(II) centre through the corresponding unsubstituted pyrazole atoms N1 and N3, with bond lengths in the 2.10−2.12 Å range. The maximum deviation of the allylic terminal atoms in these units A, B, and C, if we define the coordination plane as that containing the palladium and the two nitrogen atoms mentioned, is 0.17(1) Å for C9 in molecule A. The central allyl carbon C10 also deviates, by 0.51(9), 0.53(1), and 0.59(1) Å in A, B, and C, respectively. The dihedral angles between the allyl planes C11C10C9 and C11PdC9 in each of the A, B, and C molecules are 63.8(9), 67.4(8), and 66.6(8)°. The Pd−allyl distances are in the range expected for complexes containing *N*,*N*′-ligands coordinated *trans* to palladium-allyl fragment.[13c,21]

The crystal structure of **4** could be defined as a pseudohelical polymer, consisting of $[Pd(\eta^3\text{-}C_3H_5)(HPz^{bp2})_2]^+$ units bonding through BF_4^- anions as shown in Figure 1 (bottom). The F12 moiety of the third unit (C) is hydrogen-bonded to the N−H pyrazole group of the neighbouring A′ molecule from the new asymmetric unit (symmetry operation *x*, *y*, *z* + 1). The $[Pd(\eta^3\text{-}C_3H_5)(HPz^{bp2})_2]^+$ moiety is thus arranged pseudohelically along the *c* axis, with the pitch of the pseudohelix (i.e., the

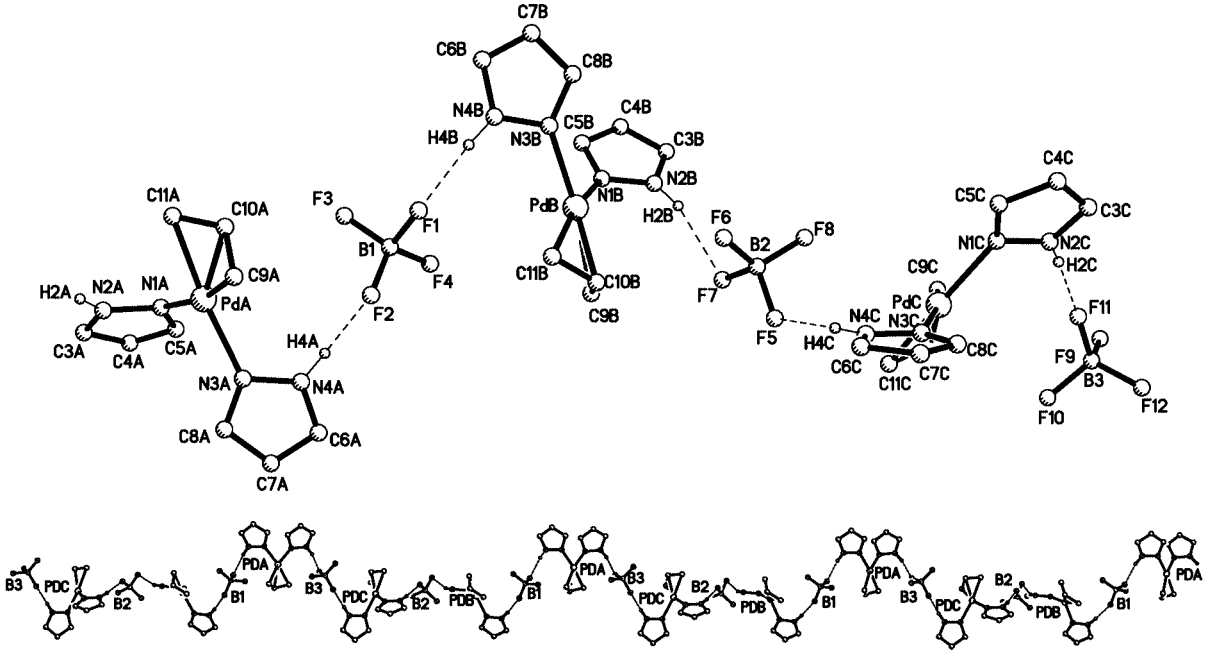

Figure 1. (top) Asymmetric unit of **4** with the atomic numbering scheme; (bottom) View of the helical distribution of **4** along *c* axis; substituents on pyrazole in both pictures are omitted for clarity

 © 2003 Wiley-VCH Verlag GmbH & Co. KGaA, Weinheim

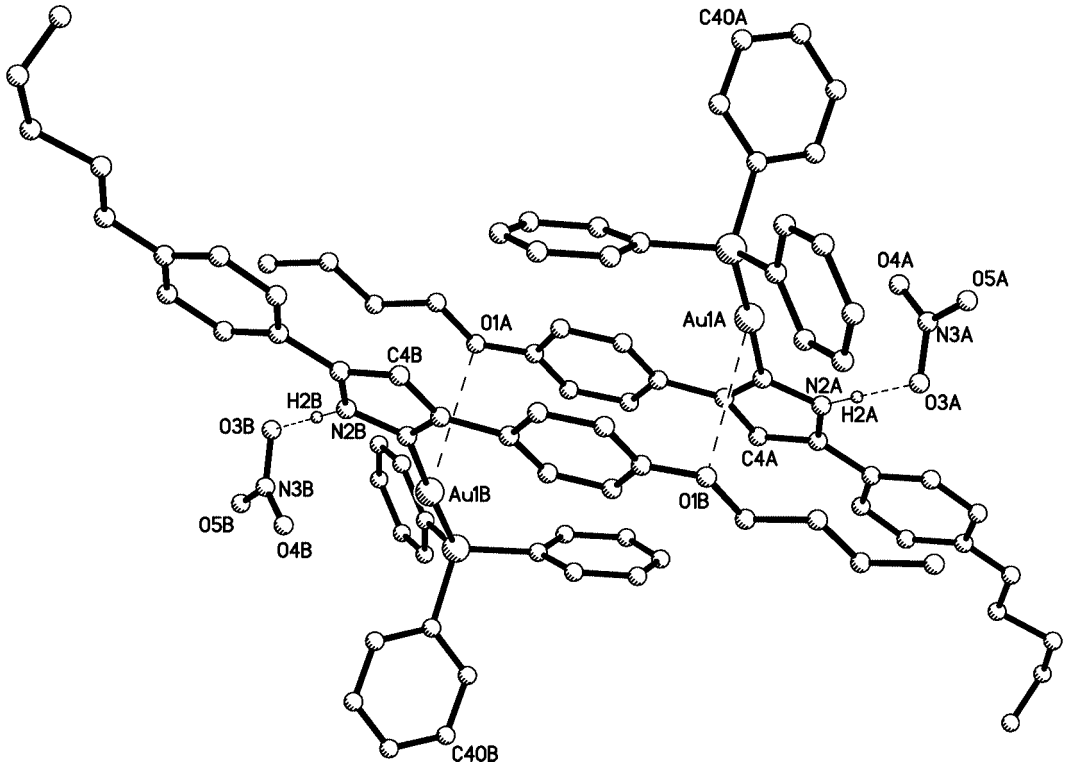

Figure 2. Molecular structure of **5** showing the dimeric unit through Au···O intermolecular bonds

distance between palladium(II) atoms of each four units) corresponding to the *c* axis. The molecular packing could be described as a columnar distribution of pseudohelical chains lying along the *c* axis. The formation of this polymer in the solid state demonstrates the important role played by intermolecular interactions through counter-ions in the supramolecular arrangements.

The crystal structure of **5** (Figure 2) consists of a mononuclear gold(I) cationic complex and a nitrate counter-ion. Both were bonded by a strong hydrogen bond (N2−H2···O3, with a N2···O3 distance of 2.764(9) Å; Table 2). The geometry around the gold(I) can be described as almost linear, the P1−Au1−N1 angle being 178.1(2)°. The Au1−N1 and Au1−P1 bond lengths are similar to

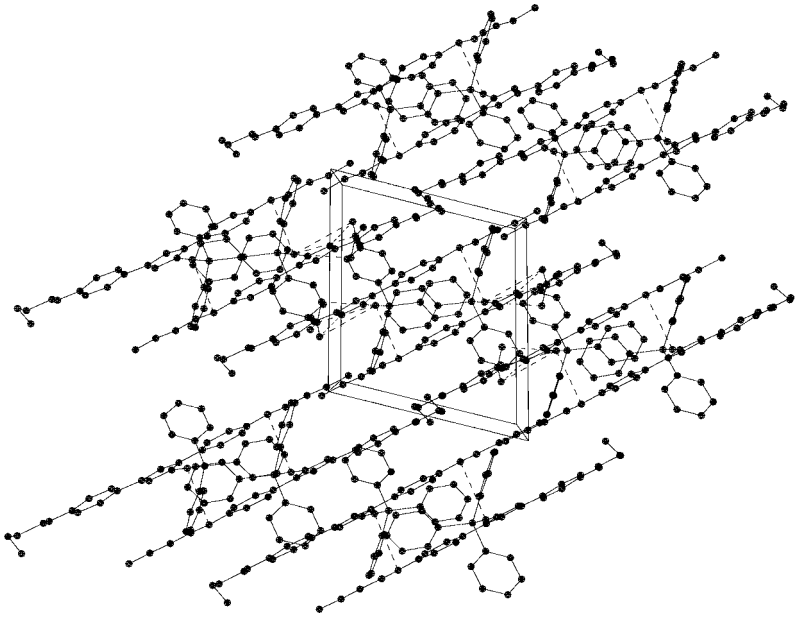

Figure 3. Molecular packing of **5** through *c* axis

 © 2003 Wiley-VCH Verlag GmbH & Co. KGaA, Weinheim

those reported for some neutral complexes of the [Au(L)(PPh_3)] type (HL = 1-methylthymine, 6-methylpyridone, 7-azaindole).[22] The most interesting feature in **5** was the presence of a very weak intermolecular coordinative interaction [Au···O, at 3.540(6) Å, ca. 0.30 Å longer than the sum of Van der Waals radii] between two neighbouring molecules. This interaction occurs through the oxygen atom of the $C_6H_4OC_4H_9$ substituent at the 5-position of the pyrazole ligand and the metal centre of the adjacent molecule and appears to be responsible for the formation of "dimers" in an antiparallel head-to-tail disposition (Figure 2). The adjacent aromatic rings of opposite substituents of each molecule of "dimers" are parallel, but are separated face-to-face by a distance of 4.4 Å. This distance suggests that π-π stacking interactions need not be considered, although they might be of help in adopting the observed dimeric arrangement.

The molecular packing could be described as a columnar distribution of these dimeric units along the *b* axis. Layers almost orthogonal to the columnar axis defined by the substituents on the pyrazole are also observed (Figure 3). New weak interactions through the O4 and O5 atoms of the NO_3^- group (not implicated in the hydrogen bond described above) between dimeric units from neighbouring columns are also present (Table 2). As a consequence, the effect of the counter-ion on the supramolecular assembly again seems to be determinant for the crystalline structure here.

Treatment of $[Pd(\eta^3\text{-}C_3H_5)]^+$ and $[Au(PPh_3)]^+$ with 2-[3,5-Bis(4-butoxyphenyl)pyrazol-1-yl]pyridine. Formation of $[Pd(\eta^3\text{-}C_3H_5)(Pz^{bp2}Py)](BF_4)$ (6) and $[Au(Pz^{bp2}Py)(PPh_3)](NO_3)$ (7)

Compounds **6** and **7** (Scheme 3) were both isolated as stable yellow solids, soluble in dichloromethane and acetone, as described in the Exp. Sect. Elemental analysis and IR and ^1H and ^{13}C NMR spectroscopy data agree with the proposed formulations. Conductivity measurements in acetone solution are consistent with 1:1 electrolytic behaviour in both cases.

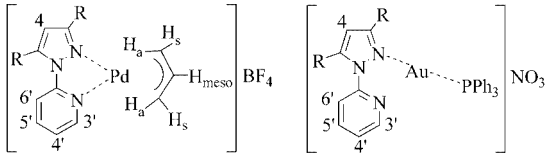

6 **7**

$R = C_6H_4OC_4H_9$

Scheme 3

On addition of an equivalent of **2** to $[Pd(\eta^3\text{-}C_3H_5)(S)_2](BF_4)$, the ionic complex **6** is formed. The gold(I) complex **7** was prepared by starting from cleavage of the chloride in [AuCl(PPh_3)] by addition of $AgNO_3$, giving rise to [Au(NO_3)(PPh_3)], and the subsequent replacement of the NO_3^- group by the *N*,*N*′-bidentate ligand **2**. The ν(C=N) absorption bands in the IR spectra of both compounds were not significantly modified in relation to that of the free ligand, indicating that the metal coordination had almost no effect on this bond, behaviour also observed for related gold(I) derivatives containing *N*-heterocyclic ligands.[23] Characteristic bands of BF_4^- and NO_3^- anions were observed for **6** and **7**, respectively.

The ^1H NMR spectrum of **6** in $CDCl_3$ at room temperature, in the allylic region, consisted of three broad signals: a multiplet at δ = 5.68 ppm, a doublet at δ = 3.87 ppm (J = 6.5) − partially overlapping with that of the OCH_2 signal at δ = 4.06 ppm − and a doublet at δ = 3.21 ppm (J = 12.8) corresponding to the H_{meso}, H_s, and H_a protons (the last of these clearly assigned from the observed coupling constant). The broadness of the allyl signals suggests a fluxional behaviour based on the asymmetry of the *N*,*N*′-coordinated ligand and attributable to a rapid *syn-syn* and *anti-anti* interchange. The remaining signals in the ^1H NMR spectrum are assigned to the pyrazolylpyridine ligand.

The ^1H NMR spectra of **7** was measured at room temperature in CD_2Cl_2. All the ligand proton signals were slightly modified by coordination. The general behaviour involves small shifts downfield for these signals, the largest shifts being observed for the 3′-H and 5′-H pyridine protons (Scheme 3). However, the position of 6′-H pyridine proton was almost unchanged (δ = 8.41 ppm for the free ligand and δ = 8.38 ppm for the complex), suggesting a very weak metal interaction towards the *N*-pyridine atom. On the other hand, the 4-H pyrazole proton shows a downfield coordination shift of δ = 0.12 ppm, and both downfield and upfield effects were observed for the phenyl substituents in positions 3 and 5. Related behaviour has also been observed for copper and ruthenium derivatives containing pyrazolylpyridine-type ligands.[24,25] The downfield shifts occurring for pyrazole protons and substituents on the 4- and 5-positions were attributed to ligand-metal coordination, whereas upfield shifts for substituents on the 3-position were attributed to ring current anisotropy effects. The above ^1H NMR results agree with a monodentate coordination of the ligand towards the pyrazole N atom, allowing the characteristic twofold coordination of gold metal centres. In this context it should be pointed out that tri- and tetracoordinate gold(I) derivatives with PPh_3 and *N*-donor ligands have also been described, although less frequently,[26] and so an interaction with the pyridine N atom should not be excluded for complex **7**. However, the well defined signals observed for all the protons suggest that exchange of gold(I) between the two nitrogen coordination sites does not occur at room temperature. This fact, probably due to steric effects of substituents on the pyrazole group, favours the linear complex.

On close examination of the ^{13}C NMR spectroscopic data and after complete assignment of all signals by means of NMR experiments with pulse field gradients — (^1H-^1H) COSY, (^1H-^{13}C) HMQC, and (^1H-^{13}C) HMBC — it can be concluded that the complexation chemical shift effects (CCSEs) in the palladium(II) and gold(I) complexes **6** and

 © 2003 Wiley-VCH Verlag GmbH & Co. KGaA, Weinheim

7 are positive, save for the carbon adjacent to the pyridine nitrogen, which bonds the pyrazole group. Such increments are larger in the palladium complex **6** (around 4 ppm) than in the gold complex **7** (around 2 ppm).

In order to establish more conclusive results regarding the metal ligand coordination, ^{15}N NMR studies were carried out by means of (^{1}H-^{15}N) HMBC experiments on the ligand and the palladium(II) and gold(I) derivatives

Table 3. ^{15}N NMR spectroscopic data (in $CDCl_3$ at 298 K) for the free ligand **2**and its Pd(η^3-C_3H_5) (**6**) and Au(PPh_3) (**7**) derivatives

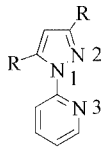

$R = C_6H_4OC_4H_9$

	Pyrazole N1	N2	Pyridine N3
2	−166.4	−84.9	−84.0
6	−167.9	−136.8	−151.0
7[a]	−168.0	−104.1	−88.0

[a] ^{15}N NMR data in CD_2Cl_2.

(Table 3). For the palladium complex **6** it was clearly observed that coordinative nitrogen atoms, N2 from pyrazole and N3 from pyridine, were significantly shifted upon coordination relative to the free ligand. For gold derivative **7**, in contrast, such an effect was only produced on the pyrazole nitrogen atom N2. Consequently, an *N*,*N*′-bidentate pyrazolylpyridine coordinative mode was proposed for the palladium derivative but only a monodentate coordination involving the pyrazole group for the gold complex **7**. Both results also agree with the expected tetracoordinate square-planar and two-coordinate linear environments around the palladium(II) and gold(I) metal centres, respectively.

Treatment of [Pd(η^3-C_3H_5)]$^+$ and [Au(PPh_3)]$^+$ with 2,4,6-Tris[3,5-bis(4-butoxyphenyl)pyrazol-1-yl]-1,3,5-triazine. Formation of [Pd_2(η^3-C_3H_5)$_2$($BPz^{bp2}TzO$)](BF_4) (8) and [Au_3($TPz^{bp2}Tz$)(PPh_3)$_3$](NO_3)$_3$ (9)

Treatment of **1** with [Pd(η^3-C_3H_5)]$^+$ or [Au(PPh_3)]$^+$ fragments resulted in bimetallic and trimetallic complexes,

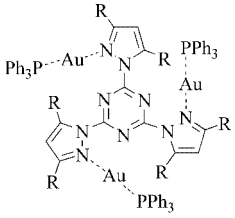

9

$R = C_6H_4OC_4H_9$

Scheme 4

respectively. The gold(I) derivative was isolated from treatment of three equivalents of [Au(NO_3)(PPh_3)] with one of **1** in dichloromethane solution as a yellow solid product, stable enough in solution for NMR purposes. It was characterized as the complex [Au_3($TPz^{bp2}Tz$)(PPh_3)$_3$](NO_3)$_3$ (**9**, Scheme 4) on the basis of its ^{1}H NMR spectroscopic and mass spectrometric data.

On the other hand, it was interesting to note that a side product, in the form of a microcrystalline white solid accompanying the main compound **9**, was also isolated from the reaction. Treatment of this mixture in dichloromethane/diethyl ether allowed crystals of this by-product to be separated, and these were identified as the pyrazolate complex [Au_2(μ-Pz^{bp2})(PPh_3)$_2$](NO_3).[10b]

The IR spectrum of **9** shows the main absorption bands of the $TPz^{bp2}Tz$ ligand. A very weak unexpected band was also observed at 1682 cm^{-1}, and was attributed to a ν(C=O) absorption arising from partial hydrolysis of the $TPz^{bp2}Tz$ ligand in the complex. This band increases after repeated attempts to purify the product confirming that the hydrolysis process is enhanced.

The structural ^{1}H NMR spectroscopic data, in relation to those obtained for [Au($Pz^{bp2}Py$)(PPh_3)](NO_3) (**7**), suggest monodentate *N*-pyrazole coordination towards the Au(PPh_3) fragment. The tris(pyrazoly)ltriazine ligand bridges three metal centres coordinated with three *N*-pyrazole atoms from the three asymmetric *N*,*N*′-chelating sites. The 15:1 relationship between the aromatic PPh_3 and the 4-H pyrazole protons agrees with the proposed formulation.

A relevant aspect of the molecular behaviour observed at room temperature is the effect that the metals induce on the pyrazole substituents, those in the proximity of Au(PPh_3) fragment (3-position) being different to those at the 5-position. The former thus show defined signals for all protons of the chains but the related signals for the latter are broad. This behaviour is consistent with the proposed monodentate coordination of gold(I) centres only towards the pyrazole groups. Rotation of the pyrazole group bonded to the Au(PPh_3) fragment around the pyrazole-triazine bonding axis is possible, and the environment of the substituents on the 3-position close to the Au(PPh_3) fragment is not modified, unlike that of 5-position substituents, which change in their spatial proximity to gold metal centres.

To confirm the proposed trimetallic formulation of **9**, a study by mass spectrometry (FAB and ESI) was carried out. Figure 4 displays a fragmentation scheme for this complex. The parent ion was not observed either by FAB or by ESI (dry acetonitrile and chloroform) mass spectra. In contrast, in all the cases mentioned above, two ion peaks at m/z = 2444.7 and 1277.2 were detected. The former (m/z = 2444.7) corresponds to the [$TPz^{bp2}Tz$ + B]$^+$ fragment (a_1) arising from the association of the $TPz^{bp2}Tz$ ligand with a metallic cluster B {B = [Au_2(PPh_3)NO_3($OH)_2$]}. From this fragment, the second ion peak (m/z = 1277.2) is formed by the loss of $TPz^{bp2}Tz$. On the other hand, the ESI spectrum (in dry acetonitrile) shows a new peak at m/z = 867.7 (0.3 mass units separated from their counterparts) for the tric-ation [{Au_3($TPz^{bp2}Tz$)(PPh_3)$_3$(NO_3)} − 2 H]$^{3+}$ (a_3) (calcd.

 © 2003 Wiley-VCH Verlag GmbH & Co. KGaA, Weinheim

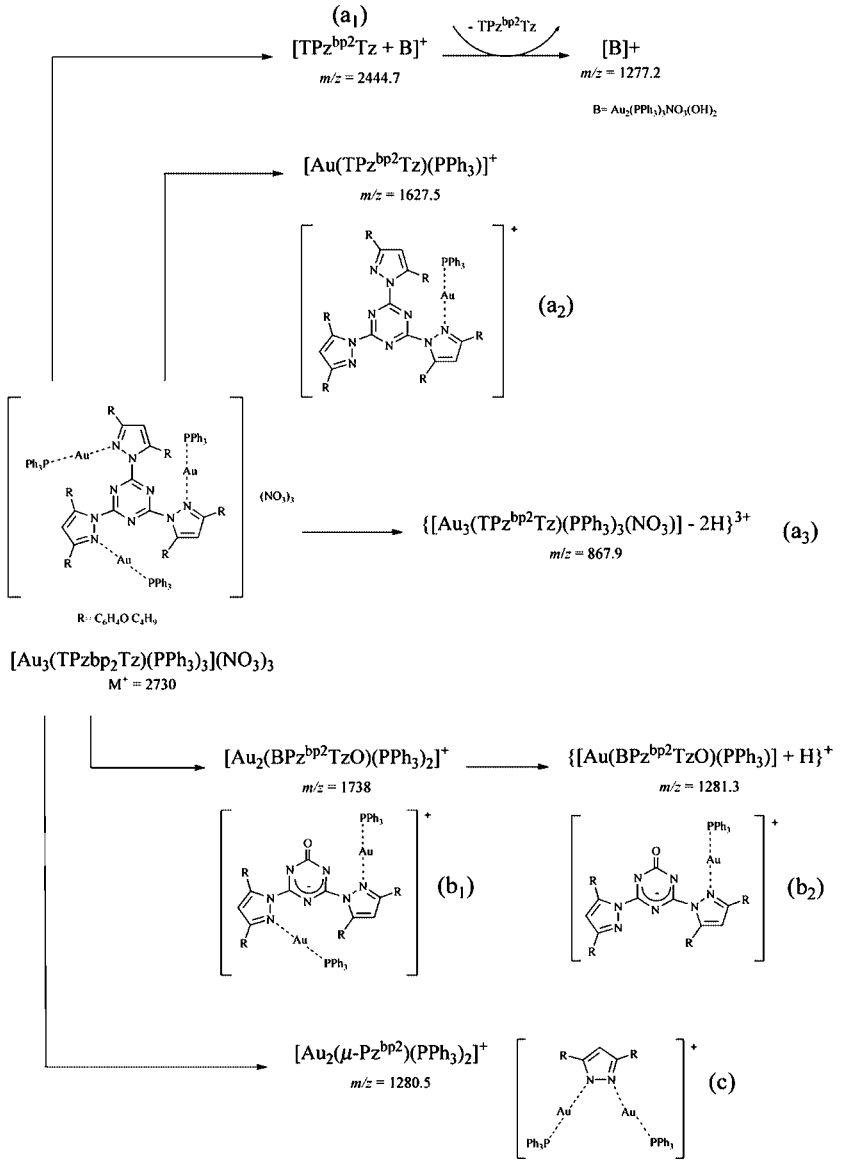

Figure 4. Fragmentation scheme for the complex $[Au_3(TPz^{bp2}Tz)(PPh_3)_3](NO_3)_3$ **9**; symbols (a), (b), and (c) indicate: (a) fragments containing the $TPz^{bp2}Tz$ ligand, (b) fragments containing the hydrolysed $TPz^{bp2}Tz$ ligand ($BPz^{bp2}TzO$), and (c) side product

2605). Another fragment, observed in all spectra, at m/z = 1627.5 was related to the mononuclear species $[Au(TPz^{bp2}Tz)(PPh_3)]^+$ (a_2). The above results agree with the presence of a $TPz^{bp2}Tz$ ligand in a trimetallic species.

On the other hand, additional ion peaks at m/z = 1738.6 and 1281.3 were also observed and related to a hydrolysis process of the $TPz^{bp2}Tz$ ligand, producing binuclear $[Au_2(BPz^{bp2}TzO)(PPh_3)_2]^+$ (b_1) and mononuclear $[\{Au(BPz^{bp2}TzO)(PPh_3)\} + H]^+$ (b_2) species, respectively. These were the sole peaks observed when the ESI spectrum was recorded in solvents favouring hydrolysis, such as methanol. Finally, the presence of the side product formulated as $[(PPh_3)Au(\mu\text{-}Pz^{bp2})Au(PPh_3)]^+$ (c) at m/z = 1280.5 was also evidenced, in agreement with the isolation of that compound from the reaction.

Several attempts to crystallise **9** from different solvents were carried out, but hydrolysis products prevent the obtention of crystals suitable for X-ray purposes.

Similar results were also obtained for the related complex $[Au_3(TPz^{bp2}Tz)(PPh_3)_3](CF_3SO_3)_3$ (**10**), containing $CF_3SO_3^-$ as counter-ion.

The binuclear complex $[Pd_2(\eta^3\text{-}C_3H_5)_2(BPz^{bp2}TzO)](BF_4)$ (**8**) was obtained by treatment of **1** with $[Pd(\eta^3\text{-}C_3H_5)(S)_2]^+$ in a 1:3 molar ratio. The suggested molecular structure (Scheme 5) was defined by bonding two $[Pd(\eta^3\text{-}C_3H_5)]^+$ fragments bound in two bidentate positions of the hydrolysed tris(pyrazolyl)triazine ligand $BPz^{bp2}TzO$, which has lost a pyrazolyl group. A related hydrolysis product has precedent in the described cationic complex $[\{(\eta^3\text{-}2\text{-}Me{-}C_3H_4)Pd\}_2(Me{-}BPzTO)]^+$,[21] and also in the estab-

 © 2003 Wiley-VCH Verlag GmbH & Co. KGaA, Weinheim

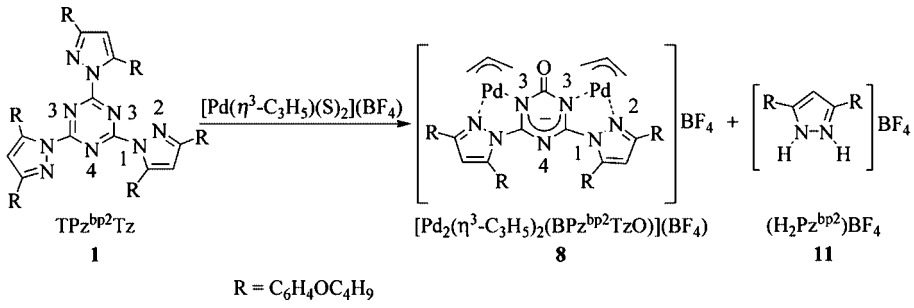

Scheme 5

lished nucleophilic displacement reactions of some 1,3,5-triazines.[27] This was the sole metal derivative isolated from the above reaction. It was interesting to note, though, that the first solid to separate from the reaction mixture was a white crystalline product, identified as the pyrazolium salt $[H_2Pz^{bp2}](BF_4)$ **11** (see Exp. Sect.).

The IR spectrum of **8** shows the characteristic bands due to the ν(C=O) absorption at 1696 cm^{-1} and the ^1H NMR spectrum present all the expected pyrazolyl signals as well as the 1:1 ratio of H4 pyrazole and H_{meso} allyl protons.

From the analysis of the ^{13}C NMR spectroscopic data and having assigned all signals by means of NMR experiments with pulse field gradients — (^1H-^1H) COSY, (^1H-^{13}C) HMQC and (^1H-^{13}C) HMBC — we observed that the CCSE signs for complexes **8** and **9** are similar, but that the absolute values of **9** are approximately half those of **8**. The appearance of the additional carbonyl signal in the spectrum of the palladium(II) complex **8** confirms the hydrolysis process.

The ^{15}N NMR spectroscopic data obtained from (^1H-^{15}N) HMBC correlation experiments for the free $TPz^{bp2}Tz$ ligand **1** and the palladium complex **8** are presented in Table 4. As in the previous $[Pd(\eta^3\text{-}C_3H_5)(Pz^{bp2}Py)](BF_4)$ complex **6**, the observed chemical shift effects on the palladium derivative in relation to the free ligand agree with a bidentate coordination by *N*-pyrazole and *N*-triazine coordinating nitrogen atoms and confirm the proposed formulation.

Table 4. ^{15}N NMR spectroscopic data in $CDCl_3$ at 298 K of the free ligand **1** and its $Pd(\eta^3\text{-}C_3H_5)$ derivative **8**

	Pyrazole[a]		Triazine[a]	
	N1	N2	N3	N4
1	−169.3	−86.0	−156.8	−156.8
8	−170.2	−138.8	−123.8	−197.4

[a] The atomic numbering as in Scheme 5.

Finally, the ESI mass spectrum (in chloroform) of **8** shows the molecular ion peak *m*/*z* = 1116.3 confirming the formation of the hydrolysis derivative $[Pd_2(\eta^3\text{-}C_3H_5)_2(BPz^{bp2}TzO)](BF_4)$.

Conclusion

The designed complexes $[Pd(\eta^3\text{-}C_3H_5)(HPz^{bp2})_2](BF_4)$ (**4**) and $[Au(HPz^{bp2})(PPh_3)](NO_3)$ (**5**) each show strong hydrogen bonding between each NH-pyrazole of one cationic unit and their corresponding counter-ions. In view of the molecular geometries around the metal centres − square-planar for the palladium derivative and linear for gold − as well as those of their counter-ions, tetrahedral BF_4^- and planar NO_3^-, these hydrogen bonds − N−H···F for **4** and N2−H2···O3, C4−H4A···O4′′ and C40−H40A···O5′′′ for **5** — are responsible for the observed supramolecular structures, of the pseudohelical type for **4** and with columnar features for **5**. In addition, **5** forms "dimers" produced by coordinative Au···O interactions between the pyrazole OR groups and the metal centres of two neighbouring molecules. We can therefore conclude that factors such as hydrogen bonding, the counter-ion effect, the presence of coordinating substituents on the ligand and a suitable molecular geometry are crucial for specific supramolecular assemblies.

Moreover, the following structural features should be pointed out:

i) The palladium complex of $TPz^{bp2}Tz$ is hydrolysed, giving rise to a bimetallic species $[Pd_2(\eta^3\text{-}C_3H_5)_2(BPz^{bp2}TzO)](BF_4)$ (**8**), containing two allyl-palladium moieties, which occupy two symmetrical *N*,*N*′-bidentate chelating positions of the ligand. The central carbon atom of the triazine core is now bonded to an oxygen, thus producing a C=O group instead of the initial C-Pz^{bp2} one, due to the nucleophilic displacement of the pyrazole group in the hydrolysis process.

ii) The formation of a trimetallic derivative $[Au_3(TPz^{bp2}Tz)(PPh_3)_3](NO_3)_3$ (**9**), containing three $Au(PPh_3)$ fragments coordinated in a monodentate fashion towards the *N*-pyrazole atoms of the $TPz^{bp2}Tz$ ligand, has been established.

The natures of the metal fragments determine the mono- or bidentate coordination of each *N*,*N*′-chelating position in the $TPz^{bp2}Tz$, analogously to what occurs in similar complexes of the related bidentate $Pz^{bp2}Py$ ligand. The presence of a square-planar or more flexible linear metal environments for **8** and **9**, respectively, appears to be correlated with the isolation of a binuclear palladium complex or a

 © 2003 Wiley-VCH Verlag GmbH & Co. KGaA, Weinheim

trinuclear gold derivative. These results offer new insights into the attainment of polymetallic complexes with supramolecular organisations.

Experimental Section

Materials and Instrumentation: The commercial starting materials $[Pd(\eta^3\text{-}C_3H_5)(\mu\text{-}Cl)]_2$ and $[AuCl(PPh_3)]$ were used as supplied. Ligands 2-[3,5-bis(4-butoxyphenyl)pyrazol-1-yl]pyridine (**2**, $Pz^{bp2}Py$)[24] and 3,5-bis(4-butoxyphenyl)pyrazole (**3**, HPz^{bp2})[16] were prepared as described in the literature. Commercial solvents were dried prior to use.

Melting points were determined on a microscope hot stage apparatus and are uncorrected.

Elemental analyses for carbon, hydrogen, and nitrogen were carried out by the Microanalytical Service of the Complutense University. IR spectra were performed on a FTIR Nicolet Magna-550 spectrophotometer in the 4000−400 cm^{-1} region with samples as KBr pellets.

^1H, ^{13}C, and ^{15}N NMR spectra were recorded on a Bruker DRX-400 at 27 °C. Chemical shifts (δ) are given in ppm from TMS for ^1H and ^{13}C NMR spectroscopy. ^{15}N NMR chemical shifts were obtained by the Inverse Gated ^1H-Decoupling Technique and are referenced to external nitromethane. *J* coupling constants are in Hz. The assignments are based on NMR experiments with pulse field gradients: (^1H-^1H) COSY, (^1H-^{13}C) HMQC, (^1H-^{13}C) HMBC, and (^1H-^{15}N) HMBC.[28]

FAB-MS positive spectra were performed on a VG AutoSpec spectrometer. ESI-MS positive spectra were carried out by the Mass Spectrometry Service of the Complutense University with a LC-SQUIRE spectrometer, in dry acetonitrile, chloroform, or methanol as solvents. The ion peaks are given in *m*/*z*.

Synthesis of 2,4,6-Tris[3,5-bis(4-butoxyphenyl)pyrazol-1-yl]-1,3,5-triazine ($TPz^{bp2}Tz$, 1): NaH (95%, 44 mg, 1.74 mmol) was added to a solution of 3,5-bis(4-butoxyphenyl)pyrazole (**3**, 600 mg, 1.65 mmol) in freshly distilled dry THF (30 mL). After 1.5 h at 90 °C, the solution was allowed to cool down, and 2,4,6-trichlorotriazine (cyanuric chloride, 90%, 102 mg, 0.55 mmol) was added. The solution, which had turned from a yellow to a white colour, was heated for 11 h at 90 °C and for 15 h at 60 °C. The solvent was evaporated and the residue was chromatographed on 60 F_{254} silica gel with chloroform/acetonitrile (95:5) as eluent. R_f = 0.55, m.p. 158−160 °C. Yield: 193 mg, 30%. Exact mass: calcd. for $C_{72}H_{81}N_9O_6$: 1168.49; found 1168.63. IR (KBr): $\tilde{\nu}$ = 1613 cm^{-1} ν(C=N). ^1H NMR (400 MHz, $CDCl_3$, 298 K): δ = 7.76 ppm (d, ^3J = 6.9 Hz, 6 H, H_o), 7.24 (d, ^3J = 6.8 Hz, 6 H, H_o), 6.98 (d, ^3J = 6.9 Hz, 6 H, H_m), 6.85 (d, ^3J = 6.8 Hz, 6 H, H_m), 6.63 (s, 3 H, H4), 4.04 (t, ^3J = 6.5 Hz, 6 H, OCH_2), 3.87 (t, ^3J = 6.6 Hz, 6 H, OCH_2), 1.82 (m, ^3J = 6.7 Hz, 6 H, CH_2), 1.72 (m, ^3J = 6.8 Hz, 6 H, CH_2), 1.51 (m, ^3J = 7.4 Hz, 6 H, CH_2), 1.43 (m, ^3J = 7.5 Hz, 6 H, CH_2), 1.01 and 0.94 (t, ^3J = 7.4 Hz, 18 H, CH_3). ^{13}C NMR (400 MHz, $CDCl_3$, 298 K): δ = 164.5 ppm (Tz), 159.9 (^3J = ^3J = 7.6 Hz, C_p), 159.2 (^3J = ^3J = 9.2 Hz, C_p), 154.3 (^2J = ^3J = ^3J = 3.7 Hz, C3), 147.8 (^2J = 8.1, ^3J = ^3J = 4.0 Hz, C5), 130.2 (^1J = 160.3, ^3J = 7.1 Hz, C_o), 127.7 (^1J = 159.5, ^3J = 7.0 Hz, C_o), 124.1 (^3J = ^3J = 7.6 Hz, C_{ipso}), 123.1 (^3J = ^3J = 8.0 Hz, C_{ipso}), 114.5 (^1J = 160.2, ^3J = 4.6 Hz, C_m), 113.9 (^1J = 160.5, ^3J = 4.2 Hz, C_m), 109.4 (^1J = 175.5 Hz, C4), 67.6 (^1J = 142.1, ^2J = 3.5 Hz, OCH_2), 31.3 and 31.2 (^1J = 126.3 Hz, CH_2), 19.2 and 19.1 (^1J = 127.2 Hz, CH_2), 13.79 and 13.77 (^1J = 125.3 Hz, CH_3).

Synthesis of $[Pd(\eta^3\text{-}C_3H_5)(HPz^{bp2})_2](BF_4)$ (4): $AgBF_4$ (35 mg, 0.18 mmol) was added under nitrogen to a solution of $[Pd(\eta^3\text{-}C_3H_5)(\mu\text{-}Cl)]_2$ (33 mg, 0.09 mmol) in freshly distilled acetone (15 mL). After stirring for 6 h in the darkness, the solution was filtered through a plug of Celite and cooled with an ice bath. Compound **3** (HPz^{bp2}, 131 mg, 0.36 mmol) was then added and the mixture was stirred for 5 h. The solvent was removed under vacuum and the white product was crystallised from dichloromethane/diethyl ether. Yield: 73 mg, 42%. $C_{49}H_{61}BF_4N_4O_4Pd$ (962.21): calcd. C 61.11, H 6.34, N 5.82; found C 60.96, H 6.11, N 5.66. IR (KBr): $\tilde{\nu}$ = 3307 cm^{-1} ν(N−H), 1613 ν(C=N), 1067 and 1039 ν(BF). ^1H NMR (400 MHz, $CDCl_3$, 298 K): δ = 11.87 ppm (s, 2 H, NH), 7.61 and 7.41 (d, ^3J = 8.5 Hz, 8 H, H_o), 6.96 and 6.78 (d, ^3J = 8.5 Hz, 8 H, H_m), 6.54 (s, 2 H, H4), 5.70 (m, ^3J_s = 6.8, ^3J_a = 12.7 Hz, 1 H, H_{meso}), 3.99 and 3.94 (t, ^3J = 6.6 Hz, 8 H, OCH_2), 3.92 (d, ^3J_s = 6.8 Hz, 2 H, H_s), 3.18 (d, ^3J_a = 12.7 Hz, 2 H, H_a), 1.87−1.70 (m, 8 H, CH_2), 1.64−1.40 (m, 8 H, CH_2), 1.00 and 0.98 (t, ^3J = 7.3 Hz, 12 H, CH_3).

Synthesis of $[Au(HPz^{bp2})(PPh_3)](NO_3)$ (5): $AgNO_3$ (34 mg, 0.20 mmol) was added under nitrogen to a solution of $[AuCl(PPh_3)]$ (100 mg, 0.20 mmol) in acetone (25 mL). After stirring for 2 h in darkness, the solution was filtered through a plug of Celite and the solvent was evaporated. Compound **3** (HPz^{bp2}, 73 mg, 0.20 mmol) was added to a solution of the obtained product in dry dichloromethane and the mixture was stirred for 5 h at room temperature. The solvent was removed under vacuum to provide a oil, from which a white solid was isolated by addition of dichloromethane and hexane. This solid was crystallised from dichloromethane/hexane. Yield: 90 mg, 51%. $C_{41}H_{43}N_3O_5AuP$ (884.94): calcd. C 55.60, H 4.86, N 4.75; found C 55.82, H 4.73, N 4.88. IR (KBr): $\tilde{\nu}$ = 3250 cm^{-1} ν(N−H), 1613 ν(C=N), 1384 $\nu_{as}(NO_3)$. ^1H NMR (400 MHz, $CDCl_3$, 298 K): δ = 7.78 ppm (d, ^3J = 8.8 Hz, 4 H, H_o), 7.57−7.40 (m, 15 H, PPh_3), 6.92 (d, ^3J = 8.8 Hz, 4 H, H_m), 6.71 (s, 1 H, H4), 3.97 (t, ^3J = 6.6 Hz, 4 H, OCH_2), 1.78 (m, 4 H, CH_2), 1.49 (m, 4 H, CH_2), 0.99 (t, ^3J = 7.3 Hz, 6 H, CH_3).

Synthesis of $[Pd(\eta^3\text{-}C_3H_5)(Pz^{bp2}Py)](BF_4)$ (6): This compound was prepared in a similar way to **4**, from $[Pd(\eta^3\text{-}C_3H_5)(\mu\text{-}Cl)]_2$ (110 mg, 0.30 mmol), $AgBF_4$ (117 mg, 0.60 mmol), and **2** ($Pz^{bp2}Py$) (265 mg, 0.60 mmol). White crystals were obtained by crystallisation from dichloromethane/hexane. Yield: 215 mg, 53%. $C_{31}H_{36}BF_4N_3O_2Pd$ (675.21): calcd. C 55.09, H 5.33, N 6.22; found C 54.75, H 5.30, N 6.21. IR (KBr): $\tilde{\nu}$ = 1609 and 1571 cm^{-1} ν(C=N), 1069 and 1027 ν(BF). ^1H NMR (400 MHz, $CDCl_3$, 298 K): δ = 8.85 ppm (m, 1 H, H6′), 7.81 (ddd, ^3J = 8.6, ^3J = 7.3, ^4J = 1.6 Hz, 1 H, H4′), 7.58 (d, ^3J = 8.6 Hz, 2 H, H_o), 7.53 (m, 1 H, H5′), 7.39 (d, ^3J = 8.5 Hz, 2 H, H_o), 7.06 (d, ^3J = 8.5 Hz, 2 H, H_m), 7.04 (d, ^3J = 8.6 Hz, 2 H, H_m), 6.99 (d, ^3J = 8.6 Hz, 1 H, H3′), 6.70 (s, 1 H, H4), 5.68 (m, ^3J_s = 6.5, ^3J_a = 12.8 Hz, 1 H, H_{meso}), 4.06 (t, ^3J = 6.5 Hz, 4 H, OCH_2), 3.87 (d, ^3J_s = 6.5 Hz, 2 H, H_s), 3.21 (d, ^3J_a = 12.8 Hz, 2 H, H_a), 1.82 (m, 4 H, CH_2), 1.54 (m, 4 H, CH_2), 1.01 (t, ^3J = 7.4 Hz, 6 H, CH_3). ^{13}C NMR (400 MHz, $CDCl_3$, 298 K): δ = 161.3 and 161.2 ppm (C_p), 157.4 (^3J = ^3J = 4.6 Hz, C3), 153.8 (^1J = 187.7 Hz, C6′), 149.7 (C2′), 147.1 (^2J = 8.8, ^3J = ^3J = 5.0 Hz, C5), 141.2 (^1J = 167.6 Hz, C4′), 130.4 (^1J = 160.5, ^3J = 7.5 Hz, C_o), 130.1 (^1J = 160.2, ^3J = 7.3 Hz, C_o), 124.5 (^1J = 170.3 Hz, C5′), 122.9 (^3J = ^3J = 7.8 Hz, C_{ipso}), 119.7 (^3J = ^3J = 7.7 Hz, C_{ipso}), 117.4 (^1J = 164.6 Hz, CH allyl), 115.7 (^1J = 161.8, ^3J = 4.7 Hz, C_m), 114.7 (^1J = 161.2, ^3J = 4.5 Hz, C_m), 114.6 (C3′), 111.3 (^1J = 181.7 Hz, C4), 68.1 (^1J = 142.7 Hz, OCH_2), 63.6 (CH_2

 © 2003 Wiley-VCH Verlag GmbH & Co. KGaA, Weinheim

allyl), 31.2 (^1J = 126.5 Hz, CH_2), 19.2 (^1J = 127.5 Hz, CH_2), 13.8 (^1J = 125.0 Hz, CH_3).

Synthesis of [Au(Pz^{bp2}Py)(PPh$_3$)](NO$_3$) (7): Compound **7** was prepared similarly to **5**, from [AuCl(PPh$_3$)] (80 mg, 0.16 mmol), $AgNO_3$ (27 mg, 0.16 mmol), and **2** (Pz^{bp2}Py) (71 mg, 0.16 mmol). The obtained yellow solid was purified by treatment with dichloromethane. Yield: 74 mg, 48%. $C_{46}H_{46}AuN_4O_5P$ (961.94): calcd. C 57.38, H 4.78, N 5.82; found C 57.48, H 4.90, N 5.62. IR (KBr): $\tilde{\nu}$ = 1611 and 1576 cm^{-1} ν(C=N), 1357 $\nu_{as}(NO_3)$. ^{1}H NMR (400 MHz, CD_2Cl_2, 298 K): δ = 8.38 ppm (m, 1 H, H6′), 7.87 (d, ^3J = 8.8 Hz, 2 H, H_o), 7.82 (ddd, ^3J = 8.1, ^3J = 7.5, ^4J = 1.6 Hz, 1 H, H4′), 7.54−7.41 (m, 15 H, PPh_3), 7.40 (m, 1 H, H5′), 7.35 (d, ^3J = 8.1 Hz, 1 H, H3′), 7.25 (d, ^3J = 8.8 Hz, 2 H, H_o), 6.91 (d, ^3J = 8.8 Hz, 4 H, H_m), 6.83 (s, 1 H, H4), 4.00 (t, ^3J = 6.5 Hz, 4 H, OCH_2), 1.78 (m, 4 H, CH_2), 1.51 (m, 4 H, CH_2), 1.00 (t, ^3J = 7.4 Hz, 6 H, CH_3). ^{13}C NMR (400 MHz, CD_2Cl_2, 298 K): δ = 161.1 and 161.0 ppm (C_p), 154.9 (^3J = ^3J = 4.1 Hz, C3), 151.7 (C2′), 149.8 (^1J = 182.9, ^3J = 7.2 Hz, C6′), 147.4 (^2J = 7.3, ^3J = ^3J = 3.7 Hz, C5), 140.1 (^1J = 166.1 Hz, C4′), 135−130 (PPh_3), 130.9 (^1J = 159.9, ^3J = 7.3 Hz, C_o), 129.1 (^1J = 159.4, ^3J = 7.4 Hz, C_o), 124.7 (^1J = 167.0 Hz, C5′), 124.4 (^3J = ^3J = 8.0 Hz or ^3J = ^3J = 7.7 Hz, C_{ipso}), 121.9 (^3J = ^3J = 8.0 Hz or ^3J = ^3J = 7.7 Hz, C_{ipso}), 120.9 (^1J = 175.2 Hz, C3′), 115.6 (^1J = 160.8 Hz or ^1J = 159.7, ^3J = 4.3 Hz, C_m), 115.5 (^1J = 160.8 Hz or ^1J = 159.7, ^3J = 4.3 Hz, C_m), 107.7 (^1J = 178.5 Hz, C4), 68.7 (^1J = 143.6 Hz, OCH_2), 32.0 (^1J = 125.3 Hz, CH_2), 20.0 (^1J = 126.2 Hz, CH_2), 14.4 (^1J = 124.7 Hz, CH_3).

Synthesis of [Pd$_2$(η^3-C$_3$H$_5$)$_2$(BPz^{bp2}TzO)](BF$_4$) (8): The synthetic procedure used for **8** was similar to that described for **4**, from [Pd(η^3-C_3H_5)(μ-Cl)]$_2$ (21 mg, 0.06 mmol), $AgBF_4$ (23 mg, 0.12 mmol), and **1** (TPz^{bp2}Tz) (46 mg, 0.04 mmol). The resulting yellow solid was purified by crystallisation in dichloromethane/hexane. Yield: 36 mg, 75%. $C_{55}H_{64}BF_4N_7O_5Pd_2$ (1201.61): calcd. C 54.93, H 5.33, N 8.15; found C 55.00, H 5.66, N 8.00. IR (KBr): $\tilde{\nu}$ = 1696 cm^{-1} ν(C=O), 1611 ν(C=N), 1066 ν(BF). ^{1}H NMR (400 MHz, $CDCl_3$, 298 K): δ = 7.59 and 6.99 ppm (d, ^3J = 6.8 Hz, 8 H, H_o), 7.03 and 6.62 (d, ^3J = 6.8 Hz, 8 H, H_m), 6.52 (s, 2 H, H4), 5.44 (m, ^3J_s = 6.5, ^3J_a = 13.0 Hz, 2 H, H_{meso}), 4.05 (t, ^3J = 6.5 Hz, 4 H, OCH_2), 3.99 (t, ^3J = 6.4 Hz, 4 H, OCH_2), 3.79 (br., ^3J_s = 6.5 Hz, 4 H, H_s), 3.21 (br., ^3J_a = 13.0 Hz, 4 H, H_a), 1.80 (m, 8 H, CH_2), 1.53 (m, 8 H, CH_2), 1.00 and 0.99 (t, ^3J = 7.5 Hz, 12 H, CH_3). ^{13}C NMR (400 MHz, $CDCl_3$, 298 K): δ = 163.1 ppm (Tz), 161.2 (^3J = ^3J = 8.9 Hz, C_p), 160.0 (^3J = ^3J = 8.8 Hz, C_p), 158.2 (^2J = ^3J = ^3J = 4.1 Hz, C3), 158.0 (CO), 149.2 (^2J = 6.5, ^3J = ^3J = 3.3 Hz, C5), 130.1 (^1J = 160.5, ^3J = 7.1 Hz, C_o), 129.9 (^1J = 160.3, ^3J = 7.0 Hz, C_o), 122.3 (^3J = ^3J = 7.8 Hz, C_{ipso}), 119.7 (^3J = ^3J = 8.0 Hz, C_{ipso}), 114.7 (^1J = 161.3, ^3J = 4.2 Hz, C_m), 114.2 (^1J = 160.8, ^3J = 4.6 Hz, C_m), 114.1 (^1J = 156.2 Hz, CH allyl), 111.9 (^1J = 181.7 Hz, C4), 68.18 (^1J = 142.2, ^2J = 4.0 Hz, OCH_2), 67.74 (^1J = 142.9, ^2J = 3.7 Hz, OCH_2), 63.8 (^1J = 162.8 Hz, CH_2 allyl), 31.26 and 31.17 (^1J = 124.7 Hz, CH_2), 19.17 and 19.15 (^1J = 125.4 Hz, CH_2), 13.8 (^1J = 124.9 Hz, CH_3).

Treatment of TPz^{bp2}Tz with [Au(NO$_3$)(PPh$_3$)]. Formation of [Au$_3$(TPz^{bp2}Tz)(PPh$_3$)$_3$](NO$_3$)$_3$ (9): This compound was prepared by a procedure analogous to that described for **5**, from [AuCl(PPh_3)] (74 mg, 0.15 mmol), $AgNO_3$ (26 mg, 0.15 mmol), and **1** (TPz^{bp2}Tz) (58 mg, 0.05 mmol). The obtained yellow solid was purified by treatment with dichloromethane/hexane. Yield: 82 mg, 60%. $C_{126}H_{126}Au_3N_{12}O_{15}P_3$ (2729.82): calcd. C 55.39, H 4.61, N 6.15; found C 55.00, H 4.39, N 6.01. IR (KBr): $\tilde{\nu}$ = 1611 cm^{-1} ν(C=N), 1384 $\nu_{as}(NO_3)$. ^{1}H NMR (400 MHz, CD_2Cl_2, 298 K): δ = 7.83 ppm (d, ^3J = 6.8 Hz, 6 H, H_o), 7.60−7.40 (m, 45 H, PPh_3), 7.3−7.5 (br., 6 H, H_o), 7.02 (br., 6 H, H_m), 6.92 (d, ^3J = 6.8 Hz, 6 H, H_m), 6.83 (s, 3 H, H4), 4.00 (t, ^3J = 6.5 Hz, 6 H, OCH_2), 3.94 (br., 6 H, OCH_2), 1.80 (m, ^3J = 7.0 Hz, 6 H, CH_2), 1.75 (br., 6 H, CH_2), 1.54 (m, ^3J = 7.5 Hz, 6 H, CH_2), 1.49 (br., 6 H, CH_2), 1.01 (t, ^3J = 7.4 Hz, 9 H, CH_3), 0.98 (br., 9 H, CH_3). ^{13}C NMR (400 MHz, CD_2Cl_2, 298 K): δ = 162.1 ppm (br., Tz), 160.9 (C_p), 156.5 (br., C_p), 154.8 (C3), 149.1 (br., C5), 135−130 (PPh_3), 129.7 (C_o), 128.9 (br., C_o), 124.9 (C_{ipso}), 122.1 (br., C_{ipso}), 115.7 (C_m), 115.1 (br., C_m), 112.1 (br., C4), 68.7 (OCH_2), 32.00 and 31.98 (CH_2), 20.04 and 19.97 (CH_2), 14.4 (CH_3).

Treatment of TPz^{bp2}Tz with [Au(CF$_3$SO$_3$)(PPh$_3$)]. Formation of [Au$_3$(TPz^{bp2}Pz)(PPh$_3$)$_3$](CF$_3$SO$_3$)$_3$ (10): $AgCF_3SO_3$ (54 mg, 0.21 mmol) was added under nitrogen to a solution of [AuCl(PPh_3)] (102 mg, 0.21 mmol) in dry THF (25 mL). After stirring for 2 h in the darkness, the solution was filtered through a plug of Celite. Compound **1** (TPz^{bp2}Tz, 80 mg, 0.07 mmol) was then added and the mixture was stirred for 4 h at room temperature. The solvent was removed under vacuum to afford an oil, from which a yellow solid was isolated by addition of diethyl ether and hexane. This solid was purified by treatment with dichloromethane. Yield: 119 mg, 57%. $C_{129}H_{126}Au_3F_9N_9O_{15}P_3S_3$ (2990.82): calcd. C 51.76, H 4.21, N 4.21; found C 52.03, H 4.28, N 4.25.

Synthesis of [H$_2$Pz^{bp2}](BF$_4$) (11): HBF_4−diethyl ether complex (85%, 37 mg, 0.36 mmol) was added to a solution of **3** (HPz^{bp2}, 131 mg, 0.36 mmol) in diethyl ether (5 mL) and the mixture was stirred for 1 h at room temperature. A white crystalline precipitate was filtered off and washed with diethyl ether. Yield: 73 mg, 45%. IR (KBr): $\tilde{\nu}$ = 3238 and 3178 cm^{-1} ν(N−H), 1619 ν(C=N), 1067 ν(BF). ^{1}H NMR (400 MHz, $CDCl_3$, 298 K): δ = 13.2 ppm (br., 2 H, NH), 7.67 (d, ^3J = 8.5 Hz, 4 H, H_o), 7.03 (d, ^3J = 8.5 Hz, 4 H, H_m), 6.86 (s, 1 H, H4), 4.02 (t, ^3J = 6.6 Hz, 4 H, OCH_2), 1.80 (m, 4 H, CH_2), 1.51 (m, 4 H, CH_2), 0.99 (t, ^3J = 7.3 Hz, 6 H, CH_3).

X-ray Structure Determination

Prismatic single crystals of [Pd(η^3-C_3H_5)(HPz^{bp2})$_2$](BF$_4$) (**4**) were obtained by crystallisation from dichloromethane/diethyl ether. Single needle crystals of [Au(HPz^{bp2})(PPh$_3$)](NO$_3$) (**5**) were obtained by crystallisation from dichloromethane/hexane.

The data for both compounds were collected on a Smart Bruker CCD detector diffractometer. A summary of the fundamental crystal data and refinement parameters for the two crystals is given in Table 5.

The structure of **4** was solved by direct methods and conventional Fourier techniques. The refinement was carried out by blocked full-matrix, least-squares on F^2.[29] The F atoms of the BF_4^- groups and some carbon atoms (including the allyl group) were refined for only two cycles anisotropically and in the last cycles the thermal factors were fixed. These carbon atoms were refined with geometrical restraints and a variable common carbon-carbon distance. The rest of the non-hydrogen atoms were refined anisotropically. The hydrogen atoms were calculated and refined as riding on the carbon bonded atom with common isotropic displacement parameters.

The molecular structure of **5** was solved by direct methods and conventional Fourier techniques and refined by full-matrix, least-squares on F^2.[29] All non-hydrogen atoms were refined anisotropically except for the oxygen atoms in the nitrate group and the last carbon atoms of the butoxy group, which were refined isotropically. The hydrogen atoms were calculated and refined as riding on the carbon-bonded atom with a common isotropic displacement parameter, except for the H2 bonded to N2, which was lo-

 © 2003 Wiley-VCH Verlag GmbH & Co. KGaA, Weinheim

Table 5. Crystal and refinement data for **4** and **5**

	4	**5**
Empirical formula	$[C_{49}H_{61}N_4O_4Pd]_3[BF_4]_3$	$[C_{41}H_{43}N_2O_2PAu]NO_3$
Formula mass	2889.68	885.72
Temperature [K]	296(2)	296(2)
Crystal system	Monoclinic	Triclinic
Space group	$P2_1/n$	$P\bar{1}$
a [Å]	21.811(1)	10.7447(9)
b [Å]	26.518(1)	11.937(1)
C [Å]	25.889(2)	15.560(1)
α [°]	90	102.475(1)
β [°]	90.783(1)	94.261(1)
γ [°]	90	102.699(2)
V [Å^3]	14973(1)	1890.5(3)
Z	4	2
F(000)	6024	888
Crystal size [mm^3]	0.22 × 0.22 × 0.14	0.30 × 0.15 × 0.07
$d_{calcd.}$ [gcm^{-3}]	1.284	1.556
μ [mm^{-1}	0.431	3.981
Scan technique	phi and omega	phi and omega
Data collected	(−19, −31, −27) to (25, 31, 30)	(−12, −14, −18) to (12, 11, 18)
θ [°]	3.82−25	1.35−25
Reflns. collected	58758	9902
Reflns. indep.	23261 (R_{int} = 0.098)	6578 (R_{int} = 0.0451)
Data/restraints/parameters	23261/45/1174	6578/0/421
Reflns.obsd. (I) > 2σ(I)	10954	4646
R_1 (reflns. obsd.)[a]	0.107	0.047
Rw_F[b]	0.336	0.098
Largest diff. peak [eA^{-3}]	1.83	1.30

[a] $R_1 = \Sigma(|F_o| - |F_c|)/\Sigma|F_o|$. [b] $Rw_F = \{\Sigma[w(F_o^2 - F_c^2)^2]/\Sigma[w(F_o^2)^2]\}^{1/2}$.

cated as one of the first peaks in a Fourier synthesis, included and its positions refined.

CCDC−194445 (**4**) and −194446 (**5**) contain the supplementary crystallographic data for this paper. These data can be obtained free of charge at www.ccdc.cam.ac.uk/conts/retrieving.html [or from the Cambridge Crystallographic Data Centre, 12 Union Road, Cambridge CB2 1EZ, UK; Fax: (internat.) +44−1223/336-033; E-mail: deposit@ccdc.cam.ac.uk].

Acknowledgments

We are indebted to the DGI/MCyT of Spain for financial support (BQU2000−0252 and PB98−0766).

[1] J. M. Lehn, *Supramolecular Chemistry: Concepts and Perspectives*, VHC, Weinheim, **1995**.
[2] M. T. Bujaci, X. Wang, S. Li, C. Zheng, *Inorg. Chim. Acta* **2002**, *333*, 152−154.
[3] N. S. Oxtoby, A. J. Blake, N. R. Champness, C. Wilson, *Proc. Natl. Acad. Sci. USA* **2002**, *99*, 4905−4910.
[4] J. Hamblin, A. Jackson, N. W. Alcock, M. J. Hannon, *J. Chem. Soc., Dalton Trans.* **2002**, 1635−1641.
[5] C. H. Chen, J. Cai, X. L. Feng, X. M. Chen, *Polyhedron* **2002**, *21*, 689−695.
[6] S.-L. Zheng, M.-L. Tong, X.-M. Chen, S. W. Ng, *J. Chem. Soc., Dalton Trans.* **2002**, 360−364.
[7] J. Yoo, Y.-K. Han, Y. S. Lee, Y. Do, *Polyhedron* **2002**, *21*, 715−719.
[8] [8a] D. Braga, F. Grepioni, *Acc. Chem. Res.* **2000**, *33*, 601−608. [8b] D. Braga, F. Grepioni, G. P. Desiraju, *Chem. Rev.* **1998**, *98*, 1375−1406. [8c] J. C. MacDonald, P. C. Dorrestein, M. M. Pilley, M. M. Foote, J. L. Lundburg, R. W. Henning, A. J. Schultz, J. L. Manson, *J. Am. Chem. Soc.* **2000**, *122*, 11692−11702. [8d] M. Munakata, L. P. Wu, M. Yamamoto, T. Kuroda-Sowa, M. Maekawa, *J. Am. Chem. Soc.* **1996**, *118*, 3117−3124. [8e] A. D. Burrows, D. M. P. Mingos, A. J. P. White, D. J. Williams, *Chem. Commun.* **1996**, 97−99. [8f] J. C. M. Rivas, L. Brammer, *New J. Chem.* **1998**, *22*, 1315−1318.
[9] [9a] J. Powell, M. J. Horvath, A. Lough, *J. Chem. Soc., Dalton Trans.* **1999**, 1569−1574. [9b] M. L. Tong, X. M. Chen, X. L. Yu, T. C. W. Mak, *J. Chem. Soc., Dalton Trans.* **1998**, 5−6. [9c] L. Carlucci, G. Ciani, D. M. Proserpio, A. Sironi, *J. Chem. Soc., Dalton Trans.* **1997**, 1801−1803. [9d] S. Kawata, S. Kitagawa, M. Kondo, I. Furuchi, M. Munakata, *Angew. Chem.* **1994**, *106*, 1861; *Angew. Chem. Int. Ed. Engl.* **1994**, *33*, 1759−1761.
[10] [10a] P. Ovejero, M. Cano, E. Pinilla, M. R. Torres, *Helv. Chim. Acta* **2002**, *85*, 1686−1690. [10b] XXth International Conference on Organometallic Chemistry, poster presentation "*Structural variety from pyrazole-based Au^{I} complexes*": P. Ovejero, M. C. Torralba, M. L. Gallego, J. A. Campo, M. Cano, J. V. Heras, E. Pinilla, M. R. Torres. Corfu (Greece) **2002**.
[11] [11a] K. Nomiya, R. Noguchi, K. Ohsawa, K. Tsuda, *J. Chem. Soc., Dalton Trans.* **1998**, 4101−4108. [11b] K. Nomiya, R. Noguchi, K. Ohsawa, K. Tsuda, M. Oda, *J. Inorg. Biochem.* **2000**, *78*, 363−370.
[12] [12a] K. Angermaier, H. Schmidbaur, *J. Chem. Soc., Dalton Trans.* **1995**, 559−564. [12b] H. Schmidbaur, *Chem. Soc., Rev.* **1995**, 391−400.
[13] [13a] R. J. Less, J. L. M. Wicks, N. P. Chatterton, M. J. Dewey, N. L. Cromhout, M. A. Halcrow, J. E. Davies, *J. Chem. Soc., Dalton Trans.* **1996**, 4055−4061. [13b] J. Elguero, A. Fruchier, A. de la Hoz, F. A. Jalón, B. R. Manzano, A. Otero, F. Gómez-de la Torre, *Chem. Ber.* **1996**, *129*, 589−594. [13c] F. Gómez-de la Torre, A. de la Hoz, F. A. Jalón, B. R. Manzano, A. M. Rodríguez, *Inorg. Chem.* **2000**, *39*, 1152−1162.
[14] [14a] M. Munakata, M. Wen, Y. Suenaga, T. Kuroda-Sowa, M. Maekawa, M. Anahata, *Polyhedron* **2001**, *20*, 2037−2043. [14b]

 © 2003 Wiley-VCH Verlag GmbH & Co. KGaA, Weinheim

P. Paul, B. Tyagi, A. K. Bilakhiya, P. Dastidar, E. Suresh, *Inorg. Chem.* **2000**, *39*, 14−22. [14c] S. R. Batten, B. F. Hoskins, B. Moubaraki, K. S. Murray, R. Robson, *Chem. Commun.* **2000**, 1095−1096. [14d] B. F. Abrahams, S. R. Batten, H. Hamit, B. F. Hoskins, R. Robson, *Angew. Chem.* **1996**, *108*, 1794−1796; *Angew. Chem. Int. Ed. Engl.* **1996**, *35*, 1690−1692. [14e] B. F. Abrahams, S. R. Batten, M. J. Grannas, H. Hamit, B. F. Hoskins, R. Robson, *Angew. Chem.* **1999**, *111*, 1538−1540; *Angew. Chem. Int. Ed.* **1999**, *38*, 1475−1477. [14f] D. Venkataraman, S. Lee, J. S. Moore, P. Zhang, K. A. Hirsch, G. B. Gardner, A. C. Covey, C. L. Prentice, *Chem. Mater.* **1996**, *8*, 2030−2040. [14g] A. J. Blake, N. R. Brooks, N. R. Champness, L. R. Hanton, P. Hubberstey, M. Schröder, *Pure Appl. Chem.* **1998**, *70*, 2351−2357. [14h] W. Clegg, M. R. J. Elsegood, L. Horsburgh, R. E. Mulvey, M. J. Ross, *Chem. Ber./Recueil* **1997**, *130*, 621−631. [14i] M. Munakata, M. Wen, Y. Suenaga, T. Kuroda-Sowa, M. Maekawa, M. Anahata, *Polyhedron* **2001**, *20*, 2321−2327. [14j] M. Bertelli, L. Carlucci, G. Ciani, D. M. Proserpio, A. Sironi, *J. Mat. Chem.* **1997**, *7*, 1271−1276.

[15] V. Milata, R. M. Claramunt, P. Cabildo, M. D. Santa María, P. Cornago, L. Infantes, F. H. Cano, J. Elguero, *Heterocycles* **2001**, *55*, 905−924.

[16] M. C. Torralba, M. Cano, J. A. Campo, J. V. Heras, E. Pinilla, M. R. Torres, *J. Organomet. Chem.* **2002**, *654*, 150−161.

[17] J. Barbera, C. Cativiela, J. L. Serrano, M. M. Zurbano, *Liq. Cryst.* **1992**, *11*, 887−897.

[18] K. Nakamoto, *Infrared and Raman Spectra of Inorganic and Coordination Compounds*, 4th edn., Wiley, New York, **1986**.

[19] L. Malatesta, L. Naldini, G. Simonetta, F. Cariati, *Coord. Chem. Rev.* **1966**, *1*, 255−262.

[20] [20a] M. Cano, J. V. Heras, M. Maeso, M. Alvaro, R. Fernández, E. Pinilla, J. A. Campo, A. Monge, *J. Organomet. Chem.* **1997**, *534*, 159−172. [20b] M. Cano, J. A. Campo, J. V. Heras, J. Lafuente, C. Rivas, E. Pinilla, *Polyhedron* **1995**, *14*, 1139−1147.

[21] F. Gómez-de la Torre, A. de la Hoz, F. A. Jalón, B. R. Manzano, A. Otero, A. M. Rodríguez, M. C. Rodríguez-Pérez, *Inorg. Chem.* **1998**, *37*, 6606−6614.

[22] [22a] R. Faggiani, H. E. Howard-Lock, C. J. L. Lock, M. A. Turner, *Can. J. Chem.* **1987**, *65*, 1568−1575. [22b] F. Bonati, A. Burini, B. R. Pietroni, B. Bovio, *J. Organomet. Chem.* **1985**, *296*, 301−313. [22c] C.-K. Chan, C.-X. Guo, K.-K. Cheung, D. Li, C.-M. Che, *J. Chem. Soc., Dalton Trans.* **1994**, 3677−3682.

[23] M. Munakata, S. G. Yan, M. Maekawa, M. Akiyama, S. Kitagawa, *J. Chem. Soc., Dalton Trans.* **1997**, 4257−4262.

[24] J. A. Campo, M. Cano, J. V. Heras, M. C. Lagunas, J. Perles, E. Pinilla, M. R. Torres, *Helv. Chim. Acta* **2002**, *85*, 1079−1095.

[25] [25a] N. Chabert-Couchouron, C. Marzin, G. Tarrago, *New J. Chem.* **1997**, *21*, 355−368. [25b] N. Chabert, L. Jacquet, C. Marzin, G. Tarrago, *New J. Chem.* **1995**, *19*, 443−452.

[26] Y. Zhao, W. Su, R. Cao, M. Hong, *Acta Crystallogr., Sect. C* **2000**, *C56*, e331−e332.

[27] [27a] A. Hunter, M. Renfrew, J. A. Taylor, J. M. J. Whitmore, A. Williams, *J. Chem. Soc., Perkin Trans. 2* **1994**, 2383−2384. [27b] A. Hunter, M. Renfrew, D. Rettura, J. A. Taylor, J. M. J. Whitmore, A. Williams, *J. Am. Chem. Soc.* **1995**, *117*, 5484−5491. [27c] N. R. Cullum, A. Hunter, M. Renfrew, D. Rettura, J. A. Taylor, J. M. J. Whitmore, A. Williams, *J. Am. Chem. Soc.* **1995**, *117*, 9200−9205. [27d] N. C. Thomas, B. L. Foley, A. L. Rheingold, *Inorg. Chem.* **1988**, *27*, 3426−3429.

[28] S. Braun, H.-O. Kalinowski, S. Berger, *150 and More Basic NMR Experiments*, Wiley-VCH, New York, **1998**.

[29] G. M. Sheldrick, *SHELXTL, Program for Refinement of Crystal Structure.* University of Göttingen, Göttingen, Germany, **1997**.

Received January 17, 2003

 © 2003 Wiley-VCH Verlag GmbH & Co. KGaA, Weinheim

Synthesis, Crystal Structure and Fluorescence of Two Novel Mixed-Ligand Cadmium Coordination Polymers with Different Structural Motifs

Junhua Luo,[a] Maochun Hong,*[a] Ruihu Wang,[a] Rong Cao,[a] Lei Han,[a] and Zhenzhong Lin[a]

Keywords: Cadmium / Coordination polymers / Fluorescence / N ligands

Two novel cadmium(II) coordination compounds, $[Cd(bpe)_{1.5}(NO_2\text{-}BDC)]\cdot 0.25H_2O$ (**1**) and $[Cd(bpp)(NO_2\text{-}BDC)(H_2O)]\cdot 0.25H_2O$ (**2**) [NO_2-$BDCH_2$ = 5-nitro-1,3-benzenedicarboxylic acid, bpe = 1,2-bis(4-pyridyl)ethane, bpp = 1,3-bis(4-pyridyl)propane] have been hydrothermally synthesized by reaction of cadmium chloride and NO_2-BDC with the homologous ligands bpe and bpp, respectively. The former compound displays a remarkable three-dimensional architecture sustained by the catenation of 2D bilayers, while the latter exhibits a unique twofold interpenetrating three-dimensional architecture. The thermal and fluorescence properties associated with their crystal structures have been measured.

(© Wiley-VCH Verlag GmbH & Co. KGaA, 69451 Weinheim, Germany, 2003)

Introduction

Polymeric coordination compounds have recently received much attention due to their interesting potential applications and various coordination architectures,[1,2] in which supramolecular polymeric architectures containing topological bonds, such as polycatenanes and polyrotaxanes, are of special interest for chemists.[3,4] The structural topology of coordination polymers can be specially designed by the careful selection of the coordination geometry of the metals, the structure of the spacer ligands, the counteranions, and the reaction conditions.[5−7] To date, of diverse elegant efforts to find key factors in the development of the polymers, the main rational synthetic strategy has been the use of unique spacer ligands where the network topology can be controlled and modified by changing the chemical structure of the organic ligand.[8,9] *N*,*N*′-bipyridine-type ligands are convenient linkers for constructing metal-organic frameworks, and a wide range of one-, two-, and three-dimensional coordination polymers has been generated with them.[10−12] At the same time, phenyldicarboxylates, which can serve as bifunctional ligands, have been effectively utilized to build coordination networks.[13,14] We anticipated using the mixed phenyldicarboxylate/*N*,*N*′-bipyridine-type ligand system [(NO_2-BDC)/(bpe or bpp); Scheme 1] to generate some coordination polymers with interesting topologies. Here, we report the crystal structure and fluorescence properties of two novel mixed organic ligand coordination polymers $[Cd(bpe)_{1.5}(NO_2\text{-}BDC)]\cdot 0.25H_2O$ (**1**) and $[Cd(bpp)(NO_2\text{-}BDC)(H_2O)]\cdot 0.25H_2O$ (**2**).

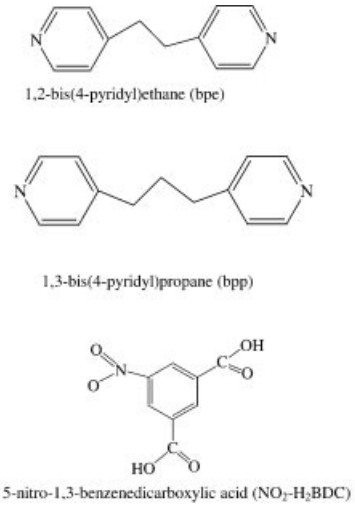

Scheme 1.

Results and Discussion

1,2-Bis(4-pyridyl)ethane (bpe) and 1,3-bis(4-pyridyl)propane (bpp) were selected as starting materials as they have different linkers between the two pyridine rings and show different structures. The two *N*,*N*′-bipyridine-type ligands react with NO_2-BDC (NO_2-$BDCH_2$ = 5-nitro-1,3-benzene-

[a] State Key Laboratory of Structural Chemistry, Fujian Institute of the Research on the Structure of Matter, Chinese Academy of Sciences,
Fuzhou, Fujian, 350002, China
Fax: (internat.) +86-591/371-4946
E-mail: hmc@ms.fjirsm.ac.cn

dicarboxylic acid) and a cadmium salt under the same reaction conditions. The two *N*,*N*′-bipyridine-type ligands have different structures, which finally results in different coordination frameworks as in **1** and **2**.

Crystal Structures

Single-crystal X-ray diffraction revealed a unique 2D bilayer structure of **1** with molecular formula $[Cd(bpe)_{1.5}(NO_2\text{-}BDC)_2]\cdot 0.25H_2O$. Each Cd^{II} center is heptacoordinated with a distorted $\{CdN_3O_4\}$ pentagonal bipyramidal coordination sphere, as shown in Figure 1. Four oxygen atoms belonging to two chelating didentate carboxylate groups from two NO_2-BDC moieties and one nitrogen atom from a bpe molecule coordinate to the cadmium center in the equatorial plane, with two nitrogen atoms from another two bpe ligands located at the axial positions of the coordination sphere. The Cd−O distances range from 2.322(10) to 2.599(9) Å, and the Cd−N distances are 2.328(13) and 2.345(12) Å. All the bpe ligands adopt an *anti* conformation and link the cadmium(II) ions into a $[Cd(bpe)_{1.5}]_n$ ladder as shown in Figure 2. The bpe ligands adopt two ligand conformations (A and B) in the ladder: the sides of the ladder adopt conformation A (bpe^A), with a dihedral angle of the two pyridyl rings of 44.1°; the rungs of the ladder adopt conformation B (bpe^B), where the two pyridyl rings are coplanar. The NO_2-BDC ligand acts as a μ_2-bridge through two chelating didentate carboxylate groups to link the ladders into a 2D bilayer (Figure 3). As seen in Figure 3b, the bpe^A and NO_2-BDC moieties in the also the link the cadmium ions into a (4,4) net sheet where the bpe^B ligands act as pillars forming bilayer galleries in which the planar sheets separated by them define 1D channels with dimensions of 13.848 × 14.054 $Å^2$. In the 2D bilayer structure of **1**, a cuboidal box containing eight cadmium(II) ions at the corners, connected by four short NO_2-BDC and eight long bpe linkers, making up the 12 edges, forms the fundamental building unit of **1** (Figure 4). This cuboidal structural motif is clearly different from the tetrahedral building blocks used to form other bilayer structures.[15,16] Interpenetration occurs in **1**, and each bilayer is interlocked by two adjacent identical frameworks (the upper and the lower identical motifs) as seen in Figure 5. This threefold interpenetration means that the void volume in **1** is very small; it is filled by the free water molecules. The resulting 3D array is, therefore, an infinite catenane of decked layers of an unprecedented interwoven type.

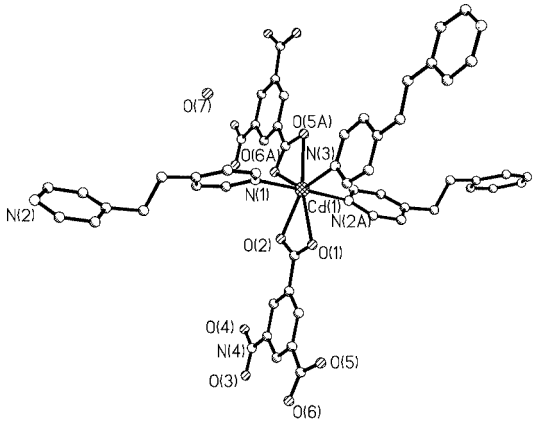

Figure 1. Perspective view of the coordination environment of the cadmium atom in **1**

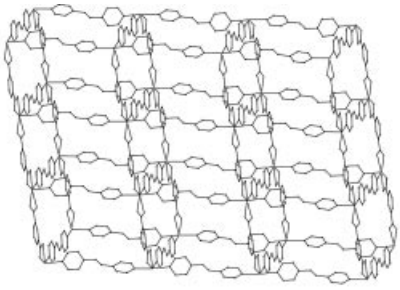

(a)

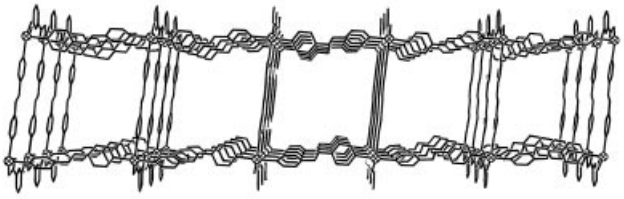

(b)

Figure 3. View of the 2D bilayer of **1**: a) along the *b* axis to show the rectangular channels; b) along the *a* axis

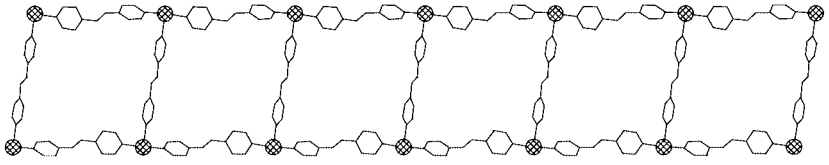

Figure 2. View of the $[Cd(bpe)_{1.5}]_n$ ladder in **1**

 © 2003 Wiley-VCH Verlag GmbH & Co. KGaA, Weinheim

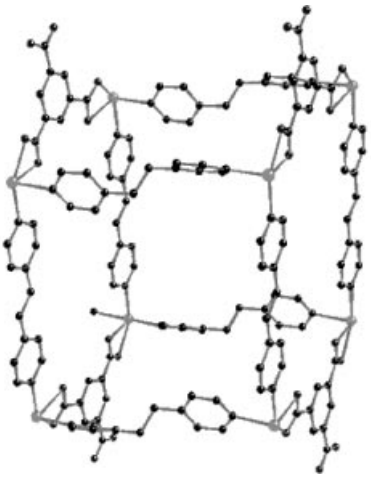

Figure 4. View of the cuboidal structural motif in **1**

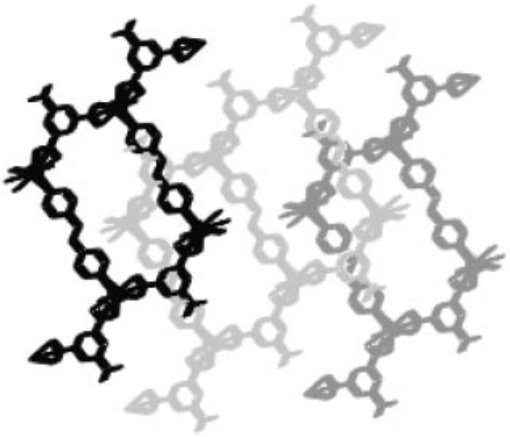

Figure 5. View of the interpenetration in **1**

The structure of **2** is a remarkable extended three-dimensional framework with molecular formula $[Cd(bpp)(NO_2\text{-}BDC)(H_2O)]\cdot 0.25H_2O$, in which the cadmium(II) atoms are bridged by mixed NO_2-BDC and bpe ligands. The asymmetric unit contains one cadmium(II) atom, one coordinated NO_2-BDC molecule, one coordinated bpp molecule, one coordinated water molecule and 0.25 free water molecules. All the Cd atoms are equivalent and each cadmium center is six-coordinate in a distorted octahedral geometry. Three carboxylate oxygens (O1, O2 and O3a) belonging to one chelating didentate carboxylate group, a monodentate carboxylate group from two NO_2-BDC molecules and one pyridyl N atom from a bpe ligand coordinate to the Cd center in the equatorial plane with *cis*-bond angles around the Cd center ranging from 54.2(2) to 128.9(2)°; the water molecule (O7) and another pyridyl N atom (N2b) from one bpe ligand are located at the axial positions of the distorted octahedral coordination sphere of Cd, with an O7−Cd−N2b bond angle of 167.7(2)° as shown in Figure 6. The $Cd-O_{carboxylate}$ distances range from 2.204(5) to 2.450(6) Å, and the Cd−N distances are 2.284(6) and 2.330(7) Å. Two NO_2-BDC and four bpp ligands link six Cd atoms to form a Cd_6 ring, which may be taken as the basic building block for the whole 3D framework of **2** (Figure 7). In the Cd_6 ring, the bpp ligands separate the Cd atoms at a distance of 11.598 Å; the two pyridine rings in dpp are almost perpendicular (dihedral angle of 97.2°), which is very different from the values found in **1** (44.1° or 0°). At the same time, the two pyridine rings coordinated to the same Cd atom are also almost perpendicular (dihedral angle of 79.4°). The Cd_6 rings are fused to form the ultimate unique 3D framework of **2**, which contains large channels with dimensions of 17.814×6.596 Å^2 (Figure 8). The 3D networks interlock with each other displaying a twofold-interpenetrating mode, which means that the void volume in **2** is very small; it is filled by the free water molecules (Figure 9).

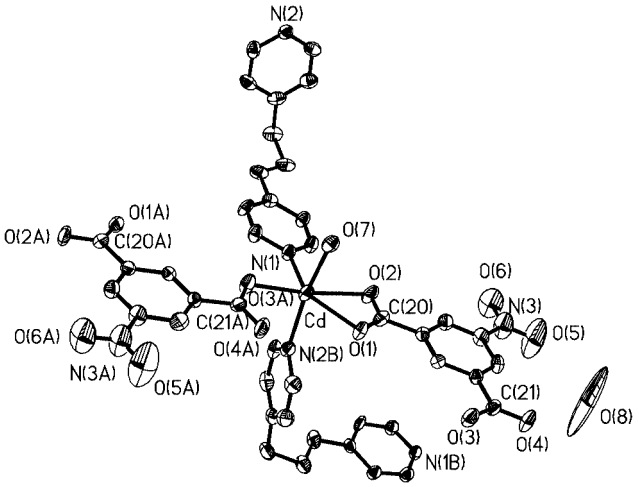

Figure 6. Perspective view of the coordination environment of the cadmium atom in **2**

IR Spectroscopy

The IR spectra of the two compounds show the characteristic bands of the dicarboxylate groups of NO_2-BDC at 1150−1620 cm^{-1} for the asymmetric vibration and at 1390−1420 cm^{-1} for the symmetric vibration. The absence of the expected absorption at 1690−1730 cm^{-1} for the protonated carboxylate groups illustrates the complete deprotonation of NO_2-BDC in the reaction with cadmium.[17]

Thermal and Fluorescent Properties

To study the thermal stability of the two compounds, thermogravimetric analysis (TGA) was performed on them. The TGA results of the two compounds are similar and show a very slow and gradual release of 0.25 water molecules in the 40−135 °C temperature range for **1** and 0.25 water molecules over the temperature range 35−120 °C for **2**. No obvious decomposition was observed until about 410 °C. Compounds **1** and **2** begin to decompose at 418 °C and 426 °C, respectively.

Metal-organic polymer compounds with a d^{10} configuration (such as Zn^{2+} and Cd^{2+}) have been found to exhibit photoluminescent properties,[18,19] and Zaworotko and co-

 © 2003 Wiley-VCH Verlag GmbH & Co. KGaA, Weinheim

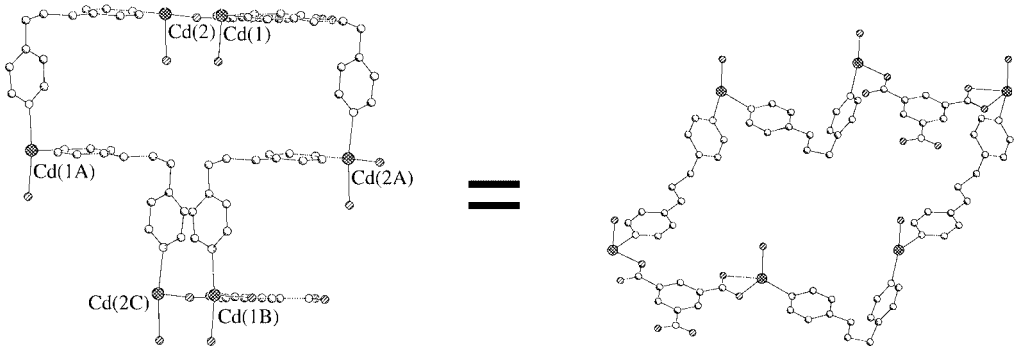

Figure 7. View of the Cd_6 ring in **2**

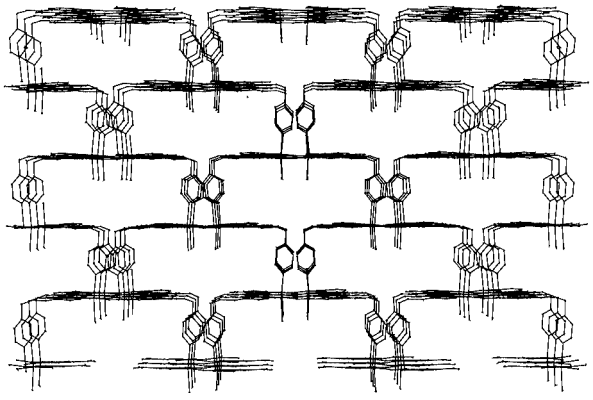

Figure 8. View of the 3D framework in **2** with large channels

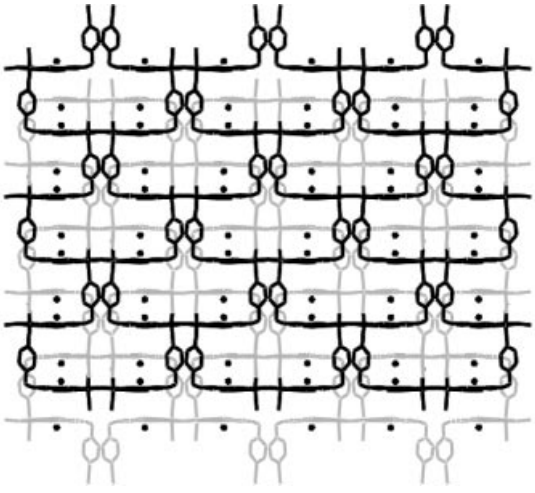

Figure 9. View of the interpenetration in **2** and the free water molecules in the void volumes

workers recently reported the first coordination polymer that traps a fluorescent guest.[20] Here, we want examine the photoluminescence of **1** and **2**. The solid-state emission spectra of complexes **1** and **2** at room temperature are shown in Figure 10. It can be seen that the maximum of the emission bands of **1** is located at 435 nm (λ_{ex} = 280 nm), while **2** also exhibits an intense photoluminescence emission at 439 nm (λ_{ex} = 310 nm). These emissions bands may be due to σ-donation from the cooperation of NO_2-BDC and bpp or bpe to the Cd center,[18a] and may be assigned to the ligand-to-metal charge-transfer (LMCT) band.[18,19] It is noticeable that **1** and **2** exhibit quenching of the fluorescence, with τ = 3.45 ns for **1** and τ = 3.64 ns for **2**.

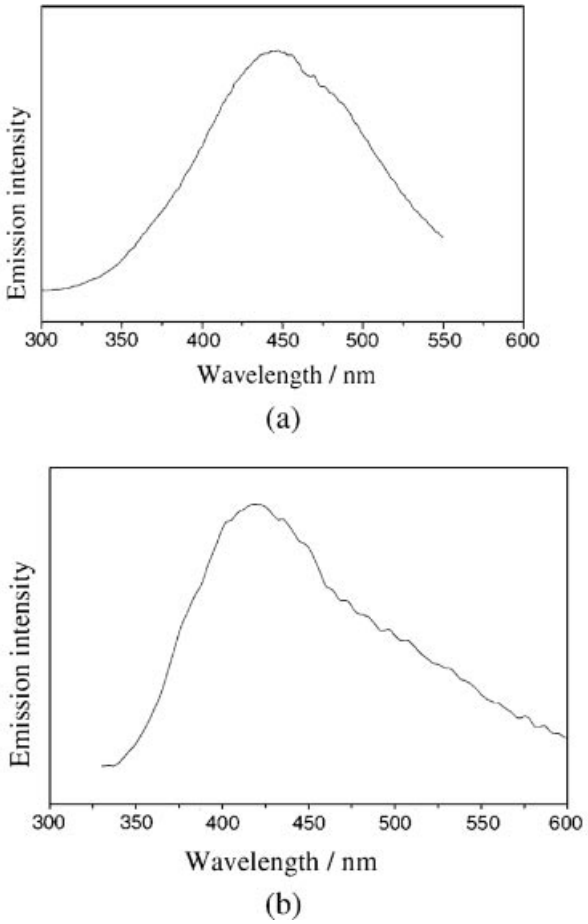

Figure 10. Solid-state emission spectra of the two compounds at room temperature: a) compound **1**; b) compound **2**

 © 2003 Wiley-VCH Verlag GmbH & Co. KGaA, Weinheim

Although **1** and **2** have different structural motifs, it is interesting to note that they exhibit similar thermal behaviors and emission bands. As the thermal behaviors and photoluminescence behaviors are closely associated with the metal ions and ligands coordinated around them, we need to compare the coordination environments of the Cd ions in **1** and **2**. The Cd atom in **1** has two chelating bis-didentate carboxylate groups and three bpp ligands, and in **2** there is one chelating bis-didentate carboylate group, one monodentate carboxylate group, and two bpp ligands. These similar environments may be the reason for the similar thermal and fluorescence behaviors of **1** and **2**.

Conclusion

Two coordination polymers formed by a cadmium salt and NO_2-BDC with the homologous ligands bpe and bpp have been prepared and characterized. Because of the different structures of the selected organic ligands (bpe for **1** and bpp for **2**), complex **1** exhibits a remarkable three-dimensional architecture sustained by the catenation of 2D bilayers, while complex **2** displays a unique twofold interpenetrating three-dimensional structural motif. Because of interpenetration, the two compounds all have small void volumes filled by free water molecules. They have similar thermal behaviors and fluorescence spectra.

Experimental Section

General: $CdCl_2 \cdot 2.5H_2O$ and NO_2-BDC were purchased commercially and used without further purification. The bpe and bpp were purchased from Fluka. C, H and N analyses were determined on a Perkin−Elmer 240C analyzer. IR spectra were measured as KBr pellets on a Nicolet Magna 750 FT-IR spectrometer in the range 200−4000 cm^{-1}. Thermogravimetric analyses were performed on a NETSCHZ STA-449C thermoanalyser under N_2 (26−750 °C range) at a heating rate of 10 °C/min. Fluorescent characterization was performed on an Edinburgh F900 analytical instrument at Fuzhou University**.** Fluorescence spectra of the solid samples were obtained by direct front-face emission from the solid powder bonded to a quartz support oriented at 40° to both the excitation and emission light paths, with excitation at 280 nm for **1** and 310 nm for **2**.

$[Cd(bpe)_{1.5}(NO_2\text{-BDC})]\cdot 0.25H_2O$ (1): The pH value of an aqueous mixture (10 mL) containing NO_2-BDC (0.5 mmol), $CdCl_2 \cdot 2.5H_2O$ (0.5 mmol) and bpe (0.5 mmol) was pre-adjusted to about 6 with a 0.1 M aqueous NaOH solution. The mixture was then transferred into an Teflon-lined, stainless-steel autoclave (18 mL), and the vessel was sealed and heated to 180 °C for 72 h, then cooled to room temperature at a rate of 10 °C/h. Colorless crystals of **1** were obtained (0.165 g, 82%). $C_{26}H_{21.5}CdN_4O_{6.25}$ (602.4): calcd. C 51.80, H 3.57, N 9.30; found C 51.41, H 3.62, N 9.24.

$[Cd(bpp)(NO_2\text{-BDC})(H_2O)]\cdot 0.25H_2O$ (2): The pH value of an aqueous mixture (10 mL) containing NO_2-BDC (0.5 mmol), $CdCl_2 \cdot 2.5H_2O$ (0.5 mmol) and bpp (0.5 mmol) was pre-adjusted to about 6 with a 0.1 M aqueous NaOH solution. The mixture was then transferred into an Teflon-lined, stainless-steel autoclave (18 mL), and the vessel was sealed and heated to 180 °C for 72 h, then cooled to room temperature at a rate of 10 °C/h. Colorless crystals of **2** were obtained (0.213 g, 78%). $C_{21}H_{19.55}CdN_3O_{7.25}$ (542.3): calcd. C 46.47, H 3.60, N 7.74; found C 45.02, H 3.67, N 7.65.

Table 1. Crystallographic data for the compounds **1** and **2**

	1	**2**
Empirical formula	$C_{26}H_{21.5}CdN_4O_{6.25}$	$C_{21}H_{19.5}CdN_3O_{7.25}$
Molecular weight	602.37	542.3
Space group	$P\bar{1}$	$C2/c$
a (Å)	10.2414(8)	14.4774(1)
b (Å)	10.9924(8)	18.3603(6)
c (Å)	13.8482(9)	17.2732(4)
α (°)	109.940(3)	90
β (°)	99.410(3)	105.561(2)
γ (°)	109.142(3)	90
V (Å^3)	1316.3(2)	4423.1(2)
Z	2	8
d_{calcd}, (Mg·m^{-3})	1.520	1.629
μ(Mo-K_α), (mm^{-1})	0.877	1.036
F(000)	607	2180
Reflections collected	3148	4582
Independent reflections	1672	2072
Parameters	343	298
Goodness-of-fit on F^2	1.120	1.129
R_1 indices [$I > 2\sigma(I)$]	0.0553	0.0425
wR_2 indices (all data)	0.1435	0.1113

Table 2. Selected bond lengths (Å) and angles (°) for **1** and **2**

$[Cd(bpe)_{1.5}(NO_2\text{-BDC})_2]\cdot 0.25H_2O$ (**1**)[a]

Cd(1)−N(2b)	2.328(13)	Cd(1)−N(1)	2.361(12)
Cd(1)−N(3)	2.345(12)	Cd(1)−O(2)	2.322(10)
Cd(1)−O(1)	2.599(9)	Cd(1)−O(6a)	2.315(11)
Cd(1)−O(5a)	2.592(10)		
O(6a)−Cd(1)−O(2)	85.0(5)	N(3)−Cd(1)−O(5a)	85.1(5)
O(6a)−Cd(1)−N(2b)	96.6(6)	N(1)−Cd(1)−O(5a)	96.3(4)
O(2)−Cd(1)−N(2b)	92.1(4)	O(6a)−Cd(1)−O(1)	137.8(4)
O(6a)−Cd(1)−N(3)	136.9(5)	O(2)−Cd(1)−O(1)	52.8(4)
O(2)−Cd(1)−N(3)	138.0(5)	N(2b)−Cd(1)−O(1)	85.4(5)
N(2b)−Cd(1)−N(3)	86.6(5)	N(3)−Cd(1)−O(1)	85.3(5)
O(6a)−Cd(1)−N(1)	89.2(5)	N(1)−Cd(1)−O(1)	89.8(4)
O(2)−Cd(1)−N(1)	87.8(4)	O(5a)−Cd(1)−O(1)	168.5(4)
O(6a)−Cd(1)−O(5a)	52.3(4)	N(2b)−Cd(1)−N(1)	174.1(6)
O(2)−Cd(1)−O(5a)	136.9(5)	N(3)−Cd(1)−N(1)	89.5(5)
N(2b)−Cd(1)−O(5a)	87.8(5)		

$[Cd(bpp)(NO_2\text{-BDC})(H_2O)]\cdot 0.25H_2O$ (**2**)[b]

Cd−O(3a)	2.204(5)	Cd−N(2b)	2.330(7)
Cd−N(1)	2.284(6)	Cd−O(1)	2.340(5)
Cd−O(7)	2.326(5)	Cd−O(2)	2.450(6)
O(3a)−Cd−N(1)	90.1(2)	N(1)−Cd−O(1)	141.0(2)
O(3a)−Cd−O(7)	86.4(2)	O(7)−Cd−O(1)	84.99(19)
N(1)−Cd−O(7)	96.8(2)	N(2b)−Cd−O(1)	84.7(2)
O(3a)−Cd−N(2b)	94.9(2)	O(3a)−Cd−O(2)	173.1(2)
N(1)−Cd−N(2b)	95.4(2)	N(1)−Cd−O(2)	86.9(2)
O(7)−Cd−N(2b)	167.7(2)	O(7)−Cd−O(2)	87.86(19)
O(3a)−Cd−O(1)	128.9(2)	N(2b)−Cd−O(2)	91.5(2)
O(1)−Cd−O(2)	54.17(19)		

[a] Symmetry codes: (a) $x - 1, y, z$; (b) $x, y, z + 1$. [b] Symmetry codes: (a) $x, -y, z + {}^1/_2$; (b) $x - {}^1/_2, -y + {}^1/_2, z - {}^1/_2$.

 © 2003 Wiley-VCH Verlag GmbH & Co. KGaA, Weinheim

X-ray Crystallography: Single crystals of **1** and **2** were selected for an X-ray diffraction study. The unit-cell parameters and intensities were collected at 299 K on a Siemens SMART CCD diffractometer with graphite-monochromated Mo-K_α radiation (λ = 0.71073Å) and a graphite monochromator using the ω-scan mode. The structures were solved by direct methods and refined on F^2 by full-matrix least-squares procedures using the SHELXTL software suite.[21] All non-hydrogen atoms were refined anisotropically. All H-atoms were located theoretically and not refined. A summary of the crystallographic data of **1** and **2** is presented in Table 1, with selected bond lengths and angles in Table 2.

CCDC-203638 (**1**) and -203639 (**2**) contain the supplementary crystallographic data for this paper. These data can be obtained free of charge at www.ccdc.cam.ac.uk/conts/retrieving.html [or from the Cambridge Crystallographic Data Centre, 12, Union Road, Cambridge CB2 1EZ, UK; Fax: (internat.) +44-1223/336-033; E-mail: deposit@ccdc.cam.ac.uk].

Acknowledgments

This work was supported by grants from NNSF of China, NSF of Fujian Province and the key project of CAS.

[1] [1a] P. J. Stang, B. Olenyuk, *Acc. Chem. Res.* **1997**, *30*, 502−518. [1b] S. Leininger, B. Olenyuk, P. J. Stang, *Chem. Rev.* **2000**, *100*, 853−908. [1c] M. Fujita, D. Oguro, M. Miyazawa, H. Oka, K. Yamaguchi, K. Ogura, *Nature* **1995**, *378*, 469−471. [1d] M. C. Hong, Y. J. Zhao, W. P. Su, R. Cao, M. Fujita, Z. Zhou, A. S. C. Chan, *Angew. Chem. Int. Ed.* **2000**, *39*, 2468−2470. [1e] O. R. Evans, W. B. Lin, *Acc. Chem. Res.* **2002**, *35*, 511−522. [1f] Y. Cui, O. R. Evans, H. L. Ngo, P. S. White, W. B. Lin, *Angew. Chem. Int. Ed.* **2002**, *41*, 1159−1160. [1g] L. Pan, N. Ching, X. Y. Huang, J. Li, *Chem. Eur. J.* **2001**, *7*, 4431−4437. [1h] M. Yoshizawa, Y. Takeyama, T. Kusukawa, M. Fujita, *Angew. Chem. Int. Ed.* **2002**, *41*, 1347−1349.

[2] [2a] J. M. Lehn, *Supramolecular Chemistry: Concepts and Perspectives*; VCH Publishers: New York, **1995**. [2b] B. F. Hoskins, R. Robson, *J. Am. Chem. Soc.* **1990**, *112*, 1546−1554. [2c] G. D. Munno, F. Cipriani, D. Armentano, M. Julve, J. A. Real, *New J. Chem.* **2001**, *25*, 1031−1036. [2d] S. S. Y. Chui, S. M. F. Lo, J. P. H. Charmant, A. G. Orpen, I. D. Williams, *Science* **1999**, *283*, 1148−1150. [2e] Y. Garcia, P. J. van Koningsbruggen, G. Brvaic, D. Chasseau, O. Kahn, *Eur. J. Inorg. Chem.* **2003**, *3*, 356−362. [2f] D. Sun, R. Cao, Y. Sun, W. Bi, X. Li, M. Hong, Y. Zhao, *Eur. J. Inorg. Chem.* **2003**, *1*, 38−41. [2g] Y. Cui, H. L. Ngo, W. Lin, *Inorg. Chem.* **2002**, *41*, 1033−1035.

[3] [3a] S. R. Batten, R. Robson, *Angew. Chem. Int. Ed.* **1998**, *37*, 1461−1494. [3b] K. N. Power, T. L. Hennigar, M. J. Zaworotko, *New J. Chem.* **1998**, 177−181. [3c] S. Noro, S. Kitagawa, M. Kondo, K. Seki, *Angew. Chem. Int. Ed.* **2000**, *39*, 2082−2084.

[4] [4a] L. Carlucci, G. Ciani, D. M. Proserpio, S. Rizzato, *Chem. Commun.* **2000**, 1319−1320. [4b] D. B. Amabilino, J. F. Stoddart, *Chem. Rev.* **1995**, *95*, 2725−2828. [4c] J.-P. Sauvage, *Acc. Chem. Res.* **1998**, *31*, 611−619. [4d] R. Ballardini, V. Balzani, A. Credi, M. T. Gandolfi, M. Venturi, *Acc. Chem. Res.* **2001**, *34*, 445−455.

[5] [5a] J. M. Knaust, S. W. Keller, *Inorg. Chem.* **2002**, *41*, 5650−5652. [5b] I. Yamaguchi, K. Osakada, T. Yamamoto, *J. Am. Chem. Soc.* **1996**, *118*, 1811−1812.

[6] [6a] O. M. Yaghi, H. Li, C. Davis, D. Richardson, T. L. Groy, *Acc. Chem. Res.* **1998**, *31*, 474−484. [6b] P. Brunet, M. Simard, J. D. Wuest, *J. Am. Chem. Soc.* **1997**, *119*, 2737−2738. [6c] X.-H. Bu, W. Chen, W.-F. Hou, M. Du, R.-H. Zhang, F. Brisse, *Inorg. Chem.* **2002**, *41*, 3472−3482. [6d] S. Lopez, M. Kaharaman, M. Harmata, S. W. Keller, *Inorg. Chem.* **1997**, *36*, 6138−6140.

[7] [7a] J. R. Black, N. R. Champness, W. Levason, G. Reid, *J. Chem. Soc., Dalton Trans.* **1995**, 3439−3435. [7b] P. Ayyappan, O. R. Evans, W. B. Lin, *Inorg. Chem.* **2001**, *40*, 4627−4632. [7c] L. Pan, N. Ching, X. Y. Huang, J. Li, *Inorg. Chem.* **2000**, *39*, 5333−5340.

[8] [8a] C.-Y. Su, Y.-P. Cai, C.-L. Chen, B.-S. Kang, *Inorg. Chem.* **2001**, *40*, 2210−2211. [8b] P. Ayyappan, O. R. Evans, W. B. Lin, *Inorg. Chem.* **2001**, *40*, 3328−3330.

[9] [9a] J. Fan, H.-F. Zhu, T. Okamura, W.-Y. Sun, W.-X. Tang, N. Ueyama, *Inorg. Chem.* **2003**, *42*, 158−162. [9b] Y. Cui, H. L. Ngo, W. B. Lin, *Inorg. Chem.* **2002**, *41*, 5940−5942.

[10] [10a] S.-I. Noro, S. Kitagawa, M. Kondo, K. Seki, *Angew. Chem. Int. Ed.* **2000**, *39*, 2082−2084. [10b] S. Subramanian, M. J. Zaworotko, *Angew. Chem. Int. Ed. Engl.* **1995**, *34*, 2127−2129. [10c] C. Inman, J. M. Knaust, S. W. Keller, *Chem. Commun.* **2002**, 156−157. [10d] O. M. Yaghi, H. Li, T. L. Groy, *Inorg. Chem.* **1997**, *36*, 4292−4293.

[11] [11a] Q. M. Wang, G. C. Guo, T. C. W. Mak, *Chem. Commun.* **1999**, 1849−1850. [11b] L. Carlucci, G. Ciani, D. M. Proserpio, S. Rizzato, *Chem. Commun.* **2000**, 1319−1320. [11c] D. Hagrman, R. P. Hammond, R. Haushalter, J. Zubieta, *Chem. Mater.* **1998**, *10*, 2091−2100.

[12] [12a] M. J. Zaworotko, *Chem. Commun.* **2001**, 1−9. [12b] K. Biradha, Y. Hongo, M. Fujita, *Angew. Chem. Int. Ed.* **2000**, *39*, 3843−3845. [12c] N. G. Pschirer, D. M. Ciurtin, M. D. Smith, U. H. F. Bunz, H.-C. zur Loye, *Angew. Chem. Int. Ed.* **2002**, *41*, 583−585.

[13] [13a] H.-X. Zhang, B.-S. Kang, A.-W. Xu, Z-N. Chen, Z.-Y. Zhou, K.-B. Yu, C. Ren, *J. Chem. Soc., Dalton Trans.* **2001**, 2559−2566. [13b] S. L. Schiavo, G. Pocsfalvi, S. Serroni, P. Cardiano, P. Piraino, *Eur. J. Inorg. Chem.* **2000**, 1371−1375. [13c] M. Eddaoudi, H. Li, O. M. Yaghi, *J. Am. Chem. Soc.* **2000**, *122*, 1391−1397.

[14] [14a] D.-F. Sun, R. Cao, Y.-C. Liang, Q. Shi, W.-P. Sui, M.-C. Hong, *J. Chem. Soc., Dalton Trans.* **2001**, 2335−2340. [14b] H. Abourahma, B. Moulton, V. Kravtsov, M. J. Zaworotko, *J. Am. Chem. Soc.* **2002**, *124*, 9990−9991. [14c] S. Valiyaveettil, K. Mullen, *New J. Chem.* **1998**, *22*, 89−95.

[15] L. Carlucci, G. Ciani, P. Macchi, D. M. Proserpio, S. Rizzato, *Chem. Eur. J.* **1999**, *5*, 237−243.

[16] F. Q. Liu, T. D. Tilley, *Inorg. Chem.* **1997**, *36*, 5090−5096.

[17] L. J. Bellamy, *The Infrared Spectra of Complex Molecules*; Wiley: New York, **1958**.

[18] [18a] J.-C. Dai, X.-T. Wu, Z.-Y. Fu, C.-P. Cui, S.-M. Hu, W.-X. Du, L.-M. Wu, H.-H. Zhang, R.-Q. Sun, *Inorg. Chem.* **2002**, *41*, 1391−1396. [18b] J. Tao, J.-X. Shi, M.-L. Tong, X.-X. Zhang, X.-M. Chen, *Inorg. Chem.* **2001**, *40*, 6328−6330. [18c] J. Zhang, W. Lin, Z.-F. Chen, R.-G. Xiong, B. F. Abrahams, H.-K. Fun, *J. Chem. Soc., Dalton Trans.* **2001**, 1806−1807.

[19] [19a] W. Chen, J.-Y. Wang, C. Chen, Q. Yue, H.-M. Yuan, J.-S. Chen, S.-N. Wang, *Inorg. Chem.* **2003**, *42*, 944−946. [19b] J. Tao, M.-L. Tong, J.-X. Shi, X.-M. Chen, S.-W. Ng, *Chem. Commun.* **2000**, 2043.

[20] B. D. Wagner, G. J. McManus, B. Moulton, M. J. Zaworotko, *Chem. Commun.* **2002**, 2176−2177.

[21] G. M. Sheldrick, *Bruker SHELSTL-PC*, University of Göttingen, Germany, **1997**.

Received February 12, 2003

 © 2003 Wiley-VCH Verlag GmbH & Co. KGaA, Weinheim

Diorganotin(IV) Complexes of a Cyclic Thiosemicarbazone Ligand: Crystal Structures of $[SnPh_2(C_{15}H_{10}N_3S)Cl]$ and $[SnMe_2(C_{15}H_{10}N_3S)_2]$

Elena López-Torres,[a] M. Antonia Mendiola,*[a] César J. Pastor,[b] and Jesús R. Procopio[c]

Keywords: Nitrogen heterocycles / S ligands / Tin

Treatment of 5-methoxy-5,6-diphenyl-4,5-dihydro-2*H*-[1,2,4]triazine-3-thione (LH_2OCH_3) with compounds SnR_2X_2 (R = Me and Ph; X = Cl and NO_3) afforded, for the first time, metal derivatives of a cyclic thiosemicarbazone. Treatment of LH_2OCH_3 with the appropriate diorganotin(IV) chloride in dichloromethane provided 1:1 complexes, but 1:2 derivatives were isolated when the nitrate salts in distilled water were used. The complexes were studied by mass spectrometry, IR and multinuclear (^1H, ^{13}C and ^{119}Sn) NMR in solution, and also by ^{119}Sn CP/MAS NMR spectroscopy and by X-ray diffraction in the solid state. In all the complexes, the thiosemicarbazone had been modified by formation of a new C=N bond. In addition, the ligand LH had lost a hydrogen atom, acting as an anion. The crystal structures of $[SnPh_2(C_{15}H_{10}N_3S)Cl]$ (**1**) and $[SnMe_2(C_{15}H_{10}N_3S)_2]$ (**4**) each consist of discrete molecules with the tin atom bonded to the sulfur and amine nitrogen atoms to give a four-membered chelate ring with the [1,2,4]triazine modified. For phenyl derivative **1**, the tin atom is in a trigonal-bipyramidal environment with the phenyl rings in equatorial positions, and for complex **4** it is in an octahedral arrangement, with the methyl groups in axial positions. The ^{119}Sn CP/MAS NMR spectra of the complexes are in accordance with these structures. The values obtained indicate a five-coordinate geometry for $[SnMe_2(C_{15}H_{10}N_3S)Cl]$ (**2**) and suggest a coordination number of six for complex **3**. The ^{119}Sn spectra of complexes in solution depend on the coordinating capacity of the solvents.

(© Wiley-VCH Verlag GmbH & Co. KGaA, 69451 Weinheim, Germany, 2003)

Introduction

The increasing interest in thiosemicarbazones (TSCs) that has arisen in the last decades is related to their wide range of biological properties as, for example, antiviral, antibacterial and anticancer agents.[1−8] In particular, the National Cancer Institute (USA) has requested from us a sample of the molecule studied in this work in order to test it against a full panel of 60 human tumours (NSC no. 711635-Y). From the data obtained, this molecule seems to be active against breast cancer. Moreover, octahedral Sn^{IV} complexes are potential anti-tumour and anti-viral agents, a number of them having been shown to be active. Diorganotin(IV) derivatives appear to be the most active.[9,10]

A combination of the ligand and the metal chemistry is therefore an interesting topic to pursue, since it involves organotin and C=S moieties, both of which should have good biological activity. The mechanism of the activity of these complexes requires understanding of their structures and isomerism. In attempts to correlate anti-tumour activity with structure, it has generally been assumed that the organic ligand should facilitate the transport of the complex across cell membranes, while the actual anti-tumour activity would be exerted by the dissociated diorganotin(IV) moieties.[11−13] Moreover, TSC ligands are very versatile as the π delocalisation (enhanced upon deprotonation) and the presence of different types of donor atoms, such as sulfur, imine and amine nitrogen atoms, makes several coordination modes possible.[14,15]

In previous work, we have studied the synthesis and characterisation of macroligands with common functional groups, but containing different numbers of donor atoms and variable structures. In particular, we have prepared open-chain [1+2] and cyclic [1+1] molecules derived from the reaction between benzil and thiosemicarbazide.[19,20] A macrocyclic [2+2] condensation product was obtained in methanol from the cyclic [1+1] species in the presence of copper(II) chloride, through a metal template macrocyclization.[21] We have also studied their complexation reactions with metal ions, in order to ascertain the structural features of the complexes relating to biological systems and to evaluate their potential use in determination of toxic metals.[22−26] Previously, the cyclic [1+1] compound 5-methoxy-5,6-diphenyl-4,5-dihydro-2*H*-[1,2,4]triazine-3-thi-

[a] Departamento de Química Inorgánica, Universidad Autónoma de Madrid,
Cantoblanco 28049, Spain
E-mail: antonia.mendiola@uam.es
[b] Servicio Interdepartamental de Investigación, Universidad Autónoma de Madrid,
Cantoblanco 28049, Spain
[c] Departamento de Química Analítica y Análisis Instrumental, Universidad Autónoma de Madrid,
Cantoblanco 28049, Spain

one (LH_2OCH_3) had been observed to undergo a macrocyclization process in the presence of copper(II) nitrate and mercury salts, yielding macrocyclic complexes.[21,27] In this paper we report the synthesis and characterisation of the first complexes from a cyclic thiosemicarbazone obtained by treatment of LH_2OCH_3 with diorganotin(IV) compounds (SnR_2X_2: R = Me, Ph; X = Cl, NO_3). We have observed that the nature of the anionic ligand (Cl and NO_3), results in complexes of different stoichiometry and geometry for the tin atom: 1:1 with a coordination number of five for chloride and 1:2 with a coordination number of six for nitrate derivatives.

Solid-state ^{119}Sn NMR is known to provide insight into the local symmetry properties of the central tin(IV) atom and, in combination with solution ^{119}Sn NMR spectroscopic data, to provide information about the structural changes occurring upon dissolution of the organotin compounds.[12,16–18] The availability of X-ray data for two structurally related complexes prompted us to complement this work with the solid-state and solution NMR spectroscopic data.

Results and Discussion

Tin complexes were prepared by the general procedure outlined in Scheme 1. The reactions with chlorides were carried out in dichloromethane in the presence of a basic medium and those from nitrates in distilled water. The presence of basic medium or of water induces the loss of methanol, probably due to acid-base reaction with the relatively highly acidic N–H bond, yielding LH (Scheme 2), which has an additional C=N bond.[20]

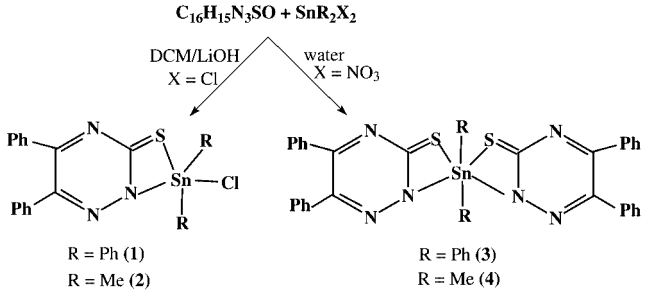

Scheme 1

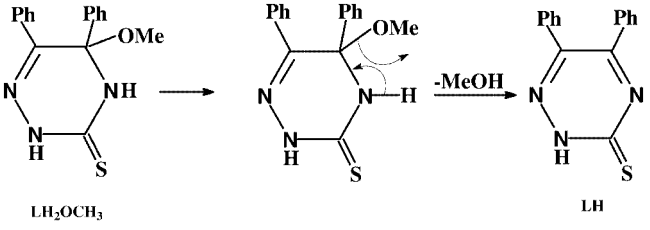

Scheme 2

Analytical data for the complexes show metal/ligand 1:1 stoichiometries for the chloride derivatives **1** and **2**, and 1:2 stoichiometries, with the absence of nitrate groups, for complexes **3** and **4**. Conductivity measurements for complex **2** in dimethylformamide and dichloromethane indicate the presence of non-ionic species in these solvents. Mass spectra confirm the molecular mass and also show fragments corresponding to the loss of R (Me or Ph), chlorine ligand or $C_{15}H_{10}N_3S$ (L^-). Experimentally measured isotopic distributions showed the same patterns as the theoretical ones in all compounds.

Crystallography

The crystal structure of **1** consists of discrete molecules of $[SnPh_2(C_{15}H_{10}N_3S)Cl]$. A perspective view of the complex, together with the atom-labelling scheme, is given in Figure 1 (hydrogen atoms are omitted for better clarity, and the thermal ellipsoids are shown at 40% probability) and selected bond angles and distances are given in Table 1. The coordination sphere of the tin atom is made up of the sulfur, amine nitrogen, chloro atoms and two phenyl rings, giving a pentacoordinate geometry. The Sn–L distances are in the range expected for this kind of complexes.[14,33] The three heteroatoms are in the same plane, with a maximum deviation of 0.1611 Å for Cl(1). The coordination mode of the ligand produces a four-membered chelate ring with the phenyl rings in the equatorial positions and the third position occupied by the sulfur atom. As is to be expected, the axial positions are occupied by nitrogen and chlorine atoms, in agreement with the polarity rule. The distortion from the ideal trigonal-bipyramidal configuration is manifested by the Cl(1)–Sn(1)–N(1) angle of 154.4°, which deviates from the ideal value of 180°, probably due to the ligand constraint. An alternative estimate of the geometry is given by the structural parameter τ introduced by Addison et al.[34] to analyse degrees of distortion from tetragonal-pyramidal (τ = 0.00) to trigonal-bipyramidal geometries (τ = 1.00). In this complex τ is 0.61. The phenyl rings form dihedral angles of 69.12, 74.14, 40.38 and 49.53° with respect to the equatorial plane for C(1)–C(6), C(7)–C(12), C(16)–C(21) and C(22)–C(27), respectively. An important change is observed with respect to LH_2OCH_3, where the dihedral angles are 36.94 [C(16)–C(21)] and 95.07° [C(22)–C(27)].[20] This change in one of the phenyl rings can be explained by the loss of the OMe group.

The crystal structure of **4** consists of discrete molecules of $[SnMe_2(C_{15}H_{10}N_3S)_2]$. A perspective view of the complex, together with the atom-labelling scheme, is given in Figure 2 (hydrogen atoms are omitted for better clarity, and thermal ellipsoids shown at 30% probability) and selected bond angles and distances are given in Table 2. Within the complex the tin(IV) ion is hexacoordinate in a distorted octahedral arrangement, four of the coordination positions belonging to the deprotonated ligands, which occupy the equatorial positions through the amine nitrogen atoms N(1) and N(4) and the sulfur atoms S(1) and S(2). The Sn–N distances are longer than in complex **1** and in other related

 © 2003 Wiley-VCH Verlag GmbH & Co. KGaA, Weinheim

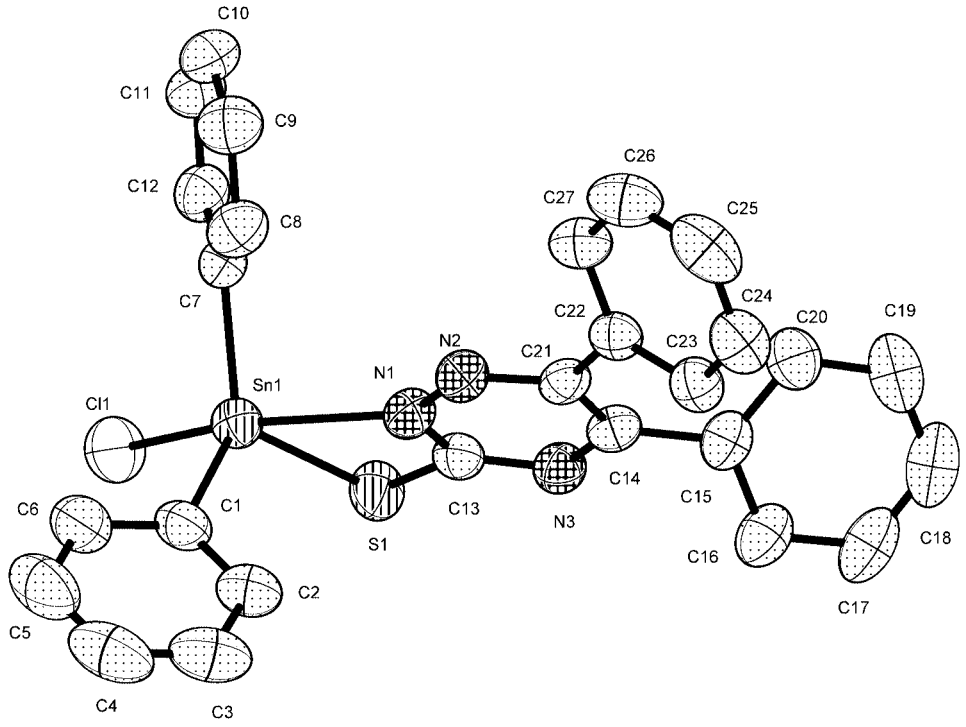

Figure 1. XSHELL view of $[SnPh_2(C_{15}H_{10}N_3S)Cl]$ (**1**)

Table 1. Selected bond lengths [Å] and angles [°] for complex **1**

S(1)−C(13)	1.746(3)	S(1)−Sn(1)	2.4597(8)
Sn(1)−C(1)	2.118(3)	Sn(1)−C(7)	2.125(2)
Sn(1)−Cl(1)	2.4113(8)	Sn(1)−N(1)	2.461(2)
C(13)−N(3)	1.328(3)	C(13)−N(1)	1.338(3)
C(14)−N(3)	1.333(3)	C(14)−C(15)	1.425(3)
C(14)−C(22)	1.484(4)	C(15)−N(2)	1.330(3)
C(15)−C(16)	1.483(3)	N(1)−N(2)	1.331(3)
C(13)−S(1)−Sn(1)	86.91(9)	C(1)−Sn(1)−C(7)	117.71(10)
C(1)−Sn(1)−Cl(1)	102.22(8)	C(7)−Sn(1)−Cl(1)	102.23(7)
C(1)−Sn(1)−S(1)	114.81(8)	C(7)−Sn(1)−S(1)	120.69(7)
Cl(1)−Sn(1)−S(1)	91.64(3)	C(1)−Sn(1)−N(1)	93.59(9)
C(7)−Sn(1)−N(1)	87.68(8)	Cl(1)−Sn(1)−N(1)	154.40(6)
S(1)−Sn(1)−N(1)	63.27(5)	C(13)−N(3)−C(14)	116.1(2)
N(3)−C(13)−S(1)	121.74(19)	N(3)−C(13)−N(1)	125.38(2)
N(3)−C(14)−C(15)	119.8(2)	N(1)−C(13)−S(1)	112.92(18)
N(2)−C(15)−C(14)	120.5(2)	N(2)−N(1)−C(13)	119.6(2)
C(13)−N(1)−Sn(1)	96.90(15)	C(15)−N(2)−N(1)	118.6(2)

compounds.[14,33] The two remaining positions in the octahedral geometry are occupied by two methyl groups, with a deviation from the expected angle of 24.4°.

The coordination mode of the ligand gives rise to two four-membered chelate rings. The core formed by the two thiosemicarbazone backbones and the tin atom can be considered planar, with a maximum deviation from the mean plane of 0.1104 Å for N(1), while the phenyl rings form dihedral angles of 41.46, 39.64, 48.2 and 42.53° with respect to this plane for C(6)−C(11), C(12)−C17), C(21)−C(26) and C(27)−C(32), respectively. These values are modified with respect to LH_2OCH_3 in the same way as in complex **1**.

Bond lengths in both complexes agree well with an iminethione form of the ligand, as does the NMR spectroscopy (see below), but with considerable electronic delocalisation through the thiosemicarbazone backbone, owing to the deprotonation of the ligands. As a consequence of this delocalisation, all the C−N bonds have almost the same length (Tables 1 and 2), which does not occur in LH_2OCH_3 (1.284−1.459 Å).[20] The thione bonds in both complexes (Tables 1 and 2) are longer than in the precursor molecule (1.628 Å in LH_2OCH_3) and are intermediate between the theoretical C−S single and double bonds,[35] as is also the case with the N−N bonds. Both S−C−N angles are also modified, especially that in which the nitrogen atom is involved in the bond to the tin atom. In addition, the N(2)−C(15)−C(14) angle in LH_2OCH_3 is 108.5°, corresponding to sp^3 hybridisation, while those in the complexes are close to 120°, as would be expected for sp^2 hybridisation. The remaining bond lengths and angles are similar to those found in similar organotin(IV) complexes and do not merit further comment.[14,33]

IR Spectroscopy

The IR assignment of LH_2OCH_3 is reported in the Exp. Sect. The absence of any band in the 2600 cm^{-1} region in all complexes suggests the absence of any thiol tautomer.[36] There are no bands in the 3000−3300 cm^{-1} region, indicating the absence of N−H bonds. In complexes **3** and **4** the absence of any band attributable to the nitrate group confirms that the organic fragment acts as an anion. The coordination through the sulfur atom can be observed in a decrease of the ν(C=S) frequency in the spectra of all the

 © 2003 Wiley-VCH Verlag GmbH & Co. KGaA, Weinheim

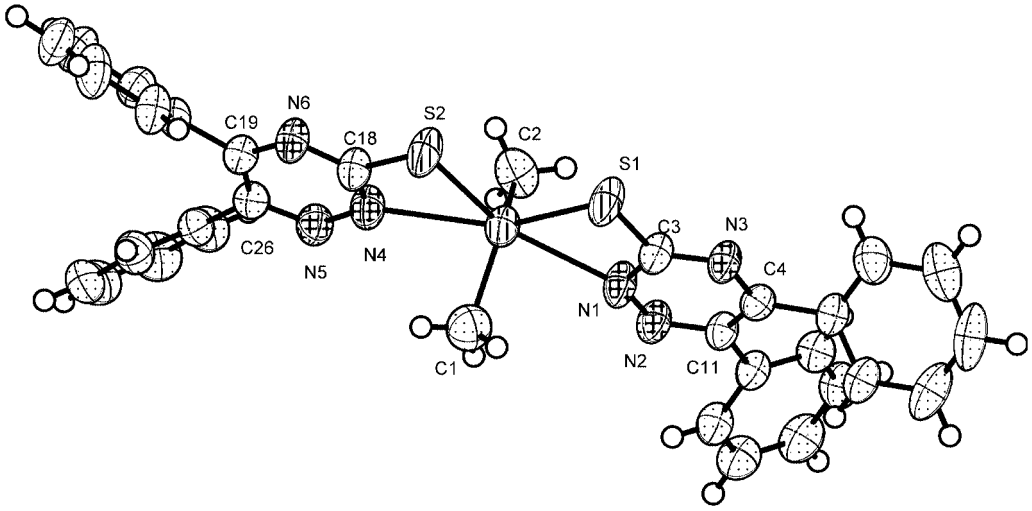

Figure 2. XSHELL view of $[SnMe_2(C_{15}H_{10}N_3S)_2]$ (**4**)

Table 2. Selected bond lengths [Å] and angles [°] for complex **4**

Sn(1)−C(1)	2.117(5)	Sn(1)−C(2)	2.123(5)
Sn(1)−S(2)	2.4938(10)	Sn(1)−S(1)	2.5091(10)
Sn(1)−N(1)	2.593(3)	Sn(1)−N(4)	2.7424(3)
S(1)−C(3)	1.733(4)	S(2)−C(18)	1.745(4)
C(3)−N(3)	1.339(4)	C(3)−N(1)	1.340(4)
C(4)−C(5)	1.423(4)	C(5)−N(2)	1.327(4)
C(4)−N(3)	1.333(4)	C(18)−N(6)	1.346(4)
C(18)−N(4)	1.324(4)	C(19)−C(20)	1.415(5)
C(19)−N(6)	1.333(4)	C(20)−N(5)	1.333(4)
[N(1)−N(2)	1.333(4)	N(4)−N(5)	1.346(4)
C(1)−Sn(1)−C(2)	131.2(3)	C(1)−Sn(1)−S(2)	107.1(2)
C(2)−Sn(1)−S(2)	103.3(2)	C(1)−Sn(1)−S(1)	107.29(18)
C(2)−Sn(1)−S(1)	108.1(19)	S(2)−Sn(1)−S(1)	92.76(3)
C(1)−Sn(1)−N(1)	84.1(2)	C(2)−Sn(1)−N(1)	85.2(2)
S(2)−Sn(1)−N(1)	153.67(7)	S(1)−Sn(1)−N(1)	60.95(7)
C(1)−Sn(1)−N(4)	80.44(19)	C(2)−Sn(1)−N(4)	82.8(2)
S(2)−Sn(1)−N(4)	60.02(7)	S(1)−Sn(1)−N(4)	152.62(7)
N(1)−Sn(1)−N(4)	146.31(9)	C(3)−S(1)−N(4)	89.25(12)
C(18)−S(2)−Sn(1)	91.25(13)	N(3)−C(3)−N(1)	124.6(3)
N(3)−C(3)−S(1)	121.2(3)	N(1)−C(3)−S(1)	114.2(3)
N(3)−C(4)−C(5)	119.7(3)	N(3)−C(4)−C(12)	116.1(3)
N(4)−C(18)−N(6)	124.9(3)	N(2)−C(5)−C(4)	120.1(3)
N(6)−C(18)−S(2)	118.6(3)	N(4)−C(18)−S(2)	116.4(3)
N(5)−C(20)−C(19)	120.2(3)	N(6)−C(19)−C(20)	120.1(3)
C(32)−C(27)−C(19)	119.0(3)	N(5)−C(20)−C(21)	114.5(3)
N(2)−N(1)−Sn(1)	144.6(2)	N(2)−N(1)−C(3)	119.1(3)
C(5)−N(2)−N(1)	119.5(3)	C(3)−N(1)−Sn(1)	95.5(2)
C(18)−N(4)−N(5)	119.3(3)	C(4)−N(3)−C(3)	116.6(3)
N(5)−N(4)−Sn(1)	148.0(2)	C(18)−N(4)−Sn(1)	92.2(2)
C(19)−N(6)−C(18)	116.2(3)	C(20)−N(5)−N(4)	118.9(3)

complexes. The presence of two bands attributable to C=N bonds indicates the formation of a new imine group, due to the loss of the methoxy group of the ligand. These moieties are non-coordinate to the tin atom. In complexes **1** and **3**, a new band at 729 cm^{-1} corresponding to phenyl rings appears. In all complexes the ν(Sn−C) bands are in the same region found in other diorganotin(IV) complexes.[37]

NMR Spectroscopy

The NMR assignments for LH_2OCH_3 are listed in the Exp. Sect. The ^1H NMR spectra of complexes **1** and **3** each show only a multiplet in the aromatic carbon atom region, corresponding to phenyl rings bonded to the tin atom and to the ligand. In each of the complexes **2** and **4** a singlet corresponding to the methyl group bonded to the metal atom can be observed, together with the multiplet for the phenyl rings of the ligand. In all complexes the absence of any signal corresponding to amine protons supports the presence of L. The loss of the methoxy group is confirmed by the absence of the singlet corresponding to the OCH_3 moiety (δ = 3.3 ppm).

In the ^{13}C NMR spectra the signals corresponding to the methoxy group carbon atoms and to the tetrasubstituted carbon atoms have disappeared and two signals attributable to imine carbon atoms have appeared. These groups are not bonded to the metal ion, as established by the X-ray diffraction. In addition, the thione group carbon atoms are deshielded in all complexes, due to the presence of metal−sulfur bonds, suggesting that the ligand retains the thione form. The numbers of signals corresponding to the phenyl carbon atoms are as expected for the proposed structures.

For methyl derivatives **2** and **4**, substitution of $^2J(^{119}Sn-^1H)$ values (72.20 and 75.02 Hz, respectively) and $^1J(^{119}Sn-^{13}C)$ values (518.69 and 557.00 Hz, respectively) into the corresponding Lockhart-Manders equations[38] (empirical relationship between the coupling constants and the C−Sn−C angle) gives C−Sn−C angle values of 122.0 and 124.4° for complex **2** and 125.0 and 125.5° for complex **4**. These similarities indicate that the data are reliable.

The ^{119}Sn chemical shifts of tin complexes appear to depend not only on coordination number, but also on the type of donor atoms bonded to the metal ion.[16,39,40] To bridge the information gap between X-ray diffraction and solution NMR spectroscopic data, solid-state NMR is an important

 © 2003 Wiley-VCH Verlag GmbH & Co. KGaA, Weinheim

routine technique.[17b] ^{119}Sn chemical shifts are summarised in Table 3. The values for the ^{119}Sn chemical shift in the solid state for complexes **1** and **4** are those expected for penta- and hexacoordinate environments for the tin atom. That obtained for complex **2** agrees with a five-coordinate structure as suggested by other measurements. The ^{119}Sn CP/MAS NMR spectrum of complex **3** is of lower resolution than the other complexes, but seems to show a δ(^{119}Sn) from −280 to δ = −335 ppm. This value corresponds to hexacoordination for the tin atom and, in comparison with the methyl derivative with the same stoichiometry, it is in the range expected.

Table 3. ^{119} Sn NMR spectroscopic data for the complexes (δ in ppm)

Compound	Solid	$CDCl_3$	[D_6]DMSO
1	−199	−181.5	−224.8
2[a]	−170	−24.5	−213.5
3	−280 to −335[b]	−206.8	−220.9
4	−251	− 84.3	−108.7

[a] −160.7 in dimethylformamide. [b] Low-resolution spectrum.

Holecek[16] established for *n*-butyl derivatives that four-coordinate compounds have δ(^{119}Sn) values in solution ranging from δ = +200 to −60 ppm, five-coordinate compounds δ = −90 to −190 ppm, and six-coordinate compounds δ = −210 to −400 ppm. The value of δ = −181.5 ppm for complex **1** is within the range expected for five-coordinate complexes, which agrees with the environment of the tin atom persisting in solution (Table 3). The value of δ = −24 ppm for complex **2** in $CDCl_3$ correlates well with a four-coordinate complex, which indicates a strong change in the coordination sphere of the metal atom, probably due to the rupture of one (Sn−L) bond (the complex is a non-electrolyte in CH_2Cl_2). The spectrum in DMF, however, shows a signal at δ = −160.7 ppm, as would be expected for pentacoordination (slightly shifted from the value in the solid state), so the five-coordination for the tin atom remains in DMF. The ^{119}Sn values observed for complex **3** are smaller than those seen in the solid state (Table 3), and could reflect a coordination number of either five or six, depending on the atoms bonded to the tin atom. For a particular geometry, relatively lower δ(Sn) values are observed with higher electronegativity of the atom directly bonded to the metal atom.[41] In comparison with complex **1** (five-coordinate by Ph_2SNCl) the elimination of the chlorine ligand and the addition of a new Sn−L bond will give a slightly more negative δ value. On the other hand, replacement of methyl by phenyl, with the same geometry, should shift the signal to a more negative value. If these factors are taken into account, the δ value in complex **3** suggests five-coordination for the tin atom in chloroform.

The chemical shift for complex **4** in $CDCl_3$ indicates a change to a lower coordination than in the solid state (Table 3). Since a value of δ = −181 ppm in solution for complex **1** corresponds to five-coordination, a value of δ = −84.3 ppm seems to indicate tetracoordination (Me_2S_2)[42] instead of hexacoordination. This change could be explained by the rupture of the weak Sn−N bonds in solution, these bonds being longer than those in other previously published complexes with related ligands[14,33] and in those presented in this work.

The ^{119}Sn chemical shift values in [D_6]DMSO are more negative than in $CDCl_3$ and − for complexes **1** and **2** − than in the solid state, as would be expected for this coordinating solvent. [D_6]DMSO can increase the coordination sphere of the tin atom and/or substitute Sn−L bonds, increasing the coordination number to six for complexes **1**−**3** and to five for complex **4**.

Conclusions

The cyclic thiosemicarbazone LH_2OCH_3 reacts with diorganotin species to give non-electrolyte complexes (**1**−**4**). The stoichiometry of the complexes depends on the organotin compound used (chloride or nitrate). X-ray diffraction studies of complexes **1** and **4** revealed that the tin atoms in both are bonded to the sulfur and to the deprotonated amine nitrogen atoms, giving a four-membered chelate ring, with the organic molecule modified. In complex **1** the tin atom is in a trigonal-bipyramid environment with the phenyl rings in equatorial positions, and in complex **4** it is in an octahedral arrangement, with the methyl groups in axial positions. We have also studied the structural changes accompanying the dissolution of the complexes by ^{119}Sn CP/MAS and multinuclear solution NMR spectroscopy. These complexes are promising from the biological point of view, because they contain organotin, the precursor molecule appearing to be active against human tumours, and also contain the C=S moiety, which displays good antimicrobial activity.

Experimental Section

Physical Measurements: Microanalyses were carried out with a Perkin−Elmer 2400 II CHNS/O Elemental Analyser. IR spectra in the 4000−400 cm^{-1} range were recorded on KBr pellets with a Jasco FT/IR-410 spectrophotometer. ^{1}H, ^{13}C and ^{119}Sn NMR spectra were recorded with a Bruker AMX 300 spectrophotometer in $CDCl_3$, [D_6]DMSO and DMF as solvents and with TMS (^{1}H, ^{13}C) and $SnMe_4$ (^{119}Sn) as internal references. Fast atom bombardment mass spectra were recorded with a VG Auto Spec instrument with Cs as the fast atom and *m*-nitrobenzyl alcohol (*m*NBA) as the matrix. ^{119}Sn MAS and CP/MAS NMR spectra were obtained at room temperature with a Bruker MSL 400 spectrometer. The external magnetic field was 9.4 T and samples were spun at 10 kHz around an axis inclined at 54°44′ with respect to this field. The spectrometer frequency was set to 149.11 MHz. For spectra recorded with use of a standard single-pulse sequence, a π/2 pulse of 6 μs and a period between successive accumulations of 10 s were used. In CP-MAS conditions, a contact time of 1 ms was used. The number of scans was 800. Chemical shift values were referenced to $Sn(CH_3)_4$. The analysis of ^{119}Sn NMR spectra was done with the WINFIT Program.

 © 2003 Wiley-VCH Verlag GmbH & Co. KGaA, Weinheim

Crystallography: Single crystals, prismatic in shape, of complexes **1** and **4** were obtained by recrystallisation from ethanol. Measurements were carried out with a Bruker SMART 6 K CCD area detector three-circle diffractometer with a Rigaku Rotating Anode (Cu-K_α radiation). For complexes **1** and **4**, the substantial redundancy in the data allows empirical absorption corrections (SADABS)[28] to be applied by use of multiple measurements of symmetry-equivalent reflections. The unit cell parameters were obtained by full-matrix, least-squares refinements of 8312 and 5730 reflections for complexes **1** and **4**, respectively. Crystallographic details are reported in Table 4. The crude intensity data frames were integrated by use of the SAINT[29] program, which also applied corrections for Lorentz and polarisation effects. The SHELXTL[30] software package, version 6.10, was used for space group determination, structure solution and refinement. The space group determination was based on a check of the Laue symmetry and systematic absences and was confirmed by the structure solution. The structure was solved by direct methods (SHELXS-97),[31] completed with difference Fourier syntheses, and refined by full-matrix, least squares by use of SHELXL-97,[32] with minimisation of $\omega(F_o^2 - F_c^2)^2$. Weighted R factors (R_w) and all goodnesses of fit S are based on F^2; conventional R factors (R) are based on F. All non-hydrogen atoms were refined with anisotropic displacement parameters. All scattering factors and anomalous dispersions factors are contained in the SHELXTL 6.10 program library. The high quality of the data set allowed all hydrogen atoms to be located by difference maps and refined isotropically in both complexes. CCDC-188698 (**4**) and -188699 (**1**) contain the supplementary crystallographic data for this paper. These data can be obtained free of charge at www.ccdc.cam.ac.uk/conts/retrieving.html [or from the Cambridge Crystallographic Data Centre, 12 Union Road, Cambridge CB2 1EZ, UK; Fax: (internat.) + 44-1223/336-033; E-mail: deposit@ccdc.cam.ac.uk].

Table 4. Crystal data and structure refinement for complexes **1** and **4**

	1	**4**
Empirical formula	$C_{27}H_{20}ClN_3SSn$	$C_{32}H_{26}N_6S_2Sn$
Formula mass	572.66	677.40
Crystal system	monoclinic	monoclinic
Space group	$P2_1/c$	$P2_1/c$
Unit cell dimensions	a = 9.72620(10) Å	a = 14.8222(2) Å
	b = 27.0583(2) Å	b = 11.62080(10) Å
	c = 9.82690(10) Å	c = 18.3507(2) Å
	β = 105.7710(10)°	β = 105.7700(10)°
Volume	2488.83(4) Å^3	3041.86(6) Å^3
Z	4	4
Absorption coefficient	10.088 mm^{-1}	8.215 mm^{-1}
Reflections collected	4543	5422
Independent reflections	4543	5422
Final R indices	$R1$ = 0.0283,	$R1$ = 0.0333,
[$I > 2\sigma(I)$]	$wR2$ = 0.0755	$wR2$ = 0.0722

Syntheses: $SnMe_2Cl_2$ and $SnPh_2Cl_2$ were used as provided by Aldrich. Dichloromethane was dried by standard procedures.

5-Methoxy-5,6-diphenyl-4,5-dihydro-2*H*-[1,2,4]triazine-3-thione (LH_2OCH_3):[20] A solution of thiosemicarbazide (1.14 g, 12.50 mmol) in methanol (150 mL), hydrochloric acid (25 mL, 2 M), concd. HCl (1 mL) and a solution of benzil (2.63 g, 12.50 mmol) in methanol (100 mL) were alternatively added dropwise and slowly, with strong stirring, to methanol (75 mL). After completion of the addition of all reactants, the mixture was stirred for 8 h. Overnight a crystalline solid formed, which was filtered off, washed and dried in vacuo (yield 95%), m.p. 222 °C. $C_{16}H_{15}N_3OS$ (297.4): calcd. C 64.64, H 5.05, N 14.14; found C 64.45, H 5.09, N 14.05. MS (FAB+): m/z (%) = 298 (35) [$C_{16}H_{15}N_3SO + 1$]$^+$. Selected spectroscopic data: IR: $\tilde{\nu}$ = 3184 s, 3131 s (NH); 1608 w (C=N); 1550 s (thioamide I); 846 w (thioamide IV) cm^{-1}. ^{1}H NMR (300 MHz, $CDCl_3$, 25 °C): δ = 3.1 (s, 3 H, OCH_3), 7.2−7.4 (m, 8 H, Ph), 7.5 (m, 2 H, Ph), 10.0 (d, 1 H, NH), 12.1 (d, 1 H, NH) ppm. ^{13}C NMR (300 MHz, $CDCl_3$, 25 °C): δ = 169.7 (C=S); 142.4 (C=N); 126.5, 129.3, 133.7, 141.7 (Ph); 83.2 (CH_3O); 50.7 (CR_3) ppm.

[$SnPh_2(C_{15}H_{10}N_3S)Cl$] (1): LH_2OCH_3 (0.50 g, 1.68 mmol) and $LiOH{\cdot}H_2O$ (0.071 g, 1.68 mmol) were stirred in dried dichloromethane (50 mL) at room temperature for 15 min. $SnPh_2Cl_2$ (0.58 g, 1.68 mmol), dissolved in the same solvent (10 mL), was then added. After the mixture had been heated at reflux for 7 d, it was filtered, and the clear yellow solution was concentrated until a yellow solid was formed (yield 95%), m.p. 170 °C. $C_{27}H_{20}ClN_3SSn$ (572.66): calcd. C 56.63, H 3.49, N 7.34, S 5.59; found C 56.44, H 3.76, N 7.14, S 5.52. MS (FAB+): m/z (%) = 537.9 (35) [$SnPh_2(C_{15}H_{10}N_3S)$]$^+$, 574.3 (5) [$SnPh_2(C_{15}H_{10}N_3S)Cl + 1$]$^+$. Selected spectroscopic data: IR (KBr): $\tilde{\nu}$ = 1598 w, 1578 w (C=N); 1489 s (thioamide I); 819 w (thioamide IV); 729 m (Ph) cm^{-1}. ^{1}H NMR (300 MHz, $CDCl_3$, 25 °C): δ = 7.31−8.07 (m, Ph). ^{13}C NMR (300 MHz, $CDCl_3$, 25 °C): δ = 128.5, 128.7, 129.3, 129.7, 129.9, 130.0, 130.6, 131.7, 134.3, 134.4, 135.8, 139.8 (Ph); 153.8, 159.8 (C=N); 175.0 (C=S) ppm; $^2J(^{119}Sn-^{13}C)$ = 60.0 Hz; $^3J(^{119}Sn-^{13}C)$ = 17.4 Hz. ^{119}Sn NMR (300 MHz, $CDCl_3$, 25 °C): δ = −181.5 ppm. ^{119}Sn NMR (300 MHz, [D_6]DMSO, 25 °C): δ = −224.8 ppm. ^{119}Sn CP/MAS NMR: δ = −199 ppm.

[$SnMe_2(C_{15}H_{10}N_3S)Cl$] (2): A solution of $SnMe_2Cl_2$ (0.37 g, 1.68 mmol) in dried dichloromethane (10 mL) was added to a boiling mixture of LH_2OCH_3 (0.80 g, 2.69 mmol) and $LiOH.H_2O$ (0.071 g, 1.68 mmol) in the same solvent (80 mL). The mixture was stirred at reflux for 10 days. The white solid was filtered off and discarded. The yellow solution was concentrated until a yellow solid was produced. Yield 90%. m.p. 186 °C. $C_{17}H_{16}ClN_3SSu$ (448.15): calcd. C 45.52, H 3.57, N 9.37, S 7.14; found C 45.29, H 3.71, N 9.12, S 6.95. MS (FAB+): m/z (%) = 414.1 (100) [$SnMe_2(C_{15}H_{10}N_3S)$]$^+$, 450.1 (9) [$SnMe_2(C_{15}H_{10}N_3S)Cl + 1$]$^+$. Selected spectroscopic data: IR (KBr): $\tilde{\nu}$ = 1597 w, 1578 w (C=N); 1489 s (thioamide I); 790 w (thioamide IV); 562 w (ν_{asy} Sn−C); 520 w (ν_{sym} Sn−C) cm^{-1}. Λ_M (DMF) = 4.5 Ω^{-1}cm^{2}mol^{-1}; Λ_M (CH_2Cl_2) = 0.7 Ω^{-1}cm^{2}mol^{-1}. ^{1}H NMR (300 MHz, $CDCl_3$, 25 °C): δ = 1.23 [s, 6 H, CH_3, $^2J(^{119}Sn-^1H)$ = 72.2 Hz]; 7.30−7.53 (m, 10 H, Ph) ppm. ^{13}C NMR (300 MHz, $CDCl_3$, 25 °C): δ = 5.8 [CH_3, $^1J(^{119}Sn-^{13}C)$ = 518.6 Hz]; 128.6, 128.8, 129.1, 129.8, 130.0, 131.6, 134.4, 134.5 (Ph); 153.7, 159.1 (C=N); 174.7 (C=S) ppm. ^{119}Sn NMR (300 MHz, $CDCl_3$, 25 °C): δ = −24.5 ppm. ^{119}Sn NMR (300 MHz, DMF, 25 °C): δ = −160.7 ppm. ^{119}Sn NMR (300 MHz, [D_6]DMSO, 25 °C): δ = −213.5 ppm. ^{119}Sn CP/MAS NMR: δ = −170 ppm.

[$SnPh_2(C_{15}H_{10}N_3S)_2$] (3) and [$SnMe_2(C_{15}H_{10}N_3S)_2$] (4): A solution of $AgNO_3$ (3.37 mmol) in distilled water (10 mL) was added to a suspension of SnR_2Cl_2 (1.68 mmol) in the same solvent (10 mL). The mixture was stirred for 30 min and filtered. The filtrate was added slowly, with stirring, to a suspension of LH_2OCH_3 (3.36 mmol) in distilled water (50 mL). After the mixture had been heated at reflux for 3 d, the solid was filtered off, washed with methanol and vacuum dried.

Complex 3: Yield 98%, m.p. 180 °C. $C_{42}H_{30}N_6S_2Sn$ (801): calcd. C 62.90, H 3.75, N 10.49, S 7.99; found C 62.58, H 3.88, N 10.81, S 8.14. MS (FAB+): m/z (%) = 538.1 (100) [$SnPh_2(C_{15}H_{10}N_3S)$]$^+$,

 © 2003 Wiley-VCH Verlag GmbH & Co. KGaA, Weinheim

725.1 (15) $[SnPh(C_{15}H_{10}N_3S)_2]^+$, 803 (10) $[SnPh_2(C_{15}H_{10}N_3S)_2 + 1]^+$. Selected spectroscopic data: IR (KBr): $\tilde{\nu}$ = 1597 w, 1578 w (C=N); 1486 s (thioamide I); 806 w (thioamide IV); 729 m (Ph) cm^{-1}. ^{13}C NMR (300 MHz, $CDCl_3$, 25 °C): δ = 128.2, 128.4, 128.8, 129.2, 129.3, 129.7, 129.8, 130.6, 134.8, 134.9, 135.5, 141.1 (Ph); 153.1, 156.6 (C=N); 173.3 (C=S); $^2J(^{119}Sn-^{13}C)$ = 56.1 Hz. ^{119}Sn NMR (300 MHz, $CDCl_3$, 25 °C): δ = −206.8 ppm; (300 MHz, $[D_6]$DMSO, 25 °C): δ = −220.9 ppm.

Complex 4: Yield 79%, m.p. 224 °C. $C_{32}H_{26}N_6SSn$ (677.40): calcd. C 56.74, H 3.84, N 12.41, S 9.45; found C 56.45, H 4.04, N 12.30, S 9.50. MS (FAB+): *m/z* (%) = 413.9 (25) $[SnMe_2(C_{15}H_{10}N_3S)]^+$, 662.8 (5) $[SnMe(C_{15}H_{10}N_3S)_2]^+$, 678.9 (5) $[SnMe_2(C_{15}H_{10}N_3S)_2 + 1]^+$. Selected spectroscopic data: IR (KBr): $\tilde{\nu}$ = 1597 w, 1578 w (C=N); 1485 s (thioamide I); 820 w (thioamide IV); 557 w (ν_{asy} Sn−C); 511 w (ν_{sym} Sn−C) cm^{-1}. ^1H NMR (300 MHz, $CDCl_3$, 25 °C): δ = 1.29 [s, 6 H, CH_3, $^2J(^{119}Sn-^1H)$ = 75.0 Hz], 7.30−7.55 (m, 20 H, Ph) ppm. ^{13}C NMR (300 MHz, $CDCl_3$, 25 °C): δ = 6.2 [CH_3, $^1J(^{119}Sn-^{13}C)$ = 557.0]; 128.4, 128.6, 129.2, 129.3, 129.8, 130.9, 135.0, 135.1 (Ph); 153.0, 157.2 (C=N); 174.2 (C=S) ppm. ^{119}Sn NMR (300 MHz, $CDCl_3$, 25 °C): δ = −84.3 ppm. ^{119}Sn NMR (300 MHz, $[D_6]$DMSO, 25 °C): δ = −108.7 ppm. ^{119}Sn CP/MAS NMR: δ = −251 ppm.

Acknowledgments

We thank the DGICYT for financial support (Project BQU2001-0151).

[1] D. X. West, A. E. Liberta, S. B. Padhye, R. C. Chikate, P. B. Sonawane, A. S. Kumbhar, R. G. Yeranda, *Coord. Chem. Rev.* **1993**, *123*, 49−71 and refs. therein.
[2] A. E. Liberta, D. X. West, *Biometals* **1992**, *5*, 121−126.
[3] D. X. West, S. B. Padhye, P. B. Sonawane, *Struct. Bonding* **1991**, *76*, 1−50.
[4] J. G. Cory, A. H. Cory, Eds.; *International Encyclopaedia of Pharmacology and Therapeutics*, Pergamon Press, New York, **1989**.
[5] D. L. Klayman, J. P. Scovill, J. F Bartosevich, J. Bruce, *J. Med. Chem.* **1983**, *26*, 35−59.
[6] J. Easmon, G. Purstinger, G. Heinish, T. Roth, H. H. Fiebig, W. Holzer, W. Jager, M. Jenny, J. Hofman, *J. Med. Chem.* **2001**, *44*, 2164−2171.
[7] Z. Iakovidou, A. Papageorgiou, M. A. Demertzis, E. Mioglou, D. Mourelatos, A. Kostis, P. N. Yadav, D. Kovala-Demertzi, *Anticancer Drugs* **2001**, *12*, 65−70.
[8] M. C. Miller III, C. N. Stineman, J. R. Vance, D. X. West, I. H. Hall, *Anticancer Res.* **1998**, *18*, 4131−4139.
[9] M. Gielen, *Coord. Chem. Rev.* **1996**, *151*, 41−51.
[10] M. Gielen, *Appl. Organomet. Chem.* **2002**, *16*, 481−494.
[11] L. Ronconi, C. Marzano, U. Russo, R. Graziani, D. Fregona, *J. Inorg. Biochem.* **2002**, *91*, 413−420.
[12] L. Pellerito, L. Nagy, *Coord. Chem. Rev.* **2002**, *224*, 111−150.
[13] J. S. Casas, A. Castiñeiras, M. C. Rodríguez-Argüelles, A. Sánchez, J. Sordo, A. Vázquez-López, S. Pinelli, P. Lunghi, P. Ciancianaini, A. Bonati, P. Dall'Aglio, R. Albertini, *J. Inorg. Biochem.* **1999**, *76*, 277−284.
[14] J. S. Casas, A. Castiñeiras, M. C. Rodríguez-Argüelles, A. Sánchez, J. Sordo, A. Vázquez-López, E. M. Vázquez-López, *J. Chem. Soc., Dalton Trans.* **2000**, 2267−2272.
[15] J. S. Casas, M. S. Tasende, J. Sordo, *Coord. Chem. Rev.* **2000**, *209*, 197−261.
[16] J. Holecek, N. Nádvorník, K. Handlír, A. Lycka, *J. Organomet. Chem.* **1986**, *315*, 299−308.
[17] [17a] B. Wrackmeyer in: M. Gielen, R. Willem, B. Wrackmeyer (Eds.), *Physical Organometallic Chemistry*, Wiley, London, **1996**, vol. 1, p. 87−96. [17b] A. Sebald in: M. Gielen, R. Willem, B. Wrackmeyer (Eds.), *Physical Organometallic Chemistry*, Wiley, London, **1996**, vol. 1, p. 123−157.
[18] B. Wrackmeyer, *Annu. Rep. NMR Spectrosc.* **1999**, *38*, 203−264.
[19] P. Souza, M. A. Mendiola, A. Arquero, V. Fernández, E. Gutiérrez-Puebla, C. Ruíz-Valero, *Z. Naturforsch., Teil B* **1994**, *49*, 263−271.
[20] A. Arquero, M. Cañadas, M. Martínez-Ripoll, M. A. Mendiola, A. Ruiz-Valero, *Tetrahedron* **1998**, *54*, 11271−11284.
[21] E. Franco, E. López-Torres, M. A. Mendiola, M. T. Sevilla, *Polyhedron* **2000**, *19*, 441−451.
[22] A. Arquero, M. A. Mendiola, P. Souza, M. T. Sevilla, *Polyhedron* **1996**, *15*, 1657−1665.
[23] Z. Duracková, M. A. Mendiola, M. T. Sevilla, A. Valent, *Bioelectrochem. Bioenerg.* **1999**, *48*, 109−116.
[24] M. J. Gismera, M. A. Mendiola, J. Rodríguez-Procopio, M. T. Sevilla, *Anal. Chim. Acta* **1999**, *385*, 143−150.
[25] M. Cañadas, E. López-Torres, A. Martínez-Arias, M. A. Mendiola, M. T. Sevilla, *Polyhedron* **2000**, *19*, 2059−2068.
[26] E. López-Torres, M. A. Mendiola, J. Rodríguez-Procopio, M. T. Sevilla, E. Colacio, J. M. Moreno, I. Sobrados, *Inorg. Chim. Acta* **2001**, *323*, 130−138.
[27] M. A. Blanco, E. López-Torres, M. A. Mendiola, E. Brunet, M. T. Sevilla, *Tetrahedron* **2002**, 1525.-1531.
[28] G. M. Sheldrick, SADABS version 2.03, *Program for Empirical Absorption Correction*, Universität Göttingen, **1997−2001**.
[29] G. M. Sheldrick, *SAINT+NT (version 6.04) SAX Area-Detector Integration Program*, Bruker AXS, Madison, WI, **1997−2001**.
[30] Bruker, *AXS SHELXTL (version 6.10) Structure Determination Package*, Bruker AXS, Madison, WI, **2000**.
[31] *SHELXS-97, Program for Structure Solution:* G. M. Sheldrick, *Acta Crystallogr., Sect. A* **1990**, *46*, 467.
[32] G. M. Sheldrick, *SHELXL-97, Program for Crystal Structure Refinement*, Universität Göttingen, **1997**.
[33] J. S. Casas, A. Castiñeiras, M. C. Rodríguez-Argüelles, A. Sánchez, J. Sordo, A. Vázquez-López, E. Vázquez-López, *J. Chem. Soc., Dalton Trans.* **2000**, 4056−4063.
[34] A. W. Addison, T. N. Rao, J. Reedijk, J. van Rijn, G. C. Verschoor, *J. Chem. Soc., Dalton Trans.* **1984**, 1349−1356.
[35] L. E. Sutton, *Tables of Interatomic Distances and Configuration in Molecules and Ions*, supplement, The Chemical Society, London, **1965**.
[36] D. E. Fenton, D. H. Cook, *J. Chem. Soc., Chem. Commun.* **1977**, 714−716.
[37] J. S. Casas, A. Sánchez, J. Sordo, A. Vázquez-López, E. E. Castellano, J. Zukerman-Schpector, M. C. Rodríguez-Argüelles, U. Russo, *Inorg. Chim. Acta* **1994**, *216*, 169−175.
[38] T. P. Lockhart, W. F. Manders, *Inorg. Chem.* **1986**, *25*, 892−895.
[39] J. Otera, *J. Organomet. Chem.* **1981**, *221*, 57−61.
[40] C. H. Yoder, L. A. Margolis, J. M. Horne, *J. Organomet. Chem.* **2001**, *633*, 33−38.
[41] A. Deák, L. Radics, A. Kálmán, L. Párkányi, I. Haiduc, *Eur. J. Inorg. Chem.* **2001**, 2849−2856.
[42] A. Tarassoli, T. Sedaghat, B. Neumüller, M. Ghassemzadeh, *Inorg. Chim. Acta* **2001**, *318*, 15−22.

Received February 14, 2003

 © 2003 Wiley-VCH Verlag GmbH & Co. KGaA, Weinheim

EurJIC
European Journal of Inorganic Chemistry

Issue 15/2003

Pages 2719–2888

Papers available ahead of print in Early View at www.interscience.wiley.com

Earliest available Table of Contents:
Automatically, free of charge by e-mail through
www.interscience.wiley.com/alerts

COVER PICTURE

The cover picture shows a hexamolybdate anion bearing a diazenido ligand. This is a member of a promising family of functionalized polyoxomolybdates $[Mo_6O_{18}(N_2Ar)]^{3-}$ with a variety of substituents on the aryl ring. The influence of these substituents on the properties of the molybdate framework is exemplified by their different ^{95}Mo NMR spectra, where a special attention should be drawn to the signal of the Mo^{II} center at very high frequencies. Details on the preparation and characterization of these and related compounds can be found in the article by P. Gouzerh et al. on p. 2757 ff.

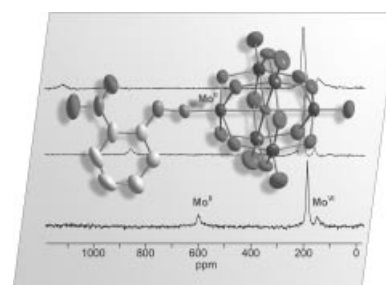

MICROREVIEW

Contents

2733 **L. Dahlenburg**

P-Modular Homochiral Bis(phosphanes) with 1,2-Disubstituted Cyclopentane Backbones in Asymmetric Hydrogenation

Keywords: Chirality / Asymmetric synthesis / Hydrogenation / Chelate phosphanes / Rhodium

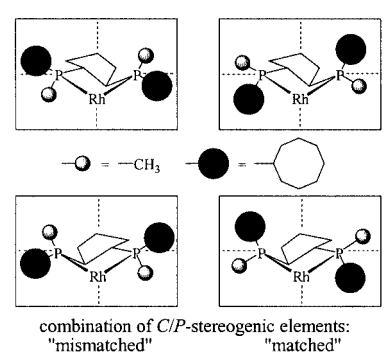

 © 2003 Wiley-VCH Verlag GmbH & Co. KGaA, Weinheim

SHORT COMMUNICATIONS

2749 **P. K. M. Siu, S.-W. Lai, W. Lu, N. Zhu, C.-M. Che***

A Diiminoplatinum(II) Complex of 4-Ethynylbenzo-15-crown-5 as a Luminescent Sensor for Divalent Metal Ions

Keywords: Crown compounds / Platinum / Luminescence / Magnesium / Sensors

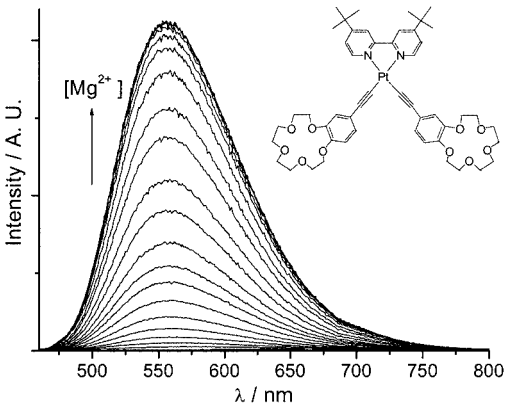

2753 **J. Lewiński,* W. Marciniak, Z. Ochal, J. Lipkowski, I. Justyniak**

A Novel Tetranuclear [MeZn(μ_3-OCH_2CH_2SMe)-Zn(μ-Cl)Me]$_2$ Adduct Derived from the Interaction of CH_2Cl_2 with an Alkylzinc Complex

Keywords: Zinc / Alkoxides / Chelates / O,S ligand / Solvent effects

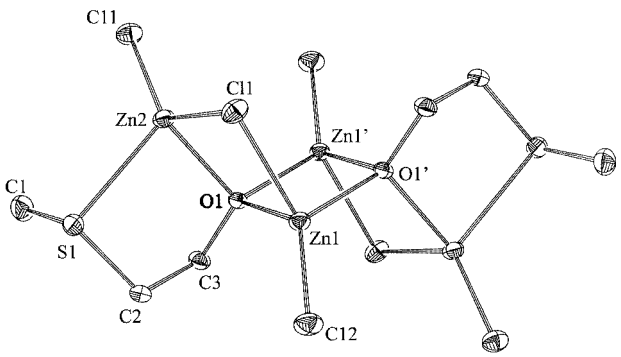

FULL PAPERS

2757 **C. Bustos, B. Hasenknopf, R. Thouvenot, J. Vaissermann, A. Proust, P. Gouzerh***

Lindqvist-Type (Aryldiazenido)polyoxomolybdates − Synthesis, and Structural and Spectroscopic Characterization of Compounds of the Type $(n\mathrm{Bu_4N})_3[Mo_6O_{18}(N_2Ar)]$

Keywords: Molybdenum / NMR spectroscopy / Polyoxometalates / N ligands

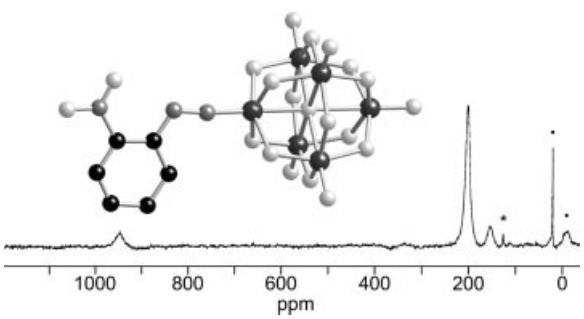

2767 **A. L. Rheingold, L. M. Liable-Sands, J. A. Golan, S. Trofimenko***

Remote Rotamer Control: The Effect of a 4-*tert*-Butyl Group on the Coordination Chemistry of Tp^R Ligands

Keywords: Scorpionates / Cobalt / Rotamer control / Borates / N ligands

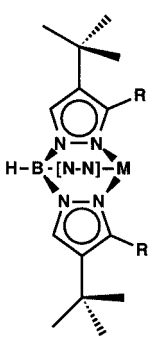

-[N-N]- is the third, hidden, 3-R-4-(*tert*-butyl)pyrazolyl ring

R = H, isopropyl, *p*-tolyl

2774 **L. Chouai, F. Wu, Y. Jang, R. P. Thummel***

Pyrene-Bridged Bis(phenanthroline) Ligands and Their Dinuclear Ruthenium(II) Complexes

Keywords: Ruthenium / Bridging ligands / Pyrene / Phenanthroline

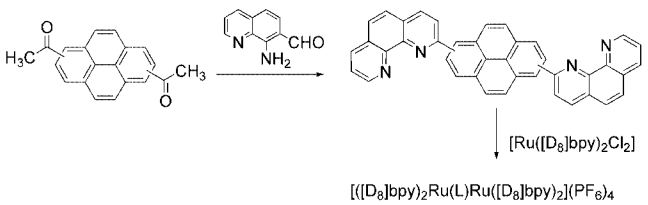

2783 **D. Görz, H. Pritzkow, W. Siebert***

Monomeric 1-Borylimidazoles: Syntheses, Structure and Reactivity of 1-[Bis(diisopropylamino)-boryl]imidazoles

Keywords: Boranes / Imidazoles / Donor-acceptor interaction / Metal complexes

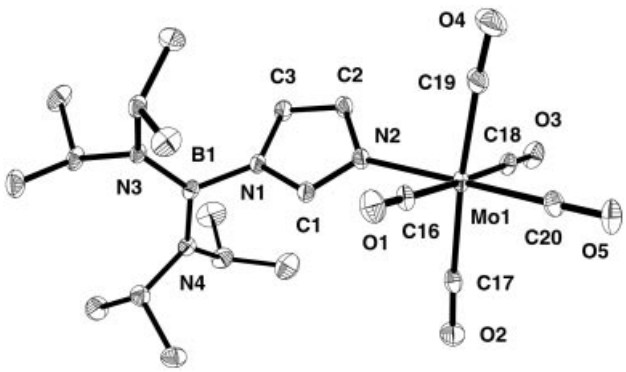

2790 **J. C. Casas, A. Castiñeiras, F. Condori, M. D. Couce, U. Russo, A. Sánchez, J. Sordo,* J. M. Varela**

Structural Characterization of *N*-Methylpyridoxine (MePN; PN = Vitamin B_6) and Its Diorganotin Complexes $[SnR_2(MePN\text{-}H)]I$ (R = Me, Et, Bu and Ph)

Keywords: Vitamins / Tin / IR spectroscopy / Mössbauer spectroscopy / NMR spectroscopy

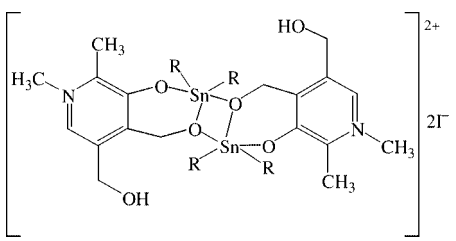

2798 **J. van den Broeke, M. Stam, M. Lutz, H. Kooijman, A. L. Spek, B.-J. Deelman,* G. van Koten**

Designing Ionic Liquids: 1-Butyl-3-Methylimidazolium Cations with Substituted Tetraphenylborate Counterions

Keywords: Ionic liquids / Cations / Anions / X-ray diffraction / Hydrogen bonds

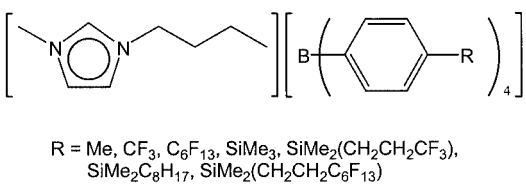

2812 **S. K. Dutta, D. Gan, M. W. Perkovic***

Allosteric Manipulation of Photoexcited State Relaxation in a Series of $Ru^{II}(bpy)_2$(bipyridine–crown ethers)

Keywords: Luminescence / Sensors / Photophysics / Lead

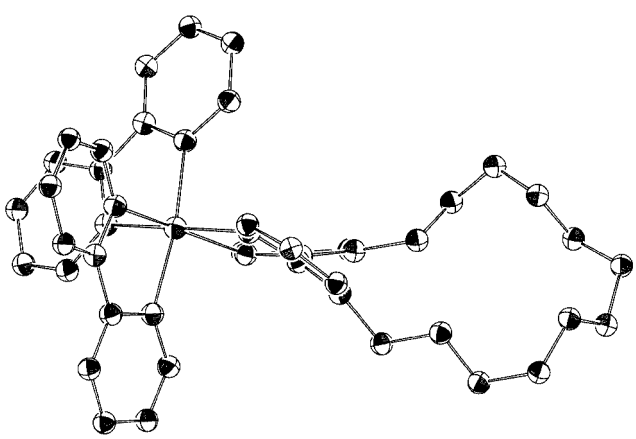

 © 2003 Wiley-VCH Verlag GmbH & Co. KGaA, Weinheim

2820 **S. Mourgues, D. Serra, F. Lamy, S. Vincendeau, J.-C. Daran, E. Manoury,* M. Gouygou***

Chiral [(Dialkylamino)methyl](phospholyl)ferrocene Ligands as a New Class of 1,2-Disubstituted Ferrocene Ligands

Keywords: Ferrocenes / Phospholes / N,P ligands / Asymmetric catalysis

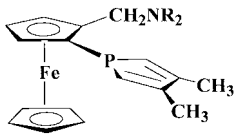

2827 **M. B. Dinger, J. C. Mol***

Degradation of the Second-Generation Grubbs Metathesis Catalyst with Primary Alcohols and Oxygen − Isomerization and Hydrogenation Activities of Monocarbonyl Complexes

Keywords: Ruthenium / Metathesis / Carbene ligands / Alcohols / Isomerization / Hydrogenation

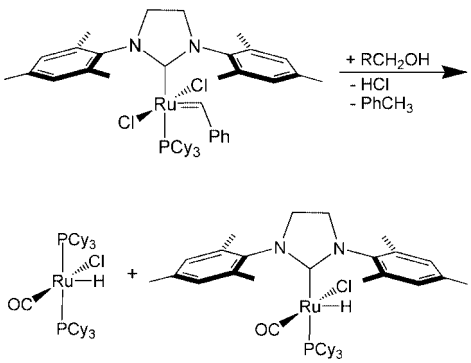

2834 **J.-M. Siaugue, A. Favre-Réguillon, F. Dioury, G. Plancque, J. Foos, C. Madic, C. Moulin, A. Guy***

Effect of Mixed Pendant Groups on the Solution Properties of 12-Membered Azapyridinomacrocycles: Evaluation of the Protonation Constants and the Stability Constants of the Europium(III) Complexes

Keywords: Macrocyclic ligands / Protonations / Stability constants / Europium / Luminescence

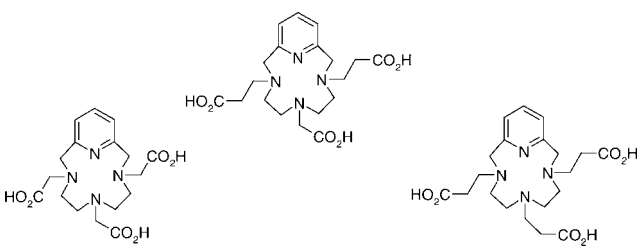

2839 **M. J. Martínez-Lope, J. A. Alonso,* M. T. Casais**

Synthesis, Crystal and Magnetic Structure of the Double Perovskites A_2NiMoO_6 (A = Sr, Ba): A Neutron Diffraction Study

Keywords: Perovskites / Neutron diffraction / Magnetic properties / Nickel

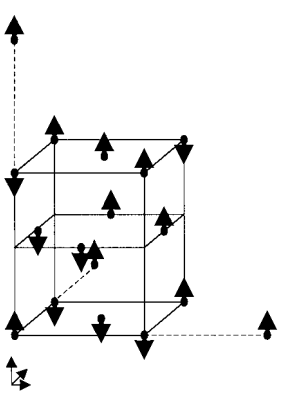

 © 2003 Wiley-VCH Verlag GmbH & Co. KGaA, Weinheim

2845 **G. Albertin,* S. Antoniutti, S. Beraldo, F. Chimisso**

Preparation of Hydroxylamine Complexes of Ruthenium(II), Osmium(II) and Iridium(III)

Keywords: Hydroxylamines / N ligands / P ligands / Ruthenium / Osmium / Iridium

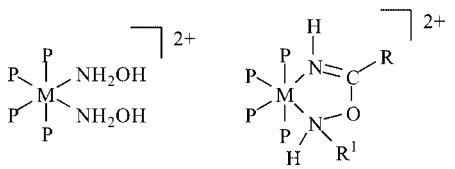

2855 **G. Albertin,* S. Antoniutti, M. T. Giorgi**

Preparation and Reactivity of Hydrazine Complexes of Rhenium: Synthesis of 1,2-Diazene (NH=NH) and Methyleneimine (CH_2=NH) Derivatives

Keywords: Hydrazine / N ligands / Oxidation / Rhenium

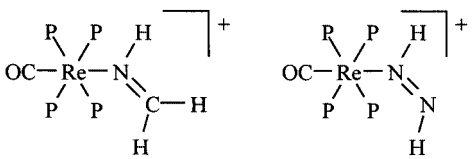

2867 **C.-D. Wu, C.-Z. Lu,* H.-H. Zhang, J.-S. Huang**

Synthesis, Crystal Structure and Characterization of a Novel Three-Dimensional Polymer: $[Cu_4V_2(OH)_2O_8]$

Keywords: Hydrothermal synthesis / Oxo ligands / Vanadium / Copper / TGA

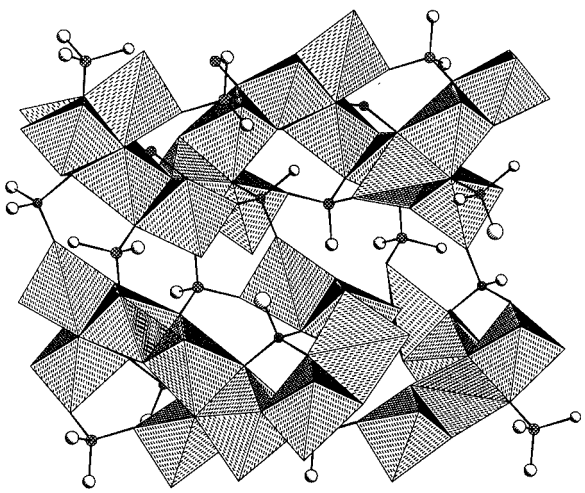

2872 **C. Ma, C. Chen, Q. Liu,* F. Chen, D. Liao, L. Li, L. Sun**

Great Framework Variation of Polymers in the Manganese(II) Maleate/α,α′-Diimine System: Syntheses, Structures, and Magneto-Structural Correlation

Keywords: Crystal structure / Maleic acid / Magnetic properties / Manganese / Structural topology

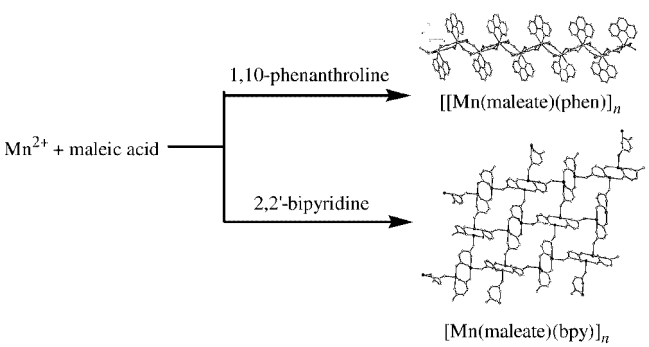

2880 **C. Faulmann,* E. Rivière, S. Dorbes, F. Senocq, E. Coronado, P. Cassoux**

Ferromagnetism in $[Mn(Cp^*)_2]^+$-Derived Complexes: the "Miraculous" Stacking in $[Mn(Cp^*)_2]$-$[Ni(dmit)_2]$

Keywords: Metallocenes / Magnetic properties / Manganese / S ligands

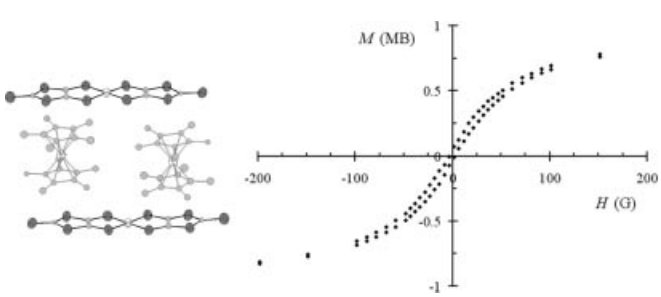

 © 2003 Wiley-VCH Verlag GmbH & Co. KGaA, Weinheim

P-Modular Homochiral Bis(phosphanes) with 1,2-Disubstituted Cyclopentane Backbones in Asymmetric Hydrogenation[‡]

Lutz Dahlenburg[a]

Keywords: Chirality / Asymmetric synthesis / Hydrogenation / Chelate phosphanes / Rhodium

The review surveys synthetic aspects of a class of bidentate phosphanes based on the *trans*-1,2-disubstituted cyclopentane framework and the application of such ligands in transition-metal-catalyzed enantioselective hydrogenation. In particular, we address the preparative potential of the isomerically pure multi-purpose P–H and P–Cl reagents (*R*,*R*)- and (*S*,*S*)-$C_5H_8(PX_2)_2$ (X = H, Cl), which can serve to construct a family of optically active bis(phosphanes) with structural components ("modules") that are easily and systematically interchanged. The so-designed chelate ligands allow access to rhodium catalysts with stereodiscriminating properties, depending on parameters such as (i) presence of P-substituents that are equal or pairwise different in steric demand, (ii) spatial orientation of such substituents as defined by the *endo*- and *exo*-chelate P–C–C–P and P–Rh–P–C torsion angles, and (iii) existence of *C*- and *P*-chirogenic stereoelements in matched (or mismatched) combination.

(© Wiley-VCH Verlag GmbH & Co. KGaA, 69451 Weinheim, Germany, 2003)

Introduction

The discovery of soluble transition metal complexes which catalyze enantioselective hydrogenation and oxidation reactions is amongst the most outstanding developments of organometallic chemistry.[2] The first homogeneously catalyzed hydrogenations of olefins were reported independently by Knowles[3] and Horner,[4] who demonstrated that the use of Wilkinson-type complexes, bearing resolved chiral monodentate phosphane ligands in place of PPh_3, resulted in the formation of enantiomerically enriched products, albeit in low optical yields. Shortly after, Kagan introduced the easily prepared (4*R*,5*R*) and (4*S*,5*S*) enantiomers of 4,5-bis[(diphenylphosphanyl)methyl]-2,2-dimethyl-1,3-dioxolane (diop) as the first C_2-symmetric chelating bis(phosphanes), which were found to control the chiral induction in rhodium-catalyzed hydrogenation reactions much more precisely than monophosphane ligands, particularly in the reduction of *N*-acylated dehydroamino acids and their esters.[5] As an equally important contribution, Knowles and co-workers subsequently established the commercial L-DOPA process using *P*-chirogenic (R_P,$R_{P'}$)-bis[(2-methoxyphenyl)phenylphosphanyl]ethane, (*R*,*R*)-DIPAMP, as a steering ligand.[2a,6] These developments gave rise to the immediate supposition that homochiral bis(phosphanes) as such are endowed with superior properties, allowing the bidentate species to control the stereochemical outcome of the rate-determining step in catalysis more precisely than a monodentate phosphane. As a result, research aimed at the improvement of chiral catalysts of low performance has predominantly been concentrated on the design of new and possibly optimized chelate phosphanes, of

[‡] Chiral Bis(phosphanes), XV. Part XIV: Ref.[1]

[a] Institut für Anorganische Chemie der Friedrich-Alexander-Universität Erlangen-Nürnberg,
Egerlandstraße 1, 91058 Erlangen, Germany
Fax: (internat.) + 49-9131/8527387
E-mail: dahlenburg@chemie.uni-erlangen.de

Lutz Dahlenburg was born in 1944 in Dresden. He received his Dr. rer. nat. in 1975 from the University of Hamburg with Prof. Reinhard Nast (topic: transition metal alkynyl complexes). In 1982 he finished his habilitation at the Institute of Inorganic and Applied Chemistry at the University of Hamburg (Prof. Heindirk tom Dieck), working in the field of metal-complex-mediated C−H activation. Since 1991, he holds a professorship in Inorganic Chemistry at the Friedrich-Alexander University of Erlangen-Nürnberg. He has authored more than 110 publications in reviewed journals. His main research interests are focused on the design of novel optically active chelate ligands, asymmetric catalysis (>C=C< hydrogenation, >C=O reduction), and heterolytic H_2 activation.

MICROREVIEWS: This feature introduces the readers to the authors' research through a concise overview of the selected topic. Reference to important work from others in the field is included.

which the DuPHOS-type *o*-phenylenebis(2,5-dialkylphospholanes)[7] and 2,2′-bis(diphenylphosphanyl)-1,1′-binaphthyl (BINAP)[2b] represent impressive examples. Note, however, that the generally accepted superiority of homochiral bidentate phosphanes in asymmetric hydrogenation has recently been challenged by the discovery that enantiopure monodentate P-ligands containing biaryl[8−13], spirobiindane,[14] oxaphosphinane[15] or carbohydrate[16] building blocks may likewise provide optical yields similar to those obtained with chelating phosphanes.[17]

Our approach to properly designed chiral hydrogenation catalysts has primarily been focussed on the construction of a class of optically active bidentate phosphanes with structural components (“modules” in Burk’s notation[7]) that can be systematically and easily interchanged in order to adapt the catalyst to a given purpose in the best possible fashion. Due to their “modular nature”[7] the so-defined ligands should be particularly suitable for adjusting the reactivity and catalytic behavior of metal complexes by judiciously selecting and changing parameters such as: (i) sets of donor groups, i.e., electronically different P−C-, P−N- or P−O-bonded substituents on the phosphorus atom; (ii) structural motifs, e.g., *P*- and/or *C*-chirality in, and steric demand of, substituent groups of that kind; (iii) torsion angles within the chelate framework, which in turn will influence the spatial orientation of selected parts of the ligand; and (iv) chelate bite angles, if variations of the backbone structure are also considered. Use of such ligands in transition-metal-mediated asymmetric catalysis can give insight into the relations and regularities existing between the performance of the catalytic system and the stereoelectronic characteristics of the metal−ligand template, provided viable synthetic schemes are available.

The traditional route to most of the widely used optically active bis(phosphanes), viz. those in which the phosphorus atoms bear two electron-withdrawing aryl groups, involves the alkylation of alkali metal diarylphosphides with disulfonates containing homochiral carbon backbones. The disadvantage of this protocol is that it cannot automatically be applied to the preparation of the more electron-rich *P*-alkylated analogues. Because of their high basicity, alkylated phosphide nucleophiles tend to engage in a number of troublesome side reactions to the effect that attempted displacement reactions using alkyl-substituted phosphide reagents will frequently result in products originating from metal−halogen exchange, P−P coupling and elimination[18] rather than substitution, especially when sterically hindered dialkylphosphides are used as nucleophiles.[18b] Previous work carried out in other laboratories has shown that these difficulties can be mastered either by the use of cyclic sulfates as substrates (particularly in displacement reactions employing relatively unhindered phosphide nucleophiles derived from primary phosphanes)[19] or, as an even more versatile method, by making use of less basic and, hence, less reactive phosphide−borane adducts.[20]

The key compounds of our synthetic strategy are the resolved enantiomers of bis(primary phosphanes), $H_2P^*\cap^*PH_2$, and bis(phosphonous dichlorides), $Cl_2P^*\cap^*PCl_2$, having their reactive $-PCl_2$ and $-PH_2$ functions supported on a rigid 1,2-*trans*-disubstituted cycloalkane backbone as represented, e.g., by the cyclopentane-based ligands $\mathbf{L^H}$ and $\mathbf{L^{Cl}}$ shown in the top row of Scheme 1. Their usefulness in the synthesis of optically active chelate phosphanes, to be discussed hereafter, is a result of the following features: First, the addition of P−H bonds across the >C=C< double bonds of different alkenes and cycloalkenes is likely to open a feasible route to various alkylated bis(secondary) and bis(tertiary) P_2 ligands with or without additional stereogenic centers at the phosphorus atom. Second, substitution reactions undergone by P−Cl functional phosphorus(III) compounds upon treatment with carbon, nitrogen or oxygen nucleophiles are among the most general and most easily accomplished coupling methods in organic chemistry. Finally, the possibility of incorporating virtually any other P−O-, P−N- or P−C-bonded residue into a homochiral bis(phosphane) framework should allow the preparation of a wide range of optically active chelate ligands having fine-tunable and, perhaps, rationally designable steric and electronic attributes.

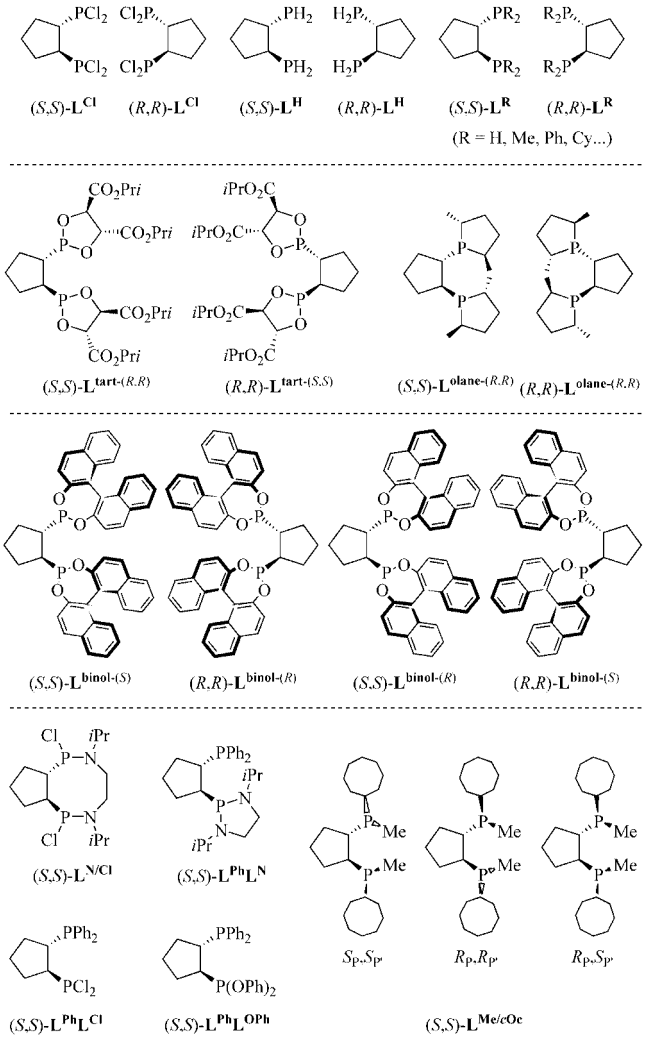

Scheme 1. Collection of ligands and abbreviations

 © 2003 Wiley-VCH Verlag GmbH & Co. KGaA, Weinheim

The Ligands

Resolution of the Enantiomers

Analogous to the preparation of $Cl_2PC_2H_4PCl_2$ from ethylene, white phosphorus, and phosphorus trichloride,[21] racemic $C_5H_8(PCl_2)_2$, *rac*-**L**^{Cl}, can be obtained easily by heating cyclopentene with P_4 and PCl_3 at 220 °C in an autoclave, as reported by Green et al. as early as 1983.[22a]

Treatment of the racemate with Grignard reagents RMgBr (R = Me, Ph) afforded (±)-$C_5H_8(PR_2)_2$, **L**^{Me} and **L**^{Ph}, as the first P−C-substituted derivatives.[22] Resolution of the isomeric mixture was originally achieved by reaction with $NiBr_2$ in dichloromethane giving [$NiBr_2$(**L**^{Ph})]·CH_2Cl_2. Upon separation from solution, the complex underwent spontaneous resolution to deposit a conglomerate of crystals which were separated by hand and treated with sodium cyanide to yield **L**^{Ph} as its (*R*,*R*) and (*S*,*S*) stereoisomers.[22a]

We entered the field in 1995 in an early attempt to accomplish stereodiscriminative C−H activation by treating 2,2′-disubstituted biphenyls and binaphthyls as racemates with the (+)- and (−)-enantiomers of the (hydrido)neopentylplatinum complex [{$C_5H_8(PCy_2)_2$}Pt(H)CH_2CMe_3] bearing the bis(dicyclohexylphosphane) ligand $C_5H_8(PCy_2)_2$ (**L**^{Cy}) in the optically active form.[23] For this particular bis(phosphane), effective resolution was brought about according to the strategy previously developed by Brunner and Pieronczyk for the separation of the stereoisomers of 2,3-bis(diphenylphosphanyl)norbornene (NORPHOS),[24] i.e., reduction with Ph_2SiH_2 of the *P*,*P*′-dioxides (+)- and (−)-C_5H_8{P(O)Cy_2}$_2$, which themselves were isolated by resolving their racemic mixture with (+)-di-*O*-benzoyltartaric acid.[23]

As an important breakthrough in the resolution of the enantiomers of the bis(phosphonous dichloride) **L**^{Cl}, we found that the cyclopentane-1,2-diyl[bis(1′,3′,2′-dioxaphospholane] **L**^{tart} resulting from the reaction of *rac*-**L**^{Cl} with (2*R*,3*R*)-(+)-diisopropyl tartrate (Scheme 2) could be crystallized from the isomeric mixture as a single (1*S*,2*S*,4′*R*,5′*R*) diastereomer, (*S*,*S*)-**L**$^{tart\text{-}(R,R)}$.[25] As expected, the (1*R*,2*R*,4′*S*,5′*S*) enantiomer, (*R*,*R*)-**L**$^{tart\text{-}(S,S)}$, was isolated, isomerically pure, from a similar reaction employing (2*S*,3*S*)-(−)-diisopropyl tartrate as the diol component.[26a] Reduction, with $LiAlH_4$, of these two phosphonites gave the bis(primary phosphane) **L**^{H} as resolved (*S*,*S*) and (*R*,*R*) enantiomers, and subsequent oxidation of the P−H bonds with bis(trichloromethyl)carbonate ("triphosgene") allowed for the routine preparation of either antipode of the multi-purpose P−Cl reagent **L**^{Cl}.[25,26b,27,28a]

In an alternative approach to the optically pure isomers of **L**^{Cl}, Brunner and co-workers preferred to hydrolyze the phosphonite enantiomers (*S*,*S*)-**L**$^{tart\text{-}(R,R)}$ and (*R*,*R*)-**L**$^{tart\text{-}(S,S)}$ to the free phosphinic acids, from which the resolved bis(phosphonous dichloride) enantiomers were recovered by chlorination with PCl_3 (Scheme 3).[29]

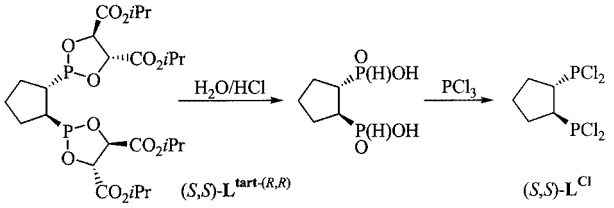

Scheme 3. Preparation of the optically pure $C_5H_8(PCl_2)_2$ enantiomers according to Brunner[29]

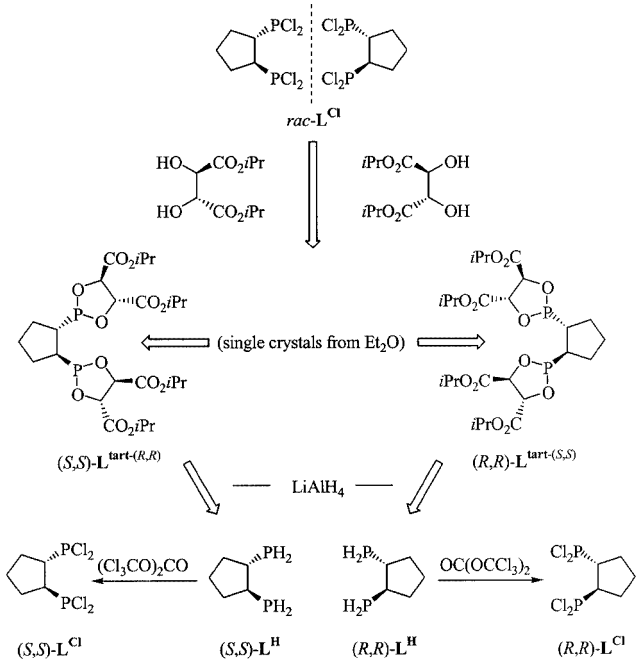

Scheme 2. Resolution of *rac*-$C_5H_8(PCl_2)_2$ into (*R*,*R*)- and (*S*,*S*)-$C_5H_8(PCl_2)_2$ via (*R*,*R*)- and (*S*,*S*)-$C_5H_8(PH_2)_2$[25,26b,27,28a]

Representative Examples

From the abundance of optically pure diphosphorus ligands containing various P−C-, P−N- and P−O-bonded donor groups that have been prepared by treating **L**^{Cl}, as either mirror image isomer, with alcohols, phenols, diols, secondary amines, Grignard reagents, or organolithium compounds,[26b,27−32] we will outline only selected cases that serve to illuminate the synthetic potential of the isomerically pure PCl_2-functional starting materials.

By combining the two enantiomers with both (*R*)-(+)- and (*S*)-(−)-1,1′-bi(2-naphthol) we were able to isolate the four diastereomeric forms of the cyclic bis(phosphonous acid diester) **L**^{binol} depicted in Scheme 1, which offered the opportunity to study matching and mismatching effects on the outcome of asymmetric hydrogenation reactions (vide infra), as caused by the mutual interaction of the different stereogenic elements in such steering ligands.[32]

The Brunner group described both divergent and convergent reaction sequences leading from enantiomers (*S*,*S*)-**L**^{Cl} and (*R*,*R*)-**L**^{Cl} to a second generation of optically active dendritically expanded bis(phosphanes).[29] These contained their stereochemically uniform dendritic extensions

 © 2003 Wiley-VCH Verlag GmbH & Co. KGaA, Weinheim

supported on a homochiral 1,2-disubstituted cycloalkane framework as defined by the phosphanes under discussion rather than on achiral 1,2-ethylene- or *ortho*-phenylene linkages as were originally used for optically active expanded P_2 ligands.[33] In the divergent synthetic approach, the enantiomerically pure $\mathbf{L^{Cl}}$ starting material was first coupled to branched aryllithium building blocks bearing acetal-protected formyl functions. Following deprotection of the acetals, multiple homochiral units were then introduced into the periphery of the expanded molecules by condensation of the aldehyde groups with different optically active amines and amino alcohols to afford branched ligands of the "$\mathbf{L^{aldimine}}$" type, as shown in Scheme 4. The alternative convergent strategy made use of pre-built branched aromatic bromides bearing (−)-borneol groups attached as benzylic ethers. Metallation followed by reaction with (*S*,*S*)-$\mathbf{L^{Cl}}$ and (*R*,*R*)-$\mathbf{L^{Cl}}$, respectively, produced the corresponding expanded "octaborneol-bis(phosphane)" ligand $\mathbf{L^{born}}$ depicted in Scheme 5 as either of the two possible diastereomers.

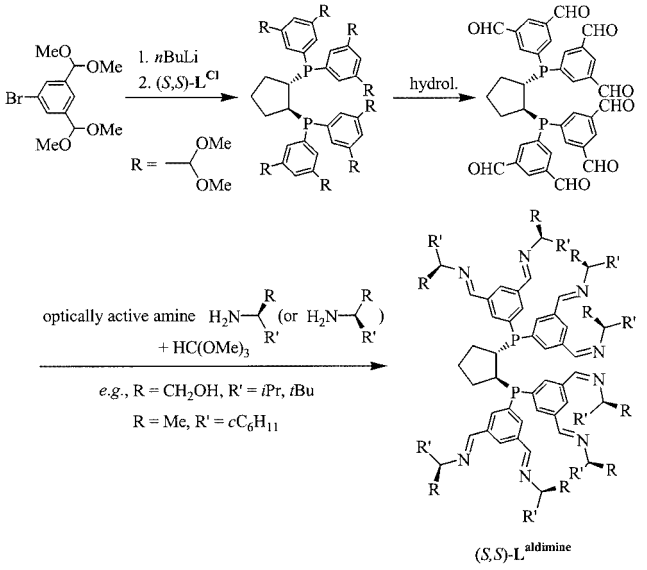

Scheme 4. Divergent approach to dendritically expanded bis(phosphanes)[29]

Dissymmetric P_2 ligands such as phosphane-phosphites[34] or bis(phosphanes) bearing different donor groups[35,36] have attracted considerable attention in homogeneous catalysis, in particular because of the impressive performance of their rhodium complexes as carbonylation and hydrogenation catalysts. Bis(phosphanes) with C_1 symmetry of the type $Ar_2PC_2H_4PAr'_2$ have previously been prepared either by base-catalyzed addition of a diarylphosphane to a suitable diarylvinylphosphane[35a] or by combining the phosphane-phosphonous dichloride $Ph_2PC_2H_4PCl_2$ with an appropriate Grignard or organolithium reagent.[35b] Analogous key intermediates having a rigid 1,2-disubstituted cyclopentane backbone rather than a flexible ethylene linkage, $C_5H_8(PPh_2)(PCl_2)$, were obtained as pure (*S*,*S*) and (*R*,*R*) enantiomers by the reaction sequence outlined in

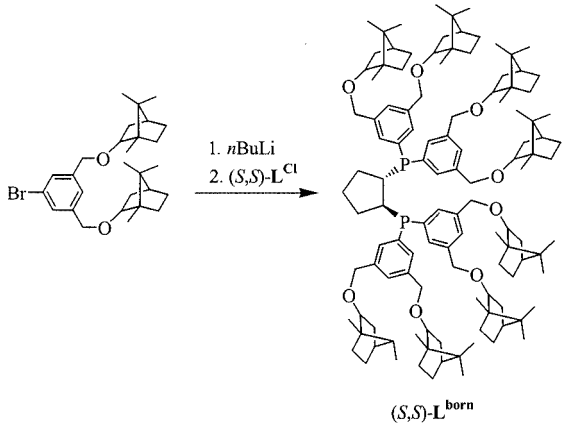

Scheme 5. Convergent approach to a dendritically expanded "octaborneol-bis(phosphane)"[29]

Scheme 6. The exclusive formation of the still C_2-symmetric initial product containing an eight-membered perhydro-1,6,2,5-diazadiphosphocine ring, $\mathbf{L^{N/Cl}}$ [$\delta(^{31}P)$ = 161.4 (s) ppm], was unexpected as was its subsequent reaction with phenylmagnesium bromide yielding the now C_1-symmetric $C_5H_8(PPh_2)\{P[N(iPr)CH_2]_2\text{-}c\}$ ($\mathbf{L^{Ph}L^{N}}$) {$\delta(^{31}P)$ = 5.7, 115.6 [both d, J(PP) = 9.3 Hz] ppm} − probably as a result of nucleophilically induced ring contraction. Cleavage of the P−N bonds with HCl proceeded smoothly to afford the desired dissymmetric phosphane-phosphonous dichloride 1,2-$C_5H_8(PPh_2)(PCl_2)$ ($\mathbf{L^{Ph}L^{Cl}}$) {$\delta(^{31}P)$ = 9.5, 211.8 [both d, J(PP) = 13.0 Hz] ppm}, which similar to 1,2-$C_5H_8(PCl_2)_2$ proved to be a convenient starting material for further derivatization, e.g., to $C_5H_8(PPh_2)_2\{P(OPh)_2\}$ ($\mathbf{L^{Ph}L^{OPh}}$).[31]

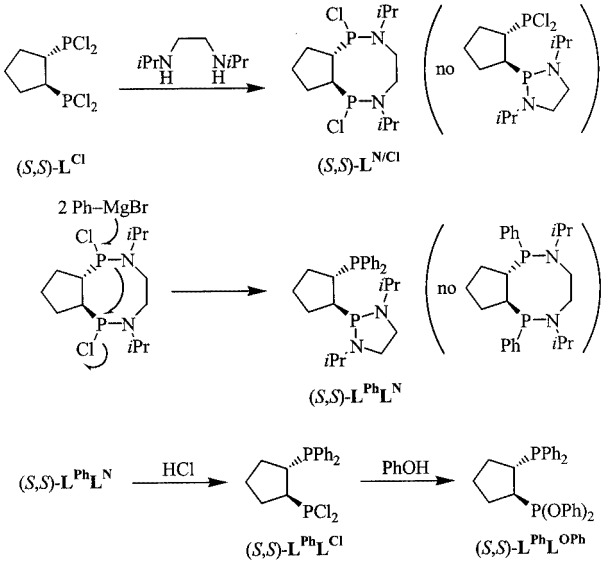

Scheme 6. Dissymmetric cyclopentane-based *P*,*P*′ ligands from C_2-symmetric $C_5H_8(PCl_2)_2$[31]

The more important diphosphorus ligands derived from the resolved bis(primary phosphane) $\mathbf{L^{H}}$ include the diastereomeric 1,2-bis(phospholano)cyclopentanes (*S*,*S*)- and

 © 2003 Wiley-VCH Verlag GmbH & Co. KGaA, Weinheim

(*R*,*R*)-$C_5H_8\{P[(R)\text{-}CH(Me)CH_2]_2\text{-}c\}_2$ [$\mathbf{L}^{\mathbf{olane}\text{-}(R,R)}$], described by Pringle et al.,[37] and the stereoisomers of the *C*- and *P*-chirogenic bis(phosphanes) $C_5H_8\{P(Me)R\}_2$ ($\mathbf{L}^{\mathbf{Me/R}}$), prepared in our laboratory.[32,38] The former were constructed in order to demonstrate how the enantioselectivity in asymmetric hydrogenation reactions of a rhodium catalyst which bears the flexible ethylene-bridged (*R*,*R*)-bis(phospholano)ethane ligand $1,2\text{-}C_2H_4\{P[(R)\text{-}CH(Me)CH_2]_2\text{-}c\}_2$ and, hence, exists in solution as an equilibrium mixture of interconverting λ and δ chelate conformers, can be rationally improved by placing an inflexible carbon skeleton between the two phosphorus atoms (vide infra). Similar to other bis(phosphanes) containing 2,5-dialkylphospholane building blocks, the two diastereomeric [$\mathbf{L}^{\mathbf{olane}\text{-}(R,R)}$] ligands resulted from consecutive treatment of the pertinent $\mathbf{L}^{\mathbf{H}}$ enantiomer with *n*BuLi (2 equiv.), followed by the required 1,4-diol cyclic sulfate and another 2 equiv. of butyllithium as summarized by Scheme 7.[37]

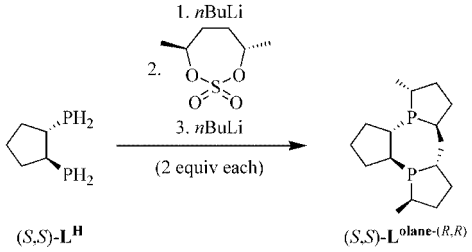

Scheme 7. Synthesis of bis(phospholane) ligands with cyclopentane skeletons[37]

In the first step of the synthesis leading to the *C*,*P*-chirogenic bis(phosphanes) $\mathbf{L}^{\mathbf{Me/R}}$, which are to be regarded as conformationally rigid counterparts of Imamoto's "(S_P,$S_{P'}$)-bisP*" ligands $1,2\text{-}C_2H_4\{(S)\text{-}P(Me)R\}_2$ (R = *i*Pr, *t*Bu, Et_3C, cC_5H_9, cC_6H_{11}, $cC_6H_{10}Me$, 1-adamantyl),[39] a radical-initiated addition of the $-PH_2$ functions of optically pure $\mathbf{L}^{\mathbf{H}}$, across the carbon−carbon double bonds of cycloalkenes C_nH_{2n-2} (n = 5−8), was employed as a method of preparation for the bis(secondary phosphanes) $C_5H_8\{P(H)R\}_2$, where R = cC_5H_9, cC_6H_{11}, cC_7H_{13}, or cC_8H_{15}.[38a]

As exemplified in Scheme 8 for the product obtained with cyclooctene ($\mathbf{L}^{\mathbf{H/cOc}}$), formation of higher alkylated byproducts originating from consecutive P−H/>C=C< addition steps did not occur. Although the dialkylated bis(phosphanes) were formed without any notable diastereoselectivity and, hence, were isolated as more or less statistical mixtures of their (R_P,$R_{P'}$), (R_P,$S_{P'}$) [= (S_P,$R_{P'}$)], and (S_P,$S_{P'}$) diastereomers, separation of these stereoisomers was feasible by further derivatization and subsequent metal complex formation.[32,38] Thus, treatment of the isomeric mixtures with alkyllithium compounds, followed by alkylation with methyl iodide, caused the diastereomeric distributions to change in favor of the (*S*,*S*)-$C_5H_8\{(S)\text{-}P(Me)C_8H_{15}c\}_2$ and (*R*,*R*)-$C_5H_8\{(R)\text{-}P(Me)C_8H_{15}c\}_2$ stereoisomers,[38a] the rhodium(I) complexes of which − $[Rh\{(S,S)\text{-}C_5H_8[(R)\text{-}P(Me)C_8H_{15}c]_2\}(COD)]O_3SCF_3$ and $[Rh\{(R,R)\text{-}C_5H_8[(S)\text{-}P(Me)C_8H_{15}c]_2\}(COD)]O_3SCF_3$, respectively − were isolated as diastereomerically pure crystals by precipitation from a THF/diethyl ether solvent mixture.[32,38b] Conversely, successive combination of the bis(secondary phosphane) isomers $\mathbf{L}^{\mathbf{H/cOc}}$ first with "triphosgene" (vide supra) and then with methylmagnesium bromide led to an enrichment of the (*S*,*S*)-$C_5H_8\{(R)\text{-}P(Me)C_8H_{15}c\}_2$ and (*R*,*R*)-$C_5H_8\{(S)\text{-}P(Me)C_8H_{15}c\}_2$ stereoisomers, which in turn were treated with $[Rh(COD)_2]O_3SCF_3$ to furnish diastereomerically pure $[Rh\{(S,S)\text{-}C_5H_8[(S)\text{-}P(Me)C_8H_{15}c]_2\}(COD)]O_3SCF_3$ and $[Rh\{(R,R)\text{-}C_5H_8[(R)\text{-}P(Me)C_8H_{15}c]_2\}(COD)]O_3SCF_3$, following chromatographic workup (Scheme 8).[32]

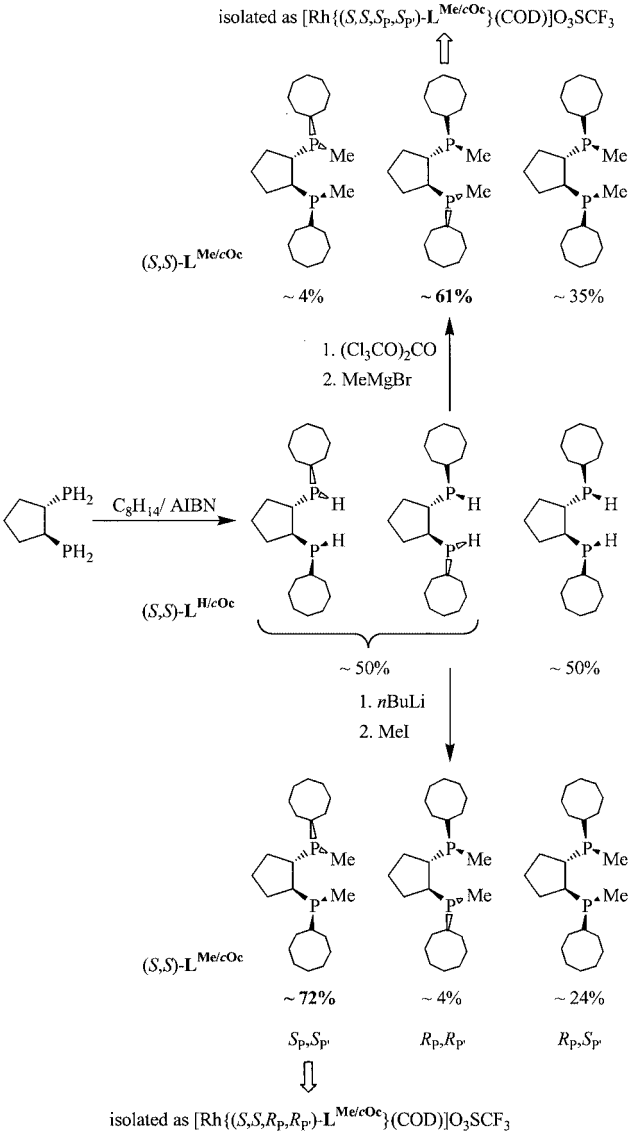

Scheme 8. Conversion of $C_5H_8(PH_2)_2$ to *C*,*P*-chirogenic bisphosphanes[32,38]

 © 2003 Wiley-VCH Verlag GmbH & Co. KGaA, Weinheim

Catalytic Hydrogenation: Results of Comparative Studies

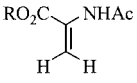

R = H: **acrH**; R = Me: **acrMe**

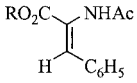

R = H: **cinH**; R = Me: **cinMe**

One of the most useful features of the ligands derived from the $\mathbf{L^H}$ and $\mathbf{L^{Cl}}$ precursors is their adjustability which enables the possibility of influencing the enantioselectivity by varying the substituents on the phosphorus atoms. Many of these optically active ligands have therefore been examined by us and others for their utility in Rh-catalyzed asymmetric hydrogenations of standard enamide substrates such as (acetylamino)acrylic (**acrH**) and -cinnamic (**cinH**) acid and their corresponding methyl esters **acrMe** and **cinMe**, respectively. The main purpose of these investigations was to reveal potential correlations between the outcome of the hydrogenation reactions and structural properties of the metal complexes in order to elucidate the factors governing the stereoselectivity of the catalysts. The results of these studies are collected in Table 1. For the sake of comparison, the catalytic results obtained with Rh catalysts derived from structurally related P_2 ligands[29,37,39a,39d,40] are also included in Table 1.

A first conclusion that can be drawn from Table 1 is that the catalytic activity of the different $[Rh(\mathbf{L})(COD)]^+$ complexes, as judged from the reaction times needed for full substrate conversion, increases with increasing electron-richness of the phosphorus atoms: $\mathbf{L^{binol}} << \mathbf{L^{Ph}} < \mathbf{L^{Me/cOc}}$. One further conclusion to be drawn for hydrogenations using either unsubstituted $\mathbf{L^{Ph}}$ steering ligands or dendritically expanded homologues with different multiple homochiral units in the periphery is that the generally high enantioselectivity for the (*S*)- or (*R*)-products displayed by the rhodium catalysts summarized under Entries **2** and **3** in Table 1 is governed by the (*R*,*R*) or (*S*,*S*) configuration and, respectively, λ or δ conformation of the chiral cyclopentane backbone rather than being controlled by the chiral dendritic expansions.[29] The rhodium chelate complexes of these ligands thus follow the empirical λ/δ rule predicting that a λ chelate will give the (*S*) enantiomer, while a δ chelate will produce the (*R*) enantiomer.[41] While this holds true for all ligands bearing two aryl substituents, the 1,1′-bi(2-naphthol)-derived bis(phosphonous acid diesters) $\mathbf{L^{binol}}$ reveal such a strong influence of the axially chiral binaphthoxy groups on the orientation of induction that their sense of chirality can override the contribution of the chiral ligand core. Thus, the catalyst complexes bearing (*R*,*R*)-

Table 1. Enantioselective hydrogenations of standard enamide substrates with [Rh(ligand)(diolefin)]X precatalysts

Entry[a]	Ligand	acrH *t* [h]	acrH *ee* [%]	acrMe *t* [h]	acrMe *ee* [%]	cinH *t* [h]	cinH *ee* [%]	cinMe *t* [h]	cinMe *ee* [%]
1a	(*S*,*S*)-$\mathbf{L^{binol\text{-}(S)}}$	16	96 (*R*)	16	89 (*R*)	16	78 (*R*)	16	85 (*R*)
1b	(*R*,*R*)-$\mathbf{L^{binol\text{-}(R)}}$	16	92 (*S*)	16	86 (*S*)	16	77 (*S*)	16	85 (*S*)
1c	(*S*,*S*)-$\mathbf{L^{binol\text{-}(R)}}$	16	28 (*S*)	16	29 (*S*)	16	24 (*S*)	16	36 (*S*)
1d	(*R*,*R*)-$\mathbf{L^{binol\text{-}(S)}}$	16	27 (*R*)		not det.	16	20 (*R*)	16	36 (*R*)
2a	(*S*,*S*)-$\mathbf{L^{Ph}}$[b]	4	91 (*R*)	4	85 (*R*)	2	93 (*R*)	2	91 (*R*)
2b	(*R*,*R*)-$\mathbf{L^{Ph}}$	4	92 (*S*)	4	86 (*S*)	2	95 (*S*)	2	91 (*S*)
3a	(*S*,*S*)-$\mathbf{L^{born}}$[c]						94 (*R*)		
3b	(*R*,*R*)-$\mathbf{L^{born}}$						96 (*S*)		
3c	(*S*,*S*)-$\mathbf{L^{aldimine}}$ [c]						93−96 (*R*)		
4a	(*S*,*S*)-$\mathbf{L^{olane\text{-}(R,R)}}$				95 (*R*)				98 (*R*)
4b	(*R*,*R*)-$\mathbf{L^{olane\text{-}(R,R)}}$				73 (*R*)				77 (*R*)
5	(*R*,*R*)-Me-BPE[d]			1	91 (*R*)			1	85 (*R*)
6a	(S,S,S_P,$S_{P'}$)-$\mathbf{L^{Me/cOc}}$[e]	1.5	21 (*S*)	1.5	29 (*S*)	2	26 (*S*)	2	35 (*S*)
6b	(R,R,R_P,$R_{P'}$)-$\mathbf{L^{Me/cOc}}$	1.5	23 (*R*)	1.5	28 (*R*)	2	28 (*R*)	2	34 (*R*)
6c	(S,S,R_P,$R_{P'}$)-$\mathbf{L^{Me/cOc}}$	1.5	90 (*R*)	1.5	82 (*R*)	2	74 (*R*)	2	86 (*R*)
6d	(R,R,S_P,$S_{P'}$)-$\mathbf{L^{Me/cOc}}$	1.5	90 (*S*)	1.5	83 (*S*)	2	73 (*S*)	2	86 (*S*)
7a	(S_P,$S_{P'}$)-*t*Bu-bisP*[e]			1	98 (*R*)	1	98 (*R*)	1	>99 (*R*)
7b	(S_P,$S_{P'}$)-1-Ad-bisP*			1	>99 (*R*)			1	>99 (*R*)
7c	(S_P,$S_{P'}$)-*c*C_5H_9-bisP*	1	33 (*R*)	1	80 (*R*)			1	43 (*R*)
8a	(R,R,R_P,$R_{P'}$)-pyrL$^{Me/Ph}$[e]						64 (*S*)		
8b	(R,R,S_P,$S_{P'}$)-pyrL$^{Me/Ph}$						34 (*S*)		
8c	(R,R,R_P,$S_{P'}$)-pyrL$^{Me/Ph}$						21 (*S*)		

[a] Diolefin = 1,5-cyclooctadiene (Entries **1**,[32] **2**,[32] **3**,[29] **4**,[37] **5**,[19a,19c] **6**,[32,38b] and **8**[40]) or norbornadiene (Entry **7**[39a,39d]); $X^- = Cl^-$ {Entry **3**: in situ catalysts generated from $[Rh(\mu\text{-}Cl)(COD)]_2$ and bis(phosphane) ligands}, BF_4^- (Entries **4**, **7**, and **8**) or $F_3CSO_3^-$ (Entries **1**, **2**, **5**, and **6**). Experimental conditions: methanol or ethanol solvents (the latter only for Entry **7c** with **acrH** or **acrMe** as substrates); ambient temperature; initial H_2 pressure either ambient (Entries **1**−**3**, **6**, and **8**) or ca. 2 bar (Entries **4**, **5**, and **7**); typical Rh/substrate ratios of about $1-2 \times 10^{-3}$ (Entries **4**, **5**, and **7**), $3-5 \times 10^{-3}$ (Entries **1** and **2**), and 10^{-2} (Entries **3**, **6**, and **8**), respectively. Reaction times given for 100% conversion; *ee* values of Entries **3**, **4**, and **8** (no reaction times detailed in the original literature) likewise determined after complete hydrogenation. [b] For the hydrogenation of (benzoylamino)acrylic and -cinnamic acid using an in situ catalyst composed of $[Rh(\mu\text{-}Cl)(COD)]_2$ and (*S*,*S*)-$\mathbf{L^{Ph}}$ in methanol, Green et al. reported *ee* values of 100 ± 2%.[22a] [c] See Schemes 4 and 5.[29] [d] 1,2-C_2H_4{P-[(*R*)-CH(Me)CH_2]$_2$-*c*}$_2$. [e] ($R_{P(P')}$) and ($S_{P(P')}$) denote the configuration at the phosphorus atom for the *free* ligands, which is inverted upon coordination to the rhodium atom as a consequence of the CIP sequence rules; see also Table 2 and Scheme 8.

 © 2003 Wiley-VCH Verlag GmbH & Co. KGaA, Weinheim

or (*S*,*S*)-$\mathbf{L}^{\mathbf{binol}\text{-}(R)}$ ligands invariably afforded hydrogenation products with (*S*) configuration (Entries **1b** and **1c**) whereas the (*R*) enantiomers predominated in the isomeric mixtures formed with the two diastereomeric Rh−$\mathbf{L}^{\mathbf{binol}\text{-}(S)}$ catalysts (**1a** and **1d**). From the results collected in Table 1 it is also clear that the optical yields achieved with (*S*,*S*)-$\mathbf{L}^{\mathbf{binol}\text{-}(S)}$ are by far superior to those obtained with (*S*,*S*)-$\mathbf{L}^{\mathbf{binol}\text{-}(R)}$ and that the (*R*,*R*)-$\mathbf{L}^{\mathbf{binol}\text{-}(R)}$ ligand is much more selective than its (*R*,*R*)-$\mathbf{L}^{\mathbf{binol}\text{-}(S)}$ diastereomer. Obviously, the (*R*,*R*)-$\mathbf{L}^{\mathbf{binol}\text{-}(R)}$ and (*S*,*S*)-$\mathbf{L}^{\mathbf{binol}\text{-}(S)}$ enantiomers represent the beneficial matched combination of stereochemical elements while the (*R*,*R*)-$\mathbf{L}^{\mathbf{binol}\text{-}(S)}$ and (*S*,*S*)-$\mathbf{L}^{\mathbf{binol}\text{-}(R)}$ forms must be looked at as the disadvantageous mismatched counterparts.[32]

Distinct matched−mismatched effects in enantioselective hydrogenation also occur for the >C=C< reductions catalyzed by the more electron-rich rhodium complexes possessing either the diastereomeric $\mathbf{L}^{\mathbf{olanc}}$ or the *C*,*P*-chirogenic $\mathbf{L}^{\mathbf{Me}/c\mathbf{Oc}}$ ligands of Entries **4**[37] and **6**.[32,38b]

The bis(phospholane) (*S*,*S*)-$\mathbf{L}^{\mathbf{olane}\text{-}(R,R)}$ clearly exhibits a stronger ability for chiral discrimination than its (*R*,*R*)-$\mathbf{L}^{\mathbf{olane}\text{-}(R,R)}$ stereoisomer. Interestingly, the enantiodiscriminating properties of the derived rhodium complex [Rh{(*S*,*S*)-$\mathbf{L}^{\mathbf{olane}\text{-}(R,R)}$}(COD)]$BF_4$ ("**Rh-4a**" hereafter) are also superior to those of the more flexible ethylene-bridged Rh−(*R*,*R*)-Me-BPE catalyst (Entry **5**[19a,19c]), which in turn is seen to be superior to [Rh{(*R*,*R*)-$\mathbf{L}^{\mathbf{olane}\text{-}(R,R)}$}(COD)]$BF_4$ (**Rh-4b**), in spite of existing, in solution, as a labile mixture of readily interconverting λ and δ conformers; Scheme 9 (a).

On the one hand, these observations further corroborate the previously drawn conclusion that greater conformational rigidity of the backbones of bis(phospholane) chelate ligands will result in a more efficient transfer of chirality during Rh^I-catalyzed asymmetric hydrogenation.[19c] On the other hand, the finding that the Rh−(*S*,*S*)-$\mathbf{L}^{\mathbf{olane}\text{-}(R,R)}$ complex with δ backbone stereochemistry proved to be much more selective for the (*R*) products than the λ-Rh−(*R*,*R*)-$\mathbf{L}^{\mathbf{olane}\text{-}(R,R)}$ catalyst was unexpected:[37] So far, the heuristic stereochemical model used for the understanding of the origin of enantioselection by Rh−(*R*,*R*)-Me-DuPHOS and Rh−(*R*,*R*)-Me-BPE catalysts was based on the premise that two of the four equatorially aligned phospholane substituents adjacent to the phosphorus atoms effectively block the top left and bottom right "coordination quadrants"[6c] indicated on the left of Scheme 9 (b).[7,19c] In the more stable (less reactive) enamide adduct, the substrate should therefore be coordinated through its *si* face, the less favored (more reactive) adduct diastereomer being that in which the enamide is *re*-face-bound. Since Rh−DuPHOS catalysts have been confirmed both experimentally[19d] and theoretically[42b,42c,42d] to nicely reproduce the Halpern-Brown-type "anti-lock-and-key"[42] mechanistic behavior in which the major product enantiomer is formed by hydrogenation of the less favorably bonded enantioface,[43,44] both the excellent (*R*)-selectivity of the Rh−(*S*,*S*)-$\mathbf{L}^{\mathbf{olane}\text{-}(R,R)}$ complex and the somewhat lower (*R*)-discriminating ability of the Rh−(*R*,*R*)-$\mathbf{L}^{\mathbf{olane}\text{-}(R,R)}$ diastereomer are indicative of *si*-face binding of the substrate in the less stable adducts and, respectively, of *re*-face binding in the sterically favored

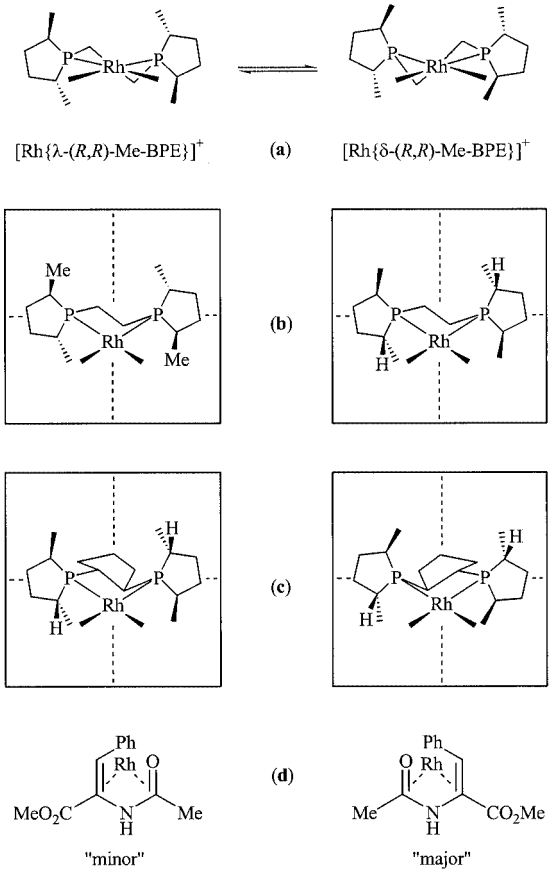

Scheme 9. (**a**): λ/δ equilibrium of Rh−(*R*,*R*)-Me-BPE catalysts; (**b**): quadrant-blocking in Rh−(*R*,*R*)-Me-BPE chelate complexes by equatorial methyl groups (left) or, alternatively, by axial hydrogen atoms (right); (**c**) and (**d**): quadrant-blocking in λ- and δ-shaped Rh−$\mathbf{L}^{\mathbf{olane}\text{-}(R,R)}$ complexes together with "minor" *si*- and "major" *re*-face binding of substrate enamides as proposed by Pringle[37]

intermediates. In sharp contrast to the original stereochemical model proposed for chelate complexes of bis(phospholane) ligands, Pringle et al. therefore concluded that it is the bottom left and top right quadrants which are more effectively blocked in the ground-state geometries of the two diastereomers than the quadrants left side up and right side down − actually, to a higher degree in matched δ-[Rh{(*S*,*S*)-$\mathbf{L}^{\mathbf{olane}\text{-}(R,R)}$}(COD)]$^+$ but to a lesser extent in mismatched λ-[Rh{(*R*,*R*)-$\mathbf{L}^{\mathbf{olane}\text{-}(R,R)}$}(COD)]$^+$. Indeed, crystal structures of two model complexes, δ-[PtI_2{(*S*,*S*)-$\mathbf{L}^{\mathbf{olane}\text{-}(R,R)}$}] (**Pt-4a**) and λ-[$PtI_2${(*R*,*R*)-$\mathbf{L}^{\mathbf{olane}\text{-}(R,R)}$}] (**Pt-4b**) confirmed that the equatorial methyl substituents of the phospholane rings shielding the top left and bottom right quadrants are ca. 0.5 Å closer to the iodo binding sites in the λ than in the δ conformer, whereas the axial α-hydrogen atoms occupying the quadrants left side down and right side up are ca. 0.3 Å closer to the other ligands in the δ than in the λ diastereomer. It was therefore proposed that it is the steric interaction of the enamide substrate with these hydrogen atoms which crucially contributes to the facially discriminating abilities of the catalyst complexes; Scheme 8 (c).[37] For a different interpretation, however, see below.

 © 2003 Wiley-VCH Verlag GmbH & Co. KGaA, Weinheim

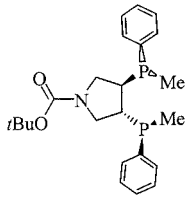

$R,R,R_P,R_{P'}$-pyrL$^{Me/Ph}$

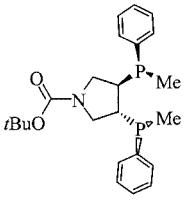

$R,R,S_P,S_{P'}$-pyrL$^{Me/Ph}$

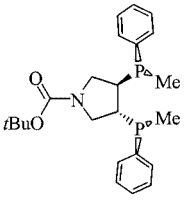

$R,R,R_P,S_{P'}$-pyrL$^{Me/Ph}$

With regard to the diastereomeric complexes bearing the four stereochemically different **L$^{Me/cOc}$** ligands, Entries **6a**−**d** of Table 1 make it clear that it is the bis(phosphanes) with opposite configuration at the carbon and phosphorus atoms (Note footnote[e] of Table 1!) that lead to the superior hydrogenation catalysts. Although less stereodiscriminating than Imamoto's catalysts with alkylated (S_P,$S_{P'}$)-bisP* ligands $C_2H_4\{(S)\text{-P(Me)R}\}_2$ having voluminous *P*-bound *tert*-butyl or 1-adamantyl groups in addition to the methyl residue (Entries **7a** and **7b**, Table 1),[39a,39d] the rhodium complexes of the two ($S,S,R_P,R_{P'}$)-**L$^{Me/cOc}$** and ($R,R,S_P,S_{P'}$)-**L$^{Me/cOc}$** enantiomers appear to perform better than those derived from (S_P,$S_{P'}$)-cC$_5$H$_9$-bisP* (Entry **7c**, Table 1), which has a cyclopentyl substituent roughly comparable in steric demand near the metal center to cyclooctyl. Also of interest is a comparison with Nagel's diastereomeric *N*-(*tert*-butoxycarbonyl)-3,4-bis[methyl(phenyl)phosphanyl]pyrrolidines ($R,R,R_P,R_{P'}$)-, ($R,R,S_P,S_{P'}$)-, and ($R,R,R_P,S_{P'}$)-pyrL$^{Me/Ph}$. Rhodium(I) chelate complexes of these ligands are λ-shaped as are Imamoto's Rh−bisP* catalysts; but unlike the latter, which yield (*R*) hydrogenation products[39a,39d] unless the enamide contains a very bulky α-substituent,[39c,39f] Nagel's catalysts induce the preferential formation of amino acids and esters as (*S*) enantiomers irrespective of the stereochemistry at the two phosphorus atoms; the different −P(Me)Ph configurations are only seen to modulate the extent of the enantiomeric excess (Entries **8a**−**c**, Table 1).[40] Thus, it is the configuration of the backbone carbon atoms that controls the sign of chiral induction imposed by the Rh−pyrL$^{Me/Ph}$ catalysts and, vice versa, it is the configuration at the phosphorus atom that outplays the influence of the carbon skeleton in hydrogenations catalyzed by Rh−bisP* complexes. In other words, while the Rh−pyrL$^{Me/Ph}$ catalysts obey the λ/δ rule (vide supra), this empirical rule is not valid for catalysts possessing the very successful electron-rich bisP* steering ligands![39b] Rhodium complexes derived from the four diastereomeric electron-rich **L$^{Me/cOc}$** bis(phosphanes) (Entries **6a**−**6d**, Table 1) and also from the more electron-poor Rh−**L^{binol}** complexes (Entries **1a**−**d**, Table 1), are intermediate in that the ligands showing the matched combination of stereoelements (Entries **1a**, **1b**, **6c**, **6d**, Table 1) follow the rule, whereas the mismatched catalysts (Entries **1c**, **1d**, **6a**, **6b**, Table 1) do not. It should be noted that the catalytic results obtained with Pringle's diastereomeric Rh−**L^{olane}** complexes **Rh-4a** and **Rh-4b** are akin: the matched δ-conformer **Rh-4a** provokes (*R*) stereoselection and thus conforms to the rule; mismatched λ-shaped **Rh-4b** similarly yields amino acids with (*R*) configuration and, hence, breaks the rule.

Although no structural data are currently at hand for metal complexes containing bis(phosphonites) of the **L^{binol}** type, substantial structural information exists on complexes possessing **L$^{Me/cOc}$** ligands and other bis(phosphanes) with P−C-bonded substituents, which strongly suggests that the very different enantioselectivities displayed by the Rh−**L$^{Me/cOc}$** systems with *like* or *unlike* stereochemistry at the donor and backbone atoms is causally related to slight differences in the spatial orientation of the bulky cycloalkyl rings in the diastereomeric complex cations.[32,38]

Molecular Structures of Complexes and Concluding Remarks on Enantioselectivity

In order to gain insight into correlations that may exist between the structural features displayed by the different

Table 2. Selected torsion angles and diene twists [°] in structurally characterized Rh and Pt complexes with optically active cyclopentane-bridged P_2 ligands

Complex[a]	P−C−C−P	P−Rh−P−R^1	P−Rh−P−R^2	P−Rh−P−R^3	P−Rh−P−R^4	COD twist	*ee*[b]
[Rh{(*S,S*)-**L^{Ph}**}(COD)]O$_3$SCF$_3$ (**Rh-2a**)[32]	+48.8 (δ)	+109.1	−129.0	+147.0	−89.2	+3.9	91 (*R*)
[Rh{(*R,R*)-**L^{Ph}**}(COD)]O$_3$SCF$_3$ (**Rh-2b**)[31][32]	−49.4 (λ)[c]	+88.5	−147.0	+129.2	−108.6	−4.1	91 (*S*)
	−57.7 (λ)[d]	+99.3	−140.4	+134.7	−99.0	+3.4	
[Rh{($S,S,R_P,R_{P'}$)-**L$^{Me/cOc}$**}(COD)]O$_3$SCF$_3$ (**Rh-6a**)[38b][e]	+52.7 (δ)	+137.2	−99.8	+131.5	−106.7	+1.5	35 (*S*)
[Rh{($R,R,R_P,R_{P'}$)-**L$^{Me/cOc}$**}(COD)]O$_3$SCF$_3$ (**Rh-6d**)[32] [e] [f]	−44.7 (λ)	+114.3	−125.1	+113.8	−125.2	+7.8	86 (*S*)
[Rh{($R_P,R_{P'}$)-*t*Bu-bisP*}(C$_7$H$_8$)]BF$_4$ (**Rh-7a**)[39a][39d] [e]	−45.5 (λ)	+109.1	−127.1	+96.8	−139.5	ca. +1	> 99 (*R*)
[PtI$_2${(*S,S*)-**L$^{olane-(R,R)}$**}] (**Pt-4a**)[37]	+58.0 (δ)	−131.2	−110.7	+143.7	−99.6		98 (*R*)
[PtI$_2${(*R,R*)-**L$^{olane-(R,R)}$**}] (**Pt-4b**)[37]	−46.3(λ)	+113.2	−131.1	+113.2	−131.1		77 (*R*)

[a] For definition of R^1−R^4, see Scheme 10. [b] Data refer to the optical yields obtained in the reduction of methyl (*Z*)-2-acetamidocinnamate (**cinMe**). [c] Crystal chosen from a recrystallized sample of optically pure [Rh{(*R,R*)-**L^{Ph}**}(COD)]O$_3$SCF$_3$.[32] [d] Specimen **Rh-2b*** separated by hand from the conglomerate obtained by crystallizing [Rh(*rac*-**L^{Ph}**)(COD)]O$_3$SCF$_3$.[31] [e] ($R_PR_{P'}$) indicates the configuration at the phosphorus atom for the *coordinated* ligands; cf. footnote[e] of Table 1 and Scheme 8. [f] Values taken from the structural analysis of racemic [Rh{(*RS,RS*,R_PS_P,$R_{P'}S_{P'}$-**L$^{Me/cOc}$**}(COD)]O$_3$SCF$_3$ (**Rh-6c/6d**); torsion and twist angles for the [Rh{($S,S,S_P,S_{P'}$)-**L$^{Me/cOc}$**}(COD)]O$_3$SCF$_3$ enantiomer (**Rh-6c**) with opposite sign.

 © 2003 Wiley-VCH Verlag GmbH & Co. KGaA, Weinheim

λ,δ conformer precatalysts $[Rh(\mathbf{L})(COD)]^+$ and the sign and the extent of the stereoinduction that can be achieved with the actual catalysts, X-ray data have been collected for several of the cationic Rh^I precursors. The most important stereochemical features of these complexes comprise (i) the chelate torsion angle P−C−C−P analytically describing the folding of the chelate ring, (ii) the exocyclic torsion angles P−Rh−P−R defining the orientation (axial or equatorial) of the four *P*-bonded substituents R with respect to the coordination plane, and (iii) the twist angle between the P−Rh−P plane and the plane spanned by the central metal and the midpoints of the two coordinated olefinic bonds. A tabulation of these values is presented in Table 2 (see also Scheme 10 and Figures 1−5) So far we have been unable to isolate the diastereomerically pure complex $[Rh\{(R,R,R_P,R_{P'})\text{-}\mathbf{L^{Me/cOc}}\}(COD)]O_3SCF_3$ (**Rh-6d**) or its enantiomer $[Rh\{(S,S,S_P,S_{P'})\text{-}\mathbf{L^{Me/cOc}}\}(COD)]O_3SCF_3$ (**Rh-6c**) as crystals suitable for X-ray crystallography. By way of alternative, we therefore derived the stereochemical features discussed below for **Rh-6d** from the structure of $[Rh\{(RS,RS,R_PS_P,R_{P'}S_{P'}\text{-}\mathbf{L^{Me/cOc}}\}(COD)]O_3SCF_3$ (**Rh-6c/6d**), made up of equal proportions of either mirror image isomer. For the sake of brevity, the salient stereochemical features of only one of the two enantiomeric forms present in the racemic crystal are considered; see also footnote [e] of Table 2.

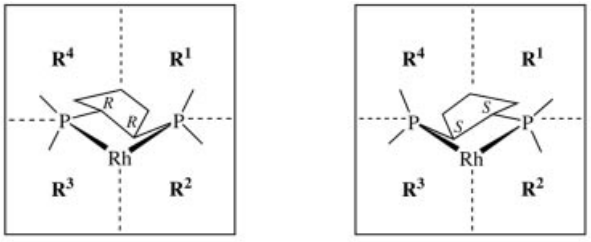

Rh-2b:	R^1–$R^4 = C_6H_5$	**Rh-2a:**	R^1–$R^4 = C_6H_5$
Rh-6d:	$R^1 = R^3 = cC_8H_{15}$	**Rh-6a:**	$R^1 = R^3 = cC_8H_{15}$
	$R^2 = R^4 = CH_3$		$R^2 = R^4 = CH_3$
Rh-7a:	$R^1 = R^3 = CH_3$		
	$R^2 = R^4 = C(CH_3)_3$	(C_2H_4-bridged)	
Rh(Pt)-4b:	$R^1 = R^3 = C^5(H)_{ax}$	**Rh(Pt)-4a:**	$R^1 = R^3 = C^5(H)_{ax}$
	$R^2 = R^4 = C^2(CH_3)_{eq}$		$R^2 = R^4 = C^2(CH_3)_{eq}$

Scheme 10. Definition of P-substituents R^1−R^4 for structurally characterized metal complexes

For the purpose of comparison, data for the two platinum compounds $[PtI_2\{(S,S)\text{-}\mathbf{L^{olane\text{-}(R,R)}}\}]$ (**Pt-4a**) and $[PtI_2\{(R,R)\text{-}\mathbf{L^{olane\text{-}(R,R)}}\}]$ (**Pt-4b**) modelling the related rhodium catalysts **Rh-4a** and **Rh-4b**[37] are also included, as are the pertinent parameters of ethylene-bridged $[Rh\{C_2H_4[(R)\text{-}P(Me)But]_2\}(C_7H_8)]BF_4$ (**Rh-7a**) (Note footnote [d] of Table 2!).[39a,39d]

As expected, all rhodium complexes containing $C_5H_8(PR_2)_2$ chelate phosphanes show torsion angles spanned by the two endocyclic P−CH bonds and the connecting ethylene chain of similar magnitude but opposite sign for the λ and δ conformations imposed by the (*R*,*R*) and (*S*,*S*) forms of the individual ligands. For λ-shaped $[Rh\{(R,R,R_P,R_{P'})\text{-}\mathbf{L^{Me/cOc}}\}(COD)]O_3SCF_3$ (**Rh-6d**), the value of the P−C−C−P torsion angle almost coincides with that of the *t*Bu-bisP* compound **Rh-7a**, in which the λ conformation is stabilized by the bulky CMe_3 substituents. A major structural difference between **Rh-7a** and **Rh-6d** arises from the contrasting orientations of the sterically demanding *tert*-butyl and cyclooctyl groups with respect to the P−Rh−P coordination plane; these are equatorial in the former (R^2 and R^4 in Scheme 10 and Table 2; torsion angles P−Rh−P−CMe_3, −127.1 and −139.5°) but tend to be axial in the latter (R^1 and R^3 in Scheme 10 and Table 2; torsion angles P−Rh−P−$C_8H_{15}c$, +114.3 and +113.8°; cf. Figure 2.)

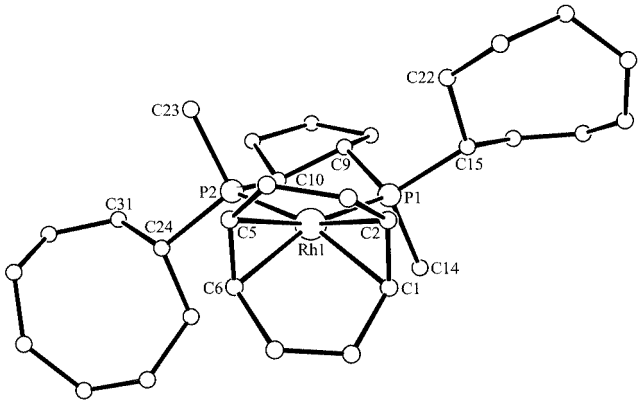

Figure 1. Perspective view of the cation $[Rh\{(S,S,R_P,R_{P'})\text{-}\mathbf{L^{Me/c\text{-}Oc}}\}(COD)]^+$ (**Rh-6a$^+$**); selected bond lengths [A] and angles [°]: Rh1−P1, 2.305(1); Rh1−P2, 2.316(1); Rh1−C1, 2.216(5); Rh1−C2, 2.226(5); Rh1−C5, 2.238(5); Rh1−C6, 2.227(6). P1−Rh−P2, 84.33(3)[38b]

$[Rh\{(S,S,R_P,R_{P'})\text{-}\mathbf{L^{Me/cOc}}\}(COD)]O_3SCF_3$ (**Rh-6a**), on the other hand, resembles **Rh-7a** in the equatorial arrangement of the large substituents (R^1 and R^3 in Scheme 10 and Table 2; torsion angles P−Rh−P−$C_8H_{15}c$, +137.2 and +131.5°; see Figure 1), with the methyl groups pointing to an axial direction in both cases. From the optical inductions achieved in the asymmetric hydrogenation of, e.g., methyl acetamidocinnamate it is clear, however, that the bisP* complex **Rh-7a** is much more enantioselective than **Rh-6a** containing the mismatched combination of *C*- and *P*-chirogenic stereoelements and is also superior in its stereodiscriminating power to that of the matched catalyst **Rh-6d**. This raises the question as to how the spatial orientation of the sterically demanding substituents in **Rh-6a**, **Rh-6d**, and **Rh-7a** contribute to the varying degrees of enantioselectivity

 © 2003 Wiley-VCH Verlag GmbH & Co. KGaA, Weinheim

observed in >C=C< hydrogenations catalyzed by these complexes.

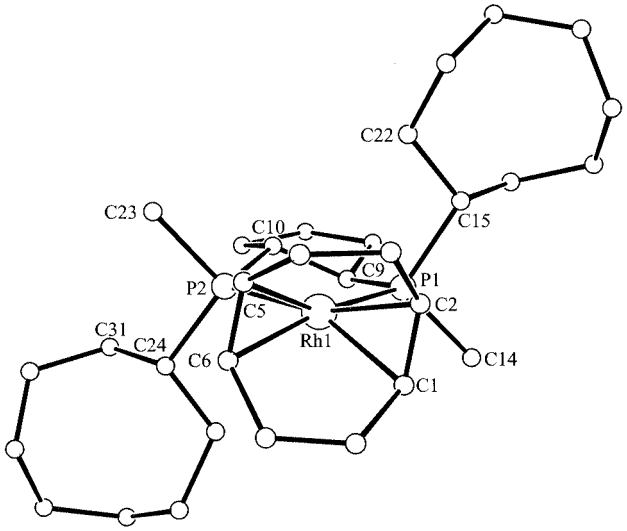

Figure 2. Perspective view of the cation [Rh{(*R*,*R*,R_P,$R_{P'}$)-$L^{Me/c\text{-}Oc}$}(COD)]$^+$ (**Rh-6d$^+$**), as present in the structure of [Rh{(*RS*,*RS*,$R_P$$S_P$,$R_{P'}$$S_{P'}$-$L^{Me/c\text{-}Oc}$}(COD)]$O_3SCF_3$ (**Rh-6c/6d**); selected bond lengths [Å] and angles [°]: Rh1−P1, 2.312(2); Rh1−P2, 2.323(2); Rh1−C1, 2.230(7); Rh1−C2, 2.237(7); Rh1−C5, 2.249(7); Rh1−C6, 2.249(7). P1−Rh−P2, 85.20(6)[32,47]

According to the "quadrant classification" established by Knowles in 1983,[6c] Gridnev and Imamoto[39b] as well as Ohashi[36d] have recently presented convincing evidence that any rhodium catalyst with C_2- or C_1-symmetric *P*-chirogenic bis(phosphanes), in which the difference in size between the terminal substituents is as apparent as in **Rh-6a**, **Rh-6d**, and **Rh-7a**, will furnish (*R*) hydrogenation products irrespective of a λ or δ conformation of the backbone, if the more voluminous groups are arranged in the upper left and lower right quadrants (cf. **Rh-7a**), while opposite orientation (as in **Rh-6a** and **Rh-6d**) will provoke (*S*) stereoselection.[39b] This is because the migratory insertion of the enamide to form an alkyl hydride, which has been identified as the enantiodetermining irreversible step of asymmetric hydrogenation both experimentally[39b−39g] and computationally,[42a] is controlled in an enantiofacially discriminating fashion by repulsive interaction between the chelate ring made up by the substrate and the bulky P-substituents in short-lived diastereomeric dihydrido enamide intermediates as depicted in Scheme 11. For **Rh-7a**, e.g., the (ethylene-connected) diastereomer λ-**A**^{eq}, containing the substrate bonded through its *si* face to give (*R*)-amino acids as observed, is definitely lower in energy than λ-**B**^{eq} because it is the smaller *P*-bound residue that undergoes direct steric repulsion with the carboxyl group attached to the chelate cycle.

For the three structurally characterized compounds under discussion, steric blocking of two diagonally arranged quadrants is most complete in the most stereoselective catalyst **Rh-7a**, where the bulky but nevertheless compact *tert*-butyl groups *exclusively* shield the quadrants left side up and right side down. Thus, the two $(H_3C)_3C$ hydrogen

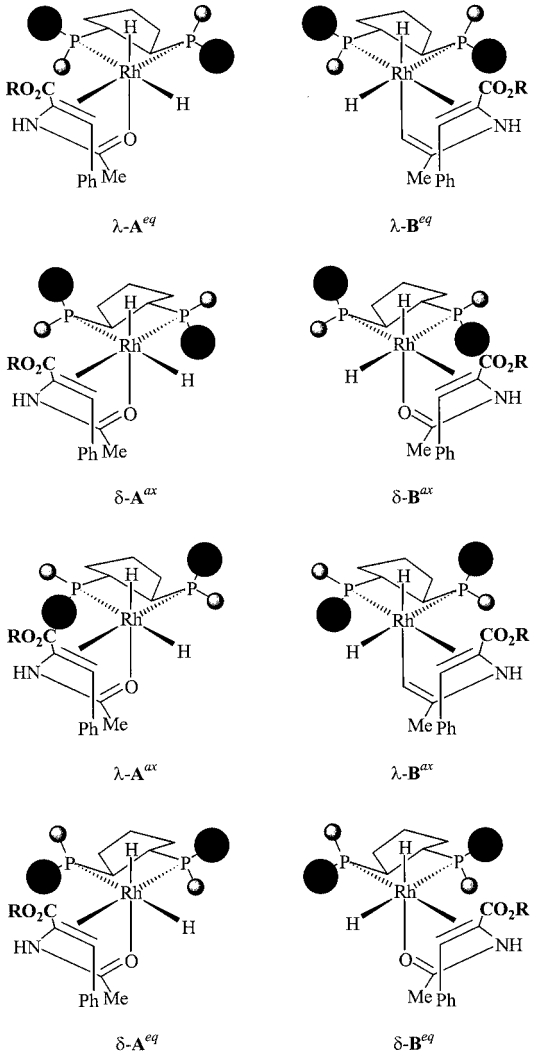

Scheme 11. Possible diastereomers of cationic dihydrido enamide intermediates with chiral bis(phosphane) ligands having P-substituents pairwise differing in size (after Gridnev and Imamoto)[39b]

atoms that are closest to the >C=C< binding sites (H-11 and H-21 in the original publication[39a]) are located *within* the area spanned by the two quadrants and − equally important − are directed towards the diolefin in such a fashion that they are almost in a straight line with the central metal atom, the distances of the three atoms from the least-squares plane defined by the four olefinic carbon atoms being 1.53 and 1.51 Å for the two hydrogen atoms and 1.73 Å for the rhodium atom (angle H···Rh··H, 169.4°). As a result of their distinct equatorial alignment, the spatially expanded cyclooctyl rings of mismatched complex **Rh-6a** (Figure 1), on the other hand, not only fill out the two top right and bottom left quadrants but slightly penetrate into the adjacent parts of the coordination sphere as well, thereby contributing to some *unwanted shielding* of the upper left and lower right quadrants.[38b] Moreover, owing to the "face-on" orientation of the equatorial pairs of cyclooctyl groups the degree of *favorable quadrant-blocking*, thought to make δ-**B**^{eq} more readily accessible than δ-**A**^{eq},

 © 2003 Wiley-VCH Verlag GmbH & Co. KGaA, Weinheim

is much less effective in **Rh-6a** than in **Rh-7a** (in this context, note also the decreased *ee* values achieved on substituting cC_5H_9 for *t*Bu or 1-Ad in Rh−bisP* catalysts!), as is evident from the deviations of the central metal atom and the *ipso*-C-bonded hydrogen atoms from the calculated least-square plane through the four coordinated >C=C< carbon atoms, which are 2.26 and 2.44 Å for the two hydrogen atoms but only 1.58 Å for rhodium (angle H···Rh··H, 155.5°). Matched catalyst **Rh-6d** which (as outlined above) is superior in stereodiscriminating power to **Rh-6a** but inferior to **Rh-7a**, differs in structure from mismatched **Rh-6a** by a more axial arrangement of the cyclooctyl rings, the methyl substituents being more equatorially aligned (Figure 2). This results in steric blocking of *only* the top right and bottom left quadrants, making λ-$\mathbf{B}^{ax}$ lower in energy than λ-$\mathbf{A}^{ax}$. Exclusive shielding of these two quadrants seems to be the main factor contributing to the stereoselective abilities of **Rh-6d**, since the "face-on" orientation of the cyclooctyl substituents is similar to **Rh-6a** and results in even slightly longer distances (2.36 and 2.70 Å) of the two *ipso*-C-bonded hydrogen atoms from the $(>C=C<)_2$ least-squares plane.

Interestingly, the Pt−$\mathbf{L}^{olane}$ complex **Pt-4a**, which served as an analogue of the matched catalyst [Rh{(*S*,*S*)-$\mathbf{L}^{olane\text{-}(R,R)}$}(COD)]$BF_4$ (**Rh-4a**),[37] similarly features quadrant-blocking methyl groups at the 2,5 positions of the phospholane ring showing a decidedly *axial* alignment in the upper left and lower right coordination quadrants (torsion angles P−Rh−P−$C^{2,5}$, −99.6/−110.7°). This arrangement should favor dihydride intermediate δ-$\mathbf{A}^{ax}$ over δ-$\mathbf{B}^{ax}$ to give high optical yields of the (*R*) hydrogenation products as observed. In marked contrast, the **Pt-4b** diastereomer, which was used to model the structure of mismatched [Rh{(*R*,*R*)-$\mathbf{L}^{olane\text{-}(R,R)}$}(COD)]$BF_4$ (**Rh-4b**), presents the same two methyl groups in the same quadrants in *equatorial* orientation (torsion angles P−Rh−P−$C^{2,5}$, −131.1° each), which can safely be predicted to lower the energy of λ-$\mathbf{A}^{eq}$ as compared to λ-$\mathbf{B}^{eq}$, but because of the equatorial alignment of the quadrant-shielding residues to a lesser degree than anticipated for δ-$\mathbf{A}^{ax}$ vs. δ-$\mathbf{B}^{ax}$. As the location of the phospholane substituents in the quadrants is independent of the λ or δ conformation of the five-membered chelate ring in the case of the two platinum complexes (large CH_3 groups top left and bottom right; small H atoms bottom left and top right) and as both rhodium analogues **Rh-4a** and **Rh-4b** induce (*R*) stereoselection, it becomes clear that Pringle's Rh−(*S*,*S*)-$\mathbf{L}^{olane\text{-}(R,R)}$ and Rh−(*R*,*R*)-$\mathbf{L}^{olane\text{-}(R,R)}$ catalysts also fit the aforementioned Gridnev/Imamoto rule for catalysts bearing *P*-chirogenic bis(phosphanes) with substituents pairwise differing in size.

We furthermore emphasize that the enhancement of enantioselectivity achieved by changing the alignment of a large substituent from a more equatorial to a more axial orientation as observed on going from **Rh-6a** to **Rh-6d** and, respectively, from **Rh-4b** to **Rh-4a** satisfies a prediction formulated by Nagel years ago: "We feel that to build a good catalyst for the hydrogenation of *N*-acylacrylic acid derivatives, it is necessary to have two large groups in the chelating diphosphane as axial as possible".[40] In view of the excellent enantioselectivities obtained with Imamoto's Rh−bisP* catalysts bearing compact bulky substituents in an equatorial arrangement, "axial" should, however, be qualified by "axial or focused to a single quadrant" rather than be understood as a sine qua non.

The results of the X-ray structure analyses carried out on the enantiomers [Rh{(*S*,*S*)-$\mathbf{L}^{Ph}$}(COD)]O_3SCF_3 (**Rh-2a**) and [Rh{(*R*,*R*)-$\mathbf{L}^{Ph}$}(COD)]O_3SCF_3 (**Rh-2b**) are worth mentioning regarding several aspects. As anticipated, single-crystals of the two complexes belonged to the same space group, $P2_1$, but because of different conditions of crystal growth, the unit-cell volumes of two of the three specimens investigated differed significantly: V = 1789.8(7) $Å^3$ and, comparably, V = 1791.1(5) $Å^3$ for the mirror image isomers taken from recrystallized samples of the enantiomerically pure complexes,[32] but V = 1772.3(5) $Å^3$ for a crystal of **Rh-2b** (**Rh-2b*** hereafter) picked from a conglomerate of [Rh(*rac*-$\mathbf{L}^{Ph}$)(COD)]O_3SCF_3, which − similar to the nickel complex [$NiBr_2$($\mathbf{L}^{Ph}$)]·CH_2Cl_2 [22a] − underwent spontaneous resolution upon crystallization from THF/*n*-pentane.[31] As a result of the different crystal packing in **Rh-2b** and **Rh-2b***, the endo- and exocyclic torsion angles measured for these two chelate systems were found to diverge considerably (Table 2) as did some of the bond lengths and angles (see captions of Figures 3−5). This demonstrates unequivocally that the two enantiomeric P_2 ligands do not build up absolutely inflexible coordination spheres but that some conformational freedom is associated with the ligand backbones. Previously, Oliver and Riley have pointed out that such adaptability of putatively stiff chiral phosphanes may be essential for high hydrogenation rates.[45] As a further and rather unexpected consequence, the diene ligand of the *same* enantiomers **Rh-2b** and **Rh-2b*** is seen to be skewed with respect to the P−Rh−P coordination plane *in opposite senses* (clockwise by +3.4° and anticlockwise by −4.1°). This clearly disproves the view that the sense of diene rotation is intimately correlated with the handedness of the catalyst pocket made up by the chiral steering ligand.[46] As complexes **Rh-2a** and **Rh-2b** catalyze the hydrogenation of standard enamide substrates giving high optical yields with opposite sign, it is furthermore concluded that no correlation whatsoever can be made between the sense of the diene twist and the enantioselectivity displayed by the catalysts. This goes against an early hypothesis of Kyba et al. that the forces causing the diolefin rotation would be the same that would induce the stereodiscrimination,[46] but corresponds to conclusions of Imamoto et al. that no interdependencies whatsoever exist between enantioselectivity and the sign of the diene skewness in the case of the bisP*−Rh catalysts, since these are highly stereoselective irrespective of an essentially ideal diene coordination with the double bonds perpendicular to the P−Rh−P plane.[39a,39b,39d]

Similar to several structures discussed in detail by Oliver and Riley already in 1983,[45] the arrangement of the phenyl rings in molecules **Rh-2a**, **Rh-2b**, and **Rh-2b*** does not obey the *ax*.−*eq*.−*ax*.−*eq*.-"edge−face−edge−face" relation[6c]

 © 2003 Wiley-VCH Verlag GmbH & Co. KGaA, Weinheim

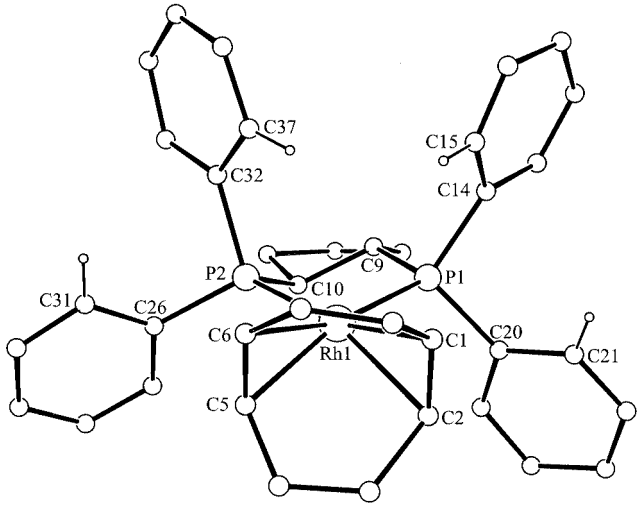

Figure 3. Perspective view of the cation [Rh{(*S*,*S*)-$\mathbf{L^{Ph}}$}(COD)]$^+$ (**Rh-2a**$^+$); selected bond lengths [Å] and angles [°]: Rh1−P1, 2.315(4); Rh1−P2, 2.306(4); Rh1−C1, 2.24(2); Rh1−C2, 2.27(2); Rh1−C5, 2.24(1); Rh1−C6, 2.25(1). P1−Rh−P2, 84.42(8); torsion angles Rh−P−C_{ipso}−C_{ortho} [°]: Rh1−P1−C14−C15, −7.1; Rh1−P1−C20−C21, −93.5; Rh1−P2−C26−C31, 91.5; Rh1−P2−C32−C37, 0.9[32,47]

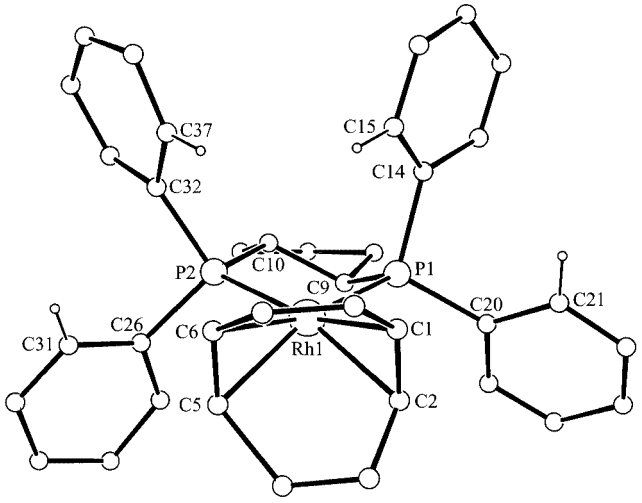

Figure 4. Perspective view of the cation [Rh{(*R*,*R*)-$\mathbf{L^{Ph}}$}(COD)]$^+$ of specimen **Rh-2b**; selected bond lengths [Å] and angles [°]: Rh1−P1, 2.328(4); Rh1−P2, 2.328(4); Rh1−C1, 2.31(4); Rh1−C2, 2.22(1); Rh1−C5, 2.24(1); Rh1−C6, 2.17(1). P1−Rh−P2, 84.19(10); torsion angles Rh−P−C_{ipso}−C_{ortho} [°]: Rh1−P1−C14−C15, 0.4; Rh1−P1−C20−C21, −93.7; Rh1−P2−C26−C31, 91.5; Rh1−P2−C32−C37, 6.9[32,47]

generally assumed for square-planar rhodium complexes with chiral bis(phosphane) ligands having terminal $-PPh_2$ donor groups: On moving from the upper right quadrant in a clockwise sense, one best describes the alignment of the phenyl substituents with respect to the five-membered chelate structures of the three molecules as *ax.*−*eq.*−*eq.*−*ax.*, as is readily evidenced from the magnitudes of the P−Rh−P−C_{ipso} torsion angles collected in Table 2. In the same sense, the Rh−P−C_{ipso}−C_{ortho} torsion angles given in the captions to Figures 3−5 define the

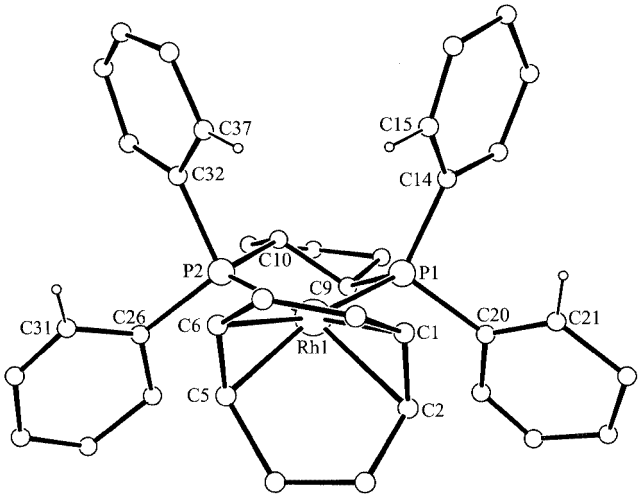

Figure 5. Perspective view of the cation [Rh{(*R*,*R*)-$\mathbf{L^{Ph}}$}(COD)]$^+$ of specimen **Rh-2b***; selected bond lengths [Å] and angles [°]: Rh1−P1, 2.309(2); Rh1−P2, 2.293(2); Rh1−C1, 2 .188(9); Rh1−C2, 2.312(7); Rh1−C5, 2.158(9); Rh1−C6, 2.264(7). P1−Rh−P2, 84.08(5); torsion angles Rh−P−C_{ipso}−C_{ortho} [°]: Rh1−P1−C14−C15, −6.2; Rh1−P1−C20−C21, −94.4; Rh1−P2−C26−C31, 91.1; Rh1−P2−C32−C37, 1.5[31,47]

orientations of the aromatic rings with respect to the binding sites of the diene as close to "edge−face−face−edge". Thus, while the backbone symmetry of the P_2 ligands in the stable conformation of the three complexes is C_2, the local symmetry at the metal atom as determined by the spatial orientation of the phenyl rings in the donor groups at first glance seems to approach C_s − were there not some subtleties that make the difference!

In **Rh-2a** we see the *ortho*-hydrogen atoms in the top right and bottom right quadrants at distances of 2.27 and 2.13 Å from the least-squares plane through the coordinated olefinic carbon atoms, the separations between that plane and the *ortho*-H atoms in the quadrants left side up and left side down amounting to 2.73 and 2.53 Å. For enantiomer **Rh-2b** (recrystallized sample), we face the opposite arrangement of the four *ortho*-hydrogen atoms with respect to the $(>C=C<)_2$ least-squares plane: 2.39 (2.28) Å and 1.96 (2.15) Å for the separations in the upper left and lower left quadrants vs. twice 2.76 (2.63, 2.48) Å for the corresponding distances in the quadrants right side up and right side down (values for specimen **Rh-2b*** picked from the conglomerate given parenthetically).

In view of the enhanced axial interactions in octahedral dihydro complexes directly preceding the enantiodetermining migratory insertion step (vide supra) it has been suggested that in RhP_2 complexes with backbone chirality and four equivalent phenyl substituents on the phosphorus atom, i.e., in catalysts *conforming* to the λ/δ rule, it is the axial phenyl rings which lend the decisive steric hindrance to the stereodiscriminating step.[39b,40] We conclude that the two phenyl groups in the top right and top left quadrants of **Rh-2a** and **Rh-2b** or **Rh-2b*** are identified by the substrate as being larger than the aryl residues in the quadrants that are bottom right and bottom left. In the critical dihydro enamide intermediates with *trans*-positioned hydride

 © 2003 Wiley-VCH Verlag GmbH & Co. KGaA, Weinheim

and acetyl ligands, steric crowding would therefore be minimized if the axial phenyl substituents point away from the equatorial plane containing the enamide chelate in addition to the five-membered metal−bis(phosphane) ring. As a consequence, the equatorially aligned aryl groups would be forced into the plane spanned by the metal atom and the >C=C< double bond of the substrate; see structures **C** and **D** in Scheme 12. Comparing the relative bulkiness of the phenyl substituents as estimated from the distances between the *ortho*-H atoms and the least-squares plane made up by the olefinic carbon atoms in the enantiomeric diene precursors, we would anticipate more steric repulsion between the enamide chelate and the phenyl groups in the top and bottom right quadrants of **Rh-2a** and, vice versa, in the upper and lower left quadrants of **Rh-2b** and **Rh-2b***, respectively. The corollary of this conclusion is that in a dihydro enamide complex resulting from **Rh-2a**, the chelated substrate should experience the least steric strain if bonded through its *si* face as in δ-**C** to give, by migratory insertion, the experimentally observed (*R*) hydrogenation products; *re*-face-bonding with formation of the (*S*) enantiomers would only be expected if the least repulsive interactions occur in the quadrants right side up and right side down, i.e., in dihydride intermediates of type λ-**D** for which **Rh-2b** and **Rh-2b*** are suitable precursors. The preferred coordination of the enamide substrate as described by structures λ-**D** and δ-**C** not only minimizes the axial repulsions but also reduces steric crowding between the enamide chelate cycle and those equatorially aligned substituents that are nearest to the olefinic binding sites in the ground state structures of the diene precursors **Rh-2a** (bottom right) and **Rh-2b** or **Rh-2b*** (bottom left). Even if the equatorial interactions have been considered as less important for stereoselection than the axial repulsions,[39b,40] they can help to make isomers λ-**D** and δ-**C** more readily accessible than their diastereomers λ-**C** and δ-**D** featuring an unfavorable close contact between the chelate cycle and the phenyl substituents. Interpreted like this, the quadrant rule changes into a "left−right" criterion, valid for RhP_2 (pre)catalysts which, from a structural point of view, do not adhere to the *ax.*−*eq.*−*ax.*−*eq.*-"edge−face−edge−face" relation.

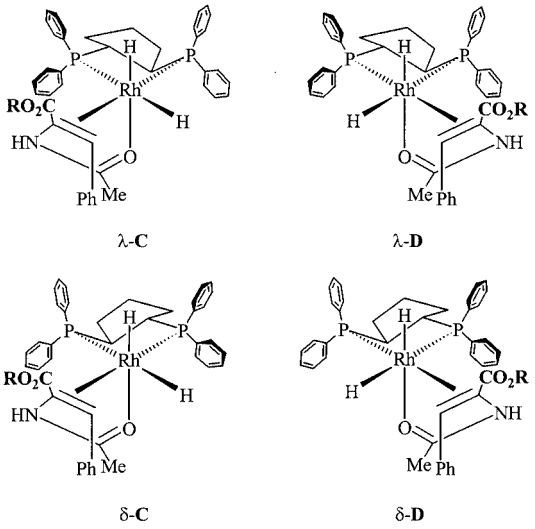

Scheme 12. Possible diastereomers of cationic dihydrido enamide intermediates with chiral bis(phosphane) ligands that have phenyl substituents of equal size but do not conform to the *ax.*−*eq.*−*ax.*−*eq.*-"edge−face−edge−face" relation

Acknowledgments

Financial support from the Deutsche Forschungsgemeinschaft and the Fonds der Chemischen Industrie is gratefully acknowledged. The author is also indebted to Degussa AG for many generous gifts of platinum salts. Furthermore, it is a pleasure to thank all coworkers who contributed to the success of this project over the past years, in particular Dr. Andrea Saare, Dr. Corinna Becker, Dr. Christine Eckert, Dr. Volker Kurth, Dr. Stefan Mertel, Dr. Nils Osthoff, Dr. Andreas Wühr, and Dipl.-Chem. Anja Kaunert. Finally, I wish to thank Mrs. Susanne Kammerer for skilful technical assistance.

[1] L. Dahlenburg, R. Götz, *Inorg. Chem. Commun.* **2003**, *6*, 443−446.
[2] For retrospective overviews, see the 2001 Nobel Lectures in Chemistry: [2a] W. S. Knowles, *Angew. Chem.* **2002**, *114*, 2096−2107; *Angew. Chem. Int. Ed.* **2002**, *41*, 1998−2007. [2b] R. Noyori, *Angew. Chem.* **2002**, *114*, 2108−2123; *Angew. Chem. Int. Ed.* **2002**, *41*, 2008−2022. [2c] K. B. Sharpless, *Angew. Chem.* **2002**, *114*, 2126−2135; *Angew. Chem. Int. Ed.* **2002**, *41*, 2024−2032.
[3] W. S. Knowles, M. J. Sabacky, *J. Chem. Soc., Chem. Commun.* **1968**, 1445−1446.
[4] [4a] L. Horner, H. Büthe, H. Siegel, *Tetrahedron Lett.* **1968**, 4023−4026. [4b] L. Horner, H. Siegel, H. Büthe, *Angew. Chem.* **1968**, *80*, 1034−1035; *Angew. Chem. Int. Ed. Engl.* **1968**, *7*, 942.
[5] [5a] H. B. Kagan, T. P. Dang, *J. Chem. Soc., D* **1971**, 481. [5b] H. B. Kagan, T. P. Dang, *J. Am. Chem. Soc.* **1972**, *94*, 6429−6433.
[6] [6a] W. S. Knowles, M. J. Sabacky, B. D. Vineyard, D. J. Weinkauff, *J. Am. Chem. Soc.* **1975**, *97*, 2567−2568. [6b] B. D. Vineyard, W. S. Knowles, M. J. Sabacky, G. L. Bachmann, D. J. Weinkauff, *J. Am. Chem. Soc.* **1977**, *99*, 5946−5952. [6c] W. S. Knowles, *Acc. Chem. Res.* **1983**, *16*, 106−112.
[7] M. J. Burk, *Acc. Chem. Res.* **2000**, *33*, 363−372, and references cited therein.
[8] C. Claver, E. Fernandez, A. Gillon, K. Heslop, D. J. Hyett, A. Martorell, A. G. Orpen, P. G. Pringle, *Chem. Commun.* **2000**, 961−962.
[9] [9a] M. T. Reetz, T. Sell, *Tetrahedron Lett.* **2000**, *41*, 6333−6336. [9b] M. T. Reetz, G. Mehler, *Angew. Chem.* **2000**, *112*, 4047−4049; *Angew. Chem. Int. Ed.* **2000**, *39*, 3889−3891.
[10] M. van den Berg, A. J. Minnaard, E. P. Schudde, J. van Esch, A. H. M. de Vries, J. G. de Vries, B. L. Feringa, *J. Am. Chem. Soc.* **2000**, *122*, 11539−11540.
[11] W. Chen, J. Xiao, *Tetrahedron Lett.* **2001**, *42*, 2897−2899.
[12] Q. Zeng, H. Lui, X. Cui, A. Mi, Y. Jiang, X. Li, M. C. K. Choi, A. S. C. Chan, *Tetrahedron: Asymmetry* **2002**, *13*, 115−117.
[13] K. Junge, G. Oehme, A. Monsees, Th. Riermeier, U. Dingerdissen, M. Beller, *Tetrahedron Lett.* **2002**, *43*, 4977−4980.
[14] Y. Fu, J.-H. Xie, A.-G. Hu, H. Zhou, L.-X. Wang, Q.-L. Zhou, *Chem. Commun.* **2002**, 480−481.
[15] M. Ostermeier, J. Prieß, G. Helmchen, *Angew. Chem.* **2002**, *114*, 625−628; *Angew. Chem. Int. Ed.* **2002**, *41*, 612−614.
[16] A. Bayer, P. Murszat, U. Thewalt, B. Rieger, *Eur. J. Inorg. Chem.* **2002**, 2614−2624.
[17] For reviews dealing with chiral monodentate phosphanes, see: [17a] T. Hayashi, *Acc. Chem. Res.* **2000**, *33*, 354−362. [17b] F. Lagasse, H. B. Kagan, *Chem. Pharm. Bull.* **2000**, *48*, 315−324.

 © 2003 Wiley-VCH Verlag GmbH & Co. KGaA, Weinheim

[17c] I. V. Komarov, A. Börner, *Angew. Chem.* **2001**, *113*, 1237−1240; *Angew. Chem. Int. Ed.* **2001**, *40*, 1197−1200.
[18] See for instance: [18a] K. Issleib, *Z. Chem.* **1962**, *2*, 163−173, and references cited therein. [18b] K. Tani, K. Suwa, E. Tanigawa, T. Ise, T. Yamagata, Y. Tatsuno, S. Otsuka, *J. Organomet. Chem.* **1989**, *370*, 203−221.
[19] [19a] M. J. Burk, *J. Am. Chem. Soc.* **1991**, *113*, 8518−8519. [19b] M. J. Burk, J. E. Feaster, R. L. Harlow, *Tetrahedron: Asymmetry* **1991**, *2*, 569−592. [19c] M. J. Burk, J. E. Feaster, W. A. Nugent, R. L. Harlow, *J. Am. Chem. Soc.* **1993**, *115*, 10125−10138. [19d] S. K. Armstrong, J. M. Brown, M. J. Burk, *Tetrahedron Lett.* **1993**, *34*, 879−882.
[20] [20a] T. Imamoto, T. Oshiki, T. Onozawa, T. Kusumoto, K. Sato, *J. Am. Chem. Soc.* **1990**, *112*, 5244−5252. [20b] L. McKinstry, T. Livinghouse, *Tetrahedron Lett.* **1994**, *35*, 9319−9312. [20c] L. McKinstry, T. Livinghouse, *Tetrahedron* **1995**, *51*, 7655−7666. [20d] F. Bitterer, O. Herd, M. Kühnel, O. Stelzer, N. Weferling, W. S. Sheldrick, J. Hahn, S. Nagel, N. Rösch, *Inorg. Chem.* **1998**, *37*, 6408−6417. [20e] M. J. Burk, A. Pizzano, J. A. Martin, L. M. Liable-Sands, A. L. Rheingold, *Organometallics* **2000**, *19*, 250−260.
[21] [21a] R. J. Burt, J. Chatt, W. Hussain, G. J. Leigh, *J. Organomet. Chem.* **1979**, *182*, 203−206. [21b] R. A. Henderson, W. Hussain, G. J. Leigh, F. B. Normanton, *Inorg. Synth.* **1985**, *23*, 141−143.
[22] [22a] D. L. Allen, V. C. Gibson, M. L. H. Green, J. F. Skinner, J. Bashkin, P. D. Grebenik, *J. Chem. Soc., Chem. Commun.* **1983**, 895−896. [22b] C. E. Davies, I. M. Gardiner, J. C. Green, M. L. H. Green, N. J. Hazel, P. D. Grebenik, V. S. B. Mtetwa, K. Prout, *J. Chem. Soc., Dalton Trans.* **1985**, 669−683.
[23] A. Saare, L. Dahlenburg, *Z. Naturforsch. B: Chem. Sci.* **1995**, *50*, 1009−1017.
[24] [24a] H. Brunner, W. Pieronczyk, *Angew. Chem.* **1979**, *91*, 655−656; *Angew. Chem. Int. Ed. Engl.* **1979**, *18*, 620. [24b] H. Brunner, W. Pieronczyk, B. Schönhammer, K. Streng, I. Bernal, J. Korp, *Chem. Ber.* **1981**, *114*, 1137−1149.
[25] C. Eckert, L. Dahlenburg, A. Wolski, *Z. Naturforsch. B: Chem. Sci.* **1995**, *50*, 1004−1008.
[26] [26a] L. Dahlenburg, A. Kaunert, *Acta Crystallogr., Sect C: Cryst. Struct. Commun.* **1998**, *C54*, 1016−1017. [26b] L. Dahlenburg, A. Kaunert, *Eur. J. Inorg. Chem.* **1998**, 885−887.
[27] L. Dahlenburg, Ger. Offen. DE 19732805 A1, **1999**, 1−29 [*Chem. Abstr.* **1999**, *130*, 168481].
[28] [28a] S. Mertel, Dissertation, Universität Erlangen-Nürnberg, **2001**. [28b] L. Dahlenburg, S. Mertel, *J. Organomet. Chem.* **2001**, *630*, 221−243.
[29] [29a] H. Brunner, S. Stefaniak, M. Zabel, *Synthesis* **1999**, 1776−1784. [29b] H. Brunner, S. Stefaniak, M. Zabel, *Synthesis* **2000**, 478 [Erratum].
[30] L. Dahlenburg, C. Eckert, *J. Organomet. Chem.* **1998**, *564*, 227−232.
[31] A. Wühr, Dissertation, Universität Erlangen-Nürnberg, **2002**.
[32] N. Osthoff, Disseration, Universität Erlangen-Nürnberg, **2003**.
[33] H. Brunner, *J. Organomet. Chem.* **1995**, *500*, 39−46, and references cited therein.
[34] For leading references, see, for example: [34a] K. Nozaki, N. Sakai, T. Nanno, T. Higashijima, S. Mano, T. Horiuchi, H. Takaya, *J. Am. Chem. Soc.* **1997**, *119*, 4413−4423. [34b] G. Franciò, K. Wittmann, W. Leitner, *J. Organomet. Chem.* **2001**, *621*, 130−142. [34c] S. Deerenberg, O. Pàmies, M. Diéguez, C. Claver, P. C. J. Kamer, P. W. N. M. van Leeuwen, *J. Org. Chem.* **2001**, *66*, 7626−7631. [34d] O. Pàmies, M. Diéguez, G. Net, A. Ruiz, C. Claver, *J. Org. Chem.* **2001**, *66*, 8364−8369. [34e] O. Pàmies, G. Net, A. Ruiz, C. Claver, *Tetrahedron: Asymmetry* **2001**, *12*, 3441−3445.
[35] For recent examples of C_1-symmetric P_2 ligands without additional stereogenic centers in the donor groups, see: [35a] C. P. Casey, E. L. Paulsen, E. W. Beuttenmueller, B. R. Proft, B. A. Matter, D. R. Powell, *J. Am. Chem. Soc.* **1999**, *121*, 63−70. [35b] C.-A. Carraz, E. J. Ditzel, A. G. Orpen, D. D. Ellis, P. G. Pringle, G. J. Sunley, *Chem. Commun.* **2000**, 1277−1278. [35c] C. Hegedüs, J. Madarász, H. Gulyás, A. Szöllősy, J. Bakos, *Tetrahedron: Asymmetry* **2001**, *12*, 2867−2873.
[36] References to dissymetric *P*-chirogenic bis(phosphanes): [36a] A. Ohashi, T. Imamoto, *Org. Lett.* **2001**, *3*, 373−375. [36b] A. Ohashi, T. Imamoto, *Tetrahedron Lett.* **2001**, *42*, 1099−1101. [36c] A. Ohashi, S. Kikuchi, A. Yasutake, T. Imamoto, *Eur. J. Org. Chem.* **2002**, 2535−2546. [36d] A. Ohashi, *Chirality* **2002**, *14*, 573−577.
[37] E. Fernandez, A. Gillon, K. Heslop, E. Horwood, D. J. Hyett, A. G. Orpen, P. G. Pringle, *Chem. Commun.* **2000**, 1663−1664.
[38] [38a] L. Dahlenburg, V. Kurth, *Eur. J. Inorg. Chem.* **1998**, 597−603. [38b] L. Dahlenburg, V. Kurth, *J. Organomet. Chem.* **1999**, *585*, 315−325.
[39] [39a] T. Imamoto, J. Watanabe, Y. Wada, H. Masuda, H. Yamada, H. Tsuruta, S. Matsukawa, K. Yamahuchi, *J. Am. Chem. Soc.* **1998**, *120*, 1635−1636. [39b] I. D. Gridnev, N. Higashi, K. Asakura, T. Imamoto, *J. Am. Chem. Soc.* **2000**, *122*, 7183−7194. [39c] I. D. Gridnev, N. Higashi, T. Imamoto, *J. Am. Chem. Soc.* **2000**, *122*, 10486−10487. [39d] I. D. Gridnev, Y. Yamamoi, N. Higashi, H. Tsuruta, M. Yasutake, T. Imamoto, *Adv. Synth. Catal.* **2001**, *343*, 118−136. [39e] I. D. Gridnev, N. Higashi, T. Imamoto, *J. Am. Chem. Soc.* **2001**, *123*, 4631−4632. [39f] I. D. Gridnev, M. Yasutake, N. Higashi, T. Imamoto, *J. Am. Chem. Soc.* **2001**, *123*, 5268−5276. [39g] M. Yasutake, I. D. Gridnev, N. Higashi, T. Imamoto, *Org. Lett.* **2001**, *3*, 1701−1704.
[40] U. Nagel, B. Rieger, *Organometallics* **1989**, *8*, 1534−1538.
[41] See, e.g.: V. A. Pavlov, E. I. Klabunovskii, Yu. T. Struchkov, A. A. Voloboev, A. I. Yanovsky, *J. Mol. Catal.* **1988**, *44*, 217−243.
[42] [42a] C. R. Landis, P. Hilfenhaus, S. Feldgus, *J. Am. Chem. Soc.* **1999**, *121*, 8741−8754. [42b] C. R. Landis, S. Feldgus, *Angew. Chem.* **2000**, *112*, 2985−2988; *Angew. Chem. Int. Ed.* **2000**, *39*, 2863−2866. [42c] S. Feldgus, C. R. Landis, *J. Am. Chem. Soc.* **2000**, *122*, 12714−12727. [42d] S. Feldgus, C. R. Landis, *Organometallics* **2001**, *20*, 2374−2386.
[43] [43a] A. S. C. Chan, J. J. Pluth, J. Halpern, *Inorg. Chim. Acta* **1979**, *37*, L477−L479. [43b] A. S. C. Chan, J. Halpern, *J. Am. Chem. Soc.* **1980**, *102*, 838−840. [43c] A. S. C. Chan, J. J. Pluth, J. Halpern, *J. Am. Chem. Soc.* **1980**, *102*, 5952−5954. [43d] J. Halpern, *Science* **1982**, *217*, 401−407. [43e] C. R. Landis, J. Halpern, *J. Am. Chem. Soc.* **1987**, *109*, 1746−1754.
[44] [44a] J. M. Brown, P. A. Chaloner, *Tetrahedron Lett.* **1978**, *21*, 1877−1880. [44b] J. M. Brown, P. A. Chaloner, *J. Chem. Soc., Chem. Commun.* **1980**, 344−346. [44c] J. M. Brown, D. Parker, *Organometallics* **1982**, *1*, 950−956. [44d] J. M. Brown, P. A. Chaloner, G. A. Morris, *J. Chem. Soc., Chem. Commun.* **1983**, 664−666. [44e] J. M. Brown, L. R. Canning, A. J. Downs, A. M. Forster, *J. Organomet. Chem.* **1983**, *255*, 103−111. [44f] J. M. Brown, P. L. Evans, *Tetrahedron* **1988**, *44*, 2905−4916.
[45] J. D. Oliver, D. P. Riley, *Organometallics* **1983**, *2*, 1032−1038.
[46] E. P. Kyba, R. E. Davis, P. N. Juri, K. R. Shirley, *Inorg. Chem.* **1981**, *20*, 3616−3623.
[47] Crystal structures: Enraf−Nonius CAD 4 (Mo-K_α radiation, λ = 0.71073 Å; T = 293 ± 2 K). **Rh-2a**: space group $P2_1$ (no. 4), a = 10.4024(9), b = 14.854(5), c = 11.665(2) Å, β = 96.803(8)°, V = 1789.8(7) Å, Z = 2, μ = 0.677 mm^{-1}; $2\theta_{max}$ = 50.36°, reflections collected (including Friedel pairs)/unique: 7048/6440 (R_{int} = 0.0324), 4720 $F_o \geq 4\sigma(F_o)$, 433 parameters, wR_2 (all data) = 0.1381, R_1 ($F \geq 4\sigma$) = 0.0566; absolute structure parameter: 0.10(7).[32] **Rh-2b**: space group $P2_1$ (no. 4), a = 10.416(1), b = 14.880(4), c = 11.631(1) Å, β = 96.50(1)°, V = 1791.1(7) Å, Z = 2, μ = 0.676 mm^{-1}; $2\theta_{max}$ = 48.56°, reflections collected (including Friedel pairs)/unique: 6398/5792 (R_{int} = 0.0570), 3252 $F_o \geq 4\sigma(F_o)$, 433 parameters, wR_2 (all data) = 0.1691, R_1 ($F \geq 4\sigma$) = 0.0761; absolute structure parameter: 0.22(11).[32] **Rh-2b***: space group $P2_1$ (no. 4), a = 10.3515(8), b = 14.827(4), c = 11.6246(8) Å, β = 96.610(7)°, V = 1772.3(5) Å, Z = 2, μ = 0.683 mm^{-1}; $2\theta_{max}$ = 47.94°, reflections collected/unique: 5787/2899 (R_{int} = 0.0482), 2163 $F_o \geq 4\sigma(F_o)$, 433 parameters, wR_2 (all data) = 0.0930, R_1 ($F \geq 4\sigma$) = 0.0371; absolute structure parameter: 0.09(10).[31] **Rh-6c/**

 © 2003 Wiley-VCH Verlag GmbH & Co. KGaA, Weinheim

6d: space group $P2_1/c$ (no. 14), $a = 9.716(1)$, $b = 19.348(2)$, $c = 18.828(4)$ Å, $\beta = 99.80(1)°$, $V = 3487.7(9)$ Å, $Z = 4$, $\mu = 0.688$ mm^{-1}; $2\theta_{max} = 52.14°$, reflections collected/unique: 14610/6889 ($R_{int} = 0.0385$), 4483 $F_o \geq 4\sigma(F_o)$, 399 parameters, wR_2 (all data) = 0.1640, R_1 ($F \geq 4\sigma$) = 0.0647.[32] CCDC-200009 (**Rh-2b***), -200010 (**Rh-6c/6d**), -200011 (**Rh-2a**) and -200012 (**Rh-2b**) contain the supplementary crystallographic data for this paper. These data can be obtained free of charge at www.ccdc.cam.ac.uk/conts/retrieving.html [or from the Cambridge Crystallographic Data Centre, 12 Union Road, Cambridge CB2 1EZ, UK; Fax: (internat.) + 44-1223/336-033; E-mail: deposit@ccdc.cam.ac.uk].

Received December 27, 2002

 © 2003 Wiley-VCH Verlag GmbH & Co. KGaA, Weinheim

A Diiminoplatinum(II) Complex of 4-Ethynylbenzo-15-crown-5 as a Luminescent Sensor for Divalent Metal Ions

Phyllis K. M. Siu,[a] Siu-Wai Lai,[a] Wei Lu,[a] Nianyong Zhu,[a] and Chi-Ming Che*[a]

Keywords: Crown compounds / Platinum / Luminescence / Magnesium / Sensors

The binding of a diiminoplatinum(II) complex of 4-ethynylbenzo-15-crown-5 to divalent metal ions such as Mg^{2+} or Zn^{2+} is accompanied by substantial enhancement of emission intensity (1035- and 870-fold increase, respectively, with 40 equivalents of metal salt) at $\lambda_{max} \approx 555$ nm; H^+, Cd^{2+} and alkali-metal ions cause minor enhancement of the photoluminescence (≤ 10-fold) under similar conditions.

(© Wiley-VCH Verlag GmbH & Co. KGaA, 69451 Weinheim, Germany, 2003)

Introduction

The design of new luminescent sensors for metal ions has continued to attract considerable interest.[1,2] An efficient luminescent probe should exhibit a substantial "switch-on" effect upon binding to metal ions. Using emission as a signalling reporter, luminescent metal complexes are of interest due to their long emission lifetimes, tunable emission energies in the visible region and large Stokes shifts between absorption and emission spectra.[3] In our design of luminescent sensors for metal ions, we were attracted to the following: (1) encapsulation of divalent metal ions such as Zn^{2+} by $[(\eta^5\text{-}C_5H_4SiMe_3)_2Ti(C{\equiv}CR)_2]$ [R = $SiMe_3$ or $(\eta^5\text{-}C_5H_4)FeCp$] via side-on coordination of alkynyl ligands has been reported;[4] (2) crown ethers are known to complex metal ions;[5] (3) neutral organoplatinum(II) complexes are known to form dative bonds with divalent metal ions;[6] and (4) square-planar cyclometalated[7] and aromatic[8,9] diiminoplatinum(II) complexes possess rich photoluminescent properties that are sensitive to the microenvironment. Herein we describe the synthesis of [Pt(4-ethynylbenzo-15-crown-5)$_2$(tBu$_2$bpy)] (**1**) (tBu$_2$bpy = 4,4′-di-*tert*-butyl-2,2′-bipyridine) and [Pt(4-ethynylbenzo-15-crown-5)(C^N^N)] (**2**) (HC^N^N = 6-phenyl-2,2′-bipyridine), and their luminescence responses towards metal ions. A dramatic photoluminescence switch-on effect has been observed for **1** in the presence of $Zn(ClO_4)_2$ and $Mg(ClO_4)_2$ and the binding of Mg^{2+} to **1** found to be selective in the presence of alkali or alkaline earth metal ions.

Results and Discussion

Treatment of [PtCl$_2$(tBu$_2$bpy)][10] with two molar equivalents of 4-ethynylbenzo-15-crown-5 (**L**)[11] in the presence of copper(I) iodide and diisopropylamine afforded **1**. The molecular structure of **1** (Figure 1) shows that the Pt^{II} core is *cis*-coordinated by two 4-ethynylbenzo-15-crown-5 moieties and the tBu$_2$bpy ligand. The cyclometalated counterpart **2** was similarly synthesised by reacting equimolar amounts of [PtCl(C^N^N)][12] and **L** (Figure 2).

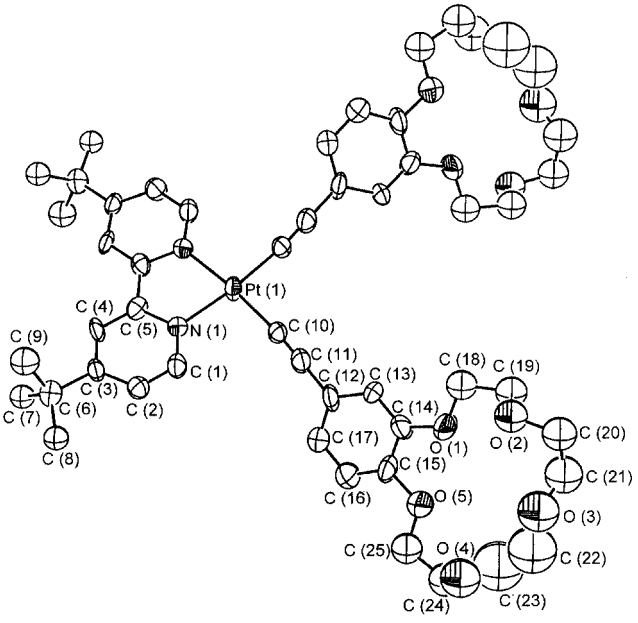

Figure 1. Perspective view of **1** (30% probability ellipsoids); selected bond lengths (Å) and angles (°): Pt(1)−C(10) 1.98(1), Pt(1)−N(1) 2.062(8), C(10)−C(11) 1.12(1); C(10)#1−Pt(1)−C(10) 90.0(6), N(1)#1−Pt(1)−N(1) 78.3(5), C(11)−C(10)−Pt(1) 172(1)

[a] Department of Chemistry and the Open Laboratory of Chemical Biology of the Institute of Molecular Technology for Drug Discovery and Synthesis, The University of Hong Kong, Pokfulam Road, Hong Kong SAR, China
Fax: (internat.) +852-2857-1586
E-mail: cmche@hku.hk

Supporting information for this article is available on the WWW under http://www.eurjic.org or from the author.

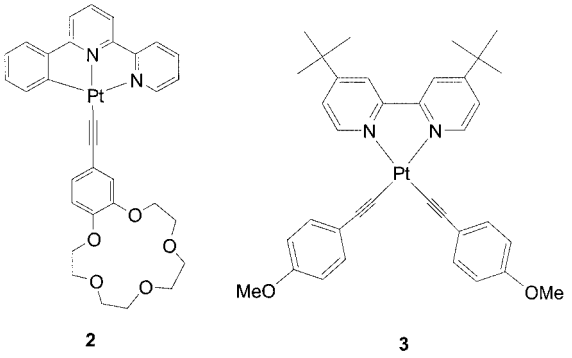

Figure 2. Structures of **2** and **3**

The absorption spectrum of **1** in acetonitrile features a moderately intense band at λ_{max} = 393 nm ($\varepsilon \approx 7900$ dm^3 mol^{-1} cm^{-1}) which is attributed to the [5d(Pt) → π* (*t*Bu$_2$bpy)] metal-to-ligand charge transfer (MLCT) transition. This absorption occurs at the same energy as that reported for [Pt(C≡CC$_6$H$_4$OMe-4)$_2$(*t*Bu$_2$bpy)] (**3**; Figure 2) in acetonitrile.[13] Complex **2** shows an intense ^{1}MLCT [5d(Pt) → π*(C^N^N)] absorption in the 400−450 nm range similar to that typically observed for cyclometalated Pt^{II} derivatives.[7] Addition of 20 equivalents of M(ClO$_4$)$_2$ (M^{2+} = Zn^{2+}, Mg^{2+}) to a 0.1 M *n*Bu$_4$NPF$_6$ acetonitrile solution of **1** (3.2×10^{-5} mol dm^{-3}) blue-shifts the MLCT absorption band from λ_{max} = 393 to 383 nm ($\varepsilon \approx 9600$ dm^3 mol^{-1} cm^{-1}); no significant change in the absorption at λ_{max} = 284 nm is observed. In contrast, addition of up to 100 equivalents of M(ClO$_4$)$_2$ to a 0.1 M *n*Bu$_4$NPF$_6$ acetonitrile solution of **2** or **3** results in no significant shift of the MLCT absorption. Thus, the presence of the *cis* crown ether moieties in **1** appears to be critical to affect the shifting of the MLCT absorption upon interaction with Mg^{2+}/Zn^{2+}.

The weak emission of **1** ($\varphi_o = 1.1 \times 10^{-4}$) in acetonitrile at λ_{max} = 635 nm is assigned as being ^{3}MLCT [5d(Pt) → π*(*t*Bu$_2$bpy)] in nature.[13] Addition of M^{2+} (as a perchlorate salt) to a 0.1 M *n*Bu$_4$NPF$_6$ acetonitrile solution of **1** induces a substantial enhancement of the emission intensity at 553 and 560 nm for Mg^{2+} and Zn^{2+}, respectively, and reaches a maximum of 1035-fold (Figure 3) and 870-fold, respectively, at 40 equivalents of M^{2+}. With reference to previous work,[14] the emission at $\lambda_{max} \approx$ 555 nm may be an admixture with both ^{3}MLCT and $^3\pi\pi^*$ character.

The effect of different Zn^{2+} salts upon binding properties was also examined. Addition of 100 equivalents of ZnCl$_2$ or Zn(NO$_3$)$_2$ to an acetonitrile solution of **1** (3.2×10^{-5} mol dm^{-3}) shows a similar blue shift in the emission maximum from 635 to approx. 560 nm, but the emission intensity was enhanced by only 105- and 250-fold, respectively. This indicates that the binding of **1** to Zn^{2+} ions weakens as the anion nucleophilicity increases in the order: ClO$_4^-$ < NO$_3^-$ < Cl$^-$ in acetonitrile. The effect of protons was investigated by addition of 200 equivalents of HBF$_4$ to a 0.1 M *n*Bu$_4$NPF$_6$ acetonitrile solution of **1**; no emission enhancement was detected. The binding properties of **1** with

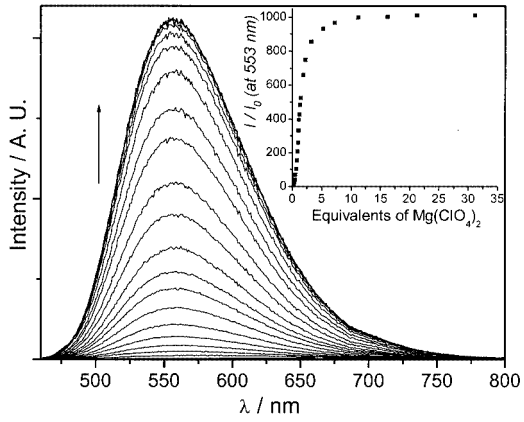

Figure 3. Emission spectral traces and (inset) luminescence enhancement factor (≡ I/I_o; monitored at 553 nm) of **1** at increasing equivalents of Mg^{2+} in 0.1 M *n*Bu$_4$NPF$_6$ acetonitrile solution at 298 K (λ_{ex} = 405 nm, [**1**] = 1.0×10^{-5} mol dm^{-3})

other metal ions have also been studied. Addition of 100 equivalents of KClO$_4$, NaClO$_4$, or Cd(ClO$_4$)$_2$ induces a relatively insignificant increase (≤ 10-fold) in the emission intensity of **1**. However, a 300-fold luminescence enhancement at λ_{max} = 563 nm was observed for **1** in the presence of 100 equivalents of Ca(ClO$_4$)$_2$. As depicted in Figure 4, the luminescence enhancement factor (LE ≡ I/I_o) induced by 40 equivalents of Mg^{2+} decreases by less than 20% in the presence of 40 equivalents of other cations, such as Na$^+$, K$^+$, Cd^{2+} and H$^+$, indicating that the binding of Mg^{2+} to **1** remains selective in their presence. For the binding of Zn^{2+} to **1**, the LE is reduced from 870 to 736 and 160 in the presence of K$^+$ and Na$^+$ respectively. This indicates that Na$^+$ is able to bind to **1** even in the presence of Zn^{2+}.

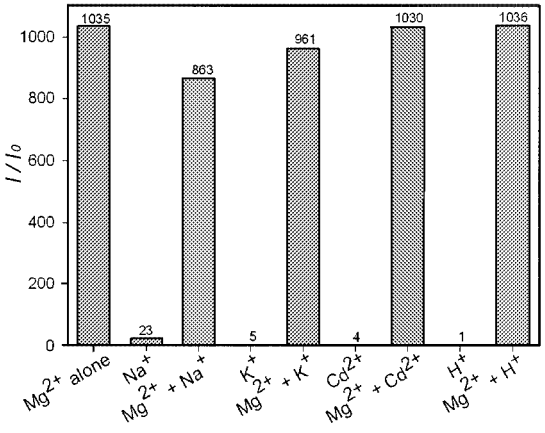

Figure 4. Luminescence enhancement factor induced by 40 equivalents of Mg^{2+} with or without the presence of M^{x+} ions in a 0.1 M *n*Bu$_4$NPF$_6$ acetonitrile solution of **1** (3.2×10^{-5} mol dm^{-3}) at 298 K

Complex **3** displays a weak ^{3}MLCT [5d(Pt) → π* (*t*Bu$_2$bpy)] emission at λ_{max} = 610 nm in acetonitrile.[13] Addition of Zn(ClO$_4$)$_2$ to **3** yields virtually no change in emission intensity with or without the presence of the free

 © 2003 Wiley-VCH Verlag GmbH & Co. KGaA, Weinheim

crown-ether ligand **L**. The ^{3}MLCT emission of the mono-crown derivative **2**, which appears at λ_{max} = 560 nm, undergoes around a 10-fold increase in intensity, together with a slight red-shift to λ_{max} = 581 nm upon addition of 100 equivalents of $Zn(ClO_4)_2$. This signifies that, as observed in the absorption studies, the two crown ether moieties in **1** are essential for the dramatic ion-induced luminescence enhancement.

In order to elucidate the ion-binding nature of **1**, we have attempted to fit the emission data to stepwise equilibrium equations, where M^{x+} ions are consecutively bound by the platinum complex.

$$\begin{aligned} Pt + M^{x+} &\rightleftharpoons PtM^{x+} & K_{11}\\ PtM^{x+} + M^{x+} &\rightleftharpoons Pt(M^{x+})_2 & K_{12}\\ \vdots \quad + M^{x+} &\rightleftharpoons \vdots & \vdots\\ Pt(M^{x+})_{n-1} + M^{x+} &\rightleftharpoons Pt(M^{x+})_n & K_{1n} \end{aligned}$$

The stepwise (K_{11}, K_{12}, K_{13}) and overall (β) binding constants for the complexation of Na^+, Mg^{2+} and Zn^{2+} ions to **1** were determined under the assumptions stated in the supporting information and compared to the total number of M^{x+} ions bound by **1** (*n*) and the β value obtained from the Hill equation (Table 1).[15] In the case of *n* = 3, the discrepancy of β values between the nonlinear least-squares fits and Hill plots for these ions suggests unreasonable data fitting, and that this can be disregarded in the analysis. The similarity in β values determined by stepwise equilibrium binding reactions and Hill plots for the case of *n* = 2 imply that two M^{x+} ions are bound per molecule of **1**. For Na^+, the values of K_{11} and K_{12} are similar, whereas for Zn^{2+} and Mg^{2+}, the K_{12} values are around 20 and 54 times larger, respectively, than the corresponding K_{11} values. The electrospray mass spectra of **1** in the presence of 20 equivalents of $M(ClO_4)_x$ (M^{x+} = Mg^{2+}, Na^+) in acetonitrile reveal peaks attributable to [**1** + nM^{x+}] species (*n* = 1 and 2). For Mg^{2+}, the intensity ratio of peaks for [**1** + M^{x+}]:[**1** +2M^{x+}] is about 2:1, whereas that for Na^+ is about 1:3.

Table 1. Stepwise and overall equilibrium constants of **1** with Na^+, Mg^{2+}, Zn^{2+}

Ions	Nonlinear least-squares fits (*n* = 2)			Hill equation	
	K_{11}	K_{12}	β[a]	n	β
Na^+	7.27×10^3	1.08×10^4	7.9×10^7	1.7	6.5×10^6
Mg^{2+}	3.11×10^3	1.69×10^5	5.3×10^8	2.2	3.7×10^9
Zn^{2+}	2.11×10^3	4.41×10^4	9.3×10^7	2.0	5.5×10^7

[a] β is the overall equilibrium constant = $\Pi^n K_{1n}$

We suggest that the electrophilic M^{2+} ion functions as a Lewis acid that can be bound by the crown ether moieties. This type of interaction induces substantial perturbation upon the luminescence but is prone to competitive interaction of M^{2+} with counteranions. The switching on of substantial emission intensity in **1** with added M^{2+} may be rationalised by the destabilisation of the ^{3}MLCT excited state, leading to an increase in ^{3}IL character for the excited state. Binding of the first M^{2+} ion by **1** may widen the *cis*-[Pt(C≡CR)$_2$] angle, which could facilitate subsequent chelation of the second M^{2+} ion by the crown ether and/or bis-alkynyl moieties. This is consistent with the increase of the K_{12} binding constant relative to K_{11}.

Experimental Section

General Remarks: Acetonitrile for photophysical measurements was distilled over potassium permanganate and calcium hydride. All other solvents were of analytical grade and purified according to conventional methods.[16] 4,4′-Di-*tert*-butyl-2,2′-bipyridine,[17] [PtCl$_2$(*t*Bu$_2$bpy)],[10] 4-ethynylbenzo-15-crown-5,[11] 6-phenyl-2,2′-bipyridine,[18] and [PtCl(C^N^N)][12] were prepared by published methods. Fast atom bombardment (FAB) and electrospray mass spectra were obtained on a Finnigan MAT 95 (3-nitrobenzyl alcohol matrix) and LCQ quadrupole ion trap mass spectrometers, respectively. ^{1}H (500 MHz) NMR spectra were recorded on DPX 500 Bruker FT NMR spectrometers; chemical shift (in ppm) are quoted relative to tetramethylsilane. Elemental analysis was performed by the Institute of Chemistry at the Chinese Academy of Sciences, Beijing. IR spectra were recorded on a BIO RAD FT-IR spectrophotometer. UV/Vis spectra were recorded on a Perkin−Elmer Lambda 19 UV/Vis spectrophotometer.

Steady-state emission spectra were recorded on a SPEX 1681 Fluorolog-2 series F111AI spectrophotometer. The emission spectra were corrected for monochromator and photomultiplier efficiency and for xenon lamp stability.

Solutions for titration experiments were prepared by mixing 5 mL of **1** (6.4×10^{-5} mol dm^{-3}) in a 0.1 M *n*Bu$_4$NPF$_6$ acetonitrile solution with the required molar equivalents of M^{x+} in the same supporting electrolyte and made up to a total of 10 mL with a 0.1 M *n*Bu$_4$NPF$_6$ acetonitrile solution. All the sample solutions were degassed with at least four freeze-pump-thaw cycles. The emission quantum yield was measured by the method of Demas and Crosby.[19] Errors for λ values (± 1 nm) and φ (± 10%) are estimated.

[Pt(4-ethynylbenzo-15-crown-5)$_2$(*t*Bu$_2$bpy)] (1): Reaction of [PtCl$_2$(*t*Bu$_2$bpy)] and two equivalents of 4-ethynylbenzo-15-crown-5 (**L**) in the presence of copper(I) iodide and diisopropylamine afforded **1** (85%). ^{1}H NMR (CD$_3$CN): δ = 1.45 (s, 18 H, *t*Bu), 3.61−3.67 (m, 16 H, CH$_2$), 3.78−3.81 (m, 8 H, CH$_2$), 4.05−4.12 (m, 8 H, CH$_2$), 6.82−6.98 (m, 6 H, C$_6$H$_3$), 7.75 (dd, *J* = 6.0, *J* = 2.0 Hz, 2 H), 8.30 (d, *J* = 1.7 Hz, 2 H), 9.54 (d, *J* = 6.0 Hz, 2 H) ppm. MS (FAB, +ve): *m*/*z* (%) = 1047 (15) [M$^+$ + H], 1069 (60) [M$^+$ + Na], 1085 (8) [M$^+$ + K]. IR (KBr disc): ν̃ = 2101 cm^{-1} (C≡C). $C_{50}H_{62}N_2O_{10}Pt$ (1046.14): calcd. C 57.41, H 5.97, N 2.68; found C 57.59, H 5.82, N 2.92.

[Pt(C^N^N)(4-ethynylbenzo-15-crown-5)] (2): The procedure for the synthesis of **1** was adopted using equimolar amounts of 4-ethynylbenzo-15-crown-5 and [Pt(C^N^N)Cl] (90%). ^{1}H NMR ([D$_6$]DMSO): δ = 3.63 (s, 8 H, CH$_2$), 3.79 (d, *J* = 1.9 Hz, 4 H, CH$_2$), 4.04−4.09 (m, 4 H, CH$_2$), 6.85−6.94 (m, 3 H, C$_6$H$_3$), 7.03−7.15 (m, 2 H), 7.62 (d, *J* = 7.1 Hz, 1 H), 7.76 (d, *J* = 7.1 Hz, 1 H), 7.86 (t, *J* = 6.3 Hz, 1 H), 7.98 (d, *J* = 7.9 Hz, 1 H), 8.10 (t, *J* = 7.9 Hz, 1 H), 8.20 (d, *J* = 7.8 Hz, 1 H), 8.33 (t, *J* = 7.7 Hz, 1 H), 8.48 (d, *J* = 7.9 Hz, 1 H), 9.06 (d, *J* = 4.8 Hz, 1 H) ppm. MS (FAB, +ve): *m*/*z* (%) = 718 (4) [M$^+$ + H], 740 (20) [M$^+$ + Na], 757 (2) [M$^+$ + K]. IR (KBr disc): ν̃ = 2097 cm^{-1} (C≡C).

 © 2003 Wiley-VCH Verlag GmbH & Co. KGaA, Weinheim

$C_{32}H_{30}N_2O_5Pt$ (717.69): calcd. C 53.55, H 4.21, N 3.90; found C 53.29, H 3.96, N 4.06.

X-ray Crystallographic Study of 1: $C_{50}H_{62}N_2O_{10}Pt$, M = 1046.11, orthorhombic, space group *Pccn*, a = 23.888(5), b = 10.653(2), c = 18.467(4) Å, V = 4699.5(16) Å^3, Z = 4, D_c = 1.479 g cm^{-3}, μ(Mo-K_α) = 3.045 mm^{-1}, F(000) = 2136. A crystal of dimensions 0.4 × 0.2 × 0.1 mm^3 mounted in a glass capillary with mother liquor was used for data collection at 20 °C on a MAR diffractometer with a 300 mm image plate detector using graphite-monochromatized Mo-K_α radiation (λ = 0.71073 Å). Data collection was made with 3° oscillation step of φ, 600 seconds exposure time and a scanner distance of 120 mm; 60 images were collected. The images were interpreted and intensities integrated using the program DENZO.[20] The structure was solved by direct methods employing the SHELXS-97 program suite[21] on a PC. Pt and many non-H atoms were located by direct methods. The positions of other non-hydrogen atoms were found after successful refinement by full-matrix least-squares using SHELXL-97[21] on a PC. The *tert*-butyl group is disordered over two kinds of positions. 2849 independent reflections from a total of 11694 reflections were used in the full-matrix least-squares refinement against F^2. R_1 = 0.044 and wR_2 = 0.103 with a goodness-of-fit of 0.853 for 1291 observed reflections with $I \geq 2\sigma(I)$. The final difference Fourier map shows maximum residual peaks and holes of 0.457 and −0.642 e·Å^{-3} respectively. CCDC-177975 contains the supplementary crystallographic data for this paper. These data can be obtained free of charge at www.ccdc.cam.ac.uk/conts/retrieving.html [or from the Cambridge Crystallographic Data Centre, 12, Union Road, Cambridge CB2 1EZ, UK; fax: (internat.) +44-1223/336-033; E-mail: deposit@ccdc.cam.ac.uk].

Supporting Information for this article (scheme for synthesis of **1**; emission spectral traces of **1** at increasing equivalents of Zn^{2+}, Ca^{2+}, Na^+ and K^+ ions; table for fluid-state emissions of **1**−**3** in acetonitrile with 100 equivalents of $M(ClO_4)_x$; analysis of the complexation of ions using nonlinear least-squares fits and Hill plots) is available (see footnote on the first page of this article).

Acknowledgments

We are grateful for financial support from the University Development Fund of The University of Hong Kong, the Research Grants Council of the Hong Kong SAR, China, Area of Excellence Scheme (AoE/P-10/01) of the University Grants Committee of the Hong Kong SAR, China, and The Chinese Manufacturers' Association of Hong Kong.

[1] S. C. Burdette, G. K. Walkup, B. Spingler, R. Y. Tsien, S. J. Lippard, *J. Am. Chem. Soc.* **2001**, *123*, 7831−7841.
[2] [2a] T. Hirano, K. Kikuchi, Y. Urano, T. Higuchi, T. Nagano, *Angew. Chem. Int. Ed.* **2000**, *39*, 1052−1054. [2b] D. A. Pearce, N. Jotterand, I. S. Carrico, B. Imperiali, *J. Am. Chem. Soc.* **2001**, *123*, 5160−5161.
[3] [3a] P. D. Beer, O. Kocian, R. J. Mortimer, C. Ridgway, *J. Chem. Soc., Dalton Trans.* **1993**, 2629−2638. [3b] A. P. de Silva, H. Q. N. Gunaratne, T. E. Rice, S. Stewart, *Chem. Commun.* **1997**, 1891−1892.
[4] H. Lang, N. Mansilla, G. Rheinwald, *Organometallics* **2001**, *20*, 1592−1596.
[5] R. M. Izatt, J. S. Bradshaw, S. A. Nielsen, J. D. Lamb, J. J. Christensen, *Chem. Rev.* **1985**, *85*, 271−339.
[6] T. Yamaguchi, F. Yamazaki, T. Ito, *J. Am. Chem. Soc.* **1999**, *121*, 7405−7406.
[7] [7a] K. H. Wong, M. C. W. Chan, C. M. Che, *Chem. Eur. J.* **1999**, *5*, 2845−2849. [7b] C. M. Che, W. F. Fu, S. W. Lai, Y. J. Hou, Y. L. Liu, *Chem. Commun.* **2003**, 118−119.
[8] S. M. Drew, D. E. Janzen, C. E. Buss, D. I. MacEwan, K. M. Dublin, K. R. Mann, *J. Am. Chem. Soc.* **2001**, *123*, 8414−8415.
[9] V. W. W. Yam, R. P. L. Tang, K. M. C. Wong, X. X. Lu, K. K. Cheung, N. Zhu, *Chem. Eur. J.* **2002**, *8*, 4066−4076.
[10] K. D. Hodges, J. V. Rund, *Inorg. Chem.* **1975**, *14*, 525−528.
[11] S. V. Klyatskaya, E. V. Tretyakov, S. F. Vasilevsky, *Mendeleev Commun.* **1998**, *8*, 201−202.
[12] [12a] E. C. Constable, R. P. G. Henney, T. A. Leese, D. A. Tocher, *J. Chem. Soc., Chem. Commun.* **1990**, 513−515. [12b] T. C. Cheung, K. K. Cheung, S. M. Peng, C. M. Che, *J. Chem. Soc., Dalton Trans.* **1996**, 1645−1651.
[13] [13a] M. Hissler, W. B. Connick, D. K. Geiger, J. E. McGarrah, D. Lipa, R. J. Lachicotte, R. Eisenberg, *Inorg. Chem.* **2000**, *39*, 447−457. [13b] S. C. Chan, M. C. W. Chan, Y. Wang, C. M. Che, K. K. Cheung, N. Zhu, *Chem. Eur. J.* **2001**, *7*, 4180−4190.
[14] V. M. Miskowski, V. H. Houlding, C. M. Che, Y. Wang, *Inorg. Chem.* **1993**, *32*, 2518−2524.
[15] *Binding Constants* (Ed.: K. A. Conners), Wiley, New York, **1987**.
[16] D. D. Perrin, W. L. F. Armarego, D. R. Perrin, *Purification of Laboratory Chemicals*; 2nd ed., Pergamon: Oxford, **1980**.
[17] G. M. Badger, W. H. F. Sasse, *J. Chem. Soc.* **1956**, 616−620.
[18] F. Kröhnke, *Synthesis* **1976**, 1−24.
[19] J. N. Demas, G. A. Crosby, *J. Phys. Chem.* **1971**, *75*, 991−1024.
[20] Z. Otwinowski, W. Minor, *Processing of X-ray Diffraction Data Collected in Oscillation Mode*, Methods in Enzymology, Volume 276: Macromolecular Crystallography, part A, 307−326, **1997** (Eds.: C. W. Carter, R. M. Sweet Jr.), Academic Press.
[21] G. M. Sheldrick, *SHELXS-97, Program for Crystal Structure Analysis*, **1997**, University of Göttingen, Germany.

Received April 14, 2003

 © 2003 Wiley-VCH Verlag GmbH & Co. KGaA, Weinheim

A Novel Tetranuclear $[MeZn(\mu_3\text{-}OCH_2CH_2SMe)Zn(\mu\text{-}Cl)Me]_2$ Adduct Derived from the Interaction of CH_2Cl_2 with an Alkylzinc Complex

Janusz Lewiński,*[a] Wojciech Marciniak,[a] Zbigniew Ochal,[a] Janusz Lipkowski,[b] and Iwona Justyniak[b]

Keywords: Zinc / Alkoxides / Chelates / O,S ligand / Solvent effects

The treatment of 2-(methylthio)ethanol (methioH) with two equivalents of Me_2Zn in CH_2Cl_2 affords a tetranuclear aggregate with two monomeric MeZn(methio) units joined by two MeZnCl moieties. This result demonstrates that transfer of a chloride ion to Zn takes place on the addition of a donor-functionalized alcohol to Me_2Zn in CH_2Cl_2 solution.
(© Wiley-VCH Verlag GmbH & Co. KGaA, 69451 Weinheim, Germany, 2003)

Introduction

Dichloromethane is one of the most commonly used solvents for organic and organometallic reactions involving alkylzinc reagents, especially the Simmons−Smith cyclopropanation of olefins[1] or the enantioselective addition of organozinc reagents to prochiral carbonyl compounds in the presence of catalytic amounts of a chiral ligand,[2] arguably the most important application of organozinc reagents in organic synthesis, as well as other types of reactions involving alkylzinc reagents.[3] The great interest and simple procedure of both reactions have motivated extensive work to better understand the reaction, including detailed mechanistic studies. For instance, very recent theoretical studies on the reaction pathways of the Simmons−Smith reaction have demonstrated that "the Lewis acid coordination to the halogen atom on the halomethyl ligand is likely to be a key event in the cyclopropanation reaction".[4] However, as far as we are aware, an influence of CH_2Cl_2 on the course or outcome of these various reactions has not been considered. Herein we report the isolation and structural characterization of the novel tetranuclear zinc adduct $[MeZn(\mu_3\text{-}OCH_2CH_2SMe)Zn(\mu\text{-}Cl)Me]_2$ (**1**), derived from the reaction of Me_2Zn with a bifunctional alcohol in the presence of CH_2Cl_2.

Results and Discussion

The treatment of 2-(methylthio)ethanol (methioH) with two equivalents of Me_2Zn in toluene/CH_2Cl_2 affords a yellow solution from which a white precipitate deposits after cooling at −15 °C for several hours. The complex could be isolated in moderate yield from the reaction, and it was studied by ^1H NMR spectroscopy and elemental analysis. ^1H NMR spectroscopy revealed two Zn-bonded methyl groups with a 1:1 Me-Zn/ligand ratio.[5] The occurrence of several sets of broad signals due to the O,S-bifunctional ligand indicated the operation of a dynamic process, likely to be the reversible dissociation of the tetranuclear complex, and the inversion of configuration at the sulfur atoms. The obtained ambiguous data of the precipitate led us to carry out a single-crystal X-ray diffraction study to elucidate the product structure. To our surprise, this study revealed **1** to be a tetranuclear aggregate with two monomeric MeZn(methio) units joined by two MeZnCl moieties (Figure 1). Interestingly, in contrast to the commonly observed μ_2-O bonding mode of the alkoxide oxygen atoms in dimeric $[RZn(\mu\text{-}O,N)]_2$ complexes,[6] the analogous oxygen atoms of **1** function as μ_3-O donors; this bonding mode is typical for the cubane-type structure of alkylzinc alkoxides $[RZn(\mu_3\text{-}OR)]_4$.[7] The aggregate **1** has C_1 symmetry with a central $Zn_2(\mu_3\text{-}O)_2$ ring. The chloride acts as a bridge between the two Zn atoms with the formation of Zn_2ClO rings which take up a trans conformation with an angle of 74.92(5)° to the Zn_2O_2 plane [the Zn_2ClO ring is slightly folded about the Zn−Zn vector with a dihedral angle of 168.72(6)°]. The geometry of the *O*,*S*-chelate may be described as an open envelope with the S−Me methyl groups trans to each other. The ligand used becomes chiral upon complexation of the SMe group to the zinc atom; the two sulfides have an opposite chirality and the resulting achiral complex possesses C_i symmetry. The geometry about the zinc centers is distorted tetrahedral. Selected bond lengths and bond angles of **1** are given in the legend of Figure 1. The Zn−O bond lengths lie in the range 2.043(2)−2.101(2) Å and are slightly longer than those in dimeric $[RZn(\mu\text{-}O,N)]_2$ complexes.[8]

[a] Department of Chemistry, Warsaw University of Technology, Noakowskiego 3, 00-664 Warsaw, Poland
E-mail: lewin@ch.pw.edu.pl
[b] Institute of Physical Chemistry, Polish Academy of Sciences, Kasprzaka 44/52, 01-224 Warsaw, Poland

The chloride bridges are essentially symmetrical with Zn−Cl distances of 2.365(1) Å and 2.370(1) Å and this fact indicates that the formation of these bridges is geometrically favorable. The Zn−C bond length of the bridging MeZnCl moiety does not differ from the value for the terminal Zn−Me group.

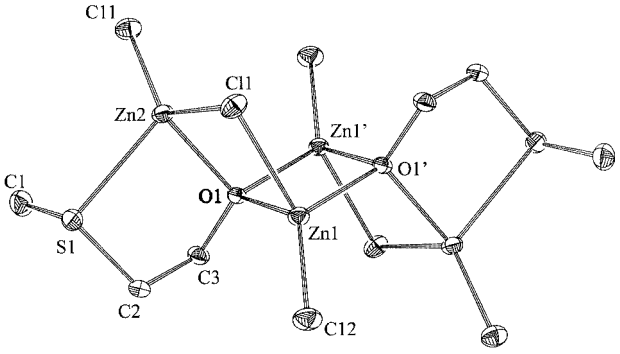

Figure 1. Molecular structure of **1** with thermal ellipsoids drawn at the 30% probability level; selected bond lengths [Å] and angles [°]: C12−Zn1 1.956(3), Zn1−O1 2.101(2), Zn1′−O1 2.043(2), Zn1−Cl1 2.370(1), Zn2−Cl1 2.365(1), Zn2−O1 2.072(2), Zn2−S1 2.475(2), Zn2−C11 1.960(3); C12−Zn1−Cl1 123.97(8), Zn1′−O1−Zn1 96.38(6), O1−Zn2−Cl1 87.59(4), Zn2−Cl1−Zn1 84.70(2)

Compound **1**, apart from being a novel organozinc aggregate, may also serve as a useful model compound for the donor-functionalized-alcohol promoted addition of dialkylzinc reagents to carbonyl compounds (vide infra). So, can related tetranuclear aggregates be formed and observed in the reaction without additional stabilization provided by the chloride bridges? In order to answer this question we conducted an analogous reaction of methioH with two equivalents of Et_2Zn in benzene as a solvent. Cryoscopic weight measurements on the post reaction mixture indicated the presence of some higher aggregated species in solution [MW found 270; for example, calcd. 309 for $EtZn(methio)ZnEt_2$]. The ^1H NMR spectrum of the same solution showed several multiple resonances, presumably due to dynamic processes and skeletal rearrangement of the resulting products in solution. Unfortunately, the above studies only confirm that zinc alkoxides have a tendency to form higher aggregates.

The reported studies revealed several important aspects of various transformations involving alkylzinc reagents. Of particular importance is the fact that on the addition of a bifunctional alcohol to R_2Zn in CH_2Cl_2 solution, the transfer of a chloride ion to Zn takes place. In this regard, our studies demonstrate that CH_2Cl_2 seems to be the least desirable solvent for reactions involving alkylzinc reagents supported by donor-functionalized alcohols and a large number of investigations reported in the literature may be invalid.[9] Furthermore, in our opinion adduct **1** mimics a potential intermediate in the donor-functionalized-alcohol promoted addition of dialkylzinc to aldehydes (especially in the case of the *O*,*X*-bifunctional auxiliary ligand with sterically non-encumbered alkyl substituents at the α-carbon atom). The commonly accepted mechanism for the latter reaction assumes the participation of the monomeric three-coordinate zinc species **II** as the sole reactive species, which exists in equilibrium with the inactive dimer **I** (Scheme 1).[2] Some uncertainties, however, in the mechanistic analysis of this reaction have been observed,[10] which are probably introduced by the presence of multiple equilibria of different Zn aggregates, and in this regard the question as to whether the reaction can proceed through different pathways arises. All the above facts indicate that a more in-depth understanding of this reaction is necessary to better interpret the results from the experiments and raises the question as to whether the reaction can proceed through different pathways. However, alternative structural models for the dormant and active species present within the donor-functionalized-alcohol promoted addition of dialkylzinc to aldehydes are lacking.

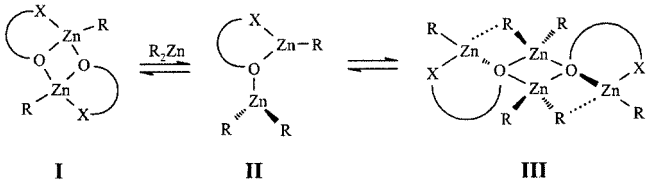

Scheme 1

Based on the isolation of **1**, we suggest that higher aggregate species, such as the tetrametallic dimer of type **III**, are possible primary reactants in the reaction. The speculated structures of the dimer **III** are presented in Scheme 1. As far as we are aware, in all the recent mechanistic discussions, as well as in the field of zinc alkoxide chemistry, such a possibility has never been taken into consideration. The considered tetrametallic species can be easily stabilized by weak intramolecular interactions resulting from metal-alkyl agostic interactions or the formation of a relatively stable carbon-bridge between zinc atoms. There is no relevant experimental evidence for this hypothesis, however, we can anticipate that both the increased nucleophilicity of the alkyl group of the R_2Zn fragment (due to the Zn coordination to two alkoxide centers) and the presence of the unsaturated three-coordinate Zn atom of the monometallic $RZn(O,X)$ subunit will favour these types of interactions.[11] The symmetrical strong chloride bridges observed for **1** also indicate that such interactions are geometrically favorable. In our opinion further studies should require serious consideration of the contribution of the associative mechanism in the case of less sterically encumbered reaction systems than the "DAIB system".[12] It seems likely that the monomeric dimetallic adduct or dimeric tetrametallic aggregate may be the active catalyst in the latter reaction depending on the nature of the auxiliary ligand and reaction conditions.[13] We fully intend to investigate this problem further based on these preliminary studies.

The reported results should be helpful for a rational catalyst design and stimulate further experimental and theoretical investigations to clarify the correlation between the structure and activity of organozinc species. Further studies on the factors controlling the degree of aggregation of

 © 2003 Wiley-VCH Verlag GmbH & Co. KGaA, Weinheim

alkylzinc chelate complexes and the extent to which CH_2Cl_2 reacts with various organozinc reagents are in progress.

Conclusion

The reported studies revealed that the transfer of a chloride ion to the zinc atom takes place upon the addition of a bifunctional alcohol to R_2Zn in CH_2Cl_2 solution. In this regard, CH_2Cl_2 seems to be the least-desirable solvent for reactions involving alkylzinc reagents supported by donor-functionalized alcohols. The reaction results in the formation of the novel tetrametallic adduct [MeZn(μ$_3$-OCH$_2$CH$_2$SMe)Zn(μ-Cl)Me]$_2$ (**1**). In our opinion, the latter compound mimics a new potential intermediate in the donor-functionalized-alcohol promoted addition of dialkylzinc to aldehydes.

Experimental Section

General Remarks: All reactions were carried out under dry nitrogen using standard Schlenk techniques. Solvents were dried and distilled prior to use. NMR spectra were recorded on a Varian Mercury 400 spectrometer.

[MeZn(μ$_3$-OCH$_2$CH$_2$SMe)Zn(μ-Cl)Me]$_2$ (1): 2-(Methylthio)-ethanol (2 mmol, 0.17 mL, 0.18 g) was added at −78 °C to a stirred toluene/CH_2Cl_2solution of Me_2Zn (2 M, 2 mL, 4 mmol). The reaction mixture was then allowed to warm to room temperature and stirred for 4 h. The solvents were then removed under vacuum, leaving a white solid that was crystallized from toluene at −15 °C. Yield 42% (0.24 g). $C_{10}H_{26}Cl_2O_2S_2Zn_4$ (574.9): calcd. C 20.89, H 4.56, Cl 12.33; found C 20.75, H 4.62, Cl 12.43. ^{1}H NMR: δ = −0.30 (s, 6 H, Zn-C*H*$_3$), 2.10 (s, 3 H, S-C*H*$_3$), 2.58 (t, 2 H, C*H*$_2$-O), 3.83 (t, 3 H, S-C*H*$_2$) ppm.

X-ray Crystallographic Study: A single crystal of **1** suitable for X-ray diffraction studies was placed in a thin-walled capillary tube (Lindemann glass 0.5 mm) under an inert atmosphere. The tube was plugged with grease, then flame-sealed and mounted on a goniometer head.

Crystal Data for 1: M = 574.86, crystal dimensions 0.40 × 0.36 × 0.16 mm^3, monoclinic, space group $P2_1/c$ (no. 14), a = 7.0040(3), b = 13.0070(6), c = 11.7400(6) Å, β = 104.5840(18)°, U = 1035.07(8) Å^3, Z = 4, F(000) = 576, D_c = 1.844 g m^3, T = 293(2) K, Mo-K_α radiation (λ = 0.71073 Å), Nonius Kappa-CCD diffractometer, θ_{max} = 27.48°, 2357 unique reflections which were used in all calculations. The structure was solved by direct methods[14] and refined by full-matrix least-squares on F^2.[15] H atoms were included in idealized positions and refined isotropically. Refinement converged at $R1$ = 0.0340, $wR2$ = 0.0624 for all data and 91 parameters [$R1$ = 0.0274, $wR2$ = 0.0606 for 2083 reflections with $I_o > 2\sigma(I_o)$]. The goodness-of-fit on F^2 was equal to 1.083. A weighting scheme $w = [\sigma^2(F_o^2 + (0.0418P)^2 + 3.1964P]^{-1}$ where $P = (F_o^2 + 2F_c^2)/3$ was used in the final stage of refinement; residual electron density = 0.42/−0.48 e·Å^{-3}. CCDC-197262 contains the supplementary crystallographic data for this paper. These data can be obtained free of charge at www.ccdc.cam.ac.uk/conts/retrieving.html [or from the Cambridge Crystallographic Data Centre, 12, Union Road, Cambridge CB2 1EZ, UK; fax: (internat.) +44-1223/336-033; E-mail: deposit@ccdc.cam.ac.uk].

Acknowledgments

This work was supported by the State Committee for Scientific Research (No. 3 T09A 066 19).

[1] A. B. Charette, *Cyclopropanation Mediated by Zinc Organometallics* (Eds.: P. Knochel, P. Jones), Oxford University Press, Oxford, **1999**, pp 263−283.
[2] K. Soai, S. Niwa, *Chem. Rev.* **1992**, *92*, 833; P. Knochel, R. D. Singer, *Chem. Rev.* **1993**, *93*, 2117; L. Pu, H. Yu, *Chem. Rev.* **2001**, *101*, 757.
[3] See for example: B. M. Trost, V. S. C. Yeh, *Angew. Chem. Int. Ed.* **2002**, *41*, 861.
[4] M. Nakamura, A. Hirai, E. Nakamura, *J. Am. Chem. Soc.* **2003**, *125*, 2507.
[5] The room temperature ^{1}H NMR spectrum exhibits an additional sharp singlet of lower intensity which was assigned to a small amount of monomeric species present upon dissolution of crystalline **1**.
[6] See for example: M. Kitamura, S. Suga, M. Niwa, R. Noyori, *J. Am. Chem. Soc.* **1995**, *117*, 4832; C. Bolm, G. Schlingloff, K. Harms, *Chem. Ber.* **1992**, *125*, 1191; M. R. P. van Vliet, G. van Koten, P. Buysingh, J. T. B. H. Jastrzebski, A. L. Spek, *Organometallics* **1987**, *6*, 537; M. R. P. van Vliet, J. T. B. H. Jastrzebski, G. van Koten, K. Vrieze, A. L. Spek, *J. Organomet. Chem.* **1983**, *251*, C17.
[7] See for example: H. M. M. Shearer, C. B. Spencer, *J. Chem. Soc., Chem. Commun.* **1966**, 194; W. A. Hermann, S. Bogdanovic, J. Behm, M. Denk, *J. Organomet. Chem.* **1992**, *430*, C33.
[8] M. Kitamura, S. Okada, S. Suga, R. Noyori, *J. Am. Chem. Soc.* **1989**, *111*, 4028.
[9] For example, it may concern a large body of work concerning a highly enantioselective addition of diethylzinc to aldehydes with the catalysis of racemic amino alcohols in the presence of chiral additives, through an asymmetric deactivation strategy with a combinatorial approach, where the reactions were carried out in CH_2Cl_2/hexane solution for 48 h; J. Long, K. L. Ding, *Angew. Chem. Int. Ed.* **2001**, *40*, 544. The same concern can be raised about other recent work using a high-throughput screening technique to find the most efficient catalyst for asymmetric reactions: R. Angelaud, Y. Matsumoto, T. Korenaga, K. Kudo, M. K. Senda. Mikami, *Chirality* **2000**, *12*, 544.
[10] See for example: T. Katagiri, Y. Fujiwara, S. Takahashi, N. Ozaki, K. Uneyama, *Chem. Commun.* **2002**, 986.
[11] There are only two structurally characterized dimeric compounds which incorporate unsaturated hydrocarbon bridges between zinc atoms, R. S. Dickson, G. D. Fallon, Q.-Q. Zhang, *J. Chem. Soc., Dalton Trans.* **2000**, 1973; E. A. Jeffery, T. Mole, J. K. Saunders, *Aust. J. Chem.* **1968**, *21*, 137.
[12] The extensive mechanistic studies carried out by Noyori et al. were supported by detailed kinetic studies involving sterically demanding camphor-derived chiral amino alcohols as auxiliary ligands, 3-*exo*-dimethylamino-*iso*-borneol (DAIB), see ref.[7]
[13] One of the most striking features of the reaction is the strong asymmetric amplification in product enantioselectivity and the central problem concerns the origin of the nonlinear effect in this catalytic reaction. The proposed novel intermediate **III** corresponds well to the theoretical idea of the ML_2 model system involving the catalytically active dimer: C. Girard, H. B. Kagan, *Angew. Chem. Int. Ed.* **1998**, *37*, 2923.
[14] G. M. Sheldrick, SHELXS-86, *Acta Crystallogr., Sect. A* **1990**, *46*, 467.
[15] G. M. Sheldrick, SHELXL-93, University of Göttingen, **1993**.

Received May 6, 2003

 © 2003 Wiley-VCH Verlag GmbH & Co. KGaA, Weinheim

Lindqvist-Type (Aryldiazenido)polyoxomolybdates − Synthesis, and Structural and Spectroscopic Characterization of Compounds of the Type $(n\mathrm{Bu_4N})_3[\mathrm{Mo_6O_{18}(N_2Ar)}]$

Carlos Bustos,[a] Bernold Hasenknopf,[b] René Thouvenot,[b] Jacqueline Vaissermann,[b] Anna Proust,[b] and Pierre Gouzerh*[b]

Keywords: Molybdenum / NMR spectroscopy / Polyoxometalates / N ligands

A series of aryldiazenido compounds of the type $(n\mathrm{Bu_4N})_3[\mathrm{Mo_6O_{18}(N_2Ar)}]$ have been prepared by treatment of $(n\mathrm{Bu_4N})_4[\mathrm{Mo_8O_{26}}]$ with the appropriate arylhydrazines in acetonitrile or in methanol. All these compounds are isostructural. Two members of the series, the *o*-nitro and the *p*-carboxy derivatives, have been characterized by single-crystal X-ray diffraction. The aryl ring in the first anion lies in a mirror plane of the polyoxometalate, while in the second one it is tilted, allowing hydrogen bonding between the carboxylic acid function and a neighbouring anion. The aryldiazenido ligands exhibit the characteristic features of the singly bent coordination mode with short Mo–N and N–N bond lengths indicative of multiple bond character. The compounds have been characterized by ^{95}Mo and ^{17}O NMR spectroscopy in acetonitrile. Their spectra indicate C_{4v} symmetry, and hence stereochemical nonrigidity in solution. The ^{95}Mo chemical shifts are mainly determined by variation in the paramagnetic shielding term, σ_{para}. The strongly deshielded resonance of the Mo^{II} centre spans a large range (600–1100 ppm).

(© Wiley-VCH Verlag GmbH & Co. KGaA, 69451 Weinheim, Germany, 2003)

Introduction

The functionalization of polyoxometalates (i.e., the replacement of one or several oxo ligands by other ligands) allows their properties to be tuned and provides a route to their application in supramolecular chemistry through the introduction of suitable pendent functions.[1,2] As part of a broad program centred on the functionalization of polyoxometalates, we have for some time been interested in the replacement of terminal oxo ligands by other multiply bonded ligands such as nitrosyl,[3−7] imido[8,9] and nitrido[10] ligands. From electronic considerations, these ligands fall into two categories, the first being the π-donor imido and nitrido ligands, RN^{2-} and N^{3-}, respectively, which can substitute for oxo ligands without a change in the oxidation state of the metal atom − although reduction of Mo^{VI} to Mo^{V} is sometimes observed in the course of the reactions of polyoxomolybdates with precursors of imido and nitrido ligands − and the second being the π-acceptor nitrosyl ligand, which cannot bind to a d^0 metal centre. Consequently, (nitrosyl)polyoxometalates always contain reduced centres, for example, d^4 (M^{II}) and d^6 (M^0) in $\{M(NO)\}^{3+}$ [3−7] and $\{M(NO)_2\}^{2+}$ [11] units (M = Mo, W), respectively. Because of the analogy between nitrosyl and diazenido ligands,[12] there should be structurally related pairs of nitrosyl and diazenido derivatives of polyoxometalates, which might be obtained − at least in principle − through analogous reactions between hydroxylamine or monosubstituted hydrazines and polyoxomolybdates. However, the reactivity of hydrazines towards polyoxomolybdates contrasts with that of hydroxylamine. Nitrosyl derivatives containing $\{M(NO)\}^{3+}$ units are quite easily obtained by treatment of polyoxomolybdates with hydroxylamine in nonaqueous solvents,[3,4,6] while the incorporation of $\{Mo(NO)_2\}^{2+}$ units in polyoxomolybdates requires the use of additional ligands, such as amidoximes.[11] In contrast, the products of the reactions between hydrazines and polyoxomolybdates most often contain $\{Mo(N_2Ar)_2\}^{2+}$ units,[13] while derivatives containing $\{Mo(N_2Ar)\}^{3+}$ units are not easily obtained. The phenyldiazenido Lindqvist-type molybdate $(n\mathrm{Bu_4N})_3[\mathrm{Mo_6O_{18}(N_2Ph)}]$ was described as early as 1986,[14] but in our hands the reported procedure failed to give the expected compound. The perfluoro derivative, $(n\mathrm{Bu_4N})_3[\mathrm{Mo_6O_{18}(N_2C_6F_5)}]$, was reported soon after, but without full details about its preparation.[15] This latter paper also included a preliminary study of these compounds by ^{95}Mo NMR spectroscopy. In our experience, the synthesis of $(n\mathrm{Bu_4N})_3[\mathrm{Mo_6O_{18}(N_2Ar)}]$ is quite sensitive to the boundary conditions. We report here the synthesis and characterization of an extended series of these compounds (Scheme 1).

[a] Instituto de Quimica, Universidad Austral de Chile, Casilla 567, Valdivia, Chile
[b] Laboratoire de Chimie Inorganique et Matériaux Moléculaires, UMR CNRS 7071, Université Pierre et Marie Curie, 4 place Jussieu, 75252 Paris cedex 05, France
E-mail: pg@ccr.jussieu.fr

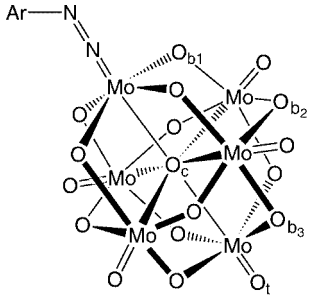

Ar	Compound	Ar	Compound
C_6H_5	**1**	C_6H_4-*m*-NO_2	**8**
C_6H_4-*p*-CH_3	**2**	C_6F_5	**9**
C_6H_4-*p*-F	**3**	C_6H_4-*o*-NO_2	**10**
C_6H_4-*p*-CN	**4**	C_6H_4-*p*-NO_2	**11**
C_6H_4-*p*-CF_3	**5**	C_6H_3-*o*,*p*-$(NO_2)_2$	**12**
C_6H_4-*p*-OCH_3	**6**	C_6H_4-*p*-CO_2H	**13**
C_6H_4-*o*-Cl	**7**		

Scheme 1

Results and Discussion

Synthesis

Arylhydrazines, $ArNHNH_2$, react with dioxomolybdenum(VI) complexes, $[MoO_2L_x]$, to give bis(aryldiazenido)molybdenum complexes of the type $[Mo(N_2Ar)_2L_x]$. While sulfur- and/or nitrogen-ligated ancillary ligands[16,17] are usually not displaced in the course of the reaction, oxygen-ligated ligands such as acetylacetone[18] and 2,3-butanediol[19] may be displaced. When the reaction is carried out in methanol this eventually produces tetranuclear complexes of the type $[Mo_4O_8(OMe)_2(N_2Ar)_4]^{2-}$.[19,20] These complexes are also easily obtained by treatment of $(nBu_4N)_4[Mo_8O_{26}]$ with arylhydrazines in refluxing MeOH,[13] and this approach can be generalized, compounds of the type $(nBu_4N)_2[Mo_4O_8(OR)_2(N_2Ar)_4]$ being obtainable from the reaction between an arylhydrazine and an isopolyoxomolybdate such as $(nBu_4N)_2[Mo_6O_{19}]$ or $(nBu_4N)_4[Mo_8O_{26}]$ in an alcohol (ROH). It was originally thought that the formation of Lindqvist-type derivatives, $(nBu_4N)_3[Mo_6O_{18}(N_2Ar)]$, would be favoured in acetonitrile, but complexes containing $\{Mo(N_2Ar)_2\}^{2+}$ moieties, such as $[Mo_8O_{20}(N_2Ar)_6]^{4-}$,[21] are again the major compounds formed. We have now found that the solvent is not critical. Indeed, $[Mo_6O_{18}(N_2C_6H_4$-*p*-$NO_2)]^{3-}$ can be obtained in acetonitrile as well as in MeOH or EtOH. In fact, the formation of the $\{Mo(N_2Ar)\}^{3+}$ unit, and hence the $[Mo_6O_{18}(N_2Ar)]^{3-}$ complexes **1**−**13**, depends critically upon the temperature and the composition of the reactant mixture. In a typical preparation, the arylhydrazine was added to a solution of $(nBu_4N)_4[Mo_8O_{26}]$ in degassed acetonitrile and the mixture was stirred at ca. 50 °C for a short period of time. Heating must not be prolonged after the colour of the mixture has changed to red-brown. Addition of triethylamine, even if the arylhydrazine was not introduced in the form of its hydrochloride, is beneficial to the reaction. It has also been found that the yield of $(nBu_4N)_3[Mo_6O_{18}(N_2Ar)]$ can be significantly increased by addition of $(nBu_4N)Br$, which is likely to help precipitation of the target compounds.

The $[Mo_6O_{18}(N_2Ar)]^{3-}$ derivatives **1**−**13** are only moderately stable in solution. In most cases, the progressive increase of the ^{95}Mo NMR signals of $[Mo_6O_{19}]^{2-}$ and α-$[Mo_8O_{26}]^{4-}$ indicates decomposition. For example, at 50 °C the parent complex $[Mo_6O_{18}(N_2Ph)]^{3-}$ was found to transform mainly into $[Mo_6O_{19}]^{2-}$ in DMF while α-$[Mo_8O_{26}]^{4-}$ was the major decomposition product in acetonitrile.

X-ray Diffraction Analysis

The *o*-nitro (**10**), *p*-nitro (**11**) and *p*-carboxy (**13**) derivatives have been characterized by single-crystal X-ray diffraction. Soon after the study of **11** had been completed, we became aware of the report by Li et al.[22] on the same compound. As there are no significant differences between the two sets of data, we will not enlarge on the crystal structure of **11**. Three other compounds of the type $(nBu_4N)_3[Mo_6O_{18}(N_2Ar)]$, namely **1**,[14] **9**[15] and **12**,[23] had been characterized previously. With the exception of **13**, all the compounds of the type $(nBu_4N)_3[Mo_6O_{18}(N_2Ar)]$ characterized to date are isomorphous (space group *Pmcn*) and the anion displays C_s symmetry with the aryl group lying in the plane of symmetry passing through the two apical Mo centres and two bridging oxygen atoms of the equatorial belt (Mo1, O33, Mo6 and O44 in Figure 1). Compound **13** crystallizes in the $P2_1cn$ space group, the noncentrosymmetric counterpart of the *Pmcn* space group. In this structure, the aromatic ring does not lie in the plane defined above. Instead, it lies almost in the plane of an $\{Mo_4O_4\}$ ring comprising Mo1, Mo2, Mo4 and Mo6 (Figure 2), the deviation being fairly small (13.5°) and the arrangement perhaps being the result of intermolecular interactions in the solid. The anions are linked into chains through O−H···O bonds involving the carboxylic acid function of one anion and a terminal oxygen atom of another anion [O···O 2.796(16) and 2.788(16) Å]. The aryldiazenido ligands in $[Mo_6O_{18}(N_2Ar)]^{3-}$ exhibit the characteristic features of the singly bent coordination mode with a linear Mo−N−N arrangement and short Mo−N and N−N bond lengths indicative of multiple-bond character (Table 1).[13−17] The bond angle at the β-nitrogen atom is around 120° as expected for an sp^2-hybridized atom. The Mo−O distance between the functionalized Mo centre and the central oxygen atom (O_c, see Scheme 1) is significantly shorter than other Mo−O_c distances. Analogous contractions have been observed in other monofunctionalized Lindqvist-type hexamolybdates such as $[Mo_6O_{18}(NNMePh)]^{2-}$,[24] $[Mo_6O_{18}(NC_6H_4$-*p*-$CH_3)]^{2-}$ [25] and $[Mo_6O_{18}(\eta^5$-$C_5Me_5)]^-$,[26] reflecting the weaker *trans* influence of diazenido, hydrazido, imido and cyclopentadienyl ligands relative to the oxo ligand. Inspection of bond lengths in the Mo_4O_4 rings going through Mo(1) (Figures 1 and 2) reveals the same pattern of bond length alternation as observed in other monosubstituted

 © 2003 Wiley-VCH Verlag GmbH & Co. KGaA, Weinheim

hexamolybdates.[24−27] Because of the disorder in the solid-state structure of $(n\mathrm{Bu_4N})_3[Mo_6O_{18}(NO)]$,[5] no accurate comparison can be made between the structural parameters of $[Mo_6O_{18}(N_2Ar)]^{3-}$ and those of $[Mo_6O_{18}(NO)]^{3-}$. However, there is no doubt that the bonding features within the $\{Mo(N_2Ar)\}^{3+}$ unit are quite similar to those of the $\{Mo(NO)\}^{3+}$ unit. In such coordination modes, diazenido and nitrosyl ligands are commonly regarded as RN_2^+ and NO^+ species, respectively. According to this formalism, $\{Mo(N_2Ar)\}^{3+}$ and $\{Mo(NO)\}^{3+}$ units contain Mo^{II} centres.

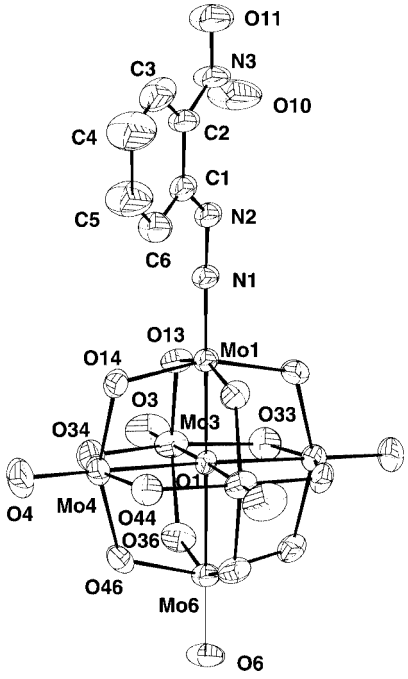

Figure 1. Molecular structure of $[Mo_6O_{18}(N_2C_6H_4\text{-}o\text{-}NO_2)]^{3-}$; thermal ellipsoids are drawn at the 30% probability level

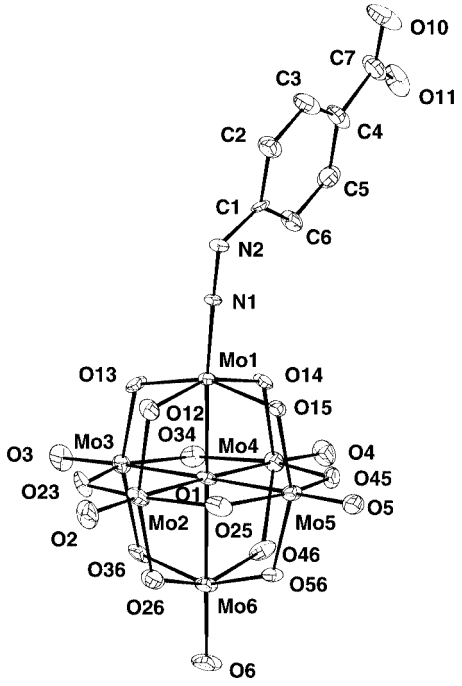

Figure 2. Molecular structure of $[Mo_6O_{18}(N_2C_6H\text{-}p\text{-}CO_2H)]^{3-}$; thermal ellipsoids are drawn at the 30% probability level

Table 1. Geometric features of the MoN_2Ar groups in $(n\mathrm{Bu_4N})_3[Mo_6O_{18}(N_2Ar)]$

Compound	Mo−N [Å]	N−N [Å]	Mo−N−N [°]	Ref.
1	1.76(2)	1.31(3)	178.7(19)	[14]
9	1.75(2)	1.30(3)	170.6(21)	[15]
10	1.75(1)	1.285(14)	173.9(10)	this work
11	1.74(2)	1.29(2)	178(2)	[22]
12	1.762	1.292	176.03	[23]
13	1.76(1)	1.246(13)	174.7(10)	this work

IR Spectroscopy

In the low-wavenumber region of the IR spectra ($\tilde{\nu} < 1000\ cm^{-1}$), all the $(n\mathrm{Bu_4N})_3[Mo_6O_{18}(N_2Ar)]$ compounds **1**−**13** display similar patterns characteristic of the Lindqvist structure. Actually, the IR bands of the aryldiazenido ligand in this region (mostly C−C and C−H deformations) are of low intensity with respect to those of the polyoxometalate framework. $(n\mathrm{Bu_4N})_3[Mo_6O_{18}(N_2Ar)]$ presents more complex features than $(n\mathrm{Bu_4N})_2[Mo_6O_{19}]$, especially in the 1000−700 cm^{-1} range characteristic of Mo−O stretchings. In particular, the strong $\nu_{as}(Mo-O_t)$ band observed at 958 cm^{-1} in $(n\mathrm{Bu_4N})_2[Mo_6O_{19}]$[28] splits into two more or less resolved bands ($\Delta\tilde{\nu} \approx 20\ cm^{-1}$) in the aryldiazenido derivatives. Similarly, the broad band observed at 796 cm^{-1} in the parent hexamolybdate and assigned to a $Mo-O_b$ stretching mode, also splits into two components ($\Delta\tilde{\nu} \approx 25\ cm^{-1}$) in $(n\mathrm{Bu_4N})_3[Mo_6O_{18}(N_2Ar)]$ (Figure 3). Such splittings are commonly observed in monofunctionalized hexamolybdates, such as imido,[8,9] nitrosyl,[4,5] and cyclopentadienyl[26] derivatives, and they have been ascribed to the reduction in symmetry of the oxometalate framework from O_h to C_{4v} upon the substitution of MoX for MoO. According to group theory, this should result in the splitting of all IR-active triply degenerated F_2 modes into A_1 and E modes. A detailed analysis, using Mo−N and $Mo-O_t$ internal coordinates, allows four IR-active modes to be predicted: one Mo−N and three $Mo-O_t$, according to the following representation:[8]

$$\Gamma(Mo-O_t) = 2A_1(IR, R) + B_1(R) + E(IR, R)$$

$$\Gamma(Mo-N) = A_1(IR, R)$$

In the approximation of separate $Mo-O_t$ and Mo−N vibrators, the stronger band, at low energy ($\tilde{\nu} \approx 940\ cm^{-1}$), should be assigned to the E-type $\nu_{as}(Mo-O_t)$ mode, whereas the less intense band ($\tilde{\nu} \approx 965\ cm^{-1}$) might correspond to an A_1-type mode, associated principally with the Mo−N vibrator. Mechanical coupling between the $Mo-O_t$ and Mo−N vibrators are not excluded, however. Isotopic

 © 2003 Wiley-VCH Verlag GmbH & Co. KGaA, Weinheim

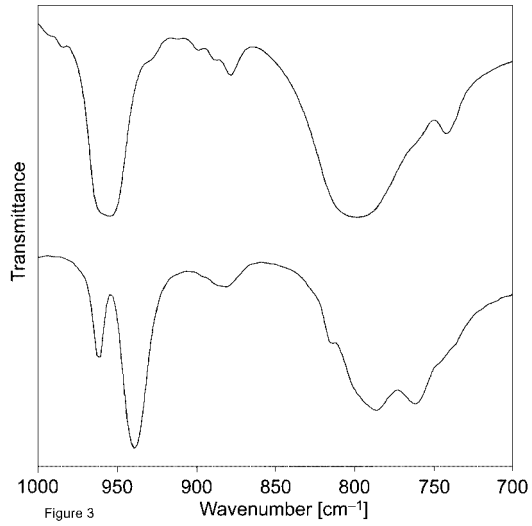

Figure 3. Part of the IR spectra of $[Mo_6O_{19}]^{2-}$ (top) and $[Mo_6O_{18}(N_2C_6H\text{-}p\text{-}CH_3)]^{3-}$ (bottom); note the splitting of the Mo=O (left) and Mo−O−Mo (right) bands in the diazenido complex

^{15}N and/or ^{18}O labelling is needed to reach a definite conclusion.

In all compounds **1**−**13**, the aromatic ν(C−H) bands ($\tilde{\nu} > 3000$ cm^{-1}) are hardly visible, due to their low intensity, and the complex pattern around 2900 cm^{-1} contains aliphatic ν(C−H) bands both of the tetrabutylammonium cation and of the substituent on the aromatic ring. The IR spectra of compounds **1**−**13** differ markedly in their band positions but also in their intensities in the medium-frequency region (1650−1300 cm^{-1}) where ν(N=N) and various bands from the arene occur.[29] It should be noted that this part of the IR absorption spectrum is more complex and more intense for a given (aryldiazenido)hexamolybdate than for the (arylimido)hexamolybdate $[Mo_6O_{18}(NAr)]^{2-}$ with the same Ar group.[8,30] By use of extensive isotopic labelling on mononuclear (aryldiazenido)metal complexes, Ibers and co-workers have shown that the intensity of the intrinsically weak ν(N=N) band may be considerably enhanced by resonance interaction with phenyl modes. This also results in differences between the experimentally observed band position and the real ν(N=N) frequency.[29] Apparently, resonance interactions also occur in the aryldiazenido hexamolybdates, because of the intense features observed between 1650 and 1300 cm^{-1}. Without isotopic labelling it is then impossible to determine the exact frequency of the N=N stretching mode, and thus the strength of the N=N bond.

UV/Vis Spectroscopy

The UV/Vis electronic spectra were recorded in acetonitrile solutions at room temperature. Slow changes were observed on standing, in line with the ^{95}Mo NMR study, indicating progressive transformation mainly into α-$[Mo_8O_{26}]^{4-}$. The electronic spectrum of the phenyldiazenido derivative **1** was recorded in different solvents, and almost identical spectra were obtained except in methanol, in which a fast transformation occurs. The electronic spectra of compounds **1**−**13** split into two groups. Those of compounds **1**−**3** and **5**−**9** exhibit two bands at ca. 390 and 290 nm, the second being more intense than the first. In addition, there are two shoulders on the lower energy side of each main band. The second group of compounds comprises the nitro derivatives **10**−**12**, for which the more intense band lies in the visible region. Compounds **4** and **13** are somewhat intermediate. The lower energy absorptions are clearly associated with the $\{Mo(N_2Ar)\}$ chromophore and their high molar absorptivity is indicative of charge-transfer character. This contrasts with $[Mo_6O_{18}(NO)]^{3-}$ and other polyoxomolybdates containing $\{Mo(NO)\}^{3+}$ units, which display a band most probably associated with a $d_{xz},d_{yz} \rightarrow d_{xy}$ transition.[3−6] Although we prefer not to speculate extensively on the origin of the absorption bands until a theoretical study has been performed, the difference between nitrosyl and diazenido derivatives might be related to the change from C_{4v} to C_s symmetry on going from $[Mo_6O_{18}(NO)]^{3-}$ to $[Mo_6O_{18}(N_2Ar)]^{3-}$. Indeed in six-coordinate complexes, bending of the diazenido ligand has a stabilizing effect on the π* N_2Ar orbital in the plane of bending.[31,32]

NMR Spectroscopy

The characterization of compounds **1**−**13**, $(n\text{Bu}_4\text{N})_3[Mo_6O_{18}(N_2Ar)]$, by multinuclear NMR ($^{17}O$ and ^{95}Mo) spectroscopy was carried out in the same way as used for the nitrosyl derivatives $(n\text{Bu}_4\text{N})_3[M_5O_{18}\{M'(NO)\}]$ (M, M′ = Mo, W)[6] and the imido derivatives $(n\text{Bu}_4\text{N})_2[Mo_6O_{19-x}(NR)_x]$ ($x = 1-6$):[8,9] in acetonitrile and at elevated temperatures (usually 50 °C). This allows the relaxation rate of the quadrupolar nuclei (^{17}O and ^{95}Mo) to be decreased and the linewidths of the resonance signals to be reduced. Even under these conditions, some of the expected ^{95}Mo resonances were not observed, probably because of extreme broadening. In some cases, such as **8**, **9** and **11**, however, full ^{95}Mo spectra could be obtained at room temperature, although the signals were significantly broadened with respect to the high-temperature spectra. Unlike the nitrosyl and imido derivatives, the diazenido compounds proved to be only fairly stable at 50 °C, even in dried acetonitrile. Decomposition was evident from the progressive growth of the ^{95}Mo NMR signals characteristic of $[Mo_6O_{19}]^{2-}$ (δ = 125 ppm) and of α-$[Mo_8O_{26}]^{4-}$ (δ = 21 and −11 ppm). In particular, decomposition could not be avoided for compounds with a donor substituent on the aryl group, and in some cases it was nearly complete during the time required for the acquisition of the ^{95}Mo spectrum, so measurement of a full set of NMR spectroscopic data was not possible for each member of the series $(n\text{Bu}_4\text{N})_3[Mo_6O_{18}(N_2Ar)]$. Results are listed in Tables 2 and 3. No significant data could be collected for **3** and **6**, and nearly complete sets of ^{17}O and ^{95}Mo data were obtained only for

 © 2003 Wiley-VCH Verlag GmbH & Co. KGaA, Weinheim

7, **8**, **9** and **12**. Nevertheless, this allows a comparison with $(n\mathrm{Bu_4N})_3[\mathrm{Mo_6O_{18}(NO)}]$ and reveals some trends within the series of diazenido compounds.

Table 2. ^{95}Mo NMR spectroscopic data for (aryldiazenido)hexamolybdates $[\mathrm{Mo_6O_{18}(N_2Ar)}]^{3-}$[a][b]

Compound	δ(Mo^{II})	δ(Mo^{VI})		Δδ$_{eq.-ax.}$
		eq.	ax.	
1	[c]	214	155	59
2	[c]	214	156	58
4	998	202	153	49
5	1100	206	153	53
7	[c]	208	155	53
8	1092	206	151	55
9	961	202	154	48
10	940	201	154	47
11	845	197	150	47
12	600	185	149	36

[a] Spectra recorded at 50 °C in acetonitrile solutions. [b] Chemical shifts in ppm with respect to external aqueous alkaline solution of 2 M Na_2MoO_4. [c] Not observed.

Table 3. ^{17}O NMR spectroscopic data for (aryldiazenido)hexamolybdates $[\mathrm{Mo_6O_{18}(N_2Ar)}]^{3-}$[a][b]

Compound	T [°C]	δ(O$_t$)		δ(O$_b$)			δ(O$_c$)
		eq.	ax.				
7	25	892.5	877.7	603.3	564.5	530.6	[c]
8	25	891.3	876.8	599.1	562.0	528.9	−37.1
9	50	892.6	878.7	603.3	563.0	531.8	ca. −30
12	50	902.6	888.8	593.1	566.6	538.6	−26

[a] Spectra recorded in acetonitrile solutions. [b] Chemical shifts in ppm with respect to neat H_2O. [c] Not observed.

Before discussing the NMR spectroscopic data in detail, let us remember briefly the two terms determining the shielding (σ) and the chemical shift (δ = −σ) of a given nucleus.[33] Shielding is usually expressed as the sum of two opposite terms: the diamagnetic term σ_{dia} (positive) and the paramagnetic term σ_{para} (negative).

$$-\delta = \sigma = \sigma_{dia} + \sigma_{para}$$

An increase in the electron density at the nucleus results in an increase in the diamagnetic contribution and hence shifts the resonance to lower chemical shifts. In contrast, an enhanced paramagnetic contribution results in reduced shielding and shifts the NMR line to higher δ values. Furthermore, σ_{para} depends on all electronic excitation energies; in favourable cases it is inversely proportional to the HOMO−LUMO gap. Then, within a congruent set of complexes, the net deshielding of the NMR signal may reflect the decrease in the HOMO−LUMO gap through the increase of the paramagnetic contribution.

^{95}Mo NMR Spectroscopy

The ^{95}Mo NMR spectrum of $(n\mathrm{Bu_4N})_3[\mathrm{Mo_6O_{18}}(\mathrm{N_2C_6H_4}$-*p*-$\mathrm{NO_2})]$ (**11**) in acetonitrile displays three signals in an approximate ratio of 1:4:1 in order of increasing shielding (Figure 4). This spectrum is quite similar to that of $(n\mathrm{Bu_4N})_3[\mathrm{Mo_6O_{18}(NO)}]$, so the two more-shielded signals at δ = 197 ppm (4 Mo, $\Delta\nu_{1/2} \approx 200$ Hz) and at δ = 150 ppm (1 Mo, $\Delta\nu_{1/2} \approx 350$ Hz) may be assigned to the equatorial and axial Mo^{VI} centres, respectively, while the strongly deshielded and broad signal ($\Delta\nu_{1/2} \approx 600$ Hz) at δ = 845 ppm may be assigned to the Mo^{II} centre. According to these data, the apparent symmetry of $[\mathrm{Mo_6O_{18}(N_2C_6H_4}$-*p*-$\mathrm{NO_2})]^{3-}$ in solution is C_{4v}, while its actual symmetry is at most C_s, as observed in the solid state.[22] Because other members of the series behave similarly, and because analysis of the ^{17}O NMR spectra suggests the same conclusion (see below), accidental degeneracy of signals can be ruled out. The NMR spectroscopic data in solution thus indicate fast rotation of the aryldiazenido ligand on NMR timescales. There is precedent for such a rotation.[34]

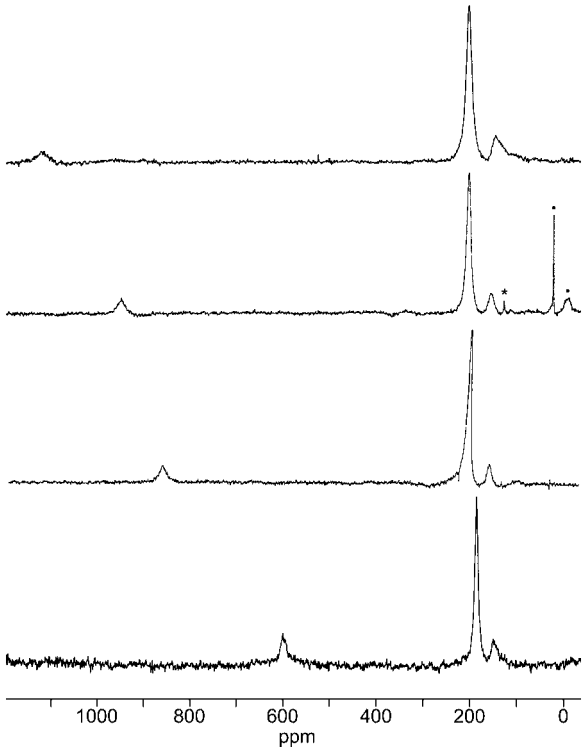

Figure 4. 32.6 MHz ^{95}Mo NMR spectra of all NO_2-substituted diazenido hexamolybdates; from top to bottom: $[\mathrm{Mo_6O_{18}(N_2C_6H_4}$-*m*-$\mathrm{NO_2})]^{3-}$ (**8**), 25 °C, 20 mM, 288·10^3 transients; $[\mathrm{Mo_6O_{18}(N_2C_6H_4}$-*o*-$\mathrm{NO_2})]^{3-}$ (**10**), 50 °C, 50 mM, 77·10^3 transients; $[\mathrm{Mo_6O_{18}(N_2C_6H_4}$-*p*-$\mathrm{NO_2})]^{3-}$ (**11**), 50 °C, 28 mM, 120·10^3 transients; $[\mathrm{Mo_6O_{18}\{N_2C_6H_3}$-*o*,*p*-$\mathrm{(NO_2)_2\}}]^{3-}$ (**12**), 50 °C, 20 mM, 54·10^3 transients; note the relative broadness of the room-temperature spectrum of **8** and the spurious signals from $[\mathrm{Mo_6O_{19}}]^{2-}$ (*) and of α-$[\mathrm{Mo_8O_{26}}]^{4-}$(·) in the spectrum of **10**; general conditions for all spectra: spectral width 45 kHz (ca. 1400 ppm); pulse width 10 μs (ca. 30° flip angle); acquisition time 45 ms; no relaxation delay; the time domain data (4 K points) were multiplied by an exponential window (LB, 20 Hz) prior to Fourier transformation without zero-filling; baseline distortions were corrected by use of the Bruker software

 © 2003 Wiley-VCH Verlag GmbH & Co. KGaA, Weinheim

The deshielding of the functionalized Mo can be attributed to the dominant role of the paramagnetic contribution. In addition, the similarity between the chemical shifts supports similar electronic structures (i.e., d^4 Mo^{II} centres) both in $[Mo_6O_{18}(N_2C_6H_4\text{-}p\text{-}NO_2)]^{3-}$ and in $[Mo_6O_{18}(NO)]^{3-}$ compounds. Any compound of the type $(n\text{Bu}_4\text{N})_3[Mo_6O_{18}(N_2Ar)]$ should display the same type of ^{95}Mo spectrum, with a strongly deshielded signal and two resonances at $\delta \approx 200$ and 150 ppm. The deshielded resonance is always quite broad and could not be observed for compounds **1**, **2** and **7**. Otherwise, all data agree with the typical spectra of Figure 4. Let us note that Zubieta and Ellis have already reported ^{95}Mo NMR spectroscopic data on compound **1**.[15] Like us, they only observed two signals, lying in a range typical of Mo^{VI} centres, though their reported chemical shifts are not in agreement with our observations. In our hands, $[Mo_6O_{18}(N_2Ph)]^{3-}$ proved to be amongst the less stable diazenido complexes, and the data reported by Zubieta and Ellis might correspond to decomposition products.

The chemical shifts for both equatorial and axial $\{^{95}MoO\}$ sites in the diazenido derivatives are uniformly deshielded with respect to those of $[Mo_6O_{19}]^{2-}$. In contrast to the wide variance of the $\{^{95}MoN_2Ar\}$ resonances, the $\{^{95}MoO\}$ resonances fall within a narrow range: δ = 185−214 ppm for the equatorial sites, and δ = 149−156 ppm for the axial site. A trend can be established for those compounds in which the three signals are observed: deshielding of the $\{^{95}MoN_2Ar\}$ resonance is accompanied by definite, albeit smaller, deshielding of the $\{^{95}MoO\}$ resonances (Figure 5). By extrapolation of this trend to all the members of the series, the $\{^{95}MoN_2Ph\}$ resonance for **1** would be expected at $\delta \approx 1300$ ppm.

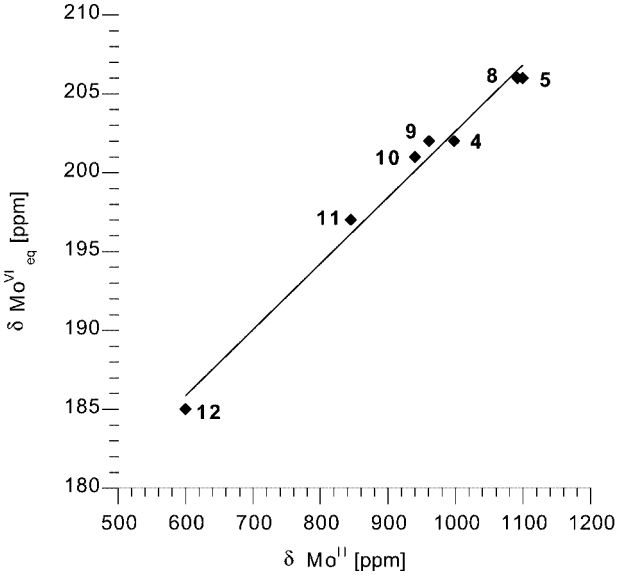

Figure 5. Plotting of the ^{95}Mo chemical shifts of the equatorial Mo^{VI} centres as a function of those of the Mo^{II} centre in the (diazenido)hexamolybdates; the heavy line represents the best fit from a linear regression $\delta(Mo^{VI}) = 4.19\cdot10^{-2}\ \delta(Mo^{II}) + 160.7$ ppm ($R = 0.993$)

It may be inferred from these observations, and from comparison with the nitrosyl complexes $[M_5O_{18}\{M'(NO)\}]^{3-}$ (M, M′ = Mo, W)[6] and the imido complexes $[Mo_6O_{18}(NR)]^{2-}$,[8,9] that all the ^{95}Mo chemical shifts for $[Mo_6O_{18}(N_2Ar)]^{3-}$ are mainly determined by variation in the paramagnetic shielding term, σ_{para}. While imido ligands are superior to oxo ligands as electron donors, nitrosyl and diazenido ligands − to be regarded as NO^+ and RN^{2+}, respectively − are strong Lewis acids and their complexes have low-lying excited states. Accordingly, there is a bathochromic shift of the lower energy absorptions of $[M_5O_{18}\{M'(NO)\}]^{3-}$ and $[Mo_6O_{18}(N_2Ar)]^{3-}$ in relation to $[Mo_6O_{18}(NR)]^{2-}$. While the $\{^{95}MoN\}$ chemical shifts correlate with λ_{max} for the arylimido complexes $[Mo_6O_{18}(NAr)]^{2-}$,[9,30] no such correlation could be found for the aryldiazenido complexes $[Mo_6O_{18}(N_2Ar)]^{3-}$, whether the lowest energy transition (which most often appears as a shoulder) or the next one is considered. Attempts were also made to correlate the ^{95}Mo chemical shifts of the *p*-substituted compounds with either Hammett function σ_p or σ_p^+: although there is no evident correlation, it is clear that both $\{^{95}MoN\}$ and $\{^{95}Mo_{eq}O\}$ resonances move to lower frequency on going from electron-donating (Me) to electron-withdrawing substituents (CN, CF_3, NO_2). For the (dinitrophenyl)diazenido species **12**, the cumulative effect of the two strongly electron-withdrawing substituents produces the most shielded spectrum of the series. A similar trend has been observed for $\delta\{^{95}MoN\}$ in the (arylimido)hexamolybdates $(n\text{Bu}_4\text{N})_2[Mo_6O_{18}(NC_6H_4\text{-}p\text{-}X)]$,[8,9,30] as well as for $\delta(^{51}V)$ in the (arylimido)vanadium(v) complexes $[VCl_3(NC_6H_4N\text{-}p\text{-}X]$,[35] and was explained by variations in the paramagnetic shielding term. We therefore suggest that the same effect is likely to apply to the aryldiazenido series. Nevertheless, further studies, in particular theoretical calculations, are needed to provide a full account of the variation of the ^{95}Mo chemical shifts in this series.

^{17}O NMR Spectroscopy

As noted above, the low solubilities and the long-term instabilities of the diazenido complexes hampered the acquisition of natural-abundance ^{17}O spectra. Moreover the sensitivity of most of these compounds to hydrolysis did not allow ^{17}O-enriched samples to be obtained. ^{17}O NMR spectra were therefore obtained only for **7**, **8**, **9** and **12** (Table 3). As a typical example, the room-temperature spectrum of $[Mo_6O_{18}(N_2C_6H_4\text{-}m\text{-}NO_2)]^{3-}$ (**8**) is displayed in Figure 6. This spectrum is very similar to that of $[Mo_6O_{18}(NO)]^{3-}$ [5] and is consistent with the C_{4v} symmetry of the species. The ^{17}O spectra of **8**, **9** and **12** all display six signals in an approximate intensity ratio of 4:1:4:4:4:1, which may be assigned to the terminal (O_t) resonances at $\delta \approx 880-900$ ppm, to the bridging (O_b) resonances between δ = 530 and 600 ppm and to the central (O_c) resonance at $\delta \approx -30$ ppm (Table 3). The signal of O_c in **7**, and also those of the nitro groups in **7** and **12**, were not detected. The four diazenido compounds measured here and the

 © 2003 Wiley-VCH Verlag GmbH & Co. KGaA, Weinheim

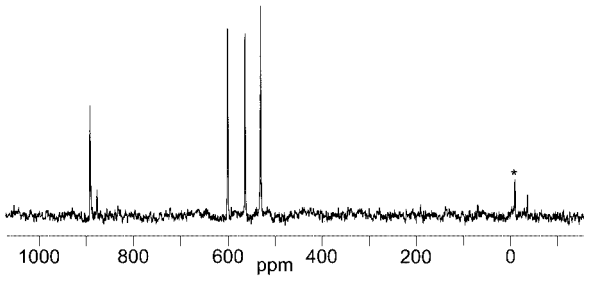

Figure 6. 67.8 MHz natural-abundance ^{17}O NMR spectrum of a 20 mM solution of $[Mo_6O_{18}(N_2C_6H_4\text{-}m\text{-}NO_2)]^{3-}$ (**8**) in CH_3CN; experimental conditions: spectral width 83 kHz (> 1200 ppm); pulse width 20 μs (ca. 45° flip angle); acquisition time 25 ms; no relaxation delay; $1.8\cdot10^6$ transients were acquired for a total spectrometer time of 12.5 h; the time domain data (4 K points) were multiplied by an exponential window (LB, 40 Hz) prior to Fourier transformation without zero-filling; baseline distortions were corrected by use of the Bruker software; the signal marked with an asterisk corresponds to H_2O

nitrosyl derivative provide a homogeneous set of ^{17}O data, again not in agreement with those reported by Zubieta and Ellis for $[Mo_6O_{18}(N_2C_6F_5)]^{3-}$.[15]

According to Klemperer,[36,37] the general pattern of the ^{17}O NMR spectra of polyoxometalates is determined by the paramagnetic shielding term, which accounts for the sequence $\delta(O_t) > \delta(O_b) > \delta(O_c)$, following decreasing π-bond order. However, variations in the diamagnetic term must be considered in order to explain the relatively subtle chemical shift modulations within each group. As with the nitrosyl derivatives, the signals of the terminal oxygen atoms in the diazenido derivatives are shielded with respect to that of $[Mo_6O_{19}]^{2-}$, in keeping with the net increase in negative charge over the polyoxometalate framework when $[Mo^{II}NO]^{3+}$ or $[Mo^{II}NNAr]^{3+}$ is substituted for $[Mo^{VI}O]^{4+}$. In contrast to the ^{95}Mo chemical shifts, the most deshielded O_t resonances in the series are shown by the dinitro derivative (**12**). This is in accordance with IR data, which indicate the highest $Mo-O_t$ stretching energy, and thus the strongest $Mo-O_t$ bond, for this compound.

With regard to the O_b signals, one appears at higher frequency than the unique O_b resonance of $[Mo_6O_{19}]^{2-}$; it had already been assigned to the oxygen atoms (O_{b1}) bridging Mo^{II} and the four equatorial Mo^{VI}.[5] The central O_b resonance does not move significantly throughout the series: it lies approximately at the same position, within ± 3 ppm, as the hexamolybate signal, a situation already encountered in the monoimido series.[8,9] Finally, the most shielded O_b signal, at −25 to −30 ppm from the previous one, seems to be the only one reflecting the overall negative charge increase.

Conclusion

A series of aryldiazenido compounds of the type $(n\text{Bu}_4\text{N})_3[Mo_6O_{18}(N_2\text{Ar})]$ has been prepared by treatment of $(n\text{Bu}_4\text{N})_4[Mo_8O_{26}]$ with the appropriate arylhydrazines in acetonitrile or in methanol. All these compounds are isostructural and belong to the family of Lindqvist-type polyoxometalates. Two members of the series, the *o*-nitro and *p*-carboxy derivatives, have been characterized by single-crystal X-ray diffraction. The first anion displays C_s symmetry, in the second one the aromatic ring is tilted and thus allows hydrogen bonding of the carboxylic acid to a neighbouring anion. The aryldiazenido ligands exhibit features characteristic of the singly bent coordination mode with short Mo−N and N−N bonds indicative of multiple-bond character. The compounds have been characterized by ^{95}Mo NMR spectroscopy in acetonitrile. Their spectra are normally composed of three signals in an intensity ratio of 1:4:1, although the strongly deshielded resonance ($\delta \approx 1100-600$ ppm) is quite broad and was not always observed. The large deshielding of the Mo^{II} centre arises from paramagnetic contributions.

We have shown here the possibility of obtaining a family of functionalized polyoxometalates differing in the substituents on the aromatic rings. These substituents influence the physical and chemical properties of the hexamolybdate, as can be seen by the spectroscopic characterization of the compounds and their different stabilities in solution. The presence of reactive groups on the aromatic ring allows further derivatization, and we are now investigating the possibilities of carbon−carbon coupling and elaboration on the carboxylic acid.

Experimental Section

General Procedures and Materials: All reactions were performed under dry nitrogen. Reagents and chemicals were purchased from commercial sources and were used as received. Solvents were purified and dried by standard procedures. $(n\text{Bu}_4\text{N})_4[Mo_8O_{26}]$ was prepared as reported in the literature.[38] IR spectra were recorded in KBr pellets with a BioRad FTS 165 FT-IR spectrophotometer. UV/Vis spectra were recorded in acetonitrile solutions (concentration ca. $2.5\cdot10^{-4}$ M) with a Shimadzu UV-2101 spectrophotometer. Natural-abundance ^{17}O and ^{95}Mo NMR spectra were recorded at 67.8 and 32.6 MHz, respectively, by use either of a Bruker AM 500 or of a Bruker DRX 500 spectrometer. All spectra were obtained without lock from nearly saturated acetonitrile solutions in 10-mm o.d. tubes. Sample concentrations ranged from 40 to 200 mg in 2.5 mL of CH_3CN (from 0.01 to 0.05 M). Chemical shifts δ are reported in ppm with respect to external H_2O (^{17}O) and external aqueous alkaline solution of 2 M Na_2MoO_4 (^{95}Mo) according to the IUPAC recommendation. Positive δ corresponds to high frequency shift (deshielding) with respect to the reference. Elemental analyses were performed by the "Service de microanalyse", Université Pierre et Marie Curie, Paris, France and by the "Service central d'analyse", CNRS, Vernaison, France.

Syntheses: The preparations of the compounds $(n\text{Bu}_4\text{N})_3[Mo_6O_{18}(N_2\text{Ar})]$ divide into two groups, differing mainly in the solvent used, and in the presence of base.

Compounds 1−8: $(n\text{Bu}_4\text{N})_4[Mo_8O_{26}]$ (2.15 g, 1.00 mmol), twice the molar amount of the appropriate arylhydrazine ($C_6H_5NHNH_3Cl$, 0.289 g; *p*-Me-$C_6H_4NHNH_3Cl$, 0.317 g; *p*-F-$C_6H_4NHNH_3Cl$, 0.325 g; *p*-NC-$C_6H_4NHNH_3Cl$, 0.339 g; *p*-F_3C-$C_6H_4NHNH_2$, 0.352 g; *p*-MeO-$C_6H_4NHNH_3Cl$, 0.349 g; *o*-Cl-$C_6H_4NHNH_3Cl$, 0.358 g; *m*-O_2N-$C_6H_4NHNH_3Cl$, 0.379 g), $(n\text{Bu}_4\text{N})Br$ (0.50 g, 1.55 mmol) and NEt_3 (2.8 mL, 20 mmol) were added to MeCN

 © 2003 Wiley-VCH Verlag GmbH & Co. KGaA, Weinheim

(15 mL). The mixture was vigorously stirred and heated at ca. 50 °C until its colour had turned dark brown (20 min at most). The product sometimes started to precipitate at this stage. Filtration was carried out after the solution had been concentrated to ca. 10 mL and cooled to room temperature. The collected solid was washed with a 1:1 mixture of MeCN and Et_2O, then with pure Et_2O, and dried under vacuo. In some cases (**1**, **3**, **5**, **6**), the solid had to be washed with cold MeCN to remove traces of $(nBu_4N)_4[Mo_8O_{26}]$. Each compound was recrystallized from MeCN by slow diffusion of Et_2O.

Compounds 9−13: $(nBu_4N)_4[Mo_8O_{26}]$ (2.15 g, 1.00 mmol) and twice the molar amount of the appropriate arylhydrazine [$C_6F_5NHNH_3Cl$, 0.408 g; *o*-O_2N-$C_6H_4NHNH_2$, 0.306 g; *p*-O_2N-$C_6H_4NHNH_2$, 0.306 g; *o*,*p*-$(O_2N)_2$-$C_6H_3NHNH_2$, 0.396 g] were added to MeOH (30 mL). The mixture was vigorously stirred and heated at reflux for 30 min at the most. The solution was concentrated to about 15 mL, and the precipitate was then collected by filtration, washed with MeOH and Et_2O, and dried in vacuo. The products were recrystallized by diffusion of Et_2O into MeCN solutions. The preparation of **13** required some modifications in the above procedure. A mixture of $(nBu_4N)_4[Mo_8O_{26}]$ (2.15 g, 1.00 mmol) and *p*-HO_2C-$C_6H_4NHNH_2$ (0.152 g, 1.00 mmol) was heated at ca. 50 °C for ca. 20 min, during which time its colour had changed to dark brown. The methanol was removed in vacuo and the residue was extracted with several portions (20 mL) of acetone. The extracts were combined and concentrated to ca. 10 mL. The insoluble material was removed by filtration and the filtrate was exposed to vapours of Et_2O. The complex may be recrystallized by diffusion of Et_2O in MeCN or Me_2CO solutions.

Only IR bands that could be unambiguously assigned are listed below. All spectra display the bands characteristic of the tetrabutylammonium cations.

$(nBu_4N)_3[Mo_6O_{18}(N_2C_6H_5)]$ (1): Yield: 1.49 g (66% based on Mo). $C_{54}H_{113}Mo_6N_5O_{18}$ (1696.17): calcd. C 38.24, H 6.72, Mo 33.94, N 4.13; found C 37.99, H 6.68, Mo 33.78, N 4.14. UV/Vis (MeCN): λ_{max} (log ε) = 486 (sh, 3.49), 383 (4.26), 331 (sh, 4.32), 286 nm (4.62). IR (KBr): $\tilde{\nu}_{max}$ = 962 (m), 939 (s) [ν(Mo=O,Mo=N)], 786 (s), 762 (s) cm^{-1} [ν(MoOMo)]. ^{95}Mo NMR: see Table 2.

$(nBu_4N)_3[Mo_6O_{18}(N_2C_6H$-*p*-Me)] (2): Yield: 1.28 g (56% based on Mo). $C_{55}H_{115}Mo_6N_5O_{18}$ (1710.19): calcd. C 38.63, H 6.78, Mo 33.66; N 4.10; found C 38.70, H 6.79, Mo 33.30, N 4.04. UV/Vis (MeCN): λ_{max} (log ε) = 498 (sh, 3.41), 385 (4.19), 331(4.26), 284 nm (4.55). IR (KBr): $\tilde{\nu}_{max}$ = 962 (m), 939 (s) [ν(Mo=O,Mo=N)], 786 (s), 762 (s) cm^{-1} [ν(MoOMo)]. ^{95}Mo NMR: see Table 2.

$(nBu_4N)_3[Mo_6O_{18}(N_2C_6H$-*p*-F)] (3): Yield: 1.33 g (58% based on Mo). $C_{54}H_{112}FMo_6N_5O_{18}$ (1714.15): calcd. C 37.84, H 6.59, F 1.17, Mo 33.58, N 4.08; found C 37.97, H 6.60, F 1.21, Mo 33.49, N 4.03. UV/Vis (MeCN): λ_{max} (log ε) = 483 (sh, 3.42), 378 (sh, 4.15), 325 (sh, 4.25), 283 nm (4.55). IR (KBr): $\tilde{\nu}_{max}$ = 963 (m), 940 (s) [ν(Mo=O,Mo=N)], 788 (s), 763 (s) cm^{-1} [ν(MoOMo)].

$(nBu_4N)_3[Mo_6O_{18}(N_2C_6H_4$-*p*-CN)] (4): Yield: 1.35 g (59% based on Mo). $C_{55}H_{112}Mo_6N_6O_{18}$ (1721.18): calcd. C 38.38, H 6.56, Mo 33.44, N 4.88; found C 38.31, H 6.49, Mo 33.52, N 4.93. UV/Vis (MeCN): λ_{max} (log ε) = 421 (4.48), 308 nm (4.30). IR (KBr): $\tilde{\nu}_{max}$ = 2207 (m) [ν(C≡N)], 965 (m), 941 (s) [ν(Mo=O,Mo=N)], 788 (s), 762 (s) cm^{-1} [ν(MoOMo)]. ^{95}Mo NMR: see Table 2.

$(nBu_4N)_3[Mo_6O_{18}(N_2C_6H_4$-*p*-$CF_3)]$ (5): Yield: 1.22 g (52% based on Mo). $C_{55}H_{112}F_3Mo_6N_5O_{18}$ (1764.16): calcd. C 37.45, H 6.40, F 3.23, Mo 32.63, N 3.97; found C 37.27, H 6.62, F 3.34, Mo 32.44, N 3.92. UV/Vis (MeCN): λ_{max} (log ε) = 481 (sh, 3.69), 400 (4.37), 330 (sh, 4.27), 296 nm (4.46). IR (KBr): $\tilde{\nu}_{max}$ = 965 (s), 942 (s) [ν(Mo=O,Mo=N)], 788 (s), 764 (s) cm^{-1} [ν(MoOMo)]. ^{95}Mo NMR: see Table 2.

$(nBu_4N)_3[Mo_6O_{18}(N_2C_6H_4$-*p*-OMe) (6): Yield: 0.86 g (38% based on Mo). $C_{55}H_{115}Mo_6N_5O_{19}$ (1726.19): calcd. C 38.27, H 6.72, Mo 33.35, N 4.05; found C 38.22, H 6.71, Mo 33.27, N 4.09. UV/Vis (MeCN): λ_{max} (log ε) = 509 (sh, 3.37), 388 (sh, 4.30), 327 (sh, 4.26), 284 nm (4.58). IR (KBr): $\tilde{\nu}_{max}$ = 961 (m), 939 (s) [ν(Mo=O,Mo=N)], 787 (s), 762 (s) cm^{-1} [ν(MoOMo)].

$(nBu_4N)_3[Mo_6O_{18}(N_2C_6H_4$-*o*-Cl) (7): Yield: 1.22 g (53% based on Mo). $C_{54}H_{112}ClMo_6N_5O_{18}$ (1730.61): calcd. C 37.48, H 6.52, Cl 2.28, Mo 33.26, N 4.05; found C 37.40, H 6.50, Cl 2.07, Mo 33.16, N 4.07. UV/Vis (MeCN): λ_{max} (log ε) = 491 (sh, 3.61); 390 (4.36), 334 (sh, 4.36), 288 nm (4.68). IR (KBr): $\tilde{\nu}_{max}$ = 963 (m), 941 (s) [ν(Mo=O,Mo=N)], 788 (s), 761 (s) cm^{-1} [ν(MoOMo)]. ^{95}Mo NMR: see Table 2. ^{17}O NMR: see Table 3.

$(nBu_4N)_3[Mo_6O_{18}(N_2C_6H_4$-*m*-$NO_2)]$ (8): Yield: 1.74 g (75% based on Mo). $C_{54}H_{112}Mo_6N_6O_{20}$ (1741.16): calcd. C 37.25, H 6.48, Mo 33.06, N 4.83; found C 37.31, H 6.52, Mo 33.12, N 4.52. UV/Vis (MeCN): λ_{max} (log ε) = 487 (sh, 3.67), 383 (4.38), 281 nm (4.71). IR (KBr): $\tilde{\nu}_{max}$ = 965 (s), 940 (s) [ν(Mo=O,Mo=N)], 788 (s), 763 (s) cm^{-1} [ν(MoOMo)]. ^{95}Mo NMR: see Table 2. ^{17}O NMR: see Table 3.

$(nBu_4N)_3[Mo_6O_{18}(N_2C_6F_5]$ (9): Yield 1.60 g (67% based on Mo). $C_{54}H_{108}F_5Mo_6N_5O_{18}$ (1786.12): calcd. C 36.31, H 6.09, F 5.32, Mo 32.23, N 3.92; found, C 36.21, H 5.95, F, 5.12, Mo 31.90, N 3.94. UV/Vis (MeCN): λ_{max} (log ε) = 467 (sh, 3.48), 379 (4.19), 279 nm (4.50). IR (KBr): $\tilde{\nu}_{max}$ = 964 (m), 942 (s) [ν(Mo=O,Mo=N)], 792 (s), 768 (s) cm^{-1} [ν(MoOMo)]. ^{95}Mo NMR: see Table 2. ^{17}O MNR: see Table 3.

$(nBu_4N)_3[Mo_6O_{18}(N_2C_6H_4$-*o*-$NO_2)]$ (10): Yield: 1.39 g (60% based on Mo). $C_{54}H_{112}Mo_6N_6O_{20}$ (1741.16): calcd. C 37.25, H 6.48, Mo 33.06, N 4.83; found C 37.14, H 6.34, N 4.79. UV/Vis (MeCN): λ_{max} (log ε) = 548 (3.76), 373 (3.88), 274 nm (4.4). IR (KBr): $\tilde{\nu}_{max}$ = 965 (s) 943 (s) [ν(Mo=O,Mo=N)], 790 (s), 762 (s) cm^{-1} [ν(MoOMo)]. ^{95}Mo NMR: see Table 2.

$(nBu_4N)_3[Mo_6O_{18}(N_2C_6H_4$-*p*-$NO_2)]$ (11): Yield: 1.74 g (75% based on Mo). $C_{54}H_{112}Mo_6N_6O_{20}$ (1741.16): calcd. C 37.25, H 6.48, Mo 33.06, N 4.83; found; C 37.62, H 6.81, Mo 32.80, N 5.04. UV/Vis (MeCN): λ_{max} (log ε) = 548 (4.59), 305 (sh, 4.25), 267 nm (4.50). IR (KBr): $\tilde{\nu}_{max}$ = 967 (m), 943 (s) [ν(Mo=O,Mo=N)], 791 (s), 762 (s) cm^{-1} [ν(MoOMo)]. ^{95}Mo NMR: see Table 2.

$(nBu_4N)_3[Mo_6O_{18}\{N_2C_6H_3$-*o*,*p*-$(NO_2)_2\}]$ (12): Yield: 1.88 g (79% based on Mo). $C_{54}H_{111}Mo_6N_7O_{22}$ (1786.16): calcd. C 36.31, H 6.26, Mo 32.22, N 5.48; found C 37.08, H 6.29, Mo 32.26, N 5.52. UV/Vis (MeCN): λ_{max} (log ε) = 525 (4.60) 300 (sh, 4.29), 258 nm (4.53). IR (KBr): $\tilde{\nu}_{max}$ = 969 (m), 946 (s) [ν(Mo=O,Mo=N)], 791 (s), 765 (s) cm^{-1} [ν(MoOMo)]. ^{95}Mo NMR: see Table 2. ^{17}O NMR: see Table 3.

$(nBu_4N)_3[Mo_6O_{18}(N_2C_6H_4$-*p*-$CO_2H)]$ (13): Yield 0.74 g (32% based on Mo). $C_{55}H_{113}Mo_6N_5O_{20}$ (1740.18): calcd. C 37.96, H 6.48, Mo 33.08, N 4.03; found C 37.67, H 6.68, Mo 32.92, N 3.89. UV/Vis (MeCN): λ_{max} (log ε) = 428 (4.16), 338 (sh, 3.86), 312 nm (3.94). IR (KBr): $\tilde{\nu}_{max}$ = 1701 (m), 1592 (s) [ν(C=O)], 966 (m), 943 (s) [ν(Mo=O,Mo=N)], 789 (s), 767 (s) cm^{-1} [ν(MoOMo)].

Crystal-Structure Analyses: Crystal-structure data are summarized in Table 4. Data were recorded at room temperature either with a

 © 2003 Wiley-VCH Verlag GmbH & Co. KGaA, Weinheim

Table 4. Crystal data and structure refinement for **10** and **13**

Compound	**10**	**13**
Empirical formula	$C_{54}H_{112}Mo_6N_6O_{20}$	$C_{55}H_{113}Mo_6N_5O_{20}$
Formula mass	1741.15	1740.16
T [K]	295	295
a [Å]	17.396(2)	17.6789(25)
b [Å]	17.431(2)	17.7551(15)
c [Å]	24.052(4)	23.5582(23)
V [Å^3]	7294(2)	7394.7(9)
Z	4	4
Crystal system	orthorhombic	orthorhombic
Space group	Pmcn	$P2_1cn$
μ [mm^{-1}]	1.067	1.05
F(000)	3560	3560
$D_{calcd.}$ [Mg·m^{-3}]	1.59	1.56
Crystal size [mm]	0.30 × 0.40 × 0.50	0.25 × 0.30 × 0.32
Diffractometer	CAD4, Enraf−Nonius	Kappa-CCD, Bruker-AXS
λ [Å]	0.71073	0.71073
θ range [°]	1−25	1.6−27.5
Index ranges (h,k,l)	$0 \le h \le 20$, $0 \le k \le 20$, $0 \le l \le 28$	$-21 \le h \le 19$, $-22 \le k \le 22$, $-30 \le l \le 28$
Reflections collected	7062	30867
Independent reflections	6643	12296 [R_{int} = 0.11]
Data [$I > 3\sigma(I)$]/parameters	3020/383	6114/690
Final R_1/wR_2 [$I > 3\sigma(I)$]	0.0511/0.0623	0.0462/0.0523
Final wR_2 (all)	0.0642	0.145
GOF	1.13	1.108
Largest diff. peak/hole [e·Å^{-3}]	0.75/−0.50	1.11/−1.05

CAD4 Enraf−Nonius or a Kappa-CCD Bruker-AXS diffractometer with use of graphite-monochromated Mo-K_α radiation (λ = 0.71073 Å). Crystals were mounted on glass fibres and sealed with an epoxy cement. Lattice parameters and the orientation matrix were obtained from a least-squares fit of 25 automatically centred reflections in the range 15−15.2° for **10** (230 reflections between 4 and 21° for **13**). Intensities were corrected for Lorentz and polarization effects. An empirical absorption correction was applied.[39] Only the reflections with $I > 3\sigma(I)$ were retained for calculations. Data processing was performed with the aid of the CRYSTALS program.[40] The structures were solved by direct methods[41] and subsequent Fourier synthesis. All atoms were refined anisotropically, except for one of the three tetrabutylammonium cations which was poorly defined in both structures. Hydrogen atoms were not included in the refinements. Neutral-atom scattering factors were used with anomalous dispersion corrections applied.[42] Molecular structures were drawn with the program CAMERON.[43] CCDC-204770 (**10**) and -204771 (**13**) contain the supplementary crystallographic data for this paper. These data can be obtained free of charge via www.ccdc.cam.ac.uk/conts/retrieving.html (or from the Cambridge Crystallographic Data Centre, 12 Union Road, Cambridge CB21EZ, UK; Fax: (internat.) + 44-1223/336-033; E-mail: deposit@ccdc.cam.ac.uk).

Acknowledgments

Financial support from the Université Pierre and Marie Curie, the CNRS and the CONICYT (PICS no. 929) and the FONDECYT (grant no. 1000437) is gratefully acknowledged.

[1] P. Gouzerh, A. Proust, *Chem. Rev.* **1998**, *98*, 77−111.
[2] A. Proust, R. Villanneau, in *Polyoxometalates From Topology via Self-Assembly to Applications* (Eds.: M. T. Pope, A. Müller), Kluwer, Dordrecht, **2001**, pp. 23−38.
[3] P. Gouzerh, Y. Jeannin, A. Proust, F. Robert, *Angew. Chem. Int. Ed. Engl.* **1989**, *28*, 1363−1364, *Angew. Chem.* **1989**, *101*, 1377−1378.
[4] A. Proust, P. Gouzerh, F. Robert, *Inorg. Chem.* **1993**, *32*, 5291−5298.
[5] A. Proust, R. Thouvenot, F. Robert, P. Gouzerh, *Inorg. Chem.* **1993**, *32*, 5299−5304.
[6] A. Proust, R. Thouvenot, S.-G. Roh, J.-K. Yoo, P. Gouzerh, *Inorg. Chem.* **1995**, *34*, 4106−4112.
[7] A. Proust, M. Fournier, R. Thouvenot, P. Gouzerh, *Inorg. Chim. Acta* **1994**, *215*, 61−66.
[8] A. Proust, R. Thouvenot, M. Chaussade, F. Robert, P. Gouzerh, *Inorg. Chim. Acta* **1994**, *224*, 81−95.
[9] J. B. Strong, G. P. A. Yap, R. Ostrander, L. Liable-Sands, A. L. Rheingold, R. Thouvenot, P. Gouzerh, E. A. Maatta, *J. Am. Chem. Soc.* **2000**, *122*, 639−649.
[10] H. Kwen, S. Tomlinson, E. A. Maatta, C. Dablemont, R. Thouvenot, A. Proust, P. Gouzerh, *Chem. Commun.* **2002**, 2970−2971.
[11] S.-G. Roh, A. Proust, P. Gouzerh, F. Robert, *J. Chem. Soc., Chem. Commun.* **1993**, 836−838.
[12] D. Sutton, *Chem. Soc. Rev.* **1975**, *4*, 443−470.
[13] T.-C. Hsieh, J. Zubieta, *Polyhedron* **1986**, *5*, 305−314.
[14] T.-C. Hsieh, J. Zubieta, *Polyhedron* **1986**, *5*, 1655−1657.
[15] S. Bank, S. Liu, S. N. Shaikh, X. Sun, J. Zubieta, P. D. Ellis, *Inorg. Chem.* **1988**, *27*, 3535−3543.
[16] M. W. Bishop, G. Butler, J. Chatt, J. R. Dilworth, G. J. Leigh, *J. Chem. Soc., Dalton Trans.* **1979**, 1843−1850.
[17] B. Debenjak, C. Bustos, D. Carrillo, F. Robert, P. Gouzerh, *Polyhedron* **1992**, *11*, 2321−2326.
[18] D. Carrillo, *C. R. Acad. Sci. Paris, Sér. IIc* **2000**, *3*, 175−181.
[19] T.-C. Hsieh, J. Zubieta, *Inorg. Chem.* **1985**, *24*, 1287−1288.
[20] B. Debenjak, C. Bustos, D. Carrillo, F. Robert, P. Gouzerh, *Bol. Soc. Chil. Quim.* **1992**, *37*, 105−113.

 © 2003 Wiley-VCH Verlag GmbH & Co. KGaA, Weinheim

[21] T.-C. Hsieh, S. N. Shaikh, J. Zubieta, *Inorg. Chem.* **1987**, *26*, 4079−4089.
[22] H.-L. Li, X.-Z. You, X.-X. Xu, J.-S. Huang, *Chin. J. Struct. Chem.* **1994**, *13*, 109−112.
[23] S. Wang, X. Wang, Y. Zhai, *Chem. Res. Chin. Univ.* **1992**, *8*, 382−387.
[24] H. Kang, J. Zubieta, *J. Chem. Soc., Chem. Commun.* **1988**, 1192−1193.
[25] Y. Du, A. L. Rheingold, E. A. Maatta, *J. Am. Chem. Soc.* **1992**, *114*, 345−346.
[26] A. Proust, R. Thouvenot, P. Herson, *J. Chem. Soc., Dalton Trans.* **1999**, 51−56.
[27] T. M. Che, V. W. Day, L. C. Francesconi, M. F. Fredrich, W. G. Klemperer, *Inorg. Chem.* **1985**, *24*, 4055−4062.
[28] C. Rocchiccioli-Deltcheff, R. Thouvenot, M. Fouassier, *Inorg. Chem.* **1982**, *21*, 30−35.
[29] B. L. Haymore, J. A. Ibers, D. W. Meek, *Inorg. Chem.* **1975**, *14*, 541−546.
[30] A. Proust, S. Taunier, unpublished results.
[31] D. L. DuBois, R. Hoffmann, *Nouv. J. Chim.* **1977**, *1*, 479−492.
[32] S. Kahlal, J.-Y. Saillard, J.-R. Hamon, C. Manzur, D. Carrillo, *New J. Chem.* **2001**, *25*, 231−242.
[33] C. J. Jameson, J. Mason, in *Multinuclear NMR* (Ed.: J. Mason), Plenum Press, New York and London, **1989**.
[34] D. Carrillo, P. Gouzerh, Y. Jeannin, *New J. Chem.* **1985**, *9*, 749−755.
[35] D. D. Devore, J. D. Lichtenhan, F. Tukusagawa, E. A. Maatta, *J. Am. Chem. Soc.* **1987**, *109*, 7408−7416.
[36] M. Filowitz, R. K. C. Ho, W. G. Klemperer, W. Shum, *Inorg. Chem.* **1979**, *18*, 93−103.
[37] W. G. Klemperer, *Angew. Chem. Int. Ed. Engl.* **1978**, *17*, 246−254, *Angew. Chem.* **1978**, *90*, 258−271.
[38] N. Hur, W. G. Klemperer, R.-C. Wang, *Inorg. Synth.* **1990**, *27*, 78−79.
[39] N. Walker, D. Stuart, *Acta Crystallogr., Sect. A* **1983**, *39*, 158−166.
[40] D. J. Watkin, J. R. Carruthers, P. W. Betteridge, *CRYSTALS*, Chemical Crystallography Laboratory, University of Oxford, **1996**.
[41] G. M. Sheldrick, *SHELXS:86, Program for the Solution of Crystal Structures*, University of Göttingen, **1986**.
[42] *International Tables for X-ray Crystallography*, Kynoch, Birmingham, England, **1974**, vol. IV.
[43] L. J. Pearce, D. J. Watkin, *CAMERON*, Chemical Crystallography Laboratory, University of Oxford, **1996**.

Received February 26, 2003

 © 2003 Wiley-VCH Verlag GmbH & Co. KGaA, Weinheim

Remote Rotamer Control: The Effect of a 4-*tert*-Butyl Group on the Coordination Chemistry of Tp^R Ligands

Arnold L. Rheingold,[a] Louise M. Liable-Sands,[a] James A. Golan,[a] and Swiatoslaw Trofimenko*[a]

Keywords: Scorpionates / Cobalt / Rotamer control / Borates / N ligands

Three novel homoscorpionate ligands containing a *tert*-butyl group in the 4-position have been synthesized: hydrotris(4-*tert*-butylpyrazol-1-yl)borate (Tp^{4tBu}), hydrotris(4-*tert*-butyl-3-*p*-tolylpyrazol-1-yl)borate ($Tp^{Tol,4tBu}$), and hydrotris(4-*tert*-butyl-3-isopropylpyrazol-1-yl)borate ($Tp^{iPr,4tBu}$). The 4-*tert*-butyl group does not alter the coordination chemistry of the first two ligands, relative to their 4-H analogues, however, the coordination chemistry of the third ligand is dramatically changed, making it a "tetrahedral enforcer". The complexes $Co[Tp^{4tBu}][Tp^{Np}]$ (**1**), $Tl[Tp^{Tol,4tBu}]$ (**2**), $Rh[Tp^{Tol,4tBu}](CO)_2$ (**3**), $Co[Tp^{iPr,4tBu}]Cl$ (**4**), $Co[Tp^{iPr,4tBu}]N_3$ (**5**) and $Co[Tp^{iPr,4tBu}]NCS$ (**6**) have been structurally characterized.
(© Wiley-VCH Verlag GmbH & Co. KGaA, 69451 Weinheim, Germany, 2003)

Introduction

Many of the reported highlights of homoscorpionate [hydrotris(pyrazol-1-yl)borate] coordination chemistry were associated with the use of Tp^R ligands containing a specific R substituent in the 3-position.[1] This defined and restricted the size and geometry of the hydrophobic pocket surrounding the coordinated metal atom. In addition to the size of the 3-substituent, it was also important to exert some control over the orientation of asymmetric substituents with regard to the pyrazolyl plane. These substituents included planar rings, such as a phenyl or substituted phenyl, or asymmetric aliphatic groups, such as isopropyl or cycloalkyl (cyclopropyl,[2] cyclobutyl,[3] cyclopentyl,[2] and cyclohexyl[4]), which could exist as different rotamers. In the case of phenyl, its coplanarity with the pyrazolyl ring was approached by means of an ethylene tether,[5] and achieved by means of an ethyne,[6] or methylene tether.[5] Conversely, approximate orthogonality of the phenyl ring to the pyrazolyl plane resulted from placing 2,6-dimethyl substituents on the phenyl group, as in Tp^{Ms},[7] or fusing two benzo rings in the 2,3- and 5,6-positions, as in Tp^{Ant}.[8] Since the last two methods of restricting the rotational freedom of the phenyl ring also altered its nature, by converting a phenyl into a mesityl or a 9-anthryl substituent, we sought to investigate the restriction of rotation of the 3-R group through "remote control", by placing a *tert*-butyl group in the 4-position of the Tp^R ligand.

To this end we have synthesized ligands of the general type $Tp^{R,4tBu}$ with R = isopropyl or *p*-tolyl, and also the ligand Tp^{4tBu}, where R = H. Some aspects of their coordination chemistry were studied, and compared with the behavior of Tp^x analogues containing either H or Br in the 4-position. Although a number of homoscorpionate ligands have been described containing 4-substituents (halide, linear alkyl groups, phenyl), none possess the steric bulk of a *tert*-butyl group.[1]

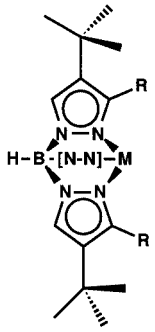

-[N-N]- is the third, hidden, 3-R-4-(*tert*-butyl)pyrazolyl ring

R = H, isopropyl, *p*-tolyl

Results and Discussion

The new ligands Tp^{4tBu}, $Tp^{Tol,4tBu}$, and $Tp^{iPr,4tBu}$ were synthesized by reaction of KBH_4 with an excess of the appropriate molten pyrazole. They were isolated, purified, and characterized as their respective Tl salts.[9]

The ligand with R = H (Tp^{4tBu}) was sterically unhindered around the 3-position, as in the parent ligand Tp. It was structurally characterized as part of the heteroleptic complex $Co[Tp^{4tBu}][Tp^{Np}]$ (**1**) by NMR spectroscopy and by X-ray crystallography (Figure 1). The Co−N bonds of the Tp^{4tBu} ligand are shorter than those of Tp^{Np} (average

[a] Department of Chemistry and Biochemistry, University of Delaware,
Newark, DE 19716, USA

bond lengths 2.13 and 2.17 Å, respectively), consistent with the unsubstituted 3-position. In the structure of Co[Tp^{4tBu}][Tp^{Np}], unidirectional sideways twisting of the neopentyl groups around the B−Co axis can be seen. This was also observed in other structurally characterized Tp^{Np} derivatives.[10] Furthermore, the paramagnetic NMR spectrum of **1** closely resembles that of the known analogue Co[Tp][Tp^{Np}][11] with each proton type uniquely defined. However, the signal in the 40−50 ppm range assigned to the 4-H proton is absent, and a new signal for the *tert*-butyl group is prominent at $\delta = -6.1$ ppm. As expected, Tp^{4tBu} forms stable octahedral M[Tp^{4tBu}]$_2$ complexes and labile tetrahedral M[Tp^{4tBu}]X complexes, which are unstable with respect to the octahedral species.

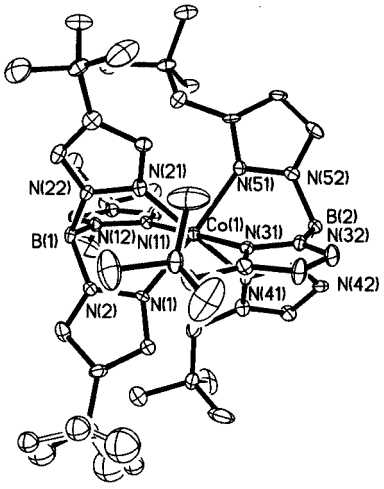

Figure 1. ORTEP plot of the structure of Co[Tp^{4tBu}][Tp^{Np}] (**1**); selected bond lengths [Å] and angles [°]: Co−N(1) 2.128(6), Co−N(11) 2.129(7), Co−N(21) 2.131(7), Co−N(31) 2.163(7), Co−N(41) 2.164(7), Co−N(1) 2.175(7); N(1)−Co−N(11) 84.8(3), N(1)−Co−N(21) 84.6(3), N(21)−Co−N(11) 87.1(3), N(31)−Co−N(41) 86.9(3), N(31)−Co−N(51) 87.4(3), N(41)−Co−N(51) 87.7(3)

Reaction of Tl[Tp^{4tBu}] with [Pd(η^3-methallyl)Cl]$_2$ yielded the stable complex Pd[Tp^{4tBu}][η^3-methallyl]. The NMR spectrum of this compound shows only one type of 3-(*tert*-butyl)pyrazolyl group, which is consistent with the rapid exchange of the coordinated and uncoordinated pyrazolyl groups, as was observed earlier in similar Pd[Tp^x][η^3-methallyl] complexes. In short, [Tp^{4tBu}] behaves similarly to the parent ligand Tp.

The ligand [Tp^{Tol,4tBu}]$^-$ was synthesized by reaction of KBH_4 with molten 4-(*tert*-butyl)-3-(*p*-tolyl)pyrazole, and it was characterized as Tl[Tp^{Tol,4tBu}] (**2**) by NMR spectroscopy and X-ray crystallography (Figure 2). The twist angles of the tolyl group with respect to the pyrazolyl plane are 101, 102, and 121°, respectively. The deviation from orthogonality of the pyrazolyl and tolyl molecular planes is, on average, 18°. Unlike the closely related Tl[Tp^{Tol}],[12] which forms a head-to-head dimer in the crystal, Tl[Tp^{Tol,4tBu}] is monomeric. The Tl−N distances are the same for both compounds (2.58 Å), and fall within the range for Tl[Tp^x] compounds (2.50−2.73 Å).[13] However, in Tl[Tp^{Tol,4tBu}], the N−Tl−N angles are smaller than those in Tl[Tp^{Tol}] (average angles 74° and approximately 77°, respectively). In other Tl[Tp^x] compounds, such angles range from 65.3 to 79.4°.[13]

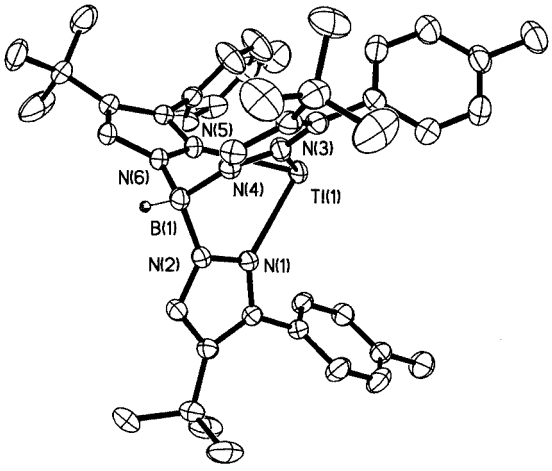

Figure 2. ORTEP plot of the structure of Tl[Tp^{Tol,4tBu}] (**2**); selected bond lengths [Å] and angles [°]: Tl−N(1) 2.580(2), Tl−N(3) 2.550(3), Tl−N(5) 2.560(2); N(1)−Tl−N(3) 73.55(8), N(5)−Tl−N(3) 74.15(8), N(1)−Tl−N(5) 73.58(8)

The reaction of Tl[Tp^{Tol,4tBu}] with anhydrous $CoCl_2$ in chloroform yielded the tetrahedral complex Co[Tp^{Tol,4tBu}]Cl, which could be used to synthesize mixed complexes. For instance, its reaction with Tl[Tp] proceeded easily, producing the heteroleptic species Co[Tp^{Tol,4tBu}][Tp]. The proton NMR spectrum of Co[Tp^{Tol,4tBu}][Tp] is in agreement with a structure that has not undergone any rearrangement. Assignment of the NMR resonances was aided by comparison with the related complex Co[Tp^{Tol}][Tp], which was synthesized from Co[Tp^{Tol}]Cl and Tl[Tp]. The *ortho*- and *meta*-protons of the tolyl substituent in both complexes appear as sharp resonances, rather than as two separate peaks or as broad resonances. This indicates a sufficient degree of oscillation of the tolyl group around the C-3 bond (despite the presence of the 4-*tert*-butyl substituent) to render them spectroscopically equivalent on the NMR timescale.

The complex Rh[Tp^{Tol,4tBu}](CO)$_2$ (**3**) was prepared by bubbling CO into a solution of the Rh[Tp^{Tol,4tBu}](COD) intermediate prepared in situ from **2** and the Rh(COD)Cl dimer. The IR spectrum of this compound contains two sets of carbonyl peaks: 2080, 2059, 2015, and 1980 cm^{-1}, with the BH stretching frequency at 2443 cm^{-1}. The presence of four CO peaks suggests that the compound contains both κ^3 and κ^2 species, which is not unusual for complexes of this general type.[14] The structure of **3** was determined by X-ray crystallography (Figure 3). The Rh center is five-coordinate, with one long (2.43 Å) and two short (2.12 and 2.13 Å) Rh−N bonds. This type of five-coordination leads to the lowest energy structure for Rh[Tp^x](CO)$_2$ complexes, as has been predicted by Webster and Hall on the basis of density functional calculations for the various structures that a Rh[Tp^x](CO)$_2$ species can adopt.[14] The deviation from orthogonality of the tolyl and pyrazolyl planes varied: 26 and 25° for the pyrazolyl arms containing the two short

 © 2003 Wiley-VCH Verlag GmbH & Co. KGaA, Weinheim

Rh−N bonds, and 10° for the arm with the long axial Rh−N bond. The N−Rh−N angles average 83.4°.

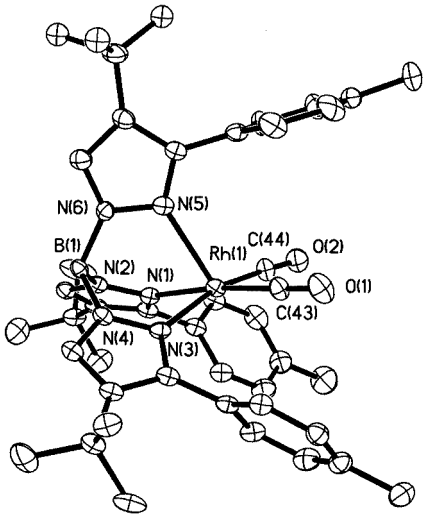

Figure 3. ORTEP plot of the structure of $Rh[Tp^{Tol,4tBu}](CO)_2$ (**3**); selected bond lengths [Å] and angles [°]: Rh−N(1) 2.116.4(4), Rh−N(3) 2.132.4(4), Rh−N(5) 2.426.4(4), Rh−C(44) 1.851(5), Rh−C(43) 1.856(5); N(1)−Rh−N(3) 85.05(13), N(1)−Rh−N(5) 84.02(13), N(5)−Rh−N(3) 81.34(13), C(43)−Rh−C(44) 85.4(2)

By comparison, the related complex $Rh[Tp^{Br3}](CO)_2$ shows only two CO bands in its IR spectrum: $\tilde{\nu}$ = 2080 and 2012 cm^{-1}, each with a hint of a shoulder at higher frequency. This compound also has one long (2.53 Å) and two short (2.12 and 2.12 Å) Rh−N bonds.[15] The somewhat longer Rh−N bond might reflect the lower nucleophilicity of the tribromopyrazolyl arm, and would be consonant with the rather high frequency of the B−H stretch, which is at 2585 cm^{-1}. In other structurally characterized $Rh[Tp^x](CO)_2$ complexes, the axial Rh−N bonds are longer, ranging from 2.55 to 2.64 Å.[14] From all the above data we can conclude that while the *tert*-butyl group in the 4-position does not permit free rotation of the 3-aryl substituent, neither does it enforce orthogonality between the pyrazolyl and tolyl planes. The 4-*tert*-butyl group allows for sufficient oscillation of the tolyl group around the C-3 bond, so that the tolyl substituent can deviate considerably from orthogonality relative to the pyrazolyl plane (we have examples which deviate by up to 31°) in order to accommodate other ligands attached to the metal atom. Thus, the difference in steric hindrance between Tp^{Tol} and $Tp^{Tol,4tBu}$ becomes rather insignificant.

While the coordination behavior of $[Tp^{Tol,4tBu}]^-$ is still fairly similar to that of $[Tp^{Tol}]^-$, major spectroscopic differences and differences in chemical reactivity can be observed between $[Tp^{iPr,4tBu}]^-$ and its closest steric analogue, $[Tp^{iPr,4Br}]^-$. The ^1H NMR spectrum of $Tl[Tp^{iPr,4Br}]$ exhibits a sharp doublet and septuplet,[11] assigned to the isopropyl groups. However, in the ^1H NMR spectrum of $Tl[Tp^{iPr,4tBu}]$, the resonances assigned to the methyl groups appear as a small broad hump at δ = 1.4 ppm. The signal for the tertiary hydrogen atom is not visible, and can only be discerned through integration in the δ = 3.1−3.5 ppm range. The difference was even more dramatic in the ^{13}C NMR spectrum. In the spectrum of $Tl[Tp^{iPr,4Br}]$, the resonance assigned to the isopropyl methyl group is only slightly broadened. However, it is split into a doublet in the spectrum of $Tl[Tp^{iPr,4tBu}]$. The value of J = 218 Hz, is the largest known ^{13}C-^{205}Tl coupling observed in $Tl[Tp^x]$ complexes. It significantly exceeds those found in $Tl[Tp^{tBu,iPr}]$ (J = 167 Hz),[16] $Tl[Tp^{tBu}]$ (J = 171 Hz),[17] $Tl[Tp^{tBu,Tn}]$ (J = 183 Hz),[11] and $Tl[Tp^{tBu,Me}]$ (J = 197 Hz).[18]

In terms of their coordination chemistry, $[Tp^{iPr,4tBu}]$ forms different complexes from those of $[Tp^{iPr,4Br}]$,[19] and resembles those of $[Tp^{tBu}]$.[20] Thus, stable compounds of the type $M[Tp^{iPr,4tBu}]X$, where X = halide or pseudohalide, are readily prepared. They do not add solvent molecules, as was observed in the case of the $M[Tp^{iPr,4Br}]X$ analogues, which readily form five-coordinate complexes with small donor molecules, such as methanol or THF (although on air-drying, the solvent is gradually lost). Thus, one could regard $[Tp^{iPr,4tBu}]$ as a bona fide "tetrahedral enforcer", no less so than $[Tp^{tBu}]$. The complex $Co[Tp^{iPr,4tBu}]Cl$ (**4**) was structurally characterized (Figure 4).

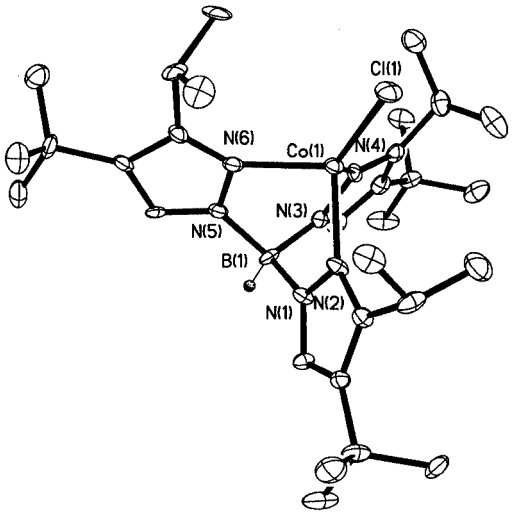

Figure 4. ORTEP plot of the structure of $Co[Tp^{iPr,4tBu}]Cl$ (**4**); selected bond lengths [Å] and angles [°]: Co−N(2) 2.040(3), Co−N(4) 2.024(6), Co−N(6) 2.058(7); N(2)−Co−N(4) 95.4(3), N(2)−Co−N(6) 94.2(3), N(4)−Co−N(6) 95.74(11)

Another distinguishing feature of $[Tp^{iPr,4tBu}]^-$, as compared with $[Tp^{iPr,4Br}]$, is the fact that while reaction of $Co[Tp^{iPr,4Br}]X$ with Tl[Tp] or Tl[Tp*] readily yields the heteroleptic complexes $Co[Tp^{iPr,4Br}][Tp]$ and $Co[Tp^{iPr,4Br}][Tp^*]$, respectively,[21] **4** does not undergo such reactions. For instance, stirring a solution of **4** with the least-hindered homoscorpionate ligand, Tl[Tp], for 26 h, did not produce the heteroleptic complex, but only a very small amount of $Co[Tp]_2$. This type of behavior was also observed for $Co[Tp^{tBu}]Cl$. Obviously, the 4-*tert*-butyl group does not permit rotation of the isopropyl substituent so as to direct the two methyl groups away from the coordinated metal atom and toward the 4-position of the pyrazolyl ring, which is a precondition for the formation of heteroleptic species

 © 2003 Wiley-VCH Verlag GmbH & Co. KGaA, Weinheim

M[Tp$^{i\mathrm{Pr,4Br}}$][Tp^{x}]. On the contrary, it locks the isopropyl substituent, so that it straddles the pyrazolyl plane with both methyl groups forking towards the coordinated metal atom. Such rotameric disposition of the isopropyl methyl groups has been established only for a few structurally characterized tetrahedral compounds of the type M[Tp$^{i\mathrm{Pr,4Br}}$]X.[19,22] However, the rotameric disposition of a 3-isopropyl group with the two methyl groups directed away from the coordinated metal atom is ubiquitous in all heteroleptic complexes M[Tp$^{i\mathrm{Pr,4Br}}$][L],[21,23] as well as in other homoscorpionate complexes containing a 3-*i*Pr substituent, such as those of Tp$^{i\mathrm{Pr,Me}}$,[24] and of Tp$^{i\mathrm{Pr2}}$.[25]

Despite the failure to form the heteroleptic complex Co[Tp$^{i\mathrm{Pr,4}t\mathrm{Bu}}$][Tp] by reaction of Co[Tp$^{i\mathrm{Pr,4}t\mathrm{Bu}}$]Cl with [Tp]$^-$, displacement of the chloride ion by other simple monodentate ions is feasible, as was demonstrated by the heterogeneous reaction of **4** with solid NaN_3 in ethyl acetate, which resulted in the formation of Co[Tp$^{i\mathrm{Pr,4}t\mathrm{Bu}}$]$N_3$ (**5**) as the only product, in good yield. Its structure, as well as that of the related complex Co[Tp$^{i\mathrm{Pr,4}t\mathrm{Bu}}$]NCS (**6**), which was prepared by the heterogeneous reaction of Tl[Tp$^{i\mathrm{Pr,4}t\mathrm{Bu}}$] and $Co(NCS)_2$, was determined by X-ray crystallography (Figures 5 and 6, respectively).

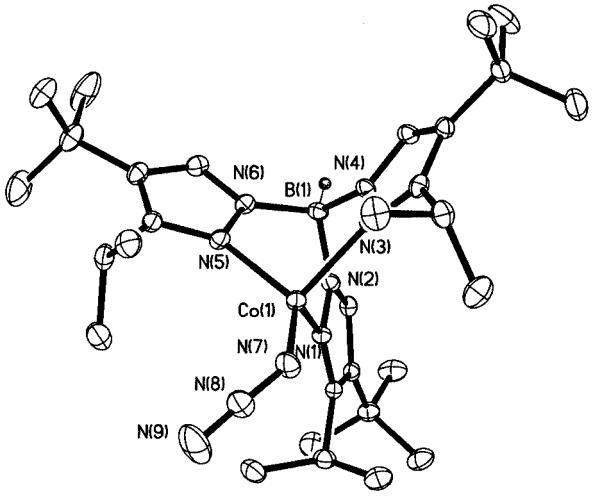

Figure 5. ORTEP plot of the structure of Co[Tp$^{i\mathrm{Pr,4}t\mathrm{Bu}}$]$N_3$ (**5**); selected bond lengths [Å] and angles [°]: Co−N(1) 2.011(2), Co−N(3) 2.044(2), Co−N(5) 2.032(2), Co−N(7) 1.911(2); N(1)−Co−N(3) 96.38(9), N(1)−Co−N(5) 93.82(9), N(5)−Co−N(3) 94.84(9), N(1)−Co−N(7) 121.61(10), N(3)−Co−N(7) 117.81(10), N(5)−Co−N(7) 125.47(10)

If one compares the Co−N bond lengths and N−Co−N angles in three related and structurally characterized complexes, Co[Tp$^{i\mathrm{Pr,4Br}}$]NCS, Co[Tp*t*Bu]NCS, and **6**, we see that **6** has the longest Co−N bond (average bond length 2.029 Å), Co[Tp$^{t\mathrm{Bu}}$]NCS has the shortest (2.019 Å), and Co[Tp$^{i\mathrm{Pr,4Br}}$]NCS has a bond length of intermediate value (2.024 Å). Compound **6** also has the widest average N−Co−N angle (95.7°), followed by Co[Tp$^{t\mathrm{Bu}}$]NCS (95.4°) and Co[Tp$^{i\mathrm{Pr,4Br}}$]NCS (95.2°).

Comparing the average Co−N bond lengths and N−Co−N angles of complex **4** with those of Co[Tp$^{i\mathrm{Pr,4Br}}$]Cl and Co[Tp$^{t\mathrm{Bu}}$]Cl, we find that the above-

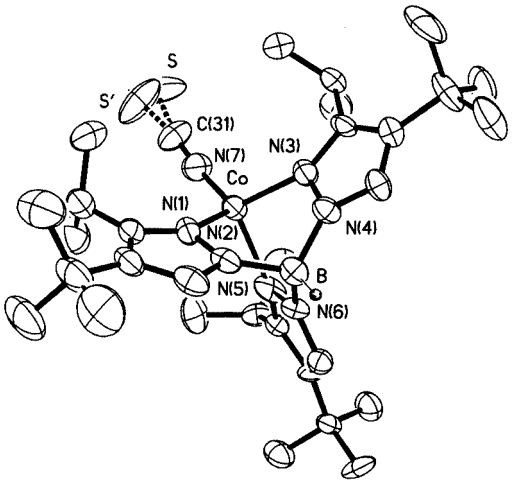

Figure 6. ORTEP plot of the structure of Co[Tp$^{i\mathrm{Pr,4}t\mathrm{Bu}}$]NCS (**6**); selected bond lengths [Å] and angles [°]: Co−N(1) 1.984(8), Co−N(3) 2.021(7), Co−N(5) 2.081(9), Co−N(7) 1.898(10); N(1)−Co−N(3) 97.0(3), N(1)−Co−N(5) 94.4(3), N(5)−Co−N(3) 95.6(3)

mentioned bond lengths and angles in **4** are closer to those of Co[Tp$^{t\mathrm{Bu}}$]C, than to those of Co[Tp$^{i\mathrm{Pr,4Br}}$]Cl. In **4**, the two values are 2.033(5) Å and 95.1°, in Co[Tp$^{t\mathrm{Bu}}$]Cl they are 2.038 Å and 95.1°,[26] while in Co[Tp$^{i\mathrm{Pr,4Br}}$]Cl they are 2.039(6) Å and 94.4°, respectively.[22] In the related complex **5**, these values are 2.029 Å and 95.0°, respectively.

Conclusion

We have prepared several Tp^{x} ligands of the general type [Tp$^{\mathrm{R,4}t\mathrm{Bu}}$]$^-$ where R = H, isopropyl, or *p*-tolyl, and found that the presence of the 4-*tert*-butyl group strongly blocks the rotational freedom of a 3-isopropyl group. Therefore, the 3-isopropyl group behaves like a 3-*tert*-butyl group (a "tetrahedral enforcer") with a fixed rotameric conformation in which the two methyl groups are forked towards the coordinated metal atom. This significantly changes the coordination chemistry of [Tp$^{i\mathrm{Pr,4}t\mathrm{Bu}}$]$^-$, relative to all other Tp^{x} ligands containing 3-isopropyl substituents. On the other hand, the effect of a 4-*tert*-butyl group on the 3-*p*-tolyl substituent in [Tp$^{\mathrm{Tol,4}t\mathrm{Bu}}$] is less pronounced, since the 4-*tert*-butyl substituent still permits substantial latitude for oscillation, if not free rotation, of the 3-tolyl group. Thus, the formation of the heteroleptic complex Co[Tp$^{\mathrm{Tol,4}t\mathrm{Bu}}$][Tp] was as easy as that of Co[Tp$^{\mathrm{Tol}}$][Tp]. When 3-R = H, [Tp$^{4t\mathrm{Bu}}$]$^-$ behaves like the parent ligand [Tp]$^-$, except that the melting points of its derivatives are higher, and its NMR spectrum is simpler.

Experimental Section

General: All chemicals were commercial reagent grade and were used as received. 4-(*tert*-Butyl)-3-isopropylpyrazole and 4-*tert*-butyl-3-(*p*-tolyl)pyrazole were prepared according to a literature procedure,[27] as was Co[Tp$^{\mathrm{Np}}$]Cl.[10] [Pd(η^3-methallyl)Cl]$_2$ was pur-

 © 2003 Wiley-VCH Verlag GmbH & Co. KGaA, Weinheim

chased from Strem. Elemental analyses were done by Microanalysis, Inc., Wilmington, DE. Infrared spectra were obtained as Nujol mulls or as KBr pellets with a Perkin−Elmer 1625 FTIR infrared spectrophotometer, using 16 scans. ^{1}H NMR spectra were obtained with a Nicolet NT360WB spectrometer. The compounds were studied under typical conditions, with 16 K data points, a sweep width of 3000−4000 Hz, 90° pulse angles, and a recycle time of 4−5 s. ^{13}C NMR: pulse width, 9.00 μs; acq. time 819.20 ns; recycle time 1.0 s; number of acq. 8192; frequency 75.43 MHz; spec. width 20000 H_3.

4-*tert*-Butylpyrazole: A mixture of pyrazole (136 g, 2 mol) and *tert*-butyl chloride (279 g, 3 mol) was heated for 6 h at 220 °C in an autoclave. After cooling, the autoclave contents were stirred in a mixture of alkaline ice water, and the products were extracted with chloroform. The extracts were filtered through alumina, stripped, and distilled under atmospheric pressure. The fraction boiling in the 176−196 °C range was obtained in 28 g yield. It was (by NMR) 40% pyrazole and 60% 1,4-di(*tert*-butyl)pyrazole. The residue obtained was almost pure 4-*tert*-butylpyrazole (90 g, 36%, by NMR spectroscopy), contaminated only by a small amount of 1,4-bis(*tert*-butyl)pyrazole. The product was purified by recrystallization the 176−196 °C range was obtained in 28 g yield. It was (by NMR) δ = 11.2 (s, broad, 1 H, NH), 7.44 (s, 2 H, H-3,5), 1.27 (s, 9 H, *t*Bu) ppm. The literature reports 4-*tert*-butylpyrazole to be a yellowish oil.[28]

K[Tp^{4tBu}]: A mixture of 4-*tert*-butylpyrazole [50 g, 0.40 mol, contaminated with traces of the innocuous 1,4-bis(*tert*-butyl)pyrazole] and KBH_4 (5.4 g, 0.10 mol) was stirred and heated gradually without any solvent. Hydrogen began to evolve at 140 °C, and evolution of the theoretical 7.5 L was completed at 220 °C. Excess 4-*tert*-butylpyrazole, and traces of 1,4-bis(*tert*-butyl)pyrazole, were removed by distillation under vacuum. The molten product was cooled, transferred to a 500-mL Erlenmeyer flask, and boiled with 300 mL of octane. The slurry was cooled, the solid was filtered off, and washed with hexane, producing the crude potassium salt in a 90% (38 g) yield. IR: $\tilde{\nu}$ = 2390 (BH, broad) cm^{-1}.

Tl[Tp^{4tBu}]: All of the above crude K[Tp^{4tBu}] was converted into Tl[Tp^{4tBu}] by dissolving it in a minimum amount of THF, and stirring the resulting solution with an excess of aqueous $TlNO_3$ solution for 1 h. Thereafter, 1 L of water was added, along with 500 mL of chloroform. The organic layer was separated, and passed through a layer of alumina. Evaporation of the solvent gave the crude product in an 86% (45 g) yield. The product was purified by recrystallization from undecane. The fine needles sintered from 280 °C, and melted and decomposed at 282−283 °C. IR: $\tilde{\nu}$ = 2450 (BH, broad) cm^{-1}. NMR: δ = 7.54 (s, 3 H, 5-H), 7.42 (s, 3 H, 3-H), 1.24 (s, 27 H, *t*Bu) ppm; BH (1 H) was detected by integration in the δ = 3.4−5.4 ppm range. ^{13}C NMR: δ = 29.6 (*C*Me_3), 32.3 (C*Me_3*), 131.4 (C-4), 132.3 (C-5), 136.4 (C-3) ppm. $C_{21}H_{37}BN_6Tl$ (588.76): calcd. C 43.1, H 5.81, N 14.4; found C 43.0, H 6.10, N 14.2.

Pd[Tp^{4tBu}][η^3-methallyl]: A mixture of Tl[Tp^{4tBu}] (1.2 g, 2 mmol) and the Pd(η^3-methallyl)Cl dimer (0.76 g, 2 mmol) was stirred in 30 mL of chloroform for 1 h. The slurry was filtered, and the filtrate concentrated to give a white solid, which was recrystallized from toluene/heptane. M.p. 154−156 °C (dec.). IR: $\tilde{\nu}$ = 2462 (BH) cm^{-1}. ^{1}H NMR: δ = 7.39 (s, 3 H, 3-H), 7.35 (s, 3 H, 5-H), 3.66 (s, 2 H, *syn*), 2 87 (2 H, *anti*), 2.09 (s, 3 H, Me), 1.21 (s, 27 H, *t*Bu) ppm. $C_{25}H_{41}BN_6Pd$ (542.88): calcd. C 55.4, H 7.56, N 15.5; found 55.6, H 7.72, N 15.3.

Co[Tp^{4tBu}][Tp^{Np}] (1): A mixture of Tl[Tp^{4tBu}] (1.2 g, 2 mmol) and Co[Tp^{Np}]Cl (1.1 g, 2 mmol) was stirred in 150 mL of dichloromethane. Within 10 min, the blue color changed to a pale yellow. The slurry was filtered through Celite, yielding a bright yellow solution, which on evaporation yielded **1** (1.3 g, 74%) as a pale yellow solid. It was recrystallized from undecane. M.p. 295−296 °C (with darkening and dec.). IR: $\tilde{\nu}$ = 2442 (BH, Tp^{Np}) and 2449 (BH, Tp^{4tBu}) cm^{-1}. ^{1}H NMR: δ = 115.6 and 113 (1 H each, BH, BH′) 93.2 and 82.2 (3 H each, 5-H and 5′-H), 44.7 (3 H, 4-H), −6.26 (27 H, 4-*t*Bu), −21.3 (27 H, neopentyl *t*Bu), −100.7 (3 H, 3-H), −103.7 (6 H, CH_2) ppm. $C_{45}H_{74}B_2CoN_{12}$ (863.72): calcd. C 62.6, H 8.57, N 19.5; found C 62.7, H 8.69, N 19.2.

Tl[$Tp^{Tol,4tBu}$] (2): A mixture of 4-(*tert*-butyl)-3-tolylpyrazole (8.9 g, 42 mmol) and KBH_4 (0.56 g, 10 mmol) was heated in a test tube until the borohydride could not be seen anymore, and the initially vigorous evolution of hydrogen ceased. The product was cooled, dissolved in DMF, and stirred with excess aqueous $TlNO_3$. The product was extracted with dichloromethane, the extracts were washed three times with water, and were passed through a bed of alumina. Concentration of the filtrate gave **2** as a fibrous white solid, which was washed with methanol to remove unchanged 4-(*tert*-butyl)-3-tolylpyrazole. **2** was obtained in a 70% (6.5 g) yield. It was recrystallized from octane. M.p. 222−224 °C. IR: $\tilde{\nu}$ = 2435, 2472 sh (BH) cm^{-1}. ^{1}H NMR: δ = 7.53 (s, 1 H, 5-H), 7.23 (d, 2 H, tolyl A_2B_2), 7.11 (d, 2 H, tolyl A_2B_2), 2.34 (s, 3 H, Me) 1.63 (s, 9 H, *t*Bu) ppm. $C_{42}H_{52}BN_6Tl$ (856.11): calcd. C 59.0, H 6.08, N 9.82; found C 59.2, H 6.17, N 9.67.

Co[$Tp^{Tol,4tBu}$]Cl: A sample of **2** (1.7 g, 2.0 mmol) was stirred in 50 mL of chloroform with excess anhydrous $CoCl_2$. After 6 h, the slurry was filtered, and the filtrate was concentrated, yielding Co[$Tp^{Tol,4tBu}$]Cl (1.2 g, 82%), which was purified by recrystallization from a toluene/octane mixture; m.p. dec. > 280 °C. IR: $\tilde{\nu}$ = 2466 (BH) cm^{-1}. $C_{42}H_{52}BClCoN_6$ (746.11): calcd. C 67.6, H 6.97, N 11.3; found C 67.9, H 7.18, N 11.1.

Co[$Tp^{Tol,4tBu}$]NCS: This complex was prepared as above; however, $Co(NCS)_2$ was used instead of $CoCl_2$. It was obtained in a 78% yield. M.p. gradual dec. > 240 °C. IR: $\tilde{\nu}$ = 2476 (BH), 2068 (NCS) cm^{-1}. $C_{43}H_{52}BCoN_7S$ (768.75): calcd. C 67.2, H 6.77, N 12.8; found C 67.6, H 6.89, N 12.6.

Co[$Tp^{Tol,4tBu}$][Tp]: A mixture of Co[$Tp^{Tol,4tBu}$]Cl (0.75 g, 1.0 mmol) and Tl[Tp] (0.42 g, 1.0 mmol) was stirred in 50 mL of chloroform for 6 h. The slurry was filtered, and the filtrate was chromatographed on alumina. On concentration of the yellow-orange eluent, yellowish-orange crystals (0.51 g, 68%) were obtained. M.p. gradual dec. > 270 °C. IR: $\tilde{\nu}$ = 2452 (BH) cm^{-1}. NMR: δ = 114 (1 H, BH), 112 (1 H, BH′), 90.1 (3 H, 5-H), 80.9 (3 H, 5′-H), −3.15 (27 H, *t*Bu), −5.9 (9 H, Me), −9.2 (6 H, *m*-H), −49.1 (6 H, *o*-H), −103.4 (3 H, 3-H H) ppm. $C_{51}H_{62}B_2CoN_{12}$ (923.63): calcd. C 66.3, H 6.72, N 18.2; found C66.5, H 6.79, N 17.9.

Co[Tp^{Tol}][Tp]: This complex was prepared as above from Co[Tp^{Tol}]Cl (0.58 g, 1 mmol) and Tl[Tp] (0.42 g, 1 mmol), in an 82% (0.62 g) yield. M.p. sintered from 265 °C, gradual dec. > 275 °C. IR: $\tilde{\nu}$ = 2470 (BH) cm^{-1}. NMR: δ = 113 (1 H, BH), 112 (1 H, BH′), 89.4 (3 H, 5-H), 77.3 (3 H, 5′-H), 44.2 (3 H, 4-H), 41.8 (3 H, 4′-H), −1.88 (9 H, Me), −2.18 (6 H, *m*-H), −55.4 (6 H, *o*-H), −99.1 (3 H, 3-H) ppm. $C_{39}H_{38}B_2CoN_{12}$ (755.36): calcd. C 62.0, H 5.03, N 22.3; found C 62.1, H 5.15, N 22.1.

Rh[$Tp^{Tol,4tBu}$]$(CO)_2$ (3): A mixture of **2** (0.86 g, 1 mmol) and the RhCl(COD) dimer (0.30 g, 1 mmol) was stirred in chloroform at room temperature for 2 h. The slurry, containing precipitated TlCl was stirred further with a stream of CO bubbling in for 1 h, and was then filtered through a pad of Celite. The filtrate was concen-

 © 2003 Wiley-VCH Verlag GmbH & Co. KGaA, Weinheim

trated and the product, obtained in a 68% (0.55 g) yield, was recrystallized from toluene/heptane. M.p. 233−235 °C (dec.). IR: $\tilde{\nu}$ = 2443 (BH); 2028, 2059, 2015, 1980 (CO) cm^{-1}. ^1H NMR: slightly broadened resonances at δ = 7.6 (1 H, 5-H), 7.3 and 7.2 (2 H each, tolyl A_2B_2 pattern), 2.4 (3 H, Me), 1.2 (9 H, *t*Bu) ppm. $C_{44}H_{52}BN_6O_2Rh$ (810.66): calcd. C 65.2, H 6.42, N 10.4; found C 65.5, H 6.57, N 10.2.

Tl[Tp^{iPr,4tBu}]: A mixture of 4-(*tert*-butyl)-3-isopropylpyrazole (24 g, 130 mmol) and KBH_4 (2.0 g, 36 mmol) was heated to 220 °C, until the theoretical amount of hydrogen evolved. Excess 4-(*tert*-butyl)-3-isopropylpyrazole was sublimed out at 220 °C/1.5 Torr. The unsublimed crude K[Tp^{iPr,4tBu}] had $\tilde{\nu}$ = 2460 (BH) cm^{-1}, and it was converted into Tl[Tp^{iPr,4tBu}] as described for **2**. M.p. 222−224 °C. IR: $\tilde{\nu}$ = 2432 (BH) cm^{-1}. ^1H NMR: δ = 7.29 (s, 3 H, 5-H), 3.1−3.5 (very broad, 1 H, tertiary CH), 1.37 (broad hump, 18 H, isopropyl Me) and 1.26 (sharp s, 27 H, *t*Bu) ppm. ^{13}C NMR: δ = 26.1 (somewhat broad d, J = 218 Hz, CH*Me*$_2$), 27.5 (s, *C*HMe$_2$), 30.1 (sharp s, *C*Me$_3$), 31.7 (sharp s, C*Me*$_3$) 125.8 (broad s, C-5), 133.3 (very sharp s, C-4), 156.9 (broad s, C-3) ppm. $C_{30}H_{52}BN_6Tl$ (711.98): calcd. C 50.6, H 7.31, N 11.8; found 50.9, H 7.46, N 11.6%.

Co[Tp^{iPr,4tBu}]Cl (4): This complex was prepared by stirring Tl[Tp^{iPr,4tBu}] (2.8 g, 4 mmol) in dichloromethane with a large excess of anhydrous $CoCl_2$. After 3 h, the blue slurry was filtered, the filtrate was chromatographed on alumina, and the deep blue eluent was concentrated. The crude product, obtained in a 73% (1.8 g) yield, was recrystallized from octane, producing deep blue needles, which did not melt up to 304 °C. IR: $\tilde{\nu}$ = 2502 (BH) cm^{-1}. NMR: δ = 34.6 (3 H, 5-H), 23.9 (3 H, C*H*Me$_2$), 10.7 (18 H, CH*Me*$_2$), 4.3 (27 H, *t*Bu) and −21.4 (1 H, BH) ppm. $C_{30}H_{52}BClCoN_6$ (601.98): calcd. C 59.8, H 8.63, N 14.0; found C 60.0, H 8.78, N 13.7.

Co[Tp^{iPr,4tBu}]N$_3$(5): This compound was obtained when **4** (0.6 g, 1 mmol) was stirred overnight in ethyl acetate with a large excess of solid NaN_3. The slurry was filtered through Celite, and the solution was concentrated, producing dark blue **5** in an 83% (0.50 g) yield. It melted at 272−274 °C, and on further heating fumes could be seen and the blue product turned purple. IR: $\tilde{\nu}$ = 2493 (BH), 2081 (N_3) cm^{-1}. NMR: δ = 42.2 (3 H, 5-H), 22.4 (3 H, C*H*Me$_2$), 9.03 (18 H, CH*Me*$_2$), 3.60 (27 H, *t*Bu), −9.2 (1 H, BH) ppm. $C_{30}H_{52}BCoN_9$ (609.12): calcd. C 59.2, H 8.55, N 20.7; found C 59.5, H 8.67, N 20.4.

Co[Tp$^{iPr,4-tBu}$]NCS (6): This compound was prepared as in the case of **4**, instead, Tl[Tp^{iPr,4tBu}] (1.4 g, 2 mmol) and a large excess of $Co(NCS)_2$ was used. It was obtained in a 65% (0.81 g) yield, as a deep blue solid. M.p. 269−271 °C. IR: $\tilde{\nu}$ = 2490 (BH), 2054 (NCS) cm^{-1}. NMR: δ = 41.3 (3 H, 5-H), 26.2 (3 H, C*H*Me$_2$), 9.18 (18 H, CH*Me*$_2$), 3.53 (27 H, *t*Bu), −6.15 (1 H, BH) ppm. $C_{31}H_{52}BCoN_7S$ (625.06): calcd. C 59.6, H 8.33, N 15.7; found C 59.7, H 8.41, N 15.5.

Attempts to Prepare the Heteroleptic Complex Co[Tp^{iPr,4tBu}][Tp]: Stirring equimolar amounts of Co[Tp^{iPr,4tBu}]Cl and TpTl in dichloromethane for 26 h showed no signs of a reaction. The greenish-blue solution was chromatographed, yielding two fractions: a minor yellow, and a dominant blue one. The material from the yellow fraction was identified as Co[Tp]$_2$ by its characteristic IR spectrum, while the blue fraction was unchanged Co[Tp^{iPr,4tBu}]Cl. A similar result was obtained when Co[Tp^{tBu}]Cl was stirred with Tl[Tp].

X-ray Crystal Structure Determinations: Diffraction intensity data were collected with Siemens P4 (**6**), Siemens P4/CCD (**1**), and

Table 1. Crystal data for compounds **1**−**6**

	1	**2**	**3**	**4**	**5**	**6**
Empirical formula	$C_{45}H_{74}B_2CoN_{12}$	$C_{42}H_{52}BN_6Tl$	$C_{44}H_{52}BN_6O_2Rh$	$C_{30}H_{52}BClCoN_6$	$C_{30}H_{52}BCoN_9$	$C_{31}H_{52}BCoN_7S$
Solvent		C_8H_{18}		$C_7H_8 + C_8H_{10}$	$CH_3CN + CH_2Cl_2$	
Formula mass	863.71	970.3	810.64	800.26	734.53	624.6
Space group	*Pbca*	*P*2$_1$/*c*	*C*2/*c*	*Pna*2$_1$	*P*2$_1$/*n*	*P*$\bar{1}$
	orthorhombic	monoclinic	monoclinic	orthorhombic	monoclinic	triclinic
a [Å]	11.807(5)	11.5083(9)	40.119(3)	19.4457(18)	19.1519(10)	12.493(3)
b [Å]	19.605(7)	13.7222(11)	11.3128(9)	9.2549(9)	18.0914(9)	12.940(4)
c [Å]	43.493(6)	31.405(3)	18.5842(15)	26.369(2)	22.5068(2)	16.688(4)
α [°]	90.00	90.00	90.00	90.00	90.00	84.17(2)
β [°]	90.00	92.837(2)	98.078(2)	90.00	94.3820(10)	83.93(2)
γ [°]	90.00	90.00	90.00	90.00	90.00	67.92(2)
V [Å^3]	10068(11)	4953.4(7)	8350.9(12)	4745.6(8)	7775.5(7)	2480.3(11)
Z, *Z*′	8, 1	4, 1	8, 1	4, 1	8, 1	2, 1
Crystal color	yellow	colorless	yellow	blue	blue	blue
Habit	plates	blocks	blocks	blocks	blocks	thin plates
Size [mm]	0.25 × 0.40 × 0.50	0.30 × 0.36 × 0.38	0.10 × 0.10 × 0.15	0.10 × 0.25 × 0.45	0.10 × 0.30 × 0.30	0.12 × 0.28 × 0.32
Temperature [K]	173	218	100	150	150	298
D(calcd.) [g·cm^{-3}]	1.140	1.301	1.290	1.120	1.147	0.836
μ (Mo-K_α) [cm^{-1}][a]	3.83	32.98	4.52	4.53	5.43	4.09
Absorption corr.	SADABS	SADABS	SADABS	SADABS	SADABS	psi scans
*T*max	0.9103	0.4378	0.9562	0.9561	0.9410	0.9525
*T*min	0.8315	0.3671	0.9353	0.8222	0.8368	0.8802
R_1 (*F*) [%][b]	12.21	3.32	6.59	6.42	5.11	10.69
wR_2 (*F*) [%][c]	27.19	8.01	15.08	16.85	9.08	26.46
Instrumentation	CCD K1	Apex	Apex	Apex	Apex	P3/4
Solution method	direct methods	direct methods	Patterson	direct methods	direct methods	direct methods

[a] Mo-K_α: λ = 0.71073 [Å] using Bruker-Siemens CCD K1, Bruker-Nonius Apex CCD, and Siemens P3/4 instruments. [b] $R = ||F_o| - |F_c||/|F_o|$. [c] $R(\omega F^2) = \{[\omega(F_o^2 - F_c^2)^2]/[\omega(F_o^2)^2]\}^{1/2}$; $\omega = 1/[\sigma^2(F_o^2) + (aP)^2 + bP]$, $P = [2F_c^2 + \max(F_o^2)]/3$.

 © 2003 Wiley-VCH Verlag GmbH & Co. KGaA, Weinheim

Bruker Smart Apex CCD (**2**−**5**) diffractometers. Crystal data collections and refinement parameters are given in Table 1. The space groups for structures **1**−**5** were chosen based on systematic absences in the diffraction, and for **6**, based on intensity statistics. Structure **3** was solved using a Patterson function and the other structures were solved by direct methods, completed by subsequent Fourier syntheses and refined by full-matrix least-squares procedures on reflection intensities (F^2). SADABS absorption corrections were applied to all data [G. M. Sheldrick, *SADABS* (2.01), Bruker/Siemens Area Detector Adsorption Correction Program, Bruker AXS, Madison Wisconsin, USA, **1998**]. In all the structures, non-hydrogen atoms were refined with anisotropic displacement coefficients and the hydrogen atoms were treated as idealized contributions. In structure **1**, carbon atoms C5−C7 of the *tert*-butyl group were disordered over two positions with 50:50 occupation. Similar disorder was found for one of the *tert*-butyl groups in structure **3**, where the disorder atoms had occupation of 47:53. In structures **2** and **4**, the solvent molecules were quite disordered and were left as isotropic in the refinement. The solvent molecules (dichloromethane and acetonitrile) in structure **5** were quite disordered and were treated using the program SQUEEZE.[29] Correction of the X-ray data for **5** by SQUEEZE (249 electrons/cell) was close to the required value of (256 electrons/cell) for the mixed solvent. Structure **6** diffracted rather poorly, and the S atom was found to be disordered over two positions with 50:50 occupation. All other software and sources, scattering factors are contained in the SHELXTL (5.10) program package (G. M. Sheldrick, Bruker AXS, Madison, WI). CCDC-198497 (**1**), -198498 (**2**), -198499 (**3**), -198500 (**4**), -198501 (**5**), and -198502 (**6**) contain the supplementary crystallographic data for this paper. These data can be obtained free of charge at www.ccdc.cam.ac.uk/conts/retrieving.html [or from the Cambridge Crystallographic Data Centre, 12 Union Road, Cambridge CB2 1EZ, UK; Fax: (internat.) + 44-1223/336-033; E-mail: deposit@ccdc.cam.ac.uk].

[1] S. Trofimenko, *Scorpionates: The Coordination Chemistry of Polypyrazolylborate Ligands*, Imperial College Press, London, **1999**.
[2] A. L. Rheingold, G. P. A. Yap, L. M. Liable-Sands, I. A. Guzei, S. Trofimenko, *Inorg. Chem.* **1997**, *36*, 6261−6265.
[3] A. L. Rheingold, G. P. A. Yap, L. N. Zakharov, S. Trofimenko, *Eur. J. Inorg. Chem.* **2002**, 2335−2343.
[4] S. Trofimenko, A. L. Rheingold, L. M. Liable-Sands, *Inorg. Chem.* **2002**, 1889−1896.
[5] A. L. Rheingold, R. L. Ostrander, B. S. Haggerty, S. Trofimenko, *Inorg. Chem.* **1994**, *33*, 3666−3676.
[6] A. L. Rheingold, B. S. Haggerty, S. Trofimenko, *J. Chem. Soc., Chem. Commun.* **1994**, 1973−1974.
[7] A. L. Rheingold, C. B. White, S. Trofimenko, *Inorg. Chem.* **1993**, *32*, 3471−3477.
[8] R. Han, G. Parkin, S. Trofimenko, *Polyhedron* **1995**, 387−391.
[9] C. Janiak, *Main Group Metal Chem.* **1998**, *21*, 33−49.
[10] J. C. Calabrese, S. Trofimenko, *Inorg. Chem.* **1992**, *31*, 4810−4814.
[11] S. Trofimenko, unpublished results.
[12] G. Ferguson, M. C. Jennings, F. J. Lalor, C. Shanahan, *Acta Crystallogr., Sect. C* **1991**, *47*, 2079−2082.
[13] C. Janiak, *Coord. Chem. Rev.* **1997**, *167*, 107−216.
[14] C. E. Webster, M. B. Hall, *Inorg. Chim. Acta* **2002**, *330*, 268−282.
[15] A. L. Rheingold, L. M. Liable-Sands, C. L. Incarvito, S. Trofimenko, *J. Chem. Soc., J. Chem. Soc., Dalton Trans.* **2002**, 2297−2301.
[16] C. López, D. Sanz, R. Claramunt, S. Trofimenko, J. Elguero, *J. Organomet. Chem.* **1995**, *503*, 265−276.
[17] A. H. Cowley, R. L. Geerts, C. M. Nunn, S. Trofimenko, *J. Organomet. Chem.* **1989**, *365*, 19−22.
[18] S. Trofimenko, J. C. Calabrese, J. K. Kochi, S. Wolowiec, F. B. Hulsbergen, J. Reedijk, *Inorg. Chem.* **1992**, *31*, 3943−3950.
[19] S. Trofimenko, J. C. Calabrese, P. J. Domaille, J. S. Thompson, *Inorg. Chem.* **1989**, *28*, 1091−1101.
[20] S. Trofimenko, J. C. Calabrese, J. S. Thompson, *Inorg. Chem.* **1987**, *26*, 1507−1514.
[21] J. C. Calabrese, P. J. Domaille, J. S. Thompson, S. Trofimenko, *Inorg. Chem.* **1990**, *29*, 4429−4437.
[22] M. D. Olson, S. J. Rettig, A. Storr, S. Trofimenko, *Acta Crystallogr., Sect. C* **1991**, *47*, 1543−1544.
[23] M. D. Olson, S. J. Rettig, A. Storr, S. Trofimenko, *Acta Crystallogr., Sect. C* **1991**, *47*, 1544−1546.
[24] M. Cano, J. V. Heras, S. Trofimenko, A. Monge, E. Gutierrez, C. J. Jones, J. A. McCleverty, *J. Chem. Soc., Dalton Trans.* **1990**, 3577−3582.
[25] See ref.[1], pp. 137−140, also: M. Akita, S. Hikichi, *Bull. Chem. Soc., Jpn.* **2002**, *75*, 1657−1679.
[26] I. B. Gorrell, G. Parkin, *Inorg. Chem.* **1990**, *29*, 2452−2456.
[27] S. Trofimenko, A. L. Rheingold, L. M. Liable-Sands, R. M. Claramunt, C. López, M. D. Santa Maria, J. Elguero, *New. J. Chem.* **2001**, *25*, 819−823.
[28] C. Cativiela, J. I. G. Laureiro, J. Elguero, *Gazz. Chim. Ital.* **1986**, *116*, 119−125.
[29] P. Van der Sluis, A. L. Spek, *Acta Crystallogr., Sect. A* **1990**, *46*, 194−201.

Received January 8, 2003

 © 2003 Wiley-VCH Verlag GmbH & Co. KGaA, Weinheim

Pyrene-Bridged Bis(phenanthroline) Ligands and Their Dinuclear Ruthenium(II) Complexes

Latif Chouai,[a] Feiyue Wu,[a] Youngchan Jang,[a] and Randolph P. Thummel*[a]

Keywords: Ruthenium / Bridging ligands / Pyrene / Phenanthroline

The Friedländer condensation of 8-amino-7-quinolinecarbaldehyde with a series of four isomeric diacetylpyrenes provides the corresponding 1,3-, 1,6-, 1,8-, and 2,7-bis(2′-[1′,10′]phenanthrolinyl)pyrenes. These ligands, along with the tetrahydro analogue to the 2,7-pyrene-bridged isomer, have been treated with $[Ru([D_8]bpy)_2Cl_2]$, where $[D_8]$bpy = $[D_8]$2,2′-bipyridine, to afford the dinuclear Ru^{II} complexes, ^{1}H NMR and X-ray crystallographic analysis of which indicate that the bridging pyrene is layered between a $[D_8]$bpy auxiliary ligand coordinated to each metal atom. Although well situated for π–π interactions, little such effect is seen on the photophysical and electrochemical properties of these complexes.

(© Wiley-VCH Verlag GmbH & Co. KGaA, 69451 Weinheim, Germany, 2003)

Introduction

Polynuclear transition metal complexes are of considerable current interest due to their potential for metal−metal cooperativity, an important design aspect in constructing molecular devices.[1] A critical component in such polynuclear complexes is the bridging ligand, which typically consists of two or more metal chelation sites connected by an appropriate linker. The most common chelators are 2,2′-bipyridine (bpy), 1,10-phenanthroline (phen), 2,2′;6′,2"-terpyridine (tpy), or closely related derivatives. These binding sites have been connected by linkers designed to control both the distance between the metal centers and the electronic communication between the sites. Distance control can be effected by using rigid linkers of known dimensions.[2] Spatial control will also depend on the point of attachment of the linker to the bpy, phen, or tpy end groups.

To attain better electronic communication between linked metal centers, substantial attention has been paid to the conjugating ability of the linker. Linkers with one or more π-bonds are common, while the inclusion of a tetrahedral center such as an sp^3-carbon atom can serve as an insulating junction.[3] Conjugated π-systems as linkers pose further problems, the most important of which is the potential for orthogonality between any two adjacent π-links. Such an orthogonal junction can also behave as an insulator, as has been noted with polyene and polyphenylene linkers.[4] Polyalkynyl linkers seem to avoid the problem and have come into use.[5]

Our interest in pyrene as part of a ligand system is due to the promising symmetry and electronic structure of this polynuclear aromatic compound. Firstly, the pyrene nucleus has three twofold axes which allow some symmetry to be retained in various mono- and disubstituted derivatives. Secondly, the pyrene nucleus is electroactive, having an oxidation potential of +1.28 V and a reduction potential of −2.09 V.[6] Thirdly, pyrene has a strong chromophore that extends over the entire molecule. It also has a reasonable excited-state lifetime (650 ns) and shows a strong emission at 372 nm.[7] Pyrene fluorescence has led to its being utilized in various sensor applications where fluorescence quenching is a useful reporter characteristic.[8] Finally the large π-surface of pyrene gives it some organizational qualities. The π-stacking of two pyrene molecules is concentration dependent, leading to the formation of an excimer which emits at lower intensity and longer wavelength than the monomer.[9]

Consequently, we sought to use pyrene as a linker in bridging ligand design. The availability of several isomers of diacetylpyrene[10] and our ability to elaborate an acetyl into a 2-phen group[11] led us to prepare and study the family of bridging ligands **1**−**5** reported here. Previously we have prepared 1,4-bis(2′-phen)benzene (**6**) and its dinuclear Ru^{II} complex,[12] and have studied the 4,4′-disubstituted biphenyl analogue **7**. Although the ligands experience free rotation about the bond connecting phen to the linker, the incorporation of an $[Ru(bpy)_2]^{2+}$ unit rigidifies the system by inhibiting this rotation. Nevertheless, the dinuclear complex of **7** can still rotate freely about the central biphenyl linkage. In addition to complexes of **6** and **7**, we have also studied the Ru^{II} complex of 1-(2′-phen)pyrene (**8**), the mononuclear analogue of the complexes derived from **3**−**5**.[13]

[a] Department of Chemistry, University of Houston, Houston, Texas 77204-5003, U.S.A.

 © 2003 Wiley-VCH Verlag GmbH & Co. KGaA, Weinheim **DOI: 10.1002/ejic.200300031**

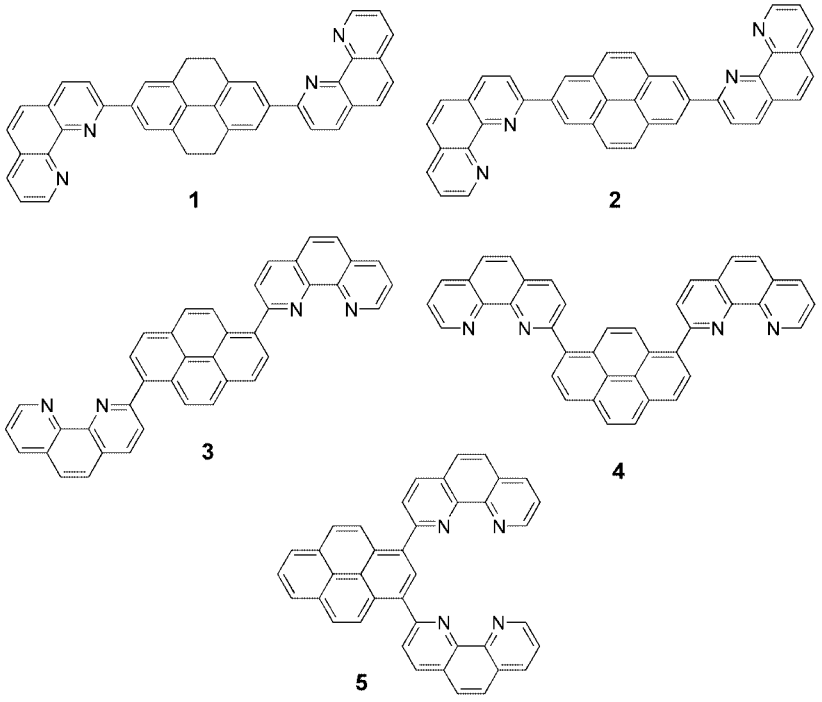

Scheme 1. Bridging pyrene-based ligands

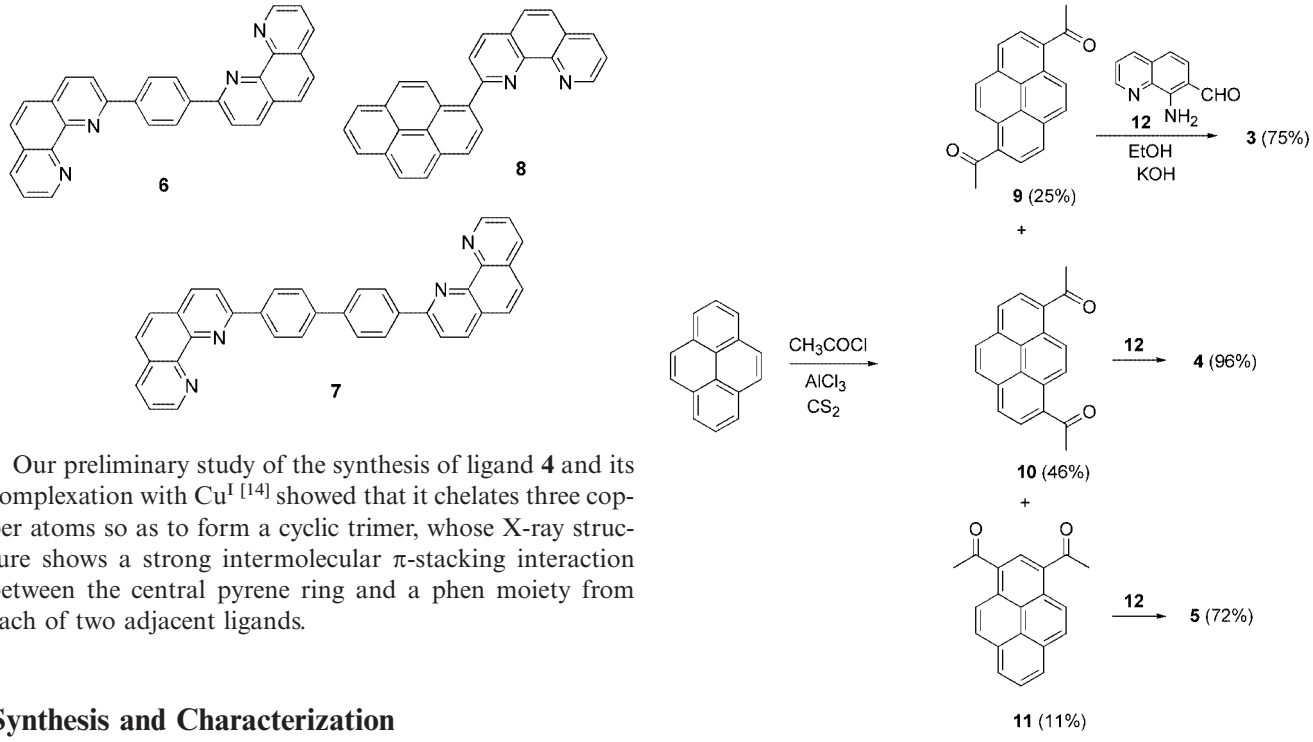

Our preliminary study of the synthesis of ligand **4** and its complexation with Cu^{I} [14] showed that it chelates three copper atoms so as to form a cyclic trimer, whose X-ray structure shows a strong intermolecular π-stacking interaction between the central pyrene ring and a phen moiety from each of two adjacent ligands.

Synthesis and Characterization

The strategic and selective introduction of acetyl groups onto the pyrene nucleus is key to the synthesis of **1**−**5**. Friedel−Crafts monoacetylation of pyrene is specific to the 1-position. Under normal conditions the 2-isomer cannot be isolated. If excess acetyl chloride is employed, a second acetyl group may be introduced at the 3-, 6-, or 8-position. Further acetylation is not readily accomplished. According to a published procedure, we produced a mixture of the three diacetyl isomers **9**−**11**, which may be separated by a combination of chromatography and crystallization.[10]

We have demonstrated that the Friedländer condensation of 8-amino-7-quinolinecarbaldehyde (**12**) with acetyl-substituted aromatic compounds is a convenient way to prepare 2-arylphen derivatives.[11] In this manner 2 equiv. of **12** were condensed with each of the diacetylpyrenes to provide the corresponding bis(phen)pyrenes **3**−**5** in yields of 72−96%.

 © 2003 Wiley-VCH Verlag GmbH & Co. KGaA, Weinheim

Each of these ligands possesses a C_2 symmetry axis so that in the ^{1}H NMR spectrum only four (**3** and **4**) or five (**5**) pyrene signals appeared along with the characteristic seven signals for the phen ring.

The more problematic substitution at the 2-position of pyrene was achieved by Harvey and co-workers by carefully controlled hydrogenation of purified pyrene to afford the 4,5,9,10-tetrahydro derivative **13**.[15] This material is actually a bis(dimethylene)-bridged derivative of biphenyl which can be specifically monoacetylated at the 2-position or diacetylated at the 2,7-positions. The reaction of 2 equiv. of **12** with the diacetyl derivative **14** provides the bis(phen)-tetrahydropyrene **1**. Alternatively, **14** may be dehydrogenated to provide the diacetylpyrene **15** which can then be converted into the bis(phen) species **2**.

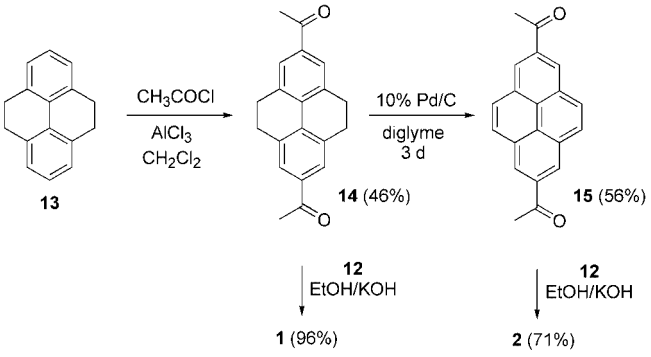

These five bis(phen)pyrenes were then treated with 2 equiv. of $[Ru([D_8]bpy)_2Cl_2]$ to incorporate two Ru^{II} centers at the vacant phen binding sites. This reaction was sluggish under the normal conditions of reflux in aqueous ethanol, due partially to poor solubility of the ligands, but when carried out in ethylene glycol under microwave irradiation[16] (30−40 min) yields of 19−60% of the purified complexes as their hexafluorophosphate salts were obtained.

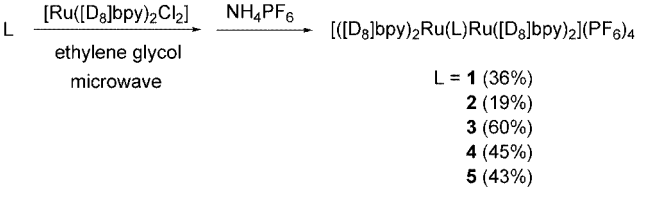

The use of $[D_8]$bpy greatly facilitates NMR characterization of the complexes by eliminating all signals from the bpy auxiliary ligands (Figure 1).[17] The phen protons could be readily identified by their characteristic coupling patterns and chemical shifts. The H-4′ to H-9′ protons were narrowly grouped in ranges spanning about 0.1 ppm. The H-3′ resonance was most affected by the adjacent linker. For the complexes of **2**−**4** the signal of this proton appeared in the range δ = 8.02−8.11 ppm. For the complex of the tetrahydropyrene ligand **1**, the H-3′ signal appeared at δ = 7.70 ppm, very similar to the δ = 7.72 ppm recorded for the analogous complex of **7**.[12]

It should be noted that each Ru^{II} center is chiral and thus may exist in either the Δ or Λ configuration. For dinuclear complexes such as those under study, this would lead to two sets of diastereomers, a *d*,*l* form (ΔΔ and ΛΛ) and a *meso* form (ΔΛ). For the dinuclear Ru^{II} complex of **6** the metal centers were sufficiently interacting that two clear sets of NMR signals were visible and could, in fact, be assigned to specific stereoisomers which were present in an approximate 1:1 ratio.[12] For the dinuclear complexes of **2**−**4**, a mixture of diastereomers was similarly evidenced by the NMR spectra. Although some enrichment may have occurred during chromatographic purification, no attempt was made to separate these diastereomers and so they were further evaluated as a mixture.

Figure 1 shows the 600 MHz ^{1}H NMR spectrum of the dinuclear complex of ligand **2**. All the peaks are clearly resolved and 2D analysis allowed their complete assignment. The phen subunits are sufficiently non-interacting that they only show one set of signals for both diastereomers. The H4′ to H7′ protons are remote from the complexation site and their signals appear in the downfield region. The H3′, H8′, and H9′ proton signals are shifted upfield due to shielding by the auxiliary $[D_8]$bpy ligands or the central pyrene ring. The multiplicities and chemical shifts of the pyrene proton signals may be explained by symmetry effects associated with the *d*,*l* or *meso* diastereoisomer. For the *meso* isomer H3 = H8 and the signal of this proton appears as a singlet at δ = 6.81 ppm, strongly shielded by an auxiliary $[D_8]$bpy ligand. For this isomer H1 = H6 and this atom is deshielded, its signal appearing at δ = 8.18 ppm. For the *meso* isomer H4 = H9 ≠ H5 and thus H4 and H9 (as well as H5 and H10) appear as doublets at δ = 7.97 and 7.56, respectively. For the *d*,*l* isomer the symmetry plane lies along the short axis of the pyrene bridge so that H3 = H6 (singlet at δ = 6.89 ppm). Likewise H4 and H5 as well as H9 and H10 are equivalent, giving the singlets at δ = 7.63 and 7.89 ppm.

Structure and Properties

We have previously described the dinuclear Ru^{II} complexes of **6** and **7**.[12] With $[(bpy)_2Ru(\mathbf{6})Ru(bpy)_2](PF_6)_4$ we had expected that π-stacking between the central benzene ring and a pyridine ring of an auxiliary bpy associated with each metal center would provide some communication between the metal atoms. Both photophysical and electrochemical data suggested that no such communication existed and the two metal centers behaved quite independently. A crystal structure analysis of this system indicated that the two π-stacked pyridine rings were bent out of a parallel arrangement and thus π−π interaction might well be diminished.

The pyrene-bridged systems might be less congested, resulting in better π-overlap. Furthermore, the 16π-electron central pyrene ring would provide better delocalization of

 © 2003 Wiley-VCH Verlag GmbH & Co. KGaA, Weinheim

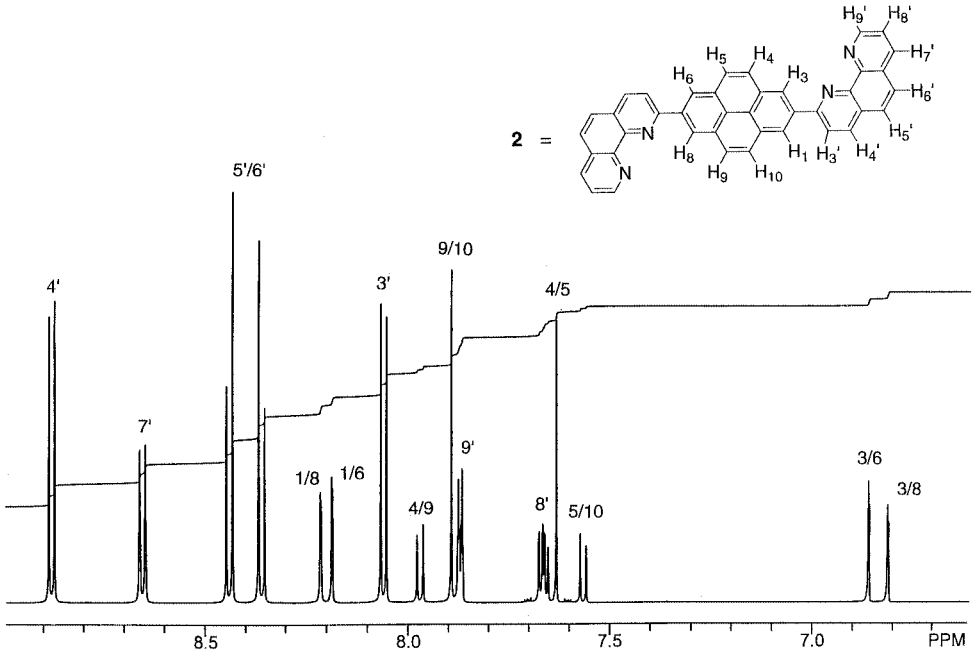

Figure 1. Downfield region of the 600 MHz ^{1}H NMR spectrum of [([D_8]bpy)$_2$Ru(**2**)Ru([D_8]bpy)$_2$](PF_6)$_4$ in CD_3CN at 25 °C

the excited state. A structural comparison between the two dinuclear complexes was made by determining the crystal structure of [([D_8]bpy)$_2$Ru(**3**)Ru([D_8]bpy)$_2$](PF_6)$_4$ (Figure 2 illustrates an ORTEP drawing of the cation). Figure 3 shows a side view of the same cation as well as the analogous dinuclear [Ru(bpy)$_2$] complex of ligand **6**.

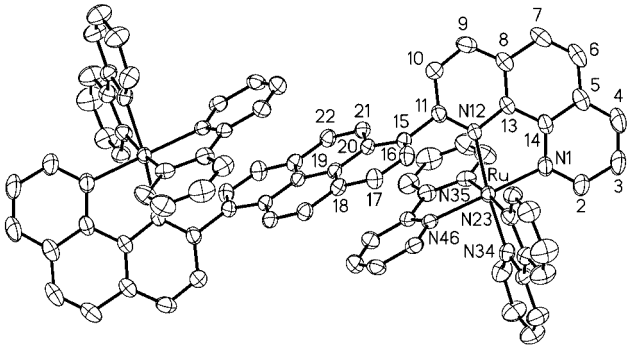

Figure 2. ORTEP drawing of the cation of [([D_8]bpy)$_2$Ru(**3**)-Ru([D_8]bpy)$_2$](PF_6)$_4$ showing the atom-numbering scheme

The larger pyrene, as compared with benzene, leads to a greater separation of the two [(phen)Ru(bpy)$_2$] halves of the molecule. All the Ru−N bond lengths fall in the range 2.05−2.07 Å, except for Ru−N12 which is 2.13 Å. This elongation is caused by interaction of pyrene with one of the auxiliary bpy groups, The bpy groups are less distorted than in the complex of **6**, and two bpy groups that form the outer layers of the central π-sandwich are more planar, with a dihedral angle between the two bpy pyridine rings of 6.6° as compared with 21.6° in the benzene-bridged complex. The other bpy is even more planar with a dihedral angle of only 1.8°, which compares to 7.5° in the benzene-bridged complex. The phen and pyrene are also more orthogonal with a dihedral angle of 76.4°, some 16° greater than for the benzene-bridged system.

The decreased congestion is due mainly to the increased distance between the inner bpy on one Ru and the phen complexed to the other Ru. In the complex of **6**, this C26′−C10 distance is 3.73 Å, pushing the pyridine out of a plane that would be parallel with the central benzene. This distortion is illustrated in Figure 2 where the C26−C26′ distance is 8.76 Å. For the pyrene complex, the bpy−phen interaction is relieved and the C43′−C10 distance lengthens to 5.19 Å while C43−C43′, at 6.73 Å, is over 2 Å less than the corresponding distance for the benzene-bridged complex. The atoms in the pyridines that form the π-sandwich and the central benzene of **6** are between 2.91 and 4.21 Å apart, while for the pyrene-bridged complex these distances are 3.09−3.39 Å. The average distance between these planes is 3.24 Å, indicating possible strong π−π interaction.

Surprisingly, the photophysical properties of the pyrene-bridged complexes do not evidence any strong coupling between the metal centers. Table 1 lists the absorption and emission data for the ligands and complexes as well as for **8** and the mononuclear model compounds [Ru(**8**)(bpy)$_2$]$^{2+}$ and [Ru(phen)([D_8]bpy)$_2$]$^{2+}$. The 1,3-, 1,6-, and 1,8-diphenpyrenes **3**−**5** all show quite similar absorption and emission spectra. The 2,7-diphen isomer absorbs at slightly higher energy, very similar to the 2-phenpyrene **8**. This is consistent with electronic decoupling of the 2,7-positions as reported by Müllen and co-workers.[18] The emission maxima for the pyrene systems appear in the range 432−488 nm and are all lower in energy than the corresponding bridged biphenyl system **1**.

Fages and co-workers have carried out a detailed photophysical study on two systems related to **3** and **8** in which a 4-(2,2′-bpy) group is attached to pyrene in place of phen.[20]

 © 2003 Wiley-VCH Verlag GmbH & Co. KGaA, Weinheim

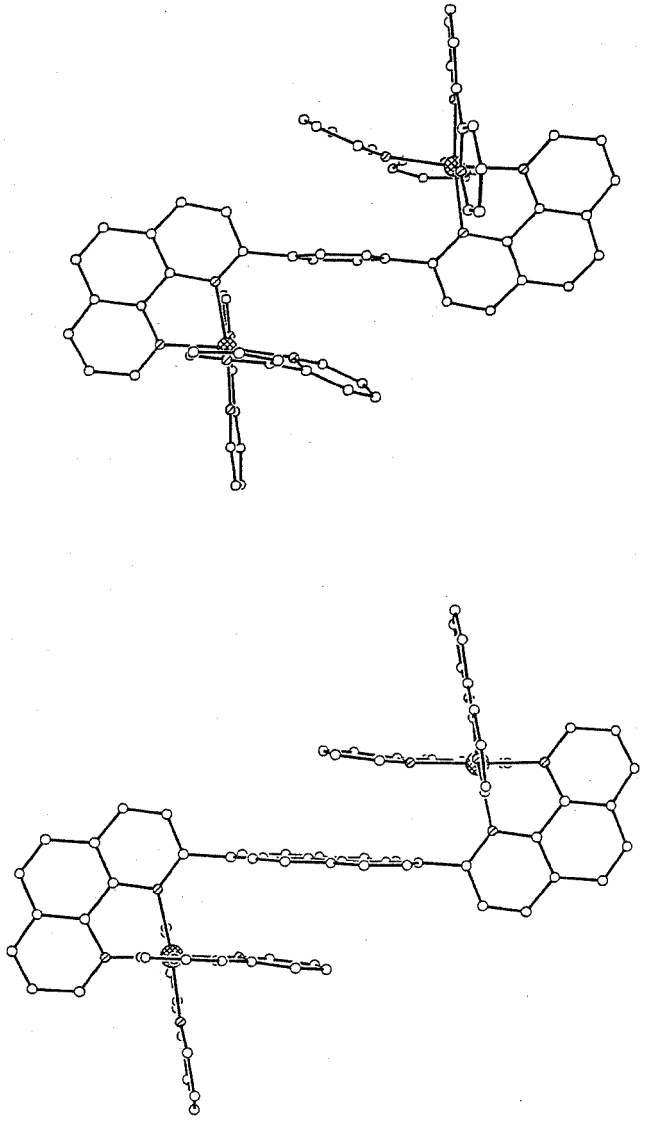

Figure 3. Analogous side views of the cation of $[(bpy)_2Ru(\mathbf{6})Ru(bpy)_2](PF_6)_4$ (top) and $[([D_8]bpy)_2Ru(\mathbf{3})Ru([D_8]bpy)_2](PF_6)_4$ (bottom)

These molecules show absorption and emission characteristics consistent with what we observe, but at higher energy, apparently due, in part, to conformational mobility about the 2,2′ bond of bpy, which thus provides less delocalization than phen. The fact that the electronegative nitrogen atom in the 4-bpy-substituted systems is two bonds further remote from pyrene than for the 2-phen of **3** and **8** may also have some influence.

The Stokes shift is the difference between the absorption and emission maxima and, to some extent, provides a measure of geometric changes that occur upon electronic excitation. For **3**−**5** we observe values of 65−71 nm which are consistent with the model compound **8** (73 nm) and slightly larger than the 58 and 67 nm Fages observed for his two bpy-based systems in acetonitrile at room temperature. A similar 5-bpy-substituted pyrene reported by Rettig and coworkers shows a Stokes shift of 92 nm.[21] The 2,7-disubstituted pyrene **2** shows a large Stokes shift of 101 nm, consistent with the more longitudinal organization of this molecule.

The longest wavelength absorption for Ru^{II} complexes of this type typically involves a metal-to-ligand charge transfer (MLCT) in which the photoexcited electron is promoted from a metal d-orbital to a low-lying ligand π*-orbital. One expectation for the pyrene-bridged complexes was that π−π interaction through the central bpy-pyrene-bpy stack would affect an MLCT state associated with the bpy ligand. Increased delocalization should produce a bathochromic shift in the MLCT absorption. For the four dinuclear pyrene complexes involving **2**−**5** as well as the mononuclear model **8** and the tetrahydropyrene **1**, the lowest energy absorption band appears at 447−450 nm. The dinuclear pyrene-containing systems also show a pyrene π−π* absorption at 367−382 nm, which is lower in energy than the mononuclear analogue **8** (357 nm). Interestingly, the complex $[Ru(phen)([D_8]bpy)_2]^{2+}$ absorbs at 448 nm, within 1−2 nm of all four pyrene-bridged complexes.

At room temperature the dinuclear complexes of **2**−**5** show weak emissions at 612−615 nm that are similar to the

Table 1. Photophysical data for phen-pyrene ligands and their Ru^{II} complexes

Compound	Absorption[a] λ_{max} [nm] (log ε)[a]	Emission[a] λ_{em} [nm] 298K	77K
1	369 (4.40), 338 (4.28), 264 (4.20)	403, 423[c]	
2[b]	359 (4.60), 341 (4.97), 342 (5.01), 311 (4.93), 260(4.68)	460, 488[c]	
3	373 (3.97), 281 (4.08), 266 (4.10), 230 (4.35)	444[c]	
4	373 (4.36), 283 (4.47), 267 (4.49), 230 (4.74)	444[c]	
5	370 (4.32), 286 (4.50), 264 (4.51), 231 (4.82)	435[c]	
8	359 (4.37), 342 (4.40), 276 (4.63), 238 (4.86)	432	
$[([D_8]bpy)_2Ru(\mathbf{1})Ru([D_8]bpy)_2]^{4+}$	450 (4.34), 443 (4.28), 422 (4.40), 287 (5.05)	613 (w)	584[d]
$[([D_8]bpy)_2Ru(\mathbf{2})Ru([D_8]bpy)_2]^{4+}$	448 (4.42), 424 (4.36), 367 (4.49), 284 (5.12), 232 (4.95)	615 (w)	605[d]
$[([D_8]bpy)_2Ru(\mathbf{3})Ru([D_8]bpy)_2]^{4+}$	447 (4.47), 380 (4.50), 284 (5.11), 267 (5.09), 228 (4.98)	614 (w)	615[d]
$[([D_8]bpy)_2Ru(\mathbf{4})Ru([D_8]bpy)_2]^{4+}$	449 (4.47), 382 (4.49), 284 (5.21), 267 (5.19), 230 (5.00)	615 (w)	615[d]
$[([D_8]bpy)_2Ru(\mathbf{5})Ru([D_8]bpy)_2]^{4+}$	449 (4.37), 382 (4.32), 282 (5.12), 230 (4.93)	612 (w)	611[d]
$[Ru(\mathbf{8})(bpy)_2]^{2+}$	448 (4.12), 337 (4.40), 268 (4.90), 233 (4.90)	610	
$[Ru(phen)([D_8]bpy)_2]^{2+}$	448 (4.31), 285 (4.91), 263 (4.87)	615	580[d] [e]

[a] 10^{-5} M in CH_3CN at 25 °C. [b] 10^{-5} M in CH_2Cl_2 at 25 °C. [c] 10^{-6} M in CH_3CN at 25 °C. [d] 10^{-5} M in EtOH/MeOH (4:1). [e] Measured for the protio-bpy analogue, ref.[19]

 © 2003 Wiley-VCH Verlag GmbH & Co. KGaA, Weinheim

Table 2. Electrochemical data for pyrene-bridged ligands and their Ru^{II} complexes

Compound	$E_{1/2}$ [a] OX	RED
$[Ru(phen)(bpy)_2]^{2+}$	+1.32 (82)	−1.30 (91), −1.49 (112)
$[Ru(\mathbf{8})([D_8]bpy)_2]^{2+}$	+1.30	
$[([D_8]bpy)_2Ru(\mathbf{1})Ru([D_8]bpy)_2]^{4+}$	+1.29 (120)	−1.31 (140), −1.49 (190)
$[([D_8]bpy)_2Ru(\mathbf{2})Ru([D_8]bpy)_2]^{4+}$	+1.32 (100)	−1.28 (180), −1.44 (150)
$[([D_8]bpy)_2Ru(\mathbf{3})Ru([D_8]bpy)_2]^{4+}$	+1.31 (240)	−1.27 (71), −1.41 (irr.)
$[([D_8]bpy)_2Ru(\mathbf{4})Ru([D_8]bpy)_2]^{4+}$	+1.31 (180)	−1.28 (240), −1.41 (irr.)
$[([D_8]bpy)_2Ru(\mathbf{5})Ru([D_8]bpy)_2]^{4+}$	+1.31 (180)	−1.28 (240), −1.41 (irr.)

[a] Solutions were 0.1 M TBAP in CH_3CN; sweep rate 200 mV s^{-1}; the number in parentheses is the difference [mV] between the anodic and cathodic waves; irr. = irreversible.

model compounds. At 77 K, the emission properties do not change appreciably for the complexes of **3**−**5** while those of the complex of **2** is shifted to 605 nm. By comparison, the dinuclear complex of the bridged biphenyl system **1**, which does not possess the pyrene chromophore, shows a stronger 77 K emission shifted to 584 nm. This 29-nm thermally induced Stokes shift compares well with that of 35 nm observed for $[Ru(phen)(bpy)_2]^{2+}$ and is characteristic for emission of a triplet MLCT state. The implication is that, due to the lack of a thermally induced Stokes shift, the emissions from the complexes involving the pyrenyl ligands **2**−**5** may not be MLCT-based but rather associated with an intraligand (IL) state, possibly a triplet IL state involving pyrene.

Schmehl and co-workers[22] have recently examined a similar dinuclear Ru^{II} complex involving the 1,6-bis(2,2′-bipyrid-4-yl)pyrene bridging ligand reported earlier by Fages.[20] A detailed photophysical study indicated that emission was not consistent with a ^{3}MLCT state, rather a triplet IL state was suggested instead. An easy test for this possibility is to measure the 77 K luminescence of the ligands **2**−**5** in the presence of an external heavy atom donor, which should promote intersystem crossing and emission of the triplet state (phosphorescence). Low-temperature spectra of the ligands were, therefore, recorded in the presence of ethyl iodide. For ligand **3** we observe a band at 615 nm, which is virtually identical to the spectrum of $[([D_8]bpy)_2Ru(\mathbf{3})Ru([D_8]bpy)_2](PF_6)_4$. The data for the other systems was less clear. Future time-resolved measurements and transient spectroscopy should help in elucidating the origin of the emissive state. It is noteworthy that other Ru^{II} complexes of bpy and phen have been reported in which each ligand contains one or two pyrene appendages attached at the 5-position.[23−24] These systems emit rather strongly and the excited state lifetime can be related to the number of pyrene appendages.

The electrochemical data summarized in Table 2 further verify the lack of metal−metal interaction. The oxidations are all in the range +1.29 to +1.32 V, as expected for the metal-based Ru^{II}-to-Ru^{III} conversion. The reductions are typically ligand-based and fall in the expected range of −1.27 to −1.31 V. It is difficult to assign this reduction to a phen or a bpy ligand in the complex. If the reduction involved a phen-type ligand, then the second reduction would involve a bpy and variation in the second reduction potential might be expected. These second reductions, however, fall in the narrow range of −1.41 to −1.44 V, excluding this possibility.

Conclusions

We have described the preparation of four new pyrene-bridged bis(phen) ligands **2**−**5** and the tetrahydro precursor **1**. Dinuclear Ru^{II} complexes prepared from all five systems, with $[D_8]$bpy as the auxiliary ligand, have been characterized by ^{1}H NMR and electronic spectroscopy and by electrochemical analysis. A crystal structure of the dinuclear complex of **3** evidences a much less congested environment than its benzene-bridged analogue. Nevertheless, the expected electronic effects of π−π interactions through the central bpy-pyrene-bpy sandwich appear to be lacking. Future studies will involve systems with pyrene more intimately involved in the 1,4-diimine chelating unit.

Experimental Section

General: Nuclear magnetic resonance spectra were recorded at 300 or 600 MHz for ^{1}H and at 75 MHz for $^{13}C\{^1H\}$ referenced to TMS in $CDCl_3$ and to the solvent peak in all other solvents (CD_3CN). Electronic spectra were obtained with a Perkin-Elmer Lambda 3B spectrophotometer. Fluorescence spectra were obtained with a Perkin-Elmer LS-50 luminescence spectrometer. Cyclic voltammetry (CV) was carried out in a conventional three-electrode cell with a BAS-27 voltammeter and a Houston Instruments model 100 X-Y recorder according to a previously described procedure.[25] Mass spectra were obtained with a Hewlett−Packard 5989B mass spectrometer (59987A electrospray) using atmospheric pressure ionization at 160 °C. Elemental analyses were performed by National Chemical Consulting, P. O. Box 99, Tenafly, NJ 07670, U.S.A. Melting points were measured with a Hoover capillary melting point apparatus and are not corrected. The microwave reactions were carried out in a household microwave oven modified according to a previously published description.[16] The 2,7-diacetyl-4,5,9,10-tetrahydropyrene,[15] 2,7-diacetylpyrene,[15] 1,6-, 1,8-, and 1,3-diacetylpyrene,[10] $[Ru([D_8]bpy)_2Cl_2]\cdot 2H_2O$,[17] and 8-amino-7-quinolinecarbaldehyde (**8**)[11] were prepared according to known procedures. CH_3CN used for cyclic voltammetry was dried by reflux with calcium hydride followed by distillation. All other solvents were used without further purification.

 © 2003 Wiley-VCH Verlag GmbH & Co. KGaA, Weinheim

2,7-Bis(2′-[1′,10′]phenanthrolinyl)-4,5,9,10-tetrahydropyrene (1): A mixture of 2,7-diacetyl-4,5,9,10-tetrahydropyrene (**14**, 300 mg, 0.69 mmol), 8-amino-7-quinolinecarbaldehyde (**12**, 240 mg, 138 mmol) and KOH (120 mg) in absolute EtOH (25 mL) was refluxed for 8 h. The solid which formed was collected, washed with H_2O (2 × 20 mL), EtOH (3 × 10 mL), and dried to provide **1** as an orange solid (370 mg, 96% yield), m.p. > 270 °C. ^{1}H NMR (300 MHz, $CDCl_3$, 25 °C): δ = 9.27 (d′, *J* = 4.7, 2.5 Hz, 2 H, H-9), 8.31 (m, 4 H), 8.18 (d, 2 H), 8.14 (s, 4 H, H-1, H-3, H-6, H-8), 7.80 (AB q, 4 H, H-5′, H-6′), 7.66 (dd, *J* = 7.9, 3.4 Hz, 2 H, H-8′), 3.13 (s, 8 H, CH_2) ppm. ^{13}C{^{1}H} NMR (75 MHz, $CDCl_3$, 25 °C): δ = 157.8, 149.9, 138.0, 136.5, 136.2, 136.0, 131.5, 128.9, 127.3, 126.3, 125.7, 125.4, 122.6, 120.5, 28.3 ppm. MS: *m*/*z* (%) = 562 (100) [M]. $C_{40}H_{26}N_4 \cdot 3H_2O$ (647): calcd. C 77.92, H 5.19, N 9.09; found C 77.08, H 4.53, N 8.74.

2,7-Bis(2′-[1′,10′]phenanthrolinyl)pyrene (2): According to the procedure described for **1**, 2,7-diacetylpyrene (**15**, 80 mg, 0.28 mmol) was condensed with **12** (100 mg, 0.58 mmol) in absolute EtOH (15 mL) for 8 h. The resultant yellow-orange residue was crystallized from chloroform to give **2** as a pale yellow solid (110 mg, 71% yield), m.p. > 270 °C. ^{1}H NMR (300 MHz, $CDCl_3$, 25 °C): δ = 9.33 (d, *J* = 4.3 Hz, 2 H, H-9′), 9.21 (s, 4 H, H-4, H-5, H-9, H-10), 8.47 (AB q, 4 H, H-3′,4′), 8.35 (d, 2 H, H-7′), 8.32 (s, 2 H, H-1, H-3, H-6, H-8), 7.86 (AB q, 4 H, H-5′, H-6′), 7.69 (dd, *J* = 7.6, 3.1 Hz, 2 H, H-8′) ppm. A ^{13}C{^{1}H} NMR spectrum could not be obtained due to poor solubility. MS: *m*/*z* (%) = 558 (100) [M]. $C_{40}H_{22}N_4 \cdot H_2O$ (576): calcd. C 83.33, H 4.16, N 9.72; found C 83.36, H 4.08, N 9.07.

1,6-Bis(2′-[1′,10′]phenanthrolinyl)pyrene (3): A mixture of 1,6-diacetylpyrene (**9**, 200 mg, 0.69 mmol), **12** (265 mg, 1.53 mmol), and KOH (120 mg) in absolute EtOH (30 mL) was refluxed overnight. After cooling to 25 °C, the residue was filtered off, washed with H_2O (2 × 20 mL) then $CHCl_3$ (2 × 20 mL). The resulting solid was then recrystallized from $CHCl_3$ to provide **3** as a pale yellow solid (290 mg, 75% yield), m.p. > 280 °C. ^{1}H NMR (300 MHz, $CDCl_3$, 25 °C): δ = 9.24 (dd, *J* = 4.4, 1.4 Hz, 2 H, H-9′), 8.53 (d, *J* = 9.5 Hz, 2 H), 8.47 (dd, *J* = 8.3, 2.9 Hz, 4 H), 8.31 (d, *J* = 8.9 Hz, 4 H), 8.12 (dd, *J* = 8.9, 4.5 Hz, 4 H), 7.95 (AB q, 4 H, H-5′, H-6′), 7.65 (dd, *J* = 8.6, 4.4 Hz, 2 H, H-8′) ppm. A ^{13}C{^{1}H} NMR spectrum could not be obtained due to poor solubility. MS: *m*/*z* (%) = 559 (100) [M + 1]. $C_{40}H_{22}N_4 \cdot H_2O$ (558): calcd. C 83.33, H 4.16, N 9.72; found C 83.83, H 3.83, N 9.85.

1,8-Bis(2′-[1′,10′]phenanthrolinyl)pyrene (4):[14] A mixture of 1,8-diacetylpyrene (**10**, 146 mg, 0.51 mmol), **12** (183 mg, 1.06 mmol), and KOH (100 mg) in absolute EtOH (20 mL) was refluxed for 12 h. After cooling to 25 °C, H_2O (20 mL) was added and the aqueous layer extracted with CH_2Cl_2 (3 × 30 mL). The organic layer was then dried ($MgSO_4$) and the solvent evaporated to dryness. The resultant residue was washed with Et_2O (2 × 25 mL) to provide **4** as a yellow solid (265 mg, 93% yield), m.p. > 270 °C. ^{1}H NMR (300 MHz, $CDCl_3$, 25 °C): δ = 9.14 (d, *J* = 3.3 Hz, 2 H, H-9′), 8.32−8.23 (m, 8 H), 8.16−8.13 (m, 4 H), 7.96 (d, *J* = 8.1 Hz, 2 H), 7.74 (d, *J* = 8.7 Hz, 2 H), 7.65−7.57 (m, 4 H) ppm. ^{13}C{^{1}H} NMR (75 MHz, $CDCl_3$, 25 °C): δ = 159, 149, 145.8, 145.7, 136.3, 136.1, 136, 131, 128.8, 128.5, 128.4, 127.9, 127.1, 126.4, 126.3, 125.7, 125.5, 125.2, 124, 123 ppm. MS: *m*/*z* (%) = 559 (100) [M + 1]. $C_{40}H_{22}N_4 \cdot 0.5H_2O$ (567): calcd. C 84.66, H 4.05, N 9.88; found C 84.73, H 3.67, N 9.50.

1,3-Bis(2′-[1′,10′]phenanthrolinyl)pyrene (5): A mixture of 1,3-diacetylpyrene (**11**, 109 mg, 0.38 mmol), **12** (131 mg, 0.76 mmol), and KOH (120 mg) in absolute EtOH (35 mL) was refluxed for 24 h. After cooling to 25 °C, H_2O (60 mL) was added and a yellow solid precipitated. The solid was purified on Al_2O_3, eluting with CH_2Cl_2, to provide **5** (152 mg, 72% yield), m.p. > 270 °C. ^{1}H NMR (300 MHz, $CDCl_3$, 25 °C): δ = 9.14 (d, *J* = 4.1 Hz, 2 H, H-9′), 8.80 (s, 1 H), 8.41 (dd, *J* = 8.0, 2.6 Hz, 4 H), 8.22 (dd, *J* = 10.3, 7.7 Hz, 4 H), 8.0−8.15 (m, 5 H), 7.84 (AB q, 4 H, H-5′, H-6′), 7.60 (dd, *J* = 8.1, 4.8 Hz, 2 H, H-8′) ppm. ^{13}C{^{1}H} NMR (75 MHz, $CDCl_3$, 25 °C): δ = 150.6, 136.6, 136.1, 136 (2 C), 131.6, 130.9, 129.7, 129.3, 129, 128.6, 127.7, 126.8 (2 C), 126.7 (2 C), 126.3, 126.2, 125.6, 125.4, 123, 120.2 ppm. MS: *m*/*z* (%) = 560 (100) [M + 2]. $C_{40}H_{22}N_4 \cdot 1.45CH_2Cl_2$ (698): calcd. C 73.30, H 3.65, N 8.22; found C 73.30, H 3.60, N 7.86.

[([D$_8$]bpy)$_2$Ru(1)Ru([D$_8$]bpy)$_2$](PF$_6$)$_4$: A mixture of **1** (60 mg, 0.10 mmol) and $[Ru([D_8]bpy)_2Cl_2] \cdot 2H_2O$ (111 mg, 0.21 mmol) in ethylene glycol (6 mL) was heated in a microwave oven under Ar for 30 min. After cooling, the mixture was poured into H_2O (20 mL). A solution of NH_4PF_6 (49 mg, 0.3 mmol) in H_2O (2 mL) was then added, and the mixture stirred for 15 min. The resultant precipitate was filtered off, dried, and purified by chromatography on alumina, eluting with toluene/CH_3CN (1:1), to provide an orange solid (75 mg, 36% yield), m.p. > 280 °C. ^{1}H NMR (600 MHz, CD_3CN, 25 °C): δ = 8.73 (d, *J* = 9.3 Hz, H-4′), 8.62 (d, *J* = 8.8 Hz, H-7′), 8.33 (AB q, H-5′, H-6′), 7.90 (d, *J* = 4.9 Hz, H-9′), 7.69 (d, *J* = 7.3 Hz, H-3′), 7.65 (dd, *J* = 6.8, 4.9 Hz, H-8′), 7.0 (s, H-2/H-5), 5.7 (s, H-4/H-9), 2.15−2.30 (CH_2 under solvent peak). MS: *m*/*z* (%) = 1857 (100) [M + 1 − PF_6].

[([D$_8$]bpy)$_2$Ru(2)Ru([D$_8$]bpy)$_2$](PF$_6$)$_4$: According to the procedure described for [([D$_8$]bpy)$_2$Ru(**1**)Ru([D$_8$]bpy)$_2$](PF$_6$)$_4$, a mixture of **2** (40 mg, 0.07 mmol) and $[Ru([D_8]bpy)_2Cl_2] \cdot 2H_2O$ (77 mg, 0.14 mmol) in ethylene glycol (6 mL) was heated in a microwave oven to provide a red solid (26.5 mg, 19% yield), m.p. > 280 °C. ^{1}H NMR (600 MHz, CD_3CN, 25 °C, two sets of peak in a 1:1 ratio for the two diastereomers): δ = 8.88 (d, *J* = 7.3 Hz, H-4′), 8.65 (d, *J* = 8.4 Hz, H-7′), 8.4 (AB q, H-5′, H-6′), 8.21 (s, H-1/H-8), 8.18 (s, H-1/H-6), 8.06 (d, *J* = 7.0 Hz, H-3′), 7.97 (d, *J* = 5.1 Hz, H-4/H-9), 7.89 (s, H-9/H-10), 7.87 (d, *J* = 5.6 Hz, H-9′), 7.66 (dd, *J* = 7.0, 5.3 Hz, H-8′), 7.63 (s, H-4/H-5), 7.56 (d, *J* = 9.0 Hz, H-5/H-10), 6.85 (s, H-3/H-6), 6.81 (s, H-3/H-8) ppm. MS: *m*/*z* (%) = 1851 (100) [M − PF_6].

[([D$_8$]bpy)$_2$Ru(3)Ru([D$_8$]bpy)$_2$](PF$_6$)$_4$: According to the procedure described for [([D$_8$]bpy)$_2$Ru(**1**)Ru([D$_8$]bpy)$_2$](PF$_6$)$_4$, a mixture of **3** (60 mg, 0.10 mmol) and $[Ru([D_8]bpy)_2Cl_2] \cdot 2H_2O$ (115 mg, 0.21 mmol) in ethylene glycol (6 mL) was heated in a microwave oven to provide a red solid (120 mg, 60% yield), m.p. > 280 °C. ^{1}H NMR (600 MHz, CD_3CN, 25 °C, two sets of peaks in a 5:1 ratio for the two diastereomers), major isomer: δ = 8.97 (d, *J* = 7.3 Hz, H-4′), 8.71 (d, *J* = 8.4 Hz, H-7′), 8.48 (AB q, H-5′, H-6′), 8.13 (d, *J* = 7.0 Hz), 8.10 (d, *J* = 7.0 Hz, H-3′), 7.97 (d, *J* = 7.0 Hz), 7.88 (d, *J* = 5.7 Hz, H-9′), 7.69 (dd, *J* = 7.0, 5.3 Hz, H-8′), 7.21 (d, *J* = 7.8 Hz, 1 H), 6.42 (d, 2 H) ppm. MS: *m*/*z* (%) = 1853 (100) [M + 2 − PF_6].

[([D$_8$]bpy)$_2$Ru(4)Ru([D$_8$]bpy)$_2$](PF$_6$)$_4$: The same procedure described for [([D$_8$]bpy)$_2$Ru(**1**)Ru([D$_8$]bpy)$_2$](PF$_6$)$_4$ was used. A mixture of **4** (60 mg, 0.10 mmol) and $[Ru([D_8]bpy)_2Cl_2] \cdot 2H_2O$ (115 mg, 0.21 mmol) in ethylene glycol (6 mL) was heated in a microwave oven to provide a red solid (89 mg, 45% yield), m.p. > 280 °C: ^{1}H NMR (600 MHz, CD_3CN, 25 °C, two sets of peaks in a 9:1 ratio for the two diastereomers), major isomer: δ = 8.94 (d, *J* = 7.3 Hz, H-4′), 8.67 (d, *J* = 8.4 Hz, H-7′), 8.45 (AB q, H-5′, H-6′), 8.10 (d, *J* = 7.0 Hz), 8.08 (d, *J* = 7.0 Hz, H-3′), 7.95 (d, *J* = 7.0 Hz), 7.87 (d, H-9′), 7.68 (dd, *J* = 7.0, 5.3 Hz, H-8′), 7.57 (d, *J* = 7.0 Hz, 1

 © 2003 Wiley-VCH Verlag GmbH & Co. KGaA, Weinheim

H), 7.18 (d, 1 H, J = 7.8 Hz), 7.40 (d, 2 H) ppm. MS: m/z (%) = 1853 (100) [M + 2 − PF_6].

[([D$_8$]bpy)$_2$Ru(5)Ru([D$_8$]bpy)$_2$](PF$_6$)$_4$: According to the procedure described for [([D$_8$]bpy)$_2$Ru(**1**)Ru([D$_8$]bpy)$_2$](PF$_6$)$_4$, a mixture of **5** (60 mg, 0.10 mmol) and [Ru([D$_8$]bpy)$_2$Cl$_2$]·2H$_2$O (115 mg, 0.21 mmol) in ethylene glycol (6 mL) was heated in a microwave oven under Ar for 30 min to provide a red solid (60 mg, 43% yield), m.p. > 280 °C. ^{1}H NMR (600 MHz, CD_3CN, 25 °C): δ = 8.81 (d, J = 7.3 Hz, H-4′), 8.69 (d, J = 8.4 Hz, H-7′), 8.45 (AB q, H-5′, H-6′), 8.38−8.31 (m, H-6, H-7), 7.85 (s, H-2), 7.82 (d, J = 7.0 Hz, H-9′), 7.67 (dd, J = 7.0, 5.3 Hz, H-8′), 7.62 (d, J = 7.0 Hz, H-3′), 7.43 (d, J = 7.8 Hz, H-3), 6.26 (d, J = 7.8 Hz, H-4) ppm. MS: m/z (%) = 1853 (100) [M + 2 − PF_6].

X-ray Determination of [([D$_8$]bpy)$_2$Ru(3)Ru([D$_8$]bpy)$_2$](PF$_6$)$_4$: All measurements were made with a Siemens SMART platform diffractometer equipped with a 1 K CCD area detector. A hemisphere of data (1271 frames at 5 cm detector distance) was collected using a narrow-frame method with scan widths of 0.30° in ω and an exposure time of 30 s per frame. The first 50 frames were re-measured at the end of data collection to monitor instrument and crystal stability, and the maximum correction on I was < 1%. The data were integrated using the Siemens SAINT program, with the intensities corrected for Lorentz factor, polarization, air absorption, and absorption due to variation in the path length through the detector faceplate. A ψ scan absorption correction was applied based on the entire data set. Redundant reflections were averaged. Final cell constants were refined using 7934 reflections having $I > 10\sigma(I)$, and these, along with other information pertinent to data collection and refinement, are listed in Table 3. The Laue symmetry was determined to be −1, and the space group was shown to be either $P1$ or $P\bar{1}$; the letter was chosen based on successful refinement. The asymmetric unit consists of one-half cation situated about an inversion center, two PF_6 anions, two acetonitrile molecules, one toluene and one dichloromethane molecule. One of the anions, and all of the various solvent molecules, are disordered and were modeled as ideal rigid bodies or by using distance constraints. Three separate orientations were found for the dichloromethane, with a total population of about 75%. It is presumed that some solvent was lost during sample handling, and all calculations are based on 100% occupancy of the solvent.CCDC-199738 contains the supplementary crystallographic data which can be obtained free of charge at www.ccdc.cam.ac.uk/conts/retreiving.html [or from the Cambridge Crystallographic Data Centre, 12 Union Road, Cambridge CB2 1EZ, UK; Fax: (internat.) + 44-1223/336-033; E-mail: deposit@ccdc.cam.ac.uk].

Table 3. Crystallographic data for [([D$_8$]bpy)$_2$Ru(**3**)Ru([D$_8$]bpy)$_2$]$^{4+}$

Empirical formula	$C_{104}H_{54}D_{32}Cl_4F_{24}N_{16}P_4Ru_2$
Formula mass	2515.90
a [Å]	12.3445(5)
b [Å]	13.9165(6)
c [Å]	18.0631(8)
α [°]	104.225(1)
β [°]	94.019(1)
γ [°]	114.575(1)
V [Å^3]	2682.7(2)
Z	1
Space group	$P\bar{1}$
T [°C]	−50
λ [Å]	0.71073
$\rho_{calcd.}$ [g cm^{-3}]	1.557
μ [cm^{-1}]	5.38
$R_1 = \Sigma\|\|F_o\| - \|F_c\|\|/\Sigma\|F_o\|$	0.0563
$wR_2 = [\Sigma w(F_o^2 - F_c^2)^2/\Sigma w(F_o^2)^2]^{1/2}$	0.1527
$w = [\sigma^2(F_o^2) + (0.0769\ P)^2 + (9.3529\ P)]^{-1}$, $P = (F_o^2 + 2F_c^2)/3$	

Acknowledgments

We thank the Robert A. Welch Foundation (E-621) and the National Science Foundation (CHE-9714998) for financial support of this work. This project made use of MRSEC/TCSUH shared experimental facilities supported by the National Science Foundation under Award Number DMR-9632667. We would also thank Dr. James Korp for assistance with the X-ray analysis and the referees for helpful comments.

[1] [1a] C. Kaes, A. Katz, M. W. Hosseini, *Chem. Rev.* **2000**, *100*, 3553−3590. [1b] U. S. Schubert, C. Eschbaumer, *Angew. Chem. Int. Ed.* **2002**, *41*, 2893−2926. [1c] P. J. Steel, *Coord. Chem. Rev.* **1990**, *106*, 227−265. [1d] V. Balzani, F. Barigelletti, P. Belser, S. Bernhard, L. De Cola, L. Flamigni, *J. Phys. Chem.* **1996**, *100*, 16786−16788. [1e] L. De Cola, P. Belser, *Coord. Chem. Rev.* **1998**, *177*, 301−346. [1f] F. Barigelletti, L. Flamigni, *Chem. Soc. Rev.* **2000**, *29*, 1−12. [1g] A. Juris, L. Prodi, A. Harriman, R. Ziessel, M. Hissler, A. El-ghayoury, F. Wu, E. Riesgo, R. P. Thummel, *Inorg. Chem.* **2000**, *16*, 3590−3598.

[2] [2a] R. N. Warrener, A. B. B. Ferreira, A. C. Schultz, F. R. Keene, L. S. Kelso, D. N. Butler, *Angew. Chem. Int. Ed. Engl.* **1996**, *35*, 2485−2487. [2b] R. N. Warrener, M. A. Houghton, A. C. Schultz, F. R. Keene, L. S. Kelso, R. Dash, D. N. Butler, *Chem. Commun.* **1996**, 1151−1152.

[3] [3a] A. I. Baba, H. E. Ensley, R. H. Schmehl, *Inorg. Chem.* **1995**, *34*, 1198−1207. [3b] E. H. Yonemoto, G. B. Saupe, R. H. Schmehl, S. M. Hubig, R. L. Riley, B. L. Iverson, T. E. Mallouk, *J. Am. Chem. Soc.* **1994**, *116*, 4786−4795. [3c] R. H. Schmehl, R. A. Auerbach, W. F. Wacholtz, C. M. Elliott, R. A. Freitag, J. W. Merkert, *Inorg. Chem.* **1986**, *25*, 2440−2445. [3d] W. F. Wacholtz, R. A. Auerbach, R. H. Schmehl, *Inorg. Chem.* **1987**, *26*, 2989−2994.

[4] [4a] A. El-Ghayoury, R. Ziessel, *Tetrahedron Lett.* **1997**, *38*, 2471−2474. [4b] A. C. Benniston, V. Grosshenny, A. Harriman, R. Ziessel, *Angew. Chem. Int. Ed. Engl.* **1994**, *33*, 1884−1885. [4c] V. Grosshenny, F. M. Romero, R. Ziessel, *J. Org. Chem.* **1997**, *62*, 1491−1500. [4d] J. R. Shaw, R. T. Webb, R. H. Schmehl, *J. Am. Chem. Soc.* **1990**, *112*, 1117−1123. [4e] R. H. Schmehl, R. A. Auerbach, W. F. Wacholtz, *J. Phys. Chem.* **1988**, *92*, 6202−6206.

[5] [5a] A. Harriman, M. Hissler, R. Ziessel, *Phys. Chem. Chem. Phys.* **1999**, *1*, 4203−4211. [5b] A. Harriman, M. Hissler, A. Khatyr, R. Ziessel, *Chem. Commun.* **1999**, 735−736. [5c] M. Hissler, A. Harriman, A. Khatyr, R. Ziessel, *Chem. Eur. J.* **1999**, *5*, 3366−3381. [5d] A. El-ghayoury, A. Harriman, R. Ziessel, *Chem. Commun.* **1999**, 2027−2028. [5e] F. M. Romero, R. Ziessel, *Tetrahedron Lett.* **1994**, *35*, 9203−9206. [5f] R. Ziessel, J. Suffert, M.-T. Youinou, *J. Org. Chem.* **1996**, *61*, 6535−6546.

[6] [6a] V. D. Parker, *J. Am. Chem. Soc.* **1976**, *98*, 98−103. [6b] M. Dietrich, J. Heinze, *J. Am. Chem. Soc.* **1990**, *112*, 5142−5145. [6c] E. S. Pysh, N. C. Yang, *J. Am. Chem. Soc.* **1963**, *85*, 2124−2130.

[7] [7a] R. Dabestani, I. N. Ivanov, *Photochem. Photobiol.* **1999**, *70*, 10−34. [7b] F. M. Winnik, *Chem. Rev.* **1993**, *93*, 587−614.

[8] L. Prodi, R. Ballardini, M. T. Gandolfi, R. Roversi, *J. Photochem. Photobio. A* **2000**, *136*, 49−52.

[9] [9a] J. B. Birks, L. G. Christophorou, *Spectrochim. Acta* **1963**, *19*, 401−410. [9b] J.-E. S. Sohna, V. Carrier, F. Fages, E. Amouyal, *Inorg. Chem.* **2001**, *40*, 6061−6063. [9c] H. Nohta, H. Satozono, K. Koiso, H. Yoshida, J. Ishida, M. Yamaguchi, *Anal. Chem.* **2000**, *72*, 4199−4204. [9d] F. D. Lewis, Y. Zhang, R. L. Letsinger, *J. Am. Chem. Soc.* **1997**, *119*, 5451−5452.

[10] [10a] L. T. Scott, A. Necula, *J. Org. Chem.* **1996**, *61*, 386−388.

 © 2003 Wiley-VCH Verlag GmbH & Co. KGaA, Weinheim

[10b] R. G. Harvey, J. Pataki, H. Lee, *Org. Prep. Proced. Int.* **1984**, *16*, 144−148.
[11] E. C. Riesgo, X. Jin, R. P. Thummel, *J. Org. Chem.* **1996**, *61*, 3017−3022.
[12] F. Wu, E. Riesgo, A. Pavalova, R. A. Kipp, R. H. Schmehl, R. P. Thummel, *Inorg. Chem.* **1999**, *38*, 5620−5628.
[13] J. A. Simon, S. L. Curry, R. H. Schmehl, T. R. Schatz, P. Piotrowiak, X. Jin, R. P. Thummel, *J. Am. Chem. Soc.* **1997**, *119*, 11012−11022.
[14] C. Bonnefous, N. Bellec, R. P. Thummel, *Chem. Commun.* **1999**, 1243−1244.
[15] [15a] R. G. Harvey, M. Konieczny, J. Pataki, *J. Org. Chem.* **1983**, *48*, 2930−2932. [15b] D. M. Conner, S. D. Allen, D. M. Collard, C. L. Liotta, D. A. Schiraldi, *J. Org. Chem.* **1999**, *64*, 6888−6890.
[16] [16a] T. Matsumura-Inoue, T. Tanabe, T. Minami, T. Ohashi, *Chem. Lett.* **1994**, 2443−2446. [16b] T. Arai, T. Matsumura, T. Oka, *Kagaku to Kyoiku* **1993**, *41*, 278 (*Chemistry and Education*). [16c] A. Musa, B. Sridharan, H. Lee, D. L. Mattern, *J. Org. Chem.* **1996**, *61*, 5481−5484.
[17] S. Chirayil, R. P. Thummel, *Inorg. Chem.* **1989**, *28*, 812−813.
[18] M. Kreyenschmidt, M. Baumgarten, N. Tyutyulkov, K. Müllen, *Angew. Chem. Int. Ed. Engl.* **1994**, *33*, 1957.
[19] J. V. Caspar, T. J. Meyer, *Inorg. Chem.* **1983**, *22*, 2444.
[20] T. Soujanya, A. Philippon, S. Leroy, M. Vallier, F. Fages, *J. Phys. Chem.* **2000**, *104*, 9408−9414.
[21] M. Beinhoff, W. Weigel, M. Jurczok, W. Rettig, C. Modrakowski, I. Brüdgam, H. Hartl, A. D. Schlüter, *Eur. J. Org. Chem.* **2001**, 3819−3829.
[22] A. Del Guerzo, S. Leroy, F. Fages, R. Schmehl, *Inorg. Chem.* **2002**, *41*, 359−366.
[23] D. S. Tyson, J. Bialecki, F. N. Castellano, *Chem. Commun.* **2000**, 2355−2356.
[24] N. D. McClenaghan, F. Barigelletti, B. Mauber, S. Campagna, *Chem. Commun.* **2002**, 602−603.
[25] V. Goulle, R. P. Thummel, *Inorg. Chem.* **1990**, *29*, 1767−1772.
Received January 10, 2003

 © 2003 Wiley-VCH Verlag GmbH & Co. KGaA, Weinheim

Monomeric 1-Borylimidazoles: Syntheses, Structure and Reactivity of 1-[Bis(diisopropylamino)boryl]imidazoles

Daniela Görz,[a] Hans Pritzkow,[a] and Walter Siebert*[a]

Dedicated to Prof. Heinrich Nöth on the occasion of his 75th birthday

Keywords: Boranes / Imidazoles / Donor-acceptor interaction / Metal complexes

Reactions of chlorobis(diisopropylamino)borane with 1-(trimethylsilyl)imidazole and 4,5-dimethyl-1-(trimethylsilyl)imidazole lead to the monomeric 1-borylimidazoles **3a** and **3b**. Treatment of **3a** with the Lewis acid BF_3 results in the quantitative formation of the corresponding trifluoroborane adduct **4a**. In contrast, **3a** reacts with the stronger Lewis acids BCl_3, BBr_3, and BI_3 to partially substitute the diisopropylamino groups and form the corresponding adducts, depending on the Lewis acidity of the reagent; **3a** forms, with $Mo(CO)_5$thf and Cp′$Mn(CO)_2$thf, the complexes 3-[$(OC)_5$Mo]**3a** (**8**) and 3-[$(OC)_2$Cp′Mn]**3a** (**6**). The product compositions agree with spectroscopic and analytical data and with X-ray structure analyses of **3a**, **3b**, **4a**, **8**, and **9**.

(© Wiley-VCH Verlag GmbH & Co. KGaA, 69451 Weinheim, Germany, 2003)

Introduction

1-(Diorganoboryl)imidazoles have been prepared either by cleavage of the silicon−nitrogen bond in silylimidazoles with haloboranes or by reaction of (dimethylamino)diethylborane with imidazole. The resulting colorless, glassy materials readily dissolve in organic solvents to form solutions of high viscosity due to intermolecular association by Lewis acid−base interactions.[1] Inherent viscosity and cryoscopical measurements, as well as mass spectrometric data, confirm the presence of polymeric structures.

Analogously, some discrete cyclic tetra-[1a,2] and -pentameric[2c] 1-(diorganoboryl)imidazoles, as well as a boryl-substituted bis(imidazole),[2d] have been obtained. Few monomeric 1-borylimidazoles are known[3] and the reactivity of their unsubstituted nitrogen atom has not been investigated.

This report describes the preparation and characterization of 1-[bis(diorganoamino)boryl]imidazoles. In contrast to former assumptions,[3] bulky substituents are necessary as the electron-donating effects of two small amino groups do not stabilize sufficiently the three-coordinate boron atom to inhibit intermolecular association. Monomeric 1-[bis(diisopropylamino)boryl]imidazoles may be obtained due to the sterically demanding boryl groups. In addition, we examined the reactivity of these compounds toward boron halides of different Lewis acidity, toward BH_3, BEt_3 and photochemically activated carbonylmetal compounds. We previously showed that *N*-borane-substituted imidazoles can be deprotonated to form anionic imidazol-2-ylidenes, which are even more nucleophilic than the classic imidazol-2-ylidenes.[2d,4] Deprotonation of 1-[bis(diisopropylamino)boryl]-3-(trifluoroborio)imidazole is, likewise, possible − despite the electrophilic three-coordinate boron atom − if bulky deprotonation reagents are used.[4d] The anionic carbene reacts with transition metal−halogen compounds to yield (diborylimidazole-2-ylidene)metal complexes containing a reactive boryl group.

[a] Anorganisch-Chemisches Institut der Universität,
Im Neuenheimer Feld 270, 69120 Heidelberg, Germany
Fax: (internat.) + 49-6221/54-5609
E-mail: ci5@ix.urz.uni-heidelberg.de

Results and Discussion

Monomeric 1-Borylimidazoles 3a,b

Chlorobis(dimethylamino)borane reacts with 1-(trimethylsilyl)imidazole (**1a**) in THF to yield colorless **2**, which is soluble in $CDCl_3$ (Scheme 1). Its ^{11}B NMR shift is in the region expected for compounds with four-coordinate boron atoms,[5] indicating that **2** undergoes intermolecular association by Lewis acid−base interactions. In contrast, the bulkier reagent chlorobis(diisopropylamino)borane affords the crystalline 1-[bis(diisopropylamino)boryl]imidazoles **3a** and **3b**, which exhibit broad ^{11}B NMR signals in the range typical for three-coordinate boron atoms.[5] The ^1H NMR spectra of **3a** and **3b** show signals for the aromatic hydrogen atoms of both molecules as singlets, the methyl substituents of the imidazole ring in **3b** exhibit only one resonance, whereas two signals appear in the ^{13}C NMR spectrum. The aliphatic resonances of **3a** coincide as a single doublet for the methyl and a septuplet for the methine protons, indicat-

ing that free rotation about the boron−imidazole as well as about the boron−diisopropylamino bonds occurs at room temperature on the NMR time scale. For the same reason the ^{13}C NMR spectrum shows only two resonances for the diisopropylamino substituents as well as three signals for the imidazole ring.

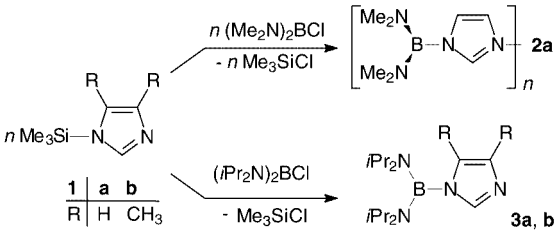

Scheme 1

By contrast, in the ^1H NMR spectrum of **3b** the methyl groups of the diisopropylamino substituents appear as two groups of diastereomeric protons, each signal split to a doublet, at slightly different fields. Likewise, two ^{13}C NMR absorptions are assigned to these chemically inequivalent methyl carbon atoms. Thus, in **3b**, due to the methyl substituent at the 5-position of the imidazole ring, free rotation of the diisopropylamino groups about the boron−imidazole bond at room temperature is assumed to be inhibited. Nevertheless, the corresponding methine carbon atoms show only one septuplet as well as one signal in the ^{13}C NMR spectrum on account of the unhindered rotation of all four isopropyl groups about the diisopropylamino−boron axis.

To determine the height of the rotation barrier for the bis(diisopropylamino)boryl group, temperature-dependent NMR experiments have been performed. From the Eyring equation,[6] using the method of the peak separation, a free energy of activation of $\Delta G^{\neq} = 84.6$ kJ/mol of the rotation barrier has been calculated. (The coalescence temperature of the corresponding peaks has been determined by temperature-dependent spectra in [D$_8$]toluene to $T_c = 318$ K; for these signals a frequency difference of up to $|\nu_A - \nu_B| = 7.1$ Hz has been ascertained.) This $\Delta G^{\neq}$ is about 20 kJ/mol higher than that obtained for (2,2′,6,6′-tetramethylpiperidino)boryl-substituted bis(imidazole).[2d]

The EI mass spectrometric data on **3a** and **3b** agree with monomeric structures for both molecules. The highest boron-containing sets of peaks in each case correspond to the respective monomeric molecules, and high-resolution spectra confirm their compositions.

Donor−Acceptor Compounds 4, 5 and 7

Imidazole−trifluoroborane adduct formation has been studied extensively,[7] whereas only one report on imidazole−trichloroborane adducts is available.[7a] We examined the reactivity of **3a** toward the haloboranes BF_3, BCl_3, BBr_3, and BI_3 as well as toward BEt_3 and BH_3 (Scheme 2).

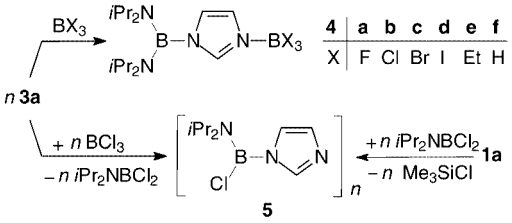

Scheme 2

Treatment of **3a** with the weak Lewis acid BF_3 in THF yields the donor−acceptor compound **4a** quantitatively. The ^{11}B NMR spectrum of **4a** has a broad signal for the three-coordinate boron atom and a sharp 1:3:3:1 quadruplet at high field. Its ^1H NMR spectrum exhibits signals for the ring protons that are slightly shifted down-field compared with the corresponding resonances of **3a**. Only a small influence on the shift of the signals of the diisopropylamino groups is observed. In the ^{13}C NMR spectrum, the imidazole carbon atoms and the diisopropylamino substituents appear nearly unchanged compared with the starting material. Mass spectrometric studies (EI, CI) on **4a** reveal that the Lewis acid−base interaction between the nitrogen and boron atoms is too weak to permit ionization without dissociation.

Treatment of **3a** with the stronger Lewis acid BCl_3 in toluene leads to a small amount of a white precipitate (**5**); NMR spectra of the crude product, obtained by evaporation of the solvent, indicate a product mixture. Recrystallization gave **4b** (68%), which shows a broad signal at low field and a sharp absorption at high field in its ^{11}B NMR spectrum. Accordingly, the ^1H NMR spectrum exhibits a doublet and a septuplet as well as three absorptions in the aromatic region. Additional signals for **3a** and for dichloro(diisopropylamino)borane are found. These observations show that, as well as the expected adduct **4b**, BCl_3 cleaves the diisopropylamino−boron bond of **3a** to give 1-[chloro(diisopropylamino)boryl]imidazole (**5**) as a white precipitate; **5** was obtained separately from **1a** and dichloro(diisopropylamino)borane (Scheme 2).[4d]

Under the same conditions, with the stronger Lewis acids BBr_3 and BI_3, the amount of side products increases, as indicated by the smaller yields of **4c** (55%) and of **4d** (< 30%). However, in contrast to **4c**, purification of **4d** by recrystallization was unsuccessful, due to the formation of [iPr$_2$NH$_2$]I. The ^1H NMR spectra showed increased low-field shifts of the aromatic protons. Additionally, the corresponding signals for the four-coordinate boron atoms are shifted to high field. Apart from the two resonances of the boron atoms of **4c** and **4d**, each ^{11}B NMR spectrum of the crude products shows an additional signal assigned to the (diisopropylamino)haloborane by-products. As (diisopropylamino)diiodoborane, not yet described, was prepared separately by treating diisopropylamine with BI_3. During crystallization of **4d**, extremely air-sensitive yellow crystals of **7** were obtained, confirming that compound **6** is formed

 © 2003 Wiley-VCH Verlag GmbH & Co. KGaA, Weinheim

by the reaction of BI_3 and **4d** (Scheme 3). Treatment of **3a** with BEt_3 and BH_3 gave the adducts **4e** and **4f** in excellent yields. Unlike the observed down-field shift of the imidazole proton signals in the ^1H NMR spectrum of the haloborane adducts **4**, the corresponding proton signals of **4e** and **4f** remain nearly unchanged compared to those of **3a**. The ^{11}B NMR resonances for the tetracoordinate boron atoms are at $\delta = -3$ (**4e**) and -20 (**4f**) ppm.

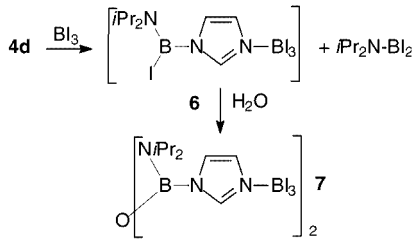

Scheme 3

Formation of Metal Complexes

Examination of the reactivity of **3a** towards photochemically generated $[Mo(CO)_5thf]$ and $Cp'Mn(CO)_2thf$ complexes ($Cp' = C_5H_4Me$)[8] revealed that THF is readily displaced by the two-electron donor ligand **3a** at low temperature to give good yields of **8** and **9**, respectively (Scheme 4).

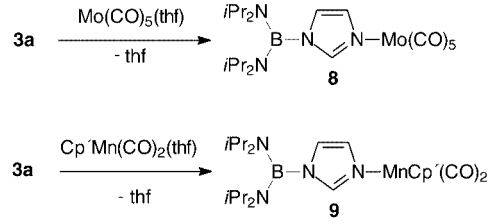

Scheme 4

In the ^1H NMR spectrum of **8** all resonances remain unchanged compared with those of the starting material, but the corresponding signals in the ^{13}C NMR spectrum appear at slightly different fields. The IR spectrum of **8** exhibits three absorptions, at $\tilde{\nu} = 1979$, 1933 and 1891 cm^{-1}.

Unlike that of **8**, the ^1H NMR spectrum of **9** exhibits clearly broadened lines that are significantly shifted in comparison with the starting material, hinting at the formation of a paramagnetic compound. The reasons for this unexpected paramagnetism at room temperature for the 18VE carbonylmetal complex of manganese(I) lie, as described by Kaim et al.,[9] in the generally small ligand-field splitting of low-valent manganese, which favors spin crossover. Other factors are the ligand strength and coordination geometry. Reduction of the symmetry of the $Cp'Mn(CO)_3$ parent to C_s in **9** and weakening of the bond to the imidazole substituent lead to an arrangement of d orbitals that favors the occupation of magnetically excited states. Conversely, the correlated ^{13}C NMR spectra exhibit all expected resonances as sharp lines at slightly different fields compared with **3a**. Infrared spectroscopy shows two CO bands at $\tilde{\nu} = 2017$ and 1928 cm^{-1}. As with the haloborane adducts **4**, no mass spectrometric data for **8** and **9** could be obtained.

Crystal Structures

To confirm their monomeric structures, we performed X-ray single-crystal analyses of the colorless and orange crystals obtained by cooling hexane solutions of **3a** and **3b**, respectively, to -80 °C. Their molecular structures are shown in Figures 1 and 2.

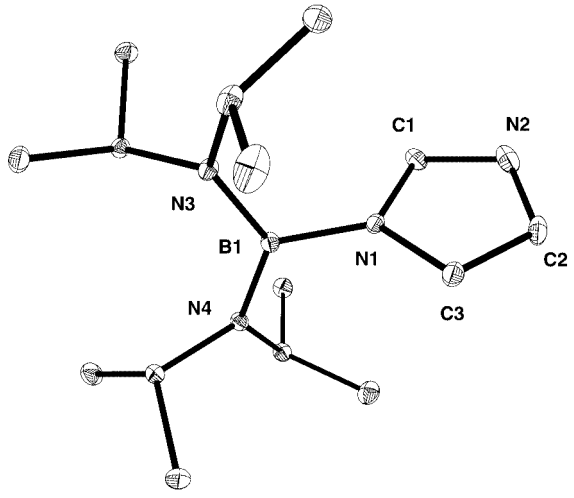

Figure 1. Molecular structure of **3a** in the crystal; hydrogen atoms are omitted for clarity; selected bond lengths [Å] and angles [°]: B1–N1 1.514(2), B1–N3 1.420(1), B1–N4 1.425(1), N1–C1 1.361(2), N1–C3 1.387(2), N2–C1 1.316(2), N2–C2 1.389(3); C1–N1–C3 104.6(1), N2–C1–N1 114.1(2), C1–N2–C2 104.4(1); angle between planes N1/B1/N3/N4 and ring 68.5

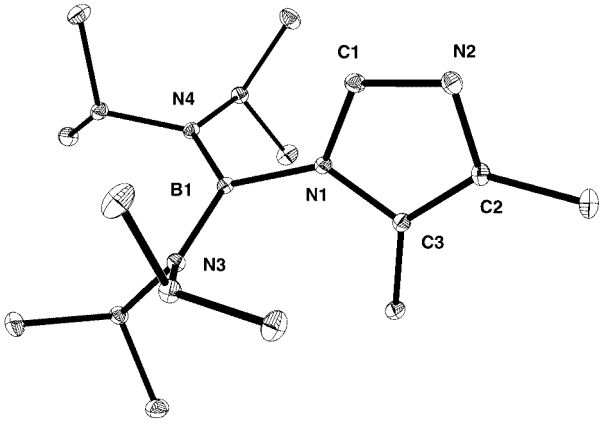

Figure 2. Molecular structure of **3b** in the crystal; hydrogen atoms are omitted for clarity; selected bond lengths [Å] and angles [°]: B1–N1 1.507(1), B1–N3 1.429(1), B1–N4 1.426(1), N1–C1 1.368(1), N1–C3 1.397(1), N2–C1 1.318(1), N2–C2 1.390(1); C1–N1–C3 105.3(1), N2–C1–N1 113.7(1), C1–N2–C2 104.5(1); angle between planes N1/B1/N3/N4 and ring 63.7

In **3a** the imidazole ring is disordered over two positions (3:1); the distances and angles of the higher occupied part are given. The imidazole rings are planar with short internal

 © 2003 Wiley-VCH Verlag GmbH & Co. KGaA, Weinheim

ring bond lengths, which are very similar to those in imidazole.[10] More significant differences are found in the ring angles, especially at N1 (decreasing) and C1 (increasing) compared with imidazole.

As expected for a substituted imidazole, the N1/2−C1 bond lengths of **3a** and **3b** show single- and double-bond character.[11] Because the B1−N1 distance is about 0.10 Å longer than that from B1 to the diisopropylamino nitrogen atoms, π-interactions of the vacant p-orbital of B1 with the free electron pair of N1 can be excluded, while the short B1−N2/N3 distances indicate strong interactions with these nitrogen atoms. This is in agreement with the angles between the planes through the imidazole ring and B1 and the adjacent nitrogen atom (**3a**: 68.5°; **3b**: 63.7°).

Single crystals of **4a** have been obtained from a toluene solution. The crystal cell contains two crystallographically independent molecules in the asymmetric unit with very similar distances and angles; only one structure is shown in Figure 3 and the average values are listed.

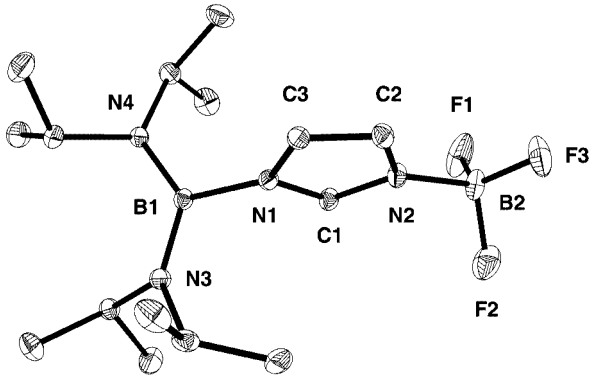

Figure 3. Molecular structure of **4a** in the crystal; hydrogen atoms are omitted for clarity; average values of selected bond lengths [Å] and angles [°]: B1−N1 1.527(2), B1−N3 1.412(2), B1−N4 1.414(2), B2−N2 1.579(2), N1−C1 1.336(2), N1−C3 1.388(2), N2−C1 1.327(2), N2−C2 1.379(2); C1−N1−C3 106.8(1), N2−C1−N1 110.7(1), C1−N2−C2 107.0(1); angle between planes N1/B1/N3/N4 and ring 73.4

Comparing the structural data of **4a** with that of **3a** enables the following observations: First, the N1/N2−C1 distances [N1−C1 1.336(2) Å and N2−C2 1.327(2) Å] exhibit significantly smaller bond-length alternations as at **3a**, indicating uninterrupted aromaticity. Second, the angles at N1 and C1 in **4a** resemble those in imidazole[10] more than in **3a** and **3b**. Third, as expected, the distance [1.577(2) Å] between N2 and the four-coordinate boron atom is longer than between N1 and B1 [1.527(2) Å].

The X-ray diffraction study of yellow **7** confirms the structure; as the quality of the data is poor, however, it will not be further discussed here. Crystals of **8** and **9** suitable for X-ray analysis were grown from a toluene solution. **8** contains four independent molecules in the asymmetric unit. As the obtained distances and angles of these molecules are similar, only one structure is shown in Figure 4, and the range of selected bond lengths and angles is listed. The values for **9** are given in the caption of Figure 5.

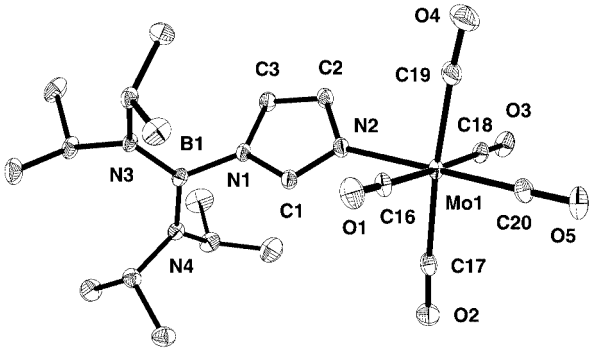

Figure 4. Molecular structure of **8** in the crystal; hydrogen atoms are omitted for clarity; selected bond lengths [Å] and angles [°]: B1−N1 1.517(5)−1.527(5), B1−N3 1.406(5)−1.412(5), B1−N4 1.404(5)−1.422(5), N1−C1 1.344(4)−1.350(5), N2−C1 1.317(5)−1.326(4); C1−N1−C3 105.0(3)−105.4(3), N2−C1−N1 112.9(3)−113.5(3), C1−N2−C2 104.2(3)−105.0(3); angle between planes N1/B1/N3/N4 and ring 108.7−117.9

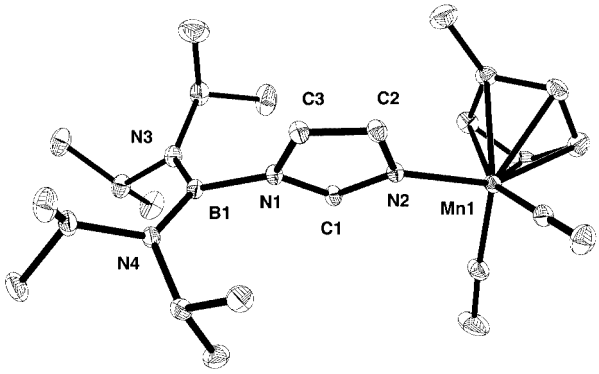

Figure 5. Molecular structure of **9** in the crystal; hydrogen atoms are omitted for clarity; selected bond lengths [Å] and angles [°]: B1−N1 1.527(2), B1−N3 1.416(2), B1−N4 1.423(2), N1−C1 1.353(2), N2−C1 1.327(2); C1−N1−C3 105.7(1), N2−C1−N1 112.5(1), C1−N2−C2 105.0(1); angle between planes N1/B1/N3/N4 and ring 118.8

Both molecules exhibit less bond-length alternations than **3a** but more than **4a** and, following this structural pattern, the angles at N1 and C1 resemble those in imidazole more than those of **3a** and **3b**. Further, the Mo−CO bonds of **8** *trans* to the nitrogen atoms (1.97 Å) are shorter than the average length of the *cis* Mo−C bonds (2.04 Å). This is due to the stronger π-bonding from Mo to CO, indicating good σ-donor and poor π-acceptor capacity of the imidazole ligand.

Conclusion

The monomeric imidazoles **3a** and **4a** are obtained by using electron-donating *and* sterically demanding boryl substituents. Contrary to **3a**, restricted rotation about the B−N(imid.) bond is observed for **4a**. X-ray structure analyses of **3a** and **4a** reveal that π-interaction of the vacant p-

 © 2003 Wiley-VCH Verlag GmbH & Co. KGaA, Weinheim

orbital of the boron atoms exists only with the diisopropylamino groups and not with the imidazole nitrogen atoms. Treatment of **3a** with the weak Lewis acids BF_3, BEt_3 and BH_3 leads to the corresponding zwitterionic adducts in excellent yields. In contrast, the stronger Lewis acids BCl_3, BBr_3, and BI_3 give decreasing yields with increasing Lewis acidity. The observed side reactions involve splitting off of the diisopropylamino groups of **3a** and the corresponding adducts. With $Mo(CO)_5$thf and $Cp'Mn(CO)_2$thf the complexes 3-[$(OC)_5$Mo]**3a** (**8**) and 3-[$(OC)_2Cp'Mn$]**3a** (**9**) are formed readily, and X-ray diffraction measurement of **8** reveals the good σ-donor and poor π-acceptor capacity of the borylimidazole ligand.

Experimental Section

General: Reactions were carried out under dry argon, using standard Schlenk techniques. Solvents were dried, distilled and saturated with nitrogen. Glassware was dried with a heat-gun under high vacuum. ^1H, ^{13}C, ^{11}B NMR: Bruker AC 200 spectrometer, with $(CH_3)_4Si$ and $BF_3{\cdot}Et_2O$ as references. IR spectra were recorded with a Bruker IFS 28 Fourier-transformation spectrometer with CaF_2 cells. Mass spectra were obtained with a Finnigan MAT 8200 plus spectrometer using the EI technique. Melting points (uncorrected) were obtained with a Büchi apparatus, using a capillary filled under argon and sealed. Chlorobis(dimethylamino)borane,[12] chlorobis(diisopropylamino)borane[13] and 4.5-dimethyl-1-(trimethylsilyl)imidazol[14] were prepared according to literature procedures. (Trimethylsilyl)imidazole, $BF_3{\cdot}Et_2O$, BBr_3, $BH_3{\cdot}THF$, $BEt_3{\cdot}THF$ and $Cp'Mn(CO)_3$ were purchased from Sigma Aldrich and $Mo(CO)_6$ from Fluka.

1-[Bis(dimethylamino)boryl]imidazole (2): Chlorobis(dimethylamino)borane (190 mg, 1.4 mmol) in THF (10 mL) was added dropwise at −30 °C to a solution of **1a** (200 mg, 1.4 mmol) in THF (40 mL). After slowly warming to room temperature and stirring for 10 h, the solvent was removed in vacuo, leaving the white crude product, m.p. (dec.) > 240 °C. ^1H NMR (200.1 MHz, $CDCl_3$): δ = 0.7−1.2 (m, CH_3), 6.8−7.5 (m, im.) ppm. ^{11}B NMR (64.2 MHz, $CDCl_3$): δ = 1.3 ($\Delta\nu_{1/2}$ = 145 Hz) ppm.

1-[Bis(diisopropylamino)boryl]imidazole (3a): Chlorobis(diisopropylamino)borane (713 mg, 2.9 mmol) in THF (10 mL) was added dropwise at −30 °C to a solution of **1a** (410 mg, 2.9 mmol) in THF (40 mL). The resultant mixture was allowed to warm to room temperature and stirred for 24 h. The solvent was then removed in vacuo, and the remaining solid extracted with hexane and filtered. The product was recrystallized from hexane solution at −80 °C. Yield: 685 mg (85%) of colorless crystals, sensitive to air and moisture, m.p. 67−68 °C. ^1H NMR (200.1 MHz, $CDCl_3$): δ = 0.98 [d, $^3J_{H,H}$ = 6.8 Hz, 24 H, $CH(CH_3)_2$], 3.41 [m, $^3J_{H,H}$ = 6.8 Hz, 4 H, $CH(CH_3)_2$], 6.85 (s, 1 H, C*H*−CH=N), 7.01, (s, 1 H, CH−C*H*=N), 7.47 (s, 1 H, N=CH−N) ppm. ^1H NMR (200.1 MHz, [D_8]THF): δ = 1.04 [d, $^3J_{H,H}$ = 6.8 Hz, 24 H, $CH(CH_3)_2$], 3.47 [m, $^3J_{H,H}$ = 6.8 Hz, 4 H, $CH(CH_3)_2$], 6.90 (s, 2 H, C*H*−C*H*=N), 7.44 (s, 1 H, N−CH=N) ppm. ^1H NMR (200.1 MHz, [D_8]toluene): δ = 1.08 [d, $^3J_{H,H}$ = 6.8 Hz, 24 H, $CH(CH_3)_2$,], 3.45 [m, $^3J_{H,H}$ = 6.8 Hz, 4 H, $CH(CH_3)_2$], 6.92 (s, 1 H, C*H*−CH=N), 7.46 (s, 1 H, CH−C*H*=N), 7.72 (s, 1 H, N−CH=N) ppm. ^{11}B NMR (64.2 MHz, $CDCl_3$): δ = 28 ($\Delta\nu_{1/2}$ = 145 Hz) ppm. ^{13}C NMR (50.3 MHz, $CDCl_3$): δ = 24.4 [$CH(CH_3)_2$], 47.0 [$CH(CH_3)_2$], 122.2 (*C*H−CH=N), 128.1 (CH−*C*H=N), 141.4 (N−CH=N) ppm. ^{13}C NMR (50.3 MHz, [D_8]THF): δ = 25.5 [$CH(CH_3)_2$], 48.5 [$CH(CH_3)_2$], 123.1 (*C*H−CH=N), 129.7 (CH−*C*H=N), 142.8 (N−CH=N) ppm. ^{13}C NMR (50.3 MHz, [D_8]toluene): δ = 24.4 [$CH(CH_3)_2$], 47.0 [$CH(CH_3)_2$], 122.2 (*C*H−CH=N), 128.1 (CH−*C*H=N), 141.4 (N−CH=N) ppm. EI-MS: *m*/*z* (%) = 278 (62) $[M]^+$, 263 (100) $[M - CH_3]^+$, 235 (82) $[M - C_3H_7]^+$, 178 (52) $[M - N(C_3H_7)_2]^+$, 43 (13) $[C_3H_7]^+$. HR-EI: *m*/*z* = 278.2670, calcd. for $C_{15}H_{31}N_4B$ 278.2698 (Δμ = 2.8).

1-[Bis(diisopropylamino)boryl]-4,5-dimethylimidazole (3b): The same procedure as for **3a** was used in treating **1b** (300 mg, 1.8 mmol) with chlorobis(diisopropylamino)borane (443 mg). After workup an air- and moisture-sensitive orange solid was obtained (484 mg; 88%), m.p. 94−95 °C. ^1H NMR (200.1 MHz, $CDCl_3$): δ = 0.96 [d, $^3J_{H,H}$ = 6.8 Hz, 12 H, $CH(CH_3)_2$], 1.01 [d, $^3J_{H,H}$ = 6.8 Hz, 12 H, $CH(CH_3)_2$]], 2.12 [2 s, 6 H, CH_3(im.)], 3.39 [m, $^3J_{H,H}$ = 6.8 Hz, 4 H, $CH(CH_3)_2$], 7.24 (s, 1 H, N=CH−N) ppm. ^{11}B NMR (64.2 MHz, $CDCl_3$): δ = 28 ($\Delta\nu_{1/2}$ = 145 Hz) ppm. ^{13}C NMR (50.3 MHz, $CDCl_3$): δ = 11.2 [CH_3 (im.)], 12.4 [CH_3 (im.)], 23.8 [$CH(CH_3)_2$], 24.6 [$CH(CH_3)_2$], 47.1 [$CH(CH_3)_2$], 124.3 (*C*Me−CMe=N), 133.9 (CMe−*C*Me=N), 138.7 (N−CH=N) ppm. EI-MS: *m*/*z* (%) = 306 (10) $[M]^+$, 211 (100) $[C_{12}H_{28}N_2B]^+$. HR-EI: *m*/*z* = 306.2953, calcd. for $C_{17}H_{35}N_4B$ 306.2947 (Δμ = 0.6).

General Procedure for the Preparation of the 1-[Bis(diisopropylamino)boryl]imidazole Adducts 4: To a solution of **1a** (200 mg, 0.7 mmol) in the corresponding solvent (40 mL), $BF_3{\cdot}OEt_2$ (120 mg, 0.84 mmol) was added at −78 °C to give **4a**; BCl_3 (81 mg, 0.7 mmol) to give **4b**; BBr_3 (174 mg, 0.7 mmol) to give **4c**; BI_3 (274 mg, 0.7 mmol) to give **4d**; $BH_3{\cdot}$thf (0.7 mL, 0.7 mmol; 1 M solution in THF) to give **4e** and $BEt_3{\cdot}$thf (0.7 mL, 1 M solution in THF) to give **4f**. The reaction mixtures were allowed to warm to room temperature and stirred for 7 h.

1-[Bis(diisopropylamino)boryl]imidazole(N^3-B)Trifluoroborane (4a): Yield after evaporation of THF: 242 mg (100%) of a white powder, sensitive to air and moisture, m.p. 112−114 °C. ^1H NMR (200.1 MHz, $CDCl_3$): δ = 1.01 [d, $^3J_{H,H}$ = 6.8 Hz, 24 H, $CH(CH_3)_2$], 3.45 [m, $^3J_{H,H}$ = 7 Hz, 4 H, $CH(CH_3)_2$], 6.98 (s, 1 H, C*H*−CH=N), 7.30 (s, 1 H, CH−C*H*=N), 7.98 (s, 1 H, N=CH−N) ppm. ^{11}B NMR (64.2 MHz, $CDCl_3$): δ = −0.3 (q, $^2J_{B,F}$ = 14 Hz, $\Delta\nu_{1/2}$ 36 Hz, BF_3), 28 [$\Delta\nu_{1/2}$ = 145 Hz, N−B(N*i*Pr$_2$)$_2$] ppm. ^{13}C NMR (50.3 MHz, $CDCl_3$): δ = 24.4 [$CH(CH_3)_2$], 47.4 [$CH(CH_3)_2$], 122.0 (*C*H−CH=N), 123.7 (CH−*C*H=N), 138.6 (N−CH=N) ppm.

1-[Bis(diisopropylamino)boryl]imidazole(N^3-B)Trichloroborane (4b): A colorless precipitate (20 mg) was filtered off and the volatile compounds of the toluene solution removed under vacuum. The NMR spectra of the crude product show signals of **4b**, **3a** and dichloro(diisopropylamino)borane. The residue was recrystallized from toluene at −18 °C. Yield: 187 mg (68%) of colorless **4b**, which is sensitive to air and moisture, m.p. 145−148 °C. ^1H NMR (200.1 MHz, [D_8]toluene): δ = 0.87 [d, $^3J_{H,H}$ = 6.8 Hz, 24 H, $CH(CH_3)_2$], 3.21 [m, $^3J_{H,H}$ = 6.8 Hz, 4 H, $CH(CH_3)_2$], 6.35 (s, 1 H, C*H*−CH=N), 7.67 (s, 1 H, CH−C*H*=N), 8.60 (s, 1 H, N−CH=N) ppm. ^{11}B NMR (64.2 MHz, $CDCl_3$): δ = 5.3 ($\Delta\nu_{1/2}$ = 30 Hz, BCl_3), 28 [$\Delta\nu_{1/2}$ = 360 Hz, N−B(N*i*Pr$_2$)$_2$] ppm. ^{13}C NMR (50.3 MHz, $CDCl_3$): δ = 23.7 [$CH(CH_3)_2$], 47.0 [$CH(CH_3)_2$], 124.7 (CH−CH=N), 128.9 (CH−CH=N), 137.4 (N−CH=N) ppm.

1-[Bis(diisopropylamino)boryl]imidazole(N^3-B)Tribromoborane (4c): A yellowish precipitate was filtered off and the volatile compounds of the toluene solution removed under vacuum. The NMR spectra of the crude product show signals of **4c**, **3a** and dibromo(di-

 © 2003 Wiley-VCH Verlag GmbH & Co. KGaA, Weinheim

isopropylamino)borane. The residue was then recrystallized from toluene at −18 °C. Yield: 202 mg (55%) of colorless **4c**, which is sensitive to air and moisture, m.p. decomp. > 150 °C. ^{1}H NMR (200.1 MHz, [D$_8$]toluene): δ = 0.90 [d, $^3J_{H,H}$ = 6.8 Hz, 24 H, CH(CH_3)$_2$], 3.23 [m, $^3J_{H,H}$ = 6.8 Hz, 4 H, CH(CH$_3$)$_2$], 6.42 (s, 1 H, CH−CH=N), 7.84 (s, 1 H, CH−CH=N), 8.81 (s, 1 H, N−CH=N) ppm. ^{11}B NMR (64.2 MHz, $CDCl_3$): δ = −11.8 (Δν$_{1/2}$ = 30 Hz, BBr_3), 28 [Δν$_{1/2}$ = 360 Hz, N−B(NiPr$_2$)$_2$] ppm. ^{13}C NMR (50.3 MHz, [D$_8$]toluene): δ = 24.1 [CH(CH_3)$_2$], 47.4 [CH(CH$_3$)$_2$], 124.0 (CH−CH=N), 129.3 (CH−CH=N), 141.1 (N−CH=N) ppm.

1-[Bis(diisopropylamino)boryl]imidazole(N^3−B)Triiodoborane (4d): A yellow precipitate was filtered off and the volatile compounds of the toluene solution were removed under vacuum. The NMR spectra of the crude product show signals of **4d**, **3a** and (diisopropylamino)diiodoborane. The residue was recrystallized from toluene at −18 °C, but was still contaminated with diisopropylammonium iodide. ^{1}H NMR (200.1 MHz, $CDCl_3$): δ = 1.06 [d, $^3J_{H,H}$ = 6.8 Hz, 12 H, CH(CH_3)$_2$], 1.58 [d, $^3J_{H,H}$ = 6.8 Hz, 24 H, CH(CH_3)$_2$], 3.48 [m, $^3J_{H,H}$ = 6.8 Hz, 4 H, CH(CH$_3$)$_2$], 3.65 [m, $^3J_{H,H}$ = 6.8 Hz, 4 H, CH(CH$_3$)$_2$], 7.11 (s, 1 H, CH−CH=N), 7.91 (s, 1 H, CH−CH=N), 8.68 (s, 1 H, N−CH=N) ppm. ^{11}B NMR (64.2 MHz, $CDCl_3$): δ = −68.5 (Δν$_{1/2}$ = 50 Hz, BI_3), 28 [Δν$_{1/2}$ = 360 Hz, N−B(NiPr$_2$)$_2$] ppm. ^{13}C NMR (50.3 MHz, $CDCl_3$): δ = 19.1 [CH(CH_3)$_2$], 24.5 [CH(CH_3)$_2$], 47.4 [CH(CH$_3$)$_2$], 48.6 [CH(CH$_3$)$_2$], 128.2 (CH−CH=N), 129.0 (CH−CH=N), 137.6 (N−CH=N) ppm.

1-[Bis(diisopropylamino)boryl]imidazole(N^3−B)Triethylborane (4e): The volatile compounds of the THF solution were removed under vacuum, leaving **4e** quantitatively as a white powder that is sensitive to air and moisture, m.p. 97−98 °C. ^{1}H NMR (200.1 MHz, $CDCl_3$): δ = 0.24 (q, 6 H, CH_2CH$_3$), 0.60 (t, 6 H, CH$_2$CH_3), 1.00 [d, $^3J_{H,H}$ = 6.8 Hz, 24 H, CH(CH_3)$_2$], 3.43 [m, $^3J_{H,H}$ = 6.8 Hz, 4 H, CH(CH$_3$)$_2$], 6.83 (s, 1 H, CH−CH=N), 7.07 (s, 1 H, CH−CH=N), 7.56 (s, 1 H, N−CH=N) ppm. ^{11}B NMR (64.2 MHz, $CDCl_3$): δ = −3 (Δν$_{1/2}$ = 380 Hz, BEt_3), 28 [Δν$_{1/2}$ = 360 Hz, N−B(NiPr$_2$)$_2$] ppm. ^{13}C NMR (50.3 MHz, $CDCl_3$): δ = 9.7 (CH$_2$$CH_3$), 15.0 ($CH_2CH_3$) 24.4 [CH($CH_3$)$_2$], 47.2 [$C$H(CH$_3$)$_2$], 122.6 ($C$H−CH=N), 123.5 (CH−$C$H=N), 138.3 (N−CH=N).

1-[Bis(diisopropylamino)boryl]imidazole(N^3−B)Trihydroborane (4f): The volatile compounds of the THF solution were removed under vacuum. The residue was then recrystallized from toluene at −18 °C. Yield: 190 mg (93%) of a white powder that is sensitive to air and moisture, m.p. 93−95 °C. ^{1}H NMR (200.1 MHz, $CDCl_3$): δ = 1.00 [d, $^3J_{H,H}$ = 6.8 Hz, 24 H, CH(CH_3)$_2$], 3.42 [m, $^3J_{H,H}$ = 6.8 Hz, 4 H, CH(CH$_3$)$_2$], 6.83 (s, 1 H, CH−CH=N), 7.05 (s, 1 H, CH−CH=N), 7.68 (s, 1 H, N−CH=N) ppm. ^{11}B NMR (64.2 MHz, $CDCl_3$): δ = −20 (Δν$_{1/2}$ = 400, $^2J_{B,H}$ = 90 Hz, BH_3), 28 [Δν$_{1/2}$ = 360 Hz, N−B(NiPr$_2$)$_2$] ppm. ^{13}C NMR (50.3 MHz, $CDCl_3$): δ = 24.4 [CH(CH$_3$)$_2$], 47.3 [CH(CH$_3$)$_2$], 123.1 (CH−CH=N), 126.7 (CH−CH=N), 140.3 (N−CH=N) ppm.

(Diisopropylamino)diiodoborane: Diisopropylamine (160 mg, 1.6 mmol) in toluene (30 mL) was added dropwise at −50 °C to a solution of BI_3 (310 mg, 0.8 mmol) in toluene (100 mL), after which the mixture was refluxed for 5 h. After removal of the diisopropylammonium iodide by filtration, the solvent of the resultant yellow solution was removed in vacuo. The product was recrystallized from hexane/toluene at −15 °C. Yield 170 mg (60%) of a yellow powder that is sensitive to air and moisture, m.p. (decomp.) > 100 °C. ^{1}H NMR (200.1 MHz, $CDCl_3$): δ = 1.4 [br., 24 H, CH(CH_3)$_2$], 4.3 [br., 4 H, CH(CH$_3$)$_2$] ppm. ^{11}B NMR (64.2 MHz,

Table 1. Crystal data and structure refinement for **3a**, **3b**, **4a**, **8** and **9**

	3a	**3b**	**4a**	**8**	**9**
Empirical formula	$C_{15}H_{31}BN_4$	$C_{17}H_{35}BN_4$	$C_{15}H_{31}B_2F_3N_4$	$C_{20}H_{31}BMoN_4O_5$	$C_{23}H_{38}BMnN_4O_2$
Formula mass	278.3	306.3	346.1	514.2	468.3
Crystal system	orthorhombic	monoclinic	triclinic	monoclinic	monoclinic
Space group	*Pbca*	$P2_1/c$	$P\bar{1}$	$P2_1/n$	$P2_1/c$
Unit cell					
a [Å]	12.5145(5)	7.5352(3)	9.1347(6)	15.525(2)	8.096(1)
b [Å]	14.4572(6)	15.9599(7)	14.3484(9)	25.507(3)	16.961(2)
c [Å]	19.3949(7)	15.9414(7)	15.693(1)	26.559(3)	18.594(3)
α [°]	90	90	82.041(1)	90	90
β [°]	90	95.843(1)	88.996(1)	101.348(3)	93.036(3)
γ [°]	90	90	81.506(1)	90	90
V [Å^3]	3509.0(2)	1907.2(1)	2014.7(2)	10311(2)	2549.6(6)
Z	8	4	4	16	4
Temperature [K]	103	100	190	190	190
Calcd. density [g/cm^3]	1.053	1.067	1.141	1.325	1.220
Absorp. coeff. [mm^{-1}]	0.06	0.06	0.09	0.54	0.54
F(000)	1232	680	744	4256	1000
Crystal size [mm]	0.30 × 0.27 × 0.14	0.28 × 0.30 × 0.31	0.40 × 0.31 × 0.15	0.41 × 0.17 × 0.07	0.52 × 0.14 × 0.12
θ_{max} [°]	32	31	30.5	26.4	32
Index ranges	0/+18, 0/+21, 0/+28	−11/+10, 0/+23, 0/+22	−13/+13, −20/+20, 0/+22	−19/+19, 0/+31, 0/+33	−12/+11, 0/+25, 0/+27
No. of reflections					
collected	37980	16411	33771	68628	23848
unique	6067	6439	12252	21094	8510
Parameters	327	339	681	1155	432
Final *R* indices					
*R*1 [$I > 2\sigma(I)$]	0.044	0.043	0.055	0.046	0.042
*wR*2	0.128	0.120	0.171	0.116	0.115
Largest diff. peak/hole [e/Å^3]	0.41/−0.17	0.49/0.20	0.86/−0.60	0.75/−0.68	0.46/−0.32

 © 2003 Wiley-VCH Verlag GmbH & Co. KGaA, Weinheim

$CDCl_3$): δ = −1 ($\Delta\nu_{1/2}$ = 30 Hz) ppm. ^{13}C NMR (50.3 MHz, $CDCl_3$): δ = 21.9 [$CH(CH_3)_2$], 58.6 [$CH(CH_3)_2$] ppm. CI-MS: *m*/*z* (%) = 238 (100) $[M - I + H]^+$.

1-Bis[diisopropylamino)boryl]imidazole(N^3−*Mo*)(Pentacarbonyl)-molybdenum (8): A solution of freshly prepared $Mo(CO)_5$thf (150 mg, 0.5 mmol) in THF (30 mL) was slowly added to **1a** (140 mg, 0.5 mmol), dissolved in THF (50 mL) at −78 °C. After warming to room temperature and stirring, a brown solution formed. The solvent was then removed in vacuo and the remaining brown oil extracted with toluene. After filtration, the product was crystallized at −30 °C. Yield 170 mg (56%) of a yellow powder that is sensitive to air and moisture (containing traces of **3a**), m.p. (decomp.) > 100 °C. ^1H NMR (200.1 MHz, $[D_8]$THF): δ = 1.04 [d, $^3J_{H,H}$ = 6.8 Hz, 24 H, $CH(CH_3)_2$], 3.47 [m, $^3J_{H,H}$ = 6.8 Hz, 4 H, $CH(CH_3)_2$], 6.90 (s, 2 H, CH−CH=N), 7.43 (s, 1 H, N−CH=N) ppm. ^{11}B NMR (64.2 MHz, $CDCl_3$): δ = 27 ($\Delta\nu_{1/2}$ = 145 Hz) ppm. ^{13}C NMR (50.3 MHz, $[D_8]$THF): δ = 24.0 [$CH(CH_3)_2$], 25.5 [$CH(CH_3)_2$], 48.2 [$CH(CH_3)_2$], 48.5 [$CH(CH_3)_2$], 123.1 (CH−CH=N), 129.1 (CH−CH=N), 129.3 (CH−CH=N), 129.7 (CH−CH=N), 132.6 (N−CH=N), 142.8 (N−CH=N) ppm. IR (THF): $\tilde{\nu}$ = 1979 (s), 1933 (vs), 1891 (w) cm^{-1}.

1-[Bis(diisopropylamino)boryl]imidazole(N^3−*Mn*)Dicarbonyl[η^5-(methylcyclopentadienyl)]manganese (9): The same procedure as for the preparation of **8** was used by treating freshly prepared Cp′$Mn(CO)_2$thf (130 mg, 0.5 mmol) with **1**(139 mg, 0.5 mmol). Crystallization from toluene yielded orange crystals (112 mg, 48%), which are sensitive to air and moisture, m.p. (decomp.) > 110 °C. ^{11}B NMR (64.2 MHz, $[D_8]$THF): δ = 32 ($\Delta\nu_{1/2}$ = 145 Hz) ppm. ^{13}C NMR (50.3 MHz, $[D_8]$THF): δ = 13.5 [$CH(CH_3)_2$], 47.8 [$CH(CH_3)_2$], 83.0 [CH_3(Cp)], 83.4 [CH_3(Cp)], 122.4 (CH−CH=N), 129.4 (CH−CH=N), 142.3 (N−CH=N), 226.7 (C=O) ppm. IR (THF): $\tilde{\nu}$ = 2017 (s), 1928 (vs) cm^{-1}.

Crystal Structure Determinations of 3a, 3b, 4a, 4f, 8, and 9: Crystal data and details of the structure determinations are listed in Table 1. Unique sets of intensity data were collected at low temperature with a Bruker−AXS SMART 1000 diffractometer (Mo-K_α radiation, λ = 0.71073 Å, graphite monochromator, ω-scan). Empirical absorption corrections were applied. The structures were solved by direct methods (SHELXS-86)[15] and refined by least-squares methods based on F^2 with all measured reflections (SHELXS-97).[16] All non-hydrogen atoms were refined anisotropically. The imidazole ring in **3a** is disordered. CCDC-193535 (**3a**), -193536 (**3b**), -193537 (**4a**), -193538 (**8**), -193539 (**9**) contain the supplementary crystallographic data for this paper. These data can be obtained free of charge via www.ccdc.cam.ac.uk/conts/retrieving.html (or from the CCDC, 12 Union Road, Cambridge CB2 1EZ, UK; Fax: (internat.) + 44-1223/336-033; E-mail: deposit@ccdc.cam.ac.uk).

Acknowledgments

This work was supported by the Deutsche Forschungsgemeinschaft and the Fonds der Chemischen Industrie.

[1] [1a] S. Trofimenko, *J. Am. Chem. Soc.* **1967**, *89*, 3903−3904. [1b] I. A. Boenig, W. R. Conway, K. Niedenzu, *Synth. React. Inorg. Met.-Org. Chem.* **1975**, *5*, 1−5. [1c] K. D. Müller, L. Komorowski, K. Niedenzu, *Synth. React. Inorg. Met.-Org. Chem.* **1978**, *8*, 149−155.

[2] [2a] K. R. Breakell, D. F. Rendle, A. STorr, J. Trotter, *J. Chem. Soc., Dalton Trans.* **1975**, 1584−1569. [2b] Niedenzu, H. Deng, D. Knoeppel, J. Krause, S. G. Shore, *Inorg. Chem.* **1992**, *31*, 3162−3164. [2c] A. Weiss, H. Pritzkow, W. Siebert, *Angew. Chem.* **2000**, *112*, 558−559; *Angew. Chem. Int. Ed.* **2000**, *39*, 547−549. [2d] A. Weiss, H. Pritzkow, W. Siebert, *Eur. J. Inorg. Chem.* **2002**, 1607−1604.

[3] W. Weber, K. Niedenzu, *J. Organomet. Chem.* **1980**, *195*, 25−28.

[4] [4a] A. Wacker, H. Pritzkow, W. Siebert, *Eur. J. Inorg. Chem.* **1998**, 843−849. [4b] A. Wacker, H. Pritzkow, W. Siebert, *Eur. J. Inorg. Chem.* **1999**, 789−793. [4c] A. Wacker, C. G. Yan, G. Kaltenpoth, A. Ginsberg, A. M. Arif, R. D. Ernst, H. Pritzkow, W. Siebert, *J. Organomet. Chem.* **2002**, *641*, 195−202. [4d] D. Görz, part of the planned PhD dissertation, **2003**.

[5] [5a] H. Nöth, B. Wrackmeyer, *Chem. Ber.* **1974**, *107*, 3070−3088. [5b] H. Nöth, H. Vahrenkamp, *Chem. Ber.* **1966**, *99*, 1049−1067.

[6] M. Hesse, H. Meier, B. Zeeh, *Spektroskopische Methoden in der Organischen Chemie*, Georg Thieme Verlag, Stuttgart, **1995**, p. 99.

[7] [7a] A. Fratiello, R. E. Schuster, *Inorg. Chem.* **1968**, *7*, 1581−1565. [7b] E. Anders, W. Will, *Tetrahedron Lett.* **1978**, *41*, 3911−3912. [7c] A. Fratiello, R. E. Schuster, M. Geisel, *Inorg. Chem.* **1972**, *11*, 11−16. [7d] I. I. Padilla-Martinez, A. Ariza-Castallo, R. Contreras, *Magn. Reson. Chem.* **1993**, *31*, 189−193.

[8] [8a] R. N. Perutz, J. J. Turner, *J. Am. Chem. Soc.* **1975**, *97*, 4791−4800. [8b] R. N. Perutz, J. J. Turner, *Inorg. Chem.* **1975**, *14*, 262−270. [8c] W. A. Herrmann, *Chem. Ber.* **1975**, *108*, 486−499. [8d] W. A. Herrmann, G. Kriechbaum, M. L. Ziegler, P. Wülknitz, *Chem. Ber.* **1981**, *114*, 276−284. [8e] B. S. Creaven, A. J. Dixon, J. M. Kelly, C. Long, M. Poliakoff, *Organometallics* **1987**, *6*, 2600−2605. [8f] R. S. Hill, M. S. Wrighton, *Organometallics* **1987**, *6*, 632−638. [8g] C. Hall, R. N. Perutz, *Chem. Rev.* **1996**, *96*, 3125−3146. [8h] J. E. Coleman, K. E. Dulaney, A. A. Bengali, *J. Organomet. Chem.* **1999**, *572*, 65−71

[9] W. Kaim, T. Roth, B. Olbrich-Deussner, R. Gross-Lannert, J. Jordanov, E. K. H. Roth, *J. Am. Chem. Soc.* **1992**, *114*, 5693−5697.

[10] R. K. McMüller, J. Epstein, J. R. Rüble, B. M. Craven, *Acta Crystallogr., Sect. B* **1979**, *35*, 688.

[11] G. Bruno, F. Nicolo, *Acta Crystallogr., Sect. C* **1994**, *50*, 428−430.

[12] J. Goubeau, M. Rahtz, M. Becher, *Z. Anorg. Allg. Chem.* **1954**, *275*, 161−175.

[13] [13a] D. W. Aubrey, M. F. Lappert, M. K. Majumdar, *J. Chem. Soc.* **1962**, 4088−4094. [13b] D. W. Aubrey, W. Gerrard, E. F. Mooney, *J. Chem. Soc.* **1962**, 1786−1789.

[14] W. A. Herrmann, *Chem. Ber.* **1975**, *108*, 486−499.

[15] G. M. Sheldrick, *SHELXS-86*, Univ. Göttingen, **1986**.

[16] G. M. Sheldrick, *SHELXS-97*, Univ. Göttingen, **1997**.

Received January 30, 2003

 © 2003 Wiley-VCH Verlag GmbH & Co. KGaA, Weinheim

Structural Characterization of *N*-Methylpyridoxine (MePN; PN = Vitamin B_6) and Its Diorganotin Complexes [SnR_2(MePN-H)]I (R = Me, Et, Bu and Ph)

José S. Casas,[a] Alfonso Castiñeiras,[a] Félix Condori,[a] María D. Couce,[b] Umberto Russo,[c] Agustín Sánchez,[a] José Sordo,*[a] and José M. Varela[a]

Keywords: Vitamins / Tin / IR spectroscopy / Mössbauer spectroscopy / NMR spectroscopy

For comparison with the corresponding pyridoxine complexes we have prepared dimethyl-, diethyl-, dibutyl- and diphenyltin(IV) complexes of *N*-methylpyridoxine (MePN). The compounds [$SnMe_2$(MePN–H)]I (**1**), [$SnEt_2$(MePN–H)]I (**2**), [$SnBu_2$(MePN–H)]I (**3**) and [$SnPh_2$(MePN–H)]I·H_2O (**4**) were isolated and characterized by IR, Raman, Mössbauer, ^1H, ^{13}C and ^{119}Sn NMR spectroscopy, and by EI and FAB mass spectrometry. The crystal structures of [HMePN]I and of compounds **1**, **2**·2H_2O and **3** were determined by X-ray diffractometry. Their lattices contain dimeric [SnR_2-(MePN–H)]$_2^{2+}$ units (R = Me, Et, Bu) in which two bridging-chelating methylpyridoxinato anions link pentacoordinate Sn atoms with coordination polyhedra closer to square pyramids than to trigonal bipyramids. NMR results show that the dimeric cations persist in $(CD_3)_2SO$.

(© Wiley-VCH Verlag GmbH & Co. KGaA, 69451 Weinheim, Germany, 2003)

Introduction

As part of our research on the interaction of diorganotin compounds with vitamins and derivatives,[1,2] we have described the interaction of pyridoxine (PN, vitamin B_6) with dimethyltin(IV) and diethyltin(IV) cations in water/ethanol mixtures in the presence of biologically relevant anions such as Cl^- and NO_3^- in various molar ratios.[3,4] These reactions led to complexes containing mono- or di-deprotonated pyridoxine ligands ([PN−H] and [PN−2H], respectively) in dimeric [SnR_2(PN−H)]$_2^{2+}$ or [SnR_2(PN−2H)]$_2$ units. In these species (**I**, **II**) the tin centre was usually pentacoordinated to the two R groups, the deprotonated phenolic oxygen atom of one PN molecule and the deprotonated 4-(hydroxymethyl) oxygen atoms of this and another PN molecule, the latter oxygen atoms bridging the tin atoms of each dimer. In some dimethyltin derivatives the tin atom was hexacoordinate owing to an additional bond with the 5-(hydroxymethyl) group of a neighbouring dimer or with a water molecule.

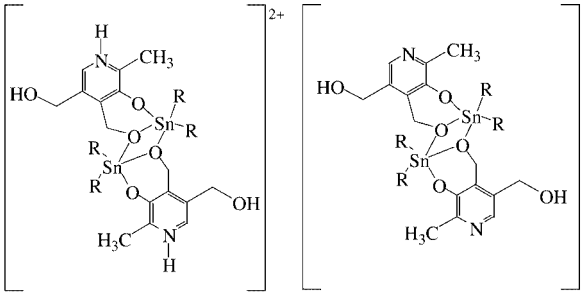

I **II**

N-Methylation suppresses the normal biological activity of PN[5] and methylation of its 4-(hydroxymethyl) group makes it toxic.[6] To find out whether *N*-methylation also significantly affects its coordination to diorganotin cations, in this work we have determined the structures of [HMePN]I and of the complexes resulting from its reaction with SnR_2O (R = Me, Et, Bu), and compared them with those of PN and its diorganotin complexes.

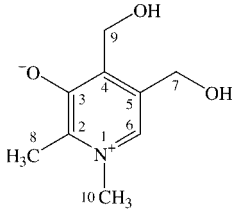

III

[a] Departamento de Química Inorgánica, Facultade de Farmacia, Universidade de Santiago de Compostela,
15782 Santiago de Compostela, Galicia, Spain
Fax: (internat.) + 34-981/594912
E-mail: qijsordo@usc.es
[b] Departamento de Química Inorgánica, Facultade de Ciencias, Universidade de Vigo,
36200 Vigo, Galicia, Spain
[c] Dipartimento di Chimica Inorganica, Metallorganica ed Analitica, Università di Padova,
Padova, Italy

 © 2003 Wiley-VCH Verlag GmbH & Co. KGaA, Weinheim **DOI: 10.1002/ejic.200200631**

We first attempted to use [HMePN]I to prepare *N*-methylpyridoxine [MePN (**III**)] with a view to treating the latter with the diorganotin oxides in reactions that parallel those previously[7] carried out with PN. However, since the resistance of MePN to deprotonation caused its reaction with SnR_2O to afford mainly impure MePN, we eventually treated the oxides (R = Me, Et, Bu and Ph) with PN and methyl iodide in a one-pot synthesis. This afforded the complexes $[SnMe_2(MePN-H)]I$, $[SnEt_2(MePN-H)]I$, $[SnBu_2(MePN-H)]I$ and $[SnPh_2(MePN-H)]I\cdot H_2O$, the first three of which were characterized, as with [HMePN]I, by single-crystal X-ray diffractometry. This appears to be the first study of MePN complexes and the first structural study of MePN.

Results and Discussion

Synthesis

The four complexes $[SnR_2(MePN-H)]I$ were prepared by adding solid SnR_2O and methyl iodide to a solution of pyridoxine in toluene/ethanol (Scheme 1). Compounds **1** and **3** crystallized as such from methanol, but compound **2** acquired two H_2O molecules during crystallization.

$$SnR_2O + PN + MeI \xrightarrow[-H_2O]{\text{toluene/ethanol}} [SnR_2(MePN\text{–}H)]I$$

R = Me (**1**)
Et (**2**)
Bu (**3**)
Ph (**4**)

Scheme 1

Description of the Structures

[HMePN]I

Figure 1 shows the structure of [HMePN]I together with the numbering scheme used. Selected distances and angles are listed in Table 1. The crystal is composed of $[HMePN]^+$ cations and iodide anions. In the cation the pyridine ring is planar and C(7), C(8), C(9), O(2) and O(3) are close to this plane, while C(10) and O(1) lie farther away.

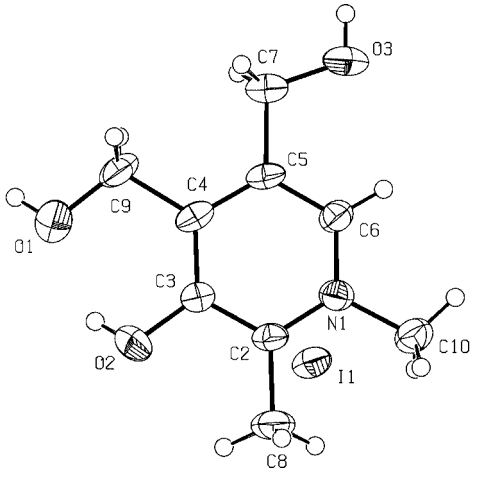

Figure 1. Crystal structure of [HMePN]I, showing the numbering scheme

Although limited by the high e.s.d.s, a comparison of bond lengths with those found for PN[8] shows that *N*-methylation and protonation do not change the ring parameters very much, even for bonds involving or close to the N atom; the most affected bond, C(3)−O(2), is shortened from 1.374(4) to 1.348(10) Å. Such changes are similar, bearing in mind the high e.s.d.s, to those caused by *N*-protonation, as observed in HPNCl[9] [except, of course, for N(1)−C(10)]. The bond angle most affected by *N*-methylation or protonation is C(2)−N(1)−C(6) [119.3(3), 123.8(5) and 122.4(7)° in PN, HPNCl and [HMePN]I, respectively].

As in HPNCl,[9] the O(2) atom of the phenolic hydroxy group and the O(1) atom of the C(4)−CH_2OH group are linked by an intramolecular hydrogen bond [0.82, 1.84 and 2.512(5) Å; 138.1°], which, by pulling O(1) out of the ring plane, is responsible for the different arrangements of the C(4)−CH_2OH and C(5)−CH_2OH groups. Each CH_2OH group is also involved in a structure-stabilizing intramolecular hydrogen bond with a neighbouring iodide ion [O(1)−H(1)···I(1)$^{\#1}$: 0.82, 2.71 and 3.423(6) Å, 146.3°; O(3)−H(3)···I(1)$^{\#2}$: 0.82, 2.86 and 3.593(8) Å, 150.0°; #1: $x + 1/2, -y + 3/2, z + 1/2$; #2: $-x, -y + 1, -z + 2$].

[SnMe$_2$(MePN−H)]I (1)

The dimethyltin derivative consists of dimeric $[SnMe_2(MePN-H)]_2^{2+}$ units and iodide ions. Figure 2 shows the structure of the dimeric unit and the numbering scheme used. Selected distances and angles are listed in Table 1.

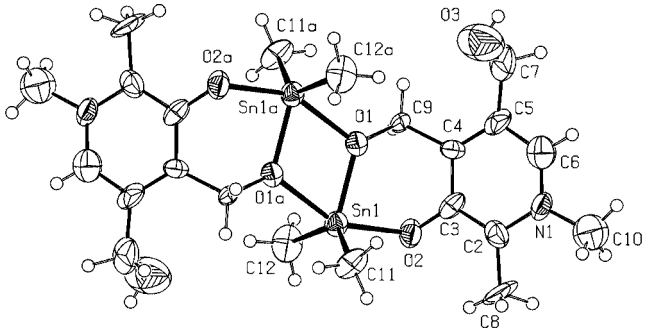

Figure 2. Crystal structure of the cation in the complex $[SnMe_2(MePN-H)]I$ (**1**), showing the numbering scheme (a: $-x, -y + 1, -z$)

In the dimeric unit the two methylpyridoxinato ligands bridge the tin atoms with their deprotonated C(4) substituents. Each tin atom coordinates to two methyl C atoms, to the deprotonated O(2) and O(1) atoms of one methylpyridoxinato ligand and to the similarly deprotonated O(1) atom of the other. As τ[10] = 0.35 for the coordination polyhedron, it is closer to a square pyramid, with the "foreign" O(1) apical, than to a trigonal bipyramid.

In the central Sn_2O_2 ring the length of one Sn−O bond, Sn−O(1), like that of Sn−O(2), is slightly less than the sum

 © 2003 Wiley-VCH Verlag GmbH & Co. KGaA, Weinheim

Table 1. Selected bond lengths [Å] and angles [°] in [HMePN]I, **1**, **2**·2H_2O and **3**, with e.s.d.s in parentheses; symmetry operations (#1): for **1**: $-x, -y + 1, -z$; for **2**·2H_2O: $-x + 1, -y + 1, -z$, for **3**: $-x + 3/2, -y, -z - 1/4$

	[HMePN]I	**1**	**2**·2H_2O	**3**
(a) Tin environment:				
Sn(1)−O(1)		2.060(9)	2.080(4)	2.171(5)
Sn(1)−O(2)		2.068(10)	2.119(4)	2.119(5)
Sn(1)−C(11)		2.090(13)	2.116(7)	2.130(8)
Sn(1)−C(12)		2.096(15)	2.117(7)	2.109(8)
Sn(1)−O(1)$^{\#1}$		2.231(9)	2.295(4)	2.073(5)
Sn(1)−Sn(1)$^{\#1}$		3.549(3)	3.5815(9)	3.5595(16)
O(1)−Sn(1)−C(11)		112.9(5)	108.1(2)	103.5(3)
O(1)−Sn(1)−C(12)		113.0(5)	104.2(2)	109.2(3)
O(1)−Sn(1)−O(2)		84.4(4)	83.20(15)	84.38(18)
O(1)−Sn(1)−O(1)$^{\#1}$		68.4(4)	70.20(16)	70.04(19)
O(2)−Sn(1)−C(11)		99.6(6)	95.1(2)	96.8(3)
O(2)−Sn(1)−C(12)		98.7(6)	99.4(3)	92.5(3)
O(2)−Sn(1)−O(1)$^{\#1}$		152.8(4)	153.21(15)	154.34(17)
C(11)−Sn(1)−C(12)		131.8(7)	145.9(3)	146.7(3)
C(11)−Sn(1)−O(1)$^{\#1}$		91.2(5)	90.3(2)	91.4(3)
C(12)−Sn(1)−O(1)$^{\#1}$		92.3(5)	90.3(3)	94.0(3)
(b) Pyridoxine ligand:				
O(1)−C(9)	1.405(11)	1.439(15)	1.436(7)	1.431(8)
C(4)−C(9)	1.506(11)	1.509(19)	1.512(8)	1.504(9)
C(3)−C(4)	1.383(11)	1.400(19)	1.397(8)	1.415(9)
C(3)−O(2)	1.348(10)	1.329(18)	1.328(6)	1.318(8)
N(1)−C(2)	1.333(11)	1.375(19)	1.352(7)	1.369(8)
N(1)−C(6)	1.348(11)	1.343(19)	1.355(8)	1.315(9)
O(1)−C(9)−C(4)	110.6(8)	110.6(11)	110.8(5)	111.9(6)
C(3)−C(4)−C(9)	123.6(9)	114.6(14)	117.2(5)	119.5(6)
C(5)−C(4)−C(3)	117.7(8)	121.9(16)	119.4(5)	118.9(6)
C(5)−C(4)−C(9)	118.7(8)	123.5(14)	123.3(5)	121.7(6)
O(2)−C(3)−C(4)	124.0(8)	122.9(14)	121.6(5)	120.9(7)
O(2)−C(3)−C(2)	115.2(7)	118.6(14)	118.8(5)	118.7(7)
C(2)−C(3)−C(4)	120.8(8)	118.5(16)	119.5(5)	120.2(6)

of the covalent radii of Sn and O (2.13 Å),[11] whereas that of the other, Sn−O(1)^a, is slightly larger [2.231(9) Å]. The parameters of this ring are similar to those in other dimeric compounds with rings based on O-bridges.[12] The ring is planar, and makes an angle of 46.26° with the pyridine rings of the [MePN−H] ligands, which are, likewise, practically planar (r.m.s. deviation = 0.0160 Å).

Although the structural parameters of $[HMePN]^+$ change upon double deprotonation and coordination, the high e.s.d.s hinder rigorous analysis of the smaller changes, such as those undergone by the C(9)−O(1) and C(3)−O(2) bonds involving the coordinating oxygen atoms. However, the C(3)−C(4)−C(9) angle narrows significantly from 123.6(9)° in [HMePN]I to 114.6(14)° in **1** due to formation of the SnO(2)C(3)C(4)C(9)O(1) chelate ring.

The iodide ion is hydrogen-bonded to the noncoordinating hydroxymethyl group, C(5)−CH_2OH [O(3)−H(3)···I(1)$^{\#2}$: 0.82, 2.75 and 3.517(15) Å, 157.0°; #2: $x, -y + 1/2, z - 1/2$].

Comparison of this structure with those[3] of [$SnMe_2$(PN−H)]NO_3·2H_2O and [$SnMe_2$(H_2O)(PN−H)]Cl·H_2O, which like **1** are composed of dimeric units, reveals similar central Sn_2O_2 rings [although Sn−O(2) is shorter in **1**] but their tin environments are different, the PN−H derivatives being hexacoordinate. They also have different hydrogen-bond networks.

[$SnEt_2$(MePN−H)]I·2H_2O (2·2H_2O)

The diethyltin derivative consists of [$SnEt_2$(MePN−H)]$_2^{2+}$ units, iodide ions and water molecules. Figure 3 shows the structure of the dimeric unit and the numbering scheme used. Selected distances and angles are listed in Table 1.

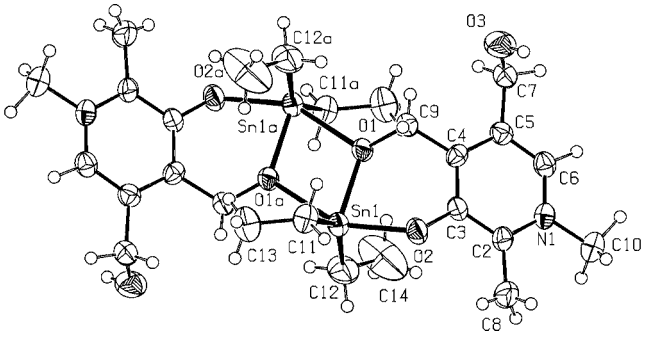

Figure 3. Crystal structure of the cation in the complex [$SnEt_2$(MePN−H)]I·2H_2O (**2**·2H_2O), showing the numbering scheme (a: $-x + 1, -y, -z + 1$)

 © 2003 Wiley-VCH Verlag GmbH & Co. KGaA, Weinheim

The essential structural features of the dimeric unit are, as in **1**, a central Sn_2O_2 ring and the two methylpyridoxinato ligands linked to this ring. However, the following differences deserve comment.

In the Sn_2O_2 ring, the Sn−O bonds are longer in **2**·$2H_2O$ than in **1**, so that even though the Sn−O(1)−Sn^i angle is narrower in **2**·$2H_2O$ than in **1** [109.80(16)° as against 111.6(4)°] the two tin atoms are separated by a greater distance in **2**·$2H_2O$ [3.5815(9) Å] than in **1**. The coordination polyhedron is closer to a square pyramid in **2**·$2H_2O$ than in **1** (τ = 0.12 versus 0.35), mainly because the C−Sn−C angle is wider in **2**·$2H_2O$ than in **1** [145.9(3)° versus 131.8(7)°]. The dihedral angles between the planar Sn_2O_2 ring and the practically planar pyridine rings (r.m.s. deviation = 0.0073 Å) are narrower in **2**·$2H_2O$ than in **1** (33.86° as against 46.26°).

The main difference in crystal packing between **1** and **2**·$2H_2O$ is the presence in **2** of a denser network of hydrogen bonds involving the iodide ion, the water molecules, and the C(5)−CH_2OH group [O(4)−H(4B)···I(1): 1.00(8), 2.52(8) and 3.501(7) Å, 168(6)°; O(4)−H(4A)···O(3)$^{\#2}$: 0.98(8), 2.33(9) and 2.839(9) Å, 112(7)°; O(3)−H(3)···O(4)$^{\#3}$: 0.82, 2.27 and 2.839(9) Å, 126.4°; #2: x, $-y$ + 1/2, z + 1/2; #3: x, $-y$ + 1/2, z − 1/2].

The structure of **2**·$2H_2O$ is very similar to that of $[SnEt_2(PN-H)]NO_3 \cdot 2H_2O$.[3] In particular, the Sn_2O_2 rings are practically identical. The most noteworthy differences are the shorter Sn−C bonds of **2**·$2H_2O$ and its narrower C−Sn−C angles [145.9(3)° versus 152.77(13)°].

[SnBu$_2$(MePN−H)]I (3)

The dibutyltin derivative consists of dimeric $[SnBu_2(MePN-H)]_2^{2+}$ units and iodide ions. Figure 4 shows the structure of the dimeric unit (for clarity the butyl carbon atoms are reduced in size) and the numbering scheme used. Selected distances and angles are listed in Table 1.

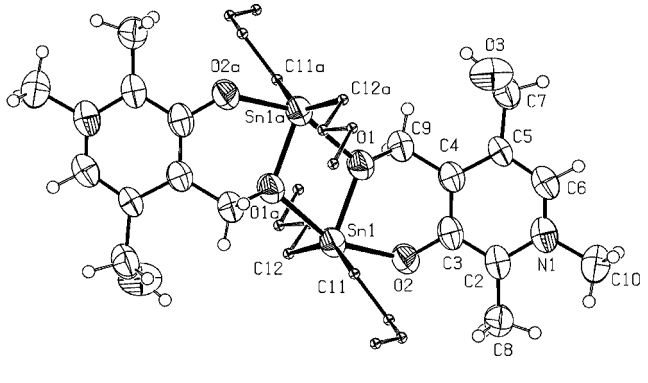

Figure 4. Crystal structure of the cation in the complex $[SnBu_2(MePN-H)]I$ (**3**), showing the numbering scheme; for clarity the butyl carbon atoms are reduced in size (a: $-x$, $-y$, $-z$)

The dimeric unit has a similar structure to **1** and **2**·$2H_2O$, its bond lengths and angles differing only very slightly from those of **2**·$2H_2O$. The Sn−O(1)^a distance is slightly shorter in **3**, but the tin environment has a similar degree of distortion. The hydrogen-bond network in **3** is practically identical to that of **1** [O(3)−H(3)···I(1)$^{\#2}$: 0.82, 2.56 and 3.372(6) Å, 172.4°; #2: x − 1/2, $-y$ + 1/2, $-z$ + 1/2].

Conversely, the angle between the planar Sn_2O_2 ring and each of the practically planar py rings (r.m.s. deviation = 0.0082 Å) is only 29.26° in **3**, falling from 46.26° for R = Me and 33.86° for R = Et, possibly due to the increasing bulk of R.

Vibrational Spectra

In addition to those given in the Exp. Sect., the IR spectrum of [HMePN]I exhibits bands at 3429, 3344, 3249 and 3150 cm^{-1}, attributed to stretching vibrations of the three OH groups. Deprotonation to [MePN] clears the IR spectrum in this region, leaving one broad band at 3160 cm^{-1} and another band at 3101 cm^{-1}, owing to the absence of phenolic ν(OH) and to alteration of the hydrogen-bonding network, which must likewise be responsible for the appearance of a broad medium-strong band at 2850 cm^{-1}.

The ν(C−O) bands for the C(4)- and C(5)−CH_2OH groups[13] of the complexes (see Exp. Sect.) are, like the vibrations of the pyridine ring, close to those of MePN. Near 1300 cm^{-1} the complexes show a strong IR band (medium in the Raman spectra) that is attributed[14] to ν(C−O) of the coordinated phenolic group.

For the methyl and ethyl derivatives the ν_{asym}(Sn−C) and ν_{sym}(Sn−C) vibrations are present in both the IR and Raman spectra, as expected for a nonlinear C−Sn−C fragment. Their positions are close to those[3,4] of unmethylated pyridoxine complexes.

Mössbauer Spectra

The Mössbauer spectra, recorded at 80 K, consist of well-resolved, slightly asymmetric doublets with isomer-shift and quadrupole-splitting values that are consistent with penta coordination around the tin(IV) centre. As usual, the isomer shifts increase on going from the methyl to the butyl derivative, while the diphenyl compound has a lower value due to its different electronegativity. Because of the marked distortion of the complexes from ideal trigonal-bipyramidal geometry, only the contributions of the covalently bonded organic groups were used in calculating Q.S. by means of the point charge model and the simplified formula[15] Q.S. = $-4[R](1-3/4\ \sin^2\ \theta)^{1/2}$. Using the experimental C−Sn−C bond angles, the Q.S. values are quite close to the experimental ones whether the p.q.s. is taken as −0.94 mm/s (valid for organic moieties in tba positions) or −1.13 mm/s (typical of tbe positions). The fact that the experimental Q.S. value of the diphenyl derivative is much lower than those calculated for the dialkyl derivatives suggests that it is even more strongly distorted.

Only the data for the diethyltin derivative can be compared with those of the corresponding PN complex,[3] the dimethyltin derivative of PN being hexacoordinate. The isomer shifts of $[SnEt_2(PN-H)]NO_3 \cdot 2H_2O$ and $[SnEt_2(PN-H)]Cl$, 1.63 and 1.61, respectively, are larger than the 1.49 found for $[SnEt_2(MePN-H)]I$, and as the iso-

 © 2003 Wiley-VCH Verlag GmbH & Co. KGaA, Weinheim

mer shift reflects the s-electron density at the tin nucleus, this suggests that MePN−H has less donor ability than PN−H (vide infra).

NMR Spectroscopy

^{1}H, ^{13}C and ^{119}Sn NMR spectroscopic data recorded in [D_6]DMSO solution, and solid-state ^{13}C CP MAS NMR spectroscopic data, are given in the Exp. Sect.

a) Solid State

Satisfactory ^{13}C CP MAS spectra were obtained for all compounds except the diphenyltin complex. Most carbon atoms afforded separate signals, which were assigned on the basis of previously reported data for similar compounds[3,7c] and on the results of solution studies (see below). *N*-Methylation of PN shifted the C(3) signal ca. 10 ppm downfield. The C(6) and C(4) signals were also deshielded (but to a lesser extent), and the other carbon atoms were shielded, especially C(5) and C(8). This re-distribution of charge in the ring must have a substantial effect on the C(3)−O(2) bond and the charge on the potential donor atom O(2). Protonation of O(2) upon formation of [HMePN]I shielded C(3) by ca. 10 ppm, and C(2), C(6) and C(4) less markedly, while the other carbon atoms were deshielded [C(5) by ca. 9 ppm and the others by ca. 3 ppm]. These results, the X-ray data and the fact that protonation of O(2) in PN to give PN·H$^+$ shifts the C(3) signal slightly downfield (from δ = 151.4 to 153.4 ppm[3]) suggest that *N*-methylation of PN increases the order of the C(3)−O(2) bond, which should affect the donor ability of O(2).

The ^{13}C NMR spectra of the ligand after deprotonation and coordination to the organometallic moieties are very similar, indicating that, as found in the X-ray study of **1**−**3**, they all have the same coordination mode. As in the PN analogues,[3] C(3) and C(4) are deshielded and all other carbon atoms are shielded.

At high field, the spectra show signals corresponding to the organometallic moieties. Compound **1** gives two peaks for the dimethyltin carbon atoms, one at a position similar to that observed in solution (vide infra), δ = 5.6 ppm, and the other slightly upfield at δ = 1.8 ppm, showing the methyl groups to be magnetically different. Similarly, the spectrum of compound **3** shows seven peaks instead of the four found in solution, in keeping with the high anisotropy exhibited by this compound in the X-ray study.

b) Solution

The published ^{1}H NMR data for the PN analogues[3,4] contain an error: the position of the H(6) signal being reported as δ = 8.17 ppm instead of δ = 7.88 ppm. In the present study, methylation of PN markedly shielded H(6), and to a lesser extent the C(9)H_2 and C(7)H_2 protons, and deshielded the C(8)H_3 protons and H(O3). ^3J for the coupling of H(O3) with C(7)H_2 is now 5.2 Hz as against 5.8 Hz in PN. The H(O2) signal was not located, the high acidity of this OH group probably resulting in fast exchange with the deuterium atoms of the solvent. In [HMePN]I, in which MePN is protonated, all the protons are deshielded with respect to MePN, especially H(6) (by 1.07 ppm).

Coordination to SnR_2^{2+} shielded all the protons of [HMePN]I except C(9)H_2, which were slightly deshielded. Flanking the C(9)H_2 singlet in the spectra of **1**, **2** and **3** were satellites corresponding to coupling between these protons and ^{119}Sn, showing that the interaction between O(1) and the tin atoms observed in the solid state persists in solution. The absence of satellites around the signal at δ ≈ 4.5 ppm, assigned to C(7)H_2, rules out interaction between O(3) and the metal atom.

The chemical shifts of the organometallic fragments are similar to those found[3,4,7c] for tin complexes in [D_6]DMSO. Substitution of the ^2J(^{1}H-^{119}Sn) value of **1** (87.0 Hz) in Equation (2) of Lockhart and Manders'[16] study of dimethyltin compounds predicts a C−Sn−C angle of 140°; this is wider than that observed in the X-ray study (131.8°) which may be due to interaction with the solvent.

The chemical shifts of the ligand carbon atoms agree well with the ^{13}C CP-MAS data (taking into account the breadth of the CP-MAS signals). This suggests that the MePN ligand has the same stereochemistry in both states.

^1J(^{13}C-^{119}Sn) constants were only measurable for **1** and **3**. The value for **3** is in the range 500−700 Hz, found[17] for other five-coordinate diorganotin complexes. That of the methyl derivative is outside this range, but also outside the 800−1000 Hz range found[17] for hexacoordinate compounds. When the value for **1** is substituted into Lockhart and Manders' equation,[18] a C−Sn−C angle of 145° is obtained, which is 5° wider than that obtained using the ^2J value but, likewise, suggests that the angle is widened due to the effect of the solvent. By contrast, substitution of ^1J(^{13}C-^{119}Sn) of **3** in the relationship obtained by Holecek et al.[19] for dibutyltin compounds predicts a C−Sn−C angle of 141°, close to the 146.7° observed in the solid state and indicative of the persistence of pentacoordination in solution. The bulky butyl groups may prevent incorporation of the solvent in **3**.

The single ^{119}Sn resonance of the complexes shows that they each have only one type of organotin moiety. Although ^{119}Sn chemical shifts are influenced by several factors,[20] the coordination number of the tin atom is one of the most important:[21] our compounds show a very narrow range, δ = −170.2 to −233.5 ppm, which is within that reported for pentacoordinate organotin compounds.[17,21,22]

Experimental Section

Material and Methods: Pyridoxine (Aldrich), methyl iodide (Aldrich), silver carbonate (Aldrich), dimethyltin oxide (Alfa) and dibutyltin oxide (Aldrich) were used as received. Diethyl- and diphenyltin oxides were obtained by treating the corresponding chlorides with sodium hydroxide. Elemental analyses were performed with a Fisons 1108 microanalyser. Melting points were determined with a Büchi Dr. Tottoli apparatus and are uncorrected. The conductivities of 10^{-3} M solutions in DMF were measured with a Crison MicroCM2202 conductivity meter. Mass spectra were recorded with a Kratos MS50TC spectrometer connected to a DS90 system,

 © 2003 Wiley-VCH Verlag GmbH & Co. KGaA, Weinheim

operating under either EI conditions (direct insertion probe, 70 eV, 250 °C) or in FAB mode (*m*-nitrobenzyl alcohol, Xe, 8 eV; ca. 1.28 × 10^{-15} J); ions were identified by DS90 software and the data characterizing the metallated peaks were calculated using the isotope ^{120}Sn. IR spectra (KBr pellets or Nujol mulls) and Raman spectra (polycrystalline samples) were recorded with a Bruker IFS66V FT-IR spectrometer equipped with an FRA-106 Raman accessory and are reported below using the following abbreviations: vs = very strong, s = strong, m = medium, w = weak, sh = shoulder, br = broad. Mössbauer spectra were recorded at 80.0 K in a Harwell cryostat; the $Ca^{119m}SnO_3$ source (15 mCi, NEN) was kept at room temperature and moved with a triangular velocity wave form; suitable computer programs were employed to fit Lorentzian lineshapes to the experimental data. Solid-state NMR spectra were recorded with a Bruker AMX 300 spectrometer at 75.40 MHz using 7-mm o.d. zirconia rotors and the standard Bruker CPTOSS or CP_2LEV pulse programs at 3 and 4 kHz spinning speeds, a contact time of 1 ms and a recycle delay of 5 s; linewidths varied between 100 and 200 Hz, and chemical shifts are referred to glycine (δ = 176.3 ppm). ^{1}H and ^{13}C NMR spectra in solution were recorded at room temperature with a Bruker AMX 300 operating at 300.14 and 75.40 MHz, respectively, by using 5-mm o.d. tubes; chemical shifts are reported relative to TMS using the solvent signal [δ(^{1}H) = 2.50 ppm; δ(^{13}C) = 39.5 ppm] as reference. ^{119}Sn NMR spectra were recorded at 186.50 MHz with a Bruker AMX 500 spectrometer by using 5-mm o.d. tubes and are reported relative to external neat $Sn(CH_3)_4$. Elemental analyses, mass, IR, Raman and NMR spectra and X-ray data were obtained at CACTUS, University of Santiago de Compostela.

Synthesis of [HMePN]I and MePN

[HMePN]I: This compound was prepared by a published procedure[23] as follows. Methyl iodide (8 mL) was added to a solution of pyridoxine (0.52 g, 3.1 mmol) in benzene/ethanol (12:1, v/v, 260 mL). The resultant solution was refluxed overnight, affording small crystals, and then concentrated to one-third of its volume; the crystals formed were filtered off, washed with diethyl ether to remove traces of hydriodic acid, and recrystallized from absolute ethanol as well-shaped single crystals. IR (Raman) : ν̃ [cm^{-1}] = 1644 w (1643 m), δ(OH); 1579 m (1583s), 1530 m (1525 w), 1460 vs (1461sh), ν(ring); 1064 s (1061 m), 1015 s (1015 w), ν(CO). ^{13}C CP MAS NMR (see **III** for numbering): δ = 152.5 [C(3)], 143.4 [C(2)], 134.5 [C(6)], 133.2 [C(4)], 131.9 [C(5)], 62.2 [C(7)], 58.4 [C(9)], 47.7 [C(10)], 15.8 [C(8)] ppm. ^{1}H NMR ([D$_6$]DMSO, TMS): δ = 8.43 [s, 1 H, C(6)−H], 5.65 [s, br, 1 H, O(3)−H], 4.80 [s, 2 H, C(9)−H], 4.68 [s, 2 H, C(7)−H], 4.23 [s, 3 H, C(10)−H], 2.59 [s, 3 H, C(8)−H] ppm. ^{13}C{^{1}H} NMR ([D$_6$]DMSO, TMS): δ = 152.6 [C(3)], 144.4 [C(2)], 139.7 [C(6)], 138.2 [C(4)], 134.9 [C(5)], 58.0 [C(7)], 56.5 [C(9)], 46.6 [C(10)], 13.8 [C(8)] ppm.

[MePN]: This compound was prepared from [HMePN]I by reaction with silver carbonate.[23] IR (Raman): ν̃ [cm^{-1}] = 1653 w, δ(OH); 1558 vs (1556 s), 1498 vs (1480 w), 1467 s (1453 m), ν(ring); 1066 m (1066 w), 1020 vs, ν(CO). ^{13}C CP MAS NMR: δ = 161.9 [C(3)], 146.9 [C(2)], 139.2 [C(6)], 134.3 [C(4)], 123.0 [C(5)], 58.4 [C(7)], 53.8 [C(9)], 44.7 [C(10)], 12.1 [C(8)] ppm. ^{1}H NMR ([D$_6$]DMSO, TMS): δ = 7.36 [s, 1 H, C(6)−H], 5.27 [t, ^3J = 5.2 Hz, 1 H, O(3)−H], 4.58 [s, 2 H, C(9)−H], 4.38 [d, 2 H, C(7)−H], 3.95 [s, 3 H, C(10)−H], 2.36 [s, 3 H, C(8)−H] ppm. ^{13}C{^{1}H} NMR ([D$_6$]DMSO, TMS): δ = 165.9 [C(3)], 142.0 [C(2)], 136.8 [C(6)], 134.6 [C(4)], 121.6 [C(5)], 58.8 [C(7)], 58.0 [C(9)], 45.0 [C(10)], 11.9 [C(8)] ppm.

Synthesis of the Complexes

[SnMe$_2$(MePN−H)]I (1): Methyl iodide (8 mL) and solid dimethyltin(IV) oxide (0.51 g, 3.1 mmol) were added to a solution of pyridoxine (0.52 g, 3.1 mmol) in toluene/ethanol (3:1, v/v, 200 mL) and the mixture was refluxed for 24 h. Water was then removed by azeotropic distillation in a Dean−Stark funnel, and the resultant yellow solid was filtered off, washed with diethyl ether and vacuum-dried. Yield 96% (1.36 g). $C_{11}H_{18}INO_3Sn$ (457.9): calcd. C 28.8, H 4.0, N 3.1; found C 28.9, H 4.2, N 3.0. M.p. 205 °C. Λ_M = 57.2 S cm^2 mol^{-1}. The main signals of metallated species in the EI spectrum are at *m*/*z* (%) = 302 (4.1) [Sn(MePN−H)], 150 (30.8) [SnMe$_2$], 135 (28.8) [SnMe] and 120 (46.9) [Sn]. In addition, the EI spectrum shows signals for pyridoxine and its fragments, and the FAB spectrum exhibits signals at *m*/*z* (%) = 664 (43.1) [SnMe$_2$(MePN−H)]$_2$, 332 (100) [SnMe$_2$(MePN−H)] and 302 (10.0) [Sn(MePN−H)]. IR (Raman): ν̃ [cm^{-1}] = 1619 w (1618 w), δ(OH); 1568 m (1568s), 1498 m (1483 w), 1451 s (1450 m), ν(ring); 1067s, 1017 m (1017 w), ν(CO); 587 sh (587 w), ν_{asym}(Sn−C); 518 w (528vs), ν_{sym}(Sn−C); 467 m (461 w), 427 m (425 w), ν(Sn−O). Mössbauer: I.S. = 1.37, Q.S. = 3.20, Γ = 0.92 mm·s^{-1}, $A_{2/1}$ = 1.00. ^{13}C CP MAS NMR: δ = 159.0 [C(3)], 149.0 [C(2)], 143.6 [C(4)], 132.8 [C(6)], 132.8 [C(5)], 60.7 [C(7)], 57.4 [C(9)], 48.4 [C(10)], 16.5 [C(8)], 5.6, 1.8 [C−Sn] ppm. ^{1}H NMR ([D$_6$]DMSO, TMS): δ = 8.05 [s, 1 H, C(6)−H], 5.53 [t, ^3J = 5.2 Hz, 1 H, O(3)−H], 4.89 [s, ^3J(^{1}H-^{119}Sn) = 60.6 Hz, 2 H, C(9)−H], 4.55 [d, ^3J = 5.2 Hz, 2 H, C(7)−H], 4.11 [s, 3 H, C(10)−H], 2.49 [s, 3 H, C(8)−H], 0.58 [s, ^2J(^{1}H-$^{119/117}$Sn) = 87.0/84.4 Hz, 6 H, CH_3−Sn] ppm. ^{13}C{^{1}H} NMR ([D$_6$]DMSO, TMS): δ = 158.9 [C(3)], 145.1 [C(2)], 142.4 [C(4)], 134.9 [C(6)], 130.8 [C(5)], 58.6 [C(7)], 57.9 [C(9)], 45.7 [C(10)], 12.6 [C(8)], 6.1 [^1J(^{13}C-^{119}Sn) = 780.5 Hz, (C−Sn)] ppm. ^{119}Sn NMR {[D$_6$]DMSO, $Sn(CH_3)_4$}: δ = −170.2 ppm. Crystals suitable for X-ray study were obtained by crystallization from methanol.

[SnEt$_2$(MePN−H)]I (2): Methyl iodide (8 mL) and solid diethyltin(IV) oxide (0.59 g, 3.1 mmol) were added to a solution of pyridoxine (0.52 g, 3.1 mmol) in toluene/ethanol (3:1, v/v, 200 mL). After refluxing for 24 h, water was removed by azeotropic distillation in a Dean−Stark funnel and the resultant yellow solid was filtered off and vacuum-dried. Yield 97% (1.46 g). $C_{13}H_{22}INO_3Sn$ (485.9): calcd. C 32.1, H 2.9, N 4.5; found C 32.4, H 2.8, N 4.5. M.p. 239 °C. Λ_M = 73.8 S cm^2 mol^{-1}. The main signals of metallated species in the EI spectrum are at *m*/*z* (%) = 302 (71.5) [Sn(MePN−H)], 178 (10.0) [SnEt$_2$], 149 (36.6) [SnEt] and 120 (30.1) [Sn]. Also, the EI spectrum shows signals for pyridoxine and its fragments, and the FAB spectrum has signals at *m*/*z* (%) = 720 (26.6) [SnEt$_2$(MePN−H)]$_2$, 360 (100) [SnEt$_2$(MePN−H)] and 302 (18.3) [Sn(MePN−H)]. IR (Raman): ν̃ [cm^{-1}] = 1619 w (1618 w), δ(OH); 1564 m (1568s), 1501 w (1500 w), 1455 s (1456 m), ν(ring); 1068 s (1064 w), 1029 m (1033 w), ν(CO); 541 m (545 w), ν_{asym}(Sn−C); 500 w (502 vs), ν_{sym}(Sn−C); 462 m (456 w), 435 m (428 w), ν(Sn−O). Mössbauer: I.S. = 1.49, Q.S. = 3.21, Γ = 0.85 mm·s^{-1}, $A_{2/1}$ = 1.08. ^{13}C CP MAS NMR: δ = 158.9 [C(3)], 147.1 [C(2)], 141.8 [C(4)], 133.9 [C(6)], 133.9 [C(5)], 54.1 [C(7)], 54.1 [C(9)], 46.5 [C(10)], 14.0 [C(8)], 9.7 [C(α)−Sn] ppm. ^{1}H NMR ([D$_6$]DMSO, TMS): δ = 8.07 [s, 1 H, C(6)−H], 5.53 [t, ^3J = 5.2 Hz, 1 H, O(3)−H], 4.91 [s, ^3J(^{1}H-^{119}Sn) = 47.7 Hz, 2 H, C(9)−H], 4.55 [d, ^3J = 5.1 Hz, 2 H, C(7)−H], 4.13 [s, 3 H, C(10)−H], 2.53 [s, 3 H, C(8)−H], 1.29 [m, 4 H, CH(α)−Sn], 1.16 [t, ^3J(^{1}H-$^{119/117}$Sn) = 135.0/128.5 Hz, 6 H, CH(β)−Sn] ppm. ^{13}C{^{1}H} NMR ([D$_6$]DMSO, TMS): δ = 159.3 [C(3)], 144.5 [C(2)], 142.0 [C(4)], 134.7 [C(6)], 130.2 [C(5)], 59.5 [C(7)], 57.7 [C(9)], 45.4 [C(10)], 17.7 [C(β)−Sn], 12.2 [C(8)], 9.6 [C(α)−Sn] ppm. ^{119}Sn NMR {[D$_6$]DMSO, $Sn(CH_3)_4$}: δ = −209.5

 © 2003 Wiley-VCH Verlag GmbH & Co. KGaA, Weinheim

ppm. Crystallization from methanol afforded crystals of **2**·2H_2O which were used for X-ray analysis.

[$SnBu_2$(MePN−H)]I (3): Methyl iodide (8 mL) and solid dibutyltin(IV) oxide (0.77 g, 3.1 mmol) were added to a solution of pyridoxine (0.52 g, 3.1 mmol) in toluene/ethanol (3:1, v/v, 200 mL). After refluxing for 24 h, water was removed by azeotropic distillation in a Dean−Stark funnel and the obtained yellow solid was filtered off and vacuum-dried. Yield 98% (1.65 g). $C_{17}H_{30}INO_3Sn$ (542.0): calcd. C 37.7, H 5.6, N 2.6; found C 38.1, H 5.9, N 2.6. M.p. 220 °C. Λ_M = 83.5 S cm^2 mol^{-1}. The main signals of metallated species in the EI spectrum are at *m*/*z* (%) = 302 (12.1) [Sn(MePN−H)], 177 (30.3) [SnBu] and 120 (42.9) [Sn]. Also, the EI spectrum shows signals for pyridoxine and its fragments, and the FAB spectrum exhibits signals at *m*/*z* (%) = 416 (100) [$SnBu_2$(MePN−H)] and 302 (12.1) [Sn(MePN−H)]. IR (Raman): $\tilde{\nu}$ [cm^{-1}] = 1613 w (1612 w), δ(OH); 1565 m (1562 m), 1500 m (1500 w), 1451 s (1443 w), ν(ring); 1063 m (1063 w), 1027 vs (1020 w), ν(CO); 570 m (573 m), ν_{sym}(Sn−C); 461 m, 442 m (450 w), ν(Sn−O). Mössbauer: I.S. = 1.58, Q.S. = 3.49, Γ = 0.77 mm·s^{-1}, $A_{2/1}$ = 1.12. ^{13}C CP MAS NMR: δ = 160.4 [C(3)], 148.2 [C(2)], 140.4 [C(4)], 134.2 [C(6)], 134.0 [C(5)], 61.6 [C(7)], 53.4 [C(9)], 49.1 [C(10)], 14.0 [C(8)], 25.6, 24.3 [C(α)−Sn], 34.4 [C(β)−Sn], 30.1, 28.8 [C(γ)−Sn], 12.8, 11.2 [C(δ)−Sn] ppm. ^{1}H NMR ([D_6]DMSO, TMS): δ = 8.07 [s, 1 H, C(6)−H], 5.54 [t, *J* = 5.0 Hz, 1 H, O(3)−H], 4.92 [s, ^3J(^{1}H-^{119}Sn) = 56.8 Hz, 2 H, C(9)−H], 4.55 [d, *J* = 5.2 Hz, 2 H, C(7)−H], 4.13 [s, 3 H, C(10)−H], 2.51 [s, 3 H, C(8)−H], 1.30 [t, 4 H, CH(α)−Sn], 1.54 [q, ^2J(^{1}H-^{119}Sn) = 85.7 Hz, 4 H, CH(β)−Sn], 1.29 [m, ^3J(^{1}H-^{119}Sn) = 93.0 Hz, 4 H, CH(γ)−Sn], 0.82 [t, 6 H, CH(δ)−Sn] ppm. ^{13}C{^{1}H} NMR ([D_6]DMSO, TMS): δ = 159.3 [C(3)], 144.5 [C(2)], 142.5 [C(4)], 135.0 [C(6)], 130.5 [C(5)], 60.0 [C(7)], 57.8 [C(9)], 45.7 [C(10)], 12.4 [C(8)], 23.9, ^1J(^{13}C-^{119}Sn) = 660.0 Hz, [C(α)−Sn], 26.9 [C(β)−Sn], 25.9 [C(γ)−Sn], 13.5 [C(δ)−Sn] ppm. ^{119}Sn NMR {[D_6]DMSO, $Sn(CH_3)_4$}: δ = −190.9 ppm.

[$SnPh_2$(MePN−H)]I·H_2O (4): Methyl iodide (8 mL) and solid diphenyltin oxide (0.90 g, 3.1 mmol) were added to a solution of pyridoxine (0.52 g, 3.1 mmol) in toluene/ethanol (3:1, v/v, 200 mL). After refluxing for 24 h, water was removed by azeotropic distillation in a Dean−Stark funnel and the resultant yellow solid was filtered off and vacuum-dried. Yield 90% (1.67 g). $C_{21}H_{22}INO_3Sn·H_2O$ (600.0): calcd. C 42.0, H 4.0, N 2.3; found C 41.6, H 4.1, N 2.6. M.p. > 250 °C. Λ_M = 70.8 S cm^2 mol^{-1}. The main signals of metallated species in the EI spectrum are at *m*/*z* (%) = 348 (72.6) [SnPh(PN−2H)], 197 (71.4) [SnPh] and 120 (55.8) [Sn]. Also, the EI spectrum shows signals for pyridoxine and its fragments, and the FAB spectrum shows signals at *m*/*z* (%) = 455 (8.8) [$SnPh_2$(MePN−H)], 302 (100) [Sn(MePN−H)], 286 (5.7) [Sn(PN−2H)], 274 (5.4) [$SnPh_2$], 197 (24.8) [SnPh] and 120 (12.2) [Sn]. IR (Raman): $\tilde{\nu}$ [cm^{-1}] = 3333 br, ν(OH); 1614 w (1614 w), δ(OH); 1562 w (1576 m), 1493 w, 1479 w (1477 w), 1450 s (1447 w), ν(ring); 1020 m (1022 m), 997 m (998 vs), ν(CO); 443 w (444 w), ν(Sn−O); 270 m (270 w), ν_{asym}(Sn−C); 233 m (230 w), ν_{sym}(Sn−C). Mössbauer: I.S. = 1.44, Q.S. = 2.87, Γ = 0.83 mm·s^{-1}, $A_{2/1}$ = 1.09. ^{1}H NMR ([D_6]DMSO, TMS): δ = 7.99 [s, 1 H, C(6)−H], 5.50 [s, br, 1 H, O(3)−H], 4.81 [s, 2 H, C(9)−H], 4.51 [s, br, 2 H, C(7)−H], 4.10 [s, 3 H, C(10)−H], 2.50 [s, 3 H, C(8)−H], 7.79 [d, ^3J = 7.3 Hz, 4 H, CH_o−Sn], 7.57 [s, 4 H, CH_m−Sn], 7.55 [s, 2 H, CH_p−Sn] ppm. ^{13}C{^{1}H} NMR ([D_6]DMSO, TMS): δ = 159.9 [C(3)], 140.0 [C(2)], (not observed) [C(4)], 135.1 [C(6)], 128.3

Table 2. Crystal data, data collection and structure refinement parameters

	[HMePN]I	**1**	**2**·H_2O	**3**
Empirical formula	$C_9H_{14}INO_3$	$C_{22}H_{36}I_2N_2O_6Sn_2$	$C_{26}H_{52}I_2N_2O_{10}Sn_2$	$C_{34}H_{60}I_2N_2O_6Sn_2$
Formula mass	311.11	915.71	1043.88	1084.02
Wavelength [Å]	1.54184	0.71073	0.71073	0.71073
Crystal system	monoclinic	monoclinic	monoclinic	tetragonal
Space group	$P2_1/n$ (no. 14)	$P2_1/c$ (no. 14)	$P2_1/c$ (no.14)	$I4_1/a$ (no. 88)
Unit-cell dimensions				
a [Å]	6.6014(6)	6.8596(8)	9.5030(12)	27.298(7)
b [Å]	11.4994(10)	12.136(2)	13.5203(10)	27.298(7)
c [Å]	14.9980(17)	18.833(8)	15.465(2)	11.738(4)
β [°]	98.129(12)	93.709(11)	107.651(14)	
V [Å^3]	1127.09(19)	1564.6(8)	1893.4(4)	8747(4)
Z	4	2	2	8
$D_{calcd.}$ [Mg·m^{-3}]	1.833	1.944	1.831	1.646
F(000)	608	872	1016	4256
μ [mm^{-1}]	22.218	3.604	2.997	2.592
Crystal size [mm]	0.25 × 0.25 × 0.15	0.25 × 0.15 × 0.10	0.20 × 0.20 × 0.20	0.35 × 0.25 × 0.10
θ range for data collection [°]	4.86−74.26	3.36−26.18	2.25−26.29	2.11−28.44
θ range (25 reflect.) [°]	14.377 < θ <42.678	9.327 < θ < 20.876	8.674 < θ < 18.086	11.882 < θ < 12.563
Index ranges	$0 \le h \le 8$	$0 \le h \le 8$	$0 \le h \le 11$	$-36 \le h \le 0$
	$-14 \le k \le 14$	$-15 \le k \le 0$	$0 \le k \le 16$	$0 \le k \le 36$
	$-18 \le l \le 18$	$-23 \le l \le 23$	$-19 \le l \le 18$	$-15 \le l \le 0$
Reflections collected	4884	3406	4072	5730
Unique reflections	2305 (R_{int} = 0.0523)	3138 (R_{int} = 0.0948)	3839 (R_{int} = 0.0283)	5503 (R_{int} = 0.0757)
Absorption correction	ψ-scan	ψ-scan	ψ-scan	ψ-scan
Max., min. transmission	0.983, 0.569	0.946, 0.790	0.975, 0.947	0.980, 0.895
Data, restraints, parameters	2305, 0, 129	3138, 0, 154	3839, 0, 264	5503, 0, 208
Goodness of fit on F^2	1.007	0.890	1.014	0.970
Final *R* indices [$I > 2\sigma(I)$]	R_1 = 0.0675, wR_2 = 0.1812	R_1 = 0.0815, wR_2 = 0.1302	R_1 = 0.0380, wR_2 = 0.0850	R_1 = 0.0514, wR_2 = 0.1205
R indices (all data)	R_1 = 0.0863, wR_2 = 0.1998	R_1 = 0.2561, wR_2 = 0.1721	R_1 = 0.0897, wR_2 = 0.0981	R_1 = 0.1957, wR_2 = 0.1558
Largest peak, hole difference [e·Å^{-3}]	2.273, −1.862	0.947, −1.14 0	1.373, −0.932	1.264, −1.153

 © 2003 Wiley-VCH Verlag GmbH & Co. KGaA, Weinheim

[C(5)], 59.6 [C(7)], 57.9 [C(9)], 45.5 [C(10)], 12.4 [C(8)], 144.2 (C_i−Sn), 136.0 (^2J = 46.8 Hz, C_o−Sn), 130.2 (C_m−Sn), 129.1 (C_p−Sn) ppm. ^{119}Sn NMR {[D_6]DMSO, $Sn(CH_3)_4$}: δ = −233.5 ppm.

Crystal Structure Determination

X-ray Data Collection and Reduction: Crystals were mounted on glass fibres for data collection with Enraf−Nonius automatic diffractometers (a CAD4 for [HMePN]I and a MACH3 for **1**, **2**·2H_2O and **3**).[24] Cell constants and an orientation matrix for data collection were calculated by least-squares refinement of the diffraction data for 25 reflections. Data were collected at 293 K by the ω-scan technique using Cu-K_α radiation (λ= 1.54184 Å) for [HMePN]I and Mo-K_α radiation (λ= 0.71073 Å) for **1**, **2**·2H_2O and **3**, and were corrected for Lorentz and polarization effects.[25] Semiempirical absorption corrections (ψ-scan) were also made.[26]

Structure Solution and Refinement: The structure was solved by direct methods[27] and subsequent Fourier maps, and was refined on F^2 by a full-matrix least-squares procedure using anisotropic displacement parameters.[28] Hydrogen atoms were placed at calculated positions (C−H 0.93−0.97 Å) and refined using a riding model. Atomic scattering factors were taken from ref.[29] Molecular graphics were generated with PLATON.[30] The crystal data, experimental details and refinement results are summarized in Table 2.

CCDC-187692 for [HMePN]I, -187693 for [$SnMe_2$(MePN−H)]I, -187694 for [$SnEt_2$(MePN−H)]I·2H_2O and -187695 for [$SnBu_2$(MePN−H)]I contain the supplementary crystallographic data for this paper. These data can be obtained free of charge at www.ccdc.cam.ac.uk/conts/retrieving.html [or from the Cambridge Crystallographic Data Centre, 12 Union Road, Cambridge CB2 1EZ, UK; Fax: (internat.) + 44-1223/336-033; E-mail: deposit@ccdc.cam.ac.uk].

Acknowledgments

We thank the Xunta de Galicia, Spain, for financial support under Project XUGA 20316 B94. F. C. thanks the Spanish Agency for International Cooperation and the University of Santiago de Compostela for grants.

[1] J. S. Casas, M. V. Castaño, M. S. García-Tasende, T. Perez Alvarez, A. Sánchez, J. Sordo, *J. Inorg. Biochem.* **1996**, *61*, 97.
[2] [2a] J. S. Casas, A. Castiñeiras, M. D. Couce, G. Martinez, J. Sordo, J. M. Varela, *J. Organomet. Chem.* **1996**, *517*, 165. [2b] J. S. Casas, E. E. Castellano, M. D. Couce, M. S. García-Tasende, A. Sánchez, J. Sordo, C. Taboada, E. M. Vázquez-López, *Inorg. Chem.* **2001**, *40*, 946.
[3] J. S. Casas, E. E. Castellano, F. Condori, M. D. Couce, A. Sánchez, J. Sordo, J. M. Varela, J. Zuckerman-Schpector, *J. Chem. Soc., Dalton Trans.* **1997**, 4421.
[4] J. S. Casas, A. Castiñeiras, F. Condori, M. D. Couce, U. Russo, A. Sánchez, J. Sordo, J. M. Varela, *Polyhedron* **2000**, *19*, 813.
[5] W. Korytnyk, in *Vitamin B_6 Pyridoxal Phosphate* (Eds.: D. Dolphin, P. Pouloon, O. Avramovich), Wiley, New York, **1986**, part A, p.371.
[6] K. Wada, S. Ishigaki, K. Veda, J. Take, K. Sasaki, M. Sakata, M. Haga, *Chem. Pharm. Bull.* **1988**, *36*, 1779.
[7] [7a] M. Gielen, R. Willem, T. Mancilla, J. Ramharter, E. Joosen, *Silicon, Germanium, Tin Lead Compd.* **1986**, *9*, 349. [7b] F. Kayser, M. Biesemans, M. Gielen, R. Willlem, *Main Group Met. Chem.* **1994**, *17*, 559. [7c] F. Kayser, M. Biesemans, M. Gielen, R. Willem, *Magn. Res. Chem.* **1994**, *32*, 358.
[8] J. Longo, K. J. Franklin, M. F. Richardson, *Acta Crystallogr., Sect. B* **1982**, *38*, 2721.
[9] G. E. Bacon, J. S. Plant, *Acta Crystallogr., Sect. B* **1980**, *36*, 1130.
[10] A. W. Addison, T. N. Rao, J. Reedijk, J. Van Rijn, G. C. Verschoov, *J. Chem. Soc., Dalton Trans.* **1984**, 1349.
[11] J. E. Huheey, E. A. Keiter, R. L. Keiter, *Inorganic Chemistry. Principles of Structure and Reactivity*, 4th ed., Harper Collins College Publishers, New York, **1993**, p. 292.
[12] C. E. Holloway, M. Melnik, *Main Group Met. Chem.* **2000**, *23*, 331.
[13] N. A. Drobinskaya, L. V. Inova, M. Ya Karpeiskii, V. L. Florent'er, *Chem. Heterocycl. Compd. (Engl. Trans.)* **1973**, *7*, 330.
[14] H. L. Sing, A. K Varshney, *Main Group Met. Chem.* **1999**, *22*, 529.
[15] R. V. Parish, "Structure and Bonding in Tin Compounds", in G. L. Long (Ed.) *Mössbauer Spectroscopy Applied to Inorganic Chemistry*, Plenum, New York, **1984**.
[16] T. P. Lockhart, W. F. Manders, *Inorg. Chem.* **1986**, *25*, 892.
[17] C. Pettinari, F. Marchetti, A. Cingolani, A. Gindulyte, L. Massa, M. Rossi, F. Caruso, *Eur. J. Inorg. Chem.* **2001**, 2171.
[18] T. P. Lockhart, W. F. Manders, *J. Am. Chem. Soc.* **1987**, *109*, 7015.
[19] J. Holecek, A. Lycka, *Inorg. Chim. Acta* **1986**, *118*, L15.
[20] R. K. Harris, J. D. Kennedy, W. McFarlane, in R. K. Harris, B. E. Mann (Eds.), *NMR and the Periodic Table*, Academic Press, London, **1978**, p. 342.
[21] J. Otera, *J. Organomet. Chem.* **1981**, *221*, 57.
[22] J. Holecek, M. Nádvorník, K. Handlír, A. Lycka, *J. Organomet. Chem.* **1986**, *315*, 299.
[23] S. A. Harris, T. J. Webb, K. Folkers, *J. Am. Chem. Soc.* **1940**, *62*, 3198.
[24] B. V. Nonius, *CAD4-Express Software*, version 5.1/1.2, Enraf−Nonius, Delft, The Netherlands, **1994**.
[25] M. Kretschmar, *GENHKL, Program for the reduction of CAD4 diffractometer data*, University of Tübingen, Germany, **1997**.
[26] A. C. T. North, D. C. Phillips, F. S. Mathews, *Acta Crystallogr., Sect. A* **1968**, *24*, 351.
[27] G. M. Sheldrick, *Acta Crystallogr., Sect. A* **1990**, *46*, 467.
[28] G. M. Sheldrick, *SHELXL-97, Program for the refinement of crystal structures*, University of Göttingen, Germany, **1997**.
[29] *International tables for crystallography*, Kluwer Academic Publishers, Dordrecht, The Netherlands, **1995**, vol. C.
[30] A. L. Spek, *PLATON, A Multipurpose Crystallographic Tool*, University of Utrecht, The Netherlands, **1997**.

Received November 15, 2002

 © 2003 Wiley-VCH Verlag GmbH & Co. KGaA, Weinheim

Designing Ionic Liquids: 1-Butyl-3-Methylimidazolium Cations with Substituted Tetraphenylborate Counterions

Joep van den Broeke,[a] Marjolijn Stam,[a] Martin Lutz,[b] Huub Kooijman,[b] Anthony L. Spek,[b] Berth-Jan Deelman,*[c] and Gerard van Koten[a]

Keywords: Ionic liquids / Cations / Anions / X-ray diffraction / Hydrogen bonds

The hydrophobic, low melting, 1-butyl-3-methylimidazolium (BMIm) salts [BMIm][BPh_4] (**1**), [BMIm][$B(C_6H_4Me\text{-}4)_4$] (**2**), [BMIm][$B\{C_6H_4(CF_3)\text{-}4\}_4$] (**3**), [BMIm][$B\{C_6H_3(CF_3)_2\text{-}3,5\}_4$] (**4**), [BMIm][$B\{C_6H_4(C_6F_{13})\text{-}4\}_4$] (**5**), [BMIm][$B\{C_6H_4(SiMe_3)\text{-}4\}_4$] (**6**), [BMIm][$B(C_6H_4\{SiMe_2(CH_2CH_2CF_3)\}\text{-}4)_4$] (**7**), [BMIm][$B\{C_6H_4(SiMe_2C_8H_{17}\text{-}4\}_4$] (**8**) and [BMIm]-[$B(C_6H_4\{SiMe_2(CH_2CH_2C_6F_{13})\}\text{-}4)_4$] (**9**) have been prepared. Systematic variation of the substituents on the tetraphenylborate anion allowed an assessment of their influence on the physical properties of the imidazolium salts. Structural investigations using NMR and IR spectroscopy, combined with single crystal X-ray structure determinations for **2**, **3**, **5** and **6**, revealed hydrogen-bonding interactions between the imidazolium ring protons and the borate anion, both in the solid state and in solution. These interactions are weakened upon the introduction of electron-withdrawing substituents in the anion and follow the order 3,5-$(CF_3)_2$ < $-C_6F_{13}$ < $-CF_3$ < $-SiMe_2CH_2CH_2C_6F_{13}$ < $-SiMe_2CH_2CH_2CF_3$ < $-H$ < $-Me$ < $-SiMe_3$. The melting points of the salts depend primarily on the bulk of the lipophilic substituents, and decrease with increasing size. Bulky lipophilic substituents dramatically enhance the solubility of the imidazolium borates **8** and **9** in hexane and reduce their relative polarity. These unique properties make imidazolium borates **8** and **9** interesting as amphiphilic ionic liquids with low polarity. Attempts to crystallise **7** resulted in decomposition. A single-crystal X-ray structure determination of the product, isolated in 6% yield, showed that a carbene–tris[4-{dimethyl(3,3,3-trifluoropropyl)silyl}phenyl]borane adduct was formed.

(© Wiley-VCH Verlag GmbH & Co. KGaA, 69451 Weinheim, Germany, 2003)

Introduction

The extremely low vapour pressure[1] of room-temperature ionic liquids (ILs) based on *N*,*N*-dialkylimidazolium cations and weakly coordinating anions (Scheme 1) makes them an interesting alternative to highly volatile organic solvents, such as CH_2Cl_2, that cause environmental concern and are subject to ever more stringent regulations.[2] The

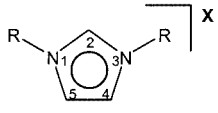

X^- = *e.g.* $AlCl_4^-$, BF_4^-, PF_6^-, $CF_3SO_3^-$

Scheme 1

miscibility of ILs with other solvents can also be controlled, through a careful choice of the ions,[3] making them attractive as easily containable solvents. Especially noteworthy is their use as a polar phase in biphasic solvent systems, which is of interest for catalyst recycling. In such a system, the advantages of both homogeneous and heterogeneous catalysis, good catalyst efficiency under mild reaction conditions and facile catalyst recovery, respectively, can be combined.[1]

The physical properties, and chemical and physical stability of an IL govern its suitability as a reaction medium. The potential of ILs as solvents for catalysis was first demonstrated with the discovery of 1-ethyl-3-methylimidazolium tetrafluoroborate,[4] which combines the favourable properties of a liquid salt with high air and water stability. Subsequently, a broad range of cation-anion combinations has been developed,[5] and their chemical and physical properties,[5,6] as well as their application as solvents in catalysis, examined[1,7] These studies focussed on varying the alkyl substitution pattern on the imidazolium ring, while the anions employed have predominantly remained limited to inorganic or small organic anions such as BF_4^-, PF_6^-, SbF_6^-, NO_2^-, $CF_3SO_3^-$, $[N(CN)_2]^-$ and $[N(SO_2CF_3)_2]^-$.[1,5a,6a] The incorporation of large and lipo-

[a] Department of Metal-Mediated Synthesis, Debye Institute, Utrecht University,
Padualaan 8, 3584 CH Utrecht, The Netherlands
[b] Department of Crystal and Structural Chemistry, Bijvoet Center for Biomolecular Research, Utrecht University,
Padualaan 8, 3584 CH Utrecht, The Netherlands
[c] ATOFINA Vlissingen B.V.,
P. O. Box 70, 4380 AB Vlissingen, The Netherlands

philic organic anions is virtually unexplored,[5a,7e,8] even though anions such as tetraphenylborates[9] and carboranes[10] efficiently delocalise their negative charge, resulting in a very low coordinating strength. The interaction of the anions, and to a lesser extent the cation, with solvent or substrate molecules plays a major role in determining the (im)miscibility of an IL with other liquids.[11] Large organic anions permit a broad range of substituents, which could allow the facile tailoring of an ionic liquid. In a first example of this approach[12] we showed that $-SiMe_2(CH_2CH_2C_6F_{13})$ substituents produced an imidazolium salt, [BMIm][$B(C_6H_4\{SiMe_2(CH_2CH_2C_6F_{13})\}\text{-}4)_4$] (**9**), that is highly miscible with apolar solvents. Furthermore, **9** displayed phase behaviour similar to perfluorinated solvents when combined with apolar organic solvents. This facilitated efficient catalyst recycling by biphasic separation following a reaction under homogeneous conditions[12] – a unique feature for ionic liquids.

After this initial demonstration a more systematic study of the effects of a range of alkyl-, perfluoroalkyl- and silyl-substituted tetraarylborates on the physical properties of the corresponding $[BMIm]^+$-salts was performed.

Results and Discussion

Synthesis: A series of 1-butyl-3-methylimidazolium salts of tetraphenylborate and alkyl-, perfluoroalkyl- and silyl-substituted derivatives thereof was prepared by metathesis of the sodium borates with dialkylimidazolium halides (Scheme 2). All imidazolium salts were purified by washing a solution in CH_2Cl_2 or toluene with demineralised water, followed by removal of residual water with $MgSO_4$ and subsequent drying of the IL in vacuo.

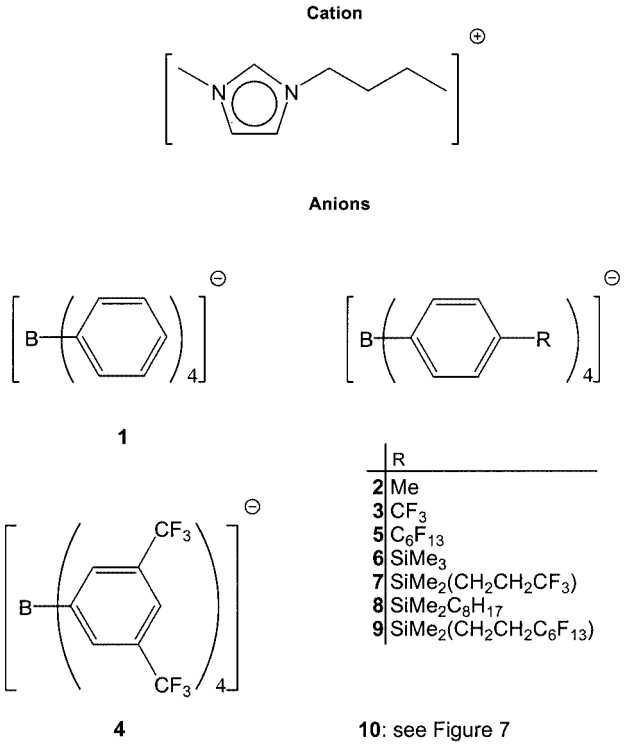

Scheme 2

The resulting compounds were characterised by ^1H, $^{13}C\{^1H\}$ and $^{11}B\{^1H\}$ NMR spectroscopy, IR spectroscopy and elemental analysis, and found to be pure. Furthermore, for **4**, **5**, **7** and the previously communicated **9**,[12] elemental analyses found no evidence of contamination by trace amounts of chloride or iodide. The remaining compounds were not analysed for halide ions. As the synthetic and workup procedures were identical, they were presumed to be halogen free at the level detectable by elemental analysis. The salts **2**–**9** are not hygroscopic, are stable in air, and are insoluble in water. Crystals suitable for single-crystal X-ray structure determination were obtained for **2**, **3**, **5** and **6**. Single crystals of **2**, **3** and **5** were grown by slow diffusion of hexane into CH_2Cl_2 solutions of these imidazolium salts. Crystals of **6** were obtained by slow evaporation of acetone from a concentrated solution. The molecular structures of **2** (Figure 1), **3** (Figure 2), **5** (Figure 3) and **6** (Figure 4) are

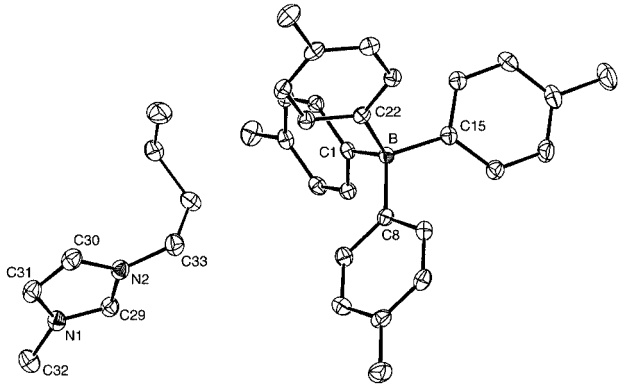

Figure 1. ORTEP drawing of the molecular structure of **2**, with ellipsoids at the 50% probability level. Hydrogen atoms are omitted for clarity

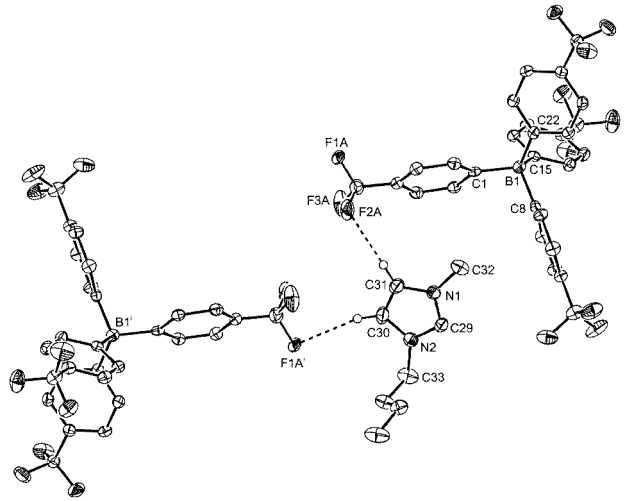

Figure 2. ORTEP drawing of the molecular structure of **3** showing hydrogen bonding between cations and anions. Ellipsoids are shown at the 50% probability level. Hydrogen atoms, except for those participating in hydrogen-bonding interactions, are omitted for clarity

 © 2003 Wiley-VCH Verlag GmbH & Co. KGaA, Weinheim

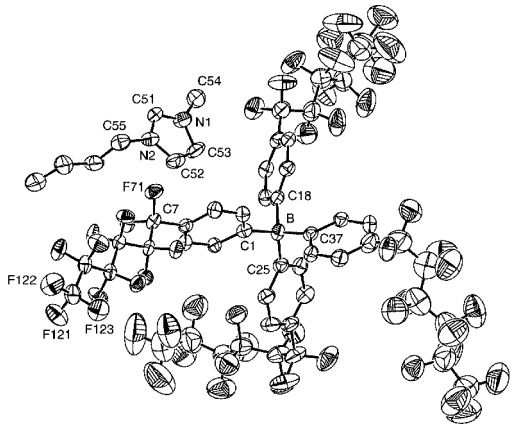

Figure 3. ORTEP drawing of the molecular structure of **5**, with ellipsoids at the 50% probability level. Hydrogen atoms are omitted for clarity

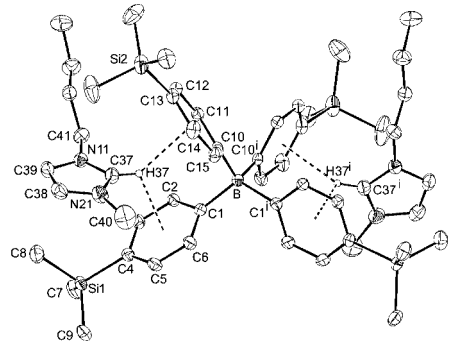

Figure 4. ORTEP drawing of the unit cell of **6**, with ellipsoids at the 30% probability level. Hydrogen atoms, except for those participating in hydrogen-bonding interactions, are omitted for clarity

represented; relevant bond angles and distances are collected in Table 1.

The 1-butyl-3-methylimidazolium cation, common to all four structures, shows little variation in bond lengths and angles for each compound, having a planar pentagonal imidazolium ring that contains two pairs of C−N bonds, with C(2)−N bonds (1.32−1.33 Å) that are shorter than the C(4)−N and C(5)−N bonds (1.37−1.40 Å). Although the precision of the bond lengths in **6** and especially in **5** is poor due to the considerable structural disorder, they are similar to those of **2** and **3**. The configuration of the imidazolium ring is identical to those observed in related structures, such as [BMIm][BPh_4],[8] [EMIm][$CB_{11}H_{(12-n)}X_n$] (X = Cl, Br, I, n = 0, 1),[13] [OMIm][$CB_{11}H_6Cl_6$],[13] and [EMIm]X (X = Br, I, $AlBr_4$)[14] [N−C(2) 1.29−1.33 Å, N−C(4) and N−C(5) 1.35−1.38 Å, N−C(2)−N 108−109°], showing that the ring's internal dimensions are largely insensitive to its environment. The orientation of the butyl substituent relative to the imidazolium ring differs with each anion due to packing effects in the respective crystal lattices.

The anions all consist of a tetraphenylborate core, with different *para* substituents. The bond lengths and angles show that substitution does not significantly affect the geometry around the boron atom, with all anions having a slightly distorted tetrahedral configuration with practically identical B−C distances (1.64−1.65 Å) and C−B−C angles (103−113°). These data correspond with that previously reported for the borate anions in [BMIm][BPh_4],[8] and [$(THF)_2$Na(18-crown-6)][B{$C_6H_4(SiMe_3)$-4}$_4$] and [Rh(dppe)$_2$][B{$C_6H_4(SiMe_3)$-4}$_4$][15] (B−C 1.64−1.72 Å, C−B−C 106−112°). Unfortunately, no molecular structures of complexes containing [$B(C_6H_4Me$-4)$_4$]$^-$, [B{$C_6H_4(CF_3)$-4}$_4$]$^-$ and [B{$C_6H_4(C_6F_{13})$-4}$_4$]$^-$ are available for comparison.

In the crystal lattice the ions in **2** and **3** form well-defined layers of cations and anions. In **2** the interlayer distances between hydrogen atoms on the imidazolium ring and the π-electron system of the phenyl groups of the anions are around 2.8 Å (Table 2), suggesting that the layers of cations

Table 1. Selected bond angles [°] and distances [Å] for **2**, **3**, **5** and **6**

[a]		**2**	**3**	**5**	**6**
	B−C(1)	1.6476(18)	1.645(3)	1.651(17)	1.641(4)
	B−C(8)	1.6422(18)	1.641(3)	1.650(17)	1.648(4)
	B−C(15)	1.6484(18)	1.647(3)	1.622(17)	1.646(4)
	B−C(22)	1.696(17)	1.647(3)	1.653(17)	1.645(4)
N(1)−C(2)	N(1)−C(29)	1.3270(17)	1.324(3)	1.327(16)	1.312(4)
N(1)−C(5)	N(1)−C(31)	1.3768(17)	1.370(3)	1.406(17)	1.376(4)
N(3)−C(2)	N(2)−C(29)	1.3325(17)	1.323(3)	1.310(16)	1.327(4)
N(3)−C(4)	N(2)−C(30)	1.3791(17)	1.374(3)	1.369(17)	1.365(4)
C(4)−C(5)	C(30)−C(31)	1.350(2)	1.343(3)	1.34(2)	1.333(5)
	C(1)−B−C(8)	103.59(9)	104.64(16)	105.2(9)	105.3(2)
	C(1)−B−C(15)	111.28(10)	112.89(16)	113.6(10)	111.5(2)
	C(1)−B−C(22)	109.85(9)	112.22(165	110.2(10)	111.7(2)
	C(8)−B−C(15)	113.30(10)	111.66(15)	112.7(10)	111.1(2)
	C(8)−B−C(22)	113.24(10)	111.95(16)	112.1(10)	113.1(2)
	C(15)−B−C(22)	105.67(9)	103.72(16)	103.2(9)	104.3(2)
	N(1)−C(29)−N(2)	108.57(11)	109.38(18)	109.7(10)	108.6(3)
	C(29)−N(1)−C(32)	125.51(12)	126.33(18)	126.1(11)	126.5(3)
	C(29)−N(2)−C(33)	125.24(11)	125.61(18)	124.4(10)	125.8(3)

[a] Atom numbers refer to atoms according to the numbering scheme used for **2** and **3** and to the equivalent atoms in **5** and **6**.

 © 2003 Wiley-VCH Verlag GmbH & Co. KGaA, Weinheim

and anions are inter-connected by weak hydrogen-bonding interactions (for a representative picture of this hydrogen-bonding pattern between layers, see Figure 5).[16,17] Similar behaviour has been reported for [BMIm][BPh_4].[8] In **3**, such layering of cations and anion was not observed. However, weak hydrogen bonding is present: The C(2)−*H* and C(4−*H* imidazolium protons are in close contact with the CF_3 groups of neighbouring anions (see Figure 2 and Table 2). Some of the inter-ionic H···F interactions may be unavoidable, due to steric congestion, but the H···F of F to C(4)−*H* (2.44 Å) clearly indicates weak hydrogen-bonding interactions.[18] The packing diagram of **6** did not reveal the separation of cations and anions into distinct layers. Nevertheless, the cations' orientation allows attractive interactions between C(2)−*H* and the π-systems of neighbouring phenyl rings (Figure 4). Their distance (2.65 Å) is similar to that for the C−H···π interactions in **2**, suggesting weak hydrogen bonding.

Table 2. Hydrogen−π interactions in the solid state of **2**, **5** and **6** and hydrogen−fluorine interactions in the solid state of **3**

	H···C_g [Å]	C···C_g [Å]	C−H···C_g [°]
2			
C(29)−H(29)···C_g5[a]	2.40	3.3506(13)	180
C(30)−H(30)···C_g3[b]	2.52	3.4076(16)	155
5			
C(51)−H(51)···C_g4[c]	3.08	3.233(13)	91
C(51)−H(51)···C_g5[c]	2.51	3.370(12)	155
C(52)−H(52)···C_g2	2.67	3.525(14)	153
C(53)−H(53)···C_g3	2.64	3.514(15)	157
6			
C(37)−H(37)···C_g4	2.81	3.340(3)	116
C(37)−H(37)···C_g6	2.65	3.331(3)	130
	H···F [Å]	C···F [Å]	C−H···F [°]
3			
C(30)−H(30)···F(1a)[d]	2.49	3.401(9)	161
C(31)−H(31)···F(2a)	2.44	3.378(6)	172

[a] $1-x, y+0.5, 0.5-z$. [b] $1-x, 1-y, 1-z$. [c] $-x$, 1-y, $z+0.5$. [d] $-x, 1-y, -z$. Note that the CF_3 group is rotationally disordered.

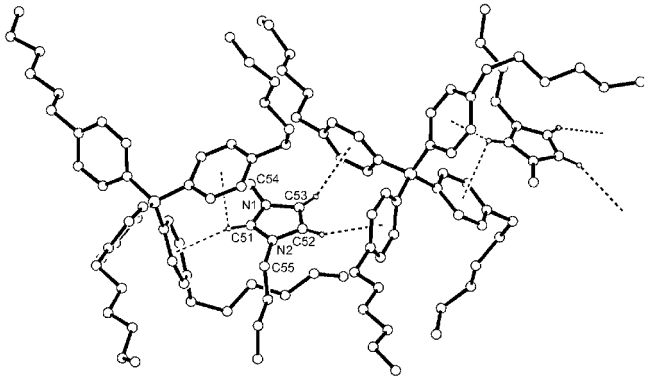

Figure 5. Representation of hydrogen bridging interactions in the crystal lattice of **5**. Hydrogen and fluorine atoms have been omitted for clarity

In the crystal lattice of fluorous borate salt **5**, an alternative ion ordering could be discerned. Instead of layers of cations and anions, a division into fluorous and non-fluorous regions is present (Figure 6). The perfluoroalkyl parts of the ions are assembled in fluorous regions, which alternate with non-fluorous layers that contain the organic and charged parts of the salts. In other words, the structure organises the imidazolium cations and the tetraarylborate cores of the anions into layers with the perfluoroalkyl groups pointing outwards (Figure 5). In these organic domains, the cations and anions form chains with each cation being connected to two anions through hydrogen···π interactions (Figure 5) and vice versa. Furthermore, the butyl substituents of the cation are also oriented towards the fluorous domains. Such layered structures are well known for perfluoroalkyl-substituted compounds,[19] and are related to the inability of the perfluoroalkyl groups to participate in stabilising interactions with other molecules. This lack of interaction excludes these substituents from the ionic organic layers, allowing optimum inter-ion interactions not involving the fluorous tails. The absence of interactions with neighbouring molecules is also reflected in the high disorder in the fluorous tails.

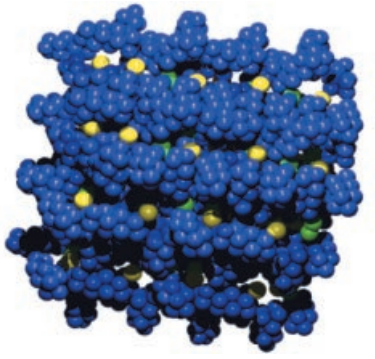

Figure 6. Packing diagram of **5** (F = blue, B = yellow, N = green, all other atoms are omitted for clarity)

During attempts to crystallise **7** from a saturated solution in warm MeOH/H_2O (v:v, 95:5), a crystalline material was isolated in low yield (6%). A single-crystal X-ray diffraction study of this material showed, unexpectedly, it to be a carbene−tris[4-{dimethyl(3,3,3-trifluoropropyl)-silyl}phenyl]borane adduct. The molecular structure **10** (formula see Figure 7) shows a carbene connected to the boron atom of a BAr_3 moiety through the C(2) carbon of the imidazolium ring, which has replaced the fourth phenyl group present in the original tetraarylborate anion. The geometry around the boron centre is a slightly distorted tetrahedral one with C−B−C angles between 105.53(11)° and 113.26(11)°, and B−C bond lengths of 1.642(2)−1.657(2) Å for the phenyl substituents and 1.659(2) Å for the carbene moiety (Table 3). These values are similar to those for the tetraarylborate anions in **2**, **3**, **5** and **6**, suggesting that the nature of the boron atom in **10** is identical and that it formally bears a single negative charge. The chemical shift in the $^{11}B\{^1H\}$ NMR supports

 © 2003 Wiley-VCH Verlag GmbH & Co. KGaA, Weinheim

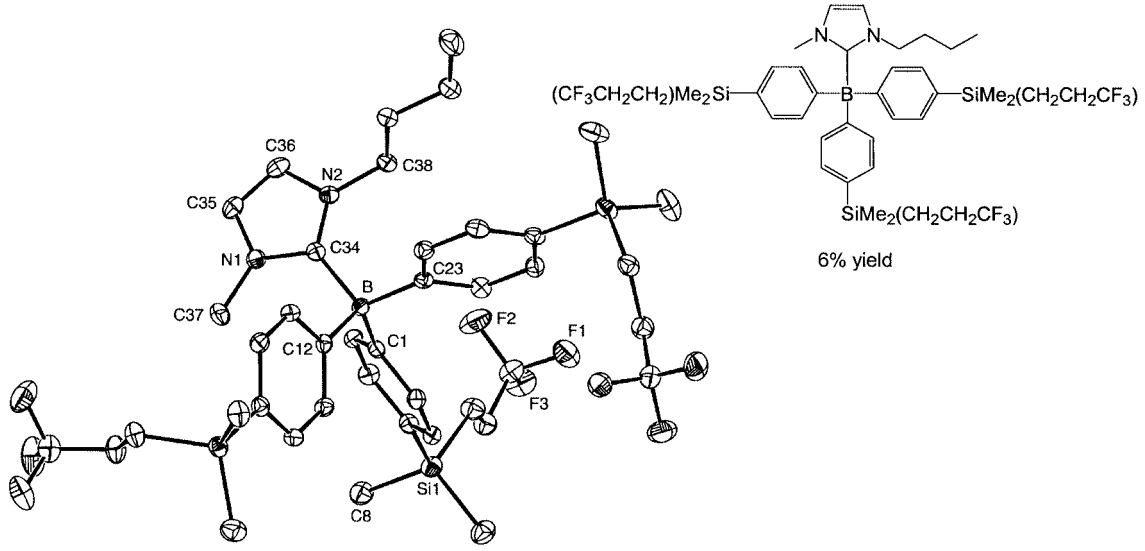

Figure 7. ORTEP drawing of the molecular structure of **10**, with ellipsoids at the 50% probability level. Hydrogen atoms are omitted for clarity

Table 3. Selected bond angles [°] and distances [Å] for **10**

Bond lengths		Bond angles	
B−C(1)	1.642(2)	C(1)−B−C(12)	113.26(11)
B−C(12)	1.645(2)	C(1)−B−C(23)	110.78(12)
B−C(23)	1.657(2)	C(1)−B−C(34)	105.53(11)
B−C(34)	1.659(2)	C(12)−B−C(34)	108.01(11)
		C(23)−B−C(34)	112.28(11)
N(1)−C(34)	1.3611(19)		
N(1)−C(35)	1.3784(19)	N(1)−C(34)−N(2)	104.20(12)
N(2)−C(34)	1.3583(18)		
N(2)−C(36)	1.3845(19)	C(34)−N(1)−C(37)	126.93(12)
C(35)−C(36)	1.337(2)	C(34)−N(2)−C(38)	128.29(12)

this suggestion, as the observed resonance corresponds with that of other $[BAr_4]^-$ (Ar = aryl) ions.[20]

However comparing the five-membered carbene ring with the imidazolium rings in the molecular structures for **2**, **3**, **5** and **6** reveals a consistent deviation in the bond lengths. The lengthening of the N−C(2) bonds in **10** compared to those in the imidazolium borate salts, N−C(34) 1.3612(19) Å (**10**) vs. N−C(2) 1.312(4)−1.3325(19) Å, combined with the shortening of the C−C bond, C(35)−C(36) 1.337(2) Å (**10**) vs. C−C 1.333(5)−1.350(2) Å, and a reduced N−C−N angle, 104.20(12)° in **10**, indicate a reduced aromatic character in the pentacycle. The bond lengths in **10** correspond with those observed for carbene adducts of transition-metals, in which the N−C bonds have single bond character and the C−C bond has a double bond character.[21] Bond lengths in such carbene moieties are around 1.36−1.40 Å for N−C(2), 1.31−1.34 Å for C(4)−C(5), with an angle of 101−104° for N(1)−C(2)−N(3). The similar angles and distances observed in **10** show it to be a carbene−borane adduct. A similar geometry has been reported for 2-borane-1,3-diethyl-4,5-dimethylimidazolin (**11**), for which N(1)−C(2) and N(3)−C(2) of 1.352(2) Å, N(1)−C(5) and N(2)−C(4) of 1.393(2) Å, C(4)−C(5) of 1.350(2) Å and N−C−N of 104.7(1)° were observed (Scheme 3).[22] However, the B−C(2) of 1.659(2) Å in **10** deviates significantly from that in **11** [1.603(3) Å] as well as that in the only related compound 2-(1,3,2-diazaborolyl)-1,3,4,5-tetramethylimidazolium bromide (**12**) that has been studied using single-crystal X-ray crystallography [1.580(11) Å].[23]

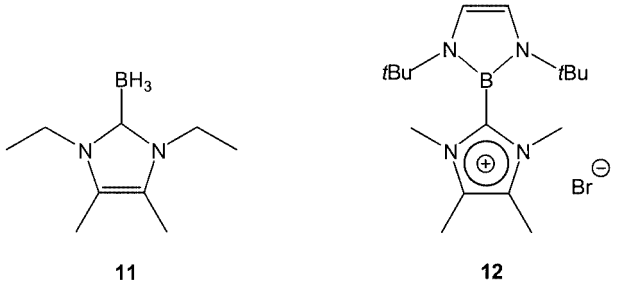

11 **12**

Scheme 3

The B−C(2) bond length is highly dependent on its σ-character.[22] Delocalisation of the electron density on the boron through the phenyl substituents in **10** results in a partial positive charge on the boron.[24] This lowers its ability to participate in the σ-bond with C(34) in comparison to the boron atom in **11** and **12**, where such a delocalisation is not possible. Hence, B−C(34) in **10** is somewhat longer than this bond in **11** and **12**.

The slightly acidic proton at C(2) of the imidazolium ring (pK_a = 7.5),[25] supplemented by the increased basicity of the borate's aryl groups due to the silyl substitution, may well be responsible for the conversion of **7** into **10**. Proton abstraction from the imidazolium moiety by one of the aryl groups will afford **10** as well as dimethyl(3,3,3-trifluoropropyl)silylbenzene. A related decomposition mode of the tetraphenylborate anion is found in the reaction of [Ru(η^3-1,2,3-η^2-5,6-(1,5-cyclooctadienyl)][BPh_4] with HF, HBF_4 and HPF_6, to form [Ru{η^3-1,2,3-η^2-5,6-(1,5-cycloocta-

 © 2003 Wiley-VCH Verlag GmbH & Co. KGaA, Weinheim

dienyl)}(η^6-$PhBF_3$)].[26] Given the weak acidity of the C(2)H proton compared to the strong acids HF, HBF_4 and HPF_6, and the absence of any transition metals that may lead to hydrides, the formation of **10** is still remarkable. Another explanation that cannot be completely ruled out is the involvement of traces of low-valent late transition metals that can oxidatively add imidazolium cations to give *N*-heterocyclic carbene hydride complexes.[27]

Infrared Spectroscopy: The aromatic C−H stretching vibrations in the imidazolium ring result in three highly characteristic infrared bands, between 3200 and 3050 cm^{-1}, that depend on the presence and strength of hydrogen-bonding interactions between these protons and the anions of the ionic liquid.[5a,28] For **1**, **2** and **6**−**9** the bands for ν[C(5)−*H*] and ν[C(4)−*H*] are observed at approximately 3140 and 3105 cm^{-1}. Furthermore, a separate stretching frequency at 3080 cm^{-1} was observed, which corresponds with ν[C(2)−*H*]. For compounds **3** and **5** these vibrations are shifted to higher frequencies, with bands at 3150, 3110 and 3091 cm^{-1}, respectively (Table 4). Furthermore, for **4**, a further shift for ν[C(5)−*H*] and ν[C(4)−*H*] to 3179 and 3130 cm^{-1} was seen, while the absorption corresponding with ν[C(2)−*H*] was not detectable. This shift is caused by a reduction in the strength of the C−H bonds in the imidazolium ring as their participation in hydrogen-bonding interactions increases.[29] Therefore, the shift of the stretching vibrations to higher frequencies in the imidazolium salts containing borate anions with electron-withdrawing substituents indicates that the hydrogen-bridging interactions are weakened by these substituents. For related imidazolium salts similar observations have been reported; [EMIm]X (X = Cl^-, Br^-, I^- and $AlBr_4^-$) shows IR bands at 3150, 3135 and 3080 cm^{-1};[14] [BMIm]X (X = BF_4^-, PF_6^-) at 3166 and 3123 cm^{-1},[28b] and [EMIm]X (X = various carboranes) at 3165, 3150 and 3110 cm^{-1}.[5a] In these salts an increase in the strength of the hydrogen bonds between the cation and the anion also resulted in lower ν(CH) stretching frequencies.

The sensitivity of the C−H stretching frequencies to the strength of the hydrogen-bonding interactions varies with the position on the imidazolium ring. Whereas ν[C(4)−*H*] and ν[C(5)−*H*] change by more than 30 cm^{-1}, a maximum shift of 20 cm^{-1} in ν[C(2)−*H*] was observed. The H(2) proton bears the largest positive charge (δ^+) of the aromatic imidazolium protons[6f,30] and is, therefore, the strongest hydrogen-bond donor. Upon reduction of the hydrogen-bonding capabilities of the anion the relatively strong C(2)H···π interactions remain intact, but the weaker bonds C(4)−*H* and C(5)−*H* are more likely to be significantly affected. This results in the relatively low sensitivity of ν[C(2)−*H*] to a reduced participation of the imidazolium cation in hydrogen bonding.

^{1}H NMR Spectroscopy: The dependence of the ^{1}H NMR chemical shifts of the imidazolium ring protons on various borate anions and different concentrations was investigated. The chemical shifts C(2)−*H*, C(4)−*H*, C(5)−*H*, NCH_2 and NCH_3 for 0.08 M solutions of **1**−**9** in dry [D_6]acetone (Table 5) proved to be highly sensitive to the substituent on the borate anion. The largest variations were observed for the C(2)−*H* resonances, which shifted by as much as 1.7 ppm, depending on the anion. With [BMIm][BPh_4] (**1**) as a reference compound, the imidazolium salts containing an anion with CF_3 or C_6F_{13} substituents exhibit a positive Δδ, i.e., the imidazolium proton resonances shift to lower field relative to **1** (Figure 8). Conversely, alkyl- or nonfluorous silyl substituents induce a negative Δδ, except for [BMIm][B{C_6H_4($SiMe_2C_8H_{17}$)-4}$_4$] (**8**) which shows no significant shifts relative to **1**. Furthermore, the largest downfield shifts were observed for the compounds with perfluoroalkyl groups connected directly to the phenyl rings of the anion.

For imidazolium compounds the chemical shifts of the protons on the ring are determined by both hydrogen-bonding interactions and shielding due to ring current effects of the tetraarylborate anions and of neighbouring imidazolium cations.[3a] Hydrogen bonding causes the protons to shift to lower field, and shielding of the protons from the magnetic field by the aromatic system of the borate and imidazolium aromatic systems results in an upfield shift.[31]

Table 4. Infrared spectroscopic data for the aromatic stretching region (3200−3050 cm^{-1}), corresponding with C−H stretching frequencies in the imidazolium cation

IL	R	ν[C(5)−*H*] and ν[C(4)−*H*]		ν[C(2)−*H*]
1	H	3132 (w)	3099 (w)	3082 (m)
2	Me	3140 (w)	3103 (w)	3078 (m)
3	CF_3	3150 (w)	3113 (w)	3088 (m)
4	3,5-$(CF_3)_2$	3179 (w)	3130 (w)	—[a]
5	C_6F_{13}	3157 (w)	3110 (w)	3094 (w)
6	$SiMe_3$	3138 (w)	3107 (w)	3079 (m)
7	$SiMe_2(CH_2)_2CF_3$	3144 (w)	3107 (m)	3077 (m)
8	$SiMe_2C_8H_{17}$	3134 (w)	3107 (w)	3074 (m)
9	$SiMe_2(CH_2)_2C_6F_{13}$	3136 (w)	3107 (w)	3074 (m)

[a] Not observed.

Table 5. ^{1}H NMR chemical shifts (δ in ppm) for 0.08 M solutions of **1**−**9** in [D_6]acetone

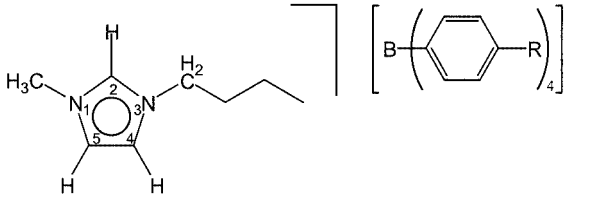

IL	R	H^2	H^4	H^5	NCH_2	NCH_3
1	H	8.08	7.48	7.40	4.08	3.74
2	Me	7.58	7.41	7.33	3.97	3.65
3	CF_3	9.06	7.77	7.71	4.37	4.06
4	3,5-$(CF_3)_2$	9.12	7.84	7.77	4.41	4.11
5	C_6F_{13}	9.07	7.78	7.72	4.38	4.06
6	$SiMe_3$	7.42	7.28	7.20	4.00	3.69
7	$SiMe_2(CH_2)_2CF_3$	8.29	7.64	7.57	4.21	3.89
8	$SiMe_2C_8H_{17}$	—[a]	—[a]	—[a]	4.04	3.77
9	$SiMe_2(CH_2)_2C_6F_{13}$	8.40	7.66	7.60	4.23	3.91

[a] Obscured by resonances of tetraarylborate anion.

 © 2003 Wiley-VCH Verlag GmbH & Co. KGaA, Weinheim

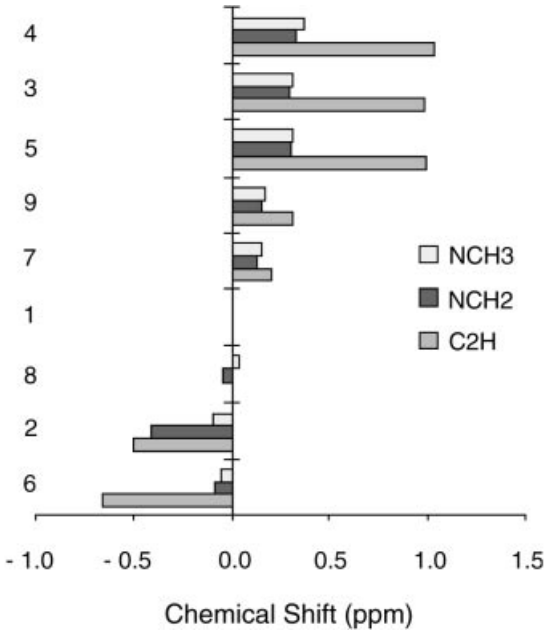

Figure 8. ^{1}H NMR chemical shifts for **2**−**9** relative to [BMIm][BPh_4] (**1**)

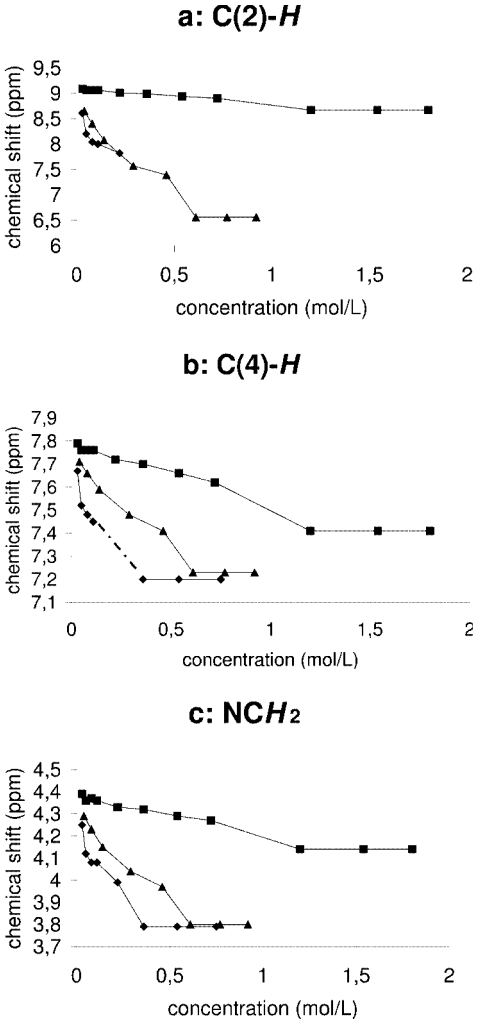

Figure 9. Concentration dependence of the ^{1}H NMR chemical shifts (δ in ppm) in [D_6]acetone for **1**, **3** and **9**. ◆ = $[BPh_4]^-$. ■ = $[B\{C_6H_4(CF_3)\text{-}4\}_4]^-$. ▲ = $[B(C_6H_4\{SiMe_2(CH_2CH_2C_6F_{13})\}\text{-}4)_4]^-$. ·-·-·-: peaks in this concentration range were obscured by resonances of the tetraarylborate anion

The IR data established that the hydrogen-bonding strength is reduced when electron-withdrawing groups are present on the borate anion. This would correspond with an upfield shift in the ^{1}H NMR spectrum;[31] however, the opposite effect is observed because the weakened cation−anion interactions reduce the proximity of the imidazolium protons to the π-orbitals of the anion. This reduces the magnetic shielding experienced by these protons. As a negative Δδ is observed with increasing hydrogen-bond strength, the effect of the shielding apparently outweighs the influence of the hydrogen-bonding interactions on the chemical shift.

Although magnetic shielding proved to be the most important factor in determining the chemical shift of C(2)−*H*, C(4)−*H* and C(5)−*H*, the C−H···π interactions affect the sensitivity of the chemical shift of the imidazolium protons to the nature of the anion. As C(2)−*H* is the strongest hydrogen-bond donor of the imidazolium ring protons it will be closer to the phenyl rings of the borate anion than C(4)−*H* and C(5)−*H*, and therefore the shielding C(2)−*H* experiences will be increased. This is reflected in the enhanced sensitivity of its chemical shift towards changes in the anion.

The concentration dependence of the chemical shifts of the imidazolium ring protons of **1**, **3** and **9** in acetone was investigated in the range 0.03−1.80 M. As reported previously,[3a] the ^{1}H NMR signals of these protons were anion- and concentration-dependent (Figure 9). The order of magnitude of these effects varied with each proton, with C(2)−*H* being the most sensitive. Smaller displacements were observed for the pairs of signals corresponding with C(4)−*H* and C(5)−*H* and with NCH_3 and NCH_2. The protons within these pairs displayed comparable concentration-related shifts.

Compounds **1** and **9** show similar behaviour − the resonances shifting to higher field at higher molarities. The C(2)−*H* signal displayed the largest Δδ (Δδ = −2.09 ppm) when increasing the concentration of **9** from 0.04 to 0.92 M (Figure 9). For **1** a similar trend could be discerned; however, broadening of the C(2)−*H* resonance at concentrations above 0.22 M prevented accurate observation. No change in the chemical shifts was observed above 0.36 M and 0.61 M for **1** and **9**, respectively. The imidazolium ring protons of **3** showed a more modest concentration-related displacement, the C(2)−*H* signal shifting by a mere −0.4 ppm over the concentration range 0.11 to 1.20 M. Below 0.11 M and above 1.20 M, all of the chemical shifts of **3** were constant.

The changes in the chemical shifts upon increasing concentration of the imidazolium salts in acetone can be explained by an equilibrium between a solvent-separated ion pair and a close-contact ion pair (Scheme 4).[3a]

 © 2003 Wiley-VCH Verlag GmbH & Co. KGaA, Weinheim

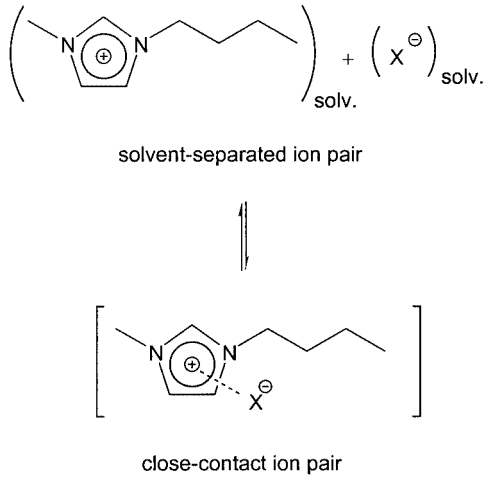

Scheme 4

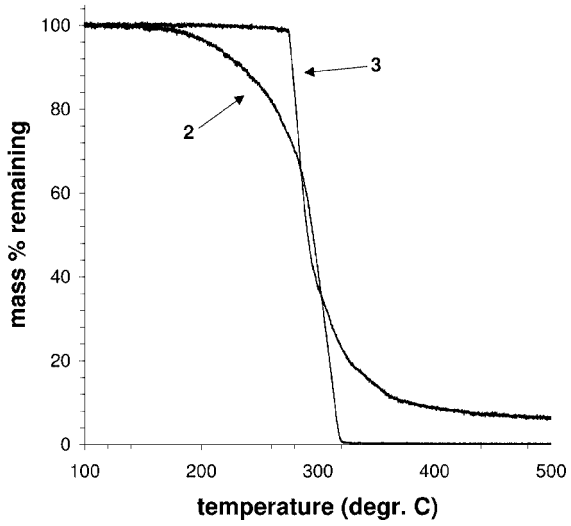

Figure 10. Thermogravimetric analysis for [BMIm][B{C_6H_4Me-4}$_4$] (**2**) and [BMIm][B{$C_6H_4(CF_3)$-4}$_4$] (**3**)

With increasing concentration, this equilibrium shifts to the right, resulting in an increase in close-contact ion pairing. In such ion-pairs the magnetic shielding of the imidazolium ring protons by the phenyl groups of the anion will be stronger than in the solvent-separated ion pairs, which explains the observed shift of the proton resonances to higher field with increasing concentrations Further increases in proton shielding in concentrated solutions are caused by ring stacking of the cations.[3a,32] This predominantly affects the C(2)−*H* proton,[3a] which could explain the high concentration sensitivity of the corresponding signal in comparison with the other imidazolium proton resonances.

The reduced cation−anion interactions in **3**, which contains the more weakly coordinating [B{$C_6H_3(CF_3)$-4}$_4$]$^-$ anion, reduces the amount of close-contact ion pairing at a given concentration. This results in weaker magnetic shielding on the imidazolium ring protons and, thus, in a smaller Δδ than observed for **1** and **9**. Furthermore, as hydrogen bonding interactions in **3** are weaker, cation−cation aggregation at higher concentration will be weaker, further reducing shielding of the imidazolium protons with respect **1** and **9**. This weakening of the inter-ionic interactions in **3** is supported by the IR data.

Melting Points and Thermal Stability: For the imidazolium salts **1**−**9** the melting points and thermal stability were determined (Table 6). All compounds are white solids that melt well above room temperature, except for **8** and **9** for which DSC measurements indicated possible glass transition temperatures in the range −20 °C to −10 °C.[33] Whereas the NMR and IR data showed an obvious influence of the electron-withdrawing CF_3 and C_6F_{13} substituents on cation−anion interactions, such a correlation with the observed melting points is difficult. However, the increasing bulk and orientational flexibility of the substituents[34] clearly depress the melting points of the imidazolium borates, as observed for **8** and **9** and to a lesser extent in **5** and **7**, since the bulky substituents disturb the most efficient packing of ions in the crystal lattice.[35]

The thermal stability of the compounds was assessed by thermogravimetric analysis under nitrogen, heating **1**−**9** from 100 to 500 °C at 5 °C/min. All compounds were stable up to 170 °C, after which the alkyl- and silyl-substituted salts **1**, **2**, **7**, **8** and **9** started to decompose. For all ionic liquids the decomposition process was complete above 450 °C (Figure 10). The only exception is $SiMe_3$-substituted **6**, which decomposes at 250 °C.

The borate anions with CF_3 or C_6F_{13} substituents directly connected to the aryl rings yielded more stable salts, with decomposition starting, on average, 70 °C higher than

Table 6. Melting points and liquid range of imidazolium salts **1**−**9**

	Anion	Melting point [°C]	Decomposition temperature [°C]	Liquid range [°C]
8	[B{$C_6H_4(SiMe_2C_8H_{17})$-4}$_4$]$^-$	−20[a]	170	190
9	[B(C_6H_4{$SiMe_2(CH_2CH_2C_6F_{13})$}-4)$_4$]$^-$	−10[a]	190	200
5	[B{$C_6H_4(C_6F_{13})$-4}$_4$]$^-$	90	225	135
7	[B(C_6H_4{$SiMe_2(CH_2CH_2CF_3)$}-4)$_4$]$^-$	104	175	71
4	[B{$C_6H_3(CF_3)_{2-}$3,5}$_4$]$^-$	109	245	136
1	[BPh_4]$^-$	126	185	59
3	[B{$C_6H_4(CF_3)$-4}$_4$]$^-$	152	275	123
2	[B(C_6H_4Me-4)$_4$]$^-$	−[b]	173	−[b]
6	[B{$C_6H_4(SiMe_3)$-4}$_4$]$^-$	−[b]	250	−[b]

[a] DSC measurements suggest a glass transition around this temperature. [b] No melting point observed before the onset of decomposition.

 © 2003 Wiley-VCH Verlag GmbH & Co. KGaA, Weinheim

for the alkyl- or silyl-substituted compounds. As the only variable in these studies is the anion, the changes in the decomposition temperature are connected with the stability of the tetraarylborate anions. The increased thermal stability for **3**−**5** is a direct result of the increased delocalisation of the negative charge due to the electron-withdrawing substituents on the phenyl groups of the anion.[9] The high stability of **6** is remarkable and remains unexplained as this anion does not contain stabilising functionalities, and because the other silyl-substituted anions do not show increased stability over $[BPh_4]^-$.

Polarity: For **8** and **9**, which are liquids at room temperature, the relative polarity was estimated by measuring λ_{max}^{abs} of the solvatochromatic dye Nile Red dissolved in these ILs. The observed solvatochromatic shifts, and the molar transition energy (E_{NR}) calculated using λ_{max}^{abs}, indicate that **8** is less polar than **9**, and that both are considerably less polar than the common ILs $[BMIm]BF_4$ and $[BMIm]PF_6$ (Table 7).[36] Nevertheless, the polarity of **8** and **9** is of the same order of magnitude as that of a polar solvent such as acetone.

Earlier work using Nile Red to assess the polarity of *N*,*N*-dialkylimidazolium ILs showed that, in general, the polarity decreased with increasing anion size. This was correlated with a reduction in electron density and, correspondingly, a reduction in the ability of the anion to interact with the dye. However, only BF_4^-, PF_6^-, NO_2^-, NO_3^- and $[N(SO_2CF_3)_2]^-$ were assessed. When comparing **8** and **9** with these anions, the increased size and efficient charge delocalisation further reduce the relative polarity of the BMIm salts. The relatively high polarity of **9** could be the result of local dipoles, caused by the electron-withdrawing C_6F_{13} substituents. Such dipole moments could lead to stronger interactions with the dye molecules and thus increase the relative polarity observed.[36]

Table 7. Polarity of **8** and **9** determined using the solvatochromatic dye Nile Red (values other than for **8** and **9** were taken from ref.[36a] and ref.[37])

	Liquid	λ_{max}^{abs} [nm]	E_{NR} [kcal/mol][a]
	H_2O	593	201.7
	$[BMIm]BF_4$	551	217.2
	MeOH	550	217.7
	$[BMIm]PF_6$	548	218.5
	$[C_{10}MIm]BF_4$[b]	546	219.2
9	$[BMIm][B(C_6H_4\{SiMe_2(CH_2CH_2C_6F_{13})\}\text{-}4)_4]$	542	220.7
8	$[BMIm][B\{C_6H_4(SiMe_2C_8H_{17})\text{-}4\}_4]$	534	224.0
	Acetone	530	225.9
	Et_2O	504	237.2
	Hexane	484	247.0

[a] Calculated from $E_{NR} = (hcN_A/\lambda_{max}^{abs}) \times 10^6$, where h is Planck's constant, c is the speed of light, N_A is Avogadro's number and λ_{max}^{abs} is the wavelength of maximum absorption for Nile Red. [b] $C_{10}MIm$ = 1-decyl-3-methylimidazolium.

Solubility and Miscibility with Other Liquids: The solubility of the imidazolium salts in a range of organic solvents was examined (Table 8). All ILs were immiscible with water and showed good solubility in acetone. Furthermore, the solubility in the solvents investigated proved to be highly dependent on the substituents present in the tetraarylborate anions. In methanol the solubility of **1**−**9** was moderate; however, the imidazolium salts with CF_3- and C_6F_{13}-substituted anions displayed significantly better solubility than those without perfluoroalkyl groups. This was especially evident in **3** and **4**, which exhibit the best solubility in methanol. In acetone, the substituent effect is less evident, with all compounds showing high solubilities. Upon going from acetone to Et_2O and hexane, the solubility of the imidazolium borates, except for **8**, decreases rapidly with decreasing solvent polarity. In Et_2O the compounds with CF_3 or large silyl substituents are still highly soluble, but only **8**, and to some extent **9**, retain significant miscibility with hexane. This is a consequence of the large, lipophilic substituents in the borate anion, which reduce the ILs to relatively apolar compounds and partially compensate the ionic character with a large lipophilic domain. The lipophilic character of **9** has been demonstrated previously,[12] where a phase behaviour resembling that of perfluorinated solvents was observed in combinations of **9** with toluene, hex-1-ene and oct-1-ene. Similar characteristics are expected for highly lipophilic **8**, but were not investigated.

The relatively low solubility in methanol and the immiscibility with water are no doubt the result of the poor hydrogen bonding character of the borate anions in **1**−**9**.[11] The

Table 8. Solubility of **1**−**9** in various organic solvents

[a]	Anion	Solubility (g/L)			
		MeOH	Acetone	Et_2O	Hexane
1	$[BPh_4]^-$	0.8	140	0.6	0.2
2	$[B(C_6H_4Me\text{-}4)_4]^-$	0.09	63	0.3	0.06
3	$[B\{C_6H_4(CF_3)\text{-}4\}_4]^-$	70	340	180	0.2
4	$[B\{C_6H_3(CF_3)_{2-}3,5\}_4]^-$	66	290	200	0.2
5	$[B\{C_6H_4(C_6F_{13})\text{-}4\}_4]^-$	3.6	82	53	0.08
6	$[B\{C_6H_4(SiMe_3)\text{-}4\}_4]^-$	0.5	96	14	0.2
7	$[B(C_6H_4\{SiMe_2(CH_2CH_2CF_3)\}\text{-}4)_4]^-$	12	160	98	0.07
8	$[B\{C_6H_4(SiMe_2C_8H_{17})\text{-}4\}_4]^-$	1.8	250	230	250
9	$[B(C_6H_4\{SiMe_2(CH_2CH_2C_6F_{13})\}\text{-}4)_4]^-$	33	580	510	19

[a] Solubility in g/L of pure solvent at 25 °C.

 © 2003 Wiley-VCH Verlag GmbH & Co. KGaA, Weinheim

comparatively high solubility of the CF_3-substituted ionic liquids could be due to the additional O−H···F hydrogen bonding possibilities such substituents introduce,[16] which would enhance solvent−solute interactions and thus enhance solubility.

Application as Solvents: Based on the melting points of the imidazolium tetraarylborate salts described here, only **8** and **9** qualify as true room-temperature ionic liquids. Although their melting point is significantly higher than that of the widely used [BMIm]BF_4 and [BMIm]PF_6 salts, which melt at −81 °C and −62 °C, [1a][7a][28b] it allows their application as solvents for reactions at room temperature. The thermal stability of **8** and **9**, up to 170 °C, is sufficient for general application in homogeneous catalysis, even though the borate anion reduces their stability relative to ionic liquids with inorganic anions such as BF_4^-.[38] Conversely, the use of the borate anions eliminates the main source of decomposition in [BMIm]BF_4 and [BMIm]PF_6. Halogen-containing inorganic anions, and especially PF_6^-, might form acids in the presence of water.[1a,39] As the conventional ionic liquids often contain trace amounts of water, HF formation is a serious concern, in particular for [BMIm]PF_6. In **8** and **9** this is prevented by the elimination of fluorine atoms that are sensitive to hydrolysis and by the possibility of removing even trace amounts of water.[40] However, isolation of **10** when attempting to crystallise **7** shows that chemical stability could be an issue. This indicates that the borate could be prone to decomposition under the influence of the acidic C(2)−*H* proton of the imidazolium cation.

The high miscibility of **8** and **9** with apolar solvents is unique amongst ionic liquids. [BMIm]PF_6 shows limited miscibility with apolar organic liquids such as oct-1-ene (65 g/L);[41] however, the high solubility of **8** and **9**, and the phase behaviour displayed by the latter, is unprecedented. In catalysis this would offer increased solubility of apolar substrates, which could be beneficial in catalytic processes that suffer from phase transfer limitations due to the high polarity of the common ILs. The lipophilic character of **8** and **9** would enable their use as a polar phase that can dissolve and immobilise ionic catalysts, with affinity for apolar substrates.

Conclusions

An interesting feature of ionic liquids that favours their use as solvents is the possibility of adapting their properties by choosing different cation−anion combinations. This concept has been applied successfully, but a thorough understanding of the effects that govern the physical properties of ionic liquids is lacking. Here the effects of systematically varying the anion on the physical properties of BMIm tetraarylborate salts are reported. The hydrogen-bonding interactions, between the imidazolium ring protons and the borate anion, that are present both in the solid state and in solution are reduced upon introducing electron-withdrawing perfluoroalkyl substituents in the anion. In addition, bulky silyl substituents depress the melting point of these salts. [BMIm][B{$C_6H_4(SiMe_2C_8H_{17}$}-4}$_4$] and [BMIm][B(C_6H_4{$SiMe_2(CH_2CH_2C_6F_{13}$)}-4)$_4$] even proved to be liquid down to −10 °C, making them true room-temperature ILs. These two imidazolium borates displayed significant solubility in hexane, due to their large lipophilic anions. As conventional ionic liquids display poor miscibility with apolar compounds, this lipophilic character makes them a unique reaction media. However, before their application as solvents, their stability under reaction conditions should be assessed carefully as they are not chemically inert.

Experimental Section

General Procedures: All reactions were performed under dry N_2 using standard Schlenk techniques. Tetrahydrofuran (THF) and diethyl ether (Et_2O) were distilled from sodium benzophenone ketyl, CH_2Cl_2 from CaH_2 and benzene from sodium. Dimethyloctylsilyl chloride,[42] 1-butyl-3-methylimidazolium chloride,[43] 1-butyl-3-methylimidazolium bromide,[44] 1-butyl-3-methylimidazolium iodide,[44] Na[B(C_6H_4Me-4)$_4$],[45] Na[B{$C_6H_4(CF_3)$-4}$_4$],[46] Na[B{$C_6H_3(CF_3)_2$-3,5}$_4$],[47] Na[B{$C_6H_4(SiMe_3)$-4}$_4$],[15] Na[B{$C_6H_4(C_6F_{13})$-4}$_4$],[48] and [BMIm][B(C_6H_4{$SiMe_2$-$(CH_2CH_2C_6F_{13})$}-4)$_4$] (**9**)[12] were prepared according to literature procedures. All other chemicals were used as received. NMR spectra were recorded with a Varian Inova 300 spectrometer at 25 °C (δ in ppm and *J* in Hz) with TMS (^{1}H, ^{13}C) and BF_3·Et_2O (^{11}B) as external references. Infrared spectra were recorded with a Mattson Galaxy FT-IR 5000 spectrometer at 25 °C under N_2 (as KBr pellets). DSC traces were recorded with a Mettler-Toledo DSC-821, and melting points were determined with a Büchi melting point apparatus. UV/Vis absorption spectra were recorded with a Perkin−Elmer Lambda 16 spectrophotometer. TGA measurements were performed with a Perkin−Elmer thermal analysis system 4 coupled to a Perkin−Elmer TGS2 thermogravimmetric system. Elemental analyses were carried out by H. Kolbe, Mikroanalytisches Laboratorium, Mülheim an der Ruhr.

4-Bromo{dimethyl(3,3,3-trifluoropropyl)silyl}benzene: *n*BuLi (17.2 mL, 1.54 M in hexanes, 26.5 mmol) was added to a solution of 1,4-dibromobenzene (6.25 g, 26.5 mmol) in Et_2O (100 mL). The resultant mixture was stirred at room-temperature for 5 min and then cooled to −78 °C. Chlorodimethyl(3,3,3-trifluoropropyl)silane (4.55 mL, 26.5 mmol) was added and the mixture warmed to room temperature over 2 h. This mixture was then poured into H_2O (100 mL), extracted with Et_2O (3 × 100 mL) and the combined organic layers dried with $MgSO_4$. Removal of the solvents in vacuo yielded 7.07 (86%) of a colourless oil. ^{1}H NMR ($CDCl_3$, 300.1 MHz): δ = 0.39 (s, SiCH_3), 1.01 (m, SiCH_2), 2.01 (m, CH_2CF_3), 7.43 (d, $^3J_{H,H}$ = 7.8 Hz, 2 Ar-H_m), 7.58 (d, $^3J_{H,H}$ = 7.8 Hz, 2 Ar-H_o) ppm. ^{13}C{^{1}H} ($CDCl_3$, 75.5 MHz): δ = −3.4 (s), 7.7 (s), 29.0 (q), 124.5 (s), 131.5 (s), 135.4 (s), 136.5 (s) ppm. $C_9H_{14}BrF_3$ (310.00): calcd. C 42.45, H 5.43, F 18.31; found C 42.22, H 4.65, F 18.18.

4-Bromo{dimethyl(octyl)silyl}benzene: Using a procedure similar to that for 4-bromo[dimethyl(3,3,3-trifluoropropyl)silyl]benzene, 1,4-dibromobenzene (14.28 g, 60.5 mmol), *n*BuLi (38 mL, 1.6 M in hexanes, 61.0 mmol) and chlorodimethyloctylsilane (12.62 g, 61.0 mmol) yielded 15.51 g (78%) of a light yellow oil. ^{1}H NMR ($CDCl_3$, 300.1 MHz): δ = 0.25 (s, SiCH_3), 0.77 (s, SiCH_2), 0.91 (m,

 © 2003 Wiley-VCH Verlag GmbH & Co. KGaA, Weinheim

$SiC_7H_{14}CH_3$), 1.31 (m, $SiCH_2C_6H_{12}CH_3$), 7.38 (d, $^3J_{H,H}$ = 7.8 Hz, 2 Ar-H_m), 7.53 (d, $^3J_{H,H}$ = 7.8 Hz, 2 Ar-H_o) ppm. $^{13}C\{^1H\}$ ($CDCl_3$, 75.5 MHz): δ = −2.8 (s), 0.7 (s), 14.4 (s), 15.9 (s), 22.9 (s), 241. (s), 29.6 (s), 32.2 (s), 33.8 (s), 123.8 (s), 131.1 (s), 135.4 (s), 138.7 (s) ppm. $C_{16}H_{27}Br$ (326.11): calcd. C 78.70, H 8.41; found C 78.56, H 8.35.

Sodium Tetrakis{4-[dimethyl(3,3,3-trifluoropropyl)silyl]phenyl}-borate: *t*BuLi (12.6 mL, 1.5 M in pentane, 20.2 mmol) was added to 4-bromo{dimethyl(3,3,3-trifluoropropyl)silyl}benzene (3.14 g, 10.1 mmol) in Et_2O (50 mL) at −78 °C. The mixture was allowed to warm to room temperature over 16 h and then cooled to −78 °C with subsequent addition of $BF_3{\cdot}Et_2O$ (0.21 mL, 1.67 mmol). This solution was then warmed to room temperature over 16 h, poured into H_2O and saturated with NaCl. After extraction with Et_2O (3 × 50 mL) the combined organic layers were dried with $MgSO_4$ and the solvents removed in vacuo. The residue was taken up in THF (25 mL), filtered through Celite and dried in vacuo, yielding 1.33 g (83%) of a white solid. ^1H NMR ([D$_4$]MeOH, 300.1 MHz): δ = 0.25 (s, 24 H, $SiCH_3$), 0.89 (m, 8 H, $SiCH_2$), 2.01 (m, 8 H, CH_2CF_3), 7.17 (d, $^3J_{H,H}$ = 7.9 Hz, 8 Ar-H_m), 7.37 (m, 8 Ar-H_o) ppm. $^{13}C\{^1H\}$ ([D$_4$]MeOH, 75.5 MHz): δ = −4.2 (s), 7.7 (s), 28.5 (s), 128.3 (s), 128.3 (s), 130.2 (s), 130.7 (s), 135.9 (s), 166.5 (q, $^1J_{BC}$ = 49.5 Hz, B−*C*) ppm. $C_{44}H_{56}BF_{12}NaSi_4$ (958.33): calcd. C 55.10, H 5.89, Na 2.40; found C 54.84, H 5.85, Na 2.48.

Sodium Tetrakis{4-[dimethyl(octyl)silyl]phenyl}borate: A procedure similar to that for sodium tetrakis{4-[dimethyl(3,3,3-trifluoropropyl)silyl]phenyl}borate and 4-bromo{dimethyl(octyl)-silyl}benzene (5.77 g, 21.5 mmol), *t*BuLi (23.5 mL, 1.5 M in pentane, 35.2 mmol) and $BF_3{\cdot}Et_2O$ (0.44 mL, 3.50 mmol) yielded a brown oil. After washing with α,α,α-trifluorotoluene (3 × 5 mL) a white solid (2.42 g; 71%) was collected. ^1H NMR ([D$_4$]MeOH, 300.1 MHz): δ = 0.21 (s, 24 H, $SiCH_3$), 0.75 (s, 8 H, $SiCH_2$), 0.92 (m, 12 H, $C_7H_{14}CH_3$), 1.32 (m, 48 H, $CH_2C_6H_{12}CH_3$), 7.19 (d, $^3J_{H,H}$ = 7.8 Hz, 8 Ar-H_m), 7.48 (m, 8 Ar-H_o) ppm. $^{13}C\{^1H\}$ ([D$_6$]-acetone, 75.5 MHz): δ = −2.9 (s), 13.9 (s), 16.2 (s), 22.8 (s), 24.2 (s), 33.9 (s), 130.4 (s), 131.3 (s), 135.9 (s), 165.8 (q, $^1J_{BC}$ = 49.5 Hz, B−*C*) ppm. $C_{64}H_{108}BNaSi_4$ (1022.75): calcd. C 75.09, H 10.63; found C 74.88, H 10.75.

1-Butyl-3-methylimidazolium Tetraphenylborate (1):[8] In a procedure adapted from the literature (2.18 g, 6.37 mmol) $Na[BPh_4]$ and (1.26 g, 5.79 mmol) [BMIm]Br were dissolved in H_2O (30 mL) and CH_2Cl_2 (30 mL). After stirring for 24 h, the layers were separated and the CH_2Cl_2 layer was washed with water (2 × 50 mL). Drying in vacuo yielded a white solid (2.12 g; 80%). ^1H NMR ([D$_6$]acetone, 300.1 MHz): δ = 0.92 (t, $^3J_{H,H}$ = 7.4 Hz, CH_2CH_3), 1.31 (m, CH_2CH_3), 1.79 (m, NCH_2CH_2), 3.75 (s, NCH_3), 4.09 (t, $^3J_{H,H}$ = 7.4 Hz, NCH_2), 6.78 (t, $^3J_{H,H}$ = 7.8 Hz, 4 Ar-H_p), 6.94 (t, $^3J_{H,H}$ = 7.5 Hz, 8 Ar-H_m), 7.36 (m, 8 Ar-H_o), 7.42 [s, C(5)*H*], 7.49 [s, C(4)*H*], 8.19 [s, C(2)*H*] ppm. $^{13}C\{^1H\}$ ([D$_6$]acetone, 75.5 MHz): δ = 13.0 (s), 19.5 (s), 32.0 (s), 35.9 (s), 49.5 (s), 122.5 (s), 124.0 (s), 131.0 (s), 135.7 (s), 136.3 (s), 165.0 (q, $^1J_{BC}$ = 49.5 Hz, B−*C*) ppm. $^{11}B\{^1H\}$ ([D$_6$]acetone, 96.3 MHz): δ = −12.21 (s) ppm. $C_{32}H_{35}BN_2$ (458.29): calcd. C 83.84, H 7.70; found C 83.17, H 7.59.

1-Butyl-3-methylimidazolium Tetrakis{4-(methyl)phenyl}borate (2): A mixture of (0.79 g, 1.98 mmol) $Na[B(C_6H_4Me\text{-}4)_4]$ and (0.58 g, 2.18 mmol) [BMIm]I was dissolved in H_2O (20 mL). After stirring for 2 d the mixture was extracted with CH_2Cl_2 (2 × 20 mL), dried with $MgSO_4$, filtered and all volatiles removed in vacuo. The resulting solid was washed with hexane (2 × 20 mL) and dried in vacuo, yielding a white solid (0.64 g; 63%). ^1H NMR ([D$_6$]acetone, 300.1 MHz): δ = 0.93 (t, $^3J_{H,H}$ = 7.4 Hz, CH_2CH_3), 1.38 (m, CH_2CH_3), 1.96 (m, NCH_2CH_2), 2.15 (s, 12 H, $ArCH_3$), 3.79 (s, NCH_3), 4.16 (t, $^3J_{H,H}$ = 7.5 Hz, NCH_2), 6.75 (d, $^3J_{H,H}$ = 7.5 Hz, 8 Ar-H_m), 7.25 (m, 8 Ar-H_o), 7.51 [s, C(5)*H*], 7.59 [s, C(4)*H*], 8.12 [s, C(2)*H*] ppm. $^{13}C\{^1H\}$ ([D$_6$]acetone, 75.5 MHz): δ = 13.0 (s), 19.3 (s), 20.6 (s), 32.1 (s), 35.9 (s), 49.5 (s), 122.5 (s), 123.9 (s), 126.2 (s), 129.5 (s), 136.3 (s), 161.2 (q, $^1J_{BC}$ = 49.4 Hz, B−*C*) ppm. $^{11}B\{^1H\}$ ([D$_6$]acetone, 96.3 MHz): δ = −12.79 (s) ppm. $C_{36}H_{43}BN_2$ (514.35): calcd. C 84.03, H 8.42; found C 83.78, H 8.54.

1-Butyl-3-methylimidazolium Tetrakis{4-(trifluoromethyl)phenyl}-borate (3): A mixture of $Na[B\{C_6H_4(CF_3)\text{-}4\}_4]$ (3.87 g, 6.30 mmol) and [BMIm]I (1.85 g, 6.93 mmol) was dissolved in CH_2Cl_2 (100 mL). After stirring for 2 d the mixture was poured into demineralised water (40 mL) and the resulting mixture was washed with demineralised water (5 × 40 mL). The organic layer was then dried with $MgSO_4$, filtered and the solvent was removed in vacuo. The resulting solid was washed with hexane (5 × 100 mL) and dried in vacuo, yielding a white solid (2.88 g; 63%). ^1H NMR ([D$_6$]acetone, 300.1 MHz): δ = 0.95 (t, $^3J_{H,H}$ = 7.4 Hz, CH_2CH_3), 1.38 (m, CH_2CH_3), 1.96 (m, NCH_2CH_2), 4.08 (s, NCH_3), 4.39 (t, $^3J_{H,H}$ = 7.2 Hz, NCH_2), 7.34 (d, $^3J_{H,H}$ = 8.4 Hz, 8 Ar-H_m), 7.42 (m, 8 Ar-H_o), 7.74 [s, C(5)*H*], 7.80 [s, C(4)*H*], 9.09 [s, C(2)*H*] ppm. $^{13}C\{^1H\}$ ([D$_6$]acetone, 75.5 MHz): δ = 13.0 (s), 19.3 (s), 32.1 (s), 36.1 (s), 49.6 (s), 120.5 (s), 122.5 (s), 124.1 (q, $^1J_{C,F}$ = 30.9 Hz, CF_3), 125.0 (s), 131.3 (s), 135.9 (s), 136.7 (s), 167.4 (q, $^1J_{BC}$ = 48.3 Hz, B−*C*) ppm. $^{11}B\{^1H\}$ ([D$_6$]acetone, 96.3 MHz): δ = −12.34 (s) ppm. $C_{36}H_{31}BF_{12}N_2$ (730.24): calcd. C 59.20, H 4.28; found C 59.00, H 4.04.

1-Butyl-3-methylimidazolium Tetrakis{3,5-(trifluoromethyl)phenyl}-borate (4): In a procedure similar to **3**, $Na[B\{C_6H_3(CF_3)_2\text{-}3,5\}_4]$ (1.40 g, 1.58 mmol) and [BMIm]I (0.39 g, 1.42 mmol) yielded a white solid (1.31 g; 82%). ^1H NMR ([D$_6$]acetone, 300.1 MHz): δ = 0.95 (t, $^3J_{H,H}$ = 6.6 Hz, CH_2CH_3), 1.38 (m, CH_2CH_3), 1.97 (m, NCH_2CH_2), 4.09 (s, NCH_3), 4.40 (t, $^3J_{H,H}$ = 7.4 Hz, NCH_2), 7.33 (d, 8 Ar-H_m), 7.47 (m, 8 Ar-H_o), 7.76 [s, C(5)*H*], 7.81 [s, C(4)*H*], 9.18 [s, C(2)*H*] ppm. ^{13}C ([D$_6$]acetone, 75.5 MHz): δ = 12.9 (s), 19.5 (s), 32.2 (s), 36.0 (s), 49.6 (s), 117.8 (s), 122.0 (s), 122.8 (s), 127.4 (s), 129.3 (q, $^1J_{C,F}$ = 31.8 Hz, CF_3), 134.8 (s), 136.8 (s), 162.5 (q, $^1J_{BC}$ = 49.9 Hz, B−*C*) ppm. $^{11}B\{^1H\}$ ([D$_6$]acetone, 96.3 MHz): δ = −12.27 (s) ppm. $C_{40}H_{27}BF_{24}N_2$ (1002.19): calcd. C 47.93, H 2.71, I 0.00; found C, 47.93, H 2.79, I 0.00.

1-Butyl-3-methylimidazolium Tetrakis{4-(perfluorohexyl)phenyl}-borate (5): In an analogous procedure to the synthesis of **3**, $Na[B\{C_6H_4(C_6F_{13})\text{-}4\}_4]$ (2.39 g, 1.44 mmol) and [BMIm]I (0.42 g, 1.59 mmol) yielded a white solid (0.48 g; 20%). ^1H NMR ([D$_6$]acetone, 300.1 MHz): δ = 0.95 (t, $^3J_{H,H}$ = 7.4 Hz, CH_2CH_3), 1.38 (m, CH_2CH_3), 1.97 (m, NCH_2CH_2), 4.09 (s, NCH_3), 4.40 (t, $^3J_{H,H}$ = 7.2 Hz, NCH_2), 7.33 (d, $^3J_{H,H}$ = 8.4 Hz, 8 Ar-H_m), 7.47 (m, 8 Ar-H_o), 7.76 [s, C(5)*H*], 7.81 [s, C(4)*H*], 9.18 [s, C(2)*H*] ppm. $^{13}C\{^1H\}$ ([D$_6$]acetone, 75.5 MHz): δ = 12.8 (s), 19.3 (s), 32.1 (s), 36.0 (s), 49.6 (s), 108.1 (m), 111.3 (m), 115.1 (m), 118.4 (m), 121.4 (m), 122.9 (m), 124.1 (s), 125.7 (s), 135.9 (s), 136.8 (s), 167.7 (q, $^1J_{BC}$ = 49.0 Hz, B−*C*) ppm. $^{11}B\{^1H\}$ ([D$_6$]acetone, 96.3 MHz): δ = −12.31 (s) ppm. $C_{56}H_{31}BF_{52}N_2$ (1730.17): calcd. C 41.67, H 3.45, Cl 0.00; found C 41.88, H 3.61, Cl 0.00.

1-Butyl-3-methylimidazolium Tetrakis{4-(trimethylsilyl)phenyl}-borate (6): A mixture of $Na[B\{C_6H_4(SiMe_3)\text{-}4\}_4]$ (1.48 g, 2.35 mmol) and [BMIm]Br (0.47 g, 2.14 mmol) was dissolved in acetone (30 mL) and H_2O (5 mL). After stirring for 24 h a white solid was collected, taken up in acetone and filtered through Celite. Slow evaporation of solvents yielded 0.61 g (38%) of a white crys-

 © 2003 Wiley-VCH Verlag GmbH & Co. KGaA, Weinheim

talline solid. ^{1}H NMR ([D$_6$]acetone, 300.1 MHz): δ = 0.16 (s, 36 H, SiC*H*$_3$), 0.95 (t, $^3J_{H,H}$ = 7.4 Hz, CH$_2$C*H*$_3$), 1.37 (m, C*H*$_2$CH$_3$), 1.90 (m, NCH$_2$C*H*$_2$), 4.00 (s, NC*H*$_3$), 4.31 (t, $^3J_{H,H}$ = 7.5 Hz, NC*H*$_2$), 7.15 (d, $^3J_{H,H}$ = 7.5 Hz, 8 Ar-*H*$_m$), 7.46 (m, 8 Ar-*H*$_o$), 7.68 [s, C(5)*H*], 7.74 [s, C(4)*H*], 8.92 [s, C(2)*H*] ppm. ^{13}C{^{1}H} ([D$_6$]acetone, 75.5 MHz): δ = −1.2 (s), 13.0 (s), 19.4 (s), 32.1 (s), 36.0 (s), 49.5 (s), 122.4 (s), 130.8 (s), 135.8 (s), 136.4 (s), 165.6 (q, $^1J_{BC}$ = 49.3 Hz, B−*C*) ppm. ^{11}B{^{1}H} ([D$_6$]acetone, 96.3 MHz): δ = −12.04 (s) ppm. $C_{44}H_{67}BN_2Si_4$ (746.45): calcd. C 70.73, H 9.04; found C, 70.86, H 8.94. Single crystals were obtained from acetone.

1-Butyl-3-methylimidazolium Tetrakis{4-[dimethyl(3,3,3-trifluoropropyl)silyl]phenyl}borate (7): A mixture of Na[B(C$_6$H$_4$-{SiMe$_2$(CH$_2$CH$_2$CF$_3$)}-4)$_4$] (0.50 g, 0.52 mmol) and [BMIm]I (0.13 g, 0.47 mmol) was dissolved in acetone (20 mL) and stirred for 4 h. A white precipitate that formed upon the addition of H$_2$O (10 mL) was then collected, washed with H$_2$O (3 × 20 mL) and dried in vacuo. The solid was taken up in toluene (50 mL), washed with demineralised water (2 × 30 mL) and dried in vacuo to yield a white solid (0.45 g; 75%). ^{1}H NMR ([D$_6$]acetone, 300.1 MHz): δ = 0.29 (s, 24 H, SiC*H*$_3$), 0.96 (m, 8 H, SiC*H*$_2$), 0.98 (t, $^3J_{H,H}$ = 7.4 Hz, CH$_2$C*H*$_3$), 1.33 (m, C*H*$_2$CH$_3$), 1.78 (m, NCH$_2$C*H*$_2$), 2.17 (m, 8 H, C*H*$_2$CF$_3$), 3.67 (s, NC*H*$_3$), 4.02 (t, $^3J_{H,H}$ = 7.5 Hz, NC*H*$_2$), 7.25 (d, $^3J_{H,H}$ = 7.9 Hz, 8 Ar-*H*$_m$), 7.36 [s, C(5)*H*], 7.45 [s, C(4)*H*], 7.49 [s, C(2)*H*], 7.56 (m, 8 Ar-*H*$_o$) ppm. ^{13}C{^{1}H} ([D$_6$]acetone, 75.5 MHz): δ = −2.7 (s), 8.7 (s), 13.9 (s), 20.2 (s), 33.0 (s), 36.8 (s), 50.4 (s), 123.5 (s), 125.0 (s), 127.7 (s), 129.3 (s), 132.0 (s), 134.6 (s), 135.9 (s), 137.0 (s), 167.0 (q, $^1J_{BC}$ = 49.2 Hz, B−*C*) ppm. ^{11}B{^{1}H} ([D$_6$]acetone, 96.3 MHz): δ = −12.15 (s) ppm. $C_{52}H_{71}BF_{12}N_2Si_4$ (1074.46): calcd. C 58.08, H 6.06, I 0.00; found C 57.86, H 6.10, I 0.00.

1-Butyl-3-methylimidazolium Tetrakis{4-[dimethyl(octyl)silyl]-phenyl}borate (8): In a procedure similar to that for **3**, Na[B{C$_6$H$_4$(SiMe$_2$C$_8$H$_{17}$)-4}$_4$] (3.78 g, 3.69 mmol) and [BMIm]I (1.47 g, 5.40 mmol) yielded a brown oil. This was washed with a hexane/methanol mixture (1:1) (3 × 60 mL), yielding a yellow oil (0.73 g; 17%). ^{1}H NMR ([D$_6$]acetone, 300.1 MHz): δ = 0.17 (s, 24 H, SiC*H*$_3$), 0.71 (s, 8 H, SiC*H*$_2$), 0.89 (t, $^3J_{H,H}$ = 7.4 Hz, NC$_3$H$_6$C*H*$_3$), 0.92 (m, 12 H, SiC$_7$H$_{14}$C*H*$_3$), 1.27 (m, NC$_2$H$_4$C*H*$_2$CH$_3$), 1.34 (m, 48 H, SiCH$_2$C$_6$*H*$_{12}$CH$_3$), 1.72 (m, NCH$_2$C*H*$_2$), 3.52 (s, NC*H*$_3$), 3.86 (t, $^3J_{H,H}$ = 7.5 Hz, NC*H*$_2$), 6.67 [s, C(2)*H*], 7.20 (d, $^3J_{H,H}$ = 7.8 Hz, 8 Ar-*H*$_m$), 7.27 [s, C(5)*H*], 7.37 [s, C(4)*H*], 7.53 (m, 8 Ar-*H*$_o$) ppm. ^{13}C{^{1}H} ([D$_6$]acetone, 75.5 MHz): δ = −2.9 (s), 13.2 (s), 13.9 (s), 16.2 (s), 19.5 (s), 22.8 (s), 24.2 (s), 32.1 (s), 33.9 (s), 35.8 (s), 49.5 (s), 122.2 (s), 123.8 (s), 130.4 (s), 131.3 (s), 134.2 (s), 135.9 (s), 165.8 (q, $^1J_{BC}$ = 49.5 Hz, B−*C*) ppm. ^{11}B{^{1}H} ([D$_6$]acetone, 96.3 MHz): δ = −12.10 (s) ppm. $C_{72}H_{123}BN_2Si_4$ (1138.89): calcd. C 75.86, H 10.88; found C 75.65, H 11.06.

Carbene−2-Tris[4-{dimethyl(3,3,3-trifluoropropyl)silyl}phenyl]-borane Adduct 10: Crystallisation of **7** (0.20 g, 0.19 mmol) from a mixture of warm MeOH/H$_2$O (95:5) yielded white crystals (0.01 g; 6%) and a yellow oil that solidified upon standing. The ^{1}H NMR spectrum of the oil was identical to that for **7**. The white crystals were suitable for X-ray single crystal analysis. ^{1}H NMR ([D$_6$]acetone, 300.1 MHz): δ = 0.34 (m, 18 H, SiC*H*$_3$), 0.67 (m, 3 H, CH$_2$C*H*$_3$), 0.76 (m, 2 H, CH$_2$C*H*$_2$CH$_3$), 0.94 (m, 6 H, SiC*H*$_2$), 1.29 (m, 2 H, NCH$_2$C*H*$_2$), 2.12 (m, 6 H, C*H*$_2$CF$_3$), 3.09 (s, 3 H, NC*H*$_3$), 3.51 (m, 2 H, NC*H*$_2$), 7.33 (m, 12 H), 7.40 (s, 1 H) ppm. ^{13}C{^{1}H} ([D$_6$]acetone, 75.5 MHz): δ = −3.9 (s), 7.7 (s), 13.1 (s), 19.6 (s), 33.1 (s), 37.8 (s), 49.3 (s), 121.1 (s), 123.3 (s), 126.6 (s), 131.7 (s), 132.2 (s), 135.0 (s) ppm. ^{11}B{^{1}H} ([D$_6$]acetone, 96.3 MHz): δ = −14.90 (s) ppm.

Solubility Studies: Saturated solutions of **1**−**9** in a solvent were prepared and allowed to settle at 25 °C for 1 h, until the solution was completely clear upon visible inspection. A sample [2.0(1) mL] was taken while ensuring that no undissolved material was

Table 9. Final unit cell parameters and structural data for **2**, **3**, **5**, **6** and **10**

	2	**3**	**5**[a]	**6**	**10**
Empirical formula	$(C_{28}H_{28}B)(C_8H_{15}N_2)$	$(C_{28}H_{16}BF_{12})(C_8H_{15}N_2)$	$(C_{48}H_{16}BF_{52})(C_8H_{15}N_2)$	$(C_{36}H_{52}BSi_4)(C_8H_{15}N_2)\cdot{}^2/_3(C_3H_6O)$	$C_{41}H_{56}BF_9N_2Si_3$
Formula mass	514.53	730.44	1730.64	785.88	842.96
Temperature [K]	110(2)	110(2)	150(2)	150(2)	110(2)
Crystal system	monoclinic	monoclinic	tetragonal	orthorhombic	monoclinic
Space group	*P*2$_1$/*c* (no. 14)	*P*2$_1$/*c* (no. 14)	*P*4$_1$ (no. 76)	*Pbcn* (no. 60)	*P*2$_1$/*c* (no. 14)
a [Å]	16.0649(1)	14.4195(1)	17.4238(10)	38.4424(2)	22.6720(2)
b [Å]	11.1877(1)	14.4595(2)		17.5784(1)	13.0435(1)
c [Å]	21.1563(1)	18.0689(2)	21.457(2)	22.1918(1)	15.2549(1)
β [°]	127.4728(3)	116.6921(6)			100.5188(3)
V [Å^3]	3017.75(4)	3365.87(6)	6514.1(8)	14996.24(13)	4435.40(6)
Z	4	4	4	12	4
$D_{calcd.}$ [g cm^{-1}]	1.133	1.441	1.765	1.044	1.262
Abs. coeff., μ [mm^{-1}]	0.065	0.130	0.208	0.151	0.175
Crystal size [mm]	0.46 × 0.36 × 0.30	0.36 × 0.09 × 0.09	0.35 × 0.21 × 0.06	0.60 × 0.30 × 0.15	0.48 × 0.21 × 0.12
θ Range [°]	1.60−27.49	3.03−24.34	1.17−25.25	1.27−22.25	1.81−27.18
Meas./unique refl.	52337/6914	50613/5500	102273/6071	90497/9463	48882/9754
Goodness-of-fit on *F*^{2}	1.046	1.087	1.262	1.049	1.041
Resid. density [e·Å^{-3}]	−0.34/0.34	−0.32/0.36	−0.72/1.51	−0.40/0.80	−0.25/0.44
R [*I* > 2σ(*I*)]	0.0453	0.0399	0.1282	0.0535	0.0365
R (all data)	0.0559	0.0635	0.1492	0.0668	0.0547
wR$_2$ (all data)	0.1218	0.1151	0.2864	0.1467	0.0922

[a] Friedel pairs were merged.

 © 2003 Wiley-VCH Verlag GmbH & Co. KGaA, Weinheim

sampled. The solvent was removed in vacuo and the residue kept under vacuum (0.1 mbar) for 1 h, after which the weight was constant to within ± 1 mg. The weight of the residue was then determined and the solubility calculated.

Polarity Measurements: A Nile Red solution in methanol (1 mL, 1.89 10^{-3} M) was added to 0.5 g of **8** or **9**. After the mixture had become homogeneous, the methanol was evaporated off in vacuo and the maximum absorbance of Nile Red determined by transmission UV/Vis spectroscopy of a thin film of the ionic liquid. An absorption maximum of 534 (**8**) or 542 nm (**9**) was observed, which corresponds to E_{NR}s of 224.0 kJ/mol (**8**) and 220.7 kJ/mol (**9**).

Structure Determination and Refinement of 2, 3, 5, 6 and 10: X-ray intensities were measured on a Nonius KappaCCD diffractometer with a rotating anode and Mo-K_α radiation (graphite monochromator). The structures were solved by direct methods with the programs SHELXS-97[49] (compounds **2** and **6**) and SIR97[50] (compounds **3**, **5** and **10**). The structures were refined with the program SHELXL-97[51] against F^2 of all reflections. Non-hydrogen atoms were refined freely with anisotropic displacement parameters, hydrogen atoms were refined as rigid groups. The drawings, structure calculations, and checking for higher symmetry were performed with the program PLATON.[52] In the crystal structure of compound **2**, the *n*-butyl group was refined with a disorder model. For compound **3**, one of the trifluoromethyl groups was rotationally disordered. The absolute structure of compound **5** could not be determined reliably. Friedel pairs were therefore merged in the refinement. In the crystal structure of compound **6**, one of the 1-butyl-3-methylimidazolium ions is located on an inversion centre and is, therefore, disordered. Further details of the crystal structure determinations are given in Table 9. CCDC-207227 (**2**), -207228 (**3**), -207229 (**5**), -207230 (**6**), and -207231 (**10**) contain the supplementary crystallographic data for this paper. These data can be obtained free of charge via www.ccdc.cam.ac.uk/conts/retrieving.html (or from the CCDC, 12 Union Road, Cambridge CB2 1EZ, UK; Fax: (internat.) +44 1223 336033; E-mail: deposit@ccdc.cam.ac.uk)

Acknowledgments

The work described here was financially supported by ATOFINA Vlissingen B.V. and the Dutch Ministry of Enonomic Affairs (B.-J. D., J. v. d. B.) and by the Council for Chemical Sciences of the Netherlands Organization for Scientific Research (CW-NWO) (A. L. S., M. L.).

[1] For recent reviews see: [1a] J. Dupont, R. F. de Souza, P. A. Z. Suarez, *Chem. Rev.* **2002**, *102*, 3667−3691. [1b] H. Olivier-Bourbigou, L. Magna, *J. Mol. Catal. A* **2002**, *182−183*, 419−437. [1c] R. Sheldon, *Chem. Commun.* **2001**, 2399−2407. [1d] P. Wasserscheid, W. Keim, *Angew. Chem. Int. Ed.* **2000**, *39*, 3772−3789. [1e] P. Wasserscheid, W. Keim, *Angew. Chemie* **2000**, *112*, 3926−3945. [1f] T. Welton, *Chem. Rev.* **1999**, *99*, 2071−2083.

[2] [2a] P. T. Anastas, M. M. Kirchhoff, *Acc. Chem. Res.* **2002**, *35*, 686−694. [2b] K. R. Seddon, *J. Chem. Tech. & Biotech.* **1997**, *68*, 351−356. [2c] European Union Council Directive 1999/13/EG of 11 March 1999, Official Journal L85, 29.03.1999. [2d] Clean Air Act and Amendments, 42 U. S. C. 7401, et seq.

[3] [3a] P. Bonhôte, A.-P. Dias, N. Papageorgiou, K. Kalyanasundaram, M. Grätzel, *Inorg. Chem.* **1996**, *35*, 1168−1178. [3b] H. Waffenschmidt, *PhD Thesis*, RWTH Aachen, Germany, **2000**.

[4] J. S. Wilkes, M. J. Zaworotko, *J. Chem. Soc., Chem. Commun.* **1992**, 965−966.

[5] [5a] A. S. Larsen, J. D. Holbrey, F. S. Tham, C. A. Reed, *J. Am. Chem. Soc.* **2000**, *122*, 7264−7272. [5b] D. R. MacFarlane, J. Golding, S. Forsyth, M. Forsyth, G. B. Deacon, *Chem. Commun.* **2001**, 1430−1431. [5c] S. V. Dzyuba, R. A. Bartsch, *Chem. Commun.* **2001**, 1466−1467. [5d] T. L. Merrigan, E. D. Bates, S. C. Dorman, J. H. Davis, *Chem. Commun.* **2000**, 2051−2052. [5e] J. H. Davis, K. J. Forrester, *Tetrahedron Lett.* **1999**, *40*, 1621−1622. [5f] L. C. Branco, J. N. Rosa, J. J. Moura Ramos, C. A. M. Afonso, *Chem. Eur. J.* **2002**, *8*, 3671−3677.

[6] [6a] R. Hagiwara, Y. Ito, *J. Fluorine Chem.* **2000**, *105*, 221−227. [6b] S. V. Dzyuba, R. A. Bartsch, *Chem. Phys. Chem.* **2002**, *3*, 161−166. [6c] J. Sun, M. Forsyth, D. R. MacFarlane, *J. Phys. Chem. B* **1998**, *102*, 8858−8864. [6d] J. D. Holbrey, K. R. Seddon, *J. Chem. Soc., Dalton Trans.* **1999**, 2133−2140. [6e] J.-F. Huang, P.-Y. Chen, I.-W. Sun, S. P. Wang, *Inorg. Chim. Acta* **2001**, *320*, 7−11. [6f] A. D. Headley, N. M. Jackson, *J. Phys. Org. Chem.* **2002**, *15*, 52−55. [6g] K. R. Seddon, A. Stark, M.-J. Torres, *Pure Appl. Chem.* **2000**, *72*, 2275−2287.

[7] [7a] P. A. Z. Suarez, J. E. L. Dullius, S. Einloft, R. F. de Souza, J. Dupont, *Polyhedron* **1996**, *15*, 1217−1219. [7b] Y. Chauvin, L. Mussmann, H. Olivier, *Angew. Chem. Int. Ed. Engl.* **1996**, *34*, 2698−2700. [7c] C. M. Gordon, *Appl. Catal. A* **2001**, *222*, 101−117. [7d] W. Keim, D. Vogt, H. Waffenschmidt, P. Wasserscheid, *J. Catal.* **1999**, *186*, 481−484. [7e] A. Bösmann, G. Franciò, E. Janssen, M. Solinas, W. Leitner, P. Wasserscheid, *Angew. Chem. Int. Ed.* **2001**, *40*, 2697−2699. [7f] M. F. Sellin, P. B. Webb, D. J. Cole-Hamilton, *Chem. Commun.* **2001**, 781−782. [7g] P. Lozano, T. De Diego, D. Carrié, M. Vaultier, J. L. Iborra, *Chem. Commun.* **2002**, 692−693.

[8] J. DuPont, P. A. Z. Suarez, R. F. De Souza, R. A. Burrow, J.-P. Kintzinger, *Chem. Eur. J.* **2000**, *6*, 2377−2381.

[9] S. H. Strauss, *Chem. Rev.* **1993**, *93*, 927−942.

[10] C. A. Reed, *Acc. Chem. Res.* **1998**, *31*, 133−139.

[11] L. Cammarata, S. G. Kazarian, P. A. Salter, T. Welton, *Phys. Chem. Chem. Phys.* **2001**, *3*, 5192−5200.

[12] J. van den Broeke, F. Winter, B.-J. Deelman, G. van Koten, *Org. Lett.* **2002**, *4*, 3851−3854.

[13] P. W. Glunz, S. Hintermann, L. J. Williams, J. B. Schwarz, S. C. Kuduk, V. Kudryashov, K. O. Lloyd, S. J. Danishefsky, *J. Am. Chem. Soc.* **2000**, *122*, 7273−7279.

[14] A. Elaiwi, P. B. Hitchcock, K. R. Seddon, N. Srinivasan, Y.-M. Tan, T. Welton, J. A. Zora, *J. Chem. Soc., Dalton Trans.* **1995**, 3467−3472.

[15] J. van den Broeke, M. Lutz, H. Kooijman, A. L. Spek, B.-J. Deelman, G. van Koten, *Organometallics* **2001**, *20*, 2114−2117.

[16] [16a] G. R. Desiraju, T. Steiner, in *The Weak Hydrogen Bond in Structural Chemistry and Biology*; Oxford University Press: Oxford, **1999**. [16b] J. F. Malone, C. M. Murray, M. H. Charlton, R. Docherty, A. J. Lavery, *J. Chem. Soc., Faraday Trans.* **1997**, *93*, 3429−3436.

[17] [17a] M. Nishio, M. Hirote, Y. Umezawa, in *The CH/π Interaction Evidence, Nature and Consequences*; John Wiley & Sons, New York, **1998**. [17b] I. Alkorta, I. Rozas, J. Elguero, *Chem. Soc. Rev.* **1998**, *27*, 163−170. [17c] S. Harder, *Chem. Eur. J.* **1999**, *5*, 1852−1861.

[18] [18a] V. R. Thalladi, H.-C. Weiss, D. Bläser, R. Boese, A. Nangia, G. R. Desiraju, *J. Am. Chem. Soc.* **1998**, *120*, 8702−8710. [18b] J. D. Dunitz, R. Taylor, *Chem. Eur. J.* **1997**, *3*, 89−98.

[19] [19a] M.-A. Guillevic, A. M. Arif, I. T. Horváth, J. A. Gladysz, *Angew. Chem. Int. Ed. Engl.* **1997**, *36*, 1612−1615. [19b] E. de Wolf, A. L. Spek, B. W. M. Kuipers, A. P. Philipse, J.D. Meeldijk, P. H. H. Bomans, P. M. Frederik, B.-J. Deelman, G. van Koten, *Tetrahedron* **2002**, *58*, 3911−3922. [19c] R. P. Singh, B. Twamley, J. M. Shreeve, *J. Chem. Soc., Dalton Trans.* **2000**, 4089−4092. [19d] E. G. Hope, A. M. Stuart, *J. Fluorine Chem.* **1999**, *100*, 75−99.

[20] Chemical shifts for tetraphenylboron compounds can be observed between δ = 0 ppm and −25 ppm: [20a] J. D. Kennedy, in *Multinuclear NMR*; (Ed.: J. Mason); Plenum Press: New York, **1987**, 221. [20b] H. Nöth, H. Vahrenkamp, *Chem. Ber.* **1966**, *99*, 1049−1067.

 © 2003 Wiley-VCH Verlag GmbH & Co. KGaA, Weinheim

[21] [21a] W. Baratta, E. Herdtweck, W. A. Herrmann, P. Rigo, J. Schwarz, *Organometallics* **2002**, *21*, 2101−2106. [21b] S. Caddick, F. G. N. Cloke, G. K. B. Clentsmith, P. Hitchcock, D. McKerrecher, L. R. Titcomb, M. R. V. Williams, *J. Organomet. Chem.* **2001**, *617−618*, 635−639. [21c] A. J. Arduengo, S. F. Gamper, J. C. Calabrese, F. Davidson, *J. Am. Chem. Soc.* **1994**, *116*, 4391−4394. [21d] A. J. Arduengo, H. V. R. Dias, F. Davidson, R. L. Harlow, *J. Organomet. Chem.* **1993**, *462*, 13−18.

[22] N. Kuhn, G. Henkel, T. Kratz, J. Kreuzenberg, R. Boese, A. H. Maulitz, *Chem. Ber.* **1993**, *126*, 2041−2045.

[23] L. Weber, E. Dobbert, H.-G. Stammler, B. Neumann, R. Boese, D. Bläser, *Chem. Ber./Recueil* **1997**, *130*, 705−710.

[24] D. S. Otkidach, I. V. Pletnev, *Theochem.* **2001**, *536*, 65−72.

[25] [25a] P. Haake, L. P. Bausher, *J. Phys. Chem.* **1968**, *78*, 2213−2217. [25b] A. J. Arduengo, R. L. Harlow, M. Kline, *J. Am. Chem. Soc.* **1991**, *113*, 361−363. [25c] A. J. Arduengo, H. V. R. Dias, R. L. Harlow, M. Kline, *J. Am. Chem. Soc.* **1992**, *114*, 5530−5534.

[26] T. V. Ashworth, M. J. Nolte, R. H. Reimann, E. Singleton, *J. Chem. Soc., Chem. Commun.* **1977**, 936−937.

[27] D. S. McGuinness, K. J. Cavell, B. F. Yates, B. W. Skelton, A. H. White, *J. Am. Chem. Soc.* **2001**, *123*, 8317.

[28] [28a] M. Koel, *Proc. Estonian Acad. Sci. Chem.* **2000**, *49*, 145−155. [28b] P. A. Z. Suarez, S. Einloft, J. E. L. Dullius, R. F. de Souza, J. Dupont, *J. Chem. Phys.* **1998**, *95*, 1626−1639.

[29] S. Bratos, H. Ratajczak, P. Voit, in *Mathematical and Physical Sciences*, (Eds.: J. C. Dore, J. Teixeira), NATO ASI Ser. C, Kluwer: Dordrecht, **1989**, vol. 329, p. 221.

[30] C. G. Hanke, N. A. Atamas, R. M. Lynden-Bell, *Green Chem.* **2002**, *4*, 107−111.

[31] [31a] M. Hesse, H. Meier, B. Zeeh, in *Spektroskopische Methoden in der Organischen Chemie, 2nd ed.*; Thieme Verlag: Stuttgart, Germany, **1984**. [31b] J. W. Akitt, in *NMR and Chemistry: an Introduction to the Fourier Transform-Multinuclear Era, 2nd ed.*; Chapman and Hall: London, **1983**.

[32] A. G. Avent, P. A. Chaloner, M. P. Day, K. R. Seddon, T. Welton, *Proceedings of the 8th International Symposium on Molten Salts*; The Electrochemical Society: Pennington, NJ, **1992**; Proceeding Vol. 92−16, p. 98.

[33] During repeated heating cycles, a slight change in the slope of the DSC trace could be observed at these temperatures.

[34] The use of the $-SiMe_2CH_2CH_2-$ linker facilitates a high degree of freedom in the orientation of the attached alkyl- and perfluoroalkyl groups.

[35] H. Bock, T. T. H. Van, H. Schödel, *J. Prak. Chem.* **1997**, *339*, 525−533.

[36] [36a] A. J. Carmichael, K. R. Seddon, *J. Phys. Org. Chem.* **2000**, *13*, 591−595. [36b] K. A. Fletcher, I. A. Storey, A. E. Hendricks, S. Pandey, S. Pandey, *Green Chem.* **2001**, *3*, 210−215.

[37] J. F. Dye, T. A. Berger, *Anal. Chem.* **1990**, *62*, 615−622.

[38] $[EMIM]BF_4$ is stable up to 300 °C: M. L. Mutch, J. S. Wilkes, *Proc. Electrochem. Soc.* **1998**, *98*, 254−260. [EMIm][$N(SO_2CF_3)_2$] is stable up to 400 °C, see ref.[3a]

[39] In particular, the PF_6^- anion decomposes relatively easily in the presence of water: P. Wasserscheid, R. van Hal, A. Boesmann, *Green Chem.* **2002**, *4*, 400−404.

[40] IR spectroscopy showed no νOH stretch frequencies.

[41] The solubility of **9** and especially **8** in hexane is an order of magnitude higher than that of the only related ionic liquid for which miscibility with an apolar liquid was reported. i.e. $[BMIm]PF_6$ in 1-octene (65 g/L): C. C. Brasse, U. Englert, A. Salzer, *Organometallics* **2000**, *19*, 3818. Fluorous ionic liquids of the type [1-R-3-($CH_2CH_2C_xF_{2x+1}$)-imidazolium]PF_6 (R = methyl or butyl, x = 5 or 7) have been reported, but no solubility data were given, ref.[5d]

[42] H. O. House, J. A. Hrabie, S. L. Narasimhan, *J. Chem. Eng. Data* **1986**, *31*, 124.

[43] J. G. Huddleston, H. D. Willauer, R. P. Swatloski, A. E. Visser, R. D. Rogers, *Chem. Commun.* **1998**, 1765−1766.

[44] P. Lucas, N. E. Mehdi, H. A. Ho, D. Belanger, L. Breau, *Synthesis* **2000**, *9*, 1253−1258.

[45] J. D. Wilkey, G. B. Schuster, *J. Org. Chem.* **1987**, *52*, 2117−2122.

[46] J. T. Vandeberg, C. E. Moore, F. P. Cassaretto, H. Posvic, *Anal. Chim. Acta* **1969**, *44*, 175−183.

[47] M. Brookhart, B. Grant, A. F. Volpe, *Organometallics* **1992**, *11*, 3920−3922.

[48] J. van den Broeke, E. de Wolf, B.-J. Deelman, G. van Koten, *Adv. Synth. Catal.* **2003**, *345*, 625−635.

[49] G. M. Sheldrick, *SHELXS-97, Program for Crystal Structure Solution*, University of Göttingen, Germany, **1997**.

[50] A. Altomare, M. C. Burla, M. Camalli, G. L. Cascarano, A. Giacovazzo, A. Guagliardi, G. G. Moliterni, G. Polidori, R. Spagna, *J. Appl. Cryst.* **1999**, *32*, 115−119.

[51] G. M. Sheldrick, *SHELXL-97, Program for Crystal Structure Refinement*, University of Göttingen, Germany, **1997**.

[52] A. L. Spek, *PLATON, A Multipurpose Crystallographic Tool*, Utrecht University, The Netherlands, **2002**.

Received January 30, 2003

 © 2003 Wiley-VCH Verlag GmbH & Co. KGaA, Weinheim

Allosteric Manipulation of Photoexcited State Relaxation in a Series of $Ru^{II}(bpy)_2$(bipyridine−crown ethers)

Subodh K. Dutta,[a] Daqing Gan,[a] and Marc W. Perkovic*[a]

Keywords: Luminescence / Sensors / Photophysics / Lead

A series of ruthenium(II) crown ether complexes containing 4-, 5-, or 6-oxygen crowns tethered to a bipyridine at the 3,3′ position were prepared and examined for their ability to act as luminescent sensors. The complexes $[(bpy)_2Ru(2,2'\text{-bipyridine-}3,3'\text{-16-crown-4})](PF_6)_2$ and $[(bpy)_2Ru(2,2'\text{-bipyridine-}3,3'\text{-19-crown-5})](PF_6)_2$ were characterized by X-ray crystallography. The 4-oxygen crown crystallizes in the $P\bar{1}$ space group. The 5-oxygen crown crystallizes in the $P\bar{1}$ space group. In both complexes, the inter-pyridine ring angle in the tethered bipyridine is twisted substantially away from 0°. Coordination of a heavy metal ion such as Pb^{2+} by the crown ether, and the geometric changes that result, were examined by UV/Vis, luminescence and NMR spectroscopy. The results show that there is a weak allosteric interaction between the Pb^{2+} ion and the Ru complexes, and that this interaction alters the luminescent behavior of the Ru complexes.
(© Wiley-VCH Verlag GmbH & Co. KGaA, 69451 Weinheim, Germany, 2003)

Introduction

The ability to manipulate the physical and chemical properties of an electronically excited molecule is widely accepted as a necessary component of developing molecular devices. The development of luminescent sensors for a host of analytes has been an active area of research.[2−5] Sensors that are based on coordination complexes of transition metals have been of particular interest.[6] Regardless of the nature of the luminophore, the mechanism by which the act of sensing results in a change in the photophysical behavior of the electronically excited molecule is of particular importance.[7] We have been investigating such mechanisms by examining molecules in which the change in photophysical behavior is the result of geometric perturbations of the transition metal center of the luminophore complex.[8]

When considering the photophysical behavior of transition metal excited state complexes, it is often difficult to distinguish between geometric and electronic effects since the two effects are rarely isolable. For example, to what extent do alterations of the substituents on a ligand effect the electron density on the metal, the electron distribution of the M−L bond, and subsequently the energy and lifetime of the photoexcited state? We have attempted to address this ambiguity by examining a series of complexes based on the well-understood $Ru(bpy)_3^{2+}$ molecule, where one of the bipyridine rings has been functionalized at the 3,3′ positions with a crown ether tethered to the bpy pyridine ring.

The oxygen atoms on the crown ethers are not part of the π-system of the bipyridine ligands to any appreciable extent, yet their motion may be telegraphed to the metal center by altering the inter-pyridine ring angle, as has been observed in the complex containing 3,3′-binicotinic acid.[9] Using this approach, we can change the geometry around the metal through an allosteric interaction between the crown ether and the free cations in solution, without changing the ligands.

Results and Discussion

Synthesis and Characterization of the Complexes

The preparation of the Ru(crown-ether) complexes proceeds via facile ligand exchange between the free crown ligands and the chloride ligands of $[cis\text{-}Ru(bpy)_2Cl_2]$. It has previously been reported that the crown ligands adopt a geometry that is unfavorable for coordination to the ru-

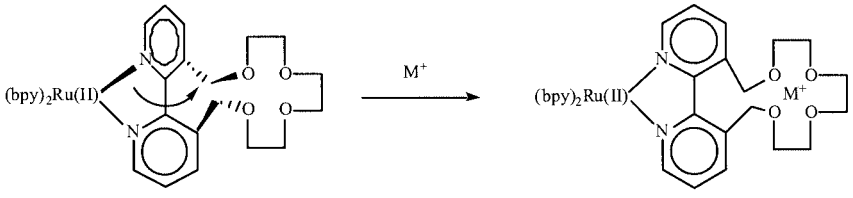

[a] Department of Chemistry, Western Michigan University, Kalamazoo, MI 49008, USA
E-mail: perkovic@wmich.edu

 © 2003 Wiley-VCH Verlag GmbH & Co. KGaA, Weinheim DOI: 10.1002/ejic.200200654

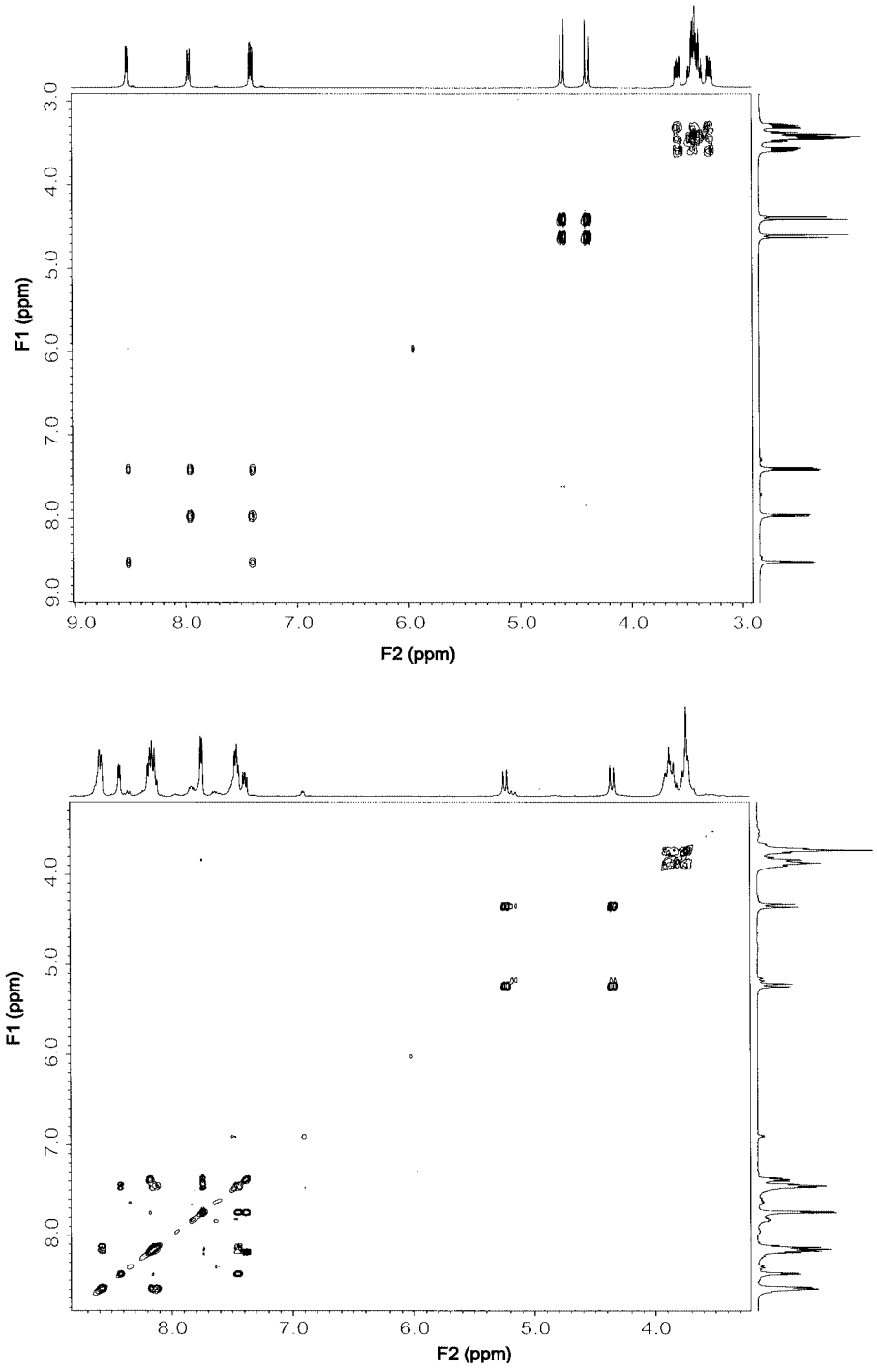

Figure 1. Proton-proton 2D COSY spectrum in CH_3CN of bipyridine-3,3′-16-crown-4 at room temperature (**A**) and $[(bpy)_2Ru(2,2'$-bipyridine-3,3′-16-crown-4)$](PF_6)_2$ at −20 °C (**B**). Changing the temperature does not alter the chemical shifts, but clarifies the coupling constants for the ruthenium complex

thenium(II) atom, with the coordinating nitrogen atoms on opposite sides of the bipyridine bridge.[15] Complex formation nevertheless readily occurs, resulting in a $[(bpy)_2Ru(crown)]^{2+}$ complex where the inter-pyridine ring angle in the crown tethered bipyridine is substantially twisted away from 0°.[9] The geometric change is reflected

 © 2003 Wiley-VCH Verlag GmbH & Co. KGaA, Weinheim

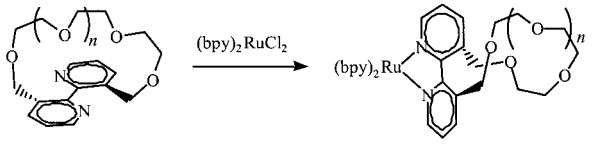

in the NMR spectrum, particularly in the resonances of the correlated benzylic protons at ≈ 5 ppm, as shown in Figure 1. Peak assignments are presented Table 5.

X-ray Structure Determination

X-ray Determination of [(bpy)$_2$Ru(2,2′-bipyridine-3,3′-16-crown-4)](PF$_6$)$_2$

X-ray quality crystals were grown by slow diffusion of diethyl ether into a solution of the crown complex in pyridine. A deep red, rectangular plate, approximately 0.25 × 0.12 × 0.1 mm, was chosen by size, habit, and polarized light microscopy. The complex crystallized in the triclinic system in the space group $P\bar{1}$(#2),[10] as determined from 25 high angle reflections. The data collection and refinement parameters are presented in Table 6. The structure was solved by direct methods using SIR,[11] and refined by full-matrix least-squares methods using SHELXL.[12] All non-hydrogen atoms were refined anisotropically. Hydrogen atoms were placed in calculated positions. The largest unassigned peak in the final difference map was 0.51e/Å^3, located near the Ru ion. No absorption correction was applied. The structure was refined to a final *R* value of 7.52%. The refined cation is shown in Figure 2, and structural details are presented in Table 1.

X-ray Determination of [(bpy)$_2$Ru(2,2′-bipyridine-3,3′-19-crown-5)](PF$_6$)$_2$

A deep red, rectangular plate, approximately 0.25 × 0.25 × 0.12 mm, crystallized from an aqueous solution of the crown complex on standing. The crystal was chosen by size, habit, and polarized light microscopy. The complex also crystallized in the triclinic system in the space group $P\bar{1}$. The structure was solved by direct methods using SIR, and refined by full-matrix least-squares methods using SHELXL. All non-hydrogen atoms were refined anisotropically. Hydrogen atoms were placed in calculated positions. The largest unassigned peak in the final difference map was 0.8 e/Å^3, located near a PF_6 anion. No absorption correction was applied. Two waters of crystallization were observed. The structure was refined to a final *R* value of 7.41%. The refined cation is shown in Figure 2, and structural details are presented in Table 2.

In both complexes, the Ru−N bond lengths and angles are typical of a ruthenium diimine, spanning a range from 2.04 to 2.08Å. The two non-crown containing bipyridine rings in both complexes are flat to within 5°. However, the bipyridine containing the tethered crown ether was distorted by about 35° for the 4-oxygen crown, and by 24° for the 5-oxygen crown. As we expected, the presence of the crown ethers caused a geometric distortion at the ruthenium center. The magnitude of the distortion reflects the flexibility in the tethered crown ether. We were unable to obtain satisfactory crystals for the 6-oxygen crown complex.

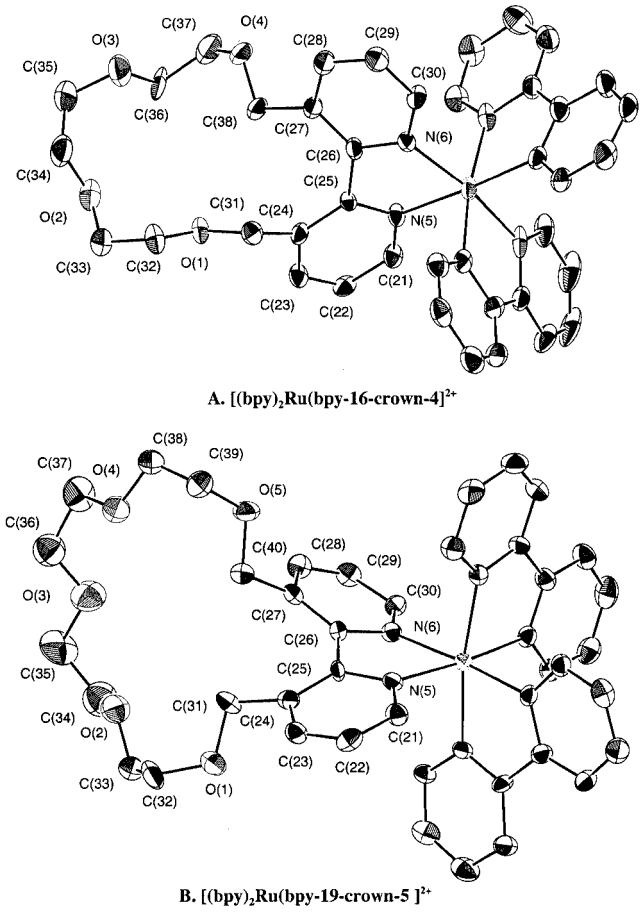

Figure 2. ORTEP diagram of [(bpy)$_2$Ru(bpy-16-crown-4)]$^{2+}$ (**A**) and [(bpy)$_2$Ru(bpy-19-crown-5]$^{2+}$ (**B**)

Electrochemistry

Half-wave potentials were determined by cyclic voltammetry (Figure 3) and are listed in Table 3. The cyclic voltammograms of each of the three [Ru(bpy)$_2$(crowns)]$^{2+}$ complex cations in CH_3CN exhibit one reversible Ru^{II}/Ru^{III} wave at a slightly lower potential than that observed for [Ru(bpy)$_3$]$^{2+}$. Three reversible reduction waves are also observed, with no significant shift in their positions relative to [Ru(bpy)$_3$]$^{3+}$. These data suggest that the slight twist of the inter-pyridine rings on the crown ligands does not alter the ground state electronics of the aromatic ring system, although the loss in angular overlap between the ligand and the ruthenium atom may slightly raise the energy of the ruthenium d-orbitals.

Emission Spectroscopy

The luminescence spectra for the three ruthenium crown complexes are also typical for ruthenium(II) *tris*-bipyridine analogs. At room temperature, the broad charge transfer spectra for the three complexes show little dependence on

 © 2003 Wiley-VCH Verlag GmbH & Co. KGaA, Weinheim

Table 1. Selected bond lengths [Å] and angles [deg] for $[(bpy)_2Ru(bpy\text{-}16\text{-}crown\text{-}4)]^{2+}$

C(1)−C(12)	1.525(13)	C(1)−O(4)	1.381(12)
C(2)−C(3)	1.52(2)	C(2)−O(4)	1.419(14)
C(3)−O(3)	1.447(14)	C(4)−C(5)	1.44(2)
C(4)−O(3)	1.45(2)	C(5)−O(2)	1.445(15)
C(6)−C(7)	1.488(15)	C(6)−O(2)	1.421(14)
C(7)−O(1)	1.408(10)	C(8)−C(17)	1.507(12)
C(8)−O(1)	1.416(10)	C(11)−C(12)	1.404(11)
C(11)−C(16)	1.462(10)	C(11)−N(2)	1.384(9)
C(12)−C(13)	1.382(13)	C(13)−C(14)	1.402(14)
C(14)−C(15)	1.348(12)	C(15)−N(2)	1.329(11)
C(16)−C(17)	1.402(11)	C(16)−N(1)	1.368(9)
C(17)−C(18)	1.390(12)	C(18)−C(19)	1.356(12)
C(19)−C(20)	1.368(12)	C(20)−N(1)	1.327(10)
N(1)−Ru(1)	2.076(6)	N(2)−Ru(1)	2.079(6)
N(4)−Ru(1)	2.071(7)	N(3)−Ru(1)	2.038(7)
N(5)−Ru(1)	2.052(8)	N(6)−Ru(1)	2.039(7)
bond angles			
N(1)−Ru(1)−N(2)	79.1(2)	N(1)−Ru(1)−N(4)	176.0(2)
N(1)−Ru(1)−N(3)	100.6(3)	N(1)−Ru(1)−N(5)	93.1(3)
N(1)−Ru(1)−N(6)	87.0(3)	N(2)−Ru(1)−N(4)	96.9(3)
N(2)−Ru(1)−N(3)	86.8(3)	N(2)−Ru(1)−N(5)	172.1(3)
N(2)−Ru(1)−N(6)	98.5(3)	N(4)−Ru(1)−N(3)	78.5(3)
N(4)−Ru(1)−N(5)	90.9(3)	N(4)−Ru(1)−N(6)	94.2(3)
N(3)−Ru(1)−N(5)	96.2(3)	N(3)−Ru(1)−N(6)	171.5(3)
N(5)−Ru(1)−N(6)	79.5(3)		

Table 2. Selected bond lengths [Å] and angles [deg] for $[(bpy)_2Ru(bpy\text{-}19\text{-}crown\text{-}5)]^{2+}$

C(21)−C(22)	1.351(13)	C(21)−N(5)	1.321(11)
C(22)−C(23)	1.360(14)	C(23)−C(24)	1.399(14)
C(24)−C(25)	1.410(12)	C(24)−C(31)	1.517(14)
C(25)−C(26)	1.497(12)	C(25)−N(5)	1.367(10)
C(26)−C(27)	1.397(12)	C(26)−N(6)	1.366(11)
C(27)−C(28)	1.404(13)	C(27)−C(40)	1.514(12)
C(28)−C(29)	1.368(15)	C(29)−C(30)	1.369(13)
C(30)−N(6)	1.348(11)	C(31)−O(1)	1.410(12)
C(32)−C(33)	1.50(2)	C(32)−O(1)	1.393(14)
C(33)−O(2)	1.42(2)	C(34)−C(35)	1.47(3)
C(34)−O(2)	1.43(2)	C(35)−O(3)	1.40(2)
C(36)−C(37)	1.50(2)	C(36)−O(3)	1.41(2)
C(37)−O(4)	1.43(2)	C(38)−C(39)	1.50(2)
C(38)−O(4)	1.395(15)	C(39)−O(5)	1.422(13)
C(40)−O(5)	1.431(12)	N(1)−Ru(1)	2.073(6)
N(2)−Ru(1)	2.062(7)	N(3)−Ru(1)	2.072(7)
N(4)−Ru(1)	2.056(6)	N(5)−Ru(1)	2.062(7)
N(6)−Ru(1)	2.066(7)		
Bond angles			
N(1)−Ru(1)−N(3)	93.9(2)	N(1)−Ru(1)−N(2)	89.6(2)
N(1)−Ru(1)−N(5)	96.0(2)	N(1)−Ru(1)−N(4)	79.1(3)
N(2)−Ru(1)−N(3)	78.7(3)	N(1)−Ru(1)−N(6)	174.5(2)
N(2)−Ru(1)−N(5)	174.3(3)	N(2)−Ru(1)−N(4)	95.7(3)
N(3)−Ru(1)−N(4)	171.1(3)	N(2)−Ru(1)−N(6)	95.6(3)
N(3)−Ru(1)−N(6)	88.6(3)	N(3)−Ru(1)−N(5)	99.7(3)
N(4)−Ru(1)−N(6)	98.9(3)	N(4)−Ru(1)−N(5)	86.6(3)
N(5)−Ru(1)−N(6)	78.8(3)		

the size of the tethered crown ether. At 77 K, only the 6-oxygen crown shows a small red shift in emission. The activation energies for the three complexes are within experimental error of each other (Table 4). The addition of Pb^{2+} ions to the complexes results in a small, but significant, increase in the emission intensity, but no significant change in the emission energy. The change in emission intensity for the three ligand complexes are similar and a typical response is shown in Figure 4. This result differs from that observed for $[(bpy)_2Ru(2,2'\text{-bipyridine-}3,3'\text{-}16\text{-crown-}4)]^{2+}$ in the presence of Group I metal ions.[13] However, it is not clear to what extent ion pairing impacts the observed emission behavior. We have observed that varying the concentration of the perchlorate ion causes shifts in the emission spectrum, similar to those previously reported.[14] For the results discussed here, the measurements were performed in DMSO/water solutions at constant ionic strength. Plotting the magnitude of the emission change over an extended range of Pb^{2+} concentrations yields a Ru−Pb complex stoichiometry of 1:1, with an equilibrium constant of $K \approx 0.4\ M^{-1}$.

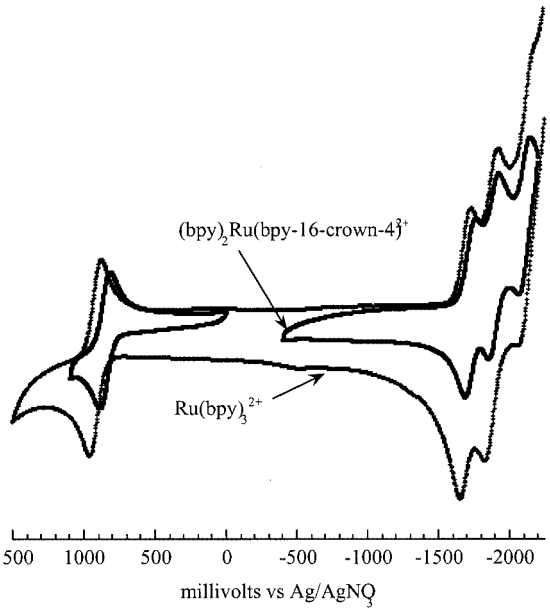

Figure 3. Cyclic voltammogram of the Ru complexes in acetonitrile

Table 3. Electrochemical data[a] for $Ru(bpy)_2(crown)^{2+}$ complexes

Ru(bpy)2(crown)	$Ru^{II/III}$ [mV]	bpy/bpy$^-$ [mV]		
2,2′-bipyridine-3,3′-16-crown-4	0.856	−1.71	−1.88	−2.09
2,2′-bipyridine-3,3′-19-crown-5	0.90	−1.75	−1.95	−2.15
2,2′-bipyridine-3,3′-21-crown-6	0.88	−1.70	−1.90	−2.12

NMR Spectroscopy

We examined the NMR spectra of the free ligands and the ruthenium complexes with and without additional metal ions such as Li^+, Na^+, K^+, Pb^{2+}, and Cs^+, in order to correlate the photophysical behavior of the ruthenium complexes with any geometric changes caused by the presence of the metal ions. Typically, a large excess of the allos-

 © 2003 Wiley-VCH Verlag GmbH & Co. KGaA, Weinheim

Table 4. Photophysical data in DMSO/water

Complex[b]	λ_{max}, nm		Lifetime		E_a	Φ_{em}[a]	
	77 K	298 K	τ_{77}, μs	τ_{298}, ns	cm^{-1}	77 K	298 K
$(bpy)_2Ru(2,2'\text{-bipyridine-}3,3'\text{-16-crown-}4)^{2+}$	589	615	3.0	680	1950	0.0332	0.0138
$(bpy)_2Ru(2,2'\text{-bipyridine-}3,3'\text{-19-crown-}5)^{2+}$	588	617	3.3	700	2260	0.0321	0.0198
$(bpy)_2Ru(2,2'\text{-bipyridine-}3,3'\text{-21-crown-}6)^{2+}$	585	622	3.4	750	2520	0.0399	0.0174

[a] Quantum yields were determined by comparing the integrated intensity of the samples to that of an absorbance-matched standard, $[Ru(bpy)_3]^{2+}$ $\Phi = 0.062$. I. Dupry, T. J. Meyer, *Inorg. Chem.* **1996**, *35*, 6299. [b] DMSO/water used because of its low temperature glass properties. Results in CH_3CN are the same to within experimental error.

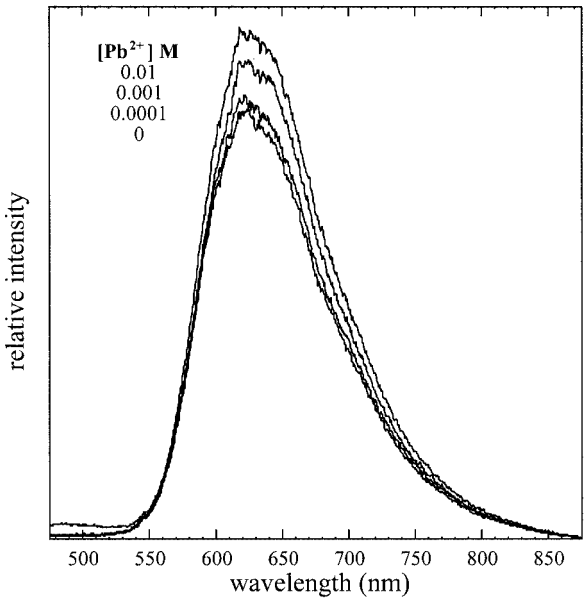

Figure 4. Emission spectrum of $(bpy)_2Ru(2,2'\text{-bipyridine-}3,3'\text{-16-crown-}4)^{2+}$ at room temperature with variable $[Pb^{2+}]$

teric ions, as their metal triflates, were added to the solution of $[Ru(bpy\text{-crown})]^{2+}$ in $CDCl_3$ and/or $[D_6]$acetone so that any equilibria present would be shifted towards the products.

The NMR spectra of the crown ethers and their ruthenium complexes have two distinct spectral features that are well-separated: the aromatic region corresponding to the bipyridine moiety of the molecule (7−9 ppm), and the aliphatic (methylene) portion of the cyclic ethers (≈ 3−5.5 ppm). As an uncoordinated molecule, the bipyridine rings are twisted such that they are *anti* to each other with respect to the pyridine−pyridine bond. On coordination to the ruthenium atom via the pyridine nitrogen atoms, the benzylic protons are forced into close proximity. The resulting anisotropic field causes an AB splitting pattern in the benzylic resonances. As has been previously reported for the free ligands,[18] we observed that all regions of the ^1H spectrum undergo considerable changes on addition of Li^+, Na^+, K^+, Pb^{2+}, and Cs^+ ions. The most dramatic changes occur in the aromatic region, followed by a smaller change in the benzylic region, and finally a relatively small change in the region of the methylene groups. However, in the case of the ruthenium complexes, a different behavior is observed. For these complexes, essentially no change is seen in the aromatic region and very small changes in the methylene resonances. The largest change is observed for the resonances of the benzylic protons. For example, $[(bpy)_2Ru(2,2'\text{-bipyridine-}3,3'\text{-19-crown-}5)]^{2+}$ shows two doublets assigned to the benzylic protons 8a-H and 8b-H, at $\delta = 4.47$ and 4.73 ppm, respectively (Figure 5 and Table 5). In the presence of Pb^{2+} ions, these two resonances shift to $\delta = 4.63$ and 4.72 ppm, respectively. The coupling constant ($J_{8a\text{-}H-8b\text{-}H}$) decreases from 12.4 to 12.1 Hz. This indicates that the Pb^{2+} ion is interacting with the crown ether oxygen atoms, but that the interaction is not telegraphed to the bipyridine ring system. Similar results were observed for the 5-crown and 6-crown complexes in the

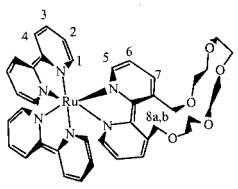

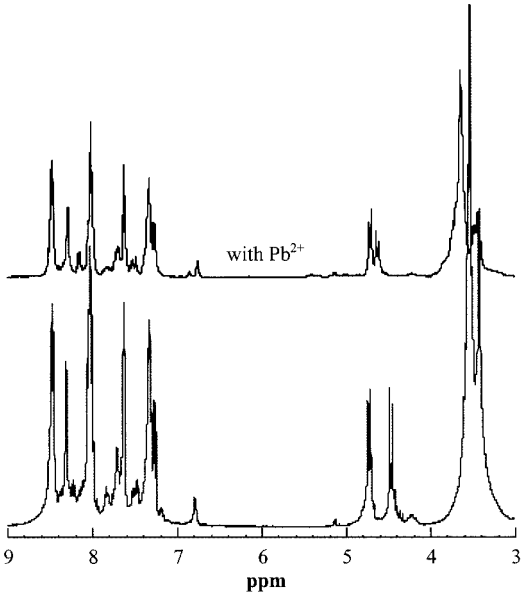

Figure 5. ^1H NMR numbering scheme and spectra recorded with and without Pb^{2+} in CH_3CN

 © 2003 Wiley-VCH Verlag GmbH & Co. KGaA, Weinheim

Table 5. ^{1}H chemical shifts (ppm) of Ru Complexes in [D_3]acetonitrile with and without Pb^{2+}

Compound	Pb^{2+}	Chemical shift[a] H1	H2	H3	H4	H5	H6	H7	H8a	H8b	Ether CH_2	
$(bpy)_2Ru(16\text{-crown-}4)^{2+}$		8.58 (d)	8.15 (m)	7.40	7.75	8.42 (d)	7.45	8.13 (m)	5.23 (d)	4.35 (d)	3.87 (b)	3.73 (b)
$(bpy)_2Ru(16\text{-crown-}4)^{2+}$	·	8.58 (d)	8.15 (m)	7.40	7.75	8.42 (d)	7.45	8.12 (m)	5.20 (d)	4.32 (d)	3.95 (b)	3.75 (b)
$(bpy)_2Ru(19\text{-crown-}5)^{2+}$		8.48 (d)	8.04 (m)	7.27	7.62	8.31 (d)	7.33	8.01	4.73 (d)	4.47 (d)	3.53 (b)	3.43 (b)
$(bpy)_2Ru(19\text{-crown-}5)^{2+}$	·	8.50 (d)	8.03 (m)	7.27	7.63	8.29 (d)	7.32	8.00 (m)	4.72 (d)	4.63 (d)	3.70 (b)	3.44 (b)
$(bpy)_2Ru(21\text{-crown-}6)^{2+}$		8.59 (m)	8.15 (m)	7.37	7.73	8.40 (m)	7.42	8.11 (m)	4.76 (m)	4.32 (b)	3.65 (b)	3.17 (b)
$(bpy)_2Ru(21\text{-crown-}6)^{2+}$	·	8.49 (m)	8.05 (m)	7.36	7.70	8.30 (m)	7.60	8.00 (m)	5.11 (m)	4.75 (m)	3.81 (b)	3.62 (b)

[a] Chemical shifts were assigned based on the ^{1}H-^{1}H COSY spectra.

presence of Pb^{2+} ions. The NMR shifts are substantially smaller for the other cations examined.

Conclusions

The smaller than expected, and previously observed,[9] photophysical response of the ruthenium crown complexes when exposed to Pb^{2+} ions is the result of stereochemical constraints exerted by the tethered crown ethers on their host bipyridine. Molecular modeling shows that in the ruthenium crown complexes, the protons on the benzylic carbon atoms (8a-,8b-H in Figure 5) are the major source of steric repulsion. These protons restrict the ability of the two pyridine rings from approaching co-planarity to less than about 15°. Regardless of the number of oxygen atoms in the ring, the oxygen atoms attached to the benzylic carbons are always positioned such that their lone pairs are no longer pointing inward towards the crown cavity.[14,15] In this way it is impossible for these two oxygen atoms to coordinate a guest ion. As the crown ring size increases, additional oxygen atoms are available to coordinate guest ions. However, these oxygen atoms are sufficiently removed from the bipyridine so as to offer little or no leverage for an allosteric perturbation of the ruthenium coordination sphere, since the flexibility of the crown framework is substantial. This, coupled with the proximity of the benzylic protons, prohibits any substantial change in the bipyridine ring geometry or motion. Without a substantial impact on the coordinated bipyridine, either in terms of geometry or electronics, no photophysical change is possible. We have prepared analogous crown complexes where the crowns are tethered directly to aromatic rings at the 3,3′ positions without a benzylic carbon and the problematic protons. The results of those studies will be reported elsewhere.

Experimental Section

Syntheses: All chemicals used were of reagent grade, or better, and used without further purification. The bipyridine crown-ether ligands 2,2′-bipyridine-3,3′-16-crown-4, 2,2′-bipyridine-3,3′-19-crown-5, 2,2′-bipyridine-3,3′-21-crown-6, and [*cis*-$(bpy)_2RuCl_2$]·$2H_2O$[16] were prepared by literature methods.[17] Metal triflates were prepared by treating the metal carbonates with neat CF_3SO_3H, (3M FC-43, technical grade), followed by recrystallization from dichloromethane.

Preparation of [$(bpy)_2$Ru(2,2′-bipyridine-3,3′-16-crown-4)]$(PF_6)_2$: [$Ru(bpy)_2Cl_2$]·$2H_2O$ (0.43 g) was added to an ethanolic solution of 2,2′-bipyridine-3,3′-16-crown-4 (0.27 g in 20 mL) in a 50-mL flask. The mixture was refluxed for 24 h, and was filtered when it was still hot. Ammonium hexafluorophosphate was added to the cooled filtrate, and the mixture was stored in a refrigerator overnight. The resulting orange−yellow precipitate was collected by filtration, washed with ether (30 mL), then dried under vacuum. The compound was purified by column chromatography (2 × 25 cm) on neutral alumina using an acetone/CH_2Cl_2 (4:7) mixture as the eluent. The first fraction was evaporated to near dryness and dissolved in a minimum volume of water. Addition of solid NH_4PF_6, followed by overnight refrigeration resulted in 500 mg of a crystalline product (86%yield). UV/Vis in (1:1) DMSO/0.1 M $NaCF_3SO_3$ [λ nm, ε ($mol^{-1}cm^{-1}$)]: 227 (61620), 290 (69714), 450 (13950). ^{1}H NMR ([D_6]acetone): δ = 8.78 (d), 8.20 (m), 7.97 (m), 7.54 (m), 5.20, 4.50, 3.80, 3.70 ppm. ^{13}C NMR ([D_6]acetone): δ = 152.2 ppm, 138.0, 127.8, 72.0, 70.4, 70.1, 69.5. MS: *m*/*z* = 889, 372, corresponding to a monocation PF_6 salt and the parent dication, respectively.

Preparation of [$(bpy)_2$Ru(2,2′-bipyridine-3,3′-19-crown-5)]$(PF_6)_2$: This compound was synthesized and purified following the same procedure as that described for the 2,2′-bipyridine-3,3′-16-crown-4 complex. Reacting 0.25 g of the crown ligand resulted in 512 mg of the ruthenium complex. (91.9% yield). UV/Vis in (1:1) DMSO/0.1 M $NaCF_3SO_3$ [λ nm, ε ($mol^{-1}cm^{-1}$)]: 236 (78126), 290 (40660), 450 (6460). ^{1}H NMR ([D_6]acetone): δ = 8.8 (d), 8.2 (m), 8.00 (m), 7.55 (m), 4.92, 4.70, 3.65, 3.00 ppm. ^{13}C NMR ([D_6]acetone): δ = 157.5 ppm, 152.2, 137.8, 127.6, 126.8, 71.0−69.0(5 peaks). MS: *m*/*z* = 395.

Preparation of [$(bpy)_2$Ru(2,2′-bipyridine-3,3′-21-crown-6)]$(PF_6)_2$: This compound was synthesized and purified following the same procedure as that described for the 2,2′-bipyridine-3,3′-16-crown-4 complex, without significant modification, except that acetone was used as the eluent. Reacting 0.31 g of the crown ligand resulted in 496 mg of the ruthenium complex. (76.2% yield). UV/Vis in (1:1) DMSO/0.1 M $NaCF_3SO_3$ [λ nm, ε ($mol^{-1}cm^{-1}$)]: 236 (30878), 290 (69714), 450 (13950). ^{1}H NMR ([D_6]acetone): δ = 8.8 (d), 8.20 (m), 8.00 (m), 7.50 (m), 5.00, 3.65, 3.55 ppm. ^{13}C NMR ([D_6]acetone): δ = 152.3 ppm, 138.5, 127.8, 124.8, 68.1−70.0. MS: *m*/*z* = 416.

Physical Measurements

Spectroscopic Measurements: IR spectra were recorded using KBr pellets on a Perkin−Elmer 1710 FTIR or a Bruker Equinox 55 FTIR. UV/Vis spectra were recorded on a Beckman 7400 diode array spectrometer. NMR spectra were recorded on a JEOL Eclipse+ 400 multinuclear NMR (400 MHz ^{1}H) equipped with a *z*-axis gradient probe. Luminescence spectra were recorded on a

 © 2003 Wiley-VCH Verlag GmbH & Co. KGaA, Weinheim

Table 6. Data collection and refinement parameters for $[(bpy)_2Ru(bpy\text{-}16\text{-}crown\text{-}4](PF_6)_2$ and $[(bpy)_2Ru(bpy\text{-}19\text{-}crown\text{-}5](PF_6)_2$

	$[(bpy)_2Ru(bpy\text{-}16\text{-}crown\text{-}4)](PF_6)_2$	$[(bpy)_2Ru(bpy\text{-}19\text{-}crown\text{-}5)](PF_6)_2$
Space group	$P\bar{1}$	$P\bar{1}$
Cell constants	a = 12.5404(0.0025) Å	a = 12.7320(0.0039) Å
	b = 12.6871(0.0047) Å	b = 13.0510(0.0043) Å
	c = 14.4495(0.0059) Å	c = 14.0350(0.0054) Å
	α = 101.2932(0.0330)°	α = 86.186(0.0288)°
	β = 102.6826(0.0161)°	β = 77.326(0.0282)°
	γ = 93.0886(0.0230)°	γ = 86.99(0.0255)°
Reflections collected	$0 < h > 12$	$0 < h > 15$
	$-13 < k > 13$	$-15 < k > 15$
	$-17 > l > 16$	$-16 > l > 16$
No. of reflections (total/unique/I_0>4Σ(I_0)]	7560/7359/4579	7737/7687/4626
Scan method	ω/2θ	ω/2θ
Empirical formula	$C_{38}H_{38}F_{12}N_6O_4P_2Ru$	$C_{40}H_{46}F_{12}N_6O_8P_2Ru$
Formula mass	1033.74 amu	1166.24 amu
Formula units per cell	Z = 2	Z = 2
Density	$d_{calcd.}$ = 1.594 g/cm^{-3}	$d_{calcd.}$ = 1.631 g/cm^{-3}
Absorption coeff.	μ = 0.54 mm^{-1}	μ = 0.52 mm^{-1}
Temperature	T = 295 K	T = 295 K
Radiation (Mo-K_α)	λ = 0.7107 Å	λ = 0.7107 Å
F_{000}	1044 e	1116 e
Structural parameters	571	607
R_1	0.0752	0.0865
wR_2	0.2075[a]	0.2373[a]

[a] Weight = $([\Sigma^2(F_o^2) + (0.1183\cdot P)^2 + 7.99\cdot P])^{-1}$ where $P = [\max(F_o^2,0) + 2F_c^2)/3$. [a] Weight = $([\Sigma^2(F_o^2) + (0.1081\cdot P)^2 + 7.99\cdot P])^{-1}$ where $P = [\max(F_o^2,0) + 2F_c^2)/3$.

PTI Quanta Master spectrometer. Spectra were corrected for wavelength response and lamp intensity fluctuations. Mass spectra were obtained from a Micromass QUATTRO II mass spectrometer by direct insertion.

Photophysical Measurements: Quantum yield determinations were performed using nitrogen purged, absorbance matched (0.1 A @450 nm) samples in DMSO/water (1:1 v/v) solutions. $[Ru(bpy)_3]^{2+}$ was used as the standard. Luminescent lifetimes were determined by exciting the samples with the third harmonic from a Continuum Surelite-I Nd:YAG laser. The laser was run at minimum flash lamp power and the beam was attenuated so that sample irradiation occurred with a less than 100 μJ/10 ns pulse @355 nm. The emitted light was filtered with a 450 nm cut-off filter to eliminate laser scatter, and collected by a fiber optic interfaced to an Acton SP300i monochromator/Hamamatsu R928 PMT. The photomultiplier was run at a constant −1000 V, and the light level was adjusted using the monochromator slits in order to provide a signal no larger than 100 mV across 50 W. Typically 16 transients were recorded on a LeCroy LT342 DSO, and the data fit by non-linear least-squares methods. Sample temperatures were maintained to ±0.5 K with an Oxford Optistat liquid-nitrogen cryostat. All device control and data manipulations were performed with a computer program developed in-house. Variable temperature lifetime data were fit to an Arrhenius function for the determination of activation energies.

Electrochemical Data: Cyclic voltammograms were recorded in nitrogen purged CH_3CN at room temperature, using a BAS 50 W potentiostat equipped with a Pt working and auxiliary electrodes and an $Ag/AgNO_3$ reference electrode. Tetrabutylammonium perchlorate was used as the supporting electrolyte.

X-ray Structure Data: Single crystal data (Table 6) were recorded on a Nonius CAD4 diffractometer at −100 °C by using graphite-monochromated Mo-$K\alpha$ radiation. The crystal was mounted on a glass fiber with epoxy and placed with a random orientation on the diffractometer. The unit cell and data collection parameters were determined from 25 high angle reflections. The space group and structural parameters were determined using the maXus suite of programs. Intensity standards were recorded after each 100 minutes of exposure.

CCDC-198711 for $[(bpy)_2Ru(bpy\text{-}16\text{-}crown\text{-}4)](PF_6)_2$ and CCDC-198712 for $[(bpy)_2Ru(bpy\text{-}19\text{-}crown\text{-}5)](PF_6)_2$ contain the supplementary crystallographic data for this paper. These data can be obtained free of charge at www.ccdc.cam.ac.uk/conts/retrieving.html [or from the Cambridge Crystallographic Data Centre, 12, Union Road, Cambridge CB2 1EZ, UK; Fax: (internat.) +44-1223/336-033; E-mail: deposit@ccdc.cam.ac.uk].

Acknowledgments

Support for this research was generously provided by the National Science Foundation (CHE-9876142), the Kalamazoo Foundation and Western Michigan University.

[1] Portions of this manuscript were submitted in partial fulfillment for the degree of Master of Arts, Western Michigan University, **1999**.
[2] See the excellent series of reviews in: L. Fabbrizzi (Ed.), *Coord. Chem. Rev.* **2000**, vol. *205*, pp. 3−228.
[3] A. W. Czarnick (Ed.), *Fluorescent Chemosensors for Ion and Molecule Recognition*; American Chemical Society: Washington DC, ACS Symposium Series 538, **1992**.
[4] A. P. de Silva, H. Q. Gunaratne, T. Gunnlaugsson, A. J. Huxley, C. P. McCoy, J. T. Rademacher, T. E. Rice, *Chem. Rev.* **1997**, *97*, 1515.
[5] [5a] O. S. Wolfbeis (Ed.), *Fiber Optic Chemical Sensors and Biosensors*; CRC Press: Boca Raton, Florida, **1991**, vol. I & II. [5b] R. A. Bissell, A. P. de Silva, H. Q. N. Gunaratne, P. L.

Lynch, G. E. M Maguire, C. P. McCoy, K. R. A. S. Sandanayake, *Chem. Soc. Rev.* **1992**, *21*, 187. [5c] R. A. Bissell, A. P. de Silva, H. Q. N. Gunaratne, P. L. Lynch, G. E. M. Maguire, K. R. A. S. Sandanayake, *Top. Curr. Chem.* **1993**, *168*, 223. [5d] A. P. de Silva, H. Q. Gunaratne, T. Gunnlaugsson, A. J. M. Huxley, C. P. McCoy, J. T. Rademacher, T. E. Rice, *Adv. Supramol. Chem.* **1997**, *4*, 127.

[6] [6a] V. Balzani, F. Scandola, *Supramolecular Photochemistry*; Ellis−Horwood: Chichester, **1991**. [6b] V. Balzani, A. Credi, F. Scandola, "Supramolecular Photochemistry and Photophysics. Energy-Conversion and Information-Processing Devices Based on Transition Metal Complexes" in: *Transition Metals in Supramolecular Chemistry* (Eds.: L. Fabbrizzi, A. Poggi), Kluwer: Dorecht, **1994**. [6c] "Perspectives in Supramolecular Chemistry-from Molecular Recognition towards Molecular Information Processing and Self-Organization": J. M. Lehn, *Angew. Chem. Int. Ed. Eng.* **1990**, *29*, 1304. [6d] L. Fabbrizzi, A. Poggi (Eds.), *Transition metals in Supramolecular Chemistry*; Kluwer: Dorecht, **1994**.

[7] M. H. Keefe, K. D. Benkenstein, J. T. Hupp, *Coord. Chem. Rev.* **2000**, *205*, 201.

[8] [8a] W. Szulbinski, J. Kincaid, *Inorg. Chem.* **1998**, *37*, 859. [8b] M. Sykora, J. Kincaid, *Inorg. Chem.* **1995**, *34*, 5852. [8c] S. Bélanger, M. Gilbeertson, D. Yoon, C. Stern, X. Dang, J. Hupp, *J. Chem. Soc., Dalton* **1999**, *19*, 3407. [8d] L. Fabrizzi, A. Poggi, *Chem. Soc., Rev.* **1995**, *24*, 197. [8e] L. Fabrizzi, M. Licchelli, P. Pallavicini, D. Sacchi, A. Taglietti, *Analyst* **1996**, *121*, 1763.

[9] M. W. Perkovic, *Inorg. Chem.* **2000**, *39*, 4962.

[10] We have determined the X-ray structure of the four oxygen crown and calculated the geometry of the four, five and six oxygen crowns. In the solid state the four oxygen crown has an inter-pyridine angle of 87°. These results will be pubished elsewhere.

[11] *International Tables for X-ray Crystallography*; Kynoch: Birmingham, **1965**.

[12] *SIR92:* A. Altomore, G. Casscarano, C. Giacovazzo, A. Guggliandi, M. C. Burla, G. Polidori, G. M. Camalli, *J. Appl. Cryst.* **1994**, *27*, 435.

[13] G. Sheldrick, *SHELXL-97* crystal structure refinement package, Unix release 97-2.

[14] M. Chiba, K. Ogawa, K. Tsuge, M. Abe, H.-B. Kim, Y. Sasaki, N. Kitamura, *Chem. Lett.* **2001**, *7*, 692.

[15] J. Rebek, T. Costello, L. Marshall, R. Watley, R. C. Gadwood, K. Onan, *J. Am. Chem. Soc.* **1985**, *107*, 7481.

[16] S. V. Luis, J. C. Frías, M. I. Burguete, M. Bolte, *Acta Crystallogr., Sect. C* **1998**, *54*, 1093.

[17] B. P. Sullivan, D. J. Salmon, T. J. Meyer, *Inorg. Chem.* **1978**, *17*, 3334.

[18] J. Rebek Jr., J. E. Trend, R. V. Watley, A. Chakravorti, *J. Am. Chem. Soc.* **1979**, *101*, 4333.

Received November 27, 2002

 © 2003 Wiley-VCH Verlag GmbH & Co. KGaA, Weinheim

Chiral [(Dialkylamino)methyl](phospholyl)ferrocene Ligands as a New Class of 1,2-Disubstituted Ferrocene Ligands

Sophie Mourgues,[a] Daniel Serra,[a] Franck Lamy,[a] Sandrine Vincendeau,[a] Jean-Claude Daran,[a] Eric Manoury,*[a] and Maryse Gouygou*[a]

Keywords: Ferrocenes / Phospholes / N,P ligands / Asymmetric catalysis

An efficient synthesis of new chiral [(dialkylamino)methyl](phospholyl)ferrocenes in an enantiomerically pure form has been developed. These new chiral N,P ligands have been tested in the palladium-catalyzed allylic substitution reaction. High activities and moderate enantioselectivities (up to 67% *ee*) were observed.
(© Wiley-VCH Verlag GmbH & Co. KGaA, 69451 Weinheim, Germany, 2003)

Introduction

Enantiopure 1,2-disubstituted ferrocene derivatives, especially ferrocenylphosphane ligands, are widely used as ligands in homogeneous transition metal catalysis.[1] Some of these ligands have proved to be especially efficient, in particular the aminophosphanes PPFA and BPPFA,[2] TRAP ligands,[3] Josiphos ligands,[4] in particular the industrially important Xyliphos,[5] pyrazolylphosphane ligands[6] or, more recently, ferrocenyloxazolines.[7] However, most of these chiral ferrocene-based ligands possess classical tertiary phosphane groups and no attention has been paid to ferrocenyl ligands with nonclassical phosphanes such as phosphole. Although phospholes are efficient ligands in homogeneous transition metal catalysis,[8] only a few enantiomerically pure chiral phospholes[9] have been used as chiral ligands for asymmetric catalysis.[10] In addition, a new approach has recently emerged where conformationally flexible ligands are intentionally used to magnify the effect of the chiral part of the catalytic system.[11] Unsymmetrically substituted phospholes can be useful in this context, because, owing to the low inversion barrier of the phosphorus in phospholes, a ligand bearing an unsymmetrically substituted phosphole could adjust the configuration of the asymmetric phosphorus atom to accommodate the metallic center through the catalytic cycle.

So, as part of our continuing interest in ferrocene chemistry[12] and in the design and synthesis of new chiral phosphole-based ligands,[13] we decided to investigate the efficiency of mixed phospholylferrocene ligands in asymmetric catalysis. Herein, we report the synthesis and characterization of the [(dialkylamino)methyl](phospholyl)-ferrocene ligands **8a,b** as a new class of 1,2-disubstituted ferrocene ligands and their use in palladium-catalyzed asymmetric allylic substitution.

[a] Laboratoire de Chimie de Coordination, UPR-CNRS 8241, 205 route de Narbonne, 31077 Toulouse Cedex, France
Fax: (internat.) +33-5/61 33 31 31
E-mail: manoury@lcc-toulouse.fr
gouygou@lcc-toulouse.fr

Results and Discussion

Synthesis of [(Dialkylamino)methyl](phospholyl)ferrocene Ligands 8a,b

The synthetic pathway used to produce enantiopure 1,2-disubstituted ferrocene derivatives **8a,b** is based on six stereochemically controlled reactions, as shown in Scheme 1. In the first step, the required planar chirality was introduced by diastereoselective ortho-lithiation of acetal **1** according to Kagan's procedure,[14] followed by treatment with 1-cyanophosphole (**2**)[15] as the electrophile, giving the expected phospholylferrocene product, which was directly converted by sulfurization to the air-stable compound **3**. This compound, isolated in 89% yield after purification by column chromatography, was obtained as an enantiomerically pure diastereoisomer. The new planar chirality in **3** was predicted to have an (*S*) configuration as the planar chirality is defined in the first step of the reaction, namely the lithiation of **1**, and is then independent of the electrophile used to quench the lithiated intermediate, as shown by Kagan et al.[14]

In the next step, the acid hydrolysis of the acetal (*S*)-**3** led quantitatively to the corresponding aldehyde (*S*)-**4**. This compound, which is slightly unstable, was only characterised by ^{1}H and ^{31}P NMR spectroscopy and then reduced with sodium tetrahydroborate to the stable alcohol (*S*)-**5**. This compound, obtained in 90% yield by column chromatography, was fully characterized by ^{1}H, ^{13}C and ^{31}P NMR spectroscopy and the (*S*)-configuration was confirmed by an X-ray diffraction analysis. A molecular view of the alcohol (*S*)-**5** is shown in Figure 1, with the atom-labelling

 © 2003 Wiley-VCH Verlag GmbH & Co. KGaA, Weinheim DOI: 10.1002/ejic.200200671

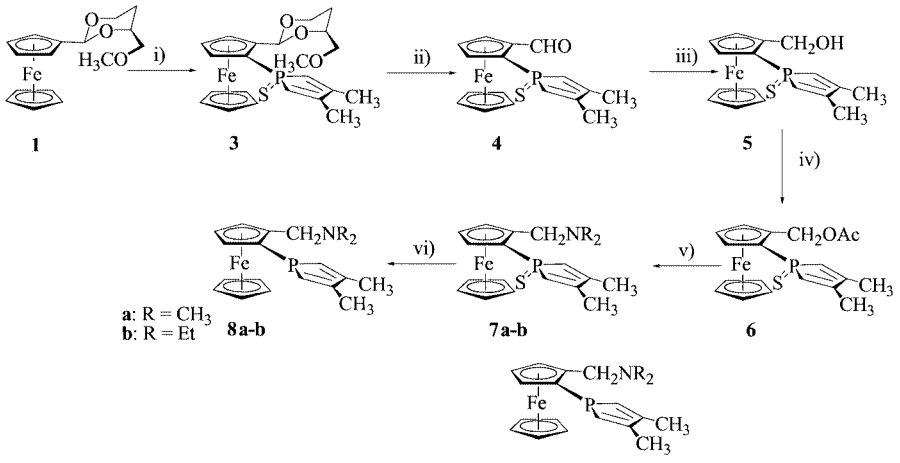

Scheme 1. Synthesis of **8**: i) *t*BuLi, −78 °C to room temp., 1-cyanophosphole (**2**), −30 °C; S_8, CH_2Cl_2, room temp.; ii) H^+, H_2O/ CH_2Cl_2, reflux; iii) $NaBH_4$, room temp.; iv) AcCl/ NEt_3, O °C to room temp., CH_2Cl_2; v) R_2NH, EtOH, reflux; vi) $P(CH_2CH_2CN)_3$, toluene, reflux

scheme. The X-ray crystal structure analysis clearly shows the nearly eclipsed conformation of the two Cp rings, with a twist angle of 4.75°. The phosphole ring is planar, with the largest deviation being 0.016 Å at C(2), and it makes a dihedral angle of 61.6° with the Cp to which it is attached. This phosphole ring is *endo* with respect to the Cp ring, whereas the S atom is *exo*. Such an arrangement is probably due to the hydrogen bond occurring between the OH of the hydroxyl group and the sulfur atom [O(1)−H(1)···S(1): O(1)−H(1) = 0.818(5) Å, O(1)···S(1) = 3.288(2) Å, H(1)···S(1) = 2.55(2) Å, O(1)−H(1)···S(1) = 150.5(8)°]. This hydrogen bond is responsible for the slight tilt angle of 4.2° observed between the Cp rings.

In the next step, the alcohol (*S*)-**5** was transformed quantitatively into the acetate (*S*)-**6** by treatment with acetyl chloride. This crude acetate was used directly for a nucleophilic substitution reaction with secondary amines, following the procedure described by Kumada et al.[16] Compounds (*S*)-**7a** and (*S*)-**7b** were obtained in 25% and 42% yield respectively. Compounds **7a,b** were fully characterized and the structure of **7a** was confirmed by X-ray analysis. A molecular view of **7a** is shown in Figure 2, with the atom-

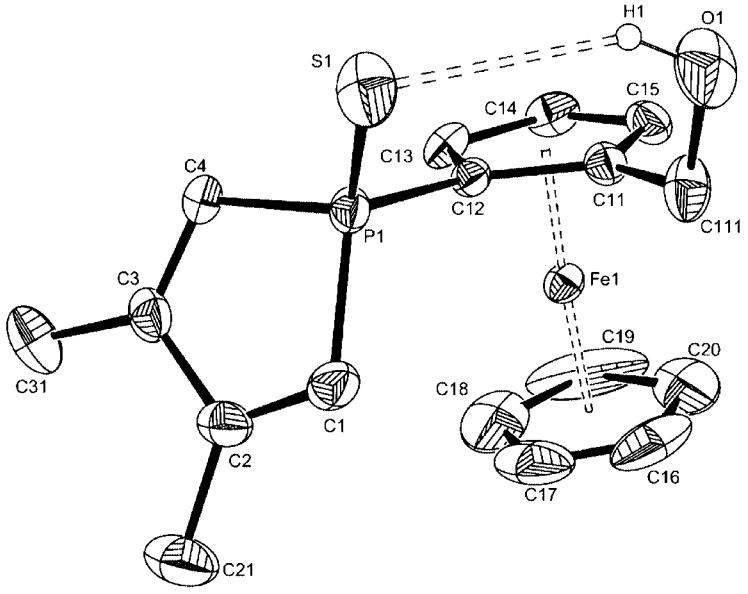

Figure 1. ORTEP drawing of **5** with atom labelling scheme; ellipsoids are drawn at 50% probability; important bond lengths (Å) and bond angles (°): Fe−Cp1(centroid) 1.633, Fe−Cp2(centroid) 1.652, C(11)−C(111) 1.489(2), C(111)−O(1) 1.425(2), C(12)−P(1) 1.7885(14), P(1)−C(1) 1.7812(17), P(1)−C(4) 1.7854(16), P(1)−S(1) 1.9645(6), C(1)−C(2) 1.341(3), C(2)−C(3) 1.501(3), C(3)−C(4) 1.334(2); Cp1(centroid)−Fe−Cp2(centroid) 176.9, S(1)−P(1)−C(1) 117.12(6), S(1)−P(1)−C(4) 116.41(5), S(1)−P(1)−C(12) 111.60(5), C(1)−P(1)−C(4) 92.83(8), C(1)−P(1)−C(12) 110.83(7), C(4)−P(1)−C(12) 106.37(7), P(1)−C(1)−C(2) 109.47(12), C(1)−C(2)−C(3) 114.08(14), C(2)−C(3)−C(4) 113.66(15), C(3)−C(4)−P(1) 109.90(12), C(11)−C(111)−O(1) 112.61(15)

 © 2003 Wiley-VCH Verlag GmbH & Co. KGaA, Weinheim

labelling scheme. As in (*S*)-**5**, the phosphole ring is planar with the largest deviation being 0.044 Å at C(3). However, there is no hydrogen bond and the phosphole is *exo* with respect to the ferrocene moiety, whereas the sulfur is *endo*. The dihedral angle between this phosphole and the Cp ring to which it is attached is 72.3°. The amine group is *exo* with respect to the ferrocene moiety and the nitrogen lone pair is oriented towards the phosphole ring. The two Cp rings are nearly eclipsed, with a twist angle of 4.71°; the tilt angle between the Cp rings is 1.7°.

In the last step, desulfuration of (*S*)-**7a,b**, performed in refluxing toluene with tris(2-cyanoethyl)phosphane as reducing agent, led to the corresponding ligands (*S*)-**8a,b** in 92% and 82% yield respectively.

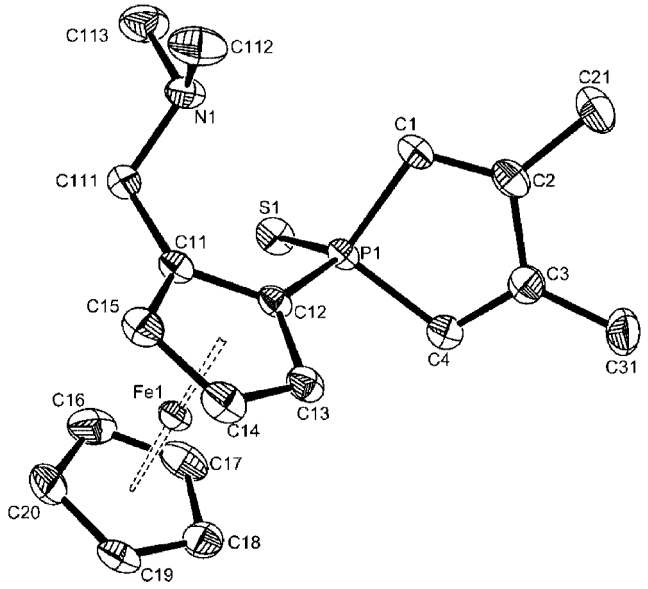

Figure 2. ORTEP drawing of complex **7a** with atom labelling scheme; ellipsoids are drawn at 50% probability; important bond lengths (Å) and bond angles (°): Fe−Cp1(centroid) 1.647, Fe−Cp2(centroid) 1.654, C(11)−C(111) 1.496(2), C(111)−N(1) 1.456(2), C(12)−P(1) 1.7951(17), P(1)−C(1) 1.8012(1), P(1)−C(4) 1.7959(17), P(1)−S(1) 1.9564(6), C(1)−C(2) 1.349(3), C(2)−C(3) 1.491(2), C(3)−C(4) 1.371(2); Cp1(centroid)−Fe−Cp2(centroid) 178.7, S(1)−P(1)−C(1) 115.14(6), S(1)−P(1)−C(4) 117.42(7); S(1)−P(1)−C(12) 116.80(6), C(1)−P(1)−C(4) 92.52(8), C(1)−P(1)−C(12) 109.23(8), C(4)−P(1)−C(12) 102.61(8), P(1)−C(1)−C(2) 110.06(13), C(1)−C(2)−C(3) 113.82(15), C(2)−C(3)−C(4) 114.05(15), C(3)−C(4)−P(1) 109.03(12), C(11)−C(111)−N(1) 110.75(13)

Application of the [(Dialkylamino)methyl](phospholyl)-ferrocenes 8a,b in Palladium-Catalyzed Asymmetric Allylic Substitution

As a preliminary evaluation of the catalytic properties of the chiral ligands **8a** and **8b**, we explored the palladium-catalyzed asymmetric allylic substitution reaction.[17] Thus, the reaction of 1,3-diphenylprop-2-enyl acetate (**9**) with the anion of dimethyl malonate in the presence of $[Pd(C_3H_5)Cl]_2$ (1mol %) and the chiral ligand **8a**,**b** (1mol %) provided the expected allylic substitution product **10** in high yields and moderate enantioselectivities (up to 67% *ee*) depending on the conditions (see Scheme 2). The results are summarised in Table 1.

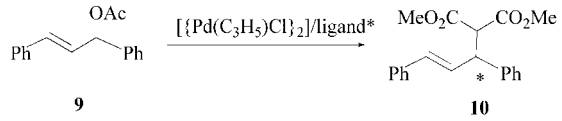

Scheme 2

This reaction occurred with 62% and 65% *ee* for **8a** and **8b**, respectively (entries 1,3), with high activities in both cases and complete conversion after 45−90 min at room temperature using CH_2Cl_2 as solvent and *N*,*O*-bis(trimethylsilyl)acetamide (BSA)/AcOK as base. The use of THF as solvent decreased the rate of the reaction (entry 2), and complete conversion was not observed even after 24 h, although the enantioselectivity was not affected.

Similar activities and enantioselectivities were observed when using NaH as base instead of the BSA/AcOK system (entries 4−5).

Conclusion

We have described a new and efficient method for the preparation of [(dialkylamino)methyl](phospholyl)ferrocenes in an enantiomerically pure form. Palladium-catalysed allylic substitution of 1,3-diphenylprop-2-enyl acetate with the anion of dimethyl malonate can be achieved with these new N,P ligands with high activities but still moderate enantioselectivities (up to 67% *ee*) compared to analogous ligands.[17,18] These new [(dialkylamino)methyl](phos-

Table 1. Results of asymmetric allylic substitution reaction of 1,3-diphenylprop-2-enyl acetate with the anion of dimethyl malonate[a]

Entry	Ligand	Base	Solvent	Reaction time	Yield[b]	*ee* (%) of **8**[c] (config.)[d]
1	**8a** (1%)	BSA/AcOK	CH_2Cl_2	1 h 30 mn	95%	65 (*S*)
2	**8a** (1%)	BSA/AcOK	THF	24 h	58%	67 (*S*)
3	**8b** (1%)	BSA/AcOK	CH_2Cl_2	0.5 h	94%	62 (*S*)
4	**8a** (1%)	NaH	CH_2Cl_2	1 h 30	96%	60 (*S*)
5	**8b** (1%)	NaH	CH_2Cl_2	1 h 30	95%	58 (*S*)

[a] Reactions conditions: 1 mmol of (*E*)-1,3-diphenylprop-2-enyl acetate, 3 mmol of dimethylmalonate with 1% palladium as $[PdCl(allyl)]_2$ at room temp. Complete conversion was confirmed by ^1H NMR spectroscopy, expect for entry 2, for which the conversion was not complete after 24 h. [b] Isolated yield. [c] Determined by ^1H NMR spectroscopy using the chiral shift reagent $Eu(hfc)_3$. [d] Determined on the basis of the sign of the specific rotation of the product.

 © 2003 Wiley-VCH Verlag GmbH & Co. KGaA, Weinheim

pholyl)ferrocenes are very modular: for example, the substituents on the phosphole ring or in the amino part can be easily changed in order to improve significantly the performances of the catalytic system. Further studies in this direction are currently in progress in our laboratory.

Experimental Section

General: All reactions were carried out under dry argon using Schlenk glassware and vacuum-line techniques. Solvents were freshly distilled from standard drying agents. ^{1}H, $^{13}C\{^{1}H, ^{31}P\}$ and $^{31}P\{^{1}H\}$ NMR spectra were recorded on a Bruker WMX 400 instrument operating at 400, 162, and 100 MHz, respectively. Chemical shifts are reported in parts per million (ppm) relative to Me_4Si (^{1}H and ^{13}C) or 85% H_3PO_4 (^{31}P). Mass spectra were obtained on a Nermag R10-10 instrument. Elemental analyses were performed by the "Service d'Analyse du Laboratoire de Chimie de Coordination" at Toulouse. Optical rotations were measured with a Perkin−Elmer 241 polarimeter.

Acetal **1**[14] and 1-cyano-3,4-dimethylphosphole (**2**)[15] were prepared as described in the literature.

(2*S*,4*S*,S_{Fc})-4-(Methoxymethyl)-2-[(3,4-dimethyl-1-thio-1*H*-1λ^5-phosphol-1-yl)ferrocenyl]-1,3-dioxane (3): In a Schlenk tube, a 1.5 M solution of *tert*-butyllithium in pentane (8.1 mL, 12.1 mmol, 1.1 equiv.) was added dropwise, at −78 °C under argon, to a solution of acetal **1** (3.47 g, 11 mmol) in 40 mL of dry diethyl ether. The solution was stirred at −78 °C during 15 minutes, then for 2 h at room temp. The solution was cooled to −30 °C and a solution of 1-cyano-3,4-dimethylphosphole (**2**; 1.81 g, 13.2 mmol, 1.2 equiv.) in 20 mL of dry diethyl ether was introduced with a cannula. The reaction mixture was stirred overnight at room temp. Dry triethylamine (0.5 mL) was then added by syringe, followed by water (2 mL). Under argon, the reaction mixture was extracted with diethyl ether and washed with brine. The organic fraction was dried over sodium sulfate and the solvents evaporated in vacuo to yield an orange oil. This oil was dissolved in 30 mL of dichloromethane. Sulfur (2 g, 62.mmol, 5.7 equiv.) was added and the mixture was stirred overnight. After evaporation, the mixture was chromatographed on silica gel using a pentane/dichloromethane mixture (7:3, v/v) to yield 4.47 g of a brown orange oil (Yield: 89%). ^{1}H NMR ([D$_6$]acetone): δ = 1.50 (d of m, J = 12.5 Hz, 1 H, CH_2-CH_2-CH), 1.66 (br. q of d, J = 12.5 Hz and 5 Hz, 1 H, CH_2-CH_2-CH), 2.03 (br. s, 3 H, CH_3), 2.12 (br. s, 3 H, CH_3), 3.33 (dd, J = 10.4 Hz and 4.2 Hz, 1 H, CH_2-OCH_3), 3.34 (s, 3 H, OCH_3), 3.43 (dd, J = 10.4 Hz and 6.5 Hz, 1 H, CH_2-OCH_3), 4.00 (br. t of d, J = 12 Hz and 2.7 Hz, 1 H, $O-CH_2CH_2$), 4.07 (m, 1 H, O−CH), 4.24 (br. dd, J = 11.2 Hz and 4.3 Hz, 1 H, $O-CH_2CH_2$), 4.33 (m, 1 H, subst Cp), 4.36 (m, 1 H, subst Cp), 4.42 (s, 5 H, Cp), 4.69 (m, 1 H, subst Cp), 6.14 (s, 1 H, O−CH−O), 6.20 (br. d, $J_{H,P}$ = 29.7 Hz, 1 H, CHP), 6.39 (br. d, $J_{H,P}$ = 29.5 Hz, 1 H, CHP) ppm. ^{13}C NMR ([D$_6$]acetone): δ = 17.0 (d, $J_{C,P}$ = 14.4 Hz, CH_3), 17.1 (d, $J_{C,P}$ = 14.1 Hz, CH_3), 28.2 (CH_2-CH_2-CH), 58.6 (OCH_3), 67.0 ($O-CH_2CH_2$), 69.0 (d $J_{C,P}$ = 10.5 Hz, subst Cp), 70.5(d, $J_{C,P}$ = 12.6 Hz, subst Cp), 71.1 (Cp), 72.2 (d, $J_{C,P}$ = 86.5 Hz, quat Cp), 75.3 (*C*H); 72.4 (d, $J_{C,P}$ = 13.5 Hz, subst Cp), 75.8 (CH_2-OCH_3), 90.1 (d, $J_{C,P}$ = 0.9 Hz, quat Cp), 99.6 (O−CH−O), 125.2 (d, $J_{C,P}$ = 85.4 Hz, CHP), 128.1 (d, $J_{C,P}$ = 84.1 Hz, CHP), 149.8 (d, $J_{C,P}$ = 18.9 Hz, $C-CH_3$), 152.6 (d, $J_{C,P}$ = 19.1 Hz, $C-CH_3$) ppm. ^{31}P NMR ([D$_6$]acetone): δ = 48.3. $[\alpha]_D$ = −2.47 (c = 0.5, $CHCl_3$). MS (DCI, NH_3): m/z (%) = 459 (100%) $[M + H]^+$. $C_{22}H_{27}FeO_3PS$ (458.34): calcd. C 57.65, H 5.94; found C 57.85, H 5.85.

(S_{Fc})-2-(3,4-Dimethyl-1-thio-1*H*-1λ^5-phosphol-1-yl)ferrocenecarbaldehyde (4): Acetal **3** (3.35 g, 7.3 mmol), dichloromethane (120 mL) and an aqueous solution (50 mL) of *p*-toluenesulfonic acid monohydrate (2 g, 10.5 mmol, 1.4 equiv.) were introduced into a round-bottomed flask equipped with a condenser and placed under argon. The reaction mixture was stirred at reflux for 20 h. After cooling back to room temp. the dark red solution was extracted with dichloromethane, washed with distilled water, dried over sodium sulfate and the solvents evaporated. Compound **4**, obtained quantitatively as a red oil, was only characterised by ^{1}H and ^{31}P NMR spectroscopy and used without purification. ^{1}H NMR ($CDCl_3$): δ = 2.10 (m, 6 H, CH_3), 4.40 (s, 5 H, Cp), 4.75 (m, 1 H, subst Cp), 4.95 (m, 1 H, subst Cp), 5.10 (m, 1 H, subst Cp), 6.20 (d, $J_{H,P}$ = 28.5 Hz, 2 H, CHP), 10.30 (s, 1 H, CHO), ppm. ^{31}P NMR ($CDCl_3$): δ = 44.9 ppm.

(S_{Fc})-[2-(3,4-Dimethyl-1-thio-1*H*-1λ^5-phosphol-1-yl)ferrocenyl]-methanol (5): The crude compound **4** was dissolved in methanol (200 mL) and an aqueous solution (140 mL) of sodium borohydride (2.78 g, 18.3 mmol) and sodium hydroxide (11.2 g, 280 mmol) was added. The solution turned rapidly from red to orange. After 15 minutes stirring at room temp. the reaction mixture was extracted with dichloromethane. The organic phase was washed with dilute hydrochloric acid then water, and finally dried over sodium sulfate. After evaporation of the solvents, the crude materials was purified by flash chromatography on silica gel using a pentane/diethyl ether mixture (2:8, v/v) to yield 2.36 g of **5** (90% from **3**) as an orange solid. Crystals suitable for X-ray analysis were obtained by diffusion of pentane into a dichloromethane solution. ^{1}H NMR ($CDCl_3$): δ = 2.08 (d, J = 1.6 Hz, 3 H, CH_3), 2.14 (d, J = 1.6 Hz, 3 H, CH_3), 3.26 (dd, J = 7.4 Hz and 6.3 Hz, 1 H, OH), 4.29−4.35 (m, 2 H, subst Cp), 4.31 (s, 5 H, Cp), 4.38 (dd, J = 12.7 Hz and 7.4 Hz, 1 H, CH_2), 4.48 (m, 1 H, subst Cp), 4.81 (dd, J = 12.7 Hz and 6.3 Hz, 1 H, CH_2), 6.16 (br. d, $J_{H,P}$ = 30.8 Hz, 1 H, CHP), 6.22 (br. d, $J_{H,P}$ = 30.4 Hz, 1 H, CHP) ppm. ^{13}C NMR ($CDCl_3$): δ = 17.80 (d, $J_{C,P}$ = 17.8 Hz, CH_3), 17.84 (d, $J_{C,P}$ = 18.0 Hz, CH_3), 59.6 (d, $J_{C,P}$ = 7.8 Hz, CH_2), 69.8 (d, $J_{C,P}$ = 10.8 Hz, subst Cp), 70.5 (d, $J_{C,P}$ = 71.5 Hz, quat Cp), 70.7 (Cp), 72.5(d, $J_{C,P}$ = 14.2 Hz, subst Cp), 74.2 (d, $J_{C,P}$ = 9.6 Hz, subst Cp), 92.1 (d, $J_{C,P}$ = 12.3 Hz, quat Cp), 125.6 (d, $J_{C,P}$ = 86.1 Hz, CHP), 126.5 (d, $J_{C,P}$ = 84.0 Hz, CHP), 151.9 (d, $J_{C,P}$ = 18.6 Hz, $C-CH_3$), 152.2 (d, $J_{C,P}$ = 18.7 Hz, $C-CH_3$) ppm. ^{31}P NMR ($CDCl_3$): δ = 49.3 ppm. $[\alpha]_D$ = −104.6 (c = 0.5, $CHCl_3$). MS (DCI, NH_3): m/z (%) = 359 (100) $[M + H]^+$. $C_{17}H_{19}FeOPS$ (358.22): calcd. C 57.00, H 5.35; found C 57.11, H 5.00.

(S_{Fc})-Acetoxy-[2-(3,4-dimethyl-1-thio-1*H*-1λ^5-phosphol-1-yl)ferrocenyl]methane (6): (*S*)-[2-(thio-3,4-dimethylphospholyl)ferrocenyl]-methanol (240 mg, 0.7 mmol) was dissolved in dry dichloromethane (7 mL) and anhydrous triethylamine (0.25 mL) in a Schlenk tube under argon. The solution was then cooled to 0 °C and acetyl chloride (70 μL, 1 mmol, 1.5 equiv.) was added with a syringe. The solution was stirred at 0 °C for 30 minutes then for 1 h at room temp. The solution was washed with dilute hydrochloric acid then water, and dried over sodium sulfate. After evaporation of the solvents, the crude compound **6** was quantitatively obtained as a yellow oil that was used without further purification in the next step. ^{1}H NMR ($CDCl_3$): δ = 1.98 [s, 3 H, $C(O)CH_3$], 2.04 (m, 6 H, CH_3), 4.34 (s, 5 H, Cp), 4.45 (m, 1 H, subst Cp), 4.50 (m, 1 H, subst Cp), 4.60 (m, 1 H, subst Cp), 4.90 (d, J = 11.8 Hz, 1 H, CH_2), 5.20 (d, J = 11.8 Hz, 1 H, CH_2), 6.05 (br. d, $J_{H,P}$ = 29.6 Hz,

 © 2003 Wiley-VCH Verlag GmbH & Co. KGaA, Weinheim

1 H, CHP), 6.15 (br. d, $J_{H,P}$ = 29.6 Hz, 1 H, CHP) ppm. ^{31}P NMR ($CDCl_3$): δ = 45.5 ppm.

(S_{Fc})-{2-[(3,4-Dimethyl-1-thio-1*H*-1λ^5-phosphol-1-yl)ferrocenyl]-methyl}dimethylamine (7a): The crude acetate, methanol (40 mL) and dimethylammonium chloride (3.58 g, 44 mmol, 40 equiv.) were introduced into a three-necked, round-bottomed flask equipped with a condenser and purged with argon. The reaction mixture was stirred at reflux for 40 h. After cooling back to room temp. the solvents were evaporated and the residue was dissolved in diethyl ether and washed with a dilute hydrochloric acid solution. Unreacted starting materials could be obtained from the organic phase after evaporation of the solvents and flash chromatography. An aqueous sodium hydroxide solution (ca. 2 M) was added to the aqueous phase in order to adjust the pH close to 13. A precipitate formed, which was dissolved by adding diethyl ether to the suspension. This second organic phase was dried over sodium sulfate and the solvents evaporated to give 105 mg of amine **7a** (yield 25%) as a yellow oil. This compound was purified by column chromatography on alumina using a pentane/diethyl ether mixture (4:6, v/v). Crystals suitable for X-ray analysis were obtained by diffusion of pentane into a dichloromethane solution. ^{1}H NMR ($CDCl_3$): δ = 2.05 (m, 3 H, CH_3), 2.10 (m, 3 H, CH_3), 2.18 (s, 6 H, N CH_3), 3.05 (d, J = 12.7 Hz, 1 H, CH_2−Cp), 4.08 (d, J = 12.7 Hz, 1 H, CH_2−Cp), 4.30 (m, 1 H, subst Cp), 4.34 (s, 5 H, Cp), 4.41 (m, 1 H, subst Cp), 4.47 (m, 1 H, subst Cp), 6.15 (br. d, $J_{H,P}$ = 29.7 Hz, 1 H, CHP), 6.21 (br. d, $J_{H,P}$ = 29.9 Hz, 1 H, CHP) ppm. ^{13}C NMR ($CDCl_3$): δ = 17.75 (d, $J_{C,P}$ = 17.9 Hz, CH_3), 17.83 (d, $J_{C,P}$ = 17.8 Hz, CH_3), 45.3 (s, N CH_3), 57.4 (s, CH_2), 69.6 (d, $J_{C,P}$ = 11.0 Hz, subst Cp), 70.8 (d, J $J_{C,P}$ = 88.4 Hz, quat Cp), 71.0 (s, Cp), 72.6 (d, $J_{C,P}$ = 14.9 Hz, subst Cp), 75.0 (d, $J_{C,P}$ = 9.4 Hz, subst Cp), 89.0 (d, $J_{C,P}$ = 12.5 Hz, quat Cp), 125.6 (d, $J_{C,P}$ = 85.5 Hz, CHP), 127.5 (d $J_{C,P}$ = 84.6 Hz, CHP), 150.8 (d, $J_{C,P}$ = 19.0 Hz, C−CH_3), 152.6 (d, $J_{C,P}$ = 18.1 Hz, C−CH_3) ppm. ^{31}P NMR ($CDCl_3$): δ = 49.1 ppm. $[\alpha]_D$ = −1.2 (c = 0.4, $CHCl_3$). $[\alpha]_{546}$ = −20.2 (c = 0.4, $CHCl_3$). MS (DCI, NH_3): m/z (%) = 386 (100) $[M + H]^+$.

(S_{Fc})-{2-[(3,4-Dimethyl-1-thio-1*H*-1λ^5-phosphol-1-yl)ferrocenyl]-methyl}diethylamine (7b): A similar procedure with 40 equiv. of pure diethylamine instead of the mixture dimethylammonium chloride/triethylamine gave compound **7b** as an orange oil (yield: 42%). ^{1}H NMR ($CDCl_3$): δ = 0.96 (t, J = 7.1 Hz, 6 H, CH_3CH$_2$), 2.01 (d, J = 1.4 Hz, 3 H, CH_3), 2.06 (d, J = 1.4 Hz, 3 H, CH_3), 2.4−2.6 (m, 4 H, CH_2CH$_3$), 3.30 (d, J = 13.2 Hz, 1 H, CH_2−Cp), 4.03 (d, J = 13.2 Hz, 1 H, CH_2−Cp), 4.24 (m, 1 H, subst Cp), 4.32 (s, 5 H, Cp), 4.36 (m, 1 H, subst Cp), 4.44 (m, 1 H, subst Cp), 6.09 (br. d, J_{H-P} = 29.7 Hz, 1 H, CHP), 6.23 (br. d, J_{H-P} = 29.7 Hz, 1 H, CHP) ppm. ^{13}C NMR ($CDCl_3$): δ = 11.6 (NCH$_2$$CH_3$), 17.77 (d, $J_{C,P}$ = 16.0 Hz, CH_3), 17.85 (d, $J_{C,P}$ = 17.7 Hz, CH_3), 45.9 (NCH$_2$CH$_3$), 52.0 (CH_2), 69.1(d, $J_{C,P}$ = 11.0 Hz, subst Cp), 70.8 (d, $J_{C,P}$ = 88.7 Hz, quat Cp), 71.0 (Cp), 72.4 (d, $J_{C,P}$ = 14.9 Hz, subst Cp), 74.9 (d, $J_{C,P}$ = 9.7 Hz, subst Cp), 90.5 (d, $J_{C,P}$ = 11.9 Hz, quat Cp), 125.5 (d, $J_{C,P}$ = 85.2 Hz, CHP), 127.7 (d, $J_{C,P}$ = 84.7 Hz, CHP), 150.5 (d, $J_{C,P}$ = 18.7 Hz, C−CH_3), 152.5 (d, $J_{C,P}$ = 18.7 Hz, C-CH_3) ppm. ^{31}P NMR ($CDCl_3$): δ = 49.3 ppm. $[\alpha]_D$ = −1.8 (c = 0.5, $CHCl_3$). $[\alpha]_{546}$ = −23.4 (c = 0.5, $CHCl_3$). MS (DCI, NH_3): m/z (%) = 414 (100) $[M + H]^+$.

(S_{Fc})-{2-[(3,4-Dimethyl-1*H*-1λ^3-phosphol-1-yl)ferrocenyl]methyl}-dimethylamine (8a): Tris(2-cyanoethyl)phosphane (0.130 mg, 0.673 mmol) was added to a solution of **7a** (0.130 mg, 0.338 mmol) in toluene (10 mL) and the resulting mixture was refluxed for 6 hours. After cooling to room temp. the mixture was filtered through celite, the solvents evaporated in vacuo and the residue extracted four times with pentane. After evaporation of the solvents, the crude compound **7a** was purified by column chromatography on alumina using a pentane/diethyl ether mixture (1:1, v/v) to yield 105 mg of amine (yield: 92%) as an orange-red oil. ^{1}H NMR ($CDCl_3$): δ = 2.08 (br. s, 3 H, CH_3), 2.16 (br. s, 3 H, CH_3), 2.22 (s, 6 H, NCH_3), 3.41 (d, J = 12.8 Hz, 1 H, CH_2−Cp), 3.63 (dd, $J_{H,P}$ = 2.6, J = 12.8 Hz, 1 H, CH_2−Cp), 3.85 (m, 1 H, subst Cp), 4.20 (m, 1 H, subst Cp), 4.21 (s, 5 H, Cp), 4.39 (m, 1 H, subst Cp), 6.40 (br. d, $J_{H,P}$ = 37.3 Hz, 1 H, CHP), 6.54 (br. d, $J_{H,P}$ = 36.5 Hz, 1 H, CHP) ppm. ^{13}C NMR ($CDCl_3$): δ = 8.2 (CH_3), 18.3 (s, CH_3), 45.3 (s, NCH_3), 58.1 (d, J_{C-P} = 6.1 Hz, CH_2), 69.9 (s, Cp), 70.0 (d, J_{C-P} = 2.4 Hz, subst. Cp), 71.7 (s, subst. Cp), 71.9 (d, $J_{C,P}$ = 7.7 Hz, quat Cp), 72.7 (d, $J_{C,P}$ = 4.1 Hz, subst Cp), 89.7 (d, $J_{C,P}$ = 22.9 Hz, quat Cp), 129.7 (CHP), 132.1 (s, CHP), 147.8 (d, $J_{C,P}$ = 7.5 Hz, C-CH_3), 148.9 (d, $J_{C,P}$ = 9.7 Hz, C-CH_3) ppm. ^{31}P NMR ($CDCl_3$): δ = −16.4 ppm. MS (DCI, NH_3): m/z (%) = 353 (100) [M + H].

(S_{Fc})-{2-[(3,4-Dimethyl-1*H*-1λ^3-phosphol-1-yl)ferrocenyl]methyl}-diethylamine (8b): The synthesis of **8b** was accomplished by the same procedure as described above for **8a.** Compound **8b** was obtained as orange-red oil (82%). ^{1}H NMR ($CDCl_3$): δ = 1.06 (t, J = 7.1 Hz, 6 H, CH_3CH$_2$), 2.08 (br. s, 3 H, CH_3), 2.20 (br. s, 3 H, CH_3), 2.4−2.6 (m, 4 H, CH_2CH$_3$), 3.50 (d, J = 13.1 Hz, 1 H, CH_2−Cp), 3.82 (m, 1 H, subst Cp), 3.84 (dd, J = 13.1, J = 2.3 Hz, 1 H, CH_2−Cp), 4.17 (t, J = 2.4 Hz, 1 H, subst Cp), 4.21 (s, 5 H, Cp), 4.37 (m, 1 H, subst Cp), 6.40 (d, $J_{H,P}$ = 36.4 Hz, 1 H, CHP), 6.54 (d, $J_{H,P}$ = 36.4 Hz, 1 H, CHP) ppm. ^{13}C NMR ($CDCl_3$): δ = 12.5 (s, NCH$_2$$CH_3$), 18.2 (s, CH_3), 18.3 (s, CH_3), 46.4 (s, NCH$_2$CH$_3$), 52.1 (d $J_{C,P}$ = 5.9 Hz, CH_2), 69.6 (s, subst Cp), 69.9 (Cp), 71.5 (s, subst Cp), 71.9 (d, $J_{C,P}$ = 26.4 Hz, quat Cp), 72.9 (d, $J_{C,P\ P}$ = 4.4 Hz, subst Cp), 90.6 (d, $J_{C,P}$ = 26.4 Hz, quat Cp), 129.6 (s, CHP), 132.4 (s, CHP), 147.7 (d, $J_{C,P}$ = 9.0 Hz, C−CH_3), 148.8 (d, $J_{C,P}$ = 10.0 Hz, C−CH_3) ppm. ^{31}P NMR ($CDCl_3$): δ = −15.9 ppm. MS (DCI, NH_3): m/z (%) = 381 (100) [M + H].

General Procedure for Palladium-Catalyzed Allylic Substitution Dimethyl Malonate/BSA/KOAc System: A mixture of ligand **8**, 1,3-diphenylprop-2-enyl acetate (0.454 g, 1.8 mmol) and $[Pd(C_3H_5)Cl]_2$ (3.3 mg, 0.009 mmol) in dry solvent (20 mL) was stirred at room temperature for 2 h. Dimethyl malonate (0.411 mL, 3.6 mmol), potassium acetate and BSA (0.880 mL, 3.6 mmol) were added to the resulting solution. The reaction was carried out at room temperature and monitored by TLC for disappearance of acetate. After complete reaction, the mixture was diluted with diethyl ether (5 mL) and quenched with a saturated aqueous solution of ammonium chloride (5 mL). The aqueous phase was extracted with Et_2O, the combined organics were dried over magnesium sulfate, filtered and the solvents evaporated. The conversion was calculated from the crude reaction mixture by ^{1}H NMR spectroscopy. Subsequent purification by chromatography on silica eluting with ethyl acetate/pentane (15:85) afforded the product as a white solid. The enantiomeric excess was determined by ^{1}H NMR spectroscopy using the chiral shift reagent Eu(hfc)$_3$.

Dimethyl Malonate/NaH System: A mineral oil dispersion of NaH (87 mg, 60% NaH, 2.17 mmol) was washed with dry pentane (3 × 5 mL). The oil-free NaH was suspended in dry dichloromethane (10 mL), cooled to 0 °C and treated dropwise with dimethyl malonate (0.297 mL, 2.6 mmol). After the reaction was complete, the resulting sodium dimethyl malonate was transferred by cannula under argon into a Schlenk tube containing a mixture of ligand **8**, 1,3-diphenylprop-2-enyl acetate (0.328 g, 1.3 mmol) and $[Pd(C_3H_5)Cl]_2$ (2.4 mg, 0.0065 mmol) in dry dichloromethane (10 mL) previously stirred at room temperature for 2 h. The reac-

 © 2003 Wiley-VCH Verlag GmbH & Co. KGaA, Weinheim

Table 2. Crystal data and structure refinement

	5	**7a**
Empirical formula	$C_{17}H_{19}FeOPS$	$C_{19}H_{24}FeNPS$
Molecular weight	358.22	385.29
Temperature	180 K	160 K
Wavelength	0.71073 Å	0.71073 Å
Crystal system	Orthorhombic	Monoclinic
Space group	$P2_12_12_1$	$P2_1$
Unit cell dimensions	a = 9.3200(8) Å α = 90°. b = 9.9140(9) Å β = 90°. c = 17.552(2) Å γ = 90°.	a = 10.0397(13) Å α = 90°. b = 9.6103(8) Å β = 113.09(1)°. c = 10.3848(13) Å γ = 90°.
Volume	1621.8(3) Å^3	921.72(17) Å^3
Z	4	2
Density (calculated)	1.467 Mg/m^3	1.388 Mg/m^3
Absorption coefficient	1.152 mm^{-1}	1.017 mm^{-1}
F(000)	744	404
Crystal size	0.43 × 0.29 × 0.22 mm^3	0.32 × 0.28 × 0.24 mm^3
Theta range for data collection	3.217 to 26.059°	2.132 to 26.15°
Reflections collected	15792	9062
Independent reflections	3126 [R(int) = 0.03]	3488 [R(int) = 0.02]
Refinement method	Full-matrix on F	Full-matrix on F
Data/restraints/parameters	3042/0/191	3407/0/209
Goodness-of-fit on F	1.0338	1.0568
Final R indices [$I > 2\sigma(I)$]	$R1$ = 0.0212, Rw = 0.0260	$R1$ = 0.0216, Rw = 0.0258
R indices (all data)	$R1$ = 0.0220, Rw = 0.0263	$R1$ = 0.0222, Rw = 0.0259
Absolute structure parameter	−0.006(13)	0.006(9)
Largest diff. peak and hole	0.47 and −0.33 e·Å^{-3}	0.51 and −0.3 e·Å^{-3}

tion was carried out at room temperature and monitored by TLC for disappearance of acetate. Treatment, extraction and purification were accomplished by the same procedure as described above.

X-ray Structure Determination: Data for **(*S*)-5** and **7a** were collected on a Stoe IPDS diffractometer. The final unit cell parameters were obtained by the least-squares refinement of 8000 reflections. Only statistical fluctuations were observed in the intensity monitors over the course of the data collections.

Both the structures were solved by direct methods (SIR97[18]) and refined by least-squares procedures on F_{obs}. All H atoms attached to carbon or oxygen were introduced at their idealised positions [d(CH) = 0.96 Å] and were refined using a riding model. They were given isotropic thermal parameters 20% higher than those of the atom to which they are attached. The absolute configuration was confirmed by the refinement of the Flack parameter[19] and careful examination of the sensitive reflections. Least-squares refinements were carried out by minimising the function $\Sigma w(F_o - F_c)^2$, where F_o and F_c are the observed and calculated structure factors. The weighting scheme used in the last refinement cycles was $w = w'[1-\{\Delta F/6\sigma(F_o)\}^2]^2$ where $w' = 1/\Sigma_i^n A_r T_r(x)$ with three coefficients A_r for the Chebyshev polynomial $A_r T_r(x)$ where x was F_c/F_c(max).[20] Models reached convergence with $R = \Sigma(F_o - F_c)/\Sigma(F_o)$ and $Rw = [\Sigma w(F_o - F_c)^2/\Sigma w(F_o)^2]^{1/2}$, with the values listed in Table 2. The calculations were carried out with the CRYSTALS programs package.[21] The views of the molecules were produced with the ORTEP-III for Windows program.[22]

Crystallographic data (excluding structure factors) for the structures reported in this paper have been deposited with the Cambridge Crystallographic Data Centre as supplementary publication no. CCDC-198748 (**5**) and CCDC-198749 (**7a**). Copies of the data can be obtained free of charge on application to CCDC, 12 Union Road, Cambridge CB2 1EZ, UK [Fax: (internat.) +44-1223/336-033; E-mail: deposit@ccdc.cam.ac.uk].

[1] [1a] A. Togni, T. Hayashi, *Ferrocenes*, VCH, Weinheim 1995. [1b] S. Borman, *Chemical and Engineering News* **1996**, July 22, 38−39. [1c] A. Togni, *Angew. Chem. Int. Ed. Engl.* **1996**, *35*, 1475−1477.

[2] [2a] T. Hayashi, M. Kumada, *Acc. Chem. Res.* **1982**, *15*, 395−401. [2b] M. Sawamura, Y. Ito, *Chem. Rev.* **1992**, *92*, 857−871. [2c] Y. Matsumoto, A. Ohno, T. Hayashi, *Organometallics* **1993**, *12*, 4051−4055.

[3] [3a] M. Sawamura, Y. Nakayama, T. Kato, Y. Ito, *J. Org. Chem.* **1995**, *60*, 1727−1732. [3b] M. Sawamura, M. Sudoh, Y. Ito, *J. Am. Chem. Soc.* **1996**, *118*, 3309−3310. [3c] R. Kuwano, H. Miyazaki, Y. Ito, *Chem. Commun.* **1998**, 71−72. [3d] R. Kuwano, H. Miyazaki, Y. Ito, *Tetrahedron Lett.* **1999**, *40*, 1327−1330. [3e] R. Kuwano, K. Sato, T. Kurokawa, D. Karube, Y. Ito, *J. Am. Chem. Soc.* **2000**, *122*, 7614−7615.

[4] H.-U. Blaser, W. Brieden, B. Pugin, F. Spindler, M. Studer, A. Togni, *Topics in Catalysis* **2002**, *19*, 3−16 and references cited therein.

[5] H.-U. Blaser, *Adv. Synth. Catal.* **2002**, *344*, 17−31 and references cited therein.

[6] [6a] A. Schnyder, L. Hintermann, A. Togni, *Angew. Chem.* **1995**, *107*, 996−998; *Angew. Chem. Int. Ed. Engl.* **1995**, *34*, 931−933. [6b] A. Togni, U. Buckardt, V. Gramlich, P. S. Pregosin, R. Salzman, *J. Am. Chem. Soc.* **1996**, *118*, 1031−1037. [6c] G. Pioda, A. Togni, *Tetrahedron: Asymmetry* **1998**, *9*, 3903−3910.

[7] [7a] Y. Nishibayashi, I. Takei, S. Uemura, M. Hidai, *Organometallics* **1998**, *17*, 3420−3422. [7b] Y. Nishibayashi, I. Takei, S. Uemura, M. Hidai, *Organometallics* **1999**, *18*, 2291−2293. [7c] K. H. Ahn, C. W. Cho, J. Park, S. Lee, *Tetrahedron: Asymmetry* **1997**, *8*, 1179−1185. [7d] C. Bolm, N. Hermans, J. P. Hildebrand, K. Muniz, *Angew. Chem.* **2000**, *110*, 3607−3609; *Angew. Chem. Int. Ed.* **2000**, *39*, 3465−3467. [7e] S.-L. You, X.-Z; Zhu,

 © 2003 Wiley-VCH Verlag GmbH & Co. KGaA, Weinheim

Y.-M. Luo, X.-L. Hou, L.-X. Dai, *J. Am. Chem. Soc.* **2001**, *123*, 7471−7472.

[8] [8a] D. E. Budd, D. G. Holah, A. N. Hughes, B. C. Hui, *Can. J. Chem.* **1974**, *52*, 775−781. [8b] Société Nationale des Poudres et Explosifs, *Patent FR 8514638*, **1980**, pp 1−19. [8c]D. Neibecker, R. Réau, S. Lecolier, *J. Org. Chem.* **1989**, *54*, 5208−5210. [8d] D. Neibecker, R. Réau, *J. Mol. Catal.* **1989**, *53*, 219−227. [8e] D. Neibecker, R. Réau, *J. Mol. Catal.* **1989**, *57*, 153−163. [8f] F. Mercier, F. Laporte, L. Ricard, F. Mathey, M. Schröder, M. Regitz, *Angew. Chem.* **1997**, *109*, 2460−2462; *Angew. Chem. Int. Ed. Engl.* **1997**, *36*, 2364−2366. [8g] Z. Csok, G. Keglevich, G. Petocz, L. Kollar, *J. Organomet; Chem.* **1999**, *586*, 79−84. [8h] P. J. Fagan, G. Li, Z. Guan, L. Wang, E. I. Du Pont De Nemours and Company, *Patent WO0021970A1*, **2000**, *640*, pp.1−44. [8i]S. Doherty, E. G. Robins, J. G. Knight, C. R. Newman, B. Rhodes, P. A. Champkin, W. Clegg, *J. Organomet. Chem.* **2001**, *640*, 182−196. [8j] M. Sauthier, F. Leca, L. Toupet, R. Réau, *Organometallics.* **2002**, *21*, 1591−1602.

[9] Some recent examples of chiral phospholes: [9a] M. Ogasawara, K. Yoshida, T. Hayashi, *Organometallics* **2001**, *20*, 1014−1019. [9b] G. Consiglio, S. C. A. Nefkens, *Eur. J. Inorg. Chem.* **2002**, 1657−1665.

[10] [10a] T. P. Dang, J.-C. Poulin, H. B. Kagan, *J. Organomet. Chem.* **1975**, *91*, 105−115. [10b] G. Consiglio, S. C. A. Nefkens, *Tetrahedron: Asymmetry* **1990**, *1*, 417−420. [10c] J. Stille, M. Su, P. Brechot, G. Parinello, L. S. Hegedus, *Organometallics* **1991**, *10*, 1183−1189. [10d] G. Consiglio, S. C. A. Nefkens, A. Borer, *Organometallics* **1991**, *10*, 2046−2051. [10e] J J. Brunet, H. Hajouji, J. C. Ndjanga, D. Neibecker, *J. Mol. Catal.* **1992**, *72*, L21−L25. [10f] T. Langer, J. Janssen, G. Helmchen, *Tetrahedron: Asymmetry* **1996**, *7*, 1599−1602. [10g] T. Langer, G. Helmchen, *Tetrahedron Lett.* **1996**, *37*, 1381−1384. [10h] T. Langer, M. Peer, J. G. de Jong, M. Kiefer, T. Langer, H. Rieck, H. Schell, P. Sennhehn, J. Sprinz, H. Steinhagen, B. Wiese, G. Helmchen, *Tetrahedron* **1996**, *52*, 7547−7583. [10i] I. Toth, C. J. Elsevier, J. G. de Vries, J. Bakos, W. J. J. Smeets, A. L. Spek, *J. Organomet. Chem.* **1997**, *540*, 15−25. [10j] W. A. Schenk, M. Stubbe, M. Hagel, *J. Organomet. Chem.* **1998**, *560*, 257−263. [10k] J. Hydrio, M. Gouygou, F. Dallemer, J.-C. Daran, G. G. A. Balavoine, *Tetrahedron: Asymmetry* **2002**, *13*, 1097−1102.

[11] [11a] S. Deerenberg, P. C. J. Kamer, P. W. N. M. van Leeuwen, *Organometallics.* **2000**, *19*, 2065−2072. [11b] M. Diéguez, O. Pamies, A. Ruiz, C. Claver, *New J. Chem.* **2002**, *26*, 827−833. [11c] A. Suárez, M. A. Méndez-Rojas, A. Pizzaro, *Organometallics.* **2002**, *21*, 4611−4621. [11d] K. Mikami, K. Aikawa, Y. Yusa, J. J. Jodry, M. Yamanaka, *Synlett* **2002**, 1561−1578 and references cited therein.

[12] [12a] G. Iftime, C. Moreau-Bossuet, E. Manoury, G. G. A. Balavoine, *Chem. Commun.* **1996**, 527−528. [12b] G. Iftime, J.-C. Daran, E. Manoury, G. G. A. Balavoine, *Organometallics* **1996**, *15*, 4808−4815. [12c] G. Iftime, J.-C. Daran, E. Manoury, G. G. A. Balavoine, *Angew. Chem.* **1998**, *110*, 1827−1829; *Angew. Chem. Int. Ed.* **1998**, *37*, 1698−1700. [12d] E. Manoury, J. S. Fossey, H. Ait-Haddou, J.-C. Daran, G. G. A. Balavoine, *Organometallics* **2000**, *19*, 3736−3739. [12e] J. Chiffre, Y. Coppel, G. G. A. Balavoine, J.-C. Daran, E. Manoury, *Organometallics* **2002**, *21*, 4552−4555.

[13] [13a] O. Tissot, M. Gouygou, J-C. Daran, G. G. A. Balavoine, *Chem. Commun.* **1996**, 2287−2288. [13b] O. Tissot, M. Gouygou, F. Dallemer, J.-C. Daran, G. G. A. Balavoine, *Angew. Chem.* **2001**, *113*, 1110−1112; *Angew. Chem. Int. Ed.* **2001**, *40*, 1076−1078. [13c] O. Tissot, M. Gouygou, F. Dallemer, J-C. Daran, G. G. A. Balavoine, *Eur. J. Inorg. Chem.* **2001**, 2385−2389. [13d] J. Hydrio, M. Gouygou, F. Dallemer, G. G. A. Balavoine, J-C. Daran, *Eur. J. Org. Chem.* **2002**, *13*, 675−685.

[14] [14a] O. Riant, O. Samuel, T. Flessner, S. Taudien, H. B. Kagan, *J. Org. Chem.* **1997**, *62*, 6733−6745. For recent use of this procedure for the synthesis of chiral ferrocenyl ligands with planar chirality only, see: [14b] A. Abiko, G. Wang, *Tetrahedron* **1998**, *54*, 11405−11420. [14c] G. Argouach, O. Samuel, H. B. Kagan, *Eur. J. Org. Chem.* **2000**, 2885−2891.

[15] S. Holand, F. Mathey, *Organometallics* **1988**, *7*, 1796−1801.

[16] T. Hayashi, T. Mise, M. Fukushima, M. Kagotani, N. Nagashima, Y. Hamada, A. Matsumoto, S. Kawakami, M. Konishi, K. Yamamoto, M. Kumada, *Bull. Chem. Soc. Jpn.* **1980**, *53*, 1138−1151.

[17] [17a] B. M. Trost, D. L. van Vranken, *Chem. Rev.* **1996**, *96*, 395−422. [17b] A. Pfalz, H. Yamamoto, *Comprehensive Asymmetric Catalysis*, Vol 1 (Eds.: E. N. Jacobsen, A. Pfalz, H. Yamamoto), Springer Verlag, Heidelberg, **1999**, p 834−884.

[18] For some recent work on allylic substitution using N,P ligands, see: [18a] T. Fukuda, A. Takehara, M. Iwao, *Tetrahedron: Asymmetry* **2001**, *12*, 2793−2799. [18b] S.-L. You, X.-Z. Zhu, Y.-M. Luo, X.-L. Hou, L.-X. Dai, *J. Am. Chem. Soc.* **2001**, *123*, 7471−7472. [18c] L. Xiao, W. Weissensteiner, K. Mereiter, M. Widhalm, *J. Org. Chem.* **2002**, *67*, 2206−2214. [18d] A. Farrell, R. Goddard, P. J. Guiry, *J. Org. Chem.* **2002**, *67*, 4209−4217. [18e] T. Mino, S. Hata, K. Ohtaka, M. Sakamoto, T. Fujita, *Tetrahedron Lett.* **2001**, *42*, 4837−4839. [18f] R. Stranne, J.-L. Vasse, C. Mobnerg, *Org. Lett.* **2001**, *32*, 2525−2528. [18g] J. Uenishi, *Tetrahedron: Asymmetry* **2001**, *12*, 2999−3006. [18h] G. Xu, S. R. Gilbertson, *Tetrahedron Lett.* **2002**, *43*, 2811−2814.

[19] A. Altomare, M. C. Burla, M. Camalli, G. L. Cascarano, C. Giacovazzo, A. Guagliardi, A. G. G. Moliterni, G. Polidori, R. Spagna. **SIR97** a program for automatic solution of crystal structures by direct methods. *J. Appl. Cryst.* **1999**, *32*, 115.

[20] [20a] H. D. Flack, *Acta Crystallogr., Sect. A* **1983**, *39*, 876. [20b] G. Bernardinelli, H. D. Flack, *Acta Crystallogr., Sect. A* **1985**, *41*, 500.

[21] E. Prince, *Mathematical Techniques in Crystallography*, Berlin, Springer-Verlag, **1982**.

[22] D. J. Watkin, C. K. Prout, J. R. Carruthers, P. W. Betteridge. *CRYSTALS Issue 11*, Chemical Crystallography Laboratory, University of Oxford, Oxford, **2001**.

[23] L. J. Farrugia. ORTEP3 for Windows, *J. Appl. Cryst.* **1997**, *30*, 565.

Received December 5, 2002

 © 2003 Wiley-VCH Verlag GmbH & Co. KGaA, Weinheim

Degradation of the Second-Generation Grubbs Metathesis Catalyst with Primary Alcohols and Oxygen − Isomerization and Hydrogenation Activities of Monocarbonyl Complexes

Maarten B. Dinger[a] and Johannes C. Mol*[a]

Keywords: Ruthenium / Metathesis / Carbene ligands / Alcohols / Isomerization / Hydrogenation

Reaction of the second-generation Grubbs metathesis catalyst [$RuCl_2$(=CHPh)(H_2IMes)(PCy_3)] (**2**) (H_2IMes = 1,3-dimethyl-4,5-dihydroimidazol-2-ylidene) with primary alcohols in the presence of a base produced the complexes [RuClH(CO)(PCy_3)$_2$] (**3**) and [RuClH(CO)(H_2IMes)(PCy_3)] (**5**). When benzyl alcohol was used, the ruthenium phenyl complexes [RuClPh(CO)(PCy_3)$_2$] (**4**) and [RuClPh(CO)(H_2IMes)(PCy_3)] (**7**) were formed in addition to **3** and **5**. Complex **7**, characterised by an X-ray structure analysis, was also formed on exposure of **2** to oxygen. The isomerization and hydrogenation activity of **7** was determined and compared with that of **3** and **4**.
(© Wiley-VCH Verlag GmbH & Co. KGaA, 69451 Weinheim, Germany, 2003)

Introduction

With the advent of the Grubbs metathesis catalysts [$RuCl_2$(=CHPh)(PCy_3)$_2$] (**1**) and [$RuCl_2$(=CHPh)(H_2IMes)(PCy_3)] (**2**) olefin metathesis has become an increasingly useful tool for organic transformations.[1] Moreover, these metathesis catalysts can catalyse a number of other reactions,[2] and can also be transformed in situ into various catalytically active species. Single-component tandem catalysis in the presence of **1** and **2** has, so far, included metathesis followed by hydrogenation,[3] dehydrogenation,[3c] and, most recently, isomerization.[4] Relatively little effort, however, has been made to identify the active species responsible for the secondary reaction(s), although various hydride species are thought to be involved.

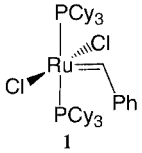

1

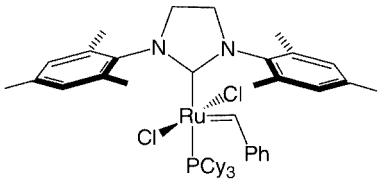

2

Recently, we[5] and others,[3a−3c,6,7] described how the transformation of the first-generation Grubbs catalyst [$RuCl_2$(=CHPh)(PCy_3)$_2$] (**1**) to the hydride species [RuClH(CO)(PCy_3)$_2$] (**3**) could be affected by aliphatic primary alcohols, and we established that the addition of a suitable base greatly facilitates this reaction. Additionally, if benzyl alcohol is used in place of the aliphatic alcohol, the phenyl complex [RuClPh(CO)(PCy_3)$_2$] (**4**) is produced in good yields. The reactions occur via an alcohol dehydrogenation pathway, with toluene and an alkane being the major organic products. Complex **4** was of particular interest because it was also formed when **1** was treated with oxygen, this reaction being especially effective in the solid state, where the undesirable oxidation of the phosphane ligands is suppressed.

Complexes **3** and **4** proved to be excellent α-olefin isomerization catalysts, producing the β-olefin with high (95%) selectivity. Extending the first-generation research to the important second-generation metathesis catalyst **2** was a natural step. The results of these studies are described here.

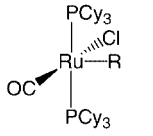

3 R = H
4 R = Ph

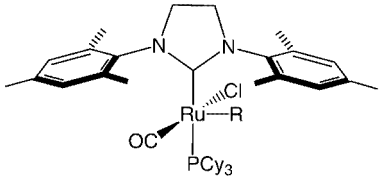

5 R = H
7 R = Ph

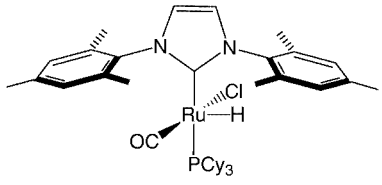

6

[a] Institute of Molecular Chemistry, Faculty of Science, Universiteit van Amsterdam
Nieuwe Achtergracht 166, 1018 WV Amsterdam, The Netherlands
Fax: (internat.) +31-20/5256456
E-mail: jcmol@science.uva.nl

Results and Discussion

Reaction of 2 with Primary Aliphatic Alcohols

When the second-generation catalyst **2** was treated with methanol in the presence of triethylamine, the initially dark brown solution slowly became dark orange. Catalyst **2** was more active than the first-generation system **1**, and the reactions proceeded readily at lower temperatures than used previously for **1** (60 vs. 80 °C).[5] However, ^{1}H and ^{31}P NMR spectroscopy revealed an unexpectedly complex reaction in which three different hydrides were produced, in marked contrast to **1** where only one hydride species was formed.[5] Two of these hydride complexes were identified spectroscopically.

The major reaction product (≈30−40% yield by NMR spectroscopy), showing a doublet at δ = −27.8 ppm in the ^{1}H NMR spectrum, was assigned as the expected mixed-ligand hydride species [RuClH(CO)(H_2IMes)(PCy_3)] (**5**). The formation of **5** was verified by comparison of ^{1}H and ^{31}P NMR spectra with those obtained from the model reaction of **3** with H_2IMes. Unfortunately, repeated attempts to isolate complex **5** from either synthetic route were unsuccessful due to the product's extremely high solubility in all common organic solvents, ranging from pentane to methanol. The surprisingly high solubility of **5** — the very closely related complex [RuClH(CO)(IMes)(PCy_3)] (**6**) was reported to be insoluble in methanol[8] — may be because it is not a solid at room temperature. Complex **5** could be precipitated from pentane solutions at −78 °C, but subsequent removal of the supernatant by syringe, followed by warming of the solid to room temperature, gave only a highly air-sensitive, oily residue.

A second hydride (about 25−30% yield by NMR spectroscopy) shows δ = −24.2 ppm as a triplet, and was determined to be complex **3** by comparison with the spectrum of an authentic sample.[5] The formation of complex **3** from **2** is especially noteworthy since it could only have originated from an unexpected H_2IMes ligand exchange with PCy_3. *N*-Heterocyclic carbene (NHC) ligands in ruthenium systems generally show stronger covalent bonds (more exothermic reaction enthalpies) than phosphanes, and so tend not to readily dissociate.[9] We were unable to unambiguously identify the reaction by-products, but the observed ligand exchange must consume the starting material (or products), and should lead to RuCl(H_2IMes) and free H_2IMes fragments which could subsequently combine to produce bis-H_2IMes complex(es). While free H_2IMes displaced PCy_3 in separate reactions (vide infra), in this case any released H_2IMes might also react with the excess alcohol, thereby limiting its immediate availability for further reaction. Reaction of the ligand with alcohol is not available for PCy_3, and so the degradation becomes considerably more complicated than that observed for **1**.

Surprisingly, the addition of an NHC ligand has virtually no effect on the ^{31}P NMR spectrum of the complexes, rendering ^{31}P NMR of less use than usual in monitoring the reaction outcomes; **3**, **5** and **6** show chemical shifts of 47.6,[5] 46.9, and 47.5[8] ppm, respectively.

The third detected hydride species shows a doublet at δ = −7.43 ppm in the ^{1}H NMR spectrum, and was only a minor product (about 10%). While the large downfield shift relative to **3** and **5** suggested a ligand *trans* to the hydride group, the $^2J_{P,H}$ coupling constant of 50.4 Hz is both too high for a phosphorus *cis* and too low for a phosphorus *trans* to the hydride moiety, indicating a distorted coordination environment. The associated phosphorus resonance appears at δ = 47.5 ppm in the ^{31}P NMR spectrum, and so was not separated from those of **3** and **5**.

A fourth, unidentified complex that was definitely not a hydride species shows a phosphorus resonance at δ = 51.2 ppm in the ^{31}P NMR spectrum, and represented about 20−25% of the total phosphorus content of the crude reaction mixture. This peak appeared in a similar location as that found for the reaction of **1** with water,[5] and might arise from the reaction of **2** with adventitious water in the reagents/solvents used.

Ethanol, 1-propanol and 1-nonanol also gave the hydrides **3** and **5** as the dominant products, but with much smaller amounts (<5%) of the unknown hydride. Interestingly, 1-propanol and 1-nonanol gave significantly higher relative yields of **5**; **3**:**5** was 15:85 for these two alcohols, compared with 40:60 and 35:65 for methanol and ethanol, respectively. Ethanol, 1-propanol and 1-nonanol also produced the unknown complex with a ^{31}P NMR peak at δ = 51 ppm, and in approximately the same quantities. Such a significant side-product was never observed in otherwise identical reactions of **1**, further highlighting the quite different behaviour of **1** and **2** in the alcoholic degradation experiments.

The volatile components of the 1-nonanol reaction were analysed by GCMS and showed that, as with **1**, toluene and octane were the major constituents, indicative of an alcohol dehydrogenation/decarboxylation mechanism.[5] Reaction with 1-^{13}C enriched ethanol ($CH_3{}^{13}CH_2OH$) confirmed that the hydride complexes were formed by this pathway. Most of the ^{13}C label was incorporated as the carbonyl groups in **3** and **5**, and the associated hydride signals clearly showed additional coupling due to an adjacent spin-active carbon isotope. A third ^{13}C-labeled carbonyl group, which showed no splitting from phosphorus (singlet), appeared at δ = 204.7 ppm; this complex may possibly be a bis-NHC complex. Interestingly, the third, unidentified, hydride species (δ = −7.43 ppm) showed no additional splitting (remaining a simple doublet), indicating that it does not contain a carbonyl group and, therefore, probably does not form from an alcohol dehydrogenation pathway.

Reaction of 2 with Benzyl Alcohol

As with aliphatic alcohols, when complex **2** was reacted with an excess of benzyl alcohol, in the presence of triethylamine, several products were observed by ^{31}P NMR spectroscopy. This was in sharp contrast to the reaction of **1** with benzyl alcohol under the same conditions, which cleanly generated the phenylruthenium complex **4** in good yield.[5] Again, the main reason for the relatively unsatisfactory reaction is the apparently significant lability of the

 © 2003 Wiley-VCH Verlag GmbH & Co. KGaA, Weinheim

H_2IMes ligand under the conditions used, which readily scrambled with the phosphane. Additionally, whereas no hydride complexes formed with **1**, catalyst **2** also produced hydride complexes. Complexes **3** and **5** represented about 25% and 10% of the total phosphorus-containing complexes, respectively, while **4** and the desired product, [RuClPh(CO)(H_2IMes)(PCy_3)] (**7**), were formed in 5% and 30% yield, respectively. The remaining about 30% was due to an unknown species that shows a ^{31}P NMR signal at δ = 51.9 ppm. This chemical shift is very similar to that of the complex(es) formed with aliphatic alcohols, although the about 0.7 ppm difference implies that it may possibly be a slightly different species.

The ^{1}H NMR spectrum revealed that a third hydride species had again formed, in addition to **3** and **5**, but this species was distinct from that present in the aliphatic alcohol reactions, showing a sharp singlet at $\delta = -6.59$ ppm that indicates the complete absence of phosphorus ligands and a substituent *trans* to the hydride atom. This complex might be the bis-carbene [RuClH(CO)(H_2IMes)$_2$], although this could not be confirmed synthetically; complex **3**, with excess H_2IMes, even at 100 °C, gave only the mono-substituted complex **5**. However, this does not rule out a bis-NHC complex; the failure of bis-phosphanes to fully substitute with NHCs can be attributed to the lowered lability of the remaining phosphane after mono-substitution.[6] To gain further insight we analysed the crude reaction mixture by FAB/MS. Unfortunately, this yielded little new information since only **4** and **7** (and their fragmentation products) were detected.

Reaction of 2 with Oxygen

Like complex **1**,[5] complex **2** also reacted with oxygen. However, the reactions were much lower yielding. Thus, **2** reacted with dry air at room temperature in toluene to give, mainly, tricyclohexylphosphane oxide, and only very low amounts of **7**. Furthermore, the diphosphane product **5** was also produced. Higher temperatures gave O=PCy_3 as the only phosphorus-containing species according to ^{31}P NMR spectroscopy.

In the solid state, the reaction of **2** with oxygen (5 bar) was cleaner. Nonetheless, only about 30% of **2** had reacted after 48 h, and, of that, only about 30% was complex **7**. The major product peak in the ^{31}P NMR spectrum appears at δ = 48 ppm, possibly due to O=PCy_3, although the lability of phosphane in the solid state should be relatively low, disfavouring the formation of this product. At higher pressures (50 bar) and 60 °C the complete reaction of **2** was achieved over three days to give, after workup, a 29% yield of the air-stable, bright pink **7**. The fate of the remaining **2** could not be determined; a phosphorus-containing material gave a ^{31}P NMR peak at δ = 54.4 ppm, but could not be isolated. The lower reactivity of **2** compared with **1** towards oxygen is foretold by its superior air tolerance; it can even be purified by chromatography using non-degassed solvents.[10] Nonetheless, the NHC ligand, being a better σ-donor than phosphanes, should render the ruthenium more electron-rich, thereby increasing the nucleophilicity of the benzylidene group toward an electrophile.[11]

Unsurprisingly, complex **7** was more easily prepared, and in better yield, by reaction of **4** with H_2IMes in toluene at 100 °C.

Crystal Structure of 7

Red blocks of **7** suitable for X-ray diffraction were grown by the slow evaporation of a CH_2Cl_2/MeOH solution in air. Figure 1 shows the structure of **7**, with selected bond lengths and angles in the caption.

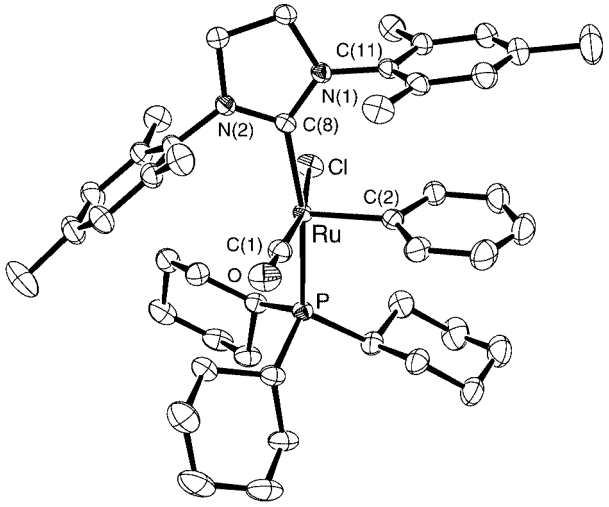

Figure 1. ORTEP representation of complex **7** with thermal ellipsoids drawn at the 30% probability level; hydrogen atoms have been omitted for clarity; selected bond lengths (Å) and angles (°): Ru−Cl 2.4542(8), Ru−P 2.4499(7), Ru−C(1) 1.805(3), Ru−C(2) 2.039(3), Ru−C(8) 2.118(3), O−C(1) 1.142(4), N(1)−C(8) 1.335(3), N(2)−C(8) 1.345(4); P−Ru−Cl 89.76(3), Cl−Ru−C(1) 168.6(1), Cl−Ru−C(2) 102.7(1), Cl−Ru−C(8) 86.05(7), P−Ru−C(1) 89.6(1), P−Ru−C(2) 94.25(8), P−Ru−C(8) 168.81(7), C(1)−Ru−C(2) 88.7(1), C(1)−Ru−C(8) 92.5(1), C(2)−Ru−C(8) 96.8(1), Ru−O−C(1) 179.2(3)

The ruthenium occupies a typical distorted square-pyramidal coordination geometry. As in related structures, the halogen is *trans* to the carbonyl moiety, so that the phosphorus is *trans* to the other neutral ligand (in this case H_2IMes). Somewhat surprisingly, few structures of complexes of the type [RuArCl(L)$_2$(CO)] (Ar = aromatic, L = phosphane) have been described,[12] and **7** is the first example containing an NHC ligand.

Overall, the structure most closely resembles that of the hydride complex **6** determined by Nolan,[8] with the phenyl group in **7** residing at the position of the hydride at the apex of the pyramid. The main distortions from an ideal square-pyramidal geometry are the P−Ru−C(8) and Cl−Ru−C(1) angles (both about 169°), which compare with analogous angles of 173.4 and 175.9°, respectively, in **6**. The increased distortion is most likely due to the higher steric influence of the phenyl group in **7** relative to the hydrogen in **6**. Surprisingly, the Ru−C(8) and Ru−P distances in **7** are significantly longer (0.035 and 0.083 Å, respectively) than in **6**; typically, these bond lengths are not greatly affected when

 © 2003 Wiley-VCH Verlag GmbH & Co. KGaA, Weinheim

saturated (H_2IMes) or unsaturated (IMes) NHC ligands are present. Conversely, the Ru−CO bond length in **7** is longer (0.021 Å) than in **6**, concomitant with a shortening (0.038 Å) of the C≡O distance. The different electronic influences of the unsaturated (in **6**) and saturated (in **7**) NHC ligands are probably not responsible for these discrepancies. The increased steric demands of the phenyl group are probably the dominant influence, since the pushing back of the neutral ligands may result in less-ideal orbital overlaps with the metal center. The phenyl ring and one of the mesityl groups are in close contact, and almost perfectly eclipse one another. Because the two rings are not quite co-planar, forming a butterfly angle of 10.0(2)°, C(2)···C(11) represents the minimum distance between the rings at 3.259 Å.

Isomerization Activity of Complexes 3, 4 and 7

Previously we reported that complexes **3** and **4**, while totally metathesis inactive, were potent C=C bond isomerization catalysts for α-olefins.[5] Wagener et al. have recently made a detailed study of the double-bond isomerization activity of the first- and second-generation Grubbs catalysts **1** and **2**, and compared that with the Mo-based Schrock metathesis catalyst.[13] Double-bond isomerization is highly relevant in metathesis chemistry because it is the primary cause of secondary metathesis products; this is generally considered to be a major limitation of olefin metathesis. Nonetheless, double-bond isomerization has also recently been deliberately exploited in a tandem metathesis-isomerization reaction for the synthesis of cyclic enol ethers[4] in which the metathesis catalysts **1** or **2** were converted by hydrogen, after metathesis had ceased, into uncharacterised isomerization catalysts. We decided to determine the isomerization activity of complex **7** towards 1-octene, and compare this with the first-generation systems **3** and **4**.

As we recently reported for metathesis catalysed by **1** and **2**,[14] additional solvents were unnecessary in the isomerization reactions. Because solvents are a major hurdle in the development of "green" chemistry, any reactions where they are not required are particularly relevant to this increasingly timely area.[15] Figure 2 summarises the 1-octene isomerization activity of **7** over a range of temperatures. In each case, the reactions were allowed to proceed to maximal conversion, and, for comparison, the results for **3** and **4** under the same conditions are included.

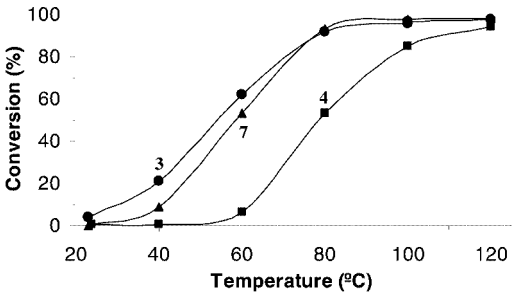

Figure 2. Double-bond isomerization of neat 1-octene (100,000 equivalents) in the presence of catalysts **3**, **4** and **7** as a function of reaction temperature; all reactions were allowed to proceed until 1-octene was no longer consumed

From Figure 2, the hydride complex **3** remains the most active catalyst with respect to turnover number. At lower temperatures, the phenyl-substituted analogue of **3**, complex **4**, displayed considerably lower activity, and was essentially inactive below 50 °C, possibly because the active species has to be generated in situ − for both **3** and **4** this active species is likely to be [RuClH(CO)(PCy_3)].[16] The NHC-substituted analogue **7** was almost as active as the hydride **3**. The loss in activity associated with substituting the hydride moiety (in **3**) for a phenyl group (in **4**) is at least partially offset by the increase in activity associated with replacing one of the tricyclohexylphosphane ligands with H_2IMes (in **7**). Unfortunately, as mentioned above, the H_2IMes-substituted hydride **5** could not be obtained in a sufficiently pure form for comparison.

Interestingly, at higher temperatures, and especially after prolonged reaction times, metathesis products (predominantly tridecene and dodecene, from the cross-metathesis of 1-octene with 2-octene and the self-metathesis of 2-octene, respectively) were detected in the reactions involving catalyst **7**. While these longer chain olefins represented only about 3−5% of the reaction products, it is noteworthy that only the NHC-containing compound initiated only metathesis, i.e. metathesis products have never been observed in reactions involving **3** and **4**.

Figure 3 depicts the relative reaction rates and selectivity over time for the isomerization of 1-octene into 2-octene at 100 °C. Catalyst **7** is clearly much more active than either **3** or **4**. Again, the presumed loss of activity due to the exchange of a hydride for a phenyl group is more than compensated for by the addition of the NHC ligand. Indeed, 97% conversion of 100,000 equivalents of 1-octene in the presence of **7** was achieved in less than 5 minutes, with 95% selectivity for 2-octene. For each catalyst, the selectivity for 2-octene formation rapidly decreased once all of the 1-octene had been consumed. Thus, the selectivity after 8 h was highest for catalyst **4**, followed by **3** and finally **7**, coinciding with their relative activities. We had previously determined that catalyst **4** could not isomerise 2-octene, and so the decrease in selectivity is primarily due to decomposition of the active catalyst into unknown ruthenium complexes that

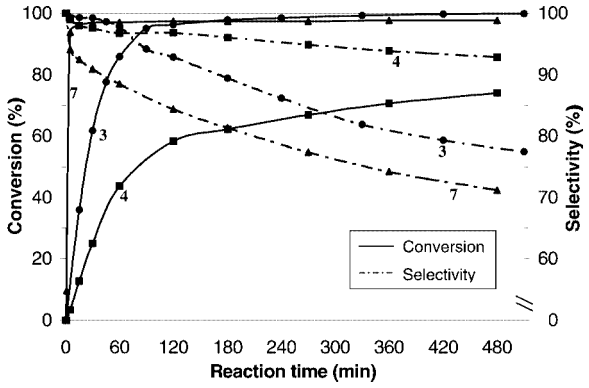

Figure 3. Double-bond isomerization of neat 1-octene (100,000 equivalents) into 2-octene at 100 °C in the presence of catalysts **3**, **4** and **7** as a function of reaction time

 © 2003 Wiley-VCH Verlag GmbH & Co. KGaA, Weinheim

Table 1. Hydrogenation of 1-octene in the presence of catalysts **3**, **4** and **7**, under various reaction conditions

T (°C)	$P(H_2)$ (bar)	Cat.	Equiv. of 1-octene[a]	Reaction time (h)	Conversion (%)	Selectivity (%)[b]	Isomerization products (%)[c]
23	4	3	100,000	18	99.9	100	0
23	4	4	100,000	18	1.6	100	0
23	4	7	100,000	18	0.4	100	0
100	4	3	100,000	3	98.7	100	0
100	4	4	100,000	3	98.5	100	0
100	4	7	100,000	3	99.3	100	0
100	4	3	350,000	2	98.3	84.1	15.6
100	4	4	350,000	2	98.5	90.2	9.7
100	4	7	350,000	2	99.1	58.9	40.7
100	1	3	250,000	3	98.5	95.3	3.2
100	1	4	250,000	3	99.6	77.8	22.1
100	1	7	250,000	3	99.1	81.4	18.4

[a] Mol of 1-octene per mol of catalyst. [b] Selectivity towards the formation of octane. [c] Isomerization products: 2-, 3-, and 4-octene.

are also catalytically active toward olefin isomerization but lack the selectivity (and activity) of the parent catalyst.[5] The *cis* to *trans* ratio of the 2-octene produced for each catalyst was approximately 30:70.

Hydrogenation Activity of 3, 4 and 7

Hydrogenation of alkenes is an important organic transformation, and can be facilitated by traditional homogeneous catalysts such as $[RhCl(PPh_3)_3]$ (Wilkinson catalyst), $[RuClH(PPh_3)_3]$ and $[RuH(CO)(PPh_3)_3]$.[17] More recently, catalyst **3** has been found to be an excellent olefin hydrogenation catalyst,[8,16,18] and has also been exploited for the hydrogenation of polybutadiene rubber.[19] Furthermore, the second-generation analogue **6** has recently been tested for hydrogenation activity, and displayed activity similar to **3** at higher temperatures.[8] Due to the current interest in single-component tandem metathesis-hydrogenation reactions,[3] we tested the efficacy of catalysts **4** and **7** for the hydrogenation of 1-octene, and compared the results with those of **3** (Table 1). Various reaction conditions were tested, and, again, the reaction proceeds very well in neat substrate, i.e. no additional solvents were required for good conversions and reaction rates.

From the data in Table 1 catalyst **3** is clearly the most active catalyst for the hydrogenation of 1-octene. Indeed, only **3** shows appreciable hydrogenation activity at room temperature. At 100 °C, **4** and **7** were "activated", and also became good hydrogenation catalysts, comparable in activity to **3**, and gave complete conversion into octane when 100,000 equivalents (mol) of 1-octene were reacted.

To better test the limits of the catalysts, reactions with lower catalyst loadings were examined. Thus, 350,000 equivalents (mol) of 1-octene were hydrogenated in the presence of **3**, **4** or **7** at 100 °C. All the catalysts consumed the 1-octene completely, but none gave selective conversion into octane. Catalysts **3** and **4** showed comparable activity and selectivity, whereas **7** produced lower amounts of octane, with isomerization clearly competing with the hydrogenation. This result is perhaps not surprising given the very high activity of **7** with regard to isomerization (vide supra), while the hydrogenation activity of **7** towards 2-octene is clearly lower.

Remarkably, the absence of solvent may benefit these reactions. Whereas Nolan reported turnover rates for the hydrogenation [$P(H_2)$ = 4 bar) of 1-hexene in benzene at 100 °C of 21,500 and 24,000 (mol product)(mol catalyst)$^{-1}h^{-1}$ for **3** and **6**, respectively,[8] we attained turnover frequencies of well over 100,000 h^{-1} for all the systems tested at 100 °C, even at only $P(H_2)$ = 1 bar.

Conclusions

The chemistry previously developed for the first-generation ruthenium metathesis catalyst **1**,[5] could be extended to include the second-generation catalyst **2**. However, the reactions were complicated by an unanticipated exchange involving the NHC ligand, even at relatively low temperatures (60 °C). The lability of the NHC ligand allowed not only the formation of the desired mixed-ligand systems, but also the corresponding diphosphane complexes. In theory these complexes could hinder olefin metathesis reactions that employ **2** in alcoholic solvents, but the higher temperatures and relatively long time needed for their formation limits their role in potential side-reactions.

Complex **7**, a fully air-stable solid, is a highly active isomerization catalyst − considerably more active than either of the first-generation systems **3** and **4**. We tentatively suggest that the higher σ-donation of the NHC ligand (relative to phosphanes), which ultimately renders the second-generation metathesis catalysts more active than their first-generation congeners, may also explain their (or their decomposition products') efficacy as isomerization catalysts. We also found that complexes **4** and **7** are efficient hydrogenation catalysts at higher temperatures, which may aid in the development of single-component tandem metathesis-hydrogenation of olefins[3a,3b] when employing the second-generation metathesis catalysts.

 © 2003 Wiley-VCH Verlag GmbH & Co. KGaA, Weinheim

Experimental Section

Unless otherwise stated, all manipulations were performed under a nitrogen atmosphere on a vacuum line using standard Schlenk techniques. Complex **1** (Fluka), potassium *tert*-pentoxide solution (1.7 M in toluene, Fluka), and 1-octene (98%, Aldrich) were obtained from commercial sources. 1,3-Dimesityl-4,5-dihydroimidazolinium chloride[20] and the complexes **2**,[21] **3**,[22] and **4**[5] were prepared by the literature procedures. NMR spectra were recorded on a Varian Mercury 300 spectrometer, at 300.14, 75.48 and 121.50 MHz for the proton, carbon and phosphorus channels, respectively. Elemental analyses were performed by H. Kolbe Mikroanalytisches Laboratorium, Germany.

[RuClH(CO)(H_2IMes)(PCy_3)] (5): Potassium *tert*-pentoxide solution (1.7 M in toluene, 260 μL, 0.442 mmol) was added to a suspension of 1,3-dimesityl-4,5-dihydroimidazolinium chloride (0.150 g, 0.437) in toluene (5 mL) and stirred for 10 min. The resulting solution was transferred, via a steel cannula fitted with a filter, to a second flask containing a toluene (2 mL) solution of **3** (0.100 g, 0.138 mmol). The mixture was then heated to 100 °C for 3 h. No colour change was observed. The solvent was removed under reduced pressure, leaving an oily residue that was miscible with all common organic solvents at room temperature. Cooling a concentrated pentane solution to −78 °C produced a yellow solid. The mother liquor was then carefully removed by syringe and the solid allowed to warm to room temperature, during which time it slowly melted. The resultant highly air-sensitive oil was spectroscopically characterised as complex **5** (≈75% purity). IR (toluene): $\tilde{\nu}$ = 1896 cm^{-1} (vs, C≡O). ^1H NMR (CD_2Cl_2): δ = 25.37 (d, J_{HP} = 21.3 Hz, 1 H, Ru-*H*), 2.5−1.1 (multiple peaks, 51 H, H-aliphatic), 3.17 (br. s, 2 H, CH_2CH_2), 3.78 (br. s, 2 H, CH_2CH_2), 6.80 (br. s, 2 H, $C_6Me_3H_2$), 6.99 (br. s, 2 H, $C_6Me_3H_2$) ppm. $^{31}P\{^1H\}$ NMR (CD_2Cl_2): δ = 46.7 ppm.

[RuClPh(CO)(H_2IMes)(PCy_3)] (7), Method A: Potassium *tert*-pentoxide solution (1.7 M in toluene, 220 μL, 0.374 mmol) was added to a suspension of 1,3-dimesityl-4,5-dihydroimidazolinium chloride (0.130 g, 0.379) in toluene (4 mL) and stirred for 10 min. The resulting solution was then transferred, via a steel cannula fitted with a filter, to a second flask containing a toluene (2 mL) solution of **4** (0.100 g, 0.125 mmol). The mixture was heated to 100 °C for 3 h, during which time the solution became a brighter orange/red. The solvent was then removed under reduced pressure, and methanol subsequently added to the residue. Rapid stirring (1 h) produced a bright pink precipitate, which was collected by filtration and then washed with methanol (4 × 10 mL) and pentane (2 × 5 mL) to give complex **7** as a crimson powder (0.072 g, 70%).

Method B: Finely powdered **2** (0.050 g, 0.059 mmol) was deposited as a solid in an autoclave that was subsequently pressurised with oxygen (50 bar) and then heated in an oil bath to 60 °C for 3 days. After releasing the pressure, workup in the same manner as Method A gave complex **7** (0.014 g, 29%). IR (KBr): $\tilde{\nu}$ = 1901 cm^{-1} (vs, C≡O). ^1H NMR (CD_2Cl_2): δ = 1.07 [m, 11 H, $P(C_6H_{11})_3$], 1.24 [m, 4 H, $P(C_6H_{11})_3$], 1.54 (s, 3 H, *p*-Me $C_6Me_3H_2$), 1.62 [br. s, 14 H, $P(C_6H_{11})_3$], 1.88 [m, 4 H, $P(C_6H_{11})_3$], 2.20 (s, 9 H, *o*-Me/*p*-Me $C_6Me_3H_2$), 2.63 (s, 6 H, *o*-Me $C_6Me_3H_2$), 3.85 (br. s, 4 H, CH_2CH_2), 5.89 (d, $^3J_{H,H}$ = 7.50 Hz, 1 H, *m*-H C_6H_5), 6.24 (d, $^3J_{H,H}$ = 7.20 Hz, 1 H, *p*-H C_6H_5), 6.30 (d, $^3J_{H,H}$ = 7.50 Hz, 1 H, *m*-H C_6H_5), 6.46 (br. s, 2 H, $C_6Me_3H_2$), 6.83 (d, $^3J_{H,H}$ = 7.80 Hz, 1 H, *o*-H C_6H_5), 6.88 (s, 2 H, $C_6Me_3H_2$), 7.14 (d, $^3J_{H,H}$ = 7.20 Hz, 1 H, *o*-H C_6H_5) ppm. $^{13}C\{^1H\}$ NMR (CD_2Cl_2): δ = 19.3, 19.4 (*o*-Me/*p*-Me $C_6Me_3H_2$), 21.2 (*o*-Me $C_6Me_3H_2$), 26.9 [s, $P(C_6H_{11})_3$], 28.4 [d, $J_{C,P}$ = 8.5 Hz, $P(C_6H_{11})_3$], 29.6 [d, $J_{C,P}$ = 16.6 Hz, $P(C_6H_{11})_3$], 34.5 [d, $J_{C,P}$ = 16.2 Hz, $P(C_6H_{11})_3$], 118.5, 124.3, 125.6, 129.6, 130.0, 136.2, 136.8, 137.1, 138.2, 139.1, 140.5 (C-Ar), 155.9 (d, $^2J_{C,P}$ = 12.0 Hz, *i*-C C_6H_5), 205.6 (d, $^2J_{C,P}$ = 13.7 Hz, Ru-*C*O), 210.8 [d, $^2J_{C,P}$ = 94.9 Hz, Ru-*C*$(N)_2$] ppm. $^{31}P\{^1H\}$ NMR (CD_2Cl_2): δ = 22.2 ppm. $C_{46}H_{64}ClN_2OPRu$: calcd. C 66.69, H 7.79, N 3.38; found C 66.78, H 7.72, N 3.31.

Isomerization Reactions: Immediately before use, the 1-octene was passed through a column (20 cm × 1.5 cm) of neutral alumina (Acros, 50-200 μm), containing 15 g of alumina per 100 mL of octene, into a Schlenk flask. The 1-octene was then deoxygenated by a series of degassings (by evacuation of the flask), followed by refilling with nitrogen. For each reaction, 20 mL (127 mmol) of 1-octene was used. The reaction vessel was immersed in an oil bath and allowed to equilibrate to the desired temperature. An appropriate quantity (six-figure analytical balance) of the catalyst under investigation was then added to the 1-octene. No additional solvents were used. All reactions were thoroughly stirred, by way of a magnetic stirrer bar, and were allowed to proceed to completion, i.e. the reported results are those obtained when 1-octene consumption had ceased. The product distribution of the isomerization reactions was measured by GC/FID (Carlo Erba 8000 Top) using a ZB-5 (5% phenyl polysiloxane) column (Zebron).

Hydrogenation Reactions: 1-Octene was prepared in the manner described above for the isomerization reactions. A small quantity of the catalyst under investigation was introduced into an autoclave fitted with a glass liner, and the autoclave was subsequently evacuated and flushed with hydrogen. 1-Octene (10 mL) was introduced by syringe, and the autoclave pressurised with the desired level of hydrogen; this pressure was maintained throughout the experiment. The autoclave was heated, where appropriate, by way of an oil bath. After completion of the reaction, the hydrogen was vented off, and the solution analysed as for the isomerization reactions.

Crystal Structure Determination of 7: Red blocks of **7** suitable for X-ray diffraction were grown by the slow evaporation of a CH_2Cl_2/MeOH solution. Intensity data were collected on an Enraf−Nonius CAD-4 diffractometer, using a crystal of dimensions 0.50 × 0.45 × 0.125 mm, with graphite-monochromated Mo-K_α X-rays (λ = 0.71069) and ω-2θ scan. A total of 7461 unique reflections in the range 1.6° < 2θ < 25° were collected at room temperature, and these were subsequently corrected for Lorentz effects, polarization effects, and for linear absorption by a Ψ-scan method. Crystal data: $C_{46}H_{64}ClN_2OPRu$, FW = 828.48, crystal class monoclinic, space group $P2_1/c$, a = 12.2573(8), b = 15.6707(12), c = 22.358(4) Å, β = 94.686(10)°, V_c = 4280.2(9) $Å^3$, D_c = 1.286 g cm^{-3}, Z = 4, $F(000)$ = 1752, μ(Mo-K_α) = 0.502 mm^{-1}.

The structure of **7** was solved using the direct methods option of SHELXS-97[23] and subsequently refined using SHELXL-97.[24] All non-hydrogen atoms were assigned anisotropic temperature factors and all hydrogen atom positions were determined by calculation. For the methyl groups of the mesityl substituents, where the location of the hydrogen atoms was uncertain, the AFIX 137 card was used to allow the hydrogen atoms to rotate to the maximum area of residual density, while fixing their geometry. The refinement converged with R_1 = 0.0422 for 6751 data with $I \geq 2\sigma(I)$, 0.0466 for all data; wR_2 = 0.1146 $\{w = 1/[\sigma^2(F_o^2) + (0.0752P)^2 + 2.3804P]$ where $P = (F_o^2 + 2F_c^2)/3\}$, and GoF = 1.046. No parameter shifted in the final cycle. The final difference map showed no peaks or troughs of electron density greater than +1.29 and −1.02 e·$Å^{-3}$ respectively, both near Ru.

CCDC-199892 contains the supplementary crystallographic data for complex **7**. These data can be obtained free of charge at

 © 2003 Wiley-VCH Verlag GmbH & Co. KGaA, Weinheim

www.ccdc.cam.ac.uk/conts/retrieving.html [or from the Cambridge Crystallographic Data Centre, 12 Union Road, Cambridge CB2 1EZ, UK; Fax: (internat.) +44-1223/336-033; E-mail: deposit@ccdc.cam.ac.uk].

Acknowledgments

We wish to thank Jan Fraanje for the collection of the X-ray data set and SASOL for funding this research.

[1] [1a] T. M. Trnka, R. H. Grubbs, *Acc. Chem. Res.* **2001**, *34*, 18−29. [1b] R. H. Grubbs, S. Chang, *Tetrahedron* **1998**, *54*, 4413−4450.
[2] B. Alcaide, P. Almendros, *Chem. Eur. J.* **2003**, *9*, 1258−1262.
[3] [3a] D. E. Fogg, D. Amoroso, S. D. Drouin, J. Snelgrove, J. Conrad, F. Zamanian, *J. Mol. Catal. A: Chem.* **2002**, *190*, 177−184. [3b] S. D. Drouin, F. Zamanian, D. E. Fogg, *Organometallics* **2001**, *20*, 5495−5497. [3c] J. Louie, C. W. Bielawski, R. H. Grubbs, *J. Am. Chem. Soc.* **2001**, *123*, 11312−11313. [3d] P. Børsting, P. Nielsen, *Chem. Commun.* **2002**, 2140−2141.
[4] A. E. Sutton, B. A. Seigal, D. F. Finnegan, M. L. Snapper, *J. Am. Chem. Soc.* **2002**, *124*, 13390−13391.
[5] M. B. Dinger, J. C. Mol, *Organometallics* **2003**, *22*, 1089−1095.
[6] T. M. Trnka, J. P. Morgan, M. S. Sanford, T. E. Wilhelm, M. Scholl, T.-L. Choi, S. Ding, M. W. Day, R. H. Grubbs, *J. Am. Chem. Soc.* **2003**, *125*, 2546−2558.
[7] A closely related reaction utilising allylic alcohols was described very recently: H. Werner, C. Grünwald, W. Stüer, J. Wolf, *Organometallics* **2003**, *22*, 1558−1560.
[8] H.-M. Lee, D. C. Smith, Z. He, E. D. Stevens, C. S. Yi, S. P. Nolan, *Organometallics* **2001**, *20*, 794−797.
[9] L. Jafarpour, S. P. Nolan, *J. Organomet. Chem.* **2001**, *617−618*, 17−27.
[10] S. B. Garber, J. S. Kingsbury, B. L. Gray, A. H. Hoveyda, *J. Am. Chem. Soc.* **2000**, *122*, 8168−8179.
[11] A. F. Hill, W. R. Roper, J. M. Waters, A. H. Wright, *J. Am. Chem. Soc.* **1983**, *105*, 5939−5940.
[12] [12a] D. Huang, W. E. Streib, J. C. Bollinger, K. G. Caulton, R. F. Winter, T. Scheiring, *J. Am. Chem. Soc.* **1999**, *121*, 8087−8097. [12b] C. E. F. Rickard, W. R. Roper, G. E. Taylor, J. M. Waters, L. J. Wright, *J. Organomet. Chem.* **1990**, *389*, 375−388.
[13] [13a] S. E. Lehman Jr., J. E. Schwendeman, P. M. O'Donnell, K. B. Wagener, *Inorg. Chim. Acta* **2003**, *345*, 190−198. [13b] J. C. Sworen, J. H. Pawlow, W. Case, J. Lever, K. B. Wagener, *J. Mol. Catal. A: Chem.* **2003**, *194*, 69−78.
[14] M. B. Dinger, J. C. Mol, *Adv. Synth. Catal.* **2002**, *344*, 671−677.
[15] [15a] A. D. Curzons, D. J. C. Constable, D. N. Mortimer, V. L. Cunningham, *Green Chem.* **2001**, *3*, 1−6. [15b] J. O. Metzger, *Angew. Chem. Int. Ed.* **1998**, *37*, 2975−2978.
[16] C. S. Yi, D. W. Lee, Z. He, A. L. Rheingold, K-C. Lam, T. E. Concolino, *Organometallics* **2000**, *19*, 2909−2915.
[17] [17a] H. Brunner, "*Hydrogenation*" in *Applied Homogeneous Catalysis with Organometallic Compounds, Second Edition* (Eds. B. Cornils, W. A. Herrmann), Wiley-VCH: Weinheim, **2002**; Vol. 1, 195−212. [17b] P. A. Chalonger, M. A. Esteruelas, F. Joó, L. A. Oro, *Homogeneous Hydrogenation*; Kluwer: Boston, **1994**. [17c] G. W. Parshall, S. D. Ittel, *Homogeneous Catalysis*, 2nd ed., Wiley: New York, **1992**. [17d] J. P. Collman, L. S. Hegedus, J. R. Norton, R. G. Finke, *Principles and Applications of Organotransition Metal Chemistry*, University Science Books: Mill Valley, CA, **1987**. [17e] *Comprehensive Coordination Chemistry* (Ed. G. Wilkinson), Pergamon: New York, **1987**, Vol. 6.
[18] C. S. Yi, D. W. Lee, *Organometallics* **1999**, *18*, 5152−5156.
[19] P. Martin, N. T. McManus, G. L. Rempel, *J. Mol. Catal. A: Chem.* **1997**, *126*, 115−131.
[20] A. J. Arduengo III, R. Krafczyk, R. Schmutzler, *Tetrahedron* **1999**, *55*, 14523−14534.
[21] M. Scholl, S. Ding, C. W. Lee, R. H. Grubbs, *Org. Lett.* **1999**, *1*, 953−956.
[22] C. S. Yi, D. W. Lee, Y. Chen, *Organometallics* **1999**, *18*, 2043−2045.
[23] G. M. Sheldrick, *SHELXS-97*, *Program for Solving X-ray Crystal Structures*, University of Göttingen, Germany, **1997**.
[24] G. M. Sheldrick, *SHELXL-97*, *Program for Refining X-ray Crystal Structures*, University of Göttingen, Germany, **1997**.

Received December 24, 2002

 © 2003 Wiley-VCH Verlag GmbH & Co. KGaA, Weinheim

Effect of Mixed Pendant Groups on the Solution Properties of 12-Membered Azapyridinomacrocycles: Evaluation of the Protonation Constants and the Stability Constants of the Europium(III) Complexes

Jean-Michel Siaugue,[a] Alain Favre-Réguillon,[b] Fabienne Dioury,[a] Gabriel Plancque,[c] Jacques Foos,[a] Charles Madic,[d] Christophe Moulin,[c] and Alain Guy*[b]

Keywords: Macrocyclic ligands / Protonations / Stability constants / Europium / Luminescence

The protonation constants ($\log K_i^H$) of new *N*-acetate or *N*-propionate substituted azamacrocycles derived from 12-membered pyridinoazamacrocycles were determined by potentiometric methods. The number of coordinated water molecules, determined from the luminescence lifetime of the Eu^{III} complexes, indicates a decreasing degree of hydration upon increasing the ring size of the pendant arms. Each ligand forms a 1:1 complex with Eu^{III}, for which the stability constants ($\log K_{therm}$) have been measured by time-resolved laser-induced europium luminescence. The replacement of acetate pendant groups by propionate increases the overall basicity of 12-membered pyridinoazamacrocycles but decreases the stability constant of the Eu^{III} complexes from $\log K = 21.1$ with three *N*-acetate pendant arms to $\log K = 13.7$ with two *N*-propionate and one *N*-acetate pendant arms and to $\log K = 10.7$ with three *N*-propionate pendant arms.
(© Wiley-VCH Verlag GmbH & Co. KGaA, 69451 Weinheim, Germany, 2003)

Introduction

Polyazamacrocyclic paramagnetic and radioactive metal ion chelates are of interest in biomedical applications such as Magnetic Resonance Imaging (MRI),[1,2] diagnostic[3] and therapeutic radiopharmaceuticals,[4] and as luminescent probes to investigate biochemical systems.[5]

Numerous 12-membered tetraazamacrocycles derived from "cyclen" with acetate, substituted acetate or propionate side chains have been studied.[2,6] The selectivity of complexation of such ligands towards various metal ions (i.e. the relative stability of the resulting complexes) can be tuned by adjusting the ring size, the number and the nature of coordinating atoms in the ring, and the type of side chains. Introduction of a pyridine in the 12-membered tetraazamacrocycles "cyclen" is expected to increase the conformational rigidity of the resulting macrocycle, and changing chelate ring size from five- to six-membered may influence the ion selectivity and properties of the macrocyclic compounds. Therefore, we studied the effect of the pendant arms (acetate versus propionate side chains) on protonation constants and Eu^{III} stability constants in a series of 12-membered pyridinoazamacrocycles L^1, L^2, and L^3 (Figure 1).

Potentiometric titrations have been used to determine the stability constants of L^1 ligands with alkaline-earth metal and first-row transition-metal ions[7] but this could not be applied to lanthanide ions due to both their extremely high constants ($\log K_{ML} > 20$) and their slow kinetics of formation. The "out-of-cell" potentiometric and competition titrations performed on cyclen derivatives are, necessarily, indirect, and the results depend on the validity of the assumptions made concerning the species present in the solution and the attainment of equilibrium at the time of the measurement. Gd^{III} complexes formed with L^1 ligand have been characterized by relaxometric experiments.[8,9]

The low extinction coefficients of Laporte-forbidden lanthanide f−f transitions mean that lanthanide ions have very small absorption coefficients, resulting in inefficient direct excitation.[10] This problem can be solved by using heterocycles as sensitizers or laser beams.[11] Tunable dye lasers excite the $^7F_0 \rightarrow {}^5D_0$ transition of the Eu^{III} ion in the range 577−581 nm, while the $^5D_0 \rightarrow {}^7F_2$ emission is monitored at 614 nm.[11] This provides an original method to directly monitor the binding of Eu^{III} to ligands in solution and has been used to determine the stability constants of lanthanides with polyaminocarboxylates.[12] However, complex and expensive tunable dye laser apparatus are required.

[a] Laboratoire des Sciences Nucléaires, Conservatoire National des Arts et Métiers,
2 rue Conté, 75003 Paris, France
[b] Laboratoire de Chimie Organique, UMR CNRS 7084, Conservatoire National des Arts et Métiers,
292 rue Saint Martin, 75141 Paris Cedex 03, France
Fax: (internat.) + 33-1/42710534
E-mail: guy@cnam.fr
[c] Laboratoire d'Analyse, de Synthèse et de Spéciation Organométallique, CEA Saclay, DEN/DPC/SCPA/LAS$_2$O,
91191 Gif-sur-Yvette, France
[d] CEA, DEN,
91191 Gif-sur-Yvette, France

 © 2003 Wiley-VCH Verlag GmbH & Co. KGaA, Weinheim **DOI: 10.1002/ejic.200300016**

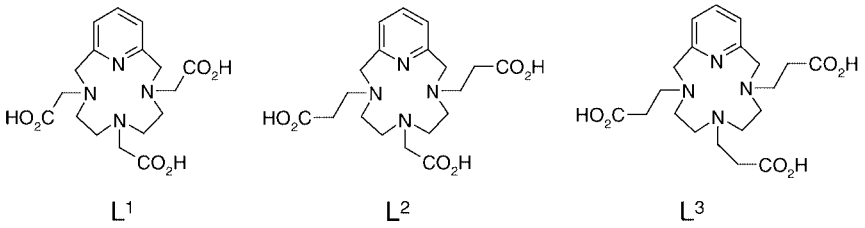

Figure 1. Structure of the ligands

Time-Resolved Laser-Induced Fluorescence (TRLIF) is widely used as a very sensitive and selective method for several luminescent actinides (U, Cm, Am) and lanthanides (Eu, Tb, Dy, Sm) in nuclear, environment, and medicinal chemistry, and is of growing interest in inorganic and organic speciation.[13,14] It is, therefore, an attractive analytical technique to apply to stability constant measurements.

Here we report, the protonation constants, the stoichiometries and the stability constants of the Eu^{III} complexes of ligands L^1, L^2, and L^3 bearing three carboxylic acid functions as well as seven potential donor atoms of various hardness.

Results and Discussion

Acidity Constants of L^1, L^2, and L^3

The ligands L^1, L^2, and L^3 each have seven basic centers, but only four constants could be determined by the potentiometric technique used. The protonation constants were found by potentiometric titrations of the fully protonated ligands. Figure 2 shows the potentiometric titration curve of macrocyclic ligands L^1, L^2, and L^3 with KOH. Analysis of the potentiometric titration curves with the Hyperquad program[15] yielded the protonation constants (Table 1).

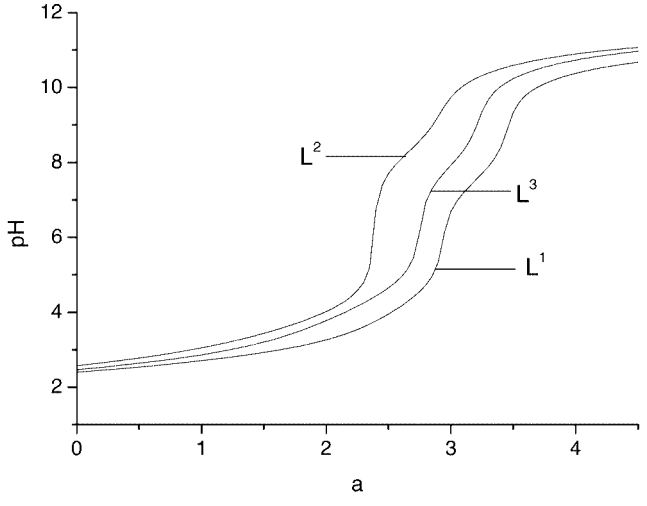

Figure 2. Potentiometric titration curve for 0.005 mM ligand: a = mol of base added per mol of ligand; solution temperature T = 25 °C, ionic strength I = 0.1 M (KCl)

Table 1. Comparison of the protonation constants of L^1, L^2, and $L^3$with the constants of an analogue (DOTA); the values in parentheses are standard deviations for the last figure given by the program[15]

Equilibrium quotient	L^1 [a]	L^2 [a]	L^3 [a]	L^1 [b]	L^1 [c]	DOTA[d]
[HL]/[H] [L]	10.73(5)	10.74(2)	10.72(3)	10.90	10.6	12.09
$[H_2L]/[HL]$ [H]	7.52(9)	8.27(6)	7.89(9)	7.11	7.6	9.76
$[H_3L]/[H_2L]$ [H]	4.2(1)	3.97(7)	4.5(1)	3.88	4.4	4.56
$[H_4L]/[H_3L]$ [H]	2.4(1)	3.26(7)	3.7(1)	2.27	–	4.09
$[H_4L]/[L]$ $[H]^4$	24.86	26.24	26.85	24.16	–	30.50

[a] 0.1 M KCl. [b] Ref.[7] 0.1 M NMe_4NO_3. [c] Ref.[16] 0.1 M KCl. [d] Ref.[17] 0.1 M NMe_4NO_3.

Ligands L^2 and L^3 differ from L^1 in their carboxylic acid side chains and, consequently, have significantly different protonation constants. All ligands have two high (or fairly high) and two low protonation constants. The first two are due to the protonation of two nitrogen atoms of the ring and the last two correspond to the protonation of carboxylate groups.[7,8] The separation of the pK_a values for a given ligand is greater than 0.7, which is consistent with non-interacting pendant arms.[18] For ligand L^3, the pK_a values are higher than those for L^1 owing to the presence of a second methylene group, which acts as an electron donor.[19]

Stoichiometry of the Complexes

The stoichiometry of the Eu^{III} complexes formed with L^1, L^2, or L^3 were determined by a mol ratio method. By monitoring the Eu^{III} luminescence at the wavelength of the $^5D_0 \rightarrow {}^7F_2$ transition peak as the function of Eu^{III} added to an aqueous solution of ligand (50 μM), at a pH such that the competition of protons is negligible (pH = 7.0), a binding curve is obtained (Figure 3). Since the ligand concentration is well above the dissociation constant for lanthanide complexes, the titration curve is expected to break sharply when the stoichiometric quantity of Eu^{III} has been added. Figure 3 shows a typical plot of the relative Eu^{III} luminescence intensity versus equivalents of added Eu^{III} with L^2 as ligand.

The macrocyclic ligands L^1, L^2, and L^3 have a 1:1 stoichiometry that is consistent with the size of the cavity as well as the number of donor atoms.

 © 2003 Wiley-VCH Verlag GmbH & Co. KGaA, Weinheim

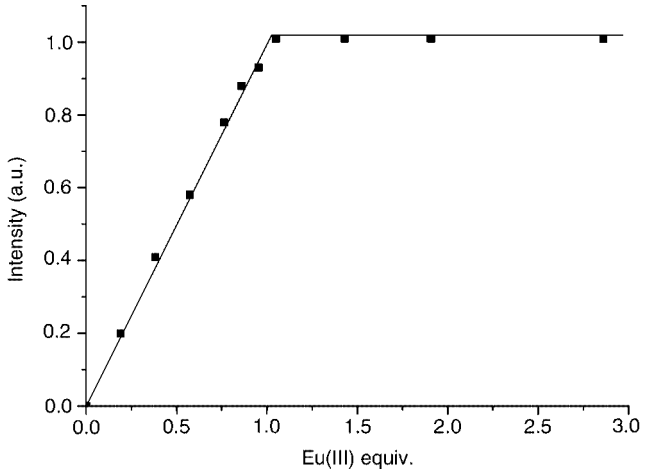

Figure 3. Intensities of the $^5D_0 \rightarrow {}^7F_2$ transition peak as the function of Eu^{III} added to an aqueous solution of ligand L^2 (50 μM), 0.085 M KCl and 0.015 M HEPES-buffered medium (pH = 7.0)

Luminescence Lifetimes, Quantum Yields

For each solution, the emission spectra are homothetical with I_{592}/I_{614} constant. Furthermore, a pulsed laser excitation source allows the measurement of characteristic Eu^{III} excited state lifetimes for each solution. The luminescence intensity of each europium complex decreases according to mono-exponential kinetics (Figure 4). Thus, under the conditions of our experiments, only 1:1 complexes for ligands L^1, L^2, and L^3 were present.

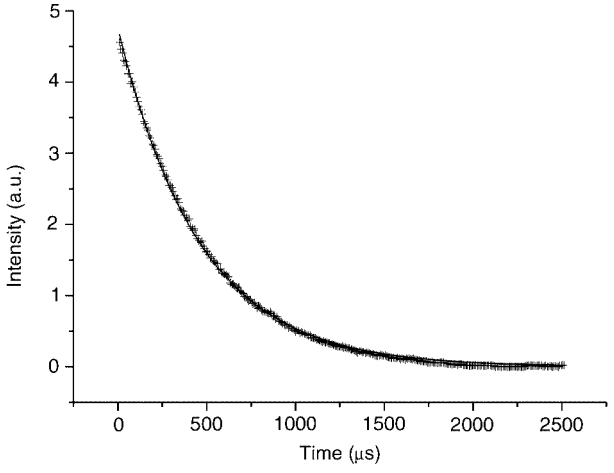

Figure 4. Excited-state luminescence decay for the system containing the macrocyclic ligand L^2 (50 μM) in the presence of $EuCl_3$ (60 μM) at pH = 5.28, [MES] = 0.015 M, [KCl] = 0.085 M

The luminescence lifetimes of Eu^{III} complexes with L^1, L^2, and L^3, and the overall quantum yields measured in H_2O and D_2O, are given in Table 2. From such measurements the estimated number of water molecules coordinated to the Eu^{III} complexes (Table 2), using the empirical relation proposed by Horrocks and co-workers,[20,21] Parker and co-workers,[22] or Kimura and co-workers,[23] show a decreasing degree of hydration with increasing ring size. The presence of 2.3, 1.6, and 1.4 coordinated water molecules for $[L^1 \subset Eu^{3+}]$, $[L^2 \subset Eu^{3+}]$, and $[L^3 \subset Eu^{3+}]$, respectively, agrees with the expected seven-coordinating nature of ligands since Eu^{III} prefers a coordination number of 8−9.

Table 2. Lifetimes of Eu^{III} complexes formed with L^1, L^2, and L^3, average number of water molecules coordinated to the complexes, and luminescence quantum yields

	Lifetimes τ [ms][a]		n H_2O[b]	n H_2O[c]	n H_2O[d]	Luminescence quantum yield[e]	
	H_2O	D_2O				H_2O	D_2O
$[L^1 \subset Eu^{3+}]$	0.37	2.12	2.3	2.3		2.32.9%	19.1%
$[L^2 \subset Eu^{3+}]$	0.43	1.35	1.7	1.7		1.94.6%	–
$[L^3 \subset Eu^{3+}]$	0.48	1.39	1.4	1.3		1.62.4%	8.1%

[a] Measured at room temperature; excitation into the lowest-energy ligand-centered absorption band in correspondence with the hypersensitive $5D_0 \rightarrow 7F_2$ transition; experimental error 5%. [b] Number of coordinated H_2O molecules estimated using Horrock's equation:[20,21] $n = 1.05 \cdot (\tau^{-1}_{H2O} - \tau^{-1}_{D2O})$. [c] Number of coordinated H_2O molecules estimated using Parker's equation:[24] $n = 1.2 \cdot [(\tau^{-1}_{H2O} - \tau^{-1}_{D2O}) - 0.25]$. [d] Number of coordinated H_2O molecules estimated using Kimura's equation:[23] $n = 1.07 \cdot (\tau^{-1}_{H2O}) - 0.62)$. [e] Measured at room temperature with reference to quinine sulfate;[25] excitation in the lowest energy ligand-centered absorption band (269 nm); experimental error 10%.

Determination of the Stability Constants of L^1, L^2, and L^3 with Eu^{III}

Since the multidentate ligands L^1 to L^3 form 1:1 complexes with Eu^{III} the general complexation equilibria apply [Equation (1)].

$$[Eu^{3+}] + [L^{3-}] \rightleftarrows [EuL] \quad (1)$$

The equilibrium constant for Equation (1) can be expressed as in Equation (2).

$$K(Eu^{3+}) = \frac{[EuL]}{[Eu^{3+}][L^{3-}]} \quad (2)$$

Depending on its intrinsic basicity, each ligand has a different response to the proton competition that limits the metal-ion binding, leading to the conditional stability constants [Equation (3)].

$$K_{cond.}(Eu^{3+}) = \frac{[EuL]}{[Eu^{3+}]\{[L^{3-}] + [HL^{2-}] + [H_2L^{-}] + [H_3L] + [H_4L^{+}]\}} \quad (3)$$

The thermodynamics and conditional stability constants are related by Equation (4)

$$K_{cond.}(Eu^{3+}) = K(Eu^{3+})\alpha_H \quad (4)$$

 © 2003 Wiley-VCH Verlag GmbH & Co. KGaA, Weinheim

with α_H defined by Equation (5)

$$\alpha_H{}^{-1} = 1 + K_{a1}\cdot[H^+] + K_{a1}\cdot K_{a2}\cdot[H^+]^2 + K_{a1}\cdot K_{a2}\cdot K_{a3}\cdot[H^+]^3 + K_{a1}\cdot K_{a2}\cdot K_{a3}\cdot K_{a4}\cdot[H^+]^4 \quad (5)$$

and K_{a1}, K_{a2}, K_{a3}, and K_{a4} being the protonation constants of the studied ligand.

Provided a constant amount of energy is furnished to the studied system, the luminescence intensity is proportional to [EuL]. Consequently, the luminescence intensity may be expressed as a function of the pH and of the stability constant of the complex (K) by Equation (6)[11]

$$I = \frac{k'}{2}\left\{[Eu]_0 + [L]_0 + \frac{\alpha_H^{-1}}{K} - \left[\left([Eu]_0 + [L]_0 + \frac{\alpha_H^{-1}}{K}\right)^2 - 4[Eu]_0[L]_0\right]^{1/2}\right\} \quad (6)$$

where $[Eu]^0$ and $[L]_0$ stand for the initial total concentrations of Eu^{III} and ligand respectively, k' is the proportionality constant between maximal intensity and $[Eu]_0$.

Plotting the luminescence intensity at the wavelength of the $^5D_0 \rightarrow {}^7F_2$ transition peak as a function of the pH after a suitable equilibration time, give a binding curve (Figure 5). The fitting (least-squares method) of the theoretical curve obtained from Equation (6) (Figure 5, solid curve) to the experimental data (Figure 5, squares) leads to a log$K$ value of 21.1, 13.7, and 10.7 for complexes with L^1, L^2, and L^3, respectively.

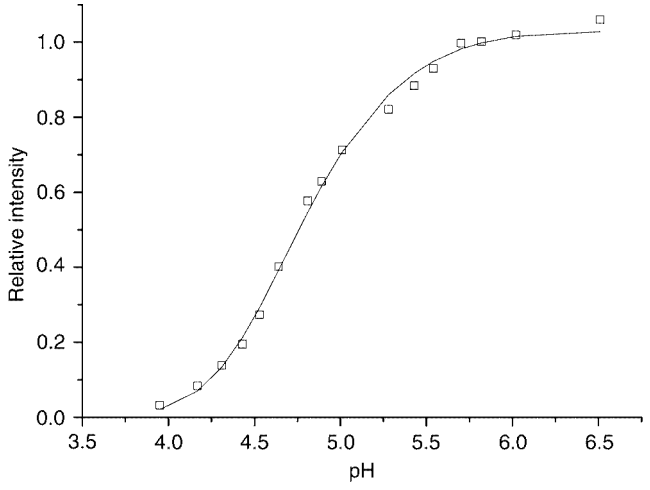

Figure 5. Binding curve obtained by monitoring the luminescence intensity (614 nm) of samples containing the macrocyclic ligand L^2 (50 μM) in the presence of $EuCl_3$ (50−60 μM) as a function of pH, [KCl] = 0.085 M, 4 < pH < 5 [HOMOPIPES] = 0.015 M, 5 < pH < 6.5 [MES] = 0.015 M; the luminescence resulted from Nd-YAG laser excitation at 266 nm; the squares represent actual data points and the solid line the theoretical fit of data with log$K$ = 13.7

Compared with L^1, an important diminution of the complexation constant is observed for L^2 and L^3 (Table 3). Thus, increasing the length of the acid group has a negative influence on the complexation of Eu^{III}.

Table 3. Stability constants (log K_{EuL}) of the complexes formed with the ligands L^1, L^2, L^3, and DOTA

Ln	L^1 [a]	L^2 [a]	L^3 [a]	DOTA
Eu^{III}	21.1	13.7	10.7	26.2 [b]
Gd^{III}	20.8 [c]			24.6 [d]

[a] 0.1 M KCl, 25 °C. [b] Ref.[12] 0.1 M KCl. [c] Ref.[8] [d] 0.1 M NaCl, ref.[26]

Conclusion

In conclusion, we report here the protonation constants of new *N*-acetate or *N*-propionate substituted azamacrocycles and an extended characterization of Eu^{III} complexes formed with these ligands based on time-resolved laser-induced Eu^{III} luminescence. This enabled us to determine the stoichiometry of the complexes, the luminescence quantum yield and the stability constant, which revealed the influence of the chelate ring size of the pendant arms on the stability constant of the Eu^{III} complex. This successful outcome has encouraged us to embark on a program to characterize various similar ligands with different macrocyclic and chelate ring sizes.

Experimental Section

Materials and Chemicals: All measurements were performed at 293 K and the solutions were prepared with deionized water (Millipore system). All glassware was thoroughly rinsed with water. The ionic strength of the solutions was adjusted to 0.1 M with KCl. Europium(III) chloride hexahydrate (Aldrich), sodium formate, 2-[*N*-(2-hydroxyethyl)piperazin-*N*′-yl]ethanesulfonic acid sodium salt (HEPES-Na), hexahydro-1*H*-1,4-diazepine-1,4-diylbis(2-ethanesulfonic acid) (Homo-PIPES) and 2-(*N*-morpholinyl)ethanesulfonic acid monohydrate (MES) were purchased as their purest form from Fluka. The potentiometric titrations were performed using an automatic titrator system DMS 716 Titrino (Metrohm) with a combined glass electrode (Metrohm, filled with saturated KCl solution) and connected to a microcomputer. $EuCl_3$ stock solutions (ca. 10 mM) were titrated by ICP-AES. The concentrations of the ligand stock solutions (ca. 0.1 M) were determined by titration with a standardized Eu^{III} solution at pH = 7 for L^1 and L^2 and at pH = 8 for L^3, on equilibrated samples using time-resolved laser-induced Eu^{III} luminescence.

Time-Resolved Laser-Induced Fluorescence: An Nd-YAG laser (Model Minilite, Continuum, Santa Clara, USA), operating at 266 nm (quadrupled) and delivering ca. 0.2 mJ of energy in a 4 ns pulse with a repetition rate of 15 Hz, was used as the excitation source. The laser output energy was monitored by a laser power meter (Scientech, Boulder, USA). The laser beam was directed into the 4-mL quartz cell of a "FLUO 2001" spectrofluorometer (Dilor, Lille, France). The radiation coming from the cell was focused on the polychromator's entrance slit. Taking into account the dispersion of the holographic grating used in the polychromator, the measurement range extended to approximately 200 nm into the visible spectrum with a resolution of 1 nm. An intensified photodiodes (1024) array, cooled by the Peltier effect (−30 °C) and posi-

 © 2003 Wiley-VCH Verlag GmbH & Co. KGaA, Weinheim

tioned at the polychromator exit, was used as detector. Spectra were recorded by integration of the pulsed light signal from the intensifier. The integration time, adjustable from 1 to 99 s, allows for variation in detection sensitivity. Logic circuits, synchronized with the laser shot, allow the intensifier to be active with a determined time delay (from 0.1 to 999 μs) and during a determined aperture time (from 0.5 to 999 μs). The whole system was controlled by a microcomputer. Data analysis was performed using the iterative least-squares fitting procedure in Microsoft Excel program. Fluorescence quantum yields were determined at 293 K by comparison with that of quinine sulfate in aqueous sulfuric acid solution (1 N), for which a reference yield of 0.55 was taken.[25] Luminescence lifetimes (at 293 K) were determined at 600 nm by excitation with a B.M. Industries frequency-quadrupled Nd-YAG laser (266 nm, pulse duration 8 ns FWHM) using an oscilloscope Tektronix 9310 to monitor the output signal of the photomultiplier.

Synthesis of Ligands: The ligands L^1, L^2, and L^3 were synthesized as reported.[8,27,28]

Potentiometric Titrations: The electrodes were calibrated to read the pH by a classical method.[29] .The ligand (5 mL, 0.001 M) was titrated with standardized 0.01 M sodium hydroxide. Argon was bubbled through the solution to exclude CO_2 and O_2. Sodium hydroxide was prepared from 0.1 M NaOH (Prolabo) and standardized against potassium hydrogen phthalate. The carbonate content was checked by Gran's method. The titration for each ligand was carried out at least three times. Each titration consisted of about 70 points collected over the pH range of 2.5−10.9. The titration data were refined by the non-linear least-squares refinement program Hyperquad[15] to determine the protonation constants. The pK_a values were calculated from the cumulative constants determined with the program. The uncertainties in the pK_a values correspond to the added standard deviations in the cumulative constants.

Spectrophotometric Experiments

Preparation of Samples for the Stoichiometry Determination: The pH of an aqueous stock solution containing HEPES (sodium salt, 0.015 M), KCl (0.085 M), and ligand (50 μM) was adjusted to pH = 7 for L^1 and L^2 and to pH = 8 for L^3 with an aqueous solution of HCl. A series of 11 samples was prepared in separate sealed containers with concentrations of $EuCl_3$ ranging from 0 to 200 μM. After overnight incubation at 60 °C, the samples were allowed to cool to room temperature and then monitored by absorption spectroscopy until no further spectral change was detected (typically 24 h). The Eu^{III} excited state lifetime was monitored and the luminescence intensity of each sample was measured at the wavelength of the $5D_0 \rightarrow 7F_2$ transition peak.

Preparation of Samples for Lifetime and Quantum Yield Measurements: Samples containing HEPES (sodium salt, 0.015 M), KCl (0.085 M), ligand (50 μM), and $EuCl_3$ (75 μM) were prepared in H_2O (D_2O). The pH (pD) was adjusted with an aqueous solution of HCl (DCl) to pH = 7.0 (7.4) (pD = pH + 0.41).

Preparation of Samples Used To Determine the Stability Constant of the Eu^{III} Complex: An aqueous stock solution containing buffer (0.015 M), KCl (0.085 M), ligand (50 μM), and a slight excess of $EuCl_3$ (55 to 60 μM) was prepared. A series of 15 samples was produced in separate sealed containers at various pH by addition of an aqueous solution of HCl (KCl/HCl buffer for pH = 1−2, HCO_2Na/HCO_2H buffer for pH =2−4, HOMOPIPES buffer for pH = 4−5, MES buffer for pH = 5−6.5, and HEPES buffer for pH = 6.5−8). After overnight incubation at 60 °C, the samples were allowed to cool to room temperature, and then monitored by absorption spectroscopy until no further change was detected. At equilibrium the samples were irradiated, and the Eu^{III} excited state lifetime monitored and the luminescence intensity of each sample measured at the wavelength of the $5D_0 \rightarrow 7F_2$ transition peak.

[1] V. Comblin, D. Gilsoul, M. Hermann, V. Humblet, V. Jacques, M. Mesbahi, C. Sauvage, J. F. Desreux, *Coord. Chem. Rev.* **1999**, *185−186*, 451−470.
[2] P. Caravan, J. J. Ellison, T. J. McMurry, R. B. Lauffer, *Chem. Rev.* **1999**, *99*, 2293−2352.
[3] C. J. Anderson, M. J. Welch, *Chem. Rev.* **1999**, *99*, 2219−2234.
[4] Z. Guo, P. J. Sadler, *Angew. Chem. Int. Ed.* **1999**, *38*, 1512−1531.
[5] D. J. Bornhop, D. S. Hubbard, M. P. Houlne, C. Adair, G. E. Kiefer, B. C. Pence, D. L. Morgan, *Anal. Chem.* **1999**, *71*, 2607−2615.
[6] C. Lecomte, V. Dahaoui-Gindrey, H. Chollet, C. Gros, A. K. Mishra, F. Barbette, P. Pullumbi, R. Guilard, *Inorg. Chem.* **1997**, *36*, 3827−3838.
[7] R. Delgado, S. Quintino, M. Teixeira, A. Zhang, *J. Chem. Soc., Dalton Trans.* **1997**, 55−63.
[8] S. Aime, M. Botta, S. G. Crich, G. B. Giovenzana, G. Jommi, R. Pagliarin, M. Sisti, *Inorg. Chem.* **1997**, *36*, 2992−3000.
[9] S. Aime, M. Botta, M. Fasano, E. Terreno, *Acc. Chem. Res.* **1999**, *32*, 941−949.
[10] N. Sabbatini, M. Guardigli, J. M. Lehn, *Coord. Chem. Rev.* **1993**, *123*, 201−228.
[11] S. L. Wu, W. D. Horrocks, Jr., *Anal. Chem.* **1996**, *68*, 394−401.
[12] S. L. Wu, W. D. Horrocks, Jr., *J. Chem. Soc., Dalton Trans.* **1997**, 1497−1502.
[13] C. Moulin, I. Laszak, V. Moulin, C. Tondre, *Appl. Spectrosc.* **1998**, *52*, 528−535.
[14] C. Moulin, C. Larpent, D. Gazeau, *Anal. Chim. Acta* **1999**, *378*, 47−54.
[15] P. Gans, A. Sabatini, A. Vacca, *Talanta* **1996**, *43*, 1739−1753.
[16] H. Stetter, W. Frank, R. Mertens, *Tetrahedron* **1981**, *37*, 767−772.
[17] M. T. S. Amorim, R. Delgado, J. J. R. Frausto da Silva, *Polyhedron* **1992**, *11*, 1891−1899.
[18] R. Viguier, G. Serratrice, A. Dupraz, C. Dupuy, *Eur. J. Inorg. Chem.* **2001**, 1789−1795.
[19] A. E. Martell, R. J. Motekaitis, *The Determination and Use of Stability Constants*, VCH, New York, **1988**.
[20] W. D. Horrocks, Jr., D. R. Sudnick, *Acc. Chem. Res.* **1981**, *14*, 384−392.
[21] R. M. Supkowski, W. D. Horrocks, *Inorg. Chim. Acta* **2002**, *340*, 44−48.
[22] A. Beeby, I. M. Clarkson, R. S. Dickins, S. Faulkner, D. Parker, L. Royle, A. S. de Sousa, J. A. G. Williams, M. Woods, *J. Chem. Soc., Perkin Trans. 2* **1999**, 493−504.
[23] T. Kimura, G. R. Choppin, *J. Alloys Compd.* **1994**, *213/214*, 313−317.
[24] A. Beeby, S. W. Botchway, I. M. Clarkson, S. Faulkner, A. W. Parker, D. Parker, J. A. G. Williams, *J. Photochem. Photobiol. B* **2000**, *57*, 83−89.
[25] W. H. Melhuish, *J. Phys. Chem.* **1961**, *65*, 229−235.
[26] W. P. Cacheris, S. K. Nickle, A. D. Sherry, *Inorg. Chem.* **1987**, *26*, 958−960.
[27] J. M. Siaugue, F. Segat-Dioury, A. Favre-Reguillon, C. Madic, J. Foos, A. Guy, *Tetrahedron Lett.* **2000**, *41*, 7443−7446.
[28] J. M. Siaugue, F. Segat-Dioury, I. Sylvestre, A. Favre-Reguillon, J. Foos, C. Madic, A. Guy, *Tetrahedron* **2001**, *57*, 4713−4718.
[29] L. Fremond, E. Espinosa, M. Meyer, F. Denat, R. Guilard, V. Huch, M. Veith, *New J. Chem.* **2000**, *24*, 959−966.

Received January 10, 2003

 © 2003 Wiley-VCH Verlag GmbH & Co. KGaA, Weinheim

Synthesis, Crystal and Magnetic Structure of the Double Perovskites A_2NiMoO_6 (A = Sr, Ba): A Neutron Diffraction Study

María J. Martínez-Lope,[a] José A. Alonso,*[a] and María T. Casais[a]

Keywords: Perovskites / Neutron diffraction / Magnetic properties / Nickel

A_2NiMoO_6 (A = Sr, Ba) perovskites have been prepared in polycrystalline form by thermal treatment, in air, of previously decomposed citrate precursors. These materials have been studied by X-ray (XRD) and neutron powder diffraction (NPD) data. At room temperature, the crystal structure is tetragonal, space group $I4/m$, for Sr_2NiMoO_6 and for Ba_2NiMoO_6 the crystal structure is cubic, space group $Fm\bar{3}m$. Both perovskites contain divalent Ni cations. The low temperature antiferromagnetic ordering has been followed from sequential neutron diffraction data. Peaks of magnetic origin appear in the NPD patterns below temperatures of T_N = 81.2 K and T_N = 64.3 K for the Sr and Ba compounds, respectively. The magnetic structures are defined by a propagation vector **k** = (1/2,0,1/2) for Sr_2NiMoO_6 and **k** = (1/2,1/2,1/2) for Ba_2NiMoO_6. The refined magnitude of the Ni magnetic moments also suggests a divalent oxidation state with $S = 1$.
(© Wiley-VCH Verlag GmbH & Co. KGaA, 69451 Weinheim, Germany, 2003)

Introduction

The double-perovskite oxides of general formula $A_2B'B''O_6$, in which A is a rare-earth metal and B′ and B″ are transition metal cations, constitute a wide family of materials displaying varied and appealing electronic and magnetic properties. More than 300 compounds with the double-perovskite structure have been synthesized so far,[1] in which the perovskite B sites are occupied alternately by different cations B′ and B″. These materials have recently attracted the interest of materials scientists for possible applications in magnetoresistive devices, since the report of room temperature colossal magnetoresistance (CMR) in the double perovskite Sr_2FeMoO_6.[2] Similar CMR properties have also been described in other complex perovskites, such as Sr_2ReMoO_6 and Ba_2FeMoO_6,[3−8] for which the CMR effect seems to be due to intergrain tunneling.[8,9]

The ideal structure of these compounds can be viewed as a regular arrangement of corner-sharing $B'O_6$ and $B''O_6$ octahedra, alternating along the three directions of the crystal, with the voluminous A cations occupying the voids between the octahedra. When the size of the A cations decreases with respect to that of B′ and B″ cations, there is a reduction in symmetry from cubic to tetragonal or even monoclinic due to the tilting of the $B'O_6$ and $B''O_6$ octahedra. For instance, Ba_2FeMoO_6 is cubic over the temperature range 2−300 K, whereas Sr_2FeMoO_6 is cubic above the ferromagnetic Curie temperature, and undergoes a structural phase-transition and becomes tetragonal ($I4/m$) below this temperature.[10−12] Sr_2CoMoO_6 is tetragonal[13] and the crystal contains alternating CoO_6 and MoO_6 octahedra, moderately tilted by 6.7° in the basal *ab* plane. Ca_2FeMoO_6 is monoclinic,[14] with a significant tilt of the FeO_6 and MoO_6 octahedra, due to the small size of the Ca cations found at the A positions.

The Ni analogues of A_2FeMoO_6 (A = Sr, Ba) have attracted our attention. The double perovskites Sr_2NiMoO_6 and Ba_2NiMoO_6 were studied in the sixties and then forgotten for more than 30 years. Sr_2NiMoO_6 was described as tetragonal,[15−17] and an antiferromagnetic behaviour has been observed below T_N = 80 K (17). Ba_2NiMoO_6 was described as cubic with a = 4.02 Å.[15−16]

In the present work we describe the synthesis of A_2NiMoO_6 (A = Sr, Ba), prepared by soft chemistry procedures, and the results of a neutron powder diffraction (NPD) study on well-crystallized samples. The crystal structures have been revised and we report complete structural data for these perovskites. Low-temperature NPD data allowed us to probe the microscopic origin of the antiferromagnetic ordering, and the evolution of the ordered Ni^{2+} magnetic moment.

Results

The double perovskites A_2NiMoO_6 (A = Sr, Ba) were obtained as nicely crystalline powders, the XRD diagrams for which are shown in Figure 1. The diffraction pattern for the Ba compound is characteristic of a cubic perovskite structure, showing superstructure peaks corresponding to the Ni/Mo ordering. The Sr_2NiMoO_6 XRD diagram shows the splitting of certain reflections, characteristic of a tetragonal distortion [for instance the (004) and (220) reflections].

[a] Instituto de Ciencia de Materiales de Madrid, CSIC, Cantoblanco, 28049 Madrid, Spain

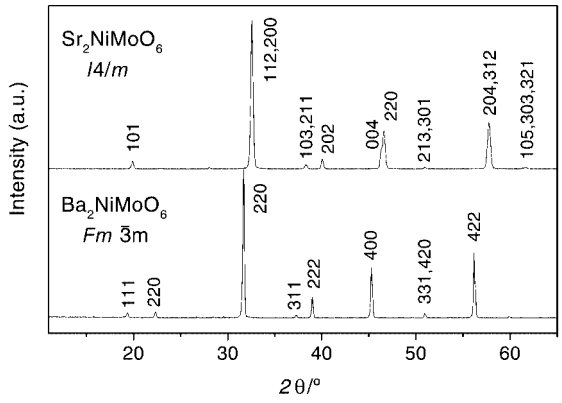

Figure 1. XRD patterns for A_2NiMoO_6 (A = Sr, Ba), indexed in a tetragonal unit cell with $a = b = \sqrt{2}a_0$, $c = 2a_0$ (A = Sr) and $a = 2a_0$, (A = Ba), $a_0 \approx 4$ Å

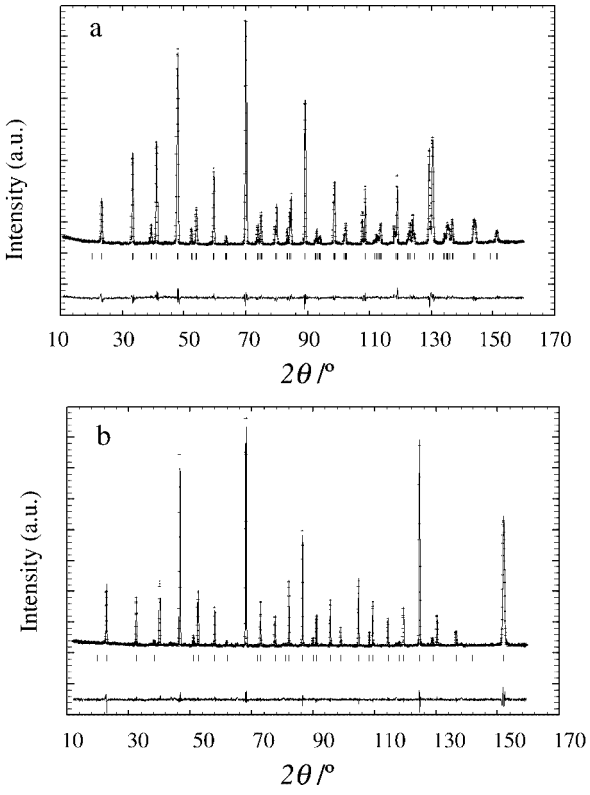

Figure 2. Observed (crosses), calculated (full line) and difference (bottom) high resolution NPD Rietveld profiles for A_2NiMoO_6 collected at 295 K with λ = 1.594 Å for (a) A = Sr, (b) A = Ba

Structural Refinement

For Sr_2NiMoO_6, the structural refinement from room temperature high resolution NPD data was performed in the *I*4/*m* space group (no. 87), $Z = 2$, with unit-cell parameters related to $\mathbf{a_o}$ (ideal cubic perovskite: $\mathbf{a_o}$ = 3.9 Å) as $\mathbf{a} = \mathbf{b} = \sqrt{2}\mathbf{a_o}$, $\mathbf{c} = 2\mathbf{a_o}$. The Sr atoms were located at 4d positions, Ni at 2a, Mo at 2b sites, and oxygen atoms at 4e and 8 h positions. For Ba_2NiMoO_6, the structural refinement from room temperature high-resolution NPD data was performed in the *Fm*$\bar{3}$*m* space group (no. 225), $Z = 4$, with unit-cell parameters related to $\mathbf{a_o}$ (ideal cubic perovskite, $\mathbf{a_o}$= 3.9 Å) as $\mathbf{a} = \mathbf{b} = \mathbf{c} = 2\mathbf{a_o}$. The Ba atoms are located at the 8c positions, Ni at 4a, Mo at 4b sites, and oxygen atoms at the 24e positions. An excellent fit was obtained for these models, as shown in Figure 2. In the final refinement, the possibility of anti-site disordering was checked by assuming that some Ni atoms could occupy Mo sites, and vice-versa: the refinement of the inversion degree led to less than 1% of anti-site disordering. The oxygen stoichiometry was also checked by refining the occupancy factors of the oxygen atoms; no deficiency was detected within the standard deviations. The most important structural parameters of the crystallographic structure at room temp. and the discrepancy factors after the refinements are listed in Table 1. The main interatomic distances and angles are included in Table 2. A view of the crystal structures is shown in Figure 3.

The tetragonal unit-cell of Sr_2NiMoO_6 is smaller than the cubic one of Ba_2NiMoO_6, normalizing per formula unit, as expected for the smaller ionic radius of Sr^{2+} (1.26 Å) versus Ba^{2+} (1.42 Å) in 12-fold coordination.[19] It is interesting to note the significant expansion of the Ni−O interatomic distances (Table 2) from the Sr compound [Ni−O: 2.024(4) Å] to the Ba perovskite [Ni−O: 2.097(2)] upon scaling the larger size of the unit cell for the Ba compound.

Magnetic Structure

The magnetic structure for A_2NiMoO_6 (A = Sr, Ba) and its thermal evolution was analyzed from a set of NPD patterns collected in the temperature range 2< T <87 K, with λ = 2.42 Å. In Sr_2NiMoO_6, on cooling to below 81.2 K, new reflections appear at positions forbidden for the Bragg reflections in the space group *I*4/*m*. These new peaks arise from the establishment of a long-range magnetic ordering defined by a propagation vector $\mathbf{k}$ = (1/2, 0, 1/2). An antiferromagnetic structure was modeled with magnetic moments at the Ni positions; after the full refinement of the profile, including the magnetic moment magnitude, a best discrepancy factor of R_{mag} = 12.6% was reached for the 2 K diagram considering the Ni moment to be approximately aligned along the [101] direction. In Ba_2NiMoO_6 the new peaks appear below T_N = 64.3 K and are indexed in the cubic cell with the propagation vector $\mathbf{k}$ = (1/2, 1/2, 1/2). The determination of the orientation of the moments is not possible in a cubic structure from powder data, therefore in the refinement we supposed that the moments lie along the [0 0 1] direction. After the refinement of the antiferromagnetic structure, a discrepancy factor of R_{mag} = 14.0% was obtained for the 2 K diagram. The goodness of both fits at 2 K is illustrated in Figures 4a and 4b.

The magnetic structure of the two compounds is stable from 2 K to T_N, as demonstrated in a sequential refinement of all the available temperature range. The thermal evolution of the Ni magnetic moments is illustrated in Fig-

 © 2003 Wiley-VCH Verlag GmbH & Co. KGaA, Weinheim

Table 1. Positional and thermal parameters for A_2NiMoO_6 (A= Sr, Ba), from NPD data at 295 K; the unit cell parameters for A = Sr (*I*4/*m* space group) are $a = b = 5.54939(5)$ Å, $c = 7.89554(9)$ Å, $V = 243.149(4)$ Å^3; for A = Ba ($Fm\bar{3}m$ space group) they are $a = b = c = 8.04862(3)$ Å, $V = 521.392(4)$ Å^3

Atoms	Positions	A = Sr	A = Ba
	x	0.00	0.25
	y	0.50	0.25
A	z	0.25	0.25
	B(Å^2)	0.70(2)	0.33(2)
	x	0.00	0.00
	y	0.00	0.00
Ni	z	0.50	0.00
	B(Å^2)	0.19(5)	0.26(5)
	x	0.00	0.50
	y	0.00	0.00
Mo	z	0.00	0.00
	B(Å^2)	0.56(9)	0.34(8)
	x	0.00	0.2605(3)
	y	0.00	0.00
O1	z	0.2426(6)	0.00
	B(Å^2)	0.86(4)	0.46(2)
	x	0.2689(4)	
	y	0.2187(5)	
O2	z	0.00	
	B(Å^2)	0.86(3)	
	R_p	4.38%	5.03%
	R_{wp}	5.83%	6.60%
	R_{exp}	3.47%	5.10%
	χ^2	2.83	1.68
	R_I	3.55%	2.11%

Table 2. Main bond lengths (Å) and selected angles (°) for tetragonal Sr_2NiMoO_6 and cubic Ba_2NiMoO_6 determined from NPD data at 295 K

	A = Sr	A = Ba
A−O1	(× 4) 2.7753(1)	(× 12) 2.8469(1)
A−O2	(× 4) 2.926(2)	
A−O2	(× 4) 2.648(2)	
<A−O>	2.783(1)	2.8469(1)
Ni−O1	(× 2) 2.032(5)	(× 6) 2.097(2)
Ni−O2	(× 4) 2.020(3)	
<Ni−O>	2.024(4)	2.097(2)
Mo−O1	(× 2) 1.916(5)	(× 6) 1.927(2)
Mo−O2	(× 4) 1.924(3)	
<Mo−O>	1.921(4)	1.927(2)
Ni−O1−Mo	180.0	180.0
Ni−O2−Mo	168.5(1)	

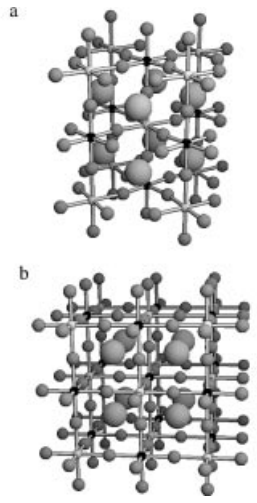

Figure 3. Two views of the crystal structure of the A_2NiMoO_6 double perovskites for (a) A = Sr, (b) A = Ba; within the octahedra, Ni atoms (small dark spheres) alternate with Mo atoms (small light spheres) in such a way that each NiO_6 octahedron is linked to six MoO_6 octahedra.

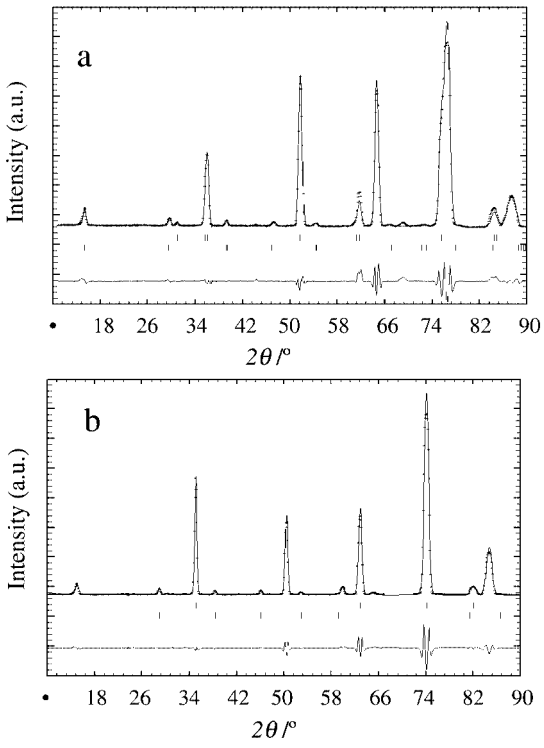

Figure 4. Observed (solid circles), calculated (solid line) and difference (bottom line) NPD patterns collected at 2 K with $\lambda = 2.42$ Å; the two series of tick marks correspond to the crystallographic and magnetic Bragg reflections: (a) Sr_2NiMoO_6 (b) Ba_2NiMoO_6

ures 5a and 5b. The ordered magnetic moments obtained at 2 K are 1.92(6) μ_B and 2.04(6) μ_B for A = Sr and A = Ba, respectively. A view of the magnetic structure of both materials is displayed in Figures 6a and 6b. In both cases, the magnetic arrangement can be described as a stacking of ferromagnetic layers of Ni moments, coupled antiferromagnetically.

 © 2003 Wiley-VCH Verlag GmbH & Co. KGaA, Weinheim

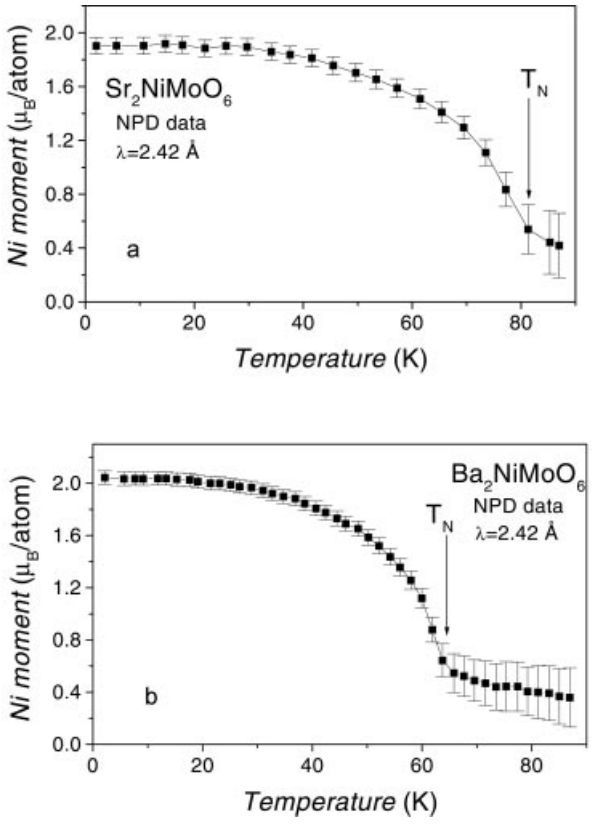

Figure 5. Thermal variation of the ordered magnetic moments for Ni in the antiferromagnetic structure of A_2NiMoO_6: (a) A = Sr (b) A = Ba

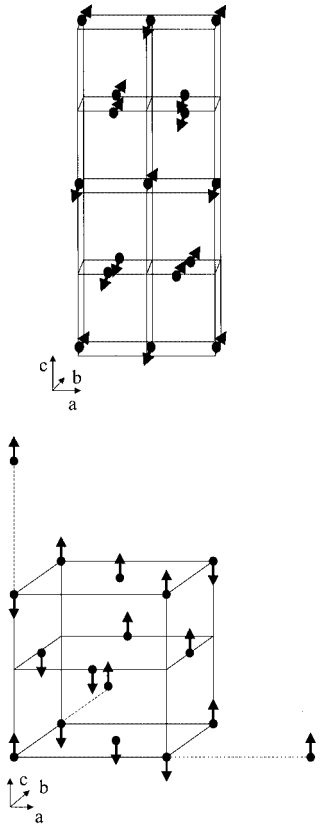

Figure 6. A sketch of the magnetic structures for: (a) Sr_2NiMoO_6, with k = (1/2 0 1/2); the magnetic unit cell consists of four crystallographic cells, and (b) Ba_2NiMoO_6, with k = (1/2 1/2 1/2); for the sake of clarity, the figure shows the chemical cell ($a \approx 8$ Å) and part of three adjacent cells

Discussion

The Ba compound adopts the well-known $(NH_4)_3FeF_6$ structure, which has been described for a large number of complex perovskites showing 1:1 long range order at the B sublattice. In this cubic structure, the BO_6 octahedra are not tilted, with B−O−B angles of 180°. The reduction of ionic size from Ba to Sr implies a reduction in symmetry from cubic to tetragonal, due to the tilting of the NiO_6 and MoO_6 octahedra along the c axis. According to Glazer's nomenclature,[20] the observed tilting is described as $a^0a^0c^-$, implying an antiphase tilting (from layer to layer) along c. The space group $I4/m$ is the one deduced by Woodward[21] for 1:1 double perovskites for the $a^0a^0c^-$ system. The magnitude of the tilting can simply be derived from the Ni−O−Mo angle (φ), as (180 − φ)/2 = 5.75°.

In both perovskites, NiO_6 and MoO_6 octahedra are almost fully ordered and alternate along the three directions of the crystal in such a way that each NiO_6 octahedron is linked to six MoO_6 octahedra, and vice versa. Figure 3 illustrates this particular feature nicely. The driving force for the Ni/Mo ordering is the charge difference between both kinds of cations, since the size difference is not too large. As shown in Table 2, the NiO_6 octahedra are only slightly larger (expanded) than the MoO_6 octahedra in both perovskites. This observation is consistent with the larger ionic size of Ni^{2+} vs. Mo^{6+}. The average Ni−O bond lengths at room temperature compare well with the expected values calculated as the sum of the ionic radii:[19] for A = Sr, <Ni−O> = 2.024(4) Å (calcd. 2.090 Å); <Mo−O> = 1.921 (4) Å (calcd. 1.99 Å); for A = Ba, <Ni−O> = 2.097(2) Å (calcd. 2.090 Å); <Mo−O> = 1.927 (2) Å (calcd. 1.99 Å).

A bond-valence calculation[22,23] from the observed bond lengths can give some insight into the actual oxidation states of the different cations present in the crystal structure. In Sr_2NiMoO_6, the calculated valences for Sr, Ni and Mo are 2.08, 2.21 and 5.78, respectively; in Ba_2NiMoO_6, the calculated valences for Ba, Ni and Mo are 2.66, 1.81 and 5.70, respectively. These values suggest an electronic configuration for these compounds at 298 K given by $Ni^{2+}(3d^8) - Mo^{6+}(4d^0)$. The electronic configuration for Ni^{2+} is in good agreement with the results of the magnetic-structure determination at 2 K. These configurations seem to exclude the presence of a mixed valence at the Ni atoms and imply a hexavalent oxidation state for the Mo cations, accounting for the electrical insulating behavior and colored aspect of these samples. The Ba cation seems to be significantly overbonded, exhibiting a valence much higher than the expected 2+ value. In fact, the observed Ba−O distances are much shorter (2.85 Å, see Table 2) than expected from the sum of the ionic radii (3.01 Å). It seems

 © 2003 Wiley-VCH Verlag GmbH & Co. KGaA, Weinheim

that the much more covalent network determined by NiO_6 and MoO_6 octahedra mainly determines the size of the unit cell; the low degree of freedom of this cubic structure constrains the Ba−O bond lengths outside of the optimal values. However, in the tetragonal structure of Sr_2NiMoO_6, the observed valence for Sr, very close to 2+, suggests that the tilt of the octahedra effectively relieves the stress at the A positions, thus optimizing the Sr−O distances.

In relation to the ordered magnetic moment obtained for Ni cations from the refinement of the magnetic structure at 2 K, it saturates to values close to 2 μ_B for both the Sr and Ba compounds. Again, this fact suggests a divalent oxidation state for the Ni cations ($t_{2g}^6e_g^2$, $S = 1$). The slightly higher Néel temperature observed for the Sr compound ($T_N = 81.2$ K) with respect to the Ba perovskite ($T_N = 64.3$ K) implies the presence of stronger magnetic interactions for the former oxide. These interactions are related to the significantly shorter Ni−O distances observed in Sr_2NiMoO_6, which account for a stronger overlap between the Ni 3d and O 2p orbitals, thus enhancing the superexchange process giving rise to the establishment of the antiferromagnetic ordering. In agreement with this observation, the saturation moment of the Ni^{2+} cations is slightly lower for the Sr compound (see Figure 5), again indicating a stronger covalent contribution to the Ni−O bonding in the Sr material, and a more ionic, weaker Ni−O bond with a larger localized magnetic moment for Ni in Ba_2NiMoO_6.

Conclusions

We have presented a detailed crystallographic study of the double perovskites A_2NiMoO_6 (A = Sr, Ba) from NPD data, allowing us to characterize subtle structural features relating the nature and strength of the Ni−O chemical bonds to the ordered magnetic moments determined by neutron diffraction. These compounds experience a low-temperature, long-range antiferromagnetic ordering, concerning the Ni^{2+} magnetic moments. For Sr_2NiMoO_6 the magnetic structure is defined by $\mathbf{k} = (1/2, 0, 1/2)$, and for Ba_2NiMoO_6 the magnetic structure is defined by $\mathbf{k} = (1/2, 1/2, 1/2)$. The slightly lower ordered magnetic moment and the greater Néel temperature observed for the Sr perovskite is related to the shorter, more covalent Ni−O bonds determined for this compound. It seems clear that Ni adopts a divalent oxidation state, and Mo is in an hexavalent $4d^0$ configuration, thus explaining the insulating behavior and the colored nature of these complex oxides.

Experimental Section

A_2NiMoO_6 (A = Sr, Ba) perovskites were prepared as ochre (A = Sr) or yellowish green (A = Ba) polycrystalline powders from citrate precursors obtained by soft chemistry procedures. Stoichiometric amounts of analytical grade $Sr(NO_3)_2$, $Ba(NO_3)_2$, $Ni(NO_3)_2{\cdot}6H_2O$ and $(NH_4)_6Mo_7O_{24}{\cdot}4H_2O$ were dissolved in citric acid. The citrate + nitrate solutions were slowly evaporated, leading to organic resins containing a random distribution of the involved cations at an atomic level. These resins were first dried at 120 °C and then slowly decomposed at temperatures up to 600 °C. All the organic materials and nitrates were eliminated in a subsequent treatment at 800 °C in air, for 2 h. This treatment gave rise to highly reactive precursor materials, which were then treated in air for 12 h at 1000 °C (Sr perovskite) or at 1100 °C (Ba perovskite).

The initial characterization of the products was carried out by laboratory X-ray diffraction (XRD) (Cu-K_α, $\lambda = 1.5406$ Å). Neutron powder diffraction (NPD) diagrams were collected at the Institut Laue-Langevin (ILL) in Grenoble (France). The crystallographic structures were refined from the high resolution NPD patterns, acquired at room temperature at the D2B diffractometer with $\lambda = 1.594$Å. For the determination of the magnetic structures and the study of their thermal variation, a series of NPD patterns were obtained at the D20 high-flux diffractometer (ILL-Grenoble) with a wavelength of 2.42 Å, in the temperature range from 2 to 87 K for (A = Sr, Ba). The refinements of both crystal and magnetic structures were performed by the Rietveld method, using the FULLPROF refinement program.[24] A pseudo-Voigt function was chosen to generate the line shape of the diffraction peaks. The coherent scattering lengths for Sr, Ba, Ni, Mo and O were 7.02, 5.70, 10.300, 4.86 and 5.803 fm, respectively.

Acknowledgments

We are grateful for financial support from the Spanish Ministry of Science and Technology under the project MAT2001−0539, and we are grateful to ILL for making all its facilities available.

[1] M. T. Anderson, K. B. Green Wood, G. A. Taylor, K. R. Poeppelmeier, *Prog. Solid State Chem.* **1993**, *22*, 197.
[2] K. I. Kobayashi, T. Kimura, H. Sawada, K. Terakura, Y. Tokura, *Nature* **1988**, *395*, 677.
[3] K. I. Kobayashi, T. Kimura, Y. Tomioka, H. Sawada, K. Terakura, Y. Tokura, *Phys. Rev. B* **1999**, *59*, 11159.
[4] B. García-Landa, C. Ritter, M. R. Ibarra, J. Blasco, P. A. Algarabel, R. Mahendiran, J. García, *Solid State Commun.* **1999**, *110*, 435.
[5] D. D. Sarma, E. V. Sampathkumaran, S. Ray, R. Nagarajam, S. Majundar, A. Kumar, G. Malini, T. N. Guru Row, *Solid State Commun.* **2000**, *114*, 465.
[6] J. Gopalakrishnan, A. Chattopadhyay, S. B. Ogale, T. Venkatesan, R. L. Greene, A. J. Millis, K. Ramesha, B. Hannoyer and Marest, *Phys. Rev. B* **2000**, *62*, 9538.
[7] D. Niebieskikwiat, R. D. Sánchez, A. Caneiro, L. Morales, M. Vázquez-Mansilla, F. Rivadulla, L. E. Hueso, *Phys. Rev. B* **2000**, *62*, 7033.
[8] A. Maignan, B. Raveau, C. Martin, M. Hervieu, *J. Solid State Chem.* **1999**, *144*, 224.
[9] H. Y. Huang, S. W. Cheong, N. P. Ong, B. Batlogg, *Phys. Rev. Lett.* **1996**, *77*, 2041.
[10] F. K. Patterson, C. W. Moeller, R. Ward, *Inorg. Chem.* **1963**, *2*, 196.
[11] F. Galasso, F. Douglas, R. J. Kasper, *Chem. Phys.* **1966**, *44*, 1672.
[12] O. Chmaissen, R. Kruk, B. Dabrowski, D. E. Brown, X. Xiong, S. Kolesnik, J. D. Jorgensen, C. W. Kimball, *Phys. Rev. B* **2000**, *6*, 14197.
[13] M. C. Viola, M. J. Martínez-Lope, J. A. Alonso, P. Velasco, J. L. Martínez, J. C. Pedregosa, R. E. Carbonio, M. T. Fernández-Díaz, *Chem. Mater.* **2002**, *14*, 812.
[14] J. A. Alonso, M. T. Casais, M. J. Martínez-Lope, J. L. Martínez, P. Velasco, A. Muñoz, M. T. Fernández-Díaz, *Chem. Mater.* **2000**, *12*, 161.

 © 2003 Wiley-VCH Verlag GmbH & Co. KGaA, Weinheim

[15] F. Galasso, Structure, *Properties and Preparation of Perovskite-Type Compounds*, Pergamon Press, Oxford **1969**.
[16] L. Brixner, *J. Phys. Chem.* **1960**, *64*, 165.
[17] M. F. Kupriyanov, E. G. Fesenko, *Soc., Phys. Cryst.* **1962**, *7*, 358.
[18] Landolt-Bornstein, *Zahlenwerte und Funktionen aus Naturwissenschaften und Technik*, Neue Serie, Band 4, Teil A, Springer-Verlag, Berlin **1970**.
[19] R. D. Shannon, *Acta Crystallogr., Sect. A* **1976**, *32*, 751.
[20] A. M. Glazer, *Acta Crystallogr.* Sect. B **1972**, *28*, 3384.
[21] P. M. Woodward, *Acta Crystallogr.* Sect. B **1997**, 5 *3*, 32.
[22] I. D. Brown, *in Structure and Bonding in Crystals* (Eds.: M. O'Keefe, A. Navrotsky) Academic Press, New York **1981**, vol. 2, p.1.
[23] N. E. Brese, M. O'Keefe, *Acta Crystallogr., Sect. B* **1991**, *47*, 192.
[24] J. Rodríguez-Carvajal, *Physica B (Amsterdam)* **1993**, *192*, 55.
Received January 31, 2003

 © 2003 Wiley-VCH Verlag GmbH & Co. KGaA, Weinheim

Preparation of Hydroxylamine Complexes of Ruthenium(II), Osmium(II) and Iridium(III)

Gabriele Albertin,*[a] Stefano Antoniutti,[a] Samuele Beraldo,[a] and Fabio Chimisso[a]

Keywords: Hydroxylamines / N ligands / P ligands / Ruthenium / Osmium / Iridium

The hydroxylamine complexes $[MH(NH_2OH)P_4]BPh_4$ (M = Ru, Os) and $[Ru(NH_2OH)_2P_4](BPh_4)_2$ [P = $P(OEt)_3$, $PPh(OEt)_2$] were prepared by allowing the triflate species $MH(\kappa^1\text{-}OSO_2CF_3)P_4$ and $[Ru(\kappa^2\text{-}O_2SOCF_3)P_4]^+$ to react with an excess of hydroxylamine. The iridium complexes $[IrCl_2(NH_2OH)PL_2]BPh_4$ [P = $P(OEt)_3$, $PPh(OEt)_2$; L = PPh_3, $AsPh_3$] and $[IrH_2(NH_2OH)(PPh_3)_3]BPh_4$ were also prepared by reacting the hydride species $[IrHCl_2PL_3]$ and $[IrH_3(PPh_3)_3]$ first with triflic acid and then with an excess of NH_2OH. The *O*-iminoacylated hydroxylamine complexes $[M\{\eta^2\text{-}NH{=}C(R)ONH_2\}P_4](BPh_4)_2$ and $[M\{\eta^2\text{-}NH{=}C(R)ONH(CH_3)\}P_4](BPh_4)_2$ (M = Ru, Os; R = CH_3, 4-$CH_3C_6H_4$) were prepared by allowing the nitrile complexes $[M(RCN)_2P_4](BPh_4)_2$ to react with hydroxylamine (NH_2OH) or *N*-methylhydroxylamine [$NH(CH_3)OH$]. The compounds were characterised spectroscopically (IR, ^1H, ^{13}C and ^{31}P NMR) and a geometry in solution was also established.

(© Wiley-VCH Verlag GmbH & Co. KGaA, 69451 Weinheim, Germany, 2003)

Introduction

Hydroxylamine is a bifunctional molecule of simple constitution and structure, which has a somewhat unexplored coordination chemistry. Apart from the proposed $[IrCl_3(NH_2OH)(PPh_3)_2]$ compound,[1] obtained by protonation of $[Ir(NO)(PPh_3)_3]$ with HCl, and the $[Fe(TPP)(NH_2OH)_2]$ derivative (TPP = tetraphenylporphyrinate),[2] prepared by reacting Fe(TPP) with NH_2OH at low temperature, only recently[3] have some examples of hydroxylamine complexes of the type $[MX(NH_2OH)(CO)_2(PPh_3)_2]CF_3SO_3$ (M = Ru, Os; X = Cl, Br) and $[Re(NH_2OH)(CO)_3(PPh_3)_2]CF_3SO_3$ been reported. In contrast with numerous studies on hydrazine derivatives,[4,5] no further studies have been reported on the chemistry of hydroxylamine complexes, although NH_2OH is isoelectronic and somewhat similar to NH_2NH_2.

We have previously reported[6] the synthesis and the reactivity of mono- and bis(hydrazine) complexes of transition metals such as Mn, Fe, Ru, Os and Ir and have now extended these studies to hydroxylamine and methylhydroxylamine with the aim of testing the behaviour of these molecules as a ligand on appropriate metal fragments and, if possible, of carrying out a comparison with related hydrazine complexes. The results of these studies, which also include hydroxylamine reactions with coordinated nitriles,[7] are reported here.

[a] Dipartimento di Chimica dell'Università Ca' Foscari di Venezia,
Dorsoduro 2137, 30123 Venezia, Italy

Results and Discussion

Preparation of Hydroxylamine Complexes

Mono- and bis(hydroxylamine) complexes of ruthenium and osmium $[MH(NH_2OH)P_4]BPh_4$ (**1**−**3**) and $[M(NH_2OH)_2P_4](BPh_4)_2$ (**4**) [P = $P(OEt)_3$, $PPh(OEt)_2$], were prepared by substituting the triflato ligand in the corresponding precursors, as shown in Scheme 1.

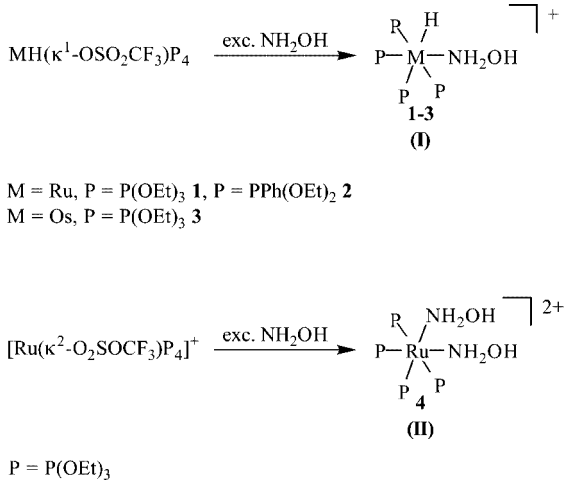

Scheme 1

The triflate precursors $[MH(\kappa^1\text{-}OSO_2CF_3)P_4]$ and $[M(\kappa^2\text{-}O_2SOCF_3)P_4]^+$ were generated in situ, in the case of ruthenium,[6a] by reacting the hydride complexes $[MH_2P_4]$ with an equimolar or an excess amount of triflic acid, while

with osmium[6c] the reaction first with methyl triflate and then with CF_3SO_3H was used (Scheme 2).

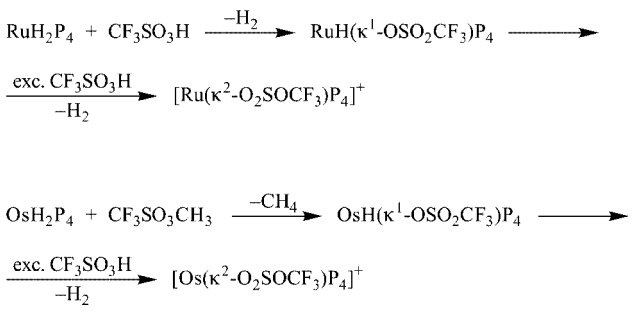

Scheme 2. P = $P(OEt)_3$, $PPh(OEt)_2$

Substitution of the triflato ligand was easy for ruthenium, allowing the preparation of both mono- (**1, 2**) and bis(hydroxylamine) (**4**) complexes. In the case of osmium, however, only the mono-substituted derivative **3** was obtained in pure form. Attempts to prepare the bis-species, in fact, gave white solids, which probably contain (by NMR) a mixture of $[Os(NH_2OH)_2P_4]^{2+}$, $[Os(\kappa^1\text{-}OSO_2CF_3)(NH_2OH)P_4]^+$ and decomposition products whose separation was unsuccessful.

The hydroxylamine complexes **1**−**4** are white or pale-yellow solids that are stable in air and in solution in polar organic solvents, where they behave as 1:1 (**1**−**3**) or as 1:2 (**4**) electrolytes.[8] Analytical and spectroscopic data (Table 1) support the proposed formulations. Both the IR and ^1H NMR spectroscopic data are diagnostic for the presence of the NH_2OH ligand. The IR spectra, in fact, show a slightly broad medium-intensity band at 3487−3318 cm^{-1}, attributed to ν(OH), and two ν(NH) absorptions at 3326−3223 cm^{-1} of the hydroxylamine ligand. In the spectra of the mono-substituted derivatives **1**−**3** one weak band is also present at 1955−1820 cm^{-1}, due to the ν(MH) absorption of the hydride ligand. Its presence is confirmed by the ^1H NMR spectra, which show the characteristic high-field multiplet due to the coupling with the phosphorus nuclei, simulated using an AB_2CX model (X = H) with the parameters reported in Table 1.

Further support for the presence of the NH_2OH ligand comes from the ^1H NMR spectra, which show, for compounds **1** and **2**, a slightly broad multiplet at δ = 6.13−6.02 ppm, attributed to the NH_2 protons, and a broad signal at δ = 4.98−4.44 ppm, attributed to the OH hydrogen atom of the hydroxylamine ligand. These assignments are confirmed by integration and ^1H COSY experiments. In the spectra of compounds **3** and **4**, on the other hand, only the NH_2 proton signal at δ = 6.61−5.80 ppm is unambiguously attributable, while the OH signal is masked by the signals of the CH_2 protons. The low-frequency values observed for our proton OH signals as compared with those (δ = 8−9 ppm) of known hydroxylamine derivatives[1,3] may suggest an O-coordination of the NH_2OH ligand. However, the ^1H NMR spectra show a small coupling ($^3J_{P,H} \approx 1$ Hz) of the NH_2 protons with the phosphorus nuclei which seems to support, like the known hydroxylamine complexes,[3] an N-bonded NH_2OH ligand. Therefore, in the absence of an X-ray structure determination, the N-coordination (Scheme 1) should be considered more likely in this case.

In the temperature range between +30 and −80 °C the $^{31}P\{^1H\}$ NMR spectra of mono-hydroxylamine complexes **1**−**3** appear as AB_2C multiplets, which can be simulated using the parameters reported in Table 1, suggesting a mutual *cis* arrangement (**I**) of the hydride and NH_2OH ligands (Scheme 1). An A_2B_2 multiplet, instead, is present in the spectra of the bis(hydroxylamine) complex **4**, in agreement with a mutually *cis* position (**II**) of the two NH_2OH ligands.

These studies on the synthesis of NH_2OH complexes have been extended to other metals with a d^6 configuration. We found that, in the case of iridium, the use of appropriate precursors containing mixed phosphite-phosphane (or arsane) ligands allows the synthesis of stable hydroxylamine derivatives. Treatment of $[IrHCl_2PL_2]$, first with triflic acid and then with an excess of NH_2OH, gives the hydroxylamine complexes $[IrCl_2(NH_2OH)PL_2]^+$ (**5**−**8**) [P = $P(OEt)_3$, $PPh(PEt)_2$; L = PPh_3, A_5Ph_3], which were isolated as their BPh_4 salts and characterised (Scheme 3).

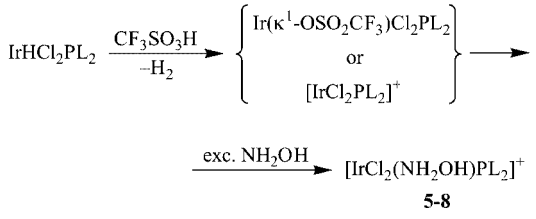

Scheme 3. L = PPh_3, P = $P(OEt)_3$ **5**, P = $PPh(OEt)_2$ **6**; L = $AsPh_3$, P = $P(OEt)_3$ **7**, P = $PPh(OEt)_2$ **8**

Protonation of $[IrHCl_2PL_2]$ with CF_3SO_3H leads[6d] to the evolution of H_2 and probable formation of either the triflate $[Ir(\kappa^1\text{-}OSO_2CF_3)Cl_2PL_2]$ or the pentacoordinate cations $[IrCl_2PL_2]^+$, which, when treated with an excess of hydroxylamine, give the final complexes **5**−**8**.

The $IrCl_2PL_2$ fragment seems to be peculiar to the formation of stable hydroxylamine complexes, since the use of other precursors such as $[IrHCl_2(PPh_3)_3]$, $[IrHCl_2(AsPh_3)_3]$ or $[IrH_2Cl(PPh_3)_3]$ does not allow the preparation of NH_2OH derivatives. The only other fragment we found to be able to bind NH_2OH is $[IrH_2(PPh_3)_3]$, which gives the stable and isolable complex $[IrH_2(NH_2OH)(PPh_3)_2]BPh_4$ (**9**). In fact, treatment of the trihydride $[IrH_3(PPh_3)_3]$, first with an equimolar amount of triflic acid and then with an excess of NH_2OH, produces the hydroxylamine complex **9**, which was isolated and characterised (Scheme 4).

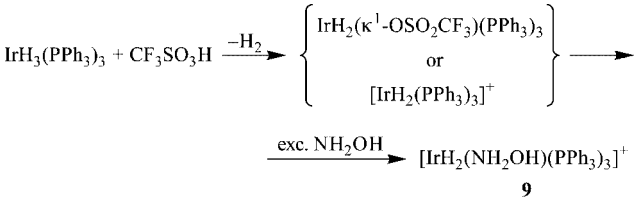

Scheme 4

 © 2003 Wiley-VCH Verlag GmbH & Co. KGaA, Weinheim

Table 1. IR and NMR spectroscopic data for hydroxylamine complexes

Complex	IR cm^{-1}	Assignment	^1H NMR[b][c] δ (*J*/Hz)	Assignment	Spin system	$^{31}P\{^1H\}$NMR[b][d] δ (*J*/Hz)
$[RuH(NH_2OH)\{P(OEt)_3\}_4]BPh_4$ (**1**)	3487 m	ν(OH)	6.13 m, br	NH_2	AB_2C	δ_A = 147.5
	3326 m	ν(NH)	4.44 br	OH		δ_B = 141.1
	3259 m		4.24−3.88 m	CH_2		δ_C = 136.7
	1820 m	ν(RuH)	1.36 t	CH_3		J_{AB} = 63.0
			1.32 t			J_{AC} = 42.2
			1.27 t			J_{BC} = 45.0
			−7.71 to −8.68 m	RuH		
			6.27 m, br [e]	NH_2		
			5.26 m	OH		
			4.19 m	CH_2		
			3.95 qnt			
			1.33 t	CH_3		
			1.30 t			
			1.26 t			
			AB_2CX	RuH		
			δ_X −8.19			
			J_{AX} = 24.2			
			J_{BX} = 24.5			
			J_{CX} = 122.1			
$[RuH(NH_2OH)\{PPh(OEt)_2\}_4]BPh_4$ (**2**)	3407 m	ν(OH)	6.02 m, br	NH_2	AB_2C	δ_A = 169.7
	3299 m	ν(NH)	4.98 br	OH		δ_B = 164.1
	3223 w		4.00−3.15 m	CH_2		δ_C = 159.4
	1946 m	ν(RuH)	1.28 t	CH_3		J_{AB} = 46.9
			1.23 t			J_{AC} = 29.7
			1.19 t			J_{BC} = 31.4
			0.92 t			
			AB_2CX	RuH		
			δ_X −8.02			
			J_{AX} = 24.5			
			J_{BX} = 24.0			
			J_{CX} = 105.2			
$[OsH(NH_2OH)\{P(OEt)_3\}_4]BPh_4$ (**3**)	3481 m, br	ν(OH)	6.61 br	NH_2	AB_2C	δ_A = 102.4
	3321 m	ν(NH)	4.22−3.84 m	CH_2		δ_B = 102.0
	3265 w		1.36 t	CH_3		δ_C = 96.3
	1955 w	ν(OsH)	1.31 t			J_{AB} = 34.3
			1.28 t			J_{AC} = 26.9
			AB_2CX	OsH		J_{BC} = 43.7
			δ_X −9.14			
			J_{AX} = 45.8			
			J_{BX} = 21.6			
			J_{CX} = −107.9			
$[Ru(NH_2OH)_2\{P(OEt)_3\}_4](BPh_4)_2$ (**4**)	3318 m	ν(OH)	5.80 m, br	NH_2	A_2B_2	δ_A = 129.6
	3290 m, br	ν(NH)	4.05 m	CH_2		δ_B = 119.8
			1.35 t	CH_3		J_{AB} = 60.3
			1.29 t			
$[IrCl_2(NH_2OH)\{P(OEt)_3\}(PPh_3)_2]BPh_4$ (**5**)	3258 m	ν(NH)	5.45 m, br	NH_2	AB_2	δ_A = 32.1
	3215 m		3.42 qnt	CH_2		δ_B = −19.2
	1601 m	δNH_2	1.00 t	CH_3		J_{AB} = 27.5
	393 m [f]	νIrCl				
$[IrCl_2(NH_2OH)\{PPh(OEt)_2\}(PPh_3)_2]BPh_4$ (**6**)	3490 m	ν(OH)	5.62 m	NH_2	AB_2	δ_A = 64.3
	3258 m	ν(NH)	3.50 m	CH_2		δ_B = −22.5
	3215 m		1.08 t	CH_3		J_{AB} = 21.0
	1616 m	$\delta(NH_2)$				
$[IrCl_2(NH_2OH)\{P(OEt)_3\}(AsPh_3)_2]BPh_4$ (**7**)	3254 m	ν(NH)	5.73 br	NH_2	A	32.84 s
	3213 m		3.55 qnt	CH_2		
	1624 m	$\delta(NH_2)$	1.00 t	CH_3		
$[IrCl_2(NH_2OH)\{PPh(OEt)_2\}(AsPh_3)_2]BPh_4$ (**8**)	3256 m	ν(NH)	5.83 m	NH_2	A	64.3 s
	3213 m		3.52 qnt	CH_2		
	1616 m	$\delta(NH_2)$	1.05 t	CH_3		
	386 m [f]	ν(IrCl)				
$[IrH_2(NH_2OH)(PPh_3)_3]BPh_4$ (**9**)	3275 m	ν(NH)	5.26 br	NH_2	A_2B	δ_A = 9.81
	3219 m		3.39 br	OH		δ_B = 5.46
	2179 w	νIrH)	A_2BXY	IrH		J_{AB} = 12.8
	2130 w		δ_X −12.19			
	1614 m	$\delta(NH_2)$	δ_Y −20.68			
			J_{AX} = 21.3			
			J_{AY} = 16.8			
			J_{BX} = 120			
			J_{BY} = 12.5			
			J_{XY} = 46.3			

 © 2003 Wiley-VCH Verlag GmbH & Co. KGaA, Weinheim

Table 1. *(Continued)*

Complex	IR[a] cm^{-1}	Assignment	^{1}H NMR[b][c] δ (*J*/Hz)	Assignment	Spin system	^{31}P{^{1}H}NMR[b][d] δ (*J*/Hz)
[Ru(η^2-NH=C(CH$_3$)ONH$_2$){P(OEt)$_3$}$_4$](BPh$_4$)$_2$ (**10a**)	3375 m 3290 m 3227 m 1668 m	ν(NH) δ(NH$_2$)	8.02 m 4.02 m 1.88 s 1.33 t 1.30 t	NH + NH$_2$ CH$_2$ CH$_3$ CH$_3$ phos	ABC$_2$	δ$_A$ = 131.9 δ$_B$ = 129.3 δ$_C$ = 116.8 *J*$_{AB}$ = 76.1 *J*$_{AC}$ = 61.4 *J*$_{BC}$ = 57.3
			9.06 br [e] 8.97 m, br 4.26 m 2.91 s 1.38 t 1.37 t	NH NH$_2$ CH$_2$ CH$_3$ CH$_3$ phos	ABC$_2$ [e]	δ$_A$ = 134.5 δ$_B$ = 131.2 δ$_C$ = 119.3 *J*$_{AB}$ = 76.8 *J*$_{AC}$ = 62.0 *J*$_{BC}$ = 57.3
{Ru(η^2-NH=C(4-CH$_3$C$_6$H$_4$)ONH$_2$)[P(OEt)$_3$]$_4$}(BPh$_4$)$_2$ (**10b**)	3381 m 3290 m 3217 m 1653 m	ν(NH) δ(NH$_2$)	8.32 m 4.17−3.94 m 2.46 s 1.36 t 1.32 t 1.24 t	NH + NH$_2$ CH$_2$ CH$_3$ CH$_3$ phos	ABC$_2$ [e]	δ$_A$ = 133.7 δ$_B$ = 131.1 δ$_C$ = 118.9 *J*$_{AB}$ = 75.9 *J*$_{AC}$ = 61.4 *J*$_{BC}$ = 57.2
			9.28 m, br [e] 8.79 br 4.28 m 2.42 s 1.42 t 1.40 t 1.29 t	NH NH$_2$ CH$_2$ CH$_3$ CH$_3$ phos		
[Ru{η^2-NH=C(CH$_3$)ONH(CH$_3$)}{P(OEt)$_3$}$_4$](BPh$_4$)$_2$ (**11**)	3408 m 3302 w 1608 m	ν(NH) δ(NH$_2$)	7.0 br 4.75 s, br 4.07 m 3.27 s 2.08 s 1.34 t 1.30 t 1.28 t	=NH NH CH$_2$ CH$_3$ CH$_3$ CH$_3$ phos	ABC$_2$	δ$_A$ = 132.4 δ$_B$ = 129.7 δ$_C$ = 120.6 *J*$_{AB}$ = 6.9 *J*$_{AC}$ = 58.8 *J*$_{BC}$ = 60.8
[Os{η^2-NH=C(CH$_3$)ONH$_2$}{P(OEt)$_3$}$_4$](BPh$_4$)$_2$ (**12a**)	3330 m 3217 w 1668 m	ν(NH) δ(NH$_2$)	7.48 s, br 4.08−6.84 m 2.07 s 1.29 t 1.25 t	NH + NH$_2$ CH$_2$ CH$_3$ CH$_3$ phos	A$_2$B$_2$	δ$_A$ = 82.7 δ$_B$ = 81.0 *J*$_{AB}$ = 41.5
			12.36 br [e,g] 8.56 s 4.04 m 2.44 s 1.21 t 1.16 t	NH NH$_2$ CH$_2$ CH$_3$ CH$_3$ phos	A$_2$BC [e,g]	δ$_A$ = 86.8 δ$_B$ = 84.7 δ$_C$ = 83.8 *J*$_{AB}$ = 41.5 *J*$_{AC}$ = 41.0 *J*$_{BC}$ = 54.2
[Os{η^2-NH=C(4-CH$_3$C$_6$H$_4$)ONH$_2$}{P(OEt)$_3$}$_4$](BPh$_4$)$_2$ (**12b**)	3481 m, br 3310 m 1636 m	ν(NH) δ(NH$_2$)	8.38 s, br 4.10−3.90 m 2.46 s 1.29 t 1.20 t	NH + NH$_2$ CH$_2$ CH$_3$ CH$_3$ phos	A$_2$BC	δ$_A$ = 81.9 δ$_B$ = 80.6 δ$_C$ = 80.4 *J*$_{AB}$ = 41.5 *J*$_{AC}$ = 41.6 *J*$_{BC}$ = 53.8
			10.12 br [g] 8.28 s 4.03−3.88 m 2.44 s 1.23 t 1.15 t	NH NH$_2$ CH$_2$ CH$_3$ CH$_3$ phos	A$_2$BC [g]	δ$_A$ = 82.9 δ$_B$ = 81.7 δ$_C$ = 81.6 *J*$_{AB}$ = 42.3 *J*$_{AC}$ = 41.5 *J*$_{BC}$ = 54.3
			11.79 s, br [e] [g] 8.71 s, br 4.17 m 2.38 s 1.29 t 1.22 t	NH NH$_2$ CH$_2$ CH$_3$ CH$_3$ phos	A$_2$BC [e,g]	δ$_A$ = 83.4 δ$_B$ = 82.9 δ$_C$ = 82.1 *J*$_{AB}$ = 41.5 *J*$_{AC}$ = 41.9 *J*$_{BC}$ = 54.5
[Os{η^2-NH=C(CH$_3$)ONH(CH$_3$)}{P(OEt)$_3$}$_4$](BPh$_4$)$_2$ (**13**)	3408 m 3294 m 1610 m	ν(NH) δ(NH$_2$)	7.4 br 5.24 s, br 4.00 m 3.29 s 2.08 s 1.28 t 1.26 t 1.24 t	=NH NH CH$_2$ CH$_3$ CH$_3$ phos	ABC$_2$	δ$_A$ = 93.8 δ$_B$ = 89.3 δ$_C$ = 82.2 *J*$_{AB}$ = 4.3 *J*$_{AC}$ = 45.4 *J*$_{BC}$ = 46.3

[a] In KBr pellets. [b] In CD_2Cl_2 at 25 °C, unless otherwise noted. [c] Phenyl proton resonances are omitted. [d] Positive shift downfield from 85% H_3PO_4. [e] In $(CD_3)_2CO$. [f] In polyethylene (far-IR). [g] At −70 °C.

 © 2003 Wiley-VCH Verlag GmbH & Co. KGaA, Weinheim

The reaction of $[IrH_3(PPh_3)_3]$ with CF_3SO_3H proceeds also in this case with the evolution of H_2 and probable formation of either κ^1-OSO_2CF_3 or pentacoordinate intermediates which, on treatment with NH_2OH, afford the final hydroxylamine derivative **9**. We also attempted to prepare bis(hydroxylamine) derivatives by reacting $[IrH_3(PPh_3)_3]$ sequentially, first with two equivalents of CF_3SO_3H and then with NH_2OH, but only a mixture of products not containing the NH_2OH ligand was isolated.

The hydroxylamine complexes of iridium (**5**−**8**) are yellow solids, while **9** is white, and all are stable in air and in solution in polar organic solvents, where they behave as 1:1 electrolytes.[8] Good analytical data were obtained for all compounds, and their IR and NMR spectroscopic data (Table 1) confirm the proposed formulations.

The IR spectra show the characteristic ν(NH) bands at 3275−3213 cm^{-1} and one of medium intensity at 1624−1607 cm^{-1}, attributed to δ(NH_2) of the NH_2OH ligands. The ν(OH) absorption in these complexes is weak and rather broad, and was unambiguously assigned only for **6** at 3490 cm^{-1}. In the spectrum of hydride complex **9** two weak bands at 2179 and 2130 cm^{-1} are also present. These were assigned to the ν(IrH) absorption of the two H^- ligands in a mutually *cis* position.

The presence of the hydroxylamine ligand in complexes **5**−**9** was further confirmed by the ^1H NMR spectra, which show the characteristic signal at δ = 5.83−5.25 ppm of the NH_2 protons of the hydroxylamine ligand. The OH proton is clearly observed at δ = 3.39 ppm only in the case of **9**; in the other complexes it is probably masked by the methylene protons of the phosphite ligands.

In the temperature range between +30 and −80 °C the $^{31}P\{^1H\}$ NMR spectra of the phosphane-phosphite complexes $[IrCl_2(NH_2OH)PL_2]BPh_4$ (**5** and **6**) [P = $P(OEt_3$, $PPh(OEt)_2$; L = PPh_3] appear as AB_2 multiplets in agreement with the magnetic equivalence of the two PPh_3 ligands. Taking into account that the far-IR spectrum of **5** shows only one ν(IrCl) band at 393 cm^{-1}, indicating that the two Cl^- ligands are in a mutually *trans* position, we may propose a *mer-trans* geometry (**III**) for our hydroxylamine derivatives **5** and **6** (Chart 1).

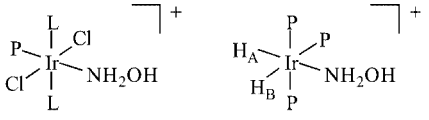

III **IV**

The $^{31}P\{^1H\}$ NMR spectra of the related arsane complexes $[IrCl_2(NH_2OH)PL_2]BPh_4$ (**7** and **8**) [P = $P(OEt)_3$, $PPh(OEt)_2$; L = $AsPh_3$] show only one singlet at δ = 32.8 and 64.3 ppm, respectively, for the phosphite ligand, and therefore no plausible hypothesis for the geometry of complexes can be made. However, taking into account that the far-IR spectra show only one ν(IrCl) band, we propose, by analogy with the related complexes **5** and **6**, a *mer-trans* geometry (**III**) for compounds **7** and **8** as well.

In the temperature range between +30 and −80 °C the $^{31}P\{^1H\}$ NMR spectra of $[IrH_2(NH_2OH)(PPh_3)_3]BPh_4$ (**9**) show an A_2B multiplet indicating the presence of two magnetically equivalent phosphanes, different from the third. In the hydride region, the ^1H NMR spectra also appear as a complicated multiplet, which can be simulated as the XY part (X, Y = H) of an A_2BXY spin system, with the parameters reported in Table 1. On this basis, we can reasonably propose a *mer-cis* geometry of type **IV** for our hydride-hydroxylamine complex **9**.

A comparison between the results for the NH_2OH complexes and those for related hydrazine NH_2NH_2 complexes shows that these two ligands are very similar in their behaviour toward metal fragments containing phosphite as supporting ligand. Similar complexes of Ru[6a] and Ir,[6d] containing either NH_2NH_2 or NH_2OH as monodentate ligand, can be isolated in the solid state. Furthermore, in the case of iridium only the mixed phosphane-phosphite fragment $IrCl_2PL_2$ can give stable hydrazine complexes, so the hydroxylamine derivative can be prepared exclusively with the same mixed-ligand fragment. Some differences, however, can be observed with osmium, which allows the synthesis of only mono-hydroxylamine complexes (**3**) with $P(OEt)_3$ phosphite ligand, whereas both mono- and bis(hydrazine) derivatives[6c] $[OsH(NH_2NH_2)P_4]^+$ and $[Os(NH_2NH_2)_2P_4]^{2+}$ can easily be prepared. In every case, although the comparison is still restricted to a few complexes, it seems that when a metal fragment is able to bind hydrazine, it can also coordinate hydroxylamine, affording the corresponding stable derivatives. Support for this hypothesis comes from the results on other complexes[3] suggesting a synthetic pathway for NH_2OH derivatives.

O-Iminoacylated Hydroxylamine Complexes

The synthesis of hydroxylamine complexes by substituting a labile ligand has prompted us to extend these studies to other precursors, such as the nitrile complexes $[M(RCN)_2P_4]^{2+}$ with the aim of testing whether new hydroxylamine derivatives may be prepared. Surprisingly, the reaction of bis(nitrile) complexes of ruthenium and osmium with hydroxylamine does not produce NH_2OH complexes, but affords a yellow solid which was characterised as containing an *O*-iminoacylated ligand of the type shown in Scheme 5.

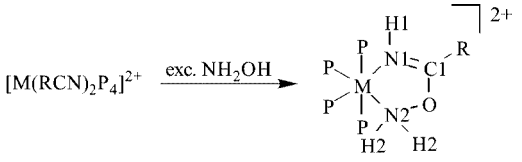

10, 12
(V)

Scheme 5. P = $P(OEt)_3$, M = Ru **10**, Os **12**, R = CH_3 **a**, 4-$CH_3C_6H_4$ **b**

The reaction proceeds easily at room temperature, affording complexes **10** and **12** in good yields. However, only the $P(OEt)_3$-containing *O*-iminoacylated complexes were pre-

 © 2003 Wiley-VCH Verlag GmbH & Co. KGaA, Weinheim

Table 2. $^{13}C\{^1H\}$ NMR spectroscopic data for selected complexes[a]

Compd.	δ	Assignment
$[Ru(\eta^2\text{-}NH{=}C(CH_3)ONH_2)\{P(OEt)_3\}_4](BPh_4)_2$ (**10a**)	172.8 s	C=N
	163−122 m	Ph
	63.4 m	CH_2
	15.9 s	CH_3C=
	16.1 m	CH_3 phos
$[Ru\{\eta^2\text{-}NH{=}C(CH_3)ONH(CH_3)\}\{P(OEt)_3\}_4](BPh_4)_2$ (**11**)	154.7 s	C=N
	164−121 m	Ph
	61.9 m	CH_2
	39.2 s	CH_3N
	19.3 s	CH_3C=
	15.9 m	CH_3 phos
$[Os\{\eta^2\text{-}NH{=}C(4\text{-}CH_3C_6H_4)ONH_2\}\{P(OEt)_3\}_4](BPh_4)_2$ (**12b**)	156.3 s	C=N
	165−122 m	Ph
	62.6 m	CH_2
	21.3 s	CH_3 *p*-tolyl
	15.8 m	CH_3 phos

[a] In $(CD_3)_2CO$ at 203 K.

pared in pure form, while with the related $PPh(OEt)_2$ compounds only intractable mixtures of product were obtained. Compounds **10** and **12** are pale-yellow solids stable in air and in solution in polar organic solvents, diamagnetic and 1:1 electrolytes.[8] The analytical and spectroscopic data (IR and NMR, Table 1 and 2) support the proposed formulation. The infrared spectra show, in the 3481−3217 cm^{-1} region, two or three medium-intensity bands, attributed to ν(NH) of the η^2-HN=C(R)ONH_2 ligand. The $\delta(NH_2)$ absorptions at 1668−1636 cm^{-1} also appear in the spectra. At room temperature, in CD_2Cl_2 as solvent, the ^1H NMR spectra of complexes **10** and **12** show, in the high-frequency region, a broad resonance at δ = 8.32−7.84 ppm. In $(CD_3)_2CO$, however, this resonance splits into two slightly broadened signals at δ = 12.36−9.06 and at 8.97−8.28 ppm, respectively, of intensity ratio 1:2. This split is observed at room temperature, except for compound **12a**, for which a lowering of the temperature to −20 °C is required. The highest frequency signal is assigned to the iminic =NH proton (H1), while the lowest is assigned to the ONH_2 (H2) group of the *O*-iminoacylated ligand. In the ^1H NMR spectra one sharp singlet between δ = 1 and 3 ppm due to the methyl group of the substituent R (CH_3 or 4-$CH_3C_6H_4$) of the η^2-ligand is also present.

Support for these assignments comes from a ^1H COSY spectrum of compound **10a**, which shows that the iminic HN= proton (H1) correlates with the methyl substituent of the iminic carbon atom HN=$C(CH_3)$ of the ligand. No correlation was observed between the iminic H1 and the aminic H2 proton resonances, in agreement with an *O*-iminoacylated molecule.

The ^{13}C NMR spectra confirm the formulation of the complexes showing, apart from the signals of the $P(OEt)_3$ and the BPh_4 anion, the imine carbon (C1) resonance of the η^2-ligand as a singlet at δ = 172.8 ppm for **10a** and at δ = 156.3 ppm for **12b**. An HMBC experiment for compound **10a** correlates the imine carbon signal at δ = 172.8 ppm with the methyl proton resonances at δ = 2.91 ppm of the methyl group bonded to the iminic C1 carbon atom, in agreement with the proposed assignment.

In the osmium complex **12b** the HMBC experiment shows a correlation between the iminic C1 carbon resonance and the signals of the phenyl protons of the *p*-tolyl substituent. On the basis of these data, and taking into account that in any solvent and in the temperature range between +20 and −80 °C the $^{31}P\{^1H\}$ NMR spectra of the *O*-iminoacylated derivatives **10**, **12** appear as an ABC_2 or A_2BC multiplet, a type-**V** geometry can reasonably be proposed.

We then thought to extend the studies to other hydroxylamines and treated the bis(nitrile) complexes $[M(CH_3CN)_2P_4]^{2+}$ with *N*-methylhydroxylamine $NH(CH_3)OH$. We observed that the reaction proceeds as with NH_2OH to give the chelated $[M(\eta^2\text{-}HN{=}C(CH_3)ONH(CH_3)\}P_4]^{2+}$ cations **11** and **13**, which were isolated as their BPh_4^- salts and characterised (Scheme 6).

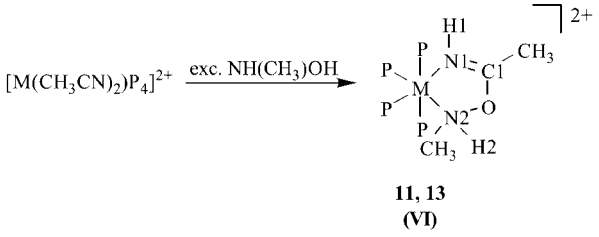

11, 13
(VI)

Scheme 6. P = $P(OEt)_3$, M = Ru **11**, Os **13**

The IR spectra of complexes **11** and **13** show the characteristic ν(NH) absorption at 3408−3294 cm^{-1} and

 © 2003 Wiley-VCH Verlag GmbH & Co. KGaA, Weinheim

$\delta[NH(CH_3)]$ at 1610−1608 cm^{-1} for the HN=$C(CH_3)ONH(CH_3)$ ligand.

In the ^1H NMR spectra (Table 1) of both compounds **11** and **13** two singlets between δ = 3.29 and 2.08 ppm appear, due to the two methyl groups of the η^2-ligand. One broad signal at δ = 4.75 ppm (**11**) and at δ = 5.24 ppm (**13**) is also present in the spectra, which was attributed to the aminic $ONHCH_3$ (H2) proton. A ^1H COSY spectrum of **11** confirms this assignment, showing a strong correlation between the signal at δ = 4.75 ppm and the methyl singlet at δ = 2.08 ppm of CH_3N2. A weak correlation was also observed between the other methyl singlet at δ = 3.27 ppm (CH_3C1) and a signal near δ = 7.0 ppm, which appears to be masked by the phenyl protons of the BPh_4 anion and can be attributed to the iminic proton (H1) of the ligand.

The $^{13}C\{^1H\}$ NMR spectrum of **11** (Table 2) shows, besides the signals of the phosphites and the BPh_4 anion, two singlets at δ = 39.2 and 19.3 ppm attributed to the two methyl carbons of the $N2CH_3$ and $C1CH_3$ groups, respectively, and one singlet at δ = 154.7 ppm due to the iminic C=N carbon atom (C1). An HMBC experiment confirms this attribution showing a strong correlation between the imino carbon signal at δ = 154.7 ppm and the proton signal at δ = 2.08 ppm of the methyl $N2CH_3$ substituent and also a weak correlation with the ^1H signal at δ = 3.27 ppm of the $C1CH_3$ methyl group. Furthermore, the methyl carbon resonance of the HN=CCH_3 group at δ = 19.3 ppm correlates with the aminic H2 proton signal at δ = 4.75 ppm, in agreement with the presence of the *O*-iminoacylated ligand.

In the temperature range between +30 and −80 °C, the $^{31}P\{^1H\}$ NMR spectra of both the ruthenium and osmium complexes **11** and **13** appear as ABC_2 multiplets; these spectra can be simulated with the parameters reported in Table 1. On the basis of these data, we can reasonably propose a geometry of type **VI** for our *O*-iminoacylated methylhydroxylamine derivatives.

Formation of *O*-iminoacylated hydroxylamine complexes from the reaction of a coordinated nitrile with NH_2OH or $NH(CH_3)OH$ is not surprising, taking into account that a metal-bonded RCN molecule can undergo nucleophilic attack by alcohols, amines and carbanions to give iminoether-, amidine- and imine derivatives.[7,9−12] Furthermore, nitrile precursors $[Ru(RCN)_2P_4]^{2+}$ are reported[6a−6c] to react with hydrazine or methylhydrazine to give amidrazone complexes $[M\{\eta^2\text{-}NH{=}C(R)N(R^1)NH_2\}P_4]^{2+}$ (R^1 = H, CH_3), probably through the nucleophilic attack of the hydrazine on the cyanide carbon atom of the coordinated nitriles, followed by an H-shift, giving a five-membered metallacycle. Finally, it is well documented[13−15] that NH_2OH can react with free nitriles through the more usual N-addition, giving amide oximes $RC(NH_2)$=NOH, or through O-addition, affording carboxamides $RC(=O)NH_2$ as the final products.

A nucleophilic attack of the hydroxylamine by the oxygen atom on the coordinated nitrile can therefore also be proposed in our case for the formation of *O*-iminoacylated hydroxylamine complexes **10**−**13**, which represents the first example[7] of the addition of hydroxylamine NH_2OH to a coordinated nitrile. Doubts remain, however, regarding the reaction path. Treatment of bis(nitrile) complexes $[M(RCN)_2P_4]^{2+}$ with $NH(R^1)OH$ (R^1 = H, CH_3) could result in the substitution of only one nitrile ligand to afford the $[M(RCN)(NH_2OH)P_4]^{2+}$ intermediate **A**. The *O*-iminoacylated hydroxylamine complex can be obtained (Scheme 7) by a nucleophilic attack of the coordinated hydroxylamine's oxygen atom on the coordinated RCN's nitrile carbon atom, followed by an H-shift.

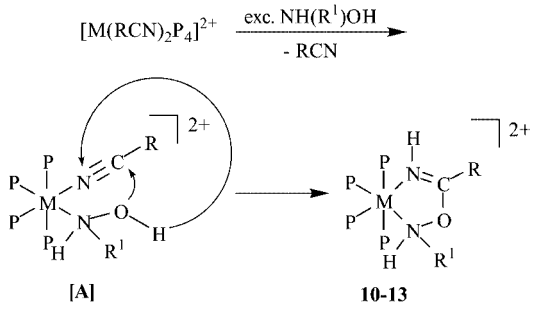

Scheme 7. P = $P(OEt)_3$, R = CH_3, 4-$CH_3C_6H_4$, R^1 = H, CH_3

The hydroxylamine, however, could react with one of the coordinated nitriles through the oxygen atom without being bonded to the central metal, resulting in the *O*-iminoacylated ligand, which, by substitution of the second RCN ligand, yields the final chelate complexes (Scheme 8).

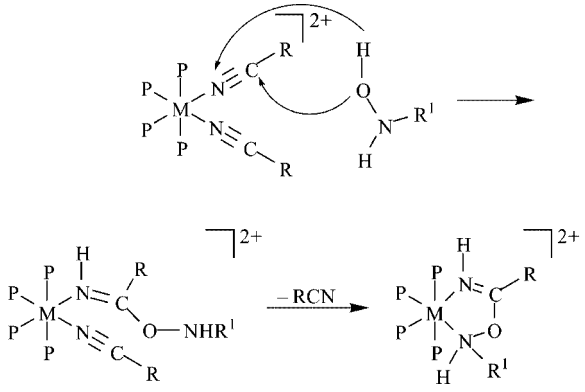

Scheme 8

The formation of complexes **10**−**13**, in fact, means that hydroxylamine, which possesses two sites of attack, reacts with the coordinated nitrile through the oxygen atom. The N-addition of hydroxylamine should give different products, such as complexes containing either the imine NH=C(R)NHOH or the tautomer amide oxime $RC(NH_2)$=NOH as a ligand (Scheme 9).

 © 2003 Wiley-VCH Verlag GmbH & Co. KGaA, Weinheim

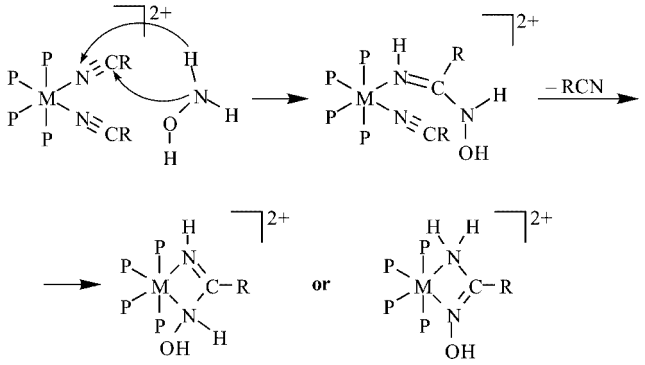

Scheme 9

We have studied the reactions between $[M(RCN)_2P_4]^{2+}$ cations and hydroxylamine by NMR spectroscopy and observed that no signals attributable to a nitrile-hydroxylamine intermediate of the type $[M(RCN)(NH_2OH)P_4]^{2+}$ were detected, with the resonances of the initial and the final products and of free nitrile being the only signals observed in the spectra. However, since the reaction of this intermediate would be intramolecular, one could expect it to be much faster than substitution of one RCN to give $[M(RCN)(NH_2OH)P_4]^{2+}$, making this intermediate undetectable. On this basis, although our data do not give conclusive information, a mechanism involving the initial substitution of one RCN with NH_2OH (Scheme 7) may be reasonably proposed.

Apart from the mechanism, the behaviour of both the hydroxylamine and the hydrazine toward a coordinated nitrile of the $[M(RCN)_2P_4]^{2+}$ cations containing $P(OEt)_3$ as ancillary ligand is very similar. In both cases they result in a nucleophilic attack on the nitrile carbon atom followed by an H-shift, yielding a new chelate ligand. A different atom, however, is used by the two nucleophiles, i.e. N-addition with hydrazine and O-addition with hydroxylamine, affording different molecules which behave, in every case, as bidentate ligands. The attack of the oxygen atom of the hydroxylamine in these reactions is rather surprising, since the reaction with free nitriles involves, in the majority of cases, N-addition.[13–15] An O-addition has been reported[16] in the reaction of the platinum complex $[PtCl_4(CH_3CN)_2]$ with *N*-substituted hydroxylamine R_2NOH, but the steric hindrance at the N-atom makes the O-attack plausible in this case. This is the only known example[16] of the reaction of a substituted hydroxylamine with coordinated RCN. In our $[M(RCN)_2P_4]^{2+}$ complexes the coordination of the nitrile to the MP_4 fragment probably makes the nitrile carbon increasingly susceptible to nucleophilic attack by the more electronegative oxygen, yielding the *O*-iminoacylated derivatives.

Conclusions

In this contribution we have reported the synthesis of several new hydroxylamine complexes of Ru, Os and Ir, including the first bis(hydroxylamine) $[Ru(NH_2OH)_2P_4](BPh_4)_2$ derivatives. The preparation of *O*-iminoacylated complexes $[M\{\eta^1\text{-}HN{=}C(R)ONHR^1\}P_4](BPh_4)_2$ (M = Ru, Os) was also achieved by O-addition of hydroxylamine to an organonitrile in a metal-assisted reaction.

Experimental Section

General: All synthetic work was carried out under an inert atmosphere using standard Schlenk techniques or a Vacuum Atmosphere dry-box. Once isolated, the complexes were found to be relatively stable in air, but were stored under an inert atmosphere at −25 °C. All solvents were dried over appropriate drying agents, degassed on a vacuum line and distilled into vacuum-tight storage flasks. The phosphite $P(OEt)_3$ (Aldrich) was purified by distillation under nitrogen, while $PPh(OEt)_2$ was prepared by the method of Rabinowitz and Pellon.[17] $RuCl_3{\cdot}3H_2O$ was obtained from Chempur, while $[(NH_4)_2(OsCl_6)]$ was purchased from Johnson Matthey and $IrCl_3{\cdot}3H_2O$ from Pressure Chemical Co.; all salts were used as received. Hydroxylamine (NH_2OH) and *N*-methylhydroxylamine [$NH(CH_3)OH$] were prepared by slight modification of a reported method,[18] involving treatment of hydroxylamine hydrochloride with sodium ethoxide in ethanol. The free NH_2OH was isolated as a white solid, while $NH(CH_3)OH$ was prepared in solution just prior to use. Other reagents were purchased from commercial sources in the highest available purity and used as received. Infrared spectra were recorded on a Nicolet Magna 750 FT-IR spectrophotometer. NMR spectra (^1H, ^{13}C, ^{31}P) were obtained on Bruker AC200 and AVANCE 300 spectrometers at temperatures varying between −90 °C and +30 °C, unless otherwise noted. ^1H and ^{13}C spectra are referred to internal tetramethylsilane, while $^{31}P\{^1H\}$ chemical shifts are reported with respect to 85% H_3PO_4, with downfield shifts considered positive. The SWAN-MR software package[19] was used to treat NMR spectroscopic data and for the simulation. The conductivity of 10^{-3} M solutions of the complexes in CH_3NO_2 at 25 °C was measured with a Radiometer CDM 83 instrument.

Preparation of the Complexes: The hydride complexes RuH_2P_4 and OsH_2P_4 and the nitrile complexes $[Ru(RCN)_2P_4](BPh_4)_2$ and $[Os(RCN)_2P_4](BPh_4)_2$ [R = CH_3, 4-$CH_3C_6H_4$; P = $P(OEt)_3$, $PPh(OEt)_2$] were prepared following the reported methods.[6,20] The iridium complexes $[IrHCl_2P(PPh_3)_2]$, $[IrHCl_2P(AsPh_3)_2]$ [P = $P(OEt)_3$, $PPh(OEt)_2$] and $[IrH_3(PPh_3)_3]$ were synthesised by published methods.[6d,21]

$[RuH(NH_2OH)P_4]BPh_4$ [P = $P(OEt)_3$ 1, $PPh(OEt)_2$ 2]: An equimolar amount of CF_3SO_3H (0.40 mmol, 35 μL) was added to a solution of the appropriate hydride RuH_2P_4 (0.40 mmol) in 10 mL of ethanol cooled to −196 °C and the reaction mixture, after warming to 0 °C, was stirred for 1 h. An excess of hydroxylamine (0.60 mmol, 0.43 mL of a 1.4 M solution in ethanol) was then added and the resulting solution stirred for about 2 h. The solvent was removed under reduced pressure to give an oil, which was treated with ethanol (2 mL) containing an excess of $NaBPh_4$ (0.8 mmol, 0.27 g). A white solid slowly separated out upon stirring the resulting solution. This solid was filtered off and recrystallised from CH_2Cl_2 and ethanol; yield 336 mg for **1** (75%); 384 mg for **2** (77%).
1: $C_{48}H_{84}BNO_{13}P_4Ru$ (1118.97): calcd. C 51.52, H 7.57, N 1.25; found C 51.41, H 7.60, N 1.18. Λ_M = 57.4 S cm^2 mol^{-1}.
2: $C_{64}H_{84}BNO_9P_4Ru$ (1247.14): calcd. C 61.64, H 6.79, N 1.12; found C 61.48, H 6.82, N 1.17. Λ_M = 58.6 S cm^2 mol^{-1}.

 © 2003 Wiley-VCH Verlag GmbH & Co. KGaA, Weinheim

$[OsH(NH_2OH)\{P(OEt)_3\}_4]BPh_4$ (3): An equimolar amount of $CF_3SO_3CH_3$ (0.12 mmol, 11 μL) was added to a solution of $[OsH_2\{P(OEt)_3\}_4]$ (0.12 mmol, 0.100 g) in 5 mL of toluene cooled to −196 °C and the reaction mixture, after warming to room temperature, was stirred for 1 h. An excess of NH_2OH (0.3 mmol, 0.48 mL of a 0.63 M solution in ethanol) was added and the solution stirred for about 4 h. The solvent was then removed under reduced pressure to give an oil which was treated with ethanol (2 mL) containing an excess of $NaBPh_4$ (0.24 mmol, 0.082 g). Upon stirring the resulting solution, a white solid separated out which was filtered off and recrystallised from CH_2Cl_2 and ethanol; yield 104 mg (72%). $C_{48}H_{84}BNO_{13}OsP_4$ (1208.10): calcd. C 47.72, H 7.01, N 1.16; found C 47.89, H 7.08, N 1.09. Λ_M = 55.0 S cm^2 mol^{-1}.

$[Ru(NH_2OH)_2\{P(OEt)_3\}_4](BPh_4)_2$ (4): An equimolar amount of CF_3SO_3H (0.40 mmol, 35 μL) was added to a solution of $[RuH_2\{P(OEt)_3\}_4]$ (0.40 mmol, 0.307 g) in 10 mL of toluene cooled to −196 °C. The reaction mixture was warmed to 0 °C, stirred for 1 h, and then cooled to −196 °C again. Triflic acid (0.40 mmol, 35 μL) was added and the solution, after warming to 0 °C, was stirred for 90 min. An excess of hydroxylamine (1.60 mmol, 1.14 mL of a 1.4 M solution in ethanol) was then added and the solution stirred for about 20 min. The solvent was removed under reduced pressure to give an oil which was treated with ethanol (2 mL). Addition of an excess of $NaBPh_4$ (1.60 mmol, 0.55 g) in ethanol (2 mL) to the resulting solution caused the separation of a white solid, which was filtered off and recrystallised from CH_2Cl_2 and ethanol; yield 476 mg (81%). $C_{72}H_{106}B_2N_2O_{14}P_4Ru$ (1470.22): calcd. C 58.82, H 7.27, N 1.47; found C 58.65, H 7.38, N 1.58. Λ_M = 119.6 S cm^2 mol^{-1}).

$[IrCl_2(NH_2OH)P(PPh_3)_2]BPh_4$ [P = $P(OEt)_3$ 5, $PPh(OEt)_2$ 6]: An equimolar amount of CF_3SO_3H (0.12 mmol, 11 μL) was added to a solution of the appropriate hydride $[IrHCl_2P(PPh_3)_2]$ (0.12 mmol) in 8 mL of CH_2Cl_2 cooled to −196 °C, and the reaction mixture was warmed to room temperature and stirred for 90 min. An excess of hydroxylamine (1.20 mmol, 1.46 mL of 0.82 M solution in ethanol) was added and the resulting mixture stirred for about 4 h. The solvent was removed under reduced pressure giving an oil, which was triturated with ethanol (2 mL) containing an excess of $NaBPh_4$ (0.24 mmol, 0.082 g). A yellow solid slowly separated out from the resulting solution, which was filtered off and recrystallised from CH_2Cl_2 in ethanol; yield 98 mg (63%) for **5**; 109 mg (68%) for **6**.
5: $C_{66}H_{68}BCl_2IrNO_4P_3$ (1306.12): calcd. C 60.69, H 5.25, N 1.07, Cl 5.43; found C 60.55, H 5.32, N 1.06, Cl 5.37. Λ_M = 58.2 S cm^2 mol^{-1}.
6: $C_{70}H_{68}BCl_2IrNO_3P_3$ (1338.17): calcd. C 62.83, H 5.12, N 1.05, Cl 5.30; found C 63.01, H 5.24, N 1.10, Cl 5.08. Λ_M = 61.6 S cm^2 mol^{-1}.

$[IrCl_2(NH_2OH)P(AsPh_3)_2]BPh_4$ [P = $P(OEt)_3$ 7, $PPh(OEt)_2$ 8]: These complexes were prepared exactly as for compounds **5** and **6**; yield 113 mg (68%) for **7**; 125 mg (73%) for **8**.
7: $C_{66}H_{68}As_2BCl_2IrNO_4P$ (1394.02): calcd. C 56.87, H 4.92, N 1.00, Cl 5.09; found C 56.64, H 5.01, N 0.92, Cl 5.27. Λ_M = 55.7 S cm^2 mol^{-1}.
8: $C_{70}H_{68}As_2BCl_2IrNO_3P$ (1426.07): calcd. C 58.96, H 4.81, N 0.98, Cl 4.97; found C 59.13, H 4.70, N 1.06, Cl 4.79. Λ_M = 59.0 S cm^2 mol^{-1}.

$[IrH_2(NH_2OH)(PPh_3)_3]BPh_4$ (9): An equimolar amount of CF_3SO_3H (0.12 mmol, 11 μL) was added to a solution of $[IrH_3(PPh_3)_3]$ (0.12 mmol, 0.118 g) in 5 mL of toluene cooled to −196 °C, and the reaction mixture warmed to room temperature and stirred for 10 min. An excess of hydroxylamine (1.20 mmol, 1.46 mL of 0.82 M solution in ethanol) was added and the solution stirred for 4 h. The solvent was removed under reduced pressure to give an oil, which was triturated with ethanol (3 mL) containing an excess of $NaBPh_4$ (0.24 mmol, 0.082 g). A white solid separated out from the resulting solution, which was filtered off and recrystallised from CH_2Cl_2 and ethanol; yield 128 mg (80%). $C_{78}H_{70}BIrNOP_3$ (1333.37): calcd. C 70.26, H 5.29, N 1.05; found C 70.35, H 5.37, N 1.11. Λ_M = 54.8 S cm^2 mol^{-1}.

$[Ru\{\eta^2\text{-}NH{=}C(R)ONH_2\}\{P(OEt)_3\}_4](BPh_4)_2$ (R = CH_3 10a, 4-$CH_3C_6H_4$ 10b): An excess of NH_2OH (0.52 mmol, 0.62 mL of a 0.84 M solution in ethanol) was added to a solution of the appropriate nitrile complex $[Ru(RCN)_2\{P(OEt)_3\}_4](BPh_4)_2$ (0.13 mmol) in 10 mL of CH_2Cl_2 and the reaction mixture was stirred for 24 h. The solvent was removed under reduced pressure to give an oil which was treated with ethanol (2 mL). The addition of an excess of $NaBPh_4$ (0.26 mmol, 0.089 g) in 2 mL of ethanol to the resulting solution caused the separation of a white solid, which was filtered off and recrystallised from CH_2Cl_2 and ethanol; yield 123 mg (64%) for **10a**; 135 mg (67%) for **10b**.
10a: $C_{74}H_{106}B_2N_2O_{13}P_4Ru$ (1478.24): calcd. C 60.13, H 7.23, N 1.90; found C 59.97, H 7.17, N 1.86. Λ_M = 117.4 S cm^2 mol^{-1}.
10b: $C_{80}H_{110}B_2N_2O_{13}P_4Ru$ (1554.34): calcd. C 61.82, H 7.13, N 1.80; found C 61.98, H 7.20, N 1.75. Λ_M = 120.7 S cm^2 mol^{-1}.

$[Ru\{\eta^2\text{-}NH{=}C(CH_3)ONH(CH_3)\}\{P(OEt)_3\}_4](BPh_4)_2$ (11): This complex was prepared similarly to **10** by reacting $[Ru(CH_3CN)_2\{P(OEt)_3\}_4](BPh_4)_2$ (0.17 mmol, 0.250 g in 10 mL of CH_2Cl_2) with an excess of $NH(CH_3)OH$ (1.7 mmol, 2.9 mL of 0.58 M solution in ethanol) for 24 h; yield 140 mg (55%). $C_{75}H_{108}B_2N_2O_{13}P_4Ru$ (1492.27): calcd. C 60.37, H 7.29, N 1.88; found C 60.49, H 7.35, N 1.80. Λ_M = 119.1 S cm^2 mol^{-1}.

$[Os\{\eta^2\text{-}NH{=}C(R)ONH_2\}\{P(OEt)_3\}_4](BPh_4)_2$ (R = CH_3 12a, 4-$CH_3C_6H_4$ 12b): An excess of hydroxylamine (1.3 mmol, 1.8 mL of a 0.72 M solution in ethanol) was added to a solution of the appropriate nitrile complex $[Os(RCN)_2\{P(OEt)_3\}_4](BPh_4)_2$ (0.13 mmol) in 8 mL of CH_2Cl_2 and the reaction mixture stirred for 20 h. The solvent was removed under reduced pressure to give an oil, which was treated with ethanol (2 mL) containing an excess of $NaBPh_4$ (0.26 mmol, 0.089 g). Upon stirring the resulting solution a white solid slowly separated out, which was filtered off and recrystallised from CH_2Cl_2 and ethanol; yield 124 mg (62%) for **12a**; 126 mg (59%) for **12b**.
12a: $C_{74}H_{106}B_2N_2O_{13}OsP_4$ (1567.37): calcd. C 56.71, H 6.82, N 1.79; found C 56.59, H 6.98, N 1.68. Λ_M = 123.4 S cm^2 mol^{-1}.
12b: $C_{80}H_{110}B_2N_2O_{13}OsP_4$ (1643.47): calcd. C 58.47, H 6.75, N 1.70; found C 58.30, H 6.81, N 1.62. Λ_M = 121.6 S cm^2 mol^{-1}.

$[Os\{\eta^2\text{-}NH{=}C(CH_3)ONH(CH_3)\}\{P(OEt)_3\}_4](BPh_4)_2$ (13): This complex was prepared similarly to **12** by reacting $[Os(CH_3CN)_2\{P(OEt)_3\}_4](BPh_4)_2$ with a 10-fold excess of *N*-methylhydroxylamine; yield 93 mg (45%). $C_{75}H_{108}B_2N_2O_{13}OsP_4$ (1581.40): calcd. C 56.96, H 6.88, N 1.77; found C 57.13, H 6.96, N 1.69. Λ_M = 115.9 S cm^2 mol^{-1}.

Acknowledgments

The financial support of MIUR (Rome) *Programmi di Ricerca Scientifica di Rilevante Interesse Nazionale, Cofinanziamento 2002−2003* is gratefully acknowledged. We thank Daniela Baldan for technical assistance.

 © 2003 Wiley-VCH Verlag GmbH & Co. KGaA, Weinheim

[1] [1a] K. R. Grundy, C. A. Reed, W. R. Roper, *J. Chem. Soc., Chem. Commun.* **1970**, 1501. [1b] R. Melenkivitz, G. Hillhouse, *Chem. Commun.* **2002**, 660.
[2] D.-W. Feng, M. D. Ryan, *Inorg. Chem.* **1987**, *26*, 2480.
[3] [3a] T.-Y. Cheng, A. Ponce, A. L. Rheingold, G. L. Hillhouse, *Angew. Chem. Int. Ed. Engl.* **1994**, *33*, 657. [3b] J. S. Southern, G. L. Hillhouse, A. L. Rheingold, *J. Am. Chem. Soc.* **1997**, *119*, 12406.
[4] [4a] D. Sutton, *Chem. Rev.* **1993**, *93*, 995. [4b] B. F. G. Johnson, B. L. Haymore, J. R. Dilworth, in *Comprehensive Coordination Chemistry*, (Eds.: G. Wilkinson, R. D. Gillard and J. A. McCleverty), Pergamon Press, Oxford, 1987, Vol. 2. [4c] R. A. Henderson, G. J. Leigh, C. J. Pickett, *Adv. Inorg. Chem. Radiochem.* **1983**, *27*, 197. [4d] F. Bottomley, *Q. Rev. Chem. Soc.* **1970**, *24*, 617.
[5] [5a] K. D. Demadis, S. M. Malinak, D. Coucouvanis, *Inorg. Chem.* **1996**, *35*, 4038. [5b] C. J. Davies, I. M. Dodd, M. M. Harding, B. T. Heaton, C. Jacob, J. Ratnam, *J. Chem. Soc., Dalton Trans.* **1994**, 787. [5c] D. Sellmann, K. Engl, F. W. Heinemann, *Eur. J. Inorg. Chem.* **2000**, 423. [5d] T. E. Glassman, M. G. Vale, R. R. Schrock, *J. Am. Chem. Soc.* **1992**, *114*, 8098. [5e] M. Kawano, C. Hoshino, K. Matsumoto, *Inorg. Chem.* **1992**, *31*, 5158.
[6] [6a] G. Albertin, S. Antoniutti, A. Bacchi, E. Bordignon, P. M. Dolcetti, G. Pelizzi, *J. Chem. Soc., Dalton Trans.* **1997**, 4435. [6b] G. Albertin, S. Antoniutti, E. Bordignon, S. Pattaro, *J. Chem. Soc., Dalton Trans.* **1997**, 4445. [6c] G. Albertin, S. Antoniutti, A. Bacchi, M. Bergamo, E. Bordignon, G. Pelizzi, *Inorg. Chem.* **1998**, *37*, 479. [6d] G. Albertin, S. Antoniutti, E. Bordignon, F. Menegazzo, *J. Chem. Soc., Dalton Trans.* **2000**, 1181. [6e] G. Albertin, S. Antoniutti, E. Bordignon, G. Perinello, *J. Organomet. Chem.* **2001**, *625*, 217.
[7] V. Yu. Kukushkin, A. J. L. Pombeiro, *Chem. Rev.* **2002**, *102*, 1771.
[8] W. J. Geary, *Coord. Chem. Rev.* **1971**, *7*, 81.
[9] R. A. Michelin, M. Mozzon, R. Bertani, *Coord. Chem. Rev.* **1996**, *147*, 299.
[10] R. Cini, F. P. Fanizzi, F. P. Intini, L. Maresca, G. Natile, *J. Am. Chem. Soc.* **1993**, *115*, 5123; P. Paul, K. Nag, *Inorg. Chem.* **1987**, *26*, 1586; D. L. Thorn, J. C. Calabrese, *J. Organomet. Chem.* **1994**, *272*, 283.
[11] A. Syamale, A. R. Chakravarty, *Inorg. Chem.* **1991**, *30*, 4699; S. G. Feng, P. S. White, J. L. Templeton, *Organometallics* **1993**, *12*, 1765; D. P. Fairlie, W. G. Jackson, *Inorg. Chem.* **1990**, *29*, 140.
[12] Z. Kanda, Y. Nakamura, S. Kawaguchi, *Inorg. Chem.* **1978**, *17*, 910; P. Braunstein, D. Matt, Y. Dusausoy, J. Fischer, *Organometallics* **1983**, *2*, 1410; J. Vicente, M.-T. Chicote, J. Fernandez-Baeza, F. J. Lahoz, J. A. Lopez, *Inorg. Chem.* **1991**, *30*, 3617; R. A. Michelin, M. Mozzon, P. Berin, R. Bertani, F. Benetollo, G. Bombieri, R. J. Angelici, *Organometallics* **1994**, *13*, 1341.
[13] S. Dayagi, Y. Degani, in *The Chemistry of the Carbon-Nitrogen Double Bond* (Ed.: S. Patai), Interscience, London, 1970, p. 111.
[14] B. P. Iudkins, D. G. Allen, T. A. Cook, B. Evans, T. E. Sardharwala, *Synth. Commun.* **1996**, *26*, 4351.
[15] L. Stephenson, W. K. Warburton, M. J. Wilson, *J. Chem. Soc., C* **1969**, 861.
[16] G. Wagner, A. J. L. Pombeiro, Y. N. Kukushkin, T. B. Pakhomova, A. D. Ryabov, V. Yu. Kukushkin, *Inorg. Chim. Acta* **1999**, *292*, 272.
[17] R. Rabinowitz, J. Pellon, *J. Org. Chem.* **1961**, *26*, 4623.
[18] C. Hurd, *Inorg. Synth.* **1939**, *1*, 87.
[19] G. Balacco, *J. Chem. Inf. Comput. Sci.* **1994**, *34*, 1235.
[20] [20a] W. G. Peet, D. H. Gerlach, *Inorg. Synth.* **1974**, *15*, 38. [20b] D. H. Gerlach, W. G. Peet, E. L. Muetterties, *J. Am. Chem. Soc.* **1972**, *94*, 4545. [20c] G. Albertin, S. Antoniutti, E. Bordignon, *J. Chem. Soc., Dalton Trans.* **1989**, 2353.
[21] S. Park, A. J. Lough, R. H. Morris, *Inorg. Chem.* **1996**, *35*, 3001 and references therein.

Received February 3, 2003

 © 2003 Wiley-VCH Verlag GmbH & Co. KGaA, Weinheim

Preparation and Reactivity of Hydrazine Complexes of Rhenium: Synthesis of 1,2-Diazene (NH=NH) and Methyleneimine (CH_2=NH) Derivatives

Gabriele Albertin,*[a] Stefano Antoniutti,[a] and Maria Teresa Giorgi[a]

Keywords: Hydrazine / N ligands / Oxidation / Rhenium

The hydrazine complexes $[Re(RNHNH_2)(CO)_nP_{5-n}]BPh_4$ [R = H, CH_3, Ar; n = 1–4; P = $P(OEt)_3$, $PPh(OEt)_2$, PPh_2OEt] were prepared by allowing the hydride species $[ReH(CO)_nP_{5-n}]$ to react first with a Brønsted acid and then with hydrazine. The reaction of either $[Re(NH_2NH_2)(CO)_nP_{5-n}]BPh_4$ or $[Re(ArNHNH_2)(CO)_nP_{5-n}]BPh_4$ with $Pb(OAc)_4$ at –40 °C proceeds with the selective oxidation of the hydrazine ligand to yield either $[Re(NH=NH)(CO)_nP_{5-n}]BPh_4$ or $[Re(ArN=NH)(CO)_nP_{5-n}]BPh_4$. The oxidation of $[Re(CH_3NHNH_2)(CO)_nP_{5-n}]BPh_4$ (n = 1, 2) with $Pb(OAc)_4$ at –40 °C gives both $[Re(CH_3N=NH)(CO)_nP_{5-n}]BPh_4$ and $[Re(\eta^1\text{-}NH=CH_2)(CO)_nP_{5-n}]BPh_4$. Reduction reactions of both hydrazine and diazene complexes with Zn amalgam were also studied and yielded ammonia in moderate yield (20–25%).

(© Wiley-VCH Verlag GmbH & Co. KGaA, 69451 Weinheim, Germany, 2003)

Introduction

Complexes containing partially reduced dinitrogen molecules such as hydrazine ($RNHNH_2$), hydrazido (RNHNH), diazene (RN=NH), and diazenido (RN_2) as ligands continue to be studied not only for their relationship with the nitrogen-fixation process intermediates, but also because their properties lead us to consider this class of compounds as having an identity and chemistry of their own,[1–3] with potentially interesting developments.

The hydrazine complexes are the least studied[1,2] among these diazo species even though NH_2NH_2 has been shown to be a substrate[4] as well as a product of functioning nitrogenase and has been isolated by quenching the enzyme.[5] Furthermore, rhenium complexes containing NH_2NH_2 or substituted hydrazine $RNHNH_2$ are very rare and include, apart from the pioneering work on $[Re(NCO)(CO)_2(NH_2NH_2)P_2]$ (P = tertiary phosphane),[6] only two papers,[7,8] one on $[ReCp^*Me_3(NH_2NH_2)]CF_3SO_3$ (Cp^* = pentamethylcyclopentadienyl) and $[Re(NH_2NH_2)(CO)_3(PPh_3)_2]CF_3SO_3$, and another on the substituted-hydrazine complex $[ReCl_2(PPh_3)_2\{NNC(O)Ph\}\{H_2NNHC(S)Ph\}]$.[9]

We have previously reported the synthesis and reactivity of mono- and bis(hydrazine) complexes of the iron triad[10] and manganese[11] of the type $[MH(RNHNH_2)P_4]BPh_4$, $[M(RNHNH_2)_2P_4](BPh_4)_2$ (M = Fe, Ru, Os) and $[Mn(RNHNH_2)(CO)_nP_{5-n}]BPh_4$ (P = phosphites). We have now extended these studies to rhenium with the aim of preparing hydrazine complexes and studying their reactivity toward oxidizing and reducing reagents in an attempt to test whether the rhenium fragments are able to stabilize diazene species. The results of these studies, which include the synthesis of stable 1,2-diazene complexes and the unprecedented methyleneimine (CH_2=NH) derivatives, are reported here. A preliminary paper on part of this work has previously been published.[12]

[a] Dipartimento di Chimica, Università Ca′ Foscari di Venezia, Dorsoduro 2137, 30123 Venezia, Italy
Fax: (internat.) +39-041/234-8917
E-mail: albertin@unive.it

Results and Discussion

Preparation of Hydrazine Complexes

The hydrazine complexes $[Re(RNHNH_2)(CO)_nP_{5-n}]BPh_4$ (**1**–**8**) were prepared by reacting the hydride species $[ReH(CO)_nP_{5-n}]$ first with an equimolar amount of a Brønsted acid (CF_3SO_3H or HBF_4) and then with an excess of hydrazine, as shown in Scheme 1.

Treatment of the hydrides $[ReH(CO)_nP_{5-n}]$ with the Brønsted acid CF_3SO_3H or HBF_4 (HY) gives the dihydrogen-containing cationic complexes $[Re(\eta^2\text{-}H_2)(CO)_nP_{5-n}]^+$,[13] which are thermally unstable and easily lose H_2 yielding either the neutral $ReY(CO)_nP_{5-n}$ species, containing the labile Y^- ligand, or the coordinatively unsaturated $[Re(CO)_nP_{5-n}]^+$ cations. Reaction of these intermediates with an excess of hydrazine gives the final derivatives $[Re(RNHNH_2)(CO)_nP_{5-n}]^+$ (**1**–**8**), which were isolated as their BPh_4^- salts and characterised. 1,1-Dimethylhydrazine reacts with these rhenium intermediates giving the final derivatives $[Re\{(CH_3)_2NNH_2\}(CO)_nP_{5-n}]BPh_4$ (**1e** and **3e**).

Good analytical data were obtained for all the hydrazine complexes **1**–**8**, which are white or pale-yellow solids,

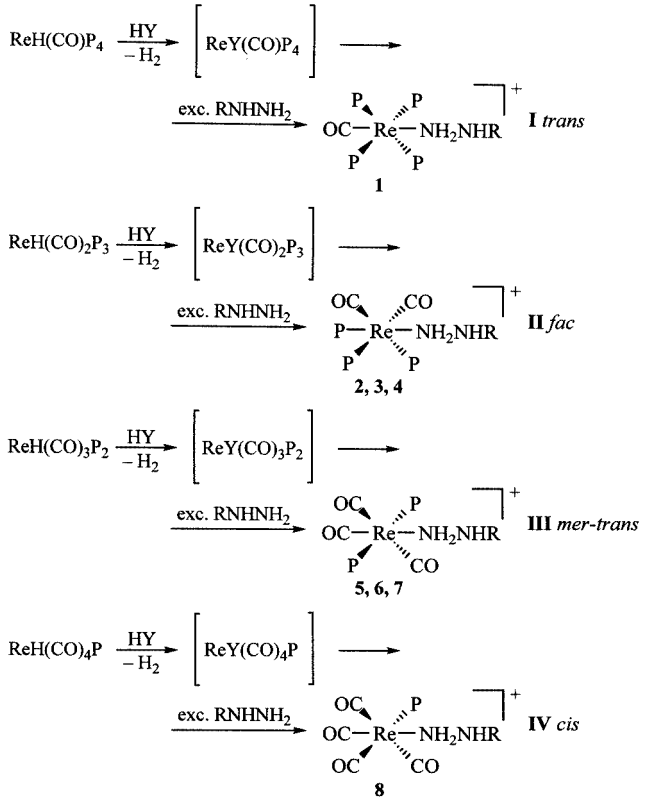

Scheme 1. P = $P(OEt)_3$ (**1**, **2**, **5**), $PPh(OEt)_2$ (**3**, **6**), PPh_2OEt (**4**, **7**, **8**); Y = $CF_3SO_3^-$, BF_4^-; R = H (**a**), CH_3 (**b**), C_6H_5 (**c**), 4-$NO_2C_6H_4$ (**d**); $(CH_3)_2NNH_2$ (**e**)

stable in air and in solution in polar organic solvents, where they behave as 1:1 electrolytes.[14] The IR and NMR spectroscopic data (Table 1) support the proposed formulation and allow a geometry in solution to be established.

The presence of a hydrazine ligand in the complexes is confirmed by the IR spectra, which show the characteristic ν(NH) bands between 3366 and 3202 cm^{-1}. In some complexes the δ(NH_2) absorption at 1624−1611 cm^{-1} is also observed. Furthermore, the ^1H NMR spectra confirm the presence of the hydrazine ligand, showing the characteristic NH and NH_2 signals, which were clearly assigned by accurate integration and homodecoupling experiments, and are reported in Table 1. The spectra also show that, in the case of the NH_2NH_2 complexes, two NH_2 proton signals are present, thus excluding the formation of a dimeric complex with an NH_2NH_2 bridging ligand.

In the temperature range between +30 and −80 °C the ^{31}P NMR spectra of the monocarbonyl complexes **1** show a sharp singlet suggesting a mutual *trans* position (geometry **I**) of the carbonyl and hydrazine ligands. This is confirmed by the IR spectra, which show the ν(CO) band at 1887−1888 cm^{-1}.

The IR spectra of the dicarbonyl complexes **2**−**4** show two strong bands in the ν(CO) region indicating the mutual *cis* position of the two carbonyl ligands. The ^{13}C NMR spectra also indicate that the two CO groups are magnetically equivalent, showing only one multiplet for **2b** in the carbonyl carbon region at δ = 194.2 ppm. Furthermore, the $^{31}P\{^1H\}$ NMR spectra display either an A_2B- or an AB_2-type coupling pattern, suggesting the magnetic equivalence of two P atoms, different from the third. On this basis a *fac* geometry (**II**) may be proposed for the dicarbonyl derivatives.

In the temperature range between +30 and −80 °C, the ^{31}P NMR spectra of the tricarbonyl compounds **5**−**7** show a sharp singlet, in agreement with two magnetically equivalent phosphane ligands. The IR spectra show three ν(CO) bands, two strong and one of medium intensity, suggesting a *mer* arrangement of the carbonyl ligands. On this basis, a *mer-trans* geometry (**III**) in solution may be reasonably proposed for the tricarbonyl derivatives.

Finally, the presence of four ν(CO) bands in the carbonyl region of its IR spectrum strongly suggests a *cis* geometry (**IV**) for the tetracarbonyl derivative $[Re(NH_2NH_2)(CO)_4(PPh_2OEt)]^+$ (**8**).

Oxidation Reactions

The hydrazine complexes $[Re(NH_2NH_2)(CO)_nP_{5-n}]BPh_4$ react with $Pb(OAc)_4$ at −40 °C to give the 1,2-diazene derivatives $[Re(NH{=}NH)(CO)_nP_{5-n}]BPh_4$, which were isolated in the solid state and characterised (Scheme 2).

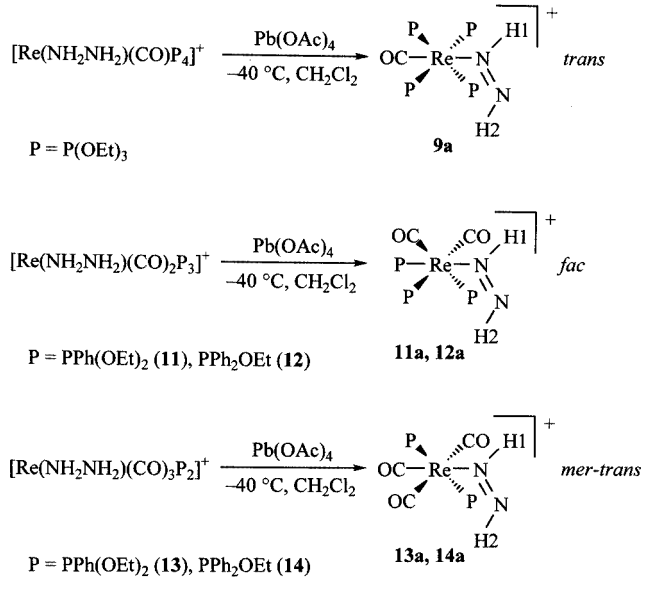

Scheme 2

The reaction proceeds with the selective oxidation of the hydrazine ligand to 1,2-diazene, which is stabilized by coordination to all the $[Re(CO)_nP_{5-n}]$ (n = 1, 2, 3) fragments, thus allowing the complexes to be isolated. The use of a temperature below −30 °C during the reaction course is crucial for a successful synthesis, as is crystallisation of the products at 0 °C. If these temperatures are not maintained, large amounts of decomposition products are obtained that contain only traces of the diazene complexes. In pure form, however, the NH=NH compounds **9**−**14** are stable at room temperature both as a solid and in solution in polar organic solvents, where they behave as 1:1 electrolytes.[14] Analytical and spectroscopic data (Table 1) support the proposed for-

 © 2003 Wiley-VCH Verlag GmbH & Co. KGaA, Weinheim

Table 1. Selected IR and NMR spectroscopic data for rhenium complexes

Compound	IR[a] $\tilde{\nu}$, cm^{-1}	Assgnt	^1H NMR[b][c] δ (*J*/Hz)	Assgnt	Spin system	$^{31}P\{^1H\}$ NMR[b] [d] δ (*J*/Hz)
$[Re(NH_2NH_2)(CO)\{P(OEt)_3\}_4]BPh_4$ (**1a**)	3366m	ν(NH)	4.45 (br. m)	$ReNH_2$	A_4	118.1 (s)
	3313m		4.07 (m)	CH_2		
	3283w		1.30 (t)	CH_3		
	3218m					
	1887s	ν(CO)				
$[Re(C_6H_5NHNH_2)(CO)\{P(OEt)_3\}_4]BPh_4$ (**1c**)	3341m	ν(NH)	6.22 (br. t)	NH	A_4	117.8 (s)
	3285m		5.16 (br. m)	$ReNH_2$		
	1888s	ν(CO)	4.08 (m)	CH_2		
	1611m	δ(NH_2)	1.31 (t)	CH_3		
$[Re\{(CH_3)_2NNH_2\}(CO)\{P(OEt)_3\}_4]BPh_4$ (**1e**)	3327w	ν(NH)	4.24 (br)	$ReNH_2$	A_4	116.7 (s)
	3283m		4.06 (m)	CH_2		
	1887s	ν(CO)	2.39 (s)	$(CH_3)_2N$		
			1.29 (t)	CH_3		
$[Re(CH_3NHNH_2)(CO)_2\{P(OEt)_3\}_3]BPh_4$ (**2b**)[e]	3325m	ν(NH)	4.44 (br)	$ReNH_2$	A_2B	δ_A = 114.7
	3285m		3.36 (br)	NH		δ_B = 113.3
	3213w		4.13 (m)	CH_2		J_{AB} = 49
	1982s	ν(CO)	2.59 (d, $J_{H,H}$ = 6)	CH_3N		
	1902s		1.38 (t)	CH_3		
			1.34 (t)			
$[Re(NH_2NH_2)(CO)_2\{PPh(OEt)_2\}_3]BPh_4$ (**3a**)	3357w	ν(NH)	3.55 (br. m)	$ReNH_2$	AB_2	δ_A = 139.3
	3298m		3.90 (m)	CH_2		δ_B = 136.4
	3262w		2.71 (br)	NH_2		J_{AB} = 35
	3219w		1.35 (t)	CH_3		
	1999s	ν(CO)	1.33 (t)			
	1905s		1.31 (t)			
$[Re(CH_3NHNH_2)(CO)_2\{PPh(OEt)_2\}_3]BPh_4$ (**3b**)	3335w	ν(NH)	3.27 (br. m)	$ReNH_2$	AB_2	δ_A = 139.4
	3289w		3.93 (m)	CH_2		δ_B = 137.1
	3276m		2.27 (m)	NH		J_{AB} = 35
	1989s	ν(CO)	1.79 (d, $J_{H,H}$ = 6)	CH_3N		
	1905s		1.38 (t)	CH_3		
			1.32 (t)			
$[Re(C_6H_5NHNH_2)(CO)_2\{PPh(OEt)_2\}_3]BPh_4$ (**3c**)	3354w	ν(NH)	4.87 (br. t)	NH	AB_2	δ_A = 139.9
	3268m		4.04 (br. m)	$ReNH_2$		δ_B = 136.6
	1982s	ν(CO)	3.88 (m)	CH_2		J_{AB} = 35
	1905s		1.31 (t)	CH_3		
	1617m	δ(NH_2)	1.30 (t)			
			1.27 (t)			
$[Re(4\text{-}NO_2C_6H_4NHNH_2)(CO)_2\{PPh(OEt)_2\}_3]BPh_4$ (**3d**)	3295m	ν(NH)	6.13 (m)	$ReNH_2$	AB_2	δ_A = 144.4
	3276w		6.10 (m)	NH		δ_B = 144.1
	1986s	ν(CO)	4.10−3.80 (m)	CH_2		J_{AB} = 40
	1894s		1.39 (t)	CH_3		
			1.32 (t)			
			1.25 (t)			
$[Re\{(CH_3)_2NNH_2\}(CO)_2\{PPh(OEt)_2\}_3]BPh_4$ (**3e**)	3299w	ν(NH)	4.05−3.80 (m)	CH_2	AB_2	δ_A = 138.7
	3262w		3.74 (m)	$ReNH_2$		δ_B = 135.1
	1980s	ν(CO)	2.05 (s)	$(CH_3)_2N$		J_{AB} = 38
	1868s		1.37 (t)	CH_3		
			1.35 (t)			
			1.28 (t)			
$[Re(NH_2NH_2)(CO)_2(PPh_2OEt)_3]BPh_4$ (**4a**)	3358m	ν(NH)	3.69 (br. m)	$ReNH_2$	AB_2	δ_A = 113.4
	3290m		3.60−3.30 (m)	CH_2		δ_B = 109.1
	3271w		2.60 (br. t)	NH_2		J_{AB} = 30
	3224w		0.99 (t)	CH_3		
	1970s	ν(CO)	0.63 (t)			
	1872s					
$[Re(CH_3NHNH_2)(CO)_2(PPh_2OEt)_3]BPh_4$ (**4b**)	3332m	ν(NH)	3.80−3.15 (m)	CH_2	AB_2	δ_A = 113.7
	3262m		2.97 (m)	$ReNH_2$		δ_B = 109.4
	1970s	ν(CO)	2.04 (m)	NH		J_{AB} = 30
	1881s		1.61 (d, $J_{H,H}$ = 6)	CH_3N		
			0.97 (t)	CH_3		
			0.62 (t)			

 © 2003 Wiley-VCH Verlag GmbH & Co. KGaA, Weinheim

Table 1 *(Continued)*

Compound	IR[a] $\tilde{\nu}$, cm^{-1}	Assgnt	^1H NMR[b][c] δ (*J*/Hz)	Assgnt	Spin system	$^{31}P\{^1H\}$ NMR[b] [d] δ (*J*/Hz)
$[Re(NH_2NH_2)(CO)_3\{P(OEt)_3\}_2]BPh_4$ (**5a**)	3347w	ν(NH)	4.11 (m)	CH_2	A_2	110.9 (s)
	3261m		3.47 (br. m)	$ReNH_2$		111.3 (s)[f]
	3223w		2.83 (br. m)	NH_2		
	2076m	ν(CO)	1.38 (t)	CH_3		
	1971s					
	1947s					
	1612m	$\delta(NH_2)$				
$[Re(NH_2NH_2)(CO)_3\{PPh(OEt)_2\}_2]BPh_4$ (**6a**)	3348m	ν(NH)	3.97 (m)	CH_2	A_2	132.3 (s)
	3287m		3.22 (br. m)	$ReNH_2$		
	3268w		2.57 (br. t)	NH_2		
	3219m		1.38 (t)	CH_3		
	2072w	ν(CO)				
	1968s					
	1944s					
	1624m	$\delta(NH_2)$				
$[Re(4\text{-}NO_2C_6H_4NHNH_2)(CO)_3\{PPh(OEt)_2\}_2]BPh_4$ (**6d**)	3285m	ν(NH)	6.30 (m)	NH	A_2	133.0 (s)
	3270sh		6.24 (m)	$ReNH_2$		
	3230w		4.10 (m)	CH_2		
	2084w	ν(CO)	1.42 (t)	CH_3		
	1984s					
	1938s					
$[Re(NH_2NH_2)(CO)_3(PPh_2OEt)_2]BPh_4$ (**7a**)	3354m	ν(NH)	3.61 (m)	CH_2	A_2	107.1 (s)
	3281w		3.43 (br. m)	$ReNH_2$		
	3267m		2.67 (br. t)	NH_2		
	3217w		1.16 (t)	CH_3		
	2075w	ν(CO)				
	1970s					
	1933s					
$[Re(CH_3NHNH_2)(CO)_3(PPh_2OEt)_2]BPh_4$ (**7b**)	3322w	ν(NH)	3.76 (br. m)	$ReNH_2$	A_2	109.0 (s)
	3263m		3.68 (m)	CH_2		
	2076m	ν(CO)	2.77 (m)	NH		
	1969s		1.97 (d, $J_{H,H}$ = 6)	CH_3N		
	1926s		1.21 (t)	CH_3		
$[Re(NH_2NH_2)(CO)_4(PPh_2OEt)]BPh_4$ (**8a**)	3328w	ν(NH)	3.58 (qnt)	CH_2	A	102.9 (s)
	3282w		2.31 (m)	$ReNH_2$		
	3267w		1.94 (br. t)	NH_2		
	3202m		1.18 (t)	CH_3		
	2113m	ν(CO)				
	2024sh					
	2009s					
	1975s					
	1614m	$\delta(NH_2)$				
$[Re(NH{=}NH)(CO)\{P(OEt)_3\}_4]BPh_4$ (**9a**)	1887s	ν(CO)	A_4XY spin syst.	NH=NH	A_4	123.6 (s)
			δ_X = 16.70	ReNH		123.4 (s)[f]
			δ_Y = 15.84	N=NH		
			J_{XY} = 33.0	CH_2		
			J_{AX} = 1.26	CH_3		
			J_{AY} = 2.86			
			4.06 (m)			
			1.32 (t)			
$[Re(C_6H_5N{=}NH)(CO)\{P(OEt)_3\}_4]BPh_4$ (**9c**)	1899s	ν(CO)	14.39 (qnt, J_{PH} = 4)	NH	A_4	116.8 (s)
			4.08 (m)	CH_2		
			1.27 (t)	CH_3		
$[Re(CH_3N{=}NH)(CO)_2\{P(OEt)_3\}_3]BPh_4$ (**10b**)[g]	1992s	ν(CO)	15.86 (br. s)	ReNH	A_2B[f]	δ_A = 114.1
	1911s		4.10 (m)	CH_2		δ_B = 111.3
			4.44 (d)	$=NCH_3$		J_{AB} = 48.3
			1.36 (t)	CH_3		
$[Re(\eta^1\text{-}NH{=}CH_2)(CO)_2\{P(OEt)_3\}_3]BPh_4$ (**10*b**)[h]	2002s	ν(CO)	13.82 (br. s)	ReNH	A_2B[f]	δ_A = 120.9
	1915s		4.05 (m)	CH_2		δ_B = 118.7
			3.75 (q)	$N=CH_2$		J_{AB} = 47.8
			1.31 (t)	CH_3		

 © 2003 Wiley-VCH Verlag GmbH & Co. KGaA, Weinheim

Table 1 *(Continued)*

Compound	IR[a] ν̃, cm^{-1}	Assgnt	^1H NMR[b][c] δ (*J*/Hz)	Assgnt	Spin system	$^{31}P\{^1H\}$ NMR[b] [d] δ (*J*/Hz)
$[Re(NH{=}NH)(CO)_2\{PPh(OEt)_2\}_3]BPh_4$ (**11a**)	1998s 1906s	ν(CO)	A_2B_2XY spin syst. δ_X = 16.07 δ_Y = 15.28 J_{XY} = 33.3 J_{AX} = 2.15 J_{AY} = 3.15 J_{BX} = 1.15 J_{BY} = 1.45 3.92 (m) 1.38 (t) 1.35 (t) 1.33 (t)	NH=NH ReNH N=NH CH_2 CH_3	A_2B	δ_A = 142.8 δ_B = 140.0 J_{AB} = 35
$[Re(CH_3N{=}NH)(CO)_2\{PPh(OEt)_2\}_3]BPh_4$ (**11b**) and $[Re(\eta^1\text{-}NH{=}CH_2)(CO)_2\{PPh(OEt)_2\}_3]BPh_4$ (**11*b**)	1992s 1911s	ν(CO)	15.94 (br. s) 12.08 (br. s) 4.29 (d) 3.90 (m) 3.70 (m) 1.35 (m)	N=NH C=NH $=NCH_3$ CH_2 $N{=}CH_2$ CH_3	AB_2 AB_2	142−140 (m) 135−132 (m)
$[Re(C_6H_5N{=}NH)(CO)_2\{PPh(OEt)_2\}_3]BPh_4$ (**11c**)	1970s 1887s	ν(CO)	12.22 (d) 3.35 (m) 0.84 (t) 0.67 (t)	NH CH_2 CH_3	AB_2	δ_A = 113.2 δ_B = 108.6 J_{AB} = 28
$[Re(NH{=}NH)(CO)_2(PPh_2OEt)_3]BPh_4$ (**12a**)	1972s 1887s	ν(CO)	AB_2XY spin syst. δ_X = 15.31 δ_Y = 14.42 J_{XY} = 33.5 J_{AX} = 2.38 J_{AY} = 3.74 J_{BX} = 1.16 J_{BY} = 1.88 3.45 (m) 0.99 (t) 0.64 (t)	NH=NH ReNH N=NH CH_2 CH_3	AB_2	δ_A = 113.5 δ_B = 109.1 J_{AB} = 30
$[Re(NH{=}NH)(CO)_3\{PPh(OEt)_2\}_2]BPh_4$ (**13a**)	2071w 1969s 1944s	ν(CO)	A_2XY spin syst. δ_X = 13.03 δ_Y = 11.89 J_{XY} = 26.5 J_{AX} = 2.4 J_{AY} = 1.3 3.88 (m) 1.30 (t)	NH=NH ReNH N=NH CH_2 CH_3	A_2	131.0 (s) 131.6 (s)[f]
$[Re(4\text{-}NO_2C_6H_4N{=}NH)(CO)_3\{PPh\{OEt)_2\}_2]BPh_4$ (**13d**)	2076m 1982s 1951s	ν(CO)	13.14 (br) 4.10 (m) 1.43 (t)	NH CH_2 CH_3	A_2	133.5 (s)
$[Re(NH{=}NH)(CO)_3(PPh_2OEt)_2]BPh_4$ (**14a**)	2069w 1967s 1940s	ν(CO)	A_2XY spin syst. δ_X = 13.16 δ_Y = 12.40 J_{XY} = 26.6 J_{AX} = 2.20 J_{AY} = 1.04 3.48 (m) 1.14 (t)	NH=NH ReNH N=NH CH_2 CH_3	A_2	110.8 (s)
$[Re(CH_3NH_2)(CO)_2\{P(OEt)_3\}_3]BPh_4$ (**15**)[i]	3329m 3283m 2005s 1894s	ν(NH) ν(CO)	4.04 (m) 2.73 (t) 2.65 (br) 1.37 (t) 1.32 (t)	CH_2 CH_3N NH_2 CH_3	A_2B	δ_A = 172.1 δ_B = 171.3 J_{AB} = 49

[a] In KBr. [b] In CD_2Cl_2 at 25 °C, unless otherwise noted. [c] Phenyl proton resonances are omitted. [d] Positive shift downfield from 85% H_3PO_4. [e] $^{13}C\{^1H\}$ NMR (**2b**): δ = 194.2 (m) CO, 165−122 (m) Ph, 62.9 (m) CH_2, 44.6 (s) CH_3N, 16.3 (m) CH_3 ppm. [f] At −80 °C. [g] $^{13}C\{^1H\}$ NMR (**10b**): δ = 196.2 (m) CO, 165−120 (m) Ph, 71.7 (s) $CH_3N{=}$, 62.7 (m) CH_2, 16.3 (m) CH_3 ppm. [h] $^{13}C\{^1H\}$ NMR (**10* b**): δ = 194.7 (m) CO, 165−122 (m) Ph, 67.8 (s) $N{=}CH_2$, 62.4 (m) CH_2, 16.1 (m) CH_3 ppm. [i] $^{13}C\{^1H\}$ NMR (**15**): δ = 194.2 (m) CO, 165−122 (m) Ph, 62.8 (m) CH_2, 38.5 (br. s) CH_3N, 16.3 (s) CH_3 ppm.

 © 2003 Wiley-VCH Verlag GmbH & Co. KGaA, Weinheim

mulation and a geometry in solution can also be established from the IR and NMR spectroscopic data.

Diagnostic evidence for the presence of the NH=NH ligand are the ^{1}H NMR spectra, which show a multiplet of the type shown in Figure 1 in the high-frequency region, which can reasonably be attributed to the H1 and H2 protons of the diazene ligand coupled to the phosphorus nucleus of the phosphane. This multiplet, in fact, can easily be simulated by using A_2XY, AB_2XY or A_4XY models (X, Y = H), with the parameters reported in Table 1. The value of $^3J_{H,H}$ was found to fall in the range 35−27 Hz, suggesting a probable *trans*-NH=NH geometry of the ligand.[16a]

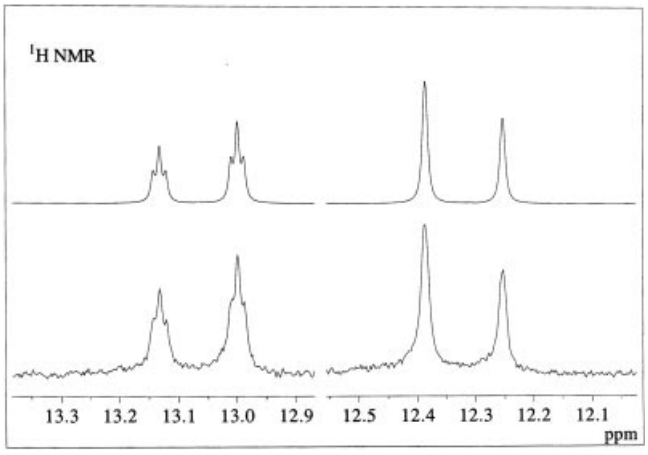

Figure 1. Observed (bottom) and calculated (top) ^{1}H NMR spectrum in the diazene region of $[Re(NH=NH)(CO)_3(PPh_2OEt)_2]BPh_4$ (**14a**), in CD_2Cl_2 at 25 °C; the simulated spectrum was obtained using the parameters reported in Table 1

IR and NMR spectroscopic data support the geometry shown in Scheme 2 for the diazene complexes **9**−**14**, which proves to be the same as that of the related hydrazine precursors. The oxidation of the NH_2NH_2 ligand does not change the geometry of the complexes, and a *trans* geometry is proposed for the monocarbonyl complex **9a** on the basis of the sharp singlet present in the ^{31}P NMR spectrum. A *fac* structure is proposed for the dicarbonyl complexes **11a** and **12a**, as their IR spectra show two ν(CO) bands, while an AB_2 multiplet appears in the ^{31}P NMR spectra. Finally, the presence of three ν(CO) bands, one medium and two strong, in the IR spectra of the tricarbonyl complexes **13a** and **14a**, and only one sharp singlet in the ^{31}P NMR spectra, suggest a *mer-trans* geometry for the complexes.

The stabilization of the very reactive molecule NH=NH by coordination to a transition metal has been achieved in a few cases, mainly in bimetallic complexes containing a μ-NH=NH ligand.[15] Stable derivatives containing a monodentate diazene have been reported,[16] but they are rather rare and include only one example for rhenium.[17] The use of a mixed-ligand phosphite-carbonyl $Re(CO)_nP_{5-n}$ fragment allows new examples of the stabilization of monodentate diazene to be achieved. It should be noted that the related manganese complexes $[Mn(NH_2NH_2)(CO)_nP_{5-n}]BPh_4$ also react with $Pb(OAc)_4$,[11] but give only thermally unstable diazene complexes, which cannot be isolated.

The arylhydrazine complexes $[Re(ArNHNH_2)(CO)_nP_{5-n}]BPh_4$ also react with $Pb(OAc)_4$ to give the corresponding aryldiazene complexes $[Re(ArN=NH)(CO)_nP_{5-n}]BPh_4$, which were isolated and characterised (Scheme 3).

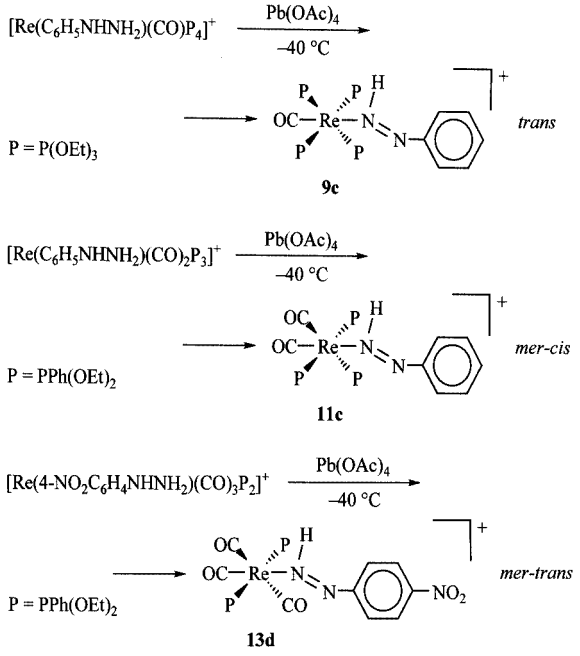

Scheme 3

These complexes are yellow or orange solids that are stable in air and in solution in polar organic solvents, where they behave as 1:1 electrolytes.[14] Analytical and spectroscopic data (Table 1) confirm the proposed formulation. Furthermore, the spectroscopic data of complex **9c** are identical to those of samples we have previously prepared by reacting the $ReH(CO)P_4$ hydride with a phenyldiazonium cation;[18] this feature strongly supports the proposed formulation. Moreover, this result highlights that stable aryldiazene complexes of rhenium can be prepared following two different methods, which involve the oxidation of a coordinated arylhydrazine, in one case, and the insertion of an aryldiazonium cation into the Re−H bond of the appropriate hydride complex, in the other.

The presence of the aryldiazene ligand in complexes **9c**, **11c** and **13d** is confirmed by the ^{1}H NMR spectra, which show the characteristic high-frequency signal of the ArN=NH ligand. The IR and NMR spectra also allow a geometry in solution to be established (Scheme 3). Apart from the *trans* geometry of the monocarbonyl complex **9c**,[18] a *mer-cis* arrangement of the ligands, like that of the related compound $[Re(C_6H_5N=NH)(CO)_2(PPh_2OEt)_3]BPh_4$,[18] can be proposed for the carbonyl complex **11c**. The IR spectra, in fact, show two ν(CO) bands, while an AB_2 multiplet is observed in the ^{31}P NMR spectrum.

 © 2003 Wiley-VCH Verlag GmbH & Co. KGaA, Weinheim

In the temperature range between +20 and −80 °C the ^{31}P NMR spectrum of the tricarbonyl compound **13d** appears as a sharp singlet, while the IR spectrum shows one medium-intensity and two strong bands in the ν(CO) region. On this basis, a *mer-trans* geometry for the complex can be proposed.

Surprisingly, the reaction of methylhydrazine complexes with an equimolar amount of $Pb(OAc)_4$ gives a mixture of methyldiazene $[Re(CH_3N{=}NH)(CO)_nP_{5-n}]^+$ and methyleneimine $[Re(\eta^1\text{-}NH{=}CH_2)(CO)_nP_{5-n}]^+$ derivatives, which were separated and characterised (Scheme 4).

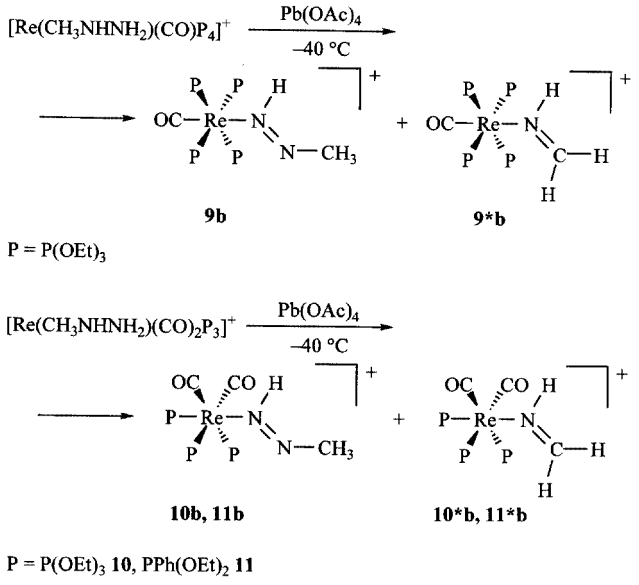

Scheme 4

The two monocarbonyl complexes **9b** and **9*b** were characterised not only spectroscopically (IR and NMR spectroscopic data) but also by two X-ray crystal structure determinations. These structures were reported in a preliminary communication[12] and will not be discussed further.

The dicarbonyl complexes **10b** and **10*b**, containing the $P(OEt)_3$ ligand, can be separated by fractional crystallisation or by the Pasteur method, obtaining the methyldiazene (**10b**) and the methyleneimine (**10*b**) species as white microcrystalline solids, while the related $PPh(OEt)_2$ derivatives **11b** and **11*b** were characterised spectroscopically as a mixture of the two species. The presence of the $CH_2{=}NH$ ligand in **10*b** is confirmed by the ^1H NMR spectrum, which shows the NH signal at δ = 13.82 ppm and the two inequivalent CH_2 protons as an AB quadruplet at δ = 3.75 ppm. The IR spectra show two strong bands at 2002 and 1915 cm^{-1} attributed to two CO ligands in a mutually *cis* position. These two carbonyls are also magnetically equivalent, since the ^{13}C NMR spectrum shows only one multiplet at δ = 194.7 ppm for the carbonyl carbon atoms. A singlet at δ = 67.8 ppm is also present in the ^{13}C NMR spectrum and is attributed to the methylene carbon atom of the $CH_2{=}NH$ ligand. A ^1H, ^{13}C HMQC experiment correlates this signal with that at δ = 3.75 ppm for the $=CH_2$ protons, in agreement with the proposed assignment. In the temperature range between +20 and −80 °C the ^{31}P NMR spectrum appears as an A_2B multiplet indicating that two of the phosphites are magnetically equivalent and different from the third. On the basis of these data a *fac* geometry (Scheme 4) can reasonably be proposed.

A similar *fac* geometry can also be proposed for the methyldiazene derivative **10b** on the basis of the presence of two ν(CO) bands in the IR spectrum and only one multiplet for the carbonyl carbon atoms at δ = 196.2 ppm in the ^{13}C NMR spectrum, indicating the magnetic equivalence of the two *cis* carbonyl ligands. A singlet at δ = 71.7 ppm is also present in the ^{13}C NMR spectrum; it was attributed, with the help of an HMQC experiment, to the methyl carbon atom of the $CH_3N{=}NH$ ligand. The presence of this ligand is confirmed by the ^1H NMR spectrum, which shows the characteristic diazene signal at δ = 15.86 ppm and the methyl protons as a doublet at δ = 4.44 ppm. The ^{31}P NMR spectrum appears as an A_2B multiplet, in agreement with the proposed geometry.

The results on the oxidation of methylhydrazine complexes seem to indicate that the formation of an η^1-NH=CH_2 ligand is general for the $[Re(CO)_nP_{5-n}]$ [n = 1, 2; P = $P(OEt)_3$, $PPh(OEt)_2$] fragments containing the CH_3NHNH_2 ligand, but appears to be specific for $Pb(OAc)_4$, as attempts to carry out the reaction with other oxidants like MnO_2 or H_2O_2 were unsuccessful. Furthermore, while oxidation of a coordinated hydrazine to the related diazene is a known reaction, the formation of the methyleneimine molecule in the reaction of methylhydrazine with $Pb(OAc)_4$ is completely new and involves the cleavage of the N−N bond.[19] Finally, it is worth noting that methyleneimine is a very reactive molecule which has never been isolated since it is unstable above −80 °C in the free state.[20] It has been detected in outer space,[21] and has been proposed as a possible precursor[22] of the simplest α-amino acid glycine. As a ligand, it has been found in only one case, through π-coordination to an osmium centre,[23] and no other report has been found on this molecule, which displays a simple constitution and structure and whose chemical properties are still unknown.

We have also investigated the products of the oxidation of methylhydrazine complexes in order to establish a stoichiometry and/or a possible reaction path. In the reaction mixture we have unambiguously identified, beside the methyldiazene complexes **9b** and **10b** and the methyleneimine complexes **9*b** and **10b***, only acetic acid, dinitrogen and traces of NH_3. Both the NMR spectra and GC analysis of the reaction mixture also revealed the presence of other species, but all were present in very small amounts and were not identified.

The oxidation of methylhydrazine to methyldiazene by $Pb(OAc)_4$ probably proceeds to give acetic acid and lead(II) acetate (Scheme 5) and should involve the loss of two hydrogen atoms and two electrons with cleavage of two N−H bonds to give the final methyldiazene species. The formation of the coordinated methyleneimine, however, seems to be much more complicated and should involve the cleavage

 © 2003 Wiley-VCH Verlag GmbH & Co. KGaA, Weinheim

of one N−N and one C−H bond (Scheme 6), with the loss of fragments such as H or NH_2 to give the final species. However, the lack of identified reaction products, as well as of any intermediates, does not allow us to determinate either the stoichiometry or to propose a path for the reaction.

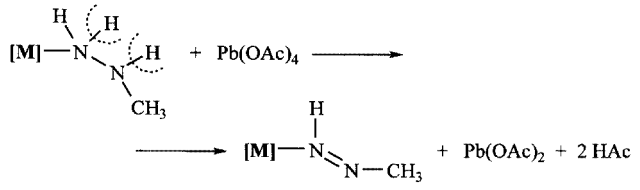

Scheme 5

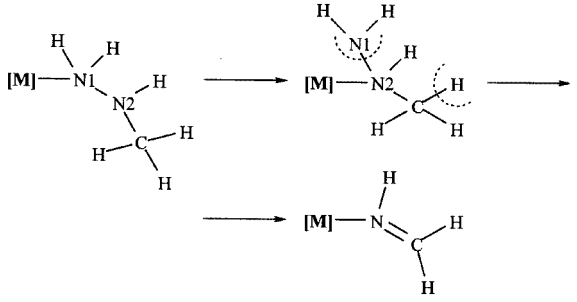

Scheme 6

In light of the reagent and the η^1-NH=CH_2 species formed, an N1 to N2 shift in the coordination of the methylhydrazine followed by N−N and C−H bond cleavage with loss of NH_3 and formation of the methyleneimine ligand may be hypothesized. The presence of only traces of NH_3 in the reaction mixture, however, seems to exclude such a mechanism in which the $Pb(OAc)_4$ does not behave as an oxidant, but only as a catalyst.

Further studies on other metal complexes will, therefore, be required to shed light on the mechanism of this new reaction.

The stabilization of the methyleneimine molecule by coordination to appropriate metal fragments prompted us to attempt to prepare similar η^1-NH=CH_2 complexes following a different method involving, for example, the reaction of a methylamine (CH_3NH_2) derivative with $Pb(OAc)_4$. The synthesis of the precursor complex $[Re(CH_3NH_2)(CO)_2\{P(OEt)_3\}_3]BPh_4$ (**15**) was achieved by reacting the hydride complex $[ReH(CO)_2\{P(OEt)_3\}_3]$ first with triflic acid and then with an excess of CH_3NH_2, as shown in Scheme 7.

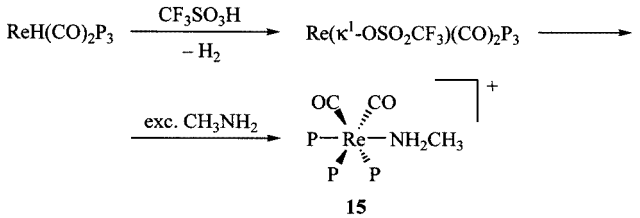

Scheme 7. P = $P(OEt)_3$

The complex was isolated as its BPh_4 salt and characterised in the usual way (Table 1). The IR spectrum shows two strong ν(CO) bands at 2005 and 1894 cm^{-1} due to two carbonyls in a mutually *cis* position. Two absorptions of medium intensity are also present at 3329 and 3283 cm^{-1}, attributed to ν(NH) of the methylamine ligand. The presence of this ligand is confirmed by the ^1H NMR spectrum, which shows a triplet at δ = 2.73 ppm for the CH_3 group and a broad signal at δ = 2.65 ppm for the NH_2 group of the CH_3NH_2 ligand. The ^{13}C NMR spectrum further supports the proposed formulation for the complex and indicates that the two CO ligands are magnetically equivalent, showing only one multiplet at δ = 194.2 ppm for the carbonyl carbon atom. In the temperature range between +20 and −80 °C, the ^{31}P NMR spectrum appears as an A_2B multiplet indicating that two of the phosphanes are magnetically equivalent and different from the third. On the basis of these data, a *fac* geometry can be proposed for our methylamine complex **15**.

The reaction of this complex with $Pb(OAc)_4$ was studied extensively in an attempt to prepare a methyleneimine complex by selective oxidation of the CH_3NH_2 ligand. Unfortunately, the reaction does not proceed under any conditions [at −40 or at +20 °C, with an equimolar or an excess amount of $Pb(OAc)_4$; Scheme 8], and the starting amine complex was recovered almost quantitatively. The coordinated methylamine does not react with $Pb(OAc)_4$ and this reaction, therefore, cannot be used to prepare methyleneimine complexes. Until a new method can be found, only the reaction of coordinated methylhydrazine can give a stable complex containing methyleneimine as a unidentate ligand, even though it is formed as a mixture.

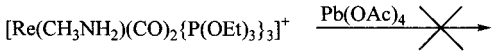

Scheme 8

Reduction Reactions

The hydrazine complexes $[Re(NH_2NH_2)(CO)_2P_3]BPh_4$ [P = $PPh(OEt)_2$ and PPh_2OEt] are reduced by zinc amalgam in tetrahydrofuran (THF) in the presence of 2,6-lutidine hydrochloride (Lu·HCl) to give NH_3 in about a 20−25% yield (Table 2). The reaction was carried out at room temperature under argon and found to be relatively slow, with the formation of NH_3 in appreciable amounts after 24 h. The conversion is, however, rather low and the addition of free NH_2NH_2 does not increase the conversion into NH_3, thus excluding any catalytic involvement of the rhenium complexes. Also, the related 1,2-diazene complex $[Re(NH{=}NH)(CO)_2\{PPh(OEt)_2\}_3]BPh_4$ is reduced by zinc amalgam to give NH_3 but, as expected, with a lower yield (about 7%) than the hydrazine precursors. Instead, a relatively high conversion (about 27%) was observed with the methylhydrazine complex $[Re(CH_3NHNH_2)(CO)_2\{PPh(OEt)_2\}_3]BPh_4$ and this result may be connected with the

 © 2003 Wiley-VCH Verlag GmbH & Co. KGaA, Weinheim

Table 2. Reduction reactions of hydrazine, methylhydrazine and diazene complexes to give ammonia

Compd	Mol	NH_3[a][b] (mol)[a]	Time (h)	Conv. (%)
$[Re(NH_2NH_2)(CO)_2\{PPh(OEt)_2\}_3]BPh_4$ (**3a**)	$1.82\cdot10^{-4}$	$1.81\cdot10^{-5}$	23	5
$[Re(NH_2NH_2)(CO)_2\{PPh(OEt)_2\}_3]BPh_4$ (**3a**)	$9.25\cdot10^{-5}$	$3.71\cdot10^{-5}$	48	20
$[Re(NH_2NH_2)(CO)_2\{PPh_2OEt\}_3]BPh_4$ (**4a**)	$8.87\cdot10^{-5}$	$4.41\cdot10^{-5}$	72	25
$[Re(CH_3NHNH_2)(CO)_2\{PPh(OEt)_2\}_3]BPh_4$ (**3b**)	$1.20\cdot10^{-4}$	$3.18\cdot10^{-5}$	26	27
$[Re(NH{=}NH)(CO)_2\{PPh(OEt)_2\}_3]BPh_4$ (**11a**)	$7.17\cdot10^{-5}$	$0.97\cdot10^{-5}$	48	7
$[Re(NH_2NH_2)(CO)_2\{PPh(OEt)_2\}_3]BPh_4$ (**3a**)[c]	$9.33\cdot10^{-5}$	$2.26\cdot10^{-4}$	96	12
Zn(Hg)/Lut·HCl		$2.6\cdot10^{-6}$	24	
NH_2NH_2/Zn(Hg)/Lut·HCl	$1.02\cdot10^{-4}$ [d]	$3.1\cdot10^{-6}$	24	1.5

[a] At 25 °C. [b] Mean value from two or three experiments. [c] Containing added NH_2NH_2 ($9.4\cdot10^{-4}$ mol, ratio 10:1). [d] Mol of NH_2NH_2.

observed easy cleavage of the N−N bond of methylhydrazine bonded to $[Re(CO)_2P_3]$ or $[Re(CO)P_4]$ fragments. In the presence of $Pb(OAc)_4$, in fact, the methyleneimine species $[Re]\eta^1$-NH=CH_2 is formed, whereas ammonia is obtained with Zn amalgam and Lut·HCl; in both cases cleavage of the N−N bond of the coordinated methylhydrazine takes place.

Although these data must be considered as preliminary results, they indicate that both hydrazine and diazene molecules bonded to the $[Re(CO)_2P_3]$ fragment can be reduced to ammonia by zinc amalgam, and this seems to be an interesting observation in organometallic diazo chemistry.

Conclusions

In this contribution we have shown that a series of hydrazine complexes of rhenium of the type $[Re(RNHNH_2)(CO)_nP_{5-n}]BPh_4$ can easily be prepared from precursor $ReH(CO)_nP_{5-n}$ hydrides. Among the properties shown by these complexes we can highlight the reaction of the methylhydrazine species with $Pb(OAc)_4$, which gives the unprecedented methyleneimine derivative $[Re(\eta^1\text{-}NH{=}CH_2)(CO)_nP_{5-n}]BPh_4$ as well as the methyldiazene derivative $[Re(CH_3N{=}NH)(CO)_nP_{5-n}]BPh_4$. Also, 1,2-diazene can be stabilized by the $Re(CO)_nP_{5-n}$ fragment, allowing stable $[Re(NH{=}NH)(CO)_nP_{5-n}]BPh_4$ complexes to be obtained through the selective oxidation of the hydrazine precursors with $Pb(OAc)_4$. Finally, reduction of hydrazine and diazene complexes with zinc amalgam in the presence of Lu·HCl was also tested and found to give NH_3 in low yield.

Experimental Section

General: All synthetic work was carried out under an inert atmosphere (Ar, N_2) using standard Schlenk techniques or a Vacuum Atmosphere dry-box. Once isolated, the complexes were found to be relatively stable in air, but were stored under an inert atmosphere at −25 °C. All solvents were dried over appropriate drying agents, degassed on a vacuum line and distilled into vacuum-tight storage flasks. $Re_2(CO)_8$ was a Pressure Chem. (USA) product, and used as received. Triethylphosphite $P(OEt)_3$ (Aldrich) was purified by distillation under nitrogen, while $PPh(OEt)_2$ and PPh_2OEt were prepared by the method of Rabinowitz and Pellon.[24] The hydrazines CH_3NHNH_2, $C_6H_5NHNH_2$, 4-$NO_2C_6H_4NHNH_2$, and $(CH_3)_2NNH_2$ are Aldrich products and were used as received. High purity (99.99%) $Pb(OAc)_4$ is an Aldrich product was used as received. Hydrazine (NH_2NH_2) was prepared by decomposition of hydrazine cyanurate (Fluka) following the reported method.[25] Other reagents were purchased from commercial sources in the highest available purity and used as received. Infrared spectra were recorded on a Nicolet Magna 750 FT-IR spectrophotometer. NMR spectra (^1H, ^{31}P, ^{13}C) were obtained on Bruker AC200 or Bruker AVANCE 300 spectrometers at temperatures varying between −90 and +30 °C, unless otherwise noted. ^1H spectra are referenced to internal tetramethylsilane, while $^{31}P\{^1H\}$ chemical shifts are reported with respect to 85% H_3PO_4, with downfield shifts considered positive. The SwaN-MR software package[26] was used in treating the NMR spectroscopic data. The conductivities of 10^{-3} M solutions of the complexes in CH_3NO_2 at 25 °C were measured with a Radiometer CDM 83 instrument.

Synthesis of Complexes: The hydrides $[ReH(CO)_nP_{5-n}]$ [n = 1−4; P = $P(OEt)_3$, $PPh(OEt)_2$, PPh_2OEt] were prepared following the method reported previously.[13]

$[Re(NH_2NH_2)(CO)\{P(OEt)_3\}_4]BPh_4$ (1a) and $[Re\{(CH_3)_2NNH_2\}(CO)\{P(OEt)_3\}_4]BPh_4$ (1e): An equimolar amount of CF_3SO_3H (0.2 mmol, 18 μL) was added to a solution of the hydride $[ReH(CO)\{P(OEt)_3\}_4]$ (0.2 mmol, 196 mg) in 8 mL of CH_2Cl_2 cooled to −196 °C, and the reaction mixture warmed to room temperature and stirred for about 1 h. An excess of the appropriate hydrazine (0.6 mmol) was added to the resulting solution which was stirred for a time varying between 3 (**1a**) and 24 (**1e**) h and then the solvent was removed under reduced pressure. The oil obtained was triturated with 3 mL of ethanol containing an excess of $NaBPh_4$ (0.4 mmol, 137 mg). Upon cooling of the resulting solution to −25 °C, a white solid separated out which was filtered off and recrystallised from CH_2Cl_2 (3 mL) and ethanol (3 mL); yield between 80% (**1a**) and 15% (**1e**).

1a: $C_{49}H_{84}BN_2O_{13}P_4Re$ (1230.11): calcd. C 47.84, H 6.88, N 2.28; found C 47.58, H 6.94, N 2.20. Λ_M = 55.4 Ω^{-1} mol^{-1} cm^2

1e: $C_{51}H_{88}BN_2O_{13}P_4Re$ (1258.17): calcd. C 48.69, H 7.05, N 2.23; found C 48.92, H 7.24, N 2.08. Λ_M = 58.6 Ω^{-1} mol^{-1} cm^2.

$[Re(C_6H_5NHNH_2)(CO)\{P(OEt)_3\}_4]BPh_4$ (1c): An equimolar amount of $HBF_4\cdot Et_2O$ (0.2 mmol, 28 μL) was added to a solution of the hydride $[ReH(CO)\{P(OEt)_3\}_4]$ (0.2 mmol, 176 mg) in 5 mL of CH_2Cl_2 cooled to −196 °C, and the reaction mixture warmed to room temperature and stirred for 1 h. An excess of $C_6H_5NHNH_2$ (0.6 mmol, 60 μL) was added to the resulting solution, which was stirred for about 150 min, and then the solvent was removed under reduced pressure. The oil obtained was treated with ethanol (3 mL), and then an excess of $NaBPh_4$ (0.4 mmol, 137 mg) in 3 mL of etha-

 © 2003 Wiley-VCH Verlag GmbH & Co. KGaA, Weinheim

nol was added. A white solid slowly separated out which was filtered off and recrystallised from CH_2Cl_2 (2 mL) and ethanol (2 mL); yield ≥40%. $C_{55}H_{88}BN_2O_{13}P_4Re$ (1306.21): calcd. C 50.57, H 6.79, N 2.14; found C 50.49, H 6.87, N 2.10. Λ_M = 55.8 Ω^{-1} mol^{-1} cm^2.

[Re(CH$_3$NHNH$_2$)(CO)$_2${P(OEt)$_3$}$_3$]BPh$_4$ (2b): An equimolar amount of $HBF_4{\cdot}Et_2O$ (0.2 mmol, 28 μL) was added to a solution of [ReH(CO)$_2${P(OEt)$_3$}$_3$] (0.2 mmol, 143 mg) in 5 mL of CH_2Cl_2 cooled to −196 °C, and the reaction mixture warmed to room temperature and stirred for 1 h. An excess of methylhydrazine (0.3 mmol, 16 μL) was added to the resulting solution which was stirred for 3 h and then the solvents evaporated to dryness. The oil obtained was treated with ethanol (2 mL) containing an excess of $NaBPh_4$ (0.4 mmol, 137 mg). Upon cooling the resulting solution to −25 °C a white solid slowly separated out which was filtered off and recrystallised from CH_2Cl_2 (2 mL) and ethanol (2 mL); yield ≥65%. $C_{45}H_{71}BN_2O_{11}P_3Re$ (1105.99): calcd. C 48.87, H 6.47, N 2.53; found C 48.80, H 6.55, N 2.48. Λ_M = 50.8 Ω^{-1} mol^{-1} cm^2.

[Re(RNHNH$_2$)(CO)$_2$P$_3$]BPh$_4$ 3, 4 [R = H a, CH$_3$ b, 4-NO$_2$C$_6$H$_4$ d; P = PPh(OEt)$_2$ 3, PPh$_2$OEt 4]: These complexes were prepared similarly to **1** by reacting the appropriate hydride $ReH(CO)_2P_3$ (0.2 mmol) first with an equimolar amount of CF_3SO_3H and then with an excess (0.6 mmol) of the appropriate hydrazine. The reaction time was 20 h for **3a**, **3b**, **4a** and 24 h for **3d** and **4b**; yields between 60 and 80%.

3a: Yield ≥ 60% $C_{56}H_{69}BN_2O_8P_3Re$ (1188.10): calcd. C 56.61, H 5.85, N 2.36; found C 56.43, H 5.89, N 2.28. Λ_M = 58.9 Ω^{-1} mol^{-1} cm^2.

3b: Yield ≥ 70% $C_{57}H_{71}BN_2O_8P_3Re$ (1202.13): calcd. C 56.95, H 5.95, N 2.33; found C 57.11, H 6.03, N 2.20. Λ_M = 58.1 Ω^{-1} mol^{-1} cm^2.

3d: Yield ≥ 80% $C_{62}H_{72}BN_3O_{10}P_3Re$ (1309.20): calcd. C 56.88, H 5.54, N 3.21; found C 56.95, H 5.62, N 3.17.. Λ_M = 49.3 Ω^{-1} mol^{-1} cm^2.

4a: Yield ≥ 75% $C_{68}H_{69}BN_2O_5P_3Re$ (1284.23): calcd. C 63.60, H 5.42, N 2.18; found C 63.46, H 5.51, N 2.15. Λ_M = 49.4 Ω^{-1} mol^{-1} cm^2.

4b: Yield ≥ 65% $C_{69}H_{71}BN_2O_5P_3Re$ (1298.26): calcd. C 63.84, H 5.51, N 2.16; found C 63.66, H 5.59, N 2.20. Λ_M = 60.0 Ω^{-1} mol^{-1} cm^2.

[Re(C$_6$H$_5$NHNH$_2$)(CO)$_2${PPh(OEt)$_2$}$_3$]BPh$_4$ (3c): This complex was prepared similarly to **2b** by treating [ReH(CO)$_2${PPh(OEt)$_2$}$_3$] (0.2 mmol) first with an equimolar mount of $HBF_4{\cdot}Et_2O$ and then with an excess of $C_6H_5NHNH_2$. The reaction time was 150 min; yield approx. 40%. $C_{62}H_{73}BN_2O_8P_3Re$ (1264.20): calcd. C 58.91, H 5.82, N 2.22; found C 59.05, H 5.90, N 2.27. Λ_M = 51.3 Ω^{-1} mol^{-1} cm^2.

[Re{(CH$_3$)$_2$NNH$_2$)(CO)$_2${PPh(OEt)$_2$}$_3$]BPh$_4$ (3e): This compound was also prepared similarly to complexes **3** and **4** using CF_3SO_3H as the protonating agent, but in this case a large excess of $(CH_3)_2NNH_2$ was used; yield approx. 75%. $C_{58}H_{73}BN_2O_8P_3Re$ (1216.15): calcd. C 57.28, H 6.05, N 2.30; found C 57.37, H 6.12, N 2.28. Λ_M = 49.5 Ω^{-1} mol^{-1} cm^2.

[Re(RNHNH$_2$)(CO)$_3$P$_2$]BPh$_4$ 5−7 [R = H a, CH$_3$ b, 4-NO$_2$C$_6$H$_4$ d; P = P(OEt)$_3$ 5, PPh(OEt)$_2$ 6, PPh$_2$OEt 7]: An equimolar mount of CF_3SO_3H (0.2 mmol, 18 μL) was added to a solution of the appropriate hydride $ReH(CO)_3P_2$ (0.2 mmol) in 7 mL of CH_2Cl_2 cooled to −196 °C, and the reaction mixture warmed to room temperature and stirred for 1 h. An excess of the appropriate hydrazine (0.6 mmol) was added and the resulting solution was stirred for 3 h for **5a**, **6a**, **7a**; 8 h for **6d** and 15 h for **7b**. The solvent was removed under reduced pressure to give a yellow oil, which was triturated with ethanol containing an excess of $NaBPh_4$ (0.4 mmol, 137 mg). Upon cooling of the resulting solution to −25 °C a white solid separated out, which was filtered off and recrystallised from CH_2Cl_2 and ethanol; yield between 55 and 80%.

5a: Yield ≥ 55% $C_{39}H_{54}BN_2O_9P_2Re$ (953.82): calcd. C 49.11, H 5.71, N 2.94; found C 48.94, H 5.80, N 3.02. Λ_M = 56.6 Ω^{-1} mol^{-1} cm^2.

6a: Yield ≥ 65% $C_{48}H_{56}BN_2O_7P_2Re$ (1031.94): calcd. C 55.87, H 5.47, N 2.71; found C 55.74, H 5.55, N 2.79. Λ_M = 54.8 Ω^{-1} mol^{-1} cm^2.

6d: Yield ≥ 80% $C_{53}H_{57}BN_3O_9P_2Re$ (1139.01): calcd. C 55.89, H 5.04, N 3.69; found C 55.71, H 5.18, N 3.59. Λ_M = 51.6 Ω^{-1} mol^{-1} cm^2.

7a: Yield ≥ 60% $C_{55}H_{54}BN_2O_5P_2Re$ (1082.00): calcd. C 61.05, H 5.03, N 2.59; found C 61.23, H 5.15, N 2.68. Λ_M = 60.2 Ω^{-1} mol^{-1} cm^2.

7b: Yield ≥ 70% $C_{56}H_{56}BN_2O_5P_2Re$ (1096.03): calcd. C 61.37, H 5.15, N 2.56; found C 61.19, H 5.25, N 2.62. Λ_M = 57.4 Ω^{-1} mol^{-1} cm^2.

[Re(NH$_2$NH$_2$)(CO)$_4$(PPh$_2$OEt)]BPh$_4$ (8a): This complex was prepared similarly to complexes **5a**, **6a** and **7a**; yield approx. 65%. $C_{42}H_{39}BN_2O_5PRe$ (879.76): calcd. C 57.34, H 4.47, N 3.18; found C 57.13, H 4.50, N 3.10. Λ_M = 57.0 Ω^{-1} mol^{-1} cm^2.

[Re(NH=NH)(CO){P(OEt)$_3$}$_4$]BPh$_4$ (9a): A solid sample of the hydrazine complex [Re(NH$_2$NH$_2$)(CO){P(OEt)$_3$}$_4$]BPh$_4$ (**1a**; 0.1 mmol, 123 mg) was placed in a three-necked 25-mL round-bottomed flask fitted with a solid-addition sidearm containing a slight excess of $Pb(OAc)_4$ (0.12 mmol, 53 mg). Dichloromethane (10 mL) was added, the solution cooled to −40 °C and the $Pb(OAc)_4$ added portionwise over 20−30 min to the cold stirring solution. The solution was then warmed to 0 °C, stirred for 15 min and the solvent removed under reduced pressure. The oil obtained was treated at 0 °C with ethanol (2 mL) containing an excess of $NaBPh_4$ (0.2 mmol, 68 mg) and the white solid separated was filtered off and recrystallised at 0 °C from CH_2Cl_2 (2 mL) and ethanol (2 mL); yield approx. 45%. $C_{49}H_{82}BN_2O_{13}P_4Re$ (1228.10): calcd. C 47.92, H 6.73, N 2.28; found C 48.01, H 6.77, N 2.19. Λ_M = 54.8 Ω^{-1} mol^{-1} cm^2.

[Re(C$_6$H$_5$N=NH)(CO){P(OEt)$_3$}$_4$]BPh$_4$ (9c): This complex was prepared by oxidation of the corresponding hydrazine derivatives with $Pb(OAc)_4$ at low temperature (−40 °C) following the method used for the related 1,2-diazene derivative **9a**; yield approx. 55%. $C_{55}H_{86}BN_2O_{13}P_4Re$ (1304.20): calcd. C 50.65, H 6.65, N 2.15; found C 50.43, H 6.70, N 2.09. Λ_M = 52.8 Ω^{-1} mol^{-1} cm^2.

[Re(CH$_3$N=NH)(CO)$_2${P(OEt)$_3$}$_3$]BPh$_4$ (10b) and [Re(η^1-NH=CH$_2$)(CO)$_2${P(OEt)$_3$}$_3$]BPh$_4$ (10*b): A sample of [Re(CH$_3$NHNH$_2$)(CO)$_2${P(OEt)$_3$}$_3$]BPh$_4$ (**2b**; 200 mg, 0.18 mmol) was placed in a three-necked 25-mL round-bottomed flask fitted with a solid-addition sidearm containing $Pb(OAc)_4$ (0.18 mmol, 80 mg). Dichloromethane (8 mL) was added, the solution cooled to −40 °C and the $Pb(OAc)_4$ added portionwise over 10−20 min to the cold stirring solution. The solution was then warmed to 0 °C, stirred for 10 min, and the solvent removed under reduced pressure. The oil obtained was treated at 0 °C with ethanol (2 mL) containing an excess of $NaBPh_4$ (0.2 mmol, 68 mg). A white solid slowly separated out, which was filtered and crystallised fractionally to separate the two complexes. A typical separation involved the slow cooling from +25 to −25 °C of a saturated solution of the complexes prepared by adding 10 mL of ethanol to the white solid and enough CH_2Cl_2 to obtain a saturated solution at room temperature. The first crystals obtained were **10b**, and the second

 © 2003 Wiley-VCH Verlag GmbH & Co. KGaA, Weinheim

a mixture, which was further recrystallised. Upon further cooling, white microcrystals of **10*b** were obtained. Pure samples of **10b** and **10*b** were also obtained by Pasteur separation of the crystals obtained by cooling a saturated solution of the reaction product in ethanol/CH_2Cl_2; yield: 38% for **10b** and 25% for **10*b**
10b: $C_{45}H_{69}BN_2O_{11}P_3Re$ (1103.98): calcd. C 48.96, H 6.30, N 2.54; found C 49.11, H 6.23, N 2.43. Λ_M = 51.1 Ω^{-1} mol^{-1} cm^2.
10*b: $C_{45}H_{68}BNO_{11}P_3Re$ (1088.96): calcd. C 49.63, H 6.29, N 1.29; found C 49.45, H 6.37, N 1.35. Λ_M = 58.9 Ω^{-1} mol^{-1} cm^2.

[Re(CH$_3$N=NH)(CO)$_2${PPh(OEt)$_2$}$_3$]BPh$_4$ (11b) and [Re(η^1-NH=CH$_2$)(CO)$_2${PPh(OEt)$_2$}$_3$]BPh$_4$ (11*b): These complexes were also prepared by oxidation of the methylhydrazine complex [Re(CH$_3$NHNH$_2$)(CO)$_2${PPh(OEt)$_2$}$_3$]BPh$_4$ (**3b**) with Pb(OAc)$_4$ at −40 °C following exactly the same method as used for the synthesis of **10b** and **10*b**. The reaction afforded a mixture of the two species which, in this case, could not be separated. The IR and NMR spectroscopic data, however, confirm the formation of both the methyldiazene (**11b**) and methyleneimine (**11*b**) derivatives.

[Re(NH=NH)(CO)$_2$P$_3$]BPh$_4$ [P = PPh(OEt)$_2$ 11a, PPh$_2$OEt 12a]: These complexes were prepared by oxidation of the hydrazine precursors [Re(NH$_2$NH$_2$)(CO)$_2$P$_3$]BPh$_4$ (**3a**, **4a**) with Pb(OAc)$_4$ at −40 °C following the method used for the related compound **9a**; yield between 40 and 55%.
11a: $C_{56}H_{67}BN_2O_8P_3Re$ (1186.09): calcd. C 56.71, H 5.69, N 2.36; found C 56.58, H 5.73, N 2.29. Λ_M = 59.2 Ω^{-1} mol^{-1} cm^2.
12a: $C_{68}H_{67}BN_2O_5P_3Re$ (1282.22): calcd. C 63.70, H 5.27, N 2.18; found C 63.56, H 5.33, N 2.08. Λ_M = 57.7 Ω^{-1} mol^{-1} cm^2.

[Re(NH=NH)(CO)$_3$P$_2$]BPh$_4$ [P = PPh(OEt)$_2$ 13a, PPh$_2$OEt 14a]: These complexes were obtained similarly to the related complexes **9a**, **11a** and **12a** by oxidation of the related hydrazine derivatives [Re(NH$_2$NH$_2$)(CO)$_3$P$_2$]BPh$_4$ (**6a**, **7a**) with Pb(OAc)$_4$ at −40 °C; yield approx. 65%.
13a: $C_{47}H_{52}BN_2O_7P_2Re$ (1015.89): calcd. C 55.57, H 5.16, N 2.76; found C 55.38, H 5.05, N 2.64. Λ_M = 58.1 Ω^{-1} mol^{-1} cm^2
14a: $C_{55}H_{52}BN_2O_5P_2Re$ (1079.98): calcd. C 61.17, H 4.85, N 2.59; found C 61.06, H 4.97, N 2.50. Λ_M = 56.5 Ω^{-1} mol^{-1} cm^2.

[Re(4-NO$_2$C$_6$H$_4$N=NH)(CO)$_3${PPh(OEt)$_2$}$_2$]BPh$_4$ (13d): This compound was prepared exactly like the related phenyldiazene compound **9c** by oxidation of the related *p*-nitrophenylhydrazine derivative; yield approx. 55%. $C_{53}H_{55}BN_3O_9P_2Re$ (1136.99): calcd. C 55.99, H 4.88, N 3.70; found C 56.17, H 5.00, N 3.79. Λ_M = 56.0 Ω^{-1} mol^{-1} cm^2.

[Re(CH$_3$NH$_2$)(CO)$_2${P(OEt)$_3$}$_3$]BPh$_4$ (15): An equimolar amount of HBF$_4$·Et$_2$O (0.27 mmol, 39 μL of a 54% solution in Et$_2$O) was added to a solution of [ReH(CO)$_2${P(OEt)$_3$}$_3$] (200 mg, 0.27 mmol) in 10 mL of CH_2Cl_2 cooled to −196 °C, and the reaction mixture warmed to room temperature and stirred for 1 h. An excess of CH_3NH_2 (0.88 mmol, 0.44 mL of a 2 M solution in THF) was added and, after 3 h of stirring, the solvent was removed under reduced pressure to give an oil which was treated with ethanol (1 mL). The addition of an excess of NaBPh$_4$ (0.54 mmol, 0.185 g) in 2 mL of ethanol to the resulting solution caused the separation of a white solid, which was filtered off and recrystallised from CH_2Cl_2 and ethanol; yield approx. 70%. $C_{45}H_{70}BNO_{11}P_3Re$ (1090.98): calcd. C 49.54, H 6.47, N 1.28; found C 49.35, H 6.55, N 1.29. Λ_M = 58.5 Ω^{-1} mol^{-1} cm^2.

Reduction Reactions: The reduction of hydrazine and diazene complexes was carried out in THF at room temperature under argon using an excess of Zn/Hg as reducing agent in the presence of lutidine hydrochloride. A typical experiment involved the addition of a 10-fold excess of Zn (20 mmol), as 2% zinc amalgam, to a solution of the appropriate diazo complex (about 0.1 mmol) in 10 mL of THF. A 16-fold excess of lutidine hydrochloride in 10 mL of THF was then added to the reaction mixture, which was stirred at room temperature under an argon atmosphere for a reaction time varying from 23 to 96 h. An excess of hydrochloric acid (1 mL of 1 M solution in Et$_2$O) was added to the reaction mixture, which was stirred for 1 h. The solvent was then removed under reduced pressure. The solid obtained was treated with five 5-mL portions of H_2O and, after filtration, ammonia from the solution was quantified by the indophenol method.[27]

Acknowledgments

The financial support of MIUR (Rome) *Programmi di Ricerca Scientifica di Rilevante Interesse Nazionale, COFIN 2002-2003* is gratefully acknowledged. We thank Daniela Baldan for technical assistance.

[1] [1a] D. Sutton, *Chem. Rev.* **1993**, *93*, 995. [1b] H. Kisch, P. Holzmeier, *Adv. Organomet. Chem.* **1992**, *34*, 67.
[2] [2a] A. E. Shilov, *Metal Complexes in Biomimetic Chemical Reactions*, CRC Press, Boca Raton, FL, **1997**. [2b] H. Zollinger, *Diazo Chemistry II*, VCH, Weinheim, Germany, **1995**. [2c] B. F. G. Johnson, B. L. Haymore, J. R. Dilworth, in *Comprehensive Coordination Chemistry* (Eds.: G. Wilkinson, R. D. Gillard, J. A. McCleverty), Pergamon Press, Oxford, UK, **1987**, vol. 2, p. 130. [2d] R. A. Henderson, G. J. Leigh, C. J. Pickett, *Adv. Inorg. Chem. Radiochem.* **1983**, *27*, 197. [2e] W. A. Nugent, B. L. Haymore, *Coord. Chem. Rev.* **1980**, *31*, 123. [2f] F. Bottomley, *Q. Rev.* **1970**, *24*, 617.
[3] [3a] M. Hidai, Y. Mizobe, *Chem. Rev.* **1995**, *95*, 1115. [3b] R. R. Eady, G. J. Leigh, *J. Chem. Soc., Dalton Trans.* **1994**, 2739. [3c] D. Sellmann, *Angew. Chem. Int. Ed. Engl.* **1993**, *32*, 14.
[4] B. K. Burgess, S. Wherland, E. I. Stiefel, W. E. Newton, *Biochemistry* **1981**, *20*, 5140.
[5] [5a] D. J. Evans, R. A. Henderson, B. E. Smith, in *Bioinorganic Catalysis* (Ed.: J. Reedijk), Marcel Dekker Inc., New York, **1993**. [5b] M. J. Dilworth, R. R. Eady, *Biochem. J.* **1991**, *277*, 465. [5c] R. N. Thorneley, R. R. Eady, D. J. Lowe, *Nature* **1978**, *272*, 557.
[6] J. T. Moelwyn-Hughes, A. W. B. Garner, A. S. Howard, *J. Chem. Soc. (A)* **1971**, 2361.
[7] M. G. Vale, R. R. Schrock, *Organometallics* **1991**, *10*, 1661.
[8] T.-Y. Cheng, J. C. Peters, G. L. Hillhouse, *J. Am. Chem. Soc.* **1994**, *116*, 204.
[9] A. Moehlenkamp, R. Mattes, *Z. Naturforsch., B: Chem. Sci.* **1992**, *47*, 969.
[10] [10a] G. Albertin, S. Antoniutti, A. Bacchi, M. Bergamo, E. Bordignon, G. Pelizzi, *Inorg. Chem.* **1998**, *37*, 479. [10b] G. Albertin, S. Antoniutti, E. Bordignon, S. Pattaro, *J. Chem. Soc., Dalton Trans.* **1997**, 4445. [10c] G. Albertin, S. Antoniutti, A. Bacchi, E. Bordignon, P. M. Dolcetti, G. Pelizzi, *J. Chem. Soc., Dalton Trans.* **1997**, 4435.
[11] [11a] G. Albertin, S. Antoniutti, A. Bacchi, E. Bordignon, F. Busatto, G. Pelizzi, *Inorg. Chem.* **1997**, *36*, 1296. [11b] G. Albertin, S. Antoniutti, E. Bordignon, G. Perinello, *J. Organomet. Chem.* **2001**, *625*, 217.
[12] G. Albertin, S. Antoniutti, A. Bacchi, E. Bordignon, M. T. Giorgi, G. Pelizzi, *Angew. Chem.* **2002**, *114*, 2296; *Angew. Chem. Int. Ed.* **2002**, *41*, 2192.
[13] G. Albertin, S. Antoniutti, S. Garcia-Fontán, R. Carballo, F. Padoan, *J. Chem. Soc., Dalton Trans.* **1998**, 2071.
[14] W. J. Geary, *Coord. Chem. Rev.* **1971**, *7*, 81.
[15] [15a] D. Sellmann, A. Brandl, R. Endell, *Angew. Chem. Int. Ed. Engl.* **1973**, *12*, 1019. [15b] G. Huttner, W. Gartzke, K. Allinger, *Angew. Chem. Int. Ed. Engl.* **1974**, *13*, 822. [15c] D. Sellmann, K. Jödden, *Angew. Chem. Int. Ed. Engl.* **1977**, *16*, 464. [15d] D.

 © 2003 Wiley-VCH Verlag GmbH & Co. KGaA, Weinheim

Sellmann, E. Böhlen, M. Waeber, G. Huttner, L. Zsolnai, *Angew. Chem. Int. Ed. Engl.* **1985**, *24*, 981. [15e] J. P. Collmann, J. E. Hutchinson, M. A. Lopez, R. Guilard, R. A. Reed, *J. Am. Chem. Soc.* **1991**, *113*, 2794. [15f] D. Sellmann, J. Käppler, M. Moll, F. Knoch, *Inorg. Chem.* **1993**, *32*, 960. [15g] D. Sellmann, A. Hennige, *Angew. Chem. Int. Ed. Engl.* **1997**, *36*, 276.

[16] [16a] M. R. Smith III, T.-Y. Cheng, G. L. Hillhouse, *J. Am. Chem. Soc.* **1993**, *115*, 8638. [16b] T.-Y. Cheng, A. Ponce, A. L. Rheingold, G. L. Hillhouse, *Angew. Chem. Int. Ed. Engl.* **1994**, *33*, 657.

[17] T.-Y. Cheng, J. C. Peters, G. L. Hillhouse, *J. Am. Chem. Soc.* **1994**, *116*, 204.

[18] G. Albertin, S. Antoniutti, A. Bacchi, G. B. Ballico, E. Bordignon, G. Pelizzi, M. Ranieri, P. Ugo, *Inorg. Chem.* **2000**, *39*, 3265.

[19] For recent papers on N−N bond cleavage see: A. K. Verma, S. C. Lee, *J. Am. Chem. Soc.* **1999**, *121*, 10838; R. G. Peters, B. P. Warner, C. J. Burns, *J. Am. Chem. Soc.* **1999**, *121*, 5585; M. A. Aubart, R. G. Bergman, *Organometallics* **1999**, *18*, 811; F. Maseras, M. A. Lockwood, O. Eisenstein, I. P. Rothwell, *J. Am. Chem. Soc.* **1998**, *120*, 6598.

[20] [20a] B. Braillon, M. C. Lasne, J. L. Ripoll, J. M. Denis, *Nouv. J. Chim.* **1981**, *6*, 121. [20b] R. Dammel, *Chem. Ber.* **1987**, *120*, 1961.

[21] [21a] J. E. Dickens, W. M. Irvine, C. H. De Vries, M. Ohishi, *Astrophys. J.* **1977**, *497*, 307. [21b] G. Winnewisser, C. Kramer, *Space Sci. Rev.* **1999**, *90*, 181.

[22] F. Hoyle, N. C. Wickramasinghe, *Nature* **1976**, *264*, 45.

[23] P. A. Shapley, J. M. Shusta, J. C. Hunt, *Organometallics* **1996**, *15*, 1622.

[24] R. Rabinowitz, J. Pellon, *J. Org. Chem.* **1961**, *26*, 4623.

[25] E. Nachbaur, G. Leiseder, *Monatsh. Chem.* **1971**, *102*, 1718.

[26] G. Balacco, *J. Chem. Inf. Comput. Sci.* **1994**, *34*, 1235.

[27] M. W. Weatherburn, *Anal. Chem.* **1967**, *39*, 971.

Received March 25, 2003

 © 2003 Wiley-VCH Verlag GmbH & Co. KGaA, Weinheim

Synthesis, Crystal Structure and Characterization of a Novel Three-Dimensional Polymer: $[Cu_4V_2(OH)_2O_8]$

Chuan-De Wu,[a] Can-Zhong Lu,*[a] Hong-Hui Zhuang,[a] and Jin-Shun Huang[a]

Keywords: Hydrothermal synthesis / Oxo ligands / Vanadium / Copper / TGA

The three-dimensional polymeric compound $[Cu_4V_2(OH)_2O_8]$ (**1**) has been synthesized by the hydrothermal reaction of sodium vanadate and copper acetate in an aqueous solution basified with a 35% aqueous ammonia solution. Detailed experiments suggest that pH values within the range 8.5–11.3 are best for the formation of crystals of compound **1**. X-ray diffraction analysis reveals that the structure of **1** is a three-dimensional polymer constructed from wave-like polymeric oxocuprate layers linked by vanadate tetrahedra, of which the sub-layer is formed by joining the zigzag ribbons together in *cis* zigzag way. Thermogravimetric analysis (TGA) suggests that the structure of compound **1** is quite stable in the temperature range 40–440 °C.

(© Wiley-VCH Verlag GmbH & Co. KGaA, 69451 Weinheim, Germany, 2003)

Introduction

As oxygen is the most abundant and highly reactive terrestrial element, the transition metal oxides represent an expanding class of materials, which are ubiquitous as both naturally existing and synthetic materials.[1−3] Because of their stability, diversity of chemical composition and variety of topological architectures, they exhibit a vast range of solid-state properties giving rise to wide applications in areas as diverse as catalysis, sorption, ion-exchange, molecular electronics, energy storage, optical materials and ceramics, heavy construction and biomineralization. The synthesis and characterization of metal oxide-based solids has provoked significant contemporary interest.[4−11]

Since the discovery of the high-temperature oxide superconductors, oxocuprates have been a focus of interest,[12] particularly the study of the relationship between crystal structures and physical properties. It has been found that the coordination environments of copper atoms and the linkages of these coordination polyhedra seem to be crucial. Inorganic chemists have devised many approaches to synthesize such kinds of materials. One very important way is the hydrothermal synthesis method, which operates at a relatively low temperature (110−220 °C) under autogenous pressure and provides a suitable technique to bring suitable metal-oxide building units together to generate polymeric oxometallic materials.[13−16]

The ability of vanadium in its higher oxidation states to form various polynuclear anionic metal-oxygen clusters is well known, and many polyvanadates with an extraordinary variety of relevant topological and electronic structures have been reported.[17−21] On the other hand, copper(II) cations tend to form various oxygen- and/or hydroxyl-bridged polymers under different reaction conditions.[12] There have been a large number of copper vanadates and related compounds reported in the past decades.[22−48] Neutral copper vanadates were first described by solid-state chemists (and later found to occur naturally; for example Blossite,[22,23] Stoiberite,[24] Ziesite,[25] McBimeyite,[26] Volborthite,[27,28] Vesignieite,[29] Calciovolborthite,[30] Mottramite,[31] Averievite,[32] Sengierite,[33] Fingerite,[34] Lyonsite,[35] Howardevansite,[36] etc.), and $Cu_3(VO_4)_2$, for instance, exists in two allotropic forms, one with the spinel structure[41] and the other[26] being isotypic with $Cu_3(PO_4)_2$.[49] Based upon the inherent properties of vanadium and copper atoms, we report here the hydrothermal synthesis, X-ray crystal structure and characterization of a three-dimensional polymeric compound $[Cu_4V_2(OH)_2O_8]$ (**1**).

Results and Discussion

Dark-blue crystals of compound **1** were synthesized by the hydrothermal reaction of sodium vanadate and copper acetate in an aqueous solution basified with 35% aqueous ammonia solution. Detailed experiments suggest that pH values within the range 8.5−11.3 are best for the formation of crystals of compound **1**. When the pH value is below 8.5, only green sediments are obtained instead of crystals. It is very interesting that the crystal size increases with the pH value of the reaction solutions. However, no product was obtained at pH values above 11.3. The aqueous ammonia solution plays a significant role in the formation of

[a] The State Key Laboratory of Structural Chemistry, Fujian Institute of Research on the Structure of Matter, the Chinese Academy of Sciences,
Fuzhou, Fujian, 350002, China
Fax: (internat.) +86-591/371-4946
E-mail: czlu@ms.fjirsm.ac.cn

compound **1**, which might help the formation of polyoxocuprate fragments and monomeric vanadate. However, if the concentration of NH_3 is above the value where the $[Cu(NH_3)_4]^{2+}$ cation is stabilzed, the formation of polyoxocuprate is prevented. A bond-valence sum calculation[50] reveals that two oxygen atoms are protonated, of which each hydroxyl group bridges three copper centers. Multiple bands from $\tilde{\nu}$ = 947 to 559 cm^{-1} in the IR spectrum of **1** are attributed to the V−O stretching or the bridging [Cu−O−V(Cu)] group absorptions, while the band at 1620 cm^{-1} is attributed to the O−H bending.[51]

The X-ray diffraction analysis reveals that the structure of **1** is a neutral three-dimensional polymeric compound constructed from wave-like polymeric oxocuprate layers linked by vanadate tetrahedra. The asymmetric unit in **1** consists of two $\{VO_4\}$ tetrahedra, two $\{CuO_5\}$ square pyramids and one $\{CuO_6\}$ octahedron (Figure 1). The oxocuprate layer is built up from three crystallographically independent copper(II) atoms, of which two copper centers exhibit a square-pyramidal geometry with Cu−O distances in the 1.881(10)−2.213(9) Å range; the other copper center has an octahedral geometry with Cu−O distances in the 1.914(7)−2.318(8) Å range. These copper atoms form a ribbon through edge sharing in a zigzag arrangement with all copper atoms coplanar (Figure 2). Adjacent ribbons are further joined together by bridging oxygen atoms also through edge sharing. Interestingly, as shown in Figure 3, these ribbons turn by an angle of 47.3(1)° and shift one polyhedral length at the "step" junction. Consequently, the adjacent ribbons are joined together in a *cis* zigzag manner to form a wave-like layered sub-framework. The wave-like oxocuprate sub-layer can also be seen as being constructed from twelve-membered copper rings, which are formed by edge sharing copper square-pyramids or octahedra. These chair-shaped rings are further attached into wave-like layers through edge-sharing copper square-pyramids or octahedra (Figure 4).

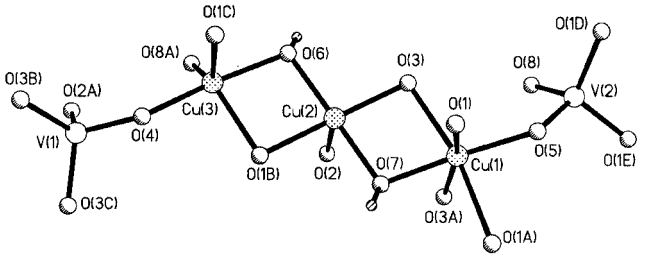

Figure 1. The symmetry-expanded unit in **1**, showing the atom connectivities and the coordination environments (the small right-hatched rings represent hydrogen atoms)

Two crystallographically independent vanadium atoms are both coordinated by four oxygen atoms in tetrahedral geometries. The V−O distances range from 1.638(8) to 1.775(9) Å, with O−V−O angles in the range 107.9(4)−111.4(5)°. The tetrahedrally coordinated vanadium(V) centers link the wave-like sub-layers together to form a three-dimensional polymeric framework (Figure 5) where each vanadate is coordinated to seven or eight $\{CuO_6\}$ octahedra and $\{CuO_5\}$square pyramids by corner sharing.

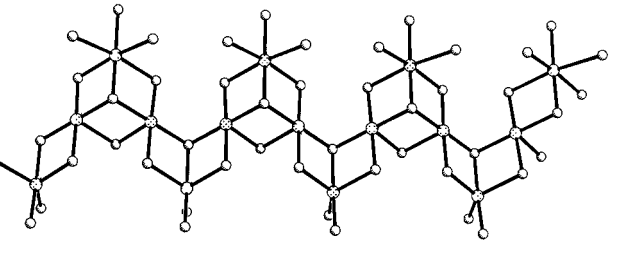

Figure 2. The one-dimensional zigzag ribbon in **1** constructed by linking $\{CuO_6\}$ octahedra and $\{CuO_5\}$ square pyramids

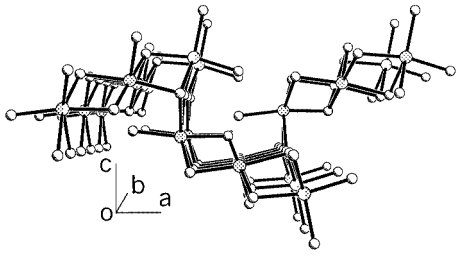

Figure 3. Side view of the linkages between the coplanar chains achieved through bridging oxygen atoms along the *b* axis (the adjacent angle between two planes is 47.3°)

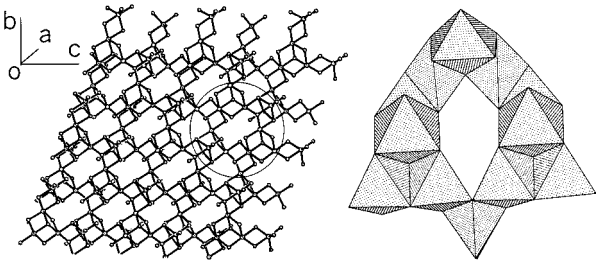

Figure 4. The layered sub-framework of **1** viewed down the *a* axis (right: polyhedral representation of a twelve-membered copper ring in **1**, which is outlined on the left-hand side)

The overall structure of **1** suggests that it should be very stable, and this was confirmed by the thermogravimetric analysis (TGA). The TGA data, recorded from 40 to 1000 °C under inflowing N_2, show that the weight of **1** is almost unchanged from 40 to 440 °C (Figure 6). Above 440 °C, compound **1** began to decompose gradually. The observed weight loss (3.32%) is slightly lower than that of losing one water molecule per empirical formula unit (3.47%). This fact suggests that the hydroxyl groups are changed into H_2O after a complicated reaction process and released from

 © 2003 Wiley-VCH Verlag GmbH & Co. KGaA, Weinheim

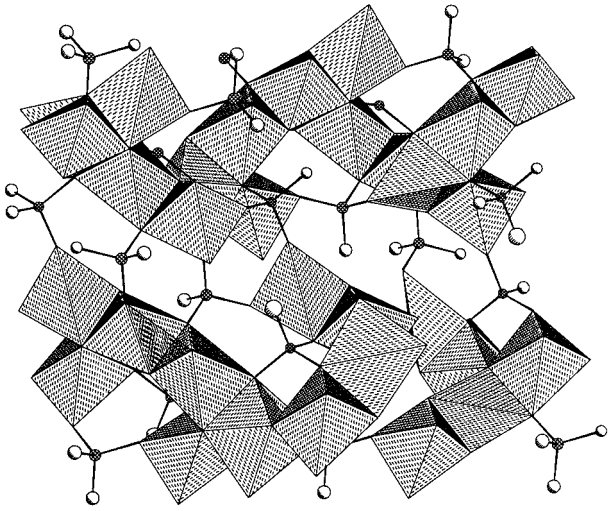

Figure 5. Polyhedral representation of the $\{CuO_6\}$ octahedra and $\{CuO_5\}$ square pyramids as well as a ball-and-stick representation of the $\{VO_4\}$ tetrahedra, showing the three-dimensional polymeric framework of **1**

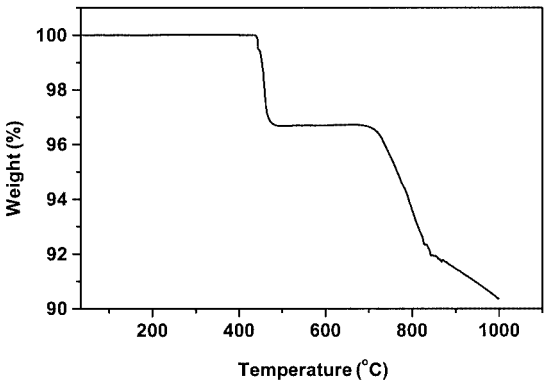

Figure 6. Thermogravimetric (TGA) analysis of **1** between 40 and 1000 °C

the sample above 440 °C. The TGA chart shows that the weight is almost unchanged in the next stage (490−700 °C). Above 700 °C, the product begins to decompose completely.

Conclusion

In conclusion, we have synthesized a three-dimensional polymeric compound under hydrothermal reaction conditions. This result shows that basic reaction conditions can help the formation of polymeric oxocuprate building blocks and monomeric vanadate, and that the pH value of the reaction conditions is a very important impact factor for the formation of novel target materials. The thermogravimetric

Table 1. Selected bond lengths (Å) and angles (°) for compound **1**[a]

Cu(1)−O(7)	1.914(7)	O(7)−Cu(1)−O(5)	172.4(4)	O(2)^{vi}−V(1)−O(4)	110.1(5)
Cu(1)−O(5)	1.943(10)	O(7)−Cu(1)−O(3)	78.8(2)	O(2)^{vi}−V(1)−O(3)^{vii}	109.3(3)
Cu(1)−O(3)	2.154(9)	O(5)−Cu(1)−O(3)	106.1(3)	O(4)−V(1)−O(3)^{vii}	108.8(3)
Cu(1)−O(1)	2.318(8)	O(3)^{i}−Cu(1)−O(3)	96.0(5)	O(3)^{vii}−V(1)−O(3)^{viii}	110.6(6)
Cu(2)−O(7)	1.939(5)	O(7)−Cu(1)−O(1)	88.0(2)	O(8)−V(2)−O(5)	107.9(4)
Cu(2)−O(3)	1.963(7)	O(5)−Cu(1)−O(1)	86.5(3)	O(8)−V(2)−O(1)^{ix}	109.1(3)
Cu(2)−O(6)	1.966(7)	O(3)−Cu(1)−O(1)	87.9(3)	O(5)−V(2)−O(1)^{ix}	109.6(3)
Cu(2)−O(1)^{ii}	2.020(6)	O(3)−Cu(1)−O(1)^{i}	165.1(3)	O(1)^{ix}−V(2)−O(1)^{x}	111.4(5)
Cu(2)−O(2)	2.213(9)	O(1)−Cu(1)−O(1)^{i}	84.9(4)	V(2)^{ii}−O(1)−Cu(2)^{ix}	120.7(5)
Cu(3)−O(4)	1.881(10)	O(7)−Cu(2)−O(3)	83.1(3)	V(2)^{ii}−O(1)−Cu(3)^{ix}	112.3(3)
Cu(3)−O(8)^{iii}	1.930(8)	O(7)−Cu(2)−O(6)	178.7(4)	Cu(2)^{ix}−O(1)−Cu(3)^{ix}	91.8(3)
Cu(3)−O(6)	1.937(10)	O(3)−Cu(2)−O(6)	97.8(4)	V(2)^{ii}−O(1)−Cu(1)	132.1(4)
Cu(3)−O(1)^{ii}	2.206(9)	O(7)−Cu(2)−O(1)^{ii}	94.4(3)	Cu(2)^{ix}−O(1)−Cu(1)	98.3(3)
V(1)−O(2)^{vi}	1.674(12)	O(3)−Cu(2)−O(1)^{ii}	172.8(3)	Cu(3)^{ix}−O(1)−Cu(1)	91.3(4)
V(1)−O(4)	1.679(10)	O(6)−Cu(2)−O(1)^{ii}	84.7(4)	V(1)^{vi}−O(2)−Cu(2)	136.6(2)
V(1)−O(3)^{vii}	1.739(9)	O(7)−Cu(2)−O(2)	86.7(3)	Cu(2)−O(2)−Cu(2)^{i}	85.1(4)
V(2)−O(8)	1.638(8)	O(3)−Cu(2)−O(2)	96.8(4)	V(1)^{xi}−O(3)−Cu(2)	121.7(5)
V(2)−O(5)	1.704(10)	O(6)−Cu(2)−O(2)	94.2(3)	V(1)^{xi}−O(3)−Cu(1)	138.9(4)
V(2)−O(1)^{ix}	1.775(9)	O(1)^{ii}−Cu(2)−O(2)	89.7(4)	Cu(2)−O(3)−Cu(1)	94.5(3)
		O(4)−Cu(3)−O(8)^{iii}	96.3(4)	V(1)−O(4)−Cu(3)	146.5(7)
		O(4)−Cu(3)−O(6)	166.6(5)	V(2)−O(5)−Cu(1)	133.2(6)
		O(8)^{iii}−Cu(3)−O(6)	97.1(4)	Cu(3)−O(6)−Cu(2)	102.2(4)
		O(4)−Cu(3)−O(1)^{ii}	90.1(3)	Cu(2)^{v}−O(6)−Cu(2)	102.6(5)
		O(8)^{iii}−Cu(3)−O(1)^{ii}	134.5(2)	Cu(1)−O(7)−Cu(2)	103.5(3)
		O(6)−Cu(3)−O(1)^{ii}	80.5(3)	Cu(2)^{i}−O(7)−Cu(2)	101.0(4)
		O(1)^{iv}−Cu(3)−O(1)^{ii}	90.3(4)	V(2)−O(8)−Cu(3)^{iii}	169.3(5)

[a] Symmetry transformations used to generate equivalent atoms: i): $x, -y + 1/2, z$; ii): $-x + 1/2, -y, z + 1/2$; iii) $-x + 1, -y, -z + 1$; iv): $-x + 1/2, y - 1/2, z + 1/2$; v): $x, -y - 1/2, z$; vi): $-x + 1, -y, -z + 2$; vii): $x, y, z + 1$; viii): $x, -y - 1/2, z + 1$; ix): $-x + 1/2, -y, z - 1/2$; x): $-x + 1/2, y + 1/2, z - 1/2$; xi): $x, y, z - 1$.

 © 2003 Wiley-VCH Verlag GmbH & Co. KGaA, Weinheim

analysis suggests that the framework of compound **1** is stable up to 440 °C.

Experimental Section

General Remarks: All chemicals were of reagent grade and were used as received. Infrared spectra were recorded on a FTS-40 spectrophotometer using pressed KBr pellets. Thermogravimetric analysis (TGA), using a universal V2.4F TA Instrument, was performed on a powdered sample of **1** under inflowing N_2 with heating rate of 10 °C·min^{-1} in the temperature range 40−1000 °C.

$[Cu_4V_2(OH)_2O_8]$ (1): $NaVO_4 2H_2O$ (0.079 g, 0.5 mmol) and $Cu(CH_3COO)_2{\cdot}H_2O$ (0.10 g, 0.5 mmol) were dissolved in H_2O (16 mL) at room temperature. The pH value of the solution was adjusted to 8.67 by adding 35% aqueous ammonia solution dropwise, resulting in a deep-blue solution. The solution was transferred into a 30 mL polytetrafluoroethylene-lined Parr acid digestion vessel. The vessel was then sealed and heated at 195 °C for five days under autogenous pressure. After cooling, dark blue crystals were filtered off and washed with water and ethanol. Yield: about 76% (based on Cu). IR (KBr pellet): $\tilde{\nu}$ = 1620 m cm^{-1}, 947 m, 877 s, 822 m, 769 s, 559 m.

X-ray Crystallographic Study: $Cu_4H_2O_{10}V_2$, M = 518.06, orthogonal, space group *Pnma*, a = 14.9251(1), b = 6.0607(1), c = 8.5460(1) Å, V = 773.04(2) Å^3, Z = 4, D_c = 4.451 g·cm^{-3}, μ = 13.167 mm^{-1}, $F(000)$ = 976, crystal size = 0.32 × 0.26 × 0.12 mm^3. The determination of the unit cell and the data collection for a dark-blue crystal of compound **1** were performed on an Enraf−Nonius CAD4 diffractometer with graphite-monochromated Mo-K_α radiation (λ = 0.71073 Å) in the ω-2θ range 2.73 < θ < 30.03°. Lorentz-polarization corrections and an empirical absorption were applied to the data. The structure was solved by direct methods and refined by full-matrix least-squares, leading to a convergence with final $R1$ = 0.0734, $wR2$ = 0.1279 and S = 1.089 for 705 reflections with $F_o > 4\sigma(F_o)$ and 87 parameters. The structure analysis and refinement were carried out using the SHELXL-97 software package.[52] Selected bond lengths and angles are listed in Table 1.

Further details of the crystal-structure investigation may be obtained from the Fachinformationzentrum Karlsruhe, 76344 Eggenstein-Leopoldshafen, Germany, on quoting the depository number CSD-412990.

Acknowledgments

We are grateful to the 973 Program of the MOST (001CB108906), the National Natural Science Foundation of China (90206040, 20073048), the NSF of Fujian (2002F015) and the Chinese Academy of Sciences for financial supports.

[1] L. L. Hench, *Inorganic Biomaterials in Materials Chemistry, An Emerging Discipline* (Eds.: L. V. Interrante, L. A. Caspar, A. B. Ellis), ACS Series 245, **1995**, ch. 21, pp. 523−547.
[2] B. Mason, *Principles of Geochemistry, 3rd ed.,* Wiley, New York, **1966**.
[3] D. W. Bruce, D. O'Hare, *Inorganic Materials*, Wiley, Chichester, **1992**.
[4] A. K. Cheetham, *Science* **1994**, *264*, 794 and references therein.
[5] A. Müller, H. Reuter, S. Dillinger, *Angew. Chem. Int. Ed. Engl.* **1995**, *34*, 2328.
[6] M. T. Pope, A. Müller, *Angew. Chem. Int. Ed. Engl.* **1991**, *30*, 34.
[7] P. A. Cox, *Transition Metal Oxides*, Clarendon Press, Oxford, **1995**.
[8] M. T. Pope, *Heteropoly and Isopoly Oxometalates*, Springer, New York, **1983**.
[9] A. Müller, F. Peters, M. T. Pope, D. Gatteschi, *Chem. Rev.* **1998**, *98*, 239.
[10] A. Clearfield, *Chem. Rev.* **1988**, *88*, 125.
[11] P. J. Hagrman, D. Hagrman, J. Zubieta, *Angew. Chem. Int. Ed.* **1999**, *38*, 2638.
[12] H. Müller-Buschbaum, *Angew. Chem. Int. Ed. Engl.* **1991**, *30*, 723.
[13] J. Gopalakrishnan, *Chem. Mater.* **1975**, *7*, 1265.
[14] A. Rabenau, *Angew. Chem. Int. Ed. Engl.* **1985**, *24*, 1026.
[15] R. A. Ludise, *Chem. Eng. News* **1987**, *65*, 30.
[16] J. Y. Lu, M. L. Lawandy, J. Li, T. Yuen, C. L. Lin, *Inorg. Chem.* **1999**, *38*, 2695.
[17] W. G. Klemperer, T. A. Marquart, O. M. Yaghi, *Angew. Chem. Int. Ed. Engl.* **1992**, *31*, 49.
[18] Y.-J. Liu, J. L. Schindler, D. C. DeGroot, C. R. Kannewurf, W. Hirpo, M. G. Kanatzidis, *Chem. Mater.* **1996**, *8*, 525.
[19] C.-G. Wu, D. C. DeGroot, H. O. Marcy, J. L. Schindler, C. R. Kannewurf, Y.-J. Liu, W. Hirpo, M. G. Kanatzidis, *Chem. Mater.* **1996**, *8*, 1992.
[20] Y. Zhang, J. R. D. DeBord, C. J. O'Connor, R. C. Haushalter, A. Clearfield, J. Zubieta, *Angew. Chem. Int. Ed. Engl.* **1996**, *35*, 989.
[21] M. I. Khan, E. Yohannes, R. J. Doedens, *Angew. Chem. Int. Ed.* **1999**, *38*, 1292.
[22] C. Calvo, R. Faggiani, *Acta Crystallogr., Sect. B* **1975**, *31*, 603.
[23] P. D. Robinson, J. M. Hughes, M. L. Malinconico, *Am. Mineralogist* **1987**, *72*, 397.
[24] R. D. Shannon, C. Calvo, *Acta Crystallogr., Sect. B* **1973**, *29*, 1338.
[25] D. Mercurio-Lavaud, B. Frit, *Comptes Rendus Hebdomadaires des Seances de l' Academie des Sciences, Serie C, Sciences Chimiques* **1973**, *277*, 1101.
[26] J. Coing-Boyat, *Acta Crystallogr., Sect. B* **1982**, *38*, 1546.
[27] R. Basso, A. Palenzona, L. Zefiro, *Neues Jahrbuch fuer Mineralogie. Monatshefte* **1988**, 385.
[28] M. A. Lafontaine, A. LeBail, G. Ferey, *J. Solid State Chem.* **1990**, *85*, 220.
[29] Z. Ma, R. He, X. Zhu, *Dizhi Xuebao* **1990**, *4*, 302.
[30] R. Basso, A. Palenzona, L. Zefiro, *Neues Jahrbuch fuer Mineralogie. Monatshefte* **1989**, 300.
[31] M. A. Cooper, F. C. Hawthorne, *Canad. Mineralogist.* **1995**, *33*, 1119.
[32] G. L. Starova, S. V. Krivovichev, V. S. Fundamenskii, S. K. Filatov, *Mineralogical Magazine* **1997**, *61*, 441.
[33] P. Piret, J. P. Declercq, D. Wauters-Stoop, *Bulletin de Mineralogie* **1980**, *103*, 176.
[34] L. W. Finger, *Am. Mineralogist* **1985**, *70*, 197.
[35] J. M. Hughes, S. J. Starkey, M. L. Malinconico, L. L. Malinconico, *Am. Mineralogist* **1987**, *72*, 1000.
[36] J. M. Hughes, J. W. Drexler, C. F. Campana, M. L. Malinconico, *Am. Mineralogist* **1988**, *73*, 181.
[37] J. Galy, D. Lavaud, *Acta Crystallogr., Sect. B* **1971**, *27*, 1005.
[38] M.-L. Ha-Eierdanz, U. Müller, *Z. Anorg. Allg. Chem.* **1993**, *619*, 287.
[39] D. Mercurio-Lavaud, B. Frit, *Acta Crystallogr., Sect. B* **1973**, *29*, 2737.
[40] C. Calvo, D. Manolescu, *Acta Crystallogr., Sect. B* **1973**, *29*, 1743.
[41] R. D. Shannon, C. Calvo, *Canad. J. Chem.* **1972**, *50*, 3944.
[42] J. R. Rea, E. Kostiner, *J. Solid State Chem.* **1973**, *7*, 163.

 © 2003 Wiley-VCH Verlag GmbH & Co. KGaA, Weinheim

[43] J. R. Rea, E. Kostiner, *J. Solid State Chem.* **1973**, *7*, 17.
[44] J. Galy, D. Lavaud, A. Casalot, P. Hagenmuller, *J. Solid State Chem.* **1970**, *2*, 531.
[45] J. R. Rea, P. W. Bless, E. Kostiner, *J. Solid State Chem.* **1972**, *5*, 446.
[46] S. Aschwanden, H. W. Schmalle, A. Reller, H. R. Oswald, *Mater. Res. Bull.* **1993**, *28*, 45.
[47] J. Galy, D. Lavaud, A. Casalot, P. Hagenmuller, *J. Solid State Chem.* **1970**, *2*, 531.
[48] M. Blanc, G. Ferey, *Acta Crystallogr., Sect. C* **1990**, *46*, 15.
[49] G. L. Shoemaker, J. B. Anderson, E. Kostiner, *Acta Crystallogr.* **1977**, *33*, 2969.
[50] N. E. Brease, M. O'Keeffe, *Acta Crystallogr., Sect. B* **1991**, *47*, 192.
[51] M. I. Khan, T. Hope, S. Cevik, C. Zheng, D. Powell, *J. Cluster Sci.* **2000**, *11*, 433.
[52] G. M. Sheldrick, Universität Göttingen, Germany, **1997**.
Received February 12, 2003

 © 2003 Wiley-VCH Verlag GmbH & Co. KGaA, Weinheim

Great Framework Variation of Polymers in the Manganese(II) Maleate/α,α′-Diimine System: Syntheses, Structures, and Magneto-Structural Correlation

Chengbing Ma,[a,d] Changneng Chen,[a] Qiutian Liu,*[a] Feng Chen,[a] Daizheng Liao,[b] Licun Li,[b] and Licheng Sun[c]

Keywords: Crystal structure / Maleic acid / Magnetic properties / Manganese / Structural topology

Three novel manganese(II) coordination polymers, $[Mn(maleate)(phen)]_n$ (**1**; phen = 1,10-phenanthroline), $[Mn(maleate)(phen)]_n \cdot nH_2O$ (**2**), and $[Mn(maleate)(bpy)]_n$ (**3**; bpy = 2,2′-bipyridine), have been synthesized by treatment of Mn^{2+} with maleic acid with participation of chelate diimine ligands, and have been identified by single-crystal X-ray diffraction to have either one-dimensional (1D) zigzag chain structures (**1** and **2**) or a two-dimensional (2D) sinuous layer structure (**3**). Each maleate dianion coordinates to three Mn centers, in different bridging modes (*syn-anti* in **1** and **2**, *syn-syn* and *anti-anti* in **3**). These compounds represent an interesting example of structural topology variation from 1D to 2D mediated by chemically similar auxiliary chelate ligands. Variable-temperature magnetic susceptibility measurements show weak anti-ferromagnetic exchange interactions between the adjacent Mn^{II} ions, with $J = -0.06$ cm^{-1} (**2**) and $J = -1.3$ cm^{-1}, $zJ' = -0.27$ cm^{-1} (**3**). The differences in the magnitudes of these coupling interactions agree well with the nature of the carboxylate-bridging coordination of maleate.
(© Wiley-VCH Verlag GmbH & Co. KGaA, 69451 Weinheim, Germany, 2003)

Introduction

There is currently great interest in the construction of metal-organic hybrid extended solids containing paramagnetic metal ions, driven to a large extent by their fascinating network topologies and their wide applications, such as in the field of molecular magnetism.[1] The key to the fabrication of such networks is the selection of appropriate bridging ligands capable of mediating magnetic interaction and coordination geometries of metal ions.[2] The recent exponential growth in the synthesis and study of such coordination polymers has provided elegant examples of how the metal ion geometry and the appropriate bridging ligand symmetry can be exploited for the design of materials with unusual structures and properties. In this respect, polycarboxylate ligands are frequently used as magnetic superexchange pathways between the metal ions, due to their versatile carboxylate-bridging coordination modes (*syn-syn*, *anti-anti*, and *syn-anti*) capable of transmitting magnetic coupling interactions to different degrees.[3]

The product architecture that will spontaneously self-assemble from a metal node and a single organic spacer can to some extent be predicted in the light of the known metal coordination preference and the ligand configuration.[4] The introduction of another ligand, however, will greatly reduce the reliability of the prediction. In this situation, the auxiliary ligand may affect the combination mode of the metal ion with a primary ligand, finally resulting in topologically different complexes.

In the course of our study on manganese complexation by polyacids, we pay special attention to the influence of auxiliary ligands on the structural topology,[5] since at present it is not possible to know for certain the differences between the compounds.[6] In this work, we selected maleate as a primary ligand, in view both of its versatile bonding modes, capable of linking more than one metal ion, and also of its specific conformation, which was predicted to yield extended structures. We obtained two types of manganese(II) polymers with 1D and 2D frameworks in the presence of phen and bpy, respectively, as the secondary ligands. The result shows profound influences of the auxiliary chelate ligand both on the structural topology and on the simultaneous adoption of maleate coordination modes (Scheme 1), followed accordingly by the alteration of the magnetic properties of the product.

[a] State Key Laboratory of Structural Chemistry, Fujian Institute of Research on the Structure of Matter, Chinese Academy of Sciences,
Fuzhou 350002, China
Fax: (internat.) + 86-591/3714946
E-mail: lqt@ms.fjirsm.ac.cn
[b] Department of Chemistry, Nankai University,
Tianjin 300071, China
[c] State Key Laboratory of Fine Chemicals, Dalian University of Technology,
Dalian, China
[d] Graduate School of the Chinese Academy of Sciences,
Beijing, China

 © 2003 Wiley-VCH Verlag GmbH & Co. KGaA, Weinheim **DOI: 10.1002/ejic.200300097**

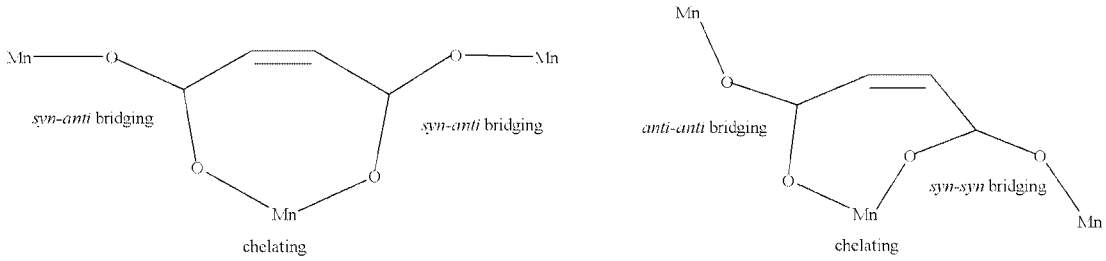

Scheme 1. A schematic illustration showing the coordination modes of maleate dianion observed in complexes **1**−**3** (left for **1** and **2**, right for **3**)

Results and Discussion

Synthesis

Three polymers were produced from the Mn^{2+}/maleate/diimine self-assembly system. Although structurally unexpected complexes are frequently encountered, as the metal−ligand self-assembly is strongly influenced by factors such as the solvent system, template, and counter-ion, as well as the preferences of metal center and organic spacer conformation, the dramatic difference derived from chemically very similar ancillary ligands, such as observed in the present work, is rather surprising. Attempts to obtain a complex topologically similar to **3** with bpy instead of phen under various reaction conditions did not succeed, and vice versa. The production of great structural variation, from 1D to 2D, for the two types of polymers (vide supra) may be due to the difference in conjugate ring area in the auxiliary ligands bpy and phen.

Structure Descriptions of Complexes 1−3

Single-crystal X-ray diffraction analysis reveals that the complex **1** is a 1D, neutral, chain-like polymer consisting of [Mn(maleate)(phen)] units. The Mn^{II} center has a distorted octahedral geometry with four O atoms of three maleate ligands [Mn−O 2.117(2)−2.208(2) Å] and two N atoms of one phen ligand [Mn−N 2.334(2) and 2.308(2) Å] at the six corners. Selected bond lengths and angles are listed in Table 1. Each Mn ion is coordinated by three maleate ions, while each maleate coordinates to three Mn ions through its two carboxylate groups in chelating and bridging modes. Two oxygen atoms of the two ends of the maleate ion chelate one Mn atom to form a seven-membered ring (**A**); meanwhile, each of the carboxylate groups bridges two Mn atoms in a *syn-anti* fashion, resulting in double μ-OCO bridges and a bridging eight-membered ring (**B**), as shown in Figure 1. Consequently, these different non-planar **A** and **B** rings alternately interlock by sharing the C−O−Mn edges to produce a one-dimensional zigzag chain (Figure 2), in which every two neighboring symmetry-related Mn atoms are separated by 4.976 Å. In addition, there is a significant π−π-stacking interaction between the phen ligands belonging to the inversion-related chains ($-x$, $1 - y$, $1 - z$) with a perpendicular ring separation of 3.363 Å, which further promotes the stabilization of the zigzag chain.

Complex **2** is made up of a one-dimensional chain and solvate water molecules. The chain is constructed from basic [Mn(maleate)(phen)] units, the structures of which are almost identical to those in **1**, and all the structural parameters are also very close to those of **1**, as can be seen from Table 1. Two hydrogen bonds link the lattice water molecule

Table 1. Selected bond lengths [Å] and angles [°] of **1** and **2** (symmetry transformations used to generate equivalent atoms: A: $-x$, $-y + 1$, $-z + 2$; B: $-x + 1$, $-y + 1$, $-z + 2$; C: $-x + 1$, $-y + 2$, $-z$; D: $-x$, $-y + 2$, $-z$)

Complex **1**							
Mn−O1	2.117(2)	Mn−O4B	2.123(2)	Mn−O2A	2.176(2)	Mn−O3	2.208(2)
Mn−N2	2.308(2)	Mn−N1	2.334(2)	O1−Mn−O4B	101.70(8)	O1−Mn−O2A	93.26(7)
O4B−Mn−O2A	89.63(7)	O1−Mn−O3	84.92(7)	O4B−Mn−O3	89.97(8)	O2A−Mn−O3	178.02(7)
O1−Mn−N2	170.56(8)	O4B−Mn−N2	87.72(8)	O2A−Mn−N2	86.11(7)	O3−Mn−N2	95.81(7)
O1−Mn−N1	98.84(8)	O4B−Mn−N1	159.14(9)	O2A−Mn−N1	92.82(8)	O3−Mn−N1	88.24(8)
N2−Mn−N1	71.80(8)						
Complex **2**							
Mn−O1	2.124(3)	Mn−O4C	2.156(3)	Mn−O2D	2.193(3)	Mn−O3	2.198(3)
Mn−N2	2.286(3)	Mn−N1	2.320(4)	O1−Mn−O4C	100.62(12)	O1−Mn−O2D	94.35(11)
O4C−Mn−O2D	86.82(11)	O1−Mn−O3	85.00(11)	O4C−Mn−O3	88.27(12)	O2D−Mn−O3	174.85(11)
O1−Mn−N2	169.65(12)	O4C−Mn−N2	89.69(13)	O2D−Mn−N2	87.02(11)	O3−Mn−N2	94.53(11)
O1−Mn−N1	97.42(12)	O4C−Mn−N1	161.8 (1)	O2D−Mn−N1	93.99(12)	O3−Mn−N1	91.16(12)
N2−Mn−N1	72.25(13)						

 © 2003 Wiley-VCH Verlag GmbH & Co. KGaA, Weinheim

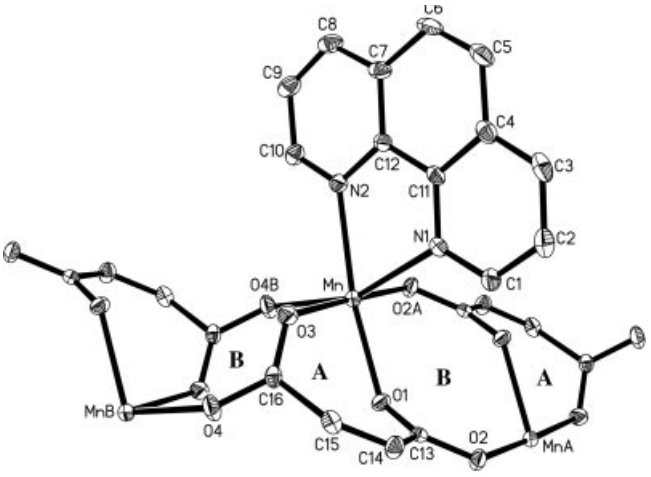

Figure 1. Structure view of **1** showing the local coordination environment of Mn^{II} with thermal ellipsoids at 30% probability (**A** and **B** represent two kinds of microcycles)

O5 and two carboxylate oxygen atoms of symmetry-related polymer chains to generate a two-dimensional network sheet (Figure 3).

Interestingly, the replacement of phen by bpy resulted in the crystallization of the architecturally significantly different complex **3**, the structure of which involves a two-dimensional layer framework composed of neutral [Mn(maleate)(bpy)] units. Selected bond lengths and angles are listed in Table 2. Each Mn^{II} ion completes its pseudoctahedral geometry with four oxygen atoms of three maleate ions and two nitrogen atoms of a chelating bpy ligand (Figure 4). Each maleate ligand is also bonded to three different Mn atoms in chelating and bridging modes, and the chelating mode results in a seven-membered ring **A**, like those in **1**. Two carboxylate groups act as triatomic bridges in two distinct bridging modes (*syn-syn* and *anti-anti*), which are greatly different from that found in **1** (*syn-anti*). The *syn-syn* bridge forms an eight-membered ring $Mn_2(\mu\text{-}OCO)_2$ unit (**B**), which is fused together with two **A** rings by shar-

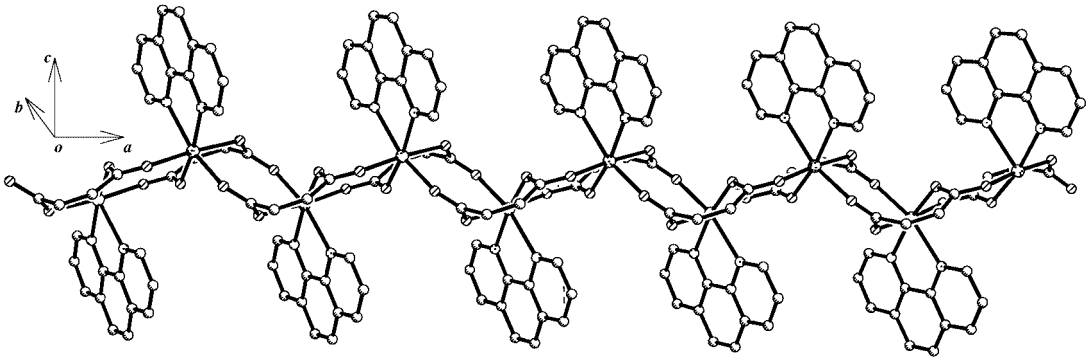

Figure 2. A view of the 1D zigzag chain in **1**, with hydrogen atoms omitted for clarity

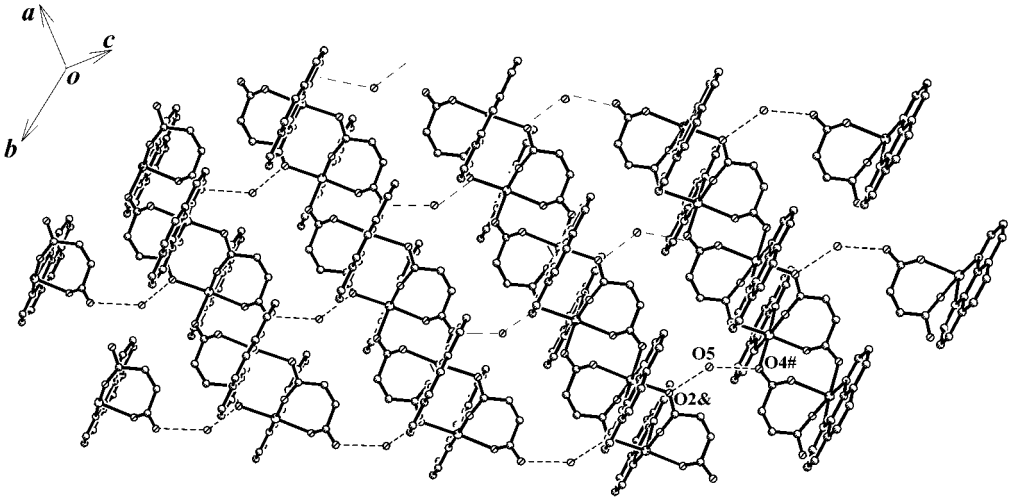

Figure 3. A packing diagram showing part of the two-dimensional hydrogen-bonded network (O5−H5B···O4# = 3.006 Å and O5−H5C···O2& = 2.943 Å); symmetric modes: #: $x - 1, y - 1, z$; &: $-x, -y + 2, -z$

 © 2003 Wiley-VCH Verlag GmbH & Co. KGaA, Weinheim

ing Mn−O−C edges to form **ABA** fused rings. The *anti-anti* bridge bridges between the two **ABA** moieties, resulting in a 22-membered macrocycle **C**, containing four Mn atoms alternately linked by four maleate ligands. The *syn-syn* and *anti-anti* bridges give rise to two spans with Mn−MnA distances of 4.666 Å and Mn−MnB distances of 6.390 Å, respectively. These rings extend sequentially to build up a two-dimensional sinuous layer-type architecture (Figures 5 and 6) with bpy ligands protruding towards the interlayer region, as shown in Figure 6. It is indicated that the **ABA-BAB**... zigzag chain of **1** arises from the mutual interlock of the **A** and **B** rings, while the linkage of the **ABA** moieties through the carboxylate group bridge gives rise to the clearly different framework topology of **3**. Surprisingly, this dramatic difference between the two complexes actually derives from chemically very similar ancillary ligands, phen and bpy. It is believed that the larger ring area of the phen ligand may be preferable for production of π−π interactions (vide supra) between the aromatic rings, albeit weak. This would favor the formation of a zigzag chain. However the larger ring area may also produce a spatial hindrance

Table 2. Selected bond lengths [Å] and angles [°] of complex **3** (symmetry codes: A: $-x + 1, -y + 1, -z$; B: $x, -y + 3/2, z + 1/2$)

Mn−O1	2.1156(18)	Mn−O4B	2.151(2)
Mn−N1	2.273(2)	Mn−N2	2.333(2)
Mn−O2A	2.1744(19)	Mn−O3	2.1821(2)
O1−Mn−O4B	99.55(8)	O1−Mn−O2A	94.64(7)
O4B−Mn−O2A	84.29(8)	O1−Mn−O3	82.92(7)
O4B−Mn−O3	94.08(8)	O2A−Mn−O3	176.81(8)
O1−Mn−N1	166.47(8)	O4B−Mn−N1	89.84(8)
O2A−Mn−N1	95.98(8)	O3−Mn−N1	86.74(8)
O1−Mn−N2	100.52(8)	O4B−Mn−N2	159.25(8)
O2A−Mn−N2	88.89(8)	O3−Mn−N2	93.56(8)
N1−Mn−N2	71.36(8)		

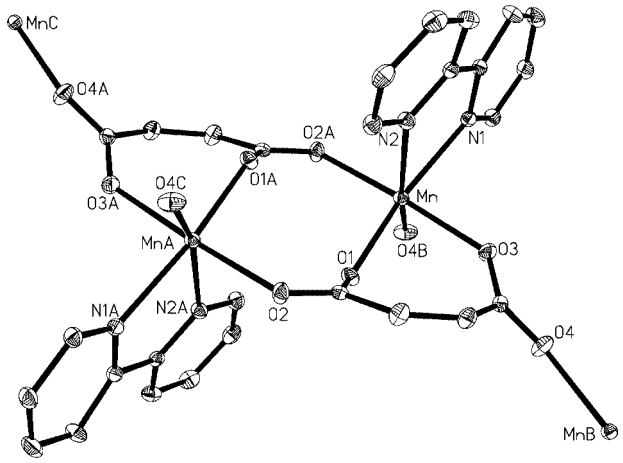

Figure 4. Structure view of **3** showing the local coordination environment of Mn^{II} with thermal ellipsoids at 30% probability

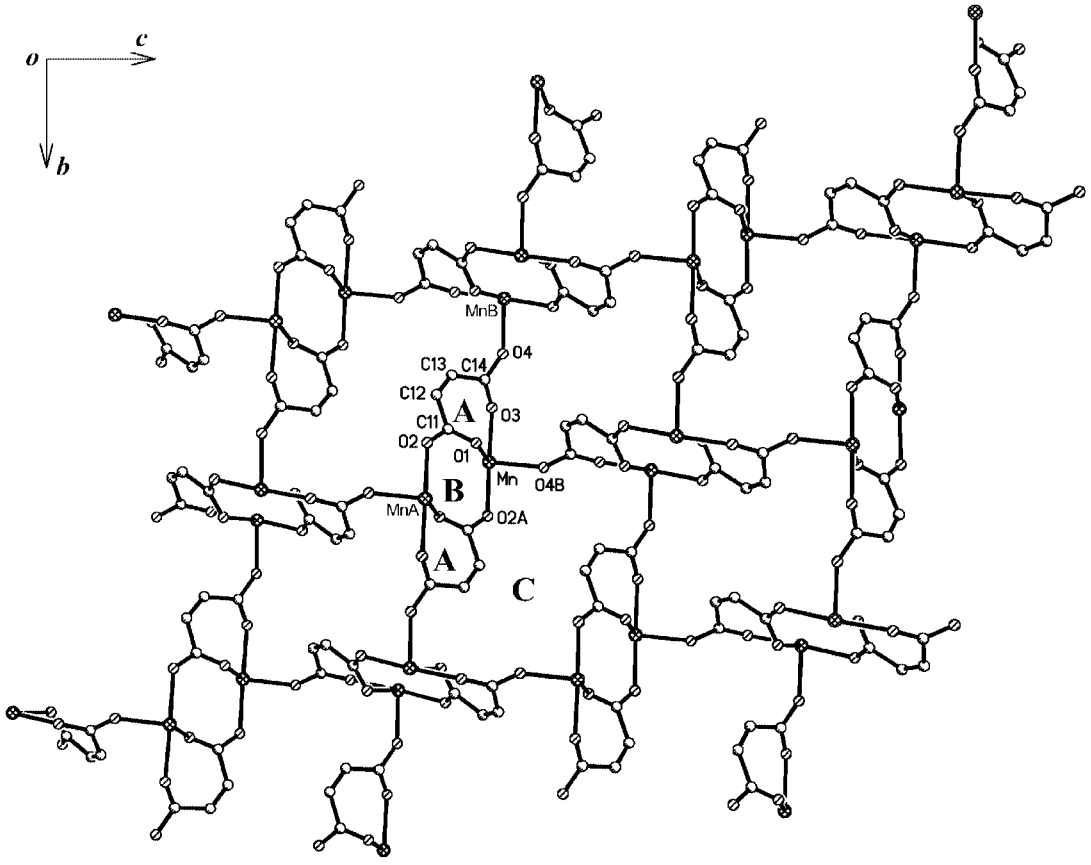

Figure 5. A view of the layer structure of **3**, with hydrogen atoms and bpy ligands omitted for clarity (**A**, **B**, and **C** represent three different subrings)

 © 2003 Wiley-VCH Verlag GmbH & Co. KGaA, Weinheim

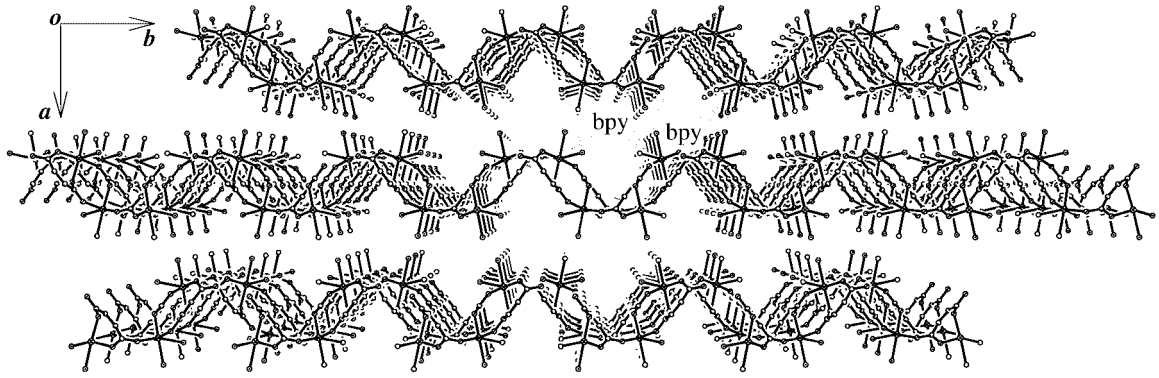

Figure 6. The packing diagram of **3** focused on the sinusoid-like layer framework; carbon atoms of bpy ligands are excluded for clarity

between the two sinuous layers (Figure 6). Consequently, the participation of the two ancillary ligands results in different framework topologies.

To the best of our knowledge, the coordination mode of maleate in **1**−**3** is unique in metal maleate/diimine systems, and different from that found in a tetramanganese cluster $[Mn_4(maleate)_2(bpy)_8](ClO_4)_4$,[7] in which each maleate ligand carboxylate group bridges two manganese ions in an *anti-anti* fashion, and also from that found in a manganese polymer $[Mn(maleate)(L)]_n$ (L = 4,4′-bipyridine),[8] in which two carboxylate groups of the maleate ligand act as a triatomic bridge in a *syn-anti* fashion and a monoatomic bridge to link two manganese ions, respectively, with the fourth carboxylate oxygen atom free. In addition, there were three previously reported dinuclear Cu/Zn maleate/bpy (or phen) complexes[9] in which the metal ions are five-coordinate and the maleate ion serves as a bidentate ligand linking two metal ions through two oxygen atoms of its two ends, and one mononuclear complex $[Co(maleate)(bpy)(H_2O)_3]\cdot H_2O$,[10] in which the maleate ion binds to the six-coordinate Co center through only one carboxylate oxygen atom. No other metal maleate/α-α′-diimine polymeric complexes have been reported so far.

IR Spectroscopy

The IR spectra of the three complexes clearly show both the presence of the maleate ion and its coordination mode. The strong absorptions at 1560 and 1425 cm^{-1} for **1**, 1558 and 1427 cm^{-1} for **2**, and 1551 and 1429 cm^{-1} for **3** correspond to asymmetric and symmetrical stretching vibrations − $\nu_{as}(COO)$ and $\nu_s(COO)$, respectively − of the coordinated carboxylate groups. The differences ($\Delta = \nu_{as} - \nu_s$) between $\nu_{as}(COO)$ and $\nu_s(COO)$ (135 cm^{-1} for **1**, 131 cm^{-1} for **2**, and 122 cm^{-1} for **3**) are significantly smaller than the corresponding value of 200 cm^{-1} for the free maleate dianions,[11] indicating a bidentate bridging coordination mode of the carboxylate groups.[12] This is in accordance with the result of X-ray diffraction analysis. In addition, the strong and broad band centered at 3450 cm^{-1} for **2** is attributable to the H−O−H stretching vibration of the lattice water molecule on the basis of the known structure. The medium absorptions at 3051 cm^{-1} for **1**, 3053 cm^{-1} for **2**, and 3046 cm^{-1} for **3** can be attributed to δ(=C−H) of maleate.

Magnetic Properties

Variable-temperature magnetic susceptibility measurements in the 5−300 K range were carried out for complexes **2** and **3**, and are shown in Figure 7. For **2**, the effective experimental magnetic moment (μ_{eff}) per Mn^{II} ion at room temperature is 5.70 μ_B, slightly lower than that of the uncoupled Mn^{2+} ion ($S = 5/2$; 5.91μ_B), remaining practically constant down to 30 K, and then gradually decreasing with decreasing temperature, reaching a value of 5.20 μ_B at 5 K. The $1/\chi_M$ vs. T plot is essentially linear (see inset in Figure 7), and obeys the Curie−Weiss law [$\chi_M = C/(T - \theta)$] with $C = 4.0\ cm^3\cdot K^{-1}\cdot mol$ and $\theta = -0.85$ K. In view of the known structure of the complex, the experimentally determined magnetic behavior was fitted by use of Equation (1) according to an isotropic Heisenberg model for a linear chain of metal ions with coefficients generated by Hiller et al.[13] for $S = 5/2$, where $A = 2.9167$, $B = 208.04$, $C = 15.543$, $D = 2707.2$, and $X = J/kT$. The best fitting parameters obtained are $J = -0.06\ cm^{-1}$, $g = 1.96$, with an agreement factor $R = 4.00\cdot10^{-4}$. This very small J value indicates very weak coupling interactions between the metal ions mediated by a triatomic *syn-anti* carboxylate group bridge, or practically a non-coupled system.

$$\chi_M = \left(Ng^2\beta^2/kT\right)(A + BX^2)(1 + CX + DX^3)^{-1} \quad (1)$$

For **3**, the experimentally determined effective magnetic moment at room temperature is 5.89 μ_B per Mn^{II} ion, very close to that of a magnetically isolated Mn^{2+} ion ($S = 5/2$; 5.91 μ_B). Upon cooling, the value decreases continuously down to 2.95 μ_B at 5 K, indicating an overall antiferromagnetic coupling interaction between the metal ions. From the known structural data, there are two types of magnetic exchange pathways between adjacent Mn^{2+} centers: one occurs between two doubly carboxylate-bridged (*syn-syn*

 © 2003 Wiley-VCH Verlag GmbH & Co. KGaA, Weinheim

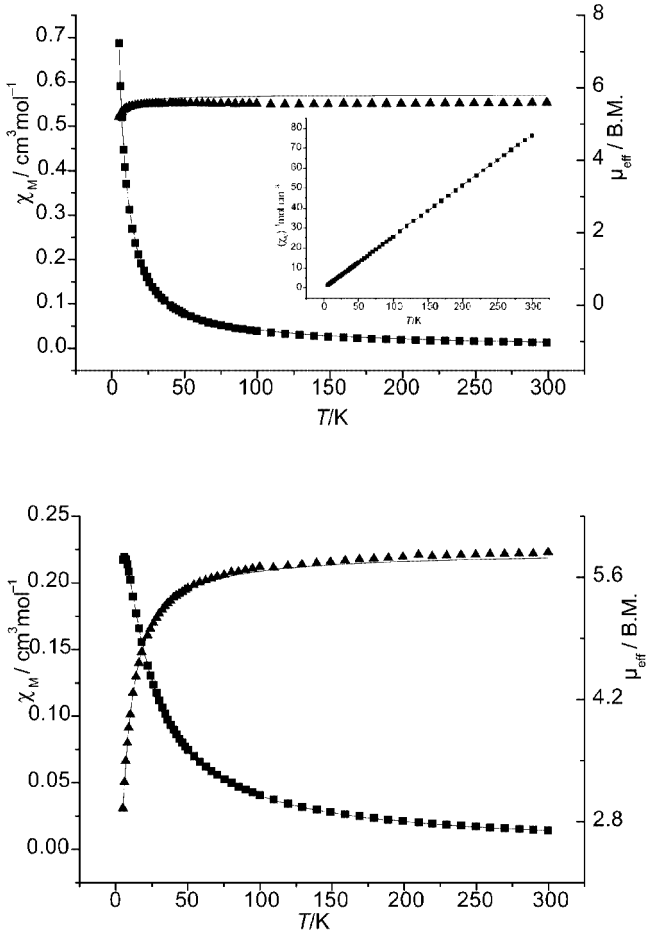

Figure 7. Experimental susceptibilities (χ_M, marked as square) and effective magnetic moment (μ_{eff}, marked as triangle) as functions of the temperature for complex **2** (top) and **3** (bottom); the solid lines represent the calculated values

mode) Mn^{2+} ions, and the other between singly carboxylate-bridged (*anti-anti* mode) Mn^{2+} ions. In view of the long separation (6.390 Å) of the *anti-anti*-bridged Mn^{2+} ions, we can simplify the coupling interaction system as a dimanganese(II) moiety, and simulate the magnetic behavior by use of Equation (2)[14] deduced from the Hamiltonian $\hat{H} = -J\hat{S}_1 \cdot \hat{S}_2$.

$$\chi_{bi} = \frac{2Ng^2\beta^2}{kT}\left[\frac{55+30\exp\left(-\frac{5J}{kT}\right)+14\exp\left(-\frac{9J}{kT}\right)+5\exp\left(-\frac{12J}{kT}\right)+\exp\left(-\frac{14J}{kT}\right)}{11+9\exp\left(-\frac{5J}{kT}\right)+7\exp\left(-\frac{9J}{kT}\right)+5\exp\left(-\frac{12J}{kT}\right)+\exp\left(-\frac{14J}{kT}\right)}\right] \quad (2)$$

To improve on the calculated expression, a mean molecular field approximation term[15] zJ' was added to describe the inter-dimer Mn^{2+} unit exchange interactions. The expression for the magnetic susceptibility becomes $\chi_M = \chi_{bi}/(1 - zJ' \cdot \chi_{bi}/Ng^2\beta^2)$. A satisfactory fitting result with parameters $J = -1.3$ cm^{-1}, $zJ' = -0.27$ cm^{-1}, $g = 1.99$, and the agreement factor $R = 3.25 \cdot 10^{-5}$ was obtained over the full temperature range.

All magnetic coupling interaction parameter values (J and zJ') fall in the normal range for two adjacent Mn^{2+} ions through the carboxylate group pathway, and the difference in the magnitude of the magnetic coupling interactions found for **2** and **3** can be explained in terms of the bridging modes of the carboxylate group and the overlap of d-p magnetic orbitals. As would be expected on the basis of the respective geometries, there is an efficient overlap between the 3d magnetic orbital of the Mn^{2+} center and the 2p magnetic orbital of the carboxylate group O in the order *syn-syn* > *anti-anti* > *syn-anti* (Scheme 2).[16] In good agreement with this, despite the larger separation of Mn···Mn (6.390 Å) in **3** than in **2** (4.976 Å), the corresponding exchange interaction value $zJ' = -0.27$ cm^{-1} in the *anti-anti* mode is larger than that of the *syn-anti* mode ($J = -0.06$ cm^{-1}, so small that the interaction is actually negligible) for **2**. Also, the *syn-syn* mode in complex **3** results in the largest J value, showing that the *syn-syn* carboxylate group bridge is more favorable than the others for transmission of the magnetic coupling interaction.[17]

Conclusion

We have obtained three novel manganese(II) polymeric complexes **1**, **2**, and **3**, variously possessing 1D zigzag chain and 2D sinuous layer structures, based on maleic acid in the presence of ancillary α,α′-diimine ligands (1,10-phenanroline and 2,2′-bipyridine). Very similar ancillary chelate ligands result in different structural topologies, which may be attributable to the different ring areas of the two delocalized aromatic diimine ligands, suggesting that the polymeric coordination framework may be designed and synthesized according to the inherent steric constraint and interactive information stored in organic ligands and metal ions,[4a,18] or modified through appropriate ancillary ligands. Studies on the magnetic properties of the complexes revealed weak antiferromagnetic coupling interactions between the paramagnetic Mn^{II} sites mediated to different degrees by the carboxylate group bridges in *syn-syn*, *anti-anti*,

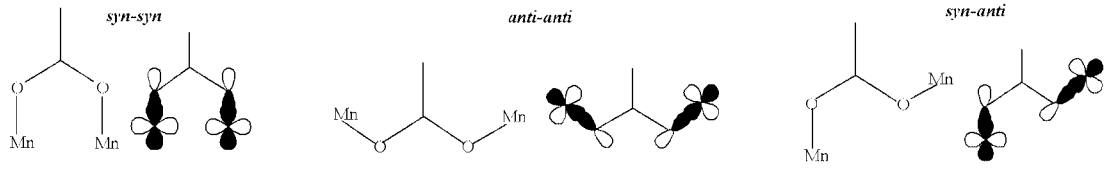

Scheme 2. Schematic representations of the coordination modes for the triatomic carboxylate bridge and the overlap of d-p magnetic orbitals

 © 2003 Wiley-VCH Verlag GmbH & Co. KGaA, Weinheim

and *syn-anti* modes. The magnitudes of the *J* values for the interactions can be explained in terms of the efficient overlap between the magnetic orbitals. Various bridging modes of the carboxylate groups give the order *J* (*syn-syn*) > *J* (*anti-anti*) > *J* (*syn-anti*) for the interactions.

Experimental Section

General: All chemicals were of reagent grade and were used as received. Elemental analyses were performed with a Vario EL III CHNOS element analyzer, and the metal analysis was carried out by standard EDTA titration methods. IR spectra of KBr pellets (4000−400 cm^{-1}) were recorded with a Magna-75-FT-IR spectrophotometer.Variable-temperature susceptibility was measured with a model CF-1 superconducting magnetometer with a crystalline sample kept in a capsule at 4.5−300 K. Diamagnetic corrections were made with Pascal's constants for all the constituent atoms of the determined complexes.

Synthesis of [[Mn($C_4H_2O_4$)($C_{12}H_8N_2$)]$_n$ (1): A solution of 1,10-phenanthroline (0.20 g, 1 mmol) in ethanol (10 mL) was added to a suspension of $MnCO_3$ (0.12 g, 1 mmol) and maleic acid (0.17 g, 1 mmol) in water (20 mL). The mixture was heated at reflux for 8 d, during which yellow crystals were produced. These were collected to afford **1** (0.08 g, yield 22.6% based on Mn). $C_{16}H_{10}MnN_2O_4$ (349.20): calcd. C 55.03, H 2.89, Mn 15.73, N 8.02; found C 54.76, H 3.07, Mn 15.98, N 8.11. IR: $\tilde{\nu}$ = 3051 (m), 1633 (m), 1620 (s), 1560 (vs), 1514 (m), 1425 (s), 1402 (w), 1346 (w), 1309 (vs), 1200 (w), 1144 (w), 1101 (w), 1088 (w), 889 (m), 850 (s), 783 (m), 731 (s), 661 (w), 634 (w), 619 (m), 550 (m), 418 (m) cm^{-1}.

Synthesis of [Mn($C_4H_2O_4$)($C_{12}H_8N_2$)]$_n$·$n$$H_2O$ (2): 1,10-Phenanthroline (0.40 g, 2 mmol) in ethanol (5 mL) was added dropwise with continuous stirring to an EtOH/H_2O (ca. 1:2, v/v, 20 mL) solution of maleic acid (0.34 g, 2 mmol), NaOH (0.16 g, 4 mmol), and $MnSO_4$·H_2O (0.34 g, 2 mmol). The resulting yellow solution was stirred for 10 min at room temperature, then filtered. The filtrate was left undisturbed for about one week to produce yellow crystals, which were collected and air-dried to afford **2** (0.48 g, yield 65.5% based on Mn). $C_{16}H_{12}MnN_2O_5$ (367.22): calcd. C 52.33, H 3.29, Mn 14.96, N 7.63; found C 52.56, H 3.13, Mn 15.21, N 7.41. IR: $\tilde{\nu}$ = 3450 (br), 3053 (m), 1635 (m), 1616 (s), 1558 (vs), 1516 (m), 1427 (s), 1394 (m), 1346 (m), 1306 (vs), 1200 (m), 1144 (m), 1101 (m), 991 (w), 891 (m), 866 (m), 850 (vs), 779 (m), 729 (s), 667 (w), 638 (w), 621 (m), 550 (m), 418 (m) cm^{-1}.

Synthesis of [Mn($C_4H_2O_4$)($C_{10}H_8N_2$)]$_n$ (3): The procedure used was similar to that for the preparation of **2**, except that 2,2′-bipyridine (0.31 g, 2 mmol) was used instead of 1,10-phenanthroline. Yellow crystals of **3** (0.26 g) were obtained in 40% yield. $C_{14}H_{10}MnN_2O_4$ (325.18): calcd. C 51.71, H 3.10, Mn 16.89, N 8.61; found C 51.64, H 2.98, Mn 16.97, N 8.54. IR: $\tilde{\nu}$ = 3046 (m), 1647 (w), 1595 (w), 1585 (w), 1551 (vs), 1491 (w), 1475 (m), 1429 (s), 1396 (s), 1317 (vs), 1284 (w), 1248 (w), 1217 (m), 1173 (w), 1157 (m), 1101 (w), 1059 (m), 1014 (s), 974 (m), 895 (m), 862 (m), 835 (w), 816 (w), 773 (s), 737 (m), 650 (m), 631 (m), 559 (m), 417 (m) cm^{-1}.

X-ray Crystallography: Intensity data were collected at 293 K with a Siemens SMART CCD diffractometer equipped with graphite-monochromated Mo-K_α radiation (λ = 0.71073 Å). Data were corrected for LP factors and empirical absorption correction was applied. The structures were solved by direct methods and refined on F^2 by the full-matrix, least-squares technique through use of the SHELXTL-97 program package.[19] All non-hydrogen atoms were refined anisotropically, and hydrogen atoms were introduced geometrically, with the exception of the lattice water hydrogen atoms, which were located from the difference Fourier syntheses. Crystallographic data of **1**−**3** are outlined in Table 3. CCDC- 201331 to -201333 contain the supplementary crystallographic data for complexes **1**−**3**. These data can be obtained free of charge at www.ccdc.cam.ac.uk/conts/retrieving.html [or from the Cambridge Crystallographic Data Centre, 12 Union Road, Cambridge CB2 1EZ, UK; Fax: (internat. + 44-1223/336-033; E-mail: deposit@ccdc.cam.ac.uk].

Acknowledgments

This work was supported by the NNSFC (No. 30170229), the State Key Basic Research and Development Plan of China

Table 3. Crystallographic data for **1**−**3**

	1	**2**	**3**
Empirical formula	$C_{16}H_{10}MnN_2O_4$	$C_{16}H_{12}MnN_2O_5$	$C_{14}H_{10}MnN_2O_4$
Formula mass	349.20	367.22	325.18
Space group	$P\bar{1}$	$P\bar{1}$	$P2_1/c$
a [Å]	8.2130(8)	8.1189(4)	11.4539(3)
b [Å]	8.4237(8)	9.3033(4)	13.3059(5)
c [Å]	10.5907(1)	10.5462(5)	8.8068(3)
α [°]	74.579(2)	104.65(1)	90
β [°]	84.621(2)	95.141(2)	111.429(1)
γ [°]	73.462(2)	105.327(1)	90
V [Å^3]	676.98(1)	732.76(6)	1249.41(7)
Z	2	2	4
T [°C]	20	20	20
λ(Mo-K_α) [Å]	0.71073	0.71073	0.71073
μ [mm^{-1}]	0.998	0.932	1.075
$\rho_{calcd.}$ [g cm^{-3}]	1.713	1.664	1.729
R[a]	0.0370	0.0621	0.0328
wR[b]	0.0928	0.1482	0.0856

[a] $R = \||F_o| - |F_c|\|/|F_o|$. [b] $wR = [w(|F_o| - |F_c|)^2/wF_o^2]^{1/2}$; **1**: $w = 1/[\sigma^2(F_o)^2 + (0.0577P)^2 + 0.2075P]$; **2**: $w = 1/[\sigma^2(F_o)^2 + (0.0985P)^2 + 0.0000P]$; **3**: $w = 1/[\sigma^2(F_o)^2 + (0.0520P)^2 + 0.8333P]$; $P = [(F_o)^2 + 2(F_c)^2]/3$ for all complexes.

 © 2003 Wiley-VCH Verlag GmbH & Co. KGaA, Weinheim

(G1998010100), and the Expert Project of Key Basic Research of the Ministry of Science and Technology.

[1] [1a] H. O. Stump, L. Ouahab, Y. Pei, D. Gradjen, O. Kahn, *Science* **1993**, *261*, 447−449. [1b] B. Moulton, M. J. Zaworotko, *Chem. Rev.* **2001**, *101*, 1629−1658. [1c] S. Konar, P. S. Mukherjee, E. Zangrando, F. Lloret, R. N. Chaudhuri, *Angew. Chem. Int. Ed.* **2002**, *41*, 1561−1563. [1d] K. Inoue, T. Hayamizu, H. Iwamura, D. Hasaizume, Y. Ohashi, *J. Am. Chem. Soc.* **1996**, *118*, 1803−1804. [1e] F. Millange, C. Serre, G. Ferey, *Chem. Commun.* **2002**, 822−823. [1f] E. W. Lee, Y. Kim, D.-Y. Jung, *Inorg. Chem.* **2002**, *41*, 501−506. [1g] R. Robson, *J. Chem. Soc., Dalton Trans.* **2000**, 3735−3744.

[2] [2a] M. Fujita, D. Oguro, M. Milyazawa, H. Oka, K. Yamaguchi, K. Oguro, *Nature* **1995**, *378*, 469−471. [2b] D. Braga, F. Grepioni, G. R. Desiraju, *Chem. Rev.* **1998**, *98*, 1375−1405. [2c] Y.-C. Liang, R. Cao, W.-P. Su, M.-C. Hong, W.-J. Zhang, *Angew. Chem. Int. Ed.* **2000**, *39*, 3304−3307. [2d] O. M. Yaghi, H. L. Li, C. Davis, D. Richardson, T. L. D. Groy, *Acc. Chem. Res.* **1998**, *31*, 474−484.

[3] T. K. Maji, S. Sain, G. Mostafa, T.-H. Lu, J. Ribas, M. Monfort, N. R. Chaudhuri, *Inorg. Chem.* **2003**, *42*, 709−716 and references therein.

[4] [4a] J. M. Lehn, *Supramolecular Chemistry − Concepts and Perspectives*, VCH, Weinheim, **1995**. [4b]P. Losier, M. J. Zaworotko, *Angew. Chem. Int. Ed. Engl.* **1996**, *35*, 2779−2782.

[5] [5a] W.-G. Wang, C.-B. Ma, X.-F. Zhang, C.-N. Chen, Q.-T. Liu, F. Chen, D.-Z. Liao, L.-C. Li, *Bull. Chem. Soc., Jpn.* **2002**, *75*, 2609−2614. [5b] C.-B. Ma, C.-N. Chen, Q.-T. Liu, D.-Z. Liao, L.-C. Li, *Eur. J. Inorg. Chem.* **2003**, 1227−1231. [5c] C.-B. Ma, C.-N. Chen, Q.-T. Liu, D.-Z. Liao, L.-C. Li, L.-C. Sun, *New J. Chem.* **2003**, *27*, 890−894.

[6] [6a] S. S. Y. Chui, S. M. F. Lo, J. P. H. Charmant, A. G. Orpen, I. D. Williams, *Science* **1999**, *283*, 1148−1150. [6b] J. D. Dunitz, *Chem. Commun.* **2003**, 545−548.

[7] M.-X. Li, G.-Y. Xie, S.-L. Jin, Y.-D. Gu, M.-Q. Chen, J. Liu, Z. Xu, X.-Z. You, *Polyhedron* **1996**, *15*, 535−539.

[8] Z. Shi, L.-R. Zhang, S. Gao, G.-Y. Yang, J. Hua, L. Gao, S.-H. Feng, *Inorg. Chem.* **2000**, *39*, 1990−1993.

[9] C.-G. Zhang, Y.-J. Leng, Z.-F. Ma, D.-Y. Yan, *J. Chem. Crystallogr.* **1999**, *29*, 1081−1084.

[10] [10a] C.-G. Zhang, K.-B. Yu, D. Wu, C.-X. Zhao, *Acta Crystallogr., Sect. C* **1999**, *55*, 1470−1473. [10b] Y.-Q. Zheng, J. Sun, J.-L. Lin, *Z. Anorg. Allg. Chem.* **2002**, *628*, 1397−1401. [10c] C.-G. Zhang, C.-X. Zhao, Z.-F. Ma, D.-Y. Yan, *J. Coord. Chem.* **2000**, *52*, 87−92.

[11] D. N. Sathyanarayana, V. V. Savant, *Z. Anorg. Allg. Chem.* **1971**, *385*, 329−331.

[12] G. B. Deacon, R. J. Phillips, *Coord. Chem. Rev.* **1980**, *33*, 227−250.

[13] W. Hiller, J. Strahle, A. Datz, M. Hanack, W. E. Hatfield, L. W. TerHaar, P. Gutlich, *J. Am. Chem. Soc.* **1984**, *106*, 329−335.

[14] O. Kahn, *Molecular Magnetism*, VCH Publishers Inc., New York, **1993**.

[15] R. L. Carlin, *Magnetochemistry*, Springer, Berlin, Heidelberg, **1986**.

[16] [16a] Z.-N. Chen, S.-X. Liu, T. Qiu, Z.-M. Wang, J.-L. Huang, W.-X. Tang, *J. Chem. Soc., Dalton Trans.* **1994**, 2989−2993. [16b] E. Colacio, J. M. Dominguez-Vera, M. Ghazi, R. Kivekäs, M. Klinga, J. M. Moreno, *Eur. J. Inorg. Chem.* **1999**, 441−445.

[17] [17a] M. Inoue, M. Kubo, *Inorg. Chem.* **1970**, *9*, 2310−2314. [17b] R. L. Carlin, K. Kopinga, O. Kahn, M. Verdauger, *Inorg. Chem.* **1990**, *29*, 4240−4246.

[18] R. Cao, D. F. Sun, Y. C. Liang, M. C. Hong, K. Tatsumi, Q. Shi, *Inorg. Chem.* **2002**, *41*, 2087−2094.

[19] G. M. Sheldrick, *SHELXL-97*, Universität Göttingen, **1997**.

Received February 19, 2003

 © 2003 Wiley-VCH Verlag GmbH & Co. KGaA, Weinheim

Ferromagnetism in $[Mn(Cp^*)_2]^+$-Derived Complexes: the "Miraculous" Stacking in $[Mn(Cp^*)_2][Ni(dmit)_2]$

Christophe Faulmann,*[a] Eric Rivière,[b] Stéphane Dorbes,[a] François Senocq,[c] Eugenio Coronado,[d] and Patrick Cassoux[a]

Dedicated to Patrick Cassoux on the occasion of his recent retirement[‡]

Keywords: Metallocenes / Magnetic properties / Manganese / S ligands

The synthesis and characterisation (X-ray structure and magnetism) of metal complexes (Ni, Au) with the $[Mn(Cp^*)_2]^+$ cation and the $dmit^{2-}$ and $dmid^{2-}$ ligands are reported. $[Mn(Cp^*)_2][Ni(dmit)_2]$ (**1**) and $[Mn(Cp^*)_2][Au(dmit)_2]$ (**2**) exhibit the same structural arrangement, built on stacks of $[Ni(dmit)_2]^-$ pairs separated by two $[Mn(Cp^*)_2]^+$ cations, showing a $\cdots D^+D^+A^-A^-D^+D^+A^-A^-\cdots$ motif. On the contrary, the $dmid^{2-}$ derivative $[Mn(Cp^*)_2][Ni(dmid)_2]\cdot CH_3CN$ (**3**) exhibits a totally different structure, built on mixed layers composed of one $[Ni(dmid)_2]^-$ unit separated by two $[Mn(Cp^*)_2]^+$ cations, showing a $\cdots D^+D^+A^-D^+D^+A^-\cdots$motif. The layers are separated from each other by perpendicular $[Ni(dmid)_2]^-$ units and solvent molecules. Compound **2** exhibits antiferromagnetic interactions, whereas **1** and **3** exhibit ferromagnetic interactions at low temperature. Moreover, as confirmed by AC and DC magnetic susceptibility measurements, **1** is a ferrimagnet, the first ever derived from a 1,2-bis-dithiolene ligand. The ferromagnetic interactions in **1** and **3** are explained using the McConnell I mechanism.

(© Wiley-VCH Verlag GmbH & Co. KGaA, 69451 Weinheim, Germany, 2003)

Introduction

Since the discovery of metamagnetism in the molecule-based solid, $[Fe(Cp^*)_2](TCNQ)$,[1] (Cp^* = pentamethylcyclopentadienyl; TCNQ = tetracyanoquinodimethane), several studies have been carried out with the aim of substituting planar metal-organic complexes with the organic TCNQ acceptor and varying the nature of the metallocene; the complexes $[Fe(Cp^*)_2](TCNE)$[2] (TCNE = tetracyanoethylene), $[Mn(Cp^*)_2](TCNQ)$[3] and $[Mn(Cp^*)_2](TCNE)$[4] have been proven to be bulk ferromagnets. These compounds are structurally analogous, and their structures consist of parallel chains of alternating donor cations (D^+) and acceptor anions (A^-), thus showing a $D^+A^-D^+A^-$ motif.

There are two possible models that may explain the ferromagnetic coupling between the metallocenium $[M(Cp^*)_2]^+$ cation and the acceptor ($TCNE^-$ or $TCNQ^-$) (see ref.[5] and papers cited therein). The first explanation was proposed by Miller et al.[2] and is based on the McConnell II mechanism[6] which involves charge transfer, whereas the second one (based on the McConnell I mechanism[7]) was proposed later by Kahn and co-workers[8] and involves spin polarisation effects. Schweizer and co-workers recently[5] showed that the McConnell I mechanism can partly explain the ferromagnetic interactions within $[Fe(Cp^*)_2](TCNE)$, however no clear-cut evidence for the first or the second mechanism has really emerged. Even more recently, the results of a solid-state NMR study on various paramagnetic metallocenium ions[9] were in agreement with all the requirements for the McConnell I mechanism. Whatever the mechanism, a 1-D structure with a $D^+A^-D^+A^-$ motif was believed to be a prerequisite for the synthesis of molecular ferromagnets.[10] The metal bis-dithiolene complexes $[M(S_2C_2R_2)_2]^-$ have been used as acceptors in order to achieve such 1D-chains, since they are able to form either alternating or segregated stacks, depending on the associated cations. These metal complexes are excellent candidates for achieving the requirements for cooperative magnetic phenomena, due to the presence of peripheral het-

[‡] For his enormous contribution in the field of the $M(dmit)_2$ systems.

[a] Equipe Précurseurs Moléculaires et Matériaux, LCC-CNRS, 205 route de Narbonne 31077 Toulouse Cedex 04, France
Fax: (internat.) +33-5/61 55 30 03
E-mail: faulmann@lcc-toulouse.fr
[b] Laboratoire de Chimie Inorganique, ICMO Bât. 420, Université Paris-Sud, 91405 Orsay Cedex, France.
[c] CIRIMAT ENSIACET, 118, Route de Narbonne, 31077 Toulouse Cedex 04, France
[d] Instituto de Ciencia Molecular (ICMol), Universitat de Valencia, Dr Moliner, 50, 46100 Burjassot, Spain

Supporting information for this article is available on the WWW under http://www.eurjoc.org or from the author.

 © 2003 Wiley-VCH Verlag GmbH & Co. KGaA, Weinheim **DOI: 10.1002/ejic.200300087**

eroatoms which might favour extended magnetic interactions. Most of the molecular charge-transfer salts previously synthesised and studied are based on the decamethylferrocenium cation, $[Fe(Cp^*)_2]^+$, in combination with metal bis-dithiolene complexes including those involving the $dmit^{2-}$ ligand[11–14] ($dmit^{2-}$ = $C_3S_5^{2-}$= 2-thioxo-1,3-dithiole-4,5-dithiolato), the mnt^{2-} ligand[15,16] [mnt^{2-} = $(NC)_2C_2S_2^{2-}$ = maleonitriledithiolato] and the tfd^{2-} ligand[15,17] [tfd^{2-} = $(F_3C)_2C_2S_2^{2-}$ = bis(trifluoromethyl)-ethylenedithiolato]. Recent studies have also focused on complexes of edt^{2-} and $dmid^{2-}$ (also called $dmio^{2-}$)[14,18–20] (edt^{2-} = $C_2H_2S_2^{2-}$ = ethylenedithiolato; $dmid^{2-}$ = $C_3OS_4^{2-}$= 2-oxo-1,3-dithiole-4,5-dithiolato).

From the studies on all these complexes, two conclusions can be drawn: their structures do not always exhibit a $D^+A^-D^+A^-$ motif (which is, a priori**,** considered as a disadvantage for producing ferromagnetic molecular compounds), and very few of them exhibit ferromagnetic interactions. Nevertheless, substituting Mn for Fe in the metallocenium part has led to complexes with interesting magnetic properties: $[Mn(Cp^*)_2][Ni(tfd)_2]$,[21] $[Mn(Cp^*)_2][Ni(bdt)_2]$[18] (bdt^{2-} = $C_6H_4S_2^{2-}$ = 1,2-benzenedithiolato) and $[Mn(Cp^*)_2][Ni(dmit)_2]$[22] (**1**) exhibit long range magnetic ordering at low temperature, whereas the $[Fe(Cp^*)_2]$-based analogues only exhibit ferromagnetic interactions. Therefore, with the intention of understanding the differences in the magnetic behaviour, and after the promising results obtained for $[Mn(Cp^*)_2][Ni(dmit)_2]$,[22] we here present a more detailed characterisation of the latter compound and the synthesis and characterisation of two new compounds based on the manganocenium cation, namely $[Mn(Cp^*)_2][Au(dmit)_2]$ (**2**) and $[Mn(Cp^*)_2][Ni(dmid)_2]\cdot CH_3CN$ (**3**).

Results and Discussion

Synthesis

Complexes **1**, **2** and **3** were obtained by slow addition of an acetonitrile solution of $[Mn(Cp^*)_2]PF_6$ [23] in slight excess to an acetonitrile or acetone solution of the appropriate $(nBu_4N)[M(ligand)_2]$ (ligand = $dmit^{2-}$, $dmid^{2-}$) complex. After concentration, a brown microcrystalline powder was collected by filtration, washed several times with acetonitrile and dried in vacuo. Recrystallisation of this powder from various solvents failed and resulted in the same brown powder. In the case of **1**, small single crystals suitable for an X-ray analysis were sometimes isolated from the microcrystalline powder. On the contrary, a large number of single crystals of **2** and **3** suitable for X-ray analyses could be easily isolated from the corresponding microcrystalline powders.

X-ray Structure of 1, 2 and 3

Although the size of the crystals of **1** was very small (0.1 × 0.1 × 0.03 mm^3), an X-ray study was undertaken and resulted in the collection of 15817 reflections, for which only 596 were observed above $2\sigma(I)$. Nevertheless, in spite of this low quality data set, we have been able to solve the structure of **1** without great difficulty. The crystal and experimental data for **1**, **2**, and **3** are summarised in Table 1.

Complexes **1** and **2** are isostructural with $[Fe(Cp^*)_2]$-$[Ni(dmit)_2]$.[11] The asymmetric unit of **1** and **2** contains one $[Mn(Cp^*)_2]^+$ cation and one $[M(dmit)_2]^-$ anion (M = Ni, Au; Figure 1).

The overall structural arrangement consists of $\cdots D^+D^+A^-A^-D^+D^+A^-A^-\cdots$ stacks comprising side-by-

Table 1. Crystallographic data for complexes **1**, **2** and **3**

	$(Cp^*_2Mn)[Ni(dmit)_2]$ (**1**)	$(Cp^*_2Mn)[Au(dmit)_2]$ (**2**)	$(Cp^*_2Mn)[Ni(dmid)_2]\cdot CH_3CN$ (**3**)
Empirical formula	$C_{26}H_{30}MnNiS_{10}$	$C_{26}H_{30}AuMnS_{10}$	$C_{28}H_{33}MnNNiO_2S_8$
M	776.75	915.01	785.68
Crystal system, space group	Triclinic, $P\bar{1}$	Triclinic, $P\bar{1}$	Monoclinic, $P2_1/a$
a (Å)	11.415(3)	11.7247(13)	16.2904(14)
b (Å)	14.940(3)	15.0702(18)	10.7906(7)
c (Å)	10.020(2)	10.0535(10)	19.3007(18)
α (°)	97.40(3)	96.240(13)	90
β (°)	94.58(3)	95.092(13)	98.570(11)
γ (°)	109.63(3)	111.128(13)	90
V (Å^3)	1582.2(6)	1631.4(3)	3354.9(5)
Z	2	2	4
$D_{calcd.}$ (g.cm^{-1})	1.567	1.863	1.556
μ(Mo-K_α) (cm^{-1})	16.70	55.36	14.63
Data collection			
Temperature (K)	160	293	160
Diffractometer	Stoe IPDS	Stoe IPDS	Stoe IPDS
Scan mode	Φ	Φ	Φ
Scan range Φ (°)	0–250	0–250	0–250
No. of collected reflns.	15817	16326	29197
No. of unique reflns.	5882 [R(int) = 0.770]	6001 [R(int) = 0.085]	6577 [R(int) = 0.039]
No. of reflns. used	5882	6001 [$I > 2\sigma(I)$]	6577
R	0.085	0.0431	0.0267
wR_2	0.12624	0.0564	0.0634
No. of parameters	223	353	505

 © 2003 Wiley-VCH Verlag GmbH & Co. KGaA, Weinheim

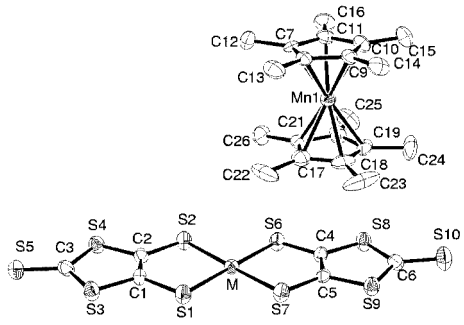

Figure 1. Atomic numbering scheme for complexes **1** and **2** (M = Ni, Au)

side $[Mn(Cp^*)_2]^+$ cations alternating with face-to-face $[M(dmit)_2]^-$ anions, the latter forming slipped dyads (Figure 2)

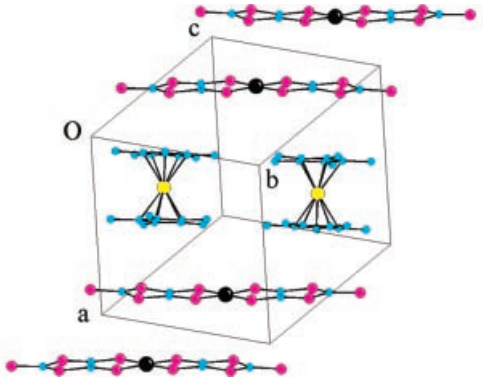

Figure 2. Structure of complexes **1** and **2** showing the ···$D^+D^+A^-A^-D^+D^+A^-A^-$··· motif

The intramolecular distances do not show any significant deviation from those observed for manganocenium-cation-based compounds[3,21] and $M(dmit)_2$-based compounds (M = Ni, Au).[11,12] The pentamethylcyclopentadienyl rings adopt approximately an eclipsed conformation, which is the opposite of the staggered conformation observed in neutral $[Mn(Cp^*)_2]$,[24] but similar to that observed in other decamethylmanganocenium-cation-containing compounds.[3,21] The planes of the Cp* rings are almost parallel to the planes of the $M(dmit)_2$ units (averaged angles of 7.84° and 5.59° for **1**; 6.27° and 4.83° for **2**) and are at averaged distances of 3.52 and 3.63 Å (for **1**) and 3.60 and 3.72 Å (for **2**).

Selected intramolecular distances and angles for **1**, **2**, $[Fe(Cp^*)_2][Ni(dmit)_2]$ and $[Fe(Cp^*)_2][Au(dmit)_2]$ are listed in Table 2. The intermolecular distances between the metal centres are very close to those found for $[Fe(Cp^*)_2]$-$[M(dmit)_2]$ (M = Ni, Au).[11,12] For an identical $M(dmit)_2$ complex, no drastic differences can be seen either between the metallic centres of a D^+D^+ pair (distance M−M in Table 2) or between the metallic centres of an A^-A^- pair (distance M′−M′ in Table 2), The largest difference (0.034 Å) occurs for the M−M′ distances, involving the metal of the cation and the metal of the anion.

Complex **3** is isostructural to $[Fe(Cp^*)_2]$-$[Ni(dmid)_2]\cdot CH_3CN$, reported in 1995 by Fettouhi and co-workers.[20] The asymmetric unit of **3** contains one molecule of acetonitrile, one $[Mn(Cp^*)_2]^+$ cation, and two halves of an $[Ni(dmit)_2]^-$ anion, each Ni atom lying on a centre of inversion (Figure 3).

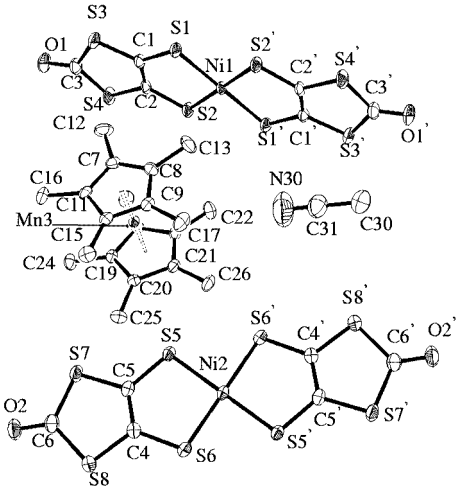

Figure 3. Atomic numbering scheme for the complex **3**

Contrary to what is observed in **1** and **2**, the overall structural arrangement of **3** consists of ···$D^+D^+A^-D^+D^+A^-$··· mixed layers parallel to the *ab* plane and separated in the *c* direction by anionic sheets of $[Ni(dmid)_2]^-$ units, which ensure neutralisation and are almost perpendicular to the mixed layers [angle of 74.35(2)° between the $Ni(dmid)_2$ units; Figure 4].

As for **1** and **2**, the planes of the Cp* rings in **3** are almost parallel to the planes of the $Ni(dmid)_2$ units in the mixed layers: they form angles of 3.38° and 3.96° and are at distances of 3.97 and 4.26 Å. Averaged and selected bond lengths and angles for **3** and $[Fe(Cp^*)_2][Ni(dmid)_2]\cdot CH_3CN$ are shown in Table 3. The Mn−Mn distance within the mixed layers is 8.250(1) Å, the shortest Mn−Ni distances are 5.911(1), 6.778(1), 6.805(1) and 7.218(1) Å and the

Table 2. Selected shortest intermolecular distances (Å) for some isostructural $[M(Cp^*)_2][M'(bis\text{-}dithiolene)_2]$ complexes

Compound	**1**	$[Fe(Cp^*)_2][Ni(dmit)_2]$	Difference	**2**	$[Fe(Cp^*)_2][Au(dmit)_2]$	Difference
M−M	8.411(8)	8.412	0.001	8.518(2)	8.523	0.005
M′−M′	5.574(8)	5.563	0.011	5.763(1)	5.755	0.008
M−M′	6.591(7)	6.557	0.034	6.564(1)	6.543	0.021
	7.330(8)	7.299	0.031	7.504(1)	7.469	0.035

 © 2003 Wiley-VCH Verlag GmbH & Co. KGaA, Weinheim

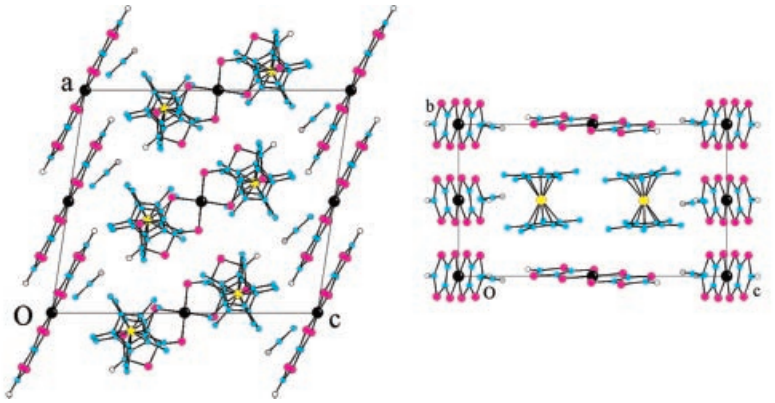

Figure 4. Projection of the structure of **3** onto the *ac* plane and onto the *bc* plane

shortest Ni−Ni distance is 9.770(1) Å. Selected intermolecular distances in **3** and in $[Fe(Cp^*)_2][Ni(dmid)_2]\cdot CH_3CN$ are also reported in Table 3. All intermolecular distances observed between metallic centres are smaller in **3** than in $[Fe(Cp^*)_2][Ni(dmid)_2]\cdot CH_3CN$, but the differences seem rather small, the largest one (0.17 Å) occurring for a large distance of ca. 11.7 Å. The Mn−S or Fe−S intermolecular distances are also similar.

Table 3. Selected shortest intermolecular distances (Å) within $[M(Cp^*)_2][Ni(dmid)_2]\cdot CH_3CN$ (M = Mn, Fe)

Compound	**3** M = Mn	$[Fe(Cp^*)_2][Ni(dmid)_2]$ M = Fe	Difference
M−M	8.250(1)	8.332(4)	0.082
Ni−Ni	9.770(1)	9.82	0.050
	11.056(1)	11.17	0.11
	11.664(1)	11.84	0.17
	13.524(1)	13.59	0.07
M−Ni	5.911(1)	6.003(2)	0.092
	6.778(1)	6.838(2)	0.060
	6.805(1)	7.268(2)	0.050
	7.218(1)		
M−S	5.426(1)	5.449(1)	0.023
	5.438(1)	5.499(6)	0.061
	5.585(1)	6.093(5)	0.010
	5.722(1)		
	6.083(1)		

Powder Diffraction

Powder diffraction was performed on sample **1** only. Analysis of the results at room temperature showed that the space group remains triclinic with the following calculated cell parameters: a = 11.5252(4) Å, b = 15.1281(5) Å, c = 10.1050(4) Å, α = 97.446(3)°, β = 94.662(3)°, γ = 109.683(3)°, to be compared with the values of 11.415(3), 14.940(3), 10.020(2) Å and 97.40(3) °, 94.58(3) °, 109.63(3)° from the single-crystal analysis at 160 K. The observed slight expansion of the lattice can be attributed to the fact that powder data were collected at room temperature, whereas the ones for single-crystal measurement were obtained at 160 K. However, the good agreement between experimental and calculated data (see Table S1 and Figure S1 in the Supporting Information) shows that the analysed powder sample retains the structure obtained from the single crystal.

Magnetic Properties of 1, 2 and 3

Magnetic studies were performed on polycrystalline powders, between 2 and 300 K.

[Mn(Cp)₂][Ni(dmit)₂] (1)*

The magnetic behaviour of **1** (in the form $\chi_M T$ versus T) is shown in Figure 5. $\chi_M T$ is equal to 1.71 emu·mol^{-1}·K at room temperature which is slightly higher than the value expected for two magnetically isolated Mn^{III} and Ni^{III} ions {1.61 emu·mol^{-1}·K, taking g values equal to 2.20 and 2.06 for $[Mn(Cp^*)_2]^+$ and $[Ni(dmit)_2]^-$, respectively}.[25,26] Such an experimental value is not surprising, since it has also been observed for several dithiolene complexes,[15,17,21,27] and is generally attributed to the anisotropic nature of the g factors of the decamethylmanganocenium[23] ion and to a partial orientation of the polycrystalline powder.

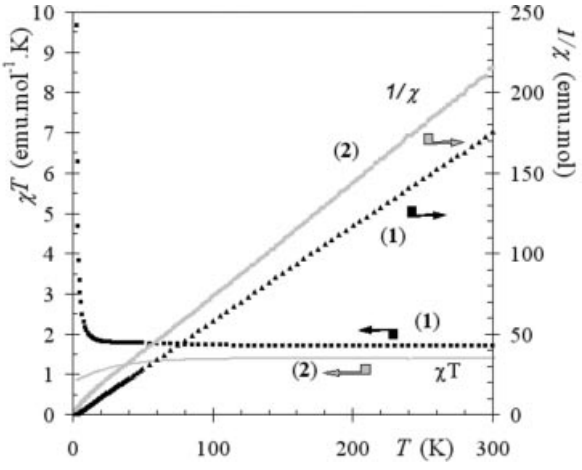

Figure 5. Temperature dependence of the magnetic susceptibility for **1** and **2**

 © 2003 Wiley-VCH Verlag GmbH & Co. KGaA, Weinheim

The $\chi_M T$ value is constant down to ca. 30 K, and the plot of χ_{M-1} versus T is linear, indicating that the susceptibility of **1** follows the Curie−Weiss law, with a Weiss parameter, θ, of 2.5 K. This positive value indicates that ferromagnetic interactions dominate. As the temperature is lowered, $\chi_M T$ increases rapidly and reaches a value of 9.65 emu K mol^{-1} at 3 K. This behaviour is typical of ferromagnetic interactions. Below this temperature, the magnetic susceptibility becomes field dependent indicating that the compound exhibits a long-range magnetic ordering. This is confirmed by the field cooled (FCM), zero field cooled (ZFC) and remnant (REM) magnetisation curves shown in Figure 6a. The FCM curve presents a break around 2.5 K and the REM vanishes at the same temperature suggesting an ordering temperature, T_c, of about 2.5 K. Magnetisation versus field behaviour at 2 K is given in Figure 6b and bears out the ferromagnetic coupling between the Mn^{III} and Ni^{III} ions. At first sight, the magnetisation increases very rapidly at low field, as expected for a magnet, and then increases smoothly above 1000 G. At 50000 G, the magnetisation is equal to 2.31 μ_B, which is below the expected saturation value (3.23 μ_B), but well above the expected value for a ferrimagnetic compound (about 1.17 μ_B). Nevertheless, by carefully checking the magnetic-field dependence of **1** (see inset in Figure 6b), one can observe that the magnetisation increases sharply only up to about 1.3 μ_B. This value is already reached around 200 G, and then increases smoothly up to 2.31 μ_B at 50000 G. Such a behaviour is not consistent with the properties of a ferromagnet. Therefore **1** must be regarded as a ferrimagnet instead of a ferromagnet. Indeed, antiferromagnetic interactions between the $[Ni(dmit)_2]^-$ units ($S = 1/2$) and the $[Mn(Cp^*)_2]^+$ cations ($S = 1$) result in an $S = 1/2$ system. This is in accordance with the observed value of about 1.3 μ_B, slightly larger than 1.17 μ_B, probably due to the large anisotropy of the g factor for the $[Mn(Cp^*)_2]^+$ unit. At higher field, the antiferromagnetic interactions between the $[Ni(dmit)_2]^-$ units and the $[Mn(Cp^*)_2]^+$ cations tend to decrease, resulting in an increase of the magnetisation. Even at high field (55000 G), a slight antiferromagnetic coupling still exists between the $[Ni(dmit)_2]^-$ units and the $[Mn(Cp^*)_2]^+$ cations, which explains why saturation is not reached.

A hysteresis curve was determined at 2 K and is shown in Figure 7. The coercive field H_c is about 3.5 G and confirms that **1** is a magnet. Since these measurements were made just below T_c, this might explain the low value of H_c. Complex **1** is indeed a ferrimagnet and not a metamagnet, as confirmed by the plot of M as a function of H that does not present any curvature at low field, as was observed for $[Fe(Cp^*)_2][Ni(edt)_2]$,[19] $[Mn(Cp^*)_2][Ni(bdt)_2]$[18] and $[Mn(Cp^*)_2][M(tfd)_2]$ (M = Ni, Pd, Pt).[21]

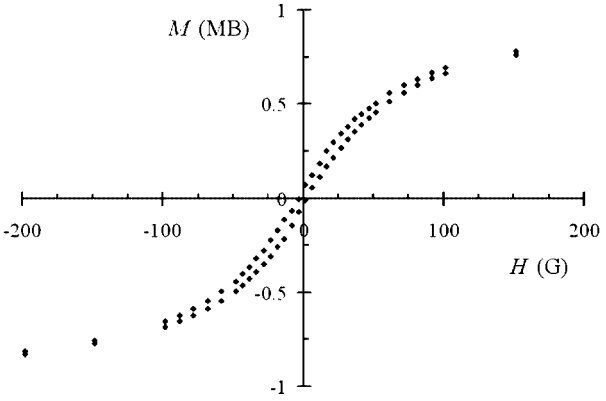

Figure 7. Hysteresis curve at 2 K for **1**

Finally, AC susceptibility measurements (Figure 8) confirm this interpretation: an out-of-phase signal is observed at 2.5 K, indicating a ferromagnetic ordering below this temperature

Such a behaviour has never been observed for any other bis-dithiolene complex. Previously studied metallocenium/metal bis-dithiolene compounds either behave as metamagnets,[18,19,21] or exhibit ferromagnetic interactions[11,15,20] but no ferromagnetic ordering has been reported. Depending on the authors, the ferromagnetic interactions in

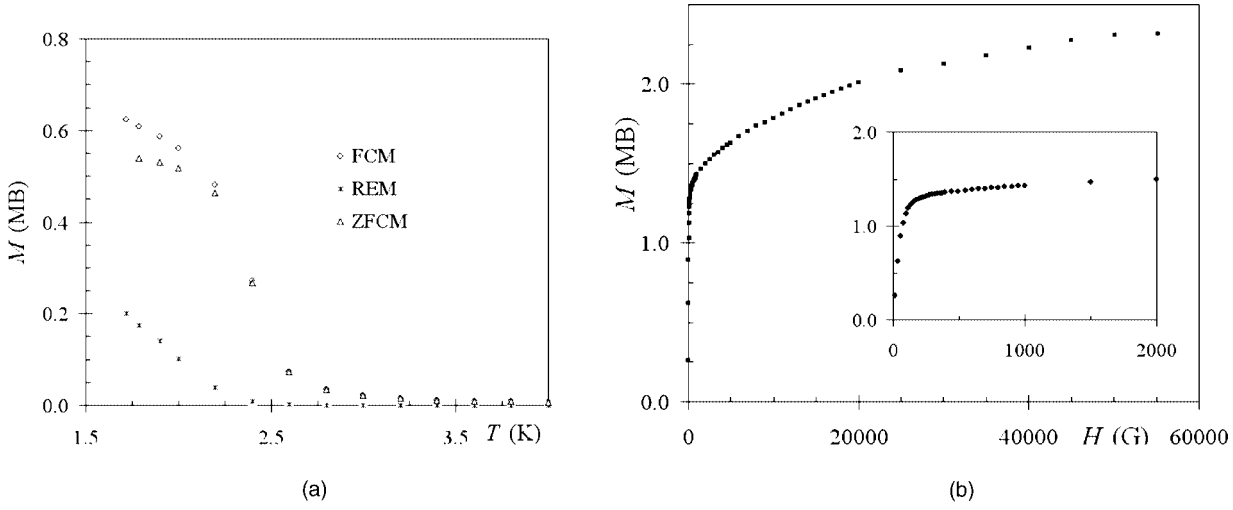

Figure 6. Temperature (a) and field dependence (b) of the magnetisation for **1**

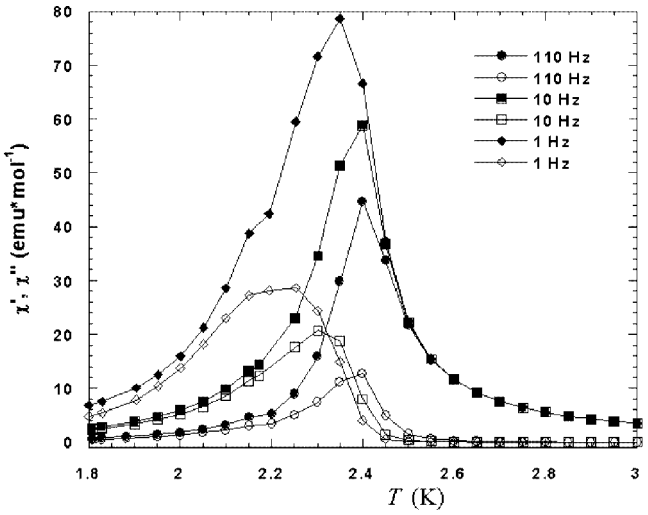

Figure 8. AC susceptibility for compound **1**

these metallocenium/metal bis-dithiolene compounds are explained by using either the McConnell mechanism II[6,11,15] (which involves charge transfer and requires the formation of $[D^{2+}]$ and $[A^{2-}]$ species) or the McConnell mechanism I[7,20] (which involves coupling between spin densities). In the latter, a global ferromagnetism arises when the interaction between spin densities of opposite sign are predominant, whereas a net antiferromagnetism results from dominant interactions between spin densities of the same sign.[28] Such a mechanism, which implies a negative spin-density located on the carbon atoms of the Cp* ring, was proposed by Kahn and co-workers[8] to explain the ferromagnetic properties in $[Fe(Cp^*)_2](TCNE)$, whereas Miller and co-workers preferred the McConnell II mechanism.[2,6] A doubt still existed as to the sign of the spin density on the carbon atoms of the Cp* ring in $[Fe(Cp^*)_2]^+$. A recent reassessment[5] of the magnetic interactions within $[Fe(Cp^*)_2](TCNE)$ has shown that a negative spin density is located on the carbon atoms of the Cp* ring, with a positive density on the carbon atoms of the methyl groups. These conclusions have been confirmed by the work of Heise and co-workers[9] on various paramagnetic metallocenium ions. Using solid-state NMR spectroscopy, these authors have shown unambiguously that a negative spin-density is located over the Cp* ring of $[Mn(Cp^*)_2]^+$ in $[Mn(Cp^*)_2](TCNE)$ and in $[Mn(Cp^*)_2](PF_6)$, and to a certain extent on the H atoms of the methyl groups, whereas a positive density on the C atoms of the methyl groups has been found, confirming previous results.[5,29] Although the stacking in **1** ($\cdots D^+D^+A^-A^-\cdots$) is different from that of $[Mn(Cp^*)_2](TCNE)$ ($\cdots D^+A^-D^+A^-\cdots$), the nature of the molecules constituting these complexes is identical: both are built from one acceptor part [TCNE or $Ni(dmit)_2$] and the same metallocenium ion. Taking these similarities and the various results into account,[5,9,29] the ferromagnetic behaviour of **1** could result from spin-polarisation effects within the McConnell I mechanism.[7] Such a mechanism is based on the interaction between the spin densities of the Cp* rings and the spin densities of the $[Ni(dmid)_2]^-$ anions.[8,30] In the $[Ni(dmit)_2]^-$ anions, positive spin-densities are observed on almost all atoms, except for the S atoms of the outer rings.[31] Three types of interaction may be considered between the spin densities of $[Mn(Cp^*)_2]^+$ and $[Ni(dmit)_2]^-$: the first interaction, between the $[Mn(Cp^*)_2]^+$ cations, should be negligible because of the large inter-cation distances ($d_{Mn-Mn} > 8.4$ Å), with the second one being between the $[Mn(Cp^*)_2]^+$ cations and the $[Ni(dmit)_2]^-$ anions and the third one between $[Ni(dmit)_2]^-$ anions within the slipped $\{[Ni(dmit)_2]_2\}^{2-}$ dyads (see Figure 2). Figure 9a clearly shows that negative-positive spin-density interactions are predominant when considering the overlap between the $[Mn(Cp^*)_2]^+$ cation and the $[Ni(dmit)_2]^-$ anion, which may result in a global ferromagnetic interaction. Within a dyad (Figure 9b), there are only two areas in which negative-positive density interactions can occur, compared to three positive-positive interactions. However, the former two zones imply the NiS_4 core, for which the spin density is larger than on the rest of the molecule, which leads to the conclusion that ferromagnetic interactions dominate also in the dyads.

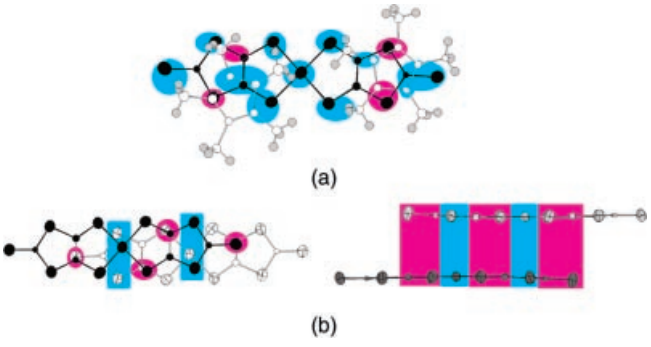

Figure 9. Modes of overlap in **1**: (a) between $[Mn(Cp^*)_2]^+$ and $[Ni(dmit)_2]^-$; (b) within a $\{[Ni(dmit)_2]_2\}^{2-}$ diad; the cyan zones represent the interactions between spin densities of opposite sign and the magenta ones represent the interactions between spin densities with the same sign

This rather qualitative approach seems to be confirmed by the preliminary results of the DFT calculations of the energy of the antiferromagnetic singlet and of the ferromagnetic triplet states as a function of the slipping within a $\{[Ni(dmit)_2]_2\}^{2-}$ dyad.[31] These calculations indicate that the minimum of energy and a ferromagnetic coupling (positive singlet-triplet gap) are observed only for slipping values close to the experimental one (3.55 Å). Consequently, the molecular arrangement in **1** could be described as favourable for ferromagnetic interactions.

$[Mn(Cp^*)_2][Au(dmit)_2]$ (2)

Magnetic measurements on **2** between 300 and 2 K lead to $\chi_M T$ values of around 1.75 emu·K·mol^{-1} at 300 K (much larger than the expected value of 1.21 emu·K·mol^{-1} calculated for an $S = 1$ isolated system, with $<g> = 2.20$). Such

 © 2003 Wiley-VCH Verlag GmbH & Co. KGaA, Weinheim

a large value has already been observed in β-$[Fe(Cp^*)_2]_2$-$[Co(mnt)_2]_2$,[16] but was attributed to contamination by a small amount of ferromagnetic impurities or to traces of other metals in the starting gold complex $HAuCl_4$. If this explanation holds true in the case of **2** (in this case, the impurity might be Fe), a more reasonable value of 1.39 emu·K·mol^{-1} for the $\chi_M T$ product is reached when subtracting this ferromagnetic contribution (see Figure 5). A perfect Curie−Weiss law is then obtained, with a Weiss temperature of −4.2 K and a Curie constant of 1.42.

When lowering the temperature, the product $\chi_M T$ decreases slightly down to ca. 70 K, below which it decreases abruptly. Such a behaviour is typical of dominant antiferromagnetic interactions and is easily explained by the absence of spin carriers (Au^{III} in the $[Au(dmit)_2]^-$ units) between the pairs of manganocenium cations, which are totally isolated from each other. Therefore, no cooperative ferromagnetic interactions can occur in this complex.

[Mn(Cp)$_2$][Ni(dmid)$_2$].CH$_3$CN (3)*

The temperature dependence of $\chi_M T$ and $1/\chi_M$ for **3** is shown in Figure 10. At room temperature, the $\chi_M T$ product is 1.87 emu·K·mol^{-1}, and it increases slightly as the temperature is lowered to about 30 K. Below this temperature $\chi_M T$ increases rapidly and reaches a value of 3.66 cm^3·K·mol^{-1} at 3 K. Below 3 K, $\chi_M T$ decreases but χ_M still continues to increase. This behaviour is similar to that reported by Fettouhi and co-workers for $[Fe(Cp^*)_2]$-$[Ni(dmid)_2]$·CH_3CN.[20] and is typical of dominant ferromagnetic interactions to which weak antiferromagnetic interactions are superimposed. The plot of χ_{M-1} versus T is linear, indicating that the susceptibility of **3** follows the Curie−Weiss law, with a Weiss temperature, θ, of 2.80 K, larger than the one obtained for $[Fe(Cp^*)_2]$-$[Ni(dmid)_2]$·CH_3CN.

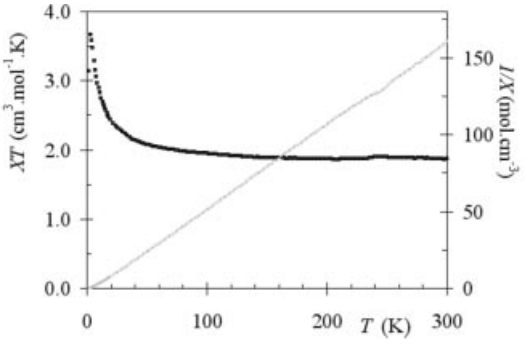

Figure 10. Temperature dependence of the magnetic susceptibility for **3**

The similarity in the behaviours of **3** and $[Fe(Cp^*)_2]$-$[Ni(dmid)_2]$·CH_3CN is not totally surprising as it is only the nature of the metal that changes in the decamethylmetallocenium ion. In contrast, we did not expect that substituting an oxygen atom for a sulfur atom when going from the $Ni(dmit)_2$ complex (**1**) to the $Ni(dmid)_2$ complex (**3**) could lead to such different structural arrangements, and consequently to very different magnetic properties. A possible explanation for the magnetic properties of **3** could be similar to that proposed by Fettouhi and co-workers in the case of $[Fe(Cp^*)_2][Ni(dmid)_2]$·CH_3CN,[20] which is based on the interaction between the negative spin-density of the Cp* rings and the positive spin-density of the sulfur atoms of the $[Ni(dmid)_2]^-$ anions.[30] Indeed, as shown in Figure 11, the overlap between $[Mn(Cp^*)_2]^+$ and $[Ni(dmid)_2]^-$ is such that interactions between spin densities of opposite sign are largely predominant. Unfortunately, however, in the case of **3** there is no clear-cut experimental evidence supporting this interpretation, as was the case for **1**.

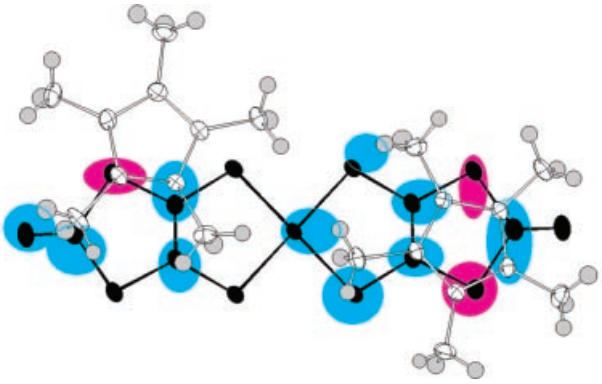

Figure 11. Modes of overlap in **3** between $[Mn(Cp^*)_2]^+$ and $[Ni(dmid)_2]^-$ in the mixed layer; the cyan zones represent the interactions between spin densities of opposite sign and the magenta ones the interactions between spin densities with the same sign

Conclusion

We have shown that by using the same cation $[Mn(Cp^*)_2]^+$ with two different 1,2-bisdithiolene metal complexes $[Ni(dmit)_2$ and $Ni(dmid)_2]$, drastic changes in the structural arrangements occur. This leads to various magnetic properties, with different behaviour. The present study has allowed us to reiterate that in compounds based on metal bis-dithiolene complexes $[M(S_2C_2R_2)_2]^-$ a $D^+A^-D^+A^-$ motif in the structural arrangement is not a prerequisite for promoting ferromagnetic interactions, let alone ferromagnetism. The selection of the $[Mn(Cp^*)_2]^+$ cation, as already recommended by Broderick et al.,[21] has led to compounds which exhibit even more interesting properties than the $[Fe(Cp^*)_2]^+$-based compounds. For example, **1** is the first ferrimagnet to be derived from a metal bis-dithiolene complex whereas $[Fe(Cp^*)_2][Ni(dmit)_2]$ exhibits only ferromagnetic interactions, and **3** presents stronger ferromagnetic interactions than its iron analogue, $[Fe(Cp^*)_2][Ni(dmid)_2]$·CH_3CN. Nevertheless, due to the complexity and diversity of the structures, and in spite of possible comparison with various compounds, the understanding of their magnetic behaviour remains at the qualitative level. Theoretical DFT calculations are currently in progress to give a better insight into

 © 2003 Wiley-VCH Verlag GmbH & Co. KGaA, Weinheim

the origin of the ferromagnetism in **1**.[31] Solid-state NMR spectroscopy, as shown by Heise and co-workers,[9] should provide qualitative as well as quantitative information on the interactions within these materials. Such a study seems to be a very promising tool, since it will take both the intra- and intermolecular effects into account. Indeed, the determination of structure-magnetism relationships in molecular magnetic materials requires not only the study of the direct overlap between neighbouring molecules, but also the consideration of the global packing of the structure, as shown by Veciana and co-workers for α-nitronyl nitroxide radicals.[32] It is important to note that only short intermolecular effects have been considered for the qualitative interpretation of the results reported here. Several complexes based on the $[Mn(Cp^*)_2]^+$ cation and metal complexes of the $dmid^{2-}$ ligand are being studied at present, in order to expand the range of compounds exhibiting such ferromagnetic interactions without the $D^+A^-D^+A^-$ motif.[33]

Experimental Section

General Remarks: Bis(pentamethylcyclopentadienyl)manganese(III) hexafluorophosphate $[Mn(Cp^*)_2]PF_6$ was synthesised from pentamethylferrocenium hexafluorophosphate $[FeCp_2]PF_6$ following the procedure reported by Robbins and co-workers.[23] Tetrabutylammonium bis(1,3-dithiol-2-thione-4,5-dithiolato)nickelate(III), $(nBu_4N)[Ni(dmit)_2]$, tetrabutylammonium bis(1,3-dithiol-2-thione-4,5-dithiolato)aurate(III), $(nBu_4N)[Au(dmit)_2]$, and tetraphenylarsonium bis(1,3-dithiol-2-one-4,5-dithiolato)nickelate(III), $(AsPh_4)[Ni(dmid)_2]$, were synthesised following the literature procedures.[26,34,35] All solvents were dried and distilled prior to use. All syntheses were carried out in an inert atmosphere box or using Schlenk techniques.

$[Mn(Cp^*)_2][Ni(dmit)_2]$ (1): This compound was obtained after slow addition of an acetonitrile solution of $[Mn(Cp^*)_2]PF_6$ (194 mg, 0.413 mmol) to an acetonitrile solution of $(nBu_4N)[Ni(dmit)_2]$ (265 mg, 0.382 mmol). Partial removal of the solvent under reduced pressure, followed by filtration, afforded a brown microcrystalline powder, which was washed several times with acetonitrile and dried in vacuo. $C_{26}H_{30}MnNiS_{10}$ (776.75): calcd. C 40.20, H 3.89, S 41.27; found C 39.62, H 3.26, S 41.15.

$[Mn(Cp^*)_2][Au(dmit)_2]$ (2): Compound **2** was synthesised following the same procedure as for **1**, using 26 mg (0.031 mmol) of $(nBu_4N)[Au(dmit)_2]$, dissolved in 15 mL of acetone and 18 mg (0.038 mmol) of $[Mn(Cp^*)_2]PF_6$ dissolved in 10 mL of acetonitrile. $C_{26}H_{30}AuMnS_{10}$ (915.01) (**2**): calcd. C 34.12, H 3.31, S 35.04; found C, 34.02, H 3.30, S 34.97.

$[Mn(Cp^*)_2][Ni(dmid)_2]\cdot CH_3CN$ (3): Compound **3** was synthesised following the same procedure as for **1**, using 196 mg (0.244 mmol) of $(AsPh_4)[Ni(dmid)_2]$ dissolved in 30 mL of acetonitrile and 122 mg (0.259 mmol) of $[Mn(Cp^*)_2]PF_6$ dissolved in 25 mL of acetonitrile. $C_{28}H_{33}MnNNiO_2S_8$ (785.68): calcd. C 42.80, H 4.24, S 32.64; found C, 42.52, H 4.16, S 31.85.

Magnetic Measurements: DC magnetic data were recorded on a MPMS5 magnetometer (Quantum Design Inc.). The calibration was made at 298 K using a palladium reference sample furnished by Quantum design Inc. AC susceptibility was measured on a SQUID magnetometer Quantum Design MPMS-XL-5.

X-ray Crystallographic Study: The experimental details and crystal data are listed in Table 1. Data collection and cell refinement were performed with a sealed Mo-K_α (λ = 0.71073 Å) X-ray source on a Stoe Imaging Plate Diffraction System (IPDS) diffractometer, using the IPDS software.[36] Crystal decay was monitored by measuring a maximum of 200 reflections per image. The structures were solved using Sir97[37] or Shelxs97[38] and refined with Shelxl97.[39] The calculations were carried out with the WinGX package program[40] running on a PC. The drawings of the molecular structures were performed with CAMERON,[41] ORTEP.[42] The atomic scattering factors are taken from the International Tables for X-ray Crystallography.[43]

$[Mn(Cp^*)_2][Ni(dmit)_2]$ (1): A brown rhombic plate (0.1 mm side and 0.02 mm thick) was selected for the X-ray study. The crystal-to-detector distance was 70 mm. 133 exposures (6 min per exposure) were obtained with $0 < \Phi < 250°$ and with the crystals rotated through 1.5° in Φ in the oscillation mode.

$[Mn(Cp^*)_2][Au(dmit)_2]$ (2): A brown elongated bar ($0.37 \times 0.05 \times 0.05$ mm^3) was selected for the X-ray study. The crystal-to-detector distance was 70 mm. 167 exposures (5 min per exposure) were obtained with $0 < \Phi < 250°$ and with the crystals rotated through 1.5° in Φ in the oscillation mode.

$[Mn(Cp^*)_2][Ni(dmid)_2]\cdot CH_3CN$ (3): A black squared-shaped thick plate (0.23 mm side and 0.1 mm thick) was selected for the X-ray study. The crystal-to-detector distance was 70 mm. 209 exposures (3 min per exposure) were obtained with $0 < \Phi < 250°$ and with the crystals rotated through 1.2° in Φ in the oscillation mode.

Full details related to every compound are given in the Supporting Information.

CCDC-203647 (**1**), -203646 (**2**) and -203645 (**3**) contain the supplementary crystallographic data for this paper. These data can be obtained free of charge at www.ccdc.cam.ac.uk/conts/retrieving.html [or from the Cambridge Crystallographic Data Centre, 12, Union Road, Cambridge CB2 1EZ, UK; Fax: (internat.) +44-1223/336-033; E-mail: deposit@ccdc.cam.ac.uk].

X-ray Powder Diffraction Studies

The sample was prepared in a side-filling cell, in order to minimise preferred orientations. The data were collected with a Seifert XRD 3000 TT diffractometer in Bragg−Brentano (Θ − Θ) configuration, using Cu-K_α radiation, fitted with a graphite diffracted-beam monochromator, in the interval $2° < \Theta < 30°$. The raw data were treated with the PowderX program,[44] in order to recalculate the cell parameters, and compared to the simulated diagram obtained with CaRine.[45]

Supporting Information [Table S1 (Miller indices and experimental and calculated $1/d^2hkl$ with the relative intensity of the experimental value], Figure S1 [experimental and calculated X-ray powder diagram for compound **1**, and the cif files for **1**, **2** and **3**] is available. See footnote on the first page of this article.

Acknowledgments

The support and sponsorship provided by COST Action D14/0003/99 are acknowledged. We are also deeply indebted to J. Cano and Y. Journaux for communicating the preliminary results of their DFT calculations and for enlightening discussions. Technical assistance by A. Mari for magnetic measurements is gratefully acknowledged. The authors are also grateful to Dr. Cheng Dong (National Labor-

 © 2003 Wiley-VCH Verlag GmbH & Co. KGaA, Weinheim

atory for Superconductivity, Institute of Physics, Chinese Academy of Science, Beijing) for free licensing his program PowderX.

[1] G. A. Candela, L. Swartzendruber, J. S. Miller, M. J. Rice, *J. Am. Chem. Soc.* **1979**, *101*, 2755−2756.
[2] J. S. Miller, J. C. Calabrese, H. Rommelmann, S. R. Chittipeddi, J. H. Zhang, W. M. Reiff, A. J. Epstein, *J. Am. Chem. Soc.* **1987**, *109*, 769−781.
[3] W. E. Broderick, J. A. Thompson, E. P. Day, B. M. Hoffman, *Science* **1990**, *249*, 401−403.
[4] G. T. Yee, J. M. Manriquez, D. A. Dixon, R. S. McLean, D. M. Groski, R. B. Flippen, K. S. Narayan, A. J. Epstein, J. S. Miller, *Adv. Mater.* **1991**, *3*, 309−311.
[5] J. Schweizer, A. Bencini, C. Carbonera, A. J. Epstein, S. Golhen, E. Lelièvre-Berna, J. S. Miller, L. Ouahab, Y. Pontillon, E. Ressouche, A. Zheludev, *Polyhedron* **2001**, *20*, 1771−1778.
[6] H. M. McConnell, *Proc. Robert A. Welch Found. Conf. Chem. Res.* **1967**, *11*, 144−145.
[7] H. M. McConnell, *J. Chem. Phys.* **1963**, *39*, 1910.
[8] C. Kollmar, M. Couty, O. Kahn, *J. Am. Chem. Soc.* **1991**, *113*, 7994−8005.
[9] H. Heise, F. H. Köhler, M. Herker, W. Hiller, *J. Am. Chem. Soc.* **2002**, *124*, 10823−10832.
[10] J. S. Miller, A. J. Epstein in *Research Frontiers in Magnetochemistry* (Ed.: C. J. O'Connor), World Scientific Publisher, Singapore, **1993**, pp 283−302.
[11] W. E. Broderick, J. A. Thompson, M. R. Godfrey, M. Sabat, B. M. Hoffman, E. P. Day, *J. Am. Chem. Soc.* **1989**, *111*, 7656−7657.
[12] G. Matsubayashi, A. Yokozawa, *Inorg. Chim. Acta* **1992**, *193*, 137−141.
[13] S. Tanaka, G. Matsubayashi, *J. Chem. Soc., Dalton Trans.* **1992**, 2837−2843.
[14] S. Rabaca, V. Gama, D. Belo, I. C. Santos, M. T. Duarte, *Synth. Met.* **1999**, *103*, 2302−2303.
[15] J. S. Miller, J. C. Calabrese, A. J. Epstein, *Inorg. Chem.* **1989**, *28*, 4230−4238.
[16] M. Fettouhi, L. Ouahab, M. Hagiwara, E. Codjovi, O. Kahn, H. Constant-Machado, F. Varret, *Inorg. Chem.* **1995**, *34*, 4152−4159.
[17] W. B. Heuer, P. Mountford, M. L. H. Green, S. G. Bott, D. O′Hare, J. S. Miller, *Chem. Mater.* **1990**, *2*, 764−772.
[18] V. Gama, D. Belo, I. C. Santos, R. T. Henriques, *Mol. Cryst. Liq. Cryst.* **1997**, *306*, 17−24.
[19] V. Gama, D. Belo, S. Rabaça, I. C. Santos, H. Alves, J. C. Waerenborgh, M. T. Duarte, R. T. Henriques, *Eur. J. Inorg. Chem.* **2000**, 2101−2110.
[20] M. Fettouhi, L. Ouahab, E. Codjovi, O. Kahn, *Mol. Cryst., Liq. Cryst.* **1995**, *273*, 29−33.
[21] W. E. Broderick, J. A. Thompson, B. M. Hoffman, *Inorg. Chem.* **1991**, *30*, 2958−2960.
[22] C. Faulmann, A. E. Pullen, E. Riviere, Y. Journaux, L. Retailleau, P. Cassoux, *Synth. Met.* **1999**, *103*, 2296−2297.
[23] J. L. Robbins, N. M. Edelstein, S. R. Cooper, J. C. Smart, *J. Am. Chem. Soc.* **1979**, *101*, 3853−3857.
[24] D. P. Freyberg, J. L. Robbins, K. N. Raymond, J. C. Smart, *J. Am. Chem. Soc.* **1979**, *101*, 892−897.
[25] J. S. Miller, R. S. McLean, C. Vazquez, G. T. Yee, K. S. Narayan, A. J. Epstein, *J. Mater. Chem.* **1991**, *1*, 479−480.
[26] R. Kirmse, J. Stach, W. Dietzsch, G. Steimecke, E. Hoyer, *Inorg. Chem.* **1980**, *19*, 2679−2685.
[27] V. Gama, S. Rabaca, C. Ramos, D. Belo, I. C. Santos, M. T. Duarte, *Mol. Cryst. and Liq. Cryst.* **1999**, *335*, 81−90.
[28] For a nice illustration based on the allyl radical, see: O. Kahn, *Molecular Magnetism* Wiley VCH, New York, **1993**, 303−309.
[29] J. Blümel, N. Hebendanz, P. Hudeczek, F. H. Köhler, W. Strauss, *J. Am. Chem. Soc.* **1992**, *114*, 4223−4230.
[30] C. Kollmar, O. Kahn, *Acc. Chem. Res.* **1993**, *26*, 259−265.
[31] Y. Journaux, J. Cano, personal communication.
[32] M. Deumal, J. Cirujeda, J. Veciana, J. J. Novoa, *Chem. Eur. J.* **1999**, *5*, 1631−1642.
[33] C. Faulmann, E. Rivière, S. Dorbes, P. Cassoux, *manuscript in preparation*.
[34] G. Steimecke, H. J. Sieler, R. Kirmse, E. Hoyer, *Phosphorus Sulfur* **1979**, *7*, 49−55.
[35] R. Vicente, J. Ribas, C. Faulmann, J. P. Legros, P. Cassoux, *C. R. Acad. Sci., Ser. II* **1987**, *305*, 1055−1058.
[36] Stoe, *IPDS Software, version 2.86*, Darmstadt, Germany, 1996.
[37] A. Altomare, M. C. Burla, M. Camalli, G. L. Cascarano, C. Giacovazzo, A. Guagliardi, A. G. G. Moliterni, G. Polidori, R. Spagna, *J. Appl. Cryst.* **1999**, *32*, 115−119.
[38] G. M. Sheldrick *SHELXS-97- A Program for Automatic Solution of Crystal Structure (Release 97−2):* Institüt für Anorganische Chemie der Universität, Tammanstrasse 4, 3400 Göttingen, Germany, **1997**.
[39] G. M. Sheldrick *SHELXL-97- Programs for Crystal Structure Analysis (Release 97−2):* Institüt für Anorganische Chemie der Universität, Tammanstrasse 4, 3400 Göttingen, Germany, **1998**.
[40] L. J. Farrugia, *J. Appl. Cryst.* **1999**, *32*, 837−838.
[41] D. M. Watkin, L. Pearce, C. K. Prout *CAMERON − A Molecular Graphics Package:* Chemical Crystallography Laboratory, University of Oxford, **1993**.
[42] L. J. Farrugia *J. Appl. Crystallogr.,* 1997; Vol. 30, pp 565.
[43] *International Tables for Crystallography, Volume A* (Ed.: T. Hahn), Kluwer Academic Publishers: Dordrecht, The Netherlands, **1995**.
[44] C. Dong *PowderX:* Institute of Physics, Beijing.
[45] ESM *CaRine Crystallography*; v; 3.1 ed.; ESM Software: Hamilton, OH 45013, USA.

Received February 13, 2003

 © 2003 Wiley-VCH Verlag GmbH & Co. KGaA, Weinheim

EurJIC
European Journal of Inorganic Chemistry

Issue 16/2003
Pages 2889–3054

Papers available ahead of print in Early View at www.interscience.wiley.com

Earliest available Table of Contents:
Automatically, free of charge by e-mail through
www.interscience.wiley.com/alerts

COVER PICTURE

The cover picture shows the multi-faceted approach required to unravel the complicated electrochemistry presented by Wells–Dawson coordinated actinide (*An*) ions, $[An(\alpha\text{-}2\text{-}P_2W_{17}O_{61})_2]^{n-}$ (*An* = Th, U, Np, Pu, Am). These *An*-polyoxometalate (POM) clusters contain two redox centers: the central *An* ion (magenta), except Th^{4+}, and the ligands, $(\alpha\text{-}2\text{-}P_2W_{17}O_{61})^{10-}$, for which P is orange, W is black, and O is teal blue. The formal potentials of the *An* ions are extracted by in situ XANES (X-ray absorption near edge structure) spectroelectrochemistry, using the Nernst formalism. This approach provides a unique avenue to quantifying the *An* redox response, because the multi-redox active centers, together with the deep blue color of the ligands upon reduction, exclude more standard experiments. The Nernst approach to XANES data provides information about the electronic influence of POM complexation, which is of fundamental interest as related to correlated electron behavior and of practical significance to separations science in nuclear waste processing. Details are presented in the article by M.-H. Chiang, L. Soderholm and M. R. Antonio on p. 2929 ff.

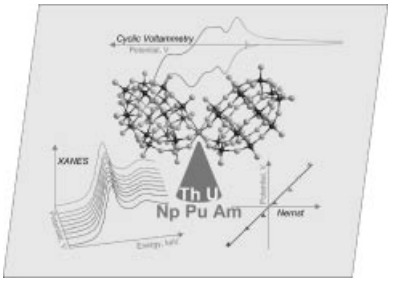

MICROREVIEW

Contents

2901 **S. B. Duckett,* D. Blazina**

The Study of Inorganic Systems by NMR Spectroscopy in Conjunction with Parahydrogen-Induced Polarisation

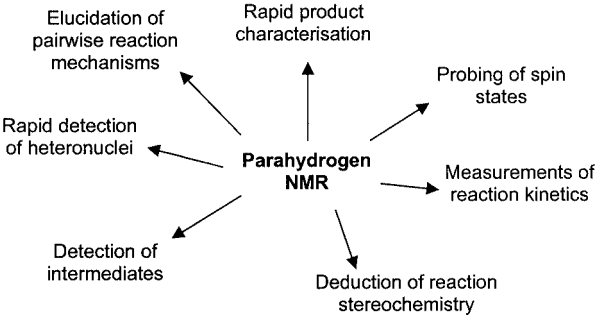

Keywords: NMR spectroscopy / Parahydrogen / Iridium / Rhodium / Ruthenium

 © 2003 Wiley-VCH Verlag GmbH & Co. KGaA, Weinheim

SHORT COMMUNICATIONS

2913 **J. Harrowfield,* Y. Kim,* Y. H. Lee, P. Thuéry**

Pendent Arm Formation and Extension accompanying Macrocycle Synthesis − A New Class of Ryongamines?

Keywords: Macrocycles / Pendent arm / X-ray diffraction

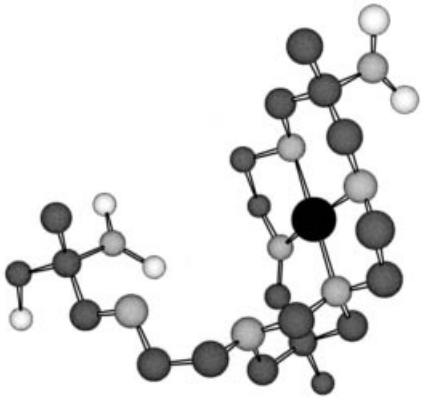

2917 **H. Arii, Y. Saito, Y. Funahashi, T. Ozawa, K. Jitsukawa, H. Masuda***

Silver(I) Complex Crystals Switched by a Water Molecule

Keywords: Coordination polymers / Hydrogen bonds / Silver

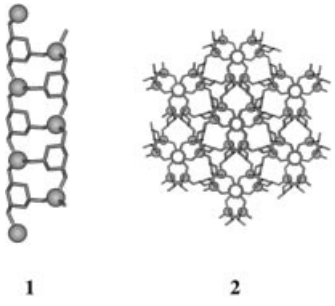

2920 **Z.-R. Qu, H. Zhao, L.-X. Xing, X.-S. Wang, Z.-F. Chen,* Z. Yu,* R.-G. Xiong,* X.-Z. You**

Two Polymeric Complexes of Norfloxacin with Iron(II) and Their Magnetic Properties

Keywords: Nofloxacin / Iron / Coordination polymers / Magnetic properties / Hydrothermal synthesis

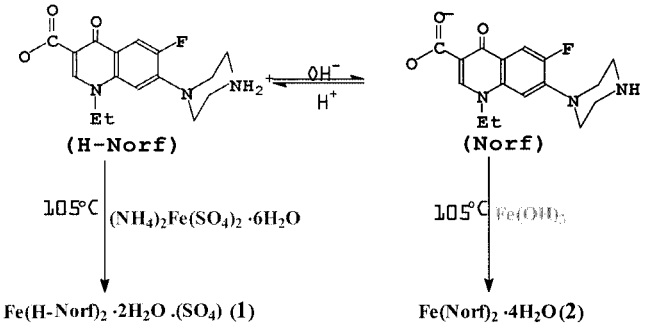

2924 **Y. Song, P. Gamez, O. Roubeau, M. Lutz, A. L. Spek, J. Reedijk***

Structural and Magnetic Characterization of a Linear Trinuclear Copper Complex Formed through Ligand Sharing

Keywords: Copper / Magnetochemistry / Bioinorganic chemistry / N,O ligands

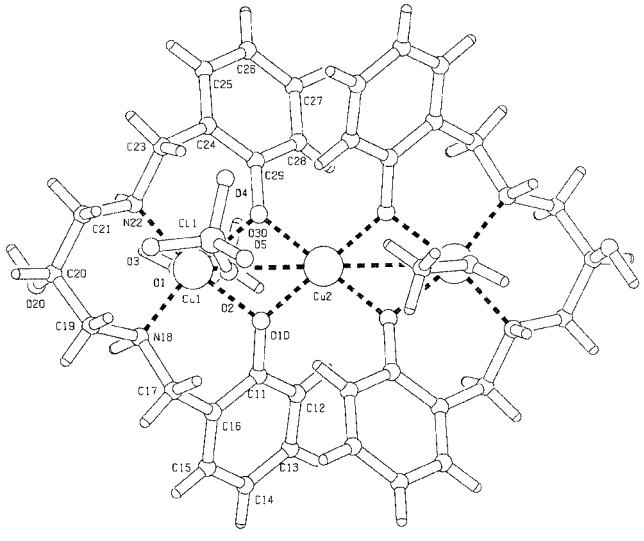

 © 2003 Wiley-VCH Verlag GmbH & Co. KGaA, Weinheim

2929 **M.-H. Chiang, L. Soderholm,* M. R. Antonio***

Redox Chemistry of Actinide Ions in Wells–Dawson Heteropolyoxoanion Complexes

Keywords: Actinides / Cyclic voltammetry / Polyoxometalates / Redox chemistry / Nernst analysis / Intermediate valence / Spectroelectrochemistry / XANES

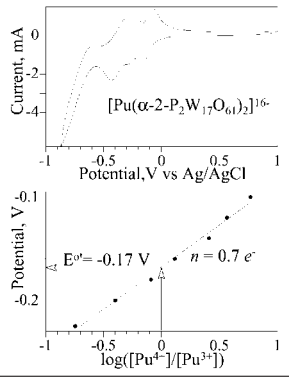

2937 **R. B. Gómez-Coca, A. Holý, R. A. Vilaplana, F. González-Vílchez, H. Sigel***

Solution Structures of Binary and Ternary Metal Ion Complexes of 9-(5-Phosphonopentyl)-adenine (3′-deoxa-PEEA). A Nucleotide Analogue Related to the Antivirally Active 9-[2-(Phosphonomethoxy)ethyl]adenine (PMEA)

Keywords: Antiviral agents / Chelates / Equilibrium constants / Nucleotides / Stacking interactions

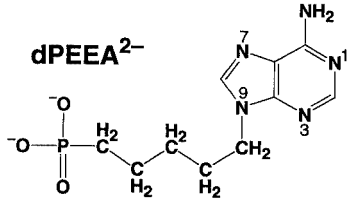

2948 **I. Gil de Muro, L. Lezama, M. Insausti, T. Rojo***

Layered $[BaM(C_3H_2O_4)_2(H_2O)_4]$ (M = Fe or Co) Complexes – Spectroscopic, Magnetic and Thermal Study

Keywords: Magnetic properties / Barium / Iron / Cobalt / Thermochemistry

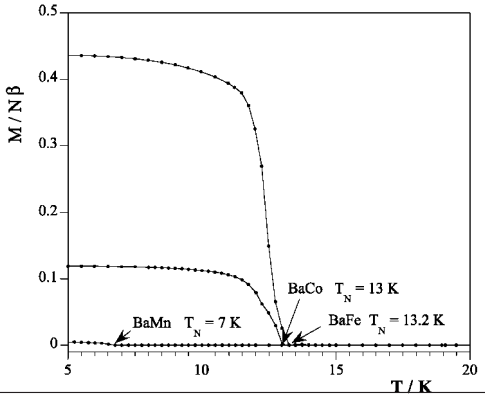

2955 **C. von Hänisch**

Synthesis and Characterisation of Ternary Cage Compounds with Adamantane-Like $M_4P_4Si_2$ (M = Al, Ga, In) Core Structures

Keywords: Aluminium / Gallium / Silicon / Indium / Phosphorus

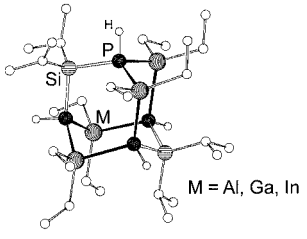

2959 **X.-M. Zhang, H.-S. Wu, X.-M. Chen***

Linear and Helical Chains in Hydrothermally Synthesized Coordination Polymers $[Co(bpdc)(H_2O)_2]$ and $[Ni(bpdc)(H_2O)_3]\cdot H_2O$ Involving in situ Ligand Synthesis

Keywords: Coordination polymers / N ligands / Helical structures / Hydrothermal synthesis / Cobalt / Nickel

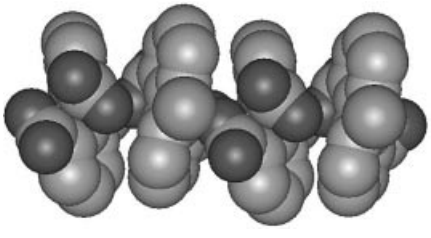

 © 2003 Wiley-VCH Verlag GmbH & Co. KGaA, Weinheim

2965 **L.-Y. Zhang, G.-F. Liu, S.-L. Zheng, B.-H. Ye, X.-M. Zhang, X.-M. Chen***

Helical Ribbons of Cadmium(II) and Zinc(II) Dicarboxylates with Bipyridyl-Like Chelates − Syntheses, Crystal Structures and Photoluminescence

Keywords: Coordination polymers / Cadmium / Zinc / N ligands / Pi interactions

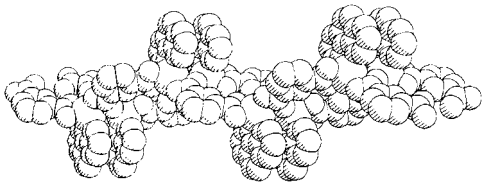

2972 **B. M. Aizoubi, M. S. A. Hamza, C. Dücker-Benfer, R. van Eldik***

Mechanistic Insight Gained into the Ligand Substitution Reactions of Bis(*o*-benzosemiquinonediiminato)(triphenylphosphane)cobalt(III) − Kinetic, Solvent, and Volume Profile Studies

Keywords: Cobalt / Kinetics / Ligand substitution / Mechanism / Pressure dependence / Solvent effects

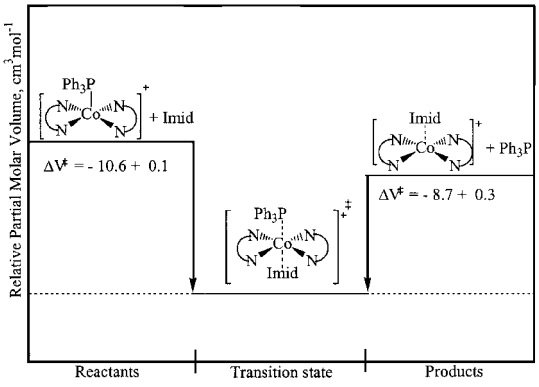

2979 **D. A. Lenev, K. A. Lyssenko, R. G. Kostyanovsky***

Rational Design, Synthesis and Crystal Structure Investigation of Hydrogen-Bonded Coordination Polymers of Bicyclic Bis-Lactam Dicarboxylates

Keywords: Carboxylate ligands / Chirality / Crystal engineering / Hydrogen bonding / Lactams

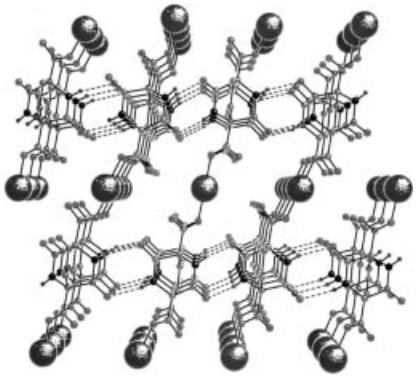

2986 **L. Ruiz-González, K. Boulahya, M. Parras, J. Alonso, J. M. González-Calbet***

HREM and CIP Characterization of Complex Superstructures in Cu-Co Related Perovskites

Keywords: Perovskite phases / Superstructures / Electron diffraction / Electron microscopy

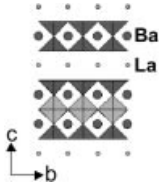

2992 **J. García-Antón, J. Pons,* X. Solans, M. Font-Bardia, J. Ros***

Synthesis, Characterisation, and X-ray Crystal Structure of New Ni^{II}, Pd^{II}, and Pt^{II} Complexes of Tridentate Pyrazole-Based Ligands with an NOS-Donor Set

Keywords: Nickel / N ligands / O ligands / Palladium / Platinum / S ligands

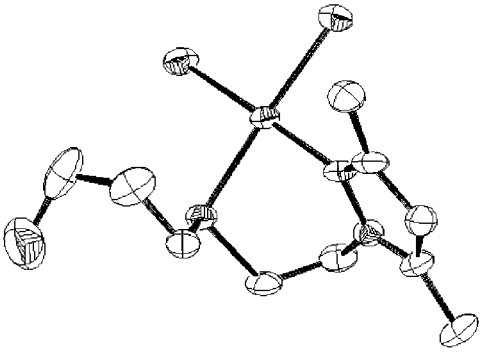

 © 2003 Wiley-VCH Verlag GmbH & Co. KGaA, Weinheim

3001 **A. Papakyriakou, N. Katsaros***

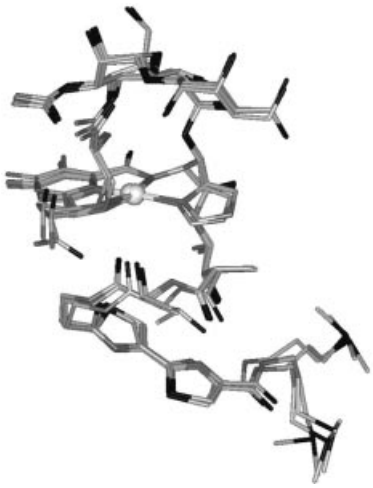

NMR and Molecular Modelling Studies on the Solution Structure of the In^{III}−Bleomycin A2 Complex

Keywords: Antitumor agents / Indium / Molecular dynamics / N ligands / NMR spectroscopy

3007 **J. Moreau, E. Guillon, P. Aplincourt, J.-C. Pierrard, J. Rimbault,* M. Port, M. Aplincourt**

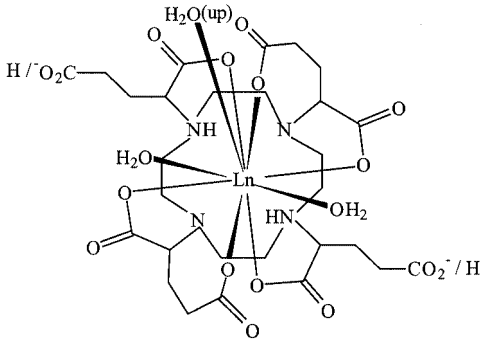

Thermodynamic and Structural Properties of Eu^{3+}, Gd^{3+} and Tb^{3+} Complexes with 1,4,7,10-Tetra(2-glutaryl)-1,4,7,10-tetraazacyclododecane in Solution: EXAFS, Luminescence, Potentiometric Studies, and Quantum Calculations

Keywords: Lanthanides / Imaging agents / EXAFS spectroscopy / Luminescence / Ab initio calculations

3021 **K. Kimpe, T. N. Parac-Vogt, S. Laurent, C. Piérart, L. V. Elst, R. N. Muller, K. Binnemans***

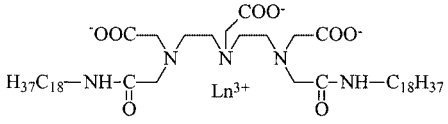

Potential MRI Contrast Agents Based on Micellar Incorporation of Amphiphilic Bis(alkylamide) Derivatives of $[(Gd-DTPA)(H_2O)]^{2-}$

Keywords: Imaging agents / Contrast agents / Lanthanides / Micelles / N,O ligands / NMR spectroscopy

3028 **K. Binnemans,* K. Lodewyckx, T. N. Parac-Vogt, R. Van Deun, B. Goderis, B. Tinant, K. Van Hecke, L. Van Meervelt**

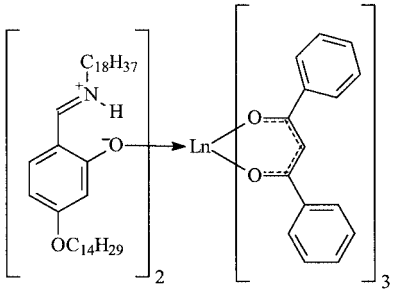

Adducts of Schiff Bases with Tris(β-diketonato)-lanthanide(III) Complexes: Structure and Liquid-Crystalline Behaviour

Keywords: Lanthanides / Liquid crystals / Metallomesogens / Supramolecular chemistry

 © 2003 Wiley-VCH Verlag GmbH & Co. KGaA, Weinheim

3034 **L. Ballester, A. M. Gil, A. Gutiérrez,* M. F. Perpiñán, A. E. Sánchez, M. Fonari, K. Suwinska, V. Belsky**

Radical Ion Salts Obtained from Substituted Ferrocene Cations and the Organic Acceptor TCNQ − Synthesis, Structure and Physical Properties

Keywords: Metallocenes / Radical ions / Stacking interactions / Supramolecular chemistry

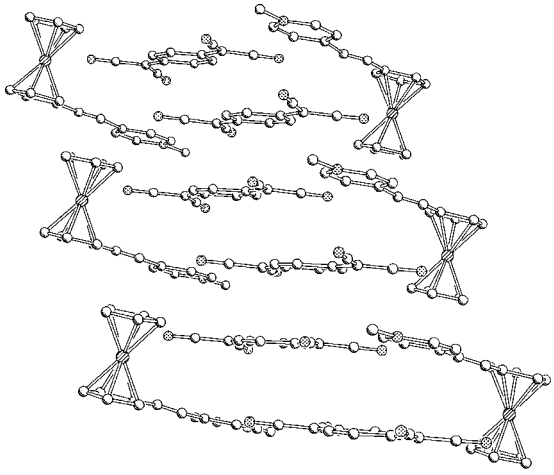

3042 **P. Comba,* A. Mayboroda, H. Pritzkow**

Homogeneous Hydrogenation Catalyzed by Trinuclear Rh^{I}-Os^{III}-Rh^{I} Complexes

Keywords: Osmium / Rhodium / Heterometallic complexes / Hydrogenation

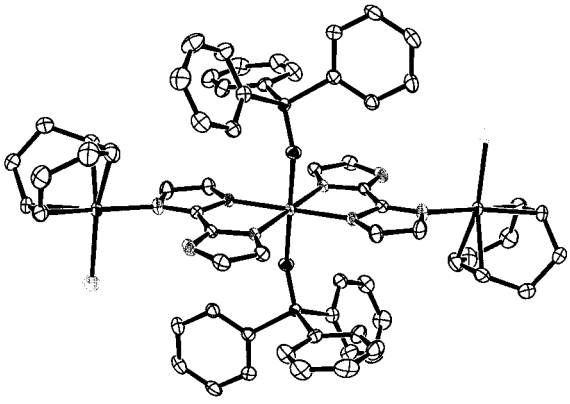

3047 **E. Valls, J. Suades,* R. Mathieu, N. Lugan**

New Rhodium(I) Complexes with Hemilabile Amphiphilic Phosphanes

Keywords: Phosphanes / Rhodium / Hemilabile ligands / Amphiphiles

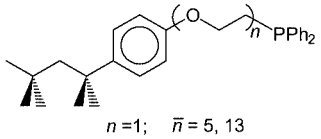

n =1; $\bar{n}$ = 5, 13

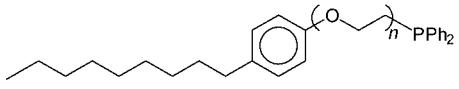

$\bar{n}$ = 1.4, 5, 11

CORRECTION

3055 **R. Caspar, H. Amouri,* M. Gruselle, C. Cordier, B. Malézieux, R. Duval, H. Leveque**

Efficient Asymmetric Synthesis of Δ- and Λ-Enantiomers of (Bipyridyl)ruthenium Complexes and Crystallographic Analysis of Δ-Bis(2,2′-bipyridine)(2,2′-bipyridine-4,4′-dicarboxylato)-ruthenium: Diastereoselective Homo- and Heterochiral Ion Pairing Revisited

Keywords: Ruthenium / Chiral resolution / Circular dichroism

 © 2003 Wiley-VCH Verlag GmbH & Co. KGaA, Weinheim

The Study of Inorganic Systems by NMR Spectroscopy in Conjunction with Parahydrogen-Induced Polarisation

Simon B. Duckett*[a] and Damir Blazina[a]

Keywords: NMR spectroscopy / Parahydrogen / Iridium / Rhodium / Ruthenium

The study of reaction mechanisms by NMR spectroscopy normally suffers from limitations in sensitivity that result in substantial difficulties in the detection and characterisation of reaction intermediates. One technique that can circumvent this problem is the use of *para*-enriched hydrogen. Here, an overview of the developments in the study of chemical reactions using parahydrogen-assisted NMR spectroscopy is presented, with the characterisation of a number of new hydride complexes of iridium, rhodium, ruthenium and tantalum being described. A number of studies involving transition metal clusters and catalytic applications are also considered.
(© Wiley-VCH Verlag GmbH & Co. KGaA, 69451 Weinheim, Germany, 2003)

1. Introduction

An obvious aim in understanding the detailed mechanism of a chemical reaction is the unambiguous detection and characterisation of any associated reaction intermediates. Unfortunately, such species are often both transient in nature and present in low concentrations. Since this makes their direct detection difficult, indirect techniques, such as reaction kinetics or isotopic labelling, are often used to impart mechanistic information. However, there will always be a degree of ambiguity associated with a mechanism that is determined in this fashion.

One technique that has found widespread use in the characterisation of compounds in all branches of chemistry is NMR spectroscopy. In many ways, NMR is an ideal technique for such studies since most important elements exhibit at least one NMR-active isotope, and isotopic labelling can be undertaken if greater sensitivity is required. The benefits of this approach when coupled with the wealth of available pulse sequences mean that it is often possible to determine molecular structures using NMR alone. Other factors, such as the ability to choose between solution and solid-state NMR and the possibility of monitoring slower dynamic processes, make this technique even more attractive for studying reactions. However, since NMR is inherently insensitive, its application in mechanistic studies has been somewhat limited.

In 1986 Bowers and Weitekamp proposed,[1] and later proved,[2] that greatly enhanced ^{1}H NMR signals could be obtained from molecules that were formed by the addition of hydrogen in the *para* spin-state. Since this report, the use of parahydrogen-enhanced NMR spectroscopy has revolutionised the study of reactions involving H_2 as a substrate by providing opportunities to study reaction intermediates directly by NMR for essentially the first time.

[a] Department of Chemistry, University of York, Heslington, York YO10 5DD, UK
E-mail: sbd3@york.ac.uk

Simon Duckett (left) was born in Preston in England in 1965. He graduated with a B.Sc. degree in Chemistry from the University of York in 1986 and was awarded a D.Phil. from the same institution in 1990 (with Prof. R. N. Perutz). During 1990 he was a postdoctoral fellow with Prof. W. D. Jones at the University of Rochester and returned there in late 1991 to work as a postdoctoral fellow with Prof. R. Eisenberg on projects relating to parahydrogen. In 1993 he returned to the University of York to take up an appointment as Lecturer in Inorganic Chemistry and in 2001 he was promoted to Reader. He has authored 30 publications in the parahydrogen field and has research interests in using NMR to probe reaction mechanisms and help develop new catalysts.

Damir Blazina (right) was born in Zagreb, Croatia in 1977. He graduated with an MChem. degree in Chemistry from the University of York in 1999 and was awarded a Ph.D. from the same institution in 2003 (with Dr. S. Duckett and Prof. P. J. Dyson). He is currently a postdoctoral fellow in the same Department. He started working in the parahydrogen area on a project sponsored by Bruker UK in 1999 and has research interests in cluster-based catalysis and NMR spectroscopy.

MICROREVIEWS: This feature introduces the readers to the author's research through a concise overview of the selected topic. Reference to important work from others in the field is included.

2. Principles Behind the Parahydrogen Effect

The existence of two isomers of molecular hydrogen derives from the symmetrisation principle of quantum mechanics, which states that the overall wave function of fermions (such as protons) must be antisymmetric with respect to exchange of nuclei. Furthermore, since the product of rotational and nuclear wave functions has to be antisymmetric, it follows that antisymmetric rotational states (odd values of J) are associated with symmetric, or *ortho*, nuclear spin-states. Likewise, antisymmetric nuclear spin-states (called *para*) are reserved for symmetric rotational states (even values of J). Hydrogen therefore might be thought to consist of a 3:1 mixture of *ortho* and *para* isomers in accordance with the threefold degeneracy of the former state (spin configurations $\alpha\alpha$, $\alpha\beta+\beta\alpha$, $\beta\beta$) over the latter (spin configuration $\alpha\beta-\beta\alpha$). However, since these two forms have different rotational (internal) energies, their populations are temperature dependent, and since interconversion between the two isomers is forbidden, the isolation of pure parahydrogen is possible. This is readily achieved by cooling H_2 in the presence of a paramagnetic species. The degree of enrichment simply depends on the temperature of the catalyst; 50% enrichment is possible at 77 K.[3,4]

An important feature of parahydrogen (p-H_2) is that it is NMR silent. However, if it adds to a metal centre in such a way that two chemically distinct hydrides are formed, the energy level diagram shown in Figure 1 is obtained. Since parahydrogen selectively populates the $\alpha\beta$ and $\beta\alpha$ spin states of the product, the population difference between the states will approach unity. This reflects a substantial increase over the normal situation where populations are controlled by the corresponding energy level separations. Because the intensity of an NMR signal depends on this population difference, enhanced signals are observed in the spectra of parahydrogen-derived molecules. Furthermore, this novel population distribution results in two of the transitions occurring in the opposite sense to that which is normally seen and the associated resonances therefore have antiphase character. This process has been termed PASADENA (Parahydrogen And Synthesis Allow Dramatically Enhanced Nuclear Alignment)[2a] and PHIP (ParaHydrogen Induced Polarisation).[2b]

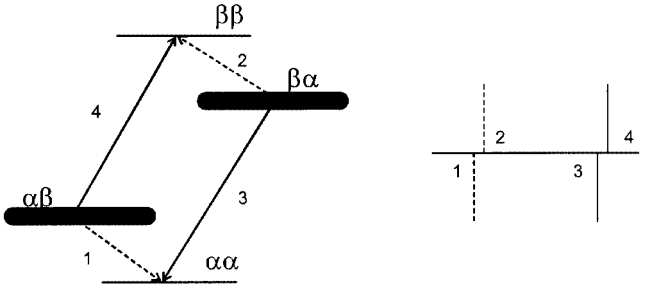

Figure 1. Idealised spin-state populations (represented by line thickness) and corresponding NMR signal patterns for an AX spin system, such as those found in $[(Me_2AsCH_2CH_2AsPh_2)Pt(H)_2]$, formed under parahydrogen-derived PASADENA conditions; the situation where $^2J_{H,H}$ is negative is illustrated

It is important to note that this situation corresponds to the chemical synthesis of an extreme spin-state, and that the system will subsequently re-establish the Boltzmann population distribution via relaxation. However, if a radio frequency pulse is applied prior to this point, the newly formed spin state can be interrogated and larger than normal coherences can be generated for detection. Scheme 1 summarises some of the ways that this approach has been harnessed in the literature.

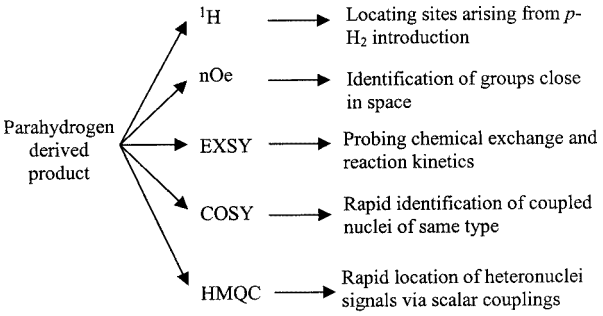

Scheme 1. NMR approaches facilitated by parahydrogen

A different effect is observed if the reaction involving parahydrogen takes place in a weak magnetic field, such as outside the NMR spectrometer. This effect, called ALTADENA (Adiabatic Longitudinal Transport After Dissociation Engenders Net Alignment)[5] occurs because under such conditions, the coupling between the nuclei is large relative to the frequency difference between them. Consequently, the added parahydrogen nuclei selectively move from their initial spin state into either the $\alpha\beta$ or $\beta\alpha$ states of the AX system, depending on which is lower in energy. Only two enhanced transitions are therefore observed in the resulting NMR spectrum. The ALTADENA effect is transitory in nature; if the reaction is not complete outside the strong magnetic field of an NMR spectrometer, PASADENA and ALTADENA effects will compete in the early stages of the reaction. Any subsequent reaction in the strong magnetic field will result in the PASADENA effect being observed.

A number of articles have appeared that have reviewed the parahydrogen effect and its chemical applications (see Scheme 2).[6] This article focuses on inorganic reports since 1999.

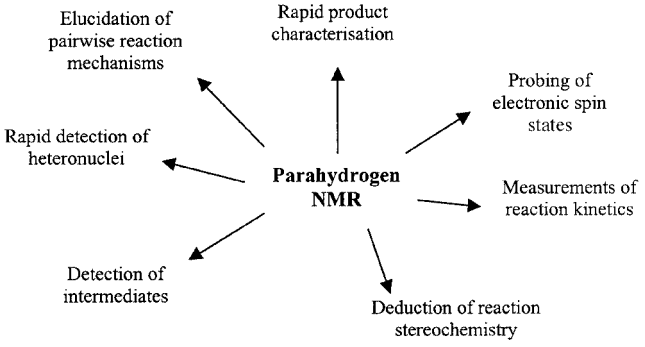

Scheme 2. Chemical applications of parahydrogen NMR methodology

 © 2003 Wiley-VCH Verlag GmbH & Co. KGaA, Weinheim

3. Applications of Parahydrogen to Mononuclear Transition Metal Complexes

If the parahydrogen effect is to be useful, it must make possible the detection of new species. For example, oxidative addition of H_2 to Vaska's Complex, *trans*-[IrCl(CO)(PPh_3)$_2$],[7] and its many analogues has been the subject of much synthetic investigation and was accepted to proceed exclusively over the OC−Ir−Cl axis. Calculations by Sargent and Hall,[8] however, revealed that H_2 addition over the OC−Ir−Cl axis rather than the P−Ir−P axis is favoured by only 9.5 kJ·mol^{-1} in the case of [IrCl(CO)(PMe_3)$_2$], and that increasing the π-accepting nature of the phosphane further favours H_2 addition across the P−Ir−P axis. Studying the oxidative addition of H_2 to Vaska's complex is therefore an ideal test of the *p*-H_2 approach, viz., is another isomer detectable? Figure 2a shows the resultant ^{1}H NMR spectrum, focusing on the hydride region, when *p*-H_2 adds to *trans*-[IrCl(CO)(PPh_3)$_2$] at 295 K. The expected resonances for *cis*-*trans*-[IrCl(H)$_2$(CO)(PPh_3)$_2$] are clearly visible, while those for a minor species are indeed detected.[9] In this case, the extra signals arise from a product with two chemically equivalent hydride protons that are magnetically distinct, i.e. *cis*-*cis*-[IrCl(H)$_2$(CO)(PPh_3)$_2$]. Further studies demonstrated that when PMe_3 was employed, a similar species could be observed, and when $AsPh_3$ was utilised, H_2 addition over the As−Ir−As axis was shown to be kinetically preferred, with slow isomerisation over the course of several days leading to the thermodynamic product *cis*-*trans*-[IrCl(H)$_2$(CO)($AsPh_3$)$_2$].

Evidence was also presented in this paper that the formation of trihydride complexes of the type [Ir(H)$_3$(CO)$_2$(L)] was possible when CO and *p*-H_2 are warmed together in the presence of [IrCl(CO)(L)$_2$] (L = PPh_3 and PMe_3). The trihydride product was shown to be formed via [IrCl(H)$_2$(CO)$_2$(L)], which undergoes competitive HCl and H_2 elimination thereby accounting for the observation of [IrH(Cl)$_2$CO(PPh_3)$_2$]. The spectral features of the associated hydride resonances of [Ir(H)$_3$(CO)$_2$(L)] are worthy of special comment (see Figure 2b) since they yield anti-phase components that have different frequency separations. This situation arises due to the internal cancellation of the central triplet feature in the unique IrH resonance.[10] Interestingly, a very different result was obtained when *trans*-[IrCl(CO)(PPh_3)$_2$] was subjected to UV radiation while un-

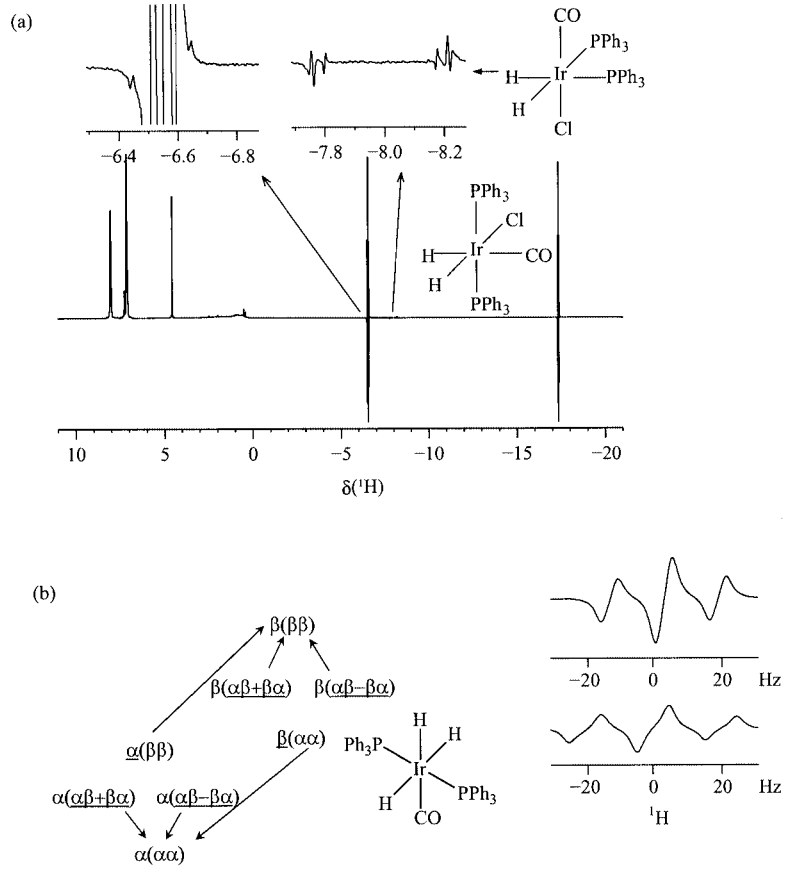

Figure 2. (a) 128 scan ^{1}H NMR spectrum obtained when a sample of [IrCl(CO)(PPh_3)$_2$] reacts with *p*-H_2 in C_6D_6 at 295 K; enhanced hydride resonances for the major isomer (corresponding to addition over the Cl−Ir−CO axis) dominate the spectrum; insets illustrate how ^{13}C satellites and signals due to the minor product, corresponding to H_2 addition over the P−Ir−P axis, are visible; (b) energy level diagram for a *p*-H_2 derived metal trihydride complex containing two magnetically equivalent hydride ligands; the *p*-H_2 enhanced hydride resonances of the inset trihydride complex are illustrated (same scale) with the lower trace containing the resonance for the hydride that is *trans* to CO, for which the central feature is missing

 © 2003 Wiley-VCH Verlag GmbH & Co. KGaA, Weinheim

der an atmosphere of *p*-H_2. Now, a dihydride product corresponding to a species containing a five-membered Ir(CO-C_6H_4-P) ring was detected. This product was suggested to form by CO insertion into an unseen *ortho*-metallation product. The above reactions are summarised in Scheme 3.

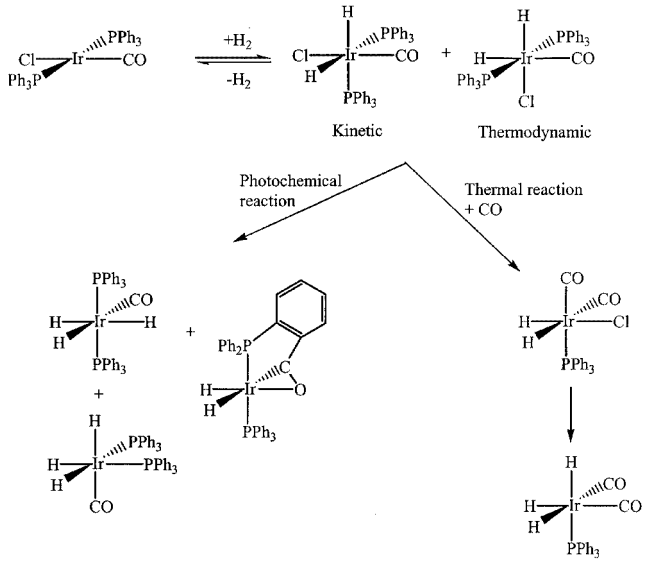

Scheme 3. Reaction pathways for [IrCl(CO)(PPh_3)$_2$] after H_2 addition as detected by *p*-H_2 NMR spectroscopy

Another example of a complex that was purported not to react with H_2 directly is the 16-electron anion $[IrI_2(CO)_2]^-$ which features in the industrially significant CATIVA process. Oxidative addition of *p*-H_2 to the tetrabutylammonium salt of $[IrI_2(CO)_2]^-$ resulted in the detection of the all-*cis* $[Ir(H)_2I_2(CO)_2]^-$.[11] Kinetic studies employing EXSY methods resulted in the demonstration that this complex eliminates H_2 on the NMR timescale with the associated activation parameters being indicative of reductive elimination from the 18-electron $[Ir(H)_2I_2(CO)_2]^-$ rather than the 16-electron $[Ir(H)_2I(CO)_2]$. Isomerisation into a second product where the two hydride ligands are *trans* to iodide was found to proceed on a slower time scale via $[I]^-$ loss. Subsequently, these species were detected using normal NMR methods, albeit in a high pressure NMR cell.[12]

More recently, Permin et al. have employed *p*-H_2 to study the related complex $(Bu_4N)[IrBr_2(CO)_2]$ and its reactions with $SnBr_2$.[13] In the absence of $SnBr_2$, oxidative addition of *p*-H_2 yields the *all-cis* product $[Ir(H)_2Br_2(CO)_2]^-$, in an analogous manner to that for the iodide complex. However, the addition of 0.5 molar equivalents of $SnBr_2$ to this system results in the formation of the dibromostannyl complex $[Ir(H)_2Br(SnBr_3)(CO)_2]^-$ which isomerises at high temperatures into two other structural forms, as identified in Scheme 4. When a large excess of $SnBr_2$ is employed initially, insertion leads instead to *cis*, *trans*, *cis*-$[Ir(H)_2(SnBr_3)_2(CO)_2]^-$. By studying the relative intensities of the associated PHIP enhanced hydride signals, the authors determined that the presence of one $SnBr_3$ ligand facilitates H_2 addition due to the enhanced σ-donating effect of the new ligand, but that the presence of two such ligands deactivates the system.

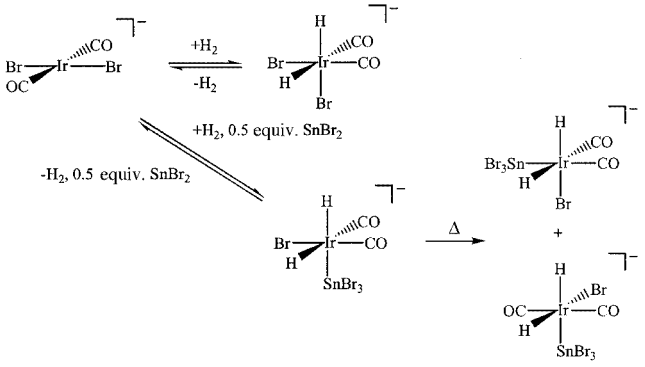

Scheme 4. Formation of iridium tribromostannyl anions as detected by PHIP[13]

The utilisation of parahydrogen-induced polarisation to detect minor isomers of metal dihydrides thus clearly marks one of the most widespread successes of the parahydrogen approach. Indeed, when the related d^8 complex [Ir(CO)-(PPh_3)(Et_2dtc)] was examined with normal H_2, three dihydride complexes were rapidly formed and their concentrations were shown to rapidly equilibrate (Scheme 5). As expected, it proved a simple matter to assign product structures based on the coupling patterns of the hydride resonances.[14] When parahydrogen was utilised, the hydride resonances of **1** were estimated to be 40-fold enhanced at 298 K and the ratio of signals for **1**:**2** was about 170:1. This implied a kinetic selectivity of ca. 170:1 for the generation of isomer **1** compared with **2**. At 358 K, exchange peaks between the inequivalent hydrides resonances of **1** and **2** were observed with the exchange pathway shown to involve phosphane dissociation. Interestingly, the dominant reaction pathway corresponds to oxidative addition of H_2 over the axis of the starting square-planar complex that contains the CO ligand.

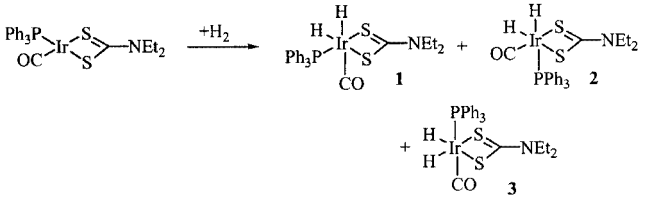

Scheme 5. Species formed by hydrogen addition to [Ir(S_2CNEt_2)-(CO)(PPh_3)]

Since the parahydrogen approach relies on NMR characterisation, complexes of ^{103}Rh, where $I = 1/2$, have proven to be extremely valuable in establishing this technique. An early example is presented by the oxidative addition of *p*-H_2 to [RhCl(PMe_3)$_4$] and [RhCl(PMe_3)$_3$],[15] where the dihydride products were used to demonstrate that two-dimensional NMR techniques such as COSY, HSQC, HMQC and NOESY could be used with *p*-H_2. In addition, this study

 © 2003 Wiley-VCH Verlag GmbH & Co. KGaA, Weinheim

laid the groundwork for many subsequent investigations by showing that rapid chemical-shift detection of ^{31}P and ^{103}Rh nuclei was possible despite the inherent insensitivity of the latter (see Figure 3), that the magnitudes and relative sizes of heteronuclear coupling constants could be determined, and that NOESY methods could be used to probe ligand arrangements and monitor hydride ligand exchange.

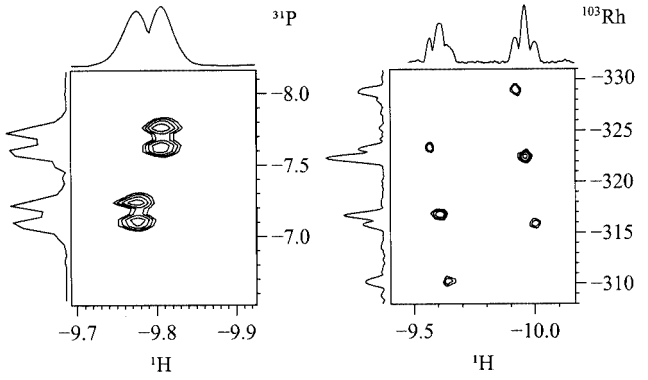

Figure 3. Selected cross-peaks (positive contours) and projections from ^{1}H-^{31}P (left) and ^{1}H-^{103}Rh (right) correlation spectra of $[Rh(H)_2Cl(PMe_3)_3]$ obtained with *p*-H_2 in CD_2Cl_2 at 313 K

As PHIP is still a relatively new NMR technique, an important part of work in this area consists of case studies that contribute to the understanding of the effect or extend its applications. One such discovery was the observation by Aime et al. that the oxidative addition of parahydrogen to a Rh^{I} centre containing a bound alkene resulted in the polarisation of the alkene protons.[16] Previously, such effects had been ascribed to exchange between the hydrides and the alkene protons.[17] However, isotopic labelling indicated that this was not the case here, and that the transfer of polarisation must occur via cross relaxation (NOE) between the hydrides and the alkene protons. This result has implications in catalytic studies since it means that it may be possible to detect unsaturated molecules bound to metal centres even in absence of hydrogenation or hydride exchange.

Recent work at York has involved extending the parahydrogen technique further via low temperature in-situ UV photolysis.[18] In this study, a 325 nm He-Cd continuous-wave laser was employed to irradiate $[Rh(\eta^5\text{-}C_5H_5)(C_2H_3SiMe_3)_2]$ at 203 K in the presence of *p*-H_2. Enhanced hydride resonances assigned to $[Rh(\eta^5\text{-}C_5H_5)(H)_2(C_2H_3SiMe_3)]$ were detected in the associated spectra (see Figure 4). This observation reflects an important result in this field since it overcomes the need for rapid thermally initiated H_2 cycling. In addition, it was concluded, on the basis of the photon flux and an estimate of the quantum yield, that the spectra illustrated the detection of 1 nmol of material.

The reactions of stable 18-electron complexes of ruthenium have also been monitored using the PHIP methodology. Indeed, the value of *p*-H_2 as a mechanistic probe is well illustrated by the highly fluxional system

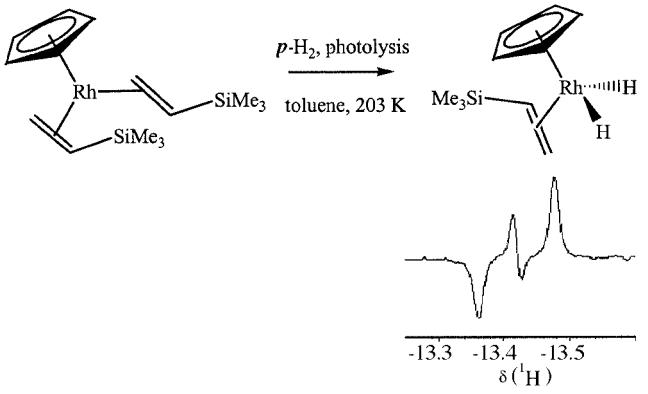

Figure 4. PHIP enhanced ^{1}H spectrum (bottom) showing hydride resonances of the inset dihydride complex obtained during concurrent UV irradiation according to the reaction illustrated

$[Ru(H)_2(CO)_2(Ph_2PCH_2CH_2PPh_2)]$.[19] In this complex, exchange between the hydride ligands and exchange of the phenyl rings was monitored quantitatively by the EXSY approach. In addition, the complex was observed to readily undergo H_2 elimination. The utilisation of *p*-H_2 indicated that H_2 loss proceeds via a diamagnetic intermediate, since a paramagnetic one would quench any enhancement, and facilitated the elucidation of the mechanism for the exchange process, which was proposed to occur via a trigonal bipyramidal transition state containing an η^2-H_2 ligand (see Scheme 6). Since H-H and P-P interchange occurred at the same rate, a concerted rotation was indicated. When $[Ru(H)_2(CO)_2(dppe)]$ was generated by the in situ photolysis of $[Ru(CO)_3dppe]$, the observation of enhanced hydride resonances was taken to indicate that the intermediate $[Ru(CO)_2dppe]$ exists in a singlet electronic state.

The application of *p*-H_2 methods to the study of early transition metal complexes is currently much less common, with one recent study involving the preparation of the dimeric tantalum dinitrogen complex $[(Cp^*_2TaCl)_2(\mu\text{-}N_2)]$.[20] Upon H_2 addition, two isomers of the dihydride complex $[Cp^*_2Ta(H)_2Cl]$ are formed, which are shown in Scheme 7. Since only the asymmetric isomer was expected to show *p*-H_2 enhancement, PHIP provided a ready means of distinguishing between the two isomers.

The oxidative addition of H_2 to the related complex $[Cp^*_2Ta(CH_2)(H)]$ has also been studied with parahydrogen.[21] This reaction leads to the formation of two enhanced products, $[Cp^*_2Ta(CH_3)(H)_2]$ and $[Cp^*_2Ta(H)_3]$. Isotopic labelling was used to show that, in both cases, the enhancement is due to two hydride ligands, and a mechanistic pathway involving the unsaturated methylene complex $[Cp^*_2Ta(CH_3)]$ was proposed.

4. Parahydrogen in the Study of Binuclear Complexes

Work at York has focused on extending the applications of PHIP methods by studying the reactions of the d^8-rho-

 © 2003 Wiley-VCH Verlag GmbH & Co. KGaA, Weinheim

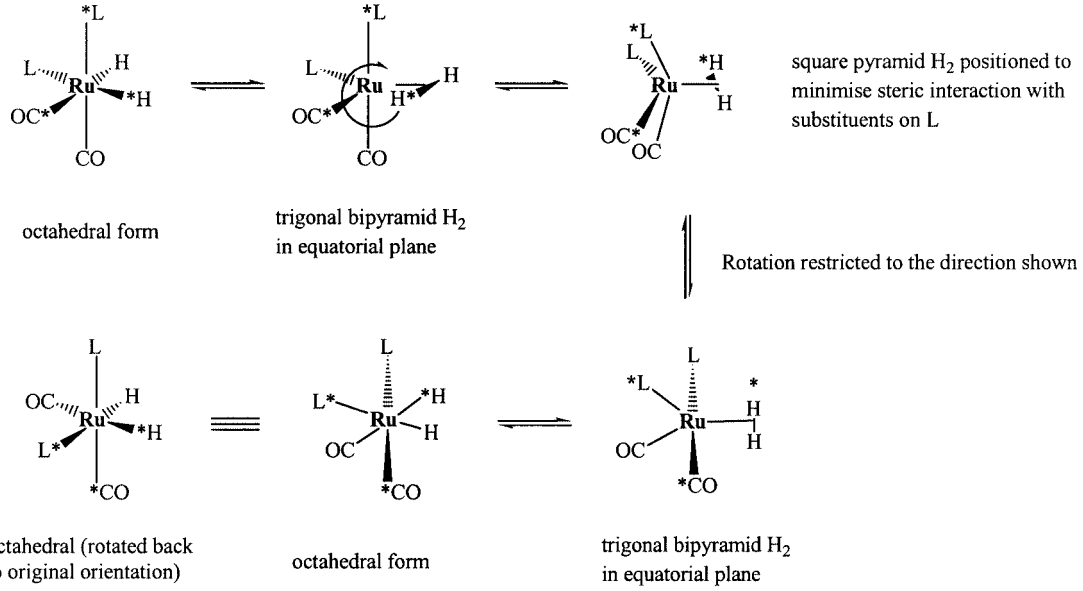

Scheme 6. Proposed mechanism of hydride ligand interchange in $[Ru(H)_2(CO)_2(L)_2]$

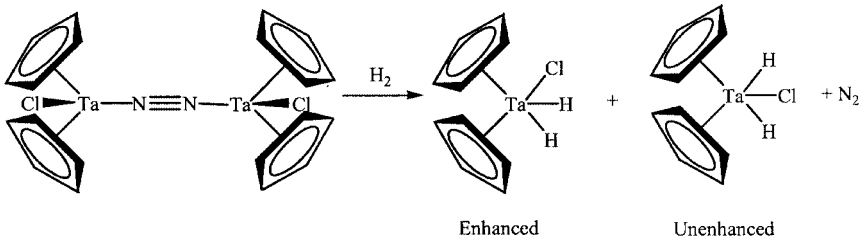

Scheme 7. Reaction of a dimeric tantalum dinitrogen complex with parahydrogen

dium complexes $[RhX(CO)(PR_3)_2]$ where X = Cl, Br, I and R = Ph, Me with *p*-H_2.[22] These complexes were previously not thought to react with hydrogen. In the case of $[RhX(CO)(PPh_3)_2]$, unexpected binuclear products of the general formula $[(H)_2Rh(PPh_3)_2(\mu\text{-}X)_2Rh(PPh_3)(CO)]$ were detected. Since the initial dihydrogen activation product $Rh(H)_2X(CO)(PPh_3)_2$ was not detected in these reactions, it was suggested that facile CO loss led to the generation of the unsaturated species $[Rh(H)_2X(PPh_3)_2]$. The proposed reaction mechanism is shown in Scheme 8.

Surprisingly, when the reaction of $[RhCl(CO)(PMe_3)_2]$ was monitored at 348 K under 3 atm of *p*-H_2, the major product corresponded to $[H(Cl)Rh(PMe_3)_2(\mu\text{-}H)(\mu\text{-}Cl)Rh(PMe_3)(CO)]$ with bridging and terminal hydride li-

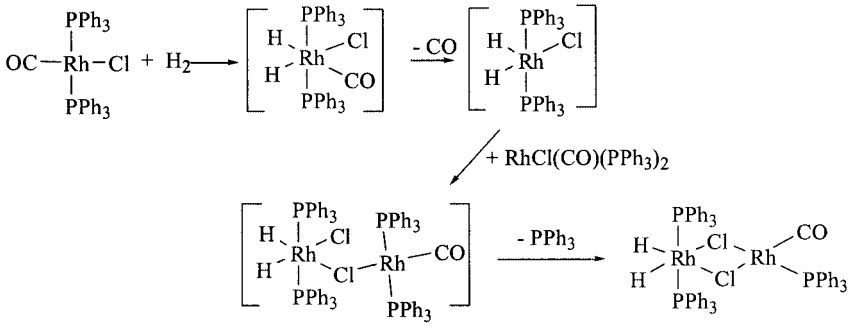

Scheme 8. Suggested route to $[(H)_2Rh(PPh_3)_2(\mu\text{-}Cl)_2Rh(PPh_3)(CO)]$, formed in the reaction of $[RhCl(CO)(PPh_3)_2]$ with *p*-H_2

 © 2003 Wiley-VCH Verlag GmbH & Co. KGaA, Weinheim

gands. However, when $RhI(CO)(PMe_3)_2$ was monitored, the reaction complexity increased still further and several new species were detected. A typical ^1H NMR spectrum from such a reaction is shown in Figure 5. Density functional theory indicated that all structural types correspond to reaction intermediates rather than transition states and Scheme 9 shows how they are formed.

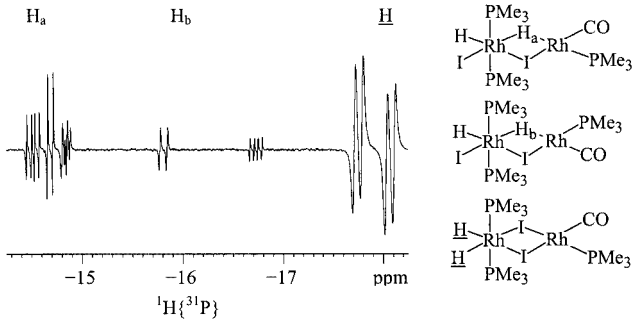

Figure 5. $^1H\{^{31}P\}$ NMR spectrum showing the hydride region after warming a sample of $[RhI(CO)(PMe_3)_2]$ with p-H_2 in C_6D_6 to 348 K; selected product resonances indicated by H_a, H_b and H are assigned according to the inset structures

Significantly, when the reaction involving $[RhCl(CO)(PMe_3)_2]$ with p-H_2 was monitored in the presence of styrene, a dramatic increase in the hydride ligand's signal enhancement was observed. This facilitated the detection of $[(H)_2Rh(PMe_3)_2(\mu\text{-}Cl)_2Rh(CO)(PMe_3)]$ and $[HRh(PMe_3)_2(\mu\text{-}H)(\mu\text{-}Cl)_2Rh(CO)(PMe_3)]$ and demonstrated that a sacrificial alkene can dramatically extend the sensitivity of the parahydrogen method by promoting H_2 cycling through the system.[22]

Koch et al. have reported a number of similar complexes that were produced by studying the reactions of the binuclear complex $[RhCl(NBD)_2]_2$ with a range of phosphanes in-situ.[23] The authors noted that if the chloride ligand was replaced by TFA, only mononuclear complexes were observed. More importantly, this paper also described the construction of an apparatus designed to monitor reactions with p-H_2 in situ, by bubbling the gas through the NMR sample via a capillary prior to data acquisition. An NMR method was also reported that eliminated the interference of resonances from unpolarised spin systems. Furthermore, when $[RhCl(NBD)_2]_2$ was examined in methanol at low temperature and in the absence of substrate, an enhanced solvent complex was detected.[24] These techniques have also been used to investigate $SnCl_3$-activated rhodium dihydride complexes.[25] For example, oxidative addition of p-H_2 to the $[RhH(SnCl_3)_5]^{3-}/PR_3$ system (where PR_3 = PPh_3, $PEtPh_2$, PEt_3) in CD_3CN and to $[RhCl(CO)_2]_2/SnCl_2$ yielded enhanced hydride resonances in neutral complexes of the type $Rh(H)_2(PR_3)_3(SnCl_3)$, anions of the form $[Rh(H)_2(PR_3)_2(SnCl_3)_2]^-$, and cations of the form $[Rh(H)_2(PR_3)_3(CD_3CN)]^+$. The relative abundance of these products was found to depend crucially on the type of phosphane. These systems were shown to be active catalysts for the hydrogenation of phenylacetylene.

Another example of the use of parahydrogen in the study of binuclear complexes involved iridium, rhodium and mixed-metal A-frame complexes.[26] For $[Ir_2(\mu\text{-}S)(CO)_2(dppm)_2]$, where dppm = bis(diphenylphosphanyl)methane, reaction with hydrogen was found to proceed by two addition pathways corresponding to oxidative addition inside (*endo*) and outside (*exo*) the pocket of the A-frame complex. The previously unseen *exo* addition pathway yields a kinetically significant dihydride that is a key intermediate in the formation of the thermodynamic product of this reaction (Scheme 10).

5. Applications to Transition-Metal Clusters

Due to the presence of multiple metal atoms in transition-metal clusters, the potential reaction pathways of these species are much more complicated than those available to mononuclear complexes. The study of such species

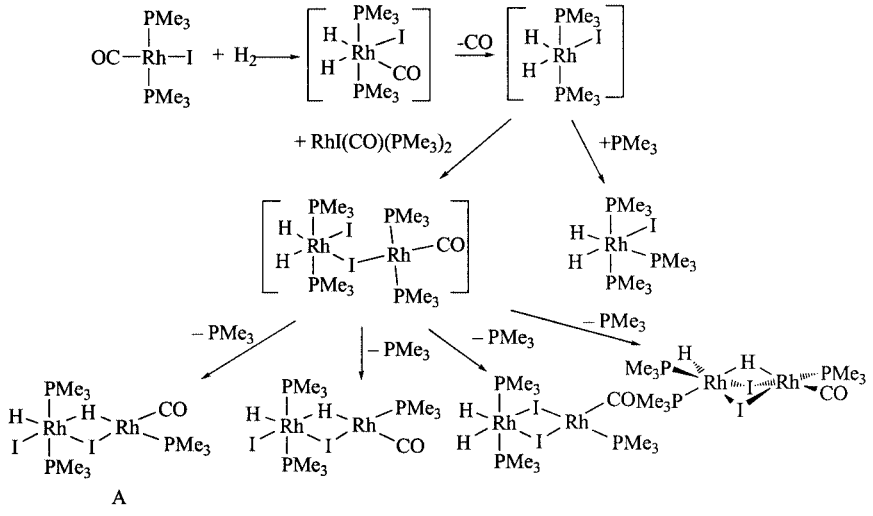

Scheme 9. Reaction pathways available to $[RhCl(CO)(PMe_3)_2]$ that are detected due to the use of p-H_2; when I is replaced by Cl, only A is detected normally, but in the presence of an alkene the four other structural types are also visible in solution

 © 2003 Wiley-VCH Verlag GmbH & Co. KGaA, Weinheim

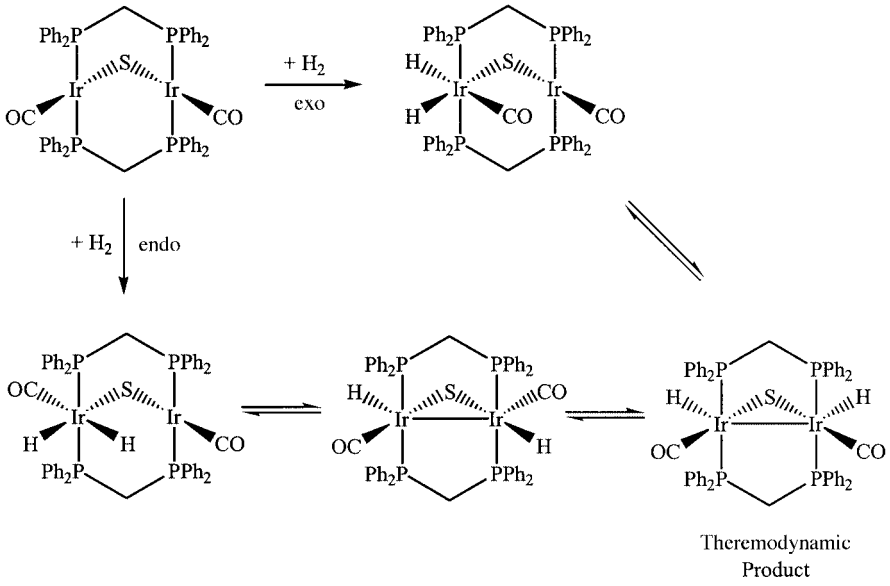

Scheme 10. Hydrogen addition reactions involving an iridium A-frame complex detected by *p*-H_2

might therefore be expected to benefit greatly from the enhanced sensitivity afforded by *p*-H_2.

Aime et al. have utilised a triruthenium system to demonstrate that the transfer of polarisation from NMR-silent *para*-hydrogen to NMR-active *ortho*-hydrogen could be achieved via an intermediate with inequivalent hydrides, as shown in Scheme 11.[27] This phenomenon occurs because the symmetry of parahydrogen is broken in the intermediate, with subsequent H_2 elimination occurring rapidly relative to proton relaxation. Under such conditions, the eliminated H_2 molecule retains a "memory" of the intermediate and is consequently polarised. In practice, under these conditions, a strong emission signal is observed for the free hydrogen resonance.

In York, our work in the area of cluster chemistry developed from the study of the reactions of $[Ru(H)_2(CO)_3(PPh_3)]$ and $[Ru(H)_2(CO)_2(PPh_3)_2]$ with *p*-H_2.[28] These complexes were prepared from $[Ru(CO)_3(PPh_3)_2]$, and two dihydride isomers were detected in both cases, as shown in Scheme 12. The former species was also generated by fragmentation of the trinuclear cluster $[Ru_3(H)(\mu\text{-}H)(CO)_9(PPh_3)_3]$.

Using the full repertoire of NMR approaches illustrated in this review, we have gained insights into the dynamic behaviour and catalytic activity of the triruthenium clusters $[Ru_3(CO)_{12-x}(PR_3)_x]$ (where PR_3 = PPh_3, PMe_2Ph, PMe_3, PCy_3; x = 1−3). Thus, when x = 2, oxidative addition of *p*-H_2 results in the formation of three isomers of $[Ru_3(H)(\mu\text{-}H)(CO)_9(PR_3)_2]$, which differ in the arrangement of their equatorial phosphanes: while one isomer contains both phosphanes on the same ruthenium centre, in the other two the phosphanes are located in different orientations on separate metal centres (see Figure 6).[29] These dihydride products were fully characterised in situ by ^1H, ^{13}C and ^{31}P NMR spectroscopy. Kinetic studies revealed the presence of intra- and inter-isomer hydride exchange processes, with activation parameters and solvent effects indicating the involvement of ruthenium−ruthenium bond heterolysis and CO loss in the respective rate-determining steps. When x = 3, reaction with H_2 proceeds to form identical products to those found with x = 2, although at a slower rate, while when x = 1 a single isomer of $[Ru_3(H)(\mu\text{-}H)(CO)_{10}(PR_3)]$ is formed.

The three isomers of $[Ru_3(H)(\mu\text{-}H)(CO)_9(PPh_3)_2]$ were shown to play a kinetically significant role in the hydrogenation of an alkyne substrate via initial CO loss (see Figure 7), with rates of H_2 transfer being explicitly determined for each isomer.[30] This was achieved by using EXSY to monitor the movement of parahydrogen-enhanced nuclei in complexes that are normally invisible. A less-significant

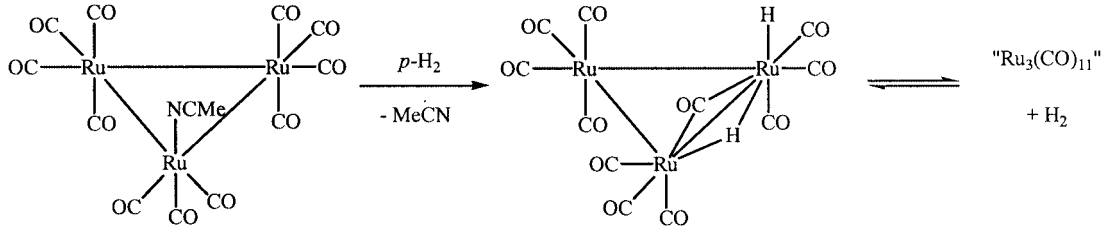

Scheme 11. Proposed mechanism for *p*-H_2 addition to $[Ru_3(CO)_{11}(NCMe)]$, yielding an enhanced emission resonance for free H_2

 © 2003 Wiley-VCH Verlag GmbH & Co. KGaA, Weinheim

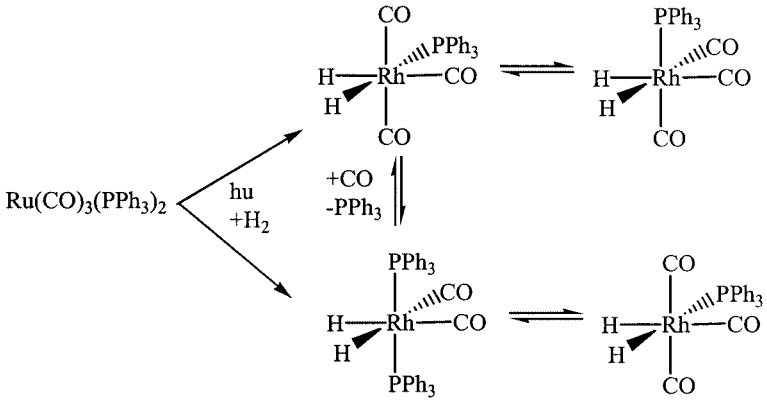

Scheme 12. Ruthenium dihydride complexes detected using parahydrogen

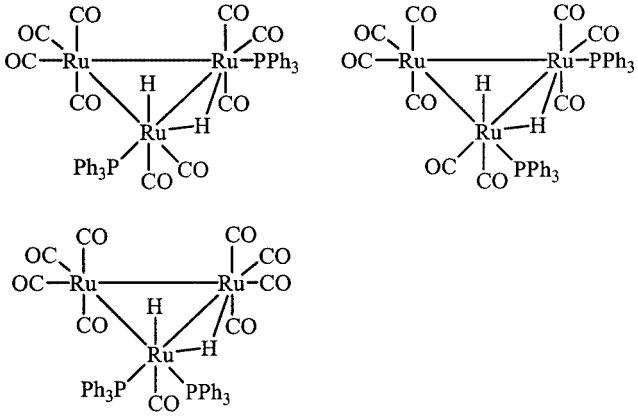

Figure 6. Isomers formed by H_2 addition to $[Ru_3(CO)_{10}(PPh_3)_2]$ detected via *p*-H_2

secondary reaction involving loss of L to yield a product containing both a pendant vinyl unit and a bridging hydride ligand was also observed, as were competing pathways involving fragmentation to form the less-active species $[Ru(H)_2(CO)_2(L)(alkyne)]$. The mechanism of catalytic hydrogenation is shown in Scheme 13. The abundance of the dihydride intermediates formed was shown to increase with the steric bulk of the phosphane, while their catalytic activity increased with the basicity of the phosphane, such that PPh_3 was the optimum phosphane for catalysis.[31] Significantly, polar solvents were found to facilitate catalysis by intact clusters while non-polar solvents led to increased cluster fragmentation. Furthermore, the activity of cluster-based intermediates was shown to be much greater than that of mononuclear fragments, a discovery with important implications for the study of catalysis by transition metal clusters.

A study of the hydrogenation of alkynes by the triosmium cluster $[Os_3(\mu\text{-}H)_2(CO)_{10}]$ led to the detection and characterisation of a range of vinyl hydride clusters.[32] Here, transfer of *p*-H_2 nuclei into the bound organic substrates was detected without alkene elimination. Parahydrogen has also been employed to support classical methods in the study of transition metal clusters during the investi-

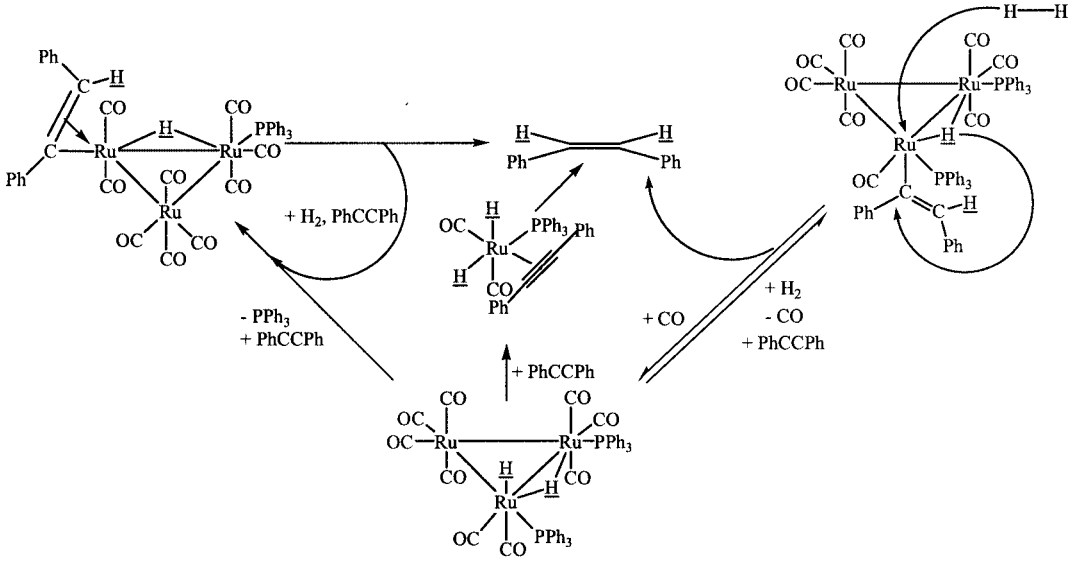

Scheme 13. Proposed catalytic cycle for the hydrogenation of diphenylacetylene by $[Ru_3(H)(\mu\text{-}H)(CO)_9(PPh_3)_2]$

 © 2003 Wiley-VCH Verlag GmbH & Co. KGaA, Weinheim

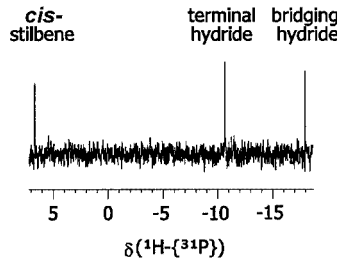

Figure 7. $^1H\{^{31}P\}$ EXSY spectrum obtained during the reaction of $[Ru_3(CO)_{10}(PPh_3)_2]$ with parahydrogen and diphenylacetylene in CD_3NO_2; the resonance corresponding to the terminal hydride of $[Ru_3(H)(\mu\text{-}H)(CO)_9(PPh_3)_2]$ was selectively excited; direct transfer of magnetisation into the bridging site on the cluster and into the hydrogenation product *cis*-stilbene are clearly evident after 700 ms

gations of hydride exchange in $[Os_3(\mu\text{-}H)_2(CO)_{10}]$.[33] Initially, studies using a mixture of H_2 and D_2 led to the proposal that the exchange proceeds via the formation of an $[Os_3(H)_2(D)_2(CO)_{10}]$ species, which is then able to undergo an H-D exchange prior to eliminating a hydrogen molecule as either H_2, HD or D_2. With the signal gain afforded by *p*-H_2, the existence of this process was confirmed and the tetrahydride intermediate was detected. In addition, a second pathway where H_2 dissociates from the cluster to yield a highly unsaturated $[Os_3(CO)_{10}]$ moiety was observed. This latter process results in no isotopic mixing. The rates for the two processes were determined via EXSY methods and subsequent kinetic simulations. It was found that the pathway involving initial hydrogen dissociation was much slower, but its efficiency and importance increased with temperature. More recently, a *p*-H_2 study involving triosmium μ_3-quinolyl trihydride clusters demonstrated that trihydride-containing clusters can be studied using this approach with all three hydride resonances showing polarisation due to fluxionality and cross polarisation effects.[34]

6. Catalytic Studies

Additional catalytic studies have been completed by Bargon et al., who have developed the DYPAS (DYnamic PASadena) method to measure reaction rates.[35] This method, based on the earlier ROCHESTER approach,[36] can be used to determine the rate of any process that involves the formation and decay of a parahydrogen signal. DYPAS involves the introduction of a variable delay between the addition of *p*-H_2 to the system and the 45° excitation pulse, yielding a plot of intensity versus time (see Figure 8). If the mechanistic scheme for the process is known, then the signal decay can be described by a series of differential equations, which can be solved to yield specific rate constants.

Hydrogenation reactions have also been studied using one-dimensional sequences involving the NOESY and ROESY effects. For example, in a study of styrene hydrogenation by $[Rh(dppb)]^+$, two sets of enhanced resonances were observed for the ethylbenzene hydrogenation product.[37] Using NOESY, it proved possible to determine that one of these signals corresponded to free ethylbenzene, while the other was due to ethylbenzene still bound to the Rh catalyst.

PHIP methodology has also been used to study stereoselective hydrogenation reactions. This approach relies on the difference between $^2J_{H,H}$ values for *E* and *Z* alkenes. For instance, Bargon et al. have shown that when [Cp* Ru(alkene)]$^+$ was the catalyst, non-phenyl-substituted alkynes selectively formed the (*E*)-alkene while phenyl-substituted alkynes did likewise at low temperature, but increasingly favoured the (*Z*) isomer as the temperature was raised.[38] The same group has also reported several investigations into the homogeneous hydrogenation of dehydroamino acids using parahydrogen.[39] This work included the determination of the reaction mechanism and the quantification of the reaction rate. Interestingly, the intermediates detected in this reaction (see Figure 9) suggested that an initial agostic hydride species was formed (as evidenced by the ^1H resonance at the unusual δ value of −1.9 ppm, which exhibited a strong $^1J_{H,C}$ coupling of 86 Hz) that subsequently yielded an alkylhydride, which is the active species in hydrogenation.

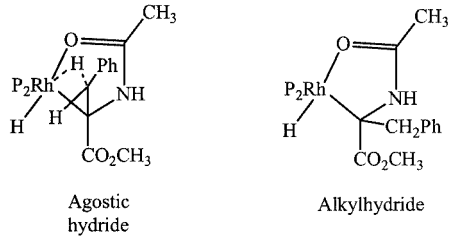

Figure 9. Intermediates detected during homogeneous hydrogenation of dehydroamino acids, where P_2 = PHANEPHOS

If a hydrogenation reaction is rapid, polarisation-transfer effects can be utilised to study secondary reactions and hence more complex catalytic transformations can be inves-

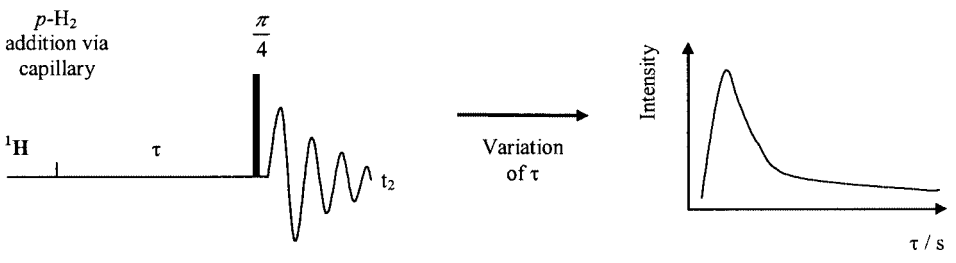

Figure 8. Pulse sequence and methodology of the DYPAS experiment

 © 2003 Wiley-VCH Verlag GmbH & Co. KGaA, Weinheim

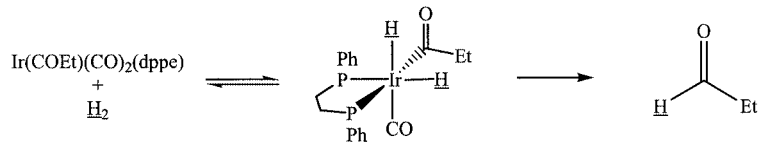

Scheme 14. System used by Eisenberg to detect one-hydrogen PHIP; the marked protons give rise to enhanced resonances

tigated. For instance, Koch et al. monitored the hydrogenation of 1-phenylpropyne by a Rh^I catalyst.[40] In the presence of parahydrogen, enhanced resonances for the product *cis*-1-phenylpropene are observed. If a dilute solution of bromine was added in situ, the subsequent alkane, 1,2-dibromo-1-phenypropane, proved also to be enhanced. This species has two chiral centres, and both diastereoisomers were detected.

This review has already illustrated how PHIP can be used to observe heteronuclei via radio frequency mediated polarisation transfer. However, if hydrogenation occurs in a weak magnetic field (i.e. outside the spectrometer), the resulting spin systems are strongly coupled and efficient polarisation transfer from ^1H to heteronuclei becomes possible via cross-relaxation and can be detected as the ALTADENA effect. A nice example of this result is provided by the hydrogenation of long-chain alkynes (4−8 carbon atoms), where polarisation of all the ^{13}C nuclei in the carbon chain of the alkene is observed.[41]

Very recently, a hydroformylation product containing a single parahydrogen atom has been successfully sensitised. This result was observed during the addition of *p*-H_2 to an acetone solution of *trans*-[PtCl(COEt)(PPh_3)$_2$] and $SnCl_2$ (see Scheme 14), as well as to [Ir(COEt)(CO)$_2$(dppe)]. These systems initially form dihydride products that subsequently eliminate propanal; this product appears with an enhanced aldehydic proton resonance.[42] This effect, termed OH-PHIP (one-hydrogen PHIP) was considerably weaker than regular PHIP and was attributed to the strong coupling that exists between the protons in the initial dihydride product.

7. Other Developments

In addition to the above examples, there have been a number of novel applications of the PHIP phenomenon that stand on their own. For example, Ulrich et al. have reported PHIP hydrogenation experiments in the presence of NMR shift-reagents.[43] The lanthanide shift-reagents cause resonance shifts due to their paramagnetic character, which unfortunately also quenches the parahydrogen enhancement. While small amounts of a racemic shift-reagent were sufficient to cause a substantial resonance shift without fully quenching the parahydrogen, the use of chiral shift-reagents yielded only a small perturbation. The authors concluded that the amount of shift-reagent required was too large to be tolerated by the parahydrogen and that optically active solvents would provide a better method to differentiate enantiomers using PHIP.

Parahydrogen has also been utilised to investigate colloidal catalysis.[44] The reaction of phenylacetylene with hydrogen using the colloidal palladium catalyst Pd_x[N(octyl)$_4$Cl]$_y$ was observed to yield enhanced signals in the product species. In another study, PHIP was used to study reversible H_2 adsorption on ZnO.[45] A prominent enhancement pattern was observed, which was attributed to *p*-H_2 chemisorbed on ZnO. Furthermore, parahydrogen has recently been employed in magnetic resonance imaging (MRI), where it was used to obtain enhanced ^{13}C resonances in vivo via initial polarisation transfer outside the strong field of the spectrometer, corresponding to the utilisation of ALTADENA.[46] Although only preliminary, these studies represent new opportunities for the PHIP effect.

Acknowledgments

D. B. acknowledges financial support from the ORS Award Scheme. S. B. D. is grateful to the University of York, the EPSRC, BBSRC, Bruker UK, BP Chemicals, SASOL and Dow Corning for financial support. Discussions with Dr. J. E. McGrady, Prof. P. J. Dyson, Prof. R. N. Perutz and Dr. R. J. Mawby are gratefully acknowledged. Finally, the most important acknowledgment goes to all the students and post-doctoral fellows whose hard work made this review possible: Ms C Elkington, Mr N. Wood, Ms K. Ampt, Dr. J Lowe, Dr. C. Kozak, Dr. C. Sleigh, Dr. S Hasnip, Dr. S. Colebrooke, Dr. M. Partridge, Dr. D. Schott and Dr. C. Goddard.

[1] C. R. Bowers, D. P. Weitekamp, *Phys. Rev. Lett.* **1986**, *57*, 2645−2648.
[2] [2a] C. R. Bowers, D. P. Weitekamp, *J. Am. Chem. Soc.* **1987**, *109*, 5541−5542. [2b] T. C. Eisenschmid, R. U. Kirss, P. A. Deutsch, S. I. Hommeltoft, R. Eisenberg, J. Bargon, R. G. Lawler, A. L. Balch, *J. Am. Chem. Soc.* **1987**, *109*, 8089−8091.
[3] S. B. Duckett, C. L. Newell, R. Eisenberg, *J. Am. Chem. Soc.* **1994**, *116*, 10548−10556.
[4] K. F. Bonhoeffer, P. Harteck, *Z. Phys. Chem.* **1929**, *B4*, 113.
[5] [5a] M. D. Pravica, D. P. Weitekamp, *Chem. Phys. Lett.* **1983**, *145*, 255−258. [5b] R. Eisenberg, T. C. Eisenschmid, M. S. Chinn, R. U. Kirss, *Adv. Chem. Ser. D* **1992**, *230*, 47−74.
[6] [6a] C. R. Bowers, D. H. Jones, N. D. Kurur, J. A. Labinger, M. G. Pravica, D. P. Weitekamp, *Adv. Magn. Reson.* **1990**, *14*, 269. [6b] R. Eisenberg, *Acc. Chem. Res.* **1991**, *24*, 110−116. [6c] J. Natterer, J. Bargon, *Prog. Nucl. Magn. Reson. Spectrosc.* **1997**, *31*, 293−315. [6d] S. B. Duckett, C. J. Sleigh, *Prog. Nucl. Magn. Reson. Spectrosc.* **1999**, *34*, 71−92.
[7] [7a] L. Vaska, M. F. Wernke, *Trans. N. Y. Acad. Sci.* **1971**, *33*, 80. [7b] R. Ugo, A. Pasini, S. Cenini, *J. Am. Chem. Soc.* **1972**, *94*, 7364−7370.
[8] A. L. Sargent, M. B. Hall, *Inorg. Chem.* **1992**, *31*, 317−321.
[9] [9a] S. K. Hasnip, S. B. Duckett, C. J. Sleigh, D. R. Taylor, G. K. Barlow, M. J. Taylor, *Chem. Commun.* **1999**, 1717−1718. [9b] S. K. Hasnip, S. A. Colebrooke, C. J. Sleigh, S. B. Duckett, D. R. Taylor, G. K. Barlow, M. J. Taylor, *J. Chem. Soc., Dalton Trans.* **2002**, 743−751.
[10] [10a] S. K. Hasnip, S. B. Duckett, D. R. Taylor, M. J. Taylor, *Chem. Commun.* **1998**, 923−924. [10b] S. P. Millar, D. L. Zubris,

 © 2003 Wiley-VCH Verlag GmbH & Co. KGaA, Weinheim

J. E. Bercaw, R. Eisenberg, *J. Am. Chem. Soc.* **1998**, *120*, 5329−5330.
[11] S. K. Hasnip, S. B. Duckett, D. R. Taylor, G. K. Barlow, M. J. Taylor, *Chem. Commun.* **1999**, 889−890.
[12] R. Churlaud, U. Frey, F. Metz, A. E. Merbach, *Inorg. Chem.* **2000**, *39*, 4137−4142.
[13] A. Permin, R. Eisenberg, *Inorg. Chem.* **2002**, *41*, 2451−2458.
[14] G. Suardi, B. P. Cleary, S. B. Duckett, C. Sleigh, M. Rau, W. E. Reed, J. A. B. Lohman, R. Eisenberg, *J. Am. Chem. Soc.* **1997**, *119*, 7716−7725.
[15] B. A. Messerle, C. J. Sleigh, M. G. Partridge, S. B. Duckett, *J. Chem. Soc., Dalton Trans.* **1999**, 1429−1435.
[16] S. Aime, D. Canet, W. Dastru, R. Gobetto, F. Reineri, A. Viale, *J. Phys. Chem. A* **2001**, *105*, 6305−6310.
[17] [17a] A. Harthun, R. Selke, J. Bargon, *Angew. Chem. Int. Ed. Engl.* **1996**, *35*, 2505−2507. [17b] A. Harthun, R. Giernoth, C. J. Elsevier, J. Bargon, *Chem. Commun.* **1996**, 2483−2484.
[18] C. Godard, P. Callaghan, J. L. Cunningham, S. B. Duckett, J. A. B. Lohman, R. N. Perutz, *Chem. Commun.* **2002**, 2836−2387.
[19] D. Schott, C. J. Sleigh, J. P. Lowe, S. B. Duckett, R. J. Mawby, M. G. Partridge, *Inorg. Chem.* **2002**, *41*, 2960−2970.
[20] D. C. Bregel, S. M. Oldham, R. J. Lachicotte, R. Eisenberg, *Inorg. Chem.* **2002**, *41*, 4371−4377.
[21] D. C. Bregel, S. M. Oldham, R. Eisenberg, *J. Am. Chem. Soc.* **2002**, *124*, 13827−13832.
[22] [22a] P. D. Morran, S. B. Duckett, P. R. Howe, J. E. McGrady, S. A. Colebrooke, R. Eisenberg, M. G. Partridge, J. A. B. Lohman, *J. Chem. Soc., Dalton Trans.* **1999**, 3949−3960. [22b] S. A. Colebrooke, S. B. Duckett, J. A. B. Lohman, *Chem. Commun.* **2000**, 685−686.
[23] A. Koch, J. Bargon, *Inorg. Chem.* **2001**, *40*, 533−539.
[24] H. Heinrich, R. Giernoth, J. Bargon, J. M. Brown, *Chem. Commun.* **2001**, 1296−1297.
[25] [25a] A. Koch, C. Ulrich, J. Bargon, *Tetrahedron* **2000**, *56*, 3177−3179. [25b] C. Ulrich, A. Permin, V. Petrosyan, J. Bargon, *Eur. J. Inorg. Chem.* **2000**, 889−894.
[26] S. M. Oldham, J. M. Houlis, C. J. Sleigh, S. B. Duckett, R. Eisenberg, *Organometallics* **2000**, *19*, 2985−2993.
[27] S. Aime, W. Dastru, R. Gobetto, A. Russo, A. Viale, D. Canet, *J. Phys. Chem. A* **1999**, *103*, 9702−9705.
[28] C. J. Sleigh, S. B. Duckett, R. J. Mawby, J. P. Lowe, *Chem. Commun.* **1999**, 1223−1224.
[29] D. Blazina, S. B. Duckett, P. J. Dyson, B. F. G. Johnson, J. A. B. Lohman, C. J. Sleigh, *J. Am. Chem. Soc.* **2001**, *123*, 9760−9768.
[30] D. Blazina, S. B. Duckett, P. J. Dyson, J. A. B. Lohman, *Angew. Chem. Int. Ed.* **2001**, *40*, 3874−3877.
[31] D. Blazina, S. B. Duckett, P. J. Dyson, J. A. B. Lohman, *Chem. Eur. J.* **2003**, *9*, 1046−1061.
[32] R. Gobetto, L. Milone, F. Reineri, L. Salassa, A. Viale, E. Rosenberg, *Organometallics* **2002**, *21*, 1919−1924.
[33] [33a] S. Aime, W. Dastru, R. Gobetto, J. Krause, L. Matas, A. Viale, *Organometallics* **1996**, *15*, 4967−4970. [33b] S. Aime, W. Dastru, R. Gobetto, F. Reineri, A. Russo, A. Viale, *Organometallics* **2001**, *20*, 2924−2927.
[34] B. Bergman, E. Rosenberg, R. Gobetto, S. Aime, L. Milone, F. Reineri, *Organometallics* **2002**, *21*, 1508−1511.
[35] P. Hübler, R. Giernoth, G. Kümmerle, J. Bargon, *J. Am. Chem. Soc.* **1999**, *121*, 5311−5318.
[36] M. S. Chinn, R. Eisenberg, *J. Am. Chem. Soc.* **1992**, *114*, 1908−1909.
[37] P. Hübler, J. Bargon, *Angew. Chem. Int. Ed.* **2000**, *39*, 3701−3703.
[38] D. Schleyer, H. G. Niessen, J. Bargon, *New J. Chem.* **2001**, *25*, 423−426.
[39] [39a] R. Giernoth, H. Heinrich, N. J. Adams, R. J. Deeth, J. Bargon, J. M. Brown, *J. Am. Chem. Soc.* **2000**, *122*, 12381−12382. [39b] S. Wildschutz, P. Hübler, J. Bargon, *Chem. Phys. Chem.* **2001**, *5*, 328−331.
[40] A. Koch, J. Bargon, *Magn. Reson. Chem.* **2000**, *38*, 216−220.
[41] M. Stephan, O. Kohlman, H. G. Niessen, A. Eichhorn, J. Bargon, *Magn. Reson. Chem.* **2002**, *40*, 157−160.
[42] A. B. Permin, R. Eisenberg, *J. Am. Chem. Soc.* **2002**, *124*, 12406−12407.
[43] C. Ulrich, J. Bargon, *Prog. Nucl. Magn. Reson. Spectrosc.* **2000**, *38*, 33−37.
[44] A. Eichhorn, A. Koch, J. Bargon, *J. Mol. Catal. A: Chem.* **2001**, *174*, 293−295.
[45] P. J. Carson, C. R. Bowers, D. P. Weitekamp, *J. Am. Chem. Soc.* **2001**, *123*, 11821−11822.
[46] K. Golman, O. Axelsson, H. Johannesson, S. Mansson, C. Olofsson, J. S. Petersson, *Magn. Reson. Med.* **2001**, *46*, 1−5.

Received March 3, 2003

 © 2003 Wiley-VCH Verlag GmbH & Co. KGaA, Weinheim

Pendent Arm Formation and Extension accompanying Macrocycle Synthesis – A New Class of Ryongamines?

Jack Harrowfield,*[a] Yang Kim,*[b] Young Hoon Lee,[b] and Pierre Thuéry[c]

Keywords: Macrocycles / Pendent arm / X-ray diffraction

Reaction of the Cu^{II} complex of the podand hexamine "sen", $CH_3C(CH_2NHCH_2CH_2NH_2)_3$, with formaldehyde and nitroethane under basic conditions provides, as one of the principal products, a complex containing a new ligand which is not only macrocyclic but which has resulted also from reactions to extend one podand arm, to introduce an aminal bridge and to oxidise one of the donor-*N* atom units to an imine.
(© Wiley-VCH Verlag GmbH & Co. KGaA, 69451 Weinheim, Germany, 2003)

Introduction

Formaldehyde has been used in a remarkable variety of reactions with polyamines to give macrocyclic and macropolycylic ligands.[1–3] Aminal formation — in general a useful pathway in macrocycle synthesis[4] — is commonly involved in these reactions, as is carbon-carbon bond formation through carbanion addition to intermediate imines, although for a particular product it is usually either one or the other that is involved. Macrocycle formation from the sexidentate amine ligand $CH_3C(CH_2NHCH_2CH_2NH_2)_3$, "sen",[5] when reacted as its Cu^{II} complex with formaldehyde and nitroethane, appears, however, as we show presently, to involve a competition between these two pathways, leading to a product macrocycle with a pendent arm which is both tied back to the macrocycle by an aminal bridge and elongated as a result of carbanion addition to a presumed imine formed at the terminal amino group. Further, the ligand then appears to have undergone alkylation by formaldehyde at the carbon atom derived from nitroethane in the extended arm, as well as partial oxidation within the macrocyclic ring to convert one N-donor unit to an imine!

For metal ions favouring octahedral coordination, the coordination chemistry of sen has been fairly well characterised[6] but surprisingly little is known of the behaviour of this ligand towards Cu^{II}. Evidence is available,[7] however, that a homologue of sen will bind to Cu^{II} through only four of its six *N*-donor atoms and, given the propensity of Cu^{II} to adopt four coordination even in systems such as those involving potentially sexidentate cage amines,[8] it was anticipated that the widely applied reaction of Cu^{II} tetraamine complexes with formaldehyde and nitroethane to give macrocycles[1–3] might, in this case, lead to a macrocycle with a pendent diamine arm. Such a macrocycle could then be used in the formation of multimetallic complexes through, for example, the formation (and capping) of a tris(bidentate) metal complex from the donor atoms in the pendent arm. There are many possible complications in this system arising from isomerism of the complex ions and thus we have attempted, as a preliminary step, to define precisely the chemistry involved in the reaction of the Cu^{II} complex of sen with nitroethane and formaldehyde. This will be described in detail elsewhere, the present report being of the remarkable structure found (Figure 1) for the leading component found during chromatographic treatment (SP Sephadex cation exchange with 0.3 M sodium citrate as eluent) of the reaction mixture inadvertently prepared with the use of a very large excess of formaldehyde.

Results and Discussion

The ligand structure (inset, Figure 1) shows that two arms of the original sen ligand have indeed become involved in the anticipated cyclisation reaction to give a cyclam-like[9] macrocycle but also that the third arm, singly protonated in the isolated complex, has become involved in elaborate related reactions leading to a partially rigidified pendent arm in which two new functional groups — hydroxyl and nitro — have been added to the diamine entity. Further, a reaction well-known with other metal ion complexes of amines but rarely observed with Cu^{II} [10] has led

[a] Chemistry, School of Biomedical and Chemical Sciences, University of Western Australia,
35 Stirling Highway, Crawley, WA 6009, Australia
[b] Department of Advanced Materials, Kosin University,
149–1, Dongsam-dong, Yeongdo-gu, Busan, 606–701, South Korea
[c] CEA/Saclay, DSM/DRECAM/SCM (CNRS URA 331),
Bâtiment 125, 91191, Gif-sur-Yvette, France

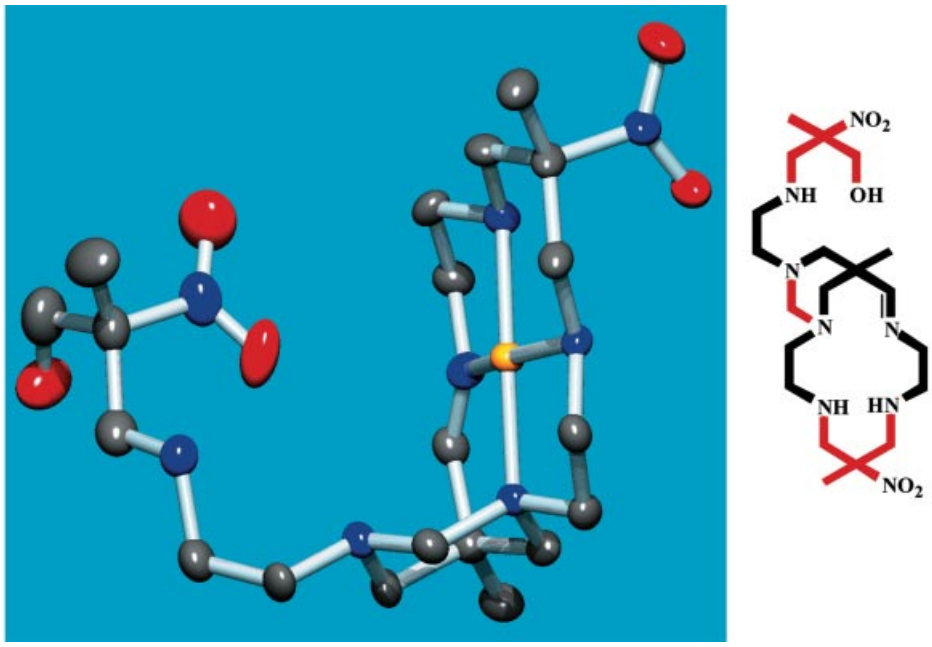

Figure 1. The complex cation found in the crystal lattice of $[Cu(LH)](ClO_4)_3 \cdot 1.5H_2O$; displacement ellipsoids are drawn at the 50% probability level; C = grey, N = blue, O = red, Cu = yellow; hydrogen atoms are not shown and one position only of the disordered parts is represented; inset is the structure of the ligand (L), with the initial sen skeleton shown in black

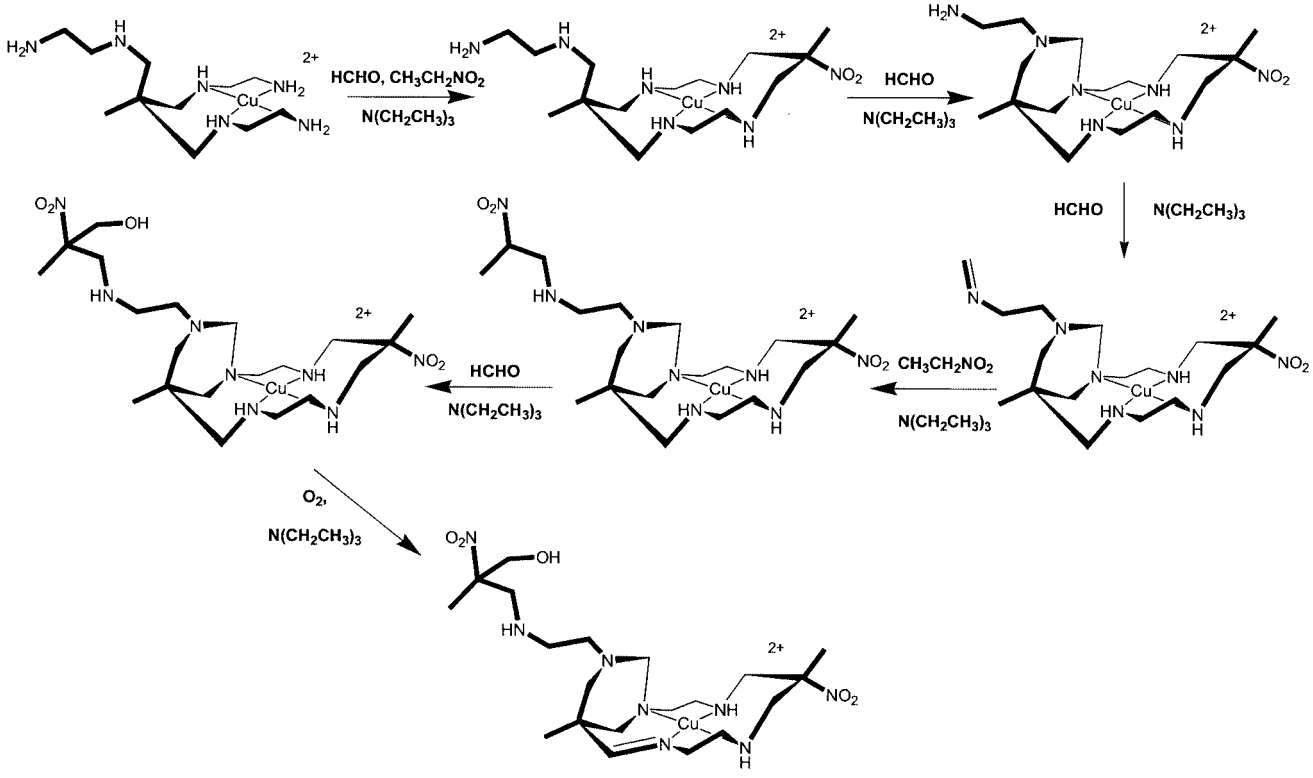

Figure 2. A possible sequence of events involved in the synthesis of a "ryongamine"

to the partial oxidation of the macrocyclic ring, converting one amine donor to an imine. As seen in many related instances,[11] the crystal structure of the complex shows the nitro and methyl substituents on the macrocyclic ring to adopt axial and equatorial orientations, respectively, on the chair six-membered ring formed by the macrocyclisation process. Despite this aspect of stereospecificity, there is disorder associated with the chiral centre generated on the

 © 2003 Wiley-VCH Verlag GmbH & Co. KGaA, Weinheim

pendent arm, indicating a complete lack of diastereoselectivity in the crystallisation process. This is perhaps in part a consequence of the rigidification of the pendent arm by aminal formation, giving a six-membered heterocyclic ring, between donor atoms N3 and N6, and which may inhibit any significant interaction between the chiral donor centres on the metal and the chiral centre near the arm terminus. A simplified representation of a possible sequence of events leading to the complex is given in Figure 2. Clearly, reduction of the product complex under acidic conditions can be expected to generate a saturated, chiral octaamine-mono-ol ligand in which a macrocyclic unit has two, very different amino-pendent arms in an *anti* (*trans*) arrangement relative to the macrocycle mean plane. The chemistry involved is a remarkably simple pathway to a ligand of such a sophisticated structure, though the detection of the product was a completely fortuitous consequence of an error made in the quantity of formaldehyde used and a systematic evaluation of procedures to optimise the yield of the complex is now in progress. The prospects are that a wide range of podand ligands might be used in similar reactions and our perception of a resemblance between the structure of the molecule presently described and classical oriental representations of a dragon (see graphical abstract), prompts us to suggest the trivial name "ryongamines" for this class of macrocycle, "ryong" being the romanised form of the Korean word for dragon.

Experimental Section

Synthesis: A methanolic solution of sen was prepared by slurrying sen·6HCl[6b] (1.20 g) with NaOH (0.62 g) in methanol (100 mL) and mixed with $CuCl_2 \cdot 2H_2O$ (0. 70 g) in 1:1 water/methanol (100 mL). The resulting blue-violet solution was filtered to remove some $Cu(OH)_2$ before HCHO (36% aqueous solution, 10 g), nitroethane (0.40 g) and triethylamine (4 g) were added and the mixture then heated at reflux for 12 h. On cooling to room temperature, the reaction mixture was acidifed to pH 6 with acetic acid and taken to dryness under vacuum. The residue was dissolved in water and chromatographed on Na^+-form SP Sephadex C25 with 0.13 M sodium citrate. Separate eluate fractions were absorbed on H^+-form Dowex 50Wx2 and elution with HCl used to recover the complexes as their chlorides after evaporation of the solvents to dryness. The first component thus obtained is the subject of the present communication and was precipitated from water as its perchlorate (50 mg) for the structure determination. $C_{20}H_{44}Cl_3CuN_8O_{18.5}$ (862.5): calcd. C 27.59, H 5.09, N 12.87; found C 27.6, H 6.7, N 12.3.

X-ray Crystallography: Data were collected on a Nonius-Kappa-CCD area detector diffractometer[12] using graphite-monochromated Mo-K_α radiation (λ = 0.71073 Å). The crystal was introduced in a glass capillary with a protecting "Paratone-N" oil (Hampton Research) coating. The unit cell parameters were determined from ten frames, then refined on all data. A 180° -range was scanned with 2° steps during data collection, with a crystal-to-detector distance fixed at 28 mm. The data were processed with DENZO-SMN.[13] The structure was solved by Patterson-map interpretation with SHELXS-97[14] and refined by full-matrix least-squares on F^2 with SHELXL-97.[14] Absorption effects were corrected empirically with the program DELABS from PLATON.[15] The terminal CH_2OH and CH_3 groups of the pendent arm are disordered so that each fragment bears a partially occupied oxygen atom site (occupancies constrained to sum to unity). One perchlorate ion is disordered over two sites sharing three oxygen atoms, the disordered chlorine and oxygen atoms having been refined with occupancy parameters constrained to sum to unity. All non-hydrogen atoms were refined with anisotropic displacement parameters, with some restraints for some oxygen atoms of the pendent arm, perchlorate ions and water molecules. Hydrogen atoms bound to nitrogen atoms were found on a Fourier-difference map and all others were introduced at calculated positions, except those bound to oxygen atoms. All protons were treated as riding atoms with a displacement parameter equal to 1.2 (NH, NH_2, CH, CH_2) or 1.5 (CH_3) times that of the parent atom. The molecular plot was drawn with SHELXTL.[16]

Crystal Data and Refinement Details: $C_{20}H_{44}Cl_3CuN_8O_{18.5}$, M = 862.52, triclinic, space group $P\bar{1}$, a = 11.8592(6), b = 12.3654(11), c = 13.3374(13) Å, α = 78.768(4)°, β = 81.703(6)°, γ = 61.386(5)°, V = 1681.1(2) Å^3, Z = 2, D_c = 1.704 g cm^{-3}, $F(000)$ = 896, μM_o = 0.979 mm^{-1}, T = 100(2) K. Refinement of 484 parameters on 5790 independent reflections out of 11446 measured reflections (R_{int} = 0.066) led to R_1 = 0.073, wR_2 = 0.183, S = 1.013, $\Delta\rho_{max}$ = 1.14 e·Å^{-3}.

CCDC-212644 contains the supplementary crystallographic data for this paper. These data can be obtained free of charge at www.ccdc.cam.ac.uk/conts/retrieving.html [or from the Cambridge Crystallographic Data Centre, 12, Union Road, Cambridge CB2 1EZ, UK; Fax: (internat.) +44-1223/336-033; E-mail: deposit@ccdc.cam.ac.uk].

Acknowledgments

This work was supported by the Brain Busan Project in 2002.

[1] P. V. Bernhardt, G. A. Lawrance, *Coord. Chem. Rev.* **1990**, *104*, 297.
[2] M. P. Suh, *Adv. Inorg. Chem.* **1997**, *44*, 93.
[3] For recent publications in this area, see: [3a] P. Comba, Y. D. Lampeka, A. Y. Nazarenko, A. I. Pridkhod'ko, H. Pritzkow, *Eur. J. Inorg. Chem.* **2002**, 1464. [3b] P. V. Bernhardt, E. J. Hayes, *Inorg. Chem.* **2002**, *41*, 2892−2902; P. V. Bernhardt, E. J. Hayes, *Inorg. Chem.* **2003**, *42*, 1371. [3c] P. V. Bernhardt, E. G. Moore, M. J. Riley, *Inorg. Chem.* **2002**, *41*, 3025−3031.
[4] M. Le Baccon, F. Chuburu, L. Toupet, H. Handel, M. Soibinet, I. Déchamps-Olivier, J.-P. Barbier, M. Aplincourt, *New J. Chem.* **2001**, *25*, 1168.
[5] See: J. M. Harrowfield, G. Jang, Y. Kim, P. Thuéry, J. Vicens, *J. Chem. Soc., Dalton Trans.* **2002**, 1241−1243 and references therein.
[6] [6a] P. V. Bernhardt, G. A. Lawrance, M. Natitupulu, G. Wei, *Inorg. Chim. Acta* **2000**, *300−302*, 604 and references therein. [6b] An optimised synthesis of the ligand is given in: R. J. Geue, G. H. Searle, *Aust. J. Chem.* **1983**, *36*, 927.
[7] R. W. Green, K. W. Catchpole, A. T. Philip, F. Lions, *Inorg. Chem.* **1963**, *2*, 597.
[8] P. S. Donnelly, J. M. Harrowfield, B. W. Skelton, A. H. White, *Inorg. Chem.* **2001**, *40*, 5645−5652.
[9] M. A. Donnelly, M. Zimmer, *Inorg. Chem.* **1999**, *38*, 1650.
[10] V. Amendola, L. Fabbrizzi, E. Mundum, P. Pallvicini, *Dalton Trans.* **2003**, 773.

 © 2003 Wiley-VCH Verlag GmbH & Co. KGaA, Weinheim

[11] M.-H. Choi, J. M. Harrowfield, B. J. Kim, I.-C. Kim, S.-H. Kim, Y. Kim, M.-K. Lee, M. Mocerino, E. Rukmini, B. W. Skelton, A. H. White, *J. Chem. Soc., J. Chem. Soc., Dalton Trans.* **2001**, 707 and references therein.
[12] *Kappa-CCD Software*, Nonius B. V., Delft, The Netherlands, 1998.
[13] Z. Otwinowski, W. Minor, *Methods Enzymol.* **1997**, *276*, 307.
[14] G. M. Sheldrick, SHELXS-97 and SHELXL-97, University of Göttingen, Germany, 1997.
[15] A. L. Spek, PLATON, University of Utrecht, The Netherlands, 2000.
[16] G. M. Sheldrick, SHELXTL, Version 5.1, Bruker AXS Inc., Madison, WI, USA, 1999.

Received June 6, 2003

 © 2003 Wiley-VCH Verlag GmbH & Co. KGaA, Weinheim

Silver(I) Complex Crystals Switched by a Water Molecule

Hidekazu Arii,[a] Yamato Saito,[a] Yasuhiro Funahashi,[a] Tomohiro Ozawa,[a] Koichiro Jitsukawa,[a] and Hideki Masuda*[a]

Keywords: Coordination polymers / Hydrogen bonds / Silver

The reaction of $AgPF_6$ and *cis*,*cis*-1,3,5-triaminocyclohexane (TACH) in a 1:1 ratio in methanol solution gave two different coordination polymer crystals depending on the presence/absence of water. The crystal structure in the absence of water is a one-dimensional, tube-like polymer with formula $\{[Ag^{I}(TACH)]PF_6\}_n$, while in the presence of water the structure is a three-dimensionally expanded complex network built up from cage units containing a water molecule, $\{[Ag^{I}_3(TACH)_4](PF_6)_3{\cdot}H_2O\}_{ni}$ this structure is induced even by a trace amount of water.
(© Wiley-VCH Verlag GmbH & Co. KGaA, 69451 Weinheim, Germany, 2003)

Introduction

Molecular regulation at the nanometer-scale level is very important and interesting from the viewpoint of the design and synthesis of nanoporous materials. The investigation of nanoporous compounds prepared by the self-assembly of metal ions and organic compounds has been investigated extensively.[1] Metal ions are often used as a junction between organic molecules as their characteristic geometries — such as trigonal planar, tetragonal planar, tetrahedral, and octahedral — allow the construction of higher-dimensional structures. Recently, some interesting compounds based on non-covalent interactions have been reported. Catenanes are formed by only a π-π interaction between aromatic rings,[2,3] and Aoyama et al. have succeeded in preparing organic zeolites linked by a hydrogen bond.[4]

The hydrogen bond is one of the most important non-covalent interactions in biological systems, and it plays an important role in the stabilization of DNA-protein structures and in mutual recognition between proteins.[5] Such non-covalent interactions contribute significantly to the formation of high-dimensional structures in DNA and/or proteins, even in water. The hydrogen bond participates clearly in such structure maintenance and recognition.[6] However, it is difficult for small molecules to interact intermolecularly in water through hydrogen bonding as the water behaves as an inhibitor. These facts imply that the water molecule is one of the essential factors in the steric interaction of DNA-proteins, although it functions as an inhibitor, too. Recently we prepared a new nanoporous material from the reaction of Cu^{I} ion and *cis*,*cis*-1,3,5-triaminocyclohexane (TACH),[7] in which we used the characteristics of the Cu^{I} ion and TACH ligand: the former prefers two-coordinate linear, three-coordinate trigonal-planar, or four-coordinate tetrahedral structures and the latter has C_{3v} symmetry. In this study, using the Ag^{I} ion instead of Cu^{I}, the reaction of $AgPF_6$ with TACH at 1:1 was carried out. Interestingly, two different complex crystals were prepared in absolute methanol and in methanol/water solutions, indicating that the formation of these silver complex crystals was discriminatively switched by the presence of a water molecule. This water-induced transformation of supramolecular structures in the crystalline state is quite novel, although it has been reported that the supramolecular structures of silver(I)-polynitrile complexes are transformed into each other by a similar anion exchange in the crystalline state.[8] Here we describe the preparation and structural characterization of their complexes in detail.

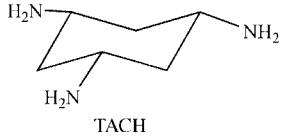

TACH

Results and Discussion

A methanol solution of TACH was added to an absolute methanol solution of $AgPF_6$ in a 1:1 ratio. Allowing the reaction solution to stand for a few hours afforded a colorless crystal suitable for an X-ray diffraction measurement, which was identified as $\{[Ag^{I}(TACH)]PF_6\}_n$ (**1**) from the elemental analysis. Complex **1** crystallizes in the monoclinic system with space group $P2_1/n$. It contains one Ag^{I} ion, one

[a] Department of Applied Chemistry, Nagoya Institute of Technology
Showa-ku, Nagoya 466−8555, Japan
Fax: (internat.) + 81-52/735-5228
E-mail: masuda@ach.nitech.ac.jp
Supporting information for this article is available on the WWW under http://www.eurjic.org or from the author.

TACH molecule, and one PF_6^- ion as crystallographically independent components of the unit cell. The Ag^I ion has a trigonal planar geometry, with coordination of three primary amine nitrogens from three TACH molecules, and the TACH molecule has a chair-form with the three amino groups oriented in the equatorial direction as expected from its *cis*,*cis*-conformation. The Ag^I and TACH units are linearly linked to each other to form a tube-like structure with a small pore of ca. 4×4 Å^2, as shown in Figure 1B, which is a one-dimensional infinite coordination polymer related by a crystallographic screw axis. The tube-like coordination polymers are weakly linked to each other by PF_6^- anions, as shown in Figure 1A. The tube-like coordination polymer may best be described by the formula $\{[Ag^I(TACH)]PF_6\}_n$. The Ag−N bond lengths agree well with those found in analogous Ag^I complexes reported hitherto (2.2−2.4 Å).[9] The nearest Ag−Ag distance is 5.689(3) Å.

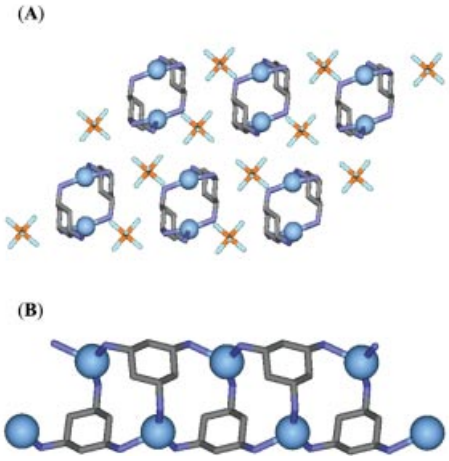

Figure 1. Wire models of the one-dimensional infinite structures of **1** viewed along the crystallographic *ac* (**A**) and *ab* planes (**B**); the blue and gray colored atoms denote nitrogen and carbon atoms, respectively; the large blue-colored atom is a silver(I) ion; hydrogen atoms have been omitted for clarity; selected bond lengths (Å) and angles (°): Ag(1)−N(1) 2.228(9), Ag(1)−N(2) 2.251(8), Ag(1)−N(3) 2.398(8); N(1)−Ag(1)−N(2) 148.4(3), N(1)−Ag(1)−N(3) 111.5(3), N(2)−Ag(1)−N(3) 100.1(3)

The addition of a methanol/water (20:1 v/v%) solution of TACH to a methanol solution of $AgPF_6$ in a 1:1 ratio and allowing the reaction solution to stand for a few hours afforded a colorless crystal suitable for an X-ray diffraction measurement. The complex was identified as $\{[Ag^I_3(TACH)_4](PF_6)_3 \cdot H_2O\}_n$ (**2**) from the elemental analysis. Complex **2** crystallizes in the cubic system with space group $I2_13$, and contains half an Ag^I ion, two units of one-third parts of TACH molecule, half a PF_6^- ion, and six units of one-sixth parts of disordered water molecules as the independent atoms in the unit cell. In spite of the same reaction conditions as for the synthesis of **1**, except for the presence of water, the crystal structure of **2** is quite different from that of **1**. The geometry around the Ag^I ion is tetrahedral, with four primary amine nitrogens from four TACH molecules, although the conformation of the cyclohexane ring and the orientation of three amino groups are the same

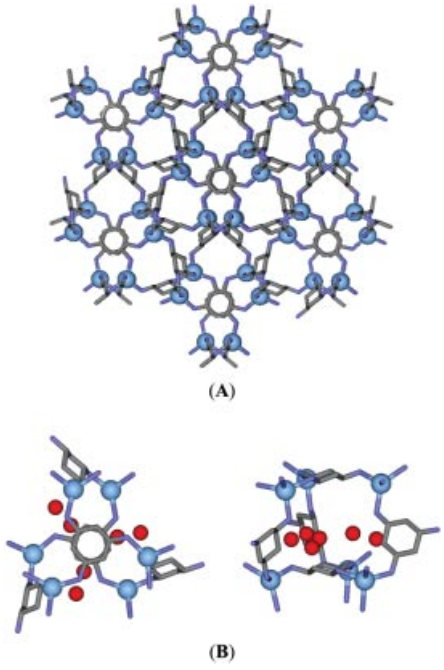

Figure 2. Wire models of the three-dimensionally expanded structure of **2** viewed along the apex of the unit cell (**A**), and top (left) and side (right) views of the cage structure (**B**) of **2** consisting of six Ag^I ions and five TACH molecules; the large blue- and red-colored atoms denote a silver ion and a disordered water molecule, respectively; the counteranions and hydrogen atoms have been omitted for clarity; selected bond lengths (Å) and angles (°): Ag(1)−N(1) 2.383(7), Ag(1)−N(2) 2.356(7); N(1)−Ag(1)−N(2) 100.9(2), N(1)−Ag(1)−N(1*) 128.8(4), N(1)−Ag(1)−N(2*) 101.0(2) (atoms with and without an asterisk are related by a crystallographic threefold axis)

as those of **1**. The dihedral angle of the two planes defined by three atoms, N(1)−Ag(1)−N(2) and N(1*)−Ag(1)−N(2*), is 69°. Judging from the bond angles (denoted in the caption of Figure 2) and the dihedral angle, the Ag^I ion is distorted from a regular tetrahedron.

As is clear from the crystal structure of **2** viewed through the apex of the unit cell (the crystallographic threefold axis), the Ag^+ ions and TACH ligands form three-dimensionally expanded networks (Figure 2). The network is made up of cage units consisting of six silver(I) ions and five TACH molecules (Figure 2B). As shown in the left and right figures of Figure 2B, exhibiting the top and side views of the cage structure, respectively, the center of the TACH molecule lies on the threefold axis and the two cyclohexane rings of the top and bottom TACHs of the cage are twisted with a rotation angle of about 30°. The cage unit is surrounded by six PF_6^- counteranions that are related by threefold axis symmetry; the inner space of the cage is occupied by disordered water molecules, which are incorporated by a hydrophilicity inside the cage. The cage contains pores with a height of about 6 Å and an inner diameter of about 4 Å based on the van der Waals radius of the atoms.[10] The existence of this porosity is also obvious from the lower density of **2** ($\rho = 1.810$ g·cm^{-3}) compared with that of **1** ($\rho = 2.054$ g·cm^{-3}).

Although **1** and **2** were prepared under the same conditions except for the absence/presence of water, respec-

 © 2003 Wiley-VCH Verlag GmbH & Co. KGaA, Weinheim

tively, **1** has a one-dimensional infinite tube-like structure, while **2** exhibits a three-dimensionally expanded network structure constructed from cage units. Both **1** and **2** were obtained from the same starting materials in the same ratio ($AgPF_6$:TACH = 1:1), and **2** was isolated even in the presence of a trace amount of water. Interestingly, a crystal obtained from a suspended solution of **1** in water showed the same X-ray diffraction pattern as the simulation pattern estimated from the single crystal X-ray diffraction measurements of **2** (Figure S1; Supporting Information, see footnote on the first page of this article). A single crystal obtained from the suspended solution also exhibited the same lattice parameters as those of **2**. It is therefore clear that water promotes such a large difference in the coordination structure and the dimensionality.[11] This may be induced by the strong hydrogen bonding ability of water and the difference in the polarity or permittivity of the solvents [H_2O (ε_r = 78.3) and CH_3OH (ε_r = 32.6) at 25 °C].[12] The difference in their formula may be due to the different coordination of TACH molecules to the Ag^I ion: **1** is three-coordinate trigonal-planar and **2** is four-coordinate tetrahedral. The above facts suggest that the water raises the Lewis acidity of the Ag^I ion and assists the linkage of the TACH ligand to the Ag^+ ion. Also, based on the O···(H)N distance of about 2.9 Å, the cage structure could be derived from the hydrogen bonding interaction between the water molecule and the hydrophilic primary amine of the TACH ligands.

In conclusion, we succeeded in the discriminative preparation and structural characterization of two kinds of Ag^I coordination polymers, which gave one- and three-dimensional infinite structures from absolute methanol and from methanol/water, respectively. These structures are switched by the presence of a water molecule.

Experimental Section

$\{[Ag^I(TACH)]PF_6\}_n$ (1): A mixture of TACH (12.9 mg, 0.100 mmol) in methanol (4 mL) was added to an absolute methanol solution (4 mL) of $AgPF_6$ (25.3 mg, 0.100 mmol). After removal of an insoluble material by filtration, allowing the reaction solution to stand for a few hours gave colorless crystals of the title compound (38 mg, 25%). $C_6H_{15}AgF_6N_3P$ (382.04): calcd. C 18.86, H 3.96, N 11.00; found C 19.05, H 3.89, N 11.08.

Crystal Data: $C_6H_{15}AgF_6N_3P$, M = 382.04, monoclinic, space group $P2_1/n$ (no. 14), a = 9.608(8), b = 7.725(6), c = 17.18(1) Å, β = 104.44(1)°, V = 1235(1) Å^3, Z = 4, $\rho_{calcd.}$ = 2.054 g cm^{-3}, μ = 18.14 cm^{-1}, $2\theta_{max}$ = 55.0 °, Mo-K_α radiation (λ = 0.71070 Å), T = 173 K, R = 0.090, Rw = 0.215 (for all reflection data), and GOF = 1.30 for 2814 independent reflections with $I > 2\sigma(I)$ and 154 variables.

$\{[Ag^I_3(TACH)_4](PF_6)_3\cdot H_2O\}_n$ (2): A mixture of TACH (12.9 mg, 0.100 mmol) in methanol (4 mL) and water (0.2 mL) was added to a methanol solution (4 mL) of $AgPF_6$ (25.3 mg, 0.100 mmol). After removal of an insoluble material by filtration, allowing the reaction solution to stand for a few hours gave colorless crystals of the title compound. $C_{24}H_{62}Ag_3F_{18}N_{12}OP_3$ (1293.33): calcd. C 22.29, H 4.83, N 13.00; found C 22.68, H 4.69, N 12.86.

Crystal Data: $C_{24}H_{62}Ag_3F_{18}N_{12}OP_3$, M = 1293.33, cubic, space group $I2_13$ (no. 199), a = 16.8048(7) Å, V = 4745.7(3) Å^3, Z = 4, $\rho_{calcd.}$ = 1.810 g cm^{-3}, μ = 14.31 cm^{-1}, $2\theta_{max}$ = 54.8°, Mo-K_α radiation (λ = 0.71070 Å), T = 173 K, R = 0.066, Rw = 0.176 (for all reflection data), and GOF = 1.36 for 911 independent reflections with $I > 2\sigma(I)$ and 102 variables.

Conversion of 1 to 2: Suspension of a crystal of **1** (10 mg) in water for four days gave colorless crystals that exhibit almost the same X-ray powder diffraction pattern as that of **2** estimated from the single-crystal X-ray diffraction measurements. The single crystal obtained has the same lattice parameters as the crystal of **2**.

CCDC-212323 (**1**) and -212322 (**2**) contain the supplementary crystallographic data for this paper. These data can be obtained free of charge at www.ccdc.cam.ac.uk/conts/retrieving.html or from the Cambridge Crystallographic Data Centre, 12, Union Road, Cambridge CB2 1EZ, UK [Fax: (internat.) +44-1223/336-033; E-mail: deposit@ccdc.cam.ac.uk].

Acknowledgments

This work was supported by a Grant-in-Aid for Scientific Research (Nos. 11228203 and 12304039) from the Ministry of Education, Science, Sports and Culture and supported in part by a grant from the NITECH 21st Century COE Program, to which our thanks are due.

[1] [1a] O. M. Yaghi, H. Li, C. Davis, D. Richardson, T. L. Groy, *Acc. Chem. Res.* **1998**, *31*, 474−484. [1b] M. Eddaoudi, D. B. Moler, H. Li, B. Chen, T. M. Reineke, M. O'Keeffe, M. Yaghi, *Acc. Chem. Res.* **2001**, *34*, 319−330.

[2] [2a] M. Fujita, M. Aoyagi, F. Ibukuro, K. Ogura, K. Yamaguchi, *J. Am. Chem. Soc.* **1998**, *120*, 611−612. [2b] F. Ibukuro, M. Fujita, K. Yamaguchi, J.-P. Sauvage, *J. Am. Chem. Soc.* **1999**, *121*, 11014−11015.

[3] D. B. Amabilino, C. O. Dietrich-Buchecker, A. Livoreil, L. Pérez-García, J.-P. Sauvage, J. F. Stoddart, *J. Am. Chem. Soc.* **1996**, *118*, 3905−3913.

[4] [4a] T. Dewa, K. Endo, Y. Aoyama, *J. Am. Chem. Soc.* **1995**, *117*, 8341−8352. [4b] K. Endo, T. Sawaki, M. Koyanagi, K. Kobayashi, H. Masuda, Y. Aoyama, *J. Am. Chem. Soc.* **1998**, *120*, 8933−8940.

[5] P. Pelletier, J. Kraut, *Science* **1992**, *258*, 1748−1755.

[6] D. E. Wilcox, *Chem. Rev.* **1996**, *96*, 2435−2458.

[7] H. Arii, Y. Saito, Y. Funahashi, K. Jitsukawa, H. Masuda, *Chem. Lett.* **2003**, 106−107.

[8] K. S. Min, M. P. Suh, *J. Am. Chem. Soc.* **2000**, *122*, 6834−6840.

[9] [9a] X.-H. Bu, H. Liu, M. Du, K. M.-C. Wong, V. W.-W. Yam, M. Shionoya, *Inorg. Chem.* **2001**, *40*, 4143−4149. [9b] M. Hong, W. Su, R. Cao, M. Fujita, J. Lu, *Chem. Eur. J.* **2000**, *6*, 427−431.

[10] G. M. Kapteijn, I. C. M. Wehman-Ooyevaar, D. M. Grove, W. J. J. Smeets, A. L. Spek, G. van Koten, *Angew. Chem. Int. Ed. Engl.* **1993**, *32*, 69−72.

[11] M. Mizutani, N. Maejima, K. Jitsukawa, H. Masuda, H. Einaga, *Inorg. Chim. Acta* **1998**, *283*, 105−110.

[12] [12a] V. Gutmann, *Coord. Chem. Rev.* **1967**, *2*, 239. [12b] V. Gutmann, *Coordination Chemistry in Non-Aqueous Solutions*, Springer, Vienna and New York, **1968**.

Received April 1, 2003

 © 2003 Wiley-VCH Verlag GmbH & Co. KGaA, Weinheim

Two Polymeric Complexes of Norfloxacin with Iron(II) and Their Magnetic Properties

Zhi-Rong Qu,[a] Hong Zhao,[a] Li-Xin Xing,[a] Xi-Sen Wang,[a] Zhen-Feng Chen,*[a] Zhi Yu,*[a] Ren-Gen Xiong,*[a] and Xiao-Zeng You[a]

Keywords: Nofloxacin / Iron / Coordination polymers / Magnetic properties / Hydrothermal synthesis

The reaction of H-Norf with $(NH_4)_2Fe(SO_4)_2{\cdot}6H_2O$ and $Fe(OH)_3$ (or Fe_2O_3) affords $Fe(H\text{-}Norf)_2(SO_4){\cdot}2H_2O$ (**1**) and $Fe(Norf)_2{\cdot}4H_2O$ (**2**), respectively, both of which have 2D polymeric structures. Their interesting magnetic properties are also reported. Crystal data for **1**: monoclinic, $P2_1/c$, a = 23.166(1), b = 10.0492(4), c = 7.7264(3) Å, β = 98.379(1)°, V = 1779.50(13) Å^3, Z = 2; for **2**: monoclinic, $P2_1/c$, a = 5.8411(12), b = 21.685(4), c = 13.265(3) Å, β = 99.20(3)°, V = 1658.6(6) Å^3, Z = 2.

(© Wiley-VCH Verlag GmbH & Co. KGaA, 69451 Weinheim, Germany, 2003)

Introduction

Norfloxacin (H-Norf, 1-ethyl-6-fluoro-1,4-dihydro-4-oxo-7-(1-piperazinyl)-3-quinoline carboxylic acid), an extremely potent antibacterial agent with a wide spectrum of activity, is increasingly used for the treatment of many infections.[1] The suggested modes of action of H-Norf are either an inhibition of metalloenzyme DNA-gyrase or an interaction with the DNA molecule via a metal complex intermediate, and it has been proposed that a copper or iron complex could be involved in these interactions with DNA.[2] Some quinolones inhibit the cytochrome P450 system, which also involves an iron(II) ion, and it has been reported that iron(II) sulfate impairs the absorption of quinolones due to the formation of chelates.[3] To date, no solid-state structure of an Fe-quinolone complex has been available to support this theory.

Iron deficiency anaemia is rather common but can be treated easily. By comparison, iron overload disease (IOLD) is relatively rare but can result in serious medical complications, including cirrhosis, primary liver cancer, diabetes, cardiomyopathy and arthritis. Since humans are unable to actively excrete iron, excess iron, once taken up, deposits in tissue in the form of solid FeOOH which then can lead to organ damage and ultimately death. More than 500000 patients world-wide who suffer IOLD (haematological defects such as β-thalassaemia major) can be treated by an iron chelator such as Desferal (siderophore desferrioxamine-B).[4] To date, no reaction product of a metal ion with quinolone derivatives is known to be a polymeric structure both in weakly acidic and basic solutions, although a number of metal ion complexes have been reported.[5] To our surprise, the reaction of H-Norf with $(NH_4)_2Fe(SO_4)_2{\cdot}6H_2O$ and $Fe(OH)_3$ (or Fe_2O_3) affords $Fe(H\text{-}Norf)(SO_4){\cdot}2H_2O$ (**1**) and $Fe(Norf)_2{\cdot}4H_2O$ (**2**) (Scheme 1), respectively, both of which have a 2D polymeric structure. Herein we report the synthesis of **1** and **2**, their solid-state structures, and magnetic properties.

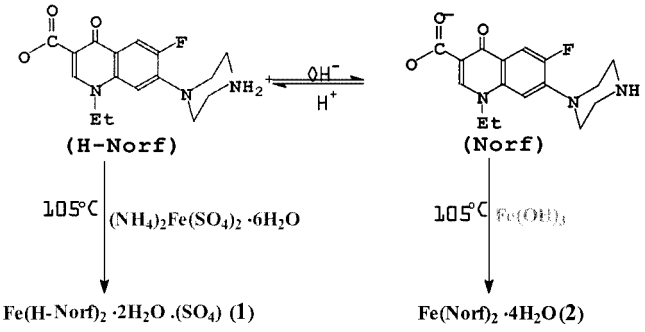

Scheme 1

Results and Discussion

Crystals of dark brown **1** and brown-red **2** were harvested from the reaction of H-Norf with $(NH_4)_2Fe(SO_4)_2{\cdot}6H_2O$ and $Fe(OH)_3$, respectively (Scheme 1). The IR spectra of both **1** and **2** show two very strong peaks at 1621 and 1571cm^{-1} for **1**, and 1621 and 1462 cm^{-1} for **2**, indicating that the carboxylic acid groups of H-Norf are deprotonated (in comparison, those of free H-Norf are at 1710 and 1621 cm^{-1}). A strong peak at 1023 cm^{-1} in the IR spectrum of **1** indicates that there is an uncoordinated SO_4^{2-}. It is

[a] Coordination Chemistry Institute, The State Key Laboratory of Coordination Chemistry, Nanjing University, 210093 Nanjing, P. R. China
Fax: (internat.) +86-25/331-7761
E-mail: xiongrg@netra.nju.edu.cn

 © 2003 Wiley-VCH Verlag GmbH & Co. KGaA, Weinheim **DOI: 10.1002/ejic.200300242**

interesting to note that in weakly basic solution the N atom of the piperidyl ring can take part in the coordination to the metal ion, while in weakly acidic solution, this N atom is protonated and does not bind to the metal ion, as evidenced by the crystal-structure determinations below. Both **1** and **2** are insoluble in common solvents. The solubilities of **1** and **2** in water were estimated by ICP-AE (Inductively Coupled Plasma-Atomic Emission) to be 0.2 and 0.03 μg/mL, respectively.

The X-ray crystal analysis of **1** revealed that the Fe^{II} ion is coordinated in a distorted octahedral geometry defined by six oxygen atoms from four different H-Norf ligands (Figure 1). Two H-Norfs afford one 4-oxo and one carboxyl oxygen to bind Fe^{II} to form two six-membered rings and one equatorial plane defined by O(1), O(2), O(1A) and O(2A), while the apical positions are occupied by two oxygen atoms [(O3B) and O(3C)] from two different carboxylates of H-Norf. Thus, the carboxylate group of H-Norf in **1** clearly binds in a bidentate manner and links the $Fe(H\text{-}Norf)_2$ unit to form a 2D framework, as shown in Figure 1 (bottom). The framework core, composed of the 4-oxo and the 3-carboxyl oxygen atoms, is like a small 2D square grid. The N atom of the piperidyl ring in **1** loses its coordination capacity as a result of protonation. The crystal packing view also indicates that the anions (sulfate) and water are intercalated between two adjacent layers (see Supporting Information). There are also many hydrogen bonds, such as those between water and sulfate (2.547 Å), and water and the protonated N atom (2.711 Å), that hold two adjacent layers together.

The apical positions in **2** (Figure 2), unlike those in **1**, are occupied by two N atoms [N(1) and N(2)] of piperidyl rings,

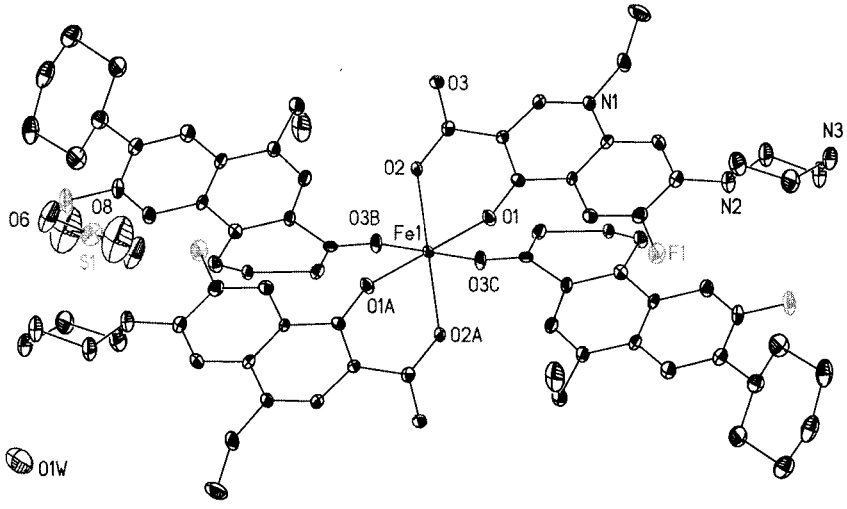

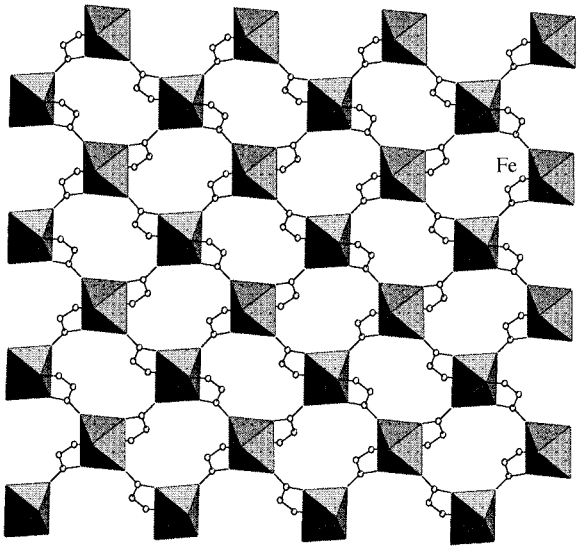

Figure 1. (top) An ORTEP symmetric unit diagram of $[Fe(H\text{-}Nor)_2]\cdot 2H_2O\cdot(SO_4)$(**1**); H atoms and sulfate are omitted for clarity; selected bond lengths [Å] and angles [°]: Fe(1)−O(1) 2.092(3), Fe(1)−O(2) 2.059(3), Fe(1)−O(3B) 2.251(3); O(1)−Fe(1)−O(2) 85.27(13), O(1)−Fe(1)−O(3B) 90.65(12), O(1)−Fe(1)−O(2A) 94.73(13), O(2)−Fe(1)−O(3B) 93.89(13), O(1)−Fe(1)−O(3C) 89.35(12); (bottom) an extended 2D network presentation of $[Fe(H\text{-}Nor)_2]\cdot 2H_2O\cdot(SO_4)$(**1**) highlighting the Fe octahedron

 © 2003 Wiley-VCH Verlag GmbH & Co. KGaA, Weinheim

resulting in the formation of a 2D square grid with a cavity dimension of 13.538 × 13.538 Å.[6] The coordination environment around Fe^{II} in **2** is also slightly distorted octahedral with an equatorial plane defined by O(2), O(3), O(2A) and O(3A) from two different Norfs. Unlike in **1**, the carboxylate group of Norf in **2** acts as monodentate ligand, and one of the O atoms of the carboxylate group is uncoordinated. This mode of bonding is similar to that of $Zn(Norf)_2{\cdot}4H_2O$.[5h]

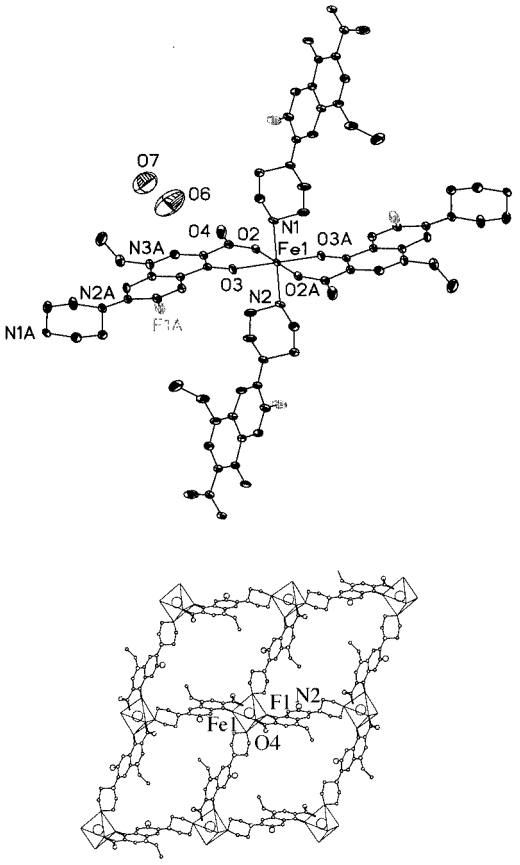

Figure 2. (top) An ORTEP symmetric unit diagram of $[Fe(Nor)_2]{\cdot}4H_2O$ (**2**); H atoms are omitted for clarity; selected bond lengths [Å] and angles [°]: Fe(1)−O(2) 2.067(2), Fe(1)−O(3) 2.105(2), Fe(1)−N(1) 2.303(3); O(2)−Fe(1)−O(3) 84.99(9), O(2)−Fe(1)−O(3A) 95.01(9), O(2)−Fe(1)−N(1B) 89.73(9), O(2A)−Fe(1)−N(1B) 90.27(9), O(3)−Fe(1)−N(1B) 92.90(10), O(3A)−Fe(1)−N(1B) 87.10(10); (bottom) an extended 2D molecular square presentation of $[Fe(Nor)_2]{\cdot}4H_2O$ (**2**) highlighting the Fe octahedron

Studies of the magnetic susceptibility of **1** versus temperature (Figure 3) show strong antiferromagnetic coupling between 20 K and 300 K and a weak ferromagnetic phenomenon at lower temperatures (5−20 K). In contrast, **2** shows a weak ferromagnetic interaction throughout this whole temperature range. This is in good agreement with the shorter distance between the Fe ions in **1** than in **2**. At room temperature the value of $\chi_{mol}T$ (≈3.5 cm^3/mol K) for both compounds is rather close to the expected value for ferrous ion ($S = 2$) in a high-spin state; this was confirmed by Mössbauer spectra at room temperature. However, $\chi_{mol}T$ for **1** is discontinuous around 15 K, which is indicative of a magnetic phase-transition originating from a spin-canting phenomenon as a consequence of neighboring spin units of iron being aligned in a canted antiparallel manner.[7] The magnetization of **1** at 5 K performed up to 50 kOe (Figure 4) shows that the field dependence of the magnetization departs from linearity. A hysteresis loop at very low magnetic field range (< 2000 Oe) was obtained. When the magnetic field was cycled, a remnant magnetization of about 0.3 μ_B and a coercive field of about 130 Oe were observed as a result of magnetic ordering at this temperature. This observation shows that **1** is a hard magnet material.

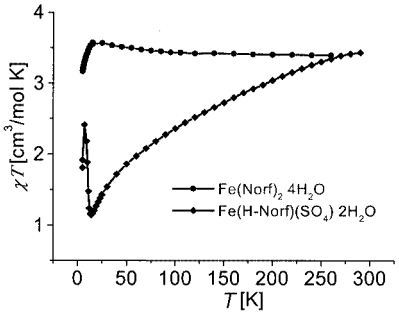

Figure 3. Temperature dependence of $\chi_{mol}T$ for **1** and **2**

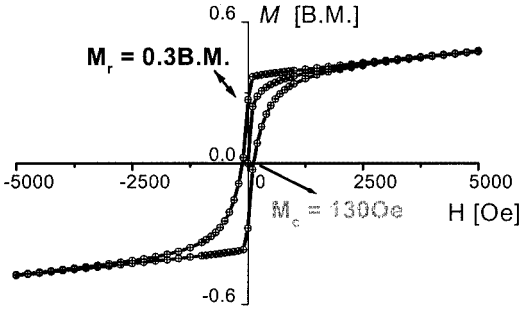

Figure 4. The magnetization of **1** in an applied field of −5 kOe to 5 kOe

In conclusion, the reaction products of H-Norf with iron(II) were found to be mainly dependent upon the pH of the solutions. In basic solution, the product is a 2D square network involving the coordination of the N atom of the piperidyl ring to iron(II), while in weakly acidic solution the product is also a 2D framework with a μ_3-carboxylate coordination mode.

Experimental Section

Compound 1: Samples of 1 mmol of $(NH_4)_2Fe(SO_4)_2{\cdot}6H_2O$ and 2 mmol of H-Norf were thoroughly mixed in a mortar with a pestle, and placed in thick-walled Pyrex tubes (ca. 20 cm long; pH ≈ 5.8 in the solution). After addition of 0.5 mL of EtOH and 1.5 mL of H_2O, the tube was frozen with liquid N_2, evacuated under vacuum and sealed with a torch. The tube was heated at 105 °C for one day to give pale-yellow block crystals (0.454 g) in 55% yield based on H-Norf. $C_{32}H_{40}F_2FeN_6O_{12}S$ (826.61): calcd. C 46.45, H 4.84,

 © 2003 Wiley-VCH Verlag GmbH & Co. KGaA, Weinheim

N 10.16; found C 46.58, H 4.90, N 10.28. The crystals showed only one phase. Solid reflectance UV/Vis (nm): 328.6, 271.7. IR (KBr): $\tilde{\nu}$ = 3402(m), 1621(s), 1462(vs), 1371(w), 1262(m), 1108(s), 1021(w), 925(w), 804(w), 791(w), 745(w) and 620(w) cm^{-1}.

Compound 2: The procedures are similar to those of **1** and $Fe(OH)_3$ was used as starting material (pH ≈ 8.2). The brown-red rod crystals (0.497 g; one phase) were harvested in 65% yield based on H-Norf. $C_{32}H_{42}F_2FeN_6O_{10}$ (764.57): calcd. C 50.22, H 5.49, N 10.99; found C 50.30, H 5.55, N 11.12. IR (KBr): $\tilde{\nu}$ = 3400(m), 1620(vs), 1578(m), 1482(s), 1380(m), 1340(m), 1261(s), 182(w),1118 (w), 1000(w), 928(m), 884(w),811(w), 790(w), 740(w) and 628(w) cm^{-1}.

Crystal Data for 1: $C_{32}H_{40}F_2FeN_6O_{12}S$, M_r = 826.61, monoclinic, $P2_1/c$, a = 23.166(1), b = 10.0492(4), c = 7.7264(3) Å, β = 98.379(1)°, V = 1779.50(13) $Å^3$, Z = 2, $\rho_{calcd.}$ = 1.543 g·cm^{-3}, T = 293(2) K, μ = 0.565 mm^{-1}, R_1 = 0.0633, $wR2$ = 0.1589 for 1975 observed reflections from 3121 independent reflections, GOF = 1.032.

Crystal Data for 2: $C_{32}H_{42}F_2FeN_6O_{10}$, M_r = 764.57, monoclinic, $P2_1/c$, a = 5.8411(12), b = 21.685(4), c = 13.265(3) Å, β = 99.20(3)°, V = 1658.6(6) $Å^3$, Z = 2, $\rho_{calcd.}$ = 1.531 g cm^{-3}, T = 293(2) K, μ = 0.534 mm^{-1}, R_1 = 0.0496, wR_2 = 0.1456 for 2033 observed reflections from 2869 independent reflections, GOF = 1.189.

The structures were solved by direct methods using the program SHELXTL. All the non-hydrogen atoms were located from the trial structure and then refined anisotropically with SHELXTL using a full-matrix least-squares procedure. The hydrogen atom positions were fixed geometrically at calculated distances and allowed to ride on the parent carbon atoms. The final difference Fourier map was found to be featureless.

CCDC-140822 (**1**) and -169760 (**2**) contain the supplementary crystallographic data for this paper. These data can be obtained free of charge at www.ccdc.cam.ac.uk/conts/retrieving.html [or from the Cambridge Crystallographic Data Centre, 12, Union Road, Cambridge CB2 1EZ, UK; Fax: (internat.) +44-1223/336-033; E-mail: deposit@ccdc.cam.ac.uk].

Acknowledgments

This work was funded by The Major State Basic Research Development Program (Grant No. G2000077500) and the National Natural Science Foundation of China. R.-G. X. thanks Prof. Dr. H.-K. Fun for the X-ray crystal structure determination of compound **1**.

[1] [1a] L. L. Shen, A. G. Pernet, *Proc. Natl. Acad. Sci. USA* **1985**, *82*, 307. [1b] G. C. Grumplin, J. M. Midgley, J. T. Smith, *Top. Antibiot. Chem.* **1980**, *8* 9. [1c] *Quinolone Antimicrobial Agents*, 2nd ed. (Eds.: D. C. Hooper, J. S. Wolfson), American Society of Microbiology, Washington DC, **1993**. [1d]G. S. Son, J.-A. Yeo, M.-S. Kim, S. K. Kim, A. Holmen, B. Akerman, B. Norden, *J. Am. Chem. Soc.* **1998**, *120*, 6451.

[2] [2a] L. L. Shen, J. Baranowski, A. G. Pernet, *Biochemistry* **1989**, *28*, 3879. [2b] A. J. Maxwell, *Antimicrob. Chemoth.* **1992**, *30*, 409. [2c] C. J. R. Willmott, S. E. Chritchlow, I. C. Eperson, A. J. Maxwell, *Mol. Biol.* **1994**, *242*, 351. [2d] P. A. Permana, R. M. Snapka, L. L. Shen, D. T. W. Chu, J. J. Clement, J. J. Platter, *Biochemistry* **1994**, *33*, 11333. [2e] H. Yu, L. H. Hurley, S. M. Kerwin, *J. Am. Chem. Soc.* **1996**, *118*, 7040. [2f] H. T. Yu, Y. Kwok, L. H. Hurley, S. M. Kerwin, *Biochemistry* **2000**, *39*, 10236.

[3] [3a] J. R. B. J. Brouwers, *Drug Safety* **1992**, *7*, 268. [3b] I. Turel, I. Leban, G. Klintschar, N. Bukovec, S. Zalar, *J. Inorg. Biochem.* **1997**, *63*, 77. [3c] F. Gao, P. Yang, J. Xie, H. Wang, *J. Inorg. Biochem.* **1995**, *60*, 61.

[4] [4a] U. Heinz, K. Hegetschweiler, P. Acklin, B. Faller, R. Lattmann, H. P. Schnebli, *Angew. Chem. Int. Ed.* **1999**, *38*, 2568. [4b] R. C. Hider, A. D. Hall, *Prog. Med. Chem.* **1991**, *28*, 40. [4c] J.-B. Galey, O. Destree, J. Dumates, S. Genard, P. Tachon, *J. Med. Chem.* **2000**, *43*, 1418. [4d] B. Crichton, M. Green, *Curr. Med. Res. Opin.* **2002**, *18*, 92. [4e] G. J. Kontoghiorghes, M. B. Agarwal, P. Tondury, J. J. M. Marx, *Lancet* **2001**, *357*, 882.

[5] [5a] C. Chulvi, M. C. Munoz, L. Perello, R. Ortiz, M. I. Arriortua, J. Via, K. Urtiaga, J. M. Amigo, L. E. Ochando, *J. Inorg. Biochem.* **1991**, *42*, 133. [5b] G. Mendoza-Diuz, L. M. R. Martinez-Aguilera, R. M. Esparza, K. H. Panell, F. C. Lee, *J. Inorg. Biochem.* **1993**, *50*, 65. [5c] M. Ruiz, R. Ortiz, A. Castinerias, M. Quiros, *Inorg. Chim. Acta* **1993**, *211*, 133. [5d] I. Turel, I. Leban, N. Bukovec, *J. Inorg. Biochem.* **1994**, *56*, 273. [5e] S, C. Wallis, L. R. Gahan, B. G. Charles, T. W. Hambley, P. A. Duckworth, *J. Inorg. Biochem.* **1996**, *62*, 1. [5f] I. Turel, K. Gruber, I. Leban, N. Bukovec, *J. Inorg. Biochem.* **1996**, *61*, 197. [5g] Z.-F. Chen, R.-G. Xiong, J.-L. Zuo, Z. Guo, X.-Z. You, H.-K. Fun, *J. Chem. Soc., Dalton Trans.* **2000**, 4013. [5h] Z.-F. Chen, R.-G. Xiong, J. Zhang, X.-T. Chen, Z.-L. Xue, X.-Z. You, *Inorg. Chem.* **2001**, *40*, 4075. [5i] Z.-F. Chen, B.-Q. Li, Y.-L. Yuan, R.-G. Xiong, X.-Z. You, X.-L. Feng, *Inorg. Chem. Commun.* **2001**, *4*, 346.

[6] [6a] M. Aoyagi, K. Biradha, M. Fujita, *J. Am. Chem. Soc.* **1999**, *121*, 7457. [6b] T. Shimizu, M. Kogiso, M. Masuda, *Nature* **1996**, *383*, 487. [6c] Z. Guo, P. J. Sadler, *Angew. Chem. Int. Ed.* **1999**, *38*, 1512. [6d] Z. Guo, P. J. Sadler, *Adv. Inorg. Chem.* **1999**, *49*, 183.

[7] [7a] C.-M. Liu, Z. Yu, R.-G. Xiong, X.-Z. You, *Inorg. Chem. Commun.* **1999**, *1*, 31. [7b] M. Martinez-Lorente, J. P. Tuchagues, V. Petrouleas, J. M. Savariault, R. Poinsot, M. Drillon, *Inorg. Chem.* **1991**, *30*, 3587. [7c] H. Oshio, N. Hoshino, T. Ito, *J. Am. Chem. Soc.* **2000**, *122*, 12602. [7d] K. L. Taft, A. Caneschi, L. E. Pence, C. D. Delfs, G. C. Papaefthymiou, S. J. Lippard, *J. Am. Chem. Soc.* **1993**, *115*, 11753. [7e] A. L. Barra, A. Caneschi, A. Cornia, F. Fabrizi de Biani, D. Gatteschi, C. Sangregorio, R. Sessoli, L. Sorace, *J. Am. Chem. Soc.* **1999**, *121*, 5302. [7f] S. M. J. Autin, M. W. Wemple, L.-C. Brunel, M. B. Maple, G. Christou, D. N. Hendrickson, *J. Am. Chem. Soc.* **1996**, *118*, 7746. [7g] J. L. Manson, Q.-Z. Huang, J. W. Lynn, H.-J. Koo, M.-H. Whangbo, R. Bateman, T. Otsuka, N. Wada, D. N. Argyriou, J. S. Miller, *J. Am. Chem. Soc.* **2001**, *123*, 162.

Received April 28, 2003

 © 2003 Wiley-VCH Verlag GmbH & Co. KGaA, Weinheim

Structural and Magnetic Characterization of a Linear Trinuclear Copper Complex Formed through Ligand Sharing

Yufei Song,[a] Patrick Gamez,[a] Olivier Roubeau,[b] Martin Lutz,[c] Anthony L. Spek,[c] and Jan Reedijk*[a]

Keywords: Copper / Magnetochemistry / Bioinorganic chemistry / N,O ligands

Reaction of bis(2-hydroxybenzyl)-1,3-diamino-2-propanol (H_2bhbdp) with copper perchlorate in methanol leads to the assembly of a trinuclear complex with the general formula $[Cu_3(bhbdp)_2(CH_3OH)_2(ClO_4)_2]$ (**1**). The complex was characterized by X-ray crystallography, Ligand Field, IR and ESR spectroscopy, and magnetic susceptibility. The structure of the complex contains a linear trinuclear array of copper ions [the Cu(1)–Cu(2)–Cu(1a) angle is 180° by symmetry], in octahedral, square planar and octahedral environments, respectively. The external Cu1 and Cu1a centers are coordinated by two amine nitrogens, two phenolate oxygen donors, one methoxide oxygen and one oxygen from a perchlorate, while the central Cu2 is coordinated by four phenolate oxygens through ligand sharing. A strong antiferromagnetic interaction between the adjacent Cu^{II} ions dominates the magnetic properties of **1** leading to an $S = 1/2$ ground state which is fully populated below 150 K.
(© Wiley-VCH Verlag GmbH & Co. KGaA, 69451 Weinheim, Germany, 2003)

Introduction

Many multinuclear copper(II) complexes have been reported during the past decades with a great number of simple and intricate bridging ligands.[1−3] This interest arises from the search for models of the active sites of multicopper proteins, like ascorbate oxidase,[4] ceruplasmin[5] or laccase,[6] and from their potential use in catalysis.[7] The trinuclear active site in laccase,[8] the ferromagnetically coupled Cu^{II} triad in the subunit of methane mono-oxygenase[9] and the angled trinuclear Cu^{II} unit as well as the mononuclear type-1 copper(II) centre of ascorbate oxidase from zucchini,[10] have drawn much attention in the study of trinuclear copper systems.[11] In addition, the study of such compounds has allowed a better understanding of the magnetic properties of molecular compounds, because copper(II) ions have the simplest magnetic spin possible i.e. 1/2. Only a limited number of linear trinuclear compounds have been structurally and magnetically characterized until now.[12−14] In particular, there is still no example of Cu−Cu bonding interactions in such closely packed multimetal systems, while many other metal ions do form M−M bonds under the same conditions.[15]

In the present study, a homometallic, linear, trinuclear complex, $[Cu_3(bhbdp)_2(CH_3OH)_2(ClO_4)_2]$ (**1**), was synthesized and characterized, in which, due to the basicity of the coordinated phenols, two octahedral Cu^{II} complexes function as didentate ligands for the square-planar central Cu^{II} ion. Strong anti-ferromagnetic exchange interactions between neighboring Cu^{II} ions are inferred from the temperature dependence of the magnetic susceptibilities of **1**.

Results and Discussion

The trinuclear copper compound of formula $[Cu_3(bhbdp)_2(CH_3OH)_2(ClO_4)_2]$ (**1**) was obtained by reaction of one equivalent of H_2bhbdp with two equivalents of copper(II) perchlorate in methanol. Diethyl ether diffusion into the methanolic solution led to the formation of deep-blue square crystals suitable for X-ray crystallography. A molecular plot representing the complex together with the atom-labeling scheme is shown in Figure 1. The hydrogen-bonding network linking the trinuclear units is presented and depicted in Figure 2.

The asymmetric unit of the coordination compound contains one $[Cu_3(bhbdp)]^{2+}$ cation, one ClO_4^- anion and one coordinated methanol molecule. The $[Cu_3(bhbdp)_2]^{2+}$ cation contains three Cu^{2+} atoms in a linear array. The two terminal Cu^{2+} atoms, Cu(1) and Cu(1a), are coordinated by two amine nitrogens and four oxygen atoms (two phenolate

[a] Leiden Institute of Chemistry, Gorlaeus Laboratories, Leiden University,
P.O. Box 9502, 2300 RA Leiden, The Netherlands
[b] Centre de Recherche Paul Pascal-CNRS;
115 avenue du Docteur Albert Schweitzer; 33600 Pessac; France
[c] Bijvoet Center for Biomolecular Research, Utrecht University,
Padualaan 8, 3584 CH Utrecht, The Netherlands
Supporting information for this article is available on the WWW under http://www.eurjic.org or from the author.

 © 2003 Wiley-VCH Verlag GmbH & Co. KGaA, Weinheim **DOI: 10.1002/ejic.200300261**

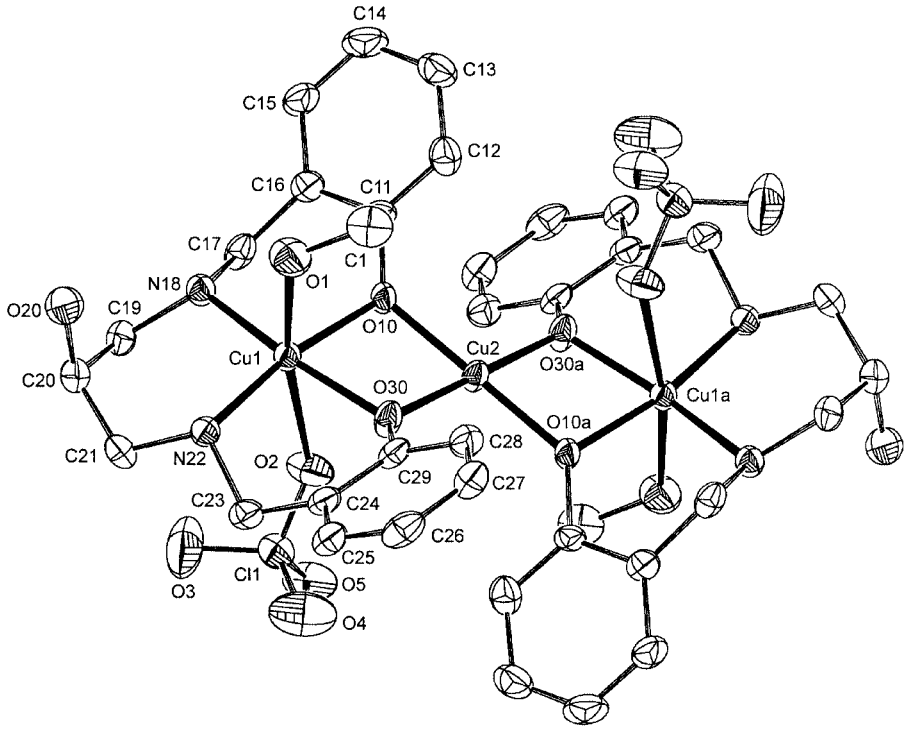

Figure 1. Displacement ellipsoid plot (50% probability level) of the trinuclear copper complex $[Cu_3(bhbdp)_2(CH_3OH)_2(ClO_4)_2]$ showing the crystallographic numbering scheme; hdrogen atoms have been omitted for clarity; symmetry operation a: $1 - x$, $1 - y$, $1 - z$; selected bond lengths and angles: Cu1−O30 1.956(3), Cu1−N18 1.996(3), Cu1−N22 2.014(3), Cu1−O10 1.958(3), Cu1−Cu2 2.9869(4), Cu1−O1 2.387(3), Cu1−O2 2.813, Cu2−O10 1.910(2), Cu2 −O30 1.911(3) Å; O10−Cu1−O30 76.59(11), O10−Cu1−N18 91.90(12), O10−Cu1−N22 169.14(11), O30−Cu1−N18 166.22(12), O30−Cu1−N22 92.58(12), N18−Cu1−N22 98.71(13), Cu2−Cu1−O1 100.27(8), Cu2−Cu1−O30 38.87(8), Cu2−Cu1−N22 130.34(9), O1−Cu1−O10 91.92(11), O1−Cu1−O30 92.81(12), O1−Cu1−N18 95.16(13), O1−Cu1−N22 89.40(12)°

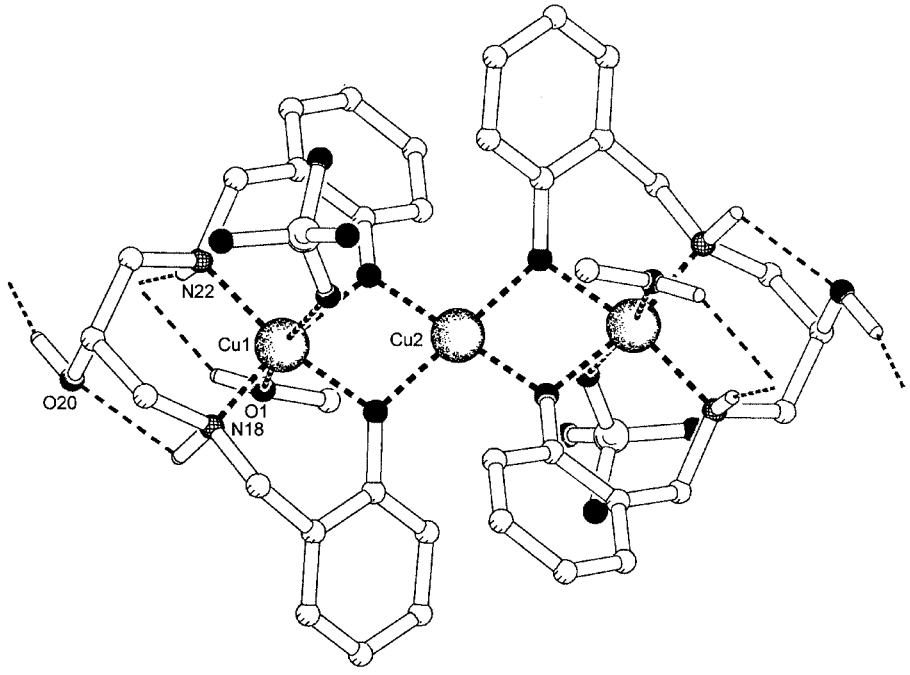

Figure 2. Perspective view exhibiting the hydrogen bonds; intramolecular D−H···A hydrogen bond (D···A, Å): N18−H18N···O20 2.735(5); intermolecular hydrogen bonds (D···A, Å): O1−H1O···O3 2.946(6); O20−H20O···O5 2.869(5); N22−H22N···O3 3.086(5)

oxygens, one methanol oxygen and one oxygen from a ClO_4^-). The central copper(II) atom, Cu(2), is coordinated by four oxygen atoms (from four phenolate oxygens). As Cu(2) occupies an inversion center, the resulting Cu(1)−Cu(2)−Cu(1a) array is linear by symmetry. The two terminal Cu(1) and Cu(1a) atoms are both coordinated by

 © 2003 Wiley-VCH Verlag GmbH & Co. KGaA, Weinheim

bhbdp^{2-} in a *cis* fashion with respect to the phenolate moieties. Thus, their coordination environment is described as an N_2O_4 donor set. Each phenolate unit further bridges to the central Cu(2) atom of the trinuclear moiety, resulting in a four-coordinate CuO4 chromophore. The central Cu^{2+} ion has a square-planar geometry due to the site symmetry, and the dihedral angle between the two Cu(1)−O(10)−Cu(2) and Cu(1)−O(30)−Cu(2) planes is 18.19(19)°. The terminal Cu(1) ions present a Jahn−Teller-distorted octahedral environment, resulting from the very long axial Cu(1)−O bonds from the semi-coordinated perchlorate O(2) and the methanol O(1). Therefore, the equatorial coordination plane is an N_2O_2 donor set [for Cu(1); N18, N22, O10, O30]. The Cu−O bond lengths of the central Cu(2) atom [1.910(2)−1.911(3) Å] are shorter than those of the equatorial Cu−O bonds of the terminal Cu(1) atoms [1.956(3)−1.958(3) Å], which is attributed to the two different coordination geometries (octahedral and square-planar, respectively). The Cu(2)−Cu(1) distance is 2.9869(4) Å, while the Cu(1)−O−Cu(2) angles of each pair of neighbors are 101.15(12)° and 101.08(12)° respectively for O(30) and O(10). Each Cu_2O_2 pair is almost planar as shown by the Cu(2)−O(30)−O(10)−Cu(1) torsion angle of 165.18(15)°.

Electronic Properties

The ligand-field spectrum of **1** shows three absorption bands centered at approximately 262 nm (38.2×10^3 cm^{-1}), 402 nm (24.8×10^3 cm^{-1}) and 567 nm (17.6×10^3 cm^{-1}). The intensity of the absorption at 402 nm clearly precludes it being a d-d transition, hence this feature is assigned as being due to a phenolate oxygen to Cu^{II} charge-transfer (CT) transition.[14] The absorption at 262 nm is another CT from phenolate oxygen to Cu^{II}. One of these phenolate oxygen to Cu^{II} CT bands is due to the terminal Cu^{II} CT and the other to the central Cu^{II} CT.[14] The transition in the visible region of the electronic spectrum of this complex is a much-less-intense absorption at 567 nm, which is assigned to d-d transitions of both square-planar and octahedral species.[16,17]

Magnetic Susceptibility and ESR

The ESR spectrum of a powered polycrystalline sample of **1** at room temperature shows a broad isotropic copper(II) signal centered around a g value of 2.0976. The main EPR signal $g_\perp = 2.0646$ sharpens upon cooling to 77 K and a very weak $g_{//}$ at ca. $g = 2.1945$ becomes visible (no $A_{//}$ resolved). The frozen solution spectrum in a CH_3CN/CH_3OH (1:1) solution shows only a broad signal at $g = 2.0794$. No structural conclusions can be drawn from these spectra.

The temperature dependence of the product $\chi_m T$ of **1** is shown in Figure 3, together with magnetization vs. field measurements at 1.8 K. Even at 390 K, $\chi_m T$ is much lower than that of three uncoupled Cu^{II} ions (0.593 cm^3·K/mol instead of 1.125 cm^3·K/mol for $g = 2$), thus indicating the presence of strong antiferromagnetic interactions. It decreases upon lowering the temperature to reach a plateau

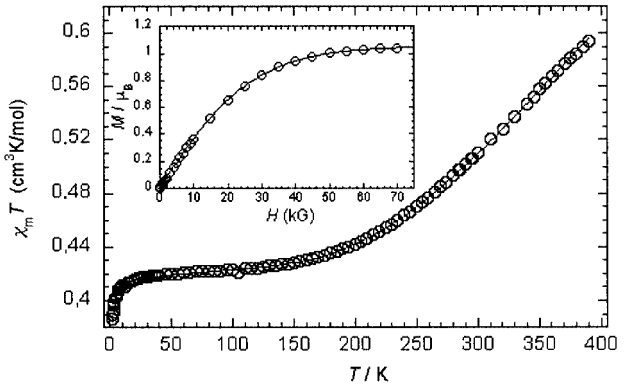

Figure 3. $\chi_m T$ vs. T plot for complex **1**; the solid line is the best fit obtained with a nearest neighbor interaction of −511(2) cm^{-1} (see text); insert: field dependence of magnetization measured at 1.83 K

below 150 K at about 0.42 cm^3·K/mol, corresponding to an $S = 1/2$ ground state (0.375 cm^3·K/mol for $g = 2$). Indeed, the magnetization vs. field data at 1.83 K (inset in Figure 3) tend to saturate at a value of 1.06. Below 10 K, a further decrease of $\chi_m T$ sets in, which can only be attributed to intermolecular interactions between $S = 1/2$ trimeric units. Therefore this behavior was modelled using the spin Hamiltonian given in Equation (1).

$$H = g\beta S_z H - J_1(S_1 \cdot S_2 + S_{1a} \cdot S_3) - J_2(S_1 \cdot S_{1a}) - zJ' \langle S_z \rangle S_z \quad (1)$$

The first term of this hamiltonian corresponds to the Zeeman term, for which a single isotropic g tensor has been considered for the two different Cu^{II} ions in **1**. The second and third terms include isotropic nearest neighbor and next-nearest neighbor interactions, respectively, with J_1 representing the exchange parameter between neighboring Cu^{II} ions and J_2 the exchange parameter between terminal Cu^{II} ions. The fourth term takes into account intermolecular interactions in the mean-field approximation,[18] with J' being the intermolecular exchange interaction and z the number of trimeric neighbors, in this case four. In cases like **1**, where the trinuclear array is perfectly linear and the dominant nearest neighbor interaction is antiferromagnetic, J_2 can be neglected, and was thus set to zero. The resulting expression of the molar magnetic susceptibility in the $\beta H/k_B T << 1$ approximation, with an additional term to take into account a Temperature-Independent Paramagnetism (TIP), is given in Equation (2).

$$\chi_M(T) = \frac{N_A g^2 \beta^2 F(T)}{4k_B(T - zJ'F(T))} + TIP$$
$$F(T) = \frac{1 + \exp(J_1/k_B T) + 10\exp(3J_1/2k_B T)}{1 + \exp(J_1/k_B T) + 2\exp(3J_1/2k_B T)} \quad (2)$$

The best set of parameters obtained (full line in Figure 3) was $J_1 = -511(2)$ cm^{-1}, $g = 2.15(1)$ and $zJ' = -1.9(1)$ cm^{-1} with a TIP value of $61(3) \times 10^{-6}$ cm^3/mol. Thus, the ground state of the trinuclear unit is, in the (S_{total}, $S_1 + S_{1a}$)

 © 2003 Wiley-VCH Verlag GmbH & Co. KGaA, Weinheim

format, the doublet (1/2,0), with the excited doublet (1/2,1) and quadruplet (3/2,1) lying 511 and 766 cm^{-1} above it, respectively. It is well-known that in planar dinuclear copper(II) complexes with di-μ-alkoxo bridges, the exchange parameter varies linearly with the Cu−O−Cu angle.[19] Indeed, the value expected for the average Cu−O−Cu angle in **1** — 101.1° — is −495 cm^{-1} and almost perfectly matches the value obtained for J_1 in the present work. In addition, the Cu−Cu separation is large (2.987 Å), indicating that no direct exchange mechanism is likely to contribute to the magnetic coupling. Therefore, the strong antiferromagnetic coupling in **1** is ascribed solely to superexchange mechanisms within the central-terminal copper(II) pairs. The moderately weak intermolecular interactions observed in **1** can be explained by the hydrogen bonding network (see Figure 2) in which the coordinated perchlorate is involved.

In summary, the ligand bis(2-hydroxybenzyl)-1,3-diamino-2-propanol allows the formation of a stable, linear, homometallic, trinuclear complex $[Cu_3(bdbhp)_2(CH_3OH)_2(ClO_4)_2]$. A strong antiferromagnetic coupling between adjacent copper(II) ions in the triad dominates the magnetic properties of this complex. Further studies of its catalytic activity for the polymerization of 2,6-dimethylphenol (DMP) and oxygen binding chemistry at room temp. and low temperature are under investigation. By developing additional model systems of copper proteins, a better insight may be obtained into the magnetic properties of multicopper proteins and the relationship between structure and activity.

Experimental Section

General Remarks: All reagents and solvents were purchased from commercial sources and used as received. The ligand bis(2-hydroxlybenzyl)-1,3-diamino-2-propanol was prepared from salicylaldehyde and 1,3-diamino-2-propanol by reductive amination in methanol with $NaBH_4$. C,H,N analyses were carried out by the Microanalysis Department of Leiden University. Infrared spectra were recorded on a Perkin−Elmer Paragon 1000 spectrophotometer equipped with a Golden Gate Diamond ATR as a sample support. X-Band EPR spectra were recorded on a JEOL ESR spectrometer equipped with an Esprit 330 data system, at room temperature and at 77 K, with dpph as an internal reference (g = 2.0036). The ligand-field spectra of the solid compounds were recorded in the 300−2000 nm range on a Perkin−Elmer Lambda 900 UV/Vis/NIR spectrometer in the diffuse reflectance mode with MgO as reference. Field cooled measurements (300 to 1.8 to 390 K) of the magnetization of smoothly powdered microcrystalline **1** (m = 23.71 mg) were performed with a Quantum Design MPMS-7XL squid magnetometer in a 1kG applied field. Corrections for diamagnetic contributions of the sample (5.26×10^{-4} cm^3/mol) to the magnetic susceptibility were calculated using Pascal's constants.

Preparation of the Compound: A solution of the ligand (12.1 mg, 0.01 mmol) in methanol (2 mL) was added to copper(II) perchlorate (29.8 mg, 0.02 mmol) in methanol (2 mL). Diffusion of diethyl ether into the solution led to the formation of brown crystals after one day. Yield 36% (1.9 mg). $C_{36}H_{48}Cl_2Cu_3N_4O_{16}$ (1054.3): calcd. C 40.97, H 4.55, H 5.31; found C 40.58, H 4.32, N 5.55. IR (solid): $\tilde{\nu}$ = 3536, 3268, 3232, 1600, 1486, 1456, 1247, 1041, 759, 625 cm^{-1}. UV/Vis/NIR (solid): λ_{max} = 24875 cm^{-1}. EPR (solid, room temp.): g = 2.0976.

Crystal structure determination: $C_{36}H_{48}Cl_2Cu_3N_4O_{16}$, mol. wt. = 1054.30, brown needle, 0.24 × 0.06 × 0.06 mm^3, monoclinic, $P2_1/c$ (no. 14), a = 11.4981(2), b = 13.7442(2), c = 16.0767(3) Å, β = 123.5141(8)°, V = 2118.26(7) $Å^3$, Z = 2, D_x = 1.653 g/cm^3, μ = 1.694 mm^{-1}. 21805 Reflections were measured on a Nonius KappaCCD diffractometer with rotating anode (λ = 0.71073 Å) at a temperature of 150(2) K up to a resolution of $(\sin\theta/\lambda)_{max}$ = 0.59 $Å^{-1}$; 3641 reflections were unique (R_{int} = 0.086). An absorption correction based on multiple measured reflections was applied (0.68−0.91 transmission). The structure was solved by direct methods (SHELXS-97[20]) and refined with SHELXL-97[21] against F^2 of all reflections. Non-hydrogen atoms were refined freely with anisotropic displacement parameters. C−H hydrogen atoms were refined as rigid groups; O−H and N−H hydrogen atoms were located in the difference Fourier map and kept fixed in that position. 278 refined parameters, no restraints. R values [$I > 2\sigma(I)$]: $R1$ = 0.0398, $wR2$ = 0.0998. R values [all refl.]: $R1$ = 0.0696, $wR2$ = 0.1142. GoF = 1.091. Residual electron density between −0.76 and 1.13 e/$Å^3$. Molecular illustration, structure checking and calculations were performed with the PLATON package.[22]

CCDC-210106 contains the supplementary crystallographic data for this paper. These data can be obtained free of charge via www.ccdc.cam.ac.uk/conts/retrieving.html (or from the CCDC, 12 Union Road, Cambridge CB2 1EZ, UK; Fax: (internat.) +44-1223/336-033; E-mail: deposit@ccdc.cam.ac.uk)

Acknowledgments

The work described here has been supported by the Leiden University Study group WFMO (Werkgroep Fundamenteeel-Materialen Onderzoek), the CNRS and the Conseil Régional d'Aquitaine. Support from the NRSC Catalysis (a Research School Combination of HRSMC and NIOK) is kindly acknowledged. This ECOX project is financially supported by the Dutch Economy, Ecology, Technology (EET) programme, a joint programme of the Ministry of Economic Affairs, the Ministry of Education, Culture and Science, and the Ministry of Housing, Spatial Planning and the Environment. This work was partially supported (M.L., A.L.S.) by The Netherlands Foundation for Chemical Sciences (CW) with financial aid from The Netherlands Organization for Scientific Research (NWO).

[1] [1a] L. Gutierrez, G. Alzuet, J. A. Real, J. Cano, J. Borras, A. Castineiras, *Inorg. Chem.* **2000**, *39*, 3608. [1b] G. A. van Albada, M. E. Quiroz-Castro, I. Mutikainen, U. Turpeinen, J. Reedijk, *Inorg. Chim. Acta* **2000**, *298*, 221. [1c] I. Riggio, G. A. van Albada, D. D. Ellis, A. L. Spek, J. Reedijk, *Inorg. Chim. Acta* **2001**, *313*, 120.
[2] V. Tangoulis, C. P. Raptopoulou, S. Paschalidou, A. E. Tsohos, E. G. Bakalbassis, A. Terzis, S. P. Perlepes, *Inorg. Chem.* **1997**, *36*, 5270.
[3] X. S. Tan, Y. Fujii, R. Nukada, M. Mikuriya, Y. Nakano, *J. Chem. Soc., Dalton Trans.* **1999**, 2415.
[4] A. Messerschmidt, A. Rossi, R. Ladenstein, R. Huber, M. Bolognesi, G. Gatti, A. Marchesini, R. Petruzzelli, A. Finazzi-Agro, *J. Mol. Biol.* **1989**, *206*, 513.
[5] P. Kyritsis, A. Messerschmidt, R. Huber, G. A. Salmon, A. G. Sykes, *J. Chem. Soc., Dalton Trans.* **1993**, 731.
[6] R. Huber, *Angew. Chem. Int. Ed. Engl.* **1989**, *101*, 849.
[7] [7a] J. Reedijk, E. Bouwman, *Bioinorganic Catalysis.* Marcel

 © 2003 Wiley-VCH Verlag GmbH & Co. KGaA, Weinheim

Dekker, Inc, **1999**. [7b] P. Gamez, P. G. Aubel, W. L. Driessen, J. Reedijk, *Chem. Soc. Rev.* **2001**, *30*, 376.
[8] D. J. Spira-Solomon, M. Allendorf, E. I. Solomon, *J. Am. Chem. Soc.* **1986**, *108*, 5316.
[9] H. H. T. Nguyen, A. K. Shiemke, S. J. Jacobs, B. J. Hales, M. E. Linstrom, S. I. Chan, *J. Biol. Chem.* **1994**, *269*, 14995.
[10] A. Messerschmidt, in *Bioinorganic Chemistry of Copper* (Eds.: K. D. Karlin, Z. Tyeklar), Chapman & Hall, New York, **1993**, p. 471.
[11] L. Gutierrez, G. Alzuet, J. A. Real, J. Cano, J. Borras, A. Castineiras, *Eur. J. Inorg. Chem.* **2002**, 2094.
[12] [12a] G. A. van Albada, I. Mutikainen, U. Turpeinen, J. Reedijk, *Eur. J. Inorg. Chem.* **1998**, 547. [12b] G. A. van Albada, P. J. van Koningsbruggen, I. Mutikainen, U. Turpeinen, J. Reedijk, *Eur. J. Inorg. Chem.* **1999**, 2269.
[13] [13a] F. Akagi, Y. Nakao, K. Matsumoto, S. Takamizawa, W. Mori, S. Suzuki, *Chem. Lett.* **1997**, *2*, 181. [13b] L. Cronin, P. H. Walton, *Inorg. Chim. Acta* **1998**, 241.
[14] [14a] M. H. W. Lam, Y. Y. Tang, K. M. Fung, X. Z. You, W. T. Wong, *Chem. Commun.* **1997**, *21*, 957. [14b] T. C. Higgs, K. Spartalian, C. J. O'Connor, B. F. Matzanke, C. J. Carrano, *Inorg. Chem.* **1998**, *37*, 2263.
[15] J. F. Berry, F. A. Cotton, P. Lei, C. A. Murillo, *Inorg. Chem.* **2003**, *42*, 377.
[16] B. J. Hathaway, in *Comprehensive Coordination Chemistry* (Eds.: G. Wilkinson, R. D. Gill and J. A. McCleverty), Pergamon Press Oxford, **1987**, Vol.5.
[17] L. P. Wu, P. Field, T. Morrissey, C. Murphy, P. Nagle, B. Hathaway, C. Simmons, P. Thornton, *J. Chem. Soc., Dalton Trans.* **1990**, 3835.
[18] O. Kahn, *Molecular Magnetism*, VCH Publishers Inc., **1991**.
[19] L. Merz, W. Haase, *J. Chem. Soc., Dalton Trans.* **1980**, 875.
[20] G. M. Sheldrick (1997). SHELXS-97. *Program for crystal structure solution.* University of Göttingen, Germany.
[21] G. M. Sheldrick (1997). SHELXL-97. *Program for crystal structure refinement.* University of Göttingen, Germany.
[22] A. L. Spek (2003). PLATON. A multipurpose crystallographic tool. Utrecht University, The Netherlands.

Received May 2, 2003

 © 2003 Wiley-VCH Verlag GmbH & Co. KGaA, Weinheim

Redox Chemistry of Actinide Ions in Wells−Dawson Heteropolyoxoanion Complexes

Ming-Hsi Chiang,[a] L. Soderholm,*[a] and Mark R. Antonio*[a]

Keywords: Actinides / Cyclic voltammetry / Polyoxometalates / Redox chemistry / Nernst analysis / Intermediate valence / Spectroelectrochemistry / XANES

The redox behavior has been characterized for several actinide (*An*) complexes with the monovacant Wells–Dawson anion, of the form $[An^{n+}(\alpha\text{-}2\text{-}P_2W_{17}O_{61})_2]^{n-20}$ (*An* = Th^{4+}, U^{4+}, Np^{4+}, Pu^{4+}, and Am^{3+}). Two complexes, with *An* = U^{4+} and Am^{3+}, show redox activity under oxidizing conditions, which is attributed to the actinide oxidation. Am^{3+} is oxidized to Am^{4+} with an $E_{1/2}$ = +1.21±0.01 V, and U^{4+} oxidizes to U^{5+} with a measured $E_{1/2}$ = +0.55±0.01 V vs. Ag/AgCl. Although the cyclic voltammetry (CV) data are consistent with a reversible redox couple, bulk oxidative electrolysis of $[U^{4+}(\alpha\text{-}2\text{-}P_2W_{17}O_{61})_2]^{16-}$ results in the decomposition of this complex to produce uranyl acetate and the free monovacant Wells–Dawson anion. In contrast, all of the CV data from the actinide coordination complexes differ from equivalent data obtained from the $[\alpha\text{-}2\text{-}P_2W_{17}O_{61}]^{10-}$ ligand itself. There are two complexed An^{4+} ions, Np and Pu, that undergo reduction over the same potential range as the ligands themselves. In situ X-ray spectroelectrochemistry is used to quantify the actinide response. The Np^{4+}/Np^{3+} redox behavior is a classically single ion process, with a formal potential of –0.84±0.01 V that was determined from a Nernst plot of X-ray absorption near-edge structure (XANES) data. The Pu^{4+}/Pu^{3+} formal reduction potential in the complex $[Pu(\alpha\text{-}2\text{-}P_2W_{17}O_{61})_2]^{n-}$ was determined to be –0.17±0.01 V using the same methodology. However, in this latter case, the slope of the Nernst plot indicates that 0.72±0.03 electrons are involved in the reduction. This is a significant deviation from the 1 electron expected for the Pu couple, and is discussed in terms of the concomitant reduction of the P–W–O framework of the Wells–Dawson anion.
(© Wiley-VCH Verlag GmbH & Co. KGaA, 69451 Weinheim, Germany, 2003)

Introduction

Polyoxometalates (POMs) are inorganic, anionic ligands with properties that have found application in such diverse areas as catalysis,[1,2] energy storage[3] and nuclear waste processing.[4−6] Unlike more familiar ligands (e.g., H_2O, NH_3, halides, carbonates, etc.), many POMs are electroactive,[7] particularly the heteropolyoxoanions of general composition $[X_aM_bO_c]^{d-}$ (X = Si, P, S; M = Mo, W). It is this intrinsic electrochemical functionality of POMs that accounts for their renowned behavior as reversible multielectron oxidants. They can accommodate substantial variation in their overall net charge without significant structural change or decomposition. The reduced species are known as heteropoly blues[7] because of their intense coloration, which arises from the delocalization of the added electrons in bands attributable to the metal oxide framework atoms (M = Mo^{6+}, W^{6+}).

The Wells−Dawson heteropolyanion $\alpha\text{-}[P_2W_{18}O_{62}]^{6-}$, shown in Figure 1, is an electroactive POM that accepts 1−6 electrons into its P−W−O framework upon reduction in aqueous media, while retaining its framework structure.[8−10] Selected $-WO^{4+}-$ units can be removed, from either the belt (α-1) or the cap (α-2) positions, to form an anion that acts as a ligand, which forms complexes with a variety of cations. Specific to our interests are complexes with 5f actinide ions, of the form $[An^{n+}(\alpha\text{-}2\text{-}P_2W_{17}O_{61})_2]^{n-20}$ (n = 3 and 4), which have been reported for Pu,[11] Am,[11−17] and Bk.[14] These actinide ions, together with U^{4+} and Np^{4+}, are known to be electroactive themselves.[18] The one-electron redox chemistry for the An^{4+}/An^{3+} aquo ions of U, Np, Pu, and Bk is generally

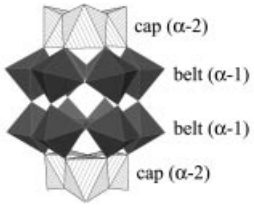

Figure 1. Polyhedral representation of the $\{W_{18}O_{62}\}$ framework of the plenary Wells−Dawson anion, $\alpha\text{-}[P_2W_{18}O_{62}]^{6-}$ showing the 6 capping W atoms (α-2 positions) as striped octahedra and the 12 belt W atoms (α-1 positions) as shaded octahedra; the two central $[PO_4]^{3-}$ tetrahedra are not shown

[a] Chemistry Division, Argonne National Laboratory,
9700 South Cass Avenue, Argonne, IL 60439-4831, USA
Fax: (internat.) + 1-630/252-4225
E-mail: ls@anl.gov, mantonio@anl.gov

facile and reversible, with tabulated standard electrode potentials in the range of $-0.773 \leq E^{\circ} \leq +1.47$ V vs. Ag/AgCl.[19]

In 1976, Saprykin et al.[11,20] reported that electroactive POMs, including the monovacant Wells–Dawson, exert a significant influence on the standard electrode potentials of the An^{4+}/An^{3+} redox couples. For example, in complexes of $[An^{4+}(\alpha\text{-}2\text{-}P_2W_{17}O_{61})_2]^{16-}$ (An^{4+} = Am, Cm, and Cf) the metal ions are stabilized toward reduction,[21] which would otherwise occur irreversibly on contact with water. From experimental measurements of the Wells–Dawson complexes of Pu^{4+},[11] Am^{3+},[11–17] and Bk^{3+},[14] the potentials for the An^{4+}/An^{3+} redox couple are approximately 1 V less than those tabulated for the standard reduction potentials, which correspond to the aquo ions in noncomplexing electrolytes.

Whereas it has been demonstrated that the substituted Wells–Dawson ligand can systematically shift the redox potential of bound 5f metal ions,[11–15,21] little work has been done to look for changes in the reduction response of the complexed anion. Of specific interest is the case, expected for the Np^{4+}/Np^{3+} and Pu^{4+}/Pu^{3+}couples, in which the reduction of the complexed *An* ion occurs over the same potential range as the reduction waves of the Wells–Dawson ligand itself. Under such conditions the localized f states are at the Fermi level of the P–W–O ligand states. Similar situations have been studied for f ions in transition-metal alloys, where correlated-electron and intermediate-valent phenomena have been observed.[22,23] Indeed, strong evidence of intermediate valence has been observed for Eu encrypted in the Preyssler anion, $[EuP_5W_{30}O_{110}]^{n-}$,[24] when the Eu f valence states are isoenergetic with the framework Fermi level. The systems under study herein provide a uniquely tunable and structurally simple model for extending studies of correlated electron behavior.

The objective of this study is to probe the electronic response of *An* Wells–Dawson complexes, in which both the f ion and the POM ligand are electroactive, to look for interactions that indicate f-state bonding or other unusual electronic responses. We report cyclic voltammetry and in situ XANES spectroelectrochemistry data on Th^{4+}, U^{4+}, Np^{4+}, and Pu^{4+} as well as Am^{3+}, some of which may give evidence of electronic interactions, but no strong evidence of intermediate valence is observed, even in cases where the P–W–O and f states are reduced concomitantly.

Results and Discussion

The CV data are shown in Figure 2 for the free ligand, $[\alpha\text{-}2\text{-}P_2W_{17}O_{61}]^{10-}$ (a, a′), and the cluster complexes, $[An^{n+}(\alpha\text{-}2\text{-}P_2W_{17}O_{61})_2]^{n-20}$ with Th^{4+} (b, b′), U^{4+} (c, c′), Np^{4+} (d, d′), Pu^{4+} (e, e′), and Am^{3+} (f, f′). These data were obtained under identical conditions, with the potential window limited by H_2 evolution at ≤ -1 V vs. Ag/AgCl and O_2 evolution at $\geq +1.4$ V vs. Ag/AgCl. The fundamental electrochemical parameters obtained from the data in Figure 2 are provided in Table 1 and compared in Table 2

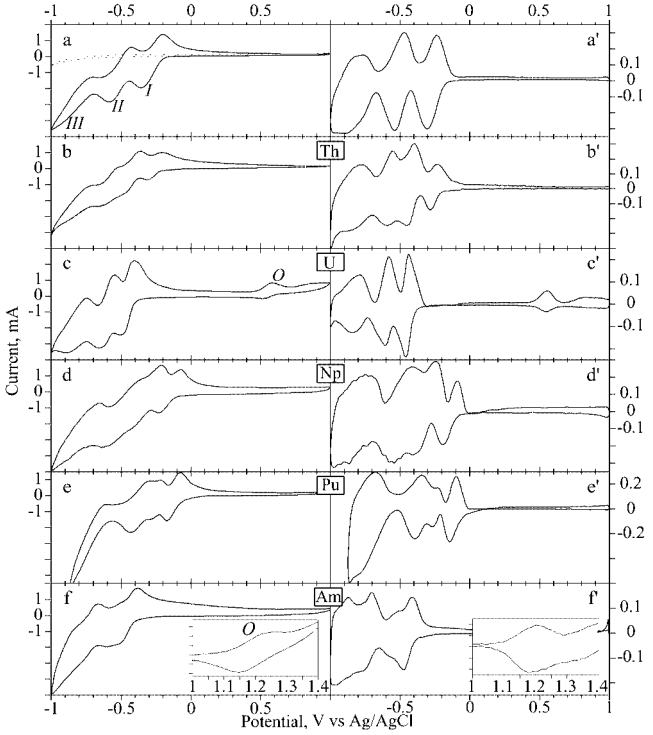

Figure 2. Left panels: cyclic voltammograms obtained at room temp. at 5 mV s^{-1} in supporting aqueous electrolytes (pH = 3.5) of 2:1 (v/v) mixtures of 0.5 M CH_3CO_2Li buffer at pH = 4.7 and 1 M $HClO_4$; right panels: the corresponding semi-differential data of the primary voltammograms; (a, a′) the uncomplexed ligand, $[\alpha\text{-}2\text{-}P_2W_{17}O_{61}]^{10-}$, including background scan (dashed line), revealing two well-resolved (*I*, *II*) redox waves and a third (*III*) less-resolved one; each arises from two-electron reduction processes of W^{6+} in the P–W–O band; by comparison, the complexes of Th^{4+} (b, b′), U^{4+} (c, c′), Np^{4+} (d, d′), Pu^{4+} (e, e′), and Am^{3+} (f, f′) with $[\alpha\text{-}2\text{-}P_2W_{17}O_{61}]^{10-}$ as $[An^{n+}(\alpha\text{-}2\text{-}P_2W_{17}O_{61})_2]^{n-20}$ cluster anions affect the reduction behavior of the ligand in significant fashion; all the solution species form heteropoly blues due to reduction of the P–W–O framework at potentials between 0 and −1 V; although the U^{4+} and Am^{3+} oxidation waves (labeled *O*) are visible in the CV data of (c, c′) and (f, f′), respectively, any evidence for the reduction of An^{4+} in $[An^{4+}(\alpha\text{-}2\text{-}P_2W_{17}O_{61})_2]^{16-}$ is not obvious because of the interfering response from the reduction of the ligand

with results from previous electrochemical investigations of $[An^{n+}(\alpha\text{-}2\text{-}P_2W_{17}O_{61})_2]^{n-20}$, as well as with the corresponding An^{n+} aquo ions.

The data in Figure 2 (a, a′) indicate that the free ligand has no electrochemical response under an oxidizing, positive, applied potential, consistent with the expectation that the W^{6+}–O valence band is empty. In contrast, the CV data for $[Am^{3+}(\alpha\text{-}2\text{-}P_2W_{17}O_{61})_2]^{17-}$, shown in Figure 2 (f, f′), exhibit an isolated redox wave under an oxidizing potential, at $E_{1/2} = +1.21 \pm 0.01$ V, that is attributed to the Am^{3+}/Am^{4+} couple. As evident from Table 2, our $E_{1/2}$ value is in agreement with previous polarographic and potentiometric measurements of the Am^{3+} oxidation potential in the $[Am^{3+}(\alpha\text{-}2\text{-}P_2W_{17}O_{61})_2]^{17-}$ complex measured in solutions with pH ranges of 2–5.[11,13–15] The measured reduction potential of +1.21 V is about 1.2 V less than the estimated standard electrode potential of +2.4 V for the Am^{4+} reduction in aqueous solution. This shift for the Am reduction potential upon complexation with the Wells–Dawson

 © 2003 Wiley-VCH Verlag GmbH & Co. KGaA, Weinheim

Table 1. Electrode potentials [V vs. Ag/AgCl] of the redox couples obtained from the cyclic voltammetry data of Figure 2 for the free ligand, $[\alpha\text{-}2\text{-}P_2W_{17}O_{61}]^{10-}$, and the *An* complexes, $[An(\alpha\text{-}2\text{-}P_2W_{17}O_{61})_2]^{n-}$; the half-wave potentials, $E_{1/2}$, are presented as $(E_{pc} + E_{pa})/2$, where E_{pc} and E_{pa} are the cathodic and anodic peak potentials, respectively; the peak separations, ΔE_p, are presented as $E_{pa} - E_{pc}$, and "nr" means "not resolved"; errors associated with the values of E_{pc}, E_{pa}, $E_{1/2}$, and ΔE_p are either ±0.01 or ±0.005 V corresponding to the precision of the tabulated potentials

Anion	Wave	E_{pc} [V]	E_{pa} [V]	$E_{1/2}$ [V]	ΔE_p [V]
$[\alpha\text{-}2\text{-}P_2W_{17}O_{61}]^{10-}$	I	−0.357	−0.200	−0.28	0.157
	II	−0.584	−0.428	−0.51	0.156
	III	nr	−0.707		
$[Th(\alpha\text{-}2\text{-}P_2W_{17}O_{61})_2]^{16-}$	I	−0.308	−0.206	−0.26	0.102
	II	−0.48	−0.366	−0.42	0.114
	III	−0.64	−0.53	−0.59	0.110
	IV	nr	−0.70		
$[U(\alpha\text{-}2\text{-}P_2W_{17}O_{61})_2]^{16-}$	O	+0.516	+0.586	+0.55	0.070
	I	−0.504	−0.402	−0.45	0.102
	II	−0.648	−0.544	−0.60	0.104
	III	−0.886	−0.745	−0.82	0.141
$[Np(\alpha\text{-}2\text{-}P_2W_{17}O_{61})_2]^{16-}$	I	−0.230	−0.072	−0.15	0.158
	II	−0.448	−0.212	−0.33	0.236
	III	−0.619	−0.361	−0.49	0.258
	IV	nr	−0.652		
$[Pu(\alpha\text{-}2\text{-}P_2W_{17}O_{61})_2]^{16-}$	I	−0.172	−0.073	−0.12	0.099
	II	−0.298	−0.213	−0.26	0.085
	III	−0.431	−0.295	−0.36	0.136
	IV	nr	−0.605		
$[Am(\alpha\text{-}2\text{-}P_2W_{17}O_{61})_2]^{17-}$	O	+1.15	+1.26	+1.21	0.11
	I	−0.50	−0.382	−0.44	0.118
	II	−0.61	−0.50	−0.56	0.11
	III	nr	−0.67		
	IV	nr	−0.85		

Table 2. Standard electrode potentials [V vs. Ag/AgCl] for the *An* aquo ions in acid solutions at room temp. from the compilation of Bratsch;[19] the original values of Bratsch[19] in V vs. SHE were converted here to V vs. Ag/AgCl with respect to the redox potential (+0.196 V vs. SHE) for the BAS Inc. Ag/AgCl reference electrode (3 M NaCl) at 25 °C;[45] estimated values for which there are no experimental data are enclosed in parentheses; "na" = "not accessible" in aqueous electrolytes; "uk" = "unknown" in aqueous electrolytes; the sources of the potentials for the *An* Wells−Dawson complexes, $[An(\alpha\text{-}2\text{-}P_2W_{17}O_{61})_2]^{n-}$, in aqueous electrolytes at room temp. are given in the footnotes

An couple	Aquo ions 4+/3+	Wells−Dawson complexes 4+/3+	Wells−Dawson complexes 5+/4+
Th	na	na	na
U	−0.773	(−1.73)[a]	+0.56±0.01[b]
			+0.55±0.01[c]
Np	−0.039	(−0.95)[d]	uk
		−0.84±0.01[e]	
Pu	+0.810	−0.12±0.01[f]	uk
		−0.17±0.01[e]	
Am	(+2.4)	+1.20−1.26[g]	uk
		+1.21±0.01[c]	
		+1.33−1.39[h]	
		+1.05−1.10[i]	
Cm	(+2.8)	(+1.9±0.2)[j]	na
Bk	+1.47	+0.44[j]	na
Cf	(+3.1)	(+2.0±0.2)[j]	na

[a] From Erine et al.[37] [b] From Maslov et al.[27] [c] This work, $E_{1/2}$ value from cyclic voltammetry. [d] From Timofeev et al.[15] [e] This work, E°′ value from Nernst analysis of XANES spectroelectrochemical data. [f] From Saprykin et al.[11] [g] Range of values for 2≤pH≤5.[11,13−15] [h] Range of values for pH≤1.[12,17] [i] Range of values for pH ≈ 7.5 from Baranov et al.[16] [j] From Baranov et al.[14]

anion is somewhat larger than the −0.9 V that is typically seen for similarly complexed *An* ions.[11,15,21] Were it not for complexation with $[\alpha\text{-}2\text{-}P_2W_{17}O_{61}]^{10-}$, Am^{4+} would not be stable in aqueous solution. This stabilization of Am^{4+} by complexation with $[\alpha\text{-}2\text{-}P_2W_{17}O_{61}]^{10-}$ is the scientific basis for the separation process known as SESAME[5] and for aspects of the PARC process[6] in nuclear waste treatment operations.

$[U(\alpha\text{-}2\text{-}P_2W_{17}O_{61})_2]^{16-}$ also shows an electrochemical response under an oxidizing applied potential, with a redox wave [labeled *O* in Figure 2 (c, c′)] centered at $E_{1/2}$ = +0.55±0.01 V. Previous work has shown that, under the synthetic conditions employed in this study, U is tetravalent in $[U(\alpha\text{-}2\text{-}P_2W_{17}O_{61})_2]^{16-}$.[25] We argue that the redox wave observed here is due to the one-electron U^{4+}/U^{5+} couple. The one-electron oxidation of U^{4+} has been previously reported in both Keggin and Wells−Dawson heteropolyoxoanion complexes, $[U^{4+}(X^nW_{11}O_{39})_2]^{2n-20}$ ($X = Si^{4+}$; P^{5+}) and $[U^{4+}(P_2W_{17}O_{61})_2]^{16-}$.[26] The oxidation was achieved through electrolytic means, with electrode potentials of $+0.23 \le E^{\circ\prime} \le +0.64$ V, and through potentiometric titrations with dichromate and permanganate.[27] Our $E_{1/2}$ value agrees with the formal potential of +0.56±0.01 V obtained through a Nernst analysis of potentiometric data for $[U^{4+}(P_2W_{17}O_{61})_2]^{16-}$ by Maslov et al.[27]

A reliable standard potential for the one-electron oxidation of U^{4+}, unaccompanied by the formation of the linear dioxo moiety $[O{=}U^{5+}{=}O]^+$ is not available for comparison with our results. U^{5+} is unstable, so that, on contact with water, it invariably takes the form of the *trans*-dioxo cation $[UO_2]^+$, which itself is unstable with respect to disproportionation.[28] The observation of an apparently reversible voltammogram indicates that the coordination provided by the two Wells−Dawson ligands[25,29] provides a stabilizing environment for the dioxo-free (i.e., the so-called nude) U^{5+} cation.

In attempts to further characterize the U^{5+} complex of $[U(\alpha\text{-}2\text{-}P_2W_{17}O_{61})_2]^{15-}$, bulk electrolysis experiments were performed with the electrode polarized at +0.80 V. The solution color, which was initially violet, changed to red and then gradually faded to light pink as a white precipitate developed over the course of 1−18 h. Powder X-ray diffraction and EXAFS (extended X-ray absorption fine structure) data of the precipitate are consistent with a uranyl(VI) acetate phase.[30] On the longer time scale needed for bulk electrolysis, the U^{4+} oxidation is seen to be irreversible. On the significantly shorter time scale of cyclic voltammetry measurements, the U^{4+}/U^{5+} redox couple [*O* in Figure 2 (c, c′)] appears reversible, with a 0.070 V peak separation. This is likely to be a kinetic effect, in that the nude U^{5+} is sterically hindered, by the bulky Wells−Dawson ligands, from access

 © 2003 Wiley-VCH Verlag GmbH & Co. KGaA, Weinheim

to the oxygen ligands necessary to form the dioxo moiety,

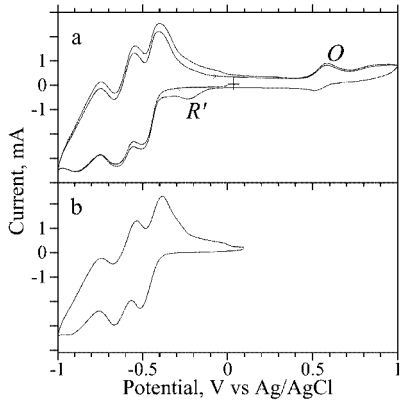

Figure 3. Cyclic voltammograms of $[U^{4+}(\alpha\text{-}2\text{-}P_2W_{17}O_{61})_2]^{16-}$; (a) starting from the initial potential of +0.1 V in a negative sweep to −1 V then to +1 V and back, showing the reversible U^{4+}/U^{5+} couple labeled *O* and the cathodic peak response labeled *R′* at −0.23 V attributed to reduction of $[UO_2]^{2+}$; (b) recorded 60 min after (a) starting from the initial potential of +0.1 V in a negative sweep to −1 V and back

$O{=}U^{5+}{=}O$. Yet, as shown in the CV data of Figure 3 (a), U demetalation is evident in successive sweeps with scan rates of 10 mV s^{-1} and slower between −1 and ≥ +0.6 V as the cathodic peak at −0.23 V labeled *R′*. This peak, which is otherwise not observed in shorter scans to ≤ +0.4 V as shown in Figure 3 (b), is the direct result of the redox couple *O* in Figure 3 (a). We suggest that peak *R′* is due to the reduction of $[UO_2]^{2+}$ (from cluster demetalation)[30] to U^{4+}, which subsequently combines with free ligand to reform the $[U^{4+}(\alpha\text{-}2\text{-}P_2W_{17}O_{61})_2]^{16-}$ complex. This would account for the absence of an anodic counterpart of *R′*, as would the irreversibility of the coupled electron transfer/chemical conversion between U^{4+} and $[UO_2]^{2+}$. No evidence is found for the reorganization of $[\alpha\text{-}2\text{-}P_2W_{17}O_{61}]^{10-}$, which can be readily reconstituted as $\alpha\text{-}[P_2W_{18}O_{62}]^{6-}$ and easily detected by CV.

In contrast to the sparse electrochemical responses of the actinide-coordinated, monovacant Wells−Dawson anions under oxidizing conditions, complicated redox responses are observed for all complexes under reducing conditions. The free ligand itself exhibits two well-resolved redox waves followed by one less-resolved wave, as indicated by *I*, *II*, and *III* in the voltammogram of Figure 2 (a). Previous work has attributed the waves to three 2-electron processes,[8,10,31−33] involving W^{6+} reduction. Extended Hückel calculations on the uncomplexed, plenary Wells−Dawson anion, $\alpha\text{-}[P_2W_{18}O_{62}]^{6-}$, indicate that the lowest unoccupied molecular orbital (LUMO) has a_1'' symmetry and is composed almost exclusively (96%) of metal orbitals derived from the 5d t_{2g} orbitals centered on the belt (α-1) tungsten atoms.[34] Symmetry requires that all 12 belt W atoms contribute with equal weight. The next higher energy state has e'' symmetry and is composed of both belt (61%) and cap (33%) positions.[34] Above these states in energy is another doubly degenerate set of orbitals that are located primarily (81%) on the cap positions, with only 12% on the belt positions.[34] The removal of a $W{=}O^{4+}$ moiety from the cap position, to form the α-2 derivative, lifts the threefold rotational symmetry of the parent ligand, and will lift the e states degeneracies. The first redox wave seen for $[\alpha\text{-}2\text{-}P_2W_{17}O_{61}]^{10-}$ in Figure 2 (a, a′) can thus be understood as arising from electron occupation in the LUMO that resides primarily on the belt (α-1) positions of Figure 1, and has a'' symmetry.[34−36]

Of the five *An* ions considered here, only Th^{4+} has no electroactivity of its own in the electrochemical region of interest. Yet, the complexation of electrochemically silent Th^{4+} modifies the voltammetric response of the P−W−O framework so that the $[Th(\alpha\text{-}2\text{-}P_2W_{17}O_{61})_2]^{16-}$ cluster has four redox waves. The first three are visible in the primary CV data of Figure 2 (b). The fourth one is less resolved but is seen clearly in the corresponding semiderivative data of Figure 2 (b′).

The reduction potentials of the An^{4+} ions coordinated by the monovacant Wells−Dawson anion are estimated by assuming a −0.9 to −1.0 V shift to the standard electrode potentials upon complexation.[15] Using this assumption, Np^{4+} and Pu^{4+} complexed with $[\alpha\text{-}2\text{-}P_2W_{17}O_{61}]^{10-}$ have reduction potentials that are expected to be accessible under our experimental conditions, whereas the estimated U^{4+}/U^{3+} potential of −1.73 V[37] is expected to be too low to be measurable. However, except for minor shifts in peak positions, the CV data for $[Np(\alpha\text{-}2\text{-}P_2W_{17}O_{61})_2]^{16-}$, shown in Figure 2 (d, d′), are essentially the same as those for $[Th(\alpha\text{-}2\text{-}P_2W_{17}O_{61})_2]^{16-}$ [Figure 2 (b, b′)], in which Th^{4+} has no redox activity. So, from the CV data alone, it is not possible to assign Np electrochemical activity to any specific feature that may otherwise arise from the redox activity of the P−W−O framework. Therefore, in order to evaluate the electrochemical response of these 5f ions under reducing conditions, optical spectroscopy and X-ray absorption experiments were undertaken.

Optical spectra were obtained for the yellow Np^{4+} solution complex and for the blue solution resulting from bulk electrolysis at −0.3 V vs. Ag/AgCl in order to assess the Np^{4+}/Np^{3+} redox activity in $[Np(\alpha\text{-}2\text{-}P_2W_{17}O_{61})_2]^{n-}$. These spectra are shown in Figure 4. The blue solution is optically dense and the electronic spectrum consists of weak bands attributable to the Np^{4+} complex superimposed on a strong and essentially featureless broad-band (460−1250 nm) ab-

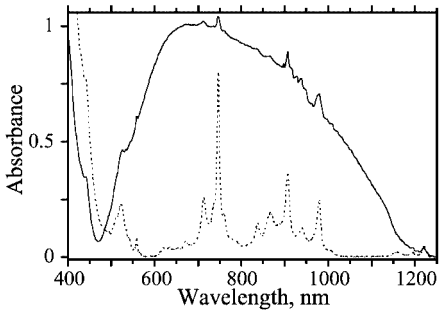

Figure 4. Optical spectrum of the transparent yellow solution of $[Np^{4+}(\alpha\text{-}2\text{-}P_2W_{17}O_{61})_2]^{16-}$ consistent with previous spectra[48−50] (dashed line) and the opaque heteropoly blue solution (solid line), following exhaustive electrolysis at −0.3 V

 © 2003 Wiley-VCH Verlag GmbH & Co. KGaA, Weinheim

sorption associated with the reduction of the ligands. Absorption bands of similar breadth are found in the spectra for the heteropoly blues of $[\alpha\text{-}1\text{-}P_2W_{17}O_{61}]^{n-}$ [38] as well as $[PMo_{12}O_{40}]^{n-}$ in protic[39] and aprotic media.[40] In the heteropoly blues of $[Np(\alpha\text{-}2\text{-}P_2W_{17}O_{61})_2]^{n-}$ produced by bulk electrolysis at potentials more negative than −0.3 V, any evidence for absorption bands due to Np was obscured by the broad, intense absorption by the P−W−O anions. Because of this, we exploited element-specific in situ XANES spectroelectrochemistry[41] to quantify the Np^{4+}/Np^{3+} redox couple.

The Np L_3-edge XANES spectra for the valence-pure α_2 Wells−Dawson complexes of Np^{3+} and Np^{4+} are shown in Figure 5 as solid lines. These spectra are discussed in detail elsewhere.[25] The data collected at intermediate potentials, after exhaustive bulk electrolysis, are shown as dashed lines. The XANES spectra can be treated as linear combinations of the two end-member, valence-pure spectra,[41,42] thereby extracting the relative ratio of the oxidized to the reduced species for each potential. These data serve as input into the Nernst equation, $E = E^{\circ\prime} + RT\{\log([ox]/[red])\}/nF$, for which [ox] and [red] are the concentrations of the oxidized and reduced species, respectively; E is the applied potential, R is the gas constant, and F is Faraday's constant.

The number of electrons (n) involved in the Np redox reaction, as well as the formal electrode potential ($E^{\circ\prime}$) for the Np^{4+}/Np^{3+} couple are determined from the Nernst plot shown in Figure 6. The variation of applied potential with $\log([Np^{4+}]/[Np^{3+}])$ shown by the solid circles has a linear dependence. The best fit, with $R^2 = 0.988$, is shown as the solid line. The slope (RT/nF) of the fitted line is 0.061±0.003 V, corresponding to $n = 0.97\pm0.05$ electrons transferred at 25 °C, and the intercept is equal to $E^{\circ\prime} = -0.84\pm0.01$ V. The observation of a slope consistent with that expected for a 1-electron transfer indicates that the Np ion in the Wells−Dawson complex is acting as a well-behaved, single-ion redox couple. The measured Np^{4+} reduction potential of −0.84 V is similar to the value of −0.95 V estimated from published trends.[37]

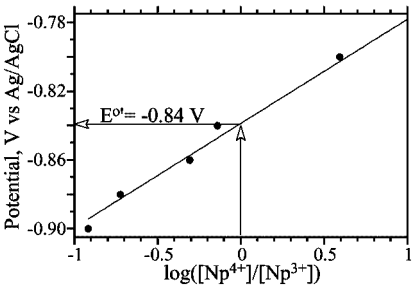

Figure 6. Nernst plot (circles) and best fit (line) with $R^2 = 0.988$ for $[Np(\alpha\text{-}2\text{-}P_2W_{17}O_{61})_2]^{n-}$; the slope, $RT/nF = 0.061\pm0.003$ V, provides the number of electrons (n) transferred in the Np^{4+}/Np^{3+} redox couple; at 25 °C, a slope of 0.05916 V corresponds to $n = 1$; we obtain $n = 0.97\pm0.05$; the X-axis intercept as indicated by the arrows provides the formal potential, $E^{\circ\prime} = -0.84\pm0.01$ V

The Pu^{4+} Wells−Dawson ion presents a situation similar to that of complexed Np^{4+} in that, under reducing conditions the CV data for $[Pu(\alpha\text{-}2\text{-}P_2W_{17}O_{61})_2]^{16-}$, shown in Figure 2 (e, e′), provide no obvious evidence for a Pu^{4+}/Pu^{3+} couple. This couple has been reported to have a formal potential of −0.12 V,[11] which is in the potential range for the observed P−W−O redox activity. Pu L_3-edge XANES experiments are used to quantify the Pu response, as a function of applied potential, from $[Pu(\alpha\text{-}2\text{-}P_2W_{17}O_{61})_2]^{n-}$. These data are shown in Figure 7. The concentrations, following bulk electrolysis, of Pu^{4+} and Pu^{3+} at each applied potential were used to construct the Nernst plot shown in Figure 8. The direct, linear dependence of potential vs. $\log([Pu^{4+}]/[Pu^{3+}]$ is evident in the primary data (solid circles) and by the best fit (solid line) with $R^2 = 0.998$. The formal potential, $E^{\circ\prime} = -0.17\pm0.01$ V, is determined from the intercept of this plot, and can be compared with that of -0.12 ± 0.01 V obtained by Saprykin et al.[11] This latter value was obtained by measurements of Eh in

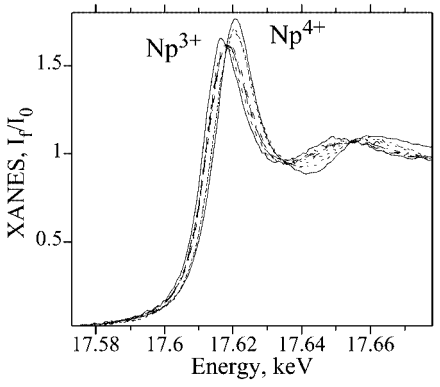

Figure 5. Normalized fluorescence XANES of the cluster anions containing valence-pure Np^{3+} and Np^{4+} (solid lines) obtained with the electrode polarized at −1.00 and +0.20 V, respectively, and with admixtures of both Np^{3+}- and Np^{4+}-containing anions (dashed lines) obtained with the electrode polarized at −0.900, −0.880, −0.860, −0.840, −0.800, and −0.780 V; as discussed elsewhere,[25] the L_3 XANES peaks for Np^{3+} and Np^{4+} are well resolved with a separation of 4.6 eV; this makes possible the quantitative analyses of the relative equilibrium concentrations of Np^{4+} and Np^{3+} in the admixtures[41]

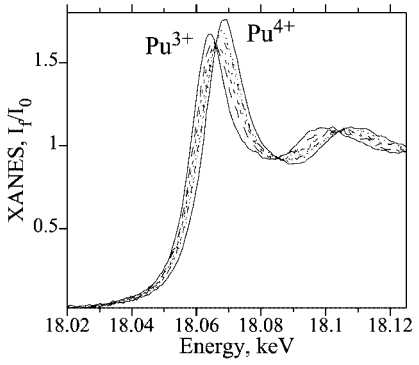

Figure 7. Normalized fluorescence XANES of the cluster anions containing valence-pure Pu^{3+} and Pu^{4+} (solid lines) obtained with the electrode polarized at −0.30 and +0.20 V, respectively, and with admixtures of both Pu^{3+}- and Pu^{4+}-containing species (dashed lines) obtained with the electrode polarized at −0.200, −0.180, −0.160, −0.140, and −0.120 V; as discussed elsewhere,[25] the L_3 XANES peaks for Pu^{3+} and Pu^{4+} are well resolved with a separation of 4.3 eV; this makes possible the quantitative analyses of the relative equilibrium concentrations of Pu^{4+} and Pu^{3+} in the admixtures[41]

 © 2003 Wiley-VCH Verlag GmbH & Co. KGaA, Weinheim

non-blue solutions containing known mixtures of $[Pu^{4+/3+}(\alpha\text{-}2\text{-}P_2W_{17}O_{61})_2]^{16-/17-}$, prepared with preformed Pu^{4+} and Pu^{3+}. The slope (0.082 ± 0.003) of the Nernst plot of Figure 8 is 38% larger than expected for a one-electron Pu^{4+}/Pu^{3+} redox couple, and provides a smaller than expected value of $n = 0.72\pm0.03$ electrons transferred in the redox reaction. This value is significantly different from that expected for a well-behaved Nernstian system.[43]

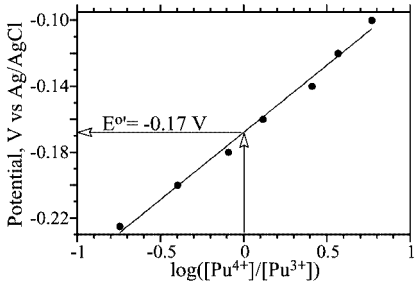

Figure 8. Nernst plot (circles) and best fit (line) with $R^2 = 0.998$ for $[Pu(\alpha\text{-}2\text{-}P_2W_{17}O_{61})_2]^{n-}$; the slope, $RT/nF = 0.082\pm0.003$ V, provides the number of electrons ($n = 0.72\pm0.03$) transferred in the Pu^{4+}/Pu^{3+} redox couple; the X-axis intercept as indicated by the arrows provides the formal potential, $E^{\circ\prime} = -0.17\pm0.01$ V

The high slope measured for the Pu^{4+} reduction may indicate weak interactions between the localized Pu f states and the P−W−O d-band states arising from correlated electron behavior. The redox couple, which has a formal potential of −0.17 V, is almost coincident with the first W-redox wave of the $[Pu(\alpha\text{-}2\text{-}P_2W_{17}O_{61})_2]^{16-}$ complex itself, which occurs at −0.12 V. This energy coincidence of localized f states with the W−O band states raises the possibility for correlated-electron behavior.[22,23] We have seen evidence for such f-P−W−O hybridization during the reduction of Eu^{3+} in the Preyssler POM, $[EuP_5W_{30}O_{110}]^{n-}$.[24] A Nernst plot, obtained from XANES data following a similar procedure to that used herein, is non-linear, with an applied potential range of 60 mV over which no change is observed in the $[Eu^{3+}]/[Eu^{2+}]$ ratio. Such behavior is consistent with that expected for a hybridization of the localized f_{Eu} states with the d_{W-O} band states because the added electrons are going into states comprised of both Eu and a large number of W. If the Pu f states and the d states on the 2 cap tungsten atoms had fully hybridized states, the electron would be shared between three centers, and the slope measured for the Pu reduction alone would be expected to be about 1/3. Therefore, an increased slope can be argued to be consistent with some degree of electron sharing among the cap-position ions. The linearity of the Pu Nernst response, as a function of applied potential, is consistent with the understanding that the W−O states that are reduced in the −0.12 V wave are those in the anion belt positions.[34−36] These states are expected to be electronically isolated from the cap-position states and therefore, although the criterion for intermediate-valent behavior is satisfied in terms of energetically isolated states in this experiment, the system symmetry prohibits the necessary spatial overlap of the appropriate wave functions.

The isolation of the first reduction wave, arising from the W atom in the belt positions, from the electronic states on the cap positions is further exemplified by the plot shown in Figure 9. The measured potentials of the W_{belt} redox waves are plotted as a function of An^{4+}−O bond length.[25] U^{4+} is not included in this plot because of the effects of the U^{5+}/U^{4+} couple (Figure 3) on cluster demetalation leading to the presence of free $[\alpha\text{-}2\text{-}P_2W_{17}O_{61}]^{10-}$ and $[UO_2]^{2+}$. The linear behavior ($R^2 = 0.999$) of this plot suggests dipolar interactions alone are primarily responsible for the slightly increased stability, of the W−O a′′ belt states, to reduction with increasing An−O bond length.

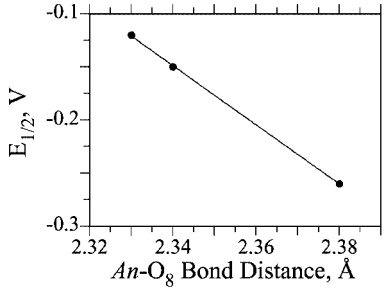

Figure 9. The decreasing half-wave, $E_{1/2}$, potentials of Table 1 for redox couple I (belt W reduction) of the Pu^{4+}, Np^{4+}, and Th^{4+} complex anions are plotted (circles) as a function of their increasing $An^{4+}-O_8$ bond lengths;[25] the best fit ($R^2 = 0.999$) is shown as a line with a slope of -2.79 ± 0.04 V/Å and an intercept of 6.37 ± 0.10 V

Conclusion

Although the reduction behaviors of both the actinide ion and the monovacant Wells−Dawson anion are altered upon their complexation, there is no evidence of significant hybridization between the An localized f states and the W−O band states. Specifically, the Pu^{4+}/Pu^{3+} redox couple is centered amongst the reduction waves of the anion itself. This situation may lead to intermediate valence[23] as has been demonstrated for $[EuP_5W_{30}O_{110}]^{n-}$ under similar conditions.[24] However, the Nernst plot obtained for Pu in $[Pu(\alpha\text{-}2\text{-}P_2W_{17}O_{61})_2]^{n-}$ is linear, although there appears to be an anomalously low number of electrons involved in the reduction. This result is interpreted in terms of electron delocalization into $Pu-W_{cap}$ states.

Experimental Section

CAUTION: Th, U, Np, Pu, and Am are radioactive elements. All experiments with these isotopes were performed in specialized laboratories using procedures designed and approved to minimize radiological and chemical hazards. For the transuranic elements, i.e., Np, Pu, and Am, their limited availability, together with radiation exposure concerns, require the use of only milligram quantities and thereby limit studies to small sample sizes. The $[An^{n+}(\alpha\text{-}2\text{-}P_2W_{17}O_{61})_2]^{n-20}$ complexes with natural Th^{4+} and U^{4+}, $^{237}Np^{4+}$, $^{242}Pu^{4+}$, and $^{243}Am^{3+}$ were prepared as described elsewhere.[25] Aqueous electrolytes of pH = 3.5, prepared from 2:1 (v/v) mixtures of 0.5 M CH_3CO_2Li buffer (pH = 4.7) and 1 M $HClO_4$, were used

 © 2003 Wiley-VCH Verlag GmbH & Co. KGaA, Weinheim

for all measurements, which included optical, in situ Np and Pu XANES spectroelectrochemistry, and cyclic voltammetry (CV). Vis/NIR data were obtained with a Cary-14 Olis-conversion spectrometer. The in situ XANES was obtained with a purpose-built cell for spectroelectrochemistry.[41,44] CV data for the dilute (ca. 1 mM) solutions of $[An^{n+}(\alpha\text{-}2\text{-}P_2W_{17}O_{61})_2]^{n-20}$ were obtained under static conditions with scan rates of 5 mV s^{-1} in a single-compartment cell. The primary voltammograms were convolved by a semi-derivative method to provide clear visual resolution of the redox waves. All electrochemical operations (bulk electrolyses and CV) were performed with a BAS 100B/W electrochemical workstation and 6.15 mm diameter graphite rod (Alfa 14739) working and auxiliary electrodes, and a BAS (RE-5B) Ag/AgCl reference electrode (3 M NaCl). Unless specified otherwise, all measured and reported potentials are with reference to this electrode, with a redox potential of +0.196 V vs. SHE at 25 °C.[45] The background voltammogram of the neat electrolyte and clean electrodes was smooth and featureless over the range of potentials from −1 to +1.4 V. Np and Pu XANES spectra were recorded at the 7 GeV APS BESSRC CAT station 12-BM-B[46] as described previously.[25] With the dilute solutions of $[Np^{4+}(\alpha\text{-}2\text{-}P_2W_{17}O_{61})_2]^{16-}$ and $[Pu^{4+}(\alpha\text{-}2\text{-}P_2W_{17}O_{61})_2]^{16-}$ in the X-ray beam under vigorous sparging with N_2, we first collected data for the fully oxidized clusters at rest potential. This was followed by exhaustive (≥ 98%) electrolysis at −1.00 V and −0.30 V to produce the reduced heteropoly blue species with valence-pure Np^{3+} and Pu^{3+}, respectively, and XANES data acquisition. Thereafter, we recorded XANES data throughout the course of the stepwise oxidation by bulk electrolyses as a function of controlled potentials with the electrode polarized at −0.900, −0.880, −0.860, −0.840, −0.800, and −0.780 V for the Np complex, and at −0.225, −0.200, −0.180, −0.160, −0.140, −0.120, and −0.100 V for the Pu complex. X-ray and electrochemical spectra, obtained from the full re-oxidation of the reduced, Wells−Dawson complex, were indistinguishable from those obtained from the starting materials. This result confirms the reversibility of the redox chemistry. The Np and Pu XANES spectra obtained at the intermediate potentials were fit in a linear combination regression analysis with the pure An^{3+} and An^{4+} spectra using procedures in WinXAS[47] that have been described in detail elsewhere.[41,42] The relative partial concentrations for An^{4+} and An^{3+} obtained therewith were used for the Nernst plots of potential vs. $\log[Np^{4+}]/[Np^{3+}]$ and $\log[Pu^{4+}]/[Pu^{3+}]$.

Acknowledgments

We thank Clayton Williams and S. Skanthakumar of the Chemistry Division Actinide Facility as well as the staff of the BESSRC CAT at the Advanced Photon Source for assistance. This work is supported by the U.S. DOE, BES−Chemical Sciences and Material Sciences and, during the initial stages, by sponsorship of the Environmental Management Science Program, Office of Science and Technology, Office of Environmental Management, all under contract No. W-31-109-ENG-38.

[1] I. A. Weinstock, *Chem. Rev.* **1998**, *98*, 113−170.
[2] M. Sadakane, E. Steckhan, *Chem. Rev. (Washington, D.C.)* **1998**, *98*, 219−237.
[3] D. E. Katsoulis, *Chem. Rev.* **1998**, *98*, 359−388.
[4] L. Bion, P. Moisy, C. Madic, *Radiochim. Acta* **1995**, *69*, 251−257.
[5] C. Madic, J. Bourges, J.-F. Dozol, *AIP Conf. Proc.* **1995**, *346*, 628−638.
[6] M. Kamoshida, T. Fukasawa, F. Kawamura, *J. Nucl. Sci. Technol.* **1998**, *35*, 185−189.
[7] M. T. Pope, in *Mixed-Valence Compounds. Theory and Applications in Chemistry, Physics, Geology, and Biology* (Ed.: D. B. Brown), D. Reidel, Dordrecht, **1980**, pp. 365−386.
[8] R. Contant, J. P. Ciabrini, *J. Chem. Res. (S)* **1977**, 222.
[9] B. Keita, L. Nadjo, *J. Electroanal. Chem.* **1987**, *227*, 77−98.
[10] B. Keita, Y. W. Lu, L. Nadjo, R. Contant, *Eur. J. Inorg. Chem.* **2000**, 2463−2471.
[11] A. S. Saprykin, V. I. Spitsyn, N. N. Krot, *Doklady Phys. Chem. Engl. Transl.* **1976**, *228*, 500−502.
[12] V. N. Kosyakov, G. A. Timofeev, E. A. Erin, V. I. Andreev, V. V. Kopytov, G. A. Simakin, *Soviet Radiochem., Engl. Transl.* **1977**, *19*, 418−423.
[13] Y. M. Kulyako, I. A. Lebedev, V. Y. Frenkel, T. I. Trofimov, V. F. Myasoedov, *Soviet Radiochem., Engl. Transl.* **1981**, *23*, 674−679.
[14] A. A. Baranov, G. A. Simakin, V. N. Kosyakov, E. A. Erin, V. V. Kopytov, G. A. Timofeev, A. G. Rykov, *Soviet Radiochem., Engl. Transl.* **1981**, *23*, 104−106.
[15] G. A. Timofeev, V. M. Chistyakov, E. A. Erin, A. A. Baranov, V. V. Kopytov, *Soviet Radiochem., Engl. Transl.* **1986**, *28*, 156−161.
[16] A. A. Baranov, A. Y. Volkov, E. A. Erin, G. A. Timofeev, V. M. Chistyakov, *Radiochem., Engl. Transl.* **1996**, *38*, 474−476.
[17] D. Chartier, L. Donnet, J. M. Adnet, *Radiochim. Acta* **1999**, *85*, 25−31.
[18] L. R. Morss, in *Handbook on the Physics and Chemistry of Rare Earths*, vol. 18 (Eds.: K. A. Gschneidner, Jr., L. Eyring, G. R. Choppin, G. H. Lander), Elsevier Science, Amsterdam, **1994**, pp. 239−291.
[19] S. G. Bratsch, *J. Phys. Chem. Ref. Data* **1989**, *18*, 1−21.
[20] A. S. Saprykin, V. P. Shilov, V. I. Spitsyn, N. N. Krot, *Doklady Chem. Engl. Transl.* **1976**, *226*, 114−116.
[21] A. B. Yusov, V. P. Shilov, *Radiochem., Engl. Transl.* **1999**, *41*, 1−23.
[22] For example, see issue 48 (25 November 1996) of *J. Phys. Condens. Matter* **1996**, *8*.
[23] P. Fulde, *Electron Correlations in Molecules and Solids*, 3rd ed., Springer, Berlin, Germany, **1995**.
[24] L. Soderholm, M. R. Antonio, S. Skanthakumar, C. W. Williams, *J. Am. Chem. Soc.* **2002**, *124*, 7290−7291.
[25] M.-H. Chiang, C. W. Williams, L. Soderholm, M. R. Antonio, *Eur. J. Inorg. Chem.*, in press.
[26] S. C. Termes, M. T. Pope, *Trans. Met. Chem.* **1978**, *3*, 103−108.
[27] L. P. Maslov, L. V. Sirotinkina, A. G. Rykov, *Soviet Radiochem., Engl. Transl.* **1985**, *27*, 679−683.
[28] S. P. Best, R. J. H. Clark, R. P. Cooney, *Inorg. Chim. Acta* **1988**, *145*, 141−147.
[29] L. Bion, P. Moisy, F. Vaufrey, S. Meot-Reymond, E. Simoni, C. Madic, *Radiochim. Acta* **1997**, *78*, 73−82.
[30] Under the aqueous conditions used here, we suggest that the U^{5+} complex succumbs to hydrolytic attack liberating U^{5+}, which is rapidly oxidized to $[UO_2]^{2+}$.
[31] S. Dong, M. Liu, *J. Electroanal. Chem.* **1994**, *372*, 95−100.
[32] B. Keita, E. Abdeljalil, L. Nadjo, B. Avisse, R. Contant, J. Canny, M. Richet, *Electrochem. Commun.* **2000**, *2*, 145−149.
[33] B. Keita, F. Girard, L. Nadjo, R. Contant, J. Canny, M. Richet, *J. Electroanal. Chem.* **1999**, *478*, 76−82.
[34] B. Keita, Y. Jean, B. Levy, L. Nadjo, R. Contant, *New J. Chem.* **2002**, *26*, 1314−1319.
[35] X. Lopez, C. Bo, J. M. Poblet, *J. Am. Chem. Soc.* **2002**, *124*, 12574−12582.
[36] X. Lopez, C. Bo, J. M. Poblet, *Inorg. Chem.* **2003**, *42*, 2634−2638.
[37] E. A. Erine, A. A. Baranov, V. A. Yu, V. M. Chistyakov, G. A. Timofeev, *J. Alloys Compd.* **1998**, *271−273*, 782−785.
[38] B. Keita, A. Belhouari, L. Nadjo, R. Contant, *J. Electroanal. Chem.* **1998**, *442*, 49−57.
[39] P. Gómez-Romero, *Solid State Ionics* **1997**, *101−103*, 243−248.
[40] H. R. Sun, S. Y. Zhang, J. Q. Xu, G. Y. Yang, T. S. Shi, *J. Electroanal. Chem.* **1998**, *455*, 57−68.

 © 2003 Wiley-VCH Verlag GmbH & Co. KGaA, Weinheim

[41] L. Soderholm, M. R. Antonio, C. Williams, S. R. Wasserman, *Anal. Chem.* **1999**, *71*, 4622−4628.
[42] M. R. Antonio, C. W. Williams, L. Soderholm, *Radiochim. Acta* **2002**, *90*, 851−856.
[43] J. O. M. Bockris, A. K. N. Reddy, *Modern Electrochemistry*, vol. 2, Plenum, New York, **1970**.
[44] M. R. Antonio, L. Soderholm, I. Song, *J. Appl. Electrochem.* **1997**, *27*, 784−792.
[45] A. W. Bott, *Curr. Sep.* **1995**, *14*, 64−68.
[46] M. A. Beno, M. Engbretson, G. Jennings, G. S. Knapp, J. Linton, C. Kurtz, U. Rütt, P. A. Montano, *Nucl. Instrum. Methods Phys. Res. A* **2001**, *467−468*, 699−702.
[47] T. Ressler, *J. Synchrotron Radiat.* **1998**, *5*, 118−122.
[48] V. P. Shilov, T. N. Bukhtiyarova, O. P. Zhuravleva, N. N. Krot, *Soviet Radiochem., Engl. Transl.* **1979**, *21*, 616−620.
[49] E. A. Erin, V. V. Kopytov, A. G. Rykov, V. Y. Vasil′ev, *Soviet Radiochem., Engl. Transl.* **1984**, *26*, 94−102.
[50] A. Y. Garnov, N. N. Krot, V. P. Perminov, *Radiochem., Engl. Transl.* **1998**, *40*, 7−10.

Received April 17, 2003

 © 2003 Wiley-VCH Verlag GmbH & Co. KGaA, Weinheim

Solution Structures of Binary and Ternary Metal Ion Complexes of 9-(5-Phosphonopentyl)adenine (3′-deoxa-PEEA). A Nucleotide Analogue Related to the Antivirally Active 9-[2-(Phosphonomethoxy)ethyl]adenine (PMEA)

Raquel B. Gómez-Coca,[a] Antonín Holý,[c] Rosario A. Vilaplana,[b] Francisco González-Vílchez,[b] and Helmut Sigel*[a]

Keywords: Antiviral agents / Chelates / Equilibrium constants / Nucleotides / Stacking interactions

The acidity constants of the twofold protonated acyclic 9-(5-phosphonopentyl)adenine, H_2(dPEEA)$^{\pm}$, as well as the stability constants of the M(H;dPEEA)$^+$ and M(dPEEA) complexes with the metal ions M^{2+} = Mg^{2+}, Ca^{2+}, Sr^{2+}, Ba^{2+}, Mn^{2+}, Co^{2+}, Ni^{2+}, Cu^{2+}, Zn^{2+} or Cd^{2+}, have been determined by potentiometric pH titrations in aqueous solution at I = 0.1 M ($NaNO_3$) and 25 °C. Application of previously determined straight-line plots of log $K^{M}_{M(R\text{-}PO_3)}$ versus p$K^{H}_{H(R\text{-}PO_3)}$ for simple phosph(on)ate ligands, R-PO_3^{2-}, where R represents a residue which cannot participate in the coordination process, proves that the primary binding site of dPEEA^{2-} is the phosphonate group with all the metal ions studied. However, for the M(dPEEA) systems with Co^{2+}, Ni^{2+}, Cu^{2+}, Zn^{2+} and Cd^{2+} a (in part rather small) stability increase is observed which is due to macrochelate formation with the adenine residue, i.e. most likely with N7. The formation degrees of the macrochelates are 17 ± 15%, 28 ± 10%, 46 ± 12%, 42 ± 28%, and 42 ± 9% (3σ), respectively. This means that in this respect dPEEA^{2-} resembles the parent nucleotide adenosine 5′-monophosphate (AMP^{2-}) more than its chain-shortened analogue 9-(4-phosphonobutyl)adenine (dPMEA^{2-}); indeed, in a first approximation macrochelate formation increases for a given metal ion within the series M(dPMEA) < M(dPEEA) < M(AMP). However, the coordinating properties of all three mentioned ligands differ significantly from those of the antivirally active 9-[2-(phosphonomethoxy)ethyl]adenine (PMEA^{2-}) which, due to the presence of an ether oxygen in the aliphatic side chain, has a different coordination chemistry which involves five-membered chelates with the ether oxygen atom. In addition, the stability constants of the mixed ligand complexes formed between Cu(Arm)$^{2+}$, where Arm = 2,2′-bipyridine (Bpy) or 1,10-phenanthroline (Phen), and the H(dPEEA)$^-$ or dPEEA^{2-} species were also measured. Detailed stability constant comparisons reveal that in the monoprotonated ternary Cu(Arm)(H;dPEEA)$^+$ complexes the proton is at the phosphonate group and that stacking between Cu(Arm)$^{2+}$ and H(dPEEA)$^-$ plays a significant role. For the Cu(Arm)(dPEEA) complexes a large increase in complex stability (compared to the stability expected on the basis of the basicity of the phosphonate group) is observed, which is due to intramolecular stack formation between the aromatic ring systems of Phen or Bpy and the purine moiety of dPEEA^{2-}. The formation degree of the stacked isomers is in the order of 65 to 80%. Comparisons of the Cu(Arm)(PA) systems, where PA^{2-} = dPEEA^{2-}, dPMEA^{2-} or AMP^{2-}, reveal that here dPEEA^{2-} resembles its parent AMP^{2-} less closely than dPMEA^{2-} does. The biological implications of these results, including antiviral activities, are shortly discussed.
(© Wiley-VCH Verlag GmbH & Co. KGaA, 69451 Weinheim, Germany, 2003)

1. Introduction

Viruses and the diseases they may cause have been studied for more than 100 years. Viruses are classified according to their genetic material into two major groups: RNA and DNA viruses. The human hepatitis A virus (HAV) and polioviruses belong to the first group, whereas the hepatitis B virus (HBV) is classified as a DNA-containing organism.[1]

Within the RNA-virus group special attention has been paid to the *Retroviridae* family to which the human immunodeficiency viruses (HIV-1 and HIV-2) belong.[2] It is well-known today[3] that, at least in theory, the viral replication cycle may be interrupted in many ways. One of the possibilities is to employ acyclic nucleotide analogues[4] and in this category 9-[2-(phosphonomethoxy)ethyl]adenine (PMEA; Figure 1),[5−7] also known as Adefovir,[8] appears to be especially promising. This compound may be con-

[a] Department of Chemistry, Inorganic Chemistry, University of Basel, Spitalstrasse 51,
CH-4056 Basel, Switzerland
Fax: (internat.) +41-61/267-1017
E-mail: Helmut.Sigel@unibas.ch
[b] Inorganic Chemistry Department, Faculty of Chemistry, University of Seville,
E-41071 Seville, Spain
[c] Institute of Organic Chemistry and Biochemistry, Academy of Sciences,
CZ-16610 Prague, Czech Republic

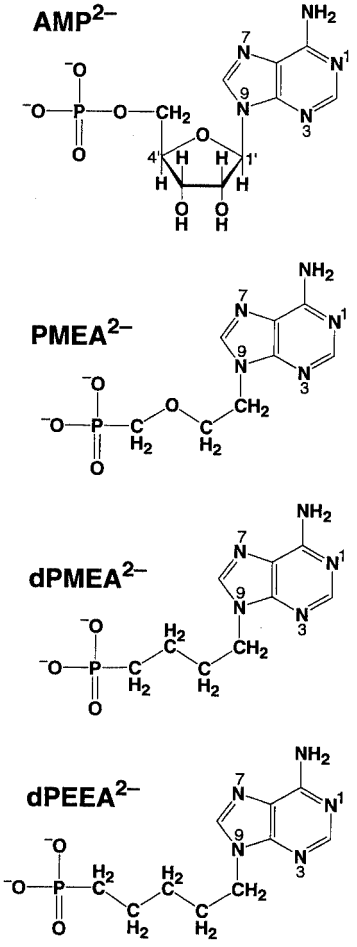

Figure 1. Chemical structures of the dianions of 9-[2-(phosphonomethoxy)ethyl]adenine (= $PMEA^{2-}$ = *Adefovir*), 9-(4-phosphonobutyl)adenine (= $dPMEA^{2-}$ = 3′-deoxa-$PMEA^{2-}$), 9-(5-phosphonopentyl)adenine (= $dPEEA^{2-}$ = 3′-deoxa-$PEEA^{2-}$) and of their parent nucleotide adenosine 5′-monophosphate (AMP^{2-}). The latter is shown in its *anti* conformation.

sidered as an analogue of (2′-deoxy)adenosine 5′-monophosphate [(d)AMP^{2-}; Figure 1]; it is active against HBV and HIV.[8,9] Indeed, its bis(pivaloyloxymethyl)ester (Adefovir dipivoxil) was very recently approved by the US Food and Drug Administration (FDA) for use in hepatitis B therapy.[10]

Since PMEA has a phosphonate group instead of a phosphate unit, it circumvents in blood plasma or in its passage through the cellular membrane the enzyme-catalyzed dephosphorylation that is suffered by nucleotide analogues which contain a monophosphate ester residue.[8,11] Instead, PMEA is diphosphorylated to give the triphosphate-like form PMEApp which is responsible for the therapeutic effect.[8,12] PMEApp is accepted as a substrate by DNA polymerases[13] and after incorporation of the nucleotidyl-like unit into the growing nucleic acid chain leads to its termination due to the lack of a 3′-hydroxyl group. It has been suggested[14,15] that the higher basicity of the phosphonyl group compared to that of a phosphoryl one, together with the presence of the ether-oxygen atom in the aliphatic side chain of $PMEApp^{4-}$, facilitate the correct positioning of the two metal ions needed in the reaction and thus make it initially an even better substrate[16,17] for DNA polymerases than $dATP^{4-}$.[14,15]

Indeed, PMEA forms with divalent metal ions (M^{2+}), like Mg^{2+}, Mn^{2+} or Zn^{2+}, five-membered chelates involving the ether oxygen as expressed in the intramolecular Equilibrium (1):

Replacement of the ether oxygen by a CH_2 unit gives 9-(4-phosphonobutyl)adenine, also termed 3′-deoxa-PMEA (dPMEA; Figure 1).[18] This compound shows no biological activity,[16] in agreement with the suggestions summarized above, and it also has a coordination pattern[18] different from that of $PMEA^{2-}$,[18–21] yet one which in fact is similar to that of AMP^{2-}.[20,22,23] This means, phosph(on)ate-coordinated metal ions may form macrochelates by interacting with N7 of the adenine residue; this is expressed in the intramolecular Equilibrium (2):[24–26]

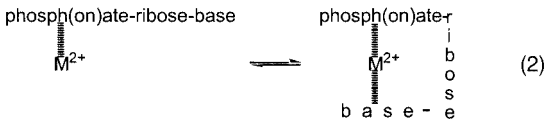

Having a broad interest in the metal ion-binding properties of nucleotide analogues,[27–30] we decided to study 9-(5-phosphonopentyl)adenine, which is also known as 3′-deoxa-PEEA (dPEEA; Figure 1), since it is the deoxa analogue of 9-[2-(2-phosphonoethoxy)ethyl]adenine.[31] As expected, dPEEA does not show a useful biological activity but its additional CH_2 group enabled the investigation of the effect that the lengthening of the side chain of dPMEA has on the metal ion-binding properties. Thus, we measured the stability constants of the binary complexes formed between dPEEA and the alkaline earth ions, the divalent ions of the second half of the 3d series as well as Zn^{2+} and Cd^{2+}. We compared the results regarding the position of Equilibrium (2) with those obtained previously for the M(dPMEA) and the M(AMP) complexes.[18,23]

Since weak interactions[32–34] like the aromatic-ring stacking are important for the anchoring process of a substrate in the active site cavity of an enzyme,[35,36] we had previously quantified the extent of intramolecular stacking according to Equilibrium (3)

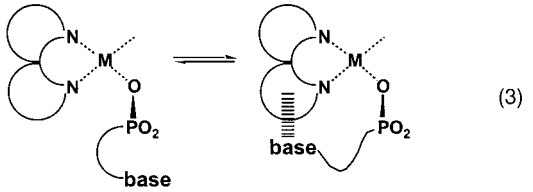

 © 2003 Wiley-VCH Verlag GmbH & Co. KGaA, Weinheim

for the ternary complexes Cu(Arm)(AMP/dPMEA),[37,38] where Arm = 2,2′-bipyridine (Bpy) or 1,10- phenanthroline (Phen). Now the corresponding Cu(Arm)(dPEEA) complexes were studied leading to the interesting result that lengthening of the aliphatic chain by a CH_2 unit diminishes intramolecular stacking [Equilibrium (3)], whereas in the binary M(dPEEA) species macrochelate formation [Equilibrium (2)] is favored.

2. Results and Discussion

2.1 Acidity Constants of $H_2(dPEEA)^{\pm}$

From the structure of $dPEEA^{2-}$ (see Figure 1) it is evident that this species can accept three protons, two at the phosphonate group and one at the N1 site of the adenine residue.[39] Further protonations at an adenine residue are possible at N7 and N3, but these protons are released with $pK_a < 0$;[39−42] similarly, release of the first proton from a twofold protonated phosphonate residue occurs with a pK_a of about 2.[18,43] Hence, in the present study, for which all potentiometric pH titrations were carried out at pH > 4.0, only the following two deprotonation reactions, in which $dPEEA^{2-}$ is abbreviated as PA^{2-}, need to be considered:

$$H_2(PA)^{\pm} \rightleftharpoons H(PA)^{-} + H^{+} \quad (4a)$$

$$K^{H}_{H_2(PA)} = [H(PA)^{-}][H^{+}]/[H_2(PA)^{\pm}] \quad (4b)$$

$$H(PA)^{-} \rightleftharpoons PA^{2-} + H^{+} \quad (5a)$$

$$K^{H}_{H(PA)} = [PA^{2-}][H^{+}]/[H(PA)^{-}] \quad (5b)$$

Indeed, all the experimental data from the pH titrations in aqueous solution (25 °C; I = 0.1 M, $NaNO_3$) could be excellently fitted by taking into account Equilibria (4) and (5). The acidity constants obtained in the present study for $H_2(dPEEA)^{\pm}$ are given in Table 1 together with some related data.[44−46]

Table 1. Negative logarithms of the acidity constants of $H_2(dPEEA)^{\pm}$ [Equations (4) and (5)] together with the corresponding values of some related systems in aqueous solution at 25 °C and I = 0.1 M ($NaNO_3$)[a][b]

No.	Protonated species	$pK^{H}_{H_2(PA)}$ $(N1)H^{+}$	$pK^{H}_{H(PA)}$ $P(O)_2(OH)^{-}$	Ref.
1	$H(9MeAde)^{+}$	4.10 ± 0.01	−	[41]
2	$CH_3P(O)(OH)_2$	−	7.51 ± 0.01	[43]
3	$CH_3OP(O)(OH)_2$	−	6.36 ± 0.01	[44]
4	$H_2(AMP)^{\pm}$	3.84 ± 0.02	6.21 ± 0.01	[22]
5	$H_2(PMEA)^{\pm}$	4.16 ± 0.02	6.90 ± 0.01	[45]
6	$H_2(dPMEA)^{\pm}$	4.17 ± 0.02	7.69 ± 0.01	[18]
7	$H_2(dPEEA)^{\pm}$	4.17 ± 0.01	7.75 ± 0.01	[c]

[a] The error limits given are three times the standard error of the mean value or the sum of the probable systematic errors, whichever is larger. [b] So-called practical, mixed or Brønsted constants are listed (see [46] for details). [c] This work.

Comparison of the values listed in Table 1 (entries 1 and 4−7) reveal that the first proton of $H_2(dPEEA)^{\pm}$ is from the $(N1)H^{+}$ site of the adenine residue and the second one from the monoprotonated phosphonate group (see entries 2−7). However, more comparisons are possible; a few are given:

(i) From the comparison of entries 3 and 4 with those of 2 and 5−7 it follows that protonated phosphonate groups are less acidic than the corresponding phosphate groups; this agrees with the lower electronegativity of a C atom compared to an O atom.

(ii) The ether oxygen, due to its electron-withdrawing effect, makes the monoprotonated phosphonate species of $PMEA^{2-}$ more acidic than those of $dPMEA^{2-}$ or $dPEEA^{2-}$ (entries 5−7).

(iii) In fact, the acid-base properties of $H_2(dPMEA)^{\pm}$ and of $H_2(dPEEA)^{\pm}$ are very similar, indicating that the additional CH_2 unit in PEEA has little effect (entries 6, 7).

Finally, it needs to be pointed out that due to the different affinities of the phosph(on)ate groups for protons, the formation degree of the free ligands, PA^{2-}, differs considerably in the physiological pH range around 7.5: Under these conditions, for example, AMP^{2-} is formed to about 95% whereas $dPEEA^{2-}$ occurs only to about 36%.

2.2 Stability Constants of the $M(H;dPEEA)^{+}$ and M(dPEEA) Complexes

The experimental data of the potentiometric pH titrations (see Section 4.3) allow the determination of the stability constants defined by Equilibria (6a) and (7a):

$$M^{2+} + H(PA)^{-} \rightleftharpoons M(H;PA)^{+} \quad (6a)$$

$$K^{M}_{M(H;PA)} = [M(H;PA)^{+}]/([M^{2+}][H(PA)^{-}]) \quad (6b)$$

$$M^{2+} + PA^{2-} \rightleftharpoons M(PA) \quad (7a)$$

$$K^{M}_{M(PA)} = [M(PA)]/([M^{2+}][PA^{2-}]) \quad (7b)$$

Together with Equilibria (4a) and (5a) they are sufficient to obtain excellent fitting of the titration data provided the evaluation is not carried into the pH range where formation of hydroxo species occurs, which was evident from titrations without ligand. Of course, Equilibria (6a) and (7a) are also connected via Equilibrium (8a)

$$M(H;PA)^{+} \rightleftharpoons M(PA) + H^{+} \quad (8a)$$

$$K^{H}_{M(H;PA)} = [M(PA)][H^{+}]/[M(H;PA)^{+}] \quad (8b)$$

and the corresponding acidity constant [Equation (8b)] may be calculated with Equation (9):[47]

$$pK^{H}_{M(H;PA)} = pK^{H}_{H(PA)} + \log K^{M}_{M(H;PA)} - \log K^{M}_{M(PA)} \quad (9)$$

The results are listed in Table 2; the stability constants given for the $M(H;dPEEA)^{+}$ complexes are in part estimates since the formation degree of these species was low (see Section 4.3). The stability constants of the M(dPEEA)

 © 2003 Wiley-VCH Verlag GmbH & Co. KGaA, Weinheim

complexes show the usual trends. For the alkaline earth ions the stability of the complexes decreases with increasing ionic radii indicating that metal ion binding at the phosphonate group is (at least) in part inner-sphere. For the divalent 3d metal ions the long-standing experience[48] is confirmed that the stabilities of phosph(on)ate-metal ion complexes often do not strictly follow[18,20,27,28,44,45,49] the Irving−Williams sequence,[50] an observation in agreement with the fact that in ligands of this kind the phosph(on)ate group is always the main stability-determining binding site.[19,22,24,25,51]

Table 2. Logarithms of the stability constants of the $M(H;dPEEA)^+$ [Equation (6b)] and M(dPEEA) complexes [Equation (7b)], together with the negative logarithms of the acidity constants of the protonated complexes [Equations (8b) and (9)] in aqueous solution at 25 °C and $I = 0.1$ M ($NaNO_3$)[a]

M^{2+}	$\log K^{M}_{M(H;dPEEA)}$	$\log K^{M}_{M(dPEEA)}$	$pK^{H}_{M(H;dPEEA)}$
Mg^{2+}	0.4 ± 0.3[b]	1.87 ± 0.05	6.28 ± 0.30
Ca^{2+}	0.2 ± 0.4[b]	1.59 ± 0.06	6.36 ± 0.40
Sr^{2+}	0.1 ± 0.4[b]	1.31 ± 0.07	6.54 ± 0.41
Ba^{2+}	0.0 ± 0.4[b]	1.25 ± 0.06	6.50 ± 0.40
Mn^{2+}	0.69 ± 0.18	2.55 ± 0.03	5.89 ± 0.18
Co^{2+}	0.86 ± 0.21	2.36 ± 0.05	6.25 ± 0.22
Ni^{2+}	1.00 ± 0.15	2.46 ± 0.03	6.29 ± 0.15
Cu^{2+}	1.92 ± 0.12	3.86 ± 0.08	5.81 ± 0.15
Zn^{2+}	1.47 ± 0.22	2.9 ± 0.2[c]	6.32 ± 0.30
Cd^{2+}	1.38 ± 0.15	3.19 ± 0.05	5.94 ± 0.16

[a] For the error limits see footnote [a] of Table 1. The error limits (3σ) of the derived data, in the present case for column 4, were calculated according to the error propagation after Gauss. [b] The constants listed for these $M(H;dPEEA)^+$ complexes are estimates (see Section 4.3). [c] The experiments with Zn^{2+} were significantly hampered by precipitation; i.e., the pH range accessible for the evaluation of the constants was severely restricted (see Section 4.3).

As far as the $M(H;dPEEA)^+$ complexes are concerned, it is evident that the evaluation of potentiometric pH titration data only allows the determination of their stability constants. Further information is required to detect the binding sites of the proton and the metal ion. At first one may ask where the proton is located because binding of a metal ion to a protonated ligand commonly leads to an acidification of the ligand-bound proton.[52,53] Indeed, the acidity constants of the $M(H;dPEEA)^+$ complexes given in column 4 of Table 2 are by about 1.2 to 1.9 log units smaller than $pK^{H}_{H(dPEEA)}$. This shows that the proton in $M(H;dPEEA)^+$ is bound to the phosphonate group, hence, one may tentatively assume that the metal ion is bound preferentially to the nucleobase, since a monoprotonated phosphonate group is only a weak binding site. Indeed, this suggestion agrees with evidence obtained previously for other related $M(H;PA)^+$ species.[20,21,45,54]

Furthermore, the stability constants of the $M(H;dPEEA)^+$ complexes are, within the error limits, identical to the values determined[45] for the corresponding $M(H;PMEA)^+$ and $M(H;dPMEA)^+$ species.[18] Considering that the basicity of the N1 sites in $H(dPEEA)^-$ and $H(dPMEA)^-$ or $H(PMEA)^-$ are also identical (see Table 1; column 3, entries 5−7) and that evidence has been provided for the $M(H;PMEA)^+$ complexes[20,21,45] that the metal ion is mainly located at the nucleobase residue, one may not only conclude that in the $M(H;dPEEA)^+$ complexes the proton is at the phosphonate group, but also that the metal ion is mainly at the adenine residue. The N1 versus N7 dichotomy for metal ion binding to the adenine residue is well-known[55] though there are indications that binding to N7 dominates.[55,56] In any case, the fact that the stabilities of the $M(H;dPEEA)^+$ complexes *follow* the Irving−Williams sequence[50] [in contrast to phosph(on)ate coordinations] also supports[48a] the above conclusion that metal ion binding in the monoprotonated species occurs preferably to a nitrogen atom.

2.3 Evaluation of the Stabilities of the M(dPEEA) Complexes

For the M(dPEEA) complexes the question arises: Does the adenine residue also participate in metal ion binding next to the phosphonate group? Should such an additional interaction with the adenine residue occur, then it has to be reflected in an increased complex stability.[57] Hence, it is necessary to define the stability of a pure $-PO_3^{2-}/M^{2+}$ interaction. This can be done by applying the previously defined[45] straight-line correlations which are based on $\log K^{M}_{M(R\text{-}PO_3)}$ versus $pK^{H}_{H(R\text{-}PO_3)}$ plots for simple phosphate monoesters[58] and phosphonates;[45] these ligands are abbreviated as $R\text{-}PO_3^{2-}$, where R represents a non-coordinating residue. The parameters for the corresponding straight-line equations, which are defined by Equation (10),

$$\log K^{M}_{M(R\text{-}PO_3)} = m \cdot pK^{H}_{H(R\text{-}PO_3)} + b \qquad (10)$$

have been tabulated,[19a,25,45,51] i.e., the slopes m and the intercepts b with the y-axis. Hence, with a known pK_a value for the deprotonation of a $-P(O)_2(OH)^-$ group an expected stability constant can be calculated for any phosph(on)ate-metal ion complex.

The plots of $\log K^{M}_{M(R\text{-}PO_3)}$ versus $pK^{H}_{H(R\text{-}PO_3)}$ according to Equation (10) are shown in Figure 2 for the 1:1 complexes of Ca^{2+}, Co^{2+}, Cd^{2+} and Cu^{2+} as examples, with the data points (empty circles) of the eight simple ligand systems used[45] for the determination of the straight base lines. The four solid circles refer to the corresponding M(dPEEA) complexes; those for the Cd^{2+} and Cu^{2+} species, and possibly also for the Co^{2+} ones, are somewhat above their reference lines, thus proving an increased stability for these complexes, whereas the data point for the Ca^{2+} complex fits within the error limits on the line. Similar properties are observed for the corresponding M(dPMEA) and M(AMP) complexes (crossed circles). In contrast, *all* of the data points[45] of the M(PMEA) complexes (solid squares) are clearly above their reference lines indicating that all these

 © 2003 Wiley-VCH Verlag GmbH & Co. KGaA, Weinheim

species are more stable than is expected on the basis of the basicity of the phosphonate group of $PMEA^{2-}$.

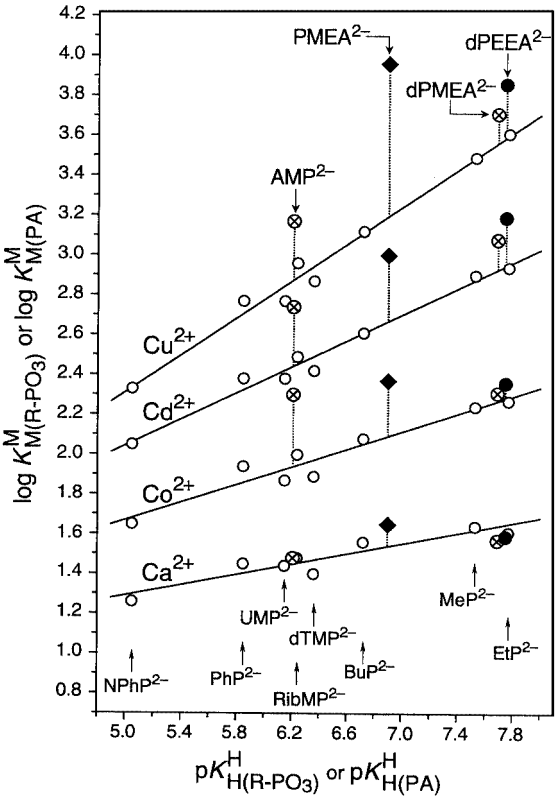

Figure 2. Evidence for an enhanced stability of the Cd(dPEEA) and Cu(dPEEA) and possibly also the Co(dPEEA) complexes, and for the lack of such an enhanced stability of the Ca(dPEEA) species (●), together with the data points for the corresponding metal ion complexes of $dPMEA^{2-}$, AMP^{2-} (⊗) and $PMEA^{2-}$ (◆) based on the relationship between log $K^{M}_{M(R\text{-}PO_3)}$ and $pK^{H}_{H(R\text{-}PO_3)}$ for M(R-PO_3) complexes of some simple phosphate monoester and phosphonate ligands (R-PO_3^{2-}) (○): 4-nitrophenyl phosphate ($NPhP^{2-}$), phenyl phosphate (PhP^{2-}), uridine 5′-monophosphate (UMP^{2-}), D-ribose 5-monophosphate ($RibMP^{2-}$), thymidine [= 1-(2-deoxy-β-D-ribofuranosyl)thymine] 5′-monophosphate ($dTMP^{2-}$), *n*-butyl phosphate (BuP^{2-}), methanephosphonate (MeP^{2-}), and ethanephosphonate (EtP^{2-}) (from left to right). The least-squares lines [Equation (10)] are drawn through the corresponding 8 data sets (○) taken from [58] for the phosphate monoesters and from [45] for the phosphonates. The points due to the equilibrium constants for the M^{2+}/dPEEA systems (●) are based on the values listed in Tables 1 and 2; those for the M^{2+}/dPMEA (⊗), M^{2+}/AMP (⊗), and M^{2+}/PMEA systems (◆) are from [18,23] and [45], respectively. The vertical broken lines emphasize the stability differences from the reference lines; they equal log $\Delta_{M/PA}$ as defined in Equation (11). All the plotted equilibrium constants refer to aqueous solutions at 25 °C and I = 0.1 M ($NaNO_3$).

The increased stability of the M(PMEA) complexes has been proven[45] to be largely due to the involvement of the ether oxygen atom in metal ion binding (see Figure 1) which gives rise to the formation of five-membered chelates and thus to the intramolecular Equilibrium (1).[15,19,45] In certain systems, like Ni(PMEA) and Cu(PMEA), a third isomer exists which involves, in addition, N3 of the adenine residue[15,19–21,45] as well as a fourth one involving N7 which, however, occurs only to a minor extent.[18]

Naturally, in the complexes of $dPEEA^{2-}$, $dPMEA^{2-}$ and AMP^{2-}, whose side chains or sugar residue is devoid of an ether oxygen atom (Figure 1), Equilibrium (1) cannot exist and therefore, any possibly observed stability increase has to be attributed to an interaction with the adenine residue. Stability enhancements, like those seen in Figure 2, can be quantified by the differences between the experimentally (exptl) measured stability constants and those calculated (calcd) according to Equation (10); this difference is defined in Equation (11),

$$\log \Delta_{M/PA} = \log K^{M}_{M(PA)_{exptl}} - \log K^{M}_{M(PA)_{calcd}} \quad (11a)$$

$$= \log K^{M}_{M(PA)} - \log K^{M}_{M(PA)_{op}} \quad (11b)$$

where the expressions log $K^{M}_{M(PA)calcd}$ and log $K^{M}_{M(PA)op}$ are synonymous because the calculated value equals the stability constant of the "open" isomer, $M(PA)_{op}$ [see, for example, Equilibria (1) and (2)], in which only a -PO_3^{2-}/M^{2+} interaction occurs. In columns 2–4 of Table 3 the values for the three terms of Equation (11) are listed. The log $\Delta_{M/dPEEA}$ values for Ni(dPEEA), Cu(dPEEA) and Cd(dPEEA) are clearly positive; the same is most likely true for those due to Co(dPEEA) and Zn(dPEEA), especially if one takes into account that the error limits refer to *three times* the standard error. Hence, in all these instances Equilibrium (2) needs to be considered.

Table 3. Stability constant comparisons for the M(dPEEA) complexes between the measured stability constants (exptl; Table 2, column 3) and the calculated stability constants (calcd) based on the basicity of the phosphonate group in $dPEEA^{2-}$ ($pK^{H}_{H(dPEEA)}$ = 7.75; Table 1) and the baseline equations established previously[25,45,51] (see Equation (10) and Figure 2), together with the stability differences log $\Delta_{M/dPEEA}$, as defined by Equation (11). The previously determined stability differences, log $\Delta_{M/dPMEA}$, for M(dPMEA) complexes[18] are given for comparison (aqueous solution; 25 °C; I = 0.1 M, $NaNO_3$)[a]

M^{2+}	log $K^{M}_{M(dPEEA)}$ exptl[b]	log $K^{M}_{M(dPEEA)}$ calcd	log $\Delta_{M/dPEEA}$	log $\Delta_{M/dPMEA}$
Mg^{2+}	1.87 ± 0.05	1.88 ± 0.03	−0.01 ± 0.06	−0.03 ± 0.05
Ca^{2+}	1.59 ± 0.06	1.65 ± 0.05	−0.06 ± 0.08	−0.07 ± 0.07
Sr^{2+}	1.31 ± 0.07	1.37 ± 0.04	−0.06 ± 0.08	−0.06 ± 0.06
Ba^{2+}	1.25 ± 0.06	1.30 ± 0.04	−0.05 ± 0.07	−0.07 ± 0.07
Mn^{2+}	2.55 ± 0.03	2.53 ± 0.05	0.02 ± 0.06	−0.04 ± 0.06
Co^{2+}	2.36 ± 0.05	2.28 ± 0.06	0.08 ± 0.08	0.04 ± 0.08
Ni^{2+}	2.46 ± 0.03	2.32 ± 0.05	0.14 ± 0.06	0.10 ± 0.08
Cu^{2+}	3.86 ± 0.08	3.59 ± 0.06	0.27 ± 0.10	0.16 ± 0.09
Zn^{2+}	2.9 ± 0.2	2.66 ± 0.06	0.24 ± 0.21	0.1 ± 0.2
Cd^{2+}	3.19 ± 0.05	2.95 ± 0.05	0.24 ± 0.07	0.15 ± 0.11

[a] Regarding the error limits (3σ) see footnote [a] of Table 2. [b] These values are from column 3 of Table 2.

A comparison of the log $\Delta_{M/PA}$ values given in columns 4 and 5 of Table 3 for the M(dPEEA) and M(dPMEA) complexes, respectively, reveals that their properties are quite alike with a slightly more enhanced stability of some of the M(dPEEA) species.

 © 2003 Wiley-VCH Verlag GmbH & Co. KGaA, Weinheim

2.4 Extent of Macrochelate Formation in M(dPEEA) Systems and Comparison with That Occurring in M(dPMEA) and M(AMP) Species

The position of the concentration-independent Equilibrium (2) between the simple phosphonate-bound species, which we designate as the "open" isomer, $M(dPEEA)_{op}$, and the macrochelated isomer involving the adenine residue, designated as the "closed" species, $M(dPEEA)_{cl}$, is defined by the intramolecular, and hence dimensionless, equilibrium constant K_I given in Equation (12):

$$K_I = [M(dPEEA)_{cl}]/[M(dPEEA)_{op}] \quad (12)$$

Values for K_I can be calculated by known procedures,[22,45,57] i.e., via Equation (13):

$$K_I = 10^{\log \Delta_{M/dPEEA}} - 1 \quad (13)$$

Knowledge of K_I allows then to obtain the percentage of the closed isomer, $M(dPEEA)_{cl}$, according to Equation (14):

$$\% M(dPEEA)_{cl} = 100 \cdot K_I/(1 + K_I) \quad (14)$$

The results are summarized in Table 4 for the M(dPEEA) complexes of the 3d ions including Zn^{2+} and Cd^{2+}. For the complexes of the alkaline earth ions the formation degree of the closed species in Equilibrium (2) is zero within the error limits as follows from the log $\Delta_{M/dPEEA}$ values listed in column 4 of Table 3.

From the results listed in columns 2−4 of Table 4 it follows that at least for Ni^{2+}, Cu^{2+}, Zn^{2+} and Cd^{2+}, which have the most pronounced affinity for N sites among the ten metal ions studied,[48a] Equilibrium (2) operates and that the adenine residue is involved in metal ion binding. From the three nitrogen atoms available in the purine ring, i.e., N1, N3 and N7 (see Figure 1), N1 cannot be reached by a metal ion already coordinated to the phosphonate group;[19] hence, N3 and N7 remain for macrochelate formation. At this stage one cannot distinguish with absolute certainty between these two possibilities, but we strongly favor an interaction of the phosphonate-coordinated metal ion with N7 because N7 is known to be considerably more basic than N3.[39−42] Furthermore, macrochelate formation in the M(AMP) complexes occurs with certainty via N7;[22,59] hence, it appears that M(dPEEA) and M(dPMEA) resemble in this respect their parent complexes, i.e., M(AMP), more than the M(PMEA) species which contain the antivirally active ligand $PMEA^{2-}$ and involve the ether oxygen atom in metal ion binding (see Section 1).

With the above evidence for macrochelate formation involving N7 in mind, it is interesting to compare the properties of the $dPEEA^{2-}$, $dPMEA^{2-}$ and AMP^{2-} ligands (Figure 1). From the results given in columns 4−6 of Table 4 it follows that the extent of macrochelate formation increases within the series M(dPMEA) < M(dPEEA) < M(AMP). The changes are not dramatic, but the trend within the series seems to be clear for each metal ion. A further interesting observation is that for Cu^{2+}, Zn^{2+} and Cd^{2+} the formation degrees of the $M(dPEEA)_{cl}$ and $M(AMP)_{cl}$ species are quite alike. Hence, it seems that $dPEEA^{2-}$ mimics AMP^{2-} even better than $dPMEA^{2-}$; most likely this is due to the by one CH_2 unit longer side chain of $dPEEA^{2-}$, compared to the one of $dPMEA^{2-}$, and that this allows the phosphonate-bound M^{2+} to reach N7 with less strain.

2.5 Stability of the Mixed Ligand Cu(Arm)(H;dPEEA)$^+$ and Cu(Arm)(dPEEA) Complexes

For the ternary complexes composed of $H(dPEEA)^-$ or $dPEEA^{2-}$, Cu^{2+} and a heteroaromatic amine (Arm), i.e., 2,2′-bipyridine (Bpy) or 1,10-phenanthroline (Phen), the same evaluation procedure holds as described in the first paragraph of Section 2.2 for the binary complexes because complex formation of $Cu(Bpy)^{2+}$ and $Cu(Phen)^{2+}$, due to their high stability,[60] is complete (see also Section 4.3) before the onset of the formation of the mixed ligand complexes occurs. This means that in the case of the ternary systems the experimental data of the potentiometric pH titrations can also be fully described by taking Equilibria (4a)−(7a) into account, but now $M^{2+} = Cu(Arm)^{2+}$. The corresponding stability constants are given in Table 5.

A comparison of the acidity constants of $H_2(dPEEA)^{\pm}$, $pK^H_{H_2(dPEEA)} = 4.17$ and $pK^H_{H(dPEEA)} = 7.75$ (Table 1), with those of the $Cu(Arm)(H;dPEEA)^+$ complexes, i.e.,

Table 4. Increased complex stability, log $\Delta_{M/dPEEA}$ [Equation (11)], and extent of chelate formation according to Equilibrium (2) for some M(dPEEA) complexes, as quantified by the dimensionless equilibrium constant K_I [Equations (12), (13)] and the percentage of $M(dPEEA)_{cl}$ [Equation (14)]. The corresponding percentages for $M(dPMEA)_{cl}$ [18] and $M(AMP)_{cl}$ [23] are given for comparison (aqueous solution; 25 °C; I = 0.1 M, $NaNO_3$)[a]

M^{2+}	log $\Delta_{M/dPEEA}$ [b]	K_I	% $M(dPEEA)_{cl}$	% $M(dPMEA)_{cl}$	% $M(AMP)_{cl}$
Mn^{2+}	0.02 ± 0.06	0.05 ± 0.14	5 ± 13	≤ 5	15 ± 11
Co^{2+}	0.08 ± 0.08	0.20 ± 0.22	17 ± 15	9 ± 17	56 ± 7
Ni^{2+}	0.14 ± 0.06	0.38 ± 0.19	28 ± 10	21 ± 15	75 ± 4
Cu^{2+}	0.27 ± 0.10	0.86 ± 0.43	46 ± 12	31 ± 14	50 ± 7
Zn^{2+}	0.24 ± 0.21[c]	0.74 ± 0.84[c]	42 ± 28	21 ± 37[d]	44 ± 12
Cd^{2+}	0.24 ± 0.07	0.74 ± 0.28	42 ± 9	29 ± 18	50 ± 8

[a] Regarding the error limits (3σ) see footnote [a] of Table 2. [b] From column 4 of Table 3. [c] See footnote [c] in Table 2. [d] The measurements for the Zn(dPMEA) systems were also affected by precipitation.[18]

 © 2003 Wiley-VCH Verlag GmbH & Co. KGaA, Weinheim

Table 5. Logarithms of the stability constants of the $M(H;dPEEA)^+$ [Equation (6b)] and M(dPEEA) complexes [Equation (7b)], where $M^{2+} = Cu^{2+}$, $Cu(Bpy)^{2+}$ or $Cu(Phen)^{2+}$, as determined by potentiometric pH titrations in aqueous solution, together with the negative logarithms for the acidity constants of $M(H;dPEEA)^+$ [Equations (8b), (9)] at 25 °C and $I = 0.1$ M ($NaNO_3$)[a]

M^{2+}	log $K^{M}_{M(H;dPEEA)}$	log $K^{M}_{M(dPEEA)}$	$pK^{H}_{M(H;dPEEA)}$
Cu^{2+}	1.92 ± 0.12	3.86 ± 0.08	5.81 ± 0.15
$Cu(Bpy)^{2+}$	1.87 ± 0.11	4.07 ± 0.07	5.55 ± 0.13
$Cu(Phen)^{2+}$	2.14 ± 0.12	4.36 ± 0.14	5.53 ± 0.18

See footnote [a] of Table 2.

$pK^{H}_{Cu(Arm)(H;dPEEA)} \approx 5.5$ (Table 5, column 4), reveals that in these complexes, just as in the binary ones, the proton must be located at the phosphonate group, since metal ion coordination must give rise to an acidification.[52,53] In fact, the acidity constants of the $Cu(Arm)(H;dPEEA)^+$ complexes are about 2.2 log units smaller than $pK^{H}_{H(dPEEA)}$, but approximately 1.4 log units larger than $pK^{H}_{H_2(dPEEA)}$.

However, where is the $Cu(Arm)^{2+}$ unit located? Indeed, the $Cu(Arm)(H{\cdot}dPEEA)^+$ species, where the notation $(H{\cdot}dPEEA)^-$ indicates that the proton is at the phosphonate group, may exist in two principally different forms: One, where $Cu(Arm)^{2+}$ is stacked with the purine system of $(H{\cdot}dPEEA)^-$, designated as $[Cu(Arm)/(H{\cdot}dPEEA)]^+_{st}$, and another one, where $Cu(Arm)^{2+}$ is simply coordinated either to the N1/N7 sites of the adenine residue (see Section 2.2), $[(H{\cdot}dPEEA){\cdot}Cu(Arm)]^+_{ade}$, or to the phosphonate group which already carries the proton. However, the formation of the latter species with both the proton and $Cu(Arm)^{2+}$ at the phosphonate group is unlikely, in agreement with the conclusions given in Section 2.2 for the binary $Cu(H;dPEEA)^+$ species, where Cu^{2+} is mainly located at the adenine residue and H^+ at the phosphonate group. Hence, we have to consider the $[(H{\cdot}dPEEA){\cdot}Cu(Arm)]^+_{ade}$ and the $[Cu(Arm)/(H{\cdot}dPEEA)]^+_{st}$ species and take into account the following intramolecular Equilibrium (15):

$$[(H{\cdot}dPEEA){\cdot}Cu(Arm)]^+_{ade} \rightleftharpoons [Cu(Arm)/(H{\cdot}dPEEA)]^+_{st} \qquad (15)$$

An evaluation of the various equilibrium constants, identical to the procedure described recently,[38,61] leads to the conclusion that the stacked species in Equilibrium (15) dominate in the $Cu(Phen)^{2+}$ system with a formation degree of about 70% for the $[Cu(Phen)/(H{\cdot}dPEEA)]^+_{st}$ species. In the case of the $Cu(Bpy)^{2+}$ system the two isomeric species of Equilibrium (15) occur in about *equal* amounts. These results are very similar to those obtained previously[38] for the $Cu(Arm)^{2+}/(H{\cdot}dPMEA)^-$ systems. Furthermore, that stacking is somewhat more pronounced in the system containing Phen is in agreement with the expectation (see also Section 2.7).

2.6 Proof of an Increased Stability of the Mixed Ligand Cu(Arm)(dPEEA) Complexes

One way to quantify the stability of mixed ligand complexes[62,63] is to consider Equilibrium (16a) with its corresponding equilibrium constant [Equation (16b)], which is calculated from Equation (17):

$$Cu(Arm)^{2+} + Cu(dPEEA) \rightleftharpoons Cu(Arm)(dPEEA) + Cu^{2+} \qquad (16a)$$

$$10^{\Delta \log K} = \frac{[Cu(Arm)(dPEEA)][Cu^{2+}]}{[Cu(Arm)^{2+}][Cu(dPEEA)]} \qquad (16b)$$

$$\Delta \log K = \log K^{Cu(Arm)}_{Cu(Arm)(dPEEA)} - \log K^{Cu}_{Cu(dPEEA)} \qquad (17)$$

According to the general rule for complex stabilities, $K_1 > K_2$, Equilibrium (16a) is expected to lie on the left with negative values for $\Delta \log K$ in agreement with statistical considerations, i.e. $\Delta \log K_{Cu/statist} \approx -0.5$.[63] The results for $\Delta \log K_{Cu/Bpy/dPEEA}$ and $\Delta \log K_{Cu/Phen/dPEEA}$ according to Equation (17) are 0.21 ± 0.11 and 0.50 ± 0.16, respectively (see Table 5). These values are clearly larger than the statistically expected value. Hence, it is clear that Equilibrium (16a) is significantly displaced to the right hand side and that these ternary complexes show an increased stability. However, it is difficult to draw quantitative conclusions from these results because the binary Cu(dPEEA) complex itself also shows an increased stability due to macrochelate formation [see Section 2.4 and Equilibrium (2)]. Yet, despite this shortcoming the given results for Equation (17) still prove definitely an increased stability for the Cu(Arm)(dPEEA) complexes.

Another way to evaluate the stability of the ternary Cu^{2+} complexes, independently of that of the corresponding binary complexes, is analogous to the procedure used in Section 2.4 for the binary systems. This means, straight-line correlations for log $K^{Cu(Arm)}_{Cu(Arm)(R\text{-}PO_3)}$ versus $pK^{H}_{H(R\text{-}PO_3)}$ plots, where $R\text{-}PO_3^{2-}$ represents phosphate monoester or phosphonate ligands in which the residue R is unable to interact with $Cu(Arm)^{2+}$, have been defined and they are valid in the pK_a range between 5 and 8.[51][61] These reference lines are seen in Figure 3 where the stability constants log $K^{Cu(Arm)}_{Cu(Arm)(dPEEA)}$ versus the acidity constant $pK^{H}_{H(dPEEA)}$ are also plotted (square symbols) together with the corresponding data[38] of the $Cu(Arm)^{2+}/dPMEA^{2-}$ systems (circles).

The data points in Figure 3 for the two ternary Cu(Arm)(dPEEA) complexes are far above their reference lines proving again the increased complex stability and this must now mean[57] that, aside from the phosphonate-$Cu(Arm)^{2+}$ coordination, further interactions occur. Such an increased stability, which in fact is even more pronounced, is also observed for the ternary Cu(Arm)(dPMEA) systems[38] as one can see in Figure 3. The vertical differences between the mentioned data points and their reference lines can be defined according to Equation (11) (Section 2.3) by keeping in mind that now $M^{2+} = Cu(Arm)^{2+}$. The needed stability of the "open" isomers, $Cu(Arm)(dPEEA)_{op}$, is calculated with $pK^{H}_{H(dPEEA)} = 7.75$ (Table 1, entry 7) and the straight-line parameters given

 © 2003 Wiley-VCH Verlag GmbH & Co. KGaA, Weinheim

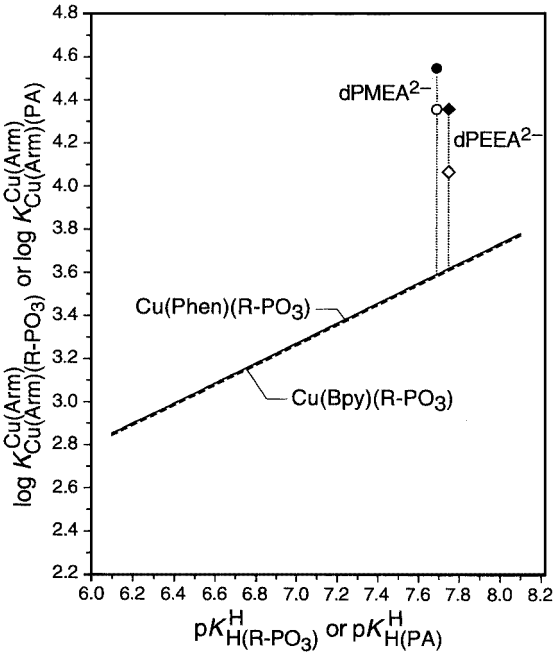

Figure 3. Evidence for an enhanced stability of the ternary Cu(Bpy)(dPEEA) (◇) and Cu(Phen)(dPEEA) (◆) as well as the Cu(Bpy)(dPMEA) (○) and Cu(Phen)(dPMEA) (●) complexes, based on the relationship between log $K^{Cu(Arm)}_{Cu(Arm)(R\text{-}PO_3)}$ or log $K^{Cu(Arm)}_{Cu(Arm)}$ and $pK^{H}_{H(R\text{-}PO_3)}$ or $pK^{H}_{H(PA)}$ in aqueous solution at $I = 0.1$ M ($NaNO_3$) and 25 °C. The plotted data corresponding to the $dPEEA^{2-}$ systems are from Tables 1 and 5 and those corresponding to $dPMEA^{2-}$ are from ref.[38] The two reference lines represent the log K versus pK_a relationship for the ternary Cu(Arm)($R\text{-}PO_3$) complexes [Equation (10)]; it should be emphasized that $R\text{-}PO_3^{2-}$ symbolizes here phosph(on)ate ligands with a group R unable to undergo any kind of hydrophobic, stacking or other type of interaction. The parameters for the straight-line equations are listed in ref.[61]

in refs.[51,61]: log $K^{Cu(Bpy)}_{Cu(Bpy)(dPEEA)op}$ = 3.61 ± 0.07 and log $K^{Cu(Phen)}_{Cu(Phen)(dPEEA)op.}$ = 3.62 ± 0.06. Application of these values together with the corresponding experimental results given in Table 5 (column 3) to Equation (11) leads to the log $\Delta_{Cu/Arm/dPEEA}$ values which quantify in an exact way the enhanced stability of the ternary Cu(Arm)(dPEEA) complexes. These values are listed in the third column of Table 6 (see below).

2.7 Evaluation of the Increased Stability of the Cu(Arm)(dPEEA) Complexes

It is clear[57] that the described enhanced complex stabilities (Table 6, column 3) must originate in additional interactions, i.e., beyond the coordination of $Cu(Arm)^{2+}$ to the phosphonate group. The ligand $dPEEA^{2-}$ offers only two such possibilities: The phosphonate-coordinated $Cu(Arm)^{2+}$ forms (i) a macrochelate with N7 of the adenine residue, as is the case with the binary Cu(dPEEA) complex (Section 2.4), or (ii) an intramolecular stack between the aromatic ring systems of Bpy or Phen and the adenine moiety. This latter type of interaction is known for many examples and can be very significant;[32,35−38,54,63] it is also evident from the results indicated in Section 2.5 for the monoprotonated $Cu(Arm)(H;dPEEA)^{+}$ species.

That the first of these two possible interactions is of no importance was demonstrated in detail recently for the $Cu(Arm)^{2+}$ systems with $dPMEA^{2-}$ [38] as well as for related analogues[36,54,61] and also for AMP^{2-} itself.[37] Hence, the enhanced complex stabilities may only be attributed to intramolecular stack formation; in fact, for Cu(Arm)(AMP) this was also proven to occur in the solid state by crystal structure analyses.[6b,64] Consequently, the Cu(Arm)(dPEEA) complexes occur in the two isomeric forms indicated in Equilibrium (3): In one, $Cu(Arm)^{2+}$ is only coordinated to the phosphonate group and this isomer is designated as $Cu(Arm)(dPEEA)_{op}$ as already indicated in Section 2.6; in the other form, designated as $Cu(Arm)(dPEEA)_{st}$, intramolecular stack formation occurs. A tentative structure of this latter isomer is shown in Figure 4. Consequently, the dimensionless equilibrium constant $K_{I/st}$ due to the intramolecular Equilibrium (3) is defined by Equation (18):

$$K_{I/st} = [Cu(Arm)(dPEEA)_{st}]/[Cu(Arm)(dPEEA)_{op}] \quad (18)$$

Values for $K_{I/st}$ as well as for the percentage of the stacked isomer, $Cu(Arm)(dPEEA)_{st}$, are calculated in analogy to Equations (13) and (14), respectively, and summarized in columns 4 and 5 of Table 6.

The results of Table 6 lead to the following conclusions: (i) Stack formation is always more pronounced in the Cu(Phen)(PA) systems, where PA^{2-} = $dPEEA^{2-}$,

Table 6. Extent of intramolecular stack formation in ternary Cu(Arm)(PA) complexes, where PA^{2-} = $dPEEA^{2-}$, $dPMEA^{2-}$ or AMP^{2-}, as calculated from stability constants determined via potentiometric pH titrations: Given are the stability enhancement log $\Delta_{Cu/Arm/PA}$ [Equation (11)], the intramolecular and dimensionless equilibrium constant $K_{I/st}$ [Equations (13), (18)], and the percentage [Equation (14)] of the stacked $Cu(Arm)(PA)_{st}$ species in aqueous solution at 25 °C and $I = 0.1$ M ($NaNO_3$)[a]

No.	Cu(Arm)(PA)	log $\Delta_{Cu/Arm/PA}$	$K_{I/st}$	%$Cu(Arm)(PA)_{st}$	Ref.
1a	Cu(Bpy)(dPEEA)	0.46 ± 0.10	1.88 ± 0.66	65 ± 8	[b]
1b	Cu(Phen)(dPEEA)	0.74 ± 0.15	4.50 ± 1.90	82 ± 6	[b]
2a	Cu(Bpy)(dPMEA)	0.78 ± 0.10	5.03 ± 1.39	83 ± 4	[29]
2b	Cu(Phen)(dPMEA)	0.96 ± 0.12	8.12 ± 2.52	89 ± 3	[29]
3a	Cu(Bpy)(AMP)	0.73 ± 0.08	4.37 ± 1.02	81 ± 4	[31]
3b	Cu(Phen)(AMP)	0.99 ± 0.08	8.77 ± 1.81	90 ± 2	[31]

[a] See footnote [a] of Table 2. [b] This work.

 © 2003 Wiley-VCH Verlag GmbH & Co. KGaA, Weinheim

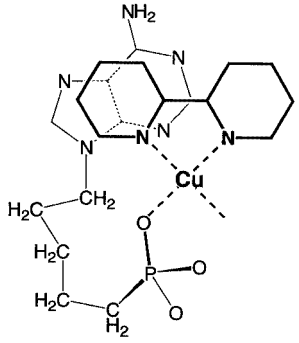

Figure 4. Tentative and simplified structure of a species with an intramolecular stack for Cu(Bpy)(dPEEA) in solution. The orientation of the aromatic rings may vary somewhat from one stacked species to the next; such a stacked complex in solution should not be considered as being rigid.

dPMEA^{2-} or AMP^{2-} (compare entries a with b). This result is understandable, since the overlap of the aromatic ring systems is expected to be more pronounced with the 3-ring system of Phen than with the 2-ring system of Bpy. (ii) The extent of stack formation for a given Arm is within the error limits clearly identical for dPMEA^{2-} and AMP^{2-} (entries 2, 3) and still similar if the Phen/dPEEA^{2-} system (entry 1b) is included in the comparisons (entries 2b, 3b). However, (iii) this is different if the Bpy systems (entries 1a, 2a, 3a) are compared; here the formation degree of Cu(Bpy)(dPEEA)$_{st}$ is clearly lower than the one for Cu(Bpy)(dPMEA) and Cu(Bpy)(AMP). Most likely the pentyl chain is too long to allow an optimal fit with one of the Bpy rings. Indeed, for C_6H_5-$(CH_2)_n$-COO^-/M^{2+}/Phen[63,65] and related systems[66] it has previously been shown that the $(CH_2)_n$ chain may become too long and reach then beyond the rings needed for the intramolecular interaction. In accord with this interpretation are the results for the Cu(Phen)(dPEEA) and Cu(Phen)(dPMEA) systems (entries 1b, 2b); Phen with its 3-ring system is less sensitive than the 2-ring Bpy with regard to the chain length, i.e., to an exchange of the butyl by a pentyl chain. Hence, as far as the stacking interaction in Cu(Arm)(PA) systems is concerned, dPMEA^{2-} mimics AMP^{2-} somewhat better than dPEEA^{2-}.

3. Conclusions

The coordinating properties of dPEEA^{2-} and dPMEA^{2-} do not differ dramatically. However, it is still interesting to note that in binary complexes of divalent 3d metal ions including Zn^{2+} and Cd^{2+}, dPEEA^{2-} resembles the parent nucleotide AMP^{2-} somewhat better than its chain-shortened analogue dPMEA^{2-} (Figure 1): In other words, macrochelate formation between the phosphonate-coordinated metal ion and N7 of the adenine moiety seems to be somewhat more favored in M(dPEEA) than in M(dPMEA) species. In fact, in a first approximation, the extent of macrochelate formation increases for a given M^{2+} within the series M(dPMEA) < M(dPEEA) < M(AMP), though, e.g., for Cu^{2+} and Cd^{2+} the extent is within the error limits identical for the dPEEA^{2-} and AMP^{2-} systems. However, the metal ion-binding properties of all three mentioned ligands differ significantly from those of the antivirally active PMEA^{2-} (see Figure 1); for all its M(PMEA) complexes an ether oxygen-M^{2+} interaction is of relevance which does not occur, of course, with its deoxa analogues or with AMP^{2-}.

In the mixed ligand Cu(Arm)(PA) complexes dPMEA^{2-} resembles its parent AMP^{2-} more closely than dPEEA^{2-}. This means, the extent of intramolecular stack formation is similar in the Cu(Arm)(dPMEA) and Cu(Arm)(AMP) systems and also more pronounced than in Cu(Arm)(dPEEA); this is especially true for Arm = Bpy. It seems that the pentyl chain is somewhat too long and does therefore not favor an ideal fit for the aromatic ring stacks as it appears to be the case with the butyl chain.

It has been suggested[14,15] that diphosphorylated PMEA^{2-}, i.e., PMEApp^{4-}, is initially an excellent substrate for DNA polymerases because of the facilitated formation of the M(P_α)-binding mode which leads then to the also facilitated formation of the reactive M(P_α)-M(P_β,P_γ) mode which is crucial for the transfer of a nucleotidyl unit in the polymerase reaction.[15] This M(P_α) binding is facilitated due to the M^{2+} interaction with the ether oxygen. At present no data are available on the metabolism of dPMEA or dPEEA but if it is assumed that dPMEA and dPEEA are transported to the cell and also diphosphorylated, like PMEA,[12,13] then it would become understandable why these two analogues lack antiviral activity. A facilitated M(P_α) binding (via the ether oxygen) is not possible[14] with dPMEApp^{4-} or dPEEApp^{4-} and thus the transfer of a nucleotidyl unit in the polymerase reaction[15] would also not be facilitated.

4. Experimental Section

4.1 Materials

Twofold protonated 9-(5-phosphonopentyl)adenine, i.e., H_2(dPEEA)$^{\pm}$, was synthesized as described below in Section 4.2 with 1,5-dibromopentane, triethyl phosphite, 1,8-diazabicyclo[1.3.0]undec-1-ene, bromotrimethylsilane and dimethylformamide, which were purchased from Sigma−Aldrich, Prague, Czech Republic.

All aqueous stock solutions for the potentiometric pH titrations were prepared by dissolving the various compounds in deionized, ultrapure (MILLI-Q185 PLUS; from Millipore S.A., 67120 Molsheim, France) CO_2-free water.

2,2′-Bipyridine and 1,10-phenanthroline monohydrate were from Merck AG, Darmstadt, FRG. All the other reagents were the same as used recently.[18]

4.2 Synthesis of 9-(5-Phosphonopentyl)adenine

This compound has been mentioned in the literature[67] in the context of enzyme-catalyzed deamination reactions but its synthesis has not been described and therefore it is given here.

The first step in the synthesis of 9-(5-phosphonopentyl)adenine [= 5-(adenin-9-yl)pentylphosphonic acid] was heating of a mixture of 1,5-dibromopentane (100 g, 0.43 mol) and triethyl phosphite (90 mL, 1.125 equiv.) for 2 days at 110 °C; the resulting ethyl bro-

 © 2003 Wiley-VCH Verlag GmbH & Co. KGaA, Weinheim

mide was distilled off. The portion volatile up to a maximum of 100 °C/2 kPa was removed. The residue, i.e. diethyl 5-bromopentylphosphonate, was utilized in the next step without further purification.

The mixture of adenine (20.0 g, 0.148 mol), 1,8-diazabicyclo[1.3.0]undec-1-ene (30 mL) and crude diethyl 5-bromopentylphosphonate (60 mL) in dimethylformamide (200 mL) was heated at 100 °C for 5 h and the solvent evaporated. The residue was extracted with hot chloroform (in total 500 mL) and the solvent evaporated to give by chromatography on a silica gel column (300 mL) in chloroform by extraction with chloroform-methanol mixtures oily diethyl 5-(adenin-9-yl)pentylphosphonate (yield: 11.6 g; 23%). This compound (34 mmol) in acetonitrile (100 mL) was stirred with bromotrimethylsilane (20 mL) till dissolution and left to stand overnight at ambient temperature. The mixture was evaporated in vacuo and the residue codistilled with toluene (2 × 25 mL). Water (150 mL) was added and, after 20 min, the mixture was basified with conc. aqueous ammonia and the solvents evaporated. The residue in minimum water was applied to a column of Dowex 50 × 8 (H^+-form) (250 mL), the column was washed with water to the loss of acidity and UV-absorption of the eluate (monitored at 254 nm). Subsequent elution of the column with diluted (1:10) aqueous ammonia gave a UV-absorbing eluate which was evaporated to dryness in vacuo. This residue in minimum water was basified with ammonia to pH 10 and applied onto a column of Dowex 1 × 2 (acetate form) prewashed with water (200 mL); the column was eluted with water (1 L) and the resin was then stirred batchwise with 1 M formic acid (500 mL), filtered off and washed with boiling water (four 500 mL portions). The combined eluates were evaporated in vacuo, the residue codistilled with water (five 50 mL portions) and crystallized from water. Yield, 5.1 g (52.5%), m.p. 330 °C. $C_{10}H_{16}N_5O_3P$ (285.2): calcd. C 42.11, H 5.65, N 25.55, P 10.86; found C 42.25, H 5.41, N 25.28, P 11.03. ^{1}H NMR (in D_2O, 500 MHz): δ = 8.28 and 8.21 (2 s, 1 H each, H2 and H8 of Ade), 4.27 (t, J = 6.9 Hz, 2 H, H1′), 1.90 (m, 2 H), 1.53 (m, 4 H), 1.36 (m, 2 H, H2′, -3′, -4′, -5′) ppm. ^{13}C NMR (in D_2O, 125.7 MHz): saturated solution − low concentration allowed the detection of proton-bearing carbons only: δ = 154.09 (s, C2), 145.90 (s, C8), 46.92 (s, C1′), 31.63 (s, C2′), 29.98 (d, $J_{C,P}$ = 5.4 Hz, C3′), 35.54 (d, $J_{C,P}$ = 4.4 Hz, C4′), 30.58 (d, $J_{C,P}$ = 121.1 Hz, C5′) ppm.

4.3 Potentiometric pH Titrations. Determination of Equilibrium Constants

The equipment for the titrations,[18] the buffers used for calibration[18] and the evaluation procedures including the computers were the same as before.[43]

The acidity constants $K^H_{H_2(dPEEA)}$ and $K^H_{H(dPEEA)}$ of $H_2(dPEEA)^{\pm}$, where one proton is at the base moiety and the other at the phosphonate group, were determined by titrating 50 mL of aqueous 0.9 m M HNO_3 (25 °C; I = 0.1 M, $NaNO_3$) in the presence and absence of 0.3 mM $dPEEA^{2-}$ under N_2 with 1.6 mL of 0.03 M NaOH. The differences in NaOH consumption between such a pair of titrations were used for the calculations. These conditions correspond to those used recently for the dPMEA system;[18] it needs to be emphasized that at a ligand concentration[22] of 3×10^{-4} M the well-known[32] self-association (via π-stacking) of purines is of no significance. The results for the acidity constants of $H_2(dPEEA)^{\pm}$ are the averages of 19 pairs of independent titrations.

The stability constants $K^M_{M(H;dPEEA)}$ and $K^M_{M(dPEEA)}$ of $M(H;dPEEA)^+$ and M(dPEEA) were determined under the same conditions as the acidity constants, but $NaNO_3$ was partly or fully replaced by $M(NO_3)_2$ (25 °C; I = 0.1 M). The conditions correspond to those given recently for the M^{2+}/dPMEA systems,[18] but the M^{2+}/dPEEA ratios were 111:1 (Mg^{2+}, Ca^{2+}, Sr^{2+}, Ba^{2+}, Mn^{2+}), 55.6:1 (Co^{2+}, Ni^{2+}), 53.3:1 (Mg^{2+}, Ca^{2+}, Sr^{2+}, Ba^{2+}), 50:1 (Mn^{2+}), 26.9:1 (Cd^{2+}), 25:1 (Co^{2+}, Ni^{2+}), 13.4:1 (Cd^{2+}), 12.3:1 (Zn^{2+}), 10.6:1 (Cu^{2+}, $Cu(Bpy)^{2+}$, $Cu(Phen)^{2+}$), 5.3:1 (Cu^{2+}, $Cu(Bpy)^{2+}$, $Cu(Phen)^{2+}$) and 5:1 (Zn^{2+}). Since the stability of the $Cu(Arm)^{2+}$ complexes is high,[60] the formation of these species is practically complete under the experimental conditions (titrations of solutions with HNO_3 and HNO_3 + Cu^{2+}/Arm were identical in the lower pH range) and therefore, the evaluation of the titration data of the ternary systems could be done in the way described for the binary ones.[28]

The evaluation of the Zn^{2+}/dPEEA systems was significantly hampered by precipitation, and therefore the pH range accessible for the calculations of the stability constants was severely restricted. In fact, for Zn(dPEEA) only a formation degree of about 2% was reached; hence, the value for Zn(dPEEA) must be considered as an estimate.

However, several of the constants given for the $M(H;dPEEA)^+$ complexes must also be considered as estimates (see Table in Section 2.2), since the formation degree of these species reached only about 3%, in the maximum 18% was reached; for the ternary $Cu(Arm)(H;dPEEA)^+$ complexes a formation degree of nearly 25% was achieved.

The individual results for the stability constants showed no dependence on pH or on the excess of metal ion concentration used. The results are in each case the average of at least five independent pairs of titration curves.

Acknowledgments

The competent technical assistance of Mrs. Rita Baumbusch and Mrs. Astrid Sigel in the preparation of this manuscript is gratefully acknowledged. Thanks are also due to Dr. M. Buděšinský (IOCB) for measurement and interpretation of NMR spectra. This study was supported by the Swiss National Science Foundation (H.S.) and the Programme of Targeted Projects (S4055109) of the Academy of Sciences of the Czech Republic (A.H.) as well as within the COST D20 programme by the Swiss Federal Office for Education and Science (H.S.) and the Ministry of Education of the Czech Republic (D.20.002; A.H.). This study is also part of a research project (No. 4055905) of the Institute of Organic Chemistry and Biochemistry (IOCB) in Prague.

[1] *Fundamental Virology* (Eds.: B. N. Fields, D. M. Knipe, P. M. Howley), 3rd Edition, Lippincott-Raven publishers, Philadelphia, New York, **1996**, pp. 1−1339.
[2] [2a] M. Popovic, M. G. Sarngadharan, E. Read, R. C. Gallo, *Science* **1984**, *224*, 497−500. [2b] R. C. Gallo, S. Z. Salahuddin, M. Popovic, G. M. Shearer, M. Kaplan, B. F. Haynes, T. J. Palker, R. Redfield, J. Oleske, B. Safai, G. White, P. Foster, P. D. Markham, *Science* **1984**, *224*, 500−503.
[3] E. De Clercq, *Collect. Czech. Chem. Commun.* **1998**, *63*, 449−479.
[4] A. Holý, J. Günter, H. Dvořáková, M. Masojídková, G. Andrei, R. Snoeck, J. Balzarini, E. De Clercq, *J. Med. Chem.* **1999**, *42*, 2064−2086.
[5] R. Tribolet, H. Sigel, *Eur. J. Biochem.* **1987**, *163*, 353−363.
[6] [6a] R. B. Martin, Y. H. Mariam, *Met. Ions Biol. Syst.* **1979**, *8*, 57−124. [6b] K. Aoki, *Met. Ions Biol. Syst.* **1996**, *32*, 91−134.
[7] Abbreviations and definitions: For AMP^{2-}, $dPEEA^{2-}$, $dPMEA^{2-}$ and $PMEA^{2-}$ see Figure 1. Arm, heteroaromatic nitrogen base like Bpy or Phen; Bpy, 2,2′-bipyridine; *I*, ionic

 © 2003 Wiley-VCH Verlag GmbH & Co. KGaA, Weinheim

strength of a solution; M^{2+}, general divalent metal ion also including in part $Cu(Arm)^{2+}$; 9MeAde, 9-methyladenine; PA^{2-} = $dPEEA^{2-}$ or any other twofold negatively charged nucleotide or nucleotide analogue; Phen, 1,10-phenanthroline; R-PO_3^{2-}, simple phosphate monoester or phosphonate ligand with R representing a non-interacting residue. Species written without a charge either do not carry one or represent the species in general (i.e. independent of their protonation degree); which of the two possibilities applies is always clear from the context. In formulas like $M(H;dPEEA)^+$, H^+ and $dPEEA^{2-}$ are separated by a semicolon to facilitate reading, yet they appear within the same parenthesis to indicate that the proton is at the ligand without defining its location (see Sections 2.2 and 2.5). The notation $(H{\cdot}dPEEA)^-$ indicates that H^+ is at the phosphonate group (see Section 2.5).

[8] L. Naesens, R. Snoeck, G. Andrei, J. Balzarini, J. Neyts, E. De Clercq, *Antiviral Chem. Chemother.* **1997**, *8*, 1−23.

[9] [9a] E. De Clercq, *Collect. Czech. Chem. Commun.* **1998**, *63*, 480−506. [9b] D. Colledge, G. Civitico, S. Locarnini, T. Shaw, *Antimicrob. Agents Chemother.* **2000**, *44*, 551−560.

[10] *Chemische Rundschau* (CH-4501 Solothurn, Switzerland), No. 19; Oct. 8, **2002**; p. 68.

[11] A. Holý, *Il Farmaco* **1991**, *46 (Suppl.* 1), 141−146.

[12] A. Merta, I. Votruba, I. Rosenberg, M. Otmar, H. Hřebabecký, R. Bernaerts, A. Holý, *Antiviral Res.* **1990**, *13*, 209−218.

[13] [13a] P. Kramata, I. Votruba, B. Otová, A. Holy, *Mol. Pharmacol.* **1996**, *49*, 1005−1011. [13b] G. Birkuš, I. Votruba, A. Holý, B. Otová, *Biochem. Pharmacol.* **1999**, *58*, 487−492.

[14] H. Sigel, B. Song, C. A. Blindauer, L. E. Kapinos, F. Gregáň, N. Prónayová, *Chem. Commun.* **1999**, 743−744.

[15] H. Sigel, *Pure Appl. Chem.* **1999**, *71*, 1727−1740.

[16] A. Holý, E. De Clercq, I. Votruba, *ACS Symp. Ser.* **1989**, *401*, 51−71.

[17] A. Holý, I. Votruba, A. Merta, J. Černý, J. Veselý, J. Vlach, K. Šedivá, I. Rosenberg, M. Otmar, H. Hřebabecký, M. Trávníček, V. Vonka, R. Snoeck, E. De Clercq, *Antiviral Res.* **1990**, *13*, 295−311.

[18] R. B. Gómez-Coca, L. E. Kapinos, A. Holý, R. A. Vilaplana, F. González-Vílchez, H. Sigel, *J. Chem. Soc., Dalton Trans.* **2000**, 2077−2084.

[19] [19a] H. Sigel, *Coord. Chem. Rev.* **1995**, *144*, 287−319. [19b] H. Sigel, *J. Indian Chem. Soc.* **1997**, *74*, 261−271 (P. Ray Award Lecture).

[20] C. A. Blindauer, A. H. Emwas, A. Holý, H. Dvořáková, E. Sletten, H. Sigel, *Chem. Eur. J.* **1997**, *3*, 1526−1536.

[21] C. A. Blindauer, A. Holý, H. Dvořáková, H. Sigel, *J. Biol. Inorg. Chem.* **1998**, *3*, 423−433.

[22] H. Sigel, S. S. Massoud, N. A. Corfù, *J. Am. Chem. Soc.* **1994**, *116*, 2958−2971.

[23] E. M. Bianchi, S. A. A. Sajadi, B. Song, H. Sigel, *Chem. Eur. J.* **2003**, *9*, 881−892.

[24] H. Sigel, *Chem. Soc. Rev.* **1993**, *22*, 255−267.

[25] H. Sigel, B. Song, *Met. Ions Biol. Syst.* **1996**, *32*, 135−205.

[26] R. K. O. Sigel, B. Song, H. Sigel, *J. Am. Chem. Soc.* **1997**, *119*, 744−755.

[27] C. A. Blindauer, A. Holý, H. Sigel, *Collect. Czech. Chem. Commun.* **1999**, *64*, 613−632.

[28] C. A. Blindauer, T. I. Sjåstad, A. Holý, E. Sletten, H. Sigel, *J. Chem. Soc., Dalton Trans.* **1999**, 3661−3671.

[29] G. Kampf, M. S. Lüth, L. E. Kapinos, J. Müller, A. Holý, B. Lippert, H. Sigel, *Chem. Eur. J.* **2001**, *7*, 1899−1908.

[30] C. F. Moreno-Luque, R. Griesser, J. Ochocki, H. Sigel, *Z. Anorg. Allg. Chem.* **2001**, *627*, 1882−1887.

[31] A. Holý, I. Rosenberg, H. Dvoraková, *Collect. Czech. Chem. Commun.* **1990**, *55*, 809−818.

[32] O. Yamauchi, A. Odani, H. Masuda, H. Sigel, *Met. Ions Biol. Syst.* **1996**, *32*, 207−270.

[33] O. Yamauchi, A. Odani, S. Hirota, *Bull. Chem. Soc. Jpn.* **2001**, *74*, 1525−1545.

[34] [34a] H. Suezawa, T. Yoshida, Y. Umezawa, S. Tsuboyama, M. Nishio, *Eur. J. Inorg. Chem.* **2002**, 3148−3155. [34b] L.-n. Ji, X. Le, *Chin. Sci. Bull.* **2002**, *47*, 1−9.

[35] H. Sigel, *Pure Appl. Chem.* **1989**, *61*, 923−932.

[36] R. B. Gómez-Coca, L. E. Kapinos, A. Holý, R. A. Vilaplana, F. González-Vílchez, H. Sigel, *Metal Based Drugs* **2000**, *7*, 313−324.

[37] S. S. Massoud, R. Tribolet, H. Sigel, *Eur. J. Biochem.* **1990**, *187*, 387−393.

[38] R. B. Gómez-Coca, L. E. Kapinos, A. Holý, R. A. Vilaplana, F. González-Vílchez, H. Sigel, *J. Inorg. Biochem.* **2001**, *84*, 39−46.

[39] C. A. Blindauer, A. Holý, H. Dvořáková, H. Sigel, *J. Chem. Soc., Perkin Trans. 2* **1997**, 2353−2363.

[40] R. L. Benoit, M. Fréchette, *Can. J. Chem.* **1984**, *62*, 995−1000.

[41] G. Kampf, L. E. Kapinos, R. Griesser, B. Lippert, H. Sigel, *J. Chem. Soc., Perkin Trans. 2* **2002**, 1320−1327.

[42] C. Meiser, B. Song, E. Freisinger, M. Peilert, H. Sigel, B. Lippert, *Chem. Eur. J.* **1997**, *3*, 388−398.

[43] H. Sigel, C. P. Da Costa, B. Song, P. Carloni, F. Gregáň, *J. Am. Chem. Soc.* **1999**, *121*, 6248−6257.

[44] A. Saha, N. Saha, L.-n. Ji, J. Zhao, F. Gregáň, S. A. A. Sajadi, B. Song, H. Sigel, *J. Biol. Inorg. Chem.* **1996**, *1*, 231−238.

[45] H. Sigel, D. Chen, N. A. Corfù, F. Gregáň, A. Holý, M. Strašák, *Helv. Chim. Acta* **1992**, *75*, 2634−2656.

[46] H. Sigel, A. D. Zuberbühler, O. Yamauchi, *Anal. Chim. Acta* **1991**, *255*, 63−72.

[47] H. Sigel, *Eur. J. Biochem.* **1968**, *3*, 530−537.

[48] [48a] H. Sigel, D. B. McCormick, *Acc. Chem. Res.* **1970**, *3*, 201−208. [48b] H. Sigel, K. Becker, D. B. McCormick, *Biochim. Biophys. Acta* **1967**, *148*, 655−664.

[49] S. A. A. Sajadi, B. Song, F. Gregáň, H. Sigel, *Inorg. Chem.* **1999**, *38*, 439−448.

[50] [50a] H. Irving, R. J. P. Williams, *Nature (London)* **1948**, *162*, 746−747. [50b] H. Irving, R. J. P. Williams, *J. Chem. Soc.* **1953**, 3192−3210.

[51] H. Sigel, L. E. Kapinos, *Coord. Chem. Rev.* **2000**, *200−202*, 563−594.

[52] [52a] H. Sigel, B. Lippert, *Pure Appl. Chem.* **1998**, *70*, 845−854. [52b] B. Song, J. Zhao, R. Griesser, C. Meiser, H. Sigel, B. Lippert, *Chem. Eur. J.* **1999**, *5*, 2374−2387.

[53] R. Griesser, G. Kampf, L. E. Kapinos, S. Komeda, B. Lippert, J. Reedijk, H. Sigel, *Inorg. Chem.* **2003**, *42*, 32−41.

[54] M. S. Lüth, L. E. Kapinos, B. Song, B. Lippert, H. Sigel, *J. Chem. Soc., Dalton Trans.* **1999**, 357−365.

[55] H. Sigel, N. A. Corfù, L.-n. Ji, R. B. Martin, *Comments Inorg. Chem.* **1992**, *13*, 35−59.

[56] R. B. Martin, *Met. Ions Biol. Syst.* **1996**, *32*, 61−89.

[57] R. B. Martin, H. Sigel, *Comments Inorg. Chem.* **1988**, *6*, 285−314.

[58] S. S. Massoud, H. Sigel, *Inorg. Chem.* **1988**, *27*, 1447−1453.

[59] H. Sigel, S. S. Massoud, R. Tribolet, *J. Am. Chem. Soc.* **1988**, *110*, 6857−6865.

[60] [60a] H. Irving, D. H. Mellor, *J. Chem. Soc.* **1962**, 5222−5237. [60b] G. Anderegg, *Helv. Chim. Acta* **1963**, *46*, 2397−2410.

[61] D. Chen, M. Bastian, F. Gregáň, A. Holý, H. Sigel, *J. Chem. Soc., Dalton Trans.* **1993**, 1537−1546.

[62] H. Sigel, *Angew. Chem.* **1975**, *87*, 391−400; *Angew. Chem. Int. Ed. Engl.* **1975**, *14*, 394−402.

[63] R. Malini-Balakrishnan, K. H. Scheller, U. K. Häring, R. Tribolet, H. Sigel, *Inorg. Chem.* **1985**, *24*, 2067−2076.

[64] K. Aoki, *J. Am. Chem. Soc.* **1978**, *100*, 7106−7108.

[65] H. Sigel, R. Malini-Balakrishnan, U. K. Häring, *J. Am. Chem. Soc.* **1985**, *107*, 5137−5148.

[66] G. Liang, R. Tribolet, H. Sigel, *Inorg. Chem.* **1988**, *27*, 2877−2887.

[67] A. L. Margolin, D. R. Borcherding, D. Wolf-Kugel, N. Margolin, *J. Org. Chem.* **1994**, *59*, 7214−7218.

Received February 19, 2003

 © 2003 Wiley-VCH Verlag GmbH & Co. KGaA, Weinheim

Layered $[BaM(C_3H_2O_4)_2(H_2O)_4]$ (M = Fe or Co) Complexes − Spectroscopic, Magnetic and Thermal Study

Izaskun Gil de Muro,[a] Luis Lezama,[a] Maite Insausti,[a] and Teófilo Rojo*[a]

Keywords: Magnetic properties / Barium / Iron / Cobalt / Thermochemistry

Complexes with formula $[BaM(C_3H_2O_4)_2(H_2O)_4]$, where M = Fe or Co, were synthesised and characterised. These two types of complexes are isostructural and crystallise in the *Pccn* space group. Their structure consists of two-dimensional networks of octahedral MO_6 polyhedra in which the transition metal ions are coordinated by bridging malonate ligands, through the O-C-O atoms. These M-malonate units are extended along the crystallographic [101] plane. Spectroscopic data are consistent with the cations being in a high-spin octahedral symmetry. The two types of compounds exhibit 2D antiferromagnetic interactions as well as weak ferromagnetism below the Néel temperature, as a result of an intralayer misalignment of the spins. Thermal treatment of the metallo-organic precursors gave rise to $BaMO_{3-y}$ oxides at lower temperatures and reaction times than those found in the literature using the ceramic method.
(© Wiley-VCH Verlag GmbH & Co. KGaA, 69451 Weinheim, Germany, 2003).

Introduction

The chemistry of heteronuclear complexes involving bridging carboxylate ligands has been exhaustively investigated using a wide variety of physical techniques such as electronic spectroscopy, susceptibility measurements, EPR spectroscopy,... with the aim of understanding the structural and chemical factors that govern the exchange coupling between paramagnetic centres.

The malonate ligand, with two neighbouring carboxylate groups, is a very flexible ligand which can adopt a monodentate mode, various bischelating coordination modes and different carboxylate bridging modes (*syn-syn, syn-anti,* and *anti-anti*).[1] It is a useful tool for connecting different metal ions and transmitting different magnetic interactions. In this way, ferromagnetically[2] or antiferromagnetically[3] coupled dimers, alternating chains,[4,5] polymeric trinuclear antiferromagnetic complexes[6,7] and two-dimensional ferromagnetic and antiferromagnetic compounds[8,9] have been obtained and studied.

On the other hand, these complexes can be used as an alternative to the ceramic method in the synthesis of mixed oxides.[10,11] In this sense, several studies with different metallo-organic precursors, employing carboxylate ligands such as edta,[12] oxalate[13] and tartrate,[14] or nitrite[15] have been carried out, and more recently using the malonate ligand.[8,16−18]

Malonate complexes such as $[AM(C_3H_2O_4)_2(H_2O)_4]$, where A is Sr or Ba and M is Mn or Cu, showed interesting spectroscopic and magnetic properties. Furthermore, their usefulness as precursors of mixed oxides was proved, and homogeneous oxides with small particles were obtained by thermal treatment of $[AM(C_3H_2O_4)_2(H_2O)_4]$.[8] In this paper we describe the synthesis and the spectroscopic and magnetic properties of the $[BaM(C_3H_2O_4)_2(H_2O)_4]$ (M = Fe or Co) compounds, together with their thermal study. These complexes will be abbreviated as BaFe and BaCo.

Results and Discussion

Crystallographic Study

Powder X-ray diffraction patterns of the microcrystalline products were recorded. Indexation of the diffraction profile and refinement of the cell parameters were made by FULLPROF (pattern-matching analysis)[19] on the basis of the space group *Pccn* and the cell parameters found for a single crystal of $[SrCu(C_3H_2O_4)_2(H_2O)_4]$, as published previously[8] (see Figure 1). The obtained crystallographic data for the $[BaM(C_3H_2O_4)_2(H_2O)_4]$ (M = Fe or Co) complexes are given in Table 1. The variation of the cell volume is in good agreement with the corresponding cation size. Taking these results into account, we have considered the two phases to be isostructural to the already characterised phase SrCu.[8] The structure consists of two-dimensional networks of transition metal ions coordinated by bridging malonate ligands. These M-malonate units are infinitely extended along the crystallographic [101] plane (see Figure 2). The metallic centres are octahedrally coordinated, with two oxygen atoms from two bidentate malonate anions at basal sites and two oxygen atoms from two malonate anions at apical sites. These bridging arrangements by carboxylate

[a] Dpto. Química Inorgánica, Facultad de Ciencias. UPV/EHU, Apdo. 644, 48080 Bilbao, Spain
Fax: (internat.) +34-94/464-8500
E-mail: qiproapt@lg.ehu.es

 © 2003 Wiley-VCH Verlag GmbH & Co. KGaA, Weinheim **DOI: 10.1002/ejic.200300077**

groups form infinite sheets where the shortest M···M distances occur through the O-C-O atoms. The alkaline earth cations are located between the M-malonate layers and are coordinated to four oxygens of different malonates and to two lattice water molecules, forming a distorted antiprism.

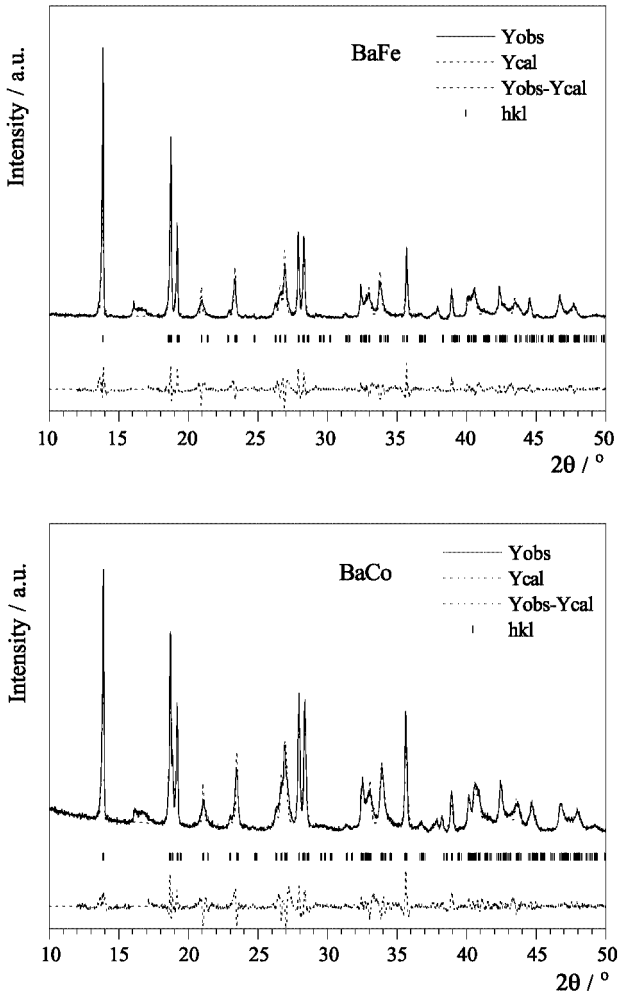

Figure 1. Observed, calculated and difference XRD profiles for the BaFe and BaCo phases

Table 1. Crystallographic data for the $[BaM(C_3H_2O_4)_2(H_2O)_4]$ (M = Fe, Co) compounds

	BaFe	BaCo	SrCu[a]
Molecular mass	469.28	472.36	427.27
Crystal system	Orthorhombic	Orthorhombic	Orthorhombic
Space group	Pccn	Pccn	Pccn
a (Å)	6.795(2)	6.782(1)	6.719(2)
b (Å)	18.948(4)	18.976(3)	18.513(7)
c (Å)	9.492(3)	9.407(2)	9.266(4)
V (Å^3)	1222.1	1210.0	1152.6

[a] Data calculated from a single crystal study.[8]

Thermal Study

The thermal decomposition steps of the compounds were obtained from the TG curves shown in Figure 3. The thermogravimetric data are summarised in Table 2. Decomposition arises from three consecutive processes: dehydration, ligand pyrolysis and inorganic residue formation.

The first process takes places in the 75−100 °C temperature range and corresponds to the loss of four water molecules. This process occurs in only one step, suggesting that all the water molecules are similar. This was also deduced from the crystallographic data of the SrCu compound. No significant differences between the treatments in air and nitrogen atmospheres were observed, except for slight displacements in the decomposition-temperature ranges.

The second stage involves the decarboxylation of the ligand, and takes place in the 250−450 °C temperature range. The following reaction schemes are the most plausible way of describing the decomposition process:$MM'L_2$ (s) → MCO_3 (s) + $M'CO_3$ (s) + R (g) (a)$MM'L_2$ (s) → MO (s) + $M'CO_3$ (s) + R (g) (b)$MM'L_2$ (s) → MO (s) + $M'O$ (s) + R (g) (c)

The main factor controlling the pyrolysis process is the nature of the cation coordinated to the ligand[20] and, depending on the stability of the metal carbonates, reactions *(a)*, *(b)* or *(c)* can occur. In our case, as alkaline-earth metal carbonates are stable, the ligand pyrolysis can be described by the second reaction. The weight loss is in good accordance with the decarboxylation of the malonate ligand to yield $BaCO_3$ and the corresponding transition metal oxide. The oxide obtained can vary depending on the applied atmosphere. Therefore, we propose that the Fe_2O_3 and Co_3O_4 oxides are formed in air while the Fe_2O_3 and CoO oxides are obtained under a nitrogen atmosphere.

Finally, a gradual mass loss is observed at temperatures above 600 °C, when carbonate decomposes and mixed oxides are formed. At this stage, the applied atmosphere plays an important role; either complete decomposition under nitrogen is not reached or more reduced mixed oxides are obtained. In fact the inorganic residues analysed by X-ray diffraction indicated the presence of different $BaFeO_{3-y}$ and $BaCoO_{3-y}$ mixed oxides.

Following this study, and in order to obtain pure phases of mixed oxides, several thermal treatments in tubular furnaces were carried out. After firing the BaFe and BaCo malonate precursors at 400 °C, investigations at higher temperatures and different atmospheres were performed for each case. The resulting products were characterised at each stage by X-ray powder diffraction (see Figure 4). The thermal decomposition of the $[BaFe(C_3H_2O_4)_2(H_2O)_4]$ precursor was carried out under an oxygen atmosphere at 800 °C to yield the non-stoichiometric oxide $BaFeO_{3-y}$.[21] In the case of the barium cobalt metallo-organic precursor, a treatment at 700 °C in air was needed in order to obtain the non-stoichiometric $BaCoO_{3-y}$ as a pure phase.[22]

Spectroscopic Properties

Infrared Spectroscopy

The IR spectra of the $[BaM(C_3H_2O_4)_2(H_2O)_4]$ (M = Fe or Co) compounds are very similar. Broad bands observed

 © 2003 Wiley-VCH Verlag GmbH & Co. KGaA, Weinheim

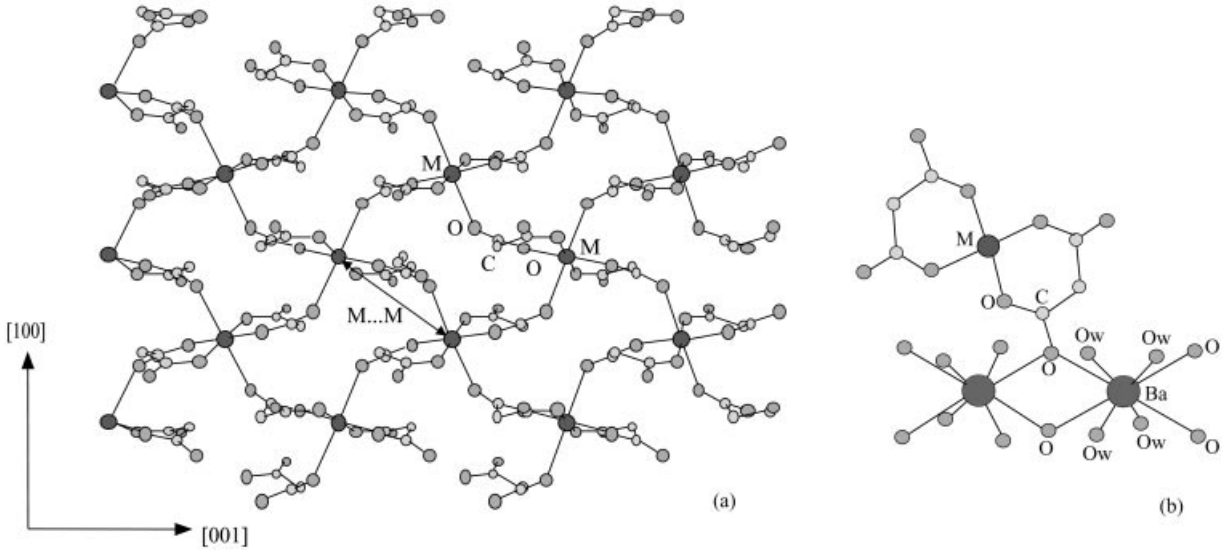

Figure 2. (a) Two-dimensional network of transition metal polyhedra and (b) alkaline earth centre and junction to transition metal polyhedra in $[AM(C_3H_2O_4)_2(H_2O)_4]$

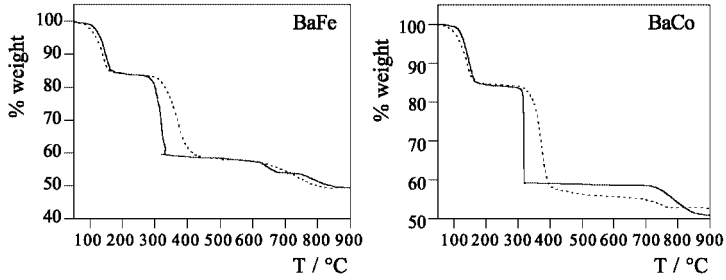

Figure 3. TG curves of the BaFe and BaCo complexes, under air (– –) and nitrogen (···)

Table 2. Thermogravimetric data of the $[BaM(C_3H_2O_4)_2(H_2O)_4]$ (M = Fe, Co) precursors

Stage			*T* (°C)	% weight[a]	Products
Dehydration	BaFe	air	100–180	84.5 (84.4)	$[BaFe(C_3H_2O_4)_2]$
		N_2	70–180	85.0 (84.4)	$[BaFe(C_3H_2O_4)_2]$
	BaCo	air	95–190	85.0 (84.7)	$[BaCo(C_3H_2O_4)_2]$
		N_2	75–175	85.5 (84.7)	$[BaCo(C_3H_2O_4)_2]$
Ligand pyrolysis	BaFe	air	275–340	59.0 (59.1)	$BaCO_3 + Fe_2O_3$
		N_2	290–450	58.8 (59.1)	$BaCO_3 + Fe_2O_3$
	BaCo	air	300–320	59.0 (58.8)	$BaCO_3 + Co_3O_4$
		N_2	310–420	57.0 (57.6)	$BaCO_3 + CoO$
Inorganic residue formation	BaFe	air	600–700, 730-	53.5 (51.4)	$BaFeO_3$
		N_2	635–865	–	$BaCO_3 + Ba_2Fe_2O_5$
	BaCo	air	685-	–	$BaCoO_3$
		N_2	690-	–	$BaCO_3 + Co_2O_3$

[a] Theoretical values in brackets.

in the 3300–3500 cm^{-1} region, can be assigned to the stretching vibration, ν(O-H), of the hydroxyl groups in the water molecules. The next group of bands appearing at around 2900 cm^{-1} corresponds to the stretching vibration, ν(C-H), of the malonate ligands. The band observed at 1730 cm^{-1} for the malonic acid is shifted in the titled compounds to 1600 cm^{-1}. This fact is indicative of the coordination of the carboxylate groups to the metal ions. This band appears together with the antisymmetric $\nu_a(OCO^-)$ vibration, whereas the band corresponding to the symmetric $\nu_s(OCO^-)$ vibration is localised at 1370 cm^{-1}. Taking the relative position of the antisymmetric $\nu_a(OCO^-)$ and symmetric $\nu_s(OCO^-)$ vibration bands into account, we can conclude that the bonding between the metal and the ligand gives rise to a chelate.[23] This observation is supported by the crystal data obtained from the SrCu compound. Finally, the bending vibration corresponding to the δ(C=O) group is observed at around 1300 cm^{-1}.

 © 2003 Wiley-VCH Verlag GmbH & Co. KGaA, Weinheim

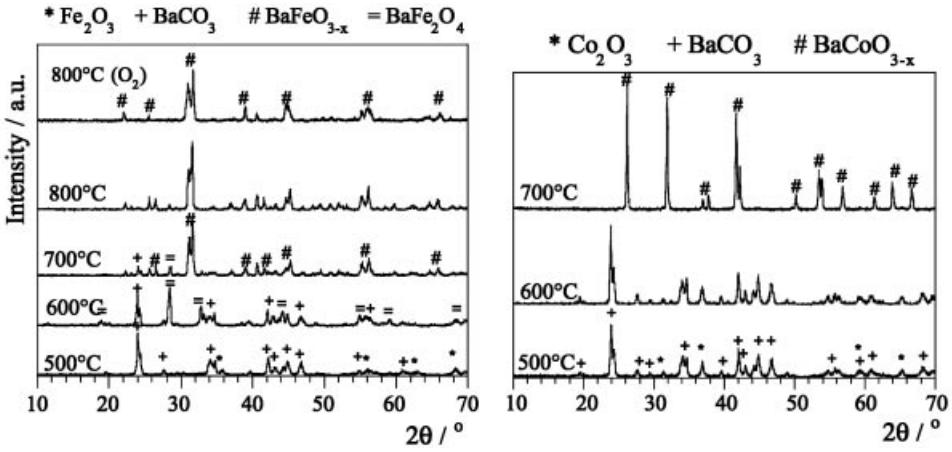

Figure 4. XRD patterns of the phases obtained from the thermal treatment of the BaFe and BaCo precursors

Diffuse Reflectance Spectroscopy

The reflectance spectra of the BaFe and BaCo complexes were recorded at room temperature in the 5000−45000 cm^{-1} range. For the iron phase, a single band appears which corresponds to the ${}^5E_g \leftarrow {}^5T_{2g}$ transition and is characteristic of a high-spin d^6 configuration in octahedral coordination. From the position of this band, the Dq parameter was calculated to be 1150 cm^{-1}, in good agreement with the usual values found for octahedrally coordinated iron(II). The spectrum of the BaCo compound shows three bands: at (ν_1) 8300, (ν_2) 15500 and (ν_3) 20600 cm^{-1}, which were assigned to the following three allowed transitions: ${}^4T_{2g} \leftarrow {}^4T_{1g}\ (F)$, ${}^4A_{2g} \leftarrow {}^4T_{1g}\ (F)$ and ${}^4T_{1g}\ (P) \leftarrow {}^4T_{1g}\ (F)$, respectively. By considering an octahedral model, the values of Dq (940) and B (753 cm^{-1}) were calculated from the ν_1 and ν_3 transitions. These values agree with those obtained for cobalt(II) compounds in an octahedral geometry.[24]

Magnetic Properties

Magnetic susceptibility measurements of powdered samples of $[BaM(C_3H_2O_4)_2(H_2O)_4]$ (where M = Fe or Co) were carried out in the 1.8−300 K temperature range, with applied magnetic fields of 1 and 0.1 kG. The χ_m and $\chi_m T$ vs. T curves of both compounds are shown in Figure 5, together with those of BaMn, given for comparison. All the calculated magnetic data are summarised in Table 3.

The μ_{eff} values measured at room temperature are 5.23 and 4.96 μ_B, for the BaFe and BaCo complexes respectively, and correspond to high-spin states for both metallic cations. In both cases, the $\chi_m T$ data decrease with decreasing temperature, reaching a minimum value at about 15 K. Then, the curves suddenly increase and at lower temperatures decrease again, reaching a maximum in $\chi_m T$ at around 12 K.

The χ_m^{-1} vs. T curves follow Curie−Weiss behaviour above 20 K, the Weiss constant, θ, being negative (−19.33 and −48.94 K), and the Curie constant, C_m, being 3.636 and 3.59 $cm^3 \cdot K \cdot mol^{-1}$ for the iron and cobalt compounds, respectively. The high value of θ found for the cobalt complex can be attributed to the spin-orbit coupling effect.

The initial progressive decrease of the $\chi_m T$ data until 15 K, together with the negative values of θ, are indicative of the presence of antiferromagnetic interactions. Considering the structural features of these compounds, the high-temperature susceptibility data were fitted to a two-dimensional Heisenberg antiferromagnetic model, employing the expansion series given by Rushbrooke and Wood.[25] Equation (1), (2) and (3) were deduced by taking into account the S = 5/2, 2 and 3/2 values for the Mn^{II}, Fe^{II} and Co^{II}, respectively, and are based on the spin Hamiltonian $H = -2J \Sigma_{<i,\ j>} S_i S_j$:

$$\chi_m = 2.91\ (Ng^2\beta^2)/(kT)\ [1 + 23.33x + 147.78x^2 + 405.48x^3 + 8171.3x^4 + 64968x^5 + 15811x^6]^{-1} \quad (1)$$

$$\chi_m = 2.00\ (Ng^2\beta^2)/(kT)\ [1 + 16x + 72x^2 + 195.067x^3 + 1781.87x^4 + 10301.4x^5 + 14736.4x^6]^{-1} \quad (2)$$

$$\chi_m = 1.25\ (Ng^2\beta^2)/(kT)\ [1 + 10x + 30x^2 + 42.6667x^3 + 262.917x^4 + 1043.85x^5 + 790.112x^6]^{-1} \quad (3)$$

where $x = J/kT$.

The BaMn susceptibility data gave the following values: g = 1.99 and J/k = −0.59 K,[8] indicating the presence of weak antiferromagnetic interactions. The best fit found for the iron and cobalt complexes is represented by the corresponding continuous lines in Figure 5. In the case of BaFe, the experimental data agree with values of g = 2.187 and J/k = −0.95 K only up to 30 K. At lower temperatures the curve clearly deviates from the theoretical model. As the maximum in χ_m is out of the fitting range, the calculated J value should be considered as a simple approximation. In this case, the zero-field splitting effect should be taken into account, especially at low temperatures. For the cobalt compound, the calculated J/k and g values are −3.24 K and 2.679, respectively, even though the inaccuracy of the model is obvious. The spin-orbit coupling effect progressively changes from a spin state S = 3/2 in the octahedral cobalt(II) ion to an effective spin state S' = 1/2 at low temperatures. Nevertheless, we can assume that until 15 K the

 © 2003 Wiley-VCH Verlag GmbH & Co. KGaA, Weinheim

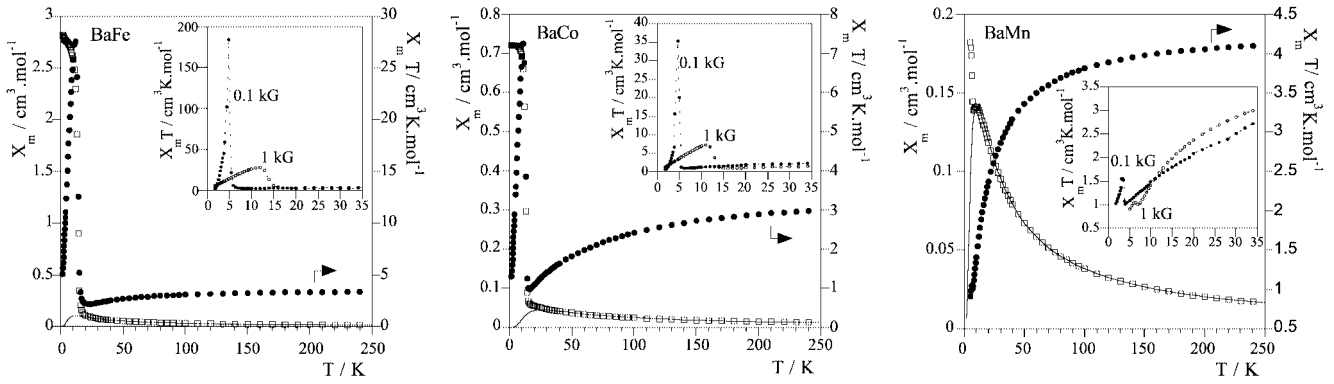

Figure 5. Thermal evolution of χ_m and $\chi_m T$ for BaFe, BaCo and BaMn, measured at 1 kG. (The $\chi_m T$ vs. T curves measured at 0.1 *k*G are represented in the insets)

Table 3. Magnetic parameters of the BaFe, BaCo and BaMn compounds

		T_N/K	C_m/cm^3·K·mol^{-1}	θ /K	μ $_{eff}$/μ_B
BaFe	AF + weak FM	13.2	3.64	−19.3	5.23
BaCo	AF + weak FM	13	3.59	−48.9	4.96
BaMn[8]	AF + weak FM	7	4.34	−13.8	5.76

three compounds show two-dimensional Heisenberg antiferromagnetic behaviour with a weak intralayer antiferromagnetic interactions between the $M^{II}\cdots M^{II}$ atoms through the O-C-O bridges. Below 15 K, the presence of the minimum in the $\chi_m T$ curve together with a sudden increase indicates that total antiparallel alignment of the spins is not reached, suggesting the presence of long-range magnetic ordering due to the existence of interlayer ferromagnetic coupling. Moreover, this is a field-dependent effect: the less intense is the applied field (0.1 kG), the sharper is the maximum observed (see insets in Figure 5). In both cases, the field dependency is more intense than that observed for the BaMn compound.

In order to study this effect, magnetization measurements were performed. The results are shown in Figure 6. The magnetization shows a linear dependence on the magnetic field at 20 K. However, at 5 K both curves became nonlinear, indicating the presence of a ferromagnetic component at this temperature. For the BaFe compound, an anomalous dependence is also observed, probably due to the zero-field splitting effect (see Figure 6a).

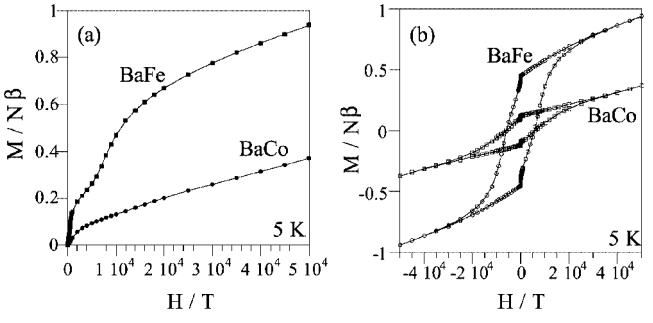

Figure 6. (a) M vs. H and (b) hysteresis curves at 5 K for the BaFe and BaCo compounds

The hysteresis curves M vs. H measured at 5 K are also indicative of the presence of ferromagnetic interactions. Both compounds show small hysteresis loops, with coercive fields of 6000 G, and remnant magnetization values of 0.44 and 0.12 in $N\beta$ units for the iron and cobalt complexes, respectively (see Figure 6b).

Finally, the thermoremnant magnetization was measured at a magnetic field of 100 G. The M_r vs. T curves are shown in Figure 7. The Néel temperatures are 13.2 K and 13 K for BaFe and BaCo, respectively. Both curves show a rapid increase reaching saturation with thermoremnant magnetization values of 0.44 and 0.12 in $N\beta$ units for the BaFe and BaCo compounds, respectively. These values agree with the M_r ones found in the hysteresis loops, and corroborate the existence of weak ferromagnetism in both samples. For BaMn, complete ordering was not reached even at 4 K (see inset in Figure 7), the ferromagnetic component in this compound being weaker than in BaFe and BaCo. Following these results, we must assume that the magnitude of the

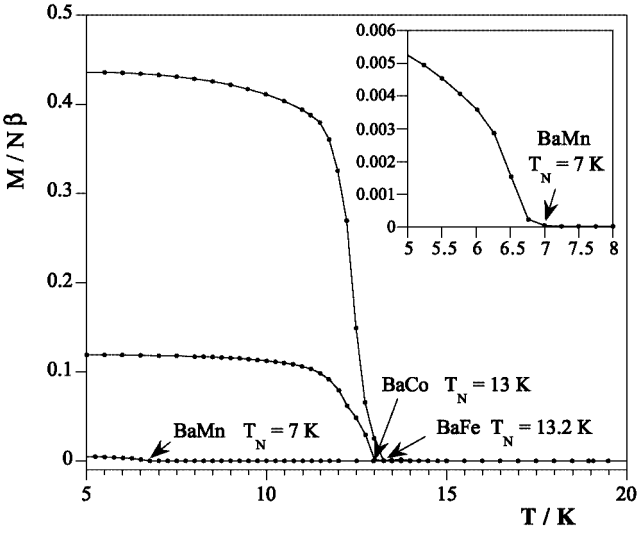

Figure 7. Zero-field magnetization vs. T curves for the BaFe, BaCo and BaMn compounds, after cooling, under a magnetic field of 100 G

 © 2003 Wiley-VCH Verlag GmbH & Co. KGaA, Weinheim

ferromagnetic component cannot depend only on the spin value of the metallic cation. Other parameters such as magnetic anisotropy of the cations, exchange angles and bond lengths should be considered in order to explain the magnetic behaviour observed in these compounds. Notwithstanding, and taking all the results into account, we can conclude that the BaMn, BaFe and BaCo compounds show 2D Heisenberg antiferromagnetic behaviour above 15 K, as a result of an intralayer antiferromagnetic interaction between M···M atoms, through the O-C-O bridges. Below this temperature, the total coupling of the antiparallel spins is not reached, probably due to the existence of an intralayer misalignment of the spins (or canting)[8] and a long-range ferromagnetic ordering between layers, with a weak ferromagnetism being observed.

Conclusions

Two new two-dimensional compounds, $[BaFe(C_3H_2O_4)_2(H_2O)_4]$ and $[BaCo(C_3H_2O_4)_2(H_2O)_4]$, have been synthesised. They are isostructural with the $[SrCu(C_3H_2O_4)_2(H_2O)_4]$ phase. These complexes exhibit two-dimensional antiferromagnetic interactions and below 12 K the presence of weak ferromagnetism has also been detected. This observation was attributed to the presence of long-range magnetic ordering of the canted spins between layers.

The thermal decomposition of the compounds occurs in three steps: dehydration, pyrolysis of the ligand and evolution of the inorganic residue to yield mixed oxides. Different thermal treatments in tubular furnaces at temperatures between 700−850 °C and under different atmospheres gave rise to non-stoichiometric $BaFeO_{3-y}$ and $BaCoO_{3-y}$ phases at temperatures and reaction times much lower than those of the ceramic method.

Experimental Section

Materials: Cobalt(II) chloride and malonic acid were purchased from Fluka, iron(II) chloride was purchased from Aldrich and sodium carbonate from Merck. They were all used without further purification.

Physical Measurements: Microanalyses were performed with a LECO CHNS-932 elemental analyser. Analytical measurements were carried out on an ARL 3410+ICP with Minitorch equipment. The powder X-ray diffraction (XRD) pattern was taken using a Philips X′pert diffractometer equipped with graphite-monochromated Cu-$K\alpha_1$ radiation. Data were collected by scanning in the range $5 < 2\theta < 70°$ with increments of 0.02° (2θ). Thermogravimetric measurements were performed on a Perkin−Elmer System-7 DSC-TGA instrument. Crucibles containing 20 mg of sample were heated at 5 °C·min^{-1} under dry nitrogen and air atmospheres. IR spectra (400−4000 cm^{-1}) were recorded on a MATTSON FTIR 1000 spectrophotometer with samples prepared as KBr pellets. Diffuse reflectance spectra were carried out on a CARY 2415 spectrometer in the range 5000−45000 cm^{-1}. Magnetic susceptibility measurements of powdered samples were carried out in the 1.8−300 K temperature range using a Quantum Design MPMS-7 Squid magnetometer. The magnetic measurements were performed at magnetic fields between 0 and 7 T.

Preparation of the Metallo-organic Precursors: To a solution of 2.5 mmol of disodium malonate, previously formed from 2.5 mmol (0.2601 g) of malonic acid neutralised with 2.5 mmol (0.7419 g) of sodium carbonate, 1 mmol of the corresponding transition metal salt was added. The mixture was stirred for 30 minutes and 1 mmol of barium chloride was added. Polycrystalline powders of the two phases were obtained in a few seconds. They were then stirred for 1−2 hours until complete precipitation was attained. For the iron compound, a closed system with a nitrogen atmosphere was needed to prevent oxidation. The powders obtained, white and light pink for the BaFe and the BaCo complexes respectively, were filtered and washed with ethanol/water followed by diethyl ether. Elemental analysis together with Inductively Coupled Plasma measurements were consistent with the following stoichiometries: $BaFeC_6H_{12}O_{12}$ and $BaCoC_6H_{12}O_{12}$. $BaFeC_6H_{12}O_{12}$: calcd. C 15.35, H 2.58, Fe 11.90, Ba 29.26; found. C 15.56, H 2.91, Fe 12.06, Ba 29.83; $BaCoC_6H_{12}O_{12}$: calcd. C 15.25, H 2.56, Co 12.48, Ba 29.07; found. C 15.10, H 2.11, Co 11.90, Ba 28.90.

Acknowledgments

This work has been carried out with the financial support of the MCYT (MAT, 2001-0064) and the Universidad del País Vasco/Euskal Herriko Unibertsitatea (Project 169.310-13494/2001).

[1] C. Ruiz-Pérez, M. Hernández-Molina, P. Lorenzo-Luis, F. Lloret, J. Cano, M. Julve, *Inorg. Chem.* **2000**, *39*, 3845.
[2] R. P. Scaringe, W. E. Hatfield, D. J. Hodgson, *Inorg. Chem.* **1977**, *16*, 1600.
[3] D. Chattopadhyay, S. K. Chattopadhyay, P. R. Lowe, C. H. Schwalke, S. K. Mazumber, A. Rana, S. Ghosh, *J. Chem. Soc., Dalton Trans.* **1993**, 913.
[4] C. Ruiz-Pérez, J. Sanchiz, M. Hernández-Molina, F. Loret, M. Julve, *Inorg. Chem.* **2000**, *39*, 1363; C. Ruiz-Pérez, J. Sanchiz, M. Hernández-Molina, F. Loret, M. Julve, *Inorg. Chim. Acta* **2000**, *298*, 202.
[5] S. H. Saadeh, K. L. Trojan, J. W. Kampf, W. E. Hatfield, V. L. Peroraro, *Inorg. Chem.* **1993**, *32*, 3034.
[6] Y.-G. Wei, S-W. Zhang, M.-C. Shao, Q. Liu, Y.-Q. Tang, *Polyhedron* **1996**, *15*, 4303.
[7] C. Ruiz-Pérez, M. Hernández-Molina, J. Sanchiz, T. López, F. Lloret, M. Julve, *Inorg. Chim. Acta* **2000**, *298*, 245.
[8] I. Gil de Muro, F. A. Mautner, M. Insausti, L. Lezama, M. I. Arriortua, T. Rojo, *Inorg. Chem.* **1998**, *37*, 3243.
[9] Y. Rodriguez-Martín, C. Ruiz-Pérez, J. Sanchiz, F. Loret, M. Julve, *Inorg. Chim. Acta* **2001**, *318*, 159.
[10] C. N. R. Rao, *Chemical Approaches to the Synthesis of Inorganic Materials*, Wiley, New York, **1994**.
[11] K. Vidyasagar, J. Gopalakrishnan, C. N. R. Rao, *Inorg. Chem.* **1984**, *23*, 1206.
[12] T. Rojo, M. Insausti, M. I. Arriortua, E. Hernández, J. Zubillaga, *Thermochim Acta* **1992**, *195*, 95.
[13] M. Insausti, R. Cortés, M. I. Arriortua, T. Rojo, E. Hernández, *Solid State Ionics* **1993**, *63*, 351.
[14] J. García-Jaca, M. Insausti, J. L. Pizarro, R. Cortés, M. I. Arriortua, T. Rojo, *Polyhedron* **1993**, *13*, 357.
[15] A. Bolivar, M. Insausti, L. Lorente, J. L. Pizarro, M. I. Arriortua, T. Rojo, *J. Mater. Chem.* **1997**, *7*, 2259.
[16] M. Insausti, I. Gil de Muro, L. Lorente, T. Rojo, E. H. Bocanegra, M. I. Arriortua, *Thermochim. Acta* **1996**, *287*, 81.

 © 2003 Wiley-VCH Verlag GmbH & Co. KGaA, Weinheim

[17] I. Gil de Muro, M. Insausti, L. Lezama, J. L. Pizarro, M. I. Arriortua, T. Rojo, *Eur. J. Inorg. Chem.* **1999**, 935.
[18] I. Gil de Muro, M. Insausti, L. Lezama, M. K. Urtiaga, M. I. Arriortua, T. Rojo, *J. Chem. Soc., Dalton Trans.* **2000**, 3360.
[19] J. Rodríguez-Carvajal, *Physica B* **1993**, *192*, 55.
[20] E. Escrivá, A. Fuertes, J. V. Folgado, E. Martínez-Tamayo, A. Beltrán-Porter, D. Beltrán-Porter, *Thermochim. Acta* **1986**, *104*, 223.
[21] Powder Diffraction File, Card No. 23−1024. Joint Committee on Powder Diffraction Standars, Swarthmore PA, **1995**.
[22] Powder Diffraction File, Card No. 10−245. Joint Committee on Powder Diffraction Standars, Swarthmore PA, **1995**.
[23] K. Nakamoto, *Infrared Spectra of Inorganic and Coordination Compounds*, 5th ed., John Wiley & Sons, New York, **1987**.
[24] A. B. P. Lever, *Inorganic Electronic Spectroscopy*, 2nd ed., Elsevier, New York, **1986**.
[25] G. S. Rushbrooke, P. Wood, *J. Mol. Phys.* **1963**, *6*, 409.
Received February 10, 2003

 © 2003 Wiley-VCH Verlag GmbH & Co. KGaA, Weinheim

Synthesis and Characterisation of Ternary Cage Compounds with Adamantane-Like $M_4P_4Si_2$ (M = Al, Ga, In) Core Structures

Carsten von Hänisch[a]

Keywords: Aluminium / Gallium / Silicon / Indium / Phosphorus

The reactions of $[LiAl(PH_2)_4]$ or $[NaAl(PH_2)_4]$ with Et_2SiCl_2 or iPr$_2$SiCl$_2$ yield the dialkyldiphosphanylsilanes $Et_2Si(PH_2)_2$ (**1**) and iPr$_2$Si(PH$_2$)$_2$ (**2**), respectively. Both compounds were identified by NMR spectroscopy as well as mass spectrometry. Compound **2** reacts with MEt_3 (M = Al, Ga, In) to form the cage compounds $[i\text{Pr}_2\text{Si}\{\text{P(H)ME}t_2\}_2]_2$ (**3**: M = Al, **4**: M = Ga, **5**: M = In). These three clusters were fully characterised by NMR and IR spectroscopy as well as by single-crystal X-ray diffraction. The central structural motif of **3**–**5** is an adamantane-like cage composed of four metal, four phosphorus and two silicon atoms. They are the first ternary clusters with these combinations of elements and crystallise isotypical in the triclinic space group $P\bar{1}$; the lattice constants are: **3**: a = 1129.0(6), b = 1164.8(8), c = 1750.6(8) pm; α = 83.63(5), β = 81.53(4), γ = 73.39(5)°; **4**: a = 1125.9(7), b = 1159.0(7), c = 1744.7(7) pm; α = 83.71(4), β = 81.89(4), γ = 73.05(5)°; **5**: a = 1147.4(2), b = 1174.7(2), c = 1753.3(4) pm; α = 85.32(3), β = 82.03(3), γ = 73.40(3)°.
(© Wiley-VCH Verlag GmbH & Co. KGaA, 69451 Weinheim, Germany, 2003)

Introduction

In the last few years reactions of primary silylphosphanes or -arsanes (R_3SiEH_2, E = P, As) with hydrido- or alkylaluminium, -gallium or -indium compounds have been applied several times to synthesise molecular compounds of these element combinations.[1−3] Cyclic and also cage-like 13/15 compounds were obtained from these reactions. The molecular structures of the reaction products can be influenced by the silyl group attached to the P or As atom. The reactions of $InEt_3$ with R_3SiPH_2 may serve as an example. Starting from iPr$_3$SiPH$_2$, the heterocubane-like compound $[EtInPSi\textit{i}Pr_3]_4$ is formed whereas the reaction of ThexMe$_2$SiPH$_2$ (Thex = CMe$_2$$i$Pr) with $InEt_3$ yields the hexagonal prismatic molecule $[EtInPSiThexMe_2]_6$.[2] By using the sterically less demanding $SiMe_3$ group a $SiMe_3$/H substituent exchange occurs and results in the formation of the cyclic compound $[Et_2InP(SiMe_3)_2]_2$.[3]

Whereas the dimethyldiphosphanylsilane $Me_2Si(PH_2)_2$ has been known in the literature for several years, dialkyldiphosphanylsilanes with sterically demanding alkyl groups such as ethyl or isopropyl are as yet unknown.[4] Reaction of these compounds with alkylaluminium, -gallium or -indium species will result in the formation of novel ternary group13/Si/P compounds. The first species of this class of compounds $[i\text{Pr}_2\text{Si}\{\text{P(H)ME}t_2\}_2]_2$ (**3**: M = Al, **4**: M = Ga, **5**: M = In), which could be obtained by the reactions of iPr$_2$Si(PH$_2$)$_2$ (**2**) with MEt_3, are described herein.

[a] Forschungszentrum Karlsruhe GmbH, Institut für Nanotechnologie
Postfach 3640, 76021 Karlsruhe, Germany
Fax: (internat.) +49-(0)7247/826-368
E-mail: carsten.vonhaenisch@int.fzk.de

Results and Discussion

A solution of $[LiAl(PH_2)_4]$ in tetraglyme reacts with Et_2SiCl_2 to form the dialkyldiphosphanylsilane $Et_2Si(PH_2)_2$ (**1**). This compound can be isolated from the reaction mixture by vacuum condensation in about 50% yield. The less volatile compound iPr$_2$Si(PH$_2$)$_2$ (**2**) can be obtained in about 70% yield from the reaction of $[NaAl(PH_2)_4]$ with iPr$_2$SiCl$_2$ in DME. The ^{31}P NMR spectra of both molecules show a triplet of higher order at δ = −242.7 (**1**) and −254.2 ppm (**2**). The high resolution spectrum of **1** (see Figure 1) allows the complete analysis of all coupling constants by an iterative process;[5] the fine structure of the

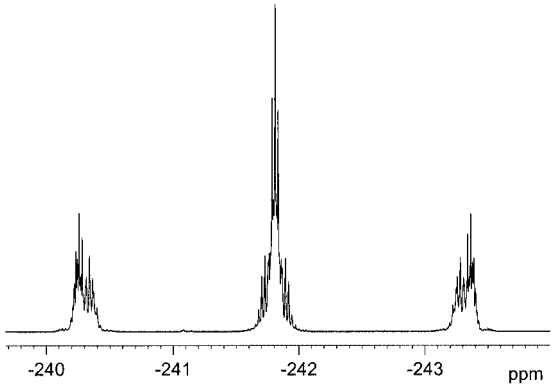

Figure 1. ^{31}P NMR Spectrum of **1** in C_6D_6

triplet of **2** cannot be fully resolved. Therefore only the $^1J_{P,H}$ coupling constants were determined. The mass spectra of both compounds show the molecule peaks at m/z = 152 (**1**) and 180 (**2**) as well as peaks for the fragments $R_2SiPH_2^+$, $RSi(H)PH_2^+$ and $H_2SiPH_2^+$.

Reaction of **1** with triethylgallium or triethylindium results in the formation of oily precipitates, which have not been characterised so far. $^{31}P\{^1H\}$ NMR investigations of the reaction mixtures showed several broad signals, which indicate that polymeric compounds have been formed. In contrast to the latter, the sterically more demanding compound **2** reacts with MEt_3 (M = Al, Ga, In) in heptane at ambient temperature with elimination of ethane and the formation of a white, crystalline precipitate. These products can be dissolved by warming the reaction mixtures slightly. Subsequent cooling of the solutions to 6 °C yields colourless crystals.[6] X-ray analysis (Table 1) confirmed that the compounds $[i\mathrm{Pr}_2\mathrm{Si}\{\mathrm{P(H)MEt}_2\}_2]_2$ (**3**: M = Al, **4**: M = Ga, **5**: M = In) had formed as described in Equation (1). Recently, Kaskel and co-workers reported reactions of $Si(NHEt)_4$ with AlR_3, which result in the formation of the ternary Al/Si/N compounds $[RAl(\mu\text{-}NHEt)(\mu\text{-}NEt)_2Si(NHEt)_2]_2$ (R = Me, Et).[7] Whereas compounds **3** and **4** are stable in solution, too, a benzene solution of the indium compound **5** decomposes after several days with further elimination of ethane. At the same time a yellow, oily, precipitate appears.

$$2\ i\mathrm{Pr}_2\mathrm{Si(PH_2)_2} + 4\ \mathrm{MEt_3} \rightarrow [i\mathrm{Pr}_2\mathrm{Si}\{\mathrm{P(H)MEt}_2\}_2]_2\ (\mathrm{M = Al, Ga, In}) + 4\ \mathrm{C_2H_6} \quad (1)$$

Compounds **3**, **4** and **5** crystallise isotypical in the triclinic space group $P\bar{1}$ (the structure of **3** is shown in Figure 2 as an example). The central structural motif is an adamantane-like cage composed of four aluminium, gallium or indium atoms, four phosphorus and two silicon atoms. Cage compounds of these element combinations have not been reported so far. In these moieties, the phosphorus atoms are in the bridgehead positions and the metal and silicon atoms are in the secondary positions. This results in an eight-membered M_4P_4 (M = Al, Ga, In) ring, where the opposite phosphorus atoms [P(1), P(3) and P(2), P(4)] are bridged by $i\mathrm{Pr}_2\mathrm{Si}$ groups on different sides of the ring. The M_4P_4 ring is therefore strongly distorted and shows a boat-like conformation.

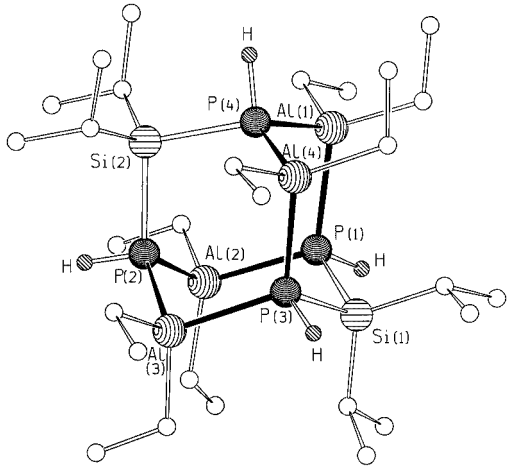

Figure 2. Molecular structure of **3**

The observed P−M and P−Si bond lengths are in the typical range for single bonds between these elements (seen Table 2).[1−3,8] The very similar Al−P and Ga−P bond

Table 1. Crystallographic data of **3**, **4** and **5** [STOE-IPDS2 (Mo-K_α radiation, λ = 0.71073 Å). The structure was solved by direct methods and refined by full-matrix least-squares techniques against F^2 (In, Ga, Al, P, Si, C refined anisotropically, H atoms at the phosphorus atoms refined isotropically, all other H atoms were calculated at ideal positions)][6]

Compound	**3**	**4**	**5**
Formula	$C_{28}H_{72}P_4Al_4Si_2$	$C_{28}H_{72}P_4Ga_4Si_2$	$C_{28}H_{72}P_4In_4Si_2$
Space group	$P\bar{1}$	$P\bar{1}$	$P\bar{1}$
Formula units	2	2	2
Temperature	200 K	200 K	200 K
Lattice constants	a = 1129.0(6) pm	a = 1125.9(7) pm	a = 1147.4(2) pm
	b = 1164.8(8) pm	b = 1159.0(7) pm	b = 1174.7(2) pm
	c = 1750.6(8) pm	c = 1744.7(7) pm	c = 1753.3(4) pm
	α = 83.63(5)°	α = 83.71(4)°	α = 85.32(3)°
	β = 81.53(4)°	β = 81.89(4)°	β = 82.03(3)°
	γ = 73.39(5)°	γ = 73.05(5)°	γ = 73.40(3)°
Volume	2176(2) Å^3	2150(2) Å^3	2240.8(8) Å^3
density	1.063 g/cm^3	1.340 g/cm^3	1.553 g/cm^3
2Θ range	3−50°	4−50°	4−54°
Reflections measured	13966	12583	17889
Independent reflections	7084 (R_{int} = 0.0563)	7104 (R_{int} = 0.0603)	9101 (R_{int} = 0.0535)
Ind. reflections with $F_0 > 4\sigma(F_0)$	5860	5611	7614
Parameter	359	359	362
μ(Mo-K_α)	0.326 mm^{-1}	1.340 mm^{-1}	2.244 mm^{-1}
R1	0.0627	0.0657	0.0382
wR2 (all data)	0.1863	0.1919	0.1088
Residual electron density	0.463 e/Å^3	0.827 e/Å^3	0.620 e/Å^3

 © 2003 Wiley-VCH Verlag GmbH & Co. KGaA, Weinheim

Table 2. Selected bond lengths (pm) and bond angles (°) for **3**−**5**

	3 [M = Al]	**4** [M = Ga]	**5** [M = In]
P−M	244.7(2) − 246.3(2)	243.0(2) − 245.4(2)	261.6(1) − 262.8(1)
P−Si	226.9(2) − 228.0(2)	227.6(2) − 229.7(2)	226.1(1) − 226.8(1)
P−M−P	94.63(7) − 95.68(7)	94.71(7) − 96.01(7)	92.12(4) − 93.08(4)
P−Si−P	103.27(7) − 103.70(7)	102.33(9) − 102.87(9)	105.18(5) − 105.41(5)
M−P−M	113.65(6) − 116.00(6)	114.01(7) − 115.98(7)	111.41(4) − 113.42(4)

lengths reflect the fact that the covalent radii of Al and Ga are almost identical due to d-block contraction. Each of the metal atoms is bound to two exocyclic ethyl groups and the silicon atoms possess two isopropyl groups each. The phosphorus atoms bind to one hydrogen atom, which was localised during the refinement of the crystal structures. Moreover, the IR spectra of **3**, **4** and **5** show strong peaks at 2306 cm^{-1} (**3**), 2305 cm^{-1} (**4**), 2303 cm^{-1} (**5**) which can be assigned to the P−H stretching vibrations. The ^{31}P NMR spectra reveal multiplets of higher order for all three compounds ([AX]$_4$ spin system). Figure 3 displays the ^{31}P NMR spectrum of **5**. Unfortunately, the comparatively broad signals in the ^{31}P NMR spectra of **3**−**5** (see Figure 3 inset) do not allow an iterative determination of the coupling constants with satisfactory accuracy. As expected, the $^{31}P\{^1H\}$ NMR spectra only show singlets at δ = −250.0 (**3**), 244.2 (**4**) and −273.5 ppm (**5**).

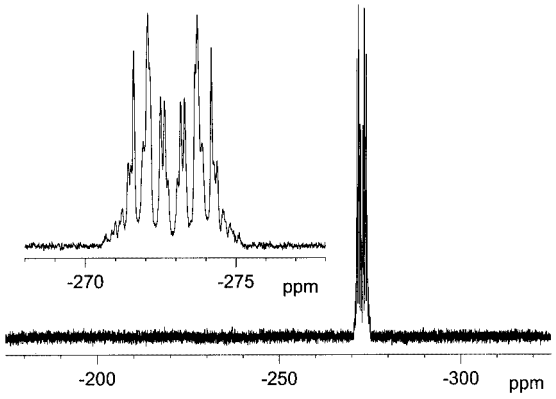

Figure 3. ^{31}P NMR Spectrum of **5** in C_6D_6

Experimental Section

All manipulations were performed with rigorous exclusion of oxygen and moisture using a Schlenk line and nitrogen atmosphere. Solvents were dried and freshly distilled before use. NMR spectra were recorded on a Bruker DPX Avance 300 or on a Bruker AC 250 instrument. $[NaAl(PH_2)_4]$, $[LiAl(PH_2)_4]$, $GaEt_3$ and $InEt_3$ were prepared according to the literature.[9−11] $AlEt_3$ was purchased from Aldrich and used as received.

1: Et_2SiCl_2 (4.0 g, 0.025 mol) was added to 100 mL of a 0.13 M solution of $[LiAl(PH_2)_4]$ in tetraglyme at −40 °C. The colour of the solution changed from slightly yellow to colourless. During this time a white precipitate also formed. After agitation for ten minutes the product was condensed into a cold trap at −196 °C under oil pump vacuum. During the condensation the reaction mixture was warmed up to room temperature. After five hours the condensation was complete. Trace amounts of solvent were removed from the product by a second condensation under a stationary vacuum of $5{\cdot}10^{-3}$ mbar. Compound **1** was obtained as a colourless, pyrophoric liquid. Yield: 2.0 g (52%). $^1H\{^{31}P\}$ NMR (C_6D_6): δ = 0.670 (q, $^3J_{H,H}$ = 7.9 Hz, 4 H, CH_2), 0.909 (t, $^3J_{H,H}$ = 7.9 Hz, 6 H, CH_3), 1.350 (m, 4 H, PH_2) ppm. $^{13}C\{^1H\}$ NMR (C_6D_6): δ = 8.4 (t $^2J_{C,P}$ = 2.6 Hz, CH_3), 10.3 (t $^3J_{C,P}$ = 7.3 Hz, CH_2) ppm. $^{29}Si\{^1H\}$ NMR (C_6D_6): δ = 12.8 (t $^1J_{Si,P}$ = 33 Hz) ppm. ^{31}P NMR (C_6D_6): δ = −242.7 [m/t, coupling constants from iterative optimisation: $^1J_{PH}$ = −184.1, $^2J_{P,P}$ = 11.9, $^3J_{PH(PH2)}$ = −4.4, $^4J_{H,H(PH2/PH2)}$ = 0.4, $^3J_{PH(CH2)}$ = 3.0 Hz (corresponds with $AA'X_2X'_2Y_2Y'_2$ spin system)].[5] MS (EI, 70 eV): *m*/*z* (%) = 152 (8.6) [M^+], 119 (56) [$M^+ - PH_2$], 95 (10) [$HSi(PH_2)_2^+$] 91 (100) [$EtSi(H)PH_2^+$], 63 (42) [$H_2Si(PH_2)_2^+$].

2: iPr_2SiCl_2 (7.4 g, 0.04 mol) was added to 100 mL of a 0.25 M solution of $[NaAl(PH_2)_4]$ in DME at −50 °C. The reaction mixture was then warmed up to room temperature over a period of 16 hours. Subsequently 100 mL pentane was added and the yellow precipitate removed by filtration. Finally, the solvent was distilled off under reduced pressure at room temperature and the residue was distilled under vacuum to give **2** as a colourless, pyrophoric liquid at 90−100 °C (25 Torr). Yield: 5.0 g (70%). ^1H NMR (C_6D_6): δ = 1.050 (s, 14 H, *i*Pr), 1.367 (m/d, $^1J_{P,H} \approx$ 190 Hz, 4 H, PH_2) ppm. $^{13}C\{^1H\}$ NMR (C_6D_6): δ = 15.2 [t $^2J_{C,P}$ = 6.3 Hz, $CH(CH_3)_2$], 18.6 (t $^3J_{C,P}$ = 2.2 Hz, CH_3) ppm. ^{31}P NMR (C_6D_6): δ = −254.2 (t, $^1J_{PH} \approx$ −190 Hz) ppm. MS (EI, 70 eV): *m*/*z* (%) = 180 (24) [M^+], 147 (100) [$M^+ - PH_2$], 105 (65 [$iPrSi(H)PH_2^+$], 43 (12.5) [iPr^+].

3: $AlEt_3$ (0.62 g, 5.4 mmol) was added to a stirred solution of $iPr_2Si(PH_2)_2$ (0.5 g, 2.78 mmol) in 20 mL of heptane. After 20 minutes a white precipitate formed. The latter was dissolved by warming the reaction mixture slightly. Compound **3** formed as large colourless crystals within three days at 6 °C. Yield: 0.9 g (96%); $C_{28}H_{72}Al_4P_4Si_2$ (696.9): calcd. C 48.26, H 10.41; found C 48.13, H 10.20. ^1H NMR (C_6D_6): δ = 0.58 (q, $^3J_{H,H}$ = 8.0 Hz, 16 H, CH_2CH_3), 1.14 [d, $^3J_{H,H}$ = 7.5 Hz, 24 H, $CH(CH_3)_2$], 1.46 (t, $^3J_{H,H}$ = 8.0 Hz, 24 H, CH_2CH_3), 1.70 [hep, $^3J_{H,H}$ = 7.5 Hz, 4 H, $CH(CH_3)_2$] ppm; P*H* not observed. $^{13}C\{^1H\}$ NMR (C_6D_6): δ = 4.1 (br. s, CH_2), 10.0 (s, CH_2CH_3), 19.4 [s, $CH(CH_3)_2$], 21.7 [s, $CH(CH_3)_2$] ppm. ^{31}P NMR (C_6D_6): δ = −250.0 (m) ppm. IR (KBr): 2945(vs) cm^{-1}, 2864(vs), 2719(w), 2306(s), 1463(vs), 1411(m), 1388(m), 1366(m), 1221(m), 1070(m), 1020(m), 976(m), 948(m), 918(m), 876(s), 822(w), 667(m), 625(s), 572(m), 537(m), 495(s), 405(s). MS (EI, 70 eV, 190 °C): *m*/*z* (%) = 695 (4) [M^+ − H], 667 (74) [M^+ − Et], 581 (13) [$M^+ - iPr_2Si - H$], 553 (95) [$M^+ - iPr_2Si$ − Et], 467 (6) [$M^+ - 2iPr_2Si - H$], 523 (33) [$M^+ - iPr_2Si - H - 2Et$], 319 (44) [$M/2^+$ − Et], 114 (61) [iPr_2Si^+], 85 (100) [Et_2Al^+].

4: $GaEt_3$ (0.85 g, 5.4 mmol) was added to a stirred solution of $iPr_2Si(PH_2)_2$ (0.5 g, 2.78 mmol) in 20 mL of heptane. After 20 mi-

 © 2003 Wiley-VCH Verlag GmbH & Co. KGaA, Weinheim

nutes a white precipitate formed. The latter was dissolved by warming the reaction mixture slightly. Compound **4** formed as large colourless crystals within three days at 6 °C. Yield: 1.1 g (94%); $C_{28}H_{72}Ga_4P_4Si_2$ (867.8): calcd. C 38.75, H 8.36; found C 38.45, H 8.40. ^{1}H NMR (C_6D_6): δ = 1.03 (q, $^3J_{H,H}$ = 8.0 Hz, 16 H, CH_2CH$_3$), 1.19 [d, $^3J_{H,H}$ = 7.5 Hz, 24 H, CH(CH_3)$_2$], 1.47 (t, $^3J_{H,H}$ = 8.0 Hz, 24 H, CH$_2$CH_3), 1.72 [hep, $^3J_{H,H}$ = 7.5 Hz, 4 H, CH(CH$_3$)$_2$] ppm; PH not observed. ^{13}C{^{1}H} NMR (C_6D_6): δ = 8.3 (br. s, CH$_2$), 11.4 (s, CH$_2$$CH_3$), 19.4 [s, CH($CH_3$)$_2$], 21.6 [s, CH(CH$_3$)$_2$] ppm. ^{31}P NMR (C_6D_6): δ = −244.2 (m) ppm. IR (KBr): 2945(vs) cm^{-1}, 2894(s), 2861(vs), 2813(w), 2721(w), 2305(s), 1459(s), 1421(m), 1388(m), 1365(m), 1286(vw), 1227(vw), 1183(w), 1070(m), 1019(s), 999(vs), 955(m), 931(vw), 917(w), 875(s), 816(w), 665(s), 631(m), 564(m), 544(m), 496(vs). MS (EI, 70 eV, 170 °C): m/z (%) = 837 (1) [M$^+$ − Et], 681 (2) [(Et$_2$Ga)$_4$(PH)$_4$$iPr^+$], 292 (100) [($iPr_2$SiPH)$_2^+$].

5: InEt$_3$ (1.1 g, 5.4 mmol) was added to a stirred solution of iPr$_2$Si(PH$_2$)$_2$ (0.5 g, 2.78 mmol) in 20 mL of heptane. After 20 minutes a white precipitate formed. The latter was dissolved by warming the reaction mixture slightly. Compound **3** formed as large colourless crystals within three days at 6 °C. Yield: 0.8 g (55%); $C_{28}H_{72}In_4P_4Si_2$ (1048.2): calcd. C 32.08, H 6.92; found C 31.15, H 6.83. ^{1}H NMR (C_6D_6): δ = 1.215 (m, overlap of iP, 44 Hr, CH_2CH$_3$), 1.656 (t, $^3J_{H,H}$ = 8.1 Hz, 24 H, CH$_2$CH_3) ppm; PH not observed. ^{13}C{^{1}H} NMR (C_6D_6): δ = 9.2 (br. s, CH$_2$), 13.7 (s, CH$_2$$CH_3$), 19.5 [s, CH($CH_3$)$_2$], 23.3 [s, CH(CH$_3$)$_2$] ppm. ^{31}P NMR (C_6D_6): δ = −273.5 (m) ppm. IR (KBr): 2944(vs) cm^{-1}, 2862(vs), 2817(w), 2722(w), 2303(s), 1462(vs), 1420(w), 1386(w), 1373(m), 1246(vw), 1225(m), 1158(s), 1070(m), 1019(w), 996(m), 956(m), 918(m), 877(s), 660(w), 634(vs), 560(w), 506(s), 492(s), 396(m).

Acknowledgments

The author thanks Dr. P. Kramkowski and Dr. E. Matern for their valuable help with the manuscript and the NMR experiments.

[1] [1a] A. H. Cowley, R. A. Jones, M. A. Mardones, J. L. Atwood, S. G. Bott, *Angew. Chem.* **1990**, *102*, 1504−1505; *Angew. Chem. Int. Ed. Engl.* **1990**, *29*, 1409−1410. [1b] M. Driess, S. Kuntz, K. Merz, H. Pritzkow, *Chem. Eur. J.* **1998**, *4*, 1628−1632. [1c] M. Driess, S. Kuntz, C. Monse, K. Merz, *Chem. Eur. J.* **2000**, *6*, 4343−4347.

[2] C. von Hänisch, B. Rolli, *Z. Anorg. Allg. Chem.* **2002**, *628*, 2255−2258.

[3] C. von Hänisch, *Z. Anorg. Allg. Chem.* **2001**, *627*, 68−72.

[4] A. D. Norman, *Inorg. Chem.* **1970**, *9*, 870−874.

[5] Programs Win NMR and Windaisy, Bruker Daltonik, Bremen 1999; G. Hägele, M. Engelhardt, W. Boenigk, Simulation und automatisierte Analyse von NMR-Spektren, VCH, Weinheim 1987.

[6] CCDC-210253 (**3**), -210254 (**4**) and -201083 (**5**) contain the supplementary crystallographic data for this paper. These data can be obtained free of charge at www.ccdc.cam.ac.uk/conts/retrieving.html or from Cambridge Crystallographic Data Centre, 12, Union Road, Cambridge CB2 1EZ, UK; Fax: (internat.) +44-1223/336-033; E-mail: deposit@ccdc.cam.ac.uk

[7] S. Kaskel, C. W. Lehmann, G. Chaplais, K. Schlichte, M. Khanna, *Eur. J. Inorg. Chem.* **2003**, 1193−1196.

[8] [8a] J. F. Janik, E. N. Duesler, W. F. William, F. McNamara, M. Westerhausen, R. T. Paine, *Organometallics* **1989**, *8*, 506−514. [8b] R. L. Wells, M. S. Self, A. T. McPail, S. R. Aubuchon, R. C. Woudenberg, J. P. Jasinski, *Organometallics* **1993**, *12*, 2832−2834. [8c] D. A. Atwood, A. H. Cowley, R. A. Jones, M. A. Mardones, *J. Organomet. Chem.* **1993**, *449*, C1−C2. [8d] K. Merzweiler, J. Spohn, *Z. Anorg. Allg. Chem.* **1993**, *619*, 318−320. [8e] R. L. Wells, A. T. McPail, M. S. Self, J. A. Laske, *Organometallics* **1993**, *12*, 3333−3339. [8f] K. Niedick, B. Neumüller, *Chem. Ber.* **1994**, *127*, 67−71. [8g] U. App, K. Merzweiler, *Z. Anorg. Allg. Chem.* **1995**, *621*, 1731−1734. [8h] B. Werner, B. Neumüller, *Organometallics* **1996**, *15*, 4258−4263. [8i] C. von Hänisch, D. Fenske, M. Kattannek, R. Ahlrichs, *Angew. Chem.* **1999**, *111*, 2900−2902; *Angew. Chem. Int. Ed.* **1999**, *38*, 2736−2738. [8j] A. Schaller, H.-D. Hausen, W. Schwarz, G. Heckmann, J. Weidlein, *Z. Anorg. Allg. Chem.* **2000**, *626*, 1047−1058.

[9] M. Baudler, G. Scholz, W. Oehlert, *Z. Naturforsch., Teil B* **1989**, *44*, 627−631.

[10] N. Muller, A. Otermat, *Inorg. Chem.* **1965**, *4*, 296−299.

[11] F. Runge, W. Zimmermann, I. Pfeiffer, *Z. Anorg. Allg. Chem.* **1951**, *267*, 37−40.

Received March 25, 2003

 © 2003 Wiley-VCH Verlag GmbH & Co. KGaA, Weinheim

Linear and Helical Chains in Hydrothermally Synthesized Coordination Polymers $[Co(bpdc)(H_2O)_2]$ and $[Ni(bpdc)(H_2O)_3]\cdot H_2O$ Involving in situ Ligand Synthesis

Xian-Ming Zhang,[a] Hai-Shun Wu,[a] and Xiao-Ming Chen*[b]

Keywords: Coordination polymers / N ligands / Helical structures / Hydrothermal synthesis / Cobalt / Nickel

Hydrothermal treatment of $M(MeCO_2)_2$ (M = Co or Ni) and 1,10-phenanthroline-5,6-dione (pdon) resulted in two chain-like coordination polymers $[Co(bpdc)(H_2O)_2]$ and $[Ni(bpdc)(H_2O)_3]\cdot H_2O$. X-ray single-crystal structural analysis revealed that the organic reagent pdon was transformed in situ into 2,2′-bipyridine-3,3′-dicarboxylate (bpdc). The different coordination modes concomitant with the difference of the dihedral angles between two bpdc pyridine rings results in simple linear chains and helical chains in **1** and **2**, respectively. The one-dimensional coordination chains of **1** and **2** are further extended into two-dimensional supramolecular arrays by hydrogen-bond interactions. A possible mechanism for the new hydrolysis reaction with the formation of bpdc under hydrothermal conditions was also discussed.
(© Wiley-VCH Verlag GmbH & Co. KGaA, 69451 Weinheim, Germany, 2003)

Introduction

The self-assembled construction of coordination polymers has become the subject of many current studies,[1−15] due to their potential optoelectronic,[16−19] magnetic,[20,21] microporous,[22−25] and catalytic applications.[26] The design of coordination polymers takes certain factors into account such as the coordination nature of the metal ion, structural features of the polydentate organic ligand, metal/ligand ratio, and possible counterion influence. A subtle alteration to any of these factors may lead to new extended network structures. Although most of these insoluble solids have been synthesized by controlled mixing of suitable soluble molecular components, hydro(solvo)thermal conditions have demonstrated increasing success in providing alternative pathways to the preparation of crystalline supramolecular solids, including metal-organic coordination networks and hydrogen-bonded systems. Hydro(solvo)thermal syntheses carried out in superheated solvent systems provide ideal conditions for the crystal growth owing to the enhanced transport ability of the solvents.[4] Besides, recent studies revealed that crystal growth under hydrothermal conditions occasionally involves in situ ligand synthesis which not only provides a powerful synthesis method for organic ligands that are difficult to synthesise but also represents a potential new direction for novel inorganic−organic hybrid network construction through crystal engineering.[16−19,27−32] Examples of in situ ligand syntheses under hydrothermal conditions include hydrolysis of −CN and −COOR groups,[16−19] hydroxylation,[27−29] carbon−carbon bond formation by reductive coupling or oxidative coupling,[30,31] and replacement of $-CO_2^-$ with $-SO_3^-$.[32]

We have paid considerable interest to the reactivity of chelate ligands such as 2,2′-bipyridine and 1,10-phenanthroline under hydrothermal conditions and found that their hydroxylation reactivity was promoted by copper(II) ions.[27,28] As an extension of our previous work, we are paying attention to 1,10-phenanthroline-5,6-dione (pdon) because of its peculiar reactivity (Scheme 1) in organic chemistry.[33,34] Two nucleophilic centers (nitrogen and oxygen lone pairs) are contained in the quinone-like pdon molecule with all the non-hydrogen atoms being sp^2-hybridized. The presence of two electronegative heteroatoms not only creates the basic properties in the Lewis sense but also, because of conjugation, makes it possible to alter the electron density in different parts of the molecule. As a result, a dramatic change in reactivity can occur, which is not observed in the case of the corresponding aromatic homocyclic analogue, phenanthrenequinone. We report herein on the in situ hydrothermal synthesis of 2,2′-bipyridine-3,3′-dicarboxylate (bpdc) from pdon and its two coordination polymers $[Co(bpdc)(H_2O)_2]$ and $[Ni(bpdc)(H_2O)_3]\cdot H_2O$.

[a] Department of Chemistry, Shanxi Normal University, Linfen, Shanxi 041004, China
[b] School of Chemistry and Chemical Engineering, Sun Yat-Sen University, Guangzhou 510275, China
Fax: (internat.) + 86-20/84112245
E-mail: cescxm@zsu.edu.cn

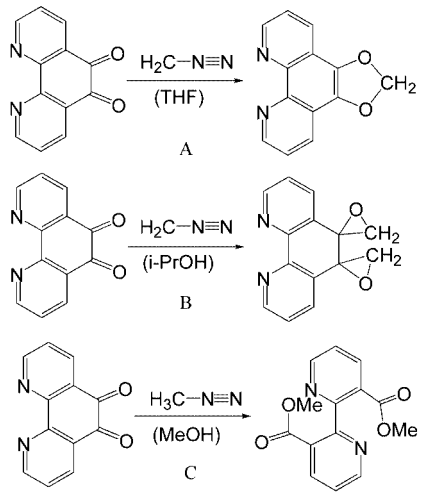

Scheme 1. Schematic representation of some known organic reactions of pdon

Results and Discussion

IR Spectra

The infrared spectra of the two compounds show strong broad bands at 3344 (**1**) or 3390 (**2**) cm^{-1} that are attributable to the stretching modes of hydrogen-bonded H_2O groups. The ν_{as}(COO) vibration is identified by the strong bands at 1566 (**1**) or 1568 (**2**), and the ν_s(COO) bands at 1394 (**1**) and 1392 (**2**) cm^{-1}. The separations Δ(COO) between the ν_{as}(COO) and ν_s(COO) bands, in both compounds, imply that the carboxylate groups act in a monodentate coordination mode.[35]

Structural Description

X-ray single-crystal structural analysis revealed that compound **1** crystallizes in the monoclinic space group *C*2/*c* and that the pdon ligand was transformed in situ into bpdc during the hydrothermal process. The asymmetric unit in **1** consists of 0.5 Co^{II}, 0.5 bpdc and 1 H_2O. The Co^{II} atom lies on a crystallographic twofold axis, which bisects one bpdc. The Co^{II} site shows a distorted octahedral geometry, being coordinated by two nitrogen atoms of one bpdc in a chelate mode and two oxygen atoms of two carboxylate groups in the equatorial plane, as well as two aqua ligands in the axial positions, as shown in Figure 1. The Co−N(1), Co−O(2) and Co−O(1w) distances are 2.123(2), 2.133(2) and 2.151(3) Å, respectively. The *cis*-L−Co−L angles are in the range of 76.70(11)−99.37(9)° and the *trans*-L−Co−L angles are 168.02(7) and 174.85(9)°. The dihedral angle between two bydc pyridine rings is 20.5°, indicating a slight non-coplanarity, which may reduce mutual repulsion between the two carboxy groups in each bpdc. Metal complexes synthesized directly from the bpdc ligand,[36,37] show the tridentate bridging and bis(monodentate) bridging coordination modes in $[Cu(bpdc)(H_2O)_2]$ and $[Mn(bpdc)(H_2O)_4]$, respectively. In contrast, each bpdc ligand utilizing the pair of nitrogen atoms and two oxygen

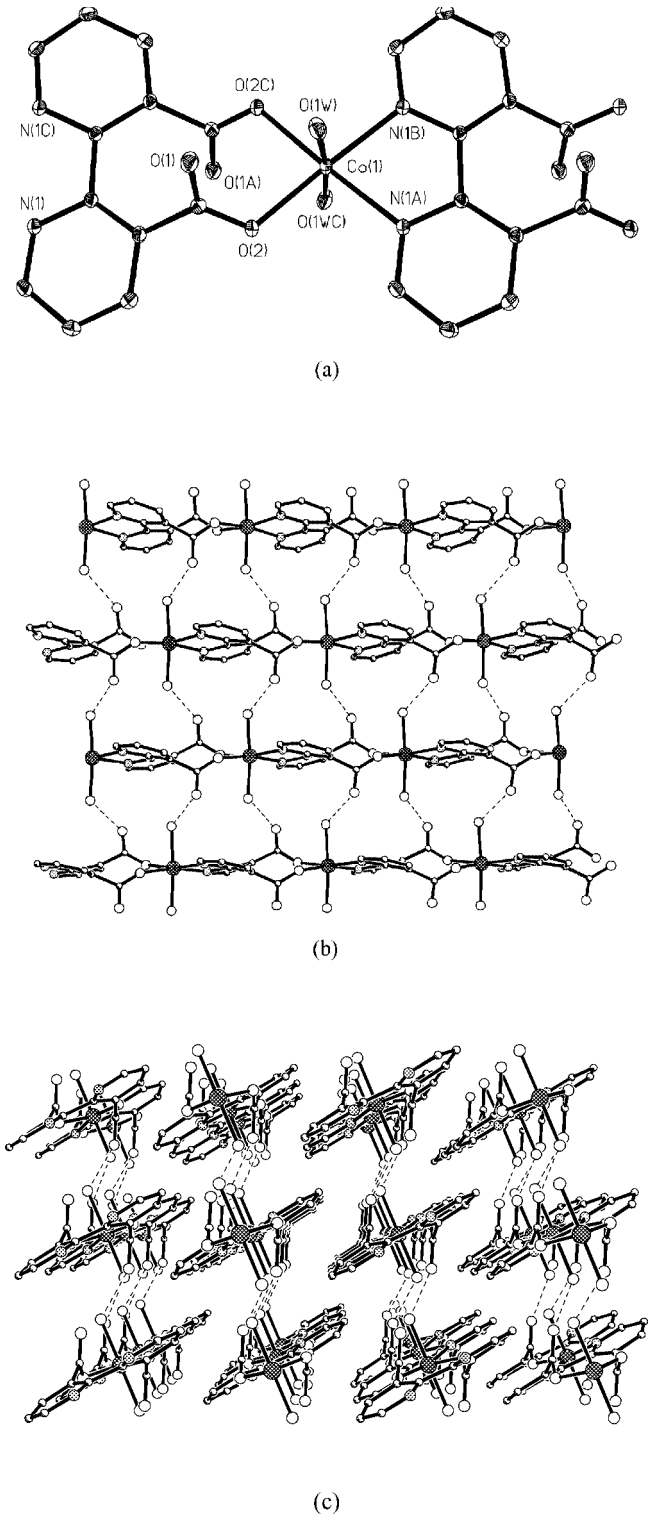

Figure 1. Perspective views of the coordination environment of the cobalt(II) atom (a), two-dimensional supramolecular network (b) and stacking array (c) in **1**

atoms of two carboxylate groups bridge two Co^{II} atoms in **1** to generate one-dimensional chains (Figure 1, b) in which all cobalt atoms are located linearly at a twofold axis. It should be noted that the aqua O(1W) atom forms a donor hydrogen bond with the uncoordinated carboxy oxygen

 © 2003 Wiley-VCH Verlag GmbH & Co. KGaA, Weinheim

atom O(1) [O(1W)···O(1) 2.786 Å], which extend the one-dimensional chains into two-dimensional supramolecular networks. Such two-dimensional networks are arranged in a repeated ···AAA··· fashion in the lattice, as shown in Figure 1, c.

In contrast to **1**, compound **2** crystallizes in the monoclinic space group $P2_1/n$ and each asymmetric unit consists of 1 Ni^{II}, 1 bpdc, 3 H_2O and one lattice H_2O. All atoms are located at general positions. The Ni^{II} site shows a distorted octahedral geometry, being ligated by two nitrogen atoms of one bpdc in a chelate mode, one carboxylate oxygen atom and three *cis*-related aqua ligands (Figure 2, a). The Ni−N and Ni−O distances are in the range of 2.080(3)−2.118(3) and 2.071(3)−2.110(3) Å, respectively, which are slightly shorter than the Co−N and Co−O distances observed in **1**. The *cis*-L−Co−L angles are in the range of 78.53(11)−96.26(12) and *trans*-L−Co−L angles are 169.35(11)−178.94(10)°, indicating that the Ni^{II} site has a more regular octahedron than the Co^{II} center in **1**. The two pyridine rings of bpdc in **2** are more twisted with a larger dihedral angle of 31.6° than that in **1**. Besides, with only one carboxylate group utilizing one oxygen atom to ligate a nickel(II) atom, the coordination mode of the bpdc molecule in **2** is different from that in **1**, in which each bpdc has two carboxylate groups coordinated, but similar to that found in $[Cu(bpdc)(H_2O)_2]$.[36] Different from the linear chain-like structure in **1**, the coordination modes of the bpdc ligand and the configuration of the Ni^{II} atom with three *cis*-related aqua ligands in **2** result in helical chains in which equivalent atoms are related by a 2_1-screw axis (Figure 2, b). This fact implies that the tridentate coordination mode of bpdc may play an important role in the

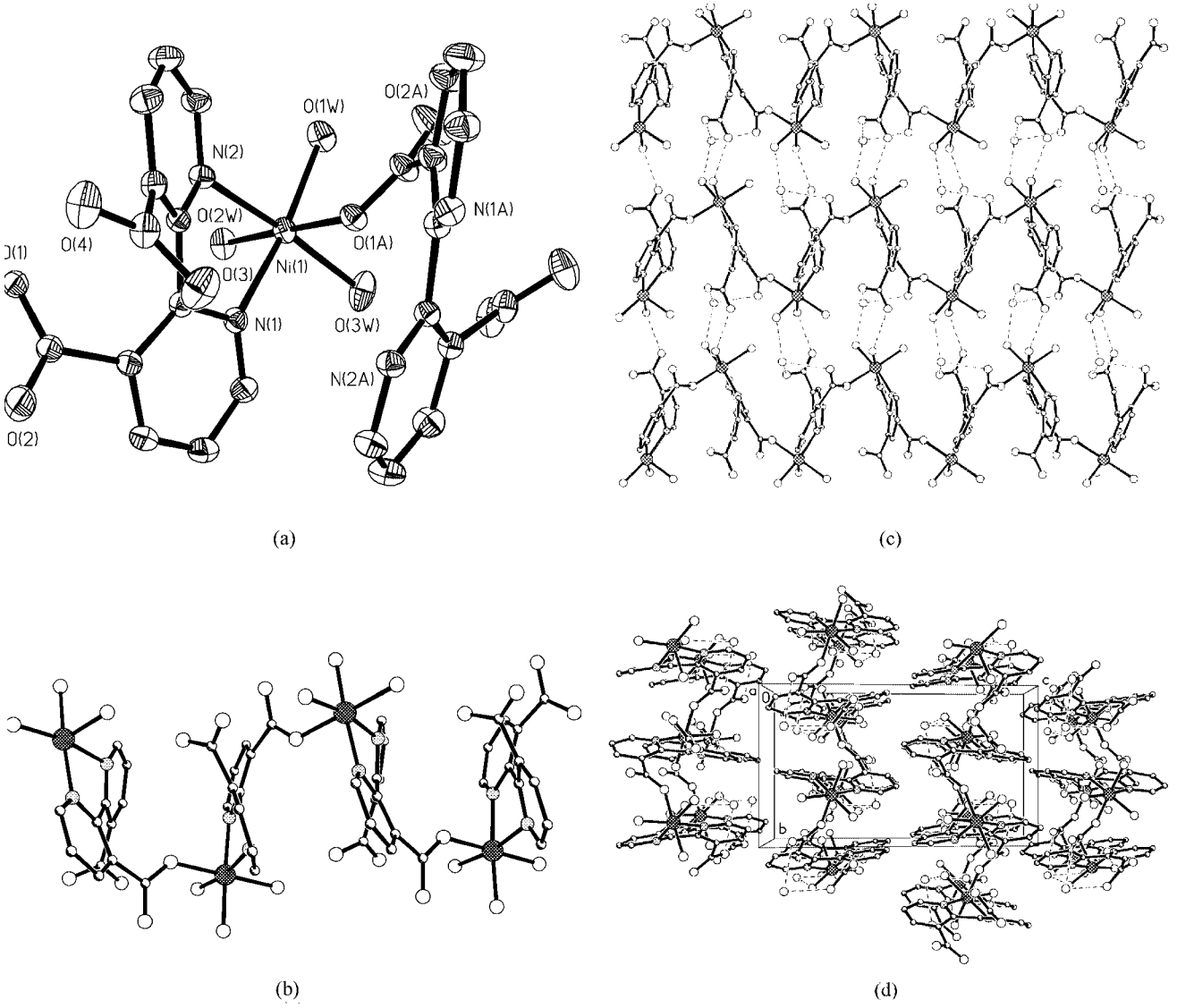

Figure 2. Perspective views of the coordination environments of the nickel atom (a), helical chain (b), and two-dimensional supramolecular network (c) and stacking array (d) in **2**

 © 2003 Wiley-VCH Verlag GmbH & Co. KGaA, Weinheim

formation of the chiral helical chains in **2**. On the other hand, there are a number of hydrogen bonds [O(1W)···O(4), 2.674; O(2W)···O(3), 2.744; O(3W)···O(4W), 2.716; O(4W)···O(3), 2.891; O(4W)···O(3W), 2.71 Å] which extend the helical chains into two-dimensional supramolecular networks (Figure 2, c). Such networks are arranged in an ···ABAB··· fashion as shown in Figure 2, d. Within each layer, all helical chains have the same chirality. However, helical chains of opposite chiralities construct adjacent layers and thus **2** crystallizes in the centrosymmetric space group.

Synthesis Chemistry

Although pdon was used as the original organic reagent in the preparation of **1** and **2** the bipyridine-3,3′-dicarboxylate ligand was unexpectedly found in the final products, which indicates an in situ transformation of pdon into bpdc during the course of hydrothermal treatment. As shown in our previous investigation[27−29] on ligand reactions under hydrothermal conditions in the presence of metal ions, the ligation of the metal ion will cause some decrease of electron density on the aromatic ring of the organic ligand, hence promote nucleophilic attack by water molecules or hydroxy groups. In this case, it seems most probable that the solvent aqua molecules act effectively as nucleophiles, attacking the carbonyl carbon atoms of pdon. As a result, the hydration of carbonyl groups of pdon furnishes an intermediate diol or even a double diol. When the sp^2 carbonyl carbon atoms become sp^3-hybridized, the carbon−carbon bond is then cleaved probably because of the crowdedness, resulting in the formation of bpdc. A recent study, indeed revealed that there is a tautomerism between a pdon complex of Co^{II} and its corresponding diol complex in aqueous solution.[38] The formation mechanism of bpdc in **1** and **2** shows some similarity to that of dimethyl 2,2′-bipyridine-3,3′-dicarboxylate in a previously reported pure organic reaction (Scheme 1, C).[34] Although the exact mechanism of ligand transformation is not yet proved, slow hydrolysis of the carbonyl groups ensures that an excess of metal ions remains in solution, thereby promoting the formation of less soluble polymeric networks. Equally important, the in situ slow bpdc formation also ensures the growth of large single crystals that are suitable for X-ray structure determination.

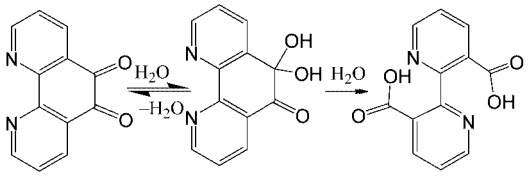

Scheme 2. Schematic representation of the possible transformation mechanism of pdon to bpdc

Conclusion

A new hydrolysis reaction of 1,10-phenanthroline-5,6-dione to 2,2′-bipyridine-3,3′-dicarboxylate has been achieved under hydrothermal conditions in the presence of metal acetates, resulting in the formation of two chain-like coordination polymers $[Co(bpdc)(H_2O)_2]$ and $[Ni(bpdc)(H_2O)_3]\cdot H_2O$. The different coordination modes concomitant with the difference of the dihedral angles between two pyridine rings of bpdc results in simple linear and helical chains, respectively.

Experimental Section

General Remarks: Elemental analyses were performed with a Perkin−Elmer 240 elemental analyzer. The FT-IR spectra were recorded from KBr pellets in the range of 400−4000 cm^{-1} with a Nicolet 5DX spectrometer.

Synthesis

$[Co(bpdc)(H_2O)_2]$ (1): A mixture of $Co(MeCO_2)_2\cdot 4H_2O$ (0.25 g, 1.0 mmol), 1,10-phenanthroline-5,6-dione (pdon) (0.208 g, 1.0 mmol), methanol (3 mL) and water (5 mL) in a molar ratio of 1:1:74:278 was stirred for 10 min in air, then transferred and sealed in a 23-ml Teflon-lined stainless steel container, which was heated to 140 °C for 72 h. After cooling to room temperature at the rate of 5 °C per hour, 0.34 g (ca. 50% yield) of brown block crystals of **1** was recovered. $C_{24}H_{20}Co_2N_4O_{12}$ (674.3): calcd. C 42.75, H 2.99, N 8.31; found C 42.67, H 3.08, N 8.23. IR (KBr): $\tilde{\nu}$ = 3751 w cm^{-1}, 3344 bs, 3102 m, 1796 w, 1566 s, 1438 m, 1394 s, 1227 w, 1152 w, 1096 wm, 826 w, 783 m, 750 m, 662 m, 518 w, 447 m.

$[Ni(bpdc)(H_2O)_3]\cdot H_2O$ (2): A mixture of $Ni(MeCO_2)_2\cdot 4H_2O$ (0.25 g, 1 mmol), pdon (0.208 g, 1 mmol), methanol (3 mL) and water (5 mL) in a molar ratio of 1:1:74:278 was stirred for 10 min in air, then transferred and sealed in a 23-ml Teflon-lined stainless steel container, which was heated to 140 °C for 72 h. After cooling to room temperature at a rate of 5 °C per hour, 0.373 g (35% yield) of blue block crystals of **1** were recovered. $C_{24}H_{28}N_4Ni_2O_{16}$ (745.9): calcd. C 38.65, H 3.78, N 7.51; found C 38.60, H 3.82, N 7.44. IR (KBr): $\tilde{\nu}$ = 3673 w cm^{-1}, 3390 bs, 1603 w, 1568 s, 1392 s, 1158 w, 1122 w, 1097 m, 772 m, 699 w, 442 w.

X-ray Crystallography: Diffraction intensities were collected at 293 K with a Siemens R3 diffractometer (Mo-K_α, λ = 0.71073 Å). Lorentz-polarization and absorption corrections were applied. The structure was solved with direct methods (SHELXS-97) and refined with a full-matrix least-squares technique (SHELXL-97).[39] Analytical expressions of neutral-atom scattering factors were employed, and anomalous dispersion corrections were incorporated. In all cases, all non-hydrogen atoms were refined anisotropically and hydrogen atoms of organic ligands were geometrically placed. CCDC-200013 and -200014 contain the supplementary crystallographic data for this paper. These data can be obtained free of charge at www.ccdc.cam.ac.uk/conts/retrieving.html [or from the Cambridge Crystallographic Data Centre, 12 Union Road, Cambridge CB2 1EZ, UK; Fax: (internat.) + 44-1223/336-033; E-mail: deposit@ccdc.cam.ac.uk].

Acknowledgments

This work was supported by the Ministry of Education of China (no. 01134).

 © 2003 Wiley-VCH Verlag GmbH & Co. KGaA, Weinheim

Table 1. Crystal and structure refinement data for complexes **1** and **2**

	1	**2**
Empirical formula	$C_{24}H_{20}Co_2N_4O_{12}$	$C_{24}H_{28}N_4Ni_2O_{16}$
Molecular mass	674.30	745.92
Temperature [K]	293(2)	293(2)
Wavelength [Å]	0.71073	0.71073
Crystal system	monoclinic	monoclinic
Space group	*C*2/*c*	$P2_1/n$
a [Å]	11.573(14)	10.045(10)
b [Å]	7.965(7)	9.285(7)
c [Å]	13.368(8)	16.155(10)
β [°]	101.21(2)	96.60(2)
V [Å^3]	1208.7(19)	1497(2)
Z	2	2
Density (calcd.) [Mg/m^3]	1.853	1.655
Absorption coefficient [mm^{-1}]	1.452	1.340
F(000)	684	768
Crystal size [mm]	0.50 × 0.26 × 0.06	0.82 × 0.64 × 0.57
Theta range for data collection [°]	3.11 to 26.68	2.28 to 27.02
Index ranges	$-14 \le h \le 10$, $-9 \le k \le 10$, $-16 \le l \le 16$	$0 \le h \le 12$, $0 \le k \le 11$, $-20 \le l \le 20$
Reflections collected	3283	3451
Independent reflections	1261 (R_{int} = 0.0227)	3268 (R_{int} = 0.0403)
Max. and min. transmission	0.9179 and 0.5304	0.5154 and 0.4061
Refinement method	full-matrix least squares on F^2	full-matrix least squares on F^2
Data/restrains/parameters	1261/0/97	3268/0/209
Goodness-of-fit on F^2	1.082	1.028
Final *R* indices [$I > 2\sigma(I)$]	0.0309, 0.0767	0.0464, 0.1207
R indices (all data)	0.0361, 0.0789	0.0620, 0.1307
Largest diff. Peak and hole [e·A^{-3}]	0.403 and −0.268	0.571 and −0.680

Table 2. Selected Bond lengths [Å] and angles [°] for complexes **1** and **2**

Complex **1**		Complex **2**	
Co(1)−N(1)[a]	2.123(2)	Ni(1)−O(3W)	2.065(3)
Co(1)−N(1)[b]	2.123(2)	Ni(1)−O(1W)	2.071(3)
Co(1)−O(2)[c]	2.133(2)	Ni(1)−O(1)[a]	2.078(3)
Co(1)−O(2)	2.133(2)	Ni(1)−N(1)	2.080(3)
Co(1)−O(1W)[c]	2.151(3)	Ni(1)−O(2W)	2.110(3)
Co(1)−O(1W)	2.151(3)	Ni(1)−N(2)	2.118(3)
N(1)[a]−Co(1)−N(1)[b]	76.70(11)	O(3W)−Ni(1)−O(1W)	95.26(13)
N(1)[a]−Co(1)−O(2)[c]	168.02(7)	O(3W)−Ni(1)−O(1)[a]	88.54(12)
N(1)[b]−Co(1)−O(2)[c]	99.37(9)	O(1W)−Ni(1)−O(1)[a]	90.51(10)
N(1)[a]−Co(1)−O(2)	99.37(9)	O(3W)−Ni(1)−N(1)	93.06(13)
N(1)[b]−Co(1)−O(2)	168.02(7)	O(1W)−Ni(1)−N(1)	171.47(11)
O(2)[c]−Co(1)−O(2)	86.65(10)	O(1)[a]−Ni(1)−N(1)	87.84(10)
N(1)[a]−Co(1)−O(1W)[c]	85.01(8)	O(3W)−Ni(1)−O(2W)	90.47(12)
N(1)[b]−Co(1)−O(1W)[c]	99.05(8)	O(1W)−Ni(1)−O(2W)	89.95(11)
O(2)[c]−Co(1)−O(1W)[c]	84.46(7)	O(1)[a]−Ni(1)−O(2W)	178.94(10)
O(2)−Co(1)−O(1W)[c]	91.79(7)	N(1)−Ni(1)−O(2W)	91.84(11)
N(1)[a]−Co(1)−O(1W)	99.05(8)	O(3W)−Ni(1)−N(2)	169.35(11)
N(1)[b]−Co(1)−O(1W)	85.01(8)	O(1W)−Ni(1)−N(2)	92.99(12)
O(2)[c]−Co(1)−O(1W)	91.79(7)	O(1)[a]−Ni(1)−N(2)	84.66(11)
O(2)−Co(1)−O(1W)	84.46(7)	N(1)−Ni(1)−N(2)	78.53(11)
O(1W)[c]−Co(1)−O(1W)	174.85(9)	O(2W)−Ni(1)−N(2)	96.26(12)

Symmetry codes for **1**: [a] $x, y + 1, z$; [b] $-x + 1, y + 1, -z + 1/2$. [c] $-x + 1, y, -z + 1/2$. Symmetry codes for **2**: $-x + 3/2, y + 1/2, -z + 1/2$.

[1] R. Robson, B. F. Abrahams, S. R. Batten, R, W. Gable, B. F. Hoskins, J. Lieu, *Supramolecular Architecture*, ACS publications, Washington, DC, **1992**, p 256.

[2] J. M. Lehn, *Supramolecular Chemistry*, Wiley-VCH, Weinheim, **1995**, chapter 9.

[3] M. Munakata, L. Wu, T. Kuroda-Sowa, *Adv. Inorg. Chem.* **1999**, *46*, 173−303.

[4] P. J. Hagrman, D. Hagrman, J. Zubieta, *Angew. Chem. Int. Ed.* **1999**, *38*, 2638−2684.

[5] J. Blake, N. R. Champness, P. Hubberstey, W.-S. Li, M. A. Withersby, M. Schröder, *Coord. Chem. Rev.* **1999**, *183*, 117−138.

[6] C. B. Aakeroy, K. R. Seddon, *Chem. Soc. Rev.* **1993**, *22*, 397−407.

 © 2003 Wiley-VCH Verlag GmbH & Co. KGaA, Weinheim

[7] O. M. Yaghi, H. Li, C. Davis, D. Richardson, T. L. Groy, *Acc. Chem. Res.* **1998**, *31*, 474−484.
[8] M. Fujita, *Acc. Chem. Res.* **1999**, *32*, 53−61.
[9] C. J. Jones, *Chem. Soc. Rev.* **1998**, *27*, 289−300.
[10] S. Leininger, B. Olenyuk, P. J. Stang, *Chem. Rev.* **2000**, *100*, 853−980.
[11] S. R. Batten, R. Robson, *Angew. Chem. Int. Ed.* **1998**, *37*, 1460−1494.
[12] T. L. Hennigar, D. C. MacQuarrie, P. Losier, R. D. Rogers, M. J. Zaworotko, *Angew. Chem. Int. Ed. Engl.* **1997**, *36*, 972−973.
[13] H. Gudbjartson, K. Biradha, K. M. Poirier, M. J. Zaworotko, *J. Am. Chem. Soc.* **1999**, *121*, 2599−2600.
[14] L. Carlucci, G. Ciani, D. M. Proserpio, A. Sironi, *Angew. Chem. Int. Ed. Engl.* **1995**, *34*, 1895−1898.
[15] G. R. Desiraju, *Angew. Chem. Int. Ed. Engl.* **1995**, *34*, 2311−2327.
[16] W.-B. Lin, O. R. Evans, R.-G. Xiong, Z.-Y. Wang, *J. Am. Chem. Soc.* **1998**, *120*, 13272−13273.
[17] W.-B. Lin, Z.-Y. Wang, L. Ma, *J. Am. Chem. Soc.* **1999**, *121*, 11249−11250.
[18] O. R. Evans, W.-B. Lin, *Chem. Mater.* **2001**, *13*, 3009−3017.
[19] O. R. Evans, W.-B. Lin, *Chem. Mater.* **2001**, *13*, 2705−2712.
[20] O. Kahn, C. J. Martinez, *Science* **1998**, *279*, 44−48.
[21] O. Kahn, *Acc. Chem. Res.* **2000**, *33*, 647−657.
[22] S. S.-Y. Chui, S. M.-F. Lo, J. P. H. Charmant, A. G. Orpen, I. D. Williams, *Science* **1999**, *283*, 1148−1150.
[23] L. Chen, M. Eddaoudi, S. T. Hyde, M. O'Keeffe, O. M. Yaghi, *Science* **2001**, *291*, 1021−1023.
[24] S.-I. Noro, S. Kitagawa, M. Kondo, K. Seki, *Angew. Chem. Int. Ed.* **2000**, *39*, 2082−2084.
[25] K. Barthelet, J. Marrot, D. Riou, G. Ferey, *Angew. Chem. Int. Ed.* **2002**, *41*, 281−284.
[26] J. S. Seo, D. Whang, H. Lee, S. I. Jun, J. Oh, Y. J. Jeon, K. Kim, *Nature* **2000**, *404*, 982−986.
[27] X.-M. Zhang, M.-L. Tong, X.-M. Chen, *Angew. Chem. Int. Ed.* **2002**, *41*, 1029−1031.
[28] X.-M. Zhang, M.-L. Tong, M.-L. Gong, H.-K. Lee, L. Luo, K.-F. Li, Y.-X. Tong, X.-M. Chen, *Chem. Eur. J.* **2002**, *8*, 3187−3194.
[29] J. Tao, Y. Zhang, M.-L. Tong, X.-M. Chen, T. Yuen, C. L. Lin, X.-Y. Huang, J. Li, *Chem. Commun.* **2002**, 1342−1343.
[30] C.-M. Liu, S. Gao, H.-Z. Kou, *Chem. Commun.* **2001**, 1670−1671.
[31] R. Evans, W. Lin, *Cryst. Growth Des.* **2001**, *1*, 9−11.
[32] R.-G. Xiong, J. Zhang, Z.-F. Chen, X.-Z. You, C.-M. Che, H.-K. Fun, *J. Chem. Soc., Dalton Trans.* **2001**, 780−782.
[33] F. Calderazzo, F. Marchetti, G. Pampaloni, V. Passarelli, *J. Chem. Soc., Dalton Trans.* **1999**, 4389−4396.
[34] W. Z. Antkowiak, A. Sobczak, *Tetrahedron* **2001**, *57*, 2799−2805.
[35] K. Nakamoto, *Infrared and Raman Spectra of Inorganic and Coordination Compounds*, John Wiley & Sons, New York, **1978**.
[36] K. Ravikumar, G. Y. S. K. Swamy, N. V. Lakshmi, *Acta Crystallogr., Sect. C* **1995**, *51*, 608−611.
[37] K. Ravikumar, N. V. Lakshmi, G. Y. S. K. Swamy, *Z. Kristallogr.* **1998**, *213*, 191−194.
[38] Y. B. Lei, C. N. Shi, F. C. Anson, *Inorg. Chem.* **1996**, *35*, 3044−3049.
[39] G. M. Sheldrick, *SHELX-97, Program for X-ray Crystal Structure Solution and Refinement*, Göttingen University, Germany, **1997**.

Received January 30, 2003

 © 2003 Wiley-VCH Verlag GmbH & Co. KGaA, Weinheim

Helical Ribbons of Cadmium(II) and Zinc(II) Dicarboxylates with Bipyridyl-Like Chelates − Syntheses, Crystal Structures and Photoluminescence

Ling-Yun Zhang,[a] Gao-Feng Liu,[a] Shao-Liang Zheng,[a] Bao-Hui Ye,[a] Xian-Ming Zhang,[a] and Xiao-Ming Chen*[a]

Keywords: Coordination polymers / Cadmium / Zinc / N ligands / Pi interactions

Four mixed-ligand complexes of $[M(mpa)(phen)]_n$ [M = Cd (**1**) or Zn (**2**) and mpa = *m*-phthalate and phen = 1,10-phenanthroline) and $[M_2(mpa)_2(2,2'\text{-bpy})_2]_n$ [M = Zn (**3**) or Cd (**4**) and 2,2′-bpy = 2,2′-bipyridine] have been synthesized and their crystal structures have been established by single-crystal X-ray diffraction. They all consist of one-dimensional ribbons featuring dinuclear units. Both **1** and **2** crystallize isomorphously in the monoclinic space group $P2/c$ and feature helical chains. While **3** and **4** crystallize in the triclinic space group $P\bar{1}$. The one-dimensional ribbons are assembled into three-dimensional networks by π–π stacking interactions. They all show strong blue photoluminescence and are stable in air up to ca. 402, 371, 365 and 370 °C, respectively.

(© Wiley-VCH Verlag GmbH & Co. KGaA, 69451 Weinheim, Germany, 2003)

Introduction

The construction of supramolecular architectures is currently of great interest owing to their intriguing network topologies and potential functions such as adsorption, ion exchange, shape-selective catalysis, non-linear and magnetic materials.[1−3] The strategies for design and tailor-making of such supramolecular architectures with dicarboxylate spacers such as terephathlate, malate, oxalate, 4,4′-oxybis-(benzoic acid) are currently interesting. Recently, we and others have reported some interesting polymeric architectures containing linear, nonlinear flexible and V-shaped dicarboxylates together with bipyridyl-like ligands.[4−11] Chelating bipyridyl-like ligands such as 1,10-phenanthroline and 2,2′-bipyridine are important in maintaining the one dimensionality of the coordination polymers and may provide potential supramolecular recognition sites for π−π aromatic stacking interactions to form interesting supramolecular structures such as double-stranded helices and molecular zippers.[7,8]

On the other hand, polynuclear d^{10} metal complexes are very attractive in that they not only exhibit intriguing structures but also photoluminescent properties.[12−17] As a sequel to our previous reports on a series of d^{10} complexes, which show strong luminescent properties,[4,5,14−16] we now describe four one-dimensional coordination polymers $[M(mpa)(phen)]_n$ [M = Cd (**1**) or Zn (**2**); mpa = *m*-phthalate and phen = 1,10-phenanthroline] and $[M_2(mpa)_2(2,2'\text{-bpy})_2]_n$ [M = Zn (**3**) or Cd (**4**) and 2,2′-bpy = 2,2′-bipyridine], which exhibit different structures compared to the related Cu^{II} complexes,[7,8] all of which show blue luminescence.

[a] School of Chemistry and Chemical Engineering, Sun Yat-Sen University,
Guangzhou 510275, China
Fax: (internat.) + 86-20/84112245
E-mail: cescxm@zsu.edu.cn

Results and Discussion

Characterization

The IR spectrum of **1** shows characteristic bands of the dicarboxylate groups in the usual region at 1564 and 1515 cm^{-1} for the asymmetric stretching and at 1400 cm^{-1} for the symmetric stretching. The separations (Δ) between $\nu_{asym}(CO_2)$ and $\nu_{sym}(CO_2)$ are at 164 and 115 cm^{-1}, which are attributed to the existence of both bridging and chelate modes of the carboxylate groups, respectively (Scheme 1, a).[18] For **2**, the bands are at 1614 and 1558 cm^{-1} for the asymmetric stretching and at 1397 cm^{-1} for the symmetric stretching; the Δ values are at 217 and 161 cm^{-1}, and are attributable to the co-existence of the monodentate and bridging modes (Scheme 1, b). For **3**, the bands of the dicarboxylate units are shown at 1562 and 1532 cm^{-1} for the asymmetric stretching and at 1431 cm^{-1} for the symmetric stretching; the Δ values are at 131 and 101 cm^{-1}, which are attributed to co-existence of the bridging and chelate modes (Scheme 1a, c). Whereas for **4**, the characteristic bands and Δ values are very similar to those found for **1**, indicating that the carboxylate groups exhibit both a bridging and chelate mode. The IR spectra indicate that the mpa carboxylate groups function in different coordination modes, consistent with the crystal structures of **1**, **2**, **3** and **4**.

Thermogravimetric analysis (TGA) was performed on polycrystalline samples in air. There was no decomposition

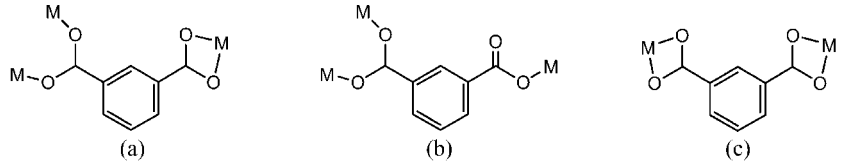

Scheme 1. Coordination modes of mpa: (a) chelate-bidentate, (b) monodentate-bidentate and (c) chelating bis(bidentate)

up to ca. 402, 371, 365 and 370 °C for **1**, **2**, **3** and **4**, respectively, suggesting that the products are more stable than the related ones synthesized by the conventional solution method, at room temperature.[17]

Crystal Structures

Complexes **1**, **2**, **3** and **4** all consist of one-dimensional ribbons. Both **1** and **2** crystallize isomorphously in the monoclinic space group $P2/c$, while **3** and **4** crystallize in the triclinic space group $P\bar{1}$ (see Tables 1 and 2).

In the crystal structure of **1**, there is one Cd^{II} atom, one mpa ligand and one phen ligand in each independent crystallographic unit. As shown in Figure 1, each Cd^{II} atom in **1** is primarily coordinated by two nitrogen atoms [Cd1−N1 = 2.395(4), Cd1−N2 = 2.377(5) Å, N2−Cd1−N1 = 70.5(2)°] of a chelating phen ligand, two oxygen atoms of two μ-carboxylate ends of two mpa ligands [Cd1−O2A = 2.255(4), Cd1−O1B = 2.301(4) Å, O2A−Cd1−O1B = 99.7(2)°] and two oxygen atoms of one chelating carboxylate end of one mpa ligand [Cd1−O4 = 2.453(4), Cd1−O3 = 2.331(4) Å, O3−Cd1−O4 = 55.2(1)°] to furnish a highly distorted octahedral geometry. Two Cd^{II} atoms related by a twofold axis are bridged by a pair of the mpa μ-carboxylate ends into a dinuclear unit [Cd1···Cd1A = 3.99 Å]. A face-to-face distance of 3.51 Å between a pair of phen ligands coordinated to the two Cd^{II} atoms is observed, showing significant intramolecular π−π interactions.

In fact, the V-shaped mpa ligand acts in the chelate-bidentate coordination mode (see Scheme 1, a) to link the adjacent Cd^{II} atoms into one-dimensional helical ribbons with a pitch of 9.55 Å running along the c axis (Figure 2, a). Pairs of phen ligands are alternately attached to both sides of the ribbon; the adjacent zigzag ribbons are packed through intercalation of the lateral phen ligands (face-to-face distance 3.32 Å), in the zipper-like fashion, into two-dimensional networks parallel to the bc plane. Adjacent ribbons also have strong intermolecular π−π interactions[19−23] between the mpa phenyl rings in an offset fashion with a face-to-face distance of ca. 3.38 Å, which

Table 1. Crystallographic data for **1**−**4**

	1	**2**	**3**	**4**
Empirical formula	$C_{20}H_{12}CdN_2O_4$	$C_{20}H_{12}N_2O_4Zn$	$C_{36}H_{24}N_4O_8Zn_2$	$C_{36}H_{24}Cd_2N_4O_8$
Formula mass	456.72	409.69	771.33	865.39
Temperature [K]	293	293	293	228
Crystal color and form	colorless prisms	pale-yellow blocks	pale-yellow blocks	colorless blocks
Crystal system	monoclinic	monoclinic	triclinic	triclinic
Space group	$P2/c$ (no. 13)	$P2/c$ (no. 13)	$P\bar{1}$ (no. 2)	$P\bar{1}$ (no. 2)
a [Å]	8.391(6)	8.730(4)	9.44(1)	9.425(2)
b [Å]	10.681(8)	10.34(1)	11.40(1)	10.267(2)
c [Å]	19.10(2)	18.57(2)	16.98(1)	18.649(4)
α [°]			100.07(1)	74.03(3)
β [°]	100.73(2)	99.65(2)	94.02(1)	85.93(3)
γ [°]			110.50(1)	64.15(3)
Volume [Å^3]	1682(2)	1652(2)	1670(2)	1558.8(6)
Z	4	4	2	2
$D_{calcd.}$ [Mg/m^3]	1.803	1.647	1.534	1.844
Absorption coefficient [mm^{-1}]	1.329	1.517	1.496	1.428
$F(000)$	904	832	784	856
Crystal size [mm]	0.30 × 0.25 × 0.20	0.35 × 0.33 × 0.27	0.50 × 0.40 × 0.35	0.52 × 0.48 × 0.42
θ_{max} [°]	26.0	28.0	26.0	28.31
Reflections collected	3554	2938	6572	10180
Independent reflections	3321	2685	6553	7385
Number of parameters	245	245	452	452
Goodness-of-fit on F^2	1.053	1.060	1.038	1.179
Final R indices [$I \geq 2\sigma(I)$][a][b]	R_1 = 0.0455, wR_2 = 0.1226	R_1 = 0.0538, wR_2 = 0.1370	R_1 = 0.0651, wR_2 = 0.1537	R_1 = 0.0342, wR_2 = 0.0827
R indices (all data)[a][b]	R_1 = 0.0621, wR_2 = 0.1331	R_1 = 0.0707, wR_2 = 0.1491	R_1 = 0.1247, wR_2 = 0.1837	R_1 = 0.0392, wR_2 = 0.0939
Largest peak and hole [e·Å^{-3}]	0.947 and −0.849	0.631 and −0.836	0.502 and −0.845	0.882 and −0.623

[a] $R_1 = (F_o - F_c)/F_o$. [b] $wR_2 = [w(F_o^2 - F_c^2)^2/w(F_o^2)^2]^{1/2}$.

 © 2003 Wiley-VCH Verlag GmbH & Co. KGaA, Weinheim

Table 2. Selected bond lengths [Å] and angles [°]; symmetry codes: (A) $x, -y, z + 1/2$, (B) $-x, -y, -z$, for **1** and **2**, (A) $-x, -y, -z + 1$, (B) $x, y + 1, z$, for **3**, (A) $-x, -y + 2, -z + 1$, (B) $x + 1, y - 1, z + 1$, for **4**

1			
Cd(1)−O(3)	2.331(4)	Cd(1)−O(4)	2.453(4)
Cd(1)−O(2A)	2.255(4)	Cd(1)−N(1)	2.395(4)
Cd(1)−O(1B)	2.301(4)	Cd(1)−N(2)	2.377(5)
O(2A)−Cd(1)−O(1B)	99.7(2)	O(3)−Cd(1)−N(2)	137.4(1)
O(2A)−Cd(1)−O(3)	100.6(2)	O(2A)−Cd(1)−N(1)	169.7(2)
O(1B)−Cd(1)−O(3)	94.7(1)	O(1B)−Cd(1)−N(1)	79.2(2)
O(2A)−Cd(1)−N(2)	101.4(2)	O(3)−Cd(1)−N(1)	89.7(2)
O(1B)−Cd(1)−N(2)	116.9(2)	N(2)−Cd(1)−N(1)	70.5(2)
O(2A)−Cd(1)−O(4)	99.2(2)	O(1B)−Cd(1)−O(4)	146.9(1)
O(3)−Cd(1)−O(4)	55.2(1)	N(2)−Cd(1)−O(4)	85.4(1)
N(1)−Cd(1)−O(4)	86.7(2)		
2			
Zn(1)−O(3)	2.026(3)	Zn(1)−N(2)	2.175(4)
Zn(1)−O(1B)	2.033(4)	Zn(1)−N(1)	2.218(4)
Zn(1)−O(2A)	2.045(3)		
O(3)−Zn(1)−O(1B)	97.4(2)	O(2A)−Zn(1)−N(2)	92.9(2)
O(3)−Zn(1)−O(2A)	101.8(2)	O(3)−Zn(1)−N(1)	92.5(2)
O(1B)−Zn(1)−O(2A)	96.2(2)	O(1B)−Zn(1)−N(1)	83.4(2)
O(3)−Zn(1)−N(2)	131.4(2)	O(2A)−Zn(1)−N(1)	165.6(1)
O(1B)−Zn(1)−N(2)	127.0(2)	N(2)−Zn(1)−N(1)	76.2(2)
3			
Zn(1)−O(1)	2.454(5)	Zn(2)−O(7)	2.066(4)
Zn(1)−O(2)	2.085(4	Zn(2)−O(8)	2.391(5)
Zn(1)−O(6)	2.095(5)	Zn(2)−O(4B)	2.012(5)
Zn(1)−O(5A)	2.039(4)	Zn(2)−O(3B)	2.469(5)
Zn(1)−N(1)	2.165(5)	Zn(2)−N(3)	2.165(6)
Zn(1)−N(2)	2.198(6)	Zn(2)−N(4)	2.086(5)
O(5A)−Zn(1)−O(2)	103.8(2)	O(4B)−Zn(2)−O(7)	101.0(2)
O(5A)−Zn(1)−O(6)	105.5(2)	O(4B)−Zn(2)−N(4)	152.3(2)
O(2)−Zn(1)−O(6)	93.6(2)	O(7)−Zn(2)−N(4)	106.4(2)
O(5A)−Zn(1)−N(1)	103.5(2)	O(4B)−Zn(2)−N(3)	98.3(2)
O(2)−Zn(1)−N(1)	151.1(2)	O(7)−Zn(2)−N(3)	105.9(2)
O(6)−Zn(1)−N(1)	88.6(2)	N(4)−Zn(2)−N(3)	77.7(2)
O(5A)−Zn(1)−N(2)	85.9(2)	O(4B)−Zn(2)−O(8)	98.4(2)
O(2)−Zn(1)−N(2)	96.9(2)	O(7)−Zn(2)−O(8)	59.7(2)
O(6)−Zn(1)−N(2)	162.3(2)	N(4)−Zn(2)−O(8)	92.4(2)
N(1)−Zn(1)−N(2)	75.5(2)	N(3)−Zn(2)−O(8)	159.8(2)
O(5A)−Zn(1)−O(1)	158.6(2)	O(4B)−Zn(2)−O(3B)	57.9(2)
O(2)−Zn(1)−O(1)	58.2(2)	O(7)−Zn(2)−O(3B)	151.0(2)
O(6)−Zn(1)−O(1)	88.3(2)	N(4)−Zn(2)−O(3B)	95.1(2)
N(1)−Zn(1)−O(1)	93.1(2)	N(3)−Zn(2)−O(3B)	97.4(2)
N(2)−Zn(1)−O(1)	85.1(2)	O(8)−Zn(2)−O(3B)	101.0(2)
4			
Cd(1)−O(1)	2.281(3)	Cd(2)−O(7)	2.245(2)
Cd(1)−O(2)	2.524(3)	Cd(2)−O(8)	2.559(3)
Cd(1)−O(6)	2.246(2)	Cd(2)−O(4B)	2.247(3)
Cd(1)−O(5A)	2.252(3)	Cd(2)−O(3A)	2.285(3)
Cd(1)−N(1)	2.379(3)	Cd(2)−N(3)	2.325(3)
Cd(1)−N(2)	2.333(3)	Cd(2)−N(4)	2.332(3)
O(5A)−Cd(1)−O(2)	87.3(1)	O(4B)−Cd(2)−O(7)	90.7(1)
O(5A)−Cd(1)−O(6)	117.1(1)	O(4B)−Cd(2)−N(4)	93.9(1)
O(2)−Cd(1)−O(6)	138.58(9)	O(7)−Cd(2)−N(4)	105.9(1)
O(5A)−Cd(1)−N(1)	84.6(1)	O(4B)−Cd(2)−N(3)	88.6(1)
O(2)−Cd(1)−N(1)	131.56(9)	O(7)−Cd(2)−N(3)	176.65(9)
O(6)−Cd(1)−N(1)	86.1(1)	N(4)−Cd(2)−N(3)	70.89(9)
O(5A)−Cd(1)−N(2)	133.8(1)	O(4B)−Cd(2)−O(8)	140.0(1)
O(2)−Cd(1)−N(2)	83.13(9)	O(7)−Cd(2)−O(8)	54.40(8)
O(6)−Cd(1)−N(2)	99.00(9)	N(4)−Cd(2)−O(8)	79.96(9)
N(1)−Cd(1)−N(2)	69.27(9)	N(3)−Cd(2)−O(8)	125.06(8)
O(5A)−Cd(1)−O(1)	100.2(1)	O(4B)−Cd(2)−O(3A)	123.2(1)
O(2)−Cd(1)−O(1)	54.08(8)	O(7)−Cd(2)−O(3A)	94.6(1)
O(6)−Cd(1)−O(1)	87.3(1)	N(4)−Cd(2)−O(3A)	137.5(1)
N(1)−Cd(1)−O(1)	173.14(9)	N(3)−Cd(2)−O(3A)	88.6(1)
N(2)−Cd(1)−O(1)	109.9(1)	O(8)−Cd(2)−O(3A)	82.64(9)

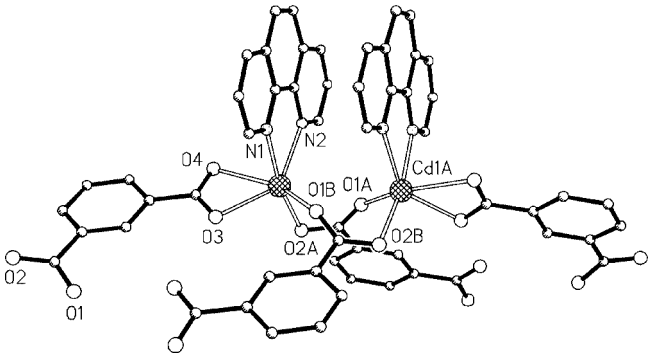

Figure 1. Perspective view of the coordination environments of the metal atoms with atomic labels in **1**

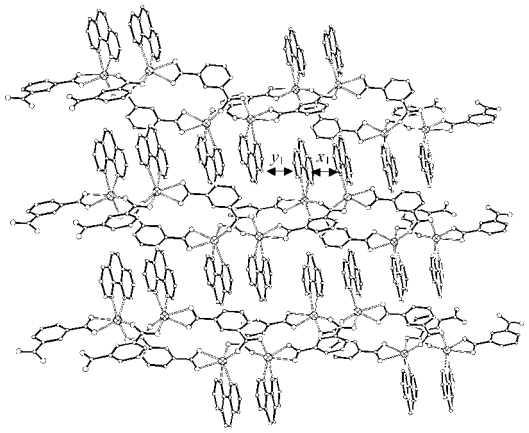

(a)

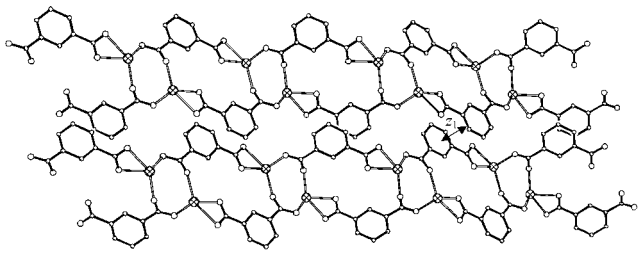

(b)

Figure 2. Perspective views of the two-dimensional networks parallel to the *bc* plane (a) and the *ac* plane (b) in **1**; the arrow in (b) highlights the intermolecular π−π interaction between the mpa phenyl rings; the face-to-face distances for the π−π interactions are x_1 = 3.51 Å, y_1 = 3.32 Å and z_1 = 3.38 Å

also extend the ribbons into two-dimensional networks (Figure 2, b) in another direction parallel to the *ab* plane. Therefore, these ribbons are in fact stacked through two different kinds of aromatic π−π stacking interactions, between phen ligands and mpa ligands, into a three-dimensional architecture in the lattice.

In the crystal structure of **2**, each Zn^{II} atom is primarily coordinated by two nitrogen atoms [Zn−N = 2.175(4) or

 © 2003 Wiley-VCH Verlag GmbH & Co. KGaA, Weinheim

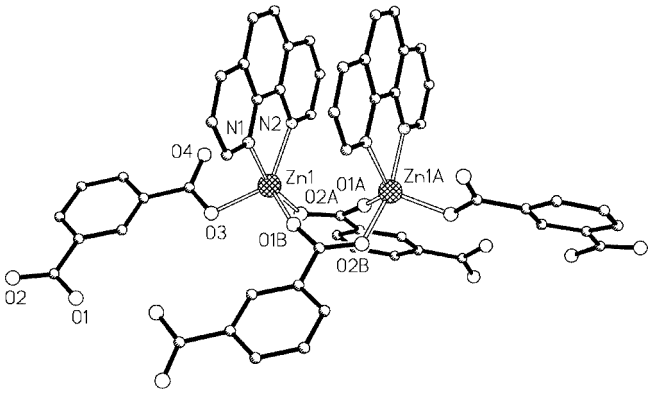

Figure 3. Perspective view of the coordination environments of the metal atoms with atomic labels in **2**

2.218(4) Å] from a chelating phen ligand and three oxygen atoms [Zn−O = 2.026(3)−2.045(3) Å] from two μ-carboxylate ends and one monodentate carboxylate end of three mpa ligands in a distorted trigonal arrangement, in which the N1 and O2A atoms occupy the axial positions and the pendant carboxy O4 atom has no significant interaction with Zn1 [Zn1···O4 = 2.675(4) Å] (Figure 3). The intradinuclear Zn···Zn distance (3.933 Å) and the face-to-face distance (3.52 Å) between the two phen ligands are similar to those found in **1**.

All the mpa ligands in **2** exhibit the monodentate-bidentate coordination mode (Scheme 1, b), and the pitch of the helical ribbon is 9.29 Å, being shorter than that in **1**. These differences may be attributed to the radius of the Cd^{II} atom being larger than that of the Zn^{II} atom, resulting in different coordination environments. On the other hand, adjacent ribbons in **2** are packed in a highly similar fashion to **1** through the π−π stacking interactions between the lateral phen ligands with face-to-face distances of ca. 3.29 Å and between the mpa phenyl rings with face-to-face distances of ca. 3.35 Å, into a three-dimensional network in the solid.

When 2,2′-bpy, an aromatic chelate ligand of smaller size, was used instead of phen, different ribbons were formed in **3** and **4** under similar reaction conditions. As illustrated in Figure 4 (a), there are two different metal coordination environments in **3**. Zn1 is coordinated by two oxygen atoms of one chelating carboxylate end of one mpa ligand [Zn1−O1 = 2.454(5), Zn1−O2 = 2.085(4) Å, O1−Zn1−O2 = 58.2(2)°], two oxygen atoms of two μ-carboxylate ends of two mpa ligands [Zn1−O5A = 2.039(4), Zn1−O6 = 2.095(5) Å, O5A−Zn1−O6 = 105.5(2)°] and two nitrogen atoms of a chelate 2,2′-bpy ligand [Zn1−N1 = 2.165(5), Zn1−N2 = 2.198(6) Å, N1 −Zn1−N2 = 75.5(2)°] to furnish a highly distorted octahedral environment, whereas Zn2 is ligated by four oxygen atoms of two chelating carboxylate ends of two mpa ligands [Zn2−O = 2.012(5)−2.469(5) Å, O3B−Zn2−O4B = 57.9(2), O7−Zn2−O8 = 59.7(2)°] and two nitrogen atoms of a chelate 2,2′-bpy ligand [Zn2−N4 = 2.086(5), Zn2−N3 = 2.165(6) Å, N3 −Zn2−N4 = 77.7(2)°] to complete a highly distorted octahedral geometry.

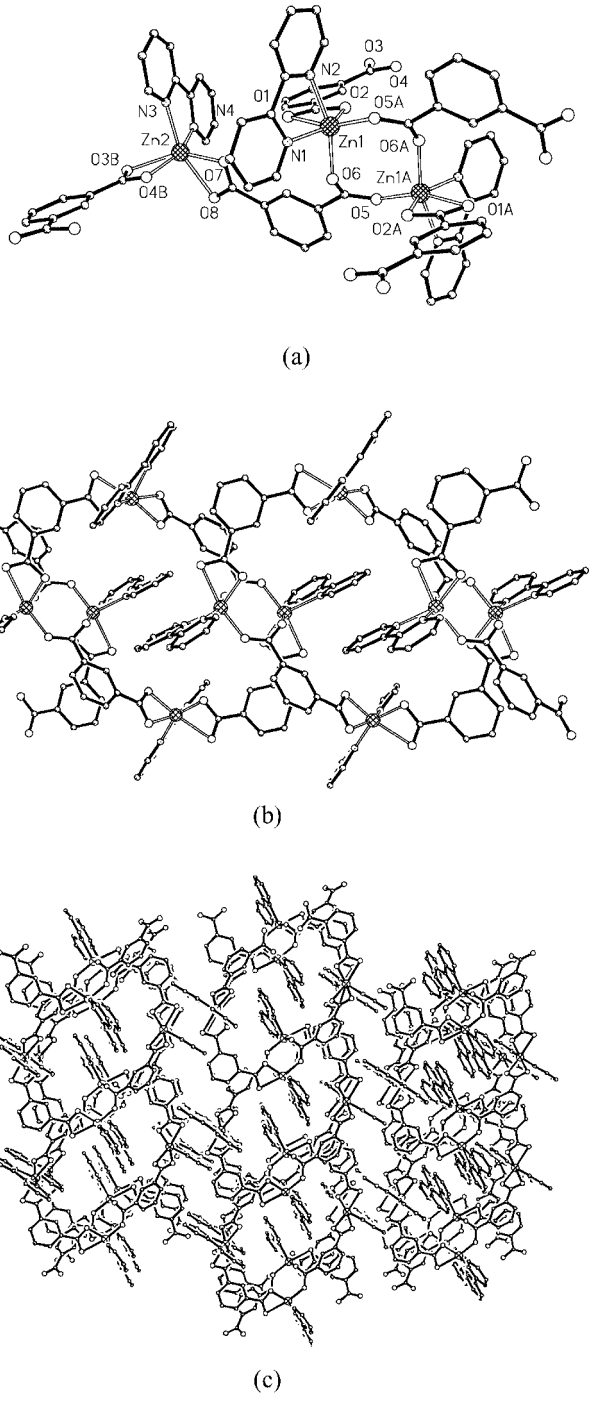

Figure 4. Perspective views of the coordination environments of the metal atoms with atomic labels (a), the one-dimensional ribbon running along the *b* axis (b) and the three-dimensional network (c) in **3**

The Zn1 atom in **3** is bridged by two μ-carboxylate ends to a crystallographically equivalent Zn^{II} atom to generate a dinuclear unit [Zn1···Zn1A = 4.324 Å] (Figure 4, a). The distance of Zn1···Zn1A is longer than in **2**, which may be attributed to the different coordination geometry and the orientation of the two 2,2′-bpy ligands around the two Zn^{II} atoms. The dinuclear units are interconnected to the mononuclear Zn2 sites, furnishing one-dimensional ribbons

 © 2003 Wiley-VCH Verlag GmbH & Co. KGaA, Weinheim

along the *b* axis, which exhibit large rings each comprising four bridging V-shaped mpa ligands, two dinuclear units and two mononuclear units. The ribbon is decorated by 2,2′-bpy ligands in four different orientations (Figure 4, b). In fact, the V-shaped mpa ligands in **3** exhibit two different modes, chelate-bidentate (Scheme 1, a) and chelating bis(bidentate) (Scheme 1, c). The bridging bidentate ends of the chelate-bidentate mpa ligands contribute to the formation of the dinuclear units, whereas the chelate ends are connected to both the mono- and dinuclear Zn^{II} sites. The 2,2′-bpy ligands are orientated outwards of the ribbon and thus play an important role in packing adjacent ribbon chains into three-dimensional networks (Figure 4, c) through π−π stacking interactions (face-to-face distance ca. 3.56 or 3.62 Å). It should be pointed out that the π−π stacking interactions for mpa ligands in **3** are insignificant compared to those of **1** and **2**.

In the crystal structure of **4**, there are two Cd^{II} atoms, two mpa ligands and two phen ligands in each independent crystallographic unit. Cd1 is coordinated by two oxygen atoms from one chelating carboxylate end of one mpa ligand [Cd1−O1 = 2.281(3), Cd1−O2 = 2.524(3) Å, O1−Cd1−O2 = 54.08(8)°], two oxygen atoms of two μ-carboxylate ends of two mpa ligands [Cd1−O5A = 2.252(3), Cd1−O6 = 2.246(2) Å, O5A−Cd1−O6 = 117.1(1)°] and two nitrogen atoms of a chelate 2,2′-bpy ligand [Cd1−N1 = 2.379(3), Cd1−N2 = 2.333(3) Å, N1−Cd1−N2 = 69.27(9)°] to furnish a highly distorted octahedral coordination. Similarly to Cd1, Cd2 is also coordinated in a highly distorted octahedral geometry (see Table 2). The two crystallographically independent Cd^{II} atoms are each bridged by two μ-carboxylate ends to its crystallographically equivalent Cd^{II} atom to generate a dinuclear unit (Figure 5, a). Such dinuclear units are further extended by the bridging mpa ligands into one-dimensional helical ribbons with a pitch of 9.71 Å running along the $(1\bar{1}1)$ direction, which are decorated by 2,2′-bpy ligands at both sides. Since the pair of 2,2′-bpy ligands are orientated in opposite directions of the dinuclear unit, the geometry of the unit is hence different, concomitant with larger intradinuclear metal−metal distances (Cd1···Cd1A = 4.364 Å, Cd2···Cd2A = 4.181 Å) compared to that in **1**. These geometric differences may be attributed to the significant intramolecular π−π stacking interactions in **1**. The V-shaped mpa ligands in **4** exhibit uniquely the chelate-bidentate coordination mode (Scheme 1, a). Adjacent ribbons are intercalated in a zipper fashion into two-dimensional layers through the π−π stacking interactions between the 2,2′-bpy ligands with face-to-face distances of ca. 3.47−3.64 Å (Figure 5, b), and the layers are further packed into a three-dimensional network by van der Waals interactions. Similar to **3**, there are no significant π−π stacking interactions from the mpa ligands.

In our previous reports, we have shown that appropriate combinations of nonlinear flexible/V-shaped dicarboxylates with chelating phen can furnish interesting one-dimensional supramolecular structures such as molecular zippers as well as single- and double-stranded helices.[7,8] In particular, a

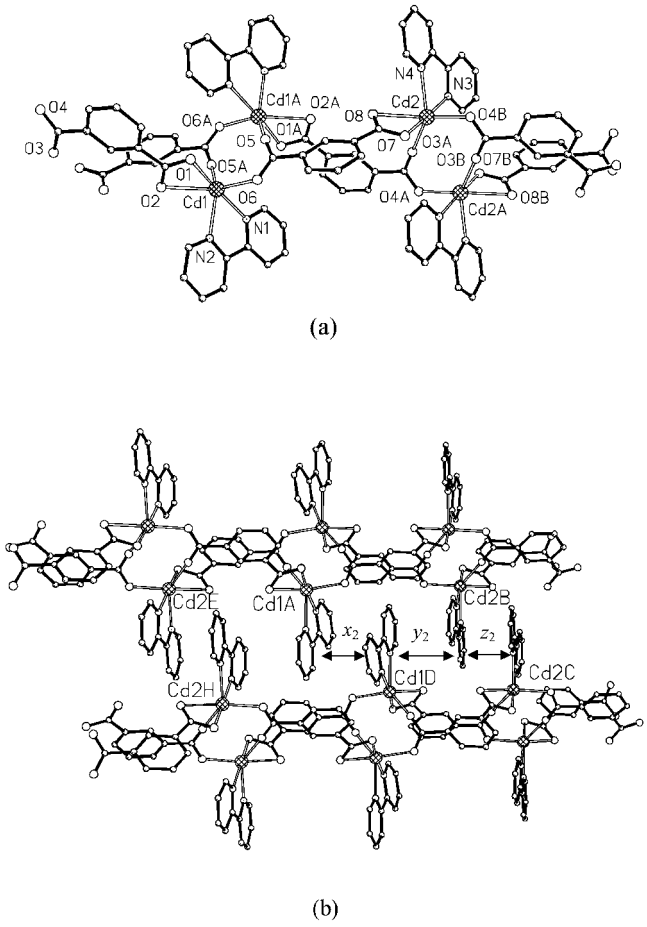

Figure 5. Perspective views of the coordination environments of the metal atoms (a) and the two-dimensional ribbons (b) in **4**; the face-to-face distances for the π−π interactions are x_2 = 3.48 Å, y_2 = 3.64 Å and z_2 = 3.47 Å

combination of V-shaped mpa ligands with chelating phen and 2,2′-bpy ligands along with the Cu^{II} ions generated single-stranded helical chains, namely $[Cu_2(mpa)_2(phen)_2(H_2O)]_n$ and $[Cu(mpa)(2,2'\text{-bpy})]_n{\cdot}2nH_2O$.[7] In contrast, using Cd^{II} or Zn^{II} atoms in place of Cu^{II} atoms under similar reaction conditions, the one-dimensional ribbons of **1**−**4** comprising dinuclear units were isolated. These observations may be attributed to the fact that the Cu^{II} has a greater tendency towards square-planar coordination tendency than the Cd^{II} and Zn^{II} atoms and the fact that Cd^{II} and Zn^{II} atoms have a tendency to form dinuclear structural units in the presence of the aromatic chelates. Actually, in $[Cu_2(mpa)_2(phen)(H_2O)]_n$ and $[Cu(mpa)(2,2'\text{-bpy})]_n{\cdot}2nH_2O$ as well as other related coordination polymers,[7] the one-dimensional chains are based on mononuclear structural units featuring primarily a square-planar geometry, compared to those in **1**, **2**, **3** and **4**. Therefore the dinuclear structural units in **1**, **2**, **3** and **4** represent new examples of building blocks among the dicarboxylate-bridged one-dimensional coordination polymers. On the other hand, different aromatic chelates also have a significant effect on the structures, as evidenced by the fact that the structure of **3** is significantly different from that of **1** and **2**.

 © 2003 Wiley-VCH Verlag GmbH & Co. KGaA, Weinheim

Photoluminescence

The solid-state photoluminescent spectra of **1**, **2**, **3** and **4** at room temperature are depicted in Figure 6. Complexes **1** and **2** both exhibit intense blue photoluminescence with an emission maximum at ca. 423 and 420 nm upon excitation at 317 and 334 nm, respectively. According to the previous observations,[4,16,24−29] these emission bands would be assigned to the emission of ligand-to-metal charge transfer (LMCT). Whereas there are two intense emission maxima at ca. 397 and 413 nm for **3**, and ca. 405 and 422 nm for **4** upon excitation at ca. 347 and 355 nm, respectively. The peaks at 413 and 422 nm would be assigned to the emission of LMCT,[4,5,26,28,29] while the peaks at 397 and 405 nm would be distributed to the intraligand emission from the 2,2′-bpy ligand.[5,30] It is known that the free 2,2′-bpy molecule displays a weak luminescence at ca. 530 nm in the solid state at room temperature. The enhancement and significant blue-shift (up to 400 nm)[30] of the luminescence of the 2,2′-bpy ligand compared to that of the free 2,2′-bpy molecule may therefore be attributed to the chelating of the 2,2′-bpy ligand to the metal ion, which effectively increases the rigidity of the ligand and reduces the loss of energy by radiationless decay of the intraligand emission excited state.[24]

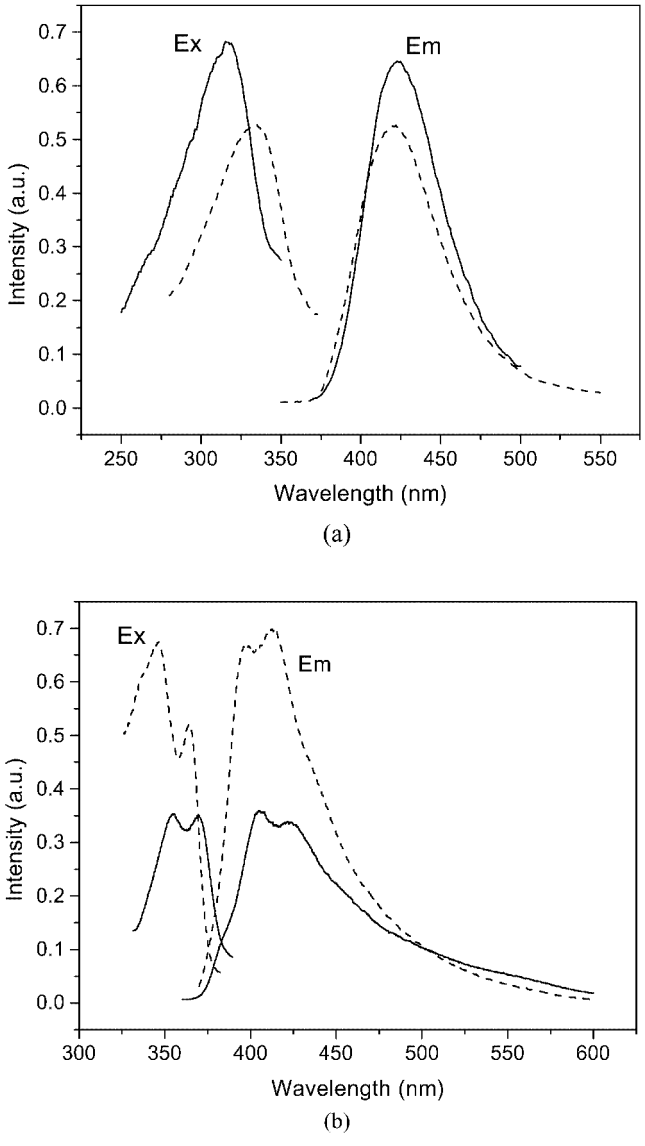

Figure 6. The excitation and emission spectra of **1**−**4** in the solid state at room temperature; the solid lines represent **1** and the dash-dot ones represent **2** in (a); the solid lines represent **4** and the dash-dot ones represent **3** in (b)

Conclusion

We have synthesized four stable one-dimensional ribbon-like coordination polymers under hydrothermal conditions, which show new dinuclear structural units as building blocks among the dicarboxylate-bridged one-dimensional coordination polymers as well as interesting photoluminescent properties. Compared to our previous one-dimensional copper(II) analogues, it has been found that different coordinations may have a very significant effect on the structures of the one-dimensional chains. Different combinations of nonlinear flexible/V-shaped dicarboxylates with chelating phen and 2,2′-bpy ligands in the presence of different metal ions, such as Cu, Cd and Zn, can furnish different one-dimensional supramolecular structures, such as molecular zippers, single- and double-stranded helices,[7,8] as well as helical ribbons.

Experimental Section

General Remarks: All chemicals were commercially available and used as received without further purification. The C, H and N microanalyses were carried out with a Perkin−Elmer 240 elemental analyzer. The FT-IR spectra were recorded from KBr pellets in the range 4000−400 cm^{-1} with a Nicolet 5DX spectrometer. All the excitation and emission spectra were measured with an Aminco Bowman Series 2 with a xenon arc lamp as the excitation light source for the solid-state samples. Thermogravimetric analysis (TGA) data were collected with a Perkin−Elmer TGS-2 analyzer in air at a heating rate of 10 °C min^{-1}.

Preparation of [Cd(mpa)(phen)]$_n$ (1): A mixture of $Cd(NO_3)_2{\cdot}9H_2O$ (1.0 mmol), H_2mpa (0.5 mmol), phen (1.0 mmol), NaOH (1.0 mmol) and water (10 mL) was stirred in air for 15 min, then transferred and sealed in a 23-mL Teflon-lined reactor, which was heated at 160 °C for 5 d and then cooled to room temperature at a rate of 5 °C h^{-1}. Colorless prisms were obtained, washed with deionized water and absolute ethanol (yield > 40% based on Cd). $C_{20}H_{12}CdN_2O_4$ (456.72): calcd. C 52.59, H 2.65, N 6.13; found C 52.70, H 2.59, N 6.20. IR (KBr, cm^{-1}): $\tilde{\nu}$ = 3417 s, 3169 s, 1979 w, 1615 s, 1564 s, 1515 m, 1481 w, 1400 s, 1145 m, 1102 m, 1049 w, 909 w, 859 s, 825 w, 783 m, 729 s and 635 m. TGA analysis of **1** shows a weight loss starting at ca. 402 °C.

Preparation of [Zn(mpa)(phen)]$_n$ (2): Complex **2** was prepared as for **1**. Pale yellow blocks of **2** were obtained, washed with deionized water and absolute ethanol (yield > 60% based on Zn). $C_{20}H_{12}N_2O_4Zn$ (409.69): calcd. C 58.63, H 2.95, N 6.84; found C 58.58, H 2.88, N 6.90. IR (KBr, cm^{-1}): $\tilde{\nu}$ = 3433 s, 3334 m, 3193 m, 3000 w, 1614 s, 1558 m, 1515 m, 1453 m, 1397 s, 1271 w, 1168 m, 1098 w, 850 s, 782 m, 744 w, 723 s, 592 m and 528 w. Decomposition of the polymeric framework of **2** began at ca. 371 °C.

 © 2003 Wiley-VCH Verlag GmbH & Co. KGaA, Weinheim

Preparation of $[Zn_2(mpa)_2(2,2'\text{-bpy})_2]_n$ (3): A mixture of $Zn(NO_3)_2{\cdot}9H_2O$ (1.0 mmol), H_2mpa (0.5 mmol), 2,2′-bpy (1.0 mmol), NaOH (1.0 mmol) and water (10 mL) was stirred in air for 15 min, then transferred and sealed in a 23-mL Teflon-lined reactor, which was heated at 160 °C for 5 d and then cooled to room temperature at a rate of 5 °C h^{-1}. Colorless prisms were obtained, washed with deionized water and absolute ethanol (yield > 35% based on Zn). $C_{36}H_{24}N_4O_8Zn_2$ (771.33): calcd. C 56.05, H 3.14, N 7.26; found C 56.11, H 3.01, N 7.33. IR (KBr, cm^{-1}): $\tilde{\nu}$ = 3424 s, 3108 s, 3069 s, 1902 w, 1943 w, 1612 s, 1562 s, 1532 s, 1431 s, 1383 s, 1159 m, 1074 m, 1020 m, 934 w, 849 m, 827 m, 750 m, 658 s, and 583 m. TGA analysis of **3** shows a weight loss starting at ca. 365 °C.

Preparation of $[Cd_2(mpa)_2(2,2'\text{-bpy})_2]_n$ (4): Complex **4** was prepared as for **3**. Colorless blocks of **4** were obtained, washed with deionized water and absolute ethanol (yield > 50% based on Zn). $C_{36}H_{24}Cd_2N_4O_8$ (856.39): calcd. C 49.96, H 2.80, N 6.47; found C 49.88, H 2.85, N 6.54. IR (KBr, cm^{-1}): $\tilde{\nu}$ = 3414 s, 3109 m, 3050 m, 1602 s, 1552 s, 1474 m, 1436 s, 1381 s, 1314 m, 1247 w, 1154 m, 1078 m, 1016 s, 908 w, 827 m, 727 m, 717 s, and 652 w. Decomposition of the polymeric framework of **4** began at ca. 370 °C.

X-ray Crystallographic Study: A summary of the crystal data for **1**, **2**, **3** and **4** is given in Table 1. Selected bond lengths and angles are listed in Table 2. Drawings were produced with SHELXTL. The intensity data of **1**, **2** and **3** were collected with a Siemens R3m diffractometer using the ω-scan technique with graphite-monochromated Mo-K_α (λ = 0.71073 Å) radiation at room temperature and the intensity data of **4** were collected with a Bruker Apex CCD diffractometer with the graphite-monochromated Mo-K_α (λ = 0.71073 Å) radiation at 228 K in the ω-2θ scan mode. Lorentz-polarization and absorption corrections were applied.[31] The structures were solved with direct methods and refined with a full-matrix least-squares technique using the SHELXS-97 and SHELXL-97 programs,[32,33] respectively. Anisotropic thermal parameters were assigned to all non-hydrogen atoms. The organic hydrogen atoms were generated geometrically (C−H 0.96 Å); the aqua hydrogen atoms were located from difference maps and refined with isotropic temperature factors. Analytical expressions of neutral-atom scattering factors were employed, and anomalous dispersion corrections were incorporated.[34] CCDC-212917 (**1**), -212918 (**2**), -212919 (**3**), -212920 (**4**) contain the supplementary crystallographic data for this paper. These data can be obtained free of charge at www.ccdc.cam.ac.uk/conts/retrieving.html [or from the Cambridge Crystallographic Data Centre, 12 Union Road, Cambridge CB2 1EZ, UK; Fax: (internat.) + 44-1223/336-033; E-mail: deposit@ccdc.cam.ac.uk].

Acknowledgments

This work was supported by the NSFC (no. 20131020) and the Ministry of Education of China (no. 01134).

[1] O. M. Yaghi, H. Li, C. David, D. Richardson, T. L. Groy, *Acc. Chem. Res.* **1998**, *31*, 474−484.
[2] S. R. Batten, R. Robson, *Angew. Chem. Int. Ed.* **1998**, *37*, 1460−1494.
[3] P. J. Hagrman, D. Hagrman, J. Zubieta, *Angew. Chem. Int. Ed.* **1999**, *38*, 2638−2684.
[4] J. Tao, M.-L. Tong, J.-X. Shi, X.-M. Chen, S. W. Ng, *Chem. Commun.* **2000**, 2043−2044.
[5] X.-M. Zhang, M.-L. Tong, M.-L. Gong, X.-M. Chen, *Eur. J. Inorg. Chem.* **2003**, 138−142.
[6] D.-F. Sun, R. Cao, Y. Liang, Q. Shi, W.-P. Su, M.-C. Hong, *J. Chem. Soc., Dalton Trans.* **2001**, 2335−2340.
[7] X.-M. Chen, G.-F. Liu, *Chem. Eur. J.* **2002**, *8*, 4811−4817.
[8] G.-F. Liu, B.-H. Ye, Y.-H. Ling, X.-M. Chen, *Chem. Commun.* **2002**, 1442−1443.
[9] M. J. Plater, M. R. St. J. Foreman, R. A. Howie, J. M. S. Skakle, S. A. McWilliam, E. Coronado, C. J. G. Garcia, *Polyhedron* **2001**, *20*, 2293−2303.
[10] S.-L. Zheng, M.-L. Tong, X.-L. Yu, X.-M. Chen, *J. Chem. Soc., Dalton Trans.* **2001**, 586−592.
[11] J. Tao, M.-L. Tong, X.-M. Chen, *J. Chem. Soc., Dalton Trans.* **2000**, 3669−3674.
[12] P. C. Ford, E. Cariati, J. Bourassa, *Chem. Res.* **1999**, *99*, 3625−3648.
[13] K. R. Kyle, C. K. Ryu, J. A. Dibenedetto, P. C. Ford, *J. Am. Chem. Soc.* **1991**, *113*, 2954−2965.
[14] W. Clegg, D. R. Harbron, C. D. Homan, P. A. Hunt, J. R. Little, B. P. Straughan, *Inorg. Chim. Acta* **1991**, *186*, 51−60.
[15] M.-L. Tong, X.-M. Chen, B.-H. Ye, L.-N. Ji, *Angew. Chem. Int. Ed.* **1999**, *38*, 2237−2240.
[16] J. Tao, J.-X. Shi, M.-L. Tong, X.-X. Zhang, X.-M. Chen, *Inorg. Chem.* **2001**, *40*, 6328−6330.
[17] S.-L. Zheng, M.-L. Tong, S.-D. Tan, Y. Wang, J.-X. Shi, Y.-X. Tong, H.-K. Lee, X.-M. Chen, *Organometallics* **2001**, *20*, 5319−5325.
[18] K. Nakamoto, *Infrared and Raman Spectra of Inorganic and Coordination Compounds*, John Wiley & Sons, New York, **1986**.
[19] M.-L. Tong, H.-J. Chen, X.-M. Chen, *Inorg. Chem.* **2000**, *39*, 2235−2238.
[20] S.-L. Zheng, M.-L. Tong, R.-W. Fu, X.-M. Chen, S. W. Ng, *Inorg. Chem.* **2001**, *40*, 3562−3569.
[21] X.-M. Zhang, M.-L. Tong, S.-H. Feng, X.-M. Chen, *J. Chem. Soc., Dalton Trans.* **2001**, 2069−2070.
[22] C. Janiak, *J. Chem. Soc., Dalton Trans.* **2000**, 3885−3896.
[23] M.-L. Tong, Y.-M. Wu, S.-L. Zheng, X.-M. Chen, T. Yuen, C.-L. Lin, X.-Y. Huang, J. Li, *New J. Chem.* **2001**, *25*, 1482−1485.
[24] H. Yersin, A. Vogler (Eds.), *Photochemistry and Photophysics of Coordination Compounds*, Springer, Berlin, **1987**.
[25] V. W.-W. Yam, K. K.-W. Lo, *Chem. Soc. Rev.* **1999**, *28*, 323−334.
[26] H. Kunkely, A. Vogler, *J. Chem. Soc., Chem. Commun.* **1990**, 1204−1205.
[27] R. Bertoncello, M. Betinelli, M. Casarin, A. Gulino, E. Tondello, A. Vittadini, *Inorg. Chem.* **1992**, *31*, 1558−1565.
[28] J.-C. Dai, X.-T. Wu, Z.-Y. Fu, C.-P. Cui, S.-M. Wu, W.-X. Du, L.-M. Wu, H.-H. Zhang, R.-Q. Sun, *Inorg. Chem.* **2002**, *41*, 1391−1396.
[29] W. Chen, J.-Y. Wang, C. Chen, Q. Yue, H.-M. Yuan, J.-S. Chen, S.-N. Wang, *Inorg. Chem.* **2003**, *42*, 944−946.
[30] G. Qian, M. Wang, *Mater. Lett.* **2002**, *56*, 71−75.
[31] A. C. T. North, D. C. Phillips, F. S. Mathews, *Acta Crystallogr., Sect. A* **1968**, *24*, 351−356.
[32] G. M. Sheldrick, *SHELXS-97, Program for X-ray Crystal Structure Solution*, Göttingen University, Germany, **1997**.
[33] G. M. Sheldrick, *SHELXL-97, Program for X-ray Crystal Structure Refinement*, Göttingen University, Germany, **1997**.
[34] *International Tables for X-ray Crystallography*, vol. C, Tables 4.2.6.8 and 6.1.1.4, Kluwer Academic Publisher, Dordrecht, **1992**.

Received January 30, 2003

 © 2003 Wiley-VCH Verlag GmbH & Co. KGaA, Weinheim

Mechanistic Insight Gained into the Ligand Substitution Reactions of Bis(*o*-benzosemiquinonediiminato)(triphenylphosphane)cobalt(III) – Kinetic, Solvent, and Volume Profile Studies

Basam M. Alzoubi,[a] Mohamed S. A. Hamza,[a][‡] Carlos Dücker-Benfer,[a] and Rudi van Eldik*[a]

Keywords: Cobalt / Kinetics / Ligand substitution / Mechanism / Pressure dependence / Solvent effects

The ligand substitution reactions of bis(*o*-benzosemiquinonediiminato)(triphenylphosphane)cobalt(III), $[Co^{III}(s\text{-}BQDI)_2(Ph_3P)]^+$, were studied with imidazole (Imid) and 4-dimethylaminopyridine (4-Me_2Npy) as entering nucleophiles in MeOH and CH_3CN as solvents (S). The complex $[Co^{III}(s\text{-}BQDI)_2(Ph_3P)S]^+$ undergoes dissociation of the solvent to form a five-coordinate intermediate, $[Co^{III}(s\text{-}BQDI)_2(Ph_3P)]^+$, which binds the entering nucleophile in a rate-determining step through a six-coordinate transition state, $[Co^{III}(s\text{-}BQDI)_2(Ph_3P)L]^+$, followed by the release of triphenylphosphane to form $[Co^{III}(s\text{-}BQDI)_2L]^+$. From the temperature and pressure dependence of the substitution of triphenylphosphane by imidazole, the activation parameters for the forward and reverse reactions of $[Co^{III}(s\text{-}BQDI)_2(Ph_3P)]^+$ with imidazole in MeOH were found to be $\Delta H^{\ddagger}$ = 58±2 and 43.4±0.5 kJ·mol^{-1}, $\Delta S^{\ddagger}$ = −116±6 and −73±2 J·K^{-1}·mol^{-1}, and $\Delta V^{\ddagger}$ = −10.6±0.1 and −8.7±0.3 cm^3·mol^{-1}, respectively. In CH_3CN, however, $\Delta H^{\ddagger}$, $\Delta S^{\ddagger}$, and $\Delta V^{\ddagger}$ for the forward reaction were found to be 50±3 kJ·mol^{-1}, −111±9 J·mol^{-1}·K^{-1}, and −12.9±0.3 cm^3·mol^{-1}, respectively. The activation parameters for the reaction between $[Co^{III}(s\text{-}BQDI)_2(Ph_3P)]^+$ and 4-dimethylaminopyridine in MeOH for the forward and reverse reactions were found to be $\Delta H^{\ddagger}$ = 76±2 and 47.9±0.4 kJ·mol^{-1}, $\Delta S^{\ddagger}$ = −51±7 and −64±2 J·K^{-1}·mol^{-1}, and $\Delta V^{\ddagger}$ = −10.5±0.3 and −11.1±0.2 cm^3·mol^{-1}, respectively. From these reported rate and activation parameters, the substitution of triphenylphosphane by imidazole and 4-dimethylaminopyridine follows an associative mechanism. The ligand substitution reactions of $[Co^{III}(s\text{-}BQDI)_2(Ph_3P)]^+$ in CH_3CN were found to be faster than those in MeOH, which is attributed to the potential for hydrogen bond formation with the entering nucleophile in the case of MeOH as solvent.

(© Wiley-VCH Verlag GmbH & Co. KGaA, 69451 Weinheim, Germany, 2003)

Introduction

The chemistry of transition metal complexes of benzosemiquinonediimine (s-BQDI), derived from *o*-phenylenediamine (OPD), are rather important because of their interesting redox properties[1,2] and their relation to biologically relevant catechol and benzoquinone derivatives.[3]

The bidentate ligand *o*-benzosemiquinonediiminato(−1), derived from the one-electron oxidation of *o*-phenylenediamine, can be stabilised by complex formation.[4] By removal of a second electron it is converted into the unstable *o*-benzoquinonediimine (BQDI) [Equation (1)], which can also be stabilised through complexation.[2]

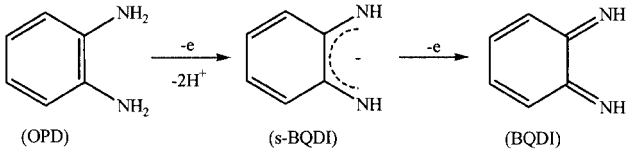

(1)

X-ray diffraction shows that the structure of $[Co^{III}(s\text{-}BQDI)_2(Ph_3P)]ClO_4$ is square-pyramidal in the solid state, with PPh_3 occupying one of the axial positions.[5] Upon dissolution in a coordinating solvent such as MeOH, the sixth position becomes occupied by a weakly bound solvent molecule, which cannot be observed in the solid-state structure.[3,6] Complexes such as $[Co^{III}(s\text{-}BQDI)_2(Ph_3P)]PF_6$, $[Co^{III}(s\text{-}BQDI)_2I]$, $[Co^{III}(s\text{-}BQDI)_2SCN]$, or $[Fe(s\text{-}BQDI)_2(Ph_3P)]$ are potentially five-coordinate in CH_3CN as solvent.[2]

We are interested generally in equilibria between five- and six-coordinate species in such complexes, since this should provide a better understanding of their mechanistic behaviour in ligand displacement processes. Alkyl cobalamines and cobinamides (vitamin B_{12} derivatives) with stronger donor ligands (e.g., vinyl, methyl, sulfite, dialkyl phosphite) exist as temperature-dependent mixtures of yellow five-coordinate and red six-coordinate aqua (solvent) complexes. Increasing the temperature favours the five-coordinate form with diethyl phosphite as ligand, whereas increasing the

[a] Institute for Inorganic Chemistry, University of Erlangen-Nürnberg,
Egerlandstr. 1, 91058 Erlangen, Germany
[‡] On leave from: Department of Chemistry, Ain Shams University, Cairo, Egypt

Supporting information for this article is available on the WWW under http://www.eurjic.org or from the author.

 © 2003 Wiley-VCH Verlag GmbH & Co. KGaA, Weinheim **DOI: 10.1002/ejic.200300107**

pressure favours the six-coordinate form.[7] The reaction volume for the formation of the six-coordinate species in water as solvent was found to be $-12.5\ cm^3\ mol^{-1}$, suggesting that the entering water molecule is fully bound in the six-coordinate complex.[7]

The ligand substitution reactions of $[Co^{III}(s\text{-}BQDI)_2L]^+$, where L = Ph_3Sb and Ph_3As, and of $[Co^{III}(s\text{-}CBQDI)_2(Ph_3As)]^+$, where s-CBQDI = 4,5-dichloro-1,2-benzosemiquinonediiminato, were studied in methanol with different nucleophiles such as pyridine, pyrrolidine, and imidazole as entering ligands.[3,6] It was found that these nucleophiles easily displace the coordinated solvent molecule to form the six-coordinate $[Co^{III}(s\text{-}BQDI)_2LL']^+$ complexes, where L′ represents the entering nucleophile.[3] In a subsequent step, substitution of L by the entering nucleophile takes place, and an associative interchange mechanism was suggested.

In this investigation we performed a detailed analysis of the axial ligand substitution reactions of $[Co^{III}(s\text{-}BQDI)_2(Ph_3P)S]^+$ by imidazole and 4-$(Me)_2$Npy, where S is MeOH or CH_3CN, in order to study the intimate nature of the ligand displacement mechanism and the effect of the selected solvent on these reactions.

Results and Discussion

We started our studies by investigating the effect of temperature and pressure on the UV/Vis spectra of $[Co^{III}(s\text{-}BQDI)_2(Ph_3P)]^+$ in methanol as solvent. The UV/Vis spectrum of $5\cdot10^{-5}$ M $[Co^{III}(s\text{-}BQDI)_2(Ph_3P)]^+$ was recorded as a function of temperature, as shown in Figure S-1 (Supporting Information). With decreasing temperature, from 60 to 5 °C, it exhibits isosbestic points at 508, 600, and 760 nm, a significant absorbance decrease at 712 and 450 nm, and an increase in absorbance at 550 nm. Similar spectra were obtained either on decreasing the temperature or on increasing the pressure.

The effect of temperature and pressure on the UV/Vis spectra suggests an equilibrium between five- and six-coordinate forms of the complex $[Co^{III}(s\text{-}BQDI)_2(Ph_3P)S]^+$, where the sixth coordination site is occupied by a solvent molecule. The six-coordinate form is favoured by increasing pressure or decreasing temperature, and vice versa for the five-coordinate complex. Similar trends could be observed in both solvents (MeOH and CH_3CN). In the case of CH_3CN as solvent, however, the change in the UV/Vis spectrum was not as significant as in that of MeOH as solvent, which is attributed to the fact that CH_3CN is a much stronger nucleophile than MeOH and will form a less labile six-coordinate species. For this reason a smaller fraction of the five-coordinate species will exist in equilibrium with the six-coordinate species in the case of CH_3CN as solvent. In the solid state the complex is square-pyramidal with a Ph_3P ligand occupying the axial position.[5]

Reaction between $[Co^{III}(s\text{-}BQDI)_2(Ph_3P)]^+$ and Imidazole in Methanol

The UV/Vis spectrum of $[Co^{III}(s\text{-}BQDI)_2(Ph_3P)]^+$ exhibits two bands at 710 and 478 nm, with a shoulder at 423 nm ($\varepsilon = 2.2\cdot10^4$, $1.1\cdot10^4$, and $7.9\cdot10^3\ M^{-1}\cdot cm^{-1}$, respectively). Upon mixing of the complex with imidazole or 4-$(Me)_2$Npy in the stopped-flow instrument, there is a small and very rapid initial increase in absorbance prior to the reaction with the entering nucleophile. This rapid increase can be ascribed to a fast equilibration between the complex and the solvent (methanol) as a result of the equilibrium between the five- and six-coordinate complexes in solution as discussed above. This rapid absorbance change is also observed in the absence of imidazole or 4-$(Me)_2$Npy, just by dilution of a solution of the complex with solvent in a stopped-flow instrument, and occurs within the mixing time of the instrument (2 ms) at room temperature. With the use of a Biologic low temperature stopped-flow unit, however, the spectral changes associated with this reaction could be recorded at −40 °C, and a typical kinetic trace (see Figure S-2, Supporting Information) indicates that this reaction is over within 2 s at −40 °C. Subsequently, there is a much larger absorbance decrease at 710 and 450 nm, and an increase at 540 nm, associated with the coordination of imidazole. The $[Co^{III}(s\text{-}BQDI)_2(Imid)]^+$ complex shows two bands at 716 and 496 nm, with a shoulder at 420 nm ($\varepsilon = 1.1\cdot10^5$, $5.7\cdot10^4$, and $3.9\cdot10^4\ M^{-1}\cdot cm^{-1}$, respectively), whereas $[Co^{III}(s\text{-}BQDI)_2(4\text{-}Me_2Npy)]^+$ has characteristic UV/Vis bands at 714 and 520 nm, with a shoulder at 422 nm ($\varepsilon = 6.7\cdot10^4$, $5.2\cdot10^4$, and $3.1\cdot10^4\ M^{-1}\cdot cm^{-1}$, respectively).

The reaction between $2.5\cdot10^{-5}$ M $[Co^{III}(s\text{-}BQDI)_2(Ph_3P)]^+$ and an excess of imidazole (0.05 to 1.0 M) was studied in methanol as a function of temperature (15−45 °C). Kinetic traces for this reaction revealed perfect pseudo-first order behaviour, and the kinetic results as a function of the imidazole concentration are shown in Figure 1. It follows that good linear plots with significant intercepts are obtained within the experimental error limits. Furthermore, the plots do not indicate any saturation at high [Imid]. This kinetic behaviour can be expressed by the rate law given in Equation (2), where k_a and k_b represent the rate constants for the forward (slope) and reverse (intercept) reactions, respectively. Values of k_a and k_b as a function of temperature, along with the corresponding activation parameters, are summarised in Table 1. Values of $\Delta H^{\ddagger}$ and $\Delta S^{\ddagger}$ for the forward reaction (k_a) were found to be $58\pm2\ kJ\cdot mol^{-1}$ and $-116\pm6\ J\cdot K^{-1}\cdot mol^{-1}$, whereas those for the reverse reaction (k_b) were found to be $68\pm1\ kJ\cdot mol^{-1}$ and $-82\pm3\ J\cdot K^{-1}\cdot mol^{-1}$, respectively.

$$k_{obsd.} = k_a[L] + k_b \quad (2)$$

The results in Figure 1 clearly indicate that we are dealing with an unfavourable displacement of triphenylphosphane by imidazole, as can be seen from the magnitude of the intercepts of the plots that represent the contribution of the reverse reaction. Under the selected experimental conditions (no free phosphane added), the reverse displacement of imidazole by phosphane will follow second-order kinetics, with the result that the kinetic data measured under

 © 2003 Wiley-VCH Verlag GmbH & Co. KGaA, Weinheim

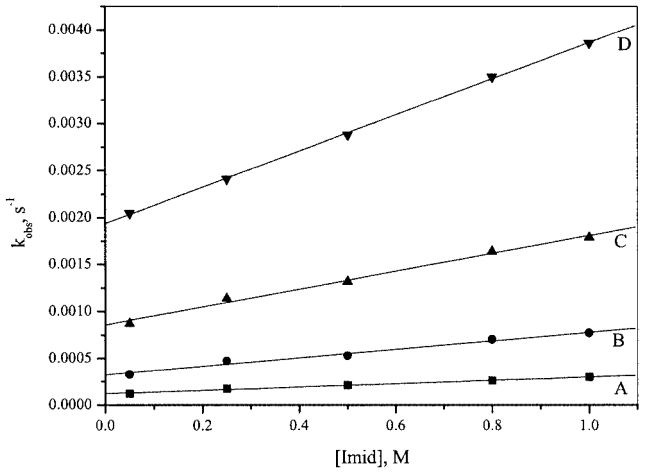

Figure 1. Plots of $k_{obsd.}$ versus [Imid] for the reaction between $[Co^{III}(s\text{-}BQDI)_2(Ph_3P)]^+$ and imidazole in methanol as a function of temperature; experimental conditions: $[Co^{III}] = 2.5\cdot10^{-5}$ M, temperature: 15.0 (A), 25.0 (B), 35.0 (C), 45.0 °C (D)

Table 1. Kinetic data for the reaction between $[Co^{III}(s\text{-}BQDI)_2(Ph_3P)]^+$ and imidazole in the absence of added phosphane in methanol as a function of temperature and pressure $\{[Co^{III}(s\text{-}BQDI)_2(Ph_3P)]^+ = 2.5\cdot10^{-5}$ M$\}$

$$[Co^{III}(s\text{-}BQDI)_2(Ph_3P)]^+ + Imid \underset{k_b}{\overset{k_a}{\rightleftharpoons}} [Co^{III}(s\text{-}BQDI)_2(Imid)]^+ + Ph_3P$$

Pressure, MPa	Temp., °C	$k_a \times 10^4$, $M^{-1}\,s^{-1}$	$k_b \times 10^4$, s^{-1} [a]
0.1	15.0	1.79±0.08	1.21±0.05
	25.0	4.5±0.3	3.2±0.2
	35.0	9.5±0.5	8.6±0.3
	45.0	19.3±1.4	19.4±0.8
10	15.0	2.39±0.06	1.30±0.04
50		2.85±0.01	1.47±0.01
90		3.41±0.08	1.63±0.05
130		4.06±0.10	1.87±0.07
$\Delta H^{\ddagger}$, $kJ\cdot mol^{-1}$		58±2	68±1
$\Delta S^{\ddagger}$, $J\cdot K^{-1}\cdot mol^{-1}$		−116±6	−82±3
$\Delta V^{\ddagger}$, $cm^3\cdot mol^{-1}$		−10.6±0.1	−7.2±0.3

[a] First-order rate constant obtained from the intercept of plots of $k_{obsd.}$ versus [Imid].

pseudo-first order conditions at low imidazole concentrations could become unreliable due to a contribution of the second-order reverse process. We therefore studied the rate and activation parameters for the reverse substitution of imidazole by Ph_3P separately, by first treating $2.5\cdot10^{-4}$ M of $[Co^{III}(s\text{-}BQDI)_2(Ph_3P)]^+$ with 1 M imidazole to form the imidazole complex, followed by the addition of an excess of Ph_3P to form the $[Co^{III}(s\text{-}BQDI)_2(Ph_3P)]^+$ complex again. Figure 2 shows a linear plot of $k_{obsd.}$ versus $[Ph_3P]$ for the reaction between $[Co^{III}(s\text{-}BQDI)_2(Imid)]^+$ and an excess of Ph_3P (0.005−0.025 M). The linear plot exhibits a negligible intercept, indicating that the displacement of imidazole by phosphane goes to completion under the selected conditions. The slope of the line in Figure 2 represents k_b, for which the results are reported as a function of temperature

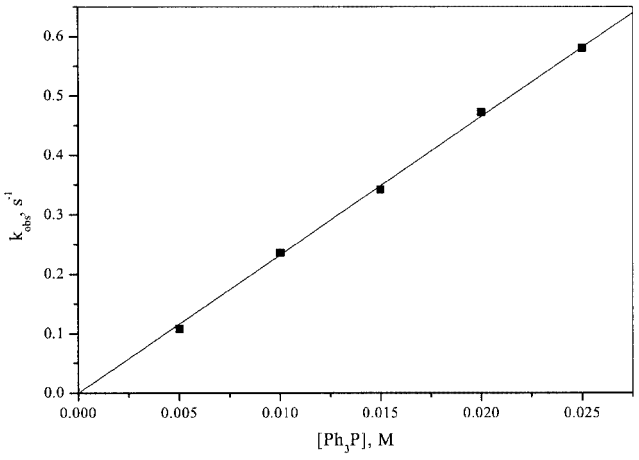

Figure 2. Plot of $k_{obsd.}$ versus $[Ph_3P]$ for the reaction between $1.25\cdot10^{-4}$ M $[Co^{III}(s\text{-}BQDI)_2(Imid)]^+$ and Ph_3P in methanol at 25 °C; the best fit (solid line) gives $k_b = 23.3\ M^{-1}\cdot s^{-1}$

Table 2. Kinetic data for the reaction between $[Co^{III}(s\text{-}BQDI)_2(Imid)]^+$ and Ph_3P in methanol as a function of temperature and pressure

$$[Co^{III}(s\text{-}BQDI)_2(Imid)]^+ + Ph_3P \underset{k_b}{\overset{k_a}{\rightleftharpoons}} [Co^{III}(s\text{-}BQDI)_2(Ph_3P)]^+ + Imid$$

Pressure, MPa	Temp., °C	$k_b/[Ph_3P]$, $M^{-1}\,s^{-1}$ [a]
0.1	5.0	6.2±0.3[b]
	10.0	8.8±0.2[b]
	15.0	12.5±0.1[b]
	20.0	17.2±0.3[b]
	25.0	23.2±0.1[b]
10	25.0	23.6±0.6[c]
50		26.9±0.3[c]
90		30.7±2.0[c]
130		36.0±1.5[c]
$\Delta H^{\ddagger}$, $kJ\cdot mol^{-1}$		43.4±0.5
$\Delta S^{\ddagger}$, $J\cdot K^{-1}\cdot mol^{-1}$		−73±2
$\Delta V^{\ddagger}$, $cm^3\cdot mol^{-1}$		−8.7±0.3

[a] Second-order rate constant calculated from the slope of plots of k_b versus $[Ph_3P]$. [b] $[Co^{III}(s\text{-}BQDI)_2(Imid)]^+ = 1.25\cdot10^{-4}$ M, $[Ph_3P] = 2.5\cdot10^{-2}$ M. [c] $[Co^{III}(s\text{-}BQDI)_2(Imid)]^+ = 1.25\cdot10^{-4}$ M, $[Ph_3P] = 1.25\cdot10^{-2}$ M.

in Table 2. The $\Delta H^{\ddagger}$ and $\Delta S^{\ddagger}$ values for k_b were found to be 43.4±0.5 $kJ\cdot mol^{-1}$ and −73±2 $J\cdot K^{-1}\cdot mol^{-1}$, respectively.

The reaction between $2.5\cdot10^{-5}$ M $[Co^{III}(s\text{-}BQDI)_2(Ph_3P)]^+$ and imidazole ([Imid] = 0.05−1 M) was studied at different pressures (10−130 MPa). The results are shown in Figure 3, from which it follows that good linear plots with significant intercepts are obtained within the experimental error limits. The values of k_a and k_b as a function of pressure, along with the corresponding activation volumes, are summarised in Table 1. Plots of ln k_a and ln k_b versus pressure were linear within the error limits (Figures S-3 and S-4, Supporting Information), and values of $\Delta V^{\ddagger}$ for the forward and the reverse reactions were found to be −10.6±0.1 and −7.2±0.3 $cm^3\cdot mol^{-1}$, respectively.

 © 2003 Wiley-VCH Verlag GmbH & Co. KGaA, Weinheim

Because of the possible unreliability of k_b under these conditions, as indicated above, its pressure dependence was also measured directly by treatment of the imidazole complex with an excess of phosphane, the results of which are included in Table 2. A plot of ln k_b versus pressure gave a good linear relationship, from which $\Delta V^{\ddagger}$ was calculated to be -8.7 ± 0.3 cm^3·mol^{-1}.

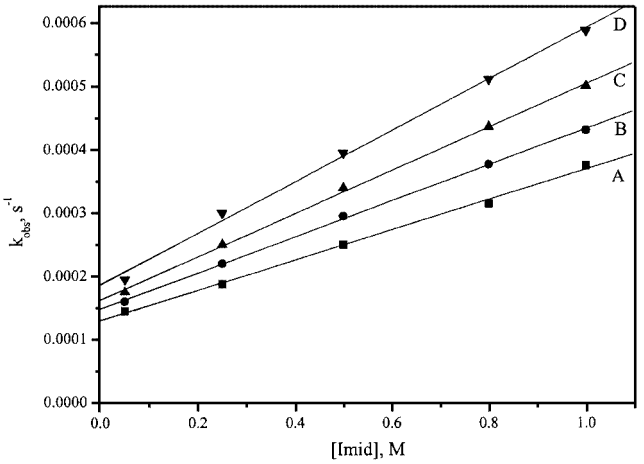

Figure 3. Plots of $k_{obsd.}$ versus [Imid] for the reaction between $[Co^{III}(s\text{-}BQDI)_2(Ph_3P)]^+$ and phosphane in methanol as a function of pressure; experimental conditions: $[Co^{III}] = 2.5\cdot10^{-5}$ M, pressure: 10 (A), 50 (B), 90 (C), 130 MPa (D)

From the available kinetic and spectroscopic data, we suggest that the reaction between $[Co^{III}(s\text{-}BQDI)_2(Ph_3P)S]^+$ and imidazole (or 4-Me_2Npy, see later) takes place in two consecutive steps. There is rapid dissociation of coordinated solvent in Equation (3) to form a five-coordinate intermediate, followed by the rate-determining associative ligand exchange process Equation (4) to form the product complex.

$$[Co^{III}(s\text{-}BQDI)_2(Ph_3P)S]^+ \rightleftarrows [Co^{III}(s\text{-}BQDI)_2(Ph_3P)]^+ + S \quad (3)$$

$$[Co^{III}(s\text{-}BQDI)_2(Ph_3P)]^+ + L \underset{k_b}{\overset{k_a}{\rightleftharpoons}} [Co^{III}(s\text{-}BQDI)_2(L)]^+ + PPh_3 \quad (4)$$

From the activation parameters and the constructed volume profile shown in Figure 4, it is reasonable to conclude that the reaction between $[Co^{III}(s\text{-}BQDI)_2(Ph_3P)]^+$ and imidazole in methanol follows an associative mechanism through the formation of a six-coordinate intermediate/transition state.

Reaction between $[Co^{III}(s\text{-}BQDI)_2(Ph_3P)]^+$ and 4-$(Me)_2$Npy in Methanol

The reaction between $2.5\cdot10^{-5}$ M $[Co^{III}(s\text{-}BQDI)_2(Ph_3P)]^+$ and an excess of 4-Me_2Npy (0.05 to 1 M) in methanol as a function of temperature (15−45 °C) was studied in a similar way. The results are presented in Figure S-5 (Supporting Information), from which it follows that good linear plots with significant intercepts are obtained

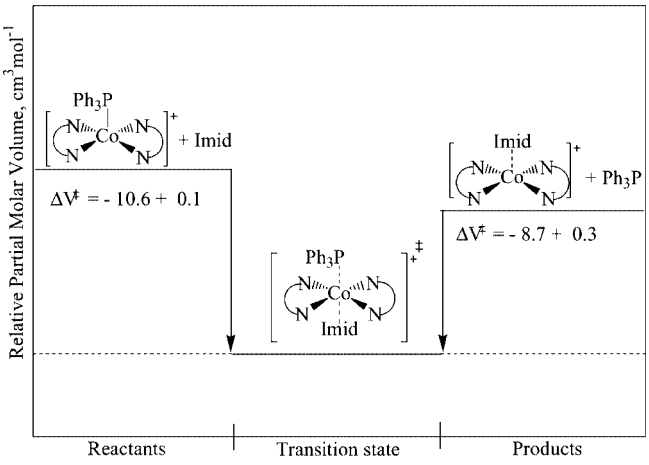

Figure 4. Volume profile for the reaction (the given structures are schematic presentations)

within the experimental error limits. Furthermore, the plots do not indicate any saturation at high 4-Me_2Npy concentrations. In this case the intercepts are smaller and the slopes of the plots larger than in the case of the reaction with imidazole, indicating that a more favourable equilibrium situation is reached in the reaction with 4-Me_2Npy. The same rate law and data treatment as used for the reaction with imidazole can be adopted, and the results are summarized as a function of temperature and pressure in Table 3. The values of $\Delta H^{\ddagger}$ and $\Delta S^{\ddagger}$ for the forward reaction (k_a) were found to be 76 ± 2 kJ·mol^{-1} and -51 ± 7 J·K^{-1}·mol^{-1}, respectively, and those for the reverse reaction to be 61 ± 4 kJ·mol^{-1} and -115 ± 12 J·K^{-1}·mol^{-1}, respectively. Because of the possible contribution of a second-order reverse reaction at low 4-Me_2Npy concentration, we also determined the rate and activation parameters for the substitution of 4-Me_2Npy by Ph_3P to form $[Co^{III}(s\text{-}BQDI)_2(Ph_3P)]^+$ directly, by treatment of $2.5\cdot10^{-4}$ M $[Co^{III}(s\text{-}BQDI)_2(Ph_3P)]^+$ with 1 M 4-Me_2Npy, followed by the reaction with phosphane. A plot of $k_{obsd.}$ versus $[Ph_3P]$ for the reaction between $[Co^{III}(s\text{-}BQDI)_2(4\text{-}Me_2Npy)]^+$ and excess Ph_3P (0.005−0.025 M) is shown in Figure S-6 (Supporting Information), from which it follows that the back reaction does not contribute significantly under these conditions. The data for k_b are summarised in Table 4. The values of $\Delta H^{\ddagger}$ and $\Delta S^{\ddagger}$ were found to be 47.9 ± 0.4 kJ·mol^{-1} and -64 ± 2 J·K^{-1}·mol^{-1}, respectively.

The reaction between $2.5\cdot10^{-5}$ M $[Co^{III}(s\text{-}BQDI)_2(Ph_3P)]^+$ and 4-Me_2Npy (0.05 to 1 M) as a function of pressure (10−130 MPa) was also studied, and the results are reported in Figure S-7 (Supporting Information). The data show good linear plots with significant intercepts within the experimental error limits. The values of k_a and k_b as a function of pressure, along with the corresponding activation parameters, are summarised in Table 3. Plots of lnk_a and lnk_b versus pressure gave good linear fits, from which the values of $\Delta V^{\ddagger}$ for the forward and reverse reactions were calculated to be -10.5 ± 0.3 and -8.7 ± 0.6

 © 2003 Wiley-VCH Verlag GmbH & Co. KGaA, Weinheim

Table 3. Kinetic data for the reaction between $[Co(s\text{-}BQDI)_2(Ph_3P)]^+$ and 4-Me_2Npy in the absence of added phosphane in methanol as a function of temperature and pressure $\{[Co^{III}(s\text{-}BQDI)_2(Ph_3P)]^+ = 2.5\cdot10^{-5}$ M$\}$

$$[Co^{III}(s\text{-}BQDI)_2(Ph_3P)]^+ + 4\text{-}Me_2Npy \underset{k_b}{\overset{k_a}{\rightleftharpoons}} [Co^{III}(s\text{-}BQDI)_2(4\text{-}Me_2Npy)]^+ + Ph_3P$$

Pressure, MPa	Temp., °C	$k_a \times 10^4$, M^{-1} s^{-1}	$k_b \times 10^4$, s^{-1} [a]
0.1	15.0	2.5±0.2	0.54±0.02
	25.0	6.7±0.5	1.6±0.2
	35.0	19±1	3.1±0.2
	45.0	54±2	6.9±0.4
10	15.0	2.5±0.1	0.54±0.04
50		3.10±0.08	0.64±0.05
90		3.65±0.09	0.74±0.06
130		4.3±0.1	0.83±0.06
$\Delta H^{\ddagger}$, kJ·mol^{-1}		76±2	61±4
$\Delta S^{\ddagger}$, J·K^{-1}·mol^{-1}		−51±7	−115±12
$\Delta V^{\ddagger}$, cm^3·mol^{-1}		−10.5±0.3	−8.7±0.6

[a] First-order rate constant obtained from the intercept of plots of $k_{obsd.}$ versus [4-Me_2Npy].

Table 4. Kinetic data for the reaction between $[Co^{III}(s\text{-}BQDI)_2(4\text{-}Me_2Npy)]^+$ and Ph_3P in methanol as a function of temperature and pressure

$$[Co^{III}(s\text{-}BQDI)_2(4\text{-}Me_2Npy)]^+ + Ph_3P \underset{k_b}{\overset{k_a}{\rightleftharpoons}} [Co^{III}(s\text{-}BQDI)_2(Ph_3P)]^+ + 4\text{-}Me_2Npy$$

Pressure, MPa	Temp., °C	$k_b/[Ph_3P]$, M^{-1} s^{-1} [a]
0.1	5.0	2.8±0.1[b]
	10.0	4.2±0.1[b]
	15.0	6.0±0.1[b]
	20.0	8.6±0.1[b]
	25.0	12.1±0.1[b]
10	25.0	15.4±0.8[c]
50		18.6±1.6[c]
90		22.0±1.3[c]
130		26.5±1.1[c]
$\Delta H^{\ddagger}$, kJ·mol^{-1}		47.9±0.4
$\Delta S^{\ddagger}$, J·K^{-1}·mol^{-1}		−64±2
$\Delta V^{\ddagger}$, cm^3·mol^{-1}		−11.1±0.2

[a] Second-order rate constant calculated from the slope of plots of k_b versus $[Ph_3P]$. [b] $[Co^{III}(s\text{-}BQDI)_2(4\text{-}Me_2Npy)]^+ = 1.25\cdot10^{-4}$ M, $[Ph_3P] = 2.5\cdot10^{-2}$ M. [c] $[Co^{III}(s\text{-}BQDI)_2(4\text{-}Me_2Npy)]^+ = 1.25\cdot10^{-4}$ M, $[Ph_3P] = 1.25\cdot10^{-2}$ M.

cm^3·mol^{-1}, respectively. The values of k_b were also measured directly as a function of pressure, with use of the displacement of 4-Me_2Npy by phosphane, and a plot of $\ln k_b$ versus pressure resulting in a $\Delta V^{\ddagger}$ value of −11.1±0.2 cm^3·mol^{-1} (see Table 4). From the reported activation parameters, we can conclude that the reverse reaction between $[Co^{III}(s\text{-}BQDI)_2(Ph_3P)]^+$ and 4-$(Me)_2$Npy follows the same associative reaction mechanism, in which the entering nucleophile is coordinated to the Co^{III} centre in the six-coordinate intermediate/transition state.

The forward rate constants for the reaction between $[Co^{III}(s\text{-}BQDI)_2(Ph_3P)]$ and 4-$(Me)_2$Npy or imidazole are $6.7\cdot10^{-4}$ and $4.5\cdot10^{-4}$ $M^{-1}\cdot s^{-1}$ at 25 °C, respectively, whereas the rate constants for the reverse reactions are 12.1 and 23.2 $M^{-1}\cdot s^{-1}$ at 25 °C, respectively. This indicates that the forward rate constant (k_a) increases with increasing basicity of the entering ligand, whereas the reversible reaction rate constant (k_b) decreases with increasing basicity due to the stronger cobalt−ligand bond.

Reaction between $[Co^{III}(s\text{-}BQDI)_2(Ph_3P)]^+$ and Imidazole in Acetonitrile

The reaction between $2.5\cdot10^{-5}$ M $[Co^{III}(s\text{-}BQDI)_2(Ph_3P)]^+$ and excess imidazole ([Imid] = 0.025−1 M) in acetonitrile was studied at different temperatures (11−32 °C). The results are presented in Figure 5 and show a significant deviation from linearity at high imidazole concentrations, as well as negligible intercepts. This behaviour can be accounted for in terms of the interchange mechanism presented in reactions according to Equations (5) and (6), for which the rate law is given in Equation (7), where K represents the equilibrium constant for precursor formation, and k the interchange rate constant. Since acetonitrile is a much more strongly coordinating solvent than methanol, this presumably prevents formation of a five-coordinate intermediate and forces the reaction to proceed through an interchange instead of an associative mechanism involving a five-coordinate intermediate.

$$[Co^{III}(s\text{-}BQDI)_2(Ph_3P)S]^+ + Imid \rightleftarrows \{[Co^{III}(s\text{-}BQDI)_2(Ph_3P)S]^+\cdot Imid\};\ K \quad (5)$$

$$\{[Co^{III}(s\text{-}BQDI)_2(Ph_3P)S]^+\cdot Imid\} \rightarrow [Co^{III}(s\text{-}BQDI)_2(Imid)S]^+ + Ph_3P;\ k \quad (6)$$

$$k_{obs} = \frac{k\cdot K[Imid]}{\{1 + K[Imid]\}} \quad (7)$$

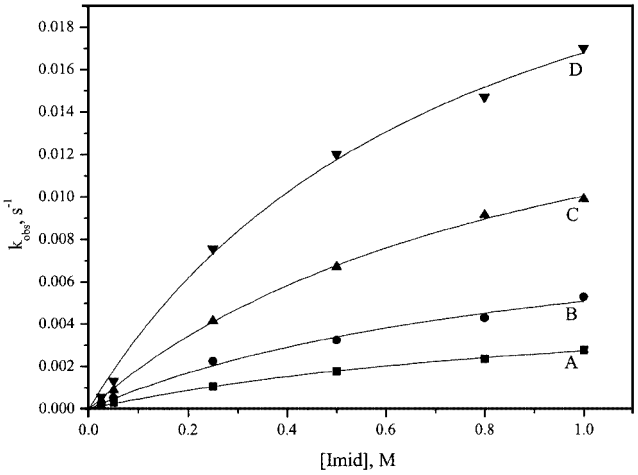

Figure 5. Plots of $k_{obsd.}$ versus [Imid] for the reaction between $[Co^{III}(s\text{-}BQDI)_2(Ph_3P)]^+$ and imidazole in acetonitrile as a function of temperature; experimental conditions: $[Co^{III}] = 2.5\cdot10^{-5}$ M, temperature: 11.0 (A), 18.0 (B), 25.0 (C), 32.0 °C (D)

 © 2003 Wiley-VCH Verlag GmbH & Co. KGaA, Weinheim

Table 5. Kinetic data for the reaction between $[Co^{III}(s\text{-}BQDI)_2(Ph_3P)]^+$ and imidazole in acetonitrile as a function of temperature and pressure

Pressure, MPa	Temp., °C	$k{\cdot}K \times 10^3$, $M^{-1}\,s^{-1}$ [a]	K, M^{-1} [b]	$k \times 10^3$, s^{-1} [b]
0.1	11.0	5.8±0.1[c]	0.9±0.1	5.8±0.5
	18.0	10.4±0.5[c]	1.0±0.2	10±2
	25.0	18±4[c]	1.1±0.1	19±1
	32.0	26±2[c]	1.3±0.1	29±3
10	5.0	4.9±0.2[d]		
50		6.1±0.3[d]		
90		7.5±0.1[d]		
130		9.6±0.1[d]		
$\Delta H^{\ddagger}$, $kJ{\cdot}mol^{-1}$		50±3[c]		
$\Delta S^{\ddagger}$, $J{\cdot}mol^{-1}{\cdot}K^{-1}$		−111±9[c]		
$\Delta V^{\ddagger}$, $cm^3{\cdot}mol^{-1}$		−12.9±0.3[d]		

[a] $k{\cdot}K$ was calculated from $k_{obsd.}$/[Imid] at [Imid] = 0.05 M. [b] K and k were calculated from the nonlinear least-squaresfit by use of Equation (7). [c] $[Co^{III}(s\text{-}BQDI)_2(Ph_3P)]^+ = 2.5{\cdot}10^{-5}$ M. [d] $[Co^{III}(s\text{-}BQDI)_2(Ph_3P)]^+ = 2.5{\cdot}10^{-5}$ M, [Imid] = 0.025 M.

The values of k and K as a function of temperature were calculated from a nonlinear fit of the measured rate constants and are summarised, along with the corresponding activation parameters, in Table 5. The values of $\Delta H^{\ddagger}$ and $\Delta S^{\ddagger}$ for the overall reaction between $[Co^{III}(s\text{-}BQDI)_2(Ph_3P)]^+$ and imidazole in CH_3CN were calculated for $k{\cdot}K = k_{obsd.}$/[Imid] at [Imid] = 0.05 M (i.e., where the imidazole concentration dependence is still linear), and were found to be 50±3 $kJ{\cdot}mol^{-1}$ and −111±9 $J{\cdot}K^{-1}{\cdot}mol^{-1}$, respectively. The pressure dependence of the reaction was studied at 0.025 M imidazole and 5 °C, and the plot of $\ln k_{obsd.}$ vs. pressure gave a good linear fit from which the value of $\Delta V^{\ddagger}$ was calculated to be −12.9±0.3 $cm^3{\cdot}mol^{-1}$. The results are summarized in Table 5. The reported activation parameters favour an associative interchange (I_a) mechanism.

Mechanistic Interpretation

Most ligand substitution reactions of Co^{III} complexes, such as those in vitamin B_{12}, its derivatives and model complexes, follow a D or I_d mechanism.[9−17] Surprisingly, the substitution reactions investigated in the current study between $[Co^{III}(s\text{-}BQDI)_2(Ph_3P)]^+$ and imidazole or 4-Me_2Npy clearly follow an associative mechanism. Simandi et al. studied the ligand substitution reactions of $[Co^{III}(s\text{-}CBQDI)_2(Ph_3As)]^+$ with pyridine, pyrrolidine, and imidazole in methanol and suggested an I_a mechanism, but no activation parameters were reported.[3]

The second-order rate constant for the reaction between $[Co^{III}(s\text{-}BQDI)_2(Ph_3P)]^+$ and imidazole in methanol at 25 °C ($4.5{\cdot}10^{-4}$ $M^{-1}{\cdot}s^{-1}$) is significantly smaller than that obtained in the case of CH_3CN as solvent ($1.78{\cdot}10^{-2}$ $M^{-1}{\cdot}s^{-1}$). This suggests either that hydrogen bonding plays an important role in methanol as solvent by deactivating the attacking nucleophile, or that the stronger donor properties of acetonitrile labilizes the *trans* position and induces a rapid displacement of phosphane.

The rates of associative substitution reactions can in principle be affected by the nature of the solvent. Especially in the case of protic solvents, partial protonation of the nucleophile, directly or through hydrogen bonding, can cause a significant decrease in the nucleophilicity of the entering nucleophile. Specific solvation of the nucleophile by a protic solvent strongly stabilizes the nucleophile and lowers its reactivity toward an electrophilic metal centre in an associative reaction mode. In contrast, polar non-protic solvents such as acetonitrile favour associative reaction modes.[8]

In the case of the benzosemiquinonediimine chelate, delocalization of electron density from the unsaturated equatorial ligand (s-BQDI) onto the Co^{III} centre could partially induce Co^{II} character, which could in turn account for the higher liability and the observed associative mechanism. The strongly negative activation entropies and volumes support the associative nature of the substitution mechanism for these complexes. By way of comparison, in complexes of ethylenediamine, the chelate is fully saturated and an I_d mechanism is more likely to account for the observed kinetic behaviour. It seems clear that the phenylenediamine ligand in the equatorial plane controls the ligand displacement mechanism. The induced electron density at the metal centre favours the unsaturated five-coordinate state and lowers the energy barrier to bind the entering nucleophile in the absence of a strongly coordinating solvent to favour the associative reaction pathway. In the presence of a more strongly coordinating solvent such as acetonitrile, the absence of a vacant coordination site will force the system to follow an interchange substitution mechanism.

Experimental Section

Materials: All chemicals were of p.a. grade and were used as received. Imidazole was purchased from Aldrich and 4-dimethylaminopyridine was purchased from Across. $[Co(s\text{-}BQDI)_2(Ph_3P)]ClO_4{\cdot}0.5C_6H_6$ was prepared as described previously[5] by treatment of $Co(ClO_4)_2{\cdot}6H_2O$ with *o*-phenylenediamine and triphenylphosphane in the presence of oxygen. The complex was characterised by elemental analysis and by IR and NMR spectroscopy, and the results were in agreement with those reported in the literature.[5]

 © 2003 Wiley-VCH Verlag GmbH & Co. KGaA, Weinheim

Instrumentation: UV/Vis spectra and kinetic measurements were recorded in thermostatted cell compartments of Shimadzu UV-2101 and Cary 5 spectrophotometers. Measurements at high pressures were carried out by use of the Shimadzu spectrophotometer equipped with a home-made high-pressure unit.[18] For faster reactions a high pressure, stopped-flow instrumentation was used.[19] Kinetic data were analysed with the OLIS KINFIT programme. All instruments used were thermostatted to the desired temperature (±0.1 °C). Kinetic measurements were carried out under pseudo-first order conditions (i.e., the ligand concentration was in at least a tenfold excess).

Acknowledgments

The authors gratefully acknowledge financial support from the Deutsche Forschungsgemeinschaft, a fellowship from the Alexander von Humboldt foundation (M. S. A. H.), and sabbatical leave from the Ain Shams University, Cairo (M. S. A. H.).

[1] S. M. Peng, C. T. Chen, D. S. Liaw, C. I. Chen, Y. Wang, *Inorg. Chim. Acta* **1985**, *101*, L31−L33.
[2] L. F. Warren, *Inorg. Chem.* **1977**, *16*, 2814−2819.
[3] L. I. Simandi, S. Nemeth, *Inorg. Chim. Acta* **1998**, *270*, 326−329.
[4] A. L. Balch, R. H. Holm, *J. Am. Chem. Soc.* **1966**, *88*, 5201−5209.
[5] S. Nemeth, L. I. Simandi, G. Argay, A. Kalman, *Inorg. Chim. Acta* **1989**, *166*, 31−33.
[6] S. Nemeth, L. I. Simandi, *Inorg. Chem.* **1994**, *33*, 5964−5966.
[7] M. S. A. Hamza, R. van Eldik, P. L. S. Harper, J. M. Pratt, E. A. Betterton, *Eur. J. Inorg. Chem.* **2002**, 580−583.
[8] J. McMurry, *Organic Chemistry*, 2nd ed., Brooks/Cole, California, USA, **1988**.
[9] B. M. Alzoubi, M. S. A. Hamza, C. Dücker-Benfer, R. van Eldik, *Eur. J. Inorg. Chem.* **2002**, 968−974.
[10] G. Stochel, R. van Eldik, *Inorg. Chem.* **1990**, *29*, 2075−2077.
[11] F. F. Prinsloo, M. Meier, R. van Eldik, *Inorg. Chem.* **1994**, *33*, 900−904.
[12] M. Meier, R. van Eldik, *Inorg. Chem.* **1993**, *32*, 2635−2639.
[13] F. F. Prinsloo, E. L. J. Breet, R. van Eldik, *J. Chem. Soc., Dalton Trans.* **1995**, 685−688.
[14] H. M. Marques, *J. Chem. Soc., Dalton Trans.* **1991**, 339−341.
[15] H. M. Marques, J. C. Bradley, L. A. Campbell, *J. Chem. Soc., Dalton Trans.* **1992**, *13*, 2019−2027.
[16] H. M. Marques, J. C. Bradley, K. L. Brown, H. Brooks, *J. Chem. Soc., Dalton Trans.* **1993**, *23*, 3475−3478.
[17] M. S. A. Hamza, C. Dücker-Benfer, R. van Eldik, *Inorg. Chem.* **2000**, *39*, 3777−3783.
[18] M. Spitzer, F. Gartig, R. van Eldik, *Rev. Sci. Instrum.* **1988**, *59*, 2092−2093.
[19] R. van Eldik, W. Gaede, S. Wieland, J. Kraft, M. Spitzer, D. A. Palmer, *Rev. Sci. Instrum.* **1993**, *64*, 1355−1357.

Received February 23, 2003

 © 2003 Wiley-VCH Verlag GmbH & Co. KGaA, Weinheim

Rational Design, Synthesis and Crystal Structure Investigation of Hydrogen-Bonded Coordination Polymers of Bicyclic Bis-Lactam Dicarboxylates[‡]

Denis A. Lenev,[a] Konstantin A. Lyssenko,[b] and Remir G. Kostyanovsky*[a]

Keywords: Carboxylate ligands / Chirality / Crystal engineering / Hydrogen bonding / Lactams

The crystal structures of the racemic coordination polymers (±)-**1** to (±)-**4** and the coordination dimers (±)-**6** and (±)-**7**, containing molecular "brick walls" with inorganic coatings and molecular "brick walls" with mixed organic-inorganic coatings, respectively, were predicted and verified on the basis of the zigzag $R_2^2(8)$ H-bonded tape columnar packing motif of the purely organic racemic dialkyl 3,6-dioxo-2,5-diazabicyclo[2.2.2]octane-1,4-dicarboxylates.
(© Wiley-VCH Verlag GmbH & Co. KGaA, 69451 Weinheim, Germany, 2003)

Introduction

H-bonded supramolecular aggregation of metal ion-coordinated assemblies is a promising approach in crystal engineering, combining a variety of coordination types and well established organic motifs of H-bonding.[1−8] In a preceding paper[9] we have shown that functionalized derivatives of chiral C_2-symmetric bicyclic dipeptide, 2,5-diazabicyclo[2.2.2]octane-3,6-dione (DBO), viz. corresponding dialkyl 1,4-dicarboxylates, form predictable heterochiral zigzag tapes with lactamic $R_2^2(8)$ H-bonding, in which molecules of different chirality alternate strictly (Scheme 1), as in the crystal structures of (±)-DBO and other bis-lactams[10−14] (for other important works on lactamic H-bonded tapes, see refs.[15−17]). A new two-dimensional motif appears in all investigated crystals of the racemic and chiral quasi-racemic esters, with homochiral columns being formed by stacking of the heterochiral tapes orthogonally to their propagation axes. We refer to this two-dimensional motif as molecular "brick walls" with non-polar coating (Scheme 1) (compare ref.[18]). An attempt to extend the "brick walls" into the third dimension (and thus explain the design of the whole crystal structure) through H-bonding, involving carboxylic acid moieties (Scheme 1, X = CO_2H)

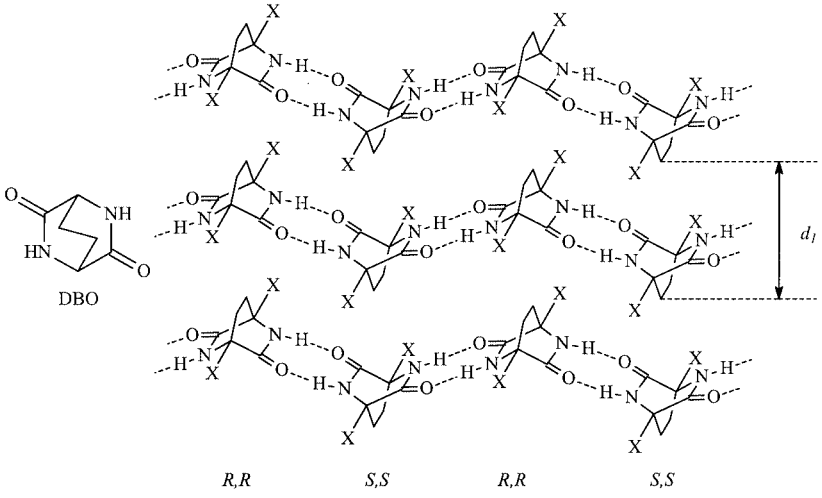

Scheme 1. Molecular "brick wall" with nonpolar coating (X = CO_2alkyl) observed in crystal structures of dialkyl DBO-1,4-dicarboxylates, where d_1 is the distance between adjacent molecules in the column and is equal to the corresponding translation (crystal lattice parameter)

[‡] Self-assembly of Cage Structures, 15. Part 14: ref.[19]
[a] N.N. Semenov Institute of Chemical Physics, Russian Academy of Sciences,
4 ul. Kosygina, 119991 Moscow, Russia
Fax: (internat.) +7-095/938-2156
E-mail: kost@center.chph.ras.ru
[b] A.N. Nesmeyanov Institute of Organoelement Compounds, Russian Academy of Sciences,
28 ul. Vavilova, 119991, Moscow, Russia
Fax: (internat.) +7-095/135-5085
E-mail: kostya@xrlab.ineos.ac.ru

failed because of hydrate formation.[9] In the case of competitive H-bonding carbamoyl substituents (X = $CONH_2$), either nanochannels or unbalanced chiral, triply interpenetrated, diamondoid networks form.[19] We therefore tried to use supramolecular forces from another field, metal−carboxylate ligand interactions, which it was hoped might direct self-assembly of the desired three-dimensional crystal structure (Scheme 2). In addition, we were also very interested in the senses of chirality of the assemblies formed. In this study we report the results of the initiated research. In fact, examples of coordination structures of cyclic dipeptides have already been published for Na and Tl^I salts of *cyclo*-(L-α-aspartyl-L-phenylalanine)[20,21] and in particular for a coordination polymer of Ag^I with *cyclo*-(L-methionyl-L-methionyl).[22] However, little attention is given in those papers to the supramolecular aspects of the structures.

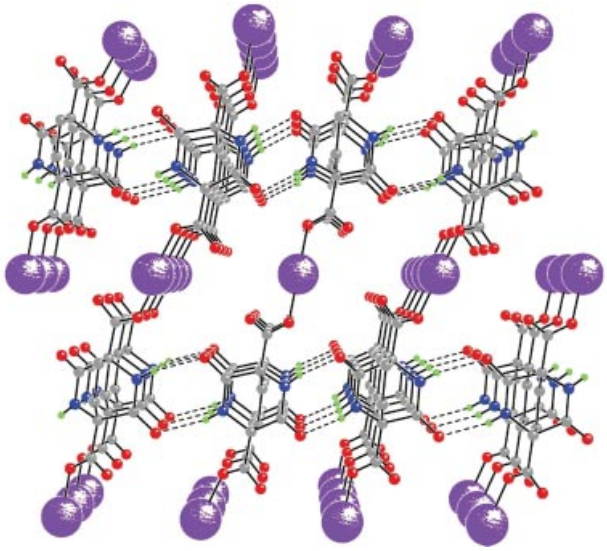

Scheme 2. Hypothetical three-dimensional self-assembly of H-bonded tapes of DBO-1,4-dicarboxylate dianions by coordination with metal cations (M lilac, C grey, N blue, O red, H green)

Results and Discussion

The synthesis of the metal DBO-1,4-dicarboxylates is depicted in Scheme 3. Metal salts of the diacid (±)-**A**[9] (±)-**1** to (±)-**3** were prepared in aqueous solution through exchange reactions. The potassium acid salt (±)-**4** was prepared by treatment of **A** with one equivalent of KOH. Monosaponification of diester (±)-**B**[9] gave compound (±)-**5**, which was converted into salts (±)-**6** and (±)-**7** through exchange reactions. All the salts were racemic. For the compounds (±)-**1** to (±)-**4**, (±)-**6** and (±)-**7**, single crystals were grown and X-ray diffraction investigation was undertaken (Table 1).

The molecular structures of the bis-lactam dicarboxylate anions in all structures studied remain practically unchanged, with variation of the bicyclic conformation from synchro- to asynchro-twist, as previously observed for the diester derivatives.[9] The dianion symmetry in **1** to **3** is close

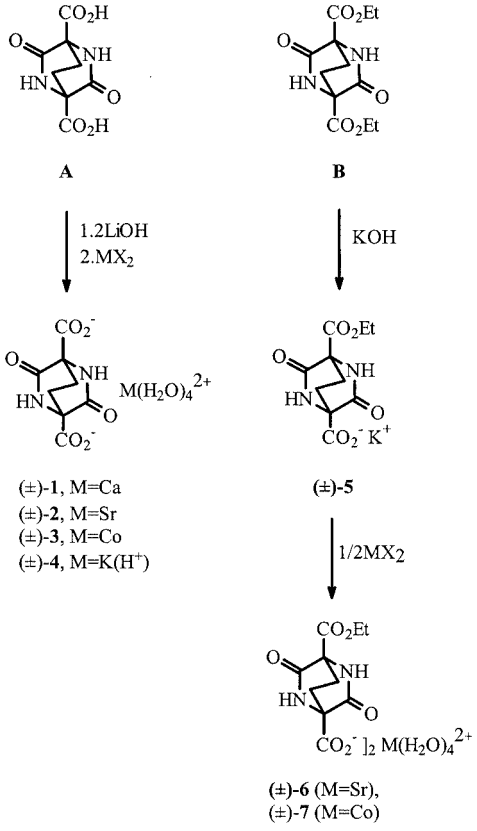

Scheme 3. Synthesis of metal DBO-1,4-dicarboxylates

to C_2 (in **1**, the dianion occupies the special position on the twofold axis) with some deviation due to variations of the disposition of the CO_2^- groups and the bicyclic skeleton. In contrast, the symmetry of the monoanionic species in the compounds **4**, **6** and **7** cannot exceed C_1.

It is remarkable that all the studied compounds **1** to **4**, **6** and **7** are tetrahydrates. X-ray diffraction investigation has shown that in **1** to **4** the bicyclic anions assemble in heterochiral zigzag tapes and form the expected "brick walls" (Scheme 1) with carboxylic groups on the outer surfaces. The carboxylic oxygen atoms of neighbouring "brick walls', together with four water molecules, form the coordination sphere of each metal ion. Metal ion coordination crosslinks the "brick walls', so the observed structures consist of alternating organic and inorganic layers (Figure 1). Consequently we may regard compounds **1** to **4** as coordination polymers. Their crystal structures differ in the building of the inorganic layers, but **1** and **2** are practically isostructural (if we do not take into account the crystallographic axis 2, which is present in **1** but missing in **2**). A change in the metal ion results only in slight deviations in lactam H-bond strength (N···O distance) and d_1 separation (Scheme 1). The N···O distance increases systematically from 2.854(4) Å in **4** to 3.042(5) Å in **2**. The same trend is observed for the d_1 separation, being 5.49 Å in **4** (even shorter than in the corresponding esters; see below) and going up to 6.12 Å in **2**. Thus, even bigger cations, such as Sr, although making lactam H-bonding weaker, do not change the observed molecular "brick wall" motif. The construction of the inor-

 © 2003 Wiley-VCH Verlag GmbH & Co. KGaA, Weinheim

Table 1. X-ray diffraction data for the compounds **1** to **4**, **6** and **7**

	(±)-**1**	(±)-**2**	(±)-**3**	(±)-**4**	(±)-**6**	(±)-**7**
Formula	$C_8H_{14}CaN_2O_{10}$	$C_8H_{14}N_2O_{10}Sr$	$C_8H_{14}CoN_2O_{10}$	$C_8H_{15}KN_2O_{10}$	$C_{20}H_{30}N_4O_{16}Sr$	$C_{20}H_{30}CoN_4O_{16}$
T, K	110	298	110	298	110	110
Crystal system	Monoclinic	Monoclinic	Triclinic	Orthorhombic	Monoclinic	Orthorhombic
Space group	*P*2/*c*	*Pc*	$P\bar{1}$	$Pca2_1$	*C*2/*c*	$Pca2_1$
a, Å	10.851(2)	11.027(2)	5.804(1)[a]	11.429(2)	43.554(5)	10.326(2)
b, Å	5.987(1)[a]	6.117(1)[a]	10.261(2)	5.493(1)[a]	5.9568(7)[a]	5.586(1)[a]
c, Å	9.980(2)	10.191(2)	11.449(3)	20.021(4)	10.371(1)	44.179(9)
α, deg			77.582(4)			
β, deg	112.393(5)	112.88(3)	79.037(4)		99.047(3)	
γ, deg			75.162(4)			
V, Å^3	599.5(2)	633.3(2)	637.1(3)	1257.0(4)	2657.1(5)	2548.3(9)
Z	2	2	2	4	4	4
M	338.29	385.83	357.14	338.32	670.10	641.41
μ, cm^{-1}	5.85	43.16	14.05	4.82	21.35	7.62
F(*000*)	352	388	366	704	1376	1332
Absorption Correction[b]	A	B	A	none	A	A
ρ_{calcd}, g·cm^{-3}	1.874	2.023	1.862	1.788	1.675	1.672
$2\theta_{max}$, deg	60	60	57	64	52	58
Diffractometer	Smart CCD	Siemens P3	Smart CCD	Siemens P3	Smart CCD	Smart CCD
Scan mode	ω	θ/2θ	ω	θ/2θ	ω	ω
No. of reflections measured	4774	3185	6068	4459	7885	12426
R_{int}	0.0286	0.0171	0.0253	0.0033	0.0639	0.0351
No. of independent reflections	1751	1837	3137	3447	2637	5206
No. of reflections with $I > 2\sigma(I)$	1465	1668	2530	2855	1860	4436
No. of parameters	124	200	249	205	240	462
R_1	0.0465	0.0203	0.0467	0.0435	0.0524	0.0496
wR_2	0.1173	0.0513	0.1040	0.1210	0.1282	0.1277
GOF	0.930	1.018	1.074	1.069	0.934	1.031
Max./min peak, e·Å^{-3}	0.83/−0.35	0.33/−0.41	0.86/−0.56	0.38/−0.40	1.23/−0.68	1.13/−0.58

[a] The translation corresponding to the d_1 distance between the DBO molecules in columns. [b] A, semiempirical absorption correction from equivalent reflections; B, ψ-scan absorption correction.

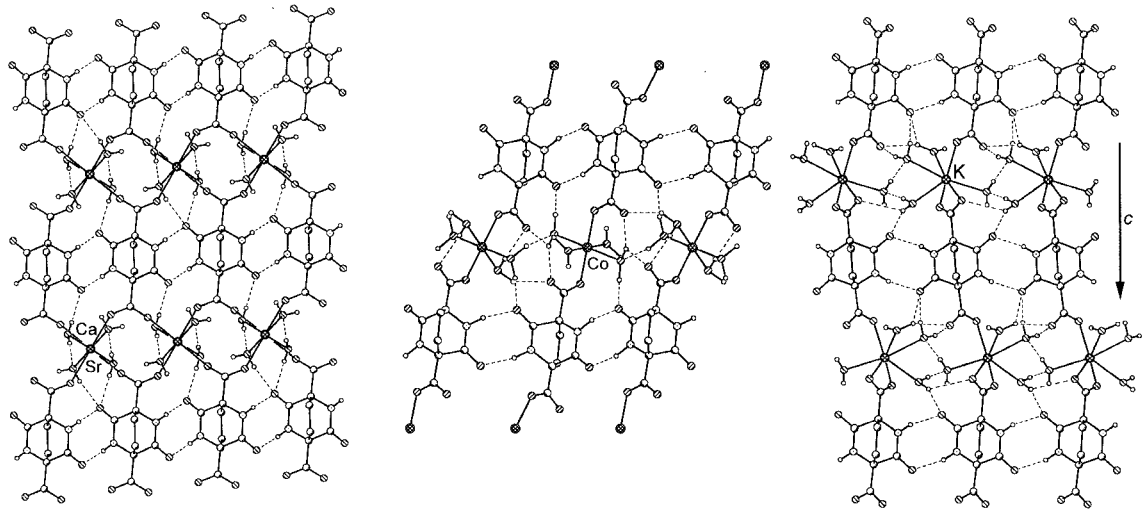

Figure 1. Projections of the crystal structures of **1** and **2** (practically isostructural) (a), **3** (b) and **4** (c), showing H-bonded heterochiral tapes of bicyclic anions united by metal ions coordination on the *ac*, *bc* and *ac* crystallographic planes, respectively

ganic layer is dictated solely by the nature of the metal cation (compare ref.[23]). The coordination numbers are 7 for K, 8 for Sr and Ca, and 6 for Co. Metal−oxygen distance ranges in the coordination polyhedra of **1** to **4**, **6** and **7** are shown in Table 2. The observed distances are not unusual, with the shortest being found in the cases of the Co complexes **3** and **7**. The inorganic layer is reinforced by H-bonds involving water molecules and carboxylic or amide carbonyl

 © 2003 Wiley-VCH Verlag GmbH & Co. KGaA, Weinheim

Table 2. Metal ion − carboxylate O_{carb} or water O_w oxygen distance ranges in coordination polyhedra of **1** to **4**, **6** and **7**

	1	**2**	**3**	**4**	**6**	**7**
M−O_{carb}	2.371(1)−2.480(1)	2.498(6)−2.615(5)	2.056(2)−2.084(2)	2.357(2)−2.437(2)	2.491(3)−2.582(3)	2.057(3)−2.092(3)
M−O_w	2.466(1)−2.497(1)	2.584(6)−2.645(6)	2.041(2)−2.125(2)	2.426(3)−2.571(3)	2.601(3)−2.604(3)	2.083(3)−2.096(3)

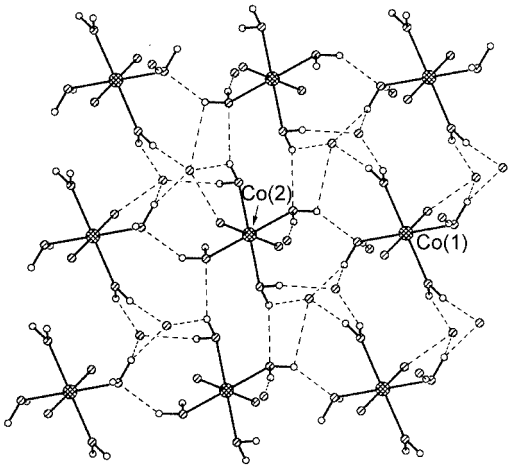

Figure 2. Projection of the H-bonded inorganic layer in **3** on the *ac* crystallographic plane

oxygens (Figure 2 shows an example of H-bonded inorganic layer in **3**). The O···O distance, which characterizes the strength of the O−H···O bonds in the inorganic layer, varies between 2.732 and 3.034 Å and is practically unaffected by the nature of the cation. If one takes only the H-bonded network into consideration, the water molecules interconnect the H-bonded tapes in **1** to **4** in a three-dimensional framework.

The number and the chirality of bicyclic bis-lactam anions coordinated by metal ions vary, thus giving rise to differences in the structures of the inorganic layers and the positioning of the "brick walls'. In the cases of **1** and **2**, the alkaline earth metal ion is surrounded by four aqua ligands and four carboxylate oxygens. Each carboxylate group of the bis-lactams in these compounds is bound to two cations and thus serves as a bridging ligand. It is noteworthy that the coordination spheres of Ca and Sr in **1** and **2** both contain two (*R*,*R*) and two (*S*,*S*) enantiomers (Figure 3, a). In contrast, in the potassium complex **4** the bicyclic monoanions have two different kinds of carboxylate groups. In the first, only one of the carboxylate oxygen atoms is coordinated by metal ion, in the second both oxygen atoms are coordinated. This molecular asymmetry is not cancelled and propagates along the screw axis 2_1, so the acentric crystal structure (space group $Pca2_1$) has a polar axis in the *c* direction (Figure 1, c). In addition, the coordination polyhedron of K is homochiral (three bicyclic ligands are characterized by the same chirality; Figure 3, b). The observed difference in the chirality of the ligands is due to the fact that potassium forms bonds with anions from three separate H-bonded tapes: one from one "brick wall' and the two others from another. The latter two anions lie in

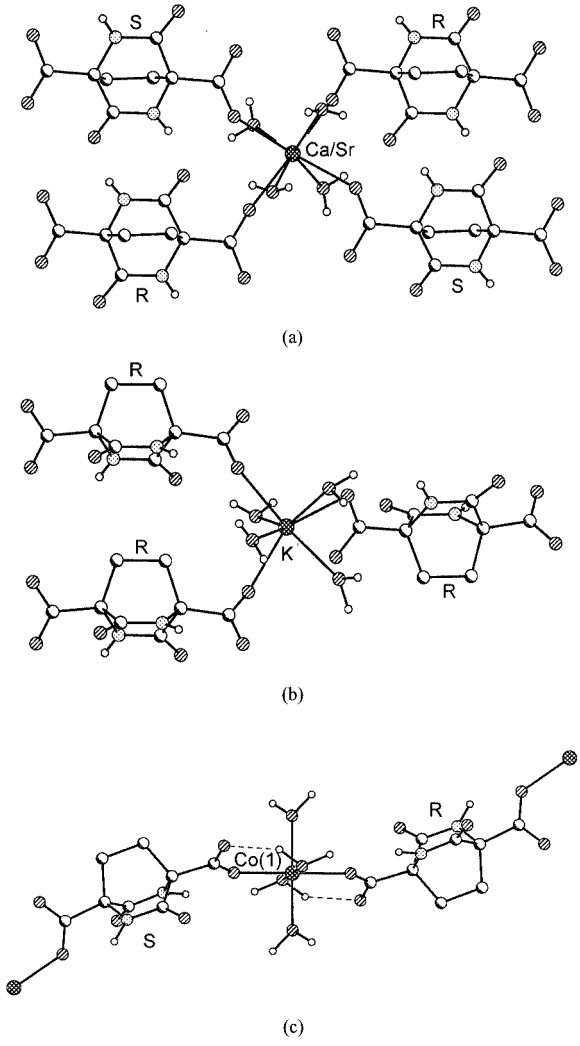

Figure 3. Coordination polyhedra and ligand chirality in **1** and **2** (a), **4** (b) and **3** (c)

the same column, one under the other, so that coordination causes a pronounced contraction of the d_1 distance (5.49 Å) in relation to the 5.57 Å in the crystal structure of the ester (±)-**B**.[9] Finally, in the crystal structure of the cobalt(II) salt **3** the metal ion (two independent cations each in the centre of symmetry) is characterized by the usual octahedral coordination with a *trans* arrangement of the monodentate ligands of opposite chirality (Figure 3, c).

If we take only the coordination connectivity into account, cations interconnect the anions, depending on the nature of the metal, in corrugated heterochiral layers (**1** and **2**) in the plane orthogonal to the axes of homochiral columns, or in the homochiral layers orthogonal to the axes

 © 2003 Wiley-VCH Verlag GmbH & Co. KGaA, Weinheim

of the heterochiral tapes (**4**), or in heterochiral chains (**3**) orthogonal to the "brick walls'.

All the coordination polymers obtained thus possessed the same general structure regardless of the type of metal (alkali, alkaline earth or transition), so that any desired property (e.g., magnetic) of the resulting material should be fine-tuneable simply by a change in the cation (compare ref.[2]).

Using the distinct and stable supramolecular organization of the "brick walls' in the crystal structures of covalent[9] (for example, (±)-**B**) and ionic DBO-1,4-dicarboxylates **1** to **4**, and also the well known analogy of the structure of biological membranes, we also tried to obtain coordination dimers **6** and **7**. In these structures, polar ionic and nonpolar alkyl residue regions should alternate, similarly to what has been observed in, for example, the structure of the monohydrate of the diketopiperazine *cyclo*-(L-leucyl-L-hystidyl).[24] Indeed, X-ray analysis has shown that the main features of packing remain unchanged, and we observe coordination dimerization of carboxylic ions. Strongly polar inorganic water-containing layers and nonpolar alkyl regions alternate as anticipated (Figure 4 shows the crystal structure of **7**). Comparison of the structures of organic and inorganic layers with those of the corresponding coordination polymers **2** and **3** has shown that the structure remains practically unchanged in the case of Sr, except for insignificant variations in the H-bonding in the inorganic layer. In **7** these changes are much more pronounced, and this is reflected in the homochirality of the coordination octahedron (Figure 5). The example of the Co complexes **3** and **7** thus implies that the chiralities of the ligands are practically independent of each other ((*RR*,*SS*) in one case and (*RR*,*RR*) in the other) and, unfortunately, are defined by peculiarities of crystal symmetry (centrosymmetric arrangement in **3** and acentric structure of **7**) and packing. It is noteworthy that the d_1 distances in **6** and **7** are approximately the average of those in the structures of (±)-**B** and **2** and **3**, respectively: in **6** d_1 equals 5.96 Å, in **7** 5.59 Å, whereas in **2** it is 6.12 Å, in **3** 5.80 Å, and in **B** 5.57 Å.

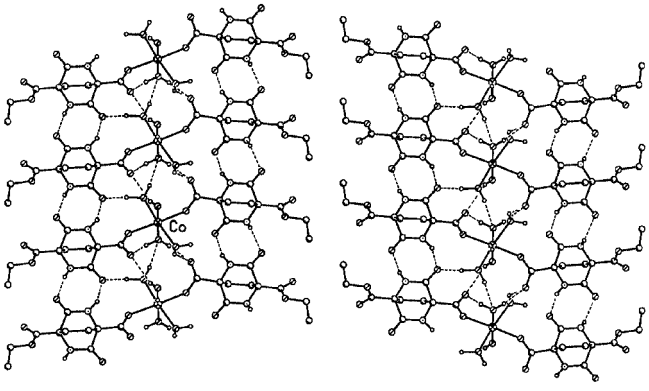

Figure 4. The projection of the crystal structure of coordination dimer **7** on the *ac* crystallographic plane

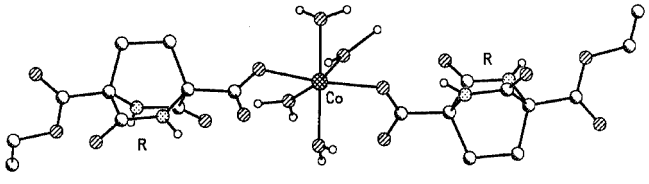

Figure 5. The coordination polyhedron and homochirality of the ligands in **7**

Compounds **6** and **7** thus represent hybrid-type materials. Firstly, the organic part makes the introduction of substituents with various functionalities possible; secondly, the nature of the cation itself may be varied. Moreover, the structures of these complexes are similar to those of biological membranes and offer perspectives for construction of ionoactive monolayers on that basis.

Conclusion

In this paper we have used a productive approach to crystal engineering − rational design of metal-organic H-bonded solids by combining a well defined H-bonded motif derived from pure organic crystal structures with the well known geometries of carboxylate metal complexes. Metal ion-assisted assembly of the bicyclic bis-lactam-dicarboxylate ions results in the predicted coordination polymers **1** to **4**, in which the molecular "brick wall" motif, found previously in dialkyl dicarboxylates (now with an inorganic ionic coating), is preserved. Formation of layers, stabilized by H-bonding of aqua ligands, is also observed. The salts' structures differ insignificantly as the coordinating centre changes. Monocarboxylate ion coordination results in other types of predicted structures, represented in the paper by coordination dimers **6** and **7**. In these compounds, "brick wall" formation is "coordinationally doubled", resulting in alternation of polar and non-polar layers (wall coatings) in the crystal.

We should also underline the limitations of our approach. Although we control the chirality of bis-lactam anions in the "brick walls", the examples of Co coordination polymer **3** and coordination dimer **7** imply that the chiralities of two anions coordinated by metal in a spatially distinct *trans* arrangement are independent of each other and depend only on the crystal symmetry and packing. Moreover, taking the strength of ionic interactions in comparison to hydrogen bonds into account, we believe that *both* organic dipole−dipole and van der Waals interaction-stabilized "brick walls" *and* inorganic H-bonded layers are responsible for the three-dimensional structure as a whole, their dimensionalities fortunately being complementary.

Finally, it should be mentioned that in the overall series of **1** to **4**, **6** and **7**, three crystal structures (**2**, **4**, **7**) are noncentrosymmetric (though achiral) and therefore offer perspectives for pyroelectric, piezoelectric and NLO applications.

Experimental Section

General Method for Preparation of Salts of (±)-A: A solution of LiOH in H_2O (2 mL, 0.2 M) was added to diacid (±)-**A** (25 mg,

 © 2003 Wiley-VCH Verlag GmbH & Co. KGaA, Weinheim

0.1 mmol), and the mixture was heated until it became clear, was filtered through cotton wool, and 1 mol equiv. of solution of metal salt [$CaCl_2$, $Sr(NO_3)_2$ or $CoCl_2$] in H_2O (1 mL) was added. On standing at ambient temperature a fine powder usually crystallized. This was filtered off, dried in air, weighed and then suspended in H_2O (2 mL). The suspension was heated at reflux with slow addition of water until complete dissolution of the precipitate (5−15 min). The clear solutions were left to cool down and were kept at ambient temperature under the conditions suitable for slow evaporation of the solvent. Separate crystals formed over several days. Besides the complexes **1** to **4**, well defined crystals also formed in the cases of Zn, Mn^{II}, Ni^{II} and Cu^{II}. The Ba and Ag^{I} salts were insoluble in hot H_2O.

Calcium 3,6-Dioxo-2,5-diazabicyclo[2.2.2]octane-1,4-dicarboxylate Tetrahydrate (±)-(1): Yield 30 mg (88%). Colourless needles, becoming turbid in air. $C_8H_{14}CaN_2O_{10}$ (338.3): calcd. C 28.4, H 4.2, N 8.3, Ca 11.6; found C 28.7, H 3.9, N 8.1, Ca 12.0.

Strontium 3,6-Dioxo-2,5-diazabicyclo[2.2.2]octane-1,4-dicarboxylate Tetrahydrate [(±)-2]: Yield 15 mg (40%). Colourless prisms. $C_8H_{14}N_2O_{10}Sr$ (385.8): calcd. C 24.9, H 3.7, N 7.3; found C 25.0, H 3.8, N 7.3.

Cobalt(II) 3,6-Dioxo-2,5-diazabicyclo[2.2.2]octane-1,4-dicarboxylate Tetrahydrate [(±)-3]: Yield 21 mg (58%). Transparent pink prisms, becoming blue and turbid in air. $C_8H_{14}CoN_2O_{10}$ (357.1): calcd. C 26.9, H 4.0, N 7.8; found C 28.0, H 4.0, N 8.1 (the significant deviation of the amount of C found from the calculated value may be attributed to water loss).

Potassium 3,6-Dioxo-2,5-diazabicyclo[2.2.2]octane-1,4-dicarboxylate Tetrahydrate [(±)-4]: For preparation of this acid salt, 1 mol equiv. of KOH was taken per mol of (±)-**A**. Yield 18 mg (52%). Colourless blocks. $C_8H_{15}KN_2O_{10}$ (338.3): calcd. C 28.4, H 4.5, N 8.3; found C 28.0, H 4.3, N 8.3.

Potassium 3,6-Dioxo-4-(ethoxycarbonyl)-3,6-dioxo-2,5-diazabicyclo[2.2.2]octane-1-carboxylate [(±)-5]: A solution of KOH in EtOH (0.0546 M, 20 mL) was slowly (10 min) added, with heating and vigorous stirring, to a boiling solution of (±)-**B** (1.551 g, 5.456 mmol) in 96% EtOH (130 mL). As soon as the mixture started to become turbid (≈ 15−20 min after the start of addition), heating was stopped, the mixture was cooled to 40 °C, and, with this temperature being maintained, KOH (0.0546 M, 80 mL) was added (slowly, 2 h). The mixture was cooled to 0°C and left for 24 h. The white precipitate of a mixture of mono- and disalts was filtered off, washed with EtOH and dried in vacuo. It was then recrystallized from the minimum possible amount of boiling water. The product crystallized as thin plates, which were filtered off, washed with cold H_2O and dried in air. Yield is 977 mg (61%), m.p. 380−390° C(dec.). ^1H NMR (400 MHz, D_2O, 60° C): δ = 1.32 (t, ^3J = 7 Hz, 3 H, CH_3,), 2.2−2.35 (m, 4 H, CH_2CH_2,), 4.38 (m, 2 H, CH_2Me) ppm. $C_{10}H_{11}KN_2O_6$ (294.3): calcd. K 13.3, C 40.8, H 3.7, N 9.5; found K 13.7, C 39.7, H 4.0, N 9.5.

Preparation of Salts (±)-6 and (±)-7: A solution of $CoCl_2$ (6.5 mg, 0.05 mmol) or $Sr(NO_3)_2$ (10.6 mg, 0.05 mmol) in H_2O (0.5 mL) was added to a hot solution of (±)-**5** (30 mg, 0.10 mmol) in H_2O (1 mL). After 1 h the precipitate was filtered off, dried in air and recrystallized from water in the same manner as for the coordination polymers.

Strontium Bis{4-(Ethoxycarbonyl)-3,6-dioxo-2,5-diazabicyclo[2.2.2]-octane-1-carboxylate} tetrahydrate [(±)-6]: Yield 8 mg (25%). Very thin colourless plates. $C_{20}H_{30}N_4O_{16}Sr$ (670.1): calcd. C 35.9, H 4.5, N 8.4; found C 36.0, H 4.3, N 8.2.

Cobalt(II) Bis{4-(Ethoxycarbonyl)-3,6-dioxo-2,5-diazabicyclo[2.2.2]-octane-1-carboxylate} Tetrahydrate (±)-7: Yield 8 mg (27%). Transparent pink prisms. $C_{20}H_{30}CoN_4O_{16}$ (641.4): calcd. C 37.5, H 4.7, N 8.7; found C 37.5, H 4.5, N 8.9.

Crystallographic data and parameters of the refinement for complexes **1** to **4**, **6** and **7** are presented in Table 1. The data collection was carried out by use of the θ/2θ scan mode for the 4-circle diffractometer (Siemens P3) and the ω-scan mode with 0.3° step in ω and 10 s (for **1** and **3**) or 20 s (**6** and **7**) exposure for SMART CCD diffractometer. The X-ray diffraction data for SMART CCD were processed by use of the SAINT PLUS program package. All structures were solved by direct methods and refined by full-matrix, least-squares against F^2 in the anisotropic (H atoms isotropic) approximation, by use of the SHELXTL-97 package. The positions of hydrogen atoms were located from the Fourier electron density synthesis and included in refinement in isotropic or riding model approximation. The hydrogen atom of the CO_2H groups in the monohydropotassium salt **4** was not located, probably due to the superposition of the CO_2^- and CO_2H groups, reflected in the equalization of the corresponding C−O bond lengths. The absolute structures in the cases of **2**, **4** and **7** were determined on the basis of the Flack parameter.

CCDC entries 204270−204275 (**1** to **4**, **6** and **7**) contain the supplementary crystallographic data for this paper. These data can be obtained free of charge at www.ccdc.cam.ac.uk/conts/retrieving.html [or from the Cambridge Crystallographic Data Centre, 12, Union Road, Cambridge CB2 1EZ, UK; fax: (internat.) +44-1223/336-033; E-mail: deposit@ccdc.cam.ac.uk].

Acknowledgments

The authors thank Prof. Dr. V. Buß (University of Duisburg) for helpful discussions. This work was supported by INTAS (grant No. 99−00157), the Russian Academy of Sciences (academician N. T. Kuznetsov programme) and the Russian Foundation for Basic Research (grant Nos. 00-03-32738, 00-03-81187 Bel, 03-03-32019 and 03-03-06525 MAS).

[1] M. Munakata, L. P. Wu, M. Yamamoto, K.-S. Takayoshi, M. Maekawa, *J. Am. Chem. Soc.* **1996**, *118*, 3117−3124.
[2] J. C. MacDonald, P. C. Dorrestein, M. M. Pilley, M. M. Foote, J. L. Lundburg, R. W. Henning, A. J. Schultz, J. L. Manson, *J. Am. Chem. Soc.* **2000**, *122*, 11692−11702.
[3] E. Breuning, U. Ziener, J.-M. Lehn, E. Wegelius, K. Rissanen, *Eur. J. Inorg. Chem.* **2001**, 1515−1521.
[4] A. D. Burrows, C.-W. Chan, M. M. Chowdhry, J. E. McGrady, D. M. P. Mingos, *Chem. Soc. Rev.* **1995**, *24*, 329−337.
[5] I. Goldberg, *Chem. Eur. J.* **2000**, *6*, 3863−3870.
[6] C. B. Aakeröy, A. M. Beatty, D. S. Leinen, *Angew. Chem.* **1999**, *111*, 1932−1936; *Angew. Chem. Int. Ed.* **1999**, *38*, 1815−1819.
[7] D. Braga, F. Grepioni, G. R. Desiraju, *Chem. Rev.* **1998**, *98*, 1375−1405.
[8] S. Ferlay, O. Felix, M. W. Hosseini, J. M. Planeix, N. Kyritsakas, *Chem. Commun.* **2002**, 702−703.
[9] K. A. Lyssenko, D. A. Lenev, R. G. Kostyanovsky, *Tetrahedron* **2002**, *58*, 8525−8537.
[10] M.-J. Brienne, J. Gabard, M. Leclercq, J.-M. Lehn, M. Cesario, C. Pascard, M. Cheve, G. Dutruc-Rosset, *Tetrahedron Lett.* **1994**, *35*, 8157−8160.
[11] D. N. J. White, J. D. Dunitz, *Isr. J. Chem.* **1972**, *10*, 249.
[12] M. Tichy, L. Ridvan, P. Holy, J. Zavada, J. Cisarova, J. Podlaha, *Tetrahedron: Asymmetry* **1998**, *9*, 227−234.
[13] C. Altomare, S. Cellamare, A. Carotti, G. Casini, M. Ferappi,

 © 2003 Wiley-VCH Verlag GmbH & Co. KGaA, Weinheim

E. Gavuzzo, F. Mazza, P.-A. Carrupt, P. Gaillard, B. Testa, *J. Med. Chem.* **1995**, *38*, 170−179.
[14] M. Czugler, A. Kalman, B. Oleksyn, M. Kajtar, *Cryst. Struct. Commun.* **1980**, 791−794.
[15] J. C. MacDonald, G. M. Whitesides, *Chem. Rev.* **1994**, *94*, 2383−2420.
[16] G. T. R. Palmore, M. T. McBride, *Chem. Commun.* **1998**, 145−146.
[17] S. Palacin, D. N. Chin, E. E. Simanek, J. C. MacDonald, G. M. Whitesides, M. T. McBride, G. T. R. Palmore, *J. Am. Chem. Soc.* **1997**, *119*, 11807−11816.
[18] H. J. Choi, M. P. Suh, *J. Am. Chem. Soc.* **1998**, *120*, 10622−10628.
[19] R. G. Kostyanovsky, K. A. Lyssenko, D. A. Lenev, I. A. Bronzova, *Tetrahedron: Asymmetry* **2002**, *13*, 2697−2701.
[20] P. Mikulcik, J. Riede, H. Schmidbaur, *Chem. Ber.* **1991**, *124*, 2743−2746.
[21] P. Mikulcik, P. Bissinger, J. Riede, H. Schmidbaur, *Z. Naturforsch., Teil B* **1992**, *47*, 952−956.
[22] Y. Kojima, T. Yamashita, Y. Ishino, T. Hirashima, K. Hirotsu, *Chem. Lett.* **1983**, 453−454.
[23] E. G. Bakalbassis, M. Korabik, A. Michailides, J. Mrozinski, C. Raptopoulou, S. Skoulika, A. Terzis, D. Tsaousis, *J. Chem. Soc., Dalton Trans.* **2001**, 850−857.
[24] I. Tanaka, T. Iwata, N. Takahashi, T. Ashida, *Acta Crystallogr., Sect. B* **1977**, *33*, 3902.

Received February 27, 2003

 © 2003 Wiley-VCH Verlag GmbH & Co. KGaA, Weinheim

HREM and CIP Characterization of Complex Superstructures in Cu-Co Related Perovskites

Luisa Ruiz-González,[a] Khalid Boulahya,[a] Marina Parras,[a] José Alonso,[b] and José M. González-Calbet*[a]

Keywords: Perovskite phases / Superstructures / Electron diffraction / Electron microscopy

Two compositions in the La-Ba-Cu-Co-O system – $La_2Ba_3Cu_2Co_3O_{13}$ and $La_2Ba_3Cu_3Co_2O_{13}$ – have been synthesized and characterized by means of SAED (Selected Area Electron Diffraction) and HREM (High Resolution Electron Microscopy). The $La_2Ba_3Cu_2Co_3O_{13}$ phase leads to a fivefold perovskite superstructure along the *c* axis, which can be described as formed by the recurrent intergrowth of the two alternating blocks ···*PP*··· and ···PO_hP··· (*P* = pyramid and O_h = octahedron). Pyramidal and octahedral sites are randomly occupied by Cu/Co cations, while La/Ba cations exhibit an ordered distribution. The $La_2Ba_3Cu_3Co_2O_{13}$ composition gives rise to a mixture of phases in which a new phase showing a threefold superstructure due to the sequence ···PO_hP··· coexists with a fivefold superstructure with the same polyhedra sequence (···*PPPO*$_h$*P*···) as the previous one, but a disordered arrangement of lanthanum-barium cations.
(© Wiley-VCH Verlag GmbH & Co. KGaA, 69451 Weinheim, Germany, 2003)

Introduction

Extensive research on compositional variations in perovskite ABO_3 related compounds has led to the stabilization of new oxygen-deficient phases $AA'BB'O_{6-x}$ as a consequence of ordered arrangement at the cation and/or oxygen sublattices. Cationic order can be found in both A and B sublattices, and is related to the size and charge differences of each set of cations. Moreover, the coordination tendencies of B cations in the host lattice of oxygen-deficient perovskites can lead to new mixed frameworks with ordered anionic vacancies in which polyhedra-sharing corners can involve octahedral (O_h), square-pyramidal (*P*), tetrahedral (T_h) or square-planar (S_p) units.

For instance, $YBaCuFeO_5$[1] can be described as being built up from the ordered stacking sequence ···*PP*···, whereas octahedra and tetrahedra alternate in an ordered way in $Ca_2(Fe,Al)_2O_5$[2] according to ···$O_hT_hO_hT_h'$··· (T_h' stands for a change of the T_h orientation), and $La_2Ni_2O_5$[3] accommodates square-planar coordination according to the stacking sequence ···O_hS_p···. Other perovskite-related types can be formed when combining the above structural units in a more complex way. For instance, $YBa_2Fe_3O_8$[4] is a threefold perovskite superstructure with iron in octahedral and square-pyramidal coordination according to the sequence ···PO_hP···. Related phases of higher periodicity are obtained if more octahedral layers are added. This is the case for $Ln_2Ba_2Cu_2M_2O_{11}$ (M = Ti, Sn)[5] and $Ln_2Ba_2Ca_2Cu_2Ti_4O_{11}$,[6] which have four- (···$PO_hO_hO_hO_h$···) and sixfold (···$PO_hO_hO_hO_hO_hO_h$···) perovskite superstructures, respectively. On the other hand, ordered intergrowths between perovskite (O_h) and brownmillerite (O_hT_h) units lead to intermediate phases, such as $Ca_2LaFe_3O_8$,[7] $Ca_4Fe_2Ti_2O_{11}$,[8] and $Ca_4YFe_5O_{13}$[9] which stabilize three-, eight-, and tenfold superstructures, exhibiting the ···$O_hO_hT_h$···, ···$O_hO_hO_hT_hO_hO_hO_hT_h'$··· and ···$O_hO_hT_hO_hT_h'O_hO_hT_h'O_hT_h$··· sequences, respectively. In a similar way, $La_4Ni_4O_{11}$[10] stabilizes the ···$O_hO_hO_hS_p$··· sequence, in the La-Ni-O system.

The above compounds are examples of perovskite-related superlattices formed by recurrent intergrowth of two different, but related, structural types. Cases in which intergrowths are non-recurrent, i.e., they do not show long-range ordering along the crystal, have also been described.[11,12] This order-disorder situation can be understood on the basis of the rather complex compositions embracing two or more types of cations for each A and B site of the perovskite sublattice $AA'BB'O_{6-x}$ and the subsequent different oxygen polyhedra. As a consequence of the local nature of such a phenomenon, some of these structures cannot be detected by X-ray powder diffraction (XRD) techniques. This makes the microstructural characterization by means of SAED and HREM essential. Furthermore, the Crystallographic Image Processing (CIP) technique, which is based on the combination of SAED and HREM, has been shown to be useful to gather more reliable structural information, after compensation of the transfer-contrast function (CTF), amplitude and phase correction and symmetry averaging.

[a] Dpto. Química Inorgánica, Facultad de Ciencias Químicas, Universidad Complutense de Madrid, 28040 Madrid, Spain
[b] Instituto de Ciencia de Materiales de Madrid, CSIC, Cantoblanco, 28049 Madrid, Spain

 © 2003 Wiley-VCH Verlag GmbH & Co. KGaA, Weinheim **DOI: 10.1002/ejic.200300136**

Among the oxygen-deficient perovskite-related phases, cobaltites and cuprates have been widely studied due to their intriguing electronic and magnetic properties. Since different coordination environments are available for both Cu and Co cations, they are suitable for rather complex pathways of vacancy ordering in non-stoichiometric phases $AA'BB'O_{6-x}$, as recently reported for $LaBaCuCoO_{5.2}$.[13] Its structure (Figure 1) can be described as formed by the recurrent intergrowth of two alternating blocks of $2a_c$, $\cdots PP\cdots$, and $3a_c$, $\cdots PO_hP\cdots$, periodicities (a_c means the basic perovskite unit cell parameter) characteristic of the $YBaCuFeO_5$[1] and $YBa_2Fe_3O_8$[4] structural types, respectively. However, evidence of a cation-ordered arrangement was not found and therefore a random distribution was assumed. In this work, we have tried to induce cation ordering by changing the cationic ratio in both A-A′ and B-B′ perovskite sublattices. In this sense, according to the polyhedra model depicted in Figure 1, corresponding to $LaBaCuCoO_{5.2}$,[13] the La/Ba ratio was kept as 2:3 taking into account the preferred twelve coordination of Ba cations,[14] while different Cu/Co ratios were considered.

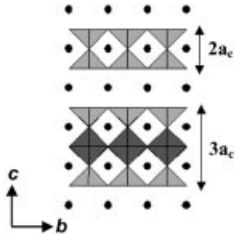

Figure 1. $LaBaCuCoO_{5.2}$ polyhedra model

Results and Discussion

$La_2Ba_3Cu_3Co_2O_y$

The XRD pattern can be indexed on the basis of an orthorhombic unit cell, $a = 0.3948$, $b = 0.3958$, and $c = 1.1683$ nm (Figure 2), characteristic of a threefold perovskite superstructure.[15] However, EDS, SAED, and HREM studies indicate that, besides the threefold superlattice, another phase is apparent. Actually, two kinds of crystals exhibiting a different Cu/Co ratio − $Cu_{0.6}Co_{0.4}$ and $Cu_{0.55}Co_{0.45}$ − have been detected. The corresponding SAED patterns along the $[100]_c$ zone axis are shown in Figure 3 a and b, respectively (subindex c refers to the cubic cell sublattice). In both cases, strong reflections appear, in agreement with the basic perovskite cell. In spite of this, weaker reflections are also present indicating different structural arrangements. In the case of the $Cu_{0.6}Co_{0.4}$ sample, spots at 1/3 and 2/3 appear along c^*, suggesting a threefold perovskite superlattice. Moreover, b^* and $c^*/3$ reciprocal parameters are clearly different, confirming the structural distortion shown in the X-ray diffraction pattern. This is in agreement with the XRD information. When the

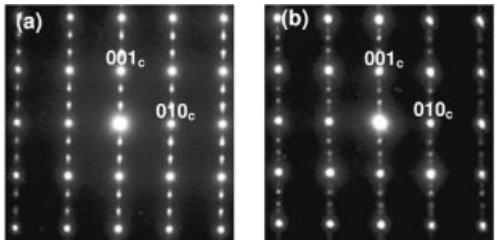

Figure 3. SAED patterns along $[100]_c$ zone axis corresponding to $La_2Ba_3Cu_3Co_2O_y$ sample (a) $Cu_{0.6}Co_{0.4}$ and (b) $Cu_{0.55}Co_{0.45}$ ratio, respectively

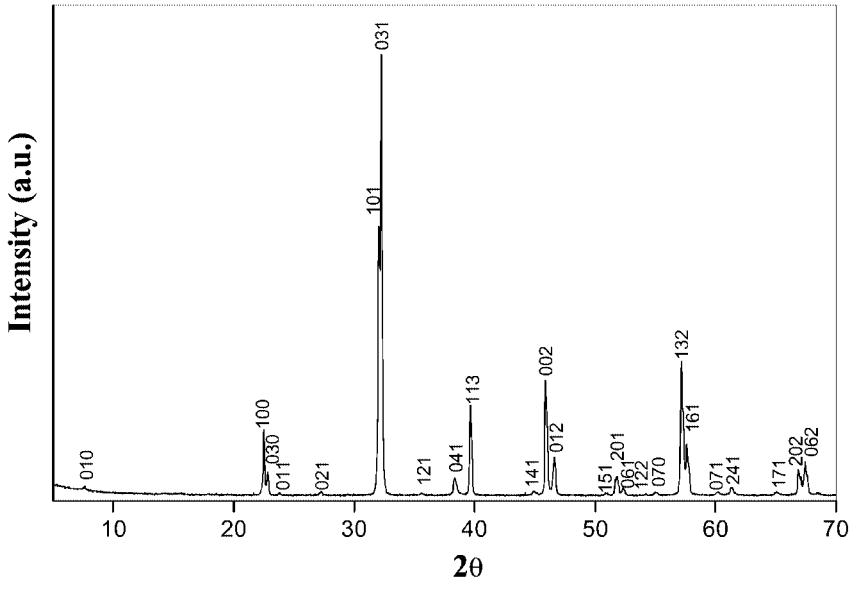

Figure 2. XRD diffraction pattern corresponding to $La_2Ba_3Cu_3Co_2O_y$

 © 2003 Wiley-VCH Verlag GmbH & Co. KGaA, Weinheim

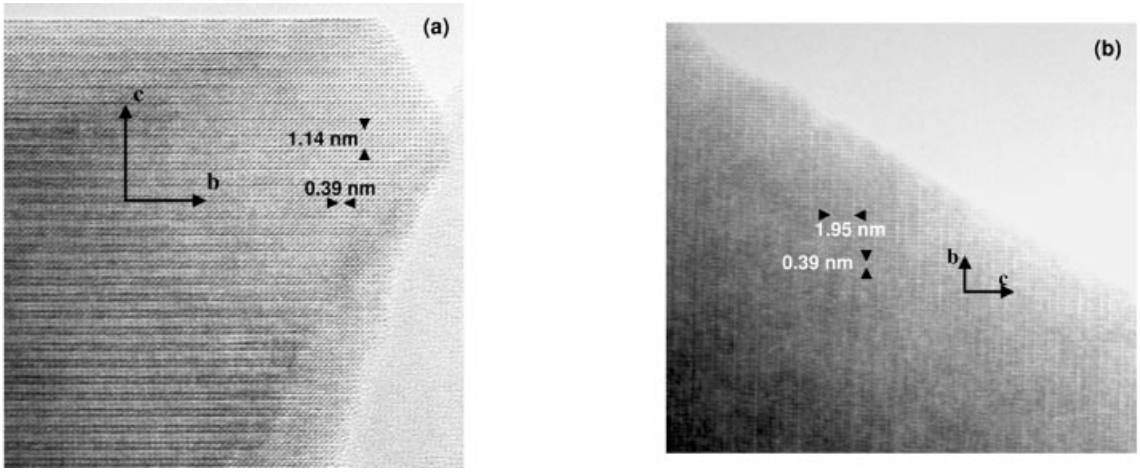

Figure 4. HREM images along $[100]_c$ zone axis corresponding to $La_2Ba_3Cu_3Co_2O_y$ sample (a) $Cu_{0.6}Co_{0.4}$ and (b) $Cu_{0.55}Co_{0.45}$ ratios, respectively

Cu/Co ratio is $Cu_{0.55}Co_{0.45}$, superlattice reflections are placed at 2/5 and 3/5 along c^*, indicating a fivefold perovskite superstructure. The corresponding HREM images (Figure 4, a and b) confirm the above periodicities, i.e, 1.14 and 1.95 nm, along c, for crystals $Cu_{0.6}Co_{0.4}$ and $Cu_{0.55}Co_{0.45}$, respectively.

The threefold order assigned to the $Cu_{0.6}Co_{0.4}$ orthorhombic phase is detected in the XRD pattern. However, the fivefold order previously reported for $LaBaCuCoO_{5.2}$,[13] is not observed. This could be related to the small X-ray powder scattering factor of the oxygen atoms together with the fact that no significant distortions from the basic perovskite sublattice are observed.[13] In this sense, the cubic pattern corresponding to the $Cu_{0.55}Co_{0.45}$ phase (related to $LaBaCuCoO_{5.2}$) must overlap with the one corresponding to $Cu_{0.6}Co_{0.4}$, thus precluding the identification of the former phase by means of XRD.

It is therefore clear that the nominal composition $La_2Ba_3Cu_3Co_2O_y$ leads to a phase mixture, in contrast to $LaBaCuCoO_{5.2}$, which stabilizes a fivefold superlattice built up from the polyhedra sequence $\cdots PO_hPPP\cdots$. The crystal showing Cu/Co = 0.6/0.4 = 1.5 is related to a threefold perovskite superstructure along c. This framework could be obtained by modifying the $2a_c$ periodicity blocks ($\cdots PP\cdots$) in the $LaBaCuCoO_{5.2}$ phase either by suppressing such a block or keeping it while adding one octahedral layer between the two square pyramids. Both pathways would give rise to the stacking sequence $\cdots PO_hP\cdots$, i.e., the basic unit of the $YBa_2Fe_3O_8$ structural type. Threefold periodicity is also found in the well-known lower-oxygen-content $YBa_2Cu_3O_7$[15] superconducting material, in which S_p instead of O_h gives rise to the polyhedra sequence $\cdots PS_pP\cdots$. Furthermore, the oxygen content can be enhanced by Co substitution, i.e., $LnBa_2Cu_{3-x}Co_xO_y$[16] leading, again, to the $\cdots PO_hP\cdots$ unit. Therefore, a similar phase, with Cu/Co = 1.5, seems to be present in this sample. However, since the Cu content in the phase Cu/Co = 0.6/0.4 (1.5) is higher than that corresponding to the fivefold ordered phase (Cu/Co = 0.5/0.5 = 1), we tentatively propose the second mechanism considering that the Cu excess is placed between the two pyramids of the $2a_c$ blocks, leading to the observed $3a_c$ periodicity. On the other hand, crystals exhibiting a higher Co content, i.e., a Cu/Co ratio close to one, Cu/Co = 0.55:0.45 (1.22), show the fivefold superlattice characteristic of $LaBaCuCoO_{5.2}$.[13] This situation could, again, be understood by adding $2a_c$ periodicity blocks, $\cdots PP\cdots$. Accordingly, since the $\cdots PP\cdots$ stacking sequence constitutes the structural unit of $LnBaCo_2O_5$ phases,[17,18] it is feasible to assume that $2a_c$ periodicity blocks are also present in the Cu/Co = 1.2 crystals as they are Co-rich.

Further annealing of this sample does not lead to a single phase. A threefold ordered superlattice is always present and attempts to avoid it were performed by changing the Cu/Co ratio. Since the excess of Cu over Co seems to stabilize a related $YBa_2Cu_3O_7$ phase, the Cu_3Co_2 ratio was reversed, i.e, the nominal $La_2Ba_3Cu_2Co_3O_y$ composition was prepared and characterized.

$La_2Ba_3Cu_2Co_3O_y$

In contrast to $La_2Ba_3Cu_3Co_2O_y$, the X ray diffraction pattern of the title material can be indexed on the basis of a cubic perovskite unit cell (Figure 5), as also reported for $LaBaCuCoO_{5.2}$.[13] EDS analysis, performed on twenty crystals, indicates an average Cu/Co ratio of 0.4:0.6 (0.66), in agreement with the nominal value. However, it is worth pointing out that small areas of some crystals showed a different ratio (Cu/Co = 0.31:0.69 = 0.45), and are therefore Cu-deficient. The oxygen content was estimated to be 13 atoms per unit formula. The compositional data fit with an average composition $La_2Ba_3Cu_2Co_3O_{13}$.

The SAED pattern along $[001]_c$ (Figure 6) is in agreement with the basic cubic perovskite cell, according to the XRD information. Further study of the reciprocal lattice indicates a more complex situation due to the presence of weaker additional reflections (Figure 7). The SAED pattern along $[100]_c$ (Figure 7, a) shows superlattice reflections at 1/5, 2/5, 3/5, and 4/5 of the c^* axis, suggesting a fivefold superstructure. It is worth recalling that this situation is similar

 © 2003 Wiley-VCH Verlag GmbH & Co. KGaA, Weinheim

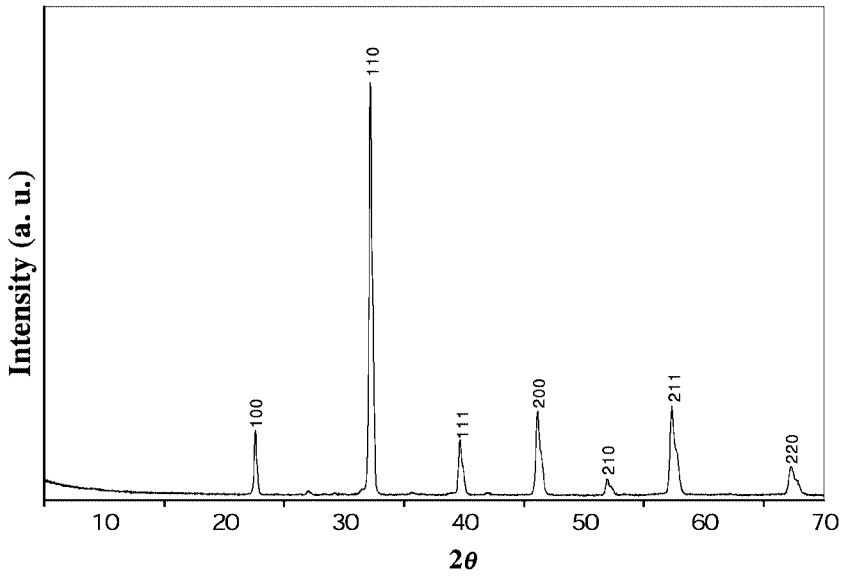

Figure 5. XRD diffraction pattern corresponding to $La_2Ba_3Cu_2Co_3O_y$

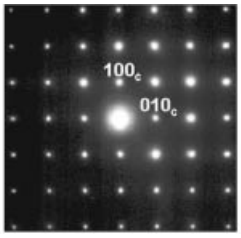

Figure 6. SAED pattern along $[001]_c$ zone axis corresponding to $La_2Ba_3Cu_2Co_3O_y$

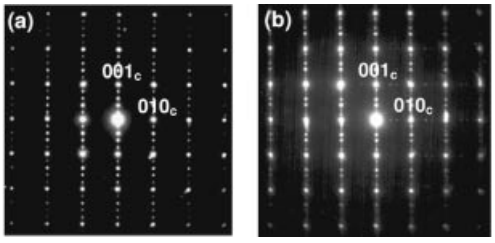

Figure 7. SAED pattern along $[100]_c$ for (a) Cu/Co = 0.4:0.6 and (b) Cu/Co= 0.31:0.69

to that reported for $LaBaCuCoO_{5.2}$,[13] although in this material superstructure streaked spots only appear at 2/5 and 3/5.[13] This difference will be discussed later. Occasionally, another kind of pattern (Figure 7, b), suggesting a sevenfold superlattice, is observed in small areas of the same crystal.

Figure 8 shows an HREM image along the $[100]_c$ zone axis. Two areas, labelled in the image as **1** and **2**, can be observed. Regarding zone **1**, the periodicity along c is 1.95 nm, i.e., related to $5a_c$, in agreement with a fivefold superlattice. FFT (Fourier Transform) performed over this area shows the presence of the corresponding superlattice spots, reinforcing the above suggestion. EDS analysis performed on this area indicates a Cu/Co ratio of 0.4:0.6. A different periodicity is observed at zone **2**, 2.73 nm, i.e., related to $7a_c$, according to the previously suggested sevenfold superstructure. Once again, FFT performed over this area confirms the indicated order. EDS analysis showed a lower Cu/Co ratio (0.31:0.69) in this area.

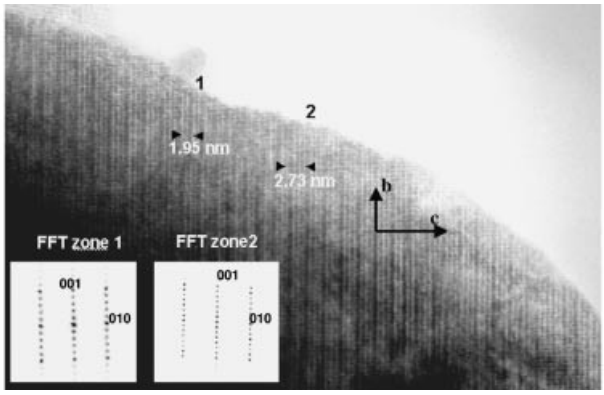

Figure 8. HREM image along $[100]_c$ zone axis corresponding $La_2Ba_3Cu_3Co_2O_y$ sample; two areas, **1** and **2**, exhibiting $5a_c$ and $7a_c$ periodicities, respectively, are labelled

According to these results, it can be concluded that $La_2Ba_3Cu_2Co_3O_{13}$ stabilizes a majority phase, showing a fivefold superlattice, as $LaBaCuCoO_{5.2}$ does. Based on this previous information and also on the structural facts described above, crystallographic image processing (CIP) was performed in order to obtain more reliable structural information. The CIP technique, which combines both SAED and HREM information, allows the gathering of potential maps after performing several corrections and symmetry averaging. In this work, the CRISP program[19] was used for image processing.

Figure 9 (a) corresponds to a thin area of the experimental image along $[100]_c$. Figure 9 (b) is a potential map obtained after the correction of tilt, CTF and the phases and amplitudes of the diffracted beams. After imposing *P2mm*

 © 2003 Wiley-VCH Verlag GmbH & Co. KGaA, Weinheim

symmetry, according to the space group *P*4/*mmm* determined by SAED and CBED (Convergent Beam Electron Diffraction), the final potential map depicted in Figure 9 (c) is obtained, in agreement with the fivefold superstructure. Moreover, differences in the black contrast (related to the cation positions) are observed in sites corresponding to La and Ba positions (pointed in Figure 9, c). Such differences are not appreciated at the corresponding B-type positions; in fact, hypothetical order of Cu and Co in these sites could not be detected by this technique, since both cations have close atomic scattering amplitudes for electrons.[20] Although it is not possible to determine the exact oxygen position by CIP, differences in white contrast are observed. It is, in fact, well known that under the optimum defocus conditions the brightest contrast corresponds to the lower potential areas, i.e., oxygen and unoccupied oxygen positions. In this sense, the superstructure must be induced, as also happens with $LaBaCuCoO_{5.2}$, by an ordered arrangement of oxygen vacancies in agreement with the polyhedral model previously mentioned $\cdots PO_hPPP\cdots$, superposed on the potential map. Cobalt and copper must be randomly arranged at the B positions of the basic $AA'BB'O_{6-x}$ perovskite structure, i.e., at the octahedral and pyramidal environments, while La and Ba seem to be ordered along the eight and twelve oxygen coordination sites. According to this, the situation in $La_2Ba_3Cu_2Co_3O_y$ is different to that observed from CIP for $LaBaCuCoO_{5.2}$,[13] whose final potential map does not reveal any cation order arrangement.

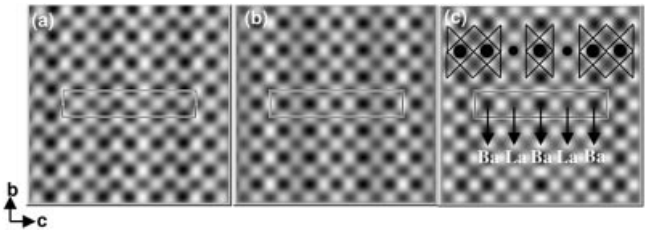

Figure 9. (a) Experimental HREM image corresponding to $La_2Ba_3Cu_3Co_2O_y$; (b) processed image; (c) potential map obtained after applying *pmm* symmetry; the unit cell and structural model are outlined

At this point, it is worth recalling the differences observed between the SAED patterns along $[100]_c$ of the $La_2Ba_3Cu_2Co_3O_{13}$ (Figure 7, a) and $LaBaCuCoO_{5.2}$ (see Figure 2c of ref.[13]) samples, respectively. The first one shows superlattice spots at 1/5, 2/5, 3/5, and 4/5 while the second one only at 2/5 and 3/5, with additional diffuse streaking. On the other hand, since atomic scattering amplitudes for electrons corresponding to La and Ba are different,[20] an ordered distribution of these cations must be detected in the SAED patterns. Accordingly, it seems clear that the observed differences in the above patterns are related to the La/Ba distribution. In order to confirm this assumption, SAED patterns corresponding to the proposed $\cdots PPPO_hP\cdots$ polyhedra sequence with La/Ba ordered and randomly arranged were calculated using the Mac Tempas software package.[21] Table 1 displays the structural parameters used in this calculation for an ordered distribution of La and Ba cations. The corresponding disordered situation has been calculated considering La and Ba distributed at 50% over the three different crystallographic positions.

Table 1. Structural parameters corresponding to $La_2Ba_3Cu_2Co_3O_{13}$ sample; an ordered La/Ba arrangement is considered [space group P4/*mmm* (123), a = 3.9352(3) Å, c = 19.538(2) Å]

Atom	*x*/*a*	*y*/*b*	*z*/*c*	Occ.
Cu/Co1	0	0	0	1
Cu/Co2	0	0	0.203	1
Cu/Co3	0	0	0.395	1
O1	0	0	0.097	1
O2	0	0.5	0.213	1
O3	0	0.5	0.414	1
O4	0	0	0.5	1
O5	0.5	0	0	1
Ba	0.5	0.5	0.1014	1
La	0.5	0.5	0.3010	1
Ba	0.5	0.5	0.5	1

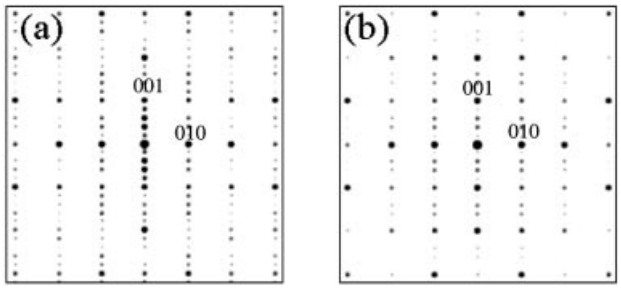

Figure 10. Calculated SAED patterns along $[100]_c$ for $La_2Ba_3Cu_3Co_2O_y$ taking into account the polyhedra sequence $\cdots PO_hPPP\cdots$ and both ordered (a) and random(b) La/Ba distributions

The calculated patterns are shown in Figure 10. When an ordered La/Ba distribution is considered all superlattice reflections are evident (Figure 10, a), while only two extra spots clearly appear when a random distribution is assumed (Figure 10, b). Finally, if La and Ba are ordered in $La_2Ba_3Cu_2Co_3O_{13}$ it could be expected that this fact should also be reflected in the XRD pattern. However, characteristic reflections of the fivefold superstructure do not appear in the experimental pattern (Figure 5). This fact can be explained by taking into account that the atomic scattering factors for X-rays corresponding to La and Ba are equal.[20] In fact, an ordered La/Ba distribution leads to the same X-ray diffraction pattern as for the disordered one.

On the other hand, areas showing sevenfold periodicity can be understood if a $2a_c$ periodicity block ($\cdots PP\cdots$) is added to the $\cdots PO_hPPP\cdots$ sequence, leading to $\cdots PO_hPPPPP\cdots$. At this point, it is worth emphasizing that these areas are Co-rich, so it is plausible to assume that additional $2a_c$ blocks are constituted by pyramidal layers, since this sequence is the basic structural unit of LnBa-

 © 2003 Wiley-VCH Verlag GmbH & Co. KGaA, Weinheim

Co_2O_5 compounds.[17,18] Attempts to isolate this sevenfold superstructure are in progress.

This set of results shows that the increase of Co content is accompanied by an increase of the square-pyramidal units in the stacking sequence. In fact, $LnBaCo_2O_{5+\delta}$ [17,18] oxides crystallize in the $\cdots PP\cdots$ stacking sequence whereas $LnBa_2Cu_{3-x}Co_xO_{7\pm\delta}$ [16] shows threefold ordering due to the sequence $\cdots PO_hP\cdots$. When Cu/Co attains a ratio around 1, the $\cdots PPPO_hP\cdots$ polyhedral sequence is stabilized and a fivefold superstructure of the cubic basic cell is observed. This is the case for both $LaBaCuCoO_{13}$[13] and $La_2Ba_3Co_3Cu_2O_{13}$. The difference between both oxides resides in the type of ordering along the A sublattice. While a random situation is obvious in the former, cationic ordering is detected in the latter. The presence of order/disorder in the A sublattice is related to the different oxygen environments involving the A cations in this fivefold superstructure: three sites of twelve coordination and two eight-coordinate sites. This is why only a La/Ba ratio of 2/3 is adequate to obtain an ordered situation.

Experimental Section

Samples of nominal compositions $La_2Ba_3Cu_3Co_2O_y$ and $La_2Ba_3Cu_2Co_3O_y$ were prepared from the apropriate amounts of $BaCO_3$, La_2O_3, Co_3O_4, and CuO. These mixtures were ground in an agate mortar and heated, after carbonate decomposition, at 960 °C for one week with intermediate milling. Cationic compositions were estimated by energy-dispersive X-ray spectroscopy (EDS) using a field-emission electron microscope (FEG) Philips CM200 equipped with an EDAX microanalytical system. Powder X-ray diffraction (XRD) was performed using a Philips X'Pert diffractometer with Cu-K_α radiation. Selected-area electron diffraction (SAED) and high-resolution electron microscopy (HREM) studies were carried out with both JEOL 2000-FX and JEOL 4000-EX electron microscopes. Oxygen content was determined by thermogravimetric analysis using a Cahn D-200 electrobalance equipped with a furnace and a two-channel recorder, allowing simultaneous recording of the weight loss and the reaction temperature. The oxygen content can be determined within $\pm 5\cdot 10^{-3}$ mg for a sample of total mass of about 50 mg.

Acknowledgments

Financial support through research project MAT2001-1440 (Spain) is acknowledged.

[1] L. Er-Rakho, C. Michel, Ph. Lacorre, N. Raveau, *J. Solid State Chem.* **1988**, *73*, 531−535.
[2] E. F. Bertaut, P. Blum, A. Sagnières, *Acta Crystallogr.* **1959**, *12*, 149−159.
[3] M. Crespin, P. Levitz, L. Gatineau, *J. Chem. Soc., Faraday Trans.* **1983**, *79*, 1181−1185.
[4] Q. Huang, P. Karen, V. L. Karen, A. Kjekhus, J. W. Lynn, A. D. Mighell, N. Rosov, A. Santoro, *Phys. Rev. B* **1992**, *45*, 9611−9619.
[5] P. A. Salvador, L. Shen, T. O. Mason, K. B. Greenwood, K. R. Poeppelmeier, *J. Solid State Chem.* **1995**, *119*, 80−89.
[6] K. D. Otzschi, K. R. Poeppelmeier, P. A. Salvador, T. O. Manson, H. Zhang, L. D. Marks, *J. Am. Chem. Soc.* **1996**, *118*, 8951−8952.
[7] J-C. Grenier, F. Ménil, M. Pouchard, P. Hagenmuller, *Mat. Res. Bull.* **1977**, *12*, 79−86.
[8] J. M. González-Calbet, M. Vallet-Regí, *J. Solid State Chem.* **1987**, *68*, 266−271.
[9] Y. Bando, Y. Sekikawa, H. Yamamura, Y. Matsui, *Acta Crystallogr., Sect. A* **1981**, *37*, 723−728.
[10] J. M. González-Calbet, M. J. Sayagués, M. Vallet-Regí, *Solid State Ionics* **1989**, *32/33*, 721−726.
[11] M. Vallet-Regí, J. M. González-Calbet, M. A. Alario-Franco, J. C. Grenier, P. Hagenmuller, *J. Solid State Chem.* **1984**, *55*, 251−261.
[12] J. M. González-Calbet, J. Alonso, M. Vallet-Regí, *J. Solid State Chem.* **1987**, *71*, 331−341.
[13] L. Ruiz-González, K. Boulahya, M. Parras, J. Alonso, J. M. González-Calbet, *Chem. Eur. J.* **2002**, *8*, 5694−5700.
[14] R. D. Shannon, *Acta Crystallogr., Sect. A* **1976**, *32*, 751−767.
[15] J. J. Caponni, C. Chaillout, A. W. Hewat, P. Lajay, P. Marezio, M. Nguyen, N. Raveau, B. Soubeyroux, J. L. Tholence, R. Tournier, *Europhys. Lett.* **1987**, *3*, 1302−1307.
[16] S. Ramesh, N. Y. Vasanthacharya, M. S. Hegde, G. N. Subbanna, H. Rajagopal, A. Sequiera, S. K. Paranjpe, *Physica C* **1995**, *253*, 243−253.
[17] L. Barbey, N. Nguyen, V. Caignaert, M. Hervieu, B. Raveau, *Mat. Res. Bull.* **1992**, *27*, 295−301.
[18] A. Maignan, C. Martin, D. Pelloquin, N. Nguyen, B. Raveau, *J. Solid State Chem.* **1999**, *142*, 247−260.
[19] S. Hovmöller, *Ultramicroscopy* **1992**, *40*, 121−135.
[20] International Tables for Crystallography, *International Union of Crystallography*, **1993**, vol. C.
[21] R. Killas, MacTempas Software 1.7.2, Berkeley Laboratory (UCLA), Berkely, CA.

Received March 12, 2002

 © 2003 Wiley-VCH Verlag GmbH & Co. KGaA, Weinheim

Synthesis, Characterisation, and X-ray Crystal Structure of New Ni^{II}, Pd^{II}, and Pt^{II} Complexes of Tridentate Pyrazole-Based Ligands with an NOS-Donor Set

Jordi García-Antón,[a] Josefina Pons,*[a] Xavier Solans,[b] Mercè Font-Bardia,[b] and Josep Ros*[a]

Keywords: Nickel / N ligands / O ligands / Palladium / Platinum / S ligands

Treatment of the ligands 1-(3-thia-5-hydroxypentyl)-3,5-dimethylpyrazole (thpd) and 1-(3-thia-6-hydroxyhexyl)-3,5-dimethylpyrazole (thhd) with $[PdCl_2(CH_3CN)_2]$, $[PtCl_2(CH_3CN)_2]$, and $NiCl_2{\cdot}6H_2O$ produces the complexes $[MCl_2(L)]$ [M= Pd, L = thpd (**1**), thhd (**2**); M = Pt, L = thpd (**3**), thhd (**4**); M = Ni, L = thpd (**5**), thhd (**6**)], which have been characterised by elemental analyses, conductivity, IR, electronic spectra, and NMR spectroscopy (when possible). The crystal structures of **2**, **3**, and **4**, determined by single-crystal X-ray diffraction, each consist of discrete $[MCl_2(L)]$ units. Each M^{II} atom is coordinated by the pyrazolyl nitrogen and the thioether sulfur from the ligand and two *cis* chloride ions in a square-planar geometry. Crystallisation of $[NiCl_2(thpd)]$ in non-anhydrous alcohols yields $[NiCl(H_2O)_2(thpd)]Cl$ ([**7**]Cl), the crystal structure of which was determined by single-crystal X-ray diffraction to reveal nickel atoms coordinated by two water molecules, one chloride ion and one thpd ligand (coordinating via all three donor atoms, N, S, and O) in a skew-trapezoidal bypyramid (distorted octahedral) geometry.
(© Wiley-VCH Verlag GmbH & Co. KGaA, 69451 Weinheim, Germany, 2003)

Introduction

The coordination chemistry of chelating ligands containing mixed functionalities is of continued importance.[1] In particular, the chemistry of ligands that contain both inert and labile groups has received considerable attention.[2] Jeffrey and Rauchfuss first introduced the term ''hemilabile ligand'' in 1979[3] to describe polydentate chelates that contain at least two different types of bonding groups — a hard and a soft donor group[4] — making them attractive for catalytic purposes.

Our group has previously synthesised and characterised pyrazolic ligands with two donor groups, in particular N−N(amine),[5] N−P,[6] N−O,[7] and N−S.[8] Our next goal is to study the coordinative properties of ligands with three donor groups.

Here, we report the synthesis and full characterisation of two new ligands, 1-(3-thia-5-hydroxypentyl)-3,5-dimethylpyrazole (thpd), and 1-(3-thia-6-hydroxyhexyl)-3,5-dimethylpyrazole (thhd), the three different donor atoms in this case being nitrogen, sulfur, and oxygen. The complexation of these ligands with $[MCl_2(CH_3CN)_2]$ (M = Pd^{II}, Pt^{II}) and $NiCl_2{\cdot}6H_2O$ is also reported, to give the complexes: $[MCl_2(L)]$ [M= Pd, L = thpd (**1**), thhd (**2**); M = Pt, L = thpd (**3**), thhd (**4**); M = Ni, L = thpd (**5**), thhd (**6**)]. Treatment of **5** with non-anhydrous alcohols produces $[NiCl(H_2O)_2(thpd)]Cl$ ([**7**]Cl). These complexes have been characterised by elemental analyses, conductivity, IR spectroscopy and, when possible, ^1H NMR, $^{13}C\{^1H\}$ NMR, and $^{195}Pt\{^1H\}$ NMR spectroscopy. The X-ray crystal structures of complexes **2**, **3**, **4**, and [**7**]Cl are also presented.

Results and Discussion

The ligands 1-(3-thia-5-hydroxypentyl)-3,5-dimethylpyrazole (thpd) and 1-(3-thia-6-hydroxyhexyl)-3,5-dimethylpyrazole (thhd), not previously reported, were synthesised to initiate a new study of pyrazole-based ligands with N1 alkyl substituents containing two different donor atoms (in this case O and S). In this respect, 2-(3,5-dimethyl-1*H*-pyrazol-1-yl)ethyl 4-methylbenzenesulfonate[9] on treatment with 2-mercaptoethanol gave thpd and 1-(2-mercaptoethyl)-3,5-dimethylpyrazole[10] on treatment with 3-chloro-1-propanol gave thhd (Scheme 1). These ligands were characterised by elemental analysis, MS spectrometry, and infrared, ^1H NMR and $^{13}C\{^1H\}$ NMR spectroscopy.

[a] Departament de Química, Facultat de Ciències, Universitat Autònoma de Barcelona,
08193 Bellaterra-Cerdanyola, Barcelona, Spain
Fax: (internat.) + 34-93/581-3101
E-mail: Josefina.Pons@uab.es
[b] Cristal.lografia, Mineralogia i Dipòsits Minerals, Universitat de Barcelona,
Martí i Franquès s/n, 08028 Barcelona, Spain

 © 2003 Wiley-VCH Verlag GmbH & Co. KGaA, Weinheim **DOI: 10.1002/ejic.200300035**

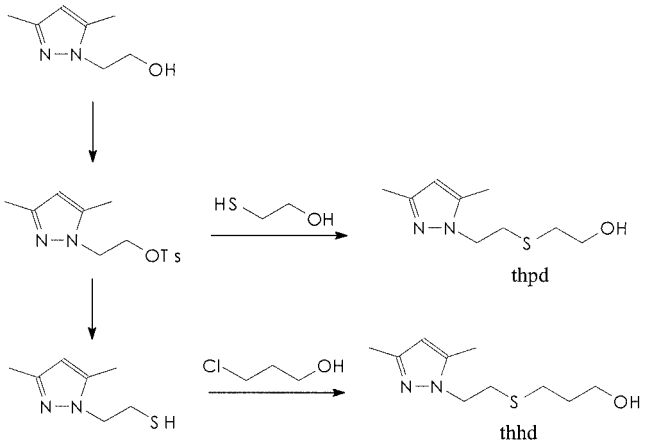

Scheme 1

Treatment of thpd and thhd with $[MCl_2(CH_3CN)_2]$ (M = Pd^{II} [11] and Pt^{II} [12]) produced four chloro complexes whose elemental analyses agree with the formula $[MCl_2(L)]$ [M = Pd, L = thpd (**1**), L = thhd (**2**); M = Pt, L = thpd (**3**), L = thhd (**4**)]. Conductivity values in acetonitrile for complexes **1**−**4** reveal a non-electrolyte nature [1.8−6.4 $\Omega^{-1}cm^2mol^{-1}$]. The reported values for 10^{-3} M solutions of non-electrolyte complexes are lower than 120 $\Omega^{-1}cm^2mol^{-1}$ in acetonitrile.[13]

The IR spectra of the complexes **1**−**4** are similar to those of the ligands, the most characteristic bands being those attributable to the pyrazolyl group, ν(C = C) and ν(C = N) between 1553 and 1548 cm^{-1} and $\delta(C-H)_{oop}$ between 828 and 785 cm^{-1}.[14]

Suitable single crystals for X-ray structure determination were obtained by recrystallisation from methanol for **2**−**4**.

^1H and ^{13}C NMR spectra of **1**−**4**, recorded in $[D_3]$acetonitrile, show the signals of the coordinated ligands (data are reported in the Exp. Sect.). HMQC spectra at 253 K were used to assign the proton signals (e.g. for **3** in Figure 1).

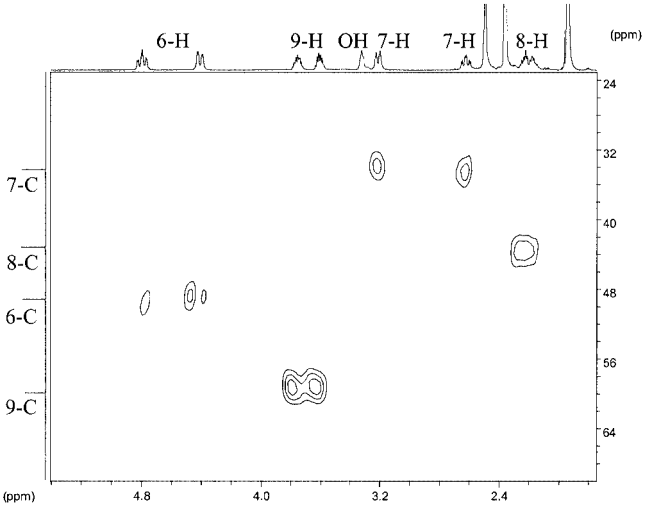

Figure 1. 250 MHz 2D HMQC spectrum of **3** at 253 K

The ^1H NMR spectra of complexes **1**−**4** at 298 K show sharp resonances for the CH and CH_3 groups of the pyrazolyl cycles. For **1** and **2**, only one broad band can be attributed to each CH_2 in the $S-(CH_2)_2-N$ and $S-(CH_2)_x-OH$ (x = 2 for **1** and x = 3 for **2**) chains, whereas at 253 K, the two protons of each CH_2 (in both chains) can be assigned to two different signals (although some of the signals are partially superposed and are given as a single multiplet in the Exp. Sect.). These two signals for each CH_2 are due to the rigidity of these chains, at 253 K, giving rise to two diastereotopic hydrogens for each CH_2.

At 298 K, for complexes **3** and **4**, two broad bands can be assigned to each CH_2 in the $S-(CH_2)_2-N$ chain but only one signal for each CH_2 in the $S-(CH_2)_x-OH$ (x = 2 for **3** and x = 3 for **4**) chain. At 253 K, signals attributable to the CH_2 in the $S-(CH_2)_2-N$ chain become well-defined multiplets and the CH_2 corresponding to the $S-(CH_2)_x-OH$ chain show two well-defined signals for each of them (but, as for the Pd^{II} complexes, some of these signals are superposed and are given as a single multiplet in the Exp. Sect.).

The broad bands for **1**−**4** at 298 K arise from fluxional processes that involve the $S-(CH_2)_2-N$ and $S-(CH_2)_x-OH$ (x = 2 for **1**, **3** and x = 3 for **2**, **4**) chains. This led us to record variable-temperature spectra for **1**−**4** (spectra for 6-H, 9-H and the alcohol group for **3** are shown in Figure 2). The two different chains [$S-(CH_2)_2-N$ and $S-(CH_2)_x-OH$] were studied separately.

For the $S-(CH_2)_2-N$ chain, the two CH_2 signals coalescence to one at 273 and 293 K for complexes **1** and **2**, respectively, whereas **3** and **4** required heating to 338 and 345 K, respectively, to bring about coalescence. These temperature coalescences and the separation of the two signals attributed to each CH_2 correspond to $\Delta G^{\ddagger}$ values of ca. 55, 59, 66, and 68 $kJ \cdot mol^{-1}$ for **1**−**4**, respectively.[15]

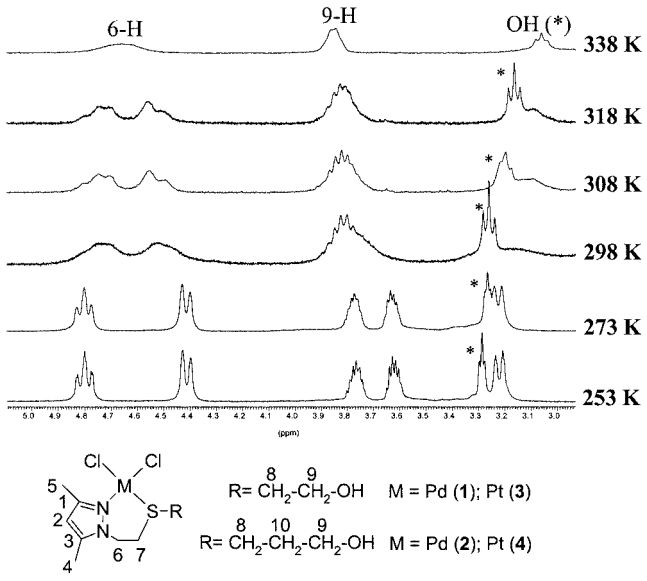

Figure 2. Numbering scheme for the complexes **1**−**4** and ^1H NMR variable-temperature experiments for 6-H and 9-H in **3**

 © 2003 Wiley-VCH Verlag GmbH & Co. KGaA, Weinheim

The $\Delta G^{\ddagger}$s are consistent with a chelate ring-flipping process due to the rocking of the pyrazolyl cycle around the M−N bond without any metal−ligand bond breaking.[5e,7c] At higher temperatures, with ring-flipping, the two hydrogens of each CH_2 are interconverted and only one signal can be observed. These energy values could also be consistent with a mechanism that implies an inversion of the sulfur atom configuration.[16,17]

For the S−$(CH_2)_x$−OH chains (x = 2 for **1** and **3** and x = 3 for **2** and **4**) the rigidity could be attributed to hydrogen bonds that occur only at low temperatures. This would explain why the hydrogens of these chains appear as diastereotopic at 253 K. Definitive evidence for O−H···Cl interactions in the solid state is given by the X-ray analyses of **2**−**4**. The existence of these interactions in solution was proved by the variable-temperature spectra of the alcohol group (example for **3** in Figure 2) in which the chemical shift of the alcohol group varied with temperature (from δ = 3.23 and 2.78 ppm at 298 K to δ = 3.36 and 3.03 ppm for **1** and **2**, respectively and from δ = 3.06 and 2.83 ppm at 338 K to δ = 3.29 and 3.09 at 253 K for **3** and **4**, respectively). The R−OH resonances shift to lower fields with decreasing temperature, as expected for this kind of process.[18]

For the S−$(CH_2)_x$−OH chains the two CH_2 signals coalescence at 298 K for complexes **1**−**4**, which, together with the separations of the two signals, corresponds to $\Delta G^{\ddagger}$s of ca. 61 kJ·mol^{-1} for **1** and **3** and ca. 63 and 66 kJ·mol^{-1} for **2** and **4**, respectively.[15]

Additional ^{195}Pt{^{1}H} NMR experiments for complexes **3** and **4** at 298 K revealed only one band for each complex (δ = −2868 ppm for **3** and −2879 ppm for **4**). This suggests that all of the bands in the ^{1}H NMR spectra belong to only one complex, as expected from the data obtained with the variable-temperature experiments.

Treatment with $NiCl_2{\cdot}6H_2O$ led to the isolation of one complex for each ligand. Their elemental analyses agree with the formula [$NiCl_2$(L)] [L = thpd (**5**) and thhd (**6**)]. The molar conductivities in absolute ethanol are consistent with non-electrolyte complexes [14.3−18.7 Ω^{-1}cm^{2}mol^{-1}]. Reported values for 10^{-3} M solutions of non-electrolyte complexes in absolute ethanol are lower than 35 Ω^{-1} cm^2 mol^{-1}.[13] The IR spectra (4000−400 cm^{-1}) of complexes **5** and **6** are similar to those of the ligands.[14] Additional spectra in the region 500−100 cm^{-1} present well-defined bands corresponding to ν(Ni−N) (450, 461 cm^{-1}), ν(Ni−Cl) (368, 387 cm^{-1}), and ν(Ni−S) (328, 344 cm^{-1}) bands for **5** and **6**, respectively, and a band attributable to ν(Ni−O) at 498 cm^{-1} for **5** and 520 cm^{-1} for **6**.[19]

Electronic spectra of the complexes **5** and **6** measured in absolute ethanol show a single d-d band at 422 nm (ε = 55 mol^{-1}cm^{-1}L) for **5** and 414 nm (ε = 75 mol^{-1}cm^{-1}L) for **6** that can be attributed to the ^{3}E′(F)→^{3}E′′(P) transition, which is characteristic for pentacoordinate Ni^{II} complexes.[20] It was not possible to obtain single crystals of these complexes.

When **5** was dissolved in methanol or ethanol it reacted with the water in the solvent to give a complex that was obtained as suitable single crystals for X-ray structure determination. This complex {[$NiCl(H_2O)_2$(thpd)]Cl ([**7**]Cl)} has an IR spectrum with bands that can be attributed to water molecules not observed for complex **5**. The electronic spectrum of complex [**7**]Cl was measured in ethanol and shows two bands in the visible region at 731 (ε = 4 mol^{-1}cm^{-1}L) and 403 nm (ε = 10 mol^{-1}cm^{-1}L), which can be attributed to $^3A_{2g}$→$^3T_{1g}$(F) and $^3A_{2g}$→$^3T_{1g}$(P) transitions, respectively, these being characteristic for octahedral Ni^{II} complexes.[20] An equivalent complex with thhd could not be isolated.

Crystal Structure of [MCl_2(L)] [M= Pd, L = thhd (2); M = Pt, L = thpd (3), thhd (4)]

The structure of **2** consists of discrete [$PdCl_2$(thhd)] units (Figure 3), while **3** and **4** consist of discrete [$PtCl_2$(L)] (L = thpd and thhd, respectively) units (Figures 4 and 5, respectively). Crystallographic data for complexes **2** and **4** indicate that they are isostructural.

The metal atom of each structure is surrounded by an identical *core* composed of the nitrogen and thioether sulfur from the pyrazole ligand and two chlorine atoms. The metal atoms have a slightly distorted square-planar geometry, with the chloride ions in a *cis* arrangement. A small tetrahedral distortion can be observed in the mean separation of the atoms linked to the metal cation in relation to the mean plane [±0.065(4) Å for **2**, ±0.001(3) Å for **3**, and ±0.050(3) Å for **4**].

Some selected bond lengths and bond angles are listed in Table 1. There are two complexes in the literature with a $PdCl_2NS$ *core* (terminal chloride ion, pyrazolic nitrogen, and tioether sulfur). For complex **2**, Pd−Cl, Pd−N, and

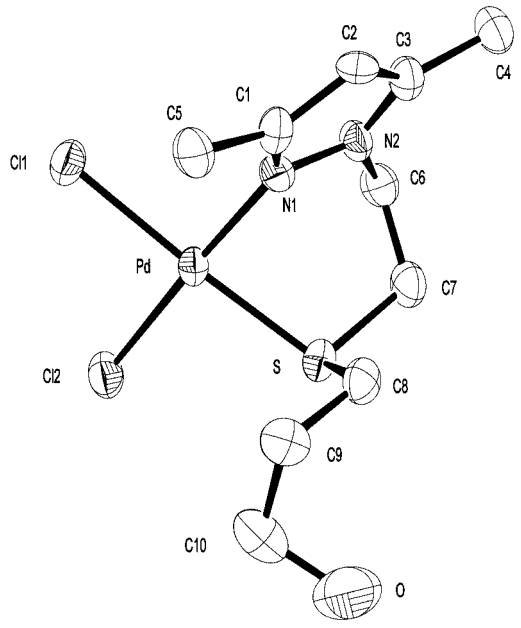

Figure 3. ORTEP drawing of [$PdCl_2$(thhd)] (**2**, 293 K determination) showing all non-hydrogen atoms and the atom-numbering scheme; 50% probability amplitude displacement ellipsoids are shown

 © 2003 Wiley-VCH Verlag GmbH & Co. KGaA, Weinheim

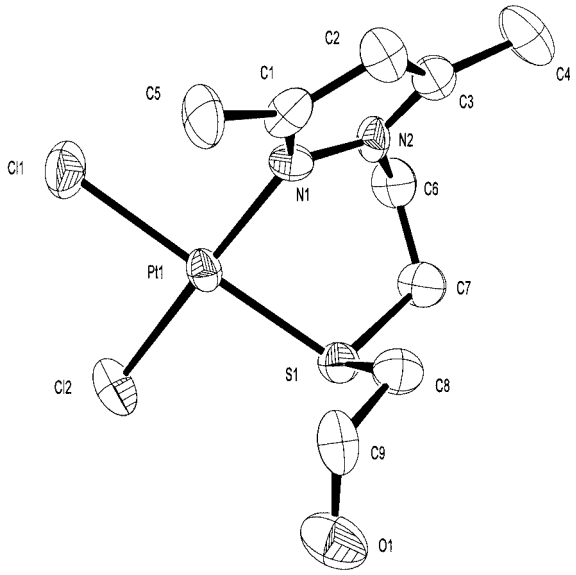

Figure 4. ORTEP drawing of $[PtCl_2(thpd)]$ (**3**, 293 K determination) showing all non-hydrogen atoms and the atom-numbering scheme; 50% probability amplitude displacement ellipsoids are shown

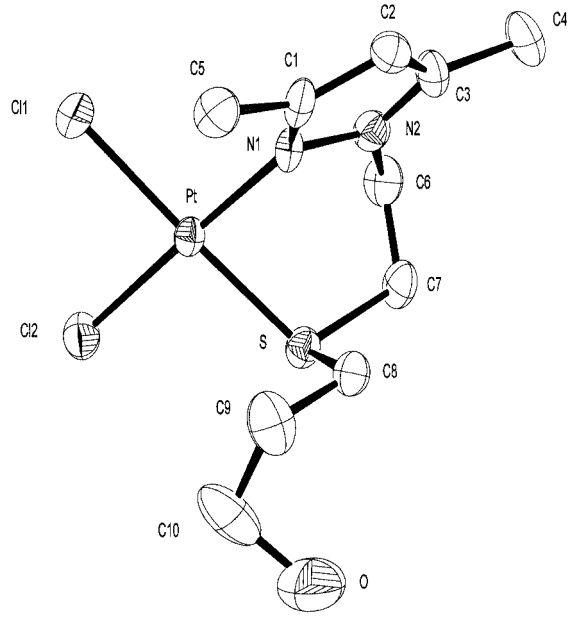

Figure 5. ORTEP drawing of $[PtCl_2(thhd)]$ (**4**, 293 K determination) showing all non-hydrogen atoms and the atom-numbering scheme; 50% probability amplitude displacement ellipsoids are shown

Pd−S bond lengths are similar to those found for the two reported complexes.[21]

No structural data for complexes with a $PtCl_2NS$ *core* (terminal chloride ion, pyrazolic nitrogen, and thioether sulfur) have been reported, although two structures with a $PtCl_2NS$ *core* (aromatic amine) have been described[22] in addition to five complexes with a PtN_2Cl_2 *core* (terminal chloride and pyrazolic nitrogen) have been described.[23] For complexes **3** and **4**, the Pt−S,[22] Pt−N,[23] and Pt−Cl[24] bond lengths are of the same order as those found in the literature.

The thpd and thhd ligands act as bidentate chelates, and form one M−S−C−C−N−N six-membered ring in each complex, all of which have a boat conformation. Bite angles are 86.9(1)° for N(1)−Pd−S in **2** and 87.7(1)° and 87.5(3)° for N(1)−Pt−S in **3** and **4**, respectively. For complex **2** this bite angle is similar to those reported for $[Pd(bddo)](BF_4)_2 \cdot H_2O$ [bddo = 1,8-bis(3,5-dimethyl-1-pyrazolyl)-3,6-dithiaoctane], 88.8(2) and 86.2(1)°,[8a] and $[Pd(pdto)](ClO_4)_2$ [pdto = 1,8-bis(2-pyridyl)-3,6-dithiaoctane], 86.9° and 87.2°.[25]

Distortion of the boat conformation in six-membered rings is observed in ΔC_s [for, **2** ΔC_s(Pd) = 6.8(4)° and ΔC_s(S−C7) = 11.0(5)°; for **3** ΔC_s(Pt) = 16.0(9)° and ΔC_s(S−C7) = 16.3(10)°; and for **4** ΔC_s(Pt) = 6.1(3)° and ΔC_s(S−C7) = 13.7(4)°; $\Phi_i + \Phi_i' =$ torsion angles related to the considered plane;[26] m = equivalent torsion angles].

$$\Delta C_s = \sqrt{\frac{\sum_{i=1}^{m} (\phi_i + \phi_i')^2}{m}}$$

Complexes **2**−**4** contain intermolecular hydrogen bonds between Cl and OH (Table 2). Complexes **2** and **4** yield infinite chains parallel to the crystallographic vector *b*, whereas the chains for complex **3** are parallel to the crystallographic vector *c* (an example for **4** is given in Figure 6).

Crystal Structure of $[NiCl(H_2O)_2(thpd)]Cl$ ([7]Cl)

The structure of [**7**]Cl consists of cationic units of $[NiCl(H_2O)_2(thpd)]^+$ and chloride anions (Figure 7). The ligand is coordinated to the metallic centre by the nitrogen, sulfur, and oxygen atoms. Nickel(II) completes its coordination with one chloride ion and two water molecules in a skew-trapezoidal bipyramid (distorted octahedral) geometry (Cl1, N1, O2, O3, and Ni atoms being in a plane) with angles at Ni^{II} in the range 83.68(8)−96.90(9)° and 168.32(6)−176.16(7)°. Water molecules are arranged *trans* to the sulfur and the nitrogen atoms, and the chloride ion is *trans* to the alcohol group.

Some selected bond lengths and bond angles are listed on Table 3. No other complex with a $NiClNO_3S$ *core* appears in the literature. The Ni−O, Ni−OH_2, Ni−S, Ni−Cl, and Ni−N bond lengths are of the same order as those found for Ni−O(alcohol),[27] Ni−OH_2 (complexes containing two water molecules),[28] Ni−S(thioether),[9,27a,29] Ni−Cl(terminal),[27b,28d,29b,29d,30] and Ni−N(pyrazole)[9,27−30] bond lengths, respectively.

The thpd ligand acts as a tridentate chelate and forms one Ni−S−C−C−O five-membered ring with an envelope conformation [C9 being ±0.457(4) Å out of the plane formed by the other four atoms] and one Ni−N−N−C−C−S six-membered ring with a boat conformation. Distortion of the boat in the six-membered ring is observed in ΔC_s(Ni) = 13.2(2)° and ΔC_s(S−C7) = 55.9(2)°.

 © 2003 Wiley-VCH Verlag GmbH & Co. KGaA, Weinheim

Table 1. Selected bond lengths (Å) and angles (°) for **2**−**4** with estimated standard deviations (e.s.d.s.) in parentheses

2		**3**		**4**	
Pd−N(1)	2.001(5)	Pt−N(1)	2.024(8)	Pt−N(1)	2.002(3)
Pd−S	2.279(2)	Pt−S	2.260(3)	Pt−S	2.2588(10)
Pd−Cl(2)	2.280(2)	Pt−Cl(2)	2.311(3)	Pt−Cl(2)	2.2909(11)
Pd−Cl(1)	2.326(2)	Pt−Cl(1)	2.321(4)	Pt−Cl(1)	2.3263(10)
N(1)−Pd−S	86.91(14)	N(1)−Pt−S	87.5(3)	N(1)−Pt−S	87.72(10)
N(1)−Pd−Cl(2)	176.03(13)	N(1)−Pt−Cl(2)	177.1(2)	N(1)−Pt−Cl(2)	177.69(10)
S−Pd−Cl(2)	90.49(6)	S−Pt−Cl(2)	90.73(16)	S−Pt−Cl(2)	90.84(4)
N(1)−Pd−Cl(1)	91.58(13)	N(1)−Pt−Cl(1)	91.7(3)	N(1)−Pt−Cl(1)	91.18(10)
S−Pd−Cl(1)	175.91(5)	S−Pt−Cl(1)	177.46(11)	S−Pt−Cl(1)	176.41(4)
Cl(1)−Pd−Cl(2)	91.21(6)	Cl(1)−Pt−Cl(2)	89.98(14)	Cl(1)−Pt−Cl(2)	90.37(4)

Table 2. Distances and angles related to hydrogen bonding

Compound	D−H	H···A	D···A	D−H···A
2				
O−H(10)···Cl(1)	0.82(8)	2.43(8)	3.235(8)	165(4)
3				
O−H(10)···Cl(2)	0.82(9)	2.40(9)	3.214(12)	174(6)
4				
O−H(10)···Cl(1)	0.82(4)	2.44(4)	3.235(5)	164(2)
[**7**]Cl				
O(1)−H(10)···Cl(2)	0.78(3)	2.44(3)	3.110(4)	145(2)
O(2)−H(20)···Cl(2)	0.78(2)	2.42(2)	3.148(4)	157(3)
O(3)−H(30)···Cl(2)	0.66(4)	2.42(4)	3.077(4)	173(4)

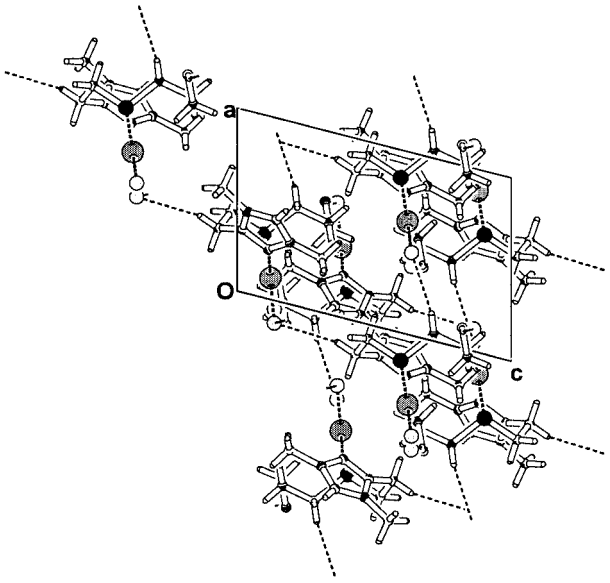

Figure 6. Partial view of the infinite chain formed by the different units of $[PtCl_2(thhd)]$ (**4**) bonded by hydrogen bonds

For the six-membered ring, the N(1)−Ni−S bite angle is 93.12(8), while for the five-membered ring the S−Ni−O(3) bite angle is 83.68(8)°. The N−Ni−S bite angle is greater and the S−Ni−O is similar to those reported in the literature for $[Ni_3(bdnol)Cl_5(EtOH)]\cdot 3EtOH$ (N−Ni−S bite angles are 89.991° and 91.634° and S−Ni−O bite angles are 82.177° and 84.090°) and $[Ni_2(bdnol)Cl_3]\cdot MeCN$ [bdnol = 1,9-bis(3,5-dimethyl-1-pyrazolyl)-3,7-dithia-5-nonanol] (N−Ni−S bite angles are 91.514°and 91.755° and S−Ni−O bite angles are 83.952° and 84.016°).[29b]

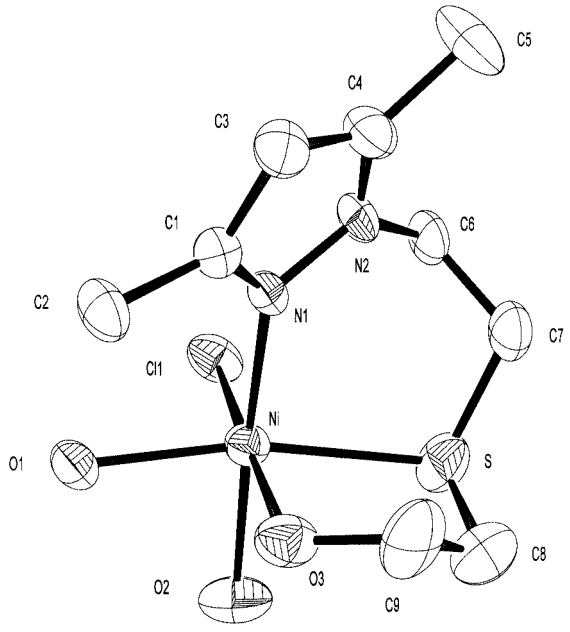

Figure 7. ORTEP drawing of $[NiCl(H_2O)_2(thpd)]^+$ ([**7**]$^+$, 293 K determination) showing all non-hydrogen atoms and the atom-numbering scheme; 50% probability amplitude displacement ellipsoids are shown

This complex contains three types of hydrogen bonds, intramolecular O(1)−H(10)···Cl(2) and intermolecular O(2)−H(20)···Cl(2) and O(3)−H(30)···Cl(2). The O(2)−H(20)···Cl(2) bonding yields a four-membered circuit and O(3)−H(30)···Cl(2) furnishes infinite chains parallel to the crystallographic vector *a* (Table 2, Figure 8).

Conclusion

The structures of the chlorocomplexes presented here were originally investigated to discover the configuration of the new potentially tridentate N, O, S ligands 1-(3-thia-5-hydroxypentyl)-3,5-dimethylpyrazole (thpd) and 1-(3-thia-6-hydroxyhexyl)-3,5-dimethylpyrazole (thhd) when com-

 © 2003 Wiley-VCH Verlag GmbH & Co. KGaA, Weinheim

Table 3. Selected bond lengths (Å) and angles (°) for $[7]^+$ with estimated standard deviations (e.s.d.s.) in parentheses

	$[7]^+$
Ni−O(1)	2.060(3)
Ni−N(1)	2.082(2)
Ni−O(2)	2.121(2)
Ni−O(3)	2.114(2)
Ni−Cl(1)	2.3881(12)
Ni−S	2.408(2)
O(1)−Ni−N(1)	96.90(9)
O(1)−Ni−O(3)	90.38(10)
N(1)−Ni−O(3)	86.83(9)
O(1)−Ni−O(2)	84.46(11)
N(1)−Ni−O(2)	172.78(9)
O(3)−Ni−O(2)	86.03(9)
O(1)−Ni−Cl(1)	91.58(8)
N(1)−Ni−Cl(1)	96.22(7)
O(3)−Ni−Cl(1)	176.16(7)
O(2)−Ni−Cl(1)	90.88(7)
O(1)−Ni−S	168.32(6)
N(1)−Ni−S	93.12(8)
O(3)−Ni−S	83.68(8)
O(2)−Ni−S	85.10(9)
Cl(1)−Ni−S	93.81(6)

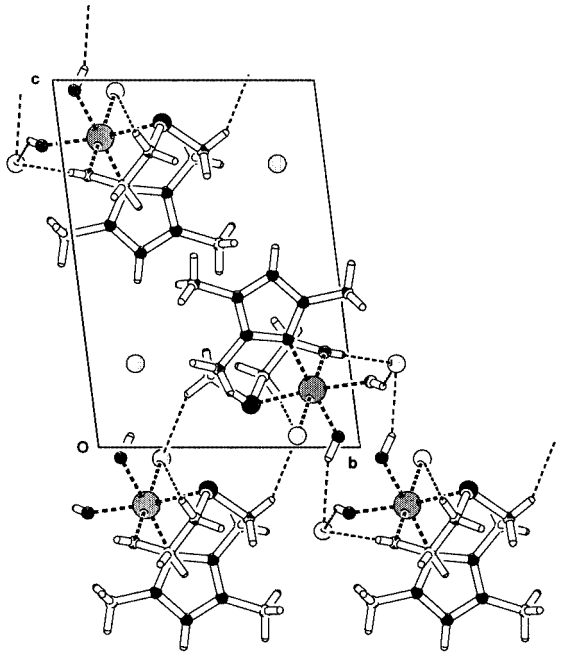

Figure 8. Partial view of the infinite 3D-structure formed by the different units of $[NiCl(H_2O)_2(thpd)]Cl$ ([7]Cl) bonded by hydrogen bonds

plexed to group 10 metals. These ligands present different coordination environments, depending on the metal ion, as observed in the X-ray structures. Hence, coordination is N, S for Pd^{II} and Pt^{II}, but N, S, O for Ni^{II}. NMR studies proved very useful in determining the configuration of ligands in the complexes. These results will enable the study of the hemilabile behaviour of these novel N, O, S ligands when coordinated to transition metals.

Experimental Section

Generals Remarks: Preparations were performed using the usual vacuum line and Schlenk techniques. All reagents were commercial grade and were used without further purification. Acetonitrile was dried and distilled by standard methods and deoxygenated in the vacuum line.

2-(3,5-Dimethyl-1*H*-pyrazol-1-yl)ethyl 4-methylbenzenesulfonate[9] and 1-(2-mercaptoethyl)-3,5-dimethylpyrazole[10] were prepared according to published methods, as were samples of $[PdCl_2(CH_3CN)_2]$[11] and $[PtCl_2(CH_3CN)_2]$.[12]

Analyses (C, N, H, S) were performed in our analytical laboratory on a Carlo Erba CHNS EA-1108 instrument. Conductivity measurements were performed at room temperature in 10^{-3} M absolute ethanol or acetonitrile solutions employing a Crison, micro CM 2200 conductimeter. Infrared spectra were recorded as KBr pellets or polyethylene mulls in the range 4000−100 cm^{-1} under a nitrogen atmosphere. Electronic spectra in solution were run on a Kontron-Uvikon 860 in acetonitrile between 750 and 350 nm. The ^1H and $^{13}C\{^1H\}$ NMR and HMQC spectra were obtained either on a Bruker AC-250 MHz or a Bruker 500 MHz instrument. $^{195}Pt\{^1H\}$ NMR spectra were obtained on a Bruker Advance DRX 250 MHz instrument. ^1H and ^{13}C chemical shifts (δ) were determined relative to internal TMS and are given in ppm. ^{195}Pt chemical shifts (δ) are relative to external 0.1 mol·dm^{-3} Na_2PtCl_6 and are given in ppm. Mass spectra were obtained on a HP 5989A apparatus.

Synthesis of 1-(3-Thia-5-hydroxypentyl)-3,5-dimethylpyrazole (thpd): A solution of 2-(3,5-dimethyl-1*H*-pyrazol-1-yl)ethyl 4-methylbenzenesulfonate (6.26 g, 21.3 mmol), mercaptoethanol (1.50 mL, 21.2 mmol) and sodium hydroxide (0.94 g, 22.8 mmol) in distilled water (30 mL) was refluxed for 5 h. After cooling to room temperature, the reaction mixture was extracted with CH_2Cl_2 (3 × 25 mL). The collected organic layers were dried with anhydrous sodium sulfate and removed in vacuo to give a brown oil that was then washed with diethyl ether to afford the desired product as a white solid. Yield: 2.70 g (61%). M.p.: 46.6−47.5 °C. $C_9H_{16}N_2OS$ (200.1) C 53.97, H 8.00, N 13.99, S 16.04; found C 54.17, H 7.93, N 14.10, S 15.91. IR (KBr, cm^{-1}): ν(O−H) 3221, $\nu(C-H)_{al}$ 2943, ν(C=C), ν(C=N) 1549, $\delta(CH_3)_{as}$ 1456, $\delta(CH_3)_s$ 1386, $\delta(C-H)_{oop}$ 792. ^1H NMR (250 MHz, $CDCl_3$ solution): δ = 2.20 (s, 3 H, *Me*), 2.25 (s, 3 H, *Me*), 2.60 (t, ^3J = 6 Hz, 2 H, CH_2-CH_2-OH), 2.95 (t, ^3J = 7 Hz, 2 H, pz-CH_2-CH_2), 3.28 (b, 1 H, OH), 3.69 (t, ^3J = 6 Hz, 2 H, CH_2-CH_2-OH), 4.14 (t, ^3J = 7 Hz, 2 H, pz-CH_2-CH_2), 5.79 (s, 1 H, pz-*CH*) ppm. $^{13}C\{^1H\}$ NMR (63 MHz, $CDCl_3$ solution): δ = 11.2 (*Me*), 13.5 (*Me*), 32.1 (pz-CH_2-CH_2), 35.6 (CH_2-CH_2-OH), 48.5 (pz-CH_2-CH_2), 61.2 (CH_2-CH_2-OH), 105.3 (pz-*CH*), 147.9 (pz-*C*) ppm. MS (CI, NH_3): *m*/*z* (%) = 201 [MH^+] (33%), 115 [pz-$(CH_2)_2-S^+$] (21), 109 [pz-CH_2^+] (88), 97 [pzH^+] (100).

1-(3-Thia-6-hydroxyhexyl)-3,5-dimethylpyrazole (thhd): A mixture of 1-(2-mercaptoethyl)-3,5-dimethylpyrazole (2.72 g, 17.4 mmol) and 3-chloro-1-propanol (1.50 mL, 17.4 mmol) in THF (40 mL) and sodium hydroxide (0.70 g, 17.0 mmol) in distilled water (30 mL) were refluxed for 4.5 h. After cooling to room temperature, the reaction mixture was extracted with CH_2Cl_2 (3 × 25 mL) and the collected organic layers were dried with anhydrous sodium sulfate and removed in vacuo. The brown oil thus formed was then washed with diethyl ether and the desired product precipitated as a white solid. Yield: 2.24 g (60%). M.p.: 53.7−54.1 °C. $C_{10}H_{18}N_2OS$ (214.1) C 56.04, H 8.46, N 13.07, S 14.91; found C 55.83, H 8.21, N 12.82, S 14.73. IR (KBr, cm^{-1}): ν(O−H) 3298, $\nu(C-H)_{al}$ 2913,

 © 2003 Wiley-VCH Verlag GmbH & Co. KGaA, Weinheim

ν(C=C), ν(C=N) 1553, $\delta(CH_3)_{as}$ 1446, $\delta(CH_3)_s$ 1386, $\delta(C-H)_{oop}$ 778. ^1H NMR (250 MHz, $CDCl_3$ solution): δ = 1.80 (qt, 2 H, ^3J = 6 Hz, CH_2-CH_2-OH), 2.20 (s, 3 H, *Me*), 2.26 (s, 3 H, *Me*), 2.55 (t, ^3J = 6 Hz, 2 H, S-$CH_2-CH_2-CH_2$), 2.92 (t, ^3J = 7 Hz, 2 H, pz-CH_2-CH_2), 3.70 (t, ^3J = 6 Hz, 2 H, CH_2-CH_2-OH), 4.15 (t, ^3J = 7 Hz, 2 H, pz-CH_2-CH_2), 5.78 (s, 1 H, pz-*CH*) ppm. $^{13}C\{^1H\}$ NMR (63 MHz, $CDCl_3$ solution): δ = 11.2 (*Me*), 13.5 (*Me*), 28.6 ($CH_2-CH_2-CH_2$), 32.1, 32.2 (pz-CH_2-CH_2, S-$CH_2-CH_2-CH_2$), 48.5 (pz-CH_2-CH_2), 61.2 (CH_2-CH_2-OH), 105.2 (pz-*CH*), 139.3, 147.9 (pz-*C*) ppm. MS (CI, NH_3): *m*/*z* [%]: 215 [MH^+] (5%), 115 [pz-$(CH_2)_2$-S^+] (22), 109 [pz-CH_2^+] (59), 97 [pzH^+] (100).

Synthesis of [$PdCl_2$(L)] [L = thpd (1), L = thhd (2)] and [$PtCl_2$L] [L = thpd (3), L = thhd (4)]: A solution of [$PdCl_2(CH_3CN)_2$] (0.101 g, 0.389 mmol) or [$PtCl_2(CH_3CN)_2$] (0.075 g, 0.215 mmol) in acetonitrile (20 mL) was added dropwise to an equimolar solution of thpd or thhd in acetonitrile (10 mL). The resulting solution was stirred for 12 h, after which the acetonitrile was evaporated and the solid residue washed with chloroform (2 × 2 mL) and then dried under vacuum. The palladium complexes were orange solids, and the platinum complexes yellow solids.

Complex 1: Yield: 0.180 (99%). Conductivity (Ω^{-1} cm^2 mol^{-1}, $1.01\cdot10^{-3}$ M in acetonitrile): 1.8. $C_9H_{16}Cl_2N_2OPdS$ (377.52) C 28.61, H 4.24, N 7.42, S 8.50; found C 28.23, H 4.11, N 7.13, S 8.26. IR (KBr, cm^{-1}): ν(O−H) 3386, $\nu(C-H)_{al}$ 2984−2937, ν(C=C), ν(C=N) 1549, $\delta(CH_3)_{as}$ 1468, $\delta(CH_3)_s$ 1402, $\delta(C-H)_{oop}$ 785. IR (polyethylene, cm^{-1}): ν(Pd−N) 467, ν(Pd−Cl) 340−335, ν(Pd−S) 292. ^1H NMR (500 MHz, [D$_3$]acetonitrile, 253 K): δ = 2.09 (b, 2 H, CH_2-CH_2-OH), 2.27 (s, 3 H, *Me*), 2.54 (s, 3 H, *Me*), 2.60 (b, 1 H, pz-CH_2-CHH), 3.20 (b, 1 H, pz-CH_2-CHH), 3.36 (t, 1 H, OH), 3.71 (b, 1 H, CH_2-CHH−OH), 3.83 (b, 1 H, CH_2-CHH−OH), 4.70 (b, 1 H, pz-*CH*H−CH_2), 4.84 (b, 1 H, pz-*CH*H−CH_2), 6.05 (s, 1 H, pz-*CH*) ppm. $^{13}C\{^1H\}$ NMR (63 MHz, [D$_3$]acetonitrile, 298 K): δ = 11.9 (*Me*), 15.4 (*Me*), 35.1, 42.6 (pz-CH_2-CH_2, CH_2-CH_2-OH), 49.8 (pz-CH_2-CH_2), 60.5 (CH_2-CH_2-OH), 109.2 (pz-*CH*) ppm.

Complex 2: Yield: 0.180 (96%). Conductivity (Ω^{-1} cm^2 mol^{-1}, $9.97\cdot10^{-4}$ M in acetonitrile): 4.1. $C_{10}H_{18}Cl_2N_2OPdS$ (391.62) C 30.64, H 4.60, N 7.15, S 8.20; found C 30.74, H 4.73, N 7.10, S 7.96. IR (KBr, cm^{-1}): ν(O−H) 3462, $\nu(C-H)_{ar}$ 3123, $\nu(C-H)_{al}$ 2975−2921, ν(C=C), ν(C=N) 1548, $\delta(CH_3)_{as}$ 1463, $\delta(CH_3)_s$ 1393, $\delta(C-H)_{oop}$ 828. IR (polyethylene, cm^{-1}): ν(Pd−N) 462, ν(Pd−Cl) 343−329, ν(Pd−S) 307. ^1H NMR (500 MHz, [D$_3$]acetonitrile, 253 K): δ = 1.82 (b, 1 H, S−*CH*H−CH_2-CH_2), 2.21 (b, 1 H, S−*CH*H−CH_2-CH_2), 2.05 (b, $CH_2-CH_2-CH_2$), − this peak could not be integrated because it is too close to the solvent signal −2.39 (s, 3 H, *Me*), 2.51 (s, 3 H, *Me*), 2.51 (b, 1 H, pz-CH_2-*CH*H), 3.03 (b, 1 H, OH), 3.24 (b, 1 H, pz-CH_2-CHH), 3.52 (b, 1 H, CH_2-CHH−OH), 3.58 (b, 1 H, CH_2-CHH−OH), 4.73 (b, 1 H, pz-C*H*H−CH_2), 4.92 (b, 1 H, pz-C*H*H−CH_2), 6.11 (s, 1 H, pz-*CH*) ppm. $^{13}C\{^1H\}$ NMR (63 MHz, [D$_3$]acetonitrile, 298 K): δ = 12.0 (*Me*), 15.3 (*Me*), 32.3 ($CH_2-CH_2-CH_2$), 35.2, 37.6 (pz-CH_2-CH_2, S-$CH_2-CH_2-CH_2$), 49.8 (pz-CH_2-CH_2), 60.4 (CH_2-CH_2-OH), 109.3 (pz-*CH*), 145.0, 153.0 (pz-*C*) ppm.

Complex 3: Yield: 0.080 (98%). Conductivity (Ω^{-1} cm^2 mol^{-1}, $1.07\cdot10^{-3}$ M in acetonitrile): 5.3. $C_9H_{16}Cl_2N_2OPtS$ (466.29) C 23.16, H 3.43, N 6.00, S 6.88; found C 23.03, H 3.48, N 6.02, S 6.73. IR (KBr, cm^{-1}): ν(O−H) 3420, $\nu(C-H)_{al}$ 2974−2924, ν(C=C), ν(C=N) 1553, $\delta(CH_3)_{as}$ 1470, $\delta(CH_3)_s$ 1409, $\delta(C-H)_{oop}$ 791. IR (polyethylene, cm^{-1}): ν(Pd−N) 496, ν(Pd-Cl) 327, ν(Pd−S) 303. ^1H NMR (500 MHz, [D$_3$]acetonitrile, 253 K): δ = 2.24 (b, 2 H, CH_2-CH_2-OH), 2.38 (s, 3 H, *Me*), 2.50 (s, 3 H, *Me*), 2.62 (b, 1 H, pz-CH_2-CHH), 3.22 (b, 1 H, pz-CH_2-CHH), 3.29 (t, 1 H, OH), 3.62 (m, 1 H, CH_2-CHH−OH), 3.76 (m, 1 H, CH_2-CHH−OH), 4.53 (m, 1 H, pz-*CH*H−CH_2), 4.72 (m, 1 H, pz-*CH*H−CH_2), 6.08 (s, 1 H, pz-*CH*) ppm. $^{13}C\{^1H\}$ NMR (63 MHz, [D$_3$]acetonitrile, 298 K): δ = 12.0 (*Me*), 15.0 (*Me*), 34.6 (pz-CH_2-CH_2), 43.5 (CH_2-CH_2-OH), 49.5 (pz-CH_2-CH_2), 60.2 (CH_2-CH_2-OH), 108.8 (pz-*CH*), 144.2 (pz-*C*) ppm. $^{195}Pt\{^1H\}$ NMR (53.8 MHz, [D$_3$]acetonitrile, 298 K): δ = −2868 ppm.

Complex 4: Yield: 0.083 (98%). Conductivity (Ω^{-1} cm^2 mol^{-1}, $9.85\cdot10^{-4}$ M in acetonitrile): 6.4. $C_{10}H_{18}Cl_2N_2OPtS$ (480.31) C 24.98, H 3.75, N 5.83, S 6.69; found C 25.25, H 3.81, N 6.11, S 6.62. IR (KBr, cm^{-1}): ν(O−H) 3477, $\nu(C-H)_{ar}$ 3124, $\nu(C-H)_{al}$ 2977−2924, ν(C=C), ν(C=N) 1549, $\delta(CH_3)_{as}$ 1466, $\delta(CH_3)_s$ 1397, $\delta(C-H)_{oop}$ 828. IR (polyethylene, cm^{-1}): ν(Pd−N) 493, ν(Pd−Cl) 322, ν(Pd−S) 305. ^1H NMR (500 MHz, [D$_3$]acetonitrile, 253 K): δ = 1.86 (b, S−*CH*H−CH_2-CH_2), 2.31 (b, S−*CH*H−CH_2-CH_2), 1.93 (b, $CH_2-CH_2-CH_2$), last three peaks could not be integrated because they were too close to the solvent signal; 2.39 (s, 3 H, *Me*), 2.51 (s, 3 H, *Me*), 2.56 (b, 1 H, pz-CH_2-CHH), 3.09 (b, 1 H, OH), 3.28 (b, 1 H, pz-CH_2-CHH), 3.51 (m, CH_2-CH_2-OH), 3.55 (m, CH_2-CH_2-OH), last two peaks integrate together 2 H, 4.50 (m, 1 H, pz-C*H*H−CH_2), 4.82 (m, 1 H, pz-C*H*H−CH_2), 6.12 (s, 1 H, pz-*CH*) ppm. $^{13}C\{^1H\}$ NMR (63 MHz, [D$_3$]acetonitrile, 298 K): δ = 11.5 (*Me*), 14.4 (*Me*), 31.3 ($CH_2-CH_2-CH_2$), 34.4 (pz-CH_2-CH_2), 38.0 (S−$CH_2-CH_2-CH_2$), 49.0 (pz-CH_2-CH_2), 59.6 (CH_2-CH_2-OH), 108.3 (pz-*CH*), 143.6, 152.5 (pz-*C*) ppm. $^{195}Pt\{^1H\}$ NMR (53.8 MHz, [D$_3$]acetonitrile, 298 K): δ = −2879 ppm.

Synthesis of [$NiCl_2$(L)] with L = thpd (5), L = thhd (6): $NiCl_2\cdot6H_2O$ (0.546 mmol) in a mixture absolute ethanol (10 mL) and triethylorthoformate (2 mL) was added dropwise, under vigorous stirring, to a solution of thpd or thhd (0.546 mmol) in absolute ethanol (10 mL). The solution turned from initial green to yellow. After 12 h of stirring, the solvent was evaporated and the desired product obtained as a pale green solid.

Complex 5: Yield: 0.176 g (98%). Conductivity (Ω^{-1} cm^2 mol^{-1}, $1.02\cdot10^{-3}$ M in absolute ethanol): 18.7. $C_9H_{16}Cl_2N_2NiOS$ (329.9) C 32.77, H 4.89, N 8.49, S 9.72; found C 32.68, H 5.06, N 8.20, S 9.43. IR (KBr, cm^{-1}): ν(O−H) 3269, $\nu(C-H)_{al}$ 2947, ν(C=C), ν(C=N) 1555, $\delta(CH_3)_{as}$ 1469, $\delta(CH_3)_s$ 1401, $\delta(C-H)_{oop}$ 724. IR (polyethylene, cm^{-1}):ν(Ni−O) 498, ν(Ni−N) 450, ν(Ni−Cl) 368, ν(Ni−S) 328. UV/Vis (absolute ethanol, $1.03\cdot10^{-3}$ M), λ(ε): 422 nm (55 mol^{-1}cm^{-1}L).

Complex 6: Yield: 0.182 (97%). Conductivity (Ω^{-1} cm^2 mol^{-1}, $9.87\cdot10^{-4}$ M in absolute ethanol): 14.3. $C_{10}H_{18}Cl_2N_2NiOS$ (343.9) C 34.89, H 5.23, N 8.14, S 9.33; found C 34.66, H 5.17, N 7.86, S 9.07. IR (KBr, cm^{-1}): ν(O−H) 3250, $\nu(C-H)_{al}$ 2922, ν(C=C), ν(C=N) 1558, $\delta(CH_3)_{as}$ 1465, $\delta(CH_3)_s$ 1387, $\delta(C-H)_{oop}$ 728. IR (polyethylene, cm^{-1}): ν(Ni−O) 520, ν(Ni−N) 461, ν(Ni−Cl) 387, ν(Ni−S) 344. UV/Vis (absolute ethanol, $9.76\cdot10^{-4}$ M), λ(ε): 414 nm (75 mol^{-1}cm^{-1}L).

Synthesis of [$NiCl(H_2O)_2$(thpd)]Cl ([7]Cl): Complex **5** (0.056 g, 0.170 mmol) was dissolved in ethanol or methanol. After 12 h, the solvent was evaporated and complex [**7**]Cl precipitated as bright green crystals.

Complex [7]Cl: Yield: 0.060 g (97%). Conductivity (Ω^{-1} cm^2 mol^{-1}, $1.07\cdot10^{-3}$ M in absolute ethanol): 41.3. $C_9H_{20}Cl_2N_2NiO_3S$ (365.94) C 29.54, H 5.51, N 7.66, S 8.76; found C 29.60, H 5.46, N 7.72, S 8.56. IR (KBr, cm^{-1}): $\nu(O-H)_{water}$ 3318, $\nu(O-H)_{alcohol}$ 3238,

 © 2003 Wiley-VCH Verlag GmbH & Co. KGaA, Weinheim

Table 4. Crystallographic data for **2**−**4**

Compound	**2**	**3**	**4**
Empirical formula	$C_{10}H_{18}Cl_2N_2OPdS$	$C_9H_{16}Cl_2N_2OPtS$	$C_{10}H_{18}Cl_2N_2OPtS$
Molecular mass	391.62	466.29	480.31
Temperature, K	293(2)	293(2)	293(2)
Crystal system	monoclinic	monoclinic	monoclinic
Space group	$P2_1/n$	Cc	$P2_1/n$
Unit cell dimensions			
a, Å	7.6360(10)	15.21(2)	7.6520(10)
b, Å	15.9160(10)	8.205(4)	15.9520(10)
c, Å	11.8370(10)	11.720(7)	11.8190(10)
β, deg	104.343(2)	111.59(8)	104.2740(10)
Volume, $Å^3$	1393.8(2)	1360(2)	1398.1(2)
Z	4	4	4
$D_{calcd.}$, $Mg·m^{-3}$	1.866	2.277	2.282
μ, mm^{-1}	18.50	10.85	10.55
F(000)	784	880	912
Crystal size (mm)	0.1 × 0.1 × 0.2	0.2 × 0.2 × 0.1	0.1 × 0.1 × 0.3
θ range, deg	3.15 to 31.51	2.87 to 30.03	2.19 to 31.58
Reflexions collected: total, independent, R_{int}	3500, 1559, 0.0273	2015, 2015, 0.0153	8103, 3162, 0.0333
Data/restraints/parameters	1559/0/161	2015/2/145	3162/0/154
Weighting coef. a, b[a]	0.0522, 4.4364	0.0469, 0	0.0576, 0
Final R1, *wR*2	0.0359, 0.0954	0.0302, 0.0715	0.0281, 0.0787
R1 (all data), *wR*2	0.0388, 0.0982	0.0348, 0.0730	0.0369, 0.0815
Residual electron density, $e·Å^{-3}$	+0.425, −0.451	+0.717, −0.743	+0.671, −0.622

[a] The function minimised was $\Sigma w(|F_o|^2 - |F_c|^2)^2$, where $w = [\sigma^2(I) + (aP)^2 + bP]^{-1}$, and $P = (|F_o|^2 + 2|F_c|^2)/3$.

Table 5. Crystallographic data for [**7**]Cl

Compound	[**7**]Cl
Empirical formula	$C_9H_{20}Cl_2N_2NiO_3S$
Molecular mass	365.94
Temperature, K	293(2)
Crystal system	triclinic
Space group	$P\bar{1}$ (n° 2)
Unit cell dimensions	
a, Å	7.206(3)
b, Å	8.611(8)
c, Å	12.661(5)
α, deg	95.97(5)
β, deg	104.97(3)
γ, deg	93.60(5)
Volume, $Å^3$	751.6(8)
Z	2
$D_{calcd.}$, $Mg·m^{-3}$	1.617
μ, mm^{-1}	17.86
F(000)	380
Crystal size (mm)	0.1 × 0.1 × 0.2
θ range, deg	2.74 to 30.20
Reflexions collected: Total, independent, R_{int}	4333, 4333, 0.0099
Data/restraints/parameters	4333/0/184
Weighting coef. *a*, *b*[a]	0.0198, 0
Final *R*1, *wR*2	0.0357, 0.0610
*R*1 (all data), *wR*2	0.1029, 0.0726
Residual electron density, $e·Å^{-3}$	+0.421, −0.347

[a] The function minimised was $\Sigma w(|F_o|^2 - |F_c|^2)^2$, where $w = [\sigma^2(I) + (aP)^2 + bP]^{-1}$, and $P = (|F_o|^2 + 2|F_c|^2)/3$.

ν(C−H)$_{al}$ 2957−2928, ν(C=C), ν(C=N) 1558, δ(CH$_3$)$_{as}$ 1467, δ(CH$_3$)$_s$ 1386, δ(C−H)$_{oop}$ 728. IR (polyethylene, cm^{-1}): ν(Ni−O) 499, ν(Ni−N) 454, ν(Ni−Cl) 368, ν(Ni−S) 322. UV/Vis (absolute ethanol, $1.02·10^{-3}$ M), λ(ε): 731 nm (4 $mol^{-1}cm^{-1}L$), 403 nm (10 $mol^{-1}cm^{-1}L$).

X-ray Crystallographic Study: Suitable crystals for X-ray diffraction experiments of compounds 2−4 and [7]Cl were obtained by crystallisation from methanol. Data for 2 and 4 were collected on a MAR345 diffractometer with an Image Plate detector, using the - scan technique. Data for 3 and [7]Cl were collected on an Enraf−Nonius CAD4 four-circle diffractometer, using the omega/2θ scan technique. All crystal data were collected using graphite-monochromated Mo-K_α radiation. The structures were solved by direct methods using the SHELXS-97 computer program[31] and refined by full-matrix least-squares method with a SHELXL-97.[32]

Fivc H atoms in structure [**7**]Cl were located from a difference synthesis and refined with an overall isotropic temperature factor. Thirteen Hs for [**7**]Cl and all hydrogen atoms for structures **2**−**4** were computed and refined using a riding model. The final *R* (on *F*) factor and ωR (on F^2) values, as well as the numbers of parameters refined and other details concerning the refinement of the crystal structure, are presented in Tables 4 and 5.

CCDC-199097 (**2**), -199096 (**3**), -199095 (**4**), and -199098 ([**7**]Cl) contain the supplementary crystallographic data for this paper. These data can be obtained free of charge at www.ccdc.cam.ac.uk/conts/retrieving.html [or from the Cambridge Crystallographic Data Centre, 12 Union Road, Cambridge CB2 1EZ, UK; Fax: (internat.) +44-1223/336-033; E-mail: deposit@ccdc.cam.ac.uk].

Acknowledgments

Support by the Spanish Ministerio de Educación y Cultura (Project BQU2000-0238 and a grant to J. G.) is gratefully acknowledged.

[1] C. S. Slone, D. A. Weinberger, C. A. Mirkin, *Prog. Inorg. Chem.* **1999**, *48*, 233.
[2] A. Bader, E. Lindner, *Coord. Chem. Rev.* **1991**, *108*, 27.
[3] J. C. Jeffrey, T. B. Rauchfuss, *Inorg. Chem.* **1979**, *18*, 2658.
[4] [4a] E. Bouwman, W. L. Driessen, J. Reedijk, *Coord. Chem. Rev.* **1990**, *104*, 143. [4b] P. Braunstein, F. Naud, *Angew. Chem. Int. Ed.* **2001**, *40*, 680.

 © 2003 Wiley-VCH Verlag GmbH & Co. KGaA, Weinheim

[5] [5a] R. Mathieu, G. Esquius, N. Lugan, J. Pons, J. Ros, *Eur. J. Inorg. Chem.* **2001**, 2683. [5b] G. Esquius, J. Pons, R. Yáñez, J. Ros, *J. Organomet. Chem.* **2001**, *619*, 14. [5c] G. Esquius, J. Pons, R. Yáñez, J. Ros, X. Solans, M. Font-Bardía, *J. Organomet. Chem.* **2000**, *605*, 226. [5d] G. Esquius, J. Pons, R. Yáñez, J. Ros, X. Solans, M. Font-Bardía, *Acta Crystallogr., Sect. C* **2002**, *58*, 133. [5e] G. Esquius, J. Pons, R. Yáñez, J. Ros, R. Mathieu, B. Donnadieu, N. Lugan, *Eur. J. Inorg. Chem.* **2002**, 2999.

[6] [6a] R. Tribó, J. Pons, R. Yáñez, J. F. Piniella, A. Álvarez-Larena, J. Ros, *Inorg. Chem. Commun.* **2000**, *3*, 545. [6b] G. Esquius, J. Pons, R. Yáñez, J. Ros, R. Mathieu, B. Donnadieu, N. Lugan, *J. Organomet. Chem.* **2003**, *667*, 126. [6c] R. Tribó, J. Ros, J. Pons, R. Yáñez, A. Álvarez-Larena, J. F. Piniella, *J. Organomet. Chem.* in press.

[7] [7a] A. Boixassa, J. Pons, A. Virgili, X. Solans, M. Font-Bardía, J. Ros, *Inorg. Chim. Acta* **2002**, *340*, 49. [7b] A. Boixassa, J. Pons, X. Solans, M. Font-Bardía, J. Ros, *Inorg. Chim. Acta* **2003**, *346*, 151. [7c] A. Boixassa, J. Pons, J. Ros, R. Mathieu, N. Lugan, manuscript submitted to *J. Organomet. Chem.*

[8] [8a] J. García-Antón, J. Pons, X. Solans, M. Font-Bardía, J. Ros, *Eur. J. Inorg. Chem.* **2002**, 3319. [8b] J. García-Antón, J. Pons, X. Solans, M. Font-Bardía, J. Ros, *Inorg. Chim. Acta* accepted.

[9] W. G. Haanstra, W. L. Driessen, J. Reedijk, U. Turpeinen, R. Hämäläinen, *J. Chem. Soc., Dalton Trans.* **1989**, 2309.

[10] E. Bouwman, P. Evans, R. A. G. de Graaf, H. Kooijman, R. Poinsot, P. Rabu, J. Reedijk, A. L. Spek, *Inorg. Chem.* **1995**, *34*, 6302.

[11] S. Komiya, *Synthesis of Organometallic Compounds: A Practical Guide*, John Wiley & Sons, New York, USA, **1997**.

[12] F. A. Cotton, *Inorganic Synthesis* **1972**, *13*, 52.

[13] [13a] W. J. Geary, *Coord. Chem. Rev.* **1971**, *7*, 81. [13b] L. K. Thompson, F. L. Lee, E. J. Gabe, *Inorg. Chem.* **1988**, *27*, 39.

[14] [14a] E. Pretsh, T. Clerc, J. Seibl, W. Simon, *Tables of Determination of Organic Compounds.* ^{13}C *NMR,* ^{1}H *NMR, IR, MS, UV/Vis, Chemical Laboratory Practice.* Springer-Verlag, Berlin, Germany, **1989**. [14b] D. H. Williams, I. Fleming, *Spectroscopic Methods in Organic Chemistry.* McGraw-Hill, London, UK, **1995**.

[15] H. Friebolin *Basic One- and Two-Dimensional NMR Spectroscopy* Wiley-VCH Verlag GmbH, Weinheim, Germany, **1998**.

[16] E. W. Abel, S. K. Bhargava, K. Orrell, *Prog. Inorg. Chem.* **1994**, *32*, 1.

[17] N. Durán, P. González-Duarte, A. Lledós, T. Parella, J. Sola, G. Ujaque, W. Clegg, K. A. Fraser, *Inorg. Chim. Acta* **1997**, *265*, 89.

[18] J. Llop, C. Masalles, C. Viñas, F. Teixidor, R. Sillanpää, R. Kivekäs, *Dalton Trans.* **2003**, 556.

[19] [19a] R. J. H. Clark, G. Natile, U. Belluco, L. Cattalini, C. Filippin, *J. Chem. Soc., (A)* **1970**, 659. [19b] K. Nakamoto, *Infrared and Raman spectra of Inorganic and Coordination Compounds.* John Wiley and Sons, New York, USA, **1986**.

[20] [20a] D. Sutton, *Electronic Spectra of Transition Metal Complexes.* McGraw Hill, London, UK, **1975**. [20b] J. C. Bailar, H. J. Emeleus, S. R. Nyttorm, A. F. T. Dickenson, *Comprehensive Inorganic Chemistry*, Pergamon Press, London, UK, **1973**. [20c] F. A. Cotton, G. Wilkinson, *Advanced Inorganic Chemistry* 5th ed., John Wiley and Sons, New York, USA, **1975**. [20d]N. F. Curtis, Y. M. Curtis, *Inorg. Chem.* **1965**, *4*, 804.

[21] D. B. Grotjahn, D. Combs, S. Van, G. Aguirre, F. Ortega, *Inorg. Chem.* **2000**, *39*, 2080.

[22] [22a] A. C. Aiub, N. R. Basso, O. L. Casagrande Jr., J. Dupont, M. Horner, A. J. Bortoluzzi, C. Maichle-Mossmer, *J. Coord. Chem.* **1996**, *40*, 35. [22b] N. K. Skvortsov, N. F. Chernov, O. M. Trofimova, V. K. Bels'skii, V. M. Svetlichnaya, M. G. Voronkov, *Zh. Obshch. Khim.* **1994**, *64*, 54.

[23] [23a] R. G. Raptis, J. F. Fackler Jr., *Acta Crystallogr., Sect. C (Cr. Str. Commun.)* **1991**, *47*, 1180. [23b] G. B. Onca, V. Moreno, M. Font-Bardia, X. Solans, J. M. Pérez, C. Alonso, *J. Inorg. Biochem.* **1999**, *75*, 205. [23c] J. A. Broomhead, L. M. Rendina, M. Sterns, *Inorg. Chem.* **1992**, *31*, 1880. [23d] M. A. Cirellu, S. Stoccoro, G. Minghetti, A. L. Bandini, G. Banditelli, B. Bovio, *J. Organomet. Chem.* **1989**, *372*, 311. [23e] K. Sakai, Y. Tomita, K. Goshima, M. Ohminato, T. Tsuboruma, K. Matsumoto, K. Ohmura, K. Kawakami, *Inorg. Chim. Acta* **2000**, *297*, 64.

[24] F. H. Allen, O. Kennard, *Chem. Des. Autom. News* **1993**, *8*, 31.

[25] S. V. Kolotilov, E. A. Goreshnik, V. V. Pavlishuk, K. B. Yatsimirskii, *Zh. Neorg. Khim.* **2000**, *45*, 967.

[26] W. L. Drax, C. M. Weeks, D. C. Roher, *Topics in Stereochemistry* (Eds.: E. L. Eliel and N. L. Allinger), John Wiley and sons, New York, **1976**.

[27] [27a] M. Konrad, F. Meyer, A. Jacobi, P. Kircher, P. Rutsch, L. Zlonai, *Inorg. Chem.* **1999**, *38*, 4559. [27b] F. Paap, E. Bouwman, W. L. Driessen, R. A. G. de Graff, J. Reedijk, *J. Chem. Soc., Dalton Trans.* **1985**, 737. [27c] Y. Sun, P. Cheng, S. Yan, Z. Jiang, D. Liao, P. Shen, *Inorg. Chem.* **2000**, *3*, 289. [27d] L. Siegfried, T. A. Kaden, F. Meyer, P. Kircher, H. Pritzkow, *J. Chem. Soc., Dalton Trans.* **2001**, 2310. [27e] J. Casabó, J. Pons, K. S. Siddiqi, F. Teixidor, E. Molins, C. Miravitlles, *J. Chem. Soc., Dalton Trans.* **1989**, 1401. [27f] B. S. Hammes, C. J. Carrano, *Inorg. Chem.* **1999**, *38*, 3562. [27g] T. C. Higgs, C. J. Carrano, *Inorg. Chem.* **1997**, *36*, 298. [27h] M. Mikuriya, K. Nakadera, T. Kotera, *Bull. Chem. Soc., Jpn.* **1996**, *69*, 399. [27i] B. Hommerich, H. Schwoppe, D. Volkmer, B. Krebs, *Z. Anorg. Allg. Chem.* **1999**, *625*, 75. [27j] S. Sheu, M. Tien, M. Cheng, T. Ho, S. Peng, Y. Lin, *J. Chem. Soc., Dalton Trans.* **1995**, 3503.

[28] [28a] L. Rosenberg, L. K. Thompson, E. J. Gabe, F. L. Lee, *J. Chem. Soc., Dalton Trans.* **1986**, 625. [28b] N. Saha, A. Saha, S. Chaudhuri, T. C. W. Mak, T. Banerjee, P. Roychoudhury, *Polyhedron* **1992**, *11*, 2341. [28c] M. Malecka, A. Rybarczyk-Pirek, T. A. Olszak, K. Malinowska, J. Ochocky, *Acta Crystallogr., Sect. C (Cr. Str. Commun.)* **2001**, *57*, 513. [28d] J. Pons, A. Chadghan, J. Casabó, A. Álvarez-Larena, J. F. Piniella, X. Solans, M. Font-Bardia, J. Ros, *Polyhedron* **2001**, *20*, 1029. [28e] A. Podder, B. P. Mukhopadhyay, N. Saha, A. Saha, B. Stensland, *J. Crystallogr. Spectrosc. Res.* **1989**, *19*, 71. [28f] L. Pan, N. Ching, X. Huang, J. Li, *Chemistry-A European Journal* **2001**, *7*, 4431. [28g] M. A. Masood, D. J. Hodgson, *Inorg. Chem.* **1994**, *33*, 3038.

[29] [29a] F. Paap, W. L. Driessen, J. Reedijk, A. L. Spek, *Inorg. Chimica. Acta* **1988**, *150*, 57. [29b] E. Bouwman, P. Evans, H. Kooijman, J. Reedijk, A. L. Spek, *J. Chem. Soc., Chem. Commun.* **1993**, 1746. [29c] S. Chiou, P. Ge, C. G. Riordan, L. M. Liable-Sands, A. L. Rheingold, *Chem. Commun.* **1999**, 159. [29d] M. Konrad, F. Meyer, K. Heinze, L. Zsolnai, *J. Chem. Soc., Dalton Trans.* **1998**, 199.

[30] [30a] I. A. Krol, V. M. Agre, V. K. Trunov, O. I. Ivanov, *Koord. Khim.* **1979**, *5*, 1569. [30b] S. Buchler, F. Meyer, A. Jacobi, P. Kircher, L. Zsolnai, *Z. Naturforsch., Teil B* **1999**, *54*, 1295. [30c] C. W. Reinmann, A. D. Mighell, F. A. Mauer, *Acta Crystallogr.* **1967**, *23*, 135. [30d] R. B. Helmholdt, W. Hinrichs, J. Reedijk, *Acta Crystallogr., Sect. C (Cr. Str. Commun.)* **1987**, *43*, 226. [30e] F. Meyer, U. RusChewitz, P. Schober, B. Antelmann, L. Zsolnai, *J. Chem. Soc., Dalton Trans.* **1998**, 1181.

[31] G. M. Sheldrick, *Acta Crystallogr., Sect. A* **1990**, *46*, 467.

[32] G. M. Sheldrick, *SHELXS-97, SHELXL-97, CIFTAB*-Program for Crystal Structure Analysis (Release 97-2), Institüt fur Anargonische Chemie der Universität, Tammanstraβe 4, 3400 Göttingen, Germany, **1998.**

Received January 16, 2003

 © 2003 Wiley-VCH Verlag GmbH & Co. KGaA, Weinheim

NMR and Molecular Modelling Studies on the Solution Structure of the In^{III}–Bleomycin A2 Complex

Athanasios Papakyriakou[a] and Nikos Katsaros*[a]

Keywords: Antitumor agents / Indium / Molecular dynamics / N ligands / NMR spectroscopy

The solution structure of the In^{III}–bleomycin A2 complex (InBLM) has been determined by NMR studies in combination with molecular modelling. Our data indicate that BLM is coordinated to In^{III} through five nitrogen ligands in a distorted tetragonal pyramid configuration. The stability and homogeneity of InBLM has allowed us to obtain a well-defined model of the complex formed at low pH, which is a very potent tumour-imaging agent.
(© Wiley-VCH Verlag GmbH & Co. KGaA, 69451 Weinheim, Germany, 2003)

Introduction

The bleomycins (BLMs) are a family of natural antibiotics, exhibiting activity against a broad spectrum of neoplasias.[1,2] Umezawa and co-workers were the first to isolate and characterize BLMs, as their copper chelates, from the culture medium of Streptomyces verticillus.[3,4] The clinically administered drug (Blenoxane or Bleocin) consists predominantly of BLM A2 (55−70%) and BLM B2 in their apo forms (Scheme 1). Their cytotoxicities were recognized to be dependent on the reaction between the ferrous BLM complex and O_2 to produce [HOO−Fe^{III}−BLM], which mediates DNA single- and double-strand scissions.[5−7] Because the biologically active species, designated as "activated bleomycin", is short-lived and unsuitable for direct structural studies, several other metallo-BLMs have been employed as models.[8,9]

The glycopeptide-derived BLM molecule can be divided into four functional domains:

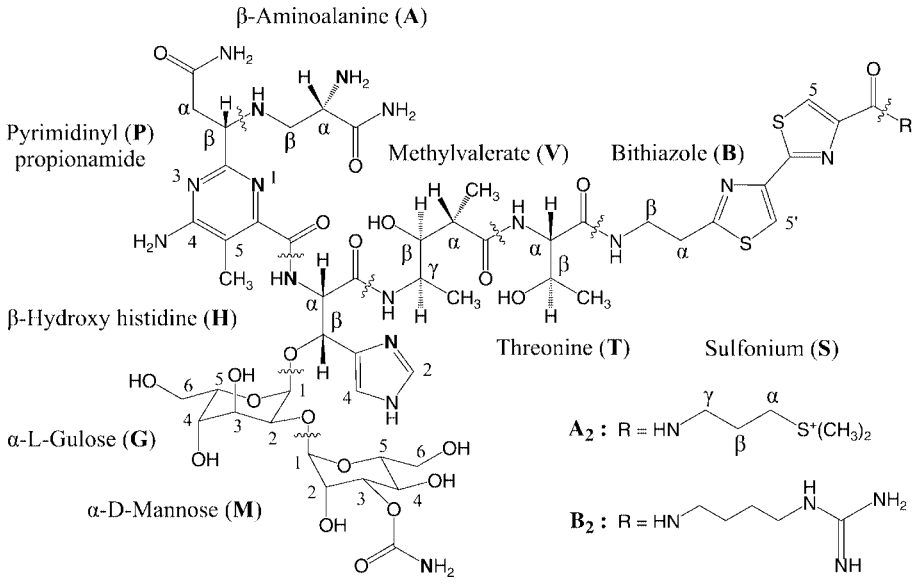

Scheme 1. Structure of bleomycin (BLM) A2 and B2; wavy lines separate their functional domains, and atoms in bold are the proposed N ligands

[a] Institute of Physical Chemistry, NCSR "Demokritos"
15310 Ag. Paraskevi Attikis, Greece
Fax: (internat.) + 30-210/6511766
E-mail: katsaros@chem.demokritos.gr
Supporting information for this article is available on the WWW under http://www.eurjic.org or from the author.

i. the metal-binding domain, made up of β-aminoalanine (**A**), pyrimidinyl propionamide (**P**) and β-hydroxy histidine (**H**)

ii. the linker domain: methyl valerate (**V**) and threonine (**T**)

iii. the DNA-binding domain, with the bithiazole moiety (**B**) intercalating mainly between G-Py base pairs and the sulfonium tail (**S**), different in each BLM

iv. the disaccharide moiety, made up of α-L-gulose (**G**) and 3-*O*-carbamoyl-α-D-mannose (**M**) and considered to be responsible for the sequence specificity of DNA recognition exhibited by the metallo-BLMs.

The equatorial planes of all the metallo-BLMs and analogues studied so far are defined by the secondary amine of **A**, the N1 of pyrimidine, the deprotonated amide of **H** and the N1 of imidazole (Scheme 1).[10−33] In most of these cases, the primary amine of **A** is an axial ligand, as is also the case in the X-ray crystal structure of Cu^{II}−BLM bound to a BLM-binding protein.[18] On the other hand, some NMR studies have introduced a controversy regarding the coordination of the **M** carbamoyl group.[19,26,31,32] Recent conformational analysis of all the binding geometries of Co^{III}−BLMs has been used to explore the configurations available in the proposed binding geometries.[34,35]

A large number of radioactive metal ion complexes of BLM have been prepared and tested as tumour imaging agents.[36−38] Most of them have failed because of a lack either of in vivo stability or of tumour affinity. Among the divalent metal cations of copper, nickel, zinc and cobalt to have demonstrated high affinity for BLM, ^{57}Co−BLM has been clinically used in lung cancer patients and exhibited high specificity. Because of the high toxicity and the inconveniently long half-life of ^{57}Co, other metals such as ^{67}Ga, ^{99m}Tc and ^{111}In have also been introduced as radiolabels. The complex formed at low pH values between ^{111}In and BLM has exhibited a remarkable stability in vivo, since it has no affinity for transferrin.[39−41] In clinical trials, ^{111}InBLM has demonstrated excellent specificity and sensitivity in head and neck cancer.[42−45]

With the aim of obtaining additional structural information for metallo-BLMs, we have undertaken the characterization of the In^{III}−BLM complex in aqueous solutions. Its high stability at low pH values has allowed us to obtain a wealth of information from 2D NMR experiments. The detection of all exchangeable amine and amide protons, especially those of the **A** primary amine, has played the key role in its structure determination. A molecular mechanics force field, specially parameterised for InBLM, was employed in combination with the experimentally obtained results in order to define the chirality of the complex formed. Structural implications and comparison with other metallo-BLMs are discussed.

Results and Discussion

The interaction between In^{III} and BLMs was monitored by ^{1}H NMR spectroscopy, with use being made both of the clinically administered form and of the pure BLM A2. Immediately after the addition of $In(NO_3)_3$ to solutions of the BLMs at room temperature, pH decreases from 4.5 to less than 2.5 were observed, a fact indicating release of protons. The reaction rate is quite high, so formation of InBLM had been completed by the time that the spectra were acquired (ca. 10 min). 1D NMR spectra of InBLM were acquired at a broad range of temperatures from 278 to 333 K, and at pH values ranging from 2.5 to 7.8. The complex demonstrated high stability even after several months at 298 K, equally well in acidic and in neutral solutions. Although 2D NMR experiments were performed at pH = 6.8 and 3.3, only the latter are presented here. Apart from the successful use of the complex formed at the lower pH as a tumour imaging agent, NMR experiments were also better resolved. In particular, the NOESY spectra acquired in H_2O at 278 K exhibited more intense signals, as the exchange and molecular tumbling rates were lower.

Assignment of the NMR Spectra

The ^{1}H and ^{13}C chemical shifts of InBLM are presented in the Supporting Information (Tables S1 and S2), in comparison with those obtained for the metal-free BLM.[19] The ^{1}H chemical shifts of the sugar moieties were assigned by complementary use of ^{1}H−^{13}C heteronuclear and homonuclear experiments. The HMQC experiment (Supporting Information; Figure S1) provides a dispersion in the carbon dimension, sufficient to spread out all the disaccharide H−C cross-peaks. In combination with the long-range couplings observed in the HMBC and TOCSY spectra, complete assignment can be carried out. The strategy for the assignment of the non-exchangeable protons has already been described in detail,[19,25−27] so we present only the assignment procedure for the exchangeable amine and amide protons, which in some cases have proved to be ambiguous.

The amide protons **V**−NH, **T**−NH, **B**−NH and **S**−NH, as well as the secondary amine proton **A**−NH, were readily assigned by observation of their vicinal scalar couplings. No resonance for the amide proton of histidine was detected, as in cases of previously studied metallo-BLMs.[19,20,25−27] This strongly suggests that this amide is deprotonated and coordinated to In^{III}. Four additional pairs of exchangeable protons, strongly coupled to each other, were detected, along with a broad singlet. The first pair of exchangeable protons with signals at δ = 3.57/5.42 ppm was assigned to the primary amine of **A**, due to the detected scalar couplings with **A**−CαH. Moreover, the δ = 5.42 ppm signal exhibits a weak cross-peak to **A**−CβH in the DQF-COSY spectrum, with a ^4J coupling implying that the bonds linking the coupled nuclei are in a sterically fixed "W" configuration (Supporting Information: Figure S2). The next pair of protons, with chemical shifts at δ = 7.13/7.90 ppm, was assigned to **P**−$CONH_2$, due to the weak couplings observed between the δ = 7.90 ppm signal and the two **P**−Cα protons, also supported by the observed NOEs (Supporting Information: Figure S3). The set of coupled protons at δ = 7.68/8.40 ppm was assigned to **A**−$CONH_2$, by virtue of the scalar coupling between the δ = 8.40 ppm signal and **A**−CαH. This ^4J coupling is also quite weak and its detection indicates a fixed conformation between the coupled nuclei. The broad signal at δ = 7.31 ppm was assigned to 4-

 © 2003 Wiley-VCH Verlag GmbH & Co. KGaA, Weinheim

NH_2 of the pyrimidine ring, in view of the medium-sized NOE exhibited with the neighbouring **P**−5-CH_3. The last pair of protons at δ = 5.96/6.63 ppm exhibits only quite weak NOEs with **P**−5-CH_3 and was assigned to the remaining **M**−$CONH_2$ group. This was also the case for Ga^{III}−BLM, while their chemical shift values are also comparable.

Analysis of the NMR Data

Detection and assignment of the exchangeable protons has revealed very important information regarding the structure of InBLM. The degeneration of the **A**−αNH_2 resonance at δ = 3.57 and 5.42 ppm is a strong indication of its coordination to the metal ion. In the opposite case, only one signal would be detected for the equivalent amine protons, due to fast rotation around the Cα−N bond. In contrast, the potential carbamoyl N ligand of **M** is disfavoured by the fact that it should be deprotonated, the histidine amide likewise. Owing to the high pK_a of **M**−NH_2 (ca. 13) and the detection of two proton resonances, **M**−CO is thus more likely to be a ligand.[46]

A wealth of structural data and distance constraints has been obtained from NOESY spectra acquired at low temperature (278 K; Supporting Information: Table S3). The observed NOEs between the protons of **H**, **V** and **T** suggest that the linker domain is folded underneath the equatorial plane from the side of the imidazole, in the same way as for the Cu^{II}, Co^{III} and Ga^{III}−BLMs.[18,25,27,33] The thiazolium rings are probably in a *trans* conformation, since through-space coupling between their aromatic protons is absent. On the other hand, **B**−5′H exhibits NOEs with the methyl groups of **V**, indicating that the bithiazole tail is close to the linker domain.

Probably the most interesting piece of information is the observation of NOEs between **A**−αNH_2 and the disaccharide protons. Medium-sized signals with **M**−C3H and **M**−C2 H, as well as weak ones with **M**−C1H and **G**−C5 H, restrain the aminoalanine moiety near the sugars. Consequently, it would be expected that both **A** and **M** moieties should share the same side of the equatorial plane. The existence only of one weak NOE between **M**−NH_2 and **P**−CH_3 points to the stacking of the carbamoyl group over the **P** ring, just as in Cu^{II}, Co^{III} and Ga^{III}−BLMs.[18,25,27,33]

Molecular Dynamics Calculations

Three different models of InBLM were used as starting structures for restrained simulated annealing calculations (Figure 1). These models were constructed with In^{III} bound to the four common N ligands of most metallo-BLMs studied so far. Only four-coordinate species were used, so as to make a direct comparison between their potential energies. Model **I** was constructed with both **A**−αNH_2 and **M**−$CONH_2$ at the same side of the equatorial plane, while in models **II** and **III** they occupy apical positions across the equatorial plane. In this way, we were able to examine whether **A**−αNH_2 and **M**−$CONH_2$ are potential axial ligands for InBLM. The coordinates of model **I** were based on the crystal structure of Cu^{II}−BLM (PDB accession no. 1JIF)[18] and models **II** and **III** were constructed on the basis of the NMR structure of Co^{II}−BLM (PDB accession no. 1DEY).[31]

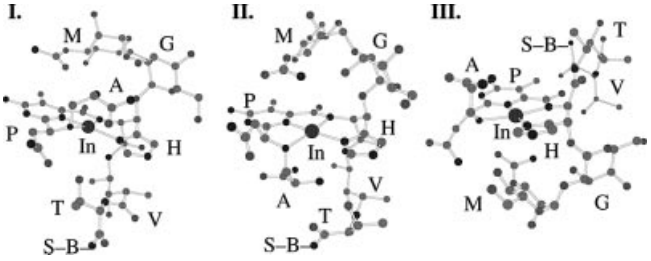

Figure 1. Starting four-coordinate models of InBLM employed in the molecular dynamics calculations; the equatorial ligands are similar in all structures, while the **A** primary amine and the **M** carbamoyl group are located at different sites: both at the same side of the equatorial plane (**I**) and each one occupying an axial position (**II** and **III**); hydrogen atoms, bithiazole and sulfonium moieties have been excluded for clarity

The results obtained by the 10 best structures, by virtue of the lowest potential energies and deviations from the NMR constraints, are summarized in Table 1. All the starting models resulted in structures with the aminoalanine and the disaccharide moieties on the same side of the equatorial plane (Supporting Information: Figure S3). In addition to

Table 1. Structural and energy statistics of the InBLM best models obtained from the simulated annealing calculations

	Structure **I**	Structure **II**	Structure **III**
Rmsd of heavy atoms [Å]	0.90 ± 0.23	0.98 ± 0.19	1.64 ± 0.37
Rmsd from distance restraints [Å]	0.019 ± 0.001	0.022 ± 0.002	0.044 ± 0.002
No. of distance restraint violations	3−5	4−7	11−16
Potential energy terms [kcal mol^{-1}]:			
Total	−28.7 ± 4.1	−18.5 ± 1.5	58.2 ± 3.6
Bond	22.5 ± 0.9	23.4 ± 1.0	25.5 ± 0.8
Angle	56.8 ± 1.2	63.2 ± 1.8	86.6 ± 6.4
Dihedral angle[a]	42.0 ± 1.6	43.7 ± 1.5	55.2 ± 2.6
Nonbonded[b]	−151.9 ± 7.0	−151.1 ± 3.7	−118.2 ± 8.9
Constraint	2.0 ± 0.1	2.2 ± 0.4	8.9 ± 0.8

[a] Including the improper angle energy term. [b] Sum of the electrostatic and van der Waals energy terms.

 © 2003 Wiley-VCH Verlag GmbH & Co. KGaA, Weinheim

this, structures resulting from model **I** exhibit lower energies and deviations from the distance constraints. Model **I** with **A**−αNH$_2$ and **M**−CONH$_2$ on the same side of the equatorial plane is therefore strongly favoured.

Coordination of **A**−αNH$_2$ is supported not only by the NMR spectroscopic data, but also by the molecular dynamics results. In most of the final structures, especially those resulting from models **I** and **II**, the primary amine is to be found at the axial site, while the carbamoyl group is stacked over the pyrimidine ring. Even though the calculated distance between In^{III} and the **A** amine nitrogen (ca. 2.9 Å) cannot be regarded as a metal−ligand bond length, it is evident that **A**−αNH$_2$ is a favoured axial ligand. The distance between the **M** carbamoyl oxygen atom and In^{III} is > 4.5 Å in all the final structures and can thus be discounted as ligand.

The average structure of the 10 best models **I** was subjected to energy minimization, but with **A**−αNH$_2$ bonded to In^{III}. All the experimental constraints were applied with no violation > 0.1 Å and the total energy was calculated to be even lower than those of the four-coordinate models. The resulting structure, as illustrated in Figure 2, represents the favourable solution structure of InBLM. On the basis of the higher thermodynamic and in vivo stabilities of the six-coordinate In^{III} complexes,[47] we can hypothesize that an H_2O molecule or a Cl^- ion might occupy an axial site *trans* to the primary amine ligand.

Structural Implications and Comparisons with Other Metallo-BLMs

An examination of InBLM structure (Figure 2) has revealed potential H bonds between different domains of BLM. A very strong one is exhibited by (**T**)O−H···O=C(**P**) (distance 1.7 Å, angle 166°). Moreover, the hydroxy oxygen atom of **T** can act as an acceptor to **A**−NH (distance 1.9 Å, angle 170°). These two H bonds, along with those between **T**−NH, **V**−NH and the potential sixth exogenous ligand (H_2O or Cl^-), might be responsible for the folded conformation of the linker domain. The result of electron shielding by the imidazole ring current is exhibited by the upfield-shifted resonances of valerate.

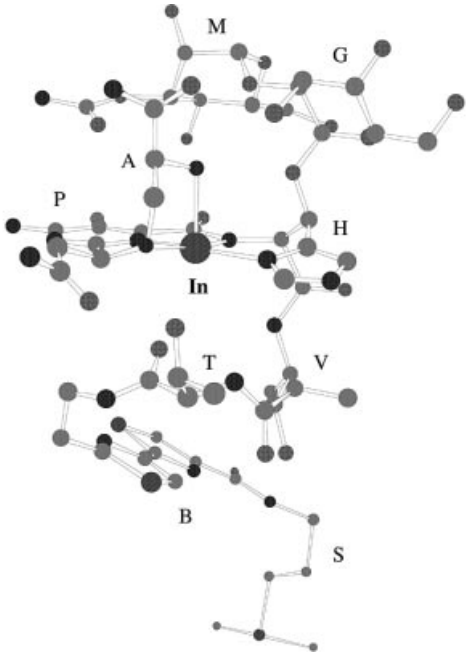

Figure 2. Favoured model for the solution structure of InBLM with the primary amine of aminoalanine occupying the axial site; this model was calculated by averaging of the coordinates of the 10 best models **I** and energy minimization with all the distance restraints

Some potential H bonds were also observed at the other side of the InBLM equatorial plane: (**M**)O4−H···O=C(**H**) (distance 1.7 Å, angle 175°), (**G**)O3−H···O=C(**A**) (distance 1.8 Å, angle 161°), (**A**)αN−H···O−C3(**G**) (distance 2.1 Å, angle 154°) and the weak (**A**)αN−H′···O=C3(**M**) (distance 2.7 Å, angle 116°). These interactions may account for an approach of the disaccharide moiety towards the axial amine ligand, which was also observed in the crystal structure of Cu^{II}−BLM,[18] as well as in the solution structures of Co^{III} and Ga^{III}−BLMs.[25,27,33] A noticeable difference between the structures of these metallo-BLMs is the location of the DNA-binding domain. While for CoBLM ("brown form") and GaBLM no NOEs were detected between **B** or **S** and any other moieties, the NMR structures of CoBLM ("green form") and InBLM have revealed some sort of folding for the BLM's tail. Since no interactions such as the H bonds mentioned above were found, we cannot provide an explanation for this variation.

Conclusion

The anticancer drug BLM forms a very stable complex with In^{III} at low pH values. Our NMR spectroscopic data indicate that InBLM is also stable at neutral pH for several months. The five N ligands of BLM form a distorted tetragonal pyramid around the metal cation, as in the case of Cu^{II}−BLM crystal structure. The carbamoyl group of mannose is not a ligand, but is constrained to the second coordination sphere of InBLM through H-bonding interactions with the axial amine ligand.

Experimental Section

Sample Preparation: Bleocin and BLM A2 were a kind gift from Nippon Kayaku Co. and were used without further purification. The complex was prepared at room temperature by addition of In(NO$_3$)$_3$·3H$_2$O (0.1 M) to aqueous solutions of BLM (10 mM) and the pH was adjusted with aliquots of dilute NaOD or DCl. For the NMR experiments, lyophilised samples were dissolved either in 90% H_2O/10% D_2O or in D_2O (99.99%) (final concentrations were 3−5 mM). The purity of InBLM was judged to be $> 95\%$ from the ^{1}H NMR spectra. All the samples were stable over a period of several months at room temperature, since no changes were detected in their periodically recorded ^{1}H NMR spectra .

NMR Experiments: NMR spectra were recorded with a Bruker Avance 500 MHz instrument and were processed by X-WIN NMR 2.6 (Bruker Analytik GmbH). The program SPARKY 3.100,[48] running on a Linux PC, was used for assignment and analysis of

 © 2003 Wiley-VCH Verlag GmbH & Co. KGaA, Weinheim

the 2D spectra. ^1H and ^{13}C chemical shifts were referenced to sulfonium tail methyl groups of BLM at $\delta = 2.93$ and 25.0 ppm, respectively. 2D NOESY (100, 200 and 400 ms mixing times), DQF COSY[49] and TOCSY experiments (MLEV-17 sequence with 35 and 70 ms mixing times)[50] were recorded at 278 and 298 K in H_2O and D_2O. Data sets with 4096 × 512 complex points were acquired with 7 kHz sweep widths in both dimensions and 32 scans per t_1 increment. $^1H-^{13}C$ HMQC[51] and HMBC[52] experiments were also recorded at 278 and 298 K in H_2O and D_2O. Data sets with 2048 × 256 points were collected with 32 or 64 scans per t_1 increment and spectral widths of 6 kHz in the proton and 25 kHz in the carbon dimension. Solvent suppression for the H_2O samples was performed by use of excitation sculpting with gradients,[53] while for the D_2O samples a presaturation pulse was used during the relaxation delay of 2.0 s. The indirect dimension was zero-filled to 2048 data points and the FIDs were processed either with a combination of exponential and Gaussian weighting functions or with a 90°-shifted sine bell function.

Distance Constraints: The NOE signals from the 200-ms NOESY spectrum of InBLM at pH = 3.3 and 278 K were classified as strong, medium and weak, by visual inspection of the cross-peak intensities. Integration of the cross-peaks was performed by the sum-over-ellipse method. The constraints were set to upper distance limits of 3.0, 4.0 and 5.0 Å, respectively, while an additional 1.0 Å was allowed for NOEs involving methyl groups and ambiguous methylene protons. A total of 88 distance constraints were applied with a 50 kcal mol^{-1} $Å^{-2}$ force constant, by use of a square bottom well function with parabolic sides out to 0.5 Å and then linear sides beyond that.

Force Field Parameters: All the molecular modelling calculations were performed with Amber 6,[54] running on a Linux PC. In order to model InBLM accurately, the Amber-1994 force field was modified according to the guidelines of its authors.[55] Standard atom types were assigned to the atoms of BLM by analogy to their chemical environment, except for the disaccharide moiety, for which we used parameters from a force field for modelling glycoproteins (GLYCAM).[56] A new atom type was created for In^{III}, with van der Waals parameters estimated as $R^* = 1.9$ Å (from Bondi crystallographic data)[57] and $\varepsilon = 0.2$ kcal mol^{-1}. The bond, angle and dihedral angle parameters of BLM were also chosen among the existing Amber force field parameter, on the basis of atom type analogy. The metal−ligand parameters were adapted from those calculated by Welch et al.[58] Bond lengths of In−N were applied with $R_o = 2.38$ Å and a 50 kcal mol^{-1} $Å^{-2}$ force constant. For the N−In−N angles we applied θ_o of 90 or 180° with 50 kcal mol^{-1} rad^{-2} force constant, while dihedral angles involving In^{III} were set with zero force constants. The atom-centred point charges of the complex were generated from the electrostatic potential of its molecular fragments. For this purpose, we used the ab initio program package GAMESS,[59] at the Hartree-Fock level of theory. The Stevens/Basch/Krauss/Jasien/Cundari-21G relativistic effective core potentials (SBKJC VDZ ECPs)[60] were used for indium, the 6-31G* basis set for all other atoms.[61] The point charges were fitted to reproduce the electrostatic potential by use of the RESP method,[62] a two-stage approach in which the equivalent methyl and methylene hydrogen atoms are restrained to have the same charge. The equatorial plane of InBLM comprising the β-aminoalanine, pyrimidinylpropionamide and histidine moieties was fitted as a whole. For the remaining domains of BLM we used the atom charges, previously calculated for GaBLM.[33]

Restrained Molecular Dynamics: Molecular dynamics calculations in vacuo were carried out at a time step of 1 fs with the Amber distance-dependent dielectric constant algorithm. The cut-off distance was set to 16.0 Å and the nonbonded pair list was updated every 10 steps. Temperature regulation was performed by use of the Berendsen algorithm. For the heating and cooling stages a bath coupling constant of 0.1−0.5 ps was applied, so as to assure a tighter coupling to the heat bath, while for the equilibration stages it was increased to 2.0 ps to allow sampling of more natural trajectories. The simulated annealing procedure used is the same as that described in the structural characterization of GaBLM.[33] Starting models were initially energy-minimized with no restraints by 500 steps of the steepest descent method and followed by the conjugate gradient method to an rms gradient < 0.1. Every model was then subjected to 20 individual runs starting with a different seed for the initial velocities assigned. A final structure from each iteration was generated by mass-weighted rms fitting and averaging of the coordinates from the last 20 ps of the trajectory (100 structures), followed by energy minimization as above but with all the restraints applied. The results presented in Table 1 are derived from the final 10 best models, by virtue of the lowest energy and deviations from the NMR constraints.

Supporting Information (see footnote on the first page of this article): Two tables with the ^1H and ^{13}C chemical shifts of InBLM in comparison with those reported for apo-BLM and a table with the categorized NOE intensities of InBLM in comparison with those obtained for GaBLM. Three figures with expanded regions from the HMQC, DQF-COSY and NOESY spectra of InBLM and a figure with ensembles of the superimposed structures calculated for each starting model.

Acknowledgments

This work was supported by the General Secretariat for Research and Technology of Greece. The authors are grateful to Prof. Ivano Bertini for his hospitality at the CERM in the framework of the European Large Research Infrastructure.

[1] F. Hutchinson, L. F. Povirk in *Bleomycin: Chemical, Biochemical, and Biological Aspects* (Ed.: S. M. Hecht), Springer-Verlag, New York, **1979**, pp. 256−266.
[2] H. Umezawa in *Anticancer Agents Based on Natural Product Models* (Eds.: J. M. Cassady, J. Douros), Academic Press, New York, **1980**, pp. 147−166.
[3] H. Umezawa, K. Maeda, T. Takeuchi, Y. Okami, *J. Antibiot.* **1966**, *19*, 200−209.
[4] H. Umezawa, Y. Suhura, T. Takita, K. Maeda, *J. Antibiot.* **1966**, *19*, 210−219.
[5] S. M. Hecht, *Acc. Chem. Res.* **1986**, *19*, 383−391.
[6] J. Stubbe, J. W. Kozarich, *Chem. Rev.* **1987**, *87*, 1107−1136.
[7] R. M. Burger, *Chem. Rev.* **1998**, *98*, 1153−1169.
[8] C. A. Claussen, E. C. Long, *Chem. Rev.* **1999**, *99*, 2797−2816.
[9] J. Stubbe, J. W. Kozarich, W. Wu, D. E. Vanderwall, *Acc. Chem. Res.* **1996**, *29*, 322−330.
[10] Y. Iitaka, H. Nakamura, T. Nakatani, Y. Muraoka, A. Fujii, T. Takita, H. Umezawa, *J. Antibiot.* **1978**, *31*, 1070−1072.
[11] T. Takita, Y. Muraoka, T. Nakatani, A. Fujii, Y. Iitaka, H. Umezawa, *J. Antibiot.* **1978**, *31*, 1073−1077.
[12] S. J. Brown, P. K. Mascharak, *J. Am. Chem. Soc.* **1988**, *110*, 1996−1997.
[13] S. J. Brown, S. E. Hudson, D. W. Stephan, P. K. Mascharak, *Inorg. Chem.* **1989**, *28*, 468−477.
[14] E. Kimura, H. Kurosaki, Y. Kurogi, M. Shionoya, M. Shiro, *Inorg. Chem.* **1992**, *31*, 4314−4321.
[15] J. D. Tan, S. E. Hudson, S. J. Brown, M. M. Olmstead, P. K. Mascharak, *J. Am. Chem. Soc.* **1992**, *114*, 3841−3853.
[16] H. Kurosaki, K. Hayashi, Y. Ishikawa, M. Goto, K. Inada, I.

 © 2003 Wiley-VCH Verlag GmbH & Co. KGaA, Weinheim

Taniguchi, M. Shionoya, E. Kimura, *Inorg. Chem.* **1999**, *38*, 2824−2832.
[17] B. Mouzopoulou, H. Kozlowski, N. Katsaros, A. Garnier-Suillerot, *Inorg. Chem.* **2001**, *40*, 6923−6929.
[18] M. Sugiyama, T. Kumagai, M. Hayashida, M. Maruyama, *J. Biol. Chem.* **2002**, *277*, 2311−2320.
[19] M. A. J. Akkerman, C. A. G. Haasnoot, C. W. Hilbers, *Eur. J. Biochem.* **1988**, *173*, 211−225.
[20] M. A. J. Akkerman, E. W. Neijman, S. S. Wijmenga, C. W. Hilbers, W. Bermel, *J. Am. Chem. Soc.* **1990**, *112*, 7462−7474.
[21] R. X. Xu, W. E. Anthroline, D. H. Petering, *J. Biol. Chem.* **1992**, *267*, 944−949.
[22] R. X. Xu, D. Nettesheim, J. D. Otvos, D. H. Petering, *Biochemistry* **1994**, *33*, 907−916.
[23] W. Wu, D. E. Vanderwall, J. W. Kozarich, J. Stubbe, C. J. Turner, *J. Am. Chem. Soc.* **1994**, *116*, 10843−10844.
[24] W. Wu, Q. Mao, P. Fulmer, W. Li, E. F. DeRose, D. H. Petering, *J. Biol. Chem.* **1996**, *271*, 6185−6191.
[25] W. Wu, D. E. Vanderwall, S. M. Lui, X.-J. Tang, C. J. Turner, J. W. Kozarich, J. Stubbe, *J. Am. Chem. Soc.* **1996**, *118*, 1268−1280.
[26] J. D. Otvos, W. E. Antholine, S. Wehrli, D. H. Petering, *Biochemistry* **1996**, *35*, 1458−1465.
[27] S. M. Lui, D. E. Vanderwall, W. Wu, X.-J. Tang, C. J. Turner, J. W. Kozarich, J. Stubbe, *J. Am. Chem. Soc.* **1997**, *119*, 9603−9613.
[28] J. Caceres−Cortes, H. Sugiyama, K. Ikudome, I. Saito, A. H. Wang, *Eur. J. Biochem.* **1997**, *244*, 818−828.
[29] T. E. Lehmann, L.-J. Ming, M. E. Rosen, L. Jr. Que, *Biochemistry* **1997**, *36*, 2807−2816.
[30] W. Wu, D. E. Vanderwall, S. Teramoto, S. M. Lui, S. T. Hoehn, X.-J. Tang, C. J. Turner, D. L. Boger, J. W. Kozarich, J. Stubbe, *J. Am. Chem. Soc.* **1998**, *120*, 2239−2250.
[31] T. E. Lehmann, M. L. Serrano, L. Jr. Que, *Biochemistry* **2000**, *39*, 3886−3898.
[32] T. E. Lehmann, *J. Biol. Inorg. Chem.* **2002**, *7*, 305−312.
[33] A. Papakyriakou, B. Mouzopoulou, N. Katsaros, *J. Biol. Inorg. Chem.* **2003**, *8*, 549−559.
[34] F. Fedeles, M. Zimmer, *Inorg. Chem.* **2001**, *40*, 1557−1561.
[35] M. Zimmer, *Coord. Chem. Rev.* **2001**, *212*, 133−163.
[36] R. B. Grove, R. C. Reba, W. C. Eckelman, M. Goodyear, *J. Nucl. Med.* **1974**, *15*, 386−390.
[37] E. B. Silberstein, *Am. J. Med.* **1976**, *60*, 226−237.
[38] D. Front, O. Israel, G. Iosilevsky, E. Even-Sapir, A. Frenkel, G. M. Kolodny, M. Feinsod, *J. Nucl. Med.* **1988**, *29*, 187−194.
[39] D. Y. Hou, H. Hoch, G. S. Johnston, K. C. Tsou, R. J. Farkas, E. E. Miller, *Eur. J. Nucl. Med.* **1983**, *8*, 535−540.
[40] D. Y. Hou, H. Hoch, G. S. Johnston, K. C. Tsou, A. E. Jones, R. J. Farkas, E. E. Miller, *J. Surg. Oncol.* **1984**, *25*, 168−175.
[41] D. Y. Hou, H. Hoch, G. S. Johnston, K. C. Tsou, R. J. Farkas, E. E. Miller, *Int. J. Nucl. Med. Biol.* **1984**, *11*, 129−39.
[42] D. A. Goodwin, C. F. Meares, L. H. DeRiemer, C. I. Diamanti, R. L. Goode, J. E. Baumert, Jr., D. J. Sartoris, R. L. Lantieri, H. D. Fawcett, *Nucl. Med.* **1981**, *22*, 787−792.
[43] A. P. Jekunen, K. J. Kairemo, H. A. Ramsay, M. J. Kajanti, *Clin. Nucl. Med.* **1996**, *21*, 129−131.
[44] K. J. Kairemo, H. A. Ramsay, T. Paavonen, S. Bondestam, *Eur. J. Cancer. B. Oral. Oncol.* **1996**, *32*, 311−321.
[45] K. J. Kairemo, H. A. Ramsay, T. K. Paavonen, H. A. Jaaskela-Saari, M. Tagesson, K. Ljunggren, S. E. Strand, *Cancer. Detect. Prev.* **1997**, *21*, 83−90.
[46] R. H. Holm, P. Kennepohl, E. I. Solomon, *Chem. Rev.* **1996**, *96*, 2239−2314.
[47] Y. Sun, C. J. Anderson, T. S. Pajeau, D. E. Reichert, R. D. Hancock, R. J. Motekaitis, A. E. Martell, M. J. Welch, *J. Med. Chem.* **1996**, *39*, 458−470.
[48] T. D. Goddard, D. G. Kneller, *SPARKY 3*, University of California, San Francisco, **2001**.
[49] A. Derome, M. Williamson, *J. Magn. Reson.* **1990**, *88*, 177−185.
[50] A. Bax, D. G. Davis, *J. Magn. Reson.* **1985**, *65*, 355−360.
[51] A. Bax, S. Subramanian, *J. Magn. Reson.* **1986**, *67*, 565−569.
[52] A. Bax, M. F. Summers, *J. Am. Chem. Soc.* **1986**, *108*, 2093−2094.
[53] T.-L. Hwang, A. J. Shaka, *J. Magn. Reson.* **1995**, *112*, 275−279.
[54] D. A. Case, D. A. Pearlman, J. W. Caldwell, T. E. Cheatham, W. S. Ross, C. L. Simmerling, T. A. Darden, K. M. Merz, R. V. Stanton, A. L. Cheng, J. J. Vincent, M. Crowley, V. Tsui, R. J. Radmer, Y. Duan, J. Pitera, I. Massova, G. L. Seibel, U. C. Singh, P. K. Weiner, P. A. Kollman, *AMBER 6*, University of California, San Francisco, **1999**.
[55] W. D. Cornell, P. Cieplak, C. I. Bayly, I. R. Gould, K. M. Jr. Merz, D. M. Ferguson, D. C. Spellmeyer, T. Fox, J. W. Caldwell, P. A. Kollman, *J. Am. Chem. Soc.* **1995**, *117*, 5179−5197.
[56] R. J. Woods, R. A. Dwek, C. J. Edge, B. Fraser-Reid, *J. Phys. Chem.* **1995**, *99*, 3832−3846.
[57] A. Bondi, *J. Phys. Chem.* **1964**, *68*, 441−451.
[58] D. E. Reichert, M. J. Welch, *Coord. Chem. Rev.* **2001**, *212*, 111−131.
[59] M. W. Schmidt, K. K. Baldridge, J. A. Boatz, S. T. Elbert, M. S. Gordon, J. J. Jensen, S. Koseki, N. Matsunaga, K. A. Nguyen, S. Su, T. L. Windus, M. Dupuis, J. A. Montgomery, *J. Comput. Chem.* **1993**, *14*, 1347−1363.
[60] W. J. Stevens, M. Krauss, H. Basch, P. G. Jasien, *Can. J. Chem.* **1992**, *70*, 612.
[61] M. M. Francl, W. J. Pietro, W. J. Hehre, J. S. Binkley, M. S. Gordon, D. J. DeFrees, J. A. Pople, *J. Chem. Phys.* **1982**, *77*, 3654−3665.
[62] C. I. Bayly, P. Cieplak, W. D. Cornell, P. A. Kollman, *J. Phys. Chem.* **1993**, *97*, 10269−10280.

Received February 5, 2003

 © 2003 Wiley-VCH Verlag GmbH & Co. KGaA, Weinheim

Thermodynamic and Structural Properties of Eu^{3+}, Gd^{3+} and Tb^{3+} Complexes with 1,4,7,10-Tetra(2-glutaryl)-1,4,7,10-tetraazacyclododecane in Solution: EXAFS, Luminescence, Potentiometric Studies, and Quantum Calculations

Juliette Moreau,[a] Emmanuel Guillon,[a] Philippe Aplincourt,[b] Jean-Claude Pierrard,[a] Jean Rimbault,*[a] Marc Port,[c] and Michel Aplincourt[a]

Keywords: Lanthanides / Imaging agents / EXAFS spectroscopy / Luminescence / Ab initio calculations

The stability of the various complexes formed by racemic solutions of the title ligand (L) with Gd^{3+}, Eu^{3+} and Tb^{3+} was investigated by potentiometry. The reaction of complexation proceeds through the quick formation of metastable species leading, after a slow reorganisation of the macrocycle, to thermodynamically stable complexes. The mean numbers of water molecules coordinated to the lanthanides were determined by luminescence and EXAFS spectroscopy. This last method, applied to solutions of complexes, allowed us to precisely determine the nature of the atoms that surround the metal atom and the distance between the lanthanide ion and the various ligands. These structural data that are in good agreement with the results found using quantum mechanics allow us to propose a reaction mechanism, from the hydrated lanthanide ion to the final stable complexes through intermediate species. The specific stability of these final complexes arises from the formation of transitory bonds between the metal ion and two pendant arms, which bear carboxylate groups. The stability constants of the final complexes have high values, close to those obtained with DOTA [log $\beta_{110}(EuL^{5-}) = 24.01$; log $\beta_{110}(GdL^{5-}) = 24.03$; log $\beta_{110}(TbL^{5-}) = 23.97$]. This induces a notable in vivo dissociation inertness, which is essential for a potential contrast agent in magnetic resonance imaging.
(© Wiley-VCH Verlag GmbH & Co. KGaA, 69451 Weinheim, Germany, 2003)

Introduction

For over two decades, there has been a continuous interest in the study of lanthanide complexes, particularly those of gadolinium(III) with tetraazamacrocyclic ligands, due to their use as paramagnetic contrast agents in diagnostic magnetic resonance imaging (MRI).[1] The main clinically approved gadolinium contrast agents have low molecular weights, and are non-specific agents, which diffuse rapidly in the vascular endothelium.[2] This property limits their use in magnetic resonance coronary angiography and functional imaging.[3] This disadvantage is overcome by the development of Blood Pool Agents, characterised by a high molecular weight, and, consequently, a limited diffusion rate through the endothelium.[4]

The potential contrast agent studied, 1,4,7,10-tetra(2-glutaryl)-1,4,7,10-tetraazacyclododecane, called P730, is a tetracarboxylated derivative of DOTA and a precursor in the synthesis of new MRI macromolecular contrast agents.[3−5] Recent publications, which involved NMR spectroscopy, relaxometry, and luminescence spectrophotometry,[6,7] and which dealt with the structure and dynamics of the numerous stereoisomers formed by this ligand with europium, gadolinium, and terbium, have highlighted the important role of the rate of water exchange.

The ligand P730 may exist as six different stereoisomers, determined by the configuration at each of the stereogenic centres of the carbon atom, (*RRRR*) [(*SSSS*)] and (*RSSS*) [(*SRRR*)] and the achiral diastereoisomers, (*RSRS*) and (*RRSS*) (Scheme 1).

For a given isomer in solution, each chelate formed with the lanthanide usually adopts the same configuration so that four stereoisomers occur, which may interconvert by concerted ring inversions ($\delta\delta\delta\delta \rightarrow \lambda\lambda\lambda\lambda$) or co-operative arm rotation ($\Delta \rightarrow \Lambda$) (Scheme 2).[6,7]

The ratio of diastereoisomers in solution also varies as a function of the lanthanide ion. For the (*RRRR*) isomer, the ratio of the twisted (m) to the regular (M) square-antiprismatic complex was measured by ^{1}H NMR spectroscopy[7] to be4:1 for Eu and 1.5:1 for Tb.

The aqua ions and simple lanthanide salts are toxic for human use. Consequently, lanthanide ions are complexed

[a] GRECI, Université de Reims Champagne-Ardenne,
B. P. 1039, 51687 Reims Cedex 2, France
Fax: (internat.) + 33-3/26913243
E-mail: jean.rimbault@univ-reims.fr
[b] Laboratoire de Chimie Théorique et des Matériaux Hybrides, UPR 5401 CNRS, Ecole Normale Supérieure de Lyon, 69364 Lyon Cedex 07, France
[c] Centre de Recherche Guerbet
Guerbet, B. P. 50400, 95943 Roissy CdG Cedex, France

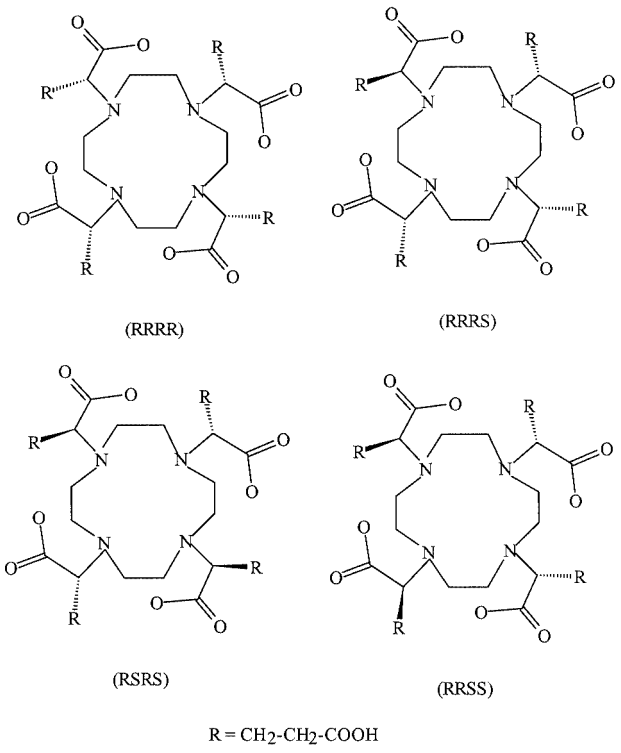

Scheme 1

in order to improve their safety and the toxicity of the lanthanide complexes is related to their stability in vivo. A high thermodynamic stability, slow kinetics, and an inertness to transmetallation, limit the dissociation of these complexes.[8,9]

Some preliminary results on transmetallation and on the stability of Gd-P730 have recently been published.[10] In this paper, we report on the thermodynamic parameters that result from potentiometric measurements performed on the complexes formed after slow complexation reactions (2−3 weeks at 40 °C) between racemic solutions of P730 and the three ions Eu^{3+}, Gd^{3+} and Tb^{3+}. The determination of the logarithms of the protonation constants, a preliminary and indispensable step, leads to the assignment of the log K_h values to the different acidic groups borne by the ligand. The mechanism of complexation of the lanthanide ions proceeds through different stages, leading to the rapid formation of metastable intermediate species, whose formation constants were also calculated.

Results and Discussion

Ligand Protonation Studies in Solution

P730 (LH_8) has 12 potential sites of protonation and, consequently, of complexation: 8 carboxylic groups and 4 tertiary ammonium groups of the macrocycle. The solubility of the neutral ligand is low, close to 10^{-3} mol·L^{-1}. The saturated racemic solution contains 70% of the neutral species LH_8 and also the minor anions LH_7^- (20%) and LH_6^{2-} (10%).

The logarithmic values of the overall protonation constants and of the corresponding successive protonation constants for DOTA and ligand P730, determined in 0.1 mol·L^{-1} Me_4NCl at 25 ± 0.1 °C from the data of 10 titrations, are listed in Table 1. An example of a titration curve is shown in Figure 1.

The protonation sequence of L^{8-} is similar that for the DOTA ligand, which was clearly evidenced by means of NMR spectroscopic studies in solution[11](Table 1). The first two protons are probably bound to two nitrogen atoms of the macrocycle (β_{011}, β_{012}) (see Scheme 1); the next four may correspond to the protonation of the external carboxylate groups [COOH(3): β_{013}, β_{014}, β_{015}, β_{016}]; at pH values < 4, the two central carboxylate groups bound to the tertiary amines are protonated [COOH(2): β_{017}, β_{018}] before the carboxylate group bound to a quaternary ammonium ion in a more acidic medium [COOH(1): β_{019}] (Scheme 3).

In the pH range 3.2−6.5, the titration curve shows a progressive increase similar to that observed with the polycarboxylic acids, which corresponds to the successive and simultaneous neutralisations of the seven carboxylic groups (see Figure 1).

Lanthanide Complexation in Solution

Preliminary tests showed that complexation of the three lanthanides with the ligand proceeds through at least two steps with very different reaction rates.

Formation of Intermediate Species

Figure 1 shows the titration curves obtained 1 h after the mixing of equal volumes of solutions of ligand and metal ion at the same concentrations of approximately 5×10^{-4} mol·L^{-1}. The waiting time between each addition of Me_4NOH is the only variable parameter. The time period is between 0.1 and 30 min. A decrease in pH, accompanying complexation, is observed between the titration curve of the ligand alone and the curves of the solutions that also contain Gd^{3+} at the same concentration.

This set of curves is composed of three parts:

pH range from 3.2 to 5.5, equiv. of OH^- from 0 to 5: The titration curves are well superimposed; the pH values are independent of the waiting time between the additions of base. Protonated metastable complexes are formed during the first and fast kinetic step (less than 30 min). Their notable stability allows the determination of their formation constants.

pH range from 5.5 to 11, equiv. OH^- from 5 to 10: The number and the position of the equivalence points are functions of the waiting time between the additions of base. For short waiting times (0.1−2 min), two equivalence points corresponding to 6 and 8 OH^- equiv. are observed. For longer times, such as 30 min, a single equivalence point remains for 7 OH^- equiv.. This pH range corresponds to the

 © 2003 Wiley-VCH Verlag GmbH & Co. KGaA, Weinheim

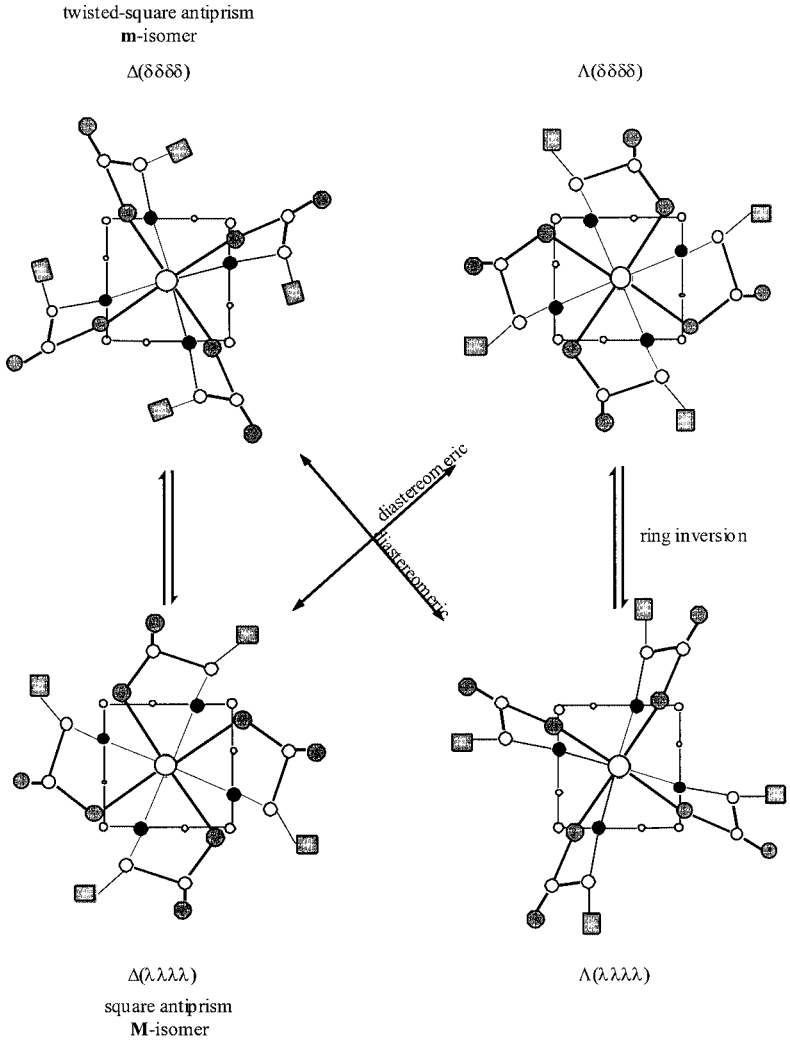

Scheme 2. Shaded squares represent alkyl groups; capped coordinated water molecule has been omitted for clarity

Table 1. Logarithmic values of the overall protonation constants and of the corresponding successive protonation constants for P730 and DOTA (0.1 mol·L^{-1} Me_4NCl; 25 ± 0.1 °C); values in parentheses represent 1 σ standard deviation; $\beta_{01h} = \prod_{1}^{h} K_i$ and log K_h refer to the equilibrium $LH_{h-1} + H^+ \rightleftarrows LH_h$

Logarithms of the overall protonation constants P730	Logarithms of the successive protonation constants P730	Logarithms of the successive protonation constants DOTA[12]	Function
log β_{011} = 12.22(11)	log K_1 = 12.22(11)	log K_1 = 11.45(2)	NH^+
log β_{012} = 21.40(14)	log K_2 = 9.18(4)	log K_2 = 9.64(1)	NH^+
log β_{013} = 27.69(15)	log K_3 = 6.29(3)	−	COOH(3)
log β_{014} = 33.38(15)	log K_4 = 5.69(3)	−	COOH(3)
log β_{015} = 38.42(16)	log K_5 = 5.04(5)	−	COOH(3)
log β_{016} = 43.22(16)	log K_6 = 4.80(5)	−	COOH(3)
log β_{017} = 47.39(16)	log K_7 = 4.17(5)	log K_3 = 4.60(1)	COOH(2)
log β_{018} = 51.32(16)	log K_8 = 3.93(3)	log K_4 = 4.11(1)	COOH(2)
log β_{019} = 54.20(16)	log K_9 = 2.88(2)	log K_5 = 2.29(2)	COOH(1)
−	log K_{10} < 2	log K_6 < 2	COOH(1)

neutralisation of one or two protons bound to nitrogen atoms (the complexation increases the acidity of these protons). These observations indicate the existence of several reaction mechanisms that lead to the formation of unstable species and to significant rearrangements of the macrocyclic ring.

 © 2003 Wiley-VCH Verlag GmbH & Co. KGaA, Weinheim

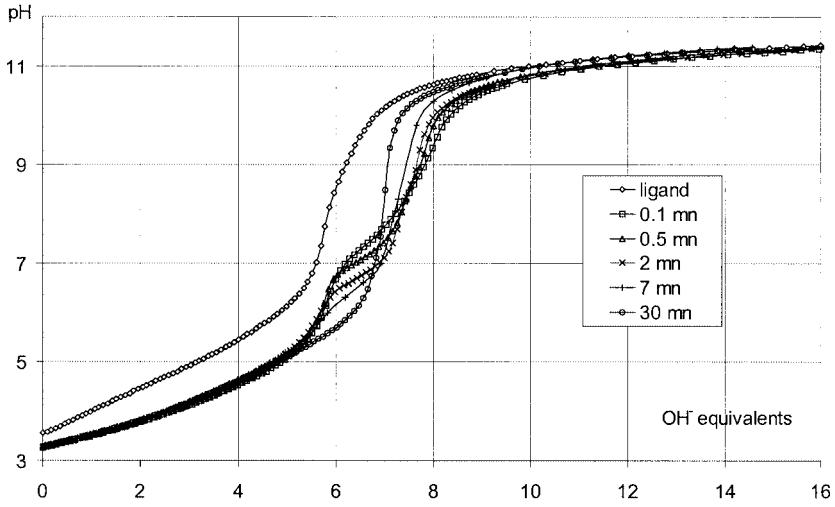

Figure 1. Titration curves of equimolar solutions of P730 and Gd^{3+} (5×10^{-4} mol·L^{-1}) (25 °C, 0.1 mol·L^{-1} Me_4NCl); the upper curve corresponds to the titration of P730 alone; the waiting times values between two successive additions of base vary from 0.1 to 30 min

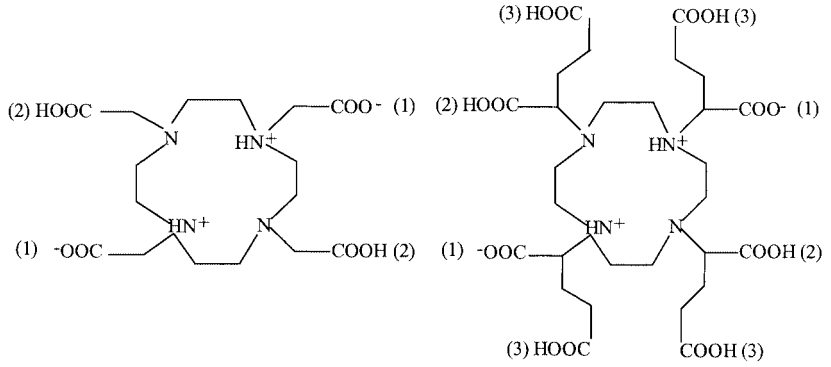

Scheme 3

pH > 11: All the curves are similar to those of the ligand.

A quantitative study is realised from the data of the first part of the titration curves, which corresponds to the formation of metastable complex species (also called intermediate complexes) with a life-time greater than 30 min. The results obtained for the three lanthanides are listed in Table 2.

The logarithms of the overall constants that correspond to the three intermediate Ln^{3+}/P730 systems are very close and follow the general trend Eu > Gd > Tb. The log K_{mh}* values correspond to the protonation of the central ($[MLH_7]^{2+}$*) or external (from $[MLH_6]^{+}$* to $[MLH_3]^{2-}$*) carboxylate groups. These values are indeed lower than those of the ligand. Figure 2 shows the variations of log K

Table 2. Logarithmic values of the overall formation constants β_{mlh}* and of the corresponding successive protonation constants K_{mh}* of the intermediate species MLH_h* (0.1 mol·L^{-1} Me_4NCl; 25 ± 0.1 °C); values in parentheses represent 1 σ standard deviation; log K_{mh}* refers to the equilibrium MLH_{h-1}* + $H^+ \rightleftarrows MLH_h$*

Species	log β_{mlh}*			log K_{mh}*		
	Eu	Gd	Tb	Eu	Gd	Tb
$[MLH_2]^{3-}$*	30.94(2)	30.30(6)	30.25(4)	–	–	–
$[MLH_3]^{2-}$*	36.15(3)	35.77(3)	35.62(4)	5.21(4)	5.46(8)	5.37(6)
$[MLH_4]^{-}$*	40.77(2)	40.36(3)	40.31(2)	4.62(4)	4.60(6)	4.70(5)
$[MLH_5]$*	45.02(3)	44.74(3)	44.59(4)	4.25(4)	4.38(5)	4.27(5)
$[MLH_6]^{+}$*	48.63(2)	48.37(2)	48.31(2)	3.62(4)	3.63(4)	3.72(5)
$[MLH_7]^{2+}$*	51.89(5)	51.70(4)	51.35(10)	3.26(5)	3.34(5)	3.04(11)

 © 2003 Wiley-VCH Verlag GmbH & Co. KGaA, Weinheim

versus the number of protonated carboxylates *h* in the case of the ligand P730 alone and of the intermediate gadolinium complexes. The maximum difference is observed at $h = 2$ and 4 ($\Delta\log K = 1.1$ and 1.2, respectively). This indicates notable interactions, maybe the formation of bonds or a network of hydrogen bonds, between two external carboxylate groups and the lanthanide ions.

Formation of Thermodynamically Stable Species

The determination of the stability of the final, stable complexes was done using batch solutions of variable pH.[8,9] Table 3 shows the logarithms of the overall formation constants and of the successive protonation constants.

The values of log β_{mlh} show little variation when the nature of the metal ion changes: the differences observed are of the same order as the calculated standard deviations. The values of log K_{mh} of the external carboxylate groups, from $[MLH]^{4-}$ to $[MLH_4]^{-}$, are only 0.2−0.5 pH units lower than the corresponding ligand log K_h values (see Figure 2). Obviously, these groups are not directly involved in the formation of bonds with the lanthanide ion. The complex $[Gd(P730)]^{5-}$ has a high thermodynamic stability (log $\beta_{110} = 24.03$) as the complex $[Gd(DOTA)]^{-}$ (in Me_4NCl 0.1 mol·L^{-1}, at 25 °C: log $\beta_{110} = 25.58$,[12] 25.30,[13] 24.70,[14] 24.0,[15] 24.67,[9] 25.4,[16] 27.0[17]).

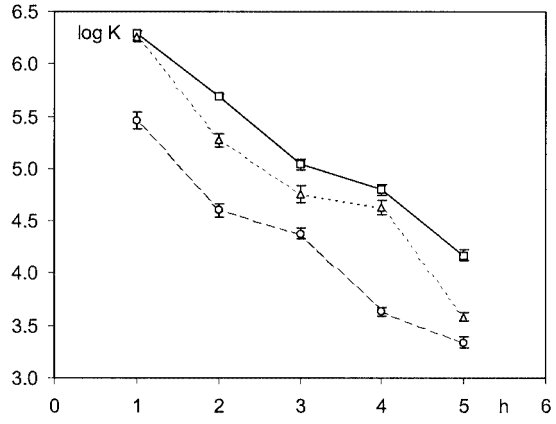

Figure 2. Variation of the logarithms of the successive protonation constants of the carboxylates versus the number of protons *h* in the case of the gadolinium (external carboxylates $h = 1-4$, central carboxylate $h = 5$); squares: ligand P730 (log K_h); circles: intermediate species (log K_{mh}*); triangles: thermodynamically stable species (log K_{mh})

Luminescence Measurements

Horrocks et al.[18,19] have established from experimental results obtained from solid lanthanide complexes that the rate of de-excitation is, to a good approximation, directly proportional to the number of OH oscillators in the first coordination sphere. More recently, an improved approach[20] including other oscillators has shown that, in solution, the intramolecular transfer of energy to the unbound water molecules constitute a significant term in the overall quenching effect. However, this improved approach has also proposed the use of empirical corrections subject to an error of around 25%. A more pragmatic process is to consider that the decay constants determined for Eu^{3+} or Tb^{3+} in D_2O/H_2O mixtures integrate the quenching of water molecules in the first and outer spheres.

The following equation describes the best least-squares lines through the experimental data Δk versus the molar fraction of H_2O in D_2O/H_2O mixtures containing low concentrations of europium or terbium chloride or P730 complexes: $Q = A^*_{Ln}\cdot(k_{H2O} - k_{D2O}) = A^*_{Ln}\cdot\Delta k$. A^*_{Ln} integrates the overall contribution of the vibronic quenching of the OH oscillators, Δk is the slope of the mean straight line, and *q* the hydration number. The values of A^*_{Ln} are calculated by using the hydration numbers determined from EXAFS data[21,22] [8 and 9 for (aquo)terbium and -europium complexes, respectively]. For europium, $A^*_{Eu} = 1.05 \pm 0.02$ ms ($k_{H2O} = 8.77$ ms^{-1}; $k_{D2O} = 0.17$ ms^{-1}) and for terbium, $A^*_{Tb} = 4.86 \pm 0.12$ ms ($k_{H2O} = 2.52$ ms^{-1}; $k_{D2O} = 0.88$ ms^{-1}).

To determine the mean hydration number of the final stable species, racemic solutions of ratio Ln/P730 = 1 were prepared one month before the measurements. The values obtained under these conditions represent a concentration-weighted average of the *q* values of each isomeric species. The results obtained by Woods et al.[7] from solutions of 4 of the 6 pure Eu-P730 stereoisomers correspond to *q* values near to unity in agreement with our average value of *q*(Eu-P730) = 1.04 ± 0.12 ($k_{H2O} = 1.66$ ms^{-1}; $k_{D2O} = 0.67$ ms^{-1}) [Eu-P730 stereoisomers: *q*(*RRRR*) = 1.06; *q*(*RRRS*) = 1.01; *q*(*RRSS*) = 0.92; *q*(*RSRS*) = 1.02]. A notable discrepancy is observed between the corresponding results ob-

Table 3. Logarithmic values of the overall formation constants β_{mlh} and of the corresponding successive protonation constants K_{mh} of the thermodynamically stable species MLH_h (0.1 mol·L^{-1} Me_4NCl; 25 ± 0.1 °C); values in parentheses represent 1 σ standard deviation; log K_{mh} refers to the equilibrium $MLH_{h-1} + H^+ \rightleftarrows MLH_h$

Species	log β_{mlh}			log K_{mh}		
	Eu	Gd	Tb	Eu	Gd	Tb
$[ML]^{5-}$	24.01(5)	24.03(13)	23.97(7)	–	–	–
$[MLH]^{4-}$	29.98(5)	30.28(13)	30.13(6)	5.97(5)	6.26(5)	6.16(6)
$[MLH_2]^{3-}$	35.14(5)	35.55(12)	35.32(6)	5.16(7)	5.27(6)	5.19(7)
$[MLH_3]^{2-}$	40.00(6)	40.31(14)	40.07(7)	4.86(8)	4.76(8)	4.75(9)
$[MLH_4]^{-}$	44.51(3)	44.94(11)	44.62(4)	4.51(6)	4.63(7)	4.54(7)
$[MLH_5]$	47.94(4)	48.52(13)	48.31(5)	3.44(3)	3.58(4)	3.70(4)

 © 2003 Wiley-VCH Verlag GmbH & Co. KGaA, Weinheim

tained with the isomers of Tb-P730[7] [Tb-P730 stereoisomers: $q(RRRR) = 0.60$; $q(RRRS) = 0.75$; $q(RRSS) = 1.00$; $q(RSRS) = 0.95$]. Our result obtained from the mixture of the conformers, q(Tb-P730) = 0.96 ± 0.06 (k_{H2O} = 0.46 ms^{-1}; k_{D2O} = 0.27 ms^{-1}), seems to point out that the isomers (*RRRR*) and (*RRRS*) are minor species.

In order to understand the mechanism of formation of the intermediate species formed between europium and the ligand, the mean number of water molecules coordinated to the metal atom was determined under various experimental conditions. The measurements of luminescence were carried out with three series of solutions of ratio P730/Eu^{3+} equal to 10 ([P730] = 10^{-3} mol·L^{-1}), to minimise the concentration of free metal ions at low pH values (Table 4).

Table 4. Experimental and calculated values of q; $q_{calcd.}$ (1): values of q calculated from the first hypothesis; $q_{calcd.}$ (2): values of q calculated from the second hypothesis; percentages of Eu^{3+} for each species (P730/Eu^{3+} = 10; [P730] = 10^{-3} mol·L^{-1}), pH = 3.46: Eu^{3+} 8.1; $[EuLH_7(OH_2)_5]^{2+}$* 0.7; $[EuLH_6(OH_2)_5]^{+}$* 43.1; $[EuLH_5(OH_2)_4]$* 43.9; $[EuLH_4(OH_2)_3]^{-}$* 3.9; $[EuLH_3(OH_2)_3]^{2-}$* 0.4; $[EuLH_2(OH_2)_3]^{3-}$* 0.0. pH = 4.87: Eu^{3+} 0.0; $[EuLH_7(OH_2)_5]^{2+}$* 0.0; $[EuLH_6(OH_2)_5]^{+}$* 0.4; $[EuLH_5(OH_2)_4]$* 10.1; $[EuLH_4(OH_2)_3]^{-}$* 22.8; $[EuLH_3(OH_2)_3]^{2-}$* 56.9; $[EuLH_2(OH_2)_3]^{3-}$* 9.8 (the numbers of molecules of water in the formula correspond to the second hypothesis)

pH	Waiting time	q_{exp}	$q_{calcd.}$ (1)	$q_{calcd.}$ (2)
3.46	none	4.6 ± 0.4	5.32	4.80
3.46	1 h	4.5 ± 0.3	5.32	4.80
4.87	1 h	2.8 ± 0.5	5.00	3.11

The q_{exp} value is a concentration-weighted average of the q values of all the intermediate species and of the (aquo)europium ion bound to 9 molecules of water. Two hypotheses for the intermediate complexes were used to simulate these experimental results. In the first hypothesis, the europium ion is bound only by the 4 central carboxylate groups and 5 water molecules, whatever the pH value and the corresponding deprotonated external carboxylate groups. Second hypothesis: the metal ion is bound by the 4 central carboxylate groups, 1 then 2 external carboxylate groups and 4 then 3 molecules of water according to the pH value. This hypothesis is relevant to the results of the potentiometric study, which points out notable interactions between the external carboxylate group and the lanthanide ion. In this case, the number of water molecules coordinated varied for each one of the protonated species: $[EuLH_7(OH_2)_5]^{2+}$*; $[EuLH_6(OH_2)_5]^{+}$*; $[EuLH_5(OH_2)_4]$*; $[EuLH_4(OH_2)_3]^{-}$*; $[EuLH_3(OH_2)_3]^{2-}$*; $[EuLH_2(OH_2)_3]^{3-}$*. The percentages of Eu^{3+} corresponding to each intermediate complex and to the free ion were calculated, from the concentrations of the reactant using the protonation constants and the stability constants, for each solution that was studied (Table 4).

The calculated values of q corresponding to the possible formation of a bond between the external carboxylate group and the metal ion are in good agreement with the experimental mean results. The similarity of the values of q obtained at pH = 3.46 immediately after preparation of the solutions and after waiting 1 h allows the exclusion of the formation of Eu−N bonds, which correspond to a slow kinetic step.

These results are consistent with the fast formation at a pH near 3.5 of an intermediate complex where the metal atom is bound to the 4 central carboxylate groups of the ligand and to 5 molecules of water. At a pH of around 5, the external carboxylic functions are neutralised which allows the formation of 2 transitory carboxylate bonds and reduces the number of coordinated molecules of water to 3.

EXAFS Measurements

EXAFS experiments were carried out on solutions of the final, stable complex formed with each lanthanide. The environment of the nine-coordinate metal ion was specified and the mean distances corresponding to each type of bond metal atom−coordinated atom determined. An additional experiment enabled the environment of the Gd^{3+} ion in a metastable intermediate complex to be specified.

The number and postulated nature of neighbours, the absorber−neighbour distances, and the Debye−Waller factors resulting from the EXAFS fitting procedure are summarised in Table 5. All four complexes have been fitted considering only single scattering paths.

The k^3-weighted EXAFS spectra and the Fourier transforms of solutions of Ln-P730 final complexes are displayed in Figure 3. Absorptions were collected at k = 12.5 $Å^{-1}$, resulting in a good resolution of peaks in the Fourier transforms. The similarity of the experimental $k\chi(k)$ values and their corresponding Fourier transforms allows us to assume that the local structure of the Ln^{3+} ions is almost the same for the three compounds, the slight differences being attributed to the Ln-P730 distance, which reflects the small ionic radius change from the Eu to the Tb ion. In particular, the amplitudes of the EXAFS oscillations appear almost unchanged. Then, there is the same number of nearest neighbours in the three compounds. In fact, Fourier transforms comprise three main peaks: the first one located at 1.2−2.1 Å (peak 1, Figure 3) corresponds to five oxygen atoms, four from the carboxylic moieties and one from a water molecule, the second one located at 2.1−2.6 Å (peak 2) corresponds to the four nitrogen atoms from the macrocyclic cavity, and the third one located at 2.6−3.4 Å is divided into two components, which correspond to the carbon atoms that belong to the macrocyclic cavity (peak 3′) and to the chains that contain the carboxylic groups (peak 3). Within the frame of the single-scattering approach, we analysed the first three coordination spheres. An additional signal is present at a distance between 3.8 and 5.0 Å for the three complexes. This signal is assigned to the multiple scattering signals on the basis of a previous investigation concerning the compound $[Gd(DOTA)]^{-}$,[22] which is confirmed by the multiple scattering paths obtained by FEFF calculations.[46]

The data available in Table 5 confirms the above qualitative discussion. Within the single-scattering approach, the lanthanide ions are surrounded by the four neighbouring nitrogen atoms of the macrocyclic cavity with an average

 © 2003 Wiley-VCH Verlag GmbH & Co. KGaA, Weinheim

Table 5. First coordination shell structural data obtained from *R*-space fits of EXAFS spectra; *N* number of neighbours, *R* absorber−neighbour distance, σ Debye−Waller factor; uncertainties are estimated in coordination numbers to ± 10%, in *R* to ± 0.02 Å, and in σ^2 to ± 0.001 $Å^2$

	Ln−O (COOH)			Ln−O (H_2O)			Ln−N		
	N	*R* [Å]	σ^2 [$Å^2$]N	*R* [Å]	σ^2 [$Å^2$]	N	*R* [Å]	σ^2 [$Å^2$]
$[Eu(P730)]^{5-}$	3.92	2.37	0.002 0.96	2.51	0.007	4.04	2.70	0.005
$[Gd(P730)]^{5-}$	4.32	2.38	0.002 1.22	2.44	0.010	4.12	2.68	0.001
$[Tb(P730)]^{5-}$	3.91	2.36	0.007 1.04	2.50	0.010	4.20	2.65	0.009
$[Gd(P730)H_n]^{(5-n)-}$* intermediate	4.07	2.40	0.009 4.98	2.42	0.010	–	–	–

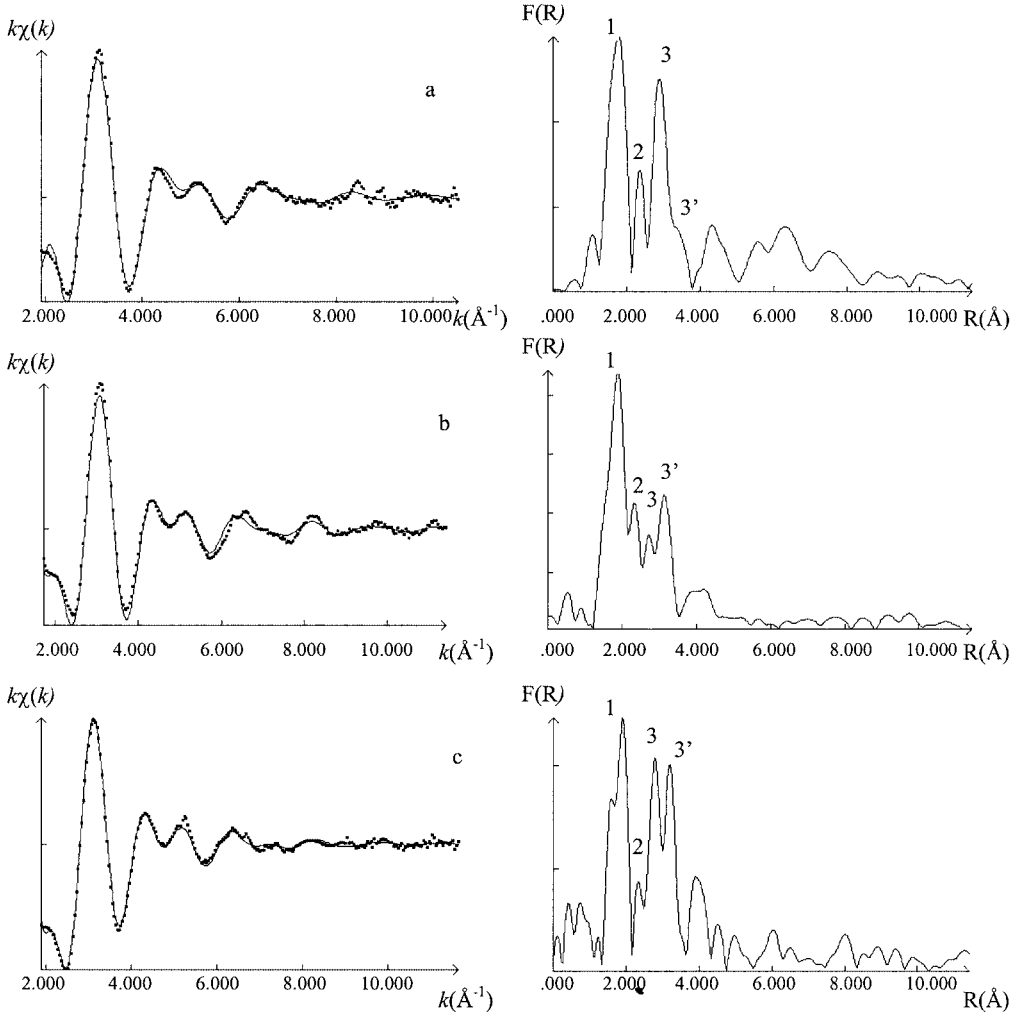

Figure 3. k^3-weighted EXAFS and the corresponding Fourier transforms of solutions containing [P730] = 0.11 mol·L^{-1} and (a) Eu^{3+} = 0.10 mol·L^{-1}, (b) Gd^{3+} = 0.10 mol·L^{-1}, and (c) Tb^{3+} = 0.10 mol·L^{-1} (stable complexes); the Fourier transforms are uncorrected for phase shift; continuous lines represent the models presented in Table 5

Ln−N bond length of 2.68 Å. The decrease of the absorber−coordinated atom distances Ln−N (Eu^{3+} > Gd^{3+} > Tb^{3+}) is in accordance with the slight decrease in ionic radius from the Eu^{3+} to the Tb^{3+} ion.

The absorber ions are also surrounded by four oxygen atoms (carboxylate) with an average Ln−O distance of 2.37 Å. A molecule of water completes the coordination sphere of the three lanthanides. The data are coherent with an EXAFS study of Gd(DOTA) which confirmed that the local environments of the Gd^{3+} centre are similar in solution and in crystals.[7] The Gd−OH_2 distance is in good agreement with the preceding result (2.44 Å), but the bond lengths corresponding to the Eu and Tb complexes are distinctly higher (Eu: 2.51 Å; Tb: 2.50 Å). This could be explained by the fact that water molecules form relatively weak and labile bonds with the lanthanide ions, which gives rise to a

 © 2003 Wiley-VCH Verlag GmbH & Co. KGaA, Weinheim

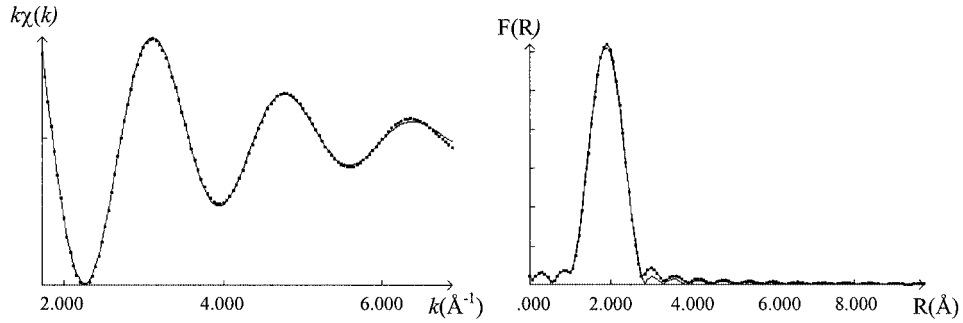

Figure 4. k^3-weighted EXAFS and the corresponding Fourier transform of the first coordination shell of a solution of the intermediate $[Gd(P730)H_n]^{(5-n)-}$* complexes; $[Gd^{3+}] = 9\times10^{-4}$ mol·L^{-1}, [P730] = 9.9×10^{-4} mol·L^{-1}

higher thermal disorder, compared to those of Ln−N or Ln−O (carboxylic), which is in accordance with a fast exchange. Moreover, the two oxygen contributions (carboxylic moieties and water molecules) are difficult to isolate due to their same scattering behaviour. These two phenomena (thermal disorder and scattering behaviour) lead to these relatively unexpected Ln−OH_2 distances.

In accordance with potentiometric studies, an intermediate gadolinium complex has been underlined. Indeed, the radial distribution function of Gd-P730 at 10 °C presents only one main peak located at 1.2−2.6 Å, which corresponds to oxygen atoms from carboxylic groups and water molecules. The k^3-weighted EXAFS, the corresponding Fourier transform, and the fitted curves of the filtered first shell of a solution of the intermediate Gd-P730 species are shown in Figure 4.

The numerical values obtained (Table 5) are in agreement with the main species of a monocapped square-antiprism geometry around the gadolinium centre with four oxygen atoms of carboxylic moieties at 2.40 Å, and five water molecules at 2.42 Å. These results are confirmed by ab initio calculations, which show a relatively stable $[GdLH_6(OH_2)_5]^+$* species with a mean Gd−O(COOH) distance equal to 2.40 Å (see Table 6).

Quantum Chemical Investigation

Quantum calculations were carried out in order to propose a mechanism for the insertion of the lanthanide ion into the ligand. All the complexes optimised by means of ab initio calculations are pictured on Figure 5 (monocapped square-antiprism geometry).The main geometrical parameters computed for these complexes are gathered in Table 6. Ab initio energies computed at the RHF level are reported in Table 7.

In this study, three different complexes {$[GdLH_6(OH_2)_5]^+$*, $[GdLH_4(OH_2)_3]^-$* and $[GdLH_4(OH_2)]^-$} have been found on the potential energy surface (see Figure 5).

The localisation of these complexes allows us to propose a mechanism for the insertion of the gadolinium atom into the ligand. At first, an initial $[GdLH_6(OH_2)_5]^+$* compound is formed in acidic solution. It is a nine-coordinate compound with five water molecules and four central carboxylate oxygen atoms linked to the gadolinium ion. When the pH increases, this complex evolves into the intermediate $[GdLH_4(OH_2)_3]^-$* complex by deprotonation of two external carboxylate groups. These two new carboxylate extremities replace two water molecules for the complexation

Table 6. Main geometrical parameters of experimental (**bold**) and RHF/3-21G (plain) structures of all the complexes optimised in this study; distances are given in Å and angles in °; Φ: twist angle between P_O and P_N planes

Parameter	$[GdLH_6(OH_2)_5]^+$*	$[GdLH_4(OH_2)_3]^-$*	$[GdLH_4(OH_2)]^-$ (*SSSS*)	$[GdLH_4(OH_2)]^-$ (*RRRR*)	**$[GdLH_4(OH_2)]^-$ (*SSSS*)**[a]
Gd−N	4.751	4.396	2.742	2.806	2.67(3)
Gd-*N*-H	4.791	4.349			
Gd−O $_W$up	2.403	2.445	2.400	2.390	2.432
Gd−O $_W$	2.503/2.540	2.508			
Gd−O cent	2.423/2.385	2.506/2.442	2.341	2.325	2.38(2)
Gd−O ext		2.410			
O1−Gd−O2		79.3	85.7	85.7	85.8
O1−Gd−O3			149.3	149.2	144.9
N−C−C−N[b]	−57.3	−61.6	−57.6	−64.2	−59.5(1.4)
Φ			39.8	34.9	38.5
Gd/O plane			0.638	0.635	0.679
Gd/N plane	4.274	3.776	1.705	1.764	

[a] Mean experimental values;[7] standard deviation in parentheses. [b] Torsion angle (for the two intermediate species: N1−C−C−N2)

 © 2003 Wiley-VCH Verlag GmbH & Co. KGaA, Weinheim

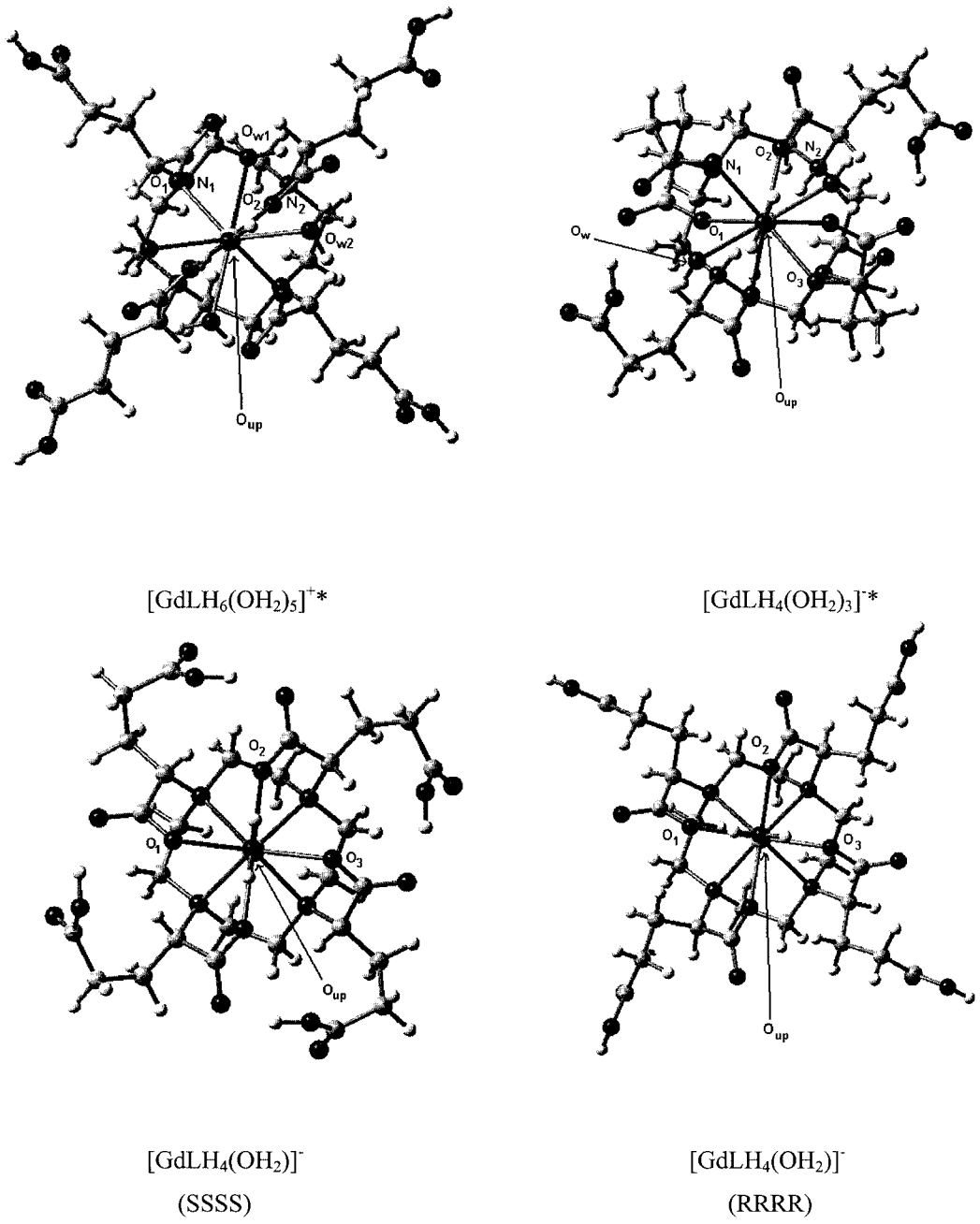

Figure 5. Representation of the three different types of complexes studied theoretically

Table 7. Absolute ab initio energies [Hartree] of all the complexes considered in this study; relative energies between the two (*RRRR*) and (*SSSS*) conformers of the final complex are also reported [kcal/mol]

	$[GdLH_6(OH_2)_5]^{+}$*	$[GdLH_4(OH_2)_3]^{-}$*	$[GdLH_4(OH_2)]^{-}$ (*SSSS*)	$[GdLH_4(OH_2)]^{-}$ (*RRRR*)
RHF/3-21G//RHF/3-21G[a]	−2900.4316609	−2748.18704751	−2597.0289135	−2596.9456351
ΔE			0.0	52.3
RHF/6-31G(d)//RHF/3-21G	−2916.1898152	−2763.0949023	−2611.1539792	−2611.1217399
ΔE			0.0	20.2

[a] See text for a definition of all the acronyms. The X//Y notation means that the energy has been computed at the X level of theory for a structure optimised at the Y level of theory.

 © 2003 Wiley-VCH Verlag GmbH & Co. KGaA, Weinheim

of Gd^{3+}. We also tried to optimise another intermediate complex $[GdLH_2(OH_2)]^{-}$* in which the four external carboxylates of the initial complex were deprotonated. However, the existence of such a compound cannot be put forward since we did not succeed in optimising it. Finally, we suggest that the $[GdLH_4(OH_2)_3]^{-}$* complex evolves to a final $[GdLH_4(OH_2)]^{-}$ one by deprotonation of the two nitrogen atoms and reprotonation of the two external carboxylate moieties. The calculation of the distances between the Gd atom and the plane defined by the four nitrogen atoms in these three successive complexes indicates that the gadolinium ion moves more and more into the plane of the ligand as the reaction path proceeds (see Table 6). However, the difference is much less marked from the initial to the intermediate complex (4.274 vs. 3.776 Å) than from the intermediate complex to the final complex (3.776 vs. 1.7−1.8 Å).

For the final $[GdLH_4(OH_2)]^{-}$ complex, two conformers (*RRRR*) and (*SSSS*) in a diastereoisomeric relationship have been optimised in monocapped square-antiprism geometry. Relative energies computed at the RHF/3-21G level show that the (*SSSS*) conformer is more stable than the (*RRRR*) one by 52.3 kcal/mol (see Table 7). It must be pointed out that the energy difference between the two conformers greatly decreases at the RHF/6-31G(d) level (20.2 kcal/mol). This underlines that it is necessary to employ an extended basis set to obtain reliable energies. The main geometrical parameters of the (*SSSS*) species have been reported in Table 6 and compared with an available crystallographic structure recently obtained by Woods et al.[7] Our calculations give Gd−O bonds that are too short and Gd−N bonds that are too long. These results are in line with those found in the case of other gadolinium complexes with similar ligands (DOTA or DOTMA).[23] These two parameters could be corrected by the use of a more extended basis set and the inclusion of the solvent by means of a continuous model[24] but such a calculation would be too time-consuming. Nevertheless, the overall agreement between experimental and theoretical data is good since the average deviation is only 0.05 Å for the distances and 2.2° for the angles. This confirms that the RHF/3-21G method was a good choice to investigate such a compound and allowed us to use this method confidently in order to optimise other complexes. The geometry of the (*RRRR*) has also been reported. The comparison with (*SSSS*) results reveals that the main structural parameters are quite similar in the two conformers. The principal difference comes from the lengthening of the Gd−N bonds in the (*RRRR*) conformer (2.806 vs. 2.742 Å). In the latter, the gadolinium atom is therefore slightly further from the ligand. This is confirmed by the calculation of the distance between this atom and the plane formed by the four nitrogen atoms.

Conclusion

The aim of the magnetic resonance imaging contrast agents is to affect the nuclear magnetic relaxation times of the water protons, increasing the contrast between normal and diseased tissues. Interpreting relaxivity data requires a detailed knowledge of the structures of the complexes in solution. This data does not necessarily correspond to the crystal data because of the lability of these species. The determination of the luminescence decay constants of the lanthanide complexes seems to provide a direct measure of the number of water molecules bound to the metal atom. However, some non-integral values have been interpreted as the result of either a mixture of eight and nine coordinated species, or of a significant contribution of the second-sphere of hydration, or the occurrence of a elongated $Ln-OH_2$ bond. In the present work, the EXAFS data agrees well with the results obtained from the luminescence study ($q \approx 1$); moreover, these results do not show the interaction of the second sphere of hydration and gives reasonable $Ln-OH_2$ bond-length values. An additional EXAFS recording at 10 °C immediately after the preparation of the solution has shown the formation of an intermediate pentahydrate species coordinated to the four central carboxylate groups. The thermodynamic data determined from the potentiometric titrations corresponding to the formation of metastable intermediate complexes indicates strong interactions between two central carboxylate groups and the metal ion. The luminescence measurements confirm the evolution of the number of water molecules coordinated to the lanthanide ion versus time; moreover, they show unambiguously the formation of transitory bonds between the metal ion and one or two external carboxylate groups, which explains the unusual stability of the intermediate complexes. These experimental results as a whole are fully compatible with the complexation mechanism suggested by the quantum chemical investigation.

This whole study allows us to determine the complexation mechanism, in solution, of the lanthanides Gd^{3+}, Eu^{3+}, and Tb^{3+} by the ligand P730. This mechanism is the same for the three lanthanides. Whereas fluorescence experiments were carried out on the europium and terbium complexes, EXAFS was performed on the complexes of the three lanthanides, and the modelling on the gadolinium complexes.

The first step consists of the formation of the species $[LnLH_6(OH_2)_5]^{+}$*, which is presented in Scheme 4.

This complex forms very rapidly, starting at pH = 3.2, in equimolar solutions of Ln^{3+} and P730. In this complex, the four central carboxylic oxygen atoms are bound to the lanthanide atom; the coordination of 9 is ensured by 5 molecules of water. Therefore, the nitrogen atoms, two of which are protonated, do not take part in the complexation. The number of water molecules is characterised by fluorescence and EXAFS experiments, and theoretical calculations predict a stable structure. This complex can be found in solution under the form $[LnLH_6(OH_2)_5]^{+}$* presented above, as well as under the form $[LnLH_7(OH_2)_5]^{2+}$*. The latter species has an additional proton, whose log K_{mh}* is close to 3−3.5. This proton is fixed on an oxygen atom that is not bound to the lanthanide atom, and which belongs to a central carboxylic group. This assumption was put forward by

 © 2003 Wiley-VCH Verlag GmbH & Co. KGaA, Weinheim

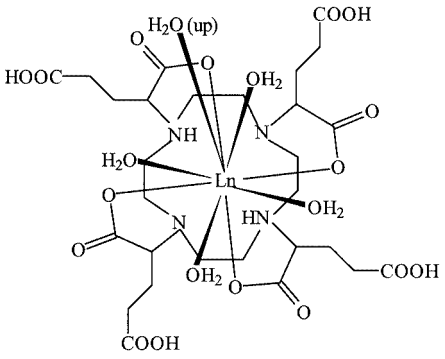

$[GdH_6L(OH_2)_5]^{+}$*

Scheme 4

Szilagyi et al.[27] in the compound Gd(HDOTA). These authors have demonstrated the position of the proton, by fluorescence, UV/Vis spectrophotometry, and NMR spectroscopy. Such a proton can also be found in the structure of the complexes Eu(HP730) in the solid state by Howard et al.[6] and Woods et al.[7]

While the pH increases from 3.2 to 5, the external carboxylic groups are gradually deprotonated. The number of water molecules bound to the lanthanide atom, calculated via fluorescence measurements, goes progressively from 5 to 3. As a result, one, then two additional oxygen atoms of the external carboxylic groups bind to form $[LnLH_5(OH_2)_3]^{2-}$* and then $[LnLH_4(OH_2)_3]^{-}$*, presented in Scheme 5.

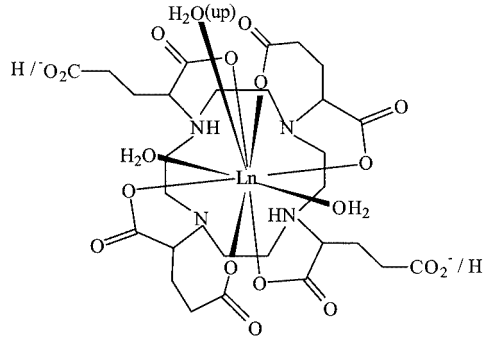

$[GdH_4L(OH_2)_3]^{-}$*

Scheme 5

These species, as well as the ones issued from the deprotonation of the external carboxylic groups $[LnLH_3(OH_2)_3]^{2-}$* and $[LnLH_2(OH_2)_3]^{3-}$*, are put in evidence by potentiometric experiments. The increase of the acidity of two carboxylic groups, shown in Figure 2 (h = 2 and 4), is in accordance with their complexation to the lanthanide. The absence of kinetics noted during these steps shows that there is no modification of the mode of complexation. The nitrogen atoms, two of which are still protonated, are not bound to the lanthanide atom. Our theoretical RHF results confirm the stability of $[GdLH_4(OH_2)_3]^{-}$*.

The coordination of the external carboxylic oxygen atoms was contemplated by Lowe et al.[28,29] in lanthanide complexes with ligands derived from P730, in which a chain $-CH(COO)-CH_2-CH_2-COOH$ linked to the nitrogen atom is replaced with a dansyl substituent.

After several weeks at ambient temperature, or 2 or 3 weeks at 40 °C, all of these compounds evolve towards a series of thermodynamically stable compounds of the formula $[LnLH_n(OH_2)]^{(5-n)-}$ with $0 \leq n \leq 5$. The kinetics corresponds to a significant modification in the nature of the coordinating atoms. The lanthanide atom, which always used to be located above the plane formed by the oxygen atoms of the central carboxylic groups, is now inserted between this plane and the one formed by the nitrogen atoms (Scheme 6).

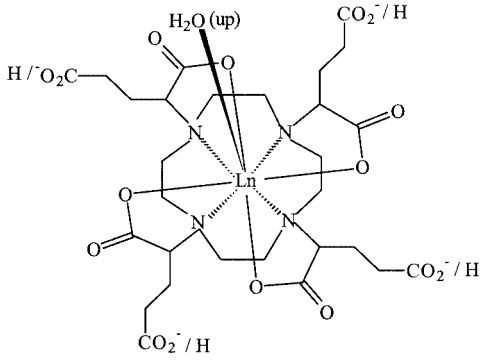

$[GdH_4L(OH_2)]^{-}$

Scheme 6

All these species are identified using potentiometric experiments. In the complex $[LnLH_4(OH_2)]^{-}$ pictured above, the four central carboxylic oxygen atoms and the four deprotonated nitrogen atoms are bound to the lanthanide atom, whereas the coordination number 9 is ensured by one water molecule. The coordinated water molecule is characterised by fluorescence and EXAFS. The latter technique also confirms the nature of the set of atoms linked to the lanthanide atom. Quantum mechanics calculations show the stability of this complex. In the complex $[LnLH_5(OH_2)]$, an additional proton (log K_{mh} close to 3.5) is fixed on the oxygen atom that is not linked to the lanthanide atom, and which belongs to a central carboxylate group.

The variations of the logarithm of the free metal ratio versus pH for the systems Gd/DOTA and Gd/P730 are drawn in Figure 6. Such a plot clearly shows the similarity in the behaviour of the two systems. At physiological pH (7.4), for the same analytical concentrations of metal ion and ligand (5×10^{-4} mol·L^{-1}), the free concentrations of gadolinium(III), in the presence of DOTA and P730, are 3.8×10^{-12} mol·L^{-1} and 3.3×10^{-11} mol·L^{-1}, respectively. These values confirm the high thermodynamic stability of

 © 2003 Wiley-VCH Verlag GmbH & Co. KGaA, Weinheim

the ligand studied, providing a potential in vivo dissociation inertness essential for medical applications.

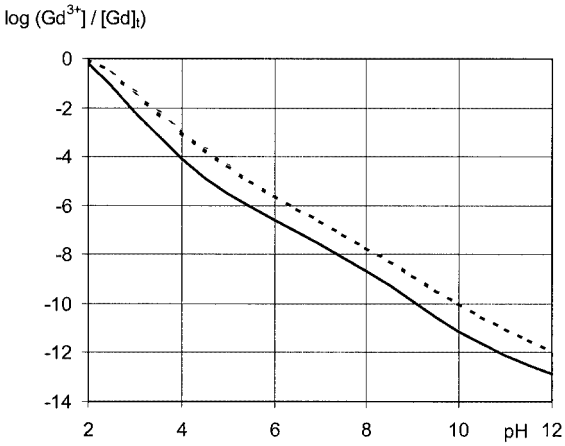

Figure 6. Variation of the logarithm of the free metal ratio versus pH; continuous line: system Gd(DOTA); dashed line: system Gd-P730

Experimental Section

Reagents: All chemicals used were of a pure analytical grade. Distilled and argon-bubbled water was used for the preparation of all solutions. Tetramethylammonium chloride (Fluka Biochemika) was used for ionic strength control in all studies. The standard solutions of the lanthanides (Eu, Gd, Tb) were prepared from trichloride hexahydrate salts (Aldrich). Their concentrations were determined by EDTA titrations using xylenol-orange indicator. Carbonate-free solutions of tetramethylammonium hydroxide (Riedel-de Haën) were used for potentiometric titrations. The ligands DOTA and P730 were a gift of Guerbet SA.

Protometric Measurements: All pH-metric measurements used in the determination of protonation and complexation constants were carried out in a thermo-regulated cell (25 ± 0.1 °C) with an argon stream over the solution to avoid the dissolution of carbon dioxide. The glass microelectrode Metrohm type T has a low alkaline error. The procedures and apparatus used for protometric measurements have been described previously.[30] Titrations of acetic acid with CO_2-free Me_4NOH allowed us to determine the ionic product of water pK_w = 13.78 (1), at 25 ± 0.1 °C in 0.1 mol·L^{-1} Me_4NCl. For each ligand, the protonation constants were determined from several experiments; DOTA: 9 titrations corresponding to 1079 pairs of data, concentration range of the ligand 10^{-3} to 3×10^{-3} mol·L^{-1} in the presence of HCl ($0 <$ [HCl]/[DOTA] < 8). P730:10 titrations corresponding to 1261 pairs of data, concentration range of the ligand 2.2×10^{-4} to 9.7×10^{-4} mol·L^{-1} in the presence of HCl ($0 <$ [HCl]/[P730] < 10.2). The complexation reactions of lanthanides with DOTA and P730 are slow at room temperature. Intermediate species formed in the first hour, after the mixing of the ligand and metal ion, transform into final and stable complexes in some weeks. Titrations performed 1 h after mixing allowed for the determination of the formation constants of the intermediate complexes. At least seven measurements (about 60 points each one) were performed for each system Ln/P730 in the pH range 3.8−6 for complexation experiments. The ligand and metal concentration were about 5×10^{-4} mol·L^{-1}, the ratio ligand/metal being slightly above 1. For each metal, in order to study the final equilibria, three or four batch experiments were performed in which 40 individual solutions, in the approximate pH range 2.8−9, corresponding to single points of conventional titrations, were stored in a thermostat at 40 ± 0.1 °C for 25 d. This time was determined from the pH of reference solutions periodically controlled to ensure the achievement of the conditions of equilibrium.

Protometric Computations: The protometric data were processed by the code Protaf[31] in order to obtain the best-fit chemical model and refined overall stability constants β_{mlh} (β_{mlh} refers to the species $M_mL_lH_h$). The program Protaf,[31] which is based on the weighted least-squares of the residues of the experimental variables (volume of titrant, pH), allows a simultaneous processing of ten titrations, each including 150 pairs of data (volume, pH).

Luminescence Measurements: The measurements were determined in D_2O/H_2O mixtures, the molar fraction of H_2O varying from a value nearing 0 to the value 1, the concentration of the lanthanide chlorides, used as references, or of the corresponding P730 complexes varying from 2×10^{-3} to 2.5×10^{-2} mol·L^{-1} in neutral or basic media. Luminescence spectra for europium and terbium complexes were recorded with a Perkin−Elmer LS50B equipped with a Hamamatsu R928 photo-multiplier and operating in time-resolved mode. Lifetimes were measured at 25 °C by excitation of the sample solution by a short pulse of light (europium species: 394 nm; terbium species: Tb^{3+} 221 nm, Tb-P730 229 nm). The emission was monitored at 616 nm for Eu^{3+} and 544 nm for Tb^{3+} using the program Lemming Ver 1.01. The gate time was 0.1 ms and the slit widths were 15 and 5 nm for Eu^{3+} and less for Tb^{3+}. The rate constants k, inverse of the lifetimes τ, are the average values from 10 series of 20−40 measurements realised for each D_2O/H_2O mixture. The luminescence decay curves were fitted by the following equation using the general curve fitting program Origin: $F = F_o\cdot\exp^{(-kt)}$. High correlation coefficients were determined. The quoted k_{D2O} values were estimated and the k_{H2O} values verified from linear extrapolation of k versus the molar fraction of H_2O.

EXAFS Study: Ln^{3+} L_3-edge spectra were recorded with the XAS4 beamline at the Laboratoire d'Utilisation du Rayonnement Electromagnétique (LURE) of the University of Paris-Sud. Standard operating conditions were a beam energy of 1.85 GeV and a mean intensity of 200−300 mA. The measurements were carried out in the transmission mode with an Si (111) channel-cut monochromator, which was de-tuned to 30% of the maximum intensity for Eu, Gd and 15% for Tb, to remove the higher-order harmonics. The detectors were low-pressure (ca. 0.2 atm) air-filled ionisation chambers. Each spectrum is the sum of three to four recordings in the range from 150 eV below to 600−700 eV above the absorption edge. Spectra were recorded using sampling steps of 2 eV with an integration time of 2.0 s per point. The EXAFS spectra at the Ln^{3+} L_3-edge were measured for the aqueous solution at room temperature at a pH around 9.0. Moreover, the intermediate Gd^{3+} complex spectra was registered at 10 °C and at a pH around 3.2 in order to slow down the kinetic formation of the final complex. The EXAFS data analysis was performed with the "EXAFS pour le Mac" and EXAFS98 programs.[32,33] The $\chi(k)$ functions were extracted from the data[34−36] with a linear pre-edge background, a combination of polynomials (of order 5) and spline atomic-absorption background, and normalised by using the Lengeler−Eisenberger method.[37] The energy threshold, E_0, was taken at the half maximum of the absorption edge. Radial distribution functions $F(R)$ were calculated by Fourier transforms of $k^3w(k)\mu(k)$ in the range 2.0−12.5 Å^{-1}; $w(k)$ is a Kaiser−Bessel apodisation window with a smoothness coefficient $\tau = 2.5$ (k is the photoelectron wave-

 © 2003 Wiley-VCH Verlag GmbH & Co. KGaA, Weinheim

number). The peaks corresponding to the successive atomic shells were then isolated and Fourier back-transformed into k space to determine the mean coordination number, N, the bond length, R, and the Debye-Waller factor, σ, by a least-squares fitting procedure using the standard EXAFS formula, without multiple scattering:

$$\chi(k) = S_0^2 \sum_i \left[\frac{N_i}{R_i^2} A_i(k) e^{-2\sigma_i^2 k^2} e^{-2R_i/\lambda(k)} \sin(2kR_i + \Phi_i(k)) \right] \quad (1)$$

The backscattering phase, $\Phi_i(k,R_i)$, and amplitude, $A_i(k,R_i)$, functions have been obtained using two approaches: the experimental and the theoretical one. The experimental back-scattering phase, $\Phi_i(k,R_i)$, and amplitude, $A_i(k,R_i)$, functions have been extracted from the EXAFS data of the model compounds of known crystallographic structure: aqueous rare earth solution,[21] $[Gd(DOTA)]^-$,[22] $[Eu(DOTA)]^-$,[38] and $[Tb(TETA)]^-$.[39] The theoretical back-scattering functions have been calculated using the ab initio code FEFF7,[46] with input data based on the X-ray crystal structure of $[Gd(DOTA)]^-$,[41,42] $[Eu(DOTA)]^-$,[38] and $[Tb(TETA)]^-$.[39]

Computational Methods: Traditional quantum mechanical methods are in general applied with great success for systems containing first-row atoms. However, they cannot be applied for systems with atoms further down the periodic table, e.g. lanthanide atoms, because of the sharp increase in computation time required to treat atoms of large atomic numbers. The effective core potential (ECP) method avoids this problem by replacing the core electrons with an approximate pseudo-potential which is only dependent upon the coordinates of the valence electrons, but takes into account the influence of the core electrons. In this study, geometries of the gadolinium complexes have been optimised in vacuo at the Restricted Hartree−Fock (RHF) level of theory using the (1s−4d, $4f^7$) ECP developed by Dolg et al.[40] with the [5s4p3d]-GTO valence basis set for the metal and the 3-21G basis set for the ligands. Previous studies have shown that inclusion of 4f electrons into the core yields a better description of large molecular systems.[23,44] For energy calculations, the 6-31G(d) basis set has also been used for the ligands. The Restricted Hartree−Fock theory is based on the resolution of the Schrödinger equation. As an exact solution of this equation is not possible, some assumptions are made within this theory. Comparison with experiments indicates that the RHF theory gives reasonably good computed structures and can be confidently used to determine the geometry of large systems. A basis set is the mathematical description of the orbitals within a system used to perform the theoretical calculation. Larger basis sets approximate the orbitals more accurately by imposing fewer restrictions on the location of the electrons in space. The 3-21G and 6-31G(d) are two standard basis sets; the 6-31G(d) one being the most extended one. The methodology described above has previously been used by Cosentino et al.[23−26] in their investigation of 5 complexes of gadolinium with macrocyclic and linear polyamino carboxylate ligands. By comparisons with experimental data, the authors concluded that geometry optimisations can be confidently performed at the RHF/3-21G level because it is a good compromise between accuracy and computational effort. In addition, they showed that RHF/6-31G(d) energy calculations on RHF/3-21G optimised geometries provide a satisfactory representation of the potential energy surface. In addition, other RHF calculations using ECP have been performed on multiply bonded transition metal complexes.[45] Computed structures are in good agreement with corresponding X-ray crystallographic data. All the calculations in this study have been carried out using the Gaussian 98 program.[47]

Acknowledgments

We would like to thank the Groupe Guerbet (Aulnay-sous-Bois, France) for their financial support and the supply of the ligands P730 and DOTA, Dr. Andrew Beeby (University of Durham, Great Britain) for the supply of the Lemming program Ver 1.01. The authors also wish to acknowledge S. Belin (Université Paris Sud, LURE, France) for her help in EXAFS data recording and for helpful discussions.

[1] S. Aime, M. Botta, M. Fasano, E. Terreno, *Chem. Soc. Rev.* **1998**, *27*, 19−29.
[2] H. Gries, *Top. Curr. Chem.* **2002**, *221*, 1−24.
[3] M. Port, C. Corot, O. Rousseaux, I. Raynal, L. Devoldère, J-M. Idée, A. Dencausse, S. Le Greneur, C. Simonot, D. Meyer, *MAGMA* **2001**, *12*, 121−127.
[4] M. Port, D. Meyer, B. Bonnemain, C. Corot, M. Schaefer, O. Rousseaux, C. Simonot, P. Bourrinet, S. Benderbous, A. Dencausse, L. Devoldère, *MAGMA* **1999**, *8*, 172−176.
[5] M. Port, C. Corot, I. Raynal, J.-M. Idée, A. Dencausse, E. Lancelot, D. Meyer, B. Bonnemain, J. Lautrou, *Invest. Radiol.* **2001**, *36*, 445−454.
[6] J. A. Howard, A. M. Kenwright, J. M. Moloney, D. Parker, M. Port, M. Navet, O. Rousseau, M. Woods, *Chem. Commun.* **1998**, 1381−1382.
[7] M. Woods, S. Aimé, M. Botta, J. A. Howard, J. M. Moloney, M. Navet, D. Parker, M. Port, O. Rousseaux, *J. Am. Chem. Soc.* **2000**, *122*, 9781−9792.
[8] A. Bianchi, L. Calabi, L. Ferrini, P. Losi, F. Ugerri, B. Valtancoli, *Inorg. Chim. Acta* **1996**, *249*, 13−15.
[9] A. Bianchi, L. Calabi, C. Giorgi, P. Losi, P. Mariani, P. Paoli, P. Rossi, B. Valtancoli, M. Virtuani, *J. Chem. Soc., Dalton Trans.* **2000**, 697−705.
[10] M. Port, O. Rousseaux, I. Raynal, M. Woods, D. Parker, J. Moreau, J. Rimbault, J-C. Pierrard, M. Aplincourt, *Acad. Radiol.* **2002**, *9 (suppl. 2)*, S300−S303.
[11] J. F. Desreux, E. Merciny, M. F. Loncin, *Inorg. Chem.* **1981**, *20*, 987−991.
[12] J. Moreau, E Guillon, J. C. Pierrard, J. Rimbault, M. Aplincourt, to be published.
[13] K. Kumar, C. A. Chang, L. C. Francesconi, D. D. Dischino, M. F. Malley, J. Z. Gougoutas, M. F. Tweedle, *Inorg. Chem.* **1994**, *33*, 3567−3575.
[14] W. P. Cacheris, S. K. Nickle, A. D. Sherry, *Inorg. Chem.* **1987**, *26*, 958−960.
[15] E. T. Clarke, A. E. Martell, *Inorg. Chim. Acta* **1991**, *190*, 37−46.
[16] M. F. Tweedle, J. J. Hagan, K. Kumar, S. Mantha, C. A. Chang, *Magn. Reson. Imaging* **1991**, *9*, 409−415.
[17] S. Aime, P. L. Anelli, M. Botta, F. Fedelli, M. Grandi, P. Paoli, F. Uggeri, *Inorg. Chem.* **1992**, *31*, 2422−2428.
[18] R. M. Supkowski,W. DeW. Horrocks, *Inorg. Chim. Acta* **2002**, *340*, 44−48.
[19] W. DeW. Horrocks, D. R. Sudnick, *Acc. Chem. Res.* **1981**, *14*, 384−392.
[20] A. Beeby, I. M. Clarkson, R. S. Dickins, S. Faulkner, D. Parker, L. Royle, A. S. de Sousa, J. A. G. Williams, M. Woods, *J. Chem. Soc., Perkin Trans. 2* **1999**, 493−503.
[21] T. Yamaguchi, M. Nomura, H. Wakita, H. Ohtaki, *J. Chem. Phys.* **1988**, *89*, 5153−5159.
[22] S. Bénazeth, J. Purans, M. C. Chalbot, M. K. Nguyen-van-Duong, L. Nicolas, F. Keller, A. Gaudemer, *Inorg. Chem.* **1998**, *37*, 3667−3674.
[23] U. Cosentino, G. Moro, D. Pitea, A. Villa, P. C. Fantucci, A. Maiocchi, F. Uggeri, *J. Phys. Chem. A* **1998**, *102*, 4606−4614.
[24] U. Cosentino, A. Villa, D. Pitea, G. Moro, V. Barone, *J. Phys. Chem. B* **2000**, *104*, 8001−8007.
[25] A. Villa, U. Cosentino, D. Pitea, G. Moro, A. Maiocchi, *J. Phys. Chem. A* **2000**, *104*, 3421−3429.

 © 2003 Wiley-VCH Verlag GmbH & Co. KGaA, Weinheim

[26] U. Cosentino, A. Villa, D. Pitea, G. Moro, V. Barone, A. Maiocchi, *J. Am. Chem. Soc.* **2002**, *124*, 4901−4909.
[27] E. Szilagyi, E. Toth, E. Brücher, A. Merbach, *J. Chem. Soc., Dalton Trans.* **1999**, 2481−2486.
[28] M. P. Lowe, D. Parker, *Inorg. Chim. Acta* **2001**, *317*, 163−173.
[29] M. P. Lowe, D. Parker, *Chem. Commun.* **2000**, 707−708.
[30] M. Aplincourt, C. Gérard, R. P. Hugel, J. C. Pierrard, J. Rimbault, A. Bertrandie, B. Magny, P. J. Siret, *Polyhedron* **1987**, *34*, 385−395.
[31] R. Fournaise, C. Petitfaux, *Talanta* **1987**, *34*, 385−395.
[32] A. Michalowicz, in *Logiciels pour la Chimie;* Société Française de Chimie: Paris, **1991**, p. 102.
[33] A. Michalowicz, *J. Chem. Phys. IV* **1997**, *7*, 235.
[34] B. K. Teo, In *Inorganic Chemistry Concepts, EXAFS: Basic Principles and Data Analysis*, Springer-Verlag, Berlin, **1986**, p. 9.
[35] D. C. Königsberger, R. Prins, in *X-ray Absorption* P*rinciples, Applications, Techniques of EXAFS, SEXAFS and XANES*, John Wiley & Sons, New York, **1988**.
[36] Co-Chairmen Report of the International Workshop on Standards and Criteria in X-ray Absorption Spectroscopy: F. W. Lytle, D. E. Sayers, E. A. Stern, *Physica* **1989**, *B158*, 701.
[37] B. Lengeler, P. Eisenberger, *Phys. Rev. B.* **1980**, *21*, 4507−4520.
[38] M. R. Spirlet, J. Rebizant, J. F. Desreux, M. F. Loncin, *Inorg. Chem.* **1984**, *23*, 359−363.
[39] M. R. Spirlet, J. Rebizant, M. F. Loncin, J. F. Desreux, *Inorg. Chem.* **1984**, *23*, 4278−4283.
[40] M. Dolg, H. Stoll, A. Savin, H. Preuss, *Theor. Chim. Acta* **1989**, *75*, 173−194.
[41] J. P. Dubost, J. M. Leger, M. H. Langlois, D. Meyer, *C. R. Acad. Sci. Ser II* **1991**, *312*, 349−354.
[42] C. A. Chang, L. C. Francesconi, M. F. Malley, K. Kumar, J. Z. Gougoutas, M. F. Tweedle, *Inorg. Chem.* **1993**, *32*, 3501−3508.
[43] M. Kaupp, P. V. R. Schleyer, M. Dolg, H. Stoll, *J. Am. Chem. Soc.* **1992**, *114*, 8202−8208.
[44] U. Cosentino, G. Moro, D. Pitea, L. Calabi, A. Maiocchi, *J. Mol. Struc. (THEOCHEM)* **1997**, *392*, 75−85.
[45] T. R. Cundari, M. T. Benson, M. Leigh Lutz, S. O. Sommerer, In Reviews in *Computational Chemistry*, VCH Publisher Inc., New York, **1996**, vol. 8, p. 145−202.
[46] S. I. Zabinsky, J. J. Rehr, A. Ankudinov, R. C. Albers, M. J. Eller, *Phys. Rev. B* **1995**, *52*, 2995−3009.
[47] M. J. Frisch, G. W. Trucks, H. B. Schlegel, G. E. Scuseria, M. A. Robb, J. R. Cheeseman, V. G. Zakrzewski, J. A. Montgomery, R. E. Stratmann, J. C. Burant, S. Dapprich, J. M. Millam, A. D. Daniels, K. N. Kudin, M. C. Strain, O. Farkas, J. Tomasi, V. Barone, M. Cossi, R. Cammi, B. Mennucci, C. Pomelli, C. Adamo, S. Clifford, J. Ochterski, G. A. Petersson, P. Y. Ayala, Q. Cui, K. Morokuma, D. K. Malick, A. D. Rabuck, K. Raghavachari, J. B. Foresman, J. Cioslowski, J. V. Ortiz, B. B. Stefanov, G. Liu, A. Liashenko, P. Piskorz, I. Komaromi, R. Gomperts, R. L. Martin, D. J. Fox, T. Keith, M. A. Al-Laham, C. Y. Peng, A. Nanayakkara, C. Gonzalez, M. Challacombe, P. M. W. Gill, B. G. Johnson, W. Chen, M. W. Wong, J. L. Andres, M. Head-Gordon, E. S. Replogle, J. A. Pople, *Gaussian 98* (Revision A.5), Gaussian Inc., Pittsburgh, PA, **1998**.

Received February 10, 2003

 © 2003 Wiley-VCH Verlag GmbH & Co. KGaA, Weinheim

Potential MRI Contrast Agents Based on Micellar Incorporation of Amphiphilic Bis(alkylamide) Derivatives of $[(Gd-DTPA)(H_2O)]^{2-}$

Kristof Kimpe,[a] Tatjana N. Parac-Vogt,[a] Sophie Laurent,[b] Corinne Piérart,[b] Luce Vander Elst,[b] Robert N. Muller,[b] and Koen Binnemans*[a]

Keywords: Imaging agents / Contrast agents / Lanthanides / Micelles / N,O ligands / NMR spectroscopy

DTPA-bisamide derivatives with alkyl chains containing 14, 16 and 18 carbon atoms were synthesized and complexes of various trivalent lanthanide ions (Ln = Gd, La, Pr, Eu) were formed. Variable temperature proton NMR spectroscopy of paramagnetic praseodymium(III) and europium(III) complexes revealed that long aliphatic substituents considerably increase the energy barrier for the intramolecular rearrangement around the lanthanide ion. The gadolinium(III) complexes were incorporated into mixed micelles, and photon correlation spectroscopy showed that the mean sizes of all the micelles were within the same range. The NMRD curves of all three DTPA-bisamide-gadolinium complexes incorporated in mixed micelles display higher relaxivity values than the commercially available Gd–DTPA contrast agent. The higher relaxivity obtained for the micellar DTPA-bisamide-gadolinium complexes with C_{14} and C_{16} chains relative to the micellar DTPA-bisamide-Gd^{III} C_{18} chain complex could be attributable to the fact that the alkyl chain containing 18 carbon atoms is longer than the alkyl chain of the major component of the micelles, DPPC, in which it is inserted. This would allow increased mobility of the polar head and hence a lower relaxivity.
(© Wiley-VCH Verlag GmbH & Co. KGaA, 69451 Weinheim, Germany, 2003)

Introduction

Complexes of lanthanides with diethylenetriamine-*N*,*N*,*N*′,*N*′′,*N*′′-pentaacetate ($DTPA^{5-}$) and with its amide derivatives have attracted considerable attention in recent years. The anionic $[Gd(DTPA)(H_2O)]^{2-}$, the first contrast agent approved for use in humans, is nowadays routinely used in clinical magnetic resonance imaging for contrast enhancement under the name Magnevist® (Schering, Berlin, Germany). This paramagnetic complex contains one inner-sphere water molecule[1−4] that exchanges rapidly[5] with the bulk water in the human body, therefore providing an efficient mechanism for the enhancement of the relaxation rates of the water protons. The negative charge of the complex, however, results in a relatively high osmolality of the clinical formulation. In order to neutralize two negative charges of $[Gd(DTPA)(H_2O)]^{2-}$, numerous bis-amide derivatives of DTPA have been developed. The bis-methylamide derivative of Gd−DTPA, Gd−DTPA-BMA, [H_3DTPA-BMA = *N*, *N*′′-bis(methylcarbamoylmethyl)−carboxymethyliminobis(ethylenediamino) diacetic acid] has been in clinical use nearly as long as its parent complex.[6] The practical application of Gd−DTPA-BMA has stimulated extensive research on the synthesis and study of new DTPA amide derivative ligands. In general, the methyl groups of DTPA-BMA have been replaced by various alkyl or aryl groups,[7−16] and in addition, macrocyclic bis(amide) derivatives of DTPA have also been successfully synthesized.[17−19] X-ray crystal structures of the lanthanide(III) complexes of some DTPA bis(amide) derivatives have revealed that the ligands coordinate to the lanthanide ion in an octadentate mode, while the ninth coordination site is occupied by a water molecule.[9,10,14,16] In solution, the presence of H_2O molecule in the inner sphere was detected in the europium(III) complex by luminescence lifetime measurements[3,20] and for some dysprosium(III) complexes by ^{17}O NMR studies.[11]

In attempt to achieve higher proton relaxivity, the Gd^{III} complexes of (DTPA-bisamide) alkyl copolymers with alkyl chains containing six, ten, or twelve $-CH_2$ groups have been synthesized.[21] The unexpectedly high proton relaxivities of these polymers were attributed to the formation of rigid, micelle-like structures in solution, these structures forming as a consequence of hydrophobic interactions between long alkyl chains. Detailed ^{17}O NMR and EPR spectroscopic studies showed that the rates and mechanisms of water exchange of all Gd (DTPA-bisamide) alkyl copolymers are the same as in the monomer chelate unit, and the proton relaxivity difference was explained in terms of differences in global motion.

[a] Katholieke Universiteit Leuven, Department of Chemistry
Celestijnenlaan 200F, 3001 Leuven, Belgium
Fax: (internat.) +32-16/327-992
E-mail: Koen.Binnemans@chem.kuleuven.ac.be
[b] NMR Laboratory, Department of Organic Chemistry,
University of Mons-Hainaut,
7000 Mons, Belgium
Fax: (internat.) +32-65/373-520
E-mail: robert.muller@umh.ac.be

Bis(amide) derivatives of Gd−DTPA containing long alkyl chains were also incorporated into the membranes of liposomal vesicles, yielding gadolinium-labelled liposomes. These liposomes, containing paramagnetic amphiphilic agents, significantly enhanced the proton relaxivity and were shown to be especially suitable for contrast enhancement in the liver, where the highly soluble parent Gd−DTPA complex does not accumulate efficiently.[22] Other attempts to slow down the rotational motion of gadolinium-based contrast agents, and thus to improve their relaxation efficiency, have included the synthesis of macromolecular gadolinium(III) chelates such as dendrimers,[23] linear polymers[24−26] or proteins.[27−29] The strategy proved rather disappointing, since the relaxivity gain obtained by increasing the molecular size is often far less than expected, as a result of internal flexibility or non-rigid attachment of the chelate to the macromolecule.[23−30] An interesting approach to high-relaxivity contrast agents is to synthesize amphiphilic gadolinium(III) complexes which can self-assemble into micelles.[30] An example is the Gd−DOTA derivative (DOTA = 1,4,7,10-tetraazacyclododecane-1,4,7,10-tetraacetic acid) with a long alkyl chain, reported by André et al.[31]

In this study we describe the synthesis of neutral, amphiphilic bisamide derivatives of DTPA with alkyl chains containing 14, 16 and 18 carbon atoms. The gadolinium complexes of these ligands were incorporated into mixed micelles to produce supramolecular structures with decreased rotational motion, and the NMRD profiles of the paramagnetic micelles are reported. The solution dynamics of europium and praseodymium complexes were investigated by NMR, and comparison was made with the related Ln-DTPA complexes.

Results and Discussion

The Ligands and Complexes

The ligands DTPA-bis-tetradecylamide (DTPA-BC14), DTPA-bis-hexadecylamide (DTPA-BC16) and DTPA-bis-octadecylamide (DTPA-BC18) were synthesized in high yields according to Scheme 1.

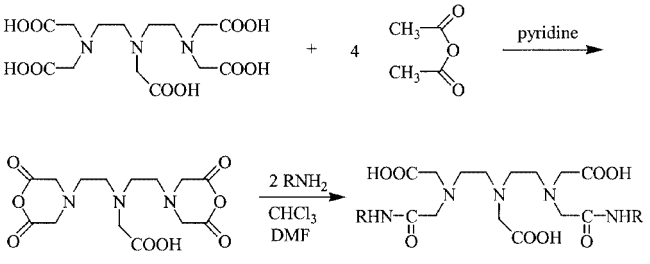

DTPA-BC14, R = $C_{14}H_{29}$
DTPA-BC16, R = $C_{16}H_{33}$
DTPA-BC18, R = $C_{18}H_{37}$

Scheme 1. Synthesis of DTPA bis(amide) derivatives

Under slightly alkaline solutions, these all readily formed complexes with lanthanide(III) ions (Ln = Gd, La, Eu, Pr), as shown in Figure 1. IR spectroscopic data of all ligands showed strong absorptions in the 3350−3360 and 1625−1670 cm^{-1} regions, corresponding to NH and CO stretching modes, respectively.[32] Shifts of around 20 cm^{-1} to lower energy were observed for the carbonyl stretching frequencies upon complexation, indicating amide oxygen coordination to the lanthanide ion. These findings are consistent with previous studies, which have shown that DTPA bis(amide) derivatives coordinate to Ln^{III} through three acetate oxygens, three nitrogen atoms and two carbonyl oxygens of the amide group, while the ninth coordination site is occupied by a water molecule.[9,10,14,16]

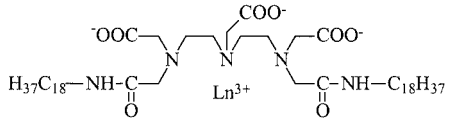

Figure 1. Schematic representation of the Ln−DTPA-BC18 complex; the ligand coordinates to lanthanide ion through three carboxylate oxygens, three nitrogen atoms and two carbonyl oxygens of the amide group, while a water molecule occupies the ninth coordination site

Solution Structures and Dynamics of Ln−DTPA-BC14, DTPA-BC16 and DTPA-BC18 Complexes

The coordination polyhedron of the nine-coordinate lanthanide complexes can best be described as a tricapped trigonal prism,[33] with the bis-amide-DTPA ligand arranged around lanthanide ion in such a way that eight different enantiomers are possible. The eight possible enantiomers of the bound ligand give rise to the complex geometries, in which four are the mirror images of the other four. Thus, in theory, four NMR signals could be detectable for each nucleus in the bis-amide-DTPA ligand. However, rapid interconversion of the bis-amide-DTPA complexes on the NMR timescale very often results in a reduction of the number of NMR signals.[11] In order to examine the solution dynamics of the lanthanide complexes with DTPA-BC14, DTPA-BC16 and DTPA-BC18, the ^1H NMR spectra were recorded at various temperatures. Unfortunately, due to the low solubility of all the complexes in the common NMR solvents we were unable to collect ^{13}C NMR spectra of good quality.

The ^1H NMR spectra of lanthanum(III) complexes with DTPA-BC14, DTPA-BC16 and DTPA-BC18 ligands at room temperature were quite complex, due to the broadening and overlapping of proton resonances originating from various isomers. This made the interpretation of the spectra quite difficult. The proton NMR spectra of the praseodymium(III) complexes were much more informative, however, since the presence of the paramagnetic ion increased the chemical shift range and resulted in separate signals for CH_2 protons. At room temperature (298 K), the praseodymium(III) complexes with DTPA-BC14, DTPA-BC16 and DTPA-BC18 show eighteen resonances for ten acetate and

 © 2003 Wiley-VCH Verlag GmbH & Co. KGaA, Weinheim

eight ethylenic protons in the range from −35 to +35 ppm. Exact distinction between ethylenic and acetate resonances was not possible, since this would require use of partially deuterated ligand. It is reasonable to assume that, analogously to the previously assigned proton NMR spectra of the parent Pr−DTPA and Eu−DTPA complexes, the acetate resonances should in general experience significant downfield shifts, while the ethylenic protons should be shifted upfield.[34]

We also extended our observation to the DTPA-BC14, DTPA-BC16 and DTPA-BC18 complexes of europium(III), because we expected that increased charge/size ratio should

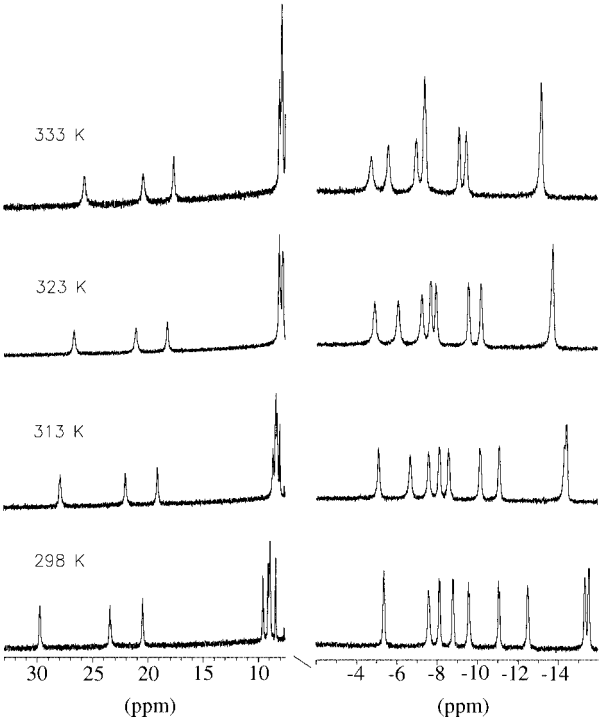

Figure 2. Variable temperature NMR spectra of Eu−DTPA-BC16 in $CDCl_3/CD_3OH$ solution; only the regions containing resonances of acetate protons (at low field) and ethylenic protons (at high field) are shown; the relative assignment was based on the assignment of the parent Eu−DTPA complex reported in ref.[34] the region containing solvent peaks as well as aliphatic proton resonances was omitted for clarity

favour even higher rigidity of the system. As Figure 2 shows, in the proton NMR spectrum of Eu-DTPA-BC16 the "frozen" structures could already be detected at 298 K. In theory, eight possible enantiomers of the bound ligand are possible, and since four of those geometries are mirror images of the other four, four signals can be expected for each group of magnetically equivalent protons in the Eu−DTPA-BC16 ligand. Examination of the NMR spectra shown in Figure 2 suggests that the spectra are consistent with the occurrence either of two static structures or of two pairs of interconverting isomers. To test this, the temperature of the solution was increased to 333 K, but only the coalescence of two pair of peaks was detected. Unfortunately, the chloroform/methanol solution in which the complexes were dissolved did not allow us to record high temperature spectra in order to observe the coalescence process. However, the broadening of the resonances supports the view that the observed spectral pattern is due to the existence of interconverting isomers.

This dynamic behaviour of the praseodymium and europium complexes with DTPA-BC14, DTPA-BC16 and DTPA-BC18 is rather surprising, since the parent Pr−DTPA and Eu−DTPA complexes are known to undergo fast intramolecular rearrangement at room temperature, so that "frozen" structures could be detected only at temperatures below 268 K, while the exchange process leading to coalescence was already observed at 338 K.[34]

Detailed kinetic study on bispropylamide-DTPA complex of neodymium(III) showed that the activation barrier for the conformational interconversion at the middle nitrogen atom in the diethylenetriamine backbone (so called "wagging" process) was virtually the same as the activation barrier of the parent DTPA complex, indicating that the replacement of two carboxylate groups by the relatively weak coordinating amide groups has no influence on this process.[11] However, the inversion of the terminal diethylenetriamine nitrogen atoms, which is characterized by a higher activation barrier, requires partial decomplexation of the ligand. It is likely that, for steric reasons, the long aliphatic substituents on DTPA-BC14, DTPA-BC16 and DTPA-BC18 ligands considerably alter the rate of this inversion, thus increasing the energy barrier for the intramolecular rearrangement around the lanthanide ion.

Mixed Micelle Formation and Size Distribution

The gadolinium(III) complexes of DTPA-BC14, DTPA-BC16 and DTPA-BC18 ligands were incorporated into mixed micelles made of phospholipid (DPPC), a surfactant (Tween 80) and the gadolinium complex. The micelle size was determined at room temperature by photon correlation spectroscopy. All micelles were monodisperse (i.e., there was only one main kind of particles in the size distribution histogram). As can be seen from Figure 3, the mean diameters of the micelles are all within the same range (15−20 nm) and can be regarded as similar. This indicates that the size of the micelles is virtually independent of the length of the bisamide chain, and that the factor that determines the size is the phospholipid DPPC.

Nuclear Magnetic Relaxation Dispersion (NMRD) Measurements

Figure 4 shows the proton NMRD profiles of the relaxivity (defined as the longitudinal relaxation rate enhancement produced by one millimole per litre of Gd complex) of Gd−DTPA-BC14, Gd−DTPA-BC16 and Gd−DTPA-BC18, incorporated in micelles, at 37 °C. As would be expected, the inclusion of the gadolinium complexes into micelles results in an increased relaxivity relative to the parent complex Gd−DTPA and in a maximum at high magnetic fields, induced on the one hand by the decreased rotational mobility of the paramagnetic complex and on the other hand by the increase in the electronic longitudinal relax-

 © 2003 Wiley-VCH Verlag GmbH & Co. KGaA, Weinheim

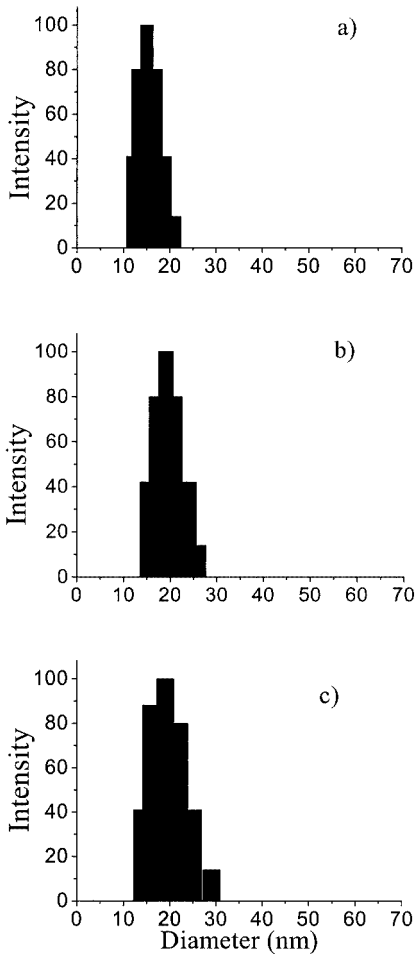

Figure 3. Histogram representing micelle size distribution, as measured by photon correlation spectroscopy: a) Gd−DTPA-BC14; b) Gd−DTPA-BC16; c) Gd−DTPA-BC18

ation time at high fields. The relaxivities of micellar Gd−DTPA-BC14 and Gd−DTPA-BC16 are quite similar, and are larger than for micellar Gd−DTPA-BC18.

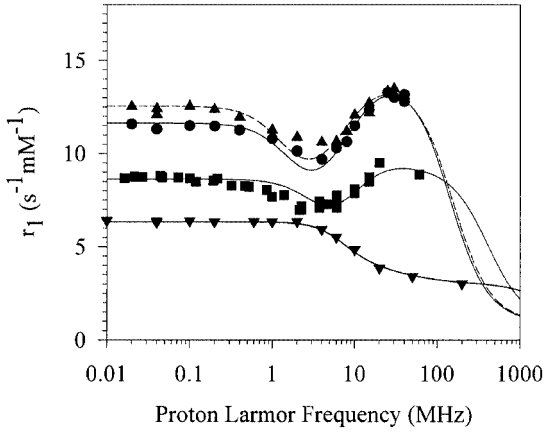

Figure 4. NMRD profile of micellar Gd−DTPA-BC14 (circles), Gd−DTPA-BC16 (triangles up) and Gd−DTPA-BC18 (squares) at 37 °C; the NMRD profile of Gd−DTPA (triangles down) has been added for comparison[47]

The data were analysed by use of the classical inner sphere[35,36] and outer sphere[37] theories. The distance of closest approach was set to 0.36 nm, the relative diffusion constant was fixed to 2.93 10^{-9} m^2s^{-1}, the distance for the inner sphere interaction was set to 0.31 nm, and the number of coordinated water molecule was assumed to be equal to 1 by analogy with other bisamide derivatives of Gd−DTPA.[35,38] The parameters describing the electronic relaxation of Gd (τ_{SO} is the electronic relaxation rate at very low magnetic field and τ_V the correlation time modulating the electronic relaxation) as well as the "global" rotational correlation time (τ_R) and the residence time of the coordinated water molecule (τ_M) were simultaneously fitted. The results are shown in Table 1.

Table 1. Parameters obtained from the theoretical fitting of the proton NMRD data (T = 37 °C)

	τ_R (ns)	τ_M (ns)	τ_{SO} (ps)	τ_V (ps)
Gd−DTPA-BC14	3.05	1300	175	30
Gd−DTPA-BC16	2.97	1280	209	30
Gd−DTPA-BC18	0.62	1470	101	27
Gd−DTPA[a]	0.059	143	82	23
Gd−DTPABMA[b]	0.047	1050	85	24

[a] From ref.[47] τ_R, τ_{SO} and τ_V obtained from the fitting of the proton NMRD data, τ_M obtained from the fitting of the ^{17}O transverse relaxation rates. [b] Calculated at 37 °C with the parameters obtained from the simultaneous fitting of EPR, ^{17}O NMR and NMRD data by Powell et al.[39]

The parameters obtained for Gd−DTPA-BC14 and Gd−DTPA-BC16 are quite similar, with a rotational correlation time of about 3 ns, a value two order of magnitude lower than the rotational correlation time calculated by the Stokes-Einstein theory for a rigid sphere (τ_R ranging between 285 and 675 ns depending on the micelle size). The observed difference can be related to the local motion of the Gd complex within the micellar structure. For micelles made of compound Gd−DTPA-BC18, which contains hydrophobic chains longer than that of DPPC, the fitted τ_R is smaller, indicating an increased local mobility in relation to the other complexes. The τ_M values are similar for the three complexes and larger than for the parent compound Gd−DTPA. Such increases in the residence time of the coordinated water molecule have already been reported for numerous Gd−DTPA bisamide derivatives.[39,40] Moreover, the insertion of both hydrophobic chains of the Gd complex in the micellar structure could also prevent the exchange of the water molecule.

Conclusions

Amphiphilic Gd−DTPA bis(amide) complexes were incorporated into mixed micelles in order to obtain supramolecular structures with decreased mobility. As already reported for other gadolinium complexes incorporated into mixed micelles,[41,42] the relaxivities of the micellar solutions

 © 2003 Wiley-VCH Verlag GmbH & Co. KGaA, Weinheim

of the three complexes Gd−DTPA-BC14, Gd−DTPA-BC16 and Gd−DTPA-BC18 are higher than that seen for the hydrophilic Gd−DPTA, as a result of the reduced mobility of the gadolinium complexes. In the case of Gd−DTPA-BC18, the immobilization inside the micellar structure is less effective, probably because the aliphatic chains of the complex are longer than the alkyl chain of DPPC, in which it is inserted. The increase in relaxivity can be related to the lower mobility of the paramagnetic complex inside the micelle. We are currently developing other amphiphilic complexes of gadolinium, which will be incorporated into micelles with the goal of achieving higher increases in relaxivity.

Experimental Section

Chemicals: Reagents were obtained from Aldrich Chemical Co. Inc., Acros Organics and Fluka, and were used without further purification. DTPA was obtained from Koch Light Laboratories. 1,2-Dipalmitoyl-sn-glycero-3-phosphocholine (DPPC) was obtained from Genzyme Pharmaceuticals (Switzerland). Gadolinium chloride hexahydrate was obtained from GFS chemicals (USA).

Instruments: Elemental analysis was performed on a CE Instruments EA-1110 elemental analyser. ^{1}H NMR spectra were run on a Bruker Avance 300, operating at 300 MHz. IR spectra were measured on a Bruker IFS66 FT IR spectrometer, in KBr discs. Mass spectra were run on a Q-tof 2 (Micromass, Manchester UK). Samples for the mass spectra were prepared as follows: the complex (2 mg) was dissolved in methanol (1 mL), and 200 μL of this solution was added to 800 μL of a mixture of a 50:50 water methanol solution. The resulting solution was injected, with a flow rate of 5 μL/min.

Synthesis of the Ligands: DTPA bisanhydride was prepared by the published procedure.[43] DTPA-BC14, DTPA-BC16 and DTPA-BC18 were prepared by the method of Jasanda and Nepveu.[44]

Analytical Data for the Ligands

DTPA-BC14: ^{1}H NMR (CF_3COOD, 298 K, ref. CF_3COOD at δ = 11.62 ppm): δ = 0.88 (t, 6 H, 2 × CH_3), 1.31 (m, 44 H, 22 × CH_2), 1.61 (m, 4 H, 2 × CH_2), 3.39 (t, 4 H, 2 × CH_2), 3.80 (m, 4 H, 2 × CH_2), 4.08 (m, 4 H, 2 × CH_2), 4.14 (s, 2 H, CH_2), 4.52 (s, 4 H, 2 × CH_2), 4.54 (s, 4 H, 2 × CH_2) ppm. IR: $\tilde{\nu}$ = 3350 cm^{-1} (N−H amide), 2960, 2920, 2850 (C−H alkyl), 1655 (CO, amide I), 1625 (COOH), 1550 (amide II). $C_{42}H_{81}N_5O_8$ (784.1): calcd. C 64.33, H 10.41, N 8.93; found C 64.42, H 10.39, N 8.99.

DTPA-BC16: ^{1}H NMR (CF_3COOD, 298 K, ref. CF_3COOD at δ = 11.62 ppm): δ = 0.91 (t, 6 H, 2 × CH_3), 1.34 (m, 52 H, 26 × CH_2), 1.64 (m, 4 H, 2 × CH_2), 3.42 (t, 4 H, 2 × CH_2), 3.88 (m, 4 H, 2 × CH_2), 4.12 (m, 4 H, 2 × CH_2), 4.18 (s, 2 H, CH_2), 4.56 (s, 4 H, 2 × CH_2), 4.58 (s, 4 H, 2 × CH_2) ppm. IR: $\tilde{\nu}$ = 3356 cm^{-1} (N−H amide), 2960, 2918, 2849 (C−H alkyl), 1666 (CO, amide I), 1624 (COOH), 1541 (amide II). $C_{46}H_{89}N_5O_8$ (840.2): calcd. C 65.76, H 10.68, N 8.34; found C 65.80, H 10.64, N 8.35.

DTPA-BC18: ^{1}H NMR (CF_3COOD, 298 K, ref. CF_3COOD at δ = 11.62 ppm): δ = 0.90 (t, 6 H, 2 × CH_3), 1.34 (m, 60 H, 30 × CH_2), 1.63 (m, 4 H, 2 × CH_2), 3.41 (t, 4 H, 2 × CH_2), 3.82 (m, 4 H, 2 × CH_2), 4.11 (m, 4 H, 2 × CH_2), 4.18 (s, 2 H, CH_2), 4.56 (s, 4 H, 2 × CH_2), 4.58 (s, 4 H, 2 × CH_2) ppm. IR: $\tilde{\nu}$ = 3350 cm^{-1} (N−H amide), 2960, 2920, 2850 (C−H alkyl), 1655 (CO, amide I), 1625 (COOH), 1550 (amide II). $C_{50}H_{97}N_5O_8$ (896.3): calcd. C 66.99, H 10.90, N 7.81; found C 66.82, H 10.85, N 7.77.

Synthesis of the Ln^{III} Complexes: All complexes were synthesized by the General Procedure as follows: a solution of hydrated $LnCl_3$ salt (1.1 mmol) in H_2O (1 mL) was added to the ligand (1 mmol) dissolved in pyridine (30 mL), and the mixture was heated at 70 °C for 3 hours. The solvents were evaporated under reduced pressure and the crude product was then heated at reflux in ethanol for 1 hour. After the mixture had cooled to room temperature, the complex was filtered off and dried in vacuo. The absence of free gadolinium was checked with xylenol orange indicator.[45]

Analytical Data for the Ln^{III} Complexes

Gd−DTPA-BC14: $C_{42}H_{78}N_5GdO_8$ (938.4): calcd. C 53.76, H 8.37, N 7.32; found C 53.49, H 8.64, N 7.28. IR: $\tilde{\nu}$ = 3093 cm^{-1} (N−H amide), 2919, 2850 (C−H alkyl), 1667 (CO, amide I), 1617 (COO^- assym. stretch), 1394 (COO^- sym. stretch). ES-MS+: *m/z* = 939 ($[M + H]^+$), 961 ($[M + Na]^+$), 1430 ($[3M + 2Na]^{2+}$).

Eu-DTPA-BC14: $C_{42}H_{80}N_5EuO_9$ (951.1): calcd. C 52.89, H 8.48, N 7.36; found C 53.04, H 8.38, N 7.25. IR: $\tilde{\nu}$ = 3093 cm^{-1} (N−H amide), 2923, 2854 (C−H alkyl), 1631 (CO, amide I), 1600 (COO^- assym. stretch), 1394 (COO^- sym. stretch). ES-MS+: *m/z* = 956.5 ($[M + Na]^+$), 1422 ($[3M + 2Na]^{2+}$), 1890 ($[2M + Na]^+$).

Pr-DTPA-BC14: $C_{42}H_{78}N_5O_8Pr$ (922.0): calcd. C 54.71, H 8.53, N 7.60; found C 55.00, H 8.63, N 7.56. IR: $\tilde{\nu}$ = 3088 cm^{-1} (N−H amide), 2920, 2850 (C−H alkyl), 1640 (CO, amide I), 1600 (COO^- assym. stretch), 1386 (COO^- sym. stretch). ES-MS+: *m/z* = 945 ($[M + Na]^+$), 1405 ($[3M + 2Na]^{2+}$), 1867 ($[2M + Na]^+$).

La-DTPA-BC14: $C_{42}H_{78}LaN_5O_8$ (920.0): calcd. C 54.83, H 8.54 , N 7.61; found C 54.37, H 8.39, N 7.44. IR: $\tilde{\nu}$ = 3089 cm^{-1} (N−H amide), 2926, 2850 (C−H alkyl), 1641 (CO, amide I), 1600 (COO^- assym. stretch), 1386 (COO^- sym. stretch). ES-MS+: *m/z* = 943 ($[M + Na]^+$), 1403 ($[3M + 2Na]^{2+}$), 1862 ($[2M + Na]^+$).

Gd−DTPA-BC16: $C_{46}H_{86}GdN_5O_8$ (994.5): calcd. C 55.56, H 8.72, N 7.04; found C 56.39, H 8.74, N 7.02. IR: $\tilde{\nu}$ = 3093 cm^{-1} (N−H amide), 2960, 2918, 2849 (C−H alkyl), 1666 (CO, amide I), 1624 (COO^- assym. stretch), 1395 (COO^- sym. stretch). ES-MS+: *m/z* = 1017 ($[M + Na]^+$), 1514 ($[3M + 2Na]^{2+}$).

Eu-DTPA-BC16: $C_{46}H_{88}EuN_5O_9$ (1007.2): calcd. C 54.86, H 8.81, N 6.95; found C 54.53, H 8.73, N 6.80. IR: $\tilde{\nu}$ = 3090 cm^{-1} (N−H amide), 2919, 2850 (C−H alkyl), 1635 (CO, amide I), 1601 (COO^- assym. stretch), 1391 (COO^- sym. stretch). ES-MS+: *m/z* = 1035 ($[M + Na]^+$), 1540 ($[3M + 2Na]^{2+}$), 2047 ($[2M + Na]^+$).

Pr-DTPA-BC16: $C_{46}H_{86}N_5O_8Pr$ (978.1): calcd. C 56.49, H 8.86, N 7.16, found C 56.61, H 8.74, N 7.09. IR: $\tilde{\nu}$ = 3094 cm^{-1} (N−H amide), 2921, 2844 (C−H alkyl), 1635 (CO, amide I), 1596 (COO^- assym. stretch), 1395 (COO^- sym. stretch). ES-MS+: *m/z* = 1001 ($[M + Na]^+$), 1490 ($[3M + 2Na]^{2+}$), 1977 ($[2M + Na]^+$).

La-DTPA-BC16: $C_{46}H_{88}LaN_5O_9$ (994.1): calcd. C 55.58, H 8.92, N 7.04; found C 55.50, H 8.73, N 6.90. IR: $\tilde{\nu}$ = 3085 cm^{-1} (N−H amide), 2920, 2850 (C−H alkyl), 1667 (CO, amide I), 1624 (COO^- assym. stretch), 1385 (COO^- sym. stretch). ES-MS+: *m/z* = 999 ($[M + Na]^+$), 1486 ($[3M + 2Na]^{2+}$), 1975 ($[2M + Na]^+$).

Gd−DTPA-BC18: $C_{50}H_{96}GdN_5O_9$ (1068.6): calcd. C 56.14, H 9.05, N 6.55; found C 56.09, H 9.55, N 6.38. IR: $\tilde{\nu}$ = 3094 cm^{-1} (N−H amide), 2960, 2920, 2850 (C−H alkyl), 1633 (CO, amide I), 1596 (COO^- assym. stretch), 1390 (COO^- sym. stretch). ES-MS+: *m/z* = 1073 ($[M + Na]^+$), 1599 ($[3M + 2Na]^{2+}$).

 © 2003 Wiley-VCH Verlag GmbH & Co. KGaA, Weinheim

Eu-DTPA-BC18: $C_{50}H_{100}EuN_5O_{11}$ (1099.3): calcd. C 54.62, H 9.16, N 6.37; found C 54.58, H 9.87, N 6.23. IR: $\tilde{\nu}$ = 3105 cm^{-1} (N−H amide), 2916, 2851 (C−H alkyl), 1634 (CO, amide I), 1595 (COO^- assym. stretch), 1386 (COO^- sym. stretch). ES-MS+: *m*/*z* = 1068 ($[M + Na]^+$)

Pr-DTPA-BC18: $C_{50}H_{96}N_5O_9Pr$ (1052.2): calcd. C 57.07, H 9.20, N 6.66; found C 57.46, H 9.19, N 6.57. IR: $\tilde{\nu}$ = 3089 cm^{-1} (N−H amide), 2915, 2844 (C−H alkyl), 1635 (CO, amide I), 1597 (COO^- assym. stretch), 1386 (COO^- sym. stretch). ES-MS+: *m*/*z* = 1057 ($[M + Na]^+$)

La-DTPA-BC18: $C_{50}H_{98}LaN_5O_{10}$ (1068.3): calcd. C 56.22, H 9.24, N 6.56; found C 56.19, H 8.82, N 6.39. IR: $\tilde{\nu}$ = 3083 cm^{-1} (N−H amide), 2925, 2850 (C−H alkyl), 1640 (CO, amide I), 1596 (COO^- assym. stretch), 1385 (COO^- sym. stretch). ES-MS+: *m*/*z* = 1055 ($[M + Na]^+$)

Sodium and Potassium Ion Content Measurements: Before the compounds were used for incorporation into micelles, the potassium and sodium ion contents were checked by flame photometry (IL, 943, Instrumentation Laboratories, Massachusetts, USA). The Na^+ and K^+ ion contents were measured on samples obtained by extraction of the solutions of complex (1.7 mg) dissolved in a 1:1 chloroform/methanol mixture with 500 μL of water. Na^+ contents (mmol:mol of the complex): (Gd−DTPA-BC14) 0.10, (Gd−DTPA-BC16) 0.15, (Gd−DTPA-BC18) 0.15. K^+ contents: no K^+ was found in any of the complexes.

Preparation of Micelles: 1,2-Dipalmitoyl *sn-glycero*-3 phosphatidyl choline (DPPC, 225 mg) and the complex (25 mg) were dissolved in a 1:1 solution of chloroform/methanol (50 mL). Evaporation under reduced pressure yielded a thin film, which was then rehydrated with hot water (5 mL, 70 °C). This solution was sonicated for 15 min with a 70-W sonicator while the temperature was maintained at 65 °C with a thermostatic bath. After the sonication, 75 mg of a surfactant was added (Tween 80® − polyoxyethylene sorbitan monooleate), followed by another 15 minutes of sonication.

Determination of Micelle Size: The mean micelle sizes were determined by photon correlation spectroscopy performed with a BIC multiangle laser light scattering system at room temperature and with a 90° scattering angle (Brookhaven Instruments Corporation, Holtsville, USA). The intensity weighted micellar diameter was measured on diluted suspensions and calculated by a non-negatively constrained least-squares (multiple pass) routine. The diameters obtained are as follows: micelles with (Gd−DTPA-BC14): 15 nm, with (Gd−DTPA-BC16): 20 nm, with (Gd−DTPA-BC18): 19 nm.

T_1 Measurements: Proton Nuclear Magnetic Relaxation Dispersion (NMRD) profiles were recorded between 0.24 mT and 1.2 T with Field Cycling Relaxometers (Field Cycling Systems, Oradell, New Jersey, USA or Stelar Spinmaster FFC-2000, Stelar S.R.L., Mede, Italy) on 0.6 mL solutions contained in 10 mm o.d. tubes. Proton relaxation rates were also measured at 0.47 T and 1.5 T on Minispec PC-120 and mq-60 instruments (Bruker, Karlsruhe, Germany). All samples were diluted 10 times and the temperature was maintained at 37 °C. ^1H NMRD data were fitted according to the theoretical inner-sphere model described by Solomon[35] and Bloembergen[36] and to the outer-sphere contribution described by Freed.[37] Calculations were performed with the aid of previously described software.[46−48]

Acknowledgments

KK, TNPV and KB thank the K.U. Leuven for financial support (VIS/01/006.01/20002−06/2004 and GOA 03/03). KB acknowledges the F.W.O.-Flanders (Belgium) for a Postdoctoral Fellowship. CHN microanalyses were performed by Mrs Petra Bloemen.

[1] C. C. Bryden, C. N. Reilley, *Anal. Chem.* **1982**, *54*, 610−615.
[2] J. A. Peters, *Inorg. Chem.* **1988**, *27*, 4686−4691.
[3] C. F. G. C. Geraldes, A. D. Sherry, W. P. Cacheris, K. T. Kuan, R. D. Brown III, S. H. Koenig, M. Spiller, *Magn. Reson. Med.* **1988**, *8*, 191−199.
[4] C. A. Chang, H. G. Brittain, J. Telser, M. F. Tweedle, *Inorg. Chem.* **1990**, *29*, 4468−4473.
[5] K. Micskei, L. Helm, E. Brucher, A. E. Merbach, *Inorg. Chem.* **1993**, *32*, 3844−3850.
[6] S. C. Quay, US Patent 4,859,451 *Paramagnetic Contrast Agents for MR Imaging.*
[7] A. D. Sherry, W. P. Cacheris, K.-T. Kuan, *Magn. Reson. Med.* **1988**, *8*, 180−190.
[8] F. Jasanada, F. Nepven, *Tetrahedron Lett.* **1992**, *33*, 5745−5748.
[9] L. Ehnebom, B. F. Pedersen, *Acta Chem. Scand.* **1992**, *46*, 126−130.
[10] S. W. A. Bligh, A. H. M. S. Chowdhury, M. McPartlin, T. J. Scowen, R. A. Bulman, *Polyhedron* **1995**, *14*, 567−569.
[11] C. F. G. C. Geraldes, A. M. Urbano, M. A. Hoefnagel, J. A. Peters, *Inorg. Chem.* **1993**, *32*, 2426−2432.
[12] C. Paul-Roth, K. N. Raymond, *Inorg. Chem.* **1995**, *34*, 1408−1412.
[13] Y.-M. Wang, T.-H. Cheng, G.-C. Liu, R.-S. Sheu, *J. Chem. Soc., Dalton Trans.* **1997**, *833−837*.
[14] S. Aime, F. Benetollo, G. Bombieri, S. Colla, M. Fasano, S. Paoletti, *Inorg. Chim. Acta* **1997**, *254*, 63−70.
[15] X. Zhao, R. Zhuo, Z. Lu, W. Lin, *Polyhedron* **1997**, *16*, 2755−2759.
[16] Y.-M. Wang, Y.-J. Wang, R.-S. Sheu, G.-C. Lin, W.-C. Lin, J.-H. Liao, *Polyhedron* **1999**, *18*, 1147−1152.
[17] J. F. Carvalho, S.-H. Kim, C. A. Chang, *Inorg. Chem.* **1992**, *31*, 4065−4068.
[18] S. J. Franklin, K. N. Raymond, *Inorg. Chem.* **1994**, *33*, 5794−5804.
[19] E. Bovens, M. A. Hoefnagel, E. Boers, H. Lammers, H. van Bekkum, J. A. Peters, *Inorg. Chem.* **1996**, *35*, 7679−7683.
[20] H. Imura, G. R. Choppin, W. P. Cacheris, L. A. deLearie, T. J. Dunn, D. H. White, *Inorg. Chim. Acta* **1997**, *258*, 227−236.
[21] E. Toth, L. Helm, K. E. Kellar, A. E. Merbach, *Chem. Eur. J.* **1999**, *5*, 1202−1211.
[22] G. W. Kabalka, M. A. Davis, E. Holmberg, K. Maruyama, L. Huang, *Magn. Res. Imaging* **1991**, *9*, 373−377.
[23] É. Tóth, D. Pubanz, S. Vauthey, L. Helm, A. E. Merbach, *Chem. Eur. J.* **1996**, *2*, 1607−1615.
[24] M. Spanoghe, D. Lanens, R. Dommisse, A. Van der Linden, F. Alderweireldt, *J. Magn. Reson. Imaging* **1992**, *10*, 913−917.
[25] V. S. Vexler, O. Clement, H. Schmitt-Willich, R. C. Brasch, *J. Magn. Res. Imaging* **1994**, *4*, 381−388.
[26] T. S. Desser, D. L. Rubin, H. H. Muller, F. Qing, S. Khodor, G. Zanazzi, S. U. Young, D. L. Ladd, J. A. Wellons, K. E. Kellar, J. L. Toner, R. A. Snow, *J. Magn. Res. Imaging* **1994**, *4*, 467−472.
[27] S. Aime, M. Botta, M. Fasano, S. G. Crich, E. Terreno, *J. Biol. Inorg. Chem.* **1996**, *1*, 312−319.
[28] É. Tóth, F. Connac, L. Helm, K. Adzamli, A. E. Merbach, *J. Biol. Inorg. Chem.* **1998**, *3*, 606−613.
[29] S. Aime, M. Botta, M. Fasano, E. Terreno, *Chem. Soc. Rev.* **1998**, *27*, 19−29.
[30] K. Binnemans, C. G. Görller-Walrand, *Chem. Rev.* **2002**, *102*, 2303−2345.

 © 2003 Wiley-VCH Verlag GmbH & Co. KGaA, Weinheim

[31] J. P. André, É. Tóth, H. Fischer, A. Seelig, H. R. Mäcke, A. E. Merbach, *Chem. Eur. J.* **1999**, *5*, 2977−2983.
[32] E. Pretsch, T. Clerc, J. Seibl, W. Simon in "*Tabellen zur Strukturaufklärung organischer Verbindungen mit spektroskopischen Methoden*", Springer, Berlin, **1976**.
[33] M. S. Konings, W. C. Dow, D. B. love, K. N. Raymond, S. C. Quay, S. M. Rocklage, *Inorg. Chem.* **1990**, *29*, 1488−1491.
[34] S. Aime, M. Botta, *Inorg. Chim. Acta* **1990**, *177*, 101−105.
[35] I. Solomon, *Phys. Rev.* **1955**, *99*, 559−565.
[36] N. Bloembergen, *J. Chem. Phys.* **1957**, *27*, 572−573.
[37] J. H. Freed, *J. Chem. Phys.* **1978**, *68*, 4034−4037.
[38] M. C. Alpoim, A. M. Urbano, C. F. G. C. Geraldes, J. A. Peters, *J. Chem. Soc., Dalton Trans.* **1992**, 463−467.
[39] D. H. Powell, O. M. Ni Dhubhghaill, D. Pubanz, L. Helm, Y. S. Lebedev, W. Schlaepfer, A. E. Merbach, *J. Am. Chem. Soc.* **1996**, *118*, 9333−9346.
[40] F. Botteman, G. M. Nicolle, L. Vander Elst, S. Laurent, A. E. Merbach, R. N. Muller, *Eur. Inorg. Chem.* **2002**, 2686−2693.
[41] H. Tournier, R. Hyacinthe, M. Schneider, *Acad. Radiol*. **2002**, *9* (suppl. 1), S20-S28.
[42] P. L. Anelli, L. Lattuada, V. Lorusso, M. Schneider, H. Tournier, F. Uggeri, *Mayn. Reson. Mater. Phys. Biol. Med.* **2001**, *12*, 114−120.
[43] V. Montembault, J. C. Soutif, J. C. Brosse, *Reactive & Function. Polym.* **1996**, *29*, 29−39.
[44] F. Jasanada, F. Nepveu, *Tetrahedron Lett.* **1992**, *33*, 5745−5748.
[45] G. Brunisholz, M. Randin, *Helv. Chim. Acta* **1959**, *42*, 1927.
[46] R. N. Muller, D. Declercq, P. Vallet, F. Giberto, B. Daminet, H. W. Fischer, F. Maton, Y. Van Haverbeke, in "Proc., ESMRMB, 7th Annual Congress, Strasbourg, France ", **1990**, p. 394.
[47] P. Vallet, PhD Dissertation, Univ. of Mons-Hainaut, Belgium **1992**.
[48] S. Laurent, L. Vander Elst, S. Houzé, N. Guérit, R. N. Muller, *Helv. Chim. Acta* **2000**, *83*, 394−406.

Received March 1, 2003

 © 2003 Wiley-VCH Verlag GmbH & Co. KGaA, Weinheim

Adducts of Schiff Bases with Tris(β-diketonato)lanthanide(III) Complexes: Structure and Liquid-Crystalline Behaviour

Koen Binnemans,*[a] Katleen Lodewyckx,[a] Tatjana N. Parac-Vogt,[a] Rik Van Deun,[a] Bart Goderis,[a] Bernard Tinant,[b] Kristof Van Hecke,[a] and Luc Van Meervelt[a]

Keywords: Lanthanides / Liquid crystals / Metallomesogens / Supramolecular chemistry

Adducts of the Schiff base 2-hydroxy-*N*-octadecyloxy-4-tetradecyloxybenzaldimine with tris(β-dibenzoylmethanato)-lanthanide(III) complexes are described. The stoichiometry of the complexes is $[Ln(dbm)_3L_x]$, where Ln is a trivalent lanthanide ion (all lanthanides except Ce and Pm), Hdbm is dibenzoylmethane and L is the Schiff base; x = 2 for Ln = La–Er and x = 1 for Ln = Tm–Lu. The Schiff-base ligands are in a zwitterionic form and coordinate through the phenolic oxygen only. The X-ray single-crystal structure of $[La(dbm)_3L'_2]$ with *L'* = *N*-butyl-2-hydroxy-4-methoxybenzaldimine is described. The solution structure of lanthanum(iii) complexes has been investigated by 1D and 2D ^{1}H NMR techniques. Although the long-chain Schiff-base ligand and the tris(β-dibenzoylmethanato)lanthanide(III) complexes are non-mesomorphic, some of the adducts exhibit a monotropic smectic A phase. The mesomorphic behaviour depends on the lanthanide ion, in the sense that only a mesophase is observed for the series Ln = La–Eu, not for the heavier lanthanides.

(© Wiley-VCH Verlag GmbH & Co. KGaA, 69451 Weinheim, Germany, 2003)

Introduction

Tris(β-diketonato)lanthanide(III) complexes are well-known as NMR shift reagents.[1−3] Examples are $[Pr(fod)_3]$ and $[Eu(fod)_3]$ (fod = anion of 6,6,7,7,8,8,8-heptafluoro-2,2-dimethyl-3,5-octanedione). The shift of the proton resonances is related to the fact that organic molecules with free electron pairs (i.e. Lewis bases) can form adducts with the tris-β-diketonate complexes of paramagnetic and magnetically anisotropic lanthanide(III) ions. The coordination sphere of the lanthanide ion in a tris(β-diketonato)lanthanide(III) complex is unsaturated, since the coordination number of the metal ion in these complexes is only six, whereas lanthanide ions prefer to be coordinated to eight or nine donor atoms.[4] The lanthanide ion in the tris-β-diketonate complexes can expand its coordination sphere by forming adducts with neutral molecules containing oxygen- or nitrogen-donor atoms. Such a molecule can be water, and therefore the tris(β-diketonato)lanthanide(III) complexes can easily be transformed into bis(hydrates). However, polydentate ligands (e.g. 1,10-phenanthroline) can replace water in the first coordination sphere, and the resulting lanthanide complexes often show a strong photoluminescence. A typical example of a luminescent lanthanide complex is $[Eu(tfa)_3(phen)]$, (tta = anion of thenoyltrifluoroacetone, phen = 1,10-phenanthroline).[5−7] These luminescent complexes can find application in organic light-emitting diodes (OLEDs).[8] Binnemans and Moors have shown that Lewis-base adducts of tris(β-diketonato)lanthanide(III) complexes can be doped into a nematic liquid-crystal mixture to obtain luminescent liquid crystals.[9] Hapiot and co-workers obtained similar results by doping cholesteryl alkanoate adducts of $[Eu(tta)_3]$ into a cholesteric liquid crystal.[10,11] Of course, it would be interesting to design lanthanide β-diketonate complexes that exhibit a liquid-crystalline phase themselves, rather than relying on host-guest systems. Earlier trials to prepare liquid-crystalline lanthanide complexes with β-diketonate ligands were unsuccessful,[12] but recently two new independent approaches gave encouraging results. Galyametdinov and co-workers made monotropic liquid-crystalline lanthanide complexes starting from mesomorphic β-diketone ligands.[13] Binnemans and Lodewyckx reported in a communication on a monotropic smectic A mesophase in adducts of salicylaldimine Schiff bases to $[Ln(dbm)_3]$ complexes (dbm = anion of dibenzoylmethane).[14] In these compounds, neither the Schiff base nor the tris(β-diketonato)lanthanide(III) complex exhibit a mesophase, but the resulting bisadducts are liquid crystalline. It should be noted that the Schiff bases are the same as the ones which have been used in the past to synthesise liquid-crystalline lanthanide complexes with Schiff-base ligands.[15−18]

In the work of Binnemans and Lodewyckx,[14] the compounds were not structurally characterised, and the mesophase was investigated by polarising optical microscopy

[a] Katholieke Universiteit Leuven, Department of Chemistry, Celestijnenlaan 200F, 3001 Leuven, Belgium
Fax: (internat.) +32-16327992
E-mail: Koen.Binnemans@chem.kuleuven.ac.be
[b] Université Catholique de Louvain, Département de Chimie, 1 Place L. Pasteur, 1348 Louvain-la-Neuve, Belgium

Supporting information for this article is available on the WWW under http://www.eurjic.org or from the author.

 © 2003 Wiley-VCH Verlag GmbH & Co. KGaA, Weinheim **DOI: 10.1002/ejic.200300245**

only. In this paper, we give a detailed description of the structural and thermal properties of Schiff-base adducts of tris(dibenzoylmethanato)lanthanide(III) complexes. The crystal structure of an adduct of a Schiff base with short alkyl chains to $[La(dbm)_3]$ is described. The solution structure of diamagnetic complexes was investigated by 1D and 2D ^1H NMR methods. A series of compounds was prepared in order to investigate the influence of the lanthanide ion on the thermal properties (Figure 1). The thermal behaviour of the lanthanide complexes was investigated by polarising optical microscopy (POM), differential scanning calorimetry (DSC) and by time-resolved temperature-dependent synchrotron X-ray diffraction measurements at the DUBBLE-beamline of the ESRF (Grenoble, F).

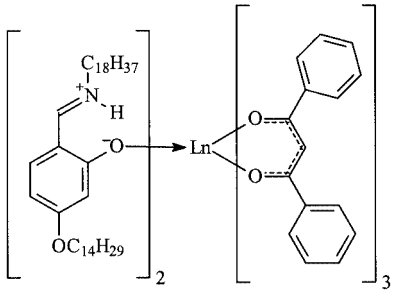

Figure 1. Schematic structure of the $[Ln(dbm)_3L_2]$ complexes

Results and Discussion

Synthesis

The Schiff-base ligands were prepared according to a literature method.[15] The tris(dibenzoylmethanato)lanthanide(III) complexes were synthesised in an ethanolic solution by first transforming dibenzoylmethane Hdbm (1,3-diphenyl-1,3-propanedione) into its sodium salt by reaction with sodium hydroxide. Secondly, the tris complexes were precipitated out of solution by addition of an aqueous solution of the corresponding lanthanide nitrate to the solution of the sodium salt of dibenzoylmethane. After drying the tris(dibenzoylmethanato)lanthanide(III) complex in a vacuum oven, the anhydrous compound was redissolved in absolute ethanol and added to two equivalents of the Schiff base dissolved in absolute ethanol. The adducts precipitated immediately. All the adducts were bisadducts (two Schiff bases bound to one lanthanide ion) whereas monoadducts were obtained for the lanthanide ions at the end of the series: thulium, ytterbium and lutetium. These ions have the smallest ionic radii among the trivalent lanthanide ions and therefore show less tendency to expand their coordination sphere. The complexes were characterised by CHN analysis and by infrared spectroscopy. The main difference between the mono- and the bis adducts is the position of the C=N stretching vibration: 1604−1606 cm^{-1} for the monoadducts and 1647−1653 cm^{-1} for the bis adducts. The stoichiometry of the complexes was not influenced by the ratio $[Ln(dbm)_3]/L$. We worked with a 1:1 ratio, so that $[Ln(dbm)_3]$ was present in excess. Complexes of all the lanthanide ions except cerium and promethium were prepared. Additionally, the lanthanum complex of the small Schiff-base ligand with methoxy and butyl chain (*N*-butyl-2-hydroxy-4-methoxybenzaldimine) was prepared for the growth of single crystals.

Crystal Structure

The X-ray single-crystal structure of $[La(dbm)_3L'_2]$ with L′ = *N*-butyl-2-hydroxy-4-methoxybenzaldimine was determined (Figure 2). According to the crystal structure, the Schiff bases coordinate as neutral ligands to the La^{III} ion i.e. the oxygen atoms of the OH group are deprotonated and the hydrogen atoms have been transferred to the nitrogen atoms. As a consequence, a zwitterionic structure (negative charge on the oxygen atom, positive charge on the imine nitrogen atom) is generated. The coordination polyhedron of the La^{III} ion, which can be described as a distorted bicapped trigonal prism, is built up of eight oxygen atoms (six oxygen atoms of the three dibenzoylmethanato ligands and two oxygen atoms of the two Schiff bases). Intramolecular N−H···O hydrogen bonds appear between the protonated nitrogen and the deprotonated oxygen atoms [average H···O distance: 1.989(8) Å]. One hydrogen (on N63) forms a second, but longer, H bond with an oxygen atom (O23) of a dibenzoylmethanato ligand [H···O distance: 2.429(5) Å]. The dihedral angle between the phenyl rings of the two Schiff-base ligands is 87.2(2)°, so the phenyl rings are positioned nearly perpendicular to each other. Both butyl chains of the Schiff bases are in the all-*trans* conformation. The dibenzoylmethanato ligands are considerably distorted: the maximum dihedral angle observed between two phenyl planes of this ligand is 24.0(2)°. A

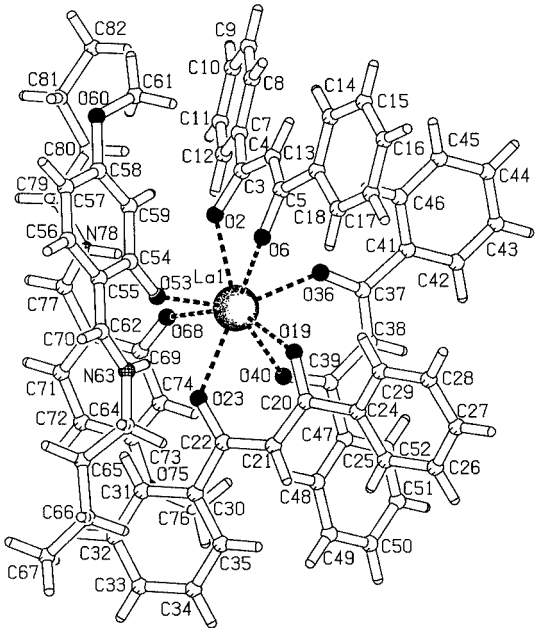

Figure 2. Molecular structure of $[La(dbm)_3L'_2]$, where L′ = *N*-butyl-2-hydroxy-4-methoxybenzaldimine

 © 2003 Wiley-VCH Verlag GmbH & Co. KGaA, Weinheim

slight stacking of phenyl rings is noticed in the packing: the shortest ring···ring distance [3.948(3) Å] is found between ring C41−C46 and ring C47−C52 of a symmetry-related complex generated by [1 − *x*, 1 − *y*, 1 − *z*]. A void of 100 Å^3 at position (0, 1/2, 1/2) contains diffuse solvent.

Structure in Solution

The coordination mode of the lanthanide ion in solution was examined by measuring one- and two-dimensional proton NMR spectra of the [La(dbm)$_3$] and [La(dbm)$_3$L$_2$] complexes (L = 2-hydroxy-*N*-octadecyloxy-4-tetradecyloxybenzaldimine) and comparing them with the ^{1}H NMR spectra of the Schiff-base ligand L and the β-diketone Hdbm. A list of all NMR resonances is given in the Exp. Sect. The proton resonances of the free ligands are sharp and show the expected splitting pattern, with the exception of the phenolic proton resonance of L, which is extremely weak and broad, due to its fast exchange with the solvent. Surprisingly, the ^{1}H NMR spectrum of the [La(dbm)$_3$L$_2$] complex at room temperature shows that the proton resonances of the dbm ligand appear as broad humps, while the proton resonances of the Schiff base L in [La(dbm)$_3$L$_2$] appear as well-resolved peaks (Figure 3). The dbm proton resonances are also very broad in the parent [La(dbm)$_3$] complex, implying either the presence of different conformers in the solution which undergo dynamic exchange, or the presence of two different modes of dbm binding to the La^{III} ion. Variable temperature ^{1}H NMR spectra of both [La(dbm)$_3$] and [La(dbm)$_3$L$_2$] complexes were measured in order to investigate the dynamic process which leads to the broadening of the dbm resonances. When the temperature of the [La(dbm)$_3$] solution was lowered to 258 K, two resolved sets of dbm peaks could be detected. The larger set of peaks, at δ = 6.85, 7.42, 7.92 and 15.52 ppm, was assigned to the free Hdbm ligand, which was confirmed by independently recording the ^{1}H NMR spectrum of the free Hdbm ligand at the same temperature. Clearly, at low temperatures the dissociation of the [La(dbm)$_3$] takes place, and at 258 K almost 95% of the complex is dissociated. However, in the [La(dbm)$_3$L$_2$] complex, dissociation at low temperatures occurs to a much smaller extent, and at 258 K only about 10% of the Hdbm ligand is dissociated from the La^{III} ion. It is likely that the adduct formation with the L ligand stabilises the binding of dbm to the central lanthanide ion.

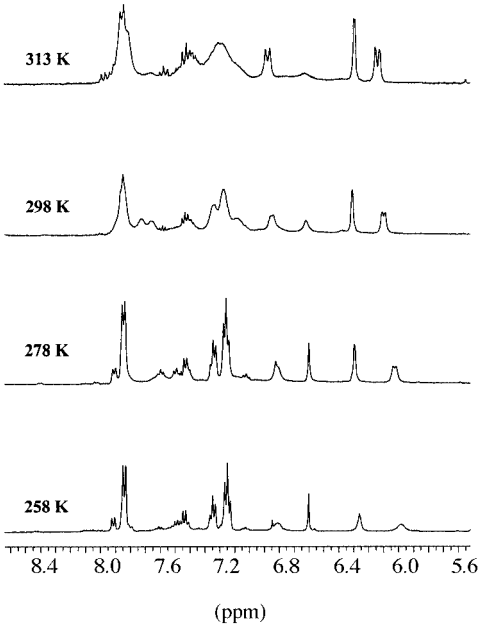

Figure 3. ^{1}H NMR spectra (400 MHz) of [La(dbm)$_3$L$_2$] in CD_2Cl_2 at different temperatures; at 313 K, the aromatic resonances of Schiff-base ligand L appear at δ = 6.16, 6.29 and 6.87 ppm; the broad humps at ca. δ = 6.65, 7.20 and 7.85 ppm belong to the diketonate ligand

The solid-state structure of the [La(dbm)$_3$L′$_2$] complex reveals the presence of intramolecular hydrogen bonding in the Schiff-base ligand. This hydrogen bonding, which occurs between the phenolic oxygen and the protonated imino nitrogen, is also found in solution. A strong, broad peak at δ = 13.3 ppm, which occurs upon complexation of the Schiff base to La^{III}, is a clear indication of the hydrogen bonding. Although the solid state structure of [La(dbm)$_3$L$_2$] suggests that the ligand L binds in a zwitterionic form, the two-dimensional ^{1}H NMR correlation spectroscopy (COSY), which was successfully used to confirm the presence of zwitterionic form of the Schiff ligand in related [LnL$_3$Cl$_3$] complexes,[19] gave no evidence that in the solution the phenolic proton has been completely transferred to the imino nitrogen. The absence of coupling between the proton at δ = 13.3 ppm and either the CH=N or N−CH$_2$ protons suggests that two extreme forms are in fast exchange: one in which the proton is bound to the phenolic oxygen, and the other in which this proton has been completely transferred to the imino nitrogen. Due to this exchange process, which takes place in the complex in solution, the N−**CH$_2$** protons appear as a broad peak (*FWHM* = 31 Hz). Even at 258 K this exchange is too fast on the NMR time scale for the two extreme forms to be distinguished by 2D COSY NMR spectroscopy.

Thermal Properties

The thermal behaviour of the complexes [Ln(dbm)$_3$L$_x$] was investigated by differential scanning calorimetry (DSC), polarising optical microscopy (POM) and high-temperature X-ray diffraction in a time-resolved mode. It should be noticed that neither L or [La(dbm)$_3$] are mesomorphic: the melting point of L is 73 °C and [La(dbm)$_3$] decomposes when heated in air.

Upon heating, [La(dbm)$_3$L$_2$] melts at 95 °C to an isotropic liquid. Upon cooling, a monotropic mesophase is formed at 81 °C. This mesophase was identified as a smectic A phase (SmA) by the typical defect texture (Figure 4): when cooling the isotropic liquid, bâtonnets formed at the clearing point and they coalesced to the focal-conic texture (fan texture). The rather low viscosity of the mesophase gives an indication that a real mesophase is present and not a plastic crystal phase. The mesophase ordering could be frozen into a glassy state. In the mesophase, the X-ray diffractograms show sharp Bragg reflections in the small angle region. The *d*-spacing values are in the ratio 1:1/2:1/3...1/*n*,

 © 2003 Wiley-VCH Verlag GmbH & Co. KGaA, Weinheim

pointing to the presence of a lamellar structure. In most of the measurements only the first-order peak and a very weak second-order peak are observable. Higher orders can be detected after longer measuring times. The *d*-spacing does not show a pronounced temperature dependence. The broad halo in the wide angle region (at $d = 4.6$ Å) shows that the alkyl chains are in a molten state. These results support identification of the phase as a smectic A phase. The *d*-spacing (ca. 27.0 Å) is much smaller than the calculated length (45.5 Å) of the Schiff-base ligand in the fully extended (all-*trans*) conformation. The most probable explanation is an interdigitation of the alkyl chains of molecules situated in adjacent smectic layers, as this is an efficient way of space filling. No major changes are seen in the X-ray diffractograms when the sample is cooled to room temperature. This is an indication that the mesophase order is frozen into a glassy state and is in agreement with the observations made on the polarising optical microscope. X-ray diffractograms of $[La(dbm)_3L_2]$ at different temperatures are shown in Figure 5.

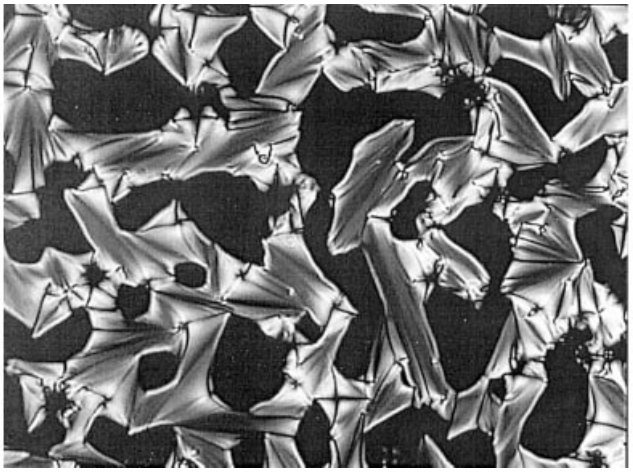

Figure 4. Texture observed for the smectic A mesophase of $[La(dbm)_3L_2]$ at 81 °C (clearing point)

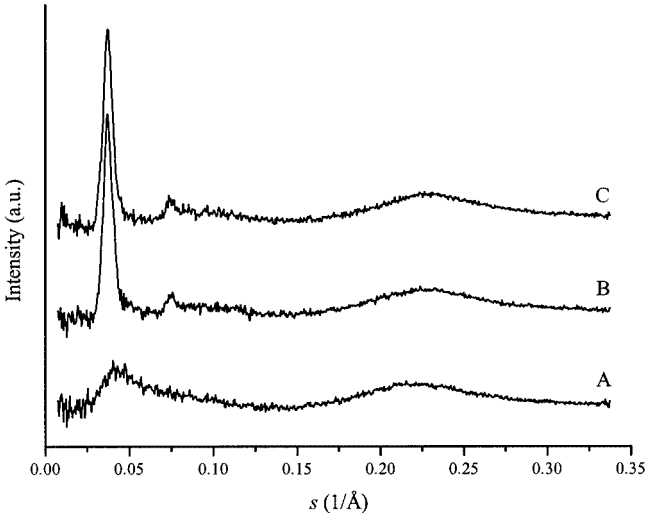

Figure 5. X-ray diffractograms for $[La(dbm)_3L_2]$. A: in isotropic liquid, B: in mesophase, C: at room temperature

The thermal behaviour of the complexes $[Ln(dbm)_3L_2]$ (Ln = Pr, Nd, Sm, Eu) resembles that of $[La(dbm)_3L_2]$ (Table 1). Hardly any variation is observed for the melting point and all these complexes form a monotropic smectic A phase. However, the temperature interval between the melting point and the clearing point becomes larger and larger when the size of the lanthanide ion decreases: $\Delta T =$ 12 °C for $[La(dbm)_3L_2]$, but $\Delta T = 30$ °C for $[Eu(dbm)_3L_2]$. The compounds of the heavier lanthanides do not form a mesophase; crystallisation occurs before a mesophase can be formed. It was difficult to decide whether or not $[Gd(dbm)_3L_2]$ and $[Tb(dbm)_3L_2]$ exhibit a mesophase, because bâtonnet-like features were observed during cooling of the melt. However, these features turned out to be very fine crystals floating in the melt. In contrast, $[Dy(dbm)_3L_2]$ and the other compounds in the lanthanide series did exhibit fast crystallisation without first forming tiny crystals. The melting point gradually decreases over the lanthanide series, with a discontinuity between Er^{III} and Tm^{III}. This can be attributed to the fact that a change in stoichiometry occurs between Er^{III} and Tm^{III} in the sense that the compounds at the end of the series contain only one Schiff-base ligand, not two.

Table 1. Transition temperatures of the $[Ln(dbm)_3L_x]$ complexes ($x = 2$ for La−Er, $x = 1$ for Tm-Lu)

Ln	Transition[a]	Temperatures (°C)
La	Cr → I	95
	I → SmA	81
Pr	Cr → I	94
	I → SmA	75
Nd	Cr → I	93
	I → SmA	71
Sm	Cr → I	93
	I → SmA	64
Eu	Cr → I	90
	I → SmA	60
Gd	Cr → I	86
Tb	Cr → I	80
Dy	Cr → I	74
Ho	Cr → I	72
Er	Cr → I	67
Tm	Cr → I	73
Yb	Cr → I	72
Lu	Cr → I	69

[a] Cr = crystalline solid; I = isotropic liquid; SmA = smectic A mesophase

These compounds are of special importance, because they form a quite unusual class of metal-containing liquid crystals (metallomesogens). It is a paradigm in metallomesogen research that in order to obtain high coordination number calamitic metallomesogens, one needs to make ligands with a very extended rigid rod-like core, or to incorporate a large number of long terminal alkyl chains.[20] None of the conditions is fulfilled in the case of the metal complexes described in this study, but nevertheless we observed a well-characterised low viscous mesophase for several of our compounds. Even more remarkable is the fact that although the size of the $[Ln(dbm)_3]$ complexes are not

 © 2003 Wiley-VCH Verlag GmbH & Co. KGaA, Weinheim

much less than that of fullerene C_{60}, it is much easier to induce a mesophase in the lanthanide complexes.[21,22] Of course, however, the [Ln(dbm)$_3$] complexes are not as space-filling as C_{60}, in the sense that free space is present between the dibenzoylmethane rings.

Conclusions

The tris(dibenzoylmethanato)lanthanide(III) complexes can form Lewis-base adducts with long-chain salicylaldimines. The number of Schiff bases bound to a metal complex depends on the size of the lanthanide ion: two for most of the lanthanides and one for the ions at the end of the lanthanide series (Tm, Yb, Lu). The molecular structure and crystal structure of an adduct of [La(dbm)$_3$] with a short-chain Schiff base were determined, and this shows that the Schiff bases line up parallel to one another. Both the X-ray crystal structure and NMR spectroscopic data show that the Schiff base in the adducts is present in a zwitterionic form. Both the stoichiometry and the thermal behaviour of the complexes depend on the size of the lanthanide ion. The complexes [Ln(dbm)$_2$L$_2$] of the series Ln = La−Eu exhibit a monotropic smectic A phase. The temperature difference between the melting point and the clearing point of the monotropic mesophase increases over the lanthanide series. The complexes of the heavier lanthanides are not liquid-crystalline. Having determined the influence of the lanthanide ion on the thermal behaviour, further studies will focus on the influence of length of the alkyl and alkoxy chain of the Schiff base and on the influence of the type of 1,3-diketone.

Experimental Section

General: ^{1}H NMR spectra were recorded with a Bruker Avance 300 and a Bruker AMX-400 spectrometer. In variable-temperature experiments the temperature error was within 0.1 K. Two-dimensional correlation spectroscopy (COSY) was used as a tool to confirm the assignment of the proton resonances. CHN elemental analyses were performed on a CE Instruments EA-1110 elemental analyser. FTIR spectra were recorded with a Bruker IFS-66 spectrometer, using the KBr pellet method. The optical textures of the mesophase were observed with an Olympus BX60 polarised optical microscope equipped with a Linkam THMS-600 hot stage and a Linkam TMS-93 programmable temperature-controller. Synchrotron X-ray measurements were made on the DUBBLE-beam line (BM26) at the European Synchrotron Radiation Facility (ESRF) in Grenoble (France).[23,24] Intensities at scattering angles between 0.134° and 6.00° were collected with a quadrant-type detector at 0.70 m from the sample.[25] Distances in real space between 133 and 2.97 Å could be covered by using an X-ray wavelength of 0.62 Å (E = 20 keV). Flat samples of 1 mm thick, placed in a brass mould and covered by aluminium foil, were mounted in a Linkam THMS600 hot stage for temperature control. The heating rate used was 10 °C min^{-1} throughout. Scattering patterns were collected sequentially for six seconds, corresponding to one pattern for each degree centigrade in the temperature ramp. The scattering angles were calibrated using the reflections of silver behenate at room temperature. No corrections were performed to account for the use of a flat detector. Data were corrected for the detector response and normalised to the intensity of the primary beam, measured at the detector position. For data reduction the XOTOKO program was used.[26]

Crystallography: Yellow crystals of [La(dbm)$_3$L′$_2$] were obtained by slow evaporation of a solution of the complex in a CH_2Cl_2/EtOH mixture. A crystal of dimensions 0.25 × 0.15 × 0.10 mm^3 was mounted in a nylon loop for data collection at 110 K on a MAR diffractometer using graphite-monochromated Mo-K_α radiation (λ = 0.71069 Å) and which was equipped with a 300 mm imaging plate detector. The images were interpreted and intensities integrated with the program DENZO.[27] The structure was solved by direct methods and refined by full-matrix least-squares on F^2 using the SHELXTL program package.[28] Non-hydrogen atoms were refined anisotropically and the hydrogen atoms in the riding mode with isotropic temperature factors fixed at 1.2-times U(eq) of the parent atoms (1.3-times for methyl groups). The disordered solvent in the void of 100 Å^3 at position 0, 1/2, 1/2 was modelled with SQUEEZE[29] (contribution of 13 electrons). Data: formula: $C_{69}H_{67}LaN_2O_{10}$; M_r = 1223.16; crystal system: triclinic, space group $P\bar{1}$, a = 10.9860(5), b = 15.4480(8), c = 19.1880(9) Å, α = 108.840(3), β = 94.240(3), γ = 103.960(4)°, V = 2949.8(2) Å^3, Z = 2; F(000) = 1264, $\rho_{calcd.}$ = 1.377 g cm^{-3}, μ = 0.786 mm^{-1}, $2\theta_{max}$ = 52.9°. No. of data collected = 34983, no. of unique data = 11756 (R_{int} = 0.075), no. of parameters refined = 744; R_1 = 0.0515 for 10049 observed reflections [$F_o > 4\sigma(F_o)$], ωR_2 = 0.1360 for all data {weighting scheme $w^{-1} = \sigma^2(F_o^2) + (0.0632P)^2 + 4.2517P$, where $P = [\max(F_o^2,0) + 2F_c^2]/3$}, S = 1.085, maximum positive and negative peaks in final difference Fourier map: 1.06 and −1.59 e·Å^{-3}. CCDC-194640 contains the supplementary crystallographic data for this paper. These data can be obtained free of charge via www.cam.ac.uk/conts/retrieving.html (or from the Cambridge Crystallographic Data Centre, 12 Union Road, Cambridge CB2 1EZ, UK; Fax: (internat.) + 44-1223/336-033; E-mail: deposit@ccdc.cam.uk).

Synthesis of Schiff-Base Ligand L (R = C$_{14}$, R′ = C$_{18}$): 2-Hydroxy-4-tetradecyloxybenzaldehyde was prepared by refluxing 2,4-dihydroxybenzaldehyde (0.1 mol, 13.82 g) with 1-bromotetradecane (0.1 mol, 27.73 g) in DMF for 4 hours, with $KHCO_3$ (0.1 mol, 10.01 g) as the base. After leaving to cool to room temperature, the reaction mixture was poured into an aqueous HCl solution (6 N). The organic layer was separated and the aqueous layer was extracted with diethyl ether. The combined organic layers were dried over anhydrous $MgSO_4$ and the solvent was removed under reduced pressure. The crude aldehyde was purified by crystallisation from hot acetonitrile. Yield: 73% (24.33 g). ^{1}H NMR (300 MHz, $CDCl_3$): δ = 0.90 (t, 3 H, CH_3), 1.02−1.60 (m, 22 H, CH_2), 1.80 (m, 2 H, CH_2−CH_2−O), 4.00 (t, 2 H, CH_2-O), 6.40 (d, 1 H, H-aryl), 9.70 (s, 1 H, CH=O) ppm. J_o = 8.5, J_m = 2.5 Hz.

The Schiff-base ligand was prepared by refluxing 2-hydroxy-4-tetradecyloxybenzaldehyde (0.05 mol, 16.72 g) with *n*-octadecylamine (0.05 mol, 13.45 g) in toluene for 3 hours. A Dean−Stark trap was used to extract the released water and a few drops of glacial acetic acid (catalyst) were added. The solvent was evaporated and the crude product was crystallised from absolute ethanol. Yield: 93% (27.20 g). ^{1}H NMR (300 MHz, $CDCl_3$): δ = 0.88 (t, 6 H, CH_3), 1.10−1.50 (m, 52 H, CH_2), 1.67 (m, 2 H, N−CH_2−CH_2), 1.77 (m, 2 H, CH_2−CH_2−O), 3.50 (t, 2 H, N−CH_2), 3.96 (t, 2 H, CH_2−O), 6.32 (dd, 1 H, H-aryl), 6.36 (d, 1 H, H-aryl), 7.06 (d, 1 H, H-aryl), 8.08 (s, 1 H, CH=N), 14.1 (s, 1 H, OH) ppm. J_o = 8.5,

 © 2003 Wiley-VCH Verlag GmbH & Co. KGaA, Weinheim

J_m = 2.5 Hz. $C_{39}H_{71}NO_2$ (585.99): calcd. C 79.94, H 12.21, N 2.39; found C 80.05, H 12.12, N 2.17.

Synthesis of [La(dbm)$_3$]: An aqueous solution of $La(NO_3)_3{\cdot}6H_2O$ (0.01 mol, 4.33 g) was added to a solution of dibenzoylmethane (0.01 mol, 2.24 g) in ethanol and 10 mL of $NaOH_{aq}$ (1 M). The mixture was stirred overnight, and then filtered and dried in vacuo. Yield: 85% (6.84 g). $C_{45}H_{33}LaO_6$ (808.7): calcd. C 66.84, H 4.11; found C 67.02, H 4.27.

Synthesis of [La(dbm)$_3$(L)$_2$]: A solution of [La(dbm)$_3$] (3 mmol; 2.42 g) in absolute ethanol was added dropwise to a solution of 2-hydroxy-*N*-octadecyloxy-4-tetradecyloxybenzaldimine (L) (3 mmol; 1.76 g) in absolute ethanol at 50 °C. The adduct precipitated immediately. After the mixture had been stirred overnight at room temperature, the precipitate was filtered off, washed with ethanol and dried in vacuo. The compound was obtained as a pale-yellow powder. Yield: 91% (2.72 g). IR (KBr): $\tilde{\nu}$ = 1654 (C=N, str.), 1552 (C=O, str.) cm^{-1}. $C_{123}H_{175}LaN_2O_{10}$ (1980.6): calcd. C 74.57, H 8.91, N 1.42; found C 74.74, H 8.97, N 1.30.

For further details of yields, elemental analysis and spectral data of the complexes, see Supporting Information (see also the footnote on the first page of this article).

Acknowledgments

KB, RVD and BG are Postdoctoral Fellows of the Fund for Scientific Research-Flanders (Belgium). Funding by the K.U.Leuven (GOA, 03/03 and a PhD grant to KL) and by the F.W.O.-Vlaanderen (G.0117.03) is gratefully acknowledged. CHN microanalyses were performed by Ms. P. Bloemen. KB, KL and BG thank FWO-Flanders and prof. H. Reynaers for their continuous support of the DUBBLE project. I.P. Dolbnya (DUBBLE, ESRF, Grenoble) assisted at the synchrotron X-ray measurements.

[1] C. C. Hinckley, *J. Am. Chem. Soc.* **1969**, *91*, 5160−5162.
[2] A. F. Cockerill, G. L. O. Davies, R. C. Harden, D. M. Rackman, *Chem. Rev.* **1973**, *73*, 553−588.
[3] J. A. Peters, J. Huskens, D. J. Raber, *Prog. Nucl. Magn. Reson. Spectrosc.* **1996**, *28*, 283−350.
[4] J. H. Forsberg, in *Gmelin Handbook of Inorganic Chemistry, Sc, Y, La-Lu Rare Earth Elements* (System Nr. 39), D3, Springer-Verlag, Berlin, **1981**, pp. 65−251 (and references therein).
[5] T. Sano, M. Fujita, T. Fujii, Y. Hamada, K. Shibata, K. Kuroki, *Jpn. J. Appl. Phys.* **1995**, *34*, 1883−1887.
[6] H. H. Li, S. Inoue, K. Machida, G. Adachi, *Chem. Mater.* **1999**, *11*, 3171−3176.
[7] K. Kuriki, Y. Koike, Y. Okamoto, *Chem. Rev.* **2002**, *102*, 2347−2356.
[8] J. Kido, Y. Okamoto, *Chem. Rev.* **2002**, *102*, 2357−2368.
[9] K. Binnemans, D. Moors, *J. Mater. Chem.* **2002**, *12*, 3374−3376.
[10] J. Boyaval, F. Hapiot, C. Li, N. Isaert, M. Warenghem, P. Carette, *Mol. Cryst. Liq. Cryst. A* **1999**, *330*, 1387−1394.
[11] J. Boyaval, C. Li, F. Hapiot, M. Warenghem, N. Isaert, Y. Guyot, G. Boulon, P. Carette, *Mol. Cryst. Liq. Cryst.* **2001**, *359*, 337−350.
[12] K. Binnemans, C. Görller-Walrand, *Chem. Rev.* **2002**, *102*, 2303−2345.
[13] Yu. G. Galyametdinov, L. V. Malykhina, W. Haase, K. Driesen, K. Binnemans, *Liq. Cryst.* **2002**, *29*, 1360−1363.
[14] K. Binnemans, K. Lodewyckx, *Angew. Chem.* **2001**, *113*, 248−250; *Angew. Chem. Int. Ed.* **2001**, *40*, 242−244.
[15] K. Binnemans, Yu. G. Galyametdinov, R. Van Deun, D. W. Bruce, S. R. Collinson, A. P. Polishchuk, I. Bikchantaev, W. Haase, A. V. Prosvirin, L. Tinchurina, I. Litvinov, A. Gubajdullin, A. Rakhmatullin, K. Uytterhoeven, L. Van Meervelt, *J. Am. Chem. Soc.* **2000**, *122*, 4335−4344.
[16] K. Binnemans, Yu. G. Galyametdinov, S. R. Collinson, D. W. Bruce, *J. Mater. Chem.* **1998**, *8*, 1551−1553.
[17] Yu. G. Galyametdinov, W. Haase, L. Malykhina, A. Prosvirin, I. Bikchantaev, A. Rakhmatullin, K. Binnemans, *Chem. Eur. J.* **2001**, *7*, 99−105.
[18] Yu. Galyametdinov, M. A. Athanassopoulou, K. Griesar, O. Kharitonova, E. A. Soto Bustamante, L. Tinchurina, I. Ovchinnikov, W. Haase, *Chem. Mater.* **1996**, *8*, 922−926.
[19] K. Binnemans, D. Moors, T. N. Parac-Vogt, R. Van Deun, D. Hinz-Hübner, G. Meyer, *Liq. Cryst.* **2002**, *29*, 1209−1216.
[20] [20a] A. M. Giroud-Godquin, P. M. Maitlis, *Angew. Chem.* **1991**, *103*, 370−398 (*Angew. Chem. Int. Ed. Engl.* **1991**, *30*, 375). [20b] S. A. Hudson, P. M. Maitlis, *Chem. Rev.* **1993**, *93*, 861−885. [20c] *Metallomesogens, Synthesis, Properties and Applications (Ed.:* J. L. Serrano) VCH, Weinheim, **1996**. [20d] D. W. Bruce, in *Inorganic Materials*, 2nd Edition, Chapter 8, p. 429 (Eds.: D. W. Bruce, D. O'Hare) Wiley,Chichester, **1996**). [20e]B. Donnio, D. W. Bruce, *Struct. Bond.* **1999**, *95*, 193−247. [20f] S. R. Collinson, D. W. Bruce, in *Transition Metals in Supramolecular Chemistry*, Chapter 7 (Ed.: J. P. Sauvage), John Wiley & Sons, New York, **1999**, p. 285).
[21] T. Chuard, R. Deschenaux, *Helv. Chim. Acta* **1996**, *79*, 736−741.
[22] T. Chuard, R. Deschenaux, *J. Mater. Chem.* **2002**, *12*, 1994−1951.
[23] M. Borsboom, W. Bras, I. Cerjak, D. Detollenaere, D. Glastra van Loon, P. Goedtkindt, M. Konijnenburg, P. Lassing, Y. K. Levine, B. Munneke, M. Oversluizen, R. van Tol, E. Vlieg, *J. Synchrotron Radiat.* **1998**, *5*, 518−520.
[24] W. Bras, *J. Macromol. Sci. Phys.* **1998**, *B37*, 557−565.
[25] A. Gabriel, F. Dauvergne, *Nucl. Instr. Meth.* **1982**, *201*, 223−224.
[26] C. Boulin, R. Kempf, M. H. J. Koch, S. M. McLaughlin, *Nuclear Instr. Meth. A* **1986**, *249*, 399−407.
[27] D. Gewirth, Z. Otwinowski, W. Minor, "*The HKL Manual − A description of programs DENZO, XDISPLAYF and SCALEPACK*" (**1995**) Yale University, New Haven (USA).
[28] SHELXTL-PC, Manual Version 5.1, Bruker Analytical X-ray Systems Inc., Madison, Wisconsin, USA, **1997**.
[29] P. van der Sluis, A. L. Spek, *Acta Crystallogr., Sect. A* **1990**, *46*, 194−201.

Received April 30, 2003

 © 2003 Wiley-VCH Verlag GmbH & Co. KGaA, Weinheim

Radical Ion Salts Obtained from Substituted Ferrocene Cations and the Organic Acceptor TCNQ − Synthesis, Structure and Physical Properties

Loreto Ballester,[a] Ana M. Gil,[a] Angel Gutiérrez,*[a] M. Felisa Perpiñán,[a] Ana E. Sánchez,[b] Marina Fonari,[c] Kinga Suwinska,[d] and Vitalii Belsky[e]

Keywords: Metallocenes / Radical ions / Stacking interactions / Supramolecular chemistry

The compounds $[Fe(C_5H_5)(C_5H_4CH_2NMe_3)][TCNQ]$ (**1**), $[Fe(C_5H_5)(C_5H_4CH_2NMe_3)][TCNQ]_2{\cdot}MeCN$ (**2**) and $[Fe(C_5H_5)(C_5H_4CH{=}CH\text{-}p\text{-}C_5H_4NMe)][TCNQ]$ (**3**) have been obtained from reaction of the corresponding ferrocene iodide and TCNQ or LiTCNQ. Their crystal structures have been determined, showing that **1** and **3** have only mononegative TCNQ radicals forming one-dimensional stacks. In compound **3** the pyridine substituent also overlaps with the stacked TCNQ. The formation reaction of **2** implies the reduction of neutral TCNQ by the iodide anion; in this reaction the reduction is partial and the formal charge of every TCNQ is approximately 0.5 e^- with some degree of electron delocalization. The TCNQs also overlap to form a one-dimensional stack in the solid. The three compounds are diamagnetic, indicating a strong antiferromagnetic coupling between the TCNQ spins.
(© Wiley-VCH Verlag GmbH & Co. KGaA, 69451 Weinheim, Germany, 2003)

Introduction

Charge-transfer salts of substituted ferrocenes with organic polynitriles have been extensively studied following the report of the bulk ferromagnetic behavior of $[Fe(C_5Me_5)_2][TCNE]$ (TCNE= tetracyanoethylene).[1] Although this is the best known derivative several other examples show a wide range of properties and stoichiometries. For example, the previously synthesized analogue $[Fe(C_5H_5)_2][TCNE]$[2−5] has a similar crystal structure, showing 1D stacks of alternating ferrocene and TCNE units, but it is, however, diamagnetic due to the higher oxidation potential of the unsubstituted ferrocene, which can not reduce the tetracyanoethylene. Consequently, the stack should be viewed as a charge-transfer complex for $[Fe(C_5H_5)_2][TCNE]$, with essentially neutral ferrocene and TCNE molecules but as an ionic salt for $[Fe(C_5Me_5)_2][TCNE]$, with alternating ferrocenium cations and $TCNE^-$ anions.[6]

The derivative with TCNQ (7,7,8,8-tetracyanoquinodimethane), $[Fe(C_5Me_5)_2][TCNQ]$, exhibits an equivalent structure, with alternating ions along the stack, and shows metamagnetic behavior.[7−8] Another phase with the same composition shows isolated dimeric $[TCNQ]_2^{2-}$ anions, with paramagnetic behaviour,[9] and a third phase with ferromagnetic behavior has a packing similar to that of the metamagnetic phase.[10] Another derivative, of formula $[Fe(C_5Me_5)_2][TCNQ]_2$, is conducting and shows a one-dimensional stack of acceptors.[11]

This variety of structural motifs and properties shows how subtle changes in electronic density or in the interionic interactions can influence the bulk properties of the material. A degenerate ground state is a necessary but not sufficient condition to obtain cooperative magnetic properties, implying the use of symmetrical ferrocenes.[12] In this way examples of ferromagnetic coupling in the stacks but without three-dimensional ferromagnetic ordering have been found in $[Fe(C_5Me_4H)_2][TCNE]$,[13] $[Fe(C_5Me_4H)_2][TCNQ]$,[13] $[Fe(C_5Me_5)_2][TCNQI_2]$,[14] or $[Fe(C_5Et_5)_2][TCNQ]$.[15] By using the stronger acceptor perfluorotetracyanoquinodimethane ($TCNQF_4$), dimerization of the anion radical similar to that in the paramagnetic phase of $[Fe(C_5Me_5)_2][TCNQ]$[9] has been observed for $[Fe(C_5Me_5)_2][TCNQF_4]$[16] and $[Fe(C_5Et_5)_2][TCNQF_4]$.[17]

Contrarily, with less symmetrically substituted ferrocenes the steric effects and intermolecular interactions determine

[a] Departamento de Química Inorgánica I, Facultad de Ciencias Químicas,
Universidad Complutense, 28040 Madrid, Spain
Fax: (internat.) + 34-913/944352
E-mail: alonso@quim.ucm.es
[b] Departamento de Ciencias Químicas, Facultad de Ciencias Experimentales y de la Salud, Universidad San Pablo C.E.U., 28668 Boadilla del Monte, Madrid, Spain
[c] Institute of Applied Physics, Academy of Science of Moldavia, Academy Str. 5, Chisinau, MD 2028, Moldavia
[d] Institute of Physical Chemistry, Polish Academy of Sciences, Kasprzaka 44/52, 01 224, Warszawa, Poland
[e] Institute of Physical Chemistry, Moscow 103064, Russia

 © 2003 Wiley-VCH Verlag GmbH & Co. KGaA, Weinheim **DOI: 10.1002/ejic.200300042**

the structural motif and the crystal packing. In this way several examples of TCNQ derivatives have been obtained. The bridged ferrocenyl $[Fe(C_5H_4)_2(CH_2)_3][TCNQ]_2$ shows dimeric anions $[TCNQ]_2^-$ stacked in non-uniform columns.[18] Substituted ferrocenes having π delocalization can overlap the π system of the TCNQ, orientating the acceptor molecules in the stack. Thus, for $[Fe(C_5H_4R)_2][TCNQ]_2$, R = CH=CHC$_6$H$_4$-*p*-SMe, the crystal structure is described as an alternating stack of TCNQ and the phenyl rings of the ferrocene substituents, giving rise to an insulating, diamagnetic derivative.[19] Similar structural features are found in $[Fe(C_5H_5)(C_5H_4CH{=}CH\text{-}9\text{-}C_{16}H_9)][TCNQ]$ with pyrene acting as both a substituent on the cyclopentadienyl ring and overlapping with the TCNQ, which remains essentially neutral.[20]

Of more interest, structurally, are compounds obtained with octamethylferrocenyl thioethers, $[Fe(C_5Me_4SR)_2]$, R = Me, *t*Bu, and TCNQ or $TCNQF_4$,[21] of which $[Fe(C_5Me_4SMe)_2]_3[TCNQ]_7$ and $[Fe(C_5Me_4S\textit{t}Bu)_2][TCNQ]_3$ show a TCNQ stack with electronic delocalization and semiconducting behaviour, while $[Fe(C_5Me_4SR)_2][TCNQF_4]$ derivatives consist of anionic dimers $[TCNQF_4]_2^{2-}$.

In designing molecular solids by controlling the crystal packing the distribution of electrostatic interactions is important. In this way we have studied the reactions of positively charged substituted ferrocenes with either neutral or anionic TCNQ. The cationic ferrocenes used are $[Fe(C_5H_5)(C_5H_4CH_2NMe_3)]^+$ and $[Fe(C_5H_5)(C_5H_4CH{=}CH\text{-}p\text{-}C_5H_4NMe)]^+$, both as iodide salts.

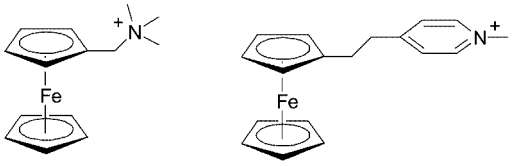

Our objective is to use these ferrocenes to build up a net of positive charges that will control the TCNQ stacking through electrostatic interactions. The size and orientation of the ferrocene cations can control the number of TCNQ units that will stack, thus inducing either the localization or the partial delocalization of electronic charges on the TCNQs. We have previously observed several examples of this modulation of charges, which gives rise to different degrees of electronic delocalization that depend on the size and packing of the counterion.[22–23]

We chose ferrocene cations as iodide salts so as to use the counterion to change the oxidation state of the TCNQ molecules involved; the half-reaction potential I_2/I^- is similar to that of TCNQ and the equilibrium $TCNQ^0 + I^- \rightleftarrows TCNQ^- + 1/2I_2$ can easily be displaced in either direction, depending on factors such as differences in solubilities of the products formed or addition of any reagents to the reaction mixture. Thus, the reaction on the right-hand side of the equilibrium is the usual method of preparing the anion radical as its lithium salt.[24] We have used the reverse reaction in forming [Cu(cyclam)(TCNQ)$_2$][TCNQ] (cyclam: 1,4,8,11-tetraazacyclotetradecane), which has one neutral and two anionic TCNQ units, from [Cu(cyclam)(TCNQ)$_2$] and I_2.[25]

The cationic charge in the ferrocene allows us to obtain derivatives of anionic TCNQ, either by iodide metathesis or by reduction from the neutral acceptor, but without any charge transfer that implies the iron atom.

Results and Discussion

The metathesis reaction of $[Fe(C_5H_5)(C_5H_4CH_2NMe_3)]^+I^-$ and LiTCNQ involves displacement of the iodide anion and crystallization of $[Fe(C_5H_5)(C_5H_4CH_2NMe_3)][TCNQ]$ (**1**). However, in the reaction of the same ferrocene salt with neutral TCNQ partial reduction of the organic molecule occurs and the derivative $[Fe(C_5H_5)(C_5H_4CH_2NMe_3)][TCNQ]_2{\cdot}MeCN$ (**2**) is formed. Since the reaction takes place in a 1:1 ratio only half of the TCNQ molecules are reduced by the iodide.

When the ferrocene salt $[Fe(C_5H_5)(C_5H_4CH{=}CH\text{-}p\text{-}C_5H_4NMe)]^+I^-$ is used $[Fe(C_5H_5)(C_5H_4CH{=}CH\text{-}p\text{-}C_5H_4NMe)][TCNQ]$ (**3**) is always obtained, either by reaction with LiTCNQ or with neutral TCNQ. In contrast to the formation of **2**, the reaction between this ferrocene salt and neutral TCNQ implies the complete reduction of the organic acceptor.

Crystal Structure Determinations

Crystal structure studies of solid compounds **1**–**3** show that they are built up of cationic ferrocene and anionic TCNQ units. Table 1 contains the more relevant bond lengths and angles.

Compound **1** crystallizes in the orthorhombic system, space group $Pna2_1$. An ORTEP view showing the labeling scheme is given in Figure 1. The structure consists of rows of TCNQ anions separated by the ferrocene cations. No close contacts between anions and cations were observed. Fe–C bond lengths are in the range 1.95(3)–2.06(2) Å and the Fe···Cp plane distances are 1.611(3) and 1.628(4) Å, the shorter distance corresponding to the substituted cyclopentadienyl ring. The Cp rings form an angle of 4.0(6)° and are within 6.7(6)° of the eclipsed conformation. All these features are similar to those previously reported for the $[Fe(C_5H_5)(C_5H_4CH_2NMe_3)]^+$ cation.[26–29]

All the TCNQ groups in the unit cell are crystallographically equivalent. Since they must neutralize the positive charges on the ferrocenes, all the TCNQ should be radical anions, bearing one negative charge per molecule. The charge located on every TCNQ can be related with the observed variation in the C–C bond lengths on reduction. The extra electron occupies an antibonding orbital and this is mainly reflected in a lengthening of the quinoid bond. A linear relation between the C–C bond lengths and the electronic charge held on the TCNQ has been established.[30–31] The values observed for compound **1** agree with the mononegative state expected for the TCNQ units. These radical-anions form a regular one-dimensional stack along the *c* axis (Figure 2) by overlap of the π clouds

 © 2003 Wiley-VCH Verlag GmbH & Co. KGaA, Weinheim

Table 1. TCNQ bond lengths [Å] for compounds **1**−**3**

1		**2**		**3**	
N2−C15	1.137(8)	N2−C15	1.144(6)	N3−C37	1.143(5)
N3−C17	1.144(8)	N3−C16	1.148(6)	N4−C39	1.144(5)
N4−C25	1.149(8)	N4−C25	1.145(6)	N5−C47	1.144(5)
N5−C26	1.145(11)	N5−C26	1.150(7)	N6−C48	1.151(6)
C15−C16	1.413(9)	C15−C17	1.434(8)	C37−C38	1.420(6)
C16−C17	1.439(10)	C16−C17	1.413(7)	C38−C39	1.415(6)
C16−C18	1.416(8)	C17−C18	1.392(6)	C38−C40	1.409(5)
C18−C19	1.420(8)	C18−C19	1.438(6)	C40−C41	1.417(5)
C18−C23	1.413(10)	C18−C23	1.432(6)	C40−C45	1.415(5)
C19−C20	1.358(7)	C19−C20	1.351(6)	C41−C42	1.359(5)
C20−C21	1.414(8)	C20−C21	1.419(6)	C42−C43	1.418(5)
C21−C22	1.407(8)	C21−C22	1.433(6)	C43−C44	1.415(5)
C21−C24	1.421(9)	C21−C24	1.381(6)	C43−C46	1.418(5)
C22−C23	1.370(9)	C22−C23	1.342(6)	C44−C45	1.358(5)
C24−C25	1.413(9)	C24−C25	1.428(8)	C46−C47	1.413(6)
C24−C26	1.422(10)	C24−C26	1.434(8)	C46−C48	1.417(6)
		N6−C27	1.146(6)	N7−C49	1.124(6)
		N7−C28	1.140(6)	N8−C51	1.144(6)
		N8−C37	1.143(7)	N9−C59	1.145(6)
		N9−C38	1.136(7)	N10−C60	1.146(6)
		C27−C29	1.415(8)	C49−C50	1.421(6)
		C28−C29	1.407(8)	C50−C51	1.407(7)
		C29−C30	1.406(6)	C50−C52	1.418(6)
		C30−C31	1.430(6)	C52−C53	1.416(5)
		C30−C35	1.413(6)	C52−C57	1.415(6)
		C31−C32	1.355(6)	C53−C54	1.365(6)
		C32−C33	1.423(6)	C54−C55	1.406(6)
		C33−C34	1.427(7)	C55−C56	1.423(5)
		C33−C36	1.387(7)	C55−C58	1.407(6)
		C34−C35	1.355(6)	C56−C57	1.357(6)
		C36−C37	1.432(8)	C58−C59	1.423(6)
		C36−C38	1.446(8)	C59−C60	1.408(7)

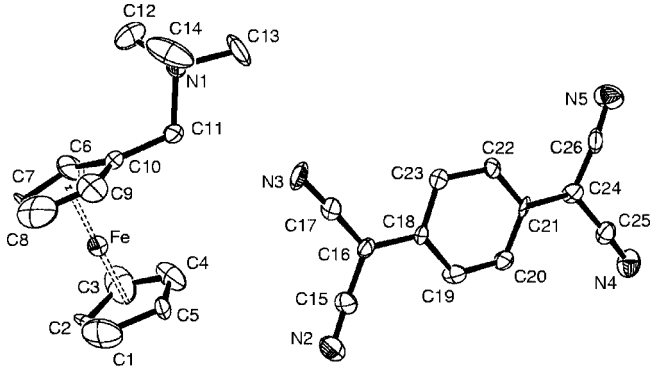

Figure 1. ORTEP view (20% probability ellipsoids) and atom labeling of compound **1**

of adjacent groups, in the ring over external bonds mode, with an intrastack separation of 3.27(1) Å. Such overlap in a regular stack of anion radicals has previously been observed;[32−33] however, dimerization is much more common, to form the dianion $[TCNQ]_2^{2-}$ which can either be isolated or form part of a non-uniform stack with alternating short and long intermolecular distances.[34−51]

Compound **2** crystallizes in the triclinic system, space group $P\bar{1}$. The asymmetric unit consists of one ferrocene cation, two TCNQ groups and one crystallization acetonitrile molecule. Figure 3 shows the numbering scheme.

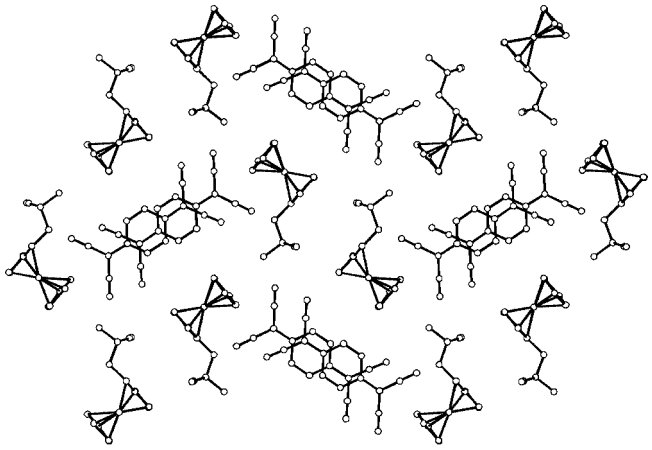

Figure 2. View of the crystal packing of compound **1** in a direction perpendicular to the *c* axis

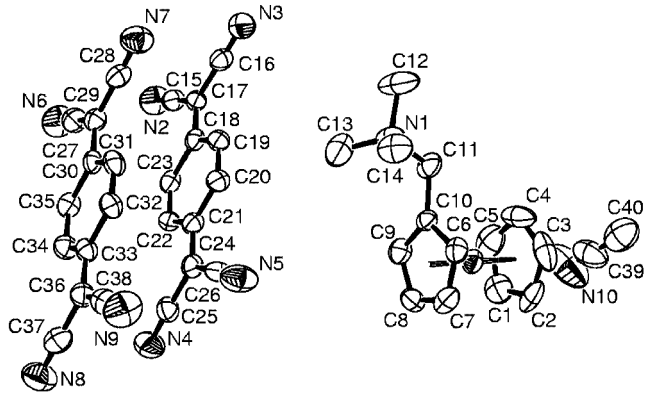

Figure 3. ORTEP view (30% probability ellipsoids) and atom labeling of compound **2**

The ferrocene cation shows similar features to those of compound **1**, with Fe−C bond lengths in the range 2.014(6)−2.048(4) Å and Fe···Cp plane distances of 1.634(6) and 1.658(5) Å − again the shortest distance corresponds to the substituted ring. The Cp rings are almost parallel, with 1.7(1)° of deviation, and are within 7.8(1)° of the eclipsed conformation.

There are two crystallographically different TCNQ molecules, types A and B. According to the Kistenmacher relation between C−C bond lengths and the negative charge located on every TCNQ,[31] we have found that TCNQ A has an approximate charge of 0.4 e^- while TCNQ B bears, approximately 0.6 e^-, i.e. two TCNQ neutralize the positive charge on the substituted ferrocene. The TCNQs are stacked in the ring over external bond mode (Figure 4) to form a one-dimensional row with the pattern ···TCNQ A···TCNQ B···TCNQ B···TCNQ A···TCNQ A···. The TCNQ As are related by inversion centers located between adjacent units. The same applies for TCNQ Bs. The angle between least-squares ring planes of TCNQ A and TCNQ B is 1.8(1)°. Thus, all the TCNQs in the stack are practically parallel since all TCNQ As are parallel, due to symmetry, as occurs with TCNQ Bs.

 © 2003 Wiley-VCH Verlag GmbH & Co. KGaA, Weinheim

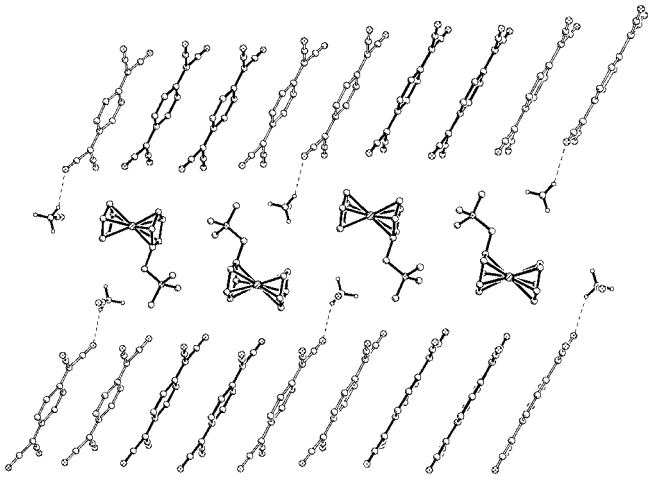

Figure 4. TCNQ stack in compound **2**; TCNQ A is depicted in black and TCNQ B in white, showing close contacts with the acetonitrile solvent molecules

The very similar intermolecular distances give rise to a quasi-uniform stack; with the shortest distance being between least-squares ring planes of TCNQ A and TCNQ B, 3.27(1) Å, followed by the separation between adjacent TCNQ As, 3.32(1) Å, and that between two TCNQ Bs, 3.34(1) Å. We can reconcile this stack with several reported examples of regularly spaced $TCNQ^{0.5-}$.[52−56]

The ferrocene cations and the acetonitrile molecules are located between the parallel rows of TCNQ. The acetonitrile molecule binds TCNQ A and B that belong to neighboring rows at the distances 3.268(9) and 3.445(8) Å

The (ethylenepyridinium)ferrocene **3** crystallizes in the triclinic system, space group $P\bar{1}$. The asymmetric unit is composed by two crystallographically independent ferrocene cations and two independent TCNQ anions. The numbering scheme is shown in Figure 5.

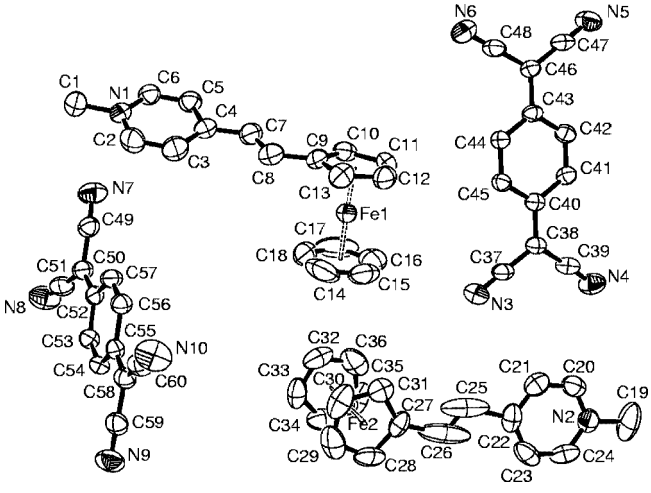

Figure 5. ORTEP view (30% probability ellipsoids) and atom labeling of compound **3**

Both ferrocene units show equivalent features and, in general terms, are similar to the trimethylammoniummethyl derivatives in **1** and **2**. For the two ferrocene units the Fe−C bond lengths are in the range 1.997(6)−2.039(4) and 2.016(5)−2.028(5) Å, respectively, with Fe···Cp plane distances of 1.630(6) and 1.647(5) Å for the first ferrocene (labeled A) and 1.642(5) and 1.649(5) Å for the second (labeled B); in both cases the shortest distance corresponds to the substituted ring. The Cp rings are almost parallel, deviating by 1.1(1)° in ferrocene A and 2.9(1)° in ferrocene B, and are, respectively, within 9.2(1)° and 22.3(1)° of the eclipsed conformation. Both ferrocene cations are almost perpendicular, forming an angle of 84(1)° between them.

There are also two crystallographically different TCNQ molecules (A and B) in the crystal; both are negatively charged to neutralize the ferrocene cations and thus bear one electron per molecule, as the C−C distances confirm.

The TCNQ As are dimerized by a ring over external bond overlap, with a distance between mean planes of 3.12(1) Å. These dimers are stacked to form a non-uniform

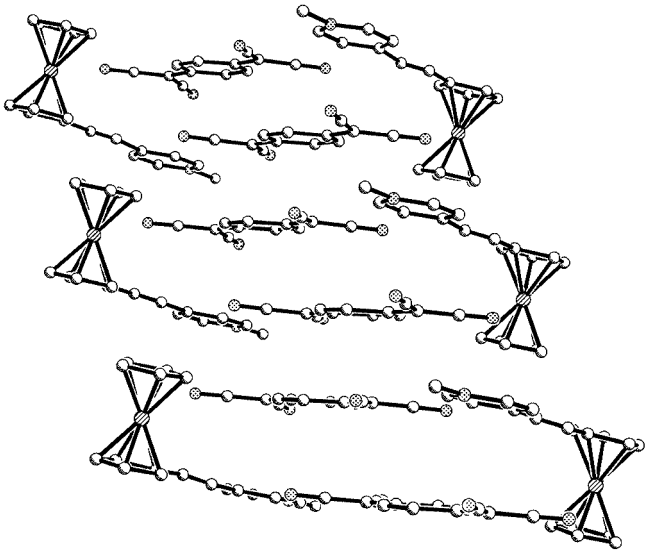

Figure 6. View of the stack of TCNQ A in compound **3** showing the overlap with the pyridine rings (see text)

one-dimensional chain (Figure 6) by overlap of the exocyclic dicyanomethyl groups of one end of the molecule, with a shortest distance of 3.35(1) Å. The other extreme of each TCNQ overlaps with the pyridine ring of the ferrocene B cations, showing a shortest contact of 3.33(2) Å. Overlap with the substituent π systems has been observed in other ferrocene derivatives, but only for neutral TCNQ[19,20] or isolated radical anions,[57] leading in all cases to alternated stacks of donors and acceptors. In our case, such overlap occurs at one end only of each TCNQ, thus allowing the formation of the TCNQ stack.

In the crystal packing, zig-zagged TCNQ chains are stacked parallel to each other, leaving holes that are occupied by the ferrocene cations. The other TCNQs, type B, form isolated dimers $[TCNQ]_2^{2-}$, with an interplanar spacing of 3.05(1) Å, and ring over external bond overlap. These dimers are oriented almost perpendicularly to the TCNQ A

 © 2003 Wiley-VCH Verlag GmbH & Co. KGaA, Weinheim

chains, forming an angle of 88.4° between the respective molecular planes (Figure 7).

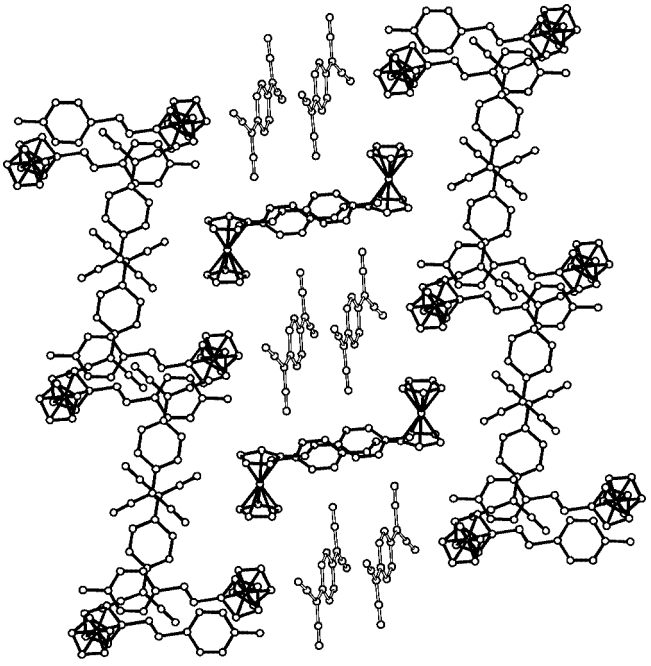

Figure 7. Crystal packing in compound **3**; TCNQ A is in black and TCNQ B in white

Finally the ferrocene A cations are located in the channels left by the stacks of TCNQ A and the dimers of TCNQ B (Figure 7). This ferrocene is perpendicular to all of the TCNQs and no π interactions are found.

Spectroscopic Studies

IR spectra are a very useful source of information about the formal oxidation state of the TCNQ molecules. The most characteristic bands[58−60] are ν(CN), which appears at 2228 cm^{-1} in neutral TCNQ and is shifted to lower frequencies and split (2194/2177 cm^{-1}) in the radical anion, the $\nu_{20}(b_{1u})$ and the $\nu_4(a_g)$ bands assignable to C−C stretching modes and which appear at 1530 and 1424 cm^{-1} in the neutral TCNQ and are shifted to 1507 and 1386 cm^{-1} in the anionic TCNQ. The last significant band is $\nu_{50}(b_{3u})$, an out-of-plane bending mode appearing at 860 cm^{-1} in neutral and 824 cm^{-1} in anionic TCNQ. The last three vibration modes are shifted almost linearly to lower frequencies with increasing negative charge on the TCNQ and are, thus, a good indication of its oxidation state.[60]

In compound **1** these bands appear at 2188, 2173, 2161, 2149, 1508, 1356 and 821 cm^{-1} respectively, clearly indicating the mononegative nature of TCNQ suggested by the crystal structure. The large split of the ν(CN) bands can be attributed to the non-equivalence of the TCNQ nitrile groups that are crystallographically different. Similar features are observed in the IR spectrum of compound **3**, with bands at 2184, 2168, 2146, 1506, 1350 and 823 cm^{-1}.

In contrast, the IR spectrum of compound **2** is dominated by the tail of an electronic absorption with broad vibrational bands superimposed on it − a typical feature of derivatives with a degree of electronic delocalization along the TCNQ stacks.[61−62] This electronic absorption is observed in the Vis/NIR spectrum centered at 4500 cm^{-1} and can be assigned to the low energy charge-transfer transition, CT_2, between radical-anion and neutral TCNQ.[63] The most significant TCNQ IR bands appear at 2197, 2156, 1519, 1410 and 833 cm^{-1}. Assuming a linear relation between the electronic charge in the TCNQ and the frequency shift of ν_{20} we can attribute a formal charge of 0.5 e^- per TCNQ, in agreement with the assignation made by crystallographic means. The other bands, ν_4 and ν_{50}, do not show this linear shift although their intermediate values clearly indicate that the TCNQ are in an intermediate oxidation state.[22−23]

Due to the partial electronic delocalization compound **2** is weakly semiconducting, with a room temperature conductivity of 10^{-4} S cm^{-1} (measured in a powder pressed sample). Conversely, compounds **1** and **3**, with only the mononegative radical anion present, have conductivities below 10^{-6} S cm^{-1} at room temperature.

The three compounds are diamagnetic, implying that the radical anions formed must interact antiferromagnetically with adjacent molecules in order to pair their spins. This is common for TCNQ derivatives that form the dimeric dianion $[TCNQ]_2^{2-}$.[25,48] The diamagnetism of compound **2** is surprising since the electronic delocalization is usually reflected in the magnetic susceptibility, either as a weak Pauli paramagnetism[64] or as the contribution of an $S = 1/2$ spin 1D system with antiferromagnetic coupling.[23,65] The unexpected diamagnetism of **2** could suggest a higher localization of the TCNQ unpaired electrons, giving rise to a stronger antiferromagnetic coupling in the bulk.

Conclusion

Cationic ferrocenium salts react with LiTCNQ by a metathesis process to form the corresponding [Ferrocene][TCNQ] derivatives **1** and **3**, which behave as typical salts of the anion radical $TCNQ^-$, forming dimeric anions, $[TCNQ]_2^{2-}$, that overlap with neighbouring dimers to give a non-uniform one-dimensional stack. A typical stack is found in **1**, but that of **3** is highly unusual as the TCNQ radical anions also overlap with the π-delocalized system of the pyridinium substituent. Such overlap is common in integrated systems of neutral TCNQ but extremely rare with anionic TCNQ, and in the reported cases the integrated stack is formed by dimeric $[TCNQ]_2^{2-}$ [66] or trimeric $[TCNQ]_3^{2-}$ [67] overlapping with the cationic donor. To the best of our knowledge there are no previous reports of overlap between 1D-stacked TCNQ and the counterion.

Compound **2** is also formed by rows of stacked TCNQ separated by the cationic ferrocenes, with only electrostatic interactions between them. The TCNQ are, however, partially reduced as a consequence of the crystal packing conditions, which will probably determine the equilibrium between the TCNQ and the iodide anion. Figure 4 shows that the TCNQ stack leaves space for two ferrocene cations and

 © 2003 Wiley-VCH Verlag GmbH & Co. KGaA, Weinheim

two acetonitrile molecules. If these solvent molecules were removed the ferrocene could be closely packed, occupying the space equivalent to three TCNQ. The resulting stoichiometry [ferrocene]$_2$[TCNQ]$_3$ is also well known,[22,51] with structures described as trimeric dianions [TCNQ]$_3^{2-}$ stacked in infinite rows. Inside the trimer every TCNQ bears approximately $^2/_3$ of an electron and the difference between this oxidation state and that found on our compound (0.5 of an electron) is small and would not determine the extent of TCNQ reduction. Therefore, we attribute the partial reduction to the need to accommodate two TCNQ groups in the stack per ferrocene and acetonitrile molecules.

The complete displacement of the reaction with iodide in the formation of **3** by either metathesis with LiTCNQ or by reduction of neutral TCNQ supports the influence of the crystal structure on the TCNQ reduction. The driving force here is the overlap between the TCNQ anions and the pyridinium substituent in the ferrocenes. Figure 6 shows that TCNQ and pyridinium alternate along the stack and that consecutive TCNQ anions overlap with ferrocenes of different rows. This packing does not allow room for extra TCNQ molecules and thus the reduction with iodide must be complete since there is only now one TCNQ per ferrocenium cation. The remaining cations and TCNQ anions in this structure are oriented perpendicularly relative to the stacks, forcing the isolation of both the anions as dimeric [TCNQ]$_2^{2-}$ and the cations, and leaving electrostatic interactions as the only force that holds them together.

Experimental Section

General Remarks: All reactions were carried out under an inert gas. LiTCNQ was obtained according to a published method[24] and its purity checked by elemental analysis. Elemental analyses were carried out by the Servicio de Microanálisis of the Universidad Complutense de Madrid. Infrared spectra were recorded as KBr pellets with a Nicolet Magna-550 FT-IR spectrophotometer. Magnetic susceptibility experiments were made on polycrystalline samples using a Quantum Design SQUID magnetometer, Model MPMS-5S in the temperature range 2−250 K and at constant field of 0.5 T. Electrical conductivity measurements at room temperature were performed by the two points method in pressed powdered samples.[68]

[Fe(C$_5$H$_5$)(C$_5$H$_4$CH$_2$NMe$_3$)][TCNQ] (1): [Fe(C$_5$H$_5$)(C$_5$H$_4$CH$_2$NMe$_3$)](I) (135 mg; 0.35 mmol) was dissolved in methanol/water (20 mL of 3:1 mixture) and then LiTCNQ (148 mg; 0.70 mmol), dissolved in methanol (35 mL), was slowly added to the double layer. After 3 d, dark blue crystals of the title compound appeared, which were filtered off and washed with methanol. The crystals were suitable for X-ray analysis. Yield: 104 mg, 64%. IR (KBr): $\tilde{\nu}$ = 2188, 2173, 2161, 2149, 1582, 1508, 1485, 1369, 1356, 1324, 1179, 881, 843, 821, 480 cm^{-1}. C$_{26}$H$_{24}$FeN$_5$ (462.3): calcd. C 67.6, H 5.2, N 15.1; found C 67.4, H 5.1, N 14.9.

[Fe(C$_5$H$_5$)(C$_5$H$_4$CH$_2$NMe$_3$)][TCNQ]$_2$·MeCN (2): A solution of TCNQ (79 mg; 0.39 mmol) in acetonitrile (40 mL) was mixed with a solution of [Fe(C$_5$H$_5$)(C$_5$H$_4$CH$_2$NMe$_3$)](I) (150 mg; 0.39 mmol) in acetonitrile/water (15 mL of a 2:1 mixture). The resulting green solution was concentrated to half of its original volume and cooled to −20 °C. Dark-violet platelets then appeared after 2 d. Yield: 48 mg, 35%. IR (KBr): $\tilde{\nu}$ = 2197, 2156, 1558, 1519, 1469, 1410, 1298, 1104, 1045, 870, 833, 683, 593, 480 cm^{-1}. C$_{40}$H$_{31}$FeN$_{10}$ (707.6): calcd. C 67.9, H 4.4, N 19.8; found C 67.8, H 4.4, N 19.6.

[Fe(C$_5$H$_5$)(C$_5$H$_4$CH=CH-*p*-C$_5$H$_4$NMe)][TCNQ] (3): This was obtained by reaction in a double layer of [Fe(C$_5$H$_5$)(C$_5$H$_4$CH=CH-*p*-C$_5$H$_4$NMe)](I) (150 mg; 0.35 mmol) in methanol (15 mL) with either an acetonitrile (20 mL) solution of TCNQ (71 mg; 0.35 mmol) or a methanolic (30 mL) solution of LiTCNQ (147 mg; 0.70 mmol). In both cases dark red prismatic crystals suitable for X-ray were obtained after 1 week. Yield: 55 mg, 31%. IR (KBr): $\tilde{\nu}$ = 2184, 2168, 2146, 1646, 1607, 1577, 1506, 1475, 1458, 1370, 1350, 1195, 1180, 950, 879, 823, 716, 475 cm^{-1}. C$_{30}$H$_{22}$FeN$_5$ (508.4): calcd. C 70.9, H 4.4, N 13.8; found C 70.6, H 4.4, N 13.4.

X-ray Crystallographic Studies: A summary of the relevant data collection parameters is given in Table 2. Data were collected with a Bruker AXS-CCD, Enraf−Nonius CAD-4, and Nonius CCD[69] for **1**, **2** and **3**, respectively, by using graphite-monochromatized Mo-K_α radiation (λ = 0.71073 Å) at room temperature. The structures were solved by Patterson or direct methods and refined by full-matrix least squares on F^2 with anisotropic thermal parameters for the non-hydrogen atoms. The hydrogen atoms were included with fixed isotropic contributions at their calculated positions determined by molecular geometry. The calculations were carried out with SHELX-97 software package.[70] CCDC-201484 (**1**), -201485 (**2**), -201486 (**3**) contain the supplementary crystallographic data for this paper. These data can be obtained free of charge at www.ccdc.cam.ac.uk/conts/retrieving.html [or from the Cambridge Crystallographic Data Centre, 12 Union Road, Cambridge CB2 1EZ, UK; Fax: (internat.) + 44-1223/336-033; E-mail: deposit@ccdc.cam.ac.uk].

Table 2. Crystal and refinement data for compounds **1**−**3**

	1	**2**	**3**
Empirical formula	C$_{26}$H$_{24}$FeN$_5$	C$_{40}$H$_{31}$FeN$_{10}$	C$_{30}$H$_{22}$FeN$_5$
Formula mass	462.3	707.6	508.3
Crystal system	orthorhombic	triclinic	triclinic
Space group	*Pna*2$_1$ (no. 33)	*P*$\bar{1}$ (no. 2)	*P*$\bar{1}$ (no. 2)
a [Å]	16.909(1)	10.562(2)	7.516(2)
b [Å]	20.748(1)	11.277(2)	14.913(3)
c [Å]	6.541(1)	15.328(3)	22.561(5)
α [°]	90	101.09(3)	100.23(3)
β [°]	90	100.74(3)	98.40(3)
γ [°]	90	91.25(3)	94.88(3)
Z	4	2	4
V [Å^3]	2294.7(4)	1757.1(6)	2445.8(10)
$D_{calcd.}$ [Mg·m^{-3}]	1.338	1.337	1.381
μ [cm^{-1}]	6.80	4.74	6.45
θ range [°]	1.55−24.97	1.84−20.95	1.52−24.97
Reflections collected	4082	7084	4480
Independent reflections	2041	3711	4105
Refined parameters	289	461	649
Goodness of fit	1.037	1.077	1.055
Absolute structure parameter	0.04(11)		
$R1$[a] [$I > 2\sigma(I)$]	0.0404	0.063	0.0359
$wR2$[b] [$I > 2\sigma(I)$]	0.0812	0.1083	0.095

[a] $R1 = \Sigma(|F_o| - |F_c|)^2/\Sigma F_o^2$. [b] $wR2 = \{\Sigma[w(F_o^2 - F_c^2)^2]/\Sigma[w(F_o^2)^2]\}^{1/2}$.

 © 2003 Wiley-VCH Verlag GmbH & Co. KGaA, Weinheim

Acknowledgments

We gratefully acknowledge the Spanish Ministerio de Ciencia y Tecnología, project BQU2002-01409, for financial support.

[1] J. S. Miller, J. C. Calabrese, H. Rommelmann, S. Chittipeddi, A. J. Epstein, J. H. Zhang, W. M. Reiff, *J. Am. Chem. Soc.* **1987**, *109*, 769−781.
[2] O. W. Webster, W. Mahler, R. E. Benson, *J. Am. Chem. Soc.* **1962**, *84*, 3678−3684.
[3] M. Rosenblum, R. W. Fish, C. Bennett, *J. Am. Chem. Soc.* **1964**, *86*, 5166−5170.
[4] E. Adman, M. Rosenblum, S. Sullivan, T. N. Margulis, *J. Am. Chem. Soc.* **1967**, *89*, 4540−4542.
[5] B. W. Sullivan, B. M. Foxman, *Organometallics* **1983**, *2*, 187−189.
[6] J. S. Miller, J. C. Calabrese, A. J. Epstein, R. W. Bigelow, J. H. Zhang, W. M. Reiff, *J. Chem. Soc., Chem. Commun.* **1986**, 1026−1028.
[7] G. A. Candela, L. J. Swartzendruber, J. S. Miller, M. J. Rice, *J. Am. Chem. Soc.* **1979**, *101*, 2755−2756.
[8] J. S. Miller, A. H. Reis, E. Gebert, J. J. Ritsko, W. R. Salaneck, L. Kovnat, T. W. Cape, R. P. Van Duyne, *J. Am. Chem. Soc.* **1979**, *101*, 7111−7113.
[9] A. H. Reis, L. D. Preston, J. M. Williams, S. W. Peterson, G. A. Candela, L. J. Swartzendruber, J. S. Miller, M. J. Rice, *J. Am. Chem. Soc.* **1979**, *101*, 2756−2758.
[10] W. E. Broderick, D. M. Eichhorn, X. Liu, P. J. Toscano, S. M. Owens, B. M. Hoffman, *J. Am. Chem. Soc.* **1995**, *117*, 3641−3642.
[11] J. J. Ritsko, P. Nielsen, J. S. Miller, *J. Chem. Phys.* **1977**, *67*, 687−690.
[12] J. S. Miller, D. T. Glatzhofer, C. Vazquez, R. S. Mclean, J. C. Calabrese, W. J. Marshall, J. W. Raebiger, *Inorg. Chem.* **2001**, *40*, 2058−2064.
[13] J. S. Miller, D. T. Glatzhofer, D. M. O'Hare, W. M. Reiff, A. Chakraborty, A. J. Epstein, *Inorg. Chem.* **1989**, *28*, 2930−2939.
[14] J. S. Miller, J. C. Calabrese, R. L. Harlow, D. A. Dixon, J. H. Zhang, W. M. Reiff, S. Chittipeddi, M. A. Selover, A. J. Epstein, *J. Am. Chem. Soc.* **1990**, *112*, 5496−5506.
[15] K. Chi, J. C. Calabrese, W. M. Reiff, J. S. Miller, *Organometallics* **1991**, *10*, 688−693.
[16] J. S. Miller, J. H. Zhang, W. M. Reiff, *Inorg. Chem.* **1987**, *26*, 600−608.
[17] D. Stein, H. Stizmann, R. Boese, E. Dormann, H. Winter, *J. Organomet. Chem.* **1991**, *412*, 143−155.
[18] C. Willi, A. H. Reis, E. Gebert, J. S. Miller, *Inorg. Chem.* **1981**, *20*, 313−318.
[19] A. Togni, M. Hobi, G. Rihs, G. Rist, A. Albinati, P. Zanello, D. Zech, H. Keller, *Organometallics* **1994**, *13*, 1224−1234.
[20] J. D. McKinney, P. A. Anderson, T. A. Hamor, C. J. Jones, K. Paxton, A. Porch, *J. Organomet. Chem.* **1998**, *558*, 147−153.
[21] S. Zürcher, J. Petrig, V. Gramlich, M. Wörle, C. Mensing, D. von Arx, A. Togni, *Organometallics* **1999**, *18*, 3679−3689.
[22] L. Ballester, A. M. Gil, A. Gutiérrez, M. F. Perpiñán, M. T. Azcondo, A. E. Sánchez, E. Coronado, C. J. Gómez-García, *Inorg. Chem.* **2000**, *39*, 2837−2842.
[23] L. Ballester, A. M. Gil, A. Gutiérrez, M. F. Perpiñán, M. T. Azcondo, A. E. Sánchez, C. Marzin, G. Tarrago, C. Bellitto, *Chem. Eur. J.* **2002**, *8*, 2539−2548.
[24] L. R. Melby, R. J. Herder, W. Mahler, R. E. Benson, W. E. Mochel, *J. Am. Chem. Soc.* **1962**, *84*, 3374−3387.
[25] L. Ballester, A. M. Gil, A. Gutiérrez, M. F. Perpiñán, M. T. Azcondo, A. E. Sánchez, U. Amador, J. Campo, F. Palacio, *Inorg. Chem.* **1997**, *23*, 5291−5298.
[26] U. Siriwardane, S. S. C. Chu, N. S. Hosmane, H. Zhu, G. Zhang, *Acta Crystallogr., Sect. C* **1989**, *45*, 333−336.
[27] G. Ferguson, J. F. Gallagher, C. Glidewell, C. M. Zakaria, *Acta Crystallogr., Sect. B* **1994**, *50*, 146−150.
[28] Z. H. Chohan, A. Howie, J. L. Wardell, R. Wilkens, S. M. S. V. Doidge-Harrison, *Polyhedron* **1997**, *16*, 2689−2696.
[29] A. E. Pullen, C. Faulmann, K. I. Pokhodnya, P. Cassoux, M. Tokumoto, *Inorg. Chem.* **1998**, *37*, 6714−6720.
[30] S. Flandrois, D. Chasseau, *Acta Crystallogr., Sect. B* **1977**, *33*, 2744−2750.
[31] T. J. Kistenmacher, T. J. Emge, A. N. Bloch, D. O. Cowan, *Acta Crystallogr., Sect. B* **1982**, *38*, 1193−1199.
[32] I. Shirotani, H. Kobayashi, *Bull. Chem. Soc. Jpn.* **1973**, *46*, 2595−2596.
[33] T. Inabe, K. Okaniwa, H. Ogata, H. Okamoto, T. Mitani, Y. Maruyama, *Acta Chim. Hung.* **1993**, *130*, 537−554.
[34] A. Hoekstra, T. Spoelder, A. Vos, *Acta Crystallogr., Sect. B* **1972**, *28*, 14−25.
[35] S. Z. Goldberg, B. D. Spivack, G. Stanley, R. Eisenberg, D. M. Braitsch, J. S. Miller, M. Abkowitz, *J. Am. Chem. Soc.* **1977**, *99*, 110−117.
[36] H. Endres, H. J. Keller, W. Moroni, D. Nothe, V. Dong, *Acta Crystallogr., Sect. B* **1978**, *34*, 1703−1705.
[37] Y. Yamamoto, H. Yamazaki, *Inorg. Chim. Acta* **1984**, *85*, 83−87.
[38] M. D. Ward, D. C. Johnson, *Inorg. Chem.* **1987**, *26*, 4213−4227.
[39] J. S. Miller, J. H. Zhang, W. M. Reiff, D. A. Dixon, L. D. Preston, A. H. Reis, E. Gebert, M. Extine, J. Troup, A. J. Epstein, M. D. Ward, *J. Phys. Chem.* **1987**, *91*, 4344−4360.
[40] A. Bencini, S. Midollini, C. Zanchini, *Inorg. Chem.* **1989**, *28*, 1963−1969.
[41] M. D. Ward, P. J. Fagan, J. C. Calabrese, D. C. Johnson, *J. Am. Chem. Soc.* **1989**, *111*, 1719−1732.
[42] M. C. Grossel, F. A. Evans, J. A. Hrijac, K. Prout, S. C. Weston, *J. Chem. Soc., Chem. Commun.* **1990**, 1494−1495.
[43] H. Oshio, E. Ino, I. Mogi, T. Ito, *Inorg. Chem.* **1993**, *32*, 5697−5703.
[44] F. Cecconi, C. A. Ghilardi, S. Midollini, A. Orlandini, *Inorg. Chim. Acta* **1993**, *214*, 13−15.
[45] M. C. Grossel, P. B. Hitchcock, K. R. Seddon, T. Welton, S. C. Weston, *Chem. Mater.* **1994**, *6*, 1106−1108.
[46] M. C. Muñoz, J. Cano, R. Ruiz, F. Lloret, J. Faus, *Acta Crystallogr., Sect. C* **1995**, *51*, 873−876.
[47] L. Ballester, A. Gutiérrez, M. F. Perpiñán, M. T. Azcondo, A. E. Sánchez, U. Amador, *An. Quim.* **1996**, *92*, 275−279.
[48] L. Ballester, A. Gutiérrez, M. F. Perpiñán, U. Amador, M. T. Azcondo, A. E. Sánchez, C. Bellitto, *Inorg. Chem.* **1997**, *36*, 6390−6396.
[49] R. Buchner, J. S. Field, R. J. Haines, *J. Chem. Soc., Dalton Trans.* **1997**, 2403−2408.
[50] S. Le Stang, F. Conan, J. Sala Pala, Y. Le Mest, M. T. Garland, R. Baggio, E. Faulques, A. Leblanc, P. Molinie, L. Toupet, *J. Chem. Soc., Dalton Trans.* **1998**, 489−496.
[51] M. T. Azcondo, L. Ballester, S. Gohlen, A. Gutiérrez, L. Ouahab, S. Yartsev, P. Delhaes, *J. Mater. Chem.* **1999**, *9*, 1237−1244.
[52] H. Kobayashi, F. Marumo, Y. Saito, *Acta Crystallogr., Sect. B* **1971**, *27*, 373−378.
[53] T. J. Kistenmacher, T. E. Phillips, D. O. Cowan, *Acta Crystallogr., Sect. B* **1974**, *30*, 763−768.
[54] R. M. Lequan, M. Lequan, G. Jaouen, L. Ouahab, P. Batail, J. Padiou, R. G. Sutherland, *J. Chem. Soc., Chem. Commun.* **1985**, 116−118.
[55] J. C. Galluci, G. Opromolla, L. A. Paquette, L. Pardi, P. F. T. Schirch, M. R. Sivik, P. Zanello, *Inorg. Chem.* **1993**, *32*, 2292−2297.
[56] M. Fourmigue, V. Perrocheau, R. Clerac, C. Coulon, *J. Mater. Chem.* **1997**, *7*, 2235−2241.
[57] V. J. Murphy, D. O'Hare, *Inorg. Chem.* **1994**, *33*, 1833−1841.
[58] R. Bozio, A. Girlando, C. Pecile, *J. Chem. Soc., Faraday Trans.* **1975**, *71*, 1237−1254.
[59] F. Bigoli, P. Deplano, F. A. Devillanova, A. Girlando, V. Lip-

 © 2003 Wiley-VCH Verlag GmbH & Co. KGaA, Weinheim

polis, M. L. Mercuri, M. A. Pellinghelli, E. F. Trogu, *Inorg. Chem.* **1996**, *35*, 5403−5406.

[60] F. Bigoli, P. Deplano, F. A. Devillanova, A. Girlando, V. Lippolis, M. L. Mercuri, M. A. Pellinghelli, E. F. Trogu, *J. Mater. Chem.* **1998**, *8*, 1145−1150.

[61] M. Inoue, M. B. Inoue, *J. Chem. Soc., Faraday Trans. 2* **1985**, *81*, 539−547.

[62] E. Ghezzal, A. Brau, J. P. Farges, P. Dupuis, *Mol. Cryst. Liq. Cryst.* **1992**, *211*, 327−330.

[63] J. B. Torrance, *Acc. Chem. Res.* **1979**, *12*, 79−86.

[64] J. M. Williams, J. R. Ferraro, R. J. Thorn, K. D. Carlson, U. Geiser, H. H. Wang, A. M. Kini, M. H. Whangbo, *Organic Superconductors. Synthesis, Structure, Properties and Theory* (Ed.: R. N. Grimes), Prentice Hall, Englewood Cliffs, New Jersey, USA, **1992**.

[65] L. Ballester, A. Gutiérrez, M. F. Perpiñán, S. Rico, M. T. Azcondo, C. Bellitto, *Inorg. Chem.* **1999**, *38*, 4430−4434.

[66] D. Gundel, H. Sixl, R. M. Metzger, N. E. Heimer, R. H. Harms, H. J. Keller, D. Nothe, D. Wehe, *J. Chem. Phys.* **1983**, *79*, 3678−3688.

[67] F. Sanz, J. J. Daly, *J. Chem. Soc., Perkin Trans. 2* **1975**, 1146−1150.

[68] F. Wudl, M. R. Brice, *J. Chem. Educ.* **1990**, *67*, 717−718.

[69] Z. Otwinowski, W. Minor, "Processing of X-ray Diffraction Data Collected in Oscillation Mode", in *Methods in Enzymology*, vol. 276 ("Macromolecular Crystallography, Part A") (Eds.: C. W. Carter, R. M. Sweet), Academic Press, New York, **1997**, p. 307−326.

[70] G. M. Sheldrick, *SHELX-97*, University of Göttingen, Germany, **1997**.

Received January 21, 2003

 © 2003 Wiley-VCH Verlag GmbH & Co. KGaA, Weinheim

Homogeneous Hydrogenation Catalyzed by Trinuclear Rh^{I}-Os^{III}-Rh^{I} Complexes

Peter Comba,*[a] Andrey Mayboroda,[a] and Hans Pritzkow[a]

Keywords: Osmium / Rhodium / Heterometallic complexes / Hydrogenation

Reaction of $[Os(Hbiim)_2(O{=}PPh_3)_2](NO_3)$ (H_2biim = 2,2′-biimidazole) with $[RhCl(cod)]_2$ (cod = 1,5-cyclooctadiene) or $[Rh(OH)(cod)]_2$ yields biimidazolato-bridged trinuclear Rh^{I}-Os^{III}-Rh^{I} complexes, which are highly efficient catalysts for the homogeneous hydrogenation of 1-hexene and cyclohexene. The reactivity of the trinuclear compounds compared with the mononuclear subunits indicates that this is due to cooperative effects. This is confirmed by spectroscopic and electrochemical data. The solid-state structure of $[\{RhCl(cod)\}_2(\mu\text{-}Hbiim)_2\{Os(O{=}PPh_3)_2\}](NO_3)$ was determined by single-crystal X-ray diffraction.

(© Wiley-VCH Verlag GmbH & Co. KGaA, 69451 Weinheim, Germany, 2003)

Introduction

Heterobimetallic complexes are receiving considerable attention in the area of homogeneous catalysis in particular;[1] the enhanced reactivity of oligonuclear complexes is thought to be due to synergistic effects.[2−5] For homogeneously catalysed hydrogenation cooperative effects have been reported for some binuclear complexes of platinum-group metals with nitrogen-containing bridging ligands, for example $[\{H(CO)(PPh_3)Ru\}(\mu\text{-}pz)_2\{Ir(TFB)\}]$ (pz = pyrazole; TFB = tetrafluorobenzobicyclo[2.2.2]octadiene)[4] and $[\{H(CO)(PPh_3)Ru\}(\mu\text{-}biim)\{M(cod)\}]$ (M = Rh, Ir).[5] Generally, the proposed mechanism involves one catalytically active site; the other metal ion provides this active site with the appropriate environment and has the role of a donor or acceptor of electron density.[6] The enhanced reactivity is believed to be due to a variation of the ligand field of the active site by the "spectator" chromophore.

2,2′-Biimidazole has been extensively studied as a bridging ligand.[5,7] The recently reported complex $[Os(H_2biim)_2(O{=}PPh_3)_2](NO_3)_3$ (**1**)[8] has two 2,2′-biimidazole ligands in the equatorial plane of the octahedral complex and, after deprotonation of the NH sites of 2,2′-biimidazole, transition metal complex fragments can be added. It is therefore a versatile building block for trinuclear complexes.[8] The use of $[Rh(cod)]^+$ as such a fragment allowed us to obtain trinuclear Rh^{I}-Os^{III}-Rh^{I} compounds. Here, we report the synthesis, characterization and catalytic properties of $[\{RhCl(cod)\}_2(\mu\text{-}Hbiim)_2\{Os(O{=}PPh_3)_2\}](NO_3)$ (**5**) and $[\{Rh(cod)\}_2(\mu\text{-}biim)_2\{Os(O{=}PPh_3)_2\}](NO_3)$ (**6**).

[a] Anorganisch-Chemisches Institut, Universität Heidelberg, Im Neuenheimer Feld 270, 69120 Heidelberg, Germany
E-mail: comba@akcomba.oci.uni-heidelberg.de

Result and Discussion

Synthesis and Characterization

The two trinuclear complexes **5** and **6** were obtained from reactions of $[Os(Hbiim)_2(O{=}PPh_3)_2](NO_3)$ (**2**)[8] with $[RhCl(cod)]_2$ (**3**) and $[Rh(OH)(cod)]_2$ (**4**), respectively (Scheme 1). The desired products were isolated as red (**5**)

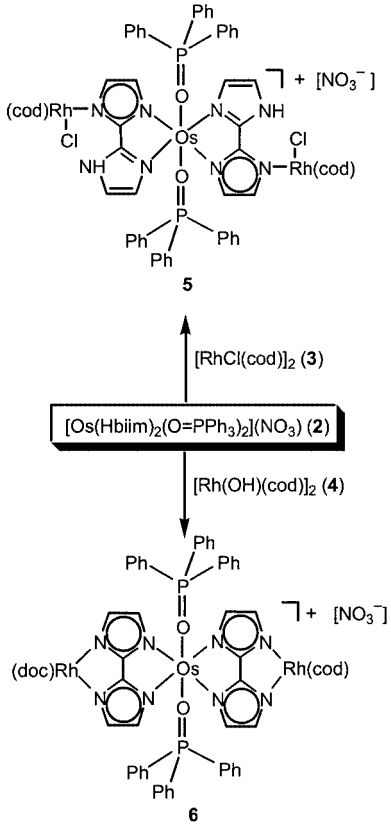

Scheme 1

 © 2003 Wiley-VCH Verlag GmbH & Co. KGaA, Weinheim DOI: 10.1002/ejic.200300177

or brown (**6**) air-stable solids that are insoluble in aromatic and aliphatic hydrocarbons but moderately soluble in dichloromethane and methanol.

Slow evaporation of a solution (dichloromethane/methanol, 4:1, 20 °C) of **5** resulted in single crystals suitable for structural analysis. The geometry of **5**, determined by the analysis of single-crystal X-ray diffraction data, is shown in Figure 1, structural parameters are given in Table 1.

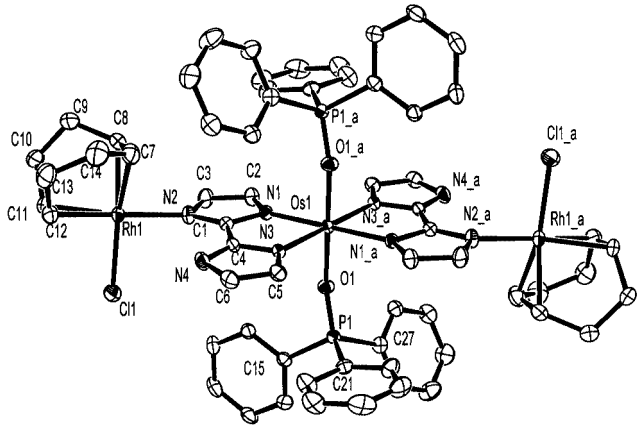

Figure 1. ZORTEP [12] drawing of the complex cation **5**; symmetry transformation used to generate equivalent atoms (a): $-x + 1, -y + 1, -z + 2$

Table 1. Selected geometric parameters of $[\{RhCl(cod)\}_2(\mu\text{-}Hbiim)_2\{Os(O{=}PPh_3)_2\}](NO_3)\cdot CH_2Cl_2$ (**5**)

Bond lengths [Å]	
Os1−O1	2.027(3)
Os1−N1	2.065(4)
Os1−N3	2.080(4)
P1−O1	1.504(3)
C2−C3	1.376(7)
Rh1−N2	2.082(4)
Rh1−C7	2.119(6)
Rh1−C8	2.107(5)
Rh1−C11	2.137(5)
Rh1−C12	2.155(5)
Rh1−Cl1	2.396(2)
Valence angles [°]	
O1−Os1−N1	85.66(14)
O1−Os1−N3	91.93(14)
N1−Os1−N3	77.85(15)
P1−O1−Os1	151.5(2)
N2−Rh1−Cl1	89.92(12)

The coordination sphere of the osmium center is approximately octahedral; the rhodium centers have a square-planar geometry. The Os(1)−N(1) and Os(1)−N(3) distances [2.065(4) and 2.080(4) Å, respectively], are in the range found in related Os^{III} biimidazole[8] and biimidazolate[9] complexes. Comparison with the molecular structure of **1**[8] reveals a distinct difference in the binding of the triphenylphosphane oxide ligand. The Os(1)−O(1) distance in **5** [2.027(3) Å] is somewhat longer than that in **1** [2.012(2) Å], and the P(1)−O(1)−Os(1) angle in **5** [151.5(2)°] is significantly larger than that in **1** [146.53(11)°]. This, together with the EPR spectra (see below), is evidence for significant differences in the electronic structure of the osmium centers between the mononuclear compound **1** and the trinuclear compounds **5** and **6**, and it is an indication of a modification of the electronic properties of the catalytically active rhodium sites.

The EPR spectra (X-band) of **1**, **5** and **6**, recorded in frozen solution [dichloromethane/methanol/tetrahydrofuran (7:1:2), 77 K], are axial, with a large anisotropy;[10] this is a common observation in EPR spectroscopy of osmium(III) complexes.[11] The large difference in $\Delta g_{1,2}$ between **1** ($\Delta g_{1,2} = 0.695$) and **5**, **6** ($\Delta g_{1,2} = 1.450, 1.372$) is attributed to the increasing axial distortion (see discussion of the X-ray structural data above) and concomitant changes in the electronic structure.

Electrochemical studies of **2**, **5** and **6** were carried out in methanol at 25 °C; cyclic voltammograms of **2** and **5** are shown in Figure 2. A comparison of the electrochemical behavior of the mononuclear complex **2** with that of the trinuclear compounds **5** and **6** indicates that the deprotonation of 2,2′-biimidazole and formation of the heterotrimetallic complexes results in a significant cathodic shift of the redox potentials of osmium. The Os^{III}/Os^{II} reduction wave, which

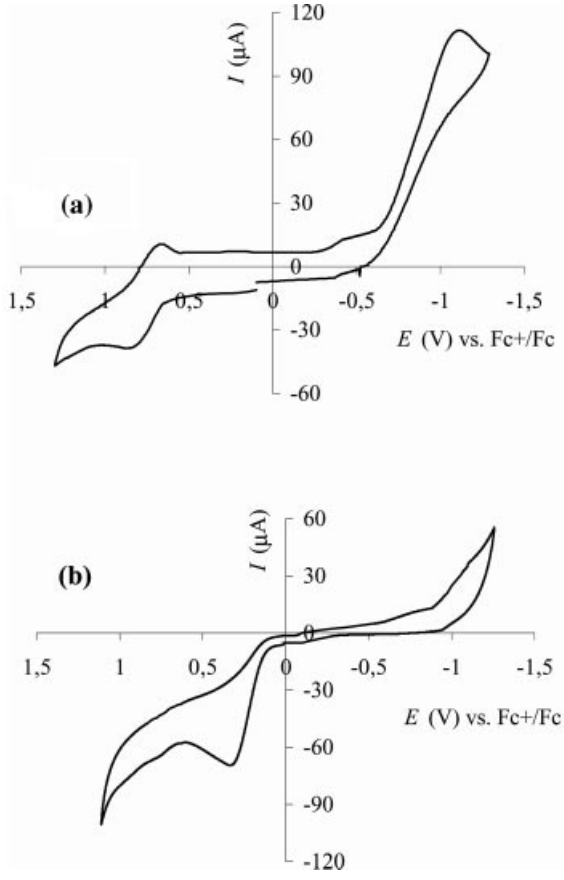

Figure 2. Cyclic voltammograms of: (a) $[Os(Hbiim)_2(O{=}PPh_3)_2](NO_3)$ (**2**) and (b) $[\{RhCl(cod)\}_2Os(\mu\text{-}Hbiim)_2(O{=}PPh_3)_2](NO_3)$ (**5**)

 © 2003 Wiley-VCH Verlag GmbH & Co. KGaA, Weinheim

is observed at −1.14 V for **2**, is beyond the accessible potential range for **5** and **6**. The Os^{III}/Os^{IV} redox couple was found at +0.77 V for **2** and seems to be shifted cathodically for **5** and **6**. These signals are broad and irreversible. The fact that they are not well resolved might be due to overlap of the cyclovoltammetric responses for Os^{III} and Rh^{I}. The oxidation wave of **5** is at +0.37 V and that of **6** is at +0.38 V. Well-resolved cyclic voltammograms have been reported for biimidazolate-bridged Pt^{II}-Os^{III}-Pt^{II} and Pd^{II}-Os^{III}-Pd^{II} complexes.[9] Under the same conditions as those reported here the Os^{III}/Os^{IV} couple was observed at +0.53 V for $[\{Pt(C_5H_3(CH_2NMe_2\text{-}2,6)\}_2Os(\mu\text{-}Hbiim)_2(O{=}PPh_3)_2](NO_3)(SO_3SF_3)_2$ [$C_5H_3(CH_2NMe_2$-2,6) = pincer ligand] and at +0.23 V for $[\{Pd(en)\}_2Os(\mu\text{-}biim)_2(O{=}PPh_3)_2](NO_3)_3$ (en = ethylene-1,2-diamine).[9] These observations and interpretations are consistent with a modification of the donor properties of 2,2′-biimidazole due to the deprotonation and coordination to a second metal ion. In agreement with the structural comparison and the EPR spectra, the electrochemical data indicate that the osmium centers in **5** and **6** act as Lewis acids and therefore modify the electronic properties of the catalytically active rhodium sites.

Catalytic Activity

Compounds **5** and **6** catalyze the hydrogenation of 1-hexene and cyclohexene under homogeneous conditions. The results are summarized in Table 2. The reactivities of the mononuclear complexes **1**, **3** and **7** (fragments of **5** and **6**) are included for comparison. The trinuclear complexes **5** and **6** are significantly more active and selective catalysts than the corresponding building blocks **1**, **3** and **7**. The mononuclear osmium complex **1** is almost inactive. This implies that the transformation of the substrate takes place at the rhodium centers of the trinuclear catalysts **5** and **6**. The observation that the mononuclear rhodium complex **7** catalyzes the migration of a double bond in the linear alkene rather than its hydrogenation is interesting. The reduction of 1-hexene in the presence of the trinuclear catalysts **5** and **6** occurs very selectively. The hydrogenation of cyclohexene is much slower than the reduction of 1-hexene. However, for cyclohexene, the enhancement of the catalytic activity by the trinuclear compounds **5** and **6** is more pronounced. A plausible catalytic pathway includes the hydrogenation of the cyclooctadiene ligand in **5** and **6**, and the formation of a coordinatively unsaturated intermediate by removal of cyclooctane.[6] The enhancement of the catalytic activity with the trinuclear complexes is due to a modification of the electronic properties of the rhodium centers, and this might occur by electrostatic effects or by electronic communication between the osmium and rhodium centers through the π-conjugated bridging ligand. Catalytic hydrogenation by rhodium complexes usually involves oxidative addition of hydrogen and formation of a π-complex with the alkene, followed by an intramolecular alkene insertion reaction, leading to a Rh-alkyl complex.[6] The last step is usually rate-determining. A decrease of the electron density on Rh^{I}, due to the Os^{III} center, must lead to a reduction of the energy barrier, and promote the nucleophilic attack of the alkene and formation of Rh-alkyl species. Here, the additional metal center is used as a weak electron acceptor and, therefore, improves the properties of the catalytically active metal ion. The osmium center provides a subtle modification of the electronic structure of rhodium, which promotes the Rh-alkyl complex formation and does not inhibit the oxidative addition of hydrogen.

In summary, we have prepared and characterized trinuclear Rh^{I}-Os^{III}-Rh^{I} complexes with 2,2′-biimidazole as a bridging ligand and shown their utility as catalysts for the homogeneous hydrogenation of 1-hexene and cyclohexene. The significant enhancement of the catalytic activity, relative to the mononuclear building blocks, is believed to be due to a variation of the ligand field induced by the "spectator" metal ion.

Experimental Section

General: $[Os(H_2biim)_2(O{=}PPh_3)_2](NO_3)_3$ (**1**) was prepared by a published procedure.[8] Its conjugate base $[Os(Hbiim)_2(O{=}PPh_3)_2](NO_3)\cdot 2H_2O$ (**2**) was obtained by reaction of **1** with KOH

Table 2. Homogeneous hydrogenation[a] of 1-hexene and cyclohexene in the presence of $[Os(H_2biim)_2(O{=}PPh_3)_2](NO_3)_3$ (**1**), $[RhCl(cod)]_2$ (**3**), $[Rh(H_2biim)(cod)](SO_3CF_3)$ (**7**), $[\{RhCl(cod)\}_2(\mu\text{-}Hbiim)_2\{Os(O{=}PPh_3)_2\}](NO_3)$ (**5**) and $[\{Rh(cod)\}_2(\mu\text{-}biim)_2\{Os(O{=}PPh_3)_2\}](NO_3)$ (**6**)

Catalyst	Cat. [mol %]	Time [h]	Hydrogenation of 1-hexene			Hydrogenation of cyclohexene
			Conversion [%]	Yield of by-products [%]		Conversion [%]
				2-hexene	3-hexene	
1	1	10	11	3	3	0
3	1	5	23	8	7	4
7	2	5	29	49	20	2
5	1	5	67	0	0	46
5	1	10	98	0	0	73
6	1	5	53	5	4	34
6	1	10	94	3	1	66

[a] Reaction conditions: 5 bar H_2, solvent: CH_2Cl_2/CH_3OH (9:1).

 © 2003 Wiley-VCH Verlag GmbH & Co. KGaA, Weinheim

in methanol/dichloromethane.[8] IR spectra (KBr pellets) were recorded on a Perkin−Elmer 16PC RT-IR instrument. UV/Vis spectra were obtained with a Cary 1E spectrophotometer. EPR spectra were recorded with a Bruker ESP300E spectrometer (9.4635 GHz) as approx. 1 10^{-3} mol·dm^{-3} frozen (liquid nitrogen temperature) solutions in dichloromethane/methanol/tetrahydrofuran (7:2:1). Electrochemical measurements (CV) were performed in solutions of [N*n*Bu$_4$]PF$_6$ (0.1 mol·dm^{-3}) in methanol at 293 K, using a BAS 100B system with a glassy-carbon working electrode, a platinum auxiliary electrode and an Ag/AgCl reference electrode. All potentials are quoted versus the ferrocene/ferrocenium couple (E = 0.0 V). Mass spectra were recorded on a Finnigan MAT 8230 instrument. GC-MS analyses were performed on a Fison GC 8000/MD 800 series instrument, equipped with a ZB-1 (Zebron) column. Melting (decomposition) points were determined with a Gallenkamp MFB 595 010 M melting point apparatus. Organic solvents (methanol, dichloromethane) were freshly distilled before use. Microanalyses were obtained from the microanalytical laboratory of the chemical institute of the University of Heidelberg.

Catalytic Hydrogenation of 1-Hexene and Cyclohexene: All experiments were performed in a 100 mL stainless steel autoclave with an inner polytetrafluorethylene vessel. In a typical experiment, 0.016 mmol of the catalyst was placed as a solid in the autoclave, supplied with a magnetic stirrer. Whilst stirring, the catalyst was dissolved in dichloromethane (6 mL) or a mixture of dichloromethane and methanol (90:10). The alkene (0.16 mmol) was then added to the solution of the catalyst. The autoclave was evacuated three times and filled with hydrogen. The pressure of hydrogen was then increased to 5 bar. The reaction mixture was stirred for 5 h. The autoclave was then degassed and all volatile materials were evaporated from the reaction mixture under oil-pump vacuum, and condensed (liquid nitrogen). The resulting solution was analysed by GC-MS.

Synthesis of [{RhCl(cod)}$_2$(μ-Hbiim)$_2${Os(O=PPh$_3$)$_2$}](NO$_3$)·CH$_2$Cl$_2$ (5): [Os(Hbiim)$_2$(O=Ph$_3$)$_2$](NO$_3$)·2H$_2$O (**2**; 300 mg, 0.27 mmol) was dissolved in a dichloromethane/methanol mixture (4:1, 15 mL) at 25 °C. [RhCl(cod)]$_2$ (**3**; 0.27 mmol), in methanol (5 mL) was added to the solution. The reaction mixture immediately turned from violet to red. The solution was stirred for 2 h, and the volume of the solution was then reduced to 4 mL. After 10 h red crystals of **5** precipitated. The slurry was decanted and the crystalline precipitate was washed twice with acetone (5 mL) and dried under an oil-pump vacuum to afford **5**. Yield: 290 mg (73% based on **2**). Mp: gradual decomposition above 150 °C. IR (KBr): ν(P=O) 1120 cm^{-1}, ν$_a$(NO$_3^-$) 1332, ν(Ar, C=C) 1438, ν(NH) 3050. UV/Vis (CH$_2$Cl$_2$): λ$_{max}$ = 360 nm (ε = 7.5 × 10^3 mol^{-1}·dm^3·cm^{-1}), 541 nm (ε = 4.7 × 10^2 mol^{-1}·dm^3·cm^{-1}). CV (CH$_3$OH, 25 °C): E_{ox} = +0.37 V (irr.). MS (FAB): *m*/*z* (%) = 1507 (21) [C$_{64}$H$_{64}$N$_8$Cl$_2$O$_2$P$_2$OsRh$_2$]$^+$, 1260 (32) [C$_{56}$H$_{52}$N$_8$ClO$_2$P$_2$OsRh]$^+$, 1014 (66) [C$_{48}$H$_{40}$N$_8$O$_2$P$_2$Os]$^+$, 736 (100) [C$_{30}$H$_{25}$N$_8$OPOs]$^+$. C$_{64}$H$_{64}$Cl$_2$N$_9$O$_5$P$_2$OsRh$_2$·CH$_2$Cl$_2$ (1653.03): calcd. C 47.23, H 4.02, N 7.64; found C 46.80, H 4.41, N 7.72.

Synthesis of [{Rh(cod)}$_2$(μ-biim)$_2${Os(O=PPh$_3$)$_2$}](NO$_3$) (6): [Os(Hbiim)$_2$(O=Ph$_3$)$_2$](NO$_3$)·2H$_2$O (**2**; 300 mg, 0.27 mmol) was treated with [Rh(OH)(cod)]$_2$ (125 mg, 0.27 mmol) in dichloromethane/methanol (4:1, 20 mL) solution at 25 °C. The reaction mixture was stirred for 2 h and the solvent was then removed under an oil-pump vacuum to afford **6** as a brown solid in quantitative yield. Mp: gradual decomposition above 150 °C. IR (KBr): ν(P=O) 1118 cm^{-1}, ν$_a$(NO$_3^-$) 1332, ν(Ar, C=C) 1436. UV/Vis (CH$_2$Cl$_2$): λ$_{max}$ = 349 nm (ε = 6.3 × 10^3 mol^{-1}·dm^3·cm^{-1}), 556 nm (ε = 4.7 × 10^2 mol^{-1}·dm^3·cm^{-1}). CV (CH$_3$OH, 25 °C): E_{ox} = +0.38 V (irr.). MS (FAB): *m*/*z* (%) = 1434 (100) [C$_{64}$H$_{62}$N$_8$O$_2$P$_2$OsRh$_2$]$^+$, 1224 (28) [C$_{56}$H$_{52}$N$_8$lO$_2$P$_2$OsRh]$^+$, 1156 (31) [C$_{46}$H$_{47}$N$_8$OPOsRh$_2$]$^+$, 946 (42) [C$_{38}$H$_{35}$N$_8$OPOsRh]$^+$. C$_{64}$H$_{62}$N$_9$O$_5$OsP$_2$Rh$_2$ (1513.3): calcd. C 51.41, H 4.18, N 8.43; found C 51.01, H 4.79, N 8.76.

X-ray Crystallographic Analysis of 5: Crystallized from CH$_2$Cl$_2$/MeOH, formula C$_{64}$H$_{64}$Cl$_2$N$_9$O$_5$OsP$_2$Rh$_2$, M = 1568.13 ([C$_{64}$H$_{64}$Cl$_2$N$_8$O$_2$OsP$_2$Rh$_2$]·NO$_3$), red crystal 0.28 × 0.25 × 0.14 mm^3, triclinic, space group $P\bar{1}$, a = 10.7225(9), b = 13.3347(11), c = 13.3707(11) Å, α = 110.312(2)°, β = 100.589(2)°, γ = 107.462(2)°, Z = 1, V = 1619.3(2) Å^3, ρ$_{calcd.}$ = 1.682 g·cm^{-3}, θ scan range 1.77 < θ < 32.05, Mo-K$_α$ radiation (λ = 0.71073 Å), T = 103(2) K. 28335 reflections collected, 10965 independent reflections, 8432 observed reflections [I ≥ 2σ(I)], 551 refined parameters, R = 0.0435, wR^2 = 0.1214, semi-empirical absorption correction from equivalents. Structure was solved by direct methods. Refinement was carried out by full-matrix least-squares techniques on F^2. Program used: structure solution and refinement: SHELXTL NT5.1 (G. M. Sheldrick, Bruker-AXS, Madison, Wisconsin, USA, 1998) Hydrogen atoms were located from the difference-Fourier map. All hydrogen atoms were fully refined. All non-hydrogen atoms were refined anisotropically.

CCDC-196197 contains the supplementary crystallographic data for this paper. These data can be obtained free of charge at www.ccdc.cam.ac.uk/conts/retrieving.html [or from the Cambridge Crystallographic Data Centre, 12, Union Road, Cambridge CB2 1EZ, UK; Fax: (internat.) +44-1223/336-033; E-mail: deposit@ccdc.cam.ac.uk].

Acknowledgments

Financial support by the Alexander von Humboldt-Stiftung is gratefully acknowledged. We also thank Degussa-Hüls AG for a generous gift of OsO$_4$ and RhCl$_3$.

[1] [1a] R. Choukroun, D. Gervais, P. Kalck, F. Senocq, *J. Organomet. Chem.* **1987**, *335*, C9−C12. [1b] R. Mutin, C. Lucas, J. Thivole-Cazat, V. Dufand, F. Dany, J. M. Basset, *J. Chem. Soc., Chem. Commun.* **1988**, 896−898. [1c] E. Sola, V. I. Bakhmutov, F. Torres, A. Elduque, J. A. Lopez, F. Lahoz, H. Werner, L. A. Oro, *Organometallics* **1998**, *17*, 683−696.

[2] L. Gelmini, D. W. Stephan, *Organometallics* **1988**, *7*, 849−855.

[3] P. Braunstein, X. Morise, *Organometallics* **1998**, *17*, 540−550.

[4] M. A. Esteruelas, M. P. Garcia, A. M. Lopez, L. Oro, *Organometallics* **1991**, *10*, 127−133.

[5] M. P. Garcia, A. M. López, M. A. Esteruelas, F. J. Lahoz, L. A. Oro, *Chem. Commun.* **1988**, 793−795.

[6] P. A. Chaloner, M. A. Esteruelas, F. Joó, L. A. Oro, *Homogeneous Hydrogenation*, Kluwer Academic Publishers, Dordrecht, **1993**.

[7] [7a] S. W. Kaiser, R. B. Saillant, W. M. Butler, P. G. Rasmussen, *Inorg. Chem.* **1976**, *15*, 2688−2694. [7b] M. S. Haddad, D. N. Hendrickson, *Inorg. Chem.* **1978**, *17*, 2622−2630. [7c] R. Usón, L. A. Oro, J. Gimeno, M. A. Ciriano, J. A. Cabeza, *J. Chem. Soc., Dalton Trans.* **1983**, 233−230. [7d] P. Majumdar, S.-M. Peng, S. Goswami, *J. Chem. Soc., Dalton Trans.* **1998**, 1569−1574. [7e] A. Maiboroda, G. Rheinwald, H. Lang, *Inorg. Chem. Commun.* **2001**, *4*, 381−383.

[8] A. Maiboroda, G. Rheinwald, H. Lang, *Eur. J. Inorg. Chem.* **2001**, 2263−2269.

 © 2003 Wiley-VCH Verlag GmbH & Co. KGaA, Weinheim

[9] A. Mayboroda, P. Comba, H. Pritzkow, G. Rheinwald, H. Lang, G. van Koten, *Eur. J. Inorg. Chem.* **2003**, 1703−1710.
[10] EPR spectroscopic data: $g_1 = 2.1755$, $g_2 = 2.8707$ (**1**); $g_1 = 1.9012$, $g_2 = 3.3511$ (**5**); $g_1 = 1.9153$, $g_2 = 3.2871$ (**6**).
[11] [11a] R. E. De-Simone, R. S. Drago, *J. Am. Chem. Soc.* **1970**, *92*, 2343. [11b] G. K. Lahiri, S. Bhattacharya, B. K. Ghosh, A. Chakravorty, *Inorg. Chem.* **1977**, *26*, 4324. [11c] E. M- Kober, T. J. Mayer, *Inorg. Chem.* **1983**, *22*, 1614. [11d] K. Majumder, S.-M. Peng, S. Bhattacharya, *J. Chem. Soc., Dalton Trans.* **2001**, 284−288.
[12] L. Zsolnai, G. Huttner, ZORTEP, Program for PC, 1994, University of Heidelberg.

Received April 16, 2003

 © 2003 Wiley-VCH Verlag GmbH & Co. KGaA, Weinheim

New Rhodium(I) Complexes with Hemilabile Amphiphilic Phosphanes

Esteve Valls,[a] Joan Suades,*[a] René Mathieu,[b] and Noel Lugan[b]

Keywords: Phosphanes / Rhodium / Hemilabile ligands / Amphiphiles

A series of Rh^I complexes was prepared and characterised with the following hemilabile amphiphilic phosphanes: R–(C_6H_4)–(OCH_2CH_2)$_n$–PPh_2 [**1** (R = *tert*-octyl, *n* = 1), **2** (R = *tert*-octyl, $\bar{n}$ = 5), **3** (R = *tert*-octyl, $\bar{n}$ = 13), **4** (R = *n*-nonyl, $\bar{n}$ = 1.4), **5** (R = *n*-nonyl, $\bar{n}$ = 5), **6** (R = *n*-nonyl, $\bar{n}$ = 11)]. The reactions between **1**–**6** and $[Rh(COD)(THF)_2]^+$, and the subsequent reaction with CO were studied by ^{31}P NMR and IR spectroscopy. The data are consistent with the formation of P-coordinated and chelated (P,O) species for ligands **2**–**6**, in agreement with the hemilabile character of these ligands. In the case of ligand **1**, the complex *trans*-$[Rh(\mathbf{1})_2(CO)_2]^+$ has been isolated and the *cis*-$[Rh(\mathbf{1})_2(CO)_2]^+$ compound has been detected. $[Rh(\mathbf{1})_2(CO)]^+$ was prepared by decarbonylation of *trans*-$[Rh(\mathbf{1})_2(CO)_2]^+$, and low-temperature NMR spectroscopic studies have shown the hemilabile character of **1** with a very weak P–O interaction. The molecular structure of *trans*-$Rh(CO)(\mathbf{1})_2Cl$ was determined by X-ray crystallography and shows that the conformation of the *tert*-octylphenoxyethyl chains is nearly identical to that previously reported in the complex *trans*-$PdCl_2(\mathbf{1})_2$.
(© Wiley-VCH Verlag GmbH & Co. KGaA, 69451 Weinheim, Germany, 2003)

Introduction

The preparation of new functionalised ligands is a central strategy for improving certain properties in transition metal complexes. Phosphanes are among the most versatile ligands, since they allow the introduction of very different functionalities by means of the different groups bound to the phosphorus atom. In this way, phosphane ligands have become water-soluble,[1] asymmetric,[2] hemilabile[3] and, more recently, amphiphilic.[4] The amphiphilic ligands contain hydrophilic and hydrophobic groups in the same molecule, and their metal complexes may aggregate forming supramolecular arrangements, such as micelles and vesicles.[5] Such micro-heterogeneous systems are attractive for improving catalytic processes, especially those that present phase-transfer limitations, such as those occurring under biphasic conditions.[6] This approach has been utilised in the study of a catalytic reaction accelerated by vesicle formation.[7]

In previous papers, we described the synthesis of neutral amphiphilic phosphanes with hemilabile properties,[8] and anionic water-soluble amphiphilic phosphanes.[9] Ligands were prepared in a straightforward manner from polyethylene glycol monoalkyl ethers, which are common starting compounds as they are used extensively as non-ionic surfactants. In subsequent papers, we have reported on the complexing properties of the neutral ligands **1**−**6** (Scheme 1) towards Ru^{II},[8] Pd^{II},[10] and hydridorhodium(I) complexes.[11] Hemilabile properties were clearly observed with the Ru^{II} complexes.[8] Here, we present a study of the reactivity of the neutral ligands **1**−**6** (Scheme 1) towards Rh^I.

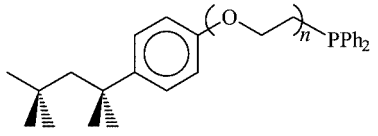

1 (n =1), **2** ($\bar{n}$ = 5), **3** ($\bar{n}$ = 13)

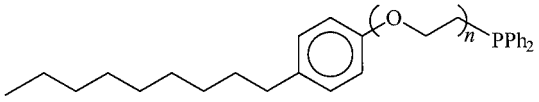

4 ($\bar{n}$ = 1.4), **5** ($\bar{n}$ = 5), **6** ($\bar{n}$ = 11)

Scheme 1

Results and Discussion

1. Ligands

Ligands **1**−**6** were synthesised from commercial non-ionic Igepal® surfactants.[12] In agreement with the nature of these starting non-ionic surfactants, the ligands were obtained as mixtures of compounds with the same structure but with different ethoxylation grades (Scheme 1). The only exception is **1**, which was obtained as a single compound

[a] Departament de Química, Universitat Autònoma de Barcelona, Edifici C, Campus UAB, 08193 Bellaterra, Spain
Fax: (internat.) +34-93-5813101
E-mail: Joan.Suades@uab.es
[b] Laboratoire de Chimie de Coordination du CNRS, 205 route de Narbonne, 31077 Toulouse Cedex 4, France
Fax: (internat.) +33-5-61553003
E-mail: mathieu@lcc.toulouse.fr

because it crystallised from the reaction mixture as a white solid.

2. Reactivity of Ligands 1−6 towards [Rh(COD)(THF)$_2$][ClO$_4$]

Two equivalents of the ligand (**1**−**6**) in THF were added to a solution of [Rh(COD)(THF)$_2$][ClO$_4$] prepared by the usual reaction between Rh(COD)(acac) and HClO$_4$ in THF. Complexation was evidenced by the change in the colour of the solution, which became darker, and by the $^{31}P\{^1H\}$ NMR spectroscopic data. Although several attempts were made, no solid compounds could be obtained. Difficulties in the isolation of solid compounds were also observed in previous complexation studies of ligands **1**−**6** with Ru^{II} [8] and Pd^{II}.[10]

The $^{31}P\{^1H\}$ NMR spectra of solutions obtained after the reactions of **1**−**6** with [Rh(COD)(THF)$_2$][ClO$_4$] show the complete absence of the corresponding free ligand, and display several doublets with coupling constants in the range 121 to 153 Hz. This result agrees with the formation of Rh−P bonds for all the ligands studied. Significant differences are also observed between the spectra for the different ligands. A comparison of the ^{31}P NMR spectroscopic data obtained from the resulting reaction mixtures with published data reporting the reactivity of related hemilabile phosphanes $Ph_2PCH_2CH_2OCH_3$[13] and $Ph_2P(CH_2CH_2O)_2CH_3$[14] is very helpful in the interpretation of our results. The spectrum of the complex obtained with ligand **1** only displays a doublet at δ = 17.6 ppm ($^1J_{PRh}$ = 144 Hz). This is in good agreement with the presence of a sole [Rh(COD)(PO)$_2$]$^+$ species (PO = P-coordinated ether−phosphane ligand). The spectra of the complexes obtained with ligands **2**−**6** also show a doublet with similar characteristics at 17−18 ppm, however, other doublets are also observed in the δ = 28 ppm region. In these spectra, as the polyether chain length increases (i.e. more oxygen atoms are added), the signal that appears at 17−18 ppm is smaller. At the same time, the signals at around δ = 28 ppm become more significant. These results agree with the simultaneous formation of the above-mentioned P-coordinated species [Rh(COD)(PO)$_2$]$^+$ (δ = 17−18 ppm region), and the chelated (P,O) complexes [Rh(COD)(P∩O)]$^+$ (δ = 28 ppm region)[14] (P∩O = chelated ligand). The absence of the signal in the δ = 28 ppm region in the spectrum with ligand **1** is consistent with the unfavourable bidentate coordination of this ligand, since it is hindered by electronic and steric effects of the aryl group bonded to the oxygen atom.[10] Finally, some observations can be made from the spectra of the complexes with ligands **4** and **6**. The spectrum of the complex with ligand **4** shows two doublets at δ = 17.5 and 17.8 ppm that can be assigned to a mixture of [Rh(COD)(PO)$_2$]$^+$ complexes, since this ligand is a mixture that contains a molecule similar to **1** and another species with a longer polyether chain. In the spectrum of the complex with ligand **6**, other signals are also observed at δ = 32.4 and 39.5 ppm. These signals could be justified by the presence of species in which the labile COD ligand could have been replaced by oxygen atoms of the polyether chain,[15] as represented in Scheme 2.

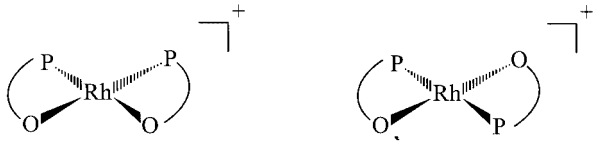

Scheme 2

3. Reaction of [Rh(COD)(L)$_2$]$^+$ Complexes with CO

a) Case where L = Ligands 2−6

After CO was bubbled into THF solutions of the Rh^I complexes described above, the colour turned from orange to yellow. After solvent evaporation, the reaction products were studied by IR and ^{31}P NMR spectroscopy, since, as in the previous section, no solids could be obtained. The $^{31}P\{^1H\}$ NMR spectra show that the previously observed signals are now absent and a new main signal at δ = 22−25 ppm, with the characteristic shape of a doublet ($J_{Rh\text{-}P}$ = 110−130 Hz) is observed for all the complexes studied. The IR spectra in the ν_{CO} region display a strong ν_{CO} band at around 1980 cm^{-1}. The position of this band is very similar to that reported for related complexes with the [Rh(CO)(P∩O)(PO)]$^+$ structure as *trans*-[Rh(CO)(Ph$_2$PCH$_2$CH$_2$OMe)$_2$]$^+$ (ν_{CO} = 1982 cm^{-1}).[13] For these last complexes, equilibrium between the κ^1 and κ^2 modes of bonding for the two ligands has been suggested (Scheme 3).[13] The $J_{Rh\text{-}P}$ coupling constant observed at room temperature in the $^{31}P\{^1H\}$ NMR spectra for our complexes is also consistent with this formulation.

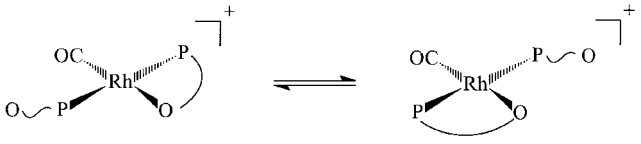

Scheme 3

b) Case where L = Ligand 1

As in previously reported studies,[8,10] more detailed work was performed with ligand **1** since it is the only compound that it is not a mixture of polyether ligands,[12] and therefore, the solid compounds can be expected to be isolated. With this aim, the COD complex with the tetrafluoroborate anion was synthesised by reaction of the [Rh(COD)Cl]$_2$ complex with two equivalents of AgBF$_4$ and four equivalents of ligand **1** in THF. A solid complex was isolated by subsequent reaction with CO, followed by crystallisation in diethyl ether. This complex displays an IR ν_{CO} band at 2040 cm^{-1}, and a broad doublet in the $^{31}P\{^1H\}$ NMR spectrum at δ = 21.0 ppm (J = 104.8 Hz). These spectroscopic parameters are in accordance with published data for *trans*-[Rh(CO)$_2$L$_2$]$^+$ complexes with related hemilabile ether ligands $Cy_2PCH_2CH_2OCH_3$[16] and $Ph_2PCH_2CH_2OPh$.[17] Although other published data indicate that formation of

 © 2003 Wiley-VCH Verlag GmbH & Co. KGaA, Weinheim

the *trans*-$[Rh(PPh_3)_2(CO)_2]^+$ is uncertain,[18] its existence has been unequivocally demonstrated with the ether ligand $Ph_2PCH_2CH_2OPh$, using ^{31}P NMR spectroscopy of ^{13}CO labelled complexes.[17] The low-temperature $^{31}P\{^1H\}$ NMR spectrum of the dichloromethane solution of the *trans*-$[Rh(\mathbf{1})_2(CO)_2]^+$ complex shows that the broad doublet becomes sharp at a temperature lower than 233 K. A plausible explanation of this could be the restricted rotation around the phosphorus−metal bond at lower temperatures as a result of hydrophobic interactions between the two *tert*-octyl chains. The two reported crystal structures of metallic complexes with this ligand (see reference[10] and section 4 of Results and Discussion) have shown that these hydrophobic interactions could be related to the configuration of the molecules in solid state. The IR spectrum of the mother solution after crystallisation of the *trans*-$[Rh(\mathbf{1})_2(CO)_2]^+$ complex shows two signals at 2040 and 1990 cm^{-1}, and suggests the existence of the kinetically favoured *cis*-$[Rh(\mathbf{1})_2(CO)_2]^+$ complex in solution.[16]

The formation of the monocarbonyl complex *trans*-$[Rh(CO)(P\cap O)(PO)]^+$ with ligands **2**−**6** and the dicarbonyl complex *trans*-$[Rh(\mathbf{1})_2(CO)_2]^+$ can be justified by the propensity of ligand **1** to avoid the P,O chelation because of electronic and steric effects.[10] To force the coordination of the oxygen atom in ligand **1**, the synthesis of the monocarbonyl complex was undertaken by refluxing a dichloromethane solution of the *trans*-$[Rh(\mathbf{1})_2(CO)_2]^+$ complex. This reaction was monitored by IR spectroscopy, which showed the quick formation of a new complex with a ν_{CO} band at 1990 cm^{-1}. The $^{31}P\{^1H\}$ NMR spectrum at room temperature shows a broad doublet at δ = 29.5 ppm (J = 120.1 Hz). The low-temperature $^{31}P\{^1H\}$ NMR spectroscopic measurements (Figure 1) show the evolution of the broad doublet to a broad band at 253 K and a very broad band (22−37 ppm) at 233 K. At lower temperatures, a sharp doublet is formed at δ = 23.8 ppm (J = 134.3 Hz) and a broad doublet at δ = 34.8 ppm (J = 110 Hz) in a 1:1 ratio. These data are consistent with the existence of a κ^1(P)-coordinated ligand (doublet at δ = 23.8 ppm) and a κ^2 (P,O)-coordinated ligand (doublet at δ = 34.8 ppm). The fact that the κ^2 (P,O) resonance remains broad at this temperature illustrates the previously mentioned unfavourable κ^2 (P,O) coordination mode for **1**. Reported studies with the $Ph_2PCH_2CH_2OPh$ ligand have shown the existence of coordinated arene complexes, and the κ^2 (P,O) coordination of this ligand has been postulated in reaction intermediates.[17] The low-temperature ^1H NMR spectra show the splitting of the signal for the two methylene groups of **1** at 193 K. Furthermore, the arene protons of the phenoxy groups show two sharp doublets at room temperature at δ = 6.63 and 7.16 ppm, which are assigned to the *ortho*- and *meta* arene hydrogen atoms of the phenoxy group, respectively. At low temperatures, the signal for the *meta* hydrogen atom shows insignificant changes. In contrast, the signal for the *ortho*-hydrogen atom shows a broad band at 213 K, which splits into two signals: a sharp band at δ = 6.38 ppm and a broad signal at δ = 6.65 ppm. All these observations − the splitting of the signal for the methylene groups that shows the existence of two different $CH_2CH_2O(C_6H_4)C_8H_{17}$ fragments and the splitting of the signal for the *ortho* hydrogen atoms of the phenoxy groups − are consistent with the co-existence of a κ^1 (P) and a κ^2 (P,O)-coordinated ligand and corroborate the $^{31}P\{^1H\}$ NMR spectroscopic data. It should be emphasised that a η^6-coordination of the arene group is not favourable for electronic reasons and a η^2-coordination of the arene is not supported by the ^1H NMR spectroscopic data.

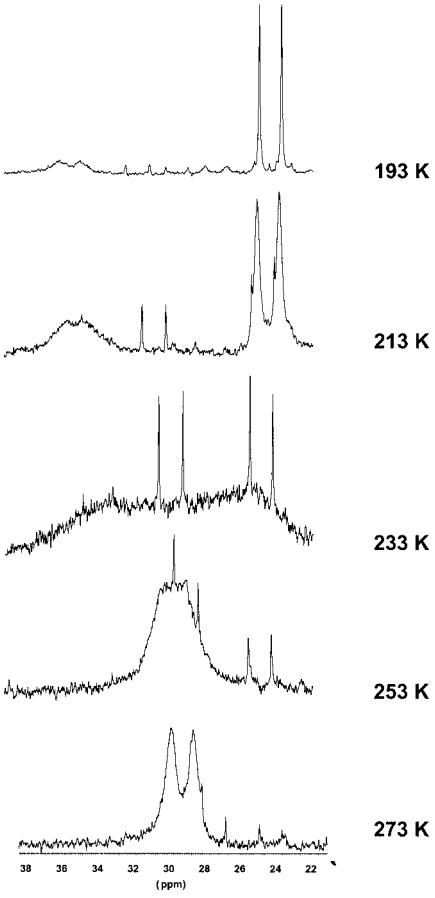

Figure 1. Low-temperature $^{31}P\{^1H\}$ NMR spectra of $[Rh(CO)(\mathbf{1})_2][BF_4]$

Finally, the attracting properties of this ligand should be noted because it can be considered as an hemilabile (P,O) ligand with a very weak, but possible, interaction between the oxygen atom and the metal atom. This observation is supported by our previous studies with Ru^{II} and Pd^{II} complexes. Those studies show the prevailing trend of this ligand to coordinate only by means of the phosphorus atom.[8,10] Finally, further support is available from the published reports on the ligand $Ph_2PCH_2CH_2OPh$, where the P,O coordination was only postulated in the reaction intermediates.[17]

4. Synthesis and X-ray Structure of *trans*-[Rh(CO)(1)$_2$Cl]

As it was not possible to get single crystals of the cationic complexes of ligand **1**, another attempt was made with neutral chloro rhodium complexes. The reaction of

 © 2003 Wiley-VCH Verlag GmbH & Co. KGaA, Weinheim

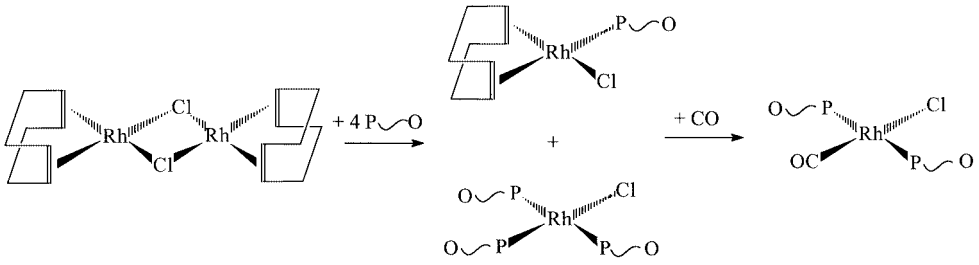

Scheme 4

$[Rh(COD)(\mu\text{-}Cl)]_2$ with four equivalents of ligand **1** leads to a mixture of two species, according to the $^{31}P\{^1H\}$ NMR spectrum of the reaction medium (Scheme 4). The first is observed as a doublet at $\delta = 28.2$ ppm ($^1J_{PRh} = 150$ Hz) and is assigned to the species [Rh(COD)(**1**)Cl]. The second complex displays a set of signals consisting of a doublet of doublets at $\delta = 22.3$ ppm ($^1J_{PRh} = 137$ Hz; $^2J_{P,P} = 39$ Hz) and a doublet of triplets centred at $\delta = 37.3$ ppm ($^1J_{PRh} = 187$ Hz; $^2J_{P,P} = 39$ Hz), and is assigned to the $[Rh(\mathbf{1})_3Cl]$ species. After bubbling CO into the previous reaction mixture, only one doublet at $\delta = 21.3$ ppm ($^1J_{PRh} = 124$ Hz) is observed. This signal and the presence of an IR band at 1975 cm^{-1} are in good agreement with the formation of a *trans*-$[Rh(CO)(\mathbf{1})_2Cl]$ species. Single crystals of this complex were obtained by crystallisation from an acetone/methanol solution, and the structure of complex was determined by X-ray methods. A perspective view of the molecule with the labelling scheme is shown in Figure 2. The rhodium atom displays a square-planar geometry with phosphane ligands in the *trans* positions, confirming previous assignment from NMR spectroscopic data. Bond lengths and angles around the metal centre are similar to other *trans*-$[Rh(CO)L_2Cl]$ complexes with monodentate phosphane ligands.[19] Note, however, that the most interesting information is attained on comparing the structure of *trans*-$[Rh(CO)(\mathbf{1})_2Cl]$ (Figure 2) with that of the previously reported *trans*-$[PdCl_2(\mathbf{1})_2]$ (Figure 3).[10] Indeed, on comparing both figures, the great similarity between the conformations of the two *tert*-octylphenoxyethyl chains in both complexes can be seen. In both complexes, the phenyl groups bonded to the phosphorus atoms are nearly eclipsed, and the values of the C2−P1−P2−C4 torsion angle in both complexes are very similar {*trans*-$[Rh(CO)(\mathbf{1})_2Cl] = 22(1)°$; *trans*-$[PdCl_2(\mathbf{1})_2] = 24.0(2)°$}. This implies that the two *tert*-octylphenoxyethyl chains are close to each other, an arrangement that could be explained by the tendency of the more hydrophobic parts of the molecule to be close together. The analysis of the structure of the $[PdCl_2(\mathbf{1})_2]$ complex led us to consider, jointly with the proposed hydrophobic interactions, that other factors should also be taken into account. Thus, hydrogen bonds between the Cl atom and the hydrogen atoms of the methylene groups bonded to the oxygen atom, or between one oxygen atom and one phenyl group were considered.[10] The noteworthy similarity between the conformation of the hydrophobic groups in the structures of these metal complexes with the two different metal fragments, $PdCl_2$ and Rh(CO)Cl, suggests that the interaction between the *tert*-octylphenoxyethyl chains can play a central role in the conformation of these complexes. It should be emphasised that in the homologous *trans*-$[PdCl_2L_2]$[20] and *trans*-$[Rh(CO)ClL_2]$[19b] complexes with the ligand PPh_2Me, which cannot lead to significant hydrophobic interactions between the methyl groups, the conformation of the two complexes is different (Figure 4). Thus, the phenyl groups

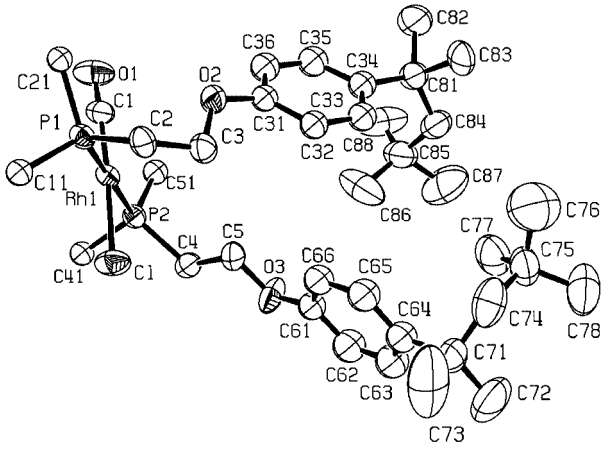

Figure 2. ORTEP diagram of *trans*-$[Rh(CO)(\mathbf{1})_2Cl]$ showing the atom numbering scheme. The phenyl rings bonded to phosphorus have been omitted

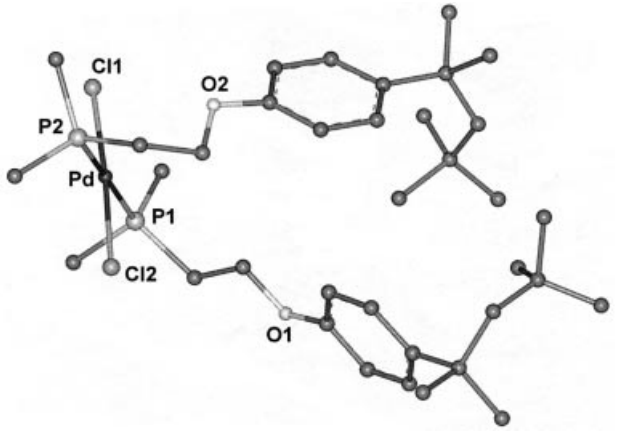

Figure 3. View of the molecular structure of *trans*-$[PdCl_2(\mathbf{1})_2]$. The phenyl rings bonded to phosphorus have been omitted

 © 2003 Wiley-VCH Verlag GmbH & Co. KGaA, Weinheim

Figure 4. Molecular structures of *trans*-[Rh(CO)(PPh_2Me)$_2$Cl][19b] (left) and *trans*-[$PdCl_2$(PPh_2Me)$_2$][10] (right) showing the different conformations of the coordinated phosphane ligands

are nearly eclipsed in the rhodium complex and the methyl groups are closer, whereas in the palladium complex the two methyl groups are located as far apart as possible.

Experimental Section

General Remarks: All reactions were performed under nitrogen by standard Schlenk tube techniques. The NMR spectra were recorded by the *Servei de Ressonància Magnètica Nuclear de la Universitat Autònoma de Barcelona* on a Bruker AC250 instrument. All chemical shift values are given in ppm and are referenced with respect to residual protons in the deuterated solvents for ^{1}H spectra, to solvent signals for ^{13}C spectra and to external phosphoric acid for ^{31}P{^{1}H} spectra. Coupling constants, in parentheses, are expressed in Hz. Infrared spectra were recorded on a Perkin−Elmer FT-2000.

Compounds **1**−**6** were prepared by published procedures.[8b] Microanalyses were performed in the Servei d'Anàlisi Química de la Universitat Autònoma de Barcelona.

Reactivity of 1−6 toward [Rh(COD)(THF)$_2$]$^+$: In a representative procedure 70% $HClO_4$ (0.16 mmol) was added to a yellow solution of [Rh(COD)(acac)] (0.16 mmol) in 10 mL of THF. The solution turned slightly orange. After stirring for several minutes, the corresponding phosphane ligand (0.32 mmol) in 5 mL of THF was added. The orange colour became more intense. The reaction mixture was stirred for over one hour at room temperature. The ^{31}P{^{1}H} NMR spectrum of the reaction mixture was recorded by adding [D$_6$]acetone to the THF solutions. **1**: 17.6 d (J = 144 Hz). **2**: 17.6 (d, J = 142 Hz), 23.8 (d, J = 122 Hz), 28.7 (d, J = 139 Hz). **3**: 17.0 (b), 28.8 (d, J = 139 Hz). **4**: 17.5 (d, J = 150 Hz), 17.8 (d, J = 142 Hz). **5**: 17.7 (d, J = 142 Hz), 26.8 (b). **6**: 17.6 (d, J = 144 Hz), 28.5 (d, J = 153 Hz), 32.4 (d, J = 121 Hz), 39.5 ppm (d, J = 130 Hz).

Reactivity of 2−6 toward [Rh(COD)(THF)$_2$]$^+$ and CO: When CO was bubbled into the previous reaction mixture its colour rapidly turned pale yellow. Bubbling was maintained for one hour after which the reaction solvents were evaporated to dryness. The ^{31}P{^{1}H} NMR and IR spectra of the resulting oily products were recorded by adding [D$_6$]acetone to the dichloromethane solutions. ^{31}P{^{1}H} NMR spectroscopic data: **2**: 22.0 (d, J = 130 Hz), 23.6 (d, J = 127 Hz). **3**: 21.8 (d, J = 124 Hz). **4**: 25.4 (broad d, $J \approx$ 110 Hz). **5**: 23.8 (d, J = 110 Hz), 30.7 (d, J = 113 Hz). **6**: 23.2 (d, J = 113 Hz), 32.5 ppm (d, J = 118 Hz). IR data (νCO, CH_2Cl_2 solution): **2**, 1980; **3**, 1972; **4**, 1980; **5**, 1979; **6**, 1983 cm^{-1}.

Reactivity of 1 toward [Rh(COD)(THF)$_2$][BF$_4$] and CO: Synthesis of *trans*-[Rh(CO)$_2$(1)$_2$][BF$_4$]: [Rh(COD)(μ-Cl)]$_2$ (100 mg, 0.2 mmol) was dissolved in 10 mL of THF and $AgBF_4$ (80 mg, 0.41 mmol) was added to the solution. The solution was stirred for 1 h. Precipitated AgCl was eliminated by filtration through a small pad of Celite. **1** (340 mg, 0.81 mmol) was added to the resulting yellow solution and the solution was stirred for 1 h. CO was bubbled into the solution for 1 h and during this time the solution lightened. THF was then evaporated under vacuum and the residue was dissolved in 5 mL of CH_2Cl_2. 15 mL of diethyl ether was added to this solution and the resulting mixture was cooled to −20 °C. 250 mg of *trans*-[Rh(CO)$_2$(**1**)$_2$][BF$_4$] was isolated as a white powder (57% yield). IR (νCO): 2041 cm^{-1} (CH_2Cl_2 solution); ^{31}P{^{1}H} NMR ($CDCl_3$): (293 K) 20.9 (bd, J = 104.8 Hz); (233 K) 20.1 ppm, (d, J = 107.1 Hz). (^{1}H) NMR (CD_2Cl_2): (293 K) 0.66 (s, 9 H), 1.31 (s, 6 H), 1.69 (s, 2 H), 3.16 (m, 2 H), 4.27 (m, 2 H), 6.57 (d, J = 8.7 Hz, 2 H), 7.21 (d, J = 8.7 Hz, 2 H), 7.44−7.65 ppm (m, 10 H). $C_{58}H_{70}BF_4O_4P_2Rh$ (1082.8): calcd. C 64.3, H 6.5; found C 63.9, H 7.0.

Synthesis of [Rh(CO)(1)$_2$][BF$_4$]: *trans*-[Rh(CO)$_2$(**1**)$_2$][BF$_4$] (250 mg) was dissolved in 15 mL of CH_2Cl_2 and the solution was refluxed for 5 h. The solution was evaporated to dryness and the residue was crystallised in a CH_2Cl_2/hexane mixture at −20 °C. 200 mg of [Rh(CO)(**1**)$_2$][BF$_4$] was isolated (82%). IR (νCO): 1990 cm^{-1} (CH_2Cl_2 solution); ^{31}P{^{1}H} NMR (CD_2Cl_2): (293 K) 29.5 (bd, J = 120.1 Hz); (193 K) 23.8, (d, J = 134.3 Hz), 34.8 ppm, (bd, J = 110 Hz). (^{1}H) NMR (CD_2Cl_2): (293 K) 0.69 (s, 9 H), 1.31 (s, 6 H), 1.69 (s, 2 H), 2.83 (m, 2 H), 4.21 (m, 2 H), 6.63 (d, J = 8.7 Hz, 2 H), 7.16 (d, J = 8.7 Hz, 2 H), 7.47−7.70 ppm (m, 10 H). (193 K) 0.56 (bs, 18 H), 1.23 (bs, 12 H), 1.62 (s, 4 H), 2.57 (b, 2 H), 3.01 (b, 2 H), 3.92 (b, 2 H), 4.22 (m, 2 H), 6.38 (2 H), 6.66 (2 H), 7.05 (b, 4 H), 7.41−7.63 ppm (m, 20 H). $C_{57}H_{70}BF_4O_3P_2Rh$ (1054.8): calcd. C 64.9, H 6.7; found C, 65.0, H 6.5.

Synthesis of *trans*-Rh(CO)(1)$_2$Cl: Ligand **1** (0.27 mmol) and [Rh(COD)(μ-Cl)]$_2$ (0.06 mmol) were dissolved in 25 mL of CH_2Cl_2. The yellow reaction mixture was stirred for one hour. The ^{31}P{^{1}H} NMR spectrum of this reaction mixture was recorded by adding [D$_6$]acetone: 22.3 (dd, $^1J_{RhP}$ = 137, $^2J_{P,P}$ = 39 Hz); 28.2 (d, $^1J_{RhP}$ = 150 Hz); 37.3 ppm (dt, $^1J_{RhP}$ = 187, $^2J_{P,P}$ = 39 Hz).

CO was bubbled into the reaction mixture for one hour and during this time the colour changed to pale yellow. The solution was evaporated to dryness and the residue was crystallised in a acetone/methanol mixture at −20 °C. 75 mg of *trans*-[Rh(CO)(**1**)$_2$Cl] was isolated (62%). IR (νCO): 1975 cm^{-1} (CH_2Cl_2 solution). ^{31}P{^{1}H} NMR (CD_2Cl_2): 21.3 ppm d ($^1J_{RhP}$ = 124 Hz). $C_{57}H_{70}O_3ClP_2Rh$: calcd. C 68.2, H 7.0; found C, 67.5, H 7.4.

 © 2003 Wiley-VCH Verlag GmbH & Co. KGaA, Weinheim

X-ray Crystallographic Study: Data were collected on an Enraf−Nonius CAD4 diffractometer at room temperature. Full crystallographic data for *trans*-[Rh(CO)(**1**)$_2$Cl] are gathered in Table 1. All calculations were performed on a PC-compatible computer using the WinGX system.[21] The structures were solved by direct methods, using the SIR92 program,[22] which revealed in each instance the position of most of the non-hydrogen atoms. All remaining non-hydrogen atoms were located by the usual combination of full-matrix least-squares refinement and difference electron density syntheses using the SHELXS-97 program.[23] One *tert*-octyl group showed structural disorder and it was split; final s.o.f. was 0.5/0.5. The phenyl rings have been refined as rigid groups (D_{6h} symmetry; C−C = 1.39 Å; C−H = 0.93 Å). Atomic scattering factors were taken from the usual tabulations.[24] Anomalous dispersion terms for Rh, P, and Cl were included in F_c.[25] All non-hydrogen atoms were allowed to vibrate anisotropically. All the hydrogen atoms were set in idealised positions (R_3CH, C−H = 0.96 Å; R_2CH_2 = 0.97 Å; C(sp^2)−H = 0.93 Å; U_{iso} 1.2 times greater than the U_{eq} of the carbon atom to which the hydrogen atom is attached) and held fixed during refinements. Final atomic coordinates for all atoms, anisotropic thermal parameters, lists of structure factor amplitude for compounds for the X-ray study are available from the authors upon request.

Table 1. Crystal data and structure refinement for *trans*-[Rh(CO)(**1**)$_2$Cl]

Empirical formula	$C_{57}H_{70}ClO_3P_2Rh$
Molecular mass	1003.43
Temperature	293(2) K
Wavelength	0.71073 Å
Crystal system	triclinic
Space group	$P\bar{1}$ (#2)
Unit cell dimensions	a = 16.2300(10) Å, α = 101.98(2)°
	b = 17.057(2) Å, β = 96.83(2)°
	c = 10.0310(10) Å, γ = 77.830(10)°
Volume	2647.2(4) Å^3
Z	1.259 Mg/m^3
Absorption coefficient	0.475 mm^{-1}
F(000)	1056
Theta range for data collection	1.24 to 21.98°
Index ranges	$0 \le h \le 17$, $-17 \le k \le 17$, $-10 \le l \le 10$
Independent reflections	6462
Completeness to theta = 21.98°	99.8%
Refinement method	Full-matrix least-squares on F^2
Data/restraints/parameters	6462/11/544
Goodness-of-fit on F^2	1.054
Final R indices [$I > 2\sigma(I)$]	$R1$ = 0.0420, $wR2$ = 0.1064

CCDC-203524 contains the supplementary crystallographic data for this paper. These data can be obtained free of charge at www.ccdc.cam.ac.uk/conts/retrieving.html [or from the Cambridge Crystallographic Data Centre, 12, Union Road, Cambridge CB2 1EZ, UK; fax: (internat.) +44-1223-336-033; E-mail: deposit@ccdc.cam.ac.uk].

Acknowledgments

We thank the DGICYT (programa de Promoción General del Conocimiento) for financial support.

[1] B. Cornils, W. A. Herrmann (Eds.), *Aqueous-Phase Organometallic Catalysis*, Wiley-VCH, Weinheim, **1998**, chapter 3.2.
[2] [2a] H. B. Kagan, in: *Asymmetric Synthesis* (Ed.: J. D. Morrison), vol. 5, Academic Press, Orlando, **1985**, chapter 1. [2b] H. Brunner, W. Zettlmeier, *Handbook of Enantioselective Catalysis with Transition Metal Compounds*, vol. II, VCH, Weinheim, **1993**. [2c] J. Holz, M. Quirmbach, A. Börner, *Synthesis* **1997**, *9*, 983.
[3] [3a] E. Lindner, S. Pautz, M. Haustein, *Coord. Chem. Rev.* **1996**, *155*, 145. [3b] H. Yang, M. Alvarez-Gressier, N. Lugan, R. Mathieu, *Organometallics* **1997**, *16*, 1401. [3c] E. Lindner, S. Pautz, R. Fawzi, M. Steimann, *J. Organomet. Chem.* **1998**, *555*, 247. [3d] I. Le Gall, P. Laurent, E. Soulier, J. Salaün, H. Abbayes, *J. Organomet Chem.* **1998**, *567*, 13. [3e] S. Borns, R. Kadyrov, D. Heller, W. Baumann, A. Spannenberg, R. Kempe, J. Holz, A. Börner, *Eur. J. Inorg. Chem.* **1998**, *9*, 1291. [3f] C. S. Slone, D. A. Weinberger, C. A. Mirkin, in: *Progress in Inorganic Chemistry* (Ed.: K. D, Karlin), Vol. 48, John Wiley & Sons, New York, **1999**, p. 233. [3g] J. L. Ruiz, T. Flor, J. C. Bayon, *Inorg. Chem. Commun.* **1999**, *2*, 484. [3h] H. Werner, J. Bank, P. Steinert, W. Wolfsberger, *Z. Anorg. Allg. Chem.* **1999**, *625*, 2178. [3i] M. Nandi, J. Jin, T. V. RajanBabu, *J. Am. Chem. Soc.* **1999**, *121*, 9899.
[4] G. Papadogiannakis, R. A. Sheldon, in ref.[1] chapter 3.2.4.
[5] [5a] J. H. Van Esch, A. L. H. Stols, R. J. M. Nolte, *J. Chem. Soc., Chem. Commun.* **1990**, 1658. [5b] G. Ghirlanda, P. Scrimin, P. Tecilla, A. Toffoletti, *Langmuir* **1998**, *14*, 1646. [5c] F. Hampl, F. Liska, F. Mancin, P. Tecilla, U. Tonellato, *Langmuir* **1999**, *15*, 405. [5d] R. Resendes, J. Massey, H. Dorn, M. A. Winnik, I. A. Manners, *Macromolecules* **2000**, *33*, 8.
[6] [6a] B. E. Hanson, H. Ding, C. W. Kohlpaintner, *Catalysis Today* **1998**, 421. [6b] G. Oehme, I. Grassert, S. Ziegler, R. Meisel, H. Fuhrman, *Catalysis Today* **1998**, *42*, 459. [6c] R. Selke, J. Holz, A. Riepe, A. Börner, *Chem. Eur. J.* **1998**, *4*, 769.
[7] M. S. Goedheijt, B. H. Hanson, J. N. H. Reek, P. C. J. Kamer, P. W. N. M. van Leeuwen, *J. Am. Chem. Soc.* **2000**, *122*, 1650.
[8] [8a] E. Valls, J. Suades, B. Donadieu, R. Mathieu, *Chem. Commun.* **1996**, 771. [8b] E. Valls, J. Suades, R. Mathieu, *Organometallics* **1999**, *18*, 5475.
[9] E. Valls, A. Solsona, J. Suades, R. Mathieu, F. Comelles, C. López-Iglesias, *Organometallics* **2002**, *21*, 2473.
[10] E. Valls, J. Suades, R. Mathieu, J. F. Piniella, A. Alvarez-Larena, *J. Organomet. Chem.* **2001**, *626*, 139.
[11] A. Solsona, J. Suades, R. Mathieu, *J. Organomet. Chem.* **2003**, *669*, 172.
[12] These products are ethoxylated alkylphenols with different ethoxylation grades.
[13] E. Lindner, H. Norz, *Chem. Ber.* **1990**, *123*, 459.
[14] V. V. S. Reddy, A. Varshney, G. M. Gray, *J. Organomet. Chem.* **1990**, *391*, 259.
[15] E. Lindner, Q. Wang, H. A. Mayer, A. Bader, *J. Organomet. Chem.* **1993**, *458*, 229.
[16] E. Lindner, Q. Wang, H. A. Mayer, R. Fawzi, M. Steimann, *Organometallics* **1993**, *12*, 1865.
[17] E. T. Singewald, X. Shi, C. A. Mirkin, S. J. Schofer, C. L. Stern, *Organometallics* **1996**, *15*, 3062.
[18] R. Schrock, J. A. Osborn, *J. Am. Chem. Soc.* **1971**, *93*, 2397.
[19] [19a] D. C. Smith Junior, E. D. Stevens, S. P. Nolan, *Inorg. Chem.* **1999**, *38*, 5277. [19b] F. Dahan, R. Choukroun, *Acta Crystallogr., Sect. C* **1985**, *41*, 704.
[20] I. Y. Guzman-Jimenez, K. H. Whitmire, *Acta Crystallogr., Sect. C* **1999**, *55*, 9900028.
[21] L. J. Farrugia, *J. Appl. Crystallogr.* **1999**, *32*, 837.
[22] A. Altomare, G. Cascarano, C. Giacovazzo, A. Guagliardi, *J. Appl. Crystallogr.* **1993**, *26*, 343.
[23] G. M. Sheldrick, *SHELXS-97, SHELXL-97, CIFTAB − Programs for Crystal Structure Analysis* (Release 97−2), Institüt für Anorganische Chemie der Universität, Tammanstrasse 4, 3400 Göttingen, Germany, **1998**.
[24] [24a] D. T. Cromer, J. T. Waber, *International Tables for X-ray*

 © 2003 Wiley-VCH Verlag GmbH & Co. KGaA, Weinheim

Crystallography; Kynoch Press: Birmingham, England, vol. 4, **1974**, Table 22B. [24b] R. F. Stewart, E. R. Davidson, W. T. Simpson, *J. Chem. Phys.* **1965**, *42*, 3175. [24c] T. Hahn (Ed.), *International Tables for Crystallography*, Volume A, Kluwer Academic Publishers, Dordrecht, The Netherlands, **1995**.

[25] D. T. Cromer and J. T. Waber, *International Tables for X-ray Crystallography*, Kynoch Press: Birmingham, England, vol. 4, **1975**, Table 2.3.1.

Received February 19, 2003

 © 2003 Wiley-VCH Verlag GmbH & Co. KGaA, Weinheim

Efficient Asymmetric Synthesis of Δ- and Λ-Enantiomers of (Bipyridyl)ruthenium Complexes and Crystallographic Analysis of Δ-Bis(2,2′-bipyridine)(2,2′-bipyridine-4,4′-dicarboxylato)ruthenium: Diastereoselective Homo- and Heterochiral Ion Pairing Revisited

Régis Caspar, Hani Amouri,* Michel Gruselle, Christine Cordier, Bernard Malézieux, Raphäel Duval, and Hubert Leveque

Keywords: Ruthenium / Chiral resolution / Circular dichroism

*In our original article,[1] the captions for Figures 2, 3 and 4 (page 501) are incorrect. We wrongly attributed the CD curves with the solid line to the Δ-enantiomers **4a**, **4a** and **5a** and those with dotted lines to the Λ-enantiomers **3b**, **4b** and **5b**. The correct captions are as follows:*

Figure 2. CD curves for **3a** (dotted line) and **3b** (solid line) in acetonitrile

Figure 3. CD curves for **5a** (dotted line) and **5b** (solid line) in acetonitrile

Figure 4. CD curves for **4a** (dotted line) and **4b** (solid line) in acetonitrile

[1] R. Caspar, H. Amouri, M. Gruselle, C. Cordier, B. Malézieux, R. Duval, H. Leveque, *Eur. J. Inorg. Chem.* **2003**, 499−505.

Received July 3, 2003
H. Amouri

 DOI: 10.1002/ejic.200300437 © 2003 Wiley-VCH Verlag GmbH & Co. KGaA, Weinheim

EurJIC
European Journal of Inorganic Chemistry

Issue 17/2003

Pages 3057–3256

Papers available ahead of print in Early View at www.interscience.wiley.com

Earliest available Table of Contents:
Automatically, free of charge by e-mail through
www.interscience.wiley.com/alerts

COVER PICTURE

The cover picture shows a disc that contains a suspension of the complex $[(C_6F_5)_2Au\{\mu\text{-}Ag(OClO_3)\}Au(C_6F_5)_2]$ (solid) (Figure 1 in the Microreview) under ultraviolet light. The border of the disc is cooled with liquid nitrogen to a temperature close to 77 K and the centre of the disc is at room temperature. The luminescence and the colour of the complex changes from red (near 77 K), through orange and yellow, to green (room temperature). Details are discussed in the Microreview by M. Bardajía and A. Laguna on p. 3069 ff.

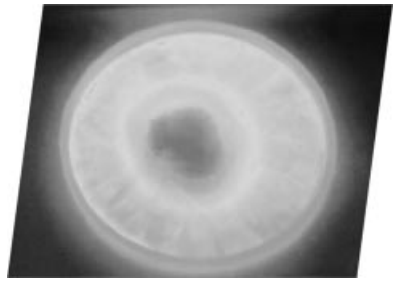

MICROREVIEWS

Contents

3069 **M. Bardají, A. Laguna***

Heteronuclear Metal–Metal Contacts between Gold(I) and Group-11, -12, and -13 Centers

Keywords: Gold / Heterometallic complexes / Metal-metal interactions / Silver

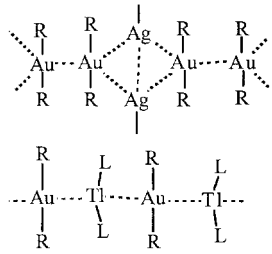

 © 2003 Wiley-VCH Verlag GmbH & Co. KGaA, Weinheim

3081 **G. Schmid,* B. Corain**

Nanoparticulated Gold: Syntheses, Structures, Electronics, and Reactivities

Keywords: Gold / Nanoparticles / Synthetic methods / Quantum dots / Self-assembly / Heterogeneous catalysis

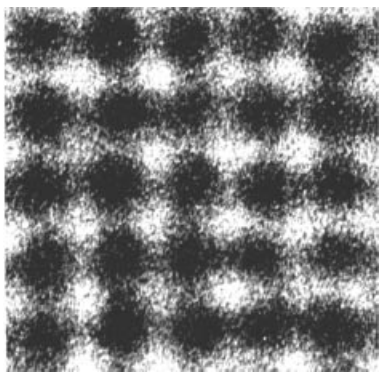

SHORT COMMUNICATION

3099 **S. Burger, B. Therrien, G. Süss-Fink***

1,2-Bis-*N*-[2′-(diphenylphosphanyl)benzoyl]diaminobenzene, a New Chelating Ligand with Versatile Coordination Properties

Keywords: Palladium / Platinum / N,P ligands / Ligand design

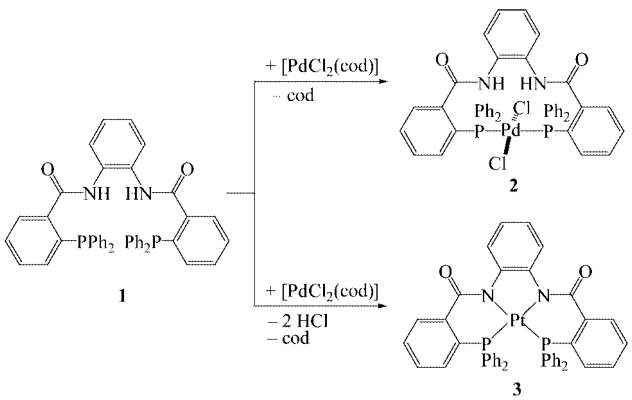

FULL PAPERS

3105 **O. Schmitt, G. Wolmershäuser, H. Sitzmann***

The Substitution Reaction of (Chloro)bis(tetraisopropylcyclopentadienyl) Complexes of La, Pr, or Nd with Silylamides

Keywords: Lanthanides / Cyclopentadienyl ligands / N ligands / Si ligands

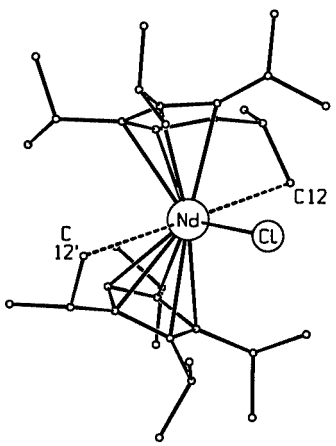

3110 **J. Rong, Y. Peng, H. W. Roesky,* J. Li, D. Vidovic, J. Magull**

The First Structurally Characterized Aluminum Squaraine Complex: $L_2(AlMe_2)_4 \cdot 2THF \cdot 2$toluene [L = Bis(2,6-diisopropylanilino)squaraine]

Keywords: Aluminum / Squaraine / N ligands / O ligands / X-ray diffraction

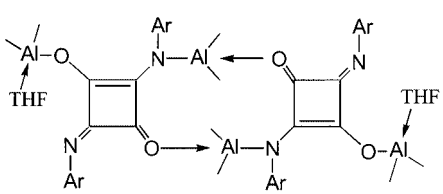

 © 2003 Wiley-VCH Verlag GmbH & Co. KGaA, Weinheim

3113 **H. Zhu, J. Chai, H. W. Roesky,* M. Noltemeyer, H.-G. Schmidt, D. Vidovic, J. Magull**

A Bulky Chelating Diamidoaluminum Monohydride. Synthesis, Structure and Reactions with Me_3SnF and Heavy Group 16 Elements

Keywords: Aluminum / Hydride / Chalcogens / Fluorine

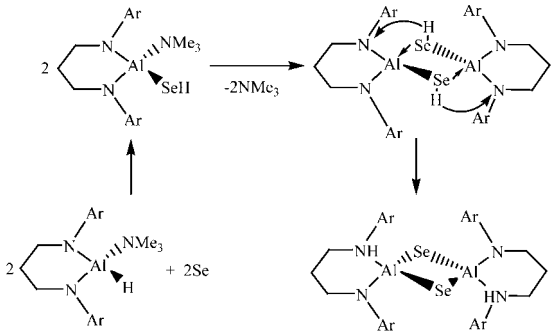

(Ar = 2,6-*i*Pr$_2$C$_6$H$_3$)

3120 **A. M. Neculai, D. Neculai, G. B. Nikiforov, H. W. Roesky,* C. Schlicker, R. Herbst-Irmer, J. Magull, M. Noltemeyer**

Partially Fluorinated Rare Earth Metal Complexes

Keywords: Lanthanides / Fluorides / Tin / N donor ligands

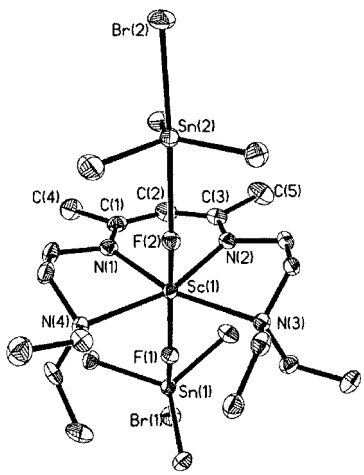

3127 **C. Bartolomé, P. Espinet,* J. M. Martín-Alvarez, F. Villafañe**

Monoarylated Fluoromesitylpalladium Complexes

Keywords: Palladium / Fluorinated ligands / Ligand substitution / Bulky ligands / Steric hindrance

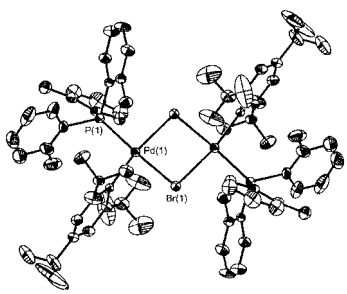

3139 **E. Lukevics, P. Arsenyan,* S. Belyakov, O. Pudova**

Synthesis, Structure and Chemical Transformations of Ethynylgermatranes

Keywords: Cobalt / Germanium / Germatrane / X-ray diffraction / Alkynes

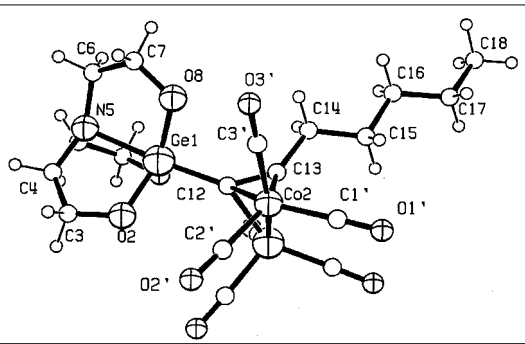

3144 **F. Schlosser, S. Krüger, N. Rösch***

Relativistic Density Functional Study of the Dinuclear Uranyl Complex $[(UO_2)_2(\mu_2\text{-}OH)_2Cl_2(H_2O)_4]$ in Its Crystalline Environment

Keywords: Actinides / Uranium / Hydrogen bonds / Relativistic density functional calculations

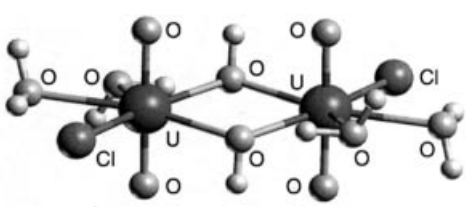

 © 2003 Wiley-VCH Verlag GmbH & Co. KGaA, Weinheim

3152 **H.-R. Wu, Y.-H. Liu, S.-M. Peng, S.-T. Liu***

Palladium(II) Complexes Containing a Pyridinyl-iminophosphorane Ligand

Keywords: N ligands / Polymerization / Palladium

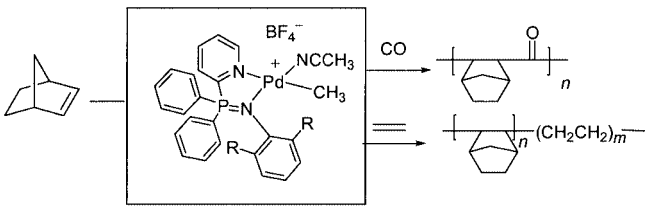

3160 **E. Alessio,* B. Serli, E. Zangrando, M. Calligaris, N. S. Panina**

Geometrical and Linkage Isomers of $[OsCl_2(dmso)_4]$ − The Complete Picture

Keywords: Density functional calculations / Dimethyl sulfoxide / Isomerizations / Osmium

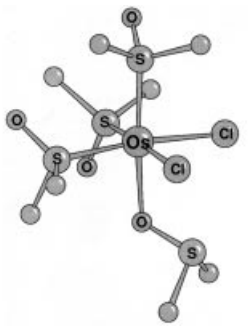

3167 **T. K. Paine, E. Rentschler, T. Weyhermüller, P. Chaudhuri***

Polynuclear Nickel(II) Complexes: Preparation and Magnetic Properties of Ni^{II}_4, Ni^{II}_5, and Ni^{II}_6 Species with Ligands containing O∩X∩O (X = S, Se or N) Donor Atoms

Keywords: Magnetic properties / Nickel / Selenium / Sulfur / Tripodal ligands

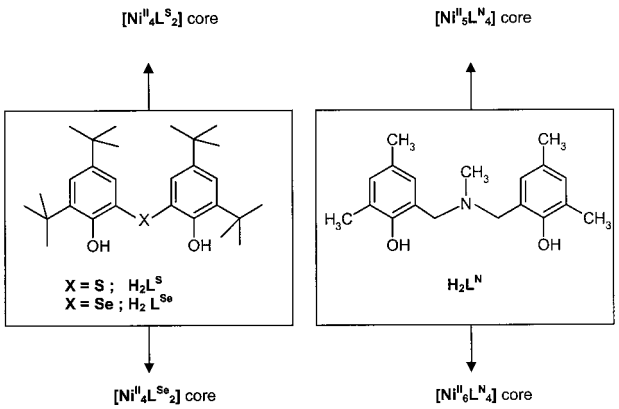

3179 **S. Burling, L. D. Field,* H. L. Li, B. A. Messerle, P. Turner**

Mononuclear Rhodium(I) Complexes with Chelating *N*-Heterocyclic Carbene Ligands − Catalytic Activity for Intramolecular Hydroamination

Keywords: Rhodium / Carbene ligands / Homogeneous catalysis / Hydroamination

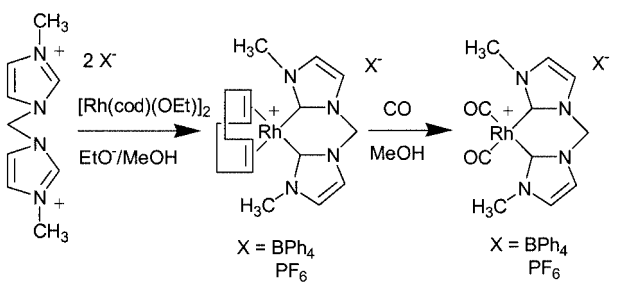

3185 **M. Di Vaira, F. Mani, S. Seniori Costantini, P. Stoppioni,* A. Vacca**

Synthesis, Kinetic Study and Molecular Orbital Investigation of Cadmium(II), Mercury(II) and Lead(II) Complexes with the Mixed Pendant-Arm Macrocyclic Ligand 1,7-Bis(carboxymethyl)-4,10-bis(1-methylimidazol-2-ylmethyl)-1,4,7,10-tetraazacyclododecane

Keywords: Macrocyclic ligands / Cadmium / Lead / Mercury / Conformational equilibrium / Density functional calculations

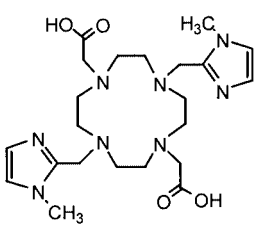

 © 2003 Wiley-VCH Verlag GmbH & Co. KGaA, Weinheim

3193 **R. Pedrido, M. R. Bermejo,* A. M. García-Deibe, A. M. González-Noya, M. Maneiro, M. Vázquez**

Metal Complexes of a Novel Achiral Symmetric Pentadentate Ligand − Crystal Structures of Monohelical Zinc(II) and Cadmium(II) Complexes

Keywords: Supramolecular chemistry / Helical structures / Schiff bases / Electrochemistry

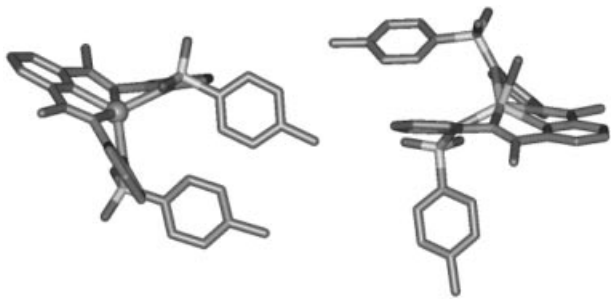

3201 **L.-C. Song,* P.-C. Liu, J.-T. Liu, F.-H. Su, G.-F. Wang, Q.-M. Hu, P. Zanello, F. Laschi, M. Fontani**

Synthesis, Characterization and Electrochemical Properties of Optically Active [60]Fullerene Organotransition Metal Complexes *mer*-[(η^2-C_{60})$M(CO)_3${(−)-DIOP}] (M = Mo, W), *mer*-[(η^2-C_{60})$M(CO)_3${(+)-DIOP}] (M = Mo, W) and [(η^2-C_{60})M{(−)-DIOP}] (M = Pd, Pt) − Crystal Structure of [(η^2-C_{60})Pt{(−)-DIOP}]

Keywords: Transition metals / Fullerenes / Electrochemistry / Optical activity

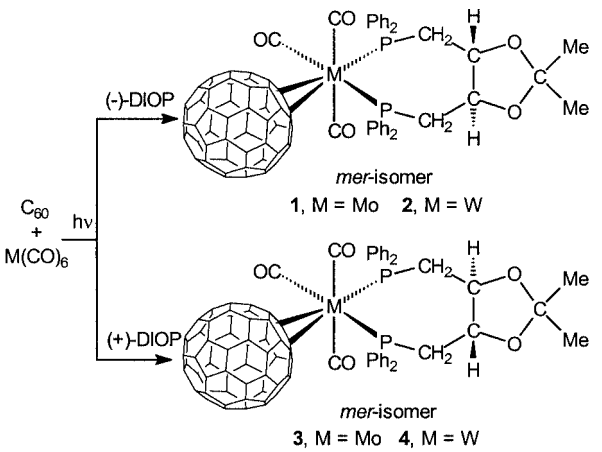

3211 **C. Knapp, E. Lork, T. Borrmann, W.-D. Stohrer, R. Mews***

Syntheses, Structures and Theoretical Investigations of 1λ⁴,3λ⁴,5λ⁴-Trithia-2,4,6,8,9-pentaazabicyclo[3.3.1]nona-1(9),2,3,5,7-pentaenes

Keywords: Sulfur / Nitrogen / Fluorine / Solid-state structures / Quantum chemistry

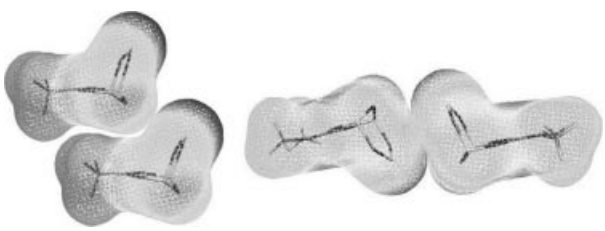

3221 **F. Caruso,* L. Massa, A. Gindulyte, C. Pettinari,* F. Marchetti, R. Pettinari, M. Ricciutelli, J. Costamagna, J. C. Canales, J. Tanski, M. Rossi**

(4-Acyl-5-pyrazolonato)titanium Derivatives: Oligomerization, Hydrolysis, Voltammetry, and DFT Study

Keywords: Titanium / Density functional calculations / Nitrogen heterocycles / Voltammetry / O ligands

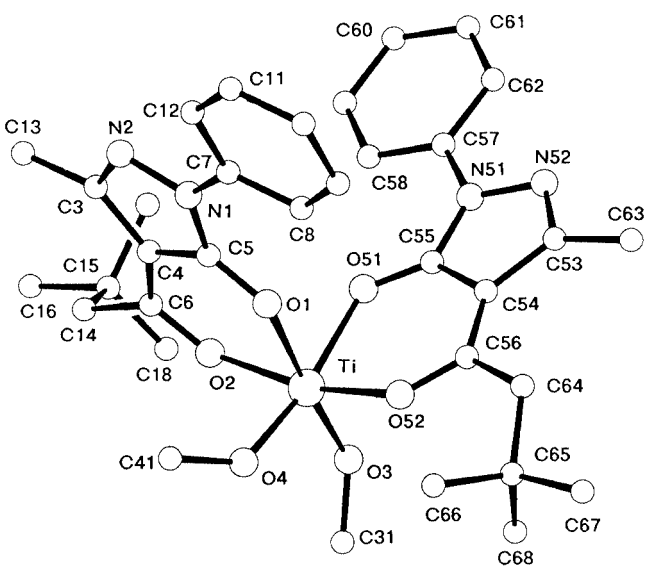

 © 2003 Wiley-VCH Verlag GmbH & Co. KGaA, Weinheim

3233 **A. Otero,* F. Carrillo-Hermosilla,* P. Terreros, T. Expósito, S. Rojas, J. Fernández-Baeza, A. Antiñolo, I. López-Solera**

Synthesis, Structure and Reactivity of New Late Transition Metal Complexes Bearing Diphosphane Ligands Derived from Bis(pyrazol-1-yl)-methane

Keywords: Nitrogen heterocycles / Phosphanes / Palladium / Platinum / Rhodium / Iridium / Hydrogenation

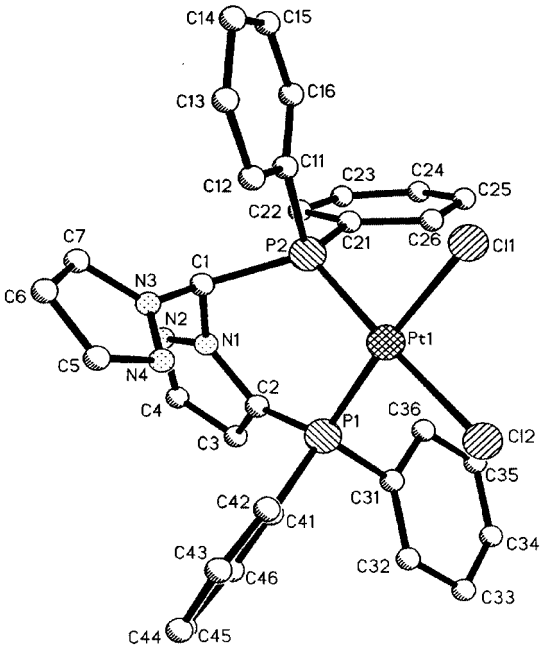

3242 **E. Y. Lee, D. Hong, H. W. Park, M. P. Suh***

Synthesis, Properties, and Reactions of Trinuclear Macrocyclic Nickel(II) and Nickel(I) Complexes: Electrocatalytic Reduction of CO_2 by Nickel(II) Complex

Keywords: Nickel / Macrocyclic compounds / Carbon dioxide / Electroreduction / Multinuclear complex

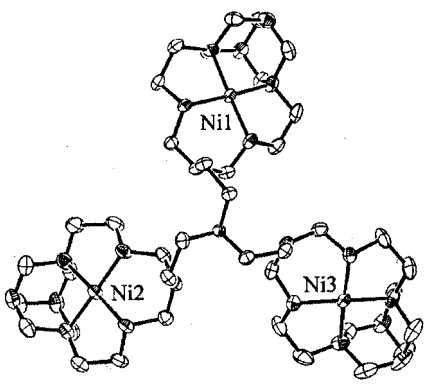

3250 **C. An, K. Tang,* X. Liu, Y. Qian**

Large-Scale Synthesis of High Quality Trigonal Selenium Nanowires

Keywords: Nanostructures / Semiconductors / Selenium

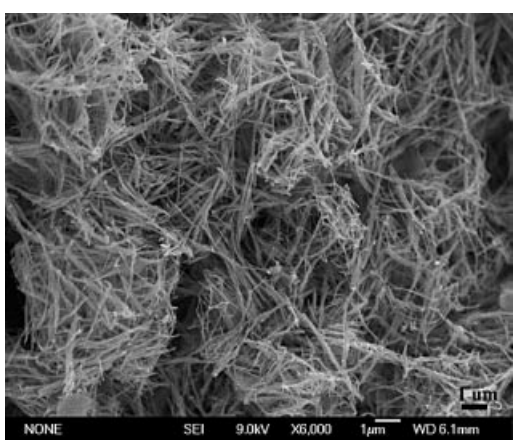

 © 2003 Wiley-VCH Verlag GmbH & Co. KGaA, Weinheim

Heteronuclear Metal−Metal Contacts between Gold(I) and Group-11, -12, and -13 Centers

Manuel Bardají[a][‡] and Antonio Laguna*[a]

Keywords: Gold / Heterometallic complexes / Metal-metal interactions / Silver

Closed-shell interactions occur mainly for some heavy late transition metals and main-group elements. In fact, these are dispersion forces reinforced by relativistic effects and by ionic components, of which the former are maximized in heteronuclear interactions. Heteronuclear compounds containing gold(I) and group-11, -12, and -13 metals display d^{10}–d^{10} or d^{10}–s^2 closed-shell interactions of intermediate strength relative to the homonuclear metal–metal interactions. The number of examples of gold(I)–gold(I) contacts is large, but representatives of heteronuclear gold(I)–metal contacts are still scarce. There are two general types of derivatives displaying short gold–metal distances: those with bridging ligands and those with unbridged ones, of which the latter are always the more indicative of the presence of a real bond. Derivatives featuring unsupported gold–metal bonds have been obtained mainly through reactions between basic gold(I) complexes and acid complexes, and also by encapsulation of metal centers in metallocryptands. Most derivatives with supported gold–metal bonds have been synthesized by use of C-donor ligands or ambidentate ligands. The gold–metal contacts dramatically affect the conformations and the aggregation of the molecules, and also their optical properties. Some of these derivatives are, in fact, intensely luminescent.
(© Wiley-VCH Verlag GmbH & Co. KGaA, 69451 Weinheim, Germany, 2003)

1. Introduction

Closed-shell species with opposite electric charges form strong ionic bonds, but such bonds should not be expected if their charges are similar. However, it has been shown experimentally that such closed-shell interactions do occur, mainly for some heavy late transition metals and main-group elements; these interactions are weaker than ionic bonds but stronger than other van der Waals bonds.[1]

The most typical case is found in gold(I) chemistry, and the term aurophilicity was coined by Schmidbaur to refer to this phenomenon. Linear two-coordinate gold(I) compounds with d^{10} configurations tend to associate into dimers, oligomers, or polymers through gold−gold contacts, showing gold−gold distances in the 2.69−3.35 Å range. The energies associated with these aurophilic interactions go from 20 to 50 kJ/mol, close to those found in hydrogen bonds.[2−4] Aurophilicity has been used in crystal engineering of homo- and heterometallic systems to design supra-

[a] Departamento de Química Inorgánica, Instituto de Ciencia de Materiales de Aragón, Universidad de Zaragoza − CSIC 50009 Zaragoza, Spain
[‡] Present and permanent address: Departamento de Química Inorgánica, Facultad de Ciencias, Universidad de Valladolid, 47005 Valladolid, Spain

Doctor Manuel Bardají completed his Ph.D. degree with Professors Antonio and Mariano Laguna in 1994 (Universidad de Zaragoza), and undertook a two-year postdoctoral stay at the Laboratoire de Chimie de Coordination (Toulouse, France) under the supervision of Bruno Chaudret. He returned to the Universidad de Zaragoza, where he has been working in the field of gold chemistry. He has been a "Profesor Titular" of Inorganic Chemistry (Profesor Titular de Química Inorgánica) at the Universidad de Valladolid since December 2002.

Professor Antonio Laguna completed his Ph.D. degree with Professor R. Usón in 1973. He also completed a postdoctoral period at the University of Bristol in 1975, under the supervision of Professor F. G. A. Stone. Since 1976 he has worked at the University of Zaragoza as Profesor Titular or Professor of Inorganic Chemistry. He is the author of more than 270 scientific papers on the organometallic and coordination chemistry of silver and gold.

MICROREVIEWS: This feature introduces the readers to the authors' research through a concise overview of the selected topic. Reference to important work from others in the field is included.

molecular structures, because it affects molecular conformations and intermolecular aggregation.[5−7]

Similarly, the terms cuprophilicity (Cu−Cu < 2.8 Å) and argentophilicity (Ag−Ag < 3.4 Å) have been used to describe this phenomenon in the cases of copper and silver, respectively, the energies involved being lower than in the case of gold but close to those of standard van der Waals interactions. The same phenomenon was also found for the close heavy metals mercury, thallium, and platinum; it was again less energetic, although some small contributions from metal−metal bonding could not be ignored.[1,8,9] Curiously, the first direct observation of a d orbital was achieved in charge-density maps of cuprite (Cu_2O), thanks to the hole in the d^{10} configuration due to Cu^I−Cu^I interactions.[10,11]

Great efforts have been devoted to theoretical studies trying to explain this phenomenon by different approaches. Pyykkö and co-workers have concluded that the aurophilic attraction is an electronic correlation effect strengthened by the relativistic effect, which has a maximum for gold. They extended their studies to other closed-shell metallic interactions in d^{10}, d^8, or s^2 systems and also to mixed systems; the term metallophilic attraction was coined to describe this phenomenon. From these, it is a dispersion force reinforced by relativistic effects (for heavy atoms) and by ionic components, the former already being important for gold−gold interactions but being more clearly seen for heteronuclear interactions.[1,12−15]

Heteronuclear compounds containing gold(I) and group-11, -12, and -13 metals display d^{10}−d^{10} or d^{10}−s^2 closed-shell interactions of intermediate strength relative to the homonuclear metal−metal interactions. The natures of the ligands and competition with other weak forces, such as hydrogen bonds or π−π interactions between aromatic rings, play an important role. It is important to note that these interactions are invoked for copper−, silver−, mercury−, indium−, and thallium−gold distances shorter than the sums of the corresponding van der Waals radii (3.06, 3.38, 3.21, 3.59 and 3.62 Å, respectively; values taken from Table 3 in ref.[1]) and are regarded as strong if they are less than or close to the sums of the metallic radii (2.72, 2.89, 3.04, 3.07 and 3.14 Å, respectively).[16]

Three general strategies are used to build these heteronuclear compounds: a) supported gold−metal bonds in which bridging ligands are present, b) unsupported gold−metal bonds through reactions between basic/donor gold(I) complexes and acid/acceptor complexes to give acid−base/acceptor−donor stacking, and c) unsupported gold−metal bonds by encapsulation of a metal center of a dinuclear gold(I) cryptand.

Moreover, there are gold−metal clusters in which the metallic centers can be formally considered to be in an oxidation state between 0 and 1, and display similar or shorter gold−metal distances. In the same kind of clusters, $Au(PR_3)^+$ fragments can be added or scrambled to give a mixture of $Au(PR_3)^+$ and $M(PR_3)^+$ (M = Cu, Ag) units. These have been reviewed elsewhere and are not considered here, at least for clusters bigger than heptanuclear.[17−19]

The metal−metal contacts dramatically affect the conformations and the aggregation of the molecules, as happens in the most typical case of aurophilicity, and this in turn affects some properties, such as the optical properties.[20] The optical properties of these derivatives (generally gold or platinum compounds) have applications in sensor technology,[21,22] and they have been used to detect oxygen,[23] volatile organic compounds,[24,25] potassium,[26] or phosphane[27] in solution, whilst other display solvoluminescence.[28] Similarly, some results for gold−silver derivatives have recently been obtained.[29]

The number of examples of gold(I)−gold(I) contacts is large, but examples of the heteronuclear gold(I)−metal contacts are still scarce. In this microreview we summarize the state of the art in heteronuclear metal−metal contacts of gold(I) with group-11, -12, and -13 centers − mainly with silver(I) and thallium(I) − for which the gold−metal distances have been determined and show the presence of d^{10}−d^{10} or d^{10}−s^2 closed-shell interactions.

The microreview is organized as follows:

2. Derivatives with Unsupported Gold−Metal Bonds
2.1. With Bis(halophenyl)aurate(I) Salts as Bases
2.1.1. Unsupported Gold−Silver Contacts
2.1.2. Unsupported Gold−Thallium Contacts
2.2. By Use of Trinuclear Cyclic Gold(I) Complexes as Bases
2.3. By Encapsulation of a Metal Center by a Dinuclear Gold(I) Cryptand
2.4. Other Cases
3. Derivatives with Supported Gold−Metal Bonds
3.1. Dinuclear Derivatives
3.2. Trinuclear Derivatives
3.3. Higher Nuclearities

2. Derivatives with Unsupported Gold−Metal Bonds

The clearest cases of metal−metal bonding are produced by the presence of short metal−metal distances in the absence of bridging ligands. In such cases, the gold−metal contacts produce aggregation, which usually dramatically affects the optical properties. Some heteronuclear derivatives, for instance, become luminescent after formation of the gold−metal bond. These derivatives can be obtained mainly by two approaches: 1) by use of bis(halophenyl)aurate(I) or trinuclear cyclic gold(I) complexes as a base, therefore maximizing the electrostatic component of these closed-shell interactions, and 2) by encapsulation of a metal center by a dinuclear gold(I) cryptand.

2.1. With Bis(halophenyl)aurate(I) Salts as Bases

Because of the number of examples, we divide this section into two parts: one for silver derivatives, and the other for

 © 2003 Wiley-VCH Verlag GmbH & Co. KGaA, Weinheim

thallium derivatives, the latter being prepared by the same type of reaction.

2.1.1. Unsupported Gold−Silver Contacts

In 1981 we characterized the first example of such a gold(I)−silver(I) interaction in a chain polymer containing the moiety $[(C_6F_5)_2Au(\mu\text{-}AgSC_4H_8)_2Au(C_6F_5)_2]_\infty$, with Ag−Au acceptor−donor (or acid−base) bonds based on dispersive and electrostatic attraction between their metal centers.[30] There is a rhomboidal arrangement of the four metallic centers, in which the gold−silver distances are as short as 2.718(2) and 2.726(2) Å, whilst the inter-unit gold−gold distance is 2.889(2) Å; for the analogue with benzene (η^2-bonded symmetrically to the silver center) in place of tetrahydrothiophene (SC_4H_8) the gold−silver distances are 2.702(2) and 2.792(2) Å, and the gold−gold distance is 3.013(2) Å (see Figure 1).[31] Therefore, the gold−silver contacts are shorter than the gold−gold contacts in these compounds.

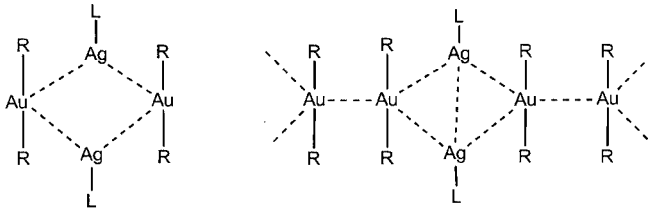

Figure 1. Complexes $[R_2Au(\mu\text{-}AgL)_2AuR_2]$ with rhomboidal geometry and unsupported gold−silver bonds; additional inter-unit gold−gold and intramolecular silver−silver contacts are possible

The basic aurate anion reacts with silver(I) to give a yellow solution. From this, through addition of ligand, yellow or orange polymers ($[R_2Au(\mu\text{-}AgL)_2AuR_2]_\infty$) are available with a variety of O-, N-, S-, or P-donors as auxiliary ligands, and R being a halophenyl ligand (R = C_6F_5, $C_6F_3H_2$ or C_6Cl_5). By this method, 35 different complexes have been prepared. These complexes are only soluble in coordinating solvents, but color loss is related to the cleavage of the gold−gold bonds.

Chain formation can be avoided by the use of bulky ligands at the gold centers, preventing aggregation through gold−gold interaction. We have thus synthesized the neutral or cationic tetrametallic phosphorus ylide gold−silver complexes $[(R_3PCH_2)_2Au(\mu\text{-}AgL)_2Au(CH_2PR_3)_2]$ (PR_3= PPh_3, PPh_2Me, $PPhMe_2$; L = $OClO_3$, PPh_3). X-ray diffraction studies carried out for L = PR_3 = PPh_3 show short gold−silver distances of 2.760(2) and 2.783(2) Å, within the previously observed range for these unsupported contacts, but there are no gold−gold interactions.[32]

We have recently revisited these polymeric derivatives in order to study their optical properties, because aggregation through gold(I)−gold(I) interactions has a dramatic effect on these properties in solution and in the solid state.[33] The absorption and emission spectra of $[(C_6F_5)_2Au(\mu\text{-}AgOCMe_2)_2Au(C_6F_5)_2]_\infty$ in acetone are consistent with molecular aggregation through gold−gold interactions when this compound goes from dilute solution conditions to concentrated ones. This derivative is also strongly luminescent in the solid state (546 nm at room temperature and 554 at 77 K). DFT calculations agree with the experimentally observed behavior and show the natures of the orbitals involved in each transition. In fact, the emission is attributable to pentafluorophenyl ππ* excited states or π-MMCT transitions in dilute solutions and to metal-centered excited states in concentrated solutions or in the solid state. Moreover, the gold−silver distances in this derivative are 2.7829(9) and 2.7903(9) Å; the gold−gold distance is 3.1674(11) Å, which is different from the previous structures. There is also a short silver−silver distance of 3.1810(13) Å.

By the same strategy, we have prepared a polymeric chain containing the dinuclear moiety $[Ag(py)_3][Au(C_6F_5)_2]$py rather than a tetranuclear one. An X-ray study showed disorder in the silver atom position, but the geometry was confirmed. Theoretical calculations reveal the presence both of metallophilic gold−silver (with ionic and dispersion contributions) and of aromatic pentafluorophenyl−pyridine interactions (dispersion effect).[34]

2.1.2. Unsupported Gold− Thallium Contacts

In 1998 we characterized the first extended unsupported gold−thallium linear chain containing the $[Tl(OPPh_3)_2][Au(C_6F_5)_2]$ moiety, with gold−thallium distances of 3.0358(8) and 3.0862(8) Å (Figure 2).[35] It was synthesized in the same way as the gold−silver polymers, through the reaction between the electron-rich $[Au(C_6F_5)_2]^-$ anion and a thallium salt in the presence of ligand.

In the same manner, we also prepared $[Tl(OPPh_3)][Tl(OPPh_3)L][Au(C_6Cl_5)_2]_2$ (L = THF, acetone), which also displayed extended unsupported chains with short gold−thallium distances, in the 3.0529(3)−3.3205(3) or 3.0937(3)−3.2705(4) Å ranges for tetrahydrothiophene or acetone, respectively (Figure 2).[36] Moreover, the thallium centers show two different types of geometrical environments, such as pseudotetrahedral and distorted trigonal-bi-

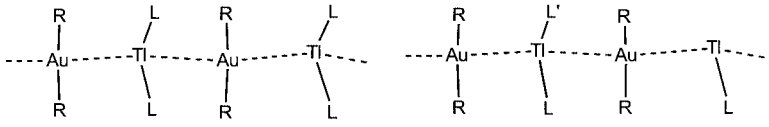

Figure 2. Asymmetric unit of linear chains with unsupported gold−thallium bonds; left: L = $OPPh_3$, R = C_6F_5; right: L = $OPPh_3$, L′ = THF, acetone; R = C_6Cl_5

 © 2003 Wiley-VCH Verlag GmbH & Co. KGaA, Weinheim

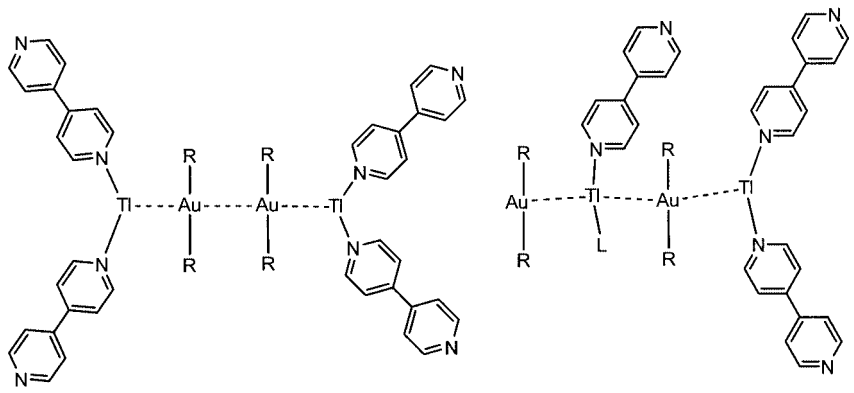

Figure 3. Tetranuclear moieties, further linked to others through bipy bridging ligands to give two-dimensional polymers; left: R = C_6F_5; right: L = THF, R = C_6Cl_5

pyramidal, due to the presence of solvent molecules that act as ligands in the solid state. Ab initio calculations, performed for the model $[Tl(OPH_3)_2][Au(C_6H_5)_2]$, are consistent with the presence of a high ionic contribution (80%) and a dispersion type with a charge-transfer contribution (20%). These three derivatives emit at 494, 497, and 501 nm, respectively, in the solid state at room temperature. Moreover, the last two derivatives show site-selective excitation at 77 K, which could be related to the different environments around the thallium centers. In fact, TD-DFT (density functional level by the time-dependent perturbation theory approach) calculations were in agreement with the experimental excitation spectra for all complexes and confirm the qualitative explanation that the excitation has $AuR_2 \rightarrow Tl$ charge-transfer character, whereby the thallium centers act as fluorophores. Again, the polymer structure is lost in donor solvents, so the colored crystals became uncolored in solution and do not luminesce.

Similar reactions resulted in the synthesis of the tetranuclear derivatives $[Tl(bipy)]_2[Au(C_6F_5)_2]_2$ (bipy = 4,4′-bipyridine) and $[Tl(bipy)][Tl(bipy)_{0.5}(THF)][Au(C_6Cl_5)_2]_2$.[37] In the first compound, a strong unsupported gold−thallium interaction of 3.0161(2) Å is found, together with gold−gold contacts of 3.409(3) Å, to give an unusual linear Tl−Au−Au−Tl arrangement in which repulsive instead of attractive forces might be expected {this non-fulfillment of the Coulomb rule was also observed[38] in $[Au(PPhMe_2)_2][Au(GeCl_3)_2]$, with the same unusual + − − + sequence}. The tetranuclear moiety is further linked through bidentate bridging bipy ligands (one bipy ligand bridging two thallium centers in two different moieties) to give a two-dimensional array. Finally, adjacent planes are connected through two additional Tl−F contacts to form an infinite three-dimensional polymer. The second compound displays a Tl−Au−Tl′−Au arrangement with two short gold−thallium distances of 3.0323(4) and 3.0540(4) Å and, again, bidentate bridging bipy ligands to form a two-dimensional polymer (Figure 3). Both complexes are strongly luminescent at room temperature, losing this property in solution (even in concentrated solutions), and so the luminescence is attributed to interactions between metal atoms. TD-DFT calculations agree with this proposal, and the obtained theoretical excitation spectra match the experimental results.

A similar reaction, however, carried out without addition of any ligand other than the solvent, produced the derivative $[Au_2Tl_2(C_6Cl_5)_4](OCMe_2)$, the crystal structure of which consists of a tetranuclear unit with four short unsupported gold−thallium contacts within the 3.0331(6)−3.1887(6) Å range and a longer thallium−thallium interaction of 3.6027(6) Å (Figure 4).[39] Two $[Au(C_6Cl_5)_2]^-$ units are held together by two thallium centers in a butterfly geometry, reminiscent of the silver−gold tetranuclear structures with unsupported gold−silver bonds, but now without additional gold−gold bonds; in addition to this, the thallium atoms show weak interaction with the oxygen atom of an acetone molecule. This complex luminesces at 556 nm at room temperature in the solid state, with lifetimes in the order of microseconds. Moreover, the starting materials do not luminesce, so this phenomenon could be assigned to the metal−metal bonds. Unlike in the case of other unsupported gold−thallium bonds, the structure of this complex is maintained in solution, in which it luminesces and shows solvent dependence. TD-DFT calculations carried out for $[Au_2Tl_2(C_6H_5)_4]$ show that the orbital from which the emission is produced is almost completely based on the two thallium(I) atoms, so these are therefore perturbed in solution by the presence of solvent molecules with donor capabilities.

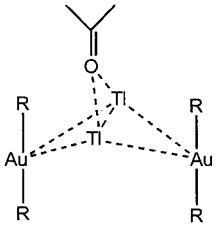

Figure 4. Butterfly tetranuclear structure; R = C_6Cl_5

 © 2003 Wiley-VCH Verlag GmbH & Co. KGaA, Weinheim

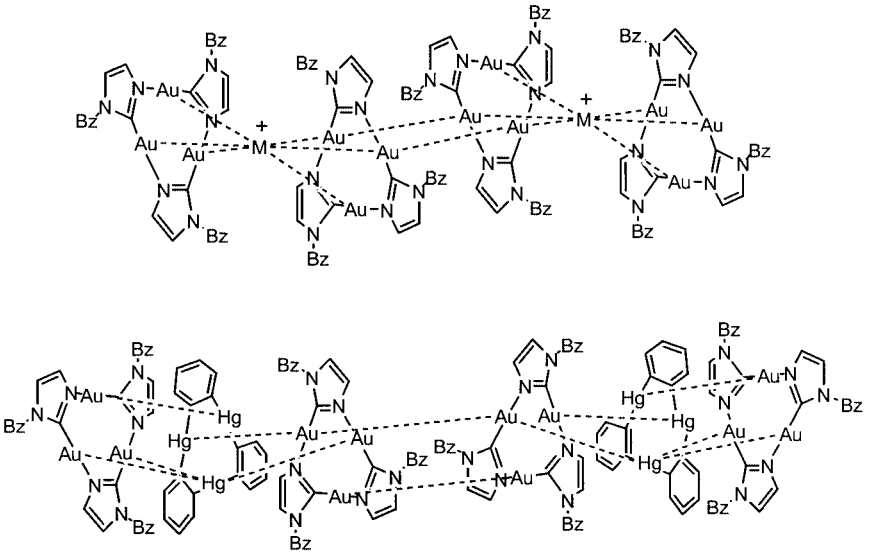

Figure 5. Sandwich heterometalllic clusters; top: silver(I)− or thallium(I)−gold(I) (M = Ag, Tl); bottom: mercury(II)−gold(I)

2.2. By Use of Trinuclear Cyclic Gold(I) Derivatives as Bases

Burini et al. have recently described[40−42] a series of sandwich derivatives obtained through the interaction between π-base trinuclear gold(I) complexes, such as $[Au(\mu\text{-}N^3,C^2\text{-bzim})]_3$ (N^3,C^2-bzim = 1-benzylimidazolate) and $[Au(\mu\text{-}C(OMe)=NCH_3)]_3$, and either acid cations such as Ag^+ or Tl^+, or the π molecular acid trinuclear complex of mercury(II) $[Hg(\mu\text{-}C,C\text{-}C_6F_4)]_3$, giving $[M\{[Au(\mu\text{-}N^3,C^2\text{-bzim})]_3\}_2]^+$ (M= Ag, Tl), $[Tl\{[Au(\mu\text{-}C(OMe)=NCH_3)]_3\}_2]PF_6$, $\{[Au(\mu\text{-}N^3,C^2\text{-bzim})]_3\}_2[Hg(C_6F_4)]_3$ or $\{[Au(\mu\text{-}C(OMe)=NCH_3)]_3\}_2[Hg(C_6F_4)]_3$, containing $[Au_3MAu_3]$ (M = Ag^I, Tl^I) or $[Au_3Hg_3Au_3]$ units (Figure 5). Additional gold−gold contacts therefore produce a supramolecular chain.

The naked silver or thallium ion center is bonded to six gold atoms to form a distorted trigonal prism, with gold−silver distances from 2.731(2) to 2.922(2) Å and gold−thallium distances from 2.9711(7) to 3.1075(4) Å. In addition to this, there are also gold−gold interactions in the cyclic trimer moiety (an average of 3.19 Å in the mixed gold−silver cluster, for instance) and between two close sandwich units [3.116 and 3.268 Å for the gold−silver cluster, or from 3.0588(4) to 3.1089(7) Å in the gold−thallium clusters].

The mercury centers interact with the gold centers in adjacent rings, with gold−mercury distances as short as 3.27 and 3.24 Å, for bzim and $C(OMe)=NCH_3$ ligands, respectively. DFT calculations showed positive electrostatic potential values above and below the plane of the mercury ring, while similar regions for the gold ring had negative values, thus clearly demonstrating the electrostatic nature of the interaction between the electron-poor mercury and the electron-rich gold rings.

The emission spectra of these compounds (silver and thallium) display low-energy phosphorescence, consistent with the extended chain structure. Furthermore, they exhibit luminescence thermochromism with red shifts in their emission maxima when they are cooled from room temperature to 77 K. The gold−mercury derivatives luminesce both at ambient and at low temperatures, the intensity of the emission increasing upon gold−mercury interaction.

2.3. By Encapsulation of a Metal Center by a Dinuclear Gold(I) Cryptand

Catalano and co-workers have recently developed an interesting approach to this subject. They have prepared metallocryptands with a cavity in which metallic centers can be encapsulated by use of metal−metal closed-shell interactions. Firstly, they synthesized a dinuclear gold(I) cryptand, employing the ligand 2,9-bis(diphenylphosphanyl)-1,10-phenantroline (P_2phen), which is able to selectively host Tl^I, Na^I (weakly; dissociates readily as there are no important closed-shell interactions), or Hg^0 (Figure 6).[43,44] Complexes $[Au_2M(P_2phen)_3](PF_6)_3$ (M = Tl, Hg) each display an almost linear arrangement with very short gold−thallium distances [2.9109(5) and 2.9171(5) Å] or gold−mercury distances [2.7807(4) and 2.7847(4) Å]. The structures contain two trigonal Au^I centers capping a D_3 symmetric cage. The gold−thallium derivative is strongly luminescent at 600 nm, both in solution and in the solid state; the emission can be attributed to metal-centered phosphorescence based on its large Stoke's shift, long lifetime, and solvent independence. The gold−mercury derivative is weakly emissive at 580 nm.

These workers have also extended the system to d^{10} Pd^0- and Pt^0-based metallocryptates [rather than gold(I)] capable of hosting a Tl^I or a Pb^{II} center through $d^{10}-s^2$ closed-shell interactions.[45−47] They have also changed the P_2phen ligand for other ligands such as 2,9-bis(diphenylphosphanyl)-1,8-naphthyridine (dppn) or PPh_2py; gold(I) centers have also been exchanged for silver(I). X-ray studies of $[Au_2$-

 © 2003 Wiley-VCH Verlag GmbH & Co. KGaA, Weinheim

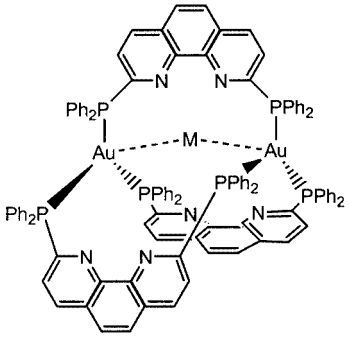

Figure 6. Metallocryptates $[Au_2M(P_2phen)_3](PF_6)_3$

$Na(dppn)_3](PF_6)_3$ display long gold−sodium interactions around 3.5 Å.[48] Moreover, these workers have also prepared a series of alkaline encapsulated derivatives $[Au_2M(dppn)_3](PF_6)_3$ (M = Li, Na, K, Cs), which also display luminescence around 580 nm in the solid state; the emission has been assigned to a gold-centered phosphorescence due to the tricoordinate gold centers.

2.4. Other Cases

Haupt and co-workers have prepared the trimetallic tetrahedron complexes $[Re_2(AuPPh_3)(MPPh_3)(\mu\text{-}PCy_2)(CO)_7(-)\text{-thiocamphanate}]$ (M = Cu, Ag), which show the short metal−metal distances of 2.584(2) Å (copper−gold) and 2.7026(18) Å (gold−silver).[49] The rhenium core is supported by phosphido ligands, but the gold−silver or gold−copper bond is unsupported. Moreover, the copper or silver center is coordinated to the sulfur atoms of the thiocamphanate ligand.

M. Laguna and co-workers have crystallographically characterized the pentanuclear derivative $[Au_4Ag(CH_2SiMe_3)_4(\mu\text{-dppm})_2]CF_3SO_3$ (dppm = $PPh_2CH_2PPh_2$) (Figure 7)[50] with an Au_4Ag core, which displays a silver atom bonded solely to four gold atoms in a distorted tetrahedral environment. The four silver−gold distances lie between the values of 2.7179(13) and 2.7822(13) Å and are almost identical to those found for our unsupported silver(I)−gold(I) bonds. Similarly, the gold−gold distances are 3.2170(9) and 3.2773(12) Å.

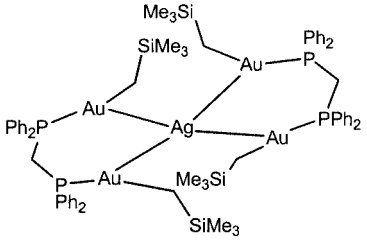

Figure 7. Pentanuclear Au_4Ag derivative with a tetrahedral geometry

The same workers have also synthesized the heptanuclear cluster $[Au_6Ag\{\mu\text{-}C_6H_2(CHMe_2)_3\}_6]CF_3SO_3$ with an almost planar Au_6Ag core, resembling a "cartwheel", in which the silver(I) atom is at the center of a regular hexagon of gold atoms (Figure 8).[51] The gold−silver distances are quite short − 2.797(1), 2.802(1), and 2.809(1) Å − whilst the gold−gold distances range from 2.795(1) to 2.817(1) Å, slightly longer than in the homoleptic pentamer $[\{Au(mes)\}_5]$ [2.692(1), 2.697(1) and 2.708(2) Å; mes = 2,4,6-$Me_3C_6H_2$].[52] The tris(isopropylphenyl) groups serve as bridges between two consecutive gold atoms within the hexagon. The derivative shows a deep green color, but it is not luminescent.

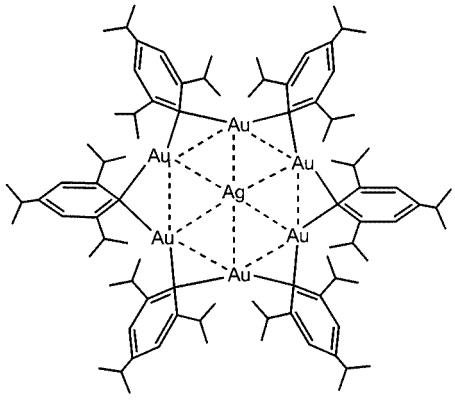

Figure 8. Heptanuclear Au_6Ag derivative with hexagonal geometry

Table 1 summarizes the gold−silver distances for this type of derivatives, their main characteristic being that all of them are quite short, often with additional gold−gold interactions. Table 2 summarizes the gold−thallium distances for unsupported bonds, which are also very short, although the presence of gold−gold interactions is less common.

3. Derivatives with Supported Gold-Metal Bonds

The use of bridging ligands favors the proximity of metal centers and therefore the presence of short distances. Moreover, these short distances are easily preserved in solution, thanks to the bridge. As is the case of unsupported gold(I)−metal bonds, the conformations of the ligands, the aggregation of the molecules, and the optical properties can be dramatically changed by the presence of these gold−metal closed-shell interactions. Very common is the use of C-donor bridging ligands that are good σ-donor ligands. These form deficient bonds and induce very short metal−metal distances. Nevertheless, ambidentate bridging ligands favor heteronuclear complexes.

3.1. Dinuclear Derivatives

For dinuclear derivatives, the simplest case, no example of copper−gold is yet known, but four gold−silver compounds have recently been crystallographically characterized. The first, reported by Schmidbaur and co-workers,[53] is $[AuAg(PPh_2py)_2](ClO_4)_2$, with a gold−silver distance of 2.820(1) Å. Two more examples − [Au-

Table 1. Ag^I-Au^I distances [Å] reported in derivatives with unsupported gold−silver interactions

Compound	Ag^I-Au^I	Au−Au	Ag−Ag	Ref.
$[(C_6F_5)_2Au(\mu\text{-}AgSC_4H_8)_2Au(C_6F_5)_2]_\infty$	2.718(2), 2.726(2)	yes	no	[30]
$[(C_6F_5)_2Au(\mu\text{-}AgC_6H_6)_2Au(C_6F_5)_2]_\infty$	2.702(2), 2.792(2)	yes	no	[31]
$[(Ph_3PCH_2)_2Au(\mu\text{-}AgPPh_3)_2Au(CH_2PPh_3)_2]$	2.760(2), 2.783(2)	no	no	[32]
$[(C_6F_5)_2Au(\mu\text{-}AgOCMe_2)_2Au(C_6F_5)_2]_\infty$	2.7829(9), 2.7903(9)	yes	yes	[33]
$[Ag\{[Au(\mu\text{-}N^3,C^2\text{-bzim})]_3\}_2]BF_4$	2.731(2)−2.922(2)	yes	no	[41]
$[Au_4Ag(CH_2SiMe_3)_4(\mu\text{-dppm})_2]CF_3SO_3$	2.7179(13), 2.7822(13)	yes	no	[50]
$[Au_6Ag\{\mu\text{-}C_6H_2(CHMe_2)_3\}_6]CF_3SO_3$	2.797(1),2.802(1), 2.809(1)	yes	no	[51]
$[Re_2(AuPPh_3)(AgPPh_3)(\mu\text{-}PCy_2)(CO)_7(-)\text{-thiocamphanate}]$	2.7026(18)	no	no	[49]

Table 2. Au^I-Tl^I distances [Å] reported in derivatives with unsupported gold−thallium interactions

Compound	Au^I-Tl^I	Au−Au	Tl−Tl	Ref.
$[Tl(OPPh_3)_2][Au(C_6F_5)_2]$	3.0358(8), 3.0862(8)	no	no	[35]
$[Tl(OPPh_3)][Tl(OPPh_3)(THF)][Au(C_6Cl_5)_2]_2$	3.0529(3)−3.3205(3)	no	no	[36]
$[Tl(OPPh_3)][Tl(OPPh_3)(acetone)][Au(C_6Cl_5)_2]_2$	3.0937(3)−3.2705(4)	no	no	[36]
$[Tl(bipy)]_2[Au(C_6F_5)_2]_2$	3.0161(2)	yes	no	[37]
$[Tl(bipy)][Tl(bipy)_{0.5}(THF)][Au(C_6Cl_5)_2]_2$	3.0323(4), 3.0540	no	no	[37]
$[Au_2Tl_2(C_6Cl_5)_4]OCMe_2$	3.0331(6)−3.1887(6)	no	yes	[39]
$[Tl\{[Au(\mu\text{-}N^3,C^2\text{-bzim})]_3\}_2]BF_4$	2.9711(7)−3.0448(7)	yes	no	[41]
$[Tl\{[Au(\mu\text{-}C(OMe)=NCH_3)]_3\}_2]PF_6$	3.0673(4)−3.1075(4)	yes	no	[41]
$[Au_2Tl(P_2phen)_3](PF_6)_3$	2.9109(5), 2.9171(5)	no	no	[43]

$Ag(PPh_2CH_2SPh)_2](CF_3SO_3)_2$ and $[AuAg(PNH_2)_2]$-$(CF_3SO_3)_2$ [PNH_2 = 2-(diphenylphosphanyl)aniline] − with longer gold−silver distances [2.9314(5) and 2.9931(12) Å, respectively] have been prepared by us.[54,55] Finally, Fackler and co-workers have prepared $[AgAu(\mu\text{-}CH_2P(S)Ph_2]_2$, with a gold−silver distance of 2.9124(13) Å and an intermolecular gold−silver distance of 3.635 Å, forming a chain structure (Figure 9, b).[56] The same strategy − use of a bridging ambidentate ligand capable of selectively coordinating to the gold(I) center through a P- or C-donor atom, whilst the silver(I) center is coordinated to the second donor atom (N or S) − was used in all four cases. According to ab initio calculations carried out on a model based in the derivative $\{[AuM(PH_2CH_2SH)_2]^{2+}$; M= Cu, Ag, Au}, the presence of only one gold atom is sufficient to induce metallophilic attractions in copper and silver, and this effect can be modulated depending on the gold ligand. It has also been shown theoretically that the isomer found (phosphorus−gold-bonded system) is not only the most stable, but it also produces the shortest gold−silver distance (3.060 Å).

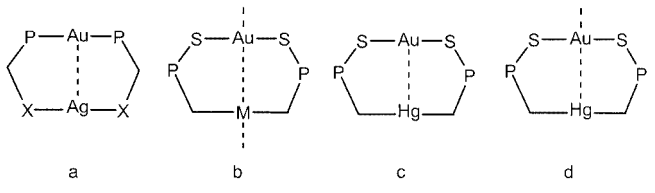

Figure 9. Doubly bridged dinuclear gold−silver(I), −mercury(II), or −thallium(I) derivatives: a) P−C−X = PPh_2py, PPh_2CH_2SPh, 2-(diphenylphosphanyl)aniline; b), c), d) M = Ag, Tl; C−P−S = $CH_2P(S)Ph_2$

Fackler and co-workers have prepared a dinuclear derivative, $[AuHg\{\mu\text{-}CH_2P(S)Ph_2\}_2]PF_6$, which displays a short gold(I)−mercury(II) distance of 3.088(1) Å (Figure 9, c).[57] It is a doubly bridged complex with the mercury centers coordinated to the ylide carbon atom and the gold centers coordinated to the sulfur atom (mercury and gold are not easy distinguished by X-ray diffraction studies, but NMR could determine the isomer: one kind of methylene signals with mercury satellites). A second X-ray structure was found for this derivative: it has a dimeric structure with gold−mercury distances of 2.9891(9) Å and a gold−gold intermolecular distance of 3.150(2) Å. These workers have also prepared the same derivative but with $[AuCl_4]$ as anion; in this case the gold(I)−mercury distance is 3.079 (2) Å and there is a gold(I)−gold(III) distance of 3.402(2) Å.[58]

Similarly, they have also prepared the dinuclear derivative $[AuTl\{\mu\text{-}CH_2P(S)Ph_2\}_2]_\infty$, a doubly bridged complex with the thallium centers coordinated to the ylide carbon atom and the gold centers coordinated to the sulfur atom. This also displays a short gold(I)−thallium(I) distance of 2.959(2) Å (Figure 9, d), but it forms an extended one-dimensional linear-chain polymer with an additional gold−thallium distance of 3.003(2) Å. This derivative is strongly photoluminescent, emitting at 575 nm (solid state 298 K) with a lifetime of 0.98 μs; the long lifetime and large separation between excitation and emission peaks indicate that the emission process is phosphorescence. This optical

 © 2003 Wiley-VCH Verlag GmbH & Co. KGaA, Weinheim

property has been related to the gold−thallium bonds by calculation by the Fenske−Hall method.[59,60]

3.2. Trinuclear Derivatives

There are no trinuclear copper−gold clusters in which the presence of short metal−metal distances has been reported. For gold−silver derivatives there are three examples, two of them using a C-donor bridging ligand and one with a diphosphane ligand.

Vicente and co-workers have structurally characterized the trinuclear derivative $[(AuPPh_3)_2\{\mu\text{-}[C(PPh_3)(C_5H_4N\text{-}2)]\}\{\mu\text{-}Ag(O_2NO)(OClO_3)\}]$, with a triangular geometry for the metallic centers (Figure 10) and the presence of supported gold−gold [3.078(1) Å] and gold−silver interactions [2.926(1) and 3.006(1) Å].[61,62] In that work, in order to distinguish clusters with weak interactions from conventional clusters in which some or all metal atoms are tightly bonded, the former were denoted as "loose" clusters. This nomenclature has been adopted by other authors.

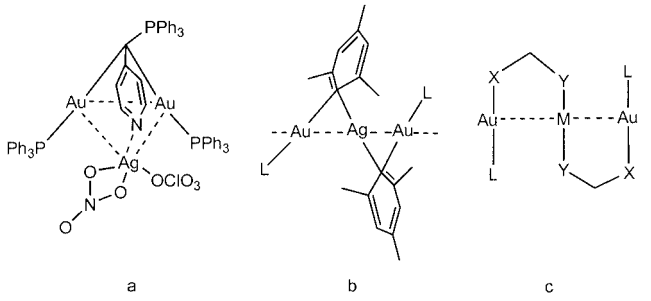

Figure 10. Molecular structures found for trinuclear Au_2Ag compounds: a) $[(AuPPh_3)_2\{\mu\text{-}[C(PPh_3)(C_5H_4N\text{-}2)]\}\{\mu\text{-}Ag(O_2NO)(OClO_3)\}]$, b) $[\{LAu(\mu\text{-mes})\}_2Ag](ClO_4)$, L = $AsPh_3$, c) M = Ag, L = mes, X−C−Y = dppm; M = Hg, L = Cl, X−C−Y = $CH_2P(S)Ph_2$

The mesityl group (2,4,6-$Me_3C_6H_2$) acts as a bridge, through three-center, two-electron bonds, and it is able to induce very short metal−metal distances, as, for instance, in the homoleptic derivatives $[\{Au(mes)\}_5]$ [2.692(1), 2.697(1) and 2.708(2) Å] and $[\{Ag(mes)\}_4]$ [2.733(3) and 2.7553(3) Å].[52] We have used this ligand to prepare heteronuclear gold−silver compounds containing trinuclear moieties $[\{(AsPh_3)Au(\mu\text{-mes})\}_2Ag](ClO_4)$ with a linear arrangement of the metallic core and a short gold−silver distance of 2.7758(8) Å; these trinuclear units are connected by gold−gold contacts of 3.132(2) Å to form a chain polymer.[63] By a similar approach, we have also prepared a diphosphane-bridged trinuclear derivative $[\{(mes)Au(\mu\text{-dppm})\}_2Ag](ClO_4)$ with longer gold−silver distances [2.944(2) and 2.946(2) Å] due to the bridging ligand (Figure 10).[64]

Fackler and co-workers have prepared the trinuclear derivative $[Au_2Hg\{\mu\text{-}CH_2P(S)Ph_2\}_2Cl_2]$, which displays a linear arrangement with a central mercury atom and gold−mercury distances of 3.310(1) and 3.361(1) Å (Figure 10). As found in the dinuclear gold−mercury derivative, the mercury center is coordinated to the ylide carbon atom and the gold centers coordinated to the sulfur atom.[58]

3.3. Higher Nuclearities

Abu-Salah et al. reported the tetranuclear cluster $[(PPh_3)Ag\{\mu\text{-}Au(CCPh)_2\}_2Ag(PPh_3)]$, with the same metallic core as in the derivatives described above (Ag_2Au_2 in section 2.1.1., Figure 1), except for a change in the positions of gold and silver (Figure 11).[65] Moreover, the main structural differences are as follows: silver centers do not aggregate (or show a lesser tendency than gold in the presence of a bulky phosphane) and so no polymer is formed; the alkyne fragments are coordinated to the silver centers, thus acting as bridging ligands. The gold−silver distances range from 2.894(1) to 3.028(1) Å, indicating appreciable metal−metal bonding; there are no gold−gold contacts (4.013 Å).

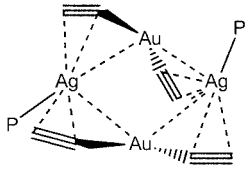

Figure 11. Rhomboidal, nearly square-planar geometry with supported gold−silver bonds; P = PPh_3

Pentanuclear clusters $[Au_3M_2(\mu\text{-}CCPh)_6]^-$ (M = Cu, Ag) displaying a trigonal-bipyramidal arrangement for the metallic core with the copper or silver centers in the apical positions have also been reported.[66−68] The gold−copper distances range from 2.783(3) to 3.016(3) Å [from 2.800 to 3.115(3) Å in a second X-ray diffraction study] whilst the gold−silver distances range from 2.911(1) to 3.096(1) Å [from 2.877(1) to 2.998(1) Å in a second X-ray determination]; there are no gold−gold contacts. Each gold center is coordinated to two alkynyl ligands, whilst the copper or silver centers are coordinated to the alkyne groups and to the gold atoms.

Eisenberg and co-workers have reported the tetranuclear heterodimetallic derivative $[\{AuCu(\mu\text{-}SPy)(\mu\text{-}PPh_2py)\}_2](PF_6)_2$, which is composed of two $AuCu(\mu\text{-}SPy)(\mu\text{-}PPh_2py)$ units (Cu bonded through N- and Au through P- and S-donor atoms) held together by bridging thiolate ligands (Figure 12).[69] There are strong gold−copper interactions of 2.6339(7) and 2.6455(7) Å in each dinuclear unit. This derivative is strongly emissive in the solid state at 77 K and in solution, whilst the mononuclear starting derivative $[Au(SPy)(PPh_2py)]$ shows weaker photoluminescence. The emitting state has been tentatively assigned to LMCT transition (from S to Au), but it has been strongly modified by the coordination of Cu to S and the formation of gold−copper bonds.

 © 2003 Wiley-VCH Verlag GmbH & Co. KGaA, Weinheim

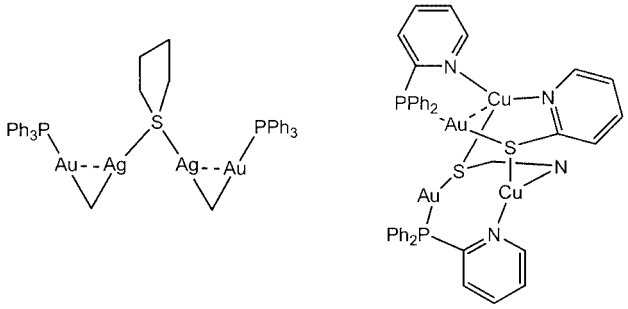

Figure 12. Two dimers bridged by ligands

We have also used the mesityl ligand to prepare heteronuclear gold−silver derivatives, such as $[(PPh_3)Au(\mu\text{-mes})\{Ag(\mu\text{-}SC_4H_8)\}_2(\mu\text{-mes})Au(PPh_3)]$, which has a gold−silver distance of 2.8245(6) Å, quite short but longer than the first unsupported bonds.[70] The structure possesses a dinuclear gold−silver core, which is bonded to an equal second unit through two tetrahydrothiophene bridges (Figure 12).

We have prepared the tetranuclear mixed derivative $[Au_2Ag_2(C_6F_5)_2(PPh_2CH_2SPh)_2(CF_3CO_2)_2]$ by treating the mononuclear *P*-bonded derivative $[Au(C_6F_5)(PPh_2CH_2SPh)]$ with $AgCF_3CO_2$.[54] The silver(I) centers are coordinated to the sulfur atom and bridged to each other by the trifluoroacetate ligands. There are two short gold−silver distances of 3.0335(8) Å and one short silver−silver distance of 2.8155(9) Å, so its geometry is a zigzag chain (Figure 13).

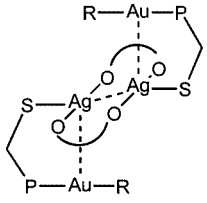

Figure 13. Tetranuclear derivative with a zigzag chain; O−O = CF_3CO_2, R = C_6F_5, P−C−S = PPh_2CH_2SPh

Henkel and co-workers have characterized the heterodimetallic clusters $[Au_3Cu_3L_4]^{2-}$ and $[Au_2Ag_4L_4]^{2-}$ (L = ethane-1,2-dithiolate), each of which displays a typical M_6S_8 cage skeleton with two gold atoms in the apical position, as shown in Figure 14.[71] The copper derivative shows short

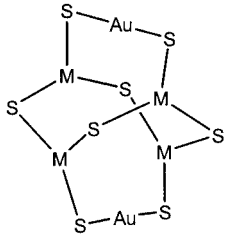

Figure 14. M_6S_8 cage skeleton

copper−gold distances of 2.862 Å on average, whilst the silver derivative displays gold−silver distances of 2.996 Å on average and silver−silver distances of 3.170 Å on average.

Salter et al. have reported the X-ray structures of heterotrimetallic hexanuclear clusters $[AuCuRu_4(\mu_3\text{-}H)_2(\mu\text{-dppf})(CO)_{12}]$ [dppf = 1,1′-bis(diphenylphosphanyl)ferrocene] and $[AuCuRu_4(\mu_3\text{-}H)_2(\mu\text{-dppe})(CO)_{12}]$ (dppe = $PPh_2CH_2CH_2PPh_2$), obtained through metal exchange reactions.[72,73] The metal-framework structures of both can be described as intermediate between a capped trigonal bipyramid and a capped square pyramid (Figure 15). There are short copper− and gold−ruthenium distances and also short copper−gold distances of 2.641(1) and 2.614(2) Å, respectively, for dppf and dppe. Moreover, the diphosphane ligand is bridging the copper and gold centers.

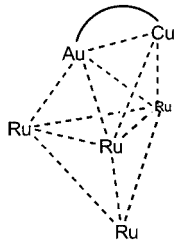

Figure 15. $AuCuRu_4$ cluster core in which a diphosphane ligand is bridging the copper and gold centers

We summarize silver(I)− and copper(I)−gold(I) distances found in mixed derivatives with supported bonds in Tables 3 and 4, respectively. Table 5 summarizes thallium−(supported bonds) and mercury−gold distances.

Finally, we describe two cases not exactly within the scope of this microreview, the first for copper(I)−gold(III) bonds, the second for gold−indium bonds. In the first case, Coucouvanis and co-workers have reported that the X-ray structure of $[AuCu_4L_4]^-$ [L = 2,2-bis(*tert*-butoxycarbonyl)-1-thiolatoethene-1-perthiolate consists of a rectangular pyramidal $AuCu_4$ core with mean $Au^{III}-Cu^{I}$ bonds of 3.029(7) Å.[74]

Now, to date there are only two clusters showing short gold−indium distances, and although the oxidation state of the starting materials is +1 for both metals, their final oxidation states are unclear. Schmidbaur and co-workers have reported the hexanuclear clusters $[Au_3In_3Cl_6(THF)_6(dppe)_2]$ and $[Au_3In_3Br_7(THF)_6(dppe)_2]^-$, obtained by the insertion of InX into the Au−X bond of $[AuXPPh_3]$.[75,76] The metallic core is formed by an isosceles triangle of three gold atoms, two indium atoms capping the gold triangle on both faces, while the third indium atom bridges the shortest edge of the gold triangle. Thus, there are two short gold−gold distances of 2.931(1) and 2.939(1) Å (for Cl), 2.860(1) and 2.858(1) Å (for Br), and one very short gold−gold distance of 2.562(1) Å and 2.571(1) Å, respectively, for Cl and Br. The gold−indium distances range from 2.761(1) to 2.973(1) Å (for Br). Theoretical investigations proposed two gold(0) and one gold(I)

 © 2003 Wiley-VCH Verlag GmbH & Co. KGaA, Weinheim

Table 3. Ag^I-Au^I distances [Å] reported in derivatives with supported gold−silver interactions

Compound	Ag^I-Au^I	Ref.
$[AuAg(PPh_2py)_2](ClO_4)_2$	2.820(1)	[53]
$[AuAg(PPh_2CH_2SPh)_2](CF_3SO_3)_2$	2.9314(5)	[54]
$[AuAg(PNH_2)_2](CF_3SO_3)_2$	2.9931(12)	[55]
$[AgAu(\mu\text{-}CH_2P(S)Ph_2]_2]$	2.9124(13)	[56]
$[(AuPPh_3)_2\{\mu\text{-}\{C\text{-}(PPh_3)(C_5H_4N\text{-}2)\}\}\{\mu\text{-}Ag(O_2NO)(OClO_3)]$	2.926(1), 3.006(1)	[61]
$[\{(AsPh_3)Au(\mu\text{-}mes)\}_2Ag](ClO_4)$	2.7758(8)	[63]
$[\{(mes)Au(\mu\text{-}dppm)\}_2Ag](ClO_4)$	2.944(2), 2.946(2)	[64]
$[(PPh_3)Ag\{\mu\text{-}Au(CCPh)_2\}_2Ag(PPh_3)]$	2.894(1)−3.028(1)	[65]
$[(PPh_3)Au(\mu\text{-}mes)\{Ag(\mu\text{-}SC_4H_8)\}_2(\mu\text{-}mes)Au(PPh_3)]$	2.8245(6)	[70]
$[Au_2Ag_2(C_6F_5)_2(PPh_2CH_2SPh)_2(CF_3CO_2)_2]$	3.0335(8)	[54]
$[Au_3Ag_2(\mu\text{-}CCPh)_6]^-$	2.911(1)−3.096(1), 2.877(1)−2.998(1)	[67,68]
$[Au_2Ag_4L_4]^{2-}$ (L = ethane-1,2-dithiolate)	average 2.996 Å	[71]

Table 4. Au^I-Cu^I distances [Å] found in derivatives with gold−copper interactions

Compound	Au^I-Cu^I	Ref.
$[Re_2(AuPPh_3)(CuPPh_3)(\mu\text{-}PCy_2)(CO)_7\{(-)\text{-thiocamphanate}\}]$	2.584(2)	[49]
$[\{AuCu(\mu\text{-}Spy)(\mu\text{-}PPh_2py)\}_2](PF_6)_2$	2.6339(7), 2.6455(7)	[69]
$[Au_3Cu_2(\mu\text{-}CCPh)_6]^-$	2.783(3)−3.016(3), 2.800−3.115(3)	[66,67]
$[Au_3Cu_3L_4]^{2-}$ (L = ethane-1,2-dithiolate)	average 2.862	[71]
$[AuCuRu_4(\mu_3\text{-}H)_2(\mu\text{-}dppf)(CO)_{12}]$	2.641(1)	[72]
$[AuCuRu_4(\mu_3\text{-}H)_2(\mu\text{-}dppe)(CO)_{12}]$	2.614(2)	[73]

Table 5. Thallium(I)−, mercury(0)−, and mercury(II)−gold(I) distances [Å] found in derivatives with gold−metal interactions

Compound	Au^I-M	Ref.
$[AuTl(\mu\text{-}CH_2P(S)Ph_2]_2]_\infty$	2.959(2)	[59]
$[AuHg(\mu\text{-}CH_2P(S)Ph_2]_2]PF_6$	3.088(1)	[57]
$[AuHg(\mu\text{-}CH_2P(S)Ph_2]_2]PF_6$	2.9891(9)	[57]
$[AuHg(\mu\text{-}CH_2P(S)Ph_2]_2][AuCl_4]$	3.079(2)	[58]
$[Au_2Hg(\mu\text{-}CH_2P(S)Ph_2]_2Cl_2]$	3.310(1), 3.361(1)	[58]
$\{[Au(\mu\text{-}N^3,C^2\text{-bzim})]_3\}_2[Hg(C_6F_4)]_3$	3.27	[42]
$\{[Au(\mu\text{-}C(OMe)=NCH_3)]_3\}_2[Hg(C_6F_4)]_3$	3.24	[42]
$[Au_2Hg(P_2phen)_3](PF_6)_2$	2.7807(4), 2.7847(4)	[44]

centers, so it is not appropriate to view them as closed-shell interactions.

Acknowledgments

We thank the Dirección General de Investigación Científica y Técnica (Project BQU2001-2409-C02-01) for financial support.

[1] P. Pyykkö, *Chem. Rev.* **1997**, *97*, 597−636.
[2] H. Schmidbaur, *Angew. Chem. Int. Ed. Engl.* **1988**, *27*, 417−419; *Angew. Chem.* **1988**, *100*, 439−441.
[3] M. Bardají, A. Laguna, *J. Chem. Educ.* **1999**, *76*, 201−203.
[4] H. Schmidbaur, *Gold Bull.* **2000**, *33*, 3−10.
[5] E. Colacio, F. Lloret, R. Kivekäs, J. Ruiz, J. Suárez-Varela, M. R. Varela, *Chem. Commun.* **2002**, 592−593.
[6] D. R. Smyth, J. Hester, V. G. Young Jr., E. R. T. Tiekink, *Cryst. Eng. Com.* **2002**, *4*, 517−521.
[7] D. B. Leznoff, B.-Y. Xue, R. J. Batchelor, F. W. B. Einstein, B. O. Patrick, *Inorg. Chem.* **2001**, *40*, 6026−6034.
[8] C.-M. Che, Z. Mao, V. M. Miskowski, M.-C. Tse, C.-K. Chan, K.-K. Cheung, D. L. Phillips, K.-H. Leung, *Angew. Chem. Int. Ed.* **2000**, *39*, 4084−4088; *Angew. Chem.* **2000**, *112*, 4250−4254.
[9] C.-M. Che, M.-C. Tse, C.-K. Chan, K.-K. Cheung, D. L. Phillips, K.-H. Leung, *J. Am. Chem. Soc.* **2000**, *122*, 2464−2468.
[10] J. M. Zuo, M. Kim, M. Okeeffe, J. C. H. Spence, *Nature* **1999**, *401*, 49−52.
[11] J. M. Zuo, M. Kim, M. Okeeffe, J. C. H. Spence, *Angew. Chem. Int. Ed.* **2000**, *39*, 3791−3794; *Angew. Chem.* **2000**, *112*, 3947−3952.
[12] N. Kaltsoyannis, *J. Chem. Soc., Dalton Trans.* **1997**, 1−11.
[13] P. Pyykkö, F. Mendizabal, *Inorg. Chem.* **1998**, *37*, 3018−3025.
[14] N. Runeberg, M. Schütz, H.-J. Werner, *J. Chem. Phys.* **1999**, *110*, 7210−7215.
[15] H. L. Hermann, G. Boche, P. Schwerdtfeger, *Chem. Eur. J.* **2001**, *7*, 5333−5342.
[16] J. Emsley, *The elements*, 2nd ed., Oxford University Press, New York, **1991**.
[17] B. K. Teo, H. Zang, *Coord. Chem. Rev.* **1995**, *143*, 611−636.
[18] L. H. Pignolet, M. A. Aubart, K. L. Craighead, R. A. T. Gould, D. A. Krogstad, J. S. Wiley, *Coord. Chem. Rev.* **1995**, *143*, 219−263.
[19] I. D. Salter, "Cluster complexes with bonds between transition elements and copper, silver and gold", in: *Comprehensive Organometallic Chemistry II* (Eds.: E. W. Abel, F. G. A. Stone, G. Wilkinson), Pergamon, Oxford, **1995**, vol. 10, p. 256−317.
[20] J. M. Forward, J. P. Fackler, Jr., Z. Assefa, "Photochemical Properties of Gold(I) Complexes", in: *Optoelectronic Properties of Inorganic Compounds* (Eds.: D. M. Roundhill, J. P. Fackler, Jr.), Plenum Press, New York, **1999**, p 195−226.
[21] J. N. Demas, B. A. Degraff, *Coord. Chem. Rev.* **2001**, *211*, 317−351.
[22] K. S. Schanze, R. H. Schmehl, *J. Chem. Educ.* **1997**, *74*, 633−698.
[23] A. Mills, A. Lepre, B. R. C. Theobald, E. Slade, B. A. Murrer, *Anal. Chem.* **1997**, *69*, 2842−2847.
[24] C. A. Daws, C. L. Exstrom, J. R. J. Sowa, K. R. Mann, *Chem. Mater.* **1997**, *9*, 363−368.

 © 2003 Wiley-VCH Verlag GmbH & Co. KGaA, Weinheim

[25] M. A. Mansour, W. B. Connick, R. J. Lachicotte, H. J. Gysling, R. Eisenberg, *J. Am. Chem. Soc.* **1998**, *120*, 1329−1330.
[26] V. W.-W. Yam, C.-K. Li, C.-L. Chan, *Angew. Chem. Int. Ed.* **1998**, *37*, 2857−2859; *Angew. Chem.* **1998**, *110*, 3041−3044.
[27] W.-H. Chan, T. C. W. Mak, C.-M. Che, *J. Chem. Soc., Dalton Trans.* **1998**, 2275−2276.
[28] J. C. Vickery, M. M. Olmstead, E. Y. Fung, A. L. Balch, *Angew. Chem. Int. Ed. Engl.* **1997**, *36*, 1179−1181; *Angew. Chem.* **1997**, *109*, 1227−1229.
[29] E. J. Fernández, A. Laguna, J. M. López de Luzuriaga, M. Monge, *Pat. Es.* P 200001391, May **2000**.
[30] R. Usón, A. Laguna, M. Laguna, P. G. Jones, G. M. Sheldrick, *J. Chem. Soc., Chem. Commun.* **1981**, 1097−1098.
[31] R. Usón, A. Laguna, M. Laguna, B. Manzano, P. G. Jones, G. M. Sheldrick, *J. Chem. Soc., Dalton Trans.* **1984**, 285−292.
[32] R. Usón, A. Laguna, M. Laguna, A. Usón, P. G. Jones, C. F. Erdbrügger, *Organometallics* **1987**, *6*, 1778−1780.
[33] E. J. Fernández, M. C. Gimeno, A. Laguna, J. M. López de Luzuriaga, M. Monge, P. Pyykkö, D. Sundholm, *J. Am. Chem. Soc.* **2000**, *122*, 7287−7293.
[34] E. J. Fernández, A. Laguna, J. M. López de Luzuriaga, M. Monge, P. Pyykkö, N. Runeberg, *Eur. J. Inorg. Chem.* **2002**, 750−753.
[35] O. Crespo, E. J. Fernández, P. G. Jones, A. Laguna, J. M. López de Luzuriaga, A. Mendía, M. Monge, M. E. Olmos, *Chem. Commun.* **1998**, 2233−2234.
[36] E. J. Fernández, A. Laguna, J. M. López de Luzuriaga, F. Mendizabal, M. Monge, M. E. Olmos, J. Pérez, *Chem. Eur. J.* **2003**, *9*, 456−465.
[37] E. J. Fernández, P. G. Jones, A. Laguna, J. M. López de Luzuriaga, M. Monge, J. Pérez, M. E. Olmos, *Inorg. Chem.* **2002**, *41*, 1056−1063.
[38] A. Bauer, H. Schmidbaur, *J. Am. Chem. Soc.* **1996**, *118*, 5324−5325.
[39] E. J. Fernández, J. M. López de Luzuriaga, M. Monge, M. E. Olmos, J. Pérez, A. Laguna, *J. Am. Chem. Soc.* **2002**, *124*, 5942−5943.
[40] A. Burini, J. P. Fackler, Jr., R. Galassi, B. R. Pietroni, R. J. Staples, *Chem. Commun.* **1998**, 95−96.
[41] A. Burini, R. Bravi, J. P. Fackler, Jr., R. Galassi, T. A. Grant, M. A. Omary, B. R. Pietroni, R. J. Staples, *Inorg. Chem.* **2000**, *39*, 3158−3165.
[42] A. Burini, J. P. Fackler Jr., R. Galassi, T. A. Grant, M. A. Omary, M. N. Rawashdeh-Omary, B. R. Pietroni, R. J. Staples, *J. Am. Chem. Soc.* **2000**, *122*, 11264−11265.
[43] V. J. Catalano, B. L. Bennett, H. M. Kar, *J. Am. Chem. Soc.* **1999**, *121*, 10235−10236.
[44] V. J. Catalano, M. A. Malwitz, B. C. Noll, *Chem. Commun.* **2001**, 581−582.
[45] V. J. Catalano, B. L. Bennett, R. L. Yson, C. Noll, *J. Am. Chem. Soc.* **2000**, *122*, 10056−10062.
[46] V. J. Catalano, B. L. Bennett, B. C. Noll, *Chem. Commun.* **2000**, 1413−1414.
[47] V. J. Catalano, B. L. Bennett, S. Muratidis, C. Noll, *J. Am. Chem. Soc.* **2001**, *123*, 173−174.
[48] V. J. Catalano, H. M. Kar, B. L. Bennett, *Inorg. Chem.* **2000**, *39*, 121−127.
[49] H.-J. Haupt, O. Seewald, U. Flörke, V. Buß, T. Weyhermüller, *J. Chem. Soc., Dalton Trans.* **2001**, 3329−3336.
[50] M. Contel, J. Garrido, M. C. Gimeno, M. Laguna, *J. Chem. Soc., Dalton Trans.* **1998**, 1083−1084.
[51] E. Cerrada, M. Contel, A. D. Valencia, M. Laguna, T. Gelbrich, M. B. Hursthouse, *Angew. Chem. Int. Ed.* **2000**, *39*, 2353−2356; *Angew. Chem.* **2000**, *112*, 2443−2446.
[52] E. M. Meyer, S. Gambarotta, C. Floriani, A. Chiesi-Villa, C. Guastini, *Organometallics* **1989**, *8*, 1067−1079.
[53] M. E. Olmos, A. Schier, H. Schmidbaur, *Z. Naturfosch. B* **1997**, *52*, 203−208.
[54] E. J. Fernández, J. M. López de Luzuriaga, M. Monge, M. A. Rodríguez, O. Crespo, M. C. Gimeno, A. Laguna, P. G. Jones, *Chem. Eur. J.* **2000**, *6*, 636−644.
[55] O. Crespo, E. J. Fernández, M. Gil, M. C. Gimeno, P. G. Jones, A. Laguna, J. M. López de Luzuriaga, M. E. Olmos, *J. Chem. Soc., Dalton Trans.* **2002**, 1319−1326.
[56] M. A. Rawashdeh-Omary, M. A. Omary, J. P. Fackler Jr., *Inorg. Chim. Acta* **2002**, *334*, 376−384.
[57] S. Wang, J. P. Fackler, Jr., *Organometallics* **1988**, *7*, 2415−2417.
[58] S. Wang, J. P. Fackler, Jr., *Organometallics* **1990**, *9*, 111−115.
[59] S. Wang, J. P. Fackler, Jr., C. King, J. C. Wang, *J. Am. Chem. Soc.* **1988**, *110*, 3308−3310.
[60] S. Wang, G. Garzón, C. King, J. C. Wang, J. P. Fackler, Jr., *Inorg. Chem.* **1989**, *28*, 4623−4629.
[61] J. Vicente, M. T. Chicote, M. C. Lagunas, P. G. Jones, *J. Chem. Soc., Chem. Commun.* **1991**, 1731−1732.
[62] J. Vicente, M. T. Chicote, M. C. Lagunas, *Inorg. Chem.* **1993**, *32*, 3748−3754.
[63] M. Contel, J. Garrido, M. C. Gimeno, P. G. Jones, A. Laguna, M. Laguna, *Organometallics* **1996**, *15*, 4939−4943.
[64] M. Contel, J. Garrido, M. C. Gimeno, J. Jiménez, P. G. Jones, A. Laguna, M. Laguna, *Inorg. Chim. Acta* **1997**, *254*, 157−161.
[65] O. M. Abu-Salah, C. B. Knobler, *J. Organomet. Chem.* **1986**, *302*, C10−C12.
[66] O. M. Abu-Salah, A.-R. A. Al-Ohaly, C. B. Knobler, *J. Chem. Soc., Chem. Commun.* **1985**, 1502−1503.
[67] M. S. Hussain, M.-U. Haque, O. M. Abu-Salah, *J. Cluster Sci.* **1996**, *7*, 167.
[68] M.-U. Haque, W. Horne, O. M. Abu-Salah, *J. Crystallogr. Spectrosc. Res.* **1992**, *22*, 421.
[69] L. Hao, H. A. Mansour, R. J. Lachicotte, H. J. Gysling, R. Eisenberg, *Inorg. Chem.* **2000**, *39*, 5520−5529.
[70] M. Contel, J. Jiménez, P. G. Jones, A. Laguna, M. Laguna, *J. Chem. Soc., Dalton Trans.* **1994**, 2515−2518.
[71] G. Henkel, B. Krebs, P. Betz, H. Fietz, K. Saatkamp, *Angew. Chem. Int. Ed. Engl.* **1988**, *27*, 1326−1329; *Angew. Chem.* **1988**, *100*, 1375−1378.
[72] I. A. Salter, V. Sik, S. A. Williams, T. Adatia, *J. Chem. Soc., Dalton Trans.* **1996**, 643−652.
[73] S. S. D. Brown, I. D. Salter, T. Adatia, *J. Chem. Soc., Dalton Trans.* **1993**, 559−566.
[74] D. Coucouvanis, S. Kanodia, D. Swenson, S. J. Chen, T. Stüdemann, N. C. Baenziger, R. Pedelty, M. Chu, *J. Am. Chem. Soc.* **1993**, *115*, 11271−11278.
[75] F. P. Gabbaï, A. Schier, J. Riede, H. Schmidbaur, *Inorg. Chem.* **1995**, *34*, 3855−3856.
[76] F. P. Gabbaï, S.-C. Chung, A. Schier, S. Krüger, N. Rösch, H. Schmidbaur, *Inorg. Chem.* **1997**, *36*, 5699−5705.

Received December 30, 2002
Early View Article
Published Online July 17, 2003

 © 2003 Wiley-VCH Verlag GmbH & Co. KGaA, Weinheim

Nanoparticulated Gold: Syntheses, Structures, Electronics, and Reactivities

Günter Schmid*[a] and Benedetto Corain[b]

Keywords: Gold / Nanoparticles / Synthetic methods / Quantum dots / Self-assembly / Heterogeneous catalysis

This microreview deals mainly with the synthesis and the electronic and chemical properties of gold nanoparticles. Modern synthetic routes, based on physical and on chemical procedures, as well as structural and optical features, are described. The bulk-to-molecule transition is discussed by studying size-controlled quantum-size effects, resulting in the determination of discrete electronic energy levels in Au_{55} clusters. Conductivity measurements of three- and two-dimensionally organized ligand-protected Au_{55} clusters are described, as well as the current techniques for the generation of ordered monolayers and artificial patterns of quantum dots. Finally, some aspects of the chemical activity of gold nanoparticles are discussed by considering ligand-exchange processes and, last but not least, the expanding role of gold nanoparticles in catalysis is considered.

(© Wiley-VCH Verlag GmbH & Co. KGaA, 69451 Weinheim, Germany, 2003)

1. Introduction

Gold: quintessence of beauty and nobility among the metals. Some time during the Stone Age man discovered and learned to appreciate gold not only for its beauty but also for its resistivity against corrosion. Moreover, because of its relative scarcity, gold has been considered a substance of great value over millennia and today it still serves as monetary parity in many countries. The Old Testament is full of stories dealing with gold and numerous wars have been started because of gold. The early historical use of gold has also to do with its natural deposits as nuggets, which meant that no chemical processes were needed to be able to use it. Due to its softness it could be hammered into articles of jewellery even in ancient times. Numerous civilizations therefore had already started gold mining by at least the 4th millennium BC. However, the mines operated by the Egyptians in Nubia surpassed all of them by far. Gold became a decisive reason for the power of the Egyptian rulers. It was, and still is, synonymous of wealth.

In contrast to the long history of gold, the development of its chemistry was retarded because of its noble character. It can only be dissolved in oxidising media like aqua regia or by complexing species such as cyanides under air. Nowadays, the chemistry of gold is rather broad, beginning with classical complex chemistry via novel organometallic chemistry up to solid-state chemistry where so-called aurides give evidence of the high electronegativity of this unique metal.

Long before the development of modern gold chemistry the special appearance of gold was appreciated by mankind: its ruby red colloids were used to color glasses and cer-

[a] Universität Duisburg-Essen,
Universitätsstrasse 5−7, 45117 Essen, Germany
E-mail: guenter.schmid@uni-essen.de
[b] Università di Padova, Dipartimento di Chimica Inorganica, Metallorganica ed Analitica,
Via Marzolo 1, 35131 Padova, Italy

Günter Schmid studied chemistry at the University of Munich. He received his Diploma in 1962 and his Doctor's Degree in Inorganic Chemistry in 1965, both at the University of Munich. In 1966 he moved to the University of Marburg, Germany, and finished his Habilitation in 1969. In 1971 he got a professorship at the University of Marburg and he then moved to the University of Essen, Germany, where he became the director of the Institute for Inorganic Chemistry (1977). His main research interests include the synthesis and investigation of large transition metal clusters and colloids, the generation of three-, two- and one-dimensional arrangements of quantum dots, and heterogeneous catalysis.

Benedetto Corain graduated in Chemistry at the University of Padova in 1965. After serving as Assistant Professor and Associate Professor in Padova, he moved to the University of L'Aquila in 1993 as full Professor of Chemistry and he was called back with the same status from his previous University in 1999 (Faculty of Sciences). He spent one year as a Research Assistant at the Department of Chemistry, Imperial College, London in 1966 and as a Visiting Professor (Humboldt fellow) at TU Munich in 1981 and 1998 and at the University of Essen in 2002. His present research interests include basic and applied metal coordination chemistry and macromolecular chemistry, with particular emphasis on reactive and functional cross-linked polymers as supports for metal nanoclusters.

MICROREVIEWS: This feature introduces the readers to the authors' research through a concise overview of the selected topic. Reference to important work from others in the field is included.

amics. Solutions of colloidal gold were also used as tonics and elixirs, especially in combination with alcohol. Colloidal gold is still applied to treat arthritis.[1]

Scientifically, the beginning of the chemistry of gold colloids dates from the middle of the nineteenth century, when Michael Faraday performed his famous experiments to generate gold colloids.[2] He reduced tetrachloroaurate using white phosphorus to yield deep-red gold sols. At the beginning of the 20th century it was Wilhelm Ostwald who contributed decisively to the further development of colloid science.[3] He was the first to point out that the properties of metal particles in the nanometer range are predominantly determined by surface atoms and he concluded that those nanoparticles, called colloids, should exhibit novel properties with respect to bulk particles. The term "colloid" has meanwhile been mostly substituted by "nanoparticle" or "cluster". Both expressions are not very precise. They simply tell us that a particle consists of an assembly of atoms, from a few up to several hundred thousands or millions, in the size range between 1 and usually not more than 50 nm.

The miniaturization of gold to the nanometer range has dramatic consequences for its physical and chemical properties. (In principle these consequences are also valid for other metals. Gold, however, is an outstanding example.) Two examples shall elucidate the change of bulk properties when the nanosize regime is reached: the melting point and the color. Figure 1 shows the melting points of gold nanoparticles from ca. 20 to 2 nm in diameter.[4]

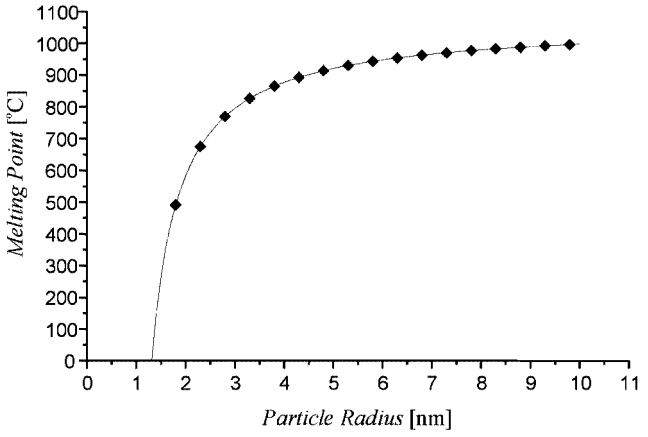

Figure 1. Relationship between particle size and melting point of gold nanoparticles

As we can see, the melting point drops below that of bulk gold (1064 °C) if the particle radius is less than 10 nm. This has to do with the increasing number of surface atoms with decreasing particle size. Surface atoms have lower coordination numbers than inner atoms and therefore become mobile more easily.

Figure 2 shows the typical color of 10 ± 5 nm gold particles.[5] In this particular case the particles are embedded in the pores of a transparent alumina membrane. The reason for the special color of metal nanoparticles is the so-called plasmon resonance, a well understood phenomenon, which is quantitatively described by the Mie theory.[6,7]

Figure 2. Photograph of a nanoporous alumina membrane, filled with 10 ± 5 nm gold nanoparticles

2. Syntheses

The number of procedures for generating gold nanoparticles is almost indeterminable. Most of them have been known for decades. For this reason only some relevant and general synthetic techniques shall be discussed here briefly. Two main routes to gold nanoparticles are available: a physical and a chemical one. Physical methods are defined as those by which gold nanoparticles are directly generated from bulk gold via atoms by various distribution techniques, whereas chemical routes use gold compounds as a starting material, linked with reduction steps.

An important aspect is the stabilization of the particles to avoid coalescence between them. This stabilization can occur in many different ways, for instance by electrostatic repulsion, steric hindrance, ligand molecules or embedding in nanocapsules such as micelles. Some of these opportunities will be discussed as part of the synthetic routes.

2.1 Physical Methods

Metal vapours usually consist of atoms. The simplest way of obtaining nanoparticles is therefore the generation of metal atoms in the gas phase followed by their controlled condensation to nanoparticles. This is the well-known metal-vapour synthesis.[8] In special cases the colloidal metals can be studied in the gas phase; however, in order to obtain them as matter, the vapours have to be condensed into a dispersing medium. Numerous modifications of this established technique have been successfully applied in the past[9] and will not be repeated in this article. Only some more recent and promising results shall be discussed.

Laser ablation methods have become commonly used techniques.[10–14] However, the size distribution of the resulting particles is usually rather broad. Improvements were obtained by the so-called "laser-induced size reduction". This is based on the well expressed plasmon resonance of

 © 2003 Wiley-VCH Verlag GmbH & Co. KGaA, Weinheim

gold nanoparticles around 520 nm and was used to change the size and geometry of the particles.[15−20] Very narrowly distributed gold nanoparticles with a diameter of 1.7 and 3.4 nm were obtained with a 532 nm pulsed laser irradiation of gold metal plates in diluted sodium dodecylsulfate solutions.[21]

A gram-scale synthesis of thiol-stabilized gold nanoparticles by solvated metal atom dispersion and digestive ripening was recently reported.[22] The method is based on the so-called solvated metal atom dispersion technique (SMAD). A well-known reactor was used to generate atoms from a piece of bulk gold.[23] The Au atoms were frozen at 77 K in acetone vapour and were then warmed up to give gold colloids, stabilized by acetone molecules. In order to attain further stabilization, they were then reacted with dodecanethiol and this enabled good dispersion in toluene. A dramatic effect on the narrowing of the gold particles was obtained by digestive ripening of the gold-toluene dispersion at 120 °C. Particles of 1−40 nm in size were narrowed down to 4−4.5 nm.

As we shall see from the following examples, wet-chemical routes to generate gold nanoparticles are much more versatile.

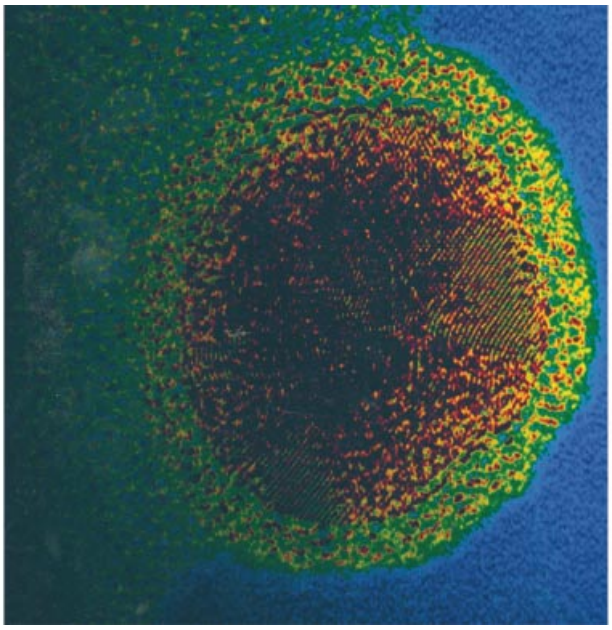

Figure 3. High-resolution transmission electron microscopic (TEM) image of a ligand-protected 11 × 13 nm gold nanoparticle; the polycrystalline gold core and the protecting shell of $P(C_6H_4SO_3Na)_3$ molecules can clearly be distinguished

2.2 Chemical Routes

As already mentioned, Michael Faraday was the first to study the formation of gold sols from a scientific point of view.[2] Phosphorus was the agent he used for the reduction of $[AuCl_4]^-$ ions. In the course of the last century numerous easier to handle reducers were found. A few of the more relevant procedures, especially the newer ones, are mentioned below.

Among the so-called salt reduction methods, the Turkevitch route still is one of the most applied procedures.[24] Sodium citrate reduces $[AuCl_4]^-$ in hot aqueous solution to give colloids of 15−20 nm. Citrate itself and its oxidation products (e.g. acetone dicarboxylate) can act as protecting agents, if no other stabiliser is used.[25,26] Dozens of variations have meanwhile been found. The use of stronger ligands than citrate was a major improvement for the synthesis and handling of gold sols. Phosphanes and thiols turned out to be excellent stabilisers due to rather strong Au−P bonds and even better Au−S bonds. These molecules allow the isolation of gold nanoparticles as solid materials that can be redispersed in appropriate solvents. This is not possible with weakly binding stabilisers such as citrate. Water-soluble phosphanes have been successfully used to shield gold colloids.[27] For instance, $P(C_6H_4SO_3Na)_3$ stabilises gold particles of 15−20 nm to such an extent that they become isolable as golden leaves that can be redispersed in deionized water with the typical purple-red color. Figure 3 shows a TEM image of an individual gold nanoparticle where the envelope of stabilizing phosphanes can be observed.[28]

PPh_3 acts as a rather good ligand for 1.4 nm Au_{55} clusters in $Au_{55}(PPh_3)_{12}Cl_6$. The latter is easily obtained by reduction of Ph_3PAuCl by gaseous B_2H_6 in benzene or toluene at elevated temperatures.[29,30] This compound will be the focus of attention of the following chapters because of its particular electronic properties. It is readily soluble in CH_2Cl_2 however, it can also be transformed into a water-soluble species by exchanging PPh_3 with $Ph_2PC_6H_4SO_3Na$ or $Ph_2PC_6H_4SO_3H$.[31]

Besides phosphanes, thiols are the most important type of stabilizing molecule for gold nanoparticles of any size. It is an accepted assumption that the use of thiols leads to the formation of RS^- thiolates that form strong covalent Au−S bonds. Since they bind more strongly to gold than phosphanes do, phosphanes can usually be substituted by thiols. However, it is also observed that the size of the original gold particles may change during the exchange process.[32,33] $[B_{12}H_{11}SH]^-Na^+$ [34] and SH-functionalized silsesquioxanes such as $(cyclopentyl)_7Si_8O_{12}(CH_2)_3SH$[35] have been successfully applied to remove phosphanes quantitatively from the surface of Au_{55} clusters. The ionic $[B_{12}H_{11}SH]^-Na^+$ transforms the CH_2Cl_2-soluble phosphane-stabilized clusters into water-soluble ones, whereas the alkyl terminated silsesquioxane makes the same particle soluble in apolar solvents such as hexane or pentane.

One of the most popular modern methods for preparing gold nanoparticles of various sizes comes from Brust et al.[36] It uses $NaBH_4$ to reduce gold salts in the presence of alkanethiols to yield gold particles of 1−3 nm. By varying the thiol concentration, the particles sizes can be controlled between 2 and 5 nm.[37] Recently, thiol-stabilized gold nanoparticles have become available following a seeding growth approach starting with 3.5 nm particles. The particle size can be varied by changing the seed-particle-to-metal-salt ratio.[38] Gold nanoparticles in the size range of about 10 to 30 nm or more have been synthesized by the $NaBH_4$

 © 2003 Wiley-VCH Verlag GmbH & Co. KGaA, Weinheim

method using mercaptosuccinic acid for stabilization.[39] By varying the succinic-acid-to-$HAuCl_4$ ratio from 2.5 to 0.5, particles of 10.2, 10.8, 12.8, 19.4, and 33.6 nm were isolated as water-redispersable powders.

11-Mercaptoundecanoic acid was also used to cover gold nanoparticles generated by the Brust method.[40] The carboxylic functions were then treated with trifluoroacetic anhydride to give the corresponding carboxylic anhydrides which are highly reactive and can, for instance, be used to anchor the nanoparticles on silica supports.

An elegant and valuable route is the generation of gold nanoparticles inside "nano-reaction vessels". Micelles can be considered appropriate chemical reactors. Due to their limited size, the control of growth by ligand concentration or other experimental conditions is not required. Möller et al. contributed decisively to this modern field of nanoscience. They used diblock co-polymers exhibiting regularly organized micelles into which tetrachloroaurates were transported, followed by a reductive step with hydrazine or $NaBH_4$ and formation of the nanoparticles.[41−45] Figure 4 shows one of those nanoparticle arrangements in a diblock co-polymer.

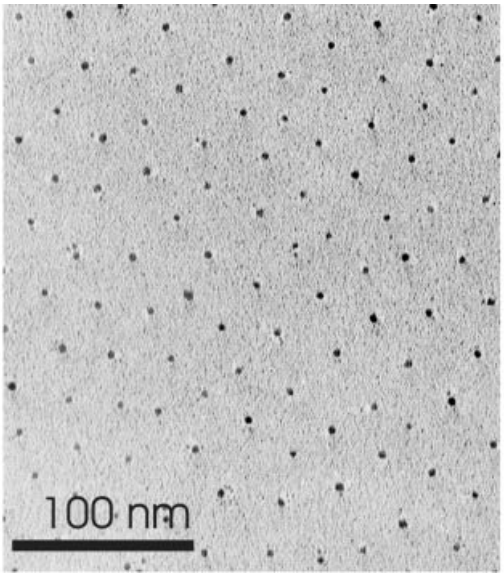

Figure 4. TEM image of 4 nm gold particles in micelles of diblock co-polymers

It must be stated that the above-mentioned examples of synthetic strategies for generating gold nanoparticles are very incomplete. A full overview of all known synthesis techniques would exceed this microreview by far. The purpose of this article is simply to report some novel improvements of well-known methods. We can conclude that since Faraday's time the syntheses have been improved, especially with respect to a better control of the particles size, however, the chemical principles are still just the same: it is the facile reduction of Au^{III} or Au^{I}. Amongst all transition metals, gold is the most electronegative one and consequently it can be generated from its salts by a huge number of reducing species. Not only classical reducers such as hydrides, hydrogen, hydrazine, hydroxylamine, alcohols etc. can be used, but any kind of organic species with some reducing character is suited to produce gold nanoparticles from salts. A so-called "green chemistry" has evolved in recent years, meaning that gold nanoparticles can be generated by natural organic materials via reduction.[46,47] Even different types of fungi have been found to work up gold salts into elemental gold.[48]

3. Structures and Optics

Transmission electron microscopy (TEM) is by far the most valuable tool for studying particle size, distribution, and structure. From thousands of TEM investigations we know that gold nanoparticles exhibit either a mono- or a polycrystalline structure of hexagonal close-packed (hcp) atoms, just like in the bulk state. Even bimetallic core-shell-structured nanoparticles can be identified by various imaging contrasts and by Energy Dispersive X-ray Analysis (EDX) of individual particles.[49,50] An example with a ca. 20 nm gold core and a palladium shell is shown in Figure 5.

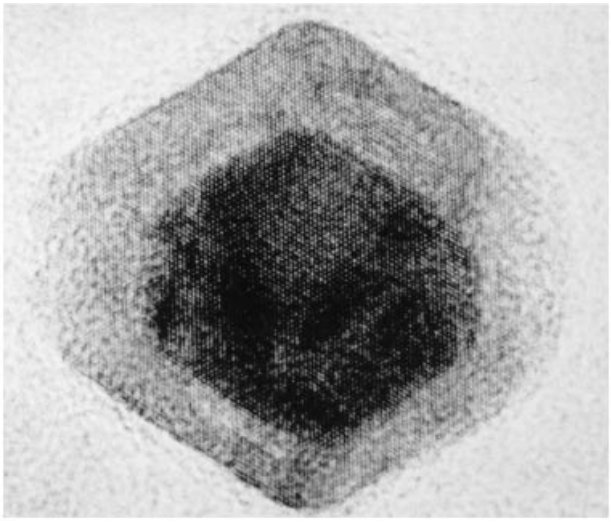

Figure 5. TEM image of a monocrystalline core-shell-structured gold-palladium particle

The smallest particle in this sense is ligand-stabilized Au_{55} which has been investigated not only by TEM, but, for instance, also by X-ray diffraction, EXAFS and Mössbauer spectroscopy. All results indicate an hcp structure.[29,51−55] However, there is an interesting transition with respect to the development of bulk structures. The smallest ligand-stabilized, so-called full-shell cluster, consists of only one central and 12 gold atoms in a first shell (Au_{13}). These have been shown to build up icosahedra.[56,57] An Au_{39} cluster has also been characterized by X-ray diffraction. It consists of a distorted hexagonal close-packed core, protected by 14 PPh_3 and 6 Cl ligands, indicating the transition to bulk structure.[58] Finally $Au_{55}(PPh_3)_{12}Cl_6$ fully reached the bulk structure. These three examples illustrate the development of the bulk state from a molecular level. However, it should

 © 2003 Wiley-VCH Verlag GmbH & Co. KGaA, Weinheim

be emphasized that these findings are only valid for ligand-stabilized particles. Conclusions on the situation in bare clusters are not possible.

A characteristic of all gold colloids is the color which can vary between light red via purple-red to bluish-red. This effect is caused by a plasmon resonance, quantitatively described by the Mie theory, as already mentioned. The plasmon resonance is initiated by the interaction of the electric field of visible light with the confined electron-gas of the particle. The wavelength, in the case of gold usually in the region of 500−600 nm, depends on the size of the particle and on the shape and the dielectric properties of the surrounding medium. These facts are quite well understood and will not be discussed here. However, a recent result shall briefly be mentioned, since it shows not only the influence of the particle size on the plasmon resonance, but also on the particles' arrangement and the nature of the surrounding medium.[59] For that purpose nanoporous alumina was filled with various gold nanoparticles. Owing to its transparency, alumina is ideally suited to study the optical properties of nanosized particles inside its pores.[60] Two approaches for placing gold nanoparticles in nanopores are available: the thermal decomposition of $Au_{55}(PPh_3)_{12}Cl_6$ clusters inside the pores to generate larger particles and the use of preformed particles to be filled into the pores by vacuum induction of solutions. An example of a membrane prepared in this manner has already been shown in Figure 2.

As expected, the size of the gold nanoparticles increases with increasing decomposition-temperature, due to the increasing melting point of larger particles (see Figure 1). In the temperature range of 100−800 °C particles with diameters of 4.5 up to 11 nm were observed in sectioned membranes by means of TEM. For example, Figure 6 shows the extinction spectra of a composite consisting of 4.5 ± 1.4 nm particles in 50 nm pores in two different media, namely in air and in toluene.

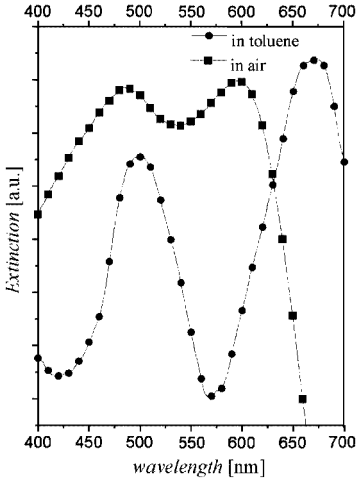

Figure 6. UV/Vis extinction spectra of 4.5 ± 1.4 nm gold nanoparticles in 50 nm alumina pores in air and in toluene, respectively

In air, two absorption peaks are observed at 480 and 600 nm. The low-energy absorbance is probably caused by the excitation of the plasmon resonance along the axis of the wire-like arranged particles. This effect can be seen even by the naked eye: when viewed perpendicularly to the membrane's surface the color is deep red (Figure 2), whereas the edge of the membrane looks blue. On immersing the sample in toluene, not only does the intensity of the peaks increase, but both peaks are red-shifted to 500 and 675 nm, respectively. This red-shift is caused by the change in the refractive index from air to toluene, whereas the increase in intensity comes from the reduction of scattering effects, since toluene has almost the same refractive index as alumina.

The use of preformed nanoparticles has the advantage of narrower size distribution and allows one to observe changes by repeated filling. If 50 nm pores are filled once with 15 nm gold colloids, only one plasmon resonance peak at 525 nm is observed because of the lack of wire-like arrangements. Repeated filling broadens out and shifts the signal to 580 and 590 nm, indicating initial formation of wire-like arrangements. Additional effects have been observed using unpolarised and polarised light with different polarization angles. Theoretical calculations, using the generalized Mie theory,[7,61−63] support the interpretation of the experimental observations.

Plasmon resonance is a size-dependent phenomenon of several metals. Bulk metals reflect light, whereas small molecular clusters do not show any kind of plasmon resonance. This is due to the lack of *quasi* delocalized electrons that are necessary for the interaction with light. On the contrary, the electrons between metal atoms in small clusters are localised. This is known for thousands of oligonuclear organometallic cluster compounds.

A decisive question, which will also be the focus of attention of the following chapters, is: how large or how small should a metal particle be in order for us to observe molecular or metallic properties? In relation to optical properties this question has to be formulated as: when does the plasmon resonance disappear if miniaturization proceeds? In this context, ligand-stabilized Au_{55} clusters play an important role. Ligand-stabilized Au_{13} and Au_{55} clusters were investigated and in both cases the vanishing of the Mie resonance was observed.[64] Again we should remember that the observed effects always include the existence of ligand shells on the particles. In spite of this restriction it can be stated that the 1.4 nm Au_{55} clusters, from an optical point of view, belong rather to the molecular world than to the metallic one. However, we will learn that such statements cannot be generalised, since the method of investigation, temperature and other experimental parameters play a decisive role with respect to what we "see". To conclude these considerations we have to accept that $Au_{55}(PPh_3)_{12}Cl_6$ and its variations do not possess enough mobile electrons to exhibit plasmon resonance. Of course, these findings are related to the special electronic situation in the Au_{55} cluster core. Therefore, the following section will deal exclusively with the electronic properties of this compound.

 © 2003 Wiley-VCH Verlag GmbH & Co. KGaA, Weinheim

4. Electronics

4.1 The Quantum Size Effect

In a bulk piece of metal the valence electrons of the participating atoms occupy energy bands instead of discrete levels, as we know from atoms and molecules. In a thought experiment we can proceed with a continuous reduction of dimensions. From a 3D situation with its typical bulk behavior we turn to a film of only a few atoms' thickness (2D). Here, the electrons can only move in two dimensions, whereas in a wire of only a few atoms in diameter, one-dimensionality (1D) of the electronic degree of freedom is enforced. If we cut off a small piece of that wire we reach the zero-dimensional (0D) situation where the remaining electrons are constrained in such a way that they begin to occupy discrete energy levels. A particle of such size no longer follows classical physical laws and has to be described by the quantum mechanical rules used to describe atoms. That is why such pieces of matter are also called "quantum dots" or, with a somewhat more popular expression, "artificial atoms". Pieces of metals following these conditions must exhibit very different physical and chemical properties compared to bulk ones and to typical molecular ones. It was the enormous interest in these novel properties that brought nanoscience to such a level that a wide public, economic and political interest arose. It is the general opinion of experts that nanotechnology will decisively influence man's life in the following century.

Back to the facts, we have to repeat the question we asked in the previous section in a more general way: how many atoms do we need, to cause metallic behavior or how small should a piece of metal be in order to see metallic properties disappearing?

4.2 Physical Tools

There are many physical methods to investigate quantum-size effects. It would exceed this article by far to mention and to discuss all of them, therefore only a few shall be selected to explain what happens when particles size is continuously reduced. It should be mentioned that many of the investigations during the last two decades involved other metals as well as gold, since quantum-size effects can be studied with any kind of metal, and, of course, also with semiconductors. However, gold played once again an important role in the process of our understanding. Some hints have already been given by the optical phenomena discussed in section 3.

One important contribution to this major problem was made by the observation of electron-phonon coupling in gold particles of different size.[65] This relation informs us on the interplay between the rate of energy transfer from electrons to lattice and the number of atoms in the particle. It was found that the electronic relaxation-speed, induced by laser pulses of 200 fs of an energy of 250 μJ/pulse at 780 nm, varies characteristically with the particle size. $Au_{13}(dppm)_6(NO_3)_4$ (dppm = $Ph_2P\text{-}CH_2\text{-}PPh_2$)[56] (core diameter 0.7 nm), $Au_{55}(Ph_2PC_6H_4SO_3Na)_{12}Cl_6$ [31] (core diameter 1.4 nm) and 15 nm colloids were tested. Figure 7 shows the results.

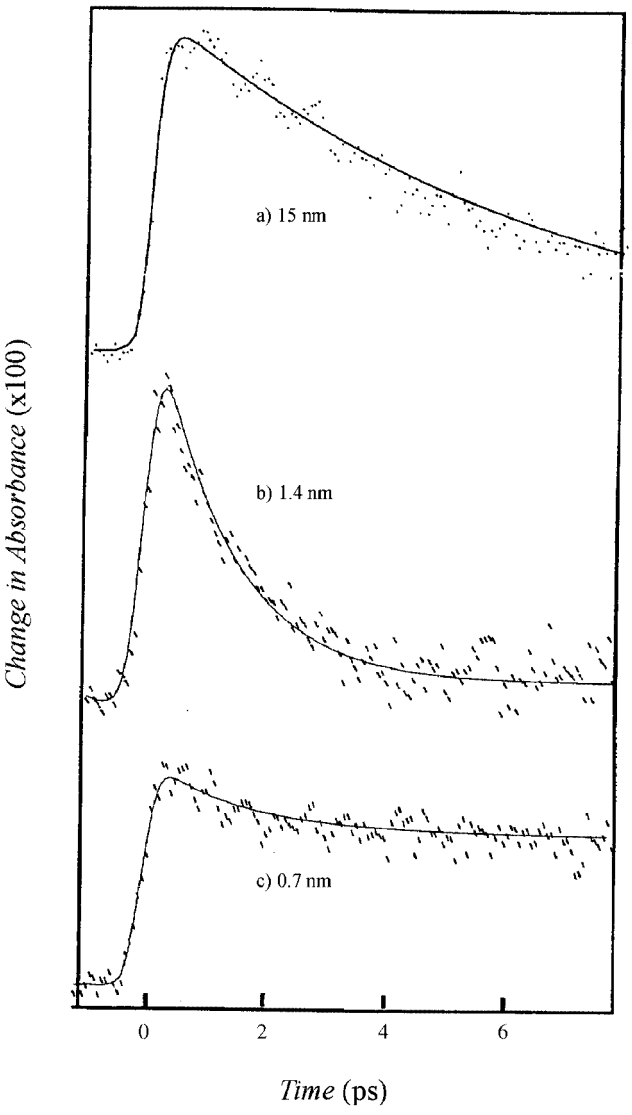

Figure 7. Relaxation behavior of gold nanoparticles of different sizes after excitation by femtosecond laser pulses

As we can see, the relaxation speed increases from the 15 nm particles to Au_{55}, also compared to the bulk. This effect is explained by the weakening of the electron-plasmon interaction, and the increase of the electronic collision-rate on the surface. For Au_{13} it decreases due to the existence of localized electrons. This cluster behaves like a molecule, whereas Au_{55} represents the very last "metal" before the typical molecular region begins. This example demonstrates that the decision "metal or not", cannot be precisely answered. As shown, optically Au_{55} is definitely no longer a colloid, and we have just learnt that it is not yet a molecule!

Probably the most informative method for studying the electronic situation inside a nanoparticle is to measure its current-voltage characteristics under different conditions. This can be performed by bringing an individual particle, bearing a non-conducting protecting shell (usually the li-

 © 2003 Wiley-VCH Verlag GmbH & Co. KGaA, Weinheim

gands), into contact with two electrodes to which a variable voltage is applied. The insulating barrier is necessary to make tunnelling of individual electrons observable, as is indicated in Figure 8.

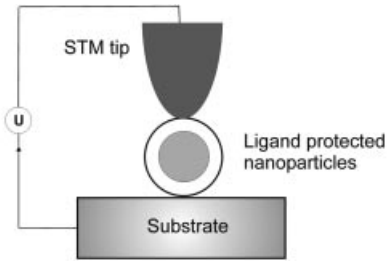

Figure 8. Sketch of a tunnelling contact consisting of an STM tip, a ligand-protected metal nanoparticle and a conducting substrate

The barrier conditions are responsible for the electron transport. Among others, they depend on the temperature. Owing to the relationship $E_C = e^2/2C >> k_BT$ (E_C = electrostatic energy, C = capacity of the island between the electrodes, k_BT = thermal energy), the thermal energy should be small in order to observe Single Electron Tunnelling (SET). If not, uncontrolled electron transitions occur. This fact was demonstrated by placing a ligand-protected 17 nm Pd particle next to two platinum tips.[66] At 295 K the particle exhibits a linear current-voltage ($I-V$) relationship and therefore indicates metallic behavior (Ohm Law). However, when measured at 4.2 K, a so-called Coulomb gap is observed: if k_BT is small enough, tunnelling of a single electron onto the particle blocks the transfer of a second one, due to Coulomb repulsion, until an appropriate voltage is reached.

$Au_{55}(PPh_3)_{12}Cl_6$ clusters on gold substrates have been investigated by bringing individual particles into contact with an STM tip so that information on $I-V$ characteristics can be gained. The result is very exciting: these particles indeed show well-expressed Coulomb blockades already at room temperature, as we can see in Figure 9.[67]

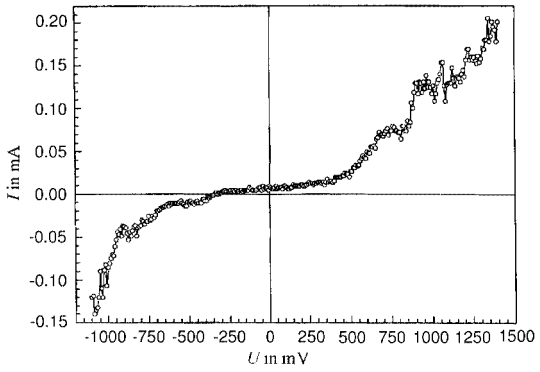

Figure 9. Room temperature $I-V$ characteristics of an individual $Au_{55}(PPh_3)_{12}Cl_6$ cluster indicating a well-expressed Coulomb blockade

This means that these 1.4 nm, ligand-protected particles behave as single electron-switches at room temperature! This opens up unexpected future applications in nanoelectronics.

The same Au_{55} species have very recently been studied by the same technique, however at 7 K under ultra high vacuum (UHV) conditions.[68] This method allows one to acquire not only tunnelling spectra, but also detailed images of individual particles. Figure 10 shows one of them together with a space-filling model in the corresponding orientation.

The light dots in Figure 11 indicate the positions of the phenyl rings of the PPh_3 ligands and **a** and **b** show two different sites where the STM tip was positioned for recording the tunnelling spectra: **a** above a C_6H_5 ring, **b** on the side of the ring, but with the same distance from the gold surface. Figure 11**A** shows the Coulomb blockade, which is the same size for both positions, indicating that the ligands do not visibly contribute to the tunnelling process;

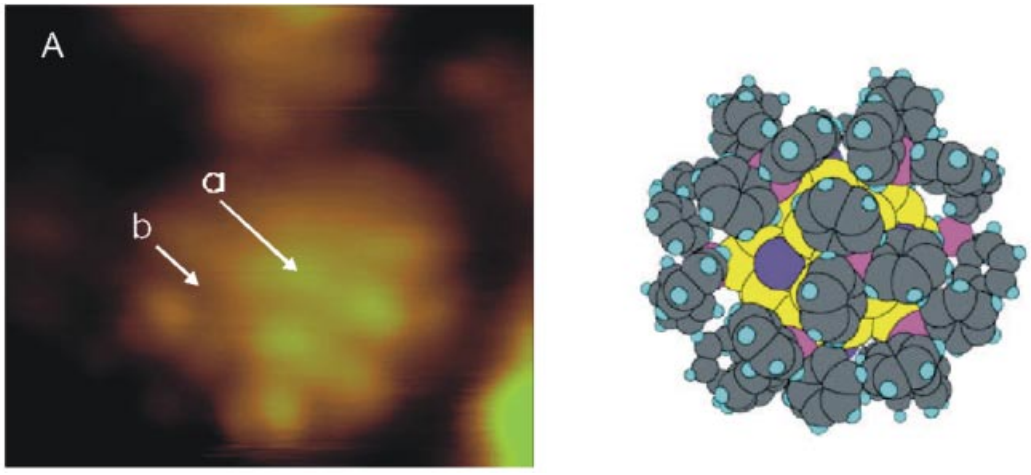

Figure 10. STM image of an individual $Au_{55}(PPh_3)_{12}Cl_6$ cluster at 7 K under UHV conditions together with a full-space model; the light dots indicate phenyl rings; the positions **a** and **b** indicate where the measurements have been performed to yield the $I-V$ characteristics in Figure 11

 © 2003 Wiley-VCH Verlag GmbH & Co. KGaA, Weinheim

they simply act as distance holders. Still more interesting is the high resolution of the blockade region by using d*I*/d*V* instead of *I* (**B**). The arrows indicate conductivity signals which coincide precisely for both positions. For the very first time the existence of discrete energy levels inside the Au_{55} core could be proven. The occupied as well as the unoccupied levels are visible, due to conductivity oscillations. The average level spacing in vicinity to the Fermi level is about 170 meV.

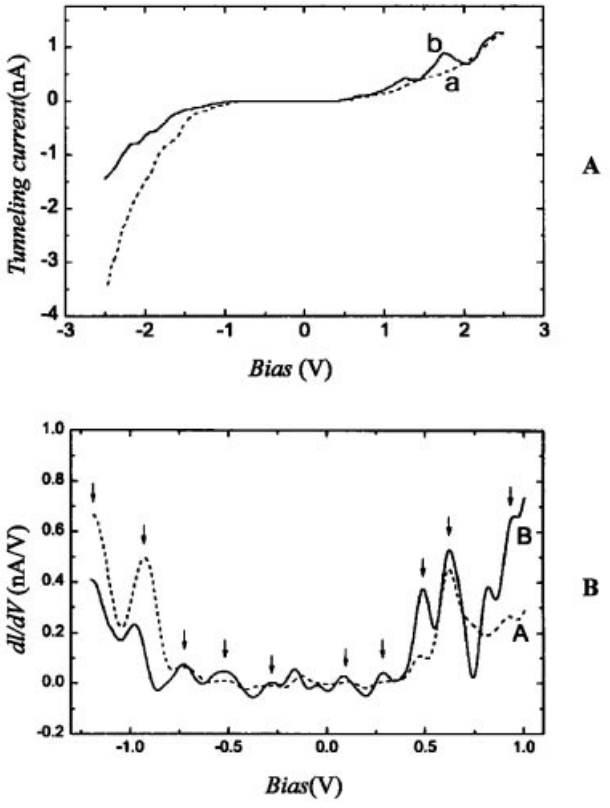

Figure 11. A) $I-V$ characteristic of an individual $Au_{55}(PPh_3)_{12}Cl_6$ cluster at 7 K under UHV conditions; **a** and **b** indicate equivalent Coulomb blockades although measured at different positions on the cluster's surface; B) d*I*/d*V* characteristic of the same particle indicating discrete electronic energy levels (arrows) in the Au_{55} cluster core

This experiment now justifies the expression "artificial atom" for those quantum dots and proves the assumptions of paragraph 4.1 that on the way from bulk to molecule at some point a situation arises where the electronic band structure begins to form discrete energy levels.

As a consequence of these unique properties it seems interesting to study the electron-transfer processes between the quantum dots. This was done for three-dimensionally organized Au_{55} clusters with variable distances.[69] However, as it turned out, it is not only the distance between the nanoclusters which determines the activation energy for the charge transfer, but also the nature of the interlinking species and the kind of linkage. If the clusters are simply separated from each other by ligand shells of different thickness or by non-covalently binding spacer molecules (ionic interactions), there is indeed only a simple linear relation between cluster-cluster distance and activation energy to be observed. On the contrary, if spacer molecules linking the particles via covalent S−Au bonds are used, it is not the distance that contributes decisively to the activation energy, but the chemical nature of the spacers. Figure 12 illustrates these results.

5. Approaches to Two-Dimensional Organizations

The two- and in some respect also the one-dimensional organization of metal nanoparticles is very relevant since one can think about the use of these particles in nanoelectronics only in an organized form. This is why numerous groups worldwide are dealing with this problem. It is again gold that plays an important role because of the easy availability of gold nanoparticles and their resistivity to air. So, there is a vast amount of reports, mainly on regular 2D arrangements of gold nanoparticles, most of them in the size regime of a few, up to 15 and 20 nm. Here we will only focus on recent results of organized Au_{55} clusters, since they are of promising electronic nature, as has been discussed in section 4.

After numerous attempts, rather extended self-assembled monolayers of $Au_{55}(Ph_2PC_6H_4SO_3H)_{12}Cl_6$ and of $Au_{55}(PPh_3)_{12}Cl_6$ became available.[70−72] The acidified cluster gives hexagonal and square structured 2D arrangements on poly(ethyleneimine) (PEI) films, whereas the neutral species is best organized at the phase transition between water and dichloromethane, supported by a layer of poly(vinylpyrrolidone) (PVP) or, still better, of poly(*p*-phenylene ethynylenes) (PPE). Although there is no doubt that PEI acts as a basic surface towards the SO_3H-modified Au_{55} cluster, the role of PVP and PPE in connection with $Au_{55}(PPh_3)_{12}Cl_6$ is somewhat more delicate. Relatively strong interactions, like those between the acidified cluster and PEI, prevent formation of extended ordered layers due to the lack of flexibility of the particles. On the contrary, PVP and PPE interact only weakly with the PPh_3-covered cluster, probably via hydrophobic-hydrophobic and π-π interactions, respectively. These weak forces between the clusters and the supports enable the formation of perfect arrangements since the particles are only weakly attracted and are allowed to find the best order. Figure 13 shows TEM images of cut-outs of square planar (**a**) and hexagonal (**b**) arrangements of Au_{55} clusters, generated on PEI and PPE, respectively.

An interesting electrical behavior of these ordered monolayers was observed when conductivity measurements were carried out.[73] Monolayers deposited between two tungsten electrodes on silica surfaces, 50−150 nm apart and 25 nm in height, and prepared on PVP films, as described above, were checked by scanning electron microscopy (SEM). Due to charging effects of the electron beam (10 keV, 10 s) the layers become conductive in the pA region in contrast to a not measurable conductivity without irradiation. However, if irradiation occurs on only one of the electrodes and part

 © 2003 Wiley-VCH Verlag GmbH & Co. KGaA, Weinheim

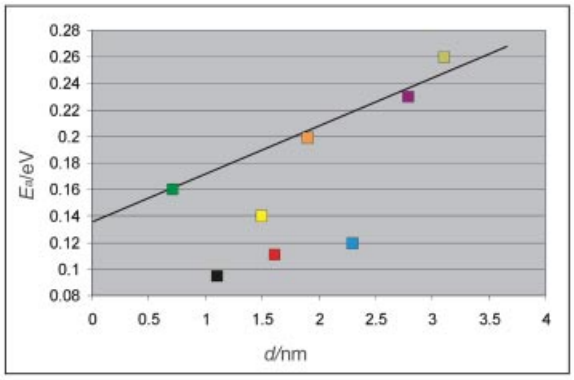

Covalently Linked **Linking System**	Distance nm	E_a (eV)
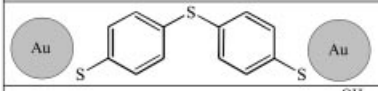	1.1	0.095
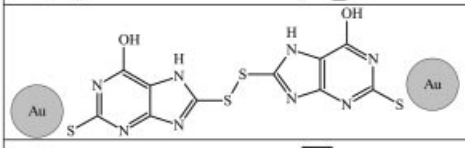	1.6	0.11
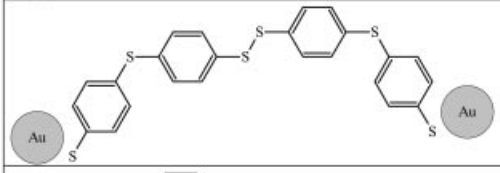	2.3	0.12
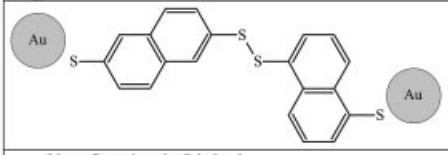	1.5	0.14
Non-Covalently Linked **Linking System**	Distance nm	E_a (eV)
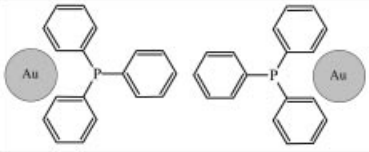	0.7	0.16
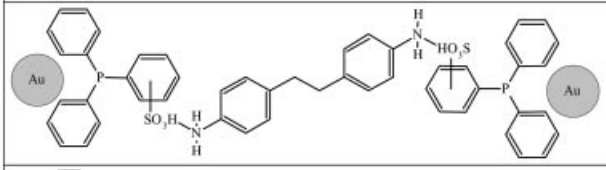	1.9	0.20
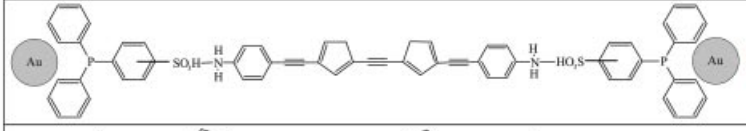	2.8	0.23
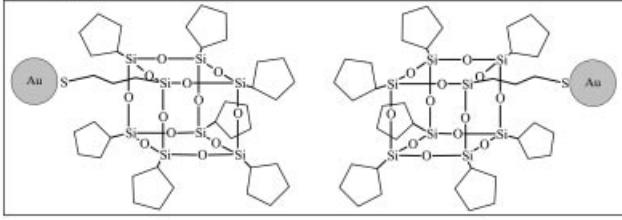	3.1	0.26

Figure 12. Activation energies for Au_{55} clusters of varying distances, covalently and non-covalently linked

 © 2003 Wiley-VCH Verlag GmbH & Co. KGaA, Weinheim

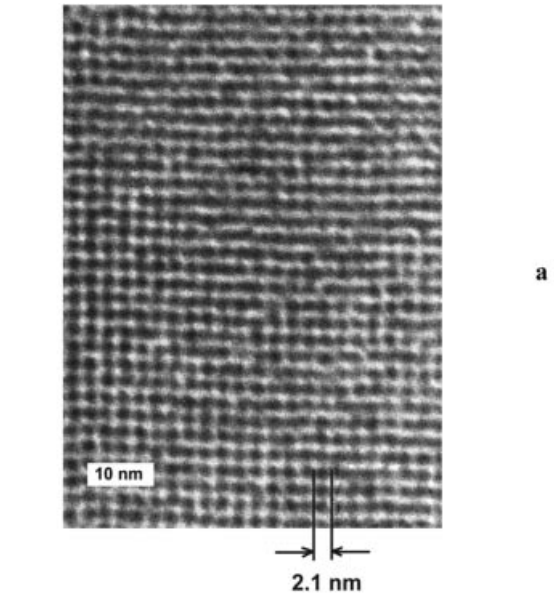

Figure 13. TEM images of square planar (**a**) and hexagonal (**b**) monolayers of ligand-stabilized Au_{55} clusters

of the monolayer, diode-like behavior is observed. The $I-V$ characteristics depend on the contact distances, the irradiation time, the energy of the electron beam, the exposure time and finally on the irradiated area. Figure 14 shows a typical diode curve (**a**) gained with a set-up of electrodes of 122 nm distance (**b**) and an exposure time of 5 s at 16 keV.

In all cases the systems relax in the course of 24−36 h after switching off the voltage. However, reactivation is possible, indicating that there is no chemical change with respect to the starting situation. In order to explain this unusual behavior we assume that electrons from irradiation, trapped in the silica layer, create so-called image charges in the cluster layer. This activation makes the particles order themselves so as to reach a minimum energy arrangement with a maximum delocalization of the additional electrons. The rearrangement of the clusters may happen very quickly due to the electron irradiation, whereas the deactivation takes much more time.

Self-organization of quantum dots must be considered only as a first step for collecting information on their electronic interchange. However, for practical use with respect to future data storage or related applications, it is necessary to create artificial architectures. A first approach as to how this high goal might be reached will be described below. It is based on the generation of appropriately modified surfaces.[74] A metallized AFM tip was used as a tool for transforming methyl groups of a self-assembled monolayer into carboxylic functions by electrical pulses under air. The total process is sketched in Figure 15.

The COOH groups are used to add silane molecules to C=C double bonds which can then be transformed to thiol-functionalized derivatives. Finally, water-soluble $Au_{55}(Ph_2PC_6H_4SO_3Na)_{12}Cl_6$ clusters are chemisorbed from solution by the thiol functions. The width of the traces simply depends on the quality of the tip. As we can see from Figure 16, arranged dots of clusters (a), as well as single gold clusters between wires made of single rows of particles (b), have been created, and of course any other structure could be created.

There is no doubt that these structures offer great advantages compared with self-assembled arrangements. How-

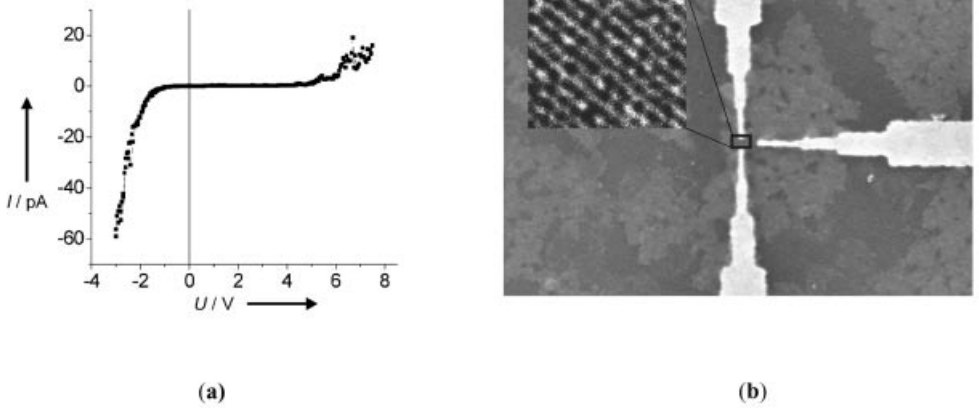

Figure 14. Diode behavior of $Au_{55}(PPh_3)_{12}Cl_6$ monolayers, in contact with tungsten electrodes on SiO_2, after partial irradiation with an electron beam

 © 2003 Wiley-VCH Verlag GmbH & Co. KGaA, Weinheim

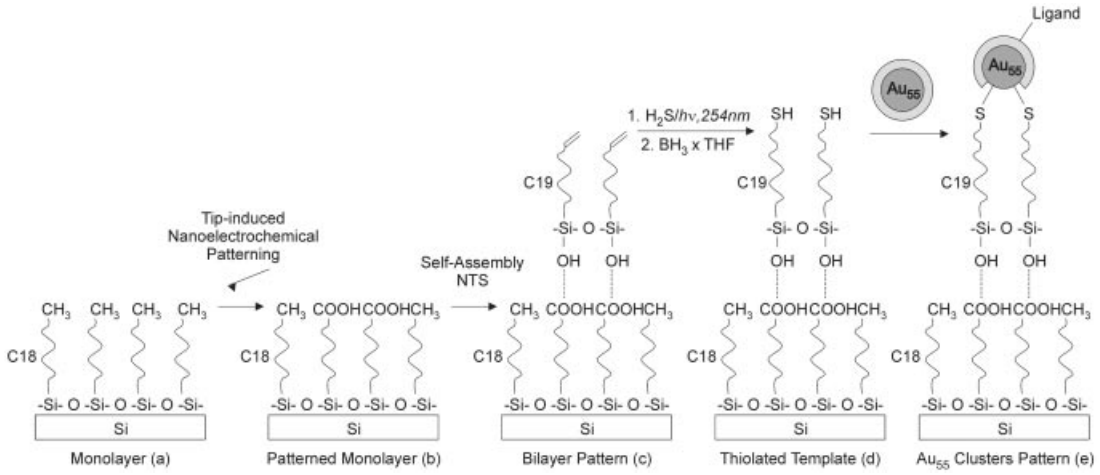

Figure 15. Sketch of the generation of SH-functionalized patterns on a Si wafer to trap Au_{55} clusters

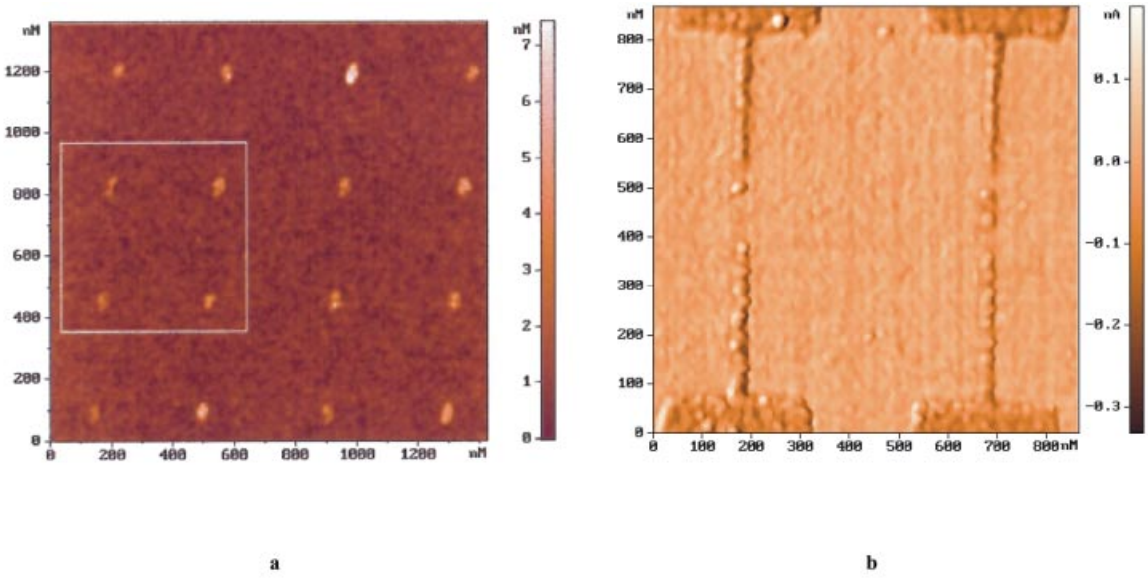

Figure 16. a, b Patterns of Au_{55} clusters deposited on chemically modified surfaces as shown in Figure 15

ever, it is also clear that there is still a lot of work to be done to develop a working system. One major problem will be to study individual quantum dots and to connect them with the outer world. There are ideas on how to do this, but many efforts will be necessary to reach this goal.

6. Chemical Activity

Two main aspects concerning chemical activity of gold nanoparticles will be treated in this chapter: ligand-exchange reactions and catalytic activity. Ligand-exchange reactions are quite common and are used to change solubility or to introduce special functions. Catalytic properties of gold nanoparticles are currently developing into an attractive and important field in gold chemistry. Therefore, a rather detailed discussion of catalytic properties will be found in this section.

6.1 Ligand-Exchange Reactions

As discussed in chapter 2.2, wet chemical syntheses of gold nanoparticles are always linked to the presence of protecting ions or molecules since without them, coalescence would quickly occur. As an example we should remember the famous citrate route for the generation of 15−20 nm gold colloids. Without any other stabilizing species the gold particles are covered by excessive citrate, but also by Cl^- ions and acetone dicarboxylate, an oxidation product of citrate. These species bind strongly enough to keep the colloids in solution for a long time. However, they can easily be substituted by stronger binding molecules. For instance, the water-soluble phosphane $P(C_6H_4SO_3Na)_3$ can easily re-

 © 2003 Wiley-VCH Verlag GmbH & Co. KGaA, Weinheim

move the original ions and molecules to form such a strong ligand-shell that these gold nanoparticles can even be isolated as solid products.[27] We must assume that phosphane molecules on the surfaces of gold nanoparticles are rather mobile in solution. This was shown long ago by ^{31}P NMR investigations of $Au_{55}(PPh_3)_{12}Cl_6$ with excess PPh_3.[75] Gradual addition of free PPh_3 to cluster solutions causes a shift of the ^{31}P signal from $\delta = 34$ ppm towards that of free phosphane ($\delta = -5.5$ ppm). This is due to the fast exchange processes between free and coordinated PPh_3 molecules. The mobility of ligand molecules is also the reason why $Au_{55}(PPh_3)_{12}Cl_6$ is rather labile in solution (due to the loss of PPh_3), and as a consequence, coalescence processes are inhibited. The formation of the water-soluble compound $Au_{55}(Ph_2PC_6H_4SO_3Na)_{12}Cl_6$, from $Au_{55}(PPh_3)_{12}Cl_6$, dissolved in dichloromethane, is also based on that ligand mobility. The fact that the water-soluble derivative is formed in quantitative amounts is due to the phase transfer from CH_2Cl_2 to H_2O and to the somewhat better coordination of $Ph_2PC_6H_4SO_3Na$ compared to PPh_3.

The high mobility of phosphanes on gold-particle surfaces can be used to substitute them with stronger ligands, above all by thiols. As already mentioned in section 2.2, the thiol-functionalized silsesquioxane $(cyclopentyl)_7Si_8O_{12}(CH_2)_3SH$, as well as the anionic thiol $[B_{12}H_{11}SH]^{2-}$, quantitatively substitute phosphanes in Au_{55} clusters with the help of phase transitions.[35,34] The alkyl-terminating silsesquioxane, readily soluble in apolar solvents such as pentane or hexane, transfers the water-soluble cluster $Au_{55}(Ph_2PC_6H_4SO_3Na)_{12}Cl_6$ into the pentane-soluble derivative with silsesquioxane ligands, whereas the dichloromethane-soluble $Au_{55}(PPh_3)_{12}Cl_6$ becomes water-soluble if reacted with $Na_2[B_{12}H_{11}SH]$. Figure 17 illustrates these transfer reactions that indicate that the same cluster particle can change its solubility from dichloromethane to pentane or even to water.

A very special kind of "phosphane substitution" in $Au_{55}(PPh_3)_{12}Cl_6$ is observed when the latter is reacted with an excess of a fourth-generation dendrimer bearing 96 terminal SH functions.[76] The excess dendrimer obviously re-

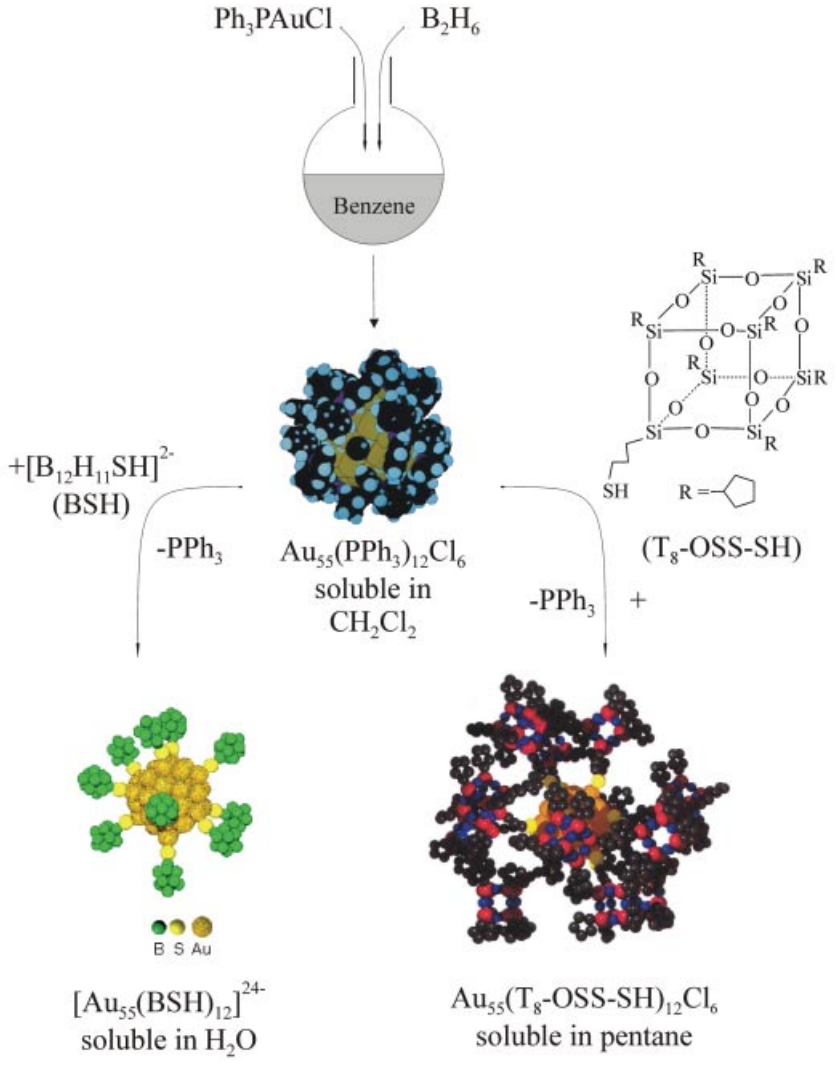

Figure 17. Sketch of synthetic routes to $Au_{55}(PPh_3)_{12}Cl_6$ and some of its derivatives

 © 2003 Wiley-VCH Verlag GmbH & Co. KGaA, Weinheim

moves all the phosphanes from the clusters' surface. However, Au−Au interactions between the bare clusters occur and the coordination of dendrimers is not observed . Consequently, naked Au_{55} particles grow to regular microcrystals inside a matrix of dendrimers.

Finally, a very unexpected behavior of naked Au_{55} clusters will be mentioned. While surfaces of bulk gold and particles of 7.9, 2.9, 1.6, 1.3, and <1 nm are all oxidized when deposited on top of a silicon wafer and exposed to atomic oxygen, bare Au_{55} resists these extreme oxidative conditions.[77] Moreover naked Au_{55} clusters are formed in oxygen plasma by burning off the ligand shell, as can clearly be followed from the X-ray photoelectron spectra. Only traces of oxides appear, as indicated by the presence of a weak shoulder, the main part of the particles remaining unchanged. Figure 18 shows the Au-4f photoelectron spectra of the oxidized particles including Au_{55} clusters.

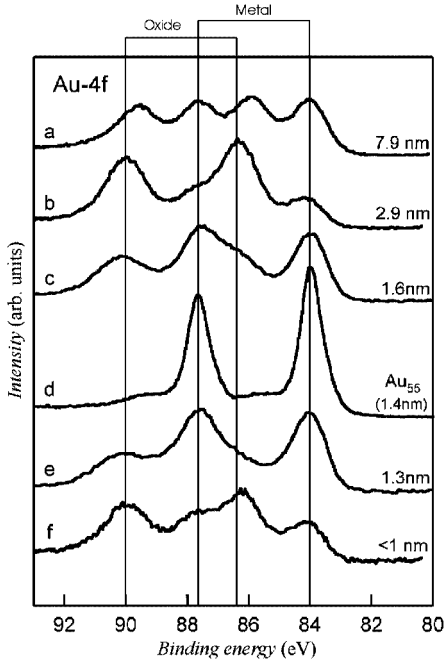

Figure 18. X-ray photoelectron spectra of various gold particles after exposure to an oxygen plasma; all particles except for Au_{55} show well expressed gold oxide signals

In all cases except for Au_{55} there are well-developed signals for gold oxides. This phenomenon has led to the formulation that Au_{55} is "nobler than bulk gold".[78] As an explanation of this unique behavior it is assumed that it is the special stability of Au_{55} as a closed-double-shell structure. It is excluded that a special electronic situation might cause this inertness. As a consequence it can be predicted that other full-shell clusters such as Au_{147} or Au_{309} etc. should also resist oxidation. Owing to the non-availability of these particles, this prediction cannot yet be proven . However, it can be suggested that these gold full-shell clusters might act as special oxidation catalysts.

6.2 Nanoparticulated Gold in Modern Catalysis

6.2.1 Historical Survey

In contrast to the catalytic potential of its neighbors silver and platinum,[79] bulk gold metal appeared for long time an essentially useless material for catalysis.[80,81]

The first documented exhibition of catalytic activity of bulk gold occurred at the beginning of the past century when Bone and Wheeler showed in 1906 that gold foils catalyse the combustion of dihydrogen and dioxygen to give water.[82] The relevant paper is remarkable in that the authors also collected good quantitative kinetic data on the same reaction. It was believed for a long time that the inability of Au^0 to activate (chemisorb) O_2 in any catalytic oxidation reaction was a straight manifestation of its thermodynamic reluctance to form metal oxides (ΔH_f^0 of Au_2O_3 = +19.3 kcal·mol^{-1} [81]). Ironically, the extremely facile Au^0-catalyzed oxidation of CO to CO_2 by O_2 is the most striking result in Au^0-catalytic chemistry, but only when Au^0 occurs as metal nanoparticles supported on suitable metal oxides.

Information on the catalytic chemistry of Au^0, obtained in the decades following Bone and Wheeler's observation, was not considered very exciting.[83] However, in the course of the seventies, three major observations were made: a) Au^0 supported on silica (0.01−0.05%) was found by Bond and Sermon to catalyse the hydrogenation of alkenes at 373 K, with no effect on the potentially concomitant double bond migration reaction,[84] b) Au^0 supported on MgO or Al_2O_3 was found by Galvagno and Parravano to catalyse oxygen- and hydrogen-transfer reactions [85] and c) a green $Au(O_2)$ molecular species with side-on bonded dioxygen could be obtained at extremely low temperatures in a solid matrix.[86,87] Most interestingly, this very remarkable molecule was found to react with CO at a suitable temperature to give eventually free Au^0 and CO_2. Indeed this was a prophetic observation!

Among the many good review papers quoted in this report, the 2002 review by Choudhary and Goodman as a general and critical reading on Au^0 catalytic chemistry is particularly recommended.[88]

6.2.2 Synthesis of Supported Gold(0) Catalysts

The overall grey scenario of Au^0 catalytic chemistry became suddenly lightened in 1989 when Haruta et al. reported on a real breakthrough in this field of research.[89] They observed, in fact, that the oxidation of CO to CO_2, a technologically relevant reaction under various circumstances, could be effectively catalyzed by supported-Au^0. Moreover, it was later observed that the reaction occurs even at 200 K.[90] It soon became apparent that the key to this success was twofold: a) the presence of gold nanoparticles in the gold catalysts and b) a strong co-catalytic role played by the support that had to be an inorganic oxide such as Fe_2O_3, TiO_2, or Co_3O_4. It also became apparent that the optimal nanocluster diameter was ca. 3 nm, the size at which metal nanoclusters start to exhibit quantum-size behavior.[91,92]

 © 2003 Wiley-VCH Verlag GmbH & Co. KGaA, Weinheim

This discovery promoted an incredible amount of research and an avalanche of papers and patents in a manifestation of a modern-day "gold rush".

We believe that the catalysis community was particularly stricken by Haruta's discovery in that it represented an unprecedented example of both extreme catalyst structure-sensitivity and of an impressive co-catalytic role played by the metal-supporting microphase (vide infra). In fact, the issue of catalyst preparation and the full understanding of the role of the support appeared immediately very complex, still to be fully evaluated nowadays and, in this connection, the reader is referred to an authoritative review paper by Bond and Thomson who critically examined the matter in the year 2000, in terms of both consensual and disputed literature observations and to other general as well as specific readings.[93−99]

Supported gold nanoparticles (1−5 nm) are currently prepared according to a dozen or so rather different methods, which can be reduced in essence to three major procedures.

The precursor of Au^0 is mixed with the precursor(s) of the supports (or with the support itself) to give a system that, after controlled calcination, produces Au^0/S catalysts. The metal nanoparticle's size is controlled by the calcination temperature, and lower temperatures seem to favor the formation of smaller particles.[100,101]

The precursor of Au^0 is deposited or grafted onto the surface of the support, which has been pre-formed from the gas or from the liquid phase,[99] and subsequently thermally decomposed to give the Au^0/S catalysts. We would like to mention, in this respect a recent outcome from these laboratories, i.e. the preparation of an Au^0/resin catalyst obtained from the chemical reduction of an $Au^{I,III}$/resin-macromolecular complex prepared simply by complexation of aqueous $AuCl_3$ with a thioethereal gel-type resin.[102]

The Au^0 nanoparticles are pre-produced in a given solution where they are stabilized by soluble polymers[103] or by kinetic conditions, and subsequently left to be adsorbed by the surface of the desired support particles.[104]

As anticipated above, it is now widely accepted that at least for CO oxidation and for the water gas shift reaction, catalytic activity depends critically on the metal nanoparticles' size, on the nature of the support and on the detailed synthetic procedure. In this context, the deposition precipitation (DP) procedure is generally widely considered the most suitable one (Scheme 1).

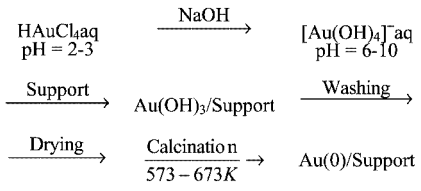

Scheme 1. Deposition precipitation procedure to give Au/S catalysts[99]

In fact, DP turns out to be particularly suitable for producing hemispherical (ca. 3 nm) nanoparticles (Figure 19) that are believed to cause a particularly strong attractive force between a given nanoparticle and the crystal lattice of the support located just underneath it.

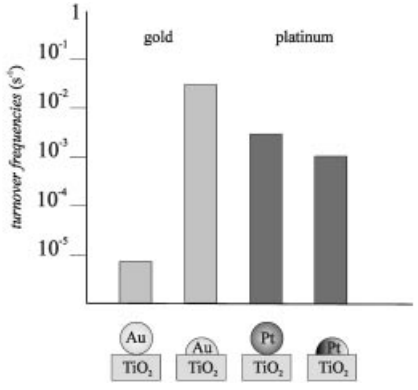

Figure 19. Dramatic effect of the Au^0-support interaction on the CO oxidation reaction rate over spherical vs. hemispherical nanoclusters; it is important to note the quite different effect of the nanoclusters's shape on the action of Pt^0

This phenomenon has two major consequences: i) a marked thermal stability of the Au^0 nanoparticles (thus contrasting the particles' coalescence) and ii) a peculiar local electronic situation at the lattice interface of the metal nanoparticles and the support, that is likely to be responsible for the particular mechanism of oxygen transfer to chemisorbed carbon monoxide to give carbon dioxide (see below).

6.2.3 Nanoparticulated-Gold(0) on Metal Oxides: Facile Oxidation of Carbon Monoxide to Carbon Dioxide

No measurable oxidation of CO by O_2 on micro-sized (in fact "bulk") supported-Au^0 is observed at ambient conditions. On the contrary, if a mixture of CO and O_2 is allowed to interact with 2−5 nm gold particles dispersed on the same support, under identical Au^0 molar fraction, a rapid and quantitative oxidation to CO_2 is observed even at 200 K.[90]

Wallace and Whetten observed an effective formation of CO_2 when CO and O_2 were reacted with Au_6^- in the gas phase (Figure 20).[105] Moreover, theoretical calculations carried out by Lopez and Norskov[106] revealed that isolated Au_{10} clusters are expected to catalyse CO oxidation even below room temperature. All these observations seem to provide an explanation of the established activity of the nanoparticles' surface gold atoms in the CO oxidation. However, reality is more complex than that!

An Au^0 nanoparticle of 2−3 nm in size, exposes ca. 50% of its atom constituents to the action of gaseous species that find possible reaction sites at the edge-, corner- or step-sites of the nanoparticle surface. Consequently, we might consider that the electronic and geometrical features of these potential activation sites are related to Au_6^- and to

 © 2003 Wiley-VCH Verlag GmbH & Co. KGaA, Weinheim

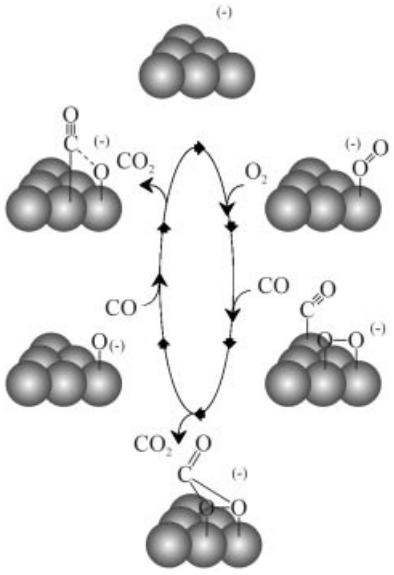

Figure 20. Schematic illustration of the formation of CO_2, catalyzed by Au_6^- in the gas phase

Au_{10} molecular clusters. However, this is probably not the case and several authors[93,88,99] provide evidence that, while CO is activated by its end-on coordination to the nanocluster surface, O_2 is activated by a combined action of the Au^0 nanoparticle surface and of the nanoparticle-support interface surface (Scheme 2).

$$CO + Au(0)/TiO_2 \text{ ---> } Au(0)(CO)/TiO_2$$

$$O_2 + Au(0)/TiO_2 \text{ ---> } Au(0)/TiO_2 \cdots O_2$$

$$CO + Au(0)/TiO_2 \cdots O_2 + Au(0)(CO)/TiO_2 \text{ ---> } CO_2 + Au(II)(CO)(O)/TiO_2 \cdots Au(0)/TiO_2$$

$$Au(II)(CO)(O)/TiO_2 \text{ ---> } CO_2 + Au(0)/TiO_2$$

Scheme 2. Reaction steps proposed for CO oxidation to CO_2 by Au^0/TiO_2

Apparently, this synergic mechanism makes Au^0/S catalysts uniquely active in CO oxidation to such an extent that Au^0/S is able to catalyse CO oxidation even more rapidly than H_2 oxidation.[107] This observation is a fundamental

Table 1. A selection of reactions relevant to chemical processing, catalyzed by supported gold(0)

Entry	Reaction	Catalyst	Remarks	Ref.
1	CH_2=CH-CH=CH_2 + H_2 → butenes	Au/S	gas phase, structure and support insensitive	[109]
2	CH_2=CH-C(O)H + H_2 → allyl alcohol	Au/ZrO_2	gas phase, structure sensitive	[110]
3	R-OH $\xrightarrow{air}$ R-C(O)H	Au/SiO_2	gas phase	[111]
4	R-OH, MeCO, Ph-CH_3 $\xrightarrow{air}$ catalytic combustion	Au/Fe_2O_3	gas phase	[112]
5	*o*-hydroxybenzyl alcohol $\xrightarrow{O_2}$ salicylic aldehyde	Au/Fe_2O_3	liquid phase, 50 °C, 1 atm, chemoselective	[113]
6	ethane-1,2-diol $\xrightarrow{O_2}$ glycolate	Au/C	liquid phase (H_2O), 70 °C, 2 atm	[114]
7	diols $\xrightarrow{O_2}$ hydroxymonocarboxylates β-amino alcohols $\xrightarrow{O_2}$ β-amino acids aliphatic aldehydes $\xrightarrow{O_2}$ carboxylic acids D-glucose $\xrightarrow{O_2}$ gluconic acid	Au/C or Au/TiO_2	liquid phase (H_2O), 70–85 °C, 1–3 atm	[103]
8	citral $\xrightarrow{H_2}$ geraniol + nerol	Au/Fe_2O_3	liquid phase, ethanol, 1 atm, 60 °C, chemoselective (95%) hydrogenation of C=O, 100% conversion	[115]
9	benzalacetone $\xrightarrow{H_2}$ phenyl-3-buten-2-ol	Au/Fe_2O_3	liquid phase, ethanol, 1 atm, 60 °C, chemoselective (60%) hydrogenation of C=O, 100% conversion	[116]
10	$H_2 + O_2 \rightarrow H_2O_2$	Au·Pd/Al_2O_3	liquid phase, methanol, 2 °C, 97 atm, chemoselective (50%)	[117]
11	aromatic amines $\xrightarrow[MeOH]{CO,\ O_2}$ carbamates	Au/resin	solvent-free, P_{CO} = 40 atm, P_{O2} = 40 atm, 175 °C. Good conversion and selectivity	[118]
12	propylene + O_2 → propylene oxide	Au/Ti-MCM48	gas phase, presently limited yields	[114]

 © 2003 Wiley-VCH Verlag GmbH & Co. KGaA, Weinheim

premise to the commercial development of fairly innovative dihydrogen-air PEM (Polymer Electrolyte Membrane) fuel cells for vehicle propulsion and auxiliary power units. In this context, CO-free dihydrogen has to be employed and various Au^0/S catalysts, in particular $Au^0/Al_2O_3/MgO/MnO$, are known to allow the removal of CO (ppm levels) from the dihydrogen stream that feeds the fuel cells at 60−100 °C (PROX reactor),[108] without a significant consumption of dihydrogen. The technical problem to be solved for a straight commercialization of PROX technology is the achievement of a suitable stability of the catalyst itself.

6.2.4 Gold(0)-Based Catalysis for Chemical Processing

Haruta's discovery, which was published in 1989, not only produced an explosion of interest for the catalytic chemistry of gold nanoparticles, mainly around the problem of CO and O_2 activation, but it also promoted a huge amount of research on a variety of possible applications of gold nanoparticles in pollution-control technologies and in chemical processing, i.e. in the potential industrial synthesis of commodities, semi-commodities, and fine and specialty chemicals.

A few recent examples of these valuable prospects are presented in Table 1.

It is apparent from Table 1 that the prospects for employing supported nano-sized-Au^0 in industrial catalysis are excellent, both in the gas and the liquid phase, with good prospects for using water as the solvent[103][114] in oxidation processes. The facile synthesis of H_2O_2 from O_2 and H_2 seems to be one of the major listed results that allow us to imagine the achievement of small-scale industrial facilities for the production of hydrogen peroxide.

6.2.5 Ongoing and Future Applications of Gold(0)-Based Catalysis

This topic is presented and discussed in references 93, 96, 99 and 119.

A peculiar current application is provided by Au^0 deposited on Fe_2O_3, supported on a zeolite wash-coated honeycomb. This sophisticated setup catalyses effectively the oxidative decomposition of bad smelling alkylamines (with a minimal production of N_2O) that are responsible for the unpleasant atmosphere in toilets ("odour eaters").[99]

Au^0/La_2O_3, integrated with Pd/SnO_2 and Ir/La_2O_3 is likely to become employed as a catalyst for the oxidative decomposition of dioxins coming from incinerator outlet gases at temperatures below 473 K.[99]

The long-awaited direct epoxidation of propylene is expected to become an Au^0-catalyzed synthetic technology once the yield in propylene oxide has been improved to ca. 10% and this goal seems to be feasible on Au^0/Ti-MCM48.[99]

Composite films of Co_2O_3 nanocrystals (5−10 nm) are expected to form the basis for optical sensors able to simultaneously detect H_2 and CO at 1% levels.[93]

Au^0/S catalysts are likely to become key components of CO safety masks and of devices for the efficient removal of CO from contaminated atmospheres.[96,119]

Finally, a little-explored and quite promising sector of gold catalytic chemistry is the employment of Au^0/S catalysts in liquid-phase synthetic processes. The brilliant results obtained by a few research groups, even in water, (Table 1) are indeed promising, quite in line with the emerging view of "Green Chemistry".

"Although we are well past the beginning of the discovery of gold's catalytic potential, the best may be yet to come, and a golden future lies ahead" (G. C. Bond, 2002).[81]

Conclusions

Nanoparticulated gold has turned out to play an important role in various fields of nanoscience. Besides their unique color, gold nanoparticles became of scientific and technological interest because of their stability to air which means that they can be used even in nanosized form for many applications. Well-expressed quantum-size effects have been observed for particles smaller than 2 nm even at room temperature, making these artificial atoms valuable candidates for future nanoelectronics once appropriate techniques allow the generation of artificial structures on surfaces. The first steps in this direction look very promising. The moderate chemical reactivity of gold atoms on particle surfaces allows them to act as catalysts for distinct reactions, for example oxidation reactions. Indeed, there are several catalytic reactions where gold nanoparticles act as highly efficient catalysts.

It can be assumed that the use of particulated gold will dramatically increase in the near future in very different fields. Gold quantum dots may act as single-electron switches and transistors, at the latest when silicon technology has reached its physical limits. Gold nanowires as conducting contacts in nanoelectronics will also contribute to the progress of nanotechnology. A renaissance in gold catalysis seems to have started. Gold nanoparticles in combination with biomolecules are already at a point where even commercial applications in medical diagnostics have become known.

Another developing field is sensorics where gold nanoparticles might play the most important role. Other applications, not yet to be foreseen, may come up and make the next decades a "golden age".

Acknowledgments

The Alexander von Humboldt Foundation is gratefully acknowledged for a Scholarship provided to one of us (B. C.) in 2002.

[1] M. T. Franklin, K. J. Klabunde, in *High Energy Process in Organometallic Chemistry* (Ed.: K. S. Suslik), *Am. Chem. Soc.,* Washington D. C., **1987**, pp 246−259.
[2] M. Faraday, *Phil. Trans. Roy. Soc.* **1857**, *147*, 145.

 © 2003 Wiley-VCH Verlag GmbH & Co. KGaA, Weinheim

[3] W. Ostwald, *Colloid-Zeitschrift* **1907**, *1*, 291.
[4] T. Castro, R. Reifenberger, E. Choi, R. P. Andres, *Phys. Rev. B* **1990**, *13*, 8548.
[5] G. L. Hornyak, M. Kröll, R. Pugin, Th. Sawitowski, G. Schmid, J.-O. Bovin, G. Karsson, H. Hofmeister, S. Hopfe, *Chem. Eur. J.* **1997**, *3*, 1951.
[6] *Optical Properties of Metal Clusters* (Eds.: U. Kreibig, M. Vollmer), Springer Series in Materials Science 25, Springer 1995.
[7] G. Mie, *Annal. Phys.* **1908**, *5*, 377.
[8] *Metal Vapour Synthesis* (Eds.: J. R. Blackborow, D. Young), Springer Verlag, New York 1979.
[9] J. S. Bradley, in *Clusters and Colloids. From Theory to Applications* (Ed.: G. Schmid), VCH, Weinheim 1994.
[10] A. Fojtik, A. Henglein, *Ber. Bunsen-Ges. Phys. Chem.* **1993**, *97*, 252.
[11] M. S. Sibbald, G. Chumanov, T. M. Cotton, *J. Phys. Chem.* **1996**, *100*, 4672.
[12] M. S. Yeh, Y. S. Yang, Y. P. Lee, H. F. Lee, Y. H. Yeh, C. S. Yeh, *J. Phys. Chem. B* **1999**, *103*, 6851.
[13] F. Mafuné, J. Kohno, Y. Takeda, H. J. Sawabe, *J. Phys. Chem. B* **2000**, *104*, 8333.
[14] F. Mafuné, J. Kohno, Y. Takeda, T. Kondow, H. J. Sawabe, *J. Phys. Chem. B* **2000**, *104*, 9111.
[15] H. Eckstein, U. Kreibig, *Z. Phys. D* **1993**, *26*, 239.
[16] Y. Niidome, A. Hori, T. Sato, S. Yamada, *Chem. Lett.* **2000**, 310.
[17] P. V. Kamat, M. Flumiani, G. W. Hartland, *J. Phys. Chem. B* **1998**, *102*, 3123.
[18] H. Kurita, A. Takami, S. Koda, *Appl. Phys. Lett.* **1998**, *72*, 789.
[19] A. Takami, H. Kurita, S. Koda, *J. Phys. Chem. B* **1999**, *103*, 1226.
[20] F. Mafuné, J. Kohno, Y. Takeda, T. Kondow, *J. Phys. Chem. B* **2001**, *105*, 9050.
[21] F. Mafuné, J. Kohno, Y. Takeda, T. Kondow, *J. Phys. Chem. B* **2002**, *106*, 7575.
[22] S. Stoeva, K. J. Klabunde, Ch. M. Sorensen, I. Dragieva, *J. Am. Chem. Soc.* **2002**, *124*, 2305.
[23] K. J. Klabunde, P. L. Timms, P. S. Skell, S. Ittel, *Inorg. Synth.* **1979**, *19*, 59.
[24] J. Turkevitch, P. C. Stevenson, J. Hillier, *Discuss. Faraday Soc.* **1951**, *11*, 55.
[25] A. Henglein, M. Giersig, *J. Phys. Chem. B* **1999**, *103*, 9533.
[26] S. Link, Z. L. Wang, M. A. El-Sayed, *J. Phys. Chem. B* **1999**, *103*, 3529.
[27] G. Schmid, A. Lehnert, *Angew. Chem. Int. Ed. Engl.* **1989**, *28*, 780.
[28] *Clusters and Colloids. From Theory to Applications* (Ed.: G. Schmid), VCH, Weinheim 1994.
[29] G. Schmid, R. Boese, R. Pfeil, F. Bandermann, S. Meyer, G. H. M. Calis, J. W. A. van der Velden, *Chem. Ber.* **1981**, *114*, 3634.
[30] G. Schmid, *Inorg. Synth.* **1990**, *7*, 214.
[31] G. Schmid, N. Klein, L. Korste, U. Kreibig, D. Schönauer, *Polyhedron* **1988**, *7*, 605.
[32] L. O. Brown, J. E. Hutchison, *J. Am. Soc., Chem.* **1997**, *119*, 12384.
[33] M. G. Warner, S. M. Reed, J. E. Hutchison, *Chem. Mater.* **2000**, *12*, 3316.
[34] G. Schmid, R. Pugin, W. Meyer-Zaika, U. Simon, *Eur. J. Inorg. Chem.* **1999**, 2051.
[35] G. Schmid, R. Pugin, J.-O. Malm, J.-O. Bovin, *Eur. J. Inorg. Chem.* **1998**, 813.
[36] M. Brust, A. Walker, D. Bethell, D. J. Schiffrin, R. Whyman, *J. Chem. Soc., Chem. Commun.* **1994**, 801.
[37] M. J. Hostetler, J. E. Wingate, C. J. Zhong, J. E. Harris, R. W. Vachet, M. R. Clark, J. D. Londono, S. J. Green, J. J. Stokes, G. D. Wignale, G. L. Glish, M. D. Porter, N. D. Evans, R. W. Murray, *Langmuir* **1998**, *14*, 17.
[38] N. R. Jana, L. Gearheart, C. J. Murphy, *Langmuir* **2001**, *17*, 6782.
[39] S. Chen, K. Kimura, *Langmuir* **1999**, *15*, 1075.
[40] K. Akamatsu, J. Hasegawa, H. Nawafune, H. Katayama, F. Ozawa, *J. Mater. Chem.* **2002**, *12*, 2862.
[41] J. P. Spatz, S. Mößmer, M. Möller, *Chem. Eur. J.* **1996**, *12*, 1552.
[42] J. P. Spatz, A. Roescher, M. Möller, *Adv. Mater.* **1996**, *8*, 337.
[43] M. Möller, J. P. Spatz, A. Roescher, S. Mößmer, S. T. Selvan, H.-A. Klok, *Macromol. Symp.* **1997**, *117*, 207.
[44] J. P. Spatz, A. Roescher, M. Möller, *Polymer Preprints, Am. Chem. Soc.* **1996**, *36*, 409.
[45] M. Möller, J. P. Spatz, *Curr. Opin. Colloid Interface Sci.* **1997**, *2*, 177.
[46] J. W. Slot, H. J. Geuze, *Eur. J. Cell Biol.* **1985**, *38*, 87.
[47] H. Mühlpfort, *Experimenta* **1982**, *38*, 1127.
[48] P. Mukherjee, A. Ahmad, D. Mandal, S. Senapati, S. R. Sainkar, M. I. Khan, R. Ramans, R. Parisaka, P. V. Ajayakumar, M. Alam, M. Sastry, R. Kumar, *Angew. Chem. Int. Ed.* **2001**, *40*, 3585.
[49] G. Schmid, A. Lehnert, J.-O. Malm, J.-O. Bovin, *Angew. Chem.* **1991**, *103*, 852; *Angew. Chem. Int. Ed. Engl.* **1991**, *30*, 874.
[50] Ch. J. Baddeley, D. A. Jefferson, R. M. Lambert, R. M. Ormerod, T. Rayment, G. Schmid, A. P. Walker, *Mat. Res. Soc., Symp. Proc.* Vol. 272, 1992 Materials Research Society.
[51] G. Schmid, R. Pugin, Th. Sawitowski, U. Simon, B. Marler, *Chem. Commun.* **1999**, 1303.
[52] M. C. Fairbanks, R. E. Benfield, R. J. Newport, G. Schmid, *Solid State Commun.* **1990**, *73*, 431.
[53] P. D. Cluskey, R. J. Newport, R. E. Benfield, S. J. Gurmann, G. Schmid, *Z. Phys. D* **1993**, *26*, 8.
[54] R. C. Thiel, R. E. Benfield, R. Zanoni, H. H. A. Smit, M. W. Dirken, *Z. Phys. D* **1993**, *81*, 1.
[55] H. H. A. Smit, R. C. Thiel, L. J. de Jongh, *Z. Phys. D* **1989**, *12*, 193.
[56] J. W. A. van der Velden, F. A. Vollenbroek, J. J. Bour, P. I. Beurskens, J. M. M. Smits, W. P. Bosman, *Recl.: J. R. Neth. Chem. Soc.* **1981**, *100*, 148.
[57] C. E. Briant, B. R. C. Theobald, J. W. White, C. K. Bell, D. M. P. Mingos, *J. Chem. Soc., Chem. Commun.* **1981**, 201.
[58] B. K. Teo, X. Shi, H. Zhang, *J. Am. Chem. Soc.* **1992**, *114*, 2743.
[59] T. Sawitowski, Y. Miquel, A. Heilmann, G. Schmid, *Adv. Funct. Mater.* **2001**, *11*, 435.
[60] G. L. Hornyak, M. Kröll, R. Pugin, Th. Sawitowski, G. Schmid, J.-O. Bovin, G. Karsson, H. Hofmeister, S. Hopfe, *Chem. Eur. J.* **1997**, *3*, 1951.
[61] *Optical Properties of Metal Clusters* (Eds.: U. Kreibig, M. Vollmer), Springer, Berlin 1995.
[62] D. Schönauer, M. Quinten, U. Kreibig, *Z. Phys. D* **1989**, *12*, 527.
[63] M. Quinten, U. Kreibig, *Appl. Opt.* **1993**, *32*, 6173.
[64] M. Herrmann, U. Kreibig, G. Schmid, *Z. Phys. D* **1993**, *26*, 1.
[65] B. A. Smith, J. Z. Zhang, U. Giebel, G. Schmid, *Chem. Phys. Lett.* **1997**, *270*, 139.
[66] A. Bezryadin, C. Dekker, G. Schmid, *Appl. Phys. Lett.* **1997**, *71*, 1273.
[67] L. F. Chi, M. Hartig, T. Drechsler, Th. Schwaack, C. Seidel, H. Fuchs, G. Schmid, *Appl. Phys. A* **1998**, *66*, 187.
[68] H. Zhang, G. Schmid, U. Hartmann, *Nano Lett.* **2003**, *3*, 305.
[69] V. Torma, O. Vidoni, U. Simon, G. Schmid, *Eur. J. Inorg. Chem.* **2003**, 1121.
[70] G. Schmid, M. Bäumle, N. Beyer, *Angew. Chem.* **2000**, *112*, 187−189; *Angew. Chem. Int. Ed.* **2000**, *39*, 181.
[71] G. Schmid, N. Beyer, *Eur. J. Inorg. Chem.* **2000**, 835.
[72] Th. Sawitowski, St. Franzka, N. Beyer, M. Levering, G. Schmid, *Adv. Funct. Mater.* **2001**, *11*, 169.
[73] V. Torma, T. Reuter, O. Vidoni, M. Schumann, C. Radehaus, G. Schmid, *ChemPhysChem.* **2001**, *8/9*, 546.
[74] S. Liou, R. Maoz, G. Schmid, J. Sagiv, *Nano Lett.* **2002**, *2*, 1055.
[75] G. Schmid, "The Way to Large Clusters", *Struct. Bonding* **1985**, *62*, 51.

 © 2003 Wiley-VCH Verlag GmbH & Co. KGaA, Weinheim

[76] G. Schmid, W. Meyer-Zaika, R. Pugin, T. Sawitowski, J.-P. Majoral, A.-M. Caminade, C.-O. Turrin, *Chem. Eur. J.* **2000**, *6*, 1693.
[77] H.-G. Boyen, G. Kästle, F. Weigl, B. Koslowski, C. Dietrich, P. Ziemann, J. P. Spatz, S. Riethmüller, C. Hartmann, M. Möller, G. Schmid, M. G. Garnier, P. Oelhafen, *Science* **2002**, *297*, 1533.
[78] *Chem. Eng. News* **2002**, *80*, p. 29.
[79] *Catalyst Handbook* (Ed.: M. V. Twigg), Manson, 1996.
[80] G. C. Bond, D. T. Thomson, *Catal. Rev. Sci. Eng.* **1999**, *41*, 319.
[81] G. C. Bond, *Catal. Today* **2002**, *72*, 5.
[82] W. A. Bone, R. V. Wheeler, *Trans. Royal Chem. Soc., A* **1906**, *206*, 1.
[83] G. C. Bond, *Gold Bull.* **1971**, *5*, 11.
[84] G. C. Bond, P. A. Sermon, *Gold Bull.* **1973**, *6*, 102.
[85] S. Galvagno, G. Parravano, *J. Catal.* **1978**, *55*, 178.
[86] D. McIntosh, G. A. Ozin, *Inorg. Chem.* **1976**, *15*, 2689.
[87] D. McIntosh, G. A. Ozin, *Inorg. Chem.* **1977**, *16*, 51.
[88] T. V. Choudary, D. W. Goodman, *Top. Catal.* **2002**, *21*, 25.
[89] M. Haruta, N. Yamada, T. Kobayashi, S. Lijima, *J. Catal.* **1989**, *115*, 301.
[90] M. Haruta, S. Tsuboda, T. Kobayashi, H. Kagehiama, M. J. Genet, B. Delmon, *J. Catal.* **1993**, *144*, 175.
[91] G. Schmid, *J. Chem. Soc., Dalton Trans.* **1998**, 1077.
[92] M. Valden, X. Lai, D. W. Goodman, *Science* **1998**, *281*, 1647.
[93] G. C. Bond, D. T. Thomson, *Gold Bull.* **2000**, *33*, 41.
[94] G. C. Bond, D. T. Thomson, *Catal. Rev.-Sci. Eng.* **1999**, *41*, 319.
[95] A. Wolf, F. Schüth, *Appl. Catal., A* **2002**, *226*, 1.
[96] M. Haruta, *Catal. Today* **1997**, *36*, 153.
[97] S. Schimpf, M. Lucas, C. Mohr, U. Rodemerk, A. Brückner, J. Radnik, H. Hofmeister, P. Claus, *Catal. Today* **2002**, *72*, 63.
[98] A. Zwijnenburg, M. Saleh, M. Makker, J. A. Moulijn, *Catal. Today* **2002**, *72*, 59.
[99] M. Haruta, *CATTECH* **2002**, *6*, 102.
[100] M. Daté, Y. Ichihashi, T. Yamashita, A. Chiorino, F. Boccuzzi, M. Haruta, *Catal. Today* **2002**, *72*, 89.
[101] T. Akita, P. Lu, S. Ichikawa, K. Tanaka, M. Haruta, *Surf. Interface Anal.* **2001**, *31*, 73.
[102] B. Corain, D. Ferrari, P. Centomo, S. Lora, W. Mayer-Zaika, G. Schmid, manuscript in preparation.
[103] F. Porta, L. Prati, M. Rossi, S. Coluccia, G. Martra, *Catal. Today* **2000**, *61*, 165.
[104] J.-D. Grunwaldt, C. Kiener, C. Wögerbauer, A. Baiker, *J. Catal.* **1999**, *181*, 223.
[105] W. T. Wallace, R. L. Whetten, *J. Am. Chem. Soc.* **2002**, *124*, 7499.
[106] N. Lopez, J. K. Norskov, *J. Am. Chem. Soc.* **2002**, *124*, 11262.
[107] R. Grisel, K.-J. Westrate, A. Gluhoi, B. Niewenhuis, *Gold Bull.* **2002**, *35*, 39.
[108] M. Okumura, S. Nakamura, S. Tsubota, T. Nakamura, M. Azuma, *Catal. Lett.* **1998**, *51*, 53.
[109] M. Okumura, T. Akita, M. Haruta, *Catal. Today* **2002**, *74*, 265.
[110] C. Mohr, H. Hofmeister, P. Claus, *J. Catal.* **2003**, *213*, 86.
[111] S. Biella, M. Rossi, *Chem. Commun.* **2003**, 378.
[112] S. Minicò, S. Sciré, C. Crisafulli, R. Maggiore, S. Galvagno, *Appl. Catal., B* **2000**, *28*, 245.
[113] C. Milone, R. Ingoglia, G. Neri, A. Pistone, S. Galvagno, *Appl. Catal., A* **2001**, *211*, 251.
[114] S. Biella, G. L. Castiglioni, C. Fumagalli, L. Prati, M. Rossi, *Catal. Today* **2002**, *72*, 43.
[115] C. Milone, M. L. Tropeano, G. Gulino, G. Neri, R. Ingoglia, S. Galvagno, *Chem. Commun.* **2002**, 868.
[116] C. Milone, R. Ingoglia, M. L. Tropeano, G. Neri, G. Galvagno, *Chem. Commun.* **2003**, 868.
[117] P. Landon, P. J. Collier, A. J. Papworth, C. J. Kiely, G. J. Hutchings, *Chem. Commun.* **2002**, 2058.
[118] F. Shi, Y. Deng, *J. Catal.* **2002**, *211*, 548.
[119] C. W. Corti, R. J. Holliday, D. T. Thomson, *Gold Bull.* **2002**, *35*, 11.

Received April 3, 2003

 © 2003 Wiley-VCH Verlag GmbH & Co. KGaA, Weinheim

1,2-Bis-*N*-[2′-(diphenylphosphanyl)benzoyl]diaminobenzene, a New Chelating Ligand with Versatile Coordination Properties

Sylvain Burger,[a] Bruno Therrien,[a] and Georg Süss-Fink*[a]

Keywords: Palladium / Platinum / N,P ligands / Ligand design

1,2-Bis-*N*-[2′-(diphenylphosphanyl)benzoyl]diaminobenzene (dppbH; **1**) was prepared by peptidic coupling and shown to exist, in the solid state, in the form of hydrogen-bonded dimers by single-crystal X-ray structure analysis. As expected, **1** reacts with [MCl_2(cod)] (M = Pd, Pt; cod = cyclooctadiene) to form square-planar complexes. However, in the case of palladium [$PdCl_2$(dppbH)] (**2**) is obtained, while in the case of platinum [Pt(dppb)] (**3**) is formed. Thus, the nature of the metal induces a completely different coordination mode: In **2**, the dppbH ligand only coordinates through the two phosphorus atoms, while in **3** a dppb ligand, formed by deprotonation of the two amino functions in dppbH, coordinates through the two phosphorus atoms and through the two nitrogen atoms. The single-crystal X-ray analyses of the two square-planar complexes reveal **2** to contain the two phosphorus atoms in a *trans* coordination mode and **3** to contain the two phosphorus atoms in a *cis* coordination mode.

(© Wiley-VCH Verlag GmbH & Co. KGaA, 69451 Weinheim, Germany, 2003)

Introduction

The synthesis of new, highly active complexes for homogeneously catalyzed processes is a challenge in coordination chemistry. Square-planar complexes of Pd^{II} and, to a minor extent, Pt^{II} have long been recognized to play a central role in catalytic reactions such as the classical Wacker process[1] and, more recently, in the co-polymerization of carbon monoxide and olefins.[2] Pd^{II} and Pt^{II} complexes are used in organic synthesis reactions such as Diels−Alder cycloadditions,[3] Baeyer−Villiger oxidation of ketones,[4] hydrogenolysis[5] or Sonogashira cross-coupling.[6]

Electron-rich ligands have been used to increase the electron density at the metal center in order to facilitate the oxidative addition step in a catalytic cycle.[7] Phosphane ligands have been extensively studied because of their electron-donating power. Diphosphane ligands have received special attention because they form, in general, more-stable (chelate) complexes than monophosphane ligands under catalytic conditions.[8] In the co-polymerization of olefins with carbon monoxide, Dosset et al.[7] showed that the catalytic activity of diphosphanylpalladium(II) complexes of the type [$PdCl_2\{Ar_2P(CH_2)_nPAr_2\}$] ($n$ = 1−3) depends upon the length of the carbon chain and upon the nature of the aryl groups. The six-membered chelate (n = 3) is an order of magnitude more active than the five-membered analogue (n = 2), while the four-membered chelate (n = 1) is essentially inactive. Complexes containing an *ortho* substituent at the aryl groups have a higher catalytic potential than those with *para* and *meta* substituents. It has been suggested that mononuclear *trans* bidentate complexes are more stable with large metallacycles than with medium-size metallacycles due to the increased flexibility of the larger ring size.[9] In general, the stability of the *trans* monomer increases with increasing chain length and reaches a maximum for a metallacycle containing 15 ring members.[10]

Herein, we report the synthesis of a new diphosphane ligand containing an *ortho*-phenylene spacer group for the synthesis of *trans*-dicoordinate as well as *cis*-tetracoordinate square-planar palladium(II) and platinum(II) complexes.

Results and Discussion

2-(Diphenylphosphanyl)benzoic acid, easily available from Wurtz coupling of sodium 2-chlorobenzoate and sodium diphenylphosphide,[11] is an attractive building block for the synthesis of diphosphane ligands by condensation of the acid function with diols, diamines or amino alcohols.[12] Peptidic coupling between *ortho*-diaminobenzene and two equivalents of 2-(diphenylphosphanyl)benzoic acid affords

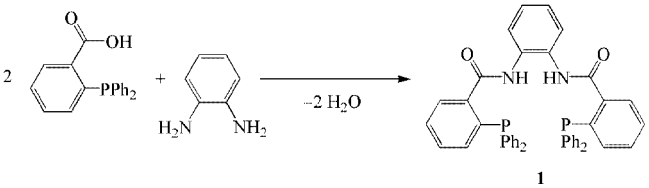

1

Scheme 1

[a] Institut de Chimie, Université de Neuchâtel
Case postale 2, CH-2007 Neuchâtel, Switzerland
Fax: (internat.) + 41-32/7182-511
E-mail: georg.suess-fink@unine.ch

1,2-bis-*N*-[2′-(diphenylphosphanyl)benzoyl]diaminobenzene (dppbH; **1**) as a microcrystalline powder in good yield (Scheme 1).

The diphosphane ligand **1** is symmetrical and shows only one resonance in the $^{31}P\{^1H\}$ NMR spectrum at $\delta = -8.83$ ppm. In the ^1H NMR spectrum, **1** gives rise to a singlet at $\delta = 8.63$ ppm (in $CDCl_3$) corresponding to the amido protons. The amido function is also easily identified in the IR spectrum by two absorptions at 3324 cm^{-1} (ν_{NH}) and 1640 cm^{-1} (ν_{CO}). The molecular structure of **1**, established by single-crystal X-ray structure analysis, is shown in Figure 1.

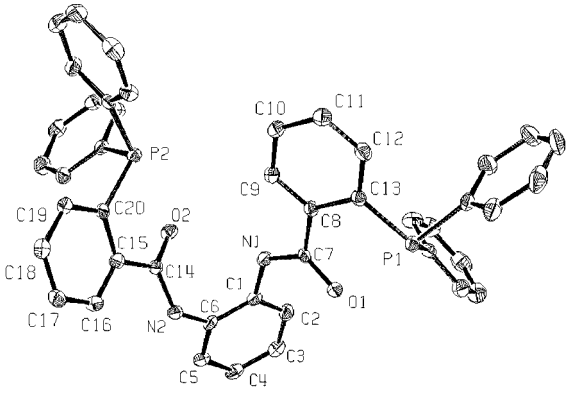

Figure 1. ORTEP view of **1**, displacement ellipsoids are drawn at the 50% probability level, hydrogen atoms are omitted for clarity; selected bond lengths (Å) and angles (°): C(7)−O(1) 1.237(3), C(14)−O(2) 1.235(3), C(7)−N(1) 1.348(4), C(14)−N(2) 1.355(4), C(13)−P(1) 1.847(3), C(20)−P(2) 1.853(3); O(1)−C(7)−N(1) 121.6(3), O(2)−C(14)−N(2) 121.8(3)

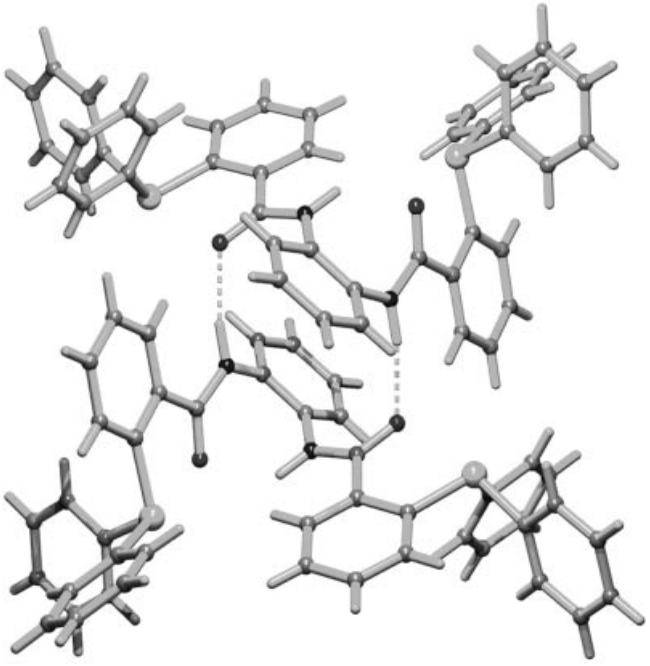

Figure 2. Dimeric structure of compound **1**

The crystal structure analysis reveals **1** to exist as a dimer in the solid state, thanks to hydrogen bonding between an NH and a CO function (see Figure 2). The N−O distance of the hydrogen bond [N(2)−H···O(1)] is 2.867(3) Å, with an N−H···O angle of 164.6°. The intramolecular distance between the two phosphorus atoms is 7.794(1) Å. In the crystal structure, there is no significant interaction between compound **1** and the dichloromethane molecule.

One equivalent of dppbH (**1**) reacts with $[MCl_2(cod)]$ (M = Pd, Pt; cod = cyclooctadiene) to afford the corresponding complexes $[PdCl_2(dppbH)]$ (**2**) and [Pt(dppb)] (**3**) in good yield (Scheme 2). The reaction was carried out in dilute solution to avoid the formation of di- or polynuclear species as observed for other diphosphane ligands.[13]

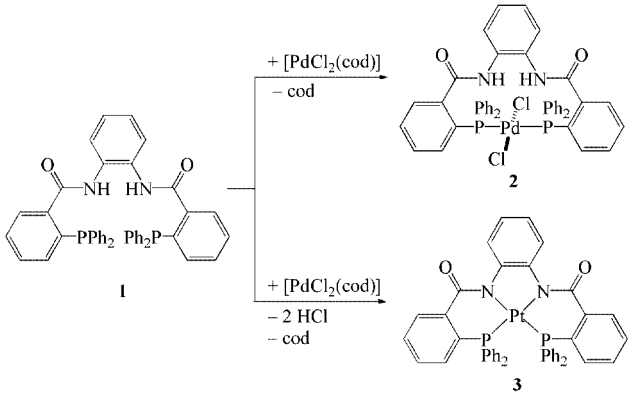

Scheme 2

$[PdCl_2(dppbH)]$ (**2**) gives only one singlet at $\delta = 24.03$ ppm in the $^{31}P\{^1H\}$ spectrum, which is indicative of the coordination of both phosphorus atoms to the metal. The mass spectrum is in accordance with the presence of a mononuclear species containing two chloride ligands. The IR spectrum shows two bands at 3324 (ν_{NH}) and 1640 cm^{-1} (ν_{CO}) assigned to the amido functions.

The molecular structure of **2** shows the palladium atom to be in a square-planar geometry, surrounded by two chlorines and two phosphorus atoms (Figure 3). The chelating diphosphane ligand adopts a *trans* coordination geometry. The Cl−Pd−Cl as well as the P−Pd−P axes are almost linear, the corresponding angles being 177.03(10)° and 178.40(9)°, respectively. The two Pd−Cl distances are equivalent [2.310(2) and 2.311(2) Å], but interestingly one Pd−P distance is slightly longer (by 0.042 Å) than the other one. There is no meaningful interaction in the apical position of the palladium atom, the shortest distance to another atom being 2.96 Å [Pd(1)−O(2)]. In the crystal structure, only one chloroform molecule interacts with complex **2**, forming a weak hydrogen bond with one of the chlorine atoms, the Cl(2)−C(1S) distance being 3.49(1) Å and the C(1S)−H···Cl(2) angle being 150.3(1)°.

The formation of **3** is best monitored by $^{31}P\{^1H\}$ spectroscopy, the complex showing a triplet centered at $\delta = 6.20$ ppm due to the coupling between the two equivalent phosphorus atoms and the platinum atom (coupling con-

 © 2003 Wiley-VCH Verlag GmbH & Co. KGaA, Weinheim

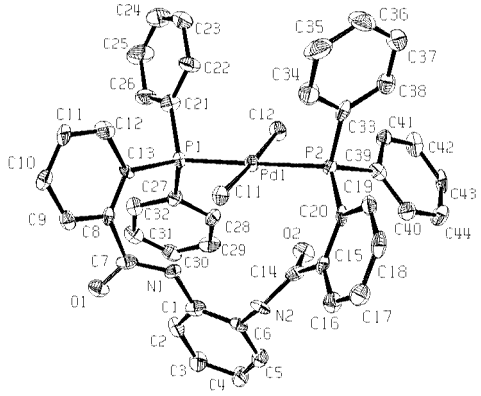

Figure 3. ORTEP view of complex **2**, displacement ellipsoids are drawn at the 50% probability level, hydrogen atoms and solvent molecules are omitted for clarity; selected bond lengths (Å) and angles (°): P(1)−Pd(1) 2.318(2), P(2)−Pd(1) 2.360(2), Cl(1)−Pd(1) 2.310(2), Cl(2)−Pd(1) 2.311(2), C(7)−O(1) 1.232(9), C(14)−O(2) 1.222(8), C(7)−N(1) 1.336(9), C(14)−N(2) 1.362(9), C(13)−P(1) 1.859(7), C(20)−P(2) 1.832(7); Cl(1)−Pd(1)−Cl(2) 177.03(10), Cl(1)−Pd(1)−P(1) 91.91(7), Cl(2)−Pd(1)−P(1) 86.27(8), Cl(1)−Pd(1)−P(2) 89.67(8), Cl(2)−Pd(1)−P(2) 92.17(8), P(1)−Pd(1)−P(2) 178.40(9), O(1)−C(7)−N(1) 123.2(7), O(2)−C(14)−N(2) 121.6(7)

stant 3120 Hz). IR spectroscopy shows that there is no ν_{NH} absorption (around 3300 cm^{-1}) any more, but a strong ν_{CO} band at 1602 cm^{-1} showing a strong bathochromic effect. It appears that the formation of **3** is accompanied by the loss of two equivalents of HCl. Unlike $[Pt\{Ph_2PC_6H_4NC(O)C_6H_4\}_2]$,[14] complex **3** does not give the dichloroplatinum complex $[PtCl_2(dppbH)]$ in the presence of HCl.

The molecular structure of **3** shows the platinum atom in a distorted square-planar geometry (Figure 4). Unlike in **2**, the chelating diphosphane ligand adopts a *cis* coordination geometry, with the two nitrogen atoms also coordinating to the metal. The formation of five- and six-membered chelate rings imposes a considerable distortion around the platinum atom. The N−Pt−P angles [83.47(16) and 89.71(16)°] are slightly acute due to the bidentate $PC_6H_4C(O)N$ units. The atoms Pt(1), P(1), P(2), N(1) and N(2) are almost coplanar, with an average deviation of 0.0674 Å; the metal lies out of the plane by 0.078(2) Å. In the crystal structure, there is no meaningful interaction between complex **3** and the chloroform molecule.

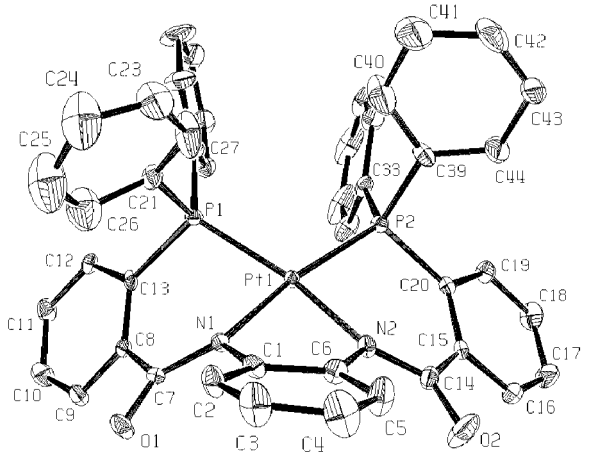

Figure 4. ORTEP view of complex **3**, displacement ellipsoids are drawn at the 35% probability level, hydrogen atoms and solvent molecules are omitted for clarity; selected bond lengths (Å) and angles (°): P(1)−Pt(1) 2.243(2), P(2)−Pt(1) 2.234(2), N(1)−Pt(1) 2.035(6), N(2)−Pt(1) 2.067(5), C(7)−O(1) 1.215(8), C(14)−O(2) 1.240(9), C(7)−N(1) 1.367(8), C(14)−N(2) 1.356(10), C(13)−P(1) 1.830(6), C(20)−P(2) 1.820(7); N(1)−Pt(1)−N(2) 80.3(2), N(1)−Pt(1)−P(1) 83.47(16), N(2)−Pt(1)−P(1) 161.74(18), N(1)−Pt(1)−P(2) 169.92(15), N(2)−Pt(1)−P(2) 89.71(16), P(1)−Pt(1)−P(2) 106.26(6), O(1)−C(7)−N(1) 125.2(6), O(2)−C(14)−N(2) 122.8(7)

The stability of complex **2** towards base attack and that of complex **3** towards acid attack has been studied in order to check the possibility of converting these *cis* or *trans* complexes into their corresponding deprotonated or protonated species. However, complex **2** is not deprotonated by an excess of triethylamine to give [Pd(dppb)], the $^{31}P\{^1H\}$ NMR signal of **2** being unchanged in $CDCl_3$ even after 24 hours in the presence of NEt_3 (100 equiv.). Likewise, complex **3** is not protonated by concentrated hydrochloric acid to give $[PtCl_2(dppbH)]$, the $^{31}P\{^1H\}$ NMR signal of **3** being unchanged in $CDCl_3$ even after 24 hours in the presence of HCl (100 equiv.).

Conclusion

We have synthesized a new diphosphane ligand, 1,2-bis-*N*-[2′-(diphenylphosphanyl)benzoyl]diaminobenzene (dppbH; **1**), which shows a different coordination pattern towards palladium(II) and platinum(II): it reacts with $[MCl_2(cod)]$ (M = Pd, Pt; cod = cyclooctadiene) to form the square-planar complexes $[PdCl_2(dppbH)]$ (**2**) and [Pt(dppb)] (**3**), respectively. In **2**, the dppbH ligand is coordinated by the two phosphorus atoms in a *trans* configuration, while in **3** the two phosphorus atoms are coordinated in a *cis* configuration, the two nitrogen atoms of the dppb ligand being coordinated as well.

Experimental Section

General Remarks: Dichloromethane was dried and distilled under nitrogen prior to use. All reactions were carried out under nitrogen, using standard Schlenk techniques. All other reagents were purchased (Aldrich, Fluka) and used as received. NMR spectra were recorded using a Varian Gemini 200BB instrument and referenced to the signals of the residual protons in the deuterated solvents. Electrospray mass spectra were obtained in positive-ion mode with an LCQ Finnigan mass spectrometer. IR spectra were recorded with a Perkin−Elmer Spectrum One FTIR spectrometer. Microanalyses were carried out by the Laboratory of Pharmaceutical Chemistry, University of Geneva, Switzerland.

Preparation of 1,2-Bis-*N*-[2′-(diphenylphosphanyl)benzoyl]diaminobenzene (dppbH; 1): A solution of 2-diphenylphosphanylbenzoic acid (1.0 g, 3.26 mmol), *N*,*N*-dicyclohexylcarbodiimide (2.7 g, 13.05 mmol), 4-(dimethylamino)pyridine (100 mg, 0.82 mmol), 4-pyrrolidinopyridine (100 mg, 0.68 mmol), and 1,2-diaminobenzene (175 mg, 1.62 mmol) in CH_2Cl_2 (40 mL) was allowed to stand at

 © 2003 Wiley-VCH Verlag GmbH & Co. KGaA, Weinheim

room temperature under nitrogen, until the esterification was complete. The resulting solution was concentrated and filtered three times to remove *N*,*N*-dicyclohexyl urea. The filtrate was then concentrated under reduced pressure. The residue was submitted to column chromatography on silica, eluting with hexane/acetone (3:1). The product was isolated from the third fraction by the evaporation of the solvent, giving **1** (550 mg, 0.81 mmol; 50%) as a white solid. ^{1}H NMR (200 MHz, $CDCl_3$): δ = 8.63 (s, 2 H, NH), 7.5−6.9 (m, 32 H, ArH) ppm. ^{13}C{^{1}H} NMR (50 MHz, $CDCl_3$): δ = 168.12, 143.45, 141.20, 141.00, 140.50, 137.62, 137.39, 134.62, 133.90, 130.84, 129.68, 128.94, 128.80, 128.65 ppm. ^{31}P{^{1}H} NMR (81 MHz, $CDCl_3$): δ = −8.83 ppm. IR (KBr): $\tilde{\nu}$ = 3324 m (N−H amide), 1640 s (C=O amide) cm^{-1}. ESI-MS: *m*/*z* = 685 [M + H$^+$]. $C_{44}H_{34}N_2O_2P_2$ (684.21): calcd. C 77.2, H 5.0, N 4.1; found C 76.8, H 4.8, N 4.3.

Preparation of [PdCl$_2$(dppbH)] (2): A solution of [$PdCl_2$(cod)] (42 mg, 0.15 mmol) and **1** (100 mg, 0.15 mmol) in CH_2Cl_2 (20 mL) was allowed to stand for 3 hours at room temperature and then filtered. The filtrate was concentrated under reduced pressure. The residue was submitted to column chromatography on silica, eluting with dichloromethane/ethanol (4:1). The product was isolated from the first fraction by the evaporation of the solvent, giving **2** (95 mg, 0.11 mmol; 79%) as a yellow-orange solid. 1H NMR (200 MHz, $CDCl_3$): δ = 8.66 (s, 2 H, NH), 8.1−6.9 (m, 32 H, ArH) ppm. ^{31}P{^{1}H} NMR (81 MHz, $CDCl_3$); δ = 24.03 ppm. IR (KBr): $\tilde{\nu}$ = 3302 m (N−H amide), 1662 s (C=O amide) cm^{-1}. ESI-MS: *m*/*z* = 885 [M + Na$^+$]. $C_{44}H_{34}Cl_2N_2O_2P_2Pd$ (861.51): calcd. C 61.3, H 4.0, N 3.3; found C 61.1, H 4.1, N 3.2.

Preparation of [Pt(dppb)] (3): A solution of [$PtCl_2$(cod)] (55 mg, 0.15 mmol) and **1** (100 mg, 0.15 mmol) in CH_2Cl_2 (20 mL) was allowed to stand for two hours at room temperature and then filtered. The filtrate was concentrated under reduced pressure. The residue was submitted to column chromatography on silica, eluting with dichloromethane/ethanol (3:1). The product was isolated from the first fraction by the evaporation of the solvent, giving **3** (80 mg, 0.09 mmol; 61%) as a yellow-green solid. ^{1}H NMR (200 MHz, $CDCl_3$): δ = 7.9−6.7 (m, 32 H, ArH) ppm. ^{31}P{^{1}H} NMR (81 MHz, $CDCl_3$); δ = 6.20 (t, $^1J_{Pt,P}$ = 3120 Hz) ppm. IR (KBr): $\tilde{\nu}$ = 1602 s (C=O amide) cm^{-1}. ESI-MS: *m*/*z* = 878 [M + H$^+$], 900 [M + Na$^+$]. $C_{44}H_{32}N_2O_2P_2Pt$ (877.28): calcd. C 60.2, H 3.7, N 3.2; found C 60.0, H 3.6, N 3.4.

X-ray Crystallographic Study

1·CH$_2$Cl$_2$: $C_{45}H_{36}Cl_2N_2O_2P_2$, *M* = 769.60 g·mol^{-1}, triclinic, *P*$\bar{1}$ (no. 2), *a* = 9.2473(8), *b* = 14.0068(14), *c* = 14.5320(16) Å, α = 89.904(12), β = 89.630(12), γ = 89.693(11)°, *U* = 1882.2(3) Å^3, *T* = 153 K, *Z* = 2, μ(Mo-K_α) = 0.300 mm^{-1}, 12481 reflections measured, 6853 unique (R_{int} = 0.0607) which were used in all calculations. The final *wR* (F^2) was 0.1126 (all data).

2·2CHCl$_3$: $C_{46}H_{36}Cl_8N_2O_2P_2Pd$, *M* = 1100.71 g·mol^{-1}, triclinic, *P*$\bar{1}$ (no. 2), *a* = 9.9013(11), *b* = 15.1734(18), *c* = 16.7870(18) Å, α = 78.059(14), β = 76.629(13), γ = 78.630(14)°, *U* = 2370.8(5) Å^3, *T* = 153 K, *Z* = 2, μ(Mo-K_α) = 0.950 mm^{-1}, 17568 reflections measured, 8657 unique (R_{int} = 0.1286) which were used in all calculations. The final *wR*(F^2) was 0.1015 (all data).

3·CHCl$_3$: $C_{45}H_{33}Cl_3N_2O_2P_2Pt$, *M* = 997.11 g·mol^{-1}, monoclinic, $P2_1/n$ (no. 14), *a* = 12.0140(17), *b* = 11.259(3), *c* = 28.720(4) Å, β = 95.026(16)°, *U* = 3870.0(13) Å^3, *T* = 153 K, *Z* = 4, μ(Mo-K_α) = 3.958 mm^{-1}, 20851 reflections measured, 7307 unique (R_{int} = 0.0544) which were used in all calculations. The final *wR*(F^2) was 0.0984 (all data).

The data were measured using a Stoe Image Plate Diffraction system equipped with a φ circle, using Mo-K_α graphite-monochromated radiation (λ = 0.71073 Å) with φ range 0−200°, increment of 1.5, 1.4 and 0.8° respectively, 2θ range from 2.0−26°, $D_{max}-D_{min}$ = 12.45−0.81 Å. The structures were solved by direct methods using the program SHELXS-97.[15] The refinement and all further calculations were carried out using SHELXL-97.[16] The H-atoms were included in calculated positions and treated as riding atoms using the SHELXL default parameters. The non-H atoms were refined anisotropically, using weighted full-matrix least-square on F^2. Figures were drawn with ORTEP.[17]

CCDC-212037 (**1**), -212039 (**2**), and -212038 (**3**) contain the supplementary crystallographic data for this paper. These data can be obtained free of charge at www.ccdc.cam.ac.uk/conts/retrieving.html [or from the Cambridge Crystallographic Data Centre, 12, Union Road, Cambridge CB2 1EZ, UK; Fax: (internat.) +44-1223/336-033; E-mail: deposit@ccdc.cam.ac.uk].

Acknowledgments

This work is supported by the Swiss National Science Foundation (grant no. 20−61227−00). We thank Professor H. Stoeckli-Evans for free access to X-ray facilities.

[1] [1a] G. W. Parshall, S. D. Ittel, *Homogeneous Catalysis*, 2nd ed.; Wiley-Interscience: New York, 1992; Chapter 6, p 137. [1b] R. A. Sheldon, J. K. Kochi, *Metal Catalyzed Oxidations of Organic Compounds*; Academic Press: New York, 1981.
[2] [2a] E. Drent, J. A. M. van Broekhoven, P. H. M. Budzelaar, in *Applied Homogeneous Catalysis with Organometallic Compounds* (Eds.: B. Cornils, W. A. Herrmann), VCH: Weinheim, 1997; Vol. 1, Chapter 2.3.4, p 233. [2b]E. Drent, P. H. M. Budzelaar, *Chem. Rev.* **1996**, *96*, 663−681. [2c] A. Sen, *Acc. Chem. Res.* **1993**, *26*, 303−310. [2d] E. Drent, Eur. Patent Appl. 251373, 1987, and references cited therein.
[3] K. Pignat, J. Vallotto, F. Pinna, G. Strukul, *Organometallics* **2000**, *19*, 5160−5167.
[4] R. Gavagnin, M. Cataldo, F. Pinna, G. Strukul, *Organometallics* **1998**, *17*, 661−667.
[5] B. L. Edelbach, D. A. Vicic, R. J. Lachicotte, W. D. Jones, *Organometallics* **1998**, *17*, 4784−4794.
[6] [6a] K. Sonogashira, Y. Tohda, N. Hagihara, *Tetraedron Lett.* **1975**, 4467−4470. [6b] S. Takahashi, Y. Kuroyama, K. Sonogashira, N. Hagihara, *Synthesis* **1980**, 627−630. [6c] E. T. Sabourin, A. Onopchenko, *J. Org. Chem.* **1983**, *48*, 5135−5137. [6d] S. J. Haven, P. M. Hergenrother, *J. Org. Chem.* **1985**, *50*, 1763−1765. [6e] S. L. Schreiber, L. L. Kiessling, *J. Am. Chem. Soc.* **1988**, *110*, 631−633. [6f] J. L. Mascarenas, L. A. Sarandeses, L. Castedo, A. Mourino, *Tetrahedron* **1991**, *47*, 3485−3498. [6g] M. L. Curtin, W. H. Okamura, *J. Am. Chem. Soc.* **1991**, *113*, 6958−6966.
[7] S. J. Dosset, A. Gillon, A. G. Orpen, J. S. Fleming, P. G. Pringle, D. F. Wass, M. D. Jones, *Chem. Commun.* **2001**, 699−700.
[8] C. M. Thomas, R. Mafua, B. Therrien, E. Rusanov, H. Stoeckli-Evans, G. Süss-Fink, *Chem. Eur. J.* **2002**, *8*, 3343−3352.
[9] A. J. Pryde, B. L. Shaw, B. J. Weeks, *J. Chem. Soc., Chem. Commun.* **1973**, 947−948.
[10] W. E. Hill, D. M. A. Minahan, J. G. Taylor, C. A. McAuliffe, *J. Am. Chem. Soc.* **1982**, *104*, 6001−6005.
[11] J. E. Hoots, T. B. Rauchfuss, D. A. Wrobleski, *Inorg. Synth.* **1982**, *21*, 178−179.
[12] [12a] B. M. Trost, D. L. Van Vranken, *Angew. Chem.* **1992**, *104*, 194−196; *Angew. Chem. Int. Ed. Engl.* **1992**, *31*, 228−230. [12b] A. Hassner, L. Krepski, V. Alexanian, *Tetrahedron* **1978**, *34*, 2069−2076. [12c] A. Hassner, V. Alexanian, *Tetrahedron Lett.* **1978**, *19*, 4475−4478. [12d] E. F. V. Scriven, *Chem. Soc. Rev.*

1983, *12*, 129−161. [12e] C. M. Thomas, A. Neels, H. Stoeckli-Evans, G. Süss-Fink, *Eur. J. Inorg. Chem.* **2001**, *12*, 3005−3008.
[13] A. R. Sanger, K. G. Tan, *Inorg. Chim. Acta* **1978**, *31*, L439−L440.
[14] D. Hedden, D. M. Roundhill, W. C. Fultz, A. L. Rheingold, *Organometallics* **1986**, *5*, 336−343.
[15] G. M. Sheldrick, *Acta Crystallogr., Sect. A* **1990**, *46*, 467−473.
[16] G. M. Sheldrick, SHELXL-97. Univ. of Göttingen, Göttingen, Germany, 1999.
[17] L. J. Farrugia, *J. Appl. Cryst.* **1997**, *30*, 565.

Received June 10, 2003

 © 2003 Wiley-VCH Verlag GmbH & Co. KGaA, Weinheim

The Substitution Reaction of (Chloro)bis(tetraisopropylcyclopentadienyl) Complexes of La, Pr, or Nd with Silylamides

Oliver Schmitt,[a] Gotthelf Wolmershäuser,[a] and Helmut Sitzmann*[a]

Keywords: Lanthanides / Cyclopentadienyl ligands / N ligands / Si ligands

The dimeric complexes $[\{(C_5HR_4)_2Ln(\mu\text{-}Cl)(\mu_3\text{-}Cl)Na(OEt_2)\}_2]$ (**1**) (R = $CHMe_2$, Ln = La, Pr, Nd) eliminate sodium chloride in toluene solution to form the (chloro)bis(cyclopentadienyl) complexes $[(C_5HR_4)_2LnCl]$ (**2**). Crystalline **2**-Nd contains monomeric molecules exhibiting two intramolecular Nd···CH_3 interactions (Nd···C = 3.32 Å) with ring substituents. Reaction of complexes **1** with bis(trimethylsilyl)amides furnishes the tetranuclear complexes $[\{(C_5HR_4)_2Ln(\mu\text{-}Cl)\}_2\{NaN(SiMe_3)_2\}_2]$ (**3**) (R = $CHMe_2$, Ln = La, Pr, Nd), which have been characterized by X-ray crystal structure analyses. In solution the La_2Na_2 complex **3**-La eliminates NaC_5HR_4 (R = $CHMe_2$) to form a mixture of **2**-La and $[(C_5HR_4)La\{N(SiMe_3)_2\}_2]$ (**4**). With less a bulky bis(dimethylsilyl)amide **1**-La yields the substitution product $[(C_5HR_4)_2LaN(SiHMe_2)_2]$ (**5**) (R = $CHMe_2$).

(© Wiley-VCH Verlag GmbH & Co. KGaA, 69451 Weinheim, Germany, 2003)

Introduction

Organometallic complexes of the early lanthanides still present a challenge because of the large ionic radii of these elements.[1] The intriguing catalytic properties of cyclopentadienyl complexes of the lanthanides in a variety of C−C, C−H, or C−N bond-formation reactions[2] warrant an investigation of the impact of extremely bulky alkylcyclopentadienyl ligands on these big cations.

The tetraisopropylcyclopentadienyl ligand[3] should be bulky enough to solve problems related to donor solvent or alkali metal salt coordination even for the early lanthanides. We therefore synthesized (chloro)bis(tetraisopropylcyclopentadienyl) complexes of lanthanum, neodymium,[4] and praseodymium (this work) as starting compounds for nucleophilic substitution.

In this paper we report on the behavior of these chloro complexes in nonpolar solvents like toluene, and their reactions with $NaN(SiMe_3)_2$, $KN(SiMe_3)_2$, and $KN(SiHMe_2)_2$.

Results and Discussion

In toluene solution the (chloro)bis(tetraisopropylcyclopentadienyl)lanthanum, -praseodymium, or -neodymium sodium chloride complex $[\{(C_5HR_4)_2Ln(\mu\text{-}Cl)(\mu_3\text{-}Cl)Na(OEt_2)\}_2]$ (**1**) (R = $CHMe_2$; Ln = La, Pr, Nd: **1**-La, **1**-Pr, **1**-Nd) (Scheme 1) eliminates sodium chloride with formation of monomeric $[(C_5HR_4)_2LnCl]$ (**2**: Ln = La, Nd; R = $CHMe_2$). **2**-Nd is the first crystallographically characterized example of a solvent-free, monomeric bis(cyclopentadienyl) halo complex of the lanthanides.

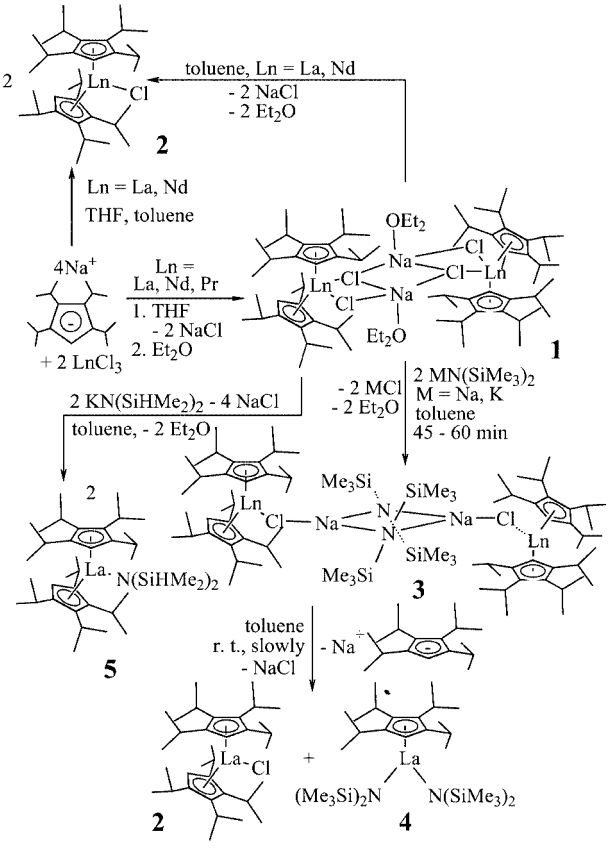

Scheme 1. Synthesis of complexes **1**−**5**

[a] FB Chemie der Universität Kaiserslautern,
Erwin-Schrödinger-Str., 67663 Kaiserslautern
Fax: (internat.) + 49-(0)631/205-4676
E-mail: sitzmann@chemie.uni-kl.de

The crystal structure of **2**-Nd (Figure 1, Table 1) shows Nd−C distances within a narrow range from 2.71 to 2.81 Å and an angle of 133.6° between the two ring planes. Two contacts to methyl groups of the ring substituents (C12 and its symmetry-equivalent atom are at an Nd···C distance of 3.32 Å) stabilize the unusually low coordination number of the central atom. The angle C12−Nd−C12′ is 179° and forms a T-shaped arrangement with the Nd−Cl vector located on the crystallographic C_2 axis. Three out of four isopropyl α-carbon atoms are bent out of the ring plane away from the metal center by 0.1−0.3 Å, but the α-carbon atom C11 carrying the methyl C12 atom is bent towards the central atom by 0.02 Å. The isopropyl substituent at C1 of the cyclopentadienyl ring seems to adopt the role of a side chain capable of an additional stabilizing interaction. The tetraisopropylcyclopentadienyl ring in **2**-Nd thus resembles the donor-functionalized cyclopentadienyl ligands in monomeric [(2-methoxyethyl-1-indenyl)$_2$NdCl][5] or [(Me$_2$NCH$_2$CH$_2$C$_5$H$_4$)$_2$NdCl].[6] Similar intramolecular Ln···CH$_3$ interactions have been found for 1,1′,3,3′-tetra(*tert*-butyl)ytterbocene.[7]

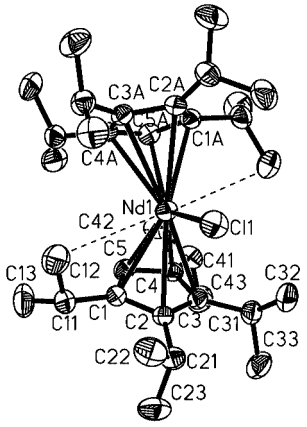

Figure 1. Crystal structure of **2**-Nd; selected bond lengths [Å] and angles [°]: Nd1−Cl1 2.713(1), Nd1−C1 2.724(4), Nd1−C2 2.801(4), Nd1−C3 2.811(4), Nd1−C4 2.782(4), Nd1−C5 2.709(4), Nd1···C12 3.318, Nd1−Cp$_{cent.}$ 2.489, Cp$_{cent.}$−Nd1−Cp$_{cent.}$ 137.3, C12···Nd1···C12a 178.7, Cl1−Nd···C12 90.6; thermal ellipsoids are at the 50% probability level

In toluene solution the (chloro)bis(tetraisopropylcyclopentadienyl)lanthanum, -praseodymium, or -neodymium sodium chloride complexes [{(C$_5$HR$_4$)$_2$Ln}$_2$(μ-Cl)$_2$(μ$_3$-Cl)$_2${Na(OEt$_2$)}$_2$] (**1**-La, **1**-Pr, **1**-Nd) react with sodium bis(trimethylsilyl)amide with formation of the tetranuclear complexes [{(C$_5$HR$_4$)$_2$Ln(μ-Cl)Na(μ-N(SiMe$_3$)$_2$)}$_2$] (**3**), which can be isolated in good yield (Scheme 1) if the reaction is stopped by solvent removal after 45−60 min. If stirring is continued for several hours, reduced yields or oily mixtures of **3** with two follow-up products are obtained. (This clean follow-up reaction of **3** will be discussed shortly.) In the solid state **3** can be stored for months at ambient temperature without noticeable decomposition.

Crystals of **3**-La, **3**-Pr, and **3**-Nd are isotypic and have been crystallographically characterized. Because of the close similarity of the structural parameters only **3**-Nd will be discussed here.

Table 1. Crystal structure determination of complexes **2**-Nd, **3**-La, **3**-Pr, and **3**-Nd

	2-Nd	**3**-La	**3**-Pr	**3**-Nd
Empirical formula	$C_{34}H_{58}ClNd$	$C_{40}H_{76}ClLaNNaSi_2$	$C_{40}H_{76}ClNNaPrSi_2$	$C_{40}H_{76}ClNNaNdSi_2$
F_w [g·mol^{-1}]	646.534	824.583	826.583	829.913
Crystal size [mm]	0.47 × 0.28 × 0.13	0.38 × 0.27 × 0.23	0.32 × 0.25 × 0.21	0.52 × 0.38 × 0.18
Space	*C*2/*c* (no. 15)	*I*2/*a* (no. 15)	*I*2/*a* (no. 15)	*I*2/*a* (no. 15)
Lattice parameters				
a [Å]	15.4470(15)	23.170(2)	23.365(2)	23.334(7)
b [Å]	12.5006(14)	17.1222(16)	17.0376(17)	17.145(4)
c [Å]	17.7273(15)	23.7779(16)	23.8476(18)	23.849(6)
β [°]	98.675(11)	102.160(9)	102.389(9)	102.53(3)
V [Å^3]	3383.9(6)	9221.5(13)	9272.2(14)	9313(4)
Z	4	8	8	8
T [K])	293(2)	293(2)	293(2)	293(2)
$D_{calcd.}$ [g·cm^{-3}]	1.269	1.196	1.181	1.179
μ [cm^{-1}9	16.32	12.70	10.65	11.89
Transmission factors	0.486−0.835	0.7124−0.8782	0.52423−0.61912	0.64602−0.74964
Θ limits [°]	2.98−24.03	2.76−25.68	2.75−25.68	2.75−25.68
Total reflections	18004	64670	64290	64551
Unique reflections	2636	8394	8628	8349
Structure solution	Direct methods	Direct methods	Direct methods	Direct methods
Program used	SIR97	SIR97	SHELXS-97	SHELXS-97
Refinement	SHELXL-97	SHELXL-97	SHELXL-97	SHELXL-97
Data/restraints/parameters	2386/0/172	6452/0/429	6697/0/599	6506/0/429
*R*1	0.0339 [$I > 2\sigma(I)$]	0.0317 [$I > 2\sigma(I)$]	0.0278 [$I > 2\sigma(I)$]	0.0348 [$I > 2\sigma(I)$]
*wR*2 (all data)	0.0926	0.0808	0.0693	0.1019
GooF (all data)	1.050	0.942	0.976	0.975
Max./min difference peak [e·Å^{-3}]	−0.842/1.345	−0.614/0.865	−0.564/0.436	−0.483/0.546

 © 2003 Wiley-VCH Verlag GmbH & Co. KGaA, Weinheim

The crystal structure of **3**-Nd (Figure 2, Table 1) shows a four-membered Na_2N_2 ring with one molecule of $[(C_5HR_4)_2NdCl]$ coordinated to each of the two sodium ions via a bridging chloro ligand (Figure 2). The Nd−Cl bond length is 2.683(1) Å in **3**-Nd and the angle between the ring planes is 137.7°. The Na−Cl distance [2.767(2) Å] is shorter than that found in crystalline sodium chloride (2.82 Å).[8] The distance Nd1···C82a is 3.37 Å, and three Nd1···C distances between 3.67 and 3.94 Å are also observed for **3**-Nd. The two NSi_2 planes are not parallel, but twisted by 37.5° relative to each other. Short Na···Si distances [3.216(2)/3.172(2) Å for Si1···Na1 and Si···Na1′] and additional Na···methyl interactions (3.023/2.915 Å for Na···C17 and Na1′···C29) are obviously the reason for this distortion. Similar Na···C distances have been found for the cyclic trimer $[NaN(SiMe_3)_2]_3$ [9] and for the sodate $Na[Na\{N(SiMe_3)_2AlMe_3\}_2]$.[10] Because of this methyl-C···Na interaction in **2**-Nd one of the three N−Si−C angles at Si1 (114.8°, 114.5°, 110.7°) or Si2 (114.8°, 114.9°, 111.1°) is significantly smaller than the others. Moreover, this interaction is strong enough to stop the silyl group rotation even in solution, as can be concluded from ^{1}H and ^{13}C NMR spectra of **3**-La, whose crystal structure shows similar methyl C···Na distances (3.019 and 2.912 Å).

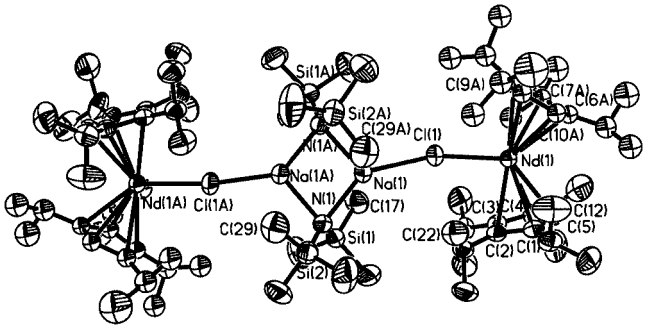

Figure 2. Crystal structure of **3**-Nd. Selected bond lengths [Å] and angles [°]: Nd1−Cl1 2.6832(9), Nd1−C1 2.757(3), Nd1−C2 2.754(3), Nd1−C3 2.766(3), Nd1−C4 2.765(3), Nd1−C5 2.720(3), Nd1−C6a 2.742(7), Nd1−C7a 2.737(7), Nd1−C8a 2.685(8), Nd1−C9a 2.709(7), Nd1−C10a 2.698(7), Nd1−$Cp_{cent.}$ 2.432, Na1···Si1 3.225, Na1···Si2a 3.172, Na1···C29a 2.912, Na1···C17 3.019, Nd1···C82a 3.372, Nd1···C62a 3.673, Nd1···C12 3.759, Nd1···C22 3.938, Cl1−Na1 2.767(2), Na1−N1 2.414(3), Na1−N1a 2.404(3), N1−Si1 1.685(3), N1−Si2 1.689(3), $Cp_{cent.}$−Nd1−$Cp_{cent.}$ 139.4, Nd1−Cl1−Na1 157.04(6), N1−Na1−N1a 101.0(2), Na1−N1−Na1a 78.38(10) thermal ellipsoids are at the 50% probability level

The NMR spectra of **3**-La are well resolved and show one set of resonances for the tetraisopropylcyclopentadienyl ring (cf. ref.[3a] for spectral pattern of C_5HR_4) and two sharp singlets at δ = 0.30 and 0.34 ppm in a 1:2 ratio for the four trimethylsilyl groups. In the ^{13}C NMR spectra two Si*C*H$_3$ signals, with an intensity ratio of 1:2, are observed for **3**-La at δ = 5.3 and 7.0 ppm. NMR spectroscopy at elevated temperatures in order to observe coalescence of the two $SiCH_3$ signals and to determine the activation barrier for $SiMe_3$ rotation was unsuccessful because **3**-La undergoes a clean follow-up reaction with deposition of 1 equiv. of sodium tetraisopropylcyclopentadienide per dimer **3** and formation of two complexes in a 1:1 ratio. One of these complexes is **2**-La, which could be identified by ^{1}H and ^{13}C NMR spectroscopy. The second component, according to the intensity of its NMR signals, contains only one tetraisopropylcyclopentadienyl and two bis(trimethylsilyl)amide ligands according to the formula $[(C_5HR_4)La\{N(SiMe_3)_2\}_2]$ (**4**-La). The observation of only one $SiCH_3$ signal of **4**-La arising from the clean decomposition of **3**-La supports the assignment stated above and rules out the possibility of an unknown impurity causing the 2:1 Si*C*H$_3$ signal pattern found for **3**-La.

In an attempt to generate a possible potassium compound analogous to **3**-Pr, potassium bis(trimethylsilyl)amide was treated with **1**-Pr instead of the sodium salt. Instead of a potassium derivative the sodium compound **3**-Pr was obtained in good yield as before. Under the conditions employed in this work the Ln_2Na_2 complexes **1** are probably not cleaved into fragments of lower nuclearity during the reaction with sodium or potassium bis(trimethylsilyl)amides. The first step could be replacement of the diethyl ether ligand coordinated to each of the sodium cations of **1** with bis(trimethylsilyl)amide anions. Elimination of alkali chloride and rearrangement then furnishes **3** as the isolable product. The attempted rare earth amide formation, a well-known reaction in lanthanide chemistry,[11] has apparently been stopped for steric reasons, and **3** can be regarded as an intermediate in the nucleophilic substitution of chloride by bis(trimethylsilyl)amide.

The composition and geometry of **3** suggests the possible formation of **3** by addition of **2** as a sort of complex ligand to sodium bis(trimethylsilyl)amide. In deuteriobenzene this reaction of **2**-La failed in our hands, however.

Since the bis(trimethylsilyl)amide ligand is obviously too bulky for nucleophilic substitution of the chloro ligand in complexes **1**, we reduced the steric bulk of the nucleophile and used potassium bis(dimethylsilyl)amide for a reaction with **1**-La. The dimer **1**-La reacts with 2 equiv. of $KN(SiHMe_2)_2$ in toluene at room temperature to form the monomeric substitution product $[(C_5HR_4)_2LaN(SiHMe_2)_2]$ (**5**) in good yield (Scheme 1).

The ^{1}H NMR spectra of **5** show the signals of two tetraisopropylcyclopentadienyl ligands, one doublet corresponding to the 12 methyl protons of two dimethylsilyl groups and one signal for the two Si*H* protons, which are coupled to the six protons of two adjacent methyl groups and to the lanthanum central atom. The coupling partner of each signal has been assigned by ^{1}H,{^{1}H}-COSY NMR spectroscopy. The spectroscopic features of the amide ligand of **5** resemble those observed very recently for the bis(dimethylsilyl)amido ligand of *ansa*-metallocene derivatives of lanthanum. Complex **5** shows a $^1J_{Si,H}$ coupling constant of 157 Hz, close to the value of 150 Hz found for $[Me_2Si(C_5Me_4)_2LaN(SiHMe_2)_2]$ indicating a β-agostic interaction of the Si−H bond with the central atom.[12]

 © 2003 Wiley-VCH Verlag GmbH & Co. KGaA, Weinheim

Conclusion

The sodium chloride adducts [{$(C_5HR_4)_2Ln(\mu\text{-}Cl)(\mu_3\text{-}Cl)Na(OEt_2)\}_2$] (**1**) (R = $CHMe_2$, Ln = La, Pr, Nd) undergo facile diethyl ether and sodium chloride elimination in nonpolar solvents. [$(C_5HR_4)_2NdCl$] (R = $CHMe_2$) (**2**-Nd) is the first crystallographically characterized bis(cyclopentadienyl)lanthanide halo complex, which crystallizes as a monomeric molecule without additional salt or heteroatom coordination. The tetraisopropylcyclopentadienyl ligand in this example provides not only steric saturation, but also offers electronic stabilization.

With bis(trimethylsilyl)amides the sodium site is attacked rather than the lanthanide cation of complexes **1** because the large cyclopentadienyl ligands around the lanthanide cation prevent the approach of this bulky nucleophile. The complex [{$(C_5HR_4)_2Ln(\mu\text{-}Cl)(Na)\mu\text{-}N(SiMe_3)_2\}_2$] (**3**) resembles a reactive intermediate of the nucleophilic substitution in nonpolar solvents as it consists of the "nucleophile" [a dimeric sodium bis(trimethylsilyl)amide core] coordinated to its designated reaction partner {a neutral [$(C_5HR_4)_2LnCl$] complex}. Two sodium chloride ion-pairs serve as a spacer between the $[(C_5HR_4)_2Ln]^+$ cations and the $[N(SiMe_3)_2]^-$ anions and steric bulk prevents salt elimination and formation of the anticipated substitution product. Instead of chloride substitution slow elimination of sodium tetraisopropylcyclopentadienide occurs and a mixture of **2** and **4** is formed. The driving force for this reaction appears to be the formation of the two Ln−N bonds of [$(C_5HR_4)Ln\{N(SiMe_3)_2\}_2$] (**4**) along with elimination of 1 equiv. of sodium chloride during this step.

With the less bulky bis(dimethylsilyl)amide the substitution reaction proceeds as usual to furnish [$(C_5HR_4)_2LnN(SiHMe_2)_2$] (**5**).

Experimental Section

General: All synthetic operations were performed under dry nitrogen in a glove box (MBraun). Tetrahydrofuran, hexane, and petroleum ether (boiling range 40−60 °C) were distilled from potassium metal, heptane and toluene from sodium metal, and pentane from a sodium/potassium alloy. NMR spectra were recorded with a Bruker AC 200 spectrometer. Chemical shifts are given in ppm and refer to the appropriate solvent signals. Mass spectra were recorded with a Finnigan MAT 90 mass spectrometer. Elemental analyses were performed with a Perkin−Elmer Elemental Analyzer 240 or 400. **1**-La, **1**-Nd[4] and sodium tetraisopropylcyclopentadienide[3d] were prepared according to published procedures.

1-Pr: A suspension of $PrCl_3$ (1.900 g, 7.6 mmol) in THF (100 mL) was stirred at ambient temperature for 30 min, then a solution of sodium tetraisopropylcyclopentadienide (4.040 g, 15.7 mmol) in THF (50 mL) was added dropwise. The mixture was stirred at room temperature for 1 h and then at reflux temperature for 13 h. The solvent was removed in vacuo and the remaining solid was extracted with two 30-mL portions of diethyl ether. After centrifugation, the orange-yellow diethyl ether extract was concentrated and stored at −35 °C to yield 2.394 g (3.1 mmol, 41%) of yellow platelets of **1**-Pr. $C_{38}H_{68}Cl_2NaOPr$ (775.77): calcd. C 58.83, H 8.83; found C 58.50, H 9.12. MS (70 eV, EI): *m/z* (%) = 642.0 (6.7) $[(C_5HR_4)_2PrCl]^+$, 607.1 (2.5) $[(C_5HR_4)_2Pr]^+$, 408.9 (100) $[(C_5HR_4)PrCl]^+$.

2-La: A solution of sodium tetraisopropylcyclopentadienide (0.512 g, 2 mmol) in tetrahydrofuran (10 mL) was added to $LaCl_3(THF)_2$ (0.390 g, 1.0 mmol) in 10 mL of tetrahydrofuran and the mixture stirred at 70 °C for 2 d. Removal of the solvent in vacuo, extraction of the residue with two 25-mL portions of hexane/toluene (3:1), centrifugation, and concentration left a foam, which slowly solidified upon storage under inert gas at ambient temperature to yield 0.280 g (0.44 mmol, 44%) of **2**-La. $C_{34}H_{58}ClLa$ (641.20): calcd. C 63.69, H 9.12; found C 60.04, H 8.16. ^{1}H NMR (200 MHz, 298 K, C_6D_6): δ = 6.18 (s, 2 H, ring-C*H*), 3.34 ("sept", 4 H, C*H*Me_2), 3.08 ("sept", 4 H, C*H*Me_2), 1.51 (d, $^3J_{H,H}$ = 7.2 Hz, 12 H, CH_3), 1.39 (d, $^3J_{H,H}$ = 6.8 Hz, 12 H, CH_3), 1.24 (d, $^3J_{H,H}$ = 7.2 Hz, 12 H, CH_3), 1.08 (d, $^3J_{H,H}$ = 6.7 Hz, 12 H, CH_3) ppm. ^{13}C NMR (50 MHz, 298 K, C_6D_6): δ = 135.5 (s, 8 C, ring-*C*$CHMe_2$), 135.0 (s, 4 C, ring-*C*$CHMe_2$), 134.5 (s, 4 C, ring-*C*$CHMe_2$), 106.1 (d, $^1J_{C,H}$ = 160 Hz, 4 C, ring-*C*H), 27.44 (d, 8 C, *C*HMe_2, *), 27.42 (d, 4 C, *C*HMe_2, *), 26.4 (q, 4 C, *C*H_3, *), 25.0 (q, 4 C, *C*H_3, *), 23.6 (q, 4 C, *C*H_3, *), 23.3 (q, 4 C, *C*H_3, *) ppm. *: Coupling constants not resolved because of signal superimposition.

2-Nd: A suspension of **1**-Nd (1.878 g, 1.2 mmol) in toluene (10 mL) was stirred at −35 °C for 1 h and at 0 °C for 17 h, then the solvents were evaporated to dryness. The green, foam-like solid was extracted with pentane (15 mL), subjected to centrifugation and concentrated to about 3 mL. Storage at −35 °C gave a green, crystalline precipitate within two weeks. A fraction of well-shaped, blue-green crystals suitable for X-ray crystallography was obtained when the mother liquor was allowed to slowly concentrate at room temperature. Combined yield 1.107 g (1.7 mmol, 71%). $C_{34}H_{58}ClNd$ (646.16): calcd. C 63.16, H 9.04; found C 62.29, H 9.02.

3-La: A solution of sodium bis(trimethylsilyl)amide (0.120 g, 0.65 mmol) in toluene (10 mL) was added to a magnetically stirred suspension of **1**-La (0.501 g, 0.32 mmol) in toluene (12 mL). Stirring was continued for 45 min, then a small amount of a gelatinous residue was separated by centrifugation and the solvents were evaporated to yield a faintly yellow, crystalline solid. The solid product was extracted with hexanes (10 mL) and traces of a colorless precipitate were removed by centrifugation. Drying in vacuo yielded 0.372 g (0.23 mmol, 70%) of faintly yellow, crystalline product. $C_{80}H_{152}Cl_2N_2Na_2La_2Si_4$ (1649.16): calcd. C 59.27, H 9.45, N 1.73; found C 57.32, H 8.81, N 1.55. ^{1}H NMR (200 MHz, 298 K, C_6D_6): δ = 6.18 (s, 2 H, ring-C*H*), 3.34 (sept, 8 H, C*H*Me_2), 3.05 (sept, 8 H, C*H*Me_2), 1.50 (d, $^3J_{H,H}$ = 7.3 Hz, 24 H, CH_3), 1.38 (d, $^3J_{H,H}$ = 6.8 Hz, 24 H, CH_3), 1.25 (d, $^3J_{H,H}$ = 7.1 Hz, 24 H, CH_3), 1.07 (d, $^3J_{H,H}$ = 6.6 Hz, 24 H, CH_3), 0.34 (s, 24 H, SiCH_3), 0.30 (s, 12 H, SiCH_3) ppm. ^{13}C NMR (50 MHz, 298 K, C_6D_6): δ = 135.5 (s, 8 C, ring-*C*$CHMe_2$), 134.7(s, 8 C, ring-*C*$CHMe_2$), 106.4 (d, $^1J_{C,H}$ = 160 Hz, 4 C, ring-*C*H), 27.44 (d, 8 C, *C*HMe_2, *), 27.42 (d, 8 C, *C*HMe_2, *), 26.5 (q, 8 C, *C*H_3, *), 25.0 (q, 8 C, *C*H_3, *), 23.6 (q, 8 C, *C*H_3, *), 23.3 (q, 8 C, *C*H_3, *), 7.0 (q, $^1J_{C,H}$ = 116 Hz, 8 C, Si*C*H_3), 5.3 (q, $^1J_{C,H}$ = 117 Hz, 4 C, Si*C*H_3) ppm. *: Coupling constants not resolved because of signal superimposition. MS (70 eV, EI): *m/z* (%) = 639.3 (5) $[(C_5HR_4)_2LaCl]^+$, 604.4 (9) $[(C_5HR_4)_2La]^+$, 531.4 (29) $[(C_5HR_4)LaN(SiMe_3)_2]^+$, 458.5 (36) $[(C_5HR_4)_2LaNSiMe_3]^+$, 406.5 (79) $[(C_5HR_4)LaCl]^+$, 233.9 (24) $[C_5H_2R_4]^+$, 145.9 (100) $[Si_2Me_6]^+$.

3-Nd: A solution of sodium bis(trimethylsilyl)amide (0.122 g, 0.66 mmol) in toluene (5 mL) was added to a magnetically stirred

 © 2003 Wiley-VCH Verlag GmbH & Co. KGaA, Weinheim

suspension of **1**-Nd (0.513 g, 0.33 mmol) in toluene (20 mL). The suspended material dissolved initially, but after about 40 min a barely visible turbidity was observed. Stirring was discontinued after 45 min, then a small amount of a sticky residue was separated by centrifugation. The solvents were evaporated and the solid product was washed with hexanes (15 mL). Drying in vacuo yielded 0.375 g (0.23 mmol, 69%) green, microcrystalline solid. The green hexane washings produced green crystals on slow concentration. $C_{80}H_{152}Cl_2N_2Na_2Nd_2Si_4$ (1659.82): calcd. C 57.89, H 9.23, N 1.69; found C 57.78, H 9.31, N 1.56. MS (70 eV, EI): *m/z* (%) = 609.2 (5) $[(C_5HR_4)_2Nd]^+$, 412.0 (11) $[(C_5HR_4)NdCl]^+$, 234.2 (84) $[C_5H_2R_4]^+$, 191.1 (100) $[C_{14}H_{22}]^+$, 146.0 (91) $[Si_2Me_6]^+$.

3-Pr: From **1**-Pr (0.500 g; 0.31 mmol) and $KN(SiMe_3)_2$ (0.130 g; 0.65 mmol), 0.390 g (0.24 mmol, 77%) of the light yellow, crystalline praseodymium complex were obtained by the same procedure. Single crystals were grown from hexane at room temperature by slow concentration. $C_{80}H_{152}Cl_2N_2Na_2Pr_2Si_4$ (1653.16): calcd. C 58.12, H 9.27, N 1.69; found C 58.06, H, 9.05, N 1.68.

4-La as a 1:1 Mixture with 2-La: A solution of sodium bis(trimethylsilyl)amide (0.118 g, 0.64 mmol) in toluene (3 mL) was added slowly to a solution of **1**-La (0.504 g, 0.32 mmol) in toluene (15 mL) at room temperature. The mixture was stirred at room temperature for 12 h. Centrifugation and evaporation of the solvents gave 0.320 g of an oily mixture of equivalent amounts of **2**-La and **4**-La (75%), which could not be separated. ^{1}H NMR for **4**-La (200 MHz, 298 K, C_6D_6): δ = 6.07 (s, 1 H, ring-C*H*), 3.08 ("sept", 4 H, C*H*Me$_2$), 1.50 (d, $^3J_{H,H}$ = 7.3 Hz, 6 H, CH_3), 1.49 (d, $^3J_{H,H}$ = 6.8 Hz, 6 H, CH_3), 1.23 (d, $^3J_{H,H}$ = 7.0 Hz, 6 H, CH_3), 1.14 (d, $^3J_{H,H}$ = 6.7 Hz, 6 H, CH_3), 0.30 (s, 36 H, SiCH_3) ppm. ^{13}C NMR (50 MHz, 298 K, C_6D_6): δ = 136.6 (s, 2 C, ring-*C*CHMe$_2$), 133.0 (s, 2 C, ring-*C*CHMe$_2$), 108.7 (d, $^1J_{C,H}$ = 159 Hz, 1 C, ring-*C*H), 27.6 (d, 2 C, *C*HMe$_2$, *), 27.1 (q, 2 C, *C*H$_3$, *), 27.0 (d, 2 C, *C*HMe$_2$, *), 25.3 (q, 2 C, *C*H$_3$, *), 25.0 (q, 2 C, *C*H$_3$, *), 24.6 (q, 2 C, *C*H$_3$, *), 5.3 (q, $^1J_{C,H}$ = 117 Hz, 12 C, Si*C*H$_3$) ppm. *: Coupling constants not resolved because of signal superimposition.

5-La: At room temperature a solution of $KN(SiHMe_2)_2$ (0.077 g; 0.45 mmol) in toluene (4 mL) was added dropwise with stirring to a solution of **1**-La (0.351 g; 0.225 mmol) in toluene (5 mL). A white precipitate formed and stirring was continued for 36 h. After centrifugation, the solvents were evaporated to dryness yielding an off-white, crystalline residue, which was redissolved in hexane (3 mL). Evaporation of the solvent, extraction with pentane (3 mL) and slow concentration of the solution gave 0.221 g (0.30 mmol, 67%) of faintly yellow crystals. $C_{38}H_{72}NLaSi_2$ (730.08): calcd. C 61.84, H 9.83, N 1.90; found C 60.17, H 9.90, N 1.86. ^{1}H NMR (200 MHz, 298 K, C_6D_6): δ = 6.33 (s, 2 H, ring-C*H*), 4.57 (m, $^1J_{Si,H}$ = 157 Hz, 2 H, Si*H*Me$_2$) 3.27 ("sept", 4 H, C*H*Me$_2$), 3.15 ("sept", 4 H, C*H*Me$_2$), 1.51 (d, $^3J_{H,H}$ = 7.2 Hz, 12 H, CH_3), 1.50 (d, $^3J_{H,H}$ = 6.8 Hz, 12 H, CH_3), 1.28 (d, $^3J_{H,H}$ = 7.0 Hz, 12 H, CH_3), 1.18 (d, $^3J_{H,H}$ = 6.7 Hz, 24 H, CH_3), 0.40 (d, $^3J_{H,H}$ = 2.8 Hz, 12 H, SiCH_3) ppm. ^{13}C NMR (50 MHz, 298 K, C_6D_6): δ = 133.3 (s, 4 C, ring-*C*CHMe$_2$), 133.2 (s, 4 C, ring-*C*CHMe$_2$), 106.6 (d, $^1J_{C,H}$ = 159 Hz, 2 C, ring-*C*H), 27.8 (d, 4 C, *C*HMe$_2$, *), 27.3 (d, 4 C, *C*HMe$_2$, *), 26.9 (q, 4 C, *C*H$_3$, *), 25.4 (q, 4 C, *C*H$_3$, *), 24.8 (q, 4 C, *C*H$_3$, *), 24.1 (q, 4 C, *C*H$_3$, *), 4.3 (q, $^1J_{C,H}$ = 118 Hz, 4 C, Si*C*H$_3$) ppm. * Coupling constants not determined due to signal superimposition, assignment confirmed by DEPT experiments.

X-ray Crystallography: Crystallographic data for the structures reported in this paper have been deposited with the Cambridge Crystallographic Data Centre as supplementary publication no. CCDC-171977 (**2**-Nd), -171978 (**3**-Nd), -171979 (**3**-Pr) amd -171980 (**3**-La). Copies of the data can be obtained free of charge on applicaton to CCDC, 12 Union Road, Cambridge CB2 1EZ, UK [Fax: (internat.) + 44-1223/336-033; E-mail: deposit@ccdc.cam.ac.uk]. A Stoe IPDS and Mo-K_α radiation were used for all structure determinations reported here.

Acknowledgments

We thank Prof. Dr. O. J. Scherer for his generous support and Dr. G. Hornung for mass spectra.

[1] [1a] R. D. Shannon, *Acta Crystallogr., Sect. A* **1976**, *32*, 751−767. [1b] The few lanthanum compounds face an overwhelming majority of yttrium compounds in the "Yttrium and Lanthanum" chapter of a recent review article: P. J. Chirik, J. E. Bercaw, in *Metallocenes* (Eds.: A. Togni, R. Halterman), Wiley-VCH, Weinheim, **1998**, vol. 1, p. 111−152. [1c]".... synthetic approaches and methodology that work well with late lanthanides become increasingly more problematic as the series is traversed to the left.": G. Jeske, H. Lauke, H. Mauermann, P. N. Swepston, H. Schumann, T. J. Marks, *J. Am. Chem. Soc.* **1985**, *107*, 8091−8103.

[2] [2a] R. Anwander, in *Applied Homogeneous Catalysis with Organometallic Compounds* (Eds.: B. Cornils, W. A. Herrmann), Wiley-VCH, Weinheim, **2000**, pp. 866−892. [2b] R. Anwander, in *Applied Homogeneous Catalysis with Organometallic Compounds* (Eds.: B. Cornils, W. A. Herrmann), VCH Publishers, Weinheim, **2000**, pp. 866−892.

[3] [3a] H. Sitzmann, *J. Organomet. Chem.* **1988**, *354*, 203−214. [3b] R. A. Williams, K. F. Tesh, T. P. Hanusa, *J. Am. Chem. Soc.* **1991**, *113*, 4843−4851. [3c] E. V. Dehmlow, C. Bollmann, *Z. Naturforsch., Teil B* **1993**, *48*, 57−60. [3d] H. Sitzmann, in *Synthetic Methods of Organometallic and Inorganic Chemistry*, (Eds.: W. A. Herrmann, A. Salzer), Thieme, Stuttgart, **1996**, vol. 1, p. 57.

[4] **1**-La and **1**-Nd have been published recently: H. Sitzmann, O. Schmitt, F. Weber, G. Wolmershäuser, *Z. Anorg. Allg. Chem.* **2001**, *627*, 12−14.

[5] C. Quian, G. Zou, J. Sun, *J. Organomet. Chem.* **1998**, *566*, 21−28.

[6] W. A. Herrmann, R. Anwander, F. C. Munck, W. Scherer, *Chem. Ber.* **1993**, *126*, 331−337.

[7] M. Schultz, C. J. Burns, D. J. Schwartz, R. A. Andersen, *Organometallics* **2000**, *19*, 781−789.

[8] N. Wiberg, *Lehrbuch der Anorganischen Chemie (Hollemann-Wiberg)*, 101st ed., Walter de Gruyter, Berlin, New York, **1995**, p. 1171.

[9] M. Driess, H. Pritzkow, M. Skipinski, U. Winkler, *Organometallics* **1997**, *16*, 5108−5112.

[10] M. Niemeyer, P. P. Power, *Organometallics* **1996**, *15*, 4107−4109.

[11] Examples are. [11a] [(EBI)YbN(SiMe$_3$)$_2$] [EBI = ethylenebis(η^5-indenyl)]: T. Gilbert, B. L. Davis, T. J. Emge, R. D. Broene, *Organometallics* **1999**, *18*, 2125−2132. [11b] [(C$_5$Me$_5$)$_2$SmN(SiMe$_3$)$_2$]: W. J. Evans, R. A. Keyer, J. W. Ziller, *Organometallics* **1993**, *12*, 2618−2633. [11c] [(C$_5$Me$_5$)Ce{N(SiMe$_3$)$_2$}$_2$]: H. J. Heeres, A. Meetsma, J. H. Teuben, R. D. Rogers, *Organometallics* **1989**, *12*, 2618−2633; review articles: [11d] H. Schumann, J. A. Meese-Marktscheffel, L. Esser, *Chem. Rev.* **1995**, *95*, 865−986. [11e] F. T. Edelmann in *Comprehensive Organometallic Chemistry II* (Eds.: E. W. Abel, F. G. A. Stone, G. Wilkinson), Pergamon, Oxford, **1995**, vol. 4, p. 11−212. [11f] F. T. Edelmann, in *Metallocenes* (Eds.: A. Togni, R. L. Halterman), Weinheim, Wiley-VCH, **1998**, vol. 1, p. 55−110.

[12] J. Eppinger, M. Spiegler, W. Hieringer, W. A. Herrmann, R. Anwander, *J. Am. Chem. Soc.* **2000**, *122*, 3080−3096.

Received March 10, 2003

 © 2003 Wiley-VCH Verlag GmbH & Co. KGaA, Weinheim

The First Structurally Characterized Aluminum Squaraine Complex: $L_2(AlMe_2)_4 \cdot 2THF \cdot 2$toluene [L = Bis(2,6-diisopropylanilino)squaraine]

Junfeng Rong,[a] Ying Peng,[a] Herbert W. Roesky,*[a] Jiyang Li,[a] Denis Vidovic,[a] and Jörg Magull[a]

Dedicated to Professor Helmut Schwarz on the occasion of his 60th birthday

Keywords: Aluminum / Squaraine / N ligands / O ligands / X-ray diffraction

Bis(2,6-diisopropylanilino)squaraine (**1**) was prepared by condensation of squaric acid and 2,6-diisopropylaniline. Treatment of **1** with trimethylaluminum affords a novel dimeric aluminum squaraine complex: $L_2(AlMe_2)_4 \cdot 2THF \cdot 2$toluene [L = bis(2,6-diisopropylanilino)squaraine] (**2**), which was characterized by X-ray diffraction.
(© Wiley-VCH Verlag GmbH & Co. KGaA, 69451 Weinheim, Germany, 2003)

Introduction

Squaraines are a class of 1,3-derivatives of squaric acid in which the substituents are amines or highly electron-donating aromatic or heterocyclic groups.[1] Their electronic structure and rich chemistry have been the subject of considerable discussion.[2] Several of them show fluorescence[3] or form self-organized films,[4] which imply their application as photosensitive films, organic solar cells, optical recording, and non-linear optical materials.[5] However, research on the organometallic chemistry of squaraines seems to be neglected. In fact, the versatility of squaraines implies that this class of compounds are ideal ligands. Only a few diamino derivatives of squaric acid have been structurally characterized.[2b,2c,6] No complex of aluminum with squaraines as ligand has been isolated and structurally characterized so far. We became interested in employing diaminosquaraines as ligands with the aim of studying their novel structure and property. Herein, we report on the first aluminum complex with the squaraine ligand.

Results and Discussion

Diamino derivatives of squaric acid can be synthesized as main products through the condensation of squaric acid with amines.[7] The ligand, bis(2,6-diisopropylanilino)squaraine (**1**) was prepared by a modified approach of refluxing squaric acid and 2,6-diisopropylaniline in ethanol with a few drops of formic acid as catalyst, as outlined in Scheme 1. The IR spectrum of **1** shows a strong absorption at 1598 cm^{-1} attributed to the squaraine carbonyl group.[2g] The 1,3-derivative of **1** is formed preferentially in this condensation reaction instead of the 1,2-species.[7b−7e] A sharp band at 3151 cm^{-1} is attributed to N−H stretching vibrations,[7b,7c] and a band at 2870 cm^{-1} to $\nu(N^+H)$.[7c] Ligand **1** is an air-stable solid which decomposes above 380 °C. The EI mass spectrum gives the molecular ion peak at $m/z = 432$ and the base peak at $[M^+ - C_3H_7]$. The composition of **1** is further supported by the ^1H and ^{13}C NMR spectra. However, an unambiguously structural assignment can only be made by an X-ray analysis. So far, we have not been able to grow suitable single crystals of **1**.

Bis(2,6-diisopropylanilino)squaraine (**1**) is sparingly soluble in most organic solvents. The reaction between trimethylaluminum and a suspension of **1** in THF was carried out at −78 °C. The acidic hydrogen of **1** is very active towards the CH_3 groups of trimethylaluminum. A clear yellow solution of **2** was readily formed upon warming to room temperature (Scheme 1). Complex **2** is much more soluble than **1** in organic solvents.

Compound **2** crystallizes in the triclinic space group $P\bar{1}$. An overview and numbering scheme is shown in Figure 1. The aluminum squaraine complex **2** turns out to be an interesting dimer with two different coordination modes for Al atoms. Two squaraine moieties are linked together by two $AlMe_2$ units, forming a ten-membered $C_4Al_2N_2O_2$ ring. Two THF molecules coordinate to the Al atoms of the two exocyclic $AlMe_2$ units by O−Al coordinative bonds, whereas the two exocyclic $AlMe_2$ units are linked to the O atoms of the squaraines by Al−O covalent bonds. In the ten-membered $C_4Al_2N_2O_2$ ring each Al atom is surrounded by the O atom, N atom and two Me groups. The N(2) atom adopts an sp^2 electron distribution and the Al−N bonds are

[a] Institut für Anorganische Chemie, Universität Göttingen, Tammannstrasse 4, 37077, Göttingen, Germany
Fax: (internat.) + 49-(0)551/393-373
E-mail: hroesky@gwdg.de

 © 2003 Wiley-VCH Verlag GmbH & Co. KGaA, Weinheim **DOI: 10.1002/ejic.200300082**

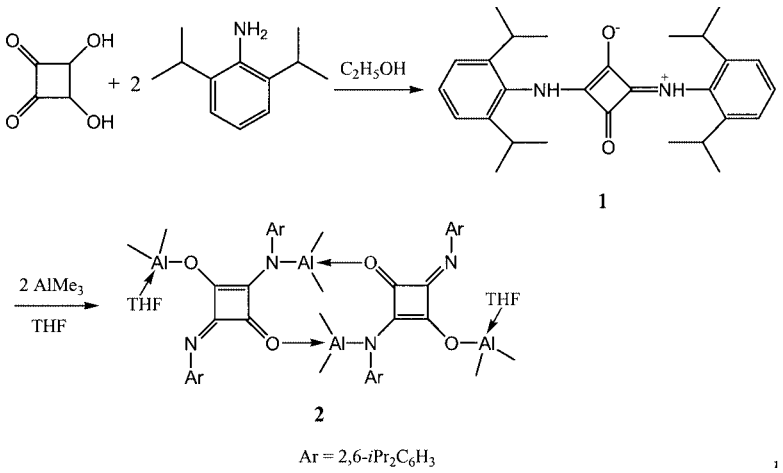

Scheme 1

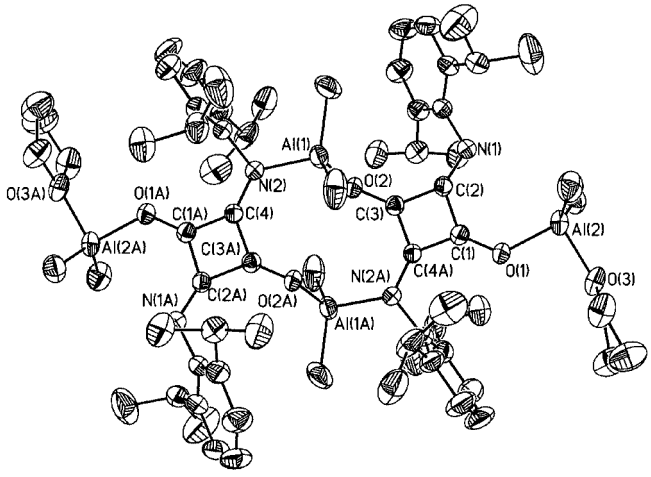

Figure 1. Molecular structure of $L_2(AlMe_2)_4$·2THF·2toluene [L = bis(2,6-diisopropylanilino)squaraine] (**2**) in the crystal (40% probability thermal ellipsoids); toluene molecules and hydrogen atoms are omitted for clarity; selected bond lengths (Å) and angles (deg.): C(1)−C(2) 1.471(3), C(2)−C(3) 1.483(3), C(1)−C(4A) 1.428(3), C(3)−C(4A) 1.446(3), C(1)−O(1) 1.279(2), C(3)−O(2) 1.267(3), C(2)−N(1) 1.281(3), N(2)−C(4) 1.335(3), Al(1)−O(2) 1.835(2), Al(2)−O(1) 1.823(2), Al(1)−N(2) 1.916(2); O(2)−Al(1)−N(2) 102.80(8), C(1)−O(1)−Al(2) 127.97(13), C(3)−O(2)−Al(1) 131.16(14), C(2)−N(1)−C(11) 119.82(18), C(4)−N(2)−Al(1) 125.16(14), C(1)−C(2)−C(3) 85.80(15), C(4A)−C(3)−C(2) 91.80(17)

covalent in nature, with a typical bond length of 1.916(2) Å. The average bond angle around N is 119.5°. The lone pairs on the O atoms coordinate to the Al atom by forming an Al−O coordinative bond. This may account for the formation of a dimer of the complex instead of a monomer, since the bond character of the O and N of the same squaraine ligand is different, and Al is more oxophilic. The two Al atoms within the ring adopt a typical tetrahedral geometry with an average bond angle of 109.3° at Al.

There are some noticeable differences in the structure of the squaraine ligands in complex **2** compared to those reported previously.[2b,2c,6] The C(2)−N(1) bond length of 1.281(3) Å is typical of a C=N double bond (1.273 Å in CH_2=NH[8]). Apparently, N(1) is sp^2 hybridized with a C(2)−N(1)−C(11) bond angle of 119.82(2)°. The C(4)−N(2) bond length of 1.335(3) Å is longer than a double bond but much shorter than a single bond (1.472 Å[9]). The C(1)−O(1) bond length of 1.279(2) Å is also much shorter than a single bond (1.426 Å[9]). These bonding characteristics can be explained by the p-π conjugation of the lone pairs on O(1) and N(2) and the carbon p orbital.[10] Like previously reported squaraines, the C atoms in the four-membered ring in **2** are all sp^2 hybridized.[2b] Delocalization of the electrons is believed to exist, and this accounts for the longer C(1)−C(4A) double bond [1.428(3) Å]. The C(1)−C(2) [1.471(3) Å], C(3)−C(4A) [1.446(3) Å], and C(2)−C(3) bond lengths [1.483(3) Å] are in the range of a C−C single bond (1.466 Å).[2b] This C-C bonding character of **2** is different from that of the reported bis(dimethylamino)squaraine[6] and dipiperidinosquaraine[2b] in which the C-C bond lengths are almost equal. This may stem from the formation of the organometallic complex of the squaraine.

In summary, bis(2,6-diisopropylanilino)squaraine shows many novel characters when it is adopted as a ligand for an aluminum complex. The rich chemistry of this ligand and its corresponding organometallic complexes have prompted us to carry out further investigation.

Experimental Section

Preparation of Complex 1: 2,6-Diisopropylaniline (9.8 mL, 52 mmol) was added to a suspension of squaric acid (2.80 g, 25 mmol) in ethanol (80 mL) at room temperature. After several minutes a few drops of formic acid were added to the suspension to form a clear colorless solution. The resulting solution was refluxed for 2 days to give a pale-yellow solution. The volatiles were then removed in vacuo to give **1** as a pale-yellow powder. Yield: 4.24 g (40%). Mp: 380 °C (decomp.). EI-MS: *m/z* (%) = 432 (38) [M^+], 417 (48) [$M^+ - CH_3$], 389 (100) [$M^+ - C_3H_7$]. ^{1}H NMR (200 MHz, [D_8]THF): δ = 1.16 (d, 12 H, CHMe_2), 1.25 (d, 12 H, CHMe_2), 3.19 (sept, 4 H, C*H*Me_2), 7.11 (m, 6 H, Ar*H*), 10.30 (s, 1 H, N*H*) ppm; N^+H was not observed. ^{13}C NMR (125.77 MHz, [D_8]THF): δ = 25.06, 25.54 (CHMe_2), 30.33 (*C*HMe_2), 67.22,

 © 2003 Wiley-VCH Verlag GmbH & Co. KGaA, Weinheim

67.56, 67.73, 67.91 (squaraine carbon), 123.71, 128.68, 133.80, 146.25 (*Ar*) ppm. IR (Nujol mull): $\tilde{\nu}$ = 1598 cm^{-1} (squaraine carbonyl), 2870 (N^+H), 3151 (N−H). $C_{28}H_{36}N_2O_2$ (432): calcd. C 77.67, H 8.32, N 6.47; found C 77.61, H 8.38, N 6.55.

The experiments below were performed using standard Schlenk techniques or in a glove box under a purified nitrogen atmosphere. Solvents were dried according to standard methods and freshly distilled prior to use.

Preparation of Complex 2: $AlMe_3$ (1.5 mL, 2 M solution in heptane, approx. 2 equiv.) was added to a suspension of **1** (0.70 g, 1.6 mmol) in THF (20 mL) at −78 °C. The suspension was warmed slowly to room temperature and stirred overnight to give a clear yellow solution. All the volatiles were removed in vacuo and the residue was recrystallized from THF/toluene (1:1) at 0 °C to give pale-yellow crystals of **2**. Yield: (0.68 g, 60%). Mp: 190 °C (decomp.). EI-MS: *m/z* (%) only small fragments. ^1H NMR (200 MHz, $CDCl_3$): δ = −1.51 (s, 12 H, Al-*Me*), −0.79 (s, 12 H, Al-*Me*), 1.07−1.17 (m, 48 H, CH*Me*$_2$), 1.85 (s, 8 H, *THF*), 2.94 (sept, 4 H, C*H*Me_2), 3.03 (sept, 4 H, C*H*Me_2), 3.75 (s, 8 H, *THF*) ppm. ^{13}C NMR (125.77 MHz, $CDCl_3$): δ = −10.24, −9.06 (Al-*Me*), 23.62, 24.02, 24.40, 24.50, 24.61, 24.81, 25.01, 25.10, 25.72, 25.75, 26.45 (CH*Me*$_2$), 29.30, 29.37 (*C*HMe_2), 25.16, 69.71 (*THF*), 77.72, 77.98, 78.18, 78.23 (*squaraine carbon*), 124.36, 124.65, 124.76, 124.94, 127.39, 128.07, 138.32, 140.50, 143.29, 144.95, 169.19 (*Ar*) ppm. IR (Nujol mull): $\tilde{\nu}$ = 1594 cm^{-1} (squaraine carbonyl). $C_{86}H_{124}Al_4N_4O_6$ (1417.81): calcd. C 72.85, H 8.82, N 3.95; found C 71.31, H 8.62, N 3.95.

X-ray Crystallographic Study of 2·2toluene: Crystal dimensions 0.30 × 0.20 × 0.15 mm^3, $C_{86}H_{124}Al_4N_4O_6$, M_r = 1417.81, triclinic, space group $P\bar{1}$, a = 10.3468(12) Å, b = 15.0508(17) Å, c = 15.6447(16) Å, α = 114.243(8)°, β = 99.359(9)°, γ = 96.321(9)°, V = 2149.1(4) $Å^3$, Z = 1, $\rho_{calcd.}$ = 1.095 $Mg·m^{-3}$, F(000) = 768, 1.58 < θ < 24.77°; of 22118 reflections collected, 7304(R_{int} = 0.0812) were independent. The R values are $R1$ = 0.0501 and $wR2$ = 0.1164 [$I > 2\sigma(I)$]; max./min. residual electron density: 0.509/−0.276 $e·Å^{-3}$.

CCDC-193657 contains the supplementary crystallographic data for this paper. These data can be obtained free of charge at www.ccdc.cam.ac.uk/conts/retrieving.html [or from the Cambridge Crystallographic Data Centre, 12, Union Road, Cambridge CB2 1EZ, UK; Fax: (internat.) +44-1223/336-033; E-mail: deposit@ccdc.cam.ac.uk].

Acknowledgments

We acknowledge the Deutsche Forschungsgemeinschaft for financial support. J. Rong and J. Li thank the Alexander von Humboldt Foundation for a research fellowship.

[1] [1a] A. H. Schmidt, *Synthesis* **1980**, 961−994. [1b] A. Treibs, K. Jacob, *Angew. Chem.* **1965**, *77*, 680−681.
[2] [2a] E. W. Neuse, B. R. Green, *J. Am. Chem. Soc.* **1975**, *97*, 3987−3991. [2b] P. H. M. Budzelaar, H. Dietrich, J. Macheleid, R. Weiss, P. R. Schleyer, *Chem. Ber.* **1985**, *118*, 2118−2126. [2c] B. Lunelli, P. Roversi, E. Ortoleva, R. Destro, *J. Chem. Soc., Faraday Trans.* **1996**, *92*, 3611−3623. [2d] A. H. Schmidt, W. Ried, P. Pustoslemsek, W. Schuckmann, *Angew. Chem.* **1975**, *87*, 879−880; *Angew. Chem. Int. Ed. Engl.* **1975**, *14*, 823−824. [2e] D. G. Farnum, M. A. Neuman, W. T. Suggs, Jr, *J. Cryst. Mol. Struct.* **1974**, *4*, 199−212. [2f] M. Tristanikendra, C. J. Eckhardt, J. Bernstein, E. Goldstein, *Chem. Phys. Lett.* **1983**, *98*, 57−61. [2g] P. M. Kazmaier, G. K. Hamer, R. A. Burt, *Can. J. Chem.* **1990**, *68*, 530−536.
[3] [3a] S. Das, P. V. Kamat, B. Delabarre, K. G. Thomas, A. Ajayaghosh, M. V. George, *J. Phys. Chem.* **1992**, *96*, 10327−10330. [3b] S. Das, K. G. Thomas, K. J. Thomas, P. V. Kamat, M. V. George, *J. Phys. Chem.* **1994**, *98*, 9291−9296.
[4] K. Y. Law, C. C. Chen, *J. Phys. Chem.* **1989**, *93*, 2533−2538.
[5] [5a] K. Y. Law, *J. Phys. Chem.* **1989**, *93*, 5925−5930. [5b] C. T. Chen, S. R. Marder, L. T. Cheng, *J. Am. Chem. Soc.* **1994**, *116*, 3117−3118. [5c] G. W. Scott, K. Tran, D. J. Funk, D. S. Moore, *J. Mol. Struct.* **1995**, *348*, 425−428. [5d] C. W. Dirk, W. C. Herndon, F. Cervantes-Lee, H. Selnau, S. Martinez, P. Kalamegham, A. Tan, G. Campos, M. Velez, J. Zyss, I. Ledoux, L. T. Cheng, *J. Am. Chem. Soc.* **1995**, *117*, 2214−2225.
[6] B. Lunelli, R. Soave, R. Destro, *Phys. Chem. Chem. Phys.* **1999**, *1*, 1469−1477.
[7] [7a] S. Cohen, S. G. Cohen, *J. Am. Chem. Soc.* **1966**, *88*, 1533−1536. [7b] G. Manecke, J. Gauger, *Tetrahedron Lett.* **1967**, *36*, 3509−3515. [7c] E. W. Neuse, B. R. Green, *J. Org. Chem.* **1974**, *39*, 3881−3887. [7d] E. Neuse, B. Green, *Justus Liebigs Ann. Chem.* **1973**, 619−632. [7e] E. Neuse, B. Green, *Justus Liebigs Ann. Chem.* **1973**, 633−635.
[8] M. D. Harmony, V. W. Laurie, R. L. Kuczkowski, R. H. Schwendeman, D. A. Ramsay, F. J. Lovas, W. J. Lafferty, A. G. Maki, *J. Phys. Chem. ref. Data* **1979**, *8*, 619−721.
[9] Table of Interatomic Distances and Configuration in Molecules and Ions, Supplement 1956−1959 (Ed.: L. E. Sutten), The Chemical Society Publ. No. 18, London **1965**.
[10] M. B. Power, S. G. Bott, J. L. Atwood, A. R. Barron, *J. Am. Chem. Soc.* **1990**, *112*, 3446−3451.

Received February 10, 2003

 © 2003 Wiley-VCH Verlag GmbH & Co. KGaA, Weinheim

A Bulky Chelating Diamidoaluminum Monohydride − Synthesis, Structure and Reactions with Me_3SnF and Heavy Group 16 Elements

Hongping Zhu,[a] Jianfang Chai,[a] Herbert W. Roesky,*[a] Mathias Noltemeyer,[a] Hans-Georg Schmidt,[a] Denis Vidovic,[a] and Jörg Magull[a]

Dedicated to Professor Helmut Werner on the occasion of his 70th birthday

Keywords: Aluminum / Hydride / Chalcogens / Fluorine

The bulky chelating diamidoaluminum monohydride $[ArN(CH_2)_3NAr]AlH(NMe_3)$ (Ar = 2,6-*i*$Pr_2C_6H_3$; **1**) was prepared in excellent yield from the reaction of the diamine $ArNH(CH_2)_3HNAr$ with a small excess of $AlH_3{\cdot}NMe_3$ in toluene. Subsequent fluorination of **1** with Me_3SnF resulted in the formation of the aluminum monofluoride $[ArN(CH_2)_3NAr]AlF(NMe_3)$ (**2**). Reaction of **1** with elemental E (E = S, Se and Te) proceeded in toluene with heating to yield the aluminum chalcogenides $\{[ArNH(CH_2)_3NAr]Al(\mu\text{-}E)\}_2$ [E = S (**3**), Se (**4**), and Te (**5**)]. The structures of complexes **1**, **2** and **4** have been determined by X-ray diffraction analyses. Compounds **1** and **2** are well-separated monomers with a central aluminum atom in a tetrahedral environment. The diamide ligand $[ArN(CH_2)_3NAr]^{2-}$ chelates the Al atom to form a distorted six-membered AlN_2C_3 ring which features a boat conformation for **1** and a flattened chair conformation for **2**. Compound **4**, however, is a dimer with a central Al_2Se_2 core bearing an ideal four-membered planar ring and two six-membered AlN_2C_3 rings, both displaying a boat conformation. The latter two rings are arranged perpendicularly to the Al_2Se_2 core in a *trans* configuration. The IR spectra and ^1H NMR spectroscopic data of compounds **3**–**5** suggest that the migration of the hydrogen from selenium to one of the nitrogens at the diamide ligand is involved in the course of the reaction.
(© Wiley-VCH Verlag GmbH & Co. KGaA, 69451 Weinheim, Germany, 2003)

Introduction

Studies of aluminum hydrides have received considerable attention due to their scientific importance and numerous applications.[1] In recent years, much work has been devoted to aluminum hydrides of low aggregation, especially the monomeric forms. The synthesis of monomeric aluminum hydrides helps us to understand the reaction chemistry of surface-bound AlH_n groups formed during thin-film growth from organoaluminum sources.[2] Moreover, aluminum hydrides of low aggregation can be very effective precursors for preparing aluminum chalcogenides.[3] However, reactions involving aluminum hydrides of low aggregation with chalcogen or organochalcogenides have been reported to a lesser extent. Raston et al.[4] have investigated the reaction of the trimethylamine adduct of alane $Me_3N{\cdot}AlH_3$ with chalcogen or organochalcogenides. Power et al.[5] have reported one example of the reaction of an aluminum dihydride with an organochalcogenide and our group has discussed the reaction of a series of aluminum dihydrides with chalcogen,[3,6] where the isolation and structural characterization of some novel compounds {such as $LAl(SeH)_2$, $LAl(SeH)Se(SeH)AlL$,[3] $LAl(SH)_2$ [6a] [L = N(Ar)C(Me)-CHC(Me)N(Ar), Ar = 2,6-*i*$Pr_2C_6H_3$); $(RAlE)_2$ (R = 2,4,6-*t*$Bu_3C_6H_2$, E = S;[5] R = $N(SiMe_3)C(Ph)C(SiMe_3)_2$,[6b] 2,6-$(Et_2NCH_2)_2C_6H_3$, 2-$Et_2NCH_2$-6-$MeC_6H_3$;[6c] E = Se, Te], *trans*-$[\{Me_3N(H)Al(\mu\text{-}E)\}_2]$ (E = Se, Te),[4b] *trans*-$[\{Me_3N(PhTe)Al(\mu\text{-}Se)\}_2]$;[4c] $[(\eta^1\text{-}3,5\text{-}t\text{Bu}_2\text{pz}(\mu\text{-Al})H]_2E$ (E = S, Se, Te);[6d] $Me_3NAl(ER)_3$ (E = Se, R = Et, Ph, CH_2Ph; E = Te, R = Ph)[4a] and $Al_4Se_5(H)_2(NMe_3)_4$ [4c]} showed a rich chemistry. Although further reaction of the dimeric chalcogenidoalane, *trans*-$[\{Me_3N(H)Al(\mu\text{-}E)\}_2]$ (E = Se, Te) with chalcogen or organochalcogenides has been investigated,[4b] studies of the reaction of bulky, monomeric aluminum monohydrides with chalcogens, which might generate the corresponding monomeric Al-EH moieties, have not been reported so far. Therefore we became interested in finding a sufficiently bulky ligand to synthesize an intramolecularly stabilized aluminum monohydride, and further studies on its reactivity with the fluorinating agent Me_3SnF and heavy group 16 elements.

The divalent bulky chelating diamide ligand $[ArN(CH_2)_3NAr]^{2-}$ (Ar = 2,6-*i*$Pr_2C_6H_3$) is increasingly being used as a ligand[7] due to its special steric and electronic properties that help to control effectively the geometry at the metal center. Known complexes containing this ligand include main group metal (Li, K, Al) and transition metal (Ti, Zr, Y, Lu) derivatives.[7−11] The only reported alumi-

[a] Institut für Anorganische Chemie der Universität Göttingen
Tammannstrasse 4, 37077 Göttingen, Germany
Fax: (internat.) +49-(0)551/393-373
E-mail: hroesky@gwdg.de

num complexes are a series of compounds containing alkyl and aryl groups [ArN(CH$_2$)$_3$NAr]AlR (R = Me, *i*Bu, C$_6$F$_5$).[11] Herein we report on the synthesis and characterization of the bulky chelating diamidoaluminum monohydride [ArN(CH$_2$)$_3$NAr]AlH(NMe$_3$) (Ar = 2,6-*i*Pr$_2$C$_6$H$_3$; **1**). The metathesis of **1** with Me$_3$SnF to give the monofluoride [ArN(CH$_2$)$_3$NAr]AlF(NMe$_3$) (**2**) and the reaction with heavy group 16 elements to afford the dimeric aluminum chalcogenides {[ArNH(CH$_2$)$_3$NAr]Al(μ-E)}$_2$ [E = S (**3**), Se (**4**), and Te (**5**)] are also described.

Results and Discussion

Syntheses and Characterization of [ArN(CH$_2$)$_3$NAr]AlH(NMe$_3$) (1) and [ArN(CH$_2$)$_3$NAr]AlF(NMe$_3$) (Ar = 2,6-*i*Pr$_2$C$_6$H$_3$) (2)

The synthesis of aluminum hydrides has been reported in a number of publications.[12] The use of AlH$_3$·NMe$_3$ as a precursor to react with *N*-substituted diamine, diimine and analogues containing N-H groups or E(SiMe$_3$)$_2$ (E = P, As) with elimination of H$_2$ or HSiMe$_3$ has been shown to be a facile route to aluminum hydrides of low aggregation.[3,13] Reaction of the diamine [ArNH(CH$_2$)$_3$HNAr] with a small excess of AlH$_3$·NMe$_3$ in toluene under heating (80 °C) affords the intramolecularly stabilized diamidoaluminum monohydride [ArN(CH$_2$)$_3$NAr]AlH(NMe$_3$) (**1**) in excellent yield. Subsequent fluorination of **1** with Me$_3$SnF either at room temperature or at high temperature (80 °C) results in the formation of the aluminum monofluoride [ArN(CH$_2$)$_3$NAr]AlF(NMe$_3$) (**2**; Scheme 1).

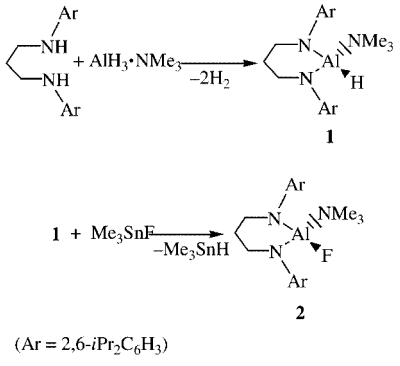

Scheme 1

Complexes **1** and **2** were characterized by NMR, MS (EI) and IR spectroscopy, and elemental analyses. The presence of the hydride in **1** is evident from the IR spectrum. The broad IR band at 1799 cm^{-1} can be assigned to the Al−H stretching absorption.[14] In the IR spectrum of **2**, this absorption disappears, indicating that compound **1** is completely fluorinated. The ^{19}F NMR spectrum of **2** exhibits one singlet resonance (δ = −175.4 ppm), which is similar to the terminal Al−F resonance in a closely related series of compounds {ArN[Si(R)Me$_2$]AlF$_2$·THF: Ar = 2,6-*i*Pr$_2$C$_6$H$_3$, R = Me, δ = −178.1; R = *i*Pr, δ = −177.0 ppm; R = *t*Bu, δ = −175.1 ppm; Ar = 2,6-Me$_2$C$_6$H$_3$, R = *t*Bu, δ = −175.0 ppm; R = 2,4,6-Me$_3$C$_6$H$_2$, δ = −175.9 ppm}.[15] In the ^{1}H NMR spectra of **1** and **2** the presence of complex resonances for the backbone protons of the diamide ligand [two isopropyl methine (C*H*Me$_2$), four isopropyl methyl (CH*Me$_2$*), two methene (N*CH$_2$*) and two methene (NCH$_2$*CH$_2$*) resonances] is consistent with a pseudotetrahedral geometry and C_s symmetry at aluminium. Similar resonances are observed in compounds [M{ArN(CH$_2$)$_3$NAr}(η-C$_5$H$_5$)Cl] (M = Zr, Y; Ar = 2,6-*i*Pr$_2$C$_6$H$_3$).[7,9] The resonance for the Al−H proton is not seen, which is typical for amidoaluminum hydride species.[13b] Substitution of Al−H in **1** by Al−F has a stronger effect on the chemical shift of the NMe$_3$ group (**1**: δ = 1.66 ppm; **2**: δ = 1.75 ppm), while a smaller effect is observed for the backbone protons of the ligand. The MS (EI) spectrum shows the molecular ion of [M$^+$ − NMe$_3$] for **1**, and [M$^+$] and [M$^+$ − NMe$_3$] for **2** and the single-crystal X-ray structural determinations of **1** and **2** confirm the composition of [ArN(CH$_2$)$_3$NAr]AlR(NMe$_3$) (R = H, **1**; F, **2**), where the former contains half a molecule of *n*-hexane per molecule of complex **1** in the asymmetric unit.

Compounds **1** and **2** are well-separated monomers both of which contain a central aluminum atom in a distorted tetrahedral environment (Figures 1 and 2). Selected bond lengths and angles are listed in Table 1. The terminal Al−H bond length (1.52 Å) is closer to those in compounds (2,4,6-*t*Bu$_3$C$_6$H$_2$)$_2$AlH[16] [1.53(4) Å] and [HAl(NMe$_2$)$_3$]$^-$[17] [1.52(2) Å], but shorter than those in AlH(Cl)-[*t*BuNCH$_2$CH$_2$N(*t*Bu)H][13a] (1.60 Å), Al$_2$(μ-NEt$_2$)$_2$-[N(*i*Pr)$_2$]$_2$H$_2$ [18] (1.67 Å) and (2,4,6-*t*Bu$_3$C$_6$H$_2$)Al(H)Cl·THF[19] [1.73(5) Å]. The terminal Al−F separation [1.678(1) Å] is in the range of 1.657−1.681 Å

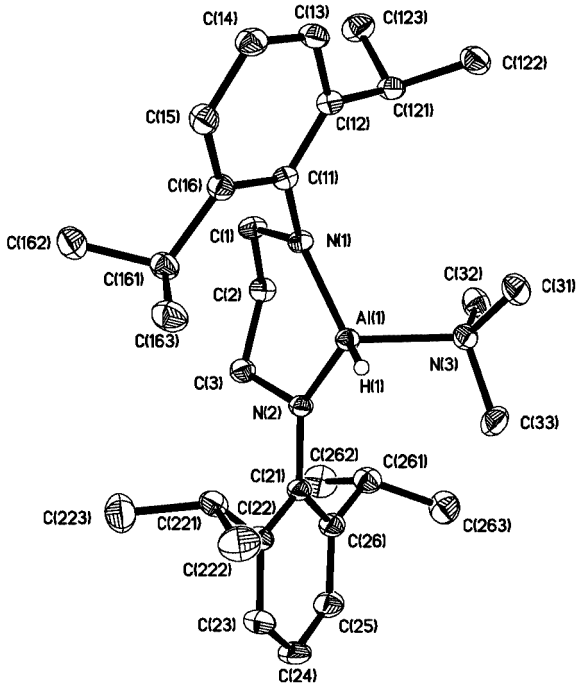

Figure 1. Molecular structure of **1** with the thermal ellipsoids at 30% probability level; H atoms are omitted for clarity except for the Al−H hydrogen atom

 © 2003 Wiley-VCH Verlag GmbH & Co. KGaA, Weinheim

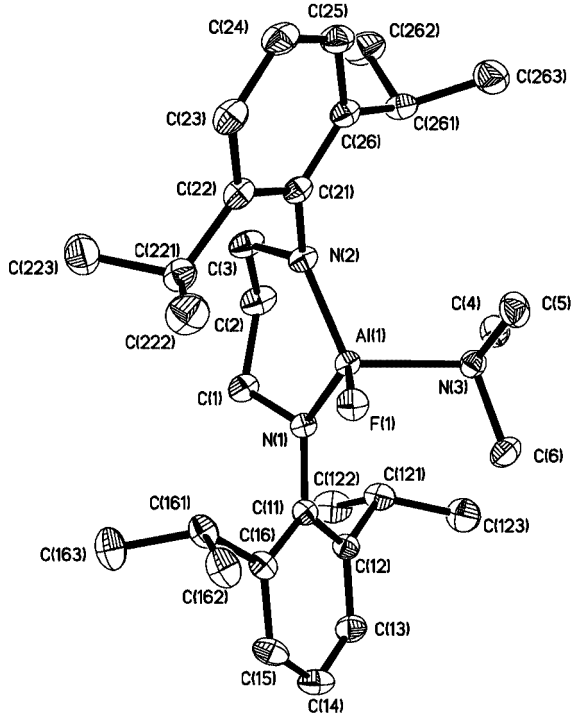

Figure 2. Molecular structure of **2** with the thermal ellipsoids at 30% probability level; H atoms are omitted for clarity

Table 1. Selected bond lengths [Å] and bond angles [°] for compounds **1**·1/2 *n*-hexane, **2** and **4**·2 toluene

Compound **1**·1/2 *n*-hexane			
Al(1)−N(1)	1.820(1)	Al(1)−N(3)	2.024(2)
Al(1)−N(2)	1.828(1)	Al(1)−H(1)	1.52
N(1)−Al(1)−N(2)	106.52(6)	H(1)−Al(1)−N(1)	116.1
N(1)−Al(1)−N(3)	111.31(7)	H(1)−Al(1)−N(2)	120.2
N(2)−Al(1)−N(3)	105.74(7)	H(1)−Al(1)−N(3)	96.0
Compound **2**			
Al(1)−F(1)	1.678(1)	Al(1)−N(2)	1.804(2)
Al(1)−N(1)	1.810(2)	Al(1)−N(3)	2.000(2)
N(1)−Al(1)−N(2)	107.45(7)	F(1)−Al(1)−N(1)	119.12(6)
N(1)−Al(1)−N(3)	108.55(8)	F(1)−Al(1)−N(2)	115.24(6)
N(2)−Al(1)−N(3)	112.69(8)	F(1)−Al(1)−N(3)	93.00(6)
Compound **4**·2 toluene			
Al(1)−Se(1)	2.339(1)	Al(1)−N(1)	1.932(11)
Al(1)−Se(1A)	2.381(1)	Al(1)−N(2)	1.916(11)
Al(1)−Al(1A)	2.988(2)	Se(1)−Al(1)−Se(1A)	101.44(5)
Al(1)−Se(1)−Al(1A)	78.56(5)	N(1)−Al(1)−N(2)	98.13(14)
N(1)−Al(1)−Se(1)	119.2(4)	N(2)−Al(1)−Se(1A)	109.7(4)
N(2)−Al(1)−Se(1)	118.6(4)	N(1)−Al(1)−Se(1A)	109.7(4)
Al(1)−N(1)−C(1)	119.6(8)	Al(1)−N(2)−C(3)	121.1(9)
Al(1)−N(1)−C(16)	126.4(8)	Al(1)−N(2)−C(4)	130.1(7)
C(1)−N(1)−C(16)	113.2(9)	C(3)−N(2)−C(4)	108.0(9)

observed in $[(Me_3Si)_3CAlF_2]_3$ [20] and somewhat longer than those in $[\{(2,6\text{-}i\text{Pr}_2C_6H_3)N(SiMe_3)AlF_2\}_3]$[15] (1.634−1.642 Å) and AlF_3 [21] (1.63 Å), as determined by electron diffraction. The diamide ligand chelates the Al atom to form an AlN_2C_3 six-membered non-planar ring, in which Al(1) and C(2) occupy the head positions with distances to the quasi-plane N(1)−N(2)−C(3)−C(1) (mean deviation Δ = 0.0716 Å) of 0.1034 and 0.6852 Å in **1** and the plane N(1)−N(2)−C(3)−C(1) (Δ = 0.0316 Å) of −0.0109 and 0.6730 Å in **2**. It is obvious that the former displays a boat conformation and the latter a flattened chair conformation, and this can be explained in terms of the strain imposed by the Ar group. The F atom has a stronger electron-attracting tendency than the H atom, which generates different charge distributions at the central Al atom of **1** and **2**. This gives rise to the small difference in the $Al-N_{diamide}$ bond length between **1** and **2** (average 1.824, **1**; 1.807 Å, **2**), as well as the $Al\text{-}N_{NMe_3}$ bond length [2.024(2), **1**; 2.000(2) Å, **2**] and the N(1)−Al(1)−N(2) chelating angle [106.52(6)°, **1**; 107.45(7)°, **2**]. The $Al-N_{diamide}$ distances in **1** and **2** can be compared with the terminal Al−N(amide) distances in $CH_2(CH_2CMe_2)_2NAlH_2{\cdot}NMe_3$ [13h] [1.838(2) Å], AlH(Cl)[*t*BuNCH$_2$CH$_2$N(*t*Bu)H][13a] [1.80(1) Å] and $\{Al(\mu\text{-}H)[N(CMe_2CH_2)_2CH_2]_2\}_2$ [22] [1.836(3) Å], and are longer than the $Al-N_{diamide}$ bond lengths in the three-coordinate aluminum compound [ArN(CH$_2$)$_3$NAr]AlMe[11] [1.760(3), 1.766(3) Å]. The $Al-N_{NMe_3}$ distances in **1** and **2** are as expected.[13h,23,24]

Syntheses of $\{[ArNH(CH_2)_3NAr]Al(\mu\text{-}E)\}_2$ [E = S (3), Se (4) and Te (5)] and X-ray Structural Analysis of Compound 4

The successful fluorination of **1** using Me_3SnF is indicative of its reactivity despite the steric hindrance of the bulky ligand. Treatment of **1** with equivalent amounts of sulfur, selenium or tellurium proceeded in toluene at elevated temperature to afford the solvated aluminum sulfide **3** as light yellow crystals, the selenide **4** as yellow crystals and the telluride **5** as green-yellow crystals. The former two compounds were obtained in good yield and the latter in moderate yield [Equation (1)].

$$2[ArN(CH_2)_3NAr]AlH(NMe_3) + 2E \rightarrow \{[ArNH(CH_2)_3NAr]Al(\mu\text{-}E)\}_2 + 2NMe_3 \quad (1)$$

E = S (**3**), 80 °C, 12 h
= Se (**4**), reflux, 12 h
= Te (**5**), reflux, 120 h

Compounds **3**−**5** are air and moisture sensitive and soluble in hot toluene and benzene, while poorly soluble in THF, $CHCl_3$ and *n*-hexane. They were characterized by IR and NMR spectroscopy and MS (EI) spectrometry, as well as by elemental analyses. The MS (EI) spectra of **3**−**5** show the dimeric molecular ion with the correct isotope pattern and their ^{1}H NMR spectra show the very similar characters of the ligand, including the resonances of solvent toluene protons. The doublets in the range of δ = 1.10−1.25 ppm, one septet centered at ca. δ = 3.38 ppm and a multiplet at δ = 7.02−7.10 ppm correspond to the protons of the 2,6-*i*Pr$_2$C$_6$H$_3$ group. One broad singlet at ca. δ = 1.36 ppm can be assigned to the NH resonance,[13a,13c] with a satisfactory integral intensity indicating two protons, and two areas of

 © 2003 Wiley-VCH Verlag GmbH & Co. KGaA, Weinheim

unresolved multiplet resonances centered at ca. δ = 1.78 and 3.00 ppm arising from the six non-equivalent methylene protons, with the latter probably coming from the overlapping proton resonances of the two amido NCH_2 and two amine HNCH_2 groups. The IR spectra exhibit the NH absorption in the $\nu_{N\text{-}H}$ region[13a,13b] (**3**: 3190; **4**: 3187; **5**: 3185 cm^{-1}). All these data indicate that compounds **3**, **4** and **5** have the same structure corresponding to the formula $\{[ArNH(CH_2)_3NAr]Al(\mu\text{-}E)\}_2$.

The reaction of aluminum dihydride with selenium has been reported by our group,[3,6b,6c] where the formation of a dimeric compound might proceed through an Al−SeH intermediate. In a similar way the reaction of the aluminum monohydride **1** with selenium might involve the formation of intermediate $[ArN(CH_2)_3NAr]Al(SeH)(NMe_3)$, which dimerizes to produce $\{[ArN(CH_2)_3NAr]Al(\mu\text{-}SeH)\}_2$ with elimination of gaseous NMe_3. However, with reference to the related Al-SeH compounds $LAl(SeH)_2$ and LAl(SeH)Se(SeH)AlL [L = N(Ar)C(Me)CHC(Me)N(Ar), Ar = 2,6-iPr$_2$C$_6$H$_3$],[25] no absorptions in the range of 2000−2500 cm^{-1} in the IR spectrum are observed to indicate the formation of an Al-SeH moiety. This suggests that the dimer $\{[ArN(CH_2)_3NAr]Al(\mu\text{-}SeH)\}_2$ is not stable under heating and the hydrogen atom attached to the selenium atom migrates quickly to one of the nitrogen atoms of the diamide ligand to afford stable compound **4**. The most likely mecha-

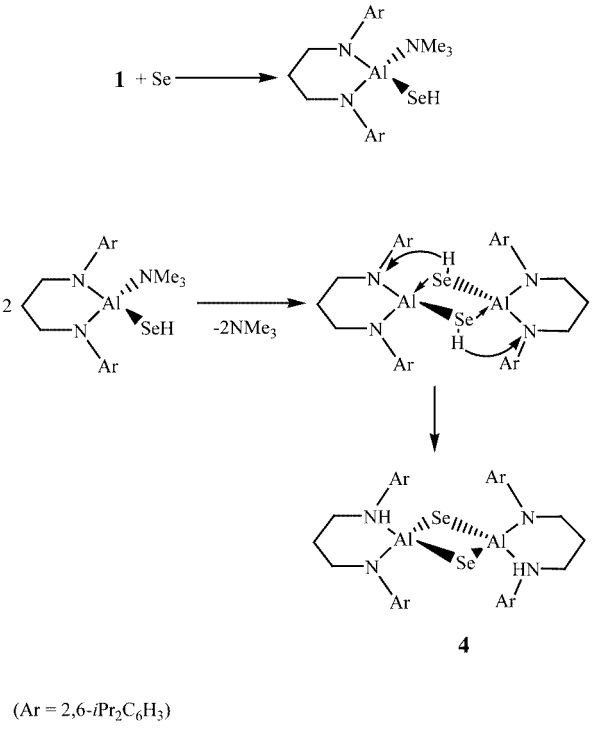

Scheme 2

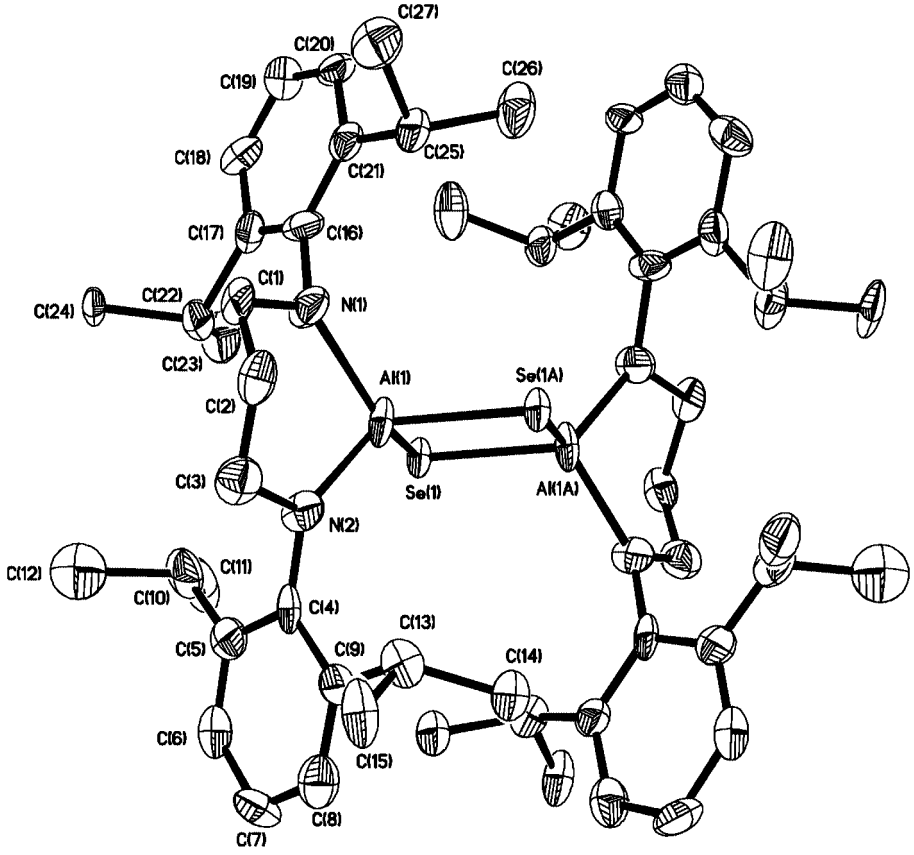

Figure 3. Molecular structure of **4** with the thermal ellipsoids at 30% probability level; H atoms are omitted for clarity

 © 2003 Wiley-VCH Verlag GmbH & Co. KGaA, Weinheim

nism is given in Scheme 2. The formation of compounds **3** and **5** is probably similar to that of **4**.

A suitable single crystal of compound **4** was measured by X-ray diffraction. The structure analysis of compound **4** shows a dimeric species containing two molecules of toluene. Unfortunately, the quality of the crystal structure did not allow the location of the hydrogen atoms on the nitrogen atoms. Nevertheless, the presence of NH groups was established by IR and ^{1}H NMR spectroscopy. The molecular structure is shown in Figure 3, and selected bond lengths and angles are listed in Table 1. The Al(1)−N(1) [1.932(11) Å] and Al(1)−N(2) [1.916(11) Å] bond lengths are midway between the Al−N_{amine} and Al−N_{amido} bond lengths observed in AlH(Cl)[*t*BuNCH$_2$CH$_2$N(*t*Bu)H][13a] [Al−N(1) (amine): 2.00(1) Å; Al−N(2) (amido): 1.80(1) Å], and are longer than those Al−N distances found in Al[*t*BuNCH$_2$CH$_2$N(*t*Bu)][*t*BuNCH$_2$CH$_2$NH(*t*Bu)],[13b] where the NH hydrogen atom is disordered over all four nitrogen centers [1.850(5), 1.870(5) Å], and much longer than Al−N_{amido} distances in **1** [1.820(1), 1.828(1) Å] and **2** [1.804(2), 1.810(2) Å]. However, compared to AlH(Cl)[*t*BuNCH$_2$CH$_2$N(*t*Bu)H],[13a] where a remarkable difference (0.20 Å) between Al−N(1) (amine) and Al−N(2) (amido) distances was observed, the very slight difference (0.016 Å) between Al(1)−N(1) and Al(1)−N(2) in **4** may imply the disorder of the two hydrogen atoms over the sides of all four nitrogen centers. Moreover, the similar coordination environments and approximately planar coordination geometries at N(1) and N(2) [at N(1), Al(1)−N(1)−C(1) 119.6(8)°, Al(1)−N(1)−C(16) 126.4(8)°, C(1)−N(1)−C(16) 113.2(9)°; at N(2), Al(1)−N(2)−C(3) 121.1(9)°, Al(1)−N(2)−C(4) 130.1(7)°, C(3)−N(2)−C(4) 108.0(9)°, (C−N−Al, C) = 359.2°] do not allow us to distinguish between the amine nitrogen and the amido nitrogen centers. In summary, it is assumed that the almost equal possibility of the hydrogen migration from the selenium atom to any nitrogen atom at the diamide ligand is included in the course of the reaction.

The Al_2Se_2 core exhibits an ideal planar ring (least-square deviation Δ of 0.0005) with an Al(1)−Se(1) distance of 2.339(1) Å, an Al(1)−Se(1A) distance of 2.381(1) Å and an Al(1)−Se(1)−Al(1A) bond angle of 78.56(5)°, which are as expected for Al_2Se_2 core compounds,[4a,4b,6b,6c] while the Al(1)−Se(1) and Al(1)−Se(1A) distances differ by ca. 0.042 Å probably due to the steric effects of the backbone ligand on the Al_2Se_2 ring. The ligand chelates the Al atom to fuse two six-membered AlN_2C_3 rings, which are arranged in *trans* positions on each side of the Al_2Se_2 core. The two AlN_2C_3 rings both display a boat conformation with Al(1) and Al(1A) at the bow and C(2) and C(2A) at the stern, respectively, and are arranged almost perpendicularly to the Al_2Se_2 ring (the dihedral angle between the ring (Al_2Se_2) and the N(1)−N(2)−C(3)−C(1) plane (Δ = 0.0238 Å) being 90.5°).

In summary we have shown that the [ArNCH$_2$CH$_2$NAr]$^{2-}$ ligand forms a stable chelate with the aluminium hydride. The hydride functionally can be replaced by a fluorine atom or substituted by a chalcogen (S, Se, Te) under migration of the hydrogen to an adjacent nitrogen of the chelating ring. The latter reaction does not yield an aluminium chalcogen double bond system but rather a four-membered ring of composition Al_2E_2 (E = S, Se, Te).

Experimental Section

General: All operations were carried out under purified nitrogen atmosphere using Schlenk techniques. Solvents were purified and dried by distillation over sodium under nitrogen prior to use. Elemental sulfur, selenium and tellurium were purchased from Aldrich and used as received. ArNH(CH$_2$)$_3$HNAr (Ar = 2,6-*i*Pr$_2$C$_6$H$_3$),[7] AlH$_3$·NMe$_3$ [26]and Me$_3$SnF[27] were prepared according to the literature.

^{1}H (200.13 MHz), ^{19}F (188.29 MHz) and ^{77}Se NMR (500 MHz) spectra were recorded on a Bruker AM 200 or a Bruker AM 250 spectrometer and the chemical shifts were externally referenced to SiMe$_4$ for ^{1}H nuclei, C$_6$F$_6$ for ^{19}F and Me$_2$Se for ^{77}Se. (In this paper the chemical shift for ^{19}F NMR spectroscopy was adjusted to the scale where CFCl$_3$ is used as external reference). The IR spectra were measured on a Bio-Rad Digilab FTS-7 spectrometer. EI (70 eV) mass spectra were measured on a Finnigan MAT 8230 or a Varian MAT CH5 instrument. Elemental analyses were performed by the Analytisches Labor des Instituts für Anorganische Chemie der Universität Göttingen. Melting points were measured in sealed glass tubes and were not corrected.

[ArN(CH$_2$)$_3$NAr]AlH(NMe$_3$) (1): A solution of ArNH(CH$_2$)$_3$HNAr (4.03 g, 10.24 mmol) (Ar = 2,6-*i*Pr$_2$C$_6$H$_3$) in toluene (20 mL) was added to a solution of AlH$_3$·NMe$_3$ (1.18 g, 13.24 mmol) in toluene (30 mL). While stirring, gas evolution was observed. The mixture was slowly heated to 80 °C and stirred for 5 h. All volatiles were removed in vacuo and the residue was extracted with *n*-hexane. After filtration through Celite, the extract was evaporated to dryness to afford [ArN(CH$_2$)$_3$NAr]AlH(NMe$_3$) as a white solid (4.41 g, 90%). X-ray quality crystals were grown from *n*-hexane. M.p. 196−197 °C. ^{1}H NMR (200.13 MHz, C$_6$D$_6$): δ = 1.22, 1.37, 1.47, 1.66 (d, 24 H, CH*Me$_2$*), 1.66 (s, 9 H, N*Me$_3$*), 2.10, 3.00 (m, 2 H, NCH$_2$*CH$_2$*), 3.25−3.45 (m, 4 H, N*CH$_2$*), 3.63, 4.25 (sept, 4 H, *CH*Me$_2$), 7.10−7.16 (m, 6 H, Ar) ppm. MS (EI): *m*/*z* = 420 [M$^+$ − NMe$_3$]. IR (KBr, Nujol mull): ν$_{Al-H}$ = 1799 cm^{-1}(br. sh.). C$_{33}$H$_{57}$AlN$_3$ (522.02) (**1**·1/2 *n*-hexane): calcd. C 75.93, H 11.00, N 8.05; found C 75.44, H 10.64, N 8.26.

[ArN(CH$_2$)$_3$NAr]AlF(NMe$_3$) (2). Method 1: A suspension of **1** (1.44 g, 3 mmol) and Me$_3$SnF (0.55 g, 3 mmol) in toluene (30 mL) was heated to 80 °C and stirred for 12 h. After filtration, the filtrate was concentrated to ca. 10 mL in vacuo and kept at 4 °C for 48 h to afford colorless block-shaped crystals of **2** (1.20 g, 80%). M.p. 220−222 °C. ^{1}H NMR (200.13 MHz, C$_6$D$_6$): δ = 1.22, 1.35, 1.47, 1.71 (d, 24 H, CH*Me$_2$*), 1.75 (s, 9 H, N*Me$_3$*), 2.00, 3.00 (m, 2 H, NCH$_2$*CH$_2$*), 3.27, 3.40 (m, 4 H, N*CH$_2$*), 3.64, 4.29 (sept, 4 H, *CH*Me$_2$), 7.10−7.32 (m, 6 H, Ar) ppm. ^{19}F NMR (188.29 MHz, C$_6$D$_6$): δ = −12.4 (adjusted value, −175.4) ppm. MS (EI): *m*/*z* = 497 [M$^+$], 438 [M$^+$ − NMe$_3$]. C$_{30}$H$_{49}$AlFN$_3$ (497.72): calcd. C 72.40, H 9.92, N 8.44; found C 72.31, H 9.71, N 8.28.

Method 2: A suspension of **1** (1.44 g, 3 mmol) and Me$_3$SnF (0.55 g, 3 mmol) in toluene (30 mL) was stirred for 4 days at room temperature until Me$_3$SnF was almost consumed. After filtration, the filtrate was concentrated to ca. 10 mL in vacuo and kept at 4 °C for a week to afford colorless crystals. All spectroscopic data confirmed the same compound as that obtained from method 1.

 © 2003 Wiley-VCH Verlag GmbH & Co. KGaA, Weinheim

Table 2. Summary of crystallographic data for compounds **1**·1/2 *n*-hexane, **2** and **4**·2 toluene

	1·1/2 *n*-hexane	**2**	**4**·2 toluene
Empirical formula	$C_{33}H_{57}AlN_3$	$C_{30}H_{49}AlFN_3$	$C_{68}H_{96}Al_2N_4Se_2$
Molecular weight	522.80	497.70	1181.37
Temperature [K]	203(2)	200(2)	133(2)
Crystal system	monoclinic	monoclinic	monoclinic
Space group	$P2_1/n$	$P2_1/n$	$C2$
a (Å)	12.285(3)	13.323(6)	19.104(4)
b (Å)	20.125(4)	12.480(2)	17.561(4)
c (Å)	14.274(3)	17.979(5)	12.286(3)
β [°]	110.47(3)	92.57(5)	129.10(3)
Volume [Å^3]	3306.2(12)	2986.5(16)	3198.5(11)
Z	4	4	2
Density (calcd.) [Mg·m^{-3}]	1.050	1.107	1.227
Absorption coefficient [mm^{-1}]	0.085	0.096	1.225
F(000)	1156	1088	1252
θ range [°]	3.52−25.00	3.61−25.04	1.80−24.81
Index ranges	$-14 \le h \le 14$	$-15 \le h \le 15$	$-22 \le h \le 22$
	$-23 \le k \le 23$	$-10 \le k \le 14$	$-20 \le k \le 20$
	$-16 \le l \le 16$	$-16 \le l \le 21$	$-14 \le l \le 13$
Reflections collected	11566	5643	18430
Independent reflections	5786 (R_{int} = 0.0346)	5249 (R_{int} = 0.1332)	5488 (R_{int} = 0.0718)
Data/restraints/parameters	5786/0/350	5249/0/327	5488/1/312
Goodness-of-fit on F^2	1.004	1.069	0.996
Final R indices [$I > 2\sigma(I)$]	R_1 = 0.0418	R_1 = 0.0486	R_1 = 0.0433
	wR_2 = 0.0994	wR_2 = 0.1282	wR_2 = 0.1112
R indices (all data)	R_1 = 0.0586	R_1 = 0.0532	R_1 = 0.0529
	wR_2 = 0.1101	wR_2 = 0.1340	wR_2 = 0.1164
Largest different peak and hole (e·Å^{-3})	0.200, −0.228	0.519, −0.300	0.694, −0.514

{[ArNH(CH$_2$)$_3$NAr]Al(μ-S)}$_2$ (3): A suspension of **1** (1.48 g, 3 mmol) and elemental S (0.096 g, 3 mmol) in toluene (30 mL) was heated to 80 °C and stirred for 12 h. After filtration, the orange-red filtrate was concentrated to ca. 10 mL and kept at 4 °C for 48 h to afford light yellow crystals of **3**·toluene (1.00 g, 67%). M.p. 278−279 °C (> 250 °C, decomp.). ^{1}H NMR (200.13 MHz, C_6D_6): δ = 1.17, 1.22 (d, 48 H, CHMe_2), 1.36 (s, 2 H, NH), 1.78 (m, 4 H, NCH$_2$$CH_2$), 2.1 (s, 3 H, MePh), 3.00 (t, 8 H, NCH_2), 3.38 (sept, 8 H, CHMe$_2$), 6.96−7.04 (m, 5 H, MePh), 7.02−7.10 (m, 12 H, Ar) ppm. MS (EI): m/z = 904 [M$^+$]. IR (KBr Nujol mull): $\tilde{\nu}_{N\text{-}H}$ = 3190 cm^{-1}. $C_{61}H_{90}Al_2N_4S_2$ (996.8) (**3**·toluene): calcd. C 73.50, H 9.10, N 5.62; found C 73.25, H 8.90, N 5.07.

{[ArNH(CH$_2$)$_3$NAr]Al(μ-Se)}$_2$ (4): A suspension of **1** (1.44 g, 3 mmol) and elemental Se powder (0.24 g, 3 mmol) in toluene (30 mL) was refluxed for 12 h until almost all the selenium was consumed. In the course of hot filtration, yellowish crystals grew from the orange filtrate, and these were collected by filtration. (0.10 g). The mother liquor was concentrated to ca. 10 mL and kept at 4 °C for 24 h to afford another crop of yellowish crystals of **4**·2 toluene (1.00 g). Total yield: 1.10 g (62%). M.p. 291 °C (> 259 °C, decomp.). ^{1}H NMR (200.13 MHz, C_6D_6): δ = 1.17, 1.22 (d, 48 H, CHMe_2), 1.36 (s, 2 H, NH), 1.78 (m, 4 H, NCH$_2$$CH_2$), 2.1 (s, 6 H, MePh), 3.00 (t, 8 H, NCH_2), 3.38 (sept, 8 H, CHMe$_2$), 6.94−7.04 (m, 10 H, MePh), 7.02−7.10 (m, 12 H, Ar) ppm. ^{77}Se NMR (500 MHz, C_6D_6, $CDCl_3$, or C_7D_8): no resonances were observed. MS (EI): m/z = 998 [M$^+$]. IR (KBr Nujol mull): $\tilde{\nu}_{N\text{-}H}$ = 3187 cm^{-1}. $C_{68}H_{98}Al_2N_4Se_2$ (1182.9) (**4**·2 toluene): calcd. C 69.04, H 8.35, N 4.74; found C 68.79, H 8.22, N 4.63.

{[ArNH(CH$_2$)$_3$NAr]Al(μ-Te)}$_2$ (5): A suspension of **1** (1.44 g, 3 mmol) and elemental Te powder (0.39 g, 3 mmol) in toluene (40 mL) was refluxed for 5 days and a small amount of unreacted Te powder still remained. After filtration, the green-yellow filtrate was concentrated to ca. 10 mL and *n*-hexane (5 mL) was added. The solution was kept at 4 °C for 24 h to afford green-yellow crystals of **5**·toluene (0.85 g, 48%). M.p. 320 °C (decomp.). ^{1}H NMR (200.13 MHz, C_6D_6): δ = 1.17, 1.22 (d, 48 H, -CHMe_2), 1.35 (s, 2 H, NH), 1.75 (m, 4 H, NCH$_2$$CH_2$), 2.1 (s, 3 H, MePh), 3.00 (t, 8 H, NCH_2), 3.37 (sept, 8 H, CHMe$_2$), 6.94−7.04 (m, 5 H, MePh), 7.02−7.10 (m, 12 H, Ar) ppm. MS (EI): m/z = 1096 [M$^+$]. IR (KBr Nujol mull): $\tilde{\nu}_{N\text{-}H}$ = 3185 cm^{-1}. $C_{61}H_{90}Al_2N_4Te_2$ (1188.1) (**5**·toluene): calcd. C 61.67, H 7.63, N 4.71; found C 61.72, H 7.61, N 4.76.

X-ray Structural Determinations and Refinements for 1, 2 and 4: The crystallographic data for compounds **1** and **2** were collected on a Stoe−Siemens−Huber four-circle diffractometer coupled to a Siemens CCD area-detector and for **4** on a Stoe IPDS II-array detector system. In both cases graphite-monochromated Mo-K_α radiation (λ = 0.71073 Å) was used. All structures were solved by direct methods (SHELXS-96)[28] and refined against F^2 using SHELXL-97.[29] In **1** and **2**, all non-hydrogen atoms were refined anisotropically and hydrogen atoms were included using the riding model with U_{iso} tied to the U_{iso} of the parent atoms, except for the Al−H hydrogen atom in **1**, which was located by difference Fourier synthesis and refined isotropically. In **4** the non-hydrogen atoms in the dimeric structure were refined anisotropically while those in the two solvent molecules were refined isotropically. Treatment of hydrogen atoms was the same as those in **1** and **2**, except for the two NH hydrogen atoms, which could not be located. A summary of cell parameters, data collections, and structure solutions is given in Table 2.

CCDC-207050 (**1**), -207051 (**2**), and -207052 (**4**) contain the supplementary crystallographic data for this paper. These data can be obtained free of charge at www.ccdc.cam.ac.uk/conts/retrieving.html [or from the Cambridge Crystallographic Data Centre, 12,

 © 2003 Wiley-VCH Verlag GmbH & Co. KGaA, Weinheim

Union Road, Cambridge CB2 1EZ, UK; fax: (internat.) +44-1223/336-033; E-mail: deposit@ccdc.cam.ac.uk].

Acknowledgments

This work was supported by the Deutsche Forschungsgemeinschaft, the Fonds der Chemischen Industrie and the Göttinger Akademie der Wissenschaften.

[1] J. J. Eisch, *Comprehensive Organometallic Chemistry II* (Eds.: E. W. Abel, F. G. A. Stone, G. Wilkinson), Elsevier: Oxford, UK, **1995**, *Vol. II*, 557−569.

[2] [2a] B. E. Bent, R. G. Nuzzo, L. H. Dubois, *J. Am. Chem. Soc.* **1989**, *111*, 1634−1644. [2b] L. Contreras, A. H. Cowley, F. P. Gabbai, R. A. Jones, C. J. Carrano, M. R. Bond, *J. Organomet. Chem.* **1995**, *489*, C1−C3.

[3] C. Cui, H. W. Roesky, H. Hao, H.-G. Schmidt, M. Noltemeyer, *Angew. Chem.* **2000**, *112*, 1885−1887; *Angew. Chem. Int. Ed.* **2000**, *39*, 1815−1817.

[4] [4a] M. G. Gardiner, C. L. Raston, V.-A. Tolhurst, *J. Chem. Soc., Chem. Commun.* **1995**, 1457−1458. [4b] M. G. Gardiner, C. L. Raston, V.-A. Tolhurst, *J. Chem. Soc., Chem. Commun.* **1995**, 2501−2502. [4c] P. D. Godfrey, C. L. Raston, B. W. Skelton, V.-A. Tolhurst, A. H. White, *Chem. Commun.* **1997**, 2235−2236. [4d] W. J. Grigsby, C. L. Raston, V.-A. Tolhurst, B. W. Skelton, A. H. White, *J. Chem. Soc., Dalton Trans.* **1998**, 2547−2556.

[5] R. J. Wehmschulte, P. P. Power, *Chem. Commun.* **1998**, 335−336.

[6] [6a] V. Jancik, Y. Peng, H. W. Roesky, J. Li, D. Neculai, A. M. Neculai, R. Herbst-Irmer, *J. Am. Chem. Soc.* **2003**, *125*, 1452−1453. [6b] C. Cui, H. W. Roesky, M. Noltemeyer, H.-G. Schmidt, *Organometallics* **1999**, *18*, 5120−5123. [6c] C. Cui, H. W. Roesky, M. Noltemeyer, H.-G. Schmidt, *Inorg. Chem.* **2000**, *39*, 3678−3681. [6d] W. Zheng, N. C. Mösch-Zanetti, H. W. Roesky, M. Noltemeyer, M. Hewitt, H.-G. Schmidt, T. R. Schneider, *Angew. Chem.* **2000**, *112*, 4446−4449; *Angew. Chem. Int. Ed.* **2000**, *39*, 4276−4279.

[7] J. D. Scollard, D. H. McConville, J. J. Vittal, *Organometallics* **1997**, *16*, 4415−4420.

[8] J. D. Scollard, D. H. McConville, *J. Am. Chem. Soc.* **1996**, *118*, 10008−10009.

[9] P. W. Roesky, *Organometallics* **2002**, *21*, 4756−4761.

[10] F. G. N. Cloke, B. R. Elvidge, P. B. Hitchcock, V. M. E. Lamarche, *J. Chem. Soc., Dalton Trans.* **2002**, 2413−2414.

[11] D. Chakraborty, E. Y.-X. Chen, *Organometallics* **2002**, *21*, 1438−1442.

[12] R. J. Wehmschulte, P. P. Power, *Polyhedron* **2000**, *19*, 1649−1661, and references therein.

[13] For some examples, see: [13a] J. L. Atwood, S. M. Lawrence, C. L. Raston, *J. Chem. Soc., Chem. Commun.* **1994**, 73−74. [13b] M. G. Gardiner, S. M. Lawrence, C. L. Raston, *J. Chem. Soc., Dalton Trans.* **1996**, 4163−4169. [13c] M. G. Gardiner, C. L. Raston, *Coord. Chem. Rev.* **1997**, *166*, 1−34. [13d] H. V. R. Dias, W. Jin, R. E. Ratcliff, *Inorg. Chem.* **1995**, *34*, 6100−6105. [13e] J. F. Janik, R. L. Wells, P. S. White, *Inorg. Chem.* **1998**, *37*, 3561−3566. [13f] W. Zheng, H. W. Roesky, M. Noltemeyer, *Organometallics* **2001**, *20*, 1033−1035. [13g] N. Kuhn, S. Fuchs, M. Steimann, *Z. Anorg. Allg. Chem.* **2000**, *626*, 1387−1392. [13h] J. L. Atwood, G. A. Koutsantonis, F.-C. Lee, C. L. Raston, *J. Chem. Soc., Chem. Commun.* **1994**, 91−92.

[14] S. Cucinella, A. Mazzei, W. Marconi, *Inorg. Chim. Acta Rev.* **1970**, *4*, 51−71.

[15] S. D. Waezsada, F. -Q. Liu, E. F. Murphy, H. W. Roesky, M. Teichert, I. Usón, H.-G. Schmidt, T. Albers, E. Parisini, M. Noltemeyer, *Organometallics* **1997**, *16*, 1260−1264.

[16] A. H. Cowley, H. S. Isom, A. Decke, *Organometallics* **1995**, *14*, 2589−2592.

[17] G. Linti, H. Nöth, P. Rahm, *Z. Naturforsch., Teil B* **1988**, *43*, 1101−1112.

[18] C.-C. Chang, M.-D. Li, M. Y. Chiang, S.-M. Peng, Y. Wang, G.-H. Lee, *Inorg. Chem.* **1997**, *36*, 1955−1960.

[19] R. J. Wehmschulte, P. P. Power, *Inorg. Chem.* **1996**, *35*, 3262−3267.

[20] C. Schnitter, K. Klimek, H. W. Roesky, T. Albers, H.-G. Schmidt, C. Röpken, E. Parisini, *Organometallics* **1998**, *17*, 2249−2257.

[21] G. Shanmugasunderan, G. Z. Nagarajan, *Phys. Chem.* **1969**, *240*, 363−370.

[22] C. Klein, H. Nöth, M. Tacke, M. Thomann, *Angew. Chem.* **1993**, *105*, 923−926; *Angew. Chem. Int. Ed. Engl.* **1993**, *32*, 886−889.

[23] Almenningen, G. Gundersen, T. Haugen, A. Haaland, *Acta Chem. Scand.* **1972**, *26*, 3928−3934.

[24] G. A. Anderson, F. R. Forgaard, A. Haaland, *Acta Chem. Scand.* **1972**, *26*, 1947−1954.

[25] See ref.[3] and some spectroscopic data are listed for [LAl(-SeH)$_2$]: ^{1}H NMR (500 MHz, C_6D_6), δ_{SeH} = −2.82 ppm. IR (KBr, Nujol): $\tilde{\nu}_{SeH}$ = 2318 cm^{-1}; [L(HSe)AlSeAl(SeH)L]: ^{1}H NMR (500 MHz, C_6D_6), δ_{SeH} = −2.83 ppm. ^{77}Se NMR (500 MHz, C_6D_6): $\delta_{Al\text{-}SeH}$ = −341 and $\delta_{Al\text{-}Se\text{-}Al}$ = −535 ppm. IR (KBr, Nujol): $\tilde{\nu}_{SeH}$ = 2276, 2292 cm^{-1}.

[26] R. A. Kovar, J. O. Callaway, *Inorg. Synth.* **1975**, *17*, 63−67.

[27] E. Krause, *Ber. Dtsch. Chem. Ges.* **1918**, *51*, 1447−1456.

[28] G. M. Sheldrick, SHELXS-90, Program for Structure Solution, *Acta Crystallogr., Sect. A* **1990**, *46*, 467−473.

[29] G. M. Sheldrick, SHELXL-97, *Program for Crystal Structure Refinement*; University of Göttingen: Göttingen, Germany, **1997**.

Received March 31, 2003

 © 2003 Wiley-VCH Verlag GmbH & Co. KGaA, Weinheim

Partially Fluorinated Rare Earth Metal Complexes

Ana Mirela Neculai,[a] Dante Neculai,[a] Grigori B. Nikiforov,[a] Herbert W. Roesky,*[a] Christine Schlicker,[a] Regine Herbst-Irmer,[a] Jörg Magull,[a] and Mathias Noltemeyer[a]

Keywords: Lanthanides / Fluorides / Tin / N donor ligands

The reaction of $LScBr_2$ (**1**), LYI_2 (**3**), $LHoI_2$ (**4**), or $LErI_2$ (**5**) [L = *N*,*N*′′-(1,3-dimethyl-1,3-propanediylidene)bis(*N*′,*N*′-diethyl-1,2-ethanediamine)] with Me_3SnF was investigated. Treatment of **1** with Me_3SnF results in the formation of $(Me_3BrSn\text{-}\mu\text{-}F)_2LSc$ (**2**) while compounds **3**–**5** give $[LSnMe_2][Me_3SnI_2]$ (**6**) as the only product that could be isolated and characterized. Metathesis reactions of **1** with $AgSO_3CF_3$ led to $LSc(SO_3CF_3)_2$ (**7**). Compounds **1**, **2**, **6** and **7** were characterized by single-crystal X-ray structural analysis.

(© Wiley-VCH Verlag GmbH & Co. KGaA, 69451 Weinheim, Germany, 2003)

Introduction

The rapid development in the chemistry of the rare earth metals has resulted in the synthesis of a plethora of original compounds with various types of ligands, along with the widely exploited cyclopentadienyl substituents. Previous published work from our group concerning β-diketiminato derivatives of these elements includes new information about derivatives of scandium,[1] praseodymium,[2] samarium,[3] terbium,[4] holmium, erbium,[5] and ytterbium[3] with the ligand *N*,*N*′′-(1,3-dimethyl-1,3-propanediylidene)-bis(*N*′,*N*′-diethyl-1,2-ethanediamine) $\{[N(CH_2CH_2NEt_2)C(Me)]_2CH\}^-$, abbreviated as L. These complexes are ideal candidates for use in a less-exploited research area of these metals, namely that of dihalo compounds as promising precursors for catalytically active species. However, we faced problems with metathesis reactions for the preparation of other derivatives when the chloro or bromo compounds were treated with alkyllithium or Grignard reagents, due to a number of side reactions. The pursuit of the complexes resulting from this kind of disubstitution reaction in which dihalo derivatives of rare-earth metals are involved[4] prompted us to study the fluorine-containing systems. More specifically, examples are known where trimethyltin fluoride is used as an effective fluorinating agent for the preparation of *d* and *f* transition metal complexes from chloride congeners.[6−8] However, reactions between other complexes and Me_3SnF are less well known. An interesting example is the oxidation of $[Sm(C_5H_4tBu)_2(THF)_2]$ with Me_3SnF for the preparation of $[(C_5H_4tBu)_2Sm(\mu\text{-}F)]_3$,[9] or the reaction of $CpTiF_3$ and $ZnMe_2$ in the presence of Me_3SnF.[10] In general, since lanthanide-fluorine bonds are very strong (124−135 kcal/mol for trivalent Eu, Yb, Er, Ho and Sm),[11] the metathesis reaction of lanthanide complexes containing Cl, Br, I, SCN or Me ligands with trimethyltin fluoride under mild conditions seemed feasible.

Besides the fluorine ion, another candidate for a successful metathesis is the quite well-known electron-withdrawing triflate group due to the oxophilic character of the rare earth metals.[12] Until now heteroleptic triflate compounds of lanthanides have been obtained using the $Ln(OTf)_3$ (Ln = lanthanide, OTf = triflate) as a starting material.[13] The synthesis of such complexes by substitution of other ligands at the coordination sphere of a metal that already contains an "ancillary" ligand (e.g. halogen) was not explored. In comparison to the homoleptic triflate derivatives, which are widely used as reusable catalysts,[14] it was expected that the heteroleptic compounds should suffer from a decrease of the Lewis acidity but still be advantageous in catalysis due to their high solubility in organic solvents.[15]

Herein, we analyze the results of the reactions of the dibromo derivative of scandium and the diiodo derivatives of yttrium, holmium, and erbium of composition $LLnX_2$ [L = *N*,*N*′′-(1,3-dimethyl-1,3-propanediylidene)bis(*N*′,*N*′-diethyl-1,2-ethanediamine); Ln = Sc, Y, Ho, Er; X = Br, I] with trimethyltin fluoride. To the best of our knowledge reactions of trimethyltin fluoride with lanthanide diiodide complexes have not been explored before in non-aqueous solvents. We also report the metathesis reaction of $LScBr_2$ and $Ag(SO_3CF_3)$ with formation of monomeric $LSc(SO_3CF_3)_2$. The precursor $LScBr_2$ will be discussed in relationship to the fluorine-containing complexes.

Results and Discussion

The precursor $LScBr_2$ (**1**) was synthesized in a similar manner as the previously reported rare earth metal com-

[a] Institut für Anorganische Chemie, Universität Göttingen, Tammannstrasse 4, 37077, Göttingen, Germany
Fax: (internat.) +49-(0)551/393-373
E-mail address: hroesky@gwdg.de

plexes with the same ligand from the lithium salt and scandium tribromide in toluene.[1,2] The X-ray structural analysis reveals the same type of coordination as the chloride congener (Figure 1, Table 1).[1]

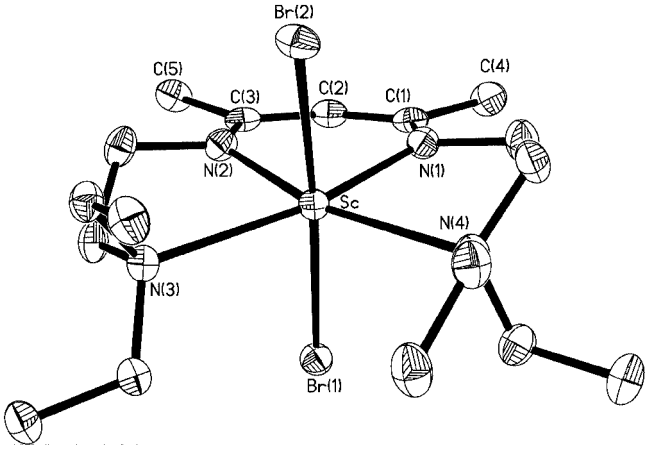

Figure 1. Molecular structure of **1**; thermal ellipsoids are drawn at the 50% probability level

Table 1. Selected bond lengths (Å) and angles (°) for **1**

C(1)−C(2)	1.394(3)	N(2)−Sc(1)−N(1)	85.21(6)
N(1)−C(1)	1.339(2)	N(1)−Sc(1)−N(4)	76.26(5)
Sc(1)−N(1)	2.155(1)	N(2)−Sc(1)−N(3)	79.44(5)
Sc(1)−N(2)	2.133(1)	N(4)−Sc(1)−N(3)	119.09(5)
Sc(1)−N(3)	2.541(1)	Br(1)−Sc(1)−Br(2)	172.274(1)
Sc(1)−N(4)	2.447(2)		
Sc(1)−Br(1)	2.610(1)		
Sc(1)−Br(2)	2.629(1)		

The reaction of $LScBr_2$ (**1**) with Me_3SnF in a 1:2 molar ratio [Equation (1)] led to compound **2** that comprises the anticipated difluorinated scandium derivative but bridged by fluorine to two Me_3SnBr molecules. The reaction of $LScCl_2$ with two equivalents of Me_3SnF gave the chloro analogue **2′** [Equation (2)].

$$\underset{\mathbf{1}}{LScBr_2} + 2\,Me_3SnF \xrightarrow[\text{room temp.}]{\text{toluene}} \underset{\mathbf{2}}{(Me_3BrSn\text{-}\mu\text{-}F)_2LSc} \quad (1)$$

$$LScCl_2 + 2\,Me_3SnF \xrightarrow[\text{room temp.}]{\text{toluene}} \underset{\mathbf{2'}}{(Me_3ClSn\text{-}\mu\text{-}F)_2LSc} \quad (2)$$

Crystals of **2** are extremely sensitive once the mother liquor is removed and they are rapidly decomposed within minutes. After that the substance cannot be dissolved again in toluene or any other solvent, indicating that decomposition and formation of insoluble fluorides has probably occurred. Therefore discussion of its structure will be based only on the X-ray analysis. Complex **2** crystallises in two phases (triclinic **2a** and monoclinic **2b**). The two phases differ only slightly in their bond lengths and angles. In the monoclinic phase **2a** the molecule lies on a twofold axis resulting in a completely planar arrangement of Sc within the β-diketiminato NCCCN plane, while deviation of the scandium atom from the same plane is 0.49 Å in **2a**. The major difference between **2a** and **2b** is found in the F−Sc−F angle [162.2 (**2a**) and 171.2° (**2b**)]. In the following discussion we will refer only to the triclinic phase due to the slightly better results of the refinement. At first glance the structure shows a trinuclear non-linear compound where the scandium atom has a pseudooctahedral geometry and the pentacoordinate tin is trigonal bipyramidal (F−Sn−Br av. 177.1°; Figure 2).

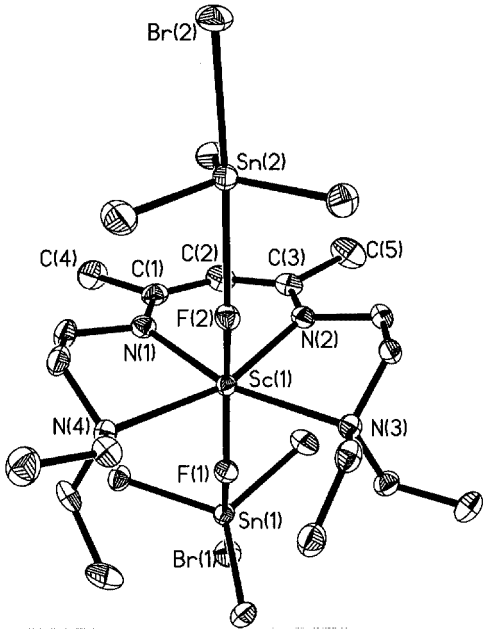

Figure 2. Molecular structure of **2a**; thermal ellipsoids are drawn at the 50% probability level

Scandium is σ-bonded to the β-diketiminato backbone similar to the dibromo derivative (distance from scandium to the backbone plane 0.49 Å). The analogous distances for **1** and **2** indicate that this kind of bonding is caused by the coordination of the metal to all four nitrogen atoms (eight-electron donor) of the ligand. Consequently the β-diketiminato backbone is acting as a four-electron donor.[16] The Sc−F bond lengths are similar to those reported in the literature (1.97 Å and 1.99 Å for **2a** and av. 2.03 Å for Cp_2ScF).[17] The Sn−F bond length (2.42 and 2.46 Å) is of the same order as the longest Sn−F distance in polymeric Me_3SnF,[18] which has the same pentacoordination. The Sc−F−Sn bond angle averages to 148.6°. A comparable intermediate was observed in the fluorination of a zirconium derivative[8a] with Me_3SnF. However, in the scandium case we cannot argue that **2** is an intermediate in the fluorination process although under electron impact conditions fragments corresponding to $LScF^+$ (359) and Me_3Sn^+ (165) are observed. Although compound **2** is quite unstable, we were not able to isolate the monomeric fluoride. Our results are in agreement with those found for the metathesis of $LScCl_2$ with Me_3SnF.

 © 2003 Wiley-VCH Verlag GmbH & Co. KGaA, Weinheim

An X-ray structural analysis of **2′** established the connectivity of the structure but this cannot be discussed in any detail due to the poor quality of the crystals. A qualitative view reveals that **2′** has the same skeletal arrangement as **2b**, with the bromine bridges being replaced by chlorine. In **2** the Me_3Sn units are coordinated in a similar manner to those reported for a zirconium compound (Table 2).[8a]

Table 2. Selected bond lengths (Å) and angles (°) for **2a**

C(1)−C(2)	1.382(7)	N(2)−Sc(1)−N(1)	84.30(16)
N(1)−C(1)	1.323(6)	N(1)−Sc(1)−N(4)	77.77(15)
Sc(1)−N(2)	2.170(4)	N(2)−Sc(1)−N(3)	76.44(15)
Sc(1)−N(1)	2.148(4)	N(4)−Sc(1)−N(3)	121.46(14)
Sc(1)−N(4)	2.421(4)	F(1)−Sc(1)−F(2)	162.20(2)
Sc(1)−N(3)	2.381(4)	Sc(1)−F(1)−Sn(1)	149.28(14)
Sc(1)−F(1)	1.967(3)	Sc(1)−F(2)−Sn(2)	147.90(14)
Sc(1)−F(2)	1.991(3)	F(1)−Sn(1)−Br(1)	177.47(7)
F(1)−Sn(1)	2.419(3)	F(2)−Sn(2)−Br(2)	176.72(6)
F(2)−Sn(2)	2.455(5)		

The variation of the rare earth metal from scandium to yttrium, holmium and erbium, and of the halide from bromine to iodine led to an entirely different behaviour of the complexes $LLnX_2$ [Ln = Y (**3**), Ho (**4**), Er (**5**)] in the reaction with Me_3SnF (1:2). Independent of whether the reaction was carried out in toluene or THF, the isolated product is the same in all three cases, namely $[LSnMe_2][Me_3SnI_2]$ (**6**). Obviously a complete substitution of the rare earth metal with tin has occurred. A solid yellow residue remained which contains non-stoichiometric amounts of Ln, C, H, F, I and N.

$$LLnI_2 + 2\,Me_3SnF \xrightarrow[\text{B. 1. THF, room temp.}]{\text{A. toluene, room temp.}} [LSnMe_2][Me_3SnI_2]$$
$$\text{2. pentane, -}Me_3SnI \qquad \textbf{6}$$
$$\text{3. toluene}$$

Scheme 1. Reaction of $LLnI_2$ with Me_3SnF (Ln = Y, Ho, Er)

Crystalline **6** (Figure 3, Table 3) consists of well-separated cations and anions and crystallizes with one molecule of toluene. In the cation of **6** the β-diketiminato ligand coordinates to the tin(IV) center through three nitrogen atoms, less than in other lanthanide compounds with this ligand but similar to a reported aluminum complex.[1−5,19,20] The Sn(2) atom has a coordination number of five that can be regarded as being distorted trigonal bipyramidal with N(1) and N(4) axial and C(71), C(72), Sn(2) and N(2) coplanar [the angle N(1)−Sn(2)−N(4) is 163.5(3)°].

Table 3. Selected bond lengths (Å) and angles (°) for **6**

C(1)−C(2)	1.413(16)	N(2)−Sn(2)−N(1)	87.3(4)
N(1)−C(1)	1.337(15)	N(1)−Sn(2)−N(4)	163.5(3)
N(2)−C(3)	1.349(16)	C(71)−Sn(2)−N(4)	94.5(4)
C(2)−C(3)	1.344(15)	C(72)−Sn(2)−C(71)	126.4(5)
Sn(2)−N(2)	2.095(9)	N(2)−Sn(2)−C(71)	115.2(4)
Sn(2)−N(1)	2.161(10)	C(61)−Sn(1)−C(62)	116.4(7)
Sn(2)−N(4)	2.381(10)	C(61)−Sn(1)−I(1)	92.0(4)
Sn(2)−C(72)	2.126(11)	I(1)−Sn(1)−I(2)	177.32(4)
Sn(2)−C(71)	2.138(11)		
Sn(1)−C(61)	2.125(15)		
Sn(1)−I(1)	2.997(14)		
Sn(1)−I(2)	3.044(14)		

Cationic tin(IV) complexes are known with N-donor ligands and a number of those have been structurally characterized.[21] In the cationic part of **6**, the Sn(2)−N bond lengths of the pendant arm are longer than those of the backbone, similar to the corresponding distances in related compounds[1−5,19,20] and in **1** and **2** [Sn(2)−N(1) 2.161, Sn(2)−N(2) 2.095, Sn(2)−N(4) 2.381 Å]. The difference between the C−C and C−N bond lengths in the NCCCN unit is greater than in **1** or **2** and other complexes with the same ligand. This may indicate the alternation of single and double bonds in the bonding pattern of the metal to the nitrogen atoms. However, the difference between Sn(2)−N(1) and Sn(2)−N(2) is just greater than the three esd's limit consistent with N(2) as an amido nitrogen and N(1) as part of a C=N unit. The Sn(2)−N bond lengths are

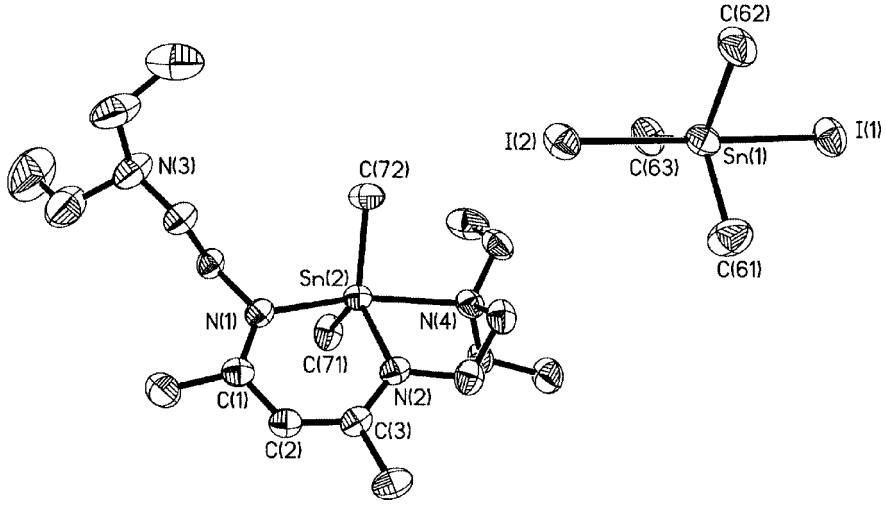

Figure 3. Molecular structure of **6**; thermal ellipsoids are drawn at the 50% probability level

 © 2003 Wiley-VCH Verlag GmbH & Co. KGaA, Weinheim

similar to those found in the literature for β-diketiminato complexes of Sn^{4+}, such as $LSnMe_2Cl$ (Sn−N 2.110, 2.112 Å)[22a] and $LSnI_3$ (Sn−N 2.163, 2.176 Å; L = β-diketiminato ligand).[22b] The NCCCN backbone of the β-diketiminato ligand remains essentially planar (the deviation from planarity is 0.024 Å) with the tin atom 0.604 Å above the plane. The nitrogen atoms of the pendant arm lie out of the NCCCN plane with N(3) 1.43 Å below and N(4) 1.07 Å above the plane. The Sn(1)−I and Sn−Me bond lengths are similar to those found for Sn^{4+} complexes.[23]

In the anion the Sn(1) atom also has a five coordinate trigonal bipyramidal environment with I(1) and I(2) axial and C(61), C(62), Sn(1) and C(63) coplanar.

The unexpected composition of $[LSnMe_2][Me_3SnI_2]$ that resulted from the X-ray analysis is consistent with the data from mass spectrometry and elemental analysis. The EI mass spectrum of **6** exhibits the $[MeSnI_2^+]$ and $[Me_2SnI_2^+]$ ions and fragments of the β-diketiminato ligand, while in the FAB mass spectrum of **6** the $[LSnMe_2^-]$ ion and fragments of $[LSnMe_2][Me_3SnI_2]$ are observed. In the ^1H NMR spectrum of **6** a set of broad and overlapping resonances is observed.

Obviously, the slight variation of the properties of the metals in complexes $LLnX_2$ between scandium and yttrium as well as the presence of iodine instead of bromine resulted in a different complex. A possible explanation for this behaviour may be due to the formation of very strong Y−F (and Ho−F and Er−F) bonds that leads to complete elimination of the ligand from the coordination sphere of the starting material and migration to the tin atom in complex **6**. The analytical data of the insoluble residues indicate the formation of very impure polymeric fluorides.

As far as the iodine precursors are concerned, the preparation of the holmium and erbium complexes was already reported.[5] The yttrium compound was obtained from the potassium salt of the ligand and yttrium triiodide. LYI_2 was characterized by ^1H, and ^{13}C NMR spectroscopy, mass spectrometry and elemental analysis and is, to the best of our knowledge, the first β-diketiminatoyttrium complex.[24]

Extending our investigation to other fluorine-containing ligands, reaction of the dibromoderivate $LScBr_2$ with $AgSO_3CF_3$ occurs, as expected, with substitution of both bromine atoms due to the oxophilic character of scandium and the thermodynamically favored formation of AgBr [Equation (3)].

$$\underset{\mathbf{1}}{LScBr_2} + 2\,Ag(SO_3CF_3) \xrightarrow[\text{room temp.}]{\text{toluene}} \underset{\mathbf{7}}{LSc(SO_3CF_3)_2} + 2\,AgBr\downarrow \quad (3)$$

Compound **7** is a yellow solid very soluble in aromatic solvents, diethyl ether and THF. The Lewis acidity of scandium is lower than in $Sc(SO_3CF_3)_3$ as a consequence of the substitution of one triflate ligand by the nitrogen-containing ligand L. Moreover, the two triflate ligands increase the electronic density on the scandium atom in **7** in comparison to **1**, documented by the substantial upfield shift of the scandium resonance in the ^{45}Sc NMR spectrum (δ = 335.8 ppm in **1** to 185.0 ppm in **7**).

The crystal structure analysis (Figure 4) reveals that the scandium atom in **7** is hexacoordinated with a pseudooctahedral geometry and the two triflate ligands are arranged in the apical positions [O(3)−Sc−O(1) 170.8° compared to Br(1)−Sc(1)−Br(2) 172.3° of **1**].

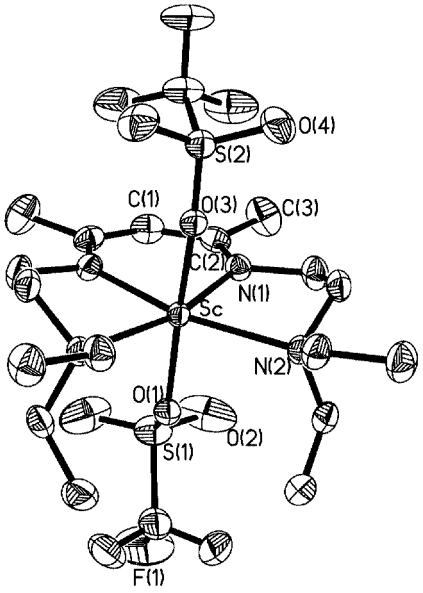

Figure 4. Molecular structure of **7**; thermal ellipsoids are drawn at the 50% probability level

For steric reasons, the triflate groups are not coordinated to scandium in a chelating fashion; they bind in a monodentate fashion through oxygen[13c,25] (Table 4). The NCCCN atoms of the β-diketiminato backbone as well as the nitrogen atoms of the ligand arms are almost coplanar. The distance from Sc to the NCCCN plane (0.28 Å) indicates a σ-bond interaction between scandium and the β-diketiminato ligand (in **1** the corresponding distance is 0.42 Å).[16]

Table 4. Selected bond lengths (Å) and angles (°) for **7** (symmetry transformations used to generate equivalent atoms #1 x, $-y + 1/2$, z)

C(1)−C(2)	1.393(2)	O(1)−Sc−O(3)	170.88(7)
N(1)−Sc	2.126(2)	N(1)−Sc−N(1)#1	85.38(8)
N(2)−Sc	2.378(1)	N(1)−Sc−N(2)	79.66(5)
O(1)−Sc	2.126(2)	N(2)#1−Sc−N(2)	115.12(7)
O(3)−Sc	2.108(2)		

A comparison of the bond lengths and angles of **1**, **2** and **7** showed that within the β-diketiminato frame these units are hardly influenced by the different substituents on scandium (see Tables 1, 2, and 4).

Conclusion

Herein we report some progress in the investigation of the reactivity of complexes of scandium, yttrium, holmium

 © 2003 Wiley-VCH Verlag GmbH & Co. KGaA, Weinheim

and erbium containing the β-diketiminato ligand L. On the basis of the hard-soft acid-base principle it is expected that rare earth metals should form very stable bonds with fluorine. Taking into account also the successful use of Me_3SnF as a fluorinating reagent, we considered that the chances of obtaining compounds of type $LLnF_2$ were realistic. However, reactions of Me_3SnF with $LScBr_2$ (**1**), LYI_2 (**3**), $LHoI_2$ (**4**), and $LErI_2$ (**5**), respectively, led to the isolation of compounds $(Me_3BrSn\text{-}\mu\text{-}F)_2LSc$ (**2**) and $[LSnMe_2][Me_3SnI_2]$ (**6**). The latter species was formed independently of the rare earth metal diiodide used as a starting material (LYI_2, $LHoI_2$, $LErI_2$) by substitution of the metal. Based on the yield of **6** we cannot argue that the fluorine derivatives of the rare earth metals were not formed but it is likely that, as in the case of compound **2**, it aggregates with formation of an insoluble product.

In view of the failure of the metathesis reaction of the scandium derivatives with the usual organometallic reagents we have reacted **1** with $AgSO_3CF_3$ to yield compound **7**.

Experimental Section

General Experimental Procedures: All operations involving air- and moisture-sensitive compounds were performed using standard Schlenk-line and dry-box techniques under purified dinitrogen atmosphere. Hexane and dichloromethane were dried from appropriate drying agents — Na/K alloy (hexane) and CaH_2 (dichloromethane) — and distilled under dinitrogen prior to use. $CDCl_3$, [D_8]THF and C_6D_6 were dried from appropriate drying agents (CaH_2 and Na/K alloy respectively) and degassed. Literature methods for the preparation of the starting materials are cited within the text. $AgSO_3CF_3$ was purchased from Aldrich and used without purification. ^1H, ^{19}F, and ^{45}Sc NMR spectra were recorded on a Bruker AM 200 instrument. Mass spectra were recorded on a Finnigan MAT 8230 instrument, and elemental analyses were carried out at the Analytical Laboratories of the Institute of Inorganic Chemistry at the University of Göttingen. Melting points were determined in sealed capillary tubes under dinitrogen and are uncorrected. IR spectra were recorded using a Perkin−Elmer Bio-Rad Digilab FTS-7.

Preparation of $LScBr_2$ (1): Toluene (30 mL) was added to LLi (2.90 g, 9.6 mmol) obtained in situ following the procedure described previously.[2] This mixture was added dropwise to a suspension of $ScBr_3$ (2.76 g, 9.7 mmol) in toluene (25 mL) in a Schlenk flask. Then, the reaction mixture was refluxed overnight. The suspension was filtered hot, the solvent removed and the crude product washed with pentane (50 mL) to yield 4.35 g (86.6%) of $LScBr_2$. Large colorless crystals were obtained upon cooling the mother liquor to −26 °C. $C_{17}H_{35}Br_2N_4Sc$ (500.3): calcd. C 40.58, H 7.30, N 10.90; found C 40.81, H 7.05, N 11.20. ^1H NMR (200.13 MHz, TMS, 300 K, C_6D_6): δ = 4.82 (s, 1 H, C*H*), 3.08 [m, 16 H, NCH_2CH_2N(CH_2)$_2$], 1.55 (s, 6 H, CHCCH_3), 0.82 (t, 12 H, CH_2CH_3) ppm. ^{13}C NMR (125.75 MHz, TMS, 300 K, C_6D_6): δ = 165.3 (*C*CHC), 100.5 (*C*H), 54.7 (CNCH_2), 47.8 (NCH_2CH_2), 30.1 (CH_2NCH_2), 22.3 (CHC*C*H_3), 8.9 (NCH_2*C*H_3) ppm. ^{45}Sc NMR (121.49 MHz, referenced to $[Sc(H_2O)_6]^{3+}$ in D_2O, 300 K, C_6D_6): δ = 335.87 ppm. M.p. 131−136 °C. EI-MS: *m*/*z* (%) = 500 (10) [M^+], 414 (100) [$M^+ - C_5H_{12}N$].

Preparation of 2 and 2′: A mixture of **1** (0.50 g, 0.98 mmol) or $LScCl_2$ (0.51 g, 0.98 mmol)[1] and Me_3SnF[26] (0.35 g, 1.96 mmol) in a Schlenk flask in toluene (50 mL) was stirred for 1 day until all the Me_3SnF dissolved. The resulting solution was concentrated under reduced pressure and kept at −26 °C. After 3 days crystals of **2** and **2′** were obtained. Cold filtration afforded 0.43 g of **2** (yield 51%) or 0.45 g of **2′** (yield 66%). Attempts to redissolve the resulting products in $CDCl_3$ or C_6D_6 for characterizing **2** and **2′** by NMR spectroscopy failed as the compounds decomposed rapidly once they were taken out of the solution.

2: EI-MS: *m*/*z* (%) = 359 (15) [$LScF^+$], 165 (5) [Me_3Sn^+], 86 (100) [$C_5H_{12}N^+$].

2′: EI-MS: *m*/*z* (%) = 359 (20) [$LScF^+$], 165 (5) [Me_3Sn^+], 86 (100) [$C_5H_{12}N^+$].

Preparation of 3: LK (0.60 g, 1.8 mmol) was obtained in situ by refluxing LH (0.53 g, 1.8 mmol) with KH (0.10 g, 2.5 mmol) in toluene (30 mL) and filtering off the excess KH. The resulting solution was added dropwise to a suspension of YI_3 (0.8 g, 1.8 mmol) in toluene (25 mL) in a 100 mL Schlenk flask. Then, the reaction mixture was refluxed for 1 day. The suspension was filtered hot, the solvent removed and the crude product was washed with pentane (50 mL) then dried in vacuo. Yield: 8.08 g (70.4%). $C_{17}H_{35}I_2N_4Y$ (638.2): calcd. C 31.99, H 5.53, N 8.78; found C 32.20, H 5.40, N 8.56. ^1H NMR (200.13 MHz, 300 K, C_6D_6): δ = 4.80 (s, 1 H, C*H*), 3.10 [m, 16 H, NCH_2CH_2N(CH_2)$_2$], 1.55 (s, 6 H, CHCCH_3), 0.78 (t, 12 H, CH_2CH_3) ppm. ^{13}C NMR (125.75 MHz, 300 K, C_6D_6): δ = 166.3 (*C*CH*C*), 101.0 (*C*H), 55.1 (CNCH_2), 46.9 (NCH_2CH_2), 30.1 (CH_2NCH_2), 22.9 (CHC*C*H_3), 8.4 (NCH_2*C*H_3) ppm. M.p. 150−155 °C. EI-MS: *m*/*z* (%) = 511 (5) [$M^+ - I$], 86 (100) [$C_5H_{12}N^+$].

Preparation of 6. A: A mixture of **3** (1.15 g, 1.8 mmol) and Me_3SnF[26] (0.64 g, 3.5 mmol) in toluene (50 mL) in a Schlenk flask was stirred for 1 day then the turbid yellow solution was filtered. The resulting solution was concentrated under reduced pressure and kept at −26 °C. After one week crystals of **6** were obtained (0.94 g, 34%).

B: Me_3SnF (0.64 g, 3.5 mmol) and THF (40 mL) were added to LYI_2 (**3**; 1.15 g, 1.8 mmol), $LHoI_2$ (**4**; 1.28 g, 1.8 mmol) or $LErI_2$ (**5**; 1.29 g, 1.8 mmol). After stirring for 1 h all the Me_3SnF had dissolved. After the reaction was complete the THF was removed in vacuo, and the residue washed with two portions (20 mL) of pentane. The solid residue was extracted with toluene (60 mL) and the toluene solution concentrated to approximately 10 mL. After standing overnight colorless crystals suitable for X-ray analysis were formed, which were separated by filtration. Another crop of crystals of **6** was obtained by washing the residue with toluene. Yield 0.83 g, 30% (for **3**), 0.75 g, 22% (for **4** and **5**). The concentration of the toluene solution of **6** should proceed slowly, otherwise two liquid layers are formed and no crystallization is observed. $C_{22}H_{50}I_2N_4Sn_2$ (861.9): calcd. C 30.66, H 5.86, N 6.50; found C 30.01, H 5.55, N 6.10. ^1H NMR (200.13 MHz, TMS, 300 K, C_6D_6): δ = 0.29 [s, 6 H, Sn(CH_3)$_2$], 0.57 [s, 9 H, Sn(CH_3)$_3$], 1.00 (t, 12 H, CH_2CH_3), 1.91 (s, 6 H, CCH_3), 2.63 [m, 12 H, CH_2N(CH_2CH$_3$)$_2$], 3.31 (m, 4 H, NCH_2CH$_2$NEt$_2$), 4.61(s, 1 H, *CH*) ppm. M.p. 222−224 °C. EI-MS: *m*/*z* (%) = 403 (2) [$Me_2SnI_2^+$], 388 (2) [$MeSnI_2^+$], 273 (6) [Me_2SnI^+], 247 (4) [SnI^+], 210 (30) [$L^+ - NC_5H_{12}$], 86 (100) [$C_5H_{12}N^+$]. EI-FAB: *m*/*z* (%) = 849 (1) [$(LSnMe_2)(Me_2SnI_2)^-$], 721 (2) [$(LSnMe_2)(Me_2SnI)^-$], 445 (8) [$LSnMe_2^-$], 297 (100) [L^-]. IR (Nujol): $\tilde{\nu}$ = 1619 cm^{-1} (w), 1659 (w), 1572 (m), 1409 (w), 1289 (w), 1261 (vs), 1205 (w), 1168 (w), 1153 (w), 1095 (vs), 1029 (vs), 967 (w), 928 (w), 873 (w), 799 (vs), 728 (m), 699 (w), 668(w), 636 (w), 534 (m), 467 (m).

 © 2003 Wiley-VCH Verlag GmbH & Co. KGaA, Weinheim

Table 5. Crystal data collection for **1**, **2**, **6**, and **7**

Complex	**1**	**2a**	**2b**	**6**·0.5C_7H_8	**7**
Formula	$C_{17}H_{35}Br_2N_4Sc$	$C_{23}H_{53}Br_2F_2N_4ScSn_2$	$C_{23}H_{53}Br_2F_2N_4ScSn_2$	$C_{25.5}H_{54}N_4Sn_2I_2$	$C_{19}H_{35}F_6N_4O_6S_2Sc$
Mol. wt.	500.27	865.85	865.85	907.91	638.59
Space group	$P2_1/n$	$P\bar{1}$	$C2/c$	$P2_1/n$	$Pnma$
Crystal system	monoclinic	triclinic	monoclinic	monoclinic	orthorhombic
a, Å	15.7672(7)	9.832(3)	10.801(2)	9.556(2)	21.6876(11)
b, Å	10.8019(3)	10.305(3)	17.220(5)	27.446(6)	14.4273(11)
c, Å	13.3651(6)	18.705(5)	18.512(5)	13.478(3)	8.9283(5)
α, deg		97.91(3)			
β, deg	107.609(4)	99.75(3)	103.87(3)	92.52(3)	
γ, deg		114.19(3)			
V, Å^3	2169.63(15)	1658.0(8)	3342.7(15)	3531.5(12)	2793.6(3)
Z	4	2	4	4	4
D_{calcd}, g/cm^3	1.532	1.734	1.721	1.708	1.518
Temp, K	133(2)	133(2)	133(2)	200(2)	133(2)
θ range, deg	2.32 to 24.71	2.23 to 27.49	2.27 to 27.53	3.66 to 24.99	1.88 to 24.71
Index ranges	$-18 \le h \le 18$	$-12 \le h \le 12$	$-14 \le h \le 11$	$-11 \le h \le 11$	$-25 \le h \le 25$
	$-12 \le k \le 12$	$-13 \le k \le 7$	$-22 \le k \le 22$	$-16 \le k \le 32$	$-16 \le k \le 16$
	$-15 \le l \le 15$	$-24 \le l \le 24$	$-24 \le l \le 23$	$-16 \le l \le 16$	$-10 \le l \le 9$
Reflections collected/unique	43718/3702	25903/7516	41276/3827	10226/6149	33172/2482
	[R(int) = 0.0657]	[R(int) = 0.0760]	[R(int) = 0.0578]	[R(int) = 0.0461]	[R(int) = 0.0519]
Completeness to θ (%)	99.9	98.8	99.4	98.8	100.0
Data/restraint/parameter	3702/0/223	7516/0/320	3827/0/161	6149/257/319	2482/0/190
GOF	1.070	0.982	1.159	1.161	1.030
Final R indices [$I > 2\sigma(I)$]	R_1 = 0.0176	R_1 = 0.0455	R_1 = 0.0573	R_1 = 0.0555	R_1 = 0.0280
	wR_2 = 0.0411	wR_2 = 0.0931	wR_2 = 0.1418	wR_2 = 0.1884	wR_2 = 0.0729
R indices (all data)	R_1 = 0.0196	R_1 = 0.0667	R_1 = 0.0678	R_1 = 0.0646	R_1 = 0.0355
	wR_2 = 0.0417	wR_2 = 0.0993	wR_2 = 0.1616	wR_2 = 0.1956	wR_2 = 0.0749
Largest diff. peak and hole (e/A^3)	0.294, −0.201	1.137 −1.048	2.723 −4.110	1.425 −1.088	0.403 −0.407

Preparation of 7: A mixture of **1** (0.50 g, 0.98 mmol) and $AgSO_3CF_3$ (0.11 g, 1.96 mmol) in toluene (35 mL) in a 50 mL Schlenk flask was stirred for 2 days. The suspension was filtered. The resulting clear solution was concentrated under reduced pressure to obtain yellow crystals of **7**, which were collected by filtration and washed with pentane (10 mL). Yield 0.31 g (68%) $C_{17}H_{35}F_6N_4O_6S_2Sc$ (614.6): calcd. C 35.74, H 5.52, N 8.77; found C 35.2, H 5.57, N 8.63. ^{1}H NMR (200.13 MHz, TMS, 300 K, C_6D_6): δ = 4.72 (s, 1 H, *CH*), 3.03 (t, J = 6.28 Hz, 4 H, N*CH*$_2$CH$_2$NEt$_2$), 2.82 (q, J = 6.47 Hz, 4 H, N*CH*$_2$CH$_3$), 2.64 (t, J = 6.24 Hz, 4 H, NCH$_2$*CH*$_2$NEt$_2$) 2.47 (m, J = 6.48 Hz, 4 H, N*CH*$_2$CH$_3$) 1.59 (s, 6 H, CHC*CH*$_3$), 0.66 (t, J = 7.16 Hz, 12 H, CH$_2$*CH*$_3$) ppm. ^{13}C NMR (125.75 MHz, TMS, 300 K, C_6D_6): δ = 165.3 (*C*CH*C*), 100.5 (*C*H), 54.7 (CN*C*H$_2$), 47.8 (NCH$_2$*C*H$_2$), 30.1 (CH$_2$N*C*H$_2$), 22.3 (CHC*C*H$_3$), 8.9 (NCH$_2$*C*H$_3$) ppm. ^{19}F NMR (188 MHz, C_6F_6 as external reference, 300 K, C_6D_6): δ = 85.01 ppm. ^{45}Sc NMR (121.49 MHz, referenced to $[Sc(H_2O)_6]^{3+}$ in D_2O, 300 K, C_6D_6): δ = 185.06 ppm. M.p. 95 °C. EI-MS: m/z (%) = 638 (74) [M$^+$], 552 (36) [M$^+$ − $C_5H_{12}N$], 489 (100) [M$^+$ − CF_3SO_3].

X-ray Crystallography: Crystal structure data were collected on a Stoe Image Plate IPDS II-system (**1**, **7**) or on a Stoe−Siemens−Huber four-circle diffractometer equipped with a Bruker AXS CCD detector (**2**, **6**). All structures were solved by direct methods (SHELXS-97)[27] and refined against F^2 using SHELXL-97.[27] The non-hydrogen atoms were refined anisotropically. Hydrogen atoms were refined using the riding model with U_{iso} tied to U_{iso} of the parent atoms. Crystal data collection details, and the solution and refinement procedures are summarized in Table 5.

CCDC-175025 (**1**), -199568 (**2a**), -199569 (**2b**), -203966 (**6**), and -199567 (**7**) contain the supplementary crystallographic data for this paper. These data can be obtained free of charge at www.ccdc.cam.ac.uk/conts/retrieving.html [or from the Cambridge Crystallographic Data Centre, 12, Union Road, Cambridge CB2 1EZ, UK; Fax: (internat.) +44-1223/336-033; E-mail: deposit@ccdc.cam.ac.uk].

[1] A. M. Neculai, H. W. Roesky, D. Neculai, J. Magull, *Organometallics* **2001**, *20*, 5501−5503.
[2] D. Neculai, H. W. Roesky, A. M. Neculai, J. Magull, H.-G. Schmidt, M. Noltemeyer, *J. Organomet. Chem.* **2002**, *643*, 47−52.
[3] D. Neculai, H. W. Roesky, unpublished results.
[4] D. Neculai, H. W. Roesky, A. M. Neculai, J. Magull, R. Herbst-Irmer, B. Walfort, D. Stalke, *Organometallics* **2003**, *22*, 2279−2284.
[5] G. B. Nikiforov, H. W. Roesky, T. Labahn, D. Vidovic, D. Neculai, *Eur. J. Inorg. Chem.* **2003**, 433−436.
[6] [6a] Review on organometallic fluoride complexes: H. W. Roesky, I. Haiduc, *J. Chem. Soc., Dalton Trans.* **1999**, 2249−2264 and references cited therein. [6b] A. Herzog, F.-Q. Liu, H. W. Roesky, A. Demsar, K. Keller, M. Noltemeyer, F. Pauer, *Organometallics* **1994**, *13*, 1251−1256.
[7] H. Dorn, E. F. Murphy, S. A. A Shah, H. W. Roesky, *J. Fluorine Chem.* **1997**, *86*, 121−125.
[8] [8a] E. F. Murphy, P. Yu, S. Dietrich, H. W. Roesky, E. Parisini, M. Noltemeyer, *J. Chem. Soc., Dalton Trans.* **1996**, 1983−1988. [8b] E. F. Murphy, T. Lübben, A. Herzog, H. W. Roesky, A. Demsar, M. Noltemeyer, H.-G. Schmidt, *Inorg. Chem.* **1996**, *35*, 23−29. [8c] S. A. A. Shah, H. Dorn, A. Voigt, H. W. Roesky,

 © 2003 Wiley-VCH Verlag GmbH & Co. KGaA, Weinheim

E. Parisini, H.-G. Schmidt, M. Noltemeyer, *Organometallics* **1996**, *15*, 3176−3181.
[9] H. Schumann, M. R. Keitsch, J. Winterfeld, J. Demtschuk, *J. Organomet. Chem.* **1996**, *525*, 279−281.
[10] P. Yu, P. Müller, H. W. Roesky, M. Noltemeyer, A. Demsar, I. Usón, *Angew. Chem.* **1999**, *111*, 3518−3520; *Angew. Chem. Int. Ed.* **1999**, *38*, 3319−3321.
[11] J. E. Huheey, *Inorganic Chemistry:* P*rinciples of Structure and Reactivity*, 2nd ed.; Harper and Row: New York, **1978**, 845.
[12] F. A. Cotton, G. Wilkinson, C. A. Murillo, M. Bochmann, *Advanced Inorganic Chemistry*, 6th ed.; John Wiley & Sons: New York **1999**, 493.
[13] [13a] U. Kilimann, M. Schäefer, R. Herbst-Irmer, F. T. Edelmann, *J. Organomet. Chem.* **1994**, *469*, C5−C18. [13b] U. Kilimann, F. T. Edelmann, *J. Organomet. Chem.* **1994**, *469*, C5−C9. [13c] H. Schumann, J. A. Meese-Marktscheffel, A. Dietrich, *J. Organomet. Chem.* **1989**, *377*, C5−C8. [13d] B. M. Chamberlain, Y. Sun, J. R. Hagadorn, E. W. Hemmesch, V. G. Young, M. Pink, M. A. Hillmyer, W. B. Tolman, *Macromolecules* **1999**, *32*, 2400−2408.
[14] S. Kobayashi, I. Hakiya, T. Takahori, *Synthesis* **1993**, 371−373.
[15] [15a] S. Kobayashi, S. Nagayama, *J. Am. Chem. Soc.* **1998**, *120*, 2985−2986. [15b] D. A. Evans, Z. K. Sweeney, T. Rovis, J. S. Tedrow, *J. Am. Chem. Soc.* **2001**, *123*, 12095−12096 and references therein. [15c] S. Kobayashi, T. Tsuchiya, I. Komoto, J. Matsuo, *J. Organomet. Chem.* **2001**, *624*, 392−394.
[16] P. G. Hayes, W. E. Piers, L. W. M. Lee, L. K. Knight, M. Parvez, M. R. J. Elsegood, W. Clegg, *Organometallics* **2001**, *20*, 2533−2542.
[17] H. Schumann, M. R. Keitsch, J. Winterfeld, J. Demtschuk, *J. Organomet. Chem.* **1996**, *525*, 279−289.
[18] H. C. Clark, R. J. O'Brien, J. Trotter, *J. Chem. Soc.* **1964**, 2332−2336.
[19] A. M. Neculai, D. Neculai, H. W. Roesky, J. Magull, M. Baldus, O. Andronesi, M. Jansen, *Organometallics* **2002**, *21*, 2590−2592.
[20] D. Neculai, H. W. Roesky, A. M. Neculai, J. Magull, B. Walfort, D. Stalke, *Angew. Chem.* **2002**, *114*, 4470−4472; *Angew. Chem. Int. Ed.* **2002**, *41*, 4294−4296.
[21] Selected references: [21a] W. J. Belcher, P. J. Brothers, A. P. Meredith, C. E. F. Rickard, D. C. Ware, *J. Chem. Soc., Dalton Trans.* **1999**, 2833−2836. [21b] C. Pettinari, M. Pellei, A. Cingolani, D. Martini, A. Drozdov, S. Troyanov, W. Panzeri, A. Mele, *Inorg. Chem.* **1999**, *38*, 5777−5787. [21c] A. Wirth, O. Moers, A. Blaschette, P. G. Jones, *Z. Anorg. Allg. Chem.* **2000**, *626*, 529−535. [21d] C. Pettinari, F. Marchetti, M. Pellei, A. Cingolani, L. Barba, A. Cassetta, *J. Organomet. Chem.* **1996**, *515*, 119−130. [21e] P. Steenwinkel, J. T. B. H. Jastrzebski, B.-J. Deelman, D. M. Grove, H. Kooijman, N. Veldman, W. J. J. Smeets, A. L. Spek, G. van Koten, *Organometallics* **1997**, *16*, 5486−5498. [21f] G. van Koten, J. T. B. H. Jastrzebski, J. G. Noltes, A. L. Spek, J. C. Schoone, *J. Organomet. Chem.* **1978**, *148*, 233−245. [21g] G. F. de Sousa, C. A. L. Filgueiras, A. Abras, S. S. Al-Juaid, P. B. Hitchcock, J. F. Nixon, *Inorg. Chim. Acta* **1994**, *218*, 139−142. [21h] K. Jurkschat, N. Pieper, S. Seemeyer, M. Schurmann, M. Biesemans, I. Verbruggen, R. Willem, *Organometallics* **2001**, *20*, 868−880. [21i] M. C. Kuchta, G. Parkin, *Polyhedron* **1996**, *15*, 4599−4602. [21j] A. Steiner, D. Stalke, *Inorg. Chem.* **1995**, *34*, 4846−4853.
[22] [22a] P. B. Hitchcock, M. F. Lappert, D.-S. Liu, *J. Chem. Soc., Chem. Commun.* **1994**, 1699−1700. [22b] B. Räke, F. Zülch, Y. Ding, J. Prust, H. W. Roesky, M. Noltemeyer, H.-G. Schmidt, *Z. Anorg. Allg. Chem.* **2001**, *627*, 836−840.
[23] C. Pettinari, M. Pellei, M. Miliani, A. Cingolani, A. Cassetta, L. Barba, A. Pifferi, E. Rivarola, *J. Organomet. Chem.* **1998**, *553*, 345−369.
[24] For a recent review on β-diketiminato ligands, see: L. Bourget-Merle, M. Lappert, J. R. Severn, *Chem. Rev.* **2002**, *102*, 3031−3065.
[25] H. Schumann, J. A. Meese-Marktscheffel, A. Dietrich, F. A. Goerlitz, *J. Organomet. Chem.* **1992**, *430*, 299−305.
[26] E. Krause, *Ber. Dtsch. Chem. Ges.* **1918**, *51*, 1447−1456.
[27] [27a] G. M. Sheldrick, *Acta Crystallogr., Sect. A* **1990**, *46*, 467−473. [27b] G. M. Sheldrick, SHELXL-97, *Program for Crystal Structure Refinement* (**1997**) University of Göttingen.
Received April 14, 2003

 © 2003 Wiley-VCH Verlag GmbH & Co. KGaA, Weinheim

Monoarylated Fluoromesitylpalladium Complexes

Camino Bartolomé,[a] Pablo Espinet,*[a] Jose M. Martín-Alvarez,[a] and Fernando Villafañe[a]

Keywords: Palladium / Fluorinated ligands / Ligand substitution / Bulky ligands / Steric hindrance

Monoarylated complexes [PdCl(Fmes)(L-L)] [Fmes = 2,4,6-tris(trifluoromethyl)phenyl or fluoromesityl] and *trans*-[PdCl(Fmes)L_2] have been obtained by arylation of [$PdCl_2$(L-L)] (L-L = tmeda) or *trans*-[$PdCl_2L_2$] (L = SMe_2), by splitting the bridging chloro ligands in [Pd(μ-Cl)(Fmes)(NCMe)]$_2$ {L-L = 4,4′-Me_2bipy, biquinolyl (2,2′-biquinoline), OPPhPy$_2$-*N*,*N*′, (OH)(CH_3)CPy$_2$-*N*,*N*′, dppe, pte [1,2-bis(phenylthio)-ethane]; L = 4-pic}, or by substitution of the diolefin in [PdCl(Fmes)(COD)] (L = *t*BuNC). A 1:1 ratio of [Pd(μ-Cl)(Fmes)(NCMe)]$_2$ and monodentate ligands affords [PdCl(Fmes)(NCMe)L] (L = 2,6-lut, 3,5-lut, PPh_3), whereas a 1:1 mixture of [{PdCl(Fmes)(NCMe)}$_2$(μ-dppe)] and [PdCl(Fmes)(dppe)] is obtained with dppe under mild conditions. The precursor [Pd(μ-Cl)(Fmes)(NCMe)]$_2$ is generated by boiling under reflux [PdCl(Fmes)(COD)] in MeCN, and has been used to obtain various binuclear monoarylated complexes [Pd(Fmes)(μ-X)L]$_2$ [X = Br, L = MeCN, P(*o*-Tol)$_3$; X = Cl, L = CO, 4-pic, 3,5-lut, P(*o*-Tol)$_3$]. Other [Pd(Fmes)(μ-X)L]$_2$ complexes have been obtained from *trans*-[PdCl(Fmes)(SMe_2)$_2$] (X = Cl, L = tht, SMe_2, PPh_3) and from K[Pd_4(Fmes)$_4I_5$] [X = I, L = P(*o*-Tol)$_3$]. Despite the steric hindrance imposed by the Fmes ligand (*ortho* effect), the ligand-substitution reactions are suggestive of associative mechanisms.

(© Wiley-VCH Verlag GmbH & Co. KGaA, 69451 Weinheim, Germany, 2003)

Introduction

The high steric demand of the 2,4,6-tris(trifluoromethyl)-phenyl (nonafluoromesityl or Fmes) group, an interesting ligand for main-group[1,2] and transition metals,[3] hinders rotation around the M−Fmes bonds, restricts rotation of other ancillary ligands on the same metal center, and shows a high degree of axial protection in square-planar complexes (*ortho* effect).[4]

Like other such ligands Fmes can stabilize species that are otherwise difficult to obtain. Thus, its coordination to palladium has resulted in an unprecedented self-assembled pyramidal tetrametallic complex with a halide apex in the [Pd_4(Fmes)$_4X_5$]$^-$ (X = Cl, Br, I), and has lead to the formation of neutral aquo complexes, and to a new halocarbon ligand that acts as a chelate.[5] Weak M···F interactions, invoked in many other complexes,[1−3] are deemed absent in our fluoromesitylpalladium(II) complexes based on analysis of a number of solid-state structures.[4,5]

The Fmes group's bulk makes its coordination by arylation difficult. In fact, our initial results on the coordination of Fmes in palladium(II) complexes indicate that arylation depends greatly on the size of the ancillary ligands in the parent complex.[4] Therefore, ligand substitution of monoarylated complexes accessible by arylation may widen the range of monoarylated species available. Here we describe the synthesis and characterization of several monoarylated Fmes palladium(II) complexes, with monodentate or bidentate ligands, as well as binuclear monoarylated complexes.

[a] Departamento de Química Inorgánica, Facultad de Ciencias, Universidad de Valladolid,
47005 Valladolid, Spain
E-mail: espinet@qi.uva.es

Results and Discussion

The synthesis and structural characterization of the parent complex [Pd(μ-Cl)(Fmes)(NCMe)]$_2$ is described first, followed by discussion of the four types of complexes prepared, i.e. [PdCl(Fmes)(L-L)], [PdCl(Fmes)L_2], [PdCl(Fmes)(NCMe)L], and [Pd(Fmes)(μ-X)L]$_2$.

Synthesis and Characterization of [Pd(μ-Cl)(Fmes)(NCMe)]$_2$

Refluxing [PdCl(Fmes)(COD)][4] in MeCN the dimeric complex [Pd(μ-Cl)(Fmes)(NCMe)]$_2$ (**1a**) was formed, which could be isolated as a yellow solid [Equation (1)].

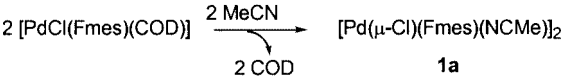

(1)

The ^{1}H and ^{19}F NMR spectra of **1a** show the presence of *cis* and *trans* isomers in solution (Scheme 1). The ^{19}F NMR spectrum in $CDCl_3$ at room temperature has two singlets (ca. 75:25 ratio) corresponding to the *para*-CF_3 groups of each isomer. The *ortho*-CF_3 groups' signals in $CDCl_3$ are coincident, and only one singlet is observed, but two sing-

lets are clearly distinguished in the spectrum recorded in [D_6]acetone. Addition of acetone to a solution of **1a** in $CDCl_3$ produces a progressive increase of the less intense resonance, indicating that it corresponds to the polar *cis* isomer, which is expected to be favored in more polar solvents.[6]

Scheme 1. The *trans* and *cis* isomers of complexes [Pd(μ-Cl)(Fmes)L]$_2$ (**1**)

When **1a** was dissolved in MeCN the initial yellow solution became nearly colorless and only one singlet for the *ortho*-CF_3 and one singlet for the *para*-CF_3 were detected by ^{19}F NMR spectroscopy. This indicates that MeCN has split the chloro bridges, giving rise to only one isomer (either *cis* or *trans*), or to a fast exchange between the two possible isomers (Scheme 2). The solid monomer could not be isolated due to its marked tendency to regenerate **1a**, releasing the MeCN ligand *trans* to the Fmes group,[7] which has a high *trans* influence.[8] The ^{19}F NMR spectrum of **1a** in $CDCl_3$ is hardly affected by the addition of MeCN (**1a**/MeCN, 1:2), and the monomer concentration is high only in the presence of a high excess of acetonitrile in solution.

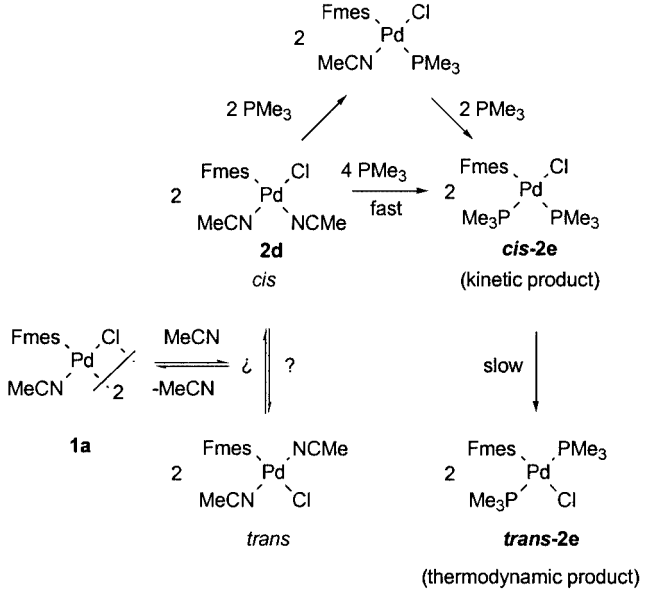

Scheme 2. Complexes detected in solutions of **1a** with MeCN and PMe_3

To understand the reaction behavior of the monomer, PMe_3 was added to a solution of **1a** in MeCN. Instantaneous formation of *cis*-[PdCl(Fmes)(PMe_3)$_2$] (*cis*-**2e**) was observed when two equivalents of PMe_3 per palladium were added, suggesting an associative substitution on *cis*-**2d** promoted by the high *trans* effect of the Fmes ligand.[9] The solution of *cis*-**2e** then isomerizes to the thermodynamic product *trans*-**2e**, according to the general antisymbiotic effect,[10] or to a high *transphobia* between the phosphane and the Fmes group.[11] The geometry of *cis*- or *trans*-**2e** is readily deduced by looking for P−F coupling between the coordinated phosphorus atom and the *ortho*-CF_3 groups. As reported for [PdCl(Fmes)(PPh_3)$_2$],[4] P−F coupling is observed when Fmes and a phosphane are coordinated *cis*, but not when these groups are coordinated *trans*.

Synthesis of [PdCl(Fmes)(L-L)]

Complexes [PdCl(Fmes)(L-L)] (**3**) were synthesized by two methods (Scheme 3): (1) arylation of the dichloro complex with Li(Fmes); or (2) bridge splitting and concomitant substitution of MeCN in **1a** by a bidentate ligand as chelate. The first method successfully furnished [PdCl(Fmes)(tmeda)] (**3a**), as we have reported for other monoarylated complexes containing bidentate chelating ligands.[4] Different neutral bidentate ligands L-L cleaved the chloro bridges and replaced MeCN from **1a** to give [PdCl(Fmes)(L-L)] (L-L= 4,4′-Me_2bipy, **3b**; biquinolyl, **3c**; OPPhPy$_2$-*N*,*N*′, **3d**; (OH)(CH_3)CPy$_2$-*N*,*N*′, **3e**; pte, **3f**; dppe, **3g**). All processes were carried out at room temperature, but to obtain [PdCl(Fmes)(dppe)] (**3g**), refluxing in toluene was needed, as milder conditions lead to a mixture of **3g** and [(μ-dppe){PdCl(Fmes)(NCMe)}$_2$] (**4d**).

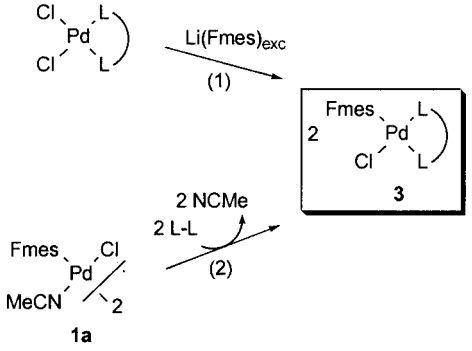

Scheme 3. Synthesis of [PdCl(Fmes)(L-L)] complexes **3**; (1) tmeda, **3a**. (2) 4,4′-Me_2bipy, **3b**; biquinolyl (2,2′-biquinoline), **3c**; OPPhPy$_2$-*N*,*N*′, **3d**; (OH)(CH_3)CPy$_2$-*N*,*N*′, **3e**; pte [1,2-bis(phenylthio)ethane], **3f**; dppe, **3g**

The ^{19}F NMR spectrum of **3g** in $CDCl_3$ shows one doublet for the *ortho*-CF_3 due to coupling with the phosphorus atom *cis* to the Fmes ($J_{P,F}$ = 5.5 Hz). The $^{31}P\{^1H\}$ NMR spectrum displays two signals, a doublet of septuplets for the phosphorus atom *cis* to the Fmes group, and a doublet for the phosphorus atoms *trans* to Fmes ($J_{P,P}$ = 23.2 Hz). Coupling between the hydrogen atoms of the Fmes group and the phosphorus atom *trans* to the Fmes ($^4J_{P,H}$ = 1 Hz) is observed in the ^1H NMR spectrum.

The ^1H NMR spectra of complexes **3** show the nonequivalence of the two halves of the bidentate ligands, confirming their coordination as a chelate with two different ligands in the other positions of the square plane. The chemical shifts detected for the H^6 of the pyridyl groups in **3b**, **3c**, **3d** and **3e** are very sensitive to the ligand coordinated *cis*. Thus, those *cis* to the chloro ligand appear at lower field than for the free ligand,[12] whereas anisotropic shielding produces an upfield shift of the H^6 signals *cis* to the Fmes ring.

 © 2003 Wiley-VCH Verlag GmbH & Co. KGaA, Weinheim

Two conformers may be proposed for **3d**, depending on whether the oxygen atom (*endo*-O) or the phenyl group (*endo*-Ph) of the $OPPhPy_2$ ligand takes the *endo* position in the boat-like metallacycle described by the chelating ligand. An *endo*-Ph conformation (Scheme 4) has been found for solid $[Pd(C_6F_5)Br(OPPhPy_2\text{-}N,N')]$,[13] which is consistent with the clear upfield chemical shift here of one of the *ortho*-CF_3 groups in the ^{19}F NMR spectrum.

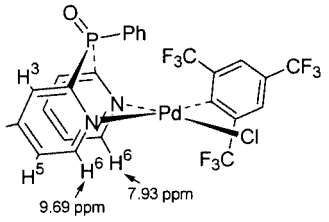

Scheme 4. Proposed conformation for $[PdCl(Fmes)(OPPhPy_2\text{-}N,N')]$ (**3d**)

Two similar conformers, (*endo*-OH) or (*endo*-Me), are possible for **3e**. A single-crystal X-ray analysis of **3e** was therefore undertaken to establish this point and other structural features. A perspective view of the molecular structure of **3e** is given in Figure 1, and selected bond lengths and angles are listed in Table 1. The square-planar geometry of Pd is distorted towards tetrahedral to some extent, as the N(1) atom is 0.196(7) Å above the plane described by the C(21), Pd(1) and Cl(1) atoms, and N(2) is 0.307(7) Å below this plane. The C−C−C angle at the *ipso* carbon is significantly less than 120° [ca. 114.4(6)°], due to the electronic effects of the electropositive metal and electronegative CF_3 substituents at these positions.[14] The fluoromesityl ligand adopts the expected coordination, essentially perpendicular to the coordination plane. The Pd···F_3C-*ortho* distances in **3e** [the shortest, Pd(1)···F(291), is 2.914(11) Å] are longer than those found in bisarylated "$Pd(Fmes)_2$" complexes. Bonding M···F interactions can be discounted in a coordinatively saturated metallic center because such contacts should involve a high energy orbital of the palladium atom as an acceptor of electronic density. Therefore, the crowding in **3e** is deemed responsible for the short nonbonding Pd···F contacts, as in other cases previously analyzed.[4]

The conformer found has the methyl group of the $(OH)(CH_3)CPy_2$ ligand oriented toward the axial position of the coordination plane (Figure 1). The hydrogen atom of the alcohol group was located in a difference Fourier map and refined;[15] it is involved in O−H···Cl intermolecular contacts. The O(1F)−Cl(1A) and H(6F)−Cl(1A) distances are 3.251(9) and 2.306(9) Å respectively, whereas the O(1F)−H(6F)−Cl(1A) angle is 165.4(8)°. The H−Cl distance is within the usual range for H−Cl hydrogen bonds,[16] suggesting that the conformation of the chelating ligand in **3e** helps to stabilize this conformer in the solid state. In solution the intermolecular hydrogen contacts probably break down and the spectroscopic evidence available does not allow us to ascertain whether the conformation of the chelating ligand found in the solid state is retained in the solution.

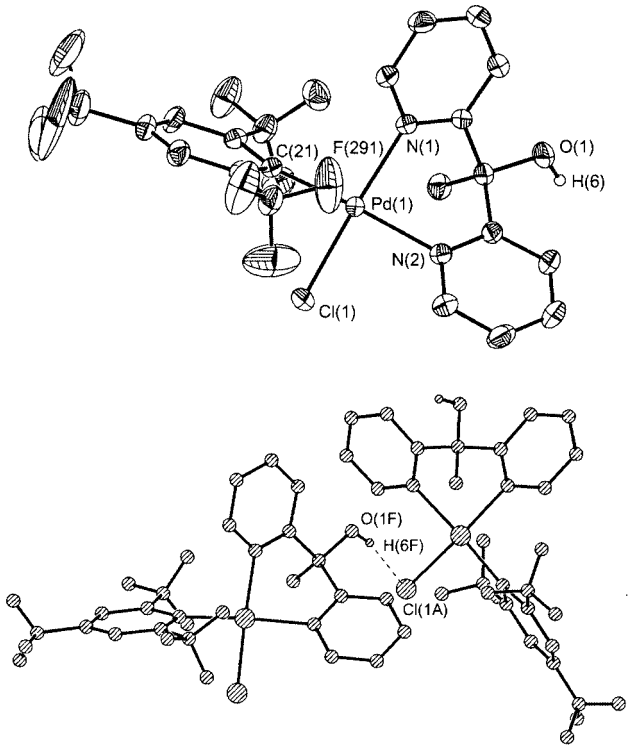

Figure 1. Top: Molecular structure of **3e** showing the atom numbering scheme. The ellipsoids are drawn at the 30% probability level. Bottom: Intermolecular H···Cl hydrogen bonds observed in **3e**

Table 1. Selected bond lengths [Å] and angles [°] for **3e**

Pd(1)−C(21)	1.988(7)	C(21)−Pd(1)−Cl(1)	86.4(2)
Pd(1)−Cl(1)	2.296(2)	N(2)−Pd(1)−Cl(1)	90.92(17)
Pd(1)−N(1)	2.068(6)	C(21)−Pd(1)−N(2)	171.2(3)
Pd(1)−N(2)	2.095(6)	N(1)−Pd(1)−Cl(1)	173.56(17)
C(21)−Pd(1)−N(1)	96.9(3)	C(26)−C(21)−C(22)	114.3(6)
N(1)−Pd(1)−N(2)	86.6(2)		

Synthesis of $[PdCl(Fmes)L_2]$

Scheme 5 shows three different ways to synthesize $[PdCl(Fmes)L_2]$ complexes: (1) by arylation of $[PdCl_2L_2]$ with Li(Fmes); (2) by bridge splitting and substitution of MeCN in **1a** by two equivalents of monodentate ligand; and (3) by substitution of the COD ligand in [PdCl(Fmes)-(COD)].[4]

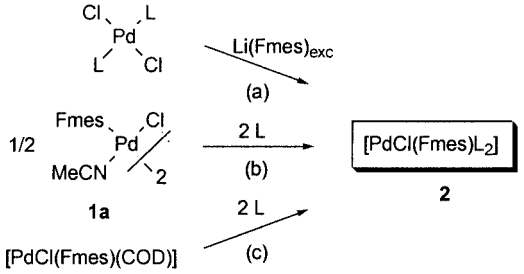

Scheme 5. Synthesis of $[PdCl(Fmes)L_2]$ (**2**). (a) L = SMe_2, **2a**. (b) L = 4-pic, **2b**. (c) L = *t*BuNC, **2c**

 © 2003 Wiley-VCH Verlag GmbH & Co. KGaA, Weinheim

The complex *trans*-[PdCl(Fmes)(SMe_2)$_2$] (**2a**) was obtained by the same procedure previously described for *trans*-[PdCl(Fmes)(tht)$_2$] (tht = tetrahydrothiophene),[4] i.e. arylation of *trans*-[$PdCl_2(SMe_2)_2$] with Li(Fmes), which also gave [Pd(μ-Cl)(Fmes)(SMe_2)]$_2$ (**1h**) and *trans*-[Pd(Fmes)$_2$(SMe_2)$_2$] as by-products. The latter can be synthesized selectively by the method reported for *trans*-[Pd(Fmes)$_2$(tht)$_2$].[4]

Treatment of **1a** with 4-pic leads to *cis*-[PdCl(Fmes)(4-pic)$_2$] (**2b**), as shown by the nonequivalence of both 4-pic ligands in the ^{1}H NMR spectrum. The solid must be isolated rapidly from its solution, otherwise a mixture with the *trans* isomer and [Pd(μ-Cl)(Fmes)(4-pic)]$_2$ (**1d**) is obtained.

The reaction of [PdCl(Fmes)(COD)] with two equivalents of *t*BuNC per palladium in refluxing acetone lead to *trans*-[PdCl(Fmes)(CN*t*Bu)$_2$] (**2c**), as evidenced by the equivalence of the two CN*t*Bu ligands in the ^{1}H NMR spectrum. Under milder conditions a mixture of the *cis* and *trans* isomers is obtained. All attempts to isolate the pure *cis* isomer were unsuccessful.

These results suggest that the *cis* isomers are the kinetic products formed initially by associative substitution of acetonitrile or COD, the reactions being controlled by the higher *trans* effect of Fmes. Whenever a *cis*-[PdCl(Fmes)L$_2$] is isolated (**2b**) or detected (*cis*-**2c**, or *cis*-**2e**) it readily isomerizes in solution to the thermodynamic product, i.e. the corresponding *trans* isomer, since Fmes is the ligand with the higher *trans* influence.[10] The *cis* to *trans* isomerization seems more favored for *cis*-**2c** than for **2b**. In fact, the isomerization of *cis*-**2c** occurs even in the solid state, because the CN*t*Bu (C-donor ligand) *trans* to Fmes is more destabilized than 4-pic (N-donor ligand). Details for these isomerizations are provided in the Exp. Sect.

Synthesis of [PdCl(Fmes)(NCMe)L]

Complexes [PdCl(Fmes)(NCMe)L] (**4**) were obtained from **1a** (Scheme 6).

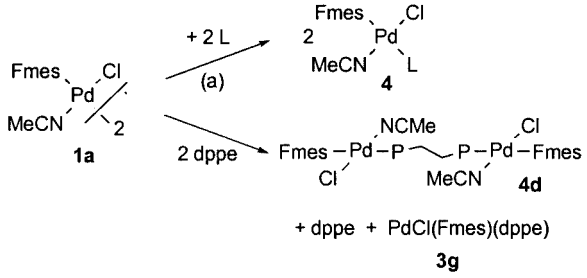

Scheme 6. Synthesis of [PdCl(Fmes)(NCMe)L] (**4**): a) L = 2,6-lut, **4a**; 3,5-lut, **4b**; PPh_3, **4c**

Treatment of **1a** with N- or P-donor ligands (1:1 ratio) in dichloromethane at room temperature leads to [PdCl(Fmes)(NCMe)L] (L = 2,6-lut, **4a**; 3,5-lut, **4b**; PPh_3, **4c**). The reaction with dppe (1:1 ratio) affords a mixture of [(μ-dppe){PdCl(Fmes)(NCMe)}$_2$] (**4d**), [PdCl(Fmes)(dppe)] (**3g**), and free dppe. The dimetallic complex **4d** is scarcely soluble in dichloromethane, which allows its separation from **3g**, which in turn can be isolated pure after free dppe is extracted with Et_2O. The formation of the kinetic product **4d** is a plausible result of the high *trans* effect of Fmes. Nevertheless, under thermodynamic conditions (in refluxing toluene), only **3g** is formed (Scheme 3).

The *trans* to Fmes coordination of the incoming ligand was confirmed by NMR spectroscopic data of the complexes containing phosphanes **4c** and **4d**, since the signals corresponding to the *ortho*-CF_3 and to the phosphorus atoms are singlets. The same geometry is expected for the complexes containing N-donor ligands, but NMR spectroscopic data do not give unequivocal support in this case. The solid IR spectra of all these complexes fit well a relative *cis* arrangement of the Fmes and chloro ligands, since the Pd−Cl stretching wavenumbers are consistently higher than those for unambiguously *trans*-[PdCl(Fmes)L$_2$] complexes.

Halogenoaryl complexes containing two different neutral ligands coordinated to the metal center, such as **4**, are not common and their disproportionation to two symmetric molecules seems to be favored [Equation (2)].[17] Although such disproportionation has not been observed for our complexes **4**, they are not indefinitely stable in solution and slowly lose MeCN to yield [Pd(Fmes)(μ-X)L]$_2$ (**1**) (Scheme 7). Details for the formation of complexes **4** in solution are provided in the Exp. Sect.

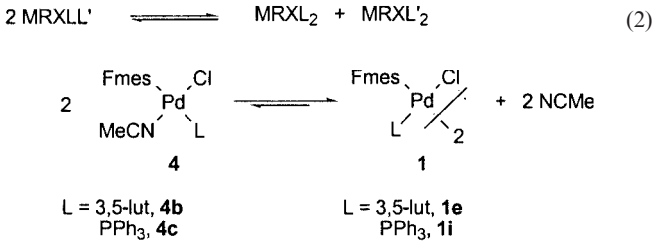

Scheme 7. Evolution of **4b** and **4c** in $CDCl_3$ solution

The destabilizing effect associated with the high "*trans-phobia*" between the phosphane and the Fmes group may help in the evolution of **4c** to **1i**.[11] Moreover, the process is entropically favored. The behavior of the complexes with N-donor ligands is remarkable: While **4a** is stable in solution, the $CDCl_3$ solutions of **4b** at room temperature are always in equilibrium with **1e**, revealing a lower tendency to give the dimer than for phosphanes. Solid **4b** is assumed to be pure, since the ^{19}F NMR spectrum of a sample dissolved at −60 °C in $CDCl_3$ showed no signals of **1e**. The different behavior of **4a** and **4b** in solution is explained upon considering that the *cis* disposition of the two bulky groups Fmes and 2,6-lut (both with *ortho* substituents) needed to form the corresponding dimer is highly destabilized.

Synthesis of [Pd(Fmes)(μ-X)L]$_2$

The syntheses of [Pd(Fmes)(μ-X)L]$_2$ (**1**) are depicted in Scheme 8. The main route to [Pd(Fmes)(μ-Cl)L]$_2$ [L = CO, **1c**; 4-pic, **1d**; 3,5-lut, **1e**; P(*o*-Tol)$_3$, **1f**] was the addition of

 © 2003 Wiley-VCH Verlag GmbH & Co. KGaA, Weinheim

neutral monodentate ligands L (Pd/L, 1:1) to solutions of **1a**. For **1c**, carbon monoxide was bubbled through the solution until a white solid precipitated. Boiling under reflux in toluene was needed to obtain **1d** and **1e**, otherwise the monometallic complexes *cis*-[PdCl(Fmes)(4-pic)$_2$] (**2b**) and [PdCl(Fmes)(NCMe)(3,5-lut)] (**4b**) were obtained as shown.

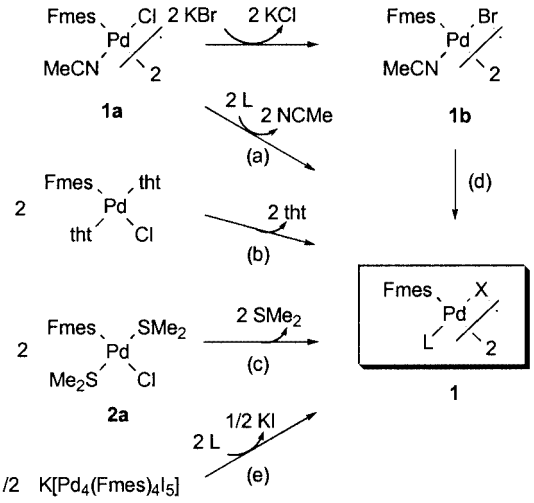

Scheme 8. Synthesis of [Pd(Fmes)(μ-X)L]$_2$ (**1**); (a) L = CO, **1c**; 4-pic, **1d**; 3,5-lut, **1e**, P(*o*-Tol)$_3$, **1f**. (b) L = tht, **1g**. (c) L = SMe$_2$, **1h**; PPh$_3$, **1i**. (d) L = P(*o*-Tol)$_3$, **1j**. (e) L = P(*o*-Tol)$_3$, **1k**

Conversely, boiling under reflux **2a** or [PdCl(Fmes)(tht)$_2$] in toluene affords [Pd(μ-Cl)(Fmes)(SMe$_2$)]$_2$ (**1h**) or [Pd(μ-Cl)(Fmes)(tht)]$_2$ (**1g**) respectively. With PPh$_3$, [Pd(μ-Cl)(Fmes)(PPh$_3$)]$_2$ (**1i**) was obtained. The latter was not selectively obtained using **1a** as starting material, as this process gives a mixture of **1i** and **4c**.

Bromo-bridged dimers can be obtained from **1a**. For instance, reaction of **1a** with KBr in MeCN yields [Pd(μ-Br)(Fmes)(NCMe)]$_2$ (**1b**), which reacts with P(*o*-Tol)$_3$ in toluene to give [Pd(μ-Br)(Fmes){P(*o*-Tol)$_3$}]$_2$ (**1j**). The similar iodo-bridged dimer [Pd(Fmes)(μ-I){P(*o*-Tol)$_3$}]$_2$ (**1k**) has been obtained by treating K[Pd$_4$(Fmes)$_4$I$_5$] with P(*o*-Tol)$_3$.[5a]

As described above for **1a**, two isomers are present in the solutions of these binuclear complexes (Scheme 1). The *trans* isomer is always the major one, but the exact *cis*:*trans* ratio in the solutions of complexes **1** seems to depend on the size of the monodentate ligand coordinated to the metal center: The bulkier the ligand, the higher the *trans*:*cis* ratio (for example, 95:5 for **1i**, L = PPh$_3$; 72:28 for **1c**, L = CO). Spectroscopic details are provided in the Exp. Sect.

All the spectroscopic and analytical data of complexes **1** confirm the geometry proposed, except for binuclear complexes with P(*o*-Tol)$_3$ (**1f**, **1j**, **1k**), where broad signals in their NMR spectra and the lack of P−F coupling prevented an unambiguous assignment. Therefore, an X-ray crystal structure analysis was carried out, revealing that the disposition of the phosphanes is *trans*. A perspective view of the molecular structure of **1j** is given in Figure 2 and selected distances and angles are listed in Table 2.

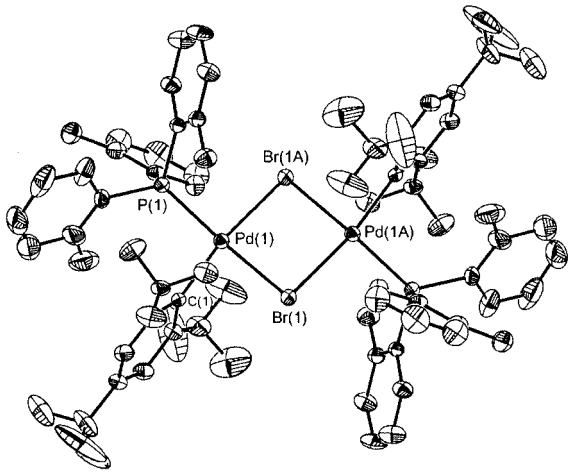

Figure 2. Molecular structure of **1j** showing the atom numbering scheme; the ellipsoids are drawn at 30% probability level

Table 2. Selected bond lengths [Å] and angles [°] for **1j**

Pd(1)−C(1)	2.036(8)	Pd(1)−P(1)	2.328(3)
C(1)−Pd(1)−P(1)	97.8(2)	P(1)−Pd(1)−Br(1)	176.48(7)
C(1)−Pd(1)−Br(1)	85.2(2)	C(1)−Pd(1)−Br(1A)	170.3(2)
Pd(1)−Br(1)	2.5119(13)	Pd(1)−Br(1A)	2.5438(13)
P(1)−Pd(1)−Br(1A)	90.51(7)	Pd(1)−Br(1)−Pd(1A)	93.35(5)
Br(1)−Pd(1)−Br(1A)	86.65(5)	C(2)−C(1)−C(6)	114.9(7)

The two palladium atoms are essentially square planar with minor distortions. Although the fluoromesityl ligand deviates by only 5.7° with respect to the perpendicular to the coordination plane, this keeps them away from the bulky phosphane, thus diminishing the steric hindrance. As usual, the C−C−C angle at the *ipso* carbon atom is less than 120° [ca. 115.0(7)°].[14] The Pd(1)−Br(1) distance at 2.5116(13) Å is smaller than Pd(1)−Br(1A) [2.5437(12) Å], and suggests a higher *trans* influence of the fluoromesityl group compared to the phosphane, as found for other aryl or alkyl phosphane complexes with bromo[18] or chloro bridges.[19]

The shortest Pd···F$_3$C-*ortho* distance found in **1j** [2.807(14) Å] is slightly longer than those found in bisarylated "Pd(Fmes)$_2$" complexes, but shorter than that in **3e**. Again this suggests that this distance is related to the degree of crowding in the fluoromesitylpalladium complexes, rather to bonding interactions.[4]

P(*o*-Tol)$_3$ has an *exo*$_2$ conformation in which an *o*-methyl group is oriented away from the metal. This reduces the rotation of the M−P−C$_{ipso}$ plane, thus also reducing the phosphane cone angle by ca. 35°.[20]

The P(1)−Pd(1)−C(1) angle is 97.8(2)°, instead of the ideal 90°, presumably due to steric constraints. The absence of a P−F coupling in the spectra of **1j** might be related to of this angle. In fact, $J_{P\text{-}F}$ is 4.6 Hz in **1i** (X = Cl, L = PPh$_3$). The involvement of increasingly bulky ligands in the

 © 2003 Wiley-VCH Verlag GmbH & Co. KGaA, Weinheim

sequence **1i** < **1j** would consistently open the X−Pd−P angle and decrease the P−F coupling.[21]

The broad signals in the NMR spectra of **1f**, **1j** and **1k** may be due to three different dynamic processes:[18,22] (1) *cis*−*trans* exchange, similar to that of the other binuclear complexes synthesized here (Scheme 1); (2) slow rotation of the Pd−P bond; (3) the so-called "two-flip mechanism" consisting of a slow rotation of the P-C_{ipso} bond which exchanges the *exo*$_2$ and *exo*$_3$ conformers.[23] The ^{19}F NMR spectra of **1f**, **1j** and **1k** show broad signals corresponding to the *ortho*-CF_3 groups. When X = Cl (**1f**) the two *ortho*-CF_3 give rise to only one broad signal at room temperature, whereas two broad signals are displayed by the *ortho*-CF_3 when X is Br (**1j**) or I (**1k**), showing their nonequivalence at room temperature. At lower temperatures many species are observed, since the three possible dynamic processes are restricted, and different conformations of the possible isomers become discernible. The main species for each complex might be assigned to the stable conformer found in the solid state structure of **1j**, but the minor species cannot be assigned only from the spectroscopic data because of the many possible rotamers.

Conclusion

Various [PdXRL_2] complexes with the bulky Fmes group can be obtained, many via ligand substitution processes under mild conditions. This suggests that a single Fmes group does not give a high degree of axial protection, probably because the group can tilt, making associative ligand substitutions kinetically accessible. The results of the ligand-substitution reactions are consistent with a high *trans* effect of the Fmes group. Thus, the kinetic product (where the incoming ligand coordinates *trans* to the Fmes) is first formed. Subsequent isomerization or evolution to the expected thermodynamic product (if only electronic factors were considered) does not always take place. In fact the stability of both isomers depends on electronic (antisymbiotic effect), steric, and entropic factors. Complexes containing two bulky ligands with *ortho* substituents mutually *cis* seem much disfavored, while mutually *trans* substituents can be tolerated.

Experimental Section

General Remarks: All reactions were carried out under dry N_2. Solvents were purified according to standard procedures.[24] 1,3,5-$C_6H_3(CF_3)_3$ (FmesH) was purchased from Fluorochem and used as received. Li(Fmes) was prepared as described in the literature,[25] and used immediately in situ without further purification. The compounds *trans*-[$PdCl_2(tht)_2$], *trans*-[$PdCl_2(SMe_2)_2$],[26] [$PdCl_2$-(tmeda)],[27] $OPPhPy_2$,[28] and $(OH)(CH_3)CPy_2$,[29] were prepared according to literature procedures.

Infrared spectra were recorded with a Perkin−Elmer 883 apparatus as Nujol mulls between polyethylene films from 4000 to 200 cm^{-1}. NMR spectra were recorded with Bruker AC-300 or ARX-300 instruments and are referred to TMS, 85% H_3PO_4, or $CFCl_3$. Elemental analyses were performed with a Perkin−Elmer 2400B microanalyzer.

[Pd(μ-Cl)(Fmes)(NCMe)]$_2$ (1a): [PdCl(Fmes)(COD)][4] (1.090 g, 2 mmol) was boiled under reflux in acetonitrile and monitored by ^{19}F NMR until the starting material disappeared (24 h). The yellow solution thus obtained was filtered through dry Celite, the solvents were pumped off and a yellow solid obtained that was washed with *n*-hexane and vacuum dried to yield 0.850 g (89%) of product. IR: $\tilde{\nu}$ = 2335 m, 2309 w, 1618 s, 1574 m, 1308 vs, 1286 vs, 1265 vs, 1189 vs, 913 vs, 1088 s, 1021 s, 914 s, 955 m, 836 m, 584 vw (br), 574 w, 438 w, 373 vw, 334 vw (sh), 323 w, 302 vw, 277 w cm^{-1}. ^{1}H NMR: δ = 7.79 [s, $C_6H_2(CF_3)_3$, 2 H, *trans*], 7.69 [s, $C_6H_2(CF_3)_3$, 2 H, *cis*], 2.17 (s, NCCH_3, 3 H, *cis*), 2.13 (s, NCCH_3, 3 H, *trans*), (*trans*/*cis*, 77:23) ppm. ^{19}F NMR: δ = −58.65 (s, *ortho*-CF_3, 6 F, *cis* and *trans*), −63.15 (s, *para*-CF_3, 3 F, *trans*), −63.29 (s, *para*-CF_3, 3 F, *cis*), (*trans*/*cis*, 77:23) ppm. $C_{22}H_{10}Cl_2F_{18}N_2Pd_2$ (928.0): calcd. C 28.47, H 1.09, N 3.02; found C 28.26, H 1.15, N 2.81.

[Pd(μ-Br)(Fmes)(NCMe)]$_2$ (1b): KBr (0.173 g, 1.45 mmol) was added to a solution of **1a** (0.135 g, 0.145 mmol) in acetonitrile (30 mL) and stirred for 1 h at room temperature. Then the solvent was removed in vacuo and the resultant yellow residue extracted with dichloromethane (30 mL), filtered, washed with *n*-hexane (3 × 10 mL) and dried to yield 0.128 g (87%) of **1b**. IR: $\tilde{\nu}$ = 2335 m, 2309 w, 1836 vw, 1646 vw, 1619 s, 1575 m, 1300 vs, 1283 vs, 1231 m, 1191 vs, 1122 vs, 1084 s, 1025 s, 954 vw, 913 s, 854 m, 835 s, 683 s, 667 w, 581 vw, 564 vw, 472 w, 438 m, 305 w, 227 w, 218 w cm^{-1}. ^{1}H NMR: δ = 7.81 [s, $C_6H_2(CF_3)_3$, 2 H, *cis*], 7.73 [s, $C_6H_2(CF_3)_3$, 2 H, *trans*], 2.18 (s, NCCH_3, 3 H, *trans*), 2.14 (s, NCCH_3, 3 H, *cis*), (*cis*/*trans*, 72:28) ppm.In the presence of MeCN, **1b** undergoes a process similar to that depicted for **1a** in Scheme 2, giving rise to different NMR signals. ^{19}F NMR: δ = −58.30 (s, *ortho*-CF_3, 6 F, *cis*), −58.31 (s, *ortho*-CF_3, 6 F, *trans*), −62.12 (s, *para*-CF_3, 3 F, *cis*), −63.26 (s, *para*-CF_3, 3 F, *trans*), (*cis*/*trans*, 72:28) ppm. ^{19}F NMR (CH_3CN/[D_6]Me_2CO): δ = −57.18 (s, *ortho*-CF_3, 6 F), −62.14 (s, *para*-CF_3, 3 F) ppm. $C_{22}H_{10}Br_2F_{18}N_2Pd_2$ (1016.9): calcd. C 25.98, H 0.99, N 2.76; found C 26.19, H 1.06, N 2.89.

[Pd(μ-Cl)(Fmes)(CO)]$_2$ (1c): Carbon monoxide was bubbled through a solution of **1a** (0.696 g, 0.75 mmol) in toluene (30 mL) at room temperature for 10 h with stirring. The resultant white solid was decanted and washed with toluene (3 × 5 mL), yielding 0.498 g (74%) of **1c**. IR: $\tilde{\nu}$ = 2149 vs, 2102 w, 1622 s, 1583 m, 1301 vs, 1283 vs, 1269 vs, 1208 vs, 1190 vs, 1130 s, 1091 s, 1023 s, 919 s, 855 m, 839 m, 749 s, 695 m, 683 m, 672 w, 585 vw, 477 m, 436 w, 395 vw, 369 vw, 301 w, 282 m cm^{-1}. ^{1}H NMR: δ = 8.00 [s, $C_6H_2(CF_3)_3$, 2 H, *trans*], 7.90 [s, $C_6H_2(CF_3)_3$, 2 H, *cis*], (*trans*/*cis*, 72:28) ppm. ^{19}F NMR: δ = −59.31 (s, *ortho*-CF_3, 6 F, *trans*), −59.35 (s, *ortho*-CF_3, 6 F, *cis*), −63.39 (s, *para*-CF_3, 3 F, *trans*), −63.53 (s, *para*-CF_3, 3 F, *cis*), (*trans*/*cis*, 72:28) ppm. $C_{20}H_4Cl_2F_{18}O_2Pd_2$ (901.9): calcd. C 26.63, H 0.45; found C 26.57, H 0.69.

[Pd(μ-Cl)(Fmes)(4-pic)]$_2$ (1d): 4-Pic (10 μL, 0.096 mg, 0.1 mmol) was added to a yellow solution of **1a** (0.046 g, 0.05 mmol) in acetone (10 mL) and boiled under reflux for 3 h. The volatiles were then pumped off and the resultant yellow solid was dissolved in dichloromethane; *n*-hexane was then added and the mixture was concentrated and cooled to −20 °C. The yellow crystals thus obtained were decanted, washed with *n*-hexane (3 × 5 mL) and vacuum dried to yield 0.041 g (79%) of product. IR: $\tilde{\nu}$ = 2343 vw (br), 2019 vw (br), 1618 m, 1572 w, 1507 w, 1298 s, 1281 vs, 1191 vs, 1126 vs, 1085 m, 1070 m, 1027 m, 911 m, 854 w, 835 w, 572 w, 696

 © 2003 Wiley-VCH Verlag GmbH & Co. KGaA, Weinheim

w, 685 m, 564 vw (br), 498 w, 438 w cm^{-1}. ^1H NMR: δ = 8.23 [d, *J* = 6.5 Hz, $NC_5H_4(CH_3)$, 2 H, *cis*], 8.19 [d, *J* = 6.5 Hz, $NC_5H_4(CH_3)$, 2 H, *trans*], 7.78 [s, $C_6H_2(CF_3)_3$, 2 H, *trans*], 7.71 [s, $C_6H_2(CF_3)_3$, 2 H, *cis*], 7.03 [d partially hidden, *J* = 6.0 Hz, $NC_5H_4(CH_3)$, 2 H, *cis*], 7.00 (d, *J* = 6.0 Hz, NC_5H_4, 2 H, *trans*), 2.32 [s, $NC_5H_4(CH_3)$, 3 H, *cis*], 2.29 [s, $NC_5H_4(CH_3)$, 3 H, *trans*], (*trans*/*cis*, 78:22) ppm. ^{19}F NMR: δ = −58.29 (s, *ortho*-CF_3, 6 F, *trans*), −58.35 (s, *ortho*-CF_3, 6 F, *cis*), −63.21 (s, *para*-CF_3, 3 F, *trans*), −63.31 (s, *para*-CF_3, 3 F, *cis*), (*trans*/*cis*, 78:22) ppm. $C_{30}H_{18}Cl_2F_{18}N_2Pd_2$ (1032.2): calcd. C 34.91, H 1.76, N 2.71; found C 34.71, H 1.79, N 2.67.

[Pd(μ-Cl)(Fmes)(3,5-lut)]$_2$ (1e): 3,5-Lut (12.5 μL, 0.012 mg, 0.11 mmol) was added to a yellow solution of **1a** (0.046 g, 0.05 mmol) in acetone (10 mL) and boiled under reflux for 3 h. The volatiles were then pumped off and the resultant yellow solid dissolved in dichloromethane; *n*-hexane was then added and the solution concentrated and cooled to −20 °C. The yellow crystals obtained were decanted, washed with *n*-hexane (3 × 5 mL) and vacuum dried to yield 0.040 g (75%) of **1e**. IR: ṽ = 2342 w, 2020 vw, 1899 vw (br), 1819 vw (br), 1617 m, 1572 m, 1298 vs, 1284 vs, 1262 s, 1187 s, 1132 vs (br), 1083 m, 1028 s, 912 s, 857 m, 833 w, 788 vw, 752 m, 696 m, 684 m, 667 m, 539 w (br), 486 vw, 419 w, 437 m, 425 w, 313 vw, 287 vw, 240 vw cm^{-1}. ^1H NMR: δ = 8.11 [s, $NC_5H_3(CH_3)_2$, H^1 and H^5, 2 H, *cis*], 8.08 [s, $NC_5H_3(CH_3)_2$, H^1 and H^5, 2 H, *trans*], 7.78 [s, $C_6H_2(CF_3)_3$, 2 H, *trans*], 7.70 [s, $C_6H_2(CF_3)_3$, 2 H, *cis*], 7.32 [s, $NC_5H_3(CH_3)_2$, H^3, 1 H, *cis*], 7.30 [s, $NC_5H_3(CH_3)_2$, H^3, 1 H, *trans*], 2.28 [s, $NC_5H_3(CH_3)_2$, 3 H, *cis*], 2.19 [s, $NC_5H_3(CH_3)_2$, 3 H, *trans*], (*trans*/*cis*, 78:22) ppm. ^{19}F NMR: δ = −58.01 (s, *ortho*-CF_3, 6 F, *trans*), −58.06 (s, *ortho*-CF_3, 6 F, *cis*), −63.21 (s, *para*-CF_3, 3 F, *trans*), −63.31 (s, *para*-CF_3, 3 F, *cis*), (*trans*/*cis*, 78:22) ppm. $C_{32}H_{22}Cl_2F_{18}N_2Pd_2$: calcd. C 36.25, H 2.09, N 2.64; found C 36.40, H 2.25, N 2.84.

[Pd(μ-Cl)(Fmes){P(*o*-Tol)$_3$}]$_2$ (1f): P(*o*-Tol)$_3$ (0.122 g, 0.4 mmol) was added to a solution of **1a** (0.186 g, 0.2 mmol) in toluene (30 mL) and the resultant solution stirred 24 h at room temperature. The volatiles were then pumped off, freshly distilled *n*-hexane was added and the mixture kept under nitrogen. The yellow solid thus obtained was decanted, washed with hexane and vacuum dried, yielding 0.197 g (68%) of **1f**. IR: ṽ = 1617 m, 1591 w, 1569 w, 1281 vs, 1180 vs, 1153 s, 1080 m, 1021 m, 910 m, 854 w, 832 w, 807 w, 753 m, 694 w, 683 m, 565 w, 536 w, 517 vw, 469 m, 292 w, 284 w, 271 w cm^{-1}. ^1H NMR: δ = 7.54 [br., $C_6H_2(CF_3)_3$], 7.47 [br., $C_6H_2(CF_3)_3$], 7.5−6.5 [br., C_6H_4, P(*o*-Tol)$_3$], 3.5−1.5 [br., CH_3, P(*o*-Tol)$_3$] ppm. ^{19}F NMR: δ = −56.8 (br., *ortho*-CF_3, 12 F, *trans*), −58.1 (br., *ortho*-CF_3, 12 F, *cis*), −63.18 (br., *para*-CF_3, 6 F, *trans*), −63.27 (br., *para*-CF_3, 6 F, *cis*) (*trans*/*cis*, 62:38) ppm. $^{31}P\{^1H\}$ NMR: δ = 22.1 (br) ppm. $C_{60}H_{46}Cl_2F_{18}P_2Pd_2$ (1454.6): calcd. C 49.54, H 3.19; found C 49.70, H 3.39.

[Pd(μ-Cl)(Fmes)(tht)]$_2$ (1g): [PdCl(Fmes)(tht)$_2$],[4] (0.060 g, 0.1 mmol) was dissolved in *n*-hexane (10 mL), and the solution boiled under reflux overnight. The yellow crystals thus formed were decanted, washed with *n*-hexane (3 × 5 mL) and dried to afford 0.036 g (71%) of **1g**. IR: ṽ = 1617 s, 1574 m, 1300 vs, 1278 vs, 1177 vs, 1132 vs (br), 1084 s, 959 w, 916 s, 880 w, 854 m, 836 m, 804 w, 751 m, 695 m, 684 s, 669 w, 582 vw, 517 vw, 470 w, 438 w, 326 vw, 297 vw. ^1H NMR: δ = 7.84 [s, $C_6H_2(CF_3)_3$, 2 H, *trans*], 7.74 [s, $C_6H_2(CF_3)_3$, 2 H, *cis*], 3.00 (br., SC_4H_8, H^α, 4 H, *cis* and *trans*), 2.00 (br., SC_4H_8, H^β, 4 H, *cis* and *trans*), (*trans*/*cis*, 90:10) ppm. ^{19}F NMR: δ = −58.84 (s, *ortho*-CF_3, 6 F, *cis* and *trans*), −63.13 (s, *para*-CF_3, 3 F, *trans*), −63.29 (s, *para*-CF_3, 3 F, *cis*), (*trans*/*cis*, 90:10) ppm. $C_{26}H_{20}Cl_2F_{18}Pd_2S_2$ (1022.2): calcd. C 30.55, H 1.97; found C 30.53, H 1.98.

[Pd(μ-Cl)(Fmes)(SMe$_2$)]$_2$ (1h): Compound **2a** (0.110 g, 0.2 mmol) was dissolved in toluene (10 mL) and the resultant solution was boiled under reflux. After 8 h the solution became yellow. It was then filtered through dry Celite, and hexane was added to the filtrate, which was concentrated and cooled to −20 °C. The yellow crystals thus obtained were decanted, washed with *n*-hexane (3 × 5 mL) and vacuum dried to yield 0.079 g (81%) of product. IR: ṽ = 1621 m, 1568 w, 1621 m, 1569 w, 1297 s, 1277 vs, 1192 vs, 1180 s, 1135 vs, 1115 vs, 1087 s, 1027 m, 950 w, 914 m, 880 vw, 851 m, 830 m, 805 vw, 754 m, 692 m, 682 s, 520 s, 462 w, 437 w, 310 vw cm^{-1}. ^1H NMR: δ = 7.85 [s, $C_6H_2(CF_3)_3$, 2 H, *trans*], 7.75 [s, $C_6H_2(CF_3)_3$, 2 H, *cis*], 2.23 [s, $S(CH_3)_2$, 6 H, *trans*], 2.17 [s, $S(CH_3)_2$, 6 H, *cis*], (*trans*/*cis*, 86:14) ppm. ^{19}F NMR: δ = −58.99 (s, *ortho*-CF_3, 6 F, *trans*), −59.10 (s, *ortho*-CF_3, 6 F, *cis*), −63.19 (s, *para*-CF_3, 3 F, *trans*), −63.32 (s, *para*-CF_3, 3 F, *cis*), (*trans*/*cis*, 86:14) ppm. $C_{22}H_{16}Cl_2F_{18}Pd_2S_2$ (970.2): calcd. C 27.24, H 1.66; found C 27.43, H 1.78.

[Pd(μ-Cl)(Fmes)(PPh$_3$)]$_2$ (1i): PPh_3 (0.052 g, 0.2 mmol) was added to a yellow solution of **2a** (0.110 g, 0.2 mmol) in toluene (20 mL) and boiled under reflux for 24 h. The volatiles were then pumped off to afford a yellow solid that was dissolved in dichloromethane; *n*-hexane was then added and the mixture concentrated and cooled to −20 °C. The yellow crystals thus obtained were decanted, washed with *n*-hexane (3 × 5 mL) and vacuum dried to furnish 0.065 g (47%) of **1i**. IR: ṽ = 1619 s, 1588 w, 1574 m, 1297 vs, 1277 vs, 1186 vs, 1143 vs (br), 1097 s, 1082 s, 1024 s, 1000 m, 972 w, 912 s, 855 m, 833 m, 747 s, 693 vs, 667 w, 532 vs, 509 s, 499 s, 469 w, 450 w, 436 w, 283 w, 277 w cm^{-1}. $^{31}P\{^1H\}$ NMR: δ = 27.3 (m, *trans*) (*cis* isomer signal not observed) ppm. ^1H NMR: δ = 7.44 [s, $C_6H_2(CF_3)_3$, 4 H, *trans*], 8.2−6.2 (br., C_6H_5, 30 H) (*cis* isomer signals not observed) ppm. ^{19}F NMR: δ = −57.74 (d, $J_{P,F}$ = 4.6 Hz, *ortho*-CF_3, 12 F, *trans*), −57.93 (d, $J_{P,F}$ = 5.0 Hz, *ortho*-CF_3, 12 F, *cis*), −63.33 (s, *para*-CF_3, 6 F, *trans*), −63.40 (s, *para*-CF_3, 6 F, *cis*), (*trans*/*cis*, 95:5) ppm. $C_{54}H_{34}Cl_2F_{18}P_2Pd_2$ (1370.5): calcd. C 47.33, H 2.50; found C 47.48, H 2.70.

[Pd(μ-Br)(Fmes){P(*o*-Tol)$_3$}]$_2$ (1j): P(*o*-Tol)$_3$ (0.018 g, 0.06 mmol) was added to a solution of **1b** (0.031 g, 0.03 mmol) in toluene (10 mL) and the solution was stirred at room temperature for 8 h. The volatiles were then pumped off to give a deep-yellow oil that was crystallized from dichloromethane/hexane under an inert atmosphere. The yellow crystals thus obtained were decanted, washed with cold hexane (2 × 5 mL) and vacuum dried to yield 0.020 g (43%) of **1j**. IR: ṽ = 1617 m, 1591 w, 1568 w, 1280 vs, 1261 s, 1161 vs, 1152 vs, 1084 s (br), 1019 s, 910 m, 855 w, 805 s, 754 s, 694 w, 683 m, 564 w, 536 w, 516 vw, 482 m, 469 m cm^{-1}. ^1H NMR: δ = 7.50 [br., $C_6H_2(CF_3)_3$, *cis* and *trans*], 7.5−6.5 [br., C_6H_4, P(*o*-Tol)$_3$], 3.5−1.5 [br., CH_3, P(*o*-Tol)$_3$] ppm. ^{19}F NMR: δ = −53.93 (br., *ortho*-CF_3), −57.44 (br., *ortho*-CF_3), −63.20 (s, *para*-CF_3, *trans*), −62.56 (s, *para*-CF_3, 6 F, *cis*) (*cis*/*trans*, 90:10) ppm. $^{31}P\{^1H\}$: δ = 21.8 (s) ppm. $C_{60}H_{46}Br_2F_{18}P_2Pd_2$ (1543.5): calcd. C 46.69, H 3.00; found C 46.67, H 3.04.

[Pd(Fmes)(μ-I){P(*o*-Tol)$_3$}]$_2$ (1k): P(*o*-Tol)$_3$ (0.031 g, 0.1 mmol) was added to a solution of $K[Pd_4(Fmes)_4I_5]$[5a] (0.056 g, 0.0025 mmol) in toluene (10 mL) and the resultant solution was stirred at room temperature for 9 h. The deep yellow solution thus obtained was filtered through dry Celite and then concentrated; hexane was then added under an inert atmosphere. The resultant orange crystals were decanted, washed with cold hexane (2 × 5 mL) and vacuum dried to furnish 0.047 g (57%) of **1k**. IR: ṽ = 2019 vw, 1616 m, 1590 w, 1568 w, 1281 vs, 1191 s, 1181 s, 1149 s, 1137 s, 1078 m, 1015 m, 910 m, 854 w, 831 w, 805 w, 754 m, 684 m, 564 w, 536 w, 517 w, 468 m, 438 w, 395 vw, 292 vw cm^{-1}. ^1H NMR: δ = 9.3 [br.,

 © 2003 Wiley-VCH Verlag GmbH & Co. KGaA, Weinheim

C_6H_4, P(*o*-Tol)$_3$], 8.0−6.5 [br., C_6H_4, P(*o*-Tol)$_3$ and $C_6H_2(CF_3)_3$], 3.3 [br., CH_3, P(*o*-Tol)$_3$], 1.4 [br., CH_3, P(*o*-Tol)$_3$] ppm. ^{19}F NMR: δ = −52.97 (br., *ortho*-CF_3), −57.09 (br., *ortho*-CF_3), −63.20 (s, *para*-CF_3) ppm. ^{31}P{^{1}H} NMR: δ = 18.3 (s) ppm. $C_{60}H_{46}F_{18}I_2P_2Pd_2$: calcd. C 44.01, H 2.83; found C 44.03, H 2.83.

***trans*-[PdCl(Fmes)(SMe$_2$)$_2$] (2a):** *trans*-[$PdCl_2(SMe_2)_2$] (0.603 g, 2 mmol) was added to a freshly prepared solution of Li(Fmes) (4.26 mmol) in Et_2O (40 mL). The reaction mixture was then maintained at 40 °C for 24 h, after which two drops of water were added to hydrolyze the excess of organolithium reagent. The volatiles were then pumped off, and the residue extracted with toluene and then filtered through silica gel. This solution afforded, after evaporation and crystallization, a mixture of **1h** and [$Pd(Fmes)_2(SMe_2)_2$].[30] The rest of the residue was extracted with dichloromethane and filtered through silica gel. The solvent was then evaporated and the resultant yellow residue was recrystallized from dichloromethane/hexane at −20 °C giving pale yellow crystals of **2a** that were decanted, washed with hexane and vacuum-dried. Yield 0.529 g (48%). IR: ṽ = 1621 s, 1572 m, 1287 vs (sh), 1262 vs, 1188 vs (sh), 1132 vs, 1085 s, 1035 s, 1026 s, 995 m, 980 s, 915 s, 853 m, 835 m, 754 m, 695 m, 684 m, 668 w, 468 w, 439 w, 377 vw, 358 vw, 306 vw, 285 w cm^{-1}. ^{1}H NMR: δ = 7.90 [s, $C_6H_2(CF_3)_3$, 2 H], 2.24 [s, S(CH_3)$_2$, 12 H] ppm. ^{19}F NMR: δ = −60.81 (s, *ortho*-CF_3, 6 F), −63.18 (s, *para*-CF_3, 3 F) ppm. $C_{13}H_{14}ClF_9PdS_2$ (547.2): calcd. C 28.53, H 2.58; found C 28.69, H 2.49.

***cis*-[PdCl(Fmes)(4-pic)$_2$] (2b):** 4-Pic (43 μL, 0.041 g, 0.44 mmol) was added to a yellow solution of **1a** (0.093 g, 0.1 mmol) in dichloromethane (10 mL) and stirred at room temperature for 15 min. Then *n*-hexane was added to the resultant colorless solution, and this was then concentrated and cooled to −20 °C. The white solid thus obtained was decanted, washed with *n*-hexane (3 × 5 mL) and vacuum dried, yielding 0.045 g (37%) of **2b**. IR: ṽ = 1617 s, 1569 w, 1504 m, 1298 vs, 1278 vs (br), 1214 m, 1195 vs (sh), 1126 vs (sh), 1083 s, 1071 s, 1040 m, 1028 m, 938 w, 914 m, 871 vw, 852 w, 834 m, 815 w, 753 w, 695 w, 683 s, 667 vw, 550 vw, 498 m, 470 vw, 436 vw, 329 w cm^{-1}. ^{1}H NMR: δ = 8.42 [d, *J* = 6.0 Hz, $NC_5H_4(CH_3)$, 2 H], 8.13 [d, *J* = 6.0 Hz, $NC_5H_4(CH_3)$, 2 H], 7.76 [s, $C_6H_2(CF_3)_3$, 2 H], 7.14 [d, *J* = 5.6 Hz, $NC_5H_4(CH_3)$, 2 H], 7.02 [d, *J* = 5.6 Hz, $NC_5H_4(CH_3)$, 2 H], 2.36 [s, $NC_5H_4(CH_3)$, 3 H], 2.31 [s, $NC_5H_4(CH_3)$, 3 H] ppm. ^{19}F NMR: δ = −58.89 (s, *ortho*-CF_3, 6 F), −63.13 (s, *para*-CF_3, 3 F) ppm. $C_{21}H_{16}ClF_9N_2Pd$ (609.2): calcd. C 41.40, H 2.65, N 4.60; found C 41.23, H 2.59, N 4.43. A solution of pure *cis*-**2b** maintained at 50 °C in $CDCl_3$ solution showed, with time, the following *cis*-**2b**/**1d**/*trans*-**2b** ratios by ^{19}F NMR: after 24 h, 20:12:68; after 48 h: 9:10:81; after 5 days: 5:9:86.

***trans*-[PdCl(Fmes)(CN*t*Bu)$_2$] (2c):** *t*BuNC (23 μL, 0.017 g, 0.2 mmol) was added to a solution of [PdCl(Fmes)(COD)][4] (0.053 g, 0.1 mmol) in acetone (10 mL), and the mixture was boiled under reflux for 3 h. The solution was then filtered through dry Celite and concentrated; *n*-hexane was subsequently added and the solution cooled to −20 °C. The colorless crystals thus obtained were decanted, washed with *n*-hexane (3 × 5 mL) and vacuum dried to yield 0.035 g (59%) of **2c**. IR: ṽ = 2221 s, 1618 m, 1571 m, 1400 w, 1299 vs, 1279 vs, 1236 m, 1196 s, 1033 s (sh), 1085 m, 1043 mw, 1024 m, 934 vw, 922 m, 852 m, 835 m, 753 m, 693 m, 683 vs, 672 w, 580 vw, 534 m, 468 m, 451 w, 438 m, 291 vw cm^{-1}. ^{1}H NMR: δ = 7.91 [s, $C_6H_2(CF_3)_3$, 2 H], 1.33 (s, CNC_4H_9, 18 H) ppm. ^{19}F NMR: δ = −61.31 (s, *ortho*-CF_3, 6 F), −63.06 (s, *para*-CF_3, 3 F) ppm. $C_{19}H_{20}ClF_9N_2Pd$: calcd. C 38.73, H 3.42, N 4.75; found C 38.75, H 3.27, N 4.74. For the same reaction in CH_2Cl_2 at −50 °C, the ^{19}F NMR spectrum of a $CDCl_3$ solution of the crude product obtained after removing immediately the volatiles in vacuo, maintaining the low temperature, showed a mixture of *cis*-**2c** (72%) and *trans*-**2c** (28%). The ^{19}F NMR spectrum of the same sample after 15 h at room temperature showed 31% of *cis*-**2c** and 69% *trans*-**2c**. This crude product was stored as a solid at room temperature and, after several weeks, the ^{19}F NMR of a $CDCl_3$ solution showed only signals due to *trans*-**2c**.

***cis*-[Pd(Fmes)Cl(NCMe)$_2$] (2d):** This complex cannot be isolated pure because it loses MeCN. It was characterized by ^{19}F NMR in CH_3CN solution: ^{19}F NMR (CH_3CN/[D_6]Me_2CO): δ = −57.63 (s, *ortho*-CF_3, 6 F), −62.17 (s, *para*-CF_3, 3 F) ppm.

***cis*-[PdCl(Fmes)(PMe$_3$)$_2$] (*cis*-2e):** This complex was detected upon addition of PMe_3 to a solution of **1a** in acetonitrile (PMe_3/**1a**, 2:1) by ^{19}F NMR (CH_3CN/[D_6]Me_2CO): δ = −58.44 (d, $J_{P,F}$ = 6.0 Hz, *ortho*-CF_3, 6 F), −62.13 (s, *para*-CF_3, 3 F) ppm. ^{31}P{^{1}H} NMR (CH_3CN/[D_6]Me_2CO): δ = −6.7 (d sept, $J_{P,P}$ = 36.0, $J_{P,F}$ = 6.0 Hz), −15.9 (d, $J_{P,P}$ = 36.0 Hz) ppm.

***trans*-[PdCl(Fmes)(PMe$_3$)$_2$] (*trans*-2e):** This was detected in similar fashion to *cis*-**2e**.^{19}F NMR (CH_3CN/[D_6]Me_2CO): δ = −61.41 (t, $J_{P,F}$ = 6.0 Hz, *ortho*-CF_3, 6 F), −62.19 (s, *para*-CF_3, 3 F) ppm. ^{31}P{^{1}H} NMR (CH_3CN/[D_6]Me_2CO): δ = −11.2 (sept, $J_{P,F}$ = 6.0 Hz). Ratios of *trans*-**2e** to *cis*-**2e**: 3:97 immediately after addition of PMe_3; 55:45 after 7 h at room temperature; 70:30 after 24 h at room temperature

[PdCl(Fmes)(tmeda)] (3a): [$PdCl_2$(tmeda)] (0.292 g, 1 mmol) was added to a recently prepared solution of Li(Fmes) (4 mmol) in Et_2O (30 mL). After stirring the solution at room temperature for 24 h, two drops of water were then added to hydrolyze the excess organolithium reagent, and the volatiles were removed in vacuo. The resultant dark residue was extracted with CH_2Cl_2 (ca. 50 mL) and filtered through dry Celite. *n*-Hexane (ca. 20 mL) was then added to the orange filtrate, which was concentrated, and cooled to −20 °C. The orange microcrystalline solid thus obtained was decanted, washed with *n*-hexane (3 × 5 mL), and dried in vacuo to furnish 0.339 g (63%) of **3a**. IR: ṽ = 1620 m, 1571 w, 1286 vs, 1262 s, 1191 vs, 1140 vs, 1128 vs, 1046 m, 957 w, 917 s, 855 m, 833 m, 804 s, 772 w, 754 w, 696 w, 684 m, 667 w, 437 w, 329 m cm^{-1}. ^{1}H NMR: δ = 7.76 [s, $C_6H_2(CF_3)_3$, 2 H], 2.73 [m, {$(CH_3)_2NCH_2$}$_2$, 6 H], 2.70 [m, {$(CH_3)_2NCH_2$}$_2$, 4 H], 2.40 [s, {$(CH_3)_2NCH_2$}$_2$, 6 H] ppm. ^{19}F NMR: −56.74 (s, *ortho*-CF_3, 6 F), −63.17 (s, *para*-CF_3, 3 F) ppm. $C_{15}H_{18}ClF_9N_2Pd$ (539.2): calcd. C 33.42, H 3.37, N 5.20; found C 32.37, H 3.46, N 5.72.

[PdCl(Fmes)(4,4′-Me$_2$bipy)] (3b): 4,4′-Me_2bipy (0.022 g, 0.12 mmol) was added to a yellow solution of **1a** (0.047 g, 0.05 mmol) in dichloromethane (15 mL) and stirred for 3 h at room temperature. Then *n*-hexane was added to the colorless solution and concentrated. The resultant white solid was washed with *n*-hexane (3 × 5 mL), vacuum dried and recrystallized from dichloromethane/hexane to yield 0.025 g (42%) of **3b** as colorless crystals. IR: ṽ = 1616 s, 1567 w, 1297 vs, 1283 vs, 1262 vs, 1242 m, 1223 w, 1187 s, 1127 vs (sh), 1083 s, 1028 s (sh), 927 w, 913 s, 896 w, 853 w, 832 s, 756 w, 696 m, 684 s, 667 vw, 564 vw, 519 m, 469 vw, 438 vw, 427 w, 337 w cm^{-1}. ^{1}H NMR: δ = 9.11 [d, $J_H{}^6{}_H{}^5$ = 5.5 Hz, {$NC_5H_3(CH_3)$}$_2$, H^6 *cis* to Cl, 1 H], 7.89 [s, $C_6H_2(CF_3)_3$, 2 H], 7.87 [s, H^3, {$NC_5H_3(CH_3)$}$_2$, 1 H], 7.39 [d, $J_H{}^5{}_H{}^6$ = 5.5 Hz, H^5, {$NC_5H_3(CH_3)$}$_2$, 1 H], 7.35 [d, $J_H{}^5{}_H{}^6$ = 5.8 Hz, H^5, {$NC_5H_3(CH_3)$}$_2$, 1 H], 7.06 [d, *J* = 5.8 Hz, H^6, {$NC_5H_3(CH_3)$}$_2$, 1 H], 2.54 (s, CH_3, 3 H), 2.48 [s, {$NC_5H_3(CH_3)$}$_2$, 3 H] ppm. ^{19}F NMR: δ = −59.21 (s, *ortho*-CF_3, 6 F), −63.00 (s, *para*-CF_3, 3 F)

 © 2003 Wiley-VCH Verlag GmbH & Co. KGaA, Weinheim

ppm. $C_{21}H_{14}N_2ClF_9Pd$ (607.2): calcd. C 41.54, H 2.32, N 4.61; found C 41.58, H 2.44, N 4.64.

[PdCl(Fmes)(biquinolyl)] (3c): 2,2′-Biquinolyl (0.056 g, 0.22 mmol) was added to a yellow solution of **1a** (0.093 g, 0.1 mmol) in dichloromethane (15 mL) and stirred for 7 h at room temperature to give a cloudy solution. The volatiles were then pumped off and the yellow residue was washed with *n*-hexane (3 × 5 mL) and vacuum dried to furnish 0.109 g (80%) of **3c**. IR: $\tilde{\nu}$ = 1619 m, 1600 m, 1575 w, 1344 m, 1300 s, 1282 vs, 1265 s, 1188 vs, 1131 vs (br), 1083 m, 1031 m, 992 w, 972 w, 915 m, 872 w, 855 w, 830 s, 784 m, 750 s, 684 m, 506 vw, 490 vw, 470 vw, 439 vw, 328 w cm^{-1}. ^{1}H NMR: δ = 9.37 [d, *J* = 8.2 Hz, $(NC_9H_6)_2$, H^6 *cis* to Cl, 1 H], 8.57 [t, *J* = 8.8 Hz, $(NC_9H_6)_2$, 2 H], 8.35 [d, *J* = 8.7 Hz, $(NC_9H_6)_2$, 1 H], 8.25 [d, *J* = 8.8 Hz, $(NC_9H_6)_2$, 1 H], 7.93 [m, $(NC_9H_6)_2$, 2 H], 7.85 [d, *J* = 7.8 Hz, $(NC_9H_6)_2$, 1 H], 7.73 [m, $C_6H_2(CF_3)_3$ and $(NC_9H_6)_2$, 4 H], 7.49 [m, $(NC_9H_6)_2$, 2 H] ppm. ^{19}F NMR: δ = −58.44 (s, *ortho*-CF_3, 6 F), −63.01 (s, *para*-CF_3, 3 F) ppm. $C_{27}H_{14}N_2ClF_9Pd$ (679.3): calcd. C 47.73, H 2.08, N 4.12; found C 47.56, H 2.12, N 4.10.

[PdCl(Fmes)(OPPhPy$_2$-*N*,*N*′)] (3d): $OPPhPy_2$ (0.031 g, 0.11 mmol) was added to a yellow solution of **1a** (0.047 g, 0.05 mmol) in dichloromethane (10 mL) and stirred at room temperature for 8 h to give a colorless solution. *n*-Hexane was then added and the solution was concentrated. The resultant white solid was washed with *n*-hexane (3 × 5 mL), vacuum dried and recrystallized from dichloromethane/hexane to yield 0.045 g (64%) of **3d** as colorless crystals. IR: $\tilde{\nu}$ = 1617 s, 1591 m, 1569 w, 1298 vs, 1275 vs, 1217 s, 1194 vs, 1136 vs, 1060 m, 1024 s, 997 w, 928 w, 906 s, 853 m, 835 m, 777 m, 756 s, 744 s, 702 m, 692 s, 684 s, 667 vw, 646 vw, 547 s, 504 w, 471 vw, 451 w, 438 vw, 326 vw, 305 vw, 285 vw cm^{-1}. ^{1}H NMR: δ = 9.69 (d, *J* = 5.5 Hz, C_5H_4N, H^6 *cis* to Cl, 1 H), 8.81 (t, *J* = 7.5 Hz, C_5H_4N, H^3, 1 H), 8.47 (t, *J* = 7.0 Hz, C_5H_4N, H^3, 1 H), 8.18 (m, C_5H_4N, H^4, 1 H), 8.08 (m, C_5H_4N, H^4, 1 H), 7.93 (d, *J* = 6.5 Hz, C_5H_4N, H^6, 1 H), 7.92 [s, $C_6H_2(CF_3)_3$, 1 H], 7.80 (m, C_6H_5, 4 H), 7.71 (m, C_5H_4N, H^5, 1 H), 7.6 (m, H^{5}of C_5H_4N, and C_6H_5, 2 H), 7.54 [s, $C_6H_2(CF_3)_3$, 1 H] ppm. ^{19}F NMR: δ = −57.13 (s, *ortho*-CF_3, 3 F), −62.42 (s, *ortho*-CF_3, 3 F), −63.19 (s, *para*-CF_3, 3 F) ppm. ^{31}P{^{1}H} NMR: δ = 20.4 (s) ppm. $C_{25}H_{15}ClF_9N_2OPPd$ (703.2): calcd. C 42.70, H 2.15, N 3.98; found C 43.04, H 2.35, N 3.91.

[PdCl(Fmes){(OH)(CH$_3$)CPy$_2$-*N*,*N*′}] (3e): $(OH)(CH_3)CPy_2$ (0.024 g, 0.12 mmol) was added to a yellow solution of **1a** (0.047 g, 0.05 mmol) in dichloromethane (10 mL) and stirred at room temperature for 2 h. Then *n*-hexane was added and the solution concentrated. The resultant yellow solid was washed with *n*-hexane (3 × 5 mL), vacuum dried and recrystallized from dichloromethane/hexane to yield 0.061 g (88%) of **3e**·CH_2Cl_2 as yellow crystals. IR: $\tilde{\nu}$ = 3371 m, 1619 m, 1603 m, 1569 w, 1283 vs, 1262 s, 1189 vw, 1126 vs, 1097 m, 1083 m, 1060 m, 1027 m, 944 w, 913 m, 854 w, 834 w, 791 w, 761 m, 694 w, 684 m, 667 vw, 654 vw, 590 vw, 468 vw, 436 vw, 332 vw cm^{-1}. ^{1}H NMR ([D$_6$]Me_2CO): δ = 9.30 (m, C_5H_4N, H^6 *cis* to Cl, 1 H), 8.36 (m, C_5H_4N, 1 H), 8.10 (m, C_5H_4N, 3 H), 8.01 [s, $C_6H_2(CF_3)_3$, 1 H], 7.91 (m, C_5H_4N, 1 H), 7.84 [s, $C_6H_2(CF_3)_3$, 1 H], 7.60 (m, C_5H_4N, 1 H), 7.23 (m, C_5H_4N, 1 H), 6.40 (s, O*H*, 1 H), 3.00 (s, CH_3, 3 H) ppm. ^{19}F NMR ([D$_6$]Me_2CO): δ = −56.17 (br., *ortho*-CF_3, 3 F), −58.86 (br., *ortho*-CF_3, 3 F), −61.96 (s, *para*-CF_3, 3 F) ppm. $C_{22}H_{16}Cl_3F_9N_2OPd$ (708.1): calcd. C 38.12, H 2.33, N 4.05; found C 38.08, H 2.34, N 3.94.

[PdCl(Fmes)(pte)] (3f): 1,2-Bis(phenylthio)ethane (0.041 g, 0.165 mmol) was added to a yellow solution of **1a** (0.067 g, 0.075 mmol) in dichloromethane (10 mL) and stirred for 5 h at room temperature. *n*-Hexane (10 mL) was then added and the dichloromethane evaporated off to give a yellow solid that was washed with *n*-hexane (3 × 5 mL), vacuum dried and recrystallized from dichloromethane/hexane [yield: 0.073 g (73%)]. IR: $\tilde{\nu}$ = 1616 m, 1571 w (sh), 1406 w, 1299 s, 1284 vs, 1262 s, 1185 vs, 1144 s, 1118 vs (sh), 1083 m, 1024 m, 924 w, 907 m, 853 vw, 834 m, 753 m, 744 s, 693 m, 684 m, 666 vw, 506 vw, 478 w, 467 vw, 455 vw, 436 vw, 322 w cm^{-1}. ^{1}H NMR: δ = 8.04 (m, C_6H_5, 2 H), 7.76 [s, $C_6H_2(CF_3)_3$, 2 H], 7.51 (m, C_6H_5, 3 H), 7.47 (m, C_6H_5, 5 H), 3.32 (m, CH_2, 2 H), 3.09 (m, CH_2, 2 H) ppm. ^{19}F NMR: δ = −57.78 (s, *ortho*-CF_3, 6 F), −63.22 (s, *para*-CF_3, 3 F) ppm. $C_{23}H_{16}ClF_9PdS_2$ (669.3): calcd. C 41.27, H 2.41; found C 41.00, H 2.42.

[PdCl(Fmes)(dppe)] (3g): The ligand dppe (0.040 g, 0.1 mmol) was added to a solution of **1a** (0.047 g, 0.05 mmol) in toluene (10 mL). The solution was then boiled under reflux for 2 h, after which the volatiles were pumped off and the resultant white residue was dissolved in dichloromethane filtered through dry Celite. Hexane (10 mL) was then added to the filtrate, which was concentrated and cooled to −20 °C. The thus obtained colorless crystals were decanted, washed with *n*-hexane (3 × 5 mL) and vacuum dried to yield 0.052 g (63%) of **3g**. IR: $\tilde{\nu}$ = 1618 m, 1569 vw, 1438 m, 1298 s, 1279 vs, 1261 s, 1186 vs, 1130 vs (sh), 1106 s, 1079 m, 1021 w, 1000 vw, 925 vw, 890 w, 852 vw, 826 w, 745 s, 706 s, 692 s, 666 w, 530 m, 498 m, 481 w, 439 vw, 329 vw, 298 vw cm^{-1}. ^{1}H NMR: δ = 8.00 (m, C_6H_5, *para*-H, 4 H), 7.60 [d, $J_{P_{trans}H_{Fmes}}$ = 1.0 Hz, $C_6H_2(CF_3)_3$, 2 H], 7.51 (m, C_6H_5, 6 H), 7.37 (m, C_6H_5, 2 H), 7.18 (m, C_6H_5, 8 H), 2.58 (m, CH_2, 2 H), 2.15 (m, CH_2, 2 H) ppm. ^{19}F NMR: δ = −58.29 (d, $J_{P,F}$ = 5.5 Hz, *ortho*-CF_3, 6 F), −63.12 (s, *para*-CF_3, 3 F) ppm. ^{31}P{^{1}H} NMR: δ = 52.9 (d sept., $J_{P,P}$ = 23.2, $J_{P,F}$ = 5.5 Hz, P_{cis} of dppe), 39.67 (d, $J_{P,P}$ = 23.2 Hz, P_{trans} of dppe) ppm. $C_{35}H_{26}ClF_9P_2Pd$ (821.4): calcd. C 51.18, H 3.19; found C 51.03, H 3.29.

[PdCl(Fmes)(2,6-lut)(NCMe)] (4a): 2,6-Lut (25 μL, 0.023 g, 0.22 mmol) was added to a yellow solution of **1a** (0.093 g, 0.1 mmol) in dichloromethane (10 mL) and stirred for 5 h at room temperature to give a colorless solution, to which *n*-hexane was added. This solution was then concentrated and cooled to −20 °C to give a white solid that was washed with *n*-hexane (3 × 5 mL) and vacuum dried to yield 0.094 g (82%) of **4a**. IR: $\tilde{\nu}$ = 2343 m, 2303 w, 1616 m, 1583 m, 1571 m, 1300 vs, 1288 vs, 1264 vs, 1180 vs (br), 1119 vs (br), 1095 m, 1029 m, 915 s, 854 m, 837 m, 781 s, 757 m, 695 m, 684 s, 668 vw, 577 vw, 470 vw, 438 w, 374 w, 340 w cm^{-1}. ^{1}H NMR: δ = 7.84 [s, $C_6H_2(CF_3)_3$, 2 H], 7.56 [t, $J_H{}^3{}_H{}^4$ = 7.7 Hz, $NC_5H_3(CH_3)_2$, H^4, 1 H], 7.11 [d, $J_H{}^3{}_H{}^4$ = 7.7 Hz, $NC_5H_3(CH_3)_2$, H^3, 2 H], 3.29 [s, $NC_5H_3(CH_3)_2$, 6 H], 2.08 (s, CH_3CN, 3 H) ppm. ^{19}F NMR: δ = −58.22 (s, *ortho*-CF_3, 6 F), −63.06 (s, *para*-CF_3, 3 F) ppm. $C_{18}H_{14}ClF_9N_2Pd$ (571.2): calcd. C 37.85, H 2.47, N 4.90; found C 37.97, H 2.54, N 4.70.

[PdCl(Fmes)(3,5-lut)(NCMe)] (4b): 3,5-Lut (25 μL, 0.023 g, 0.22 mmol) was added to a yellow solution of **1a** (0.093 g, 0.1 mmol) in dichloromethane (10 mL) and stirred for 15 min at room temperature to give a colorless solution. Then *n*-hexane was added and the solution was concentrated and cooled to −20 °C. The colorless crystals thus obtained were decanted, washed with *n*-hexane (3 × 5 mL) and vacuum dried to yield 0.060 g (53%) of **4b**. IR: $\tilde{\nu}$ = 2329 w, 2303 w, 1618 m, 1599 w, 1572 w, 1304 vs, 1292 vs, 1263 s, 1184 vs, 1157 s, 1143 s, 1117 vs, 1084 m, 1032 w, 913 m, 865 w, 856 vw, 835 w, 774 w, 755 w, 700 m, 684 m, 667 vw, 471 vw, 439 vw, 344 vw cm^{-1}. ^{1}H NMR: δ = 8.35 [s, $NC_5H_3(CH_3)_2$, H^2, 2 H], 7.80 [s, $C_6H_2(CF_3)_3$, 2 H], 7.42 [s, $NC_5H_3(CH_3)_2$, H^4, 1 H], 2.35 [s, $NC_5H_3(CH_3)_2$, 6 H], 2.14 (s, CH_3CN, 3 H) ppm. ^{19}F NMR: δ = −58.48 (s, *ortho*-CF_3, 6 F), −63.04 (s, *para*-CF_3, 3 F) ppm.

 © 2003 Wiley-VCH Verlag GmbH & Co. KGaA, Weinheim

Table 3. Crystal data and structure refinement for [Pd(Fmes)(μ-Br){P(*o*-Tol)$_3$}]$_2$ (**1j**) and [PdCl(Fmes){(OH)(CH$_3$)CPy$_2$-*N*,*N*′}] (**3e**)

	1j	**3e**
Empirical formula	$C_{30}H_{23}BrF_9PPd$	$C_{21}H_{14}ClF_9N_2OPd$
Molecular weight	771.76	623.19
Temperature	302(2) K	298(2) K
Wavelength [Å]	0.71073 Å	0.71073 Å
Crystal system	Monoclinic	Monoclinic
Space group	$P2_1/c$	$P2_1/n$
a [Å]	15.753(5)	11.567(5)
b [Å]	9.369(3)	9.696(4)
c [Å]	21.184(7)	23.001(10)
β [°]	107.803(5)	95.748(9)
V [Å^3]	2976.8(15)	2566.7(19)
Z	4	4
$D_{calcd.}$ [g·cm^{-3}]	1.722	1.613
Absorption coefficient [mm^{-1}]	2.095	0.908
F(000)	1520	1224
Crystal size [mm]	0.11 × 0.04 × 0.03	0.23 × 0.13 × 0.04
Theta range for data collection	1.36 to 23.42°	1.78 to 23.40°
Reflections collected	27367	12107
Independent reflections	4323 (R_{int} = 0.1050)	3717 (R_{int} = 0.0373)
Absorption correction	SADABS	SADABS
Data/restraints/parameters	4323/0/382	3717/0/322
Goodness-of-fit on F^2	1.000	1.002
R_1 [$I > 2\sigma(I)$]	0.0528	0.0507
wR_2 (all data)	0.1312	0.1864

$C_{18}H_{14}ClF_9N_2Pd$ (571.2): calcd. C 37.85, H 2.47, N 4.91; found C 37.62, H 2.31, N 4.72. A $CDCl_3$ solution of **4b** maintained at −20 °C for 5 days showed a **4b/1e** ratio of 81:19 by ^{19}F NMR spectroscopy. In a separate experiment, a $CDCl_3$ solution of **4b** maintained at room temperature during 24 h showed a **4b/1e** ratio of 60:40 by ^{19}F NMR spectroscopy.

[PdCl(Fmes)(NCMe)(PPh$_3$)] (4c): PPh_3 (0.058 g, 0.22 mmol) was added to a yellow solution of **1a** (0.093 g, 0.1 mmol) in dichloromethane (10 mL) and stirred at room temperature for 8 h to give a colorless solution, to which *n*-hexane was added. The resultant solution was then concentrated and cooled to −20 °C. The colorless crystals thus obtained were decanted, washed with *n*-hexane (3 × 5 mL) and vacuum dried to yield 0.060 g (52%) of **4c**·CH_2Cl_2. IR: $\tilde{\nu}$ = 2329 m, 2322 w, 1616 s, 1570 m, 1300 vs, 1286 vs, 1261 vs, 1186 vs (br), 1121 vs (br), 1099 s, 1082 s, 1024 s, 1000 m, 913 s, 852 m, 834 m, 695 vs, 684 s, 668 w, 529 s, 512 s, 494 m, 456 w, 436 w, 330 w cm^{-1}. ^1H NMR: δ = 7.85 [d, $J_{P,H}$ = 2.4 Hz, $C_6H_2(CF_3)_3$, 2 H], 7.76 (m, *ortho*-H, C_6H_5, 6 H), 7.46 (m, *meta*-H and *para*-H, C_6H_5, 9 H), 1.59 (d, $J_{P,H}$ = 1.3 Hz, CH_3CN, 3 H) ppm. ^{19}F NMR: δ = −58.40 (s, *ortho*-CF_3, 6 F), −62.98 (s, *para*-CF_3, 3 F) ppm. $^{31}P\{^1H\}$ NMR: δ = 17.6 (s) ppm. $C_{30}H_{22}Cl_3F_9NPd$ (780.3): calcd. C 44.42, H 2.73, N 1.72; found C 44.25, H 2.77, N 1.76. A $CDCl_3$ solution of **4c** maintained at room temperature for 2 days showed a **4c/1i** ratio of 58:42 by ^{19}F NMR spectroscopy.

[(μ-dppe){PdCl(Fmes)(NCMe)}$_2$] (4d): The ligand dppe (0.080 g, 0.2 mmol) was added to a yellow solution of **1a** (0.093 g, 0.1 mmol) in dichloromethane (10 mL) and stirred at room temperature for 12 h. The white solid so-formed was decanted, washed with diethyl ether (3 × 5 mL) and vacuum dried to yield 0.079 g (59%) of **4d**. IR: $\tilde{\nu}$ = 2331 w, 2304 vw, 1616 s, 1569 m, 1339 m, 1299 vs, 1278 vs, 1186 vs, 1126 vs, 1082 s, 1023 m, 1001 m, 977 vw, 913 s, 852 m, 835 m, 772 vw, 746 s, 705 s, 692 s, 682 s, 535 w, 520 s, 492 m, 450 m, 437 w, 350 w, 302 w cm^{-1}. ^1H NMR ([D$_6$]Me$_2$CO): δ = 8.2−7.7 (m, C_6H_5, 20 H), 7.94 [d, $J_{P,H}$ = 1.0 Hz, $C_6H_2(CF_3)_3$, 4 H], 3.26 (m, CH_2, 4 H), 1.93 (s, CH_3CN, 6 H) ppm. ^{19}F NMR ([D$_6$]Me$_2$CO): δ = −56.99 (s, *ortho*-CF_3, 6 F), −61.91 (s, *para*-CF_3, 3 F) ppm. $^{31}P\{^1H\}$ NMR ([D$_6$]Me$_2$CO): δ = 18.1 (s) ppm. $C_{48}H_{34}Cl_2F_{18}N_2P_2Pd_2$ (1326.4): calcd. C 43.46, H 2.58, N 2.11; found C 43.73, H 2.66, N 1.97. The filtrate was dried and the white solid thus obtained was washed with diethyl ether (3 × 5 mL) and vacuum dried to furnish 0.047 g of **3g** (29%).

X-ray Crystallographic Study: Suitable crystals of **1j** and **3e** were grown by slow diffusion of a concentrated dichloromethane (for **1j**) or acetone (for **3e**) solution of the complex into *n*-hexane at −20 °C. X-ray measurements were made using a Bruker SMART CCD area-detector diffractometer with Mo-K_α radiation (λ = 0.71073 Å).[31] Intensities were integrated from several series of exposures,[32] each exposure covering 0.3° in ω, the total data set being a hemisphere. Absorption corrections were applied, based on multiple and symmetry-equivalent measurements.[33] The structure was solved by direct methods and refined by least-squares on weighted F^2 values for all reflections (Table 3).[34] All non-hydrogen atoms were assigned anisotropic displacement parameters and refined without positional constraints. Hydrogen atoms were constrained to ideal geometries and refined with fixed isotropic displacement parameters except for the hydrogen of the alcohol group in **3e**, which was located in a difference Fourier map and refined. Refinement proceeded smoothly to give the residuals shown in Table 3. Complex neutral-atom scattering factors were used.[35]

CCDC-192421 (**1j**) and -192420 (**3e**) contain the supplementary crystallographic data for this paper. These data can be obtained free of charge at www.ccdc.cam.ac.uk/conts/retrieving.html [or from the Cambridge Crystallographic Data Centre, 12 Union

 © 2003 Wiley-VCH Verlag GmbH & Co. KGaA, Weinheim

Road, Cambridge CB2 1EZ, UK; fax: (internat.) +44-1223/336-033; E-mail: deposit@ccdc.cam.ac.uk].

Acknowledgments

The authors thank the DGI (BQU2001−2015) and the JCyL (VA17/00B) for financial support.

[1] F. T. Edelmann, *Comments Inorg. Chem.* **1992**, *12*, 259.

[2] [2a] D. Stalke, K. H. Whitmire, *J. Chem. Soc., Chem. Commun.* **1990**, 833. [2b] S. Brooker, J.-K. Buijink, F. T. Edelmann, *J. Chem. Soc., Chem. Commun.* **1991**, *10*, 25. [2c] H. Grützmacher, H. Pritzkow, F. T. Edelmann, *Organometallics* **1991**, *10*, 23. [2d] K. H. Whitmire, D. Labahn, H. W. Roesky, M. Noltemeyer, G. M. Sheldrick, *J. Organomet. Chem.* **1991**, *402*, 55. [2e] U. Lay, H. Pritzkow, H. Grützmacher, *Chem. Commun.* **1992**, 260. [2f] S. Brooker, N. Bertel, D. Stalke, M. Noltemeyer, H. W. Roesky, G. M. Sheldrick, F. T. Edelmann, *Organometallics* **1992**, *11*, 192. [2g] R. D. Schulter, A. H. Cowley, D. A. Atwood, R. A. Jones, M. R. Bond, C. J. Carrano, *J. Am. Chem. Soc.* **1993**, *115*, 2070. [2h] R. D. Schulter, H. S. Isom, A. H. Cowley, D. A. Atwood, R. A. Jones, F. Olbrich, S. Corbelin, R. J. Lagow, *Organometallics* **1994**, *163*, 4058. [2i] A. Vij, R. L. Kirchmeier, R. D. Willett, J. M. Shreeve, *Inorg. Chem.* **1994**, *33*, 5456. [2j] J.-T. Ahlemann, A. Künzel, H. W. Roesky, M. Noltemeyer, L. Markovskii, H.-G. Schmidt, *Ibid* **1996**, *35*, 6644. [2k] J. E. Bender IV, M. M. B. Holl, J. W. Kampf, *Organometallics* **1997**, *16*, 2743. [2l] J. E. Bender IV, M. M. B. Holl, A. Mitchell, N. J. Wells, J. W. Kampf, *Organometallics* **1998**, *17*, 5166. [2m] K. W. Klinkhammer, T. F. Fässler, H. Grützmacher, *Angew. Chem. Int. Ed.* **1998**, *37*, 124. [2n] J. E. Bender IV, A. J. Shusterman, M. M. B. Holl, J. W. Kampf, *Organometallics* **1999**, *18*, 1547. [2o] N. Burford, C. L. B. Macdonald, D. J. LeBlanc, T. S. Cameron, *Organometallics* **2000**, *19*, 152.

[3] [3a] M. Belay, F. T. Edelmann, *J. Organomet. Chem.* **1994**, *479*, C21. [3b] V. C. Gibson, C. Redshaw, L. J. Sequeira, K. B. Dillon, W. Clegg, M. R. J. Elsegood, *Chem. Commun.* **1996**, 2151. [3c] K. B. Dillon, V. C. Gibson, J. A. K. Howard, C. Redshaw, L. Sequeira, J. W. Yao, *J. Organomet. Chem.* **1997**, *528*, 179. [3d] P. Espinet, S. Martín-Barrios, F. Villafañe, P. G. Jones, *Organometallics* **2000**, *19*, 290. [3e] A. S. Batsanov, K. B. Dillon, V. C. Gibson, J. A. K. Howard, L. Sequeira, J. W. Yao, *J. Organomet. Chem.* **2001**, *631*, 181. [3f] G. M. Benedikt, B. L. Goodall, S. Iyer, L. H. McIntosh, III, R. Mimna, L. F. Rhodes, C. S. Day, V. W. Day, *Organometallics* **2001**, *20*, 2565.

[4] C. Bartolomé, P. Espinet, F. Villafañe, S. Giesa, A. Martín, A. G. Orpen, *Organometallics* **1996**, *15*, 2019.

[5] [5a] C. Bartolomé, R. de Blas, P. Espinet, J. M. Martín-Alvarez, F. Villafañe, *Angew. Chem. Int. Ed.* **2001**, *40*, 2521. [5b] C. Bartolomé, P. Espinet, L. Vicente, F. Villafañe, J. P. H. Charmant, G. A. Orpen, *Organometallics* **2002**, *21*, 3536. [5c] C. Bartolomé, P. Espinet, J. M. Martín-Alvarez, F. Villafañe, *Inorg. Chim. Acta* **2003**, *347*, 49.

[6] [6a] F. T. Ladipo, G. K. Anderson, *Organometallics* **1994**, *13*, 303. [6b] C. Eaborn, K. J. Odell, A. Pidcock, *J. Chem. Soc., Dalton Trans.* **1978**, 1288. [6c] R. J. Puddephatt, P. J. Thomson, *J. Chem. Soc., Dalton Trans.* **1977**, 1219. [6d] G. K. Anderson, R. J. Cross, L. Manojlovic-Muir, K. W. Muir, T. Solomun, *J. Organomet. Chem.* **1979**, *170*, 385.

[7] For R = C_6F_5, the monomer *cis*-[PdBr(C_6F_5)($NCMe)_2$] is isolated as a solid and the dimer has not been obtained: A. C. Albéniz, P. Espinet, C. Foces-Foces, R. H. Cano, *Organometallics* **1990**, *9*, 1079. This suggests that the *trans* effect of Fmes is higher than that of C_6F_5, which implies that Fmes is a stronger σ-donor than C_6F_5.

[8] K. F. Purcell, J. C. Kotz, *Inorganic Chemistry*, 1st ed., W. B. Saunders C. **1977**, Cap. 13, page 694.

[9] Fmes is a soft σ-donor ligand with a high *trans* influence, which facilitates the release of the leaving ligand in an associative ligand substitution, i.e. the high *trans* influence of Fmes induces a high *trans* effect by destabilizing the fundamental state. Probably, some π-acceptor contribution in the five-coordinate transition state will further increase the *trans* effect of Fmes.

[10] R. G. Pearson, *Inorg. Chem.* **1973**, *12*, 712.

[11] [11a] J. Vicente, A. Arcas, D. Bautista, *Organometallics* **1997**, *16*, 2127. [11b] J. Vicente, J. A. Abad, A. D. Frankland, M. C. Ramírez de Arellano, *Chem. Eur. J.* **1999**, *5*, 3066. [11c] J. Vicente, J. A. Abad, E. Martinez-Viviente, P. G. Jones, *Organometallics*, in press.

[12] [12a] P. K. Biers, A. J. Canty, *Organometallics* **1990**, *9*, 210. [12b] R. E. Rülke, J. N. Spek, C. J. Elsevier, P. W. N. M. van Leeuwen, K. Brieze, *Inorg. Chem.* **1993**, *32*, 5769.

[13] J. A. Casares, P. Espinet, J. M. Martínez-Ilarduya, Y.-S. Lin, *Organometallics* **1997**, *16*, 770.

[14] [14a] A. Domenicano, A. Vaciago, C. A. Coulson, *Acta Crystallogr., Sect. B* **1975**, *31*, 221. [14b] A. Domenicano, P. Murray-Rust, A. Vaciago, *Acta Crystallogr., Sect. B* **1983**, *39*, 457, and references therein. [14c] R. Norrestam, L. Schepper, *Acta Chem. Scand., Ser. A* **1981**, *35*, 91. [14d] A. Domenicano, P. Mazzeo, A. Vaciago, *Tetrahedron Lett.* **1976**, 1029.

[15] To correct the systematic shortening of O−H bonds measured by X-ray diffraction, normalized H-atom positions were used. An O−H distance of 0.967 Å was imposed. This value has been observed in alcohols by neutron-diffraction: F. H. Allen, O. Kennard, D. G. Watson, L. Brammer, A. G. Orpen, R. Taylor, *J. Chem. Soc., Perkin Trans. 2* **1987**, S1.

[16] G. Aullón, D. Bellamy, L. Brammer, E. A. Bruton, A. G. Orpen, *Chem. Commun.* **1998**, 653.

[17] J. P. Rourke, F. P. Fanizzi, N. J. S. Salt, D. W. Bruce, D. A. Dunmur, P. Maitlis, *J. Chem. Soc., Chem. Commun.* **1990**, 229.

[18] [18a] F. Paul, J. Patt, J. F. Hartwig, *J. Am. Chem. Soc.* **1994**, *116*, 5969. [18b] F. Paul, J. Patt, J. F. Hartwig, *Organometallics* **1995**, *14*, 3030. [18c] M. Chentit, M. Geoffroy, G. Bernardinelli, *Acta Crystallogr., Sect. C* **1997**, *53*, 866.

[19] [19a] D. A. Albisson, R. B. Bedford, S. E. Lawrence, P. N. Scully, *Chem. Commun.* **1998**, 2095. [19b] V. Dufaut, J. Thivolle-Cazat, J. M. Basset, R. Mathieu, J. Jaud, J. Waissermann, *Organometallics* **1991**, *10*, 4005. [19c] K. Tsutsumi, S. Ogoshi, S. Nishiguchi, H. Kurosawa, *J. Am. Chem. Soc.* **1998**, *120*, 1938. [19d] S. J. Geib, A. L. Rheingold, *Acta Crystallogr., Sect. C* **1987**, *43*, 1427.

[20] J. A. S. Howell, M. G. Palin, P. C. Yates, P. McArdle, D. Cunningham, Z. Goldschmidt, H. G. Gottlieb, D. Hezroni-Langerman, *J. Chem. Soc., Perkin Trans. 2* **1992**, 1769.

[21] C. A. McAuliffe, in *Comprehensive Coordination Chemistry* (Eds.: G. Wilkinson, R. D. Gillard, A. A. McCleverty), Pergamon, Oxford; **1987**, vol. 2., p. 1012.

[22] [22a] R. A. Widenhoefer, H. A. Zhong, S. L. Buchwald, *Organometallics* **1996**, *15*, 2745. [22b] J. A. S. Howell, M. G. Palin, P. McArdle, D. Cunningham, Z. Goldschmidt, H. G. Gottlieb, D. Hezroni-Langerman, *Organometallics* **1993**, *12*, 1694. [22c] J. A. S. Howell, M. G. Palin, P. McArdle, D. Cunningham, Z. Goldschmidt, H. G. Gottlieb, D. Hezroni-Langerman, *Inorg. Chem.* **1993**, *32*, 3493.

[23] [23a] A. K. Colter, I. I. Schuster, R. J. Kurland, *J. Am. Chem. Soc.* **1965**, *87*, 2278. [23b] A. K. Colter, I. I. Schuster, R. J. Kurland, *J. Am. Chem. Soc.* **1965**, *87*, 2279.

[24] D. D. Perrin, W. L. F. Armarego, *Purification of Laboratory Chemicals*, 3rd ed.; Pergamon Press: Oxford, U. K., **1988**.

[25] [25a] G. E. Carr, R. D. Chambers, T. F. Holmes, D. G. Parker, *Ibid* **1987**, *325*, 13. [25b] M. Scholz, H. W. Roesky, D. Stalke, K. Keller, F. T. Edelmann, *J. Organomet. Chem.* **1989**, *366*, 73.

[26] R. Usón, J. Forniés, F. Martínez, M. Tomás, *J. Chem. Soc., Dalton Trans.* **1980**, 888.

[27] F. L. Wimmer, S. Wimmer, P. Castan, *Inorg. Synth.* **1992**, *29*, 185.

 © 2003 Wiley-VCH Verlag GmbH & Co. KGaA, Weinheim

[28] G. R. Newkome, D. C. Hager, *J. Org. Chem.* **1978**, *43*, 947.
[29] Treatment of $OCPy_2$ with LiMe and further hydrolysis yields $(OH)(CH_3)CPy_2$, which can be recrystallized from dichloromethane/hexane. Spectroscopic data agree with those previously reported: S. Bhaduri, N. Y. Sapre, P. G. Jones, *J. Chem. Soc., Dalton Trans.* **1991**, 2539.
[30] C. Bartolomé, P. Espinet, J. M. Martín-Alvarez, F. Villafañe, manuscript in preparation.
[31] SMART V5.051 diffractometer control software, Bruker Analytical X-ray Instruments Inc., Madison, WI, **1998**.
[32] SAINT V6.02 integration software, Siemens Analytical X-ray Instruments Inc., Madison, WI, **1999**.
[33] G. M. Sheldrick. *SADABS: A program for absorption correction with the Siemens SMART system*; University of Göttingen: Germany, **1996**.
[34] *SHELXTL program system version 5.1*; Bruker Analytical X-ray Instruments Inc., Madison, WI, **1998**.
[35] *International Tables for Crystallography*, Kluwer, Dordrecht, **1992**, vol. C.

Received April 7, 2003

 © 2003 Wiley-VCH Verlag GmbH & Co. KGaA, Weinheim

Synthesis, Structure and Chemical Transformations of Ethynylgermatranes

Edmunds Lukevics,[a] Pavel Arsenyan,*[a] Sergey Belyakov,[a] and Olga Pudova[a]

Keywords: Cobalt / Germanium / Germatrane / X-ray diffraction / Alkynes

Ethynylgermatranes have been prepared from monosubstituted acetylenes by a three-step synthesis without isolation of the hydrolytically unstable intermediate chlorogermanes and ethoxygermanes. Boiling an equimolar mixture of tetrachlorogermane Cl_4Ge, acetylene RC≡CH and triethylamine in hexane leads to germylation of the C_{sp}–H bond and the formation of ethynyl-substituted trichlorogermanes. Subsequent alkoxylation of chlorogermanes by ethanol in the presence of triethylamine affords triethoxygermanes that then take part in transalkoxylation with triethanolamine to give ethynylgermatranes. The molecular structures of all ethynylgermatranes and the hexacarbonyldicobalt complex of 1-heptynylgermatrane have been determined by X-ray crystallography.
(© Wiley-VCH Verlag GmbH & Co. KGaA, 69451 Weinheim, Germany, 2003)

Introduction

Derivatives of pentacoordinate germanium are the subject of considerable current research activity, particularly germatranes that contain an intramolecular N→Ge bond.[1−4] Investigations have focused on the relationship between the transannular N→Ge bond length and such factors as the character of the substituent at the germanium atom, the atrane skeleton structure, as well as crystal packing (crystal density, *Z* of unit cell, etc). However, the scope of their synthesis is limited. The few reported examples of ethynylgermatranes (unsubstituted ethynylgermatrane, 1-octynylgermatrane, and phenylethynylgermatranes)[5−8] were obtained by the "stannyl" method, by treating ethynyltrichlorogermanes $RC{\equiv}CGeCl_3$ with the tris(trialkylstannyl) ether of triethanolamine or by addition of triethanolamine to $RC{\equiv}CGeCl_3$ in the presence of triethylamine; phenylethynylgermatrane has also been prepared by the reaction of bromogermatrane with lithium phenylacetylenide.[5] The C≡C triple bond in ethynylgermatranes should allow various chemical transformations; however, only the bromination of phenylethynylgermatrane by NBS and bromine has been studied.[5] To the best of our knowledge, only the molecular structures of 1-phenylethynylgermatrane, and its chloroform solvate, and 4-fluorophenylethynylgermatrane have been determined by X-ray crystallography.[5,6,8] In this paper we focus on the synthesis of ethynylgermatranes via germylation of monosubstituted acetylenes by tetrachlorogermane in the presence of an organic base. Various chemical transformations of the acetylene fragment have been carried out, including complexation with octacarbonyldicobalt, [2+3] dipolar cycloaddition, and electrophilic substitution. The molecular structures of all synthesized ethynylgermatranes as well as of the hexacarbonyldicobalt complex of 1-heptynylgermatrane are also reported.

[a] Latvian Institute of Organic Synthesis,
Aizkraukles 21, Riga, 1006, Latvia
Fax: (internat.) + 371/7550338
E-mail: pavel.arsenyan@lycos.com

Results and Discussion

The ethynylgermatranes **4a**−**d** were prepared from monosubstituted acetylenes **1a**−**d** by a three-step synthesis without isolation of the hydrolytically unstable intermediate chlorogermanes **2a**−**d** and ethoxygermanes **3a**−**d**. Boiling an equimolar mixture of tetrachlorogermane $GeCl_4$, acetylene RC≡CH and triethylamine in hexane[9,10] leads to germylation of the C_{sp}−H bond and formation of ethynyl-substituted trichlorogermanes **2a**−**d**. Subsequent alkoxylation of chlorogermanes by ethanol in the presence of triethylamine affords triethoxygermanes **3a**−**d** which are then involved in transalkoxylation with triethanolamine to give ethynylgermatranes **4a**−**d** (Scheme 1). The yield of germatranes **4a**−**d** depends on the structure of the substituent R. The highest yield was observed for (trimethylsilyl)ethynylgermatrane (**4d**) (85%); with 1-heptynylgermatrane (**4a**) and (1-cyclohex-1-enyl)ethynylgermatrane (**4b**) the yields were 48 and 55%, respectively. The lowest yield was for 3-methoxypropyn-1-ylgermatrane (**4c**) (12%). Our attempts to prepare germatrane from methyl propiolate failed, since tetrachlorogermane acts as a Lewis acid in the reaction with HC≡CCOOMe to form 1,3,5-tris(methoxycarbonyl)benzene by [2+2+2] cycloaddition (Scheme 2).

As with other acetylene derivatives,[11−14] 1-heptynylgermatrane (**4a**) easily reacts with octacarbonyldicobalt in hexane (20 min at −5 °C). The hexacarbonyldicobalt complex of 1-heptynylgermatrane **5**, isolated in almost quantitative yield (93%) (Scheme 1), is stable in the solid state but com-

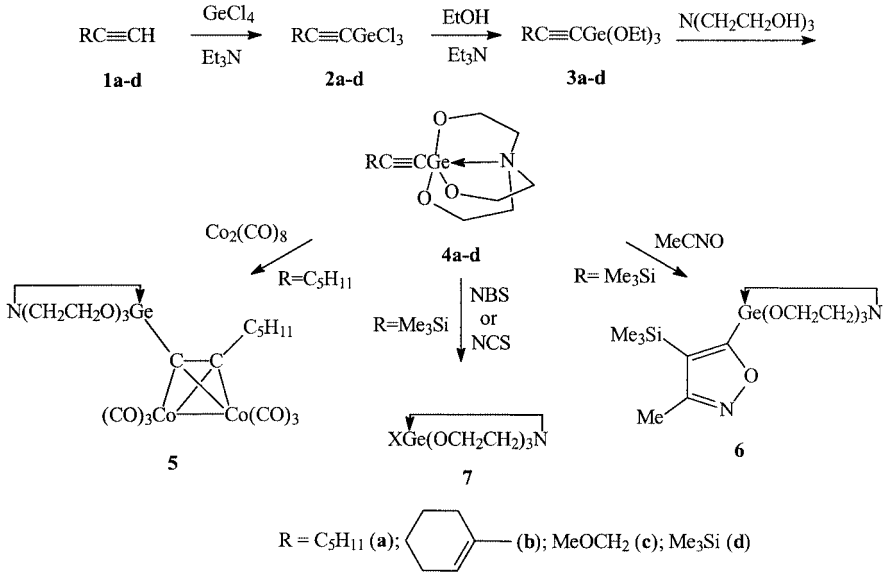

Scheme 1. Synthesis and transformations of ethynylgermatranes

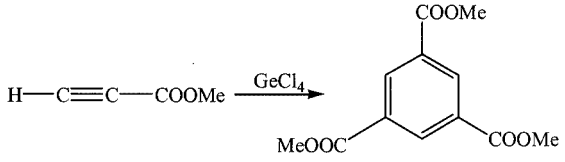

Scheme 2. [2+2+2] Cyclization of methyl propiolate in the presence of tetrachlorogermane

pletely decomposes in organic solvents (even in nonpolar ones such as hexane or benzene) after 2−3 h.

[2+3] Dipolar cycloaddition of acetonitrile oxide to the C≡C triple bonds of heptynylgermatrane (**4a**) and (trimethylsilyl)ethynylgermatrane (**4d**) has been investigated. Acetonitrile oxide, prepared in situ by the Mukaiyama−Hoshito method,[15] reacts with **4d** regioselectively to give only one of the two possible regioisomeric products, i.e. 5-germatranylisoxazole (**6**) in 75% yield. Conversely, for **4a** only a trace amount of the isoxazole derivative was detected by GC-mass spectrometry (Scheme 1).

The reaction of **4d** with NCS and NBS in DMF proceeds with cleavage of the Ge−C bond and formation of chloro- and bromogermatranes **7** (X = Cl, Br).[16] Our attempts to desilylate **4d** by different desilylation agents (Bu_4NF/Et_2O, K_2CO_3/MeOH, Amberlyst 15/THF, TsOH/MeOH) failed to cleave the Si−C bond, and so the initial germatrane **4d** was recovered.

The structures of the germatranes were confirmed by ^1H and ^{13}C NMR spectroscopy (Table 1). The ^1H spectra of

Table 1. ^1H and ^{13}C NMR spectroscopic data of ethynylgermatranes and their derivatives

Compound	δ ^1H, ppm			δ ^{13}C, ppm			
	CH_2N	CH_2O	R	CH_2N	CH_2O	GeCCR	R
4a	2.84 (t, J = 5.6 Hz, 6 H)	3.82 (t, J = 5.6 Hz, 6 H)	0.82 (t, J = 6 Hz, 3 H), 1.17−1.65 (m, 5 H), 2.20 (t, J = 6.4 Hz, 3 H)	51.5	56.6	80.5, 101.7	13.7, 19.5, 22.0, 28.2, 31.1
4b	2.87 (t, J = 5.6 Hz, 6 H)	3.84 (t, J = 5.6 Hz, 6 H)	1.45−1.60 (m, 4 H), 1.96−2.06 (m, 2 H), 2.1−2.2 (m, 2 H), 6.21 (sept, J = 1.8 Hz, 1 H)	51.3	56.5	87.0, 101.5	21.3, 22.1, 25.5, 28.8, 120.2, 136.2
4c	2.90 (t, J = 5.6 Hz, 6 H)	3.85 (t, J = 5.6 Hz, 6 H)	3.37 (s, 3 H), 4.12 (s, 2 H)	52.4	57.6	92.2, 96.5	58.4, 61.1
4d	2.87 (t, J = 5.6 Hz, 6 H)	3.84 (t, J = 5.6 Hz, 6 H)	0.15 (s, 9 H)	51.3	56.7	106.9, 108.3	−0.1
5	2.87 (t, J = 5.6 Hz, 6 H)	3.81 (t, J = 5.6 Hz, 6 H)	0.90 (t, J = 7 Hz, 3 H), 1.3−1.5 (m, 5 H), 1.6−1.7 (m, 3 H)	52.6	57.0	80.2, 108.5, 201.0 (CO), 206.7 (CO)	14.0, 22.4, 31.4, 31.5, 34.6
6	2.89 (t, J = 5.6 Hz, 6 H)	3.83 (t, J = 5.6 Hz, 6 H)	0.34 (s, 9 H), 2.41 (s, 3 H, Me-C)	51.5	56.4	119.3, 128.8, 12.1 (Me), 161.1 (C=N)	−1.1

 © 2003 Wiley-VCH Verlag GmbH & Co. KGaA, Weinheim

all germatrane derivatives (**4**–**6**) are characterized by two triplets of CH_2N (δ = 2.84–2.90 ppm) and CH_2O (δ = 3.81–3.85 ppm) groups. The signals of carbon atoms in the atrane fragment are in the δ = 51.3–52.6 and 56.4–57.6 ppm regions of the ^{13}C NMR spectra, and the signals of carbonyl-ligand carbon atoms in **5** are shifted to low field (δ = 201.0 and 206.7 ppm). As reported previously,[17] complexation of the C≡C triple bond does not strongly affect the carbon atoms' chemical shifts.

Molecular Structures of the Germatranes

Molecular structure data have been reported for more than 60 germatranes and their structural analogues.[2,18] However, only three of these structures contain an ethynylgermatrane fragment (phenylethynylgermatrane, and its $CHCl_3$ solvate, and 4-fluorophenylethynyl analogue[5,6,8]). These compounds are characterized by transannular N→Ge distances of 2.178, 2.160, and 2.175 Å, respectively, which are short in comparison with those in other alkyl-, alkenyl-, and arylgermatranes (2.20–2.24 Å). To further investigate the influence of various acetylene substituents RC≡C on the transannular N→Ge bond length the molecular structures of ethynylgermatranes **4a**–**d** and of the hexacarbonyldicobalt complex **5** have been determined by X-ray crystallography.

The germanium atom of germatranes **4a**–**d** and **5** has the typical atrane trigonal-bipyramidal geometry with nitrogen and carbon atoms in apical positions and three equatorial oxygen atoms. The axial nitrogen atom is pyramidalized so that its lone pair points towards the germanium atom. Selected bond lengths and angles are presented in Table 2. The transannular N→Ge bond length in ethynylgermatranes **4** varies between 2.202(3) Å (for the disordered germatrane **4a**) and 2.115 Å [for 3-methoxypropyn-1-ylgermatrane, (**4c**)]. The last value is one of the shortest distances detected for germatranes with Ge–C bonds. The shorter intramolecular bond length of 2.108 Å was found only for trifluoromethylgermatrane.[19] The Ge–C bonds in germatranes **4** lie between 1.905 and 1.962 Å. The longest Ge–C

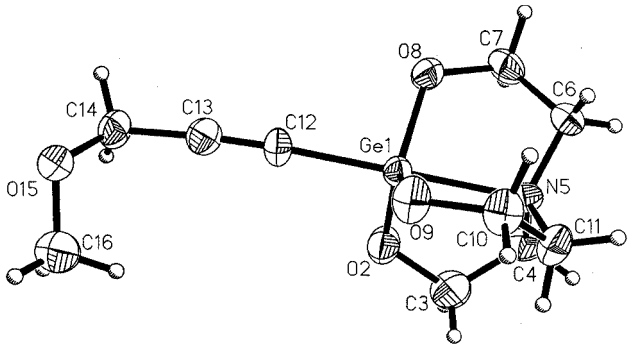

Figure 1. Molecular structure of 3-methoxypropyn-1-ylgermatrane (**4c**)

distance is observed in 3-methoxypropyn-1-ylgermatrane (**4c**) (Figure 1). This indicates that the decrease of the N→Ge bond in the fragment N→Ge–C is accompanied by elongation of the Ge–C bond.

The unit cell of germatrane **4a** contains two independent molecules; one of which is strongly disordered due to the pentyl substituent. Disorder is also observed in the crystal structure of the cyclohexenylethynyl derivative **4b**. The usual disorder for the atrane system occurs for C-4, C-6, and C-11 atoms. Carbon atom C-17 in the six-membered cycle is also disordered. The occupation *g* factor for disordered atoms is 0.5.

Crystals of (trimethylsilyl)ethynylgermatrane (**4d**) were obtained as a solvate with toluene. To prevent toluene evaporating rapidly from the crystal surface, which would destroy the mono crystal of **4d** within 1 h, the X-ray analysis was carried out under an epoxide glue film. The unit cell contains four molecules of germatrane **4d** and two of toluene.

Cobalt complex **5** (Figure 2) crystallized from light petroleum as scarlet prisms. The six-coordinate cobalt atoms have a pseudotetrahedral polyhedron. The Co–Co bond distance is 2.487(1) Å. The dihedral angle between planes C-12, C-13, Co-1 and C-12, C-13, Co-2 is 84.7(1)°. Molecules of complex **5** are in special positions: atoms Ge-1,

Table 2. Selected bond lengths and angles of ethynylgermatranes [**4** $RC{\equiv}CGe(OCH_2CH_2)_3N$] and the dicobalthexacarbonyl complex

Compound	R	r (N→Ge), Å	r (Ge – C), Å	r (C≡C), Å	∠ NGeC, deg.	∠ GeCC, deg.
4a[a]	C_5H_{11}	2.176(3)	1.914(4)	1.185(5)	178.4(2)	178.7(4)
		2.202(3)	1.908(4)	1.184(5)	179.0(2)	177.5(4)
4b		2.176(4)	1.905(6)	1.194(7)	179.1(2)	172.9(6)
4c	CH_2OMe	2.115(7)	1.962(9)	1.199(13)	179.9(3)	173.7(9)
4d	Me_3Si	2.164(7)	1.922(9)	1.185(13)	178.1(3)	179.2(10)
	(PhMe)					
5		2.195(5)	1.926(6)	1.325(8)	176.1(3)	139.6(5)

[a] For two independent molecules.

 © 2003 Wiley-VCH Verlag GmbH & Co. KGaA, Weinheim

N-5, C-12, C-13, C-14, C-15, C-16, C-17 lie in crystallographic plane *m*. However, the molecules are not symmetrical; therefore, disorder occurs in the crystal structure. The occupation *g* factor for disordered atoms is 0.5. According to the literature data, complex **5** is the first example of a cluster structure containing a germatranyl fragment.

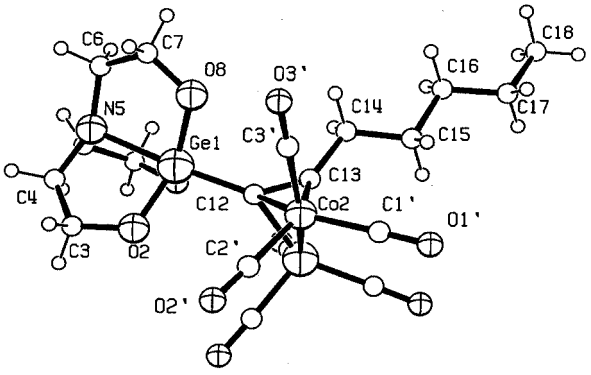

Figure 2. Molecular structure of the hexacarbonyldicobalt complex of 1-heptynylgermatrane (**5**)

Conclusions

Ethynylgermatranes have been prepared from monosubstituted acetylenes by a three-step synthesis from initial acetylenes RC≡CH. With methyl propiolate, tetrachlorogermane acts as Lewis acid to form 1,3,5-tri(methoxycarbonyl)benzene by [2+2+2] cycloaddition. 1-Heptynylgermatrane easily reacts with octacarbonyldicobalt in hexane, almost quantitatively, yielding the hexacarbonyldicobalt complex. The reaction of trimethylsilylethynylgermatrane with NCS and NBS in DMF proceeds with cleavage of the Ge−C bond and formation of chloro- and bromogermatranes. The transannular N→Ge bond lengths (2.115−2.202 Å) of the germatranes are strongly influenced by the RC≡C substituent, with 3-methoxypropyn-1-ylgermatrane having the shortest bond (2.115 Å).

Experimental Section

Instrumental: ^{1}H and ^{13}C NMR spectra were recorded with a Varian Mercury 200 spectrometer at 200.06 and 50.31 MHz, respectively, at 303 K. The chemical shifts are given relative to TMS from the solvent impurity ($CHCl_3$ in $CDCl_3$) signal (δ_H = 7.25 ppm). Mass spectra were recorded with a Hewlett Packard apparatus (70 eV). The melting points were determined with a "Digital melting point analyser" (Fisher) and are uncorrected. 1-Heptyne, 1-ethynylcyclohexene, methyl 2-propynyl ether, trimethylsilylacetylene, triethanolamine and octacarbonyldicobalt [$Co_2(CO)_8$] were purchased from Aldrich.

Table 3. Main X-ray crystallographic details for **4a−d**

	4a	**4b**	**4c**	**4d**	**5**
Crystal shape	prism	plate	needle	prism	prism
Crystal colour	colourless	colourless	colourless	colourless	purple
Crystal size (mm^3)	0.23 × 0.25 × 0.30	0.05 × 0.15 × 0.45	0.07 × 0.10 × 0.55	0.25 × 0.43 × 0.45	0.25 × 0.33 × 0.37
Chemical formula	$C_{13}H_{23}GeNO_3$	$C_{14}H_{21}GeNO_3$	$C_{10}H_{17}GeNO_4$	$C_{11}H_{21}GeNO_3Si{\cdot}(C_7H_8)_{0.5}$	$C_{19}H_{23}Co_2GeNO_9$
Molecular weight	313.92	323.91	287.84	315.97 + 0.5·92.15	599.83
Crystal system	monoclinic	orthorhombic	orthorhombic	orthorhombic	orthorhombic
Space group	$P2_1/c$	*Pbca*	$Pna2_1$	$P2_12_12_1$	*Pnma*
a (Å)	10.4850(3)	11.2133(2)	13.151(8)	6.7256(1)	16.1811(5)
b (Å)	20.2849(5)	11.8230(2)	9.824(4)	11.6160(2)	10.6651(4)
c (Å)	14.0695(4)	22.4887(4)	9.107(4)	28.2106(8)	14.0561(5)
α(°)	90	90	90	90	90
β(°)	93.448(1)	90	90	90	90
γ(°)	90	90	90	90	90
Volume ($Å^3$)	2986.98(14)	2981.44(9)	1176.6(9)	2203.94(8)	2425.7(1)
Z	8	8	4	4	4
d_{calcd}, (g/cm^3)	1.396	1.443	1.625	1.091	1.642
Absorption coefficient (mm^{-1})	2.052	2.058	2.603	1.450	2.629
F(000)	1312	1344	592	756	1208
Diffractometer used	Nonius KappaCCD	Nonius KappaCCD	Syntex $P2_1$	Nonius KappaCCD	Nonius KappaCCD
Radiation, λ (Å)	Mo-K_α (0.71073)	Mo-K_α (0.71073)	Mo-K_α (0.71073)	Mo-K_α (0.71073)	Mo-K_α (0.71073)
Temperature (K)	298(2)	298(2)	293(2)	298(2)	298(2)
Total reflections	11246	7482	1372	3758	5178
Independent reflections	7356	4348	1372	2305	2894
Used reflections	4444	3092	1155	1730	1986
Threshold expression	$I > 3.0\sigma(I)$	$I > 2.0\sigma(I)$	$I > 2.0\sigma(I)$	$I > 3.0\sigma(I)$	$I > 2.0\sigma(I)$
R(int)	0.033	0.035	–	0.039	0.036
$2\theta_{max}$(°)	55.0	60.0	55.0	50.0	55.0
Index ranges	$-13 \le h \le 13$	$-15 \le h \le 15$	$0 \le h \le 17$	$-7 \le h \le 7$	$-20 \le h \le 21$
	$-26 \le k \le 26$	$-16 \le k \le 16$	$0 \le k \le 12$	$-13 \le k \le 13$	$-13 \le k \le 13$
	$-18 \le l \le 18$	$-31 \le l \le 31$	$0 \le l \le 11$	$-33 \le l \le 33$	$-18 \le l \le 18$
Refined parameters	337	208	144	182	203
R-factor	0.0498	0.0589	0.0438	0.0671	0.0447
R(F) for all data	0.0870	0.0916	0.0535	0.0910	0.0742
w*R*(F^2) for all data	0.1281	0.1838	0.1169	0.1952	0.1145
$\Delta\rho_{max}$ ($e/Å^3$)	0.978	0.423	0.713	0.809	0.514
Deposition number CCDC	185235	186941	185234	186942	185863

 © 2003 Wiley-VCH Verlag GmbH & Co. KGaA, Weinheim

General Method for Synthesis of Ethynylgermatranes (4a−d): A solution of tetrachlorogermane (4.28 g, 0.02 mol) in dry hexane (10 mL) was added dropwise to a mixture of acetylene **1** (0.02 mol) and triethylamine (0.022 mol) in dry hexane (50 mL). The reaction mixture was boiled under reflux for 2 h and filtered from triethylamine hydrochloride. A mixture of ethanol (0.07 mol) and triethylamine (0.07 mol) was added to the filtrate. The resultant triethylamine hydrochloride precipitate was filtered off after stirring for 2 h at room temperature. The filtrate was then added to a solution of triethanolamine (0.02 mol) in hexane (10 mL). The transalkoxylation reaction was exothermic. After cooling to room temperature the resultant ethynylgermatrane (**4**) precipitate was filtered off and recrystallized from toluene. The products were obtained as white crystalline solids.

For X-ray analysis crystals of germatranes **4a−d** were grown from toluene. Crystals of the hexacarbonyldicobalt complex were obtained by rapid crystallization from dry light petroleum. The crystal structures were solved by direct methods[20−22] and refined with the help of computer programs.[23,24] The main crystallographic data of the germatranes are given in Table 3.

1-Heptynylgermatrane (4a): Yield: 3.02 g (48%). M.p. 89 °C. MS: m/z = 315 [M^+]. $C_{13}H_{23}GeNO_3$ (313.94): calcd. C 49.74, H 7.38, N 4.46; found C 49.51, H 7.30, N 4.45.

(1-Cyclohex-1-enyl)ethynylgermatrane (4b): Yield: 3.56 g (55%). M.p. 211−212 °C. MS: m/z = 325 [M^+]. $C_{14}H_{21}GeNO_3$ (323.93): calcd. C 51.91, H 6.53, N 4.32; found C 51.83, H 6.58, N 4.36.

(3-Methoxypropyn-1-yl)germatrane (4c): Yield: 0.69 g (12%). M.p. 193−194 °C. MS: m/z = 289 [M^+]. $C_{10}H_{17}GeNO_4$ (287.86): calcd. C 41.73, H 5.95, N 4.86; found C 41.77, H 5.99, N 4.84.

(Trimethylsilyl)ethynylgermatrane (4d): Yield: 5.44 g (86%). M.p. 237 °C. MS: m/z = 317 [M^+]. ^{29}Si NMR ($CDCl_3$): δ = −18.6 ppm. $C_{11}H_{21}GeNO_3Si$ (315.98): calcd. C 41.81, H 6.70, N 4.43; found C 41.76, H 6.63, N 4.44.

Hexacarbonyldicobalt Complex of 1-Heptynylgermatrane (5): A solution of octacarbonyldicobalt (0.342 g, 1 mmol) in hexane (10 mL) was added to a solution of 1-heptynylgermatrane (**4a**, 0.314 g, 1 mmol) in hexane (10 mL) at −5 °C. The reaction mixture was stirred 20 min, then hexane was removed and the crude product obtained was purified on silica gel using CH_2Cl_2 as eluent (R_f = 0.55). Yield: 0.56 g (93%). M.p. 102−104 °C. $C_{19}H_{23}Co_2GeNO_9$ (599.46): calcd. C 38.07, H 3.87, N 2.34; found C 38.06, H 3.79, N 2.29.

3-Methyl-4-trimethylsilyl-5-germatranylisoxazole (6): Nitroethane (0.005 mol) and triethylamine (two drops) in dry benzene (20 mL) were added dropwise to a mixture of trimethylsilylethynylgermatrane **4d** (1.58 g, 0.005 mol) and phenylisocyanate (0.01 mol). The mixture was heated for 5 h at 70−80 °C. After cooling to room temperature, diphenylurea was filtered off, the solvent evaporated, and the resultant residue purified on silica gel using dichloromethane as eluent (R_f = 0.45). Yield 1.39 g (75%). M.p. 115 °C. MS: m/z = 374 [M^+]. ^{29}Si NMR ($CDCl_3$): δ = −6.4 ppm. $C_{13}H_{24}GeN_2O_4Si$ (373.04): calcd. C 41.86, H 6.48, N 7.51; found C 41.81, H 6.50, N 7.54.

Method for Synthesis of 1,3,5-Tris(methoxycarbonyl)benzene: A solution of tetrachlorogermane (4.28 g, 0.02 mol) in dry hexane (10 mL) was added dropwise to a mixture of methylpropiolate (1.68 g, 0.02 mol) and triethylamine (2.22 g, 0.022 mol) in dry hexane (50 mL). The reaction mixture was refluxed for 2 h and filtered from triethylamine hydrochloride. The crude product was purified on silica using hexane as eluent. Yield: 52%. The structure was confirmed by MS-GC and ^{1}H NMR spectroscopy.

Reaction of (Trimethylsilyl)ethynylgermatrane with NCS and NBS: NCS or NBS (1 mmol) was added portion-wise, during 1 h at room temperature, to a solution of **4d** (0.315 g, 1 mmol) in DMF (10 mL). After the usual workup the crude product **7** was purified by flash chromatography using ethyl acetate/hexane (5:1) as eluent. Yield: 87−90%.

[1] S. S. Karlov, G. S. Zaitseva, *Chem. Heterocycl. Comp.* **2001**, *37*, 1325−1357.
[2] E. Lukevics, L. Ignatovich, S. Belyakov, *J. Organomet. Chem.* **1999**, *588*, 222−230.
[3] S. Belyakov, L. Ignatovich, E. Lukevics, *J. Organomet. Chem.* **1999**, *577*, 205−210.
[4] E. Lukevics, S. Belyakov, P. Arsenyan, J. Popelis, *J. Organomet. Chem.* **1997**, *549*, 163−165.
[5] S. S. Karlov, P. L. Shutov, A. V. Churakov, J. Lorberth, G. S. Zaitseva, *J. Organomet. Chem.* **2001**, *627*, 1−5.
[6] G. S. Zaitseva, S. S. Karlov, A. V. Churakov, J. A. K. Howard, E. V. Avtomonov, J. Lorberth, *Z. Anorg. Allg. Chem.* **1997**, *623*, 1144−1150.
[7] M. G. Voronkov, R. G. Mirskov, A. L. Kuznetsov, V. Yu. Vitkovskii, *Izv. Akad. Nauk SSSR, Ser. Khim.* **1979**, 1846−1849.
[8] E. Lukevics, L. Ignatovich, T. Shul'ga, S. Belyakov, *Main Group Met. Chem.* **2002**, *25*, 463−464.
[9] I. V. Efimova, B. E. Kalaganov, M. A. Kazankova, I. F. Lutsenko, *Z. Obshch. Khim.* **1984**, *54*, 459−460.
[10] M. A. Dam, W. J. Hoogervorst, F. J. J. de Rauter, F. Bickelhaupt, A. L. Spek, *Organometallics* **1998**, *17*, 1762 −1768.
[11] R. J. Baxter, G. R. Knox, M. NcLaughlin, P. L. Paulson, M. D. Spicer, *J. Organomet. Chem.* **1999**, *579*, 83−89.
[12] W.-Y. Wong, H.-Y. Lam, S.-M. Lee, *J. Organomet. Chem.* **2000**, *595*, 70−80.
[13] D. Seyferth, T. Kugita, A. L. Rheingold, G. P. A. Yap, *Organometallics* **1995**, *14*, 5362−5366.
[14] C. Kim, I. Jung, *J. Organomet. Chem.* **1999**, *588*, 9−19.
[15] T. Mukaiyama, T. Hoshito, *J. Am. Chem. Soc.* **1960**, *82*, 5339−5342.
[16] T. K. Gar, N. Yu. Chromova, S. N. Tandura, V. F. Mironov, *Z. Obshch. Khim.* **1983**, *53*, 1800−1806.
[17] B. Happ, T. Bartik, C. Zucchi, M. C. Rossi, F. Ghelfi, G. Palyi, G. Varadi, G. Szalontai, I. T. Horvath, A. Chiesi-Villa, C. Guastini, *Organometallics* **1995**, *14*, 809−819.
[18] Yu. I. Baukov, S. N. Tandura, *Hypervalent compounds of organic germanium, tin and lead*, in *The Chemistry of Organic Germanium, Tin and Lead*, (Ed. Z. Rappoport), Vol. 2, John Wiley & Sons, Chichester, England, **2002**, *963*−1240.
[19] R. Eujen, A. Roth, D. J. Brauer, *Monatsh. Chem.* **1999**, *130*, 1341−1346.
[20] A. Altomare, M. C. Burla, M. Camalli, G. L. Cascarano, C. Giacovazzo, A. Guagliardi, A. G. G. Moliterni, R. Spagna, *J. Appl. Cryst.* **1999**, *32*, 115−119.
[21] G. M. Sheldridk, *Acta Crystallogr., Sect. A* **1990**, *46*, 467−473.
[22] A. F. Mishnev, S. V. Belyakov, *Kristallografiya* **1988**, *33*, 835−837.
[23] G. M. Sheldrick, SHELXL-93. *Program for the Refinement of Crystal Structures.* (1993) University of Göttingen, Germany.
[24] S. Mackay, C. J. Gilmore, C. Edwards, N. Stewart, K. Shankland, *maXus Computer Program for the Solution and Refinement of Crystal Structures*, Bruker Nonius, The Netherlands, **1999**, MacScience, Japan & The University of Glasgow..

Received April 25, 2003

 © 2003 Wiley-VCH Verlag GmbH & Co. KGaA, Weinheim

Relativistic Density Functional Study of the Dinuclear Uranyl Complex $[(UO_2)_2(\mu_2\text{-}OH)_2Cl_2(H_2O)_4]$ in Its Crystalline Environment

Florian Schlosser,[a] Sven Krüger,[a] and Notker Rösch*[a]

Keywords: Actinides / Uranium / Hydrogen bonds / Relativistic density functional calculations

The hexavalent dinuclear uranyl dichloride complex $[(UO_2)_2(\mu_2\text{-}OH)_2Cl_2(H_2O)_4]$ was studied computationally with an all-electron scalar relativistic density functional method. This suggested hydrolysis product of uranyl in the presence of chlorine ions is one of the few polynuclear uranyl species for which a crystal structure is known. The calculated gas-phase structure is similar to the experimental crystal geometry; any major deviations are due to hydrogen bonds in the crystal. If the eight strongest hydrogen bonds are included in a model of the complex's crystalline environment, the calculated structure improves significantly. Based on this model, the hydrogen bond lengths and angles were determined, indicating that they are moderate and strong with an average binding energy of 39 kJ/mol. These computational results corroborate earlier suggestions based on experimental results concerning the location and strength of the hydrogen bonds. In addition, a valuable reference for relativistic quantum chemical methods is provided by the gas-phase results.

(© Wiley-VCH Verlag GmbH & Co. KGaA, 69451 Weinheim, Germany, 2003)

Introduction

The dinuclear complex $[(UO_2)_2(\mu_2\text{-}OH)_2Cl_2(H_2O)_4]$ (**1**) has been discussed as a polynuclear species in the initial phase of uranyl hydrolysis in the presence of chlorine ions.[1,2] While structural information about such polynuclear actinide complexes is rare, data are available from EXAFS studies that refer directly to the species in solution or from a crystal structure determination if a crystal can be grown from solution.[3−5] X-ray scattering data of a solution[1] and a crystal structure[2] determined for **1** from hydrolyzed solutions of $UO_3{\cdot}HCl{\cdot}2H_2O$ indicate the presence of the dimeric unit $(UO_2)_2(\mu_2\text{-}OH)_2^{2+}$, which has also been reported in other crystal structures.[3−5] This moiety seems to be an important structural element of dinuclear uranium species in the solid state and in solution.

Recent developments in quantum chemistry[6−12] have rendered relativistic electronic structure calculations feasible for larger compounds of very heavy elements such as the actinides and have, therefore, opened up a computational route to many of their properties. Electronic correlation as well as relativistic effects substantially affect the electronic structure of heavy-element compounds, and therefore have to be accounted for in a correct description of such systems.[13] In addition, the large number of electrons of these elements demands an efficient computational method, so that one is not restricted to small or highly symmetric model species. This renders methods based on density functional (DF) theory very attractive.

Our first goal was to describe the gas-phase structure of the title complex **1** using an appropriate all-electron scalar relativistic DF approach[7,14] that combines a geometry optimization using a local-density approximation (LDA) of the exchange-correlation functional and an energy evaluation using a generalized-gradient approximation (GGA, see Computational Details). In a second step, we modeled the packing effects in the crystal structure of **1** and compared this model with available experimental data.[2] Because **1** is neutral, long-range Coulomb interactions between the different units in the crystal should not be crucial; rather, one expects that hydrogen bonds comprise the main crystal packing effects.[2] Therefore, we chose a model approach which neglects the Madelung field. To the best of our knowledge, this work is the first attempt to model crystal packing effects of a dinuclear actinide species in a quantum chemistry investigation. Even with its simplifications, this model study represents a major challenge to the scalar relativistic DF method applied.

In the next section, we describe details of the crystal structure and present the models chosen to describe complex **1**. We then discuss results for geometry and energetics of **1** and details of the calculated hydrogen bonds, and compare the different models with experimental data. Finally, we provide computational details.

[a] Institut für Physikalische und Theoretische Chemie, Technische Universität München,
Lichtenbergstr. 4, 85747 Garching, Germany
Fax: (internat.) + 49-89/289-13468
E-mail: roesch@ch.tum.de

Supporting information for this article is available on the WWW under http://www.eurjic.org or from the author.

 © 2003 Wiley-VCH Verlag GmbH & Co. KGaA, Weinheim **DOI: 10.1002/ejic.200300024**

Crystal Structure and Models

Crystals of the diuranyl hydroxide dichloride complex $[(UO_2)_2(\mu_2\text{-}OH)_2Cl_2(H_2O)_4]$ (**1**) are monoclinic with a unit cell containing four formula units and belong to space group $P2_1/n$ (no. 14).[2] Complex **1** consists of two linear uranyl groups linked by two OH bridges, with the bridging oxygen centers denoted O_b. Both uranium centers are also surrounded by one chlorine and two further oxygen centers O_s and O_a due to coordinating aqua ligands. The index s designates O centers of aqua ligands located *syn* relative to a Cl ligand, while the index a refers to O centers of aqua ligands located *anti*, i.e. at the same uranium center, but on the side opposite to Cl (Figure 1). The two chlorine atoms, one at each U center, are *trans*-coordinated. Overall each U center is locally coordinated as a pentagonal bipyramid, which is typical for uranyl moieties.[15] The central unit $(UO_2)_2(\mu_2\text{-}OH)_2^{2+}$ is also present in the dinuclear hydrolysis product $[(UO_2)_2(\mu_2\text{-}OH)_2(H_2O)_6]^{2+}$ where the chlorine atoms are replaced by aqua ligands.[1] Although both OH and O bridges may be possible in the diuranyl species[16] previous studies[14] confirmed the presence of OH bridges at acidic pH in the initial stage of hydrolysis.

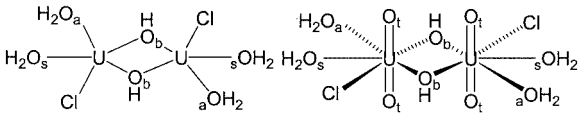

Figure 1. Schematic structure of the dinuclear complex $[(UO_2)_2(\mu_2\text{-}OH)_2Cl_2(H_2O)_4]$ (**1**): top view (left) and side-view (right); the terminal oxygen atoms of the uranyl units are not shown in the top view

Naturally, X-ray scattering data of the crystal structure do not provide explicit information about the positions of the hydrogen atoms. However, based on typical distances and angles found in the crystal structure, Åberg predicted three types of H bonds, X−H···Y, between adjacent complexes **1** (Figure 2).[2] The four strongest, i.e. shortest, bonds (A, B), extending in the *b* direction of the crystal, are assumed to exist between an oxygen center of an OH bridge and an oxygen center of an *anti*-coordinated aqua ligand, $O_b\cdots H-O_a$ (A) and $O_a-H\cdots O_b$ (B). (Frontier groups of an adjacent complex **1** are designated in *italics*.) Åberg predicted eight additional H bonds oriented mainly in the *c* direction.[2] Each of the first four H bonds (C, D) involves the same water oxygen center as H bond B and a chlorine center, $O_a-H\cdots Cl$ (C) and $Cl\cdots H-O_a$ (D); the second four H bonds (E, F) involve a bridging oxygen atom and a terminal uranyl oxygen atom, $O_t\cdots H-O_b$ (E) and $O_b-H\cdots O_t$ (F) (Figure 2). From a comparison of the corresponding X···Y distances with typical values for H bonds[17] and the van der Waals radii of the corresponding atoms,[18] we expect the bond strengths to decrease from (A, B) to (C, D) to (E, F).[2]

To determine the structure of complex **1**, we applied two models with C_i symmetry: M1 − a model of the gas-phase structure, and, to account for packing effects of the crystal,

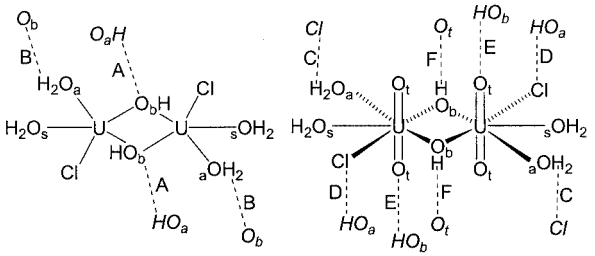

Figure 2. Schematic structure of the dinuclear complex $[(UO_2)_2(\mu_2\text{-}OH)_2Cl_2(H_2O)_4]$ (**1**), including the proposed H bonds A, B, C, D, E, and F in the crystal; see text; top view (left) and side-view (right); terminal oxygen atoms of the uranyl units are not shown in the top view; *italics* indicate frontier groups of neighboring complexes **1** in the crystal

M2 − a model including important features of the crystalline environment.

The C_i symmetry of M1 does not constrain any degree of freedom for a geometry optimization of **1**. The experimental crystal structure shows slight deviations from C_i symmetry because the local inversion symmetry of **1** is broken by the arrangement of the neighboring complexes: equivalent bond lengths scatter on average by 0.02 Å.[2] In addition, the crystal structure reveals that complex **1** exhibits approximately C_{2h} symmetry if H atoms are ommited.[2] Thus, to reduce the computational effort, we also used a model M0 with overall C_{2h} symmetry to generate a starting geometry for M1. In model M0, the OH bridges are coplanar with the $U-O_b-U-O_b$ plane and the coordinated water molecules are oriented symmetrically to this plane; these restrictions are released in model M1. To investigate the effect of the crystal hydrogen bonds on the gas-phase structure of model M1 we constructed model M2. Here, we place the gas-phase complex obtained with model M1 into a model of its crystalline environment and investigate the relaxation of the complex due to the H bonds. Comparing the optimized structure of model M2 with the crystal structure, we can check if the model environment can reproduce the main effects of crystal packing.

To model the effect of H bonds with neighboring complexes in the crystal, we represented neighboring complexes **1** by those frontier groups involved in the H bonds discussed above (Figure 2). To keep model M2 neutral, we chose H_2O and HCl molecules as the corresponding counterparts. Only the heavy atoms (O, Cl) of these model groups were placed at fixed positions derived from the experimental crystal structure.[2] Thus, the optimizations represent a relaxation of **1** in the fixed framework of heavy frontier atoms of the surrounding species in the molecular crystal. The locations of the hydrogen centers of the model groups (hence also the orientations of the H bonds) were fully optimized, subject to inversion symmetry constraint. The Mulliken charges of the corresponding centers of O (−0.62 e) in H_2O and Cl (−0.24 e) in HCl are close to those of the corresponding atoms of **1** as calculated with reference model M1, namely −0.54 e for O_a and −0.34 e for Cl. Therefore, the chemical environment of **1** in model M2 should be sufficiently similar to that of the crystal.

 © 2003 Wiley-VCH Verlag GmbH & Co. KGaA, Weinheim

Our initial, simple model of the environment accounted only for the strongest H bonds (A, B); as expected, this yielded improved distances and angles of atoms directly connected to the simulated bridges but the localized formation of these selected H bonds distorts other parts of the complex. Therefore, in model M2 we included both (A, B) and (C, D) H bonds, still applying C_i symmetry, so as to model the eight strongest out of twelve H bonds assumed to be present in the crystal. Neglect of the weak E and F bridges is supported by the good agreement of the UO_t distances with experiment in all our models, indicating only small effects of these H bonds on the strong UO_t bonds. Rotation of the complex **1** inside the "matrix" set up by the H bonds of the environment would result in further H bonds to the frontier groups of neighboring complexes; to prevent such artifacts, we constrained the equatorial ligand atoms of the uranyl groups in a plane, in agreement with the experimental crystal structure. This approximation was checked by examining the structure's relaxation (model M2′, see below), which led to changes in bond lengths of **1** of < 0.02 Å. Therefore, the following discussion will focus on model M2.

Results and Discussion

Geometry

Table 1 summarizes the calculated structures of the three models studied and compares these results with experiment. First, we shall discuss the gas-phase reference model M1. The central dimeric unit $(UO_2)_2(OH)_2^{2+}$ consists of two slightly different ($\Delta = 0.07$ Å) bonds $U-O_b$ of the bridging hydroxy groups between the uranyl units. The OH moieties show a longer bond $U-O_b$ (2.39 Å) to the uranyl where H_2O is their neighboring ligand and a shorter bond $U-O_b'$ (2.32 Å) close to a neighboring Cl ligand (Figure 1). The O_b-H bonds are bent 66.6° out of the central $U-O_b-U-O_b$ plane. The uranyl moieties of M1 are almost linear (176.7°), very close to the linear structure of a uranyl ion UO_2^{2+}. The terminal oxygen−uranium distances $U-O_t$ are significantly longer than in the corresponding gas-phase calculations of the bare uranyl ion UO_2^{2+} ($\Delta = 0.08$ Å) and even slightly longer than calculated for the solvated uranyl ion $[UO_2(H_2O)_5]^{2+}$ ($\Delta = 0.03$ Å).[19] Such bond elongation is due to increasing competition with other, equatorial ligands at the U center which bind more strongly than water (OH, Cl). For the gas-phase structure of the analogous dinuclear complex $(UO_2)_2(OH)_2(H_2O)_6^{2+}$, almost equal $U-O_t$ distances ($\Delta = -0.01$ Å) and an increased bending of the uranyl moieties (168.0°) have been calculated.[14]

The $U-O_a$, $U-O_s$ and U−Cl bonds are bent out of the $U-O_b-U-O_b$ plane by 15.9°, 0.9° and 6.2°, respectively. Therefore, the pentagonal-bipyramidal coordination of the U centers, which is typical of monomeric complexes,[15] is slightly distorted. The bonds to the aqua ligands $U-O_a$ and $U-O_s$ (2.49 Å) are slightly longer than uranium−water distances in mononuclear $UO_2(H_2O)_5^{2+}$ (2.42 Å) and dinuclear[14] species $(UO_2)_2(OH)_2(H_2O)_6^{2+}$ (2.46 Å) due to an increasing number of more strongly binding ligands. Also, the U−Cl distance (2.63 Å) indicates strong ligand bonding because it is relatively short compared to computational results for $[UO_2Cl_4]^{2-}$ where the U−Cl distances are elongated due to the competition of four strong bonds (2.68 Å). This latter result is in good agreement with EXAFS data for this complex in solution (2.67 Å)[20] while DF GGA calculations yield longer bonds, from 2.73 to 2.81 Å.[8]

As there are no experimental data for the gas phase, we compared the results of model M1 with X-ray data in solution, to obtain initial indications of solvation and crystal packing effects on geometry. Åberg has investigated solutions of hydrolyzed uranyl(VI) chloride with constant [U] (3 M) but varying OH/U ratio, i.e. the average number of OH groups per U atom (0−1.11).[1] We choose the ratio 1.11 for comparison, in agreement with the assumed structure of **1** that exhibits two U centers linked by two OH bridges. The experimental results correspond to the assumed pentagonal coordination, including one U−Cl bond [$n_r = 0.8(1)$ for

Table 1. Structure parameters (distances in Å, angles in °) of models M0 (C_{2h}), M1 (C_i), and M2 (C_i) of complex $[(UO_2)_2(\mu_2\text{-}OH)_2Cl_2(H_2O)_4]$ (**1**) in the gas phase (M0, M1) and in a model of the crystalline environment (M2); also shown are experimental values and deviations ΔMn ($n = 0, 1, 2$) of calculated quantities from the crystal structure; the last line provides the types of H bonds that directly affect the corresponding distances and angles (for the designations, see Figure 2 and text)

	U−U	$U-O_t$	$U-O_b$	$U-O_b'$	$U-O_a$	$U-O_s$	U−Cl	O_t-U-O_t	O_b-U-O_b	O_a-U-O_s	O_s-U-Cl
M0	3.785	1.792	2.254	2.332	2.463	2.495	2.700	168.7	68.8	74.8	70.5
M1	3.801	1.787	2.389	2.318	2.493	2.486	2.626	176.7	72.3	65.7	69.2
M2	3.875	1.790	2.352	2.343	2.421	2.497	2.661	174.9	68.7	68.4	68.6
Exp.[a]	3.94(0)	1.79(2)	2.40(2)	2.34(2)	2.39(2)	2.50(3)	2.75(1)	178.2(9)	67.0(7)	68.8(9)	73.4(8)
Exp.[b]	3.84(1)	1.76(1)	*2.40(1)*	*2.40(1)*	*2.40(1)*	*2.40(1)*	2.89(2)	−	−	−	−
Δ M0	−0.16	0.00	−0.15	−0.01	0.07	0.00	−0.05	−9.5	1.8	6.0	−2.9
Δ M1	−0.14	0.00	−0.01	−0.02	0.10	−0.01	−0.12	−1.5	5.3	−3.1	−4.2
Δ M2	−0.07	0.00	−0.05	0.00	0.03	0.00	−0.09	−3.3	1.7	−0.4	−4.8
H bonds		E, F	A, B, E, F	A, B, E, F	A, B, C, D		C, D	E, F	A, B, E, F	A, B, C, D	C, D

[a] Ref.[2], crystal structure (average values with respect to the assumed C_i symmetry; maximum scattering of 0.04 Å for distances and 1.7° for angles); reference for determining the deviations Δ = X(calc.) − X(exp.). [b] Ref.[1], solution (only *average* value for all equatorial U−O distances determined by experiment).

 © 2003 Wiley-VCH Verlag GmbH & Co. KGaA, Weinheim

U−Cl, where n_r is the number of corresponding bonds per U atom) and four U−O bonds [n_r = 4.3(2)], i.e. two bonds to bridging hydroxy moieties and two bonds to coordinated water molecules (Figure 1). The latter four uranium−oxygen bonds U−O_b, U−O_b', U−O_a, and U−O_s from the first hydration sphere could not be separated by experiment[1] so that only an average distance is available (2.40 Å, Table 1).

The U−O_t distance of model M1 agrees reasonably well with the solution data (Δ = 0.03 Å), indicating minimal solvation effects on the strong U−O_t bond. The U−O_t distance found in solution (1.76 Å) is short compared with other experimental data for UO_2^{2+} in solution (1.76−1.78 Å);[20,21] in fact, one would expect a longer U−O_t bond in M1 because four aqua ligands of a completely solvated uranyl complex are replaced by stronger bound ligands, namely by two Cl ligands and two OH bridges. The polar U−Cl bond, however, is notably shorter than in solution (Δ = −0.26 Å) and may be elongated by screening effects and possible H bonds in solution. The calculated average distance (2.42 Å) of all equatorial U−O bonds is only 0.02 Å longer than the experimental value. The bridging bonds U−O_b and U−O_b' are significantly shorter than the bonds U−O_a and U−O_s (Δ ≈ −0.14 Å); indicating increased bond strengths of the linking bridges.

Before judging the gas-phase model M1 against the crystal data, we briefly compare the available experimental solution and crystal structure data. Overall, they are similar, with a tendency to longer bonds in the crystal, except for the U−Cl distance. This may be because the H bonds in solution are more flexible and dynamically changing than the localized crystal H bonds; thus, the corresponding bonds are weakened and lengthened in a more pronounced fashion. The average U−O distance in the crystal is 0.01 Å longer than in solution. The U−U and U−Cl distances though are noticeably different from solution, with Δ = 0.10 Å and −0.14 Å, respectively, indicative of a weakening of the bridging bonds due to H bonds in the crystal (A and F in Figure 2). Invoking bond order conservation at the two uranyl moieties, this weakening would lengthen the U−U distance and strengthen the other equatorial bonds, including the U−Cl bond.

Model M1 is in relatively good agreement with the crystal structure, particularly considering the experimental uncertainties. Only slight deviations are found for the U−O_b (Δ = −0.01 Å) and U−O_b' (Δ = −0.02 Å) distances; also, the correct order of these two distances is reproduced (U−O_b > U−O_b'). However, the U−U distance, which does not represent an actual bond (3.80 Å), is strongly underestimated (Δ = −0.14 Å), yielding a more compact complex than the crystal structure; this is probably due to the stronger bridging bonds. The bonds to the aqua ligands U−O_a and U−O_s are almost equal in model M1, with a slightly longer distance U−O_a (Δ = 0.01 Å), whereas the crystal U−O_s bond is significantly longer, by 0.11 Å. The distance U−O_a (Δ = 0.10 Å) is too long compared to experiment whereas that of U−O_s (Δ = −0.01 Å) agrees very well. This may be traced to the effects of the H bonds involved, i.e. A, B, C, and D for U−O_a whereas the U−O_s bond length is unaffected by any of the postulated H bonds (Figure 2). The underestimation of the U−Cl distance (−0.12 Å) can be rationalized with the missing weakening effects due to H bonds C and D. The linearity of the uranyl moieties is very well reproduced (Δ = −1.5°) and deviations of other characteristic angles are small, 3−5° (Table 1).

Before turning to the computational results for model M2, where H bonds are taken into account, we briefly discuss results obtained with the highly symmetric gas-phase model M0 of C_{2h} symmetry. Model M0 shows surprisingly good overall agreement with M1 (Table 1); as expected, the main differences are with the OH bridges which are not bent due to symmetry restrictions. In addition, the order of the two distances U−O_b and U−O_b' is reversed (U−O_b < U−O_b'). The reduction in U−O_b (Δ = −0.14 Å compared to model M1) gives a shorter U−U distance (Δ = −0.02 Å) and a weakening of the U−Cl bond (Δ = 0.07 Å) due to the stronger bridging bonds. Although the U−O_t bonds are only very slightly elongated (Δ = 0.005 Å), the uranyl units are more strongly bent, 169° compared to 177° in M1, whereas deviations of other angles range from 1 to 9°.

In model M2, the H bonds A, B, C, and D were simulated to account for the crystalline environment (Figure 3). Consequently, compared to model M1, most bonds are elongated. All bond lengths except U−O_b are improved in comparison to model M1 (Table 1), with deviations Δ from experiment ranging from less than 0.01 Å up to 0.09 Å; even the U−U distance is distinctly elongated (Δ = −0.07 Å). Agreement with experimental data for U−O_a (Δ = 0.03 Å) and U−Cl (Δ = −0.09 Å) is notably improved whereas the distance U−O_s (|Δ| < 0.01 Å) is hardly affected because O_s is not involved in an H bond. Unlike model M1, the correct ordering of the lengths of the two types of aqua ligand bonds U−O_a and U−O_s is reproduced (U−O_a < U−O_s). The calculated H bond Cl···H−O_a (D) is distinctly longer than the experimental bond (see below), which reduces the effect on the corresponding U−Cl bond; this may explain the relatively strong deviation from experiment calculated for the U−Cl distance (Δ = −0.09 Å). The effect of the H bonds A on the O_b atoms is significant: the distance U−O_b (Δ = −0.05 Å) changes by 0.04 Å, the bending angle of the O_b−H bond is reduced from 66.6° in model

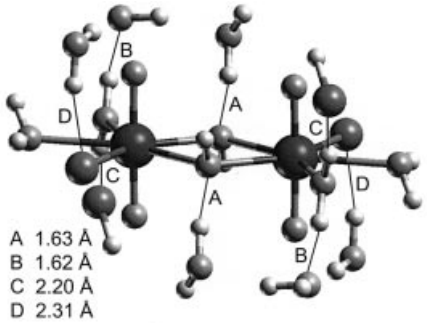

Figure 3. Optimized structure of the dinuclear complex $[(UO_2)_2(\mu_2\text{-}OH)_2Cl_2(H_2O)_4]$ (**1**), including simulated H bonds A, B, C, and D (model M2); also shown are calculated H···Y distances [Å]

 © 2003 Wiley-VCH Verlag GmbH & Co. KGaA, Weinheim

M1 to 52.9°; the distance U−O_b' is less affected and changes by 0.025 Å. Both the angle O_t−U−O_t ($\Delta = -3°$) and the remaining angles ($\Delta = 1-5°$) agree well with experiment, with deviations of the same order as in model M1.

We also find very good agreement for the strong U−O_t bonds ($\Delta < 0.01$ Å), in fact for all models M0, M1 and M2. Thus, the postulated H bonds E and F seem to affect the uranyl bonding only weakly. This corroborates our decision to neglect these weak bonds in model M2. From previous results for similar systems,[14] the expected accuracy of about ±0.02 Å for bond lengths was not reached in model M2 for the U−O_b, U−O_a, and U−Cl bonds; however, inclusion of the most important H bonds in model M2 distinctly improved the results compared to model M1. Note that the crystal structure differs slightly from the C_i symmetry assumed for the computational models, resulting in a scattering of the experimental distances by up to ±0.04 Å; this is of the same order as experimental uncertainties (0.01−0.03 Å, Table 1). Thus, for most bonds, the remaining deviations are within experimental uncertainty, but may also partly be caused by the applied symmetry restriction and the lack of H bonds E and F in model M2.

The crystal structure provides limited information on H bonds, but from model M2 we can locate the hydrogen atoms involved and the angles of the simulated H bonds (Table 2, Figure 3). The calculated H bonds A ($\Delta = -0.02$ Å) and C ($\Delta = 0.04$ Å) are in good agreement with the X···Y distances found in the crystal; this is noteworthy as H bonds are not described with high accuracy with a local-density approximation of the exchange-correlation functional (see $\Delta = 0.07$ Å for the H bonds B and D).[22] The calculated Cl···O_a distance of bridge D is too long, which seems to indicate a weaker H bond in model M2 than expected from the crystal structure. As a consequence, the calculated U−Cl bond is less destabilized and too short (see above). The agreement of both chemical bond lengths and X···Y distances of H bonds, calculated for model M2, with the corresponding data of the crystal structure confirms that the relaxation of the gas-phase structure of complex **1** (M1) is properly described in the simulated crystalline environment of model M2.

Our computational results for H bonds can also be compared to typical data[17] for H···Y distances and X−H···Y angles (Table 2). Such comparison allows us to classify the H bonds A and B as relatively strong, both resulting in almost linear bonds with O_a−H···O_b angles of 173° (Table 2). For the H bonds C and D typical weak-to-moderate bonds are indicated, with elongated distances and O_a−H···Cl angles of 171 and 156°, respectively. Charge exchange from individual H bonds to the corresponding acceptor atoms in the complex is small; the total electronic charge donation of all eight H bonds is ca. 0.4 e compared to the gas-phase model M1. According to a Mulliken population analysis, there is a slight charge donation to centers O_b (0.04 e) and Cl (0.03 e) from the H bonds A and D and also from H bonds B and C to both H atoms in H_2O_a (0.03 and 0.06 e, respectively). The calculated charge donation of ca. 0.4 e is a deficiency of our model because the molecular crystal contains neutral units of **1**. A net donation of electron charge should usually result in an elongation of bonds. However, compared to experiment, the deviations of calculated bond lengths in model M2 are the same size as found for the dinuclear species $(UO_2)_2(OH)_2(H_2O)_6^{2+}$.[14] Thus, we are confident that potential artifacts due to a net charge of complex **1** are small.

In the additional models M2′ and M2′′ we also investigated relaxation effects of complex **1** that occur on removing the constraint that all equatorial ligand atoms of the uranyl moieties be confined to one plane (see above). As the crystal structure provides no evidence for H bonds to *syn*-aqua ligands, there is no predefined orientation of the corresponding hydrogen atoms, in contrast to those of the *anti*-aqua ligands (Figure 2). Therefore, while maintaining overall C_i symmetry during relaxation of the constraint, two isomers are possible. In the first model (M2′), the hydrogen atoms of the *syn*-aqua ligands are oriented as in model M2 (Figure 3); in the second model (M2′′), these ligands are rotated by about 180° around the U−O_s bond.

Table 3 gives the geometries of the two structures M2′ and M2′′ compared with that of model M2. At first sight, the structures of the three models are very similar. Deviations between the three models are generally < 0.02 Å for distances and < 3° for angles. The most prominent geo-

Table 2. Bond lengths [Å], angles [°], and binding energies (*BE*) [kJ/mol] of modeled H bonds A, B, C, and D of model M2 in comparison with the crystal structure (in parentheses) and typical values for H bonds of various strengths; frontier groups of adjacent complexes $[(UO_2)_2(\mu_2\text{-}OH)_2Cl_2(H_2O)_4]$ (**1**) are designated in *italics*

			X···Y[a]	H···Y	X−H···Y	*BE*[b]
M2	A	O_a−*H*···O_b	2.630 (2.65)	1.632	173.2	84
	B	O_a−H···*O_b*	2.648 (2.58)	1.615	173.3	113
	C	O_a−H···*Cl*	3.177 (3.14)	2.197	171.1	14
	D	O_a−*H*···Cl	3.233 (3.16)	2.310	156.0	27
Typical values[c]		strong	2.2−2.5	1.2−1.5	175−180	60−170
		moderate	2.5−3.2	1.5−2.2	130−180	20−70
		weak	3.2−4.0	2.2−3.2	90−180	< 20

[a] Experimental values (ref.[2]) of crystal structure in parentheses. [b] Binding energies calculated from **1** (M2) → **1** (M2 − 2X) + 2X, X = H_2O for A, B, D and X = HCl for C (see text). [c] Ref.[17], typical values from various compounds.

 © 2003 Wiley-VCH Verlag GmbH & Co. KGaA, Weinheim

Table 3. Selected structure parameters (distances in Å) and stability ΔE (relative to M2, in kJ/mol) of C_i-symmetric models M2, M2′ and M2′′ (see text) of complex $[(UO_2)_2(\mu_2\text{-}OH)_2Cl_2(H_2O)_4]$ (**1**), in a model of the crystalline environment; also shown are experimental values of the structure parameters (for the designations, see Figure 2 and text)

	U−U	U−O_b	U−O_b′	U−O_a	U−O_s	U−Cl	ΔE
M2	3.875	2.352	2.343	2.421	2.497	2.661	−
M2′	3.883	2.353	2.348	2.406	2.499	2.665	−7
M2′′	3.880	2.337	2.363	2.411	2.486	2.668	12
Exp.[a]	3.94(0)	2.40(2)	2.34(2)	2.39(2)	2.50(3)	2.75(1)	

[a] Ref.[2], crystal structure (average values with respect to the assumed C_i symmetry; maximum scattering of 0.04 Å for distances and 1.7° for angles).

metrical difference relates to the U−O_b and U−O_b′ distances. Model M2′ agrees very well with model M2, concerning both length of the two bridges and their ordering (U−O_b > U−O_b′). A major improvement compared to experiment is the shortening of U−O_a by 0.02 Å (Table 3). Conversely, in model M2′′, U−O_b decreases by 0.02 Å whereas U−O_b′ increases by 0.02 Å compared to model M2; therefore the ordering of the two bridges disagrees with experiment: U−O_b < U−O_b′. Thus, also taking into account small energy disadvantages of ΔE = 12 and 19 kJ/mol over M2 and M2′, respectively, we rule out model M2′′ (Table 3).

Although model M2′ is calculated to be slightly more stable than M2 (by 7 kJ/mol; Table 3), the H bond structure favors M2 over M2′. In model M2′, the X···Y distances of the weak-to-moderate bonds C (Δ = 0.21 Å) and D (Δ = 0.19 Å) are significantly longer than in experiment; they are also overestimated in model M2 (C: Δ = 0.04 Å; D: Δ = 0.07 Å), but to a considerably smaller extent. The X···Y distances of the strong H bonds (A: Δ = −0.02 Å; B: Δ = −0.04 Å) remain similar to model M2 (see above), and the angles X−H···Y are only slightly affected, with changes below 2°. Yet, the structural relaxation of model M2′, where the equatorial ligands bend slightly out of the equatorial plane, results in notable changes in H bond lengths and removes the good agreement of the H bond network calculated for model M2 with the crystal structure.

In summary, we favor model M2 and M2′, and exclude model M2′′ based on structure and energy arguments. M2 and M2′ are very similar if one considers the internal structure of **1**. We note that the H bonds of model M2′ fit the experiment less well. These bonds are rather flexible and thus they change strongly with small geometry alterations of the central complex. Nevertheless the differences between models M2 and M2′ should not be over-interpreted, keeping in mind the approximate modeling of the crystalline environment of **1**.

Energetics

To compare the relative energies of our models, we chose the low symmetry gas-phase model M1 (C_i symmetry) as reference. Model M0, where out-of-plane bending of the OH bridges is prevented by the imposed C_{2h} symmetry, is 47 kJ/mol less stable. Contrary to this relatively small energy change, model M2 is 315 kJ/mol more stable due to the simulated eight H bonds. This calculated stabilization energy was based on the reaction **1** (M1) + 6 H_2O + 2 HCl → **1**·6H_2O·2HCl (M2). With respect to the eight H bonds formed, this energy translates into an average binding energy of 39 kJ/mol per H bond, which falls in the range 20−70 kJ/mol that is typical for moderately strong H bonds,[17] thus corroborating the previously discussed structural evidence concerning their strength.

To estimate the strengths of individual H bonds, we removed the corresponding frontier groups from model M2 and considered the model reaction **1** (M2) → **1** (M2 − 2 X) + 2 X where X = H_2O for the H bonds A, B, and D and X = HCl for H bond C. No structure relaxation was allowed. The energies of the H bonds A, B, C, and D thus estimated are 84, 113, 14, and 27 kJ/mol, respectively (Table 2). These calculated energies confirm the previous classification of the H bonds based on structural evidence: H bonds A and B, with average binding energies of about 99 kJ/mol, represent typical strong H bonds (60−170 kJ/mol)[17] whereas H bonds C and D are significantly weaker, with average binding energies of about 21 kJ/mol. Together with the good overall agreement of the detailed geometry of model M2 with the crystal structure, these energy results confirm that the simulated H bonds represent the main crystal packing effects.

Conclusion

A scalar relativistic density functional method as implemented in the parallel code PARAGAUSS was employed to study the structure of the hexavalent dinuclear uranyl chloride complex $[(UO_2)_2(\mu_2\text{-}OH)_2Cl_2(H_2O)_4]$ (**1**) in the gas phase as well as in its crystalline environment. A local-density approximation of the exchange-correlation functional was used for the geometry optimization; energies were determined with a generalized-gradient approximation (see below).

We applied different models to describe both the gas-phase structure and packing effects in the molecular crystal. The gas-phase reference model agrees reasonably well with the experimental structure; major deviations are due to the neglect of H bonds of the crystal environment. Notable deviations occur for U−O distances of an aqua ligand (too long by 0.10 Å) and U−Cl bonds (too short by 0.12 Å). We also found surprisingly good agreement for an initial high-symmetry model which enforced coplanarity of the OH bridges.

We described H bonds in the crystal environment via model H_2O and HCl moieties that mimic the effect of frontier groups of neighboring complexes **1**. In this model, the calculated structure is significantly improved. Average deviations from experiment are reduced from 0.04 to 0.03 Å for bond lengths (maximum deviation 0.09 Å for U−Cl) and from 3.5 to 2.6° for angles (maximum deviation 5°). One

 © 2003 Wiley-VCH Verlag GmbH & Co. KGaA, Weinheim

can imagine a still further improved model that includes all postulated H bonds.

Based on this model, the lengths and angles of the hydrogen bonds were determined, indicating moderate and strong H bonds with an average binding energy of 39 kJ/mol. These computational results corroborate earlier suggestions, based on experimental results, concerning the location and strength of H bonds. The good agreement of both geometry and H bonds with the crystal structure confirms the correct orientation of the complex in the simulated crystalline environment and justifies our model approach.

Computational Details

Scalar relativistic all-electron calculations were carried out by the LCGTO-FF-DF method[23] (linear combination of Gaussian-type orbitals fitting function density functional) as implemented in the parallel code PARAGAUSS.[24,25] The relativistic density functional method applied is based on the second-order Douglas-Kroll-Hess (DKH) approach[26,27] to the Dirac-Kohn-Sham problem.[7,28] Besides the standard scalar relativistic variant, a two-component version is available that includes spin-orbit interaction self-consistently.[29] Due to the closed-shell electronic structure of the U^{VI} species examined we refrained from including spin-orbit interaction.

We employed two exchange-correlation functionals: the local-density approximation (LDA) in the parameterization of Vosko, Wilk, and Nusair (VWN),[30] and the gradient-corrected functional (generalized gradient approximation, GGA) suggested by Becke and Perdew (BP).[31,32] Structures were optimized at the LDA level, invoking a quasi-Newton algorithm and analytical forces.[33,34] The LDA often yields more accurate results for molecular geometries, whereas gradient-corrected functionals perform better for binding energies.[35,36] Therefore, we applied the BP functional self-consistently to calculate binding energies at the structures optimized with the VWN functional.

The Kohn-Sham orbitals were represented by flexible Gaussian-type basis sets, contracted in a generalized fashion using atomic eigenvectors. For U, we used a basis set of the size (24*s*, 19*p*, 16*d*, 11*f*),[37] contracted to [10*s*, 7*p*, 7*d*, 4*f*]. The light atoms (Cl, O, H) were described by standard basis sets:[38] (12*s*, 9*p*, 1*d*) → [6*s*, 5*p*, 1*d*] for Cl, (9*s*, 5*p*, 1*d*) → [5*s*, 4*p*, 1*d*] for O, and (6*s*, 1*p*) → [4*s*, 1*p*] for H. To evaluate the classical Coulomb contribution to the electron-electron interaction in the LCGTO-FF-DF method, the electron density is represented with the help of an auxiliary basis set.[23] The exponents of the corresponding *s*- and r^2-type fitting functions were generated from the orbital basis by a standard procedure;[23] in addition, we chose *p*-, *d*- and *f*-type "polarization exponents" as geometric series with a factor 2.5, starting with 0.1, 0.2 and 0.3 for *p*-, *d*- and *f*-type exponents, respectively. Thus, for U, the auxiliary charge density basis set was of the size (24*s*, 9r^2, 5*p*, 5*d*, 5*f*); the auxiliary basis sets for Cl, O, and H were (12*s*, 9r^2, 5*p*, 5*d*), (9*s*, 5r^2, 5*p*, 5*d*), and (6*s*, 1r^2, 5*p*), respectively. Recently, we checked the quality of the auxiliary basis sets for uranyl; comparison with other DF calculations confirmed the accuracy of the current FF approach for actinide complexes.[39]

In the geometry optimizations, the total energy and elements of the density matrix were required to converge to 10^{-8} au; for the largest component of the displacement gradient vector and the update step length, the convergence criteria were set to 10^{-6} au. For model M1, the grid[40] for the numeric integration of the exchange-correlation functional consisted of about 26200, 16000, 10000, and 8900 points for U, Cl, O, and H centers, respectively.

Previous studies of various hexavalent actinide compounds,[39] including the dinuclear uranium species $[(UO_2)_2(OH)_2(H_2O)_x]^{2+}$ and $[(UO_2)_2O_2(H_2O)_x]$ (x = 0, 2, 4, 6),[14] showed that the computational strategy just described yields very satisfactory results. The LDA (VWN) functional provided accurate bond lengths and vibrational frequencies. Results obtained with uncontracted and contracted basis sets agreed rather well; for the dinuclear species[14] bond lengths differed by at most 0.002 Å, angles by at most 0.2° and binding energies by at most 2 kJ/mol; for mononuclear compounds,[39] deviations of distances were less than 0.0006 Å.

Acknowledgments

This work was supported by the German Bundesministerium für Wirtschaft (grant no. 02E9450) and the Fonds der Chemischen Industrie.

[1] M. Åberg, *Acta Chem. Scand.* **1970**, *24*, 2901−2915.
[2] M. Åberg, *Acta Chem. Scand.* **1969**, *23*, 791−810.
[3] A. Navaza, F. Villain, P. Charpin, *Polyhedron* **1984**, *3*, 143−148.
[4] J. Toivonen, R. Laitinen, *Acta Crystallogr., Sect. C* **1984**, *40*, 7−14.
[5] P. B. Viossat, N.-H. Dung, E. C. Soye, *Acta Crystallogr., Sect. C* **1983**, *39*, 573−579.
[6] M. Pepper, B. E. Bursten, *Chem. Rev.* **1991**, *91*, 719−741.
[7] N. Rösch, S. Krüger, M. Mayer, V. A. Nasluzov, in *Theoretical and Computational Chemistry*, vol. 4 ("Recent Developments and Applications of Modern Density Functional Theory") (Ed.: J. Seminario), Elsevier, Amsterdam, **1996**, p. 497−566.
[8] G. Schreckenbach, P. J. Hay, R. L. Martin, *J. Comp. Chem.* **1999**, *20*, 70−90.
[9] V. Vallet, U. Wahlgren, B. Schimmelpfennig, H. Moll, Z. Szabó, I. Grenthe, *Inorg. Chem.* **2001**, *40*, 3516−3525.
[10] T. Privalov, B. Schimmelpfennig, U. Wahlgren, I. Grenthe, *J. Phys. Chem. A* **2003**, *107*, 587−592.
[11] S. Spencer, L. Gagliardi, N. C. Handy, A. G. Ioannou, C.-K. Skylaris, A. Willets, A. M. Simper, *J. Phys. Chem. A* **1999**, *103*, 1831−1837.
[12] S. Tsushima, T. Yang, A. Suzuki, *Chem. Phys. Lett.* **2001**, *334*, 365−373.
[13] P. Pyykkö, *Chem. Rev.* **1988**, *88*, 563−597.
[14] F. Schlosser, M. Fuchs-Rohr, S. Krüger, N. Rösch, to be published.
[15] F. A. Cotton, G. Wilkinson, in *Advanced Inorganic Chemistry*, 5th ed., John Wiley & Sons, New York, **1988**, p. 980−993.
[16] K. A. Gschneidner, L. Eyring, G. R. Choppin, G. H. Lander, *Handbook on the Physics and Chemistry of Rare Earths*, vol. 18

 © 2003 Wiley-VCH Verlag GmbH & Co. KGaA, Weinheim

("Lanthanides/Actinides: Chemistry"), North-Holland, Amsterdam, **1994**, p. 529−558.
[17] G. A. Jeffrey, *An Introduction to Hydrogen Bonding*; Oxford University Press, New York, **1997**, p. 12.
[18] R. C. Weast, *CRC Handbook of Chemistry and Physics*, 59th ed., CRC Press, Boca Raton, **1979**, p. D-230.
[19] M. Fuchs, A. Shor, N. Rösch, *Int. J. Quant. Chem.* **2002**, *86*, 487−501.
[20] P. G. Allen, J. J. Bucher, D. K. Shuh, N. M. Edelstein, T. Reich, *Inorg. Chem.* **1997**, *36*, 4676−4683.
[21] U. Wahlgren, H. Moll, B. Schimmelpfennig, L. Maron, V. Vallet, O. Gropen, *J. Phys. Chem. A* **1999**, *103*, 8257−8264.
[22] W. Koch, M. C. Holthausen, *A Chemist's Guide to Density Functional Theory*; Wiley-VCH, Weinheim **2000**, p. 213−234.
[23] B. I. Dunlap, N. Rösch, *Adv. Quantum Chem.* **1990**, *21*, 317−339.
[24] T. Belling, T. Grauschopf, S. Krüger, M. Mayer, F. Nörtemann, M. Staufer, C. Zenger, N. Rösch, in *High Performance Scientific and Engineering Computing* (Eds.: H.-J. Bungartz, F. Durst, C. Zenger), Lecture Notes in Computational Science and Engineering, Springer, Heidelberg, **1999**, vol. 8, p. 439−453.
[25] T. Belling, T. Grauschopf, S. Krüger, F. Nörtemann, M. Staufer, M. Mayer, V. A. Nasluzov, U. Birkenheuer, A. Shor, A. Matveev, A. Hu, N. Rösch, PARAGAUSS, version 2.1, Technische Universität München, **1999**.
[26] M. Douglas, N. M. Kroll, *Ann. Phys.* **1974**, *82*, 89−155.
[27] G. Jansen, B. A. Hess, *Phys. Rev. A* **1989**, *39*, 6016−6017.
[28] O. D. Häberlen, N. Rösch, *Chem. Phys. Lett.* **1992**, *199*, 491−496.
[29] M. Mayer, S. Krüger, N. Rösch, *J. Chem. Phys.* **2001**, *115*, 4411−4423.
[30] S. H. Vosko, L. Wilk, M. Nusair, *Can. J. Phys.* **1980**, *58*, 1200−1211.
[31] A. D. Becke, *Phys. Rev. A* **1988**, *38*, 3098−3100.
[32] J. P. Perdew, *Phys. Rev. B* **1986**, *33*, 8822−8824; J. P. Perdew, *Phys. Rev. B* **1986**, *34*, 7406.
[33] V. A. Nasluzov, N. Rösch, *Chem. Phys.* **1996**, *210*, 413−425.
[34] F. Nörtemann, Dissertation, Technische Universität München, **1998**.
[35] T. Ziegler, *Chem. Rev.* **1991**, *91*, 651−667.
[36] A. Görling, S. B. Trickey, P. Gisdakis, N. Rösch, in *Topics in Organometallic Chemistry*, vol. 4 (Eds.: J. Brown, P. Hoffmann), Springer, Heidelberg, **1999**, p. 109−165.
[37] T. Minami, O. Matsuoka, *Theor. Chim. Acta* **1995**, *90*, 27−39.
[38] Cl: *s* and and *p* exponents from: A. Veillard, *Theor. Chim. Acta (Berlin)* **1968**, *12*, 405−411; *d* exponent (0.56) from: Y. Sakai, H. Tatewaki, S. Huzinaga, *J. Comput. Chem.* **1981**, *2*, 108−125. O: *s* and *p* exponents from: F. B. Van Duijneveldt, *IBM Res. Rep.* **1971**, RJ 945; *d* exponent (1.15) from: S. Huzinaga, J. Andzelm, M. Klobukowski, E. Radzio-Andzelm, Y. Sakai, H. Tatewaki, *Gaussian Basis Sets for Molecular Calculations*, Elsevier, Amsterdam, **1984**; H: *s* exponent from: F. B. Van Duijneveldt, *IBM Res. Rep.* **1971**, RJ 945; *p* exponent (1.0) from: M. J. Frisch, J. A. Pople, J. S. Binkley, *J. Chem. Phys.* **1984**, *80*, 3265−3268.
[39] M. García-Hernández, C. Lauterbach, S. Krüger, A. Matveev, N. Rösch, *J. Comp. Chem.* **2002**, *23*, 834−846.
[40] A. D. Becke, *J. Chem. Phys.* **1988**, *88*, 2547−2550.

Received January 14, 2003

 © 2003 Wiley-VCH Verlag GmbH & Co. KGaA, Weinheim

Palladium(II) Complexes Containing a Pyridinyliminophosphorane Ligand

Hung-Ren Wu,[a] Yi-Hung Liu,[a] Shie-Ming Peng,[a] and Shiuh-Tzung Liu*[a]

Keywords: N ligands / Polymerization / Palladium

A series of new pyridinyliminophosphorane bidentate ligands with different steric environments [(2-C_6H_4N)PPh_2=NAr (**NPN**)] and their methylpalladium complexes [PdClMe(**NPN**)] were prepared. From the crystal structure analysis it is evident that the alkyl ligands are always *trans* to the pyridinyl nitrogen donor, revealing a σ-donating ability of the iminophosphorane. However, the two Pd–Cl bonds in [$PdCl_2$(**NPN**)] are essentially the same length. Cationic palladium complexes catalyzed the copolymerization of norbornene/ethylene as well as CO/norbornene.
(© Wiley-VCH Verlag GmbH & Co. KGaA, 69451 Weinheim, Germany, 2003)

Introduction

Since the discovery of highly active diiminopalladium complexes for the polymerization of olefins under mild conditions by Brookhart's group,[1] the design of new ligands to fine-tune the activity of catalysts has received much attention.[2] It is documented that the steric bulkiness around the active metal center favors chain propagation, leading to higher molecular-weight and branched polymers.[1,2] Another attractive feature in this area is the possibility of employing late transition metal complexes, containing heterodonor systems, since the olefin insertion into the M−C bond can be governed by the electronic properties of donor atoms.[2] Presumably due to the reactivity of iminophosphoranes toward moisture[3] and carbonyl groups,[4] the use of this kind of donor in catalytic polymerization is less-well explored.[5] Recently, Stephan and Collins' groups have reported independently that early transition metal complexes with phosphinimide ligands can catalyze the polymerization of ethylene.[6,7] While the coordination studies involving iminophosphorane toward late transition metal complexes are well-examined,[4c,8−12] we would like to contribute our efforts in this area by investigating the behavior of palladium complexes with a series of bidentate pyridinyliminophosphorane ligands as well as their catalytic polymerization activity toward olefins.

Results and Discussion

Preparation of Complexes

The ligands (**L_a**−**L_c**) were prepared in high yield by the Staudinger reaction of 2-diphenylphosphanylpyridine with the corresponding aryl azide under anhydrous conditions (Scheme 1). Substitution reactions of [PdClMe(COD)] with pyridine-iminophosphorane (**NPN**) in dichloromethane at room temperature readily led to the formation of bidentate palladium complexes (**1a**−**c**), which were treated with $AgBF_4$ to yield the corresponding cationic species (**2a**−**c**; Scheme 1). All the palladium complexes were isolated as solids and were stable in solution under a nitrogen atmosphere.

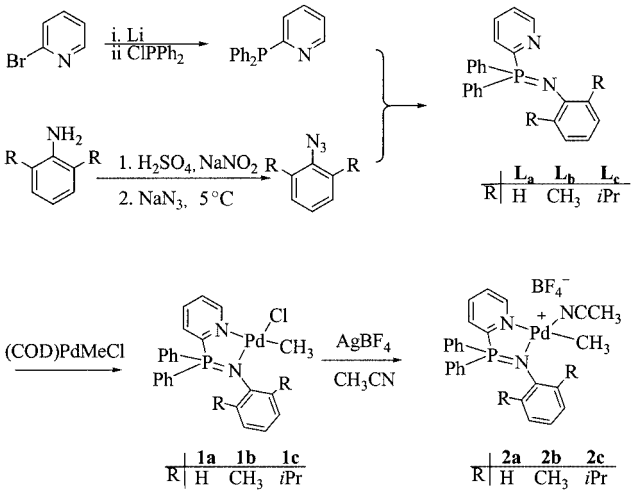

Scheme 1. Preparation of ligands and palladium complexes

In the NMR spectra of the ligands **L_a**−**L_c** and of the palladium complexes **1a**−**2c**, differences between the substituents on the benzene rings were observed. The ^1H, ^{13}C and ^{31}P NMR resonances of these related species are quite similar as shown in Table 1, and are consistent with the expected structure. It can also be seen that the ^{31}P NMR spec-

[a] Department of Chemistry, National Taiwan University, Taipei, Taiwan 106, ROC
Fax: (internat.) +886-2/2363 6359
E-mail: stliu@ntu.edu.tw

 © 2003 Wiley-VCH Verlag GmbH & Co. KGaA, Weinheim **DOI: 10.1002/ejic.200300122**

Table 1. Selected spectroscopic data of ligands and complexes

Compound	^{1}H NMR[a] Py-*H*-6	Pd-NCC*H*$_3$	Pd-C*H*$_3$	^{31}P NMR Pd-*CH*$_3$	^{13}C NMR
L$_a$	8.78 (d, J = 4.6)	–	–	14.7	–
L$_b$	8.75 (d, J = 4.8)	–	–	16.5	–
L$_c$	8.84 (d, J = 4.0)	–	–	15.6	–
1a	9.03 (d, J = 4.5)	–	0.77	26.6	−3.0
1b	9.35 (d, J = 5.1)	–	0.60	21.7	−5.79
1c	9.47 (d, J = 5.1)	–	0.69	22.5	−2.88
2a	9.03 (d, J = 4.7)	2.44	0.69	34.3	1.12
2b	9.02 (d, J = 5.1)	2.42	0.55	30.3	3.20
2c	9.13 (d. J = 4.7)	3.19	0.58	31.7	1.66

[a] Coupling constant J (in Hz).

tra for **1a−2c** show only one signal for each complex, indicating that one single stereoisomer was formed upon complexation. Fortunately, the detailed structures of **1b**, **1c** and **2a** were further confirmed by a crystal structure analysis, which showed clearly the stereo relationship of the donors around the palladium center.

Single crystals suitable for the analysis of the complexes **1b**, **1c** and **2a·CH$_2$Cl$_2$** were obtained by slow evaporation of dichloromethane/diethyl ether solutions. The crystal data of these complexes are collected in Table 2. ORTEP plots of **1b**, **1c** and **2a·CH$_2$Cl$_2$** are depicted in Figures 1−3, respectively, and selected bond lengths and angles are summarized in Table 3. All the palladium complexes are square planar with slight distortions, particularly for the angle N(1)−Pd−N(2) (ca. 84°). In all instances, the methyl group is located *trans* to the pyridinyl-nitrogen and the Pd−C distances are in the range 2.000−2.114 Å, which are typical palladium-methyl carbon lengths.[13] Examination of

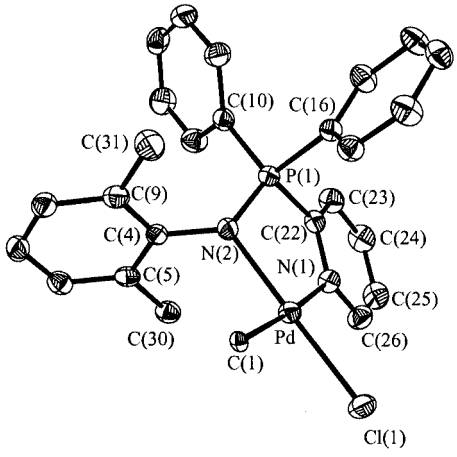

Figure 1. ORTEP plot of the cationic part of complex **1b**

Table 2. Selected crystallographic data of complexes **1b**, **1c**, **2a** and **5**

Complex	**2a**	**1b**	**1c**	**5**
Formula	$C_{27}H_{27}BCl_2F_4N_3PPd$	$C_{26}H_{26}ClN_2PPd$	$C_{30}H_{34}ClN_2PPd$	$C_{25}H_{23}Cl_2N_2PPd$
Mol. wt.	688.60	539.31	595.41	559.72
Crystal system	triclinic	monoclinic	monoclinic	monoclinic
Space group	$P\bar{1}$	$P2_1/n$	Cc	Cc
a (Å)	8.2500(1)	9.5805(1)	10.7780(6)	9.3350(1)
b (Å)	12.3890(1)	14.6296(2)	17.474(1)	17.2460(2)
c (Å)	15.4960(2)	16.6491(3)	15.0640(9)	15.2670(2)
α (°)	74.300(1)	90	90	90
β (°)	87.674(1)	98.8701(6)	91.986(3)	104.798(1)
γ (°)	82.592(1)	90	90	90
V (Å^3)	1511.99(3)	2305.61(6)	2835.4(3)	2376.33(5)
Z	2	4	4	4
D_{calcd} (Mg/m^3)	1.512	1.554	1.395	1.565
F(000)	692	1096	1224	1128
Crystal size (mm)	0.35 × 0.30 × 0.25	0.20 × 0.10 × 0.07	0.25 × 0.20 × 0.10	0.25 × 0.20 × 0.15
θ range	2.47−25.00	2.31−27.50	2.22−27.50	2.36−27.47
Refln collected	9984	32976	9688	27038
Independent refln.	5314 (R_{int} = 0.0206)	5305 (R_{int} = 0.0695)	5748 (R_{int} = 0.0713)	5396 (R_{int} = 0.0449)
Refinement method	Full-matrix least-squares on F^2			
R [$I > 2\sigma(I)$]	R_1 = 0.0418 wR_2 = 0.1194	R_1 = 0.0371 wR_2 = 0.0900	R_1 = 0.0568 wR_2 = 0.1329	R_1 = 0.0300 wR_2 = 0.0714

 © 2003 Wiley-VCH Verlag GmbH & Co. KGaA, Weinheim

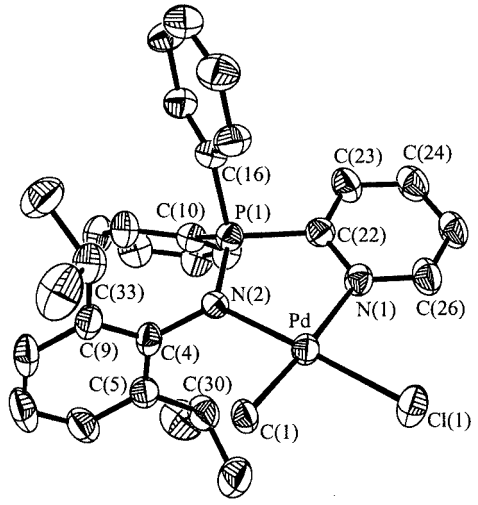

Figure 2. Molecular structure of **1c**

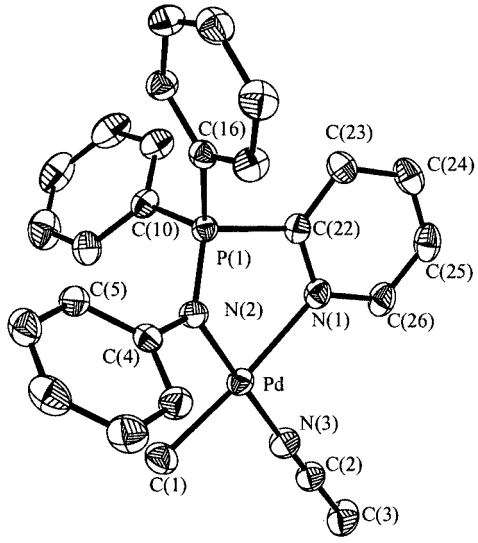

Figure 3. ORTEP drawing of **2a**

Pd−N(2)−C(4), Pd−N(2)−P(1) and P(1)−N(2)−C(4) reveals that the N(2) center is trigonal planar, indicating an sp^2 hybridization of the nitrogen atom. All other bond lengths and bond angles lie within the usual range even in the case of **1c**, with the bulky substituents on the aryl ring. However, the dihedral angles of N(1)−C(22)−P(1)−N(2) and the orientation of the imine [N(2)] aryl ring relative to the chelating ring appear to be the major differences among these crystal structures.

The small dihedral angles of N(1)−C(22)−P(1)−N(2) for **1c** [6.1(6)°] imply an almost planar geometry for this bidentate ligand, whereas a larger deviation of this angle from planar geometry in both **2a** and **1b** [**2a:** 26.9(3)°; **1b:** 28.3(3)°] is observed. In fact, the chelating ring in **1c** lies in a plane with a slight deviation of N(2) by ca. 0.12 Å, based on the calculated plane defined by P(1)−C(22)−N(1)−Pd. The dihedral angle between the chelating ring and the imino [N(2)] aryl ring for **1c** is 82.6(2)°, showing that the isopropyl groups on the aryl ring readily force this ring to lie almost perpendicular to the chelating ring in order to relieve the steric interaction between the ring substituents and the coordinated ligands.

A simple comparison of a few methylpalladium chloride complexes is summarized in Scheme 2. Several differences between these structures are: (1) the Pd−Cl bond *trans* to the phosphane donor is slightly longer than the bonds *trans* to the nitrogen donors. (2) The Pd−C bond of **1c** is longer by ca. 0.1 Å than the bonds in [PdClMe(**P~N**)]and [PdClMe(**N~N**)]. (3) The bite angle decreases in the order: **1c** < [PdClMe(**P~N**)] < [PdClMe(**N~N**)]. The shorter length of Pd−N(2) in **1c** indicates a stronger coordination of the nitrogen donor to palladium, thus showing that the iminophosphorane functionality remains intact. Indeed, the palladium complexes **1a**−**c** are fairly stable towards air or even moisture. In NMR investigations, complexes **2a**−**c** remain unchanged for several days in the presence of water with trace amounts of coordinating acetonitrile replaced by water molecules. It is known that the iminophosphorane moiety undergoes P−N bond cleavage with water,[3] but such activity is readily hindered by the chelation upon complexation, which is quite similar to that reported by Réau in palladium complexes containing 1,2-bis(triphenylphosphinimino)cyclohexane.[8]

Insertion of Carbon Monoxide and Ethylene

The insertion of carbon monoxide into the Pd−C bond of compounds **2a**−**c** was studied (Scheme 3). A dichloromethane solution of the individual complex was bubbled with CO and monitored by ^{31}P NMR spectroscopy. All three complexes, **2a**−**c**, underwent insertion to yield the corresponding acyl complexes and the insertion rate followed the order of the less steric environments (**2a** > **2b** > **2c**), as evidenced by NMR spectroscopy. The resulting acyl complexes **3b** and **3c** were isolated in stable solid form, whereas the inserted product **3a** readily decomposed in the absence of a carbon monoxide atmosphere. Selected spectroscopic data are summarized in Table 4. The presence of the ^{13}C chemical shift at $\delta = 220$ ppm and the infrared stretching frequency around 1700 cm^{-1} clearly demonstrate the formation of the acetyl group.

Subsequent insertion of ethylene into the Pd-acyl bond of **3b**−**c** can be achieved by bubbling ethylene gas through a dichloromethane solution of the respective palladium complex. The inserted products **4b**−**c** were obtained as air-stable yellow solids and the spectroscopic data (Table 4) clearly support the structure proposed. The carbonyl stretching frequency in the range of 1600−1630 cm^{-1} for **4b**−**c** suggests that the formation of the five-membered (C,O) chelate ring provides extra stability for these complexes.[13]

Complex [$PdCl_2(L_b)$]

In order to find out the difference in the *trans* influence between pyridinyl and iminophosphorane nitrogen, the palladium dichloride complex [$PdCl_2(\mathbf{L_b})$] (**5**) was prepared by

 © 2003 Wiley-VCH Verlag GmbH & Co. KGaA, Weinheim

Table 3. Selected bond lengths (Å) and angles (deg) for **1b**, **1c**, **2a** and **5**

Complex	**2a**, X = N(3)	**1b**, X = Cl(1)	**1c**, X = Cl(1)	**5,** X = Cl(1)
Pd−N(1)	2.173(3)	2.160(7)	2.170(3)	2.070(3)
Pd−N(2)	2.052(3)	2.090(6)	2.080(3)	2.048(3)
Pd−C(1)	2.008(4)	2.114(7)	2.087(3)	Pd−Cl(2): 2.291(1)
Pd−X	2.005(3)	2.302(2)	2.3085(8)	2.2877(9)
P(1)−N(2)	1.597(3)	1.595(6)	1.592(3)	1.590(3)
P(1)−C(22)	1.824(3)	1.820(8)	1.819(3)	1.834(3)
C(22)−N(1)	1.337(5)	1.36(1)	1.354(4)	1.340(5)
N(2)−C(4)	1.424(4)	1.435(9)	1.428(4)	1.426(4)
N(1)−Pd−N(2)	83.9(1)	84.9(2)	84.4(1)	85.0(1)
N(1)−Pd−C(1)	175.4(1)	175.5(3)	175.2(1)	
N(2)−Pd−C(1)	92.6(2)	92.9(2)	91.1(1)	
N(2)−Pd−X	177.9(1)	175.8(2)	178.98(7)	176.20(9)
C(1)−Pd−X	88.0(2)	88.7(2)	89.81(8)	
Pd−N(2)−C(4)	126.9(2)	124.3(4)	121.7(2)	122.5(2)
Pd−N(2)−P(1)	109.0(1)	107.7(1)	114.3(3)	108.1(3)
P(1)−N(2)−C(4)	123.8(2)	126.6(2)	120.5(5)	128.0(2)
C(22)−P(1)−N(2)	104.1(2)	107.0(3)	106.1(2)	103.4(2)

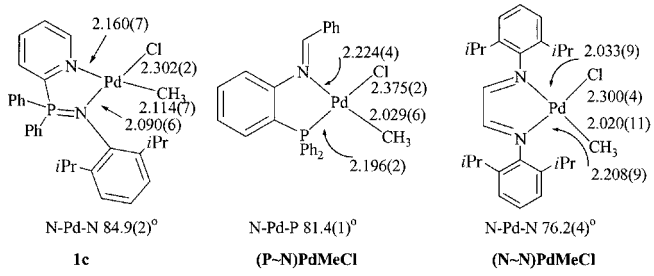

Scheme 2. Summary of bond lengths and bond angles of palladium complexes

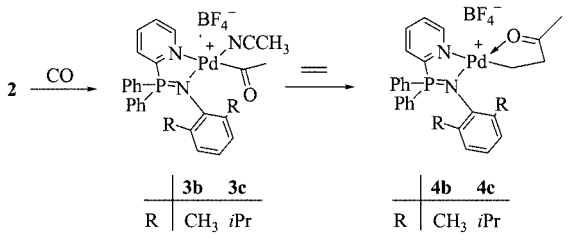

Scheme 3

Table 4. Selected spectroscopic data for **3a**−**c** and **4b**−**c**[a]

Complex	^{1}H NMR -CO-CH_3	^{13}C NMR -*C*=O	^{31}P NMR	IR (ν_{CO})[b]
3a	2.14	221.5	22.0	1728
3b	1.76	221.3	26.3	1713
3c	1.79	220.9	24.6	1713
4b	2.01	211.6	28.3	1623
4c	1.77	224.2	29.8	1660

[a] Chemical shifts in ppm, in $CDCl_3$. [b] KBr, cm^{-1}.

simple substitution of $[PdCl_2(CH_3CN)_2]$ with an equimolar amount of $\mathbf{L_b}$. The complex was readily purified by recrystallization and the crystal structure was determined. Figure 4 shows a perspective view of the complex whose selected bond lengths and bond angles are summarized in Table 3. As expected, complex **5** shows a square-planar coordination geometry around the metal center, with the N(1)−Pd−N(2) angle deviating slightly from 90° because of the constraint imposed by the chelating ring. No major deviation was observed in the bond lengths and angles with respect to **1b**, **1c** and **2a**. The lengths of both Pd−Cl bonds are essentially identical. However, the Pd−N(1) lengths in **1b**, **1c** and **2a** which is *trans* to the carbon donors, lie in the range of 2.16−2.17 Å, whereas the Pd−N(1) distance in **5** is shorter by about 0.1 Å. This variation is due to the stronger *trans* influence of carbon versus chloride ligands. From this structural analysis, both nitrogen donors (pyridinyl and iminophosphorane) have a similar *trans* influence. However, the pyridinyl-nitrogen donor appears to be somewhat stronger due to the alkyl ligands being *trans* to the nitrogen ligand in complexes **1** and **2**.

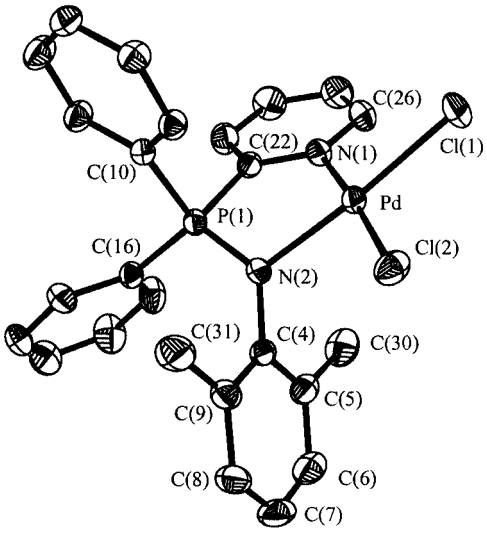

Figure 4. Molecular structure of palladium dichloride complex **5**

 © 2003 Wiley-VCH Verlag GmbH & Co. KGaA, Weinheim

Copolymerization

The catalytic activity of the cationic palladium complexes **2a**−**c** was examined. Unlike the corresponding diiminopalladium complexes,[1] this series of complexes were not good catalysts for the polymerization of ethylene. Nevertheless, complex **2b** was found to catalyze the copolymerization of carbon monoxide and norbornene (Table 5). Both the chemical shift in the ^{13}C NMR spectrum and the infrared stretching frequency of the carbonyl group (δ = 211 ppm and 1713 cm^{-1} respectively) clearly demonstrate the formation of the copolymer. As shown in Table 5, the olefin concentration does not have any effect on either the molecular weight or the yield. However, a higher pressure of carbon monoxide led to the precipitation of palladium black out of solution and to lower molecular weight copolymers. In terms of solvent effect, both a coordinating solvent such as acetonitrile (entry 6) and a non-polar solvent (entry 8) provide poor conversions. By comparing the catalysts (entries 1, 7 and 9), complex **2b** appears to be much more active than either **2a** or **2c**. The lower activity of **2c** is presumably due to the steric hindrance of the ligand, whereas in the case of **2a** it is due to the lower stability of the inserted intermediates as illustrated in the previous section. In terms of the catalytic copolymerization of CO/norbornene, complex **2b** shows a similar activity to that of [PdMe(**P~N**)(CH_3CN)]BF_4.[13a]

Table 5. Results of copolymerization of CO and norbornene[a]

Entry	CO(psi)	M_N	PDI	Yield	TOF[b]
1	14.7	5746	1.50	311 mg	24
2	200	3288	1.93	204 mg	16
3	14.7	5137	1.37	251 mg	19
4	200	2352	1.51	254 mg	20
5	50	2373	1.43	216 mg	17
6[c]	14.7	2902	1.58	125 mg	10
7[d]	14.7	2485	1.63	187 mg	14
8[e]	150	–[f]	–	76 mg	5.9
9[g]	14.7	1976	1.61	173 mg	13

[a] Catalyst: **2b** (30 mg), norbornene (5 g), 24 h, in CH_2Cl_2 (20 mL) at 30 °C except where noted; norbornene (10 g) was used in entries 3 and 4. [b] $g{\cdot}mol^{-1}{\cdot}h^{-1}$ [c] In CH_2Cl_2/CH_3CN = 4:1. [d] **2a** as the catalyst. [e] In toluene. [f] M_N was not determined due to its poor solubility in organic solvent. [g] **2c** as the catalyst.

In addition to the copolymerization of CO/norbornene, this series of complexes can also copolymerize ethylene and norbornene. In a typical reaction, **2b** (30 mg) was added to norbornene and ethylene (500 psi) in toluene (20 mL) at 30 °C and after 24 hours, 1.4 g of copolymer was produced. The results are summarized in Table 6. The appropriate reaction conditions for this polymerization appear in entry 4 with the ratio of norbornene to ethylene being 55:45. The mol percentage of the incorporated norbornene units was determined by the glass transition point (T_g) method developed by Ruchatz and Fink.[14] Among these catalysts (entries 4−6), complex **2b** appears to be the one with the highest activity. On the other hand, the phosphanylimine palladium complex [PdMe(CH_3CN)(**P~N**)]BF_4 does not show this kind of activity.

Table 6. Results of copolymerization of ethylene/norbornene[a]

Entry	norbornene	Time (h)	M_N	PDI	Yield (mg)	N%[b]	T_g (°C)	TOF[c]
1	2.5	24	31000	1.41	1431	54.2	141.8	110
2[d]	5.0	48	20000	1.75	1114	61.9	130.2	43
3	5.0	48	34000	1.61	2378	49.8	144.3	92
4	5.0	24	35000	1.59	1772	55.5	126.6	137
5[e]	5.0	24	3600	1.87	538	64.0	154.5	45
6[f]	5.0	24	2900	1.44	108	59.7	122.4	8

[a] Ethylene/Norbornene (5 g) with **2b** (30 mg) as catalyst in toluene (20 mL) at 30 °C unless noted. [b] N%: mol percent of norbornene (by T_g method). [c] $g{\cdot}mol^{-1}{\cdot}h^{-1}$ [d] Reaction temperature at 50 °C. [e] **2a** as the catalyst. [f] **2c** as the catalyst.

In summary, a series of pyridinyliminophosphorane ligands with different steric influences was prepared and their methylpalladium complexes appear to be stable toward moisture. As for the reactivity toward insertion of CO and ethylene, complexes **2b**−**c** with a sterically hindered environment can stabilize the inserted intermediates, but not **2a**. As for catalysis, complex **2b** is a good candidate for the coplymerization of CO/norbornene and ethylene/norbornene.

Experimental Section

General Information: NMR spectra were recorded in $CDCl_3$ or [D_6]acetone on either a Bruker AC-E 200 or AM-300 spectrometer. Chemical shifts are given in parts per million relative to $SiMe_4$ for ^1H and ^{13}C NMR, and 85% H_3PO_4 for ^{31}P NMR spectroscopy. Due to the complication of the aromatic region, chemical shifts of non-aromatic carbons are reported. Infrared spectra were measured on a Nicolet Magna-IR 550 spectrometer (Series-II) as KBr pellets, unless otherwise noted. Gel permeation chromatography (GPC) data were obtained from a Waters Model 590 liquid chromatograph installed with a Lab Alliance RI 2000 detector using THF as eluent at room temperature and the polystyrene calibration curve for analyses. Differential scanning calorimetric (DSC) measurement was carried out on a TA 2920 system.

All reaction, manipulation and purification steps were performed under a dry nitrogen atmosphere. Tetrahydrofuran was distilled under nitrogen from sodium benzophenone ketyl. Dichloromethane and acetonitrile were dried with CaH_2 and distilled under nitrogen. Other chemicals and solvents were of analytical grade and were used as received unless otherwise stated. 2-Diphenylphosphanylpyridine was prepared by reacting lithium diphenylphosphide with 2-bromopyridine.[15] Phenyl azide and 2,6-dialkylphenyl azide were obtained by the diazotization of the corresponding aniline followed by the substitution of azide anion.[16]

 © 2003 Wiley-VCH Verlag GmbH & Co. KGaA, Weinheim

General Procedure for the Preparation of Ligands L_a–L_c: 2-Diphenylphosphanylpyridine (0.5 g, 1.9 mmol) and dichloromethane (15 mL) were placed in a degassed round-bottomed flask. A solution of aryl azide (1.9 mmol) was transferred into the above flask under nitrogen. Nitrogen gas was generated immediately and the resulting mixture was stirred for 2.5 h. After concentration, the desired ligands were obtained as moisture-sensitive, viscous liquids.

Ligand L_a: (0.65 g, 96%), ^{1}H NMR ($CDCl_3$): δ = 8.78 (d, J = 4.6 Hz, 1 H, py-H_6), 8.34 (dd, J = 7.1, 6.1 Hz, 1 H, py-H_4), 7.99–7.94 (m, 4 H, Ar-H), 7.78–7.76 (m, 1 H, py-H), 7.51–7.35 (m, 7 H, Ar-H, py-H), 7.07 (dd, J = 9.0, 8.4 Hz, 2 H, Ar-H), 6.90 (d, J = 8.4 Hz, 2 H, Ar-H), 6.71 (t, J = 9.0 Hz, 1 H, Ar-H) ppm. ^{13}C NMR: δ = 155.2 (d, $J_{C,P}$ = 130.0 Hz), 150.2 (d, $J_{C,P}$ = 19.1 Hz), 140.0, 136.2 (d, $J_{C,P}$ = 9.0 Hz), 133.0 (d, $J_{C,P}$ = 9.3 Hz), 131.7 (d, $J_{C,P}$ = 2.7 Hz), 130.8, 129.3 (d, $J_{C,P}$ = 19.8 Hz), 128.7, 128.5 (d, $J_{C,P}$ = 11.9 Hz), 125.1 (d, $J_{C,P}$ = 3.0 Hz), 123.4 (d, $J_{C,P}$ = 18.2 Hz), 117.4 ppm. ^{31}P NMR: δ = 14.8 ppm. HRMS (EI): calcd. for $C_{23}H_{19}N_2P$ m/z = 354.1286; found: 354.1277. $C_{23}H_{19}N_2P$ (354.38): calcd. C 77.95, H 5.40; found C 77.59, H 5.38.

Ligand L_b: (0.68 g, 93%), ^{1}H NMR ($CDCl_3$): δ = 8.75 (d, J = 4.8 Hz, 1 H, py-H_6), 8.38 (dd, J = 7.0, 6.2 Hz, 1 H, py-H_4), 7.80–7.75 (m, 5 H, Ar-H), 7.50–7.48 (m, 2 H, py-H), 7.43–7.36 (m, 5 H, Ar-H), 6.95–6.93 (d, J = 7.0 Hz, 2 H, Ar-H), 6.68 (t, J = 7.0 Hz, 1 H, Ar-H), 2.07 (s, 6 H, Ar-CH_3) ppm. ^{13}C NMR: δ = 157.2 (d, $J_{C,P}$ = 133.8 Hz), 149.8 (d, $J_{C,P}$ = 20.1 Hz), 146.6, 136.1 (d, $J_{C,P}$ = 8.9 Hz), 132.8 (d, $J_{C,P}$ = 6.4 Hz), 132.5 (d, $J_{C,P}$ = 9.2 Hz), 131.3 (d, $J_{C,P}$ = 2.3 Hz), 128.2 (d, $J_{C,P}$ = 12.0 Hz), 127.8, 128.5, 124.8, 123.3, 119.0, 21.4 ppm. ^{31}P NMR: δ = 16.5 ppm. HRMS calcd. for $C_{25}H_{23}N_2P$ m/z = 382.1599; found 382.1596. $C_{25}H_{23}N_2P$ (382.44): calcd. C 78.51, H 6.06; found C 78.22, H 5.79.

Ligand L_c: (0.91 g, 91%), ^{1}H NMR ($CDCl_3$): δ = 8.84 (d, J = 4.0 Hz, 1 H, py-H_6), 7.59–7.41 (m, 7 H, py-H, Ar-H), 7.24–7.17 (m, 6 H, py-H, Ar-H), 7.09–6.98 (m, 3 H, Ar-H), 3.40–3.33 (m, 2 H, -CH-), 1.41 (d, J = 6.9 Hz, 6 H, -CH_3), 1.09 (d, J = 6.7 Hz, 6 H, -CH_3) ppm. ^{13}C NMR: δ = 156.8 (d, $J_{C,P}$ = 132.3 Hz), 150.1 (d, $J_{C,P}$ = 20.0 Hz), 143.2 (d, $J_{C,P}$ = 4.9 Hz), 140.4, 136.2 (d, $J_{C,P}$ = 8.9 Hz), 134.4, 132.7 (d, $J_{C,P}$ = 9.1 Hz), 128.4 (d, $J_{C,P}$ = 11.9 Hz), 127.1, 125.1, 124.2, 123.2, 118.8, 29.0 (-CH-), 23.8 (-CH_3), 22.7 (-CH_3) ppm. ^{31}P NMR: δ = 15.6 ppm. HRMS calcd. for $C_{29}H_{31}N_2P$ m/z = 438.2225; found 438.2233. $C_{29}H_{31}N_2P$ (438.54): calcd. C 79.42, H 7.12; found C 79.02, H 6.89.

General Procedure for the Preparation of [L_XPdClMe] (1a–c): A mixture of [PdClMe(COD)] (0.5 g, 1.89 mmol) with an equimolar amount of ligand in dichloromethane (5 mL) was stirred at room temperature under a nitrogen atmosphere. After stirring for 3 h, the solvents were evaporated and the remaining material was dissolved in dichloromethane. Pre-dried diethyl ether was slowly added to the above solution to precipitate the desired complexes as yellow solids.

Complex 1a: (0.71 g, 74%). M.p. 180–196 °C (dec). ^{1}H NMR ($CDCl_3$): δ = 9.39 (d, J = 4.5 Hz, 1 H, py-H_6), 7.84–7.81 (m, 1 H, py-H), 7.76–7.64 (m, 6 H, py-H, Ar-H), 7.57–7.51 (m, 5 H, Ar-H), 7.36 (m, 1 H, py-H), 6.99–6.93 (m, 4 H, Ar-H), 6.80–6.76 (m, 1 H, Ar-H), 0.77 (s, 3 H, Pd-CH_3) ppm. ^{13}C NMR: δ = 153.8 (d, $J_{C,P}$ = 143.9 Hz), 151.0 (d, $J_{C,P}$ = 12.8 Hz), 145.9, 137.4 (d, $J_{C,P}$ = 10.2 Hz), 133.7 133.3, (d, $J_{C,P}$ = 10.3 Hz), 129.3 (d, $J_{C,P}$ = 11.2 Hz), 128.0, 127.2 (d, $J_{C,P}$ = 9.8 Hz), 126.9, 125.2, (d, $J_{C,P}$ = 9.2 Hz), 121.8, −3.0 (s, Pd-CH_3) ppm. ^{31}P NMR: δ = 26.56 ppm. $C_{24}H_{22}ClN_2PPd$ (511.29): calcd. C 56.38, H 4.34, N 5.48; found C 56.72, H 4.34, N 5.40.

Complex 1b: (0.8 g, 79%). M.p. 185–210 °C (dec). ^{1}H NMR ($CDCl_3$): δ = 9.35 (d, J = 5.1 Hz, 1 H, py-H_6), 7.87–7.82 (m, 5 H, Ar-H), 7.57–7.55 (m, 2 H, py-H), 7.48–7.24 (m, 6 H, Ar-H, py-H), 6.75–6.66 (m, 3 H, Ar-H), 2.24 (s, 3 H, Ar-CH_3), 0.62 (s, 3 H, Pd-CH_3) ppm. ^{13}C NMR: δ = 154.4 (d, $J_{C,P}$ = 134.5 Hz), 151.3 (d, $J_{C,P}$ = 12.9 Hz), 143.1, 137.4 (d, $J_{C,P}$ = 9.52 Hz), 135.9 (d, $J_{C,P}$ = 5.5 Hz), 133.4 (d, $J_{C,P}$ = 2.8 Hz), 132.7 (d, $J_{C,P}$ = 10.1 Hz), 129.1 (d, $J_{C,P}$ = 12.5 Hz), 127.9 (d, $J_{C,P}$ = 2.7 Hz), 126.9 (d, $J_{C,P}$ = 2.7 Hz), 126.3 (d, $J_{C,P}$ = 23.0 Hz), 125.3 (d, $J_{C,P}$ = 95.0 Hz), 123.2 (d, $J_{C,P}$ = 3.2 Hz), 21.9 (s, Ar-CH_3), −5.79 (s,-$PdCH_3$) ppm. ^{31}P NMR: δ = 21.70 ppm. $C_{26}H_{26}ClN_2PPd$ (539.34): calcd. C 57.90, H 4.86, N 5.19; found C 57.39, H 4.86, N 5.20.

Complex 1c: (0.86 g, 76%). M.p. 183–190 °C (dec). ^{1}H NMR ($CDCl_3$): δ = 9.47 (d, J = 5.0 Hz, 1 H, py-H_6), 7.86–7.82 (m, 1 H, py-H), 7.80–7.75 (m, 5 H, Ar-H), 7.54–7.46 (m, 5 H, Ar-H), 7.35–7.32 (m, 2 H, py-H), 6.95–6.84 (m, 3 H, Ar-H), 3.59–3.56 (m, 2 H, -CH-), 1.34 (d, J = 6.7 Hz, 6 H, -CH_3), 0.69 (s, 3 H, Pd-CH_3), 0.55 (d, J = 6.8 Hz, 6 H, -CH_3) ppm. ^{13}C NMR: δ = 154.2 (d, $J_{C,P}$ = 136.6 Hz), 151.2 (d, $J_{C,P}$ = 12.6 Hz), 146.1 (d, $J_{C,P}$ = 5.5 Hz), 139.4 (d, $J_{C,P}$ = 2.1 Hz), 137.4 (d, $J_{C,P}$ = 9.6 Hz), 133.2 (d, $J_{C,P}$ = 2.2 Hz), 132.9 (d, $J_{C,P}$ = 9.7 Hz), 129.0 (d, $J_{C,P}$ = 12.2 Hz), 127.2, 126.9, 125.5 (d, $J_{C,P}$ = 94.1 Hz), 124.1 (d, $J_{C,P}$ = 2.9 Hz), 123.3 (d, $J_{C,P}$ = 1.8 Hz), 28.3 (−CH-),24.7 (s, Ar-CH_3),23.1 (−CH_3), −2.88 (s,-$PdCH_3$) ppm. ^{31}P NMR: δ = 22.50 ppm. $C_{30}H_{34}ClN_2PPd$ (595.45): calcd. C 60.51, H 5.76, N4.70; found C 60.23, H 5.68, N 4.73.

General Procedure for the Synthesis of [L_XPdMe(CH_3CN)]BF_4 (2a–c): An acetonitrile solution of $AgBF_4$ (0.19 g, 0.97 mmol) was added to a solution of L_xPdClMe (0.97 mmol) in dichloromethane (10 mL) under a nitrogen atmosphere. After stirring for 1 h, removal of AgCl by filtration and concentration gave the crude product, which was recrystallized from dichloromethane and diethyl ether to provide the desired products as yellow solids.

Complex 2a: (0.40 g, 66%). M.p. 121–132 °C (dec). ^{1}H NMR ($CDCl_3$): δ = 9.03 (d, J = 4.7 Hz, 1 H, py-H), 8.02–7.97 (m, 1 H, py-H), 7.93–7.89 (m, 1 H, py-H), 7.73–7.67 (m, 6 H, py-H, Ar-H), 7.59–7.53 (m, 5 H, Ar-H), 6.96 (dd, J = 7.6, 6.2 Hz, 2 H, Ar-H), 6.87 (d, J = 7.6 Hz, 1 H, Ar-H), 6.80 (t, J = 6.2 Hz, 2 H, Ar-H), 2.44 (s, 3 H, -$NCCH_3$), 0.69 (s, 3 H, Pd-CH_3) ppm. ^{13}C NMR: δ = 152.3 (d, $J_{C,P}$ = 140.5 Hz), 152.3 (d, $J_{C,P}$ = 12.7 Hz), 144.9, 139.0 (d, $J_{C,P}$ = 10.3 Hz), 134.3 (d, $J_{C,P}$ = 2.9 Hz), 133.3 (d, $J_{C,P}$ = 16.3 Hz), 129.6 (d, $J_{C,P}$ = 12.5 Hz), 128.3, 128.0 (d, $J_{C,P}$ = 23.7 Hz), 127.4 (d, $J_{C,P}$ = 8.9 Hz), 122.8, 121.1, 3.25 ($NCCH_3$), 1.12 (s, Pd-CH_3) ppm. ^{31}P NMR: δ = 34.34 ppm. $C_{26}H_{25}BF_4N_3PPd$ (603.70): calcd. C 51.73, H4.17, N 6.96; found C 51.75, H 4.18, N 6.43.

Complex 2b: (0.51 g, 84%). M.p. 182 −196 °C (dec). ^{1}H NMR ($CDCl_3$): δ = 9.02 (d, J = 5.1 Hz, 1 H, py-H), 8.01–7.98 (m, 1 H, py-H_4), 7.90–7.88 (m, 1 H, py-H), 7.78–7.73 (m, 4 H, Ar-H), 7.62–7.59 (m, 2 H, Ar-H), 7.56–7.54 (m, 1 H, py-H), 7.50–7.46 (m, 4 H, Ar-H), 6.74–6.68 (m, 3 H, Ar-H), 2.42 (s, 3 H, -$NCCH_3$), 2.14 (s, 6 H, Ar-CH_3), 0.55 (s, 3 H, Pd-CH_3) ppm. ^{13}C NMR: δ = 152.6 (d, $J_{C,P}$ = 132.8 Hz), 152.4 (d, $J_{C,P}$ = 12.5 Hz), 142.2 (d, $J_{C,P}$ = 1.5 Hz), 139.2 (d, $J_{C,P}$ = 9.4 Hz), 135.9 (d, $J_{C,P}$ = 5.2 Hz), 134.0 (d, $J_{C,P}$ = 2.7 Hz), 132.6 (d, $J_{C,P}$ = 10.1 Hz), 129.3 (d, $J_{C,P}$ = 12.3 Hz), 128.1 (d, $J_{C,P}$ = 2.3 Hz), 127.4 (d, $J_{C,P}$ = 22.5 Hz), 124.0 (d, $J_{C,P}$ = 95.6 Hz), 124.0 (d, $J_{C,P}$ = 3.0 Hz), 121.1, 21.7 (s, Ar-CH_3), 15.1 (s, -$NCCH_3$), 3.2 (s, Pd-CH_3) ppm. ^{31}P NMR: δ = 30.33 ppm. $C_{28}H_{29}BF_4N_3PPd$ (631.75): calcd. C 53.23, H 4.63, N 6.65; found C 53.42, H 4.48, N 6.46.

Complex 2c: (0.27 g, 78%). M.p. 125–140 °C (dec). ^{1}H NMR ($CDCl_3$): δ = 9.13 (d, J = 4.6 Hz, 1 H, py-H_6), 8.00–7.99 (m, 1 H, py-H), 7.93–7.92 (m, 1 H, py-H), 7.65–7.59 (m, 6 H, py-H,

 © 2003 Wiley-VCH Verlag GmbH & Co. KGaA, Weinheim

Ar-H), 7.49−7.43 (m, 5 H, Ar-H), 6.90 (t, J = 6.8 Hz, 1 H, Ar-H), 6.81 (d, J = 6.8 Hz, 2 H, Ar-H), 3.29 (m, 2 H, -CH-), 2.42 (s, 3 H, -NCCH_3), 1.22 (d, J = 6.7 Hz, 6 H, -CH_3), 0.58 (s, 3 H, Pd-CH_3), 0.47 (d, J = 6.85 Hz, 6 H, -CH_3) ppm. ^{13}C NMR: δ = 152.5 (d, $J_{C,P}$ = 134.6 Hz), 152.3 (d, $J_{C,P}$ = 12.5 Hz), 146.2 (d, $J_{C,P}$ = 5.4 Hz), 139.0 (d, $J_{C,P}$ = 9.6 Hz), 138.4 (d, $J_{C,P}$ = 2.7 Hz),133.9 (d, $J_{C,P}$ = 2.6 Hz), 132.8 (d, $J_{C,P}$ = 9.7 Hz), 129.3 (d, $J_{C,P}$ = 12.2 Hz), 128.3 (d, $J_{C,P}$ = 22.6 Hz), 125.0 (d, $J_{C,P}$ = 2.8 Hz), 124.3 (d, $J_{C,P}$ = 94.9 Hz), 123.6 (d, $J_{C,P}$ = 2.2 Hz), 121.2, 28.4 (-CH-), 24.5 (-CH_3), 23.0 (-CH_3), 3.19 (NCCH_3), 1.66 (Pd-CH_3) ppm. ^{31}P NMR: δ = 31.72 ppm. $C_{32}H_{37}BF_4N_3PPd$ (687.85): calcd. C 55.88, H 5.42, N 6.11; found C 55.62, H 5.95, N 6.53.

General Procedure for the Synthesis of [L_XPd(COMe)(CH_3CN)]BF_4: Carbon monoxide was bubbled through an acetonitrile solution of [L_XPdMe(CH_3CN)]BF_4 (0.9 mmol) for 20 min. The resulting mixture was passed through celite and the filtrate was concentrated. The crude product was dissolved in dichloromethane and diethyl ether was added to precipitate the desired insertion products as yellow solids. These complexes readily decomposed due to decarbonylation.

Complex 3b: (31 mg, 52%). IR (KBr): $\tilde{\nu}$ = 1713 cm^{-1} (ν_{CO}). ^{1}H NMR ($CDCl_3$): δ = 8.94 (d, J = 5.4 Hz, 1 H, py-H_6), 8.02−7.97 (m, 1 H, py-H), 7.87−7.77 (m, 5 H, Ar-H), 7.64−7.63 (m, 2 H, py-H), 7.54−7.53 (m, 5 H, Ar-H), 6.72−6.68 (m, 3 H, Ar-H), 2.24 (s, 6 H, Ar-CH_3), 2.01 (s, 3 H, -NCCH_3), 1.77 (s, 3 H, Pd-CO-CH_3) ppm. ^{13}C NMR: δ = 221.3 (−CO-), 152.4 (d, $J_{C,P}$ = 129.2 Hz), 152.8 (d, $J_{C,P}$ = 12.3 Hz), 143.2, 139.5 (d, $J_{C,P}$ = 9.2 Hz), 135.5 (d, $J_{C,P}$ = 5.2 Hz), 134.2, 132.9 (d, $J_{C,P}$ = 10.2 Hz), 129.5 (d, $J_{C,P}$ = 12.6 Hz), 129.0, 128.5, 127.2 (d, $J_{C,P}$ = 21.6 Hz), 124.3, 123.9 (d, $J_{C,P}$ = 97.4 Hz), 30.5 (NCCH_3), 21.8 (Ar-CH_3), 2.3 (Pd-CO-CH_3) ppm. ^{31}P NMR: δ = 26.3 ppm. HRFABMS: calcd. for [M − BF_4 − CH_3CN] m/z = 531.0818; found 531.0822.

Complex 3c: (35 mg, 59%). IR (KBr): $\tilde{\nu}$ = 1713 cm^{-1} (ν_{CO});^{1}H NMR ($CDCl_3$): δ = 8.91 (d, J = 4.8 Hz, 1 H, py-H_6), 8.02−7.97 (m, 1 H, py-H), 7.89−7.87 (m, 1 H, py-H), 7.72−7.67 (m, 6 H, Ar-H, py-H), 7.54−7.50 (m, 5 H, Ar-H), 6.93 (t, J = 7.7 Hz, 1 H, Ar-H), 6.86 (d, J = 7.7 Hz, 1 H, Ar-H), 3.38−3.30 (m, 2 H, -CH-), 2.19 (s, 3 H, -NCCH_3), 1.79 (s, 3 H, Pd-CO-CH_3), 1.40 (d, J = 5.8 Hz, 6 H, -CH_3), 0.59 (d, J = 6.8 Hz, 6 H, -CH_3) ppm. ^{13}C NMR: δ = 221.0 (−CO-), 152.6 (d, $J_{C,P}$ = 128.5 Hz), 152.6 (d, $J_{C,P}$ = 13.1 Hz), 145.8 (d, $J_{C,P}$ = 5.2 Hz), 139.6 (d, $J_{C,P}$ = 3.8 Hz), 139.4 (d, $J_{C,P}$ = 9.2 Hz), 134.2 (d, $J_{C,P}$ = 2.5 Hz), 133.2 (d, $J_{C,P}$ = 10.1 Hz), 129.5 (d, $J_{C,P}$ = 12.6 Hz), 129.0, 127.7 (d, $J_{C,P}$ = 22 Hz), 125.1 (d, $J_{C,P}$ = 2.7 Hz), 124.0 (d, $J_{C,P}$ = 90.4 Hz), 124.0, 31.30 (NCCH_3), 28.7, 24.2 (-CH_3), 23.62 (-CH_3), 2.15 (Pd-CO-CH_3) ppm. ^{31}P NMR: δ = 24.7 ppm. HRFABMS: calcd. for [M − BF_4 − CH_3CN] m/z = 587.1439; found 587.1444.

General Procedure for the Synthesis of [L_XPd(CH_2CH_2COMe)BF_4: A solution of [L_XPd(COMe)(CAN)]BF_4 in dichloromethane was bubbled through ethylene gas for 1.5 h. The purification procedure was similar to that of [L_XPd(COMe)(CAN)]BF_4. The desired complexes were obtained as yellow solids.

Complex 4b: (38 mg, 65%). M.p. 172−184 °C (dec.). IR (KBr): $\tilde{\nu}$ = 1623 cm^{-1} (ν_{CO}). ^{1}H NMR ($CDCl_3$): δ = 9.05 (d, J = 4.7 Hz, 1 H, py-H_6), 8.24−8.22 (m, 1 H, py-H), 8.07−8.04 (m, 1 H, py-H), 7.73−7.49 (m, 11 H, py-H, Ar-H), 6.91−6.78 (m, 3 H, Ar-H), 2.26 (s, 6 H, Ar-CH_3), 2.11 (m, 2 H), 2.01 (s, 3 H, -CH_3), 1.88 (m, 2 H) ppm. ^{13}C NMR: δ = 211.6 (−CO-),152.3 (d, $J_{C,P}$ = 129.3 Hz), 151.3 (d, $J_{C,P}$ = 21 Hz), 147.9, 140.0 (d, $J_{C,P}$ = 9.2 Hz), 137.4 (d, $J_{C,P}$ = 3.0 Hz), 135.1 (d, $J_{C,P}$ = 2.7 Hz), 133.8 (d, $J_{C,P}$ = 10.4 Hz), 129.5 (d, $J_{C,P}$ = 12.9 Hz), 128.2 (d, $J_{C,P}$ = 21.7 Hz), 128.0 (d, $J_{C,P}$ = 3.1 Hz), 125.1 (d, $J_{C,P}$ = 2.5 Hz), 123.8 (d, $J_{C,P}$ = 2.8 Hz), 120.0 (d, $J_{C,P}$ = 102.4 Hz), 37.9, 30.1, 19.9 (Pd-CO-CH_3) ppm. ^{31}P NMR: δ = 28.4 ppm. $C_{29}H_{30}BF_4N_2OPPd$ (646.76): calcd. C 53.85, H 4.68, N 4.33; found C 53.53, H 4.38, N 4.21.

Complex 4c: (37 mg, 64%). M.p. 170−182 °C (dec.). IR (KBr): $\tilde{\nu}$ = 1660 cm^{-1}(ν_{CO});^{1}H NMR ($CDCl_3$): δ = 8.81 (d, J = 4.3 Hz, 1 H, py-H_6), 8.22−8.20 (m, 1 H, py-H), 8.06−8.04 (m, 1 H, py-H), 7.65−7.51 (m, 11 H, py-H, Ar-H), 7.14−6.94 (m, 3 H, Ar-H), 3.01−2.96 (m, 2 H, -CH-), 2.27 (m, 2 H), 2.12 (m, 2 H), 1.77 (s, 3 H, Pd-OC-CH_3), 1.15 (d, J = 6.7 Hz, 3 H, -CH_3), 0.75 (d, J = 6.8 Hz, 3 H, -CH_3) ppm. ^{13}C NMR: δ = 224.3, (−CO-),151.3 (d, $J_{C,P}$ = 21.1 Hz), 147.9 (d, $J_{C,P}$ = 3 Hz), 147.0 (d, $J_{C,P}$ = 96.3 Hz), 139.7, 138.1 (d, $J_{C,P}$ = 10.5 Hz), 135.0 (d, $J_{C,P}$ = 2.6 Hz), 134.0 (d, $J_{C,P}$ = 14.5 Hz), 131.2 (d, $J_{C,P}$ = 24.3 Hz), 129.5 (d, $J_{C,P}$ = 13.1 Hz), 128.1 (d, $J_{C,P}$ = 3.6 Hz), 124.0, 119.8 (d, $J_{C,P}$ = 102.6 Hz), 119.6, 34.8, 29.7, 28.5, 24.7, 23.2, 19.7 (Pd-CO-CH_3) ppm. ^{31}P NMR: δ = 29.8 ppm. $C_{33}H_{38}BF_4N_2OPPd$ (702.87): calcd. C 56.39, H 5.45, N 3.99; found C 55.98, H 5.14, N 3.78.

Complex 5: A mixture of 2,6-dimethylphenyl azide (0.223 g) and 2-diphenylphosphanylpyridine (0.4 g) was placed in a degassed flask. Dichloromethane (25 mL) was introduced into the flask with a syringe under nitrogen atmosphere. The resulting mixture was stirred at room temperature for 2.5 h. [$PdCl_2$(COD)] (0.31 g) in dichloromethane was added to the above solution. The reaction mixture turned yellow immediately. After concentration to a small volume, diethyl ether was slowly added and the desired product precipitated. The latter was then re-crystallized from diethyl ether/dichloromethane to provide **5** as a yellow solid (765 mg, 90%). ^{1}H NMR ($CDCl_3$): δ = 8.74 (d, J = 4.4 Hz, 1 H, py-H_6), 8.38 (m, 1 H, Py-H_4), 7.84- 7.78 (m, 5 H, Ar-*H*), 7.64−7.62 (m, 2 H, py-H), 7.51−7.46 (m, 5 H, Ar-H), 6.91−6.88 (t, J = 7.4 Hz, 1 H), 6.81 (d, J = 7.4 Hz, 2 H), 2.15 (s, 6 H, -CH_3) ppm. ^{31}P NMR: δ = 28.42 ppm. HRFABMS: Calcd for $C_{25}H_{23}{}^{35}Cl_2N_2PPd$: m/z = 558.0011; found 558.0018. $C_{25}H_{23}Cl_2N_2PPd$ (559.76): calcd. C 53.64, H 4.14, N 5.00; found C 53.29, H 3.78, N 4.89.

Copolymerization of CO/Norbornene: The catalysts and norbornene were placed into a stainless-steel autoclave (100 mL) and dissolved in the solvent (20 mL). The reaction mixture was then pressurized with a mixture of CO and stirred at 30 °C. The reaction was stopped after the specified time and the resulting white solid was filtered and washed with 5 N HCl followed by water and acetone. The Results are listed in Table 5.

Copolymerization of Ethylene/Norbornene: The procedures for this coplymerization are similar to the ones of the copolymerization of CO/norbornene, except that ethylene is replaced by CO. The results are summarized in Table 6.

X-ray Crystallographic Study: Crystals suitable for X-ray determination were obtained for **1b**, **1c**, **2a**·CH_2Cl_2, and **5** by slow diffusion of diethyl ether into a dichloromethane solution at room temperature. The cell parameters were determined on a Siemens SMART CCD diffractometer. The crystal data for complexes **1b**, **1c**, **2a**·CH_2Cl_2 and **5** are listed in Table 2 and their ORTEP plots are shown in Figures 1−4 respectively (labels of phenyl groups are omitted for clear view).

CCDC-210737 (**1b**), -210739 (**1c**), -210738 (**2a**·CH_2Cl_2) and -210740 (**5**) contains the supplementary crystallographic data for this paper. These data can be obtained free of charge at www.ccdc.cam.ac.uk/conts/retrieving.html [or from the Cambridge Crystallographic Data Centre, 12, Union Road, Cambridge

 © 2003 Wiley-VCH Verlag GmbH & Co. KGaA, Weinheim

CB2 1EZ, UK; Fax: (internat.) +44-1223/336-033; E-mail: deposit@ccdc.cam.ac.uk].

Acknowledgments

We thank the National Science Council for financial support (NSC90-2113-M-002-038).

[1] [1a] L. K. Johnson, C. M. Killian, M. Brookhart, *J. Am. Chem. Soc.* **1995**, *117*, 6414−6415. [1b] C. M. Killian, D. J. Tempel, L. K. Johnson, M. Brookhart, *J. Am. Chem. Soc.* **1996**, *118*, 11664−11665. [1c] D. J. Tempel, L. K. Johnson, R. L. Huff, P. S. White, M. Brookhart, *J. Am. Chem. Soc.* **2000**, *122*, 6686−6700. [1d] O. Daugulis, M. Brookhart, *Organometallics* **2002**, *21*, 5926−5934.

[2] Reviews on TM-catalyzed olefin polymerization: [2a] S. D. Ittel, L. K. Johnson, M. Brookhart, *Chem. Rev.* **2000**, *100*, 1169−1203. [2b] E. Drent, P. H. M. Budzelaar, *Chem. Rev.* **1996**, *96*, 663−681. [2c] G. Consiglio, *Chimia* **2001**, *55*, 809−813. [2d] Y. Imanishi, N. Naga, *Prog. Polym. Sci.* **2001**, *26*, 1147−1198. [2e] C. Bianchini, A. Meli, *Coord. Chem. Rev.* **2002**, *225*, 35−66. [2f] J. Okuda, R. Mulhaupt, in *Synthesis of Polymers* (Ed.: A.-D. Schlueter), Wiley-VCH Verlag GmbH, Weinheim, Germany. 1999, Vol. 20, 123−162. [2g]A. Sen, *Pure Appl. Chem.* **2001**, *73*, 251−254. [2h] G. Helmchen, A. Pfaltz, *Acc. Chem. Res.* **2000**, *33*, 325−335. [2i] P. Braunstein, F. Naud, *Angew. Chem.* **2001**, *113*, 702−722; *Angew. Chem. Int. Ed.* **2001**, *40*, 680−699.

[3] H. Staudinger, E. Hauser, *Helv. Chim. Acta* **1921**, *4*, 887.

[4] [4a] A. Schmidpeter, T. von Criegern, *Angew. Chem.* **1978**, *90*, 64−65; *Angew. Chem. Int. Ed. Engl.* **1978**, *17*, 55−56. [4b] H. Alper, R. A. Partis, *J. Organomet. Chem.* **1972**, *35*, C40−C42. [4c] C.-Y. Liu, D.-Y. Chen, M.-C. Cheng, S.-M. Peng, S.-L. Liu, *Organometallics* **1995**, *14*, 1983−1991.

[5] [5a] W. Keim, R. Appel, A. Storeck, C. Kruger, R. Goddard, *Angew. Chem.* **1981**, *93*, 91−92; *Angew. Chem. Int. Ed. Engl.* **1981**, *20*, 116−117. [5b] M. Sauthier, F. Leca, R. Fernando de Souza, K. Bernardo-Gusmao, L. F. Trevisan Queiroz, L. Toupet, R. Réau, *New J. Chem.* **2002**, *26*, 630−635.

[6] [6a] N. Yue, E. Hollink, F. Guerin, D. W. Stephan, *Organometallics* **2001**, *20*, 4424−4433. [6b] N. L. S. Yue, D. W. Stephan, *Organometallics* **2001**, *20*, 2303−2308. [6c] J. E. Kickham, F. Guerin, J. C. Stewart, E. Urbanska, D. W. Stephan, *Organometallics* **2001**, *20*, 1175−1182. [6d] L. LePichon, D. W. Stephan, X. Gao, Q. Wang, *Organometallics* **2002**, *21*, 1362−1366. [6e] L. LePichon, D. W. Stephan, *Inorg. Chem.* **2001**, *40*, 3827−3829. [6f] S. Courtenay, D. W. Stephan, *Organometallics* **2001**, *20*, 1442−1450, and references therein.

[7] R. Vollmerhaus, P. Shao, N. J. Taylor, S. Collins, *Organometallics* **1999**, *18*, 2731−2733.

[8] M. Sauthier, J. Forniés-Cámer, L. Toupet, R. Réau, *Organometallics* **2000**, *19*, 553−562.

[9] [9a] J. Vicente, A. Arcas, D. Bautista, M. C. Ramirez de Arellano, *Organometallics* **1998**, *17*, 4544−4550. [9b] L. R. Falvello, S. Fernández, M. M. Garcia, R. Navarro, E. P. Urriolabeitia, *J. Chem. Soc., Dalton Trans.* **1998**, 3745−3750. [9c] S. M. Aucott, A. M. Z. Slawin, J. D. Woollins, *J. Chem. Soc., Dalton Trans.* **2001**, 2279−2287. [9d] S. Al-Benna, M. J. Sarsfield, M. Thornton-Pett, D. L. Ormsby, P. J. Maddox, P. Bres, M. Bochmann, *J. Chem. Soc., Dalton Trans.* **2000**, 4247−4257. [9e] D. M. Hankin, A. A. Danopoulos, G. Wilkinson, T. K. N. Sweet, M. B. Hursthouse, *J. Chem. Soc., Dalton Trans.* **1996**, 4063−4069. [9f] P. Imhoff, R. van Asselt, C. J. Elsevier, M. C. Zoutberg, C. H. Stam, *Inorg. Chim. Acta* **1991**, *184*, 73−87.

[10] [10a] K. V. Katti, B. D. Santarsiero, A. A. Pinkerton, R. G. Cavell, *Inorg. Chem.* **1993**, *32*, 5919−5925. [10b] R. W. Reed, B. Santarsiero, R. G. Cavell, *Inorg. Chem.* **1996**, *35*, 4292−4300.

[11] R. S. Pandurangi, K. V. Katti, L. Stillwell, C. L. Barnes, *J. Am. Chem. Soc.* **1998**, *120*, 11364−11373.

[12] [12a] M. W. Avis, C. J. Elsevier, N. Veldman, H. Kooijman, A. L. Spek, *Inorg. Chem.* **1996**, *35*, 1518−1528. [12b] M. W. Avis, C. J. Elsevier, H. Kooijman, N. Veldman, A. L. Spek, C. J. Elsevier, *Inorg. Chem.* **1995**, *34*, 4092−4105. [12c] M. W. Avis, K. Vrieze, J. M. Ernsting, C. J. Elsevier, N. Veldman, A. L. Spek, K. V. Katti, C. L. Barnes, *Organometallics* **1996**, *15*, 2376−2392. [12d] M. W. Avis, M. Goosen, C. J. Elsevier, N. Veldman, H. Kooijman, A. L. Spek, *Inorg. Chim. Acta* **1997**, *264*, 43−60.

[13] [13a] K. R. Reddy, C.-L. Chen, Y.-H. Liu, S.-M. Peng, J.-T. Chen, S.-T. Liu, *Organometallics* **1999**, *18*, 2574−2576. [13b] K. R. Reddy; K. Surekha, G.-H. Lee, S.-M. Peng, J.-T. Chen, S.-T. Liu, *Organometallics* **2001**, *20*, 1292−1299. [13c] Y.-C. Chen, C.-L. Chen, J.-T. Chen, S.-T. Liu, *Organometallics* **2001**, *20*, 1285−1286. [13d] K. R. Reddy, K. Surekha, G.-H. Lee, S.-M. Peng, S.-T. Liu, *Organometallics* **2001**, *20*, 5557−5563. [13e] P.-Y. Shi, Y.-H. Liu, S.-M. Peng, S.-T. Liu, *Organometallics* **2002**, *21*, 3203−3207. [13f] K. R. Reddy, W. W. Tsai, K. Surekha, G.-H. Lee, S.-M. Peng, J.-T. Chen, S.-T. Liu, *J. Chem. Soc., Dalton Trans.* **2002**, 1776−1782.

[14] D. Ruchatz, G. Fink, *Macromolecules* **1998**, *31*, 4674−4680.

[15] T. J. Barder, F. A. Cotton, G. L. Powell, S. M. Tetrick, R. A. Walton, *J. Am. Chem. Soc.* **1984**, *106*, 1323−1332.

[16] I. Ugi, H. Perlinger, L. Behringer, *Chem. Ber.* **1958**, *91*, 2330.

Received March 6, 2003

 © 2003 Wiley-VCH Verlag GmbH & Co. KGaA, Weinheim

Geometrical and Linkage Isomers of $[OsCl_2(dmso)_4]$ − The Complete Picture

Enzo Alessio,*[a] Barbara Serli,[a] Ennio Zangrando,[a] Mario Calligaris,[a] and Natalia S. Panina[b][‡]

Keywords: Density functional calculations / Dimethyl sulfoxide / Isomerizations / Osmium

The isomerisation between the three known isomers of the $[OsCl_2(dmso)_4]$ complex — *trans*-$[OsCl_2(dmso\text{-}S)_4]$ (**1**), *cis,fac*-$[OsCl_2(dmso\text{-}S)_3(dmso\text{-}O)]$ (**2**), and *cis*-$[OsCl_2(dmso\text{-}S)_4]$ (**3**) — has been investigated by NMR spectroscopy, X-ray crystallographic analysis, and DFT calculations. We show that the two dmso-linkage isomers **2** and **3** equilibrate slowly at room temperature in solutions of both dimethyl sulfoxide (DMSO) and light-protected chloroform. Although crystals of **2** precipitate from DMSO solutions, crystals of **3** were obtained from chloroform solutions. Compound **2** isomerises to **1** after exposure to sunlight, while **1** transforms into **2** in hot DMSO solution. The molecular energies were calculated by DFT methods, which show that in the gas phase there are small differences in the total energies (E_t), with **1** exhibiting the lowest energy, in contrast with its low population in solution. This result indicates that the stability of each isomer in solution is not simply determined by E_t, but that the solvent plays an important role. In fact, quantum chemical calculations for the isomerisation process **1** → **2** show a marked increase in the equilibrium constant with increasing the solvent polarity. The calculation of the metal–dmso binding energies, in combination with the X-ray data, shows a significantly higher strength of Os–S bonds with respect to Ru–S bonds, which explains the different behaviour of otherwise analogous osmium–dmso and ruthenium–dmso complexes.

(© Wiley-VCH Verlag GmbH & Co. KGaA, 69451 Weinheim, Germany, 2003)

Introduction

Neutral ruthenium(II) halide dimethyl sulfoxide complexes are widely used precursors in inorganic synthesis.[1] In addition, these complexes have anti-tumour[2] and radiosensitising[3] properties, as well as catalytic activity.[4]

Dimethyl sulfoxide (dmso) is an ambidentate ligand that can bind to metal centres either through the sulfur (dmso-*S*) or through the oxygen atom (dmso-*O*). The binding mode of dmso at the RuX_2 centre (X = Cl, Br) has been a matter of interest and debate since the characterisation of *cis,fac*-$[RuX_2(dmso\text{-}S)_3(dmso\text{-}O)]$ and the corresponding thermodynamically less stable geometrical/linkage isomers, *trans*-$[RuX_2(dmso\text{-}S)_4]$.[5−7] The structural and spectroscopic data for these four neutral species, together with those concerning the dinuclear compound $[Ru_2Cl_4(dmso\text{-}S)_5]$,[8] and the charged species [Y][*fac*-$RuCl_3(dmso\text{-}S)_3$] (Y = NH_2Me_2 or RR′NHOH),[9] [*fac*-$RuCl(dmso\text{-}O)_2(dmso\text{-}S)_3][BF_4]$,[10] and [*fac*-$Ru(dmso\text{-}O)_3(dmso\text{-}S)_3][BF_4]_2$,[10,11] have suggested that dmso prefers to bind to Ru^{II} through the sulfur atom for electronic reasons, and that the facial geometry of three dmso-*S* ligands seems to be a particularly stable binding motif. However, coordination of dmso through the sulfur atom is sterically more demanding, compared to coordination through the oxygen atom, and apparently the *fac*-$[Ru(dmso\text{-}S)_3]$ fragment allows coordination of further dmso ligands only through their oxygen atoms for steric reasons.[12] We have also shown that replacement of one dmso-*S* unit by a strongly π-accepting ligand, such as CO or NO, induces the S-to-O-linkage isomerisation of one or more of the remaining dmso units.[13,14] This behaviour was expected since dmso-*S* is a moderate π-acceptor ligand and, thus, it binds preferentially *trans* to pure σ donor ligands; when strong π-acceptors are present in the metal coordination sphere, dmso prefers to bind through its oxygen atom to avoid competition for π electrons.

The synthesis of *cis,fac*-$[OsCl_2(dmso\text{-}S)_3(dmso\text{-}O)]$ and of *trans*-$[OsCl_2(dmso\text{-}S)_4]$,[15] together with the X-ray crystallographic characterisation of *trans*-$[OsBr_2(dmso\text{-}S)_4]$,[16] were in perfect agreement with the previous reports on the analogous ruthenium species and suggested that Os^{II} behaves essentially as does Ru^{II}. This seemingly well-defined belief was shaken, however, in 1998 by McDonagh et al. who reported the X-ray structural characterisation of the unprecedented all-S-bonded isomer *cis*-$[OsCl_2(dmso\text{-}S)_4]$,[17] which showed that the two metal ions can behave quite differently.

[a] Dipartimento di Scienze Chimiche, Università di Trieste
Via L. Giorgieri 1, 34127 Trieste, Italy
Fax: (internat.) + 39-040/558-3903
E-mail: alessi@univ.trieste.it
[b] St. Petersburg State Technological Institute (Technical University),
Moscovsky Prospect 26, St. Petersburg 198013, Russia
[‡] Author to be addressed about quantum chemical calculations.

 © 2003 Wiley-VCH Verlag GmbH & Co. KGaA, Weinheim **DOI: 10.1002/ejic.200300132**

Here we report the results of a combined structural, spectroscopic and computational investigation of the three $[OsCl_2(dmso)_4]$ isomers that we undertook with the aim of gaining a better understanding of the system.

Results and Discussion

Solution Behaviour

The complex *trans*-$[OsCl_2(dmso\text{-}S)_4]$ (**1**) was prepared, as described by Antonov et al.,[15] by treatment of $H_2[OsCl_6]$ with $SnCl_2$ in DMSO at 100 °C (Scheme 1); complex **1** spontaneously precipitates from the hot reaction mixture. This compound was structurally and spectroscopically characterised by McDonagh et al.[17] We found, by NMR spectroscopy, that this isomer is quite stable in $CDCl_3$ solution at ambient temperature: the intensity of the resonance at $\delta = 3.44$ ppm, which accounts for the four equivalent dmso-S ligands, decreased very slowly over a period of days and the signal for free DMSO at $\delta = 2.62$ ppm increased correspondingly. No new resonance for coordinated dmso appeared as a consequence of dmso-*S* hydrolysis from **1**. A similar behaviour was found also in D_2O ($\delta = 3.47$ ppm for dmso-*S*). In contrast, the corresponding Ru^{II} isomer, which presumably binds dmso-*S* more weakly (see below), releases one dmso unit immediately upon dissolution in $CDCl_3$ and two *cis* dmso units upon dissolution in D_2O.[7a]

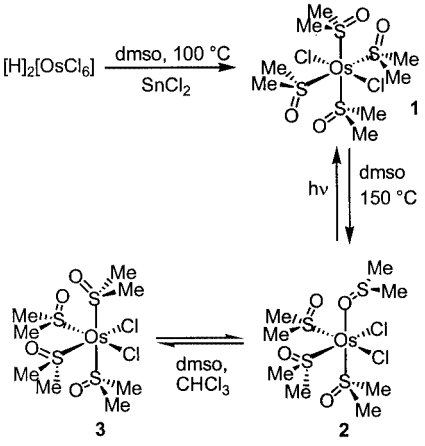

Scheme 1

As described by Antonov et al.,[15] when the above reaction was performed at higher temperature (150 °C), complete dissolution of the *trans* isomer **1** occurred and a white precipitate (**2**) formed from the DMSO solution after cooling to room temperature and addition of acetone (Scheme 1). The spectroscopic signature of this compound,[15] reported also by McDonagh et al.,[17] is typical of *cis*,*fac*-$[OsCl_2(dmso\text{-}S)_3(dmso\text{-}O)]$ (**2**); the presence of O-bonded dmso in **2** was established unequivocally by both NMR and IR spectroscopy. We monitored the isomerisation from **1** to **2** in hot DMSO by visible spectroscopy: at 90 °C the absorption band at 360 nm of the yellow isomer *trans*-$[OsCl_2(dmso\text{-}S)_4]$ (**1**) is completely replaced by that of the colourless *cis* isomer **2** (absorption maximum at 294 nm) within 8 h, with a clear isosbestic point at 282 nm. Recrystallisation of **2** from hot DMSO, followed by addition of acetone, yielded crystals of the same isomer, whose structure was determined by X-ray crystallography (see below). However, as described by McDonagh et al.,[17] crystallisation of **2** at room temperature from chloroform/diethyl ether mixtures yielded crystals that were found by X-ray crystallography to correspond to the all-S-bonded isomer, *cis*-$[OsCl_2(dmso\text{-}S)_4]$ (**3**). Thus, an isomerisation from **2** to **3** must occur in the chloroform solution, while this transformation was not observed in a DMSO solution (Scheme 1).

We found that two sets of resonances are present initially in the ^1H NMR spectrum of **2** in $CDCl_3$ (crystals from the batch used for the X-ray analysis): the major set contains four singlets of equal intensity and corresponds to **2** (dmso-*S* at $\delta = 3.57$, 3.54, and 3.43 ppm; dmso-*O* at $\delta = 2.76$ ppm), while the minor set contains only two equally intense singlets in the region of S-bonded dmso ($\delta = 3.66$ and 3.50 ppm) and corresponds to **3**. The signals of **2** are gradually replaced by those of **3**; equilibrium between the two isomers is reached after ca. 8 d at room temperature (light-protected solution); for longer observation periods (16 d) a very small signal for **1** was also apparent. The equilibrium concentrations of the three isomers correspond to ca. 66% of **3**, 33% of **2**, and less than 1% of **1**. The isomerisation is accompanied by partial hydrolysis of dmso (at equilibrium free DMSO accounts for 5% of the total DMSO) and by the growth of a new minor singlet in the region of S-bonded dmso at $\delta = 3.56$ ppm, which was not assigned. These results confirm the observations of McDonagh et al.[17] A similar behaviour was found to occur also in deuterated DMSO solution ($\delta = 3.41$, 3.38, 3.25, and 2.74 ppm for **2**; $\delta = 3.56$ and 3.40 ppm for **3**); in this case, however, the isomerisation of **2** into **3** could not be followed over a long period of time because of the concomitant exchange of coordinated dmso with the deuterated solvent that led to gradual disappearance of the signals. Thus, in both chloroform and DMSO solution, *cis*,*fac*-$[OsCl_2(dmso\text{-}S)_3(dmso\text{-}O)]$ (**2**) appears to be slightly thermodynamically less stable than *cis*-$[OsCl_2(dmso\text{-}S)_4]$ (**3**) and an equilibrium between the two isomers is established. While crystals of **2** were obtained from DMSO solutions, crystals of **3** were obtained from chloroform solutions.

Finally, as in the case of the corresponding Ru^{II} compounds,[7a] we found that exposure of **2** in solution to sunlight led to its isomerisation to the *trans* isomer **1**. This process was followed by visible spectroscopy in DMSO solution and by NMR spectroscopy in $CDCl_3$ solution.

X-ray Crystal Structure of *cis*,*fac*-$[OsCl_2(dmso\text{-}S)_3(dmso\text{-}O)]$ (2)

The results of the crystal structure determination show that *cis*,*fac*-$[OsCl_2(dmso\text{-}S)_3(dmso\text{-}O)]$ (**2**) (Figure 1) is isostructural with one of the three polymorphs (**F3**) isolated for the ruthenium analogue, *cis*,*fac*-$[RuCl_2(dmso\text{-}S)_3(dmso\text{-}O)]$.[7a] The molecular geometry of this form differs from that detected in its other monoclinic (**F1**)[5] and orthorhom-

 © 2003 Wiley-VCH Verlag GmbH & Co. KGaA, Weinheim

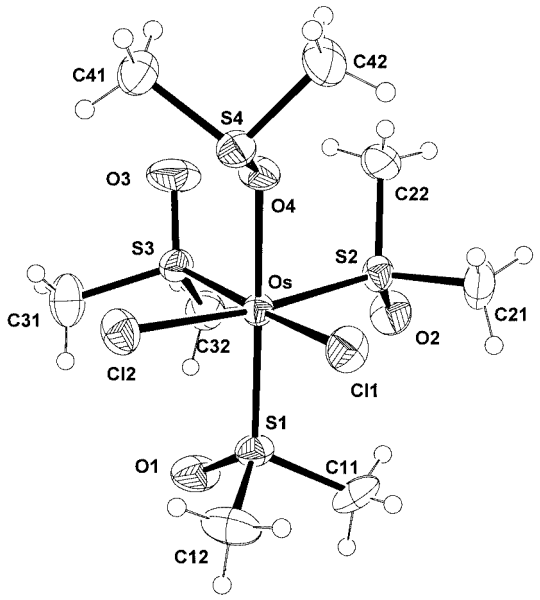

Figure 1. Molecular structure of the compound *cis,fac*-[$OsCl_2$(dmso-*S*)$_3$(dmso-*O*)] (**2**) (thermal ellipsoids drawn at a 40% probability level) with atom numbering scheme

bic (**F2**)[18] crystals, essentially by the different conformation assumed by the dmso-*S* groups upon rotation about the Ru−S bonds.[7a] Infrared spectra have shown that **F2** is the thermodynamically less stable rotamer, which transforms slowly in the solid state into **F3**, in agreement with Molecular Mechanics calculations suggesting that **F3** has the lowest molecular strain energy.[9b] The minimum-strain-energy structure is characterised by a skewed arrangement of the O and S planes of the three dmso-*S* groups (dihedral angle, $\alpha = 25.8°$) and by a *trans*−*trans* conformation of the dmso-*O* group (torsion angle Ru−O−S−C, ψ_1, in the range $-167° < \psi_1 < -90°$).[19] Owing to the similarities between the Os and Ru complexes, the experimental values of $\alpha = 24.2°$ and $\psi_1 = -121.5°$ in the osmium complex **2** suggest that the present molecular structure, found in the solid state, corresponds to the most stable rotamer for this isomer.

Comparison of the Os−S bond lengths in **2** (Table 1) with those of its isomers, *trans*-[$OsCl_2$(dmso-*S*)$_4$] (**1**) (Table 2)[20] and *cis*-[$OsCl_2$(dmso-*S*)$_4$] (**3**) (Table 3),[17] shows a lengthening of the Os−S bond lengths *trans* to S, with respect to those *trans* to Cl or O, as generally observed in metal (e.g., Ru, Rh, Pd, and Pt) sulfoxide complexes.[12,21] However, in **3** the Os−S distances, *trans* to S, are ca. 0.014 Å longer than those in **1**, probably because of stronger steric interactions. The steric demand of the four dmso-*S* groups in **3** is also indicated by the fact that the axial *trans* dmso-*S* groups are pushed away from the *cis* dmso-*S* groups, towards the less-bulky chloride ligands [av. S−Os−S angle, 93(2)°; av. Cl−Os−S angle, 87(2)°]. Similarly, in the equatorial plane, the S−Os−S and Cl−Os−Cl bond angles are 91.60(4)° and 85.42(4)°, respectively. In **1**, the bond angles between the *cis* ligands are restricted to 90°, with the four dmso-*S* groups strictly "interlocked", so that their oxygen atoms lie between the two methyl groups of the adjacent ligand. This arrangement suggests a marked reduction in flexibility on going from **2** and **3** to **1**. The greatest flexibility is to be expected in **2**, because the S→O isomerisation of one of the two *trans* dmso groups leads to a greater degree of rotational freedom.[22]

Finally, the Os−Cl and Os−O bond lengths in **2** are ca. 0.010 and 0.025 Å longer , respectively, than the corresponding distances in the Ru derivative, which is in agreement with the slightly larger covalent radius for the osmium atom. In contrast, we note that the Os−S distances are ca. 0.008 Å shorter than the corresponding Ru−S distances,

Table 1. Observed and calculated selected bond lengths [Å] and angles [°] for *cis,fac*-[$OsCl_2$(dmso-*S*)$_3$(dmso-*O*)] (**2**)

Distance	Exp.	Calcd.
Os−Cl1	2.434(2)	2.473
Os−Cl2	2.428(2)	2.475
Os−S1	2.246(2)	2.300
Os−S2	2.263(2)	2.306
Os−S3	2.277(2)	2.346
Os−O4	2.159(5)	2.168
S1−O1	1.475(6)	1.508
S3−O2	1.472(7)	1.511
S2−O3	1.451(7)	1.507
S4−O4	1.539(6)	1.568
Angle	**Exp.**	**Calcd.**
Cl1−Os−Cl2	87.25(8)	87.89
Cl1−Os−S1	90.52(8)	91.32
Cl1−Os−S2	91.98(8)	91.17
Cl1−Os−S3	173.93(8)	173.93
Cl1−Os−O4	86.0(2)	84.67
Cl2−Os−S1	90.13(9)	89.98
Cl2−Os−S2	172.75(8)	172.41
Cl2−Os−S3	89.32(8)	89.47
Cl2−Os−O4	86.4(2)	86.01
S1−Os−S2	97.09(8)	97.58
S1−Os−S3	94.50(8)	94.14
S1−Os−O4	175.2(2)	174.42
S2−Os−S3	90.79(8)	90.73
S2−Os−O4	86.4(2)	86.40
S3−Os−O4	88.8(2)	89.70

Table 2. Observed and calculated selected bond lengths [Å] and angles [°] for *trans*-[$OsCl_2$(dmso-*S*)$_4$] (**1**)

Distance	Exp.[a]	Calcd.
Os−Cl	2.415(1)	2.479
Os−S	2.3379(9)	2.396
S−O	1.485(4)	1.513
Angle	**Exp.[a][b]**	**Calcd.**
Cl−Os−Cl	180.0	180.00
Cl−Os−S	90.0	90.00
S−Os−S[c]	90.0	90.00
S−Os−S[d]	180.0	180.00

[a] From ref.[20] [b] Symmetry fixed. [c] In *cis* positions. [d] In *trans* positions.

 © 2003 Wiley-VCH Verlag GmbH & Co. KGaA, Weinheim

Table 3. Observed and calculated selected bond lengths [Å] and angles [°] for *cis*-$[OsCl_2(dmso\text{-}S)_4]$ (**3**)

Distance	Exp.[a]	Calcd.
Os−Cl1	2.424(1)	2.483
Os−Cl2	2.427(1)	2.484
Os−S1	2.349(1)	2.405
Os−S2	2.275(1)	2.350
Os−S3	2.277(1)	2.350
Os−S4	2.355(1)	2.405
S1−O1	1.474(3)	1.508
S2−O2	1.483(3)	1.511
S3−O3	1.479(3)	1.511
S4−O4	1.467(4)	1.508
Angle	**Exp.[a]**	**Calcd.**
Cl1−Os−Cl2	85.42(4)	89.56
Cl1−Os−S1	89.42(4)	86.76
Cl1−Os−S2	91.39(4)	90.00
Cl1−Os−S3	176.99(4)	177.43
Cl1−Os−S4	85.03(4)	84.95
Cl2−Os−S1	84.75(4)	84.93
Cl2−Os−S2	176.74(4)	177.42
Cl2−Os−S3	91.60(4)	90.05
Cl2−Os−S4	88.80(5)	86.71
S1−Os−S2	94.58(4)	95.79
S1−Os−S3	90.70(4)	92.50
S1−Os−S4	171.81(4)	168.26
S2−Os−S3	91.60(4)	90.51
S2−Os−S4	91.58(4)	92.50
S3−Os−S4	94.54(4)	95.73

[a] The numbering scheme for **3** and the experimental bond lengths and angles are from ref.[17]

suggesting a strengthening of the metal-to-sulfur bonds in the osmium(II) complexes.

Gas-Phase Structures of the $[OsCl_2(dmso)_4]$ Isomers 1−3

Selected bond lengths and angles calculated for the three isomers **1**, **2**, and **3** are reported in Tables 1−3, respectively, together with the experimental values. Inspection of the tables shows a good agreement between experimental and calculated bond lengths, making allowance for an average systematic 2.3% overestimate of the calculated bond lengths. On the other hand, bond angles show both positive and negative deviations, with an average difference of −0.07°.

The calculated Mulliken atomic charges in the isomers of $[OsCl_2(dmso\text{-}S)_4]$ (Table 4) show that the highest dmso-to-O electron density transfers take place for the isomers with all-S-coordinated dmso ligands, **1** and **3**. In accordance with these effects, we observe the lowest electronic energy contribution (E_e, Table 5) to the total molecular energy (E_t) for **1** and **3**. Interestingly, for the isomer **3**, *cis*-$[OsCl_2(dmso\text{-}S)_4]$, we found the highest nuclear repulsion energy contributions (E_n), which likely reflects the steric repulsion effects.

Table 5. Total molecular energy (E_t) with its electronic (E_e) and nuclear repulsion (E_n) energy components for the three isomers of $[OsCl_2(dmso)_4]$, scaled with respect to isomer **1**

Isomer	E_e (a.u.)	E_n (a.u.)	E_t (a.u.)
1 *trans*-$[OsCl_2(dmso\text{-}S)_4]$	0.00000	0.00000	0.00000
2 *cis*-$[OsCl_2(dmso\text{-}S)_3(dmso\text{-}O)]$	40.66623	−40.65683	0.00940
3 *cis*-$[OsCl_2(dmso\text{-}S)_4]$	−14.07069	14.07620	0.00551

Molecular Energies and Isomer Equilibration

The calculated molecular energies of 0.0, 24.7, and 14.4 kJ·mol^{-1}, for **1**, **2**, and **3**, respectively (Table 6), show that in the gas phase the isomer **1**, *trans*-$[OsCl_2(dmso\text{-}S)_4]$, exhibits the lowest energy. The molecular energy differences [$\Delta E_1 = E(\mathbf{2}) - E(\mathbf{1}) = 24.7$ kJ·mol^{-1}, $\Delta E_2 = E(\mathbf{3}) - E(\mathbf{2}) = -10.3$ kJ·mol^{-1}, $\Delta E_3 = E(\mathbf{3}) - E(\mathbf{1}) = 14.4$ kJ·mol^{-1}] are relatively small, yet they are indicative of a preference, in the isolated molecules, for all-S-bonded arrangements (**1** and **3**). On the other hand, a comparison with the experimental population ratios (**1/2/3** = 1:33:66) suggests that, in solution, solvent interactions lower the molecular energies of **2** and **3** with respect to **1**. In fact, the calculated values of ΔE_1 and ΔE_3 in $CHCl_3$ solution are 0.7 and 5.1 kJ·mol^{-1}, respectively, and −9.8 and 0.8 kJ·mol^{-1}, respectively, in DMSO (Table 7). Interestingly, the stabilisation of **2** and **3** relative to **1** increases with the increase in solvent polarity (from $CHCl_3$ to DMSO), paralleling the increase of the solvation energy, E_s (Table 7). The effect is particularly evident for **2**. We have to consider, however, that the equilibrium constant (K) between each pair of isomers is related to its free energy difference, according to the relationship $\ln K = -\Delta G/RT$, with $\Delta G = \Delta H - T\cdot\Delta S$. The term ΔE is only a part of ΔH, as shown by the equation $\Delta H = \Delta E + \Delta ZPE + \Delta H' + R\cdot T$, where ΔZPE is the difference in the zero-point vibration energy, and $\Delta H' = \Delta E_{vib} + \Delta E_{rot} + \Delta E_{trans}$ is the difference between the sums of the vibration, free rotation and translation energy contributions. In the present case, these additional terms can play an important role because of the small ΔE values. The values of ΔZPE, $\Delta H'$, and ΔS were calculated from the normal mode frequencies of the compounds, in the gas phase, on the basis

Table 4. Mulliken atomic electron charges, q [e], in the three isomers of $[OsCl_2(dmso)_4]$

Isomer	$q(Cl_1)$	$q(Cl_2)$	q(dmso-S_1)	q(dmso-S_2)	q(dmso-S_3)	q(dmso) [a]	q(Os)
1	−0.45	−0.45	0.45	0.45	0.45	0.45 ($-S_4$)	−0.90
2	−0.44	−0.44	0.30	0.39	0.39	0.24 (−O)	−0.44
3	−0.43	−0.43	0.47	0.40	0.40	0.47 ($-S_4$)	−0.88

[a] Coordinated atom in parentheses.

 © 2003 Wiley-VCH Verlag GmbH & Co. KGaA, Weinheim

of the DFT force field. From the data in Table 6 we obtained, for the isomerisation process **1** → **2**, ΔZPE = −7.6 kJ·mol^{-1}, $\Delta H'$ = 3.1 kJ·mol^{-1}, and ΔS = 35.3 J·mol^{-1}·K^{-1}, so that ΔG(298 K) = 9.7 kJ·mol^{-1} and K = 2.0·10^{-2}. For the isomerisation process **2** → **3**: ΔZPE = 7.3 kJ·mol^{-1}, $\Delta H'$ = −3.5 kJ·mol^{-1}, ΔS = −33.3 J·mol^{-1}·K^{-1}, ΔG(298 K) = 3.4 kJ·mol^{-1}, K = 2.5·10^{-1}; for the isomerisation process **1** → **3**: ΔZPE = −0.3 kJ·mol^{-1}, $\Delta H'$ = −0.4 kJ·mol^{-1}, ΔS = 2.0 J·mol^{-1}·K^{-1}, ΔG(298 K) = 13.1 kJ·mol^{-1}, K = 5.0·10^{-3}. The trend in the values of ΔS is consistent with that expected from the variation of the conformational entropy of each isomer pair. The highest value is calculated for the process **1** → **2**. In fact, in **2** there is the maximum degree of rotational freedom, while in **1** this rotation is strongly restricted because the four dmso-*S* groups are "blocked' in the equatorial plane (see the X-ray structure section above).

Table 6. Total molecular energy, E_t (kJ·mol^{-1}), in the gas phase, for the three isomers of [$OsCl_2$(dmso)$_4$], scaled with respect to isomer **1**. The zero-point vibration energy (ZPE, kJ·mol^{-1}), the sum of the vibration, free rotation, and translation energy contributions (H', kJ·mol^{-1}), and the entropy value (S, J·mol^{-1}), are also reported

Isomer		E_t (gas)	ZPE	H'	S
1	*trans*-$OsCl_2$(dmso-*S*)$_4$	0.0	877.0	77.6	731.8
2	*cis*-$OsCl_2$(dmso-*S*)$_3$(dmso-*O*)	24.7	869.4	80.7	767.1
3	*cis*-$OsCl_2$(dmso-*S*)$_4$	14.4	876.7	77.2	733.8

The above calculated equilibrium constants, however, which show a prevalence of isomer **1**, are not consistent with the experimental data (**1**/**2**/**3** = 1:33:66). Accounting for the solvation energy, E_s($CHCl_3$) (Table 7), in the calculations for the process **1** → **2**, leads to a lower value of ΔG(298 K) (−14.3 kJ·mol^{-1}), and a corresponding increase in the equilibrium constant to 3.2·10^2. In DMSO solution, because of the greater solvation energy, E_s(dmso) (Table 7), ΔG(298 K) = −24.8 kJ·mol^{-1}, with a further increase of the equilibrium constant (K = 2.2·10^4). For the process **2** → **3**, the corresponding values are ΔG(298 K) = 18.1 kJ·mol^{-1} and K = 6.6·10^{-4} in $CHCl_3$; in DMSO, ΔG(298 K) = 24.3 kJ·mol^{-1} and K = 5.4·10^{-5}. Thus, the calculations show that formation of isomers **2** and **3** is largely preferred, in chloroform and DMSO solutions, with respect to that of **1**. Complex **2** should prevail over **3**, however, for both entropy and solvent effects. In fact, to evaluate the equilibrium constants correctly, the terms ΔZPE, $\Delta H'$, and ΔS should be derived from the normal mode frequencies of the compounds calculated in solution, rather than in gas phase, which is a calculation that is somewhat problematic at present.

The different behaviour of the ruthenium analogue of **2**, *cis*-[$RuCl_2$(dmso-*S*)$_3$(dmso-*O*)], which does not isomerise to *cis*-[$RuCl_2$(dmso-*S*)$_4$], is likely related to the weaker metal−S bonds in the Ru complexes. In fact, the Os−S bond lengths are, on average, ca. 0.008 Å shorter than the corresponding Ru−S bond lengths. Furthermore, previous DFT calculations have shown that *cis*-[$RuCl_2$(dmso-*S*)$_4$] exhibits a molecular energy that is 56 kJ·mol^{-1} higher than that of *cis*-[$RuCl_2$(dmso-*S*)$_3$(dmso-*O*)],[24] while our present calculations show that in the corresponding Os derivatives this energy is 10.3 kJ·mol^{-1} lower.

The increased strength of the Os−S bonds relative to the Ru−S bonds, which is suggested by the trend of the bond lengths, is supported by the DFT calculations of the M−dmso binding energies, BE,[23] in the *cis*-MCl_2(dmso-*S*)$_3$(dmso-*O*) complexes, M = Ru and Os (Table 8). We note that all of the binding energies are higher in the Os derivative, but the energy differences are significantly larger for the M−S bonds [BE^S(Os) − BE^S(Ru) = 32.2 and 40.7 kJ·mol^{-1}, for dmso-*S*-*trans*-to-Cl and dmso-*S*-*trans*-to-O, respectively) than for the M−O bonds [BE^O(Os) − BE^O(Ru) = 11.6 kJ·mol^{-1}, for dmso-*O*-trans-to-S). Interestingly, in both the Ru and Os complexes, BE^S(dmso-*S*-*trans*-to-O) is larger than BE^S(dmso-*S*-*trans*-to-Cl), in agreement with the observed M−S1 distances (Os, 2.246 Å; Ru,[7a] 2.245 Å), which are significantly shorter than values of M−S2 and M−S3 (Figure 1) (Os, av. 2.270 Å; Ru,[7a] av. 2.279 Å).

Table 8. M−dmso binding energies, BE (kJ·mol^{-1}), for *cis*-[MCl_2(dmso-*S*)$_3$(dmso-*O*)]

M	dmso-*S* (*trans*-Cl)	dmso-*S* (*trans*-*O*)	dmso-*O* (*trans*-*S*)
Os	166.8	213.4	137.1
Ru	134.6	172.7	125.5

Conclusions

We have shown by NMR spectroscopy that at room temperature, both in light-protected $CDCl_3$ and [D_6]DMSO solutions, *cis*,*fac*-[$OsCl_2$(dmso-*S*)$_3$(dmso-O)] (**2**) equilibrates slowly with its linkage isomer, *cis*-[$OsCl_2$(dmso-*S*)$_4$] (**3**). For very long observation times in chloroform solution (16 d),

Table 7. Total molecular energy, E_t (kJ·mol^{-1}), in gas phase and in chloroform and DMSO solutions, for the three isomers of [$OsCl_2$(dmso)$_4$], scaled with respect to isomer **1**. The solvation energies of $CHCl_3$ and DMSO, E_s (kJ·mol^{-1}), are also reported

Isomer		E_t (gas)	E_t ($CHCl_3$)	E_s ($CHCl_3$)	E_t (DMSO)	E_s (DMSO)
1	*trans*-[$OsCl_2$(dmso-*S*)$_4$]	0.0	0.0	−63.6	0.0	−68.7
2	*cis*-[$OsCl_2$(dmso-*S*)$_3$(dmso-*O*)]	24.7	0.7	−87.6	−9.8	−103.2
3	*cis*-[$OsCl_2$(dmso-*S*)$_4$]	14.4	5.1	−72.9	0.8	−82.3

 © 2003 Wiley-VCH Verlag GmbH & Co. KGaA, Weinheim

a small amount of *trans*-$[OsCl_2(dmso\text{-}S)_4]$ (**1**) is also formed, with the equilibrium population ratio of **1/2/3** = 1:33:66. Crystals of **2** were obtained from DMSO solutions, while crystals of **3** were obtained from chloroform solutions, most likely because of solubility effects. As previously found for the well-known ruthenium analogues, **2** isomerises to **1** upon exposure of its solution to sunlight. On the other hand, the ruthenium analogue of **3** has never been observed. We attribute such behaviour to the greater preference of osmium(II) for S-bonding, as shown by the trend of the metal−sulfur bond lengths and the calculated metal−dmso binding energies. The molecular energies, calculated in gas phase by the DFT B3LYP method, show small differences between the three osmium isomers, with the lowest energy being exhibited by **1**, whereas, in solution, this isomer is only a minor product. Quantum chemical calculations show that the solvent plays an important role in determining the isomer stability in solution, together with conformational entropy effects. In fact, when taking into account both of these factors, the populations of **2** and **3** largely exceed that of **1**. A quantitative analysis of the isomer distribution is limited by the possibility of calculating the normal mode frequencies only in the gas phase.

Table 9. Crystal and refinement data for *cis*,*fac*-$[OsCl_2(dmso\text{-}S)_3(dmso\text{-}O)]$ (**2**)

Empirical formula	$C_8H_{24}Cl_2O_4OsS_4$
Formula mass	573.61
Cryst system	monoclinic
Space group	$P\ 2_1/n$ (No. 14)
a, Å	8.430(2)
b, Å	27.769(4)
c, Å	8.599(2)
β, deg	116.61(2)
V, Å^3	1799.7(5)
$D_{calcd.}$, g cm^{-3}	2.117
Z	4
μ (Mo-$K\alpha$), mm^{-1}	7.850
$F(000)$	1112
θ range, deg	2.80−27.10
No. of reflns. collcd.	5584
No. of indep. reflns.	3679
R_{int}	0.0536
No. of refined params.	176
goodness-of-fit (F^2)	1.029
$R1$ [$I > 2\sigma(I)$][a]	0.0577
$wR2$ [a]	0.1418
residuals, e/Å^3	2.764[b], −1.283

[a] $R1 = \Sigma||F_o| - |F_c||/\Sigma|F_o|$; $wR2 = [\Sigma w(F_o^2 - F_c^{2)2}/\Sigma w(F_o^2)^2]^{1/2}$. [b] Close to the Os atom.

Experimental Section

The complexes *trans*-$[OsCl_2(dmso\text{-}S)_4]$ (**1**) and *cis*,*fac*-$[OsCl_2(dmso\text{-}S)_3(dmso\text{-}O)]$ (**2**) were prepared as described by Antonov et al.[15]

Materials: Chemicals, including $H_2OsCl_6{\cdot}6H_2O$ and deuterated solvents, were purchased from Aldrich and used as received. Electronic absorption spectra were recorded in quartz cells with a Jasco UV/Vis V500 spectrophotometer equipped with a Peltier thermostatic unit. Infrared spectra (KBr) were obtained on a Perkin−Elmer 2000 NIR FT-Raman spectrometer. ^1H and $^{13}C\{^1H\}$ NMR spectra were collected at room temperature at 400 and 100.5 MHz, respectively, on a Jeol Eclipse 400 FT spectrometer, with 2,2-dimethyl-2,2-silapentane-5-sulfonate (DSS) as an internal standard for D_2O solutions and the residual non-deuterated solvent signals as references for spectra in $[D_6]$DMSO (δ = 2.50 ppm) and $CDCl_3$ (δ = 7.26 ppm).

Crystallography: Data collection was carried out on a Nonius DIP-1030H system, equipped with graphite monochromator and Mo-K_α radiation (λ = 0.71073 Å). A total of 30 frames were collected, each with a rotation of 6° about , exposure time of 20 min, detector positioned at 80 mm from the crystal. Cell refinement and data reduction were carried out using the programs Mosflm and Scala.[25] The crystals were found to be isomorphous with those of the ruthenium analogue.[7a] The structure was solved, however, by conventional Fourier methods, using SHELXS-97,[26] to avoid any bias toward any of the possible rotational isomers.[7] Anisotropic refinement was carried out by the full-matrix least-squares method based on F^2 using SHELXL-97.[26] All calculations were performed using the WinGX system, Ver 1.64.03.[27] Crystal data and details of the refinement are listed in Table 9. Bond lengths and angles are given in Table 1.

CCDC-205611 contains the supplementary crystallographic data for this paper. These data can be obtained free of charge at www.ccdc.cam.ac.uk/conts/retrieving.html [or from the Cambridge Crystallographic Data Centre, 12, Union Road, Cambridge CB2 1EZ, UK; Fax: (internat.) +44-1223/336-033; E-mail: deposit@ccdc.cam.ac.uk].

DFT Calculations: The calculations of the electronic structures of the osmium complexes were carried out by means of the DFT B3LYP method with a 6-31G(d,p) basis for main group elements, and with the HW effective core potential (ncore = 60) for the Os atom,[28] using the GAMESS-2001 program set.[29] Solvation energies of the compounds in chloroform solutions were calculated on the basis of the polarised continuum model.[30] Starting coordinates for the geometry optimisation were derived from the X-ray structures. The terms Δ*ZPE*, Δ*H′*, and Δ*S*, used to evaluate the values of Δ*G*, were calculated from the normal-mode frequencies of the compounds, in the gas phase, on the basis of the DFT force field.[29]

Atom and dmso-group charges for the three isomers of $OsCl_2(dmso)_4$ are reported in Table 4. The scaled total molecular energies, with their electronic and nuclear repulsion components, are listed in Table 5. The scaled total molecular energies in the gas phase, together with zero-point vibration energies, the sum of the vibration, free rotation, and translation energy contributions, and entropy values, are reported in Table 6. A comparison of the molecular energies, in the gas phase and in chloroform and DMSO solutions, are given in Table 7, together with the $CHCl_3$ and DMSO solvation energies. Table 8 gives the binding energies of dmso to Os and Ru in the *cis*-$[MCl_2(dmso\text{-}S)_3(dmso\text{-}O)]$ complexes.

Acknowledgments

This work has been supported by MIUR (Rome) (PRIN: 2001053898 004) and the Ministry of Education of the Russian Federation (grant E02-5.0-342).

 © 2003 Wiley-VCH Verlag GmbH & Co. KGaA, Weinheim

[1] See, for example: [1a] E. Alessio, M. Calligaris, M. Iwamoto, L. G. Marzilli, *Inorg. Chem.* **1996**, *35*, 2538−2545. [1b] T. Tanase, T. Aiko, Y. Yamamoto, *Chem. Commun.* **1996**, 2341−2342. [1c] E. Alessio, M. Macchi, S. L. Heath, L. G. Marzilli, *Inorg. Chem.* **1997**, *36*, 5614−5623. [1d] S. F. Lessing, S. Lotz, H. M. Roos, P. H. van Rooyen, *J. Chem. Soc., Dalton Trans.* **1999**, 1492−1502. [1e] J. J. Rack, H. B. Gray, *Inorg. Chem.* **1999**, *38*, 2−3. [1f] E. Iengo, G. Mestroni, S. Geremia, M. Calligaris, E. Alessio, *J. Chem. Soc., Dalton Trans.* **1999**, 3361−3371. [1g] M. Biagini Cingi, M. Lanfranchi, M. A. Pellinghelli, M. Tegoni, *Eur. J. Inorg. Chem.* **2000**, 703−711. [1h] E. Alessio, E. Iengo, E. Zangrando, S. Geremia, P. A. Marzilli, M. Calligaris, *Eur. J. Inorg. Chem.* **2000**, 2207−2219. [1i] E. Iengo, E. Zangrando, R. Minatel, E. Alessio, *J. Am. Chem. Soc.* **2002**, *124*, 1003−1013 and references therein.

[2] G. Sava, E. Alessio, A. Bergamo, G. Mestroni, in *Topics in Biological Inorganic Chemistry*, Volume 1, "*Metallo-pharmaceuticals*" (Eds.: M. J. Clarke, P. J. Sadler), Springer, Berlin, **1999**, pp. 143−169.

[3] [3a] P. K. L. Chan, B. R. James, D. C. Frost, P. K. H. Chan, H.-L. Hu, K. A. Skov, *Can. J. Chem.* **1989**, *67*, 508−516. [3b] P. K. L. Chan, P. K. H. Chan, D. C. Frost, B. R. James, K. A. Skov, *Can. J. Chem.* **1988**, *66*, 117−122.

[4] [4a] R. S. Srivastava, B. Milani, E. Alessio, G. Mestroni, *Inorg. Chim. Acta* **1992**, *191*, 15−17. [4b] B. R. James, R. S. McMillan, *Can. J. Chem.* **1977**, *55*, 3927−3932. [4c] B. R. James, R. S. McMillan, K. J. Reimer, *J. Mol. Catal.* **1976**, *1*, 439−441. [4d] D. P. Riley, *Inorg. Chem.* **1983**, *22*, 1965−1967.

[5] A. Mercer, J. Trotter, *J. Chem. Soc., Dalton Trans.* **1975**, 2480−2483.

[6] J. D. Oliver, D. P. Riley, *Inorg. Chem.* **1984**, *23*, 156−158.

[7] [7a] E. Alessio, G. Mestroni, G. Nardin, W. M. Attia, M. Calligaris, G. Sava, S. Zorzet, *Inorg. Chem.* **1988**, *27*, 4099−4106. [7b] J. S. Jaswal, S. J. Rettig, B. R. James, *Can. J. Chem.* **1990**, *68*, 1808−1817.

[8] [8a] G. A. Heath, A. J. Lindsay, T. A. Stephenson, *J. Chem. Soc., Dalton Trans.* **1982**, 2429−2432. [8b] M. Calligaris, P. Faleschini, E. Alessio, *Acta Crystallogr., Sect. C* **1993**, *49*, 663−666.

[9] [9a] R. S. McMillan, A. Mercer, B. R. James, J. Trotter, *J. Chem. Soc., Dalton Trans.* **1975**, 1006−1010. [9b] S. Geremia, M. Calligaris, Y. N. Kukushkin, A. V. Zinchenko, V. Yu. Kukushkin, *J. Mol. Struct.* **2000**, *516*, 49−56.

[10] [10a] J. D. Fotheringham, G. A. Heath, A. J. Lindsay, T. A. Stephenson, *J. Chem. Res. (S)* **1986**, 82−83. [10b] J. R. Barnes, R. J. Goodfellow, *J. Chem. Res. (S)* **1979**, 350−351.

[11] A. R. Davies, F. W. B. Einstein, N. P. Farrell, B. R. James, R. S. McMillan, *Inorg. Chem.* **1978**, *17*, 1965−1969.

[12] M. Calligaris, O. Carugo, *Coord. Chem. Rev.* **1996**, *153*, 83−154.

[13] [13a] E. Alessio, M. Bolle, B. Milani, G. Mestroni, P. Faleschini, S. Geremia, M. Calligaris, *Inorg. Chem.* **1995**, *34*, 4716−4721. [13b] E. Alessio, B. Milani, M. Bolle, G. Mestroni, P. Faleschini, F. Todone, S. Geremia, M. Calligaris, *Inorg. Chem.* **1995**, *34*, 4722−4734.

[14] [14a] B. Serli, E. Zangrando, E. Iengo, G. Mestroni, L. Yellowlees, E. Alessio, *Inorg. Chem.* **2002**, *41*, 4033−4043. [14b] B. Serli, E. Zangrando, E. Iengo, E. Alessio, *Inorg. Chim. Acta* **2002**, *339*, 265−272.

[15] P. G. Antonov, Y. N. Kukushkin, V. I. Konnov, Y. P. Kostikov, *Koord. Khim.* **1980**, *6*, 1585−1589.

[16] P. D. Robinson, C. C. Hinckley, A. Ikuo, *Acta Crystallogr., Sect. C* **1989**, *45*, 1079−1080.

[17] A. M. McDonagh, M. G. Humphrey, D. C. R. Hockless, *Aust. J. Chem.* **1998**, *51*, 807−811.

[18] W. M. Attia, M. Calligaris, *Acta Crystallogr., Sect. C* **1987**, *43*, 1426−1427.

[19] S. Geremia, M. Calligaris, *J. Chem. Soc., Dalton Trans.* **1997**, 1541−1547.

[20] M. F. C. Guedes da Silva, A. J. L. Pombeiro, S. Geremia, E. Zangrando, M. Calligaris, A. V. Zinchenko, V. Yu. Kukushkin, *J. Chem. Soc., Dalton Trans.* **2000**, 1363−1371.

[21] M. Calligaris, *Croat. Chem. Acta* **1999**, *72*, 147−169.

[22] M. Calligaris, P. Faleschini, F. Todone, E. Alessio, S. Geremia, *J. Chem. Soc., Dalton Trans.* **1995**, 1653−1661.

[23] N. S. Panina, M. Calligaris, *Inorg. Chim. Acta* **2002**, *334*, 165−171.

[24] M. Stener, M. Calligaris, *J. Mol. Struct. (Theochem)* **2000**, *497*, 91−104.

[25] Collaborative Computational Project, Number 4, *Acta Crystallogr., Sect. D* **1994**, *50*, 760−763.

[26] G. M. Sheldrick, SHELX97, *Programs for Structure Analysis*, University of Göttingen, **1998**.

[27] L. J. Farrugia, *J. Appl. Cryst.* **1999**, *32*, 837−838.

[28] P. J. Hay, W. R. Wadt, *J. Chem. Phys.* **1985**, *82*, 284−298.

[29] M. W. Schmidt, K. K. Baldrige, J. A. Boatz, S. T. Elbert, M. S. Gordon, J. H. Jensen, S. Koseki, N. Matsunaga, K. A. Nguen, S. J. Su, T. L. Windus, M. Dupuis, J. A. Montgomery, *J. Comput. Chem.* **1993**, *14*, 1347−1363.

[30] J. Tomasi, M. Persico, *Chem. Rev.* **1994**, *94*, 2027−2094.

Received March 10, 2003

 © 2003 Wiley-VCH Verlag GmbH & Co. KGaA, Weinheim

Polynuclear Nickel(II) Complexes: Preparation and Magnetic Properties of Ni^{II}_4, Ni^{II}_5, and Ni^{II}_6 Species with Ligands containing O∩X∩O (X = S, Se or N) Donor Atoms

Tapan K. Paine,[a] Eva Rentschler,[a] Thomas Weyhermüller,[a] and Phalguni Chaudhuri*[a]

Keywords: Magnetic properties / Nickel / Selenium / Sulfur / Tripodal ligands

A family of bisphenol-containing ligands with XO_2 donor atoms, where X = S, Se, or N, yields $[Ni^{II}]_4$ (**1**) and (**2**), $[Ni^{II}]_5$ (**3**), and $[Ni^{II}]_6$ (**4**) complexes. Complex **2**, **3**, and **4** have been structurally characterised by X-ray diffraction. The compounds were characterised spectroscopically and by variable-temperature (2–295 K), variable-field (1, 4, and 7 T) magnetic susceptibility measurements. Analysis of the magnetic data shows predominant ferromagnetic interactions between the nickel centres (S_{Ni} = 1) indicating "high-spin" ground states for **1**, **2**, and **3**, whereas complex **4** shows antiferromagnetic interactions. A plot of *J* vs. Ni–O–Ni angles for all structurally characterised Ni_4O_4 cubane cores, including **2**, irrespective of their symmetry, shows a large variation of *J* values within a small range of Ni–O–Ni angles. A simple two-*J* model was found to be adequate to describe the magnetic properties of the hexanuclear complex, **4**.
(© Wiley-VCH Verlag GmbH & Co. KGaA, 69451 Weinheim, Germany, 2003)

Introduction

There are several intriguing features associated with polynuclear transition metal complexes. Firstly, these complexes can have unusual electronic properties and may serve as sources of fundamental information about exchange coupling in multinuclear assemblies. A second general reason to study polynuclear metal complexes is that they may be building blocks for molecularly based magnetic materials. In another field of coordination chemistry, polynuclear complexes are important for the advancement of bioinorganic chemistry, both in their roles in advancing understanding of the chemistry of metallobiomolecules[1] and in the production of useful new biomimetic and bioinspired reactions. The magnetic molecular assemblies are therefore of interest for research areas as different as biochemistry and molecular magnetism.[2] These potential applications and issues have sparked and fuelled the interest of coordination chemists in synthesising molecules with large numbers of unpaired electrons in ground states. Consequently, the search for ligands capable of giving rise to molecules of high nuclearity is an important theme in modern coordination chemistry.

We have been exploring the feasibility of using phenol-containing ligands[3–6] to influence the nuclearity and topology of metal complexes. Since nickel(II) is known to have a large single-ion zero-field splitting and often gives rise to ferromagnetic coupling, we have especially focussed our attention on polynuclear nickel(II) complexes[7] with the aim of obtaining "high spin" species. Although polynuclear nickel(II) complexes containing up to four metal ions are not rare,[8–9] assemblies with five,[10] six,[11] and more[12] nickel(II) ions still remain a matter of curiosity. In this paper we report on the extension of our studies with the ligands containing the donor atoms (O, X, O), where X = S, Se, or N, and include the preparation and magnetochemical characterisation of

$[Ni^{II}_4L^S_2(\mu_3\text{-}OMe)_4(MeOH)_4(MeCN)_2]$ (**1**),
$[Ni^{II}_4L^{Se}_2(\mu_3\text{-}OMe)_4(MeOH)_4(MeCN)_2]$ (**2**),
$[Ni^{II}_5L^N_4(\mu_3\text{-}OH)_2(\mu_2\text{-}OH_2)_2(EtOH)_2]$ (**3**),

and

$[Ni^{II}_6L^N_4(\mu_2\text{-}OHMe)(\mu_3\text{-}OMe)_2(\mu_3\text{-}OH)_2(MeOH)_2(MeCN)_2]$ (**4**),

where H_2L^S is 2,2′-thiobis(4,6-di-*tert*-butylphenol), H_2L^{Se} is 2,2′-selenobis(4,6-di-*tert*-butylphenol), and H_2L^N is methylamino-*N*,*N*-bis(2-methylene-4,6-dimethylphenol).

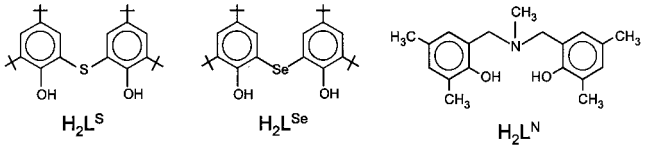

H_2L^S H_2L^{Se} H_2L^N

Results and Discussion

Depending on the solvents and the bases used during the preparations, complexes **1**–**4** were isolated in good yields (Scheme 1). The sulfur- and selenium-containing ligands, H_2L^S and H_2L^{Se}, reacted with $NiCl_2{\cdot}6H_2O$ at room tem-

[a] Max-Planck-Institut für Bioanorganische Chemie,
Stiftstrasse 34–36, 45470 Mülheim an der Ruhr, Germany
E-mail: Chaudh@mpi-muelheim.mpg.de

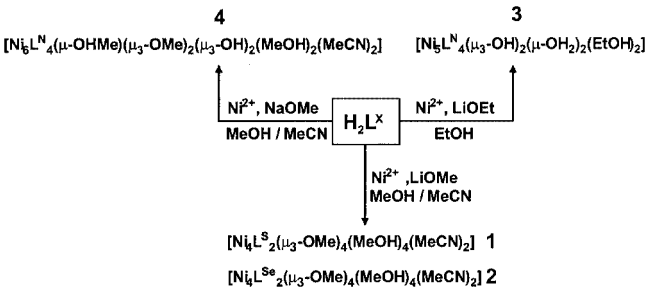

Scheme 1

perature in a solvent mixture (5:1) of methanol and acetonitrile containing $LiOCH_3$ as the base to deprotonate the phenolic −OH groups, from which complexes **1** and **2**, respectively, were isolated. On the other hand, treatment of the nitrogen-containing ligand H_2L^N with $NiCl_2{\cdot}6H_2O$ in ethanol in the presence of the base $LiOC_2H_5$ resulted in a yellow-green microcrystalline solid, which on subsequent recrystallisation from a solvent mixture (1:2) of CH_2Cl_2 and C_2H_5OH yielded pure pentanuclear material **3** in a good isolated yield of 75%. The incorporation of OH^- and H_2O in **3** presumably implies the involvement of water from the starting material. Interestingly, the isolation of the green **4**, a Ni^{II}_6 species, from a solvent mixture of methanol and acetonitrile was particularly sensitive to the use of dry solvents, although the starting material was a hydrated metal salt. This indicates that complex **4** appears in the reaction mixture only at water concentrations considerably lower than present in the case of complex **3**, and hence the absence of water as ligands in the final product **4**. That the isolated complexes **1**−**4** are thermodynamic products is shown by the reactions' insensitivity to the ligand/Ni^{II} ratios, which vary between 2:1 to 0.5:1.

Selected IR data for complexes **1**−**4** are given in the Exp. Sect. The sharp ν(OH) band around 3400 cm^{-1} for the free ligands is replaced by a broad band, indicating that the phenol character of the ligand has been lost on complexation. There are several strong bands in the 2960−2820 cm^{-1} region, due to the ν(C−H) stretchings of the *tert*-butyl groups. The weak bands in the 2300−2250 cm^{-1} region correspond to the ν(CN) vibrations of the CH_3CN molecule. The strong sharp band at 1047 cm^{-1} for both **1** and **2** is attributed to the ν(OCH_3) group of the bridging methoxide ligand.[19] The corresponding band at 1057 cm^{-1} for **4** appears as a medium band. The other ν(C−H), ν(C=C), and ν(C−O) vibrations are found in the normal ranges for these types of linkages.

Mass spectrometry in the EI and ESI mode has not proved to be a useful analytical tool for characterisation of the polynuclear Ni^{II} complexes **1**−**4**, presumably due to their decomposition at the temperatures applied in mass spectrometry.

Single-Crystal X-ray Diffraction Studies

The analytical, spectroscopic and magnetic data for **1** and **2** showed their isostructural characters, so X-ray analysis only of **2** was undertaken, to remove the doubts regarding connectivity.

Molecular Structure of 2

The crystal structure of **2** is shown in Figure 1, with selected bond lengths and angles provided in Table 1. The solid-state structure of **2**·3.5MeCN·0.5MeOH contains discrete

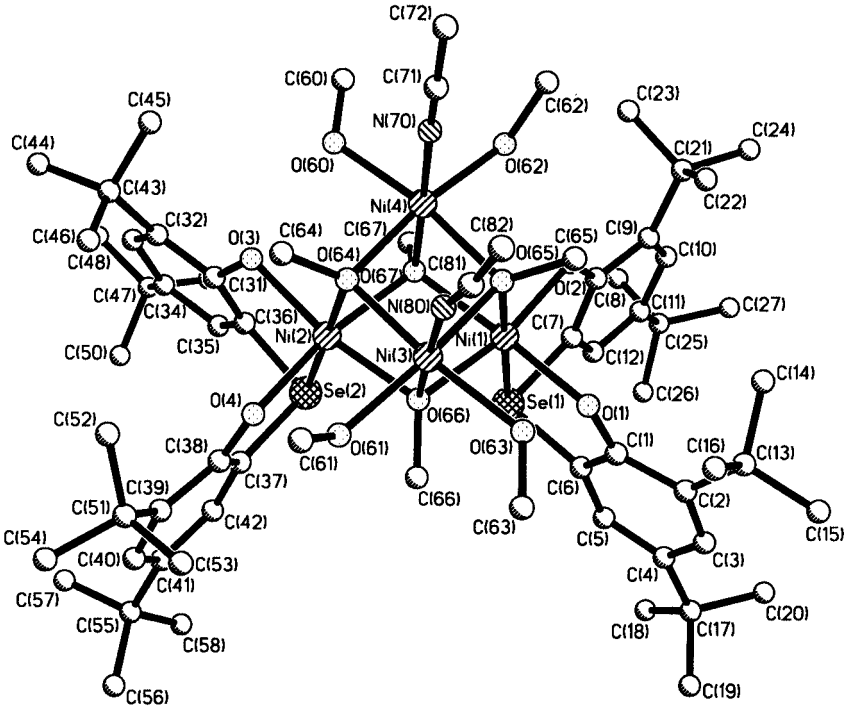

Figure 1. Molecular structure of $[Ni_4L^{Se}_2(\mu_3\text{-}OMe)_4(MeOH)_4(MeCN)_2]$ (**2**)

Table 1. Selected bond lengths [Å] and angles [deg] for $[Ni_4L^{Se}_2(\mu_3\text{-}OMe)_4(MeOH)_4(MeCN)_2]\cdot 3.5MeCN\cdot 0.5MeOH$ (**2**)

Ni(1)−O(1)	2.039(2)	O(1)−Ni(1)−O(2)	96.49(10)
Ni(1)−O(2)	2.047(2)	O(1)−Ni(1)−O(65)	90.69(9)
Ni(1)−O(65)	2.056(2)	O(2)−Ni(1)−O(65)	95.73(9)
Ni(1)−O(67)	2.073(2)	O(1)−Ni(1)−O(67)	170.61(9)
Ni(1)−O(66)	2.093(2)	O(2)−Ni(1)−O(67)	90.35(9)
Ni(1)−Se(1)	2.4452(6)	O(65)−Ni(1)−O(67)	82.20 (9)
Ni(2)−O(3)	2.054(2)	O(1)−Ni(1)−O(66)	94.52(9)
Ni(2)−O(64)	2.058(2)	O(2)−Ni(1)−O(66)	168.72(9)
Ni(2)−O(4)	2.060(2)	O(65)−Ni(1)−O(66)	81.69(9)
Ni(2)−O(66)	2.074(2)	O(67)−Ni(1)−O(66)	78.44(9)
Ni(2)−O(67)	2.082(2)	O(1)−Ni(1)−Se(1)	86.57(7)
Ni(2)−Se(2)	2.4480(6)	O(2)−Ni(1)−Se(1)	86.90(7)
Ni(3)−O(66)	2.011(2)	O(65)−Ni(1)−Se(1)	176.40(7)
Ni(3)−O(65)	2.036(2)	O(67)−Ni(1)−Se(1)	100.26(6)
Ni(3)−O(64)	2.043(2)	O(66)−Ni(1)−Se(1)	96.19(6)
Ni(3)−O(63)	2.058(3)	O(3)−Ni(2)−O(64)	92.07(9)
Ni(3)−O(61)	2.073(3)	O(3)−Ni(2)−O(4)	97.97(10)
Ni(3)−N(80)	2.074(3)	O(64)−Ni(2)−O(4)	95.42(9)
Ni(4)−O(67)	2.031(2)	O(3)−Ni(2)−O(66)	169.84(10)
Ni(4)−O(65)	2.034(2)	O(64)−Ni(2)−O(66)	82.10(9)
Ni(4)−O(64)	2.043(2)	O(4)−Ni(2)−O(66)	90.88(10)
Ni(4)−O(60)	2.054(3)	O(3)−Ni(2)−O(67)	92.34(10)
Ni(4)−N(70)	2.066(3)	O(64)−Ni(2)−O(67)	82.12(9)
Ni(4)−O(62)	2.076(3)	O(4)−Ni(2)−O(67)	169.48(10)
		O(66)−Ni(2)−O(67)	78.66(9)
		O(3)−Ni(2)−Se(2)	86.51(7)
Ni(3)−O(64)−Ni(4)	96.93(10)	O(64)−Ni(2)−Se(2)	177.83(7)
Ni(3)−O(64)−Ni(2)	95.94(10)	O(4)−Ni(2)−Se(2)	86.40(7)
Ni(4)−O(64)−Ni(2)	96.54(10)	O(66)−Ni(2)−Se(2)	99.07(6)
Ni(4)−O(65)−Ni(3)	97.44(10)	O(67)−Ni(2)−Se(2)	96.30(6)
Ni(4)−O(65)−Ni(1)	96.40(9)	O(66)−Ni(3)−O(65)	84.22(9)
Ni(3)−O(65)−Ni(1)	96.48(10)	O(66)−Ni(3)−O(64)	84.06(9)
Ni(3)−O(66)−Ni(2)	96.41(10)	O(65)−Ni(3)−O(64)	82.71(10)
Ni(3)−O(66)−Ni(1)	96.09(9)	O(66)−Ni(3)−O(63)	89.18(10)
Ni(2)−O(66)−Ni(1)	101.05(10)	O(65)−Ni(3)−O(63)	88.37(10)
Ni(4)−O(67)−Ni(1)	95.93(9)	O(64)−Ni(3)−O(63)	169.29(10)
Ni(4)−O(67)−Ni(2)	96.15(10)	O(66)−Ni(3)−O(61)	88.15(10)
Ni(1)−O(67)−Ni(2)	101.45(10)	O(65)−Ni(3)−O(61)	170.29(10)
		O(64)−Ni(3)−O(61)	90.55(10)
Ni(1)···Ni(2)	3.217(2)	O(63)−Ni(3)−O(61)	97.54(11)
Ni(1)···Ni(3)	3.052(2)	O(66)−Ni(3)−N(80)	177.73(11)
Ni(1)···Ni(4)	3.049(2)	O(65)−Ni(3)−N(80)	93.72(12)
Ni(2)···Ni(3)	3.046(2)	O(64)−Ni(3)−N(80)	96.63(12)
Ni(2)···Ni(4)	3.061(2)	O(63)−Ni(3)−N(80)	89.82(12)
Ni(3)···Ni(4)	3.058(2)	O(61)−Ni(3)−N(80)	93.99(12)
		O(67)−Ni(4)−O(65)	83.80(9)
		O(67)−Ni(4)−O(64)	83.75(9)
		O(65)−Ni(4)−O(64)	82.75(10)
		O(67)−Ni(4)−O(60)	89.06(10)
		O(65)−Ni(4)−O(60)	170.10(10)
		O(64)−Ni(4)−O(60)	89.69(10)
		O(67)−Ni(4)−N(70)	178.40(11)
		O(65)−Ni(4)−N(70)	96.09(11)
		O(64)−Ni(4)−N(70)	94.65(11)
		O(60)−Ni(4)−N(70)	90.86(12)
		O(67)−Ni(4)−O(62)	88.87(10)
		O(65)−Ni(4)−O(62)	90.73(10)
		O(64)−Ni(4)−O(62)	170.63(10)
		O(60)−Ni(4)−O(62)	95.99(11)
		N(70)−Ni(4)−O(62)	92.73(12)

tetrameric molecules of formula $[Ni_4L^{Se}_2(\mu_3\text{-}OMe)_4(MeOH)_4(MeCN)_2]$, based on a Ni_4O_4 cubane-type unit and consisting of two interpenetrating tetrahedra: one of four nickel atoms and one of four μ_3-oxygen atoms originating from bridging methoxide groups. Each Ni^{II} is in a distorted octahedral environment and bound to three μ_3-OCH_3 ligands. For Ni(1) and Ni(2), two facially coordinated $O^{\cap}Se^{\cap}O$ donor sets of the deprotonated ligands $[L^{Se}]^{2-}$ complete the sixfold coordination. Each Ni(3) and Ni(4) is coordinated to three bridging methoxide oxygens and two terminal MeOH ligands. The sixth coordination site in each nickel centre is occupied by a N-atom of a terminal MeCN molecule. Although it was not possible to locate all the hydrogen atoms in the structure, the intramolecular contacts between the oxygen atoms of the methanol molecules and the oxygen atoms of the phenolate groups of the ancillary $[L^{Se}]^{2-}$ ligand − of ca. 2.70 Å [O(1)···O(63) 2.674 Å; O(2)···O(62) 2.718 Å; O(3)···O(60) 2.702 Å; O(4)···O(61) 2.720 Å] − can be interpreted as hydrogen bonds. The intramolecular hydrogen bonds have the effect of lowering the effective symmetry of the $[Ni_4(OMe)_4]$-core from T_d *to* D_{2d}.

A similar pattern of intramolecular hydrogen bonding and structural distortions have also been observed in other alkoxide cubane complexes containing Ni^{II} and bound alcohol. The Ni−O−Ni angles in **2** vary between 95.9(1) and 101.5(1)°. The Ni···Ni distances on different cubic faces are also different, the shortest being Ni(3)···Ni(2) 3.046(2) Å and the longest Ni(1)···Ni(2) 3.217(2) Å. Average Ni−O bond lengths of 2.045 Å (phenolate) and 2.075 Å (methoxide) lie well within the range of reported[4,8] values for the corresponding bond lengths of the tetranuclear cubane-like Ni^{II}. All phenyl rings of the ligands are planar and retain their aromaticity after complexation. No substantial differences in bond lengths and angles are found between the two crystallographically independent molecules.

Molecular Structure of 3

The molecular structure of **3** is shown in Figure 2. Selected interatomic distances and bond angles are listed in Table 2. The solid-state structure of $\mathbf{3}\cdot 0.75CH_2Cl_2$ contains discrete pentanuclear molecules of formula $[Ni_5L^N_4(\mu_3\text{-}OH)_2(\mu_2\text{-}OH_2)_2(EtOH)_2]$. The structure can be regarded as a corner-shared dicubane, in which one of the corners of each cubane is missing. The pentanuclear assembly is composed of a $Ni_2-Ni-Ni_2$ array; there is a virtually twofold axis passing through the central Ni(3). There are two different types of peripheral Ni atoms: the five-coordinate Ni(2) and Ni(5) with a NO_4 square-pyramidal environment and the six-coordinate Ni(1) and Ni(4) in a distorted octahedral NO_5 environment. The peripheral metal atoms, Ni(1), Ni(2), Ni(4), and Ni(5), are bound equatorially to the deprotonated ancillary ligand $[L^N]^{2-}$. Two μ_3-hydroxide ions [O(100) for Ni(2) and O(200) for Ni(5)] act as the axial donor atoms of the square pyramids. That the donor atoms O(101) and O(201) are constituents of water molecules is discernible from the Ni−O bond lengths. Furthermore, the hydrogen atoms of the water molecules and of hydroxy groups were located from a difference map and are shown as circles of arbitrary radii in Figure 2. Two ethanol molecules, O(300) and O(400), are bound as terminal ions to Ni(1) and Ni(4), respectively, *trans* to the μ_2-OH_2 ligands.

 © 2003 Wiley-VCH Verlag GmbH & Co. KGaA, Weinheim

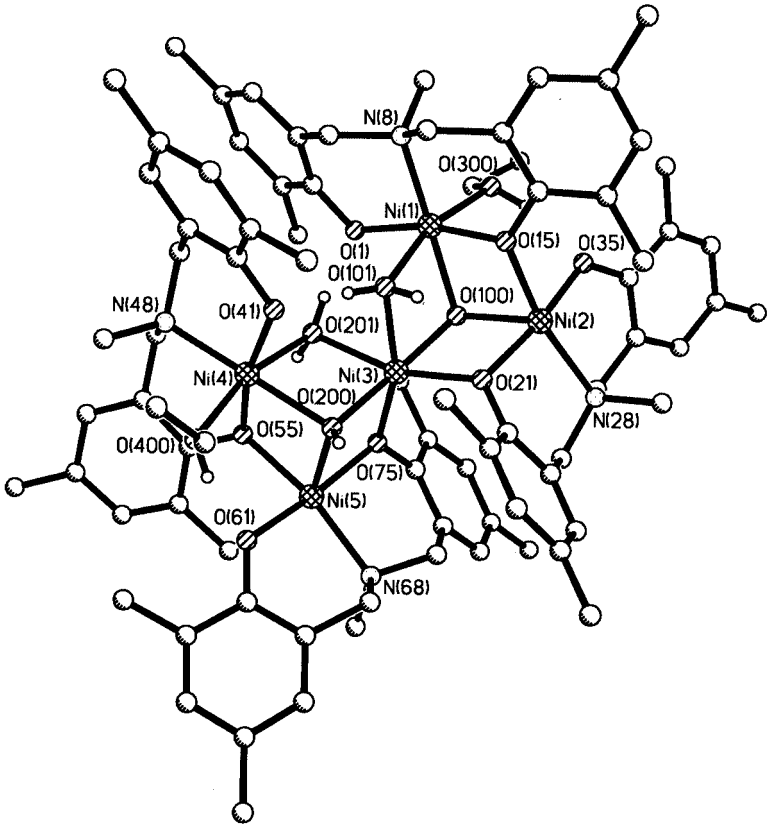

Figure 2. ORTEP representation of $[Ni_5L^N_4(\mu_3\text{-}OH)_2(\mu_2\text{-}OH_2)_2(EtOH)_2]$ (**3**)

The hydrogen atoms on the OH_2 and EtOH ligands enter into hydrogen bonding with the phenolate oxygens O(1), O(41), O(35) and O(61), with O(1)···O(201) 2.459 Å, O(41)···O(101) 2.448 Å, O(61)···O(400) 2.563 Å, and O(35)···O(300) 2.590 Å distances, thus presumably making the cluster unsusceptible to disruption. The central Ni(3) is six-coordinate, with oxygen donor atoms only. The long Ni···Ni distances (Table 2) exclude the possibility that the exchange coupling between the paramagnetic centres is transmitted directly through space. All Ni−O and Ni−N bond lengths are in conformity with the nickel ions in +II oxidation state.

Molecular Structure of 4

X-ray analysis reveals that **4** contains a Ni_6 unit and is best written as $[Ni_6L^N_4(\mu_2\text{-}OHMe)(\mu_3\text{-}OMe)_2(\mu_3\text{-}OH)_2(MeOH)_2(MeCN)_2]$, as shown in Figure 3(a). Figure 3(b) highlights the central hexanuclear core with the atom connectivity in the coordination sphere. Selected metrical parameters are given in Table 3. The structure of the Ni_6-cluster can be regarded as a face-shared distorted dicubane in which one of the corners of each cubane is missing. There is a twofold crystallographic axis passing through an oxygen atom (O60) of the bridging μ_2-methanol molecule. The nickel centres Ni(1) and Ni(1)# are five-coordinate, whereas Ni(2), Ni(3) and their symmetry related nickel centres are six-coordinate. Five-coordinated nickel centres possess square-pyramidal NO_4 geometries, with O(70) of the μ_3-OMe group as the axial ligand, whereas the six-coordinate nickel centres have NO_5 environments. The ancillary ligand $[L^N]^{2-}$, O(15), N(8) and O(1), together with the phenolate oxygen O(70) (which is a μ_2-bridging ligand) from a second ligand $[L^N]^{2-}$, form the equatorial plane for the five-coordinate Ni(1). The six-coordinate Ni(2) is bound to two μ_3-OH (O10 and O60), one μ_3-OMe (O70), one μ_2-OHMe (O60), one μ_2-phenolate (O1) and an acetonitrile (N50) ligand. On the other hand, Ni(3) is triply coordinated to the ligand $[L^N]^{2-}$ along with its monocoordination to a methanol (O80), a μ_3-hydroxide and a μ_3-methoxide group.

Magnetic Susceptibility Studies

Magnetic susceptibility data for polycrystalline samples of complexes **1**−**4** were collected in the 2−290 K temperature range in an applied magnetic field of 1 T to characterise the nature and magnitude of the exchange interaction propagated by the bridging ligands. We use the Heisenberg spin-Hamiltonian in the form $\hat{H} = -2J\,\hat{S}_A\cdot\hat{S}_B$ for an isotropic exchange coupling with $S_{Ni} = 1$ for **1**−**4**. The experimentally measured magnetic data were simulated by use of a least-squares fitting computer program[13] with a full-matrix diagonalisation of exchange coupling, Zeeman splitting, and axial single-ion zero-field interactions (DS^2_z), if necessary. The susceptibility data were corrected for diamagnetism (Pascal corrections). No temperature-independent paramagnetism (TIP) or paramagnetic impurities (PI) were used for the simulations. The experimental data are displayed in Figure 4 as the effective magnetic moment (μ_{eff})

 © 2003 Wiley-VCH Verlag GmbH & Co. KGaA, Weinheim

Table 2. Selected interatomic distances [Å] and angles [deg] for $[Ni_5L^N_4(\mu_3\text{-}OH)_2(\mu_2\text{-}OH_2)_2(EtOH)_2]\cdot 0.75\ CH_2Cl_2$ (**3**)

Ni(1)−O(1)	1.999(3)	O(1)−Ni(1)−O(15)	167.33(14)
Ni(1)−O(15)	2.047(3)	O(1)−Ni(1)−O(300)	97.52(13)
Ni(1)−O(300)	2.081(3)	O(15)−Ni(1)−O(300)	91.05(13)
Ni(1)−N(8)	2.083(4)	O(1)−Ni(1)−N(8)	92.34(15)
Ni(1)−O(100)	2.096(3)	O(15)−Ni(1)−N(8)	96.20(14)
Ni(1)−O(101)	2.159(3)	O(300)−Ni(1)−N(8)	95.07(14)
Ni(2)−O(35)	1.980(3)	O(1)−Ni(1)−O(100)	89.11(13)
Ni(2)−O(100)	2.024(3)	O(15)−Ni(1)−O(100)	81.73(12)
Ni(2)−O(15)	2.031(3)	O(300)−Ni(1)−O(100)	88.70(13)
Ni(2)−O(21)	2.044(3)	N(8)−Ni(1)−O(100)	175.75(14)
Ni(2)−N(28)	2.100(4)	O(1)−Ni(1)−O(101)	92.62(12)
Ni(3)−O(100)	2.009(3)	O(15)−Ni(1)−O(101)	77.10(12)
Ni(3)−O(200)	2.011(3)	O(300)−Ni(1)−O(101)	164.01(13)
Ni(3)−O(75)	2.097(3)	N(8)−Ni(1)−O(101)	96.84(14)
Ni(3)−O(21)	2.102(3)	O(100)−Ni(1)−O(101)	79.10(12)
Ni(3)−O(201)	2.126(3)	O(35)−Ni(2)−O(100)	93.63(13)
Ni(3)−O(101)	2.128(3)	O(35)−Ni(2)−O(15)	89.06(13)
Ni(4)−O(41)	1.999(3)	O(100)−Ni(2)−O(15)	83.91(13)
Ni(4)−O(55)	2.059(3)	O(35)−Ni(2)−O(21)	172.21(14)
Ni(4)−O(400)	2.069(4)	O(100)−Ni(2)−O(21)	78.64(12)
Ni(4)−O(200)	2.085(3)	O(15)−Ni(2)−O(21)	89.22(13)
Ni(4)−N(48)	2.087(4)	O(35)−Ni(2)−N(28)	91.50(14)
Ni(4)−O(201)	2.187(3)	O(100)−Ni(2)−N(28)	112.41(14)
Ni(5)−O(61)	1.983(3)	O(15)−Ni(2)−N(28)	163.59(14)
Ni(5)−O(200)	2.030(3)	O(21)−Ni(2)−N(28)	92.29(14)
Ni(5)−O(55)	2.046(4)	O(100)−Ni(3)−O(200)	177.78(14)
Ni(5)−O(75)	2.053(3)	O(100)−Ni(3)−O(75)	103.80(13)
Ni(5)−N(68)	2.109(5)	O(200)−Ni(3)−O(75)	77.70(13)
		O(100)−Ni(3)−O(21)	77.62(12)
Ni(2)−O(15)−Ni(1)	96.78(13)	O(200)−Ni(3)−O(21)	103.18(13)
Ni(2)−O(21)−Ni(3)	99.91(13)	O(75)−Ni(3)−O(21)	117.96(13)
Ni(5)−O(55)−Ni(4)	95.99(14)	O(100)−Ni(3)−O(201)	96.66(13)
Ni(5)−O(75)−Ni(3)	100.09(13)	O(200)−Ni(3)−O(201)	81.87(13)
Ni(3)−O(100)−Ni(2)	103.83(14)	O(75)−Ni(3)−O(201)	82.63(13)
Ni(3)−O(100)−Ni(1)	100.30(13)	O(21)−Ni(3)−O(201)	159.34(13)
Ni(2)−O(100)−Ni(1)	95.43(13)	O(100)−Ni(3)−O(101)	81.81(13)
Ni(3)−O(101)−Ni(1)	94.66(13)	O(200)−Ni(3)−O(101)	96.27(13)
Ni(3)−O(200)−Ni(5)	103.88(14)	O(75)−Ni(3)−O(101)	161.52(13)
Ni(3)−O(200)−Ni(4)	100.99(15)	O(21)−Ni(3)−O(101)	80.32(12)
Ni(5)−O(200)−Ni(4)	95.67(13)	O(201)−Ni(3)−O(101)	79.21(13)
Ni(3)−O(201)−Ni(4)	94.22(13)	O(41)−Ni(4)−O(55)	166.40(13)
Ni(1)···Ni(2)	3.049(2)	O(41)−Ni(4)−O(400)	96.86(14)
Ni(1)···Ni(3)	3.152(2)	O(55)−Ni(4)−O(400)	93.35(14)
Ni(2)···Ni(3)	3.174(2)	O(41)−Ni(4)−O(200)	89.15(13)
Ni(3)···Ni(5)	3.181(2)	O(55)−Ni(4)−O(200)	82.01(13)
Ni(3)···Ni(4)	3.160(2)	O(400)−Ni(4)−O(200)	89.24(14)
Ni(4)···Ni(5)	3.050(2)	O(41)−Ni(4)−N(48)	92.99(16)
		O(55)−Ni(4)−N(48)	95.41(16)
		O(400)−Ni(4)−N(48)	93.11(15)
		O(200)−Ni(4)−N(48)	176.61(14)
		O(41)−Ni(4)−O(201)	92.13(13)
		O(55)−Ni(4)−O(201)	76.08(13)
		O(400)−Ni(4)−O(201)	164.92(15)
		O(200)−Ni(4)−O(201)	78.77(13)
		N(48)−Ni(4)−O(201)	98.52(14)
		O(61)−Ni(5)−O(200)	92.64(14)
		O(61)−Ni(5)−O(55)	88.17(15)
		O(200)−Ni(5)−O(55)	83.69(14)
		O(61)−Ni(5)−O(75)	170.92(15)
		O(200)−Ni(5)−O(75)	78.29(13)
		O(55)−Ni(5)−O(75)	90.77(13)
		O(61)−Ni(5)−N(68)	90.97(16)
		O(200)−Ni(5)−N(68)	114.27(15)
		O(55)−Ni(5)−N(68)	162.04(15)
		O(75)−Ni(5)−N(68)	92.80(15)

versus temperature (T). The solid lines in the figure represent the simulations.

The magnetic moment μ_{eff}/molecule for **1** and **2** of 6.54 μ_B ($\chi_M{\cdot}T$ = 5.332 $cm^3{\cdot}K{\cdot}mol^{-1}$) and 6.52 μ_B ($\chi_M{\cdot}T$ = 5.233 $cm^3{\cdot}K{\cdot}mol^{-1}$), respectively, at 290 K increases monotonically with decreasing temperature, reaching a maximum at 20 K with μ_{eff} = 7.54 μ_B ($\chi_M{\cdot}T$ = 7.115 $cm^3{\cdot}K{\cdot}mol^{-1}$) for **1** and μ_{eff} = 7.15 μ_B ($\chi_M{\cdot}T$ = 6.444 $cm^3{\cdot}K{\cdot}mol^{-1}$) for **2**. Below 20 K, μ_{eff} starts to decrease, reaching a value of 6.01 μ_B ($\chi_M{\cdot}T$ = 4.60 $cm^3{\cdot}K{\cdot}mol^{-1}$) for **1** and 4.68 μ_B ($\chi_M{\cdot}T$ = 3.525 $cm^3{\cdot}K{\cdot}mol^{-1}$) for **2** at 2 K (Figure 4); it is clear that the magnetic properties of **1** and **2** are dominated by a ferromagnetic exchange interaction between four $^3A_2$ nickel(II) ions as propagated by bridging methoxides. The structural parameters of **2** strongly suggest a lower symmetry than T_d (idealised D_{2d}) for the molecule. We have assumed the same symmetry for **1**.

The most important parameter in the magnetostructural correlation of the Ni_4O_4 cubane cores has been reported in the literature[4,9i,9h,9l,9p] to be the averaged Ni−O−Ni angle of a cubane face. In accordance with the three averaged Ni−O−Ni angles of 96.2°, 97.2°, and 101.3° observed for **2**, a three-J model based on the diagram shown in Scheme 2 was used to analyse the magnetic data for **1** and **2**.

Very good fits were obtained by use of this model, the best fit parameter sets being J_1 = +2.39 cm^{-1}, J_2 = −5.77 cm^{-1}, J_3 = +6.9 cm^{-1}, g = 2.27 for **1** and J_1 = +1.05 cm^{-1}, J_2 = −4.1 cm^{-1}, J_3 = +5.5 cm^{-1}, g = 2.25 for **2**. No zero-field splitting parameter D, TIP, or PI was needed to obtain the good quality of fit shown in Figure 4 as solid lines. The differences and natures of the signs of the exchange parameters are in full agreement with the Ni−O−Ni angle correlation and support the three-J model used, which takes account of the reduced symmetry of the cubane core observed in the X-ray structure of **2**. These results for **1** and **2** thus predict a switch from ferromagnetic to antiferromagnetic coupling only for Ni−O−Ni angles above ca. 98°, as also observed by us earlier.[4] We have also plotted the observed J values for **2** and other structurally characterised $[Ni_4(OR)_4]^{4+}$ cubanes against average Ni−O−Ni angles (Figure 5 and Table 4). The solid line in Figure 5, shown only as a guide for the eyes, allows us to see that the antiferromagnetic interactions ($-J$) fall fairly well on the correlated line with respect to Ni−O−Ni angles. In contrast, the positive J values scatter appreciably.

The magnetic data indicate that **1** and **2** have complicated, low-lying magnetic structures with non-diamagnetic ground states smaller than the spin state S_t = 4 expected for a ferromagnetically coupled tetranuclear nickel(II) species (S_{Ni} = 1). We have performed magnetisation measurements at applied magnetic fields of 1, 4, and 7 T and collected most of the magnetisation data in the 2−10 K temperature range (26 data point) and only 7 data points in the 12.3−260.0 K range, which are shown in Figure 6 as plots of M/Ngβ vs. βH/kT for **1** and **2**. It is clear from Figure 6 that the saturated magnetisation value reaches a value of approximately 3.45 for **1** and 3.10 for **2** in the 2.0−2.8 K temperature range at the highest field of 7 T. Noteworthy is

 © 2003 Wiley-VCH Verlag GmbH & Co. KGaA, Weinheim

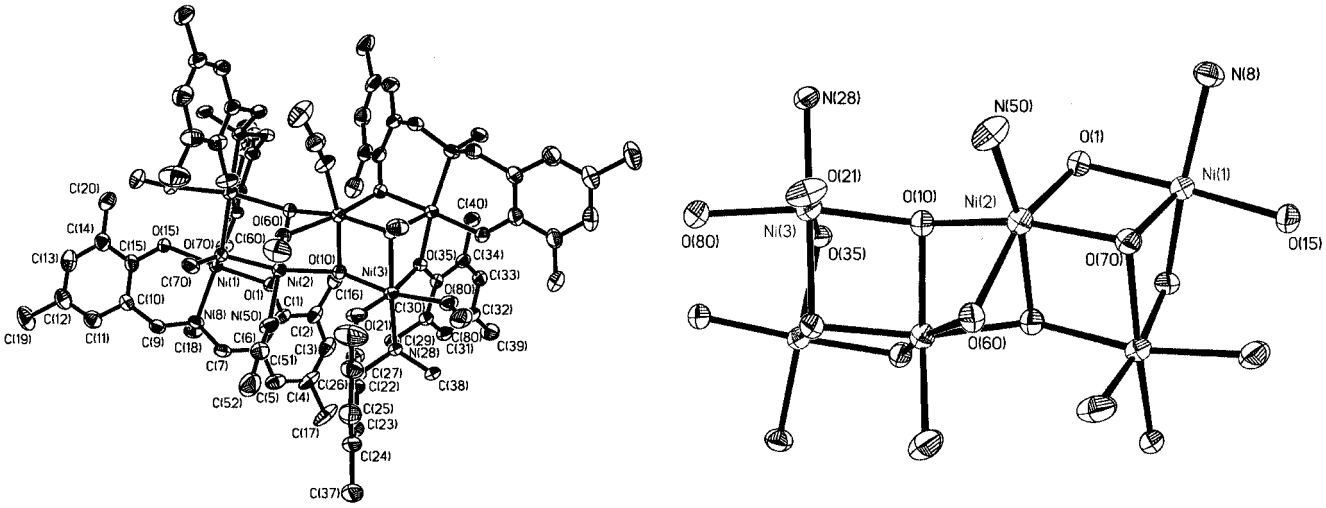

Figure 3. (a) Molecular structure of $[Ni_6L^N{}_4(\mu_2\text{-OHMe})(\mu_3\text{-OMe})_2(\mu_3\text{-OH})_2(MeOH)_2(MeCN)_2]$ (**4**); (b) a view of **4** highlighting the coordination spheres of the hexanuclear nickel core

a downward tendency of magnetisation at low temperatures and low fields, presumably due to the population of the lower component of the multiplet split in the magnetic fields.

The nature of the field dependence of the susceptibility in the present system is extreme. The first-order Zeeman splitting of the ground state $S = 4$ results in nine separate energy levels. Thus, in the absence of zero-field splittings, the energy span of the ground state is $8g\beta H$, so that at 1 T the ground state Zeeman levels span several wave numbers. It is not possible to calculate the ground state in the form of an S_t value; S is not a good quantum number to describe the ground state, but rather M_S. However, the magnetic analysis of **1** and **2** unambiguously demonstrates the overall ferromagnetic nature of the exchange interactions yielding "high-spin" ground states of $S_t > 3.0$.

The plot of μ_{eff} vs. T (Figure 4) for **3** shows the exchange coupling within the pentanuclear Ni^{II} complex to be predominantly ferromagnetic in nature. The effective magnetic moment μ_{eff} shows a maximum value of 8.52 μ_B ($\chi_M{\cdot}T$ = 9.079 $cm^3{\cdot}K{\cdot}mol^{-1}$) at 15 K and then decreases with decreasing temperature, reaching a value of 7.98 μ_B ($\chi_M{\cdot}T$ = 7.96 $cm^3{\cdot}K{\cdot}mol^{-1}$) at 5 K. The maximum μ_{eff} value of 8.52 μ_B clearly shows that both the five- and the six-coordinate nickel centres present in **3** are paramagnetic with $S_{Ni} = 1$. The maximum value of 8.52 μ_B is significantly smaller than the spin-only value of 10.95 μ_B expected for five ferromagnetically coupled Ni^{II} ions. The data were fitted by use of a two-J model based on the model shown in Scheme 3, as two different ranges of Ni−O−Ni angles of 94−96° and 100−103° prevail in **3**.

The spin-Hamiltonian used is

$$\hat{H} = -2J(\hat{S}_1{\cdot}\hat{S}_2 + \hat{S}_2{\cdot}\hat{S}_3 + \hat{S}_4{\cdot}\hat{S}_5 + \hat{S}_3{\cdot}\hat{S}_5) - 2J'(\hat{S}_1{\cdot}\hat{S}_3 + \hat{S}_3{\cdot}\hat{S}_4).$$

The best fit obtained with the parameter set $J' = +6.5$ cm^{-1}, $J = -0.24$ cm^{-1}, $g = 2.32$ is shown as a solid line in Figure 4. No zero-field splitting parameter D, TIP or PI was used to obtain the good quality of fit shown in Figure 4, suggesting that any zero-field splitting effects are small. As the value of J is very small, we checked its influence on the quality of the simulation by keeping $J = 0$ (fixed). The good quality of the simulation shown in Figure 4 could not be reproduced, indicating the importance, albeit very small, of J for the fit procedure. The spin ladder calculated by the evaluated exchange parameters exhibits clearly that the energy separation between low-lying states is very small (< 1 cm^{-1}), yielding an intermixing of the two states with $S_t = 4$ and $S_t = 5$. This is also corroborated with the magnetisation measurements at 1, 4, and 7 T, shown in Figure 6. The saturation behaviour observed at 7 T with a magnetisation value of ca. 4.5 unambiguously shows the dominant nature of the ferromagnetic coupling within the pentanuclear cluster, the nature of which is a mixture of $S_t = 4$ and $S_t = 5$ states.

Variable-temperature magnetic data for **4** (Figure 4) exhibit a steady decrease of μ_{eff} from 7.65 μ_B ($\chi_M{\cdot}T$ = 7.308 $cm^3{\cdot}K{\cdot}mol^{-1}$) at 290 K to 2.90 μ_B ($\chi_M{\cdot}T$ = 1.047 $cm^3{\cdot}K{\cdot}mol^{-1}$) at 2 K, which is indicative of an overall antiferromagnetic interaction within the hexanuclear nickel(II) complex **4**. That all five- and six-coordinate nickel(II) centres are paramagnetic with $S_{Ni} = 1$ is clearly attested to by the observed magnetic moment of μ_{eff} = 7.65 μ_B at 290 K. In accordance with the structural parameters, a three-J model, shown in Scheme 4, can be envisaged for the analysis of magnetic data.

The data were initially fit by use of g (fixed), J, J', and J'', which yielded a good fit (not shown) with $J = -1.16$ cm^{-1}, $J' = -9.11$ cm^{-1}, $J'' = -6.13$ cm^{-1}, $g = 2.269$ (fixed). To avoid overparametrisation, we did not use the zero-field splitting parameter D for the simulations. The above solution was discarded, as the Ni−O−Ni angles related to J'' are smaller than 90° and a small ferromagnetic coupling could be expected for the path. This suggested that a better fitting model should be used, so we again fitted the

 © 2003 Wiley-VCH Verlag GmbH & Co. KGaA, Weinheim

Table 4. Selected bond lengths [Å] and angles [deg] for $[Ni_6L^N_4(\mu_2\text{-OHMe})(\mu_3\text{-OMe})_2(\mu_3\text{-OH})_2(MeOH)_2(MeCN)_2]$ (**4**)

Ni(1)−O(15)	1.981(4)	Ni(1)−O(1)	2.017(4)
Ni(1)−O(35)#1[a]	2.030(4)	Ni(1)−O(70)	2.031(4)
Ni(1)−N(8)	2.121(5)	Ni(2)−O(10)	2.028(4)
Ni(2)−O(70)	2.031(4)	Ni(2)−O(1)	2.054(4)
Ni(2)−O(10)#1	2.073(4)	Ni(2)−N(50)	2.086(6)
Ni(2)−O(60)#1	2.224(9)	Ni(2)−O(60)	2.233(8)
Ni(3)−O(21)	1.989(4)	Ni(3)−O(35)	2.038(4)
Ni(3)−O(80)	2.075(5)	Ni(3)−O(10)	2.097(4)
Ni(3)−N(28)	2.101(5)	Ni(3)−O(70)#1	2.140(4)
O(15)−Ni(1)−O(1)	177.20(16)	O(15)−Ni(1)−O(35)#1	88.84(15)
O(1)−Ni(1)−O(35)#1	88.39(15)	O(15)−Ni(1)−O(70)	97.86(17)
O(1)−Ni(1)−O(70)	81.38(16)	O(35)#1−Ni(1)−O(70)	83.45(15)
O(15)−Ni(1)−N(8)	90.54(18)	O(1)−Ni(1)−N(8)	92.25(17)
O(35)#1−Ni(1)−N(8)	165.41(18)	O(70)−Ni(1)−N(8)	111.06(18)
O(10)−Ni(2)−O(70)	167.39(16)	O(10)−Ni(2)−O(1)	100.19(16)
O(70)−Ni(2)−O(1)	80.50(15)	O(10)−Ni(2)−O(10)#1	82.67(18)
O(70)−Ni(2)−O(10)#1	84.75(15)	O(1)−Ni(2)−O(10)#1	96.87(17)
O(10)−Ni(2)−N(50)	96.33(19)	O(70)−Ni(2)−N(50)	95.86(19)
O(1)−Ni(2)−N(50)	101.39(19)	O(10)#1−Ni(2)−N(50)	161.6(2)
O(10)−Ni(2)−O(60)	86.0(2)	O(70)−Ni(2)−O(60)	90.3(2)
O(1)−Ni(2)−O(60)	164.1(2)	O(10)#1−Ni(2)−O(60)	69.2(2)
N(50)−Ni(2)−O(60)	92.4(3)		
O(21)−Ni(3)−O(35)	171.31(16)	O(21)−Ni(3)−O(80)	96.2(2)
O(35)−Ni(3)−O(80)	87.87(18)	O(21)−Ni(3)−O(10)	91.09(18)
O(35)−Ni(3)−O(10)	83.68(16)	O(80)−Ni(3)−O(10)	168.10(17)
O(21)−Ni(3)−N(28)	94.36(18)	O(35)−Ni(3)−N(28)	93.27(18)
O(80)−Ni(3)−N(28)	90.36(18)	O(21)−Ni(3)−O(70)#1	91.79(16)
O(35)−Ni(3)−O(70)#1	80.60(15)	O(80)−Ni(3)−O(70)#1	88.86(16)
O(10)−Ni(3)−O(70)#1	81.52(15)	N(28)−Ni(3)−O(70)#1	173.85(18)
N(28)−Ni(3)−O(10)	98.46(17)		
Ni(1)−O(70)−Ni(3)#1	94.93(16)	Ni(2)−O(70)−Ni(3)#1	96.80(15)
Ni(2)−O(70)−Ni(1)	99.07(17)	Ni(2)#1−O(60)−Ni(2)	78.6(3)
Ni(1)#1−O(35)−Ni(3)	98.20(17)	Ni(1)−O(1)−Ni(2)	98.76(17)
Ni(2)#1−O(10)−Ni(3)	96.85(17)	Ni(2)−O(10)−Ni(3)	144.5(2)
Ni(2)−O(10)−Ni(2)#1	86.98(16)		
Ni(1)···Ni(2)	3.091(2)		
Ni(2)···Ni(3)	3.929(2)		
Ni(2)···Ni(2)#1	2.823(2)		
Ni(2)···Ni(3)#1	3.119(2)		
Ni(1)···Ni(3)#1	3.074(2)		

[a] #1 indicates the symmetry-related atom.

data with use of three different exchange parameters, but with the following constraints: g, J, and J' free for reiteration but J'' fixed between zero and a small positive value of +2.0. The quality of fit became poor, but the exchange values vary negligibly between −1.79 and −1.95 cm^{-1} for J and between −9.0 and −8.93 cm^{-1} for J', indicating that although J'' has some influence on the quality of fit, J and J' are nearly independent of J''. We therefore started another simulation, making all four parameters free to move. The quality of fit increased dramatically, yielding the following parameters: $g = 2.295$, $J = -1.15$ cm^{-1}, $J' = -9.87$ cm^{-1}, and $J'' = -9.66$ cm^{-1}. As the evaluated values for J' and J'' are nearly the same, we carried out the magnetic analysis with the constraint $J' = J''$ (i.e., a two-J model to reduce the number of fit parameters). A very good fit obtained with the parameter set $g = 2.295$, $J = -1.12$ cm^{-1} and $J' = J'' = -9.77$ cm^{-1} is shown as a solid line in Figure 4. We note that the sign of the exchange parameter J'' is not in line with the commonly accepted Ni−O−Ni angle correlation; this might be due to three different competitive exchange couplings operating on Ni(2) and Ni(2)* making the correlation more complex. Irrespective of that, the two-J model suitably describes the magnetic properties of complex **4**, which does not possess a well separated ground state of $S_t = 0$, as would be expected for an antiferromagnetically coupled hexanuclear Ni^{II} complex; the excited state of $S_t = 1$ is energetically very close to the ground state, and so a non-zero magnetic moment is observed even at 2 K. This is also corroborated by the variable-temperature magnetisation curves at 1, 4, and 7 T (Figure 6).

 © 2003 Wiley-VCH Verlag GmbH & Co. KGaA, Weinheim

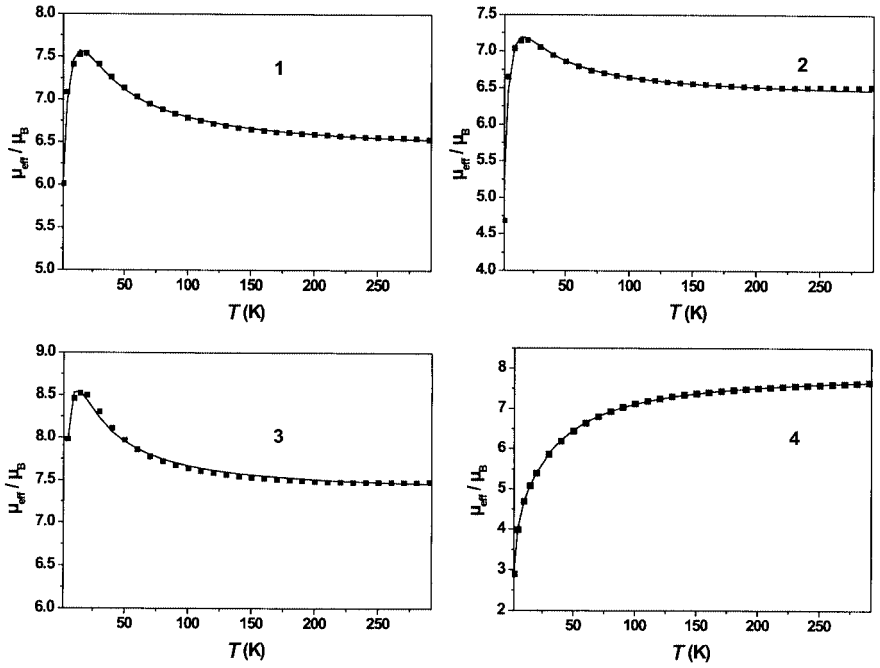

Figure 4. Plots of μ_{eff} vs. T for solid **1**−**4**; the solid lines represent the best fit of the data to the exchange coupling model

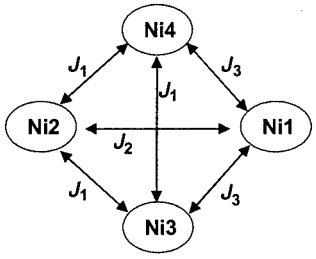

Scheme 2

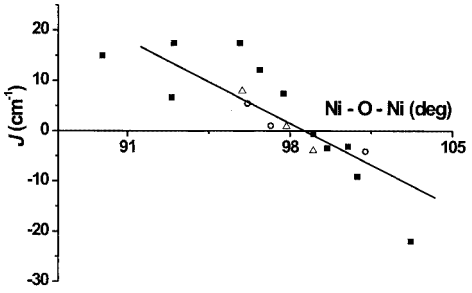

Figure 5. A plot of average Ni−O−Ni angles vs. the exchange interactions (*J*); filled squares are literature data, triangles are from ref.[4] and open circles are from this work; the solid line is drawn only as a guide

Concluding Remarks

The tridentate bisphenol ligands used in this work give rise to polynuclear nickel(II) complexes of different nuclearity: four, five or six, depending on the heterodonor atoms such as S, Se, or N. The S- and Se-containing ligands H_2L^S and H_2L^{Se} coordinate facially with five-membered chelation to a metal centre, whereas the N-containing ligand H_2L^N forms six-membered chelate rings and, presumably as a consequence of the ring size, the ligand H_2L^N coordinates meridionally. This different geometrical coordination mode seems to yield tetranuclear complexes with H_2L^S and H_2L^{Se}, but H_2L^N results in penta- and hexanuclear complexes. Thus, our starting goal of preparing polynuclear complexes with ferromagnetic exchange coupling has been partly achieved, although the hexanuclear nickel(II) complex does not belong to the class of molecules with large spin ground states.

Complexes **1** and **2** exhibit overall ferromagnetic interactions, producing ground states with "large spins". The *J* values obtained here are similar to those found for other $[Ni_4(\mu_3\text{-}OR)_4]^{4+}$ cubanes reported in the literature[9] (Table 4). The coupling between the nickel(II) ions is very close to the crossover point between antiferromagnetic and ferromagnetic coupling. In all cases, bond angles of less than ca. 98° produce ferromagnetic coupling, whilst those that are larger give rise to antiferromagnetic coupling. This correlation is similar to that in the bridged Cu−O−Cu systems,[14] in which ferromagnetic pathways of the form[15] $e_g \perp O \perp e_g$ are found to be most effective for Cu−O−Cu angles smaller than 97.5°.

Complex **2** contains the low-symmetry cubane core $[Ni_4(\mu_3\text{-methoxide})_4]^{4+}$ with differing Ni···Ni distances and Ni−O−Ni angles, resulting in three types of Ni_2O_2 faces. The observation of three discrete exchange parameters for **2** is consistent with the lower symmetry of the cubane; the symmetry of **2** is lower than that in the majority of the nickel-cubanes reported in the literature. Figure 5 shows a plot of *J* vs. Ni−O−Ni angles for all structurally characterised Ni_4O_4 cubane cores, irrespective of their symmetry; it exhibits a large variation of *J* values within a small span of Ni−O−Ni angles (90−103°). This figure also indicates that

 © 2003 Wiley-VCH Verlag GmbH & Co. KGaA, Weinheim

Table 5. J as a function of the Ni−O−Ni angles for the $[Ni_4(\mu_3\text{-}OR)_4]$ cubanes

Complex[a]	Ni−O−Ni$_{av}$ (deg)	J (cm^{-1})	Reference
$[Ni_4(\mu_3\text{-}OMe)_4(sal)_4(EtOH)_4]$	97.73	7.46	[9a,9b]
$[Ni_4(\mu_3\text{-}OH)_4(chta)_4(NO_3)_4]$	99.0	−0.57	[9c,9h]
$[Ni_4(\mu_3\text{-}OMe)_4(TMB)_4(\mu\text{-}O_2CMe)_4]$	93.0 100.9	17.5	[9e]
$[Ni_4(\mu_3\text{-}OH)_4(tzdt)_4(py)_4]$	95.89 103.2	17.5	[9i]
$[Ni_4(\mu_3\text{-}OMe)_4(dbm)_4(MeOH)_4]$	96.7 99.6	2.2	[9l]
$[Ni_4(\mu_3\text{-}OH)_2(pypentO)(pym)\text{-}(\mu\text{-}OAc)_2(NCS)_2(OH_2)]$	89.9 92.9 100.5	15.0 6.7 −3.09	[9p]
$[Ni_4(\mu_3\text{-}OMe)_2(LH)_2(OAc)_2(MeOH)_2]$	95.94 97.85 99.0	8.0 1.0 −3.8	[4]
$[Ni_4(\mu_3\text{-}OMe)_4(L^{Se})_2(MeOH)_2(MeCN)_2]$	96.17 97.17 101.25	5.50 1.05 −4.1	this work this work this work

[a] salH = salicylaldehyde; chta = *r*-1-*c*-3-*c*-5 triaminocyclohexane; TMB = 2,5-dimethyl-2,5-diisocyanohexane; dzdt = 1,3-thiazolidine-2-thione; dbmH = dibenzoylmethane; py = pyridine; pypentO = 1,5-bis[2-pyridylmethyl)amino]-3-pentanolate; pym = 2-pyridylmethoxide; L = a dinucleating Schiff-base ligand.

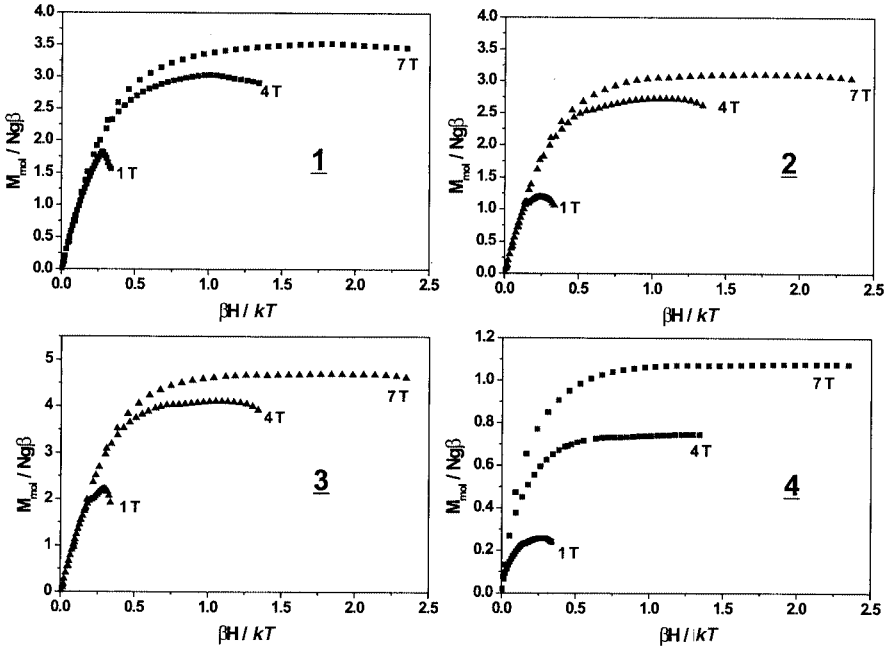

Figure 6. The field-dependent magnetisations of **1**−**4** as a function of temperature

the symmetry of the cubane core has a profound effect on the magnetostructural correlation. In particular, the scattering of the positive J values is noteworthy. This is not surprising in view of the high tolerance attached in general to the positive J values (ferromagnetic interactions) evaluated through simulation of the susceptibility data. The syn-

 © 2003 Wiley-VCH Verlag GmbH & Co. KGaA, Weinheim

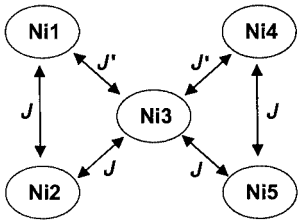

Scheme 3

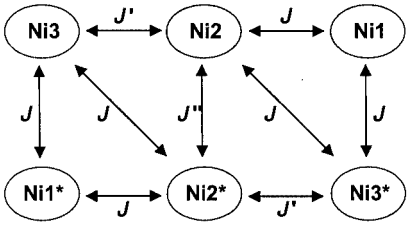

Scheme 4

thesis of more such distorted cubane-type Ni^{II} complexes would therefore be warranted in order to resolve this problem of magnetostructural correlation.

In the literature, there are only two examples of pentanuclear Ni^{II} complexes in which all five metal centres are paramagnetic with $S_{Ni} = 1$. The first example, $[Ni_5(en)_4(\mu_3\text{-}OH)_2(NO_2)_8]$,[10g] reported as early as 1981, contains a planar, pentameric arrangement of nickel(II) ions, linked by bridging hydroxide and nitrite ligands; unfortunately no magnetic data were reported. In the second example,[10a] four six-coordinate Ni^{II} ions are arranged at the apices of a tetrahedron with the fifth nickel at the centre; the compound is antiferromagnetically coupled with an admixed ground state of $S_t = 0, 1$. *Complex* **3** *constitutes the first example of a pentanuclear* Ni^{II} *complex exhibiting ferromagnetic interactions with an intermixed ground state of* $S_t = 5.0$ *and 4.0.* Pentanuclear nickel(II) complexes with five $S_{Ni} = 1$ centres still belong to the rare examples of coordination complexes.

An apparently trivial modification of the reaction, use of a mixed solvent medium, resulted in the isolation of complex **4**, a hexanuclear Ni^{II} complex, under reaction conditions otherwise the same as those used for complex **3**. The amount of water present in the reaction mixture is decisive for the isolation of complex **4**. The central nickel centres, Ni(2) and Ni(2)#, are primarily devoid of coordination to the ancillary ligand $[L^N]^{2-}$. In complex **4**, and also in **3**, the ligand $[L^N]^{2-}$ also for the first time shows the bridging functionality through one of its phenolate oxygens. The magnetic studies exhibiting predominantly antiferromagnetic exchange between the metal centres are disappointing in view of the original expectation of large-spin ground states. A simple two-*J* model shows good agreement with experimentally ascertained low-temperature magnetic data. The sign of an exchange coupling parameter J'' (-9.77 cm^{-1}) cannot be correlated with the corresponding Ni−O−Ni angles, which are appreciably smaller than 90°.

Experimental Section

Materials and Physical Measurements: Commercial grade chemicals were used for synthetic purposes, and solvents were distilled and dried before use. Fourier transform infrared spectroscopy on KBr pellets was performed on a Perkin−Elmer 2000 FT-IR instrument. Solution electronic spectra were measured on a Perkin−Elmer Lambda 19 spectrophotometer. Mass spectra were recorded either in the EI or the ESI (in CH_2Cl_2) modes with a Finnigan MAT 95 or 8200 spectrometer. Magnetic susceptibilities of the polycrystalline samples were recorded on a SQUID magnetometer (MPMS, Quantum Design) in the 2−290 K temperature range, with an applied field of 1 T. Diamagnetic contributions were estimated for each compound by use of Pascal's constants.

X-ray Crystallographic Data Collection and Refinement of the Structures: Single crystals of **2**, **3**, and **4** were coated with perfluoropolyether, picked up with glass fibres, and mounted on a Nonius Kappa-CCD diffractometer equipped with a cryogenic nitrogen cold stream operating at 100(2) K. Graphite monochromated Mo-K_α radiation ($\lambda = 0.71073$ Å) was used. Intensity data were corrected for Lorentz and polarisation effects. The intensity data set of **2** and **3**, were corrected for absorption by use of the program Gaussian face-indexed, whereas that of **4** was not corrected. The Siemens SHELXTL software package (G. M. Sheldrick, Universität Göttingen) was used for solution, refinement, and depiction of the structure, and neutral atom scattering factors of the program were used. All structures were solved and refined by direct methods and difference Fourier techniques. Non-hydrogen atoms were refined anisotropically, and hydrogen atoms were placed at calculated positions and refined as riding atoms with isotropic displacement parameters. Details of the data collection and structure refinements are summarised in Table 5.

CCDC-204445 (**2**), -204446 (**3**), and -204447 (**4**) contain the supplementary crystallographic data for this paper. These data can be obtained free of charge at www.ccdc.cam.ac.uk/conts/retrieving.html [or from the Cambridge Crystallographic Data Centre, 12, Union Road, Cambridge CB2 1EZ, UK; Fax: (internat.) +44-1223/336-033; E-mail: deposit@ccdc.cam.ac.uk].

Ligand Synthesis: The ligands H_2L^S [16] and H_2L^N [3,17] were synthesised by the published procedures. The ligand H_2L^{Se} was synthesised by a modification of the method described in the literature.[18]

2,2′-Selenobis(4,6-di-*tert*-butylphenol) (H_2L^{Se}): A suspension of 2,4-di-*tert*-butylphenol (61.89 g, 0.3 mol) and SeO_2 (11.1 g, 0.1 mol) in conc. HCl (55 mL) was heated at 80 °C with constant stirring for 2 h. The mixture was then cooled, extracted with $CHCl_3$ (3×100 mL), washed with brine solution (2×50 mL) and then with water (100 mL), dried with Na_2SO_4 and concentrated in vacuo. The crude brown product was then recrystallised from heptane and MeOH (1:1) to obtain a pure white compound. Yield: 18.5 g (25%). Melting Point: 141 °C. $C_{28}H_{42}SeO_2$ (489.6 g/mol): calcd. C 68.69, H 8.65; found C, 68.7, H 8.7%. ^{1}H NMR ($CDCl_3$): δ = 1.20 (s, 18 H); 1.38 (s, 18 H); 6.25 (s, OH, 2 H); 7.24 (m, 4 H) ppm. ^{13}C NMR ($CDCl_3$): δ = 29.5 (s, *tert*-butyl); 31.6 (s, *tert*-butyl); 34.3 (s, *tert*-butyl); 35.2 (s, *tert*-butyl); 117.0 (s), 125.4 (s); 129.6 (s); 135.7 (s); 143.3 (s), and 151.6 (s) ppm. MS (EI): The desired molecular ion ($M^+ = 490$) was observed in the ratio calculated for the naturally abundant isotope mixture of Se-74, 76, 77, 80, and 82.

General Method of Synthesis for Complexes 1 and 2: The ligand (1 mmol) was dissolved in a mixture of MeOH (12.5 mL) and

 © 2003 Wiley-VCH Verlag GmbH & Co. KGaA, Weinheim

Table 5. Crystallographic data for $[Ni_4L^{Se}_2(\mu_3\text{-}OMe)_4(MeOH)_4(MeCN)_2]\cdot 3.5MeCN\cdot 0.5MeOH$ (**2**), $[Ni_5L^{N}_4(\mu_3\text{-}OH)_2(\mu_2\text{-}OH_2)_2(EtOH)_2]\cdot 0.75CH_2Cl_2$ (**3**), and $[Ni_6L^{N}_4(\mu_2\text{-}OHMe)(\mu_3\text{-}OMe)_2(\mu_3\text{-}OH)_2(HOMe)_2(MeCN)_2]$ (**4**)

	Ni^{II}_4 **2**	Ni^{II}_5 **3**	Ni^{II}_6 **4**
Empirical formula	$C_{68}H_{114}N_2Ni_4O_{12}Se_2\cdot 3.5CH_3CN\cdot 0.5CH_3OH$	$C_{80}H_{110}N_4Ni_5O_{14}\cdot 0.75CH_2Cl_2$	$C_{85}H_{118}N_6Ni_6O_{15}$
Molecular mass	1704.08	1708.96	1816.11
Temperature	100(2) K	100(2) K	100(2) K
Wavelength (Mo-K_α)	0.71073 Å	0.71073 Å	0.71073 Å
Crystal system	Triclinic	Monoclinic	Monoclinic
Space group	$\bar{P}$	$P2_1/c$	$C2/c$
Unit cell dimensions	a = 15.4538(6) Å b = 16.6106(8) Å c = 18.2370(10) Å α = 90.31(1)° β = 108.99(1)° γ = 105.71(1)°	a = 20.6988(8) Å b = 25.7220(8) Å c = 17.8131(6) Å β = 111.65(1)°	a = 20.6998(12) Å b = 15.0379(9) Å c = 28.599(2) Å β = 110.98(1)°
Volume [Å^3]; Z	4238.7(4); 2	8814.9(5); 4	8312.2(9); 4
Density (calcd.) [Mg/m^3]	1.335	1.288	1.451
Absorption coefficient [mm^{-1}]	1.791	1.153	1.399
F(000)	1796	3606	3832
Crystal size [mm]	0.26 × 0.25 × 0.11	0.19 × 0.14 × 0.13	0.07 × 0.04 × 0.04
θ range for data collect.	4.09 to 28.50°	2.92 to 23.00°	2.11 to 24.00°
Reflections collected	96465	62882	20329
Independent reflect.	21433 [R(int.) = 0.0802]	12227 [R(int.) = 0.0938]	[6529 [R(int.) = 0.0694]
Absorption correction	Gaussian, face indexed	Gaussian, face indexed	not corrected
Data/restraints/param.	21321/150/873	12227/36/1030	6529/0/519
Goodness-of-fit on F^2	1.031	1.056	1.016
Final R indices [$I > 2\sigma(I)$]	R_1 = 0.0538; wR_2 = 0.1277	R_1 = 0.0509; wR_2 = 0.1287	R_1 = 0.0587; wR_2 = 0.1193
R indices (all data)	R_1 = 0.0851; wR_2 = 0.1441	R_1 = 0.0710; wR_2 = 0.1416	R_1 = 0.1069; wR_2 = 0.1402

MeCN (2.5 mL). LiOMe (1 M methanolic solution, 2 mL, 2 mmol) was added, and the solution was stirred for 5 min. $NiCl_2\cdot 6H_2O$ (0.24 g, 1 mol) was added to that yellow solution, and the resulting green solution was stirred for 5 min and then kept for slow evaporation of solvent under air. A green crystalline compound separated overnight.

$[Ni_4L^{S}_2(\mu\text{-}OMe)_4(MeOH)_4(MeCN)_2]$ (1): Yield: 0.42 g (58%). $C_{68}H_{114}S_2O_{12}Ni_4N_2$ (1450.54): calcd. C 56.31, H 7.92, S 4.42, N 1.93, Ni 16.18; found C 55.7, H 7.9, S 4.3, N 2.0, Ni 15.7%. IR: $\tilde{\nu}$ = 3423 cm^{-1} (br), 2957−2818 (s), 2315−2253, 1432 (s), 1298 (s), 1047 (s), 829, 731.

$[Ni_4L^{Se}_2(\mu\text{-}OMe)_4(MeOH)_4(MeCN)_2]$ (2): Yield: 0.34 g (44%). $C_{68}H_{114}Se_2O_{12}Ni_4N_2$ (1544.34): calcd. C 52.89, H 7.44, Ni 15.20; found C 49.6, H 7.3, Ni 14.9%. IR: $\tilde{\nu}$ = 3404 cm^{-1} (br), 2954−2821 (s), 2315−2253, 1429 (s), 12989 (s), 1047 (s), 828, 724.

$[Ni_5L^{N}_4(\mu_3\text{-}OH)_2(\mu\text{-}H_2O)_2(EtOH)_2]\cdot 0.75CH_2Cl_2$ (3): The ligand (1 mmol, 0.30 g) was dissolved in EtOH (15 mL). LiOEt (1 M methanolic solution, 2 mL, 2 mmol) was added, and the solution was stirred for 5 min. $NiCl_2\cdot 6H_2O$ (0.24 g, 1 mol) was added to the yellow solution, and the resulting light green solution was stirred under air. The separated yellowish green microcrystalline compound was filtered and dried. X-ray-quality crystals were grown from a solvent mixture (1:2) of CH_2Cl_2 and EtOH. Yield: 0.32 g (75%). $C_{80}H_{140}N_4O_{14}Ni_5\cdot 0.75CH_2Cl_2$ (1708.96): calcd. C 56.75, H 6.58, N 3.28, Ni 17.17; found C 56.9, H 6.7, N 3.2, Ni 17.4. IR: $\tilde{\nu}$ = 3510 cm^{-1} (br), 2915 (s), 1477 (s), 1263 (s), 1162, 801, 648, 451.

$[Ni_6L^{N}_4(\mu\text{-}MeOH)(\mu_3\text{-}OMe)_2(\mu_3\text{-}OH)_2(MeOH)_2(MeCN)_2]$ (4): The ligand (0.5 mmol, 0.15 g) was treated with NaOMe (2 mL, 0.5 M methanolic solution) in a solvent mixture of MeCN (3 mL) and MeOH (15 mL). $NiCl_2\cdot 6H_2O$ (0.12 g, 0.5 mmol) was added, and the light green solution was kept at room temperature. A green crystalline complex separated out overnight. Yield: 0.11 g (49%). $C_{85}H_{118}N_6O_{15}Ni_6$ (1816.04): calcd. C 56.22, H 6.55, N 4.63, Ni 19.39; found C 53.3, H 6.3, N 3.9, Ni 19.2. IR: $\tilde{\nu}$ = 3448 cm^{-1} (br), 2918 (s), 1475 (s), 1266 (s), 1057, 802, 453.

Acknowledgments

Financial support from the DFG, the Max-Planck Society and Fonds der Chemischen Industrie is gratefully acknowledged. Thanks are due to Mrs. H. Schucht, Mrs. R. Wagner, and Mr. A. Göbels for skilful technical assistance.

[1] For selected examples see: [1a] L. Que Jr., W. Tolman, *Angew. Chem.* **2002**, *114*, 1160; *Angew. Chem. Int. Ed.* **2002**, *41*, 1114. [1b] V. Mahadevan, R. J. M. Klein Gebbink, T. D. P. Stack, *Cur. Opin. Chem. Biol.* **2000**, *4*, 228. [1c] J. Du Bois, T. J. Mizoguchi, S. J. Lippard, *Coord. Chem. Rev.* **2000**, 200−202, 443. [1d] *Multicopper Oxidases* (Ed.: A. Messerschmidt), World Scientific, Singapore, **1997**. [1e] *Bioinorganic Chemistry of Copper* (Eds.: K. D. Karlin, Z. Tyeklar), Chapman & Hall, New York, **1993**.

[2] See for example: [2a] "*Journal of Solid State Chemistry*", Vol. 159, No. 2, July **2001** − a tribute to Olivier Kahn. [2b] *Magnetic Molecular Materials* (Eds.: D. Gatteschi, O. Kahn, J. S. Miller, F. Palacio), Kluwer, Dordrecht, The Netherlands, **1991**.

[3] T. Weyhermüller, T. K. Paine, E. Bothe, E. Bill, P. Chaudhuri, *Inorg. Chim. Acta* **2002**, *337*, 344.

[4] S. Mukherjee, T. Weyhermüller, E. Bothe, K. Wieghardt, P. Chaudhuri, *Eur. J. Inorg. Chem.* **2003**, 863.

[5] S. Mukherjee, T. Weyhermüller, E. Bothe, P. Chaudhuri, *Eur. J. Inorg. Chem.* **2003**, 1956.

[6] R. Siefert, T. Weyhermüller, P. Chaudhuri, *J. Chem. Soc., Dalton Trans.* **2000**, 4656.

[7] V. V. Pavlishchuk, F. Birkelbach, T. Weyhermüller, K. Wieghardt, P. Chaudhuri, *Inorg. Chem.* **2002**, *41*, 4405.

[8] Selected examples: [8a] K. S. Murray, *Adv. Inorg. Chem.* **1995**, *43*, 261. [8b] V. V. Pavlishchuk, S. V. Kolotilov, A. W. Addison, M. J. Prushan, D. Schollmeyer, L. K. Thompson, E. A. Goreshnik, *Angew. Chem. Int. Ed.* **2001**, *40*, 4734. [8c] J. M. Cle-

 © 2003 Wiley-VCH Verlag GmbH & Co. KGaA, Weinheim

mente-Juan, H. Andres, J. J. Borrás-Almenar, E. Coronado, H. U. Güdel, M. Eebersold, G. Kearly, H. Büttner, M. Zolliker, *J. Am. Chem. Soc.* **1999**, *121*, 10021. [8d] A. Escuer, R. Vincente, S. B. Kumar, F. A. Mautner, *J. Chem. Soc., Dalton Trans.* **1998**, 3473. [8e] H. Adams, S. Clunas, D. E. Fenton, *Chem. Commun.* **2002**, 418. [8f] M. Du, X.-H. Bu, Y.-M. Guo, L. Zhang, D.-Z. Liao, J. Ribas, *Chem. Commun.* **2002**, 1478. [8g] T. K. Karmakar, S. K. Chandra, J. Ribas, G. Mostafa, T. H. Lu, B. K. Ghosh, *Chem. Commun.* **2002**, 2364.

[9] [9a] J. E. Andrew, A. B. Blake, *J. Chem. Soc., A* **1969**, 1456. [9b] J. A. Barnes, W. E. Hatfield, *Inorg. Chem.* **1971**, *10*, 2355. [9c] B. Aurivillius, *Acta Chem. Scand., Ser. A* **1977**, *31*, 501. [9d] J. A. Bertrand, C. Marabella, D. G. Vanderveer, *Inorg. Chim. Acta* **1978**, *26*, 113. [9e] W. L. Gladfelter, M. W. Lynch, W. P. Schaefer, D. N. Hendrickson, H. B. Grey, *Inorg. Chem.* **1981**, *20*, 2390. [9f] F. Paap, E. Bouwman, W. L. Driessen, R. A. G. de Graaf, J. Reedijk, *J. Chem. Soc., Dalton Trans.* **1985**, 737. [9g] K. Bizilj, S. G. Hardin, B. F. Hoskins, P. J. Oliver, E. R. T. Tiekink, G. Winter, *Aust. J. Chem.* **1986**, *39*, 1035. [9h] P. D. Boyd, R. L. Martin, G. Schwarzenbach, *Aust. J. Chem.* **1988**, *41*, 1449. [9i] L. Ballester, E. Coronado, A. Gutiérrez, A. Monge, M. F. Perpinán, E. Pinilla, T. Rico, *Inorg. Chem.* **1992**, *31*, 2053. [9j] A. J. Atkins, A. J. Blake, M. Schröder, *J. Chem. Soc., Chem. Commun.* **1993**, 1662. [9k] A. J. Blake, E. K. Brechin, A. Codron, R. O. Gould, C. M. Grant, S. Parsons, J. M. Rawson, R. E. P. Winpenny, *J. Chem. Soc., Chem. Commun.* **1995**, 1983. [9l] M. A. Halcrow, J.-S. Sun, J. C. Huffman, G. Christou, *Inorg. Chem.* **1995**, *34*, 4167. [9m] M. S. E. Fallah, E. Rentschler, A. Caneschi, D. Gatteschi, *Inorg. Chim. Acta* **1996**, *247*, 231. [9n] A. Escuer, M. Font-Bardiá, S. B. Kumar, X. Solans, R. Vicente, *Polyhedron* **1999**, *18*, 909. [9o] M. L. Tong, H. K. Lee, S.-L. Zheng, X.-M. Chen, *Chem. Lett.* **1999**, 1087. [9p] J. M. Clemente-Juan, B. Chansou, B. Donnadieu, J.-P. Tuchagues, *Inorg. Chem.* **2000**, *39*, 5515.

[10] [10a] V. Tangoulis, C. P. Raptopoulou, A. Terzis, E. G. Bakalbassis, E. Diamantopoulou, S. P. Perlepes, *Inorg. Chem.* **1998**, *37*, 3142. [10b] S.-J. Shieh, C.-C. Chou, G.-H. Lee, C.-C. Wang, S.-M. Peng, *Angew. Chem. Int. Ed. Engl.* **1997**, *36*, 56. [10c] C. S. Velazquez, T. F. Baumann, M. M. Olmsted, H. Hope, A. G. Barrett, B. M. Hoffman, *J. Am. Chem. Soc.* **1993**, *115*, 9997. [10d] D. Fenske, H. Krautscheid, M. Müller, *Angew. Chem. Int. Ed. Engl.* **1992**, *31*, 321. [10e] B. K. Koo, E. Block, H. Kang, S. Liu, J. Jubieta, *Polyhedron* **1988**, *7*, 1397. [10f] M. Knege, G. Henkel, *Z. Naturforsch., Teil B* **1987**, *42*, 1121. [10g] A. J. Finney, M. A. Hitchman, C. L. Raston, G. L. Rowbottom, A. H. White, *Aust. J. Chem.* **1981**, *34*, 2139. [10h] F. Cecconi, C. A. Ghilardi, S. Midollini, A. Orlandini, A. Vacca, *Inorg. Chem. Commun.* **2000**, *3*, 276. [10i] C-Y. Yeh, Y. L. Chiang, G.-H. Lee, S.-M. Peng, *Inorg. Chem.* **2002**, *41*, 4096. [10j] T. Sheng, X. Wu, W. Zhang, Q. Wang, X. Gao, P. Lin, *Chem. Commun.* **1998**, 263. [10k] H. Adams, S. Clunas, D. E. Fenton, D. N. Towers, *J. Chem. Soc., Dalton Trans.* **2002**, 3933.

[11] [11a] P. Woodward, L. F. Dahl, E. W. Abel, B. C. Crosse, *J. Am. Chem. Soc.* **1965**, *87*, 5251. [11b] F. A. Cotton, B. H. Winquist, *Inorg. Chem.* **1969**, *8*, 1304. [11c] G. E. Lewis, C. S. Kraihanzel, *Inorg. Chem.* **1983**, *22*, 2895. [11d] A. Cornia, A. C. Fabretti, D. Gatteschi, G. Palyi, E. Rentschler, O. I. Shchegolikhina, A. A. Zhadanov, *Inorg. Chem.* **1995**, *34*, 5383. [11e] E. K. Brechin, W. Clegg, M. Murrie, S. Parsons, S. J. Teat, R. E. P. Winpenny, *J. Am. Chem. Soc.* **1998**, *120*, 7365.

[12] [12a] R. E. P. Winpenny, *Adv. Inorg. Chem.* **2001**, *52*, 1 and references cited therein. [12b] E. Diamantopoulou, C. P. Raptopoulou, A. Terzis, V. Tangoulis, S. P. Perlepes, *Polyhedron* **2002**, *21*, 2117. [12c] J. Faus, F. Lloret, M. Julve, J. M. Clemente-Juan, M. C. Munoz, X. Solans, M. Font-Bardia, *Angew. Chem. Int. Ed. Engl.* **1996**, *35*, 1485. [12d] I. G. Dance, M. L. Scudder, R. Secomb, *Inorg. Chem.* **1985**, *24*, 1201. [12e] M. Murrie, H. Stoeckli-Evans, H. U. Güdel, *Angew. Chem. Int. Ed.* **2001**, *40*, 1957.

[13] [13a] F. Birkelbach, C. Krebs, V. Staemmler, unpublished, Bochum, Germany, **1997**. [13b]D. Gatteschi, L. Pardi, *Gazz. Chim. Ital.* **1993**, *123*, 231.

[14] W. E. Hatfield, *Comments, Inorg. Chem.* **1981**, *1*, 105.

[15] A. P. Ginsberg, *Inorg. Chim. Acta Rev.* **1971**, *5*, 45.

[16] S. D. Pastor, J. D. Spivack, L. P. Steinhuebel, *J. Heterocycl. Chem.* **1984**, *21*, 1285.

[17] N. N. Timosheva, A. Chandrasekharan, R. O. Day, R. R. Holmes, *Inorg. Chem.* **1998**, *37*, 4945.

[18] T. Thompson, S. D. Pastor, G. Rihs, *Inorg. Chem.* **1999**, *38*, 4163.

[19] [19a] L. A. P. M. Hall, *Polyhedron* **1990**, *9*, 2575. [19b] V. Tangoulis, C. P. Raptopoulou, S. Paschalidou, A. E. Tsohos, E. G. Bakalbassis, A. Terzis, S. P. Perlepes, *Inorg. Chem.* **1997**, *36*, 5270.

Received March 27, 2003

 © 2003 Wiley-VCH Verlag GmbH & Co. KGaA, Weinheim

Mononuclear Rhodium(I) Complexes with Chelating *N*-Heterocyclic Carbene Ligands − Catalytic Activity for Intramolecular Hydroamination

Suzanne Burling,[a] Leslie D. Field,*[a] Hsiu L. Li,[a] Barbara A. Messerle,[b] and Peter Turner[a]

Keywords: Rhodium / Carbene ligands / Homogeneous catalysis / Hydroamination

The mononuclear cationic Rh^I complexes $[Rh(cod)(mdd)]^+X^-$ and $[Rh(CO)_2(mdd)]^+X^-$ (X = BPh_4, PF_6) containing the chelating bidentate *N*-heterocyclic carbene ligand 1,1′-methylene-3,3′-dimethyldiimidazoline-2,2′-diylidene (mdd) have been synthesised and spectroscopically characterised. The complexes $[Rh(cod)(mdd)]^+BPh_4^-$ and $[Rh(CO)_2(mdd)]^+PF_6^-$ have also been characterised by X-ray crystallography. The dicarbonyl complexes catalyse the intramolecular hydroamination of 4-pentyn-1-amine to 2-methyl-1-pyrroline.

(© Wiley-VCH Verlag GmbH & Co. KGaA, 69451 Weinheim, Germany, 2003)

Introduction

In 1991, Arduengo[1] synthesised and characterised the first crystalline carbene 1,3-di-1-adamantylimidazol-2-ylidene. Since then, there has been a resurgence of interest in metal complexes containing *N*-heterocyclic carbene ligands, fuelled by reports of their ability to increase catalyst activity in a range of catalytic reactions.[2,3] Our interest in Rh complexes with chelating *N*-heterocyclic carbene ligands stemmed from the synthesis of a successful hydroamination catalyst[4] $[Rh(bim)(CO)_2]^+BPh_4^-$ **1** [bim = bis(*N*-methylimidazol-2-yl)methane]; a carbene analogue might influence the catalytic activity.

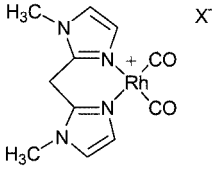

X = BPh_4 **1**
PF_6 **6**

Reactions of Rh^I precursors such as $[RhCl(cod)]_2$ or $[Rh(OEt)(cod)]_2$ (cod = 1,5-cyclooctadiene) with bidentate *N*-heterocyclic carbenes (or their precursor imidazolium halide salts) have produced dinuclear complexes where two rhodium metals are bridged by the bidentate carbene ligand.[5,6] These reactions are probably driven by the inherent insolubility of the dinuclear products. Similar reactions in the presence of OAc^- and I^- gave the mononuclear complexes, although the rhodium metal was oxidised from Rh^I to Rh^{III} [7] and the mechanism for this oxidation is as yet unknown.

In this paper, we report the successful synthesis and characterisation of mononuclear Rh^I complexes with chelating bidentate *N*-heterocyclic carbene ligands and initial studies into their activity as hydroamination catalysts.

Results and Discussion

The mononuclear Rh^I complexes were synthesised using a modification of the sodium ethoxide method introduced by Köcher et al.[6] (Scheme 1). $[RhCl(cod)]_2$ was treated with NaOEt and the product $[Rh(OEt)(cod)]_2$ was washed with methanol to remove residual chloride. The halide-free $[Rh(OEt)(cod)]_2$ was reacted with 1,1′-methylene-3,3′-dimethyldiimidazolium bis(tetraphenylborate) to form predominantly the mononuclear Rh carbene complex $[Rh(cod)(mdd)]^+BPh_4^-$ (**2**; mdd = 1,1′-methylene-3,3′-dimethyldiimidazoline-2,2′-diylidene). The removal of all

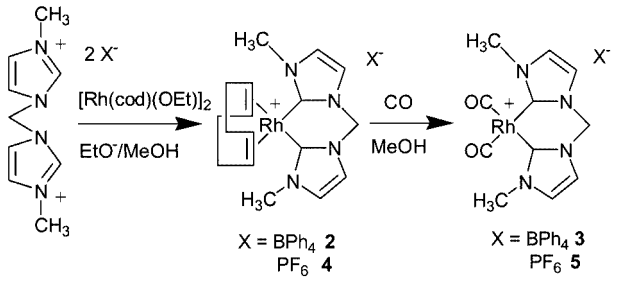

X = BPh_4 **2**
PF_6 **4**

X = BPh_4 **3**
PF_6 **5**

Scheme 1

[a] School of Chemistry, University of Sydney, New South Wales 2006, Australia
Fax: (internat.)+ 61-2/9351-5758
E-mail: l.field@chem.usyd.edu.au
[b] School of Chemical Sciences, University of New South Wales, New South Wales 2052, Australia

halide from the reaction mixture is the simple and effective key to the formation of the mononuclear complex rather than the dinuclear complex containing bridging mdd ligands. The reaction, however, was complicated by the formation of an off-white, sparingly soluble by-product which was difficult to remove. The by-product was identified as the zwitterionic compound [Rh(cod)(η^6-PhBPh$_3$)] by the four IR bands at 1478, 1458, 1426 and 1395 cm^{-1} characteristic of coordinated tetraphenylborate.[8] Complex **2** was isolated as a microanalytically pure compound after careful recrystallisation from acetone. Further reaction of **2** with carbon monoxide gas formed the Rh dicarbonyl complex [Rh(CO)$_2$(mdd)]$^+$BPh$_4^-$ (**3**). The hexafluorophosphate analogues [Rh(cod)(mdd)]$^+$PF$_6^-$ (**4**) and [Rh(CO)$_2$(mdd)]$^+$PF$_6^-$ (**5**) were synthesised in similar reactions. In the synthesis of complex **4**, it is essential to use halide-free [Rh(OEt)(cod)]$_2$ to avoid the formation of the dinuclear complex.

The ^{1}H NMR spectra of the cod complexes **2** and **4** show two separate resonances for the backbone methylene protons with a geminal splitting of 13.0 Hz, whilst the dicarbonyl complexes **3** and **5** show only a singlet for the corresponding protons. The magnetic inequivalence of the methylene protons in the cod complexes probably arises from rigidity of the non-planar metallacyclic ring imposed by the steric bulk of the cod ligand, whereas the methylene protons in the dicarbonyl complexes are more fluxional and exchange rapidly on the NMR timescale. The ^{13}C{^{1}H} NMR spectra for cod complexes **2** and **4** show the carbene resonances at δ = 181 ppm with $^1J_{Rh,C}$ in the range 52−53 Hz. The cod resonances also exhibit coupling to Rh with coupling constant values of about 8 Hz. The carbene resonances for dicarbonyl complexes **3** and **5** appear at δ = 174 ppm with $^1J_{Rh,Carbene}$ of about 45 Hz, whilst the carbonyl carbons appear at δ = 189 ppm with $^1J_{Rh,CO}$ of 57 Hz. The assignment of the carbonyl resonances was confirmed when solutions of the complexes were placed under an atmosphere of ^{13}C-labelled CO gas. There is exchange between bound and free CO and the carbonyl resonances increase in intensity relative to all resonances. The value of $^1J_{Rh,CO}$ (57 Hz) is somewhat smaller than that for the corresponding bim complexes and other related bidentate nitrogen-donor complexes where the one-bond coupling is typically in the range 66−69 Hz.[4,9] Two strong IR stretches for ν(CO) were observed for complexes **3** and **5** at 2071−2076 and 2014−2017 cm^{-1}, consistent with the *cis* geometry of the complexes.

X-ray Crystallography

A single-crystal X-ray diffraction analysis of an orange tabular section excised under a polarising microscope from a contact twinned crystal mass (grown from a concentrated [D$_6$]acetone solution at 300 K), confirmed the structure of [Rh(cod)(mdd)]$^+$BPh$_4^-$ (**2**). An ORTEP[10,11] depiction of the cation is shown in Figure 1 and selected bond lengths and angles are listed in Table 1. The structure was modelled as a pseudo-centrosymmetric structure, with $P2_1/m$ symmetry broken by a lack of mirror symmetry in the cyclooctadiene ligand. The complex molecule is bisected by a (pseudo) mirror plane, with the Rh metal and methylene carbon C(12) located in that plane. The six-membered metallacyclic ring as defined by Rh(1), C(9), N(1), C(12), N(1*) and C(9*) is boat-like with Rh and methylene carbon deviations from the boat plane of 0.94 Å and 0.58 Å, respectively. The Rh-carbene bond length [2.025(3) Å] agrees well with that found in non-chelated Rh(cod)(carbene) complexes such as [RhCl(cod)(diy)] and [Rh(cod)(diy)$_2$]Cl (diy = 1,3-dimethylimidazoline-2-ylidene) [2.023(2)−2.059(8) Å].[5,12] The Rh-cod distances [2.171(6)−2.244(6) Å] are also similar to the corresponding distances in [RhCl(cod)(diy)] and [Rh(cod)(diy)$_2$]Cl [2.095(2)−2.205(2) Å].

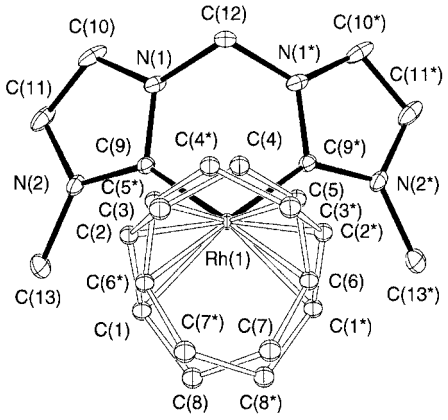

Figure 1. An ORTEP[10,11] depiction of the cation of [Rh(cod)(mdd)]$^+$BPh$_4^-$ (**2**) showing 20% displacement ellipsoids and cod ligand disorder about a (pseudo) mirror plane (see main text and Exp. Sect.); atoms labelled with an asterisk are generated from the unique sites by x, 3/2 − y, z

Single crystal X-ray diffraction analysis of an orange columnar-like crystal (grown from a methanol/diethyl ether solution) confirmed the structure of [Rh(CO)$_2$(mdd)]$^+$PF$_6^-$ (**5**). An ORTEP[10,11] depiction of the cation is shown in Figure 2 and selected bond lengths and angles are listed in Table 1. The asymmetric unit in the crystal structure of complex **5** contains the complex molecule and its hexafluorophosphate counterion, both of which are bisected by a mirror plane passing through Rh(1), C(5), P(1), F(3) and F(4). The complex has a boat-like metallacyclic ring as defined by Rh(1), C(2), N(1), C(5), N(1*) and C(2*) with Rh and methylene carbon deviations from the boat plane of 0.88 Å and 0.59 Å respectively. The Rh-carbene bond length [2.062(2) Å] is similar to that reported for [Rh(CO)(diy)$_2$Cl][13] [2.049(4) Å and 2.047(4) Å]. The Rh-carbonyl bond length [1.892(2) Å] is marginally longer than those in analogous Rh complexes with N-donor bidentate ligands [1.79(1)−1.868(7) Å].[9]

Hydroamination Catalysts

Cationic Rh^{I} complexes with chelating N-donor ligands are known to catalyse intramolecular hydroamination of aminoalkynes,[4] amino alcohols and amino carboxylic acids.[14] At a catalyst loading of 1.5%, both complexes

 © 2003 Wiley-VCH Verlag GmbH & Co. KGaA, Weinheim

Table 1. Selected bond lengths (Å) and angles (°) for $[Rh(cod)(mdd)]^+BPh_4^-$ (**2**) and $[Rh(CO)_2(mdd)]^+PF_6^-$ (**5**)

Atoms	Bond lengths (Å)	Atoms	Bond angles (°)
		[Rh(cod)(mdd)]$^+BPh_4^-$ 2	
Rh(1)−C(9)	2.025(3)	C(9)−Rh(1)−C(9*[a])	83.19(19)
Rh(1)−C(5)	2.171(6)	N(1)−C(9)−N(2)	103.0(3)
Rh(1)−C(6)	2.221(6)		
Rh(1)−C(1)	2.243(7)		
Rh(1)−C(2)	2.244(6)		
		[Rh(CO)$_2$(mdd)]$^+PF_6^-$ 5	
Rh(1)−C(1)	1.8924(17)	C(1)−Rh(1)−C(1*[b])	92.01(9)
Rh(1)−C(2)	2.0619(16)	C(2)−Rh(1)−C(2*[b])	83.48(8)
O(1)−C(1)	1.1373(19)	N(1)−C(2)−N(2)	104.3(1)

[a] x, 3/2 − y, z. [b] x, 1/2 − y, z.

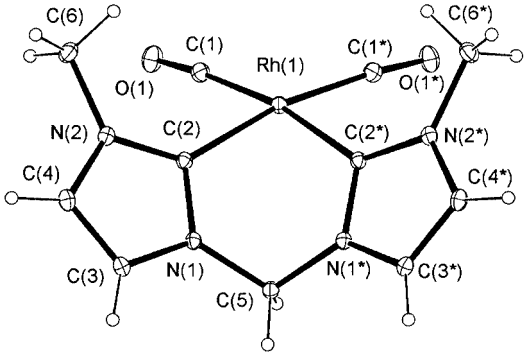

Figure 2. An ORTEP[10,11] depiction of the cation of $[Rh(CO)_2(mdd)]^+PF_6^-$ **5** showing 20% displacement ellipsoids. Atoms labelled with an asterisk are generated from the unique sites by x, 1/2 − y, z

$[Rh(CO)_2(mdd)]^+BPh_4^-$ (**3**) and $[Rh(CO)_2(mdd)]^+PF_6^-$ (**5**) catalyse the cyclisation of 4-pentyn-1-amine to 2-methyl-1-pyrroline (76% and 85% conversion, respectively, in 16 hours at 60 °C in $[D_8]$THF solution). Turnover rates[15] at 50% conversion of 6 h^{-1} and 10 h^{-1} were calculated for complexes **3** and **5** respectively (Scheme 2). The reaction rate for complex **3** was slower than that observed for the analogous bisimidazolylmethane complex $[Rh(bim)(CO)_2]^+BPh_4^-$ (**1**) (Figure 3), where conversion was complete after 12 hours (turnover rate 17 h^{-1}). In contrast, the reaction rate for complex **5** was significantly faster than that observed for $[Rh(bim)(CO)_2]^+PF_6^-$ (**6**) where the conversion was only 49% complete after 16 hours (turnover rate 2 h^{-1}) at the same catalyst loading under the same reaction conditions. Complex **6** is the PF_6^- analogue of **1**. The synthesis of **6** is analogous to that reported for the synthesis of **1**.[4]

In comparing the two carbene complexes, the PF_6^- complex **5** has a higher turnover rate for the conversion of 4-

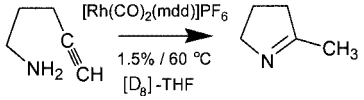

Scheme 2

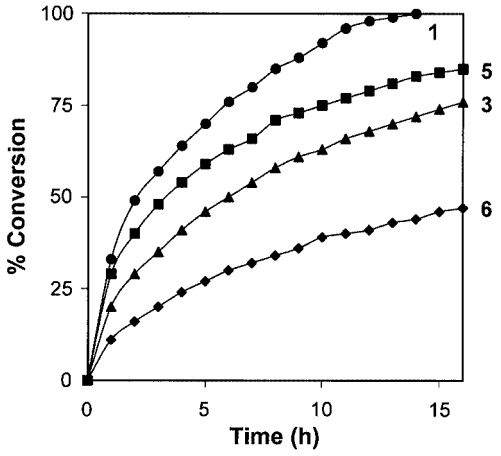

Figure 3. Comparative reaction rates for the metal-catalysed cyclisation of 4-pentyn-1-amine to 2-methyl-1-pyrroline using $[Rh(CO)_2(mdd)]^+BPh_4^-$ **3** (▲), $[Rh(CO)_2(mdd)]^+PF_6^-$ **5** (■), $[Rh(bim)(CO)_2]^+PF_6^-$ **6** (◆), and $[Rh(bim)(CO)_2]^+BPh_4^-$ **1** (●); catalyst loading 1.5% at 60 °C in $[D_8]$THF solution

pentyn-1-amine to 2-methyl-1-pyrroline than the corresponding BPh_4^- complex **3**. The dependence of the turnover rate on the counterion has also been noted previously with related catalysts and this could be the result of significant ion pairing in solution.

Conclusions

A synthetic route to mononuclear Rh^I complexes containing the bidentate bis-carbene ligand 1,1′-methylene-3,3′-dimethyldiimidazoline-2,2′-diylidene (mdd) has been developed. The complexes are robust and two Rh complexes containing the mdd ligand have been structurally characterised. Both complexes show the presence of a boat-like six-membered metallacycle containing two metal-carbon bonds. $[Rh(mdd)(CO)_2]^+$ is catalytically active for the intramolecular cyclisation of aminoalkynes and the turnover rate is similar to $[Rh(bim)(CO)_2]^+$ and other related catalysts for this conversion. Reaction conditions for this conversion are as yet unoptimised and these results demonstrate the future potential of rhodium carbenes in a range of catalytic applications.

 © 2003 Wiley-VCH Verlag GmbH & Co. KGaA, Weinheim

Experimental Section

All manipulations of metal complexes and air-sensitive reagents were carried out using standard Schlenk or vacuum techniques or in a Vacuum Atmospheres nitrogen-filled drybox. $RhCl_3 \cdot H_2O$ was purchased from Strem and used as received. $[RhCl(cod)]_2$ was prepared by the literature method.[16] 1,1′-Methylene-3,3′-dimethyldiimidazolium dibromide was synthesised by a modification of the literature procedure for the analogous diiodide salt.[17] All bulk compressed gases were obtained from BOC Gases. Nitrogen (> 99.5%) and carbon monoxide (> 99.5%) were used as supplied without further purification.

Tetrahydrofuran and diethyl ether were stored over sodium wire and distilled under nitrogen from sodium benzophenone ketyl. Methanol was distilled from magnesium methoxide under nitrogen. Acetone was distilled from calcium sulfate under nitrogen. Deuterated solvents for NMR purposes were obtained from Merck and Cambridge Isotopes. Solvents were dried over suitable drying agents, degassed using three consecutive freeze-pump-thaw cycles and vacuum distilled immediately prior to use.

Microanalyses were carried out at the Campbell Microanalytical Laboratory, University of Otago, New Zealand. Electrospray mass spectra were recorded on a Finnigan LCQ mass spectrometer. Infra-red spectra were obtained using a Perkin−Elmer 1600 Series F.T.I.R. spectrometer as KBr discs.

NMR spectra were recorded on Bruker Avance DPX 300 or DRX 400 spectrometers at 300 K. ^1H and ^{13}C NMR chemical shifts (δ/ppm) were referenced to internal solvent resonances. ^{31}P NMR chemical shifts were referenced to external neat trimethyl phosphite, taken to be at δ = 140.85 ppm. ^{19}F NMR chemical shifts were externally referenced to neat hexafluorobenzene, taken to be at δ = −163 ppm.

Synthesis of $[mddH_2]^{2+}$ $2BPh_4^-$: Sodium tetraphenylborate (2.0 g, 5.9 mmol) was added to a solution of 1,1′-methylene-3,3′-dimethyldiimidazolium dibromide (1.0 g, 3.0 mmol) in water (20 mL). The white precipitate formed was isolated by filtration and dried in vacuo overnight. 1,1′-Methylene-3,3′-dimethyldiimidazolium bis(tetraphenylborate) was recrystallised from acetone/diethyl ether as a white solid (1.4 g, 58%), m.p. 218 °C (dec). $C_{57}H_{54}B_2N_4$ (816.69): calcd. C 83.8, H 6.7, N 6.9; found C 83.7, H 6.8, N 6.9. ^1H NMR ([D$_6$]acetone, 400 MHz): δ = 8.75 (s, 2 H, NCHN), 7.75 (d, $^3J_{H,H}$ = 1.6 Hz, 2 H, NCH), 7.53 (d, $^3J_{H,H}$ = 1.6 Hz, 2 H, NCH), 7.48 (m, 16 H, *o*-H), 6.93 (t, $^3J_{H,H}$ = 7.3 Hz, 16 H, *m*-H), 6.77 (t, $^3J_{H,H}$ = 7.3 Hz, 8 H, *p*-H), 6.50 (s, 2 H, NCH_2), 3.81 (s, 6 H, NCH_3) ppm. $^{13}C\{^1H\}$ NMR ([D$_6$]acetone, 101 MHz): δ = 164.9 (q, $^1J_{C,B}$ = 49.3 Hz, *ipso*-C), 138.4 (NCHN), 136.9 (*o*-C), 126.1 (*m*-C), 126.0 (NCH), 122.9 (NCH), 122.3 (*p*-C), 59.8 (NCH_2), 37.1 (NCH_3) ppm.

Synthesis of $[mddH_2]^{2+}$ $2PF_6^-$: A solution of 1,1′-methylene-3,3′-dimethyldiimidazolium dibromide (2.6 g, 7.7 mmol) in water (15 mL) was added to a solution of potassium hexafluorophosphate (2.9 g, 15 mmol) in water (50 mL). The precipitate was isolated by filtration, washed with diethyl ether and dried in vacuo overnight to give 1,1′-methylene-3,3′-dimethyldiimidazolium bis(hexafluorophosphate) as a white solid (2.8 g, 77%), m.p. 200 °C. $C_9H_{14}F_{12}N_4P_2$ (468.24): calcd. C 23.1, H 3.0, N 12.0; found C 23.1, H 3.2, N 11.7. ^1H NMR ([D$_6$]acetone, 300 MHz): δ = 9.37 (s, 2 H, NCHN), 8.05 (s, 2 H, NCH), 7.84 (s, 2 H, NCH), 7.02 (s, 2 H, NCH_2), 4.10 (s, 6 H, NCH_3) ppm. $^{13}C\{^1H\}$ NMR ([D$_6$]acetone, 75 MHz): δ = 139.1 (NCHN), 126.0 (NCH), 123.2 (NCH), 60.1 (NCH_2), 37.2 (NCH_3) ppm. ^{19}F NMR ([D$_6$]acetone, 282 MHz): δ = −70.9 (d, $^1J_{P,F}$ = 708 Hz) ppm. ^{31}P NMR ([D$_6$]acetone, 121 MHz): δ = −146.4 (sep, $^1J_{P,F}$ = 708 Hz). Note: Spectroscopic data (^1H and ^{31}P NMR) for this compound have been reported,[18] although no microanalytical data were included.

Synthesis of $[Rh(OEt)(cod)]_2$: $[RhCl(cod)]_2$ (100 mg, 0.20 mmol) in methanol (0.6 mL) was treated with NaOEt (0.44 mL of 1 M methanol solution, 0.44 mmol) under nitrogen. After stirring for 30 min, the yellow suspension was filtered. The yellow solid obtained was washed with methanol and dried. $[Rh(cod)(OEt)]_2$ (102 mg, 98%) was used directly without further purification.

Synthesis of $[Rh(cod)(mdd)]^+$ BPh_4^- (2): Sodium ethoxide (0.40 mL of 1 M methanol solution, 0.40 mmol) and 1,1′-methylene-3,3′-dimethyldiimidazolium bis(tetraphenylborate) (290 mg, 0.36 mmol) were added to a suspension of $[Rh(cod)(OEt)]_2$ (92 mg, 0.18 mmol) in methanol (1 mL). The reaction mixture was heated at reflux for 15 minutes and then stirred at room temperature overnight, during which time the pale-yellow suspension changed to an orange suspension. The resulting precipitate was filtered and washed with methanol. (Cyclooctadiene)(1,1′-methylene-3,3′-dimethyldiimidazoline-2,2′-diylidene)rhodium(I) tetraphenylborate was recrystallised from acetone as an orange crystalline solid (159 mg, 63%), m.p. 188 °C (dec). $C_{41}H_{44}BN_4Rh$ (706.52): calcd. C 69.7, H 6.3, N 7.9; found C 69.5, H 6.5, N 8.0. ^1H NMR ([D$_6$]acetone, 400 MHz): δ = 7.45 (d, $^3J_{H,H}$ = 1.8 Hz, 2 H, NCH), 7.34 (m, 8 H, *o*-H), 7.15 (d, $^3J_{H,H}$ = 1.8 Hz, 2 H, NCH), 6.92 (t, $^3J_{H,H}$ = 7.3 Hz, 8 H, *m*-H), 6.77 (t, $^3J_{H,H}$ = 7.3 Hz, 4 H, *p*-H), 6.59 (d, $^2J_{H,H}$ = 13.0 Hz, 1 H, NCH_2), 6.26 (d, $^2J_{H,H}$ = 13.0 Hz, 1 H, NCH_2), 5.05 [m, 2 H, CH(cod)], 4.87 [m, 2 H, CH(cod)], 3.84 (s, 6 H, NCH_3), 2.54 [m, 2 H, CH_2(cod)], 2.4−2.1 [m, 6 H, CH_2(cod)] ppm. $^{13}C\{^1H\}$ NMR ([D$_6$]acetone, 101 MHz): δ = 181.1 (d, $^1J_{Rh,C}$ = 52.7 Hz, NCN), 164.9 (q, $^1J_{C,B}$ = 49.6 Hz, *ipso*-C), 137.0 (*o*-C), 126.0 (*m*-C), 123.4 (NCH), 122.3 (*p*-C), 121.8 (NCH), 92.0 [d, $^1J_{Rh,C}$ = 7.8 Hz, CH(cod)], 87.8 [d, $^1J_{Rh,C}$ = 7.8 Hz, CH(cod)], 64.1 (NCH_2), 38.0 (NCH_3), 31.2 [CH_2(cod)], 31.0 [CH_2(cod)] ppm. MS (ES+, CH_3CN): *m/z* (%) = 387 (45) $[Rh(cod)(mdd)]^+$, 361 (25) $[Rh(mdd)(CH_3CN)_2]^+$, 320 (100) $[Rh(mdd)(CH_3CN)]^+$, 279 (35) $[Rh(mdd)]^+$.

Synthesis of $[Rh(CO)_2(mdd)]^+$ BPh_4^- (3): $[Rh(cod)(mdd)]^+BPh_4^-$ (**2**; 50 mg, 71 μmol) was suspended in methanol (1 mL). The mixture was degassed using three freeze-pump-thaw cycles, flushed with carbon monoxide gas and stirred at room temperature overnight, during which time the orange suspension became a yellow suspension. The precipitate was isolated by filtration and washed with diethyl ether producing dicarbonyl(1,1′-methylene-3,3′-dimethyldiimidazoline-2,2′-diylidene)rhodium(I) tetraphenylborate as a yellow solid (41 mg, 88%), m.p. 170 °C (dec). $C_{35}H_{32}BN_4O_2Rh$ (654.36): calcd. C 64.2, H 4.9, N 8.6; found C 64.2, H 4.7, N 8.7. ^1H NMR ([D$_6$]acetone, 400 MHz): δ = 7.56 (d, $^3J_{H,H}$ = 1.8 Hz, 2 H, NCH), 7.35 (m, 9 H, NCH and *o*-H), 6.91 (t, $^3J_{H,H}$ = 7.3 Hz, 8 H, *m*-H), 6.77 (t, $^3J_{H,H}$ = 7.3 Hz, 4 H, *p*-H), 6.21 (s, 2 H, NCH_2), 3.93 (s, 6 H, NCH_3) ppm. $^{13}C\{^1H\}$ NMR ([D$_6$]acetone, 101 MHz): δ = 189.0 (d, $^1J_{Rh,C}$ = 57.0 Hz, CO), 173.6 (d, $^1J_{Rh,C}$ = 45.2 Hz, NCN), 164.9 (q, $^1J_{C,B}$ = 49.3 Hz, *ipso*-C), 137.0 (*o*-C), 126.0 (*m*-C), 124.1 (NCH), 123.2 (NCH), 122.2 (*p*-C), 63.8 (NCH_2), 38.9 (NCH_3) ppm. MS (ES+, CH_3CN): *m/z* (%) = 361 (18) $[Rh(mdd)(CH_3CN)_2]^+$, 335 (26) $[Rh(CO)_2(mdd)]^+$, 320 (100) $[Rh(mdd)(CH_3CN)]^+$, 279 (53) $[Rh(mdd)]^+$. IR: $\tilde{\nu}$ = 2071s (νCO), 2014s (νCO) cm^{-1}.

Synthesis of $[Rh(cod)(mdd)]^+$ PF_6^- (4): Sodium ethoxide (0.45 mL of 1 M methanol solution, 0.45 mmol) and 1,1′-methylene-3,3′-

 © 2003 Wiley-VCH Verlag GmbH & Co. KGaA, Weinheim

dimethyldiimidazolium bis(hexafluorophosphate) (190 mg, 0.40 mmol) were added to a suspension of $[Rh(OEt)(cod)]_2$ (100 mg, 0.20 mmol) in methanol (1 mL). The reaction mixture was stirred at room temperature for three days, during which time the yellow suspension became an orange suspension. The resulting precipitate was filtered and washed with methanol. (Cyclooctadiene)(1,1′-methylene-3,3′-dimethyldiimidazoline-2,2′-diylidene)rhodium(I) hexafluorophosphate was recrystallised from acetone as an orange-red crystalline solid (142 mg, 67%), m.p. 203 °C (dec). $C_{17}H_{24}F_6N_4PRh$ (532.28): calcd. C 38.4, H 4.5, N 10.5; found C 38.5, H 4.8, N 10.4. ^{1}H NMR ([D$_6$]acetone, 300 MHz): δ = 7.50 (d, $^3J_{H,H}$ = 1.9 Hz, 2 H, CH_2NCH), 7.17 (d, $^3J_{H,H}$ = 1.9 Hz, 2 H, CH_3NCH), 6.61 (d, $^2J_{H,H}$ = 13.0 Hz, 1 H, NCH_2), 6.31 (d, $^2J_{H,H}$ = 13.0 Hz, 1 H, NCH_2), 5.05 [m, 2 H, CH(cod)], 4.88 [m, 2 H, CH(cod)], 3.86 (s, 6 H, NCH_3), 2.54 [m, 2 H, CH_2(cod)], 2.27 [m, 4 H, CH_2(cod)], 2.08 [m, 2 H, CH_2(cod)] ppm. ^{13}C{^{1}H} NMR ([D$_6$]acetone, 75 MHz): δ = 181.1 (d, $^1J_{Rh,C}$ = 52.2 Hz, NCN), 123.4 (CH_3NCH), 121.9 (CH_2NCH), 92.0 [d, $^1J_{Rh,C}$ = 8.6 Hz, CH(cod)], 87.8 [d, $^1J_{Rh,C}$ = 7.8 Hz, CH(cod)], 64.1 (NCH_2), 38.0 (NCH_3), 31.2 [CH_2(cod)], 31.0 [CH_2(cod)] ppm. ^{19}F NMR ([D$_6$]acetone, 282 MHz): δ = −71.0 (d, $^1J_{P,F}$ = 708 Hz) ppm. ^{31}P NMR ([D$_6$]acetone, 121 MHz): δ = −146.3 (sep, $^1J_{P,F}$ = 708 Hz) ppm. MS (ES+, MeOH): *m*/*z* (%) = 387 (10) $[Rh(cod)(mdd)]^+$, 311 (100) $[Rh(mdd)(MeOH)]^+$, 279 (15) $[Rh(mdd)]^+$ ppm. MS (ES-, MeOH): *m*/*z* (%) = 145 (100) $[PF_6^-]$.

Synthesis of $[Rh(CO)_2(mdd)]^+PF_6^-$ (5): $[Rh(cod)(mdd)]^+PF_6^-$ (**4**; 70 mg, 0.13 mmol) was suspended in diethyl ether (1 mL) and methanol (1 mL). The suspension was degassed using three freeze-pump-thaw cycles, flushed with carbon monoxide gas and stirred at room temperature for 3 days, during which time the orange suspension became a yellow suspension. The precipitate was isolated by filtration and washed with diethyl ether producing dicarbonyl(1,1′-methylene-3,3′-dimethyldiimidazoline-2,2′-diylidene)-rhodium(I) hexafluorophosphate as a yellow solid (29 mg, 46%), m.p. 200 °C (dec). $C_{11}H_{12}F_6N_4O_2PRh$ (480.13): calcd. C 27.5, H 2.5, N 11.7; found C 27.7, H 2.8, N 11.6. ^{1}H NMR ([D$_6$]acetone, 400 MHz): δ = 7.68 (d, $^3J_{H,H}$ = 1.8 Hz, 2 H, CH_2NCH), 7.46 (d, $^3J_{H,H}$ = 1.8 Hz, 2 H, CH_3NCH), 6.41 (s, 2 H, NCH_2), 4.01 (s, 6 H, NCH_3) ppm. ^{13}C{^{1}H} NMR ([D$_6$]acetone, 101 MHz): δ = 189.0 (d, $^1J_{Rh,C}$ = 56.6 Hz, CO), 173.6 (d, $^1J_{Rh,C}$ = 45.4 Hz, NCN), 124.1 (CH_3NCH), 123.3 (CH_2NCH), 63.9 (NCH_2), 38.9 (NCH_3) ppm. ^{19}F NMR ([D$_6$]acetone, 282 MHz): δ = −67.7 (d, $^1J_{P,F}$ = 710 Hz) ppm. ^{31}P NMR ([D$_6$]acetone, 121 MHz): δ = −143.1 (sep, $^1J_{P,F}$ = 710 Hz) ppm. MS (ES+, MeOH): *m*/*z* (%) = 335 (100) $[Rh(CO)_2(mdd)]^+$. MS (ES-, MeOH): *m*/*z* (%) = 145 (100) $[PF_6^-]$. IR: $\tilde{\nu}$ = 2076s (νCO), 2017s (νCO) cm^{-1}.

Synthesis of $[Rh(bim)(CO)_2]^+PF_6^-$ (6): A solution of bis(*N*-methylimidazol-2-yl)methane (80 mg, 0.45 mmol) in methanol (5 mL) was added to a solution of $[RhCl(CO)_2]_2$ (88 mg, 0.22 mmol) in methanol (15 mL) at room temperature. The yellow precipitate that formed initially dissolved after the addition of the ligand was complete. The mixture was stirred for 30 minutes before adding an excess of potassium hexafluorophosphate (400 mg) in methanol (10 mL). The resulting precipitate was filtered and washed with methanol. [Bis(*N*-methylimidazol-2-yl)methane)dicarbonylrhodium(I) hexafluorophosphate was recrystallised from acetone as a dark pink solid (191 mg, 90%), m.p. 262 °C (dec). $C_{11}H_{12}F_6N_4O_2PRh$ (480.12): calcd. C 27.5, H 2.5, N 11.7; found C 27.6, H 2.2, N 11.4. ^{1}H NMR ([D$_6$]acetone, 400 MHz): δ = 7.55 (d, $^3J_{H5,H4}$ = 1.4 Hz, 2 H, H5), 7.42 (d, 2 H, H4), 4.63 (s, 2 H, CH_2), 3.97 (s, 6 H, NCH_3) ppm. ^{13}C{^{1}H} NMR ([D$_6$]acetone, 101 MHz): δ = 185.3 (d, $^1J_{Rh,C}$ = 68.2 Hz, CO), 143.9 (C2), 130.9 (C5), 124.3 (C4), 34.8 (NCH_3), 24.4 (CH_2) ppm. ^{19}F NMR ([D$_6$]acetone, 376 MHz): δ = −67.5 (d, $^1J_{P,F}$ = 708 Hz) ppm. ^{31}P{^{1}H} NMR ([D$_6$]acetone, 162 MHz): δ = −135 (sep, $^1J_{P,F}$ = 708 Hz) ppm. MS (ES+, THF): *m*/*z* (%) = 335 (100) $[Rh(bim)(CO)_2]^+$. IR: $\tilde{\nu}$ = 2084s (νCO), 2026s (νCO) cm^{-1}.

X-ray Crystallography

Low-temperature single-crystal diffraction data were collected with a Bruker SMART 1000 diffractometer using graphite monochromated Mo-K_α radiation (λ = 0.71073 Å) from a sealed tube. Crystallographic details are given in Table 2. Data integration and reduction were undertaken with SAINT and XPREP[19] and sub-

Table 2. Crystallographic data for $[Rh(cod)(mdd)]^+BPh_4^-$ (**2**) and $[Rh(CO)_2(mdd)]^+PF_6^-$ (**5**)

	2	**5**
Empirical formula	$C_{41}H_{44}BN_4Rh$	$C_{11}H_{12}F_6N_4O_2PRh$
Molecular weight (g mol^{-1})	706.52	480.13
Crystal system	Monoclinic	Orthorhombic
Space group	$P2_1/m$ (no. 11)	*Pnma* (no. 62)
a (Å)	10.457(3)	12.416(4)
b (Å)	13.108(4)	12.790(4)
c (Å)	12.295(4)	10.408(3)
β (°)	95.731(5)	
V (Å^3)	1676.9(9)	1652.7(9)
Z	2	4
T (K)	150(2)	100(2)
μ Mo-K_α (mm^{-1})	0.546	1.207
Crystal Size (mm)	0.233 × 0.154 × 0.071	0.324 × 0.121 × 0.120
T(Gaussian)$_{min,max}$	0.902, 0.962	0.820, 0.946
$2\theta_{max}$ (°)	56.50	56.60
hkl range	−13 13, −17 16, −16 16	−16 16, −17 17, −13 13
N	14318	16349
N_{ind}	4005 (R_{merge} 0.0310)	2079 (R_{merge} 0.0321)
N_{obs} [$I > 2\sigma(I)$]	3444	1888
Goodness of fit (all data)	1.499	1.316
*R*1 [*F*, $I > 2\sigma(I)$]	0.0492	0.0189
*wR*2 (F^2, all data)	0.1325	0.0549

 © 2003 Wiley-VCH Verlag GmbH & Co. KGaA, Weinheim

sequent computations were carried out with the teXsan[20] and WinGX[21] graphical user interfaces. A Gaussian absorption correction was applied to the data.[19,22] The structures were solved by direct methods with SIR97[23] and extended and refined with SHELXL-97.[24] In general the non-hydrogen atoms were modelled with anisotropic displacement parameters, and a riding-atom model with group displacement parameters was used for the hydrogen atoms. The crystal structure of complex **2** was modelled as a disordered (pseudo)centrosymmetric structure in $P2_1/m$ (no. 11). An alternative model in $P2_1$ (no. 4) had significantly higher residuals at convergence [$R1(F) = 0.0591$ and $wR2(F^2) = 0.1656$], and high levels of correlation requiring extensive geometry and displacement restraints. The Flack parameter[25] in $P2_1$ refined to 0.49(8) suggesting either an inversion twin or a centrosymmetric structure. The disordered centrosymmetric model was adopted as the better model for the crystal structure. The asymmetric unit in $P2_1/m$ contains a complex molecule bisected by a (pseudo) mirror plane, with the metal ion and C(12) atoms located in that plane. A tetraphenylborate counterion also resides on a mirror plane, with the B(1), C(14), C(15), C(16), C(17), C(18), C(19), C(20) and C(23) atoms located in the mirror plane. Two of the phenyl residues of the counterion have orientational disorder about the boron to quaternary carbon axis. The $P2_1/m$ symmetry is broken by a lack of mirror symmetry in the cyclooctadiene ligand, which is disordered about the mirror plane. The fully occupied non-hydrogen sites were modelled with anisotropic displacement parameters, and isotropic displacement parameters were used for the partially occupied non-hydrogen sites and for the fully occupied boron site. The site occupancies were refined, and then fixed and rounded to the first decimal place.

CCDC-186563 (**2**) and -186564 (**5**) contain the supplementary crystallographic data for this paper. These data can be obtained free of charge at www.ccdc.cam.ac.uk/conts/retrieving.html [or from Cambridge Crystallographic Data Centre, 12 Union Road, Cambridge CD2 1EZ, UK; Fax: (internat.) + 44-1233/336-033; E-mail: deposit@ccdc.cam.ac.uk].

Acknowledgments

We thank the Australian Research Council for financial support.

[1] A. J. Arduengo, R. L. Harlow, M. Kline, *J. Am. Chem. Soc.* **1991**, *113*, 361−363.
[2] W. A. Herrmann, *Angew. Chem. Int. Ed.* **2002**, *41*, 1290−1309.
[3] M. Muehlhofer, T. Strassner, W. A. Herrmann, *Angew. Chem. Int. Ed.* **2002**, *41*, 1745.
[4] S. Burling, L. D. Field, B. A. Messerle, *Organometallics* **2000**, *19*, 87−90.
[5] W. A. Herrmann, M. Elison, J. Fischer, C. Köcher, G. R. J. Artus, *Chem. Eur. J.* **1996**, *2*, 772−780.
[6] C. Köcher, W. A. Herrmann, *J. Organomet. Chem.* **1997**, *532*, 261−265.
[7] M. Albrecht, R. H. Crabtree, J. Mata, E. Peris, *Chem. Commun.* **2002**, 32−33.
[8] R. R. Schrock, J. A. Osborn, *Inorg. Chem.* **1970**, *9*, 2339−2343.
[9] S. Elgafi, L. D. Field, B. A. Messerle, P. Turner, T. W. Hambley, *J. Organomet. Chem.* **1999**, *588*, 69−77 and references therein.
[10] C. K. Johnson, *ORTEPII. Report ORNL-5138.*; Oak Ridge National Laboratory: Oak Ridge, Tennessee, **1976**.
[11] S. R. Hall, D. J. du Boulay, R. Olthof-Hazekamp, *Xtal3.6 System*; University of Western Australia, **1999**.
[12] W. A. Herrmann, L. J. Gooben, M. Spiegler, *J. Organomet. Chem.* **1997**, *547*, 357−366.
[13] W. A. Herrmann, J. Fischer, K. Öfele, G. R. J. Artus, *J. Organomet. Chem.* **1997**, *530*, 259−262.
[14] S. Elgafi, L. D. Field, B. A. Messerle, *J. Organomet. Chem.* **2000**, *607*, 97−104.
[15] The turnover rate was calculated as the number of mol of product/mol of catalyst/hour and was calculated at 50% conversion of substrate to product.
[16] G. Giordano, R. H. Crabtree, *Inorg. Synth.* **1979**, *19*, 218−220.
[17] R. M. Claramunt, J. Elguero, T. Meco, *J. Heterocycl. Chem.* **1983**, *20*, 1245−1249.
[18] N. E. Leadbeater, H. M. Torenius, *J. Org. Chem.* **2002**, *67*, 3145−3148.
[19] Bruker *SMART, SAINT and XPREP. Area detector control and data integration and reduction software*; Bruker Analytical X-ray Instruments Inc.: Madison, Wisconsin, USA, 2001.
[20] Molecular Structure Corporation, *teXsan for Windows: Single Crystal Structure Analysis Software.* MSC: 3200 Research Forest Drive, The Woodlands, Texas, USA, 1997−1998.
[21] L. J. Farrugia, *J. Appl. Cryst.* **1999**, *32*, 837−838.
[22] P. Coppens, L. Leiserowitz, D. Rabinovich, *Acta Crystallogr.* **1965**, *18*, 1035−1038.
[23] A. Altomare, M. C. Burla, M. Camalli, G. L. Cascarano, C. Giacovazzo, A. Guagliardi, A. G. G. Moliterni, G. Polidori, R. Spagna, *J. Appl. Cryst.* **1999**, *32*, 115−119.
[24] G. M. Sheldrick, *SHELXL-97. Program for crystal structure refinement*; University of Göttingen: Germany, 1997.
[25] [25a] H. D. Flack, *Acta Crystallogr., Sect. A* **1983**, *39*, 876−881. [25b] G. Bernardinelli, H. D. Flack, *Acta Crystallogr., Sect. A* **1985**, *41*, 500−511. [25c] H. D. Flack, G. Bernardinelli, *Acta Crystallogr., Sect. A* **1999**, *55*, 908−915. [25d] H. D. Flack, G. Bernardinelli, *J. Appl. Cryst.* **2000**, *33*, 1143−1148.

Received March 20, 2003

 © 2003 Wiley-VCH Verlag GmbH & Co. KGaA, Weinheim

Synthesis, Kinetic Study and Molecular Orbital Investigation of Cadmium(II), Mercury(II) and Lead(II) Complexes with the Mixed Pendant-Arm Macrocyclic Ligand 1,7-Bis(carboxymethyl)-4,10-bis(1-methylimidazol-2-ylmethyl)-1,4,7,10-tetraazacyclododecane

Massimo Di Vaira,[a] Fabrizio Mani,[a] Stefano Seniori Costantini,[a] Piero Stoppioni,*[a] and Alberto Vacca[a]

Keywords: Macrocyclic ligands / Cadmium / Lead / Mercury / Conformational equilibrium / Density functional calculations

The neutral $[ML^6]\cdot 3H_2O$ complexes (M = Cd^{II}, Hg^{II} and Pb^{II}) formed with the potentially octadentate ligand 1,7-bis(carboxymethyl)-4,10-bis(1-methylimidazol-2-ylmethyl)-1,4,7,10-tetraazacyclododecane (H_2L^6) in its anionic deprotonated form, which bears two pairs of different dangling groups in *trans* positions on the cyclen skeleton, have been synthesized. Their low-temperature limiting NMR spectra (^1H and ^{13}C) in D_2O show that both the dangling groups and the ethylenic moieties of the macrocycle ring are in a fixed conformation in all complexes at 273 K. These conditions are relaxed at higher temperatures, yielding a dynamic behaviour that proceeds through both ring inversion and rearrangement of the pendant arms. The kinetic parameters for ring inversion have been obtained from the temperature-dependent ^{13}C NMR spectra. Cd: k(298 K) = 236 s^{-1}; $\Delta H^{\ddagger}$ = 72.9 ± 0.6 kJ·mol^{-1}; $\Delta S^{\ddagger}$ = 45 ± 2 J K^{-1}·mol^{-1}; Hg: k(298 K) = 292 s^{-1}; $\Delta H^{\ddagger}$ = 68 ± 3 kJ·mol^{-1}; $\Delta S^{\ddagger}$ = 29 ± 10 J K^{-1}·mol^{-1}; Pb: k(298 K) = 122 s^{-1}; $\Delta H^{\ddagger}$ = 65 ± 2 kJ·mol^{-1}; $\Delta S^{\ddagger}$ = 14 ± 5 J K^{-1}·mol^{-1}. In the absence of experimental structure determinations, some insight into the geometries has been obtained by quantum-mechanical calculations.

(© Wiley-VCH Verlag GmbH & Co. KGaA, 69451 Weinheim, Germany, 2003)

Introduction

Considerable attention has been addressed to metal complexes of 1,4,7,10-tetraazacyclododecane (cyclen) bearing pendant arms.[1−6] Depending on the number of substituent groups on the macrocyclic framework, as well as on the requirements of the metal ions employed, the substituted cyclen ligands easily adapt to coordination numbers six[7−9] seven[10] or eight,[11−13] and thus they might coordinate mono-, di- and trivalent metal ions. Complexes with these ligands exhibit notable thermodynamic stability and kinetic inertia and, consequently, they have important applications in, for example,[14] (i) the design of luminescent chelates for immunoassays,[6,15,16] (ii) use of Gd-containing contrast agents in diagnostic medicine[17,18] and (iii) labelling and specific cleavage of DNA and RNA.[19−21]

Representative examples of such ligands include the 1,4,7,10-tetraazacyclododecane-tetraacetic acid (H_4DOTA), which can provide anionic donors on the dangling groups, and molecules bearing four neutral donors on the arms of functionalized tetraazacyclododecane (Scheme 1).[7,22−26] Crystal data of the complexes have revealed that the four nitrogen atoms of the macrocycle and the four donors from the dangling groups are arranged in two parallel squares that are tilted by an angle denoted as α (Scheme 2). The coordination geometry can range from a regular antiprism (α = 45°) to a prism (α = 0°). Neither limiting case has been observed so far, and most known geometries cluster around two values: α = 40° and 15° (A and B, respectively, in Scheme 2).[7,26−32]

We have synthesized potentially octadentate ligands based on tetraazacyclododecane bearing, on the pendant arms, either four pyrazoles, L^5,[33] or two pairs of different groups in *trans* positions, namely two methylimidazoles and two carboxy groups, H_2L^6 [9] (Scheme 3). The solid manganese and cadmium complexes with L^5 have nearly prismatic structures,[34,35] a geometry that is preferred in solution by some lanthanide complexes with L^6.[36] Generally, the eight donors of the octadentate ligands L^1−L^6 are also considered to be bound to the metal ion in solution, a notable exception being the seven-coordinate magnesium complex with 1,4,7,10-tetrakis(2-methoxyethyl)-1,4,7,10-tetraazacyclododecane (L^4), which has the oxygen of a pendant arm uncoordinated.[10] Most of the complexes undergo dynamic behaviour in solution, which has been rationalized in terms of an exchange process between two enantiomers,[29,30] at

[a] Dipartimento di Chimica, Università di Firenze,
Via della Lastruccia 3, 50019 Sesto Fiorentino, Italy
E-mail: piero.stoppioni@unifi.it

Supporting information for this article is available on the WWW under http://www.eurjic.org or from the author.

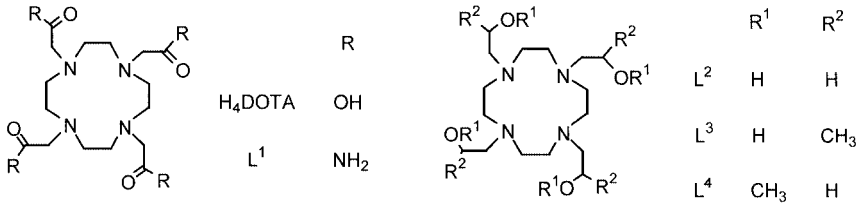

Scheme 1

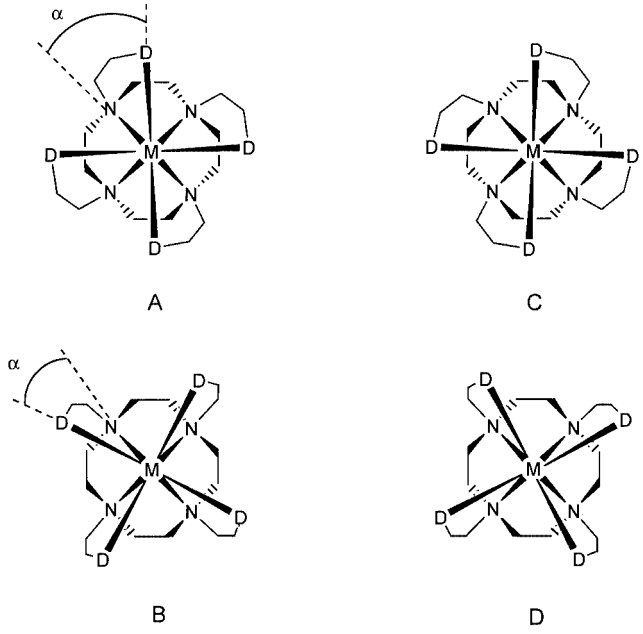

Scheme 2

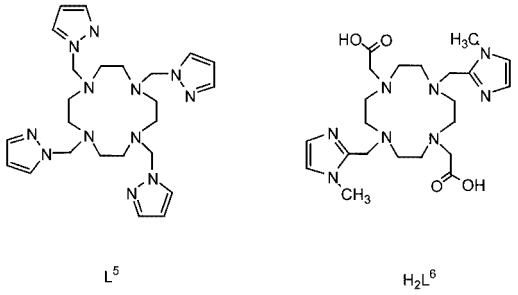

Scheme 3

rates within the ^{13}C NMR timescale. In this paper we report both on the synthesis of complexes formed by the "mixed" H_2L^6 ligand (Scheme 3) in the anionic form with different size metal ions (Cd^{II}, Hg^{II} and Pb^{II}) and on their dynamic behaviour in solution by using variable-temperature ^1H and ^{13}C NMR spectroscopy. As repeated attempts to obtain suitable crystals of the compounds for X-ray investigations failed, quantum mechanical calculations were undertaken to obtain information on their geometry and bonding.

Results and Discussion

Syntheses of the Metal Complexes

The cadmium derivative was prepared by direct reaction of cadmium carbonate with the ligand H_2L^6, dissolved in water. The mercury and lead derivatives were prepared in water by reacting the acetate of the metal with the ligand and then neutralizing the resulting solution with Na_2CO_3. The complexes obtained after workup crystallize with three water molecules, $[ML^6]\cdot 3H_2O$, and are very soluble in polar solvents (water, methanol and ethanol). As expected for such compounds, they are stable in solution for weeks in the pH range 5−10.[37]

NMR Spectra of the Complexes

The $^{13}C\{^1H\}$ spectrum of the cadmium complex at 273 K exhibits eleven peaks which, on the basis of data for lanthanide complexes with the same ligand, are assigned as δ = 177.7 ppm to the carboxylate functionalities, δ = 145.8, 125.6 and 122.5 ppm to the carbon atoms of the imidazole rings, δ = 57.4 and 48.4 ppm to the methylenic carbon atoms of the acetate and of the imidazole arms, respectively, δ = 51.8, 50.9, 48.4 and 48.1 ppm to the ethylenic carbons of the tetraazamacrocycle, and δ = 32.0 ppm to the methyl carbon of imidazole. The signals of two equivalent carbons of the macrocycle and of the two carbons of the imidazole CH_2 bridges have the same shift (δ = 48.4 ppm) and yield a resonance of comparatively higher intensity. The C^2 carbon of imidazole couples with the metal ($^2J^{13}_{C\text{-}}{}^{111}_{Cd}$ = 13.1 Hz), which does not change in the range of temperatures investigated. On increasing the temperature the four signals due to the macrocycle broaden, collapse, and then merge (Figure 1) to afford, at 358 K, two resonances at δ = 50.3 and 49.7 ppm; the signals due to the other carbon atoms remain narrow, undergoing small drifts. The proton NMR spectrum of the cadmium derivative shows thirteen resonances at 273 K (see the Exp. Sect.) which have been assigned with the aid of a 2D COSY experiment. The imidazole protons appear as a pair of doublets at low field and those of the methyl group yield a singlet at δ = 3.28 ppm. The protons of the CH_2COO^- moiety yield two doublets (δ = 3.69 and 3.34 ppm; J = 15 Hz). The CH_2 bridging the macrocycle and the imidazole yields a doublet (δ = 2.56 ppm; J = 16 Hz) and a resonance (δ = 2.28 ppm) which overlaps with those of the macrocycle. Such resonances, also seen, with minor changes, for diamagnetic lanthanide complexes with L^6,[36] are typical of two non-equivalent AB

 © 2003 Wiley-VCH Verlag GmbH & Co. KGaA, Weinheim

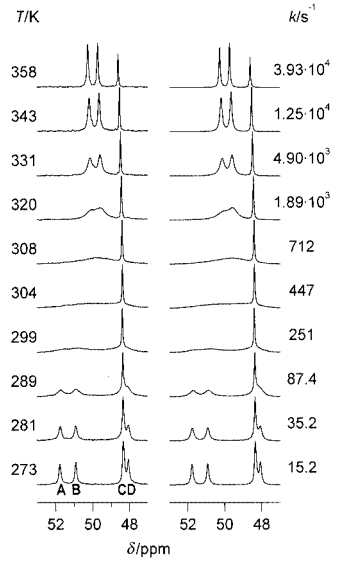

Figure 1. $^{13}C\{^1H\}$ spectra of the macrocyclic carbons of the [CdL^6] complex at different temperatures (left) compared with spectra calculated by line-shape analysis (right). The simulation has been performed by assuming an ABCD → CDAB exchange mechanism

systems.[38,39] The ethylenic moieties of the macrocycle present four triplets at δ = 3.01, 2.91, 2.67 and 2.37 ppm (coupling constants ca. 12.0 Hz), overlapping doublets centered at δ = 2.28 ppm and two doublets at δ = 2.05 and 1.86 ppm (coupling constant ca. 12.0 Hz). The chemical shifts of the resonances around δ = 2.7 and 2.1 ppm, and the multiplicity and coupling constants, are typical of two nonequivalent ABCD systems exhibiting large geminal and axial couplings, with small equatorial couplings. Such systems parallel those observed at low temperature for the ethylenic groups of lanthanum(III) and lutetium(III) complexes with L^6;[36] furthermore, each ABCD system is similar to that exhibited by diamagnetic lanthanide complexes with DOTA.[38,39] By increasing the temperature the three resonances due to the protons of methylimidazole remain narrow, undergoing a low-field shift; all the other resonances broaden, collapse, and then merge to afford a spectrum which exhibits, at 358 K, narrow signals at δ = 4.46 and 3.37 ppm for the CH_2 of the dangling groups and two unresolved resonances centered at δ = 3.54 and 3.25 ppm, due to the ethylenic moieties of the macrocycle.

The mercury and lead derivatives yield ^1H and ^{13}C NMR spectra at low temperature which parallel that of the cadmium complex; the shift of each signal is marginally affected by the nature of the metal (see the Exp. Sect.), which induces partial overlapping of some resonances so that they may appear as complex multiplets. The coupling constant between the C^2 imidazole carbon atom and mercury ($^2J^{13}_{C\text{-}^{199}Hg}$ = 54 Hz) does not change in the range of temperatures investigated. However, for no obvious reason, a similar coupling is not observed in the [PbL^6] spectrum (nor with the [PbL^1]$^+$ complex cation[7]), possibly due to either a low intensity or a small coupling constant for the ^{207}Pb satellites.[7] Both the ^{13}C and ^1H spectra of the mercury and lead complexes change with increasing temperature, as found for the cadmium derivative. At the highest temperature (Hg, 346 K, Pb 353 K) they exhibit two signals for the macrocycle (Hg, δ = 49.2 and 48.8 ppm; Pb, 49.8 and 49.7 ppm) in the ^{13}C spectra; in the proton spectra they exhibit narrow signals (Hg, δ = 4.37 and 3.27 ppm; Pb, δ = 4.50 and 3.70 ppm) for the CH_2 of the dangling groups and two unresolved resonances (Hg, δ = 3.45 and 3.20 ppm; Pb, δ = 3.55 and 3.45 ppm) due to the ethylenic moieties.

Similarities between the NMR spectroscopic data for the present cadmium, mercury and lead derivatives at the low exchange limit and the spectra of other metal complexes with L^5 and L^6, which either possess a nearly prismatic geometry in the solid state[34,35] or have been assigned that geometry in solution,[36] suggest that the same conformation should also be assigned to the present [ML^6] species. This view is supported by the quantum mechanical calculations (see below). Conversely, the variable temperature NMR experiments reveal that the conformational equilibria are thermally activated. Interconversion processes between the conformational isomers may occur via (a) simple rearrangement ("rotation") of the pendant arms (A → B or C → D, in Scheme 2), (b) macrocycle ring inversion (A → C or B → D) or (c) combinations of both types of motion,[40,53] which may afford interconversion between enantiomers. The coupling detected between the Cd or Hg atom and one imidazole carbon over the whole temperature range, which is consistent with previous results for lanthanide analogues,[36] suggests that the rearrangements occur without detachment of the pendant arms (but see below, computational results for Hg species). The above interconversion processes, particularly process (b), involve changes in the magnetic environment of the macrocycle carbon atoms, which may be characterized by a four-site line-shape analysis. Typical experimental and calculated ^{13}C NMR spectra for the cadmium complex are displayed in Figure 1. The temperature dependence of the rate constants, fitted according to the Eyring equation, yielded the parameters: Cd, k(298 K) = 236 s^{-1}, $\Delta H^{\ddagger}$ = 72.9 ± 0.6 kJ·mol^{-1}, $\Delta S^{\ddagger}$ = 45 ± 2 J^{-1}·mol^{-1}; Hg, k(298 K) = 292 s^{-1}, $\Delta H^{\ddagger}$ = 68 ± 3 kJ·mol^{-1}, $\Delta S^{\ddagger}$ = 29 ± 10 J K^{-1}·mol^{-1} and Pb, k(298 K) = 122 s^{-1}, $\Delta H^{\ddagger}$ = 65 ± 2 kJ·mol^{-1}, $\Delta S^{\ddagger}$ = 14 ± 5 J K^{-1}·mol^{-1} (details are given with the Supporting Information, see also the footnote on the first page article). The kinetic parameters for compounds with the L^1−L^4 or DOTA ligands are affected by the nature of the donor atoms on the dangling groups and by the metal, or the solvent,[7,10,41] and are higher for complexes with anionic donors on the arms. The kinetic parameters of the present [ML^6] compounds compare best with those of lanthanum complexes formed with DOTA[38] or L^6,[36] being significantly larger than those of compounds with four neutral donors on the arms. This may be due to the presence of two anionic donors on L^6 and, in part, to the nature of the metal atoms. Line shape analysis of the ^{13}C NMR peaks due to the macrocycle carbon atoms provides direct kinetic information on the macrocycle ring inversion, rather than on rotation of the arms. However, the ^1H NMR spectra show that both ring inversion and arm rotation occur sim-

 © 2003 Wiley-VCH Verlag GmbH & Co. KGaA, Weinheim

ultaneously in the temperature range studied, as indicated by the loss of rigidity of all of the NCH_2CH_2N, NCH_2COO^- and NCH_2MeIz moieties with increasing temperature. The rate constants for the above processes (a) and (b) were not measured by ^1H NMR spectroscopic data due to the complexity of the exchanging system. However, as both processes occur in the same temperature range their rate constants should be similar, so that all types of interconversions may take place.

Quantum-Mechanical Calculations

For the [ML^6] systems considered here, calculations on gas-phase models yielded two low-energy conformers, with closely spaced energies ($\leq$ 13 kJ·mol^{-1} energy differences). Their geometries broadly correspond to the idealized coordination types of Scheme 2, but precisely defined geometrical parameters (detailed below) are needed for the following discussion. The upper/lower arrangements of Scheme 2 will be, respectively, denoted by *ap* and *iap*, for "*a*nti*p*rismatic" and "*i*nverted *a*nti*p*rismatic ", as previously used to describe the analogous coordination modes in the related DOTA systems.[40,53] The cadmium conformers will, accordingly, be denoted Cd*ap* and Cd*iap*, and so on. Optimized geometries for the two Cd conformers are shown in Figure 2, and selected geometrical parameters, as well as energy differences between the low-energy conformers of each metal system, are given in Table 1.

The two fundamental geometries may be identified unambiguously by the signs of the torsion angles of the ethylenic chains of the macrocycle, τ_1 and τ_2 in Table 1, and those of the dangling groups, τ_3 and τ_4. The signs are all negative for an "idealized *iap*" conformer, such as Cd*iap* in Figure 2 (they would be all positive for its enantiomer), whereas the signs are opposite in pairs, τ_1 and τ_2 with respect to τ_3 and τ_4, for a "pure *ap*" conformer, such as Cd*ap*. These sign distributions, however, do not match the present Pb and Hg models, due to inconsistent τ_4 signs (Table 1). Therefore, the *ap*/*iap* assignments for the latter systems were based solely on consideration of the τ_{1-3} signs. Indeed, unlike the present Cd and the previous lanthanide models,[53] the angle (β in Table 1) by which the plane of the imidazole group is bent away from the line connecting the metal and the heterocycle N donor (N_{im} hereafter; the macrocycle nitrogens are collectively labelled N_{mac}) is exceedingly large for the two lowest energy conformers of both the Pb and the Hg systems. The lowest energy, Pb*iap* and Hg*iap*, conformers are shown in Figure 3 and more representations are shown in the Supporting Information. These arrangements suggest weaker interactions between the Pb or Hg atom and the "neutral" dangling groups than those between the metal and the charged carboxylates. This is particularly evident for the Hg species, where the imidazole groups lie at considerable distances from the metal (Table 1). The difference under discussion between the Pb and the Cd (or the lanthanide[53]) models may be ascribed to the smaller charge/radius ratio of the former cation and to the strain imposed

Table 1. Values of selected geometrical parameters and energy differences between conformers for the [ML^6] model systems

Model system[a]	Cd*iap*	Cd*ap*	Pb*iap*	Pb*ap*	Hg*iap*	Hg*ap*
Relative energy[b]	0	9.29	0	12.29	0	13.43
M−N1	2.687	2.634	2.809	2.732	2.600	2.575
M−N2	2.737	2.798	2.775	2.884	2.687	2.770
M−O1	2.282	2.284	2.471	2.468	2.252	2.244
M−N4	2.485	2.460	2.959	2.924	3.788	3.491
τ_1[c]	−59.1	−56.5	−58.0	−63.9	−60.8	−62.9
τ_2[d]	−57.5	−60.3	−59.1	−60.9	−56.9	−61.0
τ_3[e]	−22.7	48.2	−56.2	50.4	−43.5	43.2
τ_4[f]	−21.9	21.6	24.1	−46.8	47.4	−60.7
β[g]	21.3	15.1	63.2	68.7	61.2	68.0

[a] Distances (Å) and dihedral angles (°) from "level A" calculations (see Exp. Sect.); atomic labels as in Figure 2. [b] Energy differences (kJ·mol^{-1}) are relative to the energy of the respective M*iap* model. [c] N1−C1−C2−N2 dihedral angle. [d] N2−C3−C4−N3. [e] N1−C5−C6−O1. [f] N2−C7−C8−N4. [g] $\beta = \pi/2 - \alpha$, where α is the angle between the M−N_{im} direction and the normal to the imidazole plane (β = 14.8° for La*iap*, ref.[46]).

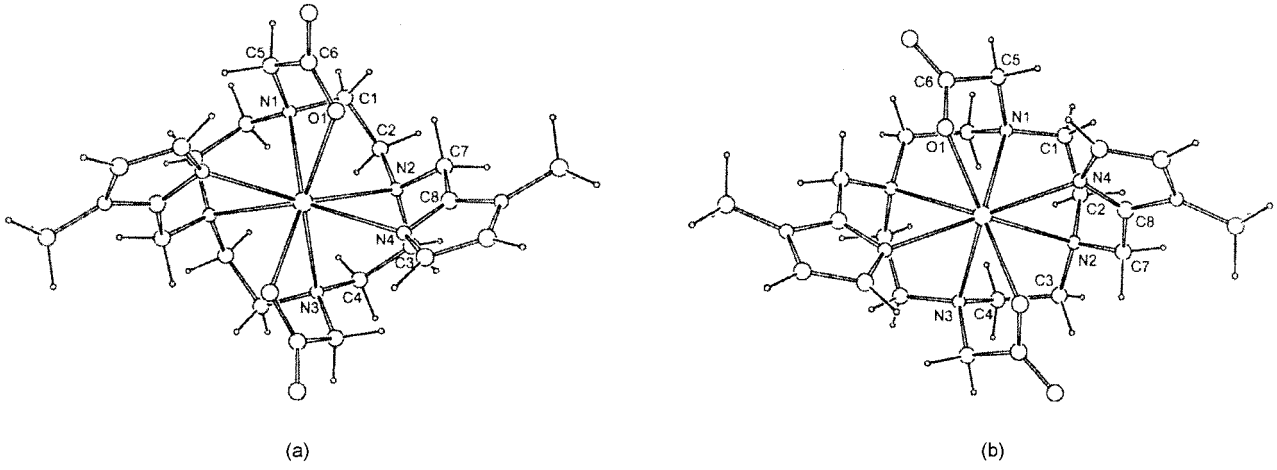

Figure 2. (a) Optimized Cd*iap* conformer geometry, showing the labelling used in Table 1 and in Supporting Information Tables. C_2 symmetry was imposed in the optimizations of all model geometries. (b) Cd*ap* conformer

 © 2003 Wiley-VCH Verlag GmbH & Co. KGaA, Weinheim

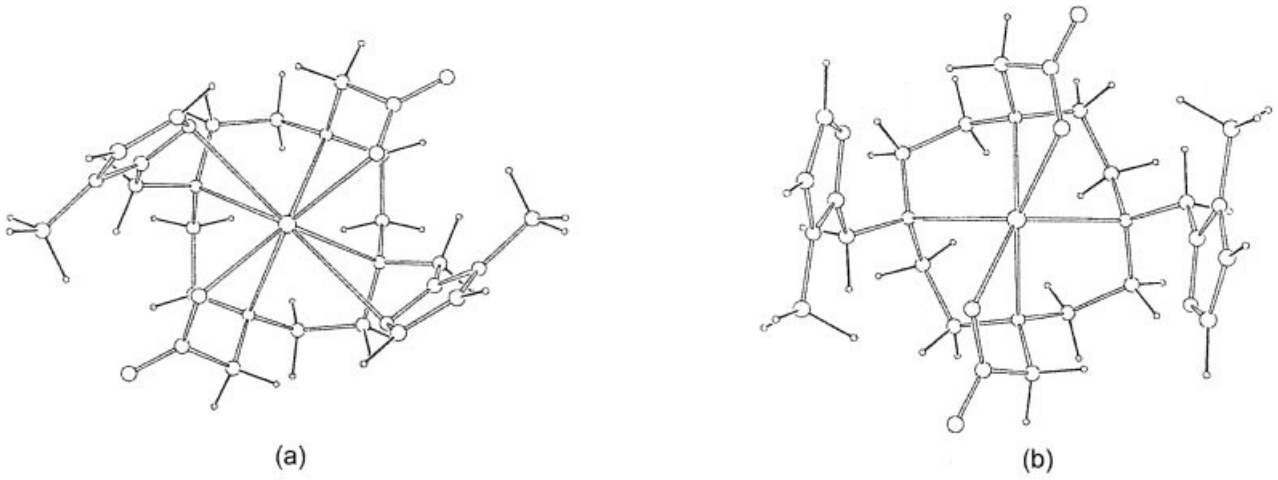

Figure 3. Geometries of the (a) Pb*iap* and (b) Hg*iap* conformers

on the chains by the overall longer metal−donor atom distances in the Pb species − factors that are obviously interrelated to some extent. The Hg conformers are peculiar, as most of their metal−donor distances are significantly shorter than those of Pb (the Hg−N_{mac} and Hg−O bond lengths are close to those of the Cd models), except for the very long Hg−N_{im} interactions (Table 1). The latter distances, which presumably affect the τ_4 values for the Hg models, may be traced to the specific electronic requirements of the Hg^{2+} cation. Indeed, the metal-based part of the HOMO for the Hg conformers has a stereochemically active d-orbital component, whereas the metal contribution to the HOMO of the Pb models has predominantly s (spherical) character; plots of sections of these electron densities are given with the Supporting Information.

Unfortunately, no experimental structure is available for detailed comparison. X-ray structures of Pb complexes formed by pyrazole-functionalized macrocycles revealed appreciable displacements of the metal atom from the planes of coordinating pyrazoles.[42] Previous computational experience with related systems[53] suggests that the overall geometrical features should be reproduced with reasonable accuracy, although individual metal−donor atom distances may be significantly in error. It may be appropriate to note here that the calculations with the SDD metal functions for the Cd systems, referred to in the Exp. Sect., yielded metal−donor atom distances that deviate by 0.012 Å (mean of absolute differences) from those obtained with the LANL2DZ metal functions (Table 1); conversely, for the less tightly bound Pb systems the considerably larger 0.070 Å mean for the absolute difference values was found, the SDD distances being consistently longer than those listed in Table 1. An indirect, but useful, test of the present procedures involves optimizing the geometries of two complex cations that are related to the present compounds and have known structures, namely the Cd[35] and Na[43] derivatives of tetraazacyclododecane functionalized with four pyrazole groups, $[CdL^5]^{2+}$ and $[NaL^5]^{+}$ in the notation of Scheme 3. These optimizations, starting from moderately idealized (C_4 symmetry constraint) but otherwise unbiased geometries [identical (enantiomeric) starting geometries for the two model systems, with parameters borrowed from parts of the present *ap*/*iap* Cd systems], and run at the same level as the present calculations, yielded results in reasonable agreement with experiment (details and graphic representations are shown in the Supporting Information), except for the Cd−N_{mac} distances, which were calculated to be as much as 0.18 Å too long. Such a discrepancy, mostly due to mispositioning of the metal cation between the two planes of donor atoms, was not unexpected for compounds of this type,[53] but should not affect too adversely other geometrical features; in particular, all computed τs are within 2° of the experimental ones. The offset of the metal atom from the heterocycle plane is 0.04 Å for the Cd model (experimental mean value: 0.51 Å) and 0.82 Å for the Na one (experimental, 1.19 Å). Good agreement cannot be expected for the latter quantity, which is very sensitive to the smallest geometrical changes, but the results seem to exclude a computational bias toward bent arrangements of the heterocycle planes, such as those found for the present Pb and Hg models. The increasing metal offset from the heterocycle plane with increasing metal size, from the Cd to the Na test model, found both experimentally and computationally, suggests that the metal−donor distance may be responsible for the predicted arrangements of the Pb and Hg models.

The calculated energy ordering consistently yielded the *iap*-type conformer as slightly more stable than the *ap* one, in agreement with the NMR results. The energy separations (Table 1) indicate that thermally activated interconversion processes between conformers may take place. Although the agreement is gratifying, the definitive assessment of such subtle features is probably beyond these calculations on gas-phase models but, limited to such models, the computed energy orderings may be trusted as merely conformational rearrangements are considered. However, the complexity of such systems may preclude the unequivocal identification of specific factors that determine such energy preferences. In fact a third conformer was found for both the Pb and Hg systems, at slightly higher energy than that of the *ap*-

 © 2003 Wiley-VCH Verlag GmbH & Co. KGaA, Weinheim

species. Interestingly, the third conformer is characterized in both cases by shorter $M-N_{im}$ but longer $M-N_{mac}$ distances than the other conformers (details are in the Supporting Information, where the third species is denoted as *ap′* or *iap′*), and features better oriented imidazole groups for coordination to the metal. All four τ signs of these *ap′*/*iap′* species conform to the expected sign distributions for the "pure" *ap* or *iap* types, at variance with results for the lower-energy Pb or Hg conformers (Table 1). Therefore, the attainment of such more regular geometries with these metals seems to involve an energy cost.

As a partial attempt to verify whether solution conditions might affect the arrangement of the dangling groups, reaction field model calculations were undertaken according to Onsager's approach,[54,55] which is based on a spherical solvent cavity and induced-dipole interactions; more explicit treatment of the solvent was difficult due to the size of the systems. Optimizations were performed with a slightly smaller basis than that used for gas-phase calculations (see the Exp. Sect., level B) and were followed by single-point energy calculations at level A. No important changes in geometries were recorded with respect to the vacuum results, and the energy ordering of the conformers was preserved. There were small contractions (< 1%) in the $M-N_{mac}$ and M−O distances and elongations (generally < 2%) of the $M-N_{im}$ distances, except that the loose $M\cdots N_{im}$ interactions of the Hg models (Table 1) decreased by < 1%. The different trends for changes in coordinative bond lengths for the two types of dangling groups might be related to the different overall negative charges localized on them. The torsion angles of the dangling groups were more affected than the metal−donor distances, but with qualitative retention of the arrangements found for the gas-phase models. Parameter values and more details are in Tables S4−S5 of the Supporting Information.

The calculated ^{13}C NMR chemical shifts broadly reproduce the experimental δ values, but are not particularly informative (Table S7). However, the calculated δ's for some carbon atoms of the pendant arms (Table 2), which appear to be sensitive to the *iap* vs. *ap* geometry differences, support the assignment of the *iap* conformer geometry to the species in solution at low temperatures. In particular, there is comparatively better agreement between experimental and calculated δ's for the *iap*-conformer carbon atoms of the acetate arms (those more tightly coordinating), irrespective of the metal atom. The computed δ value for the other arm's methylene carbon moderately favours the *iap* geometry for the Cd derivative, but is inconclusive for both Pb and Hg species. On the one hand, the GIAO calculations do not clarify the arrangement of the imidazole-bearing arms in the Hg complex; on the other hand, they suggest that signals due to those arms' carbon atoms may be insensitive to the geometrical differences predicted between the Hg and the other models.

Table 2. Comparison of computed and experimental ^{13}C NMR shifts[a]

	[CdL^6]			[PbL^6]			[HgL^6]		
	iap	*exp*	*ap*	*iap*	*exp*	*ap*	*iap*	*exp*	*ap*
C6	178.4	177.7	183.8	183.2	178.2	185.3	180.8	176.6	183.4
C5	56.6	57.4	63.1	59.5	54.7	62.9	56.3	56.6	59.7
C7	45.7	48.4	52.6	44.5	49.2	53.8	43.5	47.5	52.9

[a] Shifts (ppm) are calculated from the isotropic shielding tensor value of the Me_4Si carbon (computational level C, see the Exp. Sect.). Atomic labels are as in Figure 2.

Conclusions

Metal−C2 coupling has, perhaps surprisingly, been detected in the NMR spectra of the Cd and Hg derivatives, but not in that of [PbL^6]; however, such discrepancies are not unusual and are not easily rationalized.[7] One might invoke effects of the distinctive HOMO composition of [HgL^6] and/or effects (in the context of a ^3J, rather than ^2J coupling constant) of the shorter $Cd-N_{mac}$ and $Hg-N_{mac}$ distances compared to $Pb-N_{mac}$.

The bonding picture in these compounds set forth by the calculations, featuring two dangling groups less and less strongly bound to the metal, on going from the Cd to the Pb and the Hg derivatives appears to disagree with the similarities in their NMR properties, as well as with the similarities between their NMR behaviour and that of the L^6 lanthanide derivatives,[36] or even of DOTA complexes.[30,38] However, as may be inferred from a previous theoretical investigation,[53] the energetics of the interconversion processes between conformers may not be greatly affected by the presence of two loosely coordinating arms, as long as the other two arms are strongly bound to the metal.

Experimental Section

General Remarks: Commercial solvents were dried from appropriate drying agents just before use according to standard procedures. NMR spectra were obtained with a Varian Gemini g300bb spectrometer, equipped with variable temperature unit, operating at 300 MHz (^1H) and 75.46 MHz (^{13}C). Positive chemical shifts are to high frequency relative to Me_4Si. The variable temperature accessories were checked against methyl alcohol and ethylene glycol. CD_3OH was used as an internal reference for the ^{13}C spectra of the lead derivative. The spectra of the cadmium and mercury derivatives are referred to the CH_3 of the imidazole, whose signal is not affected by the nature of the metal. The $^{13}C\{^1H\}$ NMR spectra of the compounds in the range δ = 55−47 ppm were analyzed with the program CAHOS,[44] which can perform a line-shape fitting by simultaneous refinement of several spectral parameters. Elemental analyses were performed by the Microanalytical Laboratory of the Department of Chemistry of the University of Florence. The ligand H_2L^6 was prepared according to the published procedure.[36] Anhydrous cadmium carbonate (Aldrich), mercuric acetate (Acros) and lead acetate trihydrate (Carlo Erba) were used as received.

Synthesis of [CdL^6]·3H$_2$O: Neat $CdCO_3$ (43 mg, 0.25 mmol) was added to a solution of the ligand $H_2L^6\cdot 2H_2O$ (128 mg, 0.25 mmol) in H_2O (15 cm^3) and the resulting suspension warmed (ca. 60 °C) for 2 h; the remaining solid was eliminated by centrifugation and

 © 2003 Wiley-VCH Verlag GmbH & Co. KGaA, Weinheim

the solvent was removed in a desiccator under vacuum at room temperature. The resultant complex was recrystallized from CH_3CN and toluene; yield 65%. ^1H NMR (D_2O, 273 K, C_M = $9.2\cdot10^{-2}$, pD = 7.3): δ = 6.69 (d, J = 1.2 Hz, 2 H, H imidazole), 6.42 (d, J = 1.2 Hz, 2 H, H imidazole), 3.69 (d, J = 15.4 Hz, 2 H, CH_2 acetate), 3.34 (d, J = 15.3 Hz, 2 H, CH_2 acetate), 3.28 (s, 6 H, CH_3 imidazole), 3.01 (t, J = 11.9 Hz, 2 H, CH_2 macrocycle), 2.91 (t, J = 12.0 Hz, 2 H, CH_2 macrocycle), 2.67 (t, J = 12.5 Hz, 2 H, CH_2 macrocycle), 2.56 (d, J = 16.5 Hz, 2 H, CH_2 imidazole), 2.37 (t, J = 12.8 Hz, 2 H, CH_2 macrocycle), 2.28 (m, 6 H, CH_2 imidazole and CH_2 macrocycle), 2.05 (d, J = 12.9 Hz, 2 H, CH_2 macrocycle) and 1.86 (d, J = 12.9 Hz, 2 H, CH_2 macrocycle) ppm. $^{13}C\{^1H\}$ NMR: δ = 177.7 (COO^-), 145.8 (d, $^2J^{13}_{C\text{-}^{111}Cd}$ = 13.1 Hz, C^2 imidazole), 125.6, 122.5 (C^4, C^5 imidazole), 57.4 (CH_2COO^-), 51.8, 50.9, 48.4, 48.1 (CH_2 macrocycle), 48.4 (CH_2 imidazole) and 32.0 (CH_3 imidazole) ppm. $C_{22}H_{40}CdN_8O_7$ (641.0): calcd. C 41.2, H 6.3, N 17.5; found C 40.9, H 6.3, N 17.3.

Synthesis of $[ML^6]\cdot3H_2O$ (M = Hg, Pb): $Hg(CH_3COO)_2$ (0.25 mmol) dissolved in water (5 cm^3) was added to $H_2L^6\cdot2H_2O$ (0.25 mmol) in water (8 cm^3); the solution was then gently warmed (ca. 40 °C) for 5 h. After cooling, the pH was adjusted to 7.3 by adding Na_2CO_3 dissolved in water. The solvent was then removed at room temperature in a desiccator under vacuum and the obtained solid was recrystallized from CH_3CN and toluene; yield 60%. The lead derivative was obtained by the same procedure by adding $Pb(CH_3COO)_2\cdot3H_2O$ dissolved in water to a water solution of the ligand; yield 65%. $C_{22}H_{40}HgN_8O_7$ (729.2): calcd. C 36.2, H 5.5, N 15.4; found C 36.4, H 5.4; N. 14.6. ^1H NMR (D_2O, 273 K, c_M = $8.5\cdot10^{-2}$, pD = 7.3): δ = 6.76 (d, J = 1.3 Hz, 2 H, H imidazole), 6.44 (d, J = 1.2 Hz, 2 H, H imidazole), 3.73 (d, J = 15.6 Hz, 2 H, CH_2 acetate), 3.45 (d, J = 15.6 Hz, 2 H, CH_2 acetate), 3.29 (s, 6 H, CH_3 imidazole), 2.85 (m, 6 H, CH_2 macrocycle), 2.40 (m, 10 H, CH_2 imidazole and CH_2 macrocycle), 2.10 (d, J = 12.6 Hz, 2 H, CH_2 macrocycle) and 1.90 (d, J = 12.6 Hz, 2 H, CH_2 macrocycle) ppm. $^{13}C\{^1H\}$ NMR (D_2O, 273 K, c_M = $8.5\cdot10^{-2}$, pD = 7.3): δ = 176.6 (COO^-), 145.1 (d, $^2J^{13}_{C\text{-}^{199}Hg}$ = 54.5 Hz, C^2 imidazole), 125.6, 122.7 (C^4, C^5 imidazole), 56.6 (CH_2COO^-), 50.9, 50.6, 48.3, 47.5 (CH_2 macrocycle), 47.5 (CH_2 imidazole) and 32.0 (CH_3 imidazole) ppm.

$C_{22}H_{40}N_8O_7Pb$ (735.8): calcd. C 35.9, H 5.5, N 15.2; found C 36.0, H 5.4; N. 15.0. ^1H (D_2O, 273 K, c_M = $8.8\cdot10^{-2}$, pD = 7.2): δ = 6.74 (d, J = 1.3 Hz, 2 H, H imidazole), 6.50 (d, J = 1.3 Hz, 2 H, H imidazole), 3.98 (d, J = 15.6 Hz, 2 H, CH_2 acetate), 3.82 (d, J = 15.8 Hz, 2 H, CH_2 acetate), 3.27 (s, 6 H, CH_3 imidazole), 3.07 (m, 10 H, CH_2 macrocycle), 2.74 (t, J = 13.0 Hz, 2 H, CH_2 macrocycle), 2.48 (m, 6 H, CH_2 imidazole and CH_2 macrocycle) and 2.34 (d, J = 12.0 Hz, 2 H, CH_2 macrocycle) ppm. $^{13}C\{^1H\}$ (D_2O, 273 K, c_M = $8.8\cdot10^{-2}$, pD = 7.2): δ = 178.2 (COO^-), 145.4 (C^2 imidazole), 124.4, 123.1 (C^4, C^5 imidazole), 57.4 (CH_2COO^-), 53.3, 52.3, 49.9, 49.4 (CH_2 macrocycle), 49.2 (CH_2 imidazole) and 32.1 (CH_3 imidazole) ppm.

Computational Procedures: Calculations on the neutral $[ML^6]$ model systems (M = Cd, Pb, Hg) were performed with the GAUSSIAN 98 suite of programs,[45] generally using the hybrid HF-DFT B3LYP method.[46–48] Unless specified differently, the 6-311G(d) basis set was used for all non-metal atoms.[45,49] For the Cd and Pb atoms the LANL2DZ valence and effective core potential functions,[50] as well as their SDD counterparts,[51,52] were used for comparison purposes (only results from the former set of calculations are reported in some detail). For Hg the SDD functions were initially used and the lengthy calculations were not repeated with the alternative functions as no detailed comparisons were sought between systems formed with the different metal atoms. For brevity, the computational level B3LYP/6−311G(d) with LANL2DZ (Cd, Pb) or SDD (Hg) functions will be referred to as "level A". Geometry optimizations on gas phase models were performed with the C_2 symmetry restraint, all atoms being included. Initial geometries were from the previously investigated lanthanide analogs[53] or were applied by cross assignments, e.g. starting a Pb-model optimization from an optimized Hg-model geometry, and so on. The nature of stationary points as true minima was checked by frequency calculations, and unscaled ZPE corrections were applied to the energy values. To mimic conditions in solution, calculations (without vibrational analysis) were undertaken according to Onsager's reaction field (SCRF) approach,[54,55] at the B3LYP/6-311G(d)//B3LYP/6-31G(d) level (level B), with the above LANL2DZ/SDD metal functions. NMR shielding tensors were obtained by GIAO[56] [HF/6-311G(d) calculations on the vacuum-optimized geometries computational level C: HF/6-311G(d)//B3LYP/6-311G(d), with metal functions as above], chemical shifts for carbon atoms being calculated with respect to the 194.51 isotropic shielding tensor obtained for the Me_4Si carbon, at the same level C. For graphics, Molden[57] and ORTEP[58,59] were employed.

Acknowledgments

We acknowledge financial support by the Italian Ministero dell'Istruzione, dell'Università e della Ricerca.

[1] L. F. Lindoy, in *The Chemistry of Macrocyclic Ligand Complexes*, Cambridge University Press, Cambridge, **1989**.
[2] R. D. Hancock, A. E. Martell, *Chem. Rev.* **1989**, *89*, 1875−1914.
[3] P. V. Bernhardt, G. A. Lawrance, *Coord. Chem. Rev.* **1990**, *104*, 297−343.
[4] D. Parker, K. Pulukkody, T. J. Norman, A. Harrison, L. Royle, C. Walker, *J. Chem. Soc., Chem. Commun.* **1992**, 1441−1443.
[5] R. Dhillon, A. K. W. Stephens, S. L. Whitbread, S. F. Lincoln, K. P. Wainwright, *J. Chem. Soc., Chem. Commun.* **1995**, 97−98.
[6] D. Parker, J. A. G. Williams, *J. Chem. Soc., Dalton Trans.* **1996**, 3613−3628.
[7] H. Maumela, R. D. Hancock, L. Carlton, J. H. Reibenspies, K. P. Wainwright, *J. Am. Chem. Soc.* **1995**, *117*, 6698−6707.
[8] M. Di Vaira, F. Mani, N. Nardi, P. Stoppioni, A. Vacca, *J. Chem. Soc., Dalton Trans.* **1996**, 2679−2684.
[9] M. Di Vaira, F. Mani, P. Stoppioni, *J. Chem. Soc., Dalton Trans.* **1998**, 1879−1884.
[10] R. Dhillon, S. F. Lincoln, S. Madbak, A. K. W. Stephens, K. P. Wainwright, S. L. Whitbread, *Inorg. Chem.* **2000**, *39*, 1855−1858.
[11] M. G. B. Drew, *Coord. Chem. Rev.* **1977**, *24*, 179−275.
[12] I. Murase, I. Ueda, N. Marubayashi, S. Kida, N. Matsumoto, M. Kudo, M. Toyohara, K. Hiate, M. Mikuriya, *J. Chem. Soc., Dalton Trans.* **1990**, 2763−2769.
[13] L. H. Tan, M. R. Taylor, K. P. Wainwright, P. A. Duckworth, *J. Chem. Soc., Dalton Trans.* **1993**, 2921−2928.
[14] K. P. Wainwright, *Adv. Inorg. Chem.* **2001**, *52*, 293−334.
[15] V. Balzani, J. M. Lehn, J. Van de Loosdrecht, A. Mecati, N. Sabbatini, R. Ziessel, *Angew. Chem. Int. Ed. Engl.* **1991**, *30*, 190−191.
[16] D. Parker, J. A. G. Williams, *Chem. Commun.* **1998**, 245−246.
[17] D. Parker, *Chem. Br.,* 1994, **30**, 818−822.
[18] *Comprehensive Supramolecular Chemistry* (Eds.: J.-M. Lehn, D. D. Macnicol, J. L. Atwood, J. E. Davies, D. N. Reinhoudt, F. Vogtle), Pergamon: Oxford, 1996; Vol. 10, ch. 17.
[19] B. Barbier, A. Brack, *J. Am. Chem. Soc.* **1988**, *110*, 6880−6882.
[20] Y. Matsumoto, M. Komiyama, *J. Chem. Soc., Chem. Commun.* **1990**, 1050−1051.

 © 2003 Wiley-VCH Verlag GmbH & Co. KGaA, Weinheim

[21] K. O. A. Chin, J. R. Morrow, *Inorg. Chem.* **1994**, *33*, 5036−5041.
[22] L. Carlton, R. D. Hancock, H. Maumela, K. P. Wainwright, *J. Chem. Soc., Chem. Commun.* **1994**, 1007−1008.
[23] S. Buøen, J. Dale, P. Groth, J. Krane, *J. Chem. Soc., Chem. Commun.* **1982**, 1172−1174.
[24] C. M. Madeyski, J. P. Michael, R. D. Hancock, *Inorg. Chem.* **1984**, *23*, 1487−1489.
[25] A. K. W. Stephens, S. F. Lincoln, *J. Chem. Soc., Dalton Trans.* **1993**, 2123−2126.
[26] K. O. A. Chin, J. R. Morrow, C. H. Lake, M. R. Churchill, *Inorg. Chem.* **1994**, *33*, 656−664.
[27] M. R. Spirlet, J. Rebizant, J. F. Desreux, M. F. Loncin, *Inorg. Chem.* **1984**, *23*, 359−363.
[28] J. P. Dubost, J. M. Leger, M. H. Langlois, D. Meyer, M. Schaefer, *C. R. Acad. Sci. Paris, Ser. II* **1991**, *312*, 349−354.
[29] S. Aime, A. Barge, M. Botta, M. Fasano, J. D. Ayala, G. Bombieri, *Inorg. Chim. Acta* **1996**, *246*, 423−429.
[30] S. Aime, A. Barge, F. Benetollo, G. Bombieri, M. Botta, F. Uggeri, *Inorg. Chem.* **1997**, *36*, 4287−4289.
[31] J. R. Morrow, S. Amin, C. H. Lake, M. R. Churchill, *Inorg. Chem.* **1993**, *32*, 4566−4572.
[32] S. Aime, A. S. Batsanov, M. Botta, J. A. K. Howard, D. Parker, K. Senanayake, G. Williams, *Inorg. Chem.* **1994**, *33*, 4696−4706.
[33] M. Di Vaira, F. Mani, P. Stoppioni, *J. Chem. Soc., Chem. Commun.* **1989**, 126−127.
[34] M. Di Vaira, F. Mani, P. Stoppioni, *J. Chem. Soc., Dalton Trans.* **1992**, 1127−1130.
[35] M. Di Vaira, F. Mani, M. Menicatti, R. Morassi, P. Stoppioni, *Polyhedron* **1997**, *16*, 3585−3591.
[36] F. Mani, R. Morassi, P. Stoppioni, A. Vacca, *J. Chem. Soc., Dalton Trans.* **2001**, 2116−2120.
[37] E. Tóth, E. Brucher, I. Lázár, I. Tóth, *Inorg. Chem.* **1994**, *33*, 4070−4076.
[38] J. F. Desreux, *Inorg. Chem.* **1980**, *19*, 1319−1324.
[39] S. Aime, M. Botta, G. Ermondi, *Inorg. Chem.* **1992**, *31*, 4291−4299.
[40] S. Aime, M. Botta, M. Fasano, M. P. M. Marques, C. F. G. C. Geraldes, D. Pubanz, A. E. Merbach, *Inorg. Chem.* **1997**, *36*, 2059−2068.
[41] A. K. W. Stephens, R. S. Dhillon, S. E. Madbak, S. L. Whitbread, S. F. Lincoln, *Inorg. Chem.* **1996**, *35*, 2019−2024.
[42] M. Di Vaira, M. Guerra, F. Mani, P. Stoppioni, *J. Chem. Soc., Dalton Trans.* **1996**, 1173−1179.
[43] G. de Martino Norante, M. Di Vaira, F. Mani, S. Mazzi, P. Stoppioni, *J. Chem. Soc., Chem. Commun.* **1990**, 438−439.
[44] F. Cecconi, C. A. Ghilardi, P. Innocenti, S. Midollini, A. Orlandini, A. Ienco, A. Vacca, *J. Chem. Soc., Dalton Trans.* **1996**, 2821−2826.
[45] Frisch, M. J., G. W. Trucks, H. B. Schlegel, G. E. Scuseria, M. A. Robb, J. R. Cheeseman, V. G. Zakrzewski, J. A. Montgomery, Jr., R. E. Stratmann, J. C. Burant, S. Dapprich, J. M. Millam, A. D. Daniels, K. N. Kudin, M. C. Strain, O. Farkas, J. Tomasi, V. Barone, M. Cossi, R. Cammi, B. Mennucci, C. Pomelli, C. Adamo, S. Clifford, J. Ochterski, G. A. Petersson, P. Y. Ayala, Q. Cui, K. Morokuma, D. K. Malick, A. D. Rabuck, K. Raghavachari, J. B. Foresman, J. Cioslowski, J. V. Ortiz, A. G. Baboul, B. B. Stefanov, G. Liu, A. Liashenko, P. Piskorz, I. Komaromi, R. Gomperts, R. L. Martin, D. J. Fox, T. Keith, M. A. Al-Laham, C. Y. Peng, A. Nanayakkara, C. Gonzalez, M. Challacombe, P. M. W. Gill, B. Johnson, W. Chen, M. W. Wong, J. L. Andres, C. Gonzalez, M. Head-Gordon, E. S. Replogle, J. A. Pople, Gaussian 98, Revision A.7, Gaussian, Inc., Pittsburgh PA (USA), **1998**.
[46] A. D. Becke, *J. Chem. Phys.* **1993**, *98*, 5648−5652.
[47] A. D. Becke, *J. Chem. Phys.* **1993**, *98*, 1372−1377.
[48] C. Lee, W. Yang, R. G. Parr, *Phys. Rev. B: Condens. Matter Mater. Phys.* **1988**, *37*, 785−789.
[49] R. Krishnan, J. S. Binkley, R. Seeger, J. A. Pople, *J. Chem. Phys.* **1980**, *72*, 650−654.
[50] P. J. Hay, W. R. Wadt, *J. Chem. Phys.* **1985**, *82*, 270−283.
[51] M. Dolg, H. Stoll, A. Savin, H. Preuss, *Theor. Chim. Acta* **1989**, *75*, 173−194.
[52] A. Bergner, M. Dolg, W. Kuechle, H. Stoll, H. Preuss, *Mol. Phys.* **1993**, *80*, 1431−1441.
[53] M. Di Vaira, P. Stoppioni, *New J. Chem.* **2002**, *26*, 136−144.
[54] L. Onsager, *J. Am. Chem. Soc.* **1936**, *58*, 1486−1493.
[55] M. W. Wong, K. B. Wiberg, M. J. Frisch, *J. Am. Chem. Soc.* **1992**, *114*, 1645−1652.
[56] K. Wolinski, J. F. Hinton, P. Pulay, *J. Am. Chem. Soc.* **1990**, *112*, 8251−8260.
[57] G. Schaftenaar, J. H. Noordik, *J. Comput.-Aided Mol. Design* **2000**, *14*, 123−134.
[58] C. K. Johnson, *ORTEP*, Report ORNL-5138, Oak Ridge National Laboratory, Oak Ridge, TN, USA, **1976**.
[59] L. J. Farrugia, *J. Appl. Crystallogr.* **1997**, *30*, 565.

Received March 31, 2003

 © 2003 Wiley-VCH Verlag GmbH & Co. KGaA, Weinheim

Metal Complexes of a Novel Achiral Symmetric Pentadentate Ligand – Crystal Structures of Monohelical Zinc(II) and Cadmium(II) Complexes

Rosa Pedrido,[a] Manuel R. Bermejo,*[a] Ana M. García-Deibe,[a] Ana M. González-Noya,[a] Marcelino Maneiro,[a] and Miguel Vázquez[a]

Keywords: Supramolecular chemistry / Helical structures / Schiff bases / Electrochemistry

By both electrochemical synthesis and a traditional chemical procedure the interaction of the pentadentate ligand 2,6-bis{1-[2-(tosylamino)phenylimino]ethyl}pyridine (H_2DAPATs), with Mn^{II}, Fe^{II}, Co^{II}, Ni^{II}, Cu^{II}, Zn^{II} and Cd^{II} gives rise to neutral mononuclear complexes that have been characterised by elemental analyses, FAB mass spectrometry, IR, ^{1}H and COSY NMR spectroscopy and magnetic measurements, where appropriate. Recrystallisation of the zinc complex obtained electrochemically yielded single crystals of [Zn(DAPATs)] (**1**), while recrystallisation of cadmium complexes obtained by both techniques afforded the same structure, [Cd(DAPATs)(H_2O)] (**2**). Both **1** and **2** are monohelical single-stranded compounds with different coordination geometries. In the zinc complex, the metal ion assumes a distorted trigonal-bipyramidal geometry involving the N_5 atoms of the dianionic ligand. For cadmium complexes the metal ion is in a distorted pentagonal-pyramidal environment, as the result of coordination to the N_5 ligand donor set and an additional water molecule.

(© Wiley-VCH Verlag GmbH & Co. KGaA, 69451 Weinheim, Germany, 2003)

Introduction

Helical complexes are an active research area in supramolecular chemistry.[1–5] Nevertheless, predicting the outcome of a self-assembly process is still difficult and dependent upon numerous factors, such as the nature of the metal (coordination numbers and stereochemical preferences), the structure of the ligand, the existence of weak non-covalent interactions, etc.

Most ligands employed in the synthesis of helicates are predominantly benzimidazole,[6] catechole[7] or polypyridine types,[8] and they usually imply long and complicated synthetic routes. More recently, readily prepared Schiff-base ligands have been used to obtain helical species.[9,10]

In recent years part of our research program has focused on using pentadentate hydrazone ligands derived from 2,6-diacetylpyridine to produce helical compounds.[10–12] Previous works have demonstrated that such ligands react with metal chlorides to yield complexes containing the non-deprotonated ligand, while complexes with the bis(deprotonated) ligand could be obtained with metal acetates.[13,14] We have recently found that pentadentate ligands incorporating a rigid spacer such as pyridine yield dinuclear helical complexes for Ni[10,11] and Cu[15] and non-helical mononuclear complexes for Mn,[10,11] Co[10] and Cd[12] by electrochemical synthesis.

We have also shown that introducing bulky tosyl groups in Schiff-base ligands with different spacers is very useful in obtaining mono- and dihelical species.[16]

We then wanted to check the effect of the simultaneous presence of a bulky group, such as tosyl, and a rigid spacer, like pyridine, in a pentadentate Schiff-base ligand. Therefore, we have designed the novel pentadentate N_5 ligand 2,6-bis{1-[2-(tosylamino)phenylimino]ethyl}pyridine (H_2DAPATs).

The interaction of H_2DAPATs with Mn^{II}, Fe^{II}, Co^{II}, Ni^{II}, Cu^{II}, Zn^{II} and Cd^{II} using electrochemical and chemical procedures was investigated and the results obtained are described herein.

Results and Discussion

Synthesis of the Ligand

The Schiff base H_2DAPATs has been prepared according to a two-step synthetic route (Scheme 1) with an overall yield of 50%. The first step involves the *N*-tosylation of 1,2-diaminobenzene[17] (**I**), to obtain 2-(tosylamino)aniline (**II**). Treatment of **II** with 2,6-diacetylpyridine in a 1:2 stoichiometric ratio in ethanol under reflux yields the N_5 Schiff-base ligand H_2DAPATs.

The deep yellow powdery solid formed was satisfactorily characterised by elemental analysis, FAB mass spec-

[a] Departamento de Química Inorgánica, Facultade de Química, Universidade de Santiago de Compostela, 15782 Santiago de Compostela, Spain
Fax: (internat.) + 34-981/597525
E-mail: qimb45@usc.es

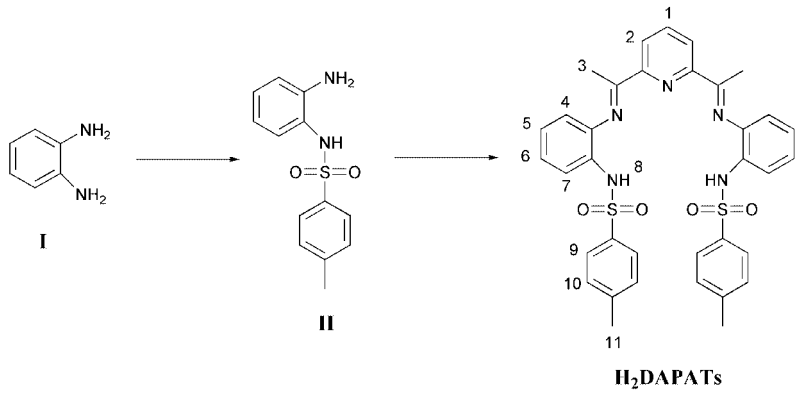

Scheme 1. Synthesis of H_2DAPATs

Table 1. Elemental analysis and selected data for the ligand and its complexes obtained by electrochemical synthesis

Compound	Yield (%)	Colour	C[a]	H[a]	N[a]	S[a]	FAB[b]	μ[c]
H_2DAPATs	50	yellow	55.3 (55.4)	5.0 (4.9)	9.0 (9.2)	8.2 (8.4)	652	–
Mn(DAPATs)$(H_2O)_3$	85	brown	55.1 (55.3)	4.7 (4.9)	9.1 (9.2)	8.5 (8.4)	705	5.6
Fe(DAPATs)$(H_2O)_3$	55	brown	57.6 (57.8)	4.6 (4.8)	9.7 (9.6)	8.8 (8.8)	706	5.0
Co(DAPATs)(H_2O)	95	black	56.3 (56.5)	4.9 (4.7)	9.4 (9.4)	8.6 (8.6)	709	3.9
Ni(DAPATs)$(H_2O)_2$	85	brown	54.7 (54.8)	4.8 (4.6)	8.0 (8.1)	8.4 (8.1)	709	2.9
Cu(DAPATs)$(H_2O)_3$	55	black	54.7 (54.8)	4.8 (4.6)	8.0 (8.1)	8.4 (8.1)	713	2.0
Zn(DAPATs)$(H_2O)_2$	95	orange	56.1 (55.9)	4.9 (4.7)	9.2 (9.3)	8.4 (8.5)	716	–
Cd(DAPATs)(H_2O)	95	orange	53.8 (53.9)	4.2 (4.3)	8.8 (9.0)	8.1 (8.2)	765	–

[a] Found (calcd.). [b] amu; peaks corresponding to $[ML]^+$. [c] In B.M.

Table 2. Selected IR data [cm^{-1}] for the ligand and its complexes obtained by electrochemical synthesis

Compound	ν(N–H)	ν(C=N)	ν(C–N)$_{py}$	$\nu_{as}(SO_2)$	$\nu_s(SO_2)$
H_2DAPATs	3273 m	1627 s	1596 s	1335 s	1167 s
Mn(DAPATs)$(H_2O)_3$	–	1656 s	1597 s	1335 s	1162 s
Fe(DAPATs)$(H_2O)_3$	–	1636 s	1596 s	1361 s	1159 s
Co(DAPATs)(H_2O)	–	1621 m	1590 s	1374 s	1154 s
Ni(DAPATs)$(H_2O)_2$	–	1656 m	1588 s	1372 s	1163 s
Cu(DAPATs)$(H_2O)_3$	–	1621 m	1590 s	1381 s	1138 s
Zn(DAPATs)$(H_2O)_2$	–	1634 m	1587 s	1370 s	1138 s
Cd(DAPATs)(H_2O)	–	1636 s	1586 s	1370 s	1130 s

trometry, IR and ^{1}H and COSY NMR spectroscopy (Tables 1, 2 and 6).

Synthesis of the Complexes

A series of neutral complexes were obtained by electrochemical oxidation of the corresponding metal anode in the presence of the ligand.[18] The electrochemical efficiency of the cell was close to 0.5 mol·F^{-1}, which is compatible with the following reaction scheme:

Cathode: $H_2DAPATs + 2\ e^- \rightarrow H_2\ (g) + DAPATs^{2-}$

Anode: $DAPATs^{2-} + M \rightarrow M(DAPATs) + 2\ e^-$

This synthetic procedure allowed us to obtain neutral complexes of the type M(DAPATs)$(H_2O)_n$ with high purity and in very good yield.

These metal compounds were also obtained by a traditional chemical procedure, in which a solution of the ligand was refluxed in the presence of a metal(II) acetate. As the characterisation patterns of these complexes are similar to those obtained by electrochemical synthesis we shall discuss only the latter ones.

Elemental analyses (Table 1) show that metal ions react with the ligand in a molar ratio of 1:1 to afford solvated complexes of the bis(deprotonated) ligand $DAPATs^{2-}$. These neutral complexes are either insoluble or sparingly soluble in water and common organic solvents, but soluble in polar coordinating organic solvents such us DMSO, DMF and pyridine. The powdery complexes appear to be stable both in the solid state and in solution, and all of them melt above 300 °C without decomposition.

X-ray Studies

The crystal structures of complexes [Zn(DAPATs)] (**1**) and [Cd(DAPATs)(H_2O)] (**2**) are shown in Figures 1, 2 and 3. Selected bond lengths and angles are given in Tables 4 and 5. The complexes are considered together here in order to comment on their structural similarities and differences.

They consist of discrete neutral molecules of [Zn(DAPATs)] (**1**) and [Cd(DAPATs)(H_2O)] (**2**), the ligand being bis(deprotonated), $DAPATs^{2-}$. In complex **1** all five nitrogen donor atoms of the ligand (two imine, two amide and one pyridine nitrogen atoms) bind to the same zinc ion. No additional ligands are coordinated to the zinc ion, resulting in a coordination number of five and a distorted bipyramidal-trigonal geometry. In this complex the Schiff-base li-

 © 2003 Wiley-VCH Verlag GmbH & Co. KGaA, Weinheim

Table 3. Crystal data and structure refinement for **1** and **2**

	[Zn(DAPATs)] (**1**)	[Cd(DAPATs)(H_2O)] (**2**)
Empirical formula	$C_{35}H_{31}N_5O_4S_2Zn$	$C_{35}H_{33}CdN_5O_5S_2$
Formula mass	715.14	780.18
Temperature [K]	293.0(2)	298.0(2)
Crystal system	triclinic	monoclinic
Space group	$P\bar{1}$	$P2_1/c$
a [Å]	9.3474(14)	11.2037(10)
b [Å]	10.8789(14)	10.6130(2)
c [Å]	17.853(3)	28.4432(3)
α [°]	73.691(3)	90
β [°]	84.882(3)	97.46(7)
γ [°]	65.678(3)	90
Z	2	4
Volume [Å^3]	1587.1(4)	3353.41(8)
Absorption coefficient [mm^{-1}]	0.954	0.826
Crystal size [mm]	0.15×0.10×0.02	0.24×0.20×0.14
Reflections collected	10909	17862
Independent reflections	3900 [R(int) = 0.0925]	8197 [R(int) = 0.0824]
Absorption correction	SADABS	SADABS
Data/restraints/parameters	3900/0/424	8197/0/437
Final R indices [$I > 2\sigma(I)$]	$R1$ = 0.0432	$R1$ = 0.0697
	$wR2$ = 0.0821	$wR2$ = 0.1099
R indices (all data)	$R1$ = 0.1343	$R1$ = 0.1533
	$wR2$ = 0.1368	$wR2$ = 0.1457

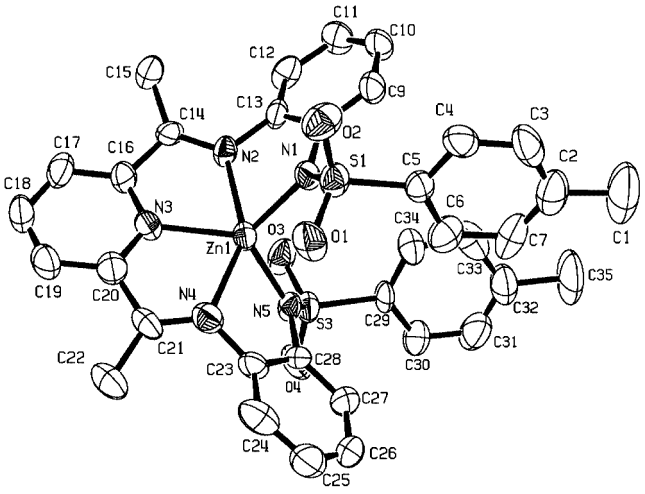

Figure 1. ORTEP view of the crystal structure of [Zn(DAPATs)] (**1**); ellipsoids are drawn at 50% of probability; hydrogen atoms have been omitted for clarity

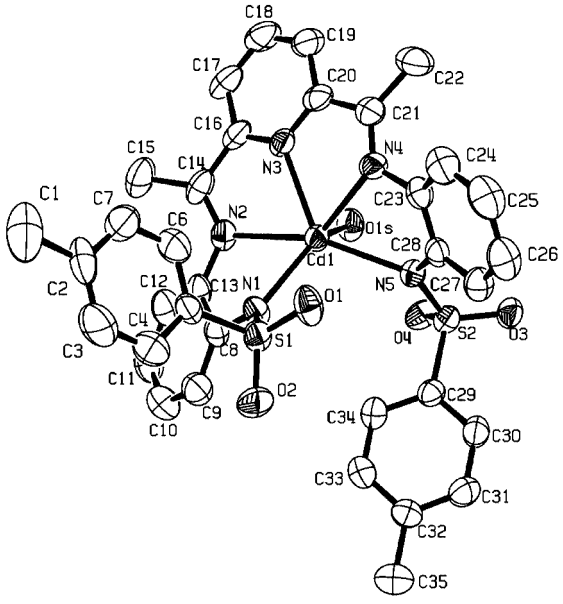

Figure 2. ORTEP view of the crystal structure of [Cd(DAPATs)-(H_2O)] (**2**); ellipsoids are drawn at 50% of probability; hydrogen atoms have been omitted for clarity

gand fulfills all the stereochemical requirements of the metal, and subsequently it can be considered a saturated compound.[4]

However, **2** is an unsaturated compound because the cadmium ion is coordinated to the same five nitrogen donor atoms of the bis(deprotonated) ligand but also needs one additional water molecule, leading to a coordination number of six and to a distorted pentagonal-pyramidal geometry.

This geometry is unusual for cadmium complexes derived from pentadentate Schiff-base ligands because, to the best of our knowledge, only one such cadmium complex with this type of geometry has been previously reported.[12] In addition, helicity in cadmium compounds is uncommon – only two monohelical cadmium complexes with Schiff-base ligands have been reported.[12,19]

For complex **1** the $Zn-N_{imine}$ distances [Zn(1)–N(2) 2.160(6) Å, Zn(1)–N(4) 2.172(7) Å] are of the order of those found for the unique monohelical zinc complex reported with similar geometry,[20] $[Zn(SpyNpy_2)]^{2+}$. The distance $Zn-N_{pyridine}$ [Zn(1)–N(3) 2.102(7) Å] is shorter than those found for penta-[21] or heptacoordinated[13,22] com-

 © 2003 Wiley-VCH Verlag GmbH & Co. KGaA, Weinheim

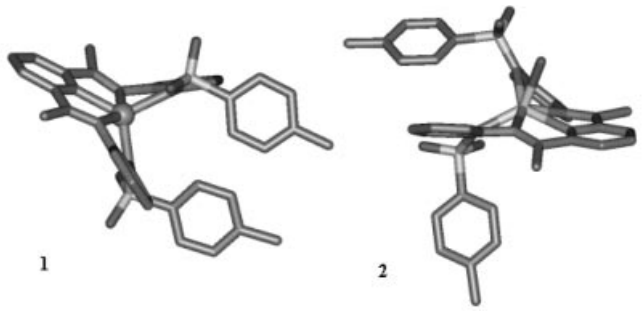

Figure 3. Stick view of [Zn(DAPATs)] (**1**) and [Cd(DAPATs)(H_2O)] (**2**), showing the screwing of the ligand

Table 4. Selected bond lengths [Å] for **1** and **2**

[Zn(DAPATs)] (**1**)		[Cd(DAPATs)(H_2O)] (**2**)	
Zn(1)−N(5)	2.006(7)	Cd(1)−N(1)	2.237(4)
Zn(1)−N(1)	2.017(6)	Cd(1)−N(5)	2.345(4)
Zn(1)−N(3)	2.102(7)	Cd(1)−N(3)	2.350(5)
Zn(1)−N(2)	2.160(6)	Cd(1)−N(4)	2.360(4)
Zn(1)−N(4)	2.172(7)	Cd(1)−O(1s)	2.377(4)
Zn(1)···O(1)	3.052	Cd(1)−N(2)	2.464(5)
Zn(1)···O(2)	4.147	Cd(1)···O(1)	3.126
Zn(1)···O(3)	3.092	Cd(1)···O(2)	4.475
Zn(1)···O(4)	4.273	Cd(1)···O(3)	4.749
		Cd(1)···O(4)	3.540

Table 5. Selected bond angles [°] for **1** and **2**

[Zn(DAPATs)] (**1**)		[Cd(DAPATs)(H_2O)] (**2**)	
N(5)−Zn(1)−N(1)	108.9(3)	N(1)−Cd(1)−N(5)	105.3(16)
N(1)−Zn(1)−N(2)	75.9(3)	N(1)−Cd(1)−N(2)	67.7(16)
N(3)−Zn(1)−N(2)	73.3(3)	N(2)−Cd(1)−N(3)	66.8(17)
N(3)−Zn(1)−N(4)	73.7(3)	N(3)−Cd(1)−N(4)	73.7(17)
N(5)−Zn(1)−N(4)	75.4(3)	N(5)−Cd(1)−N(4)	69.4(15)
C(5)−S(1)−N(1)	108.2(4)	N(1)−Cd(1)−O(1S)	125.2(15)
C(29)−N(5)−S(3)	108.4(4)	N(5)−Cd(1)−O(1S)	83.9(14)
		N(3)−Cd(1)−O(1S)	81.5(14)
		N(2)−Cd(1)−O(1S)	81.7(14)
		N(4)−Cd(1)−O(1S)	101.8(14)
		C(5)−S(1)−N(1)	107.0(3)
		C(29)−S(2)−N(5)	111.1(2)

plexes with pentadentate ligands containing $Zn-N_{pyridine}$ bonds.

For complex **2** all Cd−N distances are significantly longer than the corresponding Zn−N distances, and in both complexes $M-N_{imine}$ are longer than $M-N_{amide}$. In addition, the $Cd-N_{pyridine}$ bond [Cd(1)−N(3) 2.350(5) Å] is shorter than that of the distorted pyramidal-pentagonal cadmium complex with the pentadentate Schiff base H_4daps[12] [2.403(6) Å], but longer than those found in octahedral complexes with quite similar Schiff-base ligands (ranging from 2.310 to 2.346 Å).[23−26]

The distance Cd−O(1s) [2.377(4) Å] is of the order of those found for similar cadmium complexes.[12]

The remaining distances for both compounds are in the usual range for complexes derived from Schiff-base ligands containing tosyl groups[16,27,28] and do not merit further analysis.

The four bond angles N−Zn−N formed by the four chelate rings are close to 75°. The fifth one, N(5)−Zn(1)−N(1), is 108.9(3)°. These values explain the distorted trigonal-bipyramidal geometry adopted in **1**. In complex **2** the distortion from the ideal geometry is clearly shown by the angles between water, cadmium and the donor set of the ligand (Table 5). Four of the five angles subtended at Cd by adjacent equatorial atoms are slightly smaller than those of an ideal pentagonal-pyramidal arrangement, being close to 70°, while the fifth, N(1)−Cd(1)−N(5) is 105.33(16)°. Moreover three bond angles O(1s)−Cd(1)−N are in the range 81−84° while the other two are in the range 101−125°, reinforcing the highly distorted pyramidal-pentagonal geometry adopted by **2**.

The bond angles C(5)−S(1)−N(1) and C(29)−S(3)−N(5) are quite similar for the zinc complex [108.2(4) and 108.7(4)°, respectively]; both tosyl groups adopt a similar conformation (Figure 3). Nevertheless, in the cadmium complex these angles, C(5)−S(1)−N(1) and C(29)−S(2)−N(5), are slightly different [107.0(3) and 111.1(2)°, respectively], causing an *anti* orientation of the tosyl groups to reduce the steric hindrance.

Why do zinc and cadmium complexes show different coordination numbers and geometries? We suggest that two factors could be responsible:

i. Steric hindrance of the bulky tosyl groups.

The pentadentate dianionic ligand, $DAPATs^{2-}$, is wrapped around the metal ions to afford a helical arrangement in both complexes. This screwed disposition of the ligand seems to be clearly favoured by the two terminal bulky tosyl groups. The steric hindrance these groups induce appears to provoke a twisting of the Schiff base to minimise the sterically unfavourable interactions.

Therefore, a rigid spacer such as pyridine, containing a donor atom, and the torsion around the C=N bonds will allow the imine nitrogen atoms to be quite close (ca. 4.2 Å for **1** and 4.4 Å for **2**) and coordinate to the same metal centre. This permits the five nitrogen atoms to bind to the same metal centre, leading to the isolation of mononuclear single-stranded helical complexes.

ii. Closeness of the tosyl oxygen atoms to the metal centre.

For **1**, one oxygen atom of each tosyl group, O(1) and O(3), seems to weakly interact with the metal ion [distances O(1)···Zn(1) 3.052 Å and O(3)···Zn(1) 3.092 Å]. These Zn···O distances are too long to be true coordinated bonds, but could be considered as secondary intramolecular interactions that could be responsible for the distorted trigonal-bipyramidal disposition around the metal centre, instead of the usual bipyramidal-pentagonal or pyramidal-pentagonal geometries, because these oxygen atoms avoid coordinating additional donor ligands in the apical positions.

In complex **2** the bigger cadmium ion leads to longer metal−donor distances, in general, and in $Cd-O_{tosyl}$ especially. Thus, only one oxygen atom of one tosyl group, O(1) could weakly interact with the cadmium ion [distance

 © 2003 Wiley-VCH Verlag GmbH & Co. KGaA, Weinheim

Cd(1)···O(1) 3.126 Å], while in the other tosyl group both oxygen atoms are too far to interact with the cadmium ion [Cd(1)···O(4) 3.540 Å, Cd(1)···O(3) 4.749 Å]. Such a situation affords an easy entrance and binding for a new additional ligand such as water, increasing the coordination number to six.

Thus, the different monohelical dispositions of these two complexes can be attributed to the tosyl groups, which show different spatial orientations (Figure 3). In the zinc complex the angle between the benzene rings of the tosyl groups is 11.75°. This nearly parallel orientation for the terminal tosyl aromatic rings is unusual for complexes with Schiff-base ligands containing these bulky groups. It can be explained by the lack of superposition of the tosyl groups, which avoid the unfavourable steric interactions.

In the cadmium complex the angle between the benzene rings is 47.60°, yielding a spatial conformation quite similar to that of other monohelical complexes derived from tetradentate Schiff bases containing tosyl groups.[16]

The $DAPATs^{2-}$ thread forms four five-membered chelate rings around the metal centres. The angles between adjacent calculated chelate planes (36.65 and 37.76° for **1**; 29.48 and 26.10° for **2**) confirm the different twisting degree of the ligand for both complexes. The smaller degree of twisting for the cadmium complex is also confirmed by the angles formed between the benzylidene rings (63.45° for **1** and 37.21° for **2**).

If the tosyl groups are not considered, we can clearly observe that the wrapping angle is less than 360°, and slightly higher for the zinc complex than for the cadmium (287° for **1** and 274° for **2**). All these considerations agree with the ionic radius of the metals, as expected. The size of the cadmium ion forces the N_5 donor set of the ligand to deviate from planarity when it surrounds this metal, resulting a smaller twisting degree.

[Zn(DAPATs)] crystallises in the achiral space group $P\bar{1}$ and [Cd(DAPATs)(H_2O)] in $P(2)1/c$, so that both right- (*P*) and left-handed (*M*) helixes[4] can be simultaneously observed (in 50% yields) in their unit cells. Helicates obtained from ligands not containing chiral groups usually crystallise as racemic mixtures and self-recognition is not a very common process.

Finally, no face-to-face π-stacking interactions between the terminal tosyl aromatic rings can be identified in either complex.

FAB Mass and IR Spectra

All the FAB mass spectra show peaks due to the fragments $[M(DAPATs)]^+$, indicating ligand coordination to the metal centres (Table 1). No additional peaks appear, suggesting that the complexes are mononuclear.

The IR spectra of the complexes (Table 2) show a strong band between 1621 and 1656 cm^{-1} attributable to ν(C=N). This band appears 6 cm^{-1} shifted to lower energy from that in cobalt and copper complexes. With manganese, iron, nickel, zinc and cadmium complexes the ν(C=N) band is shifted to higher wavenumbers (7−29 cm^{-1}), indicating a slight shift of charge towards the CN group on coordination. However, the $\nu(C-N)_{py}$ stretching frequency is not shifted for manganese and iron complexes and is slightly shifted to lower energy (6−10 cm^{-1}) for the other compounds. This behaviour is compatible with the participation of both imine and amide nitrogen atoms in the coordination to the metal centres. Additionally, two bands in the ranges 1335−1381 and 1130−1167 cm^{-1} are assigned to the asymmetric and symmetric vibration modes of SO_2 groups, respectively.[29,30]

Furthermore, no bands around 3270 cm^{-1} are seen, indicating the deprotonation of the NH groups, and therefore the dianionic character of the ligand.

Finally, the ν(O−H) bands around 3400 cm^{-1} agree with the hydrate nature of these complexes.

Magnetic Characterisation

Magnetic measurements were performed at room temperature for all paramagnetic complexes. Their magnetic moments are close to those expected for magnetically dilute M^{II} ions, confirming the oxidation state II for the central atom and, therefore, that the ligands are dianionic.

^{1}H NMR Spectroscopy

The ^{1}H NMR spectra of the zinc and cadmium complexes were recorded in [D_6]DMSO at room temperature and CD_3CN at low temperatures (273 and 233 K). Selected ^{1}H NMR data are shown in Table 6. The room-temperature spectra were totally assigned by COSY experiments. The spectra do not show significant changes with temperature, being quite similar to those recorded at room temperature. All spectra show a single set of signals that could be completely assigned. This seems to indicate a single species in

Table 6. Selected ^{1}H NMR spectroscopic data for the ligand H_2DAPATs and its diamagnetic complexes (in ppm)

Compound	H1	H2	H3	H4	H5	H6	H7	H8	H9	H10	H11
H_2DAPATs	8.09 (t, 1 H)	8.31 (d, 2 H)	2.06 (s, 6 H)	6.75 (d, 2 H)	7.10 (t, 2 H)	7.09 (t, 2 H)	7.32 (d, 2 H)	9.34 (s, 2 H)	7.56 (d, 4 H)	7.21 (d, 4 H)	2.31 (s, 6 H)
Zn(DAPATs)(H_2O)$_2$	8.57 (t, 1 H)	8.47 (d, 2 H)	2.60 (s, 6 H)	7.31 (m, 2 H)	7.19 (t, 2 H)	7.28 (m, 2 H)	7.48 (d, 2 H)	–	7.36 (d, 4 H)	7.09 (d, 4 H)	2.20 (s, 6 H)
Cd(DAPATs)(H_2O)	8.50 (t, 1 H)	8.37 (d, 2 H)	2.48 (s, 6 H)	7.23−7.12 (m, 2 H)	7.23−7.12 (m, 2 H)	6.88 (t, 2 H)	7.23−7.12 (m, 2 H)	–	7.64 (d, 4 H)	7.03 (d, 4 H)	2.24 (s, 6 H)

 © 2003 Wiley-VCH Verlag GmbH & Co. KGaA, Weinheim

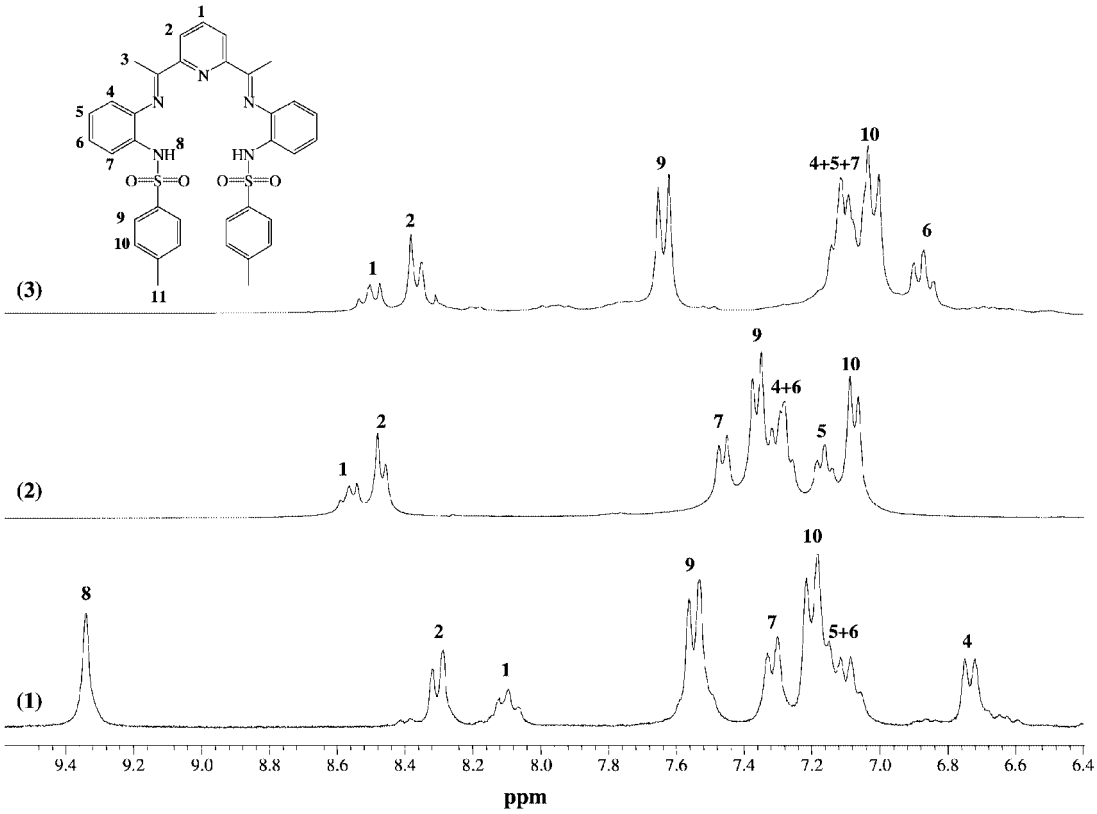

Figure 4. ^{1}H NMR spectra in [D_6]DMSO at room temperature for: (1) H_2DAPATs, (2) Zn(DAPATs)(H_2O)$_2$ and (3) Cd(DAPATs)(H_2O)

solution. Comparison of the ^{1}H NMR spectrum of the free ligand with those of the complexes (Figure 4) shows some interesting aspects:

– The NH (H8) protons present in the free ligand disappear for both complexes, in agreement with the bis(deprotonation) of the ligand.

– The aromatic proton signals of the pyridine ring are shifted downfield, and the displacements are higher for the zinc complex. The spectra show that complexation through the $N_{pyridine}$ atom affects the environments of the H1 and H2 atoms, and these signals appear with their positions exchanged with respect to the free ligand.

– The aromatic proton signals of the tosyl groups also shift on complexation, but the displacements differ for the zinc and cadmium complexes. For the zinc complex the H9 and H10 signals are shifted upfield, whilst in the cadmium compound the H10 signal is shifted upfield and the H9 signal is shifted downfield. This could be attributed to an interaction between the tosyl groups and the metal centres, as the solid-state X-ray structures of **1** and **2** seem to confirm.

– The aromatic proton signals of the benzylidene rings also appear to show different behaviour on complexation. In the zinc complex the H5 signal moves its position slightly while the H4, H6 and H7 signals are shifted downfield, with the H4 and H6 signals overlapped. With the cadmium complex the H4, H5 and H7 signals are completely overlapped. The H5 signal does not show significant changes in its position, while the H6 and H7 signals are shifted upfield and the H4 signal is strongly shifted downfield.

– Finally, in both complexes the methyl proton signals corresponding to tosyl and acetyl groups are shifted slightly downfield.

Comparison of the ^{1}H NMR spectra of zinc and cadmium complexes suggests that the tosyl groups adopt different spatial orientations in each complex, as the X-ray structures confirm, because of the size of the metal ions and their different geometrical preferences.

From the characterisation techniques employed in this work, some general points can be made. All complexes seem to be mononuclear, as FAB mass spectrometry suggests. The magnetic studies, the similar IR patterns and X-ray results agree with the coordination of the N_5 donor set of the ligand to the metal centres. In addition ^{1}H NMR studies, and other data, indicate that the solid-state structures of **1** and **2** are retained in solution.

Conclusion

The novel potentially dianionic and pentadentate Schiff-base ligand H_2DAPATs readily stabilises neutral mononuclear complexes of Mn^{II}, Fe^{II}, Co^{II}, Ni^{II}, Cu^{II}, Zn^{II} and Cd^{II} formed by either an electrochemical method or a traditional chemical procedure. The electrosynthesis is both simpler and shorter.

The rigid spacer in this ligand, such as pyridine, and the bulky terminal groups, such as tosyl, favour the formation of monohelical single-stranded compounds.

 © 2003 Wiley-VCH Verlag GmbH & Co. KGaA, Weinheim

It thus seems that careful design of the ligand is useful in controlling the selective formation of monohelical complexes.

Experimental Section

General: Elemental analyses were performed with a Carlo Erba EA 1108 analyser. NMR spectra were recorded with Bruker DPX-250 and AMX-500 spectrometers with [D_6]DMSO (296 K) and CD_3CN (273 and 233 K) as solvents. Infrared spectra were registered as KBr pellets with a Bio-Rad FTS 135 spectrophotometer in the range 4000−600 cm^{-1}. Fast atom bombardment (FAB) mass spectra were obtained with a Kratos MS-50 mass spectrometer, employing Xe atoms at 70 keV in *m*-nitrobenzyl alcohol as matrix. Room-temperature magnetic susceptibilities were measured using a Digital Measurement system MSB-MKI, calibrated by using tetrakis(isothiocyanato)cobaltate(II).

Syntheses: All solvents, 2,6-diacetylpyridine, 1,2-diaminobenzene, tosyl chloride and M^{II} acetates are commercially available and were used without further purification. Metals (Ega Chemie) were used as ca. 2 × 2 cm^2 plates and were cleaned of oxides in dilute hydrochloric acid prior to electrolysis. 2-(Tosylamino)aniline was prepared and characterised according to a method previously reported[17] (Scheme 1).

Ligand Synthesis: H_2DAPATs has been prepared by condensation of 2,6-diacetylpyridine (2 g, 12.3 mmol) with 2-(tosylamino)aniline (6.4 g, 24.6 mmol) in ethanol (250 cm^3). The solution was heated under reflux over a 5-h period, concentrated with a Dean−Stark trap to ca. 30 mL and cooled during 12 h (4 °C). The yellow precipitate that then formed was collected by filtration and purified by Soxhlet extraction (with EtOH as solvent) over a period of 12 h. The resulting solid was finally washed with diethyl ether (3 × 10 mL) and dried in vacuo.

Metal Complexes Syntheses: All complexes have been obtained by two methods: an electrochemical synthesis[18] and a traditional chemical procedure.

Electrochemical Synthesis: A warm acetone suspension of H_2DAPATs, containing tetramethylammonium perchlorate (about 10 mg) as supporting electrolyte, was electrolysed using a platinum wire as the cathode and a metal plate as anode. The cell can be summarised as: Pt(−) | H_2DAPATs + MeCOMe | M(+), where M = Mn, Fe, Co, Ni, Cu, Zn and Cd. The synthesis is typified by the preparation of Zn(DAPATs)(H_2O)$_2$: A suspension of the ligand H_2DAPATs (0.2 g, 0.46 mmol) in warm acetone (80 mL), containing tetramethylammonium perchlorate (10 mg), and using a zinc plate as anode, was electrolysed for 2.5 h using a current of 10 mA. ***Caution:*** *Although no problems have been encountered in our experiments, all perchlorate compounds are potentially explosive, and should be handled in small quantities and with great care!* The resulting orange solid was washed with diethyl ether and dried in vacuo. Slow diffusion of diethyl ether into a dichloromethane/acetone solution of Zn(DAPATs)(H_2O)$_2$ yielded orange crystals of [Zn(DAPATs)] (**1**) suitable for X-ray diffraction studies. The other complexes were obtained by the same method, using the appropriate metal anode. Orange prismatic crystals of [Cd(DAPATs)(H_2O)] (**2**), suitable for single X-ray diffraction studies, were obtained by slow concentration of acetone solutions containing Cd(DAPATs)(H_2O).

Chemical Synthesis: Complexes were obtained by refluxing the ligand and the appropriate metal(II) acetate hydrate in ethanol. A typical preparation is outlined below.

Cd(DAPATs)(H_2O): A mixture of H_2DAPATs (0.2 g, 0.31 mmol) and $Cd(C_2H_3O_2)_2\cdot 2H_2O$ (0.08 g, 0.31 mmol) in ethanol (60 mL) was refluxed for 3 h to afford a black suspension. Filtration followed by washing with diethyl ether and drying in vacuo yielded an orange powdery solid. Recrystallisation of Cd(DAPATs)(H_2O) complex in DMSO yielded [Cd(DAPATs)(H_2O)] (**2**).

X-ray Crystallographic Studies: Crystals of **1** and **2**, suitable for X-ray diffraction studies, were grown as described above. Data were collected with a Smart CCD-1000 Bruker diffractometer, using graphite-monochromated Mo-K_α radiation (λ = 0.71073 Å) from a fine focus sealed tube source. The structures were solved by direct methods[31] and DIRDIF-99.2 for Windows and finally refined by full-matrix least squares based on F^2. An empirical absorption correction was applied using SADABS.[32] All non-hydrogen atoms were anisotropically refined, and all hydrogen atoms were included in the model at geometrically calculated positions. CCDC-203518 (**1**) and -203519 (**2**) contain the supplementary crystallographic data for this paper. These data can be obtained free of charge at www.ccdc.cam.ac.uk/conts/retrieving.html [or from the Cambridge Crystallographic Data Centre, 12 Union Road, Cambridge CB2 1EZ, UK; Fax: (internat.) + 44-1223/336-033; E-mail: deposit@ccdc.cam.ac.uk].

Acknowledgments

The authors would like to thank Xunta de Galicia (Spain) (PGIDIT03PXIB20901PR) for financial support. R. P. would like to thank Xunta de Galicia for a grant.

[1] J. M. Lehn, *Supramolecular Chemistry − Concepts and Perspectives*, VCH, Weinheim, **1995**.
[2] [2a] E. C. Constable in *Comprehensive Supramolecular Chemistry*, vol. 9 (Eds.: J. P. Sauvage, M. W. Hosseini); Pergamon Press, Oxford, **1996**, p. 213−252. [2b] E. C. Constable, C. E. Housecroft, M. Neuburger, D. Phillips, P. R. Raithby, E. Schofield, E. Sparr, D. A. Tocher, M. Zehnder, Y. Zimmermann, *J. Chem. Soc., Dalton Trans.* **2000**, 2219−2228.
[3] D. Philp, J. F. Stoddart, *Angew. Chem. Int. Ed. Engl.* **1996**, *35*, 1155−1196.
[4] C. Piguet, G. Bernardinelli, G. Hopfgartner, *Chem. Rev.* **1997**, *97*, 2005−2062.
[5] G. F. Swiegers, T. J. Maleftse, *Chem. Rev.* **2000**, *100*, 3483−3537.
[6] [6a] C. Piguet, G. Bernardinelli, J. C. G. Bünzli, S. Petoud, G. Hopfgartner, *J. Chem. Soc., Chem. Commun.* **1995**, 2575−2576. [6b] N. Martin, J. C. G. Bünzli, C. Piguet, V. Mckee, G. Hopfgartner, *Inorg. Chem.* **1998**, *37*, 577−589. [6c] C. Piguet, C. Edder, S. Rigault, G. Bernardinelli, J. C. G. Bünzli, G. G. Hopfgartner, *J. Chem. Soc., Dalton Trans.* **2000**, 3999−4006.
[7] [7a] C. Piguet, G. Bernardinelli, B. Bocquet, A. Quattropani, A. F. Williams, *J. Am. Chem. Soc.* **1992**, *114*, 7440−7451. [7b] E. J. Enemark, T. D. P. Stack, *Angew. Chem. Int. Ed. Engl.* **1995**, *34*, 996−998. [7c] B. Kersting, M. Meyer, R. E. Meyers, K. N. Raymond, *J. Am. Chem. Soc.* **1996**, *118*, 7221−7222. [7d] M. Albrecht, R. Fröhlich, *J. Am. Chem. Soc.* **1997**, *119*, 1656−1661.
[8] [8a] E. C. Constable, A. J. Edwards, P. R. Raithby, J. V. Walker, *Angew. Chem. Int. Ed. Engl.* **1993**, *32*, 1465−1466. [8b] E. C. Constable, S. M. Elder, M. J. Hannon, A. Martin, P. R. Raithby, D. A. Tocher, *J. Chem. Soc., Dalton Trans.* **1996**, 2423−2433. [8c] R. Chotalia, E. C. Constable, M. Neuburger, D. R. Smith, M. Zehnder, *J. Chem. Soc., Dalton Trans.* **1996**, 4207−4216. [8d] E. C. Constable, F. Heirlitzer, M. Neuburger, M. Zehnder, *J. Am. Chem. Soc.* **1997**, *119*, 5606−5617. [8e] M. J. Hannon, C. L. Painting, W. Errington, *Chem. Commun.* **1997**, 1805−1806. [8f] G. Baum, E. C. Constable, D. Fenske, C. E.

 © 2003 Wiley-VCH Verlag GmbH & Co. KGaA, Weinheim

Housecroft, T. Kulke, M. Neuburger, M. Zehnder, *J. Chem. Soc., Dalton Trans.* **2000**, 945−959. [8g] N. W. Alcock, P. R. Barker, J. M. Haider, M. J. Hannon, C. L. Painting, Z. Pikramenou, E. A. Plummer, K. Rissanen, P. Saarenketo, *J. Chem. Soc., Dalton Trans.* **2000**, 1447−1461. [8h] C. B. Smith, E. C. Constable, C. E. Housecroft, B. Kariuki, *Chem. Commun.* **2002**, 2068−2069.

[9] [9a] G. C. Van Stein, G. Van Koten, K. Vrieze, C. Brevard, A. L. Spek, *J. Am. Chem. Soc.* **1984**, *106*, 4486−4492. [9b] M. J. Hannon, C. L. Painting, W. Errington, *Chem. Commun.* **1997**, 307−308. [9c] M. J. Hannon, C. L. Painting, A. Jackson, J. Hamblin, W. Errington, *Chem. Commun.* **1997**, 1807−1808. [9d] M. J. Hannon, S. Bunce, A. J. Clarke, N. W. Alcock, *Angew. Chem. Int. Ed.* **1999**, *38*, 1277−1278. [9e] V. Amendola, L. Fabbrizzi, L. Linati, C. Mangano, P. Pallavicini, V. Pedrazzini, M. Zema, *Chem. Eur. J.* **1999**, *5*, 3679−3688. [9f] N. Yoshida, K. Ichikawa, M. Shiro, *J. Chem. Soc., Perkin Trans.* **2000**, 17−26. [9g] J. Sanmartín, M. R. Bermejo, A. M. García-Deibe, A. L. Llamas-Saiz, *Chem. Commun.* **2000**, 795−796. [9h] L. J. Chidls, N. W. Alcock, M. J. Hannon, *Angew. Chem. Int. Ed.* **2001**, *40*, 1079−1081. [9i] M. J. Hannon, P. C. Mayers, P. C. Taylor, *Angew. Chem. Int. Ed.* **2001**, *40*, 1081−1082. [9j] J. Hamblin, L. J. Chidls, N. W. Alcock, M. J. Hannon, *J. Chem. Soc., Dalton Trans.* **2002**, 164−169.

[10] M. R. Bermejo, M. Fondo, A. M. González, O. L. Hoyos, A. Sousa, C. A. McAuliffe, W. Hussain, R. Pritchard, V. M. Novotorsev, *J. Chem. Soc., Dalton Trans.* **1999**, 2211−2117.

[11] M. R. Bermejo, A. Sousa, M. Fondo, A. M. González, O. L. Hoyos, R. Pedrido, M. Maestro, J. Mahía, *Z. Anorg. Allg. Chem.* **2000**, *626*, 506−513.

[12] M. Fondo, A. Sousa, M. R. Bermejo, A. García-Deibe, A. Sousa-Pedrares, O. L. Hoyos, M. Helliwell, *Eur. J. Inorg. Chem.* **2002**, 703−710.

[13] [13a] M. Carcelli, P. Mazza, C. Pelizzi, G. Pelizzi, F. Zani, *J. Inorg. Biochem.* **1995**, *57*, 43−62 and references therein. [13b] A. Bacchi, A. Bonardi, M. Carcelli, P. Mazza, P. Pelagatti, C. Pelizzi, G. Pelizzi, C. Solinas, F. Zani, *J. Inorg. Biochem.* **1998**, *69*, 101−112.

[14] A. Bino, N. Cohen, *Inorg. Chim. Acta* **1993**, *210*, 11−16.

[15] R. Pedrido, PhD Thesis, University of Santiago de Compostela, **2002**.

[16] [16a] M. Vázquez, M. R. Bermejo, M. Fondo, A. M. González, J. Mahía, L. Sorace, D. Gatteschi, *Eur. J. Inorg. Chem.* **2001**, 1863−1868. [16b] M. Vázquez, M. R. Bermejo, M. Fondo, A. García-Deibe, A. M. González, R. Pedrido, *Eur. J. Inorg. Chem.* **2002**, 465−472. [16c] M. Vázquez, M. R. Bermejo, J. Sanmartín, A. M. García-Deibe, C. Lodeiro, J. Mahía, *J. Chem. Soc., Dalton Trans.* **2002**, 870−877. [16d] M. Vázquez, M. R. Bermejo, M. Fondo, A. M. García-Deibe, A. M. González, R. Pedrido, J. Sanmartín, *Z. Anorg. Allg. Chem.* **2002**, *628*, 1068−1074. [16e] M. R. Bermejo, M. Vázquez, J. Sanmartín, A. M. García-Deibe, M. Fondo, C. Lodeiro, *New J. Chem.* **2002**, *26*, 1365−1370. [16f] M. R. Bermejo, J. Sanmartín, A. M. García-Deibe, M. Fondo, F. Novio, D. Navarro, *Inorg. Chim. Acta* **2003**, *347*, 53−60. [16g] M. Vázquez, M. R. Bermejo, M. Fondo, A. M. García-Deibe, J. Sanmartín, R. Pedrido, L. Sorace, D. Gatteschi, *Eur. J. Inorg. Chem.* **2003**, 1128−1135.

[17] W. U. Malik, T. C. Sharma, *J. Ind. Chem. Soc.* **1970**, *47*, 167−168.

[18] C. Oldham, D. G. Tuck, *J. Chem. Educ.* **1982**, *59*, 420−421.

[19] N. Beynek, M. McPartlin, B. P. Murphy, I. J. Scowen, *Polyhedron* **1998**, *17*, 2137−2140.

[20] T. Adatia, N. Beynek, B. P. Murphy, *Polyhedron* **1995**, *14*, 335−338.

[21] E. Amadei, M. Carcelli, S. Ianelli, P. Cozzini, P. Pelagatti, C. Pelizzi, *J. Chem. Soc., Dalton Trans.* **1998**, 1025−1029.

[22] S. Ianelli, G. Minardi, G. Pelizzi, L. Reverberi, C. Solinas, P. Tarasconi, *J. Chem. Soc., Dalton Trans.* **1991**, 2113−2120.

[23] [23a] B. Cingi, A. G. Manfredotti, C. Guastini, A. Mussatti, M. Nardelli, *Gazz. Chim. Ital.* **1971**, *101*, 315. [23b] J. Casabó, J. Colomer, A. Llobet, F. Teixidor, E. Molins, C. Miratvitlles, *Polyhedron* **1989**, *8*, 2743−2747.

[24] K. Linoh, K. L. Nagel, I. Lange, O. Moers, A. Blaschette, P. G. Jones, *Z. Anorg. Allg. Chem.* **1997**, *623*, 1175−1182.

[25] W. Dai, H. Hu, X. Wei, S. Zhu, D. Wang, K. Yu, N. Kent, X. Kou, *Polyhedron* **1997**, *16*, 2059−2065.

[26] S. Cabaleiro, E. Vázquez-López, J. Castro, J. A. García-Vázquez, J. Romero, A. Sousa, *Inorg. Chim. Acta* **1999**, *294*, 87−94.

[27] [27a] J. Romero, J. A. García-Vázquez, M. L. Durán, A. Castiñeiras, A. Sousa, A. D. Garnovskii, D. A. Garnovskii, *Acta Chem. Scand.* **1997**, *51*, 672−675. [27b] J. A. García-Vázquez, J. Romero, M. L. Durán, A. Sousa, A. D. Garnovskii, A. S. Burlov, D. A. Garnovskii, *Polyhedron* **1998**, *17*, 1547−1552. [27c] M. L. Durán, J. A. García-Vázquez, C. Gómez, A. Sousa-Pedrares, J. Romero, A. Sousa, *Eur. J. Inorg. Chem.* **2002**, 2348−2354.

[28] [28a] M. R. Bermejo, A. Sousa, M. Fondo, M. Helliwell, *New J. Chem.* **2000**, *24*, 33−38. [28b] A. Sousa, M. R. Bermejo, M. Fondo, A. García-Deibe, A. Sousa-Pedrares, O. Piro, *New J. Chem.* **2001**, *25*, 647−654.

[29] M. Morioka, M. Kato, H. Yoshida, T. Ogata, *Heterocycles* **1997**, *45*, 1173−1181.

[30] K. Nakamoto in *Infrared and Raman Spectra of Inorganic and Coordination Compounds*, John Wiley & Sons, New York, **1997**.

[31] [31a] G. M. Sheldrick, *SHELX-97 (SHELXS 97 and SHELXL 97), Programs for Crystal Structure Analyses*, University of Göttingen, Germany, **1998**. [31b] DIRDIF-99.2 for Windows: L. J. Farrugia, *J. Appl. Crystallogr.* **1999**, *32*, 837−838.

[32] G. M. Sheldrick, *SADABS, Program for Scaling and Correction of Area Detector Data*, University of Göttingen, Germany, **1996**.

Received February 13, 2003

 © 2003 Wiley-VCH Verlag GmbH & Co. KGaA, Weinheim

Synthesis, Characterization and Electrochemical Properties of Optically Active [60]Fullerene Organotransition Metal Complexes *mer*-[(η^2-C_{60})M(CO)$_3${(−)-DIOP}] (M = Mo, W), *mer*-[(η^2-C_{60})M(CO)$_3${(+)-DIOP}] (M = Mo, W) and [(η^2-C_{60})M{(−)-DIOP}] (M = Pd, Pt) − Crystal Structure of [(η^2-C_{60})Pt{(−)-DIOP}]

Li-Cheng Song,*[a] Peng-Chong Liu,[a] Jin-Ting Liu,[a] Fu-Hai Su,[a] Guang-Feng Wang,[a] Qing-Mei Hu,[a] Piero Zanello,[b] Franco Laschi,[b] and Marco Fontani[b]

Keywords: Transition metals / Fullerenes / Electrochemistry / Optical activity

This paper reports on several new optically active organometallic [60]fullerene complexes that contain a chiral (+)-DIOP or (–)-DIOP ligand [DIOP = 2,3-*O*,*O*′-isopropylidene-2,3-dihydroxy-1,4-bis(diphenylphosphanyl)butane]. The Mo/W complexes *mer*-[(η^2-C_{60})M(CO)$_3${(–)-DIOP}] (**1**, M = Mo; **2**, M = W) and *mer*-[(η^2-C_{60})M(CO)$_3${(+)-DIOP}] (**3**, M = Mo; **4**, M = W) were synthesized by a photochemical reaction of a mixture of [M(CO)$_6$], (–)-DIOP or (+)-DIOP and C_{60} in chlorobenzene in 42–51% yields, whereas the Pd/Pt complexes [(η^2-C_{60})M{(–)-DIOP}] (**5**, M = Pd; **6**, M = Pt) were prepared by a thermal reaction of C_{60} with [M(PPh$_3$)$_4$], followed by in situ treatment of the intermediate [(η^2-C_{60})M(PPh$_3$)$_2$] with (–)-DIOP, in toluene in > 90% yields. All the new complexes **1**–**6** were fully characterized by elemental analysis, ^{1}H (^{31}P, ^{13}C) NMR, IR, UV/Vis and circular dichroism (CD) spectroscopy. The structure of [(η^2-C_{60})Pt{(–)-DIOP}] (**6**) was further confirmed by X-ray diffraction techniques. The electrochemical properties of complexes **1**, **2**, **5** and **6** were studied in dichloromethane solution. Complexes **1** and **2** display the reversible, four-membered, one-electron reduction sequence typical of fullerene ligands, as well as the reversible (in the cyclic voltammetric time scale) one-electron oxidation of the outer metal fragment. Complexes **5** and **6** are less stable to the same electron transfer processes. EPR measurements suggest that in the different electrogenerated monoanions, the added electrons enter the LUMO orbitals partially contributed by the metal fragment. In addition, they confirm that the instability of the reduction intermediates is due to the release of free C_{60}.

(© Wiley-VCH Verlag GmbH & Co. KGaA, 69451 Weinheim, Germany, 2003)

Introduction

The organotransition metal derivatives of C_{60} have drawn great attention[1] since the discovery of C_{60}[2] and its synthesis in macroscopic amounts.[3] The first example of such derivatives, namely (η^2-C_{60})Pt(PPh$_3$)$_2$, was reported in 1991 by Fagan and co-workers.[4] Although a great number of such derivatives have so far appeared in the literature,[5−8] very few organotransition metal C_{60} derivatives containing chiral ligands are known to be reported.[9,10] We have been interested in the synthesis, structural characterization and properties of organotransition metal fullerene complexes.[11] In view of the theoretical and practical significance of such complexes, we recently initiated a study on optically active organometallic C_{60} complexes. This paper describes the synthesis and spectroscopic characterization of the new optically active complexes *mer*-[(η^2-C_{60})M(CO)$_3${(−)-DIOP}] (**1**, M = Mo; **2**, M = W), *mer*-[(η^2-C_{60})M(CO)$_3${(+)-DIOP}] (**3**, M = Mo; **4**, M = W) and [(η^2-C_{60})M{(−)-DIOP}] (**5**, M = Pd; **6**, M = Pt), the crystal structure of **6** and the electrochemical properties of **1**, **2**, **5** and **6**.

[a] Department of Chemistry, State Key Laboratory of Elemento-Organic Chemistry, Nankai University,
Tianjin 300071, China
Fax: (internat.) + 86-22/23504853
E-mail: lcsong@public.tpt.tj.cn
[b] Dipartimento di Chimica dell'Università di Siena,
Via Aldo Moro, 53100 Siena, Italy

Results and Discussion

Synthesis and Characterization of *mer*-[(η^2-C_{60})M(CO)$_3$-{(−)-DIOP}] (1, M = Mo; 2, M = W) and *mer*-[(η^2-C_{60})M(CO)$_3${(+)-DIOP}] (3, M = Mo; 4, M = W)

Irradiation of [M(CO)$_6$] (M = Mo, W), in the presence of an equimolar quantity of C_{60} and (−)-DIOP or (+)-DIOP in chlorobenzene, with a UV 450-W mercury vapor lamp at ambient temperature, resulted in the formation of complexes **1**−**4** in 42−51% yields, as shown in Scheme 1.

Complexes **1**−**4** as the *mer* isomers obtained from the above "one-pot" reactions might be regarded as being produced by the reaction of M(CO)$_6$ with one of the chiral

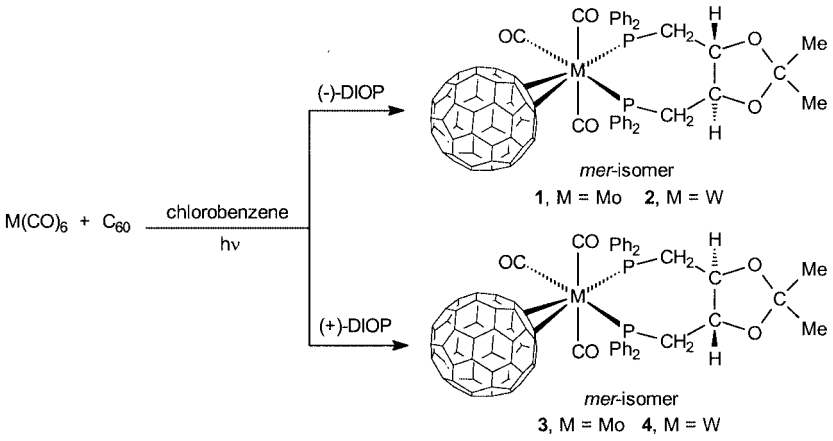

Scheme 1

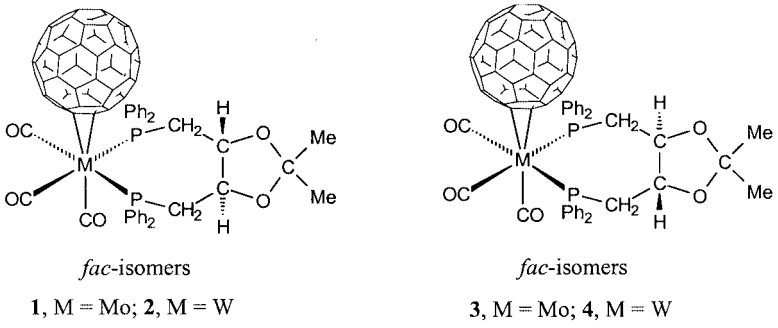

Scheme 2

diphosphane ligands (±)-DIOP, with subsequent substitution of one equatorial CO ligand from the intermediate complex [M(CO)$_4${(−)-DIOP}] or [M(CO)$_4${(+)-DIOP}] by the C_{60} ligand.

Complexes **1**−**4** are new and have been characterized by elemental analyses, ^{1}H (^{31}P, ^{13}C) NMR, UV/Vis, IR, FAB-MS and CD spectroscopy. The combustion analyses agree with their chemical formulas, and the FAB-MS spectra clearly show the molecular ion M^+ or [M^+ + 1 − 3 H] peaks. Theoretically, **1**−**4** each may have two possible isomers, namely the *fac* and the *mer* isomer. The *mer* isomers are shown in Scheme 1, and the *fac* isomers for **1**−**4** are shown in Scheme 2. However, the ^{31}P NMR spectra of **1**−**4** have indicated that they exist as the *mer* isomers. In the ^{31}P NMR spectra of **1**−**4**, two signals are present, which is consistent with the fact that *mer* isomers have two different P atoms, one *cis* to the C_{60} ligand, and the other *trans* to it (*fac* isomers have two identical P atoms, both *cis* to the C_{60} ligand). The two ^{31}P NMR signals are doublets; the doublets for the Mo complexes **1** and **3** appear at δ ≈ 20 and 15 ppm, with $J_{P\text{-}P}$ = 30−32 Hz, and the doublets for the W complexes **2** and **4** appear at δ ≈ −4 and −5 ppm, with $J_{P\text{-}P}$ ≈ 21 Hz. This can be seen from the two representative spectra of **3** and **4** (Figure 1). It is worth noting that the ^{31}P chemical shifts of complexes containing a DIOP ligand, such as **1**−**4**, usually lie at a higher field than the corre-

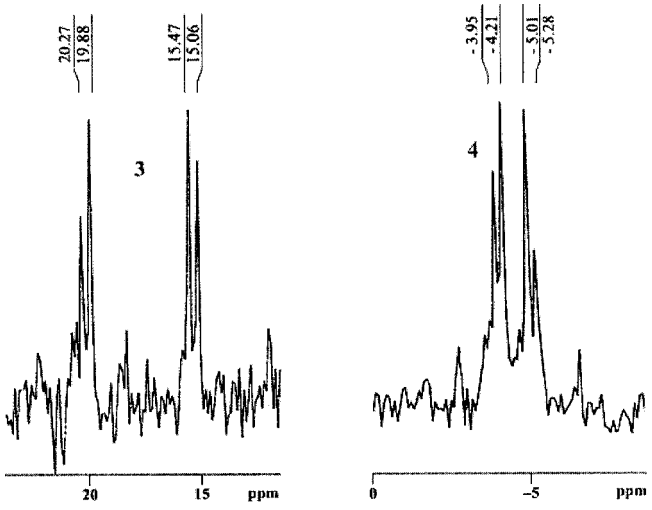

Figure 1. ^{31}P NMR spectra of **3** and **4**

 © 2003 Wiley-VCH Verlag GmbH & Co. KGaA, Weinheim

sponding complexes containing a dppe ligand {such as *mer*-[$Mo(CO)_3$(dppe)(η^2-C_{60})] and *mer*-[$W(CO)_3$(dppe)(η^2-C_{60})]: δ_P = 62.64/54.21 ppm and 41.48/38.11 ppm, respectively} or a dppb ligand {such as *mer*-[$Mo(CO)_3$(dppb)(η^2-C_{60})] and *mer*-[$W(CO)_3$(dppb)(η^2-C_{60})]: δ_P = 66.18/55.66 ppm and 49.50/43.49 ppm, respectively}. This is because δ_P of the free ligand DIOP (δ = −23.5 ppm)[12] lies at a much higher field than those of the free ligands dppe (δ = 12.5 ppm)[13] and dppb (δ = −13.41 ppm, determined by us, since no reported δ_P value is available).

The ^{1}H NMR spectra of **1**−**4** are much more complicated than those of the free ligands (−)-DIOP and (+)-DIOP. The spectra of the free ligands show a sharp singlet assigned to the two methyl groups. This singlet appears as two singlets in the spectra of their complexes. The two broad peaks in the spectra of the free DIOP ligands, assigned to the two H atoms bonded to the chiral carbon atoms, appear as two apparent triplets and two apparent quadruplets in the spectra of their complexes. Further, in the spectra of the free ligands, the multiplet assigned to the two CH_2 groups, appears as two multiplets in the spectra of their complexes. Obviously, such ^{1}H NMR spectroscopic changes are consistent with the chelation of the DIOP ligands in the *mer*-isomers of **1**−**4**.

In the ^{13}C NMR spectra of **1**−**4**, the saturated, ketal and phenyl ring carbon atoms of the DIOP ligands lie in the ranges δ = 17−27, 103−109 and 123−136 ppm, respectively. In addition, the C_{60} ligands in **1**−**4** display resonance signals in the ranges δ = 136−163 ppm for the 58 sp^2 carbon atoms, and δ = 73−80 ppm for their 2 sp^3 carbon atoms. This is consistent with known η^2-C_{60} transition metal complexes, such as [$Rh(NO)(PPh_3)_2$(η^2-C_{60})][14] and [$Fe(CO)_4$(η^2-C_{60})].[15] The ^{13}C NMR spectrum of the sp^2 and sp^3 carbon atoms of the C_{60} core in **2** is shown in Figure 2. As seen in Figure 2, there are 20 signals in the δ = 164−140 ppm region, which can be assigned to the 58 carbon atoms of the C_{60} core.[14,15] Another ^{13}C NMR signal at δ = 78.81 ppm can be assigned to the two sp^3 carbon atoms of the C_{60} core that is directly linked to the W atom.[14,15] Among the 20 signals, two signals at δ = 163.43 and 162.78 ppm are assigned to the four carbon atoms in close proximity to the carbon atoms linked to the W atom. Nine signals at δ = 147.09, 145.40, 145.05, 144.44, 144.35, 142.59, 142.49, 142.01 and 141.77 ppm can each be assigned to four carbon atoms and the other eleven signals at δ = 163.43, 162.78, 146.27, 145.28, 144.86, 143.87, 143.77, 143.64, 142.92, 141.33 and 140.03 ppm can each be assigned to two carbon atoms. Similarly, in the ^{13}C NMR spectrum of the C_{60} core, **1** displays 25 signals in the region δ = 163.42−140.95 ppm and one signal at δ = 80.01 ppm, **3** shows 19 signals in the region δ = 163.03−140.56 ppm and one signal at δ = 78.72 ppm, and **4** exhibits 22 signals in the region δ = 158.21−136.55 ppm and one signal at δ = 73.60 ppm.

The IR spectra of **1**−**4** show four characteristic absorption bands for the C_{60} core[16] in the range 1434−525 cm^{-1}, as well as three strong bands in the range 2002−1870 cm^{-1}, which can be assigned to the terminal carbonyl groups.[17] The simplicity of the carbonyl bands provides further evidence that complexes **1**−**4** consist of only one isomer (since a mixture of *fac*/*mer* isomers would exhibit more active carbonyl absorption bands).[18]

In the UV/Vis spectra of **1**−**4**, there are five absorbance bands in the range 200−610 nm. This is typical of a free C_{60} ligand that has been complexed by a transition metal moiety.[19] The largest changes in the UV/Vis spectra occur in the visible region relative to that of free C_{60}. A new weak and broad band appears at ca. 430 nm in the spectra of complexes **1**−**4**. This peak is responsible for the color change in the reaction mixture, from purple C_{60} to dark green for the corresponding complexes. In addition, the new band suggests that the C_{60} ligands are coordinated to Mo and W atoms via an η^2-coordination mode in **1**−**4**.[20]

CD spectroscopy is an important method for the characterization of chiral compounds. The CD spectra of **1**−**4** are shown in Figures 3 and 4, respectively. As can be seen in Figure 3, **1** shows the negative and positive Cotton effects at 293 (−), 326 (+), 401 (−), 451 (−) and 540 (+) nm, and **2** displays similar Cotton effects at 288 (−), 324 (+), 399 (−), 449 (−) and 537 (+) nm.

Interestingly, the CD spectra of **3** and **4** (Figure 4) appear to be the mirror images of **1** and **2**, respectively. For example, **3** shows Cotton effects at 293 (+), 326(−), 402 (+), 450 (+), and 538 (−) nm, whereas **1** shows Cotton effects at 293 (−), 326(+), 401 (−), 451 (−) and 540 (+) nm. This is consistent with the behavior of chiral compounds with the ligands (+)-DIOP and (−)-DIOP. In addition, it is worth noting that the main Cotton effects of **3** and **4**, con-

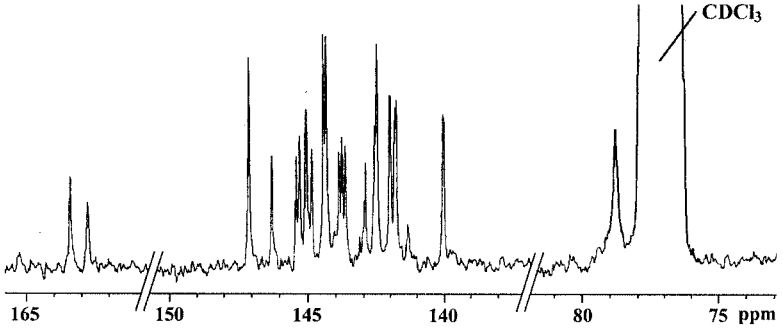

Figure 2. ^{13}C NMR spectrum of the C_{60} core in **2**

 © 2003 Wiley-VCH Verlag GmbH & Co. KGaA, Weinheim

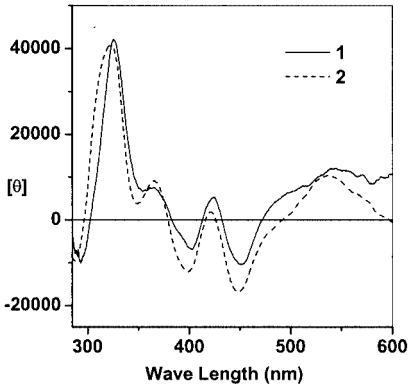

Figure 3. CD spectra of complexes **1** and **2** in THF

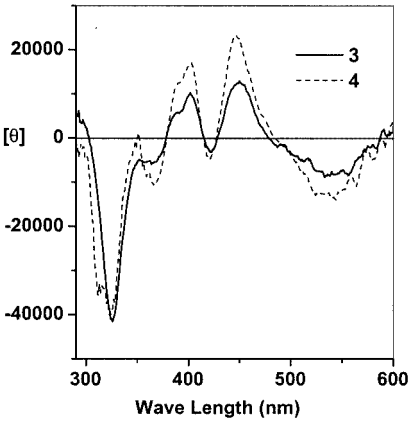

Figure 4. CD spectra of complexes **3** and **4** in THF

taining a (+)-DIOP ligand, are very similar to those of (η^2-C_{60})Pt{(+)-DIOP} and (η^2-C_{60})Pd{(+)-DIOP}.[21]

Electrochemistry of Complexes 1 and 2 and Complementary EPR Measurements

Figure 5 shows the cyclic voltammetric behavior of the W complex **2** in dichloromethane solution at −20 °C.

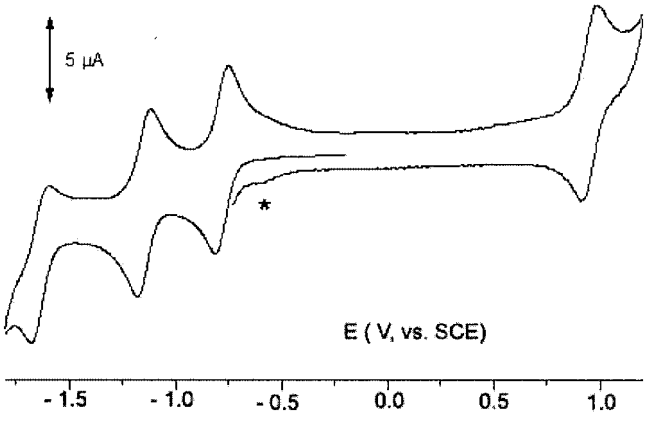

Figure 5. Cyclic voltammogram on a platinum electrode of a CH_2Cl_2 solution of **2** (0.4×10^{-3} mol·dm^{-3}); scan rate 0.2 V·s^{-1}; $T = -20$ °C; the starred peak indicates the appearance of identified by-products (see text)

Three sequential reductions appear that have features indicating chemical (i_{pa}/i_{pc} constantly equal to 1, independently from scan rate) and electrochemical (ΔE_p in the range from 58 to 70 mV with scan rate varying from 0.02 V·s^{-1} to 0.5 V·s^{-1}) reversibility. An oxidation process also occurs that shows reversibility.

In confirmation with the suggested fullerene-centered nature of the cathodic processes and their chemical reversibility, controlled potential coulometry of the first reduction step ($E_w = -0.9$ V) indicates one electron per molecule. The resulting solution displays a cyclic voltammetric profile that resembles the original one.

The anodic process is straightforwardly assigned as a one-electron process that is centered on the exohedral metal fragment. In spite of its features, which show chemical reversibility, it can be seen that in the back-scan a minor starred-peak appears at potential values coincident with the first reduction process of the free fullerene. This suggests that the monocation $[\mathbf{2}]^+$ is not indefinitely stable. At ambient temperature, the voltammetric patterns remain substantially unaltered.

The formal electrode potentials of the multiple redox changes are presented in Table 1.

As commonly seen for metallofullerenes,[22] the reduction processes are shifted towards more negative potential values, indicating that the appended metal fragment is electron-donating towards the fullerene. In the present case, these values are shifted by about 0.20 V with respect to the free fullerene.

In previous papers we have proved, by EPR spectroscopy, that the LUMO orbitals of exohedral metallofullerenes are in part contributed by the d orbitals of the metal ion itself.[23] Here, we have studied the nature of the electrogenerated paramagnetic anion radical $[\mathbf{2}]^-$ by X-band EPR spectroscopy. Figure 6 shows the spectrum recorded under glassy conditions ($T = 100$ K), relative to that of $[C_{60}]^-$.

The broad lineshape of $[\mathbf{2}]^-$ can be suitably interpreted assuming an $S = 1/2$ electron spin Hamiltonian with axial resolution either in the first or second derivative modes. The EPR features suggest that the paramagnetic species possesses significant metallic character [$g_i > g_{electron} = 2.0023$; $\Delta g = 0.083(5)$]. No evidence for a_{aniso} hyperfine (hpf) splittings of the ^{183}W nucleus (^{183}W: I nuclear spin = 1/2; natural abundance = 14.4%) has been obtained, probably as a consequence of either the broad lineshape, which masks the low intensity satellite peaks of the ^{183}W isotope, or the partial metallic character.[23] Moreover, no ^{31}P (^{31}P: $I = 1/2$; natural abundance = 100%) superhyperfine (shpf) splittings are detectable in the second derivative mode, suggesting that the unpaired electron is mainly delocalized in a SOMO basically constituted by the C_{60} and metal d atomic orbitals.

When the temperature at the glassy-fluid transition phase is raised, the anisotropic features of $[\mathbf{2}]^-$ disappear and the fluid solution becomes EPR-silent. However, rapid refreezing quantitatively restores the original glassy spectrum. This indicates the stability of the metal complex species under different experimental conditions. The absence of the absorption peaks under fluid solution conditions is not un-

 © 2003 Wiley-VCH Verlag GmbH & Co. KGaA, Weinheim

Table 1. Formal electrode potentials (V, vs. SCE) and peak-to-peak separation (mV) for the redox changes exhibited by *mer*-[(η^2-C_{60})M(CO)$_3${(−)-DIOP}] (**1**, M = Mo; **2**, M = W) in CH_2Cl_2 solution at −20 °C

Complex (M)	Fullerene-centered reductions						Metal-centered oxidation	
	$E^{\circ\prime}_{0/-}$	ΔE_p [a]	$E^{\circ\prime}_{-/2-}$	ΔE_p [a]	$E^{\circ\prime}_{2-/3-}$	ΔE_p [a]	$E^{\circ\prime}_{0/+}$	ΔE_p [a]
1 (Mo)	−0.76	62	−1.11	62	−1.60	70	+0.88	64
2 (W)	−0.78	62	−1.15	60	−1.65	58	+0.95[b]	60
C_{60}	−0.58	62	−0.96	64	−1.42	60	−	−

[a] Measured at 0.1 Vs^{-1}. [b] Coupled to relatively slow chemical complications.

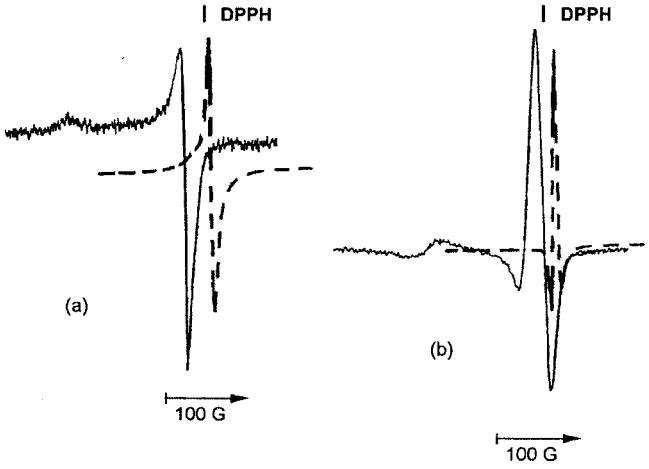

Figure 6. Low-temperature (T = 105 K) X-band EPR spectra of the electrogenerated anions [**2**]$^-$ (——) and [C_{60}]$^-$ (− −) in CH_2Cl_2 solution; (a) first derivative; (b) second derivative

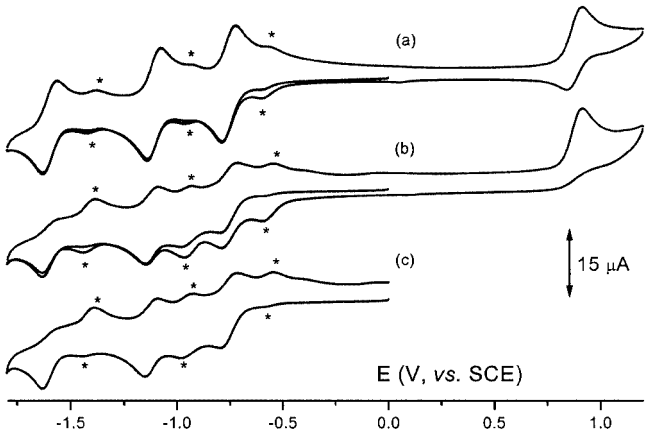

Figure 7. Cyclic voltammograms on a platinum electrode of a CH_2Cl_2 solution of **1** (0.7×10^{-3} mol·dm^{-3}); (a) T = −20 °C; (b, c) T = +20 °C; scan rate 0.2 V·s^{-1}; starred peaks indicate the appearance of identified by-products (see text)

expected in view of the increasing inter-/intramolecular dynamics induced by temperature. This in turn reflects the significant decrease in the ESR times.[24]

The X-band EPR parameters obtained by simulation procedures[25] are presented in Table 2.

Table 2. Low-temperature (100 K) X-band EPR parameters of the electrogenerated anions [2]$^-$ and [C_{60}]$^-$ in CH_2Cl_2 solution (g_i: ± *0.005)*

Anion	$g_\parallel$	$g_\perp$	$<g>$[a]	g_{iso}
[**2**]$^-$	2.093	2.010	2.034	−
[C_{60}]$^-$	2.006[b]	2.006[b]	2.006[b]	2.001[c]

[a] $<g> = (g_\parallel + 2g_\perp)/3$. [b] Averaged values. [c] T = 230 K.

The redox activity of the molybdenum analogue **1** is illustrated in Figure 7.

At low temperatures (T = −20 °C), **1** exhibits a voltammogram that is similar to that of **2** (Figure 7, a). In fact, apart from minor traces of free C_{60} initially present in solution, three fullerene-centered reductions also appear that have features indicative of chemical and electrochemical reversibility. In this case, however, the molybdenum-centered oxidation is partially chemically reversible (i_{pc}/i_{pa} = 0.4 at 0.1 V·s^{-1}). The fact that the instability of [**1**]$^+$ is due to the relatively fast release of the fullerene subunit can clearly be seen from the voltammogram in Figure 7 (b), which has been recorded at ambient temperature. Increasing amounts of the free fullerene are evident in the backscan, indicated as starred reduction processes. However, it should be noted that the monoanions [**1**]$^{-/2-/3-}$ are unstable at increasing temperatures, such that the fast release of free C_{60} occurs after traversing the respective peaks (Figure 7, c). The pertinent formal electrode potentials are given in Table 1.

Synthesis and Characterization of [(η^2-C_{60})M{(−)-DIOP}] (5, M = Pd; 6, M = Pt)

The toluene solution of the intermediate complex [(η^2-C_{60})Pd(PPh_3)$_2$] or [(η^2-C_{60})Pt(PPh_3)$_2$], formed from C_{60} and [Pd(PPh_3)$_4$] or [Pt(PPh_3)$_4$], reacted in situ with an excess amount of (−)-DIOP, through a ligand exchange process between PPh_3 and DIOP, to give **5** and **6**, as shown in Scheme 3.

Complexes **5** and **6** were isolated, as their toluene solvates **5**·PhMe and **6**·PhMe in > 90% yields, by layering the reaction mixtures with hexane.

Compounds **5** and **6** were fully characterized by elemental analysis, ^{1}H, ^{31}P NMR, IR and UV/Vis spectroscopy. The ^{31}P NMR spectrum of **5** displays a singlet at δ = 9.28 ppm assigned to its two identical P atoms, and that of **6** exhibits a singlet at δ = 11.13 ppm, along with two satellite singlets due to the ^{195}Pt-^{31}P coupling, assigned to its two identical P atoms. The Pt-P coupling constant (3749 Hz) for **6** is almost the same as that for [(η^2-C_{60})Pt{(+)-DIOP}] (3751 Hz).[10] The ^{1}H NMR spectra of

 © 2003 Wiley-VCH Verlag GmbH & Co. KGaA, Weinheim

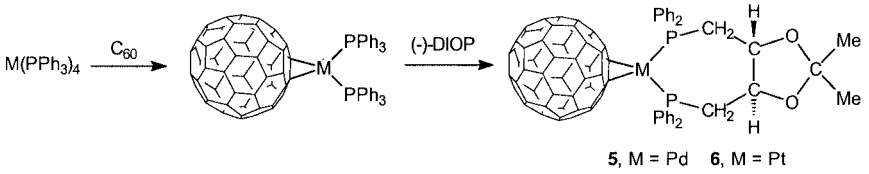

Scheme 3

5 and **6** indicate the presence of the (−)-DIOP ligand and toluene as the solvent molecule.

Compared with the UV/Vis spectrum of free C_{60}, the UV/Vis spectra of **5** and **6** display a new band at ca. 295 nm in the ultraviolet region, and a new band at 440 nm in the visible region. The former band can be attributed to the presence of phenyl groups in **5** and **6**, and the latter to the η^2-coordinating mode of C_{60} [20] with Pd and Pt, in **5** and **6**, respectively. The IR spectra of **5** and **6** show four absorption bands at 527, 576, 1184 and 1428 cm^{-1}, characteristic of the C_{60} core.

Interestingly, similar to the Mo/W complexes **1**−**4**, the CD spectra of **5** and **6**, as shown in Figure 8, display multiple Cotton effects at 298 (+), 325 (−), 366 (−) and 453 (+) nm for **5**, and 291 (+), 324 (−), 363 (−) and 450 (+) nm for **6**. The CD spectra of **5** and **6** are the mirror images of their enantiomers with (+)-DIOP in the region 280−600 nm.[21]

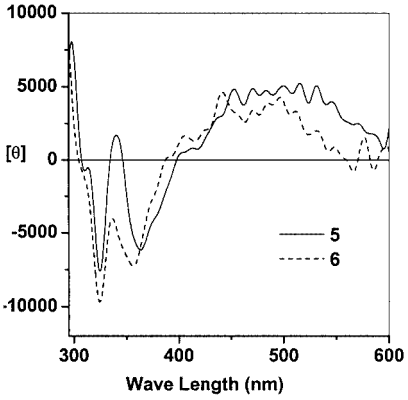

Figure 8. CD spectra of complexes **5** and **6** in toluene

Single Crystal Molecular Structure of 6

The structure of **6** has been unambiguously confirmed by X-ray diffraction methods. The molecular structure of **6** and its cell packing are demonstrated in Figures 9 and 10, respectively. As seen intuitively from Figure 9, complex **6** consists of a (4*R*,5*R*)-DIOP [i.e. (−)-DIOP] ligand chelated to platinum atom Pt(1) through its two phosphorous atoms P(1) and P(2), and a C_{60} ligand coordinated to Pt(1) through its C(1) and C(2) atoms in an η^2-fashion. The C(1)−C(2) bond length is 1.502(11) Å, similar to that of a normal C−C single bond, which suggests that C(1) and C(2) are σ-coordinated rather than π-coordinated to form a metallacyclopropane ring with the Pt(1) atom. The zerovalent platinum atom Pt(1) is at the center of a tetragon

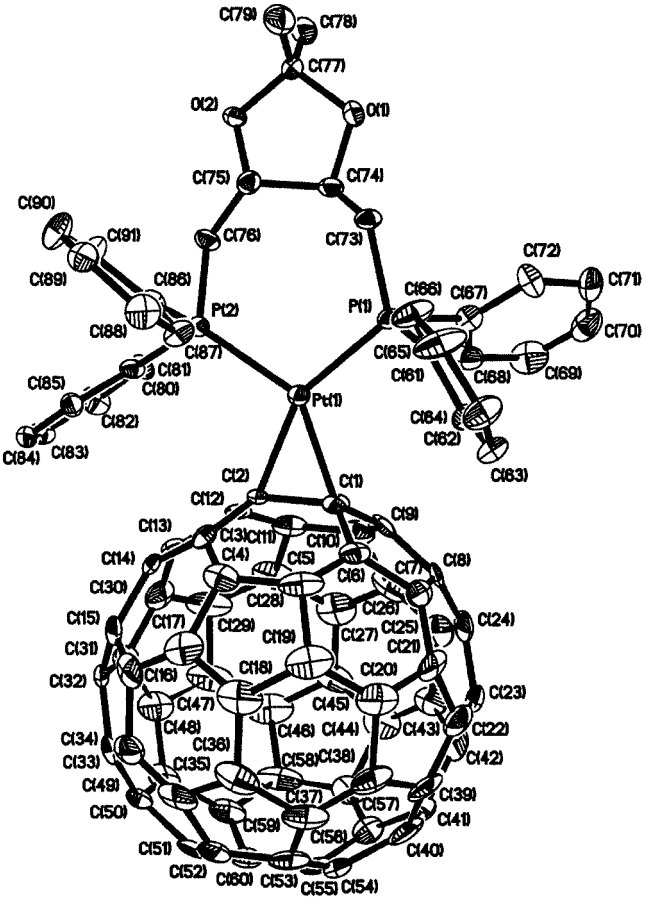

Figure 9. Structural drawing of **6** with ellipsoids drawn at the 30% probability

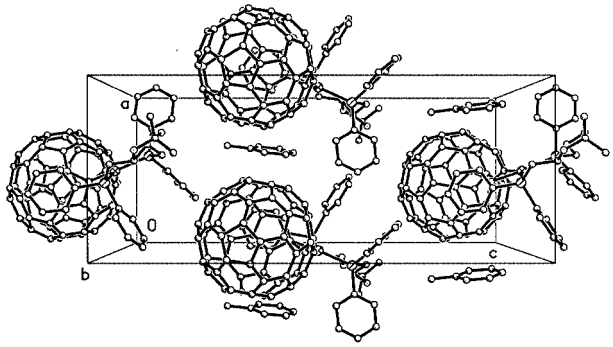

Figure 10. Molecular arrangement in a unit cell of **6**

constituted by the atoms C(1), C(2), P(1) and P(2), and all five atoms are coplanar with a mean deviation of only 0.014 Å. In addition, it is worth noting that the C_{60} ligand in **6** is slightly distorted from the perfect sphere. The two coordin-

 © 2003 Wiley-VCH Verlag GmbH & Co. KGaA, Weinheim

ating carbon atoms C(1) and C(2) are pulled out of the spherical surface by about 0.2 Å, and the distance from C(1) and C(2) to the C_{60} center (ca. 3.72 Å) is much longer than the distance from each of the other carbon atoms to the C_{60} center (3.49−3.56 Å). As a matter of fact, such a structure is typical of some diphosphane-chelated C_{60} transition metal complexes. Table 3 shows some geometric parameters of the crystal structures of **6** and its enantiomer (η^2-C_{60})Pt{(+)-DIOP}.[10] Obviously, the geometric parameters of these two platinum complexes are very similar to each other.

Table 3. Comparison of the crystal structures of **6** and its analogue with (+)-DIOP

	6	(η^2-C_{60})Pt{(+)-DIOP}
Bond length between the two coordinating carbon atoms [Å]	1.502(11)	1.51(2)
Pt−C bond length [Å]	2.107(7)	2.09(2)
	2.135(7)	2.12(2)
Pt−P bond length [Å]	2.252(2)	2.262(4)
	2.281(2)	2.279(4)
C−Pt−C bond angle [°]	41.5(3)	42.0(4)
P−Pt−P bond angle [°]	105.41(7)	109.47(13)
C−Pt−P bond angle [°]	101.2(2)	104.2(4)
	111.8(2)	104.4(4)

As seen in Figure 10, each crystal cell contains four molecules of **6** and four molecules of toluene. The closest distance between the solvent molecule toluene and the C_{60} moiety in **6** is 3.6 Å. This indicates that there are no evident interactions between them.

Electrochemistry of Complexes 5 and 6 and Complementary EPR Measurements

As exemplified in Figure 11 which refers to the Pt complex **6**, derivatives [(η^2-C_{60})M{(−)-DIOP}] exhibit a reduced redox activity compared with that of [(η^2-C_{60})M(CO)$_3${(−)-DIOP}].

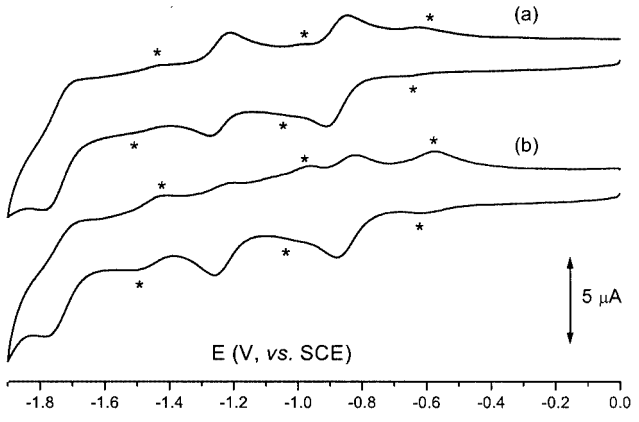

Figure 11. Cyclic voltammograms on a platinum electrode of a CH_2Cl_2 solution of **6** (0.7×10^{-3} mol·dm^{-3}); (a) $T = -20$ °C; (b) $T = +20$ °C; scan rate 0.2 V s^{-1}; starred peaks indicate the appearance of identified by-products (see text)

Complexes **5** and **6** display two fullerene-centered sequential reductions. The reduction processes show significant chemical reversibility, only at low temperatures. At ambient temperature, fast release of free C_{60} occurs on reduction. A third cathodic process is present at very negative potential values, which, based on the relative peak-height, most likely involves the metal fragment.[23] Further, these complexes show an anodic process (not shown in figure) that is completely irreversible (or, quick C_{60} release take places) at low temperatures. The formal electrode potentials are presented in Table 4.

It should be noted that the Pd/Pt fragment is slightly more electron-donating than the Mo/W unit, such that the negative shift in the redox potentials is about 0.25 V with respect to the free fullerene.

In agreement with the electrochemical findings, the liquid-nitrogen X-band EPR spectra of the electrogenerated [**5**]$^-$ monoanion show the undoubted presence of [C_{60}]$^-$ (Figure 12).

As a matter of fact, two different paramagnetic species, partially overlapped in the high-field region, are detected. The narrow, high-field (starred) signal is due to the [C_{60}]$^-$ monoanion, while the low-field signal is attributed to the parallel region of the axial absorption of [**5**]$^-$, the relevant broad parallel region is shifted at lower field. The metallofullerene anion exhibits significant metallic character [$g_i > g_{electron} = 2.0023$; $\Delta g = 0.090(5)$]. There is no evidence for a_{aniso} hpf splittings of the ^{105}Pd nucleus (^{105}Pd: I nuclear spin = 5/2; natural abundance = 22.2%), as well as no ^{31}P shpf splittings. When the temperature at the glassy-fluid transition is raised, the anisotropic features of [**5**]$^-$ disappear, while the isotropic signal of the [C_{60}]$^-$ monoanion is maintained. Rapidly refreezing the fluid solution quantitatively restores the original glassy spectrum of the complex. The X-band EPR parameters are given in Table 5.

In spite of the apparent high stability of the Pt anion [**6**]$^-$ in the cyclic voltammetric time scale, exhaustive electrolysis at the first cathodic process of **6** affords a solution which, through EPR spectroscopy, only shows the signal for [C_{60}]$^-$.

Experimental Section

General: All reactions were carried out under highly purified nitrogen using standard Schlenk or vacuum-line techniques. Chlorobenzene was dried by distillation from P_2O_5 and subsequently from CaH_2 under nitrogen. Toluene, THF, pentane and hexane were distilled under nitrogen from sodium/benzophenone ketyl. All solvents were degassed by bubbling a stream of nitrogen through them for at least 15 min before use. C_{60} (99.9%), (−)-DIOP and (+)-DIOP were of commercial grade and used as received. [$Pd(PPh_3)_4$][26] and [$Pt(PPh_3)_4$][27] were prepared according to literature procedures. Preparative thin-layer chromatography (TLC) and column chromatography were performed on glass plates coated with silica gel (10−40 μm, 20 cm × 25 cm × 0.25 cm) and glass columns packed with silica gel (200−300 mesh, 30 cm × 2.5 cm), respectively. Melting points were determined with a Yanaco MP-500 melting point apparatus. Elemental analyses and FAB-MS were performed with

 © 2003 Wiley-VCH Verlag GmbH & Co. KGaA, Weinheim

Table 4. Formal electrode potentials (V, vs. SCE) and peak-to-peak separation (mV) for the redox changes exhibited by (η^2-C_{60})M{(−)-DIOP} (**5**, M = Pd; **6**, M = Pt) in CH_2Cl_2 solution at −20 °C

Complex (M)	Fullerene-centered reductions				Metal-centered oxidation
	$E^{\circ\prime}_{0/-}$	ΔE_p [a]	$E^{\circ\prime}_{-/2-}$	ΔE_p [a]	E_p[b]
5 (Pd)	−0.83	56	−1.19	56	+0.66
6 (Pt)	−0.84	64	−1.24	63	+0.74
C_{60}	−0.58	62	−0.96	64	−

[a] Measured at 0.1 V·s^{-1}. [b] Peak potentials for irreversible processes.

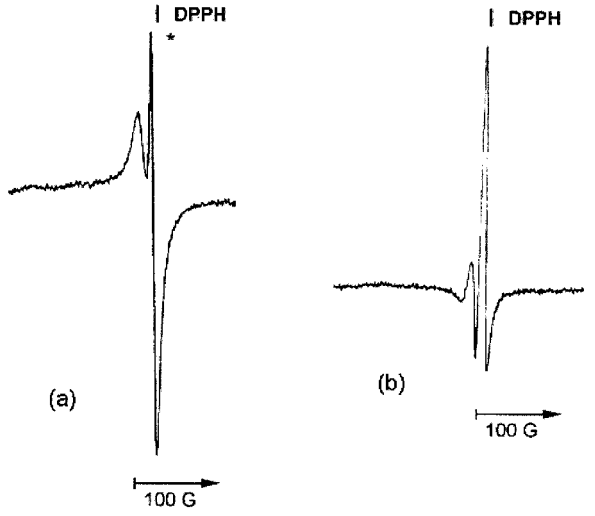

Figure 12. Low-temperature (T = 105 K) X-band EPR spectra of the solution electrogenerated at the first reduction process of **5** in CH_2Cl_2 solution; (a) first derivative; (b) second derivative

Table 5. Low-temperature (100 K) X-band EPR parameters of the electrogenerated anions $[5]^-$ in CH_2Cl_2 solution (g_i: ± 0.005)

Anion	$g_\parallel$	$g_\perp$	$<g>$	g_{iso}[a]
$[\mathbf{5}]^-$	2.094	2.004	2.038	−
$[C_{60}]^-$	2.006[b]	2.006[b]	2.006[b]	2.001[c]

[a] $<g> = (g_\parallel + 2g_\perp)/3$. [b] Averaged values. [c] T = 230 K.

an Elementar Vario EL analyzer and a Zabspec spectrometer, respectively. IR and UV/Vis spectra were recorded with a Bio-Rad FTS-135 and a Shimadzu UV-2401/PC spectrophotometer, respectively. ^{1}H NMR, ^{31}P NMR and ^{13}C NMR spectra were obtained either with a Bruker AC-P200 or a UNITY-PLUS 400 spectrometer. The CD spectra and the specific rotatory powers were determined with a JASCO 715 spectrapolarimeter and a Perkin−Elmer 241-MC polarimeter, respectively. Materials and apparatus for electrochemistry and joint EPR spectroscopy have been described elsewhere.[23] Potential values are referred to the saturated calomel electrode (SCE). Under the present experimental conditions, the one-electron oxidation of ferrocene occurs at +0.36 V.

Preparation of *mer*-[(η^2-C_{60})Mo(CO)$_3${(−)-DIOP}] (1): A 100-mL photoreactor equipped with an N_2 inlet tube and a serum cap was charged with C_{60} (0.072 g, 0.10 mmol), (−)-DIOP (0.050 g, 0.10 mmol), [Mo(CO)$_6$] (0.026 g, 0.10 mmol) and chlorobenzene (50 mL). The mixture was sonicated until all C_{60} was dissolved. The photoreactor containing the resulting purple solution was evacuated to a pressure of ca. 0.1 Torr, and was irradiated by a water-cooled UV 450-W mercury vapor lamp for 3 h to afford a dark green solution. The resulting solution was concentrated in vacuo, and the residue was separated by column chromatography using toluene/light petroleum ether (2:1, v/v) as the eluent under anaerobic conditions. From the second chlorophyll-green band, 0.059 g (42%) of **1** as a dark green solid was obtained. M.p. 300 °C (dec.). ^{1}H NMR (400 MHz, $CDCl_3$): δ = 1.35 (s, 3 H, CH_3), 1.46 (s, 3 H, CH_3), 1.60−1.88 (m, 2 H, CH_2), 2.35 (q, J = 8 Hz, 0.5 H, OCH), 3.01 (t, J = 13.2 Hz, 0.5 H, OCH), 3.26 (t, J = 13.2 Hz, 0.5 H, OCH), 3.62−3.78 (m, 2 H, CH_2), 4.93 (q, J = 8 Hz, 0.5 H, OCH), 7.10−8.00 (m, 20 H, 4 C_6H_5) ppm. ^{31}P NMR (80.96 MHz, $CDCl_3$): δ = 20.05 (d, 1 P), 15.26 (d, $J_{P\text{-}P}$ = 29.6 Hz, 1 P) ppm. ^{13}C{^{1}H} NMR (100.6 MHz, C_6D_6): δ = 211.17 (CO), 210.48 (CO), 163.42 (2 C), 162.76 (2 C), 147.59 (2 C), 147.54 (2 C), 146.63 (2 C), 146.04 (2 C), 145.93 (2 C), 145.82 (2 C), 145.67 (4 C), 145.11 (4 C), 145.04 (4 C), 144.76 (2 C), 144.70 (2 C), 144.59 (2 C), 144.05 (2 C), 143.69 (2 C), 143.62 (2 C), 143.38 (4 C), 142.97 (2 C), 142.89 (2 C), 142.75 (2 C), 142.67 (2 C), 142.30 (2 C), 141.10 (2 C), 140.95 (2 C), 80.01 (2 C) (C_{60} resonance), 135.2, 134.65, 134.45, 134.34, 133.09, 132.99, 131.62, 131.44, 131.02, 130.91, 130.81, 130.28, 129.73, 129.64, 129.51, 129.42 (4 C_6H_5P, resonance), 109.28 (−OCO−), 27.47 (CHO), 27.39 (CH_2), 23.07 (CH_3) ppm. IR (KBr disk): $\tilde{\nu}$ = 2002 (s), 1943 (s), 1883 (vs) (C≡O), 1434 (m), 1185 (w), 586 (w), 526 (s) (C_{60}) cm^{-1}. MS (FAB): m/z = 720 [C_{60}^+], 1401 {[M + H]$^+$, ^{98}Mo}. UV/Vis (THF) λ_{max} (log ε) = 237.9 (5.07), 257.1 (5.21), 330.7 (4.65), 433.9 (4.20), 600.5 (3.87) nm. $[\alpha]^{25}_{365}$ = +2.7 (c = 3.15 × 10^{-5} mol/L, THF). $C_{94}H_{32}MoO_5P_2$ (1399.17): calcd. C 80.69, H 2.31; found C 80.40, H 2.55.

***mer*-[(η^2-C_{60})W(CO)$_3${(−)-DIOP}] (2):** The same synthetic procedure was employed as for the preparation of **1**, except that [W(CO)$_6$] (0.035 g, 0.10 mmol) was used instead of the molybdenum complex [Mo(CO)$_6$], and the reaction mixture was separated by TLC using toluene/light petroleum ether (2:1, v/v) as the eluent under anaerobic conditions. From the second chlorophyll-green band, 0.076 g (51%) of **2** as a dark green solid was obtained. M.p. 300 °C (dec.). ^{1}H NMR (200 MHz, $CDCl_3$): δ = 1.33 (s, 3 H, CH_3), 1.45 (s, 3 H, CH_3), 1.72−2.00 (m, 2 H, CH_2), 2.40 (q, J = 8 Hz, 0.5 H, OCH), 3.22 (t, J = 13.2 Hz, 0.5 H, OCH), 3.39(t, J = 13.2 Hz, 0.5 H, OCH), 3.70−3.92 (m, 2 H, CH_2), 4.91 (q, J = 8 Hz, 0.5 H, OCH), 7.12−8.12 (m, 20 H, 4 C_6H_5) ppm. ^{31}P NMR (80.96 MHz, $CDCl_3$): δ = −3.97 (d, 1 P), −5.14 (d, $J_{P\text{-}P}$ = 21.5 Hz, 1 P) ppm. ^{13}C{^{1}H} NMR (100.6 MHz, $CDCl_3$): δ = 203.52 (CO), 202.58 (CO), 163.43 (2 C), 162.78 (2 C), 147.09 (4 C), 146.27 (2 C), 145.40 (4 C), 145.28 (2 C), 145.05 (4 C), 144.86 (2 C), 144.44 (4 C), 144.35 (4 C), 143.87 (2 C), 143.77 (2 C), 143.64 (2 C), 142.92

 © 2003 Wiley-VCH Verlag GmbH & Co. KGaA, Weinheim

(2 C), 142.59 (4 C), 142.49 (4 C), 142.01 (4 C), 141.77 (4 C), 141.33 (2 C), 140.03 (2 C), 78.81 (2 C) (C_{60} resonance), 134.43, 133.95, 133.83, 132.61, 132.34, 132.25, 131.54, 131.35, 130.73, 130.50, 130.41, 130.25, 129.11, 128.49, 128.40 (4 C_6H_5P, resonance), 108.84 (−OCO−), 26.95 (CHO), 26.84 (CH_2), 21.71 (CH_3) ppm. IR (KBr disk): $\tilde{\nu}$ = 2000 (s), 1938 (s), 1870 (vs) (C≡O), 1434 (m), 1186 (w), 584 (w), 526 (s) (C_{60}) cm^{-1}. MS (FAB): *m*/*z* = 720 (C_{60}^{+}), 1491 {[M + 3 H]$^+$, ^{186}W}. UV/Vis (THF): λ_{max} (log ε) = 239.3 (5.06), 256.9 (5.11), 340.5 (4.61), 429.5 (4.25), 592.1 (3.88) nm. $[\alpha]_{365}^{25}$ = +4.4 ($c = 2.16 \times 10^{-5}$ mol/L, THF). $C_{94}H_{32}O_5P_2W$ (1487.08): calcd. C 75.92, H 2.17; found C 75.80, H 2.49.

***mer*-[(η²-C_{60})Mo(CO)$_3${(+)-DIOP}] (3):** The same synthetic procedure was employed as for the preparation of **1**, except that (+)-DIOP (0.050 g, 0.10 mmol) was used instead of (−)-DIOP. The reaction mixture was separated by TLC using toluene/light petroleum ether (6:1, v/v) as the eluent under anaerobic conditions. From the second chlorophyll-green band, 0.068 g (48%) of **3** as a dark green solid was obtained. M.p. 300 °C (dec.). ^{1}H NMR (200 MHz, $CDCl_3$): δ = 1.32 (s, 3 H, CH_3), 1.43 (s, 3 H, CH_3), 1.60−1.90 (m, 2 H, CH_2), 2.30 (q, *J* = 8 Hz, 0.5 H, OCH), 3.00 (t, *J* = 16 Hz, 0.5 H, OCH), 3.30 (t, *J* = 16 Hz, 0.5 H, OCH), 3.60−3.80 (m, 2 H, CH_2), 4.90 (q, *J* = 8 Hz, 0.5 H, OCH), 7.10−8.00 (m, 20 H, 4 C_6H_5) ppm. ^{31}P NMR (80.96 MHz, $CDCl_3$): δ = 20.07 (d, 1 P), 15.27 (d, $J_{P\text{-}P}$ = 32.1 Hz, 1 P) ppm. ^{13}C{^{1}H} NMR(100.6 MHz, $CDCl_3$): δ = 163.03 (2 C), 162.43 (2 C), 147.24 (4 C), 146.39 (2 C), 145.82 (2 C), 145.70 (2 C), 145.49 (2 C), 145.36 (2 C), 144.89 (4 C), 144.80 (4 C), 144.35 (4 C), 144.19 (2 C), 143.71 (8 C), 143.40 (2 C), 143.10 (4 C), 142.68 (4 C), 142.48 (4 C), 140.67 (2 C), 140.56 (2 C), 78.72 (2 C) (C_{60} resonance), 136.22, 134.90, 134.58, 134.40, 134.02, 133.10, 131.81, 131.60, 130.97, 130.54, 129.69, 129.53, 129.21, 129.05, 128.46, 128.21 (4 C_6H_5P, resonance), 109.25 (−OCO−), 27.26 (CHO), 26.76 (CH_2), 22.79 (CH_3) ppm. IR (KBr disk): $\tilde{\nu}$ = 1997 (s), 1934 (s), 1882 (vs, C≡O), , 1430 [m, ν(C_{60})], 1185 (w), 584 (w), 523 (s, C_{60}) cm^{-1}. MS (FAB): *m*/*z* = 1395 {[M$^+$], ^{92}Mo}. UV/Vis (THF): λ_{max} (log ε) = 252.5 (5.07), 290.0 (4.80), 328.0 (4.71), 436.0 (4.23), 605.0 (3.72) nm. $[\alpha]_{365}^{25}$ = −3.74 ($c = 3.06 \times 10^{-5}$ mol/L, THF). $C_{94}H_{32}MoO_5P_2$ (1399.17): calcd. C 80.69, H 2.31; found C 80.43, H 2.60.

***mer*-[(η²-C_{60})W(CO)$_3${(+)-DIOP}] (4):** The same synthetic procedure was employed as for the preparation of **3**, except that [W(CO)$_6$] (0.035 g, 0.10 mmol) was used instead of [Mo(CO)$_6$], and the reaction mixture was separated by TLC using toluene/light petroleum ether (6:1, v/v) as the eluent under anaerobic conditions. From the second chlorophyll-green band, 0.065 g (43%) of **4** as a dark green solid was obtained. M.p. 300 °C (dec.). ^{1}H NMR (200 MHz, $CDCl_3$): δ = 1.33 (s, 3 H, CH_3), 1.45 (s, 3 H, CH_3), 1.65−1.90 (m, 2 H, CH_2), 2.40 (q, *J* = 8 Hz, 0.5 H, OCH), 3.20(t, *J* = 12 Hz, 0.5 H, OCH), 3.40 (t, *J* = 12 Hz, 0.5 H, OCH), 3.80−4.00 (m, 2 H, CH_2), 4.95 (q, *J* = 8 Hz, 0.5 H, OCH), 7.10−8.00 (m, 20 H, 4 C_6H_5) ppm. ^{31}P NMR (80.96 MHz, $CDCl_3$): δ = −4.08 (d, 1 P), −5.15 (d, $J_{P\text{-}P}$ = 21.1 Hz, 1 P) ppm. ^{13}C{^{1}H} NMR(100.6 MHz, $CDCl_3$): δ = 158.21 (2 C), 157.57 (2 C), 141.88 (4 C), 141.06 (2 C), 140.20 (2 C), 140.08 (4 C), 139.87 (2 C), 139.83 (2 C), 139.65 (2 C), 139.23 (8 C), 139.14 (4 C), 138.67 (2 C), 138.55 (2 C), 138.43 (2 C), 137.71 (2 C), 137.36 (2 C), 137.29 (4 C), 137.27 (4 C), 136.81 (2 C), 136.77 (2 C), 136.62 (2 C), 136.55 (2 C), 73.60 (2 C) (C_{60} resonance), 134.82, 129.21, 128.73, 127.02, 125.52, 125.21, 123.92, 123.28, 123.19 (4 C_6H_5P, resonance), 103.62 (−OCO−), 21.72 (CHO), 21.60 (CH_2), 17.15 (CH_3) ppm. IR (KBr disk): $\tilde{\nu}$ = 2002 (s), 1934 (s), 1870 (vs) (C≡O), ν_{C60} 1434 (m), 1181 (w), 578 (w), 523 (s) (C_{60}) cm^{-1}. MS (FAB): *m*/*z* = 1488 {[M$^+$], ^{186}W}. UV/Vis (THF): λ_{max} (log ε) = 254.0 (4.93), 291.0 (4.56), 338.5 (4.45), 432.0 (3.98), 604.0 (3.46) nm. $[\alpha]_{365}^{25}$ = −3.00 ($c = 2.02 \times 10^{-5}$ mol/L, THF). $C_{94}H_{32}O_5P_2W$ (1487.08): calcd. C 75.92, H 2.17; found C 75.64, H 2.45.

[(η²-C_{60})Pd{(−)-DIOP}] (5): A three-necked flask equipped with a magnetic stirrer bar, a rubber septum and a nitrogen inlet tube was charged with C_{60} (0.018 g, 0.025 mmol) and 8 mL of toluene. The mixture was stirred until the solids were dissolved. When [Pd(PPh$_3$)$_4$] (0.029 g, 0.025 mmol) was added, the solution turned dark green immediately. After (−)-DIOP (0.025 g, 0.050 mmol) was added, the solution was stirred for 10 min. 20 mL of hexane was then carefully layered on the reaction mixture. The flask was left to stand for 1 d without disturbing and tiny black needles precipitated. After the precipitate was filtered, washed with pentane and dried in vacuo, 0.030 g (91%) of **5**·$C_6H_5CH_3$ was obtained. M.p. > 300 °C (dec.). ^{1}H NMR (200 MHz, $CDCl_3$): δ = 1.38 (s, 6 H, 2CH_3), 2.34 (s, 3 H, PhCH_3), 2.58−2.76 (m, 2 H, 2OCH), 3.30−4.24 (m, 4 H, 2CH_2), 7.16−7.94 (m, 25 H, 5 C_6H_5) ppm. ^{31}P NMR (200 MHz, $CDCl_3$): δ = 9.28 (s, 2 P) ppm. IR (KBr disk): $\tilde{\nu}$ = 3061 (w), 3018 (w), 2983 (w), 2933 (w), 2910 (w), 2879 (w), 2860 (w), 1571 (w), 1480 (w), 1459 (w), 1433 (s), 1370 (m), 1252 (m), 1218 (m), 1183 (m), 1159(m), 1099 (m), 1055 (s), 978 (m), 885 (m), 832 (m), 749 (s, sh), 735 (s), 692 (s), 577 (m), 527 (s), 507 (s) cm^{-1}. UV/Vis (toluene): λ_{max} (log ε) = 288.5 (4.57), 294.5 (4.58), 334.5 (4.54), 447.0 (3.97) nm. $C_{98}H_{40}O_2P_2Pd$ (1417.76): calcd. C 83.02, H 2.84; found C 83.12, H 3.08.

[(η²-C_{60})Pt{(−)-DIOP}] (6): The synthesis was similar to that of **5**, except that [Pt(PPh$_3$)$_4$] (0.031 g, 0.025 mmol) was used instead of [Pd(PPh$_3$)]. 0.036 g (96%) of **6**·$C_6H_5CH_3$ as tiny black needles was obtained. M.p. > 300 °C (dec.). ^{1}H NMR (200 MHz, $CDCl_3$): δ = 1.37 (s, 6 H, 2 CH_3), 2.33 (s, 3 H, PhCH_3), 2.60−2.82 (m, 2 H, 2 OCH), 3.58−4.20 (m, 4 H, 2 CH_2), 7.10−8.04 (m, 25 H, 5 C_6H_5) ppm. ^{31}P NMR (200 MHz, $CDCl_3$): δ = 11.13 (s, $J_{Pt\text{-}P}$ = 3749 Hz, 2 P) ppm. IR (KBr disk): $\tilde{\nu}$ = 3057 (w), 3022 (w), 2983 (w), 2941 (w), 2910 (w), 2879 (w), 2860 (w), 1571 (w), 1478 (w), 1458 (w), 1434 (m), 1372 (w), 1332 (w), 1251 (m), 1218 (m), 1183 (m), 1160 (m), 1102 (m), 1057 (s), 979 (m), 884 (m), 832 (m), 784 (m), 745 (s, sh), 734 (s), 692 (s), 576 (m), 527 (s), 508 (s) cm^{-1}. UV/Vis (toluene): λ_{max} (log ε) = 288.5 (4.59), 295.0 (4.59), 334.5 (4.51), 438.5 (4.11) nm. $C_{98}H_{40}O_2P_2Pt$ (1506.42): calcd. C 78.14, H, 2.68. found C 78.40, H 2.67.

Crystal Structure Determination of 6: Single crystals of **6** suitable for X-ray diffraction analysis were obtained by slow diffusion of hexane into the toluene solution of **6** at ambient temperature. A crystal of **6** was glued to a glass fiber and mounted on a Bruker SMART-1000 automated diffractometer. Data were collected at room temperature, using graphite-monochromated Mo-K_α radiation (λ = 0.71073 Å) in the ω-2θ scanning mode. Absorption correction was performed using the SADABS method. The structure was solved by direct methods using the SHELXS-97 program[28] and refined by full-matrix least-squares techniques (SHELXL-97)[29] on F^2. Hydrogen atoms were located by using the geometric method. The crystal data and structural refinement details are listed in Table 6. The calculations were performed using the TEXSAN crystallographic software package of Molecular Structure Corporation. Crystallographic data (excluding structure factors) for the structure reported in this paper have been deposited with the Cambridge Crystallographic Data Centre as supplementary publication no. CCDC-199653. Copies of the data can be obtained free of charge on application to CCDC, 12 Union Road, Cambridge, CB2 1EZ, UK [Fax: (internat.) + 44-1223/336033; E-mail: deposit@ccdc.cam.ac.uk or www:http://www.ccdc.cam.ac.uk].

 © 2003 Wiley-VCH Verlag GmbH & Co. KGaA, Weinheim

Table 6. Crystal data and structure refinements for $6{\cdot}C_6H_5CH_3$

Empirical formula	$C_{91}H_{32}O_2P_2Pt{\cdot}C_6H_5CH_3$
Formula mass	1506.33
Temperature [K]	293(2)
Crystal system	orthorhombic
Space group	$P2_12_12_1$
a [Å]	10.058(2)
b [Å]	24.389(5)
c [Å]	25.137(6)
V [Å^3]	6166(2)
Z	4
$d_{calcd.}$ [Mg·m^3]	1.623
μ [mm^{-1}]	2.390
$F(000)$	3008
Unique reflections, R_{int}	10 833, 0.0574
Observed reflections	7092
Goodness-of-fit on F^2	0.999
R [$I > 2\sigma(I)$]	$R_1 = 0.0453$
	$wR_2 = 0.1025$
R (all data)	$R_1 = 0.0821$
	$wR_2 = 0.1165$

Acknowledgments

We are grateful to the National Natural Science Foundation of China and the Laboratory of Organometallic Chemistry for financial support of this work. P. Z. gratefully acknowledges financial support from the University of Siena.

[1] For reviews, see for example: [1a] P. J. Fagan, J. C. Calabrese, B. Malone, *Acc. Chem. Res.* **1992**, *25*, 134−142. [1b] M. L. H. Green, *Pure Appl. Chem.* **1995**, *67*, 249−256. [1c] W. Sliwa, *Transition Met. Chem.* **1996**, *21*, 583−592. [1d] A. L. Balch, M. M. Olmstead, *Chem. Rev.* **1998**, *98*, 2123−2166. [1e] J. R. Bowser, *Adv. Organomet. Chem.* **1994**, *36*, 57−94.

[2] H. W. Kroto, J. R. Heath, S. C. O'Brien, R. F. Curl, R. E. Smalley, *Nature* **1985**, *318*, 162−163.

[3] W. Kräschmer, L. D. Lamb, K. Fostiropoulos, D. R. Huffman, *Nature* **1990**, *347*, 354−358.

[4] P. J. Fagan, J. C. Calabrese, B. Malone, *Science* **1991**, *252*, 1160−1161.

[5] For mononuclear [60]fullerene derivatives, see for example: [5a] A. L. Balch, V. J. Catalano, J. W. Lee, M. M. Olmstead, *J. Am. Chem. Soc.* **1992**, *114*, 5455−5457. [5b] V. V. Bashilov, P. V. Petrovskii, V. I. Sokolov, S. V. Lindeman, I. A. Guzey, Y. T. Struchkov, *Organometallics* **1993**, *12*, 991−992. [5c] H.-F. Hsu, Y. Du, T. E. Albrecht-Schmitt, S. R. Wilson, J. R. Shapley, *Organometallics* **1998**, *17*, 1756−1761.

[6] For dinuclear [60]fullerene derivatives, see for example: [6a] A. L. Balch, J. W. Lee, B. C. Noll, M. M. Olmstead, *J. Am. Chem. Soc.* **1992**, *114*, 10984−10985. [6b] S. Zhang, T. L. Brown, Y. Du, J. R. Shapley, *J. Am. Chem. Soc.* **1993**, *115*, 6705−6709. [6c] I. J. Mavunkal, Y. Chi, S.-M. Peng, G.-H. Lee, *Organometallics* **1995**, *14*, 4454−4456.

[7] For trinuclear [60]fullerene derivatives, see for example: [7a] H.-F. Hsu, J. R. Shapley, *J. Am. Chem. Soc.* **1996**, *118*, 9192−9193. [7b] J. T. Park, H. Song, J.-J. Cho, M.-K. Chung, J.-H. Lee, I.-H. Suh, *Organometallics* **1998**, *17*, 227−236.

[8] For multinuclear [60]fullerene derivatives, see for example: [8a] P. J. Fagan, J. C. Calabrese, B. Malone, *J. Am. Chem. Soc.* **1991**, *113*, 9408−9409. [8b] M. Rasinkangas, T. T. Pakkaned, T. A. Pakkaned, M. Ahlgrén, J. Rouvinen, *J. Am. Chem. Soc.* **1993**, *115*, 4901. [8c] K. Lee, Z.-H. Choi, Y.-J. Cho, H. Song, J. T. Park, *Organometallics* **2001**, *20*, 5564−5570.

[9] V. V. Bashilov, P. V. Petrovskii, V. I. Sokolov, *Russ. Chem. Bull.* **1993**, *42*, 392−393.

[10] V. V. Bashilov, P. V. Petrovskii, V. I. Sokolov, F. M. Dolgushin, A. I. Yanovsky, Yu. T. Struchkov, *Russ. Chem. Bull.* **1996**, *45*, 1207−1213.

[11] [11a] L.-C. Song, J.-T. Liu, Q.-M. Hu, G.-F. Wang, P. Zanello, M. Fontani, *Organometallics* **2000**, *19*, 5342−5351. [11b] L.-C. Song, Y.-H. Zhu, Q.-M. Hu, *J. Chem. Res. (S)* **2000**, 316−317. [11c] P. Zanello, F. Laschi, M. Fontani, L.-C. Song, Y.-H. Zhu, *J. Organomet. Chem.* **2000**, *593−594*, 7−11. [11d] Y.-H. Zhu, L.-C. Song, Q.-M. Hu, C.-M. Li, *Org. Lett.* **1999**, *1*, 1693−1695. [11e] L.-C. Song, Y.-H. Zhu, Q.-M. Hu, *Polyhedron* **1997**, *16*, 2141−2143. [11f] L.-C. Song, Y.-H. Zhu, Q.-M. Hu, *Polyhedron* **1998**, *17*, 469−473. [11g] Y.-L. Song, G.-Y. Fang, Y.-X. Wang, S. -T Liu, C.-F. Li, L.-C. Song, Y.- H. Zhu, Q.-M. Hu, *Appl. Phys. Lett.* **1999**, *74*, 332−334. [11h] L.-C. Song, Y.-H. Zhu, Q.-M. Hu, *J. Chem. Res. (S)* **1999**, 56−57. [11i] L.-C. Song, J.-T. Liu, Q.-M. Hu, L.-H. Weng, *Organometallics* **2000**, *19*, 1643−1647.

[12] U. Hengartner, D. Valentine, Jr., K. K. Johnson, M. E. Larscheid, F. Pigott, F. Scheidl, J. W. Scott, R. C. Sun, J. M. Townsend, T. Williams, *J. Org. Chem.* **1979**, *44*, 3741−3747.

[13] H. G. Horn, K. Sommer, *Spectrochim. Acta, Part A* **1971**, *27*, 1049−1054.

[14] M. L. H. Green, A. H. H. Stephens, *Chem. Commun.* **1997**, 793−794.

[15] R. E. Douthwaite, M. L. H. Green, A. H. H. Stephens, J. F. C. Turner, *J. Chem. Soc., Chem. Commun.* **1993**, 1522−1524.

[16] J. P. Hare, T. J. Dennis, H. W. Kroto, R. Taylor, A. W. Allaf, S. Balm, D. R. M. Walton, *J. Chem. Soc., Chem. Commun.* **1991**, 412−413.

[17] D. J. Darenbourg, D. J. Zalewski, C. Plepys, C. Campana, *Inorg. Chem.* **1987**, *26*, 3727−3732.

[18] J. P. Collman, L. S. Hegedus, J. R. Norton, R. J. Finke, *Principles and Applications of Organotransition Metal Chemistry*, 2nd ed., University Science Books, Mill Valley, CA, **1987**.

[19] [19a] R. Taylor, J. P. Hare, A. K. Abdul-Sada, H. W. Kroto, *J. Chem. Soc., Chem. Commun.* **1990**, 1423−1425. [19b] J. P. Hare, H. W. Kroto, R. Taylor, *Chem. Phys. Lett.* **1991**, *177*, 394−398. [19c] T. Akasaka, W. Ando, K. Kobagashi, S. Nagase, *J. Am. Chem. Soc.* **1993**, *115*, 1605−1606.

[20] A. N. Chernega, M. L. H. Green, J. Haggitt, A. H. H. Stephen, *Dalton Trans.* **1998**, 755−767.

[21] [21a] V. I. Sokolov, *Pure Appl. Chem.* **1998**, *70*, 789−798. [21b] V. I. Sokolov, *Russ. J. Org. Chem.* **1999**, *35*, 1257−1263. [21c] V. I. Sokolov, V. V. Bashilov, *Platinum Met.Rev.* **1998**, *42*, 18−24.

[22] P. Zanello, in *Chemistry at the Beginning of the Third Millennium* (Eds.: L. Fabbrizzi, A. Poggi), Springer, Heidelberg, **2000**, pp. 247−278.

[23] [23a] P. Zanello, F. Laschi, M. Fontani, C. Mealli, A. Ienco, K. Tang, X. Jin, L. Li, *J. Chem. Soc., Dalton Trans.* **1999**, 965−970. [23b] P. Zanello, F. Laschi, A. Cinquantini, M. Fontani, K. Tang, X. Jin, L. Li, *Eur. J. Inorg. Chem.* **2000**, 1345−1350.

[24] F. E. Mabbs, D. Collison, "Electron Paramagnetic Resonance of d Transition Metal Compounds", in *Studies in Inorganic Chemistry*, Elsevier, New York, **1992**, vol. 16.

[25] G. P. Lozos, C. G. Franz, *QCPE* **1991**, *23*, 20.

[26] L. Malatesta, M. Angoletta, *J. Chem. Soc.* **1957**, 1186−1188.

[27] L. Malatesta, C. Cariello, *J. Chem. Soc.* **1958**, 2323−2328.

[28] G. M. Sheldrick, *SHELXS-97, A Program for Crystal Structure Solution*, University of Göttingen, Germany, **1997**.

[29] G. M. Sheldrick, *SHELXL-97, A Program for Crystal Structure Refinement*, University of Göttingen, Germany, **1997**.

Received February 22, 2003

 © 2003 Wiley-VCH Verlag GmbH & Co. KGaA, Weinheim

Syntheses, Structures and Theoretical Investigations of $1\lambda^4,3\lambda^4,5\lambda^4$-Trithia-2,4,6,8,9-pentaazabicyclo[3.3.1]nona-1(9),2,3,5,7-pentaenes

Carsten Knapp,[a] Enno Lork,[a] Tobias Borrmann,[b] Wolf-Dieter Stohrer,[b] and Rüdiger Mews*[a]

Keywords: Sulfur / Nitrogen / Fluorine / Solid-state structures / Quantum chemistry

The syntheses of the title compounds RCN_5S_3 with electron-withdrawing aryl substituents [R = 2-FC_6H_4 (**1m**), 4-FC_6H_4 (**1n**), 2,6-$F_2C_6H_3$ (**1o**), C_6F_5 (**1p**), 4-NCC_6H_4 (**1q**) and Cl_3C (**1r**)] are described. The X-ray structures of **1n**, **1o**, **1q** and **1r**, together with those of $Me_2NCN_5S_3$ (**1b**) and 4-$CH_3C_6H_4CN_5S_3$ (**1f**), are reported. The experimentally determined dependence of the bond lengths on the substituents R within the bicyclic system RCN_5S_3 is well-reflected in the results of the theoretical calculations (RHF, MP2, B3LYP). The bonding model developed shows that acceptor substituents do not influence bonding within the bicycle. In the solid state, two fundamentally different primary interactions of the RCN_5S_3 molecules are observed; "stacking" and "dimerisation", which can be rationalised by electrostatic interactions between the CN_5S_3 units. However, secondary effects – the interactions between the R substituents – may be even more dominant.

(© Wiley-VCH Verlag GmbH & Co. KGaA, 69451 Weinheim, Germany, 2003)

Introduction

The bicyclic carbon-sulfur-nitrogen heterocycles, $1\lambda^4,3\lambda^4,5\lambda^4$-trithia-2,4,6,8,9-pentaazabicyclo[3.3.1]nona-1(9),2,3,5,7-pentaenes **1** (Scheme 1), are multifunctional sulfur-nitrogen systems with a versatile chemistry.

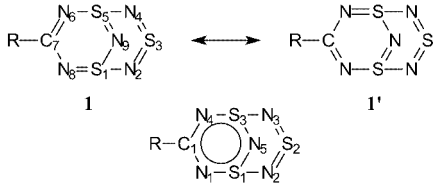

1 **1'**

R = X_3C [X = F (**1a**), Cl (**1r**)]
= R''_2N [R'' = Me (**1b**), Et (**1c**), *i*-Pr (**1d**)]
= $R'C_6H_4$ [R' = H (**1e**), 4-H_3C (**1f**), 4-Cl (**1g**), **4**-F_3C (**1h**), 4-H_3CO (**1i**), 4-C_6H_5 (**1j**), 3-F_3C (**1k**), 4-NC (**1q**)]
= Ar_F [Ar_F = 2-FC_6H_4 (**1m**), 4-FC_6H_4 (**1n**), 2,6-$F_2C_6H_3$ (**1o**), C_6F_5 (**1p**)]
= Cl (**1l**)

Scheme 1. Note: The numbering in the top left represents the IUPAC numbering scheme, the scheme below is that used consistently in this article

They are accessible via two different routes, either from the reaction of 1,3-dichloro-1,3-dithiatriazines $(RCN)(NSCl)_2$ with $Me_3SiNSNSiMe_3$ (dithiatriazine route A; Scheme 2), or from $(NSCl)_3$ and tris(trimethylsilyl)amidines $RC(NSiMe_3)[N(SiMe_3)_2]$ (amidine route B).

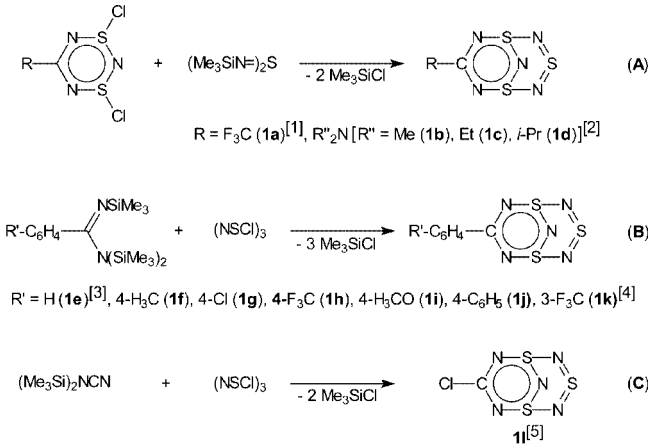

Scheme 2

The preparation of the chloro derivative, described by route C,[5] is difficult to reproduce, but the compound is also accessible via route A from $(ClCN)(NSCl)_2$.[6] Attempts to prepare the corresponding fluoro derivative from $(FCN)(NSCl)_2$ resulted in a very unstable product.[6]

[a] Institut für Anorganische und Physikalische Chemie der Universität Bremen,
Postfach 330440, Leobener Straße, 28334 Bremen, Germany
Fax: (internat.) +49-(0)421/218-4267
E-mail: mews@chemie.uni-bremen.de
[b] Institut für Organische Chemie der Universität Bremen,
Postfach 330440, Leobener Straße, 28334 Bremen, Germany
Supporting information for this article is available on the WWW under http://www.eurjic.org or from the author.

To date, the chemistry of these systems has not been well investigated. Based on MNDO calculations,[7] it has been proposed that the coordination chemistry of compounds **1** is varied. From the large number of chemically non-equivalent donor and acceptor sites in **1**, many interesting and not readily predictable reaction possibilities are expected. To date, only the F_3C derivative **1a** has been introduced as a ligand. $[Ni(F_3CCN_5S_3)_2(OSO)_2(FAsF_5)_2]$ and $[Ag(F_3CCN_5S_3)(\mu\text{-}F_3CCN_5S_3)]_2(AsF_6)_2$ have been isolated and characterised by X-ray crystallography.[7] The bicyclic system undergoes nucleophilic attack with EPh_3 (E = P, As), and **1e** is transformed into the monocyclic eight-membered imino derivatives **2** (Scheme 3),[8] with weak transannular S−S bonds.

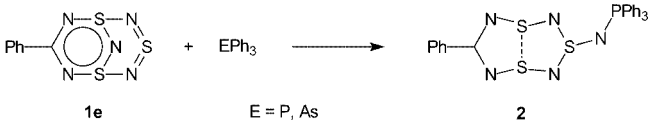

Scheme 3

Under the conditions of both thermolysis and photolysis,[9] it was recently found that the bicyclic sulfur-nitrogen heterocycles **1** afford the corresponding 1,2,3,5-dithiadiazolyl radicals, which are of high interest.[10]

The dependence of the reactivity on the substituent R is documented in the reaction of **1a** and **1e**−**k** with elemental chlorine. The aryl derivatives **1e**−**k** are readily degraded to dithiatriazines **3e**−**k** (Scheme 4),[3,4] while the trifluoromethyl derivative **1a** is not attacked under similar conditions.[11,12]

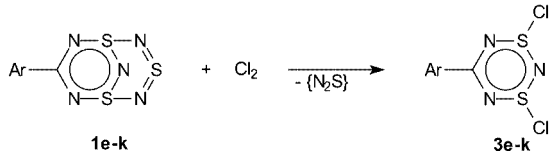

Scheme 4

From the structural and theoretical investigations we endeavoured to explain the different stabilities. Furthermore, these theoretical investigations should allow us to predict the reactivities and the properties of **1**, based on the nature of the substituent.

The X-ray structures of **1a**,[1] **1d**,[3,13] **1e**[14] and **1l**[5] have been described previously. A preliminary theoretical discussion of the bonding properties based on MNDO calculations was reported earlier by our group.[1] In this paper, the synthesis of compounds with electron-withdrawing substituents [RCN_5S_3: R = 2-FC_6H_4 (**1m**), 4-FC_6H_4 (**1n**), 2,6-$F_2C_6H_3$ (**1o**), C_6F_5 (**1p**), 4-NCC_6H_4 (**1q**) and Cl_3C (**1r**)], for which an increased stability is expected, are reported. The X-ray structures of selected compounds (**1b**, **1f**, **1n**, **1o**, **1q** and **1r**) have been determined. The experimental results are compared with the results of the theoretical calculations.

Results and Discussion

Syntheses of $1\lambda^4,3\lambda^4,5\lambda^4$-trithia-2,4,6,8,9-pentaazabicyclo-[3.3.1]nona-1(9),2,3,5,7-pentaenes

As expected, the bicyclic sulfur nitrogen systems **1m**−**1o** with partially fluorinated aryl substituents are readily prepared by the amidine route B from silylated amidines and trithiazyl trichloride. This route can also be used for the preparation of the trifluoromethyl-substituted derivative **1a** (Scheme 5). Thus, **1a** is more-readily accessible than previously reported.[1] It is not possible to use route B for the preparation of derivatives with stronger electron-withdrawing aryl groups (e.g. C_6F_5, 4-NCC_6H_4), since the corresponding *N*,*N*,*N*′-tris(trimethylsilyl)amidines cannot be prepared by silylation of lithium *N*,*N*′-bis(trimethylsilyl)amidines with Me_3SiCl. Their reactivity is greatly reduced due to the electron-withdrawing groups.[15,16] In this case, the corresponding lithium *N*,*N*′-bis(trimethylsilyl)amidines are directly reacted with $(NSCl)_3$ in diethyl ether. Under these conditions, **1p** and **1q** are also formed, but in lower yields. The compounds were obtained in a pure crystalline state by recrystallisation from acetonitrile.

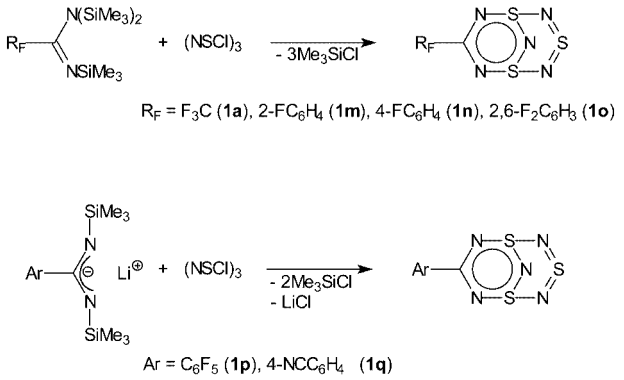

Scheme 5

Compounds **1** can be stored at room temperature in an inert atmosphere and do not decompose. The bicyclic sulfur nitrogen framework undergoes chemical, photochemical or thermal decomposition (partial or complete). In moist air, most of the bicycles are transformed into a white solid within a few hours or days. Even $PhCN_5S_3$, described in the literature as air-stable,[3] will slowly decompose under these conditions. Complete hydrolysis occurs according to Scheme 6:

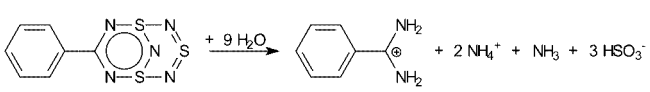

Scheme 6

The products from the direct complete hydrolysis in moist CH_2Cl_2, detected by mass spectrometry (FAB) and chemical analysis, are the corresponding amidinium ions and the NH_4^+, sulfate and thiosulfate ions; only small amounts of the sulfite ion are detected.

 © 2003 Wiley-VCH Verlag GmbH & Co. KGaA, Weinheim

The results of the mass spectrometric analysis of the pure bicyclic systems depend on the ionisation method applied. With ionisation by EI, molecular ions are mostly detected, but with low intensity. The peak representing the fragment $[M - N_3S]^+$ is always present. This corresponds to the stable 1,2,3,5-dithiadiazolylium cation b^+ (Scheme 7) The more gentle FI method also allows for the detection of molecular ions. Furthermore, the direct degradation products a^+ and b^+ are observed, together with the ions (c^+, d^+) formed by recombination of the fragments.

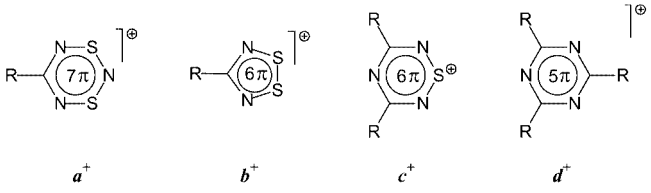

Scheme 7

Chlorine cleaves the NSN bridge of the aryl-substituted bicyclic systems, forming the 1,3-dichloro-1,3,2,4,6-dithiatriazines.[3,4] In contrast to the aryl derivatives, the trifluoromethyl derivative $F_3CCN_5S_3$ (**1a**) is astonishingly stable and does not react with elemental chlorine or with SO_2Cl_2.[4,11,12] Attempts to obtain the corresponding dithiatriazines by degradation reactions of **1a** with Br_2 or $(CF_3)_2NO$ also failed.[12] To date, no explanation for the unexpected stability could be given. In contrast to **1a**, the partially and fully fluorinated aryl derivatives **1o** and **1p** also react with chlorine in CCl_4 (the reaction occurs within a few minutes) to give the corresponding 1,3-dichloro-1,3,2,4,6-dithiatriazines. An obvious dependence of the rate of chlorination on the substituents at the aryl groups has been noted for electron-withdrawing groups (**1g**, **1h**) vs. electron-donating groups (**1f**, **1i**).[4]

Some years ago investigations on the thermal decomposition of $PhCN_5S_3$ (**1e**) in acetonitrile solution were undertaken; only benzonitrile and S_4N_4 were identified as the decomposition products.[17] More recent investigations of the thermolysis of **1e** in squalane by ESR spectroscopy have shown that the radicals b˙ and c˙ are formed as the decomposition products, in accord with the results of the mass spectrometric investigations mentioned before. Both radicals are known from the literature and can be prepared by straightforward methods.[18]

Structure Investigations

Single crystals of RCN_5S_3 [R = Me_2N (**1b**), 4-$CH_3C_6H_4$ (**1f**), 4-FC_6H_4 (**1n**), 2,6-$F_2C_6H_3$ (**1o**), 4-NCC_6H_4 (**1q**), and Cl_3C (**1r**)] were obtained by crystallisation from acetonitrile at −40 °C. They crystallise in the triclinic space group $P\bar{1}$ with the exception of $Cl_3CCN_5S_3$ (**1r**), which crystallises in the monoclinic space group $P2_1/n$ with one molecule of acetonitrile in the asymmetric unit. Crystal data and details of the structure determinations are given in Table 1. Figure 1 shows the structures and the numbering scheme of **1o** and **1q** as representative examples. In these bicycles, the different substituents only have a slight effect on the bond lengths. The C1−N1 bond lengths (131.8−135.3 pm), the N1−S1 bond lengths (158.3−164.0 pm) and the S1−N5 bond lengths (162.6−163.4 pm) lie in the range between that of single and double bonds, while the S1−N2 bonds (172.3−174.8 pm) might be considered as single bonds and the N2−S2 bonds (154.0−155.2 pm) as double bonds. In line with the mesomeric structures (Scheme 1), the bicyclic

Table 1. Crystal data and structure refinement data for **1b**, **1f**, **1n**, **1o**, **1q**, and **1r**

	1b	**1f**	**1n**	**1o**	**1q**	**1r**
Empirical formula	$C_3H_6N_6S_3$	$C_8H_7N_5S_3$	$C_7H_4FN_5S_3$	$C_7H_3F_2N_5S_3$	$C_8H_4N_6S_3$	$C_4H_3Cl_3N_6S_3$
Molecular mass	222.32	269.37	273.33	291.32	280.35	337.65
Crystal system	triclinic	triclinic	triclinic	triclinic	triclinic	monoclinic
Space group	$P\bar{1}$	$P\bar{1}$	$P\bar{1}$	$P\bar{1}$	$P\bar{1}$	$P2_1/n$
a, pm	625.90(10)	594.90(10)	594.7(2)	603.70(10)	476.60(10)	592.50(10)
b, pm	754.30(10)	736.90(10)	746.3(2)	770.90(10)	1082.9(5)	2916.5(3)
c, pm	916.2(2)	1294.1(2)	1172.4(3)	1147.80(10)	1159.3(4)	693.10(10)
α, deg	89.710(10)	78.850(10)	101.53(3)	91.460(10)	64.53(2)	90
β,deg	80.26(2)	84.540(10)	90.31(3)	90.350(10)	87.97(2)	92.500(10)
γ, deg	76.540(10)	73.640(10)	105.95(2)	107.000(10)	78.63(3)	90
V, nm³	0.41434(12)	0.53357(14)	0.4892(2)	0.51062(4)	0.5288(3)	1.1966(3)
Z	2	2	2	2	2	4
$D_{calcd.}$, Mg/m³	1.782	1.677	1.856	1.895	1.761	1.874
Crystal size	0.60 × 0.40 × 0.30	0.70 × 0.60 × 0.10	0.70 × 0.50 × 0.20	0.60 × 0.40 × 0.20	0.40 × 0.30 × 0.20	0.60 × 0.40 × 0.30
θ range	2.78−27.50	2.93−27.49	2.90−27.50	2.76−27.50	3.45−23.50	2.79−26.50
Reflections collected	2227	4994	4551	4704	2997	3394
Independent reflections	1715	2460	2247	2327	1494	2488
Absorption correction	−	−	−	−	DIFABS	−
Goodness-of-fit	1.079	1.074	1.117	1.103	1.044	1.062
Final *R* indices *R*1, *wR*2	0.0359, 0.1006	0.0267, 0.0749	0.0261, 0.0744	0.0262, 0.0726	0.0656, 0.1578	0.0490, 0.1213
R indices (all data)	0.0375, 0.1019	0.0285, 0.0768	0.0276, 0.0760	0.0280, 0.0739	0.1043, 0.1802	0.0735, 0.1307

 © 2003 Wiley-VCH Verlag GmbH & Co. KGaA, Weinheim

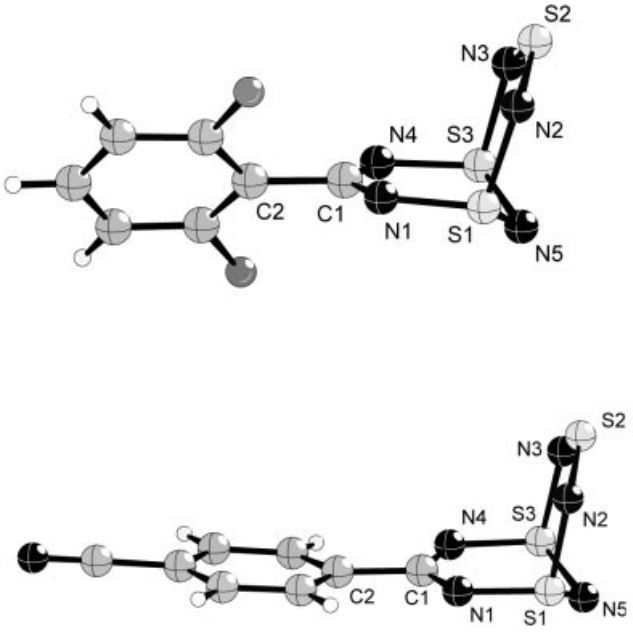

Figure 1. Crystal structures and numbering scheme of **1o** and **1q**

framework is best described as a dithiatriazine bridged by a sulfur diimide group.

Closer examination of the bonding parameters shows the effect of the substituents. The ten bicycles described in Table 2 can be divided into three groups. Strong donors or strong acceptors bonded directly to the bicycles each form one group. The third group consists of all aryl-substituted bicycles, the bond lengths of which are independent of the substituents at the aryl ring (they are equal within the range of standard deviations).

The difference between the three different groups is particularly apparent in the C1−N1 and the N1−S1 bond lengths. The C1−N1 bond length is increased by approximately 2 pm by electron-donating substituents (R = Me_2N), and shortened by approximately 1.5 pm by electron-accepting substituents (R = CF_3), relative to the weakly interacting phenyl group. The neighbouring N1−S1 bonds show the reverse effect. The effects on the other bonds in the system, except on the S1−N2 bond, are within experimental error. Directly bonded amino groups significantly increase this bond length when compared with the directly bonded electron-withdrawing groups and the aryl substituents.

The change in the C1−N1 bond lengths is accompanied by a change in the NCN angle: 127−128° for compounds with donor substituents, around 130° for the aryl derivatives, and up to 134−135° for the acceptor-substituted bicycles.

In the aryl derivatives the twist angle τ between the aromatic phenyl ring and the plane of the five atoms (C1, N1, N4, S1, S3) in the heterocycle is 26−29° for **1e**, **1f** and **1n**, i.e. the 6π-aromatic and the delocalised sulfur-nitrogen systems are not coplanar. However, in **1q**, which has a strongly electron-accepting nitrile group in the *para* position, the two rings are virtually coplanar (τ = 5.2°). However, this does not lead to an apparent shortening of the exocyclic C−C1 bond. In **1o**, the phenyl ring is 50.1° out of the plane formed by the five atoms of the heterocycle, because of the repulsive interactions between the fluorine atoms in the *ortho*-positions and the nitrogen atoms N1 and N4.

Solid-State Packing

In the crystal, the packing of the molecules varies. Two completely different arrangements of the bicycles are observed that can be described as "stacking" or "dimerisation". Stacking is found for the bicycles with R = Cl (**1l**), F_3C (**1a**) and 4-NCC_6H_4 (**1q**); a related structure is shown

Table 2. Selected bond lengths (pm) and angles (deg) for the bicyclic molecules RCN_5S_3

R	R−C1	C1−N1 C1−N4	N1−S1 N4−S3	S1−N5 S3−N5	S1−N2 S3−N3	N2−S2 N3−S2	NCN	τ	ref.
F_3C (**1a**)	152.4(4)	131.6(3) 132.5(3)	163.1(2) 163.0(2)	162.7(2) 163.3(2)	172.3(2) 172.7(2)	154.4(2) 154.6(2)	134.1(2)	–	[1]
Cl_3C (**1r**)	153.9(5)	131.6(5) 131.7(5)	163.7(3) 164.5(3)	162.9(4) 162.9(4)	172.6(3) 172.4(3)	154.1(3) 155.0(4)	133.9(4)	–	this work
Cl (**1l**)	175.1(2)	132.0(2) 131.9(2)	163.3(2) 163.2(2)	163.4(2)	173.1(2)	155.0(2)	135.2(3)	–	[5]
4-NCC_6H_4 (**1q**)	147.6(10)	132.5(9) 135.0(9)	162.0(6) 161.3(6)	163.0(6) 162.1(7)	173.9(7) 171.6(6)	152.5(7) 155.8(6)	129.2(7)	5.2	this work
2,6-$F_2C_6H_3$ (**1o**)	149.7(2)	133.3(2) 133.4(2)	162.76(14) 163.07(14)	163.37(14) 163.02(14)	172.97(16) 172.33(16)	155.02(15) 155.41(15)	131.91(15)	50.1	this work
4-FC_6H_4 (**1n**)	148.7(2)	133.8(2) 134.0(2)	162.39(14) 162.36(14)	163.15(14) 163.38(14)	173.49(16) 172.99(16)	155.09(15) 155.23(15)	133.35(15)	28.4	this work
C_6H_5 (**1e**)	148.5(3)	133.9(3) 133.3(3)	162.1(2) 162.1(2)	162.9(2) 163.0(2)	172.8(2) 172.8(2)	154.7(2) 154.6(2)	129.8(2)	26.6	[3,13]
4-$H_3CC_6H_4$ (**1f**)	148.82(19)	134.04(19) 134.17(18)	162.65(13) 162.62(13)	163.22(13) 163.52(13)	173.50(14) 173.23(15)	154.93(14) 155.32(14)	130.36(14)	27.2	this work
Me_2N (**1b**)	134.6(3)	135.2(3) 135.2(3)	159.69(18) 160.06(19)	163.51(19) 163.1(2)	175.45(19) 174.2(2)	154.66(19) 155.3(2)	128.67(19)	–	this work
iPr_2N (**1d**)	134.1(4)	135.0(5) 135.5(4)	158.8(3) 157.7(3)	163.3(3) 162.0(4)	174.5(3) 175.0(3)	153.6(3) 154.3(3)	127.0(3)	–	[2]

 © 2003 Wiley-VCH Verlag GmbH & Co. KGaA, Weinheim

by (**1d**; R = *i*Pr$_2$N). The sulfur-nitrogen rings fit into one another like stacked crates. Most of the aryl-substituted bicycles [R = 4-H$_3$CC$_6$H$_4$ (**1f**), 4-FC$_6$H$_4$ (**1n**), 2,6-F$_2$C$_6$H$_3$ (**1o**)] and the dimethylamino derivative (**1b**) form centrosymmetric dimers. The structure of Cl$_3$CCN$_5$S$_3$ (**1r**), which crystallises with one equivalent of acetonitrile, is different and cannot be assigned to either of these two types.

The stacking of the bicycles is represented by **1q** in Figure 2. Each heterocycle has one $N^{\delta-}\cdots S^{\delta+}$ and one $N^{\delta-}\cdots C^{\delta+}$ interaction with the molecule above. The $N^{\delta-}\cdots S^{\delta+}$ interacting distance between the bridging nitrogen atom and the sulfur atom of the diimide bridge is around 300−310 pm (**1q** 299.2, **1l** 304.5, **1a** 311.8 pm), depending on the substituent at the bicycle, and thereby lies within the sum of the van der Waals radii (335 pm). The $N^{\delta-}\cdots S^{\delta+}$ distance in **1d** is significantly longer (327.4 pm), which can be attributed to the repulsive steric effect of the large isopropylamino groups. The same effect is also observed for the $N^{\delta-}\cdots C^{\delta+}$ distance between the bridging nitrogen atom and the carbon atom of the heterocycle. This distance is more than 100 pm longer for **1d** (438.8 pm) than for the other three bicycles (around 315 pm). This is barely within the sum of the van der Waals radii (320−325 pm). The average distance between the planes through the parallel phenyl rings is approximately 350 pm for **1q**.

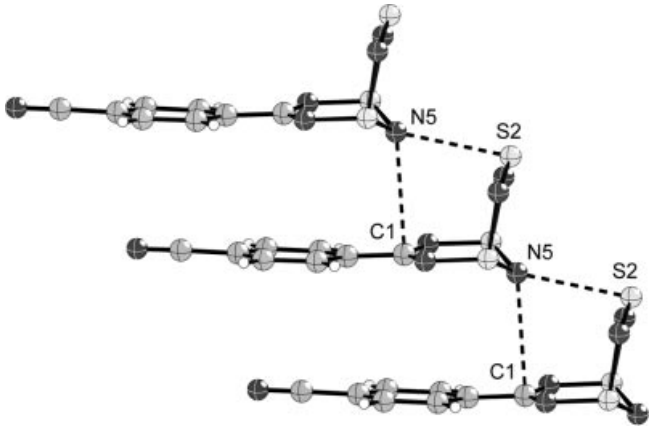

Figure 2. Stacking of **1q** in the crystal

In this case, "dimerisation" implies that two molecules are arranged with their heterocyclic heads facing each other (represented in Figure 3). The second molecule is rotated by 180° with respect to the first, so that two $N^{\delta-}\cdots S^{\delta+}$ interactions can be formed. The shortest distances between the molecules, independent of the substituent, is around 295 pm (**1o** 291.5−**11n** 296.4 pm), and is thus shorter than the sum of the van der Waals radii (335 pm).

Figures 4−6 present crystal packing diagrams that show the different arrangements of the bicycles in the crystal. Figure 4 shows details of the crystal lattice of **1q**, which is representative of the stacking arrangement. The structures of **1n** (Figure 5) and **1e** (Figure 6) show that the arrangement in the crystal is dependent on the substituents at the bicycles. The partially fluorinated aryl substituents form additional weak H-F interactions with neighbouring molecules. For example, in **1n** (Figure 5), this leads to a head-head/tail-tail arrangement of the molecules, thus forming a chain. The offset parallel chains form layers. In the phenyl derivative (**1e**), an arrangement (Figure 6) which resembles a fishbone pattern is observed.

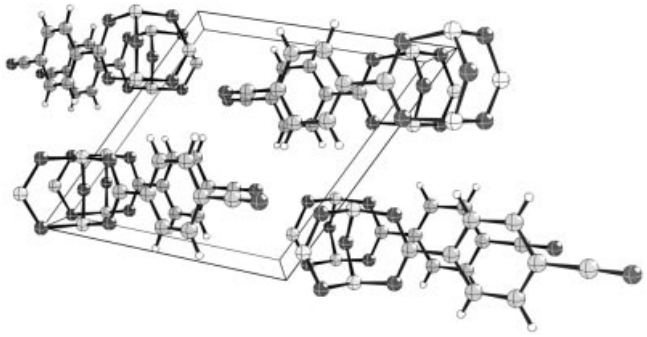

Figure 4. Crystal packing diagram of **1q**

Theoretical Calculations

Theoretical investigations were undertaken with the goal of finding explanations for the different stabilities of this bicyclic system with respect to the substituents, and for the different arrangements in the solid state. In Table 3, experimental bond lengths and bond angles for **1a** (R = CF$_3$), **1q** (R = 4-NCC$_6$H$_4$), **1e** (R = C$_6$H$_5$) and **1b** (R = Me$_2$N), representative examples for the different types of structures, are compared with the results of the RHF, MP2 and B3LYP calculations. As discussed previously, this bicyclic system is best described as a six-membered dithiatriazine with two sulfur atoms bridged by a sulfur diimide group. The experimental bond lengths within the dithiatriazine fragment are in reasonable agreement with all three methods, the best fit is found with the RHF calculations. The S1−N2 distances between the sulfur of the dithiatriazine fragment and the sulfur diimide group, obtained by the RHF method, are slightly shorter than those determined experimentally. The

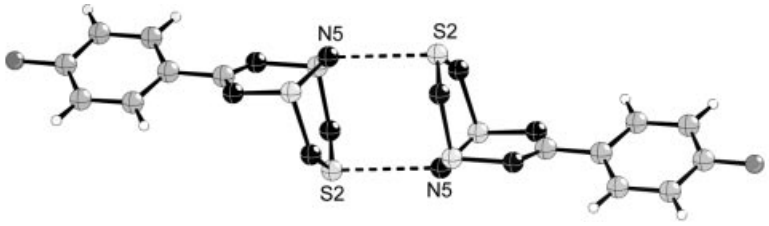

Figure 3. Centrosymmetric Dimer of **1n**

 © 2003 Wiley-VCH Verlag GmbH & Co. KGaA, Weinheim

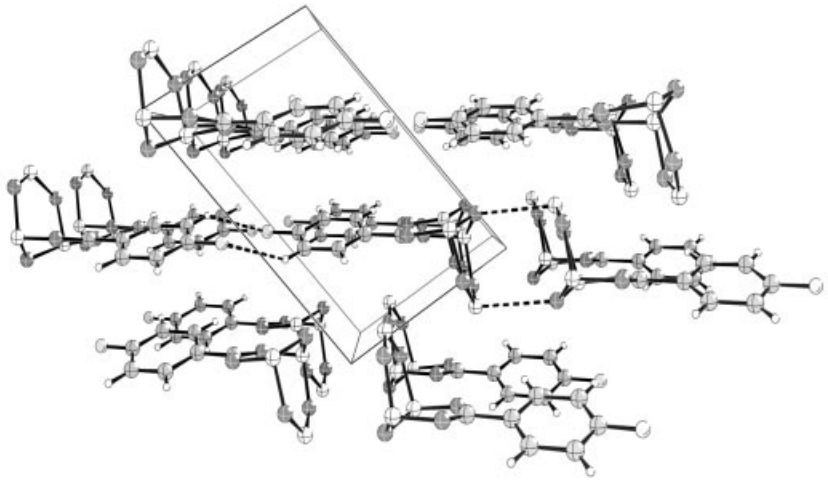

Figure 5. Crystal packing diagram of **1n**

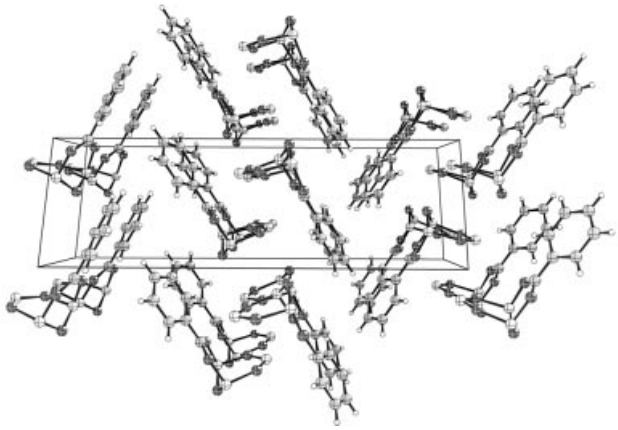

Figure 6. Crystal packing diagram of **1e**

distances resulting from the MP2 and B3LYP calculations are much larger. Similar results were obtained for the axial S−F distances in the related difluorodithiatriazines $RCN_3S_2F_2$ (R = F, CF_3). The RHF calculated distances are shorter and the MP2 and B3LYP calculated distances are much longer than those determined experimentally. The distances within the dithiatriazine are also well-reflected by all three methods.[19] The S2−N2 distances in the sulfurdiimide groups in **1**, calculated by the MP2 method, show the largest deviations (too long). Once again, the RHF calculated bond lengths are too short and those calculated by the B3LYP method are too long. Similar results have recently been obtained from the calculations of the molecular geometries of thioaminyl radicals.[20]

On the other hand, inspection of Table 3 shows that the experimentally determined influence of the different substituents on the bond lengths and on the NCN bond angle

Table 3. Averaged calculated (RHF/6−311G*, MP2/6−311G*, B3LYP/6−311G*) bond lengths and angles of **1a**, **1b**, **1e**, and **1q**

R	Method	C1−N1 (pm)	N1−S1 (pm)	S1−N5 (pm)	S1−N2 (pm)	N2−S2 (pm)	R−C1 (pm)	τ (deg)	N−C−N (deg)	NIMAG[a]
F_3C (**1a**)	Exp.	132.1	163.1	163.0	172.5	154.5	152.4(4)	−	134.1(2)	−
	RHF	130.5	162.4	161.2	170.8	151.3	153.2	−	133.3	0
	MP2	133.1	164.0	163.5	177.4	159.5	153.0	−	134.5	−
	B3LYP	132.4	165.4	165.3	178.7	156.9	154.2	−	133.8	0
H	RHF	131.3	162.4	161.5	171.1	151.3	−	−	133.0	0
	MP2	133.7	163.8	164.1	178.2	159.8	−	−	133.8	−
	B3LYP	133.0	165.5	165.8	179.1	157.0	−	−	133.8	0
4-NCC_6H_4 (**1q**)	Exp.	133.8	161.7	162.6	172.8	154.1	147.6(10)	5.2	129.2(7)	−
	RHF	131.9	161.5	161.2	171.3	151.2	149.7	0	130.0	0
	MP2	134.1	163.1	163.6	178.3	159.4	149.0	0	131.2	−
	B3LYP	133.8	164.2	165.3	179.5	156.8	149.4	0	130.3	0
C_6H_5 (**1e**)	Exp.	133.6	162.1	163.0	172.8	154.7	148.6(3)	26.6	129.8(2)	−
	RHF	132.2	161.1	161.3	171.6	151.2	149.2	0	129.5	0
	MP2	134.2	162.7	163.6	178.7	159.5	148.9	0	130.7	−
	B3LYP	134.1	163.8	165.5	180.1	156.8	149.0	0	129.7	0
Me_2N (**1b**)	Exp.	135.2	159.8	163.3	174.3	155.0	134.6(3)	−	128.67(19)	−
	RHF	133.6	159.6	161.4	172.1	151.2	134.3	−	128.5	0
	MP2	135.5	161.1	163.7	179.6	159.5	135.7	−	130.0	−
	B3LYP	135.4	162.0	165.6	180.9	156.8	135.9	−	128.7	0

[a] Number of imaginary frequencies.

 © 2003 Wiley-VCH Verlag GmbH & Co. KGaA, Weinheim

is quite well-reflected by all three methods. Compared with the CF_3 derivative **1a**, C1−N1 increases by 1−1.5 pm in the aryl derivatives **1q**, **1e**, and to 2.5−3 pm in the Me_2N compound **1b**; S1−N1 decreases by 1−1.5 pm in **1q**, **1e** and to 2.8−3.4 pm in **1b**. S1−N5 and the diimide bond N2−S2 are not affected. According to the experiments, a marginal lengthening of the axial S1−N2 bond is observed when going from **1b** to **1q** and **1e**, the calculations show a slightly larger effect. A stronger influence on the lengthening of this bond is shown by experiment and by the calculations for **1b**, but this difference can hardly account for the different stabilities of **1q**, **1e**, **1b** compared with **1a**. The larger increase in the NCN angle in **1b** relative to **1q**, **1e** is also shown by experiment and by calculations.

The influence of the substituents can already be explained in terms of the (extended) frontier orbital model. The energetically highest occupied donor orbitals of the substituents interact with the energetically lowest unoccupied acceptor orbital of the bicycles with the same symmetry, as shown in Figure 7. By this, the *a priori* empty (unoccupied) acceptor orbital with antibonding character in the CN and bonding character in the SN region is partly populated, thus explaining the lengthening of the C−N and the shortening of the S−N bonds. These results are in perfect agreement with our MNDO calculations reported earlier.[1]

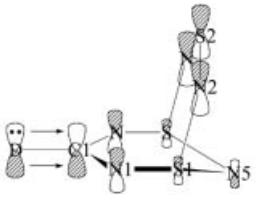

Figure 7. Interaction of the energetically highest occupied orbitals of the donor D with the energetically lowest unoccupied acceptor orbital with the same symmetry

Compared to the experimentally yet unknown hydrogen derivative included in the calculations in Table 3, acceptor substituents have no effect on the bond lengths. This is because the energetically highest occupied orbital in the bicycle with the appropriate symmetry is too low in energy for significant interaction with an empty acceptor orbital. The analysis of the orbitals with different model acceptors also confirms this. The acceptor orbital only shows negligible mixing with other orbitals. This also explains why the phenyl group acts as a donor only.

Another aim of the quantum chemical calculations was to find an explanation for the different crystallisation pattern: "stacking" and "dimerisation", and how this is dependent upon the substituents R.

The Mulliken and NBO charges (Table 4) for the atoms S2 and N5 at which the dimerisation occurs show virtually no dependency on the group R, therefore no correlation between the crystallisation pattern and the type of substituent can be observed. However, when we consider the MEP (mapped electrostatic potential),[21] which has also been utilised recently to rationalise the solid state packing of other SN systems,[22] a different picture is obtained. In Figure 8, representative examples for stacking (R = CF_3, Figure 8a) and dimerisation (R = NMe_2, Figure 8b) are shown. Positive electrostatic potential (ESP; blue) and negative ESP (red) fit perfectly together in the dimer of **1b** (R = NMe_2). For R = CF_3, the ESP's at S2 and N5 are not very pronounced. Furthermore, the negative potentials of N5 and C3 are lower than in the NMe_2 derivative, therefore "stacking" is less hindered by repulsive interactions.

Table 4. Calculated Mulliken and NBO charges (RHF/6−311G*) of **1a**, **1b**, **1e**, and **1q**

R	Method	C1	N1	S1	N5	N2	S2
F_3C (**1a**)	Mulliken	0.244	−0.608	0.998	−0.793	−0.710	1.006
	NBO	0.519	−0.899	1.546	−1.185	−1.070	1.466
4-NCC_6H_4 (**1q**)	Mulliken	0.555	−0.672	0.992	−0.793	−0.714	0.994
	NBO	0.626	−0.941	1.550	−1.189	−1.074	1.457
C_6H_5 (**1e**)	Mulliken	0.561	−0.672	0.985	−0.797	−0.716	0.985
	NBO	0.636	−0.947	1.547	−1.192	−1.072	1.450
Me_2N (**1b**)	Mulliken	0.737	−0.708	0.978	−0.807	−0.721	0.972
	NBO	0.821	−0.998	1.555	−1.199	−1.083	1.439

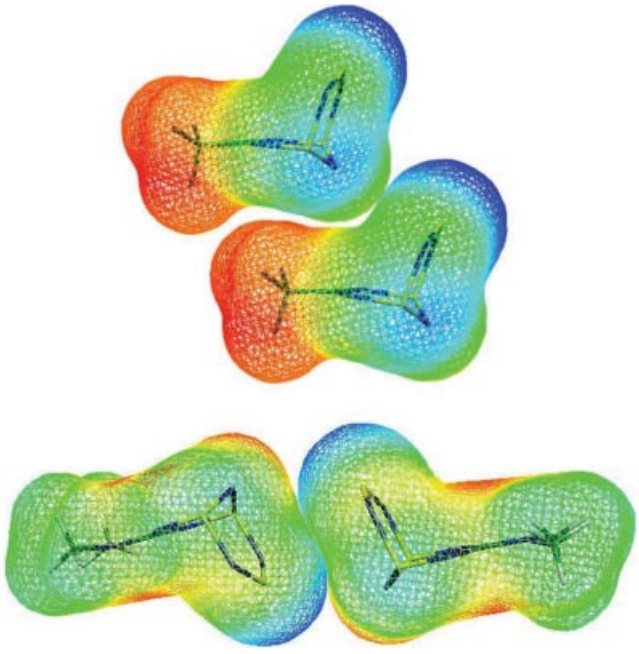

Figure 8. MEP (mapped electrostatic potential) of representative examples for stacking (R = CF_3) and for dimerisation (R = NMe_2)

Conclusions

Several new aryl 1λ⁴,3λ⁴,5λ⁴-trithia-2,4,6,8,9-pentaazabicyclo[3.3.1]nona-1(9),2,3,5,7-pentaenes RCN_5S_3 were prepared by the amidine route from $(NSCl)_3$ and $ArC(NSiMe_3)N(SiMe_3)_2$. When the persilylated amidines cannot be obtained from lithium-amidinates $RC(NSiMe_3)_2Li$ (R = C_6F_5, 4-NCC_6H_4) and Me_3SiCl, due to the decreased nucleophilicity of the amidinate, the amidinates can be used di-

 © 2003 Wiley-VCH Verlag GmbH & Co. KGaA, Weinheim

rectly as starting materials. Contrary to our expectations, the introduction of electron-withdrawing aryl groups does not increase the stability of the RCN_5S_3 system.

The results of X-ray structure investigations and the theoretical calculations are in good agreement. The influence of the substituents on bonding is readily understood from the extended frontier orbital model. Compared with the parent hydrogen derivative, acceptor substituents have no effect, since the -CN_5S_3 HOMO of appropriate symmetry is too low in energy for significant interaction. The interaction of the donor orbitals with the LUMO of appropriate symmetry will increase the C−N bond lengths and decrease the lengths of the adjacent S−N bonds because the antibonding and bonding character in these regions is increased. The influence on the other bonds is only marginal because of the nonbonding character of the LUMO in these regions. The calculations show a slight increase of the S1−N2 bond lengths when going from electron-withdrawing to aryl to amino-substituted bicycles. The experimentally observed significant lengthening of the S1−N2 bond in the amino derivatives is not reflected by the calculations.

No explanation can be given for the unusual stability of the CF_3 derivative from the structural data and the theoretical calculations (the chemistry of the CCl_3 derivative was not investigated). From the large negative charges at the nitrogen centres (Table 4), the RCN_5S_3 derivatives are expected to act as multifunctional donor ligands. When going from CF_3 to aryl to Me_2N, only the positive charges at C1 and the negative charges at N2 increase, the charges at the other centres are not affected. Therefore, *a priori* the ligand properties should not be dependent on the substituents R.

In the solid state, two fundamentally different packing patterns are observed for RCN_5S_3, stacking of the RCN_5S_3 molecules and face-to-face dimerisation of the N_3S_3 subunits of the $-CN_5S_3$ bicycle. The dependence of the packing pattern on the substituents is difficult to predict. Primary electrostatic interactions are responsible for the different packing as shown by the MEP in Figure 8, but they might be dominated by steric requirements of the substituents R and by interactions between the substituents.

Experimental Section

Materials and Methods: All manipulations of air-sensitive materials were performed under an inert atmosphere of dry nitrogen, with the absence of oxygen and moisture. The fluorinated *N,N,N′*-tris-(trimethylsilyl)amidines {R = F_3C,[15] R = 4-FC_6H_4, 2-FC_6H_4, 2,6-$F_2C_6H_3$[16]}, $[(C_6F_5C(NSiMe_3)_2Li]_2{\cdot}OEt_2$,[16] $[(Me_3Si)_2NLi{\cdot}OEt_2]_2$,[23] $Cl_3CCN(NSCl)_2$,[24] $Me_3SiNSNSiMe_3$,[25] RCN_5S_3 [R = 4-$H_3CC_6H_4$, 4-$C_6H_5C_6H_4$,[4] R = Me_2N[2]] and trithiazyltrichloride $(NSCl)_3$[26] were prepared according to published procedures. Terephthalonitrile is a commercial compound. The solvents were carefully dried and distilled prior to use. NMR spectra were recorded on Bruker DPX 200 (^1H, ^{19}F) and on Bruker AM 360 NB (^{13}C) spectrometers in [D_1]chloroform. Chemical shifts are given with respect to Me_4Si. Infrared analyses were acquired as thin Kel-F and Nujol films (with KBr cells), using a Perkin−Elmer Paragon 500 FT-IR instrument. Mass spectra were measured on a Finnigan MAT 8200, using the field ionisation (FI) technique. The high-resolution mass spectra were obtained by using the peak matching method (chemical ionisation neg.). Melting points were obtained on a Gallenkamp melting point apparatus and are uncorrected.

Preparation of $F_3CCN_5S_3$ (1a): $F_3CC(NSiMe_3)[N(SiMe_3)_2]$ (13.7 g, 42 mmol) in 50 mL of dichloromethane was added dropwise to trithiazyl trichloride (10.0 g, 41 mmol) in 100 mL of dichloromethane at 0 °C. The solution became dark red. The solvent and all volatile products were removed and the remaining residue was dissolved in 100 mL of acetonitrile and the solution was filtered. On storage at −40 °C, yellow crystals were obtained (6.35 g, 26 mmol, 63% yield). The spectroscopic data are in accordance with literature data.[1] MS-FI: *m/z* = 247 (100) [M^+]. MS-HR: found 246.92615, calcd. 246.92679.

Preparation of 2-$FC_6H_4CN_5S_3$ (1m): 2-$FC_6H_4C(NSiMe_3)[N(SiMe_3)_2]$ (14.5 g, 41 mmol) in 100 mL of acetonitrile was added dropwise to trithiazyl trichloride (10.0 g, 41 mmol) in 100 mL of acetonitrile. The solution became dark red and a precipitate formed. The solvent and all volatile products were removed and the remaining residue was dissolved in 150 mL of boiling acetonitrile and the solution was filtered. On cooling to room temperature, yellow crystals were obtained (7.7 g, 28 mmol, 69% yield), m.p. 111 °C. ^1H NMR: δ = −7.16 ppm (ddd, $^3J_{H,F}$ = 11.3, $^3J_{H,H}$ = 8.3, $^4J_{H,H}$ = 1.0 Hz, 1 H, *m*-C_6H_4F), 7.25 (td, $^3J_{H,H}$ = 7.5, $^4J_{H,H}$ = 1.0 Hz, 1 H, *m*-C_6H_4F), 7.50 (dddd, $^3J_{H,H}$ = 8.3, $^3J_{H,H}$ = 7.5, $^4J_{H,F}$ = 4.8, $^4J_{H,H}$ = 2.0 Hz, 1 H, *p*-C_6H_4F), 7.91 (td, $^3J_{H,H}$ = 7.5, $^4J_{H,F}$ = 7.5, $^4J_{H,H}$ = 2.0 Hz, 1 H, *o*-C_6H_4F ppm. $^{13}C\{^1H\}$ NMR: δ = 117.1 (d, $^2J_{C,F}$ = 22 Hz, *m*-C_6H_4F), 124.1 (s, *m*-C_6H_4F), 125.4 (d, $^2J_{C,F}$ = 8 Hz, *ipso*-C_6H_4F), 130.8 (s, *o*-C_6H_4F), 133.6 (d, $^3J_{C,F}$ = 8 Hz, *p*-C_6H_4F), 161.1 (d, $^1J_{C,F}$ = 259 Hz, *o*-C_6H_4F), 165.6 (d, $^3J_{C,F}$ = 4 Hz, NCN) ppm. ^{19}F NMR: δ = −113.3 (ddd, $^3J_{F,H}$ = 11.3, $^4J_{F,H}$ = 7.5, $J_{F,H}$ = 4.8, 1F) ppm. IR: $\tilde{\nu}$ = 1508 w, 1485 m, 1451 m, 1410 m, 1342 s, 1263 w, 1226 m, 1154 m, 1101 m, 996 s, 927 m, 843 w, 822 w, 770 s, 745 s, 721 s, 685 w, 670 m, 574 s, 551 m, 504 s, 476 m cm^{-1}. MS-FI: *m/z* = 273 (48) [M^+]. MS-HR: found 272.96192, calcd. 272.96130.

Preparation of 4-$FC_6H_4CN_5S_3$ (1n): The procedure follows that of **1m**. 4-$FC_6H_4C(NSiMe_3)[N(SiMe_3)_2]$ (14.5 g, 41 mmol) was reacted with trithiazyl trichloride (10.0 g, 41 mmol). After recrystallisation from CH_3CN, **1n** (7.8 g, 29 mmol, 71% yield) was obtained as orange crystals, m.p. 132 °C. ^1H NMR: δ = 7.07−7.19 (m, 2 H, C_6H_4F), 8.18−8.28 (m, 2 H, C_6H_4F) ppm. $^{13}C\{^1H\}$ NMR: δ = 115.5 (d, $^2J_{C,F}$ = 21 Hz, *m*-C_6H_4F), 129.9 (d, $^3J_{C,F}$ = 9 Hz, *o*-C_6H_4F), 132.4 (d, $^4J_{C,F}$ = 2 Hz, *ipso*-C_6H_4F), 164.6 (s, NCN), 166.1 (d, $^1J_{C,F}$ = 237 Hz, *p*-C_6H_4F) ppm. ^{19}F NMR: δ = −107.2 (tt, $^3J_{F,H}$ = 8.3, $^4J_{F,H}$ = 5.5 Hz, 1F) ppm. IR: $\tilde{\nu}$ = 2932 w, 1594 m, 1503 m, 1422 s, 1360 m, 1339 s, 1296 w, 1225 m, 1152 m, 1093 w, 997 s, 967 sh, 926 w, 849 m, 829 w, 814 m, 776 s, 750 s, 718 s, 688 w, 668 m, 629 w, 597 w, 573 s, 516 w, 490 s, 480 m cm^{-1}. MS-FI: *m/z* = 273 (100) [M^+]. MS-HR: found 272.96244, calcd. 272.96130.

Preparation of 2,6-$F_2C_6H_3CN_5S_3$ (1o): 2,6-$F_2C_6H_3C(NSiMe_3)[N(SiMe_3)_2]$ (9.3 g, 25 mmol) was reacted with trithiazyl trichloride (6.1 g, 25 mmol). After recrystallisation from boiling acetonitrile and storage at −40 °C, **1o** (4.9 g, 17 mmol, 68% yield) was obtained as yellow-brown crystals, m.p. 104 °C. ^1H NMR: δ = 6.92−7.04 (m, 2 H, *m*-$C_6F_2H_3$), 7.32−7.43 (m, 1 H, *p*-$C_6F_2H_3$) ppm. $^{13}C\{^1H\}$ NMR: δ = 111.9 (dd, $^2J_{C,F}$ = 23, $^4J_{C,F}$ = 2 Hz, *m*-$C_6F_2H_3$), 111.9 (t, $^2J_{C,F}$ = 13 Hz, *ipso*-$C_6F_2H_3$), 131.8 (t, $^3J_{C,F}$ = 10 Hz, *p*-$C_6F_2H_3$), 159.8 (dd, $^1J_{C,F}$ = 254, $^3J_{C,F}$ = 6 Hz, *o*-$C_6F_2H_3$), 163.5

 © 2003 Wiley-VCH Verlag GmbH & Co. KGaA, Weinheim

(s, NCN) ppm. ^{19}F NMR: δ = −114.9 (dd, $^3J_{F,H}$ = 7.8, $^4J_{F,H}$ = 6.2 Hz, 2F) ppm. IR: ṽ = 2926 w, 1622 m, 1591 m, 1566 w, 1472 m, 1344 s, 1238 m, 1148 m, 1011 s, 966 sh, 929 w, 818 w, 792 m, 776 m, 752 s, 630 m, 690 w, 670 m, 576 s, 523 w, 503 sh, 489 s, 467 m cm^{-1}. MS-FI: *m/z* = 291 (45) [M$^+$]. MS-HR: found 290.95194, calcd. 290.95187.

Preparation of $C_6F_5CN_5S_3$ (1p): $[C_6F_5C(NSiMe_3)_2Li]_2{\cdot}OEt_2$ (7.1 g, 18 mmol) in 50 mL of diethyl ether was added dropwise to trithiazyl trichloride (4.6 g, 19 mmol) in 50 mL of diethyl ether. The solution became dark red. The solvent and all volatile products were removed and the remaining residue was dissolved in 100 mL of acetonitrile and the solution was filtered. On storage at −40 °C, yellow-brown crystals were obtained (2.4 g, 7 mmol, 39% yield), m.p. 97 °C. ^{13}C{^{1}H} NMR: δ = 115.0 (t, $^2J_{C,F}$ = 17 Hz, *ipso*-C_6F_5), 138.7 (dm, $^1J_{C,F}$ = 253 Hz, *o*-C_6F_5), 143.2 (dm, $^1J_{C,F}$ = 253 Hz, *p*-C_6F_5), 145.2 (dm, $^1J_{C,F}$ = 247 Hz, *m*-C_6F_5), 162.1 (s, NCN) ppm. ^{19}F NMR: δ = −145.5 (dddd, $^3J_{FF}$ = −21.8, $^4J_{FF}$ = −4.7, $^4J_{FF}$ = 3.2, $^5J_{FF}$ = 8.0 Hz, 2F, *o*-F), −154.9 (tt, $^3J_{FF}$ = −20.2, $^4J_{FF}$ = 3.2, 1F, *p*-F), −164.3 (dddd, $^3J_{FF}$ = −21.8, $^3J_{FF}$ = −20.2, $^4J_{FF}$ = −0.8, $^5J_{FF}$ = 8.0 Hz, 2F, *m*-F) ppm. IR: ṽ = 1656 w, 1524 m,. 1504 s, 1427 sh, 1402 s, 1360 s, 1278 m, 1200 s, 1171 m, 1151 m, 1126 s, 1040 w, 1016 w, 986 m, 972 s, 901 m, 812 m, 761 sh, 722 s, 703 sh, 656 w, 626 w, 598 w, 570 w, 555 w, 531 m, 504 m, 473 m cm^{-1}. MS-FI: *m/z* = 345 (26) [M$^+$]. MS-HR: found 344.92149, calcd. 344.92361.

Preparation of 4-$NCC_6H_4CN_5S_3$ (1q): A solution of lithium bis(trimethylsilyl)amide (3.9 g, 16 mmol) and terephthalonitrile (2.1 g, 16 mmol) in 150 mL of diethyl ether was added dropwise to trithiazyl trichloride (4.4 g) in 50 mL of diethyl ether at 0 °C. The solution became brown. The solvent and all volatile products were removed and the remaining residue was dissolved in 100 mL of dichloromethane and the solution was filtered. On storage at −40 °C, orange crystals were obtained (1.4 g, 5 mmol, 31% yield), m.p. 158 °C. ^{1}H NMR: δ = 7.75 (ddd, $^3J_{H,H}$ = 8.3, $^4J_{H,H}$ = 2.0, $^5J_{H,H}$ = 1.5 Hz, 2 H, C_6H_4), 8.33 (ddd,$^3J_{H,H}$ = 8.3, $^4J_{H,H}$ = 2.0, $^5J_{H,H}$ = 1.5 Hz, 2 H, C_6H_4) ppm. ^{13}C{^{1}H} NMR: δ = 116.9 (s, *p*-C_6H_4), 119.0 (s, NC), 128.9 (s, *o*-C_6H_4), 133.0 (s, *m*-C_6H_4), 141.2 (s, *ipso*-C_6H_4), 165.4 (s, NCN) ppm. IR: ṽ = 2226 m, 1413 m, 1366 m, 1334 m, 1299 m, 1188 w, 1148 m, 1110 w, 1035 w, 1009 sh, 975 s, 921 w, 858 m, 836 w, 785 w, 768 sh, 750 m, 722 s, 692 m, 666 s, 642 sh, 561 m, 541 s, 506 m, 490 w, 467 m cm^{-1}. MS-FI: *m/z* = 280 (12) [M$^+$], 206 ($NCC_6H_4CN_2S_2^+$, 100). MS-HR: found 279.96632, calcd. 279.96597.

Preparation of $Cl_3CCN_5S_3$ (1r): $Me_3SiNSNSiMe_3$ (0.8 mL, 0.7 g, 3.5 mmol) in 10 mL of carbon tetrachloride was added dropwise to $Cl_3CCN(NSCl)_2$ (0.85 g, 2.7 mmol) in 25 mL of carbon tetrachloride. After standing overnight, the solvent and all volatile products were removed and the remaining residue was dissolved in a small amount of acetonitrile and the solution was filtered. On storage at −40 °C and after drying under vacuum, yellow crystals of **1r**·CH_3CN (0.55 g, 1.9 mmol, 68% yield) were obtained, m.p. 102 °C. ^{13}C NMR: δ = 97.3 (s, CCl_3), 168.4 (s, NCN) ppm. IR: ṽ = 1545 w, 1503 w, 1467 w, 1430 s, 1400 sh, 1362 m, 1292 s, 1265 sh, 1211 sh, 1202 m, 1171 w, 1151 m, 1127 w, 1028 m, 1004 sh, 987 m, 972 m, 946 sh, 916 sh, 872 sh, 862 m, 801 m, 758 m, 739 sh, 722 s, 702 w, 692 m, 660 m, 639 w, 567 m, 559 m, 506 s, 402 m cm^{-1}. MS-FI: *m/z* = 295 (58) [M$^+$]. MS-HR: found 294.83877, calcd. 294.83813.

Crystallographic Analysis

The single-crystal X-ray structure determinations were performed on a Siemens P4 diffractometer using Mo-K_α (0.71073 Å) radiation with a graphite monochromator. The crystals were mounted using Kel-F oil onto a thin glass fibre. Details of the data collection and refinement are given in Table 1. The programs SHELX-97[27] and DIAMOND[28] were used. The structures were solved by direct methods (SHELXS).[27] Subsequent least-squares refinement (SHELXL 97−2)[27] located the positions of the remaining atoms in the electron density maps. Non-hydrogen atoms were refined anisotropically. Hydrogen atoms were placed in calculated positions using a riding model and refined isotropically in blocks.

CCDC-205700 (**1b**) -205701 (**1f**) -205702 (**1n**) -205703 (**1r**) -205704 (**1o**) and -205705 (**1q**) contain the supplementary crystallographic data for this paper. These data can be obtained free of charge at www.ccdc.cam.ac.uk/conts/retrieving.html [or from the Cambridge Crystallographic Data Centre, 12, Union Road, Cambridge CB2 1EZ, UK; Fax: (internat.) +44-1223/336-033; E-mail: deposit@ccdc.cam.ac.uk].

Quantum Chemical Calculations: All *ab initio* calculations were performed with the GAUSSIAN′98 program package.[29] The mapped electrostatic potential (MEP) representations are made with MOLEKEL.[21]

Acknowledgments

Financial Support by the FNK, Universität Bremen is gratefully acknowledged.

[1] R. Maggiulli, R. Mews, W.-D. Stohrer, M. Noltemeyer, G. M. Sheldrick, *Chem. Ber.* **1988**, *121*, 1881−1889.
[2] T. Chivers, J. F. Richardson, N. R. M. Smith, *Inorg. Chem.* **1986**, *25*, 272−275.
[3] [3a] R. T. Boeré, A. W. Cordes, R. T. Oakley, *J. Chem. Soc., Chem. Commun.* **1985**, 929−930. [3b] R. T. Boeré, A. W. Cordes, R. T. Oakley, *Acta Crystallogr., Sect. C* **1985**, *42*, 1833−1834.
[4] R. T. Boeré, J. Fait, K. Larsen, J. Yip, *Inorg. Chem.* **1992**, *31*, 1417−1423.
[5] A. J. Banister, W. Clegg, I. B. Gorrell, Z. V. Hauptmann, R. W. H. Small, *J. Chem. Soc., Chem. Commun.* **1987**, 1611−1613.
[6] S. J. Chen, *Doctoral thesis*, Universität Bremen, Germany, **1993**.
[7] R. Maggiulli, R. Mews, W.-D. Stohrer, M. Noltemeyer, *Chem. Ber.* **1990**, *123*, 29−34.
[8] [8a] R. T. Boeré, A. W. Cordes, S. L. Craig, J. B. Graham, R. T. Oakley, J. A. J. Privett, *Chem. Commun.* **1986**, 807−808. [8b] R. T. Boeré, G. Ferguson, R. T. Oakley, *Acta Crystallogr., Sect. C* **1986**, *42*, 900−902. [8c] R. T. Boeré, A. W. Cordes, R. T. Oakley, *J. Am. Chem. Soc.* **1987**, *109*, 7781−7785.
[9] V. A. Bagryansky, N. P. Gritsan, Y. N. Molin, K. V. Shuvaev, A. V. Zibarev, personal communication.
[10] [10a] J. M. Rawson, A. J. Banister, I. Lavender, *Adv. Heterocyclic Chem.* **1995**, *62*, 137−247. [10b] J. M. Rawson, F. Palacio, *Struct. Bonding* **2001**, *100*, 93−128.
[11] R. T. Boeré, R. T. Oakley, R. W. Reed, N. P. C. Westwood, *Centenary of the Discovery of Fluorine, International Symposium*, Paris, **1986**, Abstr. I32.
[12] R. Maggiulli, *Diploma thesis*, Universität Göttingen, Germany **1986**.
[13] A. W. Cordes, R. T. Oakley, R. T. Boeré, *Acta Crstallogr., Sect. C* **1985**, *41*, 1833−1834.
[14] T. Chivers, F. Edelmann, J. F. Richardson, N. R. M. Smith, O. Treu Jr., M. Trsic, *Inorg. Chem.* **1986**, *25*, 2119−2125.
[15] R. T. Boeré, R. T. Oakley, R. W. Reed, *J. Organomet. Chem.* **1987**, *331*, 161−167.
[16] C. Knapp, E. Lork, P. G. Watson, R. Mews, *Inorg. Chem.* **2002**, *41*, 2014−2025.
[17] [17a] R. T. Boeré, R. T. Oakley, M. Shevalier, *J. Chem. Soc., Chem. Commun.* **1987**, 110−112. [17b] K. T. Bestari, R. T.

 © 2003 Wiley-VCH Verlag GmbH & Co. KGaA, Weinheim

Boeré, R. T. Oakley, *J. Am. Chem. Soc.* **1989**, *111*, 1579−1584.
[18] [18a] P. J. Hayes, R. T. Oakley, A. W. Cordes, W. T. Pennington, *J. Am. Chem. Soc.* **1985**, *107*, 1346−1351. [18b] R. T. Boeré, R. T. Oakley, R. W. Reed, N. P. C. Westwood, *J. Am. Chem. Soc.* **1989**, *111*, 1180−1185.
[19] T. Borrmann, unpublished results
[20] P. Kaszynski, *J. Phys. Chem. A* **2001**, *105*, 7615−7625.
[21] Centro Svizzero di Calcolo Scientifico (CSCS), Manno, Switzerland.
[22] e.g. [22a] T. Borrmann, A. V. Zibarev, E. Lork, G. Knitter, S.-J. Chen, P. G. Watson, E. Cutin, M. M. Shakirov, W.-D. Stohrer, R. Mews, *Inorg. Chem.* **2000**, *39*, 3999− 4005. [22b] A. D. Bond, D. A. Haynes, C. M. Pask, J. M. Rawson, *J. Chem. Soc., Dalton Trans.* **2002**, 2522− 2531; A. D. Bond, D. A. Haynes, J. M. Rawson, *Can. J. Chem.* **2002**, *80*, 1507- 1517.
[23] M. F. Lappert, M. J. Slade, A. Singh, J. L. Atwood, R. D. Rogers, R. Shakir, *J. Am. Chem. Soc.* **1983**, *105*, 302−304.
[24] A. Apblett, T. Chivers, *J. Chem. Soc., Chem. Commun.* **1989**, 96−97; A. Apblett, T. Chivers, *Phorsphorus, Sulfur, Silicon Relat. Elem.* **1989**, *41*, 439−447.
[25] C. P. Warrens, J. D. Woolins, *Inorg. Synth.* **1989**, *25*, 43−47.
[26] W. L. Jolly, K. D. Maguire, *Inorg. Synth.* **1967**, *9*, 102−109.
[27] G. M. Sheldrick, SHELX-97 *Programs for Crystal Structure Analysis (Release 97−2),* Institut für Anorganische Chemie der Universität Göttingen, Germany **1997**.
[28] *Diamond-Visual Crystal Structure Information System*, Crystal Impact, Bonn, Germany.
[29] Gaussian 98, *Revision A.7*, M. J. Frisch, G. W. Trucks, H. B. Schlegel, G. E. Scuseria, M. A. Robb, J. R. Cheeseman, V. G. Zakrzewski, J. A. Montgomery, Jr., R. E. Stratmann, J. C. Burant, S. Dapprich, J. M. Millam, A. D. Daniels, K. N. Kudin, M. C. Strain, O. Farkas, J. Tomasi, V. Barone, M. Cossi, R. Cammi, B. Mennucci, C. Pomelli, C. Adamo, S. Clifford, J. Ochterski, G. A. Petersson, P. Y. Ayala, Q. Cui, K. Morokuma, D. K. Malick, A. D. Rabuck, K. Raghavachari, J. B. Foresman, J. Cioslowski, J. V. Ortiz, A. G. Baboul, B. B. Stefanov, G. Liu, A. Liashenko, P. Piskorz, I. Komaromi, R. Gomperts, R. L. Martin, D. J. Fox, T. Keith, M. A. Al-Laham, C. Y. Peng, A. Nanayakkara, C. Gonzalez, M. Challacombe, P. M. W. Gill, B. Johnson, W. Chen, M. W. Wong, J. L. Andres, C. Gonzalez, M. Head-Gordon, E. S. Replogle, and J. A. Pople, Gaussian Inc., Pittsburgh PA, **1998**.

Received February 25, 2003

 © 2003 Wiley-VCH Verlag GmbH & Co. KGaA, Weinheim

(4-Acyl-5-pyrazolonato)titanium Derivatives: Oligomerization, Hydrolysis, Voltammetry, and DFT Study

Francesco Caruso,*[a] Lou Massa,[b,c] Asta Gindulyte,[b,c] Claudio Pettinari,*[d] Fabio Marchetti,[d] Riccardo Pettinari,[d] Massimo Ricciutelli,[d] Juan Costamagna,[e] Juan Carlos Canales,[e] Joseph Tanski,[f] and Miriam Rossi[f]

Keywords: Titanium / Density functional calculations / Nitrogen heterocycles / Voltammetry / O ligands

Twenty 4-acyl-5-pyrazolonato (Q) titanium derivatives of varied nuclearity have been synthesized from $Ti(OR)_4$ or $TiCl_4$ and characterized with spectroscopic methods (IR, NMR, ESI-MS). While Ti–(β-diketonato) cleavage is not seen in isolated solids, Ti–O(alkoxy) (or Ti–Cl) bonds cleave upon hydrolysis, leading to several structural forms, including oligomers. Ionic Q species with no Ti, i.e., obtained after Ti–Q cleavage, are seen for some Ti–Q derivatives by ESI-MS, which also indicates a varied nuclearity for a given species, e.g., the isolated polynuclear $[Q_2Ti\text{-}\mu\text{-}O]_n$ has several "*n*" values. Mononuclear Ti complexes are obtained under rigorous anhydrous conditions. The *cis* structures of the mononuclear species $(Q^T)_2Ti(OCH_3)_2$, Q^T = 3-methyl-4-(neopentylcarbonyl)-1-phenylpyrazol-5-onato have been analyzed with DFT methods. A *trans* influence is a major driving force that accounts for several sets of Ti–O bonds. One of the *cis* stereoisomers is 56 kcal/mol higher in energy than the other two. In contrast, all $(Q^T)_2TiCl_2$ *cis* isomers show similar energies. Voltammetry of the mononuclear species $(Q^T)_2Ti(OnPr)_2$ and the antitumor tetranuclear compound $[(Q^B)_2Ti\text{-}\mu\text{-}O]_4$, ($Q^B$ = 4-benzoyl-3-methyl-1-phenylpyrazol-5-onato) indicate that the Ti^{IV} is less prone to reduction to Ti^{III} in the latter (Ep_c for the Ti^{IV}/Ti^{III} couple is –1.71 V and –1.46 V versus Fc^+/Fc, respectively). Potential antitumor compounds having a Ti/Q ratio of 1:1 do not disproportionate, unlike the equivalent acetylacetonato derivatives, and are water-soluble.
(© Wiley-VCH Verlag GmbH & Co. KGaA, 69451 Weinheim, Germany, 2003)

Introduction

Titanium tetraalkoxides react with β-diketones to give products formulated as (β-diketonato)$Ti(OR)_3$ and (β-diketonato)$_2Ti(OR)_2$.[1,2] For $(bzac)_2Ti(OEt)_2$, bzac = benzoylacetonato, an equilibrium mixture of the three possible octahedral *cis* stereoisomers is seen in CH_3CN/H_2O solution.[3] Qualitatively, the *cis* configurations are more strained but are preferred due to electronic effects caused by $p_\pi - d_\pi$ (t_{2g}) bonding of the β-diketonato ligand.[4,5] $[(acac)_2TiO]_2$, acac = acetylacetonato, consists of a cyclic dimer with titanium centers linked by oxygen atoms.[5]

Other stable polynuclear oxo-bridged species have been isolated as Ti is a hard acid that forms strong metal–oxygen bonds. For example, hydrolysis of $(\eta^5\text{-}C_5H_5)_2TiCl_2$ and $(\eta^5\text{-}C_5H_5)TiCl_3$ yields the two related oxo-bridged titanium dimers $[(\eta^5\text{-}C_5H_5)_2TiCl]_2O$ and $[(\eta^5\text{-}C_5H_5)TiCl_2]_2O$, respectively.[6–8]

The success of cisplatin,[11,12] *cis*-$(NH_3)_2PtCl_2$, has prompted studies of metal-based antitumor compounds[9,10] with other metal derivatives.[13–15] The (β-diketonato)titanium species mentioned above, $(bzac)_2Ti(OEt)_2$ (Figure 1), known as budotitane,[16] was the first non-Pt metal compound to reach clinical trials.[17] It undergoes stereoisomer interconversion[3] and a theoretical[18] study shows a calcu-

[a] Istituto di Chimica Biomolecolare, Consiglio Nazionale delle Ricerche,
Piazzale Aldo Moro 5, 00185 Rome, Italy
Fax: (internat.) + 39-06/49913628
E-mail: francesco.caruso@icb.cnr.it
[b] Hunter College, Department of Chemistry,
695 Park Avenue, New York, NY 10021, USA
Fax: (internat.) + 1-212/772-5332
E-mail: lmassa@hunter.cuny.edu
[c] The Graduate School, City University of New York,
365 Fifth Avenue, New York, NY 10016, USA
Fax: (internat.) + 1-212/772-5332
E-mail: mandroji@yahoo.com
[d] Università di Camerino, Dipartimento di Scienze Chimiche,
Via S. Agostino, 1, Camerino (MC), Italy
Fax: (internat.) + 39-0737/637345
E-mail: claudio.pettinari@unicam.it
[e] Universidad de Santiago, Facultad de Quimica y Biologia,
Santiago 33, Chile
Fax: (internat.) + 56-2/6812108
E-mail: jcostama@lauca.usach.cl
[f] Vassar College, Department of Chemistry,
Poughkeepsie, NY 12604-0484, USA
Fax: (internat.) + 1-845/437-5732
E-mail: rossi@vassar.edu

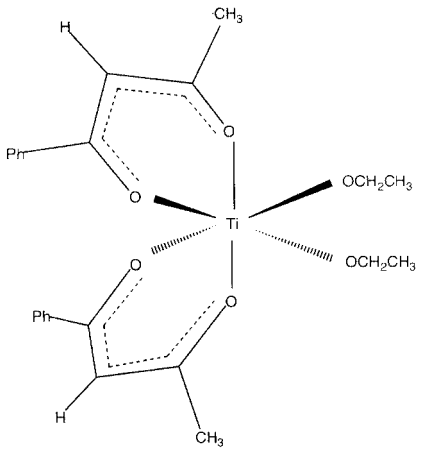

Figure 1. Isomer of budotitane, $(bzac)_2Ti(OCH_2CH_3)_2$; bzac = benzoylacetonato

lated isomer distribution that agrees with ^1H NMR spectroscopic data.

Budotitane was selected for development on the basis of structure-activity studies in which metal atom, β-diketonato substituents, and leaving groups (ethoxy in budotitane) were modified.[3] The ethoxy derivative gave the best pharmacological formulation (a limiting feature in budotitane) because hydrolysis is reduced when ethanol is added to it. These studies showed that asymmetric β-diketonates induce higher activity.[3] This structural feature is fulfilled by 4-acyl-5-pyrazolones, a sub-class of asymmetric β-diketones having a fused pyrazole ring and three useful positions for substitution (Figure 2).

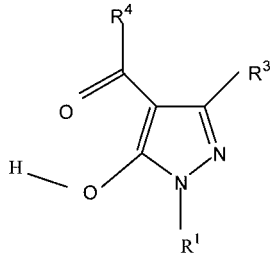

Figure 2. 4-Acyl-5-pyrazolones (keto-enol form), HQ

Recently, one such derivative, *cyclo*-tetrakis[bis(4-benzoyl-3-methyl-1-phenylpyrazolon-5-ato)(μ-oxo)titanium(IV)], $[(Q^B)_2Ti\text{-}\mu\text{-}O]_4$, has demonstrated potent and selective antitumor activity in vitro and in vivo, with an increased life span (T/C ≈ 300%), in the TA-3 mouse mammary adenocarcinoma[19] (Figure 3).

Ti−O(ethoxy) bonds in budotitane tend to hydrolyze, yielding Ti−OH derivatives. Subsequently, condensation of two Ti−OH units from different molecules produce a Ti−O−Ti linkage while releasing a molecule of water.[3] Ti−(β-diketonato) bond hydrolysis also occurs in budotitane and the system evolves towards polynuclear compounds that ultimately yield harmless titanium dioxide. While letting $TiCl_4$ react to obtain $[(Q^B)_2Ti\text{-}\mu\text{-}O]_4$ a similar hydrolytic process for the Ti−Cl bonds is seen, but without hydrolysis of the Ti−(β-diketonato) bonds.[19] This is important for the antitumor activity of Ti derivatives. In fact, budotitane and titanocene dichloride,[20] Cp_2TiCl_2 (an antitumor compound currently in clinical phase II trials),[21] are characterized by rapid hydrolysis of ethoxy and Cl^-, respectively, in comparison with a much slower hydrolysis of bzac and Cp. This slow hydrolysis was recently suggested to be a key property for biological activity in antitumor Ti compounds.[22,23] Following our interest in antitumor inorganic compounds[19,22−24] we report here the synthesis of novel Ti−(4-acyl-5-pyrazolonato) compounds with several degrees of polymerization (Table 1). Since recent results[25] show that, in addition to Ti^{IV} complexes, Ti^{III} species may also display antitumor activity (a property also shown by Pt^{II} and Pt^{IV} species),[26] we also describe the redox behavior of one mononuclear and one tetranuclear Ti−(β-diketonato) compound. Structural features are analyzed with Density Functional Theory (DFT) methods. Electrospray ionization mass spectrometry (ESI-MS) is a powerful tool with which to study charged species in the gas phase[27,28] and has been successfully applied to address

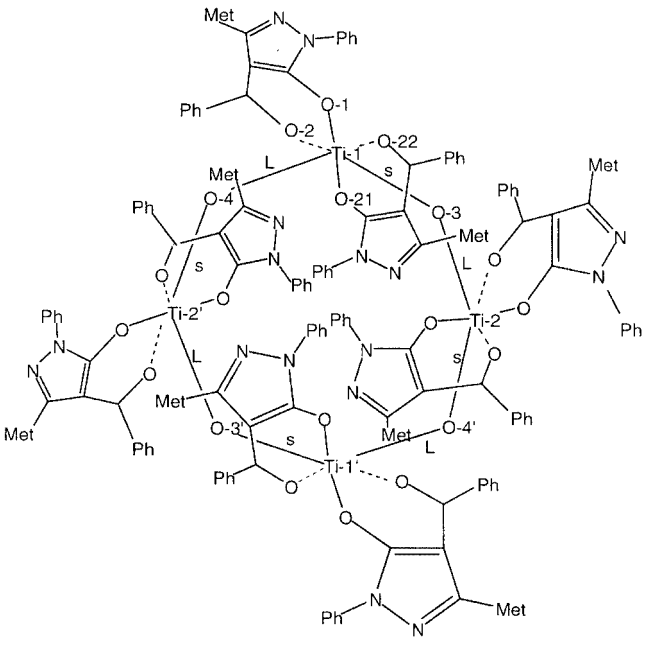

Figure 3. Tetranuclear (4-acyl-5-pyrazolonato)−Ti antitumor species, *cyclo*-tetrakis[bis(4-benzoyl-3-methyl-1-phenylpyrazolon-5-ato)(μ-oxo)titanium(IV)], $[(Q^B)_2Ti\text{-}\mu\text{-}O]_4$ (**1**) ($R^1 = R^4 = Ph$, $R^3 = CH_3$), dashed bonds indicate weak Ti−O bonds; L (s) indicate long (short) bonds in the eight-membered ring

Table 1. 4-Acyl-5-pyrazolones used

4-Acyl-5-pyrazolone	R^1	R^3	R^4
HQ^B	Ph	Me	Ph
HQ^T	Ph	Me	CH_2tBu
HQ^A	Ph	Me	C_6H_4-4-OMe
HQ^N	Ph	Me	C_6H_4-4-NO_2
HQ^C	Ph	Me	Cy
HQ^L	Ph	Me	CH_2Ph
HQ^E	Ph	Me	$[CH_2]_5Me$
HQ^P	Ph	Ph	Ph

 © 2003 Wiley-VCH Verlag GmbH & Co. KGaA, Weinheim

biochemical questions[29] and the speciation of inorganic complexes of various metals, including Ti.[30,31] We also describe here an ESI-MS study.

Results and Discussion

Synthesis and Spectroscopic Characterization

Polynuclear (oxo)titanium β-diketonates **1**−**8** (Table 2) have been obtained by treating TiX_4 (X = Cl or OR; R = Me, Et, *n*Bu, or *n*Pr) with 4-acyl-5-pyrazolones (HQ) in alcoholic solvent in the presence of KOH [see Equation (1) for tetranuclear species **1**]. KCl is removed after centrifugation of the suspension containing a soluble Ti-Q derivative. Insoluble Ti-Q products are separated from KCl after dissolution in CH_2Cl_2. Alternatively, **1**−**8** can be obtained in refluxing benzene (without addition of base) with an excess of Q ligands.

Table 2. Synthesized compounds

1	$[(Q^B)_2Ti(\mu\text{-}O)]_4$	**11**	$(Q^T)_2Ti(O\textit{n}Pr)_2$
2	$[(Q^T)_2Ti(O)(H_2O)]_n$	**12**	$(Q^T)_2Ti(O\textit{n}Bu)_2(H_2O)$
3	$[(Q^A)_2Ti(O)(H_2O)]_n$	**13**	$[(Q^A)Ti(OH)_3(H_2O)]_n$
4	$[(Q^N)_2Ti(O)(H_2O)]_n$	**14**	$[(Q^C)Ti(OH)_3]_n$
5	$[(Q^C)_2Ti(O)(H_2O)_2]_n$	**15**	$[(Q^B)Ti(OH)_2(O\textit{n}Pr)](H_2O)$
6	$[(Q^L)_2Ti(O)(H_2O)_2]_n$	**16**	$[(Q^B)Ti(OH)_2(O\textit{n}Bu)](H_2O)$
7	$[(Q^E)_2Ti(O)(H_2O)]_n$	**17**	$[(Q^L)Ti(O)(OH)]_n$
8	$[(Q^P)_2Ti(O)(H_2O)]_n$	**18**	$[(Q^E)Ti(O)(OH)]_n$
9	$(Q^B)_2Ti(O\textit{n}Pr)_2$	**19**	$(Q^B)_2TiCl_2$
10	$(Q^T)_2Ti(OMe)_2$	**20**	$(Q^T)_2TiCl_2$

X-ray data for **1** show a tetranuclear structure,[19] which agrees with the measured molecular weight of 2200 (the expected value for the tetranuclear arrangement is 2473.9). This technique suggests a mixture of di- and other polynuclear species for **4**, that is $[(Q^N)_2Ti(O)(OH_2)]_n$ (n = 2.8). In a related study of budotitane, after dissolution in CH_3CN/H_2O the species $[(bzac)_2Ti(O)]_n$ with n = 2.4 is formed.[3]

Compounds **1**−**8** are generally soluble in chlorohydrocarbons, acetonitrile, and DMSO, insoluble in ethers and alcohols, and are very stable in the air at room temperature. Compound **3**, however, is insoluble in CH_2Cl_2 and $CHCl_3$ due, probably, to the formation of bridges between different metal centers via hypervalent oxygen atoms of the OMe group.

$$8\ HQ + 16\ KOH + 4\ TiCl_4 \rightarrow [Q_2Ti(\mu\text{-}O)]_4 + 16\ KCl + 12\ H_2O \quad (1)$$

Complexes $Q_2Ti(OR)_2$ **9**−**12** have been prepared in excellent yields by treating stoichiometric amounts of the β-diketone and the titanium alkoxide in refluxing benzene according to Equation (2). These complexes are soluble in DMSO, CH_2Cl_2, and $CHCl_3$, acetonitrile and nitrobenzene, slightly soluble in benzene and acetone, and nearly insoluble in diethyl ether, water, and saturated hydrocarbons. In $CHCl_3$ they seem to hydrolyze to a large extent as several signals were found for each group of protons. Molecular weight measurements in solution further confirmed this hypothesis; the ratio between experimental and calculated molecular weights for compounds **9** and **11** being 0.62 and 0.53, respectively. Ionic species are excluded on the basis of conductivity data.

$$Ti(OR)_4 + 2\ HQ \rightarrow Q_2Ti(OR)_2 + 2\ ROH \quad (2)$$

The reaction between $Ti(OR)_4$ and HQ in a 1:1 ratio, in the presence of KOH, gave the hydroxy derivatives **13**−**16**. In addition, TiO_2 was obtained as a sub-product, probably from $Ti(OR)_4$. Compounds **13**−**16** are generally very soluble in water and behave as sol-gel precursors, a property observed in other Ti−(β-diketones) used as "modifiers" in sol-gel processing.[32] The literature is somewhat ambiguous about the structures and behavior of such species present in solution. The partially hydrolyzed hydroxy(oxo) complexes **17** and **18** are also water-soluble.

As already mentioned, compound **1** is a potent and selective cytotoxic agent that is water-insoluble and, therefore, is formulated as a liposome for pharmacological use.[19] Compounds **13**−**18** (Ti/Q = 1:1), however, are water-soluble and are thus interesting candidates for simpler formulation. They do not disproportionate, in contrast to acac-related derivatives,[33] and they resemble related Ti−Cp antitumor compounds.

$TiCl_4{\cdot}2THF$ reacts with HQ^B and HQ^T in methanol, in the presence of an equimolar amount of NaOMe, to give the mononuclear Q_2TiCl_2 complexes **19**−**20** in good yields [Equation (3)], under rigorous anhydrous conditions.

$$TiCl_4{\cdot}2THF + 2\ HQ + 2\ NaOMe \rightarrow Q_2TiCl_2 + 2\ NaCl + 2\ MeOH + 2\ THF \quad (3)$$

Therefore, reaction in basic (KOH) alcohol solution yields polynuclear products **1**−**2** whereas replacing KOH with NaOMe, under anhydrous conditions, furnishes the corresponding mononuclear compounds **19**−**20**. However, mononuclear species are more simply obtained in benzene, where hydrolysis is hindered.

Conductance data in the ionizing solvents acetone, DMSO or nitrobenzene show that complexes **1**−**20** are non-electrolytes.

Compounds **1**−**8** can be also obtained by hydrolysis of bis(4-acyl-5-pyrazolonato)dialkoxytitanium(IV) or bis(4-acyl-5-pyrazolonato)dichlorotitanium(IV). With excess β-diketone some titanium alkoxides are converted into (oxo)titanium β-diketonates. Compounds **9**−**11** also appear to hydrolyze, in solution, more rapidly than **19**−**20**.

Nujol mull IR spectra of the oxo complexes contain bands in the chelating carbonyl stretching region 1600−1300 cm^{-1}; similar frequencies are observed for other metal 4-acyl-5-pyrazolonato derivatives.[34−41] No bands were observed in the 1600−1750 cm^{-1} region, where ketonic carbonyl modes are expected for the pyrazolonato keto form. Therefore, both carbonyl groups are coordinated

 © 2003 Wiley-VCH Verlag GmbH & Co. KGaA, Weinheim

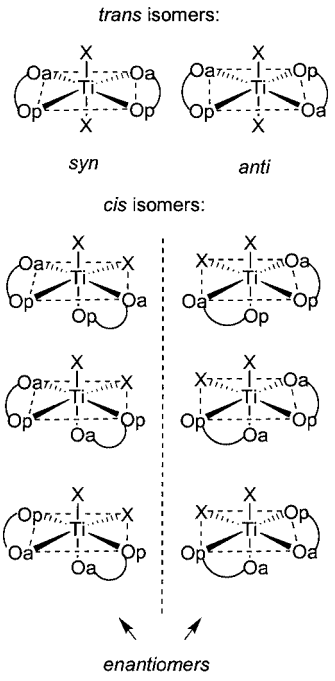

Figure 4. Possible Q_2TiX_2 stereoisomers; Oa = O(acyl), Op = O(pyrazolonato), X = Cl, OEt, O*n*Pr, O*i*Pr, or O*n*Bu; the three pairs of *cis* stereoisomers are ordered as CIS3, CIS2, and CIS1 as defined in the text

to the Ti atom. Broad bands in the 500−400 cm^{-1} region and some strong absorption in the 400−300 cm^{-1} region are associated with Ti−O bonds.[5,33−43]

Six-coordinate titanium derivatives can theoretically exist in solution as a mixture of several *cis* and *trans* isomers (Figure 4). However, for related dialkoxy- and dihalobis(acetylacetonato)titanium(IV) derivatives, steric interactions influence the relative stabilities of the isomers and *cis* forms are strongly preferred.[18,42] In particular, the low-temperature ^1H NMR spectrum of budotitane exhibits four signals for the different methyl groups due to the three *cis* isomers. Our own ^1H NMR variable-temperature experiment on compounds **9** and **11** revealed only one signal (also at 273 K) for each equivalent proton of the propoxy groups and two signals having the same integrals for the methyl group of Q^B and Q^T. This can be assigned to the equatorial and axial methyl groups of the CIS2 isomer (Figure 4) − that is only one *cis* conformer is detected under such experimental conditions. It is worth noting that 20 min after dissolution of **9** and **11** in $CHCl_3$, *n*PrOH formation was observed, i.e., hydrolysis of the Ti−O*n*Pr bond occurred. Hydrolysis is fast at high temperatures and complete 48 h after dissolution. It is also reversible as the addition of *i*PrOH or *n*PrOH to the NMR solutions showed signals due to (TiO*i*Pr)- and (TiO*n*Pr)-containing species. In contrast, derivative **10** was immediately hydrolyzed in solution, as indicated by ten signals, due to OMe groups at room temperature, seen 10 min after dissolution.

The spectrum of the monomer species $(Q^B)_2TiCl_2$ **19** carried out in non-anhydrous deuterated benzene (98%) and recorded at least 1 h after dissolution of the sample, showed some multiplets at 283 and 353 K, analogous to those in the spectrum of **1**, i.e., the mononuclear $(Q^B)_2TiCl_2$ hydrolyzed and became a polynuclear species. The same spectrum was obtained after adding H_2O (0.01 mL) to a deuterated anhydrous benzene (99.9%) solution of **19**. This shows faster hydrolysis since the spectrum was taken after 15 min.

Hydrolysis is avoided by not adding water and working under N_2 to avoid air humidity in deuterated anhydrous benzene (99.9%). This additional variable-temperature ^1H NMR of **19** shows a single sharp resonance for the methyl protons at 353 K. At 313 K line broadening is observed and the methyl resonance begins to split into two peaks. At 303 K further splitting of these peaks gives a total of four signals. The same multiplicity was found at 283 K. This sequence of increasing peaks as the temperature decreases is assigned to the four non-equivalent methyl groups of the three diastereoisomers.[18] The line broadening could be due to a rapid isomerization process. Broadening of the multiplets obscures the fine structure due to spin coupling of *ortho*, *meta*, and *para* protons.

The same experiment in $CDCl_3$ shows hydrolysis, as indicated by more than 15 lines at 218 K for the methyl groups of Q^B. Addition of MeOH to the NMR solution of **19** generates a signal at $\delta = 4.70$ ppm due to an OMe group coordinated to Ti after formation of a Ti(OMe)-containing species.

The extraordinarily high number of signals detected for each equivalent group of protons in the ^1H spectra of derivatives **1**−**3** suggests the formation of several different nuclearities (like mono-, di-, trititanium species, etc.), in solution, and perhaps even dissociation of the pyrazolonato ligands. The latter is, probably, a reversible dynamic feature, as elemental analyses of the isolated products **1**−**3** show a Ti/Q ratio of 1:2, indicating no Ti−Q cleavage in the solid. We further describe these features below.

Electrospray

Positive electrospray mass spectra of complexes **1**−**2**, **5**−**7**, **15**−**16**, **18**−**20** (the most relevant data are reported in the Exp. Sect.) indicate that, in solution, these derivatives undergo loss of the anionic pyrazolonato ligands which immediately interact with proton, sodium and/or potassium ions, yielding 1−6 polynuclear monocharged species such as $[NaH(Q)]^+$, $[NaK(Q)]^+$, $[Na_3(Q)_2]^+$, $[Na_2K(Q)_2]^+$, $[NaK_2(Q)_2]^+$, $[Na_3H(Q)_3]^+$, $[Na_2KH(Q)_3]^+$, $[NaK_2H(Q)_3]^+$, $[Na_4H(Q)_4]^+$, $[Na_3KH(Q)_4]^+$, $[Na_2K_2H(Q)_4]^+$, $[Na_4KH_2(Q)_6]^+$, $[Na_3K_2H_2(Q)_6]^+$. In general, protonated species are more abundant than Na, K, or mixed Na/K compounds. The population of polynuclear species increases as trinuclear > hexanuclear > higher isomers whereas acetonitrile derivatives containing H, Na, and K are far less abundant. Na and K adducts are common in ESI-MS spectra[44] because the O-donors immediately interact and aggregate with the small quantities of Na and K that are always present in H_2O solvent.

The aggregation behavior is strongly dependent on the ligands. For some systems, aggregation of Ti and Q is seen significantly in acetonitrile even at 10^{-3} M, and aggregates

 © 2003 Wiley-VCH Verlag GmbH & Co. KGaA, Weinheim

containing Na^+, K^+, or H^+ dominate significantly over larger adducts. Relevant peaks present in the spectra of **1** are due to the interaction of tetranuclear species with Na^+, K^+, or H^+. The most abundant Ti-containing species are the trinuclear ions $[H(Q^B)_6Ti_3O_3]^+$, $[NaTi_3(Q^B)_6O_3]^+$, and $[KTi_3(Q^B)_6O_3]^+$. For derivative **2** additional signals due to the dinuclear species $[H(Q^T)_4Ti_2O_2]^+$, $[Na(Q^T)_4Ti_2O_2]^+$, and $[K(Q^T)_4Ti_2O_2]^+$ are present. The isotopic distribution of these species agrees with the calculated composition.

The absence of ions containing MeCN indicates that there is no binding between the solvent and Ti.

The ESI-MS spectrum of **6**, recorded in the negative detection mode, is dramatically improved and simpler. It shows four main peaks, assigned to the tri- $\{[Na_3(Q)_4]^-\}$, di- $\{[Na_2(Q)_3]^-\}$, and mono-Na anions $\{[Na(Q)_2]^-\}$, and the free anionic ligand $[Q]^-$.

Since only charged species are transferred from solution to the gas phase, quantitative ESI-MS results do not represent the real relative distribution of species in solution. The strong association of Na and K cations and protons to the Q ligands concurs with an X-ray structure of an Rh^I derivative that has 4-acyl-5-pyrazolonato as a counteranion.[45]

The ESI-MS spectra clearly indicate different nuclearities within polymeric species, in agreement with the high number of NMR signals for the methyl group in **1**−**3**.

As shown in the Exp. Sect., Ti-Q compounds are isolated as mono-, tetra-, and polynuclear species, whereas the synthesis of budotitane derivatives yields only mononuclear species. However, in a biological environment for antitumor therapy, budotitane undergoes extensive hydrolysis, first on the Ti−O(ethoxy) bonds and later on the Ti−bzac moiety, to eventually yield titanium dioxide.[3] In other words, for mononuclear $(bzac)_2Ti(OEt)_2$ all of the Ti substituents, ethoxy and benzoylacetonato, are cleaved, whereas in (4-acyl-5-pyrazolonato)titanium synthesis it is the alkoxy (or Cl) bonds that cleave. Although the ESI-MS spectra suggest that the Ti−Q bonds are labile, the different environments in each case may explain such differences, as shown in the literature.[46−48]

Structural Features Obtained with DFT

As we could not obtain crystals suitable for X-ray diffraction studies, we calculated the minimum energy geometry using DFT (Density Functional Theory) theoretical methods. As shown in Figure 4 a mononuclear species can have three *cis* stereoisomer conformers, we name them CIS1, CIS2, and CIS3. For $(Q^T)_2Ti(OMe)_2$, CIS3 has the lowest energy and selected geometrical parameters are shown in Table 3. This CIS3 conformer shows both O(methoxy) groups opposite to O(pyrazolonato) atoms. A *trans* influence is seen for the two pairs of opposite bonds (Ti−O3 = 1.801 Å, Ti−O1 = 2.084 Å, and Ti−O4 = 1.816 Å, Ti−O51 = 2.046 Å) where the shorter Ti−O(methoxy) bond is opposite the longer Ti−O(pyrazolonato) bond. Completing the coordination sphere are two opposing

Table 3. Selected structural parameters of bis(4-acyl-5-pyrazolonato)titanium conformers, Q_2TiY_2, obtained with DFT methods, and related polynuclear Ti−(β-diketonato) compounds, obtained with diffraction methods

Conformer	Ti−Y3[a]	Ti−Y4[a]	Ti−O1[b]	Ti−O2	Ti−O51	Ti−O52	Y−Ti−Y	Ti ligands
			1st chelate		2nd chelate			
CIS1[c]	2.235	2.233	1.952	2.038	1.966	2.027	102.6	Q^T
	Y = Cl	Y = Cl					Y = Cl	Cl
CIS2[c]	2.233	2.236	2.021	1.968	1.955	2.048	102.3l	Q^T
	Y = Cl	Y = Cl					Y = Cl	Cl
CIS3[c]	2.234	2.237	2.041	1.950	2.047	1.957	98.8	Q^T
	Y = Cl	Y = Cl					Y = Cl	Cl
CIS3[d]	1.797	1.801	2.085	2.012	2.042	2.010	95.0	Q^B
	Y = O	Y = O					Y = O	CH_3O
CIS3[e]	1.801	1.816	2.084	1.994	2.046	1.992	95.1	Q^T
	Y = O	Y = O					Y = O	CH_3O
Polynuclear compounds	Ti−O3	Ti−O4	Ti−O1 1st chelate	Ti−O2	Ti−O51 2nd chelate	Ti−O52	O−Ti−O[f]	Ti−O−Ti[g]
$[(Q^B)_2Ti(\mu\text{-}O)]_4$[h]	1.767	1.868	1.979	2.146	1.980	2.056	99.2	150.5, 153.8
2nd Ti unit	1.758	1.859	1.983	2.163	1.978	2.076	100.2	150.5, 153.8
$[L_2Ti(\mu\text{-}O)]_4$[i]	1.804	1.818	1.969	2.116	1.969	2.117	100.5	170.3, 169.3
2nd Ti unit	1.810	1.810	1.968	2.120	1.968	2.120	100.3	170.3, 169.3
3rd unit	1.793	1.793	1.969	2.132	1.969	2.132	99.4	170.3, 169.3
$[(L')_2Ti(\mu\text{-}O)]_2$[j]	1.831	1.824	1.968	2.059	1.974	2.059	83.4	97.1, 97.1

[a] Y3 and Y4 are: O associated to methoxy groups in $(Q^T)_2Ti(OCH_3)_2$ and $(Q^B)_2Ti(OCH_3)_2$; Cl in $(Q^T)_2TiCl_2$; $Q^{[B]}$ = 4-benzoyl-3-methyl-1-phenylpyrazolon-5-ato, Q^T = 3-methyl-4-neopentylcarbonyl-1-phenylpyrazolon-5-ato. In the corresponding columns for the polynuclear compounds Ti−O(oxo) bonds are shown. [b] O1 and O2 belong to the 1st β-diketonato chelate; O51 and O52 belong to the 2nd β-diketonato chelate. [c] Energy: CIS1 has the lowest energy, followed by CIS3 (2 kcal/mol) and CIS2 (2.2 kcal/mol) for $(Q^T)_2TiCl_2$. [d] Energy: CIS1 has the lowest energy, followed by CIS2 (0.3 kcal/mol) and CIS3 (2.8 kcal/mol) for $(Q^B)_2Ti(OCH_3)_2$. [e] Energy: CIS3 has the lowest energy, followed by CIS2 (0.7 kcal/mol) and CIS1 (56 kcal/mol) for $(Q^T)_2Ti(OCH_3)_2$. [f] This parameter is O3−Ti−O4. [g] These parameters are Ti−O3−Ti and Ti−O4−Ti. [h] $[(Q^B)_2Ti(\mu\text{-}O)]_4$ has an inversion center that makes two Ti units equivalent to the other two.[19] Ti conformation is similar to CIS1. [i] $[L_2Ti(\mu\text{-}O)]_4$ has a twofold axis passing on two Ti atoms; L = 2,2,6,6-tetramethylheptane-3,5-dionato.[50] [j] The 2nd Ti unit is crystallographically related by an inversion center; L′ = acetylacetonato.[5]

 © 2003 Wiley-VCH Verlag GmbH & Co. KGaA, Weinheim

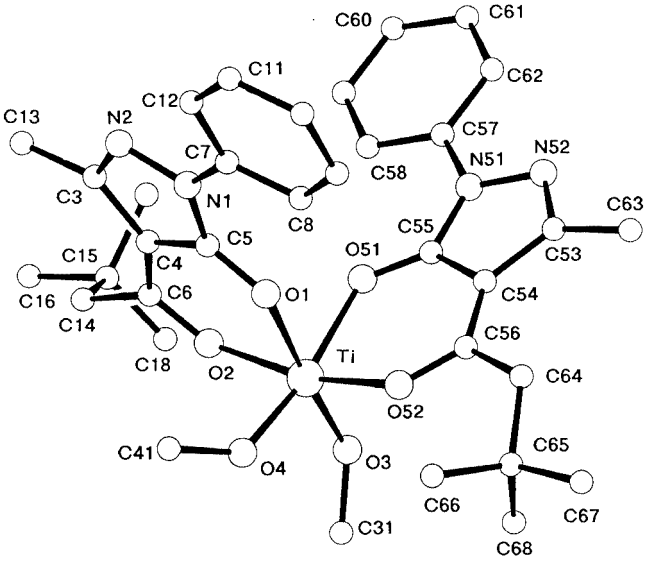

Figure 5. DFT structure of the $(Q^T)_2Ti(OCH_3)_2$ conformer having the lowest energy (CIS3); H atoms are omitted from this and all other DFT pictures

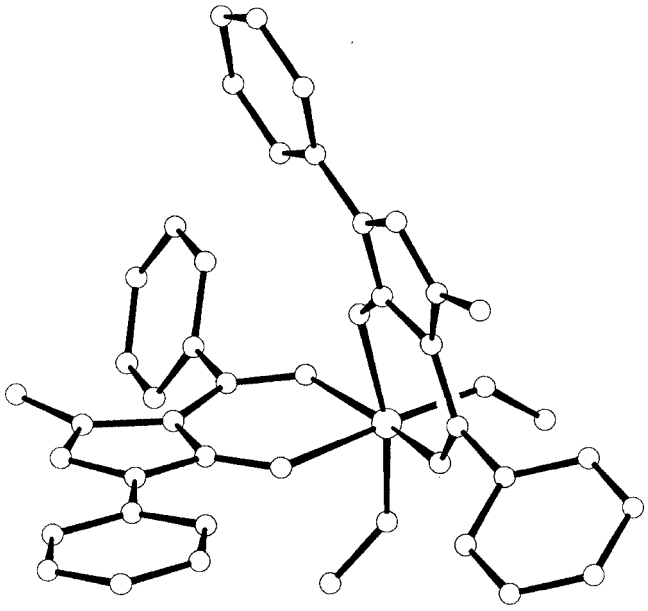

Figure 6. CIS3 DFT structure of $(Q^B)_2Ti(OCH_3)_2$

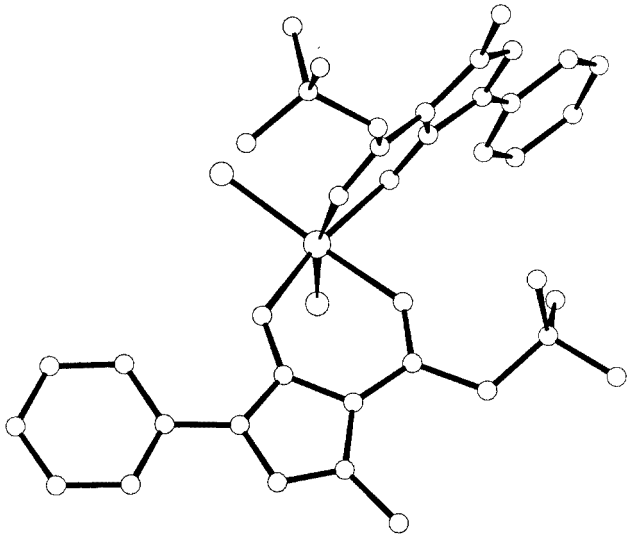

Figure 7. CIS1 DFT structure of $(Q^T)_2TiCl_2$

O(acyl) atoms; here there is no dominant *trans* influence and both Ti−O(acyl) bonds are equal (Ti−O2 = 1.994 Å, Ti−O52 = 1.992 Å).

X-ray structures of Sn-Q derivatives[34−41] show coplanarity between the pyrazole and its attached phenyl due to extended intraligand conjugation. CIS3 agrees with this experimental feature as the torsion angles C5−N1−C7−C8 and C55−N51−C57−C58 are 5.9 and −1.0° (Figure 5). Other DFT conformers studied here also show this feature.

The CIS2 conformer of $(Q^T)_2Ti(OMe)_2$ is 0.7 kcal/mol higher in energy than CIS3, whereas the CIS1 isomer shows markedly higher energy (56 kcal/mol).

We studied $(Q^B)_2Ti(OMe)_2$ and analyzed the role of the R^4 group in these complexes. In contrast with $(Q^T)_2Ti(OMe)_2$ the three *cis* conformers of $(Q^B)_2Ti(OMe)_2$ have similar energies. Thus, the CIS1 conformer shows the lowest energy followed by CIS2 (0.3 kcal/mol) and CIS3 (2.8 kcal/mol). The marked difference between the CIS1 conformers of $(Q^B)_2Ti(OMe)_2$ and $(Q^T)_2Ti(OMe)_2$ may be ascribed to the bulkiness of the neopentyl R^4 group in the latter compared with Ph in the former.

Although the CIS3 conformer of $(Q^B)_2Ti(OCH_3)_2$ (Figure 6) shows the same *trans* influence seen in $(Q^T)_2Ti(OCH_3)_2$ (both shown in Table 3), the former has slightly shorter Ti−O(methoxy) and longer Ti−O(acyl) bonds. This difference is probably related to the lower basicity of the O(acyl) atom attached to an R^4 group that is electron-withdrawing (Ph), in comparison with the more basic neopentyl group in $(Q^T)_2Ti(OCH_3)_2$. Therefore, the shortening of the Ti−O(methoxy) bond in $(Q^B)_2Ti(OCH_3)_2$ seems to arise from the weak O(acyl) basicity.

The role of leaving groups can be analyzed by comparing $(Q^T)_2Ti(OMe)_2$ and $(Q^T)_2TiCl_2$. The three *cis* conformers of the latter have similar energies; the lowest energy being CIS1 (Figure 7) followed by CIS2 (2 kcal/mol, Figure 8) and CIS3 (2.2 kcal/mol, Figure 9). Therefore, the CIS1 conformer of the Cl derivative is not as strained as that of $(Q^T)_2Ti(OCH_3)_2$. This may be associated with a longer Ti−Cl bond compared with Ti−O(methoxy). A lengthening of the Ti−Cl bond is expected due to the longer covalent radius of Cl (0.99 Å) compared to that of O (0.73 Å).[49] However, this difference (0.26 Å) is largely overcome by calculated values of about 0.42 Å (Table 3). The very short Ti−O(methoxy) bonds in $(Q^T)_2Ti(CH_3O)_2$ and $(Q^B)_2Ti(CH_3O)_2$ probably possess partial double bond character that is missing in Ti−Cl bonds. Consequently, stronger Ti−chelate bonds are induced in $(Q^T)_2TiCl_2$; see Ti−O(chelate) bonds for CIS3 isomers of $(Q^T)_2Ti(CH_3O)_2$ and $(Q^B)_2Ti(CH_3O)_2$ in Table 3.

Further agreement between our DFT calculated structures and data from diffraction studies is seen as the O(methoxy) atoms form the shortest Ti−O bonds in CIS1,

 © 2003 Wiley-VCH Verlag GmbH & Co. KGaA, Weinheim

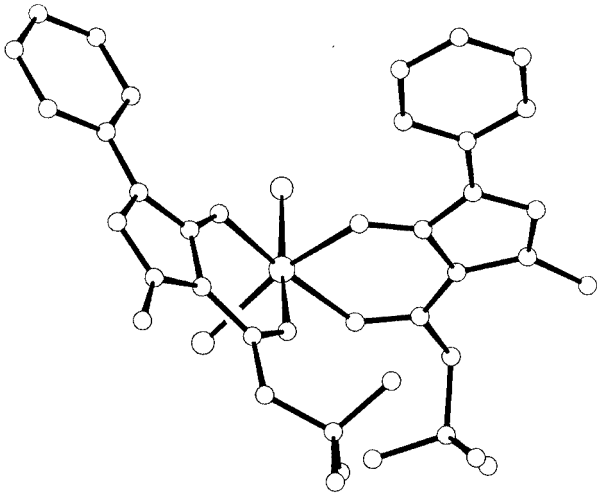

Figure 8. CIS2 DFT structure of $(Q^T)_2TiCl_2$

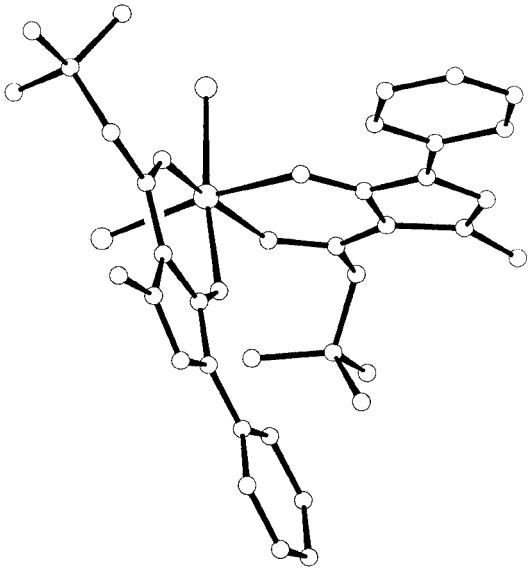

Figure 9. CIS3 DFT structure of $(Q^T)_2TiCl_2$

CIS2, and CIS3, similar to the O(oxo) atoms in the polynuclear Ti−(β-diketonates) $[(Q^B)_2Ti\text{-}\mu\text{-}O]_4$,[19] $[L_2Ti\text{-}\mu\text{-}O]_4$ (L = 2,2,6,6-tetramethylheptane-3,5-dionato)[50] and $[(acac)_2Ti\text{-}\mu\text{-}O]_2$,[5] i.e., Ti−O(β-diketonato) bonds are longer.

In conclusion, the *trans* influence determines the structural features in titanium 4-acyl-5-pyrazolonates. O(oxo) in $[(Q^B)_2Ti\text{-}\mu\text{-}O]_4$ and O(methoxy) in $Q_2Ti(OCH_3)_2$ are strong donors to Ti, resulting in the shortest Ti−O bonds and weakening their opposite Ti−O bonds in the coordination sphere.

Voltammetry

Because antitumor platinum and gold compounds exist in two metal oxidation states, Pt^{II} [11,12] and Pt^{IV} [26] and Au^{I} and Au^{III},[51−52] respectively, a redox reaction may play a role in the cytotoxic mechanism of metal derivatives. This has been demonstrated for the antitumor drug bleomycin, which forms a bleomycin−Fe^{II}−O_2 species that undergoes $Fe^{II} \rightarrow Fe^{III}$ oxidation before performing DNA cleavage.[53]

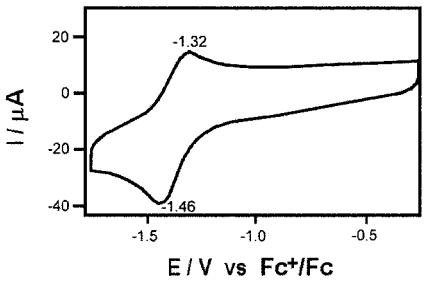

Figure 10. Voltammogram of the antitumor compound $[(Q^B)_2Ti\text{-}\mu\text{-}O]_4$(**1**)

Protein Ti-bound transferrin, believed to play a key role in the antitumor mechanism of Ti^{IV} titanocene dichloride, can also be obtained from Ti^{III} citrate.[25]

We have examined the redox behavior of Ti in the tetranuclear antitumor compound $[Q^B)_2Ti\text{-}\mu\text{-}O]_4$ (**1**) and the mononuclear species $(Q^T)_2Ti(O\textit{n}Pr)_2$ (**11**). The results, referred to Fc^+/Fc, for $[(Q^B)_2Ti\text{-}\mu\text{-}O]_4$ show a cyclic voltammogram in the cathodic region with a reversible redox couple, assigned to Ti^{IV}/Ti^{III}, with $Ep_c = -1.46$ V (Figure 10), whereas the same process for $(Q^T)_2Ti(O\textit{n}Pr)_2$ has −1.71 V (voltammogram not shown). Therefore, in the tetranuclear species all four Ti atoms undergo the same process and are indistinguishable. In addition, the Ti atom has a greater tendency to be reduced to Ti^{III} in the tetranuclear species than in the mononuclear one. In the related titanium β-diketonato compound $(Cp)_2Ti^{III}(acac)$,[54] the Ti^{IV}/Ti^{III} couple was $Ep_c = -0.85$ V (referred to Fc^+/Fc). Although comparison with the present work is difficult because of markedly different experimental conditions, it seems that the Ep_c value is highly ligand sensitive.

An initial stage in the voltammetric reduction of the mononuclear species $(Q^T)_2Ti(OCH_2CH_2CH_3)_2$ was also studied using DFT methods. Since the CIS3 stereochemistry of $(Q^T)_2Ti(OCH_3)_2$ and $(Q^B)_2Ti(OCH_3)_2$ show low energies, this conformation was expected to be favored for $(Q^T)_2Ti(OCH_2CH_2CH_3)_2$. After convergence, the anionic species $[(Q^T)_2Ti(OCH_2CH_2CH_3)_2]^-$ generally agrees with the structural trends shown by the methoxy derivatives mentioned above. However, the Ti−O*n*Pr bonds (1.840, 1.868 Å) are longer than the equivalent Ti−O(methoxy) bonds in $(Q^T)_2Ti(OCH_3)_2$ (1.801, 1.816 Å) and $(Q^B)_2Ti(OCH_3)_2$ (1.797, 1.801 Å); this seems reasonable as a leaving O*n*Pr group would induce a neutral, more stable $(Q^T)_2Ti^{III}(OCH_2CH_2CH_3)$ species.

Although Ti^{III} tends to oxidize to Ti^{IV}, the voltammetry experiment indicates a lower tendency for Ti^{IV} in the tetranuclear species $[(Q^B)_2Ti\text{-}\mu\text{-}O]_4$ and suggests a redox stability for polymeric forms stemming from $[(Q^B)_2Ti^{III}X_2]^-$ units. Such anionic forms can be water-soluble and thus improve their pharmacological formulation by avoiding the use of liposomes such as in the tetranuclear species $[(Q^B)_2Ti^{IV}\text{-}\mu\text{-}O]_4$. Biological results for the antitumor water-soluble Ti agents will be reported in a separate publication.

 © 2003 Wiley-VCH Verlag GmbH & Co. KGaA, Weinheim

Conclusion

A rich variety of (4-acyl-5-pyrazolonato)titanium(IV) compounds, with several nuclearities, is observed due to hydrolysis during synthesis. Avoiding moisture prevents polymerization and discriminates between mono- or polynuclear compounds. Spectroscopic data (NMR, ESI-MS) and molecular weight analysis describe the polymerization features. Isolated compounds do not show Ti−Q cleavage, in contrast with classical Ti−(β-diketones). The ESI-MS results indicate mild Ti−Q cleavage compared with the fast breaking of Ti−Cl (or Ti−alkoxy). These features may enhance antitumor properties as the two most investigated antitumor titanium compounds, budotitane, and titanocene dichloride, show fast hydrolysis for Ti−O(ethoxy) (or Ti−Cl) and slow hydrolysis for Ti−(β-diketonato) (or Ti−Cp) bonds. Ti-Q (1:1) derivatives possess novel water solubility, which is useful for antitumor drug formulation. Quantum mechanical calculations on mononuclear $Q_2Ti(OCH_3)_2$ species show (a) three different sets of Ti−O bonds and a strong *trans* influence; (b) no preference for a unique *cis* isomer, although one of the three *cis* conformers has a markedly higher energy for one compound with a bulky substituent. Voltammetry data on a mono- and a tetranuclear species show a lower tendency towards reduction to Ti^{III} in the latter.

Experimental Section

General: The Ti precursors were obtained from Aldrich and used without further purification. 1-Phenyl-3-R^3-4-R^4-(C=O)-pyrazol-5-ones HQ (Figure 2) were prepared according to the literature. Samples for microanalysis were dried in vacuo to constant weight (20 °C, about 0.1 Torr). Molecular weight (M.W.) determinations were performed at 40 °C with a Knauer KNA0280 vapour pressure osmometer calibrated with benzil. The solvent was Baker Analysed Spectrophotometric grade chloroform. The results were reproducible to ±2%. Elemental analyses (C,H,N) were performed inhouse with a Fisons Instruments 1108 CHNS-O Elemental Analyser. IR spectra were recorded from 4000 to 100 cm^{-1} with a Perkin−Elmer System 2000 FT-IR instrument. ^1H NMR spectra were recorded with a VXR-300 Varian spectrometer. Melting points were determined with an IA 8100 Electrothermal instrument. The positive and negative electrospray mass spectra were obtained with a Series 1100 MSI detector HP spectrometer, using an acetonitrile mobile phase. Solutions (3 mg/mL) for electrospray ionization mass spectrometry (ESI-MS) were prepared using reagent grade acetone or acetonitrile. For the ESI-MS data, mass and intensities were compared to those calculated using IsoPro Isotopic Abundance Simulator, version 2.1.[55] Peaks containing silver(I) ions are identified as the center of an isotopic cluster.

Synthesis and Spectroscopic Characterization

$[(Q^B)_2Ti(\mu\text{-}O)]_4$ (1): Compound **1** was prepared by treating $TiCl_4$ with HQ^B [56] (1:2 ratio) under reflux in basic (KOH, 1:1 regarding HQ^B) ethanol (10 mL). A yellow precipitate formed which was then dissolved in CH_2Cl_2 to remove KCl. After filtration, the solution was concentrated and the residue recrystallized from ethyl acetate/*n*-hexane under aerobic conditions, m.p. 195 °C (dec.). Yield 0.525 g (85%) for $TiCl_4$ (0.190 g) and of Q^B (0.556 g). F.W. = 2473.9 (a tetranuclear compound shown by X-ray diffraction[19]). M.W. ($CHCl_3$) = 2200 (0.5 10^{-2} M) (r = 0.89). $C_{34}H_{26}N_4O_5Ti$: calcd. C 66.03, H 4.24, N 9.06; found C 65.92, H 4.33, N 8.86. ^1H NMR ($CDCl_3$, 300 MHz, 293 K, ppm): δ = 1.3 m, 1.4 m, 1.6 m, 1.7 m (br) (6 H, 3-CH_3), 6.2 br, 6.5 br, 6.7 br, 7.0 br, 7.5 br, 8.0 br (20 H, C_6H_5). ^1H NMR ($CDCl_3$, 300 MHz, 324 K, ppm): δ = 1.3−1.8 (15 s, 6 H, 3-CH_3), 6.2 m, 6.3 m, 6.4 m, 6.6 m, 7.1 m, 7.2 m, 7.4 m, 7.6 m, 7.9 m, 8.0 m (20 H, C_6H_5). ^1H NMR ($CDCl_3$, 300 MHz, 218 K, ppm): 1.0−2.1 (25 s, 6 H, 3-CH_3), 6.0 m, 6.2 m, 6.3 m, 6.4 m, 6.6 m, 7.1 m, 7.2 m, 7.4 m, 7.6 m, 7.9 m, 8.0 m, 8.2 m, 8.8 d, 9.05 d br (20 H, C_6H_5). IR (Nujol mull, cm^{-1}): ṽ = 1606 s, 1580 s, 1568 s, 1531 s (C···O, C···C and C···N), 554 m, 518 m, 504 m, 460 s, 448 vs, 410 sh, 398 s, 357 s (Ti−O). ESI-MS (MeCN) (+): *m*/*z* (%) = 301 (95) $[Na(HQ^B)]^+$, 924 (60) $[Na_4(Q^B)_3]^+$, 940 (95) $[Na_3K(Q^B)_3]^+$, 956 (60) $[Na_2K_2(Q^B)_3]^+$, 1856 (30) $[Ti_3(Q^B)_6O_3H]^+$, 1877 (30) $[NaTi_3(Q^B)_6O_3]^+$, 1894 (45) $[KTi_3(Q^B)_6O_3]^+$, 2497 (15) $[NaTi_4(Q^B)_8O_4]^+$. Alternatively, compound **1** can be obtained by treating $TiCl_4$ (1 mmol) with HQ^B (2 mmol) in CH_2Cl_2 in the presence of excess of KOH, or by direct reaction of $Ti(OR)_4$ (1 mmol, R= Me, Et or Bu) with HQ^B (at least 4 mmol).

$[(Q^T)_2Ti(O)(H_2O)]_n$ (2): Compound **2** was prepared by treating $Ti(OEt)_4$ with HQ^T [57] (1:4 ratio) under reflux in basic (KOH) ethanol. After 2 d, the solution was concentrated under vacuum and diethyl ether was then added. A yellow precipitate formed which was identified as compound **2**; yield 0.541 g (85%), m.p. 299−302 °C. For a monomeric unit F.W. is 636.56. $C_{32}H_{38}N_5O_6Ti$: calcd. C 61.54, H 6.46, N 8.97; found C 61.78, H 6.65, N 8.98. ^1H NMR ($CDCl_3$, 300 MHz, 293 K, ppm): δ = 1.0−1.6 (18 s, 22 H, CH_3 + CH_2), 2.4 (br m, 6 H 3-CH_3), 7.2 (br, 4 H, C_6H_5), 7.4 (br m, 2 H, C_6H_5), 7.8−8.1 (br m, 4 H, C_6H_5), 2.75 (s br, 2 H, H_2O). IR (Nujol mull, cm^{-1}): ṽ = 3176 (CH), 1602 s, 1595 sh, 1574 s, 1527 s (C···O, C···C, and C···N), 506 m, 474 s, 455 s, 411 w, 381 w, 363 w, 332 w, 287 m (Ti−O). ESI-MS (MeCN) (+): *m*/*z* (%) = 295 (95) $[Na(HQ^T)]^+$, 611 (15) $[Na_3(Q^T)_2]^+$, 629 (58) $[Na_2K(Q^T)_2]^+$, 645 (8) $[NaK_2(Q^T)_2]^+$, 1235 (30) $[Ti_2(Q^T)_4O_2H]^+$, 1257 (10) $[Ti_2(Q^T)_4O_2Na]^+$, 1274 (10) $[Ti_2(Q^T)_4O_2K]^+$, 1819 (10) $[Ti_3(Q^T)_6O_3H]^+$, 1842 (100) $[Ti_3(Q^T)_6O_3Na]^+$, 1858 (15) $[Ti_3(Q^T)_6O_3K]^+$.

$[(Q^A)_2Ti(O)(H_2O)]_n$ (3): Compound **3** was obtained by the reaction of $Ti(O\textit{n}Pr)_4$ with HQ^A [58] (1:2 ratio) in *n*PrOH, in the presence of KOH (4:1 ratio regarding Ti). The reaction mixture was stirred for 3 d. The resultant clear solution was then concentrated and the residue washed with diethyl ether and shown to be compound **3**; yield 0.566 g (81%), pale yellow, m.p. 235−238 °C. For a monomeric unit F.W. is 698.57. $C_{36}H_{34}N_4O_8Ti$: calcd. C 60.51, H 4.80, N 7.84; found C 60.32, H 5.0, N 7.51. ^1H NMR (D_2O, 200 MHz, 293 K, ppm): δ = 2.16 (s, 6 H, 3-CH_3), 3.78 (s, 6 H, OCH_3), 6.90 d, 4 H, C_6H_5), 7.19 (t, 2 H, C_6H_5), 7.23 (t, 4 H, C_6H_5), 7.5 (d, 4 H, C_6H_5), 7.58 (d, 4 H, C_6H_5). IR (Nujol mull, cm^{-1}): ṽ = 1603 s br, 1530 s br (C···O, C···C, and C···N), 598 s, 536 s br, 510 s, 442 m, 432 m, 422 sh, 388 w, 368 w, 325 m, 284 w.

$[(Q^N)_2Ti(O)(H_2O)]_n$ (4): The yellow compound **4** was obtained as for **3**, using HQ^N,[58] in 54% yield (0.402 g); m.p. 334 °C (dec.). For a monomeric unit F.W. is 744.52. M.W. ($CHCl_3$) = 2100 (2.1 10^{-2} M) (r = 2.82) $C_{34}H_{28}N_6O_{11}Ti$: calcd. C 54.85, H 3.79, N 11.29; found C 54.54, H 3.52, N 11.16. ^1H NMR (D_2O, 200 MHz, 293 K, ppm): δ = 2.19 (s, 6 H, 3-CH_3), 7.19 (t, 2 H, C_6H_5), 7.31 (t, 4 H, C_6H_5), 7.39 (d, 4 H, C_6H_5), 7.63 (d, 4 H, C_6H_5), 8.18 (d, 4 H, C_6H_5). IR (Nujol mull, cm^{-1}): ṽ = 3200 br (OH) 1632 s br, 1592 s, 1500 sh br (C···O, C···C, and C···N), 566 w, 510 m, 448 m, 397 w, 376 w, 325 w, 303 w, 290 w, 279 w, 253 w, 247 w.

 © 2003 Wiley-VCH Verlag GmbH & Co. KGaA, Weinheim

$[(Q^C)_2Ti(O)(H_2O)_2]_n$ (5): Compound **5** has been obtained as for **3** using HQ^C [59] and was washed with *n*-hexane to give the pale yellow product in 62% yield (0.413 g); m.p. 268 °C (dec.). For a monomeric unit F.W. is 666.61. $C_{34}H_{42}N_4O_7Ti$: calcd. C 61.26, H 6.35, N 8.40; found C 61.18, H 6.44, N 8.26. ^1H NMR ($CDCl_3$, 200 MHz, 293 K, ppm): δ = 1.3 (br, 12 H, C_6H_{11}), 1.6−2.0 (br, 10 H, C_6H_{11}), 2.36 (s, 6 H, 3-CH_3), 2.75 (s, 4 H, H_2O), 6.90 (br, 2 H, C_6H_5), 7.20 (br, 4 H, C_6H_5), 7.53 (br, 4 H, C_6H_5). IR (Nujol mull, cm^{-1}): ṽ = 3300 br (OH) 1624 s br, 1580 sh, 1530 s, 1500 sh br (C···O, C···C, and C···N), 511 s, 494 m, 448 s, 417 w, 381 m, 334 s, 280 w. ESI-MS (MeCN) (+): *m*/*z* (%) = 613 (10) $[Na_2H(Q^C)_2]^+$, 629 (15) $[NaKH(Q^C)_2]^+$, 920 (45) $[Na_3H(Q^C)_3]^+$, 936 (100) $[Na_2KH(Q^C)_3]^+$, 952 (80) $[NaK_2H(Q^C)_3]^+$, 1226 (10) $[Na_4H(Q^C)_4]^+$, 1241 (20) $[Na_3KH(Q^C)_4]^+$, 1257 (10) $[Na_2K_2H(Q^C)_4]^+$.

$[(Q^L)_2Ti(O)(H_2O)_2]_n$ (6): Compound **6** was obtained as described for **3** using HQ^L.[59] The residue formed was washed twice with light petroleum ether (40−60 °C) to give the pale yellow product in 49% yield (0.334 g); m.p. 80 °C (dec.). For a monomeric unit F.W. is 682.57. $C_{36}H_{34}N_4O_7Ti$: calcd. C 63.35, H 5.02, N 8.21; found C 63.18, H 4.97, N 8.32. ^1H NMR ($CDCl_3$, 200 MHz, 293 K, ppm): 2.5 (br, 6 H, 3-CH_3), 3.85 (br, 4 H, CH_2), 6.90 (br, 8 H, C_6H_5), 7.20 (br, 8 H, C_6H_5), 7.7 (br, 4 H, C_6H_5). IR (Nujol mull, cm^{-1}): ṽ = 3300 br (OH) 1632 s br, 1592 sh, 1500 sh br (C···O, C···C, and C···N), 591 w, 548 m, 500 m, 457 br, 327 m, 304 w. ESI-MS (MeCN) (+): *m*/*z* (%) = 315 (40) $[NaH(Q^L)]^+$, 331 (20) $[Na_2(Q^L)]^+$, 353 (25) $[NaK(Q^L)]^+$, 651 (25) $[Na_3(Q^L)_2]^+$, 667 (25) $[Na_2K(Q^L)_2]^+$, 683 $[NaK_2(Q^L)_2]^+$, 960 (35) $[Na_2KH(Q^L)_3]^+$, 976 (100) $[NaK_2H(Q^L)_3]^+$, 991 (22) $[K_3H(Q^L)_3]^+$, 1273 (10) $[Na_3KH(Q^L)_4]^+$, 1593 (55) $[Na_6(Q^L)_5]^+$, 1610 (75) $[Na_5K(Q^L)_5]^+$, 1626 (100) $[Na_4K_2(Q^L)_5]^+$, 1641 (80) $[Na_3K_3(Q^L)_5]^+$; (−): *m*/*z* (%) = 291 (100) $[Q^L]^-$, 605 (15) $[Na(Q^L)_2]^-$, 913 (5) $[Na_2(Q^L)_3]^-$, 1233 $[Na_3(Q^L)_4]^-$.

$[(Q^E)_2Ti(O)(H_2O)]_n$ (7): Compound **7** was obtained as described for **3** using HQ^E.[56] It was recrystallized as a colorless compound from $CHCl_3$/*n*-hexane (1:1) in 50% yield (0.335 g); m.p. 260−270 °C (dec.). For a monomeric unit F.W. is 670.54. $C_{34}H_{46}N_4O_7Ti$: calcd. C 60.89, H 6.91, N 8.35; found C 61.12, H 6.87, N 8.45. ^1H NMR (D_2O, 200 MHz, 293 K, ppm): δ = 0.73 (t, 6 H, CH_3), 1.17 (br, 12 H, CH_2), 1.46 (m, 4 H, CH_2), 2.21 (s, 6 H, 3-CH_3), 2.79 (pt, 4 H, CH_2), 7.16 (t, 2 H, C_6H_5), 7.22 (t, 4 H, C_6H_5), 7.33 (d, 4 H, C_6H_5). IR (Nujol mull, cm^{-1}): ṽ = 3300 br (OH) 1624 s br, 1591 s, 1580 sh, 1500 sh br (C···O, C···C, and C···N), 512 m, 490 w, 464 w, 437 w, 390w, 386 w, 372 w, 330 w. ESI-MS (MeCN) (+): *m*/*z* (%) = 309 (100) $[NaH(Q^E)]^+$, 325 (40) $[NaK(Q^E)]^+$, 639 (20) $[Na_3(Q^E)_2]^+$, 926 (50) $[Na_3H(Q^E)_3]^+$, 942 (75) $[Na_2KH(Q^E)_3]^+$, 958 (50) $[NaK_2H(Q^E)_3]^+$, 1233 (5) $[Na_4H(Q^E)_4]^+$, 1249 (10) $[Na_3KH(Q^E)_4]^+$, 1267 (10) $[Na_2K_2H(Q^E)_4]^+$, 1845(65) $[Na_4KH_2(Q^E)_6]^+$, 1861 (80) $[Na_3K_2H_2(Q^E)_6]^+$.

$[(Q^P)_2Ti(O)(H_2O)]_n$ (8): Compound **8** was prepared by reaction of $Ti(OMe)_4$ with HQ^P [59] (1:4 ratio) in refluxing benzene. The resultant clear solution was concentrated under vacuum and the residue recrystallized twice from $CHCl_3$/*n*-hexane to give a colorless compound with an m.p. of 289−291 °C (dec.). For a monomeric unit F.W. is 786.68, yield 0.700 g (89%). $C_{46}H_{34}N_4O_6Ti$: calcd. C 70.23, H 4.36, N 7.12; found C 70.09, H 4.46, N 6.92. ^1H NMR ($CDCl_3$, 300 MHz, 293 K, ppm): 6.4−7.8 (m, 30 H, C_6H_5), 2.75 (s br, 2 H, H_2O). IR (Nujol mull, cm^{-1}): ṽ = 3400 br (OH) 1611 s br, 1565 s, 1514 s (C···O, C···C, and C···N), 562 m, 544 m, 522 m, 474 s, 443 s, 430 sh, 377 w, 340 m, 326 m, 305 m, 298 m, 280 m.

$(Q^B)_2Ti(OnPr)_2$ (9): The pale yellow compound **9** was prepared by treating $Ti(OnPr)_4$ with HQ^B [56] (1:2 ratio) in refluxing benzene under nitrogen. F.W. = 720.66; yield 0.612 g (85%), m.p. 97−105 °C (dec.). $C_{40}H_{40}N_4O_6Ti$: calcd. C 66.67, H 5.59, N 7.77; found C 67.00, H 5.89, N 7.52. M.W. ($CHCl_3$) = 450 (1.0 10^{-2} M) (*r* = 0.62). Λ_m (CH_2Cl_2, 1.0 10^3 M) = 0.3 $\Omega^{-1}\cdot mol^2\cdot cm^{-1}$. ^1H NMR ($CDCl_3$, 300 MHz, 293 K, ppm): δ = 0.9 (m, 6 H, CH_3), 1.3 (m, 4 H, CH_2), 1.95 (s, 6 H, 3-CH_3), 4.5 (t, 4 H, OCH_2), 7.0−8.0 (m, 20 H, C_6H_5). IR (Nujol mull, cm^{-1}): ṽ = 1598 s, 1560 s, 1534 s, 1526 s, 1506 s (C···O, C···C, and C···N), 550 m, 513 m, 499 m, 462 s, 446 s, 410 w, 400 w, 360 m, 340 w, 320 w, 300 w (Ti−O).

$(Q^T)_2Ti(OMe)_2$ (10): The colorless compound **10** was prepared as described for **9**, using HQ^T,[57] in 85% yield (0.552 g), F.W. = 652.63, m.p. 190 °C (dec.). $C_{34}H_{44}N_4O_6Ti$: calcd. C 62.57, H 6.80, N 8.58; found C 62.73, H 6.89, N 8.79. ^1H NMR ($CDCl_3$, 200 MHz, 293 K, ppm): δ = 0.6−1.3 (14 s, 18 H, CH_3), 1.8−2.6 (25 s, 10 H, 3-CH_3 + CH_2), 4.0−4.6 (10 s, 6 H, OCH_3), 6.7−8.3 (m, 10 H, C_6H_5). IR (Nujol mull, cm^{-1}): ṽ = 1607 s, 1576 s, 1530 s (C···O, C···C, and C···N), 595 s, 581 s, 514 s, 506 s, 465 s, 394 w, 361 m, 335 m, 316 m, 284 m (Ti−O).

$(Q^T)_2Ti(OnPr)_2$ (11): Compound **11** was prepared by treating $Ti(OnPr)_4$ with HQ^T [57] (1:2 ratio) in refluxing benzene. After 24 h of stirring, the solution was completely concentrated under vacuum. No precipitate formed when a 1:1 diethyl ether/propyl alcohol solution was added, so the solution was again concentrated and the residue washed with *n*-hexane. A colorless oil formed that was identified as compound **11**; yield 0.604 g (85%). F.W. = 710.75; M.W. ($CHCl_3$). = 380 (1.0·10^{-2} M) (*r* = 0.53). Λ_m (CH_2Cl_2, 1.0·10^3 M), 1.0 10^3 M) = 0.2 $\Omega^{-1}\cdot mol^2\cdot cm^{-1}$. $C_{38}H_{54}N_4O_6Ti$: calcd. C 64.22, H 7.66, N 7.88; found C 63.80, H 7.52, N 7.76. ^1H NMR ($CDCl_3$, 300 MHz, 293 K, ppm): δ = 0.9 (m, 24 H, CH_3), 1.3 (br m, 6 H, CH_2), 1.6 (m, 4 H, CH_2), 2.4 (s, 3 H, 3-CH_3), 2.5 (s, 3 H, 3-CH_3), 4.5 (m, 4 H, OCH_2), 7.2 (t, 2 H, C_6H_5), 7.4 (t, 4 H, C_6H_5), 8.0 (d, 4 H, C_6H_5). IR (Nujol mull, cm^{-1}): ṽ = 3193 w, 3060 m, 3048 m (CH), 1625 s, 1614 s, 1574 s, 1531 s (C···O, C···C, and C···N), 509 m, 471 s, 412 w, 394 m, 362 m, 339 sh, 314 w, 281 w.

$(Q^T)_2Ti(OnBu)_2(H_2O)$ (12): Compound **12** was prepared as described for **11**, using $Ti(OnBu)_4$ and HQ^T [57] to furnish a colorless oil in 80% yield (0.600 g), F.W. = 754.80. $C_{40}H_{58}N_4O_7Ti$: calcd. C 63.65, H 7.75, N 7.42; found C 64.00, H 7.89, N 7.52. ^1H NMR ($CDCl_3$, 200 MHz, 293 K, ppm): δ = 0.5−1.7 (m, 34 H, CH_2 + CH_3), 2.0−2.7 (br m, 10 H, CH_2 +3-CH_3), 4.5 (m, 4 H, OCH_2), 7.2 (m, 2 H, C_6H_5), 7.4 (m, 4 H, C_6H_5), 7.7 (d, 2 H, C_6H_5), 8.0 (d, 2 H, C_6H_5). IR (Nujol mull, cm^{-1}): ṽ = 3430 br (OH), 3192 w, 3070 m, 3036 m (CH), 1625 s, 1615 s, 1593 s, 1574 s, 1531 s (C···O, C···C, and C···N), 509 m, 470 s, 410 w, 392 m, 364 m, 334 sh, 312 w, 281 w.

$[(Q^A)Ti(OH)_3(H_2O)]_n$ (13): This compound was obtained by treating $Ti(OEt)_4$ with HQ^A [58] (1:1 ratio) in EtOH, in the presence of KOH (4:1 ratio regarding Ti), for 4 h. After concentration of the resultant clear solution, a residue was obtained that was washed with *n*-hexane and shown to be compound **13**; pale yellow, m.p. 84−86 °C, yield 0.385 g (95%). For a monomeric unit F.W. is 406.23. $C_{18}H_{18}N_2O_6Ti$: calcd. C 53.22, H 4.47, N 6.90; found C 53.51, H 4.44, N 6.96. ^1H NMR ($CDCl_3$, 200 MHz, 293 K, ppm): δ = 2.10 (s br, 3 H, 3-CH_3), 2.9 (br, 3 H, OH), 3.74 (br s, 3 H, OCH_3), 6.68 (t, 4 H, C_6H_5), 6.96 (d, 4 H, C_6H_5), 7.00 (d, 4 H, C_6H_5), 7.4 (t, 2 H, C_6H_5), 7.5 (d, 4 H, C_6H_5). IR (Nujol mull, cm^{-1}): ṽ = 3400−3100 br (OH), 1620 s br, 1600−1500 s br (C···O, C···C. and C···N), 539 m, 508 m, 480 m, 467 m, 362 w, 326 w.

$[(Q^C)Ti(OH)_3]_n$ (14]): This compound was obtained as described for **13**, using HQ^C,[57] as a colorless, m.p. 95−98 °C, in 73% yield (0.278 g). For a monomeric unit F.W. is 382.25. $C_{17}H_{22}N_2O_5Ti$:

 © 2003 Wiley-VCH Verlag GmbH & Co. KGaA, Weinheim

calcd. C 53.42, H 5.80, N 7.33; found C 53.46, H 5.93, N 7.23. ^{1}H NMR ($CDCl_3$, 200 MHz, 293 K, ppm): δ = 1.2 (br, 6 H, C_6H_{11}), 1.65 (br, 5 H, C_6H_{11}), 2.37 (s, 3 H, 3-CH_3) 2.74 (br, 2 H, O*H*), 7.0 (br, 3 H, C_6H_5), 7.6 (br, 2 H, C_6H_5). ^{1}H NMR ($CDCl_3$, 300 MHz, 324 K, ppm): δ = 1.2 m, 6 H, C_6H_{11}), 1.65 (br, 5 H, C_6H_{11}), 2.37 (br, 3 H, 3-CH_3) 2.8 (br, 1 H, O*H*), 4.0 (br, 2 H, OH), 7.0 (br, 2 H, C_6H_5), 7.1 (br, 1 H, C_6H_5), 7.6 (br, 2 H, C_6H_5). ^{1}H NMR ($CDCl_3$, 300 MHz, 273 K, ppm): δ = 1.2 (br, 5 H, C_6H_{11}), 1.67 (br, 5 H, C_6H_{11}), 2.34 (br, 3 H, 3-CH_3) 2.8 (br, 1 H, C_6H_{11}), 3.5 (br, 1 H, O*H*), 4.3 (br, 1 H, O*H*), 7.1 (br, 3 H, C_6H_5), 7.6 (br, 2 H, C_6H_5). ^{1}H NMR ($CDCl_3$, 300 MHz, 218 K, ppm): δ = 1.0 (m, 2 H, C_6H_{11}), 1.2 (m, 4 H, C_6H_{11}) 1.53 (m, 3 H, C_6H_{11}), 1.82 (s, 2 H, C_6H_{11}), 2.19, 2.24, 2.34, 2.39, 2.1, 2.47 (6 s, 3 H, 3-CH_3) 2.8, 2.9 (2 s br, 1 H, O*H*), 3.6 (br, 1 H, 3-CH_3), 6.6−7.6 (br, 3 H, C_6H_5), 7.9 (br, 2 H, C_6H_5). IR (Nujol mull, cm^{-1}): $\tilde{\nu}$ = 3400−3000 br (OH), 1620 s br, 1600−1550 s br, 1530 s (C···O, C···C, and C···N), 509 m, 470 m, 449 m, 361 w, 330 m, 281 w.

[(Q^B)Ti(OH)$_2$(O*n*Pr)](H$_2$O) (15): Compound **15** was obtained from the reaction of HQ^B [56] and Ti(O*n*Pr)$_4$ (1:1 ratio) in *n*PrOH at room temperature. After 12 h, a colorless precipitate (TiO_2) formed which was filtered off, and the resulting clear solution was concentarted and the residue extracted with $CHCl_3$. A green gel then formed which slowly converted into a green-black precipitate that was identified as compound **15**; F.W. = 436.30, yield 0.237 g (55%), m.p. 135−145 °C. $C_{20}H_{24}N_2O_6Ti$: calcd. C 55.06, H 5.54, N 6.43; found C 55.22, H 5.63, N 6.74. ^{1}H NMR (D_2O, 200 MHz, 293 K, ppm): 0.78 (t, 3 H, CH_3), 1.37 (m, 2 H, CH_2), 2.14 (s, 3 H, 3-CH_3), 3.48 (t, 2 H, CH_2), 7.1−7.6 (m, 5 H, C_6H_5). IR (Nujol mull, cm^{-1}): $\tilde{\nu}$ = 3400−3000 br (OH), 1621 s br, 1590 sh, 1530 s (C···O, C···C, and C···N), 543 m, 504 m, 418 m, 397 m, 374 w, 352 m, 326 br, 279 m. ESI-MS (MeCN) (+): *m*/*z* (%) = 323 (10) $[Na_2(Q^B)]^+$, 617 (15) $[NaKH(Q^B)]^+$, 917 (40) $[Na_2KH(Q^B)_3]^+$, 933 (100) $[NaK_2H(Q^B)_3]^+$, 1196 (10) $[Na_2KH_2(Q^B)_4]^+$, 1512 (100) $[Na_2K_2H_2(Q^B)_5]^+$, 1528 (45) $[NaK_3H_2(Q^B)_5]^+$, 1813 (60) $[Na_3K_2H_2(Q^B)_6]^+$, 1828 (45) $[Na_2K_3H_2(Q^B)_6]^+$.

[(Q^B)Ti(OH)$_2$(O*n*Bu)](H$_2$O) (16): Compound **16** was prepared in similar fashion to **15**, using HQ^B [56] and Ti(O*n*Bu)$_4$ to give a pale green gel in 95% yield (0.410 g); F.W. = 432.21, m.p. 88−92 °C (dec.). $C_{21}H_{24}N_2O_5Ti$: calcd. C 58.34, H 5.60, N 6.48; found C 58.22, H 5.78, N 6.38. ^{1}H NMR (D_2O, 200 MHz, 293 K, ppm): 0.78 (t, 3 H, CH_3), 1.37 (m, 2 H, CH_2), 1.41 (m, 2 H, CH_2), 2.16 (s, 3 H, 3-CH_3), 3.53 (t, 2 H, CH_2), 7.3−7.6 (m, 10 H, C_6H_5). ^{1}H NMR (D_2O, 200 MHz, 353 K, ppm): δ = 0.78 (t, 3 H, CH_3), 1.37 (m, 2 H, CH_2), 1.41 (m, 2 H, CH_2), 2.16 (s, 3 H, 3-CH_3), 3.53 (t, 2 H, CH_2), 7.3−7.6 (m, 10 H, C_6H_5).^{1}H NMR ($CDCl_3$, 300 MHz, 323 K): δ = 0.9 (t, 3 H, CH_3), 1.24 (br m, 2 H, CH_2), 1.49 (m, 2 H, CH_2), 2.11 (s, 3 H, 3-CH_3), 3.42 (t, 2 H, CH_2), 7.1 t, 7.4 t, 7.5 m, 7.6 d (br, 10 H, C_6H_5). IR (Nujol mull, cm^{-1}): $\tilde{\nu}$ = 3400−3000 br (OH), 1650 br (OH), 1624 s br, 1594 sh (C···O, C···C, and C···N), 545 m, 505 m, 4417 w, 407 w, 373 w, 357 w, 331 s, 279 m. ESI-MS (MeCN) (+): *m*/*z* (%) = 339 (18) $[NaK(Q^B)]^+$, 617 (10) $[NaKH(Q^B)]^+$, 917 (35) $[Na_2KH(Q^B)_3]^+$, 933 (100) $[NaK_2H(Q^B)_3]^+$, 949 (15) $[K_3H(Q^B)_3]^+$, 1512 (75) $[Na_2K_2H_2(Q^B)_5]^+$, 1528 (100) $[NaK_3H_2(Q^B)_5]^+$, 1544 (20) $[K_4H_2(Q^B)_5]^+$, 1813 (40) $[Na_3K_2H_2(Q^B)_6]^+$, 1828 (80) $[Na_2K_3H_2(Q^B)_6]^+$, 1846 (40) $[NaK_4H_2(Q^B)_6]^+$, 1861 (40) $[K_5H_2(Q^B)_6]^+$, 2128 (10) $[Na_3K_3H_2(Q^B)_6]^+$.

[(Q^L)Ti(O)(OH)]$_n$ (17): Compound **17** was obtained by the method described for **15**, using HQ^L,[59] and was recrystallized from $CHCl_3$/*n*-hexane as a pale-green compound in 80% yield (0.297 g), m.p. 100−110 °C (dec.). For a monomeric unit F.W. is 372.22. $C_{18}H_{16}N_2O_4Ti$: calcd. C 58.08, H 4.33, N 7.53; found C 57.80, H 4.45, N 7.43. ^{1}H NMR (D_2O, 200 MHz, 293 K, ppm): δ = 2.19 (s, 3 H, 3-CH_3), 4.16 (s, 2 H, CH_2), 7.21 (m, 6 H, C_6H_5), 7.3 (m, 4 H, C_6H_5). IR (Nujol mull, cm^{-1}): $\tilde{\nu}$ = 3400−3000 br (OH), 1650 br (OH), 1628 s br, 1594 sh, 1580 s (C···O, C···C, and C···N), 545 m, 501 m, 458 m, 446 w, 419 w, 398 m, 375 w, 357 w, 328 m, 311 m, 289 w, 276 m.

[(Q^E)Ti(O)(OH)]$_n$ (18): Compound **18** was also obtained as described for **15**, using HQ^E,[56] and was recrystallized from $CHCl_3$/*n*-hexane as the colorless product in 96% yield (0.350 g), m.p. 225−230 °C (dec.). For a monomeric unit F.W. is 366.25. $C_{17}H_{22}N_2O_4Ti$: calcd. C 55.75, H 6.05, N 7.65; found C 56.00, H 6.30, N 7.67. ^{1}H NMR ($CDCl_3$, 200 MHz, 293 K, ppm): δ = 0.8−2.0 (m, 11 H, CH_3 + CH_2), 2.42 (m, 3 H, CH_3), 3.70 (m, 2 H, CH_2), 7.0−7.6 (m, 5 H, C_6H_5). IR (Nujol mull, cm^{-1}): $\tilde{\nu}$ = 3400−3000 br (OH), 1650 br (OH), 1624 s br, 1594 sh, 1580 s, 1518 s (C···O, C···C, and C···N), 512 m, 495 m, 464 m, 438 w, 397 w, 387 w, 349 w, 331 m. ESI-MS (MeCN) (+): *m*/*z* (%) = 309 (100) $[NaH(Q^E)]^+$, 325 (40) $[NaK(Q^E)]^+$, 639 (20) $[Na_3(Q^E)_2]^+$, 655 (10) $[Na_2K(Q^E)_2]^+$, 671 (10) $[NaK_2(Q^E)_2]^+$, 926 (10) $[Na_3H(Q^E)_3]^+$, 942 (20) $[Na_2KH(Q^E)_3]^+$, 958 (10) $[NaK_2H(Q^E)_3]^+$, 1233 (5) $[Na_4H(Q^E)_4]^+$, 1249 (10) $[Na_3KH(Q^E)_4]^+$, 1266 (10) $[Na_2K_2H(Q^E)_4]^+$, 1927 (50) $[NaTi_3(Q^T)_6O_3]^+$, 1943 (100) $[KTi_3(Q^T)_6O_3]^+$.

(Q^B)$_2$TiCl$_2$ (19): Compound **19** was obtained from the reaction between $TiCl_4$·$(THF)_2$ and NaQ^B [56] in anhydrous MeOH. A yellow precipitate formed that was filtered off, washed with MeOH, and shown to be compound **19**. F.W. = 673.39, yield 0.470 g (70%); M.W. ($CHCl_3$) = 650 ($1.0\cdot10^{-2}$ M) (r = 0.96), yellow-orange, m.p. 165−166 °C. $C_{34}H_{26}Cl_2N_4O_4Ti$: calcd. C 60.64, H 3.89, N 8.32; found C 60.83, H 4.0, N 8.07. ^{1}H NMR ($CDCl_3$, 200 MHz, 293 K, ppm): δ = 1.0−2.2 (m, 6 H, 3-CH_3), 7.0−8.0 (m, 20 H, C_6H_5). ^{1}H NMR ($CDCl_3$, 300 MHz, 293 K, ppm): δ = 1.1−2.1 (14 m, 6 H, 3-CH_3), 6.9−7.4 (br m, 6 H, C_6H_5), 7.5 (3 t, 2 H, C_6H_5), 7.8 (t, 1 H, C_6H_5), 8.0 (m, 1 H, C_6H_5). ^{1}H NMR ($CDCl_3$, 300 MHz, 327 K, ppm): δ = 1.5−2.0 (br m, 6 H, 3-CH_3), 6.9−7.6 (br m, 8 H, C_6H_5), 8.0 (br, 2 H, C_6H_5). ^{1}H NMR (C_6D_6, 300 MHz, 283 K, ppm): δ = 1.5−2.0 (7 s, 6 H, 3-CH_3), 6.6−7.4 (br m, 6 H, C_6H_5), 8.0 d, 8.1 d, 8.4 t, 8.5 d, 8.6 d (4 H, C_6H_5). ^{1}H NMR (C_6D_6, 300 MHz, 303 K, ppm): δ = 1.5−2.0 (4 s, 6 H, 3-CH_3), 6.6−7.3 (br m, 6 H, C_6H_5), 8.0 br, 8.1 br, 8.4 br, 8.5 br, 8.6 br (4 H, C_6H_5). ^{1}H NMR (C_6D_6, 300 MHz, 328 K, ppm): δ = 1.6−1.9 (br, 6 H, 3-CH_3), 6.6−7.4 (br, 6 H, C_6H_5), 8.0 br, 8.3 br, 8.4 br (4 H, C_6H_5). ^{1}H NMR (C_6D_6, 300 MHz, 347 K, ppm): δ = 1.73 (s, 6 H, 3-CH_3), 6.9 (br, 6 H, C_6H_5), 7.2 (br, 2 H, C_6H_5), 8.2 (br, 2 H, C_6H_5). ^{13}C NMR (C_6D_6, 300 MHz, 293 K, ppm): δ = 15.91, 16.0, 16.3 (3 s, CH_3), 120.0, 121.0, 121.3, 121.4, 122.0, 122.1, 125.9, 126.7, 127.2, 127.7, 128.0, 128.1, 128.3, 128.7, 128.8, 128.9, 129.1, 129.5, 130.1, 131.0, 131.3, 131.9, 132.1, 132.6 (C_{arom}). IR (Nujol mull, cm^{-1}): $\tilde{\nu}$ = 3060 sh (CH), 1599 s br, 1584 s, 1574 s, 1561 s, 1553 s, 1552 s, 1518 s (C···O, C···C, and C···N), 567 br, 552 s, 517 s, 497 s, 462 m, 455 s, 376 m, 357 m, 321 w. ESI-MS (MeCN) (+): *m*/*z* (%) = 323 (10) $[Na_2(Q^B)]^+$, 623 (20) $[Na_3(Q^B)_2]^+$, 923 (10) $[Na_4(Q^B)_3]^+$, 1223 (10) $[Na_4(Q^B)_3]^+$, 1856 (30) $[Ti_3(Q^B)_6O_3H]^+$, 1878 (100) $[NaTi_3(Q^B)_6O_3]^+$, 1894 (45) $[KTi_3(Q^B)_6O_3]^+$, 2497 (40) $[NaTi_4(Q^B)_8O_4]^+$, 2514 (25) $[KTi_4(Q^B)_8O_4]^+$.

(Q^T)$_2$TiCl$_2$ (20): Compound **20** was obtained as described for **19**, using NaQ^T [57] to give the orange product in 55% yield (0.363 g). F.W. = 661.46, m.p. 189−192 °C. $C_{32}H_{38}Cl_2N_4O_4Ti$: calcd. C 58.11, H 5.79, N 8.47; found C 58.09, H 6.0, N 8.24. ^{1}H NMR ($CDCl_3$, 200 MHz, 293 K, ppm): δ = 0.7−1.3 (m, 18 H, CH_3), 1.7 (m, 4 H, CH_2), 2.5 (m, 6 H, 3-CH3), 6.4−8.2 (m, 10 H, C_6H_5). ^{1}H NMR ($CDCl_3$, 300 MHz, 218 K, ppm): δ = 0.2−1.2 (br m, 18 H,

 © 2003 Wiley-VCH Verlag GmbH & Co. KGaA, Weinheim

CH_3), 1.3−1.8 (br m, 4 H, CH_2), 2.0−2.8 (br m, 6 H, 3-CH_3), 6.6−8.4 (m, 10 H, C_6H_5). ^{1}H NMR ($CDCl_3$, 300 MHz, 273 K, ppm): δ = 0.4−1.2 (21s, 18 H, CH_3), 1.4−2.0 (20s, 4 H, CH_2), 2.0−2.7 (18s, 6 H, 3-CH_3), 6.4−8.2 (m, 10 H, C_6H_5). ^{1}H NMR ($CDCl_3$, 300 MHz, 323 K, ppm): δ = 0.4−1.1 (15 s, 18 H, CH_3), 1.6 (br, 4 H, CH_2), 2.0−2.7 (10 s, 6 H, 3-CH_3), 6.6−8.1 (5 m br, 10 H, C_6H_5). IR (Nujol mull, cm^{-1}): $\tilde{\nu}$ = 1604 s br, 1569 s, 1525 s (C···O, C···C, and C···N), 507 s, 473 s, 455 s, 412 br, 377 s br, 361 m, 331 m, 287 m. ESI-MS (MeCN) (+): *m/z* (%) = 295 10) $[Na(HQ^T)]^+$, 629 (60) $[Na_2K(Q^T)_2]^+$, 1211 (50) $[Na_2K_2H(Q^T)_4]^+$, 1235 (45) $[Ti_2(Q^T)_4O_2H]^+$, 1257 (10) $[Ti_2(Q^T)_4O_2Na]^+$, 1274 (10) $[Ti_2(Q^T)_4O_2Na]^+$, 1820 (30) $[Ti_3(Q^T)_6O_3H]^+$, 1842 (100) $[Ti_3(Q^T)_6O_3Na]^+$, 1858 (15) $[Ti_3(Q^T)_6O_3K]^+$.

Theoretical Calculations: The structural features of Q_2TiX_2 compounds were analyzed as follows. Starting coordinates were obtained from the X-ray molecular structure of the tetranuclear compound[19] $[(Q^B)_2Ti\text{-}\mu\text{-}O]_4$; three $(Q^B)_2TiO$ units were eliminated and the two former O(oxo) atoms were converted into two OH groups by adding two H atoms. Calculations on this mononuclear molecule, $(Q^B)_2Ti(OH)_2$, were preformed with the Mulliken program[60] package using an IBM/SP2 supercomputer. The MB3LYPDFT (Density Functional Theory)[61] method was used and the basis set was 6-31G*. For the titanium atom an ECP approximation[62−70] was applied, as implemented within MULLIKEN, using a double zeta basis. The starting structure was very far from that of the energy minimum reached because of the strain in the original tetranuclear molecule,[19] where *trans* O−Ti−O bond angles were as low as 163°, *cis* O(oxo)−Ti−O(oxo) bond angles were about 100° and Ti−O(oxo)−Ti bond angles were as wide as 154° − very far from the regular angle subtended at an oxygen atom. Consequently, the minimization process took about 45 d. After convergence, the H atoms in the two OH groups were replaced by methyl groups, and the two Ph groups (R^4) were replaced by neopentyl groups. This conformer, *cis*-$[(Q^T)_2Ti(OCH_3)_2]$, named CIS1, was minimized with the Accelrys program Cerius 2.4.6, subroutine DMol3,[71] using an Octane SGI computer. Standard local density was the VWN[72] functional and full geometric optimization was performed using a double numeric basis set with polarization functions (DNP)[73] on all atoms. The two other feasible *cis* isomers were analyzed after modifying the Q^T positions accordingly, and energy-minimized; these two conformers are named CIS2 and CIS3. The structure of $(Q^B)_2Ti(OH)_2$, converged with MULLIKEN, was also minimized with DMol3 and gave the same structural parameters in the coordination sphere. A related process was performed to study (a) $(Q^T)_2TiCl_2$ conformers, i.e., replacement of methoxy groups by Cl atoms in $(Q^T)_2Ti(OCH_3)_2$; (b) $(Q^B)_2Ti(OCH_3)_2$ replacing neopentyl groups by Ph groups in $(Q^T)_2Ti(OCH_3)_2$; (c) the anion $[(Q^T)_2Ti(OCH_2CH_2CH_3)_2]^-$, whose coordinates were obtained from $(Q^T)_2Ti(OCH_3)_2$ by replacing a H with a CH_2CH_3 group in each methoxy group.

Voltammetry: Electrochemical measurements were performed in a conventional three-compartment cell with three electrodes. The working electrode was vitreous carbon, the counter electrode was a platinum wire, and the reference electrode was saturated calomel. Ferrocene was used as an internal reference potential. The complex concentration was $1\cdot10^{-3}$ M, the solvent was *N*,*N*-dimethylformamide (Merck), used without further purification, and the support electrolyte was $1\cdot10^{-1}$ M tetraethylammonium perchlorate. The cyclic voltammograms were recorded with a PAR173 potentiostate/galvanostate coupled to a PAR175 universal potential programmer and a Graphtec WX4301 XY recorder.

Acknowledgments

Cristian Opazo at Vassar College SCIVIS laboratory is acknowledged for assistance with the computational aspect of this work, as is financial support by Consiglio Nazionale delle Ricerche C.N.R. − Rome, Università di Camerino, CARIMA, and Vassar College Research Committee. This research was also supported by an IBM Shared University Research (SUR) grant, a CUNY Research award, a CUNY Collaborative award, and a NASA JOVE grant.

[1] F. Schmidt, *Angew. Chem.* **1952**, *64*, 536−538.
[2] A. Yamamoto, S. Kambara, *J. Am. Chem. Soc.* **1957**, *79*, 4344−4348.
[3] B. K Keppler, C. Friesen, H. Vongerichten, E. Vogel, in: *Metal Complexes in Cancer Chemotherapy* (Ed.: B. K. Keppler), VCH, Weinheim, Germany, **1993**, p. 297.
[4] D. C. Bradley, C. E. Holloway, *J. Chem. Soc., A* **1969**, 282−285.
[5] G. D. Smith, C. N. Caughlan, J. A. Campbell, *Inorg. Chem.* **1972**, *11*, 2989−2993.
[6] S. A. Giddings, *Inorg. Chem.* **1964**, *3*, 684−687.
[7] P. Corradini, G. Allegra, *J. Am. Chem. Soc.* **1959**, *81*, 5510−5511.
[8] U. Thewalt, D. Schomburg, *J. Organomet. Chem.* **1977**, *127*, 169−174.
[9] G. Chu, *J. Biol. Chem.* **1994**, *269*, 787−790.
[10] P. M. Takahara, C. A. Frederick, S. J. Lippard, *J. Am. Chem. Soc.* **1996**, *118*, 12309−12321.
[11] B. Rosemberg, L. Van Camp, *Nature* **1969**, *222*, 385−386.
[12] P. Pil, S. Lippard, in: *Encyclopedia of Cance*r (Ed.: J. R. Bertino), Academic Press, San Diego, CA, USA, **1997**, p. 392.
[13] P. Köpf-Maier, *Eur. J. Clin. Pharmacol.* **1994**, *47*, 1−16.
[14] T. Pieper, K. Borsky, B. K. Keppler, in: *Topics in Biological Inorganic Chemistry* (Ed.: M. J. Clarke, P. J. Sadler), Springer, Berlin, Germany, **1999**, p. 172.
[15] E. Kratz, M. T. Schütte, *Cancer J.* **1998**, *11*, 176−182.
[16] BYK Gulden Lonberg, Patent WO8403042, **1984**.
[17] T. Schilling, B. K. Keppler, M. E. Heim, G. Niebch, H. Dietzfelbinger, J. Rastetter, A. R. Hanauske, *Invest. New Drugs* **1996**, *13*, 327−332.
[18] P. Comba, H. Jakob, B. Nuber, B. K. Keppler, *Inorg. Chem.* **1994**, *33*, 3396−3400.
[19] F. Caruso, M. Rossi, J. Tanski, R. Sartori, R. Sariego, S. Moya, S. Diez, E. Navarrete, A. Cingolani, F. Marchetti, C. Pettinari, *J. Med. Chem.* **2000**, *43*, 3665−3670.
[20] P. Kopf-Maier, *J. Struct. Biol.* **1990**, *105*, 35−45.
[21] C. V. Christodoulou, D. R. Ferry, D. W. Fyfe, A. Young, J. Doran, T. M. T. Sheehan, A. Eliopoulos, K. Hale, J. Baumgart, G. Sass, D. J. Kerr, *J. Clin. Oncol.* **1998**, *16*, 2761−2769.
[22] F. Caruso, M. Rossi, C. Pettinari, *Expert Opin. Ther. Patents* **2001**, *11*, 969−979.
[23] F. Caruso, M. Rossi, *J. Inorg. Biochem.* **2001**, *86*, 170−170.
[24] F. Caruso, M. Boel-Schoemakers, A. Penninks, *J. Med. Chem.* **1993**, *36*, 1168−1174.
[25] H. Sun, L. Hongzhe, R. Weir, P. J. Sadler, *Angew. Chem. Int. Ed.* **1998**, *37*, 1577−1579.
[26] L. R. Kelland, B. A. Murrer, G. Abel, C. M. Giandomenico, P. Mistry, K. R. Harrap, *Cancer Res.* **1992**, *52*, 822−828.
[27] C. E. C. A. Hop, R. Bakhtiar, *J. Chem. Ed.* **1996**, *73*, A162−A169.
[28] R. Colton, A. D'Agostino, J. C. Traeger, *Mass. Spectrom. Rev.* **1995**, *14*, 79−106.
[29] M. Fujita, F. Ibukuro, H. Hagihara, K. Ogura, *Nature* **1994**, *367*, 720−723.
[30] L. S. Bonnington, R. K. Coll, E. J. Gray, J. I. Flett, W. Henderson, *Inorg. Chim. Acta* **1999**, *290*, 213−221.
[31] M. Bonchio, G. Licini, G. Modena, O. Bortolini, S. Moro, W. A. Nugent, *J. Am. Chem. Soc.* **1999**, *121*, 6258−6268.
[32] S. Doeuff, Y. Dromzee, F. Taulelle, C. Sanchez, *Inorg. Chem.* **1989**, *28*, 4439−4445 and references therein.

 © 2003 Wiley-VCH Verlag GmbH & Co. KGaA, Weinheim

[33] R. J. Errington, J. Ridland, W. Clegg, R. A. Coxall, J. M Sherwood, *Polyhedron* **1998**, *17*, 659−674.
[34] C. Pettinari, G. Rafaiani, G. Gioia Lobbia, A. Lorenzotti, F. Bonati, B. Bovio, *J. Organomet. Chem.* **1991**, *405*, 75−92.
[35] C. Pettinari, F. Marchetti, D. Leonesi, M. Rossi, F. Caruso, *J. Organomet. Chem.* **1994**, *483*, 123−137.
[36] F. Caruso, D. Leonesi, F. Marchetti, E. Rivarola, M. Rossi, V. Tomov, C. Pettinari, *J. Organomet. Chem.* **1996**, *519*, 29−44.
[37] C. Pettinari, F. Marchetti, A. Gregori, A. Cingolani, J. Tanski, M. Rossi, F. Caruso, *Inorg. Chim. Acta* **1997**, *257*, 37−48.
[38] C. Pettinari, F. Marchetti, A. Cingolani, A. Lorenzotti, E. Mundorff, M. Rossi, F. Caruso, *Inorg. Chim. Acta* **1997**, *262*, 33−46.
[39] C. Pettinari, F. Marchetti, A. Cingolani, D. Leonesi, E. Mundorff, M. Rossi, F. Caruso, *J. Organomet. Chem.* **1998**, *557*, 187−205.
[40] F. Caruso, M. Rossi, F. Marchetti, C. Pettinari, *Organometallics* **1999**, *18*, 2398−2400.
[41] C. Pettinari, F. Marchetti, A. Cingolani, A. Gindulyte, L. Massa, M. Rossi, F. Caruso, *Eur. J. Inorg. Chem.* **2002**, 2171−2180.
[42] J. C. Huffman, J. G. Stone, W. G. Krusell, K. G. Caulton, *J. Am. Chem. Soc.* **1976**, *98*, 6733−6735.
[43] D. W. Hart, T. F. Blackburn, J. Schwartz, *J. Am. Chem. Soc.* **1975**, *97*, 679−680 and references therein.
[44] J. M. Slocik, K. V. Somayajula, R. E. Sheperd, *Inorg. Chim. Acta* **2001**, *320*, 148−158.
[45] C. Pettinari, F. Marchetti, A. Cingolani, G. Bianchini, A. Drozdov, V. Vertlib, S. Troyanov, *J. Organomet. Chem.* **2002**, *651*, 5−14.
[46] W. Henderson, G. M. Olsen, *Polyhedron* **1998**, *17*, 577−588.
[47] C. Decker, W. Henderson, B. K. Nicholson, *J. Chem. Soc., Dalton Trans.* **1999**, 3507−3513.
[48] C. F. James, R. C. Dutky, H. M. Fales, *J. Am. Soc., Mass Spectrom.* **1995**, *6*, 1226−1231.
[49] L. Pauling, *The Nature of the Chemical Bond*, 3rd ed., Cornell University Press, Ithaca, NY, **1960**, p. 260.
[50] S. I. Troyanov, O. Y. Gorbenko, *Polyhedron* **1997**, *16*, 777−780.
[51] S. J. Berners-Price, C. K. Mirabelli, R. K. Johnson, M. R. Mattern, F. L. McCabe, L. F. Faucette, C.-M. Sung, S.-M. Mong, P. J. Sadler, S. T. Crooke, *Cancer Res.* **1986**, *46*, 5486−5493.
[52] M. Coronnello, G. Marcon, S. Carotti, B. Caciagli, E. Mini, T. Mazzei, P. Orioli, L. Messori, *Oncol. Res.* **2001**, *12*, 361−371 and references therein.
[53] Y. Sugiura, T. Takita, H. Umesawa, in: *Metal Ions in Biological Systems* (Ed.: H. Sigel), Marcel Dekker, New York, **1986**, vol. 19, p. 81.
[54] A. M. Bond, R. Colton, U. Englert, H. Huegel, F. Marken, *Inorg. Chim. Acta* **1995**, *235*, 117−126.
[55] M. W. Senko, National High Magnetic Field Laboratory.
[56] B. S. Jensen, *Acta Chem. Scand.* **1959**, *13*, 1890−1896.
[57] F. Marchetti, C. Pettinari, A. Cingolani, D. Leonesi, A. Drozdov, S. I. Troyanov, *J. Chem. Soc., Dalton Trans.* **1998**, 3325−3333.
[58] F. Marchetti, C. Pettinari, A. Cingolani, D. Leonesi, *Synth. React. Inorg. Met.-org. Chem.* **1993**, *23*, 1485−1505.
[59] F. Marchetti, C. Pettinari, R. Pettinari, A. Cingolani, M. Camalli, R. Spagna, *Inorg. Chim. Acta* **2000**, *299*, 65−79.
[60] *MULLIKEN* is IBM proprietary software.
[61] P. J. Stephens, F. J. Devlin, C. F. Chabalowski, M. J. Frisch, *J. Phys. Chem.* **1994**, *98*, 11623−11627. MB3LYP is very similar to B3LYP defined in this paper, except that it uses the local correlation functional of Perdew and Wang (J. P. Perdew, Y. Wang, *Phys Rev. B* **1992**, *45*, 13244−13249) instead of the Vosko, Wilk, and Nusair functional (ref.[68]).
[62] A. D. Becke, *J. Chem. Phys.* **1993**, *98*, 5648−5652.
[63] W. Stevens, H. Basch, M. Krauss, *J. Chem. Phys.* **1984**, *81*, 6026−6033.
[64] W. Stevens, P. G. Jasien, M. Krauss, H. Basch, *Can. J. Chem.* **1992**, *70*, 612−630.
[65] T. R. Cundari, W. J. Stevens, *J. Chem. Phys.* **1993**, *98*, 5555−5565.
[66] L. F. Pacios, P. A. Christiansen, *J. Chem. Phys.* **1985**, *82*, 2664−2671.
[67] M. M. Hurley, L. F. Pacios, P. A. Christiansen, R. B. Ross, W. C. Ermler, *J. Chem. Phys.* **1986**, *84*, 6840−6853.
[68] L. A. LaJohn, P. A. Christiansen, R. B. Ross, T. Atashroo, W. C. Ermler, *J. Chem. Phys.* **1987**, *87*, 2812−2824.
[69] R. B. Ross, J. M. Powers, T. Atashroo, W. C. Ermler, L. A. LaJohn, P. A. Christiansen, *J. Chem. Phys.* **1990**, *93*, 6654−6670.
[70] W. C. Ermler, R. B. Ross, P. A. Christiansen, *Int. J. Quantum Chem.* **1991**, *40*, 829−846.
[71] B. Delley, *J. Chem. Phys.* **1990**, *92*, 508−517.
[72] S. H. Vosko, L. Wilk, M. Nusair, *Can. J. Phys.* **1980**, *58*, 1200−1200.
[73] B. Delley, *J. Phys. Chem.* **1996**, *100*, 6107−6110.

Received March 11, 2003

 © 2003 Wiley-VCH Verlag GmbH & Co. KGaA, Weinheim

Synthesis, Structure and Reactivity of New Late Transition Metal Complexes Bearing Diphosphane Ligands Derived from Bis(pyrazol-1-yl)methane

Antonio Otero,*[a] Fernando Carrillo-Hermosilla,*[a] Pilar Terreros,[b] Teresa Expósito,[a] Sergio Rojas,[b] Juan Fernández-Baeza,[a] Antonio Antiñolo,[a] and Isabel López-Solera[a]

Keywords: Nitrogen heterocycles / Phosphanes / Palladium / Platinum / Rhodium / Iridium / Hydrogenation

Modification of the multistep synthesis of the previously described bis[5-(diphenylphosphanyl)pyrazol-1-yl)]methane (bppzm, **1**) produces the novel diphosphane (diphenylphosphanyl)-[5-(diphenylphosphanyl)pyrazol-1-yl](pyrazol-1-yl)-methane (p4m, **2**). Treatment of this ligand with $[MCl_2(PhCN)_2]$ (M = Pd, Pt) or $[M(COD)(THF)_2]BF_4$ (M = Rh, Ir) produces $[MCl_2(p4m)]$ (M = Pd **3**, Pt **4**) or $[M(COD)(p4m)]BF_4$ (M = Rh **5**, Ir **6**) complexes, which chelate in a *P*,*P*-bidentate fashion. Sulfidation of bppzm and p4m produces the disulfidophosphanes $bppzmS_2$ (**7**) and $p4mS_2$ (**8**). Treatment of **7** and **8** with $[PdCl_2(PhCN)_2]$ produces $[PdCl_2(bppzmS_2)]$ (**9**) and $[PdCl_2(pmS_2)]$ (**10**), respectively, in which ligands **7** and **8** act in an *N*,*N*-bidentate chelate fashion. In contrast, ligand **8** reacts with $[Rh(COD)(THF)_2]BF_4$ to produce $[Rh(COD)(p4mS_2)]BF_4$, where ligand **7** acts in a dynamic *S*,*S*-chelate fashion. The activity of some of these complexes in the catalytic hydrogenation of olefins is reported and the single-crystal X-ray structures of **4**, **8**, and **9** have been obtained.
(© Wiley-VCH Verlag GmbH & Co. KGaA, 69451 Weinheim, Germany, 2003)

Introduction

The synthesis of polydentate phosphanes is a continuously developing field because these ligands are expected to allow greater control over the coordination sphere of a metal.[1] Increasing interest in the use of polyfunctional ligands has focused the attention of researchers on phosphanes with groups bearing nitrogen donors. Phosphorus-nitrogen hemilabile ligands are particularly useful in catalytic processes because one part of the ligand is capable of partially dissociating from the chelate form, thus allowing a substrate to coordinate to the metal centre and undergo some transformation.[2] With these precedents in mind, we have previously prepared and characterized[3] several poly(pyrazol-1-yl)methane derivatives bearing phosphane groups on the pyrazole rings, for example bis[5-(diphenylphosphanyl)-pyrazol-1-yl]methane (bppzm) (**1**). The coordinative capacity of the bppzm ligand was investigated with the metal centres niobium, palladium and platinum. In the first case, *N*,*N*-six-membered metallacyclic species were isolated. However, square-planar species with a *P*,*P*-eight-membered metallacycle were found for the late metals (see Figure 1), confirming the hard-hard, soft-soft acid-base principle.

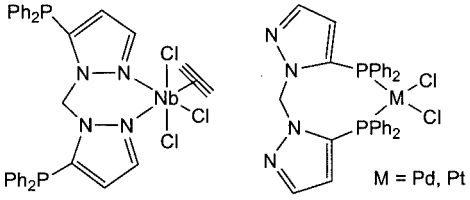

Figure 1. Complexes with the bppzm ligand

Research into the related phosphane sulfide ligands has been much less extensive.[4] Several complexes of late transition metals, namely platinum group metals, have been described with a variety of tertiary phosphane sulfides. The X-ray data suggest that $R_3P{=}S$ groups bind to the metal as simple σ-donors through the *p*-electrons of the sulfur atom, with no evidence of π-bonding between the metal *d* electrons and the empty orbitals of sulfur. This situation gives rise to weaker metal-ligand bonding than with the related phosphane ligands.

In order to extend these studies we sought to develop new functionalised bis(pyrazol-1-yl)methanes and to prepare and characterise new metal complexes formed by these ligands. Furthermore, we present here a modification of the synthesis of **1** to obtain a new chiral diphosphane. The influence of sulfidation of this new diphosphane and the previously described bppzm ligand on their coordination behaviour was also studied. One of the resulting complexes

[a] Departamento de Química Inorgánica, Orgánica y Bioquímica, Facultad de Ciencias Químicas, Universidad de Castilla-La Mancha, Campus Universitario de Ciudad Real, 13071-Ciudad Real, Spain
Fax: (internat.) +34-926/295-318
E-mail: Antonio.Otero@uclm.es
Fernando.Carrillo@uclm.es
[b] Instituto de Catálisis y Petroleoquímica, CSIC, Cantoblanco, 28049, Madrid, Spain

was found to be active in the hydrogenation of simple olefins.

Results and Discussion

We have previously described the synthesis of bis[5-(diphenylphosphanyl)pyrazol-1-yl)]methane (**1**),[3] which was prepared by reaction of bis(pyrazol-1-yl)methane (bpzm) and *n*BuLi at low temperature, followed by the addition of PPh_2Cl and warming. In many cases a minor by-product was observed in these reactions, although this was easily removed by crystallization from CH_2Cl_2/Et_2O.

The minor product has now been isolated and identified as a new asymmetric diphosphane. In an attempt to improve the yield of this new and interesting compound, the previously described synthetic procedure was modified by the addition of a slight excess of first *n*BuLi and then PPh_2Cl at room temperature, followed by recrystallization of the product from CH_2Cl_2 (Scheme 1). Similar behaviour[5] was also observed upon the modification of bis(pyrazol-1-yl)methane with MeI or $PhCH_2Br$.

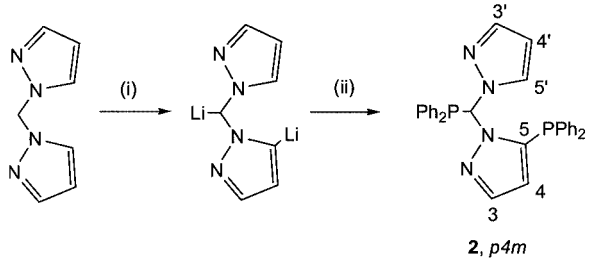

Scheme 1. (i) 2.5 *n*BuLi, THF, room temp., 30 min; (ii) 2 PPh_2Cl, THF, room temp., 16 h

This new ligand, (diphenylphosphanyl)-[5-(diphenylphosphanyl)pyrazol-1-yl](pyrazol-1-yl)methane (**2**) (p4m), can be obtained from the reaction mixture with good purity as a light brown solid (see Exp. Sect.). In this procedure compound **1** is formed as the by-product.

The ^1H NMR spectrum of **2** shows two sets of two doublets assigned to H^3 and H^4 of the two pyrazole rings, with the more shielded peak corresponding to H^4. These data indicate that the two rings are not equivalent. The signal due to the bridging CH group appears as a doublet of doublets due to coupling with the two phosphorus atoms. The $J_{H,P}$ coupling constants are similar to those found for analogous compounds described by us.[3] The ^{13}C NMR spectrum confirms the asymmetry around the CH group, which gives rise to a doublet of doublets due to coupling with phosphorus atoms. Finally, the $^{31}P\{^1H\}$ NMR spectrum exhibits two singlets at $\delta = -30.99$ and -60.94 ppm for the inequivalent phosphorus atoms.

Ligand **2** (Scheme 2) is of considerable interest on two counts; firstly due to its chiral nature and secondly because it can provide different coordination modes than compound **1**. In fact, versatile ligand **2** would form six-membered *P*,*P*-, six-membered *N*,*N*- or seven-membered *N*,*P*-chelating complexes. Chiral chelating ligands that, when complexed to a metal such as rhodium, allow homogeneous hydrogenation to proceed in an enantioselective fashion to yield chiral products are of great interest and have been the focus of many reviews.[6] Compound **2** was used in the complexation of some late transition metal fragments, namely $[MCl_2(PhCN)_2]$ (M = Pd, Pt) and $[M(COD)(THF)_2]BF_4$ (M = Rh, Ir; COD = cyclooctadiene), in order to test its coordination capacity as a chelating agent (Scheme 3).

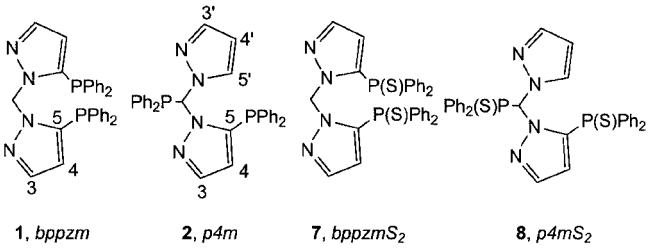

Scheme 2. Ligands **1**, **2**, **7** and **8**

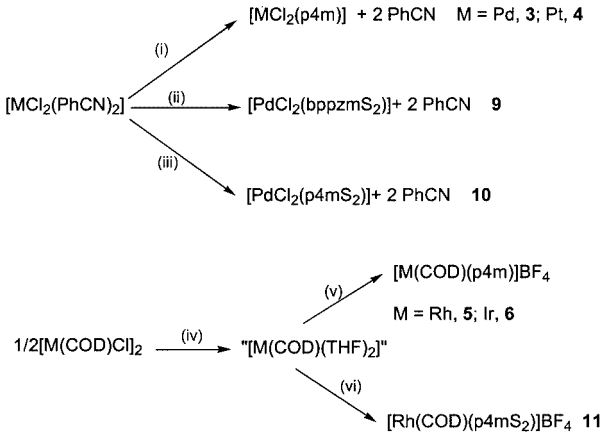

Scheme 3. (i) p4m, CH_2Cl_2, room temp., 5 h; (ii) $bppzmS_2$, CH_2Cl_2, room temp., 16 h; (iii) $p4mS_2$, CH_2Cl_2, room temp., 16 h; (iv) $AgBF_4$, THF, room temp., 30 min; (v) p4m, THF, 203 K to room temp., 3 h; (vi) $p4mS_2$, THF, 203 K to room temp., 3 h

The complexes were isolated as crystalline solids in good yields (see Exp. Sect.). Complexes **3**, **4** and **5** are very stable under an inert atmosphere but complex **6** slowly decomposes in solution.

The ^1H NMR spectra of **3**, **4**, **5** and **6** show two sets of resonances for the H^3 and H^4 protons of the pyrazolyl rings. In addition, the H^5 proton of the unsubstituted ring appears as a broad singlet. The ^{13}C NMR spectra actually exhibit the signal for the methyne carbon atom and this appears as a doublet due to coupling with the neighbouring phosphorus atom. The asymmetry of these molecules is also reflected in the COD region of the spectra. For example, the diene ligand shows two broad peaks for the =CH carbons. The $^{31}P\{^1H\}$ NMR spectra show two broad peaks for complexes **3** and **6** and these are at significantly lower fields than the corresponding peaks for the free ligand **2**, suggest-

 © 2003 Wiley-VCH Verlag GmbH & Co. KGaA, Weinheim

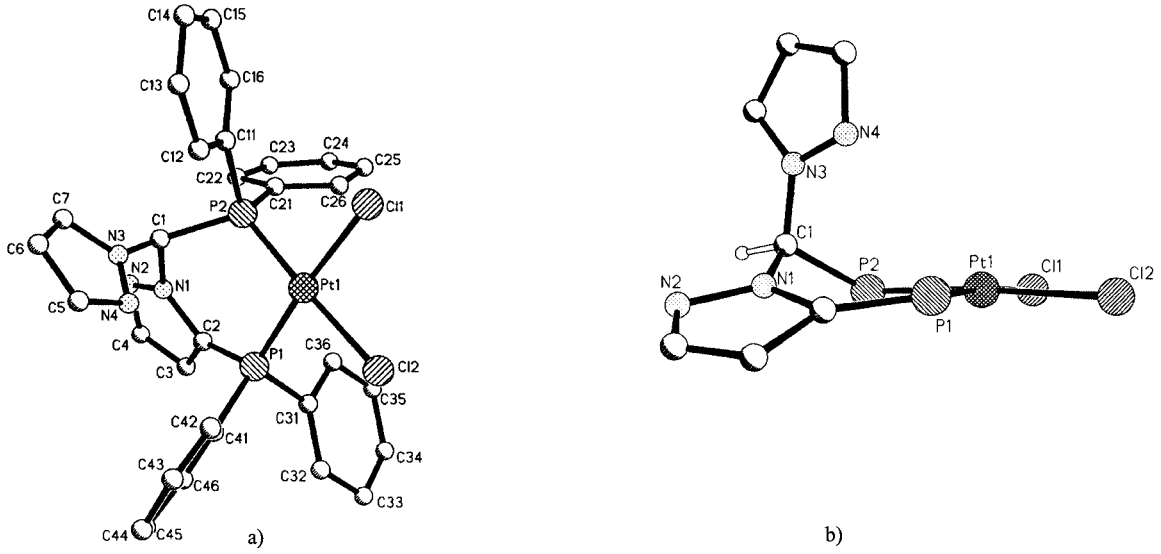

Figure 2. a) Molecular structure and atom-labelling scheme for compound 4; b) conformation of the six-membered chelate ring

ing that in these complexes a coordination of the p4m ligand takes place in a *P,P*-mode. Complex **5** also exhibits lower field signals but, in this case, the peaks appear as two doublets of doublets due to coupling between the two *cis* phosphorus atoms ($^2J_{P,P}$ = 39 Hz), through the metal, and also due to coupling with the rhodium atom ($^1J_{P,Rh}$ = 115 Hz). Complex **4** shows two doublets ($^2J_{P,P}$ = 16 Hz) at lower fields than the corresponding signals in the free ligand and these doublets are flanked by two ^{195}Pt satellites ($^1J_{Pt,P}$ = 1870 and 1791 Hz, respectively).

A crystal structure analysis of complex **4** was carried out in order to confirm the proposed coordination for these complexes. The molecular structure and atomic numbering scheme is shown in Figure 2. Selected bond lengths and angles for **4** are given in Table 1.

Table 1. Selected bond lengths [Å] and angles [deg] for **4**

Pt(1)−Cl(1)	2.34(1)
Pt(1)−Cl(2)	2.37(1)
Pt(1)−P(1)	2.23(1)
Pt(1)−P(2)	2.20(1)
P(1)−C(2)	1.66(4)
P(2)−C(1)	1.83(3)
N(1)−C(1)	1.47(5)
N(1)−C(2)	1.41(5)
Cl(1)−Pt(1)−Cl(2)	89.8(4)
Cl(1)−Pt(1)−P(1)	175.5(4)
Cl(1)−Pt(1)−P(2)	89.7(4)
Cl(2)−Pt(1)−P(1)	86.3(4)
Cl(2)−Pt(1)−P(2)	176.7(4)
P(1)−Pt(1)−P(2)	94.0(4)
Pt(1)−P(2)−C(1)	116(1)
Pt(1)−P(1)−C(2)	115(1)

The structure consists of discrete monomeric molecules separated by van der Waals distances. The platinum centre is bound to four atoms (Figure 2b) — the two phosphorus atoms from the p4m group and the two chlorine atoms — in a quasi-planar coordination. The Cl1, Cl2, P1 and P2 atoms are co-planar and Pt1 is displaced from this plane by −0.057(6) Å. The six-membered chelate ring exists in a half-boat conformation with C1 −0.96(4) Å and N1 −0.36(5) Å out of the plane defined by Pt1, P1, P2 and C2. The Pt−P and Pt−Cl distances are in reasonable agreement with the values published for related structures.[3]

In contrast to the well-known use of diphosphanes as chelating ligands, the coordination chemistry of phosphane sulfide derivatives toward platinum group metals is much less extensively studied.[7]

The sulfide derivatives (**7** and **8**) of compounds **1** and **2** (Scheme 2), respectively, were obtained by reaction with an excess of elemental sulfur (see Exp. Sect.).

In the ^{1}H NMR spectrum of **7** the signals due to the methylene protons are shifted to lower field than the precursor ligand **1**. In a similar way to **1**, compound **7** gives rise to a single set of signals for H^3 and H^4 in the ^{1}H NMR spectrum as well as the corresponding C3, C4 and C5 carbon atoms in the ^{13}C NMR spectrum. This observation confirms the equivalence of the two pyrazole rings. Sulfidation of the phosphorus atoms produces a singlet at δ = 3.22 ppm in the ^{31}P{^{1}H} NMR spectrum, at higher field than those found for the more simple diphosphane sulfides such as $dppmS_2$ (δ = 35.4 ppm),[7d] and shifted to lower field than the value found for the original diphosphane ligand **1**. A similar effect was observed in the ^{31}P{^{1}H} NMR spectrum of **8**, which exhibits two singlets at δ = 25.57 and 3.62 ppm. The ^{1}H NMR signal for the proton on the methyne bridge of compound **8** is also shifted to lower field than for **2**. The ^{1}H and ^{13}C NMR spectra of **8** confirm the non-equivalence of the pyrazole rings, with two sets of signals observed for the proton and carbon atoms of the pyrazole rings. The IR spectra of compounds **7** and **8** show characteristic[7d] broad ν(P=S) bands at 658 cm^{-1} and 633 cm^{-1}, respectively.

 © 2003 Wiley-VCH Verlag GmbH & Co. KGaA, Weinheim

The molecular structure of **8** was confirmed by X-ray crystallography. The molecular structure and atomic numbering scheme are shown in Figure 3. Selected bond lengths and angles for **8** are given in Table 2.

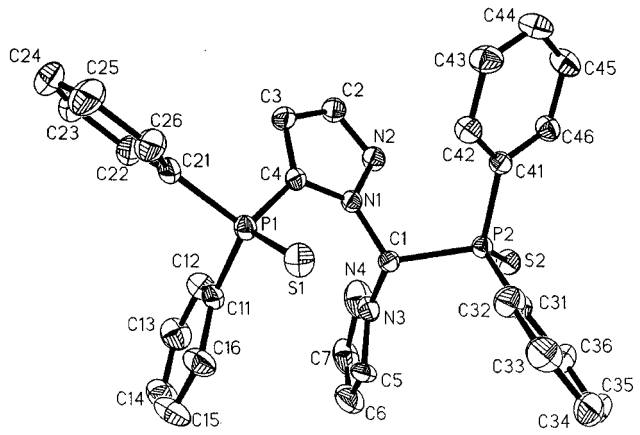

Figure 3. Molecular structure and atom-labelling scheme for compound **8**, with thermal ellipsoids at 30% probability

Table 2. Selected bond lengths [Å] and angles [deg] for **8**

P(1)−S(1)	1.955(1)
P(2)−S(2)	1.939(1)
P(2)−C(1)	1.897(2)
P(1)−C(4)	1.798(2)
N(1)−N(2)	1.354(3)
N(1)−C(1)	1.438(3)
N(1)−C(4)	1.367(3)
N(3)−C(1)	1.438(3)
S(1)−P(1)−C(4)	113.9(1)
S(1)−P(1)−C(11)	113.9(1)
S(1)−P(1)−C(21)	114.6(1)
C(4)−P(1)−C(11)	103.9(1)
C(4)−P(1)−C(21)	103.0(1)
C(11)−P(1)−C(21)	106.3(1)
S(2)−P(2)−C(1)	112.2(1)
S(2)−P(2)−C(31)	113.8(1)
S(2)−P(2)−C(41)	114.2(1)
C(1)−P(2)−C(31)	102.1(1)
C(1)−P(2)−C(41)	106.9(1)
C(31)−P(2)−C(41)	106.6(1)

Each phosphorus atom shows a distorted tetrahedral coordination. The P−S distances of 1.955(1) and 1.939(1) Å indicate a double bond between P and S. The angle between the planes of the pyrazolyl rings is 112.5(1)°.

In order to study the behaviour of these new compounds as ligands in comparison to their phosphorus precursors **1** and **2**, we explored the reactivity of the sulfide derivatives **7** and **8** towards Pd and Rh metal centres. In these cases, we expect the possibility of an *S*,*S*-, *N*,*N*- or *N*,*S*-chelating coordination. Unfortunately, attempts to prepare analogous compounds of Pt or Ir were unsuccessful.

Addition of a stoichiometric amount of **7** to a dichloromethane solution of $[PdCl_2(PhCN)_2]$ led to the formation of complex **9** as a very insoluble solid (Scheme 3). The ^1H NMR spectrum of **9** exhibits two broad singlets for H^3 and H^4, which indicates the equivalence of the two pyrazole rings. A particularly interesting result was found on examining the $^{31}P\{^1H\}$ NMR spectrum of **9**. In this case, a singlet for two equivalent phosphorus atoms appears at δ = 4.80 ppm, which is close to the value of δ = 3.22 ppm found in the free ligand. This result seems to indicate that coordination of the phosphorus atoms to the palladium centre does not take place and hence that the ligand behaves as an *N*,*N*-donor in this complex. The IR spectrum confirms this coordination mode, with a ν(P=S) band at 660 cm^{-1}, similar to the value found in the free ligand. The position of the P=S band in the IR spectrum of previously reported sulfur-coordinated complexes is shifted 20−50 cm^{-1} to lower energy relative to the corresponding band in the uncomplexed ligands.[8]

Similar Pd^{II} complexes incorporating bis(pyrazol-1-yl)methane ligands with *N*,*N*-coordination have been prepared previously[9] with the aim of studying the electronic and steric effects of these ligands on the dynamic structure and reactivity of the corresponding complexes. In some cases, cationic derivatives were used as ethylene polymerization catalysts.

The analogous complex $[PdCl_2(bppzm)]$ shows a dynamic behaviour in solution that involves a boat-to-boat inversion.[3] For this reason, we carried out a variable-temperature NMR study in order to elucidate the possible dynamic behaviour of **9**. In the $^1H\{^{31}P\}$ NMR spectrum, the signal for the CH_2 group appears as a broad singlet at δ = 7.09 ppm at room temperature. At 228 K, however, this peak disappears in the baseline but, unfortunately, a slow exchange limit could not be observed.

The molecular structure of **9** was confirmed by X-ray crystallography. The molecular structure and atomic numbering scheme is shown in Figure 4. Selected bond lengths and angles for **9** are given in Table 3.

The structure consists of discrete monomeric molecules separated by van der Waals distances. There are two molecules per asymmetric unit. The palladium atom is bound to four atoms (Figure 4b) — the two nitrogens from the $bppzmS_2$ group and the two chlorine atoms — in a square-planar coordination. The six-membered chelate ring exists in a boat conformation with C4 and Pd1 out of the plane defined by N1, N2, N3 and N4 [C4: 0.656(7) and −0.638(7) Å for molecules 1 and 2, respectively; Pd1: 0.624(7) and −0.606(7) Å for molecules 1 and 2, respectively]. The Pd−N and Pd−Cl distances are in good agreement with the previously published values.[9] The angle between the planes of the pyrazolyl rings is 47.6(2)° and 47.5(2)° for molecules 1 and 2, respectively. The angles between the N1−N2−N3−N4 and N1−Pd1−N3 planes [154.5(2)° and 155.3(2)° for molecules 1 and 2, respectively] and N1−N2−N3−N4 and N2−C4−N4 planes [128.5(2)° and 129.8(2)° for molecules 1 and 2, respectively] are similar[3] to that in the complex $[PdCl_2(bppzm)]$, in which steric interactions are not appreciable.

It is worth noting that $[PdCl_2(bppzm)]$, which was reported previously by us,[3] shows a *P*,*P*-eight-membered metallacycle in preference to a less-open *N*,*N*-six-membered

 © 2003 Wiley-VCH Verlag GmbH & Co. KGaA, Weinheim

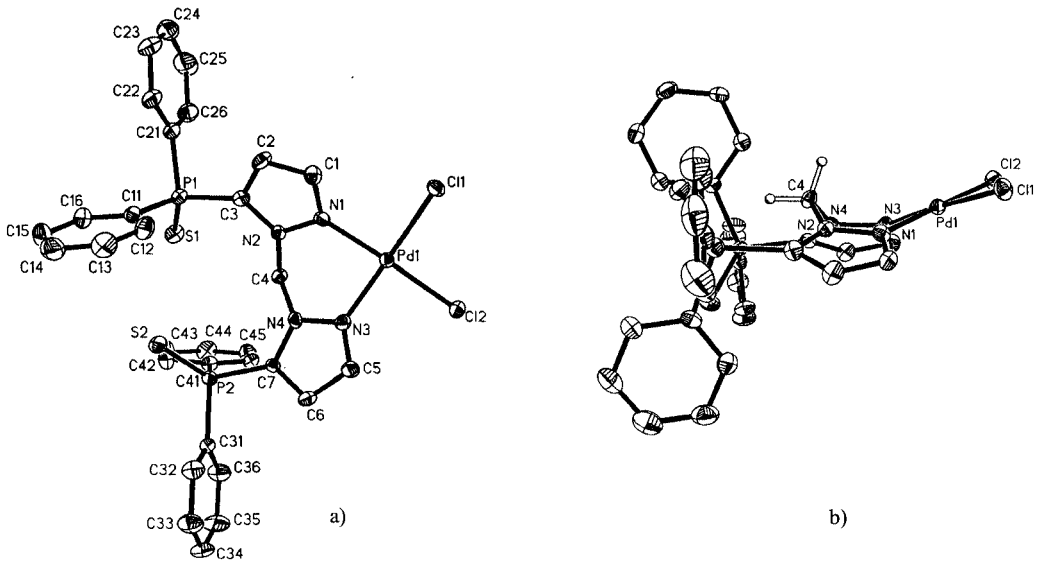

Figure 4. a) Molecular structure and atom-labelling scheme for compound **9** (molecule 1), with thermal ellipsoids at 50% probability; b) conformation of the six-membered chelate ring

Table 3. Selected bond lengths [Å] and angles [deg] for **9**

	Molecule 1	Molecule 2
Pd−Cl(1)	2.283(1)	2.282(1)
Pd−Cl(2)	2.282(1)	2.290(1)
Pd−N(1)	2.024(5)	2.016(5)
Pd−N(3)	2.012(5)	2.027(5)
S(1)−P(1)	1.939(2)	1.934(2)
S(2)−P(2)	1.937(2)	1.941(2)
Cl(1)−Pd−Cl(2)	91.76(5)	91.3(6)
Cl(1)−Pd−N(1)	90.6(1)	89.8(1)
Cl(1)−Pd−N(3)	176.7(1)	177.7(1)
Cl(2)−Pd−N(1)	177.5(1)	176.4(1)
Cl(2)−Pd−N(3)	89.4(1)	90.4(1)
N(1)−Pd−N(3)	88.2(2)	88.4(2)
S(1)−P(1)−C(3)	115.7(2)	111.9(2)
S(2)−P(2)−C(7)	112.0(2)	115.2(2)

system. This behaviour can be explained if one considers the stable soft-soft interactions between Pd^{II} and P atoms. In contrast, in complex **9** a stable *N*,*N*-six-membered chelate is preferred to the soft-soft Pd−S bonds in a ten-membered metallacycle.

The behaviour of sulfur-containing ligand **8** towards $[PdCl_2(PhCN)_2]$ was investigated in order to explore the existence of *N*,*N*-six-membered or *S*,*S*-eight-membered complexation. The reaction of **4** and $[PdCl_2(PhCN)_2]$ was performed in CH_2Cl_2 (see Scheme 3) and afforded $[PdCl_2(p4mS_2)]$ (**10**) as a very insoluble solid.

The ^1H NMR spectrum of **10** shows evidence for the non-equivalence of the pyrazole rings. The signal for the proton of the methyne group appears as a doublet at δ = 9.61 ppm due to coupling with the nearest phosphorus atom. The $^{31}P\{^1H\}$ NMR spectrum of **10** shows two singlets at δ = 26.11 and 5.70 ppm, which are closer to those of the free ligand (δ = 25.57 and 3.62 ppm). The IR spectrum confirms an *N*,*N*-coordination on the basis of the ν(P=S) absorption at 630 cm^{-1} for complex **10** — a value similar to that found in the free ligand.

Finally, reaction of **8** and the solvate moiety $[Rh(COD)(THF)_2]BF_4$ in THF afforded $[Rh(COD)(p4mS_2)]BF_4$ (**11**) as a very insoluble brown solid (see Scheme 3). This complex was prepared in order to study the influence of sulfur on the reactivity of complex **11** in comparison with the analogous complex **5** (see below).

The $^{31}P\{^1H\}$ NMR spectrum of complex **11** contains two peaks near to those of the free ligand **8**. The peak at δ = 20.64 ppm appears as a very broad multiplet, indicating that some interaction with rhodium is present and that the molecule shows a dynamic behaviour in solution. This situation was confirmed by performing a variable temperature $^{31}P\{^1H\}$ NMR study. At low temperature (213 K), the process can be frozen out and the broad peak gives rise to a pseudo-triplet at δ = 18.76 ppm (J = 9 Hz), probably due to coupling with the rhodium and the second phosphorus. On the other hand, a sharp peak at δ = 21.52 ppm was observed at 333 K. A temperature-dependent coordination/decoordination process involving one of the $P(S)Ph_2$ groups was proposed as being responsible for these changes. Additionally, the IR spectrum shows a ν(P=S) absorption at 556 cm^{-1}, which indicates an *S*,*S*-coordination mode.

Hydrogenation of Olefins

Complex **5**, which contains the ligand p4m, is an active hydrogenation catalyst for cyclohexene and 1-heptene (Table 4).

The reactions were conducted under different conditions of pressure, reaction time, solvent, and in the presence/absence of additives. In CH_2Cl_2, a conversion of 26% for cyclohexene was obtained after ca. 20 h. at 10 bar and 353 K. A similar conversion (21%) was obtained in MeOH. In contrast, addition of a small amount of KOH to the

 © 2003 Wiley-VCH Verlag GmbH & Co. KGaA, Weinheim

Table 4. Results of the catalysis experiments; reaction conditions: catalyst 0.03 mmol; substrate 3 mmol; solvent 30 mL; KOH 0.04 mmol

Complex	Substrate	Solvent	Additive	Time(h)	Temp.(K)	Pressure(bar)	Conversion (%)
5	cyclohexene	CH_2Cl_2		20	298	1	7.7
5	cyclohexene	CH_2Cl_2		20	353	10	26
5	cyclohexene	MeOH		20	353	10	21
5	cyclohexene	MeOH	KOH	1	353	10	33
5	1-heptene	MeOH	KOH	1	353	10	50

latter reaction mixture produced the highest conversion observed (33%) in only 1 h. The activity is similar to those found for other rhodium derivatives of multidentate heterocyclic ligands, of the type $[Rh(diene)(OPPy_2R)]BF_4$,[2j] under very analogous conditions. As expected, complex **5** is a better catalyst for the hydrogenation of 1-heptene, giving a conversion of 50% in 1 h. The iridium derivative **6**, probably due to its lack of stability in solution, and the rhodium complex **11**, probably due to the presence of sulfur[10] in the coordination sphere and the low solubility of this complex, did not show any catalytic activity at all, in comparison to the analogous phosphane complex **5.**

These results suggest the possibility of testing the activity and enantioselectivity of chiral complex **5** in the hydrogenation of prochiral substrates. Experiments to obtain pure enantiomers of ligand **2** are currently underway.

Conclusion

The preparation of a new chiral functionalised phosphorus-containing bis(pyrazol-1-yl)methane compound, p4m, has been carried out by modification of a previously described procedure. The coordination modes of this compound were studied towards the metal centres palladium, platinum, rhodium and iridium to produce *P*,*P*-six-membered metallacycles. Sulfidation of the previously described bppzm and the new p4m ligands produces the corresponding sulfidodiphosphanes. The compounds $p4mS_2$ and $bppzmS_2$ coordinate a palladium centre in an *N*,*N*-six-membered metallacycle and reaction of $p4mS_2$ with $[Rh(COD)(THF)_2]^+$ produces an *S*,*S*-dynamic coordination of the ligand.

Finally, complex $[Rh(COD)(p4m)]BF_4$ showed a moderate activity in the catalytic hydrogenation of simple olefins.

Experimental Section

All reactions were carried out using Schlenk-tube techniques under an atmosphere of dry nitrogen. Solvents were distilled from appropriate drying agents and degassed before use. ^1H,^{13}C and ^{31}P NMR spectra were obtained on a 300 Unity Varian spectrometer. Assignment of the signals was achieved by means of DEPT, NOE difference and two-dimensional NMR experiments, acquired using standard Varian-FT software. IR spectra were obtained in the region 500−4000 cm^{-1} using a Nicolet Magna FT-IR 550 spectrophotometer. $[MCl_2(PhCN)_2]$ (M = Pd, Pt) and bis(pyrazol-1-yl)-methane were prepared as reported previously.[11,12] $[RhCl(COD)]_2$ and $[IrCl(COD)]_2$ were purchased from Aldrich and used as received

(5-Diphenylphosphanylpyrazol-1-yl)(diphenylphosphanyl)-(pyrazol-1-yl)methane (p4m) (2): A solution of bpzm (3 g, 20 mmol) in dry THF (150 mL) in a 250 mL Schlenk tube was cooled to 203 K. A 1.6 M solution of *n*BuLi (31.3 mL, 50 mmol) in hexane was added and the solution was allowed to reach room temperature slowly. PPh_2Cl (7.27 mL, 41 mmol) was added and the reaction mixture was stirred for 16 h. The suspension was filtered and the solvent removed under vacuum. The resulting red oil was washed with hexane and the residue extracted with CH_2Cl_2. The solvent was removed and the resulting orange oil was washed with Et_2O. A pale-brown solid was obtained and was recrystallized from CH_2Cl_2. Yield 90%. $C_{31}H_{26}N_4P_2$ (516.5): calcd. C 72.08, H 5.07, N 10.85%; found C 72.20, H 5.09, N 10.49. ^1H NMR (300 MHz, $CDCl_3$, 293 K): δ = 7.87 (d, $^3J_{H,H}$ = 2.5 Hz, 1 H, H3′), 7.81 (dd, $^2J_{H,P}$ = 6.0, $^4J_{H,P}$ = 3.0 Hz, 1 H, CH), 7.58 (d, $^3J_{H,H}$ = 2.0 Hz, 1 H, H3), 7.37−7.05 (m, 20 H, Ph), 7.24 (d, $^3J_{H,H}$ = 2.0 Hz, 1 H, H5′), 6.08 (dd, $^3J_{H,H}$ = 2.0, $^3J_{H,H}$ = 2.5 Hz, 1 H, H4′), 5.87 (d, $^3J_{H,H}$ = 2.0 Hz, 1 H, H4) ppm. $^{13}C\{^1H\}$ NMR (75 MHz, $CDCl_3$, 293 K): δ = 141.05 (d, $^1J_{C,P}$ = 12.0 Hz, C5), 140.83 (d, $^3J_{C,P}$ = 3.5 Hz, C3), 139.53 (d, $^3J_{C,P}$ = 1.5 Hz C5′), 135.20−128.10 (Ph), 128.94 (s, C3′), 114.54 (d, $^2J_{C,P}$ = 2.0 Hz, C4), 107.16 (s, C4′), 73.48 (dd, $^1J_{C,P}$ = 14.0, $^3J_{C,P}$ = 5.0 Hz, CH) ppm. $^{31}P\{^1H\}$ NMR (121 MHz, $CDCl_3$, H_3PO_4 as reference): δ = −30.99 (s, PPh_2), −60.94 (s, PPh_2) ppm.

[$PdCl_2$(p4m)] (3): An equimolar quantity of p4m (0.402 g, 0.78 mmol) was added to a CH_2Cl_2 (50 mL) solution of $[PdCl_2(PhCN)_2]$ (0.300 g, 0.78 mmol). The solution was stirred for 5 h at room temperature. The solvent was removed in vacuo and the resulting pale orange solid was washed with cold CH_2Cl_2 and dried in vacuo. Yield 85%. $C_{31}H_{26}Cl_2N_4P_2Pd$ (693.8): calcd. C 53.66, H 3.78, N 8.07; found C 53.89, H 3.79, N 8.01. ^1H NMR (300 MHz, CD_2Cl_2, 293 K): δ = 7.67 (d, $^2J_{H,P}$ = 3.0 Hz, 1 H, CH), 7.65−7.26 (m, 20 H, Ph), 7.24 (br. s, 1 H, H5′), 7.13 (br. s, 1 H, H3′), 6.98 (br. s, 1 H, H3), 6.17 (br. s, 1 H, H4′), 5.92 (br. s, 1 H, H4) ppm. $^{13}C\{^1H\}$ NMR (75 MHz, CD_2Cl_2, 293 K): δ = 142.21 (s, C3′), 140.08 (d, $^1J_{C,P}$ = 13.1 Hz, C5), 136.00−128.00 (Ph), 130.80 (s, C5′), 129.80 (d, $^3J_{C,P}$ = 11.0 Hz, C3), 118.75 (d, $^2J_{C,P}$ = 7.4 Hz, C4), 107.17 (s, C4′), 68.75 (d, $^1J_{C,P}$ = 48.6 Hz, CH) ppm. $^{31}P\{^1H\}$ NMR (121 MHz, CD_2Cl_2, H_3PO_4 as reference): δ = −18.36 (s, PPh_2), 15.06 (s, PPh_2) ppm.

[$PtCl_2$(p4m)] (4): The synthetic procedure was the same as for complex 2, using $[PtCl_2(PhCN)_2]$ (0.300 g, 0.64 mmol) and p4m (0.330 g, 0.64 mmol), to give complex **4** as a white solid. Yield 90%. Crystals for X-ray diffraction were grown from a cooled saturated solution in CH_2Cl_2. $C_{31}H_{26}Cl_2N_4P_2Pt{\cdot}4CH_2Cl_2$ (1116.1): calcd. C 37.46, H 3.05, N 4.99; found C 37.50, H 3.06, N 5.02. ^1H NMR (300 MHz, CD_2Cl_2, 293 K): δ = 7.82 (d, $^2J_{H,P}$ = 3.0 Hz, 1 H, CH), 7.59−7.26 (m, 20 H, Ph), 7.24 (br. s, 1 H, H5′), 7.06 (br. s, 1 H, H3′), 6.83 (br. s, 1 H, H3), 6.16 (br. s, 1 H, H4′), 5.80 (br. s, 1 H,

 © 2003 Wiley-VCH Verlag GmbH & Co. KGaA, Weinheim

H4) ppm. $^{13}C\{^1H\}$ NMR (75 MHz, CD_2Cl_2, 293 K): δ = 141.02 (s, C3′), 139.50 (d, $^1J_{C,P}$ = 11.1 Hz, C5), 136.00−128.00 (Ph), 130.71 (s, C5′), 129.65 (d, $^3J_{C,P}$ = 11.0 Hz, C3), 118.48 (d, $^2J_{C,P}$ = 8.0 Hz, C4), 106.71 (s, C4′), 67.28 (d, $^1J_{C,P}$ = 54.3 Hz, CH) ppm. $^{31}P\{^1H\}$ NMR (121 MHz, CD_2Cl_2, H_3PO_4 as reference): δ = −34.94 (t of d, $^1J_{P,Pt}$ = 1797, $^2J_{P,P}$ = 16.0 Hz, PPh_2), −3.03 (t of d, $^1J_{P,Pt}$ = 1870, $^2J_{P,P}$ = 16.0 Hz, PPh_2) ppm.

[Rh(COD)(p4m)]BF_4 (5): An equimolar quantity of $AgBF_4$ (0.078 g, 0.40 mmol) was added to a THF (10 mL) solution of $[Rh(COD)Cl]_2$ (0.100 g, 0.20 mmol). The solution was stirred for 30 min at room temperature. The precipitated AgCl was filtered off and the filtrate was cooled to 203 K. A cooled solution of p4m (0.103 g, 0.40 mmol) in THF (10 mL) was then added slowly. The reaction was allowed to reach room temperature slowly over 3 h. The solvent was removed in vacuo and the resulting yellow solid was extracted with THF. Concentration of the solution afforded complex 5 as a bright yellow microcrystalline solid. Yield 75%. $C_{39}H_{38}BF_4N_4P_2Rh$ (814.4): calcd. C 57.51, H 4.67, N 6.88; found C 57.60, H 4.80, N 6.76. ^1H NMR (300 MHz, $CDCl_3$, 293 K): δ = 8.25 (d, $^3J_{H,H}$ = 2.0 Hz, 1 H, H5′), 8.11 (d, $^3J_{H,H}$ = 2.0 Hz, 1 H, H3′), 7.62−7.20 (m, 20 H, Ph), 7.59 (d, $^2J_{H,P}$ = 3.0 Hz, 1 H, CH), 7.43 (br. s, 1 H, H3), 6.82 (dd, $^3J_{H,H}$ = 2.0, $^3J_{H,H}$ = 2.0 Hz, 1 H, H4′), 5.99 (br. s, 1 H, H4), 4.17, 3.89 (m, 2 H, 2 H, CH, COD), 2.02, 2.33, 2.59, 2.99 (m, 2 H, 2 H, 2 H, 2 H, CH_2, COD) ppm. $^{13}C\{^1H\}$ NMR (75 MHz, $CDCl_3$, 293 K): δ = 144.08 (s, C3′), 140.63 (d, $^3J_{C,P}$ = 10.0 Hz, C3), 138.00−128.00 (Ph), 133.53 (d, $^3J_{C,P}$ = 2.0 Hz, C5′), 132.11 (d, $^1J_{C,P}$ = 15.0 Hz, C5), 116.94 (d, $^2J_{C,P}$ = 6.0 Hz, C4), 112.03 (s, C4′), 86.15 (dd, $^2J_{C,P}$ = 13.0, $^1J_{C,Rh}$ = 14.0 Hz, CH, COD), 84.16 (dd, $^2J_{C,P}$ = 10.0, $^1J_{C,Rh}$ = 10.0 Hz, CH, COD), 72.60 (d, $^1J_{C,P}$ = 60.3 Hz, CH), 35.93 (s, CH_2, COD), 28.54 (s, CH_2, COD) ppm. $^{31}P\{^1H\}$ NMR (121 MHz, $CDCl_3$, H_3PO_4 as reference): δ = 27.40 (dd, $^1J_{P,Rh}$ = 115.0, $^2J_{P,P}$ = 39.0 Hz, PPh_2), 21.10 (dd, $^1J_{P,Rh}$ = 115.0, $^2J_{P,P}$ = 39.0 Hz, PPh_2) ppm.

[Ir(COD)(p4m)]BF_4 (6): The synthetic procedure was the same as for complex **5**, using $[Ir(COD)Cl]_2$ (0.100 g, 0.15 mmol) and p4m (0.077 g, 0.30 mmol), to give complex **6** as a pale orange solid. Yield 55%. $C_{39}H_{38}BF_4IrN_4P_2$ (903.7): calcd. C 51.83, H 4.24, N 6.20; found C 51.95, H 4.30, N 6.26. ^1H NMR (300 MHz, $CDCl_3$, 293 K): δ = 8.43 (br. s, 1 H, H5′), 7.70 (d, $^2J_{H,P}$ = 3.0 Hz, 1 H, CH), 7.60−7.20 (m, 20 H, Ph), 7.40 (d, $^2J_{H,P}$ = 2.0 Hz, 1 H, H3), 7.31 (d, $^3J_{H,H}$ = 2.0 Hz, 1 H, H3′), 6.45 (br. s, 1 H, H4′), 6.01 (br. s, 1 H, H4), 3.80, 3.42 (m, 2 H, 2 H, CH, COD), 1.42, 2.45 (m, 4 H, 4 H, CH_2, COD) ppm. $^{13}C\{^1H\}$ NMR (75 MHz, $CDCl_3$, 293 K): δ = 142.43 (C3′), 139.59 (d, $^3J_{C,P}$ = 10.0 Hz, C3), 134.48 (d, $^1J_{C,P}$ = 13.0 Hz, C5), 133.10 (C5′), 128−134 (Ph), 117.00 (d, $^2J_{C,P}$ = 4.0 Hz, C4), 111.83 (C4′), 72.90 (d, $^1J_{C,P}$ = 39.2 Hz, CH), 69.12 (d, $^2J_{C,P}$ = 10.0 Hz, CH, COD), 69.09 (d, $^2J_{C,P}$ = 10.0 Hz, CH, COD), 67.45 (d, $^2J_{C,P}$ = 10.0 Hz, CH, COD), 67.43 (d, $^2J_{C,P}$ = 10.0 Hz, CH, COD), 36.22 (CH_2, COD), 36.18 (CH_2, COD), 30.42 (CH_2, COD) ppm. $^{31}P\{^1H\}$ NMR (121 MHz, $CDCl_3$, H_3PO_4 as reference): δ = −44.26 (br. s, PPh_2), 9.36 (br. s, PPh_2) ppm.

Bis(5-diphenylphosphanylpyrazol-1-yl)methane Disulfide (bppzmS_2) (7): An excess of elemental sulfur S_8 (0.640 g, 2.50 mmol) was added to a CH_2Cl_2 (50 mL) solution of bppzm (1.000 g, 2.00 mmol). The reaction mixture was stirred for 48 h at room temperature. The solvent was removed in vacuo and the resultant solid was washed with CS_2 (100 mL). The residue was washed with Et_2O and recrystallized from CH_2Cl_2/Et_2O to afford compound 7 as a pale brown solid. Yield 95%. $C_{31}H_{26}N_4P_2S_2$ (580.6): calcd. C 64.13, H 4.48, N 9.65; found C 64.17, H 4.55, N 9.75. ^1H NMR (300 MHz, $CDCl_3$, 293 K): δ = 7.76−7.40 (m, 20 H, Ph), 7.28 (d, $^3J_{H,H}$ = 1.5 Hz, H3), 7.06 (br. s, 2 H, CH_2), 5.91 (d, $^3J_{H,H}$ = 1.5 Hz, H4) ppm. $^{13}C\{^1H\}$ NMR (75 MHz, $CDCl_3$, 293 K): δ = 138.60 (d, $^3J_{C,P}$ = 14.0 Hz, C3), 138.72 (d, $^1J_{C,P}$ = 38.0 Hz, C5), 132.15−128.42 (Ph), 116.57 (d, $^2J_{C,P}$ = 15.0 Hz, C4), 63.74 (s, CH_2) ppm. $^{31}P\{^1H\}$ NMR (121 MHz, $CDCl_3$, H_3PO_4 as reference): δ = 3.22 [s, $P(S)Ph_2$] ppm. IR (KBr): $\tilde{\nu}$ = 658 cm^{-1} (s) [ν(P=S)].

(5-Diphenylphosphanylpyrazol-1-yl)(diphenylphosphanyl)-(pyrazol-1-yl)methane Disulfide (p4mS_2) (8): The synthetic procedure was the same as for compound **7**, using p4m (1.000 g, 3.88 mmol) and sulfur (1.250 g, 4.85 mmol), to give compound **8** as a pale orange solid. Yield 90%. The crystals for X-ray diffraction were grown from CH_2Cl_2/hexane. $C_{31}H_{26}N_4P_2S_2$ (580.6): calcd. C 64.13, H 4.48, N 9.65; found C 64.02, H 4.62, N 9.45. ^1H NMR (300 MHz, $CDCl_3$, 293 K): δ = 9.35 (d, $^2J_{H,P}$ = 6.8 Hz, 1 H, CH), 8.20−7.15 (m, 20 H, Ph), 7.83 (d, $^3J_{H,H}$ = 2 Hz, 1 H, H3′), 7.45 (d, $^3J_{H,H}$ = 2.0 Hz, 1 H, H5′), 6.94 (d, $^3J_{H,H}$ = 2.3 Hz, 1 H, H3), 5.96 (dd, $^3J_{H,H}$ = 2.3, $^3J_{H,H}$ = 2.0 Hz, 1 H, H4′), 5.84 (d, $^3J_{H,H}$ = 2.3 Hz, 1 H, H4) ppm. $^{13}C\{^1H\}$ NMR (75 MHz, $CDCl_3$, 293 K): δ = 139.58 (d, $^1J_{C,P}$ = 14.0 Hz, C5), 139.59 (s, C5′), 139.37 (d, $^3J_{C,P}$ = 2.0 Hz, C3), 136.60−127.80 (Ph), 130.32 (s, C3′), 116.73 (dd, $^2J_{C,P}$ = 14.4, $^4J_{C,P}$ = 10.0 Hz, C4), 105.96 (d, $^4J_{C,P}$ = 9.0 Hz, C4′), 72.40 (d, $^1J_{C,P}$ = 65.0 Hz, CH) ppm. $^{31}P\{^1H\}$ NMR (121 MHz, $CDCl_3$, H_3PO_4 as reference): δ = 25.57 [s, $P(S)Ph_2$], 3.62 [s, $P(S)Ph_2$] ppm. IR (KBr): $\tilde{\nu}$ = 633 cm^{-1} (s) [ν(P=S)].

[$PdCl_2$(bppzmS_2)] (9): An equimolar quantity of bppzmS_2 (0.452 g, 0.78 mmol) was added to a CH_2Cl_2 (50 mL) solution of $[PdCl_2(PhCN)_2]$ (0.300 g, 0.78 mmol). The solution was stirred for 16 h at room temperature. The solvent was removed in vacuo and the residue was washed with Et_2O to give an orange solid. Yield 85%. The crystals for X-ray diffraction were grown from a cooled saturated solution in CH_2Cl_2. $C_{31}H_{26}Cl_2N_4P_2PdS_2{\cdot}3.5CH_2Cl_2$ (1055.2): calcd. C 46.45, H 3.81, N 6.47; found C 46.50, H 3.84, N 6.49. ^1H NMR (300 MHz, $CDCl_3$, 293 K): δ = 8.27 (br. s, H3), 7.70−7.54 (m, 20 H, Ph), 7.09 (br. s, 2 H, CH_2), 5.99 (m, H4) ppm. $^{13}C\{^1H\}$ NMR (75 MHz, $CDCl_3$, 293 K): δ = 143.62 (d, $^1J_{C,P}$ = 27.0 Hz, C5), 138.85 (d, $^3J_{C,P}$ = 14.0 Hz, C3), 133.35−128.69 (Ph), 117.35 (d, $^2J_{C,P}$ = 14.6 Hz, C4), 63.48 (s, CH_2) ppm. $^{31}P\{^1H\}$ NMR (121 MHz, $CDCl_3$, H_3PO_4 as reference): δ = 4.80 [s, $P(S)Ph_2$] ppm. IR (KBr): $\tilde{\nu}$ = 660 cm^{-1} (s) [ν(P=S)].

[$PdCl_2$(p4mS_2)] (10): The synthetic procedure was the same as for compound **9**, using $[PdCl_2(PhCN)_2]$ (0.300 g, 0.78 mmol) and p4mS_2 (0.452 g, 0.78 mmol), to give compound **10** as an orange solid. Yield 90%. $C_{31}H_{26}Cl_2N_4P_2PdS_2$ (757.9): calcd. C 49.12, H 3.46, N 7.39; found C 49.22, H 3.50, N 7.43. ^1H NMR (300 MHz, CD_2Cl_2, 293 K): δ = 9.61 (d, $^2J_{H,P}$ = 7.0 Hz, 1 H, CH), 8.35 (m, 1 H, H5′), 8.02 (m, 1 H, H3′), 7.83−7.49 (m, 20 H, Ph), 7.45 (m, 1 H, H3), 6.15 (m, 1 H, H4), 6.13 (m, 1 H, H4′) ppm. $^{31}P\{^1H\}$ NMR (121 MHz, CD_2Cl_2, H_3PO_4 as reference): δ = 26.10 [s, $P(S)Ph_2$], 5.70 [s, $P(S)Ph_2$] ppm. IR (KBr): $\tilde{\nu}$ = 630 cm^{-1} (s) [ν(P=S)].

[Rh(COD)(p4mS_2)]BF_4 (11): An equimolar quantity of $AgBF_4$ (0.078 g, 0.40 mmol) was added to a THF (10 mL) solution of $[Rh(COD)Cl]_2$ (0.100 g, 0.20 mmol). The solution was stirred for 30 min at room temperature. The precipitated AgCl was filtered off and the filtrate was cooled to 203 K. A cooled solution of p4mS_2 (0.232 g, 0.40 mmol) in THF (10 mL) was then added slowly. The reaction was allowed to reach room temperature slowly over 3 h. The solvent was removed in vacuo and the resulting brown solid was extracted with THF. The solution was concentrated and cooled to give complex **11** as a brown microcrystalline solid. Yield 65%. $C_{39}H_{38}BF_4N_4P_2RhS_2$ (878.5): calcd. C 53.32, H 4.36, N 6.38; found

 © 2003 Wiley-VCH Verlag GmbH & Co. KGaA, Weinheim

C 53.40, H 4.42, N 6.45. ^{1}H NMR (300 MHz, $CDCl_3$, 293 K): δ = 9.67 (d, $^2J_{H,P}$ = 7.0 Hz, 1 H, CH), 8.42 (d, $^3J_{H,H}$ = 2.0 Hz, 1 H, H3), 8.20−7.10 (m, 20 H, Ph), 7.24 (d, $^3J_{H,H}$ = 2 Hz, 1 H, H3′), 6.72 (d, $^3J_{H,H}$ = 2.0 Hz, 1 H, H5′), 6.51 (d, $^3J_{H,H}$ = 2.2 Hz, 1 H, H4), 6.04 (dd, $^3J_{H,H}$ = 2.0, $^3J_{H,H}$ = 2.0 Hz, 1 H, H4′), 4.32−4.17 (m, 4 H, CH, COD), 2.75−2.54 (m, 8 H, CH_2, COD), 2.02−1.82 (m, 8 H, CH_2, COD) ppm. ^{13}C{^{1}H} NMR (75 MHz, $CDCl_3$, 293 K): δ = 143.25 (d, $^3J_{C,P}$ = 13.0 Hz, C3), 141.19 (s, C3′), 134.00−128.00 (Ph), 134.10 (d, $^1J_{C,P}$ = 12.0 Hz, C5), 133.07 (s, C5′), 118.60 (d, $^2J_{C,P}$ = 13.0 Hz, C4), 107.01 (s, C4′), 79.46 (m, CH, COD), 77.01 (m, CH, COD), 69.00 (d, $^1J_{C,P}$ = 40.1 Hz, CH), 31.35 (m, CH_2, COD), 29.65 (m, CH_2, COD) ppm. ^{31}P{^{1}H} NMR (121 MHz, $CDCl_3$, H_3PO_4 as reference): δ = 20.64 [bs, P(S)Ph_2], 4.42 [s, P(S)Ph_2] ppm. IR (KBr): $\tilde{\nu}$ = 556 (s) [ν(P=S)].

X-ray Crystallographic Study: Crystals obtained for complex **4** decomposed quickly with the loss of CH_2Cl_2, even when the data collection was performed at low temperature. We attempted this study with several crystals but data collection could not be completed. Given the importance of this structure, it was solved despite the aforementioned problems. Intensity data for complexes **4**, **8** and **9** were collected on a NONIUS-MACH3 diffractometer equipped with a graphite monochromator (Mo-K_α radiation, λ = 0.71073 Å) using the ω/2θ scan technique. The final unit-cell parameters were determined from 25 well-centered reflections and refined by the least-squares method. The space group was determined from the systematic absences and this was vindicated by the success of the subsequent solutions and refinements. Two standard reflections were measured every 60 minutes as an orientation and intensity control; significant intensity decay was not observed for compounds **8** and **9**. However, compound **4** showed an intensity decay of 56% at the end of the process. The structures were solved by direct methods using SHELXS[13] and refined on F^2 by full-matrix least-squares (SHELXL-97).[14] The CH_2Cl_2 solvate molecule could be located in complexes **4** and **9**. All non-hydrogen atoms were refined with anisotropic thermal parameters in complexes **8** and **9**. The hydrogen atoms were included in their calculated positions and were refined with an overall isotropic temperature factor using a riding model. Weights were optimized in the final cycles. Crystallographic data are given in Table 5. CCDC-207627 (**4**), -207628 (**8**) and -207629 (**9**) contain the supplementary crystallographic data for this paper. These data can be obtained free of charge at www.ccdc.cam.ac.uk/conts/retrieving.html [or from the Cambridge Crystallographic Data Centre, 12, Union Road, Cambridge CB2 1EZ, UK; fax: (internat.) +44-1223/336-033; E-mail: deposit@ccdc.cam.ac.uk].

Catalytic Activity: Hydrogenation reactions were carried out in a 100 mL stainless steel autoclave (Magnedrive Autoclave Engineers). The autoclave was evacuated for 2 h before a solution containing the catalyst and substrate was introduced by suction. Hydrogen was then introduced and the mixture was warmed to the reaction temperature. The pressure in the autoclave was monitored using a transducer. Samples were analysed by gas chromatography on a Hewlett Packard HP 6890 chromatograph equipped with an FID detector and 30 m × 0.032 mm HP-Innovax column.

Acknowledgments

We gratefully acknowledge financial support from the Dirección General de Enseñanza Superior e Investigación Científica (Ministerio de Educación y Cultura), Spain (Grant. No. 1FD97−0176).

Table 5. Crystal data and structure refinement for **4**, **8** and **9**

	4	**8**	**9**
Formula	$C_{31}H_{26}Cl_2N_4P_2Pt.4CH_2Cl_2$	$C_{31}H_{26}N_4P_2S_2$	$2C_{31}H_{26}Cl_2N_4P_2PdS_2.7CH_2Cl_2$
Mol. wt.	1116.14	580.62	2110.32
T (K)	153(2)	293(2)	153(2)
Cryst syst	Monoclinic	Monoclinic	Triclinic
Space group	$P2_1/n$	$P2_1/n$	$P\bar{1}$
a (Å)	9.229(1)	13.697(1)	12.460(1)
b (Å)	15.986(1)	14.795(1)	14.134(1)
c (Å)	29.395(1)	14.913(1)	25.799(1)
α (deg)			86.19(1)
β (deg)	92.12(1)	102.76(2)	84.98(1)
γ (deg)			72.22(1)
V (Å^3)	4333.8(6)	2947.4(4)	4306.1(5)
Z	4	4	1
Dc (g cm^{-3})	1.711	1.308	1.628
μ (mm^{-1})	3.959	0.317	1.193
F(000)	2176	1208	2116
Cryst dimens. (mm)	0.1 × 0.4 × 0.4	0.3 × 0.3 × 0.2	0.2 × 0.3 × 0.3
θ range (deg)	1.39 to 25.11	2.05 to 28.01	2.00 to 28.00
hkl ranges	$-10 \le h \le 10$	$-18 \le h \le 17$	$-16 \le h \le 16$
	$0 \le k \le 18$	$0 \le k \le 19$	$-18 \le k \le 18$
	$0 \le l \le 35$	$0 \le l \le 19$	$0 \le l \le 32$
No. of rflns measd	7756	7676	21062
No. of indep rflns	7595	7083	20607
No. of odsd rflns	3205	4693	13666
Goodness-of-fit on F^2	1.101	0.991	1.034
Final R indices [$I > 2\sigma(I)$]	R_1 = 0.1671, wR_2 = 0.3927[a]	R_1 = 0.0497, wR_2 = 0.1221	R_1 = 0.0553, wR_2 = 0.1284
Largest diff. peak (e·Å^{-3})	2.600/−3.862	0.465/−0.513	1.127/−1.094

[a] $R_1 = \Sigma F_o - F_c/\Sigma F_o$; $wR_2 = [\Sigma\{w(F_o^2 - F_c^2)^2\}/\Sigma\{w(F_0^2)^2\}]^{0.5}$.

 © 2003 Wiley-VCH Verlag GmbH & Co. KGaA, Weinheim

[1] [1a] F. A. Cotton, B. Hong, *Prog. Inorg. Chem.* **1992**, *40*, 179. [1b] H. A. Mayer, W. C. Kaska, *Chem. Rev.* **1994**, *94*, 1239. [1c] C. Bianchini, A. Meli, M. Peruzzini, F. Vizza, F. Zanobini, *Coord. Chem. Rev.* **1992**, *120*, 193. [1d] W. Levason, *The Chemistry of Organophosphorus Compounds* (Eds.: F. R. Hartley and S. Patai), Wiley, NY, **1990**.

[2] [2a] M. Álvarez, N. Lugan, R. Mathieu, *J. Chem. Soc., Dalton Trans.* **1994**, 2755. [2b] A. M. Trzeciak, T. Glowiak, J. J. Ziolkowski, *J. Organomet. Chem.* **1998**, *552*, 159. [2c] M. Valentini, K. Selvakumer, M. Worle, P. S. Pregosin, *J. Organomet. Chem.* **1999**, *587*, 244. [2d] J. D. Kostas, C. G. Screttas, *J. Organomet. Chem.* **1999**, *585*, 1. [2e] P. Pelagatti, A. Gacchi, M. Carcelli, M. Costa, A. Fochi, P. Ghidini, E. Leporati, M. Masi, C. Pelizzi, G. Pelizzi, *J. Organomet. Chem.* **1999**, *583*, 94. [2f] D. G. Grotjahn, D. Combs, S. Van, G. Aguirre, F. Ortega, *Inorg. Chem.* **2000**, *39*, 2080. [2g] G. Esquius, J. Pons, R. Yáñez, J. Ros, *J. Organomet. Chem.* **2001**, *619*, 14. [2h] P. Braunstein, M. D. Fryzuk, M. Le Dall, F. Naud, S. J. Rettig, F. Speiser, *J. Chem. Soc., Dalton Trans.* **2000**, 1067. [2i] M. L. Clarke, A. M. Z. Slawin, M. V. Wheatley, J. D. Woolins, *J. Chem. Soc., Dalton Trans.* **2001**, 3421. [2j] J. A. Casares, P. Espinet, J. M. Martín-Álvarez, G. Espino, M. Pérez-Manrique, F. Vattier, *Eur. J. Inorg. Chem.* **2001**, 289. [2k] J. T. Mague, J. L. Krinsky, *Inorg. Chem.* **2001**, *40*, 1962. [2l] V. Cadierno, P. Crochet, J. García-Álvarez, S. E. García-Garrido, J. Gimeno, *J. Organomet. Chem.* **2002**, *663*, 32. [2m] G. Esquius, J. Pons, R. Yáñez, J. Ros, R. Mathieu, B. Donnadieu, N. Lugan, *Eur. J. Inorg. Chem.* **2002**, 2999. [2n] J. García-Antón, J. Pons, X. Solans, M. Font-Bardia, J. Ros, *Eur. J. Inorg. Chem.* **2002**, 3319.

[3] A. Antiñolo, F. Carrillo-Hermosilla, E. Diez-Barra, J. Fernández-Baeza, M. Fernández-López, A. Lara-Sánchez, A. Moreno, A. Otero, A. M. Rodríguez, J. Tejeda, *J. Chem. Soc., Dalton Trans.* **1998**, 3737.

[4] [4a] T. S. Lobana, *Prog. Inorg. Chem.* **1989**, *37*, 495. [4b] J. R. Dilworth, N. Wheatley, *Coord. Chem. Rev.* **2000**, *199*, 89. [4c] P. Das, D. Konwar, P. Sengupta, D. K. Dutta, *Transition Met. Chem.* **2000**, *25*, 426.

[5] A. R. Katritzky, A. E. Abdel-Rahman, D. E. Leahy, *Tetrahedron* **1983**, *39*, 4133.

[6] [6a] R. Noyori, *Asymmetric Catalysis in Organic Synthesis*, John Wiley and Sons, NY, **1994**. [6b] H. Takaya, T. Olita, R. Noyori, *Catalytic Asymmetric Synthesis*, VCH, NY, **1993**. [6c] J. M. J. Williams, *Catalysis in Asymmetric Synthesis*, Sheffield Academic Press, Sheffield, **1999**.

[7] [7a] D. E. Berry, J. Browning, K. R. Dixon, R. W. Hilts, *Can. J. Chem.* **1988**, *66*, 1272. [7b] S. Browing, K. R. Dixon, R. W. Hilts, *Organometallics* **1989**, *8*, 552. [7c] J. Browning, K. R. Dixon, R. W. Hilts, N. J. Meanwell, F. Wang, *J. Organomet. Chem.* **1991**, *410*, 389. [7d] M. S. Abbassioun, P. A. Chaloner, C. Claver, P. B. Hitchcock, A. M. Masdeu, A. Ruiz, T. Saballs, *J. Organomet. Chem.* **1991**, *403*, 229. [7e] C. Claver, F. Gii, J. Viñas, A. Ruiz, *Polyhedron* **1987**, 1329. [7f] C. Claver, A. Ruiz, A. M. Masdeu, J. Viñas, T. Saballs, F. J. Lahoz, F. J. Plou, *J. Organomet. Chem.* **1989**, *373*, 269.

[8] [8a] P. Nicpon, D. W. Meek, *Inorg. Chem.* **1967**, *6*, 145. [8b] E. W. Ainscough, A. H. Brodie, A. R. Furness, *J. Chem. Soc., Dalton Trans.* **1973**, 2360.

[9] [9a] S. Trofimenko, *J. Am. Chem. Soc.* **1970**, *92*, 5118. [9b] G. Minghetti, M. A. Cinellu, A. K. Bandini, G. Banditelli, F. Demartin, M. Manassero, *J. Organomet. Chem.* **1986**, *315*, 387. [9c] P. K. Byers, A. J. Canty, *Organometallics* **1990**, *9*, 210. [9d] P. K. Byers, A. J. Canty; R. T. Honeyman, *Adv. Organomet. Chem.* **1992**, *34*, 1. [9e] S. Tsuji, D. C. Swenson, R. F. Jordan, *Organometallics* **1999**, *18*, 4758.

[10] C. H. Bartholomew, P. K. Agrawal, J. R. Katzer, *Adv. Catal.* **1982**, *31*, 135.

[11] J. Tsuji, *Organic Synthesis with Palladium Compounds*, Springer, Berlin, **1980**, *vol. 10*, pp. 2−3.

[12] E. Diez-Barra, A. de la Hoz, A. Sánchez-Migallón, J. Tejeda, *Heterocycles* **1992**, *34*, 1365.

[13] G. M. Sheldrick, *Acta Crystallogr., Sect. A* **1990**, *46*, 467.

[14] G. M. Sheldrick, *Program for the Refinement of Crystal Structures from Diffraction Data*, University of Göttingen, Göttingen, Germany, **1997**.

Received April 4, 2003

 © 2003 Wiley-VCH Verlag GmbH & Co. KGaA, Weinheim

Synthesis, Properties, and Reactions of Trinuclear Macrocyclic Nickel(II) and Nickel(I) Complexes: Electrocatalytic Reduction of CO_2 by Nickel(II) Complex

Eun Young Lee,[a] Daewon Hong,[a] Han Woong Park,[a] and Myunghyun Paik Suh*[a]

Keywords: Nickel / Macrocyclic compounds / Carbon dioxide / Electroreduction / Multinuclear complex

The trinuclear Ni^{II} complex of trismacrocyclic ligand **1**, $[Ni_3(\mathbf{1})](ClO_4)_6$, where **1** is 8,8′,8"-(2,2′,2"-nitrilotriethyl)-tris(1,3,6,8,10,13,15-heptaazatricyclo[11.3.1.1^{3,15}]octadecane), has been synthesized by template condensation reactions and shown to have poor axial binding ability. Cyclic voltammetry of the complex shows a three-electron reversible reduction at −1.59 V and an irreversible oxidation at +1.25 V vs. Ag/Ag^+ (0.01 M). Differential pulse voltammetry and Osteryoung square-wave voltammetry indicate that the three Ni^{II} ions are electrochemically independent. A single crystal was obtained as $[Ni_3(\mathbf{1})](ClO_4)_3{\cdot}Cl_3{\cdot}10H_2O$ and its X-ray structure was determined. When $[Ni_3(\mathbf{1})](ClO_4)_6$ was reduced to a Ni^I species by reaction with Na(Hg) in MeCN, $[Ni_3(\mathbf{1})](ClO_4)_3$ was isolated. $[Ni_3(\mathbf{1})](ClO_4)_6$ shows catalytic activity for the electrochemical reduction of CO_2 to CO in $MeCN/H_2O$ (9:1, v/v), as revealed by cyclic voltammetry and controlled-potential coulometry. The catalytic efficiency of $[Ni_3(\mathbf{1})]^{6+}$ is lower than that of $[Ni(cyclam)]^{2+}$. It gives a greater $i_p(CO_2)/i_p(N_2)$ value but produces less CO per nickel center (**3**: 8-methyl-1,3,6,8,10,13,15-heptaaza-tricyclo-[11.3.1.1^{3,15}]octadecane) compared with monometallic $[Ni(\mathbf{3})]^{2+}$.
(© Wiley-VCH Verlag GmbH & Co. KGaA, 69451 Weinheim, Germany, 2003)

Introduction

Multinuclear macrocyclic complexes can be interesting multi-electron redox catalysts and may act as models for polynuclear metalloenzymes. The synthesis and design of electrocatalyses to reduce abundant and inexpensive CO_2 may be important in lessening the greenhouse effect and in developing new sources of fuels.[1−3] CO_2 reduction may provide various products: carbon monoxide or formic acid, formaldehyde, methanol, and methane, by two-, four-, six-, and eight-electron reduction reactions, respectively. The high activation energy of CO_2 reduction at a platinum electrode, requiring a more negative potential than −2.24 V vs. SCE, is due to the high energy intermediate CO_2^- [4] but can be lowered by using catalysts. Some transition metal complexes with macrocyclic ligands − both mononuclear[5−19] and dinuclear[20−21] complexes − exhibit catalytic effects on the electrochemical reduction of CO_2 to CO or formate, shifting the CO_2 reduction potential by ca. +0.5 V. To obtain reduction products involving more than two electrons, multimetallic catalysts should be employed.

Here we report the synthesis of trinuclear Ni^{II} and Ni^I complexes of the trismacrocyclic ligand 8,8′,8"-(2,2′,2"-nitrilotriethyl)-tris(1,3,6,8,10,13,15-heptaaza-tricyclo-[11.3.1.1^{3,15}]octadecane) (**1**). We also report their electrocatalytic activity for CO_2 reduction compared with the mononuclear $[Ni(\mathbf{3})]^{2+}$ complex.

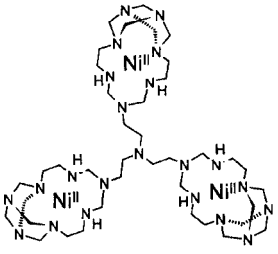

$[Ni_3(\mathbf{1})]^{6+}$

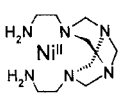

$[Ni(\mathbf{2})]^{2+}$

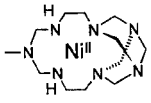

$[Ni(\mathbf{3})]^{2+}$

Results and Discussion

Synthesis and Properties of $[Ni_3(1)](ClO_4)_6$

The trinuclear trismacrocyclic complex $[Ni_3(\mathbf{1})](ClO_4)_6$ was synthesized by the template condensation of $[Ni(\mathbf{2})]^{2+}$ with tris(2-aminoethyl)amine and formaldehyde as described in Equation (1). Template condensation reactions involving amines and formaldehyde have provided various types of macrocyclic complexes that cannot be obtained in the absence of metal ions.[22−29] However, multinuclear macrocyclic complexes containing more than three metal ions are still very rare.[30]

$$3\,[Ni(\mathbf{2})]^{2+} + 6\,CH_2O + (H_2NCH_2CH_2)_3N \rightarrow [Ni_3(\mathbf{1})]^{6+} \quad (1)$$

[a] School of Chemistry and Molecular Engineering, Center for Molecular Catalysis, Seoul National University, Seoul 151−747, Republic of Korea,
Fax: (internat.) +82-2/886-8516
E-mail: mpsuh@snu.ac.kr
Supporting information for this article is available on the WWW under http://www.eurjic.org or from the author.

 © 2003 Wiley-VCH Verlag GmbH & Co. KGaA, Weinheim **DOI: 10.1002/ejic.200200543**

Although the reaction of Equation (1) seems to be entropically unfavorable, it provides the trismacrocyclic complex in ca. 50% yield. The amount of water present significantly affects the yield of $[Ni_3(\mathbf{1})](ClO_4)_6$, and the complex $[Ni_3(\mathbf{1})](ClO_4)_6$ was synthesized in MeOH/H_2O (2:1, v/v). When water was absent, the starting complex did not dissolve into the solution and provided a poor yield.

$[Ni_3(\mathbf{1})](ClO_4)_6$ is soluble in MeCN, $MeNO_2$, DMSO, and hot water, but insoluble in MeOH and diethyl ether. The ^{13}C NMR spectrum (Figure 1) is consistent with the structure of trismacrocyclic ligand **1**. The molar conductance for $[Ni_3(\mathbf{1})](ClO_4)_6$, measured in $MeNO_2$ at 25 °C, depends on the concentration of the complex; 214 $\Omega^{-1}\cdot cm^2\cdot mol^{-1}$ for a 1.13×10^{-3} M solution and 393 $\Omega^{-1}\cdot cm^2\cdot mol^{-1}$ for a 5.16×10^{-5} M solution. In MeCN, the molar conductances are 439 $\Omega^{-1}\cdot cm^2\cdot mol^{-1}$ at 2.77×10^{-4} M and 684 $\Omega^{-1}\cdot cm^2\cdot mol^{-1}$ at 1.66×10^{-5} M. A plot of molar conductance in $MeNO_2$ at various concentrations is given in Figure S1 in the Supporting Information. Extrapolation of this plot to 0 M gives 434−491 $\Omega^{-1}\cdot cm^2\cdot mol^{-1}$ for a highly diluted $MeNO_2$ solution. The highly charged (+6) cation seems to form ion-pairs even in 10^{-5} M solutions. The electronic spectrum of $[Ni_3(\mathbf{1})](ClO_4)_6$ shows a maximum absorption at 439 nm with an extinction coefficient of 273 $cm^{-1}\cdot M^{-1}$ in $MeNO_2$. The λ_{max} value of $[Ni_3(\mathbf{1})](ClO_4)_6$ is similar to that of monometallic $[Ni(\mathbf{3})](ClO_4)_2$ (438 nm)[23] but its molar absorptivity is almost three times greater than that (83 $cm^{-1}\cdot M^{-1}$) due to the existence of three Ni^{II} chromophores. The spectrum depends slightly on the solvent used. The complex does not coordinate ligands such as NCS^-, Cl^-, pyridine, NH_3, and NO_3^- at the axial site in the noncoordinating solvent $MeNO_2$, as evidenced by the UV/Vis spectra. Upon addition of CN^-, however, the solution changed from yellow to pink and then the demetallation of Ni^{II} ions took place within a few minutes.

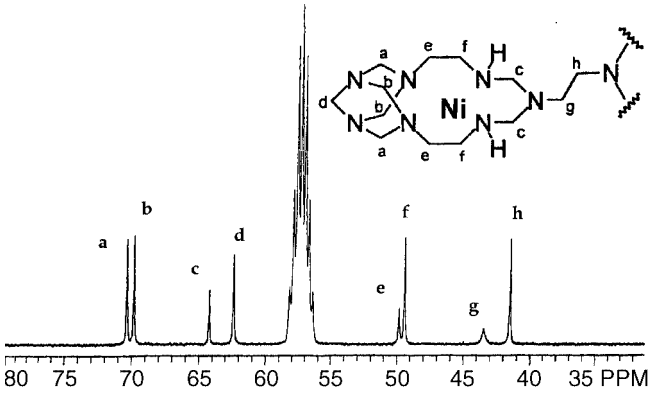

Figure 1. ^{13}C NMR spectrum of $[Ni_3(\mathbf{1})](ClO_4)_6$ in [D_3]nitromethane

Crystal Structure of $[Ni_3(\mathbf{1})](ClO_4)_3\cdot Cl_3\cdot 10H_2O$

We could not obtain single crystals of $[Ni_3(\mathbf{1})](ClO_4)_6$ by recrystallization from any solvent system. However, we acquired single crystals of $[Ni_3(\mathbf{1})](ClO_4)_3\cdot Cl_3\cdot 10H_2O$ by mixing $[Ni_3(\mathbf{1})](ClO_4)_6$ and NaCl in a hot solvent mixture of

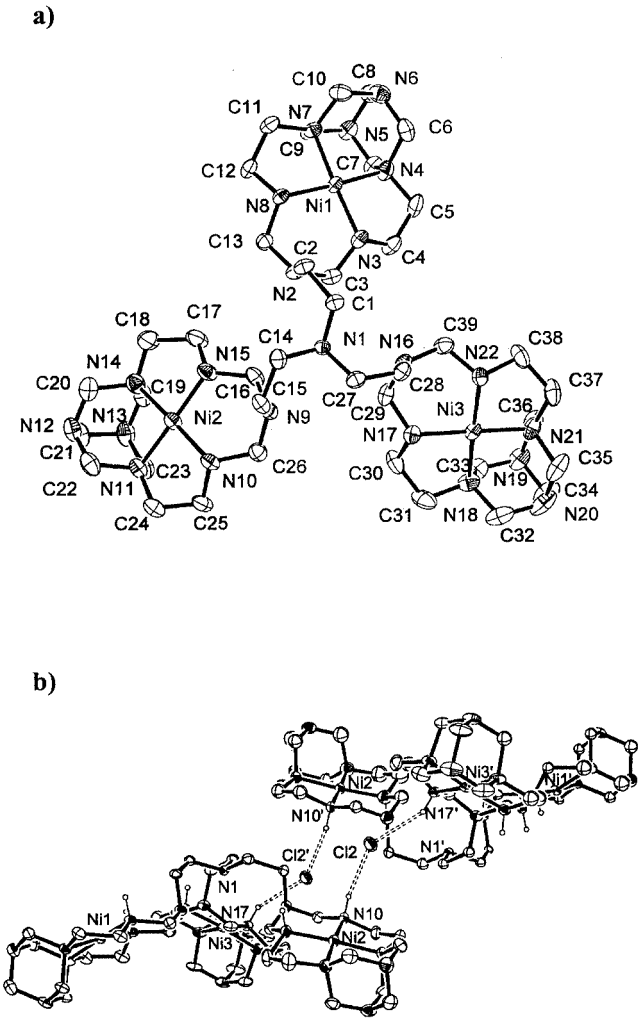

Figure 2. ORTEP views of the cation of $[Ni_3(\mathbf{1})](ClO_4)_3\cdot(Cl)_3\cdot 10H_2O$ with atomic numbering scheme: top view (a) and side view showing hydrogen bonded dimer (b); the atoms in (a) and (b) are represented by 20% probable thermal ellipsoids. Atoms marked ′ are generated by symmetry operations: $1-x$, $-1-y$, $-z$. Hydrogen bonds are indicated as dashed lines.

MeCN, MeOH, and H_2O. An ORTEP view of the cation in $[Ni_3(\mathbf{1})](ClO_4)_3\cdot Cl_3\cdot 10H_2O$ is presented in Figure 2a. The three Ni^{II} macrocycles are linked by a tren group to form a bowl-shaped molecule. Three Ni^{II} ions in the molecule are almost at the corners of a triangle. The Ni1···Ni2, Ni2···Ni3, and Ni3···Ni1 distances are 9.062(3), 9.420(2), and 8.983(2) Å, respectively. The Ni1···Ni2···Ni3, Ni2···Ni3···Ni1, and Ni3···Ni1···Ni2 angles are 58.12(2), 58.94(2), and 62.94(1)°, respectively. The central tertiary nitrogen (N1) of the tren unit is 2.624(5) Å above the triangular plane made by the Ni1, Ni2, and Ni3 atoms. The dihedral angles between the square-coordination planes involving Ni1 and Ni2, Ni2 and Ni3, and Ni3 and Ni1 are 51.15(16), 49.53(22), and 46.42(18)°, respectively. There are three ClO_4^- and three Cl^- anions per trismacrocyclic complex. The ClO_4^- anions are found at the open hollow part of the bowl, and Cl^- anions and water molecules are out of the bowls. A Cl^- anion (Cl2) connects two molecules through hydrogen bonds with the secondary amines of the

 © 2003 Wiley-VCH Verlag GmbH & Co. KGaA, Weinheim

macrocycle, involving N10 and N17 [Cl2···N10 3.204 Å, Cl2···H−N10 169.7°, Cl2···N17(1−x, −1−y, −z) 3.248 Å, Cl2···H−N17(1 − x, −1 − y, −z) 147.4°], as shown in Figure 2b.

In each macrocycle, the Ni^{II} ion exhibits square-planar coordination geometry, being coordinated with two secondary and two tertiary nitrogen atoms of the ligand. The Ni^{II} ions are displaced from their square-coordination planes by 0.057(3), 0.032(3), and 0.049(3) Å, respectively, showing a slight square-pyramidal distortion. The average Ni−N bond length is 1.927(2) Å, which falls in the range (1.86−1.94 Å) normally observed for square-planar Ni^{II} complexes.[23] In general, *N*-methylation of the secondary nitrogen donors of the macrocyclic complex decreases the ligand-field strength and increases the Ni−N distances.[23,31] However, the present complex shows no significant differences in the Ni−N distances for the secondary and tertiary amines. The local environment of every Ni^{II} ion possesses a pseudo-mirror plane that is perpendicular to the square coordination plane. The average N−C distances and average C−*N*−C angles involving coordinated tertiary nitrogens (N4, N7, N11, N14, N18, N21) are 1.504(3) Å and 109.2(1)°. The average N−C distances and average C−*N*−C angles involving uncoordinated tertiary nitrogens (N5, N6, N12, N13, N19, N20) are 1.451(3) Å and 110.4(1)°, indicating the contribution of sp^2 hybridization.[22−27]

Electrochemical Behavior of $[Ni_3(1)](ClO_4)_6$

The cyclic voltammogram of an MeCN solution of $[Ni_3(\mathbf{1})](ClO_4)_6$ shows a reversible reduction peak at −1.59 V and an irreversible oxidation peak at +1.25 V vs. Ag/Ag^+(0.01 M) (Table 1), which are very similar to those (−1.61 V and +1.10 V, respectively) for the monocyclic $[Ni(\mathbf{3})]^{2+}$ complex.[22,23] Bulk electrolysis at −1.8 V vs. Ag/Ag^+ (0.01 M) indicated n = 3.16 for the Ni^{II}/Ni^{I} reduction. The differential pulse and Osteryoung square-wave voltammograms show only one peak at −1.59 V vs. Ag/Ag^+ (0.01 M), indicating that the three Ni^{II} ions in the complex are electrochemically independent and that reduction of the three Ni^{II} centers takes place simultaneously.

Synthesis of Ni^{I} Complex

Numerous Ni^{I} azamacrocyclic complexes have been reported[32−50] but few have been isolated from solution. The trinuclear Ni^{I} complex $[Ni_3(\mathbf{1})](ClO_4)_3$ was prepared by reducing the Ni^{II} complex with Na(Hg) in MeCN under an N_2 atmosphere. The Ni^{I} complex was isolated together with the impurity $NaClO_4$, which was hardly removed by recrystallization, and so the analysis data for the Ni^{I} complex are relatively poor. The electronic absorption spectrum of the Ni^{I} complex (Table 1) shows maximum absorptions at 524 nm and 319 nm. These λ_{max} are similar to those of $[Ni(\mathbf{3})]^+$, whose X-ray structure displays the square-planar geometry around the Ni^{I} ion.[41] For Ni^{I} complexes λ_{max} is often shifted ca. 100 nm to longer wavelengths, with extinction coefficients increasing by ca. 5−10 times, compared with those of the corresponding Ni^{II} complexes.[26,41,43] The complex $[Ni^{I}_3(\mathbf{1})](ClO_4)_3$ (powder sample) shows an anisotropic axial EPR spectrum with g values of $g_\perp$ = 2.069 and g_{II} = 2.247 (Figure 3), indicating that the Ni^{I} ions have a square-planar coordination geometry with an unpaired electron in the d $d_{x^2-y^2}$ orbital.[23] The g values are similar to those of the Ni^{I} complex of **3**.[23,41]

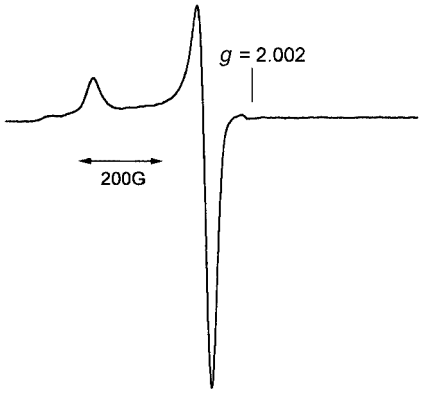

Figure 3. EPR powder spectrum of $[Ni^{I}_3(\mathbf{1})](ClO_4)_3$ at room temperature.

The Ni^{I} complex $[Ni_3(\mathbf{1})](ClO_4)_3$ is very sensitive to air and moisture. For example, a red-purple MeCN solution of the Ni^{I} complex exposed to air turned yellow, the color of

Table 1. Properties of Ni^{II} and Ni^{I} complexes

Compd.	λ_{max} nm (ε, $M^{-1}\cdot cm^{-1}$)	$Ni^{II} \rightarrow Ni^{I}$[a] $E_{cathodic}$	E_{anodic}	$E_{1/2}$	$Ni^{II} \rightarrow Ni^{III}$[a] $E_{cathodic}$	E_{anodic}	$E_{1/2}$	EPR[b]	ref.
$[Ni_3(\mathbf{1})]^{6+}$	439(265),[c] 439(283)[d]	−1.63	−1.55	−1.59(r)	+1.22	+1.37	+1.25(i)		this work
$[Ni(\mathbf{3})]^{2+}$	442(80),[c] 438(83)[d]	−1.64	−1.57	−1.61(r)			+1.10(qr)		[41]
$[Ni_3(\mathbf{1})]^{3+}$	524(1080), 319(4010)[c]							g = 2.202, $g_\perp$ = 2.058	this work
$[Ni(\mathbf{3})]^{+}$	538(600), 330(2020)[c]							g = 2.240, $g_\perp$ = 2.062	[41]

[a] Measured in MeCN with 0.1 M $(n-Bu)_4NPF_6$; volts vs. Ag/Ag^+ (0.01 M); working electrode, glassy carbon; scan rate, 50 mV s^{-1}; 20 °C; r: reversible; qr: quasi-reversible; i: irreversible. [b] Powder samples at room temperature. [c] Measured in MeCN. [d] Measured in $MeNO_2$.

 © 2003 Wiley-VCH Verlag GmbH & Co. KGaA, Weinheim

Ni^{II} complex, in less than 15 min. When CO_2 gas was bubbled through an MeCN solution, the change to yellow was abrupt, $[Ni_3(\mathbf{1})](ClO_4)_6$ was isolated from solution, and CO gas was detected in the head space of the reaction vessel.

Electrochemical Reduction of CO_2 Catalyzed by $[Ni_3(1)]^{6+}$

Some Ni^{II} tetraaza macrocyclic complexes have shown catalytic activity in the electroreduction of CO_2.[5−21] In particular, $[Ni(cyclam)]^{2+}$ is an efficient and selective catalyst on a Hg electrode in water.[5] Ni^{II} systems that can be easily reduced to Ni^{I} species are efficient electrocatalysts for reducing CO_2.[14] Since the complex $[Ni_3(\mathbf{1})]^{6+}$ exhibits a much more anodic Ni^{II}/Ni^{I} reduction potential than $[Ni(cyclam)]^{2+}$, and its trinuclear Ni^{I} species is stable enough to be isolated, we expected that $[Ni_3(\mathbf{1})]^{6+}$ would catalyze the electroreduction of CO_2, which we then investigated by cyclic voltammetry and controlled potential coulometry. In a typical cyclic voltammetric experiment, a solution of trinuclear Ni^{II} complex (2.0 mM) was prepared in a MeCN/H_2O (9:1, v/v) solution containing 0.1 M $NaClO_4$. Under N_2 atmosphere, the cyclic voltammogram of $[Ni_3(\mathbf{1})](ClO_4)_6$ showed a reversible Ni^{II}/Ni^{I} reduction peak at $E_{1/2} = -1.39$ V ($E_{cathode} = -1.44$ V and $E_{anode} = -1.35$ V) vs. SCE. When the complex solution was saturated with CO_2, the current intensity at −1.44 V increased ca. three times compared with that measured under N_2, and the anodic peak at −1.35 V disappeared (Figure 4). This indicates that the complex acts as a catalyst for the electrochemical reduction of CO_2.[51] The results of the same experiment with the mononuclear Ni^{II} complexes of cyclam and **3** are summarized in Table 2. In the cyclic voltammetry, the peak current (i_p) measured under N_2 can be described as $i_p = (2.69 \times 10^5)n^{3/2}AD_o^{1/2}v^{1/2}C_o^*$.[51] The diffusion coefficients (D_o) of $[Ni_3(\mathbf{1})]^{6+}$ and $[Ni(\mathbf{3})]^{2+}$, measured in MeCN/H_2O (9:1, v/v) by rotating disk electrode, are 1.8×10^{-5} and 8.8×10^{-5} $cm^2\,s^{-1}$, respectively. Theoretically, when the concentrations of the complexes are the same, $i_p(N_2)$ of $[Ni_3(\mathbf{1})]^{6+}$ should be 2.35 times greater than that of $[Ni(\mathbf{3})]^{2+}$. The ratio of $i_p(N_2)$ of $[Ni_3(\mathbf{1})]^{6+}$ versus that of $[Ni(\mathbf{3})]^{2+}$ is 2.1−2.3 (Table 2). Although all catalysts showed peak potentials at −1.44 to −1.49 V vs. SCE in the presence of CO_2, the trinuclear Ni^{II} complex of **1** showed a much greater catalytic current than the monometallic complex of **3**. To exclude the effect of n and D_o values on the catalytic efficiencies, the ratio of peak current measured under CO_2 vs. that measured under N_2, $i_p(CO_2)/i_p(N_2)$, was compared (Table 2). The $i_p(CO_2)/i_p(N_2)$ for $[Ni_3(\mathbf{1})]^{6+}$ is ca. 3 while those of $[Ni(\mathbf{3})]^{2+}$ and $[Ni(cyclam)]^{2+}$ are 2 and 5, respectively. This indicates that $[Ni_3(\mathbf{1})]^{6+}$ is a better catalyst than $[Ni(\mathbf{3})]^{2+}$ in terms of the catalytic current although it is not a better catalyst than $[Ni(cyclam)]^{2+}$.

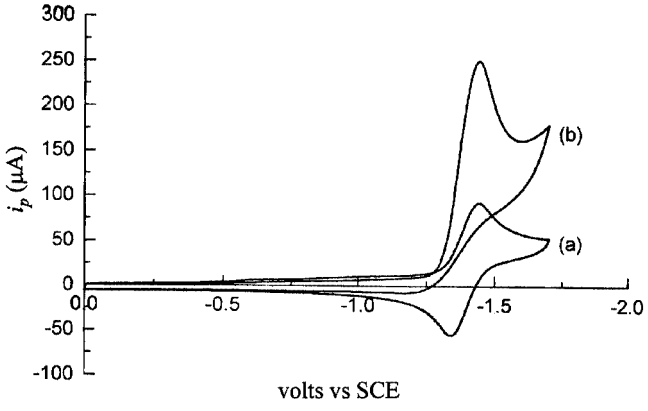

Figure 4. Cyclic voltammogram of $[Ni_3(\mathbf{1})](ClO_4)_6$ at a glassy carbon electrode in MeCN/H_2O (9:1, v/v) measured under N_2 (a) and under CO_2 (b). Volts vs. SCE; concentration of complex, 2.0 mM; electrolyte, 0.1 M $NaClO_4$; scan rate, 100 mV s^{-1}.

The solvent system as well as the electrode material dramatically affects the catalytic peak current. For example, that of $[Ni(cyclam)]^{2+}$ (10^{-3} M) increased ca. 50 times under CO_2 with H_2O as solvent and a Hg dropping mercury electrode.[5] However, here it increased by only ca. 5 times in MeCN/H_2O (9:1, v/v) at a glassy carbon electrode. In the present study, experiments could not be performed in 100% water because of the low solubility of the Ni^{II} complexes of **1** and **3** in water. In MeCN without added water, a catalytic current was not observed under CO_2 both with $[Ni_3(\mathbf{1})]^{6+}$ and $[Ni(\mathbf{3})]^{2+}$ complexes, probably due to the lack of a proton source. Protons are needed in CO_2 reduction according to Equation (2).

$$2\,Ni^{I} + 2\,H^{+} + CO_2 \rightarrow 2\,Ni^{II} + CO + H_2O \quad (2)$$

The concentration of the catalyst also affects catalytic activity and turnover number. This was especially so for a Hg electrode, where the active catalyst is a species adsorbed on the electrode, and saturation of catalytic activity occurred

Table 2. Cyclic voltammetry data for the electrocatalytic reduction of CO_2 by Ni^{II} complexes

	Under N_2[a]		Under CO_2[a]		$ip(CO_2)/ip(N_2)$[b]
catalyst	$E_{cathode}$[c] (ip)[d]	E_{anode}[c] (ip)[d]	$E_{cathode}$[c] (ip)[d]	E_{anode}[c] (ip)[d]	
$[Ni_3(\mathbf{1})]^{6+}$	−1.44 (+78.5)	−1.35 (−67.8)	−1.44 (+239)	[e]	3.04
$[Ni(\mathbf{3})]^{2+}$	−1.41 (+38.0)	−1.34 (−30.1)	−1.49 (+79.4)	[e]	2.09
$[Ni(cyclam)]^{2+}$	−1.56 (+31.8)	−1.47 (−27.3)	−1.47 (+154)	[e]	4.84

[a] In MeCN/H_2O (9:1, v/v) with 0.1 M $NaClO_4$; conc. of catalyst, 2.0 mM; working electrode, glassy carbon; scan rate, 100 mV s^{-1}. [b] Cathodic peak current ratio. [c] Volts vs. SCE. [d] μ ampere. [e] No peak was observed.

 © 2003 Wiley-VCH Verlag GmbH & Co. KGaA, Weinheim

Table 3. Effect of catalyst concentration on the electroreduction of CO_2 catalyzed by $[Ni_3(\mathbf{1})](ClO_4)_6$[a]

c (mM)	Under N_2		Under CO_2		$ip(CO_2)/ ip(N_2)$[d]
	$E_{cathode}$[b] (i_p)[c]	E_{anode}[b](ip)[c]	$E_{cathode}$[b](ip)[c]	E_{anode}[b](ip)[c]	
0.1	−1.705(0.46)	−1.621(−0.27)	−1.669(1.29)	–	2.80
0.5	−1.683(1.95)	−1.621(−1.44)	−1.677(5.40)	–	2.77
2.0	−1.685(10.1)	−1.620(−6.90)	−1.663(21.44)	–	2.12

[a] In MeCN/H_2O (9:1, v/v) with 0.1 M TBAP; working electrode, controlled growth Hg. Electrochemical measurements were made after the solution was purged with N_2 for 30 min and then with CO_2 for 30 min. [b] Volts vs. Ag/Ag^+(0.01 M). [c] μA. [d] Cathodic peak current ratio.

at 5×10^{-6}–2×10^{-3} M of catalyst.[12,52] To see if catalytic saturation took place under the present experimental conditions, $i_p(CO_2)$ was measured at various concentrations of $[Ni_3(\mathbf{1})]^{6+}$ (1.0×10^{-4}–2.0×10^{-3} M). The results obtained for a Hg electrode are summarized in Table 3, and those for a glassy carbon electrode are presented in Figure 5. For both electrode materials, saturation of catalytic activity was not observed in the concentration range employed.

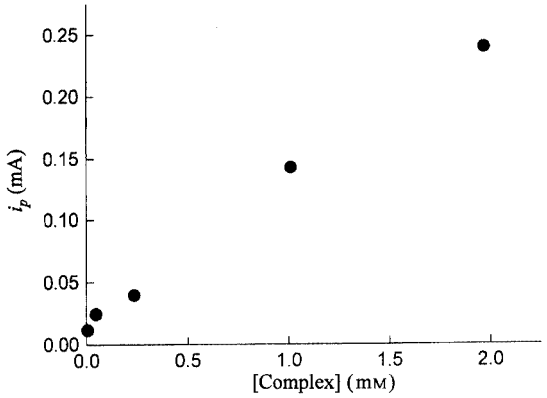

Figure 5. Effect of $[Ni_3(\mathbf{1})](ClO_4)_6$ concentration on the intensity of the catalytic wave for CO_2 electroreduction. Measured in MeCN/H_2O (9:1, v/v) with 0.1 M $NaClO_4$; glassy carbon electrode; scan rate, 100 mV s^{-1}.

It has been reported that the electrode material affects the electrocatalytic reduction of CO_2. For example, $[Ni^I(cyclam)]^+$ adsorbed on Hg is a better catalyst than that on a glassy carbon electrode.[52] For $[Ni_3(\mathbf{1})]^{6+}$ complex (2.0 mM), however, $i_p(CO_2)/i_p(N_2)$ measured on a glassy carbon electrode is 3.04 (Table 2) and that measured on the controlled growth mercury electrode is 2.12 (Table 3). This indicates that electrode-adsorption is less important for the present trinuclear catalyst.

Controlled potential coulometric experiments were carried out with CO_2-saturated MeCN/H_2O (9:1, v/v) solutions in the presence of $[Ni_3(\mathbf{1})]^{6+}$ and $[Ni(\mathbf{3})]^{2+}$ using a mercury pool electrode. The CO_2 reduction products were analyzed by GC both for gas and solution samples. Interestingly, CO was the only product, and other reduction products, including formate and H_2, were not detected. The amount of CO evolved depends on the applied voltage (Figure 6), with higher voltages producing more CO. In addition, CO production started to saturate within 0.5 h (Figure 7) and, therefore, the CO evolved after 30 min at the applied potential of −1.6 V vs. SCE was measured for various Ni^{II} catalysts (Table 4). The relative electrocatalytic efficiencies of the complexes, in terms of CO production per mol of catalyst, almost parallel the order of $i_p(CO_2)/i_p(N_2)$; $[Ni(cyclam)]^{2+} > [Ni_3(\mathbf{1})]^{6+} > [Ni(\mathbf{3})]^{2+}$ (Table 2). However, when the number of nickel centers is considered, $[Ni_3(\mathbf{1})]^{6+}$ is not as good as the monometallic complexes, $[Ni(cyclam)]^{2+}$ and $[Ni(\mathbf{3})]^{2+}$. $[Ni_2(biscyclam)]^{4+}$ produced only ca. half of the amount of CO gas or $HCOO^-$ per nickel center in DMF compared with that produced by the monometallic catalyst $[Ni(cyclam)]^{2+}$.[20] This is because an electrode(Hg)-adsorbed species was important in this electrocatalytic reaction, and only one metal center of $[Ni_2(biscyclam)]^{4+}$ was directly involved in each reaction cycle. The larger surface area of $[Ni_2(biscyclam)]^{4+}$ led to a smaller superficial surface density than that of $[Ni(cyclam)]^{2+}$, resulting in a poorer catalytic efficiency. For the present study, the TON value of $[Ni_3(\mathbf{1})]^{6+}$ (2.6) is slightly less than that of $[Ni(\mathbf{3})]^{2+}$ (3.9) (Table 4).

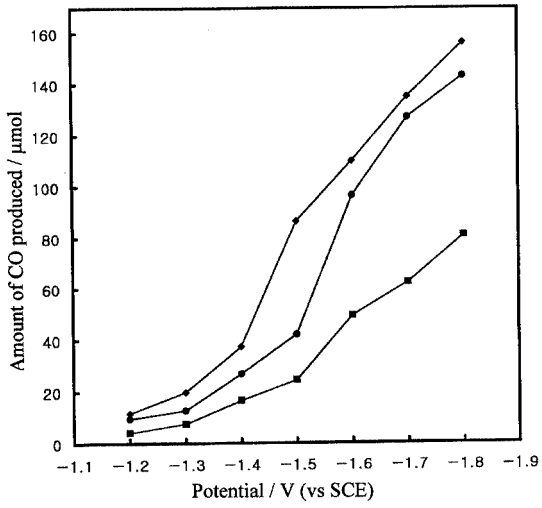

Figure 6. Effect of applied potential on CO production in the electrocatalytic reduction of CO_2. $[Ni_3(\mathbf{1})](ClO_4)_6$ (●); $[Ni(\mathbf{3})](ClO_4)_2$ (■); $[Ni(cyclam)](ClO_4)_2$, (◆). Volts vs. SCE; measured in 0.1 M $NaClO_4$ in MeCN/H_2O (9:1, v/v); electrolysis time, 30 min; 20 °C; CO_2 pressure, 1 atm; working electrode, Hg pool; concentration of catalyst, 1.0 mM.

The catalytic activity of the Ni^{II} complexes of **1** and **3** might be attributed to their ready reduction to Ni^I species. In CO_2 reduction catalyzed by cobalt macrocyclic complexes, the CO_2 adduct of the reduced complex was proposed as an intermediate, and a five-coordinate cobalt(I)–CO_2 was isolated from the reaction.[53–54] Hydrogen bonding between the coordinated CO_2 and the N–H of the macrocycle was important in stabilizing this ad-

 © 2003 Wiley-VCH Verlag GmbH & Co. KGaA, Weinheim

Table 4. CO production from the electrochemical reduction of CO_2 catalyzed by Ni^{II} complexes[a][b]

catalyst	applied potential volts vs. SCE	conc. of catalyst	CO produced in 0.5 h (μmol)	Turnovers[c] per 0.5 h at 20 °C	current efficiency (%)
$[Ni_3(\mathbf{1})]^{6+}$	−1.6	1.0 mM	96.5	2.6	96.2
$[Ni(\mathbf{3})]^{2+}$	−1.6	1.0 mM	49.2	3.9	95.3
$[Ni(cyclam)]^{2+}$	−1.6	1.0 mM	110	8.4	98.7

[a] Measured in MeCN/H_2O (9:1, v/v) with 0.1 M $NaClO_4$; 25 mL of solution with 25 μmol of complex; concentration of complex, 1.0×10^{-3} M; electrolysis time, 0.5 h. [b] Measured at 20 °C and 1 atm; working electrode, Hg pool. [c] Number corresponds to twice the number of mol of CO produced in 0.5 h per mol of nickel center.

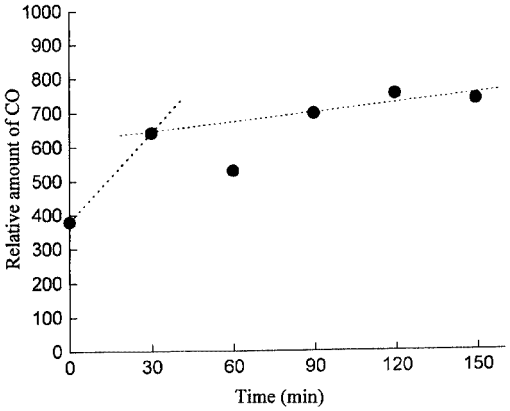

Figure 7. Relative amount of CO vs. MeCN detected by GC during the electroreduction of CO_2 catalyzed by $[Ni_3(\mathbf{1})](ClO_4)_6$; *t*, electrolysis time; applied potential, −1.6 V vs. SCE; glassy carbon electrode; data at $t = 0$ min is CO contained in the background CO_2 gas that is saturated with MeCN vapor

duct.[20] In the present study, it may be assumed that the Ni^{I} species binds CO_2 in the transition state, even though Ni^{II} species have poor coordinating ability. The secondary amines in the macrocycle **1** might promote the formation of the CO_2 adducts. It has been reported that the Ni^{II} complex of bismacrocyclic ligand **4** is highly active and selective catalyst for the photochemical reduction of CO_2[55] although the Ni^{II} species has poor binding ability for the solvent water molecule, similarly to $[Ni_3(\mathbf{1})]^{6+}$.

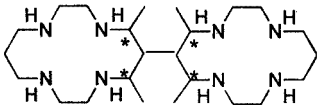

4

Conclusion

The trinuclear Ni^{II} complex $[Ni_3(\mathbf{1})]^{6+}$, in which three macrocyclic complexes are linked by a flexible tren bridge, was prepared and its X-ray structure was determined. The three Ni^{II} centers in $[Ni_3(\mathbf{1})]^{6+}$ are electrochemically independent and are easily reduced to Ni^{I} by reaction with Na(Hg) in MeCN. The complex $[Ni_3(\mathbf{1})](ClO_4)_6$ shows catalytic activity for the electrochemical reduction of CO_2 to CO in MeCN/H_2O (9:1, v/v), exhibiting a greater catalytic current than monometallic $[Ni(\mathbf{3})]^{2+}$ but producing less CO gas per nickel center. The catalytic efficiencies of $[Ni_3(\mathbf{1})]^{6+}$ and $[Ni(\mathbf{3})]^{2+}$, in terms of $i_p(CO_2)/i_p(N_2)$ and turnover number, are lower than that of $[Ni(cyclam)]^{2+}$.

Experimental Section

Reagents: All chemicals and solvents used in the syntheses were reagent grade and used without further purification. For the synthesis of Ni^{I} complex and the physicochemical measurements, reagents and solvents were purified according to the literature procedure[56] and deaerated prior to use. $[Ni(\mathbf{2})](ClO_4)_2$ and $[Ni(\mathbf{3})](ClO_4)_2$ were prepared and recrystallized according to the methods previously reported.[22] N_2 and CO_2 gases were deaerated and dried by passing through a BASF column and then a $CaCl_2$ column.

Measurements: IR spectra were recorded with a Bruker IFS48 FT IR spectrophotometer. Conductance was measured by a SUNTEX SC-170 conductivity meter. Electronic absorption spectra were obtained on a Beckman DU68 UV/Vis spectrophotometer equipped with an electronic temperature controller. ^{13}C NMR spectra were recorded on a Gemini-300 FT NMR spectrometer. EPR spectra were obtained on a Bruker ER 200E spectrometer. Elemental analyses (EA) were performed by the analytical laboratory of Seoul National University and by The Korea Basic Science Center, Seoul. Electrochemical experiments were performed on a BAS 100B/W electrochemical analyzer. Cyclic voltammetry, differential pulse voltammetry, and Osteryoung square-wave voltammetry were carried out in MeCN containing 0.1 M $(n\text{Bu})_4NPF_6$. The working electrode was a glassy carbon, the auxiliary electrode was a coiled platinum wire, and the reference electrode was Ag/Ag^+ (0.01 M in MeCN). The electrochemical reduction of the Ni^{II} complex to Ni^{I} was performed by controlled potential coulometry, carried out at −1.8 V vs. Ag/Ag^+ (0.01 M) in an MeCN solution of 0.1 M $(n\text{Bu})_4NPF_6$ under a N_2 atmosphere until the end current became 1% of the initial value.

Synthesis

Caution! *Perchlorate salts of metal complexes are potentially explosive and should be handled with care.*

$[Ni_3(\mathbf{1})](ClO_4)_6$: Tris(2-aminoethyl)amine (96%, 0.34 g, 2.2 mmol) and triethylamine (4.0 mL, 29 mmol) were added to a solution of $[Ni(\mathbf{2})](ClO_4)_2$ (3.05 g, 6.5 mmol) dissolved in hot MeOH/H_2O (2:1, v/v, 120 mL). The mixture was then heated at reflux. Excess 37% formaldehyde (3.76 mL, 50 mmol) mixed with MeOH (5 mL) was introduced dropwise over 1 hour and the solution was heated at reflux for an additional 2 h, during which time a yellow precipitate formed. The precipitate was filtered off from the hot solution and was washed with MeOH and dried in vacuo. It was then purified

 © 2003 Wiley-VCH Verlag GmbH & Co. KGaA, Weinheim

by recrystallization from H_2O/MeOH (1:1, v/v). The compound was not obtained as single crystals in any solvent. Yield: ca. 50% (5.31 g). $C_{39}H_{84}Cl_6N_{22}Ni_3O_{24}$ (1634.1): calcd. C 28.67, H 5.18, N 18.86; found C 29.29, H 5.30, N 18.87. UV/Vis: λ_{max} (ε) = 439 nm (251 cm^{-1} M^{-1}) in MeCN; 439 nm (273 cm^{-1} M^{-1}) in $MeNO_2$. IR (Nujol mull): $\tilde{\nu}$ = 3207 cm^{-1} (ν_{N-H}), 1100 cm^{-1} (br., ν_{Cl-O}). ^{13}C NMR ([D$_3$]nitromethane): δ = 41.5, 43.4, 49.4, 49.8, 62.4, 64.2, 69.8, 70.3 ppm.

Preparation of Single Crystals of $[Ni_3(1)](ClO_4)_3{\cdot}Cl_3{\cdot}10H_2O$: $[Ni_3(\mathbf{1})](ClO_4)_6$ (0.143 g) and NaCl (0.2 g) was added to a mixture of MeCN (6 mL), MeOH (6 mL), and H_2O (0.5 mL). The solution was then heated until the complex went into the solution. The resultant yellow solution was filtered while hot, and the filtrate was allowed to stand at room temperature until orange crystals formed, which were then filtered off, washed with mother liquor, and dried in air. $C_{39}H_{104}Cl_6N_{22}Ni_3O_{22}$ (1622.2): calcd. C 28.88, H 6.46, N 19.00; found C 28.17, H 6.29, N 18.69.

$[Ni^I{}_3(1)](ClO_4)_3$: The synthesis, experiments with, and manipulation of the Ni^I compound should be conducted under strict exclusion of air by using Schlenk lines since the compound is air-sensitive. **Method 1.** $[Ni_3(\mathbf{1})](ClO_4)_6$ (1.0 g, 0.6 mmol) was stirred with 5% Na(Hg) (3 g, 6.5 mmol) in MeCN (50 mL) for 20 min as the yellow complex slowly went into a red-purple solution. The solution was filtered, concentrated to one-third of the initial volume, and then allowed to stand in a refrigerator under strict exclusion of air until a red precipitate formed. The precipitate was then filtered off, washed with MeCN, and dried in vacuo. Yield: 70% (0.56 g). $C_{39}H_{84}Cl_3N_{22}Ni_3O_{12}$ (1335.7): calcd. C 35.07, H 6.34, N 23.07; found C 32.01, H 5.42, N 20.85. **Method 2.** $[Ni_3(\mathbf{1})](ClO_4)_3$ can be prepared in solution by bulk electrolysis of $[Ni_3(\mathbf{1})](ClO_4)_6$. A solution of $[Ni_3(\mathbf{1})](ClO_4)_6$ (1.0×10^{-3} M) was prepared in MeCN containing 0.1 M $(n\text{Bu})_4NPF_6$. A current was passed through the solution at -1.8 V vs. Ag/Ag$^+$ (0.01 M) for ca. 3 h until the intensity of end current became 1% of the initial value. The solution, which became reddish purple, was then frozen and its EPR spectrum was measured.

Electrochemical Reduction of CO_2: The electrochemical reduction of CO_2 was measured by cyclic voltammetry and controlled-potential coulometry. Cyclic voltammetry was performed on MeCN/H_2O (9:1, v/v) solutions of Ni^{II} complex (2.0 mM) containing 0.1 M $(n\text{Bu})_4NPF_6$ by using a glassy carbon or a controlled growth mercury electrode. Measurements were made with the solutions saturated with N_2 and then with CO_2. Controlled-potential coulometric experiments were performed at 20 °C by using a Hg pool as working electrode and a platinum plate as auxiliary electrode with a solution (25 mL) containing 1.0 mM of the Ni^{II} complex in a gas-tight electrolysis cell (internal gas volume; 32 mL). After CO_2 gas was bubbled through the solution for 30 min, a fixed potential (voltage range: -1.2 to -1.6 V vs. SCE) was applied for 30 min. The gas products were analyzed with a Hewlett−Packard 5890 Gas Chromatograph with a thermal conductivity detector. A Porapak Q column (8′ × 1/8″, 80−100 mesh) and He carrier gas were used for CO analysis. Molecular sieves, 13X column (7′ × 1/8″, 60−80 mesh), and N_2 gas were used for H_2 analysis. The CO (or H_2) peak was identified by comparing its retention time with that of standard CO (or H_2) gas. The CO was quantified by using a prepared standardization curve; the average of the three repeated experiments was obtained. Turnover frequencies were calculated as twice the number of mol of CO produced in 30 min per mol of electrocatalyst.

X-ray Crystallographic Study for $[Ni_3C_{39}H_{84}N_{22}](ClO_4)_3{\cdot}Cl_3{\cdot}10H_2O$: $C_{39}H_{104}Cl_6N_{22}Ni_3O_{22}$, M_r = 1622.27 g/mol^{-1}, a = 15.969(5) Å, b = 16.148(5) Å, c = 16.722(5) Å, α = 105.051(5)°, β = 114.812(5)°, γ = 94.227(5)°, V = 3697(2) Å^3, Z = 2, $d_{calcd.}$ = 1.457 g/cm^{-3}, triclinic, space group $P\bar{1}$ (No.2), μ = 1.052 mm^{-1}, $F(000)$ = 1708, T = 298 K. An orange rod-shaped single crystal (0.20 × 0.25 × 0.50 mm) was mounted on an Enraf Nonius Kappa CCD diffractometer. Data were collected with graphite-monochromated Mo-K_α radiation (λ = 0.71073 Å) through use of the ω-2θ scan technique. Preliminary orientation matrices and unit cell parameters were obtained from the peaks of the first ten frames and then refined using the whole data set. Frames were integrated and corrected for Lorentz and polarization effects using *DENZO*.[57] The scaling and global refinement of crystal parameters were performed by *SCALEPACK*.[57] No absorption correction was made. Of 16696 reflections measured in the range $2.68 < 2\theta < 55.22$, 9361 were assumed to be observed [$I > 2\sigma(I)$]. The crystal structures were solved by direct methods[58] and refined by full-matrix least-squares refinement using the *SHELXL-97* computer program.[59] The positions of all non-hydrogen atoms were refined with anisotropic displacement factors, except for oxygen atoms with severe thermal disorder: three from ClO_4^- anions (O4, O9, O10) and eight from water (OW2, OW3, OW5, OW6, OW7, OW8, OW9, OW10). All hydrogen atoms were allowed to ride on their bonded atoms with values of 1.2× those of the bonded atoms. Convergence of the 783 variable parameters by full-matrix, least-squares refinement on F^2 reaches R_1 = 0.0918 [$I > 2\sigma(I)$] and wR_2= 0.2554 with a goodness-of-fit of 1.061. ORTEP drawings were made with ORTEP-3 for windows.[60] Crystallographic data are summarized in Table S1, and selected bond lengths and angles are provided in Table S2, of the Supporting Information.

CCDC-194395 contains the supplementary crystallographic data for this paper. These data can be obtained free of charge at www.ccdc.cam.ac.uk/conts/retrieving.html [or from the Cambridge Crystallographic Data Centre, 12, Union Road, Cambridge CB2 1EZ, UK; Fax: (internat.) +44-1223/336-033; E-mail: deposit@ccdc.cam.ac.uk.

Acknowledgments

This work was supported by the Center for Molecular Catalysis, Korea Science and Engineering Foundation. Ms. Lee thanks the Ministry of Education, Republic of Korea for financial support through the Brain Korea 21 program.

[1] M. M. Halmann and M. Steinberg, *Greenhouse Gas Carbon Dioxide Mitigation: Science and Technology*, Lewis Publishers, Boca Raton, London, New York, Washington D. C. **1999**, Chapter 12.

[2] [2a] *Catalytic Activation of Carbon Dioxide* (Ed.: W. M. Ayers), ACS Symposium Series No 363, American Chemical Society, Washington D. C., **1988**. [2b] A. Behr, *Carbon Dioxide Activation by Metal*, VCH, New York, **1988**.

[3] H. Arakawa, M. Aresta, J. N. Armor, M. A. Barteau, E. J. Beckman, A. T. Bell, J. E. Bercaw, C. Creutz, E. Dinjus, D. A. Dixon, K. Domen, D. L. DuBois, J. Eckert, E. Fujita, D. H. Gibson, W. A. Goddard, D. W. Goodman, J. Keller, G. J. Kubas, H. H. Kung, J. E. Lyons, L. E. Manzer, T. J. Marks, K. Morokuma, K. M. Nicholas, R. Periana, L. Que, J. Rostrup-Nielson, W. M. H. Sachtler, L. D. Schmidt, A. Sen, G. A. Somorjai, P. C. Stair, B. R. Stults, W. Tumas, *Chem. Rev.* **2001**, *101*, 953−996.

[4] I. Taniguchi, in J. O′. M. Bockris (Ed.), *Modern Aspects of Electrochemistry, No. 20: Electrochemical and Photoelectrochemical Reduction of Carbon Dioxide*, Plenum Press, New York, **1989**, 327.

 © 2003 Wiley-VCH Verlag GmbH & Co. KGaA, Weinheim

[5] M. Beley, J.-P. Collin, R. Ruppert, J.-P. Sauvage, *J. Am. Chem. Soc.* **1986**, *108*, 7461.
[6] E. Kimura, M. Haruta, T. Koike, M. Shionoya, K. Takenouchi, Y. Iitaka, *Inorg. Chem.* **1993**, *32*, 2779.
[7] S. Meshitsuka, M. Ichikawa, K. Tamaru, *J. Chem. Soc., Chem. Commun.* **1974**, 158.
[8] B. Fischer, R. Eisenberg, *J. Am. Chem. Soc.* **1980**, *102*, 7361.
[9] E. Fujita, J. Haff, R. Sanzenbacher, H. Elias, *Inorg. Chem.* **1994**, *33*, 4627.
[10] S. C. Rasmussen, M. M. Richter, E. Yi, H. Place, K. J. Brewer, *Inorg. Chem.* **1990**, *29*, 3926.
[11] C. M. Bolinger, N. Story, B. P. Sullivan, T. J. Meyer, *Inorg. Chem.* **1988**, *27*, 4582.
[12] F. Abba, G. D. Santis, L. Fabbrizzi, M. Licchelli, A. M. M. Lanfredi, P. Pallavincini, A. Poggi, F. Ugozzoli, *Inorg. Chem.* **1994**, *33*, 1366.
[13] C. Arana, M. Keshavarz, K. T. Potts, H. D. Abruna, *Inorg. Chim. Acta* **1994**, *225*, 285.
[14] M. Shionoya, E. Kimura, Y. Iitaka, *J. Am. Chem. Soc.* **1990**, *112*, 9237.
[15] D. Behar, T. Dhanasekaran, T. Neta, C. M. Hosten, D. Ejeh, P. Hambright, E. Fujita, *J. Phys. Chem. A* **1998**, *102*, 2870.
[16] R. W. Hay, J. A. Crayston, T. J. Cromie, P. Lightfoot, D. C. L. de Alwis, *Polyhedron* **1997**, *16*, 3557.
[17] K. Bujno, R. Bilewicz, L. Siegfried, T. Kaden, *Electrochimica Acta* **1997**, *42*, 1201.
[18] K. Bujno, R. Bilewicz, L. Siegfried, T. Kaden, *J. Electrochim. Chem.* **1996**, *407*, 131.
[19] K. Bujino, R. Bilewicz, L. Siegfried, T. A. Kaden, *J. Electroanal. Chem.* **1998**, *445*, 47.
[20] J.-P. Collin, A. Jouaiti, J.-P. Sauvage, *Inorg. Chem.* **1988**, *27*, 1986.
[21] C. de Alwis, J. A. Crayston, T. Cromie, T. Eisenblätter, R. W. Hay, Y. D. Lampeka, L. V. Tsymbal, *Electrochimica Acta* **2000**, *45*, 2061.
[22] M. P. Suh, W. Shin, H. Kim, C. H. Koo, *Inorg. Chem.* **1987**, *26*, 1846.
[23] M. P. Suh, *Adv. Inorg. Chem.* **1997**, *44*, 93.
[24] M. P. Suh, B. Y. Shim, T.-S. Yoon, *Inorg. Chem.* **1994**, *33*, 5509.
[25] M. P. Suh, W. Shin, S.-G. Kang, M. S. Lah, T.-M. Chung, *Inorg. Chem.* **1989**, *28*, 1602.
[26] M. P. Suh, S. K. Kim, *Inorg. Chem.* **1993**, *32*, 3562.
[27] M. P. Suh, S.-G. Kang, V. L. Goedken, S. H. Park, *Inorg. Chem.* **1991**, *30*, 365.
[28] R. J. Geue, T. W. Hamblely, J. M. Harrowfield, A. M. Sargeson, M. R. Snow, *J. Am. Chem. Soc.* **1984**, *106*, 5478.
[29] G. A. Bottomley, I. J. Clark, I. I. Creasen, L. M. Engelhart, R. J. Geue, K. S. Hagen, J. M. Harrowfield, G. A. Lawrance, P. A. Lay, A. M. Sargeson, A. J. See, B. W. Skelton, A. H. White, F. R. Wilner, *Aust. J. Chem.* **1994**, *47*, 143.
[30] P. V. Bernhardt, E. J. Hayes, *J. Chem. Soc., Dalton Trans.* **1998**, 3539.
[31] M. Cheon, M. P. Suh, W. Shin, *Bull. Kor. Chem. Soc.* **1992**, *13*, 363.
[32] L. R. Furenlid, M. W. Renner, D. J. Szalda, E. Fujita, *J. Am. Chem. Soc.* **1991**, *113*, 883.
[33] F. V. Lovecchio, E. S. Gore, D. H. Busch, *J. Am. Chem. Soc.* **1974**, *96*, 3109.
[34] R. R. Gagne, D. M. Ingle, *Inorg. Chem.* **1981**, *20*, 420.
[35] N. Jurban, G. Ginzburg, H. Cohen, D. Meyerstein, *J. Chem. Soc., Chem. Commun.* **1982**, 517.
[36] N. Jubran, G. Ginzburg, H. Cohen, Y. Koresh, D. Meyerstein, *Inorg. Chem.* **1985**, *24*, 251.
[37] A. James, H. Espenson, *J. Am. Chem. Soc.* **1986**, *108*, 713.
[38] J. Lewis, M. Schroder, *J. Chem. Soc., Dalton Trans.* **1982**, 1085.
[39] P. Chmielewski, M. Grzeszczuk, L. Latos-Grazynski, J. Lisowski, *Inorg. Chem.* **1989**, *28*, 3546.
[40] A. M. Stolzenberg, M. T. Stershic, *Inorg. Chem.* **1987**, *26*, 3082.
[41] M. P. Suh, H. K. Kim, M. J. Kim, K. Y. Oh, *Inorg. Chem.* **1992**, *31*, 3620.
[42] D. J. Szalda, E. Fujita, R. Sanzenbacher, H. Paulus, H. Elias, *Inorg. Chem.* **1994**, *33*, 5855.
[43] M. P. Suh, Y. J. Lee, J. W. Jeong, *J. Chem. Soc., Dalton Trans.* **1995**, 1577.
[44] M. P. Suh, K. Y. Oh, J. W. Lee, Y. Y. Bae, *J. Am. Chem. Soc.* **1996**, *118*, 777.
[45] M. S. Ram, C. G. Riordan, R. Ostrander, A. L. Rheingold, *Inorg. Chem.* **1995**, *34*, 5884.
[46] J. S. Kim, J. H. Reibenspies, M. Y. Darensbourg, *J. Am. Chem. Soc.* **1996**, *118*, 4115.
[47] A. L. Rheingold, *Inorg. Chem.* **1996**, *35*, 5408.
[48] W. Grabarse, F. Mahlert, E. Duin, *J. Mol. Biol.* **2001**, *309*, 315.
[49] E. Pereira, L. Gomes, B. de Castro, *J. Chem. Soc., Dalton Trans.* **1998**, 629.
[50] T. Wondimagegn, A. Ghosh, *J. Am. Chem. Soc.* **2000**, *122*, 6375.
[51] A. J. Bard, L. R. Faulkner, *Electrochemical Methods, Fundamentals and Application*; John Wiley & Sons, Inc. New York, **1980**, Chapters 6 and 11.
[52] M. Fujihira, Y. Hirata, K. Suga, *J. Electroanal. Chem.* **1990**, *292*, 199.
[53] E. Fujita, D. J. Szalda, D. Creutz, N. Sutin, *J. Am. Chem. Soc.* **1988**, *110*, 4870.
[54] E. Fujita, C. Creutz, N. Sutin, D. Szalda, *J. Am. Chem. Soc.* **1991**, *113*, 343.
[55] K. Mochizuki, S. Manaka, I. Takeda, T. Kondo, *Inorg. Chem.* **1996**, *35*, 5132.
[56] D. D. Perrin, W. L. F. Armarego, *Purification of Laboratory Chemicals*, 3rd ed.; Pergamon Press: Oxford, England, **1988**.
[57] Z. Otwinowsky, W. Minor, *Processing of X-ray Diffraction Data Collected in Oscillation Mode, Methods in Enzymology* (Eds.: C. W. Carter, Jr. R. M. Sweet), Academic Press, **1996**, vol. *276* pp 307−326.
[58] G. M. Sheldrick, *Acta Crystallogr., Sect. A* **1990**, *46*, 467.
[59] G. M. Sheldrick, *SHELXL-97*, *Program for the Refinement of Crystal Structures*; University of Göttingen, Göttingen, Germany, **1997**.
[60] L. J. Farrugia, *ORTEP-3* for Windows, Version 1.07, Univerity of Glasgow, Scotland, **2001**.

Received September 30, 2002

 © 2003 Wiley-VCH Verlag GmbH & Co. KGaA, Weinheim

Large-Scale Synthesis of High Quality Trigonal Selenium Nanowires

Changhua An,[a,b] Kaibin Tang,*[a,b] Xianming Liu,[b] and Yitai Qian[a,b]

Keywords: Nanostructures / Semiconductors / Selenium

A direct and simple one-step hydrothermal reaction route has been developed for the synthesis of high quality trigonal selenium (t-Se) nanowires at 110 °C, with $(NH_4)_2S_2O_3$ and Na_2SeO_3 as starting materials in the presence of the surfactant sodium dodecyl sulfate (SDS). The diameter of the trigonal selenium nanowires can be tuned by carefully adjusting the initial feedstock concentration. The unusual chain like structure of the target material plays a key role in determining the final morphologies of the products. Several factors, such as initial concentration of the feedstock, the presence of surfactant, and the temperature which influences the quality of the t-Se nanowires, have been investigated. The optical properties of the t-Se nanowires with different diameters were examined by means of UV/Vis absorbance spectroscopy at room temperature. The investigation revealed that the absorbance peak for the t-Se nanowires with diameters of 20–40 nm shifts to the blue, relative to those for bulk t-Se nanowires (374 nm) and nanowires with diameters of 50–130 nm (306 nm).

(© Wiley-VCH Verlag GmbH & Co. KGaA, 69451 Weinheim, Germany, 2003)

Introduction

Nanoscale one-dimensional (1D) materials, such as nanotubes, nanowires and nanorods, have stimulated great interest due to their importance in basic scientific research and potential technological applications.[1−3] Moreover, new synthetic methods for the synthesis of semiconductor 1D nanostructures, such as nanowires or quantum wires, and their potential use in applications ranging from integrated circuit interconnectors to functional electronic and optical devices, have recently been investigated.[4−7] Besides significant technological advances due to their unique electrical, optical, and mechanical properties, nanowires can provide a material system to experimentally test fundamental quantum mechanical concepts.

For many applications, nanowires must be crystalline and largely defect free, with diameters in the range of 10−100 nm and lengths that greatly exceed their diameters. Many semiconductor nanowires, including Si, Ge, GaN, GaAs, InP etc., have been explored using various methods, such as laser ablation, arc-discharge, vapor phase transport processes, chemical vapor deposition and template-based routes.[8−12] On the other hand, chemical approaches (so called bottom-up techniques) may provide a more promising technique for the preparation of 1D nanostructure materials, in terms of versatility and potential for large-scale production, than conventional methods. Recently, there has been a strong trend towards the application of solution synthesis techniques for the preparation of 1D materials.[13−16] The hydrothermal method is one of the promising solution synthesis routes for the exploration of novel materials, due to the relatively mild conditions required, the one-step synthetic procedure, and the fact that the particle size can be controlled.[17] We have selectively prepared semiconducting famatinite (Cu_3SbS_4) nanofibers and tetradrite ($Cu_{12}Sb_4S_{13}$) nanoflakes via the mild solution synthesis route.[18]

Selenium is an important group VI semiconductor, which has found applications in rectifiers, solar cells, photographic exposure meters, and xerography. It is also used in the glass industry to eliminate bubbles and remove undesirable tints produced by iron.[19] In addition, selenium also has a high reactivity towards numerous chemicals that can potentially be exploited to convert selenium into other functional materials such as CdSe, ZnSe, Ag_2Se etc.[20] It is reasonable to assume that the availability of 1D selenium nanowires will introduce new types of applications or enhance the performance of currently existing devices, as a result of size restriction. The acicular and filament single crystals of selenium were studied 40 years ago.[21,22] Recently, Xia and coworkers have exploited sonochemical irradiation, and self-seeding solution-phase processes for the preparation of trigonal selenium nanowires.[23,24] Zhang et al. prepared α-monoclinic selenium nanowires via the decomposition of selenodiglutathiones.[25] Abdelouas and co-workers have also attempted to employ a reduction reaction route using cytochrome c_3 for the synthesis of monoclinic Se

[a] Department of Chemistry, University of Science and Technology of China,
Hefei, Anhui 230026, P.R. China
E-mail: kbtang@ustc.edu.cn
anch@mail.ustc.edu.cn
[b] Structure Research Laboratory, University of Science and Technology of China,
Hefei, Anhui 230026, P.R. China

nanowires.[26] More recently, Xie et al. reported a laser ablation method for the preparation of trigonal selenium nanorods at different temperatures.[27]

In this paper, we have designed a low-temperature hydrothermal synthesis route for the direct production of high quality crystalline trigonal selenium nanowires, using $(NH_4)_2S_2O_3$ and Na_2SeO_3 as starting materials in the presence of the surfactant sodium dodecyl sulfate (SDS). The initial concentration of feedstock solution is a key factor which influences the quality of the as-synthesized nanowires. The high yields of the products, without using complex apparatus, and the low reaction temperature employed, means that this simple method has good prospects for use in related future applications. The hydrothermal synthesis of t-Se nanowires is associated with the following chemical reaction.

$$(NH_4)_2S_2O_3 + Na_2SeO_3 \xrightarrow[110^{o}\,C]{SDS} Se + (NH_4)_2SO_3 + Na_2SO_3$$

In this process, the low solubility of selenium in water at 110 °C may be the driving force for this reaction to go to completion.

Results and Discussion

The obtained samples were weighed; the yields of the products were about 95%, based on the amount of Na_2SeO_3. Figure 1 (A) shows a typical XRD pattern of the sample prepared using 0.2 M feedstock in the presence of SDS at 110 °C for 18 h. All of the strong and sharp reflection peaks can readily be indexed to a single phase of trigonal-structured selenium (space group $P3_121$ (152) with infinite, helical chains of selenium atoms packed parallel to each other along the *c*-axis), with cell parameters a = 0.4364 nm and c = 0.4949 nm. These values are in agreement with the values reported in the literature (JCPDS Cards No. 73−0465). The product formed is further confirmed by XPS and Raman spectroscopy. Figure 1 (B) shows the XPS of the as-synthesized product. The binding energy at 54.8 eV, corresponding to Se3d, is the characteristic peak for elemental selenium.[28] Figure 1 (C) presents the Raman spectrum of the sample. The resonance peak at 237 cm^{-1} is a characteristic signature of trigonal selenium, which can be assigned to the vibration of the Se helical chain.[23] In comparison, the characteristic Raman peaks for monoclinic selenium and α-Se are at 256 cm^{-1} and 264 cm^{-1}, respectively.[29] These results, obtained from XRD, XPS and Raman spectroscopy, indicate that phase-pure t-Se is successfully produced via the present one-step synthetic route.

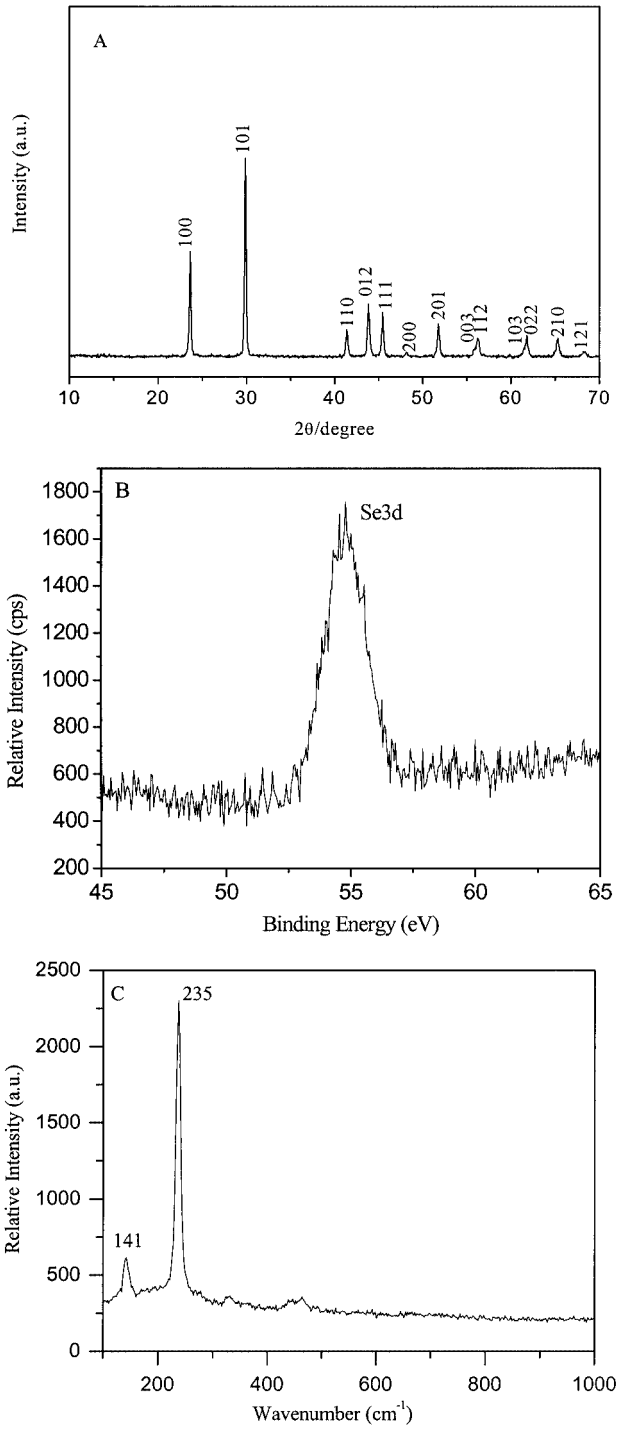

Figure 1. (A) Typical XRD pattern of the sample with 0.2 M feedstock solution in the presence of SDS; (B) XPS spectrum of the same sample as used in A; (C) Raman spectrum of the same sample as used in A

Figure 2 (A−C) provide SEM and TEM images of the same product as that presented in Figure 1. These images clearly show that the sample obtained is composed of a large number of nanowires, with a high aspect ratio (length/diameter). The uniformity in lateral dimension, the level of perfection, and the copiousness in quantity, show a good growth environment for the selenium nanowires in our system. Their lengths range from several micrometers to tens of micrometers, and their diameters are 20−40 nm, which is in agreement with that of micelles formed by SDS in aqueous solution.[30] The aspect ratio of the nanowires is in the range of several hundreds, which may be a useful feature in related applications. The inset of Figure 2 (C) shows the

 © 2003 Wiley-VCH Verlag GmbH & Co. KGaA, Weinheim

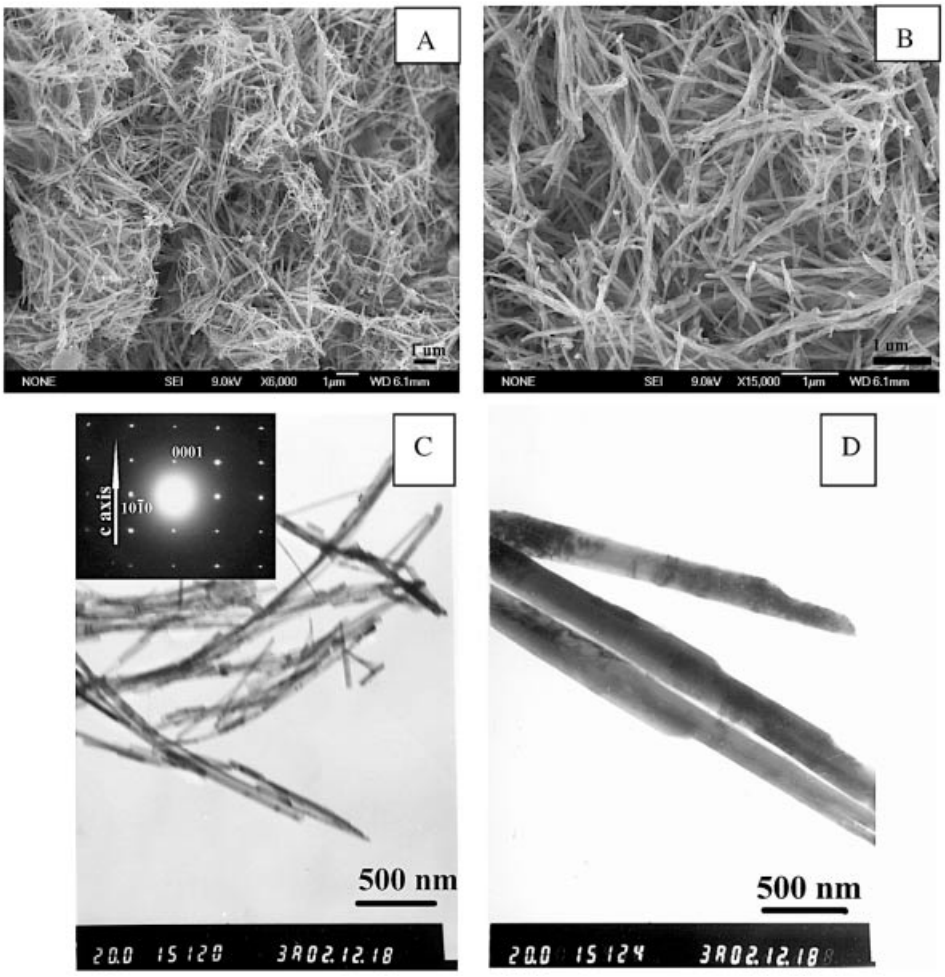

Figure 2. (A−B) Low and high magnification of the SEM images of the t-Se nanowires with 0.2 M feedstock solution in the presence of SDS; (C) TEM image of the same sample as presented in Figure 1A and ED pattern from a single nanowire (inset); (D) TEM image of the sample prepared with 0.1 M feedstock solution in the presence of SDS

selected-area electron diffraction (SAED) pattern obtained from a single nanowire, and exhibits the single-crystalline nature of nanowires. The two-fold rotational symmetry associated with this pattern indicates that these t-Se nanowires had predominately grown along the [001] direction (*c*-axis), with the helical chains of the Se atoms parallel to the longitudinal axis.[31] We have also carried out extensive investigations on more individual nanowires using ED, the results of which demonstrate that the as-synthesized sample is single-crystalline.

Selenium nanowires with larger diameters can be obtained when the initial concentration of the feedstock is reduced. Figure 2 (D) is a TEM image of the sample prepared with 0.1 M feedstock solution, whilst keeping the other conditions identical to those in the synthesis of the sample presented in Figure 1. It can be seen that the diameter (50−300 nm) of this product is much larger than that of the product synthesized at high initial concentrations. The length of the nanostructures is in the range of 2−5 μm. The corresponding aspect ratio ranges from 40 to 100. The experimental results demonstrate that the lateral dimensions of the products are strongly dependent on the initial concentrations of the feedstock. Such a dependence can be employed to control the lateral dimensions of the nanowires in the range of 20−300 nm. There have been some similar reports that show that increasing the initial concentration of reagents will favor the formation of 1D nanostructures with a high aspect ratio. Alivisatos and co-workers have systematically studied the conditions for the shape-controlled growth of CdSe nanocrystals in a mixed hexylphosphonic acid (HPA) and trioctylphosphane oxide (TOPO) surfactant system. Their results indicated that as the monomer concentration is increased, the average aspect ratio of the CdSe nanorods increase rapidly.[32] Whilst preparing Te nanorods in a sodium dodecyl benzenesulfate (NaDDBS) surfactant system, Liu et al.[33] also found that on increasing the initial concentration of $(NH_4)_2TeS_4$, the diameter of the 1D nanostructures decrease, and the nanowires will favorably be formed when a high concentration of $(NH_4)_2TeS_4$ is used. The observed phenomena in our experiments can be explained according to the previous reports.[32] At a given temperature, the high reagent concentration can provide enough selenium nuclei seeds, with a relatively narrow size distribution as the starting point. The

 © 2003 Wiley-VCH Verlag GmbH & Co. KGaA, Weinheim

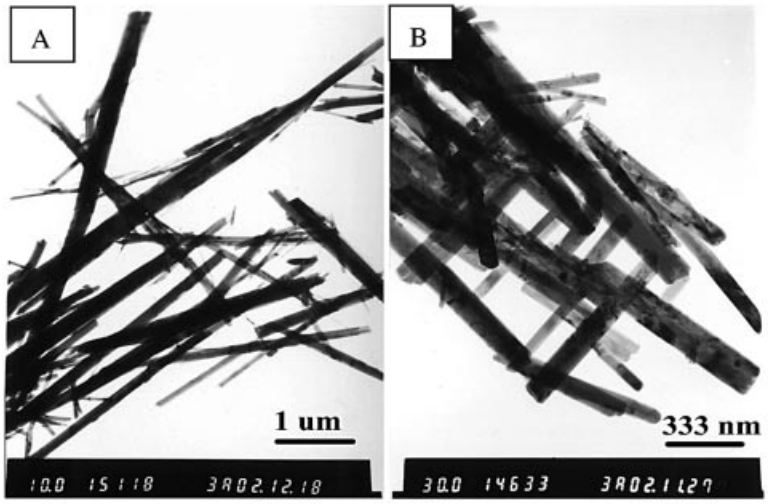

Figure 3. TEM images of the products obtained with different initial concentrations of feedstock solution in the absence of SDS (A) 0.2 M (B) 0.1 M

growth of the particles will be along the unique *c*-axis of t-Se, and finally results in high quality nanowires.

In contrast, we also prepared samples in the absence of surfactant, whilst keeping the other conditions constant. As shown in Figure 3, the TEM image of the sample synthesized using 0.2 M feedstock without using the surfactant displays uniform nanorods with diameters of 50−120 nm and lengths of up to 5 μm. When the concentration is decreased to 0.1 M, the diameters of the obtained sample are found to be 35−130 nm with lengths of about 2 μm [Figure 3 (B)]. The concentration-dependence of the diameter in the absence of surfactant is much less pronounced than that in the presence of surfactant. Hence, the surfactant is an important factor for the formation of high quality t-Se nanowires.

UV/Vis absorbance spectroscopy was used to characterize the samples. Figure 4 (A−C) shows the absorbance spectra of the obtained trigonal selenium nanowires with mean diameters of 20−40 nm, 50−120 nm and bulk t-Se, respectively. The results show that the absorbance peak for the t-Se nanowires with diameters of 20−40 nm (285 nm) is shifted to the blue, relative to those of the nanowires with diameters of 50−130 nm (306 nm) and bulk t-Se nanowires (374 nm). This shift can be attributed to the smaller diameters and larger aspect ratios of the nanowires.[34,35] Moreover, it should be noted that there is a large blue shift for both nanowires relative to that for the reported Se nanoparticles (620 nm).[19] As already known, different preparation methods have important effects on material microstructure and physical properties.[36] We believe that the optical properties of t-Se nanoparticles might be associated with its morphology and size. Thus, different optical characteristics are seen for t-Se nanowires and nanoparticles. Of course, our present understanding of the optical mechanism of crystalline t-Se nanoparticles is still limited, and more in-depth studies are underway.

Using the soft solution process, one-dimensional trigonal selenium nanostructures (nanowires or nanorods) have successfully been obtained, regardless of whether surfactants are used. In this solution-solid transformation, the morphology of the final product is determined mainly by the anisotropic nature of the target material. In other words, the 1D characteristic of the infinite, helical chains of selenium in the trigonal phase provides a natural template to define and guide the growth along one particular axis (*c*-axis). However, SDS and a relatively high initial concentration of feedstock solution are important factors for the formation of high quality trigonal selenium nanowires. The surfactant may act as a "size-tunable" reagent for the formation of selenium nanowires. A similar observation was reported for the preparation of γ-Al_2O_3 nanofibers with poly(ethylene oxide) as the surfactant.[37] We have also investigated the effect of temperature on the formation of t-Se nanowires. When the temperature is below 100 °C, the reaction is very slow and does not go to completion, and the yield is very low. When the temperature is above 130 °C, the size of the products is larger. Figure 5 shows a TEM image of the sample obtained at 150 °C using 0.2 M feedstock solution in the presence of SDS. It can be seen that the diameter of the rod-like crystal is up to 500 nm. This phenomena can be attributed to deterioration with increase in hydrothermal temperature. Therefore, 110 °C was chosen as the optimum temperature for the hydrothermal synthesis of t-Se nanowires.

Conclusion

A simple and convenient hydrothermal reaction route has been developed for the synthesis of high quality trigonal selenium nanowires in the presence of SDS. Several factors such as initial concentration of the feedstock, the presence of surfactant, and the temperature which influences the quality of the t-Se nanowires have been investigated. The unusual anisotropic structure of trigonal selenium provides a natural template to determine the morphology of the final products. The present route may be extended to the direct

 © 2003 Wiley-VCH Verlag GmbH & Co. KGaA, Weinheim

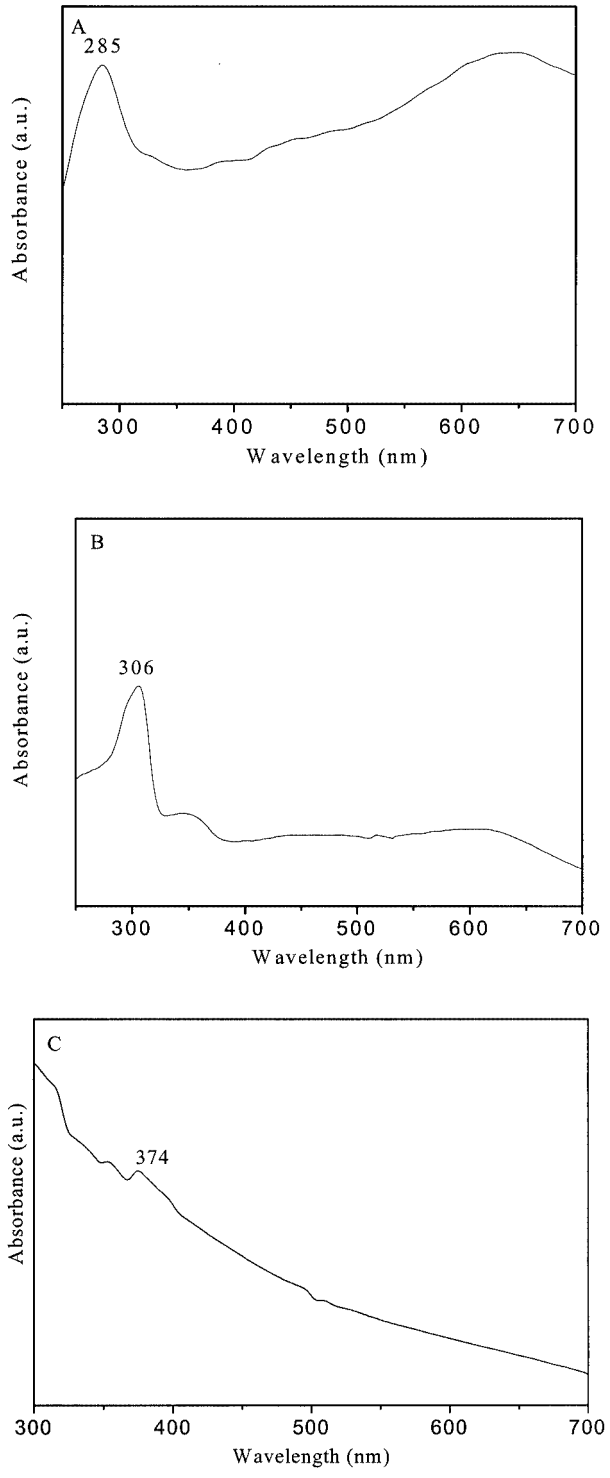

Figure 4. UV/Vis absorbance spectra of t-Se nanowires with different diameters (A) 20−40 nm; (B) 50−120 nm; (C) bulk t-Se

synthesis of 1D selenides. Moreover, the as-synthesized selenium nanowires may be useful in providing templates for the formation of 1D nanostructures of many technologically important materials, by reacting with other chemicals. The related studies are in progress and will be reported later.

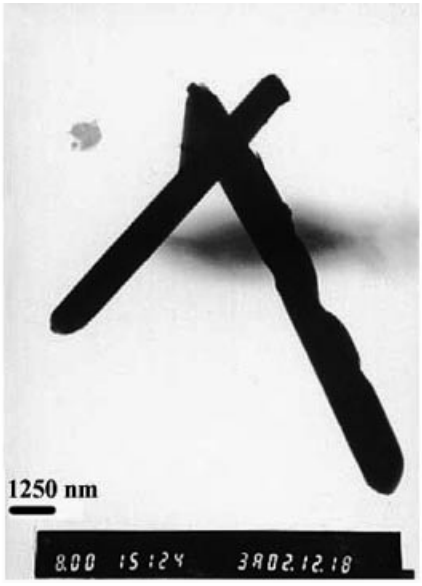

Figure 5. TEM image of the sample obtained at 150 °C

Experimental Section

All chemical reagents in this work, such as $NH_4S_2O_3$, Na_2SeO_3 and sodium dodecyl sulfate (SDS), were of A.R. grade and purchased from Shanghai Chemical Company, China. They were used as received without further purification.

Preparation of High Quality t-Se Nanowires

In a typical procedure, equivalent molar amounts of $(NH_4)_2S_2O_3$ and Na_2SeO_3 (10 mmol) were added to an aqueous solution (50 mL) of SDS (0.325 g). The solution was stirred for approximately 20 min until the solids had completely dissolved, and a 0.2 M homogeneous solution was formed. The solution was then transferred to a Teflon-lined autoclave (capacity of 60 mL). The autoclave was sealed and heated at 110 °C for 16−18 h, after which the autoclave was allowed to cool to room temperature naturally over a period of about 5 h. The resulting precipitate was rinsed with distilled water and absolute alcohol several times. After drying in vacuo at 40 °C for 4 h, the orange-red powders were collected for characterization.

For comparison, we prepared samples in the absence of surfactant whilst keeping the other conditions identical to those used in the preparation of high quality t-Se nanowires. Moreover, studies on the effect of initial concentrations (0.2 M, and 0.1 M) of feedstock solution on the resulting products were also carried out. The detailed experimental conditions were also similar to those used in the synthesis of high quality t-Se nanowires, with the exception that the initial feedstock concentrations were varied.

Sample Characterization

The phase composition and structure of the as-synthesized products were examined by X-ray powder diffraction (XRD), operating on a Japan Dmax-γA X-ray diffractometer with graphite-monochromated Cu-K_α radiation (λ = 1.54178 Å). X-ray photoelectron spectra (XPS) were recorded on a VGESCALAB MKII X-ray photoelectron spectrometer, using non-monochromated Mg-K_α radiation as the excitation source. The Raman spectra were recorded on a Jobin Yvon HR800 (Horiba group), using 514.5 nm as the excitation line. The morphology and particle size of the final

 © 2003 Wiley-VCH Verlag GmbH & Co. KGaA, Weinheim

products were determined by scanning electron microscopy (SEM), using a JEOL-6700F scanning electron microanalyzer, and Transmission electron microscopy (TEM), using a Hitachi H-800 transmission electron microscope with a tungsten filament and an accelerating voltage of 200 KV. Room temperature absorbance spectra were recorded on a Shimadzu UV/Vis absorbance diode array spectrometer, using 1 cm quartz cuvettes. The samples were prepared by dispersing t-Se nanowires in absolute alcohol.

Acknowledgments

The project was supported by the Chinese Natural Science Foundation. The 973 project of China and the State key project of fundamental research for nanomaterials and nanostructures is gratefully acknowledged.

[1] J.-F. Colomer, G. Bister, I. Willems, Z. Kónya, A. Fonseca, G. Van Tendeloo, J. B. Nagy, *Chem. Commun.* **1999**, 1343−1344.
[2] J. Hu, T. W. Odom, C. M. Lieber, *Acc. Chem. Res.* **1999**, *32*, 435−445.
[3] Y. Wu, H. Yan, P. Yang, *Chem. Eur. J.* **2002**, *8*, 1260−1268.
[4] X. Duan, Y. Huang, Y. Cui, J. Wang, C. M. Lieber, *Nature* **2001**, *409*, 66−69.
[5] Y. Q. Zhu, W. K. Hsu, H. W. Kroto, D. R. M. Walton, *Chem. Commun.* **2001**, 2184−2185.
[6] J. Hu, M. Ouyang, P. Yang, C. M. Lieber, *Nature* **1999**, *399*, 48−51.
[7] J. D. Holmes, K. P. Johnston, R. C. Doty, B. A. Korgel, *Science* **2000**, *287*, 1471−1473.
[8] M. Yazawa, M. Koyuchi, A. Muto, M. Ozaya, K. Hiruma, *Appl. Phys. Lett.* **1992**, *61*, 2051−2053.
[9] C.-C. Chen, C.-C. Yeh, *Adv. Mater.* **2000**, *12*, 738−741.
[10] Y. C. Choi, W. S. Kim, Y. S. Park, S. M. Lee, D. J. Bae, Y. H. Lee, G.-S. Park, W. B. Choi, N. S. Lee, J. M. Kim, *Adv. Mater.* **2000**, *12*, 746−750.
[11] Y. Li, G. W. Meng, L. D. Zhang, F. Philipp, *Appl. Phys. Lett.* **2000**, *76*, 2011−2013.
[12] Y. Wu, P. Yang, *J. Am. Chem. Soc.* **2001**, *123*, 3165−3166.
[13] X. Peng, L. Manna, W. Yang, J. Wickham, E. Scher, A. Kadavanich, A. P. Alivisatos, *Nature* **2000**, *404*, 59−61.
[14] J. Zhang, L. Sun, C. Liao, C. Yan, *Chem. Commun.* **2002**, 262−263.
[15] B. H. Hong, S. C. Bae, C.-W. Lee, S. Jeong, K. S. Kim, *Science* **2001**, *294*, 348−351.
[16] B. Mayers, Y. Xia, *J. Mater. Chem.* **2002**, *12*, 1875−.
[17] S. Feng, R. Xu, *Acc. Chem. Res.* **2001**, *34*, 239−247.
[18] C. An, Y. Jin, K. Tang, Y. Qian, *J. Mater. Chem.* **2003**, *13*, 301−303.
[19] J. A. Johnson, M. L. Saboungi, P. Thiyagarajan, R. Csencsits, D. Meisel, *J. Phys. Chem. B* **1999**, *103*, 59−63.
[20] D. M. ChizhiRov, V. P. Shchastlivyi, *Selenium and Selenides*, Collets publishing, London, **1968**.
[21] F. Noboru, *J. Sci. Hiroshima Univ.* **1961−1970**, 25−34.
[22] Ya. L. Stetsiv, I. D. Nabitovich, Ya. V. Voloshchuk, *Vestnik Lvovskogo Politekhnicheskogo Instituta* **1969**, *No. 34*, 31−36.
[23] B. Gates, Y. Yin, Y. Xia, *J. Am. Chem. Soc.* **2000**, *122*, 12582−12583.
[24] B. Gates, B. Mayers, A. Grossman, Y. Xia, *Adv. Mater.* **2002**, *14*, 1749−1752.
[25] X. Gao, T. Gao, L. Zhang, *J. Mater. Chem.* **2003**, *13*, 6−8.
[26] A. Abdelouas, W. Gong, W. Lutze, J. A. Shelnutt, R. Franco, I. Moura, *Chem. Mater.* **2000**, *12*, 1510−1512.
[27] Z. Jiang, Z. Xie, S. Xie, X. Zhang, R. Huang, L. Zheng, *Chem. Phys. Lett.* **2003**, *368*, 425−429.
[28] X. Gao, J. Zhang, L. Zhang, *Adv. Mater.* **2002**, *14*, 290−293.
[29] B. Gates, B. Mayers, B. Cattle, Y. Xia, *Adv. Funct. Mater.* **2002**, *12*, 219−227.
[30] Y. J. Xiong, Y. Xie, J. Yang, R. Zhang, C. Z. Wu, G. A. Du, *J. Mater. Chem.* **2002**, *12*, 3712−3716.
[31] J. Stuke, in *Selenium* (Eds: R. A. Zingaro, W. C. Cooper), Van Nostrand Reinhold, New York **1994**.
[32] L. Manna, E. C. Scher, A. P. Alivisatos, *J. Am. Chem. Soc.* **2000**, *122*, 12700−12706.
[33] Z. P. Liu, Z. K. Hu, Q. Xie, B. J. Yang, J. Wu, Y. T. Qian, *J. Mater. Chem.* **2003**, *13*, 159−162.
[34] B. M. I. Van der Zande, L. Pages, R. A. M. Hikmet, A. van Blaaderen, *J. Phys. Chem. B* **1999**, *103*, 5761−5767.
[35] Y. Liu, J. Cao, J. Zeng, C. Li, Y. Qian, S. Zhang, *Eur. J. Inorg. Chem.* **2003**, 644−647.
[36] Y. D. Li, X. F. Duan, H. W. Liao, Y. T. Qian, *Chem. Mater.* **1998**, *10*, 17−18.
[37] M. Y. Zhu, J. D. R. Riches, J. C. Barry, *Chem. Mater.* **2002**, *14*, 2086−2093.

Received March 6, 2003

 © 2003 Wiley-VCH Verlag GmbH & Co. KGaA, Weinheim

EurJIC
European Journal of Inorganic Chemistry

Issue 18/2003

Pages 3257–3500

Papers available ahead of print in Early View at www.interscience.wiley.com

Earliest available Table of Contents:
Automatically, free of charge by e-mail through
www.interscience.wiley.com/alerts

COVER PICTURE

The cover picture shows an Li_2N_2 unit which is prevented by the bulk of the aryl substituents from stacking with another to form a cubic cluster. The diethyl ether solvent traps this fragment of a molecule which, in the absence of diethyl ether, precipitates as a powder, possibly by lateral association of Li_2N_2 rings to form an infinite ladder in a manner first suggested by Ronald Snaith, whose memory is honoured in this special edition of EurJIC. Details are presented in the article by F. Mair et al. on p. 3464 ff.

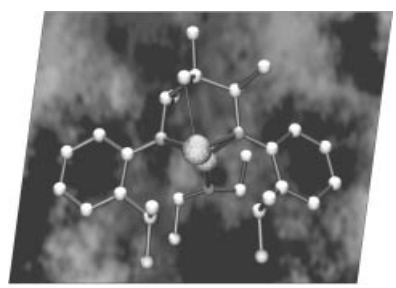

REMINISCENCE

Contents

3271 **R. E. Mulvey, K. Wade**

Ron Snaith (1947–2000), Inspirational Alkchemist and Altruist

 © 2003 Wiley-VCH Verlag GmbH & Co. KGaA, Weinheim

MICROREVIEWS

3279 **E. L. Doyle, L. Riera, D. S. Wright***

Toroidal Main Group Macrocycles: New Opportunities for Cation and Anion Coordination

Keywords: Coordination chemistry / Macrocycles / Main group elements / Synthesis

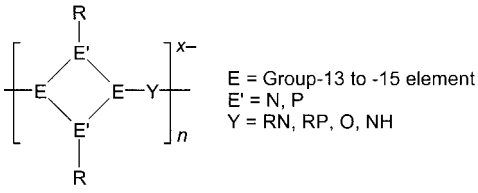

3291 **A. E. H. Wheatley**

The Directed Lithiation of Benzenoid Aromatic Systems

Keywords: Aromaticity / Directing group / Lithium / Solid-state structure / Solution structure

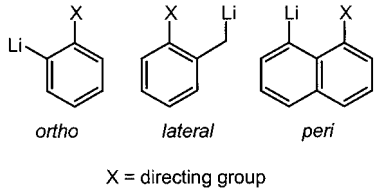

SHORT COMMUNICATIONS

3305 **P. C. Andrews*, M. Maguire, E. Pombo-Villar**

Synthesis and Structure of a Monomeric Chiral Lithium Dialkylaluminium Amide Derived from Schöllkopf's Bis-lactim Ether and α-(Methylbenzyl)benzylamine

Keywords: Lithium / Aluminium / Chirality / Amides / Structure elucidation

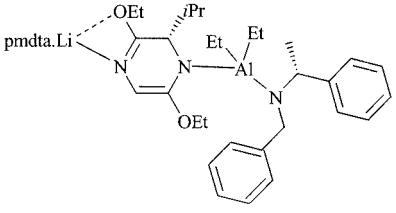

3309 **F. Rivals, A. Steiner***

Synthesis and Structure of $[\{(THF)_2Li\}_3Me_2Al\{(PhNH)_2(PhN)_4P_3N_3\}]$, the First Mixed-Metal Phosphazenate Complex

Keywords: Phosphazenes / Phosphazenates / Aluminium / Lithium / Heterometallic complexes

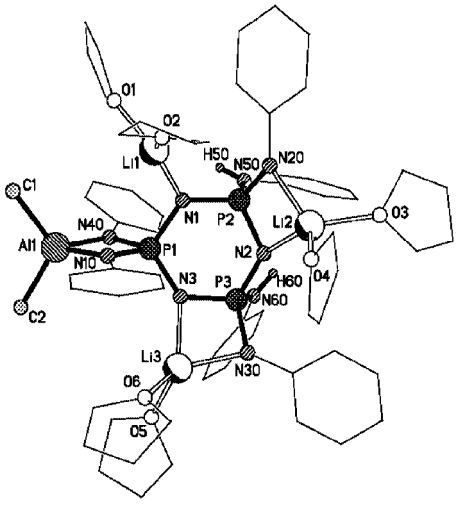

3314 **T. Chivers,* G. Schatte**

Cooperative THF Ring-Opening by $B(C_6F_5)_3$ and a Tellurium Diimide Dimer

Keywords: N ligands / Ring opening / Lewis acids / Boron / Tellurium

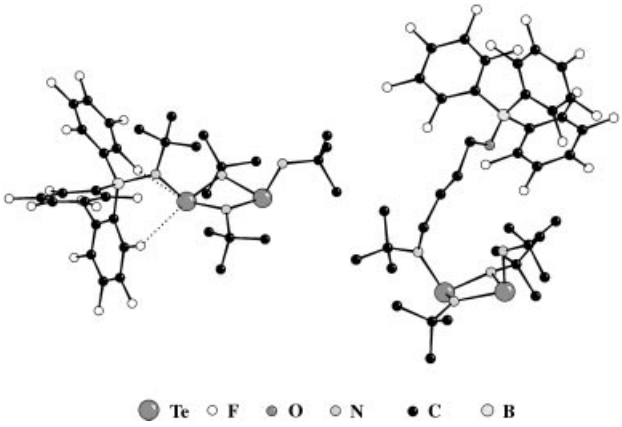

FULL PAPERS

3319 **S. Blair, K. Izod,* W. Clegg, R. W. Harrington**

Organomagnesium Phosphanide "Grignard" Analogues − Synthesis, Structural Characterisation and Solution Behaviour of [BuMg{P(CH[SiMe$_3$]$_2$)(C$_6$H$_3$-2-OMe-3R)}]$_2$ [R = H, Me]

Keywords: Magnesium / P ligands / Grignard reaction / Rearrangement

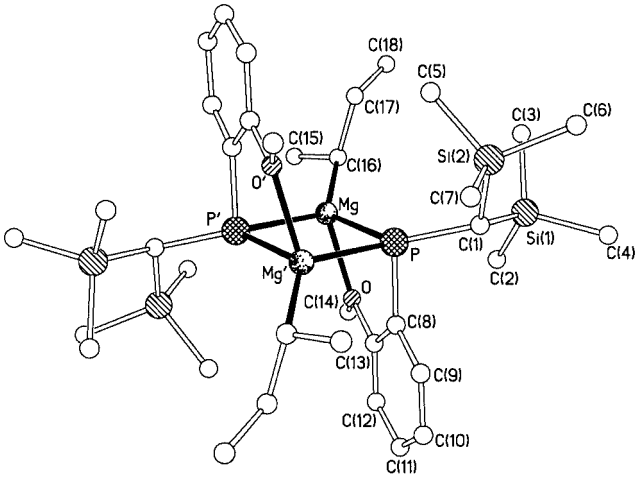

3325 **R. Nassar, A. M. Beatty, K. W. Henderson***

Sodiated β-Diphosphonate Carbanions: Characterization of the Tetrameric Cubane and the Hexameric Ladder Complexes [{(*i*PrO)$_2$P(O)}$_2$CHNa]$_4$ and [{(EtO)$_2$P(O)}$_2$CHNa]$_6$

Keywords: Alkali metals / Sodium / Cage compounds / Chelates / O Ligands

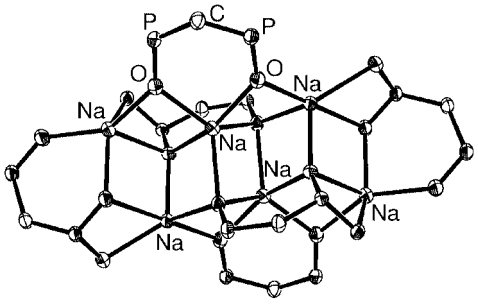

3332 **C. Eaborn, I. B. Gorrell, P. B. Hitchcock, J. D. Smith***

The First Structurally Characterized Diorganoaluminate

Keywords: Aluminum / Silicon / Hydride ligands / Lithium

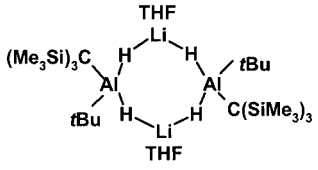

 © 2003 Wiley-VCH Verlag GmbH & Co. KGaA, Weinheim

3336 **I. L. Fedushkin,* A. A. Skatova, V. A. Chudakova, G. K. Fukin, S. Dechert, H. Schumann***

Monomeric Magnesium and Calcium Complexes Containing the Bidentate, Dianionic 1,2-Bis[(2,6-diisopropylphenyl)imino]acenaphthene Ligand

Keywords: Magnesium / Calcium / N ligands / Anions / Dianions

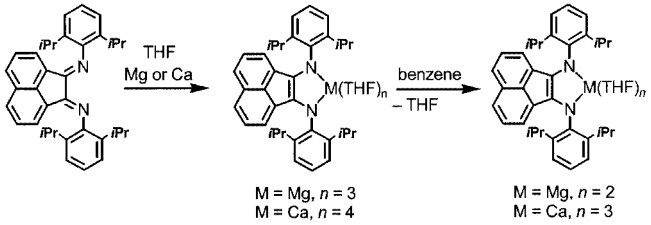

3347 **E. Hevia, F. R. Kenley, A. R. Kennedy, R. E. Mulvey,* R. B. Rowlings**

Solvent-Free and TMEDA-Solvated Mixed Alkali Metal-Magnesium Tris-diisopropylamides

Keywords: Alkali metals / N ligands / Heterometallic complexes / Potassium / Magnesium

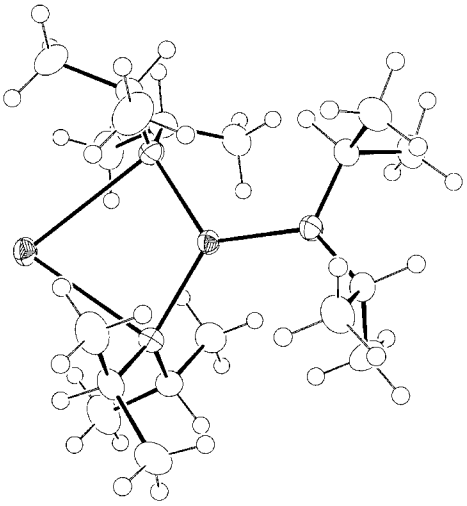

3354 **P. C. Andrikopoulos, D. R. Armstrong, A. R. Kennedy, R. E. Mulvey, C. T. O'Hara,* R. B. Rowlings**

Synthesis, Structure and Theoretical Studies of the Hydrido Inverse Crown $[K_2Mg_2(NiPr_2)_4(\mu\text{-}H)_2\cdot(toluene)_2]$: a Rare Example of a Molecular Magnesium Hydride with a Mg-$(\mu$-H$)_2$-Mg Double Bridge

Keywords: Potassium / Magnesium / N ligands / Hydride ligands / Density functional calculations

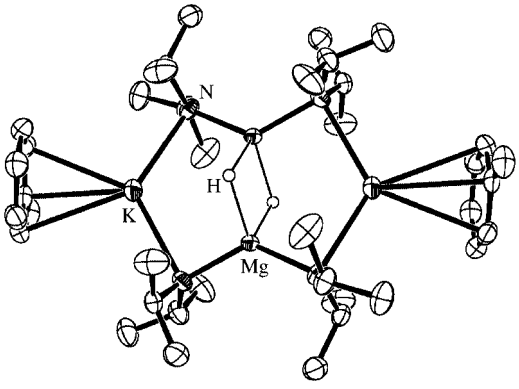

3363 **D. R. Armstrong,* R. P. Davies, R. Haigh, M. A. Hendy, P. R. Raithby, R. Snaith, A. E. H. Wheatley***

A Solid-State, Solution, and Theoretical Structural Study of Kinetic and Thermodynamic Lithiated Derivatives of a Simple Diazomethane and Their Reactivities Towards Aryl Isothiocyanates

Keywords: Density functional calculations / Diazomethane / Lithium / Solid-state structures / Solution structure

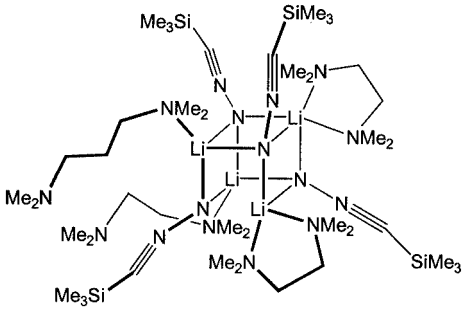

 © 2003 Wiley-VCH Verlag GmbH & Co. KGaA, Weinheim

3376 **C. Selinka, D. Stalke***

Heteroaromatic-Substituted Mono- and Bis(triimidosulfonates)

Keywords: Heterocycles / Lithium / N ligands / S ligands / Sulfur

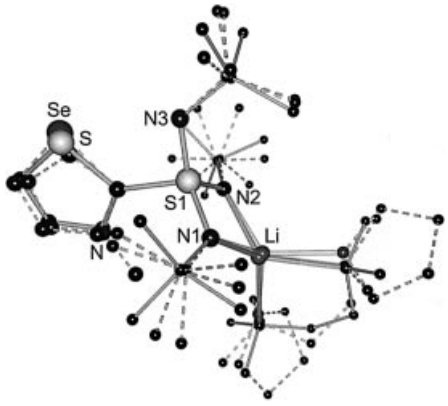

3383 **M. J. Harvey, K. T. Quisenberry, T. P. Hanusa,* V. G. Young Jr.**

A Homologous Series of Base-Free Organo-(alkaline-earth) Metallocenes: Synthesis and Molecular Structures of $[1,2,4\text{-}(SiMe_3)_3C_5H_2]_2$-(Ca, Sr, Ba)

Keywords: Alkaline-earth metals / Metallocenes / Solid-state structures

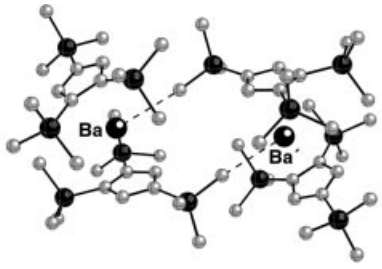

3391 **F. Antolini, P. B. Hitchcock, A. V. Khvostov, M. F. Lappert***

Alkali metals / Amides / Synthesis / NMR spectra / X-ray structures

Keywords: Synthesis and Structures of Alkali Metal Amides Derived from the Ligands $[N(SiMe_2Ph)(SiMe_3)]^-$, $[N(t\text{Bu})(SiMe_3)]^-$, $[N(Ph)(2\text{-}C_5H_4N)]^-$, and $[N(2\text{-}C_5H_4N)_2]^-$

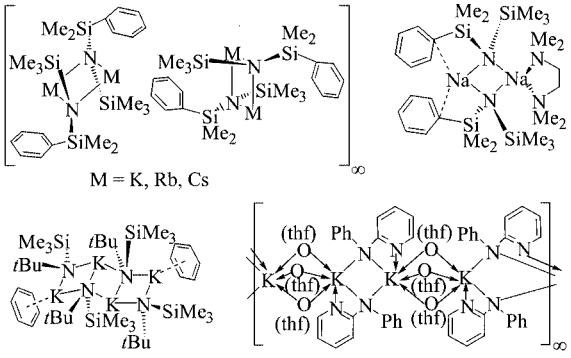

3401 **F. Feil, S. Harder***

Hypersilyl-Substituted Complexes of Group 1 and 2 Metals: Syntheses, Structures and Use in Styrene Polymerisation

Keywords: Alkali metals / Alkaline earth metals / Si ligands / Polymerization

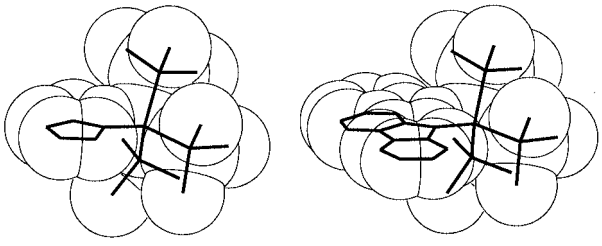

3409 **R. P. Davies,* M. G. Martinelli, A. E. H. Wheatley, A. J. P. White, D. J. Williams**

Structural Studies of Lithium Telluro- and Seleno-Phosphorus Compounds

Keywords: Lithium / Selenium / Solid-state structures / Tellurium

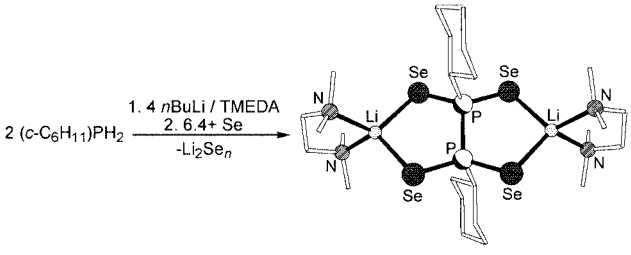

 © 2003 Wiley-VCH Verlag GmbH & Co. KGaA, Weinheim

3417 **K. W. Klinkhammer,* J. Klett, Y. Xiong, S. Yao**

Homo- and Heteroleptic Hypersilylcuprates – Valuable Reagents for the Synthesis of Molecular Compounds with a Cu–Si Bond

Keywords: Copper / Silicon / Silylcuprates / Si ligands

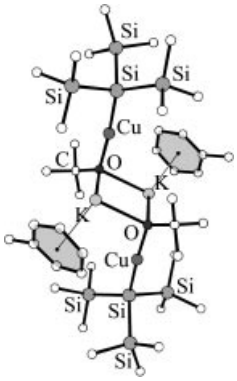

3425 **R.-D. Hoffmann, Z. Wu, R. Pöttgen***

Fluorite-Related Phases in the System Li-Pt-Sn: Synthesis and Structures of Li_2PtSn, $Li_3Pt_2Sn_3$, $Li_{2.27}Pt_2Sn_{3.73}$ and $Li_{2.43}Pt_2Sn_{3.57}$

Keywords: Lithium / Tin / Platinum / Intermetallic phases

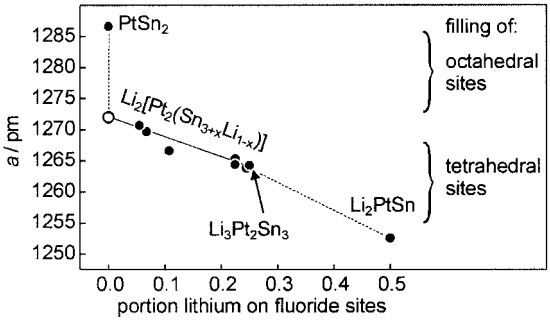

3432 **M. Westerhausen,* S. Schneiderbauer, A. N. Kneifel, Y. Söltl, P. Mayer, H. Nöth, Z. Zhong, P. J. Dijkstra, J. Feijen**

Organocalcium Compounds with Catalytic Activity for the Ring-Opening Polymerization of Lactones

Keywords: N ligands / Calcium / O ligands / Ring-opening polymerization / Tin

3440 **K. M. Fromm,* W. Maudez**

Polar Molecular Precursors for Alkali and Alkaline Earth Metal Clusters and Low-Dimensional Polymer Structures: the Solid-State Structures of $[CaI(dme)_3]I$, and *cis*-$[SrI_2(diglyme)_2]$ (dme = $CH_3OC_2H_4OCH_3$; diglyme = $CH_3(OC_2H_4)_2OCH_3$)

Keywords: Alkaline earth metals / Calcium / Halides / Polar compounds / Strontium

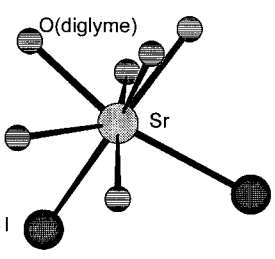

cis-$[SrI_2(diglyme)_2]$

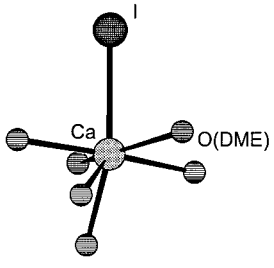

$[CaI(dme)_3]^+$

 © 2003 Wiley-VCH Verlag GmbH & Co. KGaA, Weinheim

3445 **M. G. Davidson,* P. R. Raithby, A. L. Johnson, P. D. Bolton**

Structural Diversity in Lewis-Base Complexes of Lithium Triflamide

Keywords: Lithium / Solid-state structures / Aggregation / Crystal engineering / Anions

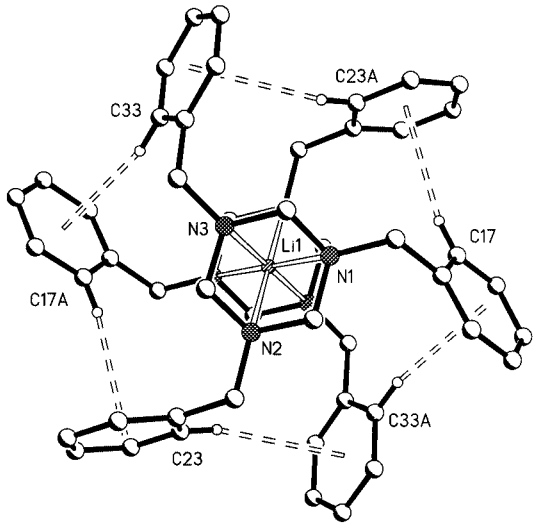

3453 **C. Strohmann,* D. H. M. Buchold, T. Seibel, K. Wild, D. Schildbach**

Syntheses and Crystal Structures of Highly Diastereomerically Enriched Lithiated Benzylsilanes in the Presence of External Donor Molecules: Experiment and Theory

Keywords: Silanes / Lithium / Diastereomers / Quantum-chemical calculations / Stereochemistry

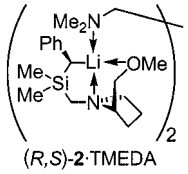

(*R*,*S*)-**2**·TMEDA

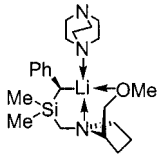

(*R*,*S*)-**2**·DABCO

3464 **D. T. Carey, F. S. Mair,* R. G. Pritchard, J. E. Warren, R. J. Woods**

Structures and Reactions of 1,3-Diamidodilithium Complexes: the Hemisolvated *l*-[CMe_2-{$CHMeN(R)\}_2Li_2{\cdot}OEt_2$], the Unsolvated 1:1 Mixed Organo-amidolithium *u*-[CMe_2{CHMeN-$(R')\}_2{\cdot}Li_2{\cdot}(n$BuLi$)_2$], and the Product of Oxidative Ring Closure, the Pyrazolidine *l*-[$(RNCHMe)_2CMe_2$] (R = 2-*i*Pr-C_6H_4; R′ = 2,6-$i Pr_2$-C_6H_3)

Keywords: Solid-state structures / Lithium / N ligands / Carbanions

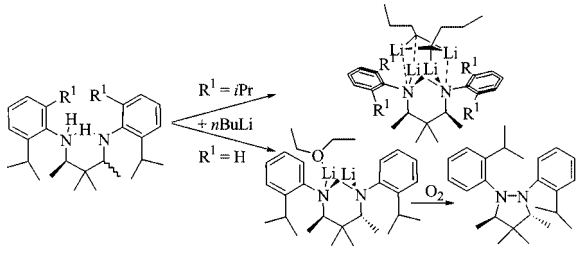

 © 2003 Wiley-VCH Verlag GmbH & Co. KGaA, Weinheim

3472 **W. Vargas, K. Ruhlandt-Senge***

Synthesis, Structures and Characterization of the Calcium Pyrrolates [Ca{(2-(dimethylaminomethyl)pyrrolyl}$_2$ donor*n*] (donor = THF and pyridine, *n* = 2; DME and TMEDA, *n* = 1) as Potential Precursors for Solid-State Applications

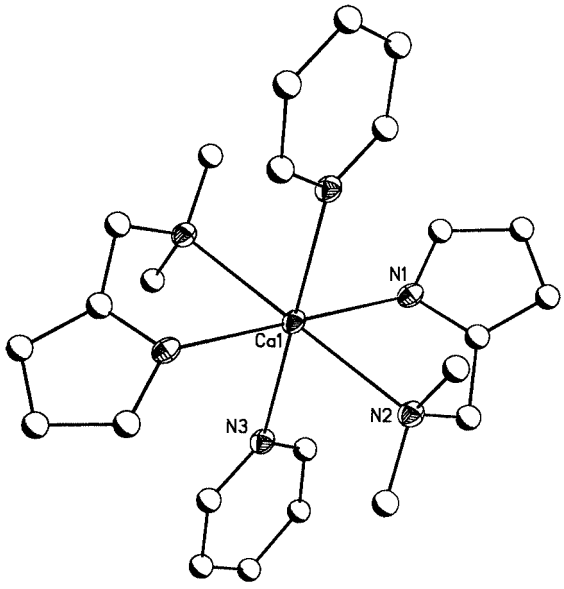

Keywords: Calcium / N ligands / Chemical vapor deposition / Transamination / Metallation / Intramolecular donation

3480 **D. L. Reger,* R. F. Semeniuc, M. D. Smith**

Influence of the Crystallization Solvent on Molecular and Supramolecular Structures of Silver(I) Tris(3-Phenylpyrazolyl)methane Complexes

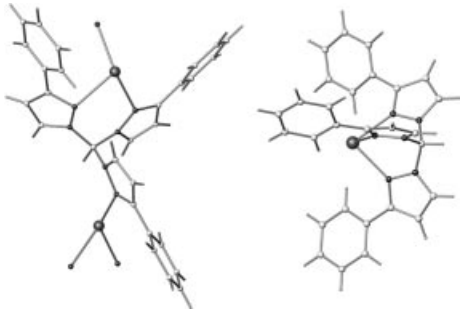

Keywords: N ligands / Solvent effects / Noncovalent interactions / Silver / Supramolecular chemistry

3495 **C. Stanciu, M. M. Olmstead, A. D. Phillips, M. Stender, P. P. Power***

Synthesis and Characterization of the Very Bulky Phenols Ar*OH and Ar′OH (Ar* = C_6H_3-2,6-Trip$_2$, Trip = C_6H_2-2,4,6-*i*Pr$_3$; Ar′ = C_6H_3-2,6-Dipp$_2$, Dipp = C_6H_3-2,6-*i*Pr$_2$) and Their Lithium and Sodium Derivatives (LiOAr′)$_2$ and (NaOAr*)$_2$

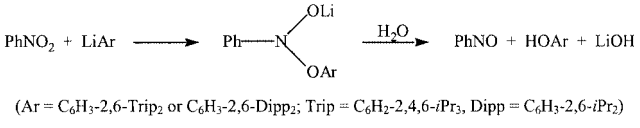

(Ar = C_6H_3-2,6-Trip$_2$ or C_6H_3-2,6-Dipp$_2$; Trip = C_6H_2-2,4,6-*i*Pr$_3$, Dipp = C_6H_3-2,6-*i*Pr$_2$)

Keywords: Phenol / Phenoxide / Terphenyl / Alkali metals

 © 2003 Wiley-VCH Verlag GmbH & Co. KGaA, Weinheim

Ron Snaith (1947−2000), Inspirational Alkchemist and Altruist

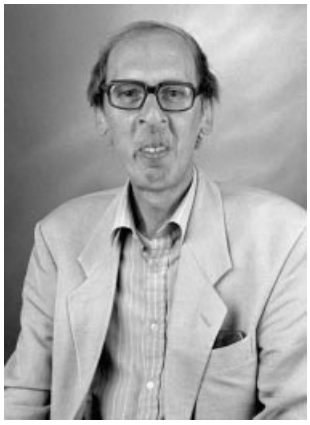

This volume is dedicated to the memory of Dr Ron Snaith, the highly respected and much-loved scientist, teacher, researcher and raconteur, whose sudden and tragic death on the first day of this millennium, January 1st 2000, shocked his family and friends throughout the world. His passing deprived his widow Jane, son Tom, and daughter Katie of a loving, adored husband and father, and the chemical community at large of a remarkably influential pioneering researcher, writer and speaker. He was an unforgettable character, regarded with great affection by all who came to know him, particularly those who had had the privilege to have been taught by him. It is a measure of the high esteem in which he and his chemistry are held that, three years after his death, an international meeting, the third in a series he founded, concerned with alkali and alkaline earth metal chemistry (ALKCHEM 3, Würzburg, Germany 28/9/03−2/10/03) should be dedicated to his memory, and that so many fellow chemists should have contributed papers to this special memorial volume.

Ron was born in Kingston-upon-Hull, Yorkshire, in 1947. Fiercely proud of the county of his birth, he showed its legendary grit, determination and spirit in all he did. A born communicator, and blessed with a sympathetic character that allowed him to see the world from others' viewpoints, he was able to turn a feeling for the pithy phrase, a gently sardonic sense of humour, and a capacity for self-mockery to excellent effect in his interactions with others, consistently instilling wit and good humour daily into their lives. In this increasingly egocentric world, he was remarkably altruistic, putting the needs of others ahead of his own, particularly the needs of those least able to help themselves. His concern for the underdog, the underprivileged, permeated his thoughts and actions.

His route into a research career in chemistry was unorthodox. Whilst studying for his BSc in chemistry at Durham University from 1965−1968, he originally intended, on graduating, to become a teacher at secondary school level (pupils aged 11−18), preferably working with pupils who were disabled. His interest in his chosen subject was, however, fired by lectures from Professor Geoffrey Coates, the charismatic pioneering organometallic chemist who headed the Department of Chemistry at Durham from 1953−1968. Subsequently, having gained a richly deserved first class honours degree in 1968, Ron stayed on at Durham (1968−1971) to secure a science Ph.D. to ensure he had some leverage later when he embarked on his career. As Coates moved in 1968 to Laramie, Ron worked for his PhD with Ken Wade, then a lecturer at Durham (formally Ron's research supervisor, Ken was soon to find himself learning more from Ron than vice versa). Having completed his PhD in 1971, Ron spent a year training as a teacher, still in Durham, before going on to teach chemistry very successfully for the next seven years at Durham Johnston Comprehensive School, putting his subject across with inspirational flair and insight, creating a generation of young enthusiasts who went on to study the subject at university and then make their own careers in chemistry. His former pupils at Johnston School (originally founded, as a technical school, by the first professor of chemistry at Durham University, J F W Johnston FRS) include some distinguished figures in UK chemistry today such as David Parker FRS, who now heads the Chemistry Department at Durham (for the second time) and Paul Attfield, chair of material science at the University of Edinburgh. It is no surprise that Ron's talent as a born teacher was recognised at Johnston School from his arrival there, and he rose rapidly to head his department.

It was from Durham Johnston School that Ron was head-hunted, in 1979, by Professor Peter Perkins, then head of inorganic chemistry at the University of Strathclyde, in Glasgow. Perkins was seeking a charismatic teacher, one able to communicate with and interest students who were required to study the subject in their first year at university but who might not go on to study the subject in depth as specialists. Ron proved so adept at this, making chemistry not only intelligible but also genuinely interesting, indeed fascinating, that he soon became a rising star in the Department of Pure and Applied Chemistry at Strathclyde. It was there that he started the researches into aspects of lithium chemistry that were soon to establish him as a leading authority on s-block chemistry.

The reputation he acquired at Strathclyde, however, prompted another university, this time Cambridge, to head-hunt him, and he moved to a lectureship there in 1986, subsequently being promoted to a Readership in Main Group Chemistry in 1998. His growing stature at Cambridge prompted many invitations for him to move again, to chairs elsewhere in the UK or abroad, but these came during a period in which another move would have been inconvenient for family reasons, and anyway he found

 DOI: 10.1002/ejic.200300559 © 2003 Wiley-VCH Verlag GmbH & Co. KGaA, Weinheim

his departmental and college work at Cambridge too fulfilling to succumb to any of these tempting invitations, for which scores of students who passed through the Chemistry Department and/or St John's College during the nineties will be most grateful. The outside world is aware of Ron's scientific work at Cambridge through his publications. His staff colleagues in the chemistry department and in St John's College will be aware of the enormous amount of work he did, whether as a brilliant lecturer and sympathetic teacher in a world-class department, as an acutely conscientious and fair admissions tutor and patient undergraduate supervisor in a historic college, or as a committee man and helper always prepared to lend a hand with many duties.

Although Ron acquired a well-deserved reputation as a chemist, his knowledge of and lectures on Egyptology probably brought him into contact with a wider public in the UK, and certainly deserve a mention here. His long-standing interest in ancient civilisations flourished through a friendship with Professor Tom Thacker, Head of Middle Eastern and Oriental Studies at Durham in the sixties and seventies. From his graduate student days, Ron soon became skilled at the specialist applied chemical techniques needed for the safe cleaning of priceless but corroded artifacts made centuries or millennia earlier. Indeed, at one time he came near to carrying out postdoctoral research in restoration work on items in the Oriental Museum at Durham. Later in his career he was in great demand on the lecture circuit on the subject of Egyptian Mummies, on which he spoke with consummate authority and brilliant wit and humour, tuning his raconteur's discourse on the subject with unerring skill to the background and interests of his audience, reducing his captivated listeners (whether schoolchildren, undergraduates, enthusiasts for the advancement of science, or members of women's institutes) to helpless laughter as he entertained them with hilarious tales about Isis, Osiris, assorted other gods and their bizarrely scattered vital parts, yet still imparting a feeling for ancient civilisations, hieroglyphics, early alchemy, and the technicalities of mummification.

As a researcher in chemistry, Ron was a thoroughly reliable experimentalist, bravely prepared to tackle systems that were so acutely air-and moisture-sensitive as to discourage others from attempting to work with them. Like his experimental work, his written or oral presentations of his work were also always meticulously well prepared, and conveyed clearly the insight and implications his results generated. He could turn his hand to preparative, spectroscopic, structural or bonding problems with equal facility, and thought laterally, making connections others had not spotted, highlighting the common characteristics of seemingly disparate species.

His early Ph.D. work on ketimino derivatives $(R_2C{=}N)_xM$, $(RC{=}N)_xMX_y$, $(R_2C{=}N)_xMLi$, etc, of such elements M as boron, aluminium and silicon, established and consolidated the link between the structures of such systems, particularly their CNM bond angles, and the number of electrons (1 or 3) the ligand provided for bonding terminally to a metal or metalloid, deduced from "sporting" methods such as IR or NMR spectroscopy if X-ray evidence was unavailable as was often the case in those days. He showed, in early examples of the method, how the state of aggregation of his products could be controlled by use of judiciously chosen bulky substituents, and was thereby responsible for preparing the first set of monomeric ketiminoboranes R_2CNBR_2, isoelectronic with allenes R_2CCCR_2, that contained linear CNB skeletons. His syntheses of these compounds entailed the use of *N*-lithio-ketimines, $R_2C{=}NLi$, as reagents, though their structures were not then known. He was later to solve their structures at Strathclyde, and show their importance in elucidating structural patterns in lithium chemistry. Also in the course of this work on ketiminates, he generated systems exhibiting significant C-H···M interactions like those found earlier by Erwin Weiss in his classic studies on lithium alkyls. Interestingly, it was to be some years before these types of interaction were detected in transition metal systems, hailed as novel, and dubbed "agostic".

In his career, Ron spent no time on conventional postdoctoral studies. However, he found time during his doctoral, teacher-training, and school-teaching years to read widely in boron cluster chemistry, on which he also became an authority and wrote a number of reviews that were well received. He later developed new methods of deducing the enthalpies of formation of such systems, initially using classical bond length-bond energy arguments but later adapting for this purpose the bond index concept developed by David Armstrong and Peter Perkins at Strathclyde. Also with David Armstrong, Ron carried out ab initio MO calculations on borane cluster systems long before such calculations became as routinely possible as they are now.

However, it is for his lithium chemistry, notably his elucidation of the patterns that permeate the structural chemistry of lithium, that he is best known. His inspired use of amino and ketimino ligands, R_2N and $R_2C{=}N$, allowed him to exploit and probe both electronic and substituent bulk effects. The twofold symmetry of these ligands, and the complementarity of the orientations of their alkyl groups (in the plane of the nitrogen lone pairs in the latter case, out of that plane in the former case) led to either laddering or stacking of the $(LiN)_n$ rings (n = commonly 2 or 3). Through Ron's ingenuity and vision, what began modestly as an esoteric study of lithium amides and lithium ketimides was transformed into ring-stacking and ring-laddering principles that could be applied with equal relevance and rigour to the structures of lithium organoelement compounds in general, including alkoxides, alkyls, aryls, alkynyls, enolates, halides and phosphides, and to the heavier alkali metal congeners. Developed through a series of key papers, these ideas were later expounded by Ron in a seminal review article on "structures of organonitrogen-lithium compounds: recent patterns and perspectives in organolithium chemistry" (*Adv. Inorg. Chem.* **1991**, *37*, 47−142), which was co-written with Karina Gregory and Paul von Ragué Schleyer (with whom

 © 2003 Wiley-VCH Verlag GmbH & Co. KGaA, Weinheim

Ron teamed up to probe the nature of the bonding in his lithium-nitrogen systems). How fitting that Ron, a son of a builder, should become an expert in the design and construction of molecular architectures.

Ron went on to show that the structural principles applicable to salts of electropositive metals with organic anions are also equally applicable to salts of the same metals with inorganic anions. This led him to develop the ''ammonium salt route'' for the synthesis of a series of novel Lewis base-captured molecular fragments of common inorganic salts. One of his great strengths was in recognising the significance of a single result, and designing a comprehensive project around it. His discovery that water and lithium, long regarded as incompatible in organolithium chemistry, can indeed coexist in an organic compound (derived from 2-mercaptobenzoxazole) is a case in point, which led him to an in-depth investigation of aqua and other protic ligand complexes of alkali and alkaline earth metal organic compounds.

Having devoted much of his career to solving and rationalising the structures of lithium reagents, Ron later turned to documenting the mechanisms by which lithio reagents operate in organic syntheses. The results were published in a string of definitive papers detailing the identities and the solid-state and (more importantly) solution structures of lithium-based intermediates isolated during the courses of several key organic syntheses, not only providing benchmarks by which such reactions can be understood, but also underlining the comprehensive, interdisciplinary nature of modern chemistry, where pooling the resources of organic, inorganic, organometallic and mechanistic investigations is necessary if we are to understand the subtleties and complexities of what initially may appear straightforward reactions between the monomeric species by which reagents are so commonly, and misleadingly, represented in equations.

Sadly, the death of Ron in his prime means that this particularly promising line of work was taken less far than he had planned. Bereft of his unique approach and originality, it will not be developed in the way he himself would have taken it. However, as a superb teacher and source of inspiration to generations of graduate students and postdoctoral co-workers, he has ensured that his ideas and philosophy will live on. Ron's own publications ensure that his very substantial contribution to science remains available to us. He has also bequeathed to academia many former students and co-workers who have themselves gone on to highly successful research careers, including Matt Davidson (Bath), Rob Davies (Imperial College, London), Rab Mulvey (Strathclyde), Andy Wheatley and Dom Wright (both Cambridge). They themselves have won a clutch of prestigious Royal Society of Chemistry Awards (Meldola/Harrison Memorial/Main Group Element Medals and Prizes). He also had a major influence on the academic careers of two former postdoctoral associates (Frank Mair, UMIST and Dietmar Stalke, Würzburg). This legacy to research chemistry is all the more remarkable given that Ron always deliberately restricted the size of his research group to a select small number.

Ron himself won the RSC Award for Main Group Element Chemistry in 1996, an award which undoubtedly would have been followed by many more awards had he survived to pursue a normal length career. Characteristically, throughout his life, he was always self-effacingly concerned to see that others gained the recognition he did not seek for himself, a true altruist. Inspirational in chemistry and in how to live one's life, Ron had a generosity of spirit and infectious good humour that enriched and transformed the lives of all who knew him, and will live long in their memories.

Throughout his career, Ron was given immense and unstinting support by Jane, whom he had met when they were both students at Durham (she herself took a PhD in engineering science). She and Tom (who followed in his father's footsteps to take a first in chemistry at Durham in 2000 before turning to law) and Katie (close to completing her studies for a Master's degree in criminology) were a source of great pride and joy to Ron, who appreciated their tolerance of his not infrequent preoccupation with chemistry. We, and the chemical community at large, share their loss, in his prime, of this highly talented, kind, considerate, lovable man.

Robert E. Mulvey and Ken Wade

[1] IR and ^{1}H NMR Spectroscopic Evidence of Dative Aluminium-Nitrogen π-Bonding in Tris(diphenylketimino) and Tris(di-*tert*-butylketimino)aluminium: R. Snaith, K. Wade, B. K. Wyatt, *Inorg. Nucl. Chem. Lett.* **1970**, *6*, 311−313.

[2] 1,1,3,3-Tetramethylguanidine Adducts of Trimethylaluminium, Triethylaluminium and Aluminium Trichloride: Dimethyl-, Diethyl- and Dichlorobis(dimethylamino)methyleneaminoaluminium: R. Snaith, K. Wade, B. K. Wyatt, *J. Chem. Soc., (A)* **1970**, 380−383.

[3] Azomethine Stretching Frequencies of some Di- and Tri-Substituted Methyleneamines, their Hydrochlorides and their Boron Trifluoride Adducts: B. Samuel, R. Snaith, C. Summerford, K. Wade:, *J. Chem. Soc., (A)* **1970**, 2019−2022.

[4] Dimeric Alkylideneaminoaluminium Dihalides and Monomeric Trialkylideneamino Derivatives of Aluminium: R. Snaith, C. Summerford, K. Wade, B. K. Wyatt, *J. Chem. Soc., (A)* **1970**, 2635−2639.

[5] Lithium Tetrakis(di-*tert*-butylmethyleneamino)aluminate: H. M. M. Shearer, R. Snaith, J. D. Sowerby, K. Wade, *J. Chem. Soc., Chem. Commun.* **1971**, 1275−1276.

[6] Monomeric Di-*tert*-butylmethyleneaminoboranes: M. R. Collier, M. F. Lappert, R. Snaith, K. Wade, *J. Chem. Soc., (D)* **1972**, 370−373.

[7] Some Diphenylmethyleneaminosilanes and Di-*tert*-butylmethyleneaminosilanes: J. B. Farmer, R. Snaith, K. Wade, *J. Chem. Soc., (D)* **1972**, 1501−1505.

[8] Diphenyl-, Di-*p*-tolyl- and Di-*tert*-butyl-Methyleneamino Derivatives of Phosphorus: B. Hall, J. Keable, R. Snaith, K. Wade, *J. Chem. Soc., Dalton Trans.* **1978**, 986−989.

[9] Bond Enthalpies of Borane Anions, $B_nH_n^{2-}$: C. E. Housecroft, R. Snaith, K. Wade, *Inorg. Nucl. Chem. Lett.* **1979**, *15*, 343−347.

[10] Preparation and X-ray Crystal Structures of the Dimeric Aldiminoborane $(PhCH{=}NBMe_2)_2$ and Monomeric Paddle-Wheel Shaped Tris(ketimino)borane $B(N{=}CtBu_2)_3$: J. R. Jennings, R. Snaith, M. M. Mahmoud, S. C. Wallwork, S. J.

 © 2003 Wiley-VCH Verlag GmbH & Co. KGaA, Weinheim

Bryan, J. Halfpenny, E. A. Petch, K. Wade, *J. Organomet. Chem.* **1983**, *249*, Cl−C5.

[11] Crystal and Molecular Structures of the Lithioketimine, $[Li(N=CtBu_2)]_6$, and Lithioguanidine, $[LiN=C(NMe_2)_2]_6$: Electron-Deficient Bridging of Li_3 Triangles by Methyleneamino-Nitrogen Atoms: W. Clegg, R. Snaith, H. M. M. Shearer, K. Wade, G. Whitehead, *J. Chem. Soc., Dalton Trans.* **1983**, 1309−1317.

[12] Crystal Structures of $[Ph_2C=NLi.NC_5H_5]_4$ and $[ClLi{\cdot}O=P(NMe_2)_3]_4$: Discrete Tetrameric Pseudo-cubane Clusters with Bridging of Li_3 Triangles by Nitrogen and by Chlorine Atoms: D. Barr, W. Clegg, R. E. Mulvey, R. Snaith, *J. Chem. Soc., Chem. Commun.* **1984**, 79−80.

[13] Crystal Structure of $\{Li[O=P(NMe_2)_3]_4\}^+{\cdot}\{Li[N=CPh_2]_6{\cdot}O=P(NMe_2)_3\}^-$: A Lithium 'Ate Complex, with a Pentanuclear Li_5 Clustered-Anion, having Both μ_2 Edge and μ_3 Face Nitrogen to Lithium Bonding: D. Barr, W. Clegg, R. B. Mulvey, R. Snaith, *J. Chem. Soc., Chem. Commun.* **1984**, 226−227.

[14] Trimeric Dibenzylamidolithium and its Dimeric Diethyl Ether and Hexamethylphosphoramide Complexes: Structural and Theoretical Studies of Reactive Organonitrogen-Lithium Oligomers: D. Barr, W. Clegg, R. E. Mulvey, R. Snaith, *J. Chem. Soc., Chem. Commun.* **1984**, 285−287.

[15] Evidence for CH···Li Interactions in the Solid-State Structure of Dibenzylamidolithium, and in Solutions of it and its Complexes: Coloured Species due to Benzyl → Lithium Charge Transfer: D. Barr, W. Clegg, R. E. Mulvey, R. Snaith, *J. Chem. Soc., Chem. Commun.* **1984**, 287−289.

[16] The Isolation and Crystal Structure of $[Ph(2\text{-}Pyr)NLi]{\cdot}[O=P(NMe_2)_3]{\cdot}[Ph(2\text{-}Pyr)NH]$: A Model Monomeric Organonitrogen-Lithium Species Containing Coordination of Lithium by both an Anchimeric Pyridyl N-Atom and by a Potentially Reactive Amine Ligand: D. Barr, W. Clegg, R. E. Mulvey, R. Snaith, *J. Chem. Soc., Chem. Commun.* **1984**, 469−470.

[17] The Structural Isomers of $\{[Ph(2\text{-}Pyr)NLi]{\cdot}[O=P(NMe_2)_3]\}_2$: Dimeric Species with Alternative $(LiN)_2$ and $(LiO)_2$ Rings, the latter involving Unprecedented Neutral Bridging Oxygen Ligands: D. Barr, W. Clegg, R. E. Mulvey, R. Snaith, *J. Chem. Soc., Chem. Commun.* **1984**, 700−701.

[18] The Isolation and Crystal Structure of $\{Li(H_2O)_2[O=P(NMe_2)_3]\}_2^{2+}{\cdot}2Cl^-$: a $(LiO)_2$ Ring Compound with Bridging Neutral Oxygen (HMPA) Ligands: D. Barr, W. Clegg, R. E. Mulvey, R. Snaith, *J. Chem. Soc., Chem. Commun.* **1984**, 974−975.

[19] Crystal and Solution Structures of $\{tBu_2C=NLi{\cdot}O=P(NMe_2)_3\}_n$: D. Barr, W. Clegg, R. E. Mulvey, D. Reed, R. Snaith, *Angew. Chem. Int. Ed. Engl.* **1985**, *24*, 328−329.

[20] Amination Reactions of Alkoxy-amidolithium Compounds: an *Ab Initio* S.C.F. M.O, Model involving an (N−O)-Lithium-bridged Intermediate: D. R. Armstrong, R. Snaith, G. T. Walker, *J. Chem. Soc., Chem. Commun.* **1985**, 789−791.

[21] Cluster Bonding and Energetics of the Borane Anions, $B_nH_n^{2-}$ (n = 5−12): a Comparative Study using Bond Length/Bond Enthalpy Relationships, MO Bond Index Calculations: C. E. Housecroft, R. Snaith, K. Moss, R. E. Mulvey, M. E. O'Neill, K. Wade, *Polyhedron* **1985**, *4*, 1875−1881.

[22] High-Field Lithium-7 Nuclear Magnetic Resonance Spectroscopic and Cryoscopic Relative Molecular Mass Studies on Solutions of Amido- and Imidolithium Compounds: D. Reed, D. Barr, R. E. Mulvey, R. Snaith, *J. Chem. Soc., Dalton Trans.* **1986**, 557−564.

[23] The Isolation of a Highly Arene-Soluble Alkali Metal Tetrafluoroborate Complex, $LiBF_4{\cdot}4HMPA$: Evidence for Strong Li···F Interactions in Solution: D. Barr, K. B. Hutton, J. H. Morris, D. Reed, R. Snaith, *J. Chem. Soc., Chem. Commun.* **1986**, 127−129.

[24] Bonding Implications of Interatomic Distances and Ligand Orientations in the Iminolithium Hexamers $\{LiN=C(Ph)tBu\}_6$ and $\{LiN=C(Ph)NMe_2\}_6$: a Stacked-Ring Approach to these and Related Oligomeric Organolithium Systems: D. Barr, R. Snaith, W. Clegg, R. E. Mulvey, K. Wade, *J. Chem. Soc., Chem. Commun.* **1986**, 295−297.

[25] Bond Indices, Enthalpies, and Relative Stabilities of Real and Hypothetical Closo-Clusters $B_nH_n^{c-}$ (n = 5−12; c = 0, 2 or 4) as Revealed by the MO Bond Index Method: R. Snaith, R. E. Mulvey, M. E. O'Neill, K. Wade, *Polyhedron* **1986**, *5*, 1437−1447.

[26] The Laddering Principle in Lithium Amide Chemistry: the Crystal and Molecular Structure of the Pyrrolididolithium Adduct $[H_2C(CH_2)_3NLi]_3{\cdot}MeN(CH_2CH_2NMe_2)_2$: D. R. Armstrong, D. Barr, W. Clegg, R. E. Mulvey, D. Reed, R. Snaith, K. Wade, *J. Chem. Soc., Chem. Commun.* **1986**, 869−870.

[27] Variable Temperature and Concentration ^1H and ^7Li NMR Studies of Solutions of Hexameric Iminolithium Compounds, $(R^1R^2C=NLi)_6$: D. Barr, R. Snaith, R. E. Mulvey, K. Wade, D. Reed, *Magn. Reson. Chem.* **1986**, *24*, 713−717.

[28] Crystal Structure of NaI·diglyme: an Unprecedented Bridging Role for Diglyme: R. E. Mulvey, W. Clegg, D. Barr, R. Snaith, *Polyhedron* **1986**, *5*, 2109−2111.

[29] The Synthesis and X-ray Structural Characterisation of the First Mixed Alkali Metal Organonitrogen Molecular Cluster $LiNa_3{\cdot}[O=P(NMe_2)_3]_3{\cdot}[N=C(NMe_2)_2]_4$: W. Clegg, R. E. Mulvey, R. Snaith, G. E. Toogood, K. Wade, *J. Chem. Soc., Chem. Commun.* **1986**, 1740−1742.

[30] The Ring-Stacking Principle in Organolithium Chemistry: its Development through the Isolation and Crystal Structures of Hexameric Iminolithium Clusters $(RR'C=NLi)_6$, (R′ = Ph, R = *t*Bu or Me_2N; R = R′ = *t*Bu or Me_2N): D. Barr, R. Snaith, W. Clegg, R. E. Mulvey, K. Wade, *J. Chem. Soc., Dalton Trans.* **1987**, 1071−1081.

[31] X-ray Crystallographic- and Solution-Studies of the PMDETA and TMEDA Adducts of Lithium Diphenylphosphide: R. E. Mulvey, K. Wade, D. R. Armstrong, G. T. Walker, R. Snaith, W. Clegg, D. Reed, *Polyhedron* **1987**, *6*, 987−993.

[32] The Syntheses and Crystal Structures of Two Iminolithium Adducts: $(Ph_2C=NLi{\cdot}Pyridine)_4$, a Tetrameric Pseudo-cubane Formed by Stacking Two $(LiN)_2$ four-membered Rings, and $(tBu_2C=NLi{\cdot}HMPA)_2$, a Dimer Prevented Sterically from Stacking: D. Barr, R. Snaith, W. Clegg, R. E. Mulvey, K. Wade, *J. Chem. Soc., Dalton Trans.* **1987**, 2141−2147.

[33] Three Model Structural Types in Lithium Amide Chemistry: the Crystal and Molecular Structures of Dimeric $(PhMeNLi{\cdot}TMEDA)_2$ and Monomeric PhNaphthylNLi·PMDETA, and of $(PhNapthylNLi{\cdot}TMEDA)_2$, a "Loose Dimer": D. Barr, W. Clegg, R. E. Mulvey, R. Snaith, D. S. Wright, *J. Chem. Soc., Chem. Commun.* **1987**, 716−718.

[34] Isolation and Solution Structures of $\{PhCH_2NLiCH_2CH_2NMe_2\}_n$ and of the Totally Rigid Dilithium Compound $\{o\text{-}LiC_6H_4CH_2NLiCH_2CH_2NMe_2\}_n$: Evidence for Li···*o*HC Interactions: D. Barr, R. Snaith, D. S. Wright, R. E. Mulvey, K. Jeffrey, D. Reed, *J. Organomet. Chem.* **1987**, *325*, C1−C6.

[35] Structure and Bonding of the Tris(diphenylmethyleneamino)aluminium Dimer, $[Al(N=CPh_2)_3]_2$: Relative Strengths of Bridging and Terminal Al−X Bonds in Systems $X_2Al(\mu\text{-}X)_2A1X_2$: S. J. Bryan, W. Clegg, R. Snaith, K. Wade, E. H. Wong, *J. Chem. Soc., Chem. Commun.* **1987**, 1223−1224.

[36] Reactions of Ammonium Salts with BuLi and with LiH: New Routes to Fully Anhydrous Inorganic Lithium Compounds: D. Barr, R. Snaith, D. S. Wright, R. E. Mulvey, K. Wade, *J. Am. Chem. Soc.* **1987**, *109*, 7891−7893.

[37] Synthesis, and Crystal and Solution Structures of the 1:1 TMEDA Complex of Lithium Thiocyanate, $(LiSCN{\cdot}TMEDA)_n$: a Polymeric Solid with Li^+ Ions Linked by Bifunctional Linear SCN^- Ligands: D. Barr, M. J. Doyle, R. E. Mulvey, P. R. Raithby, R. Snaith, D. S. Wright, *J. Chem. Soc., Chem. Commun.* **1988**, 145−147.

[38] A Li_8 Cluster of Three Edge-connected Li_4 Tetrahedra Held by Li−N, and Li···C, and Li···Li Interactions: Crystal Structure of $(o\text{-}LiC_6H_4CH_2NLiCH_2CH_2NMe_2)_4$, and Detection of

 © 2003 Wiley-VCH Verlag GmbH & Co. KGaA, Weinheim

Metal···Metal Coupling within it by ^{7}Li COSY NMR Spectroscopy: D. Barr, W. Clegg, S. M. Hodgson, R. E. Mulvey, D. Reed, R. Snaith, D. S. Wright, *J. Chem. Soc., Chem. Commun.* **1988**, 367−369.

[39] Syntheses and Solid-state Structures of Trimeric Dibenzylamidolithium and its Diethyl Ether and Hexamethylphosphoramide Complexes: an Explanation of these Structures and Evidence for Li···HC Interactions in both Solid and Solution Phases: D. R. Armstrong, R. E. Mulvey, G. T. Walker, D. Barr, R. Snaith, W. Clegg, D. Reed, *J. Chem. Soc., Dalton Trans.* **1988**, 617−628.

[40] Characterisation of the bis(Pyridine) Complex of the Butyllithium-Pyridine Adduct, 2-Bu(C_5H_5N)Li·(C_5H_5N)$_2$; its Decomposition to 2-Butylpyridine via a Dihydropyridine: D. Barr, R. Snaith, R. E. Mulvey, D. Reed, *Polyhedron* **1988**, *7*, 665−668.

[41] Oligomeric Iminolithium and Amidolithium Compounds: Comments on Previously Reported Theoretical Calculations and Experimentally Determined Structures: W. Clegg, R. Snaith, K. Wade, *Inorg. Chem.* **1988**, *27*, 3861−3862.

[42] MOBI Calculations on Selected Organolithium and Lithium 'Ate Species: Evidence for Li···HC Three-centre Interactions: D. Barr, R. Snaith, R. E. Mulvey, P. G. Perkins, *Polyhedron* **1988**, *7*, 2119−2128.

[43] Isolation, Characterisation, and Solution Structures of the Bis(Pyridine) Complex of the *n*-Butyllithium-Pyridine Adduct, *n*Bu(C_5H_5N)Li·(C_5H_5N)$_2$, its Mode of Decomposition, and *Ab Initio* Calculations on Model Systems: D. R. Armstrong, R. E. Mulvey, D. Barr, R. Snaith, D. Reed, *J. Organomet. Chem.* **1988**, *350*, 191−205.

[44] Evidence for a Radical-forming Process during the Reaction of Solid NH_4SCN with *n*BuLi and HMPA in Toluene: Crystal Structure of the Product, (LiNCS·2HMPA)$_2$: D. Barr, M. J. Doyle, S. R. Drake, P. R. Raithby, R. Snaith, D. S. Wright, *J. Chem. Soc., Chem. Commun.* **1988**, 1415−1417.

[45] Reaction of Solid NaH with Solid NH_4SCN in HMPA/Toluene: an E.S.R. Spectroscopic Investigation, and Crystal Structures of the Two Products of the Reaction, {(NaNCS·HMPA)$_2$}$_\infty$ and (NaNCS·2HMPA)$_2$: D. Barr, M. J. Doyle, S. R. Drake, P. R. Raithby, R. Snaith, D. S. Wright, *Polyhedron* **1989**, *8*, 215−218.

[46] Ladder Structures in Lithium Amide Chemistry: Syntheses, Solid-state, and Solution Structures of Donor-deficient Lithium Pyrrolidide Complexes, {[$H_2C(CH_2)_3NLi$]$_3$·PMDETA}$_2$ and {[$H_2C(CH_2)_3NLi$]$_2$·TMEDA}$_2$, and *Ab Initio* Calculations Probing Ring vs Ladder vs Stack Structural Preferences: D. R. Armstrong, D. Barr, W. Clegg, S. M. Hodgson, R. E. Mulvey, D. Reed, R. Snaith, D. S. Wright, *J. Am. Chem. Soc.* **1989**, *111*, 4719−4727.

[47] Dilithiation of *N*,*N*′-Diphenylthiourea, PhNHC(=S)HNPh: The Unexpected Structure of the Product, [PhNLiC(=NPh)SLi·2HMPA]$_2$, and Supporting *Ab Initio* MO Calculations on Model Systems: D. R. Armstrong, R. E. Mulvey, D. Barr, R. Snaith, D. S. Wright, W. Clegg, S. M. Hodgson, *J. Organomet. Chem.* **1989**, *362*, Cl−C4.

[48] A K_3-Containing Trigonal Bipyramidal Cluster: Synthesis of (KSCN)$_3$·5HMPA by Reaction of Solid NH_4SCN with Solid K or KH in Toluene/HMPA, and its Crystal Structure Revealing a Triangle of Three K^+ Ions Linked by Three Equatorial μ_2-HMPA Ligands and Bicapped by Two μ_3-HMPA Ligands: D. Barr, M. J. Doyle, S. R. Drake, P. R. Raithby, R. Snaith, D. S. Wright, *Inorg. Chem.* **1989**, *28*, 1767−1768.

[49] A Unique Lithium Halide Complex, {(LiBr)$_2$·3HMPA·Toluene}: Synthesis from Reaction of Solid NH_4Br with *n*BuLi in HMPA/Toluene Media, Crystal Structure showing Two Li−Br Units Linked by Three μ_2-HMPA Ligands, and Detection of ^{7}Li···^{31}P Coupling in Solutions of the Complex: D. Barr, M. J. Doyle, P. R. Raithby, R. Snaith, D. S. Wright, R. B. Mulvey, D. Reed, *J. Chem. Soc., Chem. Commun.* **1989**, 318−319.

[50] Synthesis and Crystal Structure of the Mixed Alkali-Metal Imide Compound $Li_{3.7}Na_{2.3}${N=C(Ph)*t*Bu}$_6$: Three (Metal-Nitrogen)$_2$ Ring Dimers in a Triple-Layered Stack: D. Barr, W. Clegg, R. E. Mulvey, R. Snaith, D. Reed, *J. Chem. Soc., Chem. Commun.* **1989**, 57−58.

[51] Two Monomeric, Octahedral Complexes of Alkaline Earth Metal Salts; Syntheses, Physical Characteristics, and Crystal Structures of SrI_2·4HMPA and Sr(NCS)$_2$·4HMPA: D. Barr, A. T. Brooker, M. J. Doyle, S. R. Drake, P. R. Raithby, R. Snaith, D. S. Wright, *J. Chem. Soc., Chem. Commun.* **1989**, 893−395.

[52] A New Coordinating Chiral Lithium Amide: J. F. Stoddart, D. J. Berrisford, R. Snaith, D. Barr, R. V. H. Jones, D. J. Williams, A. M. Z. Slawin, *Angew. Chem. Int. Ed. Engl.* **1989**, *28*, 1044−1047.

[53] [$H_2C(CH_2)_5NLi$]$_6$, The First Cyclised Lithium Amide Ladder: Synthesis and Structure of Hexamethyleneimidolithium: R. Snaith, D. Barr, D. S. Wright, W. Clegg, S. M. Hodgson, G. R. Lamming, A. J. Scott, R. E. Mulvey, *Angew. Chem. Int. Ed. Engl.* **1989**, *28*, 1241−1243.

[54] Unusual Routes to Complexes of Binary Alkali Metal−Nonmetal Compounds: Preparations and Crystal and Solution Structures of Li_2S_6·(TMEDA)$_2$ and Synthetic Extensions of the Routes: A. J. Banister, D. Barr, A. T. Brooker, W. Clegg, M. J. Cunnington, M. J. Doyle, S. R. Drake, W. R. Gill, K. Manning, P. R. Raithby, R. Snaith, K. Wade, D. S. Wright, *J. Chem. Soc., Chem. Commun.* **1990**, 105−107.

[55] The Ammonium Salt Route to Oligomeric Lanthanum Salt Complexes: Synthesis and X-ray Crystal Structure of La(NCS)$_3$·4HMPA: D. Barr, A. T. Brooker, M. J. Doyle, S. R. Drake, P. R. Raithby, R. Snaith, D. S. Wright, *Angew. Chem. Int. Ed. Engl.* **1990**, *29*, 285−287.

[56] [PhLiNCH_2CH_2NLiPh]·3HMPA, a Monomeric Dilithiumethylenediamide Complex with N_2Li_2 Double Bridging: Synthesis, Crystal Structure, and Model MO Calculations: D. R. Armstrong, D. Barr, A. T. Brooker, W. Clegg, K. Gregory, S. M. Hodgson, R. Snaith, D. S. Wright, *Angew. Chem. Int. Ed. Engl.* **1990**, *29*, 410−411.

[57] The First Lithiated Organic Compound containing Water as a Ligand: Synthesis and Crystal Structure of 2-Mercaptobenzoxazoyl(tetramethylethylenediamine)lithium Monohydrate, C_6H_4OC(···S)···NLi·(TMEDA)·H_2O, a Model Acid-Base Intermediate: D. Barr, P. R. Raithby, P. v. R. Schleyer, R. Snaith, D. S. Wright, *J. Chem. Soc., Chem. Commun.* **1990**, 643−645.

[58] Aggregation of Aza Crown Ethers by Metallation: Synthesis and Crystal Structure of 1-Lithio-1,7-diaza-12-crown-4; The First Lithiated Crown Ether: D. Barr, D. J. Berrisford, L. Méndez, A. M. Z. Slawin, R. Snaith, J. F. Stoddart, D. J. Williams, D. S. Wright, *Angew. Chem. Int. Ed. Engl.* **1991**, *30*, 82−84.

[59] Lithiations of Mercaptoamines Containing =NC(=S)NH−, −NHC(=S)S−, and −NHC(=S)NH− Units: Syntheses, Crystal Structures, and Model MO Calculations: D. R. Armstrong, R. E. Mulvey, D. Barr, R. W. Porter, P. R. Raithby, T. R. E. Simpson, R. Snaith, D. S. Wright, K. Gregory, P. Mikulcik, *J. Chem. Soc., Dalton Trans.* **1991**, 765−776.

[60] The Stabilisation of Water as a Ligand in Lithiated Organic Compounds: Inter- and Intra-Molecular Hydrogen Bonding in the Crystal Structures of [C_6H_4OC(···S)···NLi·HMPA·H_2O]$_2$ and [C_6H_4OC(···S)···NLi·HMPA]$_2$·H_2O: D. R. Armstrong, D. Barr, P. R. Raithby, P. v. R. Schleyer, R. Snaith, D. S. Wright, *Inorg. Chim. Acta* **1991**, *185*, 163−167.

[61] Alkaline Earth Metal Complexes Containing Deprotonated Organic Acids and Water: Preparation, Structures and a New Synthetic Strategy: P. Mikulcik, P. R. Raithby, R. Snaith, D. S. Wright, *Angew. Chem. Int. Ed. Engl.* **1991**, *30*, 428−430.

[62] Mixed-Anion Aggregates of Metalated Organics: Preparation and Crystal Structure of the Mixed-Anion Tetramer (PhO$^-$Li$^+$·HMPA)$_3$·(μ_3-HMPA·Li$^+$)·NCS$^-$: P. R. Raithby, D. Reed, R. Snaith, D. S. Wright, *Angew. Chem. Int. Ed. Engl.* **1991**, *30*, 1011−1013.

 © 2003 Wiley-VCH Verlag GmbH & Co. KGaA, Weinheim

[63] Capturing Platinum(II) Chloride Using a Side-arm Donating Calcium Complex: Synthesis and Structure of $[(HMPA)_3Ca(\mu_2\text{-}Cl)_3Ca(HMPA)_3]^+\cdot\{Pt[C_6H_4OC(\cdots S)\cdots N]_4\cdot CaCl]$: M. G. Davidson, P. R. Raithby, R. Snaith, D. Stalke, D. S. Wright, *Angew. Chem. Int. Ed. Engl.* **1991**, *30*, 1643−1650.

[64] Dilithiation of a Primary Amine: Synthesis and Crystal Structure of a Paramagnetic Li_{20} Aggregate $(NaphthylNLi_9)_{10}\cdot(Et_2O)_6\cdot(Et_2O)$: D. R. Armstrong, D. Barr, W. Clegg, S. R. Drake, R. J. Singer, R. Snaith, D. Stalke, D. S. Wright, *Angew. Chem. Int. Ed. Engl.* **1991**, *30*, 1707−1709.

[65] Synthesis, Structure, MO Calculational Investigations of a Highly Stable, Hydrogen-bonded Primary Amine:Phosphane Oxide Adduct, 2-aminobenzothiazole:HMPA; a Possible Model to Explain the Carcinogenicity of HMPA: D. R. Armstrong, S. Bennett, M. G. Davidson, R. Snaith, D. Stalke, D. S. Wright, *J. Chem. Soc., Chem. Commun.* **1992**, 262−264.

[66] The First Calcium-Mercury Co-Complex: Synthesis and Crystal Structure: M. G. Davidson, S. C. Llewellyn, M.-I. Lopez-Solera, P. R. Raithby, R. Snaith, D. S. Wright, *J. Chem. Soc., Chem. Commun.* **1992**, 573−575.

[67] Metal-mediated Conversion of a 5-Aminothiatriazole into a 5-Mercaptotetrazolyl Ligand by Reaction with a Solid Metal Hydroxide: Synthesis and Crystal Structure of $[NaphthylNN{=}NN\cdots C(\cdots S)]_2Ba\cdot 3HMPA$: F. A. Banbury, M. G. Davidson, A. Martin, P. R. Raithby, R. Snaith, K. L. Verhorevoort, D. S. Wright, *J. Chem. Soc., Chem. Commun.* **1992**, 1152−1154.

[68] Lithiation and Dethiacarbonylation of a Hetcrocyclic Thioamide $C_6H_4OC(=S)NH$ by Reaction with Solid Li_2S in the Presence of HMPA: Synthesis and Crystal Structure of $[C_6H_4OC(=S)NLi\cdot HMPA]_2\cdot C_6H_4(OH)NH_2$: F. A. Banbury, M. G. Davidson, P. R. Raithby, R. Snaith, D. Stalke, *J. Chem. Soc., Chem. Commun.* **1992**, 1492−1494.

[69] Investigations on a 1:1 Adduct of 2-Aminobenzothiazole and DMPU: Subtle Variations in Hydrogen-Bond Acceptors Cause Spectacular Supramolecular Differences: D. R. Armstrong, M. G. Davidson, A. Martin, P. R. Raithby, R. Snaith, D. Stalke, *Angew. Chem. Int. Ed. Engl.* **1992**, *31*, 1634−1636.

[70] A Thiouracil-Ca^{2+} Complex Which Captures $PtCl_2$: Synthesis and Crystal Structure of $[(thiouracilyl)_2Ca\cdot 2DMSO\cdot H_2O]_2$, Containing Two Tautomeric Forms of the Thiouracilyl Anion: F. A. Banbury, M. G. Davidson, A. J. Edwards, M.-I. Lopez-Solera, P. R. Raithby, R. Snaith, D. Stalke, D. S. Wright, *Inorg. Chim. Acta* **1993**, *203*, 93−95.

[71] Metalations of 1-Aminonaphthalene with $AlMe_3$ and with $ZnEt_2$: Syntheses and Crystal Structures of Cyclobutane-like $[Me_2AlNHnaphthyl]_2$ and Cyclohexane-like $[EtZnNHnaphthyl\cdot THF]_3$: M. G. Davidson, D. Elilio, S. L. Less, A. Martin, P. R. Raithby, R. Snaith, D. S. Wright, *Organometallics* **1993**, *12*, 1−3.

[72] General Equations for Determining Equilibrium Constants and Thermodynamic Data from Solution Molecular Mass Measurements: M. G. Davidson, R. Snaith, D. Stalke, D. S. Wright, *J. Org. Chem.* **1993**, *58*, 2810−2816.

[73] A New Bonding Mode for the Thiocyanate Ligand: Structure of the $[LiNCS\cdot Me_2N(CH_2)_3NMe_2]_2$ Dimer with Asymmetric NCS-Bridge Bonding: D. R. Armstrong, A. H. Khandelwal, P. R. Raithby, R. Snaith, D. Stalke, D. S. Wright, *Inorg. Chem.* **1993**, *32*, 2132−2136.

[74] Dilithiation of Aromatic Diamines Leads to Self Recognition of Monomeric Units and Assembly of "Adamantanoid" Metal Cores: The Synthesis and Structural Characterisation of the Dimeric Lithium Amide Complexes $\{[MeOCH_2CH_2N(Li)C_6H_4]_2O\}_2$ and $\{[Me_2NCH_2CH_2N(Li)C_6H_4]_2O\}_2$: I. Cragg-Hine, M. G. Davidson, O. Kocian, F. S. Mair, E. Pohl, P. R. Raithby, R. Snaith, N. Spencer, J. F. Stoddart, *Angew. Chem. Int. Ed. Engl.* **1993**, *32*, 1182−1184.

[75] Monometallation of a Di(aminoaryl)ether Induces a Smiles Rearrangement Leading to a Sodium Aryloxide Complex: the Synthesis and Crystal Structure of $[(MeOCH_2CH_2)(C_6H_4NHCH_2OMe)NC_6H_4ONa]_2$: I. Cragg-Hine, M. G. Davidson, O. Kocian, T. Kottke, F. S. Mair, R. Snaith, J. F. Stoddart, *J. Chem. Soc., Chem. Commun.* **1993**, 1355−1357.

[76] The First Structurally Characterised Early Main Group Metal Diaza-allyl Complex: Synthesis and Crystal Structure of $LiCPh(NPh)_2\cdot$PMDETA: I. Cragg-Hine, M. G. Davidson, F. S. Mair, P. R. Raithby, R. Snaith, *J. Chem. Soc., Dalton Trans.* **1993**, 2423−2424.

[77] An Unusual Co_2-Containing Anion: Synthesis and Structure of $[(OxS)Ca\cdot 4HMPA]^+\cdot[(OxS)Co\cdot\mu\text{-}(OxS)_3\cdot CoCl]^-$ $[OxS^- = C_6H_4O\cdot(C\cdots S)\cdots N^-$; $HMPA = O{=}P(NMe_2)_3]$: M. G. Davidson, M. Gerloch, S. C. Llewellyn, P. R. Raithby, R. Snaith, *J. Chem. Soc., Chem. Commun.* **1993**, 1363−1364.

[78] Structure of Bis(pentamethyldiethylenetriamine)disodium Hexasulfide: S. Besser, R. Herbst-Irmer, D. Stalke, A. T. Brooker, R. Snaith, D. S. Wright, *Acta Crystallogr., Sect. C* **1993**, *49*, 1482−1483.

[79] Synthesis and Structure of a Sixteen-Membered $Al_4(NCO)_4$ Ring Compound: C. M. Bird, C. Breheny, M. G. Davidson, A. J. Edwards, S. C. Llewellyn, P. R. Raithby, R. Snaith, *Angew. Chem. Int. Ed. Engl.* **1993**, *32*, 1433−1484.

[80] The First Lithiated Cyanamide Structure; Synthesis of $(PhNCNLi\cdot HMPA)_n$ by Extrusion of N_2 and S from 5-Phenylamino-1,2,3,4-thiatriazole $PhNHC{=}NN{=}NS$ using Various Lithium Reagents and HMPA: D. R. Armstrong, F. A. Banbury, I. Cragg-Hine, M. G. Davidson, F. S. Mair, E. Pohl, P. R. Raithby, R. Snaith, *Angew. Chem. Int. Ed. Engl.* **1993**, *32*, 1769−1771.

[81] On Enantioselective Deprotonation: Synthesis and Crystal Structure of a Chiral Amidolithium Tetrahydrofuran Complex: A. J. Edwards, S. Hockey, F. S. Mair, P. R. Raithby, R. Snaith, N. S. Simpkins, *J. Org. Chem.* **1993**, *58*, 6942−6943.

[82] Thermal Decomposition of Lithium Amides: A Matrix Isolation Investigation: R. Withnall, I. R. Dunkin, R. Snaith, *J. Chem. Soc., Perkin Trans. 2* **1994**, 1973−1977.

[83] η^3- and η^6-Bridging Cations in the Pentamethyldiethylenetriamine-Solvated Complexes of Benzylpotassium and Benzylrubidium: an X-ray, NMR and MO Study: D. Hoffmann, W. Bauer, F. Hampel, N. J. R. van Eikema Hommes, P. v. R. Schleyer, P. Otto, U. Pieper, D. Stalke, R. Snaith, D. S. Wright, *J. Am. Chem. Soc.* **1994**, *116*, 528−536.

[84] The First Structurally Characterised Sodium Primary Amide Complex: Synthesis and Crystal Structure of $2\text{-}PhOC_6H_4NHNa\cdot NMe[(CH_2)_2NMe_2]_2$: I. Cragg-Hine, M. G. Davidson, A. J. Edwards, P. R. Raithby, R. Snaith, *J. Chem. Soc., Dalton Trans.* **1994**, 2901−2902.

[85] Synthesis and Crystal Structure of a 1D-sodium Coordination Polymer: $[NaL^4(PMDETA)]_\infty$: R. W. Saalfrank, O. Struck, M. G. Davidson, R. Snaith, *Chem. Ber.* **1994**, *127*, 2489−2492.

[86] Self-Assembly in the Metallation of Bis(aminoaryl)Ethers: O. Kocian, N. Spencer, J. F. Stoddart, I. Cragg-Hine, M. G. Davidson, F. S. Mair, P. R. Raithby, R. Snaith, T. Kottke, E. Poll, *Tetrahedron* **1995**, *51*, 579−590.

[87] The First Solid-State Structure of a Mixed-Anion ROLi/LiOH Compound: $(t\text{BuOLi})_{10}\cdot(LiOH)_6$: C. Lambert, F. Hampel, P. v. R. Schleyer, M. G. Davidson, R. Snaith, *J. Organomet. Chem.* **1995**, *487*, 139−141.

[88] Aggregation of Metallated Organics by Hydrogen Bonding: Synthesis and Crystal Structures of 2-Aminophenoxy-aluminium and Salen-aluminium Ligand-separated Ion Pairs: M. G. Davidson, C. Lambert, M.-I. Lopez-Solera, P. R. Raithby, R. Snaith, *Inorg. Chem.* **1995**, *34*, 3765−3779.

[89] The Occurrence of Both Amide and Thiolate Forms of the 2-Mercaptobenzoxazolyl Anion ($C_7H_4ONS^-$) in the Same Molecule: Synthesis and Crystal Structure of $C_7H_4ONSNa[(\mu\text{-}OP(NMe_2)_3]_3NaC_7H_4ONS$: F. A. Banbury, M. G. Davidson, P. R. Raithby, D. Stalke, R. Snaith, *J. Chem. Soc., Dalton Trans.* **1995**, 3139−3142.

[90] Synthetic, Structural, Spectroscopic and Calculational Studies of a Lithium β-Diketinimate Complex: F. S. Mair, D. Scully, A. J. Edwards, P. R. Raithby, R. Snaith, *Polyhedron* **1995**, *14*, 2397−2401.

 © 2003 Wiley-VCH Verlag GmbH & Co. KGaA, Weinheim

[91] An Investigation of the Lithium Species Present during the CO_2-Protected/Directed α-Lithiation and Subsequent α-Substitution of Heterocyclic Amines: S. C. Ball, I. Cragg-Hine, M. G. Davidson, R. P. Davies, A. J. Edwards, M.-I. Lopez-Solera, P. R. Raithby, R. Snaith, *Angew. Chem. Int. Ed. Engl.* **1995**, *34*, 921−923.

[92] The First Dilithiated Salen Complexes: Chiral $(SalenLi_2{\cdot}HMPA)_2$ and Deliberate Partial Hydrolysis to give $(SalenLi_2)_3{\cdot}Li_2O{\cdot}(TMEDA)_2{\cdot}H_2O$: S. C. Ball, I. Cragg-Hine, M. G. Davidson, R. P. Davies, M.-I. Lopez-Solera, P. R. Raithby, D. Reed, R. Snaith, E. M. Vogl, *J. Chem. Soc., Chem. Commun.* **1995**, 2147−2149.

[93] The Isolation and Structure of a Highly Stable, Metallation-Resistant and Multiply Hydrogen-Bonded Sulfonylamide-Phosphane Oxide Adduct, $PhSO_2CH_2C(=O)NH_2{\cdot}O=P(NMe_2)_3$: I. Cragg-Hine, M. G. Davidson, A. J. Edwards, E. Lamb, P. R. Raithby, R. Snaith, *Chem. Commun.* **1996**, 153−154.

[94] A Stable Methyl Phosphane Oxide-Lithium Amide Complex: a Structural, MO Calculational Investigation of the Mechanism of Proton Abstraction by Alkali Metal Reagents: D. R. Armstrong, M. G. Davidson, R. P. Davies, H. J. Mitchell, R. M. Oakley, P. R. Raithby, R. Snaith, S. Warren, *Angew. Chem. Int. Ed. Engl.* **1996**, *35*, 1942−1944.

[95] The Mechanisms of Dilithiation Reactions in Organic Syntheses: a Case Study Based on the Syntheses of Ketene Dithioacetals: S. C. Ball, I. Cragg-Hine, M. G. Davidson, R. P. Davies, P. R. Raithby, R. Snaith, *Chem. Commun.* **1996**, 1581−1582.

[96] Structural Models for Lithium Intermediates During Carboxamide-Directed Metallations: M. G. Davidson, R. P. Davies, P. R. Raithby, R. Snaith, *Chem. Commun.* **1996**, 1695−1696.

[97] A Likely Intermediate During the CO_2-Induced Activation of 2-Alkylindoles Towards Electrophilic Substitution: Structure of a Unique Tetramer Formed by Joining Two Boat-shaped $(LiOCO)_2$ Rings: R. P. Davies, P. R. Raithby, R. Snaith, *Organometallics* **1996**, *15*, 4355−4356.

[98] Role of Bifunctional N/S Bridging in the Association of Metals; Syntheses and Structures of Heterobimetallic $[(Ph_3P_2)CuL_2Li(THF)_2]{\cdot}$thf and Tetrameric $[CuL(PPh_3)]_4$ (L= 1,3-benzoxazoline-2-thionate): M. A. Beswick, C. Brasse, M. A. Halcrow, P. R. Raithby, C. A. Russell, A. Steiner, R. Snaith, D. S. Wright, *J. Chem. Soc., Dalton Trans.* **1996**, 3793−3797.

[99] An Experimental, MO Calculational Study of the Stereoselective Horner−Wittig Reaction with Phosphane Oxides: Control of Stereoselectivity by Lithium: D. R. Armstrong, D. Barr, M. G. Davidson, G. Hutton, P. O'Brien, R. Snaith, S. Warren, *J. Organomet. Chem.* **1997**, *529*, 29−33.

[100] Lithiated Amidines: Syntheses and Structural Characterisations: J. Barker, D. Barr, N. D. R. Barnett, W. Clegg, I. Cragg-Hine, M. G. Davidson, R. P. Davies, S. M. Hodgson, J. A. K. Howard, M. Kilner, C. W. Lehmann, M.-I. Lopez-Solera, R. E. Mulvey, P. R. Raithby, R. Snaith, *J. Chem. Soc., Dalton Trans.* **1997**, 951−955.

[101] A Unique Li_{12}-Aggregate Containing Both $-NL_2$ and −CHLi~NLi Units: S. C. Ball, J. Cobb, R. P. Davies, P. R. Raithby, G. P. Shields, R. Snaith, *J. Organomet. Chem.* **1997**, *534*, 241−245.

[102] The Remarkable Product of Using a Large Excess of *n*-Butyllithium to Lithiate a Simple Amine: $(Ph_2NLi){\cdot}[[Ph(C_6H_4Li)NLi]_2{\cdot}(nBuLi)_2{\cdot}(Et_2O)_4$: R. P. Davies, P. R. Raithby, R. Snaith, *Angew. Chem. Int. Ed. Engl.* **1997**, *36*, 1215−1217.

[103] Inhibition of the Cyclotrimerisation of Benzonitrile: Structure of a New Tetrameric α-Amino Lithium Imide Demonstrating *Intra*-Monomer Stabilisation of the Metal Centres: R. P. Davies, P. R. Raithby, G. P. Shields, R. Snaith, A. E. H. Wheatley, *Organometallics* **1997**, *16*, 2223−2225.

[104] The First Lithiated Phosphane Oxide with Li−C Bonds: Synthesis and Structure of $[Ph_2P(O)CHLiC(H)MeEt]_4$: J. E. Davies, R. P. Davies, L. Dunbar, P. R. Raithby, M. G. Russell, R. Snaith, S. Warren, A. E. H. Wheatley, *Angew. Chem. Int. Ed. Engl.* **1997**, *36*, 2334−2335.

[105] The Synthesis and Novel Structure of the First Crystallographically Characterised Chiral α-Amino Lithium Alkoxide: J. E. Davies, P. R. Raithby, R. Snaith, A. E. H. Wheatley, *Chem. Commun.* **1997**, 1721−1722.

[106] Reaction of an Alkynyllithium Reagent with Boron Trifluoride: the Structure of a Likely Intermediate in Alkynyl Anion Chemistry: J. E. Davies, P. R. Raithby, R. Snaith, A. E. H. Wheatley, *Chem. Commun.* **1997**, 1797−1798.

[107] Lithiations of Phosphane Oxides: D. R. Armstrong, R. P. Davies, L. Dunbar, P. R. Raithby, R. Snaith, A. E. H. Wheatley, *Phosphorus, Sulfur, and Silicon* **1997**, *124−125*, 51−62.

[108] A Structural and Theoretical Study of the Mono-Lithiation of Hydroxylamines: D. R. Armstrong, W. Clegg, S. M. Hodgson, R. Snaith, A. E. H. Wheatley, *J. Organomet. Chem.* **1998**, *550*, 233−240.

[109] The Mechanism of Lithiation and Nitrile Insertion Reactions of β-Methylazines: Evidence from the Structure of $3\text{-}C_5H_4NCH{=}C(Ph)N(H)C(Ph){=}NLi{\cdot}PMDETA$, S. C. Ball: R. P. Davies, P. R. Raithby, G. P. Shields, R. Snaith, *J. Organomet. Chem.* **1998**, *550*, 457−461.

[110] The First Solid-State Structure of a Simple Lithiated Diazomethane with C−Li Bonds: $\{[Me_3SiC(Li)N_2]_2{\cdot}3THF\}_\infty$: N. Feeder, M. A. Hendy, P. R. Raithby, R. Snaith, A. E. H. Wheatley, *Eur. J. Org. Chem.* **1998**, 861−864.

[111] First Structurally Characterised Lithium Hexafluorophosphate Complexes with Acyclic Lewis Bases: Ion-separated $[Li_2(HMPA)_5]^{2+}{\cdot}2(PF_6^-)$ and Ion-contacted $[(PMDETA)LiPF_6]_2$: D. R. Armstrong, A. H. Khandelwal, L. C. Kerr, S. Peasey, P. R. Raithby, G. P. Shields, R. Snaith, D. S. Wright, *Chem. Commun.* **1998**, 1011−1012.

[112] The First Structural Studies on Trithiocyanuric Acid: the Solid-State Structures of its HMPA Adduct and its Monolithiated HMPA Complex: W. Clegg, J. E. Davies, M. R. J. Elsegood, E. Lamb, J. J. Longridge, J. M. Rawson, R. Snaith, A. E. H. Wheatley, *Inorg. Chem. Commun.* **1998**, *1*, 58−60.

[113] Reaction of *ortho*-Methylbenzonitrile with Lithium Trimethylethylenediamide: Assembly and Crystal Structure of a Primary Isoquinolinoamidolithium-Secondary Amine Complex: N. Feeder, R. Snaith, A. E. H. Wheatley, *Eur. J. Inorg. Chem.* **1998**, 879−883.

[114] The Synthesis and Solid-state and Solution Structures of an Unprecedented Mixed Chiral α-Amino Lithium Alkoxide-Lithium Alkoxide Aggregate: Evidence for Intermolecular LiH Transfer: W. Clegg, S. T. Liddle, R. Snaith, A. E. H. Wheatley, *New J. Chem.* **1998**, *22*, 1323−1326.

[115] Dynamic Processes in Organolithium Chemistry: Tetrameric and "Open" Tetrameric Chiral α-Amino Lithium Alkoxides: D. R. Armstrong, J. E. Davies, R. P. Davies, P. R. Raithby, R. Snaith, A. E. H. Wheatley, *New J. Chem.* **1999**, *23*, 35−41.

[116] Towards an Understanding of the Conjugate Addition of Organolithium Reagents to α,β-Unsaturated Ketones: the Isolation and Solid-State Structure of a Monomeric Lithium Aluminate with Very Short Agostic Li···HC Interactions: W. Clegg, E. Lamb, S. T. Liddle, R. Snaith, A. E. H. Wheatley, *J. Organomet. Chem.* **1999**, *573*, 305−312.

[117] Hexameric Chiral α-Amino Lithium Alkoxides: a Solid-state and Theoretical Structural Investigation: D. R. Armstrong, R. P. Davies, P. R. Raithby, R. Snaith, A. E. H. Wheatley, *New J. Chem.* **1999**, *23*, 499−507.

[118] Lithiated Organophosphorus Enamines: A New Synthetic Approach and the First Crystal Structures: W. Clegg, R. P. Davies, L. Dunbar, N. Feeder, S. T. Liddle, R. E. Mulvey, R. Snaith, A. E. H. Wheatley, *Chem. Commun.* **1999**, 1401−1402.

[119] The First Molecular Main Group Metal Species Containing Interstitial Hydride: W. Clegg, R. P. Davies, S. T. Liddle, D. J. Linton, P. R. Raithby, R. Snaith, A. E. H. Wheatley, *Angew. Chem. Int. Ed.* **1999**, *38*, 3367−3370.

[120] Structural studies of the chiral lithium amides $[\{PhC(H)Me\}_2NLi]$ and $[PhCH_2\{PhC(H)Me\}NLi{\cdot}THF]$ de-

 © 2003 Wiley-VCH Verlag GmbH & Co. KGaA, Weinheim

rived from α-methylbenzylamine: D. R. Armstrong, K. W. Henderson, A. R. Kennedy, W. J. Kerr, F. S. Mair, J. H. Moir, P. H. Moran, R. Snaith, *J. Chem. Soc., Dalton Trans.* **1999**, 4063−4068.

[121] Selective Oxygen Capture to give a Unique Mixed-Anion Lithium Aluminate: the Synthesis and Solid-State Structure of {[PhC(O)N(Me)Al(Me)(*t*Bu)OMe]Li·[PhC(O)N(Me)Al(Me)-(O*t*Bu)OMe]Li}$_2$: R. P. Davies, D. J. Linton, R. Snaith, A. E. H. Wheatley, *Chem. Commun.* **2000**, 193−194.

[122] Selective Oxygen Capture in Lithium Zincate Chemistry: the Syntheses and Solid-State Structures Of (μ_4-O)Zn$_4$[N(2-Pyr)Bz]$_6$ and *t*Bu(μ_3-O)Li$_3$(μ_6-O)Zn$_3$[N(2-Pyr)Me]$_6$ (Bz = benzyl): R. P. Davies, D. J. Linton, R. Snaith, A. E. H. Wheatley, *Chem. Commun.* **2000**, 1819−1820.

[123] Selective Oxygen Capture by Lithium Aluminates: a Solid-State and Theoretical Structural Study: D. R. Armstrong, R. P. Davies, D. J. Linton, P. Schooler, G. P. Shields, R. Snaith, A. E. H. Wheatley, *J. Chem. Soc., Dalton Trans.* **2000**, 4304−4311.

[124] An Investigation of the Structural Diversities of Lithiated HMPA Complexes of *o*-Mercaptopyridine and Trithiocyanuric Acid: Syntheses, Crystal Structures and Model Molecular Orbital Calculations: D. R. Armstrong, J. E. Davies, N. Feeder, E. Lamb, J. J. Longridge, J. M. Rawson, R. Snaith, A. E. H. Wheatley, *J. Mol. Mod.* **2000**, *6*, 234−247.

[125] Synthesis and Solid-State Structure of (Li$_4$Am$_3$)$^+$·{Li[(μ-Me)$_2$Al(Me)*t*Bu]$_2$}$^-$ {Am = [PhNC(Ph)NPh]$^-$}: A Polymeric Species Incorporating a Lithium-Nitrogen Cluster Cation: R. P. Davies, D. J. Linton, P. Schooler, R. Snaith, A. E. H. Wheatley, *Eur. J. Inorg. Chem.* **2001**, 619−622.

[126] The First Crystallographic Evidence for Directed Ortholithiation of an Aromatic Ring by an Amide-type Functional Group: J. Clayden, R. P. Davies, M. A. Hendy, R. Snaith, A. E. H. Wheatley, *Angew. Chem. Int. Ed.* **2001**, *40*, 1238−1240.

[127] Oxygen Capture by Lithiated Organozinc Reagents Incorporating Aromatic 2-Pyridylamide Ligands: R. P. Davies, D. J. Linton, P. Schooler, R. Snaith, A. E. H. Wheatley, *Chem. Eur. J.* **2001**, *7*, 3696−3704.

[128] Ligand Effects in the Syntheses of Molecular Main Group Metal Species Containing Interstitial Hydride: D. R. Armstrong, R. P. Davies, W. Clegg, S. T. Liddle, D. J. Linton, P. Schooler, R. Snaith, A. E. H. Wheatley, *Phosphorus, Sulfur, and Silicon* **2001**, *168*, 93−98.

[129] The Crystallographic Observation of Molecular Lithium Oxide: Synthesis and Solid-State Structure of [Ph(2-Pyr)NAlMe$_2$]$_2$(O)Li$_2$·2THF: D. R. Armstrong, R. P. Davies, D. J. Linton, P. Schooler, R. Snaith, A. E. H. Wheatley, *J. Chem. Soc., Dalton Trans.* **2001**, 2838−2843.

[130] Lithium Alkyl Selenolates and Tellurolates: a Solid-State and Solution Structural Study: W. Clegg, R. P. Davies, R. Snaith, A. E. H. Wheatley, *Eur. J. Inorg. Chem.* **2001**, 1411−1413.

[131] A Solid State and Theoretical Study of the Solvent Effects Controlling the Mono- and Dilithiation of Aromatic Primary Amines: D. R. Armstrong, S. C. Ball, D. Barr, W. Clegg, L. C. Kerr, D. J. Linton, D. Moncrieff, P. R. Raithby, R. J. Singer, R. Snaith, D. Stalke, A. E. H. Wheatley, D. S. Wright, *J. Chem. Soc., Dalton Trans.* **2002**, 2505−2511.

[132] (*trans*-Cinnamaldehyde)tris(2,6-phenylphenoxy)aluminium: W. Clegg, M. R. J. Elsegood, R. Snaith, A. E. H. Wheatley, *Acta Crystallogr. Sect. E* **2003**, E59, m225−m227.

[133] A Solid-State, Solution and Theoretical Structural Study of Kinetic and Thermodynamic Derivatives of a Simple Diazomethane and Their Reactivities Towards Aryl Isothiocyanates: D. R. Armstrong, R. P. Davies, N. Feeder, R. Haigh, M. A. Hendy, P. R. Raithby, R. Snaith, A. E. H. Wheatley, *Eur. J. Inorg. Chem.* in press.

Review Articles

[134] Carboranes and Metallocarboranes, R. Snaith, K. Wade, M.T.P. International Review of Science, Inorganic Chemistry, Series One, Volume I, Chapter 4, Butterworths, **1972**, pp. 139−183.

[135] Carboranes and Metallocarboranes, R. Snaith, K. Wade, M.T.P. International Review of Science, Inorganic Chemistry, Series Two, Volume 1, Chapter 4, Butterworths, **1975**, pp 95−134.

[136] The Chemistry of Gallium, R. Snaith, K. Wade, in "Encyclopædia of Chemistry", Utet/Sansoni (Florence), published in Italy, **1976**, pp. 3−9.

[137] Structures of Organonitrogen-Lithium Compounds; Recent Patterns and Perspectives in Organolithium Chemistry, K. Gregory, P. v. R. Schleyer, R. Snaith, *Adv. Inorg. Chem.* **1991**, *37*, 47−142.

[138] Alkali Metals: Inorganic Chemistry, F. S. Mair, R. Snaith, in "Encyclopædia of Inorganic Chemistry", ed. R. B. King; John Wiley and Sons Ltd.; **1994**, Vol. 1, Chapter 3.

[139] Complexes of Inorganic Lithium Salts, R. Snaith, D. S. Wright, in "Lithium Chemistry: A Theoretical and Experimental Overview" (Eds.: A.-M. Sapse and P. v. R. Schleyer), John Wiley and Sons Inc.; **1995**, pp. 227−293.

[140] Group One and the Coinage Metals, R. Snaith, *Specialist Periodic Reports: Organometallic Chemistry*, **1998**, *26*, 1−14.

[141] Group One and the Coinage Metals, R. Snaith, *Specialist Periodic Reports: Organometallic Chemistry*, **1999**, *27*, 419−431.

[142] Group One and the Coinage Metals, R. Snaith, A. E. H. Wheatley, *Specialist Periodic Reports: Organometallic Chemistry*, **2000**, *28*, 33−50.

Annual Reports

[143] R. Snaith, Annual Reports, Section A; Vol. 82 covering 1985. Main Groups I and II (Chapter 2), pp. 3−33.

[144] R. Snaith, Annual Reports, Section A; Vol. 83 covering 1986. Main Groups I and II (Chapter 2), pp. 3−38.

[145] R. Snaith, Annual Reports, Section A; Vol. 84 covering 1987. Main Groups I and II (Chapter 2), pp. 3−39.

Patents

[146] (a) Alkali Metal Salt Complexes Synthesised by the Ammonium Salt Route. Preliminary Patent filed by Associated Octel Co. Ltd., Ellesmere Port, U.K. Inventors named, R. Snaith, D. S. Wright. (b) European Patent No. 88309913.7, **1987**, R. Snaith, D. S. Wright.

[147] (a) Alkaline-Earth, Lanthanide, and Transition Metal Salt Complexes Synthesised by the Ammonium Salt Route. Preliminary Patent filed by the Associated Octel Co. Ltd., Ellesmere Port, U.K. Inventors named, A. T. Brooker, S. R. Drake, R. Snaith, D. S. Wright. (b) European Patent No. 8915531.1, 1989. A. T. Brooker, S. R. Drake, R. Snaith, D. S. Wright.

[148] (a) Alkali Metal Salt Complexes Synthesised by the Metal/Non-Metal *In Situ* Route. Preliminary Patent filed by the Associated Octel Co. Ltd., Ellesmere Port, U.K. Inventors named, A. T. Brooker, S. R. Drake, R. Snaith, D. S. Wright. (b) European Patent No. 8911600.8, 1989. A. T. Brooker, S. R. Drake, R. Snaith, D. S. Wright.

[149] Method for the Preparation of Aquo and other Small Protic Lewis Base Complexes of Metal Salts of Organic Acids. Preliminary Patent filed by Associated Octel Co. Ltd., Ellesmere Port, U.K. Inventors named, M. G. Davidson, R. Snaith, D. S. Wright. Filed 1991.

[150] Complexes of Metallated Organic Molecules Comprising Multiple or Mixed Metallic Species. Preliminary Patent filed by the Associated Octel Co. Ltd., Ellesmere Port, U.K. Inventors named, M. G. Davidson, P. R. Raithby, R. Snaith, D. S. Wright. Filed 1991.

[151] Method for the Deprotonation and Molecular Rearrangement of Organic Compounds, especially Heterocyclics. Preliminary Patent filed by the Associated Octel Co. Ltd., Ellesmere Port, U.K. Inventors named, F. A. Banbury, M. G. Davidson, A. Martin, R. Snaith. Filed 1992.

Miscellaneous

[152] In celebration of the sixty-fifth birthday of Professor Ken Wade, R. Snaith, *J. Organomet. Chem.* **1998**, *550*, IX−XI.

Received August 12, 2003

 © 2003 Wiley-VCH Verlag GmbH & Co. KGaA, Weinheim

Toroidal Main Group Macrocycles: New Opportunities for Cation and Anion Coordination

Emma L. Doyle,[a] Lucía Riera,[a] and Dominic S. Wright*[a]

Dedicated to the memory of Dr. Ron Snaith

Keywords: Coordination chemistry / Macrocycles / Main group elements / Synthesis

Inorganic macrocycles, possessing molecular frameworks composed entirely of elements other than carbon, are rare. Even rarer are species analogous to classical organic macrocycles (like crown ethers) that possess the potential ability to coordinate metal ions within their cavities. Recent studies reveal an emerging structural class of valence-isoelectronic main-group ligands of general formula $[\{E(\mu\text{-}E'R)\}_2Y]_n^{x-}$, which possess fascinating coordination characteristics. Such species can coordinate metal ions within their cavities (using the donor centres Y and E′), their peripheral donor centres (E′) (in an *exo* fashion) and are also capable of coordinating anions (where Y = N–H). This short review highlights the recent synthetic and structural studies of these unusual ligand systems and pinpoints potential future areas of development.

(© Wiley-VCH Verlag GmbH & Co. KGaA, 69451 Weinheim, Germany, 2003)

Introduction

Classical macrocyclic ligands based essentially on carbon backbones (such as crown ethers, calixarenes and cyclophanes) have a central role in modern coordination chemistry.[1] Modification of the donor or acceptor atoms (or groups) within these arrangements has provided an ever-growing class of ligand arrangements which are capable of coordinating cations,[2] anions or neutral guest molecules.[3] In contrast, "inorganic" counterparts whose frameworks are constructed from elements other than carbon are still relatively rare, and their coordination behaviour has been little studied. There are a number of obvious reasons for this situation. Firstly and perhaps most importantly, owing to the greater range of available orbitals and hybridisation states, a far more diverse range of bonding connectivities

[a] Chemistry Department, University of Cambridge
Lensfield Road, Cambridge CB2 1EW, U.K.

Emma L. Doyle was born in Chatham, Kent in England in 1977. She obtained her BA (Hons) in Natural Sciences in 1999 and an MSc in Chemistry in 2000 from Cambridge University. She is currently pursuing her Ph.D. at Cambridge University under the supervision of Dr. Dominic S. Wright where she is studying cyclodiphosph(III)azane chemistry. Her research interests include the study of phosphorus−nitrogen based macrocycles and the future prospects of these for host−guest and Lewis base coordination. Particular interest is in the potential selectivity of anion coordination.

Lucía Riera was born in Zaragoza, Spain in 1974. She obtained her first degree in 1997 at the University of Oviedo and completed her M.Sc. (Tesina) in Oviedo in 1998. Her Ph.D. was undertaken in Oviedo under the supervision of Julio Antonio Peréz Martínez and was obtained in 2002. She joined the Wright group in October of that year and is currently funded by an E.U. fellowship.

Dominic S. Wright obtained his first degree in Pure and Applied Chemistry at the University of Strathclyde (1982−1986). He then studied for his Ph.D. alkali metal salt complexes under the supervision of the late Dr. Ron Snaith at Cambridge University (1986−1989). After a period as a Research Fellowship at Gonville and Cauis College, Cambridge (1989−1991), he became a lecturer in Inorganic Chemistry at Cambridge. He was promoted to Reader in Inorganic Chemistry in October 2002. Dr. Wright has published extensively in the area of main-group and transition-metal chemistry, specialising in the development of new p-block element ligand systems, the chemistry of p-block cyclopentadienyl anions and the chemistry of main-group and transition-metal imido and phosphide complexes.

MICROREVIEWS: This feature introduces the readers to the authors' research through a concise overview of the selected topic. Reference to important work from others in the field is included.

and geometries are characteristic of elements after the first period of the periodic table. An associated feature is the availability of various oxidation states. These factors make rational design of cyclic systems complicated and often limit the applications of synthetic stategies. A second factor is the commonly lower thermodynamic stability and polar nature of bonds to these elements, leading to thermodynamically less robust and/or kinetically more labile ligand arrangements.

Of the few inorganic macrocycles so far investigated the most common type are acceptors (or Lewis acids), particularly those based on electropositive metals.[4−6] An example of this class recently reported are the so-called "inverse-crowns" investigated by Mulvey and co-workers.[4] These macrocyclic, (mainly) alkali or alkaline earth metal amides have been shown to be capable of coordinating various inorganic and organic anions within their cavities. The complex $[(tmp)_6Na_4Mg_2(C_6H_3CH_3)]$ (**1**) (Figure 1) is a particularly interesting example that illustrates a fascinating feature of inverse crowns, the ability to stabilise and direct the formation of highly unusual organic anions (in this case a 2,5-deprotonated $[C_5H_4CH_3]^{2-}$ dianion). Conceptually related mercury(II) metallacarborands investigated earlier by Hawthorne and co-workers are examples of rigid ligand frameworks of this type, which are capable of anion-selective behaviour (an example of which is shown in Figure 2).[5]

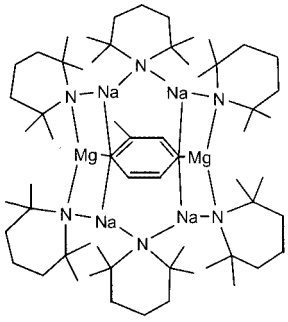

Figure 1. Structure of the inverse crown $[(tmp)_6Na_4Mg_2(C_6H_3CH_3)]$ (**1**), with coordination of a 2,5-deprotonated toluene at the center of the cavity

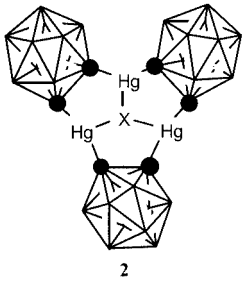

Figure 2. Structure of a trimeric mercury(II) metallacarborand coordinating a halide ion (X) within the cavity

Far rarer than Lewis acidic inorganic arrangements are macrocycles which (like crown ethers) are potentially capable of cation coordination. Examples of this type include organophosphorus macrocycles, such as the octamer $[1,2\text{-}C_6H_4P_2]_8$, composed of a 16-membered ring of P atoms, and the tetrameric anion $[1,2\text{-}C_6H_4P_2]_4^{4-}$.[7] In addition, a few macrocyclic cyclophosph(v)azanes, such as $[(Me_2N)_2PN]_6$, are also known.[8] Our interest in the area of inorganic macrocycles has derived from a general interest in inorganic donor ligands based on p-block element/nitrogen and phosphorus frameworks.[9,10] This short review aims to highlight an emerging class of structurally related, valence-isoelectronic p-block macrocycles of general formulae $[\{E(\mu\text{-}E'R)\}_2Y]^{x-}$ (Figure 3), in which dimeric $\{E(\mu\text{-}E'R)\}_2$ ring units are bridged into neutral or anionic cyclic arrangements via heteroatomic groups or atoms (Y).

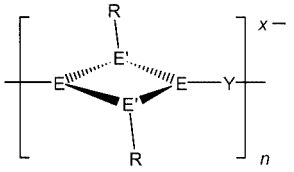

Figure 3. Structural arrangement of the macrocycles

An early indication of the existence of this structural class of macrocycles was provided by the seminal work of Scherer et al., who showed that the phosph(III)azane $[\{P(\mu\text{-}N\mathit{i}Pr)\}_2N\mathit{i}Pr]_2$ (**3**) is obtained by the thermolysis reaction of $[ClP(\mu\text{-}N\mathit{i}Pr)_2PN(\mathit{i}Pr)(SiMe_3)]$ (Scheme 1).[11] More recently, it has been shown that the similar dimeric macrocycle $[\{P(\mu\text{-}N\mathit{t}Bu)\}_2N\mathit{t}Bu]_2$ (**4**) can be obtained by the reaction of the symmetric dimer $[ClP(\mu\text{-}N\mathit{t}Bu)]_2$ with $[\mathit{t}BuNP(\mu\text{-}N\mathit{t}Bu)]_2^{2-}$ (Scheme 2).[12] A. D. Norman and co-workers were the first to suggest that smaller chain and cyclic arrangements of this kind may represent homologues of a broader family of compounds.[13] However, prior to our studies cyclic arrangements had been restricted to dimeric macrocycles of group-15 elements only.

Higher Homologues of Group 15

Our interest in macrocyclic species of this type came about by the chance discovery that the deprotonation reaction of the lithium tris(amidostannate) $[Sn(HNma)_3Li{\cdot}2thf]$ (H_2Nma = 2-methoxyaniline) (**5**) with $Sb(NMe_2)_3$ gives the hexameric macrocycle $[\{Sb(\mu\text{-}Nma)\}_2(\mu\text{-}Nma)]_6$ (**6**), rather than the anticipated heterometallic cage $[Sb(\mu\text{-}Nma)_3Sn]Li$ (**7**).[14] This reaction presumably occurs by elimination of $[Sn(NMe_2)_3Li]$ as a "leaving group" (Scheme 3).[15] Interestingly, **6** can also be obtained by the transmetallation reaction of the $[Sb(Nma)_3]^{3-}$ trianion with $SbCl_3$, a process which can be seen as an inorganic example of masked functionality (Scheme 4).[16]

The solid-state structure of **6** (Figure 4) has an all-*trans* arrangement of the dimer units and a macrocyclic cavity of ca. 13.8 Å (measured between opposite Sb^{III} centers). This was the first example of a higher oligomer of this type for

 © 2003 Wiley-VCH Verlag GmbH & Co. KGaA, Weinheim

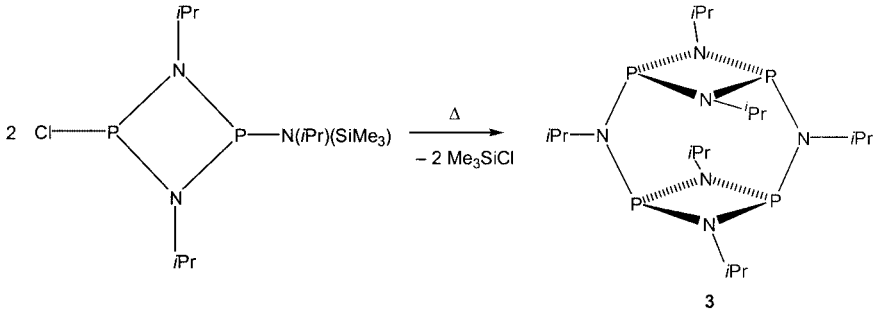

Scheme 1

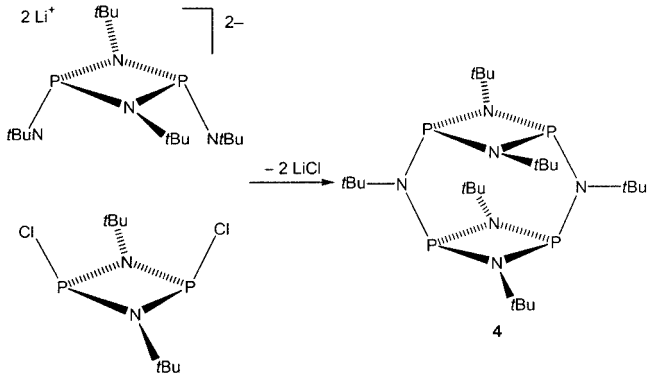

Scheme 2

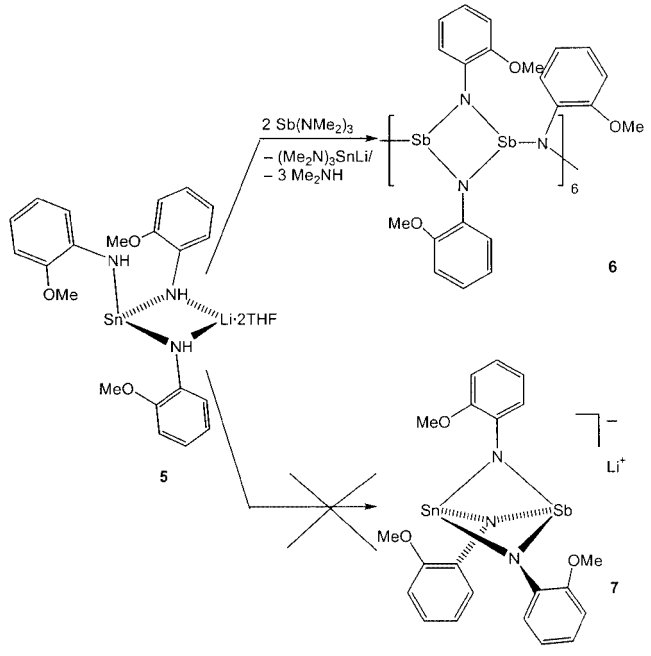

Scheme 3

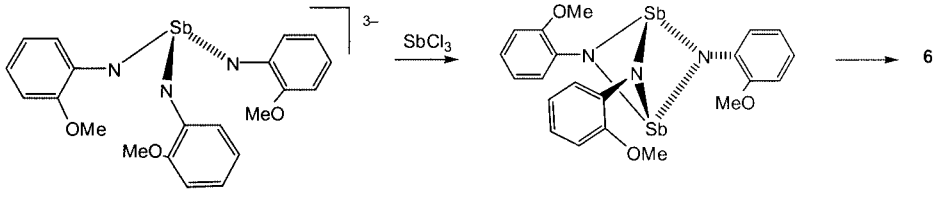

Scheme 4

group 15. More recently, N. C. Norman and co-workers showed that the similar hexameric macrocycle $[\{Sb(\mu\text{-}NPh)\}_2(\mu\text{-}NPh)]_6$ (**8**) can be readily prepared by the reaction of $SbCl_3$ with PhHLi.[17] The observation of hexameric ring units for both **6** and **8**, rather than dimeric macrocycles like **3** and **4**, gives a fundamental clue to the factors directing ring sizes of the homologues $[\{E(\mu\text{-}NR)\}_2NR]_n$.

In considering the formation of higher homologues of the type $[\{E(\mu\text{-}NR)\}_2NR]_n$ (with $n > 2$, like **7** and **8**), a number of factors need to be considered. Perhaps the most important factor influencing the size of macrocycle obtained is the steric demands of the organic substituents (R). The steric influence of the dimer-bridging NR groups is likely to be most critical in this respect. As depicted in Figure 5, for dimeric ($n = 2$) macrocycles the disposition of dimer-bridging NR groups *exo* to the cavity will minimise steric congestion. This dimeric structure is likely to be observed for R groups with moderately large steric demands (as is the case with **3** and **4**). However, in order to sustain the *exo* orientation of these groups for higher homologues ($n > 2$) some or all of the $[P(\mu\text{-}NR)]_2$ units will have to adopt *trans* orientations. This situation is likely to lead to increased ring strain for intermediately sized macrocycles. As the size of the macrocycle increases increased preference for *trans* conformations of the ring units is expected in order to minimise ring strain and at the same time prevent unfavourable *endo* orientation of the dimer-bridging NR groups. These simple considerations therefore suggest that macrocycles of the type $[\{E(\mu\text{-}NR)\}_2NR]_n$ are most likely to occur for $n = 2$ and for larger ring units, where an all-*trans* conformation of the dimeric ring units matches the geometric constraints (as presumably occurs for the hexameric macrocycles **6** and **8**).

A significantly different set of circumstances occurs where the dimer-bridging NR groups have very low steric demands. Now a *cis* configuration of the dimeric ring units can be sustained even for rings beyond $n = 2$. Such occurs

 © 2003 Wiley-VCH Verlag GmbH & Co. KGaA, Weinheim

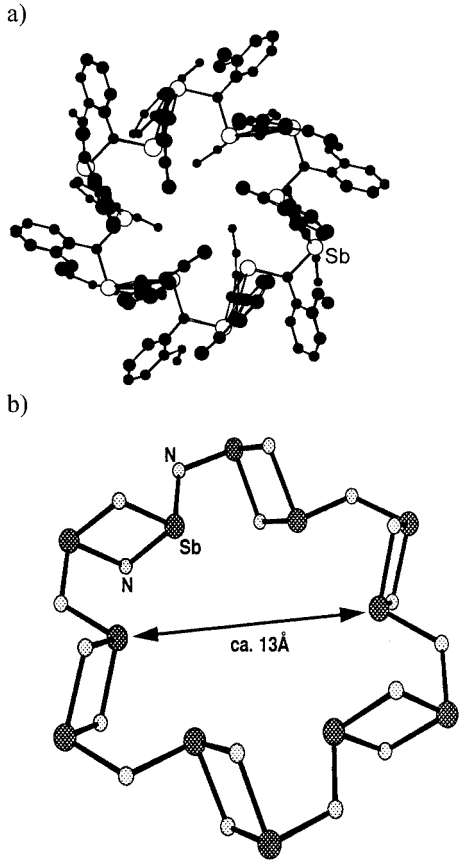

Figure 4. a) Structure of the hexamer **6**; b) core arrangement with ma groups removed

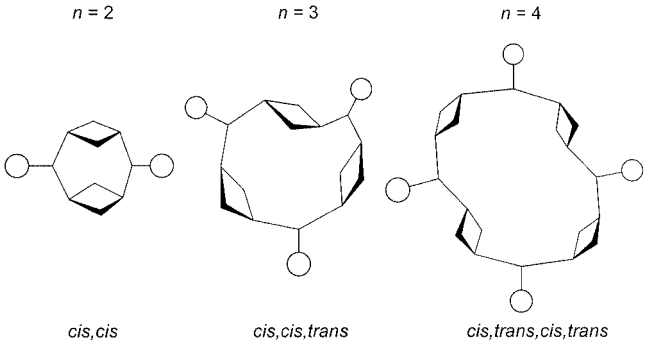

Figure 5. The transition from *cis* to *trans* conformations in macrocycles with increasing *n*

in the case of the tetrameric macrocycle $[\{P(\mu\text{-}NtBu)\}_2NH]_4$ (**9**) (Figure 6), obtained in almost quantitative yield (95−100%) from the condensation reaction of the symmetric dimers $[ClP(\mu\text{-}NtBu)]_2$ (**10**) and $[H_2NP(\mu\text{-}NtBu)]_2$ (**11**) in the presence of Et_3N (Scheme 5).[18] The *cis* conformations of the dimer ring constituents of **9** mean that the four N−H protons are now directed *endo* to the cavity, with the twelve P···P−N units defining the macrocyclic ring being almost in one plane. The transannular N···N separation between opposite pairs of N centers within the cavity of **9** differ by only ca. 0.05 Å, with the size of the cavity being ca. 5.22 Å. Presumably, the formation of a tetrameric macrocycle is a further consequence of the low steric demands of the dimer-bridging N−H groups of **9**, allowing aggegation to occur beyond simple dimers like **3** and **4.** The arrangement of **9** is reminiscent of organic ligands such as tetraazacyclotetradecanes (i.e., based on $[CH_2CH_2NH]_4$). However, the latter have significantly smaller cavities (range 4.07−4.29 Å).[19]

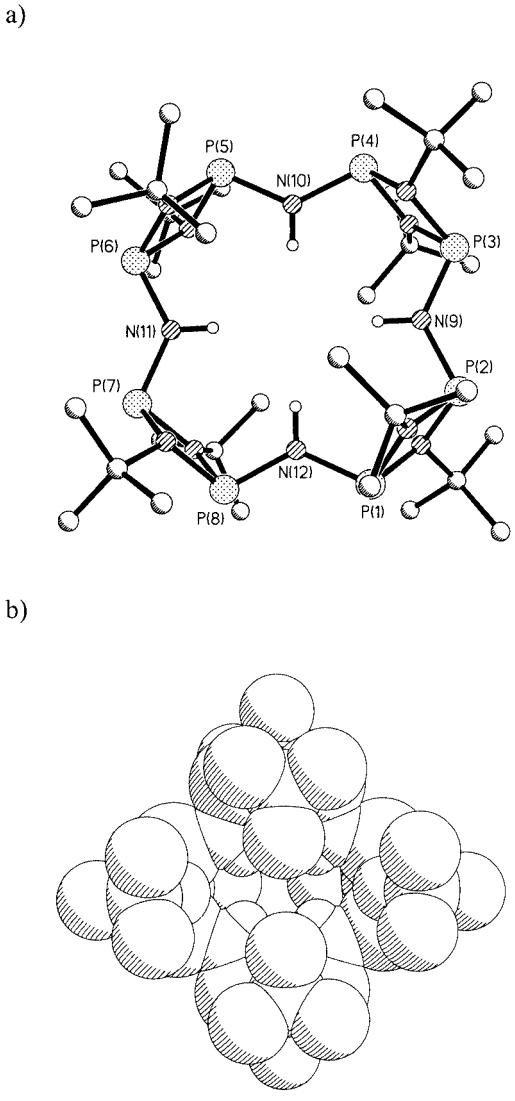

Figure 6. a) Structure of the tetramer **9**; b) space-filling diagram of **9** showing the crowding of the core

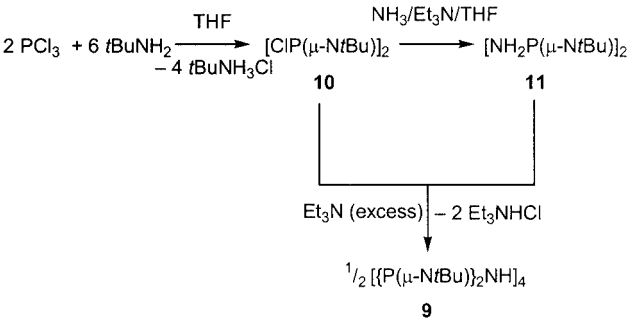

Scheme 5

 © 2003 Wiley-VCH Verlag GmbH & Co. KGaA, Weinheim

An important kinetic feature involved in the formation of **9** is "pre-organisation" of the dimer precursors **10** and **11**. The latter have both been shown to adopt *cis* conformations of the Cl and NH_2 substituents in the solid state and solution.[20,21] Indeed, in the case of **11** this *cis* conformation results in cyclisation of the dimers in the solid state via N−H···N hydrogen bonding.[20] Pre-organisation is primarily responsible for the near quantitative formation of the macrocyclic arrangement of **9**, rather than of polymeric alternatives. This is a rare (if not unprecedented) example of pre-organisation for an inorganic system. A further aspect of the mechanism by which **9** is formed is indicated by the formation of minor amounts of the host−guest complex $[\{P(\mu\text{-}NtBu)\}_2NH]_5$·HCl (**12·HCl**) along with **9** in the condensation reaction of **10** and **11** (Figure 7).[20] Like **9**, the dimer units of **12·HCl** adopt *cis* conformations, with the complex being composed of the pentameric macrocyclic ring $[\{P(\mu\text{-}NtBu)\}_2NH]_5$ (**12**) coordinating an HCl unit at the centre of the cavity via five N−H···Cl hydrogen bonds to all of the dimer-bridging N−H groups (N···Cl mean 3.6 Å, H···Cl 2.57−2.66 Å). The arrangement of the five N−H groups towards the centre of the macrocyclic unit creates a cavity of ca. 6.8 Å in diameter (measured with respect to the N atoms of the ring). The structure of **12·HCl** is similar to host−guest adducts of sapphyrins (expanded porphyrins),[22] in particular the pentapyrrole−HF complex $[\{3\text{-Me-4-Et-pyrNH}\}_5(CH_2)_4\cdot F][PF_6]$ (pyrN = pyrrole) which contains a similar arrangement of five N−H groups surrounding a central F^- anion.[22c] However, the core sizes in these complexes are significantly smaller than that in **12** (at ca. 5.5 Å in the pentaporphyrins, with respect to the five N centres[22]).

The isolation of **12·HCl** indicates that, in addition to pre-organisation, the formation of **9** may also rely on templating by Cl^- ions in the reaction. Extensive in situ ^{31}P NMR spectroscopic studies of the reactions of the dimers **10** and **11** under various conditions show that **9** and **12·HCl** are not in dynamic equilibrium with each other.[20] The most likely mechanism by which **9** and **12·HCl** are formed is by a divergent pathway like that shown in Scheme 6. The growing chain effectively competes with Et_3N as the Brønsted base in this reaction, so that N−H···Cl hydrogen bonding templates cyclisation. The pivitol intermediate **I[4]** can either eliminate HCl in the presence of Et_3N to form **9** or react with another molecule of **11** to give **12·HCl**. It is noteworthy in this regard that the formation of a pentameric macrocycle would be impossible by a simple, stepwise condensation pathway involving **9** and **10**, for which only macrocycles containing an even number of ring units (*n*) could be obtained.

A further discovery made during these ^{31}P NMR spectroscopic investigations is that the formation of the pentamer **12** can be biased by addition of excess lithium halide salts.[20] The high concentration of halide ions present presumably supresses the elimination of HX involved in the formation of **9**. The ability for the halide ions to template the formation of **12** is in the order $I^- > Br^- > Cl^-$. In the case of LiI, only the host−guest complex **12·HI** is generated

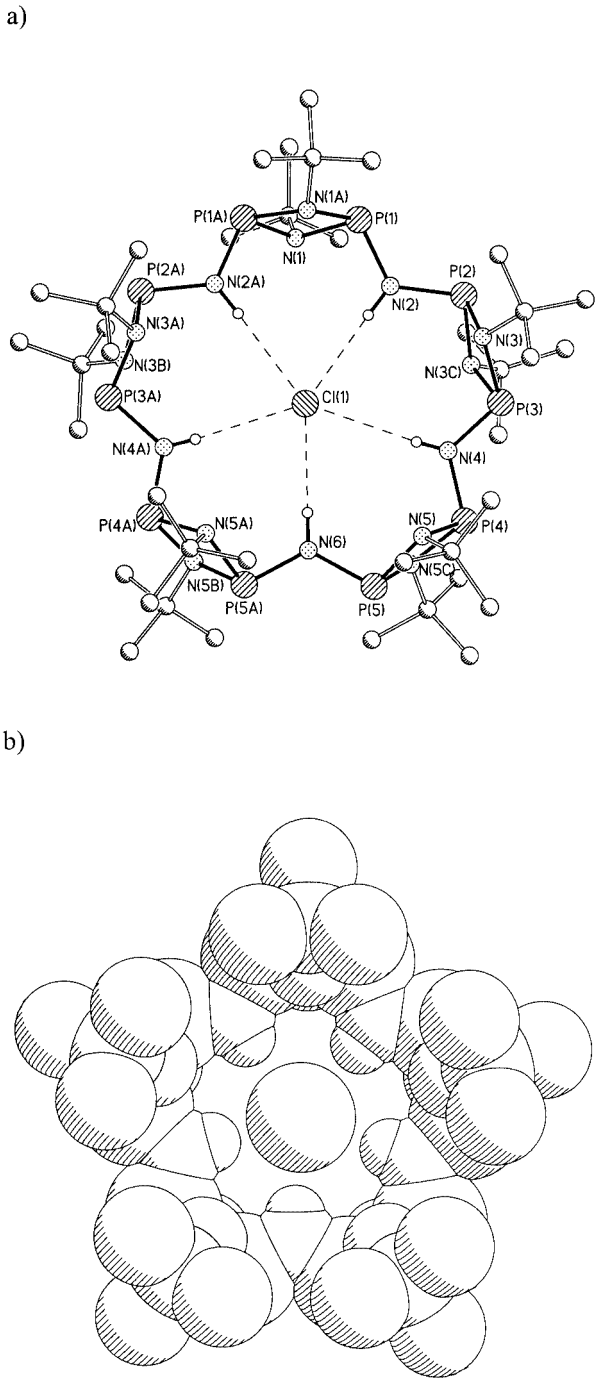

Figure 7. a) Structure of host−guest complex **12·HCl**; b) space-filling diagram of the molecule

(without **9**). This observation is broadly consistent with the size of the macrocyclic cavity of **12** (ca. 6.8 Å), which appears to be better suited to coordination of I^- (typical N···I 3.46 Å) than Cl^- (typical N···Cl 3.00−3.20 Å).[23]

At first sight, it might be expected that the presence of *cis* subunits within macrocycles of the type $[\{P(\mu\text{-}NR)\}_2NH]_n$ would limit the ring size obtainable, since beyond a particular point addition of further units would result in unfavourable ring strain. However, the formation of the tetrameric

 © 2003 Wiley-VCH Verlag GmbH & Co. KGaA, Weinheim

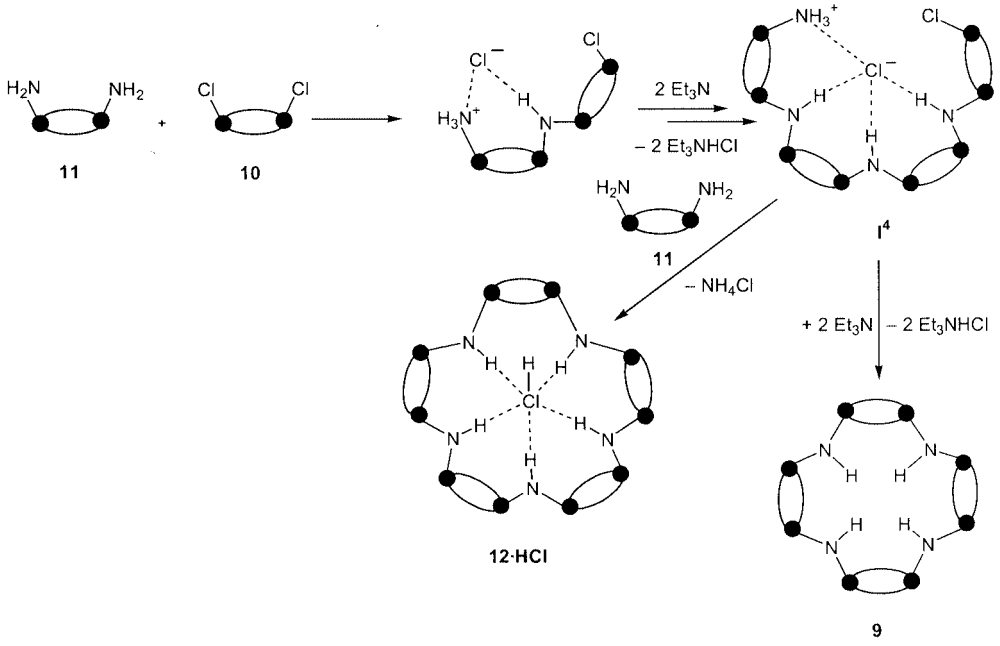

Scheme 6

and pentameric arrangements of **9** and **12** provides direct evidence that the dimeric [{P(μ-N*t*Bu)}$_2$NH] constituents of these macrocycles are in fact highly flexible. Relatively small changes in the endocyclic P−N−P and N−P−N angles within the [{P(μ-N*t*Bu)}$_2$NH] units, in the exocyclic N(*t*Bu)−P−NH angles, and in the puckering of the P_2N_2 ring units result in a significantly different bite distance (α) between adjacent N(−H) atoms within the tetramer **9** (mean 3.7 Å) compared to the pentamer **12** (mean 4.0 Å). For macrocycles like **9** and **12**, it can be shown that Equation (1) gives the relationship between the radius of the cavity (*r*) (expressed with respect to the N atoms), the number of [{P(μ-NR)}$_2$(NH)] units (*n*) and the bite distance (α). The effect of the increase in the bite distance in going from **9** to **12** (of 0.3 Å) therefore accounts for a ca. 0.2 Å increase in the size of the cavity (compared to the cavity size which would be present if the bite distance remained the same as in **9**).

$$r^2 = \frac{\alpha^2}{2(1 - \cos 2\pi/n)} \quad (1)$$

The ability of these macrocycles to coordinate anions within their cavities is witnessed in the structure of **12·HCl**. However, a more obvious potential property of macrocycles of this type is the coordination of metal cations. The attempted deprotonation of the tetramer **9** with various main-group reagents has so far failed to generate the desired tetraanion [{P(μ-N*t*Bu)}$_2$N]$_4^{4-}$ (Scheme 7).[24] In the case of s-block organometallic reagents (including MeLi, *t*BuLi and *n*BuLi), no reactions are observed. It can be noted that the dimer [*t*BuNHP(μ-N*t*Bu)]$_2$ (**13**) is fully deprotonated by *n*BuLi in toluene or THF.[12,25] Thus, the apparently low acidity of the N−H protons of **9** appears to stem from the extreme steric hindrance due to the *t*Bu groups, which fully shield the cavity to the approach of the base (Figure 6, b). With more forcing conditions, decomposition of the macrocyclic structure can arise. For example, the reaction of **9** with $PhCH_2K$ gives [*t*BuNHP(μ-N*t*Bu)]$_2$ (**13**) and/or [(*t*BuN)$_2$PK]$_\infty$ (**14**) as the only P-containing products (depending on the stoichiometry used).[24]

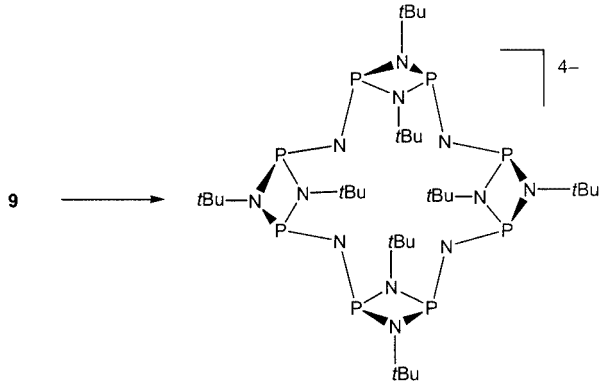

Scheme 7

Nonetheless, macrocyclic anions can be generated by alternative synthetic approaches. For example, the reaction of the dimer [Me_2NSb(μ-NCy)]$_2$ (**15**) with "active" $LiNH_2$ (generated in situ from NH_3 and *n*BuLi) gives [{Sb(μ-NCy)}$_3$(Li·THF)$_3$(LiN=NH)] (**16**).[26] Remarkably, the trimeric [({Sb(μ-NCy)}$_2$N)$_3$]$^{3-}$ trianion of **16** is produced by double-deprotonation of the NH_2^- anion (according to Scheme 8). The unexpected presence of an N=NH$^-$ anion in this arrangement has been confirmed by IR and ^{15}N NMR spectroscopic studies. The X-ray crystallographic study of **16** shows that it contains a cone-shaped [({Sb(μ-

 © 2003 Wiley-VCH Verlag GmbH & Co. KGaA, Weinheim

NCy)}$_2$N)$_3$]$^{3-}$ trianion, which is reminiscent of the arrangement of coordinated or uncoordinated calixarenes (Figure 8).[1] This trianion coordinates one Li^+ cation within the macrocyclic cavity, using the anionic μ-N centres. The remaining four, symmetry-related Li^+ cations reside above the macrocyclic cavity and are coordinated by the anionic μ-N and neutral NCy centres. The $N{=}NH^-$ anion then caps the structure, along the virtual C_3 axis of the cage.

Macrocyclic and Adamantane Alternatives

In a previous study Scherer et al. had shown that the dimeric macrocycle [{P(μ-N*i*Pr)}$_2$N*i*Pr]$_2$ (**3**) reverts to adamantane alternative [P$_4$(μ$_3$-N*i*Pr)$_6$] (**17**) on prolonged heating in the solid state (Scheme 9).[11] In contrast, a more recent study of the related macrocycle [{P(μ-N*t*Bu)}$_2$N*t*Bu]$_2$ (**4**) showed that this species does not rearrange into the adamantane under similar conditions.[22b] These limited studies

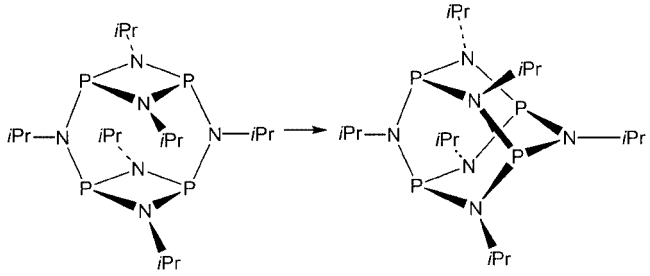
iPr
N
P
iPr
iPr
iPr

ring constituents maximise the space available. On the other hand, the six-membered ring constituents of the adamantane arrangement will result in an inherent increase in steric congestion, and such an arrangement is likely only to be formed where sterically less demanding sustituents are present. Although the mechanism by which **3** is converted into **17** is not known, as noted in Scheme 8 the rearrangement can be described by a facile "twist" of one of the (iPrN)P_2 units.

A recent study of the synthesis of the dimer [ClP(μ-Npy)]$_2$ (py = 2-pyridyl) (**18**) indicates the potential generality of this twist process in this area.[27] Attempts to prepare **18** from pyNHLi and PCl_3 in the presence of Et_3N give **18** together with the nonaphosphazane [$ClP_4(Npy)_5$] (**19**). Low-temperature ^{31}P NMR spectroscopic studies reveal that the reaction of **18** with pyNHLi/Et_3N gives **19**. The likely intermediate in this reaction is [{ClP(μ-Npy)P}$_2$(μ-Npy)] (**20**), the chain isomer of **19** which can also be detected prior to rearrangement (Scheme 10). DFT calculations on the rearrangement of the model chain species [{ClP(μ-NR)P}$_2$(μ-NR)] into the nonaphosphazanes [$ClP_4(NR)_5$] (R = H, Me) show that the thermodynamics of this reaction are dependent on the steric demands of the R group. The rearrangement being most favourable for least sterically demanding substituents.

This result gives a key insight into the relationship between various imidophosphazane frameworks that have been characterised previously. The relationship between these frameworks can be represented mechanistically in Scheme 11. It appears that there are two possible modes of reaction of imidophosphazane dimers **A**: Path I (leading to macrocyclic arrangements) or Path II (leading to adamantane arrangements). The twist process observed in the conversion of **20** into **19** is pivotal in the selection of the two alternative arrangements. As is the case in the rearrangement of the dimeric macrocycle [{P(μ-NiPr)}$_2$NiPr]$_2$ (**3**) into the adamantane [$P_4(\mu_3$-NiPr$)_6$] (**17**),[11] the steric demands of the R group is the decisive factor governing which Path (I or II) will be followed. The rearrangement of the chain isomer **B** into the nonaphosphazane **B′** is only favoured where sterically less demanding substituents are present, since otherwise the steric congestion would be too great within the six-membered ring units of the latter. Closure of **B′** with a further P center results in the adamantane structure **C**. In the case of sterically more demanding R groups, the dimeric ring units of **B** will be sustained on steric grounds. Closure with a further P center will lead to the macrocyclic isomer **C**.

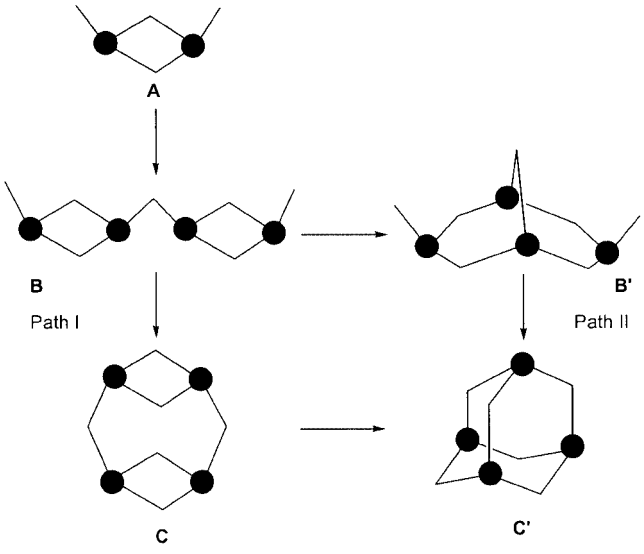

Scheme 11

Whether the importance of steric factors in the formation of macrocyclic and adamantane alternatives will limit the range of organic substituents that can be introduced into larger macrocycles of the type [{P(μ-NR)}$_2$(NH)]$_n$ is not yet known. However, a recent study indicates one potential way by which the undesired adamantane pathway may be avoided. Coordination of CuCl to the P centers of the dimer [ClP(μ-Npy)]$_2$ (**18**) before cyclisation with H_2O in the presence of pyridine gives [{P(μ-Npy)}$_2$(μ-O)]$_2${CuCl(pyridine)$_2$}$_4$ (**21**) (Figure 9), containing a dimeric macrocyclic core arrangement.[24] The potential to revert to the apparently thermodynamically more stable adamantane arrangement in this case is avoided by the increased steric demands of the *P*-coordinated metal fragments. This also has the effect of limiting the ring size of the macrocycle generated to a dimer. The structure of **21** reveals an additional property of this type of ligand arrangement not previously observed, their ability to employ the soft P centers in the coordination of metals at the periphery of the macrocycles.

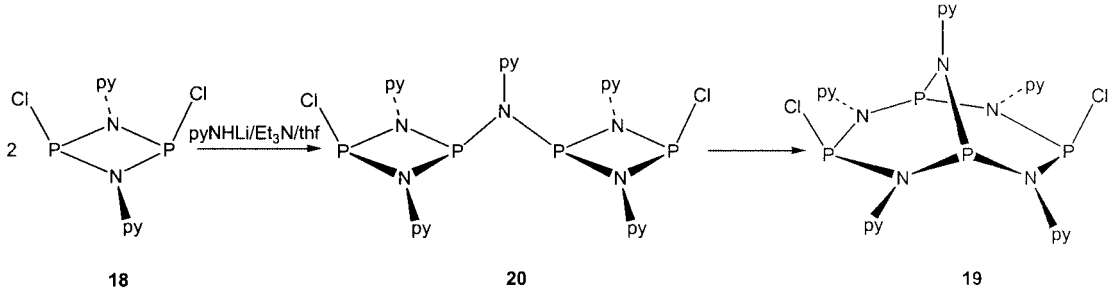

Scheme 10

 © 2003 Wiley-VCH Verlag GmbH & Co. KGaA, Weinheim

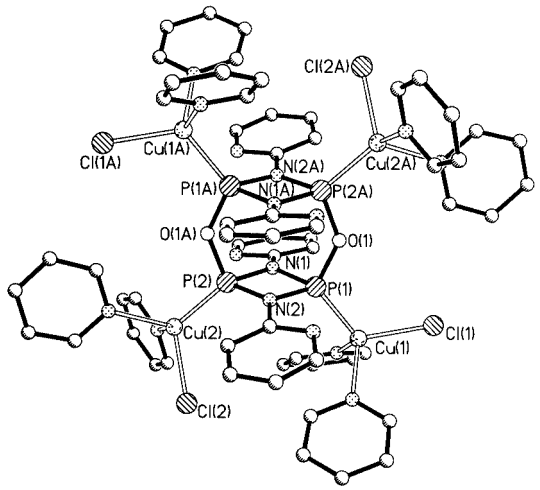

Figure 9. Structure of **21**

Valence-Isoelectronic Macrocycles Containing Other p-Block Elements

The applications of isoelectronic principles in the rationalisation and prediction of structure and bonding are long established in the area of main-group chemistry. Recently, these ideas have formed the basis of reviews concerning p-block element−N ligand systems.[28] In the context of the class of the macrocycles which the current review concerns, it can be seen that replacement of the P centers of a dimeric macrocycle of the type $[\{P(\mu\text{-}E'R)\}_2(\mu\text{-}E'R)]_2$ (E′= N or P, like **3** and **4** discussed in the previous section) with a +2 oxidation-state group-14 metal center (E) or with an organo group-13 metal fragment (R−E; E = group-13 element) would give valence-isoelectronic tetraanions of the type $[\{E(\mu\text{-}E'R)\}_2(\mu\text{-}E'R)]_2^{4-}$ and $[\{R'E(\mu\text{-}E'R)\}_2(\mu\text{-}E'R)]_2^{4-}$, respectively (Figure 10).

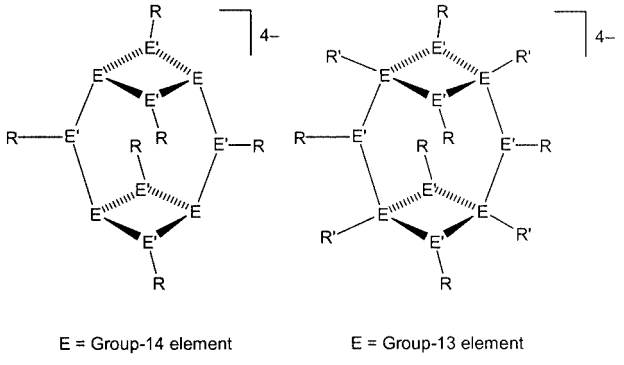

Figure 10. Valence-isoelectronic group-13 and -14 dimers

In practice the formation of isoelectronic anions of this type is not simple and different synthetic strategies have to be employed to those used in the related P−N systems. One earlier synthetic approach which we employed is the "templating" reaction of cubanes such as $[Sn(NtBu)]_4$ (**22**)[29] and $[MeAl(NMes)]_4$ (**23**)[30] with CyPHLi (Schemes 12 and 13, respectively). These reactions involve replacement of all four of the imido (RN^{2-}) ligands of the **22** and **23** with organophosphide groups (RP^{2-}). It can be noted that the related reactions with metallated primary amines (RNHLi) do not produce related macrocyclic frameworks.[29] More recently, however, we have found that group-14 frameworks of this type can be obtained in a more straightforward manner by the direct reactions of $Sn(NMe_2)_2$ with RPHLi (R= *t*Bu, Cy) (Scheme 14).[31] This strategy is restricted to aliphatic phosphides and to Li as the metal, as extensive coupling of the RP groups occurs in reactions involving aromatic phosphides or with aliphatic phosphides of the heavier alkali metals.[32] For example, the analogous reaction of MesPHLi with $Sn(NMe_2)_2$ in the presence of the Lewis base ligand TMEDA (= $Me_2NCH_2CH_2NMe_2$) gives $[\{Sn(\mu\text{-}PMes)\}_2(PMesPMes)](Li{\cdot}TMEDA)_2$ (**24**) (Mes= 2,4,6-$Me_3C_6H_3$), containing an $[Sn(\mu\text{-}PMes)\}_2(PMesPMes)]^{2-}$ dianion in which two of the MesP groups have coupled to form a $[MesPPMes]^{2-}$ unit (Scheme 15).[31]

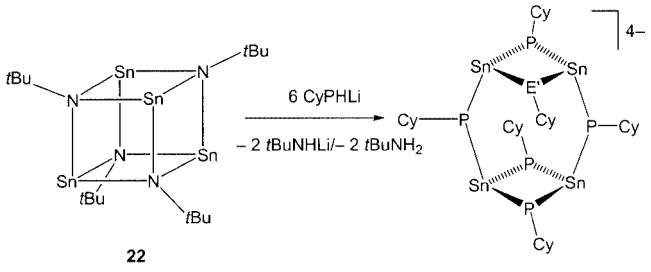

Scheme 12

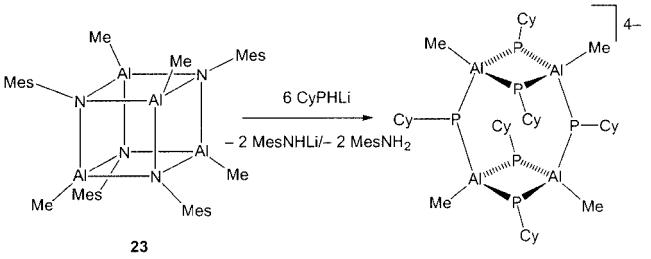

Scheme 13

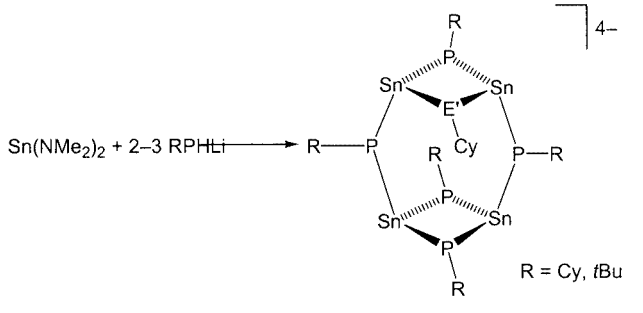

Scheme 14

The structure of $[\{Sn(\mu\text{-}PtBu)\}_2(\mu\text{-}PtBu)]_2{\cdot}(Li{\cdot}THF)_4$ (**25**) (shown in Figure 11) illustrates the mode of Li^+ coordination found in all of the lithium complexes containing macrocyclic, valence-isoelectronic group-13 and -14 anions

 © 2003 Wiley-VCH Verlag GmbH & Co. KGaA, Weinheim

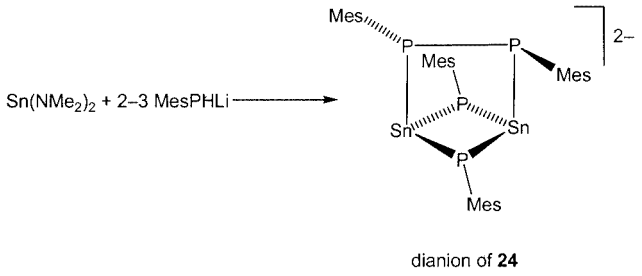

Scheme 15

of this type. The $[\{Sn(\mu\text{-}PtBu)\}_2(\mu\text{-}PtBu)]_2^{4-}$ of **25** coordinates the four Li^+ cations using both the μ-P*t*Bu groups within the dimeric ring units and those bridging the dimer units together. This coordination mode is the same as that seen for the three of the Li^+ cations by the $[(\{Sb(\mu\text{-}NCy)\}_2N)_3]^{3-}$ trianion of **16** (discussed above).[26]

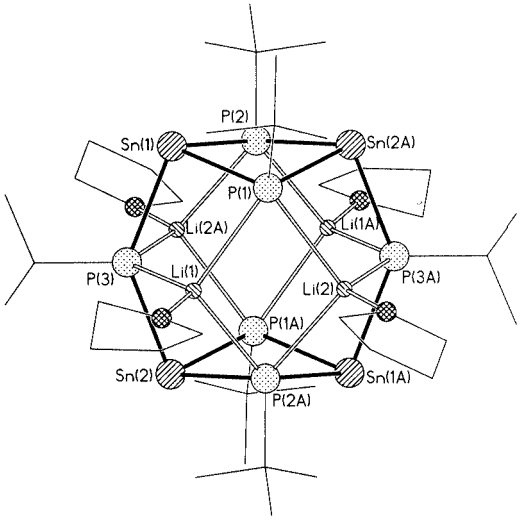

Figure 11. Structure of **25**

Future Prospects

This review has highlighted recent developments in this area. However, there is clearly much more to be done in extending the range of macrocycles available, both for group-15 systems and their valence-isoelectronic analogues, and in understanding and utilising the factors affecting the ring size of these species in general. Studies to date have pinpointed three distinctive coordination characteristics of this new class of macrocyclic ligands: the ability to coordinate metal ions within the cavity (in the case of deprotonated species), coordination of anions within the cavity (in the case of macrocycles having *endo* N−H functionality) and metal ions outside the cavity (using, for example, P centres within the macrocyclic backbone). Future studies will investigate these coordination patterns particularly with a view to (i) the synthesis of mixed-metal complexes, by utilising a combination of cavity and peripheral metal coordination, and (ii) the templating of macrocycles using anion coordination.

Acknowledgments

We thank the EPSRC (E. L. D., D. S. W.) and the European Union (L. R.) for financial support. We also thank previous and current members of the Wright group for aspects of the studies reviewed here.

[1] *Comprehensive Supramolecular Chemistry*, vol. 1, chapter 2 (crown ethers); vol. 2, chapter 4 (calixarenes); vol. 2, chapter 5 (cyclophanes), Pergamon, Oxford, **1995**.
[2] For example, involving cationic guests: R. L. E. Furlan, Y.-F. Ng, S. Otto, J. K. M. Sanders, *J. Am. Chem. Soc.* **2001**, *123*, 8876; G. R. L. Cousins, R. L. E. Furlan, Y.-F. Ng, J. E. Redman, J. K. M. Sanders, *Angew. Chem.* **2001**, *113*, 437; *Angew. Chem. Int. Ed.* **2001**, *40*, 423; R. L. E. Furlan, S. Otto, J. K. M. Sanders, *Proc. Nat. Acad. Sci.*, in press.
[3] For examples involving anionic or neutral guests. [3a] B. Hasenknopf, J.-M. Lehn, N. Boumediene, A. Dupont-Gervais, A. Van Dorsselaer, B. Kneisel, D. Fenske, *J. Am. Chem. Soc.* **1997**, *119*, 10956. [3b] P. W. Baxter, R. G. Khoury, J.-M. Lehn, G. Baum, D. Fenske, *Chem. Eur. J.* **2000**, *6*, 4140. [3c] Y. Yamanoi, Y. Sakamoto, T. Kusukawa, M. Fujita, S. Sakamoto, K. Yamaguchi, *J. Am. Chem. Soc.* **2001**, *123*, 980. [3d] S. Hiraoka, M. Fujita, *J. Am. Chem. Soc.* **1999**, *121*, 10239. [3e] M. Albrecht, O. Blau, R. Fröhlich, *Chem. Eur. J.* **1999**, *5*, 48. [3f] S. Hiraoka, Y. Kubota, M. Fujita, *Chem. Commun.* **2000**, 1509.
[4] R. E. Mulvey, *Chem. Commun.* **2001**, 1049, and references therein.
[5] M. F. Hawthorne, Z. Zheng, *Acc. Chem. Res.* **1997**, *30*, 267, and references therein.
[6] See also: [6a] R. Wang, T. Jin, Z. Zheng, R. J. Staples, *Angew. Chem.* **1999**, *111*, 1929; *Angew. Chem. Int. Ed.* **1999**, *38*, 1813. [6b] Z. Zheng, *Chem. Commun.* **2001**, 2521. [6c] A. Müller, R. Rohlfing, E. Krickemeyer, H. Bögge, *Angew. Chem.* **1993**, *105*, 916; *Angew. Chem. Int. Ed. Engl.* **1993**, *32*, 909.
[7] N. Etkin, M. C. Fermin, D. W. Stephan, *J. Am. Chem. Soc.* **1997**, *119*, 2954.
[8] W. C. Marsh, N. L. Paddock, C. J. Stewart, J. Trotter, *J. Chem. Soc., Chem. Commun.* **1970**, 1190; W. C. Marsh, J. Trotter, *J. Chem. Soc., A*, **1971**, 1482; J. P. O'Brien, R. W. Allen, H. R. Allcock, *Inorg. Chem.* **1979**, *18*, 2230.
[9] M. A. Beswick, D. S. Wright, *Coord. Chem. Rev.* **1998**, *176*, 373.
[10] A. D. Hopkins, J. A. Wood, D. S. Wright, *Coord. Chem. Rev.* **2001**, *216*, 155.
[11] O. J. Scherer, K. Andres, C. Krüger, Y.-H. Tsay, G. Wolmerhäuser, *Angew. Chem.* **1980**, *92*, 563; *Angew. Chem. Int. Ed. Engl.* **1980**, *19*, 571.
[12] J. K. Brask, T. Chivers, M. Krahn, M. Parvez, *Inorg. Chem.* **1999**, *38*, 290.
[13] H. J. Chen, R. C. Haltiwanger, T. G. Hill, M. L. Thomson, D. E. Coons, A. D. Norman, *Inorg. Chem.* **1985**, *24*, 4725.
[14] M. A. Beswick, M. K. Davies, M. A. Paver, P. R. Raithby, A. Steiner, D. S. Wright, *Angew. Chem.* **1996**, *108*, 1660; *Angew. Chem. Int. Ed. Engl.* **1996**, *35*, 1508.
[15] M. A. Beswick, S. J. Kidd, P. R. Raithby, D. S. Wright, *Inorg. Chem. Commun.* **1999**, *2*, 419.
[16] M. K. Davies, C. N. Harmer, D. S. Wright, unpublished results.
[17] R. Bryant, S. C. James, J. C. Jeffery, N. C. Norman, A. G. Orpen, U. Weckenmann, *J. Chem. Soc., Dalton Trans.* **2000**, 4007.
[18] A. Bashall, E. L. Doyle, C. Tubb, S. J. Kidd, M. McPartlin, A. D. Wood, D. S. Wright, *Chem. Commun.* **2001**, 2542.
[19] For example J. H. Reibenspies, *Acta Crystallogr., Sect. C* **1992**, *48*, 1717; T. Sakuri, K. Kobayashi, K. Tsuboyama, S. Tsuboyama, *Acta Crystallogr.* **1978**, *34B*, 1144.
[20] A. Bashall, A. D. Bond, E. L. Doyle, F. García, S. Kidd, G. T. Lawson, M. McPartlin, M. Parry, A. D. Woods, D. S. Wright, *Chem. Eur. J.* **2002**, *8*, 3377.

 © 2003 Wiley-VCH Verlag GmbH & Co. KGaA, Weinheim

[21] K. W. Muir, J. F. Nixon, *J. Chem. Soc., Chem. Commun.* **1971**, 1405.
[22] [22a] J. L. Sessler, J. M. Davis, *Acc. Chem. Res.* **2001**, *34*, 989. [22b] J. L. Sessler, M. J. Cyr, V. Lynch, E. McGhee, J. A. Ibers, *J. Am. Chem. Soc.* **1990**, *112*, 2810. [22c] M. Shionoya, H. Furuta, A. Harriman, V. Lynch, J. L. Sessler, *J. Am. Chem. Soc.* **1992**, *114*, 5714.
[23] W. C. Hamilton, J. A. Ibers, *Hydrogen Bonding in Solids*, W. A. Benjamin, New York, **1968**; A. F. Wells, *Structural Inorganic Chemistry*, 4th ed., Oxford University Press, Oxford, **1975**.
[24] E. L. Doyle, D. S. Wright, unpublished work.
[25] I. Schranz, L. Stahl, R. J. Staples, *Inorg. Chem.* **1998**, *37*, 1493.
[26] F. García, D. J. Linton, M. McPartlin, A. Rothenberger, A. E. H. Wheatley, A. D. Woods, D. S. Wright, *J. Chem. Soc., Dalton Trans.* **2002**, 481.
[27] A. Bashall, E. L. Doyle, F. García, G. T. Lawson, M. McPartlin, D. Moncrieff, D. S. Wright, *Chem. Eur. J.*, in press.
[28] For example: J. K. Brask, T. Chivers, *Angew. Chem.* **2001**, *113*, 4082; *Angew. Chem. Int. Ed.* **2001**, *40*, 3960.
[29] R. E. Allan, M. A. Beswick, N. L. Chromhout, M. A. Paver, P. R. Raithy, A. Steiner, M. Trevithick, D. S. Wright, *Chem. Commun.* **1996**, 1501.
[30] R. E. Allan, M. A. Beswick, P. R. Raithby, A. Steiner, D. S. Wright, *J. Chem. Soc., Dalton Trans.* **1996**, 4153.
[31] A. D. Bond, A. Hopkins, A. Rothenberger, A. D. Wood, D. S. Wright, *Chem. Commun.* **2001**, 525.
[32] A. D. Bond, A. D. Hopkins, G. T. Lawson, M. McPartlin, A. D. Wood, D. S. Wright, *Chem. Eur. J.*, manuscript in preparation.

Received December 16, 2002
Early View Article
Published Online July 17, 2003

 © 2003 Wiley-VCH Verlag GmbH & Co. KGaA, Weinheim

The Directed Lithiation of Benzenoid Aromatic Systems

Andrew E. H. Wheatley[a]

Dedicated to the memory of Ron Snaith. An inspirational teacher and a great friend

Keywords: Aromaticity / Directing group / Lithium / Solid-state structure / Solution structure

Directed metallation using organolithium bases is one of the best ways of regiospecifically elaborating aromatic systems and their substituents. For benzenoid arenes, deprotonation occurs at the ortho, lateral or peri positions. The reasons for each type of reaction will be considered in the context of the propensities of different directing groups for complex formation with the incoming organolithium base, acidification of the reactive site(s) and post-reaction stabilisation of the metal ion(s). Discussion will concentrate on structural investigations, for the most part by single-crystal X-ray diffraction and/or by multinuclear NMR spectroscopy. Theoretical studies will also be incorporated.
(© Wiley-VCH Verlag GmbH & Co. KGaA, 69451 Weinheim, Germany, 2003)

Introduction

Directed metallation using Group 1 organometallic bases in general, and organolithium substrates in particular, represents one of the most selective ways of regiospecifically elaborating benzenoid aromatic rings and substituents thereon, with deprotonation generally taking one of three forms: ortho, lateral or peri (Figure 1). The synthetic applications of the first of these have formed the basis for several review articles.[1] Orthometallation occurs both because the directing group can raise the acidity of the ortho hydrogen and also because the incoming organometallic substrate closely approaches this position. It is in the context of this reactivity that, for example, the recent total syntheses of phomactin, narciclasine, and analogues of meridine and atpenin B have been achieved.[2] The elaboration of aromatic substituents by means of directed lateral lithiation, that is metallation of, for example, alkyl groups located ortho to a directing group,[3] has facilitated the preparation of many polycyclic products, including corydalic acid methyl ester and fredericamycin.[4] Selectivity for ortho- vs. lateral lithiation is poorly understood, though kinetic, thermodynamic and steric effects all seem to play a role. Stereochemical aspects of the formation and reaction of laterally lithiated amides have been investigated,[5] with enantio-[6] and atroposelective lateral lithiations[7] having been published. Less

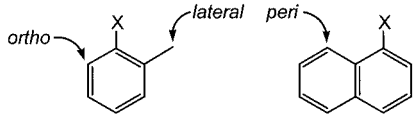

Figure 1. Schematic showing ortho-, lateral, and perilithiation sites

[a] Department of Chemistry, University of Cambridge, Lensfield Road, Cambridge, CB2 1EW, U. K.
Fax: (internat.) +44-1223/336-362
E-mail: aehw2@cam.ac.uk

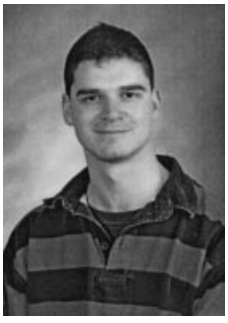

Dr. Andrew Wheatley graduated from the University of Kent and did his Ph.D. (University of Cambridge, 1995−1998) for the late Dr. Ron Snaith after which he became a Research Fellow at Gonville & Caius College (1998−2002). In 1999 he was awarded the Harrison Memorial Medal by the Royal Society of Chemistry and in 2000 he was made a University Assistant Lecturer at Cambridge. In 2002 he became a Fellow of Fitzwilliam College and he was made University Lecturer in 2003. He has published extensively in the field of Main Group organometallic chemistry. He specialises in the elucidation of organolithium reaction intermediates and the development of alkali metal 'ate complexes and Main Group metal interstitial hydrides.

MICROREVIEWS: This feature introduces the readers to the author's research through a concise overview of the selected topic. Reference to important work from others in the field is included.

commonly employed as a synthetic tool, the perimetallation of arenes occurs not because of directing group acidification of this position (*cf.* orthometallation) but because the incoming organometallic substrate closely approaches it.

The manifold synthetic applications that have been developed in light of the reactivities discussed above have recently been the subject of comprehensive review.[8] Nevertheless, it is remarkable that little is known of the organometallic products of metallation reactions involving demonstrably useful directing groups. The success of such synthetic protocols, involving metallation in general and lithiation specifically, have been interpreted in terms of promotion of the "complex-induced proximity effect",[9] with kinetic isotope effect evidence suggesting that rate-determining deprotonation of the arene proceeds in the wake of the formation of an equilibrating substrate-organometallic complex.[10]

The aim of the present article is to amalgamate the reported structural data for the products of the directed deprotonation of benzenoid aromatic systems by organolithium substrates. "Complex bases" have been used to occasion the derivatization of aromatic substrates as heterometallic Li-Group 1,[11] Li-Cu,[12] Li-Zn[13] and other Li-(d-block)[14] salts. However, only homometallic lithium derivatives will be considered by the present article since it is with these compounds that the synthetic utility of alkali metallated arenes lays.[8] The three main parts of the text will each deal with a different deprotonation position and, thereafter, the article is sub-divided firstly into solution studies and, secondly, into solid-state structural studies. Each of these two sub-sections will be ordered, with homoaromatics preceding heteroaromatics and with further categorisation occurring by directing group. Discussion of both solution and solid-state studies will be augmented by that of theoretical investigations where appropriate.

Orthometallation

Since the seminal studies that established the ability of substituted aromatic systems to undergo regioselective reaction[15] many synthetic procedures have been developed that utilise ortholithiation,[1a] and extensive studies have been undertaken into the relative directing abilities of a wide variety of substituents, many of which contain heteroatoms.[16] It is acknowledged that the best directors of orthometallation—and also the most versatile—are the so-called "N+O class" amide-type functional groups such as secondary and tertiary amides, carbamates and oxazolines.[1a] Other powerful (though less synthetically useful) orthodirecting groups include "S+O class" sulfones, sulfonamines[17] and *tert*-butyl sulfoxides.[18] Less potent are "O class" (e.g. ether) and "N class" (e.g. amine) substituents.[8] Halogens ("X class") are of importance, though prone to undergo halogen-metal exchange.[19]

The orthometallation of electron-deficient benzenoid heterocycles has been utilised synthetically,[8] though competition between deprotonation of and addition to the ring has been noted.[20] In the context of heterocyclic arenes, by far the most commonly employed systems are those of pyridyl derivatives. In spite of this, there are no reported structural characterisations of pyridines that have undergone alkali metallation at the ortho position.

Solution Studies

The ^{13}C NMR spectrum of 2,4,6-tri-*tert*-butylphenyllithium (**1**) in THF has been studied in some detail, with electric quadrupole relaxation of ^{7}Li incurring the partial averaging of $^{1}J(^{13}C,^{7}Li)$ while metal-carbon bond exchange has been reported between ^{6}Li enriched isotopomeric monomers.[21] In a similar vein, mesityllithium has been probed as a PMDETA complex (**2**), with data suggesting an asymmetric structure in which the metal is chiral at low temperature.[21]

The ortholithiation of anisole by *n*BuLi has been extensively studied by NMR spectroscopy.[22] Low temperature ^{1}H and ^{13}C NMR spectroscopy suggests that upon the addition of organolithium substrate a tetramer of the complex *n*BuLi·MeOPh (**3**) forms with the introduction of TMEDA causing its replacement by dimers of *n*BuLi·TMEDA (**4**). The spectroscopic benefits of ^{6}Li enrichment having been previously demonstrated,[23] the conversion of **3** to **4** has been corroborated by $^{6}Li,^{1}H$ HOESY and it has been suggested that orthometallation only proceeds in the presence of (more reactive) **4**.[22] This interpretation of the metallation of anisole, depending on the conversion of **4** to $(n\text{BuLi})_2$·TMEDA·MeOPh (**5**), has also been scrutinised theoretically with MNDO calculations suggesting that the orthodirecting functionality stabilises the transition state during deprotonation.[24] More recently, the reactivity of 1-methoxynaphthalene towards various organolithium substrates has been probed.[25] Whereas it has been previously noted that 1-methoxynaphthalene reacts with a 1:1 mixture of *n*BuLi and TMEDA to give an almost uniquely orthometallated product **6**, regioselectivity has proved less easy to control if an excess of Lewis base is present.[26] Accordingly, ^{1}H, ^{13}C and $^{6}Li,^{1}H$ HOESY spectra suggest that in the absence of a donor a 1-methoxynaphthalene-(*n*BuLi) complex **7** forms initially, whereas in the presence of TMEDA such complexation is precluded. The observation that ortholithiation nevertheless results from the employment of *n*BuLi/TMEDA, when taken in conjunction with the detection of an isotope effect (in $[D_8]$THF) whereby the exchange of hydrogen at the ortho position by deuterium incurs a slower lithiation process, suggests kinetic control. This view is reinforced by the observation that at elevated temperatures, the ortholithiated complex slowly converts into the corresponding perimetallate **8**.[25]

The ability of a [2-(dimethylamino)]-containing substituent to exhibit chelation control[27] during an orthometallation reaction has been demonstrated by the structural elucidation of $[Me_2NN(Me)]C_6H_4Li\cdot{}^{1}/_{2}$TMEDA (**9**)[28] and 2-(dimethylaminomethyl)phenyllithium (**10**)[29] in various media. The asymmetric solid-state structure of **9** (see below) is based on a $(CLi)_2$ metallacyclic core, the integrity of

 © 2003 Wiley-VCH Verlag GmbH & Co. KGaA, Weinheim

which in [D_6]benzene is suggested by the observation of a septet [$^1J(^{13}C,^7Li)$ = 20 Hz] for the metallated carbon centre by ^{13}C NMR spectroscopy at room temperature.[28] While it is known that **10** takes the form of a chelated tetramer in hydrocarbon solution[30] it had been formerly suggested that the introduction of etherate solvent not only incurred separation into dimers[31] but also disrupted internal coordination.[32] However, more recent work using the doubly labelled ($^6Li,^{15}N$) compound, indicates that three interconverting isomeric and fully chelated dimers are retained in the presence of THF, and that internal coordination is not depleted even upon treatment with HMPA.[29]

The ability of lithium itself to direct subsequent metallation has applications in the lateral deprotonation of aromatics (see below) but is also revealed in the context of ortholithiation by the reaction of 2-lithio-1-phenylpyrrole (**11**), a solid-state dimer,[32] with *n*BuLi.[33] $^6Li,^1H$ HOESY suggests that in [D_8]THF/TMEDA a co-complex forms in which the ortho position of the benzenoid ring may be agostically activated.[32] In a like vein, *trans*-1-lithio-1,2-diphenylhex-1-ene (**12**) undergoes orthometallation of the 2-phenyl substituent upon treatment with *n*BuLi. In the same way as for **11**, $^6Li,^1H$ HOESY points to activation of the position of ultimate dilithiation.[34] Low temperature ^1H and ^{13}C NMR spectroscopy suggests that the dissolution of (*n*Bu)[C_6H_4(Li·TMEDA)-2]C=C(Li·TMEDA)Ph (**13**) in [D_8]THF yields a mixture of essentially unaltered **13** and a pseudo-cubic dimer of (*n*Bu)[C_6H_4(Li·[D_8]THF)-2]C=C(Li·[D_8]THF)Ph (**14**).[34] $^6Li,^6Li$ COSY with fixed delays reveals scalar coupling between the two chemically inequivalent metal locations in this last species[35] and interchange of the metal centres between **13** and **14** has been demonstrated by $^6Li,^6Li$ EXSY.[36]

Solid-State Studies

Several straightforward examples of substituted phenyllithium compounds have been fully characterised, both in their pure forms and as complexes with Lewis bases. Dilithiated biphenyl has been characterised as the TMEDA solvate μ_2-biphenyl-C2,C2, C2′,C2′-bis(lithium-TMEDA) (**15**).[37] Concerning polysubstituted arenes, various dimers of unsolvated 2,6-$R_2C_6H_3Li$ are known. Whereas for R = mesityl (**16**)[38] the structure is based on a normal $(CLi)_2$ core, for the more sterically congested ligand in which R = 2,6-(*i*Pr)$_2C_6H_4$ (**17**) dimerisation occurs by the η^6-interaction of one R group on each ligand with the metal component of an adjacent monomer.[39] Solvated analogues exhibit even more diverse behaviour; 2,6-$(C_{10}H_7)_2C_6H_3Li$·2THF (**18**),[40] 2,6-$Ph_2C_6H_3Li$·2OEt_2 (**19**),[41] 2,6-[4-(*t*Bu)C_6H_4]$_2C_6H_3Li$·2OEt_2 (**20**),[42] 2,6-(4-$MeOC_6H_4)_2C_6H_3Li$·2OEt_2 (**21**) (wherein the methoxy groups are passive with respect to the metal),[43] 2,6-[2,4,6-(*i*Pr)$_3C_6H_2$]C_6H_3Li·L (L = OEt_2 **22**,[44] η^6-C_6H_6 **23**[39]) and 2,4,6-$Ph_3C_6H_2Li$·2OEt_2 (**24**)[45] are monomers in the solid state while 2,4,6-(*i*Pr)$_3C_6H_2Li$·OEt_2 (**25**)[46] and 2,4,6-$Me_3C_6H_2Li$·2THF (**26**)[47] form differently solvated dimers. The complex 2,4,6-$Ph_3C_6H_2Li$·$^1/_2$THF (**27**) is unusual by virtue of its asymmetry. While both metal ions in its dimeric structure straddle the formal charge centres, one is mono-THF solvated and the other is bis(η^2-Ph) supported.[40] In a like vein, the dimer of 2,6-$Ph_2C_6H_3Li$·$^1/_2$THF, **28**, reveals Lewis base stabilisation of one metal centre and the η^2-interaction of two phenyl rings with the other.[40] Whereas the simple monolithiate **21** is formed by lithium-halogen exchange with the corresponding iodide,[19] application of *excess* *n*BuLi to the related substrate 2,6-[2-Me-4-(*t*Bu)C_6H_3]$_2$-C_6H_3I has yielded the dilithium complex 2-[2-CH_2Li-4-(*t*Bu)C_6H_3]-6-[2-Me-4-(*t*Bu)C_6H_3]C_6H_3Li·OEt_2 (**29**).[42] As part of the same study, a 1:1 co-complex (**30**) between *t*BuLi and 2,6-[2,4,6-(*i*Pr)$_3C_6H_2$]$_2C_6H_3Li$ (*cf.* **22**, **23**) has been reported to incorporate a $(CLi)_2$ core.[42] As already mentioned, **21** reveals coordinatively inactive methoxy substituents.[43] However, in the THF-solvated co-complex (**31**) between lithium iodide and 2,6-bis(2-methoxyphenyl)phenyllithium each metal centre is singly MeO-bonded.[48] Just as the tetramer of 2,4,6-tris(isopropyl)phenyllithium, **32**, reveals η^6-support of the metal centres[39] so the butyllithium-phenyllithium complex *n*BuLi·[2,4,6-(*t*Bu)$_3C_6H_2Li$] (**33**) exhibits a dimeric solid-state structure by virtue of there being η^6-links between the component monomers.[38] Lastly, as previously pointed out the extensively conjugated system *trans*-1-lithio-1,2-diphenylhex-1-ene (**12**) has been reported to react with one equivalent of *n*BuLi at the 2-phenyl substituent to give **13**.[34] This last complex reveals a solid-state structure similar to that of μ_2-biphenyl-C2,C2, C2′,C2′-bis-(lithium-TMEDA) **15**.[37]

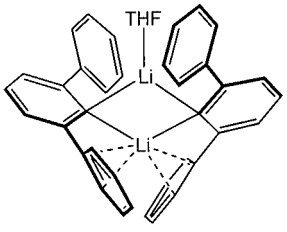

(28)$_2$

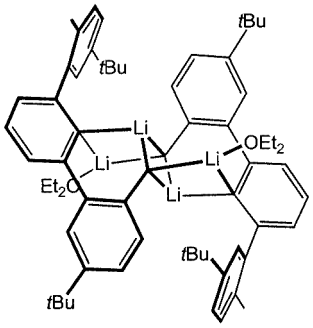

(29)$_2$

The potential for passivity on the part of MeO groups towards lithium has already been alluded to in the context of the diethyl ether solvate **21**.[43] However, the lithiation of anisoles is more commonly known to proceed at the position ortho to this weak "O class" director, with internal Li−O stabilisation of the metal occurring. While solution

 © 2003 Wiley-VCH Verlag GmbH & Co. KGaA, Weinheim

studies into such processes have already been discussed (see above), several examples of chelated lithioalkoxyarenes have been characterised in the solid state. The metallation of anisole itself using *n*BuLi has long been known to yield a tetramer of the simple orthometallate 2-$MeOC_6H_4Li$ (**34**),[49] with the methylcyclopropane solvate 2-$MeOC_6H_4Li{\cdot}OCH_2CHMe$ (**35**) having a similar structure[50] and 2-$MeOC_6H_4Li{\cdot}{}^1/_8$TMEDA (**36**) revealing pairs of tetramers that are TMEDA bridged.[51] While the simplest poly(methoxy) example of such species is a dimer of 2,6-(dimethoxy)phenyllithium (**37**), in which each metal is supported by interaction with both charge centres and one oxygen atom on each ligand,[52] more extensive (tetrameric) aggregation of **37** has also been reported.[53] Meanwhile, increasing the steric demands of alkoxy groups [in 2,6-di-(*tert*-butoxy)phenyllithium (**38**)] has been noted to incur the formation of a rare cyclic trimer based on a $(CLi)_3$ core.[54]

Remaining with chalcogen-based directing groups, polymeric chains based on $(CLi)_2$-centred dimers of 2-(tBu)$SC_6H_4Li{\cdot}{}^1/_2$TMEDA (**39**) have been noted to form by virtue of the ability of TMEDA to adopt a dimer-bridging motif.[55] Biphenyl sulfide has been shown to undergo dimetallation in TMEDA (in a manner analogous to that revealed by biphenyl, *cf.* **15**)[37] to yield μ_2-biphenyl sulfide-C2,C2′,C2′-bis(lithium-TMEDA) (**40**).[56] In the context of "S+O class" directing agents, 3-fluorophenyl(phenyl)sulfone has been shown to undergo lithiation on the fluorinated ring between the two substituents to afford 3-FC_6H_3(Li·PMDETA-2)SO_2Ph (**41**).[57] Of the two possible coordinating substituents, it is the SO_2 moiety that dominates, with one of its two oxygen centres interacting with the metal [Li−O = 2.170(8) Å; Li···F = 3.672(7) Å]. Nevertheless, in spite of the lack of Li−F coordination, the arene-fluorine distance is, at 1.389(5) Å, longer than normal. This has been interpreted in terms of the observation that **41** eliminates LiF at +60 °C.[57] The dilithiated sulfone 2-[$(Me_3Si)_2C$(Li·OEt_2)SO_2]$C_6H_4Li{\cdot}OEt_2$ (**42**) has been reported, wherein both O-directed ortholithiation (the solid-state structure reveals Li−C_{ortho} and Li−O coordination) and deprotonation of the sulfone α-carbon are seen.[58] Reaction of racemic EtS(=O)(Ph)=NMe with *n*BuLi/TMEDA in the presence of a trace oxide source[59] yields the heterochiral mixed α-mono- and α,orthodilithiated sulfoximine [MeCHLiS(=O)(Ph)=NMe]$_2$·[MeCHLiS(=O)(C_6H_4Li-2)=NMe]$_2$·Li_2O·3TMEDA (**43**),[60] the solid-state structure of which reveals chiral resolution. Consequently, the aggregate is composed of two (*S*)-configured α-metallated sulfoximine monoanions and two (*R*)-configured α,orthometallated dianions. At the structure core, and interacting with six of the eight metal centres present, is a rogue oxide dianion (thought to arise from LiOH contamination of the organolithium reagent). The α-Li centre in the monolithiated moiety interacts with neither the oxygen nor the nitrogen centres in the same unit but sits *gauche* with respect to these atoms and bonds, instead, to TMEDA and the O-centre of a dianionic sulfoximine unit (Figure 2a). Each of these dianions interact with both metal counterions *via* their deprotonated ortho positions — the corresponding

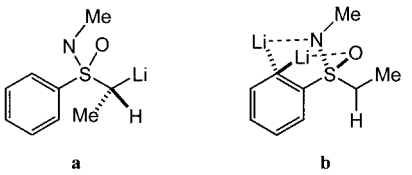

Figure 2. a) Li^+ in the monolithiated component of **40** bonds to TMEDA and the O-centre of a dianionic sulfoximine unit and, b) the α-C lone pair in the dianion adopts a *gauche* conformation with respect to nitrogen and arene[60]

two metals being stabilised by intramolecular N,O-coordination. The α-C lone pair in the dianion adopts a *gauche* conformation with respect to both nitrogen and deprotonated arene (Figure 2b).[61]

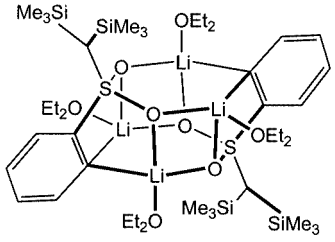

$(42)_2$

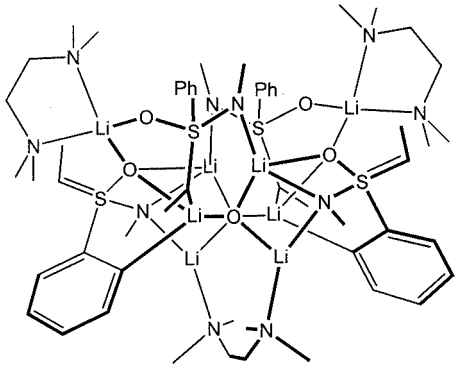

43

The solution structures incurred by the action of the purely "N class" directing group in 2-(dimethylaminomethyl)-phenyllithium (**10**) have already been discussed[29] in the context of retention of the pseudo-cubic tetramer noted in the solid state.[30a] The substrate 3,5-dimethyl(dimethylaminomethyl)benzene has been shown to undergo orthodirected metallation upon treatment with *n*BuLi/OEt_2. The result is a dimer of 2-Me_2NCH_2−4,6-$Me_2C_6H_2Li{\cdot}{}^1/_2OEt_2$ (**44**), an asymmetric species in which one metal centre in a $(CLi)_2$ core is supported by two amine N-donors while the other metal is mono(diethyl ether) solvated (*cf.* **28**). This species is thermally unstable with respect to the formation of (2-Me_2NCH_2−4,6-$Me_2C_6H_2Li$)·(Me_2NCH_2−3,5-$Me_2C_6H_3$) (**45**).[28] As part of the same study, the TMEDA-solvated structural analogue of **44** has been obtained using trimethylhydrazine directors. Whereas *n*BuLi/OEt_2 fails to

 © 2003 Wiley-VCH Verlag GmbH & Co. KGaA, Weinheim

effect lithiation of $Me_2NN(Me)Ph$, the use of *n*BuLi/TMEDA affords the asymmetric complex **9**, which is known to retain its solid-state structure in hydrocarbon solution (see above).[28] Extensive crystallographic work has been done on bis(amine) compounds of the type 2,6-$(R_2NCHR')_2C_6H_nR''_{3-n}Li$. For $n = 3$, the pure ortholithiates 2,6-bis(*N*,*N*-diethylaminomethyl)phenyllithium (**46**)[61] and 2,6-bis[1′-(dimethylaminoethyl)]phenyllithium (**47**)[62] have both been shown to adopt dimeric structures in the solid state. The 1:1 co-complex of 2,6-bis[1′-(dimethylaminopropyl)]phenyllithium with *n*BuLi **48** is based on a more complicated $(CLi)_4$ ladder, in which the *n*-butyl ions reside in the ladder middle while the ortho deprotonated aromatic systems both intercept laddering and straddle ladder edges.[62] The compound 2,3,5,6-$(Me_2NCH_2)_4C_6HLi$ (i.e., $n = 1$) (**49**) exists as a dimer in which each metal in the core $(CLi)_2$ ring is supported by the 2- and 6-aminomethyl groups in either ligand, the remaining substituents being coordinatively inactive.[63] In a related vein, 2-Me_2N-6-$Me_2NCH_2C_6H_3Li$ (**50**) reveals a dimer incorporating both four- and five-membered chelate rings,[64] whereas 2,6-$(Me_2N)_2C_6H_3Li$ (**51**) is a $(CLi)_3$-based trimer incorporating only four-membered C_2NLi chelate rings.[65] Just as (O-directed) 2,6-di-(*tert*-butoxy)phenyllithium (**38**)[54] and (N-directed) **51** are unusual by virtue of the fact that they exist as cyclic trimers in the solid state, in 2-(*t*Bu)O-6-$Me_2NC_6H_3Li$ (**52**) trimerisation is noted to result from the employment of both N- and O-directing groups.[66] In contrast to the intramolecular N-stabilisation revealed by **50** and **51**, 2-[(4-methylpiperazinyl)phenyl-C,N]lithium-THF (**53**) exhibits a dimeric structure based on an eight-membered $(C_2NLi)_2$ core by virtue of intermolecular stabilisation of the metal ions by piperazinyl α-nitrogen atoms.[67] The investigation of orthometallated compounds incorporating polyfunctional substituents has been extended to cover the solid-state structure of 2-(dimethylaminoethoxy)phenyllithium (**54**)[68]and also that of 2-[*N*-alkyl(*N*′,*N*′-diethylaminoethyl)aminomethyl]phenyllithium (alkyl = methyl **55**,[69] ethyl **56**[70]). The use of α-aminolithium alkoxides[71] has allowed the regiospecific metallation of arylaldehydes. Hence, in situ protection of variously substituted benzaldehydes and heterocyclic arylaldehydes[72] has been reported[71,73] by reaction with lithium dialkylamides, and has been followed by ring lithiation, affording a convenient one-pot route to orthosubstituted arylaldehydes. In a comparable area, **54** exhibits a tetrameric structure in the solid state. Unusually, for such an aggregation state, a straightforward pseudo-cubane does not result. Instead, two boat-shaped eight-membered $(C_2OLi)_2$ rings are found to be stacked with one being inverted and twisted by approximately 90° to the other. In a manner analogous to *N*,*N*,*N*′-trialkylethylenediamine-substituted aromatics,[70] the 2-(dimethylaminoethoxy)phenyl anion acts as an N,O-chelating ligand in **54** such that each metal is rendered four-coordinate by the action of nitrogen.[68] Compounds **55** and **56** have revealed a $(CLi)_2$-based dimer with both donor centres on each side-chain chelating a given metal centre.[69,70] A related co-complex has been reported; that of 2,6-bis[*N*-methyl(*N*′,*N*′-dimethylaminoethyl-)aminomethyl]phenyllithium with BrLi (**57**) is centred on a four-membered $CBrLi_2$-ring.[74] The polyfunctional ligand *N*-(2-phenoxyphenyl)-*N*-(trimethylsilyl)amine has been used to afford a variety of structural motifs upon dilithiation.[75] As such, simple deprotonation in DME to give, for example, N,O-chelated 2-$PhOC_6H_4N(Li{\cdot}DME)SiMe_3$ (**58**), can be followed by reaction with further *n*BuLi in the presence of different Lewis bases to give the dimer of diglyme-bridged 2-$(C_6H_4Li\text{-}2')OC_6H_4N(Li{\cdot}OEt_2)SiMe_3{\cdot}{}^1/_2$-$O(CH_2CH_2OMe)_2$ (**59**), the dimer of 2-$(C_6H_4Li\text{-}2')OC_6H_4N(Li{\cdot}DME)SiMe_3$ (**60**) or *n*BuLi-containing co-complex *n*BuLi·2-$(C_6H_4Li\text{-}2')OC_6H_4N(Li{\cdot}OEt_2)SiMe_3$ (**61**).[76] Attempts to react dilithiates such as **59** or **60** with $LaCl_3$ in Et_2O have serendipitously afforded a decalithium cluster that comprises two units of formulation EtOLi·[2-$(C_6H_4Li\text{-}2')OC_6H_4N(Li{\cdot}OEt_2)SiMe_3]_2$ (**62**).[76] The dilithiation of *N*-phenylcarbazole in TMEDA gives μ_2-*N*-phenylcarbazole-C1,C1, C2′,C2′-bis(lithium-TMEDA) (**63**)[56] (*cf.* **15**[37] and **40**[56]). Whereas previous studies into the propagation of reactions between organolithium substrates and amines have typically utilised an excess of amine and so generated species of the type $R_2NLi{\cdot}HNR_2$,[77] a recent probe has investigated the reaction of *n*BuLi with Ph_2NH using as much as a sixfold excess of organolithium substrate. Such work has afforded the remarkable (*n*BuLi)-containing (mixed anion)-dianion co-complex $(n\text{BuLi})_2{\cdot}[Ph(C_6H_4Li\text{-}2)NLi{\cdot}OEt_2]_2{\cdot}Ph_2NLi$ (**64**).[78] The structure of **64** incorporates three connected units. The first two are $(CLi)_2$-based $(n\text{BuLi}{\cdot}OEt_2)_2$ and a dimer of dilithiated $Ph(C_6H_4Li\text{-}2)NLi{\cdot}OEt_2$. The four negative charge centres of the latter fragment interact with the third component of the structure; a single Ph_2NLi molecule.[78]

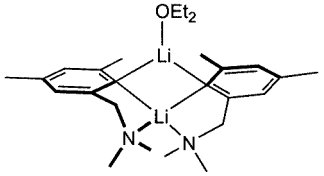

$(\mathbf{44})_2$

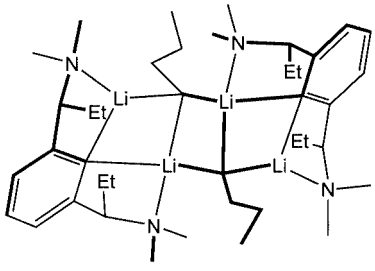

$(\mathbf{48})_2$

 © 2003 Wiley-VCH Verlag GmbH & Co. KGaA, Weinheim

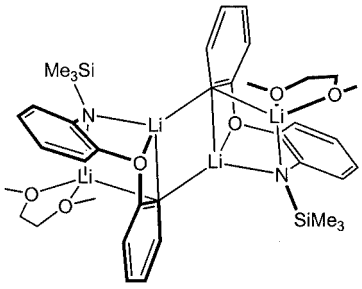

$(\mathbf{60})_2$

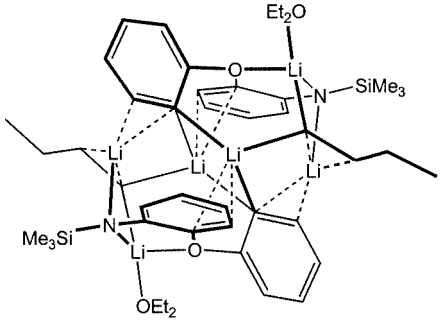

$(\mathbf{61})_2$

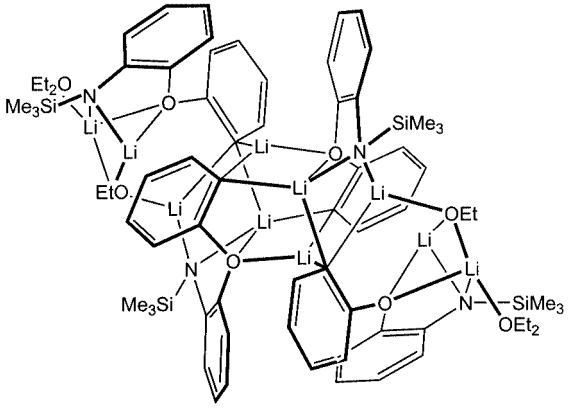

$(\mathbf{62})_2$

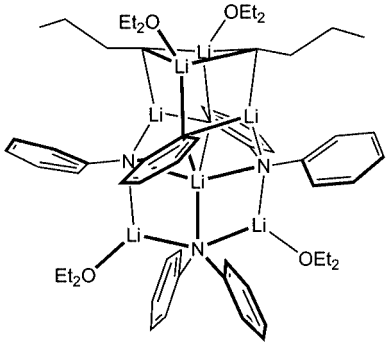

64

Remaining with the nitrogen-based chelation of metal centres, two common ligand types have been found to exhibit a predilection for stabilising lithium cations; those that contain separate "N class" and "O class" directing groups and those that feature "N+O class" directors. In the context of the first of these, compounds **52** and **59**−**62** have already been discussed.[66−76] Concerning the latter, mixed "N+O class", it has already been mentioned that about the best and most versatile orthodirecting substituents of all are those incorporating amide-type groups in general[1a] and tertiary amides specifically.[16a] In spite of this utility it is only recently that the propensity of even the simple amides $(i\text{Pr})_2\text{NC(O)Ar}$ (Ar = Ph, $C_{10}H_7$) for directing lithiation has been adequately explained with reference to the known sterically induced amide-arene twist-angle.[79] While it is well documented that this angle has a bearing on the rate of lithiation,[79a] even these two relatively rigid and nearly perpendicular amides undergo efficient orthometallation.[79b][80] Accordingly, treatment of $(i\text{Pr})_2\text{NC(O)Ph/OEt}_2$ with *t*BuLi yields crystalline $(i\text{Pr})_2\text{NC(O)C}_6\text{H}_4(\text{Li}\cdot\text{OEt}_2)$-2 (**65**) with X-ray diffraction revealing a $(\text{CLi})_2$-centred dimer in which the core is stabilised by the O-centres of OEt_2 and of the amide carbonyl functionalities (amide-arene twist-angle of 47°). A similar structural motif is noted for $(i\text{Pr})_2\text{NC(O)C}_{10}\text{H}_6(\text{Li}\cdot\text{THF})$-2 (**66**; twist-angle 65°), which is obtained from the 1:1 reaction of $(i\text{Pr})_2\text{NC(O)C}_{10}\text{H}_7$ with *t*BuLi in THF.[81] More complicated is the behaviour of 2-ethyl-*N*,*N*-diisopropylbenzamide with respect to *t*BuLi. Recent crystallographic results suggest that ortho- and lateral lithiation are in strongly solvent-dependent competition, with the formation of $(i\text{Pr})_2\text{NC(O)-2-Et-C}_6\text{H}_3\text{Li}\cdot\text{THF}$ (**67**) − a dimer in the solid state − and $(i\text{Pr})_2\text{NC(O)C}_6\text{H}_4\text{CH(Li}\cdot\text{PMDETA)Me-2}$ (**68**; see below) being made possible by the employment of different reaction media.[82]

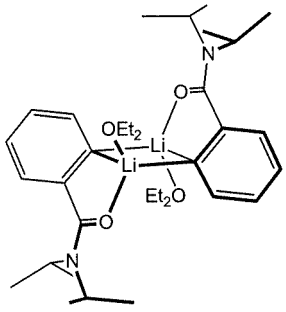

$(\mathbf{65})_2$

Unsurprisingly, 2-(*P*,*P*-dimethylphosphanylmethyl)phenyllithium-OEt_2 (**69**)[83] and 2,6-bis(*P*,*P*-dimethylphosphanylmethyl)phenyllithium (**70**)[84] reveal solid-state dimers related to that of internally coordinated "N class"-controlled **46**.[61] Triphenylphosphane also undergoes efficient "P class" orthodirected metallation in the presence of *n*BuLi/OEt_2. However, while 2-$\text{Ph}_2\text{PC}_6\text{H}_4(\text{Li}\cdot\text{OEt}_2)$-2 (**71**) is a dimer in the solid state, its structure contrasts with that of **69** insofar as it fails to demonstrate Li−P bonding.[85] Bis(2-bromobenzyl)methylphosphane undergoes lithiation of both aromatic benzylic positions in the presence

 © 2003 Wiley-VCH Verlag GmbH & Co. KGaA, Weinheim

of TMEDA. This is of note in the context of the recently reported ring-activating properties of lithium substituents themselves.[86] Hence, bis(orthometallation) of the phosphane proceeds, upon treatment with *n*BuLi and via a lithium-halogen exchange mechanism,[19] to give MeP[$CH_2(C_6H_4Li$-2)]$_2$·2TMEDA (**72**). However, the monolithiation of each benzyl α-carbon centre in **72** occurs readily upon the subsequent introduction of *n*BuLi/TMEDA. The product (**73**) is a dimer in the solid state with four metal ions adopting a near planar equilateral rhombus, the edges of which are bridged both by as many deprotonated ortho carbon centres and two phosphane Group 15 donors. Peripheral to this core, four TMEDA-chelated metal ions are positioned: two are η^4-bonded to ligand phosphorus and benzyl centres and one ipso carbon centre while two more are each η^6-stabilised by the two remaining aromatic rings.[87]

A single crystallographic example of "P+N class" ortho-directed lithiation has been reported. Whereas reaction of the iminophosphorane (2-$C_5H_4N)_3P{=}NSiMe_3$ with MeLi proceeds via nucleophilic attack on the phosphorus, the same is not true of $Ph_3P{=}NSiMe_3$. In this latter case, the direction of ortholithiation affords an asymmetric dimer of $Me_3SiN{=}PPh_2C_6H_4Li{\cdot}{}^1/_2OEt_2$ (**74**) (*cf.* **44**).[28] The solid-state structure of **74** reveals that the orthometallated iminophosphorane anions N,C_{ortho}-chelate one of the two metal centres.[88]

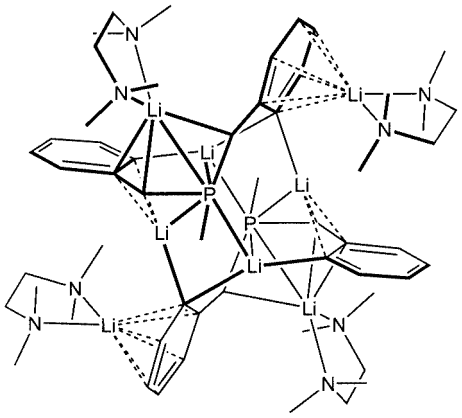

$(\mathbf{73})_2$

Whereas an example in which "S+O class" direction supersedes "X class" direction of an ortholithiation process has already been discussed (*cf.* **41**)[57] it is, nonetheless, the case that the fluorine-based direction of orthometallation has been reported in synthetic contexts[26b] and, in rare instances, in the solid state. As part of an investigation into the magnitude of carbon-fluorine bond extension upon ortholithiation both 1,2,3,4-tetrafluorobenzene and (from it) the benzyne precursor (2,3,4,5-tetrafluoro)phenyllithium-tris(THF) (**75**) have been prepared. Complex **75** is a monomer in the solid state wherein external solvation of the metal obviates the need for lithium-fluorine interaction. However, at 3.448(4) Å Li···F_{ortho} is less than in **41**,[57] and this is consistent with the observation that **75** undergoes LiF elimination at temperatures as low as −40 °C.[89] Conversely, in spite of the inclusion of coordinating diethyl ether, metal-fluorine interactions are noted in the dimer of (2,4,6-trifluoromethyl)phenyllithium-OEt_2 (**76**).[90] In this case each metal centre is in part stabilised by two fluorine atoms on ortho-CF_3 groups.

Lateral Metallation

Lateral or benzylic metallation results from the ability of a directing group situated ortho to a given lateral group to both coordinate an organometallic substrate and withdraw electrons from the lateral group in question. The result is that ortho- and lateral metallation are competitive processes that result from the presence of the same classes of directing group.[3] The promotion of lateral metallation by a directing group is emphasised by the observation that whereas toluene can be laterally metallated by *n*BuLi/TMEDA,[91] 2-(dimethylaminomethyl)toluene affects the same reaction much more rapidly on treatment with *n*BuLi/OEt_2.[27][92]

Solution Studies

Fluorenyllithium (FlLi; **77**) has been studied with a view to understanding whether it exists as a contact ion pair (CIP) or a solvent-separated ion pair (SSIP). SSIP and CIP solid-state structures have been reported for fluorenyl derivative $Fl^-(Li^+{\cdot}4THF)$ (**78**)[93] and the related complex FlLi·2N$(CH_2CH_2)_3CH$ (**79**),[94] respectively (see below). It has been noted that **77** affords SSIPs in THF solution at low temperature.[93] This view has been reinforced by ^{6}Li,^{1}H HOESY. Data suggest that **78** dissolves in [D_8]THF to give mostly SSIPs at low temperature but a higher proportion of CIPs in which the metal η^5-interacts with the central Cp ring at elevated temperatures.[95] In contrast, analysis of a [D_{10}]diethyl ether solution of **78** reveals that in this inferior solvent a CIP structure in which the metal is η^1-bonded to fluorenyl-C9 is preferred.[95]

The lateral direction of metallation by a lithium aryloxide moiety has been noted in 2,6-$(CH_2Li)_2C_6H_3OLi$·TMEDA (**80**).[96] The solid-state structure (see below) reveals a tetramer, the solution integrity of which is implied (in hydrocarbon media at room temperature) by the ^{1}H NMR spectroscopic discrimination of aromatic 3- and 5-positions and the observation of three different metal environments in the ^{7}Li NMR spectrum. At elevated temperatures and in [D_8]THF symmetry about the Ar−O axis is implied spectroscopically.[96]

Whereas the ortho-directing capacities of 2-(dimethylaminomethyl) fragments have already been discussed,[29] their ability to incur lateral deprotonation has been probed by NMR spectroscopic study of the co-complex *n*BuLi·[2,6-$(Me_2NCH_2)_2$−3,5-$Me_2C_6HCHLiR$]. (R = H **81**,[97] $SiMe_3$ **82**, *t*Bu **83**, 4-toloyl **84**[98]). At low temperature, a ^{6}Li-enriched sample of **81** reveals two signals, with ^{6}Li,^{6}Li INADEQUATE spectroscopy[99] affording a homonuclear scalar coupling and suggesting retention of the tetranuclear co-complex noted in the solid state (see below).[100] Unambigu-

 © 2003 Wiley-VCH Verlag GmbH & Co. KGaA, Weinheim

ous assignment of the two ^{6}Li resonances is enabled by ^{6}Li,^{13}C HMQC spectroscopy[35c] on the basis that the metal ions bonded to *two* butyl anions show the higher intensity ^{6}Li,$^{13}C_\alpha$ correlation; assignment of these ^{6}Li resonances also allows interpretation of the ^{15}N and ^{6}Li,^{15}N HMQC[101] NMR spectra (natural abundance with respect to ^{15}N). Accordingly, 1:1:1 triplets observed in the first of these experiments are attributable to ^{6}Li,^{15}N interactions.[29] For **81**−**84**, reaction of 1,3-bis(dimethylaminomethyl)-2,4,6-trimethylarene with *n*BuLi has yielded a 2:2 mixed butyllithium-aryllithium cluster. However, whereas that noted for **81** is pseudo-cubic, the use of **82** gives a ladder structure (see below). NMR spectroscopy and cryoscopic relative molecular mass measurements combine to suggest that **81** retains its pseudo-cubane structure in hydrocarbon solution. Hence, at low temperatures (< −10 °C) the ^{1}H NMR spectrum of **81** reveals four signals for the two NMe_2 functions, two signals for the two ArMe groups, two AB multiplets for the two CH_2N units and an ArH singlet. Such diastereotopicity of the dimethylaminomethyl moieties suggests the absence of a symmetry plane through ipso and para positions perpendicular to the arene. Such a symmetry element is, however, manifest above room temperature, where a single AB pattern, two NMe signals and one ArMe singlet are seen. If the sample is heated to above +100 °C then the AB pattern and NMe peaks coalesce into single lines. In conjunction with the ^{6}Li NMR spectrum, which reveals a single peak, these data suggest rapid scrambling of the four organic anions.[97] For **82**, ^{1}H NMR spectroscopy points — through the observation of two AB patterns for the NCH_2 groups — to asymmetric interaction of the benzylic anion with two Li^+ ions (see below) and to the static nature of Li−N interactions at and below room temperature. However, a rapid fluxional process involving the dissociation/association of these bonds is evidently manifest at higher temperatures, with one singlet and one AB pattern observed for the two NMe_2 and NCH_2 groups, respectively.[98] In solution, both **83** and **84** appear to be close structural analogues of **82**.[98]

The establishment that lateral metallation occurs under the influence of a tertiary amide directing group has recently been probed both theoretically and in the solid state (see below).[102] This follows on from formative studies, which established that enantiomerically pure α-stanyllated anilides undergo tin-lithium exchange and electrophilic workup with retention and inversion of configuration, respectively.[103] Thus, 2-ethyl-*N*,*N*-diisopropyl-1-naphthamide has been metallated using *s*-BuLi to give a pair of configurationally stable diastereomeric *syn* atropisomers of $(i\text{Pr})_2NC(O)C_{10}H_6CHLiMe$-2 (**85a**). Reaction of **85a** with Bu_3SnCl yields the corresponding *syn* and *anti* stannylated atropisomers in the kinetic ratio 89:11, with subsequent heating establishing a 4:96 equilibrium.[104] While lithiation of the thermodynamic *anti* stannylated atropisomer yields *syn*-**85a**, the *syn* stannylated atropisomer itself lithiates to give a 60:40 *syn*:*anti* (**85a**:**85b**) mixture. ^{1}H NMR studies have corroborated the non-stereospecific nature of each of these two reaction steps, revealing the existence of non-interconverting *syn* and *anti* stannylated diastereoisomers in THF at −40 °C.[104] In contrast, the dissolution of preformed $(i\text{Pr})_2NC(O)C_{10}H_6CH(Li{\cdot}3THF)Me$-2 (**86**; see below) in [D_8]THF appears to yield (by ^{1}H NMR spectroscopy) one dominant solution species, with the observation of two diastereotopic *i*Pr groups at −25 °C pointing to slow rotation about the amide C−N bond below room temperature. Two diastereotopic *i*Pr moieties are also noted at −25 °C in [D_8]-toluene, as are signals attributable to the deprotonated α-CH group. However, at −48 °C in [D_8]-toluene all ^{1}H NMR resonances split into two in a 60:40 ratio, suggesting that diastereoisomers interconvert very much faster, with NMR spectroscopy showing rapid exchange in solution above this temperature.[102]

Metallation of the tertiary phosphane $MeP(C_6H_4CH_2NMe_2{-}2)_2$ using *t*BuLi yields a dimer of the benzyllithium product $MeP(C_6H_4CH_2NMe_2{-}2)$-$(C_6H_4CHLiNMe_2{-}2)_2$ (**87**) that exhibits novel dynamics in [D_8]toluene solution.[105] In spite of this it is apparent that the main features of the solid-state structure are retained at 203 K. However, ^{31}P and ^{7}Li NMR spectroscopy reveal that at elevated temperatures each metal can be associated with either phosphorus atom in the dimeric structure, but not with both simultaneously.

Solid-State Studies

Several solid-state structures have been published in which metallation has been laterally directed by the acidifying (delocalising) action of a 1-aryl substituent. In this context, the biphenyl derivatives 2-($CH_2Li{\cdot}$PMDETA)-6-$MeC_6H_3(C_6H_3Me_2{-}2,6)$ (**88**)[106] and (the dimer of) 2-(CHRLi·TMEDA)C_6H_4 (R = H **89**, $SiMe_3$ **90**)[107] have been characterised. Moreover, the structure of 2,2′-bis(TMEDA)lithiomethyl-1,1′-binaphthyl (**91**) has also been reported.[106] Just as ortholithiation has been noted in aromatic alkenes (*cf.* **13**),[34] so the 1,3-dialkyl lateral direction of metallation has been noted in the α-deprotonation of styrene. Hence, simple dimers of $2,6\text{-}Me_2C_6H_3C(Li{\cdot}L)=CH_2$ [L = OEt_2 **92**, MeO(*t*Bu) **93**] have been reported.[108] Whereas both SSIP and CIP structures have been noted for fluorenyllithium complex **78** upon dissolution in Lewis base media,[95] X-ray crystallography has established an ion-separated structure in the solid state.[93] Meanwhile, the related species **79** has been found to be a CIP with η^3-stabilisation of the metal via the 1-, 9- and 10-fluorenyl positions.[94] More recently, two lithium complexes have been generated from the substituted fluorenyl ligand 9-(dimethylaminoethyl)fluorenyl (Fl^N). In either case deprotonation at the 9-position is accompanied by internal amine-coordination, the presence of etherate solvent also supporting the metal. In $Fl^NLi{\cdot}OEt_2$ (**94**) the metal exhibits η^5-interaction with the anion, while this is reduced to η^2-bonding in $Fl^NLi{\cdot}2THF$ (**95**).[109]

In contrast to **92** and **93**, where external solvation combined with the lack of directing group donor sites to obviate the possibility of clear metal-directing group interaction, a single example of a (2-methoxy)-stabilised aromatic allene has been reported. In $2\text{-}MeOC_6H_4C(Li{\cdot}OEt_2)=C=CPh_2$

 © 2003 Wiley-VCH Verlag GmbH & Co. KGaA, Weinheim

(**96**) the metal forms part of a five-membered ring incorporating both the methoxy oxygen atom and the site of formal deprotonation.[110] Whereas a methoxy directing-group is itself passive to direct metallation, the other common "O class" director hydroxyl is, of course, itself susceptible to deprotonation. As such, this latter group will only act as a director of subsequent reaction in its phenoxide form and in the presence of excess metal. Sterically congested 2-methyl-6-(*tert*-butyl)phenol undergoes just such a reaction to give a hexalithium aggregate of 2-CH_2Li-6-(*t*Bu)C_6H_3OLi·$Me_2N(CH_2)_2N(Me)CH_2$Li·TMEDA (**97**). This complex contains a laterally lithiated aromatic system and both deprotonated and unchanged TMEDA.[111] Dimerisation of **97** occurs *via* the formation of an $(OLi)_2$ ring, each metal component of which is also supported by interaction with $ArCH_2^-$ (that is, chelated by the aryl dianion) and NCH_2^-. An investigation of "superbase" structural chemistry[112] has led to the deprotonation of 2,6-dimethylphenol in the presence of TMEDA and the unexpected formation of a dodecalithium tetramer of 2,6-$(CH_2Li)_2C_6H_3$OLi·TMEDA (**80**) wherein the lack of steric congestion [relative to that noted for 2-methyl-6-(*tert*-butyl)phenol] combines with the introduction of a second acidic methyl substituent on each aromatic ring to allow the generation of organic trianions.[96] The tetramer core is defined by an elongated eight-membered $(OLi)_4$ boat-shaped ring, at either end of which reside Li^+·TMEDA units. Such a structure contains three unique metal environments; an observation consistent with solution studies (see above).[96]

The lateral directing capacity of "N class" substituents such as R_2N- and $R_2N(CH_2)_n$- have been the subject of investigation. As already discussed, extensive solution studies have been carried out on the various lateral lithiates obtained utilising the directing abilities of 2,6-bis(dimethylaminomethyl) substituents. As part of these studies, the (*n*-butyllithium)-containing co-complexes *n*BuLi·[2,6-$(Me_2NCH_2)_2$−3,5-$Me_2C_6HCHLiR$] (R = H **81**,[97] $SiMe_3$ **82**, *t*Bu **83**, 4-toloyl **84**[98]) have been prepared and fully characterised. The solid-state structure of **81** reveals a $(CLi)_4$ pseudo-cubic dimer of dimers with each metal centre being supported by a single dimethylaminomethyl donor centre.[97] Attempts to overcome pseudo-cubane formation have revolved around the introduction of a non-hydrogen α-substituent, with R = trimethylsilyl affording **82**. The solid-state structure of **82** reveals a $(CLi)_4$ ladder, at either end of which resides an asymmetrically bonded benzylic anion.[98] The straightforward lithium salt 2-Me_2N-

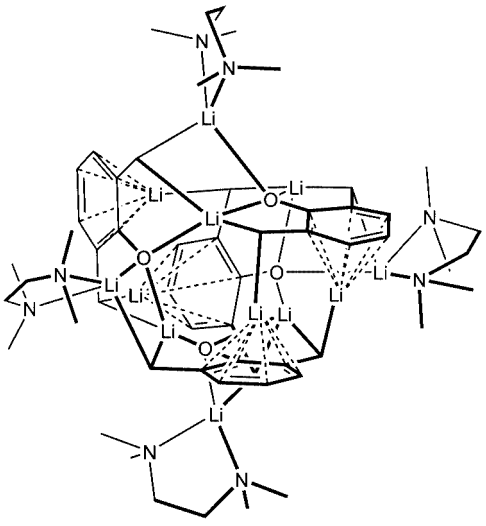

$(80)_4$

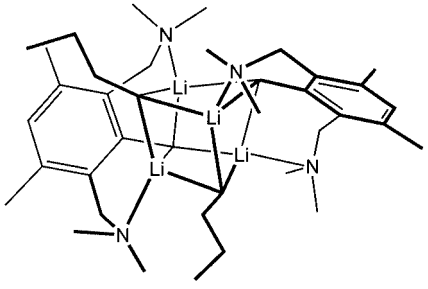

$(81)_2$

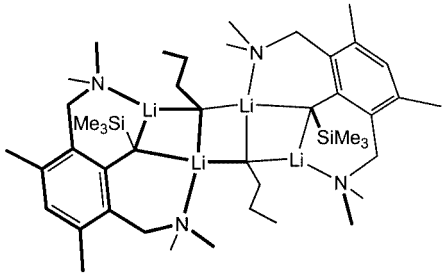

$(82)_2$

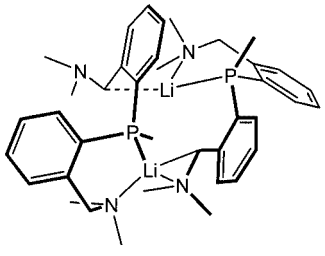

$(87)_2$

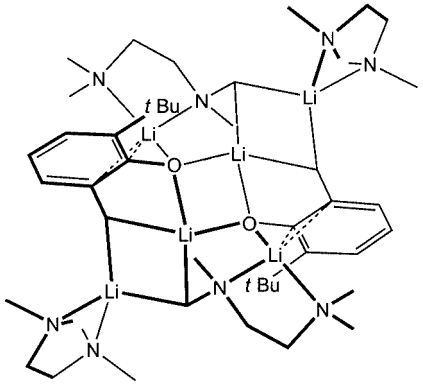

$(97)_2$

 © 2003 Wiley-VCH Verlag GmbH & Co. KGaA, Weinheim

$Me_3Si(TMEDA{\cdot}Li)CHC_6H_4$ (**98**) is a solid state monomer incorporating N-centre chelation of the metal, with transmetallation yielding the potassium congener as a precursor to the bis(benzyl)strontium species.[113] Moreover, the higher Group 15 analogue $2\text{-}Ph_2P\text{-}Me_3Si(TMEDA{\cdot}Li)CHC_6H_4$ (**99**) has been reported.[114] Nitrogen and phosphorus donor centres can, of course, act in tandem and, as such, the previously discussed benzyllithium dimer of $MeP(C_6H_4CH_2NMe_2{-}2))C_6H_4CHLiNMe_2{-}2)_2$ (**87**) reveals both intra- and intermolecular direction of lithiation in the solid state. Whereas one metal centre is η^2-bonded by both the benzylic carbon with which it is formally associated and the adjacent α-nitrogen, the second metal ion shows no intramolecular N-stabilisation. It instead exhibits a weak intermolecular interaction with a benzylic carbon centre. Both alkali metal ions are intermolecularly chelated by P- and N-donors.[105]

Concerning "N+O class" directing agents, the competitive formation of $(i\text{Pr})_2NC(O)\text{-}2\text{-}Et\text{-}C_6H_3Li{\cdot}THF$ (**67**) and $(i\text{Pr})_2NC(O)C_6H_4CH(Li{\cdot}PMDETA)Me\text{-}2$ (**68**) has already been alluded to.[82] This latter compound is structurally analogous to the product of reaction between 2-ethyl-*N*,*N*-diisopropyl-1-naphthamide and *t*BuLi in toluene/THF. Crystallography reveals that $(i\text{Pr})_2NC(O)C_{10}H_6CH(Li{\cdot}3THF)Me\text{-}2$ (**86**) is monomeric in the solid state, there being no Li−C interaction and the metal instead being entirely oxygen-supported.[102] Calculations (at the 6-311G**/B3LYP level) on $(i\text{Pr})_2NC(O)C_{10}H_6CH(Li{\cdot}3OMe_2)Me\text{-}2$ corroborate the stability of the crystallographically characterised tris(solvate) and suggest that cleavage of the $Li{-}C_\alpha$ interaction occurs in order to allow coordination of the third solvent molecule. In consequence, the calculated enthalpy of complexation for the introduction of this donor molecule is largely negated.[102]

Whereas the absence of structural data on ortholithiated pyridines has already been mentioned, 2-[bis(trimethylsilyl)methyl]pyridine is known to undergo lateral deprotonation. It is now several years since the solid-state structure of the dimeric product was first revealed.[115] Recently, however, this species has been revisited, with a topological analysis of single crystal neutron diffraction data being combined with DFT calculations to reveal that in the dimer of $2\text{-}(Me_3Si)_2CLiC_5H_4N$ (**100**) delocalisation of the C−Li bonding electrons over the agostic alkyl group controls the geometry of the Si−C−Li bond angle.[116] Just as ortho- and lateral deprotonation represent competing reactions in the case of 2-[bis(trimethylsilyl)methyl]pyridine, the lithiation of 2,6-disubstituted analogues has led to the elucidation of both the monolithiate $[2\text{-}Me\text{-}6\text{-}CH_2LiC_5H_4N]_2$ (**101**)[117] and the monomeric dilithiate $2,6\text{-}[Me_3SiCH(Li{\cdot}TMEDA)]_2C_5H_4N$ (**102**).[118] In this last complex the aromatic dianion acts as a η^2-donor to each of the two metal ions, utilising its formal charge centres and pyridyl nitrogen to do this. More complicated is the mixed anion-dianion product of reaction between 2-hydroxy-6-methylpyridine and *n*BuLi. Deprotonation is effected not only at the hydroxy position in all ligands within the cluster, but also at the orthomethyl group in four of these ligands, making the product $(2\text{-}OLi\text{-}6\text{-}CH_2LiC_5H_3N)_4{\cdot}(2\text{-}OLi\text{-}6\text{-}MeC_5H_3N)_6{\cdot}9THF$ (**103**).[119]

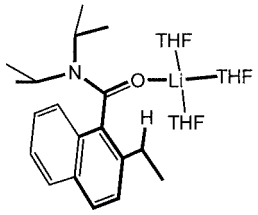

86

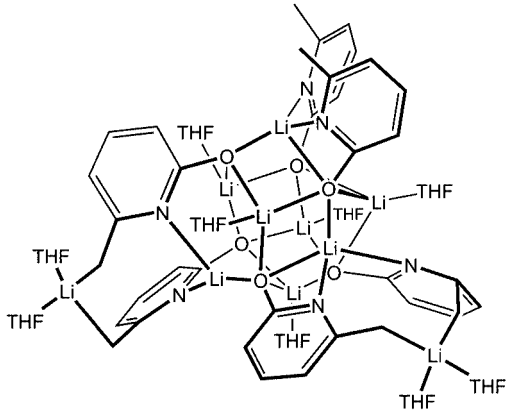

103

Perimetallation

Contrary to ortho- and lateral metallation, perimetallation occurs in the absence of electron-withdrawing properties in the directing group. Instead, whereas evidence exists (see above) for the kinetic nature of deprotonation at the ortho position, a perimetallated salt represents the thermodynamic product of reaction between organolithium and substituted arene.

Solution Studies

The THF-solvated and perilithiated derivative of 1-(dimethylamino)naphthalene has been probed by low-temperature ^{13}C NMR spectroscopy, with both the observed $^1J(^{13}C,^7Li)$ coupling constant of 20.5 Hz and the sevenfold multiplicity of the peri carbon resonance suggesting that 1-(dimethylamino)-8-naphthyllithium·THF (**104**) is dimeric in $[D_8]THF$ at −90 °C.[120]

In light of formative MNDO studies,[121] the perimetallation of 1-naphthol in THF to give $LiOC_{10}H_6Li\text{-}8{\cdot}THF$ (**105**) has been studied both as a function of the *n*BuLi:1-naphthol ratio and (for reaction in a 4:1 ratio) as a function of temperature. Moreover, $^6Li,^1H$ HOESY[122] has revealed the presence of a strong correlation for the peri hydrogen and has thus established the intermediacy of a mixed aggregate in the deprotonation of 1-naphthol.[123] Whereas the ortholithiation of 1-methoxynaphthalene by *n*BuLi/TMEDA (to give **6**) has already been alluded to effect per-

 © 2003 Wiley-VCH Verlag GmbH & Co. KGaA, Weinheim

imetallation. Moreover, the isotope effect suggestive of kinetic control in the former reaction is not observed in the latter case, pointing to perimetallated product **8** representing the thermodynamic one.[25]

The ability of lithium itself to direct perimetallation has been investigated in the context of the dilithiation of naphthalene. $^{6}Li,^{1}H$ HOESY[122] and one-dimensional $^{6}Li\{^{1}H\}$ spectroscopy[36b] have been employed to probe the 1:1 complex between 1-naphthyllithium and TMEDA (**106**) with data suggesting chelation of the metals in a dimeric aggregate. Treatment of **106** with *n*BuLi has long been known to effect the formation of 1,8-$Li_2C_{10}H_6$ (**107**),[124] with $^{6}Li,^{1}H$ HOESY more recently revealing a cross-peak involving the peri hydrogen atom prior to reaction and suggesting activation of this position.[122]

Solid-State Studies

Little structural work has been done on perimetallated systems in the solid state. The simple dimers of 1-(dimethylamino)-8-naphthyllithium·THF (**105**) and 1-methoxy-8-naphthyllithium·THF (**108**) obtained from the reaction of *n*BuLi with "N class" and "O class" directors 1-(dimethylamino)naphthalene[120] and 1-methoxynaphthalene,[120,125] respectively, have been crystallographically characterised. In each case the metal components of a core $(C_{peri}Li)_2$ ring are supported by reaction-directing amine or methoxy heteroatoms and, for **105**, this renders the structure analogous to that noted in Lewis base solution (see above). The core-naphthyl twist-angle of 63° in the crystal structure of **105** is decreased to 38° in that of **108**. If the inferior Lewis base OEt_2 is used in place of THF then the twist-angle is reduced further, such that dimeric 1-(dimethylamino)-8-naphthyllithium·OEt_2 (**109**) reveals an 11° twist.[69,126] This trend is backed up by semi-empirical (PM3) calculations.[120]

Conclusions

Directed metallation using Group 1 organometallic bases in general and organolithium substrates in particular has been shown to be of great efficacy in regiospecifically elaborating benzenoid rings (ortho-, perimetallation) and their substituents (lateral metallation). While the manifold synthetic applications of this chemistry have been extensively reviewed[1,3,8] the structural parameters surrounding lithiated species of types salient to such processes have been discussed here.

Of interest in interpreting the ability of directing groups to interact with incoming organolithium substrates are the structural elucidation of several species that incorporate either *tert*- (*cf.* **30**)[42] or *n*BuLi. The latter have taken the form of both organolithium-organic complexes (*cf.* **3**, **4**, **7**)[22,23,25] that represent precursors to directed reaction and mixed-anion organolithium co-complexes (*cf.* **33**, **48**, **61**, **64**, **81**–**84**).[38,62,75,78,97,98] This latter class of aggregates pose interesting questions about the nature of multilithiation processes.[78]

In the context of straightforward monolithiates many of the compounds discussed reveal structural characteristics normal to the field of organolithium chemistry. However, the inclusion of various mono- (e.g. "O class" or "N class") or polyheteroatom (e.g. "N+O class") directing groups has had significant effects in several cases. The ability of various electron-rich directors to interact with metals at ortho, lateral and peri sites is richly demonstrated and has been shown to effect observed chemistries in synthetically important transformations such as tertiary amide directed metallation.[81–82] Less predictable are polymetallated species. Nevertheless, fundamentally similar chelation-control processes to those noted in monolithiates dictate their structures. Overall, the synthetic utility of directed metallation is well established and promises to facilitate the development of new methodologies and total syntheses in the future. Central to the understanding of these processes is the understanding of organolithium complexes of the types discussed here.

[1] [1a] H. W. Gschwend, H. R. Rodriguez, *Org. React.* **1979**, *26*, 1–360. [1b] P. Beak, R. A. Brown, *J. Org. Chem.* **1982**, *47*, 34–46. [1c] P. Beak, V. Snieckus, *Acc. Chem. Res.* **1982**, *15*, 306–312. [1d] V. Snieckus, *Chem. Rev.* **1990**, *90*, 879–933. [1e] T. G. Gant, A. I. Meyers, *Tetrahedron* **1994**, *50*, 2297–2360.

[2] [2a] D. L. Boger, J. Y. Dong, M. Hikota, M. Ishida, *J. Am. Chem. Soc.* **1999**, *121*, 2471–2477. [2b] G. E. Keck, T. T. Wager, J. F. D. Rodriquez, *J. Am. Chem. Soc.* **1999**, *121*, 5176–5190. [2c] M. A. Brimble, S. A. Chan, *Aust. J. Chem.* **1998**, *51*, 235–242. [2d] C. Cochennec, P. Rocca, F. Marsais, A. Godard, G. Quéguiner, *Synthesis* **1995**, 321–324. [2e] F. Trécourt, M. Mallet, O. Mongin, G. Quéguiner, *J. Org. Chem.* **1994**, *59*, 6173–6178.

[3] R. D. Clark, A. Jahangir, *Org. React.* **1995**, *47*, 1–314.

[4] [4a] R. D. Clark, A. Jahangir, *J. Org. Chem.* **1989**, *54*, 1174–1178. [4b] T. R. Kelly, N. Ohashi, R. J. Armstrong-Chong, S. H. Bell, *J. Am. Chem. Soc.* **1986**, *108*, 7100–7101.

[5] [5a] J. Clayden, J. H. Pink, *Tetrahedron Lett.* **1997**, *38*, 2565–2568. [5b] J. Clayden, M. Helliwell, J. H. Pink, N. Westlund, *J. Am. Chem. Soc.* **2002**, *123*, 12449–12457.

[6] S. Thayumanavan, A. Basu, P. Beak, *J. Am. Chem. Soc.* **1997**, *119*, 8209–8216.

[7] J. Clayden, J. H. Pink, N. Westlund, C. S. Frampton, *J. Chem. Soc., Perkin Trans. 1* **2002**, 901–917.

[8] J. Clayden, *Organolithiums: Selectivity for Synthesis*, Pergamon, (Oxford) **2002**.

[9] [9a] P. Beak, A. I. Meyers, *Acc. Chem. Res.* **1986**, *19*, 356–363. [9b] P. Beak, J. E. Hunter, Y. M. Jun, *J. Am. Chem. Soc.* **1983**, *105*, 6350–6351.

[10] D. R. Anderson, N. C. Faibish, P. Beak, *J. Am. Chem. Soc.* **1999**, *121*, 7553–7558.

[11] [11a] S. Harder, A. Streitwieser, *Angew. Chem.* **1993**, *105*, 1108–1110, *Angew. Chem. Int. Ed. Engl.* **1993**, *32*, 1066–1068. [11b] S. Harder, M. Lutz, T. Kremer, *Organometallics* **1995**, *14*, 2133–2135.

[12] [12a] G. van Koten, J. T. B. H. Jastrzebski, F. Muller, C. H. Stam, *J. Am. Chem. Soc.* **1985**, *107*, 697–698. [12b] M. Niemeyer, *Organometallics* **1998**, *17*, 4649–4656.

[13] E. Rijnberg, J. T. B. H. Jastrzebski, J. Boersma, H. Kooijman, N. Veldman, A. L. Spek, G. van Koten, *Organometallics* **1997**, *16*, 2239–2245.

[14] [14a] J. J. H. Edema, S. Gambarotta, F. van Bolhuls, W. J. J. Smeets, A. L. Spek, M. Y. Chiang, *J. Organomet. Chem.* **1990**, *389*, 47–59. [14b] P. J. Bailey, L. A. Mitchell, P. R. Raithby, M.-A. Rennie, K. Verhorevoort, D. S. Wright, *Chem. Commun.* **1996**, 1351–1352. [14c] J. A. Brandts, M. van Leur, R. A. Goss-

 © 2003 Wiley-VCH Verlag GmbH & Co. KGaA, Weinheim

age, J. Boersma, A. L. Spek, G. van Koten, *Organometallics* **1999**, *18*, 2633−2641.
[15] [15a] H. Gilman, R. V. Young, *J. Am. Chem. Soc.* **1934**, *56*, 1415−1416. [15b] G. Wittig, U. Pockels, H. Dröge, *Ber.* **1938**, *71B*, 1903−1912.
[16] [16a] P. Beak, R. A. Brown, *J. Org. Chem.* **1979**, *44*, 4463−4464. [16b] A. I. Meyers, K. Lutomski, *J. Org. Chem.* **1979**, *44*, 4464−4466. [16c] A. I. Meyers, P. D. Pansegrau, *Tetrahedron Lett.* **1983**, *24*, 4935−4938. [16d] R. R. Fraser, M. Bresse, T. S. Mansour, *J. Am. Chem. Soc.* **1983**, *105*, 7790−7791.
[17] M. Iwao, T. Iihama, K. K. Mahalanabis, H. Perrier, V. Snieckus, *J. Org. Chem.* **1989**, *54*, 24−26.
[18] C. Quesnelle, T. Iihama, T. Aubert, H. Perrier, V. Snieckus, *Tetrahedron Lett.* **1992**, *33*, 2625−2628.
[19] R. Snaith, D. S. Wright, in *Lithium Chemistry: A Theoretical and Experimental Overview*, Ed. A.-M. Sapse, P. v. R. Schleyer, John Wiley & Sons, (New York) **1995**.
[20] W. Clegg, L. Dunbar, L. Horsburgh, R. E. Mulvey, *Angew. Chem.* **1996**, *108*, 815−816, *Angew. Chem. Int. Ed. Engl.* **1996**, *35*, 753−755.
[21] G. Fraenkel, S. Subramanian, A. Chow, *J. Am. Chem. Soc.* **1995**, *117*, 6300−6307.
[22] W. Bauer, P. v. R. Schleyer, *J. Am. Chem. Soc.* **1989**, *73*, 7191−7198.
[23] G. Fraenkel, A. M. Fraenkel, M. J. Geckle, F. Schloss, *J. Am. Chem. Soc.* **1979**, *101*, 4745−4747.
[24] N. J. R. van Eikema Hommes, P. v. R. Schleyer, *Angew. Chem.* **1992**, *104*, 768−771, *Angew. Chem. Int. Ed. Engl.* **1992**, *33*, 755−758.
[25] J. Betz, W. Bauer, *J. Am. Chem. Soc.* **2002**, *124*, 8699−8706.
[26] [26a] C. Kiefel, A. Mannschreck, *Synthesis* **1995**, *8*, 1033−1037. [26b] M. Schlosser, *Eur. J. Org. Chem.* **2001**, 3975−3984.
[27] F. N. Jones, M. F. Zinn, C. R. Hauser, *J. Org. Chem.* **1963**, *28*, 663−665.
[28] J. Belzner, D. Schar, U. Dehnert, M. Noltemeyer, *Organometallics* **1997**, *16*, 285−288.
[29] H. J. Reich, B. Ö. Gudmundsson, *J. Am. Chem. Soc.* **1996**, *118*, 6074−6075.
[30] [30a] J. T. B. H. Jastrzebski, G. van Koten, M. Konijn, C. H. Stam, *J. Am. Chem. Soc.* **1982**, *104*, 5490−5492. [30b] E. Wehman, J. T. B. H. Jastrzebski, J.-M. Ernsting, D. M. Grove, G. van Koten, *J. Organomet. Chem.* **1988**, *353*, 145−155.
[31] D. Grandjean, P. Pale, *Tetrahedron Lett.* **1993**, *34*, 1155−1158.
[32] W. Bauer, G. Müller, R. Pi, P. v. R. Schleyer, *Angew. Chem.* **1986**, *98*, 1130−1131, *Angew. Chem. Int. Ed. Engl.* **1986**, *25*, 1103−1104.
[33] G. W. H. Cheeseman, S. G. Greenberg, *J. Organomet. Chem.* **1979**, *166*, 139−152.
[34] W. Bauer, M. Feigel, G. Müller, P. v. R. Schleyer, *J. Am. Chem. Soc.* **1988**, *110*, 6033−6046.
[35] [35a] G. A. Morris, *Magn. Reson. Chem.* **1986**, *24*, 371−403. [35b] H. Günther, D. Moskau, R. Dujardin, A. Maercker, *Tetrahedron Lett.* **1986**, *27*, 2251−2254. [35c] D. Moskau, F. Brauers, H. Günther, A. Maercker, *J. Am. Chem. Soc.* **1987**, *109*, 5532−5534.
[36] [36a] B. H. Meier, R. R. Ernst, *J. Am. Chem. Soc.* **1979**, *101*, 6441−6442. [36b] H. Günther, D. Moskau, P. Bast, D. Schmalz, *Angew. Chem.* **1987**, *99*, 1242−1250, *Angew. Chem. Int. Ed. Engl.* **1987**, *26*, 1212−1220.
[37] U. Schubert, W. Neugebauer, P. v. R. Schleyer, *J. Chem. Soc., Chem. Commun.* **1982**, 1184−1185.
[38] K. Ruhlandt-Senge, J. J. Ellison, R. J. Wehmschulte, F. Pauer, P. P. Power, *J. Am. Chem. Soc.* **1993**, *115*, 11353−11357.
[39] B. Schiemenz, P. P. Power, *Angew. Chem.* **1996**, *108*, 2288−2290, *Angew. Chem. Int. Ed. Engl.* **1996**, *35*, 2150−2152.
[40] G. W. Rabe, R. D. Sommer, A. L. Rheingold, *Organometallics* **2000**, *19*, 5537−5540.
[41] R. C. Crittendon, B. C. Beck, J. Su, X.-W. Li, G. H. Robinson, *Organometallics* **1999**, *18*, 156−160.
[42] N. J. Hardman, B. Twamley, M. Stender, R. Baldwin, S. Hino, B. Schiemenz, S. M. Kauzlarich, P. P. Power, *J. Organomet. Chem.* **2002**, *643*, 461−467.
[43] G. L. Wegner, R. J. F. Berger, A. Schier, H. Schmidbaur, *Z. Naturforsch., Teil B* **2000**, *55*, 995−999.
[44] B. Schiemenz, P. P. Power, *Organometallics* **1996**, *15*, 958−964.
[45] [45a] M. M. Olmstead, P. P. Power, *J. Organomet. Chem.* **1991**, *408*, 1−6. [45b] G. S. Girolami, M. E. Riehl, K. S. Suslick, S. R. Wilson, *Organometallics* **1992**, *11*, 3907−3910.
[46] R. A. Bartlett, H. V. R. Dias, P. P. Power, *J. Organomet. Chem.* **1988**, *341*, 1−9.
[47] M. A. Beno, H. Hope, M. M. Olmstead, P. P. Power, *Organometallics* **1985**, *4*, 2117−2121.
[48] G. W. Rabe, M. Zhang-Presse, G. P. A. Yap, *Acta Crystallogr., Sect. E* **2002**, *58*, m434−m435.
[49] S. Harder, J. Boersma, L. Brandsma, G. P. M. van Mier, J. A. Kanters, *J. Organomet. Chem.* **1989**, *364*, 1−15.
[50] S. Harder, J. Boersma, L. Brandsma, J. A. Kanters, A. J. M. Duisenberg, *Organometallics* **1990**, *9*, 511−516.
[51] S. Harder, J. Boersma, L. Brandsma, J. A. Kanters, *J. Organomet. Chem.* **1988**, *339*, 7−15.
[52] H. Dietrich, W. Mahdi, W. Storck, *J. Organomet. Chem.* **1988**, *349*, 1−10.
[53] S. Harder, J. Boersma, L. Brandsma, A. van Heteren, J. A. Kanters, W. Bauer, P. v. R. Schleyer, *J. Am. Chem. Soc.* **1988**, *110*, 7802−7806.
[54] S. Harder, J. Boersma, L. Brandsma, J. A. Kanters, A. J. M. Duisenberg, J. H. van Lenthe, *Organometallics* **1991**, *10*, 1623−1627.
[55] [55a] S. Harder, L. Brandsma, J. A. Kanters, A. J. M. Duisenberg, *Acta Crystallogr., Sect. C* **1987**, *43*, 1535−1537. [55b] W. Bauer, P. A. A. Klusener, S. Harder, J. A. Kanters, A. J. M. Duisenberg, L. Brandsma, P. v. R. Schleyer, *Organometallics* **1988**, *7*, 552−555.
[56] M. Kranz, H. Dietrich, W. Mahdi, G. Müller, F. Hampel, T. Clark, R. Hacker, W. Neugebauer, A. J. Kos, P. v. R. Schleyer, *J. Am. Chem. Soc.* **1993**, *115*, 4698−4704.
[57] F. Bosold, P. Zulauf, M. Marsch, K. Harms, J. Lohrenz, G. Boche, *Angew. Chem.* **1991**, *103*, 1497−1499, *Angew. Chem. Int. Ed. Engl.* **1991**, *30*, 1455−1457.
[58] W. Hollstein, K. Harms, M. Marsch, G. Boche, *Angew. Chem.* **1987**, *99*, 1279−1280, *Angew. Chem. Int. Ed. Engl.* **1987**, *26*, 1287−1288.
[59] A. E. H. Wheatley, *Chem. Soc. Rev.* **2001**, 265−273.
[60] J. F. K. Müller, M. Neuburger, M. Zehnder, *Helv. Chim. Acta* **1997**, *80*, 2182−2190.
[61] R. Schlengermann, J. Sieler, S. Jelonek, E. Hey-Hawkins, *Chem. Commun.* **1997**, 197−198.
[62] J. G. Donkervoort, J. L. Vicario, E. Rijnberg, J. T. B. H. Jastrzebski, H. Kooijman, A. L. Spek, G. van Koten, *J. Organomet. Chem.* **1998**, *550*, 463−467.
[63] W. J. J. Smeets, A. L. Spek, A. A. H. van der Zeijden, G. van Koten, *Acta Crystallogr., Sect. C* **1987**, *43*, 1429−1430.
[64] A. L. Spek, N. Veldman, CCDC ref. JUKDAU.
[65] S. Harder, J. Boersma, L. Brandsma, J. A. Kanters, W. Bauer, P. v. R. Schleyer, *Organometallics* **1989**, *8*, 1696−1700.
[66] S. Harder, P. F. Ekhart, L. Brandsma, J. A. Kanters, A. J. M. Duisenberg, P. v. R. Schleyer, *Organometallics* **1992**, *11*, 2623−2627.
[67] A. L. Spek, M. T. Lakin, R. den Besten, CCDC ref. LEDQUG.
[68] R. den Besten, M. T. Lakin, N. Veldman, A. L. Spek, L. Brandsma, *J. Organomet. Chem.* **1996**, *514*, 191−196.
[69] M. H. P. Rietveld, I. C. M. Wehmann-Ooyevaar, G. M. Kapteijn, D. M. Grove, W. J. J. Smeets, H. Kooijman, A. L. Spek, G. van Koten, *Organometallics* **1994**, *13*, 3782−3787.
[70] A. L. Spek, N. Veldman, CCDC ref. HIGQOD.
[71] D. L. Comins, J. D. Brown, *J. Org. Chem.* **1984**, *49*, 1078−1083.
[72] D. L. Comins, M. O. Killpack, *J. Org. Chem.* **1987**, *52*, 104−109.
[73] [73a] D. L. Comins, J. D. Brown, *Tetrahedron Lett.* **1981**, *22*, 4213−4216. [73b] D. L. Comins, J. D. Brown, N. B. Mantlo,

 © 2003 Wiley-VCH Verlag GmbH & Co. KGaA, Weinheim

Tetrahedron Lett. **1982**, *23*, 3979−3982. [73c] D. L. Comins, J. D. Brown, *J. Org. Chem.* **1989**, *54*, 3730−3732.
[74] I. C. M. Wehman-Ooyevaar, G. M. Kapteijn, D. M. Grove, A. L. Spek, G. van Koten, *J. Organomet. Chem.* **1993**, *452*, C1−C3.
[75] G. B. Deacon, C. M. Forsyth, N. M. Scott, *J. Chem. Soc., Dalton Trans.* **2001**, 2494−2501.
[76] P. C. Andrews, G. B. Deacon, C. M. Forsyth, N. M. Scott, *Angew. Chem.* **2001**, *113*, 2166−2169, *Angew. Chem. Int. Ed.* **2001**, *40*, 2108−2111.
[77] G. Boche, I. Langlotz, M. Marsch, K. Harms, N. E. S. Nudelman, *Angew. Chem.* **1992**, *104*, 1239−1240, *Angew. Chem. Int. Ed. Engl.* **1992**, *31*, 1205−1207.
[78] R. P. Davies, P. R. Raithby, R. Snaith, *Angew. Chem.* **1997**, *109*, 1261−1263, *Angew. Chem. Int. Ed. Engl.* **1997**, *36*, 1215−1217.
[79] [79a] P. Beak, S. T. Kerrick, D. J. Gallagher, *J. Am. Chem. Soc.* **1993**, *115*, 10628−10636. [79b] P. Bowles, J. Clayden, M. Helliwell, C. McCarthy, M. Tomkinson, N. Westlund, *J. Chem. Soc., Perkin Trans. 1* **1997**, 2607−2616.
[80] J. Clayden, C. S. Frampton, C. McCarthy, N. Westlund, *Tetrahedron* **1999**, *55*, 14161−14184.
[81] J. Clayden, R. P. Davies, M. A. Hendy, R. Snaith, A. E. H. Wheatley, *Angew. Chem.* **2001**, *113*, 1282−1285, *Angew. Chem. Int. Ed.* **2001**, *40*, 1238−1240.
[82] A. E. H. Wheatley, unpublished results.
[83] G. Müller, H.-P. Abicht, M. Waldkircher, J. Lachmann, M. Lutz, M. Winkler, *J. Organomet. Chem.* **2001**, *622*, 121−134.
[84] A. Pape, M. Lutz, G. Müller, *Angew. Chem. Int. Ed. Engl.* **1994**, *33*, 2281−2284.
[85] S. Harder, L. Brandsma, J. A. Kanters, A. Duisenberg, J. H. van Lenthe, *J. Organomet. Chem.* **1991**, *420*, 143−154.
[86] M. Schlosser, L. Guio, F. Leroux, *J. Am. Chem. Soc.* **2001**, *123*, 3822−3823.
[87] M. Winkler, M. Lutz, G. Müller, *Angew. Chem.* **1994**, *106*, 2372−2374, *Angew. Chem. Int. Ed. Engl.* **1994**, *33*, 2279−2281.
[88] A. Steiner, D. Stalke, *Angew. Chem.* **1995**, *107*, 1908−1910, *Angew. Chem. Int. Ed. Engl.* **1995**, *34*, 1752−1755.
[89] T. Kottke, K. Sung, R. J. Lagow, *Angew. Chem.* **1995**, *107*, 1612−1614, *Angew. Chem. Int. Ed. Engl.* **1995**, *34*, 1517−1519.
[90] D. Stalke, K. H. Whitmire, *J. Chem. Soc., Chem. Commun.* **1990**, 833−834.
[91] [91a] C. D. Broaddus, *J. Am. Chem. Soc.* **1966**, *88*, 4174. [91b] C. D. Broaddus, *J. Org. Chem.* **1970**, *35*, 10−15.
[92] R. L. Vaulx, F. N. Jones, C. R. Hauser, *J. Org. Chem.* **1964**, *29*, 1387−1391.
[93] W. Bauer in *Lithium Chemistry: A Theoretical and Experimental Overview* (Ed.: A.-M. Sapse, P. v. R. Schleyer), John Wiley & Sons, (New York) **1995**.
[94] R. Zerger, W. Rhine, G. D. Stucky, *J. Am. Chem. Soc.* **1974**, *96*, 5441−5448.
[95] D. Hoffmann, W. Bauer, P. v. R. Schleyer, *J. Chem. Soc., Chem. Commun.* **1990**, 208−211.
[96] S. Harder, M. Lutz, A. Streitweiser, *J. Am. Chem. Soc.* **1995**, *117*, 2361−2362.
[97] P. Wijkens, E. M. van Koten, M. D. Janssen, J. T. B. H. Jastrzebski, A. L. Spek, G. van Koten, *Angew. Chem. Int. Ed. Engl.* **1995**, *107* 239−242, *Angew. Chem. Int. Ed. Engl.* **1995**, *34*, 219−222.
[98] P. Wijkens, J. T. B. H. Jastrzebski, N. Veldman, A. L. Spek, G. van Koten, *Chem. Commun.* **1997**, 2143−2144.
[99] [99a] O. Eppers, H. Günther, K.-D. Klein, A. Maercker, *Magn. Reson. Chem.* **1991**, *29*, 1065−1067. [99b] O. Eppers, T. Fox, H. Günther, *Helv. Chim. Acta* **1992**, *75*, 883−891. [99c] N. Chandrakumar, H.-E. Mons, D. Hüls, H. Günther, *Magn. Reson. Chem.* **1996**, *34*, 715−718.
[100] D. Hüls, H. Günther, G. van Koten, P. Wijkens, J. T. B. H. Jastrzebski, *Angew. Chem. Int. Ed. Engl.* **1997**, *36*, 2629−2631.
[101] J. H. Gilchrist, A. T. Harrison, D. J. Fuller, D. B. Collum, *Magn. Reson. Chem.* **1992**, *30*, 855−859.
[102] D. R. Armstrong, J. Clayden, R. Haigh, D. J. Linton, P. Schooler, A. E. H. Wheatley, *Chem. Commun.* **2003**, 1694−1695.
[103] A. Basu, P. Beak, *J. Am. Chem. Soc.* **1996**, *118*, 1575−1576.
[104] [104a] J. Clayden, J. H. Pink, *Tetrahedron Lett.* **1997**, *38*, 2565−2568. [104b] J. Clayden, M. Helliwell, J. H. Pink, N. Westlund, *J. Am. Chem. Soc.* **2002**, *123*, 12449−12547.
[105] W. Clegg, K. Izod, W. McFarlane, P. O'Shaughnessy, *Organometallics* **1999**, *18*, 3950−3952.
[106] L. M. Engelhardt, W.-P. Leung, C. L. Raston, G. Salem, P. Twiss, A. H. White, *J. Chem. Soc., Dalton Trans.* **1988**, 2403−2409.
[107] L. M. Engelhardt, W.-P. Leung, C. L. Raston, P. Twiss, A. H. White, *J. Chem. Soc., Dalton Trans.* **1984**, 321−330.
[108] R. Knorr, C. Behringer, H. Nöth, M. Schmidt, E. Lattke, E. Rapple, *Chem. Ber./Recueil* **1997**, *130*, 585−592.
[109] R. D. Culp, A. H. Cowley, *Organometallics* **1996**, *15*, 5380−5384.
[110] P. Dem'yanov, G. Boche, M. Marsch, K. Harms, G. Fyodorova, V. Petrosyan, *Liebigs Ann.* **1995**, 457−460.
[111] S. Harder, M. Lutz, *Organometallics* **1994**, *13*, 5173−5176.
[112] W. Bauer, L. Lochmann, *J. Am. Chem. Soc.* **1992**, *114*, 7482−7489.
[113] F. Feil, S. Harder, *Organometallics* **2001**, *20*, 4616−4622.
[114] L. T. Byrne, L. M. Engelhardt, G. E. Jacobsen, W.-P. Leung, R. I. Papasergio, C. L. Raston, B. W. Skelton, P. Twiss, A. H. White, *J. Chem. Soc., Dalton Trans.* **1989**, 105−113.
[115] [115a] R. I. Papasergio, C. L. Raston, A. H. White, *J. Chem. Soc., Chem. Commun.* **1983**, 1419−1420. [115b] R. I. Papasergio, B. W. Skelton, P. Twiss, A. H. White, C. L. Raston, *J. Chem. Soc., Dalton Trans.* **1990**, 1161−1172.
[116] [116a] W. Scherer, P. Sirsch, M. Grosche, M. Spiegler, S. A. Mason, M. G. Gardiner, *Chem. Commun.* **2001**, 2072−2073. [116b] W. Scherer, P. Sirsch, D. Shorokhov, G. S. McGrady, S. A. Mason, M. G. Gardiner, *Chem. Eur. J.* **2002**, *8*, 2324−2334.
[117] P. v. R. Schleyer, R. Hacker, H. Dietrich, W. Mahdi, *J. Chem. Soc., Chem. Commun.* **1985**, 622−624.
[118] R. Hacker, P. v. R. Schleyer, G. Reber, G. Müller, L. Brandsma, *J. Organomet. Chem.* **1986**, *316*, C4−C8.
[119] S. T. Liddle, W. Clegg, *Chem. Commun.* **2001**, 1584−1585.
[120] J. Betz, F. Hampel, W. Bauer, *J. Chem. Soc., Dalton Trans.* **2001**, 1876−1879.
[121] [121a] G. A. Suñer, P. M. Deyá, J. M. Saá, *J. Am. Chem. Soc.* **1990**, *112*, 1467−1471. [121b] J. M. Saá, J. Morey, A. Frontera, P. M. Deyá, *J. Am. Chem. Soc.* **1995**, *117*, 1105−1116.
[122] W. Bauer, T. Clark, P. v. R. Schleyer, *J. Am. Chem. Soc.* **1987**, *109*, 970−977.
[123] J. M. Saá, G. Martorell, A. Frontera, *J. Am. Chem. Soc.* **1996**, *61*, 5194−5195.
[124] W. Neugebauer, T. Clark, P. v. R. Schleyer, *Chem. Ber.* **1983**, *116*, 3283−3292.
[125] J. Betz, F. Hampel, W. Bauer, *Org. Lett.* **2000**, *2*, 3805−3807.
[126] [126a] J. T. B. H. Jastrzebski, G. van Koten, K. Goubitz, C. Arlen, M. Pfeffer, *J. Organomet. Chem.* **1983**, *246*, C75−C79. [126b] K. Sorger, P. v. R. Schleyer, R. Fleischer, D. Stalke, *J. Am. Chem. Soc.* **1996**, *118*, 6924−6933.

Received May 27, 2003

 © 2003 Wiley-VCH Verlag GmbH & Co. KGaA, Weinheim

Synthesis and Structure of a Monomeric Chiral Lithium Dialkylaluminium Amide Derived from Schöllkopf's Bis-lactim Ether and α-(Methylbenzyl)benzylamine

Philip C. Andrews,*[a] Melissa Maguire,[a] and Esteban Pombo-Villar[b]

Dedicated to the memory of Ron Snaith in recognition of his great contribution to lithium chemistry

Keywords: Lithium / Aluminium / Chirality / Amides / Structure elucidation

Crystals of a monomeric lithium dialkylaluminium amide containing two different chiral amide moieties have been isolated from the reaction of lithiated Schöllkopf's bis-lactim ether complexed by pmdta with the diethylaluminium amide of (*S*)-α-(methylbenzyl)benzylamine, with single crystal X-ray diffraction revealing a migration of the Li cation in the aluminate from its initial position on the pyrazine ring of the lactim ether precursor.
(© Wiley-VCH Verlag GmbH & Co. KGaA, 69451 Weinheim, Germany, 2003)

Introduction

Lithium aluminates can show significantly different reactivity and selectivity when compared to that of their constituent parts — the nucleophilic alkyllithium or lithium hydride and the organoaluminium species — the reactivity of the latter being dominated primarily by its Lewis acidic properties.[1a−1c] By analogy, lithium dialkylaluminium amides have the potential to play a similar role, although synthetic activity has largely focused on the amidohydroaluminates.[2a,2b] However, some interest in their solid-state structures has developed since they fall within an important broader group of main-group heterobimetallic complexes containing group 1 metals, a family of complexes whose reactivity and selectivity is only gradually coming to be understood and exploited.[3a−3e] The lithium dialkylaluminium amide complexes that have been structurally characterised to date are comprised primarily of (N_2MM') rings,[4a−4d] the two metals not surprisingly being bridged by the N_{amido} atoms, for example $[Me_2Al(Bn_2N)_2]Li\cdot(THF)$],[5] although further association into a ladder-type structure[6] and bridging through Me groups has also been observed.[7]

Recently, we have been interested in two related areas dealing with the structural chemistry of chiral lithium amide bases which are important in the synthesis of biologically active compounds. The first area is the alkali-metal complexes of α-(methylbenzyl)benzylamine,[8a−8c] which have become prominent in β-amino acid and β-lactam syntheses,[9a−9d] and we have been extending our studies to the reactions of this and similar chiral amines with group 13 organometallic compounds. The second area concerns the lithium complexes of Schöllkopf's bis-lactim ether, 1-lithio-3,6-diethoxy-2-isopropyl-1,2-dihydropyrazine,[10a−10c] and we recently reported the structure of the complex coordinated by the tridentate donor pmdta, (*R*)-**1**, represented in Figure 1.[11]

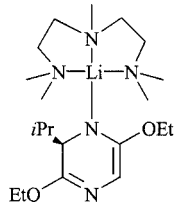

Figure 1. Lithiated Schöllkopf's bis-lactim ether, (*R*)-**1**, coordinated by pmdta

In bringing these two "precursor" areas together we have now synthesised and structurally characterised, by single-crystal X-ray diffraction, the first lithium dialkylaluminium amide, **2**, which is both monomeric in the solid state and comprised of two completely different chiral amide bases.

Results and discussion

Prompted by extensive studies on the formation of aluminium amides from dibenzylamine[12] we found that the thermal elimination of EtH from the reaction of Et_3Al and

[a] School of Chemistry, Monash University,
PO Box 23, Melbourne, Vic. 3800, Australia
Fax:(internat.) +61-3/9905-4597
E-mail: p.andrews@sci.monash.edu.au
[b] Preclinical Research, Novartis Pharma Ltd.,
4002 Basel, Switzerland

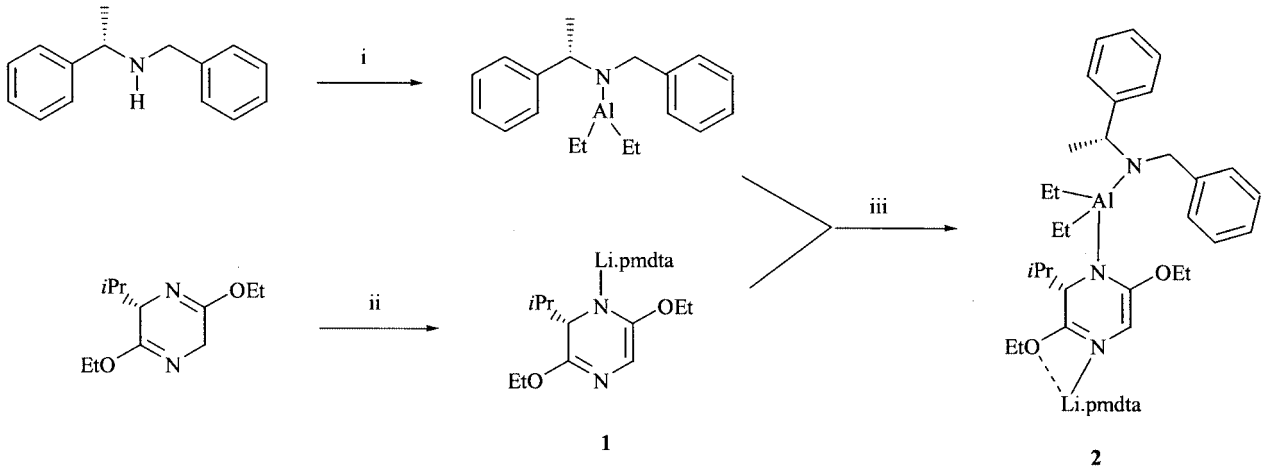

Scheme 1. Reaction conditions; i. Et_3Al, toluene, 120 °C, 4−6 h; ii. *n*BuLi, pmdta, toluene, −30 °C to room temp.; iii toluene, −30 °C to room temp.

(*S*)-α-(methylbenzyl)benzylamine occurs on heating to 120 °C (Scheme 1), although no crystalline product has yet been obtained from this reaction. This may be influenced by the fact that EtH elimination does not appear to occur quantitatively.

Following an analogous procedure to that described for the synthesis of $[Me_2Al(Bn_2N)_2]Li\cdot(py)]$,[13] a toluene solution of the lithiated Schöllkopf's bis-lactim ether, (*S*)-**1**, was added to a toluene solution of the aluminium amide generated in situ. A deep orange coloured solution was formed from which a low yield of orange crystals were isolated after approximately one week at −25 °C. By this time the solution had become dark red.

A second crop of crystals was then extracted after refrigeration at 4 °C over several days. However, the collective yield was still not high (32%) and no further solid product was obtained even at lower temperatures, with a dark red oil being observed to have formed. The crystals melt to a deep red between 142−144 °C and, as would be expected, are highly sensitive to atmospheric moisture and oxygen. Elemental analysis, multi-dimensional NMR studies, and single crystal X-ray diffraction identified the crystals as the chiral heterobimetallic species **2** (Figure 2).

Complex **2** crystallises in the orthorhombic space group $P2_12_12_1$ with four molecules in the unit cell. Although the crystal quality was not exceptionally high, leading to a large amount of weak intensities and high R_{int} value, the structural solution was of sufficient quality to allow us to assign definitive atom connectivities. The first striking feature of the structure comes directly from a comparison with the parent lithiated bis-lactim ether **1**. As can be seen, the Li cation, with its accompanying pmdta molecule, migrates from one N in the pyrazine ring in **1** to the opposite one in **2** as the lithium aluminate is formed. The Li(1)−O(2) bond at 2.543(11) Å would be considered long, however, an analysis of the bond angles at the sp^2 pyrazine nitrogen attached to Li reveals a high degree of asymmetry [Li(1)−N(3)−C(22) 108.7(5)°, Li(1)−N(3)−C(21)

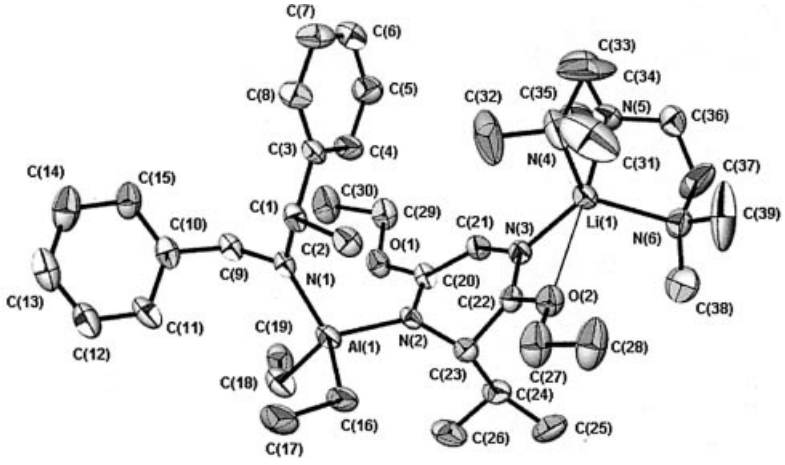

Figure 2. Molecular structure of (*S,S*)-**2**; thermal ellipsoids shown at 50% probability; all H atoms omitted for clarity; selected bond length (Å) and angles (°); Li(1)−N(3) 2.014(12), Li(1)−N(4) 2.117(14), Li(1)−N(5) 2.127(13), Li(1)−O(2) 2.543(11), Al(1)−N(1) 1.860(5), Al(1)−N(2) 1.939(5), C(21)−N(3) 1.423(8), C(22)−N(3) 1.265(7), N(2)−C(23) 1.449(7) N(2)−C(20) 1.352(7); Al(1)−N(2)−C(23) 122.0(4), Al(1)−N(2)−C(20) 126.4(4), Li(1)−N(3)−C(22) 108.7(5), Li(1)−N(3)−C(21) 136.2(5), C(21)−N(3)−C(22) 114.1(5), C(20)−N(2)−C(23) 111.5(5), N(2)−C(23)−C(22) 105.2(5)

 © 2003 Wiley-VCH Verlag GmbH & Co. KGaA, Weinheim

136.4(5)°] with the Li cation clearly associating itself preferentially with the C=N bond [C(21)−N(3) 1.423(8) Å, C(22)−N(3) 1.265(7) Å] and the ethoxy O atom. The Li−N_{amido} distance in **2** of 2.014(12) Å is only marginally longer than that in **1** [1.965(3) Å] and is typical of four-coordinate Li complexed by pmdta. Not unexpectedly there are two significantly different Al−N bond lengths. They are 1.860(5) Å and 1.939(5) Å for Al(1)−N(1, 2) respectively indicating that the tetravalent Al center is bound more tightly to the α-(methylbenzyl)benzylamido group than to the pyrazine ring. Though there are no direct structural comparisons available for **2** since all analogous compounds contain bridging N rather than terminal, the Al(1)−N(1) distance is nevertheless similar to those commonly found in complexes with a dialkylaluminium dibenzylamido moiety in which Al is four coordinate (e.g. 1.982 Å in $[Bn_2NAlMe_2]_2$),[14] while the bond from Al(1)−N(2) is longer than that commonly found {e.g. 1.934(2) Å in $[Me_2Al(Bn_2N)_2]Li\cdot(py)$]}.[13] This is undoubtedly to relieve steric interactions between the Al centre and the pyrazine ring and is compensated for by the shorter Al(1)−N(1) bond.

It is hard to reason the migration of the Li^+ solely on steric grounds, i.e. avoidance of the *i*Pr group, since the presence of the two Et and the α-(methylbenzyl)benzylamido groups on the Al centre amounts to a substantial degree of steric bulk, most likely equivalent to that offered by pmdta on the Li cation. However, it is notable that in both **1** and **2** the metals locate themselves on the side of the pyrazine ring opposite the *i*Pr group, and, indeed, in **2** both Li and Al are located on the same side of the slightly buckled ring. If we assume the precursor to the aluminate is an intermediate containing a mixed-metal aggregate structured around the formation of a (Li-*N*-Al-N) four-membered ring then the steric strain could easily influence the cleavage of the Li^+-N^- bond and separation of the pmdta-bound Li cation. We had speculated when reporting the solution studies on (*R*)-**1** that, even without any additional chemical factors, a relocation of the Li cation was possible though our evidence was circumstantial.[11] As such, several co-incident factors may effect the migration of the lithium ion and aluminate formation: the possibility of solvent-separated ion pairs in **1** facilitated by the ethoxy groups, the sterically assisted weakening and ultimate cleavage of the Li^+-N^- bond, and the greater electrophilicity of Al^{3+} over that of Li^+. The Li cation then satisfies its coordinative demands by bonding with the available electron density associated with the N=C bond and the OEt group.

It is important to note that it would not be possible to form complex **2** by the alternate route which would involve swapping the metals on the constituent components, principally because the pmdta complex of α-(methylbenzyl)-benzylamidolithium undergoes facile transformation to an aza-allyl complex at low temperature.[8c] However, this could indicate one possibility for the gradual presence of the red oil in the reaction mixture if an electronic rearrangement in solution occurs which allows for the formation of (*S*)-[{Ph(Me)CH}($PhCH_2$)NLi·(pmdeta)] and its subsequent decomposition.

From this structural study there is no doubt that **1**, **2** and any Lewis base (L) complexes of α-(methylbenzyl)benzylamidolithium, $[\{PhC(Me)H\}(PhCH_2)NLi\cdot(L)_k]_n$, would behave very differently to each other in synthetic procedures, an aspect which needs to be further explored.

Experimental Section

Crystallographic Data for (*S,S*)-2: $C_{35}H_{68}AlLiN_6O_2$, M = 686.91, T = 123 K, orthorhombic $P2_12_12_1$, a = 14.300(3), b = 16.848(3), c = 17.659(4) Å, V = 4254.5(15) Å^3, D_c = 1.072 g·cm^{-3}, Z = 4; $F(000)$ = 1504, $\mu_{Mo\text{-}K\alpha}$ = 0.85 cm^{-1}, $2\theta_{max}$ = 56.6°, N_{tot} = 43347, N = 10455 [R(int) = 0.2173], N_o = 5801, final R, R_w = 0.076, 0.17 [$I > 2\sigma(I)$], GooF 0.938. Crystals were coated in oil, mounted on a fibre,[15] and data collected on an Enraf−Nonius KappaCCD at 123 K with Mo-K_α radiation (λ = 0.71073Å). The structure was solved by direct methods (SHELXS-97)[16] and refined by full-matrix least-squares on F^2 using the X-Seed interface.[17] All H atoms were placed in calculated positions (C−H 0.95 Å) and included in the final least-squares refinement. All other atoms were located and refined anisotropically. The absolute stereochemistry could not be accurately determined since the Flack parameter was indeterminate and the final assignment was based on a knowledge of the starting materials.

CCDC-197094 contains the supplementary crystallographic data for this paper. These data can be obtained free of charge at www.ccdc.cam.ac.uk/conts/retrieving.html [or from the Cambridge Crystallographic Data Centre, 12, Union Road, Cambridge CB2 1EZ, UK; Fax: (internat.) +44-1223/336-033; E-mail: deposit@ccdc.cam.ac.uk].

Synthesis of (*S,S*)-2: Et_3Al (5 mmol, 5 mL of a 1 M solution in hexanes) was added to a toluene solution of (*S*)- α-(methylbenzyl)-benzylamine (5 mmol, 1.05 mL) and heated to 120 °C for 6 h. On cooling to room temperature this was then added to a chilled (−30 °C) equimolar toluene solution of (*S*)-**1**, prepared by the method previously described for (*R*)-**1**.[11] The reaction mixture was allowed to warm slowly to room temperature and stirred overnight before being placed in the freezer at −25 °C. After approximately one week a moderate crop of yellow crystals were obtained. These were isolated and washed with cold toluene. A further crop of crystals were obtained after a further duration at 4 °C. These were analytically identical to the first crop. Yield 32% (1.1 g), m.p. 142−144 °C (decomp. to dark red melt). ^{1}H NMR (300 MHz, 25 °C, [D_6]benzene): δ = 7.79 (d, 2 H, *o*), 7.73 (d, 2 H, *o*), 7.34 (m, 4 H, *m*), 7.15 (m, 2 H, *p*), 4.84 (s, 1 H, C=C*H*), 4.68 (d, 1 H, PhCH_2), 4.47 [q, 3 H, Ph(Me)C*H*), 4.40 (d, 1 H, *i*Pr-C*H*), 4.06 (d, 1 H, PhCH_2), 3.95 (q, 2 H, CH_2O···Li), 3.66 (q, 2 H, CH_2O), 2.45 (m, 1 H, Me_2CH), 1.87 (m, 6 H, $AlCH_2CH_3$), 1.80 (br., 3 H, PhC(*Me*)H], 1.79, 1.71, 1.65, 1.58 (br., 4 × s, 23 H, pmdta), 1.39 (d, 3 H, Me_2CH), 1.00 (d, 3 H, Me_2CH), 0.68 (m, 4 H, $AlCH_2CH_3$) ppm. ^{13}C NMR (75.5 MHz, 25 °C, [D_6]benzene): δ = 158.1 (*q*C), 148.1 (*q*C), 147.5 (*q*C), 128.0 (*o*CH), 127.5 (*m*CH), 123.9 (*p*CH), 123.8 (*p*CH), 81.5 (N-*C*=C), 61.7 (C=*C*-O), 61.0 (CH_2O), 58.0 [Ph*C*(Me)], 56.4 (CH_2O), 54.6 (CH_2N), 52.7 ($PhCH_2$), 51.9 (MeN), 43.8 (Me_2N), 25.4 (Me_2C), 24.5 (Me_2C), 18.4 (CH_3), 14.0 (CH_3), 11.1 (CH_2Al) ppm. $C_{35}H_{68}AlLiN_6O_2$ (638.9): calcd. C 68.20, H 9.98, N 12.23; found C 67.89, H 9.79, N 12.07.

 © 2003 Wiley-VCH Verlag GmbH & Co. KGaA, Weinheim

Acknowledgments

We thank the Australian Research Council and Monash University for financial support.

[1] [1a] H. Yamamoto, *Organometallics in Synthesis; A Manual (2nd Ed)*. Chap. IV (Ed.: M. Schlosser), John Wiley & Sons Ltd, UK, 2002. [1b] J. J. Eisch, *Comprehensive Organometallic Chemistry II*, Vol 11, Chap. 6 (Eds.: E. W. Abel, F. G. A. Stone, G. Wilkinson), Elsevier Science Inc, 1995. [1c] J. R. Hauske, *Comprehensive Organic Chemistry*, Vol 1. Chap. 3 (Eds.: B. M. Trost), Pergamon Press, 1991.

[2] [2a] G. Bringmann, T. Hartung, *Tetrahedron* **1993**, *49*, 7891. [2b] J. S. Cha, J. C. Lee, J. M. Kim, W. Jeong, K. S. Park, S. E. Lee, H. S. Lee, *Bull. Kor. Chem. Soc.* 1992, **13**, 581.

[3] [3a] E. Jung, S. H. Yoo, T. M. Chung, C. G. Kim, D. Y. Jung, *Inorg. Chem. Commun.* **2002**, *5*, 439. S. T. Liddle, W. Clegg, *J. Chem. Soc., Dalton Trans.* **2001**, 3549. [3b] R. E. Mulvey, *Chem. Commun.* **2001**, 1049. [3c] D. J. Linton, P. Schooler, A. E. H. Wheatley, *Coord. Chem. Rev.* **2001**, *223*, 53. R. P. Davies, *Inorg. Chem. Commun.* **2000**, *3*, 13. [3d] G. Manickam, G. Sundararajan, *Tetrahedron* **1999**, *55*, 2721. [3e] M. A. Beswick, N. Choi, C. N. Harmer, A. D. Hopkins, M. Mepartlin, M. A. Paver, P. R. Raithby, A. Steiner, M. Tombul, D. S. Wright, *Inorg. Chem.* **1998**, *37*, 2177.

[4] [4a] D. A. Atwood, D. Rutherford, *Main Group Chem.* **1997**, *2*, 5. [4b] D. Rutherford, D. A. Atwood, *J. Am. Chem. Soc.* **1996**, *118*, 11535. [4c] D. A. Atwood, D. Rutherford, *Organometallics* **1996**, *15*, 436. [4d] M. A. Petrie, K. Ruhlandt-Senge, P. P. Power, *Inorg. Chem.* **1993**, *32*, 1135.

[5] D. R. Armstrong, F. J. Craig, A. R. Kennedy, R. E. Mulvey, *J. Organomet. Chem.* **1998**, *550*, 355.

[6] E. Horchler, E. Parisini, H. W. Roesky, H.-G. Schmidt, M. Noltemeyer, *J. Chem. Soc., Dalton Trans.* **1997**, 2761.

[7] D. R. Armstrong, R. P. Davies, D. J. Linton, R. Snaith, P. Schooler, A. E. H. Wheatley, *J. Chem. Soc., Dalton Trans.* **2001**, 2838.

[8] [8a] P. C. Andrews, G. D. Fallon, M. Maguire, A. C. Peatt, *Angew. Chem. Int. Ed.* **2000**, *39*, 4516. [8b] P. C. Andrews, P. J. Duggan, G. D. Fallon, T. D. McCarthy, A. C. Peatt, *J. Chem. Soc., Dalton Trans.* **2000**, 2505. [8c] P. C. Andrews, P. J. Duggan, G. D. Fallon, T. D. McCarthy, A. C. Peatt, *J. Chem. Soc., Dalton Trans.* **2000**, 1937.

[9] See, for example. [9a] S. G. Davies, G. D. Smyth, *J. Chem. Soc., Perkins Trans. 1* **1996**, 2467. S. G. Davies, O. Ichihara, *Tetrahedron: Asymmetry* **1996**, *7*, 1919. [9b] S. G. Davies, D. J. Dixon, *Chem. Commun.* **1996**, 1797. [9c] S. G. Davies, G. Bhalay, *Tetrahedron: Asymmetry* **1996**, *7*, 1959. S. G. Davies, D. R. Fenwick, *J. Chem. Soc., Chem. Commun.* **1995**, 1109. [9d] S. G. Davies, A. S. I. Walters, *J. Chem. Soc., Perkins Trans. 1* **1994**, 1129.

[10] [10a] U. Schöllkopf, D. Pettig, E. Schulze, M. Klinge, E. Egert, B. Benecke, M. Noltemeyer, *Angew. Chem. Int. Ed. Engl.* **1988**, *27*, 1194. [10b] D. Pettig, U. Schöllkopf, *Synthesis* **1988**, 173; U. Schöllkopf, J. Schröder, *Liebigs Ann. Chem.* **1988**, 87. [10c] U. Schöllkopf, W. Kühnle, E. Egert, M. Dyrbusch, *Angew. Chem. Int. Ed. Engl.* **1987**, *26*, 480.

[11] P. C. Andrews, M. Maguire, E. Pombo-Villar, *Helv. Chim. Acta* **2002**, *85*, 3516−3524.

[12] E. K. Styron, C. H. Lake, D. H. Powell, C. L. Watkins, L. K. Krannich, *Polyhedron* **2002**, *21*, 1747 and references therein.

[13] W. Clegg, S. T. Liddle, K. W. Henderson, F. E. Keenen, A. R. Kennedy, A. E. McKeown, R. E. Mulvey, *J. Organomet. Chem.* **1999**, *572*, 283.

[14] E. K. Styron, C. H. Lake, C. L. Watkins, L. K. Krannich, *Organometallics* **1998**, *17*, 4319.

[15] D. Stalke, *Chem. Soc. Rev.* **1998**, *27*, 171−178.

[16] SHELXS-97, Program for the Solution of Crystal Structures, G. M. Sheldrick, 1997, Göttingen, Germany.

[17] XSEED: A graphical interface for use with the SHELXS program suite, L. J. Barbour, University of Missouri, 1999.

Received April 3, 2003

 © 2003 Wiley-VCH Verlag GmbH & Co. KGaA, Weinheim

Synthesis and Structure of $[\{(THF)_2Li\}_3Me_2Al\{(PhNH)_2(PhN)_4P_3N_3\}]$, the First Mixed-Metal Phosphazenate Complex

Frederic Rivals[a] and Alexander Steiner*[a]

In memory of Ron Snaith

Keywords: Phosphazenes / Phosphazenates / Aluminium / Lithium / Heterometallic complexes

Reaction of the trilithium phosphazenate $[\{(THF)_2Li\}_3\{(PhNH)_3(PhN)_3P_3N_3\}]$ with one equivalent of trimethylaluminium yields the first mixed-metal phosphazenate complex $[\{(THF)_2Li\}_3Me_2Al\{(PhNH)_2(PhN)_4P_3N_3\}]$. X-ray structure analysis showed that the Me_2Al group is accommodated in an N(exo)–P–N(exo) chelation site of the phosphazenate ligand. Two lithium ions reside in N(ring)–P–N(exo) sites, while the third lithium ion interacts with the ligand solely via an N(ring) atom. NMR spectroscopic data obtained from THF solution indicate a fluxional behaviour of the lithium ions, which oscillate between mono- and bidentate coordination sites.

(© Wiley-VCH Verlag GmbH & Co. KGaA, 69451 Weinheim, Germany, 2003)

Introduction

Multianionic ligand systems containing extended arrays of coordination sites often enable the accommodation of well-defined and kinetically stable multinuclear metal ion and mixed-metal ion arrangements. Prominent examples are multianionic calixarinates[1] and calixpyrrolates[2] comprising cyclic structures of repeating monoanionic phenolate and pyrrolate units, respectively. Recently, we introduced phosphazenates as multianionic ligands. They are assembled from repeating tridentate dianionic $[-N{=}P(NR)_2-]^{2-}$ units and facilitate the accommodation of large numbers of metal ions around the ligand backbone in a variety of bi- and tridentate coordination sites.[3] The highly selective sequential deprotonation patterns of the multiprotic phosphazene precursors enable the synthesis of well-defined partially metallated phosphazenate complexes. For example, threefold deprotonation of the hexaprotic phosphazene $(PhNH)_6P_3N_3$ (**1**) by *n*BuLi occurs in a *cis*-fashion yielding the monomeric trilithium phosphazenate $[\{(THF)_2Li\}_3\{(PhNH)_3(PhN)_3P_3N_3\}]$ (**2**), which hosts three lithium ions in alternating N(ring)−P−N(exo) chelation sites on one face of the central phosphazenate ring.[4] The other face of the ring is equipped with three protonated N(exo) functions. Organoaluminium compounds were also applied as metallating agents. Trimethylaluminium fully deprotonates $(CyNH)_6P_3N_3$ to give the monomeric pentanuclear organoaluminium complex $[(THFMeAl)(Me_2Al)_4\{(CyN)_6P_3N_3\}]$ (**3**). All five Al atoms in **3** occupy bidentate chelation sites.[5] Threefold deprotonation generates the trinuclear complex $[(Me_2Al)_3\{(CyNH)_3(CyN)_3P_3N_3\}]$.[3a] The characteristic sequential metallation pattern leading to multinuclear metal phosphazenates is an ideal platform for the preparation of mixed-metal complexes by subsequent treatment of multiprotic phosphazenes with different metallating agents. Herein, we discuss further metallation of the trilithium complex **2** with Me_3Al. This reaction yields the complex $[\{(THF)_2Li\}_3Me_2Al\{(PhNH)_2(PhN)_4P_3N_3\}]$ (**4**), the first example of a mixed-metal phosphazenate.

Results and Discussion

The trilithium phosphazenate **2** reacts with one equivalent of trimethylaluminium in THF as indicated by the appearance of a doublet at $\delta = 3.7$ ppm and a triplet at $\delta = 7.9$ ppm, with an intensity ration of 2:1, in the ^{31}P NMR spectrum. The reaction product was crystallised from THF solution and an X-ray structure analysis showed the formation of the monomeric complex $[\{(THF)_2Li\}_3Me_2Al\{(PhNH)_2(PhN)_4P_3N_3\}]$ (**4**; Figure 1). In addition, the crystal lattice contains two non-bonded THF molecules per formula unit. The crystal structure reveals that one NH group of **2** has been deprotonated by Me_3Al, with evolution of methane (Scheme 1). One exocyclic N−P−N unit chelates the resulting Me_2Al group by forming a planar four-membered PN_2Al ring system. Both N−Al bonds are of equal length (selected bond lengths and angles are listed in Table 1). The chelation of an Me_2Al group in an exocyclic N−P−N site of a phosphazenate ligand also occurs in the solid-state structure of the pentaalu-

[a] Department of Chemistry, University of Liverpool
Crown Street, Liverpool L69 7ZD, UK
Fax: (internat.) +44-151/794-3588
E-mail: a.steiner@liv.ac.uk

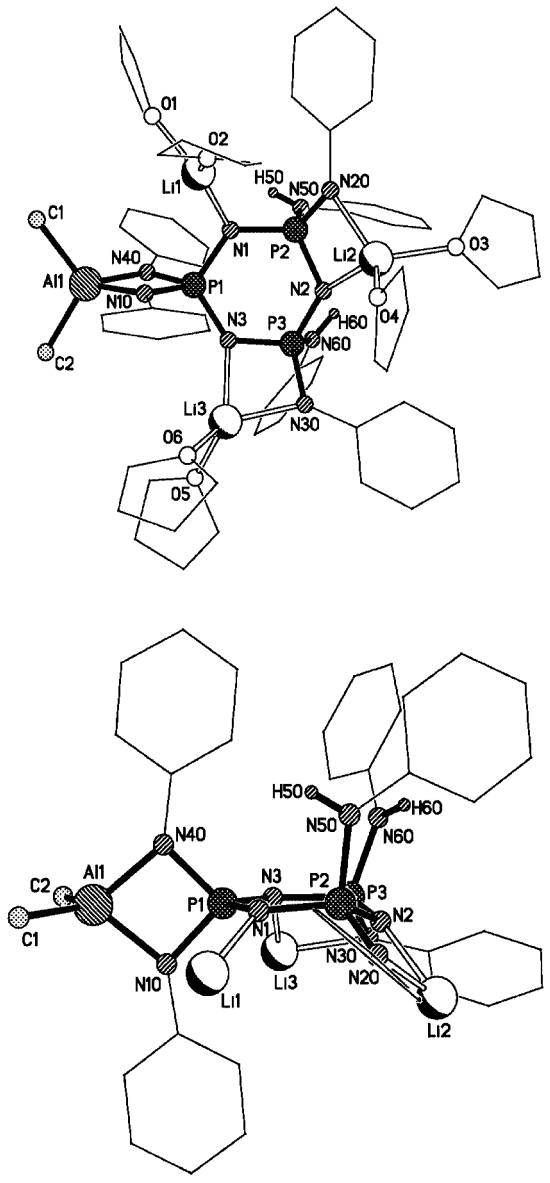

Figure 1. Two different orientations of the crystal structure of **4**; the THF molecules have been omitted from the bottom diagram for clarity

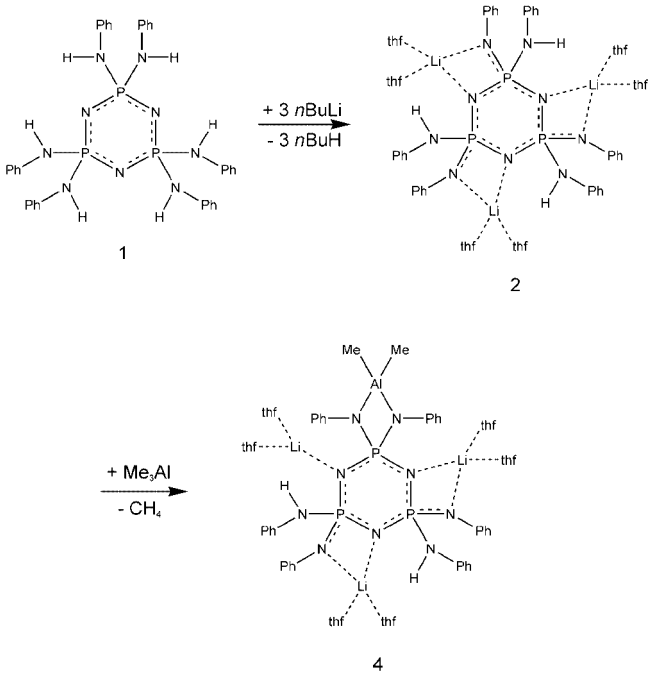

Scheme 1. Mixed metallation pathway leading to complex **4**

Table 1. Selected bond lengths [Å] and angles [°] for **4**

P1−N1	1.622(3)	N1−P1−N3	113.3(2)
P1−N3	1.605(3)	N10−P1−N40	89.8(2)
P1−N10	1.666(3)	N1−P1−N10	111.1(2)
P1−N40	1.659(3)	N1−P2−N2	113.9(2)
P2−N1	1.618(3)	N20−P2−N50	111.0(2)
P2−N2	1.618(3)	N2−P2−N20	102.6 (2)
P2−N20	1.593(3)	N2−P3−N3	114.2(2)
P2−N50	1.709(2)	N30−P3−N60	111.8(2)
P3−N2	1.611(3)	N3−P3−N30	102.7(2)
P3−N3	1.616(3)	P1−N1−P2	123.6(2)
P3−N30	1.595(3)	P2−N2−P3	118.5(2)
P3−N60	1.701(3)	P1−N3−P3	125.6(2)
Al1−N10	1.903(3)	N10−Al1−N40	76.2(2)
Al1−N40	1.900(3)	C1−Al1−C2	112.4(2)
Li1−N1	1.989(7)	P1−N10−Al1	96.7(2)
Li2−N2	2.065(6)	P1−N40−Al1	97.1(2)
Li2−N20	2.031(6)		
Li3−N3	2.099(7)		
Li3−N30	2.021(8)		

minium phosphazenate **3**.[5] The two lithium ions Li2 and Li3 reside in the N(ring)−P−N(exo) sites of **4**, while Li1 is interacting with the ligand solely via an N(ring) atom. In addition, each lithium ion is coordinated by two THF molecules. This results in a trigonal planar coordination at Li1 and distorted tetrahedral environments at Li2 and Li3. The Li−N(ring) distance at Li1 is shorter than the Li−N distances of Li2 and Li3, reflecting the low coordination number of Li1. Within the bidentate chelates Li−N(exo) bonds are slightly shorter than Li−N(ring) bonds. The coordination of Li2 and Li3 is similar to that of the lithium ions in the C_3 symmetrical precursor complex **2**.[4] In **4** there are no interactions between the Al-coordinated N(exo) centres and the lithium ions, presumably due to the strong acceptor behaviour of the aluminium atom. This reduces the number of N-donor sites available for Li coordination. As a result, the ligand provides only a monodentate interaction to one of the lithium ions.

The central P_3N_3 ring in **4** adopts a half-chair conformation. The ring atom N2 deviates by 0.43 Å from the planar arrangement of the other five ring atoms. The P−N(ring) bond lengths are similar throughout the ring, ranging from 1.605(3) to 1.622(3) Å. Conversely, the P−N(exo) bond lengths have a broader range: short P−N(exo) bonds are found at lithiated N(exo) positions [P−N(Li) 1.593(3), 1.595(3) Å], while P−N(exo) bonds within the chelate coordinating Al1 are of intermediate length [P−N(Al) 1.659(3), 1.666(3) Å] and P−N(exo) bonds associated with NH functions are relatively long [P−N(H) 1.701(3), 1.709(3) Å]. Equally short P−N(Li)

 © 2003 Wiley-VCH Verlag GmbH & Co. KGaA, Weinheim

bonds and long P−N(H) bonds were observed in **2**, but somewhat shorter P−N(H) bonds were found in the hexaprotic phosphazene **1**.[6] Interestingly, the average P−N bond length of the four P−N bonds surrounding one phosphorus atom is almost the same for all three P atoms (av. P−N at P1: 1.638, at P2: 1.635 and at P3: 1.631 Å). This cooperative "seesaw" effect suggests that the P−N bond orders within each PN_4 tetrahedron vary, but the overall sum of P−N bond orders around each P atom is finely balanced. A similar effect has been observed for the S−N bonds in iminosulfonate complexes.[7] The shortness of the P−N(Li) bonds indicates delocalisation of the negative charge from the P−N(Li) onto the P−N(ring) bond and a mainly ionic character of the N−Li interactions. This extra amount of negative charge around the PN_4 tetrahedra is compensated by an elongation of the P−N(H) bond. On the other hand the N−Al bonds in **4** are covalent, as indicated by P−N(Al) bonds of intermediate lengths. The range of exocyclic N−P−N angles mirrors the flexibility of the phosphazenate ligand towards metal coordination. The N−P−N angle of the exocyclic chelate hosting the aluminium centre is very sharp [89.9(2)°] compared to the other two exocyclic N−P−N angles [111.0(2), 111.8(2)°]. The N−P−N angles within the ring are similar and range from 113.3(2)° to 114.2(2)°. The two N(ring)−P−N(exo) angles of lithium binding chelates are identical [102.6(2), 102.7(2)°], but not as acute as that of the Al binding site.

A variety of complexes containing both lithium and aluminium centres have been described,[8] although the accommodation of three Li and one Al centre around one ligand system has not been reported so far. The coordination modes exhibited in **4** are closely related to those of other ligands containing N−P−N chelates.[3a] Several metal complexes have been described featuring four-membered PN_2M ring systems where M is either Li[9] or Al.[10] Monodentate coordination of N-donor ligands towards tricoordinate lithium ions in monomeric complexes, like Li1 in **4**, is usually achieved by bulky ligands with sterically demanding substituents.[11] On the contrary, the phosphazenate ligand **4** gains its steric demand by accommodating a larger number of metal ions rather than providing bidentate chelation sites.

In contrast to the solid-state structure, which contains three chemically different phosphorus nuclei, the ^{31}P NMR spectrum of a solution of complex **4** in THF exhibits an AX_2 system. Variable-temperature NMR studies were hampered by the low solubility of **4** in THF at low temperatures. However, NMR spectroscopic data obtained from measurements at room temperature suggest a fluctuating behaviour of the lithium ions in solution, as illustrated in Scheme 2. The three lithium ions oscillate in a concerted manner around the three N(ring) and the two lithiated N(exo) sites. The two chemically equivalent lithium ions, Li^a, oscillate between a bidentate N(ring)−P−N(exo) chelate and the monodentate N(ring) site, whilst Li^b oscillates between two neighbouring N(ring)−P−N(exo) sites. This mechanism is backed up by the ^7Li NMR spectrum, which consists of two signals at δ = 2.83 and 3.40 ppm displaying an intensity

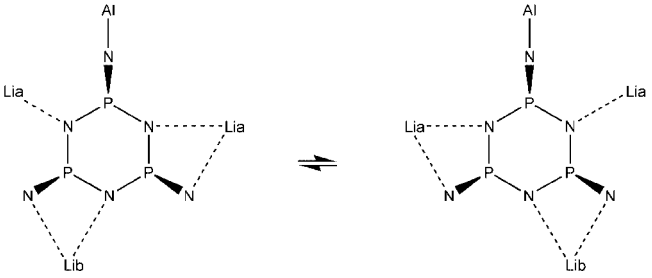

Scheme 2. Proposed mechanism of fluctuation of lithium ions within complex **4** in THF solution (for clarity, only P, Al, Li and coordinating N atoms are shown)

ratio of 2:1. Also, four sets of chemically distinct phenyl groups are evident from the ^{13}C NMR spectrum, reflecting the mirror symmetry of the fluctuating structure. These four sets consist of: (i) the two PhNH groups, (ii) the two PhNLi groups, (iii) the PhNAl group at the "NH face" of the phosphazenate ring, and (iv) the PhNAl group at the "NLi face" of the ring. The ^1H NMR spectrum exhibits one singlet at δ = −0.89 ppm for the Me_2Al, unit indicating the chemical equivalence of both methyl groups, and one signal at δ = 6.21 ppm for the two NH groups.

Further metallation of the phosphazenate ligand in **4** appears possible, since it holds two potentially acidic NH functions. The stepwise addition of excess Me_3Al to **2** was monitored by ^{31}P NMR spectroscopy (Figure 2). The familiar AX_2 pattern of **4** emerges upon addition of one equivalent Me_3Al. After further addition of Me_3Al several other species appear, exhibiting either an AX_2 or AXY pattern, indicating the presence of either two or three distinct phosphorus nuclei. So far, we have been unsuccessful in isolating mixed Li-Al complexes showing higher metallation grades than **4**. Moreover, complex **4** proved to be a rather stable member of a possible series of mixed Li-Al phosphazenates, since higher metallated species slowly degrade in THF solu-

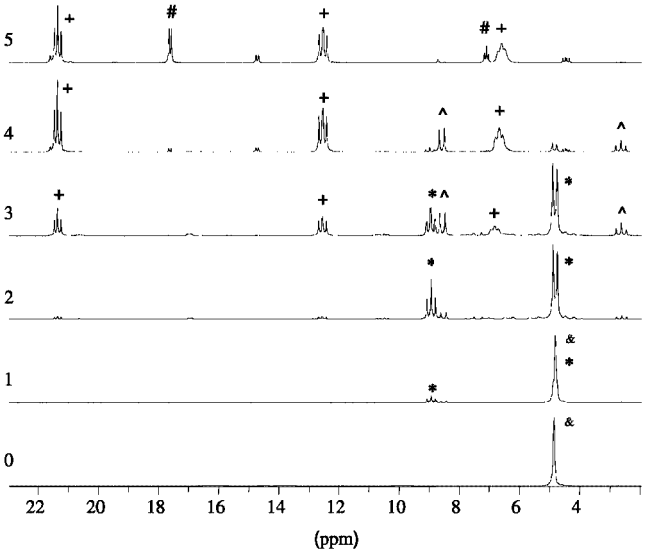

Figure 2. ^{31}P NMR spectrum of stepwise reaction of **2** with *n* equivalents of Me_3Al in THF at room temperature; & represents complex **2** and * complex **4**; +, ^ and # indicate further metalated species

 © 2003 Wiley-VCH Verlag GmbH & Co. KGaA, Weinheim

tion to give **4**. The fluctuating behaviour of lithium ions could be a stabilising factor for **4**.

In summary, we have presented the first phosphazenate complex that accommodates a mixed-metal array. The synthesis of the mixed Li-Al complex was achieved by successive deprotonation of a hexaprotic phosphazene with *n*BuLi and Me_3Al. It looks as if a variety of other stable mixed-metal species can be generated by exploiting the selective metalation pattern of multiprotic phosphazenes. Metal ions and organometallic fragments occupy specific coordination sites around the phosphazenate core. The ligand provides both rigid metal chelation and allows a fluctuating behaviour of the metal ions within the ligand sphere. This concept could lead to tailor-made, mixed-metal complexes for homogeneous catalysis.

Experimental Section

All synthetic procedures were carried out under a dry N_2 atmosphere. Compounds **1**[6] and **2**[4] were prepared according to literature methods. Organometallic reagents were applied as standard solutions: *n*BuLi (1.6 M in hexane) and Me_3Al (2 M in hexane).

Synthesis of 4: *n*BuLi (0.85 mL, 1.35 mmol) was added at −78 °C to a solution of **1** (300 mg, 0.45 mmol) in 20 mL of THF. After stirring for one hour at room temperature, Me_3Al (0.22 mL, 0.45 mmol) was added dropwise and the solution was stirred overnight at room temperature. Subsequently the reaction solution was filtered and the volume of the filtrate reduced by half in vacuo. Single crystals were obtained after three days. In the absence of mother liquor the crystals degrade to give a white powder. Yield 215 mg (73%). ^{1}H NMR (300 MHz, [D$_8$]THF SiMe$_4$): δ = −0.87 (s, 3 H, AlC*H*$_3$), 6.21 (br., 2 H, N*H*), 6.98−6.51 (m, 30 H, Ph) ppm. ^{7}Li NMR [97.16 MHz, THF, $(CD_3)_2CO$, LiCl in D_2O ext.] δ = 2.83 (2 Li), 3.40 (Li) ppm. $^{13}C\{^1H\}$ NMR (75.46 MHz, [D$_8$]THF, SiMe$_4$): δ = −9.94 (Me_2Al), 113.6, 114.7, 115.3, 116.7 (*ortho*), 117.4, 120.0, 120.1, 120.2 (*para*), 127.6, 127.7, 127.8 128.1, (*meta*), 143.8, 148.5, 148.7, 153.1 (*C*N) ppm. ^{31}P NMR (101.25 MHz, [D$_8$]THF, 85% H_3PO_4 in D_2O ext.): δ = 3.7 (t, $^2J_{P,P}$ = 21.8 Hz, 1 P), 7.9 (d, $^2J_{P,P}$ = 21.8 Hz, 2 P) ppm. IR (nujol): $\tilde{\nu}$ = 3380.5 (N−H), 1588.2, 1335.3, 1300.2, 1242.5, 1109.2 (P−N), 1073.5, 1030.9, 1005.9, 891.9, 860.8, 797.2, 748.6, 692 cm^{-1}. $C_{62}H_{86}AlLi_3N_9O_6P_3$ (1193.62): calcd. C 62.4, H 7.26, N 10.6; found C 62.0, H 7.01, N 11.1.

Crystal data for **4**·2THF were recorded on a Stoe-IPDS diffractometer using Mo-K_α radiation (λ = 0.71073 Å), T = 200 K. The structure was solved by direct methods and refined by full-matrix least-squares against F^2 using all data (SHELX-97). $C_{70}H_{102}AlLi_3N_9O_8P_3$: M = 1338.32, triclinic, $P\bar{1}$, a = 12.431(2), b = 14.467(2), c = 23.663(4) Å, α = 91.97(2)°, β = 101.62(2)°, γ = 114.46(2)°, V = 3760.9(9) Å^3, Z = 2, D_c = 1.182, μ(Mo-K_α) = 0.147, number of reflections: 23726 (total), 11018 (unique), R_{int} = 0.057, R_1 [$I > 2\sigma(I)$] = 0.057, wR_2 (all data) = 0.160. One THF molecule bonded to Li3 and the two non-bonded lithium ions are disordered over two positions and were refined using similar distance and similar U restraints. Non-hydrogen atoms were refined anisotropically, except for the disordered positions, which were treated isotropically. H-atoms were placed geometrically in accordance with the hybridisation of their parent atoms.

CCDC-208395 contains the supplementary crystallographic data for this paper. These data can be obtained free of charge at www.ccdc.cam.ac.uk/conts/retrieving.html [or from the Cambridge Crystallographic Data Centre, 12, Union Road, Cambridge CB2 1EZ, UK; Fax: (internat.) +44-1223/336-033; E-mail: deposit@ccdc.cam.ac.uk].

Acknowledgments

This work was supported by EPSRC and The Royal Society.

[1] [1a] C. Floriani, *Chem. Eur. J.* **1999**, *5*, 19. [1b] C. Floriani, R. Floriani-Moro, *Adv. Organomet. Chem.* **2001**, *47*, 167. [1c] G. Guillemot, E. Solari, C. Rizzoli, C. Floriani, *Chem. Eur. J.* **2002**, *8*, 2072. [1d] J. M. Smith, S. G. Bott, *Chem. Commun.* **1996**, 377.

[2] [2a] T. Dube, G. Jingwen, S. Gambarotta, G. P. A. Yap, *Chem. Eur. J.* **2001**, *7*, 374. [2b] T. Dube, S. Gambarotta, G. P. A. Yap, *Organometallics* **2000**, *19*, 817. [2c] S. De Angelis, E. Solari, C. Floriani, A. Chiesi-Villa, C. Rizzoli, *J. Chem. Soc., Dalton Trans.* **1994**, 2467.

[3] [3a] A. Steiner, S. Zacchini, P. I. Richards, *Coord. Chem. Rev.* **2002**, *227*, 193. [3b] F. Rivals, A. Steiner, *Chem. Commun.* **2001**, 1426. [3c] V. Chandrasekhar, S. Nagendran, *Chem. Soc. Rev.* **2001**, *30*, 193.

[4] G. T. Lawson, F. Rivals, M. Tascher, C. Jacob, J. F. Bickley, A. Steiner, *Chem. Commun.* **2000**, 341.

[5] G. T. Lawson, C. Jacob, A. Steiner, *Eur. J. Inorg. Chem.* **1999**, 1881.

[6] J. F. Bickley, R. Bonar-Law, G. T. Lawson, P. I. Richards, F. Rivals, A. Steiner, S. Zacchini, *Dalton Trans.* **2003**, 1235−1244.

[7] B. Walfort, A. P. Leedham, C. A. Russell, D. Stalke, *Inorg. Chem.* **2001**, *40*, 5668.

[8] See for example: [8a] M. Driess, S. Kuntz, C. Monse, K. Merz, *Chem. Eur. J.* **2000**, *6*, 4343. [8b] R. E. Allan, M. A. Beswick, P. R. Raithby, A. Steiner, D. S. Wright, *J. Chem. Soc., Dalton Trans.* **1996**, 4153. [8c] J. K. Brask, T. Chivers, G. Schatte, M. Krahn, *Organometallics* **2000**, *19*, 5683. [8d] A. Heine, D. Stalke, *Angew. Chem. Int. Ed. Engl.* **1992**, *31*, 854. [8e] M. Veith, M. Jarczyk, V. Huch, *Angew. Chem. Int. Ed.* **1998**, *37*, 105. [8f] H. Nöth, A. Schlegel, J. Knizek, I. Krossing, W. Ponikwar, T. Seifert, *Chem. Eur. J.* **1998**, *4*, 2191. [8g] J. Storre, C. Schnitter, H. W. Roesky, H.-G. Schmidt, M. Noltemeyer, R. Fleischer, D. Stalke, *J. Am. Chem. Soc.* **1997**, *119*, 7505. [8h] W. Uhl, J. Molter, R. Koch, *Eur. J. Inorg. Chem.* **1999**, 2021. [8i] P. Böttcher, H. W. Roesky, M. G. Walawalkar, H.-G. Schmidt, *Organometallics* **2001**, *20*, 790. [8j] H. Nöth, A. Schlegel, M. Suter, *J. Organomet. Chem.* **2001**, *621*, 231.

[9] [9a] A. Steiner, D. Stalke, *Inorg. Chem.* **1993**, *32*, 1977. [9b] P. R. Raithby, C. A. Russell, A. Steiner, D. S. Wright, *Angew. Chem. Int. Ed. Engl.* **1997**, *36*, 649. [9c] L. T. Burke, E. Hevia-Freire, R. Holland, J. C. Jeffrey, A. P. Leedham, C. A. Russell, A. Steiner, A. Zagorski, *Chem. Commun.* **2000**, 1769. [9d] L. Stahl, *Coord. Chem. Rev.* **2000**, *210*, 203. [9e] I. Schranz, L. Stahl, R. J. Staples, *Inorg. Chem.* **1998**, *37*, 1493. [9f] G. G. Briand, T. Chivers, M. Krahn, *Coord. Chem. Rev.* **2002**, *233*, 237. [9g] A. Armstrong, T. Chivers, M. Krahn, M. Parvez, G. Schatte, *Chem. Commun.* **2002**, 2332. [9h] B. Eichhorn, H. Nöth, T. Seifert, *Eur. J. Inorg. Chem.* **1999**, 2355. [9i] E. Niecke, M. Frost, M. Nieger, V. von der Gönna, A. Ruban, W. W. Schoeller, *Angew. Chem. Int. Ed. Engl.* **1994**, *33*, 2111. [9j] R. Detsch, E. Niecke, M. Nieger, W. W. Schoeller, *Chem. Ber.* **1992**, *125*, 1119. [9k] A. Steiner, D. S. Wright, *Angew. Chem. Int. Ed. Engl.* **1996**, *35*, 636. [9l] A. Steiner, D. S. Wright, *Chem. Commun.* **1997**, 283.

[10] [10a] L. Mahalakshmi, D. Stalke, *Struct. Bonding* **2002**, *103*, 85. [10b] G. R. Lief, C. J. Carrow, L. Stahl, R. J. Staples, *Organometallics* **2001**, *20*, 1629. [10c] P. Blais, T. Chivers, G. Schatte, M. Krahn, *J. Organomet. Chem.* **2002**, *646*, 107. [10d] M. Veith, M. Kross, J.-F. Labarre, *J. Mol. Struct.* **1991**, *248*, 345. [10e] P. B. Hitchcock, H. A. Jasim, M. F. Lappert, H. D. Williams, *J. Chem. Soc., Chem. Commun.* **1986**, 1634. [10f] A. N. Chernega,

 © 2003 Wiley-VCH Verlag GmbH & Co. KGaA, Weinheim

M. Yu. Antipin, Yu. T. Struchkov, I. E. Boldeskul, V. F. Shul′gin, V. D. Romanenko, *Zh. Strukt. Chim.* **1985**, *26*, 120. [10g] P. Braunstein, R. Hasselbring, D. Stalke, *New J. Chem.* **1996**, *20*, 337.

[11] [11a] K. Gregory, P. v. R. Schleyer, R. Snaith, *Adv. Inorg. Chem.* **1991**, *37*, 47. [11b] R. E. Mulvey, *Chem. Soc. Rev.* **1991**, *20*, 167. [11c] H. Chen, R. A. Bartlett, H. V. R. Dias, M. M. Olmstead, P. P. Power, *J. Am. Chem. Soc.* **1989**, *111*, 4338. [11d] M. Westerhausen, M. Wieneke, H. Nöth, T. Seifert, A. Pfitzner, W. Schwarz, O. Schwarz, J. Weidlein, *Eur. J. Inorg. Chem.* **1998**, 1175.

Received April 16, 2003
Early View Article
Published Online July 17, 2003

 © 2003 Wiley-VCH Verlag GmbH & Co. KGaA, Weinheim

Cooperative THF Ring-Opening by $B(C_6F_5)_3$ and a Tellurium Diimide Dimer

Tristram Chivers*[a] and Gabriele Schatte[a]

Dedicated to the memory of Professor Ron Snaith

Keywords: N ligands / Ring opening / Lewis acids / Boron / Tellurium

The tellurium diimide dimer [*t*BuNTe(μ-N*t*Bu)$_2$TeN*t*Bu] (**1**) and $B(C_6F_5)_3$ form a 1:1 adduct which instigates THF ring-opening to give [*t*BuNTe(μ-N*t*Bu)$_2$TeN(*t*Bu)$(CH_2)_4OB(C_6F_5)_3$] (**3**) quantitatively; complex **3** is also formed rapidly when **1** is added to a THF solution of $B(C_6F_5)_3$.

(© Wiley-VCH Verlag GmbH & Co. KGaA, 69451 Weinheim, Germany, 2003)

The perfluorinated borane $B(C_6F_5)_3$ was first reported in 1963.[1] During the past decade this strong Lewis acid has attracted wide attention as a co-catalyst for olefin polymerization.[2] While early work established that $B(C_6F_5)_3$ forms 1:1 adducts with NH_3 and NMe_3,[1] more recent studies with nitrogen bases have included cyano derivatives,[3] imidazole,[4] pyridines,[5] amines,[6] and the anions CN^- [7] and NH_2^-.[8] As part of our studies of the Lewis base behaviour of the tellurium diimide dimer *t*BuNTe(μ-N*t*Bu)$_2$TeN*t*Bu (**1**),[9] we have investigated the reaction of this bidentate ligand with $B(C_6F_5)_3$. We report here the formation of the 1:1 adduct **2**, which engenders rapid THF ring-opening to produce [*t*BuNTe(μ-N*t*Bu)$_2$TeN(*t*Bu)$(CH_2)_4OB(C_6F_5)_3$] (**3**). Complex **2** is also generated when **1** is added to a THF solution of $B(C_6F_5)_3$. Although various transition-metal and uranium complexes promote THF ring-opening,[10] main-group element Lewis acids are rarely involved[11,12] and, to the best of our knowledge, this is the first example involving $B(C_6F_5)_3$.

The reaction of **1** with $B(C_6F_5)_3$ in a 1:1 molar ratio in *n*-pentane at 23 °C produced the adduct **2** as a moisture-sensitive yellow-orange adduct in almost quantitative yield. The same reaction with a 1:2 molar ratio affords an equimolar mixture of **2** and $B(C_6F_5)_3$. The ^{11}B NMR chemical shift of **2** ($\delta = -6.1$ ppm) is consistent with the formation of a four-coordinate boron complex [cf. $\delta^{11}_B = 59.5$ ppm for $B(C_6F_5)_3$ in CD_2Cl_2].

An X-ray structural determination of **2**, on crystals obtained from a saturated CH_2Cl_2 solution at −20 °C, confirmed the formation of a 1:1 adduct and revealed a *cis*(*endo*, *exo*) arrangement of the exocyclic N*t*Bu groups

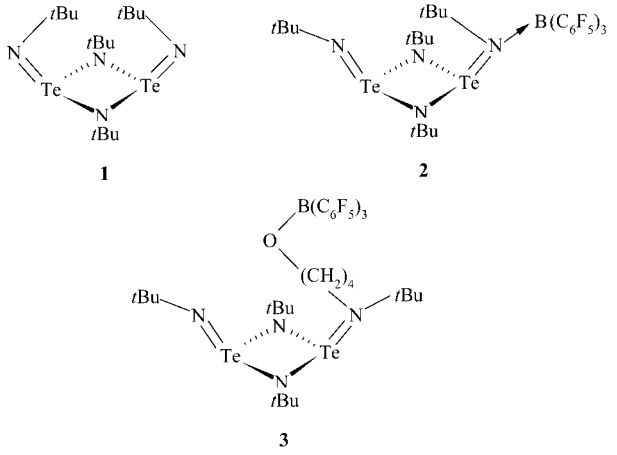

(Figure 1).[13] This conformation is also found in **1**·HCl, whereas a *cis*(*endo*, *endo*) arrangement is observed for **1** in the solid state.[14] Pertinent bond lengths and bond angles for **2** are given in the caption to Figure 1. Coordination of **1** to $B(C_6F_5)_3$ lengthens one of the exocyclic Te−N bonds involving the coordinated nitrogen by ca. 0.10 Å, whereas the other exocyclic Te−N bond is unchanged. Concomitantly, the endocyclic Te−N bond lengths involving the tellurium atom connected to the three-coordinate nitrogen are elongated by ca. 0.04 Å. The Te_2N_2 ring is puckered, with a torsion angle N(2)−Te(1)−N(1)−Te(2) of −21.17(11)°, and the geometry at the bridging N atoms is distinctly non-planar $\Sigma\angle N(1) = 344.8°$ and $\Sigma\angle N(2) = 341.3°$. The B−N bond length of 1.632(4) Å in **2** is identical to that in $(C_6F_5)_3B{\cdot}NH_2tBu$.[15] As indicated in Figure 1 the tellurium atom Te(1) engages in weak Te···F interactions [3.136(2) and 3.112(2) Å; sum of van der Waals radii is 3.53 Å[16]] with one of the *ortho*-fluorine atoms of two C_6F_5 groups. Similar intramolecular M···F contacts have been observed in transition-metal complexes.[17]

[a] Department of Chemistry, University of Calgary
Calgary, Alberta T2N 1N4, Canada
Fax: (internat.) +1-403/289-9488
E-mail: chivers@ucalgary.ca

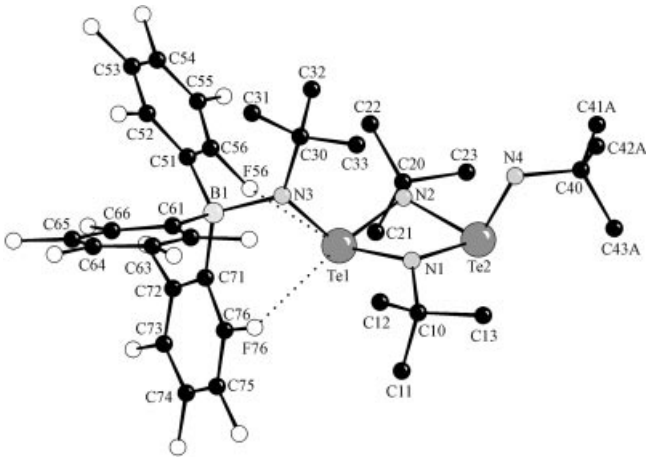

Figure 1. X-ray structure of **2** showing the weak intramolecular Te···F interactions; selected bond lengths (Å) and bond angles (deg): Te(1)−N(1) 2.035(2), Te(1)−N(2) 2.040(2), Te(1)−N(3) 1.970 (2), Te(2)−N(1) 2.061(3), Te(2)−N(2) 2.081(2), Te(2)−N(4) 1.875(3), B(1)−N(3) 1.632(4)

Surprisingly, an attempt to recrystallize **2** from THF/*n*-pentane (1:1) produced X-ray quality orange-yellow needles, within 20 min at 23 °C, of a complex identified as **3** by CHN analysis, multinuclear NMR spectroscopy and an X-ray structural analysis. The ^1H and ^{13}C NMR spectra of **3** in [D_8]THF show the characteristic ($CH_2CH_2CH_2CH_2O$) resonances of a ring-opened THF molecule[10d,11] in addition to resonances corresponding to the N*t*Bu groups. In the ^1H NMR spectrum two of these resonances are almost isochronous (δ = 1.479 and 1.477 ppm) and have a relative intensity corresponding to 27 H compared to 9 H for the third resonance at δ = 1.503 ppm. In the ^{13}C NMR spectrum three environments are readily distinguishable because of their well-separated chemical shifts. The ^{11}B NMR chemical shift of this product in [D_8]THF is δ = −3.6 ppm. Collectively, the NMR spectroscopic data suggest that complex **2** promotes THF ring-opening to give the adduct **3**, which is isolated in essentially quantitative yield. Subsequently, it was shown that **3** can also be obtained in high yield by addition of a THF solution of **1** to a solution of $B(C_6F_5)_3$ in THF at 23 °C.

X-ray crystallography[18] confirmed the molecular structure of **3** (Figure 2), with the ring-opened THF molecule linked to boron through the oxygen atom and to one of the terminal N*t*Bu groups via a carbon atom. In contrast to **2**, the $(CH_2)_4OB(C_6F_5)_3$ substituent occupies an *endo* position with respect to the Te_2N_2 ring while both terminal N*t*Bu groups are in *exo* configurations. The trends in Te−N bond lengths in **3** compared to those in **1**[14] are similar to, but less pronounced than, those described above for **2**. An interesting feature of the solid-state structure of **3** is the intermolecular Te···F interactions of 2.991(2) and 3.275(2) Å (Figure 2) that produce molecular strands parallel to the *b* axis. These strands are separated by THF solvent molecules. The shorter contact involves Te(1), which has a larger formal positive charge than Te(2) (Scheme 1). The Te_2N_2 ring in **3**, with a torsion angle of 14.0(1)°, is less puckered than that of **1** and **2**, and the geometry at the bridging nitrogen atoms is closer to planarity [$\Sigma\angle$N(1) = 352.3° and $\Sigma\angle$N(2) = 356.8°]. The B−O bond length in **3** is 1.444(5) Å {cf. 1.480(11) Å in the anion $[HOB(C_6F_5)_3]^-$}.[19]

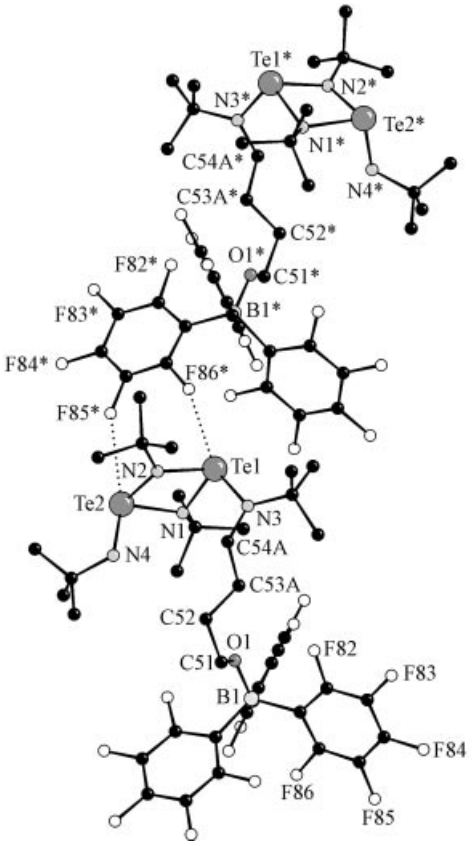

Figure 2. X-ray structure of **3** showing the weak intermolecular Te···F interactions; selected bond lengths (Å) and bond angles (deg): Te(1)−N(1) 2.020(3), Te(1)−N(2) 2.012(3), Te(1)−N(3) 1.922 (3), Te(2)−N(1) 2.036(3), Te(2)−N(2) 2.053(3), Te(2)−N(4) 1.905(3), B(1)−O(1) 1.444(5); the THF molecule in the lattice is not shown

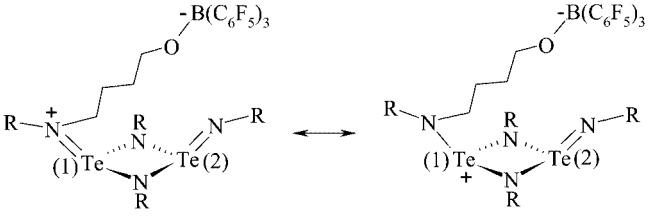

Scheme 1

The NMR spectra for **3** in [D_8]THF at 23 °C indicate that the Te···F contacts are not maintained in solution. Thus, the ^{19}F NMR spectrum shows only one set of resonances at δ = 131.3, 163.8 and 166.7 ppm, corresponding to the *ortho*, *para* and *meta* fluorine atoms, respectively, of the three C_6F_5 groups. By contrast, the complex NMR spectra for **2** in CD_2Cl_2 at 23 °C indicate intramolecular Te···F interactions. Thus, the ^{19}F NMR spectrum exhibits multiple resonances in each of the regions characteristic of *ortho*,

 © 2003 Wiley-VCH Verlag GmbH & Co. KGaA, Weinheim

meta and *para*-fluorines of a C_6F_5 group. The ^{13}C NMR spectrum of **2** is especially difficult to assign due to numerous overlapping doublets. The ^1H NMR spectrum of **2** exhibits four equally intense singlets that are consistent with the inequivalence of the bridging N*t*Bu groups as well as the terminal N*t*Bu groups. Variable-temperature NMR studies indicated the presence of conformational isomers, but the spectra could not be unequivocally assigned.

The strong Lewis acid $B(C_6F_5)_3$ forms a complex with THF.[20] Over a few hours at room temperature, the THF is polymerized by $B(C_6F_5)_3$, as reported for some other Lewis acids, for example $AlCl_3$.[21] The addition of **1** to a freshly prepared solution of $B(C_6F_5)_3$ in THF preempts this polymerization and, instead, generates the ring-opened complex **3**. By analogy with transition-metal systems,[10] it is proposed that coordination of the THF oxygen atom to the electrophilic boron centre polarizes the C−O bond so that the α-carbon atom is susceptible to nucleophilic attack. As a result, and in contrast to the THF ring-opening mode observed for $PPh_3/TeBr_4$,[12] the carbon atom of the THF fragment is bonded to the nucleophilic centre in **3**.

Experimental Section

2: A solution of $B(C_6F_5)_3$ (0.285 g, 0.556 mmol) in *n*-pentane (20 mL) was added to an orange-red solution of sublimed [*t*BuNTe(μ-N*t*Bu)$_2$TeN*t*Bu][19] (0.300 g, 0.556 mmol) in *n*-pentane (20 mL) at −78 °C. After 3.5 h at 23 °C the solvent was removed from the reaction mixture under vacuum to give analytically pure [*t*BuNTe(μ-N*t*Bu)$_2$TeN(*t*Bu)B$(C_6F_5)_3$] (0.546 g, 0.519 mmol, 93%) as a yellow-orange solid. $C_{34}H_{36}BF_{15}N_4Te_2$ (1051.68): calcd. C 38.83, H 3.45, N 5.33; found C 38.13, H 3.24, N 4.93. All NMR spectroscopic data were recorded in CD_2Cl_2 solution at 23 °C. ^1H NMR: δ = 1.617 (s, 9 H, *t*Bu), 1.589 (s, 9 H, *t*Bu), 1.501 (s, 9 H, *t*Bu), 1.426 (s, 9 H, *t*Bu) ppm. ^{11}B NMR: δ = −6.06 (s) ppm. ^{19}F NMR: δ = −116.10 (m, *ortho*), −124.30 (m, *ortho*), −130.10 (m, *ortho*), −130.50 (m, *ortho*), −130.90 (m, *ortho*), −157.24 (m, *para*), −159.60 (m, *para*), −161.65 (m, *para*), −161.90 (m, *meta*), −164.56 (m, *meta*), −166.42 (m, *meta*), −166.88 (m, *meta*) ppm. ^{125}Te NMR: δ = 1552.9 (s) ppm.

3: A solution of **1** (0.300 g, 0.556 mmol) in THF (10 mL) was added to a solution of $B(C_6F_5)_3$ (0.285 g, 0.556 mmol) in THF (10 mL) at −78 °C. After 2 h at 23 °C the solvent was removed under vacuum to give **3**·THF (0.533 g, 0.474 mmol, 85%) as an orange solid. Analytical and spectroscopic data were obtained for crystals of **3**·THF obtained from the attempted recrystallization of **2** from THF/*n*-pentane (1:1). $C_{42}H_{52}BF_{15}N_4O_2Te_2$ (1195.89): calcd. C 42.18, H 4.38, N 4.68; found C 42.11, H 4.21, N 4.61. All NMR spectroscopic data were recorded in [D_8]THF at 23 °C. ^1H NMR: δ = 4.02 (t, 2 H, CH_2-CH_2-CH_2-CH_2-O), 3.61 (4 H, THF, CH_2-CH_2-O), 3.17 (t, 2 H, CH_2-CH_2-CH_2-CH_2-O), 1.96 (q, 2 H, CH_2-CH_2-CH_2-CH_2-O), 1.77 (4 H, THF, CH_2-CH_2-O), 1.59 (q, 2 H, CH_2-CH_2-CH_2-CH_2-O), 1.50 (s, 9 H, *t*Bu), 1.479 and 1.477 (both s, 27 H, *t*Bu) ppm. ^{11}B NMR: δ = −3.64 (s) ppm. ^{13}C NMR: δ = 149.09 [d, $^1J_{C,F}$ = 235.0 Hz, *ortho*], 138.91 [d, $^1J_{C,F}$ = 245.9 Hz, *para*], 137.20 [d, $^1J_{C,F}$ = 249.1 Hz, *meta*], 126.64 (br, *ipso*), 68.27 (THF, CH_2-CH_2-O), 66.44 (CMe_3), 64.03 (CH_2-CH_2-CH_2-CH_2-O), 63.23 (CMe_3), 60.23 (CMe_3), 44.83 (CH_2-CH_2-CH_2-CH_2-O), 36.83 (CMe_3), 35.75 (CMe_3), 34.32 (CH_2-CH_2-CH_2-CH_2-O), 32.79 (CMe_3), 30.85 (CH_2-CH_2-CH_2-CH_2-O), 26.43 (THF, CH_2-CH_2-O) ppm. ^{19}F NMR: δ = −131.34 (m, *ortho*), −163.84 (m, *para*), −166.71 (m, *meta*) ppm. ^{125}Te NMR: δ = 1395.7 (s) ppm.

X-ray data were collected on a Nonius Kappa CCD diffractometer using Mo-K_α radiation (λ = 0.71073 Å) at 173 K. The non-hydrogen atoms were refined anisotropically. Hydrogen atoms were included at geometrically idealized positions and not refined.

Acknowledgments

The authors gratefully acknowledge financial support from the Natural Sciences and Engineering Research Council (Canada).

[1] A. G. Massey, A. J. Park, F. G. A. Stone, *Proc. Chem. Soc.* **1963**, 212.
[2] For reviews, see: [2a] W. Piers, T. Chivers, *Chem. Soc. Rev.* **1997**, *26*, 345−354. [2b] E. Y.-X. Chen, T. J. Marks, *Chem. Rev.* **2000**, *100*, 1391−1434.
[3] [3a] W. Fraenk, T. M. Klapötke, B. Krumm, P. Mayer, H. Piotrowski, M. Vogt, *Z. Anorg. Allg. Chem.* **2002**, *628*, 745−750. [3b] H. Jacobson, H. Berke, S. Döring, G. Kehr, G. Erker, R. Fröhlich, O. Meyer, *Organometallics* **1999**, *18*, 1724−1735.
[4] D. Röltger, G. Erker, R. Fröhlich, S. Kotila, *J. Organomet. Chem.* **1996**, *518*, 17−19.
[5] M. J. G. Lesley, A. Woodward, N. J. Taylor, T. B. Marder, I. Cazenobe, I. Ledoux, J. Zyss, A. Thornton, D. W. Bruce, A. K. Kakhar, *Chem. Mater.* **1998**, *10*, 1355−1365.
[6] N. Millot, C. C. Santini, B. Fenet, J. M. Basset, *Eur. J. Inorg. Chem.* **2002**, 3328−3335.
[7] S. J. Lancaster, D. A. Walker, M. Thornton-Pett, M. Bochmann, *Chem. Commun.* **1999**, 1533−1534.
[8] S. J. Lancaster, A. Rodriguez, A. Lara-Sanchez, M. D. Hannant, D. A. Walker, D. H. Hughes, M. Bochmann, *Organometallics* **2002**, *21*, 451−453.
[9] [9a] T. Chivers, M. Parvez, G. Schatte, *Angew. Chem.* **1999**, *111*, 2355−2357; *Angew. Chem. Int. Ed.* **1999**, *38*, 2217−2219. [9b] T. Chivers, M. Parvez, G. Schatte, *Inorg. Chem.* **1999**, *38*, 5171−5177. [9c] T. Chivers, M. Parvez, G. Schatte, *Inorg. Chem.* **2001**, *40*, 540−545.
[10] For recent examples, see [10a] A. Mommertz, R. Leo, W. Massa, K. Harms, K. Dehnicke, *Z. Anorg. Allg. Chem.* **1998**, *624*, 1647−1652. [10b] M. Polamo, I. Multikainen, M. Leskelä, *Acta Crystallogr., Sect. C* **1997**, *53*, 1036−1037. [10c] L. R. Avens, D. M. Barnhart, C. J. Burns, S. D. McKee, *Inorg. Chem.* **1996**, *35*, 537−539. [10d] W. J. Evans, J. T. Leman, J. W. Ziller, *Inorg. Chem.* **1996**, *35*, 4283−4291. [10e] M. P. C. Campello, A. Domingos, J. Santos, *J. Organomet. Chem.* **1994**, *484*, 37−46. [10f] Z. Guo, P. K. Bradley, R. F. Jordan, *Organometallics* **1992**, *11*, 2690−2693. [10g] T. L. Breen, D. W. Stephan, *Inorg. Chem.* **1992**, *31*, 4019−4022.
[11] J. P. Campbell, W. L. Gladfelter, *Inorg. Chem.* **1997**, *36*, 4094−4098.
[12] S. M. Kunnari, R. Oilunkaniemi, R. S. Laitinen, M. Ahlgren, *J. Chem. Soc., Dalton Trans.* **2001**, 3417−3418.
[13] Crystal data for **2**: crystal size 0.12 × 0.12 × 0.10 mm^3, monoclinic $P2_1/c$ (No. 14) a = 12.3660(2) Å, b = 18.3420(4) Å, c = 17.1050(3) Å, β = 98.3940(8)°, V = 838.15(12) Å^3, Z = 4. The three methyl carbon atoms [labelled C(41A), C(42A), C(43A), C(41B), C(42B) and C(43B)] of one of the *tert*-butyl groups were disordered over two positions with refined site-occupancy factors of 0.581(9) and 0.419(9), respectively. The final cycle of full-matrix least-squares refinement using F^2 was based on 8683 reflections [6763 reflections with $I > 2\sigma(I)$], 533 variable parameters and converged with R = 0.0338.
[14] [14a] T. Chivers, X. Gao, M. Parvez, *J. Am. Chem. Soc.* **1995**, *117*, 2359−2360. [14b] T. Chivers, X. Gao, M. Parvez, *Inorg. Chem.* **1996**, *35*, 9−15.
[15] T. Chivers, G. Schatte, *Inorg. Chem.* to be submitted.
[16] [16a] N. W. Alcock, *Adv. Inorg. Chem. Radiochem.* **1972**, *15*,

 © 2003 Wiley-VCH Verlag GmbH & Co. KGaA, Weinheim

1−58. [16b] L. Pauling, *The Nature of the Chemical Bond*, 3rd edn. Cornell University Press, Ithaca, NY, 1960, p. 260.
[17] For a recent example, see: H.-C. Liang, E. Kim, C. D. Incarvito, A. L. Rheingold, K. D. Karlin, *Inorg. Chem.* **2002**, *41*, 2209−2212.
[18] Crystal data for **3**·THF: crystal size 0.10 × 0.10 × 0.05 mm^3, monoclinic $P2_1/c$ (No. 14), a = 10.9920(1) Å, b = 24.3640(3) Å, c = 18.8900(2) Å, β = 102.4600(7)°, V = 4939.76(9) Å^3, Z = 4. Two of the carbon atoms [labelled C(53A), C(54A) and C(53B), C(54B)] of the ring-opened THF molecule were disordered over two sites with refined site-occupancy factors of 0.647(6) and 0.353(6), respectively. Least-squares refinement on F^2 based on 10081 reflections and 614 variable parameters [7186 reflections with $I > 2\sigma(I)$] gave a final R_1 of 0.039. CCDC-211059 (**2**) and -208709 (**3**) contain the supplementary crystallographic data for this paper. These data can be obtained free of charge via www.ccdc.cam.ac.uk/conts/retrieving.html (or from the Cambridge Crystallographic Data Centre, 12 Union Road, Cambridge CB2 1EZ, UK; Fax: (internat.) +44-1223/336-033; or E-mail: deposit@ccdc.cam.ac.uk).
[19] A. A. Danopoulus, J. R. Galsworthy, M. L. H. Green, S. Cafferkey, L. H. Doerrer, M. B. Hursthouse, *Chem. Commun.* **1998**, 2529−2530.
[20] L. H. Doerrer, A. J. Graham, D. Haussinger, M. L. H. Green, *J. Chem. Soc., Dalton Trans.* **2000**, 813−820.
[21] F. Johnson, *Friedel−Crafts and Related Reactions* (Ed.: G. A. Olah), Interscience: New York, **1965**, Vol. IV, p. 1.

Received June 1, 2003
Early View Article
Published Online August 11, 2003

 © 2003 Wiley-VCH Verlag GmbH & Co. KGaA, Weinheim

Organomagnesium Phosphanide "Grignard" Analogues − Synthesis, Structural Characterisation and Solution Behaviour of $[BuMg\{P(CH[SiMe_3]_2)(C_6H_3\text{-}2\text{-}OMe\text{-}3R)\}]_2$ [R = H, Me]

Stuart Blair,[a] Keith Izod,*[a] William Clegg,[a] and Ross W. Harrington[a]

In memory of Ron Snaith

Keywords: Magnesium / P ligands / Grignard reaction / Rearrangement

The reaction between either one or two equivalents of the secondary phosphane $\{(Me_3Si)_2CH\}PH(C_6H_3\text{-}2\text{-}OMe\text{-}3\text{-}R')$ [R′ = H (**1a**), Me (**1b**)] and Bu_2Mg yields the heteroleptic complexes $[BuMg\{P[CH(SiMe_3)_2](C_6H_3\text{-}2\text{-}OMe\text{-}3\text{-}R')\}]_2$ [R′ = H (**2a**), Me (**2b**)], irrespective of the ratio of **1** to Bu_2Mg. X-ray crystallography shows that **2a** and **2b** crystallise as dimers containing a central Mg_2P_2 core. Dissolution of either **2a** or **2b** in THF results in complex degradation and formation of the tertiary phosphanes $\{(Me_3Si)_2CH\}P(Me)(C_6H_3\text{-}2\text{-}OMe\text{-}3\text{-}R')$ and unidentified magnesium-containing products.
(© Wiley-VCH Verlag GmbH & Co. KGaA, 69451 Weinheim, Germany, 2003)

Introduction

Although the synthesis of the parent calcium phosphanide $Ca(PH_2)_2$, by metallation of PH_3 with calcium in liquid ammonia, was reported as early as 1942,[1] little progress was made in the synthesis of other alkaline earth metal phosphanides until 1987, when Raston and co-workers reported that the reaction between *n*Bu*s*BuMg and $PhPH_2$ in the presence of tmeda gave the adduct [(tmeda)$Mg(PHPh)_2$] in good yield (tmeda = *N*,*N*,*N*′,*N*′-tetramethylethylenediamine).[2] However, the last two decades have seen growing interest in such species, with Westerhausen and co-workers making a particularly important contribution to this area.[3,4] With few exceptions, crystallographically characterised alkaline-earth metal phosphanides are limited to complexes containing phosphanide ligands in which the donor phosphorus atom is directly bonded to a silyl substituent. Such species typically crystallise as solvated monomers, symmetrical or unsymmetrical dimers, or linear trimers. We recently reported the synthesis, structural characterisation and dynamic behaviour of a homologous series of mononuclear alkaline-earth metal phosphanides without a direct Si−P bond.[5] We now describe the synthesis and structural characterisation of two related, heteroleptic organomagnesium phosphanide "Grignard analogues" and their behaviour in solution.

[a] Chemistry, School of Natural Sciences, University of Newcastle, Newcastle upon Tyne, NE1 7RU, UK
E-mail: k.j.izod@ncl.ac.uk

Results and Discussion

The reaction between Bu_2Mg and one equivalent of the secondary phosphanes $\{(Me_3Si)_2CH\}PH(C_6H_3\text{-}2\text{-}OMe\text{-}3\text{-}R')$ [R′ = H (**1a**), Me (**1b**)][6] gives the heteroleptic dimeric organomagnesium phosphanides $[BuMg\{P[CH(SiMe_3)_2](C_6H_3\text{-}2\text{-}OMe\text{-}3\text{-}R')\}]_2$ [R′ = H (**2a**), Me (**2b**)] in good yields (Scheme 1).

Unexpectedly, when Bu_2Mg was reacted with *two* equivalents of **1** under the same conditions only **2** and one equivalent of unchanged **1** were recovered. This is in marked contrast to the reaction between Bu_2Mg and two equivalents of the related secondary phosphane $\{(Me_3Si)_2CH\}PH(C_6H_4\text{-}2\text{-}CH_2NMe_2)$, which proceeds cleanly to give the bis(phosphanide) $[Mg\{P[CH(SiMe_3)_2](C_6H_4\text{-}2\text{-}CH_2NMe_2)\}_2]$ (**3**) in essentially quantitative yield.[5] The reason for this mono-substitution is, as yet, unclear, although it is possible that the five-membered chelate ring in **2** engenders greater steric hindrance at the metal centre than the six-membered chelate ring present in **3**, disfavouring substitution of the second Bu group.

Compounds **2a** and **2b** are unusual examples of "Grignard analogues", RMgX, in which the halide X has been replaced by a phosphanide ligand. Although there are several examples of amide analogues of these species, $RMg(NR_2)$,[7] to the best of our knowledge there has been only one previous report of an organomagnesium phosphanide $RMg(PR_2)$: Westerhausen and co-workers found that the reaction between $Mg\{P(SiMe_3)_2\}_2$ and diphenylbutadiyne in toluene gave an unusual organomagnesium phosphanide addition product (**4**).[8]

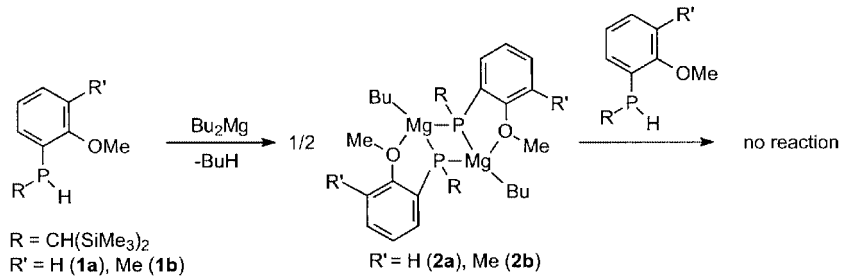

Scheme 1

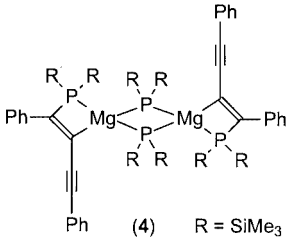

Compounds **2a** and **2b** are initially precipitated as colourless solids from reactions conducted in light petroleum and freshly prepared samples of either compound may be recrystallised from cold (6 °C) diethyl ether as colourless blocks suitable for X-ray crystallography. Compounds **2a** and **2b** are insoluble in hydrocarbon solvents such as light petroleum, benzene or toluene, but dissolve readily in THF to give deep yellow solutions. However, dissolution in donor solvents is accompanied by decomposition (see below), preventing satisfactory characterisation of these compounds by NMR spectroscopy.

The crystals of compounds **2a** and **2b** studied by X-ray diffraction differ both in the substitution of the aromatic ring and in the nature of the butyl group. This latter effect is a consequence of the mixture of isomers present in the commercially sourced Bu_2Mg used in their synthesis. Compounds **2a** and **2b** have very similar molecular structures but they do not form isomorphous crystals; the molecule of **2a** has crystallographic inversion symmetry, but **2b** occupies a general position in its crystal structure. The molecular structures of **2a** and **2b** are shown in Figure 1 and details of bond lengths and angles are given in Table 1. Both compounds crystallise as dimers in which each Mg centre is bound by the P and O atoms of a chelating phosphanide ligand, forming five-membered chelate rings with bite angles of 80.76(4)° (**2a**) and 81.13(9) and 81.23(9)° (**2b**). The P atoms of the ligands further bridge the two Mg centres, forming a planar, parallelogram-shaped Mg_2P_2 core with Mg−P−Mg angles of 97.16(2)° (**2a**) and 95.83(5)° (two crystallographically independent but equal values in **2b**). The two, essentially planar, chelate rings adopt a *transoid* conformation, generating a pseudo-ladder arrangement; the dihedral angles between the Mg_2P_2 core and the chelate rings in the two compounds are 80.8° (**2a**) and 81.8 and 82.9° (**2b**).

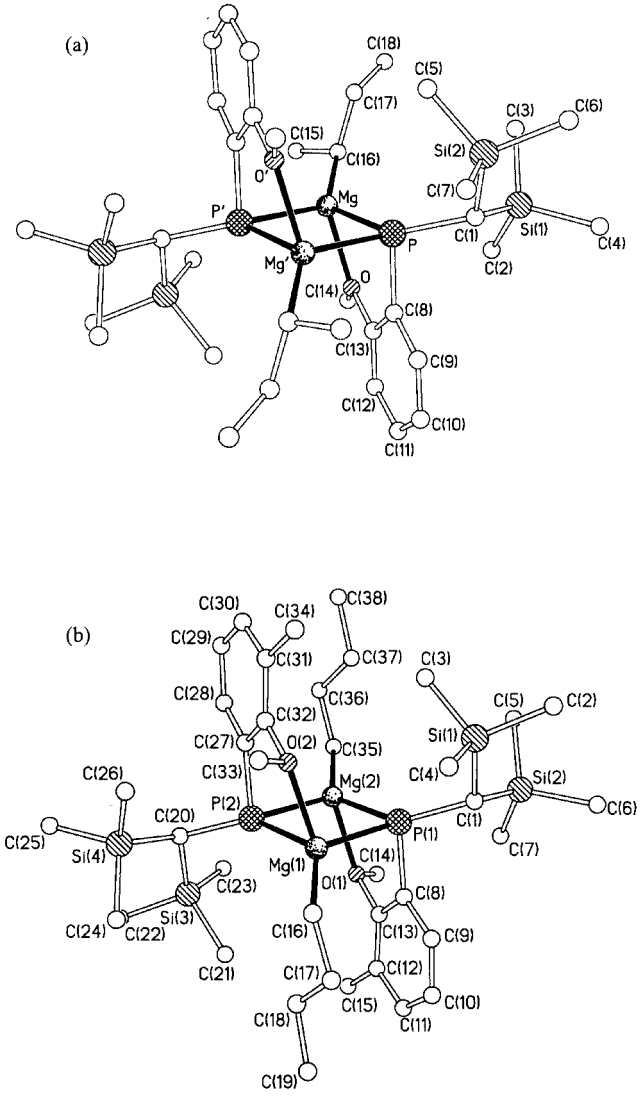

Figure 1. Molecular structures of (a) **2a** and (b) **2b**; H atoms omitted for clarity

In both **2a** and **2b** the phosphorus atoms bridge the two Mg centres in a slightly unsymmetrical fashion; the Mg−P distances in **2a** are 2.5760(8) and 2.5978(8) Å, whilst in **2b** they are 2.5765(17)/2.5730(16) Å [Mg(1)−P(2)/

 © 2003 Wiley-VCH Verlag GmbH & Co. KGaA, Weinheim

Table 1. Selected bond lengths (Å) and angles (deg.) for **2a** and **2b**[a]

2a					
Mg−O	2.1088(15)	Mg−C(16)	2.127(2)	Mg−P	2.5760(8)
Mg−P′	2.5978(8)	P−C(8)	1.847(2)	P−C(1)	1.8745(19)
O−C(14)	1.444(2)	Si(1)−C(1)	1.884(2)	Si(1)−C(2)	1.868(2)
Si(1)−C(3)	1.865(2)	Si(1)−C(4)	1.873(2)	Si(2)−C(1)	1.890(2)
Si(2)−C(5)	1.860(3)	Si(2)−C(6)	1.870(3)	Si(2)−C(7)	1.867(3)
O−Mg−C(16)	109.54(9)	O−Mg−P	80.76(4)		
C(16)−Mg−P	133.81(8)	O−Mg−P′	104.21(5)		
C(16)−Mg−P′	132.83(8)	P−Mg−P′	82.84(2)		
C(8)−P−C(1)	102.68(9)	C(8)−P−Mg	92.88(6)		
C(1)−P−Mg	131.99(6)	C(8)−P−Mg′	92.49(6)		
C(1)−P−Mg′	126.62(6)	Mg−P−Mg′	97.16(2)		
C(13)−O−C(14)	117.54(16)	C(13)−O−Mg	123.01(12)		
2b					
Mg(1)−P(1)	2.6138(16)	Mg(1)−P(2)	2.5765(17)	Mg(1)−O(2)	2.113(3)
Mg(1)−C(16)	2.141(5)	Mg(2)−P(1)	2.5730(16)	Mg(2)−P(2)	2.6105(17)
Mg(2)−O(1)	2.121(3)	Mg(2)−C(35)	2.136(5)	P(1)−C(1)	1.869(4)
P(1)−C(8)	1.850(4)	P(2)−C(20)	1.878(4)	P(2)−C(27)	1.846(4)
Si(1)−C(1)	1.881(4)	Si(1)−C(2)	1.863(5)	Si(1)−C(3)	1.868(5)
Si(1)−C(4)	1.878(5)	Si(2)−C(1)	1.901(4)	Si(2)−C(5)	1.865(5)
Si(2)−C(6)	1.879(5)	Si(2)−C(7)	1.856(5)	Si(3)−C(20)	1.887(4)
Si(3)−C(21)	1.865(5)	Si(3)−C(22)	1.880(5)	Si(3)−C(23)	1.868(5)
Si(4)−C(20)	1.880(4)	Si(4)−C(24)	1.859(5)	Si(4)−C(25)	1.887(5)
Si(4)−C(26)	1.875(5)				
P(1)−Mg(1)−P(2)	84.09(5)	P(1)−Mg(1)−O(2)	103.64(9)		
P(1)−Mg(1)−C(16)	131.37(15)	P(2)−Mg(1)−O(2)	81.13(9)		
P(2)−Mg(1)−C(16)	136.88(16)	O(2)−Mg(1)−C(16)	107.15(16)		
P(1)−Mg(2)−P(2)	84.22(5)	P(1)−Mg(2)−O(1)	81.23(9)		
P(1)−Mg(2)−C(35)	137.76(16)	P(2)−Mg(2)−O(1)	102.93(9)		
P(2)−Mg(2)−C(35)	130.34(16)	O(1)−Mg(2)−C(35)	107.89(16)		
Mg(1)−P(1)−Mg(2)	95.83(5)	Mg(1)−P(1)−C(1)	123.25(14)		
Mg(1)−P(1)−C(8)	91.51(13)	Mg(2)−P(1)−C(1)	135.42(14)		
Mg(2)−P(1)−C(8)	93.69(13)	C(1)−P(1)−C(8)	104.72(18)		
Mg(1)−P(2)−Mg(2)	95.83(5)	Mg(1)−P(2)−C(20)	136.44(15)		
Mg(1)−P(2)−C(27)	93.15(13)	Mg(2)−P(2)−C(20)	122.36(14)		
Mg(2)−P(2)−C(27)	92.84(14)	C(20)−P(2)−C(27)	104.01(19)		

[a] The prime denotes an atom generated by inversion symmetry.

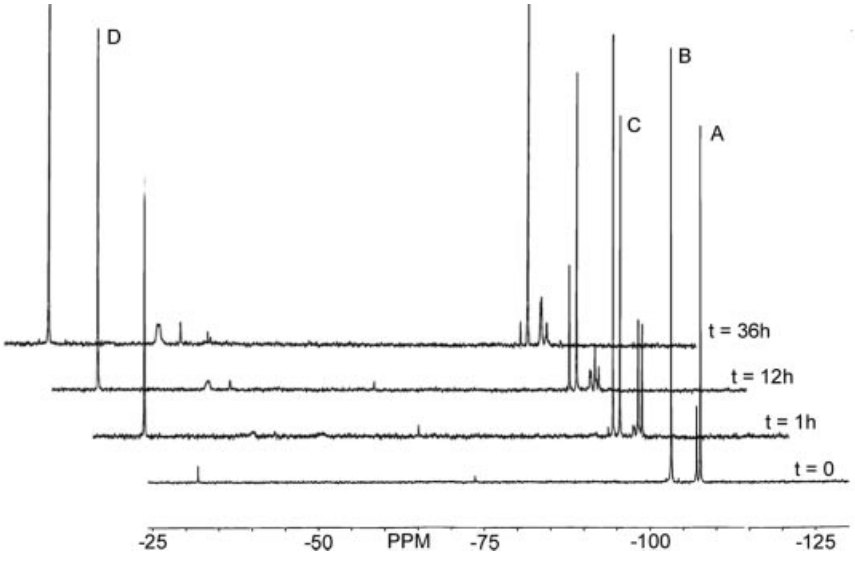

Figure 2. $^{31}P\{^{1}H\}$ NMR spectra of **2a** in [D_8]THF recorded over 36 h

 © 2003 Wiley-VCH Verlag GmbH & Co. KGaA, Weinheim

Mg(2)−P(1)] and 2.6138(16)/2.6105(17) Å [Mg(1)−P(1)/Mg(2)−P(2)]. These distances compare with Mg−P distances of 2.592(5) and 2.587(5) Å in [(tmeda)Mg(PHPh)$_2$],[2] 2.5031(6) Å in [(THF)$_2$Mg{P(SiMe$_3$)$_2$}$_2$],[4b] and 2.5555(11) and 2.5557(11) Å in **3**.[5] The Mg−C distances of 2.127(2) Å (**2a**) and 2.141(5) and 2.136(5) Å (**2b**) are similar to Mg−C distances in typical diorganomagnesium or Grignard-type compounds; for example, the Mg−C distance in {(1,4-dioxane)MgEt$_2$}$_n$ is 2.142(2) Å.[9]

The ^{31}P{^{1}H} NMR spectra of **2a** and **2b** in [D$_8$]THF recorded shortly after sample preparation show rapid decomposition at room temperature, preventing precise characterisation of these compounds by NMR spectroscopy. A ^{31}P{^{1}H} NMR spectrum of a solution of **2a** in [D$_8$]THF obtained immediately after sample preparation (Figure 2) exhibits two main peaks at δ = −107.0 (**A**) and −103.1 ppm (**B**), both signals arising from magnesium phosphanide species. After one hour peak **A** has decreased markedly in intensity and new signals have appeared at δ = −104.4 and −31.8 ppm (**C** and **D**, respectively). Peak **C** is likely to be due to a magnesium phosphanide species, whereas peak **D** is consistent with the presence of a tertiary phosphane. After a period of 36 hours peaks **A** and **B** have almost disappeared, leaving only peaks **C** and **D** with significant intensity (Figure 2). The ^{1}H NMR spectra of **2a** in [D$_8$]THF solution recorded at several intervals over a period of 24 hours are very complicated, with numerous peaks due to SiMe$_3$, aromatic and OMe protons; however, a clear doublet at δ = 1.43 ppm (J_{PH} = 6.4 Hz) is visible in the later spectra, consistent with the presence of a PMe group.

We recently reported that the metathesis reaction between [{(Me$_3$Si)$_2$CH}(C$_6$H$_4$-2-OMe)P]K and CaI$_2$ in THF yields the novel alkoxophosphanide cluster complex [{([Me$_3$Si]$_2$CH)(C$_6$H$_4$-2-O)P}Ca(THF)]$_4$·4THF via an unusual ligand degradation reaction, involving rapid migration of a methyl group from the oxygen atom of one phosphanide ligand to the phosphorus atom of another (Scheme 2).[10] This process yields the tertiary phosphane {(Me$_3$Si)$_2$CH}P(Me)(C$_6$H$_4$-2-OMe) (**5a**) as the sole phosphorus-containing side product [this phosphane has a ^{31}P chemical shift of δ = −31.8 ppm and a ^{1}H chemical shift of δ = 1.41 ppm (d, J_{PH} = 6.1 Hz) due to the PMe group].

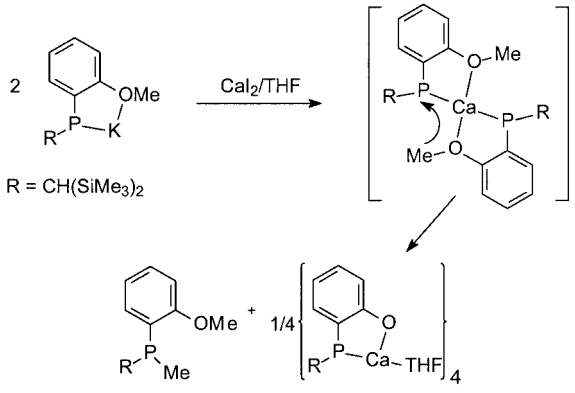

Scheme 2

Thus, the ^{31}P and ^{1}H NMR spectra of **2a** are consistent with rapid complex degradation upon dissolution in [D$_8$]THF and formation of a new magnesium phosphanide species and the tertiary phosphane **5a** (peak **D**). Unfortunately, in spite of repeated attempts, it was not possible to separate the new magnesium phosphanide species from the tertiary phosphane **5a** for further characterisation; in contrast to **2a**, this new species appears to be highly soluble, even in the extremely poor solvent hexamethyldisiloxane. Compound **2b** displays similar behaviour to **2a** in THF solution. NMR spectra recorded shortly after sample preparation suggest the presence of two magnesium phosphanide species and the corresponding tertiary phosphane {(Me$_3$Si)$_2$CH}P(Me)(C$_6$H$_3$-2-OMe-3-Me) (**5b**). After several hours compound **2b** appears to have completely degraded to a new magnesium phosphanide and **5b**.

We therefore propose that in THF solution compounds **2a** and **2b** undergo a ligand degradation reaction, possibly forming a magnesium alkoxophosphanide complex of the form [{[(Me$_3$Si)$_2$CH](C$_6$H$_3$-2-O-3-R′)P}Mg(THF)$_n$]$_m$ (**6**; R′ = H, Me) and the corresponding tertiary phosphane **5**. This process may occur via the Grignard-type compounds **2**, or else these compounds may be subject to a Schlenk-type equilibrium in solution, generating the homoleptic phosphanides [{[(Me$_3$Si)$_2$CH](C$_6$H$_3$-2-OMe-3-R′)P}$_2$Mg] (**7**) and one equivalent of Bu$_2$Mg (Scheme 3). The homoleptic compound **7** may then undergo a methyl migration reaction analogous to that observed in the formation of [{[(Me$_3$Si)$_2$CH](C$_6$H$_4$-2-O)P}Ca(THF)]$_4$·4THF to give the alkoxophosphanide complex **6**.

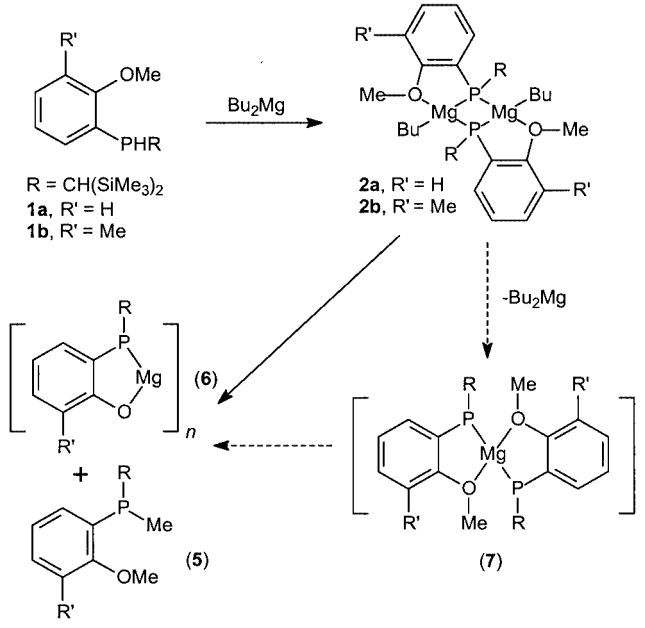

Scheme 3

At present the available evidence does not allow these two reaction pathways to be distinguished. However, if such a Schlenk-type equilibrium were slow on the NMR time scale, this may account for the two magnesium phosphanide

 © 2003 Wiley-VCH Verlag GmbH & Co. KGaA, Weinheim

species present in initially prepared samples of **2a**, peaks **A** and **B** perhaps arising from the Grignard analogue **2a** and the homoleptic bis(phosphanide) **7a**.

Experimental Section

General Comments: All manipulations were carried out using standard Schlenk techniques under an atmosphere of dry nitrogen. Diethyl ether and light petroleum (b.p. 40−60 °C) were distilled from sodium/potassium alloy under an atmosphere of dry nitrogen and were stored over a potassium film. Bu_2Mg was obtained from Aldrich as a 1.0 M solution of a mixture of isomers in heptanes. The compounds $\{(Me_3Si)_2CH\}PH(C_6H_3\text{-}2\text{-}OMe\text{-}3\text{-}R')$ (R′ = H, Me) were prepared by a previously published procedure.[6] All other compounds were obtained from commercial sources and were used as supplied.

Due to the poor solubility of **2a** and **2b** in non-donor solvents and their rapid degradation in THF, satisfactory NMR spectroscopic data could not be obtained. The constitutions of compounds **2a** and **2b** were confirmed by elemental analyses and X-ray crystallography. Elemental analyses for **2a** and **2b** were obtained by the Elemental Analysis Service of London Metropolitan University, UK.

Preparation of $[BuMg\{P[CH(SiMe_3)_2](C_6H_4\text{-}2\text{-}OMe)\}]_2$ (2a): Bu_2Mg (4.33 mL, 4.33 mmol) was added to a solution of $\{(Me_3Si)_2CH\}PH\{C_6H_4\text{-}2\text{-}OMe\}$ (1.29 g, 4.33 mmol) in light petroleum (10 mL) and the solution was stirred for 16 h. The colourless precipitate was isolated by filtration and dissolved in diethyl ether (10 mL). The resulting solution was concentrated and cooled to −30 °C for 48 h, yielding colourless blocks of **2a**. Yield 0.94 g, 57%. $C_{36}H_{70}Mg_2O_2P_2Si_4$ (757.84): calcd. C 57.05, H 9.31; found C 56.93, H 9.20.

Preparation of $[BuMg\{P[CH(SiMe_3)_2](C_6H_3\text{-}2\text{-}OMe\text{-}3\text{-}Me)\}]_2$ (2b): Bu_2Mg (1.70 mL, 1.70 mmol) was added to a solution of $\{(Me_3Si)_2CH\}PH\{C_6H_3\text{-}2\text{-}OMe\text{-}3\text{-}Me\}$ (0.53 g, 1.70 mmol) in light petroleum (10 mL). The solution was stirred for 16 h and the resulting colourless precipitate was isolated by filtration. The solid was dissolved in diethyl ether, concentrated and cooled to −30 °C for 60 h, to yield **2b** as colourless blocks. Yield 0.41 g, 61%. $C_{38}H_{74}Mg_2O_2P_2Si_4$ (785.89): calcd. C 58.07, H 9.49; found C 57.94, H 9.43.

Crystal Structure Determination of 2a and 2b: All measurements were made at 150 K on a Bruker AXS SMART CCD diffractometer using graphite-monochromated Mo-K_α radiation (λ = 0.71073 Å) and narrow (0.3° in ω) frame exposures. Cell parameters were refined from the observed positions of all strong reflections in each data set. The structures were solved by direct methods and refined on F^2 values for all unique data. Table 2 gives further details. All non-hydrogen atoms were refined anisotropically, and H atoms were constrained with a riding model; U(H) was set at 1.2 (1.5 for methyl groups) times U_{eq} for the parent atom. Programs were Bruker AXS SMART (control) and SAINT (integration), and SHELXTL for structure solution, refinement, and molecular graphics.[11] CCDC-207042 (**2a**) and -207043 (**2b**) contain the supplementary crystallographic data for this paper. These data can be obtained free of charge at www.ccdc.cam.ac.uk/conts/retrieving.html [or from the Cambridge Crystallographic Data Centre, 12 Union Road, Cambridge CB2 1EZ, UK; Fax: (internat.) +44-1223/336-033; E-mail: deposit@ccdc.cam.ac.uk].

Table 2. Crystallographic data for **2a** and **2b**

	2a	**2b**
Molecular formula	$C_{36}H_{70}Mg_2O_2P_2Si_4$	$C_{38}H_{74}Mg_2O_2P_2Si_4$
Formula mass	757.8	785.9
Crystal system	monoclinic	orthorhombic
Space group	$P2_1/c$	$Pbc2_1$
a (Å)	10.9511(6)	10.8569(5)
b (Å)	10.6790(5)	18.8044(9)
c (Å)	19.4682(10)	23.9371(11)
β (deg.)	98.563(2)	
Volume (Å^3)	2251.4(2)	4886.9(4)
Z	2	4
Density (calculated) (g cm^{-3})	1.118	1.068
μ (mm^{-1})	0.259	0.240
Crystal size (mm)	0.36 × 0.26 × 0.14	0.36 × 0.34 × 0.30
Reflections collected	18668	33963
Independent reflections	5314 [R_{int} = 0.0315]	8554 [R_{int} = 0.0542]
Parameters	217	451
R (F, $F^2>2\sigma$)	0.0421	0.0448
R_w (F^2, all data)	0.1095	0.1174
Goodness-of-fit	1.082	1.085
Largest diff. peak and hole (e/Å^3)	0.60 and −0.32	0.40 and −0.27
Absolute structure parameter		−0.15(12)

Acknowledgments

The authors gratefully acknowledge the support of the University of Newcastle, the EPSRC and the Royal Society.

[1] C. Legoux, *Ann. Chim.* **1942**, *17*, 100.
[2] E. Hey, L. M. Engelhardt, C. L. Raston, A. H. White, *Angew. Chem. Int. Ed. Engl.* **1987**, *26*, 81; *Angew. Chem.* **1987**, *99*, 61.
[3] For recent reviews see: [3a] M. Westerhausen, *Trends Organomet. Chem.* **1997**, *2*, 89. [3b] M. Westerhausen, *Coord. Chem. Rev.* **1998**, *176*, 157 and references therein.
[4] [4a] M. Westerhausen, M. H. Digeser, B. Wieneke, H. Nöth, J. Knizek, *Eur. J. Inorg. Chem.* **1998**, 517. [4b] M. Westerhausen, A. Pfitzner, *J. Organomet. Chem.* **1995**, *487*, 187. [4c] M. Westerhausen, W. Schwarz, *Z. Anorg. Allg. Chem.* **1994**, *620*, 304. [4d] M. Westerhausen, M. Hartmann, W. Schwarz, *Inorg. Chem.* **1996**, *35*, 2421. [4e] M. Westerhausen, *J. Organomet. Chem.* **1994**, *479*, 141. [4f] M. Westerhausen, G. Lang, W. Schwarz, *Chem. Ber.* **1996**, *129*, 1035. [4g] M. Westerhausen, M. Krofta, P. Mayer, *Z. Anorg. Allg. Chem.* **2000**, *626*, 2307. [4h] M. Westerhausen, M. H. Digeser, M. Krofta, N. Wiberg, H. Nöth, J. Knizek, W. Ponikwar, T. Seifert, *Eur. J. Inorg. Chem.* **1999**, 743. [4i] M. Westerhausen, W. Schwarz, *J. Organomet. Chem.* **1993**, *463*, 51. [4j] M Westerhausen, R. Low, W. Schwarz, *J. Organomet. Chem.* **1996**, *513*, 213. [4k] M. Westerhausen, M. H. Digeser, H. Nöth, J. Knizek, *Z. Anorg. Allg. Chem.* **1998**, *624*, 215. [4l] M. Westerhausen, G. Lang, W. Schwarz, *Chem. Ber.* **1996**, *129*, 1035.
[5] S. Blair, K. Izod, W. Clegg, *Inorg. Chem.* **2002**, *41*, 3886.
[6] W. Clegg, K. Izod, S. T. Liddle, P. O'Shaughnessy, J. M. Sheffield, *Organometallics* **2000**, *19*, 2090.
[7] For examples see: [7a] M. Westerhausen, T. Bollwein, N. Makropolous, S. Schneiderbauer, M. Suter, H. Nöth, P. Mayer, H. Piotrowski, K. Polborn, A. Pfitzner, *Eur. J. Inorg. Chem.* **2002**,

 © 2003 Wiley-VCH Verlag GmbH & Co. KGaA, Weinheim

389. [7b] L. M. Engelhardt, B. S. Jolly, P. C. Junk, C. L. Raston, B. W. Skelton, A. H. White, *Aust. J. Chem.* **1986**, *39*, 1337. [7c] N. Kuhn, M. Schulten, R. Boese, D. Blaser, *J. Organomet. Chem.* **1991**, *421*, 1. [7d] M. M. Olmstead, W. J. Grigsby, D. R. Chacon, T. Hascall, P. P. Power, *Inorg. Chim. Acta* **1996**, *251*, 273. [7e] K.-C. Yang, C.-C. Chang, J.-Y. Huang, C.-C. Lin, G.-H. Lee, Y. Wang, M. Y. Chiang, *J. Organomet. Chem.* **2002**, *648*, 176. [7f] K. W. Henderson, R. E. Mulvey, W. Clegg, P. A. O'Neil, *J. Organomet. Chem.* **1992**, *439*, 237.

[8] M. Westerhausen, M. H. Digeser, H. Nöth, T. Seifert, A. Pfitzner, *J. Am. Chem. Soc.* **1998**, *120*, 6772.

[9] R. Fischer, D. Walther, P. Gebhardt, H. Gorls, *Organometallics* **2000**, *19*, 2532.

[10] K. Izod, W. Clegg, S. T. Liddle, *Organometallics* **2000**, *19*, 3640.

[11] [11a] SMART and SAINT software for CCD diffractometers; Bruker AXS Inc., Madison, WI, **1997**. [11b] G. M. Sheldrick, SHELXTL user manual, version 5.1; Bruker AXS Inc. Madison, WI, **1997**.

Received March 28, 2003
Early View Article
Published Online July 22, 2003

 © 2003 Wiley-VCH Verlag GmbH & Co. KGaA, Weinheim

Sodiated β-Diphosphonate Carbanions: Characterization of the Tetrameric Cubane and the Hexameric Ladder Complexes $[\{(i\text{PrO})_2\text{P(O)}\}_2\text{CHNa}]_4$ and $[\{(\text{EtO})_2\text{P(O)}\}_2\text{CHNa}]_6$

Roger Nassar,[a] Alicia M. Beatty,[a] and Kenneth W. Henderson*[a]

In memory of the late Dr. Ron Snaith, an independent thinker and spirit

Keywords: Alkali metals / Sodium / Cage compounds / Chelates / O Ligands

Reaction of the methylene diphosphonates $[(\text{RO})_2\text{P(O)}]_2\text{CH}_2$, where R = *i*Pr or Et, with the metalating reagents NaH, *n*BuNa or the superbasic mixture *t*BuONa/*n*BuLi leads to monodeprotonation, and formation of the complexes $[\{(i\text{PrO})_2\text{P(O)}\}_2\text{CHNa}]_4$ (**1**) and $[\{(\text{EtO})_2\text{P(O)}\}_2\text{CHNa}]_6$ (**2**). Single-crystal X-ray diffraction studies revealed that **1** is tetrameric in the solid state, with a central Na_4O_4 cubane core. Each metal in **1** is rendered pentacoordinate by binding to three μ_3-O phosphoryl bridges within the cubane, a chelating phosphoryl unit, and also a single *i*PrO group. In contrast, the structure of **2** is hexameric, and is composed of an unusual six-rung Na_6O_6 ladder core. Three distinct sodium environments as well as μ_1-, μ_2- and μ_3-O phosphoryl units are present within the ladder framework. No Na–C interactions are present in either **1** or **2**. All of the six-membered NaOPCPO chelate rings display localized P=O double bonds and partial multiple bonding on the P–C–P linkages (mean P–O: 1.49 Å, and mean P–C: 1.69 Å). Ab initio molecular orbital calculations (HF/6–31G*) on model complexes indicate that the hexameric arrangement found for **2** is thermodynamically more stable than the cubane structure of **1**, in the absence of steric effects.
(© Wiley-VCH Verlag GmbH & Co. KGaA, 69451 Weinheim, Germany, 2003)

Introduction

Metallated β-diphosphonates, $[\{(\text{RO})_2\text{P(O)}\}_2\text{CH}]^-\ \text{M}^+$, have been receiving continuous attention since their first reported synthesis and subsequent usage in 1953 by Kosolapoff.[1] The presence of two stabilizing groups adjacent to a methylene unit of the parent neutral diphosphonate allows straightforward access to the carbanion by deprotonation using a variety of bases. In turn, these carbanions have proven highly useful in the formation of new carbon-carbon bonds, in particular via alkylation and also Horner−Wadsworth−Emmons-type reactions.[2−4] Interest in β-diphosphonates has resulted from their potent biological activity,[5] and they have found applications as agrochemicals,[6] and in medicinal chemistry.[7] In addition, they are used in several industrial processes including as detergents,[8] sequestrates[9] and as fixing agents in photography.[10]

From a coordination chemistry perspective, there are clear parallels between β-diphosphonates and the widely studied β-diketonates,[11] β-enaminoketonates[12] and β-diketiminates,[13] as metal binding ligands (Figure 1). However, relatively few solid-state studies of metallated β-diphosphonates have been reported, and these have generally been limited to transition metal complexes.[14,15] This is somewhat surprising considering that the vast majority of the reaction chemistry involving these ligands has been developed using their alkali metal salts as reactive intermediates.

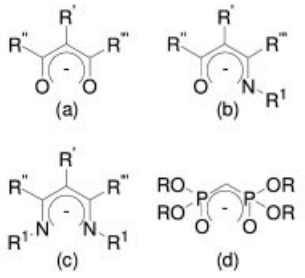

Figure 1. Generalized (a) β-diketonato, (b) β-enaminoketonato, (c) β-diketiminato, and (d) β-diphosphonato ligand frameworks

Of particular relevance to this study is the finding that the nature of the alkoxyl sidearms can strongly influence the reactivity of the β-diphosphonates.[3a] For example, whereas the tetraisopropyl esters react to give almost quantitative yields of *C*-alkylated esters, the methyl and ethyl esters give very low yields (>20%) under similar conditions.

[a] University of Notre Dame, Department of Chemistry and Biochemistry
251 Nieuwland Science Hall, Notre Dame, IN 46556-5670, USA
Fax: (internat.) + 1-574/631-6652
E-mail: khenders@nd.edu

Moreover, the rates of alkylation are higher and less side products are formed when the larger alkoxy groups are used in these reactions. Such large and unexpected discrepancies between apparently very similar types of ligands still remains to be fully explained.[3b] In an effort to shed light on some of these issues we wish to report the single-crystal X-ray diffraction studies of the two sodium β-diphosphonate complexes $[\{(RO)_2P(O)\}_2CHNa]_n$, where R = *i*Pr and *n* = 4 (**1**) and where R = Et and *n* = 6 (**2**).

Results and Discussion

Synthetic and Solid-State Studies

Three alternative metalating reagents, NaH, *n*BuNa and *t*BuONa/*n*BuLi,[16] were reacted with hexane solutions of the parent phosphonates $[(RO)_2P(O)]_2CH_2$ [R = *i*Pr (**3**), Et (**4**)] in stoichiometries varying from 1:1 to 3.5:1 (Scheme 1). In all instances, the only crystalline material precipitated from the resulting solutions (or filtrates) was the monosodiated complex **1** or **2**, as determined by NMR spectroscopy. Previous spectroscopic studies of both **1** and **2** have been reported and will not be elaborated upon here.[3b,15] Single crystals suitable for X-ray diffraction were prepared for both complexes and their structures elucidated.

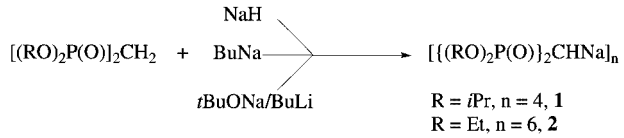

Scheme 1

The core of cage complex **1** is composed of four sodium and four oxygen centers arranged in an approximate cubane structure (Figure 2 and 3). In addition to the three Na−O contacts associated with the Na_4O_4 unit, each metal binds to one chelating phosphoryl group and also to a single *i*PrO group, rendering the sodium centers pentacoordinate. Hence, within **1**, each phosphonate forms five Na−O bonds and bridges between three different metal centers. Tetra-

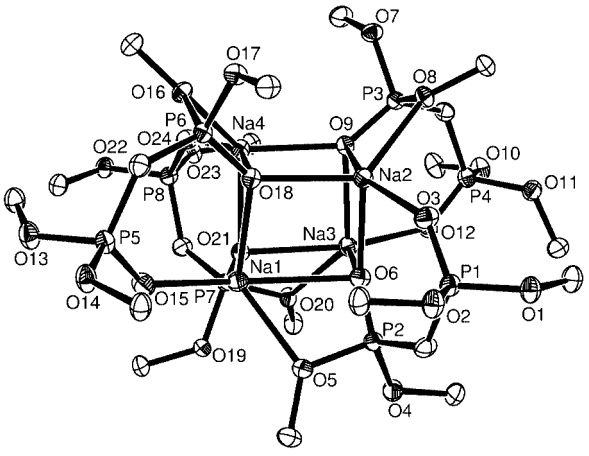

Figure 2. Molecular structure of $[\{(iPrO)_2P(O)\}_2CHNa]_4$, **1**, with hydrogen atoms and methyl groups removed for clarity

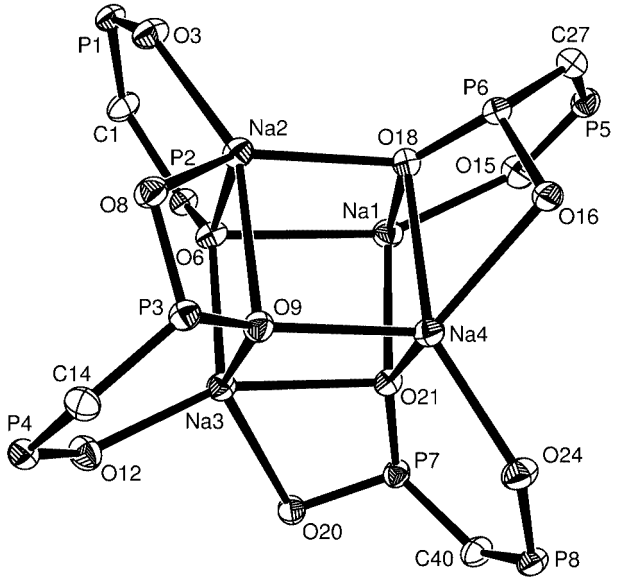

Figure 3. Core of the molecular structure of **1**, showing only the atoms involved with binding to the metal centers

meric cubane aggregates are comparatively common for sodium complexes, in particular when alkoxy or aryloxy ligands are employed.[17] The closest structural analog to **1** is the complex $[4\text{-Me-2,6-}(Me_2NCH_2)_2C_6H_2ONa]_4$, in which the "pincer phenolate" ligands coordinate to three sodium centers of a Na_4O_4 cubane.[18] However, the phenolate possesses approximate D_2 symmetry, whereas **1** is rendered closer to C_2 symmetry due to the "secondary" chelation of the *i*PrO groups.

There are no significant interactions present between the carbanionic carbons and the sodium centers, with all Na−C distances greater than 3.8 Å (see Table 1 for a list of pertinent bond lengths and angles). This bonding arrangement is commonly found for alkali metal complexes of α-stabilized carbanions, where the highly electropositive cations preferentially bind to the electronegative groups of the anion.[19,20] In fact, the phosphoryl unit has proved to be an excellent bridge for group 1 metals even when present as part of a neutral ligand.[21] For example, the crystal structure of the dimeric lithium chloride complex $[\{(iPrO)_2P(O)\}_2CH_2{\cdot}LiCl]_2$ contains a central Li_2O_2 ring and terminal chloride anions.[22]

Complex **2** was the focus of an early ^1H NMR spectroscopic study by Cotton in 1962.[15a] As part of these investigations cryoscopic measurements indicated that **2** is hexameric in benzene solution. However, at that time he did not speculate on the structure of the complex. Our X-ray diffraction studies of **2** confirm that it is indeed hexameric in the solid state and that it adopts a highly unusual centrosymmetric six-rung ladder framework (Figure 4 and 5, and Table 2). Each sodium is bound to five oxygen centers, however, three distinct metal and ligand environments are present within the structure. The three different types of sodium centers present can be related to their position within the ladder framework, i.e. rung-one, rung-two or rung-three. The three crystallographically unique phosphonate li-

 © 2003 Wiley-VCH Verlag GmbH & Co. KGaA, Weinheim

Table 1. Selected bond lengths (Å) and angles (°) within **1**

Na(1)−O(15)	2.222 (1)	Na(1)−O(21)	2.286 (1)
Na(1)−O(18)	2.296 (1)	Na(1)−O(5)	2.344 (1)
Na(1)−O(6)	2.623 (1)	Na(2)−O(3)	2.235 (1)
Na(2)−O(6)	2.270 (1)	Na(2)−O(18)	2.346 (1)
Na(2)−O(8)	2.396 (1)	Na(2)−O(9)	2.534 (1)
Na(3)−O(12)	2.202 (1)	Na(3)−O(6)	2.298 (1)
Na(3)−O(9)	2.340 (1)	Na(3)−O(20)	2.424 (1)
Na(3)−O(21)	2.434 (1)	Na(4)−O(24)	2.221 (1)
Na(4)−O(9)	2.329 (1)	Na(4)−O(21)	2.333 (1)
Na(4)−O(16)	2.436 (1)	Na(4)−O(18)	2.480 (1)
P(1)−O(3)	1.485 (1)	P(2)−O(5)	1.612 (1)
P(2)−O(6)	1.490 (1)	P(3)−O(8)	1.608 (1)
P(3)−O(9)	1.500 (1)	P(4)−O(12)	1.484 (1)
P(5)−O(15)	1.480 (1)	P(6)−O(16)	1.617 (1)
P(6)−O(18)	1.502 (1)	P(7)−O(20)	1.616 (1)
P(7)−O(21)	1.495 (1)	P(8)−O(24)	1.482 (1)
P(2)−O(6)−Na(2)	131.22 (6)	P(2)−O(6)−Na(3)	131.79 (6)
Na(2)−O(6)−Na(3)	96.23 (4)	P(2)−O(6)−Na(1)	95.89 (5)
Na(2)−O(6)−Na(1)	90.24 (4)	Na(3)−O(6)−Na(1)	91.23 (4)
P(3)−O(9)−Na(4)	140.52 (6)	P(3)−O(9)−Na(3)	127.37 (6)
Na(4)−O(9)−Na(3)	90.60 (4)	P(3)−O(9)−Na(2)	97.59 (5)
Na(4)−O(9)−Na(2)	93.33 (4)	Na(3)−O(9)−Na(2)	88.41 (4)
P(6)−O(18)−Na(1)	128.43 (6)	P(6)−O(18)−Na(2)	132.38 (6)
Na(1)−O(18)−Na(2)	96.99 (4)	P(6)−O(18)−Na(4)	100.16 (5)
Na(1)−O(18)−Na(4)	87.83 (4)	Na(2)−O(18)−Na(4)	94.34 (4)
P(7)−O(21)−Na(1)	133.90 (6)	P(7)−O(21)−Na(4)	131.02 (6)
Na(1)−O(21)−Na(4)	91.71 (4)	P(7)−O(21)−Na(3)	100.58 (5)
Na(1)−O(21)−Na(3)	96.57 (4)	Na(4)−O(21)−Na(3)	88.20 (4)
O(15)−Na(1)−O(21)	118.87 (4)	O(15)−Na(1)−O(18)	88.65 (4)
O(21)−Na(1)−O(18)	92.67 (4)	O(15)−Na(1)−O(5)	111.65 (4)
O(21)−Na(1)−O(5)	116.66 (4)	O(18)−Na(1)−O(5)	124.90 (4)
O(15)−Na(1)−O(6)	156.01 (4)	O(21)−Na(1)−O(6)	83.98 (4)
O(18)−Na(1)−O(6)	82.69 (4)	O(5)−Na(1)−O(6)	57.79 (3)
O(3)−Na(2)−O(6)	87.08 (4)	O(3)−Na(2)−O(18)	120.46 (4)
O(6)−Na(2)−O(18)	89.80 (4)	O(3)−Na(2)−O(8)	104.85 (4)
O(6)−Na(2)−O(8)	122.96 (4)	O(18)−Na(2)−O(8)	125.53 (4)
O(3)−Na(2)−O(9)	153.15 (4)	O(6)−Na(2)−O(9)	85.59 (4)
O(18)−Na(2)−O(9)	85.32 (4)	O(8)−Na(2)−O(9)	59.04 (3)
O(12)−Na(3)−O(6)	116.61 (4)	O(12)−Na(3)−O(9)	89.11 (4)
O(6)−Na(3)−O(9)	89.68 (4)	O(12)−Na(3)−O(20)	103.88 (4)
O(6)−Na(3)−O(20)	123.49 (4)	O(9)−Na(3)−O(20)	130.19 (4)
O(12)−Na(3)−O(21)	155.12 (4)	O(6)−Na(3)−O(21)	88.19 (4)
O(9)−Na(3)−O(21)	89.14 (4)	O(20)−Na(3)−O(21)	59.69 (3)
O(24)−Na(4)−O(9)	121.50 (4)	O(24)−Na(4)−O(21)	86.72 (4)
O(9)−Na(4)−O(21)	91.89 (4)	O(24)−Na(4)−O(16)	104.48 (4)
O(9)−Na(4)−O(16)	120.73 (4)	O(21)−Na(4)−O(16)	128.30 (4)
O(24)−Na(4)−O(18)	151.03 (4)	O(9)−Na(4)−O(18)	86.96 (4)
O(21)−Na(4)−O(18)	87.00 (4)	O(16)−Na(4)−O(18)	59.08 (3)

gands within **2** can be distinguished by the number of Na−O contacts they make and the number of metals they bind to, i.e. (i) four Na−O contacts, and bridging two metals [terminal ligand carrying P(5) and P(6)]; (ii) four Na−O contacts, and bridging three metals [central ligand carrying P(1) and P(2)]; and (iii) seven Na−O contacts, and bridging five metals [central ligand carrying P(3) and P(4)]. The remarkable coordination flexibility of the β-diphosphonate ligands found within **1** and **2** is illustrated in Figure 6.

The coordination modes labeled (a), (b) and (d) in Figure 6 have not previously been observed for either neutral or anionic complexes of β-diphosphonates.[14] In fact, to the best of our knowledge, there are no reported examples of ester phosphonates that utilize an attached alkoxy unit as a

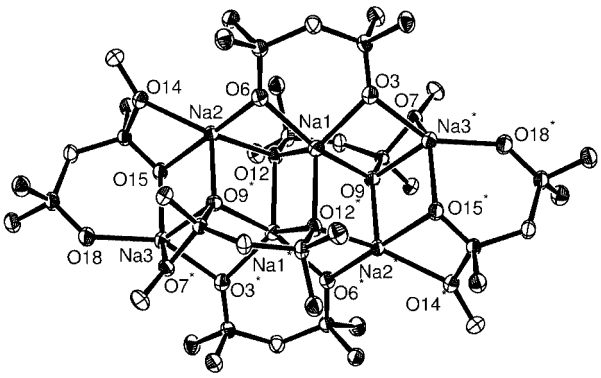

Figure 4. Molecular structure of $[\{(EtO)_2P(O)\}_2CHNa]_6$, **2**, with hydrogen atoms and ethyl groups (except for the α-Cs of the ethoxy groups involved in metal binding) removed for clarity

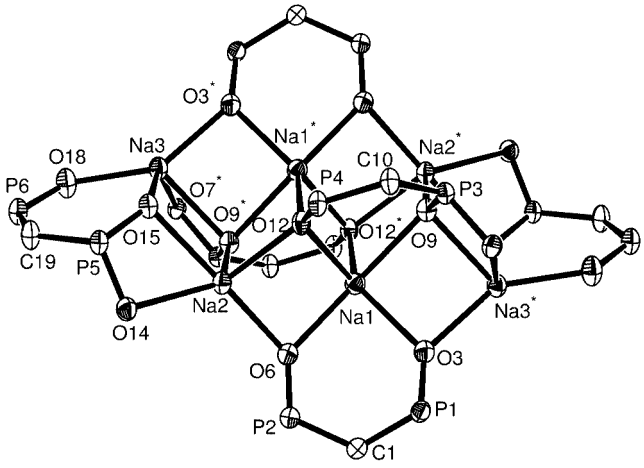

Figure 5. Alternative view of **2** showing the six-rung step ladder core, with only the atoms involved with binding to the metal centers displayed

ligating site to a metal center.[23] However, simple chelation by the phosphoryl units and also binding mode (c) in Figure 6 have previously been found for several transition metal and lanthanide complexes of β-diphosphonates.[14,24,25]

Although hexameric aggregates for sodium complexes have previously been characterized,[26] the six-rung ladder arrangement found in **2** is unusual. Most commonly, sodium hexamers adopt either double-stacked trimeric[27] or triple-stacked dimeric[28] structures (Figure 7). The closest structural analog to **2** is the imidophosphate complex $[\{(PhO)_2P(O)\}_2NNa]_6$, which has a similar Na_6O_6 ladder core but has only very long range interactions between the metals and the phenoxy groups (>2.8 Å).[29] A simple six-rung ladder aggregate of a group 1 complex has also been characterized, the lithium phosphane $[(Me_3Si)_2PLi]_6$.[30] Most commonly, four-rung (association of two dimers) or polymeric ladders are formed for these metal complexes.[31] The seminal work of Snaith and others in developing the ring-laddering and ring-stacking principles has been essential to our understanding of such systems.[32,33]

Looking in detail at the key geometric parameters within the cages **1** and **2**, the Na−O bond lengths vary over a

 © 2003 Wiley-VCH Verlag GmbH & Co. KGaA, Weinheim

Table 2. Selected bond lengths (Å) and angles (°) within **2**

Na(1)−O(3)	2.268 (2)	Na(1)−O(6)	2.291 (2)
Na(1)−O(12)	2.374 (2)	Na(1)−O(12*)	2.386 (2)
Na(1)−O(9)	2.441 (2)	Na(2)−O(9*)	2.244 (2)
Na(2)−O(6)	2.291 (2)	Na(2)−O(12)	2.347 (2)
Na(2)−O(14)	2.396 (2)	Na(2)−O(15)	2.450 (2)
Na(3)−O(18)	2.225 (2)	Na(3)−O(15)	2.267 (2)
Na(3)−O(3*)	2.296 (2)	Na(3)−O(7*)	2.437 (2)
Na(3)−O(9*)	2.451 (2)	P(1)−O(3)	1.493 (2)
P(2)−O(6)	1.489 (2)	P(3)−O(7)	1.613 (2)
P(3)−O(9)	1.496 (2)	P(4)−O(12)	1.504 (1)
P(5)−O(14)	1.615 (2)	P(5)−O(15)	1.489 (2)
P(6)−O(18)	1.489 (2)		
P(3)−O(9)−Na(2*)	139.16 (9)	P(3)−O(9)−Na(1)	123.63 (8)
Na(2*)−O(9)−Na(1)	94.77 (6)	P(3)−O(9)−Na(3)*	100.65 (7)
Na(2*)−O(9)−Na(3*)	95.91 (6)	Na(1)−O(9)−Na(3)*	84.57 (5)
P(4)−O(12)−Na(2)	125.44 (8)	P(4)−O(12)−Na(1)	126.83 (8)
Na(2)−O(12)−Na(1)	85.02 (5)	P(4)−O(12)−Na(1)*	130.79 (9)
Na(2)−O(12)−Na(1)*	93.62 (6)	Na(1)−O(12)−Na(1)*	79.76 (5)
P(5)−O(15)−Na(3)	130.96 (9)	P(5)−O(15)−Na(2)	99.57 (8)
Na(3)−O(15)−Na(2)	95.37 (6)	O(10)−C(15)−C(16)	109.1 (3)
O(3)−Na(1)−O(6)	87.79 (6)	O(3)−Na(1)−O(12)	131.70 (7)
O(6)−Na(1)−O(12)	87.49 (6)	O(3)−Na(1)−O(12*)	123.61 (6)
O(6)−Na(1)−O(12)*	119.09 (6)	O(12)−Na(1)−O(12*)	100.24 (5)
O(3)−Na(1)−O(9)	88.22 (6)	O(6)−Na(1)−O(9)	155.94 (7)
O(12)−Na(1)−O(9)	77.60 (5)	O(12*)−Na(1)−O(9)	82.50 (5)
O(9*)−Na(2)−O(6)	94.75 (6)	O(9*)−Na(2)−O(12)	87.76 (6)
O(6)−Na(2)−O(12)	88.13 (6)	O(9*)−Na(2)−O(14)	120.65 (6)
O(6)−Na(2)−O(14)	119.21 (6)	O(12)−Na(2)−O(14)	135.57 (6)
O(9*)−Na(2)−O(15)	84.62 (6)	O(6)−Na(2)−O(15)	178.19 (7)
O(12)−Na(2)−O(15)	93.55 (6)	O(14)−Na(2)−O(15)	59.88 (5)
O(18)−Na(3)−O(15)	87.84 (6)	O(18)−Na(3)−O(3*)	145.54 (7)
O(15)−Na(3)−O(3*)	113.41 (6)	O(18)−Na(3)−O(7*)	90.11 (6)
O(15)−Na(3)−O(7*)	133.60 (6)	O(3*)−Na(3)−O(7*)	93.31 (6)
O(18)−Na(3)−O(9*)	122.99 (7)	O(15)−Na(3)−O(9*)	84.10 (6)
O(3*)−Na(3)−O(9*)	87.36 (6)	O(7*)−Na(3)−O(9*)	58.91 (5)

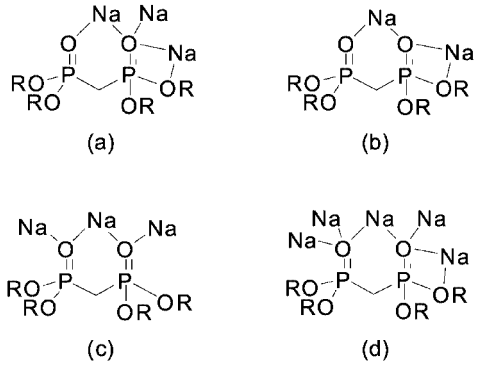

Figure 6. The different bonding modes found for the ligands in **1** (a), and **2** (b-d)

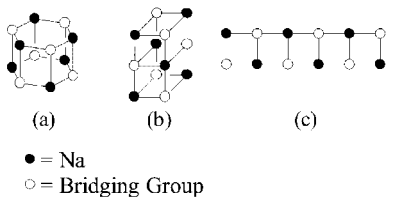

Figure 7. Hexameric aggregation states of sodium complexes: (a) double-stacked trimeric, (b) triple-stacked dimeric, (c) six-rung ladder

relatively wide range, from 2.202(1) to 2.623(1) Å. The shortest Na−O distances are associated with the chelating phosphoryl units, which ligate to a single sodium center [mean 2.220 Å in **1** and Na(3)−O(18): 2.225(2) Å in **2**]. Within the cubane framework of **1** each metal has two relatively short Na−O contacts (mean 2.312 Å) and a third longer contact (mean 2.518 Å) along the edges of the cube containing the chelating *i*PrO groups. The Na−O distance involving the *i*PrO groups lies in between these values at 2.400 Å (mean). A similar pattern is observed in **2**, where the Na−O distances lengthen, as expected, as the number of metals bridged by the phosphoryl increases (μ_1 to μ_3). The exceptions are the phosphoryl to sodium bonds Na(2)−O(15) at 2.450(2) and Na(3)−O(9*) at 2.451(2) Å, which are longer than expected. These elongated bonds are again associated with the four-membered NaOPO rings formed by the chelating OEt groups. Hence, the alkoxy-to-metal interactions in both **1** and **2** are relatively strong, and in fact the structures are significantly distorted in order to accommodated this mode of bonding.

The P=O distances lie in a relatively narrow range from 1.480(1) to 1.504(1) Å (mean 1.491 Å) over the two complexes, with the bonds lengthening as the number of metals bridged increases, i.e. μ_1, μ_2 and μ_3. These distances correspond well with those of previously characterized transition metal complexes of neutral β-diphosphonates,[14a,14b] and are consistent with localized P=O double bonds. The P−C distances in **1** and **2** range between 1.679(2) and 1.705(2) Å (mean 1.692 Å), and are substantially shorter than single P−C bonds in neutral β-diphosphonates (approximately 1.79 Å).[14] The shorter P−C bonds are associated with phosphoryl units that are involved in bridging multiple sodium centers. However, for the set of symmetrically bound ligands in **2** the P−C distances are identical, i.e. where P(1)−C(1) and P(2)−C(1) are both 1.694(2) Å. For comparison, the P−C distances in the ylides $Ph_3P{=}CH_2$ and mesitylP=CPh_2 are 1.67 and 1.69 Å respectively.[34] Overall, the bonding within the ligand backbone is best described as localized double bonding for the P=O units and delocalized partial multiple bonding over the P−C−P fragment.

It is also worth noting that although there are four different modes of ligation found for the β-diphosphonates in **1** and **2** (Figure 6), all the ligands contain synperiplanar phosphoryl units that chelate a metal center. It has previously been speculated that the reactivity differences between the anions of **3** and **4** may be due to the steric bulk of the isopropyl groups prohibiting coplanarity of the phosphoryl and carbanion groups.[3a] However, the six-membered OPCPONa chelate rings in both complexes are all similarly non-planar, with the range of the rms deviations from the planes being between 0.077 and 0.277 Å (mean 0.117). Again, these results are in agreement with the mostly localized bonding model described above.

Ab Initio Calculations

In an effort to determine the relative stabilities of the tetrameric and hexameric aggregations states found for **1** and **2** a set of ab initio calculations performed at the HF/

 © 2003 Wiley-VCH Verlag GmbH & Co. KGaA, Weinheim

6−31G* level were undertaken on model systems.[35,36] The tetramethoxy complexes $[\{(MeO)_2P(O)\}_2CHNa]_4$ (**I**) and $[\{(MeO)_2P(O)\}_2CHNa]_6$ (**II**) were geometry optimized using the relevant crystal structure data for **1** and **2** as starting positions. The geometries of the calculated and experimentally determined structures are in excellent agreement, with differences of less than 0.01 Å (mean) for the bonds involving the metals. The key finding from these calculations was that the hexamer is more stable than the tetramer by 12.08 kcal mol^{-1} according to Equation (1) (or by 2.01 kcal mol^{-1} on a per-monomer basis).

$$3/2\ [\{(MeO)_2P(O)\}_2CHNa]_4 \xrightarrow{-12.08\ kcal\ mol^{-1}} [\{(MeO)_2P(O)\}_2CHNa]_6 \quad (1)$$

Considering that all the metals are pentacoordinate, and in the absence of any significant steric effects, the stability of the aggregates is most likely related to differences in the types of metal-to-ligand interactions present. In **I** each metal binds to four phosphoryl oxygen centers and a single *i*PrO group. Two of the metals in **II** also have this bonding pattern but the third metal bonds solely to five phosphoryl units. The increased coulombic component resulting from this bonding mode may, in turn, favor the formation of the hexamer. Furthermore, formation of the more open ladder framework will result in a decrease in ring strain compared with the cubane but without necessitating a reduction in the coordination number at the metals.

Conclusions

The main findings from this work are: (i) complexes **1** and **2** are the first examples of simple alkali metal derivatives of β-diphosphonates to be crystallographically characterized, and were found to form tetrameric cubane and hexameric ladder structures respectively, (ii) the β-diphosphonate ligands display four distinct ligation modes, three of which have not been described previously, (iii) the bonding within the β-diphosphonate backbones in both complexes are similar, and are composed of localized P=O double bonds and partial delocalization of the charge over the P−C−P units, and (iv) the hexameric six-rung ladder structure has been determined by calculations to be thermodynamically preferred over the tetrameric cubane structure for the model complexes **I** and **II**.

In summary, formation of the cubane **1** is most likely a consequence of the increased steric encumbrance of the attached alkoxy sidearms precluding the multiple bridging ligand environments required for construction of the hexameric framework found for **2**. Nevertheless, each individual β-diphosphonate ligand within **1** and **2** still adopts relatively similar local geometries, with synperiplanar phosphoryl units. Finally, in view of the different aggregation states found for **1** and **2**, it is unsurprising that there are differences in the reactivity of the β-diphosphonates. While it is true that the smaller tetrameric aggregate **1** has increased reactivity compared to the larger hexameric **2**, it may be too simplistic to attribute the reactivity differences solely to aggregate size.[37] Rather, the ability of the electrophile to approach the carbanion has to be considered. Also, the increased strain within the cubane compared to the ladder may lead to an attenuation in its reactivity.[38]

Experimental Section

General Procedures: All manipulations were carried out under a protective dinitrogen atmosphere using standard Schlenk techniques.[39] All glassware was flame-dried under vacuum before use. Hexane was purified by passage through copper-based catalyst and molecular sieves columns (Innovative Technology). The sodium hydride was supplied by Alfa Aesar as an oil dispersion, and was washed with dry hexane prior to use. The sodium butoxide was used as supplied by Acros Organics. *n*BuLi was purchased from Aldrich as a 1.6 M solution in hexane and was standardized by titration with salicylaldehyde phenylhydrazone directly before use.[40] Butylsodium (*n*BuNa) was prepared according to modified literature procedures and stored in an argon-filled glove box before use.[41] The phosphonate ligands $[(RO)_2P(O)]_2CH_2$ (R = *i*Pr, Et), **1** and **2**, were supplied by Lancaster and were purified by distillation from over calcium hydride and stored over 4 Å molecular sieves.

Although reactions using stoichiometries ranging between 1:1 and 3.5:1 of the three metalating reagents — NaH, *n*BuNa and *t*BuONa/*n*BuLi — and the parent phosphonates **3** and **4** were conducted, the only single crystals gleaned were the monodeprotonated complexes **1** or **2**. It has been reported previously that these ligands undergo cleavage in the presence of excess base and at elevated temperatures.[3g] Complexes **1** and **2** could be prepared in a rational manner as described below.

Synthesis of 1 and 2: The parent phosphonate (**3** or **4**, 10 mmol) was dissolved in 5 mL of hexane and the solution cooled to 0 °C. *n*BuNa (10 mmol) was added to the reaction mixture via a solids addition tube over several minutes, and the resulting mixture was slowly warmed to room temperature. The mixture was heated gently, filtered and the filtrate was stored at −45 °C. After one day, small colorless blocks of the complexes **1** or **2** were precipitated. Formation of **1** and **2** was confirmed by their ^1H and ^{13}C NMR spectra, which were in agreement with previously published data.[3b,15a]

1: Yield = 52%. ^1H NMR (300 MHz, [D$_5$]pyridine, 25 °C): δ = 1.05 (t, $^2J_{H,P}$ = 6.3 Hz, 1 H, PCH), 1.33 (d, $^3J_{H,H}$ = 6.0 Hz, 12 H, CH_3), 1.37 (d, $^3J_{H,H}$ = 6.0 Hz, 12 H, CH_3), 4.80 (m, 4 H, CH) ppm. $^{13}C\{^1H\}$ NMR (300 MHz, [D$_5$]pyridine, 25 °C): δ = 12.8 (t, $^1J_{C,P}$ = 213.4 Hz, CP), 24.7 (t, $J_{C,P}$ = 4.5 Hz, CH_3), 24.9 (t, $J_{C,P}$ = 4.5 Hz, CH_3), 67.7 (s, CH) ppm.

2: Yield = 46%. ^1H NMR (300 MHz, [D$_5$]pyridine, 25 °C): δ = 1.13 (t, $^2J_{H,P}$ = 6.4 Hz, 1 H, PCH), 1.28 (t, $^3J_{H,H}$ = 7.0 Hz, 12 H, CH_3), 4.16 (m, 8 H, CH_2) ppm. $^{13}C\{^1H\}$ NMR (300 MHz, [D$_5$]pyridine, 25 °C): δ = 10.2 (t, $^1J_{C,P}$ = 217.1 Hz, CP), 17.1 (t, $J_{C,P}$ = 3.7 Hz, CH_3), 60.4 (s, CH_2) ppm.

X-ray Structure Determination: Table 3 contains details of the data collection. In both cases the crystalline sample was placed in inert oil, mounted on a glass pin, and transferred to the cold N_2 gas stream of the diffractometer. Crystal data were collected and integrated using a Bruker Apex system, with graphite monochromated Mo-K_α (λ = 0.71073 Å) radiation at 100 K. The structures were

 © 2003 Wiley-VCH Verlag GmbH & Co. KGaA, Weinheim

solved by direct methods using SHELXS-97 and refined using SHELXL-97.[42] Non-hydrogen atoms were found by successive full-matrix least-squares refinement on F^2 and refined with anisotropic thermal parameters. All hydrogen atoms were placed at idealized positions and a riding model was applied, with fixed thermal parameters [uij = 1.2*U*ij(eq) for the atom to which they are bonded]. The asymmetric unit contains one tetrameric cage for **1** and one half of a hexameric cage for **2**.

Table 3. Crystallographic data for **1** and **2**

Compound	**1**	**2**
Formula	$C_{52}H_{116}Na_4O_{24}P_8$	$C_{54}H_{126}Na_6O_{36}P_{12}$
Molecular weight	1465.17	1861.13
Temperature (K)	100 (2)	100 (2)
Crystal System	Monoclinic	Triclinic
Space Group	$P2_1/c$	$P\bar{1}$
a (Å)	7.5772 (10)	12.4357 (9)
b (Å)	21.6203 (13)	13.9757 (11)
c (Å)	12.8075 (15)	14.1637 (11)
α (°)	90	73.5970 (10)
β (°)	90.8460 (10)	73.3650 (10)
γ (°)	90	83.0830 (10)
Volume (Å^3)	7812.9 (8)	2260.5 (3)
Z	4	1
Density (calcd.) (Mg/m^3)	1.246	1.367
Absorption Coefficient (mm^{-1})	0.266	0.331
F(000)	3136	984
Crystal Size (mm)	0.3 × 0.1 × 0.1	0.4 × 0.3 × 0.3
Reflections Collected/ unique	82239/19424 [*R*(int) = 0.0559]	24137/11236 [*R*(int) = 0.0244]
Data/Restraints/Parameters	5574/0/277	11236/0/487
Goodness-of-fit on F^2	1.023	1.043
R_1	0.0345	0.0503
wR_1	0.0967	0.1467

CCDC-209651 (**1**) and -209652 (**2**) contain the supplementary crystallographic data for this paper. These data can be obtained free of charge at www.ccdc.cam.ac.uk/conts/retrieving.html [or from the Cambridge Crystallographic Data Centre, 12 Union Road, Cambridge CB2 1EZ, UK; Fax: (internat.) +44-1233/336-033; E-mail: deposit@ccdc.cam.ac.uk].

Computational Details: The Gaussian 98 series of programs were used for the calculations.[35] No symmetry constraints were imposed and the molecules were allowed to freely optimize at the HF/6−31G* level using the relevant crystal structure data for **1** and **2** as starting geometries.[36] Frequency analysis was used to ensure that true minima were located. The total energies for **I** and **II** are 5958.4381 and 8937.6764 Hartrees respectively.

Acknowledgments

We wish to thank the University of Notre Dame for financial support.

[1] G. M. Kosolapoff, *J. Am. Chem. Soc.* **1953**, *75*, 1500.
[2] [2a] *Comprehensive Organic Synthesis* (Eds.: B. M. Trost, I. Fleming), Pergamon, Oxford, U. K., 1991, Vols. 1 and 2. [2b] *Comprehensive Carbanion Chemistry Part B* (Eds.: E. Buncel, T. Durst), Elsevier, Amsterdam, 1984.
[3] For examples of alkylation reactions see: [3a] D. W. Hutchinson, G. Semple, *J. Organomet. Chem.* **1985**, *291*, 145. [3b] D. W. Hutchinson, G. Semple, *J. Organomet. Chem.* **1986**, *309*, C7−C10. [3c] J. R. Hanrahan, D. W. Hutchison, *Tetrahedron Lett.* **1993**, *34*, 3767. [3d] D. Seyferth, R. S. Manor, *J. Organomet. Chem.* **1973**, *59*, 237. [3e] A. Bakalarz-Jeziorna, J. Heliński, B. Krawiecka, *J. Chem. Soc., Perkin Trans. 1* **2001**, 1086. [3f] C. Viornery, P. Péchy, M. Boegli, B. O. Aronsson, P. Descouts, M. Grätzel, *Phosphorus Sulfur and Silicon* **2002**, *177*, 231. [3g] O. T. Quimby, J. D. Curry, D. A. Nicholson, J. B. Prentice, C. H. Roy, *J. Organomet. Chem.* **1968**, *13*, 199.
[4] For examples of Horner−Wadsworth−Emmons reactions see: [4a] W. S. Wadsworth, Jr., W. D. Emmons, *J. Am. Chem. Soc.* **1961**, *83*, 1733. [4b] J.-P. Gourves, H. Couthon, G. Sturtz, *Eur. J. Org. Chem.* **1999**, *9* 3489. [4c] G. Wang, Y. Shen, *Heteroatom Chem.* **2002**, *13*, 116. [4d] B. Bessières, A. Schoenfelder, C. Verrat, A. Mann, P. Ornstein, C. Pedregal, *Tetrahedron Lett.* **2002**, *43*, 7659. [4e] H. Streicher, C. Bohner, *Tetrahedron* **2002**, *58*, 7573.
[5] [5a] W. Eubank, R. R. Reeves, *J. Parasitol.* **1982**, 599. [5b] P. A. Cload, D. W. Hutchinson, *Nucleic Acids Res.* **1983**, *11*, 5621. [5c] J. S. Oxford, D. D. Perin, *Ann. N. Y. Acad. Sci.* **1977**, *284*, 613. [5d] T. S. T. Wang, R. A. Fawwaz, L. J. Johnson, G. E. Majdehi, P. M. Johnson, *J. Nucl. Med.* **1980**, *21*, 767.
[6] [6a] F. Szuki, Y. Fujikawa, S. Yamamoto, H. Mizutani, T. Ohya, T. Ikai, T. Oguchi, Nissan Chemical Industries Ltd., U. S. Pat. 4,447,256, 1984. [6b] R. S. Edmundson, *Dictionary of Organophosphorus Compounds*, Chapman and Hall Ltd., London, 1988. [6c] R. Engel, *Handbook of Organophosphorus Compounds*, M. Dekker, New York, 1992, vol. 15−16, pp739.
[7] [7a] H. Fleisch, *Bisphosphonates in Bone Disease. From the Laboratory to the Patient*, Pathernon, New York, 1997, 3rd Edn. [7b]P. David, H. Nguyen, A. Barbier, R. Baron, *J. Bone Miner. Res.* **1996**, *11*, 1498. [7c] G. Golomb, J. M. van Gelder, I. S. Alferev, A. Ornoy, A. Hoffman, A. Schlossman, A. Friedman-Erza, N. El-H. Rozen, R. Chen, V. Solomon, H. Cohen, L. Rabinovich, E. Breuer, *Phosphorus Sulfur and Silicon* **1996**, *109/110*, 221. [7d] I. Shinkai, Y. Ohta, *Bioorg. Med. Chem.* **1996**, *4*, 3.
[8] [8a] O. T. Quimby, U. S. Pat. 3,400,176, **1968**. [8b] O. T. Quimby, C. Township, H. County, The Proctor & Gamble Co., U. S. Pat. 3,551,339, **1970**. [8c] L. Maier, *Chimia* **1969**, *23*, 323.
[9] [9a] J. B. Prentice, I. Batesville, The Procter & Gamble Co., U. S. Pat. 3,641,126, **1972**. [9b] O. T. Quimby, The Proctor & Gamble Co., U. S. Pat. 6,617,575, **1971**. [9c] S. J. Fitch, R. R. Irani, Fr. Pat. 1,394,386, **1965**.
[10] Y. Fujita, S. Ueda, T. Ishikawa, A. Abe, Fuji Photo Film Co., Eur. Pat. 0.330,043 B1, **1989**.
[11] R. C. Mehrotra, R. Bohra, D. P. Gaur, *Metal* β-*Diketonate and Allied Derivatives*, Academic Press, New York, **1978**
[12] [12a] R. H. Holm, G. W. Everett, A. Chakravorty, *Prog. Inorg. Chem.* **1966**, *7*, 83. [12b] M. Calligaris, L. Randaccio, *Comprehensive Coordination Chemistry* (Eds.: G. Wilkinson, R. D. Gillard, J. A. McCleverty), Pergamon: Oxford, **1987**, vol. 2, p21.
[13] L. Bourget-Merle, M. F. Lappert, J. R. Severn, *Chem. Rev.* **2002**, *102*, 3031.
[14] [14a] B. Bremer, A. A. Pinkerton, J. A. Walmsley, *Inorg. Chim. Acta* **1990**, *174*, 27. [14b] P. T. Miller, P. G. Lenhert, M. D. Joesten, *Inorg. Chem.* **1973**, *1*, 218. [14c] J. Browning, G. W. Bushnell, K. R. Dixon, *Inorg. Chem.* **1981**, *20*, 3912.
[15] For early work regarding the nature of the bonding in β-diphosphonates see: [15a] J. D. Baldeschwieler, F. A. Cotton, B. D. Nageswara Rao, R. A. Schunn, *J. Am. Chem. Soc.* **1962**, *84*, 4454. [15b] F. A. Cotton, R. A. Schunn, *J. Am. Chem. Soc.* **1963**, *85*, 2394.
[16] For a recent review of superbases see: L. Lochmann, *Eur. J. Inorg. Chem.* **2000**, *6*, 1115.
[17] [17a] Y. Chi, S. Ranjan, P.-W. Chung, C.-S. Liu, S.-M. Peng, G.-H. Lee, *J. Chem. Soc., Dalton Trans.* **2000**, 343. [17b] P. Sobota, M. Klimowicz, J. Utko, L. B. Jerzykiewicz, *New J. Chem.* **2000**, *7*, 523. [17c] Z. Hou, X. Jia, A. Fujita, H. Tezuka, H. Yamazaki, Y. Wakatsuki, *Chem. Eur. J.* **2000**, *6*, 2994. [17d] I. Abrahams, M. Lazell, M. Motevalli, S. A. A. Shah, A. C. Sullivan, *J. Organomet. Chem.* **1998**, *553*, 23. [17e] M. Kunert, E. Dinjus, M.

Nauck, J. Sigler, *Chem. Ber./Recueil* **1997**, *130*, 1461. [17f] M. Veith, E.-C. Yu, V. Huch, *Chem. Eur. J.* **1995**, *1*, 26. [17g] W. J. Evans, R. E. Golden, J. W. Ziller, *Inorg. Chem.* **1993**, *32*, 3041. [17h] E. Solari, S. De Angelis, C. Floriani, A. Chiesi-Villa, C. Rizzoli, *J. Chem. Soc., Dalton Trans.* **1991**, 2471.

[18] P. A. van der Schaaf, J. T. B. H. Jastrzebski, M. P. Hogerheide, W. J. J. Smeets, A. L. Spek, J. Boersma, G. van Koten, *Inorg. Chem.* **1993**, *32*, 4111.

[19] For a review see: G. Boche, *Angew. Chem. Int. Ed. Engl.* **1989**, *28*, 277.

[20] For the structures of other group one metallated α,α′-stabilized carbanions see: [20a] K. W. Henderson, A. R. Kennedy, A. E. McKeown, D. Strachan, *J. Chem. Soc., Dalton Trans.* **2000**, 4348. [20b] K. W. Henderson, A. R. Kennedy, D. J. MacDougall, D. Shanks, *Organometallics* **2002**, *21*, 606. [20c] K. W. Henderson, A. R. Kennedy, D. J. MacDougall, *Inorg. Chem.* **2003**, *42*, 2736. [20d] K. W. Henderson, A. R. Kennedy, L. Macdonald, D. J. MacDougall, *Inorg. Chem.* **2003**, *42*, 2839.

[21] [21a] D. Barr, W. Clegg, R. E. Mulvey, R. Snaith, *J. Chem. Soc., Chem. Commun.* **1984**, 700. [21b] D. Barr, W. Clegg, R. E. Mulvey, R. Snaith, *J. Chem. Soc., Chem. Commun.* **1984**, 974. [21c] K. Jens, J. Kopf, N. P. Lorenzen, E. Weiss, *Chem. Ber.* **1988**, *121*, 1201. [21d] P. C. Andrews, W. Clegg, R. E. Mulvey, *Angew. Chem. Int. Ed. Engl.* **1990**, *29*, 1440. [21e] J. Barker, D. Barr, N. D. R. Barnett, W. Clegg, I. Cragg-Hine, M. G. Davidson, R. P. Davies, S. M. Hodgson, J. A. K. Howard, M. Kilner, C. W. Lehmann, I. Lopez-Solera, R. E. Mulvey, P. R. Raithby, R. Snaith, *J. Chem. Soc., Dalton Trans.* **1997**, 951. [21f] D. R. Armstrong, A. H. Khandelwal, L. C. Kerr, S. Peasey, P. R. Raithby, G. P. Shields, R. Snaith, D. S. Wright, *Chem. Commun.* **1998**, 1011. [21g] D. R. Armstrong, F. A. Banbury, M. G. Davidson, P. R. Raithby, R. Snaith, D. Stalke, *J. Chem. Soc., Chem. Commun.* **1992**, 1492. [21h] F. A. Banbury, M. G. Davidson, P. R. Raithby, D. Stalke, R. Snaith, *J. Chem. Soc., Dalton Trans.* **1995**, 3139.

[22] K. W. Henderson, A. R. Kennedy, D. J. MacDougall, D. Strachan, *Acta Crystallogr., Sect. C* **2003**, *59*, m49.

[23] For related structures containing both phosphoryl and alkoxyl to metal ligation see: [23a] C. G. Lugmair, T. D. Tilley, *Inorg. Chem.* **1998**, *37*, 1821. [23b] G. Balazs, J. E. Drake, C. Silvestru, I. Haiduc, *Inorg. Chim. Acta* **1999**, *287*, 61. [23c] R. Shakir, J. L. Atwood, T. S. Janik, J. D. Atwood, *J. Organomet. Chem.* **1980**, *190*, C14.

[24] [24a] A. W. G. Platt, D. Simpson, J. Fawcett, D. R. Russell, *Inorg. Chim. Acta* **1994**, *223*, 43. [24b] A. M. J. Lees, J. M. Charnock, R. A. Kresinski, A. W. G. Platt, *Inorg. Chim. Acta* **2001**, *312*, 170. [24c] A. M. J. Lees, A. W. G. Platt, R. A. Kresiski, *Acta Crystallogr., Sect. C* **1997**, *53*, 581.

[25] A dimeric tin complex containing a bridging β-diphosphonate has also been characterized: J. Lorberth, S.-H. Shin, M. Otto, S. Wocadlo, W. Massa, N. S. Yashina, *J. Organomet. Chem.* **1991**, *407*, 313.

[26] For hexameric sodium aggregates see: [26a] Yu Yang, J. Pinkas, M. Noltemeyer, H. W. Roesky, *Inorg. Chem.* **1998**, *37*, 6404. [26b] M. Driess, G. Huttner, N. Knopf, H. Pritzkow, L. Zsolnai, *Angew. Chem. Int. Ed. Engl.* **1995**, *34*, 316. [26c] H. Bock, H. Schödel, Z. Havlas, E. Herrmann, *Angew. Chem. Int. Ed. Engl.* **1995**, *34*, 1355. [26d] B. W. F. Gordon, M. J. Scott, *Inorg. Chim. Acta* **2000**, *297*, 206.

[27] [27a] T. Gröb, C. Müller, W. Massa, T. Miekisch, G. Seybert, K. Harms, K. Dehnicke, *Z. Anorg. Allg. Chem.* **2001**, *627*, 2191. [27b] S. Schütte, U. Klingebiel, D. Schmidt-Bäse, *Z. Naturforsch., Teil B* **1993**, *48*, 263. [27c] R. den Besten, M. T. Lakin, N. Veldman, A. L. Spek, L. Brandsma, *J. Organomet. Chem.* **1996**, *514*, 191. [27d] D. J. Rose, Y. Da Chang, Q. Chen, P. B. Kettler, J. Zubieta, *Inorg. Chem.* **1995**, *34*, 3973.

[28] [28a] U. Englich, S. Chadwick, K. Ruhlandt-Senge, *Inorg. Chem.* **1998**, *37*, 283. [28b] S. Chadwick, U. Englich, K. Ruhlandt-Senge, *Organometallics* **1997**, *16*, 5792. [28c] J. Knizek, I. Krossing, H. Nöth, H. Schwenk, T. Seifert, *Chem. Ber./Recueil* **1997**, *130*, 1053. [28d] M. Kunert, E. Dinjus, M. Nauck, J. Sieler, *Chem. Ber./Recueil* **1997**, *130*, 1461. [28e] M. P. Hogerheide, S. N. Ringelberg, M. D. Janssen, J. Boersma, A. L. Spek, G. van Koten, *Inorg. Chem.* **1996**, *35*, 1195.

[29] H. Bock, H. Schödel, Z. Havlas, E. Herrmann, *Angew. Chem. Int. Ed. Engl.* **1995**, *34*, 1355.

[30] E. Hey-Hawkins, E. Sattler, *J. Chem. Soc., Chem. Commun.* **1992**, 775.

[31] For a review on lithium compounds see: *Lithium Chemistry, A Theoretical and Experimental Overview* (Eds.: A. M. Sapse P. v. R. Schleyer), John Wiley & Sons, New York, 1995.

[32] [32a] D. Barr, W. Clegg, R. E. Mulvey, R. Snaith, K. Wade, *J. Chem. Soc., Chem. Commun.* **1986**, 295. [32b] D. R. Armstrong, D. Barr, W. Clegg, R. E. Mulvey, D. Reed, R. Snaith, K. Wade, *J. Chem. Soc., Chem. Commun.* **1986**, 869. [32c] D. R. Armstrong, D. Barr, W. Clegg, S. M. Hodgson, R. E. Mulvey, D. Reed, R. Snaith, D. D. Wright, *J. Am. Chem. Soc.* **1989**, *111*, 4719.

[33] [33a] A. Downard, T. Chivers, *Eur. J. Inorg. Chem.* **2001**, 2193. [33b] R. E. Mulvey, *Chem. Soc. Rev.* **1998**, 339. [33c] E. Weiss, *Angew. Chem. Int. Ed. Engl.* **1993**, *32*, 1501. [33d] R. E. Mulvey, *Chem. Soc. Rev.* **1991**, *20*, 167. [33e] K. Gregory, P. v. R. Schleyer, R. Snaith, *Adv. Inorg. Chem.* **1988**, *27*, 1624. [33f] D. Seebach, *Angew. Chem. Int. Ed. Engl.* **1988**, *27*, 1624. [33g] J. L. Rutherford, D. B. Collum, *J. Am. Chem. Soc.* **1999**, *121*, 10198.

[34] [34a] J. C. J. Bart, *J. Chem. Soc., B* **1969**, 350. [34b] H. Schmidbaur, J. Jeong, A. Schier, W. Graf, D. L. Wilkinson, G. Muller, *New J. Chem.* **1989**, *13*, 341. [34c] T. A. van der Knaap, T. C. Klebach, F. Visser, F. Bickelhaupt, P. Ros, E. J. Baerends, C. H. Stam, M. Konijn, *Tetrahedron* **1984**, *40*, 765.

[35] M. J. Frisch, G. W. Trucks, H. B. Schlegel, G. E. Scuseria, M. A. Robb, J. R. Cheeseman, V. G. Zakrzewski, J. A., Jr., Montgomery, R. E. Stratmann, J. C. Burant, S. Dapprich, J. M. Millam, A. D. Daniels, K. N. Kudin, M. C. Strain, O. Farkas, J. Tomasi, V. Barone, M. Cossi, R. Cammi, B. Mennucci, C. Pomelli, C. Adamo, S. Clifford, J. Ochterski, G. A. Petersson, P. Y. Ayala, Q. Cui, K. Morokuma, D. K. Malick, A. D. Rabuck, K. Raghavachari, J. B. Foresman, J. Cioslowski, J. V. Ortiz, B. B. Stefanov, G. Liu, A. Liashenko, P. Piskorz, I. Komaromi, R. Gomperts, R. L. Martin, D. J. Fox, T. Keith, M. A. Al-Laham, C. Y. Peng, A. Nanayakkara, C. Gonzalez, M. Challacombe, P. M. W. Gill, B. G. Johnson, W. Chen, M. W. Wong, J. L. Andres, M. Head-Gordon, E. S. Replogle, J. A. Pople, Gaussian 98, Gaussian, Inc., Pittsburgh, PA, **1998**.

[36] [36a] J. D. Dill, J. A. Pople, *J. Chem. Phys.* **1975**, *62*, 2921. [36b] P. C. Hariharan, J. A. Pople, *Theor. Chim. Acta* **1973**, *28*, 213. [36c] W. J. Hehre, R. Ditchfield, J. A. Pople, *J. Chem. Phys.* **1972**, *56*, 2257.

[37] P. Zhao, D. B. Collum, *J. Am. Chem. Soc.* **2003**, *125*, 4008.

[38] The relationship between cage ring strain and reactivity has previously been discussed: [38a] C. J. Harlan, S. G. Bott, A. R. Barron, *J. Am. Chem. Soc.* **1995**, *117*, 6465. [38b] Y. Koide, S. G. Bott, A. R. Barron, *Organometallics* **1996**, *15*, 5514.

[39] D. F. Shriver, M. A. Drezdzon, *The Manipulation of Air-Sensitive Compounds*; Wiley, New York, **1986**.

[40] B. E. Love, E. G. Jones, *J. Org. Chem.* **1999**, *64*, 3755.

[41] M. Schlosser, in, *Organometallics in Synthesis*; M. Schlosser, M., Ed., Wiley, New York, 2002, Chapter 1.

[42] G. M. Sheldrick, University of Göttingen.

Received May 1, 2003
Early View Article
Published Online July 22, 2003

 © 2003 Wiley-VCH Verlag GmbH & Co. KGaA, Weinheim

The First Structurally Characterized Diorganoaluminate

Colin Eaborn,[a] Ian B. Gorrell,[b] Peter B. Hitchcock,[a] and J. David Smith*[a]

Dedicated to the memory of our friend and colleague Ron Snaith

Keywords: Aluminum / Silicon / Hydride ligands / Lithium

The first structurally characterized dialkylaluminate $[\{Li(THF)\}(Al\textit{t}Bu\{C(SiMe_3)_3\}H_2)]_2$ (**3**) is dimeric in the solid state with $[Li(THF)]^+$ and $[Al\textit{t}Bu\{C(SiMe_3)_3\}H_2]^-$ fragments linked by Li···H–Al bridges.

(© Wiley-VCH Verlag GmbH & Co. KGaA, 69451 Weinheim, Germany, 2003)

Introduction

Dialkylaluminates − compounds containing the $[AlR_2H_2]^-$ fragment − have been known as useful intermediates in syntheses for nearly 50 years.[1] The $NaAlEt_4$-$NaAlH_4$ phase diagram shows that sodium diethylaluminate is a thermodynamically stable species,[2] and both this and sodium dimethylaluminate are commercially available reducing agents.[3] Several routes to dialkylaluminates have been reported but evidence for individual species has been confined to elemental analysis (R = Me,[4−6] Et,[2,4,5,7,8] *n*Pr,[4] *i*Bu [4,5,9]), IR spectroscopy[6,8,10] and ^{27}Al NMR spectroscopy.[11] Dialkylaluminates are sometimes obtained from reaction mixtures that might be expected to yield monoalkylaluminates. For example, attempts to make sodium ethylaluminate $Na[AlEtH_3]$ give $Na[AlEt_2H_2]$ and $Na[AlH_4]$, suggesting that any initially formed $Na[AlEtH_3]$ rearranges as shown in Equation (1) (R = Et).

$$2Na[AlH_3R] \rightarrow Na[AlH_2R_2] + Na[AlH_4] \quad (1)$$

Diorganoaluminates are much less well characterized than the corresponding dialkoxo- and diaryloxoaluminates, which contain the ions $[Al(OR)_2H_2]^-$,[12,13] or aluminates containing the ions $[Al(ER_2)_2H_2]^-$ (E = N, P or As).[14,15] As far as we are aware, no diorganoaluminate has previously been structurally characterized, though the $[AlR_2H_2]^-$ fragment has been identified in titanium[16] and rhenium[17] hydride complexes and an aluminacarborane.[18]

In a footnote to a paper describing the alkylaluminate $[\{Li(THF)_2\}\{Al\{C(SiMe_2Ph)_3\}H_3\}]_2$ (**1a**), we mentioned briefly the di-*tert*-butylaluminate $Li[Al\textit{t}Bu_2H_2]\cdot 2THF$ (**2**).[19] This was obtained from the reaction of $LiAlH_4$ with one equivalent of Li*t*Bu, indicating that any initially formed $Li[Al\textit{t}BuH_3]$ either reacted more rapidly than $LiAlH_4$ with Li*t*Bu, or rearranged according to Equation (1) (R = *t*Bu). Treatment of $LiAlH_4$ with LiR (R = $C_6H_2\textit{i}Pr_3$-2,4,6) followed by $SiMe_3Cl$ gave AlR_2H, again suggesting that a diarylaluminate intermediate was formed from the monoaryl species.[20]

We have not been able to obtain crystals of **2** suitable for an X-ray structure determination, but we report the synthesis of the related compound $[\{Li(THF)\}(Al\textit{t}Bu\{C(SiMe_3)_3\}H_2)]_2$ (**3**) and its crystal structure. The iodide $Al\textit{t}Bu_2I\cdot THF$ (**4**) and the compounds $Li(TMEN)_n[Al\textit{t}Bu_2H_2]$ (n = 2, **5**; n = 1, **6**; TMEN = tetramethylethylenediamine), are also described.

Results and Discussion

Treatment of $Li[AlH_4]$ with $LiC(SiMe_3)_3(THF)_2$ or $LiC(SiMe_2Ph)_3(THF)$ gave the alkylaluminates **1b** and **1a**, in each of which one of the four hydride ligands has been replaced by a bulky organic group. Treatment of $Li[AlH_4]$ with the smaller Li*t*Bu led to the replacement of two hydride ligands and the formation of a dialkylaluminate **2**. The formation of a di- rather than a mono-substituted aluminate appears, therefore, to depend on the size of the attacking lithium derivative. We surmised that the reaction between **1b** and Li*t*Bu might yield the dialkylaluminate **3**, and this proved to be the case. Compound **3** was isolated in good yield as an air- and moisture-sensitive solid.

[a] Department of Chemistry, School of Life Sciences, University of Sussex,
Brighton, BN1 9QJ, UK
E-mail: J.D.Smith@sussex.ac.uk
[b] Department of Chemical and Forensic Sciences, University of Bradford,
Bradford, West Yorkshire, BD7 1DP, UK

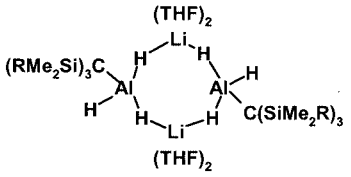

1a R = Ph, **1b** R = Me
1c R = NMe_2

$Li[AltBu_2H_2].2THF$

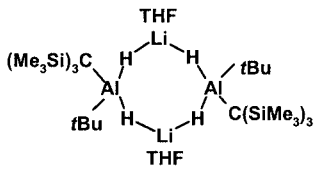

2 **3**

The molecular structure is shown in Figure 1 and selected bond lengths and angles in Table 1. The molecules of **3** are dimeric with a twofold axis through O2Li2···Li1O1. As in the organoaluminates **1a**[19] and **1c**,[21] the arylaluminates $Li[Al\{C_6H_2R_3\text{-}2,4,6\}H_3]$ with R = Ph (**1d**) or *t*Bu (**1e**),[22] the aryloxyaluminate $[Li(Et_2O)_2][Al\{OC_6H_3tBu_2\text{-}2,6\}H_3]$,[12] the bis(trimethylsilyl)amido derivatives $[Li(Et_2O)_2][Al\{N(SiMe_3)_2\}H_3]$[15] and $[Li(Et_2O)_2][Al\{PhNN(SiMe_3)_2\}H_3]$,[23] and the tetrahydoaluminates $[LiL\{AlH_4\}]_2$ {L = HN(*t*Bu)CH(*t*Bu)CH=N*t*Bu,[24] HN(*t*Bu)CH(*t*Bu)CH_2N(H)*t*Bu,[25] or TMEN[26]}, the cationic lithium and anionic aluminum fragments are held together by hydride bridges to give an eight-membered puckered $Li_2Al_2H_4$ ring. However, the conformation of this ring differs from those in the previously described compounds. In these the rings are in a chair conformation **I** with the aluminum atoms bent away from the almost planar Li_2H_4 array so that the large organic groups R on the periphery of the molecule point outwards. In **3** the $Li_2Al_2H_4$ ring adopts a skew-boat configuration **II** in which the atoms H1a′ and H1b lie above and H1a and H1b′ lie below the plane containing the Li, Al and O atoms; the larger ligands R are *trans* with respect to the ring. We cannot at present say whether the conformation is determined by other than crystal packing forces. In contrast to **1a**, there are no problems with crystallographic disorder.

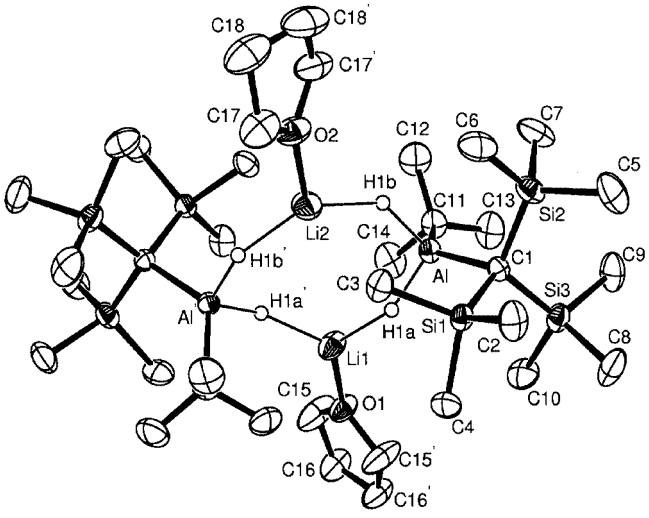

Figure 1. The molecular structure of **3** with thermal ellipsoids 50% probability

Table 1. Selected bond lengths [Å] and angles [°] in $[\{Li(THF)\}(AltBu\{C(SiMe_3)_3\}H_2)]_2$ (**3**)

Al−CSi_3	2.041(2)	Li−H1a	1.79(3)
Al−CC_3	2.043(2)	Li−H1b	1.82(3)
Al−H1a	1.55(3)	Li−O1	1.862(6)
Al−H1b	1.59(3)	Li−O2	1.891(6)
Si−C1[a]	1.878(2)	Si−Me[a]	1.881(3)
C−Al−C	130.23(10)	Al−C−Si	105.11(10) −110.26(11)
H−Al−H	101(1)	Si−C1−Si	109.37(11) −112.64(11)
H−Li1−H	114(2)	Me−Si−Me	102.42(13) −106.36(14)
H−Li2−H	141(2)	C1−Si−Me	112.07(11) −115.24(12)
O1−Li1−H1a	123(1)	C−Al−H	103(1) −109(1)
O2−Li2−H1b	110(1)		

[a] Average value, with esd's of individual measurements in parentheses. None differs significantly from the mean.

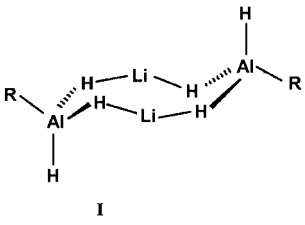

I

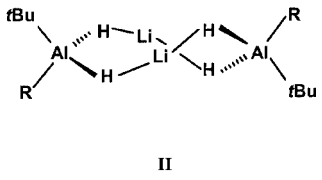

II

The distances from aluminum to the central carbon atoms of the *t*Bu [2.043(2) Å] and $C(SiMe_3)_3$ groups [2.041(2) Å] are the same within the experimental uncertainty and identical to those in **1a** [2.046(4) Å]. Similar distances [2.001(2) to 2.081(4) Å] are found in the *tert*-butylaluminium compounds $(AltBu_2H)_3$ (**7**) and $Li[AltBu_3H]$ (**8**).[27] The Li−H bond lengths are greater than the Al−H bond lengths and cover a wider range, indicating that the ionic formulation $[Li(THF)][AltBu\{C(SiMe_3)_3\}H_2]$ accurately describes the structure. The experimental uncertainties in the mean Al−H and Li−H distances are considerably greater than those in the exocyclic Al−C bonds, but the endocyclic bonds in **3** [Al−H 1.57(3) and Li−H 1.80(3) Å] are not significantly different from the bridging bonds in **1a** [1.62(4) and 1.93(4) Å, respectively], other compounds containing $Li_2Al_2H_4$rings,[12,15,22−26] or **8** [1.68(3) and 1.92(3) Å].[27] The increased crowding from the replacement of an exocyclic hydrogen in **1b** by a *tert*-butyl group to give **3** results in the displacement of one molecule of coordinated THF. The conformations of the bulky groups attached to aluminum are such that the crowding at Li1 is different from that at Li2; the mean planes of the attached THF molecules are orthogonal and the H−Li−H angles [114(2)° at Li1 and 141(2) at Li2] are significantly different. The C−Al−C angle [130.23(10)°] in **3** is considerably wider and

 © 2003 Wiley-VCH Verlag GmbH & Co. KGaA, Weinheim

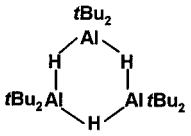

7

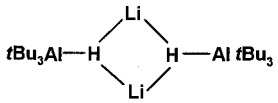

8

the H−Al−H angle within the ring [101(1)°] narrower than the tetrahedral value.

The NMR spectra of **3** at 298 K are consistent with the structure found in the solid state but, as we have not collected data over a range of temperatures, we cannot comment on whether isomeric species are obtained under different conditions. The ^{27}Al resonance (δ = 137 ppm) is at higher frequencies than those in **1a** and **1b** (δ = 113−115); similar shifts (δ = 132−141) have been reported in **2**[19] and other diorganoaluminates.[11]

The organoaluminates **1a**−**1e** are versatile starting materials for the synthesis of a range of organoaluminum derivatives bearing bulky groups,[20,28,29] since the Al−H bonds are considerably more reactive than the more protected Al−C bonds towards a variety of reagents. The reactions of the diorganoaluminates **2** and **3** can be expected to lead to a similar range of products containing AlR_2 or AlRR′ fragments, in which R and R′ are bulky or fairly bulky organic groups. We report two preliminary results here.

Treatment of **2** with iodomethane gave a good yield of Al*t*Bu$_2$I·THF (**4**) as an air- and moisture-sensitive solid [Equation (2)]. Although di-*tert*-butylaluminum fluoride, chloride,[30] bromide[31] and hydride[27] have been described we cannot find any previous report of the iodide.

$$\underset{\mathbf{2}}{\text{Li[Al}t\text{Bu}_2\text{H}_2\text{].2THF}} + \text{MeI} \longrightarrow \underset{\mathbf{4}}{\text{Al}t\text{Bu}_2\text{I.THF}} + \text{CH}_4 + \text{LiH} \qquad (2)$$

$$\underset{\mathbf{1e}}{[\{\text{Li(THF)}_2\}\{\text{AlRH}_3\}]_2} + 2\text{MeI} \longrightarrow (\text{AlRH}_2)_2 + 2\text{CH}_4 + 2\text{LiI} + 4\text{THF} \qquad (3)$$

$$\text{R} = \text{C}_6\text{H}_2\,t\text{Bu}_3\text{-2,4,6}$$

The reaction of **3** with iodomethane gave a complex mixture but reaction of the compound [{Li(THF)$_2$}{AlH$_3${C$_6$H$_2$*t*Bu$_3$-2,4,6}}]$_2$ (**1e**) gave [AlH$_2$C$_6$H$_2$-*t*Bu$_3$-2,4,6]$_2$ and LiI cleanly [Equation (3)].[29] These results can be attributed to effects of steric hindrance to attack at bonds in the eight-membered $Li_2Al_2H_4$ rings. In **2** the two *t*Bu groups attached to aluminum are not large enough to prevent coordination of the iodine of MeI and consequent reaction at Al−H bonds. In **1d**, however, coordination of iodine at aluminum is inhibited by the bulky aryl group so that the iodomethane attacks at Li−H rather than Al−H bonds. In **3** the rates of attack by MeI at Al−H and Li−H bonds appear to be similar so that a complex mixture of products is formed. The fact that the aluminum iodide rather than the hydride is isolated in reaction (2) indicates that under the conditions that we employed LiH is an ineffective reagent for reduction of Al*t*Bu$_2$I.

Reaction of **2** with an excess of TMEN gave a colorless solid that was shown by chemical analysis and NMR spectroscopy to be [Li(TMEN)$_2$][Al*t*Bu$_2$H$_2$] (**5**). One equivalent of TMEN was lost when the compound was sublimed at 120 °C in a way that is reminiscent of the behavior of [Li(TMEN)$_2$][AlH$_4$]. This was shown to crystallize in an extended ionic lattice, but the species obtained after loss of one mol of TMEN was [{Li(TMEN)}{(μ-H)$_2$AlH$_2$}]$_2$, which formed a lattice of dimeric ion pairs having Li···H−Al bridges like those in **3**.[26] With the elucidation of the structure of **3**, examples of compounds containing each of the species [AlR$_n$H$_{4-n}$]$^-$ with n = 0−4 (R = alkyl or aryl) are now known. However, when n = 1−3, the group R varies from compound to compound[19,21,22,27,31,32] so that it is not possible at this stage to draw meaningful conclusions about trends in bond lengths and angles.

Experimental Section

Air and moisture were excluded by Schlenk-tube techniques with Ar as blanket gas. All glassware was flame-dried immediately before use and solvents were carefully dried by standard methods. NMR spectra were recorded at 300.13 (^{1}H), 75.43 (^{13}C), 194.5 (^{7}Li), 130.4 (^{27}Al) or 99.36 MHz (^{29}Si) and chemical shifts are given relative to SiMe$_4$, aqueous LiCl or Al(NO$_3$)$_3$. IR spectra are for Nujol mulls.

The compound [Li(THF)$_2$][AlH$_2$*t*Bu$_2$] (**2**) has been made previously.[19]

[{Li(THF)}(Al*t*Bu{C(SiMe$_3$)$_3$}H$_2$)]$_2$ (3): A solution of Li*t*Bu (0.97 mmol) in pentane (0.6 mL) was added dropwise to a stirred solution of **1b** (0.40 g, 0.97 mmol) in toluene (20 mL) at room temperature. The mixture was stirred for 15 h, then the white precipitate was filtered off, solvent was removed from the filtrate and the residue was recrystallised from benzene to give **3** as a white air- and moisture-sensitive solid (0.28 g, yield 74%), m.p. 160 °C. C$_{18}$H$_{46}$AlLiOSi$_3$ (396.7): calcd. C 54.4, H 11.7; found C 53.3, H 11.4. IR: $\tilde{\nu}_{max}$ = 1731m, 1612br, (Al−H), 1253s, 1205w, 1168w, 1043m, 1008w, 855s, 782w, 670m cm^{-1}. ^{1}H NMR (C$_6$D$_6$, 298 K): δ = 0.48 (s, 27 H, SiMe$_3$), 1.23 (m, 4 H, THF), 1.39 (s, 9 H, *t*Bu), ca. 2.9 (br. s, 2 H, AlH), 3.42 (m, 4 H, THF) ppm. ^{7}Li NMR: δ = −0.37 ppm. ^{13}C NMR: δ = −2.9 (CSi$_3$), 5.8 ($^1J_{SiC}$ = 50 Hz, SiMe$_3$), 25.1 (THF), 34.6 (*t*Bu), 68.9 (THF) ppm. ^{27}Al NMR: δ = 137 ppm ($\Delta\nu_{1/2}$ = 3 kHz). ^{29}Si NMR: δ = −3.9 ppm.

Reaction of 2 with MeI: Iodomethane (0.20 g, 3.2 mmol) was added dropwise to a stirred solution of **2** (0.70 g, 2.4 mmol) in toluene (25 mL) at room temperature. After 15 h the solvent was pumped from the white suspension and the residue was extracted with heptane (25 mL). The extract was filtered and the filtrate reduced to ca. 10 mL in volume to give Al*t*Bu$_2$I.THF (**4**) as a white crystalline solid, m.p. 46 °C, which was filtered off and dried (0.64 g, 79%). C$_{12}$H$_{26}$AlIO (340.2): calcd. C 42.4, H 7.6; found C 42.4, H 7.7. IR: $\tilde{\nu}$ = 1359s, 1301w, 1252m, 1177m, 1044s, 1004s, 923m, 854m, 812s, 683m cm^{-1}. ^{1}H NMR (C$_6$D$_6$, 298 K): δ = 0.94 (m, 4 H, THF), 1.20 (s, 18 H, CMe$_3$), 3.63 (m, 4 H, THF) ppm. ^{13}C NMR: δ = 17.4 (CMe$_3$), 24.8 (THF), 30.5 (CMe$_3$), 74.8 (THF) ppm. ^{27}Al NMR: δ = 158 ppm ($\Delta\nu_{1/2}$ = 3.4 kHz). MS: *m*/*z* = 268 (69) [M − THF], 211 (100) [M − THF − *t*Bu], 169 (90), 154 (70).

[Li(TMEN)$_2$][Al*t*Bu$_2$H$_2$] (5) and [Li(TMEN)][Al*t*Bu$_2$H$_2$] (6): TMEN (4.5 mL, 29.8 mmol) was added to a stirred solution of **2** (2.20 g,

 © 2003 Wiley-VCH Verlag GmbH & Co. KGaA, Weinheim

7.5 mmol) in toluene (30 mL) at room temperature. After 30 min the solvent was removed until the solution became cloudy, then the mixture was cooled to give colorless air-sensitive crystals of **5** (2.40 g, 84%). $C_{20}H_{52}AlLiN_4$ (382.6): calcd. C 62.8, H 13.7, N 14.6; found C 62.2, H 13.3, N 13.5. IR: $\tilde{\nu}_{max}$ = 1651vs, br (Al−H), 1361s, 1291s, 1251m, 1187m, 1166m, 1132s, 1103m, 1070m, 1036s, 1018s, 1003sh, 948s, 811m, 788m, 750m cm^{-1}. ^1H NMR (C_6D_6, 298 K): δ = 1.48 (s, 18 H, *t*Bu), 1.95 (s, 8 H) and 1.99(s, 24 H) (TMEN) ppm. ^7Li NMR: δ = 0.37 ppm. ^{13}C NMR: δ = 15.0 (CMe_3), 32.3 (CMe_3), 45.9 and 75.4 (TMEN) ppm. ^{27}Al NMR: δ = 152 ppm ($\Delta\nu_{1/2}$ 1.37 kHz).

With the same experimental procedure, the reaction between **2** (1.65 g, 5.6 mmol) and TMEN (0.85 mL, 5.6 mmol) gave colorless crystals of **6** (1.32 g, 89%), m.p. 140 °C. $C_{14}H_{36}AlLiN_4$ (294.4): calcd. C 63.1, H 13.6, N 10.5; found C 62.5, H 13.0, N, 10.5. IR: $\tilde{\nu}_{max}$ 1740s, 1633s, br (Al−H), 1358s, 1291s, 1250m, 1208w, 1180sh, 1160s, 1130s, 1101m, 1069m, 1035s, 1021s, 1002m, 974s, 811w cm^{-1}. ^1H NMR: δ = 1.44 (s, 18 H, *t*Bu), 1.66 (s, 4 H) and 1.94 (s, 12 H, TMEN) ca. 2.7 (vb s, 2 H, AlH) ppm. ^7Li NMR: δ = 0.26 ppm. ^{13}C NMR: δ = 15.8 and 32.3 (*t*Bu), 45.9 and 56.8 (TMEN) ppm. ^{27}Al NMR: δ = 151 ppm ($\Delta\nu_{1/2}$ 1.57 kHz). Compound **6** was also obtained by sublimation of **5** at 120 °C/0.01 Torr.

Crystal Data for Compound 3: $C_{36}H_{92}Al_2Li_2O_2Si_6$: M = 793.5; T = 173(2) K; orthorhombic, $C222_1$ (no. 20); a = 15.705(4), b = 19.977(6), c = 17.089(5) Å; U = 5361(3) Å^3; Z = 4; μ = 0.21 mm^{-1}. Data from 9405 reflections, 4721 unique [R(int) = 0.038], were collected on an Enraf−Nonius CAD4 diffractometer by use of Mo-K_α radiation and full-matrix least-squares refinement was by use of SHELXL-97 programs. All non-H atoms were isotropic, the hydrogen atoms attached to Al were refined freely, and the others were refined in riding mode to give $R1$ = 0.034, $wR2$ = 0.080 [$I > 2\sigma(I)$] and $R1$ = 0.041, $wR2$ = 0.083 (all data).
CCDC-208982 contains the supplementary crystallographic data for this paper. These data can be obtained free of charge at www.ccdc.cam.ac.uk/conts/retrieving.html [or from the Cambridge Crystallographic Data Centre, 12 Union Road, Cambridge CB2 1EZ, UK: Fax +44-1223/336-033; E-mail: deposit@ccdc.cam.ac.uk].

Acknowledgments

We thank the Engineering and Physical Sciences Research Council for financial support.

[1] K. Ziegler, H.-G. Gellert, H. Martin, K. Nagel, J. Schneider, *Justus Liebigs Ann. Chem.* **1954**, *589*, 91−121.
[2] P. Kobetz, W. E. Becker, R. C. Pinkerton, J. B. Honeycutt, *Inorg. Chem.* **1963**, *2*, 859−861.
[3] J. March, *Advanced Organic Chemistry*, 4th ed., Wiley, New York, **1992**. p. 1208.
[4] L. I. Zakharkin, V. V. Gavrilenko, *J. Gen. Chem. USSR* **1962**, *32*, 688−690.
[5] L. I. Zakharkin, V. V. Gavrilenko, *Bull. Acad. Sci. USSR, Div. Chem. Sci.* **1965**, 624−628 and references therein.
[6] A. B. Goel, E. C. Ashby, *Inorg. Chim. Acta* **1984**, *87*, 61−65.
[7] E. C. Ashby, G. J. Brendel, H. E. Redman, *Inorg. Chem.* **1963**, *2*, 499−504.
[8] S. C. Srivastava, E. C. Ashby, *Inorg. Chem.* **1971**, *10*, 186−192.
[9] H. E. Podall, H. E. Petree, J. R. Zietz, *J. Org. Chem.* **1959**, *24*, 1222−1226.
[10] E. C. Ashby, R. G. Beach, *Inorg. Chem.* **1970**, *9*, 2300−2302.
[11] V. V. Gavrilenko, M. I. Vinnikova, V. A. Antonovich, L. I. Zakharkin, *Bull. Acad. Sci. USSR, Div. Chem. Sci.* **1982**, 2084−2087.
[12] H. Nöth, A. Schlegel, J. Knizek, I. Krossing, W. Ponikwar, T. Seifert, *Chem. Eur. J.* **1998**, *4*, 2191−2203.
[13] M. Veith, *J. Chem. Soc., Dalton Trans.* **2002**, 2405−2412. H. Nöth, A. Schlegel, M. Suter, *J. Organomet. Chem.* **2001**, *621*, 231−241. H. Nöth, A. Schlegel, S. R. Lima, *Z. Anorg. Allg. Chem.* **2001**, *627*, 1793−1800.
[14] J. Pauls, B. Neumüller, *Inorg. Chem.* **2001**, *40*, 121−124. J. F. Janik, R. L. Wells, P. S. White, *Organometallics* **1998**, *17*, 2361−2365.
[15] A. Heine, D. Stalke, *Angew. Chem.* **1992**, *104*, 941, *Angew. Chem. Int. Ed. Engl.* **1992**, *31*, 854−855.
[16] L. J. Guggenberger, F. N. Tebbe, *J. Am. Chem. Soc.* **1973**, *95*, 7870−7872.
[17] W. A. Skupiński, J. C. Huffman, J. W. Bruno, K. G. Caulton, *J. Am. Chem. Soc.* **1984**, *106*, 8128−8136.
[18] D. M. Schubert, M. A. Bandman, W. S. Rees, C. B. Knobler, P. Lu, W. Nam, M. F. Hawthorne, *Organometallics* **1990**, *9*, 2046−2061.
[19] C. Eaborn, I. B. Gorrell, P. B. Hitchcock, J. D. Smith, K. Tavakkoli, *Organometallics* **1994**, *13*, 4143−4144.
[20] R. J. Wehmschulte, W. J. Grigsby, B. Schiemenz, R. A. Bartlett, P. P. Power, *Inorg. Chem.* **1996**, *35*, 6694−6702.
[21] C. Eaborn, S. M. El-Hamruni, M. S. Hill, P. B. Hitchcock, M. Hopman, A. Le Gouic, J. D. Smith, *J. Organomet. Chem.* **2000**, *597*, 3−9.
[22] R. J. Wehmschulte, J. J. Ellison, K. Ruhlandt-Senge, P. P. Power, *Inorg. Chem.* **1994**, *33*, 6300−6306.
[23] H. Nöth, T. Seifert, *Eur. J. Inorg. Chem.* **1998**, 1931−1938.
[24] M. G. Gardiner, S. M. Lawrence, C. L. Raston, *Inorg. Chem.* **1999**, *38*, 4467−4472.
[25] M. G. Gardiner, S. M. Lawrence, C. L. Raston, *Inorg. Chem.* **1996**, *35*, 1349−1354.
[26] M. M. Andrianarison, A. G. Avent, M. C. Ellerby, I. B. Gorrell, P. B. Hitchcock, J. D. Smith, D. R. Stanley, *J. Chem. Soc., Dalton Trans.* **1998**, 249−253.
[27] W. Uhl, *Z. Anorg. Allg. Chem.* **1989**, *570*, 37−53.
[28] A. G. Avent, W.-Y. Chen, C. Eaborn, I. B. Gorrell, P. B. Hitchcock, J. D. Smith, *Organometallics* **1996**, *15*, 4343−4345. W.-Y. Chen, C. Eaborn, I. B. Gorrell, P. B. Hitchcock, M. Hopman, J. D. Smith, *J. Chem. Soc., Dalton Trans.* **1997**, 4689−4693. W.-Y. Chen, C. Eaborn, I. B. Gorrell, P. B. Hitchcock, J. D. Smith, *J. Chem. Soc., Dalton Trans.* **2000**, 2313−2317. S. S. Al-Juaid, C. Eaborn, I. B. Gorrell, S. A. Hawkes, P. B. Hitchcock, J. D. Smith, *J. Chem. Soc., Dalton Trans.* **1998**, 2411−2415. R. J. Wehmschulte, P. P. Power, *Inorg. Chem.* **1996**, *35*, 3262−3267. R. J. Wehmschulte, P. P. Power, *Polyhedron* **2000**, *19*, 1649−1661. A. G. Avent, C. Eaborn, I. B. Gorrell, P. B. Hitchcock, J. D. Smith, *J. Chem. Soc., Dalton Trans.* **2002**, 3971−3974.
[29] R. J. Wehmschulte, P. P. Power, *Inorg. Chem.* **1994**, *33*, 5611−5612.
[30] H. Lehmkuhl, O. Olbrysch, H. Nehl, *Leibigs Ann. Chem.* **1973**, 708−714.
[31] W. Uhl, J. E. O. Schnepf, *Z. Anorg. Allg. Chem.* **1991**, *595*, 225−238.
[32] W. Uhl, E. Schnepf, J. Wagner, *Z. Anorg. Allg. Chem.* **1992**, *613*, 67−75. G. Hencken, E. Weiss, *J. Organomet. Chem.* **1974**, *73*, 35−39.

Received April 30, 2003
Early View Article
Published Online August 1, 2003

 © 2003 Wiley-VCH Verlag GmbH & Co. KGaA, Weinheim

Monomeric Magnesium and Calcium Complexes Containing the Bidentate, Dianionic 1,2-Bis[(2,6-diisopropylphenyl)imino]acenaphthene Ligand

Igor L. Fedushkin,*[a] Alexandra A. Skatova,[a] Valentina A. Chudakova,[a] Georgy K. Fukin,[a] Sebastian Dechert,[b] and Herbert Schumann*[b]

Dedicated to Prof. Irina P. Beletskaya on occasion of her anniversary

Keywords: Magnesium / Calcium / N ligands / Anions / Dianions

The reduction of 1,2-bis[(2,6-diisopropylphenyl)imino]-acenaphthene (2,6-*i*Pr$_2$C$_6$H$_3$-BIAN) with metallic magnesium or calcium in THF affords the monomeric complexes (2,6-*i*Pr$_2$C$_6$H$_3$-BIAN)Mg(THF)$_3$ (**1**) and (2,6-*i*Pr$_2$C$_6$H$_3$-BIAN)-Ca(THF)$_4$·(THF)$_{1/2}$ (**2**). The crystallisation of **1** and **2** from benzene causes the removal of one of the coordinated THF molecules, yielding (2,6-*i*Pr$_2$C$_6$H$_3$-BIAN)Mg(THF)$_2$·(C$_6$H$_6$)$_{1/2}$ (**3a**) and (2,6-*i*Pr$_2$C$_6$H$_3$-BIAN)Ca(THF)$_3$ (**4**). Repeated recrystallisation of **1** from benzene gives (2,6-*i*Pr$_2$C$_6$H$_3$-BIAN)Mg(THF)$_2$·(C$_6$H$_6$)$_2$ (**3b**). Although the crystals of **3a** and **3b** differ in colour and in their crystallographic parameters, their molecular dimensions are very similar. Recrystallisation of **1** from pyridine produces (2,6-*i*Pr$_2$C$_6$H$_3$-BIAN)Mg(py)$_3$·(py)$_2$ (**5**). Complexes **1**–**5** have been characterised by elemental analysis, UV, IR and ^{1}H NMR spectroscopy, as well as by single-crystal X-ray diffraction.
(© Wiley-VCH Verlag GmbH & Co. KGaA, 69451 Weinheim, Germany, 2003)

Introduction

The first reports on the preparation of bis(arylimino)acenaphthenes (Ar-BIAN) were published in the late sixties.[1] However, the complex chemistry of these ligands was not explored before the early nineties, when van Asselt and Elsevier reported in a series of papers on the synthesis and application of Ar-BIAN complexes.[2] In the last decade, Ar-BIAN complexes of the transition metals, mainly of the late transition metals, have been studied extensively[3−7] due to the wide range of their applications, for example in the catalytic hydrogenation of alkynes,[3] C−C[4] and C−Sn[5] bond formation, and especially in olefin polymerisation.[6] While metal complexes containing radical-anionic or -dianionic ligands generated by reduction of 2,2′-bipyridyl[8] or of diimines like 1,4-diaza-1,3-dienes (DAD)[9] are well-known, investigations concerning Ar-BIAN were unknown until now. However, it is to be supposed that Ar-BIAN will be easily reduced forming not only radical-monoanions or -dianions, but also radical-trianions or even -tetraanions, since these ligands can be considered as hybrids of naphthalene and diazadienes, components which either can be reduced to radical-anions and -dianions (Scheme 1). Thus, several metal complexes with DAD[9f−9i] or naphthalene[10] dianions have been previously reported. According to the reduction potentials of acenaphthylene (−1.63 V),[11] 1,4-di-*tert*-butyl-1,4-diaza-1,3-diene (−1.82 V),[12] and naphthalene (−2.6 V),[11] the alkali metals lithium, sodium, or potassium, possessing reduction potentials of −3.05, −2.71, or −2.92 V,[13] respectively, should be suitable for the reduction of Ar-BIAN ligands. Actually, we were able to synthesise and to determine the structures

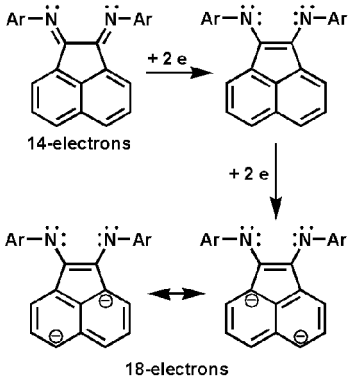

Scheme 1

[a] G. A. Razuvaev Institute of Organometallic Chemistry of Russian Academy of Sciences
Tropinina 49, 603950 Nizhny Novgorod GSP-445, Russia
Fax: (internat.) +7-8312/661-497
E-mail: igorfed@imoc.sinn.ru
[b] Institut für Chemie der Technischen Universität Berlin
Straße des 17. Juni 135, 10623 Berlin, Germany
Fax: (internat.) +49-(0)30/3142-2168
E-mail: schumann@chem.tu-berlin.de

 © 2003 Wiley-VCH Verlag GmbH & Co. KGaA, Weinheim **DOI: 10.1002/ejic.200300181**

of the sodium salts of the mono-, di-, tri- and tetraanions of Ar-BIAN.[14]

In this paper, we report on the products obtained by the reduction of 2,6-*i*$Pr_2C_6H_3$-BIAN with metallic magnesium and calcium. In this context the successful synthesis of heteroleptic magnesium β-diketiminato complexes,[15] homoleptic alkaline-earth bis-β-diketiminates,[16] and alkaline-earth metal complexes containing diazadiene ligands[17–19] should be mentioned.

Results and Discussion

(2,6-*i*$Pr_2C_6H_3$-BIAN)$Mg(THF)_3$ (1) and (2,6-*i*$Pr_2C_6H_3$-BIAN)$Ca(THF)_4\cdot(THF)_{1/2}$ (2)

The reduction of 2,6-*i*$Pr_2C_6H_3$-BIAN by activated metallic magnesium or calcium in THF affords the complexes (2,6-*i*$Pr_2C_6H_3$-BIAN)$Mg(THF)_3$ (**1**) and (2,6-*i*$Pr_2C_6H_3$-BIAN)$Ca(THF)_4\cdot(THF)_{1/2}$ (**2**), each in high yield.

(2,6-*i*$Pr_2C_6H_3$-BIAN) + M $\xrightarrow{\text{THF}}$ (2,6-*i*$Pr_2C_6H_3$-BIAN)$M(THF)_n\cdot(THF)_x$

1, 2

1 M = Mg, $n = 3$, $x = 0$

2 M = Ca, $n = 4$, $x = 1/2$

The reactions require the use of an excess of the respective metal, the activation of the metal shavings or granules, and a short reflux of the reaction mixture. The activation of the metals can be achieved by the addition of CH_2I_2 or CH_3I. The presence of the diiodides in a molar amount similar to that of the ligand causes the intermediate formation of the mixed ligand complexes (2,6-*i*$Pr_2C_6H_3$-BIAN)$MI(THF)_n\cdot(THF)_x$ (M = Mg, Ca), which, however, on refluxing the reaction mixtures react with the respective metal being present in excess to give **1** or **2**. In our experiments, we used CH_2I_2 to activate the metals. The formation of species in which the metals are coordinated to two 2,6-*i*$Pr_2C_6H_3$-BIAN radical anions has not been observed. The preferential formation of **1** and **2** is confirmed by the fact that the isolated complexes do not react further with the free ligand in THF. Nevertheless, it is to be expected that such complexes will be formed under changed conditions and, very recently, we successfully synthesised and characterised the solvent-free homoleptic complexes (2,6-*i*$Pr_2C_6H_3$-BIAN)$_2$M (M = Mg, Ca).[20] Complex **2** can also be prepared by reacting K_2(2,6-*i*$Pr_2C_6H_3$-BIAN) in situ with CaI_2 in THF or by reduction of 2,6-*i*$Pr_2C_6H_3$-BIAN with calcium naphthalenide, $(C_{10}H_8)Ca(THF)_2$, but its synthesis starting from pure calcium metal proved to be the most convenient method for laboratory use.

At the temperature of refluxing THF, the reaction mixtures show a green (**1**) or green-brown colour (**2**) and the time at which the colour of the mixtures does not become more intense can be considered as the end of the reactions. On cooling the mixtures below 0 °C, their colour turns to red-brown.

Both compounds crystallise from concentrated THF solutions as block-like, deep-red crystals, which are highly sensitive towards oxygen and water. In addition to the 2,6-*i*$Pr_2C_6H_3$-BIAN ligand, THF molecules complete the coordination sphere of the metal atoms. Owing to the difference in the ionic radii of the cations, three THF molecules are coordinated to the Mg^{II} cation in **1** and four THF molecules to the Ca^{II} cation in **2**.

In the ^{1}H NMR spectrum of **1**, the methyl protons of the four isopropyl groups give rise to two doublets centred at δ = 1.16 and 1.03 ppm due to the restricted rotation of the 2,6-*i*$Pr_2C_6H_3$ groups and the methine protons appear as a septet at δ = 3.85 ppm. All the aromatic protons appear as a broad signal at δ = 4.5 to 8.0 ppm with only four peaks, one of them showing a spin-spin coupling structure (doublet at δ = 6.81 ppm). The broadening of these signals may be explained by a dynamic process in the coordination sphere of the metal associated with an equilibrium between complex molecules with three or two coordinated THF ligands (Scheme 2). The assumption of such a dynamic process seems to be justified by the molecular structure of **1**, which shows that one of the three Mg-O_{THF} bonds is significantly longer than the other two (see Figure 2).

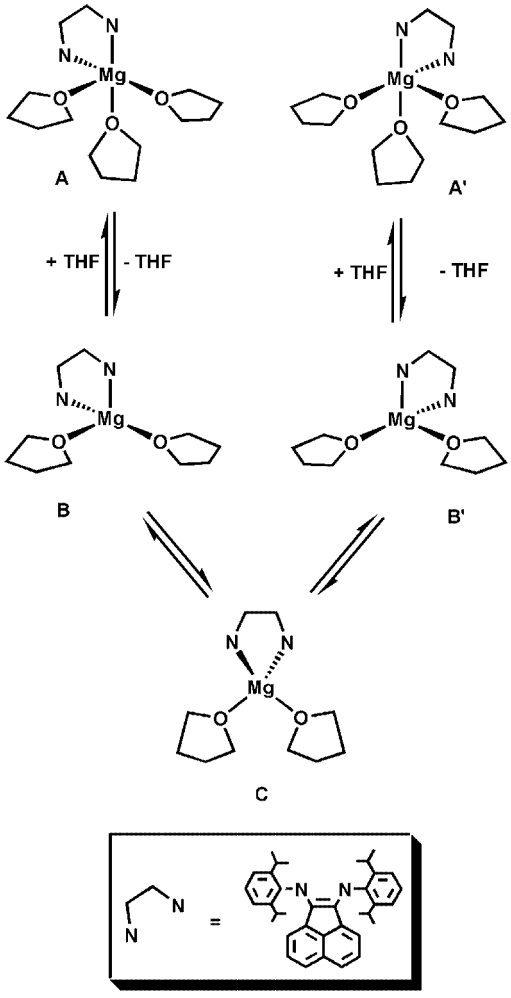

Scheme 2

 © 2003 Wiley-VCH Verlag GmbH & Co. KGaA, Weinheim

The IR spectra of the complexes **1** and **2** confirm the dianionic character of the 2,6-*i*$Pr_2C_6H_3$-BIAN ligand. The strongest absorptions in the IR spectrum of the free ligand are the C=N stretching vibrations at 1671, 1652, and 1642 cm^{-1}.[7a,7b] In the Cu^I complex [(2,6-*i*$Pr_2C_6H_3$-BIAN)-$CuBr]_2$ in which the 2,6-*i*$Pr_2C_6H_3$-BIAN ligand acts as a neutral bidentate ligand, the corresponding absorptions are shifted only slightly to lower wavenumbers (1669 and 1633 cm^{-1}),[7a,7b] whereas these vibrations are totally absent in the spectra of **1** and **2** which show the C-N stretching vibration at ca. 1300 cm^{-1} (broad band) as the most intensive absorption associated with the 2,6-*i*$Pr_2C_6H_3$-BIAN ligand.

(2,6-*i*$Pr_2C_6H_3$-BIAN)$Mg(THF)_2\cdot(C_6H_6)_n$ [$n = 0.5$ (**3a**), $n = 2$ (**3b**)] and (2,6-*i*$Pr_2C_6H_3$-BIAN)$Ca(THF)_3$ (**4**)

The starting point of our research on magnesium and calcium Ar-BIAN complexes was the preparation of coordinatively unsaturated, highly reactive complexes. In the case of the coordinatively saturated complexes **1** and **2**, this corresponds to the elimination of coordinated THF ligands. Several methods are known to eliminate coordinated solvent molecules from metal complexes, including the sublimation of the compounds in high vacuum or the distillation of solutions of the compounds in non-coordinating media. Since initial attempts to eliminate THF molecules from **1** or **2** by heating the complexes in vacuo up to 180 °C failed, we used the "wet" method. Crude **1** and **2**, dried in vacuo, were dissolved in benzene forming green solutions which were heated to 60−80 °C. Cooling of these solutions to ambient temperature resulted in the separation of khaki-coloured cubic crystals when starting from **1** or of red prismatic crystals when starting from **2**. The ratio of the THF protons to the methyl protons of the 2,6-*i*$Pr_2C_6H_3$-BIAN ligand, estimated by integration of the respective ^1H NMR signals, indicates that both **1** and **2** lost one THF ligand in the course of this dissolution-crystallisation procedure, thus changing into (2,6-*i*$Pr_2C_6H_3$-BIAN)$Mg(THF)_2\cdot(C_6H_6)_{1/2}$ (**3a**) and (2,6-*i*$Pr_2C_6H_3$-BIAN)$Ca(THF)_3$ (**4**). In the case of **1**, the repetition of this procedure again leads to a different complex, the emerald-green, rhombic crystals of (2,6-*i*$Pr_2C_6H_3$-BIAN)$Mg(THF)_2\cdot(C_6H_6)_2$ (**3b**). Complex **3b** differs from **3a** only in the number of C_6H_6 lattice molecules. Surprisingly, crystallisation of **3b** from benzene again affords crystals of different colour and shape: thin, square, deep-brown coloured plates (**3c**). The NMR spectrum of **3c** is almost identical to that of **3b** and indicates the presence of two THF molecules coordinated to the magnesium. Unfortunately, the crystals of **3c** were not suitable for X-ray diffraction. However, based on the data of the crystal structures of **3a** and **3b**, one can suggest that **3c** differs from **3a** and **3b** only with regard to its crystal packing.

Since the molecular structures of **3a** and **3b** differ only with respect to their dihedral angles between the N(1)−Mg−N(2) and N(1)−C(1)−C(2)−N(2) planes, being, as expected, rather small in both cases, [6.7° (**3a**), 14.6° (**3b**)], one can suggest that the different colours of their crystals may be a result of the difference in ligand-to-metal charge transfer. Alternatively, the difference in colour may be attributed to differences in the mutual arrangement of the complex molecules and the lattice benzene molecules and thus to differences in the kind of charge transfer between them. The question as to why **3a**, **3b** and **3c** never jointly crystallise in one and the same crop and what forces determine the kind of crystal growth cannot yet be answered. The repeated crystallisation of **4** from benzene did not cause any change in the complex.

The dissolution of **1** in hot pyridine (60 to 70 °C) results in a replacement of the THF ligands by pyridine ligands and formation of (2,6-*i*$Pr_2C_6H_3$-BIAN)$Mg(py)_3\cdot(py)_2$ (**5**), which separates as black prismatic crystals on cooling the concentrated pyridine solution to ambient temperatures.

Molecular Structures of 1, 2, 3a, 3b, 4, and 5

Prior to the detailed discussion of each structure, some general remarks on the structure of the complexes should be made:

a) The 2,6-*i*$Pr_2C_6H_3$-BIAN molecule acts as a rigid, chelating ligand. Probably due to the bulkiness of the 2,6-*i*$Pr_2C_6H_3$ groups, the complexes crystallise from different solvents as monomers. The metal atoms deviate to a varying degree from the 1,2-diimonoacenaphthene plane, forming dihedral angles of 5.7° (**1**), 10.3° (**2**), 6.7° (**3a**), 14.6° (**3b**), 11.1° (**4**), and 12.3° (**5**) (Figure 1). These dihedral angles are somewhat larger than those in the magnesium DAD complexes [RN(Ph)CC(Ph)NR]$Mg(DME)_2$ (3.0°, R = Ph; 5.0°, R = *p*-MeC_6H_4), but much smaller than those in the analogous calcium complex (40.0°, R = *p*-MeC_6H_4).[18]

b) The two-electron reduction of the diimine moiety causes a reorganization of the bonds from Ar-N=C(R)-(R)C=N-Ar to $[(Ar)N\text{-}(R)C{=}C(R)\text{-}N(Ar)]^{2-}$. Thus, the dianionic nature of the 2,6-*i*$Pr_2C_6H_3$-BIAN ligand in the complexes **1** to **5** must be apparent from a shortening of the C(1)−C(2) bond and an elongation of the N(1)−C(1) and N(2)−C(2) bonds compared to the respective bond lengths in metal complexes containing the ligand in the neutral form. Actually, the C(1)−C(2) bonds in **1**−**5**, ranging from 1.389 to 1.409 Å, are shorter than those in (2,6-*i*$Pr_2C_6H_3$-BIAN)$CuCl_2$(AcOH) (1.500 Å)[7a] and [(2,6-*i*$Pr_2C_6H_3$-BIAN)$CuBr]_2$ (1.517 Å),[7b] and the N(1)−C(1) and N(2)−C(2) bonds in **1**−**5** (1.378 to 1.402 Å) are longer than those in the above $CuCl_2$ (av. 1.287 Å)[7a] and CuBr complexes (1.285 Å).[7b]

c) Another general feature of the molecular structure of complexes **1**−**5** is the fact that one of the solvent ligands fits into the pocket formed by two isopropyl groups, one of each *N*-phenyl moiety (Figure 1). The angles between the diiminoacenaphthene moiety, the metal atom, and the donor atom of the ligand located in this pocket range from 92 to 116°. A similar situation has been observed in the complex (2,6-*i*$Pr_2C_6H_3$-BIAN)$CuCl_2$(AcOH)[7a] in which the acetic acid molecule occupies the vertex of a square pyramid (O−Cu−N 95.4 and 94.6°) and two N and two Cl atoms form the square plane.

The molecular structures of **1**, **2**, **3a**, **4**, and **5** are depicted in Figures 2−6, respectively (the figure of the molecular

 © 2003 Wiley-VCH Verlag GmbH & Co. KGaA, Weinheim

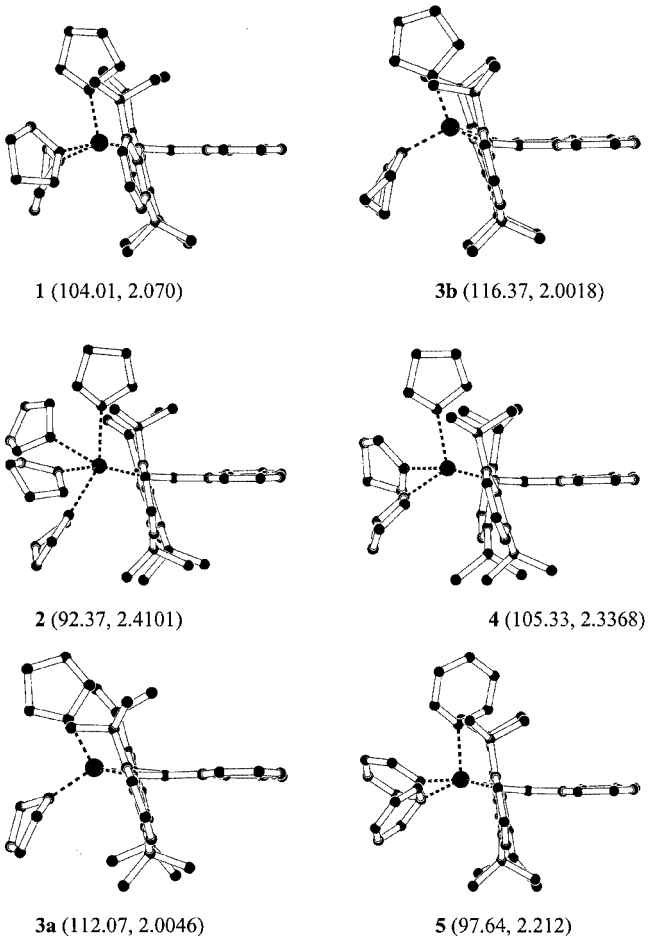

Figure 1. View of the molecules **1**−**5** along the acenaphthylene plane; the angles (deg) between the plane formed by the acenaphthene moiety, the metal, and the solvent donor atom, which is located between two isopropyl groups of the N bonded aryls, are given in parentheses along with the respective M−O(THF) and M−N(pyridine) distances (Å)

structure of **3b** is omitted since it is almost identical to that of **3a**). The crystal data collection and structure refinement data for **1**, **2**, **3a**, **3b**, **4**, and **5** are listed in Tables 1 and 2, selected bond lengths and bond angles of the molecules of these complexes are listed in Table 3 and 4. A comparison of the main bond lengths and angles in **1**−**5** is given in Figure 7.

(2,6-*i*Pr$_2$C$_6$H$_3$-BIAN)Mg(THF)$_3$ (1): Assuming that in **1** the ligand arrangement around the Mg atom is that of a square pyramid, the basal plane, made up by the atoms N(1), N(2), O(2), and O(3), is strongly distorted towards a rhombus because the Mg−O(3) bond (2.224 Å) is significantly longer than the Mg−O(1) (2.070 Å) and the Mg−O(2) bonds (2.084 Å) and the Mg−N(2) bond (2.105 Å) is longer than the Mg−N(1) bond (2.045 Å). Furthermore, the longer Mg−O(3) bond and the longer Mg−N(2) bond are in opposite positions relative to the magnesium atom. Thus, the atoms N(2) and O(3) match much better with the axial positions of a trigonal bipyramid, the equatorial plane of which is formed by the atoms N(1), O(1) and O(2) (Figure 2). The sum of the angles (359.3°) between the Mg atom and the equatorial atoms corresponds almost exactly with the ideal value of 360°, thus indicating the absence of an umbrella-like distortion of the trigonal bipyramid. Owing to the higher rigidity of the 2,6-*i*Pr$_2$C$_6$H$_3$-BIAN ligand compared to the β-diketiminate ligand, the bite angle N(1)−Mg−N(2) in **1** (84.8°) is smaller than that of the β-diketiminate ligand in (2,6-*i*PrC$_6$H$_3$NCMe)$_2$CHMg(R)(THF) (98.8° for R = O-*t*Bu, 92.8° for R = N-*i*Pr$_2$).[15e]

(2,6-*i*Pr$_2$C$_6$H$_3$-BIAN)Ca(THF)$_4$·(THF)$_{1/2}$ (2): Due to the larger ionic radius of Ca^{2+} compared to Mg^{2+} (1.00 and 0.72 Å, respectively, for six-coordinate ions[22]), the calcium atom is coordinated by four THF molecules which, along with the bidentate 2,6-*i*Pr$_2$C$_6$H$_3$-BIAN ligand, surround the calcium atom in a distorted octahedral fashion (Figure 3). One of the four Ca−O(THF) bonds is longer [Ca−O(4) 2.619 Å] than the other three which are in a fairly narrow range (2.410−2.458 Å). In contrast to the Mg−N bonds in **1**, the two Ca−N bonds (2.396 and 2.382 Å) are almost of the same length, but, as expected, longer by about 0.3 Å. The distorted octahedron is made up by O(4) and N(1) in the axial positions and O(1), O(2), O(3), and N(2) forming the equatorial plane. This distortion is caused by both the crowding around the calcium atom and the small bite angle N(1)−Ca−N(2) (75.8°), this angle being the smallest among complexes **1**−**5**.

(2,6-*i*Pr$_2$C$_6$H$_3$-BIAN)Mg(THF)$_2$·(C$_6$H$_6$)$_{1/2}$ (3a) and (2,6-*i*Pr$_2$C$_6$H$_3$-BIAN)Mg(THF)$_2$·(C$_6$H$_6$)$_2$ (3b): Despite the different crystallographic parameters, the different crystal packing and the difference in the number of the lattice solvent molecules, **3a** and **3b** exhibit almost the same molecular structure, showing a distorted tetrahedral ligand arrangement around the central Mg atom. For this reason only the structure of **3a** is depicted (Figure 4) and discussed. The two Mg−O bonds and the two Mg−N bonds do not differ markedly in length [Mg−O(1) 2.005, Mg−O(2) 1.999 Å; Mg−N(1) 1.994, Mg−N(2) 2.004 Å]. The Mg−N bonds are notably shorter than those in **1**, and, as a consequence, the bite angle N(1)−Mg−N(2) in **3a** (90.7°) is larger than in **1** (84.8°). Although the sum of the angles N(1)−Mg−N(2), N(1)−Mg−O(2) and N(2)−Mg−O(2) of 332.7° approaches the value of 328.5° for an ideal tetrahedral MgN_2O_2 moiety, a considerable distortion of the tetrahedron is apparent from the bite angle (90.7°) and the angle O(1)−Mg−O(2) (96.2°), both of which deviate significantly from the ideal value of 109.5°.

(2,6-*i*Pr$_2$C$_6$H$_3$-BIAN)Ca(THF)$_3$ (4): Except for the fact that all bonds in **4** are longer than the respective bonds in **1**, the molecular structures of **1** and **4** (Figure 5) are very similar and correspond to a trigonal bipyramid. Similar to **1**, the two Ca−N bonds differ in their length [Ca−N(1) 2.290 Å, Ca−N(2) 2.345 Å] and one of the Ca−O(THF) bonds, the Ca−O(3) bond (2.445 Å), is considerably longer than the other two, which in turn are essentially equal in length [Ca−O(1) 2.337 Å, Ca−O(2) 2.338 Å]. Thus, O(3) and N(2) are the apical atoms of the trigonal bipyramid and the equatorial plane is formed by the atoms N(1), O(1), and O(2). Also, the sum of the basal bond angles N(1)−Ca−O(1), N(1)−Ca−O(2) and O(1)−Ca−O(2)

 © 2003 Wiley-VCH Verlag GmbH & Co. KGaA, Weinheim

Table 1. Crystal data and structure refinement details for **1**, **4** and **5**

Compound	(BIAN)Mg(THF)$_3$ (**1**)	(BIAN)Ca(THF)$_3$ (**4**)	(BIAN)Mg(py)$_3$ (**5**)
Empirical formula	$C_{48}H_{64}MgN_2O_3$	$C_{48}H_{64}CaN_2O_3$	$C_{51}H_{55}MgN_5{\cdot}2(C_5H_5N)$
Molecular weight	741.32	757.09	920.51
Temperature, K	173(2)	100(2)	173(2)
Crystal system	monoclinic	orthorhombic	monoclinic
Space group	*Cc* (No.9)	$P2_12_12_1$ (No.19)	$P2_1/c$ (No.14)
Unit cell dimensions	a = 22.6706(3), b = 10.8552(2) c = 18.6094(3) Å; β = 111.038(1)°	a = 11.3799(7), b = 18.6296(11) c = 20.2251(12) Å	a = 20.6168(4), b = 13.1957(3) c = 19.3918(3) Å; β = 92.416(1)°
Volume, Å^3	4274.39(12)	4287.8(4)	5270.91(18)
Z	4	4	4
Density (calculated), g/cm^3	1.152	1.173	1.160
Absorption coefficient, mm^{-1}	0.084	0.188	0.079
F(000)	1608	1640	1968
Crystal size, mm^3	0.40 × 0.38 × 0.10	0.50 × 0.50 × 0.50	0.40 × 0.38 × 0.28
θ range for data collection, deg	1.92 to 25.00	2.01 to 24.00	0.99 to 25.00
Index ranges	$-22 \le h \le 26$, $-12 \le k \le 12$, $-22 \le l \le 22$	$-13 \le h \le 13$, $-21 \le k \le 21$, $-23 \le l \le 23$	$-16 \le h \le 24$, $-15 \le k \le 15$, $-16 \le l \le 23$
Reflections collected	10447	29339	14996
Independent reflections	4982 [R(int) = 0.0999]	6695 [R(int) = 0.0320]	9004 [R(int) = 0.1138]
Max/min transmission	0.9924/0.7456	0.9117/0.9117	0.9655/0.5598
Data/restraints/parameters	4982/2/505	6695/38/647	9004/0/630
Goodness-of-fit on F^2	1.000	1.136	1.033
Final R indices [$I > 2\sigma(I)$]	$R1$ = 0.0641, $wR2$ = 0.1151	$R1$ = 0.0432, $wR2$ = 0.1078	$R1$ = 0.0798, $wR2$ = 0.1474
R indices (all data)	$R1$ = 0.1214, $wR2$ = 0.1356	$R1$ = 0.0464, $wR2$ = 0.1094	$R1$ = 0.2300, $wR2$ = 0.1923
Absolute structure parameter	−0.5(5)	0.03(3)	−
Largest diff. peak and hole, e/Å^3	0.242 and −0.273	0.394 and −0.185	0.291 and −0.295

Table 2. Crystal data and structure refinement details for **2**, **3a** and **3b**

Compound	(BIAN)Ca(THF)$_4$ (**2**)	(BIAN)Mg(THF)$_2$ (**3a**)	(BIAN)Mg(THF)$_2$ (**3b**)
Empirical formula	$C_{52}H_{72}CaN_2O_4{\cdot}1/2(C_4H_8O)$	$C_{44}H_{56}MgN_2O_2{\cdot}1/2(C_6H_6)$	$C_{44}H_{56}MgN_2O_2{\cdot}2(C_6H_6)$
Molecular weight	865.25	708.27	825.43
Temperature, K	173(2)	100(2)	100(2)
Crystal system	monoclinic	monoclinic	orthorhombic
Space group	$P2_1/n$ (No.14)	$P2_1/n$ (No.14)	*Pbca* (No.61)
Unit cell dimensions	a = 13.3251(1), b = 18.7219(3) c = 19.9719(3) Å; β = 99.857(1)°	a = 11.8702(7), b = 16.7665(10) c = 20.7019(12) Å; β = 96.0960(10)°	a = 18.7994(13), b = 21.1341(15) c = 24.4612(17) Å
Volume, Å^3	4908.86(11)	4096.8(4)	9718.6(12)
Z	4	4	8
Density (calculated), g/cm^3	1.171	1.148	1.128
Absorption coefficient, mm^{-1}	0.175	0.083	0.079
F(000)	1880	1532	3568
Crystal size, mm^3	0.56 × 0.24 × 0.20	0.10 × 0.10 × 0.10	0.40 × 0.40 × 0.20
θ range for data collection, deg	1.50 to 27.50	1.90 to 29.02	1.66 to 23.30
Index ranges	$-17 \le h \le 17$, $-24 \le k \le 18$, $-25 \le l \le 25$	$-10 \le h \le 16$, $-22 \le k \le 22$, $-28 \le l \le 26$	$-20 \le h \le 20$, $-23 \le k \le 23$, $-27 \le l \le 27$
Reflections collected	36143	29759	62079
Independent reflections	11270 [R(int) = 0.0875]	10865 [R(int) = 0.0191]	6997 [R(int) = 0.0409]
Max/min transmission	0.9766/0.6809	0.9918/0.9918	0.9844/0.9692
Data/restraints/parameters	11270/4/578	10865/0/705	6997/6/809
Goodness-of-fit on F^2	1.010	1.027	1.040
Final R indices [$I > 2\sigma(I)$]	$R1$ = 0.0646, $wR2$ = 0.1357	$R1$ = 0.0425, $wR2$ = 0.1066	$R1$ = 0.0377, $wR2$ = 0.0984
R indices (all data)	$R1$ = 0.1265, $wR2$ = 0.1624	$R1$ = 0.0548, $wR2$ = 0.1158	$R1$ = 0.0499, $wR2$ = 0.1109
Absolute structure parameter	−	−	−
Largest diff. peak and hole, e/Å^3	0.425 and −0.453	0.448 and −0.187	0.274 and −0.196

(359.8°) coincides with that of **1** (359.3°) and corresponds with the ideal value of 360°. Because of the longer Ca−N bonds compared to the Mg−N bonds in **1**, the bite angle N(1)−M−N(2) in **4** (M = Ca; 77.0°) is smaller than in **1** (M = Mg; 84.8°). A closer look at the structures of **1** and **4** establishes that the molecules are enantiomorphic (see

 © 2003 Wiley-VCH Verlag GmbH & Co. KGaA, Weinheim

Table 3. Selected bond lengths (Å) and angles (deg) for Mg complexes **1**, **3a**, **3b** and **5**

	1	3a	3b	5
Mg−N(1)	2.045(5)	1.9945(9)	1.9937(11)	2.103(4)
Mg−N(2)	2.105(5)	2.0038(9)	1.9951(12)	2.071(4)
Mg−C(1)	2.811(6)	2.6778(11)	2.6515(13)	2.828(5)
Mg−C(2)	2.817(6)	2.6900(11)	2.6520(14)	2.805(5)
Mg−L(1)[a]	2.070(4)	2.0046(9)	2.0018(10)	2.198(5)
Mg−L(2)	2.084(4)	1.9994(8)	2.0001(10)	2.212(5)
Mg−L(3)	2.224(4)			2.271(5)
N(1)−C(1)	1.401(6)	1.3965(13)	1.3933(17)	1.400(6)
N(1)−C(13)	1.408(7)	1.4166(12)	1.4192(17)	1.431(6)
N(2)−C(2)	1.378(7)	1.3893(13)	1.3945(17)	1.386(6)
N(2)−C(25)	1.419(7)	1.4170(12)	1.4125(17)	1.422(6)
C(1)−C(2)	1.389(7)	1.3976(13)	1.3916(18)	1.392(6)
N(1)−Mg−N(2)	84.77(18)	90.71(4)	91.12(5)	84.94(17)
N(1)−Mg−L(1)	105.83(18)	115.30(4)	118.72(5)	91.47(17)
N(1)−Mg−L(2)	154.17(18)	117.74(4)	117.78(5)	95.44(18)
N(1)−Mg−L(3)	90.42(17)			168.27(19)
N(2)−Mg−L(1)	102.14(18)	114.19(4)	115.61(5)	149.89(18)
N(2)−Mg−L(2)	95.95(19)	124.32(4)	115.45(5)	106.43(18)
N(2)−Mg−L(3)	164.16(18)			95.24(18)
L(1)−Mg−L(2)	99.28(17)	96.24(4)	99.45(4)	103.67(18)
L(1)−Mg−L(3)	93.69(16)			82.48(17)
L(2)−Mg−L(3)	81.89(17)			95.75(17)
C(1)−N(1)−Mg	107.9(3)	102.89(6)	101.57(8)	105.9(3)
C(13)−N(1)−Mg	130.2(3)	139.01(7)	140.86(9)	137.8(3)
C(2)−N(2)−Mg	106.0(3)	103.40(6)	101.49(8)	106.8(3)
C(25)−N(2)−Mg	134.2(4)	138.08(7)	139.82(9)	134.3(3)

[a] For **1** and **5** L(1), L(2), L(3) are O(1), O(2), O(3) and N(3), N(4), N(5), respectively; for **3a** and **3b** L(1) and L(2) are O(1) and O(2).

Figure 7). One can suggest that in solutions of the compounds, the structures may interconvert by splitting off and recoordinating a THF ligand, thus forming four-coordinate species B and B′ as intermediates (Scheme 2). We propose such a process in order to explain the broadened aryl signals in the ^{1}H NMR spectrum of **1** (see below).

(2,6-*i*Pr$_2$C$_6$H$_3$-BIAN)Mg(py)$_3$·(py)$_2$ (5): The structure of complex **5** (Figure 6) corresponds with the trigonal-bipyramidal structures of the five-coordinate complexes **1** and **4** except that the axial and equatorial positions in **5** are not as pronounced as in **1** and **4**. The axial positions of N(1) and N(5) are apparent from the angle N(1)−Mg−N(5) of 168.3°, but the distances of N(1) and N(5) to the magnesium atom [Mg−N(1) 2.103 Å, Mg−N(5) 2.271 Å] do not differ all that much from those of the other three N−Mg distances [Mg−N(2) 2.071, Mg−N(3) 2.198 Å, Mg−N(4) 2.212 Å]. The sum of the bond angles between the Mg atom and N(2), N(3), and N(4) is exactly 360°, thus indicating that the Mg atom lies perfectly in the equatorial plane of the bipyramid. The bite angle N(1)−Mg−N(2) (84.9°) can be considered to be equal to that in complex **1** (84.8°). A closer inspection of the crystal structure of **5** shows that one of the CH_3 groups of the 2,6-*i*Pr$_2$C$_6$H$_3$-BIAN ligand is turned towards the magnesium atom, but keeps away from the metal by ≥ 3 Å (Figure 8). In the case of complex **1** this contact is less evident due to the overcrowding around the magnesium atom arising from the shorter Mg−O distances and the non-flat shape of the THF ligands.

Table 4. Selected Bond lengths (Å) and Angles (deg) for Ca complexes **2** and **4**

	2	4
Ca−N(1)	2.396(2)	2.2901(18)
Ca−N(2)	2.382(2)	2.3454(18)
Ca−C(1)	3.118(2)	3.041(2)
Ca−C(2)	3.123(2)	3.056(2)
Ca−O(1)	2.4101(18)	2.3368(16)
Ca−O(2)	2.439(2)	2.3380(17)
Ca−O(3)	2.4578(19)	2.4449(17)
Ca−O(4)	2.6187(18)	
N(1)−C(1)	1.391(3)	1.384(3)
N(1)−C(13)	1.423(3)	1.407(3)
N(2)−C(2)	1.402(3)	1.384(3)
N(2)−C(25)	1.418(3)	1.405(3)
C(1)−C(2)	1.409(3)	1.397(3)
N(1)−Ca−N(2)	75.76(7)	77.04(6)
N(1)−Ca−O(1)	91.27(7)	115.23(6)
N(1)−Ca−O(2)	91.11(7)	140.12(7)
N(1)−Ca−O(3)	117.68(7)	93.31(6)
N(1)−Ca−O(4)	163.44(7)	
N(2)−Ca−O(1)	106.00(7)	102.12(6)
N(2)−Ca−O(2)	160.10(7)	98.00(7)
N(2)−Ca−O(3)	90.66(7)	166.24(6)
N(2)−Ca−O(4)	111.68(7)	
O(1)−Ca−O(2)	88.91(7)	104.55(7)
O(1)−Ca−O(3)	149.70(7)	90.82(6)
O(1)−Ca−O(4)	72.60(6)	
O(2)−Ca−O(3)	82.17(7)	83.03(6)
O(2)−Ca−O(4)	85.02(7)	
O(3)−Ca−O(4)	77.80(6)	
C(1)−N(1)−Ca	107.85(14)	109.19(13)
C(13)−N(1)−Ca	135.38(16)	129.79(13)
C(2)−N(2)−Ca	108.47(14)	107.20(13)
C(25)−N(2)−Ca	133.24(16)	133.49(14)

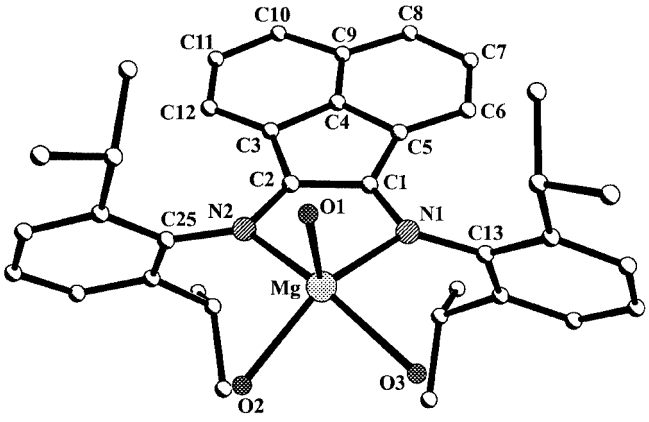

Figure 2. PLATON plot[21] of the molecular structure and the numbering scheme of **1**; all hydrogens and the carbon atoms of the THF ligands have been omitted

NMR Studies on Solutions of 1 and 5: The solution behaviour of the five-coordinate complexes **1** in [D$_8$]THF and **5** in [D$_5$]pyridine is rather different. The broadening of the aromatic signals in the ^{1}H NMR spectrum of **1** (see Figure 9a) can be explained by a dynamic process in the metal coordination sphere connected with a change in the coordination number of the magnesium atom from five to four (Scheme 2). Similar processes have been observed for THF

 © 2003 Wiley-VCH Verlag GmbH & Co. KGaA, Weinheim

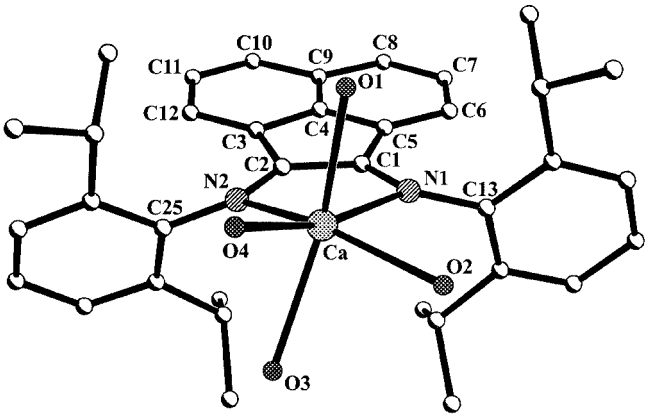

Figure 3. PLATON plot[21] of the molecular structure and the numbering scheme of **2**; all hydrogens and the carbon atoms of the THF ligands have been omitted

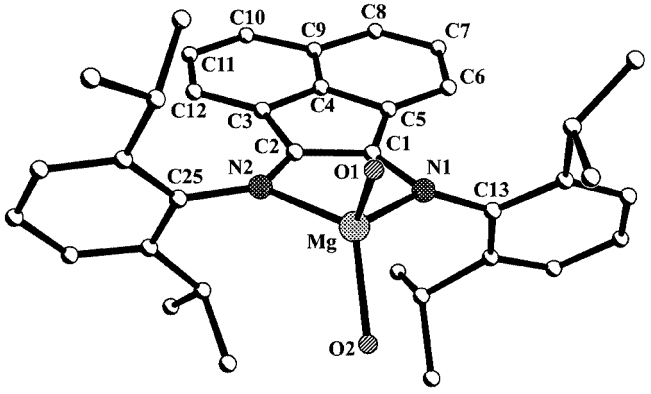

Figure 4. PLATON plot[21] of the molecular structure and the numbering scheme of **3a**; all hydrogens and the carbon atoms of the THF ligands have been omitted

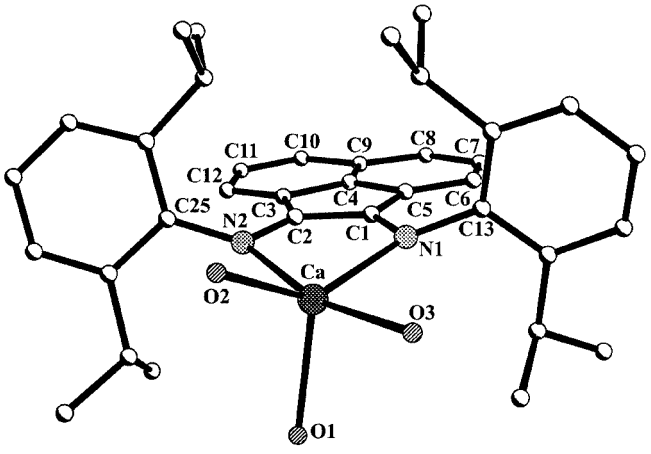

Figure 5. PLATON plot[21] of the molecular structure and the numbering scheme of **4**; all hydrogens and the carbon atoms of the THF ligands have been omitted

solutions of the β-diketiminato complexes (2,6-iPrC$_6$H$_3$NCMe)$_2$CHMgR (R = N-iPr$_2$, O-tBu).[15e] The change in the coordination number of the magnesium effects the electronic properties of the planar diiminoacenaphthene system and explains the broadening of its proton

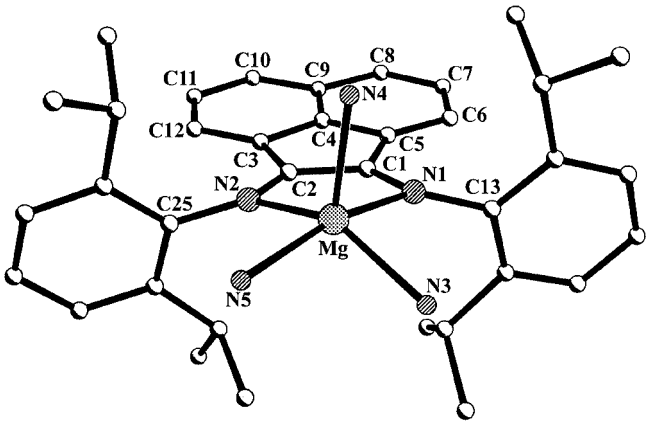

Figure 6. PLATON plot[21] of the molecular structure and the numbering scheme of **5**; all hydrogens and the carbon atoms of the py ligands have been omitted

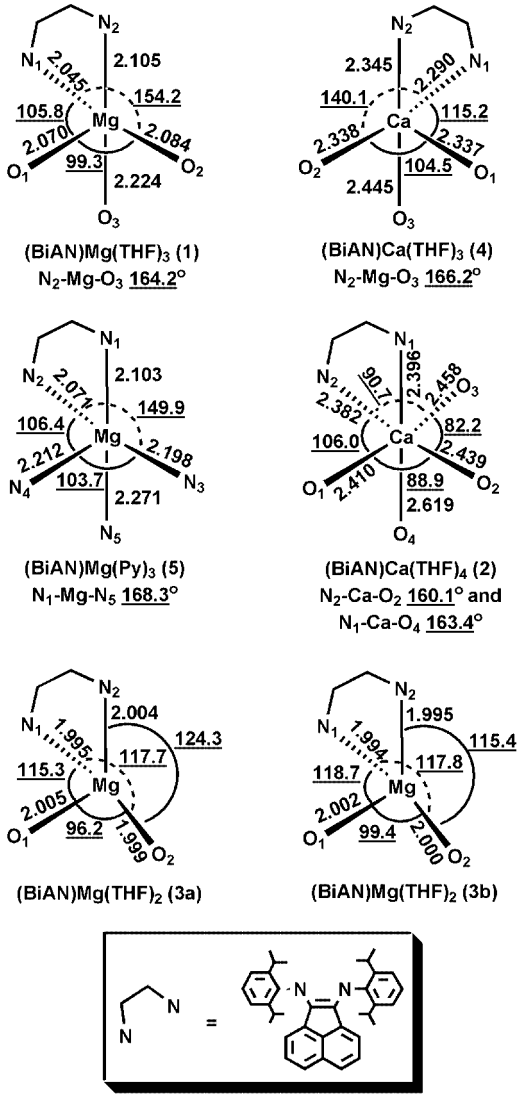

Figure 7. Comparison of the main bond lengths (Å) and angles (deg) in **1**–**5**

 © 2003 Wiley-VCH Verlag GmbH & Co. KGaA, Weinheim

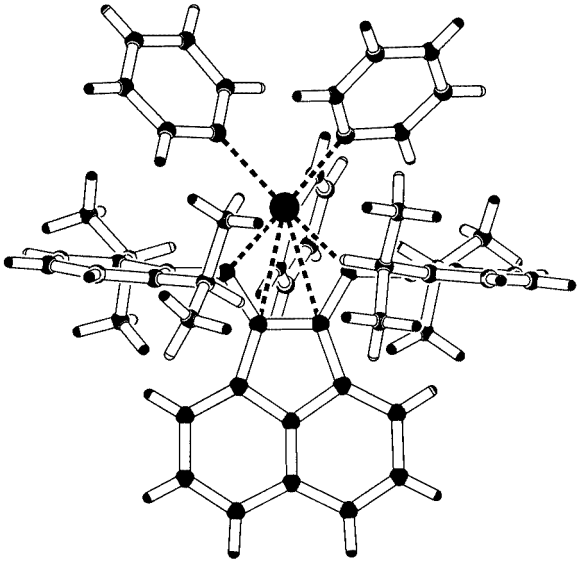

Figure 8. View of **5**, emphasising the tendency of one CH_3 group to interact with the Mg atom

signals. Since the 2,6-*i*$Pr_2C_6H_3$ groups are attached in an almost orthogonal fashion to the five-membered metallacycle C_2N_2Mg [due to the restricted rotation around the C(*ipso*)−N bond] the electronic changes at the metal do not influence the 2,6-*i*$Pr_2C_6H_3$ groups substantially, thus causing a normal shape of the isopropyl methyl and the isopropyl methine signals (two doublets and a septet, respectively). On going from THF to benzene as the solvent, the NMR spectrum of **1** does not change significantly. At this point it should be noted that the ^{1}H NMR spectrum of (2,6-*i*PrC_6H_3-BIAN)$Mg(THF)_2\cdot(C_6H_6)_{1/2}$ (**3a**) (Figure 9b), containing four-coordinate magnesium, does not indicate the formation of a three-coordinate species by splitting off of one of the two THF ligands.

The ^{1}H NMR spectrum of **5** in [D_5]pyridine (Figure 9c) exhibits four isopropyl methyl signals of different intensity at δ = 1.26 (bs), 1.19 (d), 1.13 (d), and 0.86 ppm (bs), two of which are significantly broadened. The isopropyl methine proton signal centred at δ = 3.84 ppm (spt) corresponds to the two methyl doublets at δ = 1.19 and 1.13 ppm, whereas the chemical shift of the methine proton signal corresponding to the two broadened isopropyl methyl signals is

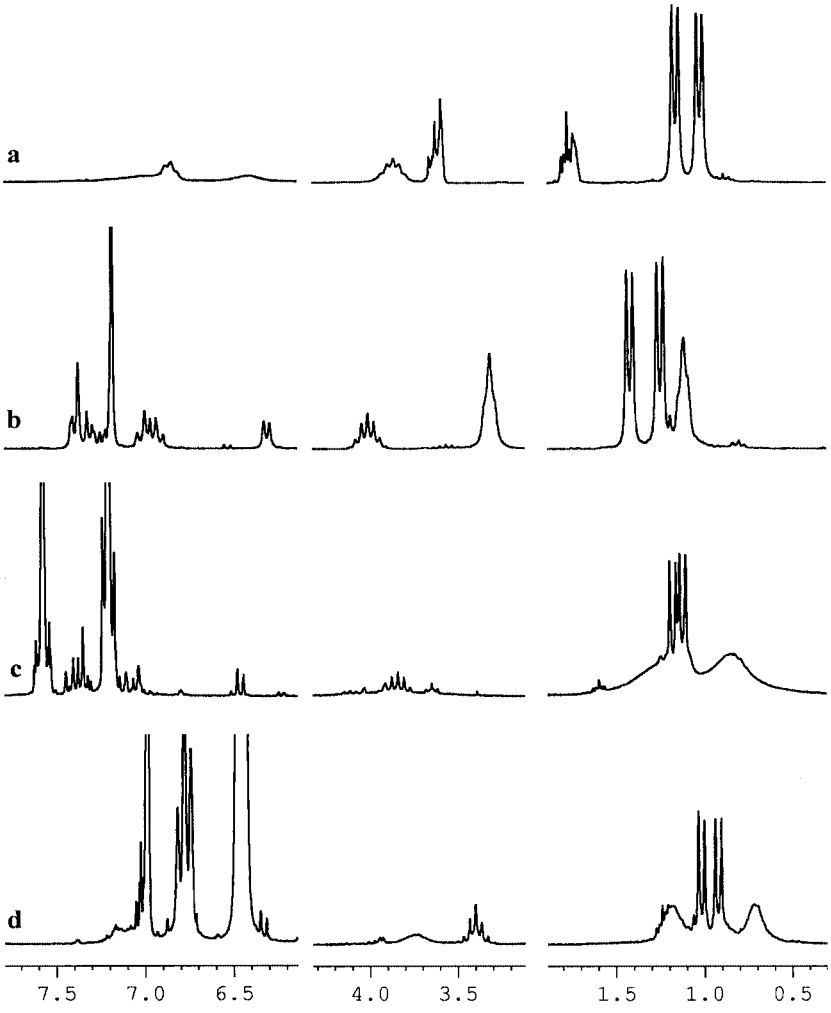

Figure 9. ^{1}H NMR spectra (200 MHz) of **1** in [D_8]THF (a) and C_6D_6 (b) and of **5** in [D_5]pyridine (c) and C_6D_6 (d)

 © 2003 Wiley-VCH Verlag GmbH & Co. KGaA, Weinheim

impossible to ascertain because of its extreme broadening. However, in the ^{1}H NMR spectrum of **5** in C_6D_6 (Figure 9d), the two methine proton signals corresponding to the four isopropyl methyl proton signals at δ = 1.38 (bs), 1.21 (d), 1.12 (d), and 0.91 ppm (bs) can be located at δ = 3.93 (bs) and 3.59 ppm (spt). In this case, the four methyl signals are approximately of equal intensity, whereas in the spectrum of **5** recorded in pyridine (Figure 9c), the broadened methyl signals are more intense. For comparison, in the ^{1}H NMR spectrum of the free 2,6-*i*Pr$_2$C$_6$H$_3$-BIAN ligand in [D$_5$]pyridine three signals represent the isopropyl protons, two doublets at δ = 1.27 (12 H) and 1.07 ppm (12 H) for the methyl protons and a septet at δ = 3.24 ppm (4 H) for the methine protons. The difference in the integrals of the four methyl signals in the spectra of **5** in [D$_5$]pyridine and in C_6D_6 evidently indicates the presence of two different species in both solutions. When using pyridine as the solvent for **5**, the removal of one of the three pyridine ligands from the magnesium atom, and thus the formation of a four-coordinate species, as discussed in the case of complex **1** for a THF ligand (see Scheme 2), should be considerably suppressed. Furthermore, the Mg−N(py) bonds are stronger than the Mg−O(THF) bonds due to the higher donor strength of pyridine compared to THF (33.1 and 20.0, correspondingly vs. $SbCl_5$).[23] Therefore, we suggest that besides the dynamic dissociation-recoordination process connected with a change in the coordination number of the magnesium atom, a second process (slow on the NMR time scale) will take place in solutions of **5** in pyridine, as well as in benzene, consisting of a distortion of the coordination sphere of the metal without a change of its coordination number. In the case of **5**, the well-known Berry pseudorotation[24,25] of five-coordinate complexes cannot serve as an explanation because of the constraints imposed by the chelating ring system and the molecular structure of **5**, which is best described as a distorted trigonal bipyramid and not as a square pyramid. We therefore suppose that in solutions of **5**, a distortion of the trigonal bipyramid occurs, in the course of which the nitrogen atoms N(1) and N(2) change their positions from axial to equatorial and vice versa (Scheme 3). A weak interaction between the Mg atom and the CH_3 groups may play some role in this process.

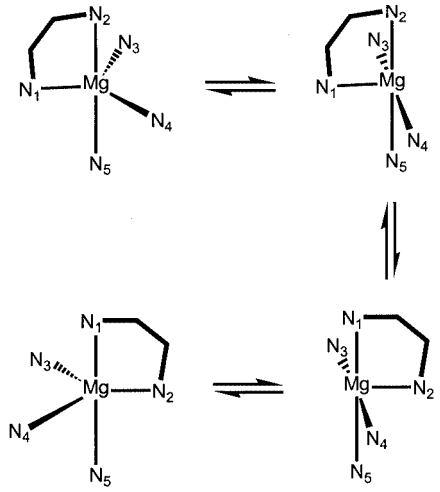

Scheme 3

Conclusion

We have synthesised and characterised magnesium and calcium complexes with the dianionic 1,2-bis[(2,6-diisopropylphenyl)imino]acenaphthene ligand. The sterically demanding substituents at both nitrogen atoms cause the formation of monomeric species. In the near future, we intend to investigate the reactivity of these complexes towards different organic substrates, such as ketones, organic halides and unsaturated organic compounds in order to find out whether these magnesium and calcium complexes may serve as one- and two-electron reductants. Preliminary studies have shown that the reactions of complex **1** with $Ph_2C{=}O$ or Me_3SiCl afford a pinacone coupling product or a product formed by the two-electron oxidative addition of Me_3SiCl to the complex, respectively.

Experimental Section

General Remarks: All manipulations were carried out under vacuum in Schlenk tubes. Tetrahydrofuran and benzene were distilled from sodium/benzophenone. Pyridine was distilled and further treated with small amounts of sodium and then condensed in vacuo immediately prior to use. The deuterated solvents [D$_8$]THF, C_6D_6, and [D$_5$]pyridine (Aldrich) were dried at ambient temperature over sodium/benzophenone (THF, benzene) or sodium (pyridine) and, just prior to use, condensed under vacuum into the NMR tubes containing the compounds. Melting points were measured in sealed capillaries. 1,2-Bis[(2,6-diisopropylphenyl)imino]acenaphthene (2,6-*i*Pr$_2$C$_6$H$_3$-BIAN) was prepared according to the published procedure.[7a] The excess of Mg and Ca left after the preparation of **1** and **2** was used without further activation by CH_2I_2 for the repeated synthesis of these complexes. The IR spectra were recorded on a Specord M80 spectrometer and the UV/Vis spectra on a Specord M80. The ^{1}H and ^{13}C{^{1}H} NMR spectra were recorded on a Bruker DPX-200 NMR spectrometer (^{1}H, 200 MHz; ^{13}C, 50.32 MHz). Chemical shifts are reported in ppm relative to the ^{1}H and ^{13}C{^{1}H}- residues of the deuterated solvents.

(2,6-*i*Pr$_2$C$_6$H$_3$-BIAN)Mg(THF)$_3$ (1): Magnesium shavings (2.4 g, 100 mmol) and CH_2I_2 (0.8 g, 2.98 mmol) were placed in a Schlenk-like ampoule (ca. 100 mL volume) equipped with a Teflon stopcock. After evacuation of the ampoule (10^{-1} Torr within ca. 1 min), THF (40 mL) was added by condensation and the mixture was stirred for 2 h. The $MgI_2(THF)_n$ formed was decanted together with the solvent and the residual metal was washed three times with THF (40 mL). A suspension of 2,6-*i*Pr$_2$C$_6$H$_3$-BIAN (0.5 g, 1.0 mmol) in THF (30 mL) was then added to the activated magnesium metal and the mixture was refluxed. In the course of about 10 min reflux, the reaction mixture turned deep green. The solution was then cooled to ambient temperature and decanted from the excess of magnesium. Crude **1** (0.69 g, 93%) was obtained as a deep-red crystalline solid on removal of the volatiles from the solution in vacuo. Recrystallisation of **1** from THF (15 mL) yielded large block-like crystals (0.27 g, 37%) and further **1** (0.31 g, 42%)

 © 2003 Wiley-VCH Verlag GmbH & Co. KGaA, Weinheim

was obtained by concentration of the mother liquor. M.p. 176 °C (decomp.). ^{1}H NMR ([D$_8$]THF, 20 °C): δ = 8.0−4.5 (br. m, 12 H, C$_{arom}$), 3.85 (spt, 4 H, C*H*Me$_2$), 3.61 [m, 8 H, α-C*H*$_2$(THF)], 3.58 [s, 8 H, α-C*H*$_2$(THF)], 1.76 [m, 4 H, β-C*H*$_2$(THF)], 1.73 [s, 4 H, β-C*H*$_2$(THF)], 1.16 [d, ^3J = 8.0 Hz, 12 H, CH(C*H*$_3$)$_2$], 1.03 [d, ^3J = 6.0 Hz, 12 H, CH(C*H*$_3$)$_2$]. IR (Nujol): $\tilde{\nu}$ = 1580 s, 1410 s, 1315 vs, 1250 s, 1170 m, 1105 w, 1020 s, 910 m, 875 s, 800 m, 760 vs, 615 m cm^{-1}. UV/Vis (THF, 20 °C): λ_{max} = 822, 370 nm. $C_{48}H_{64}MgN_2O_3$ (741.32): calcd. C 77.77, H 8.70, Mg 3.28; found C 77.02, H 8.13, Mg 3.26.

(2,6-*i*Pr$_2$C$_6$H$_3$-BIAN)Ca(THF)$_4$·(THF)$_{1/2}$ (2): Calcium metal granules (5.5 g, 137 mmol) were activated by CH_2I_2 (0.8 g, 2.98 mmol) as described for **1**. The activated Ca was treated with 2,6-*i*Pr$_2$C$_6$H$_3$-BIAN (0.5 g, 1.0 mmol) in THF (30 mL) and the mixture was stirred under reflux for 1 h. After cooling the mixture to ambient temperature, the solution was decanted from the excess of Ca metal. Evaporation of the solvent in vacuo afforded 0.75 g (85%) of crude **2** as deep-red crystals. Analytically pure, black coloured **2** was isolated by concentration of the decanted solution under reflux to 15 mL and cooling of the concentrate to ambient temperature. M.p. >160 °C (decomp.). ^{1}H NMR ([D$_8$]THF, 20 °C): δ = 8.0−5.0 (br. m, 12 H, C$_{arom}$), 3.9 (br. m, 4 H, C*H*Me$_2$), 3.63 (m, 8 H, α-C*H*$_2$(THF)], 3.60 [s, 8 H, α-C*H*$_2$(THF)], 1.78 [m, 8 H, β-C*H*$_2$(THF)], 1.75 [s, 8 H, β-C*H*$_2$(THF)], 1.18 [s, 24 H, CH(C*H*$_3$)$_2$]. IR (Nujol): $\tilde{\nu}$ = 1585 s, 1405 s, 1310 vs, 1250 s, 1170 m, 1100 w, 1020 m, 1010 m, 910 m, 870 s, 800 m, 760 vs, 620 m cm^{-1}. $C_{52}H_{72}CaN_2O_4(C_4H_8O)_{1/2}$ (865.25): calcd. C 74.96, H 8.85, Ca 4.63; found C 74.13, H 8.47, Ca 4.41.

(2,6-*i*Pr$_2$C$_6$H$_3$-BIAN)Mg(THF)$_2$·(C$_6$H$_6$)$_{1/2}$ (3a): Complex **1** (0.69 g, 0.93 mmol) dried in vacuo for 1 h, was dissolved in benzene (20 mL) and the solution was heated to 70−80 °C. The volume of the green benzene solution was than reduced to 10 mL by evaporation in vacuo at 70 °C. After cooling the solution to ambient temperature khaki-green crystals of **3a** (0.31 g, 47%) separated within 24 h. M.p. > 260 °C. ^{1}H NMR (C$_6$D$_6$, 20 °C): δ = 7.38−7.20 (m, 6 H, C$_{arom}$), 7.02−6.87 (m, 4 H, C$_{arom}$), 6.29 (d, ^3J = 8.0 Hz, 2 H), 3.99 (spt, 4 H, C*H*Me$_2$), 3.30 [s, 8 H, α-C*H*$_2$(THF)], 1.41 [d, ^3J = 6.0 Hz, 12 H, CH(C*H*$_3$)$_2$], 1.23 [d, 12 H, ^3J = 6.0 Hz, CH(C*H*$_3$)$_2$], 1.08 [s, 4 H, β-C*H*$_2$(THF)]. IR (Nujol): $\tilde{\nu}$ = 1605 w, 1575 s, 1415 vs, 1300 vs, 1250 s, 1170 m, 1100 w, 1020 s, 910 m, 905 s, 870 s, 800 m, 760 vs, 680 s, 615 m cm^{-1}. UV/Vis (C$_6$H$_6$, 20 °C): λ_{max} = 750, 370 nm. $C_{44}H_{56}MgN_2O_2(C_6H_6)_{1/2}$ (708.27): calcd. C 79.70, H 8.40, Mg 3.43; found C 78.61, H 7.48, Mg 3.29.

(2,6-*i*Pr$_2$C$_6$H$_3$-BIAN)Mg(THF)$_2$·(C$_6$H$_6$)$_2$ (3b): Complex **1** (0.65 g, 0.87 mmol) was heated in vacuo to 80 °C for 10 min. The solid was then dissolved in hot benzene (20 mL) and after its dissolution the solvent was evaporated in vacuo. The remaining solid was redissolved in hot benzene (20 mL), followed by evaporation of the solvent. The residue was crystallised from benzene (10 mL) at ambient temperature affording 0.25 g (34%) of **3b** as thin emerald-green crystals. M.p. ca. 180 °C (decomp.). ^{1}H NMR (C$_6$D$_6$, 20 °C): δ = 7.38−7.20 (m, 6 H, C$_{arom}$), 7.02−6.87 (m, 4 H, C$_{arom}$), 6.29 (d, ^3J = 8.0 Hz, 2 H), 3.99 (spt, 4 H, C*H*Me$_2$), 3.30 [s, 8 H, α-C*H*$_2$(THF)], 1.41 [d, ^3J = 6.0 Hz, 12 H, CH(C*H*$_3$)$_2$], 1.23 [d, ^3J = 6.0 Hz, 12 H, CH(C*H*$_3$)$_2$], 1.08 [s, 4 H, β-C*H*$_2$(THF)] ppm. IR (Nujol): $\tilde{\nu}$ = 1580 s, 1415 vs, 1300 vs, 1250 s, 1170 m, 1100 w, 1020 s, 910 m, 905 s, 870 s, 800 m, 760 vs, 680 vs, 615 m cm^{-1}. UV/Vis (C$_6$H$_6$, 20 °C): λ_{max} = 750, 370 nm. $C_{44}H_{56}MgN_2O_2(C_6H_6)_2$ (825.43): calcd. C 81.48, H 8.30, Mg 2.94; found C 81.67, H 7.88, Mg 2.62.

(2,6-*i*Pr$_2$C$_6$H$_3$-BIAN)Ca(THF)$_3$ (4): Crude **2** (0.7 g, 0.81 mmol) was dried in vacuo at ambient temperature for 10 min and was then dissolved in hot benzene (15 mL; 60−80 °C). Cooling the benzene solution to ambient temperature caused the precipitation of **4** as deep red-brown crystals within 36 h (0.38 g, 63%). M.p. 178 °C (decomp.). ^{1}H NMR (C$_6$D$_6$, 20 °C): δ = 7.38−7.21 (m, 6 H, C$_{arom}$), 6.99−6.88 (m, 4 H, C$_{arom}$), 6.35 (d, ^3J = 6.0 Hz, 2 H), 3.98 (spt, 4 H, C*H*Me$_2$), 3.39 [s, 12 H, α-C*H*$_2$(THF)], 1.41 [d, ^3J = 6.4 Hz, 12 H, CH(C*H*$_3$)$_2$], 1.32 [d, ^3J = 6.6 Hz, 12 H, CH(C*H*$_3$)$_2$], 1.17 [s, 4 H, β-C*H*$_2$(THF)]. IR (Nujol): $\tilde{\nu}$ = 1580 s, 1550 w, 1400 vs, 1320 vs, 1220 s, 1170 m, 1100 w, 1020 s, 910 s, 870 s, 850 s, 800 s, 755 vs, 680 w, 610 m cm^{-1}. $C_{48}H_{64}CaN_2O_3$ (757.09): calcd. C 76.15, H 8.52, Ca 5.29; found C 75.94, H 8.13, Ca 4.89.

(2,6-*i*Pr$_2$C$_6$H$_3$-BIAN)Mg(py)$_3$·(py)$_2$ (5): Crude **1** (0.65 g, 0.87 mmol) was dissolved in pyridine (30 mL) and the solution was heated to 60 °C. The brown solution formed was concentrated to 10 mL by evaporation of the solvent in vacuo. After one day, black crystals of **5** (0.56 g, 69%) had precipitated. M.p. 171 °C (decomp). ^{1}H NMR (C$_6$D$_6$, 20 °C): δ = 3.93 [s, 4 H, C*H*(CH$_3$)$_2$], 3.59 [spt, ^3J = 6.0 Hz, 4 H, C*H*(CH$_3$)$_2$], 1.38 [br. s, 12 H, CH(C*H*$_3$)$_2$], 1.21 [d, ^3J = 6.6 Hz, 12 H, CH(C*H*$_3$)$_2$], 1.12 [d, ^3J = 6.8 Hz, 12 H, CH(C*H*$_3$)$_2$], 0.91 [br. s, 12 H, CH(C*H*$_3$)$_2$] ppm; the signals of the aromatic protons are broadened and covered by the pyridine resonances. IR (Nujol): $\tilde{\nu}$ = 1600 m, 1580 vs, 1485 m, 1310 vs, 1250 s, 1210 m, 1170 s, 1100 w, 1070 m, 1040 m, 990 w, 910 s, 890 w, 800 m, 750 vs, 705 vs cm^{-1}. $C_{51}H_{55}MgN_5(C_5H_5N)_2$ (920.51): calcd. C 79.59, H 7.12, Mg 2.64; found C 78.94, H 6.82, Mg 2.63.

Single-Crystal X-ray Structure Determination of 1−5: The crystal data and details of data collection are given in Table 1 and 2. The data for **1**, **2**, **5**, and **3a**, **3b**, **4** were collected on a SMART CCD and a SMART APEX diffractometer, respectively (graphite-monochromated Mo-K_α radiation, ω- and ψ-scan technique, λ= 0.71073 Å). The structures were solved by direct methods using SHELXS-97[26] and were refined on F^2 using all reflections with SHELXL-97.[27] All non-hydrogen atoms were refined anisotropically and the hydrogen atoms were placed in calculated positions and assigned to an isotropic displacement parameter of 0.08 Å^2. Absolute structure parameters were determined according to the method of Flack[28] with SHELXL-97.[27] For **1**, the determination of the correct absolute structure was not possible. SADABS[29] was used to perform area-detector scaling and absorption corrections. The geometrical aspects of the structures were analysed with the PLATON program.[21]

CCDC-206142 (**1**) -206143 (**2**) -206144 (**3a**) -206145 (**3b**) -206146 (**4**) and -206147 (**5**) contain the supplementary crystallographic data for this paper. These data can be obtained free of charge at www.ccdc.cam.ac.uk/conts/retrieving.html or from the Cambridge Crystallographic Data Centre, 12, Union Road, Cambridge CB2 1EZ, UK; Fax: (internat.) +44-1223/336-033; E-mail: deposit@ccdc.cam.ac.uk.

Acknowledgments

This work was supported by the Russian Foundation for Basic Research (Grant No. 03-03-32246a), the Alexander von Humboldt Stiftung (ILF), the Fonds der Chemischen Industrie, and the Deutsche Forschungsgemeinschaft.

[1] [1a] I. Matei, T. Lixandru, *Bull. Inst. Politeh. Iasi* **1967**, *13*, 245−255. [1b] G. Manecke, J. Gauger, *Chem. Ber.* **1968**, *101*, 3326−3328. [1c] I. Matei, T. Lixandru, *Bull. Inst. Politeh. Iasi* **1969**, *15*, 57−66.

[2] [2a] R. van Asselt, E. E. C. G. Gielens, R. E. Rulke, C. J. Elsevier, *J. Chem. Soc., Chem. Commun.* **1993**, 1203−1205. [2b] R.

 © 2003 Wiley-VCH Verlag GmbH & Co. KGaA, Weinheim

van Asselt, K. Vrieze, C. J. Elsevier, *J. Organomet. Chem.* **1994**, *480*, 27−40. [2c] R. van Asselt, C. J. Elsevier, W. J. J. Smeets, A. L. Spek, R. Benedix, *Recl. Trav. Chim. Pays-Bas* **1994**, *113*, 88−98. [2d] R. van Asselt, C. J. Elsevier, *Organometallics* **1994**, *13*, 1972−1980. [2e] R. van Asselt, C. J. Elsevier, W. J. J. Smeets, A. L. Spek, *Inorg. Chem.* **1994**, *33*, 1521−1531. [2f] R. van Asselt, E. Rijnberg, C. J. Elsevier, *Organometallics* **1994**, *13*, 706−720. [2g] R. van Asselt, E. E. C. G. Gielens, R. E. Rulke, K. Vrieze, C. J. Elsevier, *J. Am. Chem. Soc.* **1994**, *116*, 977−985.

[3] M. W. van Laren, C. J. Elsevier, *Angew. Chem.* **1999**, *111*, 3926−3929; *Angew. Chem. Int. Ed.* **1999**, *38*, 3715−3717.

[4] R. van Belzen, H. Hoffmann, C. J. Elsevier, *Angew. Chem.* **1997**, *109*, 1833−1835; *Angew. Chem. Int. Ed. Engl.* **1997**, *36*, 1743−1745.

[5] E. Shirakawa, T. Hiyama, *J. Organomet. Chem.* **2002**, *653*, 114−121.

[6] [6a] D. Pappalardo, M. Mazzeo, S. Antinucci, C. Pellecchia, *Macromolecules* **2000**, *33*, 9483−9487. [6b] D. J. Tempel, L. K. Johnson, R. L. Huff, P. S. White, M. Brookhart, *J. Am. Chem. Soc.* **2000**, *122*, 6686−6700. [6c] D. P. Gates, S. A. Svejda, E. Onate, Ch. M. Killian, L. K. Johnson, P. S. White, M. Brookhart, *Macromolecules* **2000**, *33*, 2320−2334. [6d] S. A. Svejda, M. Brookhart, *Organometallics* **1999**, *18*, 65−74.

[7] [7a] A. A. Paulovicova, U. El-Ayaan, K. Shibayama, T. Morita, Y. Fukuda, *Eur. J. Inorg. Chem.* **2001**, 2641−2646. [7b] A. A. Paulovicova, U. El-Ayaan, K. Umezava, C. Vithana, Y. Ohashi, Y. Fukuda, *Inorg. Chim. Acta* **2002**, *339*, 209−214. [7c] D. S. Tromp, M. A. Duin, A. M. Kluwer, C. J. Elsevier, *Inorg. Chim. Acta* **2002**, *327*, 90−97. [7d] R. J. Maldanis, J. S. Wood, A. Chandrasekaran, M. D. Rausch, J. C. W. Chien, *J. Organomet. Chem.* **2002**, *645*, 158−167. [7e] M. Gasperini, F. Ragaini, S. Cenini, *Organometallics* **2002**, *21*, 2950−2957.

[8] [8a] *Gmelin Handbook of Inorganic Chemistry, Sc, Y, La-Lu: Rare Earth Elements*, 8th Ed.; Springer-Verlag; Berlin, **1980**; Vol. D1. [8b] I. L. Fedushkin, M. N. Bochkarev, V. I. Nevodchikov, *Russ. Chem. Bull. Int. Ed.* **1995**, *44*, 2185−2186. [8c] M. N. Bochkarev, I. L. Fedushkin, V. I. Nevodchikov, V. K. Cherkasov, H. Schumann, H. Hemling, R. Weimann, *J. Organomet. Chem.* **1996**, *524*, 125−131. [8d] M. N. Bochkarev, B. I. Petrov, I. L. Fedushkin, T. V. Petrovskaya, V. I. Nevodchikov, N. B. Patrikeeva, L. N. Zakharov, Yu. T. Struchkov, *Russ. Chem. Bull. Int. Ed.* **1997**, *46*, 371−373. [8e] T. V. Petrovskaya, I. L. Fedushkin, M. N. Bochkarev, H. Schumann, R. Weimann, *Russ. Chem. Bull. Int. Ed.* **1997**, *46*, 1766−1768. [8f] T. V. Petrovskaya, I. L. Fedushkin, V. I. Nevodchikov, M. N. Bochkarev, N. V. Borodina, I. L. Eremenko, S. E. Nefedov, *Russ. Chem. Bull. Int. Ed.* **1998**, *47*, 2271−2273. [8g] H. Bock, J.-M. Lehn, J. Pauls, S. Holl, V. Krenzel, *Angew. Chem.* **1999**, *111*, 1004−1008; *Angew. Chem. Int. Ed.* **1999**, *38*, 952−955. [8h] I. L. Fedushkin, T. V. Petrovskaya, F. Girgsdies, R. D. Köhn, M. N. Bochkarev, H. Schumann, *Angew. Chem.* **1999**, *111*, 2407−2409; *Angew. Chem. Int. Ed.* **1999**, *38*, 2262−2264. [8i] I. L. Fedushkin, T. V. Petrovskaya, F. Girgsdies, V. I. Nevodchikov, R. Weimann, H. Schumann, M. N. Bochkarev, *Russ. Chem. Bull. Int. Ed.* **2000**, *49*, 1869−1876. [8j] M. Schultz, J. M. Boncella, D. J. Berg, T. D. Tilley, R. A. Andersen, *Organometallics* **2002**, *21*, 460−473. [8k] D. J. Berg, J. M. Boncella, R. A. Andersen, *Organometallics* **2002**, *21*, 4622−4631.

[9] [9a] F. G. N. Cloke, H. C. de Lemos, A. A. Sameh, *J. Chem. Soc., Chem. Commun.* **1986**, 1344−1345. [9b] A. Recknagel, M. Noltemeyer, F. T. Edelmann, *J. Organomet. Chem.* **1991**, *410*, 53−61. [9c] F. G. N. Cloke, *Chem. Soc. Rev.* **1993**, 17−24. [9d] M. N. Bochkarev, A. A. Trifonov, F. G. N. Cloke, C. I. Dally, P. T. Matsunaga, R. A. Andersen, H. Schumann, J. Loebel, H. Hemling, *J. Organomet. Chem.* **1995**, *486*, 177−182. [9e] A. Scholz, K.-H. Thiele, J. Scholz, R. Weimann, *J. Organomet. Chem.* **1995**, *501*, 195−200. [9f] A. A. Trifonov, L. N. Zakharov, M. N. Bochkarev, Yu. T. Struchkov, *Izv. Akad. Nauk, Ser. Khim* **1994**, 148−151. [9g] H. Görls, B. Neumüller, A. Scholz, J. Scholz, *Angew. Chem.* **1995**, *107*, 732−735; *Angew. Chem. Int. Ed. Engl.* **1995**, *34*, 673−676. [9h] M. Haaf, A. Schmiedl, T. A. Schmedake, D. R. Powell, A. J. Millevolte, M. Denk, R. West, *J. Am. Chem. Soc.* **1998**, *120*, 12714−12719. [9i] J. Scholz, H. Görls, H. Schumann, R. Weimann, *Organometallics* **2001**, *20*, 4394−4402.

[10] [10a] J. J. Brooks, W. Rhine, G. D. Stucky, *J. Am. Chem. Soc.* **1972**, *94*, 7346−7351. [10b] A. V. Protchenko, L. N. Zakharov, M. N. Bochkarev, Yu. T. Struchkov, *J. Organomet. Chem.* **1993**, *447*, 209−214. [10c] I. L. Fedushkin, M. N. Bochkarev, H. Schumann, L. Esser, G. Kociok-Köhn, *J. Organomet. Chem.* **1995**, *489*, 145−151. [10d] M. N. Bochkarev, I. L. Fedushkin, R. B. Larichev, *Russ. Chem. Bull. Int. Ed.* **1996**, *45*, 2443−2444. [10e] M. N. Bochkarev, I. L. Fedushkin, A. A. Fagin, H. Schumann, J. Demtschuk, *Chem. Commun.* **1997**, 1783−1784. [10f] A. V. Protchenko, O. G. Almazova, L. N. Zakharov, G. K. Fukin, Yu. T. Struchkov, M. N. Bochkarev, *J. Organomet. Chem.* **1997**, *536−537*, 457−463. [10g] M. N. Bochkarev, *Chem. Rev.* **2002**, *102*, 2089−2117.

[11] E. de Boer, *Adv. Organomet. Chem.* **1964**, *2*, 115−155.

[12] H. tom Dieck, I. W. Renk, *Chem. Ber.* **1971**, *104*, 110−130.

[13] W. von Schröter, K.-H. Lautenschläger, H. Bibrack, A. Schnabel, *Chemie*, VEB Verlag, Fachbuchverlag Leipzig, **1986**.

[14] I. L. Fedushkin, A. A. Skatova, V. A. Chudakova, G. K. Fukin, *Angew. Chem.*, in press.

[15] [15a] V. C. Gibson, J. A. Segal, A. G. P. White, D. J. Williams, *J. Am. Chem. Soc.* **2000**, *122*, 7120−7121. [15b] P. J. Bailey, R. A. Coxall, C. M. Dick, S. Fabre, S. Parsons, *Organometallics* **2001**, *20*, 798−801. [15c] P. J. Bailey, S. T. Liddle, C. A. Morrison, S. Parsons, *Angew. Chem.* **2001**, *113*, 4595−4598; *Angew. Chem. Int. Ed.* **2001**, *40*, 4463−4466. [15d] M. H. Chisholm, J. C. Huffman, K. Phomphrai, *J. Chem. Soc., Dalton Trans.* **2001**, 222−224. [15e] M. H. Chisholm, J. C. Huffman, K. Phomphrai, *Inorg. Chem.* **2002**, *41*, 2785−2794.

[16] S. Harder, *Organometallics* **2002**, *21*, 3782−3787.

[17] V. Lorenz, B. Neumüller, K.-H. Thiele, *Z. Anorg. Allg. Chem.* **1994**, *620*, 691−695.

[18] V. Lorenz, B. Neumüller, K.-H. Thiele, *Z. Naturforsch., Teil B* **1995**, *50*, 71−75.

[19] M. Rieckhoff, U. Pieper, D. Stalke, F. T. Edelmann, *Angew. Chem.* **1993**, *105*, 1102−1104; *Angew. Chem. Int. Ed. Engl.* **1993**, *32*, 1079−1081.

[20] I. L. Fedushkin, A. A. Skatova, V. A. Chudakova, V. K. Cherkasov, S. Dechert, H. Schumann, *Chem. Eur. J.*, accepted for publication.

[21] A. L. Spek, *PLATON A Multipurpose Crystallographic Tool*, Utrecht University **2000**.

[22] R. D. Shannon, *Acta Crystallogr., Sect. A* **1976**, *32*, 751−767.

[23] V. Gutmann, *Coordination Chemistry in Non-Aqueous Solutions*, **1968**, Springer-Verlag, Wien-New York, 30. Dielectric constants for THF −7.6 and pyridine −12.3.

[24] R. S. Berry, *J. Chem. Phys.* **1960**, *32*, 933−938.

[25] S. Alvarez, M. Llunell, *J. Chem. Soc., Dalton Trans.* **2000**, 3288−3303.

[26] G. M. Sheldrick, *SHELXS-97 Program for the Solution of Crystal Structures*; Universität Göttingen **1990**.

[27] G. M. Sheldrick, *SHELXL-97 Program for the Refinement of Crystal Structures*; Universität Göttingen **1997**.

[28] H. D. Flack, *Acta Crystallogr., Sect. A* **1983**, *39*, 876−881.

[29] G. M. Sheldrick, *SADABS Program for Empirical Absorption Correction of Area Detector Data*; Universität Göttingen **1996**.

Received April 1, 2003
Early View Article
Published Online August 11, 2003

 © 2003 Wiley-VCH Verlag GmbH & Co. KGaA, Weinheim

Solvent-Free and TMEDA-Solvated Mixed Alkali Metal-Magnesium Tris-diisopropylamides

Eva Hevia,[a] Fiona R. Kenley,[a] Alan R. Kennedy,[a] Robert E. Mulvey,*[a] and René B. Rowlings[a]

Dedicated to the memory of Ron Snaith

Keywords: Alkali metals / N ligands / Heterometallic complexes / Potassium / Magnesium

A trio of heterobimetallic tris-diisopropylamides, the solvent-free potassium-magnesium amide [{KMg(N*i*Pr$_2$)$_3$}$_\infty$], its TMEDA solvate [KMg(N*i*Pr$_2$)$_3$·TMEDA] and the sodium congener [NaMg(N*i*Pr$_2$)$_3$·TMEDA] has been synthesised by mixing the appropriate metal alkyl reagents with three molar equivalents of diisopropylamine in a hydrocarbon medium, to which, in the last two cases, TMEDA is added. All three amides have been successfully crystallographically characterised by X-ray diffraction studies. Representing the first pure *s*-block mixed-metal diisopropylamide free of solvent molecules or other stabilising anionic co-ligands, the first compound adopts an infinite spiral chain of ···K-(μ-N)$_2$-Mg-N··· links, the metal-N framework of which is supported by agostic K···C intra-dinuclear and inter-dinuclear contacts. The dinuclear tris-amido motif is maintained in both TMEDA complexes, the metal-N cores of which are essentially isostructural, but the presence of the chelating diamine blocks the propagating terminal site on the alkali metal and so gives rise to discrete molecular structures.

(© Wiley-VCH Verlag GmbH & Co. KGaA, 69451 Weinheim, Germany, 2003)

Introduction

Generally dispensed in the form of its lithium compound, the sterically demanding diisopropylamido ligand (*i*Pr$_2$N$^-$, DA; with lithium, LDA) has long commanded a high-ranking position in synthesis on account of its good (kinetic) basicity and poor nucleophilicity. These complementary properties combine to make LDA the shelf reagent of choice in a legion of proton abstraction applications (especially with weakly acidic organic compounds).[1] When planning a synthesis it would be a tactical error to view LDA as simply a convenient source of DA, as the presence of the lithium counterion imparts (or affects) certain characteristics of the amide [including, for example, aggregation state/s; extent and nature of solvation; polarity and strength of the metal-N bond; hybridisation of the anionic N centre; solubility; thermal stability; susceptibility to β-hydride elimination from the Me$_2$C(H)- branches], which can have a profound effect on the outcome and rate of a reaction with a substrate.[2] Though patterns can be discerned and rationalised in certain systems, in general metal effects in metal-mediated reactions can be a minefield of complexity, which can only be safely trodden through by assessing the influence of each metal on an individual basis.[3] It follows that changing the metal supporting the DA ligand from lithium to another metal can bring about significant differences in the reactivity/selectivity and kinetics of the amido functionality. This is one reason for synthesising new metal complexes of DA. We have an additional incentive for pursuing such a goal. The DA ligand has played a major role in advancing our work in *s*-block metal synergy and "inverse crown" chemistry. So called because of their inverse topological relationship to conventional crown ether complexes, inverse crowns are poly-mixed-metal amide cationic ring compounds with anionic centres.[4] DA has served as the metal atom linking unit in inverse crowns with alkoxo [{MMg(DA)$_2$OR}$_2$] (M = Li, R = *n*Oct; M = Na, R = *n*Bu or *n*Oct),[5] hydrido [Na$_2$Mg$_2$(DA)$_4$(H)$_2$·(toluene)$_2$][6] or ferrocenetetrayl [Na$_4$Mg$_4$(DA)$_8${Fe(C$_5$H$_3$)$_2$}] cores,[7] where it performs a μ$_2$ bonding role. The "super" inverse crown structure of [{NaMg(DA)(O)·(THF)}$_6$][8] also has μ$_2$-DA ligands in the sodium amide appendages to the hexameric (MgO)$_6$ cage. Common to the synthesis of each of these species is a synergic tris-amide of general formula [MMg(DA)$_3$], though hitherto no structural information has been available on these inverse crown precursors. Here we report the first isolated and crystallographically characterised such tris-diisopropylamides in the solvent-free, mixed potassium-magnesium polymer [{KMg(DA)$_3$}$_\infty$] **1**, its diamine-solvated analogue [KMg(DA)$_3$·TMEDA] **2**, and for comparison the mixed sodium-magnesium solvate [NaMg(DA)$_3$·TMEDA] **3** [where TMEDA = *N*,*N*,*N*′,*N*′-tetramethylethylenediamine,

[a] Department of Pure and Applied Chemistry, University of Strathclyde,
Glasgow, G1 1XL, U.K.

$Me_2N(CH_2)_2NMe_2$]. A survey of the literature also reveals that the significance of **1** goes beyond its relevance to inverse crown chemistry as, to the best of our knowledge, it represents the first pure *s*-block heterobimetallic diisopropylamide, pure in the sense that it is free of stabilising anionic co-ligands or neutral solvent ligands. Such a pure form is also unknown in homometallic systems if one discounts the crystal structure of LDA itself, as this was determined from a sample which contained small, non-stoichiometric quantities of TMEDA and the parent amine DAH.

Results and Discussion

The new compounds **1**−**3** were prepared by the same mixed-metallation strategy [Equation (1)]: metal alkyl reagents are stirred together in a hydrocarbon medium, before the introduction of the required quantity of DAH to convert all of the alkyl substituents to gaseous alkane (or to an arene in the case of the benzyl substituents), leaving the desired heterobimetallic amide mixture in solution. The preparation of **1** from *n*-butylpotassium is not straightforward. While crystals of **1** can be grown reproducibly in low yields, they are invariably accompanied by variable amounts of an oily residue and a black waxy solid, the characterisation of which was not pursued. This decomposition is almost certainly triggered by β-hydride elimination from *n*-butylpotassium in the main (prior to the alkane generation stage) and possibly from DA ligands — it has been reported previously that homometallic $Mg(DA)_2$ suffers a thermally induced hydride elimination from one of its β-C atoms, in a process which can be subsequently exploited to reduce aldehydes or ketones to alcohols.[9] Heating the reaction solution of **1** above ambient temperature proves particularly detrimental, leading to more black waxy solid residue. Switching to benzylpotassium seems to produce a cleaner reaction, though the yield of **1**, whilst better, does not improve vastly. When toluene is added as a co-solvent the reaction solution can even tolerate reflux conditions using this resonance-stabilised reagent, however, under such conditions the reaction follows a different course, generating hydride ions, which ultimately end up in the new inverse crown species $[K_2Mg_2(DA)_4(H)_2\cdot(toluene)_2]$, as discussed in the following paper in this issue.[10] To complete the formation of both **2** and **3**, TMEDA is added in an additional step. While in comparison to that for **1** it is a more routine task to crystallise these TMEDA complexes (by cooling the resulting solutions to −28 °C) it is not easy to collect all of the crystalline product/s by vacuum filtration. This is because the crystals of both **2** and **3** readily dissolve in hexane/heptane solution at ambient temperature, hence the isolation procedure is best carried out at subambient temperature (even then, a large proportion of the crystalline material is visibly lost). Such exceptionally good solubility in hydrocarbon media pointed to a synergic effect with both metal atoms intimately involved in the crystalline structures (as confirmed later by the X-ray crystallographic studies, vide infra), as on their own NaDA/KDA exhibit little or no solubility in hexane/heptane and their solvated offspring $[(NaDA\cdot TMEDA)_2]$[11] and $[(KDA\cdot TMEDA)_2]$[12] only limited solubility. The solubilising effect of mixing alkali metal and magnesium compounds in certain systems has also been noted in alkoxide chemistry.[13] As expected, the synergic influence has no bearing on the air instability of **1**−**3** as all are highly sensitive to moisture and oxygen.

$$RM + Bu_2Mg + 3iPr_2NH \rightarrow \text{“}MMg(NPr^i_2)_3\text{”} + 2BuH + RH \quad (1)$$

Solvent-free **1** dissolves in arene solvents allowing a ^1H NMR spectrum to be recorded in [D_6]benzene solution. At room temperature a single type of amide *i*Pr group [$(CH_3)_2CH$ septet at δ = 3.38 ppm; $(CH_3)_2CH$ doublet at δ = 1.27 ppm] is revealed. This is consistent with either chemically distinct amide ligands undergoing a fast exchange process or chemically equivalent ligands. With respect to the crystal structure, the former scenario could involve the exchanging of bridging and terminal groups within a “$K(\mu\text{-}DA)_2MgDA$” molecule, while the latter scenario could be envisioned as a discrete $[Mg(DA)_3]^-$ “ate” with the K^+ counterion sequestered by π-binding arene solvent ligands (alkali metal π-arene interactions, which have been observed in several inverse crown complexes, are believed to be of fundamental structural importance to a wide range of materials).[14,15] In both these scenarios the agostic $K\cdots C(H)(CH_3)_2$/$K\cdots C(H_3)C(H)(CH_3)$ intermolecular interactions extending the molecular structure in the solid state would be absent in solution. The corresponding spectrum of **3** also reveals a single type of amido *i*Pr group, but the chemical shifts of the $CH(CH_3)_2$ septet (δ = 3.50 ppm) and the $CH(CH_3)_2$ doublet (δ = 1.38 ppm) show a modest yet significant move to higher frequency compared to those in **1** (by 0.12 and 0.11 ppm respectively) suggesting that a $[Mg(DA)_3]^-$ “ate” anion is not common to both species. These chemical shifts in **3** also differ from those in homometallic $[(NaDA\cdot TMEDA)_2]$[11] (corresponding values δ = 3.66 and 1.26 ppm) where the DA ligand bridging is exclusively to Na^+ centres. In $[(NaDA\cdot TMEDA)_2]$ it was reasoned that TMEDA is not bound to the Na^+ centres in [D_6]benzene solution at room temperature on account of the relative positioning of the TMEDA resonances [CH_2CH_2N at δ = 2.13 ppm; $(CH_3)_2N$ at δ = 2.08 ppm]; when TMEDA is ligated to the metal the situation is reversed. Significantly, the latter case, and at notably lower chemical shift values [$(CH_3)_2N$ at δ = 1.81 ppm; CH_2CH_2N at δ = 1.72 ppm], is observed for **3**, indicative of metal-bound TMEDA ligands. This evidence points to the molecular structure within the crystal (vide infra) being retained in solution. Strong support for this viewpoint was gained from a variable temperature study in [D_8]toluene solution. At room temperature two broad resonances are observed for the $(CH_3)_2CH$ and $(CH_3)_2CH$ hydrogen atoms at δ = 3.43 and 1.31 ppm, respectively. However, on cooling the solution to −30 °C, the former resonance separates into two distinct ones at δ = 3.77 and 3.38 ppm in a 1:2 inte-

 © 2003 Wiley-VCH Verlag GmbH & Co. KGaA, Weinheim

gration ratio. These resonances can be confidently assigned to terminal and bridging DA groups, respectively, and thus it can be concluded that these groups undergo a rapid dynamic equilibration at room temperature in the manner of that seen in classic dimeric structures such as $[(A1Me_3)_2]$.[16] The ^1H (and ^{13}C) NMR spectra of the potassium analogue **2** show enough similarity to those of **3** to suggest that it too retains its crystalline molecular structure in arene solution. Thus in deutero-toluene solution the $(CH_3)_2CH$ and $(CH_3)_2CH$ resonances of **2** shift by only 0.03 and 0.02 ppm respectively (to lower frequency) than those in **3** and the corresponding ^{13}C resonances differ by only 0.6 and 0.2 ppm (shifted to higher and lower frequency respectively) than those in **3**. A slight anomaly seemingly exists when considering the ^1H resonances associated with TMEDA: the order of the CH_2 and Me_2N resonances (at $\delta = 1.91$ and 1.89 ppm respectively) is reversed compared to that for **3** (corresponding values $\delta = 1.76$ and 1.84 ppm). However, the limited chemical shift range of all the signals involved (covering a mere 0.15 ppm), and, more importantly, the substantial margin between these and those of free TMEDA (i.e., CH_2, $\delta = 2.32$ ppm; Me_2N $\delta = 2.11$ ppm) would appear to refute any notion that the TMEDA is not attached to the K^+ centre in **2**.

Figure 1 shows the asymmetric unit of the crystal structure of **1**, while Figure 2 captures a view of a section of the infinite, one-dimensional arrangement. Its primary feature is the familiar tris-amido motif, here consisting of a [K(μ-$N)_2$Mg] ring (strictly planar) with an additional amide N "terminus" on the Mg centre. Connected by the N terminus on one interacting with the K centre of the other, two such tris-amido motifs make up the asymmetric units, which interconnect through similar K−N linkages to generate an infinite spiral chain. All the intermolecular tris-amido connection points are reinforced by agostic K···C interactions. Table 1 records the principal bond lengths and bond angles for **1**. A noteworthy observation is the lack of distinction in the Mg−N bond lengths. The notional terminal ones (Mg1−N3; Mg2−N6) display a mean length (2.046 Å) longer, not shorter, than that of the bridging type (2.037 Å), but by a mere 0.009 Å. This reflects the fact that the former DA ligands are not actually terminal but bridging (through intermolecular contacts between tris-amido units). A similar lack of distinction is found for the K−N bond lengths (mean: intramolecular bridges, 2.9351 Å; intermolecular bridges, 2.9297 Å). Thus with the intramolecular and intermolecular bridging having approximately equal weighting, the bonding can therefore be best described as genuinely supramolecular (polymeric) in nature, as opposed to that of a single tris-amido molecule with weak extended forces. An army of short, agostic K···C contacts involving both methyne and methyl groups helps to strengthen the K-(μ-$N)_2$-Mg-N framework. Disorder in two of the *i*Pr branches (those labelled C16/17/18 and C34/35/36) precludes discussion of bond lengths involving them, though they almost certainly make as important a contribution as those now mentioned. For both K atoms, the shortest of these contacts involve intramolecularly bound methyne groups [K1···C8, 3.126(2) Å; K2···C23, 3.135(3) Å]. The closest such intermolecular contacts are again to methyne C atoms [K1···C32, 3.420(2) Å; K2···C14, 3.288(2) Å]. Other K···C contacts range from 3.138(2)−3.516(3) Å for K1 and 3.167(2)−3.506(3) Å for K2. Though hydrogen atoms were not independently refined in this study, it can be assumed from the short K···C contact distances that the K atoms also lie in close proximity to CH_3 and/or CH hydrogen atoms. This may have some bearing on the propensity of **1** to undergo β-hydride elimination.[10] Turning to bond angles, the Mg atoms display distorted trigonal planar geometries. To make the bridge within the [K(μ-$N)_2$Mg] ring, the endocyclic N−Mg−N bond angle must compress (mean value, 112.78°). A concomitant widening occurs at the exocyclic N−Mg−N positions (mean value, 123.58°), but not symmetrically as one bond angle (mean, 125.72°) is significantly more obtuse than the other (mean, 121.43°). The coordination geometry of the K centres is less well-defined in keeping with its softer, Lewis acidic character (compared to that of Mg). With respect to N atoms, the K atoms are trigonal pyramidal (sum of bond angles: 352.64° for K1; 356.08° for K2) with two obtuse (mean, 141.87°) and one acute (mean, 70.61° belonging to the [K(μ-$N)_2$Mg] ring) N−K−N bond angles, but including the close K···C contacts the coordination number of the alkali metal could be considered as high as twelve.

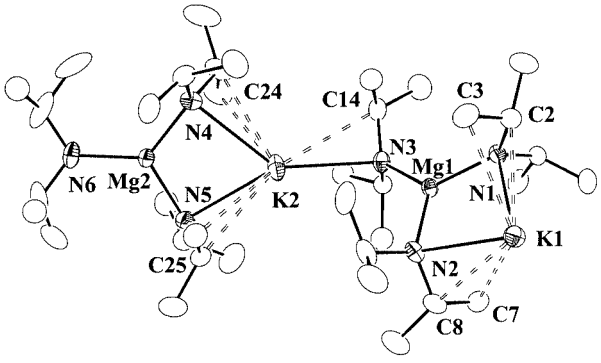

Figure 1. Asymmetric unit of the molecular structure of **1** with agostic contacts shown as broken lines; hydrogen atoms are omitted for clarity

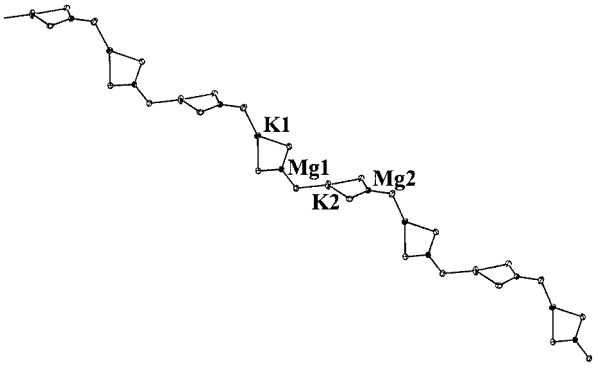

Figure 2. A section of the extended structure of **1**

 © 2003 Wiley-VCH Verlag GmbH & Co. KGaA, Weinheim

Table 1. Selected bond lengths (Å) and bond angles (°) for $[\{KMg(NiPr_2)_3\}_\infty]$ (**1**)

Bond lengths (Å)		Bond angles (°)	
K(1)−N(6)′	2.9379(18)	N(2)−K(1)−N(6)′	136.80(5)
K(1)−N(1)	2.9595(17)	N(2)−K(1)−N(1)	70.53(5)
K(1)−N(2)	2.9181(17)	N(6)′−K(1)−N(1)	145.31(5)
K(1)···C(2)	3.138(2)	N(3)−K(2)−N(5)	146.08(5)
K(1)···C(3)	3.270(2)	N(3)−K(2)−N(4)	139.31(5)
K(1)···C(8)	3.126(2)	N(5)−K(2)−N(4)	70.69(5)
K(1)···C(7)	3.285(2)	N(1)−Mg(1)−N(2)	112.83(7)
Mg(1)−N(1)	2.0301(17)	N(1)−Mg(1)−N(3)	125.04(7)
Mg(1)−N(2)	2.0435(18)	N(2)−Mg(1)−N(3)	122.10(7)
Mg(1)−N(3)	2.0524(18)	N(5)−Mg(2)−N(4)	112.74(8)
K(2)−N(3)	2.9215(17)	N(5)−Mg(2)−N(6)	120.77(8)
K(2)−N(4)	2.9332(19)	N(4)−Mg(2)−N(6)	126.41(8)
K(2)−N(5)	2.9215(17)	Mg(1)−N(1)−K(1)	87.87(6)
K(1)···C(24)	3.167(2)	Mg(1)−N(2)−K(1)	88.76(6)
K(1)···C(14)	3.288(2)	Mg(2)−N(4)−K(2)	88.18(6)
K(1)···C(15)	3.506(3)	Mg(1)−N(5)−K(2)	88.39(6)
K(1)···C(25)	3.301(3)		
Mg(2)−N(4)	2.0395(18)		
Mg(2)−N(5)	2.0340(19)		
Mg(2)−N(6)	2.0396(19)		

The tris-amido motif also dominates the structure of **2** though now it is contained within a discrete molecular arrangement (Figure 3). This modification is due to the introduction of the didentate, chelating TMEDA ligand. By completing a distorted tetrahedral coordination sphere around K^+, the TMEDA ligation kills the need for any intermolecular K−N interactions. Table 2 records the principal bond lengths and bond angles for **2**. The distorted trigonal planar Mg coordination sphere is marked by long Mg-(μ-N) (mean length, 2.0418 Å) and short terminal Mg−N bonds [length, 1.9722(13) Å], in line with coordination number differences (i.e., 3 for N1; 4 for N2/N3). Only the latter bond shows a significant shortening compared to those in **1**, reflecting its genuine terminal nature. Adding to the asymmetry of the essentially planar $[K(\mu\text{-}N)_2Mg]$ trapezoidal ring, there is one long and one short K-(μ-N) bond (difference in length, 0.054 Å). These bonds clearly represent the weak points of the tris-amido motif given that their Mg-(μ-N) counterparts are on average 0.848 Å shorter. A comparison with the series of potassium hexamethyldisilazide $[(Me_3Si)_2N^-$; HMDS] complexes $[\{K(ar)_2\}^+\{Mg(HMDS)_3\}^-]$[17] (ar = benzene, toluene or *para*-xylene) shows that it is possible to completely cleave the large alkali metal from its tris-amido magnesiate partner (severing all K−N linkages, but retaining agostic K···C connections) by introducing π-binding arene ligands. It is significant that the K atoms in **2** ignored the toluene solvent molecules generated in the reaction by protonation of benzylpotassium. This is because TMEDA fulfils the donor responsibility in **2**, and effectively at that going on the lengths of the dative K−N bonds (mean, 2.8759 Å) which, unusually, are of the same magnitude (mean, 2.8899 Å) as their anion-containing K-(μ-N) comrades. In the aforementioned homometallic relative $[(KDA{\cdot}TMEDA)_2]$,[12] the K−N "anionic" bonds are significantly shorter than their dative counterparts (mean values, 2.771 and 2.886 Å respectively). Worthy of comment is the marked variation between the length of the shortest K−N (from DA) bond in this homodimer [2.706(2) Å] and that of the corresponding shortest bond in heterodimeric **2** [K−N2, 2.8630(13) Å]: this emphasises the profound proximal effect that the introduction of a Mg atom can exert on the dimensions of an identical K coordinative environment (here involving four N atoms, two from DA and two from TMEDA). The presence of TMEDA in **2** also lessens the need for reinforcement K···C agostic bonding. This is manifested in fewer K···C contacts and much longer contact distances than those previously discussed for **1**. There are only three such contacts below 4 Å in length: the shortest is to the methyl C17 at 3.277 Å, the next shortest is to the methyne C10 at 3.303 Å, and the remaining contact is to the methyl C11 at 3.475 Å. There are no intermolecular K···C contacts present, in keeping with the monomeric (dinuclear) constitution of the structure.

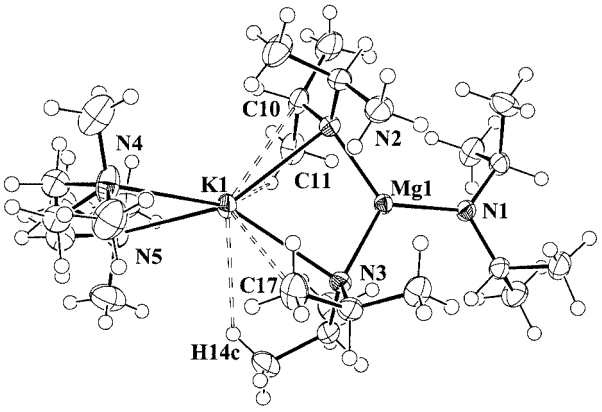

Figure 3. Molecular structure of **2** with agostic contacts shown as broken lines

Table 2. Selected bond lengths (Å) and bond angles (°) for $[KMg(NiPr_2)_3(TMEDA)]$ (**2**)

Bond lengths (Å)		Bond angles (°)	
Mg(1)−N(1)	1.9722(13)	N(4)−K(1)−N(2)	131.82(4)
Mg(1)−N(2)	2.0381(13)	N(2)−K(1)−N(5)	132.33(4)
Mg(1)−N(3)	2.0454(13)	N(4)−K(1)−N(3)	139.84(4)
K(1)−N(2)	2.8630(13)	N(2)−K(1)−N(3)	72.60(3)
K(1)−N(3)	2.9169(13)	N(5)−K(1)−N(3)	126.64(4)
K(1)−N(4)	2.8413(15)	N(1)−Mg(1)−N(2)	126.56(6)
K(1)−N(5)	2.9105(14)	N(1)−Mg(1)−N(3)	119.51(6)
K(1)···C(10)	3.303(2)	N(2)−Mg(1)−N(3)	113.87(6)
K(1)···C(11)	3.475(2)	Mg(1)−N(2)−K(1)	86.96(4)
K(1)···C(17)	3.303(2)	Mg(1)−N(3)−K(1)	131.82(4)

Since the metal-N core of the molecular structure of the sodium congener **3** (Figure 4) is essentially isostructural to that of **2**, it merits only a brief discussion. Table 3 records the principal bond lengths and bond angles for **3**. There is a marginally greater deviation in the bridging and terminal Mg−N (from DA) bond lengths [2.0613 Å (mean) and

 © 2003 Wiley-VCH Verlag GmbH & Co. KGaA, Weinheim

1.9679(13) Å, respectively] than that in **2**. Comparison with the dimensions of the homodimeric structure of $[(NaDA{\cdot}TMEDA)_2]$,[11] where the mean Na−N (from DA) bond length is 2.447 Å, reveals again the strong bonding power of the proximate Mg atom in **3** as it draws the amido N bridges away from the Na atom to elongate the Na−N bonds (mean length, 2.5313 Å). To compensate the Na atom in **3** for this loss in valency, there is a concomitant strengthening of the dative bonding to TMEDA as reflected by short Na−N bonds (mean length, 2.5504 Å; *cf.* 2.6195 Å in the homodimer). Within the Na-$(\mu\text{-}N)_2$-Mg trapezoidal ring, the obtuse bond angle is at Mg [110.44(5)°] and the acute one is at the larger Na centre [83.94(4)°], with a mean angle at N of 82.72°. Switching to the yet larger K centre in **2**, as expected, exacerbates this trapezoidal distortion to give corresponding values of 113.87(6)°, 72.60(3)°, and 86.17° respectively. Finally it should be noted that there are no Na···C agostic interactions in **3**, with the shortest such contact being 3.239 Å.

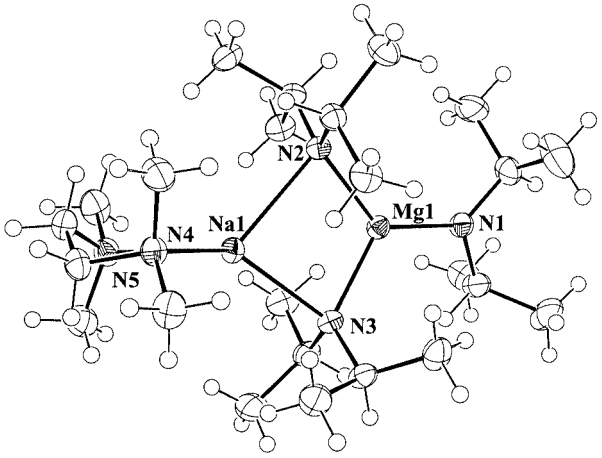

Figure 4. Molecular structure of **3**

Table 3. Selected bond lengths (Å) and bond angles (°) for $[NaMg(N\textit{i}Pr_2)_3(TMEDA)]$ (**3**)

Bond lengths (Å)		Bond angles (°)	
Mg(1)−N(1)	1.9679(13)	N(2)−Na(1)−N(5)	126.82(5)
Mg(1)−N(2)	2.0638(13)	N(2)−Na(1)−N(4)	134.30(5)
Mg(1)−N(3)	2.0587(13)	N(2)−Na(1)−N(3)	83.94(4)
Na(1)−N(2)	2.4988(13)	N(5)−Na(1)−N(3)	125.29(4)
Na(1)−N(3)	2.5638(13)	N(4)−Na(1)−N(3)	116.98(4)
Na(1)−N(4)	2.5537(13)	N(1)−Mg(1)−N(3)	131.34(6)
Na(1)−N(5)	2.5472(14)	N(1)−Mg(1)−N(2)	118.00(5)
		N(3)−Mg(1)−N(2)	110.44(5)
		Mg(1)−N(3)−Na(1)	81.95(4)
		Mg(1)−N(2)−Na(1)	83.49(4)

Structural differences in the solid state, if maintained in solution, can influence the reaction chemistry of the DA anion given the close correlation that exists between structure and reactivity. A brief survey of a selection of previously determined *s*-block metal-based DA structures (see Figure 5) is therefore warranted to enable the novelty of the structures of **1**−**3** to be put into perspective. Pure crystalline LDA exists as a helical polymer (**A**) with near linear NLiN segments, eight of which constitute a turn of the helix.[18] More relevant to the solution phase, the solvated derivative $[(LDA{\cdot}THF)_2]$ (**B**) exhibits a planar $(LiN)_2$ dimeric ring, the Li corners of which carry monodentate THF ligands.[19] A similar discrete four-membered ring structure (**B**) is observed in both the aforementioned $[(NaDA{\cdot}TMEDA)_2]$[11] and $[(KDA{\cdot}TMEDA)_2]$,[12] though the wider exocyclic coordination arcs offered by the larger alkali metals allows for the chelation of didentate TMEDA ligands. Combining LDA with the same diamine molecule in $[\{(LDA{\cdot}TMEDA)_2\}_\infty]$[20] again generates a $(LiN)_2$ dimeric ring, but the reduced space about the Li centres forces the TMEDA ligands into bridging (non-chelating) roles to create an infinite chain of linked dimers (**C**). It may be significant from a reactivity standpoint that the exclusively bridging mode of the DA ligands in all of the last four structures discussed contrasts with the combination of bridging and terminal modes encountered in both **2** and **3** (and possibly in **1** depending on its fragmentation process in solution). The opportunity for **1**−**3** to dissociate in the form of a complex "ate" anion $[Mg(DA)_3]^-$, which is unavailable to the homometallic compositions, may also cause them to react differently towards protic substrates. To the best of our knowledge, this tris-DA coordination about Mg is unique to the structures of **1**−**3** though it is known with other metals both discretely, for example with A1 in neutral monomeric $[A1(DA)_3]$ (**D**),[21] or linked into the common dimeric motif as with Mn in $[\{Mn(DA)_2\}_2]$ (**E**).[22] On the other hand bis-DA coordination of Mg is well-known when auxiliary ligands are present to fill the remaining sites: it is only rarely observed in homomagnesium structures such as the mixed alkynyl/DA dimer $[\{Mg(DA)(C{\equiv}CPh){\cdot}THF\}_2]$ (**E**),[23] where the linearity of the alkynyl ligand allows for a tetrahedral Mg coordination, but is much more common in heterometallic examples, and these can exhibit three (trigonal planar), or more usually, four (tetrahedral) Mg coordination depending on the steric characteristics of the ligand sets, as illustrated by the alkide $[Me_2A1(DA)_2MgMe]$ (**G**)[24] and the amidinate $[Me_2A1(DA)_2Mg\{\textit{t}BuNC(Me)N\textit{t}Bu\}]$ (**H**)[25] respectively. While mixed aluminium-magnesium complexes of this type are commonplace, in general, the range of heterometallic magnesium-containing DA-based crystal structures is rather limited. Extending the search to other related amide ligands reveals a far higher number of hits of "ate" complexes with the general formula $[Mg(amide)_3]^-$. HMDS complexes of this type are particularly commonplace as exemplified by the aforementioned π-arene series $[\{K(ar)_2\}^+\ \{Mg(HMDS)_3\}^-]$.[17] The recent report of the trimetallic lithium-potassium-(bis)magnesium N-metallated/N,C-dimetallated amide $[Li_2K_2Mg_4\{\textit{t}Bu(Me_3Si)N\}_4\{\textit{t}Bu[Me_2(H_2C)Si]N\}_4]$,[26] an inverse crown molecule with an atomless cavity, suggests there is every possibility that the rich structural variety found within the s-block chemistry of the DA ligand is far from exhausted.

 © 2003 Wiley-VCH Verlag GmbH & Co. KGaA, Weinheim

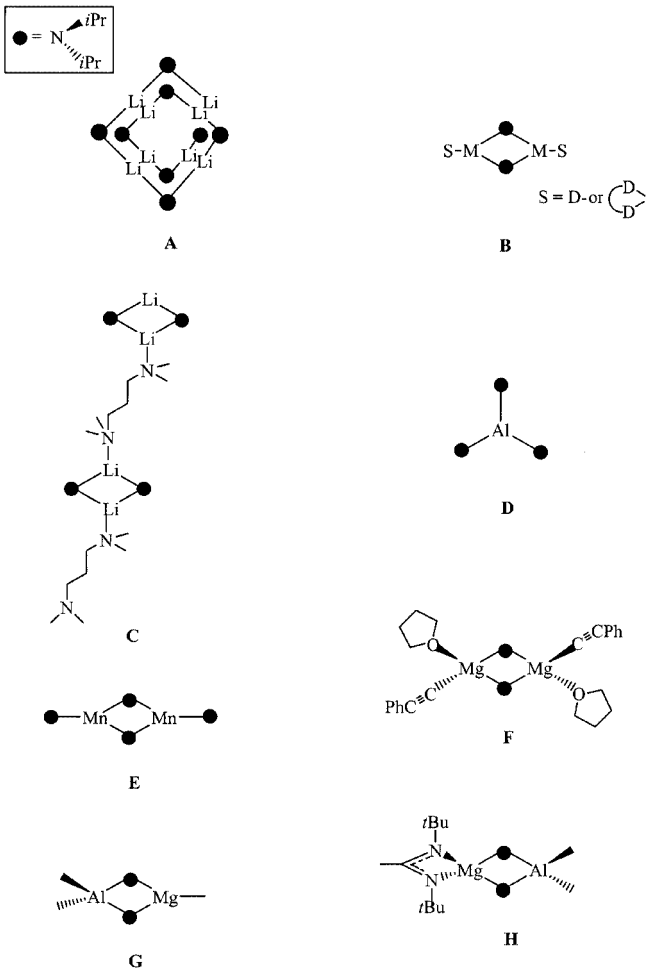

Figure 5. Selected structures in the *s*-block chemistry of the DA ligand and related structures

Experimental Section

General: All reactions were performed under a protective argon atmosphere using standard Schlenk techniques. Hexane was dried by heating to reflux over sodium benzophenone ketyl and distilled under nitrogen prior to use. Diisopropylamine was dried by heating to reflux over calcium hydride and stored over 4 Å molecular sieves. *n*,*s*-Dibutylmagnesium was purchased from Aldrich Chemicals as a 1 M solution in heptane and standardised immediately prior to use using salicylaldehyde phenylhydrazone.[27] Benzylpotassium,[28] butylpotassium[29] and butylsodium[30] were prepared according to the literature methods. Melting points were determined in sealed argon-filled capillary tubes and are uncorrected. NMR experiments were carried out on a Bruker DPX 400 MHz spectrometer, operating at 400.13 MHz for ^{1}H and 100.62 MHz for ^{13}C.

[{KMg(DA)$_3$}$_\infty$] (1): (From butylpotassium) A 1:1:3 stoichiometric mixture of *n*BuK (0.4 g, 5 mmol)/*n*,*s*-Bu_2Mg (5 mL of a 1 M solution in heptane, 5 mmol)/*i*Pr_2NH (2.1 mL, 15 mmol) in hexane (15 mL) was stirred at ambient temperature overnight. This resulted in the formation of a brown oily solution with a trace amount of a black waxy solid. The solid was removed by filtering the mixture through Celite. The filtrate was reduced in volume in vacuo, then placed in the freezer at −28 °C. Overnight this solution deposited a crop of colourless crystals of **1** (yield 0.49 g, 27%). M.p. 96−98 °C (decomposes to brown oil). Satisfactory microanalyses could not be obtained due to samples losing weight rapidly on the balance.^{1}H NMR ([D$_6$]benzene solution; 25 °C): δ = 3.38 (sep., 1 H, Me_2CH), 1.27 (d, 6 H, Me_2CH).
(From benzylpotassium) Benzylpotassium (0.65 g, 5 mmol) was suspended in hexane (20 mL). *n*,*s*-Bu_2Mg (5 mL of a 1 M solution in heptane, 5 mmol) and *i*Pr_2NH (2.1 mL, 15 mmol) were then added. The reaction mixture was stirred for 12 hours at ambient temperature. The resulting cloudy red mixture was filtered through Celite and the filtrate was concentrated by removing some solvent in vacuo. Freezer cooling of the solution at −28 °C afforded a crop of colourless crystals of **1** (yield 0.62 g, 34%). Characterisation as above but in addition: ^{1}H NMR ([D$_8$]toluene solution; 25 °C): δ = 3.30 (sep., 1 H, Me_2CH), 1.21 (d, 6 H, Me_2CH) ppm. ^{13}C NMR ([D$_8$]toluene solution; 25 °C): δ = 49.7 (Me_2CH), 27.92 (Me_2CH) ppm.

[KMg(DA)$_3$·TMEDA] (2): Benzylpotassium (0.65 g, 5 mmol) was suspended in hexane (20 mL). *n*,*s*-Bu_2Mg (5 mL of a 1 M solution in heptane, 5 mmol) and *i*Pr_2NH (2.1 mL, 15 mmol) were then introduced. The resulting red solution was stirred for 30 minutes after which time TMEDA (0.75 mL, 5 mmol) was added. After stirring for a further 60 minutes, the solution was concentrated by removing some solvent in vacuo. Freezer cooling of the remaining solution at −28 °C produced a crop of colourless crystals of **2**. These were partially covered by a red oil which hindered the isolation of the pure crystalline material and precluded a meaningful determination of its yield. Satisfactory microanalyses could not be obtained due to contamination by the red oily coating. ^{1}H NMR ([D$_8$]toluene solution; 25 °C): δ = 3.40 [m (broad), 6 H, Me_2CH], 1.91 (s, 4 H, CH_2, TMEDA), 1.89 (s, 12 H, CH_3, TMEDA), 1.29 [d (broad), 36 H, Me_2CH] ppm. ^{13}C NMR ([D$_8$]toluene solution; 25 °C): δ = 57.2 (CH_2, TMEDA), 49.8 (Me_2CH), 45.4 (CH_3, TMEDA), 27.9 (Me_2CH) ppm.

[NaMg(DA)$_3$·TMEDA] (3): *n*BuNa (0.4 g, 5 mmol) was suspended in hexane (10 mL) and placed in an ultrasonic bath for 10 minutes. *n*,*s*-Bu_2Mg (5 mL of a 1 M solution in heptane, 5 mmol) was introduced slowly to give a brown gum, which dissolved upon the addition of *i*Pr_2NH (2.1 mL, 15 mmol). The resulting pale yellow solution was stirred for 20 minutes at which time TMEDA (0.75 mL, 5 mmol) was added. Turning cloudier, the solution was stirred for a further 20 minutes, filtered through Celite, reduced in volume in vacuo, and left to cool in the freezer at −28 °C. After several days a crop of colourless crystals of **3** was obtained (isolated yield 0.51 g, 22% − the bulk of the crystalline product redissolved during the isolation procedure). M.p. 103−105 °C. Satisfactory microanalyses (C,H,N) were obtained. ^{1}H NMR ([D$_6$]benzene solution; 25 °C): δ = 3.50 (sep., 6 H, Me_2CH), 1.81 (s, 12 H, CH_3, TMEDA), 1.72 (s, 4 H, CH_2, TMEDA), 1.38 (d, 36 H, Me_2CH) ppm. ^{1}H NMR ([D$_8$]toluene solution; 25 °C): δ = 3.43 [m (broad), 6 H, Me_2CH], 1.84 (s, 12 H, CH_3,TMEDA), 1.76 (s, 4 H, CH_2, TMEDA), 1.31 [d (broad), 36 H, Me_2CH] ppm. ^{1}H NMR ([D$_8$]toluene solution; −30 °C): δ = 3.77 [s (broad), 2 H, Me_2CH], 3.38 [s (broad), 4 H, Me_2CH, μ-DA] 1.75 [s, 12 H, CH_3, TMEDA], 1.60 [d, 4 H, CH_2, TMEDA], 1.27[s (broad), 36 H, Me_2CH] ppm. ^{13}C NMR ([D$_8$]toluene solution; 25 °C): δ = 57.4 (CH_2, TMEDA), 49.2 (Me_2CH), 46.2 (CH_3, TMEDA), 28.1 (Me_2CH) ppm.

X-ray Structure Determinations: Measurements were made on a Nonius Kappa CCD diffractometer at 123 K with Mo-K_α radiation (λ = 0.71073 Å). Structures were refined on F^2 using all reflections with the Shelxl-97 program. All non-H atoms were treated anisotropically except for the disordered components in **1** and **2**. H atoms were not refined except for those involved in agostic interac-

 © 2003 Wiley-VCH Verlag GmbH & Co. KGaA, Weinheim

tions in **2**. Further crystallographic data and refinement parameters are given in Table 4. CCDC-213563 (**1**), -213564 (**2**) and -213565 (**3**) contain the supplementary crystallographic data for this paper. These data can be obtained free of charge at www.ccdc.cam.ac.uk/conts/retrieving.html [or from the Cambridge Crystallographic Data Centre, 12, Union Road, Cambridge CB2 1EZ, UK; Fax: (internat.) +44-1223/336-033; E-mail: deposit@ccdc.cam.ac.uk].

Table 4. Crystallographic data for compounds **1**−**3**

	1	**2**	**3**
Empirical formula	$C_{18}H_{42}KMgN_3$	$C_{24}H_{58}KMgN_5$	$C_{24}H_{58}MgN_5Na$
Molecular weight	363.96	480.16	464.05
Crystal system	triclinic	monoclinic	orthorhombic
Space group	$P\bar{1}$	$P2_1/n$	Pbca
a (Å)	9.9818 (1)	10.1715 (1)	18.2113 (5)
b (Å)	14.3537 (2)	20.5215 (3)	16.9186 (4)
c (Å)	15.8388 (3)	15.4082 (2)	20.0492 (6)
α (°)	92.479 (1)	90	90
β (°)	91.747 (1)	101.598 (1)	90
γ (°)	90.414 (1)	90	90
V (Å^3)	2266.06 (6)	3150.55 (7)	6177.4 (3)
Z	4	4	8
2θ max.	27.64	27.87	26.79
No. of reflections	10414	7500	6554
No. of parameters	430	295	296
$R1$	0.0516	0.0453	0.0438
$wR2$	0.1273	0.1046	0.1045
S	1.031	1.025	1.057

Acknowledgments

We thank the UK EPSRC for funding this research through grant award number GR/R81183/01.

[1] For reviews of the uses of lithium amides in synthesis see: J. K. Crandall, M. Apparu, *Org. React.* **1983**, *29*, 345−443; V. Snieckus, *Chem. Rev.* **1990**, *90*, 879−933; C. H. Heathcock, in *Comprehensive Organic Synthesis* (Eds: B. M. Trost, I. Fleming), Pergamon, New York, **1991**, vol. 2, chapter 1.6; T. Satoh, *Chem. Rev.* **1996**, *96*, 3303−3326.

[2] Collum has made a colossal contribution to correlating the complicated structural chemistry of LDA in solution to its performances and kinetics in organic reactions. For leading papers see: Y.-J. Kim, M. P. Bernstein, A. S. Galiano Roth, F. E. Romesberg, P. G. Williard, D. J. Fuller, A. T. Harrison, D. B. Collum, *J. Am. Chem. Soc.* **1991**, *56*, 4435−4439; J. F. Remenar, B. L. Lucht, D. B. Collum, *J. Am. Chem. Soc.* **1997**, *119*, 5567−5571; X. Sun, D. B. Collum, *J. Am. Chem. Soc.* **2000**, *122*, 2459−2463; J. L. Rutherford, D. B. Collum, *J. Am. Chem. Soc.* **2001**, *123*, 199−202.

[3] For an excellent general monologue on the multivariate factors which determine the course of an organoalkali metal-mediated reaction see: M. Schlosser, in *Organometallics in Synthesis A Manual*, 2nd Edn (Ed.: M. Schlosser), John Wiley and Sons Ltd, Chichester, England, **2002**, chapter 1, 1−352.

[4] R. E. Mulvey, *Chem. Commun.* **2001**, 1049−1056.

[5] K. J. Drewette, K. W. Henderson, A. R. Kennedy, R. E. Mulvey, C. T. O'Hara, R. B. Rowlings, *Chem. Commun.* **2002**, 1176−1177.

[6] D. J. Gallagher, K. W. Henderson, A. R. Kennedy, C. T. O'Hara, R. E. Mulvey, R. B. Rowlings, *Chem. Commun.* **2002**, 376−377.

[7] W. Clegg, K. W. Henderson, A. R. Kennedy, R. E. Mulvey, C. T. O'Hara, R. B. Rowlings, D. M. Tooke, *Angew. Chem.* **2001**, *113*, 4020−4023; *Angew. Chem. Int. Ed.* **2001**, *40*, 3902−3905.

[8] A. M. Drummond, L. T. Gibson, A. R. Kennedy, R. E. Mulvey, C. T. O'Hara, R. B. Rowlings, T. Weightman, *Angew. Chem.* **2002**, *114*, 2488−2490; *Angew. Chem. Int. Ed.* **2002**, *41*, 2382−2384.

[9] R. Sanchez, W. Scott, *Tetrahedron Lett.* **1988**, *29*, 139−142.

[10] P. Andrikopoulos, D. R. Armstrong, A. R. Kennedy, R. E. Mulvey, C. T. O'Hara, R. B. Rowlings, *following paper in this issue.*

[11] P. C. Andrews, N. D. R. Barnett, R. E. Mulvey, W. Clegg, P. A. O'Neil, D. Barr, L. Cowton, A. J. Dawson, B. J. Wakefield, *J. Organomet. Chem.* **1996**, *518*, 85−95.

[12] W. Clegg, S. Kleditzsch, R. E. Mulvey, P. O'Shaughnessy, *J. Organomet. Chem.* **1998**, *558*, 193−196.

[13] M. Micha-Screttas, C. G. Screttas, B. R. Steele, G. A. Heropoulos, *Tetrahedron Lett.* **2002**, *43*, 4871−4873.

[14] G. W. Gokel, L. Barbour, S. L. DeWall, E. S. Meadows, *Coord. Chem. Rev.* **2001**, *222*, 127−154.

[15] E. S. Meadows, S. L. DeWall, L. J. Barbour, G. W. Gokel, *J. Am. Chem. Soc.* **2001**, *123*, 3092−3107.

[16] Ch. Elschenbroich, A. Salzer, in *Organometallics A Concise Introduction*, 1st Edn, VCH, Weinheim, **1989**, pp 80−81.

[17] G. C. Forbes, A. R. Kennedy, R. E. Mulvey, B. A. Roberts, R. B. Rowlings, *Organometallics* **2002**, *21*, 5115−5121.

[18] N. D. R. Barnett, R. E. Mulvey, W. Clegg, P. A. O'Neil, *J. Am. Chem. Soc.* **1991**, *113*, 8187−8188.

[19] P. G. Williard, J. M. Salvino, *J. Org. Chem.* **1993**, *58*, 1−3.

[20] M. P. Bernstein, F. E. Romesberg, D. J. Fuller, A. T. Harrison, D. B. Collum, Q.-Y. Liu, P. G. Williard, *J. Am. Chem. Soc.* **1992**, *114*, 5100−5110.

[21] P. J. Brothers, R. J. Wehmschulte, M. M. Olmstead, K. Ruhlandt-Senge, S. R. Parkin, P. P. Power, *Organometallics* **1994**, *13*, 2792−2799.

[22] A. Belforte, F. Calderazzo, U. Englert, J. Strahle, K. Wurst, *J. Chem. Soc., Dalton Trans.* **1991**, 2419−2427.

[23] K.-C. Yang, C.-C. Chang, J.-Y. Huang, C.-C. Lin, G.-H. Lee, Y. Wang, M.-Y. Chiang, *J. Organomet. Chem.* **2002**, *648*, 176−187.

[24] T.-Y. Her, C.-C. Chang, L.-K. Liu, *Inorg. Chem.* **1992**, *31*, 2291−2294.

[25] M.-D. Li, C.-C. Chang, Y. Wang, G.-H. Lee, *Organometallics* **1996**, *15*, 2571−2574.

[26] G. C. Forbes, F. R. Kenley, A. R. Kennedy, R. E. Mulvey, C. T. O'Hara, J. A. Parkinson, *Chem. Commun.* **2003**, 1140−1141.

[27] B. E. Love, E. G. Jones, *J. Org. Chem.* **1999**, *64*, 3755−3756.

[28] D. Hoffmann, W. Bauer, F. Hampel, N. J. R. van Eikema Hommes, P. v. R. Schleyer, P. Otto, U. Pieper, D. Stalke, D. S. Wright, R. Snaith, *J. Am. Chem. Soc.* **1994**, *116*, 528−536.

[29] R. Pi, W. Bauer, B. Brix, C. Schade, P. v. R. Schleyer, *J. Organomet. Chem.* **1986**, *306*, C1−C4.

[30] C. Schade, W. Bauer, P. v. R. Schleyer, *J. Organomet. Chem.* **1985**, *295*, C25−C28.

Received June 27, 2003

 © 2003 Wiley-VCH Verlag GmbH & Co. KGaA, Weinheim

Synthesis, Structure and Theoretical Studies of the Hydrido Inverse Crown $[K_2Mg_2(NiPr_2)_4(\mu\text{-}H)_2\cdot(toluene)_2]$: a Rare Example of a Molecular Magnesium Hydride with a Mg-$(\mu\text{-}H)_2$-Mg Double Bridge

Prokopis C. Andrikopoulos,[a] David R. Armstrong,[a] Alan R. Kennedy,[a] Robert E. Mulvey,[a] Charles T. O'Hara,*[a] and René B. Rowlings[a]

Dedicated to the memory of Ron Snaith who for DRA and REM was an inspirational teacher, a pre-eminent researcher and a revered colleague and friend

Keywords: Potassium / Magnesium / N ligands / Hydride ligands / Density functional calculations

Reaction of benzylpotassium, *n*,*s*-dibutylmagnesium and diisopropylamine in boiling toluene produces a rare example of a molecular magnesium hydride with a Mg-$(\mu\text{-}H)_2$-Mg double bridge, in $[K_2Mg_2(NiPr_2)_4(\mu\text{-}H)_2\cdot(toluene)_2]$ (**1**). In an effort to rationalise the formation of **1**, a series of DFT calculations were performed. This report of **1** establishes the first isostructural pair of Na and K complexes solvated by toluene to be reported in the Cambridge Crystallographic Database. In comparison with its previously reported Na analogue, **2**, the metal-arene centroid distances are considerably *shorter* (by 0.159 Å) in the new complex reported here. It was found that a hydrocarbon solution of **1** is capable of reducing benzophenone to benzhydrol in moderate yields (74%).

(© Wiley-VCH Verlag GmbH & Co. KGaA, 69451 Weinheim, Germany, 2003)

Introduction

Main group metal hydrides, in particular those containing aluminium are widely utilised by the synthetic chemist as highly efficient reducing agents.[1] Commercially available reagents such as lithium aluminium hydride, lithium tri-*tert*-butoxyaluminohydride and Red-Al® [sodium bis(2-methoxyethyoxy)aluminium hydride] can effect the reduction of many polarised organic functional groups easily and efficiently. The structural chemistry of molecules containing an Al−H−Al linkage is also well developed.[2] However, unlike their aluminium counterparts, magnesium hydrides have thus far not been the subject of intensive research. To the best of our knowledge, only one genuine molecular magnesium hydride, which contains a Mg−H−Mg bridge, has been prepared and crystallographically characterised[3] (see below). Synthetically, it has been shown that magnesium hydride-containing species (such as RMgH, ROMgH or R_2NMgH; where R = Me, Et, *i*Pr or C_5H_5 for the alkylmagnesium hydrides and R = Me, *i*Pr, *t*Bu, *t*$BuCH_2$, $PhCH_2CH_2$, Ph, Ph_3C, 2,6-$Me_2C_6H_3$, 2,6-$iPr_2C_6H_3$ or 2,6-tBu_2-4-MeC_6H_2 for the alkoxy or aryloxymagnesium hydrides and R = Et, *i*Pr, *n*Bu or Ph for the dialkyl or diarylaminomagnesium hydrides) are useful in effecting reductive transformations.[4] Unsolvated magnesium bis(diisopropylamide)[5] is also capable of converting aldehydes/ketones to alcohols and converting nitro compounds to amines via hydride transfer from the carbon positioned beta to the magnesium centre.

Herein we report the synthesis and structural analysis of $[K_2Mg_2(NiPr_2)_4(\mu\text{-}H)_2\cdot(toluene)_2]$ (**1**). Complex **1** represents the first structurally characterised potassium-containing heterobimetallic diisopropylamide and only the second molecular magnesium hydrido species which contains an Mg−H−Mg bridge, the first being the Na analogue of **1**, $[Na_2Mg_2(NiPr_2)_4(\mu\text{-}H)_2\cdot(toluene)_2]$ (**2**). This complex was reported in a recent communication.[3] Here we provide further details of the structure of **2**. Complex **1** is only the second example of a crystallographically characterised potassium diisopropylamide, the first example being the simple dimeric, TMEDA solvate $[(KNiPr_2\cdot TMEDA)_2]$ (**3**).[6] Recent work in our laboratory has focused on the synergistic chemistry of combining an alkali metal amide with its magnesium (or zinc) bis(amide) analogue. The major consequence of these studies thus far has been the development of a series of heterobimetallic macrocyclic amide complexes that have become known collectively as "inverse crowns."[7] A subset of the inverse crowns (IC) are the inverse crown ethers (ICE). This non-precise nomenclature was chosen because the ICE complexes show an inverse topological relationship to conventional crown ether complexes — the Lewis acidic metal sites and Lewis basic oxygen centres are mutually interchanged. IC complexes are distinguished

[a] Department of Pure and Applied Chemistry, University of Strathclyde,
Glasgow, G1 1XL, UK

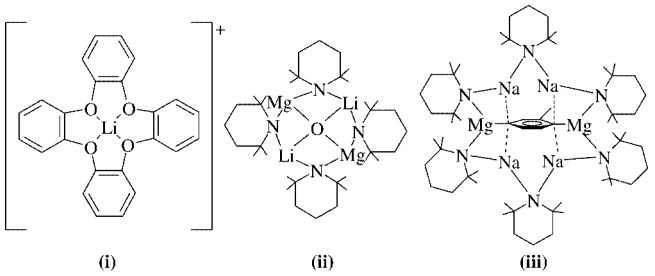

Figure 1. Examples of a conventional crown ether complex (i), an inverse crown ether (ii)[8] and an "oxygen-free" inverse crown complex (iii)[9]

from ICE complexes by the fact that the former do not contain any oxygen-containing anions (Figure 1).

As well as forming complexes with aesthetically pleasing crystal structures, a special chemistry that is otherwise irreproducible has been uncovered using these synergistic metal amide bases. Employing "$NaMg(NiPr_2)_3$", the tris(amido) species prepared from the in situ reaction of BuNa, Bu_2Mg and $HNiPr_2$ in a 1:1:3 molar ratio, the unprecedented 1,1′,3,3′-tetrametallation of ferrocene was accomplished.[10] Returning to **1**, this molecule is the most recent addition to the inverse crown family. Although essentially isostructural with its sodium analogue, in the potassium variant, the alkali metal exhibits stronger coordination to the arene molecule, indicated by the fact that the mean arene-M (where M = Na or K) length is *shorter* for the K analogue. Alkali metal-π interactions have recently been the subject of considerable research.[11] The importance of these interactions has been realised in zeolite-supported processes,[12] in the interaction of alkali metal cations with aromatic side chains of proteins,[13] and in the selectivity of superbases,[14] via the coordination of an arene molecule to a group 1 metal centre.

Results and Discussion

Preparation and Spectra

Complex **1** was prepared by heating a 1:1:3 mixture of benzylpotassium, *n*,*s*-dibutylmagnesium and diisopropylamine, in a toluene/heptane medium. This synthesis marks a significant departure from that of most of the other members of the inverse crown family prepared to date[15] — a M*n*Bu (where M = Li, Na or K) reagent has not been utilised in the preparation. The synthesis of **1** was initially attempted using *n*-butylpotassium; however, on the addition of amine to the heterobimetallic alkyl mixture, a significant quantity of an insoluble, black solid was obtained. The formation of this impurity can be attributed to the fact that *n*-butylpotassium is not thermally stable being readily susceptible to β-hydride elimination. Ironically, a similar decomposition pathway is vital to the formation of **1** (vide infra), but at this early stage in the synthetic procedure, it appears to be highly detrimental. On changing the potassiating reagent from butyl- to benzyl- (i.e. ruling out β-hydride elimination as a potential decomposition pathway) the reaction proceeded in a seemingly more controlled manner, resulting in the observation of a discernible colour change without the precipitation of an undesired solid by-product. Although less reactive than its butyl counterpart, the activity of benzylpotassium is adequate for our needs, and this easily prepared reagent will undoubtedly be utilised by our group in various reactions in the future. Interestingly, if the heterobimetallic amide mixture is not subjected to intense heating, complex **1** is not formed — instead the unsolvated tris(amido) species $KMg(NiPr_2)_3$ is produced. Details of the preparation and structural analysis of this complex and two other related compounds can be found in the preceding paper in this issue.[16]

The by-product of amine deprotonation by benzylpotassium is toluene and since the bulk of the reaction medium is composed of this solvent, the by-product does not have a disadvantageous effect on the reaction. Indeed, toluene is actually incorporated into the molecular structure of **1**. The shielding of the potassium and magnesium centres by the isopropyl groups and the former by toluene molecules results in the entire molecule being highly lipophilic.[17] As a consequence the complex is highly hydrocarbon soluble, explaining why the isolated yield of the crystals of **1** was relatively low.

Table 1 contains the ^1H NMR spectroscopic data for **1** along with those of **2** for comparison. The chemical shifts for the potassium analogue **1** are systematically at a higher frequency than those for the sodium variant **2**, although the differences are rather small. The hydride shift in both complexes is similar indicating that changing the alkali metal has little effect on the Mg−H−Mg bridge. This supports our interpretation that there is essentially no K−H bonding in **1** (see below). Unfortunately, the relative chemical shifts of the complexed toluene molecules in **1** and **2** cannot be directly compared. For **1** the acquired spectrum in C_6D_6 clearly shows that the correct stoichiometric amount of toluene is present, consistent with that in the crystal structure; however, for **2** in the same solvent virtually no toluene can be observed, meaning that the vast majority of the toluene is lost on isolation. When **2** is dissolved in $C_6D_5CD_3$, two distinct methyl resonances are observed. These are attributed to uncomplexed toluene (δ = 2.09 ppm) and toluene which has been incorporated into the structure of **1** (δ = 2.11 ppm).

Table 1. ^1H NMR spectroscopic data for **1** and **2**; spectra acquired at 400.13 MHz in [D_6]benzene

Fragment	Chemical shift for **1**	Chemical shift for **2**
$(CH_3)_2CH$	1.29	1.22
$(CH_3)_2CH$	3.35	3.19
Mg-*H*-Mg	3.78	3.76
CH_3-Ph	2.11	2.11 (in $C_6D_5CD_3$)

 © 2003 Wiley-VCH Verlag GmbH & Co. KGaA, Weinheim

X-ray Crystallography

The molecular structure of **1** (Figure 2) is essentially isostructural with its sodium analogue **2**. Listed in Table 2 are the key structural dimensions of **1**, alongside those of **2** for comparison.

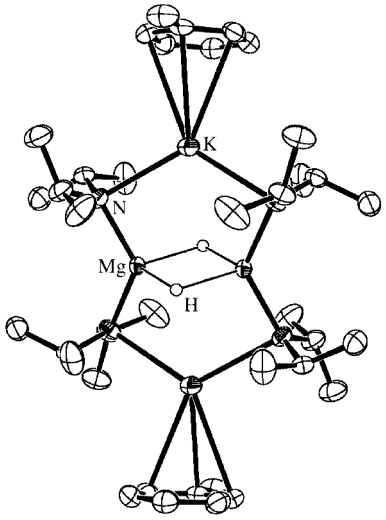

Figure 2. Molecular structure of **1**

Table 2. Key structural dimensions of **1** and **2**

Selected bonds and bond angles	Bond lengths (Å) and bond angles (°) M = K (**1**)	M = Na (**2**)
M1−N1	2.7754(16)	2.4807(18)
Mg1−N1	2.0595(15)	2.0651(18)
M···H	2.96(3)	2.68(3)
Mg1−H1	1.94(2)	1.89(2)
Mg···Mg	2.9437(14)	2.8921(19)
M-*ipso*-C	3.107(3)	3.157(4)
M-*ortho*-C	3.1840(19)	3.275(3)
M-*meta*-C	3.339(2)	3.531(3)
M-*para*-C	3.422(3)	3.663(4)
M-centroid	2.955	3.114
N−M−N	119.55(6)	132.08(10)
N−Mg−N	126.55(9)	133.16(11)
Mg−H−Mg	98.7(14)	100(2)

The eight-membered metal-amide ring of **1** is chair-shaped. As for **2**, the N−Mg−N···N−Mg−N "chair-seat" is strictly planar, whilst the "head-" and "foot-rest" positions (signified by N−K−N in **1**) are tilted at an angle of 154.70(11)° compared to 153.5(2)° in **2** (Figure 3). At this juncture it is important to mention that the bridging hydride ions were independently refined. The Mg−H bond length in **1** is the same within experimental error as that in **2**. These dimensions resemble those of the Mg−H bonds present in a selection of other heterobimetallic hydride complexes: $[\{(C_5Me_5)_2Ti(\mu\text{-}H)_2\}_2Mg]$,[18] (mean, 1.88 Å); $[\{(C_5HMe_4)_2Ti(\mu\text{-}H)_2Mg(THF)(\mu\text{-}Cl)\}_2]$,[19] (mean, 1.91 Å); and $[(\{Me_2Si(C_5Me_4)_2\}Zr\{\eta^2\text{-}C_2H_4\}H)_2Mg]$,[20] (mean, 1.82 Å). The magnesium atoms in **1** are forced into a highly distorted tetrahedral coordination environment [the angles around the magnesium centres range from 104.1(9) to 126.55(9)°; mean, 115.57°].

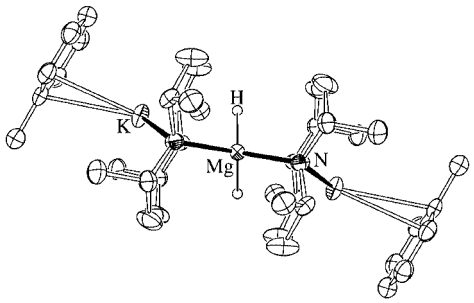

Figure 3. Alternative view of the molecular structure of **1** highlighting the planar "seat" and tilted "head-" and "foot-rest" arrangements

The closest K···H contact in **1** is 2.96(3) Å. This value can be compared with those in [K(*fac*-$RuH_3\{Cy_2P(CH_2)_4PCy_2\}\{CO\}$)$KBHsBu_3$],[17] [mean, 2.63 Å; range, 2.44(6)−2.82(5) Å], and in $[\{(C_5Me_5)Sm(\mu\text{-}H)_2\}_6\{(\mu\text{-}H)K(THF)_2\}_3]$,[21] [2.58(4) and 2.89(7) Å]. Unlike **1**, these complexes exhibit both short and long K···H contacts. The short contacts are significantly shorter than those found in **1**; however, the longer contacts, especially those in the latter complex, are similar to those in **1**. Therefore it appears that the K···H contacts in **1** appear to be too long to be considered significant.

The K−N bond length in **1** [2.7754(16) Å] is of the same order as those in the aforementioned TMEDA solvate **3** (mean, 2.7715 Å). The K centres in each form two bonds to diisopropylamido bridges, therefore it can be assumed that the TMEDA chelation and toluene π-interactions stabilise the respective molecules to a similar extent. To elaborate, the K coordination sphere in **1** is completed by an η^3 (*ipso* and two equivalent *ortho* C atoms) π-interaction to a toluene molecule [bond lengths: K−C_{ipso}, 3.107(3) Å; K−C_{ortho}, 3.1840(19) Å; all other K···C separations are 3.339(2) Å or longer]. There are no agostic bonds evident in the molecule, presumably as a consequence of the strong K-arene interactions which are present. Arguably the most interesting feature of the dimensions is that the K−C_{ipso} bond lengths are approximately 0.05 Å *shorter* than the corresponding Na−C_{ipso} bonds in **2**. Also, the K−C_{ortho} bonds are approximately 0.09 Å shorter than their Na counterparts in **2**, seemingly contrary to the fact that the ionic radius of K (1.52 Å) is larger than that of Na (1.16 Å).[22] These short metal-carbon contacts may help to explain some anomalies in the chemical analysis of **1** and **2**. Firstly, the elemental analysis results for **2** were found to be extremely variable — this was attributed to the rapid loss of toluene upon isolation of the inverse crown. In contrast, the elemental analysis results for **1** were reproducible and accurate, possibly as a reflection of the stronger complexation of the toluene to the larger alkali metal. Secondly, the ^1H NMR spectroscopic studies of **1** and **2** in C_6D_6 seem to confirm this assertion, namely that the spectra indicate

 © 2003 Wiley-VCH Verlag GmbH & Co. KGaA, Weinheim

that for the sodium analogue **2**, there is much less toluene present than expected in comparison from the stoichiometry in the crystal structure, whereas for **1**, the spectrum indicates that no toluene had been lost during the isolation procedure.

To determine whether or not this apparently surprising anomaly in the M-arene distances has been observed previously, a search of the Cambridge Crystallographic Database[23] was conducted. This search uncovered no examples of an isostructural pair of Na and K toluene solvated species that could be used as a direct comparison to **1** and **2**. However, it revealed five complexes[3,24] that contain a sodium atom solvated by a neutral toluene molecule — as opposed to a benzyl fragment — and there are fourteen examples[11c,24a,25] of complexes that contain a potassium atom solvated by a toluene molecule. Examples of such Na−toluene(centroid) distances found in the search are 2.664[24a] and 2.746 Å[24b] for the hexameric thiolate $[(NaSSiPh_3)_6 \cdot (toluene)_2]$ and the monomeric aluminate $[NaAl(SiMe_3)_4 \cdot (toluene)_2]$, respectively. These are 0.368−0.450 Å shorter than the Na−toluene(centroid) distances found for **2**. In the former complex two of the six sodium centres interact strongly with a molecule of toluene, whilst in the latter complex the Na cation is sandwiched between two arene molecules rendering it separate from its aluminate anion. The range of K−toluene(centroid) distances is 2.936[25d]−3.128[25f] Å. It is therefore evident that the K−toluene(centroid) distance in **1** is representative of those for the other complexes, whilst the Na−toluene(centroid) distance in **2** is much longer (and by implication weaker) than previously observed.

The N−K−N endocyclic bond angle in **1** [119.55(6)°] compares to that of 100.54(5)° in **3**, and the N−Na−N angles of 132.08(10)° in **2**. Therefore on changing from Na to K there is a significant narrowing of the N−M−N angle. The consequence of this narrowing, coupled with the longer K−N bonds, creates a greater N···N separation of 4.796 Å compared to 4.534 Å in **2**, resulting in the K atom being pushed out further from the core of the structure. Concomitantly, a wider separation of the diisopropylamido groups occurs to give a larger coordination arc, which allows for a closer approach of the toluene molecule compared to that in **2**. The N−Mg−N bond angles in **1** are also less obtuse than those in **2** [126.55(9)° vs. 133.169(11)°].

Returning to the point made earlier, the formation of **1** and **2** can be explained by a β-hydride elimination process (Scheme 1). Thus, on heating a solution of the heterobimetallic tris(amide) species to reflux, it is proposed that hydride elimination could take place from an amido group to yield a hydrido intermediate and a molar equivalent of imine [*i*Pr-N=C(Me)$_2$]. The resultant relaxation in steric crowding about the magnesium centre would then allow dimerisation to take place. To ascertain whether the process proposed is a realistic possibility, a series of ab initio MO calculations were performed. The findings of this theoretical study are discussed in the next subsection.

DFT Calculations

As described previously, complex **1** was prepared by reacting a 1:1:3 mixture of benzylpotassium and dibutylmagnesium with diisopropylamine, and then boiling in toluene. Although the reaction was carried out in situ, according to the proposed mechanism it can be thought of as proceeding in five stages. Stage I involves the formation of the monometallic amides, which is accompanied by butane and toluene generation. Stage II involves the formation of the single tris(amide) species from its two component monometallic amides. Stage III involves the β-hydride elimination from a diisopropylamide group and transfer of the hydride ion to the magnesium centre with concomitant elimination of imine. Stage IV involves ring opening and dimerisation to give the eight-membered inverse crown ring. The final stage,

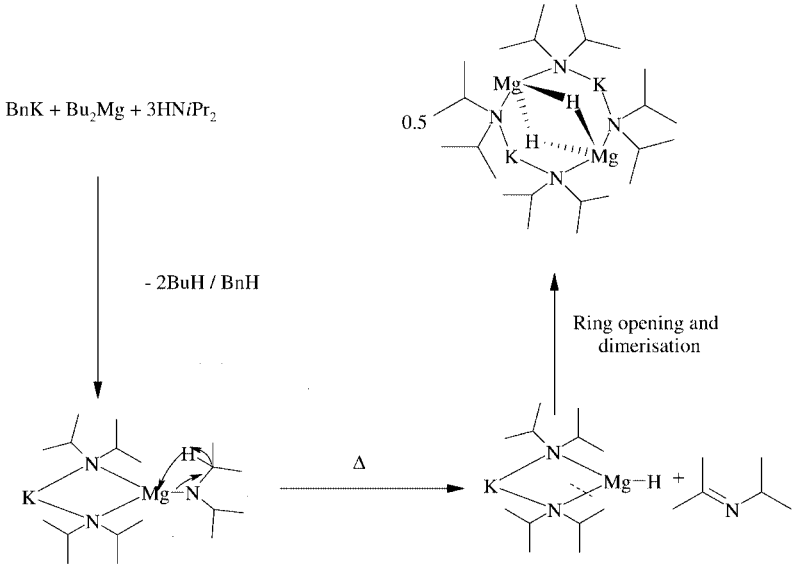

Scheme 1. Proposed reaction pathway for the preparation of **1**; for clarity, the solvating toluene molecules in the final product have been omitted

 © 2003 Wiley-VCH Verlag GmbH & Co. KGaA, Weinheim

stage V, involves the completion of the K coordination sphere by the docking of a toluene solvent molecule.

Relevant starting molecules, intermediates and final products (Figure 4) were initially modelled[26] at the Hartree−Fock (HF) level, using the 6−31G(d)[27−31] basis set and subjected to a frequency analysis. Using the HF-optimised structures, the geometry of molecules were then refined at the DFT[32] level, using the B3LYP[33,34] method and the 6−311G(d, p)[35,36] basis set. The geometrical values reported here are taken exclusively from the DFT calculations while the energy values[37] are the DFT results modified by the scaled (0.91) zero point energy correction abstracted from the corresponding HF calculation. All the molecules have C_1 symmetry except for **11** (C_{2h}) and **1a** (C_i).

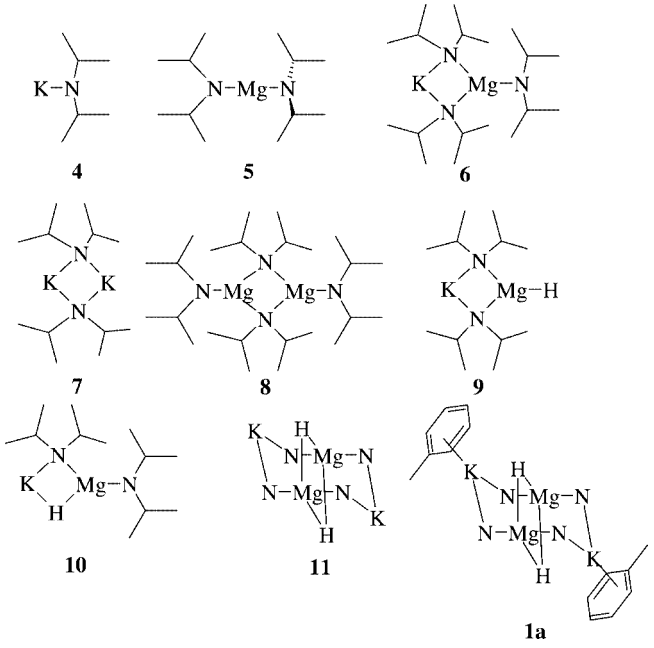

Figure 4. Schematic diagram of **1a** (modelled version of the experimental complex **1**) and other key complexes which were modelled by DFT calculations

In Stage I, KN*i*Pr$_2$ (**4**) and Mg(N*i*Pr$_2$)$_2$ (**5**) are assumed to be the initial products along with toluene and butane [Equations (1) and (2)]. To aid calculational simplicity, the metallo products were modelled as monomers. For the potassium amide **4** the K−N bond length was found to be 2.438 Å and the N centre was distorted trigonal planar with KNC angles of 123.0° and a CNC angle of 114°. For the magnesium amide **5** the Mg−N bond length is 1.935 Å, whilst the diisopropylamide ligands lie essentially perpendicular to each other. The N−Mg−N bond angle is near-perfect linear (179.6°). The combined calculated energy for the formation of the monometallic amides from the monomeric alkyl reagents was found to be −44.0 kcal mol^{-1}. The formation of **4** is a much less exothermic process than the formation of **5**. This can be partially attributed to the fact that for the formation of **4**, only one new metal-N bond is being formed whereas for **5**, two new metal-N bonds are formed. However, even if the energy of formation value for the latter process [Equation (2)] is halved, to account for the formation of only one new metal-N bond, the energy derived from the monoamination of Bu$_2$Mg (19.8 kcal mol^{-1}) is significantly higher than for the amination of BnK (4.4 kcal mol^{-1}). Intuitively, it would be expected that an alkylpotassium reagent would react more exothermally than an alkylmagnesium; however, in the case of the BnK model, the K centre is stabilised by coordination to the π-system of the benzyl fragment.

$$\mathrm{BnK} + \mathrm{HN}i\mathrm{Pr}_2 \rightarrow \mathbf{4} + \mathrm{BnH}\ (\Delta E_f = -4.4\ \mathrm{kcal\ mol^{-1}}) \quad (1)$$

$$\mathrm{Bu_2Mg} + 2\mathrm{HN}i\mathrm{Pr}_2 \rightarrow \mathbf{5} + 2\mathrm{BuH}\ (\Delta E_f = -39.6\ \mathrm{kcal\ mol^{-1}}) \quad (2)$$

In Stage II, the mixed metal tris(amido) species **6** is formed [Equation (3)]. Largely as a consequence of forming two new (one K−N and one Mg−N) bonds, **6** was calculated to be 26.5 kcal mol^{-1} more stable than its monometallic components. The optimised structure indicates asymmetric K−N bonds (2.690 and 2.737 Å) whilst the Mg−N$_{bridging}$ bonds are more uniform in length (2.097 and 2.100 Å). As expected from coordination number considerations, the Mg−N$_{terminal}$ bond length is shorter and calculated to be 2.000 Å. A general elongation of approximately 0.2 Å is observed in all of the M−N$_{bridging}$ bonds in comparison with the terminal ones in the respective monometallic species. Another possibility at this stage would be the formation of the monometallic dimers **7** and **8** [Equation (4) and (5) respectively]. The energies for the formation of **7** and **8** are −34.2 kcal mol^{-1} and −19.3 kcal mol^{-1} respectively. The energy of formation of **6** is intermediate between these two values, hence either outcome could be considered as a viable possibility.

$$\mathbf{4} + \mathbf{5} \rightarrow \mathbf{6}\ (\Delta E_f = -26.5\ \mathrm{kcal\ mol^{-1}}) \quad (3)$$

$$\mathbf{4} + \mathbf{4} \rightarrow \mathbf{7}\ (\Delta E_f = -34.2\ \mathrm{kcal\ mol^{-1}}) \quad (4)$$

$$\mathbf{5} + \mathbf{5} \rightarrow \mathbf{8}\ (\Delta E_f = -19.3\ \mathrm{kcal\ mol^{-1}}) \quad (5)$$

In Stage III, a hydride anion is transferred from a β-carbon of a diisopropylamide unit to the magnesium centre with the elimination of the imine *i*Pr-N=C(Me)$_2$, which, as previously noted, was detected in the experimental study. Two possible pathways for this elimination have been investigated, one where the hydride elimination occurs via a terminal amide group, giving **9** [Equation (6)], and one where the hydride elimination occurs via a bridging amide group, giving **10** [Equation (7)]. In an effort to determine which pathway hydride transfer favours, the optimised geometries of both intermediates were calculated. Since a C−H and a Mg−N bond are broken while a Mg−H and a C−N bond are formed, it would be expected that the reaction would be endothermic. This was indeed found to be the case [this

 © 2003 Wiley-VCH Verlag GmbH & Co. KGaA, Weinheim

is in agreement with the experimental work, as **1** can only be prepared if the tris(amido) intermediate **6** is heated strongly] with the formation of **9** having a calculated energy of +13.1 kcal mol^{-1}, while the corresponding value for **10** is +13.8 kcal mol^{-1} (i.e. +0.7 kcal mol^{-1} higher in energy). Hence, hydride transfer is most likely to occur via the terminal amide. As a further comparison, it was observed that the β-hydride elimination reaction from the terminal amide of magnesium bis(diisopropylamide) (**5**) — a known experimentally observed process[5] [Equation (8)] — was found to be considerably higher in energy (+22.4 kcal mol^{-1}).[38] Therefore it appears that on synergistically combining the two metal amides, β-hydride elimination occurs more readily for either **9** or **10** than for when the diisopropylamide moiety resides on the Mg centre in the monometallic Mg(N*i*Pr$_2$)$_2$. Intermediate **9** has a greater degree of symmetry than **6**, due to the absence of the terminal, sterically demanding diisopropylamido group. Focusing on the planar, four-membered [Mg-(μ-N)$_2$-K] ring in **9**, the Mg−N bonds span 2.087 Å, whilst the K−N bond lengths are symmetrical (unlike those previously mentioned for **6**) and have a length of 2.714 Å. The former bonds are slightly shorter, whilst the latter are longer than the calculated values in **6** due to the presence of the terminal Mg−H bond (length, 1.743 Å).

6 → **9** + *i*Pr-N=C(Me)$_2$ (ΔE_f = +13.1 kcal mol^{-1}) (6)

6 → **10** + *i*Pr-N=C(Me)$_2$ (ΔE_f = +13.8 kcal mol^{-1}) (7)

5 → *i*Pr$_2$NMgH + *i*Pr-N=C(Me)$_2$ (ΔE_f = +22.4 kcal mol^{-1}) (8)

In Stage IV, it has been assumed that two equivalents of **9** (since the formation of **9** was slightly preferred over **10**) combine to produce the dimeric inverse crown **11** [Equation (9)]. The calculated energy of dimerisation is −35.3 kcal mol^{-1}. This can be rationalised in terms of the formation of new Mg−H bonds and also in the formation of a less sterically demanding larger eight-membered ring.

9 + **9** → **11** (ΔE_f = −35.3 kcal mol^{-1}) (9)

In Stage V, one toluene molecule coordinates to each K centre and, as expected, this process is exothermic resulting in the calculated structure corresponding to **1a** [Equation (10)]. The data from the calculated structure were found to closely resemble the crystal data. For instance, the K−N bonds from the X-ray crystallographic data were found to be 2.7754(16) Å whilst the theoretical value is 2.777 Å. Good agreement was also found in the Mg−N bond lengths [2.0595(15) Å vs. theoretical value of 2.103 Å), the N−K−N bond angle [119.55(6)° vs. theoretical value of 122.30°] and the N−Mg−N bond angle [126.55(9)° vs. theoretical value of 128.40°]. As expected the docking of the toluene molecules is exothermic (−1.45 kcal mol^{-1} per coordinating toluene molecule). However, the energy gain calculated by this study is much lower than would have been predicted considering the strength of the K-arene interaction which is evident from the crystal data. This is related to the substantial difference between the K-arene bond lengths for the calculated structure and those found experimentally [shortest K···C$_{tol}$ approach 3.730 Å vs. 3.107(3) Å from the X-ray data].

11 + 2 PhCH$_3$ → **1a** (ΔE_f = −2.9 kcal mol^{-1}) (10)

Reduction of Benzophenone

Preliminary studies have shown that a heptane/toluene solution of **1** has the ability to act as a reducing agent. As mentioned previously, Sanchez and Scott[5] report that, like **1**, Mg(N*i*Pr$_2$)$_2$ can reduce benzophenone to benzhydrol [Equation (11)].

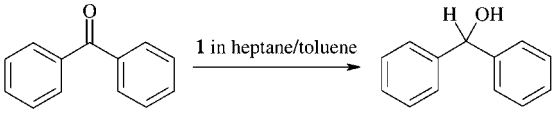

(11)

A 1:4 molar ratio of benzophenone to an in situ solution of **1** was chosen, in accordance with the work of Ashby et al.[4] On work up of the reaction mixture using standard protocols, a ^{1}H NMR spectrum of the crude product was obtained. The spectrum indicated that, as well as the reduction product benzhydrol, some unchanged benzophenone was present (26% by NMR spectroscopy). The spectrum of the crude product also indicated the presence of the imine *i*Pr-N=C(Me)$_2$ produced as a secondary product of the β-hydride elimination. The yield of benzhydrol (74%) is similar to that obtained using monometallic Mg(N*i*Pr$_2$)$_2$ [5] as the reducing agent (73%).

To provide further evidence that the reduction is taking place as a consequence of β-hydride elimination, 2,2,6,6-tetramethylpiperidide (TMP) — an amide in which it is impossible for β-hydride elimination to take place — was utilised instead of diisopropylamide. Previously, BuK, Bu$_2$Mg and TMPH in a 1:1:3 mixture in toluene has been used to prepare the hexapotassium-hexamagnesium twenty-four membered inverse crown [K$_6$Mg$_6$(TMP)$_{12}$(C$_6$H$_4$CH$_3$)$_6$], where the 6+ charge of the "host" heterobimetallic cationic ring is balanced by the encapsulation of six monodeprotonated "guest" arene molecules.[39] For the experiment outlined here, BuK was exchanged for BnK. The reaction was carried out in an analogous fashion to that shown for the benzophenone reduction using **1** in the Exp. Sect. As for the reaction reported earlier, a dramatic colour change occurred upon addition of the ketone. Similarly, when quenched with water, a white suspension of NaOH and Mg(OH)$_2$ was produced. After work up, a ^{1}H NMR spectrum of the crude reaction mixture was obtained. While this spectrum contained a large number of resonances it was

 © 2003 Wiley-VCH Verlag GmbH & Co. KGaA, Weinheim

clear that benzhydrol was not present although some unchanged benzophenone remianed. As found in the study by Sanchez and Scott,[5] it proved impossible to identify the other products present, presumably due to their intractable polymeric nature. This evidence coupled with both the X-ray data and the detection of *i*Pr-N=C(Me)$_2$ by ^{1}H NMR spectroscopy, unequivocally proves that the reduction must be taking place as a consequence of a β-hydride elimination pathway.

Experimental Section

The synthesis of **1** was carried out under a protective atmosphere of argon using standard Schlenk techniques. Hexane and toluene were dried by heating to reflux over sodium benzophenone ketyl and distilled under nitrogen prior to use. Diisopropylamine was dried by heating to reflux over calcium hydride, distilled under nitrogen and stored over 4 Å molecular sieve. *n*,*s*-Dibutylmagnesium in the form of a 1 M solution in heptane was purchased from Aldrich Chemicals and standardised immediately prior to use using salicylaldehyde phenylhydrazone.[40] Benzylpotassium was prepared according to literature methods.[41] Benzophenone was used as received from Aldrich Chemicals. The melting point was determined in a sealed argon-filled capillary tube and is uncorrected. NMR spectroscopic experiments were carried out on a Bruker DPX 400 MHz spectrometer.

[K$_2$Mg$_2$(N*i*Pr$_2$)$_4$(μ-H)$_2$.(toluene)$_2$] (1): A flame-dried, argon-filled Schlenk tube was charged with benzylpotassium (0.65 g, 5 mmol). This orange/red solid was subsequently suspended in toluene (10 mL). *n*,*s*-Dibutylmagnesium in heptane (5 mL, 5 mmol) was added, followed by diisopropylamine (2.1 mL, 15 mmol) to give an orange solution. The solution was heated to reflux for 35 minutes and an orange to red colour change was observed. The solution was then concentrated by removal of some solvent in vacuo and then placed in a freezer operating at −28 °C. After 48 hours, colourless needle-like crystals were deposited from the solution. Due to their high solubility, the crystals proved difficult to isolate in high yields (first batch = 0.26 g, 15%). m.p. >280 °C. $C_{38}H_{74}K_2Mg_2N_4$ (713.8): calcd. C 63.9, H 10.4, N 7.8; found C 64.7, H 10.3, N 7.6. ^{1}H NMR (400.13 MHz, C_6D_6, 300 K): δ = 1.29 [d, 48 H, CH(C*H*$_3$)$_2$], 2.11 (s, 6 H, C_6H_5C*H*$_3$), 3.35 [sept, 8 H, C*H*(CH$_3$)$_2$], 3.78 (s, 2 H, Mg*H*), 6.94 (d, 4 H, *o*-tol), 7.05 (t, 2 H, *p*-tol), 7.15 (m, 4 H, *m*-tol) ppm. ^{13}C NMR (100.62 MHz, C_6D_6, 300 K): δ = 21.75 (C_6H_5*C*H$_3$), 27.29 [CH(*C*H$_3$)$_2$], 49.50 [*C*H(CH$_3$)$_2$], 126.03 (*p*-tol), 129.67 (*o*-tol), 138.00 (*ipso*-tol) ppm. The *m*-tol resonance is obscured by the solvent C_6D_6 resonance at δ = 128 ppm.

X-ray Crystal Structure Determination of 1: The X-ray structural analysis was carried out at 123 K on a Nonius Kappa CCD diffractometer (Mo-K_α, λ = 0.71073 Å, graphite monochromator, standard techniques). Crystal data: $C_{38}H_{74}K_2Mg_2N_4$, mol. wt. 713.83, orthorhombic, space group *Pnnm*, *a* = 9.9080(2) Å, *b* = 12.5553(3) Å, *c* = 17.4310(4) Å, *U* = 2168.38(8) Å^3, *Z* = 2, D_c = 1.093 g cm^{-3}. A total of 5567 reflections were collected out to θ_{max} = 29.16°, of which 3018 were unique (R_{int} = 0.0204). The structure was solved by direct methods and refined by full-matrix least-squares on F^2 with all non-H atoms anisotropic and using SHELX-97.[42] The bridging hydride H-atoms were refined isotropically but all other H-atoms were placed in calculated positions. Final *R* values: *R*1 = 0.0508, *wR*2 = 0.1422, GOF = 1.043.

CCDC-213617 contains the supplementary crystallographic data for this paper. These data can be obtained free of charge at www.ccdc.cam.ac.uk/conts/retrieving.html [or from the Cambridge Crystallographic Data Centre, 12, Union Road, Cambridge CB2 1EZ, UK; Fax: (internat.) +44-1223/336-033; E-mail: deposit@ccdc.cam.ac.uk].

Reduction of Benzophenone: A flame-dried, argon-filled Schlenk tube was charged with benzylpotassium (0.65 g, 5 mmol). This orange/red solid was subsequently suspended in toluene (10 mL). *n*,*s*-Dibutylmagnesium in heptane (5 mL, 5 mmol) was added, followed by diisopropylamine (2.1 mL, 15 mmol) to give an orange solution. The solution was heated to reflux for 35 minutes and an orange to red colour change was observed. Benzophenone (0.2275 g, 1.25 mmol) was added, immediately producing a deep purple coloured oil. This mixture was allowed to stir for thirty minutes before being quenched with distilled water (5 mL). The resulting white suspension was washed with three aliquots of diethyl ether (10 mL). The organic phase was dried over anhydrous $MgSO_4$. All volatiles were removed in vacuo and the reduction product — benzhydrol, Ph_2CHOH — was recrystallised from petroleum ether 60−80 (0.11 g, 48% not optimised: yield obtained from NMR analysis relative to recovered benzophenone was 74%). The purity of the product was confirmed by ^{1}H NMR spectroscopy. ^{1}H NMR (400.13 MHz, $CDCl_3$, 300 K): δ = 2.20 (d, 1 H, O*H*), 5.87 (d, 1 H, C*H*), 7.25−7.41 (overlapping multiplets, 10 H, Ph) ppm. As well as obtaining the yield with respect to benzophenone from the ^{1}H NMR spectrum of the crude product, the presence of *i*Pr-N=C(Me)$_2$, the by-product from the formation of **1**,[43] was also noted: δ = 1.12 (d, 6 H, C*H*$_3$), 1.85 (s, 3 H, *H*$_3$C′-C=N), 1.99 (s, 3 H, *H*$_3$C-C=N), 3.62 (sept, 1 H, C*H*) ppm.

Acknowledgments

The authors gratefully acknowledge the financial support of the UK EPSRC through grant award GR/R81183/01.

[1] First preparation of $LiAlH_4$: [1a] A. E. Finholt, A. C. Bond, Jr., H. I. Schlesinger, *J. Am. Chem. Soc.* **1947**, *69*, 1199−1203. First use of $LiAlH_4$ as a reducing agent: [1b] R. F. Nystrom, W. G. Brown, *J. Am. Chem. Soc.* **1947**, *69*, 1197−1199. Selected recent uses of aluminium-containing hydride reagents in reduction reactions: [1c] J. T. Kuethe, A. Wong, J. Wu, I. W. Davies, P. G. Dormer, C. J. Welch, M. C. Hillier, D. L. Hughes, P. J. Reider, *J. Org. Chem.* **2002**, *67*, 5993−6000. [1d] M. Harding, R. Hodgson, A. Nelson, *J. Chem. Soc., Perkin Trans. 1* **2002**, 2403−2413. [1e] F. Benedetti, F. Berti, S. Norbedo, *J. Org. Chem.* **2002**, *67*, 8635−8643. [1f] S. Kim, R. Kavali, *Tetrahedron Lett.* **2002**, *43*, 7189−7191. [1g] P. Sairam, R. Puranik, B. S. Rao, P. V. Swamy, S. Chandra, *Carbohydrate Res.* **2003**, *338*, 303−306.

[2] 48 Compounds in the Cambridge crystallographic database contain an Al−H−Al unit within their molecular structure. For selected examples of homometallic species see: [2a] W. Uhl, J. Molter, B. Neumuller, F. Schmock, *Z. Anorg. Allg. Chem.* **2001**, *627*, 909−917. [2b] U. Fooken, M. A. Khan, R. J. Wehmschulte, *Inorg. Chem.* **2001**, *40*, 1316−1322. [2c] U. Dumichen, T. Gelbrich, J. Sieler, *Z. Anorg. Allg. Chem.* **2001**, *627*, 1915−1920. [2d] W. Uhl, F. Breher, A. Lutzen, W. Saak, *Angew. Chem. Int. Ed.* **2000**, *39*, 406−409; *Angew. Chem.* **2000**, *112*, 414−416. [2e] N. Kuhn, S. Fuchs, M. Steimann, *Z. Anorg. Allg. Chem.* **2000**, *626*, 1387−1392. [2f] G. S. Hair, S. L. Battle, A. Decken, A. H. Cowley, R. A. Jones, *Inorg. Chem.* **2000**, *39*, 27−31. [2g] W. Uhl, F. Breher, *Angew. Chem. Int. Ed.* **1999**, *38*,

 © 2003 Wiley-VCH Verlag GmbH & Co. KGaA, Weinheim

1477−1479; *Angew. Chem.* **1999**, *111*, 1578−1580. [2h] J. F. Janik, R. L. Wells, A. L. Rheingold, I. A. Guzei, *Polyhedron* **1998**, *17*, 4101−4108. [2i] H. Nöth, A. Schlegel, J. Knizek, I. Krossing, H. Schwenk, *Angew. Chem. Int. Ed. Engl.* **1997**, *36*, 2640−2643; *Angew. Chem.* **1997**, *109*, 2754−2758. [2j] P. C. Andrews, M. G. Gardiner, C. L. Raston, V.-A. Tolhurst, *Inorg. Chim. Acta* **1997**, *259*, 249−255. [2k] R. J. Wehmschulte, W. J. Grigsby, B. Schiemenz, R. A. Bartlett, P. P. Power, *Inorg. Chem.* **1996**, *35*, 6694−6702. [2l] I. B. Gorrell, P. B. Hitchcock, J. D. Smith, *J. Chem. Soc., Chem. Commun.* **1993**, 189−190. [2m] W. Uhl, *Z. Anorg. Allg. Chem.* **1989**, *570*, 37−53. [2n] G. Perego, M. Cesari, G. del Piero, A. Balducci, E. Cernia, *J. Organomet. Chem.* **1975**, *87*, 33−41. For selected examples of heterometallic species see: [2o] C. Eaborn, S. M. El-Hamruni, M. S. Hill, P. B. Hitchcock, M. Hopman, A. Le Gouic, J. D. Smith, *J. Organomet. Chem.* **2000**, *597*, 3−9. [2p] N. Etkin, A. J. Hoskin, D. W. Stephan, *J. Am. Chem. Soc.* **1997**, *119*, 11420−11424. [2q] V. K. Belsky, Yu. K. Gun'ko, B. M. Bulychev, G. L. Soloveichik, *J. Organomet. Chem.* **1991**, *420*, 43−52. [2r] G. S. Girolami, C. G. Howard, G. Wilkinson, H. M. Dawes, M. Thornton-Pett, M. Motevalli, M. B. Hursthouse, *J. Chem. Soc., Dalton Trans.* **1985**, 921−929. [2s] E. B. Lobkovskii, G. L. Soloveichik, A. I. Sizov, B. M. Bulychev, *J. Organomet. Chem.* **1985**, *280*, 53−66.

[3] D. J. Gallagher, K. W. Henderson, A. R. Kennedy, C. T. O'Hara, R. E. Mulvey, R. B. Rowlings, *Chem. Commun.* **2002**, 376−377.

[4] [4a] E. C. Ashby, A. B. Goel, *J. Chem. Soc., Chem. Commun.* **1977**, 169. [4b] E. C. Ashby, A. B. Goel, *J. Org. Chem.* **1977**, *42*, 3480−3485. [4c] A. B. Goel, E. C. Ashby, *J. Organomet. Chem.* **1981**, *214*, C1−C6. [4d] E. C. Ashby, A. B. Goel, *Inorg. Chem.* **1979**, *18*, 1306−1311. [4e] E. C. Ashby, A. B. Goel, J. J. Lin, *J. Org. Chem.* **1978**, *43*, 1564−1566. [4f] E. C. Ashby, A. B. Goel, J. J. Lin, *Tetrahedron Lett.* **1977**, *36*, 3133−3136. [4g] R. G. Beach, E. C. Ashby, *Inorg. Chem.* **1971**, *10*, 906−910.

[5] [5a] R. Sanchez, W. Scott, *Tetrahedron Lett.* **1988**, *29*, 139−142. [5b] R. Sanchez, G. Vest, W. Scott, P. S. Engel, *J. Org. Chem.* **1989**, *54*, 4026−4027.

[6] W. Clegg, S. Kleditzsch, R. E. Mulvey, P. O'Shaughnessy, *J. Organomet. Chem.* **1998**, *558*, 193−196.

[7] R. E. Mulvey, *Chem. Commun.* **2001**, 1049−1056.

[8] A. R. Kennedy, R. E. Mulvey, R. B. Rowlings, *Angew. Chem. Int. Ed.* **1998**, *37*, 3180−3183; *Angew. Chem. Int. Ed.* **1998**, *110*, 3321−3323.

[9] D. R. Armstrong, A. R. Kennedy, R. E. Mulvey, R. B. Rowlings, *Angew. Chem. Int. Ed.* **1999**, *38*, 131−133 *Angew. Chem. Int. Ed.* **1999**, *111*, 231−233.

[10] W. Clegg, K. W. Henderson, A. R. Kennedy, R. E. Mulvey, C. T. O'Hara, R. B. Rowlings, D. M. Tooke, *Angew. Chem. Int. Ed.* **2001**, *40*, 3902−3905; *Angew. Chem.* **2001**, *113*, 4020−4023.

[11] [11a] G. W. Gokel, L. J. Barbour, S. L. De Wall, E. S. Meadows, *Coord. Chem. Rev.* **2001**, *222*, 127−154. [11b] E. S. Meadows, S. L. De Wall, L. J. Barbour, G. W. Gokel, *J. Am. Chem. Soc.* **2001**, *123*, 3092−3107. [11c] G. C. Forbes, A. R. Kennedy, R. E. Mulvey, B. A. Roberts, R. B. Rowlings, *Organometallics* **2002**, *21*, 5115−5121.

[12] S. Hashimoto, M. Hagiri, N. Matsubara, S. Tobita, *Phys. Chem. Chem. Phys.* **2001**, *3*, 5043−5051.

[13] [13a] D. A. Dougherty, *Science* **1996**, *271*, 163−168. [13b] D. Sun, V. L. Davidson, *Biochemistry* **2001**, *40*, 12285−12291. [13c] J. Wouters, *Protein Sci.* **1998**, 2472−2475. [13d] G. W. Gokel, S. L. De Wall, E. S. Meadows, *Eur. J. Org. Chem.* **2000**, 2967−2978.

[14] A. R. Kennedy, J. G. MacLellan, R. E. Mulvey, *Angew. Chem. Int. Ed.* **2001**, *40*, 3245−3247; *Angew. Chem.* **2001**, *113*, 3345−3347.

[15] For the first inverse crown to be prepared from a benzyl-alkali metal reagent see: G. C. Forbes, F. R. Kenley, A. R. Kennedy, R. E. Mulvey, C. T. O'Hara, J. A. Parkinson, *Chem. Commun.* **2003**, 1140−1141.

[16] E. Hevia, F. R. Kenley, A. R. Kennedy, R. E. Mulvey, R. B. Rowlings, *preceding paper in this issue.*

[17] S. D. Droulin, D. Amoroso, G. P. A. Yap, D. E. Fogg, *Organometallics* **2002**, *21*, 1042−1049.

[18] S. I. Troyanov, V. Varga, K. Mach, *J. Chem. Soc., Chem. Commun.* **1993**, 1174−1175.

[19] M. HorÆček, I. Czsařová, J. Čejka, J. Karban, L. Petrusová, K. Mach, *J. Organomet. Chem.* **1999**, *577*, 103−112.

[20] H. Lee, T. Hascall, P. J. Desrosiers, G. Parkin, *J. Am. Chem. Soc.* **1998**, *120*, 5830−5831.

[21] Z. Hou, Y. Zhang, O. Tardif, Y. Wakatsuki, *J. Am. Chem. Soc.* **2001**, *123*, 9216−9217.

[22] Values quoted are for six coordinate cations and were obtained from: R. D. Shannon, *Acta Crystallogr., Sect. A* **1976**, *32*, 751−767.

[23] F. H. Allen, O. Kennard, *Chem. Des. Autom. News* **1993**, *8*, 31. CSD Version 5.24, April 2003 update.

[24] Due to the large range of metal-arene distances found in the crystal structures, and the ambiguity of whether the contact is a meaningful interaction or simply the random presence of a molecule of solvent of crystallisation, the inclusion or exclusion of molecules here is subjective. [24a] S. Chadwick, U. Englich, K. Ruhlandt-Senge, *Organometallics* **1997**, *16*, 5792−5803. [24b] L. Rösch, G. Altnau, C. Kruger, Y. H. Tsay, *Z. Naturforsch., Teil B* **1983**, *38*, 34−41. [24c] R. Wochele, W. Schwarz, K. W. Klinkhammer, K. Locke, J. Weidlein, *Z. Anorg. Allg. Chem.* **2000**, *626*, 1963−1973. [24d] K. W. Klinkhammer, *Chem. Eur. J.* **1997**, *3*, 1418−1431.

[25] [25a] C. J. Schaverien, J. B. van Mechelen, *Organometallics* **1991**, *10*, 1704−1709. [25b] E. Leiner, O. Hampe, M. Scheer, *Eur. J. Inorg. Chem.* **2002**, 584−590. [25c] M. A. Beswick, N. Choi, A. D. Hopkins, M. McPartlin, M. A. Paver, D. S. Wright, *Chem. Commun.* **1998**, 261−262. [25d] M. Unverzagt, H.-J. Winkler, M. Brock, M. Hofmann, P. v. R. Schleyer, W. Massa, A. Berndt, *Angew. Chem. Int. Ed. Engl.* **1997**, *36*, 853−855; *Angew. Chem.* **1997**, *36*, 879−882. [25e] S. Chitsaz, B. Neumüller, *Organometallics* **2001**, *20*, 2338−2343. [25f] P. B. Hitchcock, M. F. Lappert, G. A. Lawless, B. Royo, *J. Chem. Soc., Chem. Commun.* **1993**, 554−555. [25g] C. Kayser, R. Fischer, J. Baumgartner, C. Marchner, *Organometallics* **2002**, *21*, 1023−1030. [25h] H-J. Gosink, F. Nief, L. Ricard, F. Mathey, *Inorg. Chem.* **1995**, *34*, 1306−1307. [25i] I. Korobkov, G. Aharonian, S. Gambarotta, G. P. A. Yap, *Organometallics* **2002**, *21*, 4899−4901. [25j] G. Bai, H. W. Roesky, M. Noltemeyer, H.-G. Schmidt, *J. Chem. Soc., Dalton Trans.* **2002**, 2437−2440. [25k] G. Bai, H. W. Roesky, M. Noltemeyer, H.-G. Schmidt, *Organometallics* **2002**, *21*, 2789−2792.

[26] Gaussian 98 (Revision A.9); M. J. Frisch, G. W. Trucks, H. B. Schlegel, G. E. Scuseria, M. A. Robb, J. R. Cheeseman, V. G. Zakrzewski, J. A. Montgomery, Jr., R. E. Stratmann, J. C. Burant, S. Dapprich, J. M. Millam, A. D. Daniels, K. N. Kudin, M. C. Strain, O. Farkas, J. Tomasi, V. Barone, M. Cossi, R. Cammi, B. Mennucci, C. Pomelli, C. Adamo, S. Clifford, J. Ochterski, G. A. Petersson, P. Y. Ayala, Q. Cui, K. Morokuma, P. Salvador, J. J. Dannenberg, D. K. Malick, A. D. Rabuck, K. Raghavachari, J. B. Foresman, J. Cioslowski, J. V. Ortiz, A. G. Baboul, B. B. Stefanov, G. Liu, A. Liashenko, P. Piskorz, I. Komaromi, R. Gomperts, R. L. Martin, D. J. Fox, T. Keith, M. A. Al-Laham, C. Y. Peng, A. Nanayakkara, M. Challacombe, P. M. W. Gill, B. Johnson, W. Chen, M. W. Wong, J. L. Andres, C. Gonzalez, M. Head-Gordon, E. S. Replogle, J. A. Pople, Gaussian, Inc., Pittsburgh PA, 2001.

[27] R. Ditchfield, W. J. Hehre, J. A. Pople, *J. Chem. Phys.* **1971**, *54*, 724−728.

[28] W. J. Hehre, R. Ditchfield, J. A. Pople, *J. Chem. Phys.* **1972**, *56*, 2257−2261.

[29] P. C. Hariharan, J. A. Pople, *Mol. Phys.* **1974**, *27*, 209−212.

[30] M. S. Gordon, *Chem. Phys. Lett.* **1980**, *76*, 163−168.

[31] P. C. Hariharan, J. A. Pople, *Theo. Chim. Acta* **1973**, *28*, 213−216.

 © 2003 Wiley-VCH Verlag GmbH & Co. KGaA, Weinheim

[32] W. Kohn, A. D. Becke, R. G. Parr, *J. Phys. Chem.* **1996**, *100*, 12974−12980.
[33] A. D. Becke, *Phys. Rev. A* **1988**, *38*, 3098−3100.
[34] C. T. Lee, W. T. Yang, R. G. Parr, *Phys. Rev. B* **1998**, *37*, 785−789.
[35] A. D. McLean, G. S. Chandler, *J. Chem. Phys.* **1980**, *72*, 5639−5648.
[36] R. Krishnan, J. S. Binkley, R. Seeger, J. A. Pople, *J. Chem. Phys.* **1980**, *72*, 650−654.
[37] The DFT total energies (in a.u.) including the zero point energy correction for calculated molecules are as follows: (**1a**) −3311.320228, (**4**) −891.646686, (**5**) −783.566645, (**6**) −1675.255643, (**7**) −1783.347845, (**8**) −1567.164098, (**9**) −1384.115447, (**10**) −1384.114410, (**11**) −2768.287148.
[38] The β-hydride elimination from K*N*i*Pr*$_2$ to give KH and *i*Pr-N=C(Me)$_2$ was also modelled. The energy of the reaction was calculated to be +20.9 kcal mol^{-1}.
[39] P. C. Andrews, A. R. Kennedy, R. E. Mulvey, C. L. Raston, B. A. Roberts, R. B. Rowlings, *Angew. Chem. Int. Ed.* **2000**, *39*, 1960−1962; *Angew. Chem.* **2000**, *112*, 2036−2038.
[40] B. E. Love, E. G. Jones, *J. Org. Chem.* **1999**, *64*, 3755−3756.
[41] D. Hoffmann, W. Bauer, F. Hampel, N. J. R. van Eikema Hommes, P. v. R. Schleyer, P. Otto, U. Pieper, D. Stalke, D. S. Wright, R. Snaith, *J. Am. Chem. Soc.* **1994**, *116*, 528−536.
[42] SHELXL-97; G. M. Sheldrick, University of Göttingen, Germany.
[43] Synthetic procedure and NMR spectroscopic data for *i*Pr-N=C(Me)$_2$: W. H. Bunnelle, P. R. Singam, B. A. Narayanan, C. W. Bradshaw, J. S. Liou, *Synthesis* **1997**, 439−442.

Received June 27, 2003

 © 2003 Wiley-VCH Verlag GmbH & Co. KGaA, Weinheim

A Solid-State, Solution, and Theoretical Structural Study of Kinetic and Thermodynamic Lithiated Derivatives of a Simple Diazomethane and Their Reactivities Towards Aryl Isothiocyanates

David R. Armstrong,*[a] Robert P. Davies,[b] Robert Haigh,[c] Mark A. Hendy,[c] Paul R. Raithby,[d] Ronald Snaith,[†] and Andrew E. H. Wheatley*[c]

Dedicated to the memory of Ron Snaith

Keywords: Density functional calculations / Diazomethane / Lithium / Solid-state structures / Solution structure

(Trimethylsilyl)diazomethane (**1-H**) reacts with *n*BuLi in THF at elevated temperature to afford (previously reported) **1-Li·$^3/_2$THF**. However, reaction in hexane/TMEDA at low temperature affords instead the *N*-lithiate $Me_3SiCNNLi$·TMEDA (**9**), which is a novel "open" pseudo-cubic tetramer in the solid state. Variable-temperature NMR spectroscopy suggests that *N*-metallated **9**, apparently the kinetic product of the reaction, irreversibly rearranges at high temperature in solution to give the thermodynamically preferred *C*-lithiated isomer. These observations, supported by DFT calculations, influence our understanding of the reactivity of lithiated diazomethanes towards aryl isothiocyanates, suggesting as they do that previously observed product selectivity in these reactions is critically dependent on temperature control exercised during the process.

(© Wiley-VCH Verlag GmbH & Co. KGaA, 69451 Weinheim, Germany, 2003)

Introduction

(Trimethylsilyl)diazomethane (**1-H**), a safe and stable analogue of diazomethane, has many applications in, for example, Arndt−Eistert syntheses,[1] the homologation of ketones[2] and aldehydes,[3] cycloaddition reactions,[4] and the methyl esterification of carboxylic acids.[5] Moreover, the chemistry of its lithiated derivative (**1-Li**) has also been extensively studied due to its synthetic utility. This derives from its combination of reactivity (greater than that of **1-H**) and safety (relative to diazomethane).[6] In consequence, **1-Li** has found ready use in the preparation of substituted triazoles[7] and tetrazoles,[8] the syntheses of aldehydes from ketones,[9] Colvin rearrangements[10] and the formation of synthetically useful[11] silyl ketenes.[12] These last species react with phosphorus ylides and so afford a simple route to silyl allenes.[13] In this context, central to the synthesis[13] of the disubstituted silyl ketene **3**, is the formation, by the sequential treatment of **1-H** with *n*-butyllithium and carbon monoxide, of a lithium ynolate **2**. This latter species is considered to result from the insertion[14] of CO into the proposed C−Li bond in **1-Li**, whereupon N_2 is eliminated (Scheme 1), the addition of triethylsilyl trifluoromethanesulfonate (Et_3SiOTf) and subsequent work-up affording **3**.

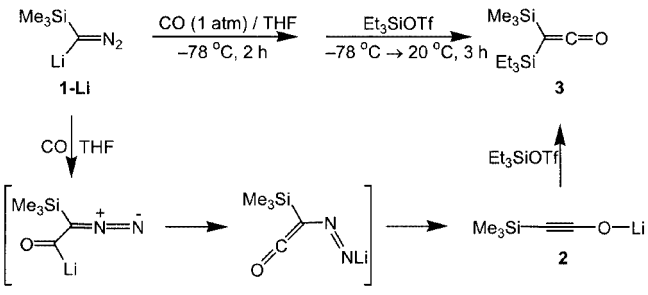

Scheme 1. Proposed mechanism for the preparation of the disubstituted silyl ketene **3**[13]

[a] Department of Pure and Applied Chemistry, University of Strathclyde,
295 Cathedral Street, Glasgow, G1 1XL, U. K.
Fax: (internat.) +44-141/548-4822
E-mail: drarmstrong@strath.ac.uk
[b] Department of Chemistry, Imperial College London,
South Kensington, London, SW7 2AZ, U. K.
Fax: (internat.) +44-20/7594-5804
E-mail: r.davies@imperial.ac.uk
[c] Department of Chemistry, University of Cambridge,
Lensfield Road, Cambridge, CB2 1EW, U. K.
Fax: (internat.) +44-1223/336-362
E-mail: rh293@cam.ac.uk, aehw2@cam.ac.uk
[d] Department of Chemistry, University of Bath,
Claverton Down, Bath, BA2 7AY, U. K.
Fax: (internat.) +44-1225/386-231
E-mail: p.r.raithby@bath.ac.uk
Supporting information for this article is available on the WWW under http://www.eurjic.org or from the author.
[†] Deceased.

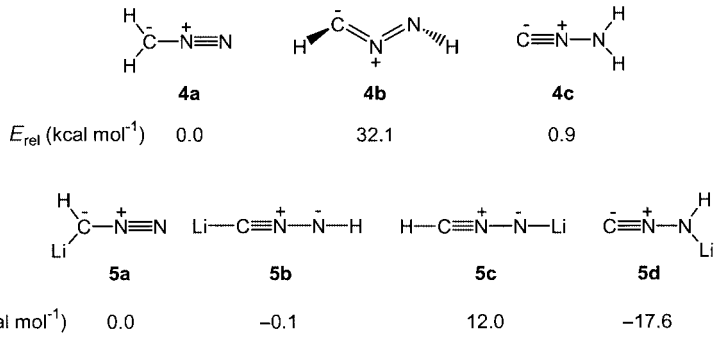

Figure 1. Possible isomers of **1-H**[15] (and their relative energies)[17] and **1-Li** (and their relative energies, 1 kcal = 4.184 kJ)

The chemistry of metallated (mono-substituted) diazomethane has been previously investigated[15] (Figure 1) with results indicating that deprotonation/reprotonation of diazomethane **4a** affords the *less* stable CH_2N_2 *N*-isocyanoamine isomer **4c**, which undergoes base-induced reversion to **4a**. The other possible non-cyclic CH_2N_2 isomer (nitrile imine **4b**) has not been detected experimentally. The structures and energies of the CH_2N_2 isomers **4a**−**c**, as well as those of their lithiated derivatives, **5a**−**d**, have recently been modelled theoretically.[16,17] From these calculations it was suggested that while N-protonation of **5d** would give **4c**, C-protonation of **5a** would yield **4a**. Further, consistent with experiment, theory pointed to the most stable **1-H** isomer (**4a**) being obtainable, in the presence of base, from energetically less favourable **4c** (Scheme 2). This is in spite of the suggestion, based on calculation, that **5a** (precursor to **4a**) is less stable than **5d**; in other words that the reaction is thermodynamically controlled by the stability of the final protonated product. In contrast to the parent diazomethane structures discussed above, calculations[17] have shown that for the lithiated mono-substituted (trimethylsilyl)diazomethanes **1-Li** and **6** (Figure 2), the *N*-metallated nitrile imine isomer was slightly more stable than the *C*-lithiate. However, previous attempts to isolate and crystallographically characterise **6** have resulted only in the isolation and structural elucidation of {hexakis[lithio(trimethylsilyl)-diazomethane]·bis[lithio{4,5-bis(trimethylsilyl)triazole}]·heptakis(diethyl ether)} [(**7**)$_2$·OEt_2; Figure 3].[17] This species is composed both of **6** and lithiotriazole **8**, this last component evidently being formed by the reaction of **6** with **1-H**.

Suggestions[12,18] that the reactivity of lithiated **1-H** is solvent dependent have been borne of the observation that whereas it reacts with RNCS (R = alkyl, aryl) in OEt_2 to afford 2-amino-1,3,4-thiadiazole (**13**), in THF thio-1,2,3-triazoles **10**−**12** result (Scheme 3).[18b] However, such differing behaviour has not hitherto been explained in detail and this has led us to attempt the isolation and structural characterisation of *pure* lithiated (trimethylsilyl)diazomethane (cf. **7**) in order to clarify which of the proposed model structures, *C*- or *N*-lithiated, better describes the true structure of lithiated **1-H**. In this context, we report here on the observation of both kinetic [giving $Me_3SiCNNLi$·TMEDA, **9**] and thermodynamic [giving **1-Li·$^3/_2$THF**] metallation. The latter observation has led to the isolation and structural characterisation of an intermediate in the synthesis of disubstituted silyl ketene **3** (Scheme 1). Finally, we report here on the reactions of lithiodiazomethanes with different isothiocyanates with a view to understanding the relationship between the site of lithiation in the substrate and the structure of the final cyclised product.

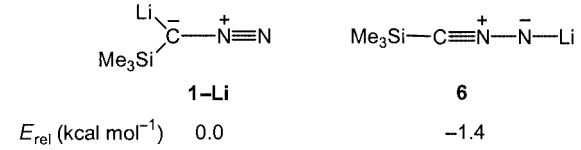

Figure 2. *C*- and *N*-lithiated isomers of **1-Li** and their relative energies[17]

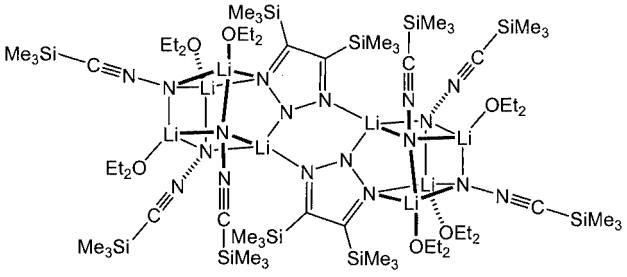

Figure 3. The molecular structure of (**7**)$_2$

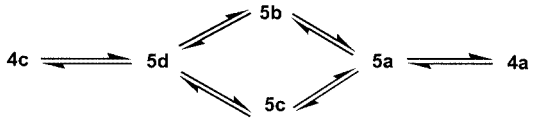

Scheme 2. Equilibria in the interconversion of diazomethane isomers

Results and Discussion

Solid-State and Theoretical Studies on 1-Li·$^3/_2$THF and 9

The reaction of **1-H** with *n*BuLi in THF yielded large yellow crystals of pure lithiated (trimethylsilyl)diazomethane $^1/_2$[{$Me_3SiC(Li)N_2$}$_2$·3THF] (**1-Li·$^3/_2$THF**), the solid-state structure of which we have previously reported.[19] X-

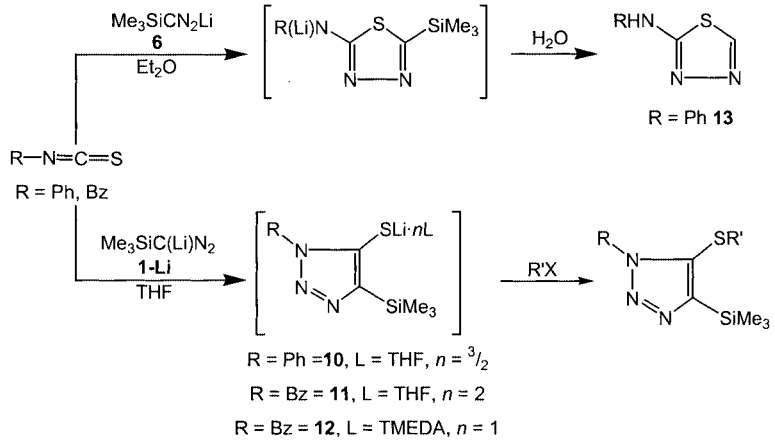

Scheme 3. Proposed pathways for the reaction of different **1-Li** isomers with RNCS (R = Ph, Bz)[12,18]

ray crystallography has shown **1-Li·$^3/_2$THF** to be a polymer based on a repeating tetramer unit (Figure 4), consisting of two (*mono*-THF) complexed lithiodiazomethane molecules and two (*bis*-THF) complexed ones i.e. $\{[Me_3SiC(Li{\cdot}THF)N_2]{\cdot}[Me_3SiC(Li{\cdot}2THF)N_2]\}_2$. This revelation of two types of lithiodiazomethane molecule in the solid-state structure of **1-Li·$^3/_2$THF** is consistent with the observation of two sets of C=N=N stretching modes by IR spectroscopy (ν_{sym} = 2149, 2116 cm^{-1} and ν_{asym} = 2092, 2052 cm^{-1}) which collapse to a single set upon hydrolysis to **1-H**. The ambiguity surrounding the preferred site of lithiation in **1-H** that results from the contrasting structures noted for **1-Li·$^3/_2$THF** and **7** made it desirable to theoretically probe the relative stabilities and geometries of both *N*- and *C*-lithiates. DFT calculations[20] based on a variety of models were undertaken (B3LYP[21]/6-311G**[22]). Energetic results for $XCN_2Li{\cdot}nL$ (X = H_3Si, Me_3Si; n = 0, 1, 2; L = OEt_2, THF) are summarised in Table 1 with selected calculated geometrical parameters in Table E1 (see Electronic Supporting Information; see footnote on the first page of this article).

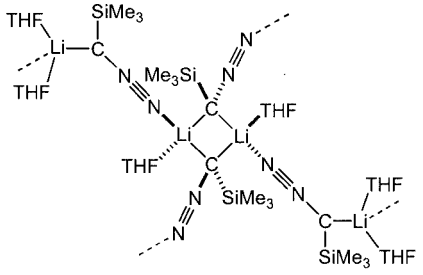

Figure 4. The molecular structure of polymeric **1-Li·$^3/_2$THF**

Overall, calculations reported here on lithiodiazomethanes and their complexes suggest that, while *N*-metallation is thermodynamically preferred, *C*-metallation becomes increasingly favourable in the presence of strongly coordinating media. For unsolvated diazomethanes XCN_2Li (X = H_3Si, Me_3Si) *C*-lithiation is 2.5 kcal·mol^{-1} (**I**; 1 kcal = 4.184 kJ) more energetic than *N*-lithiation (**II**) for X = H_3Si (Table 1 and Figure 5) while for X = Me_3Si the computed preference for *N*- (**IV**) over *C*-metallation (**III**) is 4.0 kcal·mol^{-1}, illustrating the electron-donating nature of the methyl groups over hydrogen atoms yet still suggesting a fine energetic balance between the differently metallated, unsolvated monomers. Calculated molecular geometries show little dependence upon X. Whereas *C*-lithiates **I** and **III** both show relatively long C−N (1.283 and 1.282 Å, respectively) and short N−N (1.141 and 1.144 Å, respectively) bonds, the opposite is true of *N*-lithiates **II** and **IV** (C−N = 1.195 Å in both, N−N = 1.201 and 1.205 Å, respectively). The structural feature most significantly dependent on X is the Si−C bond length. This increases significantly from a mean of 1.798 Å to one of 1.817 Å on replacing H atoms with Me groups−presumably reflecting both the increased steric requirements of the trimethylsilyl group and its aforementioned inductive effect. The metallo−organic bonds show no significant variation with X. Hence, while the C−Li bonds are 1.906 Å in both **I** and **III**, the N−Li ones in **II** and **IV** are 1.697 and 1.692 Å, respectively.

The extension of calculations to the simple mono-solvated, monomeric lithiates $Me_3SiCN_2Li{\cdot}L$ (L = OEt_2, THF) shows that, irrespective of the choice of L, the *C*-lithiates (**V**, **VII**) are higher in energy than the *N*-lithiates (**VI**, **VIII**; Table 1 and Figure 5). All of the resultant structure types are significantly more stable than either **III** or **IV** by virtue of Lewis base coordination [$\Delta E_{Complexation}$ (ΔE_C) = −21.5 (**V**), −22.9 (**VII**), −21.5 (**VI**), −22.7 (**VIII**) kcal·mol^{-1}]. Of note (see below) for both types of L, *C*-lithiated models show more negative ΔE_C values than their *N*-lithiated counterparts. Moreover, for both *C*- and *N*-lithiates, both the magnitude of and differences between ΔE_C values are enhanced for coordination of the stronger Lewis base (THF). Thus, $-\Delta E_C$(**V**) = $-\Delta E_C$(**VI**) and $-\Delta E_C$(**VII**) > $-\Delta E_C$(**VIII**), $-\Delta E_C$(**VII**) > $-\Delta E_C$(**V**) and $-\Delta E_C$(**VIII**) > $-\Delta E_C$(**VI**) and, whereas for *mono*-OEt_2 solvation **VI** is preferred to **V** by 4.0 kcal·mol^{-1}, for *mono*-THF solvation **VII** is 3.8 kcal·mol^{-1} more stable than **VIII**. This implies that *N*-metallation is less strongly favoured over *C*-metal-

 © 2003 Wiley-VCH Verlag GmbH & Co. KGaA, Weinheim

Table 1. Summary of DFT calculations (B3LYP/6-311G**)[21,22] based on $XCN_2Li{\cdot}nL$ (X = H_3Si, Me_3Si; n = 0, 1, 2; L = OEt_2, THF, TMEDA). (1 kcal = 4.184 kJ.) ΔE_c/L quoted as enthalpy of complexation per Lewis base *donor atom*

Model	Figure	Formula	Total Energy (incl. ZPE; Hartrees)	ΔE_c (kcal mol^{-1})	ΔE_c/L (kcal mol^{-1} L^{-1})	Relative Energy (kcal mol^{-1} L^{-1})
I	E1	$H_3SiC(Li)N_2$	−446.410355	–	–	2.5
II	E1	H_3SiCN_2Li	−446.414282	–	–	0.0
III	E1	$Me_3SiC(Li)N_2$	−564.343445	–	–	4.0
IV	E1	Me_3SiCN_2Li	−564.349859	–	–	0.0
V	E1	$Me_3SiC(Li{\cdot}OEt_2)N_2$	−797.976187	−21.5	−21.5	4.0
VI	E1	$Me_3SiCN_2Li{\cdot}OEt_2$	−797.982585	−21.5	−21.5	0.0
VII	E1	$Me_3SiC(Li{\cdot}THF)N_2$	−796.779249	−22.9	−22.9	3.8
VIII	E1	$Me_3SiCN_2Li{\cdot}THF$	−796.785302	−22.7	−22.7	0.0
IX	E2	$Me_3SiC(Li{\cdot}2OEt_2)N_2$	−1031.594155	−33.7	−16.9	3.0
X	E2	$Me_3SiCN_2Li{\cdot}2OEt_2$	−1031.598894	−32.6	−16.3	0.0
XI	E2	$Me_3SiC(Li{\cdot}2THF)N_2$	−1029.205798	−40.1	−20.1	2.6
XII	E2	$Me_3SiCN_2Li{\cdot}2THF$	−1029.209892	−38.7	−19.3	0.0
XIII	E2	$Me_3SiC(Li{\cdot}TMEDA)N_2$	−912.022702	−35.1	−17.6	1.7
XIV	E2	$Me_3SiCN_2Li{\cdot}TMEDA$	−912.025424	−32.8	−16.4	0.0

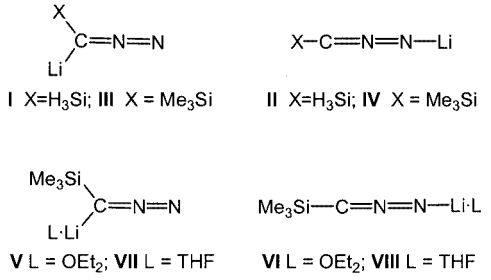

Figure 5. Theoretically modelled structures of the simple *C*- (**I**, **III**) and *N*-lithiated (**II**, **IV**) diazomethanes XCN_2Li (X = H_3Si, Me_3Si) and **III**·L and **IV**·L complexes (**V**−**VIII**; L = OEt_2, THF)

lation as external solvation increases; an important inference given the previously reported reactivities of lithiated (trimethylsilyl)diazomethanes in different Lewis base media.[12,18] Differences in the calculated energies of the variously coordinated *mono*-solvates do not, however, translate into significant differences in bonding parameters. Slight changes are noticeable relative to unsolvated **III** and **IV** on the inclusion of Lewis base and this is most apparent in increments to C−Li lengths (to, 1.959 and 1.956 Å for **V** and **VII**, respectively, cf. 1.906 Å in **III**) and N−Li distances (to, 1.735 and 1.732 Å for **VI** and **VIII**, respectively, cf. 1.692 Å in **IV**).

Calculations on $Me_3SiCN_2Li{\cdot}2$ L (L = OEt_2, THF; Table 1 and Figure 6) reinforce the view that, irrespective of the choice of L, the preference for *N*- over *C*-lithiation is diminished as external solvation of the metal is introduced. The resultant structure types (**IX**−**XII**) are all significantly more stable than models **V**−**VIII** [ΔE_C = −33.7 (**IX**), −40.1 (**XI**), −32.6 (**X**), −38.7 (**XII**) kcal·mol^{-1}]. As for **V**−**VIII**, ΔE_C is most negative for solvation by THF while the predilection for *N*-metallation is minimised in this medium [$Me_3SiC(Li{\cdot}2THF)N_2$ (**XI**) is only 2.6 kcal·mol^{-1} less stable than $Me_3SiCN_2Li{\cdot}2THF$ (**XII**)]. The addition of a second Lewis base molecule causes the further extension of C−Li (to, 2.055 and 2.038 Å for **IX** and **XI**, respectively) and N−Li bonds (to 1.801 Å for both of **X** and **XII**).

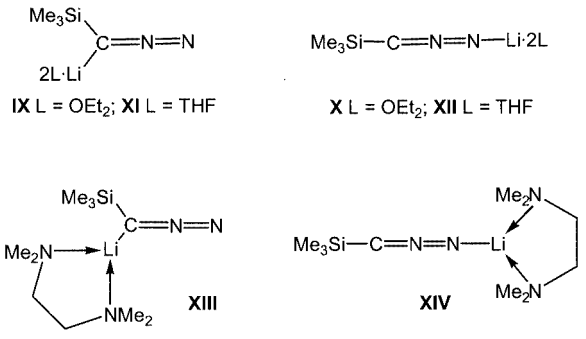

Figure 6. Modelled structures of monomeric **III**·2L and **IV**·2L complexes **IX**−**XII**; L = OEt_2, THF) and **III**·L and **IV**·L (L = TMEDA)

While the gas phase calculations do not account for the aggregation behaviour either of **1-Li·$^3/_2$THF** or of **7** it is nonetheless apparent that some useful correlations exist between theory and experiment. Table E1 (Supp. Inf.) indicates close carbon−nitrogen and the nitrogen−nitrogen bond length agreement both between **1-Li·$^3/_2$THF** and **I** (Figure 5) and between **7** and **II**. Clearly, in **1-Li·$^3/_2$THF** the carbon−nitrogen bond (mean 1.326 Å) is longer than a double one and the nitrogen−nitrogen bond (1.182 Å) is shorter than a double one.[23] Furthermore in **7**, the

 © 2003 Wiley-VCH Verlag GmbH & Co. KGaA, Weinheim

carbon−nitrogen bond (mean 1.202 Å) is longer than a triple one and the nitrogen−nitrogen bond (1.208 Å) is slightly longer than a double one.

Previously reported calculations on H_3SiCN_2Li [6-31G(d)/MP2] have suggested (in the light of structurally characterising **7**) an energetic preference of 1.4 kcal·mol^{-1} for the *N*- over the *C*-lithiate.[17] However, calculations presented here clearly suggest that any such preference is eroded by the introduction of external solvation. This leads us to the view that in the presence of excess donor (either solvent or, by aggregation, other molecules of lithiated **1-H**) the *C*-metallated product represents the thermodynamic product of lithiation whereas the *N*-metallate reveals kinetic control. Consistent with this is the fact that, whereas **1-Li·$^3/_2$THF** is afforded after having heated the reaction mixture to reflux (approx. 65 °C), **7** results from a process in which the temperature never exceeds −25 °C.

In order to further probe the question of thermodynamic versus kinetic control in the metallation of **1-H** and also in an attempt to obtain pure lithiated derivatives based on oligo- rather than complex polymeric structures, we have effected the crystallisation of lithiated (trimethylsilyl)diazomethanes from polydentate Lewis bases. The best results have been obtained by the reaction of **1-H** with *n*BuLi in TMEDA (= *N*,*N*,*N*′,*N*′-tetramethylethylenediamine) at low temperature (< −25 °C). This process achieves yellow crystals of a single isolable product and these analyse as Me_3SiCN_2Li·TMEDA (**9**). Not only does ^{1}H NMR spectroscopy support the 1:1 TMEDA/lithiate ratio but it also, by displaying just a single trimethylsilyl resonance, suggests the adoption of a single aggregation state, symmetrical species in solution. In line with the kinetic control exercised during the reaction, the solid-state structure of **9** reveals a tetramer (Table 2 and Figures 7 and 8) consisting of *N*-lithiated (trimethylsilyl)diazomethane molecules arranged as an "open" pseudo-cubane. Unusually, stabilisation of the metal centres by TMEDA takes two distinct forms with both *mono*- and *bi*dentate coordination modes being observed. Notably, such a structure is incompatible with the symmetry suggested by NMR spectroscopy, suggesting that the structure is either rapidly fluxional and/or significantly deaggregated in solution (see below).

While Li(1), Li(2), and Li(4) are each coordinated by three diazomethane terminal N-centres, Li(3) is coordinated by just two; there being no interaction with N(1) [Li(3)···N(1) = 2.839(9) Å]. *Bis*-coordination by the two TMEDA molecules that exhibit bidentate behaviour renders Li(3) and Li(4) four and five coordinate, respectively. The remaining two Li^+ ions are tetra-coordinate, each being *mono complexed* by one N-centre of a monodentate TMEDA molecule. Thus the aggregate can be viewed as a dimer of dimeric pairs [each one based on a $(NLi)_2$ ring, i.e. Li(3)N(5)Li(4)N(7) and Li(1)N(1)Li(2)N(3)] whereby each one is defined by the characteristic behaviour of its TMEDA components (Figure 8). Nevertheless, the combination of pseudo-cubane opening and differences in the coordinative modes adopted by TMEDA incurs significant variations in core Li−N interactions (Table 2). Perhaps most significantly, and presumably symptomatic of the predilection of lithium for forming four bonds,[24] pentacoordinate Li(4) forms long[25] interactions both with bidentate TMEDA [mean Li(4)−N = 2.264 Å] and with three deprotonated diazomethane monomers [mean Li(4)−N = 2.204

Table 2. Selected bond lengths [Å] and angles [°] in **9**

Li(1)−N(1)	1.991(7)	Li(4)−N(5)	2.211(8)
Li(1)−N(3)	2.108(7)	Li(4)−N(7)	2.288(8)
Li(1)−N(7)	2.045(8)	Li(4)−N(15)	2.324(8)
Li(1)−N(9)	2.067(7)	Li(4)−N(16)	2.203(8)
Li(2)−N(1)	2.010(7)	N(1)−N(2)	1.204(5)
Li(2)−N(3)	2.042(7)	N(2)−C(1)	1.210(6)
Li(2)−N(5)	2.046(7)	N(3)−N(4)	1.216(5)
Li(2)−N(11)	2.091(7)	N(4)−C(5)	1.212(6)
Li(3)−N(5)	2.058(8)	N(5)−N(6)	1.219(5)
Li(3)−N(7)	2.011(7)	N(6)−C(9)	1.209(6)
Li(3)−N(13)	2.208(9)	N(7)−N(8)	1.218(5)
Li(3)−N(14)	2.146(8)	N(8)−C(13)	1.193(6)
Li(4)−N(3)	2.113(8)		
N(1)−Li(1)−N(3)	97.4(3)	N(3)−Li(2)−N(5)	97.1(3)
Li(1)−N(1)−Li(2)	81.9(3)	Li(2)−N(3)−Li(4)	135.6(3)
Li(1)−N(3)−Li(2)	78.4(3)	Li(2)−N(5)−Li(4)	84.8(3)
N(1)−Li(2)−N(3)	98.9(3)	N(3)−Li(4)−N(5)	90.3(3)
N(3)−Li(1)−N(7)	97.0(3)	N(5)−Li(3)−N(7)	98.4(3)
Li(1)−N(3)−Li(4)	87.9(3)	Li(3)−N(5)−Li(4)	86.8(3)
Li(1)−N(7)−Li(4)	84.8(3)	Li(3)−N(7)−Li(4)	85.8(3)
N(3)−Li(4)−N(7)	89.9(3)	N(5)−Li(4)−N(7)	86.4(3)

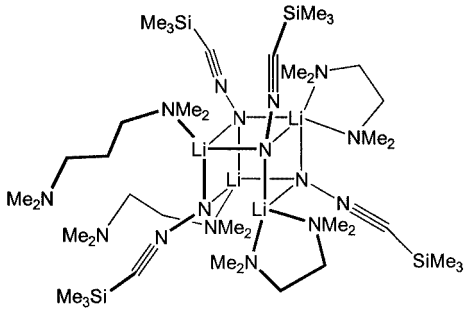

Figure 7. The molecular structure of $(\mathbf{9})_4$

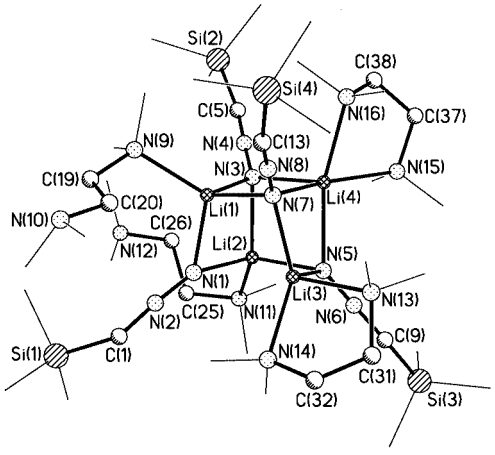

Figure 8. Solid-state structure of tetrameric **9**; hydrogen atoms and minor disorder omitted for clarity

 © 2003 Wiley-VCH Verlag GmbH & Co. KGaA, Weinheim

Å]. The remaining TMEDA-chelated metal shows similar, though less pronounced, lengthening of Li−N(TMEDA) bonds [Li(3)−N(13) and Li(3)−N(14) = 2.208(9) and 2.146(8) Å, respectively] but rather stronger bonds to the cluster core [mean Li(3)−N = 2.035 Å]. It may be the case that the discrepancy between these two Li−N(TMEDA) interactions has its origins in the orientation of the Lewis base since the shorter of the two interactions is associated with N(14), which can presumably closely approach Li(3) by virtue of diminished steric interactions with the N(1)-containing diazomethane unit−a result of the extended Li(3)···N(1) distance. A further consequence of bond-cleavage in the aggregate core is that N(1) becomes unique among the terminal diazomethane N-centres in that it stabilises just two metal ions [mean Li−N(1) = 2.001 Å]. Finally, shorter than the Li−N(TMEDA) bonds previously noted for the *bis*-coordinating Lewis base molecules are those in which the TMEDA acts only as a monodentate donor [mean Li−N = 2.079 Å]. A comparison of the solid-state structural parameters observed for **9** with those noted in **7** reveals that both C−N (mean 1.206 and 1.202 Å respectively for **9** and **7**) and N−N (mean 1.214 and 1.208 Å) bond lengths correlate well but differ significantly from those in *C*-lithiated **1-Li·$^3/_2$THF**.[19]

Coincidentally, the only other known example of an "open" $(LiN)_4$ pseudo-cubane in which a single core bond is absent is **7**. However, bond cleavage in **7** derives from the mixed-anion nature of the cluster, with one vertex of the [otherwise lithio(trimethylsilyl)diazomethane-based] cube being defined by the deprotonated N-centre in the triazole ring, the neighbouring ring-nitrogen inserting into a cubane edge. The only other discrete, related "open" pseudo-cubanes reported are the $(LiO)_4$-based structures $(PhOLi{\cdot}THF)_4{\cdot}PhOH$ (wherein a single core interaction is absent),[26] $[2\text{-}MeOC_6H_4C(H)(OLi)NMe(CH_2)_2NMe_2]_4$[27] and $[PhC(O)N(Ph)Li{\cdot}THF]{\cdot}[PhC(O)N(Ph)Zn(t\text{Bu})_2\text{-}Li{\cdot}THF]$[28] (in each of which two eclipsed core bonds are absent). This latter mode of separation is also noted in polymeric $(BrLi{\cdot}THF)_\infty$.[29] The remaining rare feature of $(\mathbf{9})_4$ in the solid state is highlighted by $Cl_6Li_6{\cdot}2TMEDA{\cdot}{}^4/_2TMEDA$.[30] Here variations in the mode of external solvation by TMEDA allow four of the six Lewis base molecules associated with each hexamer to bridge between aggregates affording a three-dimensional network. Contrastingly, in $(\mathbf{9})_4$, Li(1) and Li(2) are each stabilised by just one TMEDA N-centre [N(9), N(11)]; these donors being strictly monodentate with neither N(10) nor N(12) bridging to adjacent aggregates.

Complex **9** (like **7**) results from the employment of kinetic control during the reaction and this, perhaps, overshadows the true aim of employing TMEDA here. Nevertheless, the solid-state structure of **9** affords us the first glance of a discrete molecular lithiodiazomethane [cf. $(\mathbf{1\text{-}Li\cdot{}^3/_2THF})_\infty$] which incorporates no other by-products (cf. **7**) and a theoretical probe has been undertaken [B3LYP/6-311G**;[21,22] Figure 6 and Table 1 and Table E2 (Supp. Inf.)].[20−22] The stabilities of $Me_3SiC(Li{\cdot}TMEDA)N_2$ (**XIII**) and $Me_3SiCN_2Li{\cdot}TMEDA$ (**XIV**) are significantly enhanced by the coordination of TMEDA [ΔE_C = −35.1 (**XIII**), −32.8 (**XIV**) kcal·mol^{-1}] relative to unsolvated **III** and **IV**. In line with earlier calculations reported here (see above) $-\Delta E_C$(**XIII**) > $-\Delta E_C$(**XIV**), pointing again to the chances of *C*-metallation being enhanced by external solvation. Whilst *C*-lithiate **XIII** is still less stable than *N*-lithiated analogue **XIV** the introduction of TMEDA has almost completely negated the energy difference (1.7 kcal·mol^{-1}). The structural parameters in diazomethane anions in **9** correlate well with those of computed **XIV**. Notably, in **9** (as in **7**) the carbon−nitrogen and the nitrogen−nitrogen bond lengths are very similar (in contrast to those in *C*-lithiated **1-Li·$^3/_2$THF**, wherein the carbon−nitrogen distance was significantly greater than the nitrogen−nitrogen one).

Solution Studies on 1-Li·$^3/_2$THF and 9

The observation of **1-Li·$^3/_2$THF** and **9** demonstrates the viability of both *C*- and *N*-lithiated derivatives of **1-H** in the solid state. However, the details of their syntheses suggest that the regiospecificity of metallation is critically dependant on reaction conditions. This observation made it desirable to elucidate the structures of species obtained on dissolution of both **1-Li·$^3/_2$THF** and **9** and to probe the possible interconversion between *N*- and *C*-lithiates. Cryoscopic relative molecular mass (CRMM) measurements[31] on **1-Li·$^3/_2$THF** in benzene show both that the complex deaggregates significantly in non-donor solution and that the molecular mass (M_r) and aggregation state (n) remain essentially constant at 177 ± 10 and n = 0.77 ± 0.04, respectively [assuming n = 1 for $Me_3SiC(Li)N_2{\cdot}{}^3/_2THF$, M_r = 228] over a wide concentration range ($4.55{\cdot}10^{-3}$ to $3.20{\cdot}10^{-2}$ mol·dm^{-3}, Table E3, Supp. Inf.). This may signify the polymer (M_r = 912) breaking down (the chain-linking Li−N bonds cleaving) such that $[Me_3SiC(Li{\cdot}THF)N_2]_2$ dimers (M_r = 384) and $Me_3SiC(Li{\cdot}2THF)N_2$ monomers (M_r = 264) result. Dimerisation of these monomers, concomitant with the evolution of THF molecules yields fundamental *mono*-THF solvated dimers in solution (M_r = 228). Deaggregation of — and/or loss of THF from — these species can then explain the observed M_r. For **9**, CRMM measurements suggest significant deaggregation of the tetramer. Over the concentration range $4.80{\cdot}10^{-2}$ to $2.60{\cdot}10^{-1}$ mol·dm^{-3} (Table E4, Supp. Inf.) M_r increases from 425 ± 5 (n = 1.80 ± 2 assuming n = 1 for $Me_3SiCN_2Li{\cdot}TMEDA$) to 494 ± 3 (n = 2.14 ± 2). This points to substantial dislocation of the tetramer (M_r = 945) to give $(Me_3SiCN_2Li{\cdot}TMEDA)_2$ (M_r = 473), with limited dissociation of dimers and/or de-coordination of TMEDA occurring at lower concentrations. Data indicates some tetramer retention at higher concentrations.

Variable-temperature ^{1}H NMR spectra of **9** in $[D_8]$PhMe (Figure 9) reveal broadening of the TMEDA peaks and downfield movement of the Me_3Si signal as the temperature is reduced. By −25 °C new sets of Me_3Si and (both) TMEDA resonances develop, suggesting the evolution of a second species and, as the temperature is further reduced, these new signals become dominant. Such behaviour is consistent with the aggregation of $(Me_3SiCN_2Li{\cdot}TMEDA)_2$

 © 2003 Wiley-VCH Verlag GmbH & Co. KGaA, Weinheim

(see above) to give tetramers at low temperature and, as such, these spectral changes are thermally reversible. If, instead, this sample is heated above room temperature the Me_3Si singlet (δ = 0.28 ppm at 35 °C) is replaced by a second one (δ = 0.34 ppm at 52 °C; both signals are present in the range 45−51 °C) suggesting a significant change in the lithiodiazomethane molecule whereby kinetically favoured *N*-lithiate **9** rearranges to the (thermodynamic) *C*-lithiate in situ. This view is supported by the observation that subsequent cooling of the sample to room temperature fails to incur any further significant changes in the appearance of the spectrum, suggesting that this thermal rearrangement is irreversible.

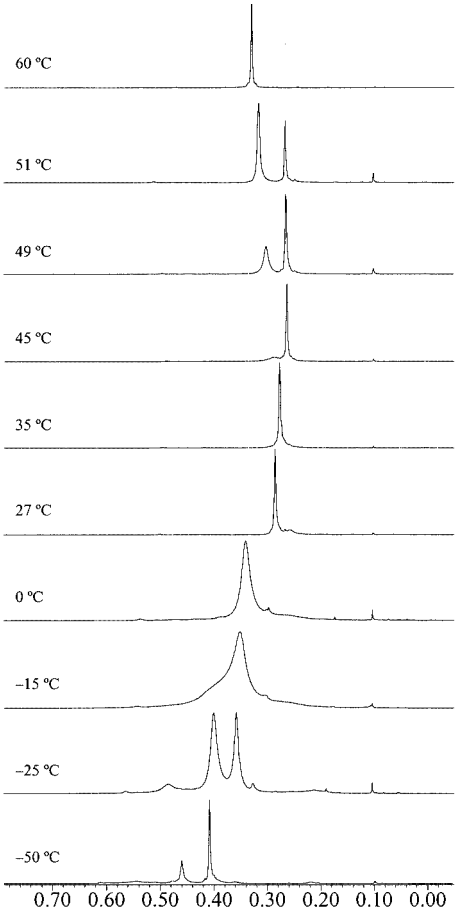

Figure 9. ^{1}H NMR spectroscopic data for the Me_3Si group in **9** in [D_8]PhMe over the range 60 °C to −50 °C

The room temperature ^{13}C NMR spectrum of **9** in [D_8]PhMe (Figure 10) shows a dominant Me_3Si signal at δ = 2.2 and a significantly smaller one at δ = −0.8. (This latter signal may represent a small amount of the sample converting slowly to the thermodynamic isomer at room temperature.) Cooling the sample to −30 °C (below the temperature at which ^{1}H NMR spectroscopy showed the effects of aggregation, see above) causes both the main Me_3Si and the TMEDA CH_2-peak to split into two. (The trace signal tentatively attributed to Me_3Si in the *C*-lithiate at room temperature is not observed at this lower temperature. However, at −30 °C all peaks are noticeably broader and it seems reasonable that this already weak resonance becomes difficult to detect.) If the same sample is heated to +95 °C it is found that the Me_3Si resonance (dominant at room temperature) is completely replaced by one at high field (δ = −0.7 ppm, cf. the weak δ = −0.8 ppm signal at room temperature). In the same way as for ^{1}H NMR spectroscopic data, this encourages the view that whereas the dominant species both at and below room temperature is the *N*-lithiate, it is converted into the *C*-metallated isomer at higher temperature. While the signal for the C=N carbon centre does not move in a manner that might be expected for such a rearrangement, it should be noted that the ^{13}C NMR spectra of both (*C*-lithiated) **1-Li·$^3/_2$THF** and (*N*-lithiated) **9** (in [D_6]DMSO at room temperature) show extremely similar chemical shifts for this carbon nucleus.

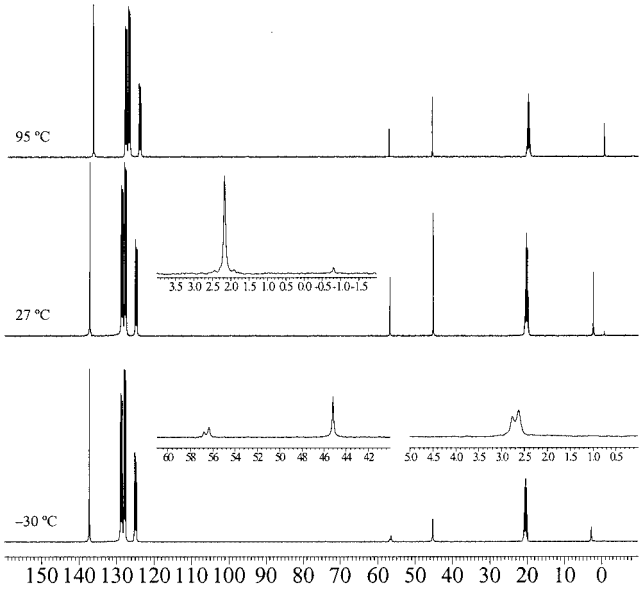

Figure 10. ^{13}C NMR spectroscopic data for **9** in [D_8]PhMe over the range 95 °C to −30 °C

Variable-temperature ^{7}Li NMR spectra (Figure 11) reinforce the information gained from ^{1}H and ^{13}C NMR spectroscopy. The single resonance observed at δ = −1.59 ppm at room temperature broadens as the temperature is lowered until at −20 °C it splits into two separate signals, consistent with the dimer-tetramer system implicated by cryoscopy. If the temperature is reduced still further this new peak becomes the dominant one. As the sample is heated to above room temperature a significant alteration in the position of the sole lithium signal can be seen. Consistent with the ^{1}H NMR spectra, this latter thermal change is irreversible.

The observation of both **1-Li·$^3/_2$THF** and **9** suggests a complicated chemistry for lithiated diazoalkanes and (in tandem with calculations) challenges previous assertions that **1-H** is necessarily preferentially *N*- rather than *C*-lithiated. Rather, calculations now suggest metallation of the carbon centre in the presence of excess donor. Indeed, further synthetic work, culminating in the isolation and structural characterisation of *N*-lithiated **9** suggests that the

 © 2003 Wiley-VCH Verlag GmbH & Co. KGaA, Weinheim

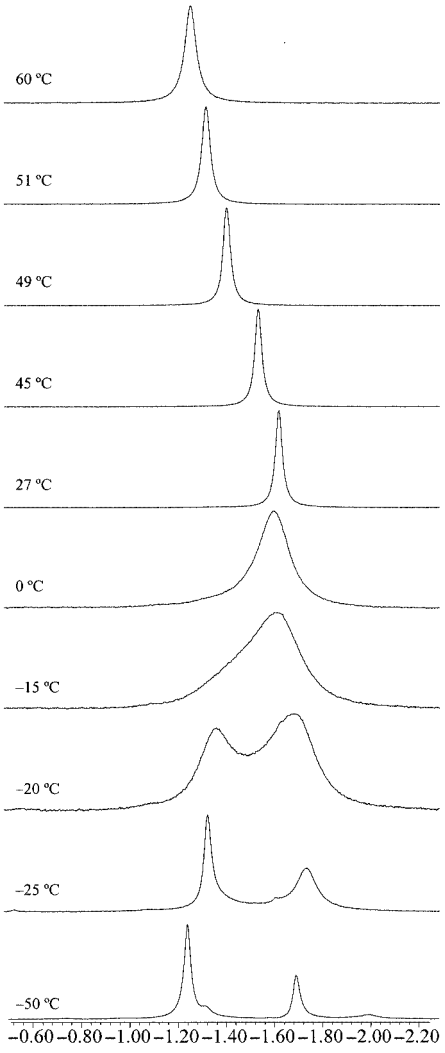

Figure 11. ^{7}Li NMR spectroscopic data for **9** in [D_8]PhMe over the range 60 °C to −50 °C

regiospecificity of metallation is temperature dependant. Clearly, such variability in the behaviour of **1-H** towards organolithium species has consequences for our understanding of the reactions undergone by the subsequently formed lithiate, and this has led us to probe the details of representative processes.

Reactions of Lithio(trimethylsilyl)diazomethane with Aryl Isothiocyanates

i) Treatment of 1-H with *n*BuLi and RNCS in THF: Syntheses of 10 (R = Ph) and 11 (R = PhCH$_2$ = Bz)

Reaction of lithio(trimethylsilyl)diazomethane with phenyl isothiocyanate (PhNCS)[18] in THF affords a product that analyses as PhNNNC(Me_3Si)C(SLi·$^3/_2$THF) **10** (Scheme 3). This shows a 1:1 Ph/Me_3Si ratio by ^{1}H NMR spectroscopy − consistent with expectation for the intended cyclised product. That ring-formation has occurred is also suggested by ^{13}C NMR spectroscopy, which reveals peaks for the sp^2 ring-carbons. However, the failure of **10** to afford crystals suitable for an unambiguous structure determination led to the replacement of phenyl isothiocyanate with its benzylic analogue (BzNCS).

Employment of BzNCS in the above reaction sequence yields a crystalline material that analyses as *S*-lithio-1-benzyl 4-trimethylsilyl-5-thio-1,2,3-triazole [BzNNNC(Me_3Si)C(SLi·2THF)], **11**. X-ray crystallography affords the first full characterisation of a lithiated thio-1,2,3-triazole (Figure 12 and Table 3; the asymmetric unit incorporates two crystallographically independent but structurally similar molecules of **11** of which a representative one is discussed). The species is rendered polymeric in the solid state through the coordination of lithium by, for example, N(3) [Li−N = 2.050(9) Å] in the almost planar (internal angles sum to 540.1°), aromatic triazole ring. The anion is formally metallated at sulfur and, at 2.460(8) Å, Li(1)−S(1) is consistent with metal-sulfur distances reported for lithium-containing thiolates,[32] thioimidates,[32j,33] and thioureas.[34] The only other solid-state structures to incorporate an alkali metallated 1,2,3-triazole ring are those of lithiated[35] and potassiated[36] benzotriazole (the triazole ring being pre-formed in both cases). In **7** a triazole ring is incorporated as a neutral adduct.[17a] The observation of a triazole ring in **11** has ramifications for our interpretation of the cyclisation process by which lithiodiazomethanes and RNCS combine to give 1-substituted 5-alkylthio-1,2,3-triazoles suggesting, as it does, the action of *C*-lithio(trimethylsilyl)diazomethane in THF solution (Scheme 4).

ii) Treatment of 1-H with *n*BuLi and RNCS in OEt$_2$: Syntheses of 12 (R = Bz) and 13 (R = Ph)

According to previous reports, the sequential combination of **1-H** with *n*BuLi and BzNCS in OEt$_2$ affords, via a postulated lithio-2-benzylamino-5-trimethylsilyl-1,3,4-thiadiazole intermediate, 2-amino-1,3,4-thiadiazoles with redirection of the reaction being attributed to an ambiguous

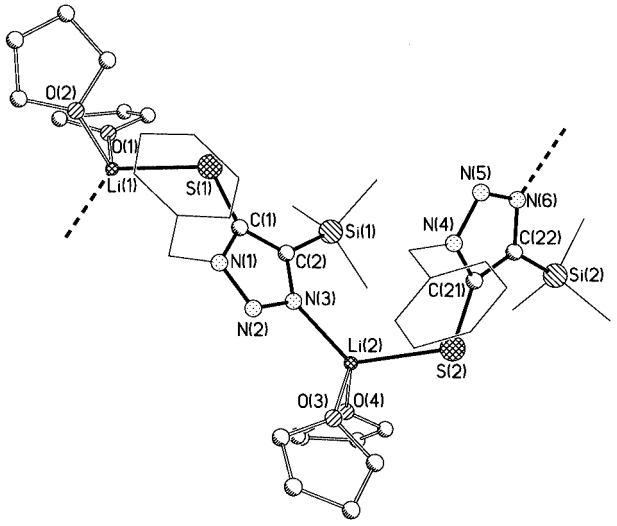

Figure 12. The solid state structure of polymeric **11**, showing the association of two crystallographically independent monomer units via *N*-stabilisation of the metal; for clarity hydrogen atoms have been omitted

 © 2003 Wiley-VCH Verlag GmbH & Co. KGaA, Weinheim

Table 3. Selected bond lengths [Å] and angles [°] in **11**

Li(1)−N(6)	2.052(8)	Li(2)−N(3)	2.050(9)
Li(1)−S(1)	2.460(8)	Li(2)−S(2)	2.482(8)
S(1)−C(1)	1.717(4)	S(2)−C(21)	1.726(4)
C(1)−N(1)	1.363(5)	C(21)−N(4)	1.347(5)
C(1)−C(2)	1.383(6)	C(21)−C(22)	1.395(6)
N(1)−N(2)	1.365(5)	N(4)−N(5)	1.369(5)
N(2)−N(3)	1.314(5)	N(5)−N(6)	1.308(5)
N(3)−C(2)	1.380(5)	N(6)−C(22)	1.374(5)
S(1)−Li(1)−N(6)	124.7(4)	S(2)−Li(2)−N(3)	124.4(4)
Li(1)−S(1)−C(1)	115.8(2)	Li(2)−S(2)−C(21)	116.5(2)
N(1)−C(1)−C(2)	104.2(4)	N(4)−C(21)−C(22)	104.8(4)
C(1)−C(2)−N(3)	107.8(4)	C(21)−C(22)−N(6)	106.8(4)
C(1)−N(1)−N(2)	111.9(3)	C(21)−N(4)−N(5)	111.7(4)
N(1)−N(2)−N(3)	105.9(3)	N(4)−N(5)−N(6)	105.8(3)
N(2)−N(3)−C(2)	110.3(4)	N(5)−N(6)−C(22)	111.0(4)

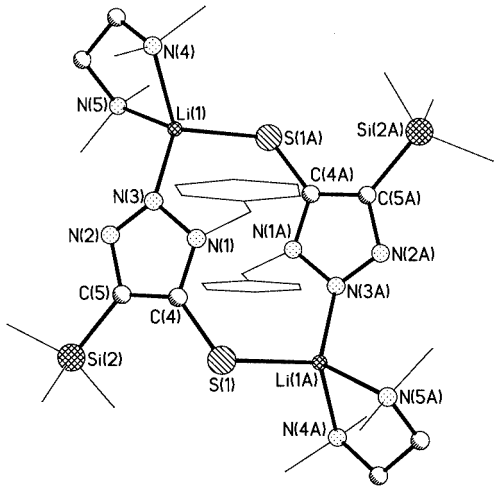

Figure 13. Molecular structure of the dimer of **12**; hydrogen atoms omitted for clarity

Table 4. Selected bond lengths [Å] and angles [°] in **12**

Li(1)−S(1A)	2.422(6)	N(1)−C(4)	1.342(4)
Li(1)−N(3)	2.053(6)	N(2)−C(5)	1.377(4)
N(3)−N(1)	1.377(4)	C(4)−C(5)	1.385(5)
N(3)−N(2)	1.285(4)	C(4)−S(1)	1.722(4)
S(1A)−Li(1)−N(3)	113.8(3)	N(1)−C(4)−C(5)	104.6(3)
Li(1)−N(3)−N(1)	124.8(3)	N(2)−C(5)−C(4)	107.7(3)
N(1)−N(3)−N(2)	107.1(3)	N(1)−C(4)−S(1)	124.0(3)
N(3)−N(1)−C(4)	110.7(3)	C(4)−S(1)−Li(1A)	111.4(2)
N(3)−N(2)−C(5)	109.9(3)		

solvent effect.[1] However, we report here that (for R = Bz) such a reaction, if followed by reflux and the addition of TMEDA affords *S*-lithio-1-benzyl 4-trimethylsilyl-5-thio-1,2,3-triazole, BzNNNC(Me_3Si)C(SLi·TMEDA) (**12**) as the only isolable product. In the solid state **12** is dimeric (Figure 13) and consists of two (mono-TMEDA) complexed metallo-1-benzyl-5-thio-4-trimethylsilyl-1,2,3-triazole molecules. Akin to **11**, **12** is an *S*-lithiate [Li−S = 2.422(6) Å], with metal centre stabilisation [Li(1)−N(3) = 2.053(6) Å] incurring dimerisation. The two planar triazole systems show aromatic character (Table 4) and, as such, are essentially similar to those in **11** notwithstanding that the N−N distances in the triazole component of **12** are consistent with greater localisation of electron density [viz. C(4)−N(1), N(1)−N(2), N(2)−N(3) in **11** and C(1)−N(1), N(1)−N(3), N(2)−N(3) in **12**]. Dimerisation of **12** results in these triazole systems being linked by (and participating in) a hitherto unknown type of 10-membered $(NNCSLi)_2$ heterocycle.

Of mechanistic importance is the observation that **12** is not the expected lithio-2-benzylamino-5-trimethylsilyl-1,3,4-thiadiazole,[1] but rather a lithio-1-benzyl 4-trimethylsilyl-5-thio-1,2,3-triazole. This is, of course, inconsistent with the reaction of *N*-lithio(trimethylsilyl)diazomethane (cf. **9**) with BzNCS but rather suggests that the reactive species in solution is the *C*-lithiate (cf. **1-Li**) instead (Scheme 4). This observation suggests several things. That the reaction is refluxed in the presence of TMEDA prior to the recrystallisation and isolation of **12** agrees with the view that preference for the *N*-lithiate is diminished in the presence of sufficiently strong external donation. Furthermore, the reaction of BzNCS with **1-Li** is apparently not facile. Hence, treatment of the lithiated diazomethane in (relatively poorly donating) OEt_2 with BzNCS at low temperature presumably gives only a slow reaction via the *N*-lithiate. However, heating of the reaction mixture immediately after introducing BzNCS (but *before* the application of TMEDA) affords the lithio-1-benzyl-5-thio-4-trimethylsilyl-1,2,3-triazole, strongly suggesting that the N-isomer has been converted into its C-congener prior to significant reaction hav-

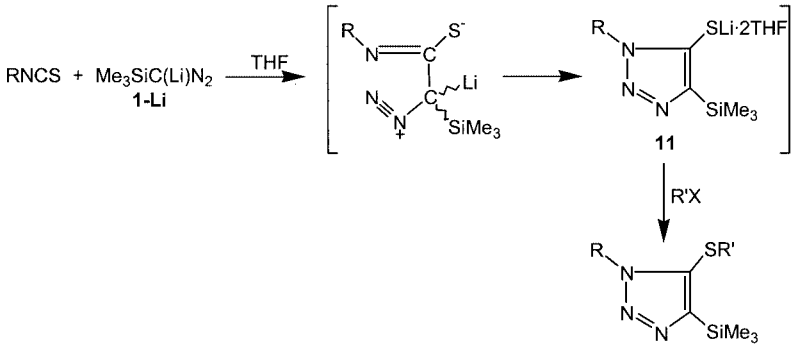

Scheme 4. Proposed mechanism for the formation of **11** from a *C*-lithiated diazomethane precursor[18]

 © 2003 Wiley-VCH Verlag GmbH & Co. KGaA, Weinheim

ing occurred. Notably the synthesis of **12** can be reproduced in THF/TMEDA (with reflux prior to introduction of the bidentate donor) whereas if the literature preparation (no reflux) is closely adhered to then **1-H**, *n*BuLi and PhNCS can be sequentially combined in OEt_2 at 0 °C and worked up to give PhNHCSCHNN **13** in high yield (its formation requiring a lithio-2-phenylamino-1,3,4-thiadiazole precursor). While it has been noted that four types of cyclic system could reasonably result from the reaction of lithiodiazomethanes with aryl isothiocyanates,[37] only two such classes have been reported.[1] Reaction of the *C*-lithiate has been considered (Scheme 4) to require the initial formation of a C−C bond between the diazomethane carbanionic centre and the isothiocyanate carbon atom. However, 2-amino-5-trimethylsilyl-1,3,4-thiadiazole production necessitates that the *N*-lithio(trimethylsilyl)diazomethane molecule forms a N−C bond prior to ring closure by C−S bond formation (Scheme 5).

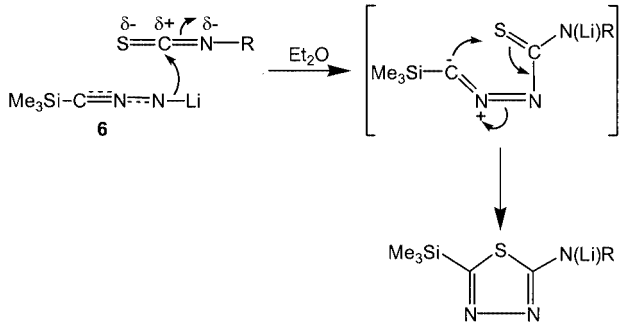

Scheme 5. Proposed mechanism for the production of lithio-2-amino-5-trimethylsilyl-1,3,4-thiadiazole from an *N*-lithiated diazomethane precursor

Conclusions

This work clearly demonstrates for the first time the viability of both the *C*- and *N*-lithiated isomers of a simple diazomethane both in the solid state (as, **1-Li·$^3/_2$THF** and **9**, respectively) and in solution. X-ray crystallographic characterisations of these two species point to bonding in the two types of molecule being quite different (Figure 14). New calculations corroborate these bonding patterns and also suggest that while the *C*-lithiated isomer of **1-Li** is less stable than its *N*-metallated analogue, the energetic difference between the two decreases with the extent of solvation by progressively stronger donors. Reaction conditions employed in the syntheses of these compounds point to the regiospecificity of metallation being significantly temperature dependent. Thus, *C*- and *N*-metallation result from the exercise of thermodynamic and kinetic control, respectively. Consistent with this is the observation, by variable temperature NMR spectroscopy, of the *irreversible* conversion of *N*- to *C*-lithiate at high temperature, a result that has significant consequences for our view of the reactivity of this lithiodiazomethane with aryl isothiocyanates.

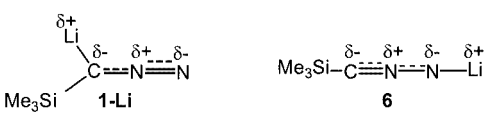

Figure 14. A review of bonding in *C*- and *N*-lithiated isomers of (trimethylsilyl)diazomethane

The solid-state structures of both **1-Li·$^3/_2$THF** and **9** indicate why it is that organic syntheses which involve the elimination of N_2 from diazomethanes require formation of the *C*-lithiate with its weak C−N and strong N=N bond. Finally, such reactivity has been probed and has resulted in the crystallographic characterisation of lithiothiotriazoles **11** and **12**. Details of their syntheses and structures bear out the view that product selectivity in these reactions, rather than being directly solvent dependent, is in fact influenced by temperature.

Experimental Section

General Remarks: All operations were carried out using standard Schlenk techniques. Toluene (freshly distilled from sodium) was added direct to the nitrogen-filled Schlenk tube using standard syringe techniques. NMR spectroscopy: Bruker DPX 250 (250.133 MHz for ^{1}H, 62.533 MHz for ^{13}C), DRX 400 (400.136 MHz for ^{1}H, 100.614 MHz for ^{13}C, 155.508 MHz for ^{7}Li), DRX 500 (500.050 MHz for ^{1}H) at 27 °C unless otherwise stated. For NMR spectroscopy, [D_6]DMSO, [D_8]THF, or [D_8]PhMe as solvents, TMS at 27 °C as external standard (for ^{1}H and ^{13}C) and PhLi in [D_8]PhMe at 27 °C as external standard (for ^{7}Li).

Synthesis of $^1/_2$[{$Me_3SiC(Li)N_2$}$_2$·3THF] (1-Li·$^3/_2$THF): Preparation as previously reported.[19] IR (Nujol): $\tilde{\nu}$ = 2149 cm^{-1} w, 2116 m (C=N=N sym. str.), 2092 m, 2052 m (C=N=N asym. str.), 838 w [$SiMe_n$ (n = 3)[38] str.], after air exposure 2160 w (C=N=N sym. str.), 2116 m (C=N=N asym. str.). ^{1}H NMR (250 MHz, [D_6]DMSO): δ = 3.60 (m, 6 H, THF), 1.76 (m, 6 H, THF), 0.05 (s, 3 H, Me), −0.18 (s, 6 H, Me) ppm. ^{13}C NMR (63 MHz, [D_6]DMSO): δ = 103.9 (C=N), 67.1 (THF), 25.2 (THF), 2.1 (SiMe), 0.4 (SiMe) ppm.

Synthesis of 6(Me_3SiCN_2Li)·2[($Me_3SiC)_2N_3Li$]·7OEt_2 [(7)$_2$·OEt_2]: Based on the literature preparation.[17a] *n*BuLi (2.5 mL, 3.2 M in hexanes, 4 mmol) was added to an OEt_2 (0.5 mL) solution of **1-H** (2 mL, 2 M in hexanes, 4 mmol) at −78 °C. The resultant orange solution was frozen in liquid nitrogen and then kept at −25 °C. Crystals of (**7**)$_2$·OEt_2 were afforded after 2 days at this temperature. The crystal structure of this compound has been reported,[17a] but supporting data has not been given previously. Yield 201 mg (30% based on **1-H**), m.p. 106−110 °C. $C_{68}H_{160}Li_8N_{18}O_7Si_{10}$ (1677): calcd. C 48.66, H 9.61, N 15.02; found C 44.93, H 9.11, N 15.34. IR (Nujol): $\tilde{\nu}$ = 2085 cm^{-1} m, 2066 m (C=N=N sym. str.), 2047 m, 2000 br (C=N=N asym. str.), 1632 m (C=C), 839 m [$SiMe_n$ (n = 3)[38] str.], after air exposure 2066 w (C=N=N sym. str.). ^{1}H NMR (500 MHz, [D_6]DMSO): δ = 3.36 (q, 15 H, OEt_2), 1.07 (t, 22.5 H, OEt_2), 0.18 (s, 36 H, Me), −0.14 (s, 12 H, Me), −0.18 (s, 42 H, Me) ppm. ^{13}C NMR (100 MHz, [D_6]DMSO): δ = 144.2 (C=C), 104.1 (C=N), 65.0 (OEt_2), 15.3 (OEt_2), 2.1 ($SiMe_3$), 0.4 ($SiMe_3$) ppm.

Synthesis of Me_3SiCN_2Li·TMEDA (9): *n*BuLi (2.5 mL, 1.6 M in hexanes, 4 mmol) was added to a TMEDA (0.9 mL, 6 mmol) solu-

 © 2003 Wiley-VCH Verlag GmbH & Co. KGaA, Weinheim

tion of **1-H** (2 mL, 2 M in hexanes, 4 mmol) at −78 °C. The resultant orange solution was frozen in liquid nitrogen and then kept at −25 °C. Crystals of **9** were afforded after storage for 24 hours at this temperature. Yield 500 mg (53%), m.p. 122−124 °C. $C_{10}H_{25}LiN_4Si$ (236): calcd. C 50.82, H 10.66, N 23.70; found C 50.56, H 10.79, N 23.84. IR (Nujol): $\tilde{\nu}$ = 2129 cm^{-1} w (C=N=N sym. str.), 2042 s (C=N=N asym. str.), 835 m [$SiMe_n$ (n = 3)[38] str.], after air exposure 2171 w (C=N=N sym. str.), 2092 m (C=N=N asym. str.). ^1H NMR (400 MHz, [D_6]DMSO): δ = 2.27 (s, 4 H, CH_2), 2.11 (s, 12 H, NMe), −0.18 (s, 9 H, Me) ppm. ^{13}C NMR (100 MHz, [D_6]DMSO): δ = 104.1 (C=N), 57.0 (TMEDA), 45.6 (TMEDA), 0.3 ($SiMe_3$) ppm.

Synthesis of PhNNNC(Me_3Si)C(SLi·$^3/_2$THF) (10): nBuLi (1.25 mL, 1.6 M in hexanes, 2 mmol) was added to a THF (3.0 mL) solution of **1-H** (1 mL, 2 M in hexanes, 2 mmol) at −78 °C whereupon the solution was treated with phenyl isothiocyanate (PhNCS) (0.24 mL, 2 mmol). The orange precipitate formed on allowing the solution to warm to room temperature was dissolved at reflux and the reaction mixture was then cooled slowly to room temperature. After 1 day needles of PhNNNC(Me_3Si)C(SLi·$^3/_2$THF) (**10**) were deposited. Yield 225 mg (31%), m.p. > 116−118 °C (decomp.). $C_{34}H_{52}Li_2N_6O_3S_2Si_2$ (726): calcd. C 56.17, H 7.21, N 11.56; found C 55.82, H 7.40, N 10.46. IR (Nujol): $\tilde{\nu}$ = 2116 cm^{-1}, 2044, 1600, 1499, 1402, 1378, 839 m [$SiMe_n$ (n = 3)[38] str.], after air exposure 2053, 2028, 1625 br (C=C str.), 1499. ^1H NMR spectroscopy (400 MHz, [D_8]THF): δ = 8.12 (m, 2 H, Ph), 7.30 (m, 2 H, Ph), 7.17 (tt, 1 H, Ph), 3.59 (m, 6 H, THF), 1.75 (m, 6 H, THF), 0.33 (s, 9 H, Me) ppm. ^{13}C NMR (100 MHz, [D_8]THF): δ = 158.7 (C−S), 143.1 (C−Si), 140.7, 129.9, 128.2, 126.5, 126.1, 125.4 (Ph), −0.8 (Me) ppm.

Synthesis of BzNNNC(Me_3Si)C(SLi·2THF) (11): nBuLi (1.25 mL, 1.6 M in hexanes, 2 mmol.) was added to a THF (2.0 mL) solution of **1-H** (1 mL, 2 M in hexanes, 2 mmol) at −78 °C after which the solution was treated with benzyl isothiocyanate (BzNCS) (0.27 mL, 2 mmol). The orange precipitate formed on allowing the solution to warm to room temperature dissolved at reflux. The reaction mixture was then allowed to cool slowly to room temperature whereupon it was stored for 2 days, affording crystals of BzNNNC(Me_3Si)C(SLi·2THF) (**11**). Yield 256 mg (31%), m.p. > 168−170 °C (decomp.). $C_{20}H_{32}LiN_3O_2SSi$ (413): calcd. C 58.08, H 7.80, N 10.16; found C 57.15, H 7.76, N 10.39. IR (Nujol): $\tilde{\nu}$ = 1720 cm^{-1} w, 1403, 1217, 917, 841 [$SiMe_n$ (n = 3)[38] str.], after air exposure 1719 w, 1625 br (C=C stretch). ^1H NMR (400 MHz, [D_8]THF): δ = 7.28 (d, 2 H, Ph), 7.13 (m, 2 H, Ph), 7.08 (tt, 1 H, Ph), 5.35 (s, 2 H, CH_2), 0.29 (s, 9 H, Me) ppm. ^{13}C NMR (100 MHz, [D_8]THF): δ = 160.4 (C−S), 141.5 (C−Si), 140.2, 129.0, 128.5, 127.2 (Ph), 48.8 (CH_2), −0.8 (Me) ppm.

Preparation of BzNNNC(Me_3Si)C(SLi·TMEDA) (12): (a) nBuLi (1.25 mL, 1.6 M in hexanes, 2 mmol) was added to an OEt_2 (2.0 mL) solution of **1-H** (1 mL, 2 M in hexanes, 2 mmol) at −78 °C. BzNCS (0.27 mL, 2 mmol) was then added to the chilled solution, affording a clear yellow solution at room temperature. This was heated to reflux whereupon TMEDA (0.3 mL, 2 mmol) was added. Storage of the resultant solution for 2 days at room temperature afforded crystals of BzNNNC(Me_3Si)C(SLi·TMEDA), **12**.

(b) nBuLi (1.25 mL, 1.6 M in hexanes, 2 mmol) was added to a THF (1.8 mL) solution of **1-H** (1 mL, 2 M in hexanes, 2 mmol) at −78 °C. BzNCS (0.27 mL, 2 mmol) was then added to the chilled solution, affording a yellow precipitate at room temperature. The mixture was heated to reflux and TMEDA (0.3 mL, 2 mmol) was added, providing an orange solution. Storage of the resultant solution for 2 days at room temperature afforded crystals of **12**: Yield 154 mg (20%; route a), 62 mg (8%; route b), m.p. > 163−165 °C (decomp.). $C_{18}H_{32}LiN_5SSi$ (385): calcd. C 56.07, H 8.37, N 18.16; found C 55.99, H 8.94, N 21.43. IR (Nujol, cm^{-1}): $\tilde{\nu}$ = 1735, 1403, 1377, 842 [$SiMe_n$ (n = 3)[38] str.], after air exposure 1734, 1627 br (C=C str.), 1377. ^1H NMR (400 MHz, [D_8]THF): δ = 7.52 (d, 2 H, Ph), 7.17 (m, 2 H, Ph), 7.10 (tt, 1 H, Ph), 5.66 (s, 2 H, CH_2), 2.32 (s, 8 H, TMEDA), 2.17 (s, 24 H, TMEDA), 0.32 (s, 9 H, Me) ppm. ^{13}C NMR (100 MHz, [D_8]THF): δ = 159.9 (C−S), 140.1 (C−Si), 139.7, 128.5, 127.4, 126.0 (Ph), 57.8 (TMEDA) 47.8 (CH_2), 45.3 (TMEDA), −1.6 (Me_3Si) ppm.

Synthesis of PhNHCSCHNN (13): nBuLi (0.75 mL, 1.6 M in hexanes, 1.2 mmol) was added to an OEt_2 (10.0 mL) solution of **1-H** (0.6 mL, 2 M in hexanes, 1.2 mmol) at 0 °C. After stirring for 20 minutes PhNCS (0.12 mL, 1.2 mmol) was added to the chilled solution and the mixture stirred for a further 2 hours at this temperature. The solution was allowed to warm to room temperature and NH_4Cl (20 mL) was added. The resultant mixture was extracted with OEt_2 (2 × 10 mL) washed with water (2 × 10 mL) and dried ($MgSO_4$). Removal of excess solvent afforded **13** as a white powder. Yield 160 mg (75%), m.p. > 170−172 °C (decomp.). $C_8H_7N_3S$ (177): calcd. C 54.22, H 3.98, N 23.71; found C 53.49, H 5.43, N 21.05. IR (Nujol, cm^{-1}): $\tilde{\nu}$ = 3411, 3245 w, 3195 w (N−H str.), 1715, 1597, 1573 (C=N str.). ^1H NMR (400 MHz, [D_6]DMSO): δ = 10.42 (s, 1 H, N−H) 8.90 (s, 1 H, N=C−H), 7.65 (d, 2 H, Ph), 7.32 (m, 2 H, Ph), 7.00 (t, 1 H, Ph), 2.32 (s, 8 H, TMEDA), 2.17 (s, 24 H, TMEDA), 0.32 (s, 9 H, Me) ppm. ^{13}C NMR (100 MHz, [D_6]DMSO): δ = 164.3 (N=C(N)−S), 144.1 (S−C(H)=N), 140.8, 129.1, 121.9, 117.4 (Ph) ppm.

X-ray Crystallography: Data to check the unit cell of (**7**)$_2$·OEt_2 ($C_{68}H_{160}Li_8N_{18}O_7Si_{10}$, monoclinic, space group $C2/m$, a = 23.05, b = 15.77, c = 15.05 Å, β = 101.9°) were collected on a Rigaku R-Axis II imaging plate diffractometer[39] at 200(2)K using graphite monochromated Mo-K_α radiation (λ = 0.71069 Å). This compared with the previously published[17a] unit cell and so the full data were not collected. Data for **9** were collected on a Rigaku R-Axis II imaging plate diffractometer using 45 frames, each frame covering a 4° oscillation with an exposure time of 30 minutes per frame, in each of four orientations. Data for **11** were collected by the ω/2θ method on a Rigaku AFC-7R four circle diffractometer[39] and data for **12** were collected on a Stoe−Siemens four circle diffractometer. All structures were solved by direct methods[40] and subsequent Fourier difference syntheses and refined by full-matrix least-squares[41] on F^2 with anisotropic thermal parameters for Li, N, Si, and most C atoms. A riding model with idealised geometry was employed for H-atom refinement. For **9**, one terminal methyl group of a TMEDA molecule and three of the $SiMe_3$ groups showed positional disorder with respect to the position of the C atoms and were refined isotropically over two different sites with partial occupancies. Crystallographic data for **9**, **11** and **12** are given in Table 5. CCDC-207850 (**9**), -207849 (**11**), and -207848 (**12**) contain the supplementary crystallographic data for this paper. These data can be obtained free of charge at www.ccdc.cam.ac.uk/conts/retrieving.html [or from the Cambridge Crystallographic Data Centre, 12, Union Road, Cambridge CB2 1EZ, UK; Fax: (internat.) +44-1223/336-033; E-mail: deposit@ccdc.cam.ac.uk].

Computational Methods: Preliminary geometry optimisation calculations[20] based on XCN_2Li·nL (X = H_3Si, Me_3Si; n = 0, 1, 2; L = OEt_2, THF) were done using the 6-31G* basis set[22] at the HF level. A frequency analysis was performed on the most stable conformation of each structure and the geometry was refined using

 © 2003 Wiley-VCH Verlag GmbH & Co. KGaA, Weinheim

Table 5. Crystallographic data for **9**, **11**, and **12**

	9	**11**	**12**
Formula	$C_{40}H_{100}Li_4N_{16}Si_4$	$C_{20}H_{32}LiN_3OSSi$	$C_{18}H_{32}LiN_5SSi$
M	945.48	413.58	385.58
Crystal system	Triclinic	Triclinic	Monoclinic
Space group	$P\bar{1}$	$P\bar{1}$	$C2/c$
a [Å]	14.836(2)	11.147(4)	19.705(4)
b [Å]	19.893(3)	20.679(7)	11.210(2)
c [Å]	11.880(1)	10.151(3)	23.186(5)
α [°]	99.77(1)	97.62(3)	90
β [°]	113.15(1)	90.49(4)	114.81(3)
γ [°]	84.15(1)	94.42(3)	90
U [Å^3]	3175.7(7)	2311.9(13)	4649(2)
Z	2	4	8
D_c [g cm^{-3}]	0.989	1.188	1.102
λ [Å]	0.71073	0.71069	0.71073
μ [mm^{-1}]	0.131	0.211	0.201
T [K]	180(2)	180(2)	180(2)
Refl., unique	12251, 7118	8322, 7889	4337, 4076
Refl. $F^2 > 2\sigma(F^2)$	4822	4542	2875
θ [°]	3.59−22.02	2.60−25.01	4.12−25.00
R_{int}	0.0645	0.0843	0.0567
R, $wR2$	0.0692, 0.1813	0.0707, 0.1755	0.0665, 0.1891
Parameters	606	511	235
Peak, hole [e·Å^{-3}]	0.371, −0.353	0.369, −0.304	0.839, −0.285

DFT methods (B3LYP/6-311G**).[21,22] The structural parameters reported here were taken from the DFT calculations while the electronic energy of the DFT calculation was modified by the scaled (0.91) ZPE correction taken from the HF calculation. Geometries modelled are shown in Figure 5 [XCN_2Li (X= H_3Si, Me_3Si), Me_3SiCN_2Li·L (L = OEt_2, THF)] and Figure 6 [Me_3SiCN_2Li·2 L (L = OEt_2, THF), (Me_3SiCN_2Li·TMEDA)]. The results are summarised in Table 1 and selected computed bonding parameters are given in Tables E1 and E2 (Supporting Information, see footnote on page 1 of this article).

Acknowledgments

We gratefully thank the U. K. EPSRC (R. H., M. A. H.) for financial support and Dr. Neil Feeder for collecting X-ray data for $(\mathbf{7})_2$·OEt_2, **9**, **11**, and **12**.

[1] [1a] T. Aoyama, T. Shioiri, *Tetrahedron Lett.* **1980**, *21*, 4461−4462. [1b] T. Aoyama, T. Shioiri, *Chem. Pharm. Bull.* **1981**, *29*, 3249−3255.

[2] [2a] N. Hashimoto, T. Aoyama, T. Shioiri, *Tetrahedron Lett.* **1980**, *21*, 4619−4622. [2b] N. Hashimoto, T. Aoyama, T. Shioiri, *Chem. Pharm. Bull.* **1982**, *30*, 119−124.

[3] N. Hashimoto, T. Aoyama, T. Shioiri, *Heterocycles* **1981**, *15*, 975−979.

[4] C. Baldoli, P. D. Buttero, E. Licandro, S. Maiorana, A. Papagni, A. Zanotti-Gerosa, *J. Organomet. Chem.* **1994**, *476*, C27−C29.

[5] N. Hashimoto, T. Aoyama, T. Shioiri, *Chem. Pharm. Bull.* **1981**, *29*, 1475−1478.

[6] E. W. Colvin, B. J. Hamill, *J. Chem. Soc., Perkin. Trans. 1* **1977**, 869−874.

[7] [7a] T. Aoyama, M. Kabeya, A. Fukushima, T. Shioiri, *Heterocycles* **1985**, *23*, 2363−2366. [7b] T. Aoyama, K. Sudo, T. Shioiri, *Chem. Pharm. Bull.* **1982**, *30*, 3849−3851.

[8] T. Aoyama, T. Shioiri, *Chem. Pharm. Bull.* **1982**, *30*, 3450−3452.

[9] K. Miwa, T. Aoyama, T. Shioiri, *SynLett* **1994**, 109−109.

[10] K. Miwa, T. Aoyama, T. Shioiri, *SynLett* **1994**, 107−108.

[11] R. A. Ruden, *J. Org. Chem.* **1974**, *39*, 3607−3608.

[12] H. Kai, K. Iwamoto, N. Chatani, S. Murai, *J. Am. Chem. Soc.* **1996**, *118*, 7634−7635.

[13] Y. Kita, Y. Tsuzuki, S. Kitagaki, S. Akai, *Chem. Pharm. Bull.* **1994**, *42*, 233−236.

[14] D. Seyferth, R. C. Hui, W.-L. Wang, *J. Org. Chem.* **1993**, *58*, 5843−5845.

[15] [15a] E. Müller, H. Disselhoff, *Justus Liebigs Ann. Chem.* **1934**, *512*, 250−263. [15b] E. Müller, W. Kreutzmann, *Justus Liebigs Ann. Chem.* **1934**, *512*, 264−275. [15c] E. Müller, D. Ludsteck, *Chem. Ber.* **1954**, *87*, 1887−1895. [15d] E. Müller, D. Ludsteck, *Chem. Ber.* **1955**, *88*, 921−933. [15e] E. Müller, W. Rundel, *Chem. Ber.* **1956**, *89*, 1065−1071. [15f] E. Müller, P. Kastner, R. Beutler, W. Rundel, H. Suhr, B. Zeeh, *Justus Liebigs Ann. Chem.* **1968**, *713*, 87−95. [15g] E. Müller, R. Beutler, B. Zeeh, *Justus Liebigs Ann. Chem.* **1968**, *719*, 72−79. [15h] R. Beutler, B. Zeeh, E. Müller, *Chem. Ber.* **1969**, *102*, 2636−2639.

[16] [16a] A. I. Boldyrev, P. v. R. Schleyer, A. Higgins, C. Thompson, S. S. Kamarenko, *J. Comput. Chem.* **1992**, *13*, 1066−1078. [16b] M. W. Wong, C. Wentrup, *J. Am. Chem. Soc.* **1993**, *115*, 7743−7746.

[17] [17a] G. Boche, K. Harms, M. Marsch, F. Schubert, *Chem. Ber.* **1994**, *127*, 2193−2195. [17b] G. Boche, J. C. W. Lohrenz, F. Schubert, *Tetrahedron* **1994**, *50*, 5889−5902.

[18] [18a] T. Aoyama, M. Kabeya, A. Fukushima, T. Shioiri, *Heterocycles* **1985**, *23*, 2367−2369. [18b] T. Aoyama, M. Kabeya, T. Shioiri, *Heterocycles* **1985**, *23*, 2371−2374.

[19] N. Feeder, M. A. Hendy, P. R. Raithby, R. Snaith, A. E. H. Wheatley, *Eur. J. Inorg. Chem.* **1998**, 861−864.

[20] M. J. Frisch, G. W. Trucks, H. B. Schlegel, P. M. W. Gill, B. G. Johnson, M. A. Robb, J. R. Cheeseman, T. Keith, G. A. Petersson, J. A. Montgomery, K. Raghavachari, M. A. Al-Laham, V. G. Zakrzewski, J. V. Ortiz, J. B. Foresman, J. Cioslowski, B. B. Stefanov, A. Nanayakkara, M. Challacombe, C. Y. Peng, P. Y. Ayala, W. Chen, M. W. Wong, J. L. Andres, E. S. Replogle, G. Gomperts, R. L. Martin, D. J. Fox, J. S. Brinkley, D. J. Defrees, J. Baker, J. J. P. Stewart, M. Head-Gordon, C. Gonzalez, J. A. Pople, *GAUSSIAN 94 Revision C. 3*, Gaussian, Inc., Pittsburgh, P. A., **1995**.

 © 2003 Wiley-VCH Verlag GmbH & Co. KGaA, Weinheim

[21] [21a] A. D. Becke, *Phys. Rev. A* **1988**, *38*, 3098−3100. [21b] A. D. Becke, *J. Chem. Phys.* **1993**, *98*, 5648−5652.
[22] [22a] W. J. Hehre, R. Ditchfield, J. A. Pople, *J. Chem. Phys.* **1972**, *56*, 2257−2261. [22b] P. C. Hariharan, J. A. Pople, *Theor. Chim. Acta* **1973**, *28*, 213−222. [22c] J. D. Dill, J. A. Pople, *J. Chem. Phys.* **1975**, *62*, 2921−2923.
[23] [23a] R. D. Harrison, H. Ellis, *Revised Nuffield Advanced Science Book of Data*; Longman Group Ltd., Harlow, **1984**. [23b] J. G. Stark, H. G. Wallace, *Chemistry Data Book*; 2nd Edn. in SI, John Murray, London, **1992**.
[24] P. G. Williard, G. J. MacEwan, *J. Am. Chem. Soc.* **1989**, *111*, 7671−7672.
[25] N. Feeder, R. Snaith, A. E. H. Wheatley, *Eur. J. Inorg. Chem.* **1998**, 879−883.
[26] M. Pink, G. Zahn, J. Sieler, *Z. Anorg. Allg. Chem.* **1994**, *620*, 749−752.
[27] D. R. Armstrong, J. E. Davies, R. P. Davies, P. R. Raithby, R. Snaith, A. E. H. Wheatley, *New J. Chem.* **1999**, 35−41.
[28] S. R. Boss, R. Haigh, D. J. Linton, P. Schooler, G. P. Shields, A. E. H. Wheatley, *Dalton Trans.* **2003**, 1001−1008.
[29] A. J. Edwards, M. A. Paver, P. R. Raithby, C. A. Russell, D. S. Wright, *J. Chem. Soc., Dalton Trans.* **1993**, 3265−3266.
[30] C. L. Raston, B. W. Skelton, C. R. Whitaker, A. H. White, *Aust. J. Chem.* **1988**, *41*, 1925−1934.
[31] M. G. Davidson, R. Snaith, D. Stalke, D. S. Wright, *J. Org. Chem.* **1993**, *58*, 2810−2816.
[32] [32a] D. R. Armstrong, A. J. Banister, W. Clegg, W. R. Gill, *J. Chem. Soc., Chem. Commun.* **1986**, 1672−1673. [32b] A. J. Banister, W. Clegg, W. R. Gill, *J. Chem. Soc., Chem. Commun.* **1987**, 850−852. [32c] G. A. Sigel, P. P. Power, *Inorg. Chem.* **1987**, *25*, 2819−2822. [32d] K. Ruhlandte-Senge, P. P. Power, *Bull. Soc. Chim. Fr.* **1992**, *129*, 594−598. [32e] N. Frölich, P. B. Hitchcock, J. Hu, M. F. Lappert, J. R. Dilworth, *J. Chem. Soc., Dalton Trans.* **1996**, 1941−1946. [32f] K. Ruhlandte-Senge, U. Englich, M. O. Senge, S. Chadwick, *Inorg. Chem.* **1996**, *35*, 5820−5827. [32g] M. D. Janssen, E. Rijnberg, C. A. de Wolf, M. P. Hogerheide, D. Kruis, H. Kooijman, A. L. Spek, D. M. Grove, G. van Koten, *Inorg. Chem.* **1996**, *35*, 6735−6741. [32h] M. Niemeyer, P. P. Power, *Inorg. Chem.* **1996**, *35*, 7264−7272. [32i] S. Chadwick, U. Englich, K. Ruhlandte-Senge, *Organometallics* **1997**, *15*, 5792−5803. [32j] S. Chadwick, K. Ruhlandte-Senge, *Chem. Eur. J.* **1998**, *4*, 1768−1780. [32k] J. Knizek, A. Schlegel, H. Nöth, *Eur. J. Inorg. Chem.* **2001**, 181−187.
[33] [33a] H. L. van Maanen, J. T. B. H. Jastrzebski, H. Kooijman, A. L. Spek, G. van Koten, *Tetrahedron* **1994**, *50*, 11509−11526. [33b] T. Chivers, A. Downard, G. P. A. Yap, *Inorg. Chem.* **1998**, *37*, 5708−5709. [33c] T. Chivers, A. Downard, M. Parvez, *Inorg. Chem.* **1999**, *38*, 5565−5570. [33d] C. Kimblin, B. M. Bridgewater, T. Hascall, G. Parkin, *J. Chem. Soc., Dalton Trans.* **2000**, 891−897.
[34] D. R. Armstrong, R. E. Mulvey, D. Barr, R. Snaith, D. S. Wright, W. Clegg, S. M. Hodgson, *J. Organomet. Chem.* **1989**, *362*, C1−C4.
[35] C. Lambert, F. Hampel, P. v. R. Schleyer, *J. Organomet. Chem.* **1993**, *455*, 29−35.
[36] P. C. Andrews, W. Clegg, R. E. Mulvey, P. A. O'Neil, H. M. M. Wilson, *J. Chem. Soc., Chem. Commun.* **1993**, 1142−1144.
[37] M. Usher, A. Rybar, A. Martvon, J. Lesko, *Collect. Czech. Chem. Commun.* **1976**, *41*, 1182−1187.
[38] D. H. Williams, I. Fleming, *Spectroscopic Methods in Organic Chemistry*; 4th Edn., McGraw-Hill International (U. K.) Ltd., England, **1989**.
[39] *TEXSAN*, Version 1.7−1, Molecular Structure Corporation, The Woodlands, TX, **1985, 1992, 1995**.
[40] [40a] G. M. Sheldrick, *Acta Crystallogr., Sect. A* **1990**, *46*, 467−473. [40b] G. M. Sheldrick, *SHELXL-PLUS*, Program for Structure Solution and Refinement, University of Göttingen, **1991**.
[41] G. M. Sheldrick, *SHELXL-97*, Program for Crystal Structure Refinement, University of Göttingen, **1997**.

Received April 30, 2003

 © 2003 Wiley-VCH Verlag GmbH & Co. KGaA, Weinheim

Heteroaromatic-Substituted Mono- and Bis(triimidosulfonates)

Carola Selinka[a] and Dietmar Stalke*[a]

Dedicated to the memory of Ron Snaith

Keywords: Heterocycles / Lithium / N ligands / S ligands / Sulfur

In this paper we present the syntheses and structures of the metal complexes $[(THF)_2Li\{(NtBu)_3S(C_4H_3NMe)\}]$ (**1**), $[(tmeda)Li\{(NtBu)_3S(C_4H_3S)\}]$ (**2**), $[(tmeda)Li\{(NtBu)_3S(C_4H_3Se)\}]$ (**3**), $[(THF)_4Li_2\{(tBuN)_3S(SC_4H_2)S(NtBu)_3\}]$ (**4a**) and $[(tmeda)_2Li_2\{(tBuN)_3S(SC_4H_2)S(NtBu)_3\}]$ (**4b**). The lithium salts form non-aggregated soluble molecules rather than infinite insoluble solid-state lattices like their oxo analogues. The metals are *N*,*N*-chelated rather than tripodally coordinated. Although the S–N bond to the one pendant spectator *t*BuN group is considerably shorter than in the metal-coordinated *t*BuN groups, conjugation of the S–N bonds to the heteroaromatic rings could not be deduced unambiguously from the experimental structures.

(© Wiley-VCH Verlag GmbH & Co. KGaA, 69451 Weinheim, Germany, 2003)

Introduction

Arylsulfonates ($ArSO_2^-$) and arylsulfamides $[ArS(NR)_2^-]$ are used in various fields of modern chemistry. Sulfonic acids (RSO_2OH) and their metal salts (RSO_3M) are versatile catalysts used on a large scale for industrial cyclization and polymerization processes. A catalytic transfer-hydrogenation process is provided by sulfonates.[1] The preparation of inclusion compounds based on lamellar host frameworks constructed from guanidinium and organodisulfonate ions has been reported.[2] With this and the recent progress in isoelectronic replacement of oxygen atoms in simple *p*-block element oxoanions in mind, we aimed to synthesise aryltriimidosulfonates $ArS(NR)_3^-$ with Ar = $MeNC_4H_3$, SC_4H_3 and SeC_4H_3. To envisage oligo- or even polymeric molecules two $S(NR)_3^-$ moieties were linked by a 2,5-disubstituted thiophenyl ring. Thiophenesulfonamides and their alkali metal or non-toxic acid addition salts are useful as insecticides, acaricides and larvicides.[3] Molecules like 5-substituted thiophene-2-sulfonamides are promising drugs that are currently being used as carbonic anhydrase inhibitors for the treatment of glaucoma.[4] This industrial relevance combined with the recent progress in isoelectronic replacement of oxygen atoms in simple *p*-block element oxoanions[5] encouraged us to generate the unprecedented aryltriimidosulfonates $ArS(NR)_3^-$. Substitution of the oxygen atom in the aryloxoanions $ArSiO_3^{3-}$, $ArPO_3^{2-}$, $ArAsO_3^{2-}$, $ArSbO_3^{2-}$, $ArPO_2^{2-}$, $ArSO_2^-$, $ArSeO_3^-$ or $ArTeO_3^-$ by an NR imido group gives the polyimido anions $ArP(NR)_2^{2-}$, $ArS(NR)_2^-$, $ArSi(NR)_3^{3-}$, $ArP(NR)_3^{2-}$ and $ArAs(NR)_2^{2-}$.[6] However, to the best of our knowledge, related species with Sb, Se, Te and S^{VI} have not yet been reported in the literature. By contrast to the simple oxoanions, these species should be soluble because they form contact ion pairs in cage complexes surrounded by a lipophilic layer of organic residues rather than infinite solid-state lattices by multiple oxygen/cation contacts. Furthermore, their redox potential and coordination behaviour is tuneable by variation of the organic substituents.

To date the *S*-alkyl-[7] $[MeS(NR)_2]^-$ and *S*-phenyl diimidosulfinates[8] $[PhS(NR)_2]^-$ and *S*-alkyltriimidosulfonates[9] $[MeS(NR)_3]^-$ have been studied in detail. The CH-acidic organic substituent at the sulfur atom in the first and the latter species can be deprotonated to give dianionic alkylenediimidosulfites[10] and alkylenetriimidosulfates[11] in which the CR_2 group replaces the oxygen or NR group isoelectronically. They can both be rationalized as S^{IV}- and S^{VI}-ylides. Until recently the direct reaction of thiols with chloroamines or, better, bromoamines was the only known synthetic access to *S*-alkyltriimidosulfonates.[12] In this paper we present a new straightforward synthetic route which involves the nucleophilic addition of aryllithiums to the formal S=N double bond of sulfur triimides.[13] Presumably due to the steric crowding in the products, only sterically less-demanding alkyls could be added (e.g. MeLi) to the few structurally known sulfur triimides $[S(NR)_3$, R = *t*Bu, $SiMe_3$).[14] Addition reactions with *n*BuLi and *t*BuLi failed. In principle, the resulting $[MeS(NR)_3]^-$ anion possesses C_{3v} symmetry prompting feasible tripodal cap-shaped metal coordination. While the triimidosulfite[15] $S(NR)_3^{2-}$ and the triimidosulfate[16] $OS(NR)_3^{2-}$ dianions show this

[a] Institut für Anorganische Chemie der Universität Würzburg
Am Hubland, 97074 Würzburg, Germany
Fax: (internat.) +49-(0)931/888-4619
E-mail: dstalke@chemie.uni-wuerzburg.de

 © 2003 Wiley-VCH Verlag GmbH & Co. KGaA, Weinheim **DOI: 10.1002/ejic.200300194**

anticipated tripodal behaviour even in mixed-metal complexes,[17] only (*N*,*N*)-SN_2 chelation has been observed for the $[MeS(NR)_3]^-$ monoanion.[18]

In this paper we aimed both to evaluate the reactivity of the sulfur triimide towards organolithium reagents and to introduce an additional coordination site in the S-bound organic substituent. Experimental charge-density investigations of $S(NtBu)_3$ suggested that only flat carbanions are suitable for addition across the polar S−N bond as the reactive surface at $\nabla^2\rho(\mathbf{r}) = 0$ shows holes in the SN_3 plane on the NSN bisectors and maxima above and below the central sulfur atom. Hence, the carbanion needs to approach the electrophilic sulfur along the bisectors and slot in between the *t*BuN groups.[19] Thus we decided to react $S(NtBu)_3$ with lithiated furan, pyrrole, thiophene and selenophene.

Results and Discussion

[Li{(N*t*Bu)$_3$SAr}] Complexes

The aromatic heterocycles were lithiated first with BuLi and then reacted at low temperatures with a stoichiometric amount of the sulfur triimide. Although addition reactions of organolithiums like *n*BuLi and *t*BuLi to $S(NtBu)_3$ failed in the past, presumably because of steric crowding in the sulfonates, methylpyrrolyl-, thiophenyl-, and selenophenyllithium react smoothly to give the related products $[(THF)_2Li\{(NtBu)_3S(C_4H_3NMe)\}]$ (**1**), $[(tmeda)Li\{(NtBu)_3S(C_4H_3S)\}]$ (**2**), and $[(tmeda)Li\{(NtBu)_3S(C_4H_3Se)\}]$ (**3**). Due to the reactivity and thermal instability of 2-lithiofuran all attempts to add it to sulfur triimide failed. Upon addition of $S(NtBu)_3$ to $Li(C_4H_3O)$ the reaction mixture polymerises instantaneously. The organic substituents (C_4H_3NMe), (C_4H_3S) and (C_4H_3Se) bond in the 2-position to the electropositive sulfur while the lithium cation is coordinated to the nitrogen atoms (Scheme 1). This reactivity is not surprising in view of the S^{2+} charge and the sp^3-hybridization of the nitrogen atoms.[20]

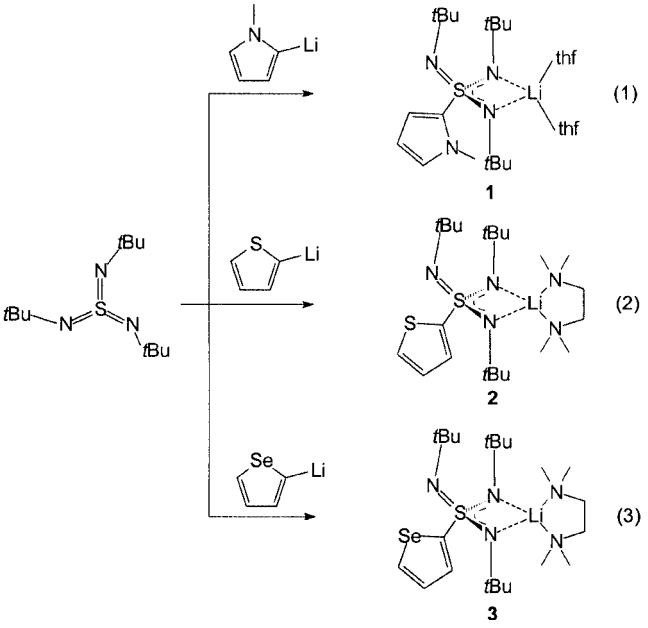

Scheme 1. Preparation of $[(THF)_2Li\{(NtBu)_3S(C_4H_3NMe)\}]$ (**1**), $[(tmeda)Li\{(NtBu)_3S(C_4H_3S)\}]$ (**2**), and $[(tmeda)Li\{(NtBu)_3S(C_4H_3Se)\}]$ (**3**)

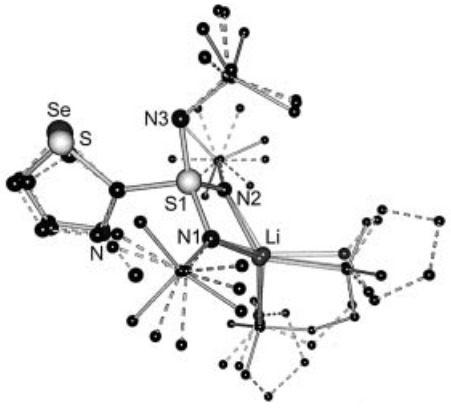

Figure 1. Superposition plot of the solid-state structures of **1**−**3**

Structures of 1−3

The solid-state structures of the lithium *S*-aryl-tri(*tert*-butyl)triimidosulfonates **1**, **2** and **3** (Figure 1) show that neither tripodal coordination nor additional coordination of the heteroatom in the aromatic five-membered ring to the lithium cations is accomplished. Like in the coordination of $PhS(NSiMe_3)_2^-$ [8] and $PhCCS(NtBu)_3^-$,[18] the ligand coordinates one hemisphere of the metal, leaving the two THF donor molecules coordinated to the other in **1**. In **2** and **3** the tetragonal coordination sphere is completed by one tmeda molecule each. Like the methyl derivatives, these anions coordinate in a bidentate manner with only two nitrogen atoms orientated towards the metal. No further coordination of the third *t*BuN group could be detected. In all three complexes one *tert*-butyl group is turned in the direction of the N_3 face, away from the heteroaromatic group, so one nitrogen atom is blocked from conceivable metal coordination. The methyl group of the heteroaromatic ring in **1** points towards the chelated lithium atom while the sulfur and selenium atoms in the heterocycles of **2** and **3** point towards the pendant *t*BuN group. The negative charge is distributed over both nitrogen atoms of the chelating SN_2 unit, as indicated by the almost ideal planar arrangement of the C1−N1−S1−N2−C5−Li1 moiety (mean deviation from best plane only 4.6 pm for **1**, 8.31 pm for **2** and 8.45 pm for **3**) and the S−N bond lengths, half-way between an S−N single and an S−N double bond [**1**: av. 158.5(6) pm; **2**: av. 157.7(4) pm; **3**: av. 157.91(30) pm]. The nitrogen atoms of the pendant *t*BuN group show significantly shorter S−N distances [**1**: 153.6(3) pm; **2**: 154.3(2) pm; **3**: 154.72(14) pm]. They are similar to the S=N double bonds in $S(NtBu)_2$ (153.2 pm),[21] but notably longer than in $S(NtBu)_3$ (151.5 pm).[14] In general, the S−N bond lengths in **1**, **2** and **3** match the standard range for S^{VI}−N

 © 2003 Wiley-VCH Verlag GmbH & Co. KGaA, Weinheim

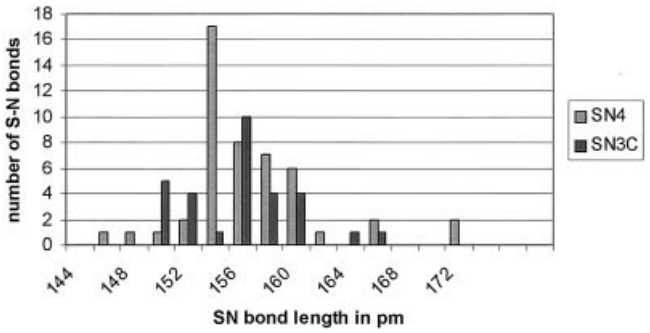

Scheme 2. $S^{VI}-N$ bond lengths from the CCDC (dark: SN_3C compounds; light: SN_4 compounds).

bond lengths found in the CCDC (Scheme 2).[22] The S−N bond lengths of non-coordinating nitrogen atoms are in the range of 150−156 pm, and the S−N bond lengths of coordinating nitrogen atoms are in the range of 156−168 pm. The S−C bond lengths of 179.6(3) pm in **1**, 179.2(3) pm in **2** and 179.29(19) pm in **3** are only marginally longer than a typical S−C(sp^2) single bond of 176 pm.[23] The Li−N bond lengths of about 200 pm match those normally observed in lithium amides.[24] The geometrical features of **1**, **2** and **3** (Table 1) reveal that the mean metric parameters of the $ArS(NtBu)_3^-$ anion (i.e. S−N and S−C-distances, N−S−N and S−N−C-angles, etc.) are almost independent of the nature of the aromatic system. In addition, the delocalisation in the heteroaromatic ring seems not to be perturbed by the metalated $S(NtBu)_3$ moiety.

In all known metal complexes the alkyltriimidosulfonate chelates as a bidentate ligand,[18] although tripodal coordination occurs with the triimidosulfite[13,15] and the oxotriimidosulfate $OS(NtBu)_3^{2-}$.[15] In these dianions, tripodal coordination is facilitated by all the *tert*-butyl groups pointing towards the sulfur atom, leaving the lone pairs of the nitrogen atoms pointing in the opposite direction. A comparison with the tripodal $OS(NtBu)_3^{2-}$ dianion proves that tripodal coordination is primarily caused by the higher negative charge than by steric or electronic effects:[18] for a single negative charge in the triimidosulfonates it is sufficient to be distributed over two nitrogen atoms rather than over all three. To stabilise a double negative charge in the triimidosulfite and the oxotriimidosulfate three S-bound nitrogen atoms are required.

[Li{(N*t*Bu)$_3$S(C$_4$H$_3$S)S{(N*t*Bu)$_3$}Li] Complexes

Thiophene was lithiated twice with BuLi and subsequently reacted with two equivalents of sulfur triimide. Despite the anticipated steric strain in the disubstituted product the reaction works under mild conditions. The non-optimised yields for both complexes were about 65%. Dependant on the donating solvent used in the reaction, two different complexes $[(THF)_4Li_2\{(tBuN)_3S(SC_4H_2)S(NtBu)_3\}]$ (**4a**), and $[(tmeda)_2Li_2\{(tBuN)_3S(SC_4H_2)S(NtBu)_3\}]$, (**4b**) could be obtained (Scheme 3).

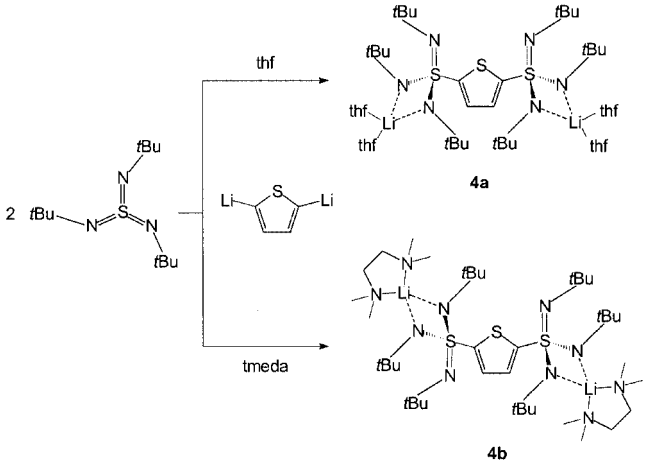

Scheme 3. Preparation of $[(THF)_4Li_2\{(tBuN)_3S(SC_4H_2)S(NtBu)_3\}]$ (**4a**), and $[(tmeda)_2Li_2\{(tBuN)_3S(SC_4H_2)S(NtBu)_3\}]$ (**4b**)

Table 1. Selected bond lengths [pm] and angles [°] of **1**−**3**

	1 R = *N*-methylpyrrolyl	**2** R = thiophenyl	**3** R = selenophenyl
S1−C13	179.6(3)	179.2(3)	179.29(19)
C13−C14	137.4(5)	140.2(4)	138.5(3)
C14−C15	142.0(6)	143.5(4)	142.4(3)
C15−C16	135.6(6)	134.8(5)	134.2(3)
C16−E	137.0(5) (E = N4)	170.0(4) (E = S2)	186.5(2) (E = Se1)
E−C13	138.5(5) (E = N4)	171.1(3) (E = S2)	186.11(17) (E = Se1)
S1−N1	158.4(3)	157.8(2)	157.94(15)
S1−N2	158.5(3)	157.6(2)	157.88(15)
S1−N3	153.6(3)	154.3(2)	154.72(14)
Li−N1	201.9(7)	198.9(5)	198.5(3)
Li−N2	196.9(6)	201.3(5)	201.6(3)
N1−S1−N2	96.52(15)	97.85(9)	97.63(8)
N2−S1−N3	122.03(6)	122.46(11)	122.14(8)
N1−S1−N3	123.79(17)	121.77(12)	121.71(8)
C13−S1−N1	109.24(15)	109.34(12)	109.54(8)
C13−S1−N2	108.97(16)	108.97(12)	109.61(8)
C13−S1−N3	95.85(16)	96.04(12)	95.99(8)
N1−Li−N2	72.7(2)	72.91(16)	72.88(12)

 © 2003 Wiley-VCH Verlag GmbH & Co. KGaA, Weinheim

Crystal Structures of 4a and 4b

Each central thiophenyl ring is 2,5-disubstituted by a triimidosulfite group coordinated to a single lithium atom. Like in the complexes **1**−**3** only two nitrogen atoms of each (tBuN)$_3$S moiety chelate the metal while the third tBuN group acts as a pendant spectator. The preferred tetragonal coordination of each lithium cation is completed by two THF molecules (**4a**) or one tmeda molecule (**4b**; Figure 2).

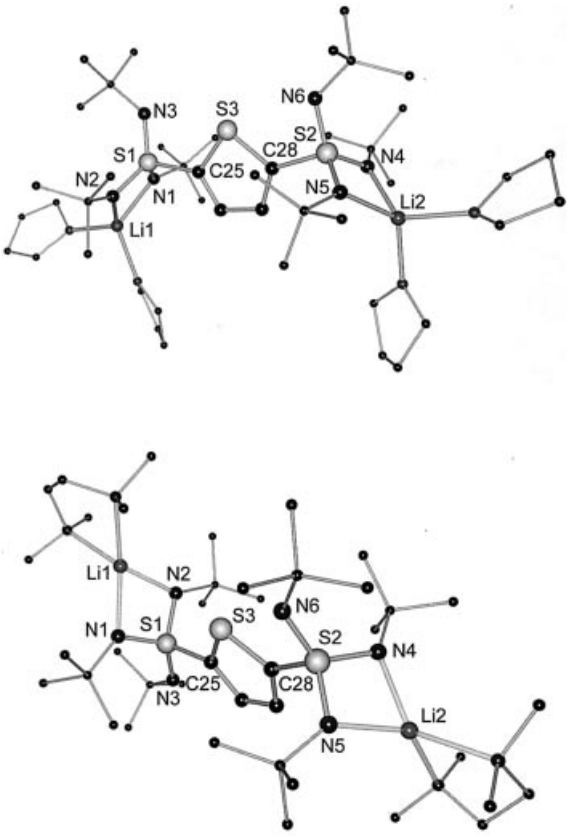

Figure 2. Solid-state structures of [(THF)$_4$Li$_2${(tBuN)$_3$S(SC$_4$H$_2$)S(NtBu)$_3$}] (**4a**; top), and [(tmeda)$_2$Li$_2${(tBuN)$_3$S(SC$_4$H$_2$)S(NtBu)$_3$}] (**4b**; bottom); selected bond lengths [pm] and angles [°] are compiled in Table 2

Although **4a** and **4b** are isostructural they differ in the arrangement of the NtBu groups. In **4a** the uncoordinated NtBu groups are pointing exactly in the same direction toward the thiophene ring sulfur atom S3, while in **4b** they are located opposite to each other like the lithium atoms. The S1−N3 and the S2−N6 bonds of both molecules are in the same plane as the thiophene ring. In addition, the N1−S1−N2 and the N4−S2−N5 bisectors are almost coplanar with the thiophene plane.

The negative charge in the (tBuN)$_3$S sulfonate unit is distributed over both nitrogen atoms of the chelating N−S−N unit [(S−N(av.): **4a** 157.2(5); **4b** 156.7(3) pm], and therefore the S−N bonds are equal to those in the monosubstituted aryltriimidosulfonates **1**−**3**. The S−N bonds of the pendant NtBu group are much shorter than the other S−N bonds [S−N(av.): **4a** 151.4(3); **4b** 153.8(5) pm]. Most remarkably, the S1−N3 bond in **4b** of 149.4(3) pm is the shortest S−N bond ever observed in SN$_3$C moieties (see Scheme 2), possibly due to hyperconjugation[25] to the SC$_4$ thiophenyl perimeter, as it is the only one in-plane and next to a C=C bond in the C$_4$S perimeter. Donation of the electron density via p(N3) → σ*(C25) in the S(NR)$_3^-$ moiety (anionic or negative hyperconjugation[25d]) would result in shortening of the S1−N3 bond and an elongation of the S1−C25 bond. The latter, however, could not be confirmed experimentally. Clearly NBO and NRT analysis are required to elucidate that problem. In [(THF)Li$_2${O$_2$S(NtBu)$_2$}]$_8$·2LiOH·2LiCl [av. S−N: 155.0(4) pm] and [{(THF)Li}$_2${O$_2$S(NtBu)$_2$]·(THF)LiCl}$_2$ [av. S−N: 155.7(2) pm] the S−N bonds are about 6 pm longer.[26] The S−C$_{ipso}$ distances in **4a** and **4b** of 180.1(5) and 178.8(4) pm, respectively, are considerably longer than the S−C bond in [(tmeda)$_2$Li$_2${(CH$_2$)S(NtBu)$_3$}] of 172.5(2) pm (see also Table 2).[11]

Table 2. Selected bond lengths [pm] and angles [°] of [(THF)$_4$Li$_2${(tBuN)$_3$S(SC$_4$H$_2$)S(NtBu)$_3$}] (**4a**), and [(tmeda)$_2$-Li$_2${(tBuN)$_3$S(SC$_4$H$_2$)S(NtBu)$_3$}] (**4b**)

	4a	**4b**
S1−N1	157.4(5)	156.5(3)
S1−N2	157.0(5)	156.9(3)
S1−N3	153.3(5)	149.4(3)
S3−N4	156.9(5)	156.9(3)
S3−N5	157.1(5)	156.3(3)
S3−N6	154.4(5)	153.4(3)
S1−C25	180.1(5)	178.8(4)
C25−C26	134.3(8)	136.7(5)
C26−C27	139.2(8)	141.4(5)
C27−C28	135.5(8)	135.4(5)
S3−C28	173.4(6)	170.3(4)
S3−C25	172.4(6)	171.9(4)
S2−C28	178.7(6)	178.2(4)
Li1−N1	197.7(11)	198.6(7)
Li1−N2	196.2(11)	196.6(8)
Li2−N4	198.5(11)	198.4(7)
Li2−N5	196.3(12)	198.7(8)
N1−S1−N2	97.0(2)	98.02(17)
N2−S1−N3	122.7(3)	122.64(19)
N1−S1−N3	122.6(3)	122.42(19)
N4−S3−N5	97.9(3)	97.91(17)
N5−S3−N6	121.1(3)	123.16(17)
N4−S3−N6	121.6(3)	121.97(17)

Conclusions from the Structural Comparisons

Comparison of the structures of **1**, **2** and **3** reveals that the geometrical features of the ES(NtBu)$_3^-$ unit (e.g. S−N distances, N−S−N and N−S−C angles) are almost independent of the nature of the heteroaromatic substituent and vice versa. The S or Se atom in the heteroaromatic ring is not involved in lithium coordination. Linkage of two sulfonate units via an S-heteroaromatic ring is possible, but conjugation of the S−N bonds to the SC$_4$ perimeter seems unlikely as the S−C and C−C bonds match the range of the related bond lengths in the parent thiophene. The negative charge in each sulfonate unit is distributed over both

 © 2003 Wiley-VCH Verlag GmbH & Co. KGaA, Weinheim

nitrogen atoms of the chelating N−S−N unit; the third N*t*Bu group remains non-coordinating. Tripodal metal coordination of the SN_3 unit is necessary for a double negative charge in the $S(NR)_3^{2-}$ triimidosulfite and the oxotriimidosulfate $OS(NR)_3^{2-}$, whereas for a single negative charge in $RS(NR)_3^-$ *N*,*N*-chelation seems to be sufficient.

Experimental Section

All manipulations were performed under inert-gas atmosphere of dry N_2 with Schlenk techniques or in an argon glove box. All solvents were dried over Na/K alloy and distilled prior to use. NMR spectroscopic data were obtained on either a Bruker AMX 400 or a Bruker AMX 300 instrument in the FT mode in C_6D_6 solvent. Elemental analyses were performed by the Microanalytisches Labor der Universität Würzburg. $S(NtBu)_3$ was obtained as described previously in ref. 15.

[(THF)$_2$Li{(H$_3$CNC$_4$H$_3$)S(N*t*Bu)$_3$}] (1): A solution of butyllithium in hexane (1.6 M, 2.44 mmol, 1.52 mL) was added dropwise to a solution of *N*-methylpyrrole (2.44 mmol, 0.2 g) in 3.5 mL THF at −78 °C. The reaction mixture was allowed to warm to room temperature and finally refluxed gently for 30 min. *N*,*N*′,*N*′′-Tris(*tert*-butyl)sulfur triimide (2.44 mmol, 0.6 g) was added to the solution and stirred for 12 h. All volatile material was removed under vacuum and the residue was dissolved in 3 mL of hexane and 1 mL of THF. Crystallisation at −36 °C gave colourless crystals. Yield: 0.76 g (65%). ^{1}H NMR (400 MHz, C_6D_6): δ = 1.31 [q, 4 H, (CH_2CH$_2$)$_2$O], 1.44 [s, 18 H, C(CH_3)$_3$], 1.50 [s, 9 H, C(CH_3)$_3$], 3.47 [t, 4 H, (CH$_2$CH_2)$_2$O], 3.52 (s, 3 H, NCH_3), 6.02 (t, 1 H, H2), 6.19 (t, 1 H, H4), 6.83 (q, 1 H, H3) ppm. ^{7}Li (155 MHz, C_6D_6): δ = 0.87 ppm. ^{13}C NMR (100 MHz, C_6D_6): δ = 25.48 [(*C*H$_2$CH$_2$O)$_2$], 30.57 [C(*C*H$_3$)$_3$], 33.11 [C(*C*H$_3$)$_3$], 37.05 (N-*C*H$_3$), 53.83 [*C*(CH$_3$)$_3$], 54.82 [*C*(CH$_3$)$_3$], 68.23 [(CH$_2$*C*H$_2$O)$_2$], 105.76 (C3), 114.91 (C4), 126.00 (C2), 128.28 (C1) ppm. $C_{25}H_{49}LiN_4O_2S$ (476.37): calcd. C 62.99, H 10.36, N 11.75, S 6.73; found C 60.69, H 9.6, N 12.77, S 7.12. Mp.: 60 °C.

[(tmeda)Li{(SC$_4$H$_3$)S(N*t*Bu)$_3$}] (2): Thiophene (5 mmol, 0.42 g) was added slowly to a mixture of tmeda (5 mmol, 0.58 g), 2 mL of diethyl ether and butyllithium in hexane (1.6 M, 5 mmol, 3.125 mL) and stirred for 30 min. A solution of *N*,*N*′,*N*′′-tris(*tert*-butyl)sulfur triimide (4.5 mmol, 1.1 g) in 2 mL of hexane was added to the solution and stirred for 12 h. After the small amount of precipitate was filtered off, 5 mL of hexane and 1.5 mL of THF were added. The solution was stored at +6 °C and after 1 day colourless crystals were obtained. Yield: 1.60 g (70%). ^{1}H NMR (400 MHz, C_6D_6): δ = 1.42 [s, 18 H, C(CH_3)$_3$], 1.74 [s, 9 H, C(CH_3)$_3$], 1.82 (s_{br}, 4 H, Me$_2$NCH_2CH_2NMe$_2$), 1.99 (s, 12 H, *Me*$_2$NCH$_2$CH$_2$N*Me*$_2$), 6.80, 6.95, 7.26 (C$_4$*H*$_3$S) ppm. ^{7}Li (155 MHz, C_6D_6): δ = 0.64 (s) ppm. ^{13}C NMR (100 MHz, C_6D_6): δ = 33.02 [C(*C*H$_3$)$_3$], 33.83 [C(*C*H$_3$)$_3$], 46.72 (*Me*$_2$NCH$_2$CH$_2$N*Me*$_2$), 51.82 [*C*(CH$_3$)$_3$], 56.80 (Me$_2$N*C*H$_2$*C*H$_2$NMe$_2$) ppm. $C_{22}H_{46}LiN_5S_2$ (451.34): calcd. C 58.50, H 10.26, N 15.50, S 14.20; found C 55.63, H 9.45, N 14.11, S 13.01. Mp.: 141 °C.

[(tmeda)Li{(SeC$_4$H$_3$)S(N*t*Bu)$_3$}] (3): A solution of selenophene (3.8 mmol, 0.5 g) in 4.77 mL of hexane was added dropwise to a solution of tmeda (3.8 mmol, 0.45 g) and butyllithium in hexane (1.6 M, 3.8 mmol, 2.4 mL) at −78 °C. The reaction mixture was allowed to warm to room temperature and stirred for 1 h. *N*,*N*′,*N*′′-Tris(*tert*-butyl)sulfur triimide (3.8 mmol, 0.94 g) in 1 mL hexane was added at 0 °C. After 12 h stirring at room temperature, the small amount of precipitate was filtered off. Crystallisation from the resulting solution at +6 °C yielded colourless crystals after 1 day. M = g/mol. (yield 1.74 g, 91%). ^{1}H NMR (400 MHz, C_6D_6): δ = 1.45 [s, 18 H, C(CH_3)$_3$], 1.72 (s_{br}, 4 H, Me$_2$NCH_2CH_2NMe$_2$), 1.80 [s, 9 H, C(CH_3)$_3$], 1.97 (s, 12 H, *Me*$_2$NCH$_2$CH$_2$N*Me*$_2$), 7.15 (s_{br}, 1 H, H2), 7.34 (s_{br}, 1 H, H4), 7.66 (dd, 1 H, H3) ppm. ^{7}Li NMR (155.5 MHz, ext. sat. LiCl solution): δ = 0.62 (s) ppm. ^{13}C NMR (100 MHz, C_6D_6): δ = 33.69 [C(*C*H$_3$)$_3$], 33.98 [C(*C*H$_3$)$_3$], 46.71 (*Me*$_2$NCH$_2$CH$_2$N*Me*$_2$), 51.82 [*C*(CH$_3$)$_3$], 53.17 [*C*(CH$_3$)$_3$], 56.75 (Me$_2$N*C*H$_2$*C*H$_2$NMe$_2$), 127.87, 128.11, 128.35, 129.06 (*C*$_4$H$_3$Se) ppm. $C_{22}H_{46}LiN_5SSe$ (499.30): calcd. C 53.00, H 9.30, N 14.05, S 6.43; found C 49.21, H 8.57, N 13.62, S 6.01. Mp.: 134 °C (dec).

[(THF)$_4$Li$_2${(*t*BuN)$_3$S(SC$_4$H$_2$)S(N*t*Bu)$_3$}] (4a): Thiophene (2.08 mmol, 0.18 g) was added slowly to a mixture of tmeda (4.15 mmol, 0.48 g), 2 mL of diethyl ether and butyllithium in hexane (1.6 M, 4.15 mmol, 2.60 mL) and stirred for 30 min. A solution of *N*,*N*′,*N*′′-tris(*tert*-butyl)sulfur triimide (4.15 mmol, 1.0 g) in 1 mL of hexane was added to the solution and stirred for 3 days. The suspension was dissolved by addition of 4 mL of THF and 1 day storage at +6 °C yielded yellow crystals. M = 875.28 g/mol. (yield 1.43 g, 84%). All spectroscopic and analytical data are virtually identical to those of the tmeda derivative **4b**.

[(tmeda)$_2$Li$_2${(*t*BuN)$_3$S(SC$_4$H$_2$)S(N*t*Bu)$_3$}] (4b): Thiophene (2.08 mmol, 0.18 g) was added slowly to a mixture of tmeda (4.15 mmol, 0.48 g), 2 mL of diethyl ether and butyllithium in hexane (1.6 M, 4.15 mmol, 2.60 mL) and stirred for 30 min. A solution of *N*,*N*′,*N*′′-tris(*tert*-butyl)sulfur triimide (4.15 mmol, 1.0 g) in 1 mL of hexane was added to the solution and stirred for 3 days. The white precipitate was filtered off. The clear reaction mixture was stored at +6 °C and after 1 day light-yellow crystals could be obtained. M = g/mol. (yield 1.46 g, 86%). ^{1}H NMR (400.13 MHz, C_6D_6): δ = 1.55 [s, 18 H, C(CH_3)$_3$], 1.77 (s, 4 H, Me$_2$NCH_2CH_2NMe$_2$), 1.83 [s, 9 H, C(CH_3)$_3$], 2.07 (s, 12 H, *Me*$_2$NCH$_2$CH$_2$N*Me*$_2$), 6.95, 7.34 (2s, 2 H, C$_4$*H*$_2$S) ppm. ^{7}Li NMR (155.5 MHz, ext. sat. LiCl solution): δ = 0.70 (s) ppm. ^{13}C NMR (100 MHz, C_6D_6): δ = 33.10 and 33.92 [C(*C*H$_3$)$_3$], 46.58 (*Me*$_2$NCH$_2$CH$_2$N*Me*$_2$), 51.91 [*C*(CH$_3$)$_3$], 53.58 [*C*(CH$_3$)$_3$], 55.03 (Me$_2$N*C*H$_2$*C*H$_2$NMe$_2$), 130.27, 130.69, 133.16, 148.89 (*C*$_4$H$_2$S). $C_{40}H_{88}Li_2N_{10}S_3$ (819.26): calcd. C 58.64, H 10.83, N 17.10, S 11.74; found C 55.33, H 10.42, N 15.54, S 10.98. Mp.: 152 °C (dec).

Crystal Structure Determinations: Crystal data for the structures **1**−**4b** are presented in Table 3. Data for structures were collected on a Bruker Apex CCD diffractometer at low temperature using oil-coated shock-cooled crystals[27] and Mo-K_α radiation (λ = 0.71073 Å). The structures were solved by direct methods using SHELXS 97.[28] The structures were refined by full-matrix least-squares procedures on F^2, using SHELXL 97.[29] All non-hydrogen atoms were refined anisotropically, and a riding model was employed in the refinement of the hydrogen atom positions. Data were corrected for absorption using SADABS2.[30] In complex **2** one disordered tmeda molecule (C20−C22) was refined to a split site occupancy factor of 0.51/0.49. In complex **4a** the disordered THF molecule (O4−C44) was refined to a split site occupancy factor of 0.51/0.32/0.17, and the *tert*-butyl groups to 0.51/0.49 (C2−C4), 0.67/0.33 (C14−C16) and 0.78/0.22 (C22−C24), respectively. In complex **4b** the disordered tmeda molecule (C32−C34) was refined to a split site occupancy factor of 0.67/0.33, and the *tert*-butyl groups to 0.85/0.15 (C5−C8) and 0.69/0.31 (C13−C16), respectively. In all these refinements bond length and similarity restraints were applied.

 © 2003 Wiley-VCH Verlag GmbH & Co. KGaA, Weinheim

Table 3. Crystal data and structure refinement for complexes **1**−**4** at T = 173(2) K

	1	**2**	**3**	**4a**	**4b**
Empirical formula	$C_{25}H_{49}LiN_4O_2S$	$C_{22}H_{46}LiN_5S_2$	$C_{22}H_{46}LiN_5SSe$	$C_{44}H_{88}Li_2N_6O_4S_3$	$C_{40}H_{88}Li_2N_{10}S_3$
M	476.37	451.70	498.60	875.26	819.26
Space group	$P2_1/n$	$P2_1/n$	$P2_1/n$	$P2_1/c$	$P2_1/c$
a [pm]	1012.92(9)	995.32(8)	9970.1(9)	1092.68(8)	1060.86(10)
b [pm]	1601.06(14)	1591.64(13)	1606.39(15)	1769.00(14)	1787.60(16)
c [pm]	1796.99(16)	1779.67(14)	1773.06(17)	2755.8(2)	2727.6(3)
β [°]	91.5070(10)	91.5970(10)	92.610(2)	94.869(2)	92.533(2)
V [nm^3], Z	2.9133(4), 4	2.8182(4), 4	2.8368(5), 4	5.3076(7), 4	5.1676(8), 4
D_c [Mg·m^{-3}]	1.087	1.065	1.167	1.095	1.053
μ [mm^{-1}]	0.137	0.205	1.413	0.182	0.179
θ range [°]	1.70 to 25.07	1.72 to 25.03	1.71 to 26.40	1.37 to 23.82	1.36 to 23.26
Data/restraints/parameter	5128/0/308	4973/126/323	5796/0/284	8147/712/736	7400/396/641
$R1$[a] [$I > 2\sigma(I)$]	0.0901	0.0627	0.0336	0.1225	0.0540
$wR2$[b] (all data)	0.1796	0.1468	0.0930	0.2619	0.1171
Largest diff. peak and hole [e nm^{-3}]	418, −301	365, −327	427, −266	670, −500	288, −175
CCDC no	208432	208429	208430	208431	208428

[a] $R1 = \Sigma||F_o| - |F_c||/\Sigma|F_o|$. [b] $wR2 = [\Sigma w(F_o^2 - F_c^2)^2/\Sigma w(F_o^2)^2]^{1/2}$ with $w = 1/[\sigma^2(F_o^2) + (g_1P)^2 + g_2P$ and $P = (F_o^2 + 2F_c^2)/3$.

CCDC-208432, -208429, -208430, -208431 and -208428 (see also Table 3) contain the supplementary crystallographic data for this paper. These data can be obtained free of charge at www.ccdc.cam.ac.uk/conts/retrieving.html [or from the Cambridge Crystallographic Data Centre, 12, Union Road, Cambridge CB2 1EZ, UK; Fax: (internat.) +44-1223/336-033; E-mail: deposit@ccdc.cam.ac.uk].

Acknowledgments

The financial support of the Deutsche Forschungsgemeinschaft, the Fonds der Chemischen Industrie, BRUKER Nonius, Karlsruhe, and CHEMETALL, Frankfurt/Main, is kindly acknowledged.

[1] J. M. J. Williams, C. Bubert, S. M. Brown, A. J. Blacker, Avecia Ltd., UK, Internat. Patent, WO 0244111 A1 **2002**.
[2] K. T. Holman, S. M. Martin, D. P. Parker, M. D. Ward, *J. Am. Chem. Soc.* **2001**, *123*, 4421.
[3] B. J. Banks, M. R. G. Leeming, A. B. Penrose, N. D. A. Walshe, Pfizer Ltd., UK, European Patent, EP 42731 A1 **1981**.
[4] S. L. Graham, T. H. Scholz, *J. Org. Chem.* **1991**, *56*, 4260.
[5] Reviews: [5a] M. A. Beswick, D. S. Wright, *Coord. Chem. Rev.* **1998**, *176*, 373. [5b] R. Fleischer, D. Stalke, *Coord. Chem. Rev.* **1998**, *176*, 431. [5c] D. Stalke, *Proc. Indian Acad. Sci.* **2000**, *112*, 155. [5d] T. Chivers, J. K. Brask, *Angew. Chem.* **2001**, *113*, 4082; *Angew. Chem. Int. Ed.* **2001**, *40*, 3988. [5e] G. M. Aspinall, M. C. Copsey, A. P. Leedham, C. A. Russell, *Coord. Chem. Rev.* **2002**, *227*, 217.
[6] $ArP(NR)_2^{2-}$: [6a] B. Eichhorn, H. Nöth, T. Seifert, *Eur. J. Inorg. Chem.* **1999**, 2355. $ArS(NR)_2^-$: [6b] J. Kuyper, K. Vrieze, *J. Chem. Soc., Chem. Commun.* **1976**, 64. [6c] F. T. Edelmann, F. Knösel, F. Pauer, D. Stalke, W. Bauer, *J. Organomet. Chem.* **1992**, *438*, 1. $ArSi(NR)_3^{3-}$: [6d] D. J. Brauer, H. Bürger, G. R. Liewald, *J. Organomet. Chem.* **1986**, *308*, 119. $ArP(NR)_3^{2-}$: [6e] V. D. Romanenko, V. F. Shul'gin, V. V. Skopenko, L. N. Markovskii, *Zh. Obshch. Khim.* **1985**, *55*, 538. $ArAs(NR)_2^{2-}$: [6f] D. B. Sowerby, J. R. Tillott, *J. Chem. Soc., Dalton Trans.* **1977**, 455. [6g] B. W. Ross, W. B. Marzi, *Chem. Ber.* **1975**, *108*, 1518. [6h] G. G. Briand, T. Chivers, M. Parvez, *J. Chem. Soc., Dalton Trans.* **2002**, 3785. [6i] G. G. Briand, T. Chivers, M. Parvez, *Can. J. Chem.* **2003**, *81* 169.
[7] [7a] D. Hänssgen, R. Steffens, *J. Organomet. Chem.* **1982**, *236*, 53. [7b] D. Hänssgen, R. Steffens, *Z. Naturforsch., Teil B* **1985**, *40*, 919. [7c] D. Hänssgen, R. Plum, *Chem. Ber.* **1987**, *120*, 1063.
[8] [8a] F. Pauer, D. Stalke, *J. Organomet. Chem.* **1991**, *416*, 127. [8b] F. Pauer, J. Rocha, D. Stalke, *J. Chem. Soc., Chem. Commun.* **1991**, 1477. [8c] F. T. Edelmann, F. Knösel, F. Pauer, D. Stalke, W. Bauer, *J. Organomet. Chem.* **1992**, *438*, 1. [8d] S. Freitag, W. Kolodziejski, F. Pauer, D. Stalke, *J. Chem. Soc., Dalton Trans.* **1993**, 3779. [8e] R. Fleischer, D. Stalke, *J. Organomet. Chem.* **1998**, *550*, 173.
[9] R. Fleischer, B. Walfort, A. Gburek, P. Scholz, W. Kiefer, D. Stalke, *Chem. Eur. J.* **1998**, *4*, 2266.
[10] [10a] D. Hänssgen, H. Hupfer, M. Nieger, M. Pfendtner, R. Steffens, *Z. Anorg. Allg. Chem.* **2001**, *627*, 17. [10b] B. Walfort, R. Bertermann, D. Stalke, *Chem. Eur. J.* **2001**, *7*, 1424. [10c] C. Selinka, D. Stalke, *Z. Naturforsch., Teil B* **2003**, *58*, 291.
[11] B. Walfort, D. Stalke, *Angew. Chem.* **2001**, *113*, 3965; *Angew. Chem. Int. Ed.* **2001**, *40*, 3846.
[12] [12a] R. C. Laughlin, *Chem. Ztg.* **1968**, *92*, 383. [12b] R. C. Laughlin, *J. Am. Chem. Soc.* **1968**, *90*, 2651. [12c] R. Appel, J. Kohnke, *Chem. Ber.* **1971**, *104*, 3875. [12d] D. Hänssgen, W. Roelle, *J. Organomet. Chem.* **1974**, *71*, 231.
[13] R. Mews, P. J. Watson, E. Lork, *Coord. Chem. Rev.* **1996**, *158*, 233.
[14] S. Pohl, B. Krebs, U. Seyer, G. Henkel, *Chem. Ber.* **1979**, *112*, 1751.
[15] R. Fleischer, S. Freitag, F. Pauer, D. Stalke, *Angew. Chem.* **1996**, *108*, 208; *Angew. Chem. Int. Ed. Engl.* **1996**, *35*, 204.
[16] R. Fleischer, S. Freitag, D. Stalke, *J. Chem. Soc., Dalton Trans.* **1998**, 193.
[17] R. Fleischer, D. Stalke, *Organometallics* **1998**, *17*, 832.
[18] B. Walfort, A. P. Leedham, C. A. Russell, D. Stalke, *Inorg. Chem.* **2001**, *40*, 5668.
[19] D. Leusser, PhD thesis, Universität Würzburg, **2002**.
[20] D. Leusser, B. Walfort, D. Stalke, *Angew. Chem.* **2002**, *114*, 2183; *Angew. Chem. Int. Ed.* **2002**, *41*, 2079.
[21] M. Herberhold, S. Gerstmann, W. Milius, B. Wrackmeyer, H. Borrmann, *Phosphorus, Sulfur, Silicon, Relat. Elem.* **1996**, *112*, 261.
[22] [22a] Cambridge Structural Database, May 2002. [22b]F. H. Allen, O. Kennard, *Chem. Des. Automat. News* **1993**, *8*, 131.
[23] P. Rademacher, in *Strukturen organischer Moleküle*, VCH, Weinheim, **1987**.
[24] [24a] K. Gregory, P. v. R. Schleyer, R. Snaith, *Adv. Inorg. Chem.* **1991**, *37*, 47. [24b] R. Snaith, D. S. Wright, in *Lithium Chemistry: A Theoretical and Experimental Overview*, Chap. 8 (Eds.: A.-M. Sapse, P. v. R. Schleyer), John Wiley & Sons, New York, **1994**.

 © 2003 Wiley-VCH Verlag GmbH & Co. KGaA, Weinheim

[25] [25a] W. Kutzelnigg, *Angew. Chem.* **1984**, *96*, 262; *Angew. Chem. Int. Ed. Engl.* **1984**, *23*, 272. [25b] A. E. Reed, F. Weinhold, *J. Am. Chem. Soc.* **1986**, *108*, 3586. [25c] D. A. Bors, A. Streitwieser, *J. Am. Chem. Soc.* **1986**, *108*, 1397. [25d] A. E. Reed, P. v. R. Schleyer, *J. Am. Chem. Soc.* **1990**, *112*, 1434. [25e] U. Salzner, P. v. R. Schleyer, *J. Am. Chem. Soc.* **1993**, *115*, 10231. [25f] T. Stefan, R. Janoschek, *J. Mol. Model.* **2000**, *6*, 282.
[26] J. K. Brask, T. Chivers, G. P. A. Yap, *Inorg. Chem.* **1999**, *38*, 5588.
[27] [27a] T. Kottke, D. Stalke, *J. Appl. Crystallogr.* **1993**, *26*, 615. [27b] T. Kottke, R. J. Lagow, D. Stalke, *J. Appl. Crystallogr.* **1996**, *29*, 465. [27c] D. Stalke, *Chem. Soc. Rev.* **1998**, *27*, 171.
[28] G. M. Sheldrick, *Acta Crystallogr., Sect. A* **1990**, *46*, 467.
[29] G. M. Sheldrick, SHELXL-97, *Program for Crystal Structure Refinement*, University of Göttingen, **1997**.
[30] SADABS2: G. M. Sheldrick, Universität Göttingen **2000**, *Program for empirical absorption correction*.

Received April 16, 2003

 © 2003 Wiley-VCH Verlag GmbH & Co. KGaA, Weinheim

A Homologous Series of Base-Free Organo(alkaline-earth) Metallocenes: Synthesis and Molecular Structures of [1,2,4-$(SiMe_3)_3C_5H_2]_2$(Ca, Sr, Ba)

Melanie J. Harvey,[a] Keith T. Quisenberry,[a] Timothy P. Hanusa,*[a] and Victor G. Young Jr.[b]

Dedicated to the memory of Professor Ronald Snaith

Keywords: Alkaline-earth metals / Metallocenes / Solid-state structures

Bis[1,2,4-tris(trimethylsilyl)cyclopentadienyl] complexes [1,2,4-$(SiMe_3)_3C_5H_2]_2$Ae [$(Cp^{3Si})_2$Ae; Ae = Ca (**1**), Sr (**2**), Ba (**3**)] are isolated from the 2:1 reaction of K[Cp^{3Si}] and AeI_2 in diethyl ether. Under the same reaction conditions used for the heavier metallocenes, the corresponding $(Cp^{3Si})_2$Be compound was not formed, although calculations suggest that the beryllocene would be sterically feasible. Compound **1** crystallizes as a bent monomer from hexanes (ring centroid–Ca–ring centroid = 166.7°) with two η^5-Cp^{3Si} ligands on the calcium atom [Ca–C(av) = 2.63(2) Å]. Metallocene **2**, the first crystallographically characterized example of an unsolvated strontocene, is also isolated as a bent monomer (159.4°) from hexanes with two η^5-Cp^{3Si} ligands on the strontium atom [Sr–C(av) = 2.819(2) Å]. Compound **3** crystallizes on sublimation as a coordination dimer in which each barium atom is flanked by two η^5-Cp^{3Si} rings [Ba–C(av) = 3.01(2) Å] and one methyl group from a neighboring Cp′ ring; the intermolecular Ba···C(methyl)′ distance is 3.275(6) Å. The amount of bending observed in **1**–**3** and other Group-2 metallocenes varies with the metals, the steric bulk of the cyclopentadienyl ligands, and crystal packing effects, and is not easily predictable.
(© Wiley-VCH Verlag GmbH & Co. KGaA, 69451 Weinheim, Germany, 2003)

Introduction

A characteristic feature of nearly all base-free metallocenes of the heavy alkaline-earth (Ca, Sr, Ba) and lanthanide (Sm, Eu, Yb) elements is a distinctly "bent" geometry, with ring centroid−metal−ring centroid angles as small as 131°.[1−8] The non-linear structures are found in both the solid state and the gas phase,[9,10] and their origin is not easily explained on steric or electrostatic grounds alone. One analysis of the bending phenomenon found that a strongly linear correlation existed between metal−ring distances and the ring−metal−ring bending angles in decamethylmetallocenes of the alkaline-earth, lanthanide, and p-block elements;[8] larger metals (with longer M−C distances) were associated with greater bending angles. The distance/bending correlation partially reflects the fact that decamethylmetallocenes with long metal−ring distances can bend proportionally farther back before encountering appreciable van der Waals resistance between the methyl groups (Figure 1).

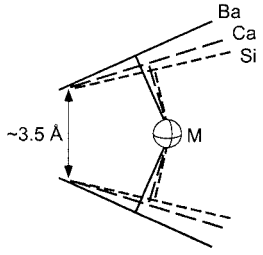

Figure 1. Origin of the strongly linear correlation between metal radius and bending angles in Cp^*_2M (M = Ae, Ln, Group 14) complexes; with longer M−C distances, greater bending is allowed before CH_3···CH_3′ repulsions on the "closed" side of the metallocene prevent further bending

With cyclopentadienyl rings less symmetrical than Cp*, the bending angle/metal radius relationship is less easily modeled. Although it can be expected that metallocenes with bulkier rings, i.e., [(*i*Pr)$_4C_5H]_2$(Ca, Ba), would be less bent than Cp_2M or Cp^*_2M complexes,[11] it is not simple to compare the relative bulkiness of cyclopentadienyl rings when both the number and sizes of the substituents are different. In addition, there are still many gaps within the series of structurally characterized metallocenes containing a particular cyclopentadienyl ligand; in fact, until this re-

[a] Department of Chemistry, Vanderbilt University, Nashville, TN 37235, U.S.A.
Fax: (internat.) + 1-615/343-1234
E-mail: t.hanusa@vanderbilt.edu
[b] X-ray Crystallographic Laboratory, Chemistry Department, University of Minnesota, Minneapolis, MN 55455, U.S.A.
Fax: (internat.) + 1-612/626-7541
E-mail: young@chemsun.chem.umn.edu

port, there were no published crystallographic data for any base-free strontocene.

We have been examining the properties of 1,2,4-tris(trimethylsilyl)cyclopentadiene (HCp^{3Si})[12,13] as a sterically bulky ligand in s-block metal chemistry.[14,15] In conjunction with the previously reported structure of the substituted magnesocene [1,2,4-$(SiMe_3)_3C_5H_2]_2Mg$ [$(Cp^{3Si})_2Mg$],[16] a homologous series of unsolvated Group-2 metallocenes from Mg to Ba has now been synthesized and crystallographically authenticated. Such data provide a means for testing the strength of the M−C bond length/ring bending relationship when the metal radius is varied by nearly a factor of two (for 6-coordination, $r_{Mg^{2+}}$ = 0.72 Å; $r_{Ba^{2+}}$ = 1.35 Å).[17]

Results and Discussion

The bis[tris(trimethylsilyl)cyclopentadienyl]alkaline-earth metallocenes, $(Cp^{3Si})_2Ae$ (Ae = Ca, Sr, Ba), can be isolated from the 2:1 reaction of $K[Cp^{3Si}]$ and AeI_2 in diethyl ether [Equation (1)].

$$2\ K[Cp^{3Si}] + AeI_2 \xrightarrow{Et_2O} (Cp^{3Si})_2Ae + 2\ KI\downarrow \quad (1)$$

Ae = Ca (**1**), Sr (**2**), Ba (**3**)

The metallocenes were characterized with spectroscopic methods and X-ray crystallography, which supported the proposed formulations. The complexes are thermally stable and begin to sublime at temperatures ranging from 125 to 140 °C at between 10^{-5} and 10^{-7} Torr. These complexes must be formed in diethyl ether, since in the presence of even small amounts of THF, the mono(ring) complexes $(Cp^{3Si})AeI(THF)_n$ are isolated as the exclusive products.[15] Once formed, however, the complexes can be recrystallized as base-free metallocenes from THF solution. The hexakis(trimethylsilyl)metallocenes visibly decompose upon exposure to air after only a few seconds, turning from white to dark brown. In contrast, enhanced air stability has been reported for both the octa- and decaisopropylated alkaline-earth metallocenes.[18,19]

The magnesium compound $(Cp^{3Si})_2Mg$ was reported some time ago by Jutzi and co-workers.[16] Of the remaining Group-2 elements, only the radium and beryllium analogues remain unknown. We attempted to synthesize $(Cp^{3Si})_2Be$ with methods similar to those used recently to prepare $(Me_4C_5H)_2Be$ and Cp^*_2Be;[20] viz., the reaction of $BeCl_2$ and $K[Cp^{3Si}]$ in diethyl ether (3 d at room temperature) or in a 1:1 diethyl ether/toluene mixture at reflux for 3 d. The reaction at room temperature yielded only starting materials; the refluxed reaction mixture produced a black residue from which no metallocene was isolated.

Solid State Structures

$(Cp^{3Si})_2Ca$ (1)

A crystal of **1** grown from hexanes was used to determine its structure with X-ray crystallography. A summary of bond lengths and angles for **1** is given in Table 1. An ORTEP is provided in Figure 2.

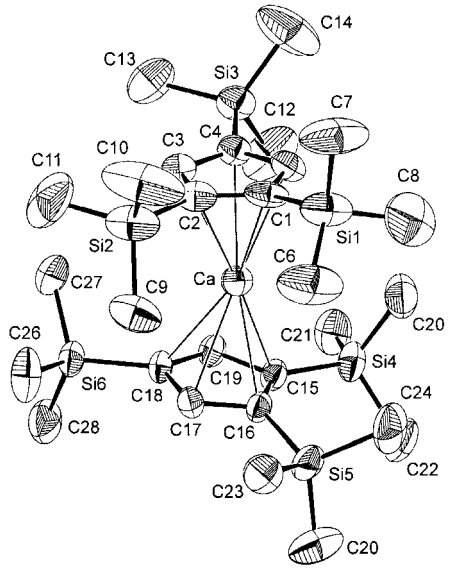

Figure 2. ORTEP of the non-hydrogen atoms of **1**; Ca−C bond lengths [A] to C1, C2, C3, C4, C5, C15, C16, C17, C18, and C19 are 2.619(7), 2.607(7), 2.618(6), 2.665(6), 2.631(6), 2.625(6), 2.618(6), 2.638(6), 2.650(6), and 2.612(6), respectively

The compound exists as a monomeric species with two nearly eclipsed (twist angle of 8°) η^5-Cp^{3Si} ligands framing a Ca core in a bent geometry. The average Ca−C distance

Table 1. Selected bond lengths [Å] and angles [°] for $(Cp^{3Si})_2Ae$ (Ae = Mg, Ca, Sr, Ba)

	Mg (a)[a]	Mg (b)	**1**	**2**	**3**
Ae−C(ring) (av)	2.37	2.37	2.63(2)	2.812(9)	3.01(2)
Ae−ring centroid (av)	2.03(1)	2.03(1)	2.35	2.54	2.75
Ring centroid−Ae−ring centroid	171.8(2)	170.4(2)	166.7	159.4	162.2
C−C(Cp ring) (av)	1.45(3)	1.44(5)	1.42(3)	1.42(1)	1.42(2)
C(ring)−Si (av)	1.88(2)	1.88(2)	1.86(2)	1.860(7)	1.87(1)
Closest inter-ring Me···Me′ contact	4.0	4.0	4.0	3.8	3.7
Twist angle between rings	1	5	8	18	2
Ref.	[16]	[16]	this work	this work	this work

[a] Two independent molecules (a and b) are found in the unit cell.

 © 2003 Wiley-VCH Verlag GmbH & Co. KGaA, Weinheim

in **1** is 2.63(2) Å. This distance is within experimental error of the average Ca−C length observed in the other structurally characterized base-free calcocenes, i.e., $(Cp^{4i})_2Ca$,[18] $(Cp^{3i})_2Ca$ {Cp^{ni} = $[(iPr)_nC_5H_{5-n}]$},[21] and Cp^*_2Ca[2] [2.64(1) Å, 2.62(2) Å, and 2.64(2) Å, respectively]. Although the two complexes belong to structurally distinct classes of compounds, the Ca−centroid distance of 2.35 Å in **1** is indistinguishable from the analogous distance in $[(Cp^{3Si})Ca(\mu\text{-}I)(THF)]_2$, which also contains a formally six-coordinate calcium center.[15] The ring centroid−Ca−ring centroid angle of 166.7° is more linear than the analogous angles found in $(Cp^{4i})_2Ca$[18] and Cp^*_2Ca[2] (162.3° and 147.0°, respectively). There is no evidence for excessive steric crowding in the complex, however, as the closest intramolecular methyl···methyl′ contact is at 4.0 Å; this is equal to the sum of the van der Waals radii of two methyl groups.[22] In addition, the greatest silyl group displacement from the cyclopentadienyl ring plane is 8.3°, which is similar to the maximum displacement of 8.7° found in the relatively uncrowded $[(Cp^{3Si})Ca(\mu\text{-}I)(THF)]_2$.[15]

$(Cp^{3Si})_2Sr$ (2)

A crystal of **2** grown from hexanes was used to determine its structure with X-ray crystallography. A summary of bond lengths and angles for **2** is given in Table 1. An ORTEP is provided in Figure 3.

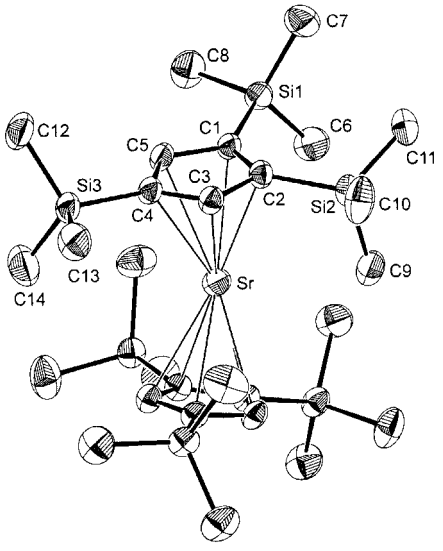

Figure 3. ORTEP of the non-hydrogen atoms of **2**; Sr−C bond lengths [Å] to C1, C2, C3, C4, and C5 are 2.811(4), 2.773(4), 2.784(4), 2.850(4), and 2.841(4), respectively

The compound exists as a monomer in which the strontium atom is coordinated by two partially staggered (twist angle of 18°) Cp^{3Si} rings. The strontium atom resides on a crystallographic C_2 axis, so that only half the molecule is unique. Although no other unsolvated strontocenes exist for direct comparison, useful structural parallels exist with divalent organolanthanide species, as Sm^{2+} and Eu^{2+} have six-coordinate radii (1.17 Å) that are almost identical to that of Sr^{2+} (1.18 Å).[17] The average Sr−C distance of 2.812(9) Å in **2** is similar to the analogous distances observed in Cp^*_2Sm and Cp^*_2Eu [Ln−C = 2.79(1) Å],[1] or $(Cp^{4i})_2Sm$ (Sm−C = 2.79 Å)[23] and $(Cp^{4i})_2Eu$ [Eu−C = 2.782(6) Å].[24] Giving consideration to the difference between the six- vs. seven-coordinate radii of Sr^{2+} (Δ = 0.03 Å), the Sr−ring centroid distance of 2.54 Å in **2** is also equivalent to the 2.57 Å distance found in $(Cp^{3i})_2Sr(THF)$.[25] The ring centroid−Sr−ring centroid angle of 159.4° represents a substantially more linear structure than is found in Cp^*_2Sm and Cp^*_2Eu (140.1° and 140.3°).[1] This is not unexpected, given the increase in steric bulk in going from Cp* to Cp^{3Si} ligands. Even so, the closest interring methyl···methyl contact is at 3.78 Å, which is 95% of the sum of the van der Waals radii of two methyl groups,[22] and as with compound **1**, **2** does not display any significant silyl group displacements from the cyclopentadienyl ring planes (maximum of 7.7°; cf. 8.7° in the dimer $[(Cp^{3Si})Sr(\mu\text{-}I)(THF)_2]_2$.[15]

$(Cp^{3Si})_2Ba$ (3)

A crystal of **3**, grown by sublimation, was used to determine its structure with X-ray crystallography. A summary of bond lengths and angles for **3** is given in Table 1. An ORTEP is provided in Figure 4.

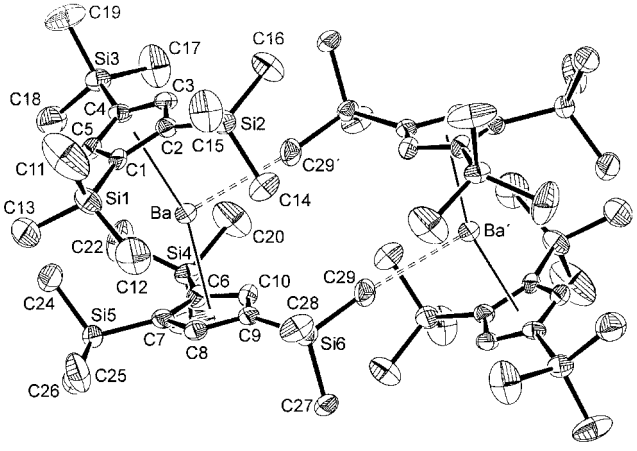

Figure 4. ORTEP of the non-hydrogen atoms of **3**, giving the numbering scheme used in the text; Ba−C bond lengths [Å] to C1, C2, C3, C4, C5, C6, C7, C8, C9, C10, and C29′ are 2.975(5), 2.977(5), 2.988(5), 3.044(5), 3.012(5), 2.981(5), 2.976(5), 3.007(5), 3.076(5), 3.036(5), and 3.275(6), respectively

Unlike the calcium and strontium analogues, **3** crystallizes as a coordination dimer in which each barium atom is surrounded by two nearly eclipsed η^5-1,2,4-tris(trimethylsilyl)cyclopentadienyl rings and one methyl group from a neighboring Cp^{3Si} ring. The average Ba−C(Cp′) distance in **3** of 3.01(2) Å and the Ba−ring centroid distance of 2.75 Å are longer than those observed in the formally six-coordinate $(Cp^{4i})_2Ba$ [2.94(2) Å and 2.68 Å, respectively].[18] The Ba−C distance is similar to that found in the sterically crowded metallocene $[(iPr)_5C_5]_2Ba$ [2.997(4) Å].[19] Based on the additional bridging interaction, however, **3** could be considered a formally seven-coordinate complex; consistent with this, the average Ba−C and Ba−ring centroid dis-

 © 2003 Wiley-VCH Verlag GmbH & Co. KGaA, Weinheim

tances are indistinguishable from those observed in the seven-coordinate $\{[(Cp^{3Si})BaI(THF)_2]\cdot C_7H_8\}_\infty$ [3.00(2) and 2.76(1), respectively].[18] The ring centroid−Ba−ring centroid angle of 162.2° in **3** is considerably wider than the angle in either $(Cp^{4i})_2Ba$ (154.2°)[18] or Cp^*_2Ba (131.0°).[2] In contrast, $(Cp^{5i})_2Ba$ is strictly linear with a ring centroid−Ba−ring centroid angle of 180°.[19]

The intermolecular contact between each barium metal center and a methyl group from an adjacent metallocene unit [Ba(1)−C(29′)] is at 3.275(6) Å, a shorter distance than the sum of the van der Waals radius of a methyl group and the ionic radius of seven-coordinate Ba^{2+} (= 3.4 Å). Similar interactions between cyclopentadienyl ring substituents and neighboring metallocenes have been observed in Group-2 and lanthanide metallocene structures. For example, in Cp^*_2Ba, there are two methyl groups with Ba···CH_3′ distances of 3.35 and 3.36 Å.[2] There is a related interaction observed in the polymeric structure of $[\{1,3\text{-}(SiMe_3)_2C_5H_3\}_2Yb]_\infty$,[26] i.e., a close contact is present between the metal and a methyl group of a neighboring metallocene unit at 2.872(7) Å (the radii of seven-coordinate Yb^{2+} and Ba^{2+} differ by 0.30 Å[17]). The europium derivative $[\{1,3\text{-}(SiMe_3)_2C_5H_3\}_2Eu]_\infty$ displays the same type of intermolecular metal···methyl contact at 3.091(6) Å;[26] the difference in Eu^{2+} and Ba^{2+} radii is 0.18 Å, so that the contact distances in the europium and barium structures are equivalent.[17]

The trimethylsilyl group with the bridging interaction in **3** (Si6) is displaced from the cyclopentadienyl ring plane by 0.33 Å (equivalent to 10.3°), which is only slightly more than the maximum displacements observed in **1** and **2**; the next largest displacement in **3** is at 0.26 Å (= 8.1°), involving Si3. The closest intramolecular methyl···methyl′ contact is found between the eclipsed trimethylsilyl groups containing Si2 and Si6 at 3.66 Å (C14···C28).

Relative Orientations of Tris(trimethylsilyl) Rings

The presence of three trimethylsilyl groups on a Cp^{3Si} ring allow for six distinct possible relative orientations of the two rings in a metallocene (with three eclipsed C_5 rings and three staggered rings).[27] Among those possibilities, three different orientations are observed in the $(Cp^{3Si})_2Ae$ series. The magnesium[16] and calcium complexes both adopt the same eclipsed configuration [Figure 5(a)] with twist angles of 1° [for Mg(a)], 5° [for Mg(b)] and 8° [for Ca (**1**)] (Table 1). The analogous germanium complex adopts the same arrangement of silyl groups in the solid state,[27] as does the ferrocene derivative $(Cp^{3Si})_2Fe$.[28] Calculations with $(Cp^{3Si})_2Ge$ demonstrated that this conformation lies in a steric energy minimum.[27] The two rings in $(Cp^{3i})_2Ca$ also adopt the same relative orientation;[21] this seems to be a favored arrangement for 1,2,4-substituted rings in complexes with metal radii ≤ 1.0 Å. The orientation probably reflects a balance between steric repulsions and van der Waals attractive forces in these complexes; with larger metals and greater separation of the rings, steric repulsions between substituents are less energetically costly, and more eclipsing of substituents is possible.

Figure 5. Orientation of the tris(trimethylsilyl)cyclopentadienyl rings in $(Cp^{3Si})_2Ae$ [Ae = Mg, Ca (**1**): (a); Sr (**2**): (b); Ba (**3**): (c)]

The rings in **2** crystallize in a staggered conformation [Figure 5(b)] with a twist angle of 18° between them (Table 1). In contrast, **3** adopts an orientation with two sets of eclipsed trimethylsilyl substituents [Figure 5(c)]; the cyclopentadienyl rings are in correspondingly close alignment (twist angle of 2°). The bending of the metallocene occurs so that the staggered substituents are on the "closed" side of the metallocene. The interaction of the barium metal center with the bridging methyl group takes place from the "open" side.

Degree of Bending in Cp'_2Ae Complexes

Despite the controversy that still surrounds the issue, the bending observed in many base-free main-group and lanthanide metallocenes is probably most readily understood through the use of various polarization models of bonding, although the participation of low-lying d-orbitals has also been proposed.[3,29−31] The amount of possible bending is limited by steric repulsions between the substituent groups, and therefore the bending angle changes not only with the metal radius and polarizability, but also with the bulk of the cyclopentadienyl ligands. Consequently, before the bending observed in metallocenes with differently substituted Cp′ rings can be compared in a meaningful way, possible ring orientations, the existence of coordination oligomers, and distortions from crystal packing all need to be taken into account.

The complexes reported here illustrate the difficulties involved in establishing such metal/bending correlations. For example, the bending angles (ring centroid−metal−ring centroid) of the four known $(Cp^{3Si})_2Ae$ compounds decrease as the metal radii increase from Mg to Sr [i.e., 171.1°, 166.7°, and 159.4° for $(Cp^{3Si})_2Mg$, $(Cp^{3Si})_2Ca$ and $(Cp^{3Si})_2Sr$, respectively] but then increase slightly for barium (162.2°). The break in the trend reflects the change from the mononuclear structures to the dimeric geometry of the barium compound, whose ring bending angle is evidently influenced by the bridging methyl group.

Comparisons of bending angles using metallocenes with only a single type of metal suffer from similar anomalies, although the difficulties may not always be apparent in small sets of compounds. For instance, the bending angles of calcocenes open from Cp^*_2Ca (147.0°) to $(Cp^{4i})_2Ca$ (162.3°) to $(Cp^{3Si})_2Ca$ (166.7°). The order is repeated with barocenes [i.e., Cp^*_2Ba (131°) < $(Cp^{4i})_2Ba$ (154°) < $(Cp^{3Si})_2Ba$ (162.2°)], even though Cp^*_2Ba exists as a coordination polymer and $(Cp^{3Si})_2Ba$ is a coordination dimer in the solid state. Based on the progression in bending angles,

 © 2003 Wiley-VCH Verlag GmbH & Co. KGaA, Weinheim

there might be a temptation to conclude that the Cp^{3Si} ring is effectively more bulky than Cp^{4i}. However, the structure of bis(1,2,4-triisopropylcyclopentadienyl)calcium, $(Cp^{3i})_2Ca$, despite having two fewer isopropyl groups than $(Cp^{4i})_2Ca$, has a wider bending angle (169.7°) than either $(Cp^{4i})_2Ca$ or $(Cp^{3Si})_2Ca$.[32] This counterexample demonstrates that the approach to linearity in the solid state is not solely a function of the number and size of ring substituents, but that packing effects may be involved as well. Great care is needed when proposing the existence of quantitative relationships between steric bulk and bending angles in such conformationally flexible molecules.

The Case of Bulky Beryllocenes

Almost all crystallographically characterized magnesocenes, including Cp_2Mg,[33] $[(t\mathrm{Bu})C_5H_4]_2Mg$,[34] $[(PhCH_3CH)C_5H_4]_2Mg$,[35] and $(Me_4C_5H)_2Mg$[36] have parallel rings. The slight tilting of the rings observed in $(Cp^{3Si})_2Mg$ (7.8°) has been ascribed to the large amount of steric encumbrance around the Mg^{2+} center generated by the two Cp^{3Si} rings.[16] The steric pressure on a beryllocene with Cp^{3Si} rings might be even greater, and could conceivably destabilize the complex through the operation of "steric oversaturation."[37] Although we were not successful in isolating a beryllocene containing two Cp^{3Si} rings, combination DFT/semiempirical (ONIOM) calculations were performed on several possible conformations of $(Cp^{3Si})_2Be$, including η^1/η^1, η^1/η^5, and η^5/η^5, to try to establish the steric feasibility of such a structure.

The η^1/η^1 geometry shown in Figure 6(a) was used as a starting geometry in optimization. The unsubstituted position on the rings was chosen as the site of ligation, both to minimize steric interactions between the rings and from the fact that in $(\eta^5\text{-}C_5Me_4H)(\eta^1\text{-}C_5Me_4H)Be$,[20] the beryllium atom is attached to the unsubstituted carbon atom in the η^1-bonded ring. Nevertheless, during optimization one ring rotated relative to the other, and the structure collapsed to an η^1/η^5 geometry [Figure 6(b)]. The beryllium atom is now attached to a carbon atom bearing a trimethylsilyl group; the Be−C(η^1) distance is 1.781 Å (cf. 1.827 Å in Cp_2Be[38]),

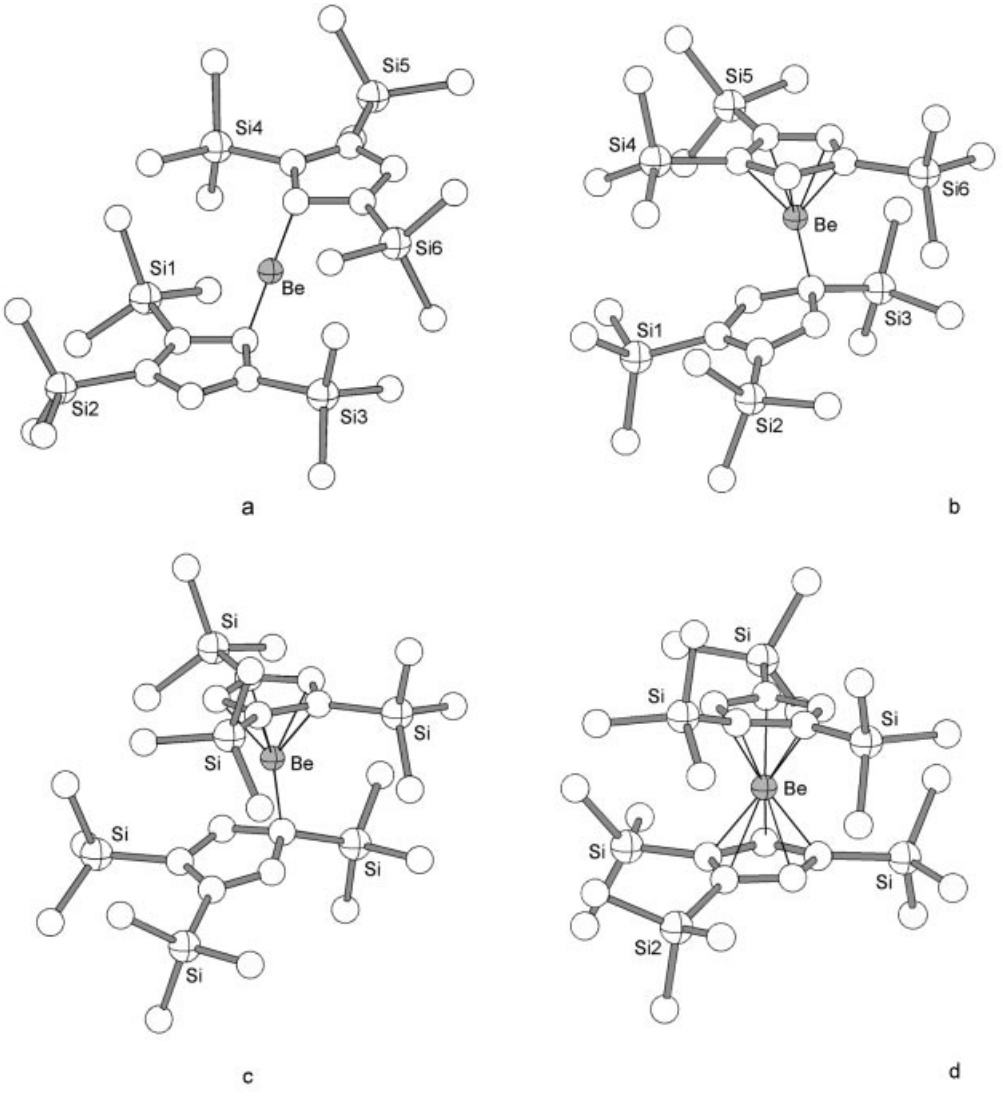

Figure 6. ONIOM-optimized geometries (H atoms omitted) for $(Cp^{3Si})_2Be$

 © 2003 Wiley-VCH Verlag GmbH & Co. KGaA, Weinheim

and Si3 is bent out of the C_5 plane by 1.03 Å (32.8°). Such a rearrangement can be rationalized on electronic grounds, as silicon atoms help stabilize negative charges on adjacent atoms; the bending distortion also serves to increase the negative charge on the carbon atom.[39] The Be−C(η^5) bonds are in the narrow range from 1.901 to 1.934 Å, and average 1.923 Å, nearly matching the average Be−C(η^5-Cp) bond length in the parent molecule (1.93 Å[38]). The structure is a local minimum on the potential energy surface (PES) (no imaginary frequencies), but a similar η^1/η^5 structure can be obtained that is formally related to the first by a ring rotation [Figure 6(c)]. The latter geometry is also a minimum on the PES, and has nearly identical geometric parameters [Be−C(η^1) = 1.780 Å; Be−C(η^5) = 1.921 Å (av)]. Structure (b) in Figure 6 is 1.9 kcal mol^{-1} higher in enthalpy ($\Delta H°$) than structure (c) a difference that is not meaningful at this level of theory. The height of the energy barrier that might separate the two forms, however, is not known.

The stability of an η^5/η^5 configuration was evaluated by starting from an eclipsed conformation similar to that in Figure 5(a). The sandwich geometry was retained during optimization [Figure 6(d)]; a frequency calculation indicated that it was a local minimum (N_{imag} = 0). The angle between the ring planes is 6.9°, and the metallocene is somewhat slipped, with Be−C bonds ranging from 2.04 to 2.14 Å; the latter distance is slightly longer than the maximum distance observed in Cp*$_2$Be (2.11 Å), which is already long compared to the Be−C bond length in the parent molecule.[38] Even so, there are no intermolecular methyl···methyl′ contacts closer than 3.64 Å; the closest analogous contact in Cp*$_2$Be is at 3.63 Å. The η^5/η^5 structure is 3.3 kcal mol^{-1} higher in enthalpy ($\Delta H°$) than structure (c) in Figure 6; the height of the energy barrier that separates the η^1/η^5 and η^5/η^5 forms is not known. In any case, the failure of the reactions designed to produce (Cp^{3Si})$_2$Be (like the initial attempts to form Cp*$_2$Be[40,41]) is probably best ascribed to kinetic difficulties, rather than to fundamental steric limitations on the geometry of the beryllocene.

Conclusion

The 1,2,4-tris(trimethylsilyl)cyclopentadienyl ligand has now been incorporated into unsolvated metallocenes containing metals from magnesium to barium. A balance between steric repulsions and van der Waals attractive forces evidently directs the relative ring orientations. A configuration with a single eclipsed substituent seems to be a favored arrangement in complexes with smaller metals ($r \leq 1.0$ Å); the larger metals adopt arrangements that may be influenced more by intermolecular interactions. With the exception of (Cp^{3Si})$_2$Mg, whose rings are non-parallel owing to high steric pressure within the complex, the other metallocenes are all bent less than their Cp, Cp* or Cp^{4i} counterparts, although the trends are not uniform for all combinations of metals and cyclopentadienyl rings. In addition, three trimethylsilyl substituents do not block access to the metal center as completely as do four isopropyl groups; **3** forms a coordination dimer, for example, whereas (Cp^{4i})$_2$Ba remains rigorously monomeric. Hence the bending angle of a metallocene, although reflecting the steric bulk of the cyclopentadienyl rings, is not a completely reliable indicator of the shielding of the metal center.

Experimental Section

General Remarks: All manipulations were performed with the rigorous exclusion of air and moisture using high vacuum, Schlenk, or drybox techniques. Anhydrous calcium, strontium or barium iodide (Strem Chemicals or Cerac, 95%) were heated under vacuum (150 °C, 10^{-6} Torr) to remove residual amounts of free iodine. K[1,2,4-(SiMe$_3$)$_3$C$_5$H$_2$] was prepared as described previously.[15] Solvents for reactions were distilled under nitrogen from sodium or potassium benzophenone ketyl. NMR solvents were vacuum-distilled from Na/K (22:78) alloy and stored over molecular sieves (4 Å). Proton (^{1}H) and carbon (^{13}C) NMR spectra were obtained with a Bruker NR-300 spectrometer at 300 and 75.5 MHz, respectively, and were referenced to the residual resonances of C_6D_6 (δ = 7.15 and 128.0 ppm) or [D_8]THF (δ = 3.58 and 67.4 ppm). Infrared data were measured with KBr pellets as described previously.[18] Elemental analyses were performed by Desert Analytical Laboratory, Tucson, AZ; the low carbon value found for **1** reflects a not uncommon problem with highly air-sensitive organo(alkaline-earth) compounds.[42]

Synthesis of [1,2,4-(SiMe$_3$)$_3$C$_5$H$_2$]$_2$Ca (1): CaI_2 (0.145 g, 0.49 mmol) and K[1,2,4-(SiMe$_3$)$_3$C$_5$H$_2$] (0.291 g, 0.91 mmol) were added to a flask under nitrogen at room temperature. Diethyl ether (45 mL) was added to the flask, and the reaction mixture was stirred overnight, concentrated to dryness under vacuum, and the residue extracted with hexanes. The extract was filtered, and the filtrate concentrated to an oil that crystallized upon standing, yielding **1** as air-sensitive, colorless crystals (0.100 g, 37%). This material sublimed at 125−140 °C and 10^{-5} Torr to give a white powder (0.093 g, 34%), m.p. 164 °C. $C_{28}H_{58}CaSi_6$ (603.36): calcd. C 55.74, H 9.69; Ca, 6.64; found C 54.41, H 10.20; Ca, 6.70. ^{1}H NMR (C_6D_6, 20 °C): δ = 6.96 (s, 2 H, ring-C*H*), 0.38 [s, 27 H, Si(CH_3)$_3$] ppm. ^{1}H NMR ([D_8]THF, 20 °C): δ = 6.76 (s, 2 H, ring-C*H*), 0.28 [s, 18 H, Si(CH_3)$_3$], 0.17 [s, 9 H, Si(CH_3)$_3$] ppm. ^{13}C NMR (75.5 MHz, C_6D_6, 20 °C): δ = 133.1 (2C, ring-*C*H), 131.7 [ring-*C*Si(CH$_3$)$_3$], 126.5 [ring-*C*Si(CH$_3$)$_3$], 2.0 [Si(*C*H$_3$)$_3$], 1.1 [Si(*C*H$_3$)$_3$]. Selected IR bands (KBr): $\tilde{\nu}$ = 2956 (s), 2904 (m), 1633 (m), 1556 (m), 1250 (vs), 1116 (w), 1016 (m), 977 (m), 833(vs), 526 (w) cm^{-1}. Crystals for X-ray structural analysis were grown by slow concentration of a saturated hexanes solution of **1** at room temperature.

Synthesis of [1,2,4-(SiMe$_3$)$_3$C$_5$H$_2$]$_2$Sr (2): SrI_2 (0.100 g, 0.29 mmol) and K[1,2,4-(SiMe$_3$)$_3$C$_5$H$_2$] (0.176 g, 0.54 mmol) were added to a flask under nitrogen at room temperature. Diethyl ether (55 mL) was added to the flask, and the reaction mixture was stirred overnight, concentrated to dryness, and the residue extracted with hexanes. The extract was filtered, and the filtrate concentrated to an oil that crystallized upon standing, yielding **2** as air-sensitive, colorless crystals (0.125 g, 71%). Analytically pure material was obtained by sublimation at 140−165 °C and 10^{-6} Torr to give a white crystalline solid (71 mg, 40%), m.p. 94−96 °C. $C_{28}H_{58}Si_6Sr$ (650.90): calcd. C 51.67, H 8.98; found C 51.93, H 9.20. ^{1}H NMR (300 MHz, C_6D_6, 20 °C): δ = 6.89 (s, 2 H, ring-C*H*), 0.37 [s, 9 H, Si(CH_3)$_3$],

 © 2003 Wiley-VCH Verlag GmbH & Co. KGaA, Weinheim

0.34 [s, 18 H, Si(CH_3)$_3$] ppm. ^{1}H NMR ([D$_8$]THF, 20 °C): δ = 6.69 (s, 2 H, ring-C*H*), 0.27 [s, 18 H, Si(CH_3)$_3$], 0.17 [s, 9 H, Si(CH_3)$_3$] ppm. ^{13}C NMR (75.5 MHz, C_6D_6, 20 °C): δ = 132.4 (2C, ring-*C*H), 130.0 (ring-*C*Si(CH$_3$)$_3$], 125.5 (ring-*C*Si(CH$_3$)$_3$], 1.9 [Si(*C*H$_3$)$_3$], 1.1 [Si(*C*H$_3$)$_3$]. Selected IR bands (KBr): $\tilde{\nu}$ = 2957 (vs, br), 1247 (vs, sh), 1091 (ms), 1005 (ms), 850 (vs, br), 751 (s) cm^{-1}. Crystals for X-ray structural analysis were grown by slow concentrated of a saturated hexanes solution of **2** at room temperature.

Synthesis of [1,2,4-(SiMe$_3$)$_3$C$_5$H$_2$]$_2$Ba (3): BaI_2 (0.455 g, 1.2 mmol) and K[1,2,4-(SiMe$_3$)$_3$C$_5$H$_2$] (0.794 g, 2.5 mmol) were added to a flask under nitrogen at room temperature. Diethyl ether (65 mL) was added to the flask, and the reaction mixture was stirred overnight, concentrated to dryness, and the residue extracted with hexanes. The extract was filtered, and the filtrate concentrated to dryness to yield a beige powder (0.42 g, 50%). The crude product was sublimed at 140 °C and 10^{-7} Torr to give air-sensitive, colorless crystals of **3** (0.206 g, 24%), m.p. 139−140 °C. $C_{28}H_{58}BaSi_6$ (700.61): calcd. C 48.00, H 8.34; found C 47.97, H 8.40. ^{1}H NMR (C_6D_6, 20 °C): δ = 6.78 (s, 2 H, ring-C*H*), 0.35 [s, 18 H, Si(CH_3)$_3$], 0.33 [s, 9 H, Si(CH_3)$_3$] ppm. ^{1}H NMR ([D$_8$]THF, 20 °C): δ = 6.60 (s, 2 H, ring-C*H*), 0.25 [s, 18 H, Si(CH_3)$_3$], 0.17 [s, 9 H, Si(CH_3)$_3$] ppm. ^{13}C NMR (75.5 MHz, C_6D_6, 20 °C): δ = 133.1 (2 C, ring-*C*H), 130.5 (ring-*C*Si(CH$_3$)$_3$], 125.4 (ring-*C*Si(CH$_3$)$_3$], 2.0 [Si(*C*H$_3$)$_3$], 0.9 [Si(*C*H$_3$)$_3$]. Selected IR bands (KBr): $\tilde{\nu}$ = 2955 (s), 2897 (m), 1436 (w), 1250 (s), 1092 (m), 1005 (m), 978 (m), 830 (vs), 752 (m), 689 (w), 629 (w) cm^{-1}. Crystals for X-ray structural analysis were obtained from the sublimation of **3**.

Attempted Syntheses of [1,2,4-(SiMe$_3$)$_3$C$_5$H$_2$]$_2$Be: $BeCl_2$ (0.031 g, 0.39 mmol) and K[1,2,4-(SiMe$_3$)$_3$C$_5$H$_2$] (0.252 g, 0.79 mmol) were added to a flask under nitrogen at room temperature. Diethyl ether (20 mL) was added to the flask, and the reaction mixture was stirred at room temperature for 3 d, concentrated to dryness under vacuum, and the residue extracted with hexanes. ^{1}H NMR analysis of the extract indicated that only starting materials were present. The reaction was repeated in a 1:1 diethyl ether/toluene mixture, which was refluxed under nitrogen for 3 days. A black residue was left at the completion of the reaction, and no metallocene was isolated on workup of the reaction mixture.

X-ray Crystallographic Studies: The crystal structure measurement and refinement data for **1**−**3** are given in Table 2. Measurements on **1** and **2** were performed with a Rigaku AFC6S diffractometer at Vanderbilt University with graphite-monochromated Cu-K_α radiation (λ = 1.54178 Å). A crystal of each compound was sealed in a glass capillary tube. Selected crystal and data collection parameters for the present study are given in Table 2. The space groups were determined from reflection conditions and intensity statistics. Data collection was performed using continuous ω-2θ scans with stationary backgrounds (peak/background counting time = 2:1). The structures were solved by direct methods and Fourier techniques with TEXSAN software. All non-hydrogen atoms were refined anisotropically. Hydrogen atoms were inserted in calculated positions based on packing considerations and *d*(C−H) = 0.95 Å. The positions were fixed for the final cycles of refinement. Measurements on **3** were performed on a Siemens SMART system at the X-ray Crystallography Laboratory at the University of Minnesota. A crystal of **3** was attached to a glass fiber, and mounted for data collection at 173(2) K. Data collection and structure solution were conducted at the X-ray Crystallography Laboratory at the University of Minnesota. All calculations were performed using the SHELXTL V5.0 suite of programs. A successful direct-methods solution was calculated which provided most non-hydrogen atoms from the E-map. Several full-matrix least-squares/difference Fourier cycles were performed that located the remainder of the non-hydrogen atoms. All non-hydrogen atoms were refined with anisotropic displacement parameters. All hydrogen atoms were placed in ideal positions and refined as riding atoms with relative isotropic dis-

Table 2. Crystal data and summary of X-ray data collection

	1	**2**	**3**
Empirical formula	$C_{28}H_{58}CaSi_6$	$C_{28}H_{58}Si_6Sr$	$C_{28}H_{58}BaSi_6$
Molecular mass [g·mol^{-1}]	603.36	650.90	700.62
Color of crystal	colorless	colorless	colorless
Cryst dimension [mm]	0.68 × 0.35 × 0.30	0.80 × 0.45 × 0.38	0.25 × 0.15 × 0.06
Space group	$P2_1/n$	$C2/c$	$C2/c$
Temperature [K]	293	293	173(2)
a [Å]	12.928(2)	20.616(3)	20.3972(5)
b [Å]	18.463(2)	20.304(3)	11.1368(2)
c [Å]	17.049(2)	9.697(3)	33.9370(8)
β [°]	95.09(1)	105.79(2)	97.552(1)
V [Å^3]	4053(2)	3906(2)	7642.2 (3)
Z	4	4	8
D(calcd.) [g/cm^3]	0.989	1.107	1.218
Radiation type	Cu-K_α	Cu-K_α	Mo-K_α
Abs. coeff [cm^{-1}]	31.65	38.3	12.42
Scan speed [°/min]	8.0	4.0	
Scan width	0.94 + 0.30 tan θ	1.73 + 0.30 tan θ	
F(000)	1329	1392	2928
Limits of data collection [°]	6 ≤ 2θ ≤ 120	6 ≤ 2θ ≤ 120	1.21 ≤ θ ≤ 25.03
Total reflections	6559	3093	22 399
Unique reflections	6250	2999	6736
No. with $I > n\sigma(I)$	2698 (n = 3)	2164 (n = 3)	4849 (n = 2)
R_1 indices [$I > n\sigma(I)$]	0.053 (n = 3; F)	0.040 (n = 3; F)	0.052 (n = 2; F^2)
wR_2 indices [$I > n\sigma(I)$]	0.062 (F)	0.044 (F)	0.117 (F^2)
Goodness of fit	1.87 (F)	1.69 (F)	1.015 (F^2)
Max/min peak (final diff. map) [e/Å^3]	0.19/−0.35	0.48/−0.32	1.4/−0.81

 © 2003 Wiley-VCH Verlag GmbH & Co. KGaA, Weinheim

placement parameters. SAME restraints were applied to the disordered Si(4)/C(20)/C(21)/C(22) group, which was found to be occupied in a 0.53:0.47 ratio. CCDC-210464 (**1**), -210465 (**2**) and -210466 (**3**) contain the supplementary crystallographic data for this paper. These data can be obtained free of charge at www.ccdc.cam.ac.uk/conts/retrieving.html [or from the Cambridge Crystallographic Data Centre, 12 Union Road, Cambridge CB2 1EZ, UK; Fax: (internat.) + 44-1223/336-033; E-mail: deposit@ccdc.cam.ac.uk].

Computational Details: Calculations on $(Cp^{3Si})_2Be$ were performed using the Gaussian 03 W suite of programs.[43] A full geometry optimization using even the relatively modest 6-31G(d,p) basis set would have involved a computationally expensive set of 839 basis functions. An ONIOM calculation[44] was performed instead, using the 6-31G(d,p) basis set on Be, the ten carbon atoms of the cyclopentadienyl rings, and the directly attached atoms (hydrogen or silicon). The semi-empirical PM3 method was used for the 18 methyl groups. The B3PW91 functional, which incorporates Becke's three-parameter exchange functional[45] with the 1991 gradient-corrected correlation functional of Perdew and Wang,[46] was used; this hybrid functional has previously been shown to provide realistic geometries for organometallic species.[47,48] Frequency calculations were used to establish that all optimized geometries were local minima ($N_{imag} = 0$).

Acknowledgments

Acknowledgment is made to the National Science Foundation for support.

[1] W. J. Evans, L. A. Hughes, T. P. Hanusa, R. J. Doedens, *Organometallics* **1986**, *5*, 1285−1291.
[2] R. A. Williams, T. P. Hanusa, J. C. Huffman, *Organometallics* **1990**, *9*, 1128−1134.
[3] T. P. Hanusa, *Organometallics* **2002**, *21*, 2559−2571.
[4] P. Jutzi, N. Burford, *Chem. Rev.* **1999**, *99*, 969−990.
[5] M. Kaupp, *Angew. Chem. Int. Ed.* **2001**, *40*, 3535−3565.
[6] M. Kaupp, P. v. R. Schleyer, M. Dolg, H. Stoll, *J. Am. Chem. Soc.* **1992**, *114*, 8202−8208.
[7] T. K. Hollis, J. K. Burdett, B. Bosnich, *Organometallics* **1993**, *12*, 3385−3386.
[8] D. J. Burkey, T. P. Hanusa, *Comments, Inorg. Chem.* **1995**, *17*, 41−77.
[9] R. A. Andersen, J. M. Boncella, C. J. Burns, R. Blom, A. Haaland, H. V. Volden, *J. Organomet. Chem.* **1986**, *312*, C49−C52.
[10] R. A. Andersen, R. Blom, C. J. Burns, H. V. Volden, *J. Chem. Soc., Chem. Commun.* **1987**, 768−769.
[11] T. V. Timofeeva, J.-H. Lii, N. L. Allinger, *J. Am. Chem. Soc.* **1995**, *117*, 7452−7459.
[12] P. Jutzi, W. Leffers, S. Pohl, W. Saak, *Chem. Ber.* **1989**, *122*, 1449−1456.
[13] P. Jutzi, R. Sauer, *J. Organomet. Chem.* **1973**, *50*, C29−C30.
[14] M. J. Harvey, T. P. Hanusa, M. Pink, *J. Chem. Soc., Dalton Trans.* **2001**, 1128−1130.
[15] M. J. Harvey, T. P. Hanusa, *Organometallics* **2000**, *19*, 1556−1566.
[16] C. P. Morley, P. Jutzi, C. Krüger, J. M. Wallis, *Organometallics* **1987**, *6*, 1084−1090.
[17] R. D. Shannon, *Acta Crystallogr., Sect. A* **1976**, *32*, 751−767.
[18] R. A. Williams, K. F. Tesh, T. P. Hanusa, *J. Am. Chem. Soc.* **1991**, *113*, 4843−4851.
[19] H. Sitzmann, T. Dezember, M. Ruck, *Angew. Chem. Int. Ed.* **1998**, *37*, 3114−3115.
[20] M. Del Mar Conejo, R. Fernandez, E. Gutierrez-Puebla, A. Monge, C. Ruiz, E. Carmona, *Angew. Chem. Int. Ed.* **2000**, *39*, 1949−1951.
[21] D. J. Burkey, T. P. Hanusa, J. C. Huffman, *Adv. Mater. Opt. Electron.* **1994**, *4*, 1−8.
[22] L. Pauling, *The Nature of the Chemical Bond*, 3rd ed., Cornell University Press, Ithaca, New York, **1960**.
[23] M. Visseaux, D. Barbier-Baudry, O. Blacque, A. Hafid, P. Richard, F. Weber, *New J. Chem.* **2000**, *24*, 939−942.
[24] H. Sitzmann, T. Dezember, O. Schmitt, F. Weber, G. Wolmershauser, M. Ruck, *Z. Anorg. Allg. Chem.* **2000**, *626*, 2241−2244.
[25] D. J. Burkey, T. P. Hanusa, *Acta Crystallogr., Sect. C* **1996**, *52*, 2452−2454.
[26] P. B. Hitchcock, J. A. K. Howard, M. F. Lappert, S. Prashar, *J. Organomet. Chem.* **1992**, *437*, 177−189.
[27] P. Jutzi, E. Schlueter, M. B. Hursthouse, A. M. Arif, R. L. Short, *J. Organomet. Chem.* **1986**, *299*, 285−295.
[28] J. Okuda, E. Herdtweck, *Chem. Ber.* **1988**, *121*, 1899−1905.
[29] I. Bytheway, P. L. A. Popelier, R. J. Gillespie, *Can. J. Chem.* **1996**, *74*, 1059−1071.
[30] V. N. Sapunov, K. Kirchner, R. Schmid, *J. Organomet. Chem.* **2001**, *214*, 143−185.
[31] V. M. Rayon, G. Frenking, *Chem. Eur. J.* **2002**, *8*, 4693−4707.
[32] D. J. Burkey, R. A. Williams, T. P. Hanusa, *Organometallics* **1993**, *12*, 1331−1337.
[33] W. Bünder, E. Weiss, *J. Organomet. Chem.* **1975**, *92*, 1−6.
[34] M. G. Gardiner, C. L. Raston, C. H. L. Kennard, *Organometallics* **1991**, *10*, 3680−3686.
[35] M. Westerhausen, N. Makropoulos, B. Wieneke, K. Karaghiosoff, H. Noeth, H. Schwenk-Kircher, J. Knizek, T. Seifert, *Eur. J. Inorg. Chem.* **1998**, 965−971.
[36] H. Schumann, J. Gottfriedsen, M. Glanz, S. Dechert, J. Demtschuk, *J. Organomet. Chem.* **2001**, *617−618*, 588−600.
[37] T. P. Hanusa, *Chem. Rev.* **1993**, *93*, 1023−1036.
[38] K. W. Nugent, J. K. Beattie, T. W. Hambley, M. R. Snow, *Aust. J. Chem.* **1984**, *37*, 1601−1606.
[39] S. Harder, M. Lutz, A. W. G. Straub, *Organometallics* **1997**, *16*, 107−113.
[40] C. J. Burns, R. A. Andersen, *J. Organomet. Chem.* **1987**, *325*, 31−37.
[41] S. J. Pratten, M. K. Cooper, M. J. Aroney, *J. Organomet. Chem.* **1990**, *381*, 147−153.
[42] H. Sitzmann, F. Weber, M. D. Walter, G. Wolmershaeuser, *Organometallics* **2003**, *22*, 1931−1936.
[43] M. J. Frisch, G. W. Trucks, H. B. Schlegel, G. E. Scuseria, M. A. Robb, J. R. Cheeseman, J. A. Montgomery, Jr., T. Vreven, K. N. Kudin, J. C. Burant, J. M. Millam, S. S. Iyengar, J. Tomasi, V. Barone, B. Mennucci, M. Cossi, G. Scalmani, N. Rega, G. A. Petersson, H. Nakatsuji, M. Hada, M. Ehara, K. Toyota, R. Fukuda, J. Hasegawa, M. Ishida, T. Nakajima, Y. Honda, O. Kitao, H. Nakai, M. Klene, X. Li, J. E. Knox, H. P. Hratchian, J. B. Cross, C. Adamo, J. Jaramillo, R. Gomperts, R. E. Stratmann, O. Yazyev, A. J. Austin, R. Cammi, C. Pomelli, J. W. Ochterski, P. Y. Ayala, K. Morokuma, G. A. Voth, P. Salvador, J. J. Dannenberg, V. G. Zakrzewski, S. Dapprich, A. D. Daniels, M. C. Strain, O. Farkas, D. K. Malick, A. D. Rabuck, K. Raghavachari, J. B. Foresman, J. V. Ortiz, Q. Cui, A. G. Baboul, S. Clifford, J. Cioslowski, B. B. Stefanov, G. Liu, A. Liashenko, P. Piskorz, I. Komaromi, R. L. Martin, D. J. Fox, T. Keith, M. A. Al-Laham, C. Y. Peng, A. Nanayakkara, M. Challacombe, P. M. W. Gill, B. Johnson, W. Chen, M. W. Wong, C. Gonzalez, J. A. Pople, *Gaussian 2003*, Revision B.01, Gaussian, Inc., Pittsburgh PA, **2003**.
[44] S. Dapprich, I. Komaromi, K. S. Byun, K. Morokuma, M. J. Frisch, *J. Molec. Struct. THEOCHEM* **1999**, *462*, 1−21.
[45] A. D. Becke, *J. Chem. Phys.* **1993**, *98*, 5648−5652.
[46] J. P. Perdew, Y. Wang, *Phys. Rev. B* **1992**, *45*, 13244−13249.
[47] T. Ziegler, *Chem. Rev.* **1991**, *91*, 651−667.
[48] J. D. Smith, T. P. Hanusa, *Organometallics* **2001**, *20*, 3056−3062.

Received May 13, 2003

 © 2003 Wiley-VCH Verlag GmbH & Co. KGaA, Weinheim

Synthesis and Structures of Alkali Metal Amides Derived from the Ligands $[N(SiMe_2Ph)(SiMe_3)]^-$, $[N(tBu)(SiMe_3)]^-$, $[N(Ph)(2\text{-}C_5H_4N)]^-$, and $[N(2\text{-}C_5H_4N)_2]^-$

Floria Antolini,[a] Peter B. Hitchcock,[a] Alexei V. Khvostov,[a] and Michael F. Lappert*[a]

Dedicated to the memory of Ron Snaith

Keywords: Alkali metals / Amides / Synthesis / NMR spectra / X-ray structures

The following crystalline complexes are reported: $[(M\{\mu\text{-}N(SiMe_2Ph)(SiMe_3)\})_2]_n$ [the *cis* complex for $n = 1$ and M = Li (**1**); and the *trans* complexes with $n = \infty$ and M = Na (**2**), K (**4**), Rb (**5**), Cs (**6**)], $[(Na\{\mu\text{-}trans\text{-}N(SiMe_2Ph)(SiMe_3)\})_2(tmeda)]$ (**3**), $[(K\{\mu\text{-}trans\text{-}N(tBu)(SiMe_3)\})_4(\eta\text{-}C_6H_6)_2]$ (**7**), $[(K\{\mu\text{-}trans\text{-}N(Ph)(2\text{-}C_5H_4N)\})_2(\mu'\text{-}thf)_3]_\infty$ (**8**), and $[K\{\mu\text{-}N(2\text{-}C_5H_4N)_2\}]_\infty$ (**9**). Each, except **3**, was obtained by metallation of the appropriate secondary amine with Li*n*Bu (for **1**), MBzl [M = Na (for **2**), K (for **4** and **7**), Rb (for **5**), Cs (for **6**)], or KH (for **8** and **9**); treatment of **2** with an excess of tmeda yielded **3**. Each of **1**–**9** has an unusual, and in some cases unprecedented, molecular structure.
(© Wiley-VCH Verlag GmbH & Co. KGaA, 69451 Weinheim, Germany, 2003)

Introduction

Bulky alkali metal amides MNR_2 (especially M = Li and R = *i*Pr or $SiMe_3$, or NR_2 = 2,2,6,6-Me_4-piperidyl) are widely used as proton abstractors in organic synthesis, by virtue of their strong basicity but low carbon-centred nucleophilicity; and as reagents for the synthesis (including enantioselective) of compounds containing C−C bonds.[1−11] In coordination chemistry they are of synthetic interest as (i) ligand-transfer reagents; as substrates for (ii) reactions with protic compounds, thereby eliminating amine and generating new alkali metal compounds, and (iii) insertion of heterocumulenes or α-H-free organic cyanides.[12] They are also of major structural interest.[13−15]

We have a long-standing interest in the chemistry of metal and metalloid amides.[12] Many are prepared from the corresponding metal or metalloid chlorides, or other leaving groups such as triflates, by treatment with an alkali metal amide. Whereas lithium amides are the most readily available, the heavier alkali metal congeners, especially the sodium or potassium compounds, are often to be preferred because of the ease of separation of the target metal amide from the alkali metal halide coproduct.

Our most recent contributions have dealt with the crystalline dimeric dilithium diamide $[Li_2\{(1,3\text{-}CH_2NC_6H_3iPr_2\text{-}2',6')_2C_6H_4\}]_2$ [16] and crystalline polymeric lithium amides $[(Li\{\mu\text{-}N(Ph)R\}\text{-}trans)_2(\mu\text{-tmeda})]_\infty$ (R = $SiMe_3$ or *t*Bu).[17]

Results and Discussion

Synthesis and Characterisation

In a preliminary communication, we described the conversion of $HN(SiMe_2Ph)(SiMe_3)$ into the crystalline lithium (**1**) and sodium (**2**) amides [as well as related chemistry based on $HN(Ph)SiMe_3$].[18] An objective was to compare their structures with those of the metal amides of the better known C_2-symmetric ligand $[N(SiMe_3)_2]^-$. In this paper we report (i) full details of the synthesis and characterisation of **1** and **2**; (ii) extensions to **3**, the crystalline tmeda complex of **2**, and the potassium (**4**), rubidium (**5**) and caesium (**6**) analogues of **1** and **2**; (iii) the synthesis of the potassium salt of another C_1-symmetric trimethylsilylamide $K[N(tBu)(SiMe_3)]$ **7a** and its crystalline benzene adduct **7**; (iv) the preparation of the crystalline potassium 2-pyridylamides $[K\{N(Ph)(2\text{-}C_5H_4N)\}\cdot 11/2thf]_\infty$ (**8**) and $[K\{N(2\text{-}C_5H_4N)_2\}]_\infty$ (**9**); and (v) X-ray structural data on the crystalline compounds **3**−**9** (those of **1** and **2** are in the literature[18]). As for (iv), the crystalline X-ray-characterised tmeda analogue of **8** $[K\{N(Ph)(2\text{-}C_5H_4N)\}(tmeda)]$ has been reported.[19] The first metal complexes of the ligand $[N(2\text{-}C_5H_4N)_2]^-$ to be described were the crystalline $[Cu_3\{N(2\text{-}C_5H_4N)_2\}X_2]\cdot H_2O$ chloride and bromide,[20] and further transition metal analogues have been much studied.[21]

[a] The Chemical Laboratory, University of Sussex, Brighton BN1 9QJ, UK
Fax: (internat.) +44-1273/677-196
E-mail: M.F.Lappert@sussex.ac.uk

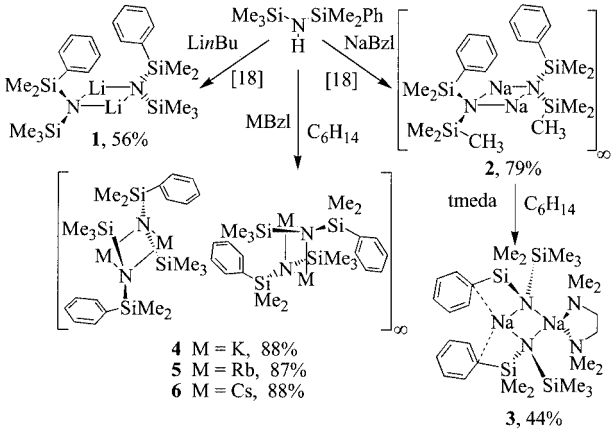

Scheme 1. Synthesis of the crystalline alkali metal phenyldimethylsilyl(trimethylsilyl)amides **1**−**6**; yields of **1**−**3** refer to X-ray quality specimens

The syntheses of the new alkali metal amides $[(M\{\mu\text{-}N(SiMe_2Ph)(SiMe_3)\})_2]_n$ [n = 1 with M = Li (**1**); and n = ∞ with M = Na (**2**), K (**3**), Rb (**5**), Cs (**6**)], as well as that of the tmeda adduct **3** of **2**, are shown in Scheme 1. For each of **1**, **2**, **4**, **5**, and **6**, the parent silazane was metallated at −78 °C in hexane (**1**) or pentane, using *n*-butyllithium (**1**) or the appropriate heavier alkali metal benzyl (MBzl). The latter were prepared as solids from M*O*t*Bu (M = Na, K, Rb), Li*n*Bu and toluene in hexane at −78 °C, the precipitated MBzl then thoroughly washed with hexane; CsBzl was obtained by carefully heating Cs in toluene at ca. 60 °C. Complex **3** was made from **2** and an excess of tmeda in hexane at ambient temperature, removal of volatiles and extraction of the residue with benzene; it is surprising that the dinuclear complex **3** contains only a single sodium-bound tmeda ligand.

The alkali metal amides **1**, **2**, **4**, **5** and **6** were found to be more soluble in hydrocarbon solvents than the corresponding compounds having the $[N(SiMe_3)_2]^-$ ligand, possibly in part due to the phenyl substituent assisting in delocalising the negative charge on the nitrogen atom. Each of the compounds **1**−**5** gave satisfactory microanalyses for hydrogen and nitrogen, although values for carbon were invariably low (as we have generally found for silicon-containing compounds, which is attributed to incomplete combustion). The caesium amide **6** proved to be too moisture-sensitive to give reproducible analytical data. Each of **1**−**6** gave satisfactory NMR and EI-mass spectra.

Treatment of trimethylsilyl(*tert*-butyl)amine with benzylpotassium, under identical conditions to those used for the preparation of **4**, yielded the potassium amide **7a** as a powder, which from benzene afforded the crystalline tetranuclear potassium amide as the bis(benzene) adduct **7** (Scheme 2). In a similar fashion, but using benzylsodium, the product was the sparingly hydrocarbon-soluble amorphous sodium amide **7b**, from which X-ray quality crystals were not obtained.

Values for $^{29}Si\{^1H\}$ NMR spectral chemical shifts in $C_6D_5CD_3$ for **1** or C_6D_6 for **2**−**6** and $M[N(SiMe_3)_2]$ (M = Li, Na) at ambient temperature are shown in Table 1.

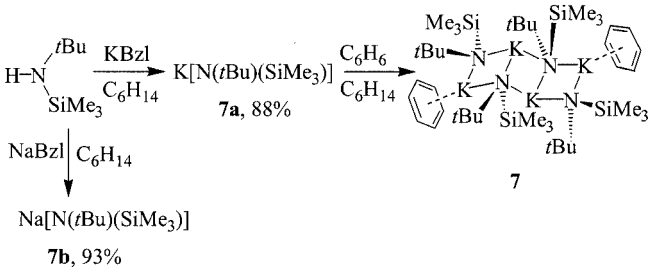

Scheme 2. Synthesis of the colourless solid sodium (**7b**) and potassium (**7a**) *tert*-butyl(trimethylsilyl)amides and the crystalline benzene adduct (**7**) of **7a**

Addition of *N*-2-pyridylaniline to potassium hydride in THF at ambient temperature yielded, after filtration and concentration of the filtrate, pale-yellow crystals of the corresponding potassium amide **8**, as a triply THF-bridging polymer of a tetranuclear array chain structure. The colourless, polymeric, crystalline bis(2-pyridyl)amidopotassium complex **9**, of layer structure, was obtained similarly, from bis(2-pyridyl)amine and KH in THF (Scheme 3). Each of the amides **8** and **9** was characterised by microanalyses (C, H, N) and ^1H and $^{13}C\{^1H\}$ NMR spectra in $[D_8]$THF, as well as their X-ray structures.

Crystal Structures

The structures of $[Li\{\mu\text{-}cis\text{-}N(SiMe_2Ph)(SiMe_3)\}]_2$ (**1**) and $[(Na\{\mu\text{-}trans\text{-}N(SiMe_2Ph)(SiMe_3)\})_2]_\infty$ (**2**) have been published.[18] In summary, **1** is unusual in that it appears to be only the second example of a neutral donor-free binuclear lithium amide,[18] albeit of opposite stereochemistry to that of $[Li\{\mu\text{-}trans\text{-}N(C_6H_3iPr_2\text{-}2,6)(SiMe_3)\}]_2$.[22] The LiNLi′N′ core in the C_2-symmetric **1**, unlike in the latter (which is centrosymmetric), deviates from a planar rhombus, the Li−N bonds ranging from 1.980(3) to 2.019(3) Å, the four atoms alternating above and below the plane by ca. 0.033 Å. The endocyclic angles subtended at the nitrogen atoms (71.75 ± 0.05°) are narrower than those at the lithium atoms (106.6 ± 0.3°), and are similar to those in $[Li\{\mu\text{-}trans\text{-}N(C_6H_3iPr_2\text{-}2,6)(SiMe_3)\}]_2$.[22] Crystalline **2** is a polymer of linked C_2-symmetric, planar dinuclear units, each attached to its neighbour by close Na···C contacts.[18] Neutral donor-free dinuclear sodium amides are, we believe, unprecedented. Each of **1** and **2** has close M···C contacts (see Table 9 below).

The crystalline dinuclear sodium amide − mono-tmeda adduct **3** is unusual in that the two four-coordinate sodium atoms of the central Na1N1Na2N2 core are in different environments: Na1 has an exocyclic chelating tmeda ligand, whereas Na2 has close Na2···C_{ipso} contacts of 2.698 ± 0.006 Å (Figure 1); as a corollary, the endocyclic Na−N bonds are longer for Na1 than Na2 (Table 2) and both are significantly longer than those in **2** (2.420 ± 0.012 Å[18]) or in $[Na\{\mu\text{-}trans\text{-}N(Ph)(SiMe_3)\}(tmeda)]_2$ (av. 2.475 Å[18]), while the endocyclic bond angle at N2 is much wider than that at N1 and their mean is close to that in **2** (102.2 ± 0.7 Å[18]).

Table 1. $^{29}Si\{^1H\}$ NMR spectral chemical shifts (δ) in C_6D_6 at 298 K of $M[N(SiMe_3)_2]$ (M = Li, Na) and of compounds **1**−**7**

Compound	δ	Compound	δ
$Li[N(SiMe_3)_2]$	−10.7	$[(K\{\mu\text{-}trans\text{-}N(SiMe_2Ph)(SiMe_3)\})_2]_\infty$ (**4**)	−24.0, −19.5
$Na[N(SiMe_3)_2]$	−14.5	$[(Rb\{\mu\text{-}trans\text{-}N(SiMe_2Ph)(SiMe_3)\})_2]_\infty$ (**5**)	−[a]
$[Li\{\mu\text{-}cis\text{-}N(SiMe_2Ph)(SiMe_3)\}]_2$ (**1**)	−13.9, −10.6	$[(Cs\{\mu\text{-}trans\text{-}N(SiMe_2Ph)(SiMe_3)\})_2]_\infty$ (**6**)	−26.3, −21.8
$[(Na\{\mu\text{-}trans\text{-}N(SiMe_2Ph)(SiMe_3)\})_2]_\infty$ (**2**)	−18.1, −13.2	$K[N(tBu)(SiMe_3)]$ (**7a**)	−18.2
$[(Na\{\mu\text{-}trans\text{-}N(SiMe_2Ph)(SiMe_3)\})_2(\mu\text{-tmeda})]$ (**3**)	−20.9, −16.6	$Na[N(tBu)(SiMe_3)]$ (**7b**)	−25.4

[a] Not determined.

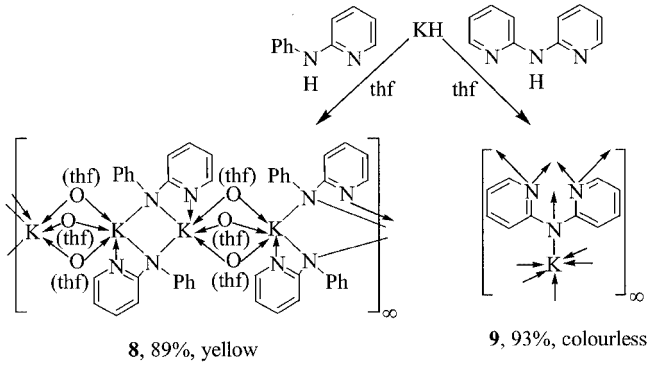

Scheme 3. Synthesis of the crystalline potassium 2-pyridylamides **8** and **9**

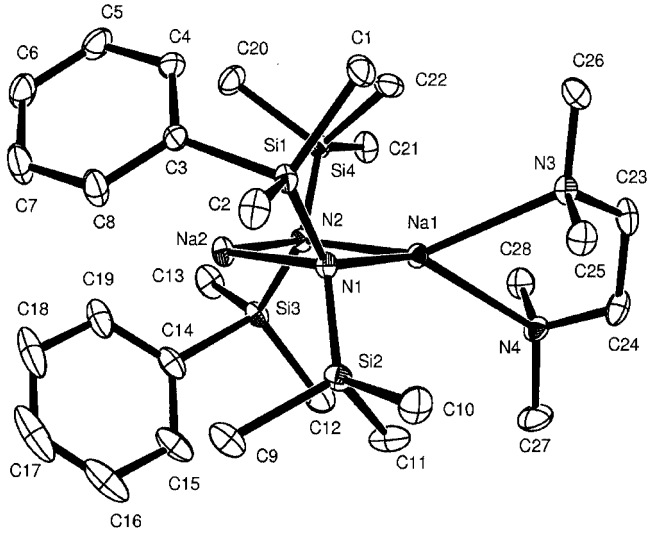

Figure 1. Molecular structure of $[(Na\{\mu\text{-}trans\text{-}N(SiMe_2Ph)(SiMe_3)\})_2(tmeda)]$ (**3**)

Table 2. Selected bond lengths (Å) and angles (°) for **3**

Bond		Angles	
Na(1)−N(1)	2.5070(19)	N(1)−Na(1)−N(2)	97.50(6)
Na(1)−N(2)	2.5987(19)	N(3)−Na(1)−N(4)	69.23(7)
Na(1)−N(3)	2.624(2)	N(2)−Na(2)−N(1)	106.26(7)
Na(1)−N(4)	2.637(2)		
Na(2)−N(2)	2.387(2)		
Na(2)−N(1)	2.4118(19)		

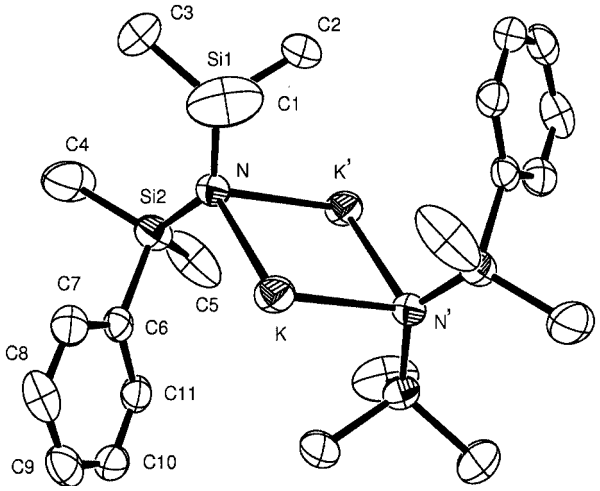

Figure 2. Molecular structure of $[(K\{\mu\text{-}trans\text{-}N(SiMe_2Ph)(SiMe_3)\})_2]_\infty$ (**4**), showing one of the dimeric units

Each of the crystalline alkali metal amides bearing the $[N(SiMe_3)(SiMe_2Ph)]^-$ ligand adopts a dinuclear structure. The heavier alkali metal amides $[(M\{\mu\text{-}trans\text{-}N(SiMe_2Ph)(SiMe_3)\})_2]_\infty$ (M = K, Rb, Cs) have a very similar crystal architecture. Two molecules are situated in the unit cell, which are orientated in such a way that the cations are stabilised by both intra- and intermolecular interactions with the methyl and/or phenyl substituents (Table 9), responsible for the polymeric aggregation. Descending the group, the $[MN]_2$ central core becomes progressively more rectangular.

X-ray quality crystals of $[(K\{\mu\text{-}trans\text{-}N(SiMe_2Ph)(SiMe_3)\})_2]_\infty$ (**4**) were obtained by sublimation at 180 °C and 5×10^{-4} Torr. The molecular structure of one dimeric unit is shown in Figure 2; there are two independent dimers **A** and **B** in the unit cell, each lying on an inversion centre. The phenyl groups in **A** are orthogonal to those in **B**. A list of selected interatomic bond lengths (Å) and angles (°) together with those of a related compound $[K\{\mu\text{-}N(SiMe_3)_2\}]_2$ [23] are in Table 3. The structural parameters describing the internal core $[KN]_2$ in **4** are unexceptional. Comparing **4** with $[K\{\mu\text{-}N(SiMe_3)_2\}]_2$,[23,24] only the Si(1)−N−Si(2) and SiB(1)−NB−SiB(2) [133.49(13) and 132.56(12)° [23]] angles show significant differences.

As shown by a portion of the structure of **4** depicted in Figure 3, close contacts between a potassium atom (say in **B**) and the phenyl ring of the neighbouring unit (say **A**) are present: [K−C(2) 3.512(2), K−C(3) 3.119(2), K−C(4)

 © 2003 Wiley-VCH Verlag GmbH & Co. KGaA, Weinheim

Table 3. Selected bond lengths (Å) and angles (°) for **4** and $[K\{\mu\text{-}N(SiMe_3)_2\}]_2$ [23]

Bond or angle	**4** **A**, [**B**]	Bond or angle	$[K\{\mu\text{-}N(SiMe_3)_2\}]_2$ [23]
K-N, [KB-NB]	2.778(2), [2.790(2)]	K−N	2.770(3)
K−N′, [KB-NB′]	2.808(2), [2.826(2)]	K−N′	2.803(3)
K−N−K′, [KB-NB-KB′]	83.59(6), [83.47(5)]	K−N−K′	85.53(9)
N−K−N′, [NB-KB-NB′]	96.42(6), [96.53(5)]	N−K−N	94.47(9)
Si(1)−N−Si(2), [SiB(1)−NB−SiB(2)]	133.49(13), [132.56(12)]	Si−N−Si′	129.18(18)

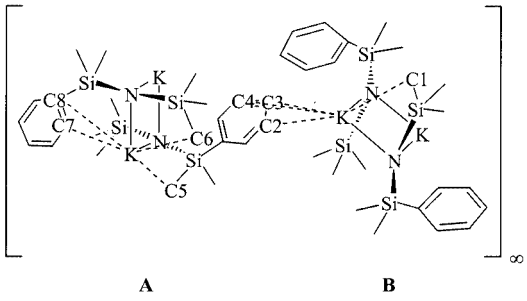

Figure 3. Schematic view of intra- and intermolecular K···C interactions in compound **4**

3.225(2) Å]. The same potassium atom is involved in an intramolecular K-methyl interaction, K−C(1), of 3.231(2) Å. In the other dimer (say **A**) the potassium atom has intramolecular contacts with the phenyl and methyl substituents: [K−C(5) 3.450(2), K−C(6) 3.357(2), K−C(7) 3.587(2) and K−C(8) 3.381(2) Å]. A higher coordination number with increasingly heavier alkali metal complexes is to be expected. The C_2-symmetric analogue $[K\{\mu\text{-}N(SiMe_3)_2\}]_2$ exhibits close intramolecular agostic-type contacts of 3.34 Å,[23] and also, as a referee (but not refs. 23 or 24) has noted, close intermolecular contacts.

Crystals of the rubidium amide **5** were obtained from a saturated toluene solution. There are two independent dimers **A** and **B** in the unit cell, as shown in Figure 4. A list of selected geometrical parameters for a single dimeric unit is shown in Table 4, together with comparative data for $[Rb\{\mu\text{-}N(SiMe_3)_2\}]_2$.[25] Crystalline **5** is similar to **4**, but the coordination sphere at the metal is different; thus the rubidium in the **A** molecule is involved in an η^6-bonding mode with the phenyl substituent of the **B** molecule [Rb−C(1B) 3.716(7), Rb−C(2B) 3.640(8), Rb−C(3B) 3.466(8), Rb−C(4B) 3.339(7), Rb−C(5B) 3.407(7), Rb−C(6B) 3.570(7) Å], as shown schematically in Figure 5.

Crystals of the caesium amide **6** were obtained from a solution in benzene and hexane. As for **4** and **5**, there are two independent dimers **A** and **B** in the unit cell, as shown in Figure 6. A list of selected geometrical parameters for a single dimeric unit is shown in Table 5, together with comparative data for $[Cs\{\mu\text{-}N(SiMe_3)_2\}]_2$ (**C**) and $[Cs\{\mu\text{-}N(SiMe_3)_2\}]_2(\mu'\text{-}\eta^6,\eta^6\text{-}PhMe)]_\infty$ (**D**).[25] The caesium atom in each of **A** and **B** has a different coordination environment, as shown schematically in Figure 7. In **A**, there are two close intra-**A** and three inter-**A/B** Cs···Ph contacts: Cs−C(1) 3.473(2), Cs−C(2) 3.556(2), Cs−C(3) 3.682(2), Cs−C(4) 3.487(2), Cs−C(5) 3.586(2) Å. In **B**, only intra-**B**

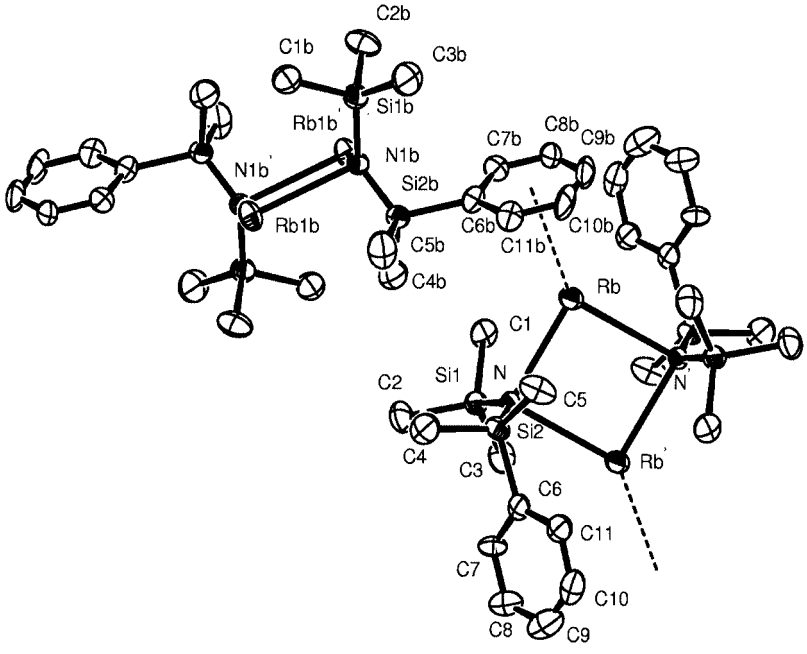

Figure 4. Molecular structure of $[(Rb\{\mu\text{-}trans\text{-}N(SiMe_2Ph)(SiMe_3)\})_2]_\infty$ (**5**), showing adjacent dimeric units

 © 2003 Wiley-VCH Verlag GmbH & Co. KGaA, Weinheim

Table 4. Selected bond lengths (Å) and angles (°) for **5** and $[Rb\{\mu\text{-}N(SiMe_3)_2\}]_2$ [23]

Bond or angle	**5 A**, [**B**]	Bond or angle	$[Rb\{\mu\text{-}N(SiMe_3)_2\}]_2$ [23]
Rb−N, [RbB-NB]	2.898(6), [2.901(6)]	Rb−N	2.878(2)
Rb−N′, [RbB-NB′]	3.056(5), [2.914(6)]	Rb−N′	2.956(3)
Rb−N−Rb′, [RbB-NB-RbB′]	87.81(15), [85.56(17)]		
N−Rb−N′, [NB-RbB-NB′]	92.19(15), [94.44(17)]	N−Rb−N′	92.01(1)
Si(1)−N−Si(2), [SiB(1)−NB−SiB(2)]	133.1(4), [128.2(4)]	Si−N−Si′	130.7(1)

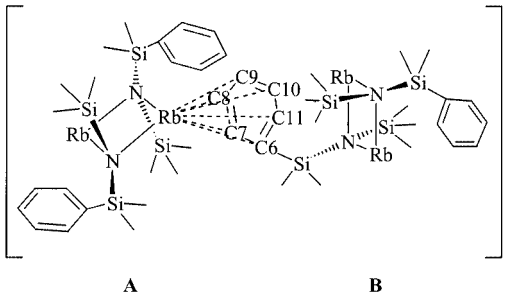

Figure 5. Schematic view of **5**, which highlights the Rb-phenyl contacts

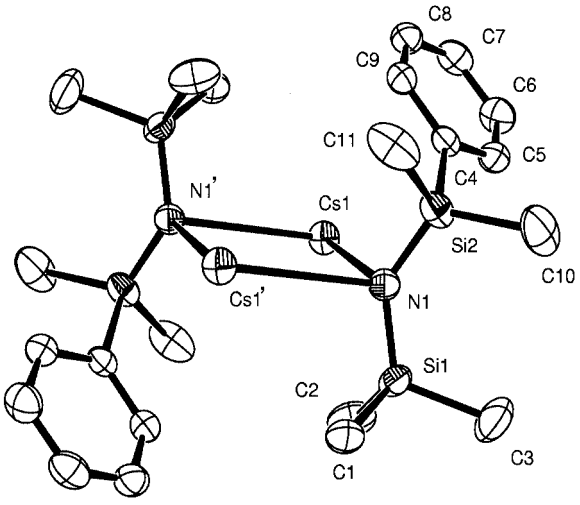

Figure 6. Molecular structure of $[(Cs\{\mu\text{-}trans\text{-}N(SiMe_2Ph)(SiMe_3)\})_2]_\infty$ (**6**), showing one of the dimeric units

Cs···Ph contacts are present: Cs−C(8) 3.451(2), Cs−C(9) 3.653(2) Å; but additionally there are two Cs···CH_3 close contacts: Cs−C(7) 3.624(2), Cs−C(6) 3.556(2) Å.

Compound **7** is a centrosymmetric tetramer, comprising a fusion of three rhomboidal planes, arranged in ladder fashion. The conformational order of the ladder in the molecule is *cisoid-transoid* with angles between the planes of 151.21° (Figure 8). The use of benzene as crystallisation solvent, which is η^6-coordinated to each terminal K^+ cation, may have caused the partial rupture of the probable infinite polymeric chain adopted by the solid $[K\{\mu\text{-}N(t\text{Bu})(SiMe_3)\}]_\infty$. We believe that **7** is the first oligomeric potassium amide having a ladder structure. The central rhomboid K2N2 K2′N2′ is flanked by terminal planar K1N1 K2N2 and K1′N1′K2′N2′ rings. The K2 and K2′ ions have three nitrogen atom neighbours and close K2···C3, K2′···C3′ contacts, while K1 and K1′ have two nitrogen neighbours and also are η^6-C_6H_6-bound. Selected bond lengths and angles are listed in Table 6, along with some comparative data for $[K\{\mu\text{-}N(SiMe_3)_2\}]_2$.[23]

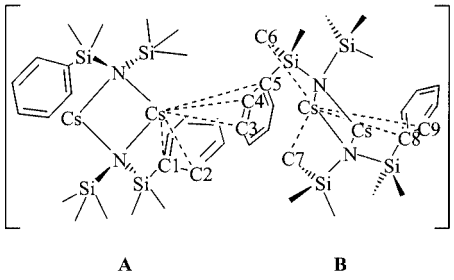

Figure 7. Schematic view of caesium-carbon contacts in a dimeric pair **A** and **B** of $[(Cs\{\mu\text{-}trans\text{-}N(SiMe_2Ph)(SiMe_3)\})_2]_\infty$ (**6**)

The crystalline complex $[(K\{\mu\text{-}trans\text{-}N(Ph)(2\text{-}C_5H_4N)\})_2(\mu'\text{-thf})_3]_\infty$ (**8**) has a polymeric chain structure generated by alternation of inversion centres (relating N1 and N1′) and C_2 axes (through O3; Figure 9). Thus, the potassium ions in the chain are connected to one another by alternating bridges of three THF ligands (average K−O bond length, 2.79 Å) and two amido ligands (average K−NPh, 2.81 Å and average K−NC_5H_4, 2.90 Å). A similar [K-(μ-amido)]$_2$ motif is present in $[K\{\mu\text{-}trans\text{-}[N(Ph)(2\text{-}C_5H_4N)]\}(tmeda)]_2$,[19] but the bridging is symmetrical [K−NPh, 2.805(3) Å; K−NC_5H_4-2, 2.841(2) and 2.877(3) Å]; in both this compound [K−N−K′, 73.9(1)° and

Table 5. Selected bond lengths (Å) and angles (°) for **6**, $[Cs\{\mu\text{-}N(SiMe_3)_2\}]_2$ (**C**) and $(\mathbf{C}_2(\mu'\text{-}\eta^6,\eta^6\text{-PhMe})]_\infty$ (**D**)

Bond or angle	**6 A**, [**B**]	Bond or angle	**C** [25]	**D** [25]
Cs(1)−N(1), [Cs(1B)−N(1B)]	3.199(2), [3.111(2)]	Cs−N	3.047(4)	3.016(2)
Cs−N′, [CsB-NB′]	3.200(2), [3.218(2)]	Cs−N′	3.149(2)	3.139(2)
Cs−N−Cs′, [CsB-NB-CsB′]	92.47(6), [94.74(5)]			
N−Cs−N′, [NB-CsB-NB′]	*av.* 91.13, [85.56]	N−Cs−N′	89.6(1)	90.71(1)
Si(1)−N−Si(2), [SiB(1)−NB−SiB(2)]	133.9(1), [132.69(1)]	Si−N−Si′	129.4(1)	128.02(1)

 © 2003 Wiley-VCH Verlag GmbH & Co. KGaA, Weinheim

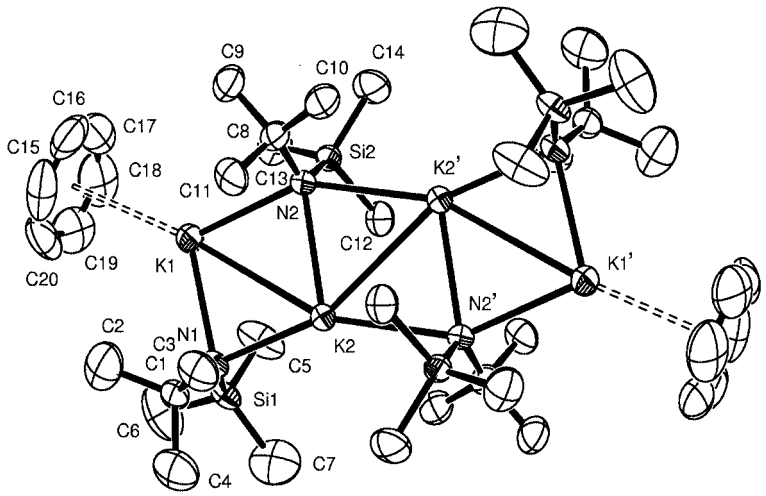

Figure 8. Molecular structure of $[(K\{\mu\text{-}trans\text{-}N(t\text{Bu})(SiMe_3)\})_4(\eta\text{-}C_6H_6)_2]$ (**7**)

Table 6. Selected bond lengths (Å) and angles (°) for **7** and $[K\{\mu\text{-}N(SiMe_3)_2\}]_2$ [23]

Bond or angle	**7**	$[K\{\mu\text{-}N(SiMe_3)_2\}]_2$ [23]
K1−N1	2.726(2)	2.770(3)
K1−N2	2.934(2)	2.803(3)
K2−N1	2.701(2)	
K2−N2	2.821(2)	
N1−Si1	1.633(2)	1.678(3)
N2−Si2	1.616(2)	1.685(3)
K1−N1−K2	82.93(5)	85.53(9)
N1−K1−N2	98.15(5)	94.47(9)
N2−K2−N2′	107.10(4)	
K2−N2−K2′	72.89(4)	

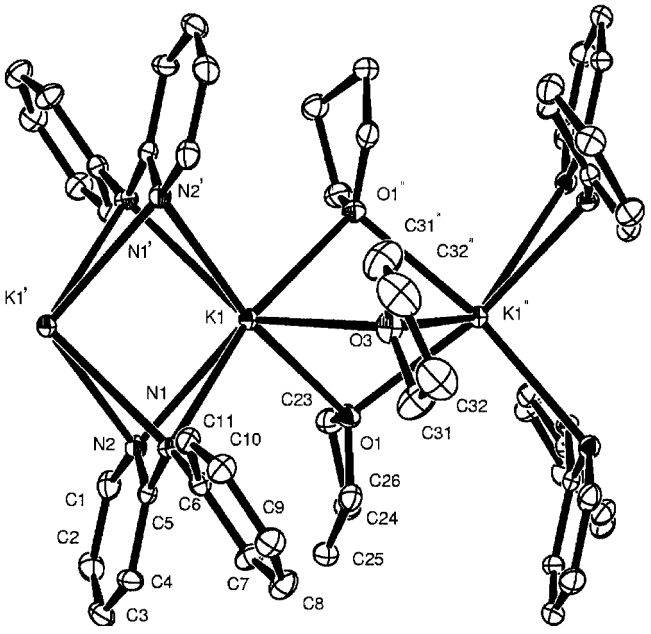

Figure 9. Polymeric chain crystal structure of $[(K\{\mu\text{-}trans\text{-}N(Ph)(2\text{-}C_5H_4N)\})_2(\mu'\text{-thf})_3]_\infty$ (**8**)

N−K−N′, 106.0(1)°] and **8**, the central potassium amido KNK′N′ planar ring has comparable endocyclic bond angles. Similar endocyclic geometric parameters are also found in $[K\{\mu\text{-}trans\text{-}[N(SiMe_3)(2\text{-}C_5H_4N)]\}(12\text{-crown-}4)]_2$ but the K-NSiMe$_3$ distances [2.858(2), 2.912(2) Å] are almost identical to the K−NC$_5$H$_4$-2 distance of 2.853(2) and 2.858(2) Å.[26] An unprecedented feature in the structure of **8** is the presence of the three bridging THF ligands in the M(μ-thf)$_3$M′ moiety; THF-bridging between two metals is well documented, as for M = K.[27−36] Table 7 lists selected geometric parameters for **8**.

Table 7. Selected bond lengths (Å) and angles (°) for **8**

Bond		Angles	
K(1)−O(1)	2.760(2)	O(1)−K(1)−O(1)′′	73.83(8)
K(1)−O(1)′′	2.817(2)	O(1)−K(1)−O(3)	77.48(6)
K(1)−O(3)	2.885(2)	O(1)′′−K(1)−O(3)	76.58(6)
K(1)−N(1)	2.836(2)	N(1)−K(1)−N(1)′	106.64(6)
K(1)−N(2)′	2.870(2)	N(2)−K(1)−N(2)′	106.90(6)
K(1)−N(2)	2.908(2)		
K(1)−N(1)′	2.924(2)		

The complex $[K\{\mu\text{-}N(2\text{-}C_5H_4N)_2\}]_\infty$ (**9**) crystallises from THF as a THF-free polymer of layer structure (Figure 10); selected geometric parameters are given in Table 8. Complex **9** differs from each of **1**−**8** in being free from a central cyclic MNM′N′ core. Each potassium ion is in a six-coordinate KN$_6$ environment; for K, four of the nitrogen atoms (N2#1 and N2#2; N2#3 and N2#4) are from μ_2-bridging pyridine atoms on adjacent *cisoid* $[N(C_5H_4N\text{-}2)_2]^-$ ligands, while the other two are from μ_2-amido nitrogen atoms (N1 and N1#5) of another pair of *cisoid* $[N(C_5H_4N\text{-}2)_2]^-$ ligands. Each of the $[N(C_5H_4N\text{-}2)_2]^-$ ligands is thus hexadentate.

Conclusion

The synthesis and structures of the following crystalline alkali metal amides is reported:

 © 2003 Wiley-VCH Verlag GmbH & Co. KGaA, Weinheim

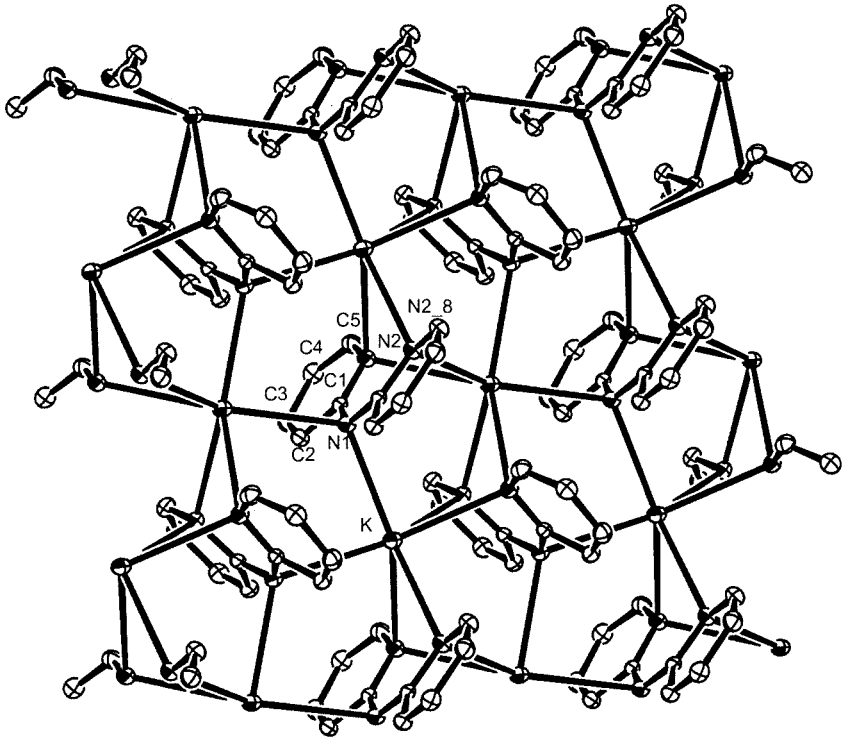

Figure 10. Polymeric layer crystal structure of $[K\{\mu\text{-}N(2\text{-}C_5H_4N)_2\}]_\infty$ (**9**)

Table 8. Selected bond lengths (Å) and angle (°) for **9**

Bond		Angle	
K−N(1)	2.8911(17)	N(1)−K−N(1)#5	84.62(3)
K−N(2)#1	2.8949(12)		
K−N(2)#2	2.8949(12)		
K−N(2)#3	2.9744(12)		
K−N(2)#4	2.9744(12)		
K−N(1)#5	3.0729(17)		

1. the homologous series of compounds $[(M\{\mu\text{-}N(SiMe_2Ph)(SiMe_3)\})_2]_n$ [the *cis* complex for $n = 1$ and M = Li (**1**); and the *trans* complexes with $n = \infty$ and M = Na (**2**), K (**4**), Rb (**5**), Cs (**6**)];
2. $[(Na\{\mu\text{-}trans\text{-}N(SiMe_2Ph)(SiMe_3)\})_2(tmeda)]$ (**3**);
3. $[(K\{\mu\text{-}trans\text{-}N(t\text{Bu})(SiMe_3)\})_4(\eta\text{-}C_6H_6)_2]$ (**7**);
4. $[(K\{\mu\text{-}trans\text{-}N(Ph)(2\text{-}C_5H_4N)\})_2(\mu'\text{-thf})_3]_\infty$ (**8**);
5. $[K\{\mu\text{-}N(2\text{-}C_5H_4N)_2\}]_\infty$ (**9**).

Each of **1**−**9** has an unusual, and in some cases unprecedented, molecular structure. Thus **1** is only the second example of a neutral donor-free binuclear lithium amide, while **2** has no antecedents as a neutral donor-free sodium amide. Complex **3** is remarkable in having only one of its two sodium ions bound by a chelating tmeda ligand. Each of the isoleptic amides **4**, **5** and **6** adopts a similar polymeric chain structure made up of a tetranuclear aggregate of two independent dimers **A** and **B**. The centrosymmetric tetranuclear potassium amide **7** is the first potassium amide of ladder structure. The polymeric chain complex **8** provides the first example of a complex in which two metal ions are bridged by three THF ligands. Complex **9**, although crystallised from THF, is a THF-free sheet polymer and is the first X-ray-characterised alkali metal bis(2-pyridyl)amide.

Table 9 provides a summary of the metal coordination environment, as well as M···L contacts, in which L represents a non-nitrogen-centred neutral ligand.

Experimental Section

General Remarks: All manipulations were performed under argon using standard Schlenk techniques. Toluene was dried using sodium. Pentane, benzene and hexane were dried using sodium-potassium alloy; THF was dried and distilled from sodium-benzophenone and stored over a sodium mirror under argon; tmeda (Aldrich) was distilled from CaH_2 prior to use. The NMR spectra were recorded on a Bruker DPX 300 (300.1 MHz for ^1H, 75.5 MHz for ^{13}C and 116.6 MHz for ^7Li) or AMX 500 (49.7 MHz for ^{29}Si) instruments and referenced externally (^7Li, using LiCl; ^{29}Si, using $SiMe_4$) or internally to the residual solvent resonances (chemical shift data in δ). Unless otherwise stated, all NMR spectra were measured at 298 K and other than ^1H were proton-decoupled. Electron impact mass spectra were taken from solid samples using a Kratos MS 80 RF instrument. Melting points were taken in sealed capillaries and are uncorrected. Elemental analyses were determined by Medac Ltd., Brunel University. The amines HN(*t*Bu)SiMe_3 and HN($SiMe_2Ph$)($SiMe_3$) (Aldrich) were dried over KOH and distilled therefrom, while HN(Ph)(2-C_5H_4N) and HN(2-$C_5H_4N)_2$ (Aldrich) were used without purification.

$[Li\{\mu\text{-}cis\text{-}N(SiMe_2Ph)(SiMe_3)\}]_2$ (1): L*i*nBu (6 mL of a 1.6 mol·dm^{-3} solution in hexane, 9.60 mmol) was added dropwise to a cooled (−70 °C) and stirred solution of HN($SiMe_2Ph$)($SiMe_3$) (2.13 g, 9.53 mmol) in pentane (35 mL) over a period of 15 min. The reaction mixture was warmed to room temperature and stirred

 © 2003 Wiley-VCH Verlag GmbH & Co. KGaA, Weinheim

Table 9. Metal ligating atoms and coordination numbers (CN) and M···C close and K−O (**8**) contacts for compounds **1**−**9**

Compound	CN of M	M···Ph/ M···Me/ K···η^6-C_6H_6/ K−O/ Å
1	2N + C, 3	2.444(3) and 2.430(3), *ipso*-C.
2	2N +3C, 5	2.947(2) × 2, Me and 3.059(2), Me adjacent dimer.
	2N +4C, 6	2.868(1) × 2, *ipso*-C and 2.884(2) × 2, *ortho*-C.
3	2N +2C, 4	2.692(2), *ipso*-C and 2.730(3), *ipso*-C.
	4N, 4	
4	2N +4C, 6	3.381(2), *ipso*-C; 3.587(2), *o*-C; 3.450(2) and 3.357(2), Me.
	2N +4C, 6	3.512(2), *m*-C; 3.225(2), *m*-C; 3.119(2), *p*-C; 3.231(2), Me.
5	2N +6C, 8	3.339(7), *ipso*-C; 3.407(7), *o*-C; 3.466(8), *o*-C; 3.716(7), *m*-C; 3.640(8), *m*-C; and 3.570(7), *p*-C.
6	2N +5C, 7	3.473(2), *ipso*-C; 3.586(2), *ipso*-C; 3.556(2), *o*-C; 3.487(2), *o*-C; and 3.682(2), *m*-C.
	2N +4C, 6	3.451(2), *ipso*-C; 3.653(2), *o*-C; 3.556(2), Me; 3.642(2), Me.
7	2N +6C, 9	3.032, centroid of η-C_6H_6.
	3N +2C, 5	3.301(5) and 3.231(5), Me.
8	4N +3O, 7	2.760(2), 2.817(2) and 2.885(2), O
9	6N, 6	

for 12 h. The mixture was filtered and the filtrate was concentrated and stored at −25 °C for two days yielding tiny white crystals. Recrystallisation from hexane afforded colourless crystals of **1** (1.22 g, 56%), m.p. 60−65 °C. $C_{22}H_{40}Li_2N_2Si_4$ (458.8): calcd. C 57.6, H 8.79, N 6.10; found C 56.6, H 8.30, N 5.81. ^{1}H NMR ($C_6D_5CD_3$): δ = 0.02 (s, 9 H, $SiMe_3$), 0.27 (s, 6 H, $SiMe_2Ph$), 7.07−7.17 (m, 1 H, *p*-H), 7.20−7.25 (t, $^3J_{H,H}$ = 6.4 Hz, 2 H), 7.45 (dd, $^3J_{H,H}$ = 6.4, $^4J_{H,H}$ = 1.4 Hz, 2 H) ppm. ^{13}C NMR ($C_6D_5CD_3$): δ = 3.5 ($SiMe_3$), 4.7 ($SiMe_2Ph$), 129.7, 129.9, 133.2, 143.8 (*ipso*-C) ppm. ^{29}Si NMR ($C_6D_5CD_3$): δ = −13.9, −10.6 ppm. ^{7}Li NMR ($C_6D_5CD_3$): δ = −2.0 ppm. MS (*M* denotes the monomer): *m*/*z* (%) = 271 (10) [M_2 − $SiMe_2Ph$ −3Me − Li]$^+$, 208 (100) [$SiMe_2Ph$ + $SiMe_3$]$^+$, 192 (57) [271 − $SiMe_3$ − Li + H]$^+$.

[(Na{μ-*trans*-N($SiMe_2Ph$)($SiMe_3$)})$_2$]$_\infty$ (2): Benzylsodium (0.43 g, 3.80 mmol) was added in small portions to a cooled (−78 °C) and stirred solution of HN($SiMe_2Ph$)($SiMe_3$) (0.963 mL, 3.74 mmol) in hexane (50 mL). The reaction mixture was warmed to room temperature and stirred for 12 h. The volatiles were removed at 35 °C/10^{-2} Torr for 30 min. The residue was washed with hexane to yield compound **2** as a white fluffy powder (0.72 g, 79%). $C_{22}H_{40}N_2Na_2Si_4$ (491.0): calcd. C 53.8, H 8.21, N 5.71; found C 52.5, H 8.28, N 5.49%. Recrystallisation from benzene after 1 day at 15 °C afforded colourless plates of **2** (0.57 g, 62%), m.p. 130−133 °C. ^{1}H NMR (C_6D_6): δ = 0.05 (s, 9 H, $SiMe_3$), 0.31 (s, 6 H, $SiMe_2Ph$), 7.14−7.23 (m, 3 H), 7.50 (d, $^3J_{H,H}$ = 7.7 Hz, 2 H) ppm. ^{13}C NMR (C_6D_6): δ = 5.1 ($SiMe_3$), 6.9 ($SiMe_2Ph$), 128.5 (*p*-C), 128.8, 132.7, 148.7 (*ipso*-C) ppm. ^{29}Si NMR (C_6D_6): δ = −18.1, −13.2 ppm. MS (*M* denotes the monomer): *m*/*z* (%) = 342 (50) [M_2 − $PhSiMe_3$ +2H]$^+$, 270 (55) [Na_2M +2H]$^+$, 192 (100) [M − Na]$^+$, 135 (70) [$SiPhMe_2$]$^+$.

[(Na{μ-*trans*-N($SiMe_2Ph$)($SiMe_3$)})$_2$(tmeda)] (3): Addition of tmeda (0.57 mL, 3.75 mmol) to a milky suspension of Na[N($SiMe_2Ph$)($SiMe_3$)] (0.46 g, 1.87 mmol) in hexane (40 mL) immediately gave a colourless mixture, which was stirred for 2 h at room temperature, then filtered. The volatiles were removed at 25 °C/10^{-2} Torr for 30 min. The residue was extracted with benzene (20 mL) and the extract was concentrated (to ca. 1 mL); hexane (10 mL) was added. Storage at −25 °C for two weeks yielded compound **3** (0.52 g, 44%) as transparent crystals, m.p. 55−60 °C. $C_{28}H_{56}N_4Na_2Si_4$ (607.1): calcd. C 55.4, H 9.30, N 9.22; found C 54.1, H 9.32, N 8.95. ^{1}H NMR (C_6D_6): δ = 0.23 (s, 9 H, $SiMe_3$), 0.47 (s, 6 H, $SiMe_2$), 1.52 (s, 4 H, CH_2, tmeda), 1.62 (s, 12 H, Me, tmeda), 7.23 (m, 3 H, *p*-H and *m*-H), 7.66 (d, $^3J_{H,H}$ = 7.77, $^4J_{H,H}$ = 1.37 Hz, 2 H, *o*-H) ppm. ^{13}C NMR (C_6D_6): δ = 5.3 ($SiMe_3$), 7.1 ($SiMe_2Ph$), 45.3 (CH_3, tmeda), 56.6 (CH_2, tmeda), 132.95, 128.1, 128.6 (Ph), 149.8 (*ipso*-C) ppm. ^{29}Si NMR (C_6D_6): δ = −20.9 ($SiMe_3$), −16.6 ($SiMe_2Ph$) ppm. MS (*M* denotes the monomer of **3**): *m*/*z* (%) = 530 (8) [M_2 − Ph]$^+$, 500 (13) [M_2 − Ph − 2Me]$^+$, 475 (63) [M_2 − $SiMe_2Ph$ − 3H]$^+$, 459 (80) [M_2-2$SiMe_3$]$^+$, 399 (35) [M_2 − amine − Me]$^+$, 230 (100) [*M* − tmeda − Me]$^+$, 208 (95) [*M* − tmeda − Na − Me]$^+$, 192 (82) [208 − Me]$^+$, 58 (100) [1/2 tmeda]$^+$.

[(K{μ-*trans*-N($SiMe_2Ph$)($SiMe_3$)})$_2$]$_\infty$ (4): Benzylpotassium (1.0 g, 7.68 mmol) was added in small portions to a cooled (−78 °C) and stirred solution of HN($SiMe_2Ph$)($SiMe_3$) (2.1 mL, 8.06 mmol) in hexane (60 mL). The reaction mixture was allowed to warm up to room temperature and stirred for 12 h. The volatiles were removed at 35 °C/10^{-2} Torr for 30 min. The residue was washed with hexane (4 × 15 mL) to yield compound **4** (1.76 g, 88%) as a white fluffy powder, m.p. 131−135 °C. $C_{22}H_{40}K_2N_2Si_4$ (532.1): calcd. C 50.5, H 7.71, N 5.35; found C 48.7, H 7.81, N 5.35. Sublimation at 180 °C/5 × 10^{-4} Torr afforded a few X-ray quality crystals. ^{1}H NMR (C_6D_6): δ = 0.12 (s, 9 H, $SiMe_3$), 0.28 (s, 6 H, $SiMe_2Ph$), 7.18 (dd, $^3J_{H,H}$ = 1.50, $^4J_{H,H}$ = 1.37 Hz, 2 H), 7.23 (d, $^3J_{H,H}$ = 7.23 Hz, 2 H), 7.55 (dd, $^3J_{H,H}$ = 7.51, $^4J_{H,H}$ = 1.35 Hz, 2 H) ppm. ^{13}C NMR (C_6D_6): δ = 5.6 ($SiMe_3$), 7.2 ($SiMe_2Ph$), 127.8, 128.3, 133.1 (Ph) ppm. ^{29}Si NMR (C_6D_6): δ = −24.0, −19.5 ppm. MS (*M* denotes the monomer): *m*/*z* (%) = 270 (22) [M_2 − $SiMe_2Ph$ − $SiMe_3$-3Me + H]$^+$), 208 (100) [$SiMe_3$ + $SiMe_2Ph$]$^+$, 194 (72) [208 − Me + H]$^+$.

[(Rb{μ-*trans*-N($SiMe_2Ph$)($SiMe_3$)})$_2$]$_\infty$ (5): Benzylrubidium (0.23 g, 1.30 mmol) was added in small portions to a cooled (−78 °C) and stirred solution of HN($SiMe_2Ph$)($SiMe_3$) (0.35 mL, 1.36 mmol) in hexane (25 mL). The reaction mixture was allowed to warm up to room temperature and stirred for 12 h. The volatiles were removed at 25 °C/10^{-2} Torr for 30 min. The residue was washed with hexane (4 × 5 mL) to yield compound **5** (0.35 g, 87%) as a grey fluffy powder. $C_{22}H_{40}N_2Rb_2Si_4$ (615.9): calcd. C 42.9, H 6.55, N 4.55; found C 39.8, H 6.59, N 4.49. Compound **5** was extracted into hot toluene (10 mL) and the extract was filtered; the filtrate was concentrated and stored at 15 °C for 12 h to afford tiny transparent crystals, m.p. 150−152 °C. ^{1}H NMR ($C_6D_5CD_3$): δ = 0.03 (s, 9 H, $SiMe_3$), 0.22 (s, 6 H, $SiMe_2Ph$), 7.12 (m, 3 H, *p*-H and *m*-H), 7.49 (dd, $^3J_{H,H}$ = 7.84, $^4J_{H,H}$ = 1.46 Hz, 2 H) ppm. ^{13}C NMR ($C_6D_5CD_3$): δ = 5.4 ($SiMe_3$), 7.2 ($SiMe_2$), 127.6, 128.2, 133.2 (Ph) ppm. MS (*M* denotes the monomer): *m*/*z* (%) = 344 (10)

 © 2003 Wiley-VCH Verlag GmbH & Co. KGaA, Weinheim

$[\{RbN\}_2(SiMe_3)_2]^+$, 270 (95) $[\{RbN\}_2(SiMe_3) - H]^+$, 208 (100) [*M* − Rb − Me]$^+$, 192 (85) [*M* − Rb − 2Me]$^+$.

[(Cs{μ-*trans*-N(SiMe$_2$Ph)(SiMe$_3$)})$_2$]$_\infty$ (6): Benzylcaesium (0.49 g, 2.20 mmol) was added in small portions to a cooled (−78 °C) and stirred solution of HN(SiMe$_2$Ph)(SiMe$_3$) (0.59 mL, 2.31 mmol) in hexane (40 mL). The reaction mixture was allowed to warm up to room temperature and stirred for 12 h. The volatiles were removed at 35 °C/10^{-2} Torr for 30 min. The residue was washed with hexane (4 × 10 mL) to yield compound **6** (0.67 g, 88%), as a cream fluffy powder, m.p. (decomp.) 125 °C. Compound **6** was extracted into hot toluene and the extract was filtered; the filtrate was concentrated and stored at room temperature for 12 h to furnish a few X-ray quality crystals. ^{1}H NMR (C_6D_6): δ = 0.19 (s, 9 H, SiMe$_3$), 0.39 (s, 6 H, SiMe$_2$Ph), 7.10 (m, 1 H, *p*-H), 7.18 (m, 2 H, *m*-H), 7.67 (d, $^3J_{H,H}$ = 6.02 Hz, 2 H, *o*-H) ppm. ^{13}C NMR (C_6D_6): δ = 5.4 (SiMe$_3$), 7.4 (SiMe$_2$Ph), 127.4, 128.05, 133.9 (Ph), 150.8 (*ipso*-C) ppm. ^{29}Si NMR (C_6D_6): δ = −26.3, −21.8 ppm. MS (*M* denotes the monomer): *m*/*z* (%) = 355 (9) $[M_2]^+$, 281 (12) [M_2 − SiMe$_3$]$^+$, 208 (100) [M_2 − Cs − Me]$^+$, 192 (53) [M_2 − Cs − 2Me]$^+$, 133 (81) [PhMe$_2$Si − 2H]$^+$, 78 (67) [SiMe$_3$]$^+$.

[(K{μ-*trans*-N*t*Bu(SiMe$_3$)})$_4$(η-C$_6$H$_6$)$_2$] (7): Benzylpotassium (0.59 g, 4.56 mmol) was added in small portions to a cooled (−78 °C) and stirred solution of HN*t*Bu(SiMe$_3$) (1.18 mL, 4.80 mmol) in hexane (45 mL). The reaction mixture was warmed to room temperature and stirred for 12 h. The volatiles were removed at 25 °C/10^{-2} Torr. The residual cream solid was washed with hexane (4 × 10 mL). Filtration and drying of the residue for 30 min at 25 °C/10^{-2} Torr yielded K[N*t*Bu(SiMe$_3$)] (**7a**; 0.77 g, 88%), as a white powder. $C_7H_{18}KNSi$ (367.0): calcd. C 45.8, H 9.01, N 6.98; found C 43.8, H 8.71, N 6.50. X-ray-suitable crystals were obtained by dissolving K[N*t*Bu(SiMe$_3$)] (0.49 g) in a mixture of hexane (40 mL) and benzene (20 mL). The solution was concentrated and stored at 15 °C for seven days yielding compound **7** as a few transparent, plate-shaped crystals, m.p. 131−135 °C. ^{1}H NMR (C_6D_6): δ = 0.18 (s, 9 H, SiMe$_3$), 1.26 (s, 9 H, *t*Bu) ppm. ^{13}C NMR (C_6D_6): δ = 7.8 (SiMe$_3$), 39.15 (*t*Bu), 52.4 (C, *t*Bu) ppm. ^{29}Si NMR (C_6D_6): δ = −25.4 ppm. MS (*M* denotes the monomer): *m*/*z* (%) = 423 (3) [M_2 + *t*Bu]$^+$, 281 (5) [M_2 − *t*Bu − 2Me + H]$^+$, 222 (29) [K_2M]$^+$, 167 (40) [K(N*t*Bu)$_2$ − Me + H]$^+$, 147 (50) [222 − SiMe$_3$]$^+$, 73 (83) [SiMe$_3$]$^+$.

Na[N*t*Bu(SiMe$_3$)] (7b): Benzylsodium (0.54 g, 4.76 mmol) was added in small portions to a cooled (−78 °C) and stirred solution of HN*t*Bu(SiMe$_3$) (0.96 mL, 5.01 mmol) in hexane (45 mL). The mixture was warmed to room temperature and stirred for 5 h. The volatiles were removed at 25 °C/10^{-2} Torr. The residual cream solid was washed with hexane (4 × 10 mL). Filtration and drying of the residue in vacuo for 30 min at 25 °C/10^{-2} Torr yielded compound **7b** (0.78 g, 93%), as a white powder, m.p. 185−187 °C. ^{1}H NMR (C_6D_6): δ = 0.19 (s, 9 H, SiMe$_3$), 1.21 (s, 9 H, *t*Bu) ppm. ^{13}C NMR (C_6D_6): δ = 7.4 (SiMe$_3$), 39.0 (*t*Bu), 51.9 (C, *t*Bu) ppm. ^{29}Si NMR (C_6D_6): δ = −18.2 ppm. MS (*M* denotes the monomer): *m*/*z* (%) = 229 (8) [M_2 − SiMe$_3$-2Me + 2H]$^+$), 207 (10) [229 − Na]$^+$, 149 (12) [207 − SiMe$_2$]$^+$.

[(K{μ-*trans*-N(Ph)(2-C$_5$H$_4$N)})$_2$(μ-thf)$_3$]$_\infty$ (8): *N*-2-Pyridylaniline (0.51 g, 3.00 mmol) was added in small portions to a stirred suspension of KH (0.13 g, 3.22 mmol) in THF (100 mL). The light yellow suspension was stirred for 2 h and filtered. The filtrate was concentrated to yield pale-yellow crystals of compound **8**, which, after drying in a vacuum, gave K{N(Ph)(2-C$_5$H$_4$N)} (0.56 g, 89%). $C_{11}H_9KN_2$ (208.3): calcd. C 63.4, H 4.35, N 13.45; found C 63.35, H 4.38, N 13.51. ^{1}H NMR ([D$_8$]THF): δ = 7.78 (ddd, $J_{6\text{-H},5\text{-H}}$ = 4.97, $J_{6\text{-H},4\text{-H}}$ = 2.23, $J_{6\text{-H},3\text{-H}}$ = 0.90, 1 H, *6-H* of 2-C$_5$H$_4$N), 6.96 (m, 4 H, *o*- and *m*-*H* of Ph), 6.89 (ddd, $J_{4\text{-H},3\text{-H}}$ = 8.76, $J_{4\text{-H},5\text{-H}}$ = 6.59, $J_{4\text{-H},6\text{-H}}$ = 2.23, 1 H, *4-H* of 2-C$_5$H$_4$N), 6.71 (dt, $J_{3\text{-H},4\text{-H}}$ = 8.72, $J_{3\text{-H},5\text{-H}}$ = $J_{3\text{-H},6\text{-H}}$ = 0.99, 1 H, *3-H* of 2-C$_5$H$_4$N), 6.42 (m, 1 H, *p*-*H* of Ph), 5.83 (ddd, $J_{5\text{-H},4\text{-H}}$ = 6.35, $J_{5\text{-H},6\text{-H}}$ = 4.97, $J_{5\text{-H},3\text{-H}}$ = 1.05 Hz, 1 H, *5-H* of 2-C$_5$H$_4$N) ppm. ^{13}C NMR ([D$_8$]thf): δ = 166.6 (*ipso*-*C* of Ph), 156.4 (*2-C* of 2-C$_5$H$_4$N), 149.9 (*6-C* of 2-C$_5$H$_4$N), 136.0 (*4-C* of 2-C$_5$H$_4$N), 128.9 (*m*-*C* of Ph), 121.45 (*o*-*C* of Ph), 116.1 (*5-C* of 2-C$_5$H$_4$N), 107.9 (*3-C* of 2-C$_5$H$_4$N), 105.5 (*p*-*C* of Ph) ppm.

[K{μ-N(2-C$_5$H$_4$N)$_2$}]$_\infty$ (9): Colourless complex **9** (0.46 g, 93%) was synthesised by a procedure similar to that used for compound **8**, from HN(2-C$_5$H$_4$N)$_2$ (0.40 g, 2.36 mmol), KH (0.10 g, 2.49 mmol) in THF (100 mL). $C_{10}H_8KN_3$ (209.3): calcd. C 57.4, H 3.85, N 20.08; found C 57.45, H 3.89, N 20.07. ^{1}H NMR ([D$_8$]THF): δ = 7.92 (d, *J* = 4.39 Hz, 2 H, *6-H*), 7.21 (d, *J* = 8.78 Hz, 2 H, *3-H*), 7.09 (t, *J* = 8.78 Hz, 2 H, *4-H*), 6.14 (t, *J* = 5.86 Hz, 2 H, *5-H*) ppm. ^{13}C NMR ([D$_8$]THF): δ = 167.1 (*2-C* of 2-C$_5$H$_4$N), 149.0 (*6-

Table 10. Crystallographic data for compounds **3**−**9** at *T* = 173(2) K

	3	**4**	**5**	**6**	**7**	**8**	**9**
Formula	$C_{28}H_{56}N_4Na_2Si_4$	$C_{22}H_{40}K_2N_2Si_4$	$C_{22}H_{40}N_2Rb_2Si_4$	$C_{22}H_{40}Cs_2N_2Si_4$	$C_{40}H_{84}K_4N_4Si_4$	$C_{34}H_{42}K_2N_4O_3$	$C_{10}H_8KN_3$
M	607.11	523.12	615.86	710.74	889.87	632.92	209.29
Crystal system	Monoclinic	Monoclinic	Triclinic	Monoclinic	Triclinic	Monoclinic	Orthorhombic
Space group	$P2_1/n$ (No. 14)	$P2_1/c$ (No. 14)	$P\bar{1}$ (No. 2)	$P2_1/c$ (No. 14)	$P\bar{1}$ (No. 2)	$C2/c$ (No. 15)	*Pnma* (No. 62)
a (Å)	11.3850(4)	13.5077(3)	11.4685(11)	11.5066(2)	10.9027(5)	23.705(2)	6.7598(3)
b (Å)	17.7048(6)	13.4679(2)	11.9751(12)	15.8809(4)	11.0047(4)	10.8276(10)	20.6744(14)
c (Å)	18.7964(4)	16.9813(3)	12.0417(9)	17.8558(4)	12.8942(5)	14.8147(9)	6.6776(4)
α (°)	90	90	82.850(5)	90	72.333(2)	90	90
β (°)	90.754(2)	99.365(1)	69.220(6)	106.499(2)	77.825(2)	115.378(5)	90
γ (°)	90	90	78.061(4)	90	65.383(2)	90	90
V (Å^3)	3788.4(2)	3048.1(1)	1510.4(2)	3128.5(1)	1333.73(9)	3435.5(5)	933.23(9)
Z	4	4	2	4	1	4	4
μ (mm^{-1})	0.20	0.48	3.41	2.49	0.45	0.31	0.53
Unique reflections, R_{int}	6661, 0.070	5336, 0.053	5269, 0.090	8942, 0.040	4560, 0.035	3007, 0.062	1388, 0.047
Reflections with $I > 2\sigma(I)$	4939	4524	2823	7692	3767	2011	1191
Final *R* indices	*R*1 = 0.045	*R*1 = 0.038	*R*1 = 0.069	*R*1 = 0.033	*R*1 = 0.042	*R*1 = 0.051	*R*1 = 0.036
[$I > 2\sigma(I)$]	*wR*2 = 0.098	*wR*2 = 0.114	*wR*2 = 0.116	*wR*2 = 0.072	*wR*2 = 0.102	*wR*2 = 0.107	*wR*2 = 0.088
R indices	*R*1 = 0.072	*R*1 = 0.047	*R*1 = 0.157	*R*1 = 0.041	*R*1 = 0.055	*R*1 = 0.093	*R*1 = 0.045
(all data)	*wR*2 = 0.109	*wR*2 = 0.127	*wR*2 = 0.144	*wR*2 = 0.076	*wR*2 = 0.108	*wR*2 = 0.122	*wR*2 = 0.092

 © 2003 Wiley-VCH Verlag GmbH & Co. KGaA, Weinheim

C of 2-C_5H_4N), 135.95 (*4*-*C* of 2-C_5H_4N), 114.1 (*5*-*C* of 2-C_5H_4N), 109.45 (*3*-*C* of 2-C_5H_4N) ppm.

X-ray Crystallographic Study: Diffraction data for compounds **3**−**9** were collected on an Enraf−Nonius Kappa-CCD diffractometer using monochromated Mo-K_α radiation (λ = 0.71073 Å). Crystals were directly mounted on the diffractometer under a stream of cold nitrogen gas. For compound **7**, the [N(*t*Bu)$SiMe_3$] groups are predominantly as shown in Figure 5 but with a small occupancy having the *t*Bu and $SiMe_3$ groups reversed; the disorder is 0.75:0.25 for the N1 group and 0.87:0.13 for the N2 group; the disorder was not resolved and hence the dimensions within these groups are unreliable. The structures were refined on all F^2 using SHELXL 97.[37] Further details are given in Table 10.

CCDC-209646 (**3**), -209647 (**4**), -209648 (**5**), -209649 (**6**), -209650 (**7**), -202589 (**8**), and -202590 (**9**) contain the supplementary crystallographic data for this paper. These data can be obtained free of charge at www.ccdc.cam.ac.uk/conts/retrieving.html [or from the Cambridge Crystallographic Data Centre, 12, Union Road, Cambridge CB2 1EZ, UK; fax: (internat.) +44-1223/336-033; E-mail: deposit@ccdc.cam.ac.uk].

Acknowledgments

We thank the EU and the University of Bologna for provision of a studentship for F. A. and the Royal Society for the award of an R.S./NATO fellowship for A. V. K. and EPSRC for financial support.

[1] B. J. Wakefield, *Best Synthetic Methods: Organolithium Methods*, Academic Press, London, **1988**.
[2] L. Brandsma, H. Verkuijsse, *Preparative Polar Organometallic Chemistry 1*, Springer, Berlin, **1987**.
[3] D. Seebach, *Angew. Chem. Int. Ed. Engl.* **1988**, *27*, 1624−1654.
[4] G. Boche, *Angew. Chem. Int. Ed. Engl.* **1989**, *28*, 277−297.
[5] V. Snieckus, *Chem. Rev.* **1990**, *90*, 879−933.
[6] *Lithium Chemistry* (Eds.: A. M. Sapse, P. v. R. Schleyer), Wiley, New York, **1994**.
[7] P. J. Cox, N. S. Simpkins, *Tetrahedron: Asymmetry* **1991**, *2*, 1−26.
[8] P. Beak, A. Basu, D. J. Gallagher, Y. S. Park, S. Thayumanavan, *Acc. Chem. Res.* **1996**, *29*, 552−560.
[9] D. Hoppe, T. Hense, *Angew. Chem. Int. Ed. Engl.* **1997**, *36*, 2282−2316.
[10] P. O'Brien, *J. Chem. Soc., Perkin Trans. 1* **1998**, 1439−1457.
[11] P. O'Brien, *J. Chem. Soc., Perkin Trans. 1* **2001**, 95−113.
[12] M. F. Lappert, P. P. Power, A. R. Sanger, R. C. Srivastava, *Metal and Metalloid Amides*, Horwood-Wiley, Chichester, **1980**.
[13] R. E. Mulvey, *Chem. Soc. Rev.* **1991**, *20*, 167−209.
[14] R. E. Mulvey, *Chem. Soc. Rev.* **1998**, *27*, 339−346.
[15] K. Gregory, P. v. R. Schleyer, R. Snaith, *Adv. Inorg. Chem.* **1991**, *37*, 47.
[16] S. Daniele, P. B. Hitchcock, M. F. Lappert, T. A. Nile, C. M. Zdanski, *J. Chem. Soc., Dalton Trans.* **2002**, 3980−3984.
[17] J. P. Bezombes, P. B. Hitchcock, M. F. Lappert, P. G. Merle, *J. Chem. Soc., Dalton Trans.* **2001**, 816−821.
[18] F. Antolini, P. B. Hitchcock, M. F. Lappert, P. G. Merle, *Chem. Commun.* **2000**, 1301−1302.
[19] P. C. Andrews, D. R. Barker, R. E. Mulvey, W. Clegg, P. A. O'Neil, *Polyhedron* **1991**, *10*, 1839−1841.
[20] L.-P. Wu, R. Field, T. Morrissey, C. Murphy, P. Nagle, B. Hathaway, C. Simmons, P. Thornton, *J. Chem. Soc., Dalton Trans.* **1990**, 3835−3840.
[21] R. Clérac, F. A. Cotton, L. M. Daniels, K. R. Dunbar, K. Kirschbaum, C. A. Murillo, A. A. Pinkerton, A. J. Schultz, X. Wang, *J. Am. Chem. Soc.* **2000**, *122*, 6226−6236, and refs. therein.
[22] D. K. Kennepohl, S. Brooker, G. M. Sheldrick, H. W. Roesky, *Chem. Ber.* **1991**, *124*, 2223−2225.
[23] K. F. Tesh, T. P. Hanusa, J. C. Huffman, *Inorg. Chem.* **1990**, *29*, 1584−1586.
[24] P. G. Williard, *Acta Crystallogr., Sect. C* **1988**, *44*, 270−272.
[25] S. Neander, U. Behrens, *Z. Anorg. Allg. Chem.* **1999**, *625*, 1429−1434.
[26] S. T. Liddle, W. Clegg, *J. Chem. Soc., Dalton Trans.* **2001**, 402−408.
[27] C. Frenzel, F. Somoza, S. Blaurock, E. Hey-Hawkins, *J. Chem. Soc., Dalton Trans.* **2001**, 3115−3118.
[28] N. Hu, L. Gong, Z. Jin, W. Chen, *J. Organomet. Chem.* **1988**, *352*, 61−66.
[29] M. C. Fermin, J. Ho, D. W. Stephan, *J. Am. Chem. Soc.* **1994**, *116*, 6033−6034.
[30] M. C. Fermin, J. Ho, D. W. Stephan, *Organometallics* **1995**, *14*, 4247−4256.
[31] Z. Hou, X. Jia, A. Fujita, H. Tezuka, H. Yamazaki, Y. Wakatsuki, *Chem. Eur. J.* **2000**, *6*, 2994−3005.
[32] S. Brooker, F. T. Edelmann, T. Kottke, H. W. Roesky, G. M. Sheldrick, D. Stalke, K. H. Whitmire, *J. Chem. Soc., Chem. Commun.* **1991**, 144−146.
[33] K. Dippel, U. Klingebiel, T. Kottke, F. Pauer, G. M. Sheldrick, D. Stalke, *Chem. Ber.* **1990**, *123*, 237−241.
[34] H. Bock, K. Gharagozloo-Hubmann, M. Sievert, T. Prisner, Z. Havlas, *Nature (London)* **2000**, *404*, 267−269.
[35] P. Müller, S. Huck, H. Köppel, H. Pritzkow, W. Siebert, *Z. Naturforsch., Teil B* **1995**, *50*, 1476−1484.
[36] Y. Liu, T. C. Stringfellow, D. Ballweg, I. A. Guzei, R. West, *J. Am. Chem. Soc.* **2002**, *124*, 49−57.
[37] G. M. Sheldrick, *SHELXL-97*, Universität Göttingen, **1997**.

Received May 13, 2003

 © 2003 Wiley-VCH Verlag GmbH & Co. KGaA, Weinheim

Hypersilyl-Substituted Complexes of Group 1 and 2 Metals: Syntheses, Structures and Use in Styrene Polymerisation

Florian Feil[a] and Sjoerd Harder*[a]

In memory of Professor Ron Snaith

Keywords: Alkali metals / Alkaline earth metals / Si ligands / Polymerization

Alkali and alkaline-earth metal complexes with sterically demanding hypersilyl-substituted cyclopentadienyl or fluorenyl ligands [hSi-Cp or hSi-Flu; hSi = $(Me_3Si)_3Si$] were prepared. The crystal structures of $[Li(hSi\text{-}Flu)(THF)_2]$, [K(hSi-Flu)(THF)], $[Ca(hSi\text{-}Flu)_2(THF)_2]$, $[Sr(hSi\text{-}Flu)_2(THF)_2]$ and $[Ca(hSi\text{-}Cp)_2(THF)]$ were determined. All structures show the enormous steric bulk of the hypersilyl substituent, which either results in a reduction in the number of solvent molecules in the coordination sphere of the metal or in a distortion of the ligand-metal interaction. Heteroleptic calcium and strontium complexes with a benzyl ligand (2-Me_2N-α-Me_3Si-benzyl) and a sterically demanding hSi-Flu ligand were prepared and used as initiators in the polymerization of styrene. The polymers produced with the heteroleptic benzylcalcium initiator are enriched in syndiotactic sequences, although they show the same tacticities as polymers obtained with benzylcalcium initiators containing the less bulky Me_3Si-Flu ligand. Introduction of the bulky hypersilyl group in heteroleptic benzylstrontium initiators resulted in a slight increase of the syndiotacticity of the polymers.
(© Wiley-VCH Verlag GmbH & Co. KGaA, 69451 Weinheim, Germany, 2003)

Introduction

We recently introduced novel heteroleptic benzylcalcium complexes (e.g. **1**)[1] as initiators for the living anionic polymerization of styrene. The polymers obtained show a high degree of syndiotacticity.[2] Syndioselective chain growth arises from a chain-end controlled insertion mechanism (**2**) in which communication between the chiral chain-end and the chiral carbon of a coordinated styrene monomer is responsible for stereocontrol. The 9-Me_3Si-fluorenyl group in **1** is a spectator ligand, i.e. it fills one side of the coordination sphere around calcium and is passive during the polymerization. We are currently studying the influence of the spectator ligand on the syndioselectivity in styrene polymerization.

A highly sterically demanding spectator ligand, like 9-hypersilyl-fluorenyl [9-$(Me_3Si)_3Si$-fluorenyl), would confine the remaining coordination sphere around calcium and decrease the distance between the chiral centers in the polymerization active species **3**. This might lead to a more efficient communication between chain-end and monomer, thus improving stereocontrol.

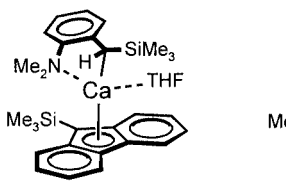

1

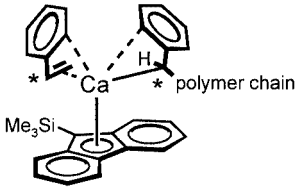

2

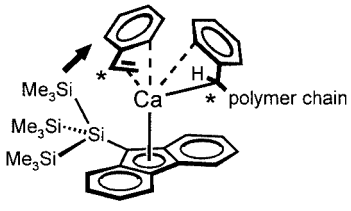

3

Here we describe the syntheses and structures of hypersilyl-substituted fluorenyl and cyclopentadienyl complexes of alkali and alkaline-earth metals. Also, the syntheses and applications in styrene polymerization of heteroleptic benzylcalcium and -strontium complexes containing the hypersilyl-substituted ligands are described.

[a] University of Konstanz
Postfach 5560 (M738), 78457 Konstanz, Germany
Fax: (internat.) +49-7531/883-137
E-mail: harder@chemie.uni-konstanz.de
Supporting information for this article is available on the WWW under http://www.eurjic.org or from the author.

Results and Discussion

Direct lithiation of 9-hypersilyl-fluorene (hSi-FluH) with *n*BuLi in THF gave the lithium complex 9-hypersilyl-fluorenyllithium Li(hSi-Flu) in quantitative yield. Recrystallization of the crude product yielded bright-red, plate-like crystals with the composition [Li(hSi-Flu)(THF)$_2$]. The monomeric lithium complex (Figure 1) contains a Li^+ ion with a nearly planar trigonal coordination sphere: the sum of the valence angles between O1, O2 and ring$_{center}$ is 357.2°. The Li^+ ion is bonded over the five-membered ring of the hSi-Flu ligand and, despite the steric bulk of the hypersilyl group, is situated slightly closer to the carbon attached to Si. This situation has also been observed in Me_3Si-fluorenyl complexes of the alkaline-earth metals[1,3] and is likely attributed to the higher charge-density at the silyl-substituted carbon. A space-filling model of Li(hSi-Flu) (Figure 1b) shows the extraordinary steric bulk of the hypersilyl substituent. This substituent is efficiently shielding a large part of the metal's coordination sphere, although no indication of agostic $SiCH_3\cdots Li^+$ interactions is found (the shortest C···Li distance observed is 3.975 Å).

The number of THF ligands attached to Li^+ is another measure of the steric bulk of the hSi-Flu anion. The *ansa*-lithocene anion $[Me_2Si(Flu)_2Li]^-$ also crystallizes with two THF ligands bonded to Li^+.[4] Likewise, a fluorenyllithium complex with a pendant chelating $CH_2CH_2NMe_2$ arm in the 9-position crystallizes with two THF ligands at the Li^+ ion.[5] Therefore, the steric demand of the hSi-Flu$^-$ ligand is similar to that of 9-$(Me_2NCH_2CH_2)$Flu$^-$ or to that of the dianionic *ansa*-ligand $Me_2Si(Flu)_2{}^{2-}$.

Reaction of 9-hypersilyl-fluorene with the superbase mixture *n*BuLi/KOCMe(Et)$_2$ yielded 9-hypersilyl-fluorenylpotassium K(hSi-Flu) in 85% isolated yield. Recrystallization of the raw product from a benzene/THF mixture gave orange needle-like crystals with the composition [K(hSi-Flu)(THF)(C_6H_6)]. The K(hSi-Flu) units form a polymer chain (Figure 2) in which the K^+ ions are sandwiched between the six-membered rings of neighbouring hSi-Flu anions. The large hypersilyl substituents of neighbouring hSi-Flu anions point in opposite directions. The THF ligands complete the planar trigonal coordination of the K^+ ions (the sum of the valence angles between O and the aryl ring centers is 359.4°). Vacant sites in the coordination sphere of K^+ are shielded by the bulk of the hypersilyl groups. Short $Si-CH_3\cdots K^+$ contacts (Figure 2) point to weak agostic interactions. The benzene solvent fills channels between the chains; there is no interaction between benzene and K^+. A similar chain structure was observed

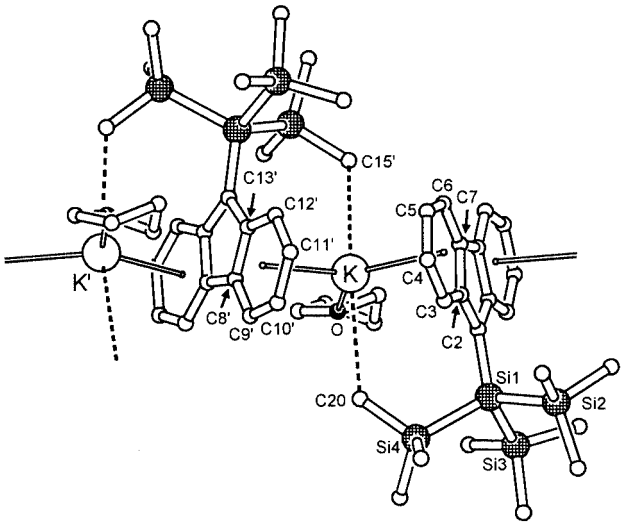

Figure 2. The crystal structure of {K(hSi-Flu)(THF)}$_\infty$ (hydrogens omitted for clarity); C−K bond lengths (Å) for atoms in the ring C2, C3, C4, C5, C6, C7 are respectively 3.053(4), 3.258(6), 3.391(8), 3.385(7), 3.210(6) and 3.015(4), ring$_{center}$−K = 2.903(3) Å; C−K bond lengths (Å) in the ring C8′, C9′, C10′, C11′, C12′, C13′ are respectively 3.114(4), 3.209(6), 3.240(7), 3.187(7), 3.117(6) and 3.072(4), ring$_{center}$−K 2.829(3) Å; O−K 1.919(4) Å; weak agostic $Si-CH_3\cdots K^+$ interactions: C15′···K 3.80(1) Å and C20···K 3.40(1) Å

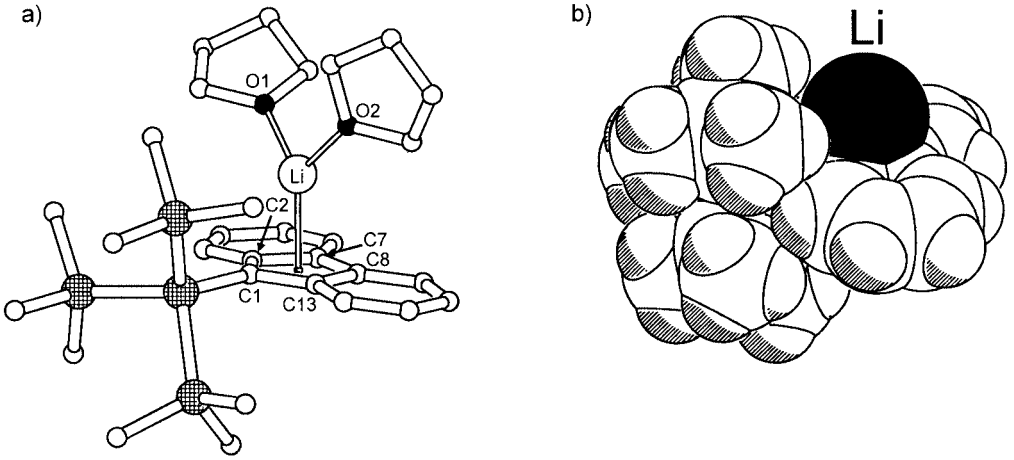

Figure 1. a) The crystal structure of [Li(hSi-Flu)(THF)$_2$] (hydrogens omitted for clarity); C−Li bond lengths (Å) for atoms in the ring C1, C2, C7, C8, C13 are respectively 2.321(5), 2.400(4), 2.486(4), 2.503(4) and 2.389(4), ring$_{center}$−Li 2.088(4) Å, O1−Li 1.919(4) Å and O2−Li 1.919(4) Å; b) space-filling model of the hSi-FluLi unit

 © 2003 Wiley-VCH Verlag GmbH & Co. KGaA, Weinheim

for K(9-*t*Bu-Flu),[6] which crystallizes with two, instead of one, THF ligands coordinated to K^+, again showing the steric bulk of the hypersilyl substituent.

Reaction of two equivalents of K(hSi-Flu) with CaI_2 in THF gave bis[9-hypersilyl-fluorenyl]calcium, Ca(hSi-Flu)$_2$. Recrystallization of the crude product from hot benzene yielded red, needle-like crystals with the composition [Ca(hSi-Flu)$_2$(THF)$_2$(C_6H_6)]. The crystal structure of this monomeric calcium complex is shown in Figure 3. One of the hSi-Flu$^-$ ligands binds the Ca^{2+} ion in an η^5 fashion with Ca−C bond lengths in the narrow range of 2.722(4)−2.785(4) Å. The second hSi-Flu$^-$ ligand binds to Ca^{2+} only with the outer edge of the fluorenyl ring. This is a rather unusual and hitherto unseen bonding mode for a fluorenyl ligand in a non-polymeric coordination complex. The enormous bulk of the hypersilyl group apparently blocks η^5 coordination of a second hSi-Flu ligand. Also, the shallow potential energy surface of the fluorenyl anion allows easy migration of the metal cations.[7] The structure of [Ca(hSi-Flu)$_2$(THF)$_2$] can be interpreted as an intermediate on the pathway for formation of the solvent-separated ion-pair (ssip) [hSi-FluCa$^+$·(THF)$_3$] [hSi-Flu$^-$]. Structures of the first ssip's with calcium have been reported only recently: the structure of [Cp*Ca$^+$·(O=PPh$_3$)$_3$][I$^-$][8] and the structure of a complete ssip [Me_3Si-Flu$^-$]$_2$ [C_6H_6]$_2$ [Ca^{2+}·(THF)$_6$], which was described with the "metal-in-a-box" model.[9]

The analogous Sr complex, Sr(hSi-Flu)$_2$, was obtained by reacting two equivalents of hSi-FluK with SrI_2 in THF. Recrystallization from hot hexane yielded dark-red crystals with the composition [Sr(hSi-Flu)$_2$(THF)$_2$]. The crystal structure of [Sr(hSi-Flu)$_2$(THF)$_2$] (Figure 4) is similar to that of its Ca analogue. One of the hSi-Flu$^-$ ligands is coordinated through the five-membered ring, whereas the other ligand coordinates through the aryl part of the fluorenyl ring. Despite the larger radius of Sr^{2+} (Ca: 0.99 Å, Sr 1.12 Å), a second coordination through the five-membered ring is still not possible on the basis of steric congestion. However, the larger Sr^{2+} ion allows a more extended aryl-metal interaction than in the Ca complex.

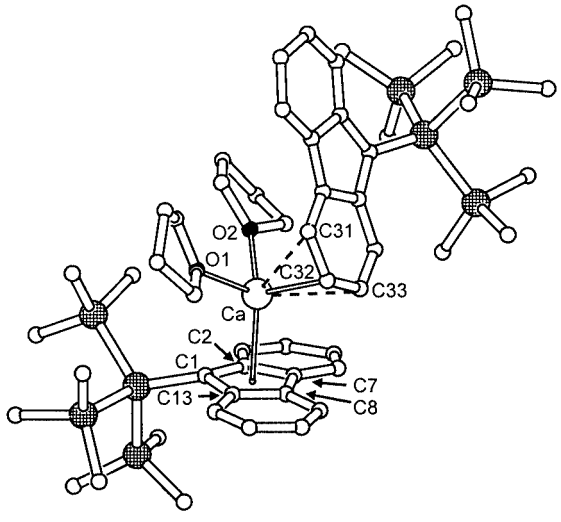

Figure 3. The crystal structure of [Ca(hSi-Flu)$_2$(THF)$_2$] (hydrogens omitted for clarity); C−Ca bond lengths (Å) for atoms in the ring C1, C2, C7, C8, C13 are respectively 2.748(4), 2.785(4), 2.766(4), 2.735(4) and 2.722(4), ring$_{center}$−Ca = 2.462(2) Å; Ca−O1 2.296(3), Ca−O2 2.376(4), Ca−C31 2.993(4), Ca−C32 2.662(4), Ca−C33 2.833(4)

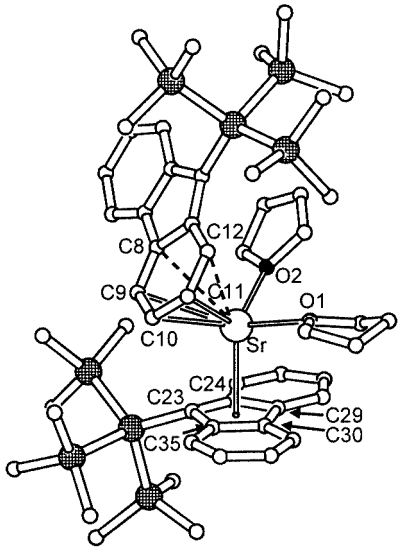

Figure 4. The crystal structure of [Sr(hSi-Flu)$_2$(THF)$_2$] (hydrogens omitted for clarity); C−Sr bond lengths (Å) for atoms in the ring C23, C24, C29, C30, C35 are respectively 2.913(3), 2.891(3), 2.852(3), 2.863(3) and 2.876(3), ring$_{center}$−Sr = 2.606(2) Å; Sr−C8 3.095(3), Sr−C9 2.927(4), Sr−C10 2.853(4), Sr−C11 2.929(4), Sr−C12 3.099(3), Sr−O1 2.466(3), Sr−O2 2.551(2)

The various crystal structures of alkali and alkaline-earth metal complexes with the hSi-Flu ligand show the enormous steric bulk of the hypersilyl substituent. The $(Me_3Si)_3Si$ substituents all display normal Si−Si and Si−C bond lengths, as well as expected tetrahedral Si−Si−Si, Si−Si−C and C−Si−C angles. This means that steric stress is relieved rather by deformation of the metal coordination sphere than by deformation of the hypersilyl substituent. It should be mentioned, however, that whereas the $(Me_3Si)_3Si$ geometry itself is practically undisturbed, the (Flu)C−Si bond is slightly elongated: bond lengths in the complexes reported here vary from 1.864(4) to 1.885(3) Å. In comparison, a typical (sp^2)C−Si bond length is tabulated as 1.84(1) Å[10] and the (Flu)C−Si bond length in **1** is 1.851(2) Å.[1] A similar situation was observed in the sterically congested $(Me_3Si)_3Si$-fluorene itself: the (Flu)C−Si bond of 1.947(4) Å[11] is significantly longer than an average (sp^3)C−Si bond [1.865(8) Å].[10] All structures reported here also show a similar rotation of the $(Me_3Si)_3Si$ substituent with respect to the fluorenyl plane: typically, one of the Me_3Si groups eclipses the plane of the fluorenyl ring, whereas the other two are in gauche positions. Especially noteworthy are the geometries of the (η^5)hSi-Flu ligands in the complexes [Ca(hSi-Flu)$_2$(THF)$_2$] and [Sr(hSi-Flu)$_2$(THF)$_2$]. The fluorenyl rings show deviations from planarity, with the aryl

 © 2003 Wiley-VCH Verlag GmbH & Co. KGaA, Weinheim

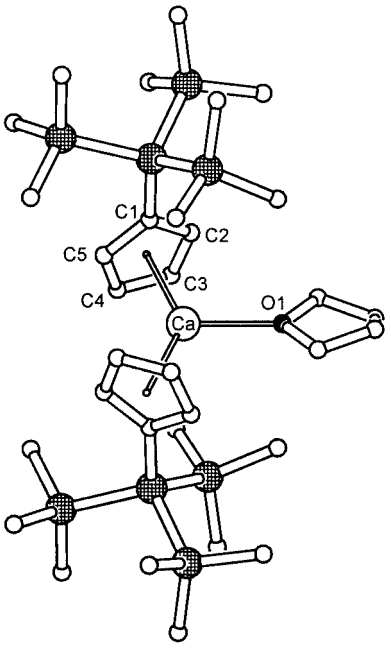

Figure 5. The crystal structure of [Ca(hSi-Cp)$_2$(THF)] (hydrogens omitted for clarity; crystallographic C_2 axis through Ca−O); C−Ca bond lengths (Å) for atoms in the ring C1, C2, C3, C4, C5 are respectively 2.667(3), 2.655(3), 2.657(3), 2.649(3) and 2.649(3), ring$_{center}$−Ca = 2.371(2) Å; Ca−O1 2.381(3)

parts being slightly bent away from the metal. More importantly, the $(Me_3Si)_3Si$ substituents are bent out of the C_5 plane away from the metal [Ca: 16.1(2)° and 13.9(2)°; Sr: 20.2(2) and 10.3(2)°]. Out-of-plane bending of silyl substituents costs only half the energy of that of alkyl substituents[4] and maximizes the Coulomb attraction between Flu^- and M^{2+}.[12] We attribute these deviations also partly to steric stress between the hypersilyl substituent and the rest of the structure.

In order to evaluate the effect of a large hypersilyl substituent in a Cp ring, we also prepared Ca(hSi-Cp)$_2$ from K(hSi-Cp) and CaI_2. The compound crystallized from a hexane/THF mixture in the form of colourless plates with the composition [Ca(hSi-Cp)$_2$(THF)]. The crystal structure (Figure 5) shows a C_2-symmetric sandwich complex with a perfectly trigonal planar coordination at Ca.

The hSi-Cp ligands coordinate to the Ca^{2+} ion in an η^5 fashion with Ca−C bond lengths in the narrow range of 2.649(3) to 2.667(3) Å. Steric stress is avoided by the orientation of the two hypersilyl substituents in different directions rather than by a distortion of the Cp-Ca coordination. The two sterically demanding hSi-Cp ligands leave room for coordination of only one THF ligand [all other monosubstituted calcocenes, Ca(RCp)$_2$, possess two THF ligands]. The steric bulk of the hSi-Cp ligand can be compared to that of 1,3-$(Me_3Si)_2$Cp or *i*Pr$(Me)_4$Cp, which both form calcocenes with only one THF ligand.[13,14]

The heteroleptic alkaline-earth metal complexes containing the hypersilyl-substituted ligands are of particular interest as initiators in stereoselective styrene polymerization.[1] These initiators were prepared by mixing the homoleptic bis-fluorenyl and bis-cyclopentadienyl complexes of Ca (or Sr) with a polymerization-active homoleptic dibenzylcalcium (or strontium) complex.

Reaction of [Ca(hSi-Flu)$_2$(THF)$_2$] with [Ca(DMAT)$_2$(THF)$_2$] in C_6D_6 [Equation (1)] resulted in the quantitative formation of the heteroleptic calcium complex [Ca(DMAT)(hSi-Flu)(THF)$_x$] with x = 1 or 2. The heteroleptic nature of the newly formed complex is clear from NOE's observed between protons of the hSi-Flu ligand and protons of the DMAT ligand. Low temperature NMR spectra (0 °C) of the heteroleptic complex show unique signals for all fluorenyl protons, which are diastereotopic due to the chirality of the benzylic carbon [$\Delta G^{\ddagger}$(20 °C) = 15.3 kcal

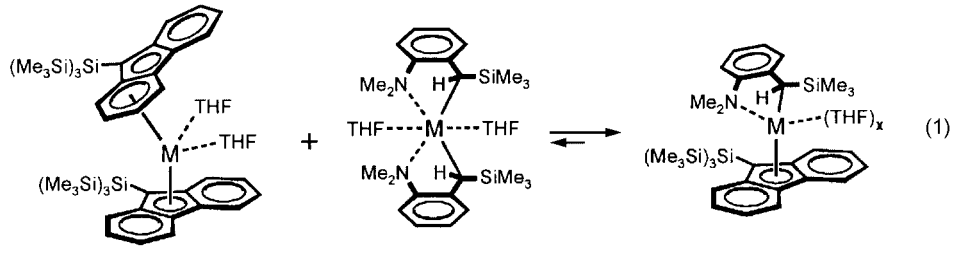

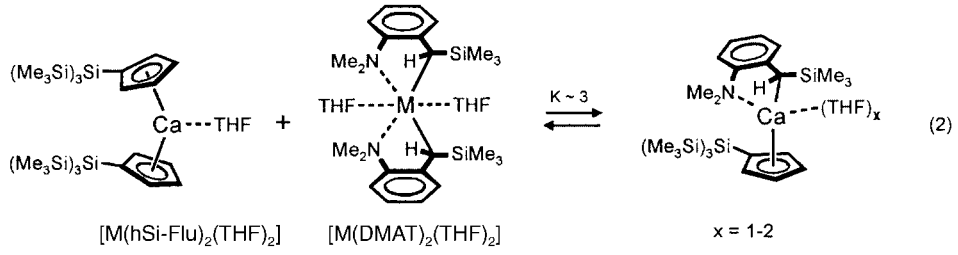

 © 2003 Wiley-VCH Verlag GmbH & Co. KGaA, Weinheim

mol^{-1}]. Fast exchange proceeds either by inversion of the chiral benzyl carbon or by a dissociation/association process of the hSi-Flu$^-$ ligand. It is unclear how many THF molecules coordinate at the Ca^{2+} ion. Evaporation of the solvent and drying of the complex under vacuum (0.01 Torr) at 60 °C yielded the complex [Ca(DMAT)(hSi-Flu)(THF)]. The NMR spectra of [Ca(DMAT)(hSi-Flu)(THF)] redissolved in C_6D_6 also display signals originating from small amounts of the homoleptic precursors ($K \approx 20$). This means that the Schlenk equilibrium is dependent on the Ca/THF ratio.

Reaction of the homoleptic complexes [Ca(hSi-Cp)$_2$(THF)] and [Ca(DMAT)$_2$(THF)$_2$] in C_6D_6 [Equation (2)] resulted in a mixture of both a homoleptic and a heteroleptic calcium complex ($K \approx 3$). In this case no strong preference for the formation of the heteroleptic complex was found. The use of fluorenyl ligands seems therefore to be essential in directing the Schlenk equilibrium to the heteroleptic side. This might originate from the steric stress observed in the crystal structure of homoleptic [Ca(hSi-Flu)$_2$(THF)$_2$], making this particular homoleptic species energetically unfavourable. Steric stress is less severe in homoleptic [Ca(hSi-Cp)$_2$(THF)]: the Cp-Ca coordination observed for both hSi-Cp ligands is not distorted from an ideal η^5 geometry.

Reaction of the homoleptic complexes [Sr(hSi-Flu)$_2$(THF)$_2$] and [Sr(DMAT)$_2$(THF)$_2$] in C_6D_6 [Equation (1)] resulted in the formation of the heteroleptic strontium complex as the major product. Only traces of the homoleptic compounds were detected ($K \approx 800$). Evaporation of the solvent and drying of the complex under vacuum (0.01 Torr) at 60 °C yielded the complex [Sr(hSi-Flu)(DMAT)(THF)]. The Schlenk equilibrium for this compound dissolved in C_6D_6 is similar as above ($K \approx 800$). The heteroleptic complex shows NOE's between the two different ligands. Also, at lower temperatures diastereotopic fluorenyl signals were observed [$\Delta G^{\ddagger}$(5 °C) = 14.2 kcal mol^{-1}].

Styrene polymerizations with a mixture of [Ca(hSi-Flu)$_2$(THF)$_2$] and [Ca(DMAT)$_2$(THF)$_2$], i.e. with the pure heteroleptic compound, were carried out. ^{13}C NMR analyses of the polymers obtained show that there is no significant improvement in the syndiotacticity when compared with polymers obtained by polymerization with **1** (r = 92%, rr = 85%).[2] However, it was found that, under the same reaction conditions, the chain lengths of the polymers obtained with the more bulky hypersilyl-substituted initiator are only 10% of those of polymers obtained with initiator **1**. Apparently, the chain-growth step for the hypersilyl-substituted species **3** is significantly slower than that for the less bulky active species **2**. It should be mentioned that a discussion on the relation of polymer tacticity and spectator ligand is hampered by the possible existence of small quantities of homoleptic polymerylcalcium species which might influence the overall stereoselectivity of monomer insertion.

Styrene polymerization with a mixture of [Sr(hSi-Flu)$_2$(THF)$_2$] and [Sr(DMAT)$_2$(THF)$_2$], i.e. with a predominantly heteroleptic compound, were carried out. ^{13}C NMR analyses of the polymers obtained show that there is a slight improvement in syndiotacticity when compared with polymers obtained by polymerization with a mixture of [Sr(Me$_3$Si-Flu)$_2$(THF)] and [Sr(DMAT)$_2$(THF)$_2$].[15] The syndiotacticity of the polymers is, however, lower than that of polymers obtained with analogous Ca initiators and no estimation of r and rr J-ades could be made. The use of the bulky hSi-Flu ligand in Sr initiators also resulted in short chain lengths, indicative of a sluggish chain growth.

Conclusion

Homoleptic hypersilyl-substituted cyclopentadienyl and fluorenyl complexes of alkali and alkaline-earth metals are readily accessible in crystalline purity. All crystal structures of these compounds show the enormous bulk of the hypersilyl substituent, which either limits the number of THF ligands coordinated at the metal center or distorts the metal-anion coordination geometry. The homoleptic [M(hSi-Flu)$_2$(THF)$_2$] complexes of Ca and Sr, both show structures in which one of the hSi-Flu$^-$ ligands is only weakly bound through the edge of the aryl ring. These compounds are intermediates on the reaction path to the solvent-separated ion-pair [hSi-FluM$^+$(THF)$_3$] [hSi-Flu$^-$].

Heteroleptic benzylcalcium and -strontium complexes with hSi-Flu spectator ligands were generated by ligand exchange between the homoleptic compounds. The Schlenk equilibrium for the fluorenyl complexes lies largely towards the heteroleptic side. Exchange of the fluorenyl group for a cyclopentadienyl group resulted in mixtures of homo- and heteroleptic complexes.

Styrene polymerization with benzylcalcium initiators containing the sterically demanding hSi-Flu spectator ligand gave predominantly syndiotactic polymers (r = 92%, rr = 85%). However, no improvement was observed in comparison with polymers obtained with **1**, i.e. with Me$_3$Si-Flu as a spectator ligand. Only in the case of benzylstrontium initiators containing the hSi-Flu spectator ligand was a slight improvement in the syndiotacticity of the obtained polymer observed. In all cases the large hypersilyl substituent retarded the chain growth step.

Experimental Section

General Remarks: All experiments were carried out under argon using dry solvents and Schlenk techniques. The following compounds were prepared according to literature procedures: 9-tris(trimethylsilyl)silylfluorene,[11] bis(2-dimethylamino-α-Me$_3$Si-benzyl)-bis(tetrahydrofuran)calcium[16] and bis(2-dimethylamino-α-Me$_3$Si-benzyl)bis(tetrahydrofuran)strontium.[17] NMR spectra were recorded on Bruker AC250 (250 MHz) and Bruker DRX600 (600 MHz) machines.

Polymerizations of styrene were performed in a thermostatted 100 mL stainless-steel reactor at normal pressure. Polymerizations were either carried out in a 1 M styrene solution (90 mL cyclohexane and 11.5 mL styrene at 50 °C) or in pure styrene (at 20 °C).

 © 2003 Wiley-VCH Verlag GmbH & Co. KGaA, Weinheim

Styrene was freshly distilled from CaH_2 and kept over dry aloxperls. A solution of the initiator (0.1 mmol of active benzyl anion) in 1.0 mL of benzene/cyclohexane was added via a port. After a polymerization time of 30 minutes the mixture was quenched with oxygen-free methanol. The tacticity of the polymer was checked by analyzing the ^{13}C NMR signal (solvent: [D_2]tetrachloroethane) for the C_{ipso} phenyl ring carbon.[2]

[Li(hSi-Flu)(THF)$_2$]: *n*-Butyllithium (1.6 M in hexane, 1.06 mL, 1.70 mmol) was added dropwise to a solution of 9-tris(trimethylsilyl)silylfluorene (0.70 g, 1.70 mmol) in 10 mL of THF at −68 °C. The solution was stirred at this temperature for 1 h and slowly turned orange. Thereafter the solution was warmed slowly to room temperature, and the solvents were removed. The sticky orange product was washed with 10 mL of hexane and dissolved in a mixture of warm benzene (10 mL) and THF (2 mL). Cooling to room temperature overnight afforded bright-red, plate-like crystals of the title compound (98%, 0.94 g). ^1H NMR (250 MHz, [D_6]benzene): δ = 0.48 [s, 27 H, $(Me_3Si)_3Si$], 1.03 (m, 8 H, THF), 2.67 (m, 8 H, THF), 7.07 (dd, *J* = 7.2 Hz, 2 H, fluorenyl), 7.39 (dd, *J* = 7.5 Hz, 2 H, fluorenyl), 8.12 (d, *J* = 8.3 Hz, 2 H, fluorenyl), 8.28 (d, *J* = 7.8 Hz, 2 H, fluorenyl) ppm. $^{13}C\{^1H\}$ NMR ([D_8]THF): δ = 4.0 [$(Me_3Si)_3Si$], 25.2 (THF), 67.4 (THF), 87.2 (fluorenyl), 114.4 (fluorenyl), 119.9 (fluorenyl), 121.2 (fluorenyl), 122.2 (fluorenyl), 124.4 (fluorenyl), 141.7 (fluorenyl) ppm.

[K(hSi-Flu)(THF)]: *n*-Butyllithium (1.6 M in hexane, 2.27 mL, 3.63 mmol) was added dropwise to a mixture of 9-tris(trimethylsilyl)silylfluorene (1.50 g, 3.63 mmol) and potassium 3-methyl-3-pentanolate in 30 mL of THF at −68 °C. The solution was stirred at this temperature for about one hour and slowly turned red. Thereafter the solution was warmed slowly to room temperature and the solvents were removed. The orange residue was washed five times with 10 mL portions of hexane and was dissolved in a mixture of warm benzene (10 mL) and THF (2 mL). Cooling to 20 °C overnight yielded orange-red needles of a benzene solvate of the title compound (85%, 1.85 g) which can be freed from THF and benzene under vacuum. ^1H NMR (250 MHz, [D_6]benzene/[D_8]THF 10:1): δ = 0.44 [s, 27 H, $(Me_3Si)_3Si$], 1.43 (m, 4 H, THF), 3.56 (m, 4 H, THF), 6.90 (dd, *J* = 7.6 Hz, 2 H, fluorenyl), 7.28 (dd, *J* = 7.1 Hz, 2 H, fluorenyl), 7.64 (d, *J* = 8.3 Hz, 2 H, fluorenyl), 8.19 (d, *J* = 7.7 Hz, 2 H, fluorenyl) ppm. $^{13}C\{^1H\}$ NMR ([D_8]THF): δ = 3.6 [$(Me_3Si)_3Si$], 25.8 (THF), 67.8 (THF), 83.0 (fluorenyl), 111.1 (fluorenyl), 119.0 (fluorenyl), 120.2 (fluorenyl), 120.3 (fluorenyl), 125.9 (fluorenyl), 144.0 (fluorenyl) ppm.

[Ca(hSi-Flu)$_2$(THF)$_2$]: A mixture of THF-free K(hSi-Flu)$_2$ (0.80 g, 1.77 mmol) and CaI_2 (0.27 g, 0.92 mmol) in 20 mL of THF was stirred for two days at room temperature. The THF solvent was then evaporated and the remaining residue was extracted with two 10 mL portions of dry benzene. Evaporation of the solvent from these combined extracts resulted in a red solid, which was crystallized from 12 mL of warm hexane. Cooling to 4 °C yielded red needles of a benzene solvate of the title compound in 49% yield (0.47 g). ^1H NMR (250 MHz, [D_6]benzene): δ = 0.37 [s, 54 H, $(Me_3Si)_3Si$], 1.01 (m, 8 H, THF), 2.77 (m, 8 H, THF), 6.80 (dd, *J* = 7.2 Hz, 4 H, fluorenyl), 7.10 (dd, *J* = 7.6 Hz, 4 H, fluorenyl), 7.86 (dd, *J* = 7.1 Hz, 8 H, fluorenyl) ppm. $^{13}C\{^1H\}$ NMR ([D_8]THF): δ = 3.3 [$(Me_3Si)_3Si$], 26.1 (THF), 70.4 (THF), 83.1 (fluorenyl), 113.5 (fluorenyl), 120.7 (fluorenyl), 121.9 (fluorenyl), 122.6 (fluorenyl), 124.6 (fluorenyl), 142.8 (fluorenyl) ppm.

[Sr(hSi-Flu)$_2$(THF)$_2$]: A mixture of THF-free K(hSi-Flu)$_2$ (1.50 g, 3.33 mmol) and SrI_2 (0.58 g, 1.70 mmol) in 20 mL of THF was stirred for three days at room temperature. The THF solvent was evaporated and the remaining residue was extracted with two 10 mL portions of dry benzene. Evaporation of the solvent from these combined extracts resulted in a red solid, which was crystallized from 30 mL of warm hexane. Cooling to 20 °C yielded dark-red blocks of the title compound in 72% yield (1.27 g). ^1H NMR (250 MHz, [D_6]benzene): δ = 0.40 [s, 54 H, $(Me_3Si)_3Si$], 1.05 (m, 8 H, THF), 2.62 (m, 8 H, THF), 6.82 (dd, *J* = 7.2 Hz, 4 H, fluorenyl), 7.18 (dd, *J* = 7.5 Hz, 4 H, fluorenyl), 7.83 (d, *J* = 7.6 Hz, 4 H, fluorenyl), 7.91 (d, *J* = 8.3 Hz, 4 H, fluorenyl) ppm. $^{13}C\{^1H\}$ NMR ([D_8]THF): δ = 3.6 [$(Me_3Si)_3Si$], 25.1 (THF), 68.4 (THF), 80.5 (fluorenyl), 112.9 (fluorenyl), 120.5 (fluorenyl), 121.6 (fluorenyl), 122.1 (fluorenyl), 126.0 (fluorenyl), 143.2 (fluorenyl) ppm.

[K(hSi-Cp)(THF)]: A solution of tris(trimethylsilyl)silyl chloride (1.00 g, 3.55 mmol) and cyclopentadienylsodium (0.30 g, 3.40 mmol) in 15 mL of THF was stirred for 16 hours at room temperature. The THF solvent was evaporated and the remaining residue was extracted with two 10 mL portions of dry diethyl ether. Potassium bis(trimethylsilyl)amide (0.60 g, 3.00 mmol) dissolved in 15 mL of THF was added to the combined ether extracts of [tris(trimethylsilyl)silyl]cyclopentadiene and the resulting solution was stirred for 15 hours at room temperature. The solvent was evaporated and the remaining white residue was crystallized from 30 mL of hot THF. Cooling to −30 °C yielded crystalline [K(hSi-Cp)(THF)] in the form of white needles (98%, 1.25 g, 2.95 mmol) which can be freed from THF under vacuum. ^1H NMR (250 MHz, [D_8]THF): δ = 0.17 [s, 27 H, $(Me_3Si)_3Si$], 1.78 (m, 4 H, THF), 3.63 (m, 4 H, THF), 5.88 (dd, *J* = 1.9 Hz, 2 H, Cp), 5.89 (dd, *J* = 1.9 Hz, 2 H, Cp) ppm. $^{13}C\{^1H\}$ NMR ([D_8]THF): δ = 2.0 [$(Me_3Si)_3Si$], 25.3 (THF), 67.4 (THF), 98.8 (Cp), 109.0 (Cp), 116.6 (Cp) ppm.

[Ca(hSi-Cp)$_2$(THF)]: A mixture of THF-free K(hSi-Cp) (0.70 g, 2.00 mmol) and CaI_2 (0.30 g, 1.02 mmol) in 50 mL of THF was stirred for two days at room temperature. The THF solvent was evaporated and the remaining residue was extracted with two 20 mL portions of dry benzene. Evaporation of the solvent from these combined extracts resulted in a white solid, which was crystallized from a mixture of warm toluene (10 mL) and THF (1 mL). Cooling to −80 °C yielded colourless crystals of [Ca(hSi-Cp)$_2$(THF)] in 60% yield (0.44 g). ^1H NMR (250 MHz, [D_6]benzene/[D_8]THF 10:1): δ = 0.36 [s, 54 H, $(Me_3Si)_3Si$, 1.43 (m, 4 H, THF), 3.56 (m, 4 H, THF), 6.20 (dd, *J* = 2.3 Hz, 4 H, Cp), 6.39 (dd, *J* = 2.3 Hz, 4 H, Cp) ppm. $^{13}C\{^1H\}$ NMR ([D_8]THF): δ = 1.9 [$(Me_3Si)_3Si$], 25.8 (THF), 67.8 (THF), 104.8 (Cp), 111.0 (Cp), 120.1 (Cp) ppm.

[Ca(DMAT)(hSi-Flu)(THF)$_x$]: [Ca(DMAT)$_2$(THF)$_2$] (7.1 mg, 12 μmol) and [Ca(hSi-Flu)$_2$(THF)$_2$] (12 mg, 12 μmol) were mixed in an NMR tube and dissolved in [D_6]benzene (0.5 mL). Heating to 60 °C immediately resulted in the quantitative formation of [Ca(DMAT)(hSi-Flu)(THF)$_x$] (*x* = 1 or 2). Evaporation of the solvent and drying under vacuum yielded the complex [Ca(DMAT)(hSi-Flu)(THF)]. Upon redissolving this complex in [D_6]benzene the constant of the Schlenk equilibrium is approximately 20. NMR spectra before and after removal of one equivalent of THF are similar and show maximum chemical shift differences of 0.02 ppm. ^1H NMR (600 MHz, [D_6]benzene): δ = 0.34 [s, 27 H, $(Me_3Si)_3Si$], 0.42 (s, 9 H, Me_3Si-benzyl), 0.74 [s, 1 H, $CH(SiMe_3)$], 1.06 (m, 4 H, THF), 1.93 (s, 3 H, Me_2N), 2.04 (s, 3 H, Me_2N), 2.71 (m, 4 H, THF), 6.14 (dd, *J* = 7.0 Hz, 1 H, benzyl), 6.31 (d, *J* = 7.8 Hz, 1 H, benzyl), 6.63 (dd, *J* = 7.3 Hz, 1 H, benzyl), 6.85 (d, *J* = 7.9 Hz, 1 H, benzyl), 6.99 (dd, *J* = 8.3 Hz, 1 H, fluorenyl), 7.02 (dd, *J* = 8.3 Hz, 1 H, fluorenyl), 7.27 (dd, *J* = 7.1 Hz, 1 H, fluorenyl), 7.30

 © 2003 Wiley-VCH Verlag GmbH & Co. KGaA, Weinheim

Table 1. Crystal data

Compound	[Li(hSi-Flu)(THF)$_2$]	[K(hSi-Flu)(THF)]	[Ca(hSi-Flu)$_2$(THF)$_2$]	[Sr(hSi-Flu)$_2$(THF)$_2$]	[Ca(hSi-Cp)$_2$(THF)]
Formula	$C_{30}H_{51}LiO_2Si_4$	$C_{32}H_{49}KOSi_4$	$C_{58}H_{92}CaOSi_8$	$C_{52}H_{86}SrO_2Si_8$	$C_{32}H_{70}CaOSi_8$
Weight	563.01	601.17	1086.12	1055.55	735.68
Crystal system	monoclinic	monoclinic	triclinic	monoclinic	monoclinic
Space group	$P2_1/c$	$P2_1/c$	$P\bar{1}$	$P2_1/c$	$C2/c$
a (Å)	11.4724(15)	14.407(2)	9.860(6)	9.7034(15)	14.648(3)
b (Å)	16.5382(14)	13.1977(10)	17.554(6)	31.200(4)	10.2742(16)
c (Å)	19.716(2)	22.810(5)	20.475(12)	20.391(3)	30.436(5)
α (°)	90	90	67.02(5)	90	90
β (°)	113.277(7)	124.26(1)	84.59(4)	108.42(1)	93.11(2)
γ (°)	90	90	83.90(4)	90	90
V (Å^3)	3437.6(7)	3584(1)	3239(3)	5857(1)	4574(1)
Z	4	4	2	4	4
μ(MoKa) (mm^{-1})	0.196	0.304	0.282	1.120	0.369
Crystal size	0.5 × 0.4 × 0.4	0.6 × 0.2 × 0.2	0.5 × 0.4 × 0.3	0.5 × 0.5 × 0.5	0.5 × 0.4 × 0.2
T (°C)	−90	−90	−90	−90	−90
θ max (°)	26.0	25.0	25.0	26.0	25.0
Data(total)	7077	6617	12048	11871	4208
Data(unique), R_{int}	6728, 0.016	6347, 0.041	11324, 0.039	11534, 0.029	4036, 0.039
Data[$I > 2\sigma(I)$]	4695	3825	6560	9404	3121
R1	0.039	0.077	0.054	0.037	0.043
$wR2$	0.103	0.234	0.137	0.136	0.132
GOF	1.02	1.03	1.00	1.05	1.04
ρ−/ρ+ (e.A^{-3})	−0.35/+0.36	−0.50/+0.65	−0.32/+0.46	−0.57/+0.79	−0.32/+0.40
Abs. corr.	−	−	−	psi scan	−
$T_{min.}/T_{max.}$	−	−	−	0.90/0.97	−

(dd, J = 7.6 Hz, 1 H, fluorenyl), 8.00 (d, J = 8.0 Hz, 1 H, fluorenyl), 8.04 (d, J = 7.7 Hz, 1 H, fluorenyl), 8.21 (d, J = 7.5 Hz, 1 H, fluorenyl), 8.21 (d, J = 7.5 Hz, 1 H, fluorenyl) ppm. $^{13}C\{^1H\}$ NMR ([D$_6$]benzene): δ = 2.6 (Me$_3$Si-benzyl), 3.5 [(Me$_3$Si)$_3$Si-fluorenyl], 24.9 (THF), 41.9 (Me$_2$N), 45.0 (Me$_2$N), 47.6 [CH(Me$_3$Si)], 68.9 (THF), aromatics: 81.6, 113.3, 115.0, 115.7, 119.4, 121.6, 121.9, 122.2, 122.3, 123.4, 123.9, 124.9, 125.5, 126.5, 128.2, 135.2, 142.3, 143.4 147.4 ppm.

[Sr(DMAT)(hSi-Flu)(THF)$_x$]: [Sr(DMAT)$_2$(THF)$_2$] (10.5 mg, 16 μmol) and [Sr(hSi-Flu)$_2$(THF)$_2$] (16 mg, 16 μmol) were mixed in an NMR tube and dissolved in [D$_6$]benzene (0.5 mL). Heating to 60 °C immediately resulted in the formation of the heteroleptic strontium complex as the major product. Only traces of the homoleptic starting materials were detected (Schlenk equilibrium $K \approx$ 800). Evaporation of the solvent and drying under vacuum yielded the complex [Sr(DMAT)(hSi-Flu)(THF)]. NMR spectra and the constant of the Schlenk equilibrium of this compound are similar as with two equivalents of THF. ^1H NMR (600 MHz, [D$_6$]benzene): δ = 0.39 [s, 27 H, (Me$_3$Si)$_3$Si], 0.44 (s, 9 H, Me$_3$Si-benzyl), 0.76 [s, 1 H, CH(SiMe$_3$)], 1.18 (m, 4 H, THF), 2.05 (s, 3 H, Me$_2$N), 2.15 (s, 3 H, Me$_2$N), 3.00 (m, 4 H, THF), 6.10 (dd, J = 7.2 Hz, 1 H, benzyl), 6.36 (d, J = 7.8 Hz, 1 H, benzyl), 6.67 (dd, J = 7.3 Hz, 1 H, benzyl), 6.91 (d, J = 8.0 Hz, 1 H, benzyl), 7.02 (t, broad, 2 H, fluorenyl), 7.34 (t, broad, 2 H, fluorenyl), 8.04 (d, J = 6.9 Hz, 2 H, fluorenyl), 8.15 (d, broad, 2 H, fluorenyl) ppm. $^{13}C\{^1H\}$ NMR ([D$_6$]benzene): δ = 2.8 (Me$_3$Si-benzyl), 3.6 [(Me$_3$Si)$_3$Si-fluorenyl], 25.2 (THF), 41.8 (Me$_2$N), 43.7 (Me$_2$N), 50.2 [CH(Me$_3$Si)], 68.2 (THF), aromatics: 85.2, 111.2, 113.8, 120.0, 120.8, 121.6, 122.4, 123.5, 126.3 128.3, 134.3, 143.4, 147.3 ppm.

X-ray Crystallographic Studies: Crystals protected with a layer of dry paraffin oil were mounted in the cold nitrogen stream (−90 °C) on an Enraf−Nonius CAD4 diffractometer. Structures were solved with SHELXL-97[18] and the PLATON program package[19] (the latter was also used for geometrical calculations and illustrations). All crystal data are summarized in Table 1. CCDC entries 205469−205473 contain the supplementary crystallographic data for this paper. These data can be obtained free of charge at www.ccdc.cam.ac.uk/conts/retrieving.html [or from the Cambridge Crystallographic Data Centre, 12, Union Road, Cambridge CB2 1EZ, UK; fax: (internat.) +44-1223/336-033; E-mail: deposit@ccdc.cam.ac.uk].

Acknowledgments

We are grateful to the Deutsche Forschungsgemeinschaft, the Fonds der Chemischen Industrie and the BASF AG (Ludwigshafen, Germany) for financing this project. Prof. Dr. H.-H. Brintzinger (Konstanz) and Dr. K. Knoll (Ludwigshafen) are kindly acknowledged for helpful discussions. Mrs. A. Friemel is thanked for measuring 600 MHz spectra.

[1] S. Harder, F. Feil, K. Knoll, *Angew. Chem.* **2001**, *113*, 4391; *Angew. Chem. Int. Ed.* **2001**, *40*, 4261.
[2] The tacticity reported by us earlier (r = 84%, rr = 76%)[1] is based on the generally accepted pentad assignment. A new assignment based on heptads results in a higher syndiotacticity (r = 92%, rr = 85%): F. Feil, S. Harder, *Macromolecules* **2003**, *36*, 3446.
[3] S. Harder, F. Feil, *Organometallics* **2002**, *21*, 2268.
[4] S. Harder, M. Lutz, A. W. G. Straub, *Organometallics* **1997**, *16*, 107.
[5] R. D. Culp, A. H. Cowley, *Organometallics* **1996**, *15*, 5380.
[6] C. Janiak, *Chem. Ber.* **1993**, *126*, 1603.
[7] D. Hoffmann, F. Hampel, P. v. R. Schleyer, *J. Organomet. Chem.* **1993**, *456*, 13.
[8] K. C. Jayaratne, L. S. Fitts, T. P. Hanusa, V. G. Young Jr., *Organometallics* **2001**, *20*, 3638.
[9] S. Harder, F. Feil, T. Repo, *Chem. Eur. J.* **2002**, *8*, 1991.
[10] *Handbook of Chemistry and Physics 64th Ed.* (Ed.: R. C. Weast), CRC Press, Boca Raton, Florida, **1984**, F-171.

 © 2003 Wiley-VCH Verlag GmbH & Co. KGaA, Weinheim

[11] A. Rengstl, U. Schubert, *Chem. Ber.* **1980**, *113*, 278.
[12] S. Alexandratos, A. Streitwieser Jr., H. F. Schaefer III, *J. Am. Chem. Soc.* **1976**, *98*, 7959.
[13] L. M. Engelhardt, P. C. Junk, C. L. Raston, A. H. White, *J. Chem. Soc., Chem. Commun.* **1988**, 1500.
[14] H. Schumann, J. Gottfriedsen, M. Glanz, S. Dechert, J. Demtschuk, *J. Organomet. Chem.* **2001**, *617*, 588.
[15] F. Feil, S. Harder, unpublished results.
[16] S. Harder, F. Feil, A. Weeber, *Organometallics* **2001**, *20*, 1044.
[17] F. Feil, S. Harder, *Organometallics* **2001**, *20*, 4616.
[18] G. M. Sheldrick, *SHELXL-97*, Universität Göttingen, **1997**.
[19] A. L. Spek, *PLATON*, A Multipurpose Crystallographic Tool, Utrecht University, The Netherlands, **2000**.

Received March 19, 2003

 © 2003 Wiley-VCH Verlag GmbH & Co. KGaA, Weinheim

Structural Studies of Lithium Telluro- and Seleno-Phosphorus Compounds

Robert P. Davies,*[a] M. Giovanna Martinelli,[a] Andrew E. H. Wheatley,[b] Andrew J. P. White,[a] and David J. Williams[a]

Dedicated to the memory of Ron Snaith

Keywords: Lithium / Selenium / Solid-state structures / Tellurium

Lithium tellurophosphinite $[Ph_2PTe][Li(TMEDA)_{1.33}(THF)_{1.33}]$ (**4**), ditellurophosphinate, $[Ph_2PTe_2][Li(THF)_{3.5}(TMEDA)_{0.25}]$ (**5**), and selenotellurophosphinate $[Ph_2P(Se)Te][Li(THF)_2(TMEDA)]$ (**6**) complexes have been prepared from the insertion/oxidation reactions of lithiated secondary phosphanes with elemental chalcogens and characterised by X-ray crystallography. Compounds **4**–**6** contain no tellurium–lithium bonding interactions in the solid state, instead existing as ion-separated species with THF/TMEDA-solvated lithium cations. Reaction of dilithiated primary phosphanes with more than three equivalents of elemental selenium gives $[\{(c\text{-}C_6H_{11})P(Se)(SeLi)\}_2\cdot 2TMEDA]$ (**7**) via a phosphorus-phosphorus coupling reaction. Solid state characterisation of **7** reveals the organo groups in the tetradentate tetraselenohypodisphosphinate ligand to be in an anti conformation to one another and each lithium atom to be coordinated by two selenium atoms, one from each of the diselenophosphinate groups. Multinuclear NMR spectroscopic data are consistent with retention of the solid-state structures of **4**–**7** in solution.
(© Wiley-VCH Verlag GmbH & Co. KGaA, 69451 Weinheim, Germany, 2003)

Introduction

Thiophosphorus ligands, in particular dithiophosphates and -phosphinates, have been reported extensively in the literature[1] and have found many applications including as lubricant oil additives[1,2] and as extraction agents for separation procedures.[3] In addition they have been shown to exhibit a broad variety of coordination patterns leading to a wide range of molecular and supramolecular structures.[1] However, the chemistry of the heavier group 16 homologues, the seleno- and telluro-phosphorus ligands, is less well documented. This is despite the growing interest in using selenolates and tellurolates as precursors to semiconducting metal selenides and tellurides,[4] and also as new reagents for the synthesis of selenium- and tellurium-containing organics.[5] Furthermore, triorganophosphane tellurides have been employed as more reactive sources of tellurium than elemental tellurium metal itself in, for example, the low-temperature synthesis of transition metal tellurium clusters and nanoclusters.[6] We have been interested in the synthesis and characterisation of new selenolate and tellurolate complexes utilising the insertion reaction of elemental chalcogens into carbon−lithium[7] or heteroatom−lithium bonds[8] and have recently reported the synthesis and structural characterisation of a lithium selenophosphinite, $[Ph_2PSeLi\cdot TMEDA]_2$ **1** [TMEDA = $(Me_2NCH_2)_2$], a lithium diselenophosphinate, $[Ph_2PSe_2Li\cdot THF\cdot TMEDA]$ **2**, and a dilithium triselenophosphonate, $[(c\text{-}C_6H_{11})PSe_3Li_2\cdot 2TMEDA]$ **3** (Figure 1).[8] In these systems the ligands were shown to exhibit a variety of novel coordination modes to the lithium centres which differed from those exhibited by their thio-phosphorus counterparts. This observation has now led us to turn our attention to the corresponding tellurium and mixed selenium/tellurium analogues.

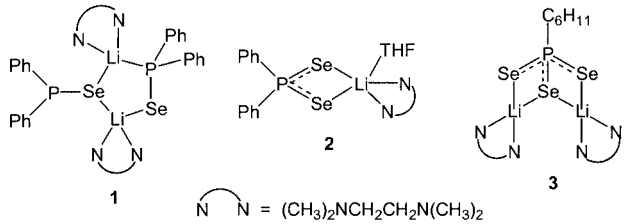

Figure 1. Lithium seleno-phosphorus complexes **1**, **2**, and **3**

Although the syntheses of ditellurophosphinates and selenotellurophosphinates have been reported previously by Sladky and Bildstein[9] there are to date no solid-state

[a] Dept of Chemistry, Imperial College London, South Kensington, London SW7 2AZ, U.K.
Fax: (internat.) +44-20/7594-5804
E-mail: r.davies@imperial.ac.uk
[b] Dept of Chemistry, University of Cambridge, Lensfield Road, Cambridge, CB2 1EW, U.K.
Fax: (internat.) +44-1223/336-362
E-mail: aehw2@cam.ac.uk
Supporting information for this article is available on the WWW under http://www.eurjic.org or from the author.

characterisations of these species. Indeed, a search of the Cambridge Structural Database[10] reveals fewer than twenty structures containing any form of phosphorus−tellurium bond, and of these the only metal-containing examples are the triorganophosphane telluride complexes $[(CO)_5WTeP{t}Bu_3]$[11] and $[(HgTeP{n}Bu_3)_3Br_5]_2$-$[Hg_2Br_6]$,[12] the tellurobisphosphane complex $[(CO)_4Cr(\mu$-$P{t}Bu_2)_2Te]$,[13] a 1,2,4-telluradiphosphole ring complex $[W(CO)_5(P_2TeC_2{t}Bu_2)]$,[14] a binuclear iron species $[Fe_2(CO)_6(\mu_2$-TeMes$)\{\mu_2$-P(iPr)TeMes$\}]$[15] and, most recently, a magnesium cyclodiphosphazane monotelluride $[{t}BuN(Te)P(\mu$-NtBu$)_2PN{t}Bu\cdot Mg(THF)_2]$.[16]

We present here the first solid-state characterisations of anionic telluro-phosphorus ligands, namely a tellurophosphinite $[Ph_2PTe][Li(TMEDA)_{1.33}(THF)_{1.33}]$ (**4**), a ditellurophosphinate $[Ph_2PTe_2][Li(THF)_{3.5}(TMEDA)_{0.25}]$ (**5**), and a mixed chalcogen selenotellurophosphinate $[Ph_2P(Se)Te]$-$[Li(THF)_2(TMEDA)]$ (**6**). In addition we report on the reactions of dilithiated primary phosphanes with an excess of selenium. It has been shown previously that reaction of dilithio organylphosphides, $RPLi_2$, with elemental tellurium leads, via a series of phosphorus-phosphorus coupling reactions, to the formation of cyclic organylpolyphosphanes $(RP)_n$.[9] In contrast, reaction of $RPLi_2$ with three equivalents of selenium leads to formation of the dilithio triselenophosphonate **3**.[8] We now report how reaction of (c-C_6H_{11})PLi_2 with an excess (>3.2 equivalents) of selenium results in a single phosphorus-phosphorus coupling reaction to yield the novel tetraselenohypodiphosphonate complex $[\{(c$-$C_6H_{11})P(Se)(SeLi)\}_2\cdot 2TMEDA]$ (**7**).

Results and Discussion

Using a synthetic route analogous to that employed to prepare the seleno-phosphorus compounds **1** and **2**,[8] and also in accordance with literature procedures,[9] reaction of one equivalent of elemental tellurium with lithium diphenylphosphide in THF gave insertion of the tellurium into the phosphorus-lithium bond to yield the tellurophosphinite, $[Ph_2PTe][Li(TMEDA)_{1.33}(THF)_{1.33}]$ (**4**). Reaction of $LiPPh_2$ with two equivalents of elemental tellurium gave insertion followed by oxidation to yield the ditellurophosphinate $[Ph_2PTe_2][Li(THF)_{3.5}(TMEDA)_{0.25}]$ (**5**). A mixed selenotellurophosphinate $[Ph_2P(Se)Te][Li(THF)_2$-$(TMEDA)]$ (**6**) was prepared from reaction of lithium diphenylphosphide with elemental selenium and tellurium in a one-pot reaction, although we were also able to prepare **6** from reaction of **1** or **4** with one equivalent of tellurium or selenium respectively (Scheme 1). All of these tellurium-containing compounds (**4**−**6**) are much more reactive than their selenium analogues (**1**, **2**), being highly air, moisture, and light sensitive, and readily decompose to deposit amorphous tellurium.

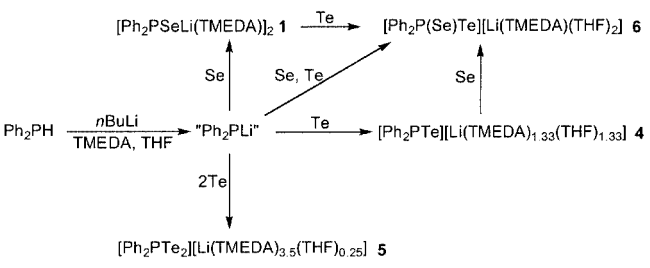

Scheme 1

X-ray structural analysis of $[Ph_2PTe][Li(TMEDA)_{1.33}(THF)_{1.33}]$ (**4**) shows it to crystallise as an ion-separated species consisting of the tellurophosphinite anion $[Ph_2PTe]^-$ and a solvated lithium cation (Figure 2); two different lithium cations are present in the crystal lattice, $[(TMEDA)(THF)_2Li]^+$ (67% occupancy, depicted in Figure 2) and $[(TMEDA)_2Li]^+$ (33% occupancy). The tellurophosphinite anion contains a distorted pyramidal phosphorus atom with angles of 97.8(1), 105.8(1) and 107.6(1)° (Table 1), the most "acute" corresponding to the Ph−P−Ph angle (i.e. between the two least sterically demanding substituents). The P−Te bond length of 2.447(1) Å is slightly shorter than previously reported P−Te single bonds: 2.565 Å (av.) in $[(i$Pr$)_2P]_2Te$;[17] 2.481(1) and 2.491(1) Å in $[(CO)_4Cr(\mu$-PtBu$_2)_2Te]$;[13] 2.4728(9) and 2.4790(5) Å in the phosphorus-tellurium cage $P_6C_4{t}Bu_4Te$.[18] This shortening suggests that the species exists predominately as its Ph_2P-Te^- tautomer with a P−Te single bond and the negative charge localised on the tellurium centre, with possibly some minor contribution from the $Ph_2P(=Te)^-$ tautomer resulting in a slight shortening of the P−Te bond. Given the weakness of phosphorus−tellurium double bonds[1c] it is perhaps not unexpected that the equilibrium lies well on the side of the Ph_2P-Te^- tautomer and this is also in agreement with our observations with the selenium analogue **1**, which also exists in a similar tautomeric form.[8] The ^{31}P NMR spectrum of **4** consists of a single peak with ^{125}Te satellites ($^1J_{P,Te}$ = 747 Hz). As expected the coupling constant is approximately two to three times larger than the corresponding P−Se coupling constants in **1**, and is also at the top end of the range of values expected for P−Te single bonds (reflecting the slightly shorter P−Te distance), for example 451 Hz in $({t}Bu_2P)_2Te$.[19] It is interesting to note the absence of any Te−Li or P−Li bonding interactions in the solid-state structure of **4**, especially when compared to the analogous Se complex **1** where two distinct coordination modes were observed: end-on bridging from Se to two Li and side-on bridging from Se to one Li and P to another Li.[8] Low-temperature ^{31}P NMR spectroscopic studies were carried out on **4**, but even at −70 °C we were unable to verify the existence of any metal−tellurophosphinite bonding, there being only one constant peak observed as the temperature was lowered (cf. **1**[8]). Although lithium−tellurium bonds are expected to be weak due to the size mismatch of the atoms, Li−Te bonds have previously been reported in both Si−Te−Li[20] and C−Te−Li systems[7,20d,21] and, to the best of our knowledge, the only example of an ion-separated lithium tellurolate is $[(Me_3Si)_3$-$SiTe][Li(12\text{-crown-}4)_2]$ where the lithium cation is stabilised by crown ether ligands. It therefore seems likely that stabil-

 © 2003 Wiley-VCH Verlag GmbH & Co. KGaA, Weinheim

isation of the negative charge on the tellurium by the phosphorus in **4** is responsible for the lack of Te−Li bonding, presumably due to the $Ph_2P(=Te)^-$ tautomer formed from donation of a lone pair in a p orbital on the tellurium into an empty d orbital on the phosphorus. However, it is also possible that overlap of the p orbitals on tellurium with σ* orbitals on the Ph_2P moiety is occurring, similar to that previously reported for triorganophosphane tellurides.[6,22] Both of these interactions would result in a shortening of the P−Te bond as observed in the solid state and in solution.

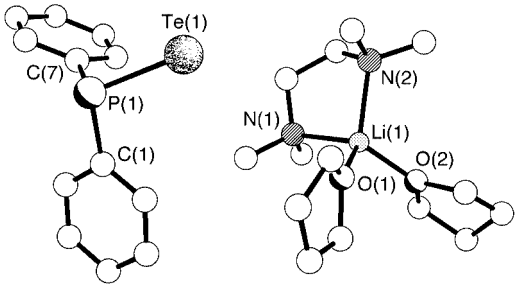

Figure 2. The molecular structure of $[Ph_2PTe][Li(TMEDA)_{1.33}(THF)_{1.33}]$ (**4**) showing the major occupancy $[(TMEDA)(THF)_2Li]^+$ cation

The solid-state characterisation of dark red crystals of $[Ph_2PTe_2][Li(THF)_{3.5}(TMEDA)_{0.25}]$ (**5**) reveals an ion-separated species comprising a $[Ph_2PTe_2]^-$ anion and a combination of $[(THF)_4Li]^+$ (75%) and $[(TMEDA)(THF)_2Li]^+$ (25%) solvated lithium cations. The crystals contain two crystallographically independent cation-anion pairs in the asymmetric unit (see Figure 3 and Figure S1 (Supporting Information, see footnote on page 1 of this article); selected bond lengths and angles for the major component are given in Table 1). The phosphorus atoms in both of the independent anions in **5** are distorted tetrahedral with Te−P−Te angles of 118.6(2) and 117.3(2)°, and Ph−P−Ph angles of 100.6(5) and 101.8(6)°; the Ph−P−Te angles range between 107.9(4) and 110.3(5)°. The four P−Te bond lengths (av. 2.391 Å) do not differ significantly, ranging between 2.380(4) and 2.399(3) Å. These values are concordant with delocalisation of the negative charge throughout the ditellurophosphinate group and would suggest a formal bond order of 1.5 for each of the P−Te bonds, analogous to the bonding observed in lithium diselenophosphinates and di-

Table 1. Selected bond lengths [Å] and angles [°] for **4**−**7**

4	P(1)−Te(1)	2.4471(9)	P(1)−C(1)	1.857(8)
	P(1)−C(7)	1.851(3)		
	Te(1)−P(1)−C(1)	107.57(11)	Te(1)−P(1)−C(7)	105.78(10)
	C(1)−P(1)−C(7)	97.82(14)		
5	P(1)−Te(1)	2.399(3)	P(1)−Te(2)	2.380(4)
	P(1)−C(1)	1.843(8)	P(1)−C(7)	1.851(12)
	Te(1)−P(1)−Te(2)	118.56(15)	Te(1)−P(1)−C(1)	107.9(3)
	Te(1)−P(1)−C(7)	110.0(4)	Te(2)−P(1)−C(1)	110.1(3)
	Te(2)−P(1)−C(7)	108.2(4)	C(1)−P(1)−C(7)	100.6(5)
6	P(1)−Te(1)	2.379(3)	P(1)−Se(1)	2.137(6)
	P(1)−C(1)	1.847(5)	P(1)−C(7)	1.848(5)
	Te(1)−P(1)−Se(1)	116.8(2)	Te(1)−P(1)−C(1)	110.7(2)
	Te(1)−P(1)−C(7)	111.0(2)	Se(1)−P(1)−C(1)	110.5(3)
	Se(1)−P(1)−C(7)	106.7(3)	C(1)−P(1)−C(7)	99.8(2)
7	Se(1)−P(1)	2.0719(16)	Se(1)−Li(1)	2.561(4)
	Se(1′)−P(1)	2.2290(16)	Se(1′)−Li(1)	2.561(4)
	P(1)−C(1)	1.858(5)	P(1)−Se(1A)	2.0719(16)
	P(1)−Se(1D)	2.2290(16)	P(1)−P(1A)	2.2516(18)
	Li(1)−N(1)	2.084(6)	Li(1)−N(1B)	2.084(6)
	Li(1)−Se(1B)	2.561(4)	Li(1)−Se(1F)	2.561(4)
	P(1)−Se(1)−Li(1)	99.33(14)	P(1)−Se(1′)−Li(1)	95.24(13)
	C(1)−P(1)−Se(1A)	113.30(16)	C(1)−P(1)−Se(1)	91.16(15)
	Se(1)−P(1)−Se(1A)	120.10(9)	C(1)−P(1)−Se(1D)	126.81(16)
	Se(1)−P(1)−Se(1D)	116.33(5)	C(1)−P(1)−Se(1′)	104.20(15)
	Se(1A)−P(1)−Se(1′)	116.33(5)	Se(1D)−P(1)−Se(1′)	109.58(8)
	C(1)−P(1)−P(1A)	105.09(16)	Se(1A)−P(1)−P(1A)	112.24(5)
	Se(1)−P(1)−P(1A)	112.24(5)	Se(1D)−P(1)−P(1A)	104.61(5)
	Se(1′)−P(1)−P(1A)	104.61(5)	Se(1B)−Li(1)−Se(1′)	104.0(2)
	Se(1)−Li(1)−Se(1B)	104.6(3)	Se(1′)−Li(1)−Se(1F)	106.0(3)
	Se(1)−Li(1)−Se(1F)	104.0(2)		

 © 2003 Wiley-VCH Verlag GmbH & Co. KGaA, Weinheim

thiophosphinates.[1,8] However, although these phosphorus−tellurium bonds are shorter than, for example, the P−Te single bond observed in **4** [2.447(1) Å], they do not differ considerably in length from formal "double" bonds [such as those in triorganophosphane tellurides, $TePR_3$, i.e. 2.368 Å in $TeP{t}Bu_3$,[23] 2.365 Å in $TeP{i}Pr_3$,[24] and 2.371 Å in $t{Bu}_2P(Te)NH(C_6H_{11})$[25]]. There has been considerable debate in the literature concerning the nature of the multiple bonding in phosphorus-tellurium compounds,[6] particularly the triorganophosphane tellurides, with ^{125}Te NMR and Mössbauer spectroscopy being interpreted as showing no P−Te multiple bonding in these compounds,[26] whereas density functional theory calculations have shown contributions from resonance structures consistent with substantial multiple bonding.[22] The P−Te bonds in **5** are the first crystallographically characterised P−Te bonds with a "formal" bond order of 1.5 (assuming complete delocalisation of the negative charge throughout the ditellurophosphinate) and therefore allow us speculate that, due to the similarity in bond lengths, the correct bond order for triorganophosphane tellurides is also 1.5. This conclusion agrees with the calculations carried out by Sandblom, Ziegler and Chivers.[22] It is also worthwhile noting that the ^{31}P NMR spectrum of **5** has a $^1J_{P,Te}$ coupling constant of 1530 Hz which is close to the range observed elsewhere for triorganophosphane tellurides (1548−1743 Hz),[19] indicating that the P−Te bonds in these two species are of similar length both in solution and in the solid-state ($^1J_{P,Te}$ coupling constants are known to correlate very strongly with bond lengths[19]).

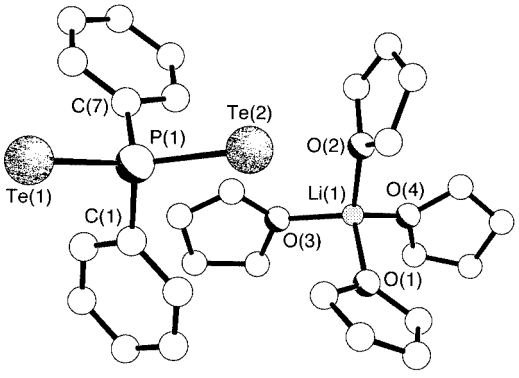

Figure 3. The molecular structure of one of the crystallographically independent cation:anion pairs present in the crystals of $[Ph_2PTe_2][Li(THF)_{3.5}(TMEDA)_{0.25}]$ (**5**) showing the major occupancy $[(THF)_4Li]^+$ cation

Crystals of $[Ph_2P(Se)Te][Li(THF)_2(TMEDA)]$ (**6**) were shown by X-ray analysis to contain a mixed chalcogen selenotellurophosphinate anion (Figure 4). The positions of the Te(1) and Se(1) centres are sometimes reversed (ca. 63:37, see Figure S2), and this disorder means that the possibility of a certain amount of the diseleno and ditellurophosphinate species also being present in the crystal cannot be ruled out, though NMR spectroscopic data (see later) suggests that any contribution from these species is likely to be minor. Again the species is ion separated, this time containing a $[Li(THF)_2(TMEDA)]^+$ cation. The geometry at phosphorus is distorted tetrahedral with, for the major occupancy atoms, a Ph−P−Ph angle of 99.8(2)° and a Te−P−Se angle of 116.8(2)°; the other angles are in the range 106.7(3)−111.0(2)° (Table 1). The P−Se bond lengths of 2.137(6) to Se(1), and 2.136(8) Å to Se(1′), are similar in length to those observed in the diselenophosphinate **2** [2.141(1) and 2.147(1) Å][8] and the P−Te bonds of 2.379(3) to Te(1), and 2.378(6) Å to Te(1′), are similar to those observed in the ditellurophosphinate **4** (av. 2.391 Å). Together these bond lengths point to delocalisation of the negative charge over the selenotellurophosphinate group to give P−Se and P−Te bonds of order 1.5. This interpretation is further supported by ^{31}P NMR spectroscopy (Figure 5) which shows one main phosphorus peak ($\delta = -43.0$ ppm) with both ^{77}Se and ^{125}Te satellites and coupling constants similar to those observed in the dichalcogenophosphinates **2** and **5**; $^1J_{P,Se} = -635$ Hz and $^1J_{P,Te} = 1485$ Hz in **6** cf. $^1J_{P,Se} = -585$ Hz in **2** and $^1J_{P,Te} = 1585$ Hz in **5**. Small peaks (< 10%) can also be seen in the ^{31}P NMR spectra at $\delta = 24.0$ and -121.8 ppm due to the presence of the dichalcogenophosphinate species **2** and **5** respectively, which are present in equilibrium with the asymmetric species **6**.[9] Low temperature ^{31}P NMR spectroscopy of this mixture shows the signals at $\delta = 24$ and -122 ppm to increase in size (20% at −70 °C) due to the equilibrium being shifted more towards the symmetrical chalcogenophosphinates **2** and **5** at lower temperatures.

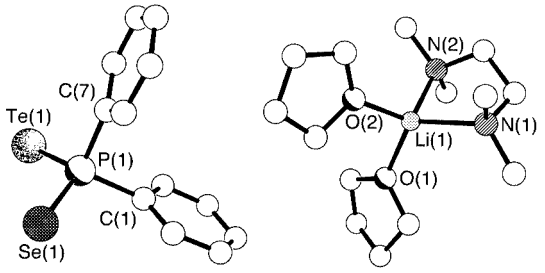

Figure 4. The molecular structure of $[Ph_2P(Se)Te][Li(THF)_2(TMEDA)]$ (**6**) showing the major occupancy orientation of the $[Ph_2PSeTe]^-$ anion

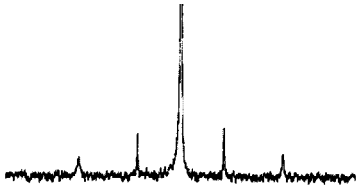

Figure 5. ^{31}P NMR spectrum of **6** showing the main truncated peak at $\delta = -43.0$ ppm with ^{77}Se and ^{125}Te satellites

Previously we have shown how reaction of dilithiated primary phosphanes, $RPLi_2$, with three equivalents of elemental selenium gives triselenophosphonates such as **3**. However, similar attempts to prepare tritellurophosphonates from reaction of $RPLi_2$ with elemental Te failed, instead forming cyclic poylphosphanes $(RP)_n$ and lithium telluride

 © 2003 Wiley-VCH Verlag GmbH & Co. KGaA, Weinheim

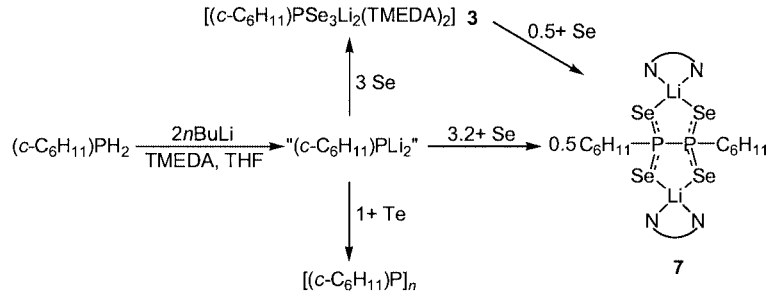

Scheme 2

(Li_2Te_n) (Scheme 2). We therefore turned our attention to the reaction of $CyPLi_2$ and a greater than threefold excess of selenium powder to see if similar phosphorus-phosphorus coupling reactions[27] would occur. Indeed, reaction of $CyPLi_2$ with a greater than threefold excess of selenium was observed to give the dilithium tetraselenohypodiphosphonate complex [{(*c*-C_6H_{11})P(Se)(SeLi)}$_2$·2TMEDA] **7** via reduction of **3** with concomitant elimination of Li_2Se_n (Scheme 2), as well as some cyclic phosphane by-products. It also proved possible to prepare **7** by direct reaction of the triselenophosphonate **3** with 0.5 equivalents of selenium verifying that **3** is indeed an intermediate in this reaction. Further tests showed the reaction to proceed from (*c*-C_6H_{11})PLi_2 to **7** with between three (with reflux) and six equivalents of selenium, although the best yields with least contamination from cyclic polyphosphanes (<5% by ^{31}P NMR spectroscopy) were achieved with 3.2 equivalents of selenium at room temperature. There is only one other published example of a tetraselenohypodiphosphonate, that of the diphenyl analogue formed from the reaction of LiP(Ph)$SnPh_3$ (itself prepared from the reaction of PPh_5 with $LiSnPh_3$) with four equivalents of selenium, although no solid-state characterisation was reported and there was significant contamination with cyclic phosphanes (57%).[28]

X-ray structural characterisation of [{(*c*-C_6H_{11})P(Se)(SeLi)}$_2$·2TMEDA] (**7**, Figure 6) showed it to be disordered about a crystallographic C_{2h} position (with the twofold axis passing along the Li···LiA vector and the mirror pane bisecting the two Se−P−Se angles). As a consequence only the phosphorus, lithium, and nitrogen centres are ordered. In particular, each of the selenium centres is disordered over two 50% occupancy sites (shown in Figure S3, see Supporting Information) so that there are two distinctly different P−Se bond lengths [2.072(2) and 2.229(2) Å]; by contrast, all of the Li−Se distances are the same (Table 1). The 50:50 nature of this disorder means that for each of the two phosphorus centres it is crystallographically impossible to distinguish between i) the disorder of a single PSe_2 unit having one "short" and one "long" P−Se linkage, and ii) the superimposition of two different PSe_2 units, one that has two "short" P−Se linkages and one in which both bonds are "long". Although the presence of this disorder precludes an in-depth analysis of the bond lengths and angles, the structure clearly shows two lithium coordination sites on either side of the phosphorus-phosphorus backbone with each lithium bonding to two selenium atoms (one from each of the diselenophosphinate groups) and a TMEDA molecule, whilst the two cyclohexyl groups are in an *anti* conformation to one another. The two P−Se bond lengths are very disparate (differing by ca. 0.16 Å) with the longer bond [2.229(2) Å] being close to the length expected for a P−Se single bond [cf. P−Se bond lengths of 2.233(1) and 2.200(8) in **1**][8] and the shorter [2.072(16) Å] being within the range expected for a P−Se double bond.[29] This therefore suggests disorder of type i) with one selenium singly and one doubly bonded to each phosphorus atom and no, or very little, charge delocalisation occurring within the diselenophosphinate moieties. This behaviour therefore contrasts with that observed for the dichalcogenophosphinate groups in **2**, **5**, and **6** where complete charge delocalisation was present. The P−P bond, 2.252(2) Å, is in the range expected for a single bond (2.20 to 2.35 Å);[27] the Li−Se distances are all equal at 2.561(4) Å and are similar to previously reported Li−Se bond lengths in lithium seleno-phosphorus complexes.[8] Characterisation in solution by ^{31}P NMR spectroscopy showed just one predominate phosphorus signal (δ = 53.4 ppm) with satellites exhibiting AA′X splitting (where A is ^{31}P and X is ^{77}Se) due to the 23.9% abundant ^{77}Se isotopomer (Figure 7, a). ^{77}Se NMR spectroscopy also reveals an AA′X splitting pattern due to the same isotopomer (Figure 7, c). These ^{31}P and ^{77}Se NMR spectra correlate very accurately with compu-

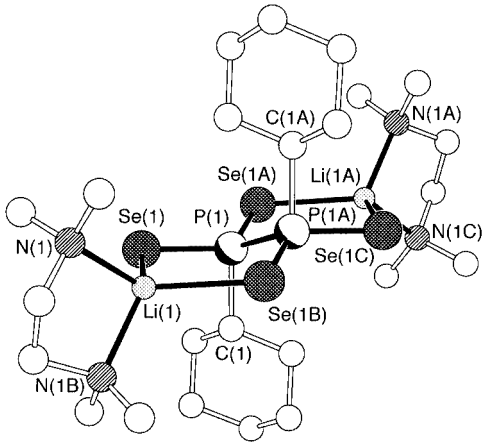

Figure 6. The molecular structure of [{(*c*-C_6H_{11})-P(Se)(SeLi)}$_2$·2TMEDA] (**7**)

 © 2003 Wiley-VCH Verlag GmbH & Co. KGaA, Weinheim

tationally simulated spectra (Figure 7, b and d) with assignment iterated coupling constants of $^1J_{P,Se} = -623.2$, $^1J_{P,P} = -175.2$ and $^3J_{P,Se} = 2.0$ Hz (± 0.2 Hz).[30] The value of the $^1J_{P,Se}$ coupling constant is indicative of a phosphorus-selenium bond of order 1.5 and is similar to the $^1J_{P,Se}$ values observed for **2** (−585 Hz) and **6** (−635 Hz). Therefore, in contrast to the behaviour observed for **7** in the solid state, in solution all P−Se bonds are of equal length (on the NMR time scale), signifying that charge delocalisation within the diselenophosphinate groups is now taking place. The P-P NMR coupling constant is within the range expected for a single bond.[27]

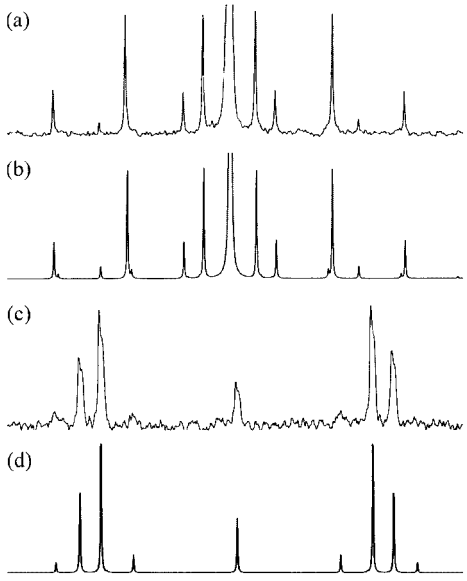

Figure 7. (a) ^{31}P NMR spectrum of **7** in C_6H_6; (b) Computationally simulated[30] ^{31}P NMR spectrum of **7**; (c) ^{77}Se NMR spectrum of **7** in C_6H_6; (d) Computationally simulated[30] ^{77}Se NMR spectrum of **7**

Conclusion

In summary, we have shown the first solid-state characterisations of a tellurophosphinite complex **4**, a ditellurophosphinate complex **5** and a mixed chalcogen selenotellurophosphinate complex **6**. Although these compounds are all ion-separated species with solvated lithium cations and therefore do not exhibit such a range of coordination modes with lithium as observed for their selenium or sulfur analogues, they do provide some valuable and rare structural insights into phosphorus tellurium multiple bonding. We are now investigating the coordination chemistry of these ligands with a range of transition metal centres as it is envisaged that stronger ligand-metal coordination will render these ligands more stable, and such complexes would be of potential use as chemical vapour deposition (CVD) precursors to metal chalcogenolides.[4] Related phosphinotellurgenoic amidato complexes [M{tBu$_2$P(Te)NR}$_2$] (M = Fe, Mn, and Co) have already shown promise is this area as suitable agents for the gas-phase deposition of metal chalcogenolide films.[31]

In addition we have demonstrated a new, clean synthetic route to a tetraselenohypodiphosphonate complex by reaction of dilithiated primary phosphanes with greater than three equivalents of elemental selenium, and have presented the first full characterisation of such a species. The tetradentate nature of these ligands should allow them to form wide range of coordination compounds and we are currently investigating their transmetallation reactions.

Experimental Section

General Procedures: All reactions and manipulations were carried out under an inert atmosphere of dry nitrogen or argon using standard double manifold and glove-box techniques. Purification and drying of the solvents were done using standard methods.[32] Ph_2PH and $CyPH_2$ were purchased from Strem and all other chemicals from Lancaster.

NMR spectra were recorded on either a Bruker DPX400 (^{1}H and ^{31}P) or a Joel EX270 Delta Upgrade (^{77}Se and low temperature ^{31}P) spectrometer. External standards used were TMS (^{1}H, ^{13}C), 85% H_3PO_4 (^{31}P) or Me_2Se (^{77}Se). Melting points were measured in sealed capillaries under argon.

Synthesis of [Ph$_2$PTe][Li(TMEDA)$_{1.33}$(THF)$_{1.33}$] (4): nBuLi (1.6 M in hexanes, 3.2 mL, 5 mmol) was added to Ph_2PH (0.86 mL, 5 mmol) and TMEDA (1.0 mL, 6.7 mmol) in 5 mL THF. The resulting solution was then transferred onto powdered Te (0.64 g, 5 mmol) in 3 mL of toluene at −78 °C and allowed to warm slowly to room temperature to give a dark red solution which was filtered through celite and left at −30 °C for 48 h to yield red crystals of **4** (1.52 g, 54%). M.p. 76−78 °C. Note that 0.66 THF was lost from **4** during the isolation procedure in the glove-box, so all spectroscopic characterisation is for [Ph$_2$PTe][Li(TMEDA)$_{1.33}$(THF)$_{0.67}$]. ^{1}H NMR (250 MHz, [D$_6$]DMSO, 25 °C): δ = 1.74 (m, 2.7 H, THF), 2.09 (s, 16 H, TMEDA), 2.25 (s, 5.3 H, TMEDA), 3.59 (m, 2.7 H, THF), 6.97−7.63 (m, 10 H, Ph_2P-) ppm. ^{13}C NMR (101 MHz, [D$_6$]DMSO, 25 °C): δ = 145.7, 134.0, 126.9, 125.7 (Ph_2P-), 67.1 (THF), 57.3, 45.6 (TMEDA), 25.2 (THF) ppm.^{31}P NMR (162 MHz, [D$_6$]DMSO, 25 °C): δ = −32.5 (s + d satellites, $^1J_{P,Te}$ = 747 Hz) ppm. $C_{22.66}H_{36.66}LiN_{2.66}O_{0.66}PTe$ (522.7): calcd. C 52.08, H 7.07, N 7.15; found C 51.99, H 6.98, N 7.18.

Synthesis of [Ph$_2$PTe$_2$][Li(THF)$_{3.5}$(TMEDA)$_{0.25}$] (5): nBuLi (1.6 M in hexanes, 1.6 mL, 2.5 mmol) was added to Ph_2PH (0.43 mL, 2.5 mmol) in 5 mL of THF. The resulting solution was then reacted with a suspension of powdered Te (0.64 g, 5 mmol) in 5 mL of THF at −78 °C followed by further stirring for 12 h at room temperature to give a dark red-brown solution. This solution was filtered through celite and reduced in volume to 5 mL in vacuo. Highly air- and moisture-sensitive dark-red crystals of **5** grew from this solution on storage at −30 °C over 72 h. Due to the extreme air, moisture and thermal instability of **5** we were unable to isolate it as a stable solid long enough to achieve full characterisation. Therefore ^{31}P NMR was carried out on a 1 mL aliquot of the reaction mixture to show qualitative production of **5**. ^{31}P NMR (162 MHz, THF, 25 °C): δ = −123.8 (s + d satellites, $^1J_{P,Te}$ = 1530 Hz) ppm.

Synthesis of [Ph$_2$P(Se)Te][Li(THF)$_2$(TMEDA)] (6): nBuLi (1.6 M in hexanes, 1.6 mL, 2.5 mmol) was added to Ph_2PH (0.43 mL, 2.5 mmol) and TMEDA (0.37 mL, 2.5 mmol) in 2 mL of toluene/2 mL of THF to give a clear yellow solution. This solution was then transferred onto a mixed suspension of Te powder (0.64 g,

 © 2003 Wiley-VCH Verlag GmbH & Co. KGaA, Weinheim

Table 2. Crystal data, data collection and refinement parameters for compounds **4**−**7**

	4	**5**	**6**	**7**
Formula	$(C_{14}H_{32}LiN_2O_2)_{0.67}$-$(C_{12}H_{32}LiN_4)_{0.33}$-$(C_{12}H_{10}PTe)$	$(C_{16}H_{32}LiO_4)_{0.75}$-$(C_{14}H_{32}LiN_2O_2)_{0.25}$-$(C_{12}H_{10}PTe_2)$	$(C_{14}H_{32}LiN_2O_2)$-$(C_{12}H_{10}PSeTe)$	$C_{24}H_{54}Li_2N_4P_2Se_4$
Molecular mass	570.8	728.7	659.1	790.4
Crystal size [mm]	0.21 × 0.18 × 0.18	0.23 × 0.21 × 0.21	0.12 × 0.12 × 0.09	0.20 × 0.20 × 0.17
Temperature [K]	180	220	180	183
Crystal system	monoclinic	monoclinic	triclinic	orthorhombic
Space group	$P2_1/c$ (no. 14)	$P2_1/c$ (no. 14)	$P\bar{1}$ (no. 2)	*Cmca* (no. 64)
a [Å]	15.7655(6)	15.974(3)	10.7603(10)	16.9716(8)
b [Å]	9.9042(3)	22.957(5)	12.0722(9)	12.4529(4)
c [Å]	18.6989(18)	17.372(4)	12.8144(12)	16.9878(10)
α [deg]	−	−	74.935(5)	−
β [deg]	91.150(2)	91.79(3)	76.817(4)	−
γ [deg]	−	−	73.593(4)	−
V [Å^3]	2919.15(18)	6367(2)	1520.3(2)	3590.3(3)
Z	4	8[a]	2	4[b]
D_c [g cm^{-3}]	1.299	1.520	1.440	1.462
Radiation used[c]	Mo-K_α	Mo-K_α	Mo-K_α	Cu-K_α[d]
μ [mm^{-1}]	1.09	1.91	2.25	5.87
2θ max [deg]	55.0	49.7	50.0	120.0
No. of unique reflns.				
Measured	6673	10763	5220	1367
Obsd., $\|F_o\| > 4\sigma(\|F_o\|)$	4381	6982	3458	1187
No. of variables	378	784	330	133
R_1, wR_2[d]	0.042, 0.105	0.097, 0.273	0.050, 0.098	0.029, 0.070

[a] There are two crystallographically independent cation:anion pairs in the asymmetric unit. [b] The molecule has crystallographic C_2h symmetry. [c] Details in common: graphite-monochromated radiation, refinement based on F^2. [d] Rotating anode source. [e] $R_1 = \Sigma||F_o| - |F_c||/\Sigma|F_o|$; $wR_2 = \{\Sigma[w(F_o^2 - F_c^2)^2]/\Sigma[w(F_o^2)^2]\}^{1/2}$; $w^{-1} = \sigma^2(F_o^2) + (aP)^2 + bP$.

5 mmol) and Se powder (0.40 g, 5 mmol) in 5 mL of THF at −78 °C, allowed to warm to room temperature slowly and stirred for a further 12 h. Orange crystals of **2** grew from this solution at room temperature over 72 h in 42% yield (1.39 g). M.p. 95−98 °C. ^{1}H NMR (250 MHz, [D$_6$]DMSO, 25 °C): δ = 1.75 (m, 8 H, THF), 2.10 (s, 12 H, TMEDA), 2.27 (s, 4 H, TMEDA), 3.60 (m, 8 H, THF), 7.21−8.00 (m, 10 H, Ph$_2$P) ppm. ^{13}C NMR (101 MHz, [D$_6$]DMSO, 25 °C): 142.0, 132.4, 128.5, 126.8 (Ph$_2$P-), 67.1 (THF), 57.3, 45.7 (TMEDA), 25.2 (THF) ppm. ^{31}P NMR (162 MHz, [D$_6$]DMSO, 25 °C): δ = 24.0 (5%, s + d satellites, $^1J_{P,Se}$ = −647; **2**), −43.0 (90%, s +2 × d satellites, $^1J_{P,Se}$ = −635, $^1J_{P,Te}$ = 1485 Hz; **6**), −121.8 (5%, s + d satellites, $^1J_{P,Te}$ = 1510; **5**) ppm. Due to contamination of **6** by small amounts of **2** and **5** we were unable to obtain satisfactory elemental analyses.

Synthesis of [{(*c*-C$_6$H$_{11}$)P(Se)(SeLi)}$_2$·2TMEDA] (7): *n*BuLi (1.6 M in hexanes, 3.2 mL, 5 mmol) was added to CyPH$_2$ (0.33 mL, 2.5 mmol) and TMEDA (0.75 mL, 5 mmol) in 4 mL of toluene/6 mL of THF at −78 °C. The resulting solution was then slowly warmed to room temperature and then transferred onto powdered grey Se (0.635 g, 8 mmol) and stirred for 15 min. Colourless crystals of **4** grew from the solution after 3 days at −27 °C 0.71 g, 72% yield). M.p. 166−168 °C. ^{1}H NMR (270 MHz, [D$_6$]DMSO, 25 °C): δ = 0.82−2.10 (m, 11 H, C$_6$H$_{11}$), 2.12 (s, 4 H, TMEDA), 2.28 (s, 12 H, TMEDA) ppm. ^{13}C NMR (101 MHz, [D$_6$]DMSO, 25 °C): δ = 57.3, 45.7 (TMEDA), 44.9, 27.3, 26.7, 26.5, 26.4, 26.3, 26.0 (*c*-C$_6$H$_{11}$) ppm. ^{31}P (109 MHz, [D$_6$]DMSO, 25 °C): δ = 53.4 (m) ppm. ^{77}Se (51.5 MHz, [D$_6$]DMSO, 25 °C): δ = −504 (m) ppm. $C_{24}H_{54}Li_2N_4P_2Se_4$ (790.4): calcd. C 36.47, H 6.89, N 7.09; found C 38.46, H 7.00, N 7.07.

X-ray Structure Determinations of 4−7: Table 2 provides a summary of the crystallographic data for compounds **4**−**7**. Data were collected on Nonius Kappa CCD (compounds **4**−**6**) and Siemens P4/RA (compound **7**) diffractometers, and the structures were refined based on F^2 using the SHELXTL and SHELX-97 program systems.[33] The crystals of **4** contain two different cations, there being a ca. 67:33 mixture of [(TMEDA)(THF)$_2$Li]$^+$ and [(TMEDA)$_2$Li]$^+$. A similar situation is seen in the crystals of **5**, though here the two cations [(THF)$_4$Li]$^+$ and [(TMEDA)(THF)$_2$Li]$^+$ are present in a ca. 75:25 ratio. In the structure of **6** the positions of the Te(1) and Se(1) centres are occasionally reversed (ca. 63:37). The structure of **7** is substantially disordered about the crystallographic C_{2h} position (refinement in lower symmetry space groups does not remove the disorder) such that only the P(1), Li(1), and N(1) positions are ordered.

CCDC-208127−208130 (**4**−**7**) contain the supplementary crystallographic data for this paper. These data can be obtained free of charge at www.ccdc.cam.ac.uk/conts/retrieving.html [or from the Cambridge Crystallographic Data Centre, 12 Union Road, Cambridge CB2 1EZ, UK; fax: (internat.) +44-1223/336-033; E-mail: deposit@ccdc.cam.ac.uk].

Acknowledgments

This work was supported by a studentship from the Dept of Chemistry, Imperial College, London (M.G.M), a CRF grant from the University of London and a Royal Society Research Grant. The authors also wish to thank Dr J. Davies, University of Cambridge, for his assistance in the collection of the X-ray crystallographic data on compounds **4**−**6**.

 © 2003 Wiley-VCH Verlag GmbH & Co. KGaA, Weinheim

[1] [1a] I. Haiduc, *J. Organomet. Chem.* **2001**, *623*, 29−42. [1b] B. Walther, *Coord. Chem. Rev.* **1984**, *60*, 67−105. [1c] R. C. Mehrotra, G. Srivastava, B. P. S. Chauhan, *Coord. Chem. Rev.* **1984**, *55*, 207−259.
[2] C. N. Rowe, J. J. Dickert, *ASLE Trans.* **1967**, *10*, 85−90.
[3] For examples see: [3a] A. P. Fernandes, M. de Moraes, J. A. G. Neto, *Eclet. Quim.* **2001**, *26*, 211−222. [3b] M. Curtui, I. Haiduc, L. Ghizdavu, *J. Radioanal. Nucl. Ch.* **2002**, *251*, 163−166.
[4] [4a] H. B. Singh, N. Sudha, *Polyhedron* **1996**, *15*, 745−763. [4b] J. Arnold, in *Prog. Inorg. Chem. vol. 43* (Ed.: K. D. Karlin), John Wiley & Sons: New York, **1995**, p. 353−418. [4c] A. N. Gleizes, *Chem. Vap. Deposition* **2000**, *6*, 155−173. [4d] M. Bochmann, *Chem. Vap. Deposition* **1996**, *2*, 85−96.
[5] [5a] H. J. Gysling, in *The Chemistry of Organic Selenium and Tellurium compounds, vol. 1* (Eds.: S. Patai, Z. Rappoport), John Wiley & Sons: New York, **1986**, 679−855. [5b] N. Petragnani, *Tellurium in Organic Synthesis*; Academic Press: London, **1994**. [5c] C. Paulmier, *Selenium Reagents and Intermediates in Organic Synthesis*; Pergamon: Oxford, **1986**. [5d] J. V. Comasseto, R. E. Barrientos-Astigarraga, *Aldrichimica Acta* **2000**, *33*, 66−78.
[6] T. Chivers, *J. Chem. Soc., Dalton Trans.* **1996**, 1185−1194.
[7] W. Clegg, R. P. Davies, R. Snaith, A. E. H. Wheatley, *Eur. J. Inorg. Chem.* **2001**, 1411−1413.
[8] R. P. Davies, M. G. Martinelli, *Inorg. Chem.* **2002**, *41*, 348−352.
[9] B. Bildstein, F. Sladky, *Phosphorus, Sulfur and Silicon* **1990**, *47*, 341−347.
[10] Cambridge Structural Data Centre, 12 Union Road, Cambridge CB2 1EZ, UK. Database version: February **2003**.
[11] N. Kuhn, H. Schumann, G. Wolmershaeuser, *J. Chem. Soc., Chem. Commun.* **1985**, 1595−1597.
[12] L. Huang, R. A. Zingaro, E. A. Meyers, J. H. Reibenspies, *Heteroatom Chem.* **1996**, *7*, 57−65.
[13] R. Hensel, W. W. du Mont, R. Boese, D. Wewers, L. Weber, *Chem. Ber.* **1985**, *118*, 1580−1587.
[14] M. D. Franics, D. E. Hibbs, P. B. Hitchcock, M. B. Hursthouse, C. Jones, T. Mackewitz, J. F. Nixon, L. Nyulaszi, M. Regitz, N. Sakarya, *J. Organomet. Chem.* **1999**, *580*, 156−160.
[15] D. Buchholz, G. Huttner, L. Zsolnai, W. Imhof, *J. Organomet. Chem.* **1989**, *377*, 25−41.
[16] G. G. Briand, T. Chivers, M. Parvez, G. Schatte, *Inorg. Chem.* **2003**, *42*, 525−531.
[17] H. Westermann, M. Nieger, E. Neicke, *Chem. Ber.* **1991**, *124*, 13−16.
[18] M. M. Al-Ktaifani, D. P. Chapman, M. D. Francis, P. B. Hitchcock, J. F. Nixon, L. Nyulászi, *Angew. Chem. Int. Ed.* **2001**, *40*, 3474−3478.
[19] [19a] H. Duddeck, in *Encyclopedia of Nuclear Magnetic Resonance, vol. 7* (Eds.: D. M. Grant, R. K. Harris); Wiley: New York, **1996**, p. 4623−4635. [19b] H. Duddeck, *Prog. Nucl. Mag. Res. Spec.* **1995**, *27*, 1−323. [19c] H. C. E. McFarlane, W. McFarlane, in *NMR of Newly Accessible Nuclei, vol. 2* (Ed.: P. Laszlo) Academic: New York, **1983**, 275−299.
[20] [20a] G. Becker, K. W. Klinkhammer, S. Lartiges, P. Bottcher, W. Poll, *Z. Anorg. Allg. Chem.* **1992**, *613*, 7−18. [20b] G. Becker, K. W. Klinkhammer, W. Massa, *Z. Anorg. Allg. Chem.* **1993**, *619*, 628−640. [20c] P. J. Bonasia, D. E. Gindelberger, B. O. Dabbousi, J. Arnold, *J. Am. Chem. Soc.* **1992**, *114*, 5209−5214. [20d] P. Bonasia, J. Arnold, *J. Organomet. Chem.* **1993**, *449*, 147−157. [20e] P. J. Bonasia, V. Christou, J. Arnold, *J. Am. Chem. Soc.* **1993**, *115*, 6777−6781.
[21] H. Gornitzka, S. Bresser, R. Herbst-Irmer, U. Kiliman, F. T. Edelmann, *Angew. Chem. Int. Ed. Engl.* **1992**, *31*, 1260−1261.
[22] N. Sandblom, T. Ziegler, T. Chivers, *Can. J. Chem.* **1996**, *74*, 2363−2371.
[23] N. Kuhn, H. Schumann, G. Wolmerhäuser, *Z. Naturforsch., Teil B* **1987**, *42*, 674−678.
[24] N. Kuhn, G. Henkel, H. Schumann, R. Fröhlich, *Z. Naturforsch., Teil B* **1990**, *45*, 1010−1018.
[25] [25a] M. Bochmann, G. C. Bwembya, N. Whilton, X. Song, M. B. Hursthouse, S. J. Coles, A. Karanlov, *J. Chem. Soc., Dalton Trans.* **1995**, 1887−1892. [25b] M. Bochmann, G. C. Bwembya, M. B. Hursthouse, S. J. Coles, *J. Chem. Soc., Dalton Trans.* **1995**, 2813−2817.
[26] C. H. W. Jones, R. D. Sharma, *Organometallics* **1987**, *6*, 1419−1423.
[27] A. H. Cowley, *Compounds Containing Phosphorus − Phosphorus Bonds*, Dowden, Hutchingson and Ross Inc.: Pennsylvania, USA, **1973**.
[28] A. Schmidpeter, K-H. Zirzow, *Phosphorus and Sulfur* **1988**, *36*, 15−21.
[29] Mean P−Se double bond length from literature values = 2.093(19) Å. See: *Handbook of Chemistry and Physics 75th Ed.* (Chief Ed.: D. R. Lide); CRC Press: Boca Raton, Fl., **1995**, p. **9**−12.
[30] gNMR v4.01, Cherwell Scientific publishing, The Magdalen Centre, Oxford Science Park, Oxford OX4 4GA, UK.
[31] X. Song, M. Bochmann, *J. Chem. Soc., Dalton Trans.* **1997**, 2689−2692.
[32] D. D. Perrin, W. L. F. Armarego, D. R. Perrin, *Purification of Laboratory Chemicals*, 2nd ed.; Pergamon Press: Oxford, U. K., **1980**.
[33] *SHELXTL PC version 5.1*, Bruker AXS, Madison, WI, **1997**; *SHELX-97*, G. Sheldrick, Institut Anorg. Chemie, Tammannstr. 4, 37077 Göttingen, Germany, **1998**.

Received April 24, 2003

 © 2003 Wiley-VCH Verlag GmbH & Co. KGaA, Weinheim

Homo- and Heteroleptic Hypersilylcuprates — Valuable Reagents for the Synthesis of Molecular Compounds with a Cu−Si Bond

Karl W. Klinkhammer,*[a] Jan Klett,[a] Yun Xiong,[a] and Shenglai Yao[a]

Dedicated to the memory of Ron Snaith

Keywords: Copper / Silicon / Silylcuprates / Si ligands

Unsolvated hypersilanides MHyp [Hyp = $Si(SiMe_3)_3$] of the heavier alkali metals (M^I = Na, K, Cs) react with copper *tert*-butoxide in toluene to yield crystalline heteroleptic cuprates [M^I(toluene)][*t*BuOCuHyp]. These cuprates proved to be valuable sources for pure hypersilylcopper and other cuprates bearing hypersilyl ligands such as the di(hypersilyl)-cuprates $M^I[CuHyp_2]$.

(© Wiley-VCH Verlag GmbH & Co. KGaA, 69451 Weinheim, Germany, 2003)

Introduction

Molecular compounds with a Cu−Si bond are very important reagents in modern organic chemistry.[1] However, since they are usually prepared in situ for this purpose, only limited information about their composition and molecular structures is available. This information has mainly been derived from NMR experiments.[2] Only very few structural data for pure compounds are available to date.[3−8] This is partially related to the low kinetic stability of these cuprates and/or the fact that the reaction mixtures often contain various additives to get better regiospecificity and stereoselectivity. The first report of a crystal structure came from Cowley et al. in 1988 , who succeeded in preparing a kinetically stabilized triphenylphosphane complex of a neutral silylcopper complex and determined its structure by X-ray diffraction.[3] All efforts to isolate the pure silylcopper complex in the absence of any stabilizing donor failed however. A few years later Stalke et al. synthesized two silylcuprates as crystalline materials.[4,5] The yields were low, however, and in spite of the bulky hypersilyl substituent employed one of these cuprates, a polynuclear chlorocuprate, is extremely kinetically unstable and decomposes below −20 °C. Until 1999 when we finally succeeded in preparing the first kinetically stable unsolvated silylcopper complex as well as stable lithium cuprates in very good yields,[6,7] a few further reports were published concerning the synthesis of pure Cu^I compounds bearing silyl groups.[9−11] To the best of our knowledge, no detailed structural information about such species had been provided with the exception of two cuprates synthesized very recently by Lerner et al. by a procedure similar to the one used by Stalke.[8] We again used the mentioned hypersilyl group, but in contrast to Stalke and Lerner avoided the presence of halide anions which are thought to have a destabilizing influence on related copper derivatives with hydrocarbyl substituents. As alternative copper(I) source we used either copper *tert*-butoxide or a very bulky arylcopper derivative.

$$7\ LiHyp + 6\ CuO\mathit{t}Bu \longrightarrow [Li_7(O\mathit{t}Bu)_6][Cu_7Hyp_3] + 4\ CuHyp \quad (1)$$

$$9\ LiHyp + 6\ CuO\mathit{t}Bu \longrightarrow [Li_7(O\mathit{t}Bu)_6][Cu_2Hyp_3] + 2\ LiCu_2Hyp_3 \quad (2)$$

$$11\ LiHyp + 6\ CuO\mathit{t}Bu \longrightarrow [Li_7(O\mathit{t}Bu)_6][Cu_2Hyp_3] + 4\ LiCuHyp_2 \quad (3)$$

$$PbHyp_2 + CuAr \longrightarrow CuHyp + Pb(Ar)Hyp \quad (4)$$

The employed silanide nucleophiles were unsolvated hypersilanides of lithium [Equations (1)−(3)] and lead(II) [Equation (4)], respectively. Both reaction types, however, are not suitable for preparing large quantities of pure silylcopper derivatives. We now report the synthesis of novel hypersilyl complexes of Cu^I, the heteroleptic *tert*-butoxy(hypersilyl)cuprates of the heavier alkali metals M^I[*t*BuOCuHyp], which are easily accessible in high quantities and excellent yields. They are fairly stable under controlled conditions and, as will be seen below, have proved to be valuable starting compounds for other silyl derivatives of Cu^I.

[a] Institut für Anorganische und Analytische Chemie der Johannes-Gutenberg-Universität Mainz,
Duesbergweg 10−14, 55099 Mainz, Germany
Fax: (internat.) +49-(0)6131/392-5745
E-mail: klink@uni-mainz.de

Table 1. Crystallographic data for M^I(toluene)[HypCuO*t*Bu] [M^I = K (**1**), Na (**2**), Cs(**3**)] and M^ICuHyp_2 [M^I = K (**4**), Na (**5**)]

	1	**2**	**3**	**4**	**5**
Formula	$C_{40}H_{88}Cu_2K_2O_2Si_8$	$C_{40}H_{88}Cu_2Na_2O_2Si_8$	$C_{40}H_{88}Cs_2Cu_2O_2Si_8$	$C_{18}H_{54}CuKSi_8$	$C_{18}H_{54}CuNaSi_8$
Molecular mass	1031.10	998.88	1218.72	597.97	581.86
Crystal System	monoclinic	triclinic	triclinic	monoclinic	triclinic
Space Group	$P2_1/n$	$P\bar{1}$	$P\bar{1}$	$P2_1$	$P\bar{1}$
a [Å]	13.6489(14)	9.916(2)	9.400(2)	9.134(2)	9.442(2)
b [Å]	12.498(2)	12.329(2)	11.478(2)	12.619(3)	13.164(2)
c [Å]	18.619(2)	12.469(2)	15.454(3)	15.827(3)	16.689(3)
α [°]	90	90.82(3)	71.41(3)	90	108.495(9)
β [°]	107.762(10)	101.99(3)	81.59(3)	91.87(3)	96.201(10)
γ [°]	90	91.03(3)	81.37(3)	90	108.919(9)
V [Å^3]	3024.7(7)	1490.6(5)	1553.8(5)	1823.3(7)	1808.9(6)
Z	2	1	1	2	2
F(000)	1104	536	624	644	628
$D_{calcd.}$ [gcm^{-1}]	1.132	1.113	1.302	1.089	1.068
μ [mm^{-1}]	1.026	0.916	2.019	0.982	0.886
Crystal Size [mm^{-3}]	0.4 × 0.3 × 0.1	0.8 × 0.6 × 0.3	0.6 × 0.5 × 0.5	0.8 × 0.3 × 0.3	0.6 × 0.3 × 0.2
θ range	2.7 < θ < 28°	3.4 < θ < 27.5°	2 < θ < 28°	2 < θ < 30°	2.3 < θ < 28°
hkl ranges	$-1 < h < 18$	$0 < h < 12$	$0 < h < 12$	$-12 < h < 12$	$0 < h < 12$
	$-1 < k < 16$	$-16 < k < 16$	$-14 < k < 14$	$-8 < k < 17$	$-15 < k < 15$
	$-24 < l < 23$	$-16 < l < 15$	$-20 < l < 20$	$-22 < l < 22$	$-22 < l < 21$
No. of reflns measd.	8910	7207	7799	6919	8777
No. of unique reflns, R_{int}	7303, 0.057	6819, 0.0399	7354, 0.045	6919, 0.059	8286, 0.045
Reflections with $I > 2\sigma(I)$	2600	3891	4923	4134	4075
Parameters, restraints	320, 90	320, 220	257, 0	254, 1	368, 66
Final *R* indices [$I > 2\sigma(I)$]	R_1 = 0.046,	R_1 = 0.050,	R_1 = 0.050,	*R*1 = 0.039,	*R*1 = 0.064,
	wR_2 = 0.071	wR_2 = 0.116	wR_2 = 0.112	*wR*2 = 0.085	*wR*2 = 0.146
Final *R* indices (all data)	R_1 = 0.154,	R_1 = 0.092,	*R*1 = 0.091,	*R*1 = 0.061,	*R*1 = 0.137,
	wR_2 = 0.085	wR_2 = 0.125	wR_2 = 0.131	*wR*2 = 0.089	*wR*2 = 0.166
Goodness-of-fit	0.680	0.880	0.987	0.866	0.925
Residual electron density [e·Å^{-3}]	−0.301, 0.327	−0.389, 0.739	−1.003, 0.802	−0.396, 0.441	−0.311, 0.457

Results and Discussion

Potassium hypersilanide [KHyp; Hyp = -Si(SiMe$_3$)$_3$][12] readily reacts with copper *tert*-butoxide in toluene to give a pale yellow solution from which, on cooling to −20 °C, colorless crystals precipitate. The NMR spectroscopic data indicate that the toluene solvate of heteroleptic potassium *tert*-butoxy(hypersilyl)cuprate [K(toluene)][*t*BuOCuHyp] (**1**) had formed quantitatively [Equation (5)]. This assumption was verified by an X-ray diffraction experiment on a single crystal (Table 1 and 2). Whereas in the crystalline state cuprate **1** may be stored for several months, in solution

Table 2. Selected bond lengths [pm] and angles [°] in M^I(toluene)[HypCuO*t*Bu] [M^I = K (**1**), Na (**2**), Cs(**3**)]

	1	**2**	**3**
Cu1−Si1	222.59(2)	223.47(11)	223.0(2)
Cu1−O1	188.0(3)	188.7(2)	188.1(3)
Si−Si (range)	233.2(2)−234.68(14)	233.8(2)−234.6(2)	233.5(2)−233.9(2)
M^I−O1	259.1(3)	225.5(3)	290.1(3)
M^I−O1′	266.0(2)	229.4(3)	298.5(3)
M^I···C_{arom} (range)	315(4)−338(4)	294.2(12)−356.9(8)	359.7(9)−388.4(9)
M^I···C_T [a]	302	295.2	346.5
Si1−Cu1−O1	171.70(7)	177.05(8)	174.59(11)
Cu1−O1−C1	120.4(2)	122.8(2)	119.0(3)
Cu1−O1−M^I	106.24(12)	104.55(10)	104.87(13)
Cu1−O1−$M^{I\prime}$	91.51(9)	97.85(10)	93.64(12)
M^I−O1−C1	121.1(2)	117.5(2)	119.2(3)
$M^{I\prime}$−O1−C1	118.0(2)	117.0(2)	116.8(3)
M^I−O1−$M^{I\prime}$	92.65(8)	91.24(10)	98.75(10)
O1−M^I−O1′	87.35(8)	88.76(10)	81.25(10)
Cu−Si−Si (range)	104.98(5)−120.50(6)	107.96(5)−118.76(6)	106.29(7)−117.26(7)
Si−Si−Si (range)	105.26(6)−106.63(6)	105.69(5)−106.71(5)	106.81(8)−107.49(8)

[a] C_T denotes the centroid of the carbon atoms of the aromatic ring.

 © 2003 Wiley-VCH Verlag GmbH & Co. KGaA, Weinheim

it decomposes slowly even at −20 °C with precipitation of a black powder within a few weeks; this process is even faster when the solution is exposed to ambient light.

$$M^{I}Hyp + CuO\mathit{t}Bu \xrightarrow[-20°C]{\text{toluene}} [M^{I}(\text{toluene})][\mathit{t}BuOCuHyp]$$

M^{I} = Na (**2**), K (**1**), Cs (**3**) (5)

In the solid state the heterocuprate **1** consists of centrosymmetric dimers (Figure 1), where two *tert*-butoxy(hypersilyl)cuprate anions with almost linear Si−Cu−O backbones [171.70(7)°] are linked via two $[K(\text{toluene})]^{+}$ cations, thus forming planar K_2O_2 rings with alternating short and long K−O distances of 259.1(3) and 266.0(2) pm, respectively. The coordination sphere of each alkali cation is completed by an η^6-bonded toluene molecule. Due to twofold disordering of the toluene ligand the K···C distances cannot be determined to a great accuracy, but observed values between 315 and 352 pm lie in the expected range. An intriguing feature of the cuprate anion is a very short Cu−Si bond of 222.59(12) pm, which is thus far the shortest among all structurally characterized compounds with Cu−Si bonds (Table 3). The Cu−O distance, on the other hand, is comparatively long, giving rise to the description of cuprate **1** as a *loose* Lewis-acid/base adduct of hypersilylcopper and potassium *tert*-butoxide. Replacing the relatively hard Lewis base *tert*-butoxide for a softer one such as a second hypersilanide anion, or neutral ligands such as phosphanes, leads to substantial lengthening of the Cu−Si bond. We were able to synthesize and structurally characterize di(hypersilyl)cuprates with Na, K and Cs as countercations and therein found Cu−Si distances of about 230 ± 1 pm (see below).

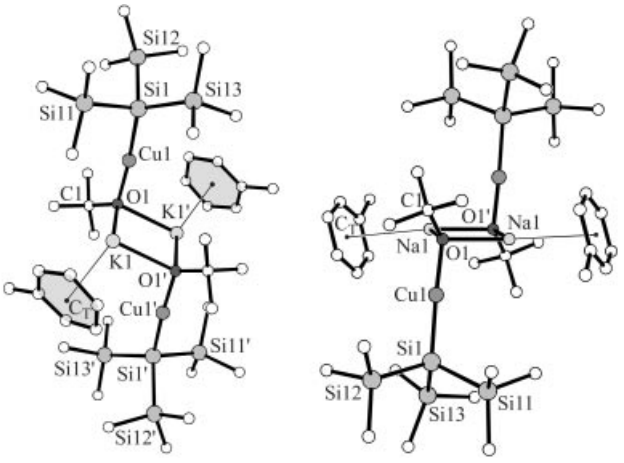

Figure 1. Molecular structures of heterocuprates **1** (left) and **2** (right); slightly differing orientations have been chosen for better illustrating the structural details; atoms are represented by spheres of arbitrary radii; the centroids of the aromatic rings are denoted by C_T; selected structural parameters are given in Table 2

Replacing K^{+} for Na^{+} or Cs^{+} does not significantly change the basicity and availability of the butoxide anion. The respective heterocuprates **2** and **3** again form dimers in the solid state (Figure 1 and 2) and in spite of different crystal structures display very similar molecular structures to the potassium derivative **1**. The observed differences such as different M^{I}−O bond lengths and different M^{I}···C distances (Table 2) can all be related to the strongly differing ionic radii of the alkali metals. Due to the much larger radius of Cs^{+} the cesium cuprate **3** exhibits — other than its relatives **1** and **2** — further aggregation in the solid state. This is accomplished by a Cs···CH_3 agostic interaction with methyl groups of neighboring cuprate dimers [Cs···C122′ 372.8(6) pm] and finally leads to one-dimensional coordination polymers (Figure 2). The cesium cuprate also differs in the fact that the solvating toluene, again bonded in an η^6-fashion, is now well ordered.

Replacing potassium for lithium, i.e. reacting lithium hypersilanide with copper *tert*-butoxide, dramatically changes the type of products obtained. Lithium *tert*-butoxide, which is presumably formed at first, doesn't give any isolable adduct with hypersilylcopper. Instead it catches Li^{+} cations from excess lithium hypersilanide to give the unique cation $[Li_7(O\mathit{t}Bu)_6]^{+}$, and — with simultaneously generated hypersilylcopper — gives rise to the formation of different homocuprates [Equations (1) − (3)], details of which have been published in a previous paper.[7]

The structural parameters of the hypersilyl group present in the cuprates **1**, **2** and **3** differ only slightly. Relatively short Si−Si bonds and Si−Si−Si angles significantly smaller than ideal tetrahedral values indicate negative charge accumulation on the hypersilyl group. An almost complete charge transfer is expected, and found, for the parent alkali metal silanides. Consequently, Si−Si bond lengths of 233 pm and Si−Si−Si angles down to 102° are observed for these compounds, whereas almost ideal tetrahedral angles are found for the derivatives of elements with a similar electronegativity as silicon (e.g. $HgHyp_2$ [13]). A relatively high negative charge of about −0.5 is verified by NBO analysis of the density derived from ab initio or DFT calculations, and is in agreement with the position of the ^{29}Si NMR resonance for the central silicon atom, which is observed at high field (δ = −147 ppm) for all cuprates **1**−**3**.

Next we discuss preliminary results for the utilization of the heterocuprates **1**−**3** in the synthesis of other cuprates. From the outcome of the reaction of lithium hypersilanide with copper *tert*-butoxide, we assumed that in the presence of (unsolvated) Li^{+} cations *tert*-butoxide anions usually do not bind to a Cu−SiR_3 moiety to form heterocuprates. Therefore we supposed that the addition of lithium salt might lead to substitution of the *tert*-butoxide ligand for the co-anion of lithium [Equation (6)].

$$[M^{I}(\text{toluene})][\mathit{t}BuOCuHyp] + LiX \longrightarrow [M^{I}][XCuHyp] + LiO\mathit{t}Bu + \text{toluene}$$

M^{I} = Na (**2**), K (**1**), Cs (**3**) (6)

 © 2003 Wiley-VCH Verlag GmbH & Co. KGaA, Weinheim

Table 3. Cu−Si bond lengths [pm] in molecular compounds

Compound	Cu−Si	CN(Cu)	CN(Si)	Ref.
$Ph_3SiCu(PPh_3)_3$	234.0	4	4	3
$(HypCu)_3$	av 235.0/av 249.2	2	5	6
$HypCu(PPh_3)_2$	234.5	3	4	16
HypCuSn(Hyp)Ar[a]	227.3	2	4	6
[(toluene)Na][*t*BuOCuHyp] (**2**)	223.5	2	4	
[(toluene)K][*t*BuOCuHyp] (**1**)	222.6	2	4	
[(toluene)Cs][*t*BuOCuHyp] (**3**)	223.0	2	4	
$NaCuHyp_2$ (**5**)	av. 228.8	2	4	
$KCuHyp_2$ (**4**)	av 229.9	2	4	
$[(THF)_6K][CuHyp_2]$	av 229.3	2	4	16
$(toluene)_2Cs[CuHyp_2]$	229.1	2	4	16
$[Li_7(OtBu)_6][Cu_2Hyp_3]$	av 231.4, av 238.7	2	4 (2 ×), 5 (1 ×)	7
$LiCu_2Hyp_3$	av 232.9, av 240.0	2	4 (2 ×)[b], 5 (1 ×)	7
$[(THF)_4Li][Cu_5Cl_4Hyp_2]$	av 233.4/av 234.8	3	5	5
$[(THF)_3Li][Cu_2BrHyp_2]$	226.6/240.6	2	4/5	4
$[(THF)_2Na][CuSup_2]$	236.1 (2 ×)	2	4	8
$[(THF)_4Na][CuSup_2]$	231.1 (2 ×)	2	4	8

[a] Ar = C_6H_3-2,6-Mes_2; Mes = C_6H_2-1,3,5-Me.

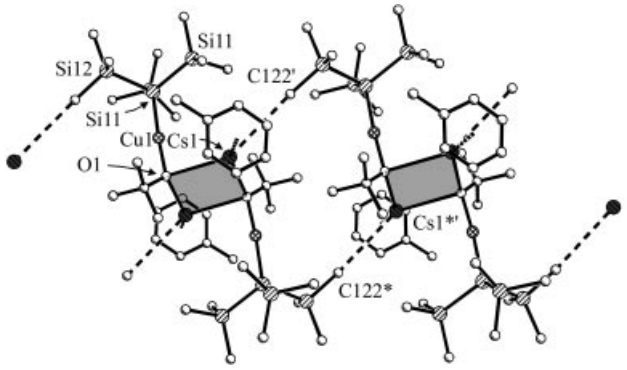

Figure 2. Molecular and crystal structure of heterocuprate **3**; intermolecular contacts are symbolized as dashed lines; atoms are represented by spheres of arbitrary radii; selected structural parameters are given in Table 2

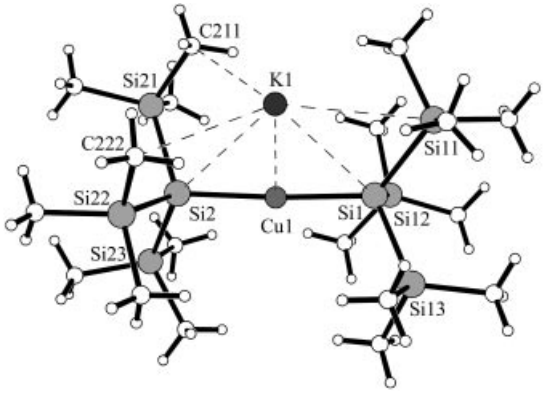

Figure 3. Molecular structure of potassium di(hypersilyl)cuprate (**4**); atoms are represented by spheres of arbitrary radii; dashed lines are used to symbolize interatomic distances markedly smaller than the sum of the corresponding van der Waals radii; selected structural parameters are given in Table 2

At first we investigated the reaction of unsolvated lithium hypersilanide with toluene solutions of the heterocuprates **1**−**3**. In the course of all these reactions the heterocuprates are fully consumed and one very soluble compound, probably unsolvated lithium *tert*-butoxide, is detected as a major product. The ^1H NMR spectra of the non-volatile products reveal the presence of at least one novel species present in all three reaction mixtures, in each case giving a resonance near $\delta = 0.38$ ppm (C_6D_6). The same resonances are found if pure hypersilylcopper is reacted with solvated or unsolvated lithium or potassium hypersilanide in a 1:1 molar ratio. Only for potassium has the respective product — potassium di(hypersilyl)cuprate $K[CuHyp_2]$ (**4**) — been isolated almost pure and in high yields after crystallization from pentane/toluene mixtures [according to Equation (6) with X = Hyp] as a colorless crystalline compound that could be fully characterized by X-ray diffraction (Table 1 and 4; Figure 3 and 4) and NMR spectroscopy.

The colorless solid material from the reaction of heterocuprate **2** contains at least three different compounds. Beside the desired $Na[CuHyp_2]$ (**5**), which again could be structurally characterized, varying amounts of crystalline sodium hypersilanide and one further unidentified product are present in the recrystallized material; from the reaction of cesium derivative **3**, solid mixtures of the desired $Cs[CuHyp_2]$ (**6**), cesium hypersilanide, hypersilylcopper, $Si(SiMe_3)_4$ and at least one other unidentified product are obtained. We concentrate here on the discussion of solid-state structures for the di(hypersilyl)cuprates **4** and **5** which could be determined from single crystals. A thorough comparison of molecular structures and spectroscopic data for all three dihypersilyl cuprates **4**−**6** will be discussed in a later paper, since only during the writing of the present report were we able to isolate the di(hypersilyl)cuprates **5** and **6** as pure compounds from direct reactions of hypersilylcopper and the appropriate alkali metal hypersilanide.[14]

 © 2003 Wiley-VCH Verlag GmbH & Co. KGaA, Weinheim

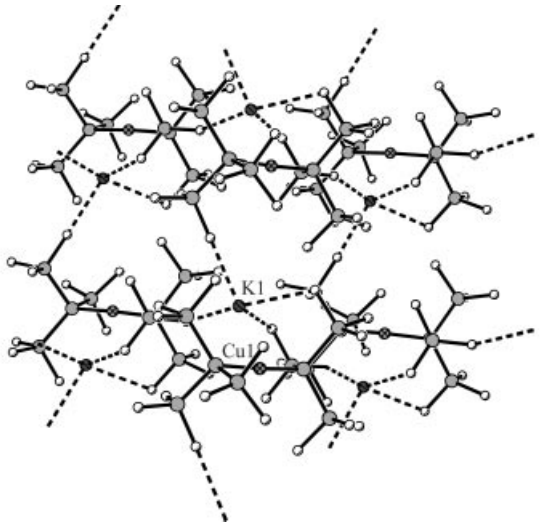

Figure 4. View parallel to [001] of the puckered two-dimensional coordination polymer of cuprate **4**; dashed lines indicate agostic-type intermolecular K···C contacts

The colorless crystal needles of potassium di(hypersilyl)-cuprate (**4**) comprise discrete molecules (Figure 3) interlinked weakly by agostic-type interactions (Figure 4). The potassium ion is located above the center of the dumbbell-like di(hypersilyl)cuprate fragment, thus giving short K−Si distances to the central silicon atoms of the hypersilyl groups of nearly equal length (380 pm), and a short K−Cu distance of 305 pm. The copper atom is slightly bent away from the potassium atom giving a Si−Cu−Si angle of about 176.4°. We assume the most adequate description of the molecule to be as an intimate ion-pair with a predominantly ionic binding mode between the K^+ cation and the cuprate anion. The anion is isoelectronic with di(hypersilyl)-zinc and, in spite of the additional K^+ ion present in **4**, adopts an almost ideal staggered conformation (approximate local D_{3d} symmetry) and has similar structural parameters.[15] According to the somewhat larger atomic radius of zinc the Cu−Si bonds found in the cuprate **4** (2 × 230 pm) are slightly shorter (by 4 pm) than the corresponding Zn−Si bonds in di(hypersilyl)zinc (2 × 234 pm).

The only structural differences between the cuprate anion and di(hypersilyl)zinc worth mentioning are markedly widened Cu−Si−Si angles to those trimethylsilyl groups in the neighborhood of the intruding K^+ cation (Table 4). The electrostatic bond between the K^+ cation and $[Hyp_2Cu]^-$ anion is further amended by agostic-type interaction to two methyl groups within the molecular unit [K···CH_3: 331.2(6) and 336.0(5) pm]. Two further, but intermolecular, K···CH_3 contacts of 321.8(5) and 342.1(5) pm complete the coordination of the K^+ cation, leading to puckered infinite two-dimensional coordination polymers (Figure 4).

The structural parameters of the related sodium di(hypersilyl)cuprate (**5**) are very similar (Table 4). Significant differences occur only for the location and coordination of the markedly smaller Na^+ cation. Other than the K^+ ion in compound **5**, which is located above the center of the dumbbell anion, the Na^+ ion is statistically disordered about two positions. The sites are located on opposite sites of the $CuSi_2$ dumbbell and slightly displaced from the center of the dumbbell in opposite directions (Figure 5). Again, due to the smaller ionic radius of Na^+, the sodium derivative **5** does not form coordination polymers but only dimers, as illustrated in Figure 6.

Very recently the synthesis of related sodium di(supersilyl)cuprates Na[Cu(Si*t*Bu$_3$)$_2$] was reported by Lerner et al.[8] They were obtained as THF solvates from CuCl and sodium supersilanide in tetrahydrofuran at −78 °C. However, similar to the findings of Stalke the overall yields were relatively low (47%), perhaps again due to the presence of halide. Interestingly two *different* solvates were isolated from the reaction mixture. The first, [Na(THF)$_4$][Cu(Si*t*Bu$_3$)$_2$], consists of separated ions, whereas the second, [Na(THF)$_2$][Cu(Si*t*Bu$_3$)$_2$], displays similar structural features to potassium di(hypersilyl)cuprate, i.e. contact ion-pairs, but now with two additional THF molecules coordinated to the sodium cation.

Unexpectedly, the Cu−Si bonds shorten markedly from ca. 236 pm to 231 pm on going from the contact ion-pair to

Table 4. Selected bond lengths [pm] and angles [°] in M^I[HypCuHyp] [M^I = K (**4**), Na (**5**)]

	4	**5**
Cu1−Si1	229.88(13)	228.09(14)
Cu1−Si2	230.01(13)	228.63(14)
Si−Si (range)	232.6(2) −234.2(2)	232.5(2) −233.7(2)
M^I−Si1	379.9(2)	305.3(7) *(Na1)*
M^I−Si2	380.3(2)	323.1(5) *(Na2)*
M^I···Cu1	305.18(13)	267.9(4) *(Na1)*; 252.2(7) *(Na2)*
Si1−Cu1−Si2	176.44(4)	177.45(6)
Cu1−Si1−Si11	123.69(5)	114.45(7)
Cu1−Si1−Si12	108.77(6)	111.59(7)
Cu1−Si1−Si13	103.06(6)	106.00(7)
Cu1−Si2−Si21	109.57(5)	113.70(6)
Cu1−Si2−Si22	115.19(6)	109.69(7)
Cu1−Si2−Si23	108.40(6)	111.07(7)
Si−Si−Si (range)	106.26(6)−109.42(7)	104.70(7) −109.92(8)

 © 2003 Wiley-VCH Verlag GmbH & Co. KGaA, Weinheim

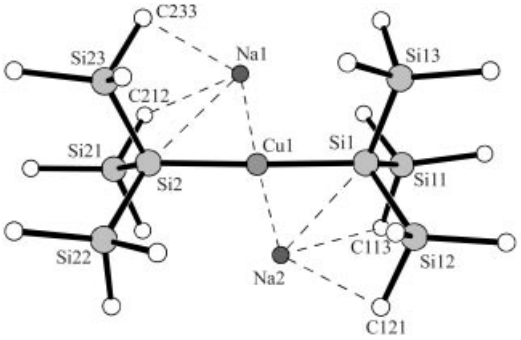

Figure 5. Molecular structures of sodium di(hypersilyl)cuprate (**5**), atoms are represented by spheres of arbitrary radii; dashed lines are used to symbolize interatomic distances markedly smaller than the sum of the corresponding van der Waals radii; the sodium atoms are statistically disordered about the sites Na1 and Na2; selected structural parameters are given in Table 3

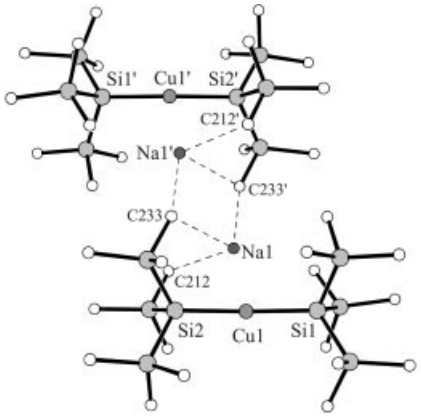

Figure 6. Coordination dimer of cuprate **5**; dashed lines indicate intra- and intermolecular agostic-type Na···C contacts

the separated anion, although we do not see a comparable shortening of the Cu−Si bonds on going from the contact ion-pair in cuprate **4** to separated ions in $[K(THF)_6][CuHyp_2]$, which is obtained by reaction of potassium hypersilanide with copper *tert*-butoxide in tetrahydrofuran (Table 3).[16]

It should be noted, finally, that a mixture of lithium hypersilanide and other lithium silanides may be used as a reactant in the reaction with the heterocuprates **1**−**3**, leading to cuprates with two different silyl ligands. In some cases mixed bis(silyl)cuprates may be isolated, whereas in other cases ligand redistribution takes place and the two symmetric species are formed. Detailed investigations are currently in progress.

Finally, we report a rational synthesis of large amounts of pure hypersilylcopper[6] — a compound ideal for the study of prototypic reactions of the Cu−Si bond towards organic or inorganic substrates — and for which no straightforward synthesis is known to date. Since the cuprates **1**, **2**, and **3** in turn are very easily accessible, we looked for a possible transformation of those cuprates into the neutral silylcopper complex. We finally succeeded with the reaction of the cuprates with chlorotrimethylsilane in toluene or pentane at low temperatures [Equation (7)].

$$\underset{(\mathbf{1})}{[K(\text{toluene})][t\text{BuOCuHyp}]} + Me_3SiCl \longrightarrow CuHyp + KCl + Me_3SiO t\text{Bu} + \text{toluene} \quad (7)$$

At ambient temperature both nucleophiles — the *tert*-butoxide and the hypersilanide anion — are stripped simultaneously from the heterocuprate anion leading to mixtures of hypersilylcopper and undesired non-volatile side-products such as copper *tert*-butoxide, the mixed tetramers $Cu_4Hyp_2(OtBu)_2$ (**7**) and $Cu_4Hyp_3(OtBu)$ (**8**) as well as tetrakis(trimethylsilyl)silane [Equation (8) and (9)]. At temperatures below −20 °C solutions of almost pure hypersilylcopper are obtained, however, from which crystalline material is obtained after removing all volatile components in vacuo and subsequent crystallization of the residue from toluene. To get very clean hypersilylcopper the cuprate **1** should be recrystallized before use and the ratio of the reactants should be as close as possible to 1:1. The mixed tetramers **7** and **8**, which are found as major side-products if the temperature chosen is too high, represent the first *heteroleptic* neutral Cu^I species bearing silyl substituents. A rational synthesis, spectroscopic data and structural details will be discussed in a subsequent paper.

$$\underset{(\mathbf{1})}{[K(\text{toluene})][t\text{BuOCuHyp}]} + Me_3SiCl \longrightarrow CuOtBu + KCl + Me_3SiHyp + \text{toluene} \quad (8)$$

$$x\ CuOtBu + y\ CuHyp \longrightarrow Cu_4(OtBu)_xHyp_y \quad [x = 2, y = 2\ (\mathbf{7}); x = 1, y = 3\ (\mathbf{8})] \quad (9)$$

Conclusion

We have shown that copper *tert*-butoxide reacts with the hypersilanides of the heavier alkali metals Na, K, and Cs in toluene solution to yield heterocuprates of the type $M^I[t$-BuOCuHyp] (**1**−**3**). They form dimers in the solid state and contain the shortest Cu−Si bond ever determined for molecular compounds. These cuprates can be used as valuable sources for the parent hypersilylcopper complex and other silylcopper reagents. Due to the fact that Li^+ cations bind to the *tert*-butoxide anion very strongly, reactions of cuprates **1**−**3** with lithium salts often leads to a replacement of the *tert*-butoxide anion for the counteranion of the employed salt. Therefore di(hypersilyl)cuprates, or even unsymmetrically substituted bis(silyl)cuprates, are obtained if the heterocuprates **1**−**3** are treated with a mixture of lithium hypersilanide and other lithium silanides. If the *tert*-butoxide anion is completely removed from the heterocuprate anion pure hypersilylcopper is obtained.

 © 2003 Wiley-VCH Verlag GmbH & Co. KGaA, Weinheim

Experimental Section

General Remarks: All experiments were carried out under dry oxygen-free argon using standard Schlenk techniques. Solvents were freshly distilled under Ar from $LiAlH_4$ prior to use. NMR: Bruker AM 200 and AC 250 instruments and referenced to solvent resonances.

$[M^I(C_7H_8)][t$BuOCuSi(SiMe$_3$)$_3$] [M^I = K (1), Na (2), Cs(3)]: In a typical experiment unsolvated $M^ISi(SiMe_3)_3$ (2 mmol) dissolved in toluene (10 mL) was slowly added to a well-stirred solution of CuO*t*Bu (0.27 g, 2 mmol) in toluene (20 mL) at −20 °C. The reaction mixture was stirred for 30 min at −20 °C and then rapidly heated for a few minutes to about 40 °C. After filtration from small amounts of copper powder the now pale-yellow solution was concentrated under dynamic vacuum to a volume of about 20 mL and cooled to −60 °C for 24 h. The cuprates **1**−**3** were obtained as colorless (**1** and **2**) or pale-yellow (**3**) crystalline toluene solvates. Some more crystalline material was obtained after subsequent concentration and crystallization at −60 °C. Typical yields lie between 85 and 96%.

1: $C_{40}H_{88}Cu_2K_2O_2Si_8$ (1031.10): calcd. C 46.59, H 8.6; found C 46.23, H 8.52. ^{1}H NMR (C_6D_6): δ = 0.49 (s, 27 H, $SiMe_3$) 1.12 [s, 9 H, Me (O*t*Bu)] ppm. ^{13}C NMR (C_6D_6): δ = 5.53 ($SiMe_3$, $^1J_{C,Si}$ = 42.1 Hz), 37.4 [C(*C*H$_3$)], 70.1 [*C*(CH$_3$)] ppm. ^{29}Si NMR: δ = −7.40 [Si(*Si*Me$_3$)$_3$], 141.2 [*Si*(SiMe$_3$)$_3$] ppm.

2: $C_{40}H_{88}Cu_2Na_2O_2Si_8$ (998.88): calcd. C 48.09, H 8.88; found C 47.92, H 8.91. ^{1}H NMR (C_6D_6): δ = 0.49 (s, 27 H, $SiMe_3$) 1.06 [s, 9 H, Me (O*t*Bu)] ppm. ^{13}C NMR (C_6D_6): δ = 5.43 ($SiMe_3$, $^1J_{C,Si}$ = 42.0 Hz), 37.4 [C(*C*H$_3$)], 69.8 [*C*(CH$_3$)] ppm. ^{29}Si NMR: δ = −7.60 [Si(*Si*Me$_3$)$_3$, $^1J_{Si,Si}$ = 47.3 Hz), 139.6 [*Si*(SiMe$_3$)$_3$] ppm.

3: $C_{40}H_{88}Cu_2Cs_2O_2Si_8$ (1218.72): calcd. C 39.42, H 7.28; found C 39.12, H 7.24. ^{1}H NMR (C_6D_6): δ = 0.48 (s, 27 H, $SiMe_3$) 1.13 [s, 9 H, Me (O*t*Bu)] ppm. ^{13}C NMR (C_6D_6): δ = 6.20 ($SiMe_3$, $^1J_{C,Si}$ = 41.4 Hz), 36.5 [C(*C*H$_3$)], 70.4 [*C*(CH$_3$)] ppm. ^{29}Si NMR: δ = −7.40 [Si(*Si*Me$_3$)$_3$], 141.5 [*Si*(SiMe$_3$)$_3$] ppm.

KCu[Si(SiMe$_3$)$_3$]$_2$ (4): Unsolvated lithium hypersilanide (2.5 g, 9.82 mmol) dissolved in toluene (10 mL) was added to a solution of cuprate **1** [5.06 g, 4.91 mmol (dimer)] in toluene (20 mL) at −20 °C and stirred for 30 min at this temperature, then warmed to room temperature and stirred for another 20 min. The volatiles were removed at 25 °C/10^{-2} Torr and the oily residue extracted with 3 × 10 mL of *n*-pentane. The pentane solution was concentrated under dynamic vacuum at 20 °C until a few colorless crystals appeared and then placed at −60 °C for 24 h. The cuprate **4** was obtained in 65% yield as colorless crystal blocks. $C_{18}H_{54}CuKSi_8$ (597.97): calcd. C 36.15, H 9.10; found C 35.95, H 9.13. ^{1}H NMR (C_6D_6): δ = 0.38 (s, 27 H, $SiMe_3$) ppm. ^{13}C NMR (C_6D_6): δ = 6.1 ($SiMe_3$, $^1J_{C,Si}$ = 41.6 Hz) ppm. ^{29}Si NMR: δ = −7.5 [Si(*Si*Me$_3$)$_3$], 147.5 [*Si*(SiMe$_3$)$_3$].

NaCu[Si(SiMe$_3$)$_3$]$_2$ (5): Unsolvated lithium hypersilanide (2.5 g, 9.82 mmol) dissolved toluene (10 mL) was added to a solution of cuprate **2** [4.90 g, 4.91 mmol (dimer)] in toluene (20 mL) at −20 °C and stirred for 30 min at this temperature, then warmed to room temperature and stirred for another 20 min. The volatiles were removed at 25 °C/10^{-2} Torr and the oily residue extracted with 3 × 10 mL of *n*-pentane. The pentane solution was concentrated to 5 mL and then placed at −60 °C for several days. The cuprate **5** was obtained as a solid mixture with sodium hypersilanide and one unidentified product. ^{1}H NMR (C_6D_6): δ = 0.38 (s, 27 H, $SiMe_3$) ppm. ^{13}C NMR (C_6D_6): δ = 5.9 ($SiMe_3$, $^1J_{C,Si}$ = 41.7 Hz) ppm. ^{29}Si NMR: δ = −7.3 [Si(*Si*Me$_3$)$_3$], 147.3 [*Si*(SiMe$_3$)$_3$] ppm.

Synthesis of Hypersilylcopper [CuSi(SiMe$_3$)$_3$] from [K(C$_7$H$_8$)][*t*BuOCuSi(SiMe$_3$)$_3$] (1): A solution of Me_3SiCl (0.466 g, 4.29 mmol) in toluene (20 mL) was added dropwise to a stirred solution of cuprate **1** [2.21 g, 2.14 mmol (dimer)] in the same solvent (15 mL) at −20 °C. The solution was slowly warmed to room temperature and stirred for 0.5 h. Then all volatiles were removed at 25 °C/10^{-2} Torr. After addition of 25 mL of *n*-pentane to the residue, the resulting suspension was filtered through a glass filter. The solution was concentrated in dynamic vacuum to approximately 5 mL and cooled to −30 °C for 24 h. Hypersilylcopper was obtained as colorless crystal plates or needles in about 80% yield. The yield may be improved by another 5−10% by subsequent cooling of the mother liquor to −60 °C for several days. The identity and purity of the product were verified by comparison with published NMR spectroscopic data.

X-ray Crystallographic Study: Diffraction data for compounds **1**−**5** were collected on a Siemens P4 four-circle diffractometer using monochromated Mo-K_α radiation (λ = 0.71073 Å) at 173 K. Crystals were covered with nujol, placed on the tip of a glass fiber and mounted on the diffractometer under a stream of cold nitrogen gas. The cell dimensions were determined from the positions of 35−52 selected reflections ($20 < 2\theta < 25°$). The structures were solved by direct methods and refined against all F^2 using the SHELXTL-PC 5.03 program package on a local PC. Anisotropic thermal parameters were included for all non-hydrogen atoms. Hydrogen atoms were placed at ideal positions using appropriate HFIX procedures and refined with riding models. The isotropic displacement parameters were constrained to 1.5 (aliphatic) or 1.2 (aromatic) times the U_{eq} of the connected carbon atom. Further details can be found in Table 1.

CCDC-213800 (**1**), -213801 (**2**), -213802 (**3**), -213803 (**4**), and -213804 (**5**) contain the supplementary crystallographic data for this paper. These data can be obtained free of charge at www.ccdc.cam.ac.uk/conts/retrieving.html [or from the Cambridge Crystallographic Data Centre, 12, Union Road, Cambridge CB2 1EZ, UK; fax: (internat.) +44-1223/336-033; E-mail: deposit@ccdc.cam.ac.uk].

Acknowledgments

We thank the Deutsche Forschungsgemeinschaft and the Fonds der Chemischen Industrie for financial support.

[1] See for example: I. Fleming in *Organocopper Reagents: A Practical Approach* (Ed.: R. J. K. Taylor), Oxford University Press, Oxford, **1994**, chapter 12, p. 257; R. K. Dieter, in *Modern Organocopper Chemistry* (Ed.: N. Krause), Wiley-VCH, Weinheim, **2002**, chapter 3, p. 79.

[2] See for example: S. Sharma, A. C. Oehlschlager, *J. Org. Chem.* **1991**, *56*, 770. S. Sharma, A. C. Oehlschlager, *Tetrahedron* **1989**, *45*, 557. R. D. Singer, A. C. Oehlschlager, *J. Org. Chem.* **1991**, *56*, 3510.

[3] A. H. Cowley, T. M. Elkins, R. A. Jones, C. M. Nunn, *Angew. Chem.* **1988**, *100*, 1396; *Angew. Chem. Int. Ed. Engl.* **1988**, *27*, 1349.

[4] A. Heine, R. Herbst-Irmer, D. Stalke, *J. Chem. Soc., Chem. Commun.* **1993**, 1731.

[5] A. Heine, D. Stalke, *Angew. Chem.* **1993**, *105*, 90; *Angew. Chem. Int. Ed. Engl.* **1993**, *32*, 121.

[6] J. Klett, K. W. Klinkhammer, M. Niemeyer, *Chem. Eur. J.* **1999**, *5*, 2531.

 © 2003 Wiley-VCH Verlag GmbH & Co. KGaA, Weinheim

[7] K. W. Klinkhammer, *Z. Anorg. Allg. Chem.* **2000**, *626*, 1217.
[8] H.-W. Lerner, S. Scholz, M. Bolte, *Organometallics* **2001**, *20*, 575.
[9] H. M. Chen, J. P. Oliver, *J. Organomet. Chem.* **1986**, *316*, 255.
[10] H. F. Klein, J. Montag, U. Zucha, U. Flörke, H.-J. Haupt, *Inorg. Chim. Acta* **1990**, *177*, 35.
[11] U. Schubert, B. Mayer, C. Ruß, *Chem. Ber.* **1994**, *127*, 2189.
[12] K. W. Klinkhammer, *Chem. Eur. J.* **1997**, *3*, 1418.
[13] K. W. Klinkhammer, J. Weidlein, *Z. Anorg. Allg. Chem.* **1996**, *622*, 1209.
[14] Due to a pseudo-symmetry problem, which has still not been resolved, no reliable structural data are available for **6**. Preliminary crystallographic data show that the compound is again a monomer with similar structural features as the potassium derivative **4**, but now has two toluene molecules solvating each cesium cation. These data can be obtained from the authors.
[15] J. Arnold, T. D. Tilley, A. L. Rheingold, S. J. Geib, *Inorg. Chem.* **1987**, *26*, 2106.
[16] J. Klett, K. W. Klinkhammer, Y. Xiong, unpublished results.
Received June 30, 2003

 © 2003 Wiley-VCH Verlag GmbH & Co. KGaA, Weinheim

Fluorite-Related Phases in the System Li-Pt-Sn: Synthesis and Structures of Li_2PtSn, $Li_3Pt_2Sn_3$, $Li_{2.27}Pt_2Sn_{3.73}$ and $Li_{2.43}Pt_2Sn_{3.57}$

Rolf-Dieter Hoffmann,[a] Zhiyun Wu,[a] and Rainer Pöttgen*[a]

In memory of Ron Snaith

Keywords: Lithium / Tin / Platinum / Intermetallic phases

The intermetallic compounds Li_2PtSn, $Li_3Pt_2Sn_3$, $Li_{2.27}Pt_2Sn_{3.73}$ and $Li_{2.43}Pt_2Sn_{3.57}$ were synthesised by reaction of the elements in sealed tantalum tubes. They were investigated by X-ray diffraction on powders and single crystals: $F\bar{4}3m$, a = 626.0(1) pm, $wR2$ = 0.0834, 70 F^2 values, 7 variables for Li_2PtSn; $Ia\bar{3}$, a = 1264.3(1) pm, $wR2$ = 0.0340, 416 F^2 values, 23 variables for $Li_3Pt_2Sn_3$; $Ia\bar{3}$, a = 1269.7(1) pm, $wR2$ = 0.1130, 521 F^2 values, 24 variables for $Li_{2.27(1)}Pt_2Sn_{3.73(1)}$; $Ia\bar{3}$, a = 1266.6(1) pm, $wR2$ = 0.1094, 620 F^2 values, 25 variables for $Li_{2.43(1)}Pt_2Sn_{3.57(1)}$. The latter refinement was based on a crystal twinned by merohedry. Li_2PtSn crystallises with an ordered variant of the BiF_3 type. The other stannides adopt a superstructure of the fluorite type where all three subcell axes are doubled. In $Li_3Pt_2Sn_3$ the platinum atoms are located on the calcium sites while the tin and 1/3 of the lithium atoms are ordered on the fluorine site. The remaining lithium atoms fill octahedral voids of the *fcc* arrangement of platinum. The superstructure is discussed on the basis of a group-subgroup scheme and experimental evidence is given for a solid solution $Li_{3-x}Pt_2Sn_{3+x}$.
(© Wiley-VCH Verlag GmbH & Co. KGaA, 69451 Weinheim, Germany, 2003)

Introduction

The binary fluoride BiF_3[1] has three crystallographic positions, Bi on the Wyckoff site 4*a*, F1 at 4*b*, and F2 at 8*c*. This structure type may be described as a filled fluorite variant with F1 in the octahedral voids or as a filled blende-type structure with half of the F2 atoms in the remaining tetrahedral voids and the F1 atoms in the octahedral voids. A variety of intermetallic lithium compounds adopt BiF_3-related structures. According to the different Wyckoff positions, the compositions Li_2TX, LiT_2X and $LiTX_2$ (T = late transition metal; X = *p*-block element of the 3rd or 4th group) are possible. Indeed, examples are known for all of them.[2] A large variety of such intermetallics were synthesised in the groups of Schuster[3,4] and Weiss[5] 30 years ago. Most of these intermetallics, however, have only been characterised on the basis of X-ray powder diffraction data.

Depending on the composition as well as on the T and X components, the compounds Li_2TX, LiT_2X and $LiTX_2$ have different electron counts, leading to a variety of interesting physical properties. Susceptibility and resistivity measurements reveal metallic behaviour and Pauli paramagnetism.[3,6] One of the most interesting properties of these intermetallics is the intrinsic colour,[3,6,7] which varies with the valence electron concentration. To give an example, in the solid solution $Li_{2-x}Mg_xPdSn$, the colour changes from brass yellow via copper red to red violet with increasing x.[7] The optical constants have been determined from reflection spectroscopic data.[3,6,7] At least some of the Li_2TX, LiT_2X and $LiTX_2$ compounds show lithium mobility.[8,9] Chemical bonding in various Li_2TX and $LiTX_2$ (T = Rh, Pd, Ir, Pt; X = Al, Ga, In) intermetallics has been investigated by X-ray photoelectron and X-ray excited Auger spectroscopy paralleled by DFT electronic structure calculations.[10,11]

In the course of our systematic studies on structure/property relation of Li-*T*-Sn stannides,[12–14] we have investigated the ternary system lithium-platinum-tin in more detail. It turned out that a large solid solution $Li_{3-x}Pt_2Sn_{3+x}$ (x = 0–1) exists with a fluorite subcell structure. $PtSn_2$ [15] crystallises with a fluorite structure and Li_2PtSn has a fluorite type subcell as well. In the superstructure with the ideal formula $Li_3Pt_2Sn_3$ the lithium and tin atoms are well ordered in a 2 × 2 × 2 cubic supercell. The process of lithium filling and Sn/Li substitution is formally done in two steps. At first the octahedral sites in $PtSn_2$ are filled to get "$LiPtSn_2$" and secondly tin is substituted by lithium on the tetrahedral sites up to Li_2PtSn.[16,17] The synthesis and crystal chemistry of these stannides is reported herein.

[a] Institut für Anorganische und Analytische Chemie and Sonderforschungsbereich 458, Universität Münster, Wilhelm-Klemm-Straße 8, 48149 Münster, Germany, E-mail: pottgen@uni-muenster.de

Results

A fluorite-type arrangement heavily governs the structural chemistry in the ternary system Li-Pt-Sn. The binary stannide $PtSn_2$ crystallises in the CaF_2 type. From the literature it is not known whether $PtSn_2$ has a noticeable range of homogeneity. This is also suggested by our own phase-analytical investigations within this work.

In the ternary compounds Li_2PtSn and $Li_3Pt_2Sn_3$ (better formulated as $Li_{3-x}Pt_2Sn_{3+x}$ with $x = 0-1$) the *ccp* arrangement of platinum atoms remains fixed, while lithium fills the octahedral voids and in addition substitutes tin atoms on the tetrahedral sites (Table 1 and 2, Figure 1). This filling is done in two steps. First, the octahedral sites are filled and then the Sn/Li substitution sets in. This conclusion can be drawn from Figure 2. For comparison reasons the lattice parameters of $PtSn_2$ and Li_2PtSn have been doubled to compare to the supercell of $Li_3Pt_2Sn_3$ (Table 3). Binary $PtSn_2$ has the largest lattice parameter, leading to a Sn−Sn distance of 321 pm which nicely matches the distance in elemental tin: 4×302 and 2×318 pm in β-Sn.[18] The Pt−Sn contacts are 278 pm comparing well to the sum of Pauling's single bond radii.[19] Incorporation of lithium at octahedral voids lets the lattice parameter sharply drop by about 16 pm resulting in shorter Pt−Sn distances (Table 4) than those in binary $PtSn_2$. The excess electrons from the lithium atoms, therefore, presumably fill bonding Pt−Sn states. The ideal structure $LiPtSn_2$, where only octahedral voids are filled by lithium, was not obtained. The extrapolated lattice parameter is indicated by an open circle in Figure 2. The composition with the lowest lithium content was $Li_{1.11}PtSn_{1.89}$ with 5.5% lithium on the tin site, whereas the highest lithium content in the superstructure was 25% corresponding to the ideal composition $Li_3Pt_2Sn_3$.

Table 1. Crystal data and structure refinement parameters for Li_2PtSn, $Li_3Pt_2Sn_3$, $Li_{2.43}Pt_2Sn_{3.57}$ and $Li_{2.27}Pt_2Sn_{3.73}$

Empirical formula	Li_2PtSn	$Li_3Pt_2Sn_3$	$Li_{2.43}Pt_2Sn_{3.57}$	$Li_{2.27}Pt_2Sn_{3.73}$
Formula mass	333.25	767.07	830.41	848.79
Crystal system	cubic	cubic	cubic	cubic
a (pm) single crystal	626.1(1)	1264.3(1)	1266.6(1)	1269.7(2)
a (pm) powder sample	626.0(1)	1264.4(2)	1266.6(2)	1270.2(4)
Volume (nm^3)	0.02453	0.20214	0.20320	0.20494
Space group	$F\bar{4}3m$	$Ia\bar{3}$	$Ia\bar{3}$	$Ia\bar{3}$
Pearson Symbol	c*F*16	c*I*128	c*I*128	c*I*128
Z	4	16	16	16
ρ_{calc} (gcm^{-3})	9.018	10.084	10.859	11.017
Crystal size (μm^3)	50 × 60 × 90	40 × 40 × 40	80 × 50 × 8	15 × 25 × 55
Transmission ratio (max/min)	4.04	1.65	3.22	2.92
λ (Mo-K_α) pm	71.073	71.073	71.073	71.073
μ (mm^{-1})	67.2	69.62	71.98	72.22
F(000)	545	5040	5466	5590
Detector distance (mm)	60	60	60	50
Exposure time (min)	35	8	12	20
ω range (°); increment (°)	0−180; 1.0	−	0−180; 1.0	−
range (°); increment (°)	360	2−200/1.2	360	0−180/1.5
Profile/pixel	−	9−21	−	9−25
Pixelsize (mm)	0.15	−	0.15	−
Profile parameters				
A, B,	15.0/6.0	−/−	15.8, 3.8	−/−
EMS	0.024	0.010	0.039	0.011
θ range (°)	5−33	3−28	3−32	3−30
Total data collected	822	7566	12098	10123
Range in *hkl*	±9, ±9, ±9	±16, ±16, ±16	±19, ±19, ±19	±17, ±17, ±17
Unique data	70	416	620	521
Observed data [$I > 2\sigma(I)$]	70	389	561	167
Refinement method	Full-matrix least-squares on F^2			
$R_{internal}$ / R_{sigma}	0.2439/0.0962	0.0521/0.0172	0.1114/0.0318	0.1140/0.0406
R indices [$I > 2\sigma(I)$]				
R_1, *wR*2	0.0461/0.0834	0.0166/0.0335	0.0411/0.1043	0.0321/0.0795
R (all data)				
R_1, *wR*2	0.0461/0.0834	0.0192/0.0340	0.0483/0.1094	0.1131/0.1130
Weight parameters *a*, *b*	0.0358/0.8761	0.0208/0	0.0394/80.625	0.0380/0
Goodness of fit (S_{obs})	1.191	1.001	1.098	0.770
No. of variables, restraints	7/0	23/0	25/0	24/0
Twin, *BASF*	−	−	−	0.487(7)
Extinction coefficient	0.0013(8)	0.000062(5)	0.00011(2)	0.00016(2)
Largest diff. peak and hole e·Å^{-3}	4.120/−2.965	1.002/−1.025	2.074/−1.925	1.593/−1.982

 © 2003 Wiley-VCH Verlag GmbH & Co. KGaA, Weinheim

Table 2. Atomic coordinates and isotropic displacement parameters [pm^2] for $Li_{1.96(2)}PtSn_{1.04(2)}$, $Li_3Pt_2Sn_3$, $Li_{2.27(1)}Pt_2Sn_{3.73(1)}$ and $Li_{2.43(1)}Pt_2Sn_{3.57(1)}$; U_{eq} is defined as one third of the trace of the orthogonalized U_{ij} tensor

Atom	Occ.	Wyckoff position	x	y	z	U_{eq}/U_{iso}
			$Li_{1.96(2)}PtSn_{1.04(2)}$			
Li1	0.96(2)	4*b*	1/2	0	0	20(10)[a]
Li2	1	4*d*	3/4	3/4	3/4	71(95)
Pt	1	4*a*	0	0	0	23.4(6)
Sn1	1	4*c*	1/4	3/4	3/4	26(1)
Sn2	0.04(2)	4*b*	1/2	0	0	20(10)[a]
			$Li_3Pt_2Sn_3$			
Li1	1	16*c*	0.121(1)	x	x	25(5)
Li2	1	8*a*	0	0	0	31(8)
Li3	1	24*d*	1/4	0.253(2)	0	69(13)
Pt1	1	8*b*	1/4	1/4	1/4	8.3(1)
Pt2	1	24*d*	1/4	0.47895(3)	0	8.5(1)
Sn	1	48*e*	0.11611(3)	0.35634(4)	0.12176(3)	11.7(1)
			$Li_{2.27(1)}Pt_2Sn_{3.73(1)}$			
Li1	0.27(1)	16*c*	0.1241(1)	x	x	12.2(8)[a]
Li2	1	8*a*	0	0	0	22(21)
Li3	1	24*d*	1/4	0.251(4)	0	26(13)
Pt1	1	8*b*	1/4	1/4	1/4	8.6(4)
Pt2	1	24*d*	1/4	0.49513(8)	0	10.8(4)
Sn1	1	48*e*	0.1228(1)	0.3706(1)	0.1243(1)	16.9(4)
Sn2	0.73(1)	16*c*	0.1241(1)	x	x	12.2(8)[a]
			$Li_{2.43(1)}Pt_2Sn_{3.57(1)}$			
Li1	0.43(1)	16*c*	0.1246(2)	x	x	18.7(7)[a]
Li2	1	8*a*	0	0	0	2(7)
Li3	1	24*d*	1/4	0.2472(16)	0	12(7)
Pt1	1	8*b*	1/4	1/4	1/4	13.0(3)
Pt2	1	24*d*	1/4	0.49013(7)	0	17.3(3)
Sn1	1	48*e*	0.12086(7)	0.3663(1)	0.1230(1)	21.4(3)
Sn2	0.57(1)	16*c*	0.1246(2)	x	x	18.7(7)[a]

[a] The displacement parameters are constrained to be equal and the sum of Li1 and Sn2 are set to 100% occupancy.

Thus, the content of lithium can be increased further. This is done by substitution of tin at the tetrahedral sites by lithium atoms. Gradually the lithium content can be increased from $LiPtSn_2$ to $Li_3Pt_2Sn_3$, where 2/8 of the tin atoms are replaced. The general formula of the new ternary compound may be written as $Li_{octahedra}[Pt(Sn_{1.5+x}Li_{tetrahedra\ 0.5-x})]$ with $x = 0-0.5$ for the fluorite-type subcell i.e. $Li_2[Pt_2(Sn_{3+x}Li_{1-x})]$ with $x = 0-1$ for the superstructure.

Seven single crystals were refined and their lattice parameters found to correlate nicely with the amount of lithium on the tetrahedral sites (Figure 2). Decreasing the tin content lets the lattice parameter drop mainly because the smaller lithium atoms substitute the larger tin atoms (123 pm and 140 pm for lithium and tin, respectively).[19] Along with this substitution the intensities of the superstructure reflections increase in intensity to reach a maximum at the ideal composition for the superstructure of $Li[Pt(Sn_{1.5}Li_{0.5})]$ i.e. $Li_3Pt_2Sn_3$.

The following discussion reflects on the consequences of the ordered arrangement of lithium and tin for the near neighbour environment (Figure 3). The filling of octahedral sites by lithium in a fluorite-type subcell increases the coordination numbers (CN) of platinum and tin and lithium as well. CNs of 8, 9 and 10 are found for Pt1, Pt2 and Sn, respectively. The CNs for the lithium atoms are 14, 8 and 9 for Li1, Li2 and Li3, respectively. The high CN of Li1 can be explained as follows. The lithium atom Li1 replaces 2/8 of the tin positions of the subcell. This would lead to CN 8 i.e. four tetrahedrally oriented platinum atoms and four lithium atoms on octahedral sites. In the superstructure, however, shorter Pt−Sn distances of 270−276 pm (Table 4) occur as compared to those in binary $PtSn_2$ (278 pm). This shrinkage allows extra atoms to be in contact with the Li1 atoms. Due to the additional lithium on octahedral voids of the *fcc* arrangement of the platinum atoms and the order of tin and lithium on tetrahedral voids, all near-neighbour environments are basically strongly distorted cubes with six additional atoms on faces and edges increasing the CN.

In Li_2PtSn the lithium content seems to reach the maximum possible, where 4/8 of the tin positions are occupied by lithium atoms. The lattice parameter fits well in the *a* vs. *portion Li* plot of Figure 2, indicating again that the drop of the lattice parameter is due to the size difference of Li/Sn of 123/140 pm (Pauling's radii).

Li_2PtSn constitutes the second ordered superstructure in the large range of fluorite-related structures in the Li-Pt-Sn system. It derives from the binary BiF_3 (a filled fluorite type) where bismuth forms a *fcc* arrangement and the two different fluoride sites occupy the tetrahedral and octahedral voids on 4*b* and 8*c* in $Fm\bar{3}m$, respectively (Figure 1). As compared to CaF_2, the Li2 atoms replace 4/8 of the fluoride positions in an ordered manner. This leads to a reduction in symmetry. The structure becomes non-centro-

 © 2003 Wiley-VCH Verlag GmbH & Co. KGaA, Weinheim

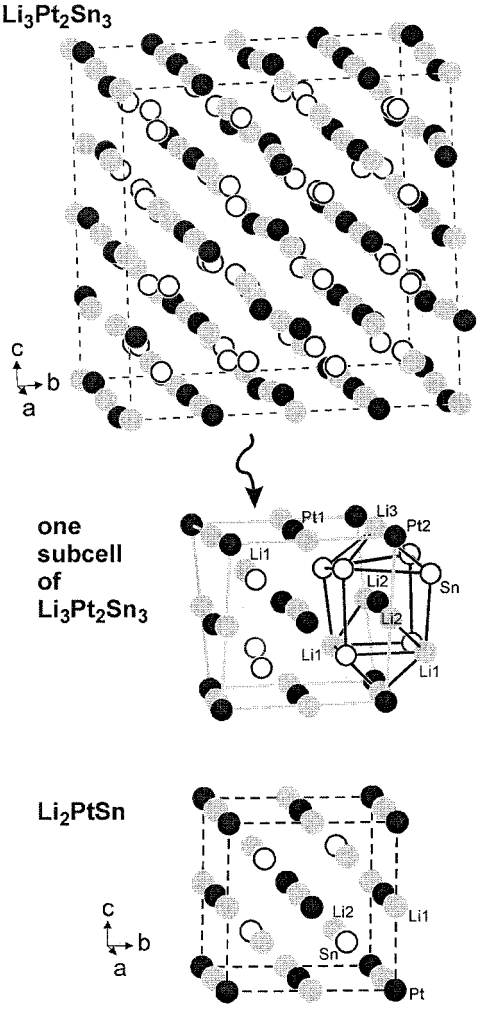

Figure 1. The crystal structures of $Li_3Pt_2Sn_3$ and Li_2PtSn; the lithium, platinum and tin atoms are drawn as grey, filled and open circles, respectively; at the top the $2 \times 2 \times 2$ supercell of $Li_3Pt_2Sn_3$ is shown; one subcell of $Li_3Pt_2Sn_3$ is outlined in the middle; note that in the solid solution $Li_{3-x}Pt_2Sn_{3+x}$ the Li1 position is additionally occupied by tin atoms; the similarity of the subcell with the ternary ordered BiF_3-type Li_2PtSn is emphasised below

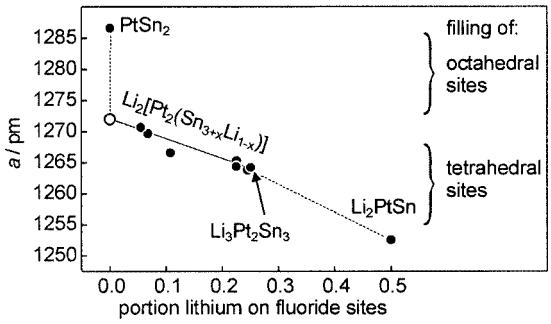

Figure 2. Course of the cubic lattice parameter of the solid solution $Li_{3-x}Pt_2Sn_{3+x}$, $PtSn_2$ and Li_2PtSn; for the latter two compounds the lattice parameters are doubled for comparison; the open circle marks the composition with the lowest lithium content possible of the solid solution where no tin/lithium mixing on the tetrahedral sites occur; the different filling mechanisms by lithium atoms are indicated on the right hand side of the drawing; filling of tetrahedral sites corresponds to a replacement of tin atoms

symmetric and it crystallises in the space group $F\bar{4}3m$, a *translationengleiche* subgroup of index 2 of $Fm\bar{3}m$ (Figure 4, upper right-hand side). The indide $LiPdIn_2$[12] actually crystallises in $Fm\bar{3}m$ representing a ternary ordered version of BiF_3. In Figure 4 the substitution of tin by lithium can be seen by the splitting of the 8*c* site of $Fm\bar{3}m$ into two fourfold sites 4*c* and 4*d* of $F\bar{4}3m$.

There is no direct group-subgroup relation between $F\bar{4}3m$ and $Ia\bar{3}$ because $F\bar{4}3m$ is non-centrosymmetric and one cannot gain symmetry. In addition, following the Bärnighausen formalism strictly,[20,21] filled structures are also excluded from a symmetry tree. Li_2PtSn and $Li_3Pt_2Sn_3$ have the same aristotype (BiF_3), but both are situated on different branches.

BiF_3 is a filled CaF_2 type. For clarity the empty octahedral sites are left out on the CaF_2 branch (left hand side of Figure 4). Within the CaF_2 branch it is improbable that the interim AX_2 phases exist, and in actual fact they do not have to. So far no intermetallics with the symmetry $Pm\bar{3}m$ or $Pm\bar{3}$ and the atomic positions given in Figure 4 are known. One might speculate that a ternary stannide with two different transition metals on the sites 1*a* (A1) and 3*c* (A′2) of $Pm\bar{3}m$ exists. The necessary distortions are already

Table 3. Lattice parameters of $PtSn_2$[26] and the various ternary lithium-platinum stannides Li_2PtSn and $Li_{3-x}Pt_2Sn_{3+x}$

Compound	*Octahedra*[Pt(*Tetrahedra*)]	*a*/pm	Portion of tetrahedral Li
$PtSn_2$	[Pt(Sn_2)]	1286.62	0
Li_2PtSn	Li[Pt(SnLi)]	1252.2(2)	0.5
$Li_3Pt_2Sn_3$	Li_2[Pt_2(Sn_3Li)]	1264.2(1)	0.25
$Li_{2.98}Pt_2Sn_{3.02}$	Li_2[Pt_2($Sn_{3.02}Li_{0.98}$)]	1263.89(8)	0.245
$Li_{2.9}Pt_2Sn_{3.1}$	Li_2[Pt_2($Sn_{3.1}Li_{0.9}$)]	1265.3(2)	0.225
$Li_{2.9}Pt_2Sn_{3.1}$	Li_2[Pt_2($Sn_{3.1}Li_{0.9}$)]	1264.94(9)	0.225
$Li_{2.43}Pt_2Sn_{3.57}$	Li_2[Pt_2($Sn_{3.57}Li_{0.43}$)]	1266.6(1)	0.1075
$Li_{2.27}Pt_2Sn_{3.73}$	Li_2[Pt_2($Sn_{3.73}Li_{0.27}$)]	1269.7(2)	0.0675
$Li_{2.22}Pt_2Sn_{3.78}$	Li_2[Pt_2($Sn_{3.78}Li_{0.22}$)]	1270.7(2)	0.055

 © 2003 Wiley-VCH Verlag GmbH & Co. KGaA, Weinheim

Table 4. Interatomic distances [pm], calculated with the lattice parameters taken from the single crystal diffractometer measurements of Li_2PtSn and $Li_3Pt_2Sn_3$; all distances of the first coordination spheres are listed; standard deviations are all equal or less than 1 pm

			Li_2PtSn				
Li1	4	Li2	271.1				
	4	Sn	271.1				
	6	Pt	313.1				
Li2	4	Li1	271.1				
	4	Pt	271.1				
	6	Sn	313.1				
Pt	4	Li2	271.1				
	4	Sn	271.1				
	6	Li1	313.1				
Sn	4	Li1	271.1				
	4	Pt	271.1				
	6	Li2	313.1				
			$Li_3Pt_2Sn_3$				
Li1	1	Li2	265.4	Pt2	2	Sn	268.7
	3	Li3	278.9		2	Sn	271.5
	1	Pt1	282.1		2	Sn	276.4
	3	Pt2	287.0		1	Li3	285.7
	3	Sn	297.4		2	Li1	287.0
	3	Sn	301.4		2	Li2	317.2
Li2	2	Li1	265.4		2	Li3	317.2
	6	Sn	279.7		1	Li3	346.5
	6	Pt2	317.2	Sn	1	Li3	259.1
Li3	2	Sn	259.1		1	Li3	263.5
	2	Sn	263.5		1	Pt2	268.7
	2	Li1	278.9		1	Pt1	270.2
	1	Pt2	285.7		1	Pt2	271.5
	2	Sn	294.4		1	Pt2	276.4
	2	Pt1	316.1		1	Li2	279.7
	2	Pt2	317.2		1	Li3	294.4
	1	Pt2	346.5		1	Li1	297.4
Pt1	6	Sn	270.2		1	Li1	301.4
	2	Li1	282.1		2	Sn	334.4
	6	Li3	316.1		2	Sn	337.4

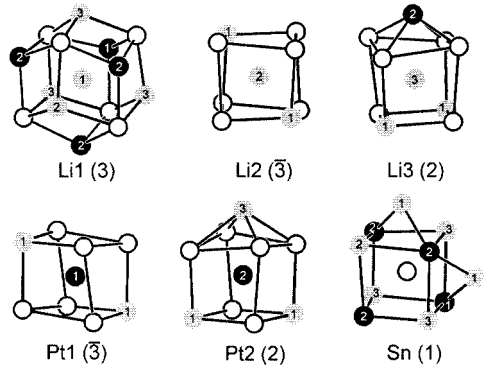

Figure 3. Near neighbour environment in the structure of $Li_3Pt_2Sn_3$; the lithium, platinum and tin atoms are drawn as grey, filled and open circles, respectively; the numbers correspond to the atom designations; the site symmetries are given in parentheses

taken care of by the extra parameter x of the X (Sn) position in 8*g*. Nevertheless, at this point the two different platinum sites of $Li_3Pt_2Sn_3$ already come into play. Both have different average distances to lithium and tin (Table 4).

The gain of the next *klassengleiche* symmetry reduction of index 4 (doubling in all three directions) is the most important one. It allows ordering of the tin and lithium atoms in the ratio 3:1. This was the key in solving the superstructure. It also means that this reduction is a one-way direction. The tin/lithium ratio on the tetrahedral sites is now fixed to 3:1 and cannot be changed unless further symmetry reductions occur. The consequence of this is that there is no solid solution between $Li_3Pt_2Sn_3$ and Li_2PtSn, because Li_2PtSn crystallises with a higher symmetry. Nevertheless, as Figure 2 suggests, the different volume increments of tin/lithium determine the course of the lattice parameters of $Li_3Pt_2Sn_3$ and Li_2PtSn.

To sum up, the crystal chemical relation between the different ternary lithium stannides is nicely depicted by the symmetry tree given in Figure 4. There are different mechanisms of establishing a certain lithium/tin ratio by filling octahedral and tetrahedral voids with lithium and lithium/tin mixtures, respectively, in the *fcc* arrangement of platinum.

Experimental Section

General: Starting materials for the preparation of the lithium-platinum-stannides were lithium rods (Merck, >99%), platinum powder (Degussa-Hüls, 200 mesh, >99.9%) and a tin bar (Heraeus, 99.9%). The lithium rods were cut into smaller pieces under dry paraffin oil and subsequently washed with *n*-hexane. The paraffin oil and *n*-hexane were previously dried over sodium wire. The lithium pieces were kept in Schlenk tubes under argon prior to the reactions. Argon was purified over titanium sponge (900 K), silica gel and molecular sieves.

The lithium pieces were mixed with cold-pressed pellets of platinum powder and pieces of the tin bar in the respective atomic ratios and sealed in tantalum ampoules under an argon pressure of about 800 mbar in an arc-melting apparatus.[22] The tantalum tubes were then sealed in evacuated silica tubes to prevent oxidation, rapidly heated at 1070 K and held at this temperature for between three hours and one day. The temperature was then lowered to 720 K or 820 K within four days followed by slow cooling to room temperature by switching off the furnace. The samples could be readily separated from the tubes. No reaction with the container material was observed. The light grey, polycrystalline compounds are stable in air over several weeks. Single crystals exhibit a metallic lustre.

X-ray investigations

The samples were characterised from Guinier patterns or powder diffractograms (Stoe StadiP) using Cu-$K\alpha_1$ radiation and silicon (a = 543.07 pm) as external standard or α-quartz (a = 491.30 pm, c = 540.46 pm) as internal standard. The cubic lattice parameters (Table 1) were obtained from least-squares fits of the powder data. The correct indexing of the patterns was facilitated by intensity calculations[23] taking the atomic positions from the structure refinements. The lattice parameters determined from the powders and the single crystals agreed well.

Several silvery, irregularly shaped single crystals of the solid solution were isolated from the annealed samples by mechanical fragmentation. They were examined on a Buerger precession camera equipped with an image plate system (Fujifilm BAS-2500 and -1800) in order to establish suitability for intensity data collection.

 © 2003 Wiley-VCH Verlag GmbH & Co. KGaA, Weinheim

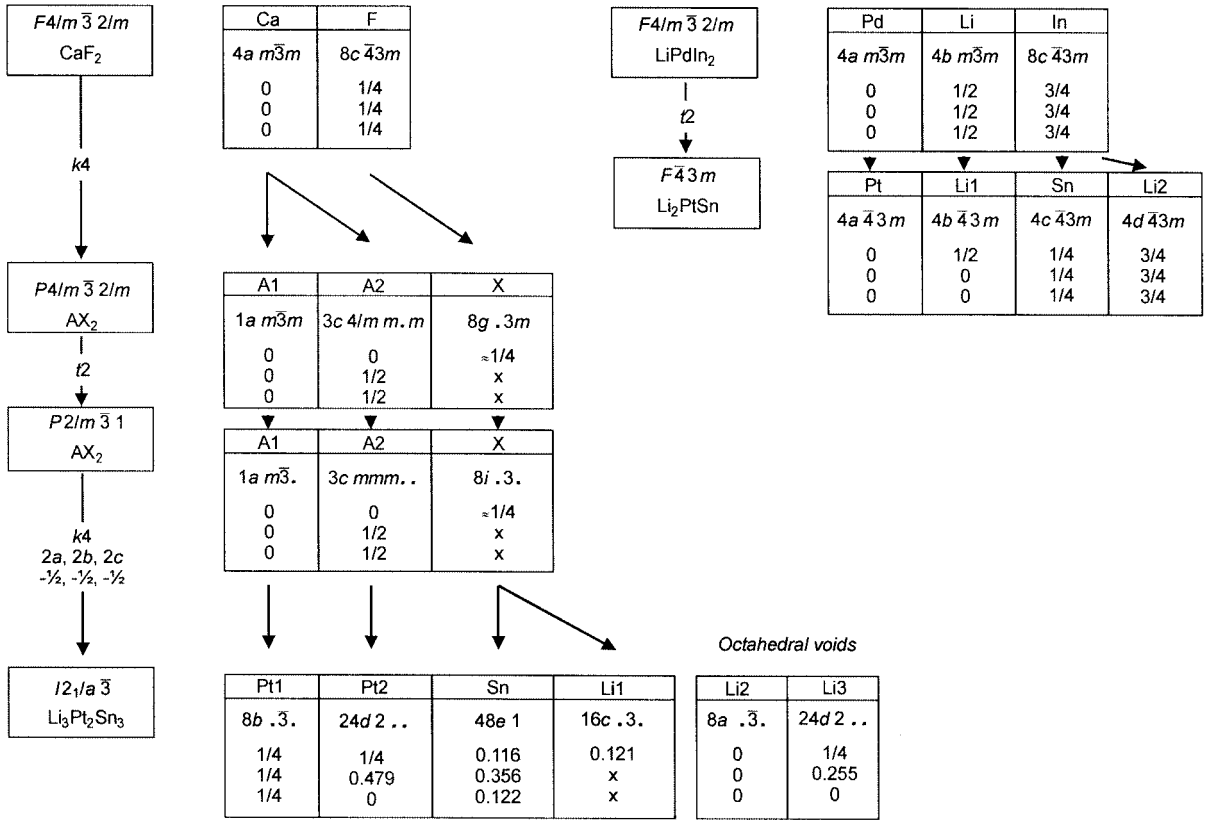

Figure 4. Group-subgroup relation in the Bärnighausen formalism[20,21] for the structures of CaF_2, $Li_3Pt_2Sn_3$, $LiPdIn_2$ and Li_2PtSn; the indices of the *klassengleiche* (k) and *translationengleiche* (t) transitions, the unit cell transformations with origin shifts and the evolution of the atomic parameters are given; the octahedral voids in CaF_2 and the interim structures are left out for clarity; $LiPdIn_2$ constitutes a ternary ordered version of BiF_3, which is a filled fluorite type

Single-crystal intensity data were collected at room temperature by use of a four-circle diffractometer (CAD4) with graphite-monochromated Mo-K_α radiation (71.073 pm) and a scintillation counter with pulse height discrimination. The scans were performed in the $\omega/2\theta$ mode. Empirical absorption corrections were applied on the basis of Ψ-scan data. Some data sets were collected on a Stoe IPDS-I and IPDS-II diffractometer with graphite monochromated Mo-K_α radiation. All relevant crystallographic data and experimental details for the data collections are listed in Table I.

Structure Refinements

The starting atomic parameters for the platinum and tin atoms were deduced from automatic interpretations of direct methods with SHELXS-97.[24] The lithium positions were determined from subsequent difference Fourier analyses. The structures were then refined using SHELXL-97 (full-matrix least-squares on F_o^2)[25] with anisotropic atomic displacement parameters for tin and platinum while isotropic refinement was carried out for the lithium atoms.

Refinement of Li_2PtSn

The determination of the space group for Li_2PtSn was carried out as follows. Reciprocal space revealed only the extinction conditions for a cubic face centred lattice. No extra extinctions were observed. Therefore, $Fm\bar{3}m$ was chosen as the highest symmetry space group possible. The refinement went smoothly to low R values ($R1$ = 0.032) assuming a fluorite-type structure with platinum occupying the calcium sites and a 1:1 mixture of tin and lithium on the fluoride sites. The drawback of this refinement, of course, is the mixed Sn/Li occupancy and that the occupation of additional octahedral sites by lithium could not be detected in a difference Fourier synthesis. However, the subgroup $F\bar{4}3m$ of $Fm\bar{3}m$ allows ordering of the tin/lithium atoms on the fluoride positions. This refinement yielded a reasonable R value, but not as low as the refinement in $Fm\bar{3}m$. In addition, a final difference Fourier synthesis revealed the occupancy of the octahedral voids leading to the composition Li_2PtSn. Careful inspection of the displacement parameters and the difference Fourier synthesis suggested a slight mixing of tin and lithium on the octahedral sites resulting in the composition $Li_{1.96(2)}PtSn_{1.04(2)}$. Despite the fact that the final R value is actually higher than the refinement in $Fm\bar{3}m$, the structure is correctly described in $F\bar{4}3m$. This is also undermined by the refined Flack parameter of 0.01(6), indicating the correct absolute orientation. In addition, the Flack parameter is expected to be 0.5 in the case where $Fm\bar{3}m$ is the correct space group.

$Li_{3-x}Pt_2Sn_{3+x}$: Refinement of $Li_3Pt_2Sn_3$, $Li_{2.27}Pt_2Sn_{3.73}$ and $Li_{2.43}Pt_2Sn_{3.57}$

The strongly dominating subcell of $Li_3Pt_2Sn_3$ with $a' = 1/2a$ belongs to a fluorite type as does Li_2PtSn. Indeed, the atomic positions of the binary fluorite phase $PtSn_2$ served as a starting point. Both lithium and tin occupy the fluoride positions with a refined ratio of approximately 3:1. The difference Fourier synthesis indicated additional occupation of octahedral voids by lithium, but in the subcell those positions were not refinable. This is due to the high cubic symmetry and parameter correlations. However, these correlations were nicely resolved in the superstructure.

 © 2003 Wiley-VCH Verlag GmbH & Co. KGaA, Weinheim

All three lattice parameters are doubled in the superstructure. This means in terms of symmetry reduction that one has to decentre the *F*-lattice first to get a primitive lattice and subsequently double a', b' and c'. The extinction conditions of the many weak superstructure reflections were compatible with a body centred lattice and showed the presence of an *a*-glide plane. Only one cubic space group was possible, $Ia\bar{3}$, in which the superstructure was refined successfully. Also, $Ia\bar{3}$ allows ordering of the lithium and tin atoms on the fluoride positions of the subcell in the ratio 1:3.

The ternary stannide follows the general formula $Li_{3-x}Pt_2Sn_{3+x}$. To cover the whole range of homogeneity a total of seven single crystals were refined for which x varied between $x = 0$ and $x = 0.78$. The crystals originated from samples with four different starting compositions, Li:Pt:Sn = 1:1:4, 1:1:2, 1:1:1 and 3:2:3.

The lattice parameters were refined from powder data as well and matched those obtained for the single crystal. We did not obtain pure samples in all cases as the starting compositions suggest. Therefore the lattice parameters obtained from the single crystal were taken to calculate atomic distances for the various structures refined. Apparently inhomogeneity with respect to the composition $Li_{3-x}Pt_2Sn_{3+x}$ could not be avoided as additional shoulders next to the strongest reflections suggested. Nevertheless, the lattice parameters in a single powder sample were within a narrow range and smaller than the variation of the lattice parameters over the whole range of homogeneity.

Two of the seven data sets were collected from crystals that showed twinning by merohedry. This twinning is suggested by the *translationengleiche* symmetry reduction t2 i.e. losing the high Laue symmetry. Consequently the twin matrix is 0 1 0, 1 0 0, 0 0 −1. Only three refinements are reported here, corresponding to the compositions, $Li_3Pt_2Sn_3$, $Li_{2.27}Pt_2Sn_{3.73}$ and $Li_{2.43}Pt_2Sn_{3.57}$. The other four data sets were refined to similar results, but give only redundant information.

The course of the structure refinement will be discussed for $Li_3Pt_2Sn_3$ as an example. The platinum and tin positions were calculated in going from the subcell positions to the supercell positions according to the symmetry reductions given in a Bärnighausen scheme[20,21] (Figure 4). The three lithium positions were clearly revealed by a difference Fourier synthesis. For the ideal composition $Li_3Pt_2Sn_3$ no remaining electron density on the lithium sites was observed and the displacement parameters of the lithium atoms behaved well. This occurred quite differently within the solid solution. Here, large difference Fourier peaks on the lithium site 16*c* could be observed. The only explanation, supported by the varying lattice parameters, was a mixed occupancy by tin atoms. The 16*c* site was occupied by Li1 and additional Sn2 atoms assuming that the sum was 100% (Table 2). The atomic positions and displacement parameters were constrained to be equal. Thus, the refinement of the lithium content was riding on the larger scattering power of tin on the site 16*c*, even though increasing tin/lithium mixing lets the intensity of the superstructure reflections gradually diminish.

Final difference Fourier syntheses revealed no significant residual peaks (see Table 1). The positional parameters of the refinements are listed in Table 2. Table 3 contains additional information regarding the range of homogeneity. In Table 4 the interatomic distances of the ideal structures are listed. Listings of the observed and calculated structure factors are available.
Further details of the crystal-structure investigation(s) may be obtained from the Fachinformationszentrum Karlsruhe, 76344 Eggenstein-Leopoldshafen, Germany, on quoting the depository number(s) CSD-413190 (Li_2PtSn), -413187 ($Li_3Pt_2Sn_3$), -413188 ($Li_{2.27}Pt_2Sn_{3.73}$) and -413189 ($Li_{2.43}Pt_2Sn_{3.57}$).

Acknowledgments

We thank the Degussa-Hüls AG for a generous gift of platinum powder. This work was financially supported by the Fonds der Chemischen Industrie and by the Deutsche Forschungsgemeinschaft through SFB 458 Ionenbewegung in Materialien mit ungeordneten Strukturen.

[1] F. Hund, R. Fricke, *Z. Anorg. Allg. Chem.* **1949**, *258*, 198.
[2] P. Villars, L. D. Calvert, *Pearson's Handbook of Crystallographic Data for Intermetallic Phases*, second ed. and desk ed., ASM International, Materials Park, OH, **1991** and **1997**.
[3] H.-U. Schuster, D. Thiedemann, H. Schönemann, *Z. Anorg. Allg. Chem.* **1969**, *370*, 160.
[4] A. Czybulka, D. Last, H.-U. Schuster, *Metall−Metall-Wechselwirkungen in Zintl-Verbindungen und intermetallischen Phasen verwandter Struktur*, in B. Krebs, *Unkonventionelle Wechselwirkungen in der Chemie metallischer Elemente*, VCH, chapter 17, **1992**.
[5] H. Pauly, A. Weiss, H. Witte, *Z. Metallkd.* **1968**, *59*, 47.
[6] A. Czybulka, A. Petersen, H.-U. Schuster, *J. Less-Common Met.* **1990**, *161*, 303.
[7] J. Drews, U. Eberz, H.-U. Schuster, *J. Less-Common Met.* **1986**, *116*, 271.
[8] M. M. Thackeray, K. D. Kepler, J. T. Vaughey, Patent No. WO 2000003443, Application No. WO 1999-US12868.
[9] Zh. Wu, R.-D. Hoffmann, D. Johrendt, B. D. Mosel, H. Eckert, R. Pöttgen, *J. Mater. Chem.* in press.
[10] L. Drews-Nicolai, G. Hohlneicher, *J. Alloys Compd.* **2001**, *316*, 1.
[11] L. Drews-Nicolai, G. Hohlneicher, U. Hoppe, W. Jung, *Z. Anorg. Allg. Chem.* **2001**, *627*, 1157.
[12] R. Pöttgen, Zh. Wu, R.-D. Hoffmann, G. Kotzyba, H. Trill, J. Senker, D. Johrendt, B. D. Mosel, H. Eckert, *Heteroatom Chem.* **2002**, *6*, 506.
[13] Zh. Wu, H. Eckert, J. Senker, D. Johrendt, G. Kotzyba, B. D. Mosel, H. Trill, R.-D. Hoffmann, R. Pöttgen, *J. Phys. Chem. B* **2003**, *107*, 1943.
[14] Zh. Wu, H. Eckert, B. D. Mosel, R. Pöttgen, *Z. Naturforsch., Teil B* **2003**, *58*, 501.
[15] H. J. Wallbaum, *Z. Metallkd.* **1943**, *35*, 200.
[16] C. J. Kistrup, H. U. Schuster, *Z. Anorg. Allg. Chem.* **1974**, *410*, 113.
[17] C. J. Kistrup, H. U. Schuster, *Z. Naturforsch., Teil B* **1972**, *27*, 324.
[18] J. Donohue, *The Structures of the Elements*, Wiley, New York, **1974**.
[19] J. Emsley, *The Elements*, Oxford University Press, 3rd edn, **1999**.
[20] H. Bärnighausen, *Commun. Math. Chem.* **1980**, *9*, 139.
[21] H. Bärnighausen, U. Müller, *Symmetriebeziehungen zwischen den Raumgruppen als Hilfsmittel zur straffen Darstellung von Strukturzusammenhängen in der Kristallchemie*, University of Karlsruhe and University/GH Kassel, Germany, **1996**.
[22] R. Pöttgen, Th. Gulden, A. Simon, *GIT-Laborfachzeitschrift* **1999**, *43*, 133.
[23] K. Yvon, W. Jeitschko, E. Parthé, *J. Appl. Crystallogr.* **1977**, *10*, 73.
[24] G. M. Sheldrick, SHELXS-97, *Program for the Solution of Crystal Structures*, University of Göttingen, Germany, **1997**.
[25] G. M. Sheldrick, SHELXL-97, *Program for Crystal Structure Refinement*, University of Göttingen, Germany, **1997**.
[26] J. S. Charlton, M. Cordey-Hayes, I. R. Harris, *J. Less-Common Metals* **1970**, *20*, 105.

Received May 27, 2003

 © 2003 Wiley-VCH Verlag GmbH & Co. KGaA, Weinheim

Organocalcium Compounds with Catalytic Activity for the Ring-Opening Polymerization of Lactones

Matthias Westerhausen,*[a] Stefan Schneiderbauer,[a] Alexander N. Kneifel,[a] Yvonne Söltl,[a] Peter Mayer,[a] Heinrich Nöth,[a] Zhiyuan Zhong,[b] Pieter J. Dijkstra,[b] and Jan Feijen[b]

Dedicated to the memory of Ron Snaith

Keywords: N ligands / Calcium / O ligands / Ring-opening polymerization / Tin

The equimolar reaction of calcium bis[bis(trimethylsilyl)-amide] with 2,2,6,6-tetramethylheptane-3,5-dione (Htmhd) in THF yields liquid mononuclear [Ca(tmhd){N-$(SiMe_3)_2$}$(THF)_3$] (**1**). A similar reaction in toluene with a stoichiometric ratio of 2:3 gives the dinuclear complex [{$(THF)Ca\}_2(tmhd)_2$(μ-tmhd){μ-$N(SiMe_3)_2$}] (**2**). The calcium atoms of these complexes are in a distorted octahedral environment. In **2** the complex consists of two octahedra connected by a common face of one nitrogen base and two oxygen atoms; the bridging Ca–N bond lengths are extremely large. The metalation of the tetradentate Jacobsen reagent with calcium bis[bis(trimethylsilyl)amide] in 1,2-dimethoxyethane (DME) gives the corresponding calcium complex **3**, nearly quantitatively, as its DME adduct. The calcium atom is in an unusual trigonal prismatic coordination sphere. The metathesis reaction of **3** with tin(II) chloride yields the corresponding yellow tin(II) complex with the metal atom in a distorted square-pyramidal environment. Complexes **2** and **3** show catalytic reactivity in the ring-opening polymerization of cyclic esters such as lactones and lactides.
(© Wiley-VCH Verlag GmbH & Co. KGaA, 69451 Weinheim, Germany, 2003)

Introduction

The expectations that organocalcium chemistry might have a wide variety of applications[1] has led to intensive research efforts on this topic. Organocalcium compounds have been investigated for use as combustion improvers and smoke inhibitors, and as an additive for diesel fuels and fuel oils.[2] Another field of interest is the MOCVD (*M*etal *O*rganic *C*hemical *V*apour *D*eposition) process to produce, for example, thin films of calcium sulfide[3] or titanate.[4] There are also investigations on these compounds as sol-gel precursors.[5] Another important application for organocalcium compounds focuses on their use as initiators for the anionic ring-opening polymerization of cyclic esters and lactones.[6] These arbitrarily chosen examples illustrate the wide spectrum of interest in these compounds. Whereas for the MOCVD processes the main requirements of these compounds are volatility and thermal stability, the demands for ring-opening polymerization concern their reactivity towards cyclic esters and their solubility in common organic solvents such as ethers and hydrocarbons.

Due to the lack of redox reactivity, which is the key step in many catalytic cycles with transition metals, the alkaline-earth metals always show the oxidation state of +2. For their use as polymerization initiators and catalysts the organocalcium complexes should therefore have vacant coordination sites, which can be filled by weakly bonding ligands, or have unusual or distorted coordination spheres at the metal center. Furthermore, we have to design organocalcium compounds in a special reactivity range to have sufficient reactivity for the ring opening of cyclic esters but to prevent side reactions with the already formed polymer or with the solvent (such as ether cleavage reactions).

Polymeric cyclic esters such as D,L-lactide or ε-caprolactone are used for tissue engineering and as materials for surgical sutures. Orthopedic applications as well as the use for controlled-release systems for pharmaceuticals are also under investigation. The demand for these materials is extremely high with respect to toxicity and immunogenic, allergic and thrombogenic reactions. Furthermore, the polymeric materials should be sterilizable and have suitable mechanical properties.[7] Polylactides are amongst the most important biodegradable polymers. Due to the fact that the anionic polymerization initiator remains in the polymeric material, organometallic compounds based on calcium are the ideal starting materials for ring-opening polymerization.

For the purpose of investigating organocalcium compounds with respect to ring-opening polymerization we have chosen heteroleptic β-diketonates of calcium with reactive bis(trimethylsilyl)amide ligands. Homoleptic calcium

[a] Department Chemie, Ludwig-Maximilians-Universität Munich München, Germany
[b] Department of Chemical Technology and Institute for Biomedical Technology, University of Twente, Enschede, The Netherlands

 © 2003 Wiley-VCH Verlag GmbH & Co. KGaA, Weinheim **DOI: 10.1002/ejic.200300286**

bis(tetramethylheptane-3,5-dionate) was prepared from calcium diethoxide and tetramethylheptane-3,5-dione (Htmhd) and crystallized as a dimeric bis(ethanol) complex or as a solvent-free trimer.[8] This trimer was monomerized by addition of strong mono- or bidentate N-donors.[9]

Results and Discussion

Synthesis

Until now the synthesis of β-diketonato complexes of calcium started from the alkoxides. However, the soluble and readily accessible {by transmetalation of $Sn[N(SiMe_3)_2]_2$} bis(tetrahydrofuran)calcium bis[bis(trimethylsilyl)-amide][10,11] is a more reactive metalation reagent. The equimolar reaction of $Ca[N(SiMe_3)_2]_2$ with Htmhd in tetrahydrofuran yielded the liquid, mononuclear complex tris-(tetrahydrofuran)(2,2,6,6-tetramethylheptane-3,5-dionato)-calcium bis(trimethylsilyl)amide (**1**) according to Equation (1) with a surprisingly low melting point of 4 °C. The prolonged exposure of this complex to vacuum gave a brown and nearly insoluble oil. The metalation of Htmhd with $[Ca\{N(SiMe_3)_2\}_2(THF)_2]$ in a stoichiometric ratio of 3:2 in toluene gave binuclear bis[(tetrahydrofuran)calcium]-tris(2,2,6,6-tetramethylheptane-3,5-dionato)bis(trimethylsilyl)amide (**2**) according to Equation (2) in good yield. This complex reacts in THF with alcohols such as methanol, ethanol and 2-propanol by substitution of the amide ligand by an alkoxide anion. However, recrystallization from toluene gave the homoleptic dismutation product $[Ca(tmhd)_2]_3$ and a mixture of alkoxide-rich complexes of yet unknown composition. However, the structure of **2** was maintained upon alcoholysis with sterically demanding alcohols such as 2,6-di(*tert*-butyl)phenol and 1-phenylethanol, and compounds of the type $[(THF)Ca]_2(tmhd)_3OR$ were isolated.

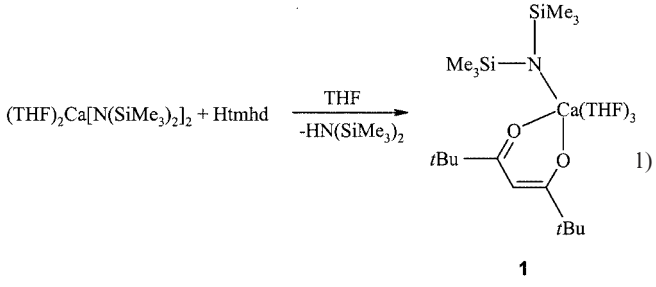

1) **1**

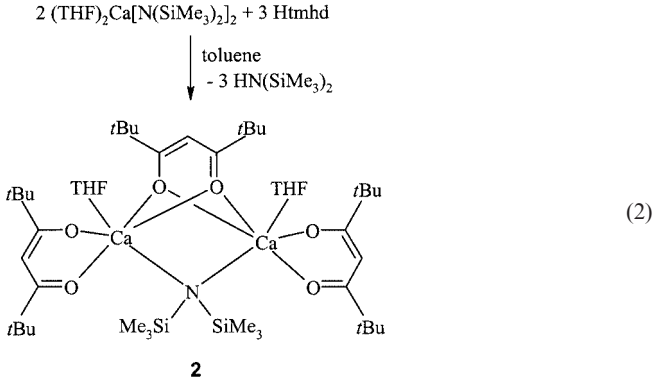

(2) **2**

The different coordination spheres of the nitrogen atoms of the bis(trimethylsilyl)amido ligands is clearly shown by the $^{29}Si\{^1H\}$ NMR chemical shifts.[12] For **1** the $N(SiMe_3)_2$ substituent with a triply coordinated nitrogen atom shows a chemical shift of $\delta = -15.9$ ppm which is a characteristic value for a terminally bonded amido group. The low-field shifted $^{29}Si\{^1H\}$ NMR resonance of **2** at $\delta = -8.0$ ppm proves the bridging position of the bis(trimethylsilyl)amido ligand. Similar characteristic shifts have been found for the calcium bis[bis(trimethylsilyl)amides].[12]

In order to investigate the reactive coordination sites of the calcium-containing complexes the molecular structures of **1** and **2** were determined (see below). We have already shown that **2** shows catalytic activity in anionic ring opening polymerization of cyclic esters.[13]

Another possibility to enhance the reactivity of organocalcium compounds is to embed the calcium center in an unusual coordination sphere. Vacant coordination sites at the Lewis-acid metal center lead immediately to coordination of Lewis bases such as ethers or to a dimerization of the calcium-containing compound. Therefore, the unusual coordination sphere has to be fixed by employing a multidentate ligand which shows very restricted flexibility and enforces a non-octahedral coordination sphere of the calcium atom.

In order to investigate the coordination sphere the Jacobsen ligand[14] was chosen due to its nearly square-planar tetradentate N_2O_2 coordination site and its dianionic charge to ensure a stable complex with *tert*-butyl groups at the periphery to ensure solubility in common organic solvents such as ethers. The metalation of the Jacobsen reagent with calcium bis[bis(trimethylsilyl)amide] in 1,2-dimethoxyethane (DME) yielded (1,2-dimethoxyethane-*O*,*O*′)calcium (*R*,*R*)-(−)-*N*,*N*′-bis[3,5-di(*tert*-butyl)salicylate]-1,2-cyclohexenediimine (**3**) according to Equation (3).

In order to investigate the suitability of the calcium complex **3** for metathesis reactions a well-known tin(II) complex was prepared. Compound **3** was reacted with tin dichloride to give nearly quantitatively the corresponding yellow tin(II) (*R*,*R*)-(−)-*N*,*N*′-bis[3,5-di(*tert*-butyl)salicylate]-1,2-cyclohexenediimine (**4**) according to Equation (3). The $^{119}Sn\{^1H\}$ NMR chemical shift of $\delta = -536.0$ ppm is similar to the published value ($\delta = -524.5$ ppm[15]). This compound was prepared earlier by metalation of the Jacobsen reagent with $Sn[N(SiMe_3)_2]_2$, however, only the oxidation product with 3,5-di(*tert*-butyl)-1,2-benzoquinone[15] and the addition products to metal carbonyl fragments[16] were characterized by X-ray crystallography. The metal centers of organometallic tin(II) compounds usually display coordination numbers of two and three. Monomeric molecules such as $Sn[N(SiMe_3)_2]_2$ are bent due to the lone pair at the metal center.[17] The dimeric molecules can either form a tin-tin bond in a trans-bent fashion, as for example observed for $[Sn\{CH(SiMe_3)_2\}_2]_2$,[18] or can exhibit a Sn_2X_2 cycle, as for example in $[RSn(\mu\text{-}Cl)_2SnR][R = N(SiMe_3)_2, N(CMe_2CH_2)_2CH_2]$.[19] In all compounds with a triply coordinated tin(II) atom the metal atoms show a strongly pyramidal coordination sphere because stannanediyls of the

 © 2003 Wiley-VCH Verlag GmbH & Co. KGaA, Weinheim

type SnR_2 are Lewis acids as well as Lewis bases.[20] Due to the geometry of the Jacobsen ligand the formation of a distorted tetragonal pyramid has to be expected, as found for a similar complex.[21] The molecular structure of **4** was determined by X-ray crystallography.

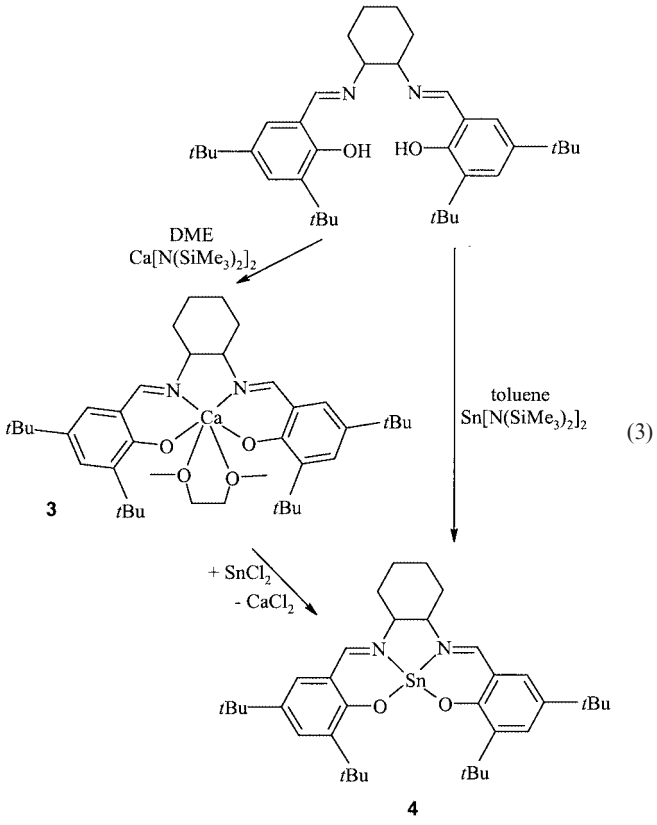

Molecular Structures

Due to their low melting point single crystals of **1** have to be handled at temperatures below −20 °C during isolation from the mother liquor and mounting on the diffractometer. The molecular structure of **1** and the numbering scheme is represented in Figure 1. Selected structural parameters are summarized in Table 1. The calcium center is in a distorted octahedral environment with a meridional arrangement of the three anionic donors.

The Ca−O distances of the anionic diketonate ligand are approximately 12 pm smaller than those of the THF molecules. The Ca−N bond length of 237.7 pm is rather large in comparison to Ca−N bonds of terminally bonded bis(trimethylsilyl)amido substituents in $[Ca\{N(SiMe_3)_2\}_2(THF)_2]$ (230 pm[11]) and $[Ca\{N(SiMe_3)_2\}_2(DME)]$ (227 pm[22]).

The distortion of the octahedral coordination sphere of the calcium atom is caused by the bite of the β-diketonate ligand, with an O1···O2 distance of 278.8 pm, which gives an O1−Ca1−O2 angle of only 74.2°. The anionic charge is delocalized within the planar diketonate fragment. Therefore, average C−O and C−C bond lengths of 128 and 139 pm, respectively, are observed.

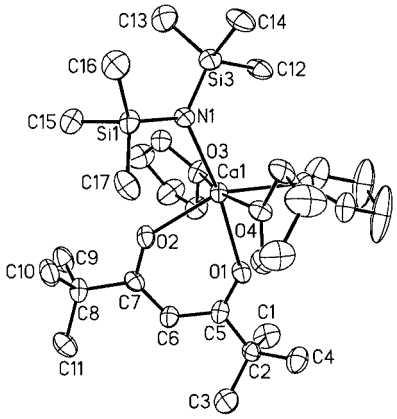

Figure 1. Molecular structure of **1**; the ellipsoids represent a probability of 40%; the hydrogen atoms are omitted for clarity; selected bond lengths (pm) of the coordination sphere of calcium: Ca1−O1 232.0(6), Ca1−O2 230.1(6), Ca1−O3 243.5(6), Ca1−O4 239.8(6), Ca1−O5 247.0(6), Ca1−N1 237.7(6); bond angles (°): O1−Ca1−O2 74.2(2), O1−Ca1−O3 94.6(2), O1−Ca1−O4 84.1(2), O1−Ca1−O5 77.1(2), O1−Ca1−N1 165.4(2), O2−Ca1−O3 82.6(2), O2−Ca1−O4 108.8(2), O2−Ca1−O5 147.4(2), O2−Ca1−N1 97.3(2), O3−Ca1−O4 167.5(2), O3−Ca1−O5 84.7(2), O3−Ca1−N1 96.1(2), O4−Ca1−O4 82.9(2), O4−Ca1−N1 87.6(2), O5−Ca1−N1 113.9(2)

Table 1. Selected structural parameters of the compounds **3** (M = Ca) and **4** (M = Sn)

	3	**4** (molecule A)	**4** (molecule B)
M−O1	218.8(2)	209.6(4)	210.7(5)
M−O2	219.4(2)	211.9(4)	212.3(5)
M−O3	244.2(2)	–	–
M−O4	245.2(2)	–	–
M−N1	247.0(3)	235.0(4)	232.5(5)
M−N2	240.2(3)	236.1(5)	238.0(5)
O1−M−O2	104.46(7)	80.4(2)	79.9(2)
O1−M−O3	89.97(9)	–	–
O1−M−O4	140.98(9)	–	–
O1−M−N1	75.83(9)	76.6(2)	78.0(2)
O1−M−N2	133.13(9)	110.5(2)	118.9(2)
O2−M−O3	149.90(8)	–	–
O2−M−O4	87.11(9)	–	–
O2−M−N1	123.79(9)	129.2(2)	120.7(2)
O2−M−N2	74.79(9)	78.4(2)	76.2(2)
N1−M−O3	85.03(8)	–	–
N1−M−O4	128.20(9)	–	–
N1−M−N2	67.64(8)	68.6(2)	68.3(2)
N2−M−O3	114.21(9)	–	–
N2−M−O4	85.73(9)	–	–
O3−M−O4	65.98(7)	–	–

The molecular structure of **2** and the numbering scheme are represented in Figure 2. In this dinuclear molecule the calcium atoms are in distorted octahedral environments. The molecule contains two octahedra connected by a common face. The bridging ligands are the bis(trimethylsilyl)-amido and one of the β-diketonato substituents, which

 © 2003 Wiley-VCH Verlag GmbH & Co. KGaA, Weinheim

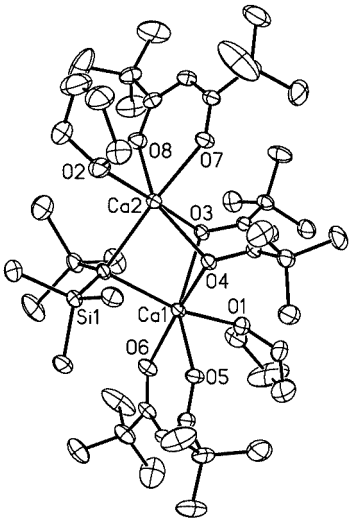

Figure 2. Molecular structure of **2**; the ellipsoids represent a probability of 40%; the hydrogen atoms are omitted for clarity; selected bond lengths (pm): Ca1−N 246.5(2), Ca1−O1 243.7(2), Ca1−O3 248.1(2), Ca1−O4 243.7(2), Ca1−O5 226.4(2), Ca1−O6 229.2(2), Ca2−N 251.2(2), Ca2−O2 241.8(2), Ca2−O3 244.8(2), Ca2−O4 239.7(2), Ca2−O7 231.5(2), Ca2−O8 225.9(2), Ca1···Ca2 337.46(7)

leads to coordination numbers of four for the nitrogen atom and three for the bridging oxygen atoms O3 and O4.

The Ca−N bonds, with an average length of 249 pm, are extraordinarily long. Likewise, the bridging Ca−O bonds have an average length of 244 pm, which is even slightly larger than the distance between the metal centers and the THF molecules. The terminally bonded β-diketonate ligands display much shorter Ca−O bonds, with an average value of 228 pm. These Ca−O distances are the smallest due to the electrostatic attraction and the small coordination numbers of the oxygen atoms. The N−Si distances, with a mean value of 172 pm, are in the expected region found for other calcium bis[bis(trimethylsilyl)amides] and do not support an ionic picture where extremely short N−Si bonds are to be expected, as, for example, for barium bis[bis(trimethylsilyl)amide].[12]

For multidentate ligands with a fixed arrangement of the Lewis donors several possibilities of coordination behaviour are possible (Scheme 1). Depending on the ratio of the radii of the metal atoms and the coordination gap an in-plane or out-of-plane coordination is realized. Furthermore, doming of the ligand is often observed, with the metal atom on the outside, or a saddle-like arrangement, with the metal on the inside of the ligand. Sometimes a twisting or ruffling of the multidentate base is also observed. To enhance the reactivity, a doming of the ligand with the metal center bonded from the outside is necessary.

The Jacobsen ligand retains its stereochemical centers and therefore centrosymmetric space groups have been excluded during the structure determination and refinement procedures of the calcium complex **3**. The geometry of the unit cell and the reflection conditions lead to the acentric orthorhombic space group $P2_12_12_1$. Surprisingly, other authors have found centrosymmetric space groups for solid-state structures of complexes of the Jacobsen ligand with divalent metals such as zinc,[23] even though the synthesis was performed with a stereochemically pure starting material.

The molecular structure of the calcium compound **3** with the Jacobsen ligand is shown in Figure 3. Here also the alkaline-earth metal center displays a coordination number of six, although the calcium atom is in an unusual distorted trigonal prismatic environment. The Ca−O distances of 219 pm to the alkoxide groups are extremely small due to the anionic charge, whereas in **2** the anionic charge on the oxygen atoms is reduced because it is delocalized within the β-diketonate fragment. In Figure 3 the doming of the Jacobsen ligand can clearly be seen.

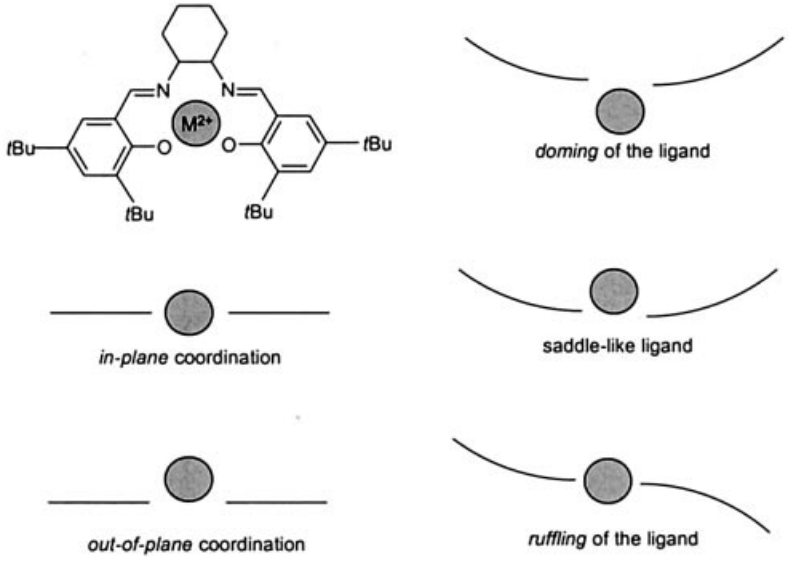

Scheme 1. Coordination behaviour of potentially multidentate ligands with reference to the flexibility of compounds **3** (M^{2+} = Ca·DME) and **4** (M^{2+} = Sn)

 © 2003 Wiley-VCH Verlag GmbH & Co. KGaA, Weinheim

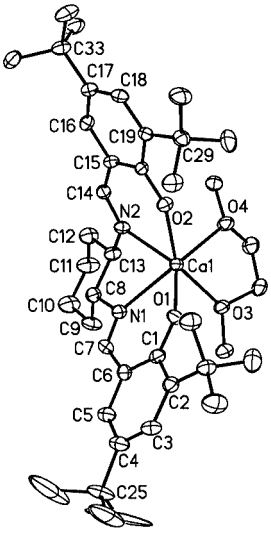

Figure 3. Molecular structure of **3**; the ellipsoids show a probability of 40%; the hydrogen atoms are omitted for clarity

The square-planar fragment is slightly distorted, as can be seen from the widening of the O1−Ca1−O2 angle (104.5°), whereas the other (endocyclic) angles are much smaller (O1−Ca1−N1 75.8°, N1−Ca1−N2 67.6°, N2−Ca1−O2 74.8°). However, the smallest angle is observed to the bidentate DME ligand. The calcium atom is larger than the O_2N_2 gap, and therefore it is located above the plane containing O1, O2, N1, and N2. Furthermore, the Jacobsen ligand is not planar but arched. Nevertheless, the nitrogen atoms are coordinated in a trigonal planar manner by two carbon atoms and the alkaline earth metal dication. The Ca1−O1−C1 and Ca1−O2−C20 fragments are bent (average 142.2°). The cyclohexane backbone shows the favoured chair conformation with a slightly elongated C8−C13 bond (154.3 pm) compared to the other C−C bonds of the cyclohexane moiety (average value of 152 pm).

The distances between the calcium center and the oxygen atoms of the DME molecule are approximately 25 pm longer than those to the alkoxide anions. In solution exchange reactions with solvent molecules are observed. Dissolving **3** in tetrahydrofuran immediately leads to the THF adduct, which can be isolated as a powder after standard workup procedures. Another coordination sphere of this molecule which contains monodentate Lewis bases has to expected. Atwood and co-workers[24] found a heptacoordinate calcium center for [Ca(*t*Bu-salen)(HOEt)$(THF)_2$] with a distorted pentagonal bipyramidal coordination. The use of a bidentate ligand is necessary to enforce the trigonal prismatic environment of the alkaline-earth metal atom. This easily exchangeable DME molecule offers the possibility of creating a coordination vacancy for the initial step of the polymerization reaction namely the coordination of the cyclic ester such as lactide or ε-caprolactone. Detailed studies of the polymerization process are under investigation and will be published elsewhere.

Compound **4** (M.p. 291−293 °C) crystallizes in the acentric orthorhombic space group $P2_12_12_1$ with two crystallographically independent molecules which are distinguished by the letters A and B. The molecular structure of molecule A is shown in Figure 4. Both the molecules show nearly identical structural parameters. Therefore, the discussion of this structure is limited to molecule A; however, in Table 1 selected bond lengths and angles of both molecules are listed together with the data of the calcium complex **3**.

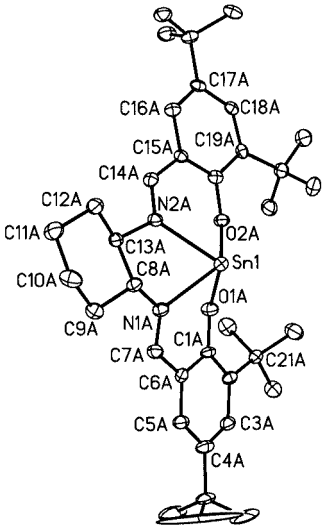

Figure 4. Molecular structure of **4**; the ellipsoids show a probability of 40%; the hydrogen atoms are omitted for clarity

The tin atom is bonded above the N_2O_2 plane with Sn−O bond lengths of 209.6 and 211.9 pm which are larger than in tin(II) bis[2,6-di(*tert*-butyl)phenolate] (200.3 and 204.4 pm[25]) and tin(II) bis[2,6-di(*tert*-butyl)-4-methylphenolate] (200.8 pm[26]). In dimeric Sn(O*t*Bu)$_2$, with a central Sn_2O_2 ring, endocyclic and exocyclic Sn−O bonds of 214.7 (average) and 200.9 pm, respectively, were found.[27] The Sn−N distances are coordinative bonds with large values of 235.0 and 236.1 pm. The Sn−O−C angles display an average value of 127°. The oxidation of tin(II) to tin(IV) leads to a drastic contraction of the bonding parameters, even though the enhancement of the coordination number to six is realized in an octahedral environment of the tin(IV) atom.[15] Also, the Sn−N bonds show a smaller average length of 218.3 pm, with the Sn−O bonds having average values of 201.8 pm. The Jacobsen ligands of **2** and **3** display nearly the same orientation and structural features. This observation shows that an inflexible ligand can enforce unusual coordination spheres at the metal atoms, namely a trigonal prism for the calcium center and the tin(II) atom being the apex of a distorted square pyramid.

Perspective

The catalytic reactivity of **2** was tested towards the polymerization of lactide and ε-caprolactone in THF solution. A fast gel formation as a sign of polymerization was observed. The polymeric materials show high molecular weights of approximately 1.67×10^5 g·mol^{-1} and a broad mass distribution. The substitution of the bis(trimethylsilyl)-

 © 2003 Wiley-VCH Verlag GmbH & Co. KGaA, Weinheim

amide by an alkoxide substituent, or the polymerization in the presence of an alcohol, leads to a living polymerization. The preparative details of the ring-opening polymerization and the concept that labile anionic ligands support the catalytic activity of this polymerization reaction will be presented in detail elsewhere. The preformed coordination gap by enforcing a trigonal prismatic coordination sphere at the calcium atom as realized in **3** is also a promising working hypothesis. Usually an octahedral environment of the alkaline earth metal atoms is preferred, and therefore the 1,2-dimethoxyethane ligand is immediately substituted by monodentate ligands, which is the first step in the polymerization process. On the other hand, the liquid complex **1** also loses neutral coligands very easily at room temperature during handling under an inert gas atmosphere or in hydrocarbons; a brown, nearly insoluble oil forms which separates from solution. Therefore, it is not recommended to use this calcium compound as an initiator or catalyst for the anionic polymerization of lactones and lactides. In a short communication Chisholm[28] has reported calcium compounds with four-coordinate calcium centers which can be used as catalysts for the ring-opening polymerization of lactides.

The advantage of the catalytically active complexes **2** and **3** in comparison to the already investigated calcium bis[bis(trimethylsilyl)amide][6,29] lies in the reduced sensitivity towards air and moisture and, therefore, an easier handling outside of a glove box seems to be possible during the polymerization experiments. Preliminary experiments support the expectation that these compounds are valuable initiators for the anionic polymerization of lactones and other cyclic ester.

Experimental Section

General Remarks: All experiments and manipulations were carried out under an atmosphere of argon. Reactions were performed using standard Schlenk techniques and dried, thoroughly deoxygenated solvents. Calcium bis[bis(trimethylsilyl)amide] was prepared according to a literature procedure.[10,11] NMR spectra were recorded on Jeol spectrometers GSX270 and EX400. A Nicolet 520 FT-IR spectrophotometer was used to record the IR spectra; solid substances were measured in nujol between KBr plates (vs very strong, s strong, m medium strong, w weak, vw very weak, sh shoulder).

Tris(tetrahydrofuran)(2,2,6,6-tetramethylheptane-3,5-dionato)-calcium Bis(trimethylsilyl)amide (1): A solution of [Ca{N-$(SiMe_3)_2$}$_2$$(THF)_2$] (2.40 g, 4.76 mmol) in 20 mL of THF was cooled to 0 °C. Then 2,2,6,6-tetramethylheptane-dione (0.99 mL, 4.76 mmol) was added. After stirring for an additional hour the solution was warmed to room temperature and the volume reduced to a few milliliters. After cooling to approximately −20 °C 1.74 g of colorless crystals of **1** (yield 66%) were collected. M.p. 4 °C. ^{1}H NMR ([D$_6$]benzene/THF mixture): δ = 0.19 ($SiMe_3$), 1.13 (*t*Bu), 5.68 (CH), 1.51 and 3.57 (THF) ppm. ^{13}C{^{1}H} NMR ([D$_6$]benzene/THF mixture): δ = 5.42 ($SiMe_3$), 28.46 (C*Me*$_3$), 40.69 (*C*Me$_3$), 89.00 (CH), 199.29 (CO), 25.40 and 67.65 (THF) ppm. ^{29}Si{^{1}H} NMR ([D$_6$]benzene/THF mixture): δ = −15.9 (NSi_2) ppm. IR: $\tilde{\nu}$ = 1693 m, 1660 s, 1562 w, 1538 m, 1505 s, 1480 w, 1450 w, 1417 s, 1390 m, 1360 m, 1250 m, 1224 w, 1183 w, 1131 w, 956 w, 932 m, 881 w, 867 m, 841 m, 794 w, 479 w, 403 w. $C_{25}H_{45}CaNO_4Si_2$ (527.95) [bis(THF) complex due to loss of THF during handling and combustion]: calcd. C 57.76, H 8.72, N 2.69; found C 57.48, H 8.71, N 2.69.

Bis[(tetrahydrofuran)calcium] Tris(2,2,6,6-tetramethylheptane-3,5-dionate) Bis(trimethylsilyl)amide (2): A solution of [Ca{N$(SiMe_3)_2$}$_2$$(THF)_2$] (4.41 g, 8.74 mmol) in 50 mL of toluene was cooled to 0 °C and then 2,2,6,6-tetramethylheptane-3,5-dione (1.82 mL, 8.74 mmol) was added. After warming to room temperature the solution was stirred for an additional 12 hours. All volatile materials were removed under vacuum and the residue redissolved in 50 mL of *n*-pentane. The remaining solid materials were removed and the volume of the solution reduced to 10 mL. At −30 °C 3.25 g of colorless crystals of **2** (yield 80%) precipitated. Dec. 74 °C (without melting). ^{1}H NMR ([D$_6$]benzene): δ = 0.53 ($SiMe_3$), 1.26 (*t*Bu), 5.89 (CH), 1.37 and 3.63 (THF) ppm. ^{13}C{^{1}H} NMR ([D$_6$]benzene): δ = 5.12 ($SiMe_3$), 28.63 (C*Me*$_3$), 41.11 (*C*Me$_3$), 91.24 (CH), 200.84 (CO), 28.63 and 68.09 (THF) ppm. ^{29}Si{^{1}H} NMR ([D$_6$]benzene): δ = −8.0 (NSi_2) ppm. IR: $\tilde{\nu}$ = 1693 m, 1660 s, 1562 w, 1537 m, 1505 s, 1450 w, 1419 s, 1390 m, 1360 m, 1249 w, 1224 w, 1183 w, 1131 w, 933 m, 867 m, 843 w, 793 w, 479 w. $C_{47}H_{91}Ca_2NO_8Si_2$ (934.57): calcd. C 60.40, H 9.80, N 1.50; found C 60.38, H 9.81, N 1.41.

(1,2-Dimethoxyethane-*O*,*O*′)calcium (*R*,*R*)-(−)-*N*,*N*′-bis[3,5-di(*tert*-butyl)salicylate]-1,2-cyclohexenediimine (3): A solution of Htmhd (1.08 g, 1.98 mmol) in 10 mL of toluene was added to a solution of (1,2-dimethoxyethane-*O*,*O*′)calcium bis[bis(trimethylsilyl)amide] (1.07 g, 1.98 mmol) in 10 mL of toluene. The yellow solution was stirred for one day at room temperature and then all volatile materials were removed under vacuum. The yellow residue was redissolved in a few milliliters of toluene. At 5 °C 0.82 g of yellow plates of **3** (1.2 mmol, 61%) precipitated. M.p. 255−257 °C. ^{1}H NMR ([D$_6$]benzene): δ = 8.04 (s, 2 H, CH=N), 7.71 (s, H, aryl), 7.24 (s, 2 H, aryl), 3.05 (s, 6 H, DME), 2.96−2.78 (m, 6 H, DME, CH), 1.84 (s, 18 H, *t*Bu), 1.61 (s, 4 H, CH_2), 1.49 (s, 18 H, *t*Bu), 1.24−1.12 (m, 4 H, CH_2) ppm. ^{13}C{^{1}H} NMR ([D$_6$]benzene): δ = 168.1, 166.3 (CH=N), 139.9, 132.3, 129.9, 128.3, 126.3, 122.0 (aryl), 70.4 (DME), 69.5 (CH), 59.5(DME), 35.8, 33.8 (*C*Me$_3$), 31.9 (C*Me*$_3$), 31.4, 30.9 (CH_2), 29.9 (C*Me*$_3$), 29.5, 25.4 (CH_2) ppm. IR: $\tilde{\nu}$ = 1633 vs, 1615 vs, 1523 vs, 1479 vs, 1462 vs, 1439 vs, 1412 vs, 1398 vs, 1380 vs, 1361 vs, 1348 vs, 1334 vs, 1313 m, 1276 s, 1257 vs, 1230 s, 1199 s, 1158 vs, 1128 w, 1114 m, 1101 m, 1067 vs, 1030 m, 1023 m, 984 w, 974 w, 953 w, 927 w, 915 w, 882 s, 866 s, 857 m, 836 m, 810 w, 794 s, 743 m, 729 w, 637 w, 520 m, 475 w, 440 s, 421 w, 380 w, 336 w, 307 w.

X-ray Structure Determinations of 1−4: Data were collected on a Siemens P4 diffractometer with a Siemens SMART-CCD area detector using oil-coated rapidly cooled single crystals.[30,31] Graphite monochromated Mo-K_α radiation (λ = 71.073 pm) was used. Crystallographic parameters, details of data collection and refinement procedures are summarized in Table 2. The structures were solved by direct methods and refined with the software packages SHELXL-93 and SHELXL-97.[33] Neutral scattering factors were taken from Cromer and Mann[34] and for the hydrogen atoms from Stewart et al.[35] The non-hydrogen atoms were refined anisotropically. The H-atoms were considered with a riding model under restriction of ideal symmetry at the corresponding carbon atoms or refined isotropically. Crystallographic details can be obtained from the Cambridge Crystallographic Data Centre quoting the CCDC numbers given in Table 2.[36] One of the *tert*-butyl groups of **3** and **4** shows a rotatory disordering which was not resolved by split-positions of the corresponding atoms because neither the *R*

 © 2003 Wiley-VCH Verlag GmbH & Co. KGaA, Weinheim

Table 2. Crystallographic data of **3** and **5** as well as details of the structure solution and refinement procedures

Compound	**1**	**2**	**3**	**4**
Formula	$C_{29}H_{61}CaNO_5Si_2$	$C_{47}H_{91}Ca_2NO_8Si_2$	$C_{40}H_{62}CaN_2O_4$	$C_{36}H_{52}N_2O_2Sn$
Formula mass [g·mol^{-1}]	600.05	934.554	675.00	663.485
T [K]	193(2)	200(2)	193(2)	193(2)
Space group[32]	$P2_1/n$ (No. 14)	$P2_1/n$ (No. 14)	$P2_12_12_1$ (No. 29)	$P2_12_12_1$ (No. 29)
a [pm]	976.8(1)	1270.91(2)	1353.97(9)	1080.78(5)
b [pm]	2082.7(2)	2432.61(4)	1568.33(9)	2347.7(1)
c [pm]	1818.9(2)	1865.35(2)	1944.9(1)	2676.3(2)
β [°]	93.129(2)	97.708	90	90
V [nm^3]	3.6949(7)	5.7149(1)	4.1299(4)	6.7907(7)
Z	4	4	4	8
$d_{calcd.}$ [g·cm^3]	1.079	1.086	1.086	1.298
μ [mm^{-1}]	0.267	0.285	0.190	0.785
F(000)	1320	2048	1472	2784
Scan range [°]	$10.2 < 2\theta < 44.0$	$4.4 < 2\theta < 55.0$	$3.3 < 2\theta < 46.5$	$2.3 < 2\theta < 46.6$
Collected data	14049	64185	18551	30937
Unique data	4318	12758	5850	8668
Data with $I > 2\sigma(I)$	1452	7990	4910	7123
Parameters	356	541	518	771
Restraints	0	0	0	0
wR_2[a] (all data, on F^2)	0.2102	0.1759	0.1071	0.0970
wR_2 [a] [$I > 2\sigma(I)$]	0.1977	0.1421	0.1010	0.0907
R_1 [a] [$I > 2\sigma(I)$]	0.0914	0.0553	0.0416	0.0376
GOF[b] on F^2	0.681	1.057	1.046	1.035
Residual dens. [e·Å^{-3}]	510/-350	597/-501	342/-328	712/-490
CCDC number	210028	210029	210030	210031

[a] $R_1 = (\Sigma||F_o| - |F_c||)/\Sigma|F_o|$; $wR_2 = \{\Sigma[w(F_o^2 - F_c^2)^2]/\Sigma[w(F_o^2)^2]\}^{1/2}$ with $w^{-1} = \sigma^2(F_o^2) + (aP)^2$. [b] $S = \{\Sigma[w(F_o^2 - F_c^2)^2]/(N_o - N_p)\}^{1/2}$.

values nor the standard deviations of the molecular parameters were improved.

Acknowledgments

This work was financially supported by the Deutsche Forschungsgemeinschaft and the Fonds der Chemischen Industrie. We thank Prof. Dr. P. Klüfers for his kind support.

[1] J. J. Eisch, R. B. King, *Organometallic Synthesis*, Vol. 2, Academic Press, New York, **1981**; p. 101.
[2] L. S. Cook, M. W. Rush, P. J. Richards, D. Barr, *PCT Int. Apl.* **1995**.
[3] T. Haenninen, I. Mutikainen, V. Saanila, M. Ritala, M. Leskelae, J. C. Hanson, *Chem. Mater.* **1997**, *9*, 1234−1240.
[4] G. Ghandari, T. E. Glassman, D. B. Studebaker, G. Stauf, T. H. Baum, *Mater. Res. Soc., Symp. Proc.* **1997**, *446*, 327−332.
[5] V.-C. Arunasalam, I. Baxter, S. R. Drake, M. B. Hursthouse, K. M. Abdul Malik, D. J. Otway, *Inorg. Chem.* **1995**, *34*, 5295−5306.
[6] Z. Zhong, S. Schneiderbauer, P. J. Dijkstra, M. Westerhausen, J. Feijen, *J. Polym. Environ.* **2001**, *9*, 31−38.
[7] Z. Zhong, P. J. Dijkstra, J. Feijen, *Angew. Chem.* **2002**, *114*, 4692−4695; *Angew. Chem. Int. Ed. Engl.* **2002**, *41*, 4510−4513 and literature cited therein.
[8] V.-C. Arunasalam, S. R. Drake, M. B. Hursthouse, K. M. Abdul Malik, A. S. Stewart, D. M. P. Mingos, *J. Chem. Soc., Dalton Trans.* **1996**, 2435−2442.
[9] S. Daniele, L. G. Hubert-Pfalzgraf, C. Bavoux, *Polyhedron* **2001**, *20*, 1065−1070.
[10] M. Westerhausen, *Inorg. Chem.* **1991**, *30*, 96−101.
[11] M. Westerhausen, M. Hartmann, N. Makropoulos, B. Wieneke, M. Wieneke, W. Schwarz, D. Stalke, *Z. Naturforsch., Teil B* **1998**, *53*, 117−125.
[12] M. Westerhausen, *Coord. Chem. Rev.* **1998**, *176*, 157−210.
[13] Z. Zhong, S. Schneiderbauer, P. J. Dijkstra, M. Westerhausen, J. Feijen, manuscript in preparation.
[14] Selected examples may show the wide use of this ligand: W. Zhang, J. L. Loebach, S. R. Wilson, E. N. Jacobsen, *J. Am. Chem. Soc.* **1990**, *112*, 2801−2803. W. Zhang, E. N. Jacobsen, *J. Org. Chem.* **1991**, *56*, 2296−2298. J. F. Larrow, E. N. Jacobsen, Y. Gao, Y. Hong, X. Nie, C. M. Zepp, *J. Org. Chem.* **1994**, *59*, 1939−1942. S. Chang, J. M. Galvin, E. N. Jacobsen, *J. Am. Chem. Soc.* **1994**, *116*, 6937−6938. L. E. Martínez, J. L. Leighton, D. H. Carsten, E. N. Jacobsen, *J. Am. Chem. Soc.* **1995**, *117*, 5897−5898. M. Palucki, N. S. Finney, P. J. Pospisil, M. L. Güler, T. Ishida, E. N. Jacobsen, *J. Am. Chem. Soc.* **1998**, *120*, 948−954. D. A. Annis, E. N. Jacobsen, *J. Am. Chem. Soc.* **1999**, *121*, 4147−4154. E. N. Jacobsen, *Acc. Chem. Res.* **2000**, *33*, 421−431. J. M. Ready, E. N. Jacobsen, *J. Am. Chem. Soc.* **2001**, *123*, 2687−2688. J. M. Ready, E. N. Jacobsen, *Angew. Chem. Int. Ed.* **2002**, *41*, 1374−1377. S. E. Schaus, B. D. Brandes, J. F. Larrow, M. Tokunaga, K. B. Hansen, A. E. Gould, M. E. Furrow, E. N. Jacobsen, *J. Am. Chem. Soc.* **2002**, *124*, 1307−1315. R. T. Ruck, E. N. Jacobsen, *J. Am. Chem. Soc.* **2002**, *124*, 2882−2883.
[15] D. Agustin, G. Rima, H. Gornitzka, J. Barrau, *J. Organomet. Chem.* **1999**, *592*, 1−10.
[16] [16a] D. Agustin, G. Rima, H. Gornitzka, J. Barrau, *Eur. J. Inorg. Chem.* **2000**, 693−702. [16b] D. Agustin, G. Rima, H. Gornitzka, J. Barrau, *Inorg. Chem.* **2000**, *39*, 5492−5495.
[17] [17a] T. Fjeldberg, H. Hope, M. F. Lappert, P. P. Power, A. J. Thorne, *J. Chem. Soc., Chem. Commun.* **1983**, 639−641. [17b] T. Fjeldberg, A. Haaland, B. E. R. Schilling, M. F. Lappert, A. J. Thorne, *J. Chem. Soc., Dalton Trans.* **1986**, 1551−1556.
[18] D. E. Goldberg, D. H. Harris, M. F. Lappert, K. M. Thomas, *J. Chem. Soc., Chem. Commun.* **1976**, 261−262. See also: P. P. Power, *Chem. Rev.* **1999**, *99*, 3463−3503.
[19] R. W. Chorley, P. B. Hitchcock, B. S. Jolly, M. F. Lappert, G. A. Lawless, *J. Chem. Soc., Chem. Commun.* **1991**, 1302−1303.
[20] [20a] M. F. Lappert, *Main Group Met. Chem.* **1994**, *17*, 183−207. [20b] J. W. Connolly, C. Hoff, *Adv. Organomet. Chem.* **1981**, *19*, 123−153.
[21] D. Agustin, G. Rima, H. Gornitzka, J. Barrau, *Main Group Met. Chem.* **1999**, *22*, 703−711.

 © 2003 Wiley-VCH Verlag GmbH & Co. KGaA, Weinheim

[22] M. Westerhausen, W. Schwarz, *Z. Anorg. Allg. Chem.* **1991**, *604*, 127−140.
[23] G. A. Morris, H. Zhou, C. L. Stern, S. T. Nguyen, *Inorg. Chem.* **2001**, *40*, 3222−3227.
[24] M. Sánchez, M. J. Harvey, F. Nordstrom, S. Parkin, D. A. Atwood, *Inorg. Chem.* **2002**, *41*, 5397−5402.
[25] D. M. Barnhart, D. L. Clark, J. G. Watkin, *Acta Crystallogr., Sect. C* **1994**, *50*, 702−704.
[26] B. Cetinkaya, I. Gumrukcu, M. F. Lappert, J. L. Atwood, R. D. Rogers, M. J. Zaworotko, *J. Am. Chem. Soc.* **1980**, *102*, 2088−2089.
[27] M. Veith, P. Hobein, R. Rösler, *Z. Naturforsch., Teil B* **1989**, *44*, 1067−1081.
[28] M. H. Chisholm, *Polym. Mater. Sci. Eng.* **2002**, *87*, 85.
[29] Z. Zhong, P. J. Dijsktra, C. Birg, M. Westerhausen, J. Feijen, *Macromolecules* **2001**, *34*, 3863−3868.
[30] T. Kottke, D. Stalke, *J. Appl. Crystallogr.* **1993**, *26*, 615−619.
[31] D. Stalke, *Chem. Soc. Rev.* **1998**, *27*, 171−178.
[32] *International Tables for Crystallography* (Ed.: T. Hahn), Vol. A, *Space Group Symmetry*, 2nd Ed., D. Reidel, Dordrecht, **1984**.
[33] G. M. Sheldrick, *SHELXL-93*, Universität Göttingen, **1993**; *SHELXL-97*, Universität Göttingen, **1997**.
[34] D. T. Cromer, J. B. Mann, *Acta Crystallogr.* **1968**, *24*, 321−324.
[35] R. F. Stewart, E. R. Davidson, W. T. Simpson, *J. Chem. Phys.* **1965**, *42*, 3175−3187.
[36] CCDC-210028, -210029, -210030 and -210031 (as given in Table 2) contain the supplementary crystallographic data for this paper. These data can be obtained free of charge at www.ccdc.cam.ac.uk/conts/retrieving.html [or from the Cambridge Crystallographic Data Centre, 12, Union Road, Cambridge CB2 1EZ, UK; Fax: (internat.) +44-1223/336-033; E-mail: deposit@ccdc.cam.ac.uk].

Received May 15, 2003

 © 2003 Wiley-VCH Verlag GmbH & Co. KGaA, Weinheim

Polar Molecular Precursors for Alkali and Alkaline Earth Metal Clusters and Low-Dimensional Polymer Structures: the Solid-State Structures of $[CaI(dme)_3]I$, and *cis*-$[SrI_2(diglyme)_2]$ (dme = $CH_3OC_2H_4OCH_3$; diglyme = $CH_3(OC_2H_4)_2OCH_3$)

Katharina M. Fromm*[a] and William Maudez[a]

Keywords: Alkaline earth metals / Calcium / Halides / Polar compounds / Strontium

Two new alkaline earth metal halide adducts with oxygen-donor polyether ligands are described. One of them, *cis*-$[SrI_2(diglyme)_2]$, features two terminally bonded anions in vicinal positions, and at an angle of ca. 90°. The low bond valence sum of ca. 1.9 indicates how well the cation is shielded by its ligands in the solid state, and that ligand exchange can be expected in solution and upon reaction. The second compound, $[CaI(dme)_3]I$, consists of an ion pair formed by the cationic complex $[CaI(dme)_3]^+$ with one anion in terminal position, and one iodide. Both compounds possess a strong dipole moment at the molecular level, but crystallize in centrosymmetric space groups.
(© Wiley-VCH Verlag GmbH & Co. KGaA, 69451 Weinheim, Germany, 2003)

Introduction

We are interested in molecular compounds, especially oxygen donor adducts of alkaline earth metal iodides, because they are used as starting materials in the synthesis of low-dimensional polymeric compounds, including clusters.[1−10] The latter are used in the low-cost synthesis of superconductors and other oxide materials by the sol-gel technique, or as volatile precursors in CVD processes.[2,10] Furthermore, alkaline earth metal iodides complexed with polyether ligands have also been shown to have a dramatic effect on the dealkylation reactions of phosphinic esters.[11] We have also started to investigate the synthesis of polar materials for possible applications in NLO, for instance second harmonic generation. We became interested in these compounds because we wished to understand how they were formed and discover whether polar molecules can be forced to crystallize in polar space groups.

Compounds that have so far been isolated in the class of molecular species are, for instance, the zero-dimensional compounds *trans*-$[CaI_2(THF)_4]$[12] or *trans*-$[MI_2(THF)_5]$ (M = Sr,[13] Ba[1]), in which the metal cation is always surrounded in a linear or quasi-linear fashion by the two anions, whereas the THF ligands are found in the equatorial positions of a square or pentagonal bipyramid. They are commonly used as starting materials for substitution reactions of at least one iodide. Other compounds can also be molecular, but without any direct M−I contacts left to be reactive. Instead, the halide ions are replaced in the first coordination sphere by neutral water or polyether oxygen donor ligands for instance, leading to compounds such as $[Ba(OH_2)(triglyme)_2]I_2$ [triglyme = $CH_3(OC_2H_4)_3OCH_3$],[7] in which the anions are linked to the cationic complex by hydrogen bonding to the protons of the water molecules remaining in a second coordination sphere.

We now present some new exceptional molecular compounds that possess either two M−I bonds in *cis*-positions or only one M−I bond, leading in both cases to polar molecular precursors of alkaline earth metal iodides.

Results and Discussion

When SrI_2 is dissolved and re-crystallised from freshly dried and distilled diglyme ($CH_3OC_2H_4OC_2H_4OCH_3$), only the compound *cis*-$[SrI_2(diglyme)_2]$ (**1**) is obtained. Compound **1** crystallises in the monoclinic space group $P2_1/c$ with two independent molecules A and B per asymmetric unit (Figure 1).[14] Both molecules consist of a strontium cation to which two diglyme ligands and two anions are directly linked, with Sr−I distances between 3.314(3) and 3.335(3) Å, the shorter bonds being found in the first molecule A with Sr1. They are 0.11 Å longer than the Sr−I bonds in other molecular strontium iodide adducts, firstly due to the higher coordination number in **1** (eight instead of seven), and secondly due to the intra-ionic repulsion between the iodides in the *cis*-positions.[10,13] On the other hand, they are shorter than the bonds in compounds where iodide plays the role of a μ-bridging ligand between two strontium cations.[10] The I1−Sr1−I2 angle is, at 91.26(9)°, slightly smaller than that in the second molecule,

[a] University of Karlsruhe, Institute for Inorganic Chemistry, Engesserstr., 76128 Karlsruhe, Germany
E-mail: katharina.fromm@chiam.unige.ch

 © 2003 Wiley-VCH Verlag GmbH & Co. KGaA, Weinheim DOI: 10.1002/ejic.200300241

I3−Sr2−I4 [91.78(9)°]. In addition to the anions, each alkaline earth metal cation is surrounded by two diglyme ligands, their oxygen atoms coordinating to the strontium ion with distances ranging between 2.614(7) and 2.731(8) Å. This results in a severely distorted square antiprismatic coordination sphere around the cation in each molecule. In molecule A, the bite angles of the diglyme ligand are 58.6(7)° and 60.8(7)° for the first, and 58.8(6)° and 60.6(6)° for the second ligand. In molecule B, the corresponding values are 61.1(7)°, 60.3(7)°, 60.7(6)° and 59.2(6)°, slightly larger than in molecule A. The O−Sr−O angles closest to linear are O1−Sr1−O6 [166.9(7)°] and O9−Sr2−O12 [165.6(7)°]. The other angles between the two diglyme ligands of each molecule are 74.3(6)° and 74.3(7)° for O1−Sr1−O4 and O3−Sr1−O6, respectively, and 80.9(3)° for O3−Sr1−O4 in molecule A, and 74.1(7)°, 74.3(7)° and 81.2(7)° for O9−Sr2−O10, O7−Sr2−O12 and O7−Sr2−O10, respectively, in molecule B. The C−O and C−C bonds are normal at 1.42 and 1.55 Å, respectively, on average, but with the general tendency of being slightly longer in molecule B than in molecule A. The molecules A and B can be considered as isolated as there aren't any close contacts between, for instance, the iodide of one molecule and hydrogen atoms of a neighbouring unit (>3 Å). Only one intramolecular H-bond can be found in molecule B, with a I3−H24B distance of 2.958(6) Å. There are no contacts between the iodides of one unit and the strontium cations of another, as the cation is completely protected by the organic ligands and its own anions. Thus, the shortest distance between the anions of one molecule and the cation of another is greater than 6 Å. Although there is some similarity between the two molecules A and B of **1**, no correlation matrix was found linking the two in order to indicate a higher symmetry. Furthermore, careful analysis of the X-ray data gave no hints for the presence of a higher symmetry. The relatively high *R* value is due to slight disorder in the polyether ligands as well as — and more importantly — to strong absorption effects, which could unfortunately not be corrected. This is not unusual for structures containing heavy elements such as iodine, and residual electron density as high as three electrons close to the anions in **1** has also been reported in other structures.[1]

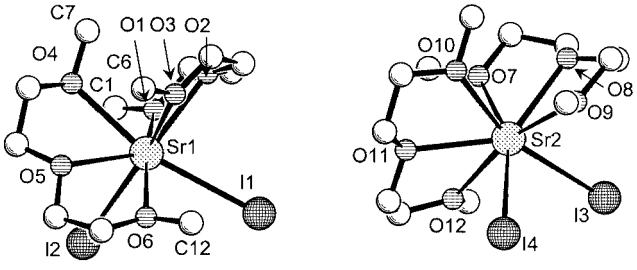

Figure 1. Two independent molecules of **1**; H atoms not shown

The coordination number of eight for the strontium cation is common. Generally, the strontium cation usually behaves more like barium than calcium as far as coordination numbers are concerned. Examples are found with a coordination number of seven in the compounds *trans*-$[MI_2(THF)_5]$ (M = Sr, Ba) whereas the corresponding calcium compound possesses a coordination number of six in *trans*-$[CaI_2(THF)_4]$, or for coordination number five as in $[IM(OtBu)_4(Li\{thf\})_4(OH)]$ for M = Sr and Ba, whereas the corresponding Ca compound has not been reported.[6,10] Barium compounds with sterically similar polyether ligands exist, and they all show a coordination number of nine for the alkaline earth metal cation, the corresponding bond valence sums being greater than two to satisfy the charge requirements.[7] In **1**, however, we observe a coordination number of eight for the strontium cation, and, more importantly, a bond valence sum of 1.95 and 1.91 for Sr1 and Sr2, respectively, which is obviously less than two.[15] This means that the cation is not sufficiently coordinated and would therefore be an excellent starting material for further synthesis, as it would tend to complete its coordination sphere by exchanging ligands for instance. However, the space-filling model of molecule A (Figure 2) shows how well the cation is shielded by its ligands, explaining why the bond valence sum remains below two.

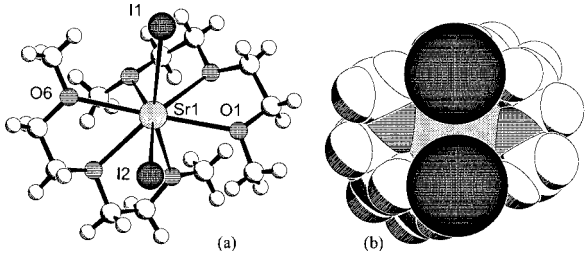

Figure 2. Molecule A of **1**: Sr1 and its coordination sphere as ball-and-stick model (a) and as space-filling representation (b)

The most intriguing fact about this structure is the fact that both anions occupy vicinal positions. This has never been observed before in a molecular species of the heavier alkaline earth metal halides, but only in two- or three-dimensional compounds with H-bonding involved,[5,7,16] or forming polymers or dimers with other anions of the neighbouring units.[1,17,18] For small alkaline earth metal cations, like Mg, with a coordination number of four, two anions are automatically in the vicinal positions, although with a larger angle between the anions than in **1**.[19] In general, to obtain such structures with the anions in *cis*-positions a sterically important ligand, which shields one side of the cation, such as slightly too small crown ethers, is required.[16] In these cases the X−M−X angles are usually much larger, the M−X bonds are longer than in **1**, and the anions are involved in H-bonding to build up a polymeric structure. Compound **1** is therefore the first example of a polar molecular alkaline earth metal iodide precursor. The strongly bent I−Sr−I feature in this structure is reminiscent of the alkaline earth metal halides, especially the heavier ones with strontium, barium and iodide as counterions, in the gas phase. Indeed, experimental as well as theoretical data show bent structures for the molecules in the gas

 © 2003 Wiley-VCH Verlag GmbH & Co. KGaA, Weinheim

phase.[20] So, **1** could be compared to a gas phase species stabilised by oxygen donor ligands. The bent structure is also reminiscent of the cyclopentadienyl derivatives of the alkaline earth metals. They have bent structures as well, although in the solid state they form polymers via contacts to neighbouring units. The THF-solvated cyclopentadienyl species are more similar to **1**.[21] More generally, other neutral complexes of alkaline earth metal cations, with coordination numbers greater than or equal to six, where two anions, such as halides or bulky amides for instance, are directly linked to the cation, preferentially show the anions organised in *trans*-positions. If the anions and further coordinating ligands are sterically more demanding, a distortion from the quasi-linear arrangement is observed, although it never reaches as small angles between the anions as in **1**.[17−19,22] Unfortunately, the polarity of the molecules of **1** is not maintained in the overall solid state as the compound crystallizes in a centrosymmetric space group.

The second compound presented here, $[CaI(dme)_3]I$ (**2**), was obtained by crystallizing CaI_2 from freshly dried and distilled DME.[14] It is built up from two independent cationic molecules A and B per asymmetric unit, each consisting of a calcium cation, Ca1 and Ca2, to which one iodide and three DME ligands are bonded terminally via both oxygen atoms, with two separate iodides as counterions (Figure 3). Thus, the cation reaches a coordination number of seven, that is, between six and eight, which are the most common coordination numbers for the calcium atom in general. The coordination geometry can roughly be described as a distorted pentagonal bipyramid with one iodide and an oxygen atom in axial positions. The corresponding I−Ca−O angle is, however, far from linear with an average value of 155°. This is due to the bite angles of the DME ligands, which vary from 63.7(4)° to 68.8(3)°. Of the five oxygen atoms in equatorial positions, one is clearly more out of the mean plane (formed by Ca and the five oxygen atoms) than the other four oxygen atoms, as has been described for a calcium compound with a similar coordination sphere.[9,23] The Ca−O bonds vary between 2.375(11) and 2.496(11) Å, the shorter bonds on average being found in molecule A around Ca1. The Ca−I bond is 3.120(3) Å and 3.121(3) Å for Ca1 and Ca2, respectively. This gives a cationic species for each molecule, the counterions I2 and I4 not being bonded at all to the cationic unit since all further Ca−I contacts are larger than 5.8 Å. In fact, there are no H−I contacts to I2 and I4 of less than 3.7 Å. Therefore, these anions can be considered as independent and not H-bonded to the cationic units. A similar compound can be obtained by replacing the three DME ligands of **2** by two, larger diglyme molecules. The number of oxygen atoms then remains identical, and so does their arrangement around the cation. The compound which is then obtained can be written as $[CaI(diglyme)_2]I$.[24] Unfortunately, crystals of both polar compounds are difficult to grow, as mentioned by Rogers et al.,[25] and the single crystal data is not yet of sufficient quality for publication. However, we have shown before that small polyether molecules (such as DME) can easily be replaced by larger ones (diglyme or triglyme for instance), as long as the number of oxygen atoms remains constant, without changes in the structure except for higher symmetries.[7]

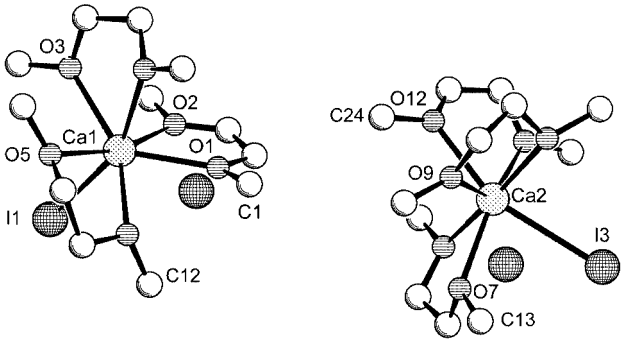

Figure 3. Two independent molecules of **2**; H atoms omitted for clarity

A heavier analogue to **2** with pseudo-halides is $[Sr(NO_3)(EO3)_2](NO_3)$ (EO3 = triethylene glycol)[25] where one anion is directly bonded to the cation whereas the other is weakly linked via H-bonds to an OH group of one of the polyglycols. In contrast to **2**, the H-bonding allows connections between anions and cationic units to form an overall threedimensional network. This is not observed in **2**.

The $[CaI(dme)_3]^+$ cations of **2** possess a strong dipole moment along the Ca−I bond vector, as can be seen from Figure 4. Such polar species are scarce: in the literature, only one example with calcium and iodide has been described so far to the best of our knowledge, $[CaI(THF)_5]^+$,[26] in which the cation possesses a coordination number of six, the counterion being an extremely bulky phosphonium diylide. The bond lengths in **2** are generally longer than in $[CaI(THF)_5]^+$, which is readily explained by the larger coordination number. In fact, the bond-valence sums for the calcium cations in **2** are, at 2.227 and 2.266, larger than the charge of the cation, indicating a more than satisfying bonding situation. The cation is indeed well wrapped up by its ligands, as shown in the space-filling model (Figure 4). Other polar compounds of alkaline earth metal cations linked to one halide and other neutral ligands can only be achieved when one coordination side of the cation is efficiently shielded by a sterically bulky ligand.[18,27] In some cases, formation of dimers occurs when

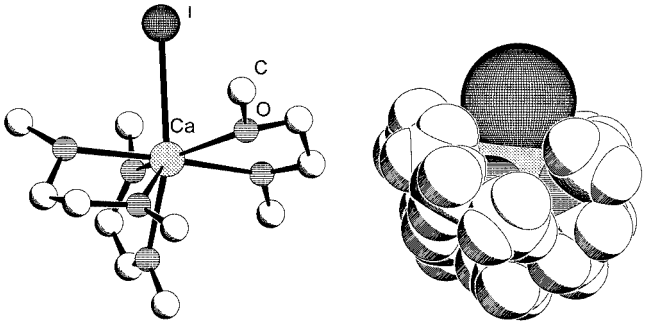

Figure 4. Cationic unit A $[CaI(dme)_3]^+$ of **2** and its space filling model

 © 2003 Wiley-VCH Verlag GmbH & Co. KGaA, Weinheim

coordination sites on the cation remain empty, in order to avoid single polar units,[28,29] whereas other complexes form infinite polymer structures via H-bonding of the neutral ligands toward both of the linked and free anions.[24,30]

Conclusions

We have synthesised two adducts of alkaline earth metal halides, one of which carries both anions connected to the cation in mutual *cis*-positions, and the other with only one iodide bound to the cation with the second anion showing no interaction with the cationic units. Both compounds possess a strong dipole moment at the molecular level, although this vanishes in the overall solid-state structure as both crystallize in centrosymmetric space groups. Both type of species are rare in the chemistry of the heavier alkaline earth metal halides, and could therefore be useful alternatives for precursors in new substitution reactions as have been described in the literature on *trans*-alkaline earth metal iodide adducts.[10,12,13,17] In all of the examples cited above, the polarity remains a local phenomenon, whereas the compounds crystallize in centrosymmetric space groups, so that the dipole moment vanishes in the solid state. We are now investigating the possibilities of crystallizing these compounds, **1** and **2**, in polar space groups, relying on the presence of polar ion pairs in solution.

Experimental Section

General: All experiments were carried out under an inert nitrogen atmosphere, using Schlenk techniques. The solvents DME and diglyme (diethylene glycol dimethyl ether) were dried over Na/benzophenone and distilled under nitrogen prior to use. IR spectra were carried out on a Perkin−Elmer Spectrum One IR spectrometer.

1: SrI_2 (0.174 g, 0.51 mmol) was dried for 30 min under vacuum at 300 °C and then dissolved in 30 mL of freshly dried and distilled diglyme, heating to reflux. The solution was filtered while hot and was then left to stand at room temperature. After two days, colourless single crystals grow in a yield of 78% with respect to SrI_2. $C_{24}H_{56}I_4O_{12}Sr_2$ (1219.6): calcd C 23.64, H 4.63; found C 25.97, H 5.27. The differences between found and calculated values are due to solvent, which remains on the crystals as they can't be dried under vacuum, and decompose rapidly if left in air. IR (nujol, CsI plates): $\tilde{\nu}$ = 2849 cm^{-1} (Nujol), 2077(w), 1971(w), 1939(w), 1605, 1459(Nujol), 1380(m), 1354(Nujol), 1286(m), 1269(w), 1249(vs), 1203(vs), 1129(s, sh), 944(m), 870(s), 839(s), 723(Nujol), 559(s), 489(w), 461(m), 367(w)

2: CaI_2 (0.24 g, 0.817 mmol) was dried under vacuum for half an hour at 300 °C, and then dissolved in 30 mL of freshly dried and distilled DME by heating to reflux for 15 minutes. The solution was filtered while hot, and colourless single crystals of **2** formed within one day at room temperature. Out of the mother liquor, crystals quickly lose solvent, as can be observed under the microscope, where they turn from clear colourless to opaque. The yield has therefore been estimated at 70% with reference to CaI_2. The lower evaporation temperature of DME compared to diglyme explains the values found for elemental analysis, where values are generally too low. $C_{24}H_{60}Ca_2I_4O_{12}$ (1128.5): calcd. C 25.54, H 5.36; found C 21.47, H 4.9. IR (nujol, CsI plates): $\tilde{\nu}$ = 863 cm^{-1} (Nujol), 2059(w), 1915(w), 1622(m), 1465(Nujol), 1374(Nujol), 1285(s), 1247(s), 1192(s), 1123(w, sh), 937(w), 859(vs), 721(Nujol), 569(m), 387(s)

[1] K. M. Fromm, *Angew. Chem.* **1997**, *109*, 2876−2878; *Angew. Chem. Int. Ed. Engl.* **1997**, *36*, 2799−2801.
[2] K. M. Fromm, *Chem. Commun.* **1999**, *17*, 1659−1660.
[3] K. M. Fromm, G. Bernardinelli, H. Goesmann, M.-J. Mayor-Lopez, J. Weber, *Z. Anorg. Allg. Chem.* **2000**, *626*, 1685−1691.
[4] K. M. Fromm, G. Bernardinelli, H. Goesmann, *Polyhedron* **2000**, *19*, 1783−1789.
[5] K. M. Fromm, H. Goesmann, *Acta Crystallogr., Sect. C* **2000**, *56*, 1179−1180.
[6] K. M. Fromm, E. D. Gueneau, H. Goesmann, *Chem. Commun.* **2000**, 2187−2188.
[7] K. M. Fromm, *Chem. Eur. J.* **2001**, *7*, 2236−2244.
[8] K. M. Fromm, G. Bernardinelli, *Z. Anorg. Allg. Chem.* **2001**, *627*, 1626−1630.
[9] K. M. Fromm, *Cryst. Eng. Commun.* **2002**, *4*, 318−322.
[10] K. M. Fromm, E. D. Gueneau, G. Bernardinelli, H. Goesmann, J. Weber, M.-J. Mayor-López, P. Boulet, H. Chermette, *J. Am. Chem. Soc.* **2003**, *125*, 3593−3604.
[11] D. Albanese, D. Landini, A. Maia, *J. Org. Chem.* **2001**, *66*, 3249−3252.
[12] K. F. Tesh, D. J. Burkey, T. P. Hanusa, *J. Am. Chem. Soc.* **1994**, *116*, 2409−17.
[13] K. Ruhlandt-Senge, K. Davis, S. Dalal, U. Englich, M. O. Senge, *Inorg. Chem.* **1995**, *34*, 2587−92; K. M. Fromm, unpublished results.
[14] **Structural Data for 1**: $C_{24}H_{56}I_4O_{12}Sr_2$, M = 1219.52 g·mol^{-1}, monoclinic, space group $P2_1/c$, a = 19.723(4), b = 15.262(3), c = 14.066(3) Å, β = 90.50(3)°, V = 4233.9(2)Å^3, Z = 4, $\rho_{calcd.}$ = 1.913 Mg·m^3, F(000) = 2336, T = 203 K, λ = 0.71069 Å, μ(Mo-K_α) = 5.482 mm^{-1}, 3.38° < 2θ < 45.08°, 5539 reflections of which 5539 unique and 5304 observed, 388 parameters refined, *GOOF* (on F^2) = 1.010, $R1 = \Sigma|F_o - F_c|/\Sigma F_o$ = 0.1119, $wR2$ = 0.2749 for $I > 2\sigma(I)$ and $R1$ = 0.1701, $wR2$ = 0.3213 for all data.
Structural Data for 2: $C_{24}H_{60}Ca_2I_4O_{12}$, M = 1128.48 g·mol^{-1}, monoclinic, space group $P2_1/n$, a = 13.594(3), b = 17.256(4), c = 18.638(4) Å, β = 91.91(3)°, V = 4369.6(15)Å^3, Z = 4, $\rho_{calcd.}$ = 1.715 Mg·m^3, F(000) = 2208, T = 203 K, λ = 0.71069 Å, μ(Mo-K_α) = 3.131 mm^{-1}, 3.22° < 2θ < 50.16°, 14562 reflections of which 7691 unique, 392 parameters refined, *GOOF* (on F^2) = 1.813, $R1 = \Sigma|F_o - F_c|/\Sigma F_o$ = 0.1217, $wR2$ = 0.3208 for $I > 2\sigma(I)$ and $R1$ = 0.2172, $wR2$ = 0.3908 for all data.
Crystal data for **1** and **2** were measured on a STOE CAD-4 diffractometer equipped with monochromated graphite Mo-K_α radiation (λ = 0.71073 Å) and an Oxford Cryosystems open flow cryostat.[31] No absorption correction was possible due to decomposition of the crystals during measurement. The structures were solved with direct methods and refined by full-matrix least-squares on F^2 with the SHELX-99 package.[32] All heavy atoms could be refined anisotropically. Disorder was observed for the ethyl groups of the polyether ligands in **1** and **2**. CCDC-206570 (**1**) and -206569 (**2**) contain the supplementary crystallographic data for this paper. These data can be obtained free of charge at www.ccdc.cam.ac.uk/conts/retrieving.html [or from the Cambridge Crystallographic Data Centre, 12, Union Road, Cambridge CB2 1EZ, UK; Fax: (internat.) +44−1223/336−033; E-mail: deposit@ccdc.cam.ac.uk].
[15] M. O'Keeffe, N. E. Brese, *J. Am. Chem. Soc.* **1991**, *113*, 3226−3229. G. J. Palenik, *Inorg. Chem.* **1997**, *36*, 122.
[16] P. C. Junk, L. M. Louis, M. K. Smith, *Z. Anorg. Allg. Chem.* **2002**, *628*, 1196−1209.

 © 2003 Wiley-VCH Verlag GmbH & Co. KGaA, Weinheim

[17] M. J. Harvey, T. P. Hanusa, *Organomet.* **2000**, *19*, 1556−1566.
[18] B. W. Skelton, A. F. Waters, A. H. White, *Austr. J. Chem.* **1996**, *49*, 99−115.
[19] A. F. Waters, A. H. White, *Aust. J. Chem.* **1996**, *49*, 35−46.
[20] M. Kaupp, P. v. R. Schleyer, H. Stoll, H. Preuss, *J. Am. Chem. Soc.* **1991**, *113*, 6012−6020; M. Kaupp, P. v. R. Schleyer, *J. Am. Chem. Soc.* **1993**, *115*, 11202−11208 and references cited therein.
[21] R. Zerger, G. Stucky, *J. Organomet. Chem.* **1974**, *80*, 7−17. M. J. Mc Cormick, R. A. Williams, L. J. Levine, T. P. Hanusa, *Polyhedron* **1988**, *7*, 725−730. M. Westerhausen, C. Gückel, H. Pietrowski, P. Mayer, M. Warchhold, H. Nöth, *Z. Anorg. Allg. Chem.* **2001**, *627*, 1741−1750.
[22] M. Westerhausen, *Coord. Chem. Rev.* **1998**, 157−210. M. Westerhausen, S. Weinrich, M. Ossberger, N. W. Mitzel, *Z. Anorg. Allg. Chem.* **2003**, *629*, 575−577 and references cited therein.
[23] K. M. Fromm, *Chimia* **2002**, *56*, 676−680.
[24] K. M. Fromm, W. Maudez, unpublished results.
[25] R. D. Rogers, M. J. Jezl, C. B. Bauer, *Inorg. Chem.* **1994**, *33*, 5682−5692.
[26] E. D. Brady, T. P. Hanusa, M. Pink, V. G. Young, Jr., *Inorg. Chem.* **2000**, *39*, 6028−6037.
[27] D. Fenske, G. Baum, H. Wolkers, B. Schreiner, F. Weller, K. Dehnicke, *Z. Anorg. Allg. Chem.* **1993**, *619*, 489−499. A. N. Chekhlov, *Russ. J. Coord. Chem.* **2001**, *27*, 381−386.
[28] Y. Yokota, R. A. Jacobson, B. C. Logsdon, S. Ringrose, A. T. Setterdahl, J. G. Verkade, *Polyhedron* **1999**, *18*, 2519−2532.
[29] A. F. Waters, A. H. White, *Aust. J. Chem.* **1996**, *49*, 147−154, and therein.
[30] A. F. Waters, A. H. White, *Aust. J. Chem.* **1996**, *49*, 61−72.
[31] J. Cosier, A. M. Glazer, *J. Appl. Crystallogr.* **1986**, *19*, 105.
[32] G. M. Sheldrick, SHELX-99, *Program for Crystal Structure Refinement*, University of Göttingen, Göttingen, **1999**.

Received April 28, 2003

 © 2003 Wiley-VCH Verlag GmbH & Co. KGaA, Weinheim

Structural Diversity in Lewis-Base Complexes of Lithium Triflamide

Matthew G. Davidson,*[a] Paul R. Raithby,*[a] Andrew L. Johnson,[a] and Philip D. Bolton[a]

Dedicated to the memory of Dr Ron Snaith

Keywords: Lithium / Solid-state structures / Aggregation / Crystal engineering / Anions

Complexation of the salt lithium triflamide [$LiNTf_2$; NTf_2 = $N(SO_2CF_3)_2$], with a range of nitrogen donor ligands results in the formation of a series of coordination complexes [$(Tf_2N)Li{\cdot}N(H)PPh_2Me$] (**1**), [$(Tf_2N)Li{\cdot}N(H)PPh_3$] (**2**), [$(Tf_2N)Li{\cdot}TMEDA$] (**3**), [$(Tf_2N)Li{\cdot}PMDTEA$] (**4**) and [$(Bz\text{-}TAC)_2\text{-}Li][NTf_2$] (**5**). The molecular structures of **1**, **3**, **4** and **5** have been determined by single-crystal X-ray diffraction. The resulting solvated structures are discussed in terms of solvent-separated ion pairs, contact ion pairs and higher aggregates, with the degree of aggregation and ion contact being dependent on the relative coordinating abilities and steric demands of the donor ligand and the anion, and provide an insight into the possible structures of lithium aggregates present in complex systems such as polymer electrolytes and synthetic reaction media.

(© Wiley-VCH Verlag GmbH & Co. KGaA, 69451 Weinheim, Germany, 2003)

Introduction

The structural chemistry of organolithium compounds has attracted significant and sustained interest, primarily because of their extensive use as reagents in synthetic chemistry and the perceived close relationship between structure and reactivity.[1−6] Principles such as ring stacking and laddering[2,3] have been developed to explain the structural types of organolithiums that are found in the gas phase,[4] the solid state[5] and in solution.[6] Furthermore, these structures have been useful in accounting for the observed reactivity of even quite complex systems.[6] In contrast, the systematic study of simple inorganic lithium salts has attracted considerably less attention. The development of "in situ" synthetic routes (in particular the so-called "ammonium salt route")[7] has provided facile and high yielding methodologies for the controlled synthesis of hydrocarbon-soluble molecular complexes of inorganic lithium salts. However, these methodologies have yet to be fully exploited in terms of providing well-defined materials with specific reactivities and/or material properties.

Two areas of research that may benefit from systematic structural studies of inorganic lithium salts are polymer electrolytes[8] and Lewis acid-mediated organic synthesis.[1,9] Both of these areas utilise inorganic lithium salts containing weakly coordinating anions, such as $LiPF_6$, $LiClO_4$, $LiBF_4$ and $LiAsF_6$.

[a] Department of Chemistry, University of Bath, Claverton Down, Bath. BA2 7AY, UK
Fax: (internat.) +44-(0)1225/826-231
E-mail: M.G.Davidson@Bath.ac.uk
P.R.Raithby@Bath.ac.uk

In order to understand more fully the role of these weakly coordinated lithium salts in complex environments (such as in homogeneous liquid-phase reactions or a coordinating polymer electrolyte) it is useful to investigate systems in the solid state in which we can more easily and unambiguously assign the coordination geometry about the lithium ion and extrapolate these studies to "real" systems.

Of late, studies in these areas have begun to focus on salts that incorporate much more stable, larger and more weakly coordinating anions such as $CF_3SO_3^-$ (OTf^-, triflate), $[N(SO_2CF_3)_2]^-$ (NTf_2^-, triflamide), $[HC(SO_2CF_3)_2]^-$ and $[C(SO_2CF_3)_3]^-$, all of which show remarkable chemical and electrochemical stability, and provide alternatives to potentially dangerous salts such as $LiClO_4$.

In this context, we report herein a systematic study of the coordination chemistry of lithium triflamide. Although structural studies of the parent salt, $LiNTf_2$,[10] and its hydrate, $LiNTf_2{\cdot}H_2O$,[11] have been performed, this work represents the first systematic structural study of $LiNTf_2$ in the presence of a range of nitrogen-donor ligands, with the aim of investigating the extent and range of anion binding within these systems and their more general structural diversity.

Results and Discussion

In order to study the coordination chemistry between $LiNTf_2$ and donor ligand systems, and the extent of anion-cation contact in the presence of strongly competing donor ligands, we first chose specific donor ligands that could provide a varied number of coordination environments from

mono- to polydentate in order to mimic the possible coordination environments in systems such as conducting polymer electrolytes. The nitrogen-based ligands, selected on the basis of their synthetic utility and availability, are shown below.

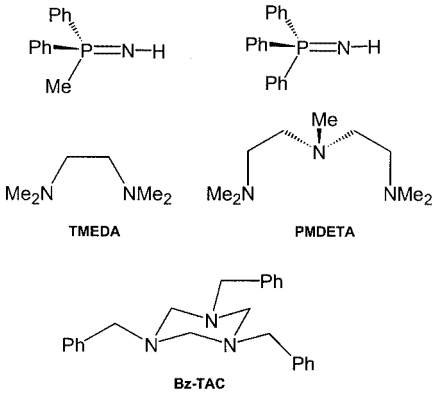

All lithium complexes **1**−**5** were initially synthesised using the "ammonium-salt route",[7] in which ammonium triflamide, $[NH_4][NTf_2]$, and the ligand are combined in toluene and a stoichiometric amount of *n*-butyllithium is added. The ammonium triflamide was prepared by passing ammonia gas through a toluene solution of the parent acid, Tf_2NH (see Exp. Sect.).

In some scenarios, the "ammonium-salt route" is the only rigorous method of synthesis for complexes of lithium salts, e.g. halides.[7] However, direct methods, whereby solid salts are treated with the Lewis base (donor ligand), either neat or in hydrocarbon solution, can be applied to more soluble lithium salts, such as lithium triflamide. Both direct and in situ methods of lithium complex preparation were employed in our investigation in order to reveal any differences between the products formed by the two methods, i.e. stoichiometries, different ligand coordination modes, different polymorphs, etc.

Our investigation has shown that for the compounds discussed here, both methodologies (Scheme 1) are equally effective, and for comparable experiments, the products were found to be identical by multinuclear NMR spectroscopy, elemental analysis, melting point analysis and unit cell determination.

In solution, ^{1}H, ^{13}C, ^{19}F and ^{31}P NMR experiments performed on complexes **1**−**5** indicate that, in all cases, on the NMR timescale, the lithium ion appears to remain coordinated to the nitrogen donor ligand in solution, as indicated by the moderate change in ^{1}H and ^{13}C NMR chemical shift between free and ligated nitrogen-donor ligand. As with the closely related triflate anions $[OTf]^-$, ^{19}F NMR experiments on **1**−**5** provide little information about the coordination state of the triflamide anion, $[NTf_2]^-$, in the solution state.[12]

Compound **1** was found to have the empirical formula $[(Tf_2N)Li{\cdot}N(H)PPh_2Me]$. Crystallisation of the complex from hot toluene resulted in the formation of colourless crystals. Single crystal X-ray diffraction experiments reveal the asymmetric unit cell of **1** to consist of a central lithium cation coordinated by both the nitrogen atom of the iminophosphorane ligand and one oxygen atom of the triflamide

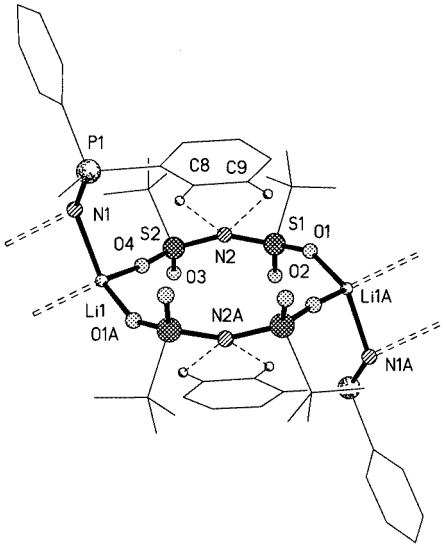

Figure 1. Molecular structure of (**1**), highlighting the weak N···H−C hydrogen bonding interaction between the C−H of a iminophosphorane bound phenyl group and the central nitrogen atom of the triflamide anion; CF_3 groups on the triflamide anion and the iminophosphorane ligand are shown as wire frames and hydrogen atoms omitted for clarity; symmetry transformations used to generate equivalent atoms: $(-x, -y+1, -z+2)$, $(x+1, y, z)$ and $(x-1, y, z)$; selected bond lengths (Å): Li(1)−N(1) 2.036(13), Li(1)−N(1A) 2.051(12), Li(1)−O(4) 1.980(13), Li(1)−O(1A) 1.934(12), O(1)−S(1) 1.427(5), O(2)−S(1) 1.415(5), S(1)−N(2) 1.562(6), N(1)−S(2) 1.573(5), S(2)−O(3), 1.424(5), S(2)−O(4) 1.429(5), P(1)−N(1) 1.589(6), P(1)−C(15) 1.782(7), P(1)−C(1) 1.806(7), P(1)−C(7) 1.805(7), C(8)−H(8) 0.93, N(2)−H(8) 2.79, C(8)−N(2) 3.465(9), C(9)−H(9) 0.93, N(2)−H(9) 2.96, C(9)−N(2) 3.541(9); selected bond angles (°): Li(1)−N(1)−Li(1A) 80.6(5), N(1)−Li(1)−N(1A) 99.4(5), O(4)−Li(1)−O(1A) 119.2(6), S(1)−N(2)−S(2) 127.5(3), C(15)−P(1)−N(1) 109.7(3) C(8)−H(8)−N(2) 130.7, C(9)−H(9)−N(2) 122.3

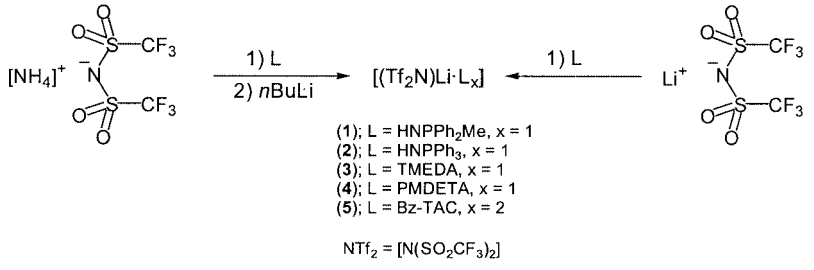

Scheme 1

 © 2003 Wiley-VCH Verlag GmbH & Co. KGaA, Weinheim

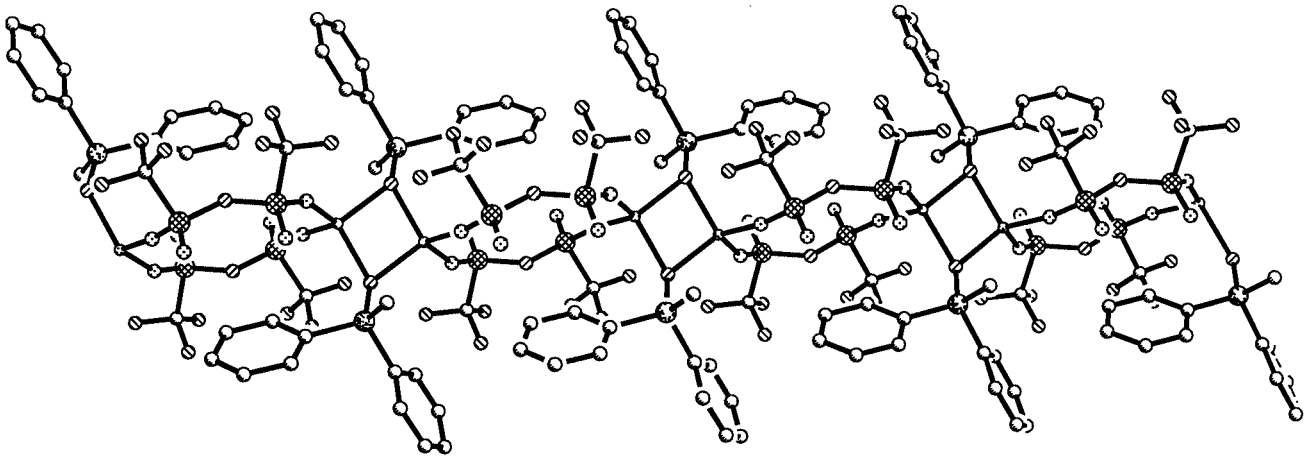

Figure 2. View of the polymeric chain in **1**

anion. Crystallographic symmetry renders the asymmetric unit part of an infinite polymeric chain, in which each lithium triflamide unit forms one half of a twelve-membered ring system (Figure 1). Each twelve-membered ring is subsequently linked by lithium-bridging iminophosphorane groups to propagate the polymeric chain through alternate, and approximately orthogonal, corner-sharing twelve-membered and four-membered rings (Figure 2).

Searches of the literature and the Cambridge Structural Database reveal this twelve-membered ring system to be unique in terms of both its composition and as a bonding mode for the triflamide anion.[13] The CF_3 groups of each NTf_2^- anion within the dimer are found to be mutually *cisoid* with respect to the twelve-membered ring, whereas those of different anions are mutually *transoid*. This unexpected conformation allows a close approach between one of the iminophosphorane-based phenyl groups and the lone pair of the central nitrogen atom of the triflamide anion, facilitating the formation of two C−H···N···H−C hydrogen bonds [C(8)···N(2): 3.464(9) Å; H(8)···N(2): 2.77 Å; C(8)−H(8)···N(2): 130.3°; and C(9)···N(2): 3.540(9) Å; H(9)···N(2): 2.94 Å; C(9)−H(9)···N(2), 122.0°; Figure 1].[14]

Neutral iminophosphorane ligands, which are isoelectronic with phosphane oxides,[15] have been observed previously as ligands to s-block metals.[15,16] The iminophosphorane P−N bond length [P(1)−N(1): 1.589(6) Å] is little changed on coordination to Li from that of the parent ligand,[17] [P−N: 1.563(4)], and in the solid state the ligands are arranged *trans* to each other across the $[Li_2N_2]$ core. Whilst the Li−N bond lengths in **1** [Li(1)−N(1): 2.036(13) Å; Li(1)−N(1A): 2.051(12) Å] are fairly typical of Li−N bonds in a wide range of compounds, the Li−O bonds [Li(1)−O(1): 1.934(12) Å; Li(1)−O(4): 1.980(13) Å] are longer than generally observed in systems containing oxygen-based anions, such as lithium aryloxides,[18] and are closer to typical bond lengths for Li···THF and Li···OEt_2 contacts, implying rather weak anion-cation interactions. The binding of triflamide to the lithium atoms via the oxygen atoms, and not the nitrogen, would suggest that the centre of electronegativity does not reside solely at the nitrogen centre, and close inspection of the bond lengths and bond angles in the triflamide anion reveals only a small degree of asymmetry.

We believe that the preference for Li−O rather than Li−N coordination is electronic in nature rather than steric. This theory is supported by both the structural characterisation of bulkier bis(fluorobenzylsuphonyl)imido systems, $[N(SO_2C_6H_4F)_2]^-$,[19] which possess M−N interactions and the observation by others that strong electron-withdrawing effects of the -CF_3 groups result in a large degree of pπ-dπ bonding within the N−S backbone, resulting in charge delocalisation over the whole of the anion.[20,21]

Compound **2**, $[(Tf_2N)Li{\cdot}N(H)PPh_3]_n$, was prepared in an identical manner to **1** using triphenyliminophosphorane as the nitrogen donor ligand. Characterisation by multinuclear NMR spectroscopy and elemental analysis showed **2** to have the empirical formula $[(Tf_2N)Li{\cdot}N(H)PPh_3]$. Single-crystal X-ray diffraction studies were not undertaken on **2**, but the complex is assumed to be isostructural with the methyldiphenyliminophosphorane complex **1**.

In order to examine further the coordination chemistry of the triflamide anion we reasoned that addition of a bidentate N-donor ligand would enable us to isolate and characterise a single dimeric $[Li_2(NTf_2)_2]$ twelve-membered ring system. Indeed, reaction of TMEDA with $LiNTf_2$ in toluene (or reaction of $[NH_4][NTf_2]$ with *n*BuLi in the presence of TMEDA) results in the isolation of the complex **3**, which has been shown by X-ray diffraction studies to be a discrete dimeric lithium species, $[(Tf_2N)Li{\cdot}TMEDA]_2$, as predicted (Figure 3).

The asymmetric unit of **3** contains half of the dimer, the second half being generated by a crystallographic centre of symmetry that lies at the centre of the twelve-membered $[Li_2(NTf_2)_2]$ ring such that the two lithium centres are bridged by two triflamide ligands as in **1**. However, unlike in **1**, distortion of the twelve-membered ring results in increased cation-anion contact, such that a secondary coordination of the triflamide ligand results, and the geometry about each lithium ion in **3** is pseudo-trigonal bipyramidal rather than the pseudo-tetrahedral geometry observed in **1**.

 © 2003 Wiley-VCH Verlag GmbH & Co. KGaA, Weinheim

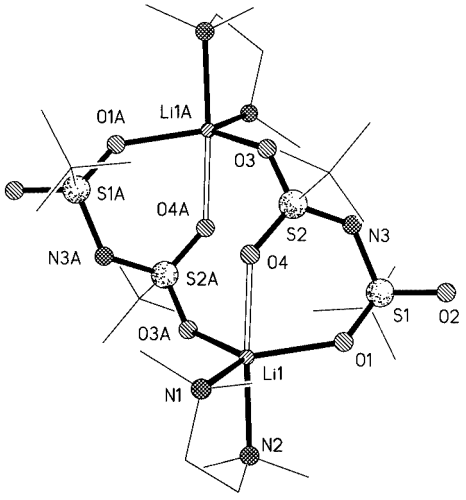

Figure 3. Molecular structure of **3**; symmetry transformations used to generate equivalent atoms: ($-x$, $-y$, $-z$); CF_3 groups and the TMEDA ligands are shown as wire frames and hydrogen atoms omitted for clarity; selected bond lengths (Å): Li(1)−N(1) 2.077(3), Li(1)−N(2) 2.175(3), Li(1)−O(1) 2.070(3), Li(1)−O(3A) 2.008(3), Li(1)−O(4) 2.230(3), O(1)−S(1) 1.4382(13), S(2)−O(3) 1.4332(12), S(2)−O(4) 1.4326(13), S(1)−N(3) 1.5779(15), S(2)−N(3) 1.5628(15); selected bond angles (°): N(1)−Li(1)−N(2) 86.63(12), O(1)−Li(1)−O(4) 79.66(12) O(1)−Li(1)−O(3A) 126.33(16), O(1)−Li(1)−N(1) 118.71(16), O(3A)−Li(1)−N(1) 113.68(15), N(2)−Li(1)−O(4) 175.53(17), S(1)−N(3)−S(2) 124.74(10)

The nitrogen atoms of the TMEDA ligand occupy equatorial and axial positions [Li(1)−N(1): 2.077(3) Å; Li(1)−N(2): 2.175(3) Å], with the axial Li−N bond being the longer. Each lithium centre within the dimer is also coordinated by two oxygen atoms of separate triflamide anions, creating the twelve-membered ring. These oxygen atoms occupy equatorial positions about the lithium ion [Li(1)−O(1): 2.007(3) Å; Li(1)−O(3A): 2.008(3) Å], leaving the axial position available for secondary coordination by an oxygen atom from one of the two bound triflamide anions. This axial Li−O distance [Li(1)−O(4): 2.230(3) Å] is significantly longer than any of the other interactions with lithium, implying a significantly weaker ligation compared to other Li−O contacts. These observations are in contrast to the related complex $[(Tf_2N)Li{\cdot}DME]_\infty$ [22] (DME = dimethoxyethane) in which the central lithium possesses a five-coordinate square-based pyramidal geometry with both the DME ligand and triflamide anion coordinating in an η^2-fashion to the lithium ion. The fifth coordination about the lithium ion site is filled by a long Li−O interaction from a neighbouring η^2-bound triflamide ligand. This bonding motif continues throughout the complex forming a polymeric chain of $[(Tf_2N)Li{\cdot}DME]$ units.[22]

In contrast to **1** the central nitrogen atom of the triflamide anion does not participate in any hydrogen bonding in the absence of suitable acidic C−H donor groups, and it is unclear whether the change in NTf_2^- coordination mode between **1** and **3** is a result of the lack of suitable hydrogen-bonding interactions or due to the steric differences in the N-donor ligands. The different conformations of the twelve-membered rings found in **1** and **3** are highlighted in Figure 4.

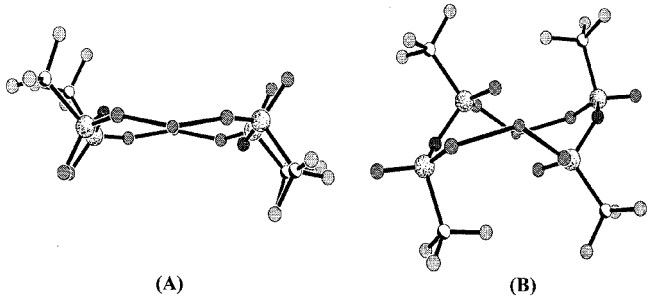

Figure 4. Structure of the central twelve-membered rings found in **1** (**A**) and **3** (**B**)

On changing the nitrogen donor ligand from bidentate TMEDA to the tridentate ligand PMDETA (pentamethyldiethylenetriamine), the aggregation state of the lithium triflamide is further reduced with the formation of a monomeric complex $[(Tf_2N)Li{\cdot}PMDETA]$ (**4**). The central lithium cation in this monomeric species possesses a five-coordinate pseudo-trigonal bipyramidal geometry as in **3** with the PMDETA ligand and the triflamide anion bound to the lithium centre in a tridentate and bidentate fashion, respectively. The molecular structure of **4** is shown in Figure 5.

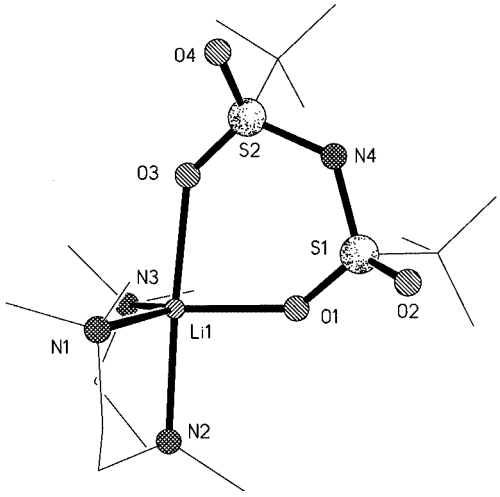

Figure 5. Molecular structure of **4** highlighting the coordination geometry about the central lithium ion; hydrogen atoms have been omitted and selected groups (PMDETA and CF_3) are shown as wire frames for clarity; selected bond lengths (A): Li(1)−N(1) 2.118(4), Li(1)−N(2) 2.173(4), Li(1)−N(3) 2.132(4) Li(1)−O(1) 1.997(4), Li(1)−O(3) 2.151(4), O(1)−S(1) 1.4251(17), S(2)−O(3) 1.4322(15), S(1)−N(4) 1.5705(17), S(2)−N(4) 1.5658(17); selected bond angles (°): O(1)−L(1)−O(3) 83.84(13), N(1)−Li(1)−N(3) 123.62(17), N(1)−Li(1)−N(2) 86.23(13), N(1)−Li(1)−N(3) 84.12(13), N(1)−Li(1)−O(1) 110.06(17), O(1)−Li(1)−N(3) 125.98(17), N(2)−Li(1)−O(3) 175.04(18), S(1)−N(4)−S(2) 126.99(11)

The distortion away from an ideal trigonal bipyramidal geometry in **4** is manifest in the axial-equatorial bond angles and is presumably the result of constrained bite angles within the PMDETA ligand and the triflamide anion [N(1)−Li(1)−N(2): 86.32(13)°; N(2)−Li(1)−N(3): 84.12(13)°; O(1)−Li(1)−O(3): 83.84(13)°]. However the

 © 2003 Wiley-VCH Verlag GmbH & Co. KGaA, Weinheim

O−Li−N angle is close to linear [N(2)−Li(1)−O(3): 175.04(18)°].

The PMDETA ligand binds to the lithium in a facial configuration, with three Li−N contacts, two of which correspond to the outer nitrogen atoms [Li(1)−N(1): 2.118(4) Å; Li(1)−N(3): 2.132(4) Å] and lie in the equatorial plane of the trigonal bipyramid. The third nitrogen atom, which is the central nitrogen of the PMDETA ligand, occupies an axial position with a comparatively longer Li−N contact [Li(1)−N(2): 2.173(4) Å]. The triflamide anion, which binds to the lithium in an η^2-fashion [Li(1)−O(1): 1.997(4) Å; Li(1)−O(3): 2.151(4) Å] fills the remaining two coordination sites about the lithium ion, with the longer of the two Li−O contacts in the axial position. In the absence of any further intra- or intermolecular bonding the CF_3 groups of the triflamide anion maintain the *cis*- conformation observed in **1**.

It is noteworthy when considering the conceptual deaggregation of a dimeric complex containing a bidentate donor ligand, such as **3**, to a monomeric complex containing a tridentate donor ligand, such as **4**, that it is the short Li−O bond [Li(1)−O(3A) in **3**] that generates the dimer that is replaced rather than the longer (secondary) Li−O interaction [Li(1)−O(4) in **3**].

Finally, we wished to investigate the effect of variation in the nature of the tridentate donor ligand by synthesising complexes of *N*-tribenzyltriazocyclohexane (Bz-TAC). Although both PMDETA and Bz-TAC contain three donor atoms we expected the more compact ligand set of Bz-TAC relative to PMDETA to influence the nature of NTf_2^- coordination to the lithium ion.[23]

Attempted synthesis of the Bz-TAC analogues of **4**, using the direct addition of ligand to $LiNTf_2$ in toluene, were unsuccessful, with all stoichiometries of starting materials resulting in the isolation of the ion-separated bis-ligand complex $[(Bz\text{-}TAC)_2Li][NTf_2]$, (**5**), in which each lithium ion is coordinated by two TAC ligands.

Complex **5** was characterised by single-crystal X-ray diffraction (Figure 6). The asymmetric unit cell contains two independent half $[\eta^3\text{-}(Bz\text{-}TAC)_2Li]^+$ cations, with the Li atom in each case sitting on a centre of symmetry. The asymmetric unit is completed by one non-coordinating NTf_2^- anion. For both cations all Li−N distances are similar, spanning a small range [2.2411(15) to 2.3031(15) Å].

The six benzyl groups of the $[(Bz\text{-}TAC)_2Li]^+$ cation wrap around the central lithium ion and participate in an intricate *ortho*-(C−H···π) arene hydrogen bonding motif, in which each benzyl group is hydrogen bonded to its nearest neighbour on the other Bz-TAC ligand (Figure 7). The two ligands are thus interlocked in a paddlewheel motif about the central lithium ion.

$[(R\text{-}TAC)_2Li]^+$ cations, where R = Bz[24] or R = Me,[24,25] have been characterised previously, although the hydrogen-bonding network that is present in the benzyl system has not been commented upon. The presence of two TAC ligands around the lithium ion provides sufficient steric protection to preclude any cation-anion interactions in **5**.

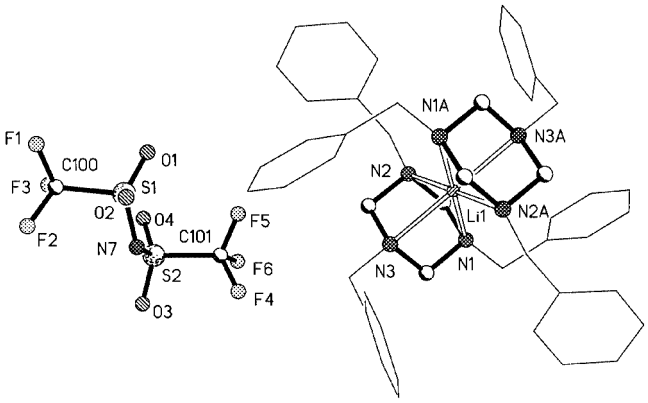

Figure 6. Molecular structure of one of the two centrosymmetric $[Li(Bz\text{-}TAC)_2]^+$ cations and an NTf_2^- anion in (**5**); symmetry transformations used to generate equivalent atoms: (x, y, z), & ($-x$, $-y$, $-z$); benzyl groups of the $[Li(Bz\text{-}TAC)_2]^+$ cation are shown as wire frames and hydrogen atoms omitted for clarity; selected bond lengths (Å): Li(1)−N(1) 2.2411(15), Li(1)−N(2) 2.2602(15), Li(1)−N(3) 2.2471(16), S(1)−N(7) 1.5731(17), S(2)−N(7) 1.5736(18), S(1)−O(1) 1.4259(16), S(1)−O(2) 1.4239(15), S(2)−O(3) 1.4286(15), S(2)−O(4) 1.4223(15); selected bond angles (°): N(1)−Li(1)−N(2) 63.64(6), N(1)−Li(1)−N(3) 63.53(6), N(2)−Li(1)−N(3) 63.06(6), S(1)−N(7)−S(2) 125.41(11)

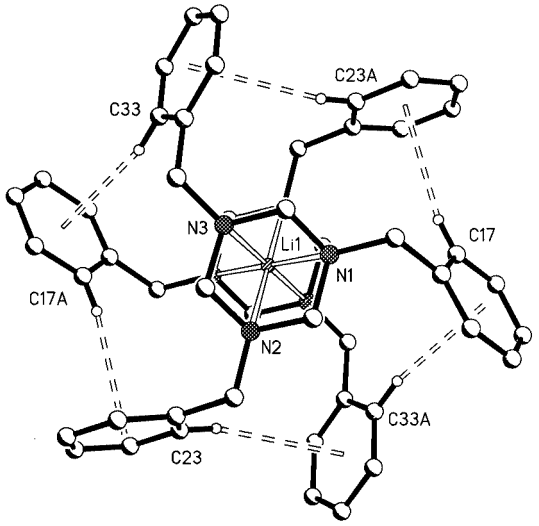

Figure 7. Diagram highlighting the C−H···π arene hydrogen-bonding network within one of the two centrosymmetric cations in **5**; hydrogen atoms not involved in the hydrogen-bonding network omitted for clarity; C−(H)···X distances (where X = centroid of the relevant aryl ring) (Å): C(17)−X 3.802, C(23)−X 3.956, C(33)−X 3.593; selected C−(H)···X angles (°): C(17)−H(17)−X 167, C(23)−H(23)−X 155, C(33)−H(33)−X 166

Close inspection of the bond lengths and angles about the NTf_2^- anion in **5** (Figure 6), shows a remarkable similarity to the coordinated anions in $[(Tf_2N)Li{\cdot}N(H)Ph_2Me]$, $[(Tf_2N)Li{\cdot}TMEDA]$, $[(Tf_2N)Li{\cdot}PMDETA]$, and other non-coordinated anions in complexes such as $[Li(12\text{-}C\text{-}4)_2][NTf_2]$,[26] $[Li(C\text{-}2,2,2)][NTf_2]$,[26] $[Mg(H_2O)_6][NTf_2]_2$,[27] $[Im][NTf_2]$,[28] $[R_4N][NTf_2]$[29] and $[Me_3NH][NTf_2]$.[30]

It is noteworthy that even using the high degree of control provided by the ammonium salt route, it has not been possible to isolate mono Bz-TAC complexes, such as [(*i*Pr-

 © 2003 Wiley-VCH Verlag GmbH & Co. KGaA, Weinheim

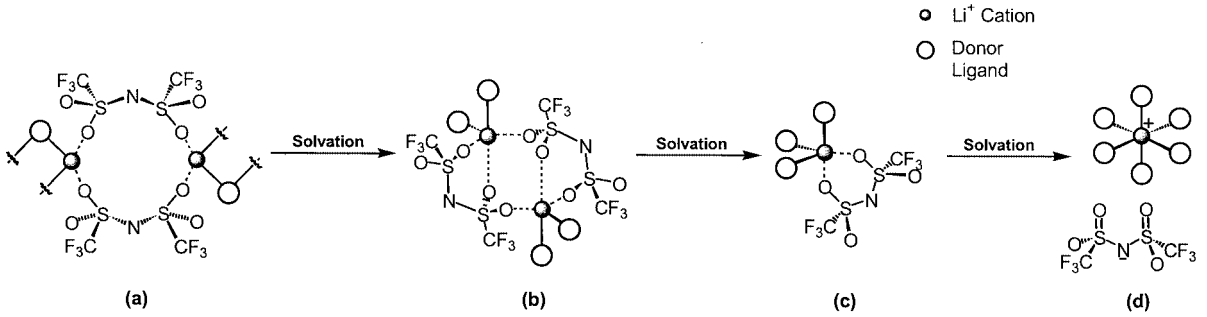

Figure 8. Schematic illustration of the sequential solvation and deaggregation of lithium triflamide complexes: (a) higher aggregate (polymeric) structures, (b) dimeric contact ion pair, (c) a contact ion pair and (d) donor ligand-separated ion pair

TAC)Li·BH_4]$_2$,[24] highlighting the high stability of the [(Bz-TAC)$_2$Li]$^+$ cation.

Conclusions

The single crystal structures of the four lithium triflamide salts have been determined. The resulting solvated structures can be thought of in terms of solvent-separated ion pairs, contact ion pairs and higher aggregates (Figure 8), with the degree of aggregation and ion contact being dependent on the relative coordinating abilities and steric demands of the donor ligand and the anion. These results provide an insight into the possible structures of lithium aggregates present in complex systems such as polymer electrolytes and synthetic reaction media.

The degree to which lithium ions will engage in intimate contact with the triflamide anions has little effect on the electronic structure of the anion, which remains reasonably impassive. However, conformational changes within the very flexible anion are observed.

The observation of ion separation in lithium triflamide salts contrasts directly with more coordinating (less delocalised) anions such as triflate, $CF_3SO_3^-$, in which contact between anion and cation persists to the extent that the coordination number of the metal cation is expanded rather than loss of contact with the anion.

Experimental Section

General Remarks: All manipulations were carried out under an atmosphere of dry argon using standard Schlenk and glove-box techniques. Solvents were purified by conventional procedures and distilled prior to use. $LiNTf_2$ was purchased from Aldrich and used as received, without further purification. The ligand systems were prepared using standard literature techniques or purchased from Aldrich.

Solution ^{1}H, ^{19}F and ^{31}P NMR experiments were performed at ambient temperature using a Varian 400 or a Bruker Advance-300 Spectrometer. ^{1}H NMR chemical shifts are referenced to $SiMe_4$, and ^{31}P NMR shifts relative to 85% H_3PO_4. All chemical shifts (δ) are in ppm and coupling constants in Hz.

[NH_4][NTf_2]: Ammonia gas was bubbled through an ethereal solution (50 mL) of bis(trifluoromethylsulfonyl)amine (Tf_2NH; 10 mmol, 2.8 g) for 10 min. The solvent was then allowed to evaporate at room temperature, yielding a white crystalline material which was isolated and washed with hexane (3 × 5 mL). Yield: 2.9 g (98%). Colourless blocks. $C_2H_4F_6N_2O_4S_2$ (298.2): calcd. C 8.1, H 1.4, N 9.4; found C 8.1, H 1.3, N 9.9.

The lithium complexes **1**−**5** were prepared using standard procedures for both the direct and in situ synthesis, examples of both procedures are given below.

[(Tf_2N)Li·N(H)Ph_2Me] (1). (in situ Method): Methyldiphenyliminophosphorane (0.22 g, 1 mmol) was added to a suspension of ammonium trifluoromethanesulfonimide (0.30 g, 1 mmol) in 5 mL of toluene. The mixture was stirred for 20 min at room temperature, and then cooled to −78 °C. One mole-equivalent of *n*BuLi (0.63 mL, 1.6 M) was then added to the cooled suspension. Warming to room temperature caused the solution to undergo several colour changes, and a fine colourless precipitate to be deposited on the walls of the vessel. The precipitate was re-dissolved by heating, and the solution was left to cool to room temperature to yield a crop of crystals, which where isolated by filtration and washed with 5 mL of cold hexane and dried in vacuo. Yield: 0.30 g (60%). Colourless blocks. Mp: 120−122 °C. $C_{15}H_{14}F_6LiN_2O_4P_1S_2$ (502.3): calcd. C 35.9, H 2.8, N 5.6; found C 36.2, H 3.2, N 4.9. ^{1}H NMR (400 MHz, 23 °C, C_6D_6): δ = 1.11 (s, 1 H, N*H*), 1.45 (d, $^2J_{P,H}$ = 13.3 Hz, 3 H, P−CH_3), 6.8−7.0 (m, 6 H, *m*- & *p*- aromatic C*H*), 7.1−7.3 (m, 4 H, *o*-aromatic C*H*) ppm. ^{19}F NMR (376 MHz, 23 °C, C_6D_6): δ = −79.9 (s, CF_3) ppm. ^{31}P NMR (162 MHz, 23 °C, C_6D_6): δ = 33.7 (s, Ph_2Me*P*NH) ppm.

(Direct Method): A toluene solution (2 mL) of methyldiphenyliminophosphorane (0.22 g, 1 mmol) was added to a sample of *N*-lithiotrifluoromethanesulfonimide (0.29 g, 1 mmol) in 2 mL of toluene. The reaction was stirred for 1 h under an argon atmosphere and a further 3 mL of toluene was added. The mixture was then heated to reflux, to aid dissolution, and the solution left to crystallise at room temperature to yield a crop of crystals suitable for X-ray analysis, which where isolated by filtration and washed with 5 mL of cold hexane and dried in vacuo. Yield: 0.36 g (71%). Analysis showed the product to be identical to that prepared by the in situ method.

[(Tf_2N)Li·N(H)PPh_3] (2): Triphenyliminophosphorane (0.28 g, 1 mmol). in situ method: yield 0.30 g (60%); direct method: yield 0.37 g (73%). Colourless blocks. Mp: 85−87 °C. $C_{20}H_{16}F_6Li_1N_2O_4P_1S_2$ (564.4): calcd. C 42.5, H 2.9, N 5.0; found C 43.2, H 3.34, N 4.8. ^{1}H NMR (400 MHz, 23 °C, C_6D_6): δ = 1.35 (s, 1 H, N*H*), 7.0−7.2 (m, 9 H, *m*- & *p*- aromatic C*H*), 7.4−7.6 (m, 6 H, *o*-aromatic C*H*) ppm. ^{19}F NMR (376 MHz, 23 °C, C_6D_6): δ = −79.7 (s, CF_3) ppm. ^{31}P NMR (162 MHz, 23 °C, C_6D_6): δ = 33.0 (s, Ph_3*P*NH) ppm.

 © 2003 Wiley-VCH Verlag GmbH & Co. KGaA, Weinheim

Table 1. Crystallographic data for $[NH_4][NTf_2]$ and compounds **1**, **3**, **4** and **5**

Compound	$[NH_4][NTf_2]$	$[(Tf_2N)Li{\cdot}N(H)PPh_2Me]$ (1)	$[(Tf_2N)Li{\cdot}TMEDA]$ (3)	$[(Tf_2N)Li{\cdot}PMDETA]$ (4)	$[(Bz\text{-}TAC)_2Li][NTf_2]$ (5)
Formula	$C_2H_4F_6N_2O_4S_2$	$C_{15}H_{14}F_6LiN_2O_4PS_2$	$C_{16}H_{32}F_{12}Li_2N_6O_8S_4$	$C_{11}H_{23}F_6LiN_4O_4S_2$	$C_{50}H_{54}F_6LiN_7O_4S_2$
Molecular weight	298.19	502.31	806.64	460.39	1002.06
T (K)	150(2)	150(2)	150(2)	150(2)	150(2)
Crystal system	Orthorhombic	Triclinic	Triclinic	Orthorhombic	Triclinic
Space group	*Pnba*	$P\bar{1}$	$P\bar{1}$	*Pcab*	$P\bar{1}$
a (Å)	13.0150(2)	8.988(4)	8.9560(2)	13.48100(10)	11.2890(2)
b (Å)	13.8460(2)	11.094(4)	9.6970(2)	16.4720(2)	11.6820(2)
c (Å)	22.1410(3)	11.858(5)	10.7950(3)	18.3100(2)	21.1100(5)
α (°)		67.90(3)	81.4230(10)		97.5620(10)
β (°)		77.14(2)	75.6930(10)		97.1280(10)
γ (°)		69.02(2)	70.9400(10)		111.8580(10)
U (Å^3)	3989.93(10)	1017.6(7)	856.23(4)	4065.90(7)	2515.60(9)
Z	16	2	1	8	2
D_c (g cm^{-3})	1.986	1.639	1.564	1.504	1.323
μ (mm^{-1})	0.629	0.420	0.389	0.339	0.179
F(000)	2368	508	412	1904	1048
Crystal size (mm)	0.32 × 0.20 × 0.10	0.20 × 0.10 × 0.10	0.25 × 0.15 × 0.13	0.13 × 0.10 × 0.08	0.38 × 0.25 × 0.25
Theta range (°)	3.81 to 25.57	3.66 to 24.28	3.77 to 27.47	3.75 to 27.50	3.78 to 27.47.
Reflections collected	39131	4004	12900	73535	39239
Independent reflections	3705 [*R*(int) = 0.0532]	2864 [*R*(int) = 0.0448]	3903 [*R*(int) = 0.0492]	4657 [*R*(int) = 0.0828]	11382 [*R*(int) = 0.0866]
Reflections [$I > 2\sigma(I)$]	3096	2221	3328	3748	6163
Data/restraints/parameters	3705/0/322	2864/0/286	3903/0/222	4657/0/259	11382/0/635
Goodness-of-fit on F^2	1.056	1.132	1.041	1.034	0.967
Final *R*1, *wR*2 [$I > 2\sigma(I)$]	0.0329, 0.0770	0.0852, 0.1851	0.0395, 0.1005	0.0427, 0.1032	0.0536, 0.1037
Final *R*1, *wR*2 (all data)	0.0425, 0.0828	0.1124, 0.2010	0.0475, 0.1066	0.0583, 0.1125	0.1272, 0.1250
Max, min diff. (e·Å^{-3})	0.444, −0.395	0.394, −0.406	0.564, −0.390	0.604, −0.491	0.325, −0.500

$[(Tf_2N)Li{\cdot}TMEDA]$ (3): *N*,*N*,*N*′,*N*′-Tetramethylethylenediamine (0.15 mL, 0.12 g, 1 mmol); in situ method: yield 0.28 g (69%); direct method: yield 0.4 g (85%). Colourless blocks. Mp: 110−112 °C. $C_8H_{16}F_6Li_1N_3O_4S_2$ (403.3): calcd. C 23.8, H 4.0, N 10.4, Found: calcd. C 23.6, H 4.0, N 10.9. ^{1}H NMR (400 MHz, 23 °C, C_6D_6): δ = 1.8 (br. s, 4 H, NCH_2CH_2N), 1.9 (br. s, 12 H, N−CH_3) ppm. ^{19}F NMR (376 MHz, 23 °C, C_6D_6): δ = −80.0 (s, CF_3) ppm.

$[(Tf_2N)Li{\cdot}PMDETA]$ (4): *N*,*N*,*N*′,*N*′′,*N*′′-Pentamethyldiethylenetriamine (0.20 mL, 0.17 g, 1 mmol); in situ method: yield 0.34 g (74%); direct method: yield 0.38 g (83%). Colourless blocks. Mp: 122−123.5 °C. $C_{11}H_{23}F_6LiN_4O_4S_2$ (460.4): calcd. C 28.7, H 5.0, N 12.2; found C 28.8, H 5.1, N 12.3. ^{1}H NMR (400 MHz, 23 °C, C_6D_6): δ = 2.19 (s, 12 H, NMe_2), 2.23 (s, 3 H, N*Me*), 2.28−2.56 [br. m, 8 H, (Me_2NCH_2CH_2)NMe] ppm. ^{19}F NMR (376 MHz, 23 °C, C_6D_6): δ = −78.9 (s, CF_3) ppm.

$[(Bz\text{-}TAC)_2Li][NTf_2]$(5): *N*-tribenzyltriazocyclohexane (0.36 g, 1 mmol); in situ method: yield 0.36 g (36% with respect to Li); direct method: yield 0.48 g (48% with respect to Li). Colourless blocks. Mp: 141−143 °C. $C_{50}H_{54}F_6Li_1N_7O_4S_2$ (1002.1): calcd. C 59.9, H 5.4, N 9.8; found C 59.9, H 5.6, N 9.8. ^{1}H NMR (400 MHz, 23 °C, $CDCl_3$): δ = 3.32 (br. s, 12 H, N−CH_2-N), 3.46 (br. s, 12 H, N−CH_2-Ph), 7.1−7.4 (br. m, 30 H, aromatic-C*H*) ppm. ^{19}F NMR (376 MHz, 23 °C, $CDCl_3$): δ = −78.8 (s, CF_3) ppm.

X-ray Crystallographic Study: Suitable single crystals of $[NH_4][NTf_2]$ and compounds **1**, **3**, **4** and **5** were mounted on glass fibres using perfluoroether oil. Data collections were carried out on an Enraf Nonius Kappa CCD diffractometer, equipped with a Oxford Cryosystems cooling device, and graphite-monochromated Mo-K_α radiation (λ = 0.71069 Å). Data were corrected for Lorentz and polarisation effects and for absorption. The structures were solved by direct methods, and refined using full-matrix least-squares on F^2 with all non-hydrogen atoms assigned anisotropic displacement parameters. Hydrogen atoms were included at calculated positions throughout and refined using a riding model, with U_{iso} set to 1.2-times (1.5-times for methyl-H) U_{equiv} of the carrier atom, with the exception of the nitrogen-bound hydrogen atoms in $[NH_4][NTf_2]$. In the final stages of refinement a weighting scheme was introduced and refinement continued until convergence was achieved. Programs used were SHELXS-86[31] and SHELXL-97.[32] Experimental data relating to all the structure determinations are presented in Table 1.

CCDC-212575−212579 ($[NH_4][NTf_2]$, **1**, **3**, **4** and **5**) contain the supplementary crystallographic data for this paper. These data can be obtained free of charge at www.ccdc.cam.ac.uk/conts/retrieving.html [or from the Cambridge Crystallographic Data Centre, 12, Union Road, Cambridge CB2 1EZ, UK; fax: (internat.) +44-1223/336-033; E-mail: deposit@ccdc.cam.ac.uk].

Acknowledgments

The authors would like to thank the EPSRC (studentship to P.D.B, JREI Award for M.G.D.) and the Royal Society (Industrial Fellowship for M.G.D.).

[1] [1a] *Organometallics in Synthesis* (Ed.: M. Schlosser), J. Wiley & Son, New York, 1994. [1b] E. Weiss, *Angew. Chem.* **1993**, *105* 1565−1587; *Angew. Chem. Int. Ed. Engl.* **1993**, *32*, 1501−1523.

[2] [2a] D. R. Armstrong, D. Barr, R. Snaith, W. Clegg, R. E. Mulvey, K. Wade, D. Reed, *J. Chem. Soc., Dalton Trans.* **1987**, 1071−1081. [2b] R. E. Mulvey, *Chem. Soc. Rev.* **1991**, *20*, 167−209. [2c] R. E. Mulvey, *Chem. Soc. Rev.* **1998**, *27*, 339−346.

[3] *Lithium Chemistry* (Eds.: A. M. Sapse and P. von R. Schleyer), Wiley Interscience, New York, London, Sydney, 1996, and references cited therein.

[4] For recent examples see: [4a] L. M. Pratt, A. Streitwieser, *J. Org. Chem.* **2003**, *68*, 2830−2838. [4b] K. W. Henderson, A. R. Kennedy, D. J. MacDougall, *Inorg. Chem.* **2003**, *42*, 2736−2741. [4c] O. Parisel, C. Fressigne, J. Maddaluno, C. Giessner-Prettre, *J. Org. Chem.* **2003**, *68*, 1290−1294.

 © 2003 Wiley-VCH Verlag GmbH & Co. KGaA, Weinheim

[5] For recent examples see. [5a] A. Johansson, O. Davidsson, *Chem. Eur. J.* **2001**, *7*, 3461−3465. [5b] A. E. H. Wheatley, *Chem. Soc. Rev.* **2001**, *30*, 265−273. [5c] G. C. Forbes, F. R. Kenley, A. R. Kennedy, R. E. Mulvey, C. T. O'Hara, J. A. Parkinson, *Chem. Commun.* **2003**, 1140−1141. [5d] D. R. Armstrong, S. C. Ball, D. Barr, W. Clegg, D. J. Linton, L. C. Kerr, D. Moncrieff, P. R. Raithby, R. J. Singer, R. Snaith, D. Stalke, A. E. H. Wheatley, D. S. Wright, *J. Chem. Soc., Dalton Trans.* **2002**, 2505−2511.

[6] For recent examples see: [6a] H. J. Reich, W. S. Goldenberg, A. W. Sanders, K. L. Jantzi, C. C. Tzschucke, *J. Am. Chem. Soc.* **2003**, *125*, 3509−3521. [6b] J. L. Rutherford, D. Hoffmann, D. B. Collum, *J. Am. Chem. Soc.* **2002**, *124*, 264−271. [6c] R. L. Parsons, J. M. Fortunak, R. L. Dorow, G. D. Harris, G. S. Kauffman, W. A. Nugent, M. D. Winemiller, T. F. Briggs, B. S. Xiang, D. B. Collum, *J. Am. Chem. Soc.* **2001**, *123*, 9135−9143. [6d] I. Keresztes, P. G. Williard, *J. Am. Chem. Soc.* **2000**, *122* 10228−10229.

[7] R. Snaith, D. S. Wright, *Lithium Chemistry* (Eds.: A. M. Sapse and P. von R. Schleyer), Wiley Interscience, New York, London, Sydney, 1996, chapter 8, p 227−293.

[8] [8a] W. H. Meyer, *Adv. Mater.* **1998**, *10*, 439−448. [8b] R. Frech, S. Chintapalli, P. G. Bruce, C. A. Vincent, *Chem. Commun.* **1997**, 157−158. [8c] A. Lauenstein, J. Tegenfeldt, *J. Phys. Chem. B* **1998**, *102*, 6702−6709. [8d] P. G. Bruce, *Phil. Trans. R. Soc., Lon. A* **1996**, *354*, 415−436.

[9] [9a] J. S Yadav, B. V. S. Reddy, D. Narsimhaswamy, K. Narsimulu, A. C. Kunwar, *Tetrahedron. Lett.* **2003**, *44*, 3697−3700. [9b] B. Karimi, W. Maleki, *Tetrahedron. Lett.* **2002**, *43*, 5353−5355. [9c] *Lewis Acids in Organic synthesis* (Ed.: H. Yamamoto), Wiley-VCH, New York, **2000**.

[10] J. L. Nowinski, P. Lightfoot, P. G. Bruce, *J. Mater. Chem.* **1994**, *4*, 1579−1580.

[11] L. Xue, C. W. Padgett, D. D. DesMarteau, W. T. Pennington, *Solid State Sci.* **2002**, *4*, 1535−1545.

[12] G. A. Lawrance, *Chem. Rev.* **1986**, *86*, 17−33.

[13] [13a] F. H. Allen, O. Kennard, *Chem. Des. Autom. News* **1993**, *8*, 1. [13b] F. H. Allen, O. Kennard, *Chem. Des. Autom. News* **1993**, *8*, 31.

[14] G. R. Desiraju, T. Steiner, *The Weak Hydrogen Bond*, Oxford Science Publications, Oxford, **1999**.

[15] A. S. Batsanov, M. G. Davidson, J. A. K. Howard, S. Lamb, C. Lustig, R. D. Price, *Chem. Commun.* **1997**, 1211−1212.

[16] D. R. Armstrong, M. G. Davidson, D. Moncrieff, *Angew. Chem.* **1995**, *107* 514−517; *Angew. Chem. Int. Ed. Engl.* **1995**, *34*, 478−481.

[17] P. D. Bolton, M. G. Davidson, unpublished results.

[18] *Alkoxo and Aryloxo Derivatives of Metals* (Eds.: D. C. Bradley, R. C. Mehrotra, I. P. Rothwell, A. Singh), Academic Press, London, **2001**.

[19] O. Moers, A. Blaschette, P. G. Jones, *Z. Anorg. Allg. Chem.* **2000**, *626*, 2409−2418.

[20] J. Foropoulos, D. D. DesMarteau, *Inorg. Chem.* **1984**, *23*, 3720−3723.

[21] D. W. Cruickshank, *Inorganic Sulfur Chemistry* (Ed.: G. Nickless) Elsevier, Amsterdam, **1998**.

[22] D. Brouillette, D. E. Irish, N. J. Taylor, G. Perron, M. Odziemkowski, J. E. Desnoyers, *Phys. Chem. Chem. Phys.* **2002**, *4*, 6063−6071.

[23] Indeed, gas-phase ab initio calculations of lithium with PMDETA, and its parent complex DTA, have shown them to have a much greater ability to solvate lithium ions than the TAC [$(CH_2NH)_3$] and Me-TAC [$(CH_2NMe)_3$] ligands. See: E. Kaufmann, J. Gose, P. von R. Schleyer, *Organometallics* **1989**, *8*, 2577−2584.

[24] H. H. Giese, T. Habereder, J. Knizek, H. Nöth, M. Warchhold, *Eur. J. Inorg. Chem.* **2001**, 1195−1205.

[25] [25a] W. Uhl, R. Gerding, F. Hannemann, *Z. Anorg. Allg. Chem.* **1998**, *624*, 937−944. [25b] W. Uhl, F. Hannemann, W. Saak, R. Wartchow, *Eur. J. Inorg. Chem.* **1998**, 921−926. [25c] W. Uhl, M. Koch, S. Pohl, W. Saak, *Z. Anorg. Allg. Chem.* **1994**, *620*, 1619−1626. [25d] M. Westerhausen, B. Rademacher, W. Schwartz, S. Henkel, *Z. Naturforsch., Teil B* **1994**, *49*, 199−210. [25e] W. Uhl, M. Koch, J. Wagner, *Z. Anorg. Allg. Chem.* **1995**, *621*, 249−257. [25f] W. Uhl, U. Schutz, W. Kaim, E. Waldhor, *J. Organomet. Chem.* **1995**, *501*, 79−85.

[26] R. E. A. Dillon, C. L. Stern, D. F. Shriver, *Solid State Ionics* **2000**, *133*, 247−255.

[27] A. Haas, Ch. Klare, P. Betz, J. Bruckmann, C. Kruger, Y. H. Tsay, F. Aubke, *Inorg. Chem.* **1996**, *35*, 1918−1925.

[28] D. R. McFarlane, J. Sun, J. Golding, P. Meakin, M. Forsyth, *Electrochim. Acta* **2000**, *45*, 1271−1278.

[29] D. R. McFarlane, J. Huang, M. Forsyth, *Nature* **1999**, *402*, 792−794.

[30] C. M. Forsyth, D. R. McFarlane, J. Golding, J. Huang, J. Sun, M. Forsyth, *Chem. Mater.* **2002**, *14*, 2103−2108.

[31] G. M. Sheldrick (**1986**). SHELX-86. Program for the solution of crystal structures, Univ. of Göttingen, Germany.

[32] G. M. Sheldrick (**1997**). SHELX-97. *Program for crystal structure refinement*, Univ. of Göttingen, Germany.

Received June 17, 2003

 © 2003 Wiley-VCH Verlag GmbH & Co. KGaA, Weinheim

Syntheses and Crystal Structures of Highly Diastereomerically Enriched Lithiated Benzylsilanes in the Presence of External Donor Molecules: Experiment and Theory

Carsten Strohmann,*[a] Daniel H. M. Buchold,[a] Timo Seibel,[a] Kerstin Wild,[a] and Daniel Schildbach[a]

In memory of Ron Snaith

Keywords: Silanes / Lithium / Diastereomers / Quantum-chemical calculations / Stereochemistry

The solid-state structures of the lithiated (aminomethyl)benzylsilanes $Me_2Si[(R)$-(CHPhLi·0.5TMEDA)$](CH_2SMP)$ [{(*R*,*S*)-**2**}$_2$·TMEDA] and $Me_2Si[(R)$-(CHPhLi·DABCO)$](CH_2SMP)$ [(*R*,*S*)-**2**·DABCO] [CH_2SMP = (*S*)-2-(methoxymethyl)pyrrolidinomethyl] and the absolute configurations at the stereogenic metallated carbon centres of these compounds were determined by single-crystal X-ray diffraction methods. The crystal structures of the TMEDA-bridged dimer [(*R*,*S*)-**2**]$_2$·TMEDA and monomeric (*R*,*S*)-**2**·DABCO were compared to that of the parent compound (*R*,*S*)-**2**, a coordination polymer. By computational methods [B3LYP/6–31+G(d)], the mechanism of the deprotonation of the starting compound, (aminomethyl)benzylsilane [(*S*)-**1**], as well as the stability of configuration of the lithiated derivatives of (*R*,*S*)-**2**, were examined. For the highly diastereoselective substitution reactions of the derivatives of (*R*,*S*)-**2** with iodomethane, inversion of the configuration at the metallated carbon centre was observed and correlated with the results of the quantum-chemical studies.

(© Wiley-VCH Verlag GmbH & Co. KGaA, 69451 Weinheim, Germany, 2003)

Introduction

The synthesis of enantiomerically or diastereomerically enriched[1] alkyllithium compounds, in which the metallated carbon centre is the stereogenic centre, has been intensively studied for the last 20 years.[2] Among these compounds are several enantiomerically enriched benzyllithium reagents.[2–5] Stereogenic metallated carbon centres are usually generated by deprotonation using alkyllithium bases, like *tert*-butyllithium. The stereochemical information can be introduced *prior* to the deprotonation reaction by using enantiomerically enriched C–H acidic precursors bearing only one proton at the stereogenic carbon centre. In contrast, methods for the introduction of the stereochemical information *during* the deprotonation reaction are either *inter*molecular by chiral auxiliaries, like (–)-sparteine, or *intra*molecular by the side-arm donation of chiral substituents, like the (*S*)-2-(methoxymethyl)pyrrolidinomethyl substituent (CH_2SMP). This latter method is used in our laboratory.

Two different reaction conditions for the synthesis of the studied diastereomerically enriched benzyllithium compounds are applicable. *Kinetically controlled synthesis:* Diastereotopos-differentiating deprotonation at low temperatures, mostly observed in non-polar solvents (e.g. in toluene, *n*-pentane); *Thermodynamically controlled synthesis:* Epimerisation between two diastereomeric alkyllithiums at higher temperatures, mostly observed in polar solvents (e.g. in THF) (Scheme 1). Kinetically controlled deprotonation and thermodynamically controlled epimerisation will be discussed in detail in the section "Quantum-Chemical Studies".

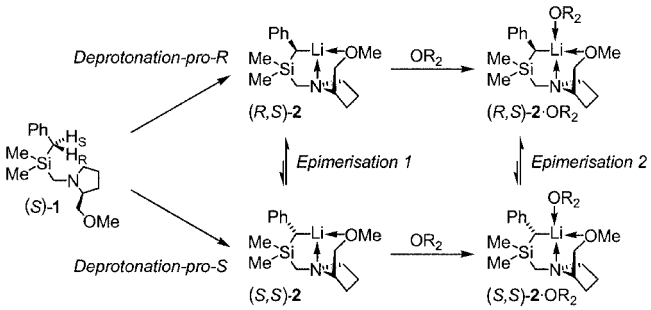

Scheme 1. Relevant deprotonation reactions and epimerisation equilibria starting from (*S*)-**1**

[a] Institut für Anorganische Chemie der Universität Würzburg
Am Hubland, 97074 Würzburg, Germany
Fax: (internat.) +49-(0)931/888-4605
E-mail: mail@carsten-strohmann.de

The focus of this article will be particularly on the lithiated (aminomethyl)benzylsilane (*R*,*S*)-**2** in the presence of external coordinating donor molecules. The synthesis, the stability of configuration at the metallated carbon centre and further transformations (stereochemical course) have been investigated thoroughly.

The lithiation of [(benzyldimethylsilyl)methyl]-(*S*)-2-(methoxymethyl)pyrrolidine [(*S*)-**1**] with *sec*-butyllithium in THF and selective substitution reactions with alkyl halides, which showed very high diastereomeric ratios (*dr*), were first reported by Chan and co-workers.[4a] A significant solvent effect on the diastereomeric ratios of the transformations with iodomethane was observed when the reaction was carried out in THF (*dr* = 75:25) and diethyl ether (*dr* ≥ 98:2). Thus, it was of great interest to determine the solid-state structure (and the absolute configuration) of lithiated organosilane (*R*,*S*)-**2** in the crystal,[6] especially since only very few enantiomerically pure alkyllithiums have been investigated in the solid state up to now.[2a,3d,3g,3h,7–9]

The lithiation of (aminomethyl)benzylsilane [(*S*)-**1**] was carried out with *tert*-butyllithium at −90 °C in a toluene/*n*-pentane mixture (Scheme 2). At −30 °C, yellow needles of the metallated product (*R*,*S*)-**2** could be isolated as single crystals in 80% yield. The result of the single-crystal X-ray diffraction study is shown in Figure 1.[6]

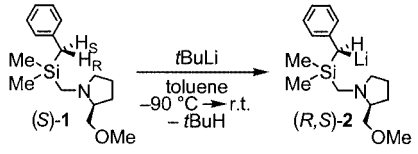

Scheme 2

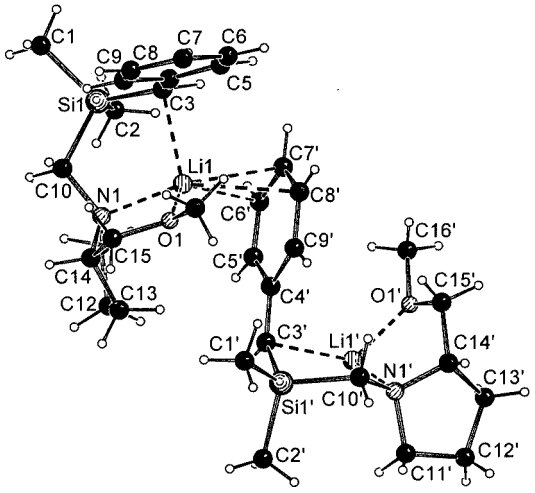

Figure 1. Molecular structure and numbering scheme of compound (*R*,*S*)-**2** in the crystal (Schakal plot);[10] selected bond lengths (Å) and angles (°): Si(1)−C(3) 1.797(7), Li(1)−C(3) 2.269(14), C(3)−C(4) 1.419(9), N(1)−Li(1) 2.183(12); C(3)−Si(1)−C(10) 107.9(3)

For the substitution reaction of (*R*,*S*)-**2** with iodomethane in toluene/*n*-pentane, inversion of the configuration at the metallated carbon centre was observed with a high diastereoselectivity (*dr* = 96:4). The absolute configuration of methylated (aminomethyl)benzylsilane (*S*,*S*)-**3** was determined by X-ray structural analysis of the corresponding ammonium iodide (Scheme 3).[6]

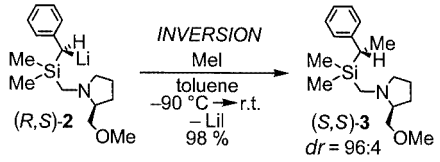

Scheme 3

Due to the difference in the stereoselectivities of the mentioned substitution reactions, when switching from non-polar solvents to polar solvents, the molecular structures of (*R*,*S*)-**2** with external (intermolecularly) coordinating molecules, blocking a potential vacant coordination site at the lithium centre, were to be examined. Therefore, the solid-state molecular structures of the two donor-stabilised adducts (*R*,*S*)-**2**·DABCO and [(*R*,*S*)-**2**]$_2$·TMEDA are presented, as well as the results of substitution reactions with the electrophile iodomethane. The stereochemical aspects of these transformations will be explained by quantum-chemical studies.

Results and Discussion

Synthesis of the Diastereomerically Enriched Alkyllithiums

[(*R*,*S*)-**2**]$_2$·TMEDA and (*R*,*S*)-**2**·DABCO were generated by lithiation with *tert*-butyllithium in a toluene/*n*-pentane mixture in the presence of the corresponding diamine ligand at low temperatures. After warming to room temperature, single crystals of both compounds were obtained that were suitable for X-ray structural analysis. According to this, a monomeric molecular structure was observed for (*R*,*S*)-**2**·DABCO, with only one nitrogen centre coordinating to one lithium centre, while a dimeric structure was determined for [(*R*,*S*)-**2**]$_2$·TMEDA with the diamine in a bridging mode [both molecular structures, with an (*R*) configuration at the lithiated carbon centre, will be discussed]. The bridged dimer [(*R*,*S*)-**2**]$_2$·TMEDA is formed indepen-

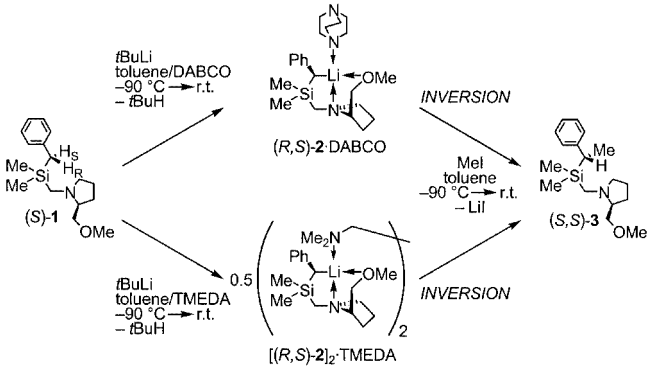

Scheme 4

dently of the molar ratio between the alkyllithium compound and TMEDA (1:1 or 2:1), and the use of half an equivalent of DABCO (molar ratio of 2:1) does not force this ligand into a bridging position (Scheme 4).

After dissolving the solids of [(*R*,*S*)-**2**]$_2$·TMEDA and (*R*,*S*)-**2**·DABCO in toluene, the trapping reactions with iodomethane were carried out at −90 °C and the reaction mixture was subsequently warmed to room temperature. Methylated silane (*S*,*S*)-**3**/(*R*,*S*)-**3** was formed in maximum yields of 98%. Higher diastereomeric ratios were observed when the substitution reactions with iodomethane were carried out in the coordinating solvent diethyl ether (*dr* > 98:2), than for the corresponding reactions in a toluene/*n*-pentane mixture (*dr* = 96:4). Surprisingly, THF as a solvent gave only poor diastereomeric ratios (*dr* = 75:25).[4a,6] Unfortunately, no single-crystals of (*R*,*S*)-**2** from the two ethereal solvents have been obtained up to now. Thus, the absolute configurations at the lithiated carbon centres of compounds of the formal type (*R*,*S*)-**2**·OR$_2$ (OR$_2$ = THF, Et$_2$O) have not been confirmed for these two solvents. Due to the difference in the stereoselectivities of the substitution reaction with iodomethane in the two ethereal solvents, different reaction conditions for the methylation were applied and the diastereomeric ratios studied. The results are summarised in Table 1.

Table 1. Diastereoselectivities of substitution reactions with iodomethane in different solvents

Compound	Solvent	*dr* [(*S*,*S*)-**3**:(*R*,*S*)-**3**]
[(*R*,*S*)-**2**]$_2$·TMEDA	toluene	>98:2
(*R*,*S*)-**2**·DABCO	toluene	>98:2
(*R*,*S*)-**2**	toluene +1 equiv. THF *before* metallation	>98:2
(*R*,*S*)-**2**	toluene +1 equiv. THF *after* metallation	>98:2
(*R*,*S*)-**2**	Et$_2$O	>98:2
[(*R*,*S*)-**2**]$_2$·TMEDA	THF	69:31
(*R*,*S*)-**2**·DABCO	THF	62:38
(*R*,*S*)-**2**	THF	75:25

For the reactions of the defined donor adducts [(*R*,*S*)-**2**]$_2$·TMEDA and (*R*,*S*)-**2**·DABCO as well as for reactions where the external donor molecule is added stoichiometrically (THF), high diastereoselectivities were observed. In contrast to the methylation in the solvent diethyl ether, methylations of (*R*,*S*)-**2**, [(*R*,*S*)-**2**]$_2$·TMEDA and (*R*,*S*)-**2**·DABCO in THF as a solvent give only poor diastereoselectivities. Obviously, the high selectivities of reactions of (*R*,*S*)-**2** are only diminished by the highly polar environment of THF as a solvent, while reactions of defined mixtures/adducts of (*R*,*S*)-**2** with external coordinating donor molecules in less or non-polar solution give high diastereomeric ratios. Moreover, the stereochemical course of the transformations with the lithiated (aminomethyl)benzylsilanes is not affected by crystallisation and isolation of these compounds; reactions starting with the lithium compound as prepared and maintained in solution gave the same *dr* values.

Discussion of the X-ray Structural Analyses of [(*R*,*S*)-**2**]$_2$·TMEDA and (*R*,*S*)-**2**·DABCO

The alkyllithium compound [(*R*,*S*)-**2**]$_2$·TMEDA crystallised from a toluene/*n*-pentane mixture in the orthorhombic crystal system, space group $P2_12_12_1$ (see also Table 2). The asymmetric unit of [(*R*,*S*)-**2**]$_2$·TMEDA contains one molecule, representing a TMEDA-bridged dimer, where each nitrogen centre of the bidentate diamine ligand coordinates to one lithium centre of a silane unit (Figure 2). (Due to the similarity of the structural parameters of these two bridged silane units, only one unit is discussed; selected bond lengths are given in Table 3).

The lithium centre, with a distorted tetrahedral coordination sphere, has contacts to the metallated carbon centre C(3), to the oxygen centre O(1) and the nitrogen centre N(1) of the SMP substituent, as well as to N(3) of the TMEDA ligand. The metallated carbon centre C(3) is slightly pyramidalised: the sum of the angles at the "carbanionic" unity, consisting of Si(1), C(3), C(4) and H(3), is 354°. Nevertheless, the tetracoordinate C(3) is a stereogenic centre with the (*R*) configuration due to the Li(1)−C(3) contact; the Li(1)−C(3) distance is 2.254(4) Å. The *intra*molecular nitrogen-lithium contact [N(1)−Li(1) = 2.185(4) Å] and the *inter*molecular nitrogen-lithium contact [N(3)−Li(1) = 2.171(4) Å] are equal within the margin of error. As a consequence of the stabilisation effect of silicon centres on vicinal metallated carbon centres (polarisability of the silicon centre in addition to the stabilisation effect by the phenyl substituent), the Si(1)−C(3) bond length [1.817(2) Å] is significantly shorter than the Si(1)−C(10) bond [1.916(2) Å]. Moreover, when the C−C distances in the phenyl ring are compared to a similar (aminomethyl)-(lithiomethyl)benzylsilane that is not lithiated at the benzyl position, the influence of the metallation at C(3) is noticeable. Thus, the C−C distances between the *ipso*- and the two *ortho* carbon centres are longer [C(4)−C(5) = 1.419(4) and C(4)−C(9) = 1.427(3) Å] than the values found previously [1.378(4) and 1.390(4) Å].[11,12]

The related alkyllithium compound (*R*,*S*)-**2**·DABCO crystallised from a toluene/*n*-pentane mixture in the monoclinic crystal system, space group $P2_1$. The asymmetric unit of (*R*,*S*)-**2**·DABCO contains one molecule of the alkyllithium as well as one molecule of toluene from the solvent (due to the lack of interactions between the alkyllithium compound and the toluene, the solvent molecule is omitted in Figure 3). In contrast to the TMEDA adduct [(*R*,*S*)-**2**]$_2$·TMEDA, the bidentate DABCO ligand does not bridge two silane units, but coordinates to the lithium centre Li through the nitrogen centre N(2), while the nitrogen centre N(3) remains in a non-coordinating mode [the shortest intermolecular distance N(3)···H(10a) is 2.678(7) Å]. The reason for this is probably the lack of flexibility of the more rigid DABCO, compared to the TMEDA ligand; steric interactions between bridged silane units would be the consequence. The distorted tetrahedral coordination sphere of the lithium centre is built up by one contact to the metallated carbon centre C(3), as well as to O(1) of the meth-

 © 2003 Wiley-VCH Verlag GmbH & Co. KGaA, Weinheim

Table 2. Crystal data and structure refinement for [(*R*,*S*)-**2**]$_2$·TMEDA and (*R*,*S*)-**2**·DABCO

Compound	[(*R*,*S*)-**2**]$_2$·TMEDA	(*R*,*S*)-**2**·DABCO
Empirical formula	$C_{38}H_{68}Li_2N_4O_2Si_2$	$C_{22}H_{38}LiN_3OSi·C_6H_5CH_3$
Molecular weight (g·mol^{-1})	683.02	487.72
Data collection temperature *T* (K)	173(2)	173(2)
Wavelength (Å)	0.71073	0.71073
Crystal system	orthorhombic	monoclinic
Space group (no.)	$P2_12_12_1$ (19)	$P2_1$ (4)
a (Å)	13.882(3)	10.1371(19)
b (Å),	17.225(3)	11.711(2)
c (Å)	17.575(4)	13.055(3)
β (°)	–	112.297(3)
Volume (Å^3)	4202.6(15)	1433.9(5)
Z	4	2
Calculated density ρ (g·cm^{-1})	1.080	1.130
Absorption coefficient μ (mm^{-1})	0.119	0.107
F(000)	1496	532
Crystal size [mm^3]	0.20 × 0.20 × 0.20	0.20 × 0.20 × 0.10
Range for data collection 2θ (°)	4.42–50.00	3.38–50.00
Index ranges	$-16 \le h \le 16$ $-20 \le k \le 20$ $-20 \le l \le 20$	$-11 \le h \le 11$ $-13 \le k \le 13$ $-14 \le l \le 14$
Collected reflections	36683	21995
Independent reflections	7407 (R_{int} = 0.1065)	4486 (R_{int} = 0.0867)
Refinement method	full-matrix least-squares on F^2	full-matrix least-squares on F^2
H atom refinement	riding model; H(3) and H(19) refined independently	riding model; H(3) refined independently
Data/restraints/parameters	7407/0/451	4486/1/324
Goodness-of-fit on F^2	1.018	1.062
Final *R* indices [$I > 2\sigma(I)$]	*R*1 = 0.0439, *wR*2 = 0.1052	*R*1 = 0.0685, *wR*2 = 0.1544
R indices (all data)	*R*1 = 0.0517, *wR*2 = 0.1088	*R*1 = 0.0711, *wR*2 = 0.1560
Absolute structure factor	−0.01(10)	0.2(2)
Largest diff. peak and hole (e·Å^{-3})	0.380 and −0.276	0.292 and −0.299

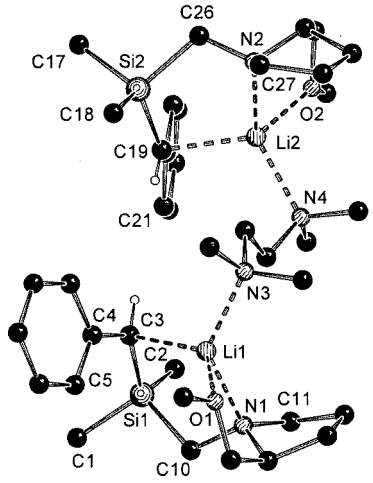

Figure 2. Molecular structure and numbering scheme of compound [(*R*,*S*)-**2**]$_2$·TMEDA in the crystal (Schakal plot);[10] selected bond lengths (Å) and angles (°): Si(1)–C(3) 1.817(2), Li(1)–C(3) 2.254(4), C(3)–C(4) 1.430(3), N(1)–Li(1) 2.185(4), N(3)–Li(1) 2.171(4), O(1)–Li(1) 1.993(4); C(3)–Si(1)–C(10) 110.19(10), Li(1)–C(3)–Si(1)–C(4) 96.5(2), Si(2)–C(19) 1.809(2), Li(2)–C(19) 2.254(5), C(19)–C(20) 1.437(3), N(2)–Li(2) 2.185(4), N(4)–Li(2) 2.161(4), O(2)–Li(2) 2.013(4), C(19)–Si(2)–C(26) 109.75(12)

oxymethyl substituent and two lithium-nitrogen contacts to nitrogen centres N(1) and N(2) of the SMP substituent and the DABCO ligand. In (*R*,*S*)-**2**·DABCO, the metallated carbon centre C(3) is also slightly pyramidalised: At the "carbanionic" unit, consisting of Si(1), C(3), C(4) and H(3), a sum of the angles of 358° is found. The tetracoordinate metallated carbon centre C(3), a stereogenic centre due to the Li(1)–C(3) contact, has an (*R*) configuration; the Li(1)–C(3) distance is 2.279(9) Å. The two nitrogen-lithium distances are slightly shorter than in the TMEDA adduct [(*R*,*S*)-**2**]$_2$·TMEDA, but equal within the margin of error [N(1)–Li(1) = 2.138(9) Å (*intra*molecular), N(2)–Li(1) = 2.102(9) Å (*inter*molecular)]. As a consequence of the stabilizing effect of the silicon centre on metallated C(3) (in addition to the stabilisation of the phenyl substituent), the Si–C(3) distance, which amounts to 1.814(5) Å, is significantly shorter than the Si(1)–C(10) distance, which is 1.895(5) Å. In a related non-chiral lithiated benzyl(piperidinomethyl)silane, whose synthesis and crystal structure were reported previously,[11,12] the corresponding Si(1)–C(3) bond length [1.821(3) Å] is of a similar value, indicating an analogous stabilising effect by the silicon centre of this molecule. The C–C bonds between the *ipso*- and both *ortho* carbon centres [C(4)–C(5) = 1.419(7) and C(4)–C(9) = 1.425(7) Å] are longer than the previously reported values [1.378(4) and 1.390(4) Å].[11,12]

All three lithiated (aminomethyl)benzylsilanes [(*R*,*S*)-**2**, (*R*,*S*)-**2**·DABCO and [(*R*,*S*)-**2**]$_2$·TMEDA] are metallated at the benzyl position; the benzylic carbon centre, being the stereogenic metallated carbon centre, has an (*R*) configura-

 © 2003 Wiley-VCH Verlag GmbH & Co. KGaA, Weinheim

Table 3. Selected X-ray structural parameters for (*R*,*S*)-**2**,[6] [(*R*,*S*)-**2**]$_2$·TMEDA (second silane unit in brackets) and (*R*,*S*)-**2**·DABCO

Compound	(*R*,*S*)-**2**	[(*R*,*S*)-**2**]$_2$·TMEDA	(*R*,*S*)-**2**·DABCO
Absolute configuration at C(3)	(*R*)	(*R*) [(*R*)]	(*R*)
Sum of the angles at C(3) [°]	360	354 (354)	358
Si(1)−C(3)*/Si−C(3) [Å]	1.797(7)*	1.817(2)* [1.809(2)]	1.814(5)
Li(1)−C(3)*/Li−C(3) [Å]	2.269(14)*	2.254(4)* [2.254(5)]	2.279(9)
Li(1)−N(1)*/Li−N(1) [Å]	2.183(12)*	2.185(4)* [2.185(4)]	2.138(9)
Li(1)−N(3)*/Li−N(2) [Å]	−	2.171(4)* [2.161(4)]	2.102(9)
Li(1)−O(1)*/Li−O [Å]	1.949(13)*	1.993(4)* [2.013(4)]	1.992(9)
C(3)−C(4) [Å]	1.419(9)	1.430(3) [1.437(3)]	1.428(7)
C(4)−C(5) [Å]	1.422(9)	1.419(4) [1.427(4)]	1.419(7)
C(5)−C(6) [Å]	1.412(11)	1.386(4) [1.385(4)]	1.372(7)
C(6)−C(7) [Å]	1.390(12)	1.394(4) [1.350(5)]	1.375(8)
C(7)−C(8) [Å]	1.405(11)	1.370(5) [1.389(6)]	1.387(8)
C(8)−C(9) [Å]	1.369(10)	1.400(4) [1.394(4)]	1.368(8)
C(9)−C(4) [Å]	1.446(9)	1.427(3) [1.405(4)]	1.425(7)
Li(1)−C(3)−Si(1)−C(4)*/Li−C(3)−Si−C(4) [°]	104.1(7)*	96.5(2)* [100.1(3)]	101.6(6)

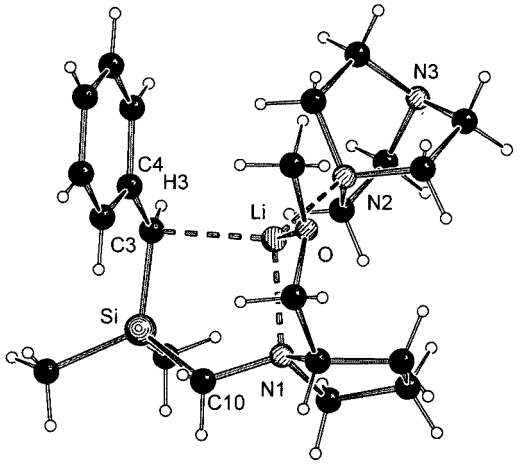

Figure 3. Molecular structure and numbering scheme of compound (*R*,*S*)-**2**·DABCO in the crystal (Schakal plot)[10] selected bond lengths (Å) and angles (°): Si−C(3) 1.814(5), Si−C(10) 1.895(5), Li−C(3) 2.279(9), C(3)−C(4) 1.428(7), N(1)−Li 2.138(9), N(2)−Li 2.102(9), O−Li 1.992(9); C(3)−Si(1)−C(10) 109.7(2), Li−C(3)−Si−C(4) 101.6(6)

tion in all three cases. The carbon-lithium distances of the three compounds are equal within the margin of error. This fact underlines — especially in the case of the two *inter*molecularly coordinated compounds [(*R*,*S*)-**2**]$_2$·TMEDA and (*R*,*S*)-**2**·DABCO — that these compounds do not have the properties of lithium-carbanion pairs. The lithium centre is not separated from the metallated carbon centre, either by the DABCO or by the strongly chelating TMEDA ligand. In the case of compound (*R*,*S*)-**2**, which is only *intra*molecularly coordinated by donor centres, the ''carbanionic'' unit is planar (sum of the angles of 360°), thus the adjoining centres H(3), C(4) and Si are coplanar with C(3). The two externally coordinated compounds [(*R*,*S*)-**2**]$_2$·TMEDA and (*R*,*S*)-**2**·DABCO are slightly pyramidalised at C(3) (sum of the angles of 354° and 358° respectively), although the sums of the angles should not be overvalued. The torsion angles, incorporating the lithium, the silicon, the metallated carbon and the *ipso* carbon centres, are in the range of 96.5(2)° and 104.1(7)° and demonstrate that the lithium centres are located almost orthogonal to the planes of the ''carbanionic'' units. Moreover, the periplanar conformation of the C(3)−C(4) bond shows that this ''carbanionic'' unit is in the same plane as the aromatic ring system. The most important structural parameters of the three alkyllithium compounds (*R*,*S*)-**2**,[6] [(*R*,*S*)-**2**]$_2$·TMEDA and (*R*,*S*)-**2**·DABCO are summarised in Table 3.

An investigation of the molecular structures of (*R*,*S*)-**2**, (*R*,*S*)-**2**·DABCO and [(*R*,*S*)-**2**]$_2$·TMEDA in solution by low-temperature NMR techniques is not possible due to the poor solubility of the compounds in the essential non-polar solvents at reduced temperatures. At room temperature, no carbon-lithium coupling was observed, although this is not a reliable probe for the carbon-lithium distance.

Quantum-Chemical Studies

Kinetically Controlled Deprotonation

An insight into the deprotonation reaction of (*S*)-**1** with *tert*-butyllithium can be gained by computational methods.[13] Experimentally, this reaction is effected at very low temperatures (−70 to −90 °C) under kinetically controlled conditions. Under these conditions, the reaction will proceed via the energetically more stable transition state. Two reaction paths are possible, resulting in the formation of the two possible epimers (*R*,*S*)-**2** and (*S*,*S*)-**2** (Scheme 1). Each of these reaction paths will be considered separately. With the implication of the complex induced proximity effect (CIPE),[14] the reaction is believed to start with a pre-coordinated *tert*-butyllithium molecule, whose lithium centre is coordinated by the oxygen and nitrogen atoms of the SMP ligand. From the specific conformation of the Si−C bond in **MIN-1**, the *pro*-R hydrogen atom (H_R) is being abstracted in the deprotonation reaction, proceeding via the transition state **TS-1**, in which the carbon-lithium contact is formed simultaneously with the carbon-hydrogen bond cleavage. The reaction products (metallated silane and *tert*-

 © 2003 Wiley-VCH Verlag GmbH & Co. KGaA, Weinheim

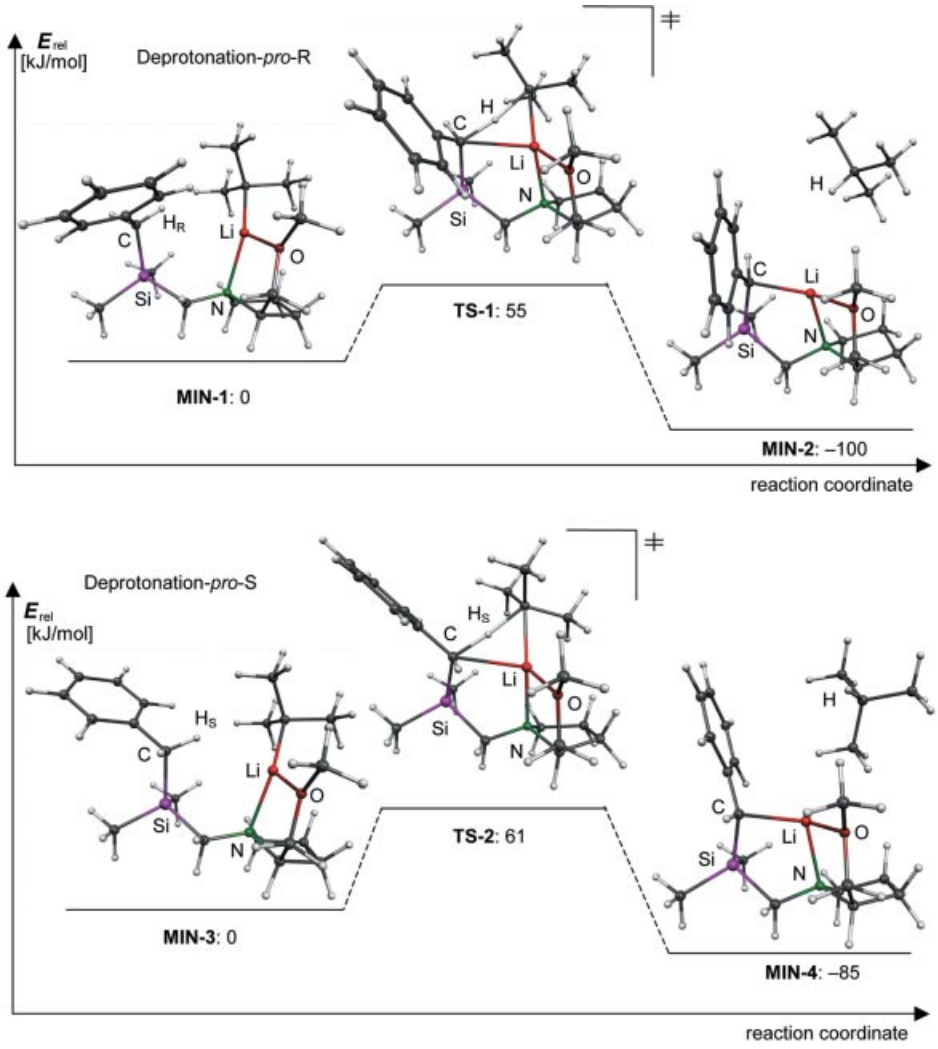

Figure 4. (a) Relative-energy profile of stationary points **MIN-1**, **TS-1** and **MIN-2** for the deprotonation reaction towards the (*R*,*S*)-epimer, deprotonation-*pro*-*R*, B3LYP/6−31+G(d); (b) relative-energy profile of stationary points **MIN-3**, **TS-2** and **MIN-4** for the deprotonation reaction towards the (*S*,*S*)-epimer, deprotonation-*pro*-*S*, B3LYP/6−31+G(d)

butane) form the stationary point **MIN-2** (Deprotonation-*pro*-R; Scheme 1, Figure 4a, Table 4). The results of this calculation, together with the analogous deprotonation reaction, where the abstraction of the *pro*-*S* hydrogen atom (H_S) gives the other epimer **MIN-4** (deprotonation-*pro*-*S*; Scheme 1, Figure 4b, Table 4), are summarised in Table 4.

Table 4. Calculated energies for the stationary points **MIN-1** to **MIN-4**, **TS-1** and **TS-2** of the deprotonation reactions towards the (*R*,*S*)/(*S*,*S*)-epimer, B3LYP/6−31+G(d) (ZPVE = Zero-Point Vibrational Energy)

Deprotonation reaction towards (*R*,*S*)-/(*S*,*S*)-epimer		Electronic Energy relative to **MIN-1**	
		corrected by ZPVE	uncorrected
Deprotonation 1 **MIN-1** → **MIN-2**	**MIN-1**	0	0
	TS-1	55	65
	MIN-2	−100	−102
Deprotonation 2 **MIN-3** → **MIN-4**	**MIN-3**	0	0
	TS-2	61	71
	MIN-4	−85	−88

The energies of the two conformers **MIN-1** and **MIN-3** are equal within the margin of error of the DFT method used.[15] On the reasonable assumption of an equilibrium between **MIN-1** and **MIN-3**, the stereoselectivity of the reaction would be influenced by the difference between the two activation barriers of the potential energy surface of deprotonation-*pro*-*R* and deprotonation-*pro*-*S*. This activation barrier for deprotonation-*pro*-*R* is 6 kJ/mol smaller than the one for the abstraction of the *pro*-*S* hydrogen atom. This reflects the trend of the kinetically controlled experiment, where the epimer with the (*R*)-configured metallated centre is highly enriched (Scheme 2).[16] After the deprotonation reaction, two equilibria (epimerisations 1 and 2 in Scheme 1) can influence the distribution of the stereoisomers. This will be examined in the following subsection.

Thermodynamically Controlled Epimerisation — Stability of Configuration

In general, "carbanions" have a low barrier of inversion (they are isoelectronic with tertiary amines). Therefore, un-

 © 2003 Wiley-VCH Verlag GmbH & Co. KGaA, Weinheim

substituted systems of this type lose their stereochemical information even at low temperatures. For the racemisation, the following process is assumed (Scheme 5), where the two enantiomeric alkyllithiums **A** and *ent*-**A** are interconverting by separation/fixation of the lithium centre (steps a and d) and the inversion of the configuration via the planar transition state **C** (steps b and c):

The two equilibria (epimerisations 1 and 2 in Scheme 1) can influence the distribution of the stereoisomers after the deprotonation reaction. The situations in non-polar and polar solution are, of course, different. While it is reasonable to imply a vacant coordination site at the lithium centre for non-polar solvents (Figure 5a, see also crystal structure in Figure 1), a polar solvent molecule, like diethyl ether, will complete the coordination sphere of the metal centre. This has been demonstrated in the case of amines by the X-ray structural analyses of $[(R,S)\text{-}\mathbf{2}]_2$·TMEDA and (*R*,*S*)-**2**·DABCO. Thus, the energies of the stationary points of the epimerisation were calculated with a three-coordinate lithium centre (epimerisation 1, Scheme 1; Figure 5a, Table 5) and a four-coordinate lithium centre with an additionally coordinated dimethyl ether and DABCO molecule (epimerisation 2, Scheme 1; Figure 5b and Figure 6, Table 5), to take this into account.

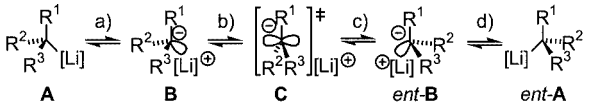

Scheme 5. Proposed racemisation process of enantiomerically enriched alkyllithiums: a) separation of the Li fragment; b) and c) inversion of the "carbanion" via a planar transition state; d) fixation of the Li centre

The two reaction products (*R*,*S*)-**2** and (*S*,*S*)-**2** (equivalent to **MIN-5** and **MIN-6**, epimerisation 1, Scheme 1; Figure 5a, Table 5) might be involved in an equilibrium process of interconversion. This process, which is undesirable for the kinetically controlled synthesis, is required for the

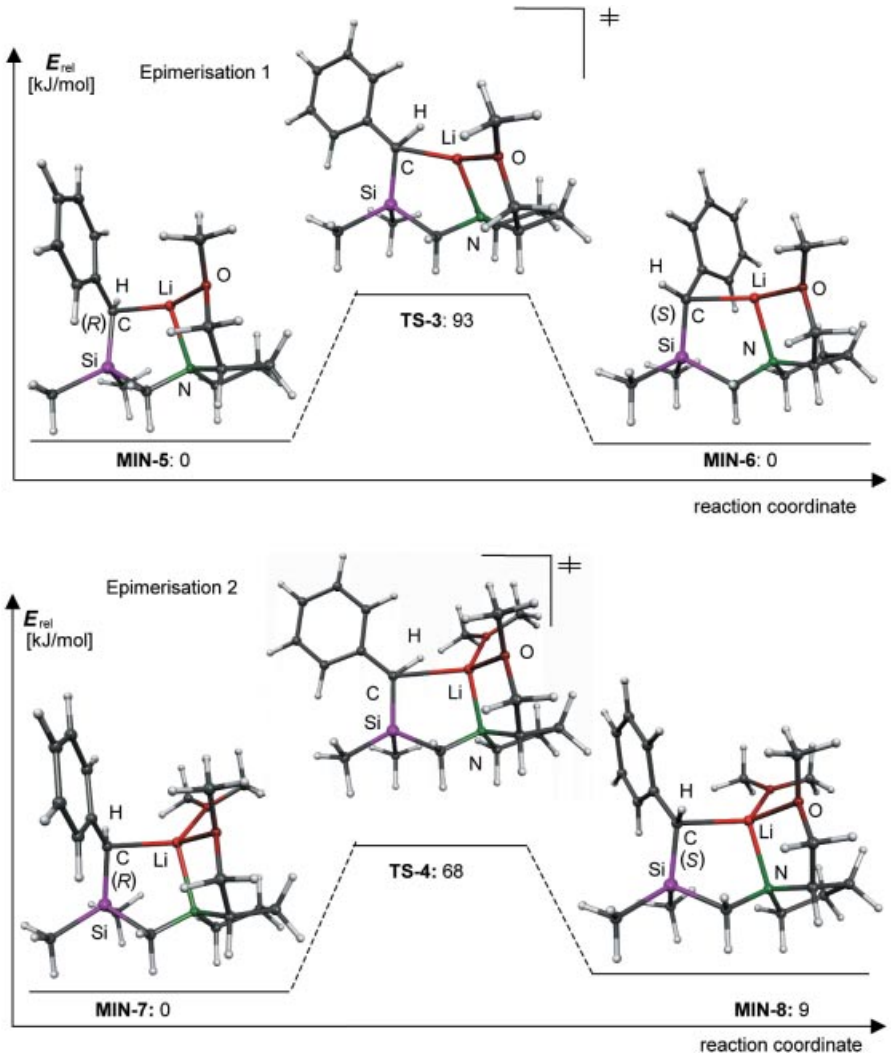

Figure 5. (a) Relative-energy profile of stationary points **MIN-5**, **TS-3** and **MIN-6** for the epimerisation reaction (vacant coordination site) between the (*R*,*S*)/(*S*,*S*) epimer, epimerisation 1, B3LYP/6-31+G(d); (b) relative-energy profile of stationary points **MIN-7**, **TS-4** and **MIN-8** for the epimerisation reaction (dimethyl ether molecule coordinated) between the (*R*,*S*)/(*S*,*S*) epimer, epimerisation 2, B3LYP/6-31+G(d)

 © 2003 Wiley-VCH Verlag GmbH & Co. KGaA, Weinheim

Table 5. Calculated energies for the stationary points **MIN-5** to **MIN-10** and **TS-3** to **TS-5** of the epimerisation reactions between the (*R*,*S*)/(*S*,*S*) epimers, B3LYP/6-31+G(d) (ZPVE = Zero-Point Vibrational Energy)

Epimerisation Reaction in non-polar/polar solvent		Electronic Energy relative to **MIN-5/MIN-7/MIN-9**	
		corrected by ZPVE	uncorrected
Epimerisation 1 **MIN-5** ⇌ **MIN-6**	**MIN-5**	0	0
	TS-3	93	95
	MIN-6	0	0
OMe_2 *Epimerisation 2* OMe_2 **MIN-7** ⇌ **MIN-8**	**MIN-7**	0	0
	TS-4	68	71
	MIN-8	9	9
DABCO *Epimerisation 3* DABCO **MIN-9** ⇌ **MIN-10**	**MIN-9**	0	0
	TS-5	76	79
	MIN-10	6	6

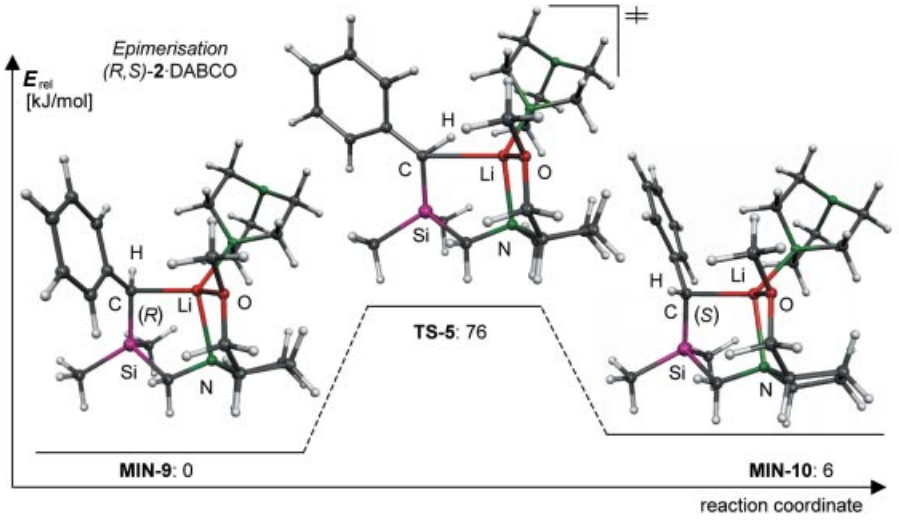

Figure 6. Relative-energy profile of stationary points **MIN-9**, **TS-5** and **MIN-10** for the epimerisation reaction (DABCO molecule coordinated) between epimers (*R*,*S*)- and (*S*,*S*)-**2**·DABCO, B3LYP/6-31+G(d)

thermodynamically controlled route, where typically a polar solvent is added.

Previous calculations and experimental NMR studies[5] have shown that the energies for removing the intramolecularly coordinating ligands from the lithium centre and for removing the lithium centre from the metallated carbon centre, are much higher than the energies discussed in Table 4 and 5. Therefore, it is reasonable to exclude a racemisation proceeding via dimeric structures or carbanions.

The energy differences of the stationary points **MIN-5**, **TS-3** and **MIN-6** (Figure 5a, Table 5) indicate that an epimerisation process at room temperature is unlikely to occur in a non-polar solvent. In this model system for (*R*,*S*)-**2** in that type of solvent with a vacant coordination site at the lithium centre, the activation barrier on the potential energy surface of epimerisation 1 is 93 kJ/mol.

In the model system for (*R*,*S*)-**2** in a polar solvent with a coordinating dimethyl ether molecule at the lithium centre (epimerisation 2 in Scheme 1), the energy difference between **MIN-7** and **TS-4** is smaller by 25 kJ/mol. Furthermore, in contrast to the described non-polar case, there is an energy difference of 9 kJ/mol between both diastereomeric minimum structures **MIN-7** and **MIN-8**. Concluding these studies, in an ethereal solution, highly diastereomerically enriched (*R*,*S*)-**2** should be obtained by epimerisation at room temperature, while a diastereotopos-differentiating deprotonation without noticeable epimerisation should be possible in non-polar solution (under the described reaction conditions).

For (*R*,*S*)-**2**·DABCO, the corresponding calculations have been performed and lead to similar results. [Although a slightly increased inversion barrier is calculated for this

 © 2003 Wiley-VCH Verlag GmbH & Co. KGaA, Weinheim

compound, compared to the results with dimethyl ether, the energy difference between both epimers (*R*,*S*)-**2**·DABCO and (*S*,*S*)-**2**·DABCO decreases slightly]. For this experimentally accessible compound, the more stable epimer (*R*,*S*)-**2**·DABCO is the stereoisomer found in the solid state. Thus, experimental structural information can be correlated with the results of selective transformations and the corresponding quantum-chemical investigations.

The experiments with coordinating amine ligands and potentially coordinating ether molecules that have been described in the previous section show very high diastereoselectivities for substitution reactions in non-polar solvents. These results are supported by the quantum-chemical calculations applied on systems of this type (Scheme 6). The poor selectivities of reactions carried out in highly polar solvents, like THF, might not be explained by the calculation of gas-phase structures, since more polar structures are stabilised by the polar solvent environment. Phenomena like this do have an obvious impact on the equilibria and inversion barriers involved and could in an extreme case lead to a change in the reaction mechanism (e.g. orbital control, CIPE control, ionic reaction mechanisms).

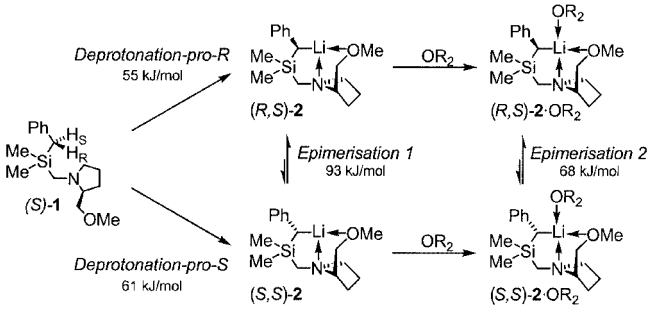

Scheme 6. Relevant deprotonation reactions and epimerisation equilibria starting from (*S*)-**1** (including the quantum chemically calculated activation barriers for R = Me)

Stereochemical Course

The literature reveals that both retention and inversion of the configuration have been observed for the reactions of lithiated benzylic and related systems with various electrophiles.[17,3a,3e] In most cases no solid-state structure of the corresponding alkyllithium could be determined to support the absolute configuration of the stereogenic metallated carbon centre. The stereochemical course (inversion of the configuration) of the reaction of our alkyllithiums with the electrophile iodomethane in toluene can be understood on the basis of the solid-state structure of compound (*R*,*S*)-**2**·DABCO (crystallised from the same solvent as was used in the substitution reaction with the alkyl iodide) in combination with the computational studies.

The modelling of monomeric (*R*,*S*)-**2**·DABCO [B3LYP/6−31+G(d)] indicates that the highest occupied molecular orbital (HOMO) is chiefly located at the metallated carbon centre and the aromatic ring system (Figure 7). It can be deduced from the calculated orbital coefficients that both inversion and retention of the configuration are almost equally likely to result from electrophilic attack. Only the fact that the site opposite to the lithium centre is sterically accessible to attack by electrophiles makes it possible for (*R*,*S*)-**2**·DABCO to react selectively with inversion of configuration at C(3) under kinetic control in non-polar solvents.

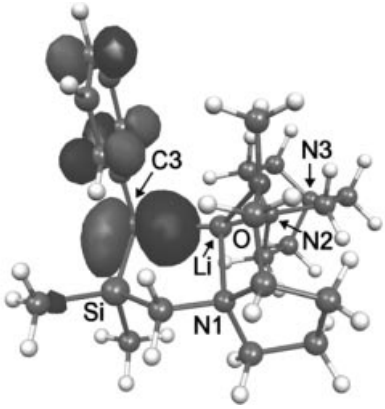

Figure 7. B3LYP/6−31+G(d)-optimised structure of monomeric (*R*,*S*)-**2**·DABCO and visualisation of the highest occupied molecular orbital (HOMO) (Molekel plot;[18] numbering scheme adopted from Figure 3)

Outlook

In a recent review article by Basu and Thayumanavan, the following quote on the main challenges in this research field can be found: "We believe that the first of these challenges is the development of a systematic structure-function relationship for the stereochemical behaviour of organolithium compounds. There have only been a few instances in which structural information about organolithium aggregates have been used as the starting point for the design of stereoselective lithiation/substitution sequences."[2a]

It is hoped that the correlation of experimental data, like stereoselectivities and the stereochemical pathways — especially results from solid-state structural analyses — will lead to a deeper understanding of the transformations of (highly diastereomerically enriched) alkyllithium compounds. It must always be of general interest to determine whether the results of such investigations may be of use in understanding the reaction pathways of alkyllithium systems, or if studies of systems like (*R*,*S*)-**2** and its derivatives are too specialised to set up common rules for the stereochemistry of this class of compounds.[19]

Experimental Section

Experimental Procedures: All reactions were carried out under an argon atmosphere using Schlenk tubes that had been flame-dried in vacuo. The solvents, including the NMR solvents, were dried according to common procedures. All NMR spectra were measured on a Bruker DRX-300 NMR spectrometer. Assignment of the signals was supported by DEPT135 and C,H-COSY experiments and

 © 2003 Wiley-VCH Verlag GmbH & Co. KGaA, Weinheim

the relative intensities of the resonance signals. Crystal structure determination of [(*R*,*S*)-**2**]$_2$·TMEDA: Stoe IPDS diffractometer (Stoe & Cie GmbH); data collection: Expose (Stoe & Cie, 1997); cell determination and refinement: Cell (Stoe & Cie, 1997); integration: Integrate (Stoe & Cie, 1999); numerical absorption correction: Faceit (Stoe & Cie, 1997). Crystal structure determination of (*R*,*S*)-**2**·DABCO: Bruker APEX-CCD (D8 three-circle goniometer) (Bruker AXS); data collection, cell determination and refinement: Smart version 5.622 (Bruker AXS, 2001); integration: SaintPlus version 6.02 (Bruker AXS, 1999); empirical absorption correction: Sadabs version 2.01 (Bruker AXS, 1999). The determination of the absolute configurations at the metallated stereogenic carbon centres of both compounds is unambiguous due to the fixed (*S*) configuration at the SMP substituent; for the achieved crystal quality of (*R*,*S*)-**2**·DABCO, the lack of a heavier atom than silicon does not allow a refinement of the absolute structure factor (Flack parameter) better than 0.2(2), indicating yet the overall refinement of the correct stereoisomer. The crystals of both compounds were mounted at −100 °C (N_2 stream), using the X-TEMP 2 device.[20] Both structures were solved applying direct and Fourier methods, using SHELXS-90[21] and SHELXL-97.[22] CCDC-210324 {[(*R*,*S*)-**2**]$_2$·TMEDA} and CCDC-210325 [(*R*,*S*)-**2**·DABCO] contain the supplementary crystallographic data for this paper. These data can be obtained free of charge at www.ccdc.cam.ac.uk/conts/retrieving.html [or from the Cambridge Crystallographic Data Centre, 12, Union Road, Cambridge CB2 1EZ, UK; Fax: (internat.) +44-1223/336-033; E-mail: deposit@ccdc.cam.ac.uk].

Computational Methods: All calculations were carried out on gas-phase structures. Structure optimisations at the B3LYP/6−31+G(d) level were performed using GAUSSIAN 98.[13] The basis for the starting structures were the coordinates of the X-ray structural analyses of (*R*,*S*)-**2** and (*R*,*S*)-**2**·DABCO; different starting conformers [C(3)−C(4) bond] were also investigated. Selected bond lengths [Å] and angles [°] of the optimised structure (*R*,*S*)-**2**·DABCO: Si−C(3) 1.832, Si−C(10) 1.941, Li−C(3) 2.211, Li−N(1) 2.206, Li−N(2) 2.170, Li−O 2.047, C(3)−C(4) 1.451, C(3)−Si−C(10) 108.5. For all transition states, only one imaginary frequency was found. For the deprotonation reactions, the vibrational modes corresponding to the imaginary frequency were in the direction of the C(3)−H bond dissociation. For the epimerisation reactions, the vibrational modes corresponding to the imaginary frequency were in the direction of the inversion of the configuration at C(3). IRC calculations (intrinsic reaction coordinate) were performed at the HF/3−21G level of theory.

[(*R*,*S*)-2]$_2$·TMEDA: A solution of (aminomethyl)benzylsilane [(*S*)-**1**; 450 mg, 1.62 mmol] and TMEDA (94.0 mg, 810 μmol) in *n*-pentane was combined with 950 μL (1.62 mmol) of a solution of *t*BuLi in *n*-pentane (1.7 M) at −90 °C. Upon warming to room temp. the lithium compound [(*R*,*S*)-**2**]$_2$·TMEDA was obtained as a microcrystalline orange powder. Whilst stirring at room temp., toluene was added dropwise until a solution was obtained. The yellow solution was kept at −30 °C. After 14 days at −30 °C [(*R*,*S*)-**2**]$_2$·TMEDA was obtained as orange-coloured single-crystals suitable for X-ray structural analysis (yield: 509 mg, 745 μmol, 92%). ^{1}H NMR (300.1 MHz, $C_6D_5CD_3$): δ = 0.27 (s, 6 H, SiCH_3), 0.31 (s, 6 H, SiCH_3), 1.29−1.58 (m, 8 H, CH_2), 1.82 [br, 2 H, SiC(*H*)Li], 1.89−2.04 (m, 18 H, NCH_3, NCH_2C, NC*H*), 2.11−2.28 (m, 4 H, NCH_2CH_2N), 1.45, 2.56 (AB-System, $^2J_{A,B}$ = 14.3 Hz, 2 H, SiCH_2N), 2.64 (ABX-System, unresolved, 2 H, CH_2O), 2.67 (s, 6 H, OCH_3), 3.03−3.19 (m, 2 H, CH_2), 3.24 (ABX-System, unresolved, 2 H, CH_2O), 6.19−6.23 (m, 2 H, aromat. H), 6.64−6.67 (m, 4 H, aromat. H), 6.90−6.97 (m, 4 H, aromat. H) ppm. ^{7}Li{^{1}H} NMR (116.6 MHz, $C_6D_5CD_3$): δ = 0.46 ppm. ^{13}C{^{1}H} NMR (75.5 MHz, $C_6D_5CD_3$): δ = −1.6 (2C, Si*C*H$_3$), 0.9 (2C, Si*C*H$_3$), 22.1 (2C, *C*H$_2$), 26.6 (2C, *C*H$_2$), 36.7 (2C) [Si*C*(H)Li], 45.8 (4C, N*C*H$_3$), 47.8 (2C, Si*C*H$_2$N), 57.1 (2C, N*C*H$_2$*C*H$_2$N), 57.8 (2C, N*C*H$_2$C), 58.7 (2C, O*C*H$_3$), 67.3 (2C, N*C*H), 70.8 (2C, *C*H$_2$O), 108.6 (2C, *C*-p), 119.9 (4C, *C*-m or *C*-o), 137.4 (4C, *C*-o or *C*-m), 157.3 (2C, *C*-i) ppm. ^{29}Si{^{1}H} NMR (59.6 MHz, $C_6D_5CD_3$): δ = −13.2 ppm.

(*R*,*S*)-2·DABCO: A solution of (aminomethyl)benzylsilane [(*S*)-**1**; 440 mg, 1.59 mmol] and DABCO (179 mg, 1.59 mmol) in *n*-pentane was combined with 935 μL (1.59 mmol) of a solution of *t*BuLi in *n*-pentane (1.7 M) at −90 °C. Upon warming to room temp. lithium compound (*R*,*S*)-**2**·DABCO was obtained as a microcrystalline yellow powder. Whilst stirring at room temp., toluene was added dropwise until a solution was obtained. The yellow solution was kept at −30 °C. After 21 days at −30 °C (*R*,*S*)-**2**·DABCO was obtained as yellow single-crystals suitable for X-ray structural analysis (yield: 744 mg, 1.53 mmol, 96%). ^{1}H NMR (300.1 MHz, $C_6D_5CD_3$): δ = 0.24 (s, 3 H, SiCH_3), 0.41 (s, 3 H, SiCH_3), 1.19−1.41 (m, 4 H, CH_2), 1.43, 2.60 (AB-System, $^2J_{A,B}$ = 14.2 Hz, 2 H, SiCH_2N), 1.78 [br, 1 H, SiC(*H*)Li], 1.85−2.07 (m, 2 H, NC*H*, NCH_2), 2.42 (s, 12 H, NCH_2CH_2N), 2.60 (s, 3 H, OCH_3), 2.97−3.00 (ABX-System, unresolved, 1 H, CH_2O), 2.97−3.06 (m, 1 H, NCH_2), 3.33−3.39 (ABX-System, unresolved, 1 H, CH_2O), 6.31−6.36 (m, 1 H, aromat. H), 6.69−6.72 (m, 2 H, aromat. H), 7.10−7.19 (m, 2 H, aromat. H) ppm. ^{7}Li{^{1}H} NMR (116.6 MHz, $C_6D_5CD_3$): δ = 0.45 ppm. ^{13}C{^{1}H} NMR (75.5 MHz, $C_6D_5CD_3$): δ = −2.2 (br., Si*C*H$_3$), 0.7 (Si*C*H$_3$), 22.8 (*C*H$_2$), 26.6 (*C*H$_2$), 34.5 [Si*C*(H)Li], 47.8 (6C, N*C*H$_2$*C*H$_2$N), 48.1 (Si*C*H$_2$N), 57.9 (N*C*H$_2$), 58.8 (O*C*H$_3$), 67.7 (N*C*H), 70.3 (*C*H$_2$O), 108.6 (*C*-p), 124.3 (2C, *C*-m or *C*-o), 128.9 (2C, *C*-o or *C*-m), 157.5 (*C*-i) ppm. ^{29}Si{^{1}H} NMR (59.6 MHz, $C_6D_5CD_3$): δ = −13.6 ppm.

Absolute electronic energies [B3LYP/6−31+G(d)] including ZPVE correction (uncorrected values in brackets): **MIN-1** −1210.329989 (−1210.85396686), **MIN-2** −1210.367902 (−1210.89273147), **TS-1** −1210.309066 (−1210.82931116), **MIN-3** −1210.330119 (−1210.85397884), **MIN-4** −1210.362321 (−1210.88757733), **TS-2** −1210.306980 (−1210.82688289), **MIN-5** −1052.035771 (−1052.42846659), **MIN-6** −1052.035924 (−1052.42849744), **TS-3** −1052.000391 (−1052.39218728), **MIN-7** −1207.002773 (−1207.47727275), **MIN-8** −1206.999447 (−1207.47375891), **TS-4** −1206.973602 (−1207.44687856), **MIN-9** −1397.204510 (1397.78271366), **MIN-10** −1397.202535 (−1397.78059515), **TS-5** −1397.175908 (−1397.75282437).

Acknowledgments

We are grateful to the Institut für Anorganische Chemie der Universität Würzburg, the Deutsche Forschungsgemeinschaft (DFG), the Sonderforschungsbereich 347, the Graduiertenkolleg 690, and the Fonds der Chemischen Industrie (FCI) for financial support. D. S. and K. W. thank the FCI for the grant of two scholarships. Furthermore we acknowledge Wacker-Chemie GmbH for providing us with special chemicals.

[1] Remark: In general, we speak of *enantiomerically enriched* metal alkyls when we focus our interest on the stereogenic metallated carbon centre, whereas these molecules are almost always *diastereomerically enriched* metal alkyls, due to the presence of more stereogenic centres than only the metallated one.

[2] [2a] A. Basu, S. Thayumanavan, *Angew. Chem. Int. Ed.* **2002**, *41*, 716, and literature cited therein. [2b] D. Hoppe, T. Hense,

Angew. Chem. Int. Ed. Engl. **1997**, *36*, 2282, and literature cited therein.

[3] For examples see: [3a] O. Stratmann, B. Kaiser, R. Fröhlich, O. Meyer, D. Hoppe, *Chem. Eur. J.* **2001**, *7*, 423. [3b] P. Beak, D. R. Anderson, M. D. Curtis, J. M. Laumer, D. J. Pippel, G. A. Weisenburger, *Acc. Chem. Res.* **2000**, *33*, 715. [3c] G. A. Weisenburger, N. C. Faibish, D. J. Pippel, P. Beak, *J. Am. Chem. Soc.* **1999**, *121*, 9522. [3d] D. J. Pippel, G. A. Weisenburger, S. R. Wilson, P. Beak, *Angew. Chem. Int. Ed.* **1998**, *37*, 2522. [3e] D. Hoppe, B. Kaiser, O. Stratmann, R. Froehlich, *Angew. Chem. Int. Ed. Engl.* **1997**, *36*, 2784. [3f] H. Ahlbrecht, J. Harbach, R. W. Hoffmann, T. Ruhland, *Liebigs Ann.* **1995**, 211. [3g] G. Boche, M. Marsch, J. Harbach, K. Harms, B. Ledig, F. Schubert, J. C. W. Lohrenz, H. Ahlbrecht, *Chem. Ber.* **1993**, *126*, 1887. [3h] R. I. Papasergio, B. W. Skelton, P. Twiss, A. H. White, C. L. Raston, *J. Chem. Soc., Dalton Trans.* **1990**, 1161.

[4] [4a] T. H. Chan, P. Pellon, *J. Am. Chem. Soc.* **1989**, *111*, 8737. [4b] T. H. Chan, S. Lamothe, *Tetrahedron Lett.* **1991**, *32*, 1847. [4c] T. H. Chan, K. T. Nwe, *J. Org. Chem.* **1992**, *57*, 6107.

[5] [5a] G. Fraenkel, J. H. Duncan, K. Martin, J. Wang, *J. Am. Chem. Soc.* **1999**, *121*, 10538. [5b] G. Fraenkel, K. Martin, *J. Am. Chem. Soc.* **1995**, *117*, 10336.

[6] C. Strohmann, K. Lehmen, K. Wild, D. Schildbach, *Organometallics* **2002**, *21*, 3079.

[7] M. Marsch, K. Harms, O. Zschage, D. Hoppe, G. Boche, *Angew. Chem. Int. Ed. Engl.* **1991**, *30*, 321.

[8] I. Hoppe, M. Marsch, K. Harms, G. Boche, D. Hoppe, *Angew. Chem. Int. Ed. Engl.* **1995**, *34*, 2158.

[9] H. Ahlbrecht, G. Boche, K. Harms, M. Marsch, H. Sommer, *Chem. Ber.* **1990**, *123*, 1853.

[10] E. Keller, Schakal 99, University of Freiburg (Germany): Freiburg 1999.

[11] D. Schildbach, *Doctoral Thesis*, University of Würzburg **2002**.

[12] C. Strohmann, K. Lehmen, A. Ludwig, D. Schildbach, *Organometallics* **2001**, *20*, 4138.

[13] Gaussian 98, Revision A.9, M. J. Frisch, G. W. Trucks, H. B. Schlegel, G. E. Scuseria, M. A. Robb, J. R. Cheeseman, V. G. Zakrzewski, J. A. Montgomery, Jr., R. E. Stratmann, J. C. Burant, S. Dapprich, J. M. Millam, A. D. Daniels, K. N. Kudin, M. C. Strain, O. Farkas, J. Tomasi, V. Barone, M. Cossi, R. Cammi, B. Mennucci, C. Pomelli, C. Adamo, S. Clifford, J. Ochterski, G. A. Petersson, P. Y. Ayala, Q. Cui, K. Morokuma, D. K. Malick, A. D. Rabuck, K. Raghavachari, J. B. Foresman, J. Cioslowski, J. V. Ortiz, A. G. Baboul, B. B. Stefanov, G. Liu, A. Liashenko, P. Piskorz, I. Komaromi, R. Gomperts, R. L. Martin, D. J. Fox, T. Keith, M. A. Al-Laham, C. Y. Peng, A. Nanayakkara, M. Challacombe, P. M. W. Gill, B. Johnson, W. Chen, M. W. Wong, J. L. Andres, C. Gonzalez, M. Head-Gordon, E. S. Replogle, J. A. Pople, Gaussian, Inc., Pittsburgh PA, 1998.

[14] F. Haeffner, P. Brandt, R. E. Gawley, *Org. Lett.* **2002**, *4*, 2101.

[15] All corrected and uncorrected electronic energies are given relative to **MIN-1**.

[16] At this point, the influence of the indispensable correction of all optimised structures by the *zero-point vibrational energy* (ZPVE) becomes obvious, since it decreases the absolute energies of the transition states more than those the minimum structures. This, and the computational method itself, significantly affect the electronic part of the activation energy. Thus, conclusions, deriving from too accurate comparisons of calculations with experimental data have to be drawn very carefully but can be found in the literature time and time again.

[17] For examples see: [17a] F. Marr, R. Fröhlich, D. Hoppe, *Org. Lett.* **1999**, *1*, 2081. [17b] N. C. Faibish, Y. S. Park, S. Lee, P. Beak, *J. Am. Chem. Soc.* **1997**, *119*, 11561. [17c] M. D. Curtis, P. Beak, *J. Org. Chem.* **1999**, *64*, 2996. [17d] F. Hammerschmidt, A. Hanninger, B. C. Simov, H. Völlenkle, A. Werner, *Eur. J. Org. Chem.* **1999**, 3511.

[18] S. Portmann, Molekel, Version 4.1.win-32, ETH Zürich (Switzerland), Zürich 2001.

[19] C. Strohmann, B. C. Abele, K. Lehmen, F. Villafañe, L. Sierra, S. Martín-Barrios, D. Schildbach, *J. Organomet. Chem.* **2002**, *661*, 149.

[20] T. Kottke, D. Stalke, *J. Appl. Cryst.* **1993**, *26*, 615.

[21] G. M. Sheldrick, SHELXS-90, *A Program for the Solution of Crystal Structures*, Universität Göttingen 1990.

[22] G. M. Sheldrick, SHELXL-97, *A Program for Crystal Structure Refinement*, Universität Göttingen 1997.

Received May 29, 2003

 © 2003 Wiley-VCH Verlag GmbH & Co. KGaA, Weinheim

Structures and Reactions of 1,3-Diamidodilithium Complexes: the Hemisolvated *l*-[$CMe_2\{CHMeN(R)\}_2Li_2\cdot OEt_2$], the Unsolvated 1:1 Mixed Organo-amidolithium *u*-[$CMe_2\{CHMeN(R')\}_2\cdot Li_2\cdot(n$BuLi$)_2$], and the Product of Oxidative Ring Closure, the Pyrazolidine *l*-[$(RNCHMe)_2CMe_2$] (R = 2-*i*Pr-C_6H_4; R′ = 2,6-*i*Pr$_2$-C_6H_3)

David T. Carey,[a] Francis S. Mair,*[a] Robin G. Pritchard,[a] John E. Warren,[a] and Rebecca J. Woods[a]

In memory of Ron Snaith, an inspired teacher, an inspiring researcher, and a humorous, kind and generous man.

Keywords: Solid-state structures / Lithium / N ligands / Carbanions

The hemi-solvated C_2-symmetric 1,3-diamidolithium *l*-[$CMe_2\{CHMeN(R)\}_2Li_2\cdot OEt_2$] has been crystallographically characterized. It reacts with oxygen to form the N-N ring-closed pyrazolidine *l*-[$(RNCHMe)_2CMe_2$]. The slightly bulkier C_s-symmetric amidolithium *u*-[$CMe_2\{CHMeN(R')\}_2\cdot Li_2$] forms an unsolvated 1:2 heterocubane complex with *n*BuLi in the solid state and in solution, as determined by X-ray crystallography and multinuclear NMR spectroscopy (R = 2-*i*Pr-C_6H_4; R′ = 2,6-*i*Pr$_2$-C_6H_3).

(© Wiley-VCH Verlag GmbH & Co. KGaA, 69451 Weinheim, Germany, 2003)

Introduction

The basis for the solid-state study of the aggregation behaviour of secondary amidolithium and organolithium compounds was set in two major reviews some years ago.[1,2] Given the massive growth of interest in the intervening years, it comes as little surprise that investigation of mixed aggregates containing each of these two key weapons in the modern arsenal of synthetic chemistry has developed rapidly. There are now a good number of mixed lithium aggregates containing both carbanions and secondary amido groups. Seminal solution-phase studies[3] have been augmented by theory[4] and by a number of X-ray crystallographically characterized examples. The solution-phase studies indicate that a complicated, equilibrating mixture, containing some unmixed homo-aggregate of one or both components, is commonly in existence, such that attempts to crystallise components of the mixture offer no guarantee of isolation of a mixed aggregate. Most crystallographic studies circumvent this problem by placing the carbanion and nitrogen-anion centres on the same covalent framework.[5] There are only a very small number of solid-state studies not invoking such C/N dianions in order to isolate mixed species.[6] We present here an additional example, different in a number of key respects from those reported previously. We have isolated this first solid-sate unsolvated 2:2 amido/organolithium tetralithium cluster by lithiation of a new class of diamine ligand. Diamines,[7] including, as in our examples, 1,3-diamines,[8] have also enjoyed much previous interest from lithium structural chemists, but ours differ from almost all previous structurally characterized examples in that they are C_2 or C_s symmetric, as opposed to the common C_{2v} case, and incorporate a higher degree of substitution into the chain linking the two amido centres than has previously been the case. There is but a single precedent for a crystallographically characterized C_2-symmetric dilithiodiamide.[7c] We report a hemi-solvated dilithiated diamine, and its novel oxidative ring-closure reaction to yield a C_2-symmetric pyrazolidine. The isolation of this product has implications for the mechanism of formation of the remarkable "inverse crown ether" class of compounds developed by Mulvey and co-workers.[9]

In addition to the above-cited precedents in organo/amido mixed aggregates, there are increasing numbers of examples where *n*BuLi is incorporated into P-N, As-N, Al-N and other main-group cluster species.[10] These have yet to mirror the synthetic utility of more conventional secondary amidolithiums, though,[3d,4b,11] and so it is secondary amidolithium compounds which remain our focus.

[a] Department of Chemistry, UMIST,
PO Box 88, Manchester M60 1QD, UK
Fax: (internat.) +44-161/200-4559
Email frank.mair@umist.ac.uk

 © 2003 Wiley-VCH Verlag GmbH & Co. KGaA, Weinheim **DOI: 10.1002/ejic.200300373**

Results and Discussion

Lithiation in hexane of *l*-(2-*i*Pr-$C_6H_4NHCHMe)_2CMe_2$, an amine derived from a diastereoselective hydroboration[12] of a 1,3-diimine,[13] produced a pale cream precipitate, which would only redissolve upon addition of a coordinating solvent. From a solution containing diethyl ether, crystals of *l*-[(2-*i*Pr-$C_6H_4NHCHMe)_2CMe_2Li_2{\cdot}OEt_2$] (**1**·$OEt_2$), deposited. Its structure was determined by X-ray crystallography, and is depicted in Figure 1; selected geometric parameters are listed in Table 1.

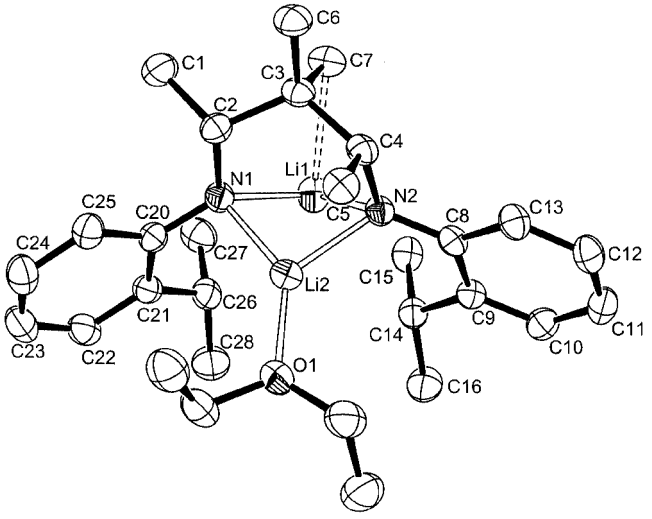

Figure 1. Molecular structure of **1**·OEt_2; hydrogen atoms are omitted

Table 1. Selected bond lengths [Å] and angles [°] for **1**·OEt_2

N(1)−Li(1)	1.945(3)	C(20)−N(1)−C(2)	115.89(11)
N(1)−Li(2)	2.029(3)	C(20)−N(1)−Li(1)	136.55(12)
N(2)−Li(1)	1.953(3)	C(2)−N(1)−Li(1)	106.73(11)
N(2)−Li(2)	2.008(3)	C(20)−N(1)−Li(2)	100.04(11)
Li(2)−O(1)	1.865(3)	C(2)−N(1)−Li(2)	105.74(11)
Li(1)−C(7)	2.487(3)	Li(1)−N(1)−Li(2)	75.21(11)
Li(2)−C(4)	2.593(3)	C(8)−N(2)−C(4)	115.92(11)
Li(2)−C(20)	2.652(3)	C(8)−N(2)−Li(1)	130.13(11)
Li(2)−C(5)	2.669(3)	C(4)−N(2)−Li(1)	107.47(11)
N(1)−C(2)	1.4754(17)	C(8)−N(2)−Li(2)	121.63(11)
N(1)−C(20)	1.3901(17)	C(4)−N(2)−Li(2)	95.03(10)
N(2)−C(4)	1.4742(17)	Li(1)−N(2)−Li(2)	75.51(11)
N(2)−C(8)	1.3778(17)	N(1)−Li(1)−N(2)	95.61(12)
C(1)−C(2)	1.537(2)	O(1)−Li(2)−N(2)	130.62(14)
C(2)−C(3)	1.5640(19)	O(1)−Li(2)−N(1)	137.21(14)
C(3)−C(6)	1.5393(19)	N(2)−Li(2)−N(1)	91.31(11)
C(3)−C(7)	1.545(2)	N(1)−C(2)−C(1)	110.50(12)
C(3)−C(4)	1.566(2)	N(1)−C(2)−C(3)	111.79(11)
C(4)−C(5)	1.541(2)	C(1)−C(2)−C(3)	111.12(12)
O(1)−C(31)	1.439(2)	C(6)−C(3)−C(7)	106.97(12)
O(1)−C(30)	1.4509(19)	C(6)−C(3)−C(2)	108.39(12)
C(6)−C(3)−C(4)	106.83(12)	C(7)−C(3)−C(2)	111.79(12)
C(2)−C(3)−C(4)	114.09(11)	C(7)−C(3)−C(4)	108.42(12)
N(2)−C(4)−C(5)	111.18(11)	C(3)−C(7)−Li(1)	80.05(10)
C(5)−C(4)−C(3)	112.79(11)	N(2)−C(4)−C(3)	112.43(11)

Only a single diethyl ether molecule is incorporated into the structure, which is comprised of a single diamido unit with a central Li_2N_2 ring. This most common motif[1] is in this case rather puckered [torsion angle Li(1)−N(3)−Li(2)−N(1) = −34°]. This butterfly conformation is characteristic of *di*amides,[7,8] where the linking group draws together the two N-vertices of the Li_2N_2 ring, pushing the lithium atoms downwards as shown below. Also apparent from this scheme is the reason that cyclic diamidolithium complexes often defy the ring-laddering prediction, since the projection of one of the substituents of the secondary amine into an axial position, which prevents ring stacking, thus favouring ring laddering,[1] is converted into an equatorial projection by the constraint of the diamido ring.

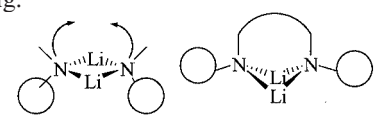

Evident from a comparison of the structures of **1**·OEt_2 and its protonated secondary amine precursor[12] is the fact that the conformational preferences of the organic portion are dominant. The organic portions of the structures map closely, since in the diamine, an H-bonded ring is present. The N−N distance of 2.89 Å in **1**·OEt_2 matches that of 2.84 Å in the NH precursor.[12] Because of the two lithium atoms bonded to each nitrogen atom, the ring in **1** can at once be described as both a boat and a chair. The axial/equatorial arrangement of the methyls attached to the two chiral centres is also identical in metallated and unmetallated forms. Crystallographic symmetry generates the molecule of opposite polarity in this racemic crystal. In the only other dilithiated C_2-symmetric diamine,[7c] the 1,2 diamidolithium *l*-[Li{*t*BuN$(CHMe)_2$N*t*Bu}Li], which, like most dilithiated diamines, defies Snaith's laddering principle by adopting a stacked, dimeric structure, disorder of both enantiomers confused the issue of conformation, and of whether in its dimeric structure, like or unlike enantiomers aggregated. It was synthesised by the rather different route of diastereoselective double carbolithiation[7c] of the parent 1,2-diimine *t*BuN$(CH)_2$N*t*Bu. The parent 1,3-diimines from which **1** is derived do not undergo similar carbolithiation or carbozincation reactivity.[14]

Included in the previous examples of stacked diamidolithium structures is a case involving a 1,3-diamine linkage: [Li{$Me_3SiN(CH_2)_3NSiMe_3$}Li]$_2$ was obtained as an unsolvated stack, reminiscent of the 1,2 cases discussed above.[8b] Complex **1** differs from all of these cases in the fact that it precipitates as an insoluble (presumably polymeric) powder from hexane. In this behaviour, it mimics the less-bulky amides which gave rise to the ring laddering principle.[1] The possibility that **1** aggregates in a ladder form is supported by close inspection of its structure. Unusually for an arylamidolithium,[15] the aryls are almost coplanar with the CNC planes (dihedral angles of −16.4° on the side bearing the equatorial methyl, and 2.1° on the axial methyl side). This facilitates π-interaction of the amido density into the

 © 2003 Wiley-VCH Verlag GmbH & Co. KGaA, Weinheim

aromatic ring, as shown by the relatively short (aryl)C−N bonds (mean 1.38 Å, cf. 1.43 Å for orthogonal rings; see later). This coplanarity is optimal for lateral packing (laddering), while both isopropyl groups are in a position which would make stacking difficult. This perhaps explains the insolubility of **1** in non-donor solvents, despite its relative bulk.

Nevertheless, **1** crystallizes with only a single molecule of diethyl ether coordinated to Li(2), rendering it three-coordinate, while Li(1) remains merely two-coordinate. A fairly close CH···Li interaction is present across the boat-ring. This sort of interaction is quite frequently found to low-coordination number lithium atoms,[16] but it is more usually a C_α or C_β interaction, as in [(*n*BuLi)$_6$], for example (see later).[17] To find a C···Li distance of 2.49 Å to a C_δ carbon is without precedent.[16] However, we tend toward the view that the short "δ-agostic" interaction is a consequence of the high degree of puckering of the boat conformation in the C_2N_2Li ring, rather than a cause of it. The hemisolvated nature of the Li_2N_2 ring has some precedent; in [$C_{10}H_6$(N{Li(THF)}$SiMe_3$){N(Li)$SiMe_3$}], also a 1,3-diamidolithium, though one with a planar aromatic core, a single lithium is coordinated by THF, while the other engages in π-interactions with a neighbouring molecule.[8a] Similar situations obtain in doubly lithium-reduced diazadiene complexes.[7e] In **1**, the only such stabilizing interaction is the aforementioned "δ-agostic" one.

The exposed nature of the low-coordinate lithium may be a factor in the reactivity of compound **1**. Interestingly, a similarly exposed, bent two-coordinate lithium is present in [LiMg{N($SiMe_3$)$_2$}$_3$],[9a] which has been shown to be extremely sensitive to traces of oxygen, generating the first case of the remarkable oxo-centred "inverse crown ether" cluster class.[9b] It has, however, never been established without doubt that the oxo-centre of the clusters was a result of reduction of dioxygen, because it was not possible to unambiguously identify the partner product of oxidation, the presumed substituted hydrazine {N($SiMe_3$)$_2$}$_2$, in the reaction mixtures.

We find the opposite scenario to pertain for **1**: significant amounts of the stable, crystalline product of oxidative N-N ring closure, the substituted pyrazolidine **2**, were found in aged solutions of **1**, and in reaction products where **1** was employed as an intermediate, whereas we have not isolated oxide-containing aggregates. It was subsequently shown that exposure of solutions of **1** to dry oxygen generated significant yields of **2**. While we have yet to identify oxo-centred lithium clusters in our products, this first clear proof of oxidative N-N coupling of secondary amidolithium compounds is strong indirect evidence supporting the mechanism proposed by Mulvey and co-workers for the generation of inverse crown ethers.[9]

Normal routes to pyrazolidines involve additions across an N−N π-bond.[18] In 1994, Nelsen et al. reported a curious reaction in which two molar equivalents of *t*BuLi were reacted with a polycyclic secondary bis(chloroamine) to yield an N−N bonded species,[19] but in this case the rings formed in the ring closure were four- and six-membered. The mechanism of this reaction was not discussed. It seems that our route to pyrazolidines is new. Structurally (see Figure 2), there is little remarkable in **2**; the conformation and bonding parameters (Table 2) are as expected; an approximate C_2 axis passes through the mid-point of the N−N bond and the C(3) atom. C(2), C(3), and C(4) are coplanar; the ring puckers above and below this plane at the pyramidalized N(1) and N(2) centres, in which the neighbouring lone pairs adopt an antiperiplanar arrangement.[19] This allows both methyls on the chiral carbon to adopt equatorial positions. The crystals are racemic.

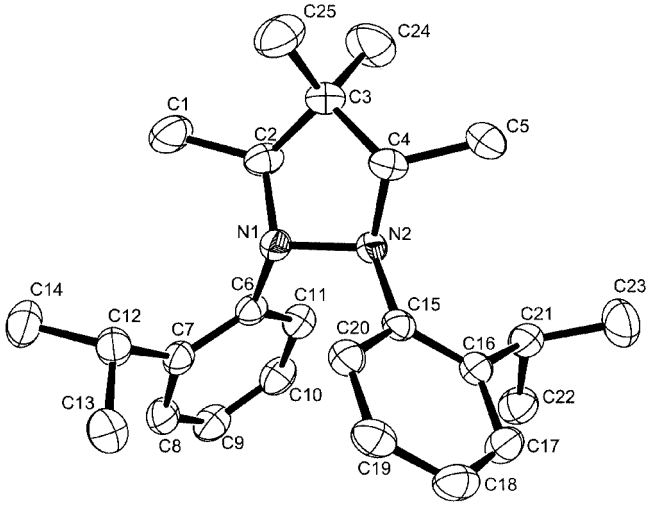

Figure 2. Molecular structure of **2**; hydrogen atoms are omitted

Table 2. Selected bond lengths [Å] and angles [°] for **2**

N(1)−C(6)	1.4505(17)	C(15)−N(2)−C(4)	111.52(10)
N(1)−C(2)	1.4757(17)	C(15)−N(2)−N(1)	109.79(9)
N(1)−N(2)	1.4846(15)	C(4)−N(2)−N(1)	100.94(10)
N(2)−C(15)	1.4510(17)	N(1)−C(2)−C(1)	111.25(13)
N(2)−C(4)	1.4773(17)	N(1)−C(2)−C(3)	104.44(11)
C(1)−C(2)	1.507(2)	C(1)−C(2)−C(3)	116.97(13)
C(2)−C(3)	1.543(2)	C(25)−C(3)−C(24)	109.35(15)
C(3)−C(25)	1.518(2)	C(25)−C(3)−C(2)	114.47(14)
C(3)−C(24)	1.522(2)	C(24)−C(3)−C(2)	108.18(14)
C(3)−C(4)	1.5450(19)	C(25)−C(3)−C(4)	109.23(13)
C(4)−C(5)	1.504(2)	C(24)−C(3)−C(4)	113.02(14)
		C(2)−C(3)−C(4)	102.55(11)
C(6)−N(1)−C(2)	111.75(10)	N(2)−C(4)−C(5)	111.67(12)
C(6)−N(1)−N(2)	109.17(10)	N(2)−C(4)−C(3)	104.36(10)
C(2)−N(1)−N(2)	100.97(10)	C(5)−C(4)−C(3)	116.61(12)

Turning now to mixed aggregates containing amido units akin to **1**, by far the most common means of achieving mixed carbanion/N-aggregation in the solid state is to tie both anionic centres together in the same molecule, i.e. to use heterodentate C/N dianions.[5a−5e] Rather less common are genuine mixed aggregates of independent carbanion and amido anion, where the thermodynamic balance between homo-aggregates and mixed aggregates is often a fine one, as evidenced by the observance of mixtures in solution.[3] The enthalpy-neutrality of the formation of mixed dimer

 © 2003 Wiley-VCH Verlag GmbH & Co. KGaA, Weinheim

over homodimer has been demonstrated computationally for simple amido and carbanion groups.[4a] However, by appropriate choice of ancillary donor atoms and/or steric bulk, it has proven possible in a few cases to isolate heterocomponent amidolithium/*n*-butyllithium aggregates.[6] In addition, there are two examples where C/N dianions are co-aggregated with Ph_2N monoanions and/or *n*-butyl carbanions in a large cluster,[5f,5g] and another example where an anti-fluorite-like cluster of $(C_6H_5C_6H_4)NLi_2$ is stabilized by a methanide anion.[20] All of these are ether-solvated.

We restrict our discussion to simple cases of solid-state co-aggregation of secondary amidolithium species with organolithium species. In this category there are only two structural types in existence (see below), **3** and **4**.[6] Isostructural analogues of **3** containing *sec*- and *tert*-butyllithium are also known.[6a] The structure of the homoaggregate, $[(n\text{BuLi})_6]$ (**5**) is shown for comparison.[17]

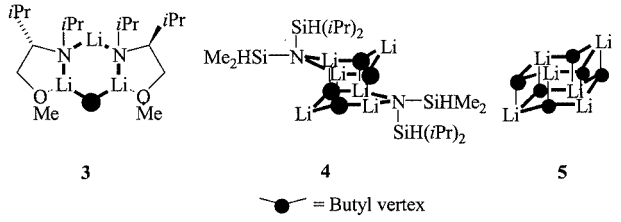

Use of an excess of *n*BuLi in the metallation of the bulkier, C_s-symmetric *u*-(2,6-$i\text{Pr}_2$-C_6H_3NHCHMe)$_2$$CMe_2$ in hexane afforded a solution from which the mixed organo/amidolithium compound **6** crystallized. Its structure (Table 3 and Figure 3) is that of a heterocubane, in which a dimer of *n*BuLi stacks with a diamidodilithium unit similar to that in **1**. The incorporation of bulk in both *ortho* positions on the phenyl rings, and the *u*-(*meso*) diastereochemistry of the diamide, results in conformational differences: both of the chiral carbons can now direct their methyl substituents into equatorial positions while maintaining the dual boat/chair character of the ring. This forces both aryls to pack in an approximately orthogonal disposition with respect to the average plane of the $N_2C_3Li_2$ pair of rings. In turn, this facilitates a stacked packing arrangement. However, key to the isolation of a mixed organo-amido complex is the fact that the extreme bulk of the 2,6-diisopropylphenyl substituents still precludes such a stacking arrangement in a homo-aggregate of amidolithium units; in order to relieve steric strain, it is the less demanding *n*BuLi units which are pressed into service to complete the stable, heterocubane arrangement. Looking from the other perspective, this is a case where the extra bulk of the amido unit forces *n*BuLi to adopt a role in a tetrameric aggregate, whereas in a homo-aggregate of *n*BuLi a hexameric stack of two trimeric rings is preferred.[17]

Unfortunately, attempts to isolate a homoaggregate of the 1,3-diamido unit in **6** resulted only in isolation of oils, though a similar 1,2-diamidolithium, with identical 2,6-diisopropylphenyl substituents, has been characterized.[7b] It is a rare example of an unsolvated four-runged step-ladder (the extreme bulk limits growth of the ladder in this case),

Table 3. Selected bond lengths [Å] and angles [°] for **6**

N(1)−Li(2)	1.997(3)	C(3)−C(7)−Li(1)	77.58(10)
N(1)−Li(1)	2.041(3)	N(2)−C(8)−Li(3)	66.40(9)
N(1)−Li(4)	2.180(3)	N(1)−C(20)−Li(4)	64.62(9)
N(2)−Li(1)	1.977(3)	C(33)−C(32)−Li(4)	75.60(11)
N(2)−Li(2)	2.031(3)	Li(4)−C(32)−Li(2)	68.21(10)
N(2)−Li(3)	2.182(3)	C(33)−C(32)−Li(3)	121.69(13)
C(2)−N(1)	1.4851(18)	Li(4)−C(32)−Li(3)	69.42(11)
C(2)−C(3)	1.5715(19)	Li(2)−C(32)−Li(3)	67.57(10)
C(3)−C(4)	1.581(2)	C(32)−C(33)−Li(4)	64.66(10)
C(4)−N(2)	1.4916(18)	C(37)−C(36)−Li(4)	126.78(13)
C(7)−Li(1)	2.402(3)	Li(1)−C(36)−Li(4)	65.20(10)
C(8)−N(2)	1.4267(18)	C(37)−C(36)−Li(3)	140.59(13)
C(8)−Li(3)	2.318(3)	Li(1)−C(36)−Li(3)	66.19(10)
C(20)−N(1)	1.4301(18)	Li(4)−C(36)−Li(3)	68.83(10)
C(20)−Li(4)	2.369(3)	C(20)−N(1)−C(2)	113.94(11)
C(21)−Li(4)	2.500(3)	C(20)−N(1)−Li(2)	104.58(11)
C(32)−Li(4)	2.178(3)	C(2)−N(1)−Li(2)	110.26(11)
C(32)−Li(2)	2.185(3)	C(20)−N(1)−Li(1)	144.50(11)
C(32)−Li(3)	2.222(3)	C(2)−N(1)−Li(1)	97.41(11)
C(33)−Li(4)	2.334(3)	Li(2)−N(1)−Li(1)	77.95(11)
C(36)−Li(1)	2.182(3)	C(20)−N(1)−Li(4)	79.04(10)
C(36)−Li(4)	2.209(3)	Li(2)−N(1)−Li(4)	71.53(10)
C(36)−Li(3)	2.224(3)	Li(1)−N(1)−Li(4)	68.09(10)
		N(1)−Li(2)−N(2)	93.23(11)
C(8)−N(2)−C(4)	116.82(11)	C(8)−N(2)−Li(1)	136.84(11)
C(4)−N(2)−Li(2)	91.95(10)	C(4)−N(2)−Li(1)	101.78(11)
Li(1)−N(2)−Li(2)	78.66(11)	C(32)−Li(4)−C(33)	39.74(7)
C(8)−N(2)−Li(3)	76.79(10)	N(1)−Li(4)−C(36)	108.66(12)
Li(1)−N(2)−Li(3)	70.51(11)	C(32)−Li(4)−C(36)	105.74(12)
Li(2)−N(2)−Li(3)	71.05(10)	C(32)−Li(4)−N(1)	104.85(11)
N(2)−Li(1)−N(1)	93.54(11)	C(32)−Li(3)−C(36)	103.73(12)
N(2)−Li(1)−C(36)	114.41(13)	N(2)−Li(3)−C(36)	105.07(12)
N(1)−Li(1)−C(36)	115.20(12)	N(2)−Li(3)−C(32)	106.22(12)
N(2)−Li(1)−C(7)	87.03(10)	N(2)−Li(2)−C(32)	113.31(12)
N(1)−Li(1)−C(7)	94.07(11)	N(1)−Li(2)−C(32)	111.28(12)

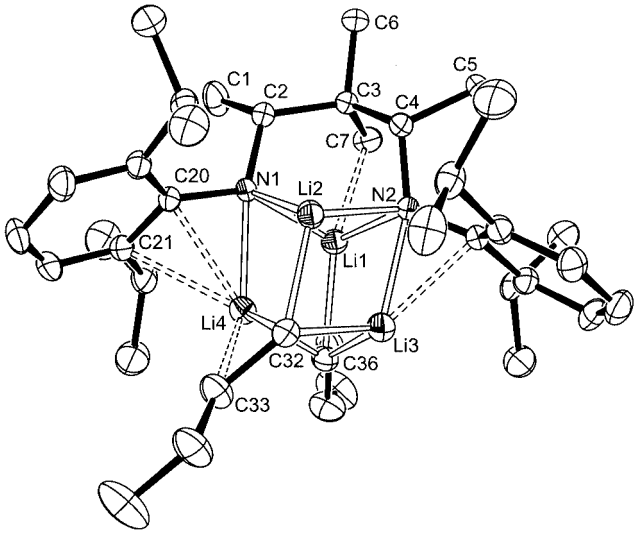

Figure 3. Molecular structure of **6**; hydrogen atoms are omitted

and it seems reasonable to assume a similar arrangement would occur for the 1,3 analogue. In such an aggregation mode, only two lithiums attain three coordination, the other two having to limit themselves to two-coordination, augmented by aryl-Li interactions. Just such a situation occurs

 © 2003 Wiley-VCH Verlag GmbH & Co. KGaA, Weinheim

in an arched unsolvated limited ladder attained by lithiation of a trimethylsilyl-substituted benzyldiamine.[8c] Incorporation of *n*BuLi into the aggregate **6** allows for more stabilizing electrostatic interactions, all four lithium atoms attaining three coordination. The energetic cost of this to the *n*BuLi fragment is modest. It finds itself in a very similar arrangement to that of its homoaggregate, capping a triangular face of lithium atoms, to use the traditional terminology for the description of organolithium structures.[17] In this mode of description, **5** is viewed as an octahedral array of lithium atoms with six of its faces capped by butyl anions. In the same way, the mixed aggregate **4** is described as an octahedron in which four faces are capped by butyl anions, and two edges are capped by amido anions. We prefer to describe the structures on the basis of the electrostatic interaction which hold them together, rather than the Li−Li framework, which has been shown not to be involved in bonding.[21] Re-examination of **5** in this way reveals a view of it as a stack of cyclic trimers. The inter-trimer distances are systematically longer than the intra-trimer ones.[22] Each six-membered ring adopts a flattened chair conformation. The extra bulk of the amido groups in **4** is inconsistent with stacking, but they can be accommodated without distorting the structure unduly simply by flipping one corner of each six-membered ring, so that each is in a boat, rather than a chair, conformation. This generates room for all four butyl groups to direct their secondary interaction to the two lithium atoms that are left two-coordinate by the cleavage of the two stacking interactions. Further stabilization through SiH−Li interactions help to favour the mixed aggregate **5**, despite the fact that the stoichiometry employed in its preparation was far from 1:2.[6b] In the synthesis of **6**, we originally employed a 2:1 N:*n*Bu ratio, hoping to isolate unsolvated versions of compound **3**, but in our hands also, there was no stoichiometric control over the product identity. This is generally true of all mixed aggregate syntheses in s-block chemistry. The key to the unusual stoichiometry of **3** is clearly in the internal solvation and high degree of bulk, which destabilize the homoamide aggregate in favour of incorporation of a single unit of organolithium.[6a] All of these factors must be considered for the successful isolation of solid state mixed aggregates. Though in ether solutions, cubic amido-organoaggregates similar to **6** have been previously characterized by NMR spectroscopy,[3b,3c,3e] they are generally components of mixtures. Synthetic studies have shown that incorporation of *n*BuLi into the mixed aggregates often increases its reactivity, and where the amidolithium unit is chiral, asymmetric induction can be observed in additions of *n*BuLi across carbonyl bonds.[11]

This might be partially explained by a closer inspection of the structure of **6**. It has a δ-agostic interaction between C(7) and Li(1) even shorter (2.40 Å) than that in **1**, possibly as a result of flattening of the butterfly (torsion = −31°, a decrease of 3° with respect to **1**·OEt_2) by the steric influence of the $(n\text{BuLi})_2$ ring, and a more conventional β-agostic interaction between C(33) and Li(4), separated by 2.33 Å. This is longer than the β-agostic distances in **5** (2.28 Å on average), because all those distances in **5** involved interactions *within* each trimeric ring.[17] The Li−C−Li angles at the bridging carbons in the trimeric rings of **5** average 85°, whereas those in the dimeric ring found in **6** average 69°. Lithium-β-carbon distances are therefore trigonometrically predetermined to be longer in tetramers (stacks of dimers) than in hexamers (stacks of trimers), as shown schematically below. This may be linked to higher reactivity.

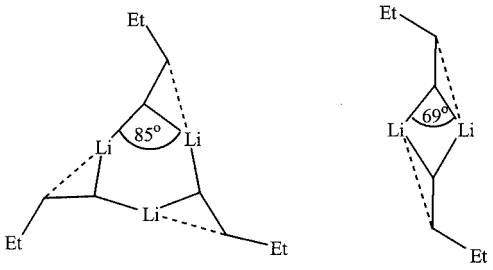

Similar β-agostic distances to that in **6** are found in $[(n\text{BuLi})_4(t\text{BuOLi})_4]$, in which $(n\text{BuLi})_2$ units cap either end of a folded (*t*BuOLi) octagon.[23] In fact, there is only a single conventional β-agostic interaction in **6**, shown in Figure 4. The other butyl chain is excluded by the bulky substituents, a result of the C_s symmetry of the backbone, telegraphed via the conformation of the aryl rings, and the δ-agostic interaction to C(7) differentiating either side of the $(n\text{BuLi})_2$ unit. Aryl-Li interactions are probably more important in stabilizing the structure of **6**: *ipso*-C(aryl)···Li distances of 2.318(3) and 2.369(3) Å are in the normal range for such interactions.[7b] Despite the fact that in all structures the hydrogen atoms were freely refined, no statistically meaningful systematic lengthening of C−H bonds is seen for hydrogens with short H···Li contacts.[16]

The above discussion presupposes that **6** can be rationalized as a stack of amidolithium dimers with butyllithium dimers. The Li−N distances support this view, those within the Li_2N_2 butterfly [1.977(3)−2.041(3) Å] being systematically shorter than the stacking N−Li distances [2.180(3) and 2.182(3) Å].[1] However, the Li−C distances involving the carbanionic centres of the $(n\text{BuLi})_2$ unit are in the range 2.178(3)−2.224(3) Å, and the stacking interactions lie within the *lower* part of that range [2.182(3) and 2.185(3) Å]. There is, therefore, little basis for viewing the $(n\text{BuLi})_2$ unit as an independent entity within the cluster. Rather, the molecule is an integrated whole. The rather longer-than-expected C−Li distances within the $(n\text{BuLi})_2$ "dimer" might be explained by a slight elongation of the Li(3)···Li(4) distance {2.506(4) Å, cf 2.42 Å in $[(n\text{BuLi})_4(t\text{BuOLi})_4]$ and 2.43 Å in **5** for the equivalent distances}[17,23] in order for those two lithium atoms to engage most effectively in the stacking interactions with N(1) and N(2).

Given the extent of previous interest in the solution-phase behaviour of mixed amidolithium/butyllithium aggregates,[3] and the fact that reactions of such aggregates have hitherto been performed only in solution,[11] a limited NMR investigation of **6** was undertaken. The signals in the NMR spectra are broad at room temperature. The best-

 © 2003 Wiley-VCH Verlag GmbH & Co. KGaA, Weinheim

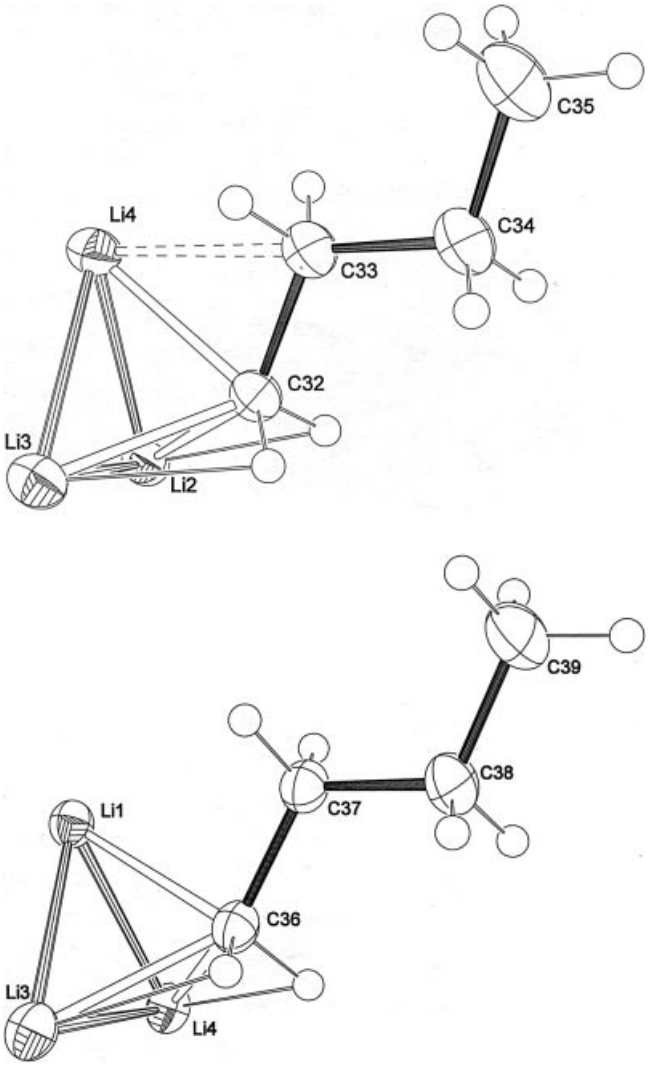

Figure 4. Views of the two butyl anions (top) including normal Cβ interaction to the lithium with shortest bond to Cα and (bottom) lacking Cβ interaction due to steric effect of C(7)

resolved data were obtained at −40 °C. It is reasonable to assume that the puckering of the central $C_3N_2Li_2$ ring is maintained, since flexing into the alternative conformation [C(7) equatorial] would place a total of three methyl groups and one lithium atom, as well as the isopropyl substituents on each aryl, into axial positions. It is deemed highly unlikely that this conformation would be populated to any appreciable extent. Therefore, the environments of Li(1) and Li(2) should remain well-distinguished. Li(3) and Li(4), being related by the approximate molecular C_s symmetry plane, are less likely to exhibit distinct chemical shifts. At −40 °C a ^{7}Li NMR spectrum consistent with this model, i.e. three signals in the ratio 1:1:2, is observed. In the ^{1}H NMR spectrum at −40 °C, two high-field signals in the *n*BuLi C_α region are observed. Both show a characteristic non-first-order envelope which has previously been associated with restricted rotation about the $C_\alpha-C_\beta$ bond of the butyl anions.[24] It is observed here at significantly higher temperature than in the other studies, which were performed in ether solvents.[3,24] It may be that the bulky amide substituents help to hinder such rotation. In any case, the presence of two types of butyl is consistent with the molecular symmetry of **6**. The other butyl signals are partially obscured by the methyl region, but the integrals of the resolved peaks match for two distinct α-carbons for each amido ligand, of which there is only one type. The observance of two distinct isopropyl methine resonances in the ratio 1:1 shows that the aryl-N bonds are fixed. An interesting feature of the ^{1}H NMR spectrum is the observance of a quintet at δ = 0.2 ppm. This is tentatively assigned (attempts at ^{1}H-^{1}H COSY failed for these broad, weak peaks) to the β-carbon of an atypical butyl group. For **5** in toluene, and for $(n\text{BuLi})_4$ in THF, this proton environment resonates around δ = 1.5 ppm. The marked shift in what must either be the β- or the γ-proton environment into a region which is silent in all other observed spectra of *n*BuLi fragments suggests an unusual situation.[3,24] Given that close β-C(H)···Li contacts are reported in all other *n*BuLi fragments discussed above, but are absent in one of the butyls in **6**, we tentatively ascribe the anomalous shift to the absence of the agostic-type interaction. More normal β, γ and δ environments were also observable, but not all eight expected butyl peaks could be identified due to crowding in the δ = 0.9−1.7 ppm region. The different butyl environments were less-easily distinguished in the ^{13}C NMR spectrum, but such resonances as could be discerned were consistent with the maintenance of the structure **6** in solution. It should be stressed, however, that alternative models of behaviour, such as expulsion of one *n*BuLi unit from **6** to form one sixth of an equivalent of **5** (matching of some of the butyl resonances to **5** in toluene was quite close, but not identical), and reversion of the remaining cluster to a structure analogous to **3**,[6a] cannot be ruled out. There was fluxionality evident (e.g. coalescence of the different butyl environments at 0 °C), but detailed solution studies lie outside the scope of this predominantly solid-state investigation.

Unfortunately, the *l*-diastereomer of the bulkier amine used in **6** is inaccessible due to the difficulty in deboronating the hydroboration intermediate,[12] but, given the encouraging results that have been obtained by others in enantioselective syntheses using mixed aggregates of chiral amines,[11] we feel justified in pressing on with resolution of the amine used in **1**, and its employment in mixed aggregate synthesis. There may yet prove to be a role for the C_s-symmetric amine used in **6** in the promotion of syndiotacticity in alkene polymerization, where titanium complexes of 1,3-diamido ligands identical to that in **6** but for the de-symmetrizing methylene backbone substituents, have shown promise.[25]

Experimental Section

All manipulations were carried out under a protective argon blanket, either in a double manifold argon/vacuum line or argon-filled recirculating glovebox. Argon was dried over phosphorus pentoxide supported on vermiculite. Toluene and diethyl ether were used freshly distilled under argon from sodium-benzophenone ketyl; in the case of hexane, approximately 5% tetraglyme was added in order to dissolve the sodium-benzophenone ketyl. $CDCl_3$, C_6D_6,

 © 2003 Wiley-VCH Verlag GmbH & Co. KGaA, Weinheim

C_7D_8 and [D_8]THF were stored over freshly activated 4 Å molecular sieves. The hexane solution of *n*BuLi was used as received and standardised using *N*-benzylbenzamide.[26] *u*-*N*,*N*′-bis(2,6-diisopropylphenyl)-3,3′-dimethylpentane-2,4-diamine and *l*-*N*,*N*′-bis(2-isopropylphenyl)-3,3′-dimethylpentane-2,4-diamine were prepared by literature methods.[12] All other reagents were obtained from standard commercial vendors and used as received.

Melting points were determined in sealed glass capillaries under argon. Elemental analyses were performed by the microanalytical group in the Chemistry Department at UMIST.

Chemical shifts are given in ppm and referenced to residual solvent shifts for ^{13}C and ^{1}H; ^{7}Li spectra were referenced to 0.1 M LiCl in D_2O. Assignments were made with the aid of DEPT and HMQC experiments. Infrared spectra were recorded on a Nicolet Nexus-FTIR/Raman spectrometer using NaCl plates and nujol mulls.

***l*-[(2-*i*Pr-C_6H_4NCHMe)$_2$CMe$_2$Li$_2$·OEt$_2$] (1·OEt$_2$):** *n*BuLi (16.0 mL of a 1.51 M hexane solution, 24.16 mmol) was added to a stirring solution of *l*-[(2-*i*Pr-C_6H_4NHCHMe)$_2$CMe$_2$ (4.03 g, 11.0 mmol) in hexane (30 mL) at room temperature. Initially, a pale orange solution was obtained, but over a stirring period of 5 minutes, a cream precipitate deposited. Heating to boiling did not induce re-dissolution. To the cream precipitate was added diethyl ether (65 mL, in 5 mL volumes) over a 10 minute period until the precipitate had dissolved. The resulting dark orange solution was cooled to −45 °C yielding crystals of dilithiated amido complex **1**·OEt$_2$. Isolation by filtration in vacuo resulted in a decrease in crystal quality, associated with loss of coordinated diethyl ether. Isolated material (2.84 g, 57% based on the formulation [2-*i*Pr-C_6H_4NCHMe)$_2$CMe$_2$Li$_2$.OEt$_2$]) was poorly soluble in deuterobenzene. M.p. 160−163 °C dec. $C_{29}H_{46}Li_2N_2O$ (452.6): calcd. C 77.0, H 10.2, N 6.2; found C 79.0, H 10.1, N 6.6. Poor agreement due to diethyl ether loss. ^{1}H NMR (300 MHz; [D_8]THF, 35 °C): δ = 1.08 [br. s, 6 H, NCHMeC(*Me*)$_2$CHMeN],1.12 (d, 6 H, *Me*CHMe), 1.17 [d, 6 H, NCH*Me*C(Me)$_2$CH*Me*N], 1.31 (d, 6 H, MeCH*Me*), 2.69 (sept., 2 H, MeC*H*Me), 3.96 [q, 2 H, NC*H*MeC(Me)$_2$C*H*MeN], 7.00 (dd, 2 H), 7.10 (td, 2 H), 7.20 (td, 2 H) and 7.35 (dd, 2 H, aromatic C*H*) ppm. ^{13}C NMR (75 MHz; [D_8]THF, 35 °C): δ = 15.6 [NCH*Me*C(Me)$_2$CH*Me*N], 21.3 [NCHMeC(*Me*)$_2$CHMeN, broad; accidental coincidence], 23.4 and 24.6 [CH(*Me*)$_2$], 29.8 [*C*H(Me)$_2$], 42.7 [NCHMe*C*(Me)$_2$CHMeN], 65.3 [N*C*HMeC(Me)$_2$*C*HMeN], 114.0, 118.4, 127.2 and 129.1 (aromatic CH), 133.2 (*C*-N, aromatic C), 151.9 {*C*[CH(Me)$_2$], aromatic C}. Peaks due to free Et$_2$O could also be observed at substoichiometric levels.

1,2-(2-Isopropylphenyl)-3,4,4,5-tetramethylpyrazolidine (2): *n*BuLi (1.6 mL of a 1.51 M hexane solution, 2.42 mmol) was added to a stirring solution of *l*-[(2-*i*Pr-C_6H_4NHCHMe)$_2$CMe$_2$] (0.40 g, 1.1 mmol) in hexane (5 mL) at room temperature. The suspension was vented to the atmosphere via a drying tube freshly charged with anhydrous $CaCl_2$, and stirred for 12 h. Removal of solvent yielded a brown oil. Its NMR spectrum was dominated by peaks listed below, but contained some other unidentified impurities. Flash column chromatography on silica (eluting with hexane) yielded **2** as the major fraction, R_f = 0.7. Large colourless crystals of 1,2-(2-isopropylphenyl)-3,4,4,5-tetramethyl pyrazolidine (**2**) were grown from a hexane solution at −25 °C. M.p.: 118−120 °C. Yield: 0.19 g, 48%. ^{1}H NMR (300 MHz. $CDCl_3$): δ = 0.97 (d, $^{3}J_{H,H}$ = 6.8 Hz, 6 H, *Me*CHMe), 0.91 [d, $^{3}J_{H,H}$ = 6.8 Hz, 6 H, NCH*Me*C(Me$_2$)CH*Me*N], 1.10 [s, 6 H, NCHMeC(*Me*$_2$)CHMeN], 1.19 (d, $^{3}J_{H,H}$ = 6.8 Hz, 6 H, MeCH*Me*), 2.80 [q, $^{3}J_{H,H}$ = 6.8 Hz, 2 H, NC*H*MeC(Me$_2$)C*H*MeN], 3.94 (septet, $^{3}J_{H,H}$ = 6.8 Hz, 2 H, MeC*H*Me), 6.96−7.11 and 7.76−7.82 (8 H, non-first-order m, aromatic protons) ppm. ^{13}C NMR (75 MHz; C_6D_6): δ = 14.4 [NCH*Me*C(Me$_2$)CH*Me*N], 24.3 [NCHMeC(*Me*$_2$)CHMeN], 24.4 (*Me*CHMe), 25.5 (MeCH*Me*), 25.9 (Me*C*HMe), 42.6 [NCHMe*C*-(Me$_2$)CHMeN], 73.7 [N*C*HMeC(Me$_2$)*C*HMeN], 125.6, 126.1, 126.2 and 126.4 (aromatic CH), 147.4 and 147.8 {*C*-N, aromatic C and *C*[CH(Me$_2$)]}. $C_{25}H_{36}N_2$ (364.6): calcd. C 82.4, H 10.0, N 7.7; found C 82.7, H 10.2, N 7.8. IR: $\tilde{\nu}$ = 1521 cm^{-1}, 1485 cm^{-1} and 1445 cm^{-1} (s, aromatic C−C stretch), 1345 cm^{-1} [s, ν(C−N)].

{*N*,*N*′-Bis(2,6-diisopropylphenyl)-3,3′-dimethylpentane-2,4-diamido}dibutyltetralithium (6): *n*BuLi (4.2 mL of a 1.58 M hexane solution, 6.7 mmol) was added dropwise to a stirring solution of *N*,*N*′-bis(2,6-diisopropylphenyl)-3,3′-dimethylpentane-2,4-diamine (1.00 g, 2.2 mmol) in toluene (20 mL) at 22 °C and the solution was stirred for 2 h. Large, colourless crystals were grown overnight from the solution at −4 °C. The crystals were filtered from the solution and dried under vacuum. Yield: 0.42 g, 32%. M.p. 80−83 °C dec. The UMIST microanalysis facility could not handle this extremely sensitive compound; results indicated hydrolysis. Large crystal size and reproducibility and purity of NMR spectroscopic data indicated acceptable sample purity and homogeneity. ^{1}H NMR (200 MHz; [D_8]toluene, −40 °C): δ = −1.6 [br. m, 2 H, CH$_3$(CH$_2$)$_2$C*H*$_2$Li], −0.9 [br. m, 2 H, CH$_3$(CH$_2$)$_2$C*H*$_2$Li], 0.2 (br. quint., 2 H, CH$_3$CH$_2$C*H*$_2$CH$_2$Li or CH$_3$C*H*$_2$CH$_2$CH$_2$Li), 0.75 [t, $^{3}J_{H,H}$ = 7.2 Hz, 3 H, C*H*$_3$(CH$_2$)$_2$CH$_2$Li], 1.0 [two broad d overlapped, 6 H +6 H, NCH*Me*C(Me$_2$)CH*Me*N and *Me*C$_A$HMe], 1.1 [s, 3 H +3 H, unresolved NCHMeC(*Me*$_2$)CHMeN], 1.31 (br. d, 6 H, MeC$_B$H*Me*), 1.45 (apparent br. d, two d overlapped, 6 H +6 H, *Me*C$_A$HMe and MeC$_B$H*Me*), 1.75 [non-first-order br. m, 4 H, CH$_3$(C*H*$_2$)$_2$CH$_2$Li], 3.01 (br. septet, 2 H, MeC$_A$*H*Me), 3.89 [br. q, $^{3}J_{H,H}$ = 6.8 Hz, 2 H, NC*H*MeC(Me$_2$)C*H*MeN], 4.16 (br septet, 2 H, MeC$_B$*H*Me), 7.02−7.22 (non-first-order br. m, 6 H, aromatic protons) ppm. ^{7}Li NMR (78 MHz, [D_8]toluene, −40 °C): δ = 1.0 (br. s, 2 Li), 2.6 (br. s, 1 Li), 3.3 (br. s, 1 Li) ppm. ^{13}C NMR (75 MHz; C_6D_6, 22 °C): δ = 10 [br. overlapped m, Me(CH$_2$)$_2$*C*H$_2$Li], 14.2 [NCHMeC(*Me*$_2$)CHMeN], 20.4 [NCH*Me*C(Me$_2$)CH*Me*N], 25.6, 26.5 and 30.8 (*Me*CH*Me*), 27.1 and 31.2 (Me*C*HMe), 32 [br. overlapped m, Me(*C*H$_2$)$_2$CH$_2$Li], 44.1 [NCHMe*C*(Me$_2$)CHMeN], 69.7 [N*C*HMeC(Me$_2$)*C*HMeN], 123.2, 126.0 and 128.0 (aromatic CH), 145.6, 149.1 and 151.4 [*C*(CHMe$_2$) and *C*-N, aromatic C] ppm.

X-ray Structure Determinations: Low-temperature X-ray diffraction data for **1**·OEt$_2$, **2** and **6** were recorded from perfluoropolyether-coated crystals on a Nonius KappaCCD instrument fitted with an Oxford Instruments Cryostream (**1**·OEt$_2$ and **6**), or a Nonius MACH 3 diffractometer (**2**) fitted with a liquid-nitrogen boil-off device. Collection and solution methods and programs have been detailed elsewhere.[14] All hydrogens were found in difference maps and freely refined. Collection and refinement summaries are shown in Table 4. CCDC-212782 (**1**·OEt$_2$), -212783 (**2**) and -212784 (**6**) contain the supplementary crystallographic data for this paper. These data can be obtained free of charge at www.ccdc.cam.ac.uk/conts/retrieving.html [or from the Cambridge Crystallographic Data Centre, 12, Union Road, Cambridge CB2 1EZ, UK; fax: (internat.) +44-1223/336-033; E-mail: deposit@ccdc.cam.ac.uk].

Acknowledgments

We are indebted to the EPSRC for studentships (RJW, JEW) and NMR and X-ray diffraction equipment grants, to the Royal Society (FSM) for small equipment and consumables, and to Creators Ltd for Total Technology support (JEW).

Table 4. Crystal data

Compound	**1**·OEt_2	**2**	**6**
Formula	$C_{29}H_{46}Li_2N_2O$	$C_{25}H_{36}N_2$	$C_{39}H_{66}Li_4N_2$
M_w	452.56	364.56	590.70
Crystal system	Monoclinic	Triclinic	Monoclinic
a (Å)	13.8928(3)	10.352(2)	19.8740(6)
b (Å)	12.9728(3)	10.791(2)	13.0540(5)
c (Å)	15.5382(4)	11.134(3)	30.2390(11)
α (°)	(90)	63.35(2)	(90)
β (°)	98.1100(10)	79.18(2)	98.9750(10)
γ (°)	(90)	84.357(18)	(90)
Space group	$P2_1/c$, No. 14	$P\bar{1}$, No. 2	$C2/c$, No. 15
Z	4	2	8
Temp. (K)	150(2)	203(2)	123(2)
μ (mm^{-1})	0.063	0.064	0.056
Reflns. measd.	27311	3995	9366
Reflns. obsd[a] (R_{int})	6158 (0.0469)	3770 (0.0421)	9366 (0.000)
R_1(observed)	0.0505	0.0391	0.0542
wR_2(all data)[b]	0.1237	0.0964	0.1327

[a] $I > 2\sigma(I)$. [b] $wR_2 = \{\sigma[w(F_o^2 - F_c^2)^2]/\sigma[w(F_o^2)^2]\}^{1/2}$.

[1] K. Gregory, P. v. R. Schleyer, R. Snaith, *Adv. Inorg. Chem.* **1991**, *37*, 47.

[2] W. N. Setzer, P. v. R. Schleyer, *Adv. Organomet. Chem.* **1985**, *24*, 353.

[3] [3a] G. Hilmersson, Ö. Davidsson, *J. Organomet. Chem.* **1995**, *489*, 175. [3b] G. Hilmersson, Ö. Davidsson, *Organometallics* **1995**, *14*, 912. [3c] G. Hilmersson, P. I. Arvidsson, Ö. Davidsson, M. Håkansson, *Organometallics* **1997**, *16*, 3352. [3d] P. I. Arvidsson, G. Hilmersson, Ö. Davidsson, *Chem. Eur. J.* **1999**, *5*, 2348. [3e] P. I. Arvidsson, P. Ahlberg, Ö. Davidsson, *Chem. Eur. J.* **1999**, *5*, 1348. [3f] A. Johansson, G. Hilmersson, Ö. Davidsson, *Organometallics* **2002**, *21*, 2283. [3g] A. Corruble, J.-Y. Valnot, J. Maddaluno, Y. Iprgnet, D. Davoust, P. Duhamel, *J. Am. Chem. Soc.* **1997**, *119*, 10042. [3h] A. Corruble, D. Davoust, S. Desjardins, C. Fressigné, C. Giessner-Prettre, A. Harrison-Marchand, H. Houte, M.-C. Lasne, J. Maddaluno, H. Oulyadi, J.-Y. Valnot, *J. Am. Chem. Soc.* **2002**, *124*, 15267.

[4] [4a] C. Fressigné, A. Corruble, J.-Y. Valnot, J. Maddaluno, C. Giessner-Prettre, *J. Organomet. Chem.* **1997**, *549*, 81. [4b] Y. Balamraju, C. D. Sharp, W. Gammill, L. M. Pratt, *Tetrahedron* **1998**, *54*, 7357. [4c] C. Fressigné, J. Maddaluno, A. Marquez, C. Giessner-Prettre, *J. Org. Chem.* **2000**, *65*, 8899. [4d] O. Parisel, C. Fressigné, J. Maddaluno, C. Giessner-Prettre, *J. Org. Chem.* **2003**, *68*, 1290.

[5] [5a] D. Barr, W. Clegg, S. M. Hodgson, R. E. Mulvey, D. Reed, R. Snaith, D. S. Wright, *J. Chem. Soc., Chem. Commun.* **1988**, 367. [5b] S. Harder, M. Lutz, T. Kremer, *Organometallics* **1995**, *14*, 2133. [5c] M. Konemann, G. E. Erker, R. Frohlich, E.-U. Wurthwein, *J. Am. Chem. Soc.* **1997**, *119*, 11155. [5d] P. C. Andrews, S. M. Calleja, M. Maguire, *J. Chem. Soc., Dalton Trans.* **2002**, 3640. [5e] P. G. Williard, M. A. Jacobsen, *Org. Lett.* **2000**, *2*, 2753. [5f] R. P. Davies, P. R. Raithby, R. Snaith, *Angew. Chem.* **1997**, *109*, 1261; *Angew. Chem. Int. Ed. Engl.* **1997**, *36*, 1215. [5g] G. B. Deacon, C. M. Forsyth, N. M. Scott, *J. Chem. Soc., Dalton Trans.* **2001**, 2494.

[6] [6a] P. G. Williard, C. Sun, *J. Am. Chem. Soc.* **1997**, *119*, 11693. [6b] J. Schneider, E. Popowski, H. Reinke, *Z. Anorg. Allg. Chem.* **2002**, *628*, 719.

[7] [7a] D. J. Brauer, H. Bürger, G. R. Liewald, *J. Organomet. Chem.* **1986**, *308*, 119. [7b] H. Chen, R. A. Bartlett, H. V. R. Dias, M. M. Olmstead, P. P. Power, *Inorg. Chem.* **1991**, *30*, 2487. [7c] M. G. Gardiner, C. L. Raston, *Inorg. Chem.* **1995**, *34*, 4206. [7d] M. G. Gardiner, C. L. Raston, *Inorg. Chem.* **1996**, *35*, 4047. [7e] M. Haaf, A. Schmiedl, T. A. Schmedake, D. R. Powell, A. J. Millerolte, M. Denk, R. West, *J. Am. Chem. Soc.* **1998**, *120*, 12714.

[8] [8a] K. W. Hellmann, C. Galka, L. H. Gade, A. Steiner, D. S. Wright, T. Kottke, D. Stalke, *Chem. Commun.* **1998**, 549. [8b] K. W. Hellmann, A. Bergner, L. H. Gade, I. J. Scowen, M. McPartlin, *J. Organomet. Chem.* **1999**, *573*, 156. [8c] R. M. Gauvin, N. Kyritsakas, J. Fischer, J. Kress, *Chem. Commun.* **2000**, 965. [8d] S. Danielle, C. Drost, B. Gerhus, S. M. Hawkins, P. B. Hitchcock, M. F. Lappert, P. G. Merle, S. G. Bott, *J. Chem. Soc., Dalton Trans.* **2001**, 3179.

[9] [9a] A. R. Kennedy, R. E. Mulvey, R. B. Rowlings, *J. Am. Chem. Soc.* **1998**, *120*, 7816. [9b] R. E. Mulvey, *Chem. Commun.* **2001**, 1049.

[10] [10a] J. K. Brask, T. Chivers, G. P. A. Yap, *Chem. Commun.* **1998**, 2543. [10b] J. K. Brask, T. Chivers, G. Schatte, G. P. A. Yap, *Organometallics* **2000**, *19*, 5683. [10c] M. A. Beswick, B. R. Elvidge, N. Feeder, S. J. Kidd, D. S. Wright, *Chem. Commun.* **2001**, 379. [10d] M. C. Copsey, J. C. Jeffery, A. P. Leedham, C. A. Russell, J. M. Slattery, *Dalton Trans.* **2003**, 2103.

[11] [11a] M. B. Eleveld, H. Hogeveen, *Tetrahedron Lett.* **1984**, *25*, 5187. [11b] A. Corruble, J.-Y. Valnot, J. Maddaluno, P. Duhamel, *J. Org. Chem.* **1998**, *63*, 8266. [11c] P. I. Arvidsson, Ö. Davidsson, G. Hilmersson, *Tetrahedron: Asymmetry* **1999**, *10*, 527. [11d] K. Flinois, Y. Yuan, C. Bastide, A. Harrison-Marchand, J. Maddaluno, *Tetrahedron* **2002**, *58*, 4707. [11e] J. Granander, R. Sott, G. Hilmersson, *Tetrahedron* **2002**, *58*, 4717.

[12] D. T. Carey, F. S. Mair, R. G. Pritchard, J. E. Warren, R. J. Woods, *Dalton Trans.* in press.

[13] D. T. Carey, E. K. Cope-Eatough, E. Vilaplana-Mafé, F. S. Mair, R. G. Pritchard, J. E. Warren, R. J. Woods, *Dalton Trans.* **2003**, 1083.

[14] E. K. Cope-Eatough, F. S. Mair, R. G. Pritchard, J. E. Warren, R. J. Woods, *Polyhedron* **2003**, *22*, 1447.

[15] D. K. Kennepohl, S. Brooker, G. M. Sheldrick, H. W. Roesky, *Chem. Ber.* **1991**, *124*, 2223.

[16] D. Braga, F. Grepioni, K. Biradha, G. R. Desiraju, *J. Chem. Soc., Dalton Trans.* **1996**, 3925.

[17] T. Kottke, D. Stalke, *Angew. Chem.* **1993**, *105*, 619; *Angew. Chem. Int. Ed. Engl.* **1993**, *32*, 580.

[18] See, for example: K. N. Zelenin, A. V. Dovgilevich, I. P. Bezhan, G. A. Golubeva, L. A. Sviridova, *Chem. Heterocycl. Compd.* **1984**, *20*, 529; J. L. Vennerstrom, T. J. Holmes, *J. Med. Chem.* **1987**, *30*, 563; A. R. Katritzky, G. Qiu, B. Yang, *J. Org. Chem.* **1997**, *62*, 8210.

[19] S. F. Nelsen, M. R. Willi, *J. Org. Chem.* **1984**, *49*, 1.

[20] C. Neumann, A. Schulz, T. Siefert, W. Storch, M. Vosteen, *Eur. J. Inorg. Chem.* **2002**, 1040.

[21] J. P. Ritchie, S. M. Bachrach, *J. Am. Chem. Soc.* **1987**, *109*, 5909.

[22] R. E. Mulvey, *Chem. Soc. Rev.* **1991**, *20*, 167.

[23] M. Marsch, K. Harms, L. Lochmann, G. Boche, *Angew. Chem.* **1990**, *102*, 334; *Angew. Chem. Int. Ed. Engl.* **1990**, *29*, 308.

[24] [24a] J. F. McGarrity, C. A. Ogle, *J. Am. Chem. Soc.* **1984**, *107*, 1805. [24b] W. Bauer, T. Clark, P. v. R. Schleyer, *J. Am. Chem. Soc.* **1987**, *109*, 970.

[25] J. D. Scollard, D. H. McConville, N. C. Payne, J. J. Vittal, *Macromol.* **1996**, *29*, 5241; J. D. Scollard, D. H. McConville, *J. Am. Chem. Soc.* **1996**, *118*, 10008; J. Jin, S. Tsubaki, T. Uozumi, T. Sano, K. Soga, *Makromol. Chem. Rapid Commun.* **1998**, *19*, 597.

[26] A. F. Burchatt, J. M. Chong, N. Nielsen, *J. Organomet. Chem.* **1997**, *542*, 281.

Received June 17, 2003

 © 2003 Wiley-VCH Verlag GmbH & Co. KGaA, Weinheim

Synthesis, Structures and Characterization of the Calcium Pyrrolates [Ca{(2-(dimethylaminomethyl)pyrrolyl}$_2$ donor$_n$] (donor = THF and pyridine, n = 2; DME and TMEDA, n = 1) as Potential Precursors for Solid-State Applications

Wilda Vargas[a] and Karin Ruhlandt-Senge*[a]

In memory of the late Ron Snaith

Keywords: Calcium / N ligands / Chemical vapor deposition / Transamination / Metallation / Intramolecular donation

The synthesis and characterization of novel alkaline earth metal pyrrolyl derivatives is described. The target molecules were synthesized using transamination and metallation protocols, involving either the treatment of calcium bis[bis(trimethylsilyl)]amide with two equivalents of 2-(dimethylaminomethyl)pyrrole (2-DMAMP) or the reaction of elemental calcium with two equivalents of 2-DMAMP. Different donors, namely THF, pyridine (py), DME (dimethoxyethane), and TMEDA (*N*,*N*,*N*′,*N*′-tetramethylethylenediamine) were utilized to study their influence on the structural chemistry of the target compounds. In order to compare the influence of the metal coordination on the pyrrole ligand, we included the crystal structure of the free 2-DMAMP ligand. All new compounds were characterized using ^{1}H, ^{13}C NMR and IR spectroscopy in addition to X-ray crystallography**.** Crystal data with Mo-K_α radiation (λ = 0.71073 Å) are as follows: **1**: [Ca(2-DMAMP)$_2$(THF)$_2$], a = 15.440(2) Å, b = 14.992(2) Å, c = 10.175(1) Å, β = 94.9(3)°,V= 2346.6(6) Å^3, Z = 4, monoclinic, space group $P2_1/c$, $R1$(all data) = 0.0981; **2**: [Ca(2-DMAMP)$_2$(py)$_2$], a = 9.168(6) Å, b = 10.418(7) Å, c = 13.329(8) Å, α = 85.9(1)°, β = 72.9(1)°, γ = 86.2(1)°, V = 1212.2(1) Å^3, Z = 2, triclinic, space group $P\bar{1}$, $R1$ (all data) = 0.0711; **3**: [Ca(2-DMAMP)$_2$(DME)], a = 10.814(1) Å, b = 12.907(1) Å, c = 15.170(1) Å, V = 2117.3(3) Å^3, Z = 4, orthorhombic, space group $P2_12_12_1$, $R1$ (all data) = 0.0729; **4**: [Ca(2-DMAMP)$_2$(TMEDA)], a = 9.403(6) Å, b = 15.810(1) Å, c = 15.417(1) Å, V = 2292.0(3) Å^3, Z = 4, orthorhombic, space group $Pbcn$, $R1$ (all data) = 0.0997; **5**: 2-DMAMP, a = 10.8820(7) Å, b = 15.2186(10) Å, c = 9.7578(6) Å, β = 109.736(2)°,V = 1521.05(17) Å^3, Z = 2, monoclinic, space group Cc, $R1$ (all data) = 0.0382.

(© Wiley-VCH Verlag GmbH & Co. KGaA, 69451 Weinheim, Germany, 2003)

Introduction

Calcium-containing solid-state materials showing huge negative resistance or colossal magnetoresistance (CMR) have become prominent not only for fundamental physics but also for their possibilities in device applications.[1] Amongst these materials, the doped manganates $A_{1-x}Ca_xMnO_3$ (A = rare earth metals) are especially interesting for their potential employment in the development of magnetic recording heads.[2,3] The production of these materials by CVD procedures requires precursors with a high volatility. The well-established β diketonate[4] derivatives decompose cleanly, but their volatility is not sufficient for these applications. Conventional means to improve the volatility by -$SiMe_3$ or -CF_3 substitution are not applicable since small amounts of fluorine or silicon impurities are detrimental to electronic applications.[5]

Nitrogen-based precursors are ideally suited for the production of a wide array of solid-state materials. In addition, the structural flexibility of the ligand system, since two not one organic groups (as in oxygen-based precursors) are linked to a monoanionic, secondary amido ligand, significantly increases ligand design opportunities. The most intensively studied nitrogen-based calcium derivatives carry the sterically demanding hexamethyldisilazane ligand in conjunction with various mono and bidentate donors. A number of donor-containing monomers in addition to a donor-free dimer have been reported and recently summarized in an excellent review article.[6] However, the promise of the calcium bis[bis(trimethylsilyl)]amides as potential precursor materials has not been fulfilled due to the facile acid-promoted cleavage of the N−Si bonds[7] and consequent silicon contamination of the final products. Derivatives of the hexamethyldisilazane ligand replacing one trimethylsilyl group by a bulky aromatic substituent display a reduced

[a] Syracuse University, Department of Chemistry, 111 College Place, Rm. 1-014 Center for Science & Technology, Syracuse, NY 13244-4100, USA
Fax: (internat.) +1-315/443-4070
E-mail: kruhland@syr.edu

 © 2003 Wiley-VCH Verlag GmbH & Co. KGaA, Weinheim **DOI: 10.1002/ejic.200300311**

tendency towards N−Si bond cleavage and have partially fulfilled the aim for volatile precursors.[8] Still, advanced amido-based precursors would avoid the presence of silyl groups altogether, but synthetic difficulties have so far precluded the preparation of these highly reactive materials.[9]

Volatile precursor materials will likely consist of monomeric compounds. However, heavy alkaline earth metal derivatives exhibit a pronounced tendency towards oligomerization due to their large ionic radii.[10] Multiple strategies exist to prevent the formation of oligomers, most prominently the use of sterically demanding ligands, and application of donors and intramolecularly coordinating ligands. Since the use of bulky ligands alone does not ensure the presence of monomeric molecules,[11] a combined approach of multiple strategies is advantageous. As an added incentive, intramolecular coordination is likely to increase the solubility of the target compounds in common organic solvent systems, thus facilitating the delivery of the target compounds in CVD applications.

Amongst the array of nitrogen ligands with intramolecular stabilization capabilities, we identified the monoanionic bidentate pyrrole derivative 2-(dimethylaminomethyl)pyrrole (2-DMAMP), as shown in Scheme 1, as being ideally suited for our purpose, with the $(CH_3)_2NCH_2$- linker providing the desired intramolecular stabilization to allow for the isolation of monomeric species.

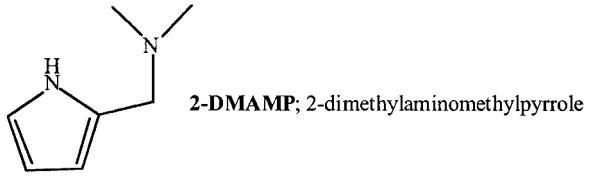

2-DMAMP; 2-dimethylaminomethylpyrrole

Scheme 1. Schematic drawing of the 2-DMAMP ligand

Although first reported in the 1940′s,[12] 2-DMAMP has received little attention as a ligand system. In fact, well-characterized main group derivatives are limited to aluminum,[13] gallium and indium[14] in addition to some recently published mixed magnesium cyclopentadienide/amido derivatives.[15] Other metal complexes bearing DMAMP-type ligands include titanium,[16] tungsten,[16] zirconium,[17−19] vanadium,[19] thallium,[20] chromium,[19] molybdenum,[21] cobalt[19] and nickel.[19]

Pyrrolylcalcium and -strontium derivatives with two *tert*-butyl substituents have been reported.[22] This sterically demanding ligand disfavors the η^1-type bonding observed in the 2-DMAMP compounds; instead, π-bonding involving an η^5 arrangement is observed. A related metal geometry is also observed in a calcium porphyrinogen derivative. Here, four pyrrolyl rings are arranged in a macrocycle, each binding in an η^3 fashion to calcium.[23] If, instead, calcium is coordinated to a pyrollyl ring in a porphyrin system, η^1 binding is ensured by the planar nature of the macrocycle.[24] Studies focusing on the unsubstituted pyrrole ligand in conjunction with the heavier alkaline earth metals have been limited to the gas-phase synthesis of the monopyrrolylcalcium and -strontium free radicals.[25]

We report here on a group of monomeric pyrrolylcalcium derivatives carrying the 2-(dimethylaminomethyl)pyrrolyl ligand (2-DMAMP), in addition to mono- and bidentate donors, namely $[Ca(2\text{-DMAMP})_2(THF)_2]$ (**1**), $[Ca(2\text{-DMAMP})]_2(py)_2]$ (**2**), $[Ca(2\text{-DMAMP})]_2(DME)]$ (**3**), and $[Ca(2\text{-DMAMP})_2(TMEDA)]$ (**4**). The crystal structure of the free 2-DMAMP ligand **5** is also reported.

Results and Discussion

Synthetic Aspects and Reactivity

Multiple synthetic methods were probed to identify the most facile route that allows the production of the target compounds in a simple and efficient manner. The initial starting point was salt elimination, used successfully for the preparation of amidocalcium derivatives.[6,8] Following a similar procedure, we obtained an inseparable precipitate containing the pyrrolyl target compound and potassium iodide. A change in reaction conditions did not improve this result.

Two reaction schemes, transamination[26] (Scheme 2) and metallation[27] (Scheme 3) were identified as viable alternatives, since both have been used successfully to prepare a host of alkaline earth metal derivatives. Limitations of the transamination scheme are based on the required pK_a difference between the liberated amine and the reagent, and only substrates with a higher acidity than the secondary amine may be successfully utilized. If, on the other hand, the acidity would be too high, as for example observed in aromatic thiols, consumption of acid, with protonation of the liberated amine and formation of primary amine and silylated substrate, is observed.[7]

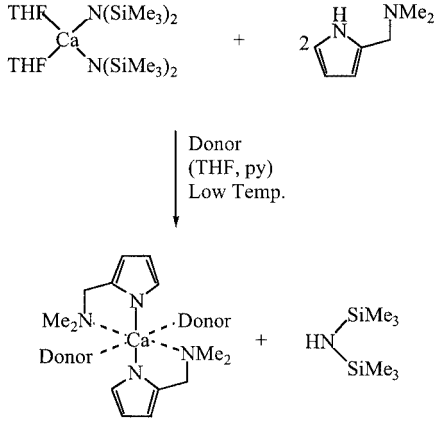

Scheme 2. The synthesis of calcium pyrrolates by transamination

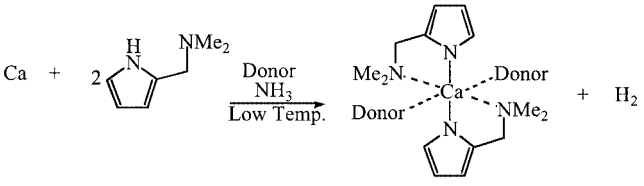

Scheme 3. The synthesis of calcium pyrrolates by direct metallation

 © 2003 Wiley-VCH Verlag GmbH & Co. KGaA, Weinheim

Compounds **1** and **2** were prepared using transamination (Scheme 2), although the purity of the resulting products was not consistently high. A common technique to obtain high quality products by transamination is the removal of $HN(SiMe_3)_2$ in vacuo to shift the equilibrium to the product side and assure the quantitative release of $HN(SiMe_3)_2$.[26c] Still, elimination of amine was occasionally incomplete as evidenced by ^1H NMR analysis. Attempts to remove the amine at elevated temperature and under vacuum resulted in the removal of the donor and consequent formation of insoluble precipitates. This was also observed if the acid and the amide were combined too rapidly, or donors were omitted, despite the use of very dilute solutions and low reaction temperatures.

Metallation, used successfully to prepare the target compounds in a facile, reproducible manner, requires the activation of calcium since the oxide layer in commercially available calcium effectively passivates the metal. Several methods are available to activate the metal. Westerhausen et al. successfully use the distillation of the metals for this purpose,[28] while recent collaborative work between the Deacon group and our group showed mercury activation, as used frequently for the rare earth metals, to be effective.[29] Alternatively, dissolving the metals in anhydrous, liquid ammonia followed by addition of acid, as shown with the preparation of a selection of alkaline earth metal derivatives, is also a viable method.[27] As an example, the preparation of the barium amide $[Ba\{N(SiMe_3)_2\}_2(THF)_2]$ by metallation in the presence of ammonia proceeds smoothly,[30] whereas no product is observed if ammonia is omitted. Since the reactivity of the alkaline earth metals increases upon descending the group, metallation is most efficient for barium, whereas no reaction, even after extended reflux in liquid ammonia (dry-ice condenser), is observed for calcium.

With these parameters in mind, we proceeded by dissolving calcium in anhydrous, condensed ammonia, followed by addition of the acid and extended reflux of the reaction mixture. Consistently, the reaction mixture turned dark, and intractable, insoluble solids were obtained. If, however, a small amount of ammonia is condensed onto the reaction mixture to dissolve the metal (as indicated by the formation of deep-blue solutions), followed by the evaporation of most of the ammonia and brief heating, the reaction proceeds smoothly, as evidenced by the vigorous evolution of gas. This method produces the target compounds in excellent yield and purity.

The initially surprising fact that compounds **1**−**4** may be prepared in good yields and purity, while the reaction of calcium metal with $HN(SiMe_3)_2$ does not yield the amide, may be explained by the lower pK_a of the pyrrole vs. the amine, its reduced steric demand and the pyrrole's capability for intramolecular stabilization yielding a thermodynamically favored five-membered ring.

Spectroscopic Studies

The ^1H NMR spectra of compounds **1**−**4** show a consistent change from the spectrum of the free 2-DMAMP ligand **5**. Due to limited solubility of the target compounds, all NMR spectra were recorded in $[D_8]$THF. The most prominent difference is observed for the proton in the 5-position, which shifts from δ = 6.57 ppm in the free ligand **5** to δ = 6.63−6.67 ppm in compounds **1**−**4**. The protons in the 3- and 4-positions in the free ligand lie very close together at δ = 5.90 and 5.85 ppm. In **1**−**4** these signals are shifted slightly upfield, moving even closer together; they are observed at δ = 5.79 and 5.78 ppm. In the free ligand the CH_2 and $N(Me)_2$ protons are observed as singlets at δ = 3.31 and 2.13 ppm, respectively. Upon deprotonation both signals experience a slight downfield shift to δ = 3.46 and

Table 1. Crystallographic data for compounds **1**−**5**

	1	**2**	**3**	**4**	**5**
Formula	$CaN_4O_2C_{22}H_{38}$	$CaN_6C_{24}H_{32}$	$CaN_4O_2C_{18}H_{32}$	$CaN_6C_{20}H_{38}$	$C_{14}H_{24}N_4$
Fw	430.64	444.64	376.56	402.64	99.35
a (Å)	15.440(2)	9.168(6)	10.814(1)	9.403(6)	10.8820(7)
b (Å)	14.992(2)	10.418(7)	12.907(1)	15.810(1)	15.2186(10)
c (Å)	10.175(1)	13.329(8)	15.170(1)	15.417(1)	9.7578(6)
α (deg)		85.9(1)	90	90	90
β (deg)	94.916(3)	72.9(1)	90	90	109.736(2)
γ (deg)		86.2(1)	90	90	90
V (Å^3)	2346.6(6)	1212.2(1)	2117.3(3)	2292.0(3)	1521.05(17)
Z	4	2	4	4	2
Space group	$P2_1/c$	$P\bar{1}$	$P2_12_12_1$	*Pbcn*	*Cc*
d_{calc} (g/cm^3)	1.219	1.218	1.181	1.167	1.085
Linear abs coeff (mm^{-1})	0.291	0.281	0.314	0.290	0.067
T (K)	93(2)	93(2)	87(2)	85(2)	96(2)
2θ range (deg)	3.80 −50.0	3.20−65.78	4.14−50.00	5.14−65.76	4.80- 65.64
Indep reflns	4048	8176	3712	4120	2979
No. of params	265	283	226	199	259
*R*1, *wR2* (all data)[a]	0.0981, 0.1730	0.0700, 0.1253	0.0729, 0.1096	0.0997, 0.0766	0.0382, 0.0770
*R*1, *wR*2 (>2σ)	0.0515, 0.1345	0.0505, 0.1253	0.0568, 0.1074	0.0401, 0.0674	0.0349, 0.0760

[a] $R1 = \Sigma||F_0| - |F_c||/\Sigma|F_0|$; $wR2 = [\Sigma w(F_0^2 - F_c^2)^2/\Sigma w(F_0^2)^2]^{1/2}$.

 © 2003 Wiley-VCH Verlag GmbH & Co. KGaA, Weinheim

2.25 ppm. These values are in good agreement with literature data.[13−15]

Structural Aspects

Crystallographic information and data collection parameters for compounds **1**−**4** are summarized in Table 1 and the Exp. Sect. A compilation of selected geometrical parameters for the compounds is given in Table 2 and 3, while Figures 1−5 illustrate the structural principles displayed in compounds **1**−**5**. Compounds **1** and **2**, bearing the monodentate donors THF and pyridine, and **3** and **4**, carrying bidentate donors DME and TMEDA, display very similar structural features and will be described together.

Table 2. Selected bond lengths (Å) and angles (°) for **1**−**4**

	1[a]	**2**[a]	**3**	**4**
Ca−N*p*[b]	2.386(6)	2.394(2)	2.384(6)	2.404(1)
Ca−N*id*	2.523(6)	2.532(2)	2.523 (6)	2.584(1)
Ca−O*nd*	2.372(4)		2.378(4)	
Ca−N*nd*		2.524(2)		2.595(1)
N*p*1−Ca−N*p*2	180.0	180.0	112.26(1)	115.95(5)
N*id*1−Ca−N*id*2	180.0	180.0	166.75(1)	148.88(4)
N*p*1−Ca−N*id*1	75.22(2)	75.71(8)	73.16(2)	72.59(4)
N*p*1−Ca−O*nd*1	91.99(9)		156.51(1)	
N*p*1−Ca−N*nd*1		89.68(8)		87.47(4)
O*nd*1−Ca−O*nd*2	180.0		67.55(8)	
N*nd*1−Ca−N*nd*2		180.0		69.38(6)

[a] Independent molecules averages. [b] N*p* = pyrrolyl nitrogen; N*id* = intramolecular donor nitrogen; O*nd* = neutral donor oxygen; N*nd* = neutral donor nitrogen.

Table 3. Selected bond lengths (Å) and angles (°) for **5**

C1−N1	1.37(2)
C1−C2	1.37(3)
C2−C3	1.42(2)
C5−N2	1.47(2)
C6−N2	1.46(2)
C1−N1−C4	108.9(2)
C6−N2−C7	110.0(1)
N1−C1−C2	108.1(1)
C1−C2−C3	107.3(2)
N1−C1−C5	120.4(2)
N2−C5−C1	113.7(1)

[Ca(2-DMAMP)$_2$(THF)$_2$] (1) and [Ca(2-DMAMP)$_2$(py)$_2$] (2): Compounds **1** (Figure 1) and **2** (Figure 2) exhibit monomeric six-coordinate calcium centers. The two independent metal centers in compounds **1** and **2** are located on inversion centers, thus, two half molecules are located in each asymmetric unit, of which only one is shown. The coordination geometry around calcium is distorted octahedral with a center of symmetry requiring a linear geometry of the trans oriented ligands and donors. The distortion from octahedral geometry stems from the narrow bite angles within the intramolecularly coordinating ligand, with values of 75.22(2)° for **1** and 75.71(8)° for **2**. Ca−N(pyrrolate) and Ca−N(NMe$_2$) distances in **1** are 2.386(6) Å and 2.523(6) Å, respectively, with closely related values [2.394(2) Å and 2.532(2) Å] for **2**. The Ca−O(THF) distances in **1** are 2.372(4) Å, while the Ca−N(pyridine) distances in **2** are 2.524(2) Å.

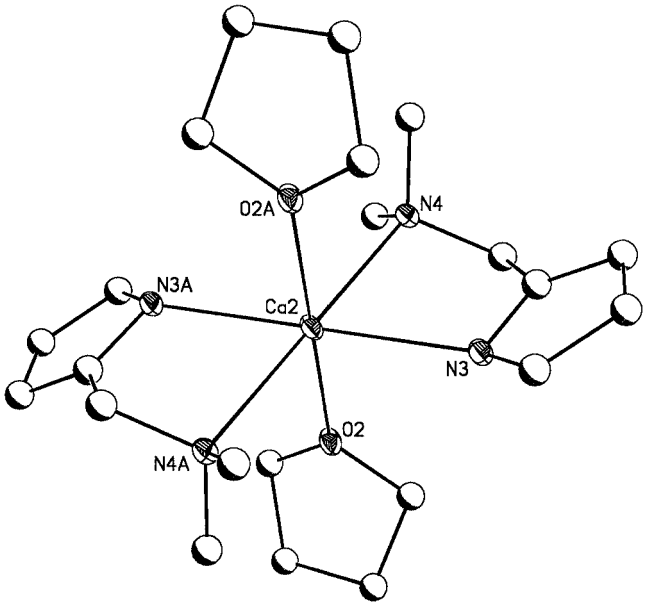

Figure 1. Computer-generated plot of **1** with anisotropic displacement parameters depicting 30% probability for all non-carbon atoms; the hydrogen atoms have been omitted for clarity

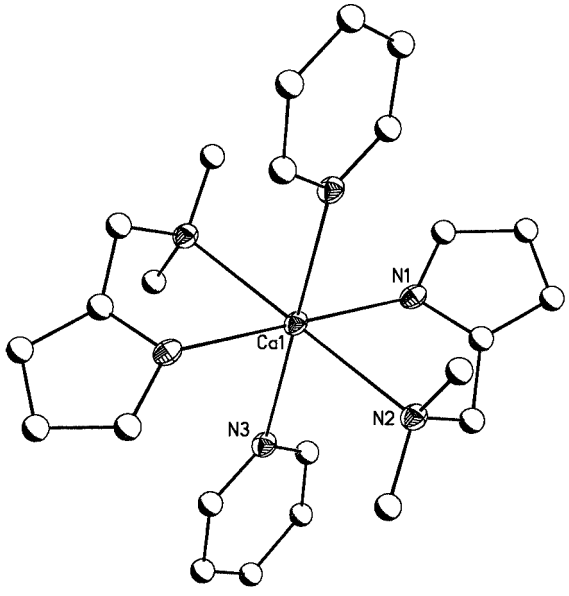

Figure 2. Computer-generated plot of **2** with anisotropic displacement parameters depicting 30% probability for all non-carbon atoms; the hydrogen atoms have been omitted for clarity

[Ca(2-DMAMP)$_2$(DME)] (3) and [Ca(2-DMAMP)$_2$-(TMEDA)] (4): Compounds **3** and **4,** represented in Figures 3 and 4, respectively, feature monomeric, six-coordinate metal centers with two 2-DMAMP ligands and one DME or TMEDA donor. In compound **4** the metal center is located on a twofold axis, generating the second half of the

 © 2003 Wiley-VCH Verlag GmbH & Co. KGaA, Weinheim

molecule. In both **3** and **4** the 2-DMAMP ligands adopt a *cisoid* conformation to accommodate the bidentate donors, resulting in a significant distortion from ideal octahedral geometry, as reflected in N1−Ca1−N1A, N2−Ca1−N2A and O1−Ca1−O2 angles of 112.35(1)°, 166.65(1)° and 67.82(8)°, respectively, in **3**, and N1−Ca1−N3, N2−Ca1−N4 and N5−Ca1−N6 angles of 115.95(5)°, 142.23(5)° and 69.38(6)°, respectively, in **4**. The calcium center and the 2-DMAMP ligand form five-membered rings with N−Ca−N angles of 73.22(2)° in **3**, and 72.59(4)° in **4**, which are in part responsible for the distortion from octahedral geometry. The Ca−N(pyrrolate) and Ca−N(NMe_2) distances are 2.378(6) Å and 2.522(6) in **3** and 2.384(6) Å and 2.523(6) Å in **4**, respectively. The calcium-oxygen bond lengths in **3** average 2.378(4) Å, while Ca−N(TMEDA) contacts in **4** are 2.595(1) Å.

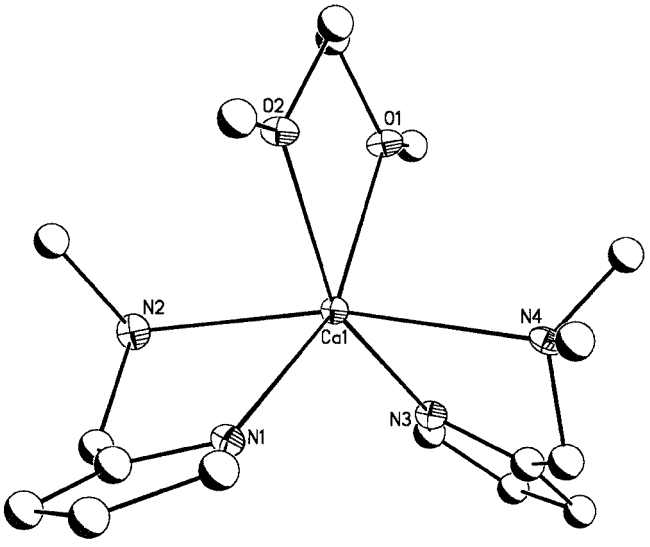

Figure 3. Computer-generated plot of **3** with anisotropic displacement parameters depicting 30% probability for all non-carbon atoms; the hydrogen atoms have been omitted for clarity

DMAMP-2 (5): The free ligand is depicted in Figure 5; pertinent bond lengths and angles are summarized in Table 3. Compound **5** crystallizes with two independent molecules per asymmetric unit which are connected through a hydrogen bond (2.024 Å) involving the pyrrole hydrogen atom on one molecule and the dimethylamine fragment on the second pyrrole. The geometrical parameters in the two independent molecules are very similar, therefore only one is described. Pyrrole nitrogen-carbon bond lengths are observed at 1.370(2) Å, the C−C bond lengths between carbons 2 and 3 and 4 and 5 are slightly shorter, at 1.356(3) and 1.361(2) Å, while the C−C bond between carbons 3 and 4 is the longest, at 1.422(2) Å. This is consistent with the location of the double bonds. The angle at nitrogen is 108.81(16)°. The (CH_2)NMe_2 linker is attached to carbon 2, with a C2−C6 bond length of 1.497(2) Å.

The observed calcium-pyrrolate binding mode in **1**−**4** is a sigma-type η^1-bond through the nitrogen atom on the pyrrole ring. η^5 Coordination, as observed for di-*tert*-butyl-substituted pyrrolates of calcium and strontium,[22] or calcium porphyrinogen,[23] is not observed. The differences in coordination mode can be explained by the steric bulk of the di-*tert*-butyl-substituted pyrrolate, or the arrangement of pyrrolyl groups in the macrocycle, which effectively block the σ-type Ca−N(pyrrolyl) bonding observed here. In addition, the formation of a thermodynamically favored five-membered ring utilizing the intramolecularly coordinating $(CH_3)_2NCH_2$- linker also favors the σ-type bonding observed in compounds **1**−**4**.

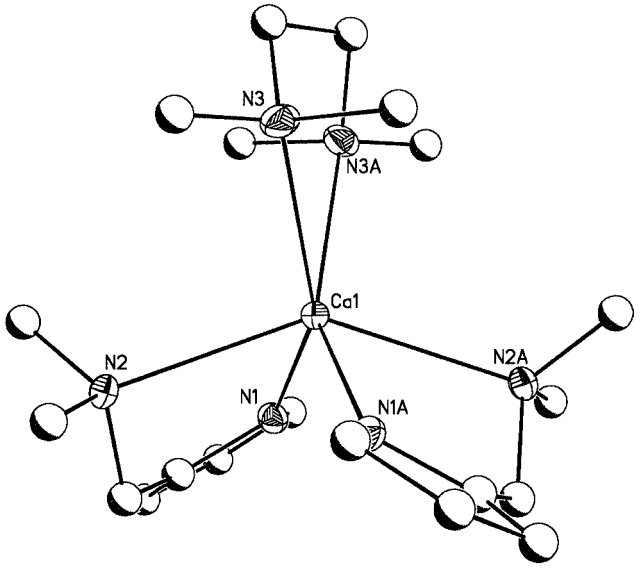

Figure 4. Computer-generated plot of **4** with anisotropic displacement parameters depicting 30% probability for all non-carbon atoms; the hydrogen atoms have been omitted for clarity

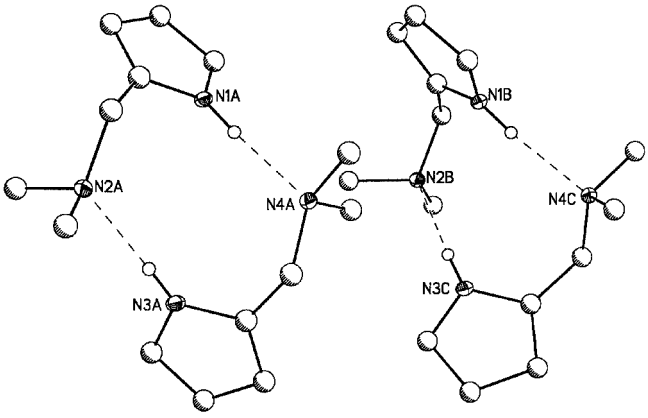

Figure 5. Computer-generated plot of **5** with anisotropic displacement parameters depicting 30% probability for all non-carbon atoms; the hydrogen atoms, except on the pyrrole nitrogen have been omitted for clarity

In compounds **1** and **2** the two 2-DMAMP ligands occupy the equatorial plane, with the two monodentate donors occupying the axial positions. In the case of the bidentate donors DME and TMEDA, this arrangement is no longer possible, since the donor bite angle prevents the coordination to both axial positions. Instead, a *cisoid* ligand arrangement is observed.

 © 2003 Wiley-VCH Verlag GmbH & Co. KGaA, Weinheim

Calcium-pyrrolyl nitrogen bond lengths in **1**−**4** lie in a narrow range [2.378(6)−2.404(1) Å], as do the calcium-nitrogen [Ca−N(CH_3)$_2$] contacts involving the intramolecular linker [2.522(2)−2.584(1) Å]. As expected, the Ca−N bond lengths to the anionic pyrrolyl ligand are significantly shorter than to those to the neutral -N(CH_3)$_2$ donor. The Ca−N(pyrrolyl) values compare favorably with the four-coordinate calcium amides [Ca{N($SiMe_3$)$_2$}$_2$(THF)$_2$] [2.301(6) Å],[31] and [Ca{N($SiMe_3$)(2,6-*i*Pr$_2$$C_6H_3$)}$_2(THF)_2$] [2.326(8) Å],[8] despite the lower coordination number observed in these compounds. The only marginally longer Ca−N(pyrrolyl) bond lengths in compounds **1**−**4** are an expression of the larger steric demand of the amido ligands as compared to the pyrrolyl system. The ligand size is based on the narrow N(pyrrolyl)−Ca−N[N(CH_3)$_2$] bite angle [72.59(4) to 75.71(8)°], effectively reducing the steric bulk of the ligand. The Ca−N(pyrrolyl) bond lengths also compare favorably with the seven coordinate tris-pyridine solvated calcium porphyrin with Ca−N(pyrrolyl) distances of 2.382(4)−2.416(3) Å.[23]

Metal binding has only a negligible influence on the overall features of the pyrrolyl ring, and the structural parameters of **1**−**4** are within standard deviations compared to the free 2-DMAMP ligand **5**. Compounds **1**−**4** may be compared with a family of furfurylsilylamides, of which the magnesium compound is closest to the calcium species presented here.[32] In this ligand system, a furan ring is connected in the 2-position to a methyltrimethylsilylamine linker. This linker is deprotonated yielding an amido function with the opportunity for intramolecular furan coordination. In the presence of non-coordinating solvents, both the furan oxygen and the amido function are coordinated to the magnesium. If, however, donating solvents such as THF are utilized, only the amide coordinates to the metal. In the pyrrole system presented here, the intramolecular coordinating ability of the ligand is used in all cases, even in the presence of strong or multidentate donors such as pyridine, TMEDA or DME, with analogous results for a series of magnesium compounds.[33] Clearly then, without relying on silyl substitution, the 2-DMAMP ligand displays excellent capabilities to stabilize monomeric heavy alkaline earth metal derivatives, as needed for solid-state applications.

Solid-State Studies

Compounds **1**−**4** were analyzed for their capacity as CVD precursor molecules. To this effect, TGA and sublimation studies were conducted. Remarkably, the compounds involving nitrogen donation by either pyridine (compound **2**) or TMEDA (compound **4**) show a clean decomposition pattern in the TGA, whereas **1** and **3** display a complex decomposition behavior, with a significant amount of residue remaining at 450 °C. The TGA pattern for compound **4** is shown in Figure 6, indicating a clean decomposition process at low temperatures. To confirm the usefulness of the material as a CVD precursor, extended sublimation studies were conducted with the most promising material, the TMEDA adduct **4**. It was shown that compound **4** sublimes cleanly into a uniform calcium-containing solid-state species, demonstrating the potential of these compounds as precursor materials.

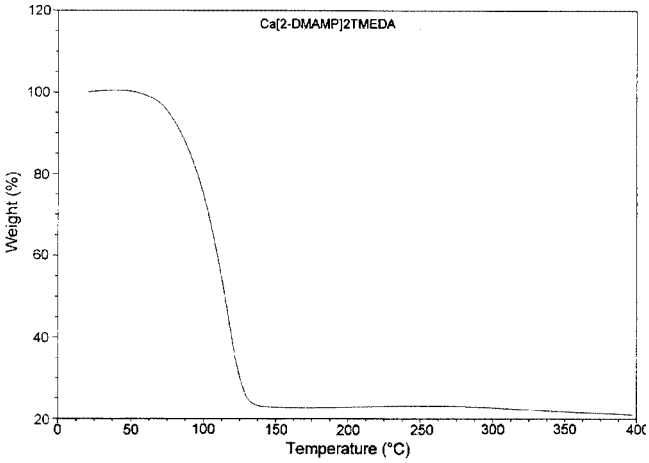

Figure 6. TGA profile for compound **4**

Conclusion

Four new calcium pyrrolates containing intramolecularly coordinating linkers were synthesized and characterized. The compounds exhibit monomeric structures in the solid state as shown by X-ray crystallography. Extended studies involving TGA and sublimation showed that compounds **2** and **4** show considerable promise as precursor materials for the production of calcium-containing solid-state materials. This result is especially important in the light of desirable silicon-free calcium source material.

We have probed salt-elimination, transamination, and metallation procedures and found that calcium pyrrolate derivatives are most conveniently accessible by metallation. This method also holds the greatest promise of a facile large-scale preparation.

Experimental Section

General Procedures: All reactions were performed using standard procedures using a purified nitrogen atmosphere by utilizing either modified Schlenk techniques and/or a Braun Labmaster 100 dry box. Pyridine, THF, DME, TMEDA, hexamethyldisilazane and pyrrole were distilled prior to use from CaH_2 or Na/K alloy. Ca[N($SiMe_3$)$_2$]$_2$$THF_2$ [31] and 2-DMAMP[12] were synthesized according to literature procedures. Formaldehyde and dimethylamine hydrochloride were obtained from commercial sources and used as received. Anhydrous ammonia was further dried by condensing over sodium metal. ^{1}H NMR and ^{13}C NMR spectra were recorded on a Bruker DPX-300 or -500 spectrometer. Spectra were recorded in deuterated THF and are referenced to residual solvent resonances. Use of C_6D_6 or $CD_3C_6D_5$ as NMR solvents did not allow for the dissolution of the target compounds, precluding the recording of quality spectra. Infrared spectra were recorded as Nujol mulls between NaBr plates on a Perkin−Elmer PE 1600 FI-IR spectrometer. Thermogravimetric analysis (TGA) was performed on

 © 2003 Wiley-VCH Verlag GmbH & Co. KGaA, Weinheim

vacuum dried samples kept under inert conditions and loaded manually onto a Auto TGA2950HR thermogravimetric analyzer. The TGA experiments were performed under an N_2 atmosphere using a heating rate of 10 °C /min. Reliable elemental analyses could not be obtained, even when glove-box handling was attempted, due to the high moisture and oxygen sensitivity of all compounds reported. Repeated elemental analysis of high quality samples with clean ^{1}H NMR spectra and perfect integration afforded large deviations between duplicate runs, even when V_2O_5 was added as a combustion aid. This is a well-known problem in alkaline earth metal chemistry.[34]

Procedure A, Transamination: In a typical experiment, a Schlenk tube was charged with one equivalent of $[Ca\{N(SiMe_3)_2\}_2(THF)_2]$ (typically 3.6 mmol), dissolved in 40 mL of donor solvent (THF, pyridine or DME) and stirred at low temperature for half an hour. To this, a solution of two equivalents of 2-DMAMP in 20 mL of the same solvent was added dropwise with vigorous stirring. The resulting clear solution was stirred for three hours at low temperature, −78 °C (acetone/dry ice) for THF or DME, or −40 °C (acetonitrile/dry-ice) for the pyridine reactions, due to the higher melting point of pyridine. The clear, yellow solution was slowly warmed to room temperature before being filtered through a fine filter frit. The filtrate was reduced in volume to about 30 mL, followed by storage at −23 °C.

Procedure B, Metallation: In a typical experiment, a Schlenk tube was charged with calcium metal (typically 1 mmol) and two equivalents of 2-DMAMP. To this, about 60 mL of solvent (THF, pyridine or a toluene/TMEDA (10:1 v/v mixture) was added and stirred at −78 °C (THF, DME or toluene/TMEDA), or at −40 °C if pyridine was utilized. Into this mixture approximately 20 mL of ammonia was condensed. The solution was then removed from the cold bath and allowed to warm up to room temperature. After most of the ammonia had evaporated, the presence of ammoniates was indicated by a characteristic bronze color. Heat was applied briefly, initiating vigorous bubbling. The evolution of gas persisted for several minutes. After the formation of bubbles had ceased, the homogeneous clear solution was filtered through a fine filter frit. The volume of the filtrate was reduced to about 30 mL followed by storage at −23 °C (unless otherwise noted).

[Ca(2-DMAMP)$_2$(THF)$_2$] (1). Procedure A: $[Ca\{N(SiMe_3)_2\}_2(THF)_2]$ (1.89 g, 3.6 mmol) in 40 mL of THF and 2-DMAMP (0.93 g, 7.5 mmol) in 20 mL of THF stirred at −78 °C. Within a week colorless block-shaped crystals suitable for X-ray crystallography studies formed. Yield: 47% (0.73 g, 1.70 mmol).

Procedure B: Calcium metal (0.04 g, 1 mmol) and 2-DMAMP (0.25 g, 2 mmol), stirred at −78 °C. Within a day colorless block-shaped crystals suitable for X-ray crystallography studies formed. Yield: 65% (0.28 g, 0.65 mmol).

$C_{22}H_{38}CaN_4O_2$ (430.64): calcd. C 61.36, H 8.89, Ca 9.31, N 13.01; found C 54.88, H 8.24, Ca 10.34, N 18.41. M.p.: turns opaque at 80 °C (presumably loss of donor solvent), turns dark above 135 °C. ^{1}H NMR ([D]$_8$THF): δ = 1.80 (m, 4 H), 2.25 (s, 12 H), 3.46 (s, 4 H), 3.64 (m, 4 H), 5.79 (s, 4 H), 6.63 (s, 2 H) ppm. ^{13}C NMR ([D]$_8$THF): δ = 23.63 (THF), 45.70 (NMe_2), 57.63 (CH_3), 62.25 (CH_2), 68.28 (THF), 106.34 (CH), 107.77 (CH), 127.21 (CH) ppm. IR (Nujol): $\tilde{\nu}$ = 3084.4 cm^{-1}, 1353.3, 1294.5, 1261.8, 1160, 1136, 1086, 1037, 767.2, 623.5.

[Ca(2-DMAMP)$_2$(py)$_2$] (2). Procedure A: $[Ca\{N(SiMe_3)_2\}_2(THF)_2]$ (1.89 g, 3.6 mmol) in 40 mL of pyridine and 2-DMAMP (0.93 g, 7.5 mmol) in 20 mL of pyridine (−40 °C). The solution turned cloudy and was removed from the cold bath and warmed to room temperature upon which it turned clear. Within a week, colorless block-shaped crystals suitable for X-ray crystallography studies formed. Yield: 55% (0.88 g, 1.97 mmol).

Procedure B: Calcium metal (0.04 g, 1 mmol) and 2-DMAMP (0.25 g, 2 mmol). Stirred at −40 °C. Yield: 72% (0.32 g, 0.72 mmol).

$C_{24}H_{32}CaN_6$ (444.64): calcd. C 64.82, H 7.25, Ca 9.01, N 18.90; found C 55.20, H 7.63, Ca 9.88, N 18.00.. M. p.: turns opaque at 95 °C (presumably loss of donor solvent), turns dark above 120 °C, sublimes above 200 °C. ^{1}H NMR ([D]$_8$THF): δ = 2.25 (s, 12 H), 3.46 (s, 4 H), 5.79 (s, 4 H), 6.68 (s, 2 H), 7.25 (m, 4 H), 7.66 (t, 2 H), 8.53 (d, 4 H) ppm. ^{13}C NMR ([D]$_8$THF): δ = 45.82 (NMe_2), 62.36 (CH_2), 106.3 (CH), 106.4(CH), 124.5 (py), 127 (CH), 136.4 (py), 151 (py) ppm. IR (Nujol): $\tilde{\nu}$ = 2723.1 cm^{-1}, 1591.9, 1345.6, 1169.6, 1021, 947.8, 729.4, 627.9.

[Ca(2-DMAMP)$_2$(DME)] (3). Procedure A: $[Ca\{N(SiMe_3)_2\}_2(THF)_2]$ (1.89 g, 3.6 mmol) in 40 mL of DME and 2-DMAMP (0.93 g, 7.5 mmol) in 20 mL of dimethoxyethane stirred at −78 °C. The solution turned cloudy and was removed from the cold bath, first warmed up to room temperature and subsequently heated to reflux temperature. On reaching reflux temperature, the solution turned clear. Upon cooling to room temperature, colorless needle-shaped crystals suitable for X-ray crystallography studies formed. Yield: 44% (0.59 g, 1.56 mmol).

$C_{18}H_{32}CaN_4O_2$ (376.56): M.p.: turns opaque at 80 °C (presumably loss of donor solvent), turns dark above 155 °C. ^{1}H NMR ([D]$_8$THF): δ = 2.25 (s, 12 H), 3.27 (s, 6 H), 3.43 (s, 4 H), 3.60 (s, 4 H), 5.79 (s, 4 H), 6.68 (s, 2 H), 7.25 (m, 4 H) ppm. ^{13}C NMR ([D]$_8$THF): δ = 45.40 (NMe_2), 57.63 (CH_3), 59.00 (CH_2), 72.83 (OCH_2), 107.6 (CH), 107.8(CH), 127 (CH) ppm. IR (Nujol): $\tilde{\nu}$ = 1261.2 cm^{-1}, 1242.9, 1224, 1172.4, 11.38.2, 1100.8, 1069.6, 1025.9, 992.9, 827.9.

[Ca(2-DMAMP)$_2$(TMEDA)] 4. Procedure B: Calcium (0.04 g, 1 mmol) and 2-DMAMP (0.25 g) in 5 mL of TMEDA and 50 mL of toluene (−78 °C). Block-shaped crystals suitable for X-ray crystallography formed within 24 hours. Yield: 67% (0.17 g, 0.44 mmol).

$C_{20}H_{38}CaN_6$ (402.64): calcd. C 59.65, H 9.51, Ca 9.95, N 20.89; found C 51.82, H 8.30, Ca 12.35, N 21.24. M.p.: turns opaque at 85 °C (presumably loss of donor solvent), turns dark above 145 °C, sublimes above 200 °C. ^{1}H NMR ([D]$_8$THF): δ = 1.73 (s, 12 H), 3.27 (s, 6 H), 3.30 (s, 4 H), 3.45 (s, 4 H), 5.79 (s, 4 H), 6.68 (s, 2 H), 7.25 (m, 4 H), 7.66 (t, 2 H), 8.53 (d, 4 H) ppm. ^{13}C NMR ([D]$_8$THF): δ = 45.50 (TMEDA, NMe_2), 45.82 (NMe_2), 57.73 (TMEDA, CH_2), 62.03 (CH_2), 106.29 (CH), 106.45(CH), 127.4 (CH) ppm. IR (Nujol): $\tilde{\nu}$ = 3361.8 cm^{-1}, 1506.1, 1376.4, 1096.0, 1027.2, 947.8, 714.1.

X-ray Crystallographic Study: X-ray quality crystals for all compounds were grown as described in the Exp. Sect. The crystals were removed from the Schlenk tube under a stream of N_2 and immediately covered with a layer of viscous hydrocarbon oil (Infineum). A suitable crystal was selected with the aid of a microscope, attached to a glass fiber, and immediately placed in the low temperature N_2 stream of the diffractometer.[35] The intensity data sets for all compounds were collected using a Siemens SMART system, complete with three-circle goniometer and CCD detector operating at −54 °C. Data for compounds **1** and **2** were collected at 93(2)K and for **3**, **4** and **5** at 87(2), 85(2) and 96(2) K, respectively, using a custom-built low temperature device from Professor H. Hope (UC Davis). In all cases graphite-monochromated Mo-K_α radiation (λ = 0.71073Å) was employed. The data collections nominally covered a hemisphere of reciprocal space utilizing a combination of three

 © 2003 Wiley-VCH Verlag GmbH & Co. KGaA, Weinheim

sets of exposures, each with a different angle, and each exposure covering 0.3° in φ. Crystal decay was monitored by repeating the initial frames at the end of the data collection and analyzing the duplicate reflections. In all cases, no decay was observed. An absorption correction was applied for all compounds utilizing the program SADABS.[36] The crystal structures of all compounds were solved by Direct Methods, as included in the SHELXTL-Plus program package.[37] Missing atoms were located in subsequent difference Fourier maps and included in the refinement. The structures of all compounds were refined by full-matrix least-squares refinement on F^2 (SHELX-93). Hydrogen atoms were placed geometrically and refined using a riding model, including free rotation about C−C bonds for methyl groups with U_{iso} constrained at 1.2 for non-methyl groups, and 1.5 for methyl groups times U_{eq} of the carrier C atom. The crystallographic programs used for structure refinement and solution were installed on a PC clone. Scattering factors were those provided with the SHELX program system. All non-hydrogen atoms were refined anisotropically.

CCDC-210044−210047 (**1**−**4**) and -217175 (**5**) contain the supplementary crystallographic data for this paper. These data can be obtained free of charge at www.ccdc.cam.ac.uk/conts/retrieving.html or from the Cambridge Crystallographic Data Centre, 12, Union Road, Cambridge CB2 1EZ, UK; fax: (internet.) +44-1223/336-033; E-mail: deposit@ccdc.cam.ac.uk].

Acknowledgments

We are grateful for support from the National Science Foundation (CHE-9702246 and CHE-0108098), SHARP Corporation of North America and Syracuse University. Purchase of the X-ray diffractometer was made possible with grants from NSF (CHE-9527898), the W. M. Keck Foundation and Syracuse University. We thank Professor W. Winter (SUNY ESF, Syracuse) for his help in obtaining TGA analyses.

[1] [1a] K. H. Kim, M. Uehara, V. Kiryukhin, S.-W. Cheong,, *Condensed Matter* **2002**, 1−83 (Los Alamos National Laboratory, Preprint Archive). [1b] B. Raveau, A. Maignan, C. Martin, M. Hervieu, *J. Supercond.* **1999**, *12*, 247.
[2] A. P. Ramirez, *J. Phys.: Condens. Matter* **1997**, *9*, 8171.
[3] S. Jin, T. H. Tiefel, M. McCormack, R. A. Fastnacht, R. Ramesh, L. H. Chen, *Science* **1994**, *264*, 413.
[4] [4a] V. C. Arunasalam, S. R. Drake, M. B. Hursthouse, K. M. A. Malik, S. A. S. Miller, D. M. P. Mingos, *J. Chem. Soc., Dalton Trans.* **1996**, 2435. [4b] V. C. Arunasalam, I. Baxter, S. R. Drake, M. B. Hursthouse, K. M. A. Malik, D. J. Otway, *Inorg. Chem.* **1995**, *34*, 5295. [4c] R. E. Sievers, S. B. Turniseed, I. Huang, A. F. Lagante, *Coord. Chem. Rev.* **1993**, *128*, 285.
[5] W. A. Wojtczak, P. F. Fleig, M. J. Hampden-Smith, *Adv. Organomet. Chem.* **1996**, *40*, 215.
[6] M. Westerhausen, *Coord. Chem. Rev.* **1998**, *176*, 157, and references cited therein.
[7] S. Chadwick, U. Englich, K. Ruhlandt-Senge, *Angew. Chem. Int. Ed.* **1998**, *37*, 3007, and references cited therein.
[8] W. Vargas, U. Englich, K. Ruhlandt-Senge, *Inorg. Chem.* **2002**, *41*, 5602.
[9] W. Vargas, M. Gillett-Kunnath, K Ruhlandt-Senge, unpublished results.
[10] [10a] R. Shannon, C. T. Previtt, *Acta Crystallogr., Sect. B* **1969**, *25*, 925. [10b] R. D. Shannon, *Acta Crystallogr., Sect. A*, **1976**, *32*, 751.
[11] T. P. Hanusa, *Chem. Rev.* **1993**, *93*, 1023.
[12] W. Herz, K. Dittmer, S. J. Cristol, *J. Am. Chem. Soc.* **1947**, *69*, 1698.
[13] J. Huang, H. Chen, J. Chang, C. Zhou, G. Lee, S. Peng, *Organometallics* **2001**, *20*, 2647.
[14] P. Kuo, J. Huang, C. Hung, G. Lee, S. Peng, *Eur. J. Inorg. Chem.* **2003**, *7*, 1440.
[15] A. Xia, M. J. Heeg, C. H. Winter, *Organometallics* **2002**, *21*, 4718.
[16] J. Huang, L. Chi, F. Huang, P. Kuo, C. Zhou, G. Lee, S. Peng, *J. Chinese. Chem. Soc.* **2000**, *47*, 895.
[17] J. Huang, P. Kuo, G. Lee, S. Peng, *J. Chinese Chem. Soc.* **2000**, *47*, 1191.
[18] J. Huang, L. Chi, R. Yu, G. Jiang, W. Yang, G. Lee, S. Peng, *Organometallics* **2001**, *20*, 5788.
[19] H. Drevs, A. Schmeiβer, H. Hartung, U. Baumeister, *Chem. Ber.* **1996**, *129*, 853.
[20] C. Zhou, J. Huang, M. Wang, T. Lee, G. Lee, S. Peng, *Inorg. Chim. Acta* **2003**, *342* 59.
[21] J. Huang, H. Chen, C. Hsieh, G. Lee, S. Peng, *Inorg. Chim. Acta* **2001**, *321*, 142.
[22] H. Schumann, J. Gottfriedsen, J. Demtsschuk, *Chem. Commun.* **1999**, 2091.
[23] L. Bonomo, O. Dandin, E. Solari, C. Floriani, R. Scopelliti, *Angew. Chem. Int. Ed.* **1999**, *38*, 914.
[24] [24a] G. Guillemot, E. Solari, C. Rizzoli, C. Floriani, *Chem. Eur. J.* **2002**, *8*, 2072. [24b] L. Bonomo, M. Lehaire, E. Solari, R. Scopelliti, C. Floriani, *Angew. Chem. Int. Ed.* **2001**, *40*, 771.
[25] A. M. R. P. Bopegedera, W. T. M. L. Fernando, P. F. Bernath, *J. Phys. Chem.* **1990**, *94*, 4476.
[26] [26a] D. E. Gindelberger, K. W. Klinkhammer, W. Schwarz, M. Westerhausen, T. Hildendrand, *Z. Naturforsch., Teil B* **1992**, *47*, 1225. [26b] D. E. Gindelberg, J. Arnold, *Inorg. Chem.* **1994**, *33*, 6293. [26c] W. Teng, U. Englich, K. Ruhlandt-Senge, *Inorg. Chem.* **2000**, *39*, 3875. [26d] D. C. Green, U. Englich, K. Ruhlandt-Senge, *Angew. Chem. Int. Ed.* **1999**, *38*, 354.
[27] [27a] S. Chadwick, U. Englich, B. Noll, K. Ruhlandt-Senge, *Inorg. Chem.* **1998**, *37*, 4718. [27b] S. Chadwick, U. Englich, K. Ruhlandt-Senge, *Chem. Commun.* **1998**, 2149. [27c] U. Englich, K. Ruhlandt-Senge, *Chem. Eur. J.* **2000**, *6*, 4063.
[28] [28a] M. Westerhausen, C. Gueckel, H. Piotrowski, M. Vogt, *Z. Anorg. Allg. Chem.* **2002**, *628*, 735. [28b] M. Westerhausen, M. H. Digeser, H. Noeth, W. Ponikwar, T. Seifert, K. Polborn, *Inorg. Chem.* **1999**, *38*, 3207. [28c] M. Westerhausen, M. H. Digeser, C. Gueckel, H. Noeth, J. Knizek, J. W. Ponikwar, *Organometallics* **1999**, *18*, 2491.
[29] J. Hitzbleck, A. O'Brien, C. Forsyth, G. B. Deacon, K. Ruhlandt-Senge, *in preparation*.
[30] [30a] S. R. Drake, D. J. Otway, *J. Chem. Soc., Chem. Commun.* **1991**, 517. [30b] S. R. Drake, P. Hall, D. J. Otway, *Inorganic Experiments* (Ed.: J. D. Woolins), VCH, **1994**. [30c] R. L. Kuhlman, B. A. Vaartstra, K. G. Caulton, *Inorg. Synth.* **1997**, *31*, 8.
[31] M. Westerhausen, *Trends Organomet. Chem.* **1997**, *2*, 89.
[32] H. Sachdev, C. Wagner, C. Preis, V. Huch, M. Veith, *J. Chem. Soc., Dalton Trans.* **2002**, 4709.
[33] N. Fry, W. Vargas, K. Ruhlandt-Senge, in preparation.
[34] M. L. Hays, T. P. Hanusa, T. A. Nile, *J. Organomet. Chem.* **1996**, *514*, 73 and references cited therein.
[35] H. Hope, *Prog. Inorg. Chem.* **1994**, *41*, 1.
[36] G. M. Sheldrick, *SADABS: Program for Absorption Correction Using Area Detector Data:* University of Göttingen: Göttingen, Germany, **1996**.
[37] G. M. Sheldrick, *SHELXTL-Plus: Program package for Structure Solution and Refinement; Siemens:* Madison, WI, **1999**.

Received May 23, 2003

 © 2003 Wiley-VCH Verlag GmbH & Co. KGaA, Weinheim

Influence of the Crystallization Solvent on Molecular and Supramolecular Structures of Silver(I) Tris(3-Phenylpyrazolyl)methane Complexes

Daniel L. Reger,*[a] Radu F. Semeniuc,[a] and Mark D. Smith[a]

Keywords: N ligands / Solvent effects / Noncovalent interactions / Silver / Supramolecular chemistry

The compound [{HC(3-Phpz)$_3$}Ag](BF$_4$) (pz = pyrazolyl ring) has been prepared and shown to crystallize in four different forms depending on the solvent. Vapor-phase diffusion of diethyl ether into nitromethane solutions of the complex produces two polymorphs, an orthorhombic form (**1**) and triclinic form (**2**). Both polymorphs are coordination polymers constructed by a κ^2–κ^1 coordination of the tris(3-Phpz)methane units and have similar, but different, supramolecular structures. In **1** there are two independent chains linked by C–H···π interactions. In **2** only one type of chain is present, with a different internal structure than in **1**. Non-covalent forces, mainly C–H···π interactions, organize the chains into sheets and the sheets into a final 3-D supramolecular structure in the case of **1**, while in the case of **2** only a 2-D supramolecular structure forms. In contrast, vapor-phase diffusion of diethyl ether into acetonitrile or acetone solutions produces [{HC(3-Ph-pz)$_3$}Ag{(CH$_3$)$_2$CO}](BF$_4$) (**3**) and [{HC(3-Phpz)$_3$}-Ag{CH$_3$CN}](BF$_4$) (**4**). In these compounds, the ligand shows tripodal coordination to a single silver center and coordination of one solvent molecule to the metallic center. Both compounds form 3-D supramolecular structures organized by both C–H···π interactions and weak C–H···F hydrogen bonds and in the case of **4** π–π stacking.

(© Wiley-VCH Verlag GmbH & Co. KGaA, 69451 Weinheim, Germany, 2003)

Introduction

In 1966 Trofimenko introduced the tripodal hydrotris(pyrazolyl)borate family of ligands. They remain an important class of N_3 tripodal ligands in many fields of coordination chemistry, supramolecular chemistry, and catalysis.[1−5] Substituted hydrotris(pyrazolyl)borates, especially in the 3-position of the pyrazolyl ring, offer the possibility of controlling steric factors, making them suitable ligands in various enzyme models.[6−9] We have recently been investigating the isoelectronic tris(pyrazolyl)methane ligands and wish to demonstrate the ability of these neutral ligands to control the coordination chemistry of various metals through careful choice of substituents on the pyrazolyl rings.[10−15] With silver(I), we have reported the solid-state structures of [{HC(3,5-Me$_2$pz)$_3$}$_2$Ag](O$_3$SCF$_3$), [{HC(3-Butpz)$_3$}Ag](O$_3$SCF$_3$), and [{HC(3-Butpz)$_3$}Ag(CNBut)](O$_3$SCF$_3$).[12] Recently, others reported a series of silver derivatives of simple tris(pyrazolyl)methane ligands[16] and structures based on linking pyrazolyl rings with organic spacers.[17,18]

We have expanded the chemistry of simple tris(pyrazolyl)-methane ligands with the synthesis of a new class of multitopic ligands of the general formula C_6H_{6-n}[CH$_2$OCH$_2$C(3-Rpz)$_3$]$_n$, (R = H or Ph, n = 2, 4). These ligands are based on semi-rigid organic spacers that link two or more tris(pyrazolyl)methane units in a single molecule.[19−25] We have shown that metal complexes of these ligands form an array of unusual supramolecular structures supported by a multitude of non-covalent interaction, such as weak hydrogen bonds,[19−22] intermolecular[20,25] or intramolecular[22,24] π−π stacking, and C−H···π interactions.[20,24,25] This versatility is a consequence of the presence of the aromatic pyrazolyl rings and linking arene rings that can act as acceptors in C−H···π interactions or participate in π−π stacking. Another factor is that the hydrogen atoms within the pyrazolyl rings are acidic enough to be involved in weak hydrogen bonds. Additional structural diversity is derived from the ability of the tris(pyrazolyl)methane units to act as (a) a κ^3-tripodal ligand, (b) a κ^2-ligand, with the third pyrazolyl not coordinated to a metal, and (c) a bridge between two metals in a $\kappa^2-\kappa^1$ coordination mode, see Scheme 1. We defined these ligands as *structurally adaptive*.[24,25] A structurally adaptive ligand can adjust its shape to maximize covalent and non-covalent interactions and the overall structure of the supramolecular array will be the resultant of the interplay amongst all forces. While rigid ligands allow a better prediction of the overall structure, shape and porosity of the resulting array,[26,27] these semi-rigid, structurally adaptive ligands offer new insights into the self-assembly process. For example, [*o*-C$_6$H$_4${CH$_2$OCH$_2$C(3-Phpz)$_3$}$_2$Ag$_2$(BF$_4$)$_2$]$_n$ forms a 1-D organometallic coordination polymer that contains two different types of silver(I) cations arranged in bimetallic units. The bimetallic units show three different types of bridging

[a] Department of Chemistry and Biochemistry University of South Carolina,
Columbia South Carolina 29208, USA
Fax: (internat.) +1-803/777-9521
E-mail: Reger@mail.chem.sc.edu

Supporting information for this article is available on the WWW under http://www.eurjIc.org or from the author.

 © 2003 Wiley-VCH Verlag GmbH & Co. KGaA, Weinheim **DOI: 10.1002/ejic.200300141**

interactions, including a $\kappa^2-\kappa^1$ coordination mode of a tris(3-Ph-pyrazolyl)methane unit, a silver η^2-bonded to a phenyl group and $\pi-\pi$ stacking interactions.[23]

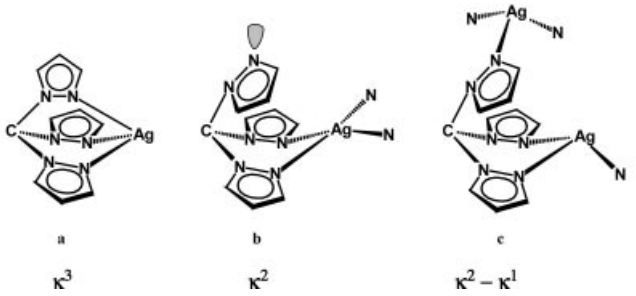

Scheme 1. Observed coordination modes of the $[HC(pz)_3]$ unit in silver(I) chemistry: a) κ^3 — tripodal; b) κ^2 — chelating one metal with the third pyrazolyl ring not coordinated; c) $\kappa^2-\kappa^1$ — bridging two metallic centers

In an attempt to elucidate the intimate processes that lead to the formation of these supramolecular species containing multitopic tris(pyrazolyl)methane ligands, we focused our attention back on simple tris(pyrazolyl)methane ligands, ligands that have the same potential to enter into non-covalent interactions and poses the same structural diversity in the modes of covalent bonding, to study the molecular and supramolecular structures of complexes of the tris(pyrazolyl)methane unit without the organizational feature of the linking, semi-rigid organic spacer. We have shown that $[\{HC(pz)_3\}CuPPh_3](NO_3)$ and $[\{HC(3\text{-}Phpz)_3\}CuPPh_3](NO_3)$ form a two dimensional supramolecular network of dimeric units.[28] Reported here are the synthesis and spectral characterization of $[\{HC(3\text{-}Phpz)_3\}_2Ag](BF_4)$, and the solid state structures of four different crystallographic forms of the complex with emphasis on the importance of the crystallization solvent and the role played by the counterion in influencing the types of covalent and non-covalent forces that organize the supramolecular networks.

Results and Discussion

Syntheses and Characterization

$HC(3\text{-}Phpz)_3$ was prepared in high yield using a modified procedure of the published preparation[13] that avoids the chromatography step. The compound $[\{HC(3\text{-}Phpz)_3\}Ag](BF_4)$ (Scheme 2) was prepared by mixing a THF solution of the ligand with a THF solution of $AgBF_4$ in a 1:1 ratio. The same product is formed in a reaction using a 1:2 metal to ligand ratio, with one equivalent of the ligand recovered from the filtrate. The compound is an air and light stable solid. It is soluble in acetone, acetonitrile, and nitromethane but insoluble in halogenated solvents, water, or alcohols.

The ^1H NMR spectrum of the solid in CD_3CN shows that the acetonitrile completely replaces the ligand in solution; the spectrum of the compound in CD_3CN is the same as the free ligand in this solvent. However, the ^1H NMR spectra of the compound in deuterated acetone or nitromethane are clearly different from the free ligand, showing the coordination of the ligand to the silver(I) in these solutions. Although the X-ray structures of all crystalline forms of $[\{HC(3\text{-}Phpz)_3\}Ag](BF_4)$ show that in the solid state the pyrazolyl rings are non-equivalent (vide infra), the NMR spectra of $[\{HC(3\text{-}Phpz)_3\}Ag](BF_4)$ and similar complexes of silver containing the $[C(pz)_3]$ unit[20,21,23,25] all show equivalent rings, presumably because of fast exchange of the ligands and metals on the NMR timescale. This fast exchange process is maintained even at low temperatures.

An interesting solvent dependence was observed in the chemical shifts of the hydrogen atoms of the silver complex when they were compared with their initial position in the free ligand. In deuterated acetone the resonances that corresponds to the methine hydrogen and the 5-H (pz) were shifted ca. 0.4 ppm while the other resonances [the 4-H(pz) and phenyl hydrogens] were found at almost the same positions as in the free ligand. In deuterated nitromethane the only peak that was found shifted significantly was the 5-H(pz) with a shift of ca. 0.25 ppm. The greater shifts in acetone are likely due to hydrogen bonding of the acetone with the acidic methine hydrogen, an effect that has been observed previously.[29,30]

Electrospray mass spectroscopy (ES/MS) has emerged as a technique for investigating solution aggregation of covalent and noncovalent species. In the case of coordination polymers, ES/MS was used to probe the aggregation between the ligands and silver(I) salts in solution, aggregates that might be related to the building blocks and subsequently to the final supramolecular structure of the coordination polymers.[31] We performed the ES/MS experiment in three different solvents to establish such a connection,

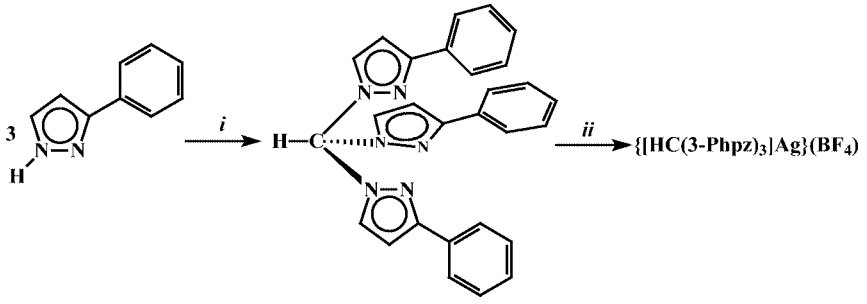

Scheme 2. Preparation of $[\{HC(3\text{-}Phpz)_3\}Ag](BF_4)$: i: $HCCl_3$, Na_2CO_3, nBu_4NBr; ii: $AgBF_4$, THF

 © 2003 Wiley-VCH Verlag GmbH & Co. KGaA, Weinheim

especially given the important influence the crystallization solvent has over the solid state structures (vide infra).

In nitromethane, four peaks were identified at 551, 610, 991, and 1187 *m*/*z*, corresponding to $[LAg]^+$, $[LAg(nitromethane)]^+$, $[L_2Ag]^+$, and $[L_2Ag_2(BF_4)]^+$ respectively. The spectrum is presented in Figure 1. The most abundant peak is the one that corresponds to $[LAg]^+$ species. The least abundant peak corresponds to the species that contains two ligands, two silver(I) ions and one BF_4^-, a peak that presumably arises from a species related to the presence of a coordination polymer in solution. When acetone was used, three peaks were identified at 551, 607, and 991 *m*/*z*, corresponding to $[LAg]^+$, $[LAg(acetone)]^+$, and $[L_2Ag]^+$ respectively. In this case the most abundant peak is the one that corresponds to the $[LAg(acetone)]^+$ species. The same situation was observed when acetonitrile was used as solvent. Three peaks at 551, 590, and 991 *m*/*z* were observed, corresponding to $[LAg]^+$, $[LAg(acetonitrile)]^+$, and $[L_2Ag]^+$ respectively. Interestingly, the most abundant species observed here is the one that corresponds to $[L_2Ag]^+$ species. These $[L_2Ag]^+$ species in all solvents could indicate individual species with a metal to ligand ratio of 1:2 in solution, but given that such species have only been observed for $[\{\kappa^3\text{-HC(3,5-Me}_2\text{pz)}_3\}_2\text{Ag}]^+$ [12] they more likely arise from solution coordination polymers. While the observation of $[L_2Ag_2(BF_4)]^+$ in the spectrum taken from the non-coordinating solvent nitromethane almost certainly arises from a solution coordination polymer, further studies are needed to definitively establish the relationship between ES/MS results and solution aggregation. What is clear from the NMR and ES/MS studies and the fact that coordination compounds of the ligand crystallize from acetonitrile and acetone (vide infra) is that in solutions of coordinating solvents a complicated series of equilibria take place between $[LAg]^+$ species (either aggregated or not), and species in which the solvent has partially or completely displaced the ligands.

Solid-State Studies

Given the versatility of the tris(3-Ph-pyrazolyl)methane ligand (L) we determined the solid state structure of the free ligand for comparison purposes. The molecular structure of the ligand together with the crystallographic and structure refinement data and selected bond lengths and angles are presented as supplementary information (Figure S1 and Tables S1 and S2, Supporting Information, see footnote on page 1 of this article). The ligand structure consists of discrete molecules without significant intermolecular associations. The orientation of the three pyrazolyl rings is a propeller arrangement with only one of the donor nitrogen atoms oriented toward the potential bonding "pocket" of the ligand. The pyrazolyl and phenyl rings are not in the same plane, the N(*n*1)−C(*n*1)−C(*n*4)−C(*n*5) (where *n* denotes the ring number) torsion angles between the rings ranging from 155 to 172 degrees.

We have grown crystals of $[\{HC(3\text{-Phpz})_3\}Ag](BF_4)$ from vapor phase diffusion of diethyl ether into nitromethane, acetonitrile, and acetone solutions of the complex in order

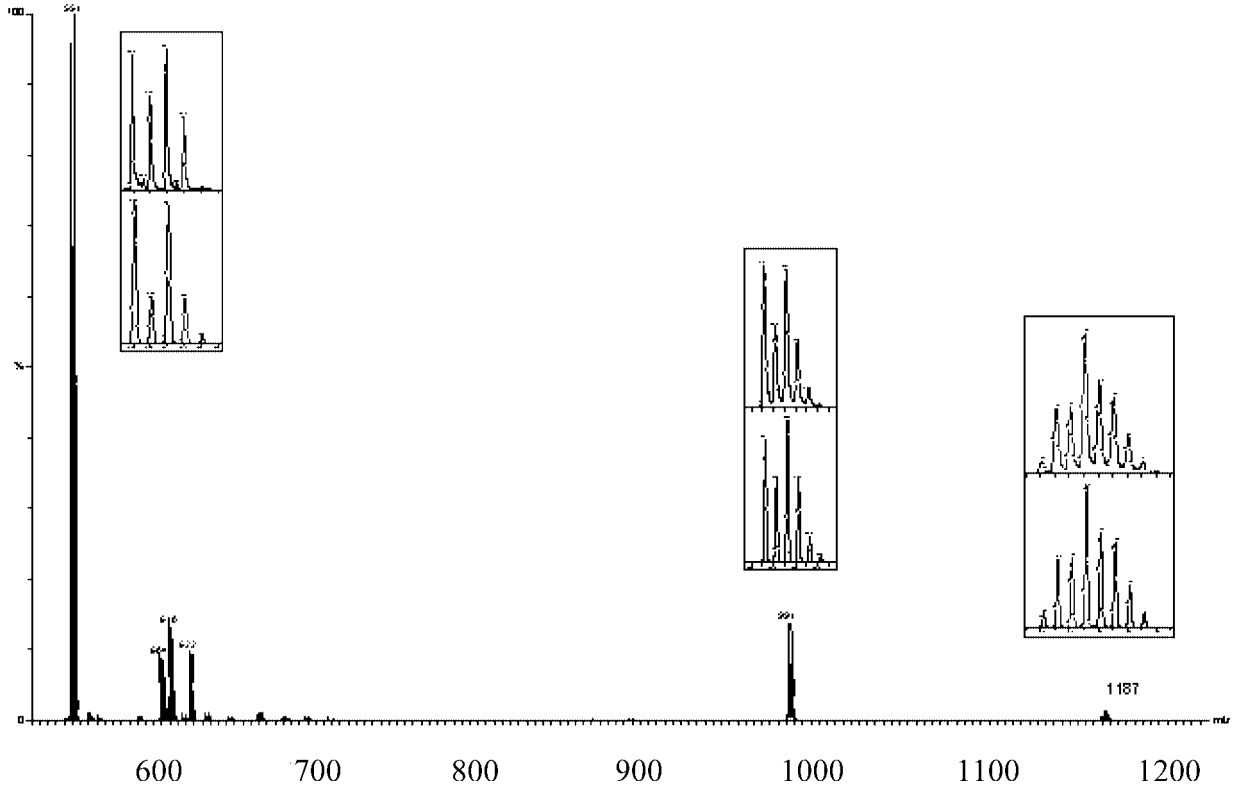

Figure 1. Portion of ES/MS spectra of $[\{HC(3\text{-Phpz})_3\}Ag](BF_4)$ in nitromethane; the insets show the observed (top) and calculated (bottom) isotopic patterns

 © 2003 Wiley-VCH Verlag GmbH & Co. KGaA, Weinheim

to ascertain the effects of non-coordinating and coordinating solvents on molecular and the subsequent supramolecular structures. When nitromethane was used, two polymorphs were found, an orthorhombic form (**1**) and triclinic form (**2**). Both polymorphs are coordination polymers constructed by a κ^2-κ^1 coordination of the tris(3-Ph-pyrazolyl)methane units, with a metal to ligand ratio of 1:1. In contrast, when acetonitrile or acetone was used, two new discrete compounds were obtained, with the same metal to tris(pyrazolyl)methane ligand ratio, of the formula [{HC(3-Phpz)$_3$}Ag{$(CH_3)_2CO$}](BF_4) (**3**) and [{HC(3-Phpz)$_3$}Ag{CH_3CN}](BF_4) (**4**). In these compounds, the ligand shows tripodal coordination to a single silver center. In addition one solvent molecule is coordinated to the metallic center. The metrical parameters for all four compounds (bond lengths and angles) are given in Table 1.

The two crystallographically independent [{HC(3-Phpz)$_3$}Ag]$^+$ units and two BF_4^- anions of **1** are pictured in Figure 2 (a and b) together with their partial crystallographic numbering scheme (for a full crystallographic numbering scheme see the ORTEP representation of **1** in the Supplementary Information, Figure S2). Each ligand is κ^2-κ^1 coordinated to silver(I) centers. The polyhedra about Ag(1) and Ag(2) atoms are flattened trigonal pyramids [sum of the N−Ag−N bond angles = 332° for Ag(1) and 341° for Ag(2)], with a large distortion caused by the restricted bite angle [82.55(11)° for Ag(1) and 84.11(10)° for Ag(2)] of the κ^2-bonded ligand. The BF_4^- anions are located along the polymeric strand in the vicinity of the silver atoms. There are several close contacts between the silver and fluorine atoms in both chains, interactions that are best described as secondary bonds.[32] The Ag···F distances, shown as blue dotted lines in Figure 2, are listed in Table 2, together with other non-covalent parameters for **1**.[33−37] Interestingly, in **1** the BF_4^- anions are not involved in the organization of the extended structure, a structural feature frequently observed with other similar complexes.[21,23,25] There are several C−H···F weak hydrogen bonds (see Table 2), but they are interstrand only and pictured in Figure 2 (a and b) also as blue dotted lines. The H···F distances are all well below the sum of van der Waals radii for hydrogen and fluorine and are typical for this type of hydrogen bonding.

Table 1. Selected bond lengths and angles for **1**−**4**

1			
Ag(1)−N(11)	2.381(3)	N(11)−Ag(1)−N(21)	82.55(11)
Ag(1)−N(21)	2.304(3)	N(11)−Ag(1)−N(31)′	111.52(11)
Ag(1)−N(31)′	2.255(3)	N(21)−Ag(1)−N(31)′	137.59(10)
Ag(2)−N(41)	2.379(3)	N(41)−Ag(2)−N(51)	84.11(10)
Ag(2)−N(51)	2.294(3)	N(41)−Ag(2)−N(61)′	117.38(10)
Ag(2)−N(61)′	2.230(2)	N(51)−Ag(2)−N(61)′	139.13(11)
2			
Ag(1)−N(11)	2.324(3)	N(11)−Ag(1)−N(61)	140.11(10)
Ag(1)−N(21)	2.353(3)	N(21)−Ag(1)−N(61)	112.61(10)
Ag(1)−N(61)	2.221(3)	N(11)−Ag(1)−N(21)	86.08(9)
Ag(2)−N(31)′	2.217(3)	N(31)′−Ag(2)−N(41)	145.96(10)
Ag(2)−N(41)	2.255(3)	N(31)′−Ag(2)−N(51)	111.54(10)
Ag(2)−N(51)	2.479(3)	N(41)−Ag(2)−N(51)	85.17(9)
3			
Ag(1)−N(111)	2.412(3)	O(101)−Ag(1)−N(131)	138.57(12)
Ag(1)−N(121)	2.381(3)	O(101)−Ag(1)−N(121)	123.95(12)
Ag(1)−N(131)	2.338(3)	N(131)−Ag(1)−N(121)	79.48(11)
Ag(1)−O(101)	2.231(3)	O(101)−Ag(1)−N(111)	131.25(12)
Ag(2)−N(211)	2.358(3)	N(131)−Ag(1)−N(111)	82.00(11)
Ag(2)−N(221)	2.413(3)	N(121)−Ag(1)−N(111)	80.46(11)
Ag(2)−N(231)	2.363(3)	O(201)−Ag(2)−N(211)	135.12(12)
Ag(2)−O(201)	2.172(4)	O(201)−Ag(2)−N(231)	123.60(13)
		N(211)−Ag(2)−N(231)	83.19(11)
		O(201)−Ag(2)−N(221)	133.98(12)
		N(211)−Ag(2)−N(221)	81.95(10)
		N(231)−Ag(2)−N(221)	78.74(10)
4			
Ag(1)−N(111)	2.337(2)	N(101)−Ag(1)−N(111)	132.15(8)
Ag(1)−N(121)	2.4047(19)	N(101)−Ag(1)−N(131)	131.32(8)
Ag(1)−N(131)	2.353(2)	N(111)−Ag(1)−N(131)	80.34(7)
Ag(1)−N(101)	2.137(2)	N(101)−Ag(1)−N(121)	132.63(8)
Ag(2)−N(211)	2.3549(18)	N(111)−Ag(1)−N(121)	78.73(7)
Ag(2)−N(221)	2.394(2)	N(131)−Ag(1)−N(121)	81.13(7)
Ag(2)−N(231)	2.361(2)	N(201)−Ag(2)−N(211)	136.49(8)
Ag(2)−N(201)	2.149(2)	N(201)−Ag(2)−N(231)	133.62(8)
		N(211)−Ag(2)−N(231)	81.89(7)
		N(201)−Ag(2)−N(221)	123.46(8)
		N(211)−Ag(2)−N(221)	78.63(6)
		N(231)−Ag(2)−N(221)	81.82(7)

There are two crystallographically independent chains (Figure 2, c and e), that run along the *a* axis, associated with the independent atoms Ag(1) and Ag(2). As pictured in Figure 2 (c), the chain associated with Ag(1) has an intrastrand π−π stacking interaction (black double dotted lines) between the [N(31)−N(32)−C(31)−C(32)−C(33)] pyrazole ring that is κ^1 coordinated to silver(I) and the [C(14)−C(15)−C(16)−C(17)−C(18)−C(19)] phenyl ring attached to the [N(11)−N(12)−C(11)−C(12)−C(13)] pyrazolyl ring that is κ^2 coordinated to the same silver. The two rings are parallel displaced, resulting in a centroid−centroid distance of 3.83 Å, but with a perpendicular distance between the rings of 3.47 Å. These values are typical for a π−π stacking interaction.[35] There is no similar interaction in the chains associated with Ag(2). Figure 2 (d and f) show a view of both chains along the *a* axis, illustrating the overall similarity in the chains, where the only important difference is the orientation of the phenyl rings involved in the π−π stacking in the Ag(1) chain.

These non-covalent forces appear to be correlated with a twisting of the pyrazolyl rings. For maximum overlap with the lone pair on the donor nitrogen atoms the metal would lie in the plane of each pyrazole ring. Any deviation where the metal lies out of this plane can be measured by the Ag−N(*n*1)−N(*n*2)−C(*n*1) (where *n* denotes the ring number) torsion angle, an angle that is 180° for a metal located in the same plane as the ring. We have shown[38] that these deviations are related to the size of the metal when the tris(pyrazolyl)methane ligand is tripodal. For **1**, where the ligand is not tripodal, the angles associated with the Ag(1) chain are 160°, 145°, and 122° and those associated with Ag(2) chain are 165°, 143°, and 134° respectively. The greatest value (least twisting) in this series (165°) is correlated with a pyrazolyl and its associated phenyl ring that are *not*

 © 2003 Wiley-VCH Verlag GmbH & Co. KGaA, Weinheim

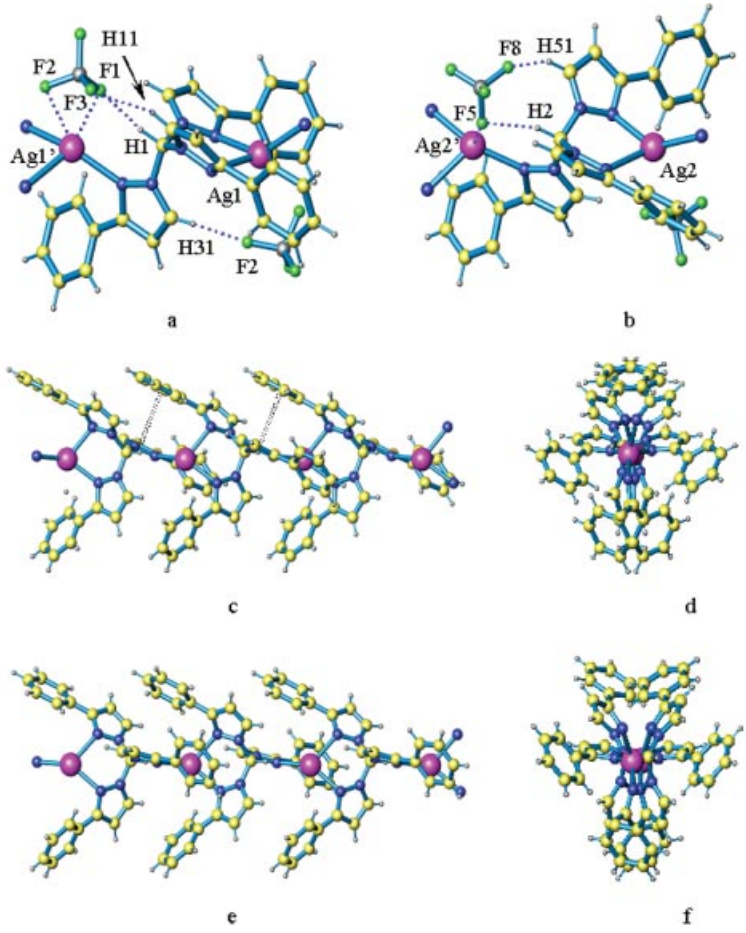

Figure 2. a, b) Formation of the two independent chains in **1** based on the κ^2-κ^1 coordination mode of the HC(3-Phpz)$_3$ ligand; secondary Ag···F bonds and C−H···F weak hydrogen bonds are shown as blue dotted lines; color scheme: silver purple, carbon yellow, nitrogen blue, fluorine green; c) Ag(1) chain with the π−π stacking between pyrazolyl and phenyl rings showed as black double dotted lines; d) end-on view of the same chain; e) Ag(2) chain, with no intrastrand interactions; f) view down the Ag(2) chain

involved in any non-covalent interaction. In contrast, the smallest value in this series (122°) is related to the [N(11)−N(12)−C(11)−C(12)−C(13)] pyrazolyl ring that has its associated phenyl ring involved in the intrachain π−π stacking as showed above. Furthermore, this pyrazolyl ring participates in a C−H···F hydrogen bond, see Figure 2 (a).

The non-equivalent chains of **1** are organized into a 3-D supramolecular structure by C−H···π interactions. The chains are organized into corrugated sheets by two interactions of this type, with phenyl rings acting as both donors and acceptors. The sheets are situated in the *ab* plane of the crystal. Further, the sheets are held together by another C−H···π interaction, with a pyrazolyl ring acting as donor and a phenyl ring acting as acceptor. The metrical parameters for these interactions are given in Table 2 and are represented by red dotted lines in Figure 3, which shows partial views of two of the sheets down the polymer chains.

Compound **2** is also a coordination polymer, built by the same κ^2−κ^1 coordination mode of the HC(3-Phpz)$_3$ ligand. Figure 4 (a) shows a portion of this coordination polymer together with the partial numbering scheme (for a full crystallographic numbering scheme see the ORTEP representation of **2** in the Supplementary Information, Figure S3). Selected bond lengths and angles are summarized in Table 1. The polyhedra around the silvers are again flattened trigonal pyramids [sum of the N−Ag−N bond angles = 339° for Ag(1) and 343° for Ag(2)], with a large distortion caused by the restricted bite angle [86.08(9)° for Ag(1) and 85.17(9)° for Ag(2)] of the κ^2-bonded ligand. The difference between **1** and **2** is that in **2** there is only one independent chain containing two independent silver atoms, while in **1** there are two independent chains, associated with two independent silver atoms. A similarity with **1** is that the BF_4^- anions are located along the polymeric strand in the vicinity of silver atoms, leading to close contacts between the silver and fluorine atoms along the chain. The Ag···F distances (blue dotted lines) are listed in Table 2, together with other non-covalent parameters for **2**. Another similarity between **1** and **2** is that the BF_4^- anions are not involved in the organization of the supramolecular structure and all the C−H···F weak hydrogen bonds are intrastrand. They are pictured in Figure 4 (a) as blue dotted lines and their metrical parameters are given in Table 2.

In the case of **2** there are several additional non-covalent interactions within the polymeric strands, also represented

 © 2003 Wiley-VCH Verlag GmbH & Co. KGaA, Weinheim

Table 2. Non-covalent interactions present in **1**−**4**

	H−A	D−A	D−H−A	Role
1				
Ag(1)−F(1)	2.604(3)	−	−	Intrastrand, secondary bond
Ag(1)−F(2)	3.124(4)	−	−	Intrastrand, secondary bond
Ag(2)−F(5)	2.578(3)	−	−	Intrastrand, secondary bond
C(1)−H(1)−F(1)	2.02	3.00	167.6	Intrastrand, no organization function
C(2)−H(2)−F(5)	2.35	3.30	159.8	Intrastrand, no organization function
C(11)−H(11)−F(3)	2.44	3.34	158.9	Intrastrand, no organization function
C(31)−H(31)−F(2)	2.25	3.00	135.4	Intrastrand, no organization function
C(51)−H(51)−F(8)	2.33	3.13	142.3	Intrastrand, no organization function
C(16)−H(16) − Ct	2.61	3.55	169.5	Organize the strands in sheets
C(36)−H(36) − Ct	2.94	3.76	144.9	Organize the strands in sheets
C(42)−H(42) − Ct	2.66	3.46	142.2	Organize the sheets in 3D
2				
Ag(1)−F(1)	2.761(3)	−	−	Intrastrand, secondary bond
Ag(1)−F(2)	2.988(3)	−	−	Intrastrand, secondary bond
Ag(2)−F(5)	2.481(3)	−	−	Intrastrand, secondary bond
C(1)−H(1)−F(5)	2.31	3.28	165.1	Intrastrand, no organization function
C(2)−H(2)−F(1)	2.09	3.06	160.3	Intrastrand, no organization function
C(21)−H(21)−F(8)	2.30	3.20	157.9	Intrastrand, no organization function
C(51)−H(51)−F(4)	2.24	3.18	174.8	Intrastrand, no organization function
C(37)−H(37) − Ct	2.71 (2.68)	3.60	154.6	Formation of dimers
C(46)−H(46) − Ct	2.67 (2.59)	3.51	147.2	Formation of dimers
C(57)−H(57) − Ct	2.83 (2.82)	3.65	145.8	Organize the dimers into sheets
3				
C(101) − H(101) − F(8)	2.33	3.23	150.1	Formation of Ag(1) chains
C(138) − H(138) − F(5)	2.39	3.24	148.4	Formation of Ag(1) chains
C(201) − H(201) − F(2)	2.04	3.02	166.3	Organize the Ag(2) dimers into sheets
C(211) − H(211) − F(3)	2.28	3.23	172.1	Organize the Ag(2) dimers into sheets
C(238) − H(238) − F(4)	2.45	3.40	172.9	Organize the Ag(2) dimers into sheets
C(222) − H(222) − F(1)	2.45	3.31	150.8	Organize the Ag(2) dimers into sheets
C(143) − H(14E) − F(1)	2.26	3.22	165.3	Support the 3D architecture
C(127) − H(127) − Ct	2.81 (2.73)	3.47	127.7	Organize the Ag(1) chains into sheets
C(217) − H(217) − Ct	2.90 (2.84)	3.75	148.6	Formation of Ag(2) dimers
C(115) − H(115) − Ct	2.90 (2.85)	3.78	152.9	Support the 3D architecture
4				
C(121) − H(121) − F(3)	2.33	3.04	131.6	Bridges one Ag(1) chain and one Ag(2) dimer
C(201) − H(201) − F(1)	2.38	3.30	152.4	Bridges one Ag(1) chain and one Ag(2) dimer
C(211) − H(211) − F(3)	2.34	3.26	162.3	Bridges one Ag(1) chain and one Ag(2) dimer
C(231) − H(231) − F(2)	2.42	3.21	141.2	Bridges one Ag(1) chain and one Ag(2) dimer
C(116) − H(116) − Ct	2.81 (2.74)	3.43	124.0	Formation of Ag(1) chains
C(135) − H(135) − Ct	2.81 (2.79)	3.56	135.7	Formation of Ag(1) chains
C(126) − H(126) − Ct	2.88 (2.84)	3.66	139.4	Organize the Ag(1) chains into sheets
C(216) − H(216) − Ct	3.02 (2.74)	3.96	171.5	Formation of Ag(2) dimers

in Figure 4 (a). There are two π−π stacking interactions involving both pyrazolyl and phenyl rings. One interaction (shown as black double dotted line) involves one of the κ^2 bonded pyrazolyl ring [N(21)−N(22)−C(21)−C(22)−C(23)] and the phenyl ring associated with one of the κ^1 bonded pyrazolyl ring [containing N(61)] with a perpendicular distance between the rings of 3.73 Å. Another π−π interaction involves the second κ^1 bonded pyrazolyl ring [N(31)−N(32)−C(31)−C(32)−C(33)] and a phenyl ring attached to another κ^2 bonded pyrazolyl ring [containing N(51)] with a perpendicular distance between the rings of 3.63 Å. This interaction is shown in Figure 4 (a) by two black arrows pointing toward where the respective group would be located if more of the strand were shown. There are additional C−H···π interactions within the strand (red dotted lines) with the metrical parameters listed in Table 2.

There is substantial tilting of the pyrazolyl rings from the ideal value of 180°. The torsion angles around the Ag(1) atom are 164°, 144°, and 124° and those around the Ag(2) atom are 170°, 151°, and 118°, respectively. As in **1**, these angles are correlated to the non-covalent interactions within the strand. For example, the Ag(1)−N(11)−N(12)−C(11) angle of 124° is related to a C−H···π interaction formed by the [N(11)−N(12)−C(11)−C(12)−C(13)] ring, acting as acceptor, with one of the phenyl rings involved in the π−π stacking interaction. The associated phenyl ring acts also as the acceptor in another C−H···π interaction where the donor is the [N(41)−N(42)−C(41)−C(42)−

 © 2003 Wiley-VCH Verlag GmbH & Co. KGaA, Weinheim

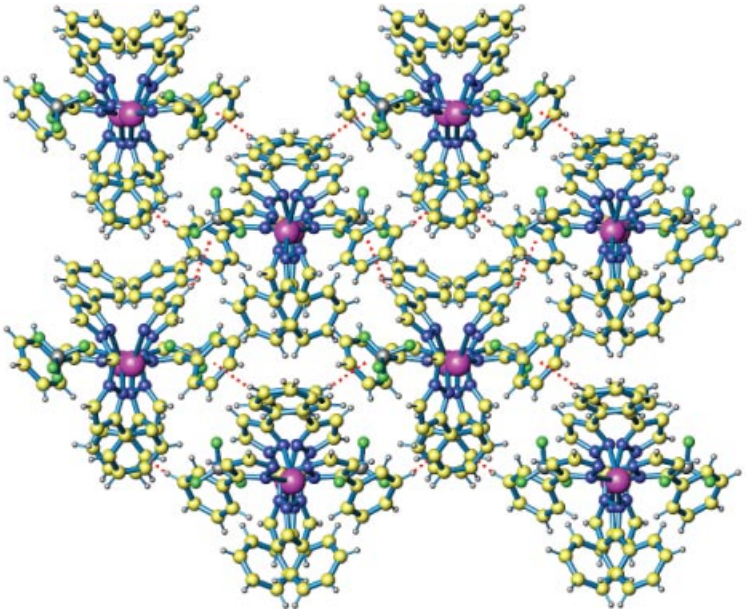

Figure 3. The supramolecular structure of **1** viewed down the *a* axis; the C−H···π interactions that organize the 3-D architecture are shown as red dotted lines

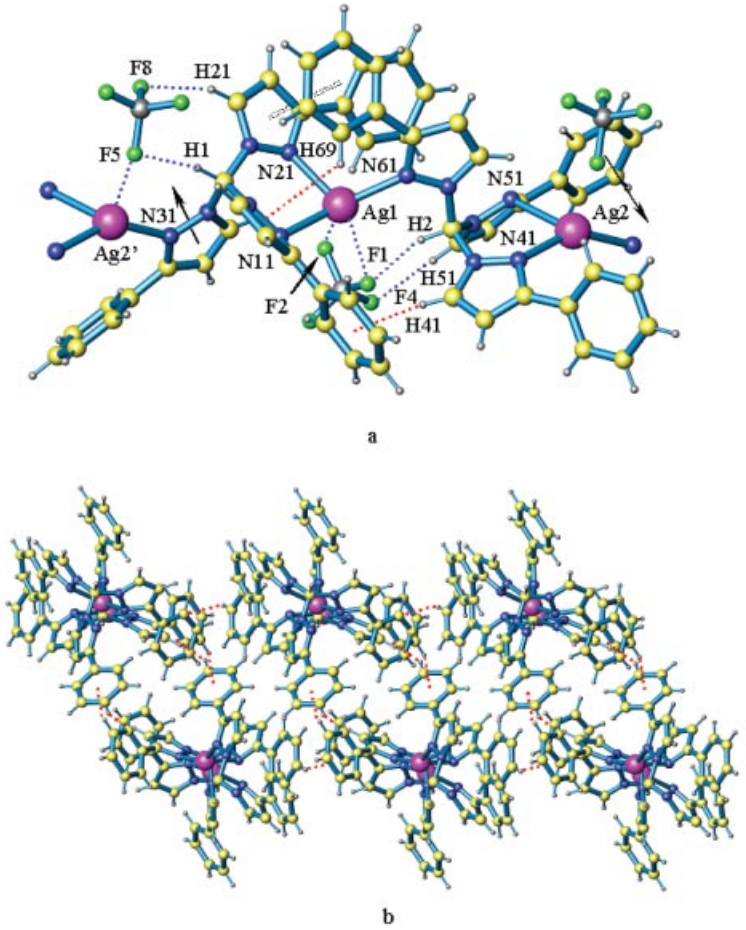

Figure 4. a) Part of the coordination polymer **2**; secondary Ag···F bonds and weak C−H···F hydrogen bonds shown as blue dotted lines and C−H···π interactions as red dotted lines; one π−π stacking is shown as double black dotted lines; the second π−π stacking is pictured by two black arrows. The tilting of the pyrazolyl ring containing N(11) is clearly visible in this orientation; b) formation of the dimeric sheets in **2** via C−H···π interactions, shown as red dotted lines; three dimeric chains are shown, down the *a* axis of the unit cell

 © 2003 Wiley-VCH Verlag GmbH & Co. KGaA, Weinheim

C(43)] pyrazolyl ring. The Ag(2)−N(51)−N(52)−C(51) torsion angle of 118° is influenced by four non-covalent interactions. The pyrazolyl ring associated with the largest angle is not involved in any non-covalent interactions.

The supramolecular structure of **2** is only 2-D and is again organized by C−H···π interactions, Table 2. A pair of these interactions organizes the strands into dimers that are oriented in the direction of the *c* axis. A third interaction organizes the dimers into sheets placed parallel to the *ab* plane of the crystal. Figure 4 (b) depicts a 2-D sheet built up from three dimers with the C−H···π interactions represented by red dotted lines.

The replacement of nitromethane with acetone or acetonitrile as the crystallization solvent leads to a dramatic change in the structure of the compound. The coordination of one molecule of solvent to the silver atom, together with a tripodal, κ^3-coordination of the (3-Ph-pyrazolyl)methane ligand leads to the formation of discrete complexes of the formula $[\{HC(3\text{-}Phpz)_3\}Ag\{(CH_3)_2CO\}](BF_4)$ (**3**) and $[\{HC(3\text{-}Phpz)_3\}Ag\{CH_3CN\}](BF_4)$ (**4**).

The crystal structure of **3** contains two symmetry independent units of virtually identical conformation about the silver(I) (see Table 1), but which have different supramolecular contacts. The two units and their partial numbering schemes are represented in Figure 5 (a and b) (for a full crystallographic numbering scheme see the ORTEP representation of **3** in the Supplementary Information, Figure S4; see also footnote on the first page of this article). The silver atoms have a distorted tetrahedral arrangement. For the first unit the average Ag(1)−N distance is 2.37 Å with a corresponding N−Ag(1)−N average angle of 80.64°. The Ag(1)−O distance is 2.231(3) Å, with an average N−Ag(1)−O angle of 131.25°. For the second unit the average Ag(2)−N distance is the same as for the first, 2.37 Å, but with a corresponding N−Ag(2)−N average angle of 81.29°. The Ag(2)−O distance is 2.172(4) Å with the corresponding average N−Ag(2)−O angle of 130.9°.

In contrast with **1** and **2**, where the counterions interacted with the silvers and were not involved in interchain interactions, the cations in **3** are organized into a 3-D structure using both weak C−H···F hydrogen bonds and C−H···π interactions (Table 2). The unit containing the Ag(1) atom is organized into chains via C−H···F hydrogen bonds, Figure 5 (c). The BF_4^- counterion makes two hydrogen bonds, shown as blue dotted lines, one with the methine hydrogen H(101) and another with H(138), a hydrogen situ-

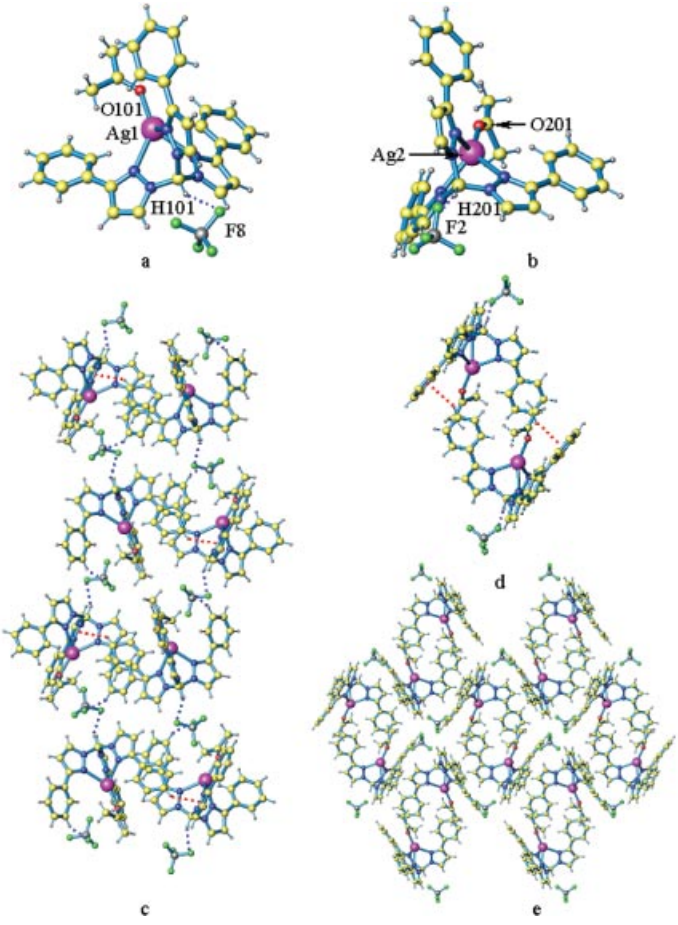

Figure 5. a, b) Two silver(I) building blocks in **3** with their BF_4^- counterions positioned close to the methine hydrogen; color scheme as in Figure 2, plus oxygen red; c) formation of Ag(1) chains and sheets in **3** by the means of C−H···F hydrogen bonds (blue dotted lines) and C−H···π interactions (red dotted lines); d) dimeric association of Ag(2) units, connected by C−H···π interactions, shown as red dotted lines; e) the 2-D network of Ag(2) dimers: view perpendicular to the sheet, showing seven dimers connected by C−H···F weak hydrogen bonds

 © 2003 Wiley-VCH Verlag GmbH & Co. KGaA, Weinheim

ated on one of the phenyl rings. The (C)H···F distances to H(101) and H(138) are 2.33 and 2.39 Å with the corresponding C−H−F angles of 150 and 148°. Both these distances are below the sum of van der Waals radii for hydrogen and fluorine[33,34] and are typical for this type of hydrogen bonding.[39,40] These interactions build up chains that run along *c* axis of the unit cell. The chains are arranged into sheets by means of C−H···π interactions, as can be seen also in Figure 5 (c) as red dotted lines. One hydrogen atom from a phenyl group in one cationic unit is pointed toward a pyrazolyl ring within another chain thus generating a sheet in the *bc* plane of the unit cell.

The unit containing the Ag(2) atom has a different supramolecular organization, based again on both C−H···π interactions and weak C−H···F hydrogen bonds. One C−H···π interaction is between H(217), located in a phenyl ring and the pi cloud of a phenyl ring on an adjacent silver(I) unit, Figure 5 (d). The hydrogen to centroid distance is 2.90 Å with the corresponding C−H-centroid angle of 149° see also Table 2. This distance is typical for C−H···π interactions.[36,37] A pair of these interactions, showed as red dotted lines, links two Ag(2) units forming a dimer.

The BF_4^- ions connect these dimers into a 2-D supramolecular network (see Table 2 for metrical parameters) via C−H···F hydrogen bonds. Figure 5 (e) shows seven dimeric assemblies viewed in the same orientation as in Figure 5 (d), connected by the BF_4^- anions. At the corners of each square shaped dimeric unit, each dimer is bonded to four other dimers arranged in a square around it through four BF_4^- anions. The two "outside" dimers in Figure 5 (e) are not connected to the central dimer but to the two dimeric units above and below them in the figure.

The sheets associated with Ag(1) and Ag(2) are arranged in a 3-D architecture again by weak C−H···F hydrogen bonds and C−H···π interactions, Figure 6. One fluorine atom that is part of the BF_4^- anion involved in the organization of the Ag(2) units in chains makes a close contact with a hydrogen located on an acetone molecule coordinated to an Ag(1) unit. The H···F contact is 2.26 Å (C···F contact of 3.22 Å) with a corresponding C−H−F angle of 165°. A second interaction holding the sheets together is a C−H···π interactions formed between a hydrogen atom situated on a phenyl ring within the Ag(1) unit and another phenyl ring that is part of Ag(2) unit. The H···centroid distance is 2.90 Å and the C···centroid distance of 3.78 Å, with the corresponding C−H-centroid angle of 153°.

When acetone was replaced with acetonitrile in the crystallization procedure, the structures of the two silver(I) units of the resulting compound (**4**) are similar to those of **3**. The crystal structure of **4** contains two symmetry independent units of virtually identical conformation but which have different supramolecular contacts. The two units and their partial numbering schemes are represented in Figure 7 (for a full crystallographic numbering scheme see the ORTEP representation of **4** in the Supplementary Information, Figure S5). The silver atoms again have a distorted tetrahedral arrangement. For the first unit the average $Ag(1)-N_{pz}$ distance is 2.36 Å with a corresponding $N_{pz}-Ag-N_{pz}$ average angle of 80.06°. The Ag(1)−N(101) distance is 2.137(2) Å, with an average $N_{pz}-Ag(1)-N(101)$ angle of 132.03°. For the second unit the average $Ag(2)-N_{pz}$ distance is 2.37 Å, with a corresponding $N_{pz}-Ag-N_{pz}$ average angle of 80.78°. The Ag(2) − N(201) distance in this case is 2.149(2) Å with the corresponding average $N_{pz}-Ag(2)-N(201)$ angle of 131.19°. For further details on the bond lengths and angles see Table 1. The BF_4^- counterions make hydrogen bonds with the hydrogen atoms attached to the central methine carbon atoms. The BF_4^- anion associated with Ag(1) was found to be disordered over two closely spaced positions so further discussions about its role in the extended structure of **4** are precluded; Figure 7 (a) pictures one component of the disordered counterion, but in further discussions this counterion will not be mentioned.

The units containing the Ag(1) silver atoms are organized in chains running along the *b* axis by means of two C−H···π interactions (see Table 2 for details). In both cases, two pyrazolyl rings act as acceptors and two phenyl rings as hydrogen donors. Figure 8 (a) illustrates three chains, that are further connected in a 2-D network, again through C−H···π interactions, with pyrazolyl rings acting as acceptors and phenyl rings as hydrogen donors. The interactions responsible for the formation of the chains and sheets are pictured as red dotted lines in Figure 8 (part a). Figure 8 (part b) is a view end-on of the Figure 8 (part a), showing the orientation of the sheets in the *bc* plane of the unit cell.

The units containing the Ag(2) atoms are arranged in a different way. A double π−π/C−H···π interaction organizes these units in dimers, as pictured in Figure 9. The metrical

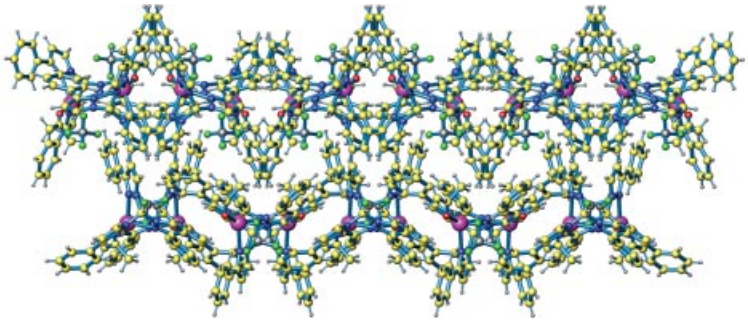

Figure 6. The 3-D architecture of **3** formed by combining the Ag(1) and Ag(2) sheets

 © 2003 Wiley-VCH Verlag GmbH & Co. KGaA, Weinheim

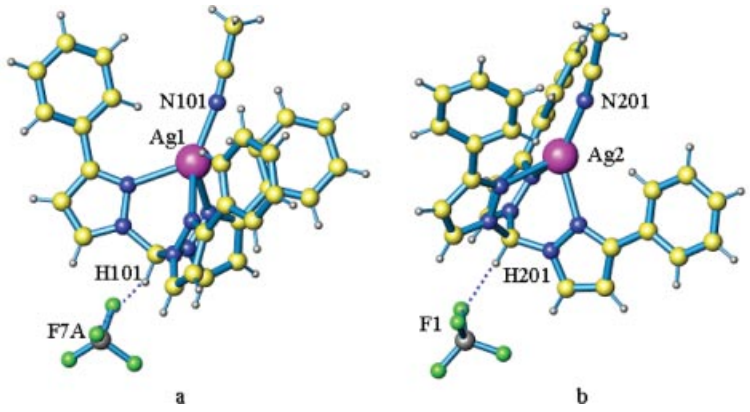

Figure 7. Two silver(I) building blocks in **4** with the BF_4^- counterions positioned close to the methine hydrogen; the BF_4^- anion in (a) is disordered over two positions; only one component is shown here

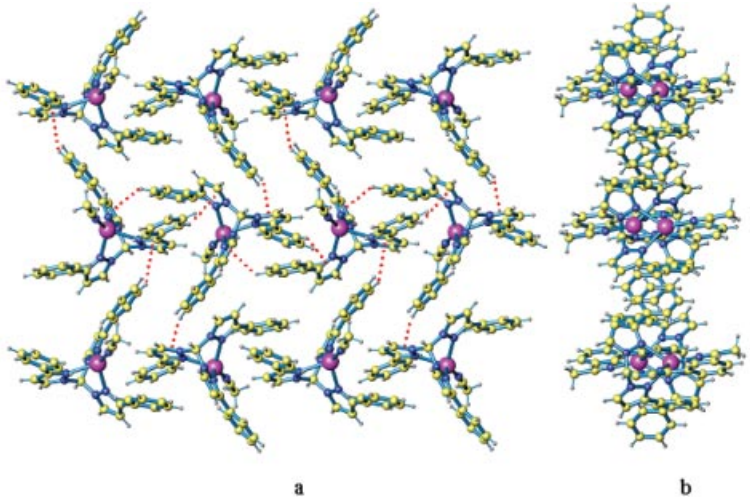

Figure 8. Formation of Ag(1) sheets in **4**: a) view perpendicular to the sheet, illustrating three interconnected chains; the C−H···π interactions that form the chains are represented only within the middle chain; b) end-on view of the same sheet in the *bc* plane of the unit cell

parameters for these non-covalent interactions are listed in Table 2. The π−π stacking is between two phenyl rings that also act as hydrogen donors in the C−H···π interaction, with two other phenyl rings acting as acceptors. The stacked phenyl rings are parallel, but displaced in order to maximize the C−H···π interaction, the angle formed by the centroid−centroid vector with the ring normal being 30°. The centroid−centroid distance is 3.9 Å and the perpendicular distance between the planes is 3.4 Å.[35] There is also a shift from an ideal geometric arrangement for the C−H···π interaction. The presence of the π−π stacking between the parallel displaced phenyl rings leads to a rather long H···centroid distance of 3.02 Å, but the perpendicular distance from the hydrogen atom to the acceptor phenyl planes is 2.7 Å, with the corresponding C−H−centroid angle of 171°.[36,37]

These two units are arranged into a supramolecular structure by the means of weak (C)H···F hydrogen bonds. The ordered BF_4^- counterion act as a bridge between one Ag(1) chain and one Ag(2) dimer, Figure 10 (a). The F(3) atom within the BF_4^- counterion is involved in a bifurcated hydrogen bond with two hydrogen atoms located on the fifth carbon atom of the pyrazolyl rings. As it can be seen in Table 2, the H···F contacts are short, with C−H−F angles approaching to linearity. The resultant architecture is further connected into a 3-D network by the non-covalent C−H···π interactions that connects the Ag(1) chains into sheets, as pictured in Figure 10 (b). There is no non-coval-

 © 2003 Wiley-VCH Verlag GmbH & Co. KGaA, Weinheim

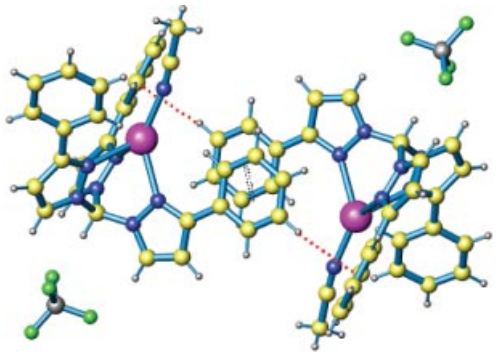

Figure 9. Dimeric association of Ag(2) building blocks in **4** via a double π−π stacking (black double dotted line)/C−H···π (red dotted lines) interaction

ent interaction holding the dimers associated with Ag(2) together. The sheets in Figure 10 (b) are in the same orientation as in Figure 8 (b).

Comparison of Molecular and Supramolecular Structures

Our systematic X-ray crystallographic studies reveal that a coordinating solvent dramatically changes the molecular structures and/or the supramolecular structures of the four forms of [{HC(3-Phpz)$_3$}Ag](BF_4) studied here. In the absence of a coordinating solvent, the tris(3-phenyl-pyrazolyl)methane ligand bridges two silver atoms in the κ^2-κ^1 bonding mode forming coordination polymers arranged in argentachains. This arrangement of the ligands allows room for the BF_4^- counterion to be located in the vicinity of the silver atoms, with close silver−fluorine contacts (see Table 2 and Figure 2, a, b and Figure 4, a). This secondary interaction between the silver and fluorine atoms completes the fourth coordination site and prevents the anions from participating in the organization of the subsequent supramolecular structures of the polymeric chains. Two polymorphs with the same basic κ^2-κ^1 coordinating mode have been crystallized that have different supramolecular structures based on similar types of non-covalent interactions. In compound **1** there are two independent chains having different shapes (Figure 2, d and f) and in **2** only one type of chain is present, with a different internal structure than in **1**. Noncovalent forces organize the chains into sheets and the sheets into a final 3-D supramolecular structure in the case of **1**, while in the case of **2** only a 2-D supramolecular structure forms (compare Figures 3 and 4, b).

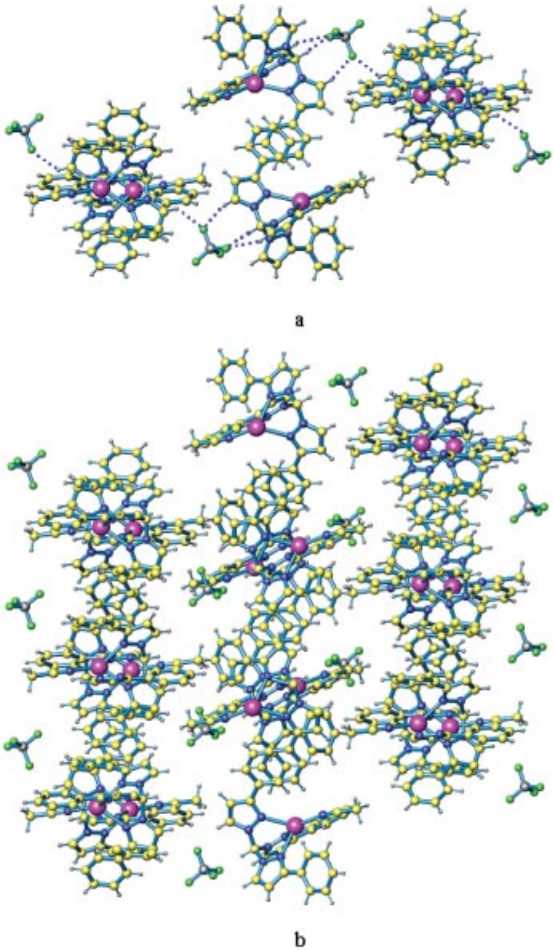

Figure 10. a) Two Ag(1) chains and one Ag(2) dimer in **4** bridged by the counterions, with the C−H···F hydrogen bonds shown as blue dotted lines; one fluorine atom makes a bifurcated hydrogen bond with hydrogen atoms situated on the fifth position of pyrazolyl rings; b) the extended 3-D structure of **4**, showing six Ag(1) chains in two Ag(1) sheets (left and right, view down the chains) and three Ag(2) dimers (middle) bridged by six BF_4^- counterions

 © 2003 Wiley-VCH Verlag GmbH & Co. KGaA, Weinheim

The structures of the same complex crystallized from the coordinating solvents acetone and acetonitrile are very different from **1** and **2**. The structures feature a κ^3 tripodal coordination mode of the tris(3-phenylpyrazolyl)methane ligand with the fourth coordination site on the silver filled with the solvent, thus generating the discrete compounds **3** (Figure 5, a, b) and **4** (Figure 7) rather than coordination polymers. In both cases the structures of the silver cationic units are very similar. Their asymmetric units contain two chemically similar but crystallographically independent [HC(3-Phpz)$_3$Ag(solvent)] cations. The coordination environment around the silver atom is also similar − a distorted tetrahedron.

The supramolecular structures of **3** and **4** are also similar. In both cases one type of silver(I) unit associates in chains and then in sheets (Figure 5, c, and Figure 8). The second type of silver(I) forms dimeric units (Figure 5, d, and Figure 9). Association between the sheets and dimers leads in both cases to a 3-D supramolecular structure. However, the connection pattern and the resulting extended structures are different. In the case of **3** the chains are supported by weak H···F hydrogen bonds with the BF_4^- counterion acting as a bridge between the cationic units, whereas in **4** the chains are formed only by the means of C−H···π interactions with phenyl rings acting as hydrogen donors and pyrazolyl rings acting as acceptors. The sheets that result from the association of the chains are in both cases supported by C−H···π interactions where the phenyl rings are the donors and pyrazolyl rings are the acceptors.

The mode of formation of the dimeric units in each structure is also different. The self-assembly of the dimeric units in **3** are supported by C−H···π interactions with phenyl rings acting as hydrogen donors and acceptors, while in **4** there is an additional π−π stacking between the phenyl rings that are the hydrogen donors in the C−H···π interaction. The shape of the acetone molecule (two methyl groups, see Figure 5, d) prevents the donor phenyl rings involved in the C−H···π interaction from getting close enough for the additional π−π stacking observed in the case of **4**, where an acetonitrile molecule (one methyl group, see Figure 9) does not have such a pronounced steric effect.

The role of the dimers is also different. In **3**, the dimers are arranged in chains by the non-covalent forces, forming a 2-D array of dimers (Figure 5, e) and the association of these sheets forms the overall supramolecular structure pictured in Figure 6. In contrast, in **4** the dimers are not arranged into an extended structure, their contribution to the 3-D supramolecular structure is that they act, together with the BF_4^- anions, as a bridge between two sheets, as shown in Figure 10 (a).

Conclusion

An important conclusion of this work is that in silver(I) chemistry the non-linked, tris(pyrazolyl)methane ligand HC(3-Phpz)$_3$ supports complex supramolecular structures using the same types of covalent and non-covalent forces observed in the silver(I) complexes of the linked multitopic ligands studied earlier. In the absence of a coordinating solvent, [{HC(3-Phpz)$_3$}Ag](BF$_4$) forms two polymorphs with structures dominated by polymeric argentachains that are constructed from the κ^2-κ^1 bonding mode of each ligand, a bonding mode that is frequently observed in the structures of the linked ligands.[20,21,25] In these structures, the weakly coordinating counterion BF_4^- bonds to the silvers completing the coordination spheres. This interaction removes the BF_4^- groups from the ability to support the supramolecular structure through weak H···F hydrogen bonds with the acid hydrogen atoms located on the ligands of different cationic units.

When [{HC(3-Phpz)$_3$}Ag](BF$_4$) is crystallized from coordinating solvents, the solvent bonds directly to silver. The presence of the coordinating solvent changes the bonding mode of the HC(3-Phpz)$_3$ ligand to tripodal. Even in the absence of a coordination polymer formed by either the κ^2-κ^1 coordinating mode or from the linking component of the multitopic ligands, complex supramolecular structures form from an interesting array of non-covalent interactions. In these structures, the BF_4^- does not interact with the metal, but contributes to the supramolecular structures through weak H···F hydrogen bonds.

Tris(pyrazolyl)methane ligands, whether monotopic or multitopic, clearly contain functionality that supports 2D and 3D supramolecular structures organized by weak hydrogen bonds, π−π stacking, and C−H···π interactions. Their ability to act as (a) κ^3 tripodal, (b) κ^2 bonded to a single metal with the third pyrazolyl not coordinated, and (c) κ^2-κ^1 bonded bridging two metals adds to the structural diversity observed for silver(I) complexes of these ligands. The 3-phenyl substituents on the pyrazolyls add to the structural diversity of HC(3-Phpz)$_3$ complexes in comparison to those of the parent HC(pz)$_3$ ligand.

An understanding of how the covalent and non-covalent forces organize the supramolecular self-assembly process is a prerequisite for the progress of crystal engineering. This study shows that although the same types of forces are involved in building the supramolecular structures of **1**−**4**, differences were found when the extended structures of even similar building blocks were compared. A good example is given by the formation of the dimeric units of **3** and **4** and their role in the extended structures. In one case they are formed only by a C−H···π interaction and in the other there is an additional π−π stacking as a supporting interaction. Also, each has a different role in the resulting supramolecular structure. Further studies are clearly needed in order to ascertain the influence of *all* factors on the outcome of a supramolecular arrays if one hopes to fully understand/control the self-assembly process.

Experimental Section

General Remarks: All manipulations involving uncomplexed silver tetrafluoroborate were carried out either in a Vacuum Atmospheres HE-493 dry box under a N_2 atmosphere or by using standard

 © 2003 Wiley-VCH Verlag GmbH & Co. KGaA, Weinheim

Schlenk techniques. After complexation of the silver salt by the ligand no precautions were taken to exclude moisture or oxygen. All solvents were dried using conventional procedures and distilled prior to use. The ^{1}H NMR spectra were recorded on a Varian AM300 spectrometer using a broad-band probe. Proton chemical shifts are reported in ppm vs. internal Me_4Si. Mass spectroscopic data were recorded on a MicroMass QTOF spectrometer. Clusters assigned to specific ions show appropriate isotopic patterns as calculated for the atoms present. Robertson Microlit Laboratories, Inc. (Madison, NJ) performed the elemental analyses. Silver tetrafluoroborate and 3-Ph-pyrazole (3-PhpzH) were used as purchased from Aldrich. Samples for melting point determinations were contained in flame sealed capillaries and the reported temperatures are uncorrected.

HC(3-Phpz)$_3$: Distilled water (400 mL) was added to a 1000 mL flask containing a mixture of 3-phenylpyrazole (28.8 g, 0.20 mol) and tetra-*n*-butylammonium bromide (3.2 g, 9.9 mmol). With vigorous stirring, sodium carbonate (127 g, 1.2 mol) was added gradually to the reaction mixture. Then chloroform (150 mL) was added and the flask was equipped with a reflux condenser. This mixture was heated at reflux for 3 days over which time it became a dark yellow emulsion. The mixture was allowed to cool to room temp. and filtered to remove the solid Na_2CO_3. The organic layer was separated from the aqueous layer and the latter extracted with diethyl ether (3 × 75 mL). The combined organic layers were washed with distilled water (2 × 150 mL) and dried over sodium sulfate. The solution was filtered and the solvent was removed by rotary evaporation. The resulting off-white solid containing 3/5-substituted isomers was then dissolved in the minimum required amount of boiling toluene and poured into a 100 mL flask containing a small amount of *p*-toluenesulfonic acid monohydrate (ca. 0.1 g). The golden solution was heated at reflux temperature overnight. After it had cooled to room temp., an off-white precipitate appeared that was filtered with suction. The moist powder was taken into a beaker and 200 mL of distilled water added. After 2 hours of stirring the suspension was filtered (suction), washed twice with water and once with hexanes, to afford 15 g (52%) of pure HC(3-Phpz)$_3$ as a white powder. M.p. 125−126 °C. ^{1}H NMR ([D$_6$]acetone): δ = 8.86 (s, 1 H, *H*C), 8.10 (d, *J* = 2.1 Hz, 3 H, 5-H *pz*), 7.90 (m, 6 H, *o*-H *Ph*), 7.42 (m, 6 H, *m*-H *Ph*), 7.35 (m, 3 H, *p*-H *Ph*), 6.90 (d, *J* = 2.1 Hz, 3 H, 4-H *pz*) ppm. ^{1}H NMR ([D$_3$]nitromethane): δ = 8.64 (s, 1 H, *H*C), 7.95 (d, *J* = 2.7 Hz, 3 H, 5-H *pz*), 7.87 (m, 6 H, *o*-H *Ph*), 7.42 (m, 9 H, *m*-H, *p*-H *Ph*), 6.86 (d, *J* = 2.7 Hz, 3 H, 4-H *pz*) ppm.

[{HC(3-Phpz)$_3$}Ag](BF$_4$): *Reaction A (1:1 metal to ligand ratio):* Silver tetrafluoroborate, $AgBF_4$ (0.195 g, 1.0 mmol) was dissolved in dry THF (15 mL). To this solution was added via syringe a solution of HC(3-Phpz)$_3$ (0.442 g, 1.0 mmol) in THF (15 mL). After stirring the reaction mixture overnight, hexanes were added (75 mL) and a white precipitate appeared. The mixture was kept 1 hour at −20 °C, and then quickly filtered to afford 0.592 g (93%) of a white powder identified by elemental analysis as [{HC(3-Phpz)$_3$}Ag](BF$_4$): $C_{28}H_{22}AgBF_4N_6$ calcd. C 52.79, H 3.45, N 13.18%, found C 52.43, H 3.65, N 13.09%. *Reaction B (1:2 metal to ligand ratio):* The second procedure involved the same steps as procedure A, using 0.097 g of $AgBF_4$ (0.50 mmol) and 0.442 g of HC(3-Phpz)$_3$ (1.0 mmol). The white compound obtained was identified by elemental analysis as [{HC(3-Phpz)$_3$}Ag](BF$_4$): $C_{28}H_{22}AgBF_4N_6$ calcd. C 52.79, H 3.45, N 13.18, found C 52.93, H 3.36, N 12.79. In addition, 0.5 mol of the ligand was recovered from the filtrate. The ^{1}H NMR spectra of the two samples were identical and they are listed below [D$_6$]acetone: δ = 9.30 (s, 1 H, *H*C), 8.42 (d, *J* = 2.4 Hz, 3 H, 5-H *pz*), 7.92 (m, 6 H, *o*-H *Ph*), 7.43 (m, 9 H, *m*-H, *p*-H *Ph*), 6.98 (d, *J* = 2.4 Hz, 3 H, 4-H *pz*) ppm; [D$_3$] nitromethane: δ 8.67 (s, 1 H, *H*C), 8.19 (d, *J* = 2.4 Hz, 3 H, 5-H *pz*), 7.83 (m, 6 H, *o*-H *Ph*), 7.41 (m, 9 H, *m*-H, *p*-H *Ph*), 6.87 (d, *J* = 2.7 Hz, 3 H, 4-H *pz*) ppm.

X-ray Crystallographic Study: Suitable colorless single crystals of **1**−**4** were selected and mounted onto thin glass fibers. Low-temperature X-ray intensity data were measured on a Bruker SMART APEX CCD-based diffractometer (Mo-*Kα* radiation, λ = 0.71073 Å). After preliminary crystal quality and unit cell parameter determination, a full sphere (**1**, **2**) or hemisphere (**3**, **4**) of raw frame data was collected. Raw data frame integration was performed with SAINT+,[41] which also applied corrections for Lorentz and polarization effects. Analysis of each data set showed negligible crystal decay during data collection. Empirical absorption corrections were applied to each data set (SADABS)[41] in the case of **1**, **2**, and **4**, while in the case of **3** no correction for absorption was applied. The reported final unit cell parameters are based on the least-squares refinement of all reflections from each data set with $I > 5\sigma(I)$. The structures were solved by a combination of direct methods and difference Fourier syntheses and refined by full-matrix least-squares against F^2 (SHELXTL).[42] Non-hydrogen atoms in each structure were refined with anisotropic displacement parameters; hydrogen atoms were placed in idealized positions and included as riding atoms. For **1** systematic absences in the intensity data were consistent with the space groups *Pcam* and *Pca*2$_1$; intensity statistics indicated acentricity. The structure was solved in the polar space group *Pca*2$_1$. Upon successful solution and refinement in *Pca*2$_1$, a check for missed symmetry using the ADDSYM program in PLATON[43] verified the space group choice. All atoms reside on positions of general crystallographic symmetry. The structure contains two crystallographically independent polymeric chains, associated with the independent atoms Ag(1) and Ag(2). At the end of the refinement, the Flack parameter was 0.24(2), indicating that both orientations of the polar axis are present and the crystal is an inversion twin. Refinement of the data accounting for the twinning[42] yielded twin fractions of 0.76/0.24. Compound **2** crystallizes in the triclinic system. The space group $P\bar{1}$ was assumed and confirmed by the successful solution and refinement of the structure. The asymmetric unit contains two ligands, two silver atoms and two BF_4^- counterions with all of them residing on positions of general crystallographic symmetry. Systematic absences in the data sets for **3** and **4** were consistent with the space group $P2_1/c$, and the structures were readily solved in this space group. The asymmetric unit of **3** contains two chemically similar but crystallographically independent [{HC(3-Phpz)$_3$Ag}(CH$_3$)$_2$CO]$^+$ cations, two BF_4^- anions and one acetone molecule of crystallization. All atoms reside on positions of general crystallographic symmetry. The asymmetric unit of **4** contains two chemically similar but crystallographically independent [{HC(3-Phpz)$_3$Ag}(CH$_3$CN)]$^+$ cations, two BF_4^- anions, and one diethyl ether molecule of crystallization. All atoms reside on positions of general crystallographic symmetry. One BF_4^- anion is disordered over two closely spaced positions; a total of 30 geometric restraints (SHELX SAME) were used to assist in modeling the disorder. Crystal data and structure refinement for all compounds are presented in Table 3. CCDC 203781−203784 (**1**−**3**) and -205526 (**4**) contains the supplementary crystallographic data for this paper. These data can be obtained free of charge at www.ccdc.cam.ac.uk/conts/retrieving.html [or from the Cambridge Crystallographic Data Centre, 12, Union Road, Cambridge CB2 1EZ, UK; fax: (internat.) +44-1223/336-033; E-mail: deposit@ccdc.cam.ac.uk].

 © 2003 Wiley-VCH Verlag GmbH & Co. KGaA, Weinheim

Table 3. Crystal data and structure refinement for **1**−**4**

	1	**2**	**3**	**4**
Empirical formula	$C_{28}H_{22}AgBF_4N_6$	$C_{28}H_{22}AgBF_4N_6$	$C_{32.50}H_{31}AgBF_4N_6O_{1.50}$	$C_{32}H_{30}AgBF_4N_7O_{0.50}$
Molecular mass	637.20	637.20	724.31	715.31
Temperature [K]	150.0(2)	150.0(2)	190(2)	173(2)
Wavelength	0.71073	0.71073	0.71073 Å	0.71073 Å
Crystal system	Orthorhombic	Triclinic	Monoclinic	Monoclinic
Space group	$Pca2_1$	$P\bar{1}$	$P2_1/c$	$P2_1/c$
a [Å]	14.3467(7)	12.3992(6)	19.1516(11)	21.7605(9)
b [Å]	15.7777(8)	13.9575(7)	16.2130(10)	15.9462(7)
c [Å]	24.1775(12)	16.4625(8)	21.3959(13)	18.7512(8)
α [deg]	90°	93.2900(10)	90°	90°
β [deg]	90°	95.2510(10)	105.6890(10)	99.2920(10)
γ [deg]	90°	109.9850(10)	90°	90°
V [Å^3]	5472.8(5)	2654.2(2)	6396.0(7)	6421.2(5)
Z	8	4	8	8
Density (calcd.) [Mg·m^{-3}]	1.547	1.595	1.504	1.480
Absorption coefficient [mm^{-1}]	0.793	0.818	0.692	0.687
F(000)	2560	1280	2944	2904
Crystal size [mm]	0.40 × 0.26 × 0.14	0.56 × 0.10 × 0.04	0.28 × 0.24 × 0.16	0.56 × 0.42 × 0.40
Reflections collected	48614	24621	42399	46296
Independent reflections	11181[R(int) = 0.0408]	10827[R(int) = 0.0350]	13102 [R(int) = 0.0545]	13149 [R(int) = 0.0484]
Data/restraints/parameters	11181/1/722	10827/0/721	13102/2/835	13149/30/861
Goodness-of-fit on F^2	1.033	1.011	0.943	1.013
Final *R* indices [$I > 2\sigma(I)$]	$R1 = 0.0346, wR2 = 0.0762$	$R1 = 0.0418, wR2 = 0.0899$	$R1 = 0.0494, wR2 = 0.1001$	$R1 = 0.0340, wR2 = 0.0742$
R indices (all data)	$R1 = 0.0375, wR2 = 0.0774$	$R1 = 0.0565, wR2 = 0.0993$	$R1 = 0.0854, wR2 = 0.1090$	$R1 = 0.0473, wR2 = 0.0777$

Acknowledgments

We thank the National Science Foundation (CHE-0110493) for support. The Bruker CCD Single Crystal Diffractometer was purchased using funds provided by the NSF Instrumentation for Materials Research Program through Grant DMR:9975623.

[1] S. Trofimenko, *J. Am. Chem. Soc.* **1966**, *88*, 1842.
[2] S. Trofimenko, *Scorpionates: The Coordination Chemistry of Polypyrazolylborate Ligands*, Imperial College Press, London, 1999.
[3] F. T. Edelman, *Angew. Chem.* **2001**, *113*, 1704; *Angew. Chem. Int. Ed.* **2001**, *40*, 1656.
[4] C. Janiak, S. Temizdemir, S. Dechert, *Inorg. Chem. Commun.* **2000**, *3*, 271.
[5] M. M. Diaz-Requejo, T. R. Belderrain, M. C. Nicasio, P. J. Perez, *Organometallics* **2000**, *19*, 285.
[6] N. Kitajima, Y. Moro-oka, *Chem. Rev.* **1994**, *94*, 737.
[7] G. Parkin, *Adv. Inorg. Chem.* **1995**, *42*, 291.
[8] H. Vahrenkamp, *Acc. Chem. Res.* **1999**, *32*, 589.
[9] A. M. Santos, F. E. Kuhn, K. Bruus-Jensen, I. Lucas, C. C. Romao, E. Herdtweck, *J. Chem. Soc., Dalton Trans.* **2001**, 1332.
[10] D. L. Reger, *Comment, Inorg. Chem.* **1999**, *21*, 1.
[11] D. L. Reger, J. E. Collins, A. L. Rheingold, L. M. Liable-Sands, G. P. A. Yap, *Organometallics* **1996**, *15*, 2029.
[12] D. L. Reger, J. E. Collins, A. L. Rheingold, L. M. Liable-Sands, G. P. A. Yap, *Organometallics* **1997**, *16*, 349.
[13] D. L. Reger, T. C. Grattan, K. J. Brown, C. A. Little, J. J. S. Lamba, A. L. Rheingold, R. D. Sommer, *J. Organomet. Chem.* **2000**, *607*, 120.
[14] D. L. Reger, C. A. Little, M. D. Smith, A. L. Rheingold, L. M. Liable-Sands, G. P. A. Yap, L. A. Guzei, *Inorg. Chem.* **2002**, *41*, 19.
[15] D. L. Reger, C. A. Little, M. D. Smith, G. J. Long, *Inorg. Chem.* **2002**, *41*, 4453.
[16] A. Cingolani, M. D. Effendy, M. Pellei, C. Pettinari, B. W. Skelton, A. H. White, *Inorg. Chim. Acta* **2002**, *328*, 87.
[17] D. A. McMorran, P. J. Steel, *Inorg. Chem. Commun.* **2003**, *6*, 43.
[18] D. A. McMorran, S. Pfadenhauer, P. J. Steel, *Aust. J. Chem.* **2002**, *55*, 519.
[19] D. L. Reger, T. D. Wright, R. F. Semeniuc, T. C. Grattan, M. D. Smith, *Inorg. Chem.* **2001**, *40*, 6212.
[20] D. L. Reger, R. F. Semeniuc, M. D. Smith, *Inorg. Chem.* **2001**, *40*, 6545.
[21] D. L. Reger, R. F. Semeniuc, M. D. Smith, *Eur. J. Inorg. Chem.* **2002**, 543.
[22] D. L. Reger, R. F. Semeniuc, M. D. Smith, *J. Chem. Soc., Dalton Trans.* **2002**, 476.
[23] D. L. Reger, R. F. Semeniuc, M. D. Smith, *Inorg. Chem. Commun.* **2002**, *5*, 278.
[24] D. L. Reger, R. F. Semeniuc, M. D. Smith, *J. Organomet. Chem.* **2003**, *666*, 87.
[25] D. L. Reger, R. F. Semeniuc, M. D. Smith, *Dalton Trans.* **2003**, 285.
[26] A. N. Khlobystov, A. J. Blake, N. R. Champness, D. A. Lemenovskii, G. Majouga, N. V. Zyk, M. Schröder, *Coord. Chem. Rev.* **2001**, *222*, 155.
[27] A. J. Blake, N. R. Champness, P. Hubberstey, W.-S. Li, M. A. Withersby, M. Schröder, *Coord. Chem. Rev.* **1999**, *183*, 117.
[28] D. L. Reger, R. F. Semeniuc, M. D. Smith, *Rev. Roumaine Chim.* **2002**, *47*, 1035.
[29] D. L. Reger, K. J. Brown, M. D. Smith, *J. Organomet. Chem.* **2002**, *658*, 50.
[30] S. B. Seymore, S. N. Brown, *Inorg. Chem.* **2000**, *39*, 325.
[31] K. A. Hirsch, S. R. Wilson, J. S. Moore, *J. Am. Chem. Soc.* **1997**, *119*, 10401.
[32] N. W. Alcock, R. M. Countryman, *J. Chem. Soc., Dalton Trans.* **1977**, 217.
[33] A. Bondi, *J. Phys. Chem.* **1964**, *68*, 441.
[34] R. S. Rowland, R. Taylor, *J. Phys. Chem.* **1996**, *100*, 738.

 © 2003 Wiley-VCH Verlag GmbH & Co. KGaA, Weinheim

[35] C. Janiak, *J. Chem. Soc., Dalton Trans.* **2000**, 3885 and references cited therein.
[36] M. Nishio, M. Hirota, Y. Umezawa, *The CH/π interaction Evidence, Nature and Consequences*, Wiley-VCH, New York, **1998**.
[37] H. Takahashi, S. Tsuboyama, Y. Umezawa, K. Honda, M. Nishio, *Tetrahedron* **2000**, *56*, 6185.
[38] D. L. Reger, T. D. Wright, C. A. Little, J. J. S. Lamba, M. D. Smith, *Inorg. Chem.* **2001**, *40*, 3810.
[39] V. R. Thalladi, H. C. Weiss, D. Blaser, R. Boese, A. Nangia, G. R. Desiraju, *J. Am. Chem. Soc.* **1998**, *120*, 8702.
[40] F. Grepioni, G. Cojazzi, S. M. Draper, N. Scully, D. Braga, *Organometallics* **1998**, *17*, 296.
[41] *SMART* Version 5.625, *SAINT+* Version 6.02a, and *SADABS*. Bruker Analytical X-ray Systems, Inc., Madison, Wisconsin, USA, **1998**.
[42] G. M. Sheldrick, *SHELXTL* Version 5.1; Bruker Analytical X-ray Systems, Inc., Madison, Wisconsin, USA, **1997**.
[43] A. L. Spek, *PLATON*, A Multipurpose Crystallographic Tool, Utrecht University, Utrecht, The Netherlands, **2003**.

Received March 13, 2003

 © 2003 Wiley-VCH Verlag GmbH & Co. KGaA, Weinheim

Synthesis and Characterization of the Very Bulky Phenols Ar*OH and Ar′OH (Ar* = C_6H_3-2,6-$Trip_2$, Trip = C_6H_2-2,4,6-*i*Pr_3; Ar′ = C_6H_3-2,6-$Dipp_2$, Dipp = C_6H_3-2,6-*i*Pr_2) and Their Lithium and Sodium Derivatives $(LiOAr')_2$ and $(NaOAr^*)_2$

Corneliu Stanciu,[a] Marilyn M. Olmstead,[a] Andrew D. Phillips,[a] Matthias Stender,[a] and Philip P. Power*[a]

Dedicated to the memory of Ron Snaith, a pioneer in alkali metal chemistry

Keywords: Phenol / Phenoxide / Terphenyl / Alkali metals

The very bulky phenols Ar*OH (**1**) and Ar′OH (**2**), where Ar* = C_6H_3-2,6-$Trip_2$ (Trip = C_6H_2-2,4,6-*i*Pr_3) and Ar′ = C_6H_3-2,6-$Dipp_2$ (Dipp = C_6H_3-2,6-*i*Pr_2), as well as their lithium and sodium derivatives $(LiOAr^*)_2$ (**3**), $(LiOAr')_2$ (**4**) and $(NaOAr^*)_2$ (**5**) have been synthesized and characterized. The terphenols **1** and **2** were obtained by the reaction of the aryllithium reagents with nitrobenzene and were isolated in *ca.* 70% yield. The lithium or sodium salts **3**–**5** were isolated by the reaction of **1** or **2** with *n*BuLi or sodium metal. All compounds were characterized spectroscopically, and by X-ray crystallography in the case of **1**, **2**, **4** and **5**. The large terphenyl substituents prevent hydrogen-bonded association of the phenols **1** and **2**. Instead, the O–H hydrogens interact with the π-electron cloud on one of the flanking Trip or Dipp rings. The dimeric structures of **4** and **5** are relatively rare examples of structurally characterized alkali metal phenoxides that are unsolvated by internal electron pair donors or classical Lewis bases such as ethers or amines.
(© Wiley-VCH Verlag GmbH & Co. KGaA, 69451 Weinheim, Germany, 2003)

Introduction

The continuing interest in sterically encumbered phenols is mainly due to use of their deprotonated derivatives (aryloxides) as protecting ligands for a large variety of metallic and non-metallic reactive centers.[1] Such ligands have been extensively used to stabilize low coordinate compounds,[1,2] persistent odd-electron species[3] and heavier main group compounds with multiple bonds.[4] Aryloxides have been used as supporting ligands in metal catalysts as exemplified by the employment of Zn^{II} and Cd^{II} aryloxide derivatives in the copolymerization of epoxides and carbon dioxide.[5] In addition, aryloxide ligands have been employed to synthesize bowl-shaped Lewis acid host molecules as in $Al\{OC_6H_3$-2,6-$Ph_2\}_3$ which can encapsulate Lewis base guests and protect and accelerate chemical reactions with various substrates.[6] The most common, currently used, sterically hindered aryloxides are those that employ either *t*Bu or Ph substituents at the ortho positions of the phenoxide aryl ring. Some members of these ligand classes are commercially available as illustrated by the examples 1-HOC_6H_2-2,4,6-*t*Bu_3 and 1-HOC_6H_3-2,6-Ph_2. In both of these ligands, however, the ortho *t*Bu or Ph groups are susceptible to activation either to form oxametallacycle rings, or dehydrogenation can occur in the alkyl-substituted species. For the phenyl-substituted -OC_6H_3-2,6-Ph_2 activation of the ortho phenyls by close approach of the phenyl CH groups to the reactive center can occur by rotation of the ortho phenyl ring so that it is almost coplanar with the central phenoxide moiety. Recent work by Rothwell and coworkers has shown that when large meta substituents are also present at the central ring, as in -OC_6H-2,6-Ph_2-3,5-*t*Bu_2,[7] resistance or immunity to the cyclometallation reaction is induced because the ortho phenyl rings cannot become coplanar with the central ring due to the steric effects of the *t*Bu substituents. In related work we have pursued the use of very bulky terphenyl ligands in the stabilization of several new compound classes.[8] In these ligands, bulky substituents have been introduced on the flanking aryl rings [e.g., *i*Pr groups in -C_6H_3-2,6-*i*Pr_2(Dipp) or -C_6H_2-2,4,6-*i*Pr_3(Trip)] to prevent them from becoming coplanar with the central phenyl ring. In this way an approximately perpendicular orientation of the flanking rings is maintained which protects the wedge shaped cavity containing the reactive center. In much of this work the terphenyl ligand has been attached directly to the reactive center. However, we have also shown that several derivatives of terphenyl ligands (or their precursors) can be synthesized by attachment of

[a] Department of Chemistry, University of California, Davis, One Shields Avenue, Davis, CA 95616, USA
Fax: (internat.) +1-530/752-8995
E-mail: pppower@ucdavis.edu

-NH_2,[9] PH_2,[9] AsH_2,[9] SbH_2,[9] -SH,[10] or SeH[10] groups to the central phenyl ring at the C-1 position to give very bulky terphenylamines, phosphanes, thiols, etc. A notable omission from this list are the corresponding phenol derivatives. Their absence can be partially explained on the basis of synthetic difficulties due to steric hindrance and solubility effects. In seeking a route to such compounds we have examined several synthetic routes to the two bulky terphenols and show that they can be synthesized in good yield and that they readily form alkali metal salts in essentially quantitative yields.

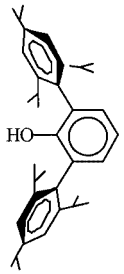

1-HOC_6H_3-2,6-$Trip_2$, Ar*OH

1

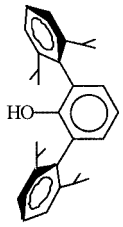

1-HOC_6H_3-2,6-$Dipp_2$, Ar'OH

2

Results and Discussion

Synthesis

There exist several methods for the synthesis of phenols on a laboratory scale.[11] Among the most prominent of these are the diazotization of arylamines followed by hydrolysis, conversion of halides to phenols in the presence of concentrated KOH or NaOH, and the sulfonation-alkaline melting process. The synthesis of the bulky phenols **1** and **2** was attempted by each of these methods. None afforded yields that were useful. It seems likely that the steric effects of the flanking aryl rings and the low solubility of the aryl halide precursors in aqueous phases prevent efficient reactions in these cases. There are other routes to terphenols in the literature[12,13] but since we already had terphenyllithium reagents to hand, we were drawn to the, apparently little used, anhydrous route,[14] which involves the reaction between nitrobenzene and an aryllithium derivative and afforded as products the nitrosobenzene and the lithium aryloxide salt as depicted below.

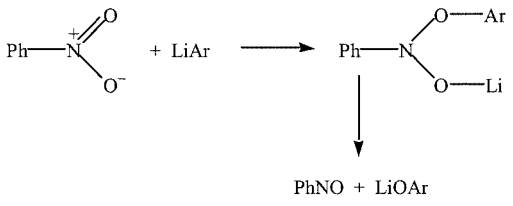

It may be noted that the addition of the bulky aryl group, Ar, to nitrogen is disfavored for steric reasons, although it seems likely that products in which the Ar group is bound to nitrogen will be obtained under appropriate reaction conditions. Quenching of the reaction with a methanol/water mixture affords ArOH in ca. 70% yield for both of the very bulky aryl substituents Ar = Ar* and Ar′. The above route was discovered in 1966−67[14] during the investigation of the reactions of various substituted benzenes with organolithium compounds. The reaction of *o*-nitrobromobenzene with phenyllithium readily afforded the expected *o*-nitrophenyllithium.[15] However, it was found that for pure nitrobenzene the nitro group rather than the aryl ring was attacked. Investigations showed that the addition of one equivalent of phenyllithium to nitrobenzene in THF, with cooling to ca. −95 °C, afforded nitrosobenzene and lithium phenoxide in good yield. We found that a similar reaction result is obtained upon treatment of nitrobenzene with the very bulky lithium reagents LiAr*[11] or LiAr′[12] which afford nitrosobenzene and LiOAr* or LiOAr′ which can then be hydrolysed to give the terphenols **1** and **2**. The terphenols may then be readily converted into their lithium or sodium salts by reaction with *n*BuLi or sodium metal.

Structures

The main feature of the structures of **1** (Figure 1) and **2** (Figure 2) is that they are monomers and contain no inter-

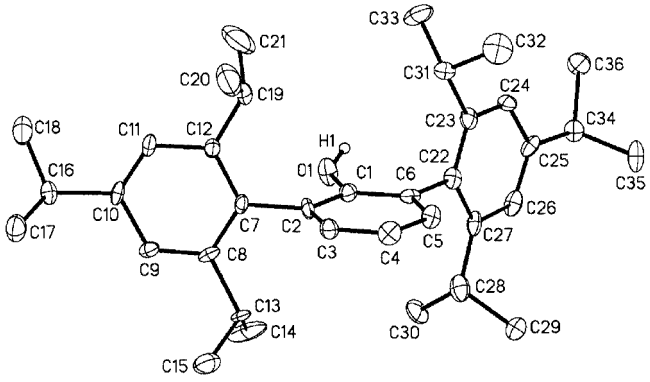

Figure 1. Thermal ellipsoid (35%) plot of **1**. H atoms (except O−H) are not shown; selected bond lengths and angles are given in Table 2

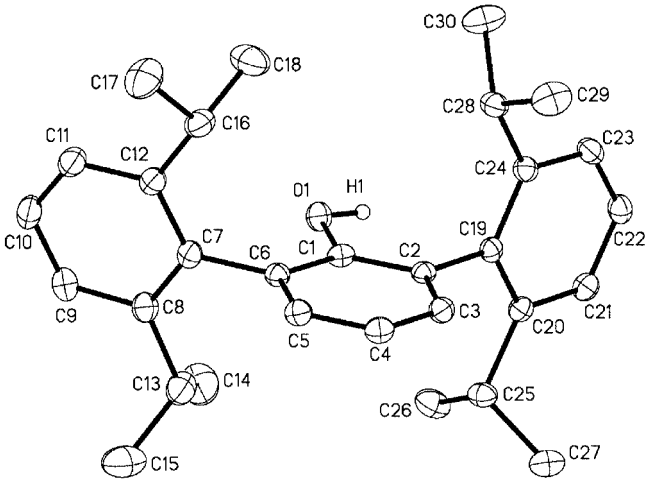

Figure 2. Thermal ellipsoid (35%) plot of **2**. H atoms (except O−H) are not shown; selected bond lengths and angles are given in Table 2

 © 2003 Wiley-VCH Verlag GmbH & Co. KGaA, Weinheim

molecular hydrogen bonding. Although alcohols and phenols are prone to intermolecular hydrogen bonding, this is prevented in **1** and **2** by the steric effects of the ortho Trip or Dipp substituents. Instead, the structures of **1** and **2** show evidence of interaction between the O−H hydrogens and the π-electrons of an ortho phenyl ring. The coordination planes of the O(1) atom and the central aryl ring plane are essentially coincident in each molecule. In **1** the H(1)···C(22) distance is 2.64 Å and in **2** the corresponding H(2)···C(19) separation is 2.39 Å. In addition there is a long H(2) to Dipp(centroid) contact of 3.30 Å to a Dipp ring in an adjacent molecule in **2**, although an interaction of this length may not be significant. The intramolecular O−H···Ar distances resemble those found in the structure of 2,6-diphenylphenol [2.40(4) and 2.43 Å].[16] The O−H stretching frequencies observed in **1** and **2** (3520 and 3530 cm^{-1}) also support the existence of an O−H···π interaction since they are red shifted by 70−80 cm^{-1} in comparison to the O−H stretching frequency observed for phenol in dilute CCl_4 solution.[17] However, there is no clear pattern in the angles and distances surrounding the O(1), C(1), C(2) and C(6) atoms in the molecules that suggests that the O−H···π interaction has any systematic effect on the geometry in the remainder of the molecule. A previous publication has noted that the O−C(1)−C(ortho) angle on the side of the hydroxyl group is wider.[16] While this is true for **2** [120.8(1) vs. 117.1(1)°], the opposite is the case for **1** [116.9(5) vs. 120.7(5)°]. The internal angle at the ipso−C(1) atom exceeds the idealized 120° value by ca. 2° and this is consistent with previous structures of phenols,[16,18,19] and the fact that the very electronegative oxygen substituent removes electron density from C(1) toward itself, thereby permitting a widening of the C(2)−C(1)−C(6) angle. The C−O bond lengths in **1** and **2** are similar to those observed in other sterically encumbered phenols.[14,16,17] As in most structures with bulky terphenyl ligands[8] the flanking aryl rings subtend almost vertical angles (83.1−85.7°) with the central ring and this is maintained in solution, as evidenced by the observation of two sets of methyl doublets for the *i*Pr groups.

Both **1** and **2** react immediately with *n*BuLi to form the lithium salts LiOAr* (**4**) or LiOAr′ (**5**). However, only crystals of the LiOAr′ species were suitable for X-ray crystallography. These proved to exist as dimers, as shown in Figure 3. This structure is a relatively rare example of an alkali metal aryloxide unsolvated[20−24] by internal Lewis base donors or molecules such as Et_2O, THF or pyridine. It consists of centrosymmetric dimers in which the lithiums bridge two OAr′ groups. The lower degree of aggregation in **5** may be contrasted with the trimer structure observed for (Li-OC_6H-2,6-Ph_2-3,5-$t Bu_2$)$_3$ [24] which has the less crowded phenyl substituents in the ortho positions. The planar Li_2O_2 rhombic core features two different Li−O distances of 1.807(3) and 1.979(3) Å and LiOLi and OLiO angles of 81.2(1)° and 98.8(1)°. These distances lie near the lower and upper extremities of the known Li−O range for dimeric solvated and unsolvated LiOR species.[18−25] Each lithium further interacts with the ipso (Li−C = 2.39 Å) and ortho carbons (Li−C = 2.54 and 2.65 Å) of a flanking Dipp ring. The Ar′ groups are tilted toward the side which interacts with the lithiums as indicated by the ca. 22° difference between the LiOC angles. The oxygen atoms have almost stanar coordination. The O−C bond length of 1.335(2) is 0.05−0.07 Å shorter than the corresponding distances in **1** and **2** probably as a result of the increased ionic contribution to the O−C bond strength when hydrogen is replaced by lithium. The flanking aryl rings subtend angles of 88.3° (C7 ring) and 82.8° (C19 ring) with respect to the central ring. A notable difference between the structure of $(LiOAr')_2$ and **1** and **2** concerns the internal angle at the ipso carbon of the central aryl ring of the terphenyl substituent. The much more negative character of the oxygen in the lithium salt means that, relatively speaking, it is less electronegative than the oxygens in **1** and **2**. This is reflected in the C(2)−C(1)−C(6) angle, which, at 117.55(14)°, is ca. 4.5° narrower than the corresponding angle in **2**.

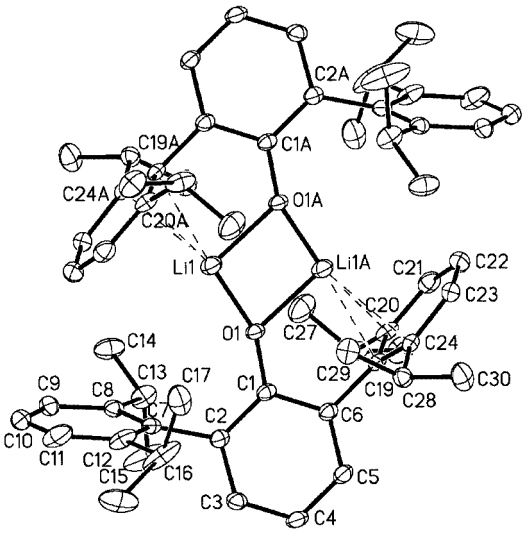

Figure 3. Thermal ellipsoid (35%) plot of **5**. H atoms are not shown; selected bond lengths and angles are given in Table 2

The structure of NaOAr* (**4**; Figure 4) is a relatively rare example of a structurally characterized unsolvated (by internal or external Lewis base donors) sodium phenolate. It crystallizes as two slightly different sodium-bridged dimeric units. One dimer incorporates a twofold rotational axis along the Na···Na [Na(1) and Na(2)] vector, whereas the other involves a twofold rotational axis along the O···O [O(2) and O(3)] vector. The planar Na_2O_2 cores are very similar in each molecule, having Na−O−Na angles near 94.5° and O−Na−O angles near 85.5°. The Na−O bonds are in the narrow range 2.221(2)−2.237(2) Å. The sodiums also display close interactions to the ipso carbons of the flanking Trip rings in the range 2.995(3)−3.076(3) Å. The Na−O−C(ipso) angles are symmetric and lie within the narrow limits 132.1(2)−132.78(6)°.

The unassociated dimeric structural motif in **4** provides a good illustration of the disruption of the stacking of dimeric units[26] in the polymeric structures of $(NaOPh)_n$ [22,23] or $(NaOC_6H_4$-4-$Me)_n$.[20] The Na−O bond lengths in

 © 2003 Wiley-VCH Verlag GmbH & Co. KGaA, Weinheim

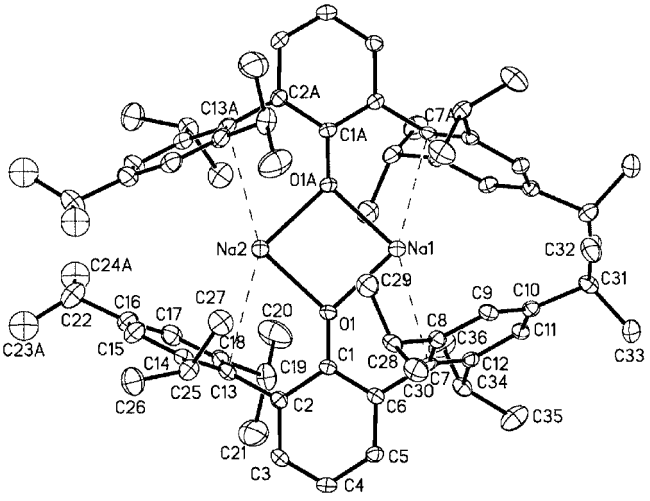

Figure 4. Thermal ellipsoid (35%) plot of one of the molecules in the asymmetric unit of **4**. H atoms are not shown; selected bond lengths and angles are given in Table 2

4 are at the shorter end of the range previously observed in species such as $(NaOC_6H_4\text{-}4\text{-}Me)_n$,[20] $[(MeOCH_2CH_2O\text{-}Me)NaOC_6H_4\text{-}4\text{-}Me]_4$ [18] or $(NaOPh)_n$.[22,23] The Na···C interactions are similar to the average Na−C(arene) distance of 2.94(11) Å observed in $(NaOC_6H_4\text{-}4\text{-}Me)_n$ [20] and 3.05(8) Å in $(NaOPh)_n$.[23] The basic structural motif in **4** resembles that observed for the dimer $(NaSAr^*)_2$.[10] However, in the latter species the sodium displays unequal and weaker interactions with the aryl rings. Apparently, the Na^+ ions are a better fit for the cavity generated by the flanking aryl rings in the case of **4**. As in the structure of **5**, and for the same reasons, the internal angles at the ipso carbons of the central aryl rings [117.6(3) and 117.7(4)°] are less than the idealized 120° and the flanking aryl rings subtend high angles with respect to the central aryl ring.

Conclusions

The reaction of LiAr* or LiAr′ with nitrobenzene at low temperature, followed by hydrolysis, is an effective, high-yield route to very bulky terphenols from their lithium terphenyl precursors. The latter are available in essentially quantitative yield from the reaction of terphenyl iodide with *n*BuLi thereby permitting the terphenols to be isolated in *ca*. 70% from the terphenyl iodide starting material.

Experimental Section

General Procedures: All manipulations were carried out (except where otherwise noted) by using modified Schlenk techniques under an atmosphere of Ar or N_2 or in Vacuum Atmospheres HE-43 or NEXUS dryboxes. All solvents were distilled from molten Na/K alloy and degassed prior to use. Nitrobenzene was distilled off P_2O_5 and stored over molecular sieves. The lithium compounds $Et_2O{\cdot}LiC_6H_3\text{-}2,6\text{-}Trip_2$ (LiAr*)[27] and $LiC_6H_3\text{-}2,6\text{-}Dipp_2$ (LiAr′)[28] were prepared as described previously. The ^1H and ^{13}C NMR spectra were recorded on a Varian 300 or 400 MHz spectrometer and referenced to known standards. Melting points were recorded in glass capillaries under N_2 and are uncorrected. Infrared spectra were recorded as Nujol mulls between CsI plates on a Perkin−Elmer-1430 spectrometer.

1-HOC_6H_3-2,6-$Trip_2$ (Ar*OH, 1): $Et_2O{\cdot}$LiAr* (1.7 g, 3.0 mmol) was dissolved in diethyl ether (20 mL) with rapid stirring. This solution was cooled in a CH_2Cl_2/liquid N_2 slush bath, and nitrobenzene (1.5 mL, ca. 15 mmol) was added dropwise by syringe. A red solution was formed immediately upon the addition of nitrobenzene, and after stirring for ca. 5 min, methanol (20 mL) was added with a syringe. The resulting amber colored mixture was warmed to room temperature and water (25 mL) was added to afford a solution with two layers. The upper layer was separated and the aqueous alcohol layer was acidified with concentrated HCl (1.0 mL), extracted with 2 × 20 mL portions of diethyl ether and combined with the upper layer. The combined organic layers were washed with 2 × 100 mL portions of water and 2 × 100 mL saturated NaCl/H_2O solution. The ethereal layer was separated, dried over $MgSO_4$, filtered and concentrated to ca. 10 mL. Column chromatography on silica gel with use of pentane eluent afforded, upon concentration to ca. 10 mL, large orange-yellow crystals of the crude product upon standing overnight. These were purified by recrystallization from diethyl ether to afford colorless crystals of **1**. Yield: 1.12 g, 2.25 mmol, (75%), m.p. 148−150 °C. The crystals proved suitable for X-ray crystallographic studies. ^1H NMR (300 MHz, C_6D_6, 25 °C): δ = 1.21 [d, $^3J_{H,H}$ = 7.50 Hz, 12 H, *o*-CH(CH_3)$_2$], 1.24 [d, $^3J_{H,H}$ = 6.60 Hz, 12 H, *o*-CH(CH_3)$_2$], 1.27 [d, $^3J_{H,H}$ = 6.90 Hz, 12 H, *p*-CH(CH_3)$_2$], 2.82 [sept, $^3J_{H,H}$ = 6.90 Hz, 2 H, *p*-*CH*(CH_3)$_2$], 3.02 [sept, $^3J_{H,H}$ = 6.90 Hz, 4 H, *o*-*CH*(CH_3)$_2$], 4.57 [s, 1 H, −OH], 6.89 [t, $^3J_{H,H}$ = 7.50 Hz, 1 H, *p*-Ph], 7.06 [d, $^3J_{H,H}$ = 7.50 Hz, 2 H, *m*-Ph], 7.23 [s, 4 H, *m*-Trip] ppm. ^{13}C NMR (300 MHz, $CDCl_3$, 25 °C): δ = 24.36 [*o*-CH(CH_3)$_2$], 24.43 [*o*-CH(CH_3)$_2$], 24.69 [*p*-CH(CH_3)$_2$], 31.04 [*o*-*CH*(CH_3)$_2$], 34.65 [*p*-*CH*(CH_3)$_2$], 120.07 (*p*-Ph), 121.29 (m-Trip), 126.64 (i-Trip), 130.23 (*o*-Ph), 131.02 (p-Trip), 147.79 (*m*-Ph), 148.83 (o-Trip), 150.96 (i-Ph) ppm. IR (Nujol): $\tilde{\nu}$ = 3520 cm^{-1} (ν_{OH}, sharp).

1-HOC_6H_3-2,6-$Dipp_2$ (Ar′OH, 2): In a similar manner to that described for **1**, nitrobenzene (3.5 mL, ca. 35 mmol) was syringed into a rapidly stirred solution of LiAr′ (2.93 g, 7.0 mmol) dissolved in diethyl ether (20 mL) with cooling to ca. −95 °C. Quenching with MeOH (20 mL), followed by warming to room temperature, and water addition, afforded two layers, which were worked up as described for **1**, to yield colorless crystals of **2**. Yield: 2.0 g, 4.83 mmol (69%); m.p. 164−166 °C. ^1H NMR (300 MHz, $CDCl_3$, 25 °C): δ = 1.08 [d, $^3J_{H,H}$ = 6.9 Hz, 12 H, *o*-CH(CH_3)$_2$], 1.13 [d, $^3J_{H,H}$ = 6.9 Hz, 12 H, *o*-CH(CH_3)$_2$], 2.72 [sept, $^3J_{H,H}$ = 6.9 Hz, 4 H, *o*-*CH*(CH_3)$_2$], 4.46 [s, 1 H, −O*H*], 7.03−7.09 [m, 2 H, *p*-Ph and *p*-Dipp], 7.25 [d, $^3J_{H,H}$ = 7.5 Hz, 4 H, *m*-Dipp], 7.37 [d, $^3J_{H,H}$ = 7.8 Hz, 2 H, *m*-Ph] ppm. ^{13}C NMR (300 MHz, $CDCl_3$, 25 °C): δ = 24.14 [*o*-CH(CH_3)$_2$], 24.50 [*o*-CH(CH_3)$_2$], 30.86 [*o*-*CH*(CH_3)$_2$], 120.08 (*p*-Ph), 123.10 (m-Dipp), 126.36 (i-Dipp), 128.76 (p-Dipp), 129.91 (*m*-Ph), 133.36 (0-Ph), 147.97 (o-Dipp), 150.86 (i-Ph) ppm. IR (Nujol): $\tilde{\nu}$ = 3530 cm^{-1} (ν_{OH}, sharp).

LiOAr* (3): MeLi (1.1 mmol, 0.65 mL, 1.6 M in ether) was added from a syringe to a well-stirred solution of **1** (0.5 g, *ca*. 1 mmol) in diethyl ether (20 mL) at room temperature. After 10 minutes, the solution became a pale red and the reaction was stirred for another 4 h. The diethyl ether was pumped off and hexane (20 mL) was added. The volume of the clear red solution was reduced to ca. 10 mL under reduced pressure and the flask was placed in a ca. −20 °C freezer overnight. Colorless crystals (stable up to 260 °C) had formed after 24 h, but they were found to be unsuitable for X-

 © 2003 Wiley-VCH Verlag GmbH & Co. KGaA, Weinheim

ray crystallography. Several efforts were made to grow crystals from other solvents without success. The isolated yield of **3** was 0.465 g, 0.92 mmol (92%). ^{1}H NMR (300 MHz, C_6D_6, 25 °C): δ = 0.92 [d, $^3J_{H,H}$ = 11.1 Hz, 12 H, *o*-CH(*CH*$_3$)$_2$], 1.10 [d, $^3J_{H,H}$ = 11.1 Hz, *o*-CH(*CH*$_3$)$_2$], 1.40 [d, $^3J_{H,H}$ = 11.1 Hz, 12 H, *p*-CH(*CH*$_3$)$_2$], 3.00 [m, 6 H, o+*p*-*CH*(CH$_3$)$_2$], 6.61 [t, J_{ortho} = 8.1 Hz, 1 H, *p*-Ph], 6.73 [d, J_{ortho} = 10.5 Hz, 2 H, *m*-Ph], 7.16 (s, 4 H, *m*-Tripp) ppm. ^{13}C NMR (300 MHz, C_6D_6, 25 °C): δ = 24.10 [*o*-CH(*CH*$_3$)$_2$], 24.40 [*o*-CH(*CH*$_3$)$_2$], 24.85 [*p*-*CH*(CH$_3$)$_2$], 31.02 [*o*-*CH*(CH$_3$)$_2$], 34.41 [*p*-*CH*(CH$_3$)$_2$], 115.05 (*p*-Ph), 121.91 (m-Trip), 126.51 (i-Trip), 131.04 (p-Trip), 137.38 (*o*-Ph), 147.11 (*m*-Ph), 147.25 (o-Trip), 161.41 (i-Ph) ppm.

NaOAr* (4): A solution of Ar*OH (**1**; 0.5 g, 1 mmol) in toluene was added via cannula to sodium metal 0.050 g (ca. 2 mmol) suspended in toluene (5 mL). The mixture was refluxed overnight. The red solution obtained was pumped to dryness and the residue was extracted in diethyl ether (15 mL) and the resultant solution allowed to settle. The clear, red supernatant solution was decanted off, and pumped down to ca. 5 mL, and stored in a ca. −20 °C freezer. After three weeks, colorless crystals of **4** were formed which were suitable for X-ray analysis. Yield: 0.45 g, 0.86 mmol (86%). m.p. 230−232 °C. ^{1}H NMR (300 MHz, C_6D_6, CD_3, 25 °C): δ = 1.01 [d, $^3J_{H,H}$ = 6.0 Hz, 12 H, *o*-CH(*CH*$_3$)$_2$], 1.20 [d, $^3J_{H,H}$ = 6.0 Hz, 12 H, *o*-CH(*CH*$_3$)$_2$], 1.47 [d, $^3J_{H,H}$ = 6.0 Hz, 12 H, *p*-CH(*CH*$_3$)$_2$], 3.17 [s broad, 6 H, o+*p*-*CH*(CH$_3$)$_2$], 6.61 [s, 1 H, *p*-Ph], 6.83 [s, 2 H, *m*-Ph], 7.19 [s, 4 H, *m*-Trip] ppm. ^{13}C NMR (300 MHz, [D$_8$]toluene, 25 °C): δ = 23.87 [*o*-CH(*CH*$_3$)$_2$], 24.14 [*o*-CH(*CH*$_3$)$_2$], 24.75 [*p*-CH(*CH*$_3$)$_2$], 30.56 [*o*-*CH*(CH$_3$)$_2$], 33.96 [*p*-*CH*(CH$_3$)$_2$], 111.97 (*p*-Ph), 120.92 (m-Trip), 128.55 (i-Trip), 130.26 (p-Trip), 138.67 (*o*-Ph), 146.53 (o-Trip), 147.27 (*m*-Ph), 166.02 (i-Ph) ppm.

LiOAr′ (5): Ar′OH (**2**; 0.36 g, 0.86 mmol) was dissolved in diethyl ether (15 mL) and the resulting solution was cooled to 0 °C. *n*-Butyllithium (0.6 mL, 0.96 mmol, 12% excess of a 1.6 M solution in hexane) was slowly added with a syringe. Evolution of gas (*n*BuH) was seen during addition. The solution was stirred at room temperature for an additional 2 h, the diethyl ether was pumped off, and hexane (*ca*. 20 mL) was added. The resulting yellow solution was concentrated to about 10 mL and let stand in a ca. −20 °C freezer. After three days small, colorless crystals were obtained. They were suitable for X-ray analysis. Yield: 0.334 g, 0.79 mmol (92%). M.p. 198−200 °C. ^{1}H NMR (300 MHz, C_6D_6, 25 °C): δ = 0.92 [d, $^3J_{H,H}$ = 6.9 Hz, 12 H, *o*-CH(*CH*$_3$)$_2$], 1.02 [d, $^3J_{H,H}$ = 6.9 Hz, 12 H, *o*-CH(*CH*$_3$)$_2$], 2.89 [sept, $^3J_{H,H}$ = 6.9 Hz, 4 H, *o*-*CH*(CH$_3$)$_2$], 6.67 [t, $^3J_{H,H}$ = 6.3 Hz, 1 H, *p*-Ph], 6.84 [d, $^3J_{H,H}$ = 7.5 Hz, 2 H, *m*-Ph], 7.03 [d, $^3J_{H,H}$ = 7.5 Hz, 4 H, *m*-Dipp], 7.14 [t, $^3J_{H,H}$ = 6.3 Hz, 2 H, *p*-Dipp] ppm. ^{13}C NMR (300 MHz, $CDCl_3$, 25 °C): δ = 24.54 [*o*-CH(*CH*$_3$)$_2$], 24.62 [*o*-CH(*CH*$_3$)$_2$], 30.71 [*o*-*CH*(CH$_3$)$_2$], 114.76 (*p*-Ph), 124.30 (*m*-Dipp), 128.57 (*p*-Dipp), 129.17 (i-Dipp), 130.26 (*m*-Ph), 139.17 (*o*-Ph), 146.71 (*o*-Dipp), 161.13 (i-Ph) ppm.

X-ray Crystallographic Studies: Sample preparation consisted of removing the crystal from the Schlenk tube under a rapid flow of Argon and immediately submerging it in hydrocarbon oil. A suitable crystal was selected, attached to a glass fiber, mounted on a copper pin and rapidly placed in the cold stream of N_2 of the diffractometer for data collection.[29] Data were collected at 293 K (**1**), 130 K (**2**) or 90 K (**4**) and (**5**) with Mo-K_α (λ = 0.71073Å) radiation (**1**, **4** and **5**) or Cu-K_α (λ = 1.54178Å) (**2**) on a Bruker SMART 1000 (**1**, **4** and **5**) or Siemens P4 (**2**) diffractometers. Data collection and processing were performed using the Bruker programs SMART and SAINT (**1**, **4** and **5**) or Siemens P3-PC (**2**). Empirical absorption corrections were applied using SADABS,[30a] XABS.[30b] The crystal structures were solved using either direct methods or the Patterson option in SHELXS program and refined by the full-matrix least-squares procedure in the SHELXL program.[31] All non-hydrogen atoms were refined anisotropically while hydrogen atoms (with the exception of those attached to oxygen in **1** and **2** which were located) were placed at calculated positions and included in refinement using a riding model. Some details of the data collection and refinement are given in Table 1. Further details can be found in the supporting information.

CCDC-218873 (**1**), -218874 (**2**) -218875 (**4**) and -218876 (**5**) contain the supplementary crystallographic data for this paper. These data

Table 1. Selected crystallographic data for compounds **1**, **2**, **4**, and **5**

Compound	**1**	**2**	**4**	**5**
Formula	$C_{36}H_{50}O$	$C_{30}H_{38}O$	$C_{36}H_{49}NaO$	$C_{60}H_{78}Li_2O_2$
Mol. wt.	498.76	414.60	520.74	845.1
Color, habit	colorless, block	colorless, plate	colorless, plate	colorless, block
Cryst syst	orthorhombic	monoclinic	monoclinic	monoclinic
Space group	*Pna*2$_1$	*P*2$_1$/*n*	*P*2/*c*	*P*2$_1$/*n*
a, Å	8.6426(8)	10.8581(10)	19.1061(18)	10.9610(4)
b, Å	14.3044(16)	20.8313(15)	17.2110(16)	19.8181(7)
c, Å	25.501(3)	11.1785(8)	19.6114(18)	11.3802(4)
α, °				
β, °		94.474(7)	90.100(2)	91.352(1)
γ, °				
V, A^3	3152.7(6)	2520.7(3)	6448.9(10)	2471.39(15)
Z	4	4	8	2
Cryst dims, mm	0.10 × 0.07 × 0.05	0.60 × 0.28 × 0.08	0.37 × 0.29 × 0.09	0.31 × 0.31 × 0.17
D calc, g cm^{-3}	1.051	1.092	1.073	1.136
μ, mm^{-1}	0.061	0.480	0.074	0.065
No. of rflns	9958	3307	11638	4868
No. of obsd rflns	5236	2871	7600	3746
R, obsd rflns	0.0499	0.0383	0.0579	0.0529
wR$_2$, all rflns	0.1197	0.0954	0.1479	0.1560

 © 2003 Wiley-VCH Verlag GmbH & Co. KGaA, Weinheim

Table 2. Selected bond lengths (Å) and angles (°) for **1**, **2**, **4**, and **5**

1 (Ar*OH)		**2** (Ar′OH)	
O(1)−C(1)	1.381(2)	O(1)−C(1)	1.407(2)
O(1)−H(1)	0.83(3)	O(1)−H(1)	0.85(1)
C(1)−C(2)	1.398(7)	C(1)−C(2)	1.394(2)
C(1)−C(6)	1.396(7)	C(1)−C(6)	1.396(2)
C(2)−C(7)	1.514(6)	C(2)−C(19)	1.502(2)
C(6)−C(22)	1.479(6)	C(6)−C(7)	1.499(2)
C(1)−O(1)−H(1)	129(2)	C(1)−O(1)−H(1)	107(2)
C(2)−C(1)−C(6)	122.4(1)	C(2)−C(1)−C(6)	122.1(1)
C(2)−C(1)−O(1)	120.7(5)	C(2)−C(1)−O(1)	120.8(1)
C(6)−C(1)−O(1)	116.9(5)	C(6)−C(1)−O(1)	117.1(1)
C(1)−C(2)−C(7)	117.8(4)	C(1)−C(2)−C(19)	121.0(1)
C(1)−C(6)−C(22)	121.8(4)	C(1)−C(6)−C(7)	119.8(1)
4 $(NaOAr^*)_2$		**5** $(LiOAr')_2$	
Na(1)−O(1)	2.237(2)	Li(1)−O(1)	1.807(3)
Na(2)−O(1)	2.225(2)	Li(1)−O(1A)	1.979(3)
Na(3)−O(3)	2.221(2)	O(1)−C(1)	1.335(2)
Na(3)−O(2)	2.226(2)	C(1)−C(2)	1.415(2)
O(1)−C(1)	1.320(4)	C(1)−C(6)	1.420(2)
C(1)−C(2)	1.420(4)	C(2)−C(7)	1.502(2)
C(1)−C(6)	1.408(4)	C(6)−C(19)	1.494(2)
C(2)−C(13)	1.497(5)	Li(1)−C(19)	2.390(3)
C(6)−C(7)	1.495(5)	Li(1)−C(20)	2.647(3)
O(2)−C(37)	1.313(5)	Li(1)−C(24)	2.543(3)
O(3)−C(56)	1.308(5)	Li(1)···Li(1A)	2.468(6)
C(37)−C(38)	1.415(4)	O(1)−C(1)−C(2)	123.43(14)
C(56)−C(57)	1.424(4)	O(1)−C(1)−C(6)	119.01(14)
C(57)−C(60)	1.497(5)	C(2)−C(1)−C(6)	117.55(14)
C(38)−C(41)	1.499(5)	C(1)−C(2)−C(7)	124.63(14)
Na(1)−C(7)	2.995(3)	C(1)−C(6)−C(19)	117.44(14)
Na(2)−C(13)	3.074(3)	Li−O(1)−Li(1A)	81.22(14)
Na(3)−C(14)	3.015(3)	O(1)−Li−O(1A)	98.78(14)
Na(3)−C(46)	3.043(3)	Li(1)−O(1)−C(1)	155.11(14)
Na(3)−C(60)	3.076(3)	Li(1A)−O(1)−C(1)	122.91(13)
Na(1)···Na(2)	3.269(2)		
Na(3)···Na(3A)	3.268(2)		
O(1)−Na(1)−O(1A)	85.49(12)		
O(1)−Na(2)−O(1A)	86.07(12)		
Na(1)−O(1)−Na(2)	94.22(9)		
Na(1)−O(1)−C(1)	132.1(2)		
Na(2)−O(1)−C(1)	132.7(2)		
O(1)−C(1)−C(2)	121.2(3)		
O(1)−C(1)−C(6)	121.2(3)		
C(1)−C(2)−C(6)	117.6(3)		
C(1)−C(2)−C(13)	119.6(3)		
C(1)−C(6)−C(7)	120.0(3)		
Na(3)−O(2)−C(37)	132.78(6)		
Na(3)−O(3)−C(56)	132.64(6)		
Na(3)−O(2)−Na(3A)	94.44(12)		
Na(3)−O(3)−Na(3A)	94.72(12)		
O(2)−Na(3)−O(3)	85.42(8)		
Na(3)−O(2)−C(37)	132.78(6)		
Na(3)−O(3)−C(56)	132.64(6)		
C(38)−C(37)−C(38A)	117.7(4)		
O(2)−C(37)−C(38)	121.14(3)		
C(38)−C(37)−(38A)	117.7(4)		
O(3)−C(56)−C(57)	121.37(19)		
C(57)−C(56)−C(57A)	117.3(4)		

can be obtained free of charge at www.ccdc.cam.ac.uk/conts/retrieving.html [or from the Cambridge Crystallographic Data Centre, 12, Union Road, Cambridge CB2 1EZ, UK; Fax: (internat.) +44-1223/336-033; E-mail: deposit@ccdc.cam.ac.uk].

Acknowledgments

We are grateful to the National Science Foundation (CHE-0096913) for financial support.

[1] D. C. Bradley, R. C. Mehrotra, I. P. Rothwell, A. Singh. *Alkoxo and Aryloxo Derivatives of Metals*, Academic, San Diego, 2001.
[2] B. Cetinkaya, I. Gumrukcu, M. F. Lappert, J. L. Atwood, R. D. Rogers, M. J. Zawarotko, *J. Am. Chem. Soc.* **1980**, *102*, 2088.
[3] B. Cetinkaya, A. Hudson, M. F. Lappert, P. P. Power, H. Goldwhite, *J. Chem. Soc., Chem. Commun.* **1982**, 609.
[4] P. P. Power, *Chem. Rev.* **1999**, *99*, 3463.
[5] D. J. Darensbourg, M. W. Holtcamp, G. E. Struck, M. S. Zimmer, S. A. Niezgoda, P. Rainey, J. B. Robertson, J. D. Draper, J. H. Reibenspies, *J. Am. Chem. Soc.* **1999**, *121*, 107.
[6] T. Ooi, Y. Kondo, K. Maruoka, *Angew. Chem. Int. Ed.* **1998**, *37*, 3039.
[7] J. S. Vilardo, M. A. Lockwood, L. G. Hanson, J. R. Clark, B. C. Parker, P. E. Fanwick, I. P. Rothwell, *J. Chem. Soc., Dalton Trans.* **1997**, 3353.
[8] B. Twamley, S. T. Haubrich, P. P. Power, *Adv. Organomet. Chem.* **1999**, *44*, 1.
[9] B. Twamley, C.-S. Hwang, N. J. Hardman, P. P. Power, *J. Organomet. Chem.* **2000**, *609*, 152.
[10] M. Niemeyer, P. P. Power, *Inorg. Chem.* **1996**, *35*, 7264.
[11] M. B. Smith, J. March. *March's Advanced Organic Chemistry*, 5th ed.; Wiley, New York, 2001, p. 874, 1685.
[12] S. Ueji, *J. Org. Chem.* **1985**, *50*, 2711.
[13] S. Saito, T. Kano, K. Hatanaka, H. Yamamoto, *J. Org. Chem.* **1997**, *62*, 5651.
[14] P. Buck, G. Köbrich, *Tetrahedron Lett.* **1967**, 1563.
[15] G. Köbrich, P. Buck, *Angew. Chem. Int. Ed. Engl.* **1966**, *5*, 1044.
[16] K. Nakatsu, H. Yoshioka, K. Kunimoto, T. Kinugasa, S. Ueji, *Acta Crystallgr.* **1978**, *B34*, 2357.
[17] S. Ueji, N. Ueda, T. Kinugasa, *J. Chem. Soc., Perkin Trans. 2* **1976**, 178.
[18] Y. Iimure, T. Sakurai, Y. Ohno, K. Asahi, K. Isono, *Acta Crystallogr., Sect. C* **1983**, *39*, 778.
[19] K. Bekkouch, M. Perrin, A. Thozet, *Acta Crystallogr., Sect. C* **1988**, *44*, 2161.
[20] W. J. Evans, R. E. Golden, J. W. Ziller, *Inorg. Chem.* **1993**, *32*, 3041.
[21] F. Pauer, P. P. Power, *Lithium Chemistry* (Eds.: A.-M. Sapse, P. v. R. Schleyer), J. Wiley, New York, 1995, Chapter 9.
[22] R. E. Dinnebier, M. Pink, J. Sieler, P. W. Stephens, *Inorg. Chem.* **1997**, *36*.
[23] M. Kunert, E. Dinjus, M. Nauck, J. Sieler, *Chem. Ber./Receuil* **1997**, *130*, 1461.
[24] J. S. Vilardo, P. E. Fanwick, I. P. Rothwell, *Polyhedron* **1998**, *17*, 769.
[25] M. B. Dinger, M. J. Scott, *Inorg. Chem.* **2000**, *39*, 1238.
[26] K. Gregory, P. v. R. Schleyer, R. Snaith, *Adv. Inorg. Chem.* **1991**, *37*, 47.
[27] B. Schiemenz, P. P. Power, *Organometallics* **1996**, *15*, 958.
[28] B. Schiemenz, P. P. Power, *Angew. Chem. Int. Ed. Engl.* **1996**, *35*, 2150.
[29] H. Hope, *Prog. Inorg. Chem.* **1995**, *41*, 1.
[30] [30a] SADABS: Area Detector Absorption Connections: Bruker AXS Inc: Madison, WI, 1996. [30b] XABS 2 an empirical absorption correction program: S. R. Parkin, B. Moezzi, H. Hope, *J. Applied Crystallogr.* **1995**, *28*, 53.
[31] SHELXL Version 5.1: Bruker AXS Inc: Madison, WI, 1997.

Received May 23, 2003

 © 2003 Wiley-VCH Verlag GmbH & Co. KGaA, Weinheim

EurJIC
European Journal of Inorganic Chemistry

Issue 19/2003

Pages 3501–3668

Papers available ahead of print in Early View at www.interscience.wiley.com

Earliest available Table of Contents:
Automatically, free of charge by e-mail through
www.interscience.wiley.com/alerts

COVER PICTURE

The cover picture shows, as one representative out of the carbene-analogue family, a novel heteroleptic lead(II) compound containing an O,C,O-coordinating pincer-type ligand. Details are discussed in the article by K. Jurkschat et al. on p. 3563 ff.

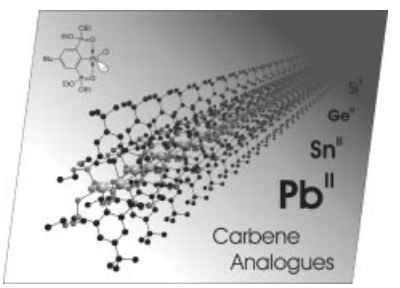

MICROREVIEW

Contents

3513 **M. Sundermeier, A. Zapf, M. Beller***

Palladium-Catalyzed Cyanation of Aryl Halides: Recent Developments and Perspectives

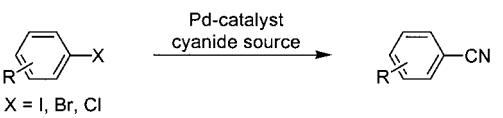

Keywords: Palladium / Cyanation / Benzonitriles / Homogeneous catalysis

 © 2003 Wiley-VCH Verlag GmbH & Co. KGaA, Weinheim

SHORT COMMUNICATIONS

3527 **Z. Fei, R. Scopelliti, P. J. Dyson***

Synthesis and Structural Elucidation of a "Free" Phosphinoamide Anion

Keywords: N,P ligands / Potassium / Crown ether / X-ray structure

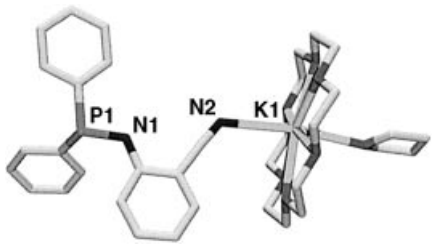

3530 **E. Terreno, P. Boniforte, M. Botta, F. Fedeli, L. Milone, A. Mortillaro, S. Aime***

The Water-Exchange Rate in Neutral Heptadentate DO3A-Like Gd^{III} Complexes: Effect of the Basicity at the Macrocyclic Nitrogen Site

Keywords: Gadolinium / Water exchange / Imaging agents / Kinetics

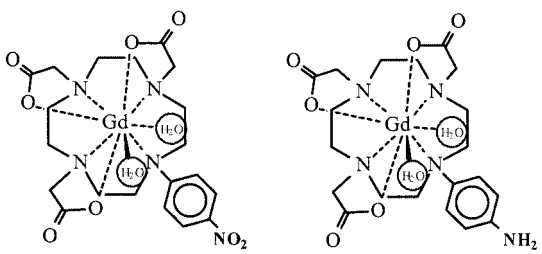

3534 **C. Li, X. Yang, B. Yang, Y. Yan, Y. Qian***

A Template-Interface Co-Reduction Synthesis of Hollow Sphere-like Carbides

Keywords: Nanostructures / Carbides / Titanium / Vanadium / Synthesis design

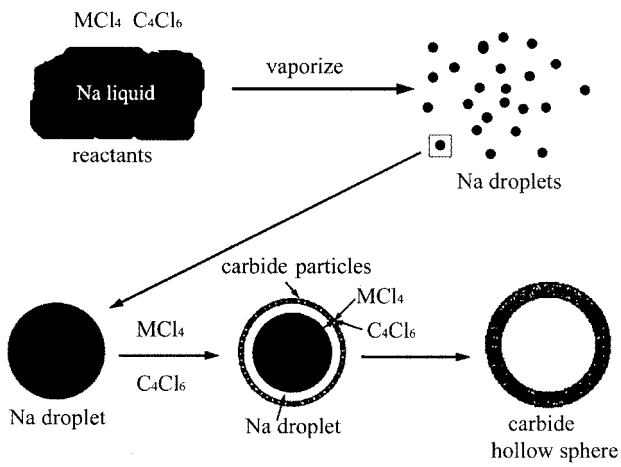

FULL PAPERS

3539 **W. K. Wong,* X.-P. Chen, T.-W. Chik, W.-Y. Wong, J.-P. Guo, F.-W. Lee**

Synthesis of Chiral Cationic (Diimino- and diaminodiphosphane)ruthenium Complexes and Their Applications in Catalytic Oxidation − Crystal Structures of *cis*-[RuCl(py){κ^4-$Ph_2PC_6H_4CH{=}NC_6H_{10}N{=}CHC_6H_4PPh_2$}]$BF_4$ and *cis*-[RuCl(py){κ^4-$Ph_2PC_6H_4CH{=}NC_6H_{10}N$-(H)$CH_2C_6H_4PPh_2$}]$BF_4$

Keywords: Catalysis / Chiral complexes / Oxidation / N,P ligands / Ruthenium

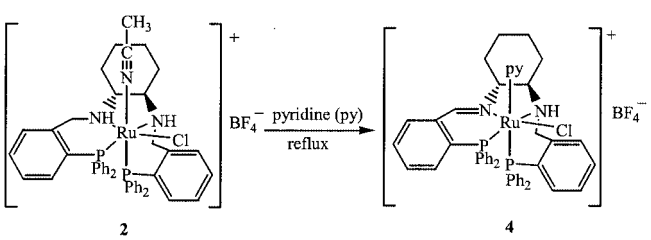

3547 **D. Brown, S. Muranjan, R. P. Thummel***

The Preparation and Study of Bis(2-quinolyl) and Bis(2-[1,8]naphthyridyl) Derivatives of Pyrimidine and Pyrazine as Bridging Ligands for Ru^{II}

Keywords: Bridging ligands / Ruthenium / N ligands

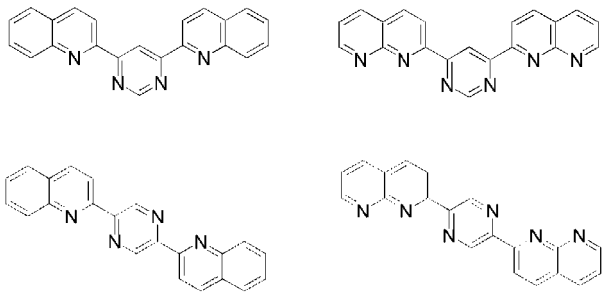

3554 **J. G. Alvarado-Rodríguez,* N. Andrade-López, S. González-Montiel, G. Merino, A. Vela**

Study of the D→Sb (D = O, S) Transannular Interaction in Sb-Monohalogenated Dibenzostibocines − An Experimental and Theoretical Study

Keywords: Antimony / Density functional calculations / Halogens / Hypervalent compounds / Structure elucidation

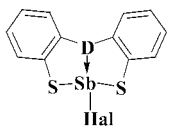

D = O, S

3563 **K. Jurkschat,* K. Peveling, M. Schürmann**

Synthesis, Structure, and Reactivity of Novel Intramolecularly Coordinated Organolead(II) Compounds

Keywords: Lead / Chain structures / Carbene homologues / Phosphorus / Hypervalent compounds

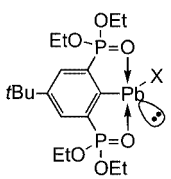

2, X = Cl; **3**, X = SPh

3572 **Y. Wang, X. Zheng, W. Zhuang, L. Jin***

First Examples of Ternary Lanthanide 2,2′-Diphenyldicarboxylate Complexes: Hydrothermal Syntheses and Structures of Lanthanide Coordination Polymers of 2,2′-Diphenyldicarboxylic Acid and 1,10-Phenanthroline

Keywords: Complexes / Hydrothermal synthesis / Lanthanides / Hydrogen bonds / X-ray diffraction

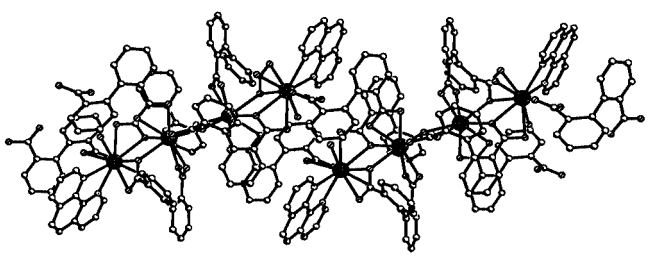

 © 2003 Wiley-VCH Verlag GmbH & Co. KGaA, Weinheim

3583 **M. Hill, G. Kehr, R. Fröhlich, G. Erker***

Organic Functional Group Transformations in the Periphery of a Group-4 Metallocene Complex: 2*H*-Pyrrole Formation at a Pendant Boron Lewis Acid

Keywords: Boron / Hydroboration / Lewis acids / Tautomerism / Zirconium

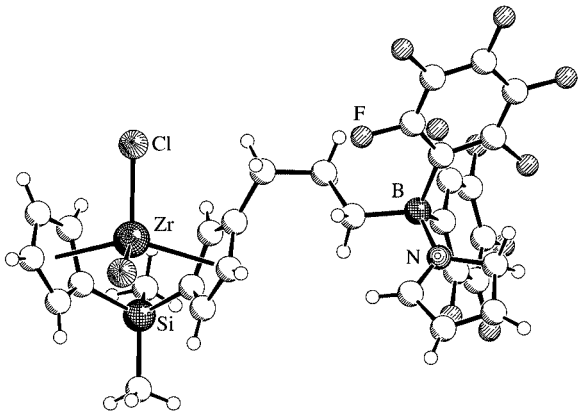

3590 **P. Liptau, L. Tebben, G. Kehr, B. Wibbeling, R. Fröhlich, G. Erker***

Preparation of Optically Active α-Amino[3]-ferrocenophanes − Building Blocks for Chelate Ligands in Asymmetric Catalysis

Keywords: Ferrocenes / Ferrocenophanes / Chelate ligands

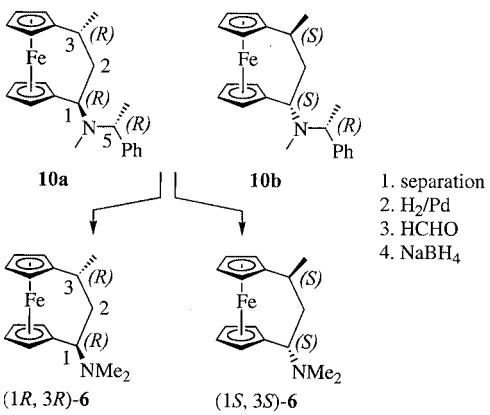

3601 **Z. Jászberényi, E. Brücher,* J. Jekő, K. Hideg, T. Kálai, R. Király**

Synthesis, Equilibrium and Kinetic Properties of Gd^{3+} Complexes of Three DTPA-Bis(Amide) Derivatives Containing Stable Nitroxide Free Radical Substituents

Keywords: Chelates / Imaging agents / Kinetics / Lanthanides / Radicals

$$GdL + M^{z+} \rightarrow ML^{(z-3)+} + Gd^{3+} \quad (M = Lu^{3+}, Zn^{2+})$$

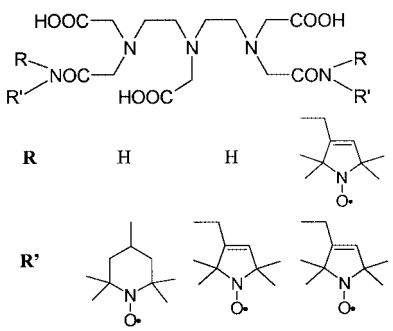

3609 **P. C. R. Soares-Santos, H. I. S. Nogueira, F. A. A. Paz, R. A. Sá Ferreira, L. D. Carlos, J. Klinowski, T. Trindade***

Lanthanide Complexes of 2,6-Dihydroxybenzoic Acid: Synthesis, Crystal Structures and Luminescent Properties of $[nBu_4N]_2[Ln(2,6\text{-dhb})_5(H_2O)_2]$ (Ln = Sm and Tb)

Keywords: Lanthanides / O ligands / Luminescence / Triboluminescence

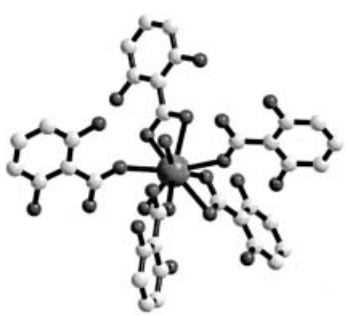

 © 2003 Wiley-VCH Verlag GmbH & Co. KGaA, Weinheim

3618 **C.-M. Liu,* D.-Q. Zhang,* J.-L. Luo, N.-L. Wang, H.-M. Hu, D.-B. Zhu***

A Novel Mixed-Valence Cu^{I}/Cu^{II} Coordination Polymer: Solvothermal Synthesis, Crystal Structure, and Magnetic Properties of $Cu^{I}Cu^{II}$-(2-Pyrazinecarboxylate)$_2$(H_2O)(ClO_4)

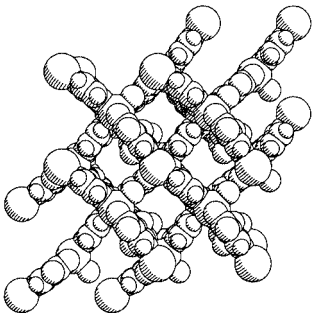

Keywords: Copper / Magnetic properties / N ligands / Solvothermal synthesis

3623 **J. Luo, M. Hong,* R. Wang, D. Yuan, R. Cao, L. Han, Y. Xu, Z. Lin**

Self-Assembly of Three Cd^{II}- and Cu^{II}-Containing Coordination Polymers from 4,4′-Dipyridyl Disulfide

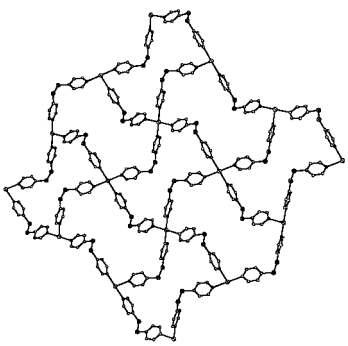

Keywords: Cadmium / Coordination polymers / Copper / Fluorescence / Magnetic properties / N ligands

3633 **V. G. Vaidyanathan, B. U. Nair***

Synthesis, Characterization, and DNA Binding Studies of a Chromium(III) Complex Containing a Tridentate Ligand

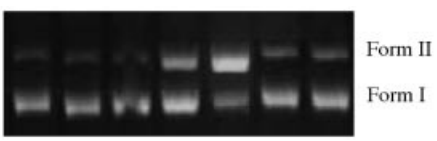

Keywords: Chromium / Tridentate ligands / DNA cleavage / Radicals

3639 **D. J. Darensbourg,* M. J. Adams, J. C. Yarbrough, A. L. Phelps**

Synthesis and Structural Characterization of Potassium Salts of Phosphane-Substituted (Cyclopentadienyl)iron Dicyanides, and Their Use as Bridging Ligands for Copper(I) Phosphane Derivatives

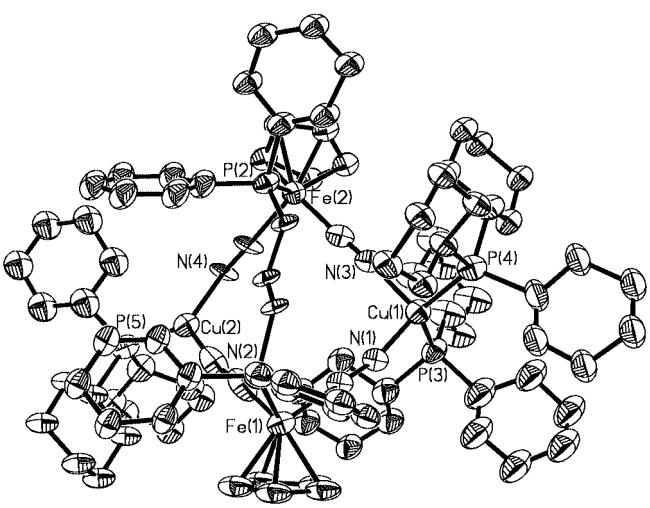

Keywords: Cyanides / Heterometallic complexes / Bridging ligands / Iron / Copper / Potassium

 © 2003 Wiley-VCH Verlag GmbH & Co. KGaA, Weinheim

3649 **D. Pucci,* G. Barberio, A. Crispini, O. Francescangeli, M. Ghedini, M. La Deda**

Self-Organization of Dipolar 4,4′-Disubstituted 2,2′-Bipyridine Metal Complexes into Luminescent Lamellar Liquid Crystals

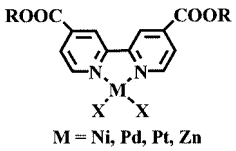

Keywords: N ligands / Platinum / Zinc / Nickel / Metallomesogens

3662 **L. Beneš,* V. Zima, K. Melánová, J. Dybal, M. Trchová, P. Matějka**

Intercalates of Vanadyl Phosphate with Benzonitrile and Tolunitrile

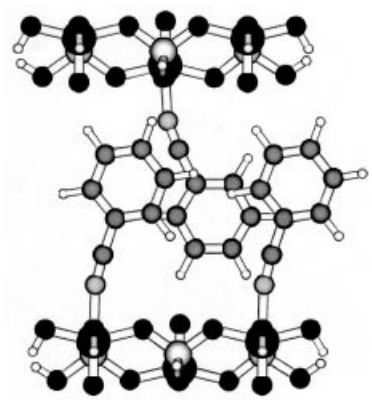

Keywords: Intercalations / X-ray diffraction / Vibrational spectroscopy / Ab initio calculations / Semiempirical calculations

 © 2003 Wiley-VCH Verlag GmbH & Co. KGaA, Weinheim

Palladium-Catalyzed Cyanation of Aryl Halides: Recent Developments and Perspectives

Mark Sundermeier,[a][‡] Alexander Zapf,[a] and Matthias Beller*[a]

Keywords: Palladium / Cyanation / Benzonitriles / Homogeneous catalysis

The palladium-catalyzed cyanation of aryl halides is an elegant method for the preparation of benzonitriles. Since its discovery in 1973, this reaction has been the topic of several investigations. Nevertheless, the general methodology is still somewhat underdeveloped compared to other palladium-catalyzed coupling reactions. Here, we summarize important developments from 1997 until 2003 in this area. Recent contributions from our group include the development of palladium/phosphane/amine catalyst systems for the cyanation of aryl chlorides, the successful cyanation of aryl halides with acetone cyanohydrin and trimethylsilyl cyanide as cyanation reagents, and a general improvement of catalyst efficiency by using a continuous dosage of cyanide sources.

(© Wiley-VCH Verlag GmbH & Co. KGaA, 69451 Weinheim, Germany, 2003)

Introduction

Benzonitriles are of considerable interest for organic chemistry as an integral part of dyes, herbicides, agrochemicals, pharmaceuticals, and natural products. The nitrile group also serves as an important intermediate structure for a multitude of possible transformations into other functional groups. As an example the synthesis of Fluvoxamine is shown in Scheme 1. Here, 4-(trifluoromethyl)-

[a] Leibniz-Institut für Organische Katalyse an der Universität Rostock e.V.
Buchbinderstr. 5−6, 18055 Rostock, Germany
Fax: (internat.) + 49-381/46693-24
E-mail: matthias.beller@ifok.uni-rostock.de
[‡] Present address: Mark Sundermeier, Colorado State University, Department of Chemistry,
Fort Collins, CO 80523, Colorado, USA

Mark Sundermeier was born in Herford, Germany in 1972. He studied chemistry at the Friedrich-Schiller-University in Jena, where he has done his diploma thesis in 1998 under directions of Prof. R. Beckert on the field of 1,2-dioxetanes and their luminescence. Under the supervision of Prof. M. Beller he started his PhD studies in 1998 on the field of palladium-catalyzed cyanation of aryl−X derivatives at the Leibniz-Institut für Organische Katalyse in Rostock, where he completed his PhD degree in 2002. He focused his research on the cyanation of aryl chlorides and bromides. Since 2003 he is a postdoctoral fellow at the Colorado State University in the group of Prof. T. Rovis working on the field of asymmetric O→C rearrangements.

Alexander Zapf was born in Coburg, Germany, in 1970. After studying chemistry at the Technical University of Munich he worked on his PhD thesis in the area of Heck and Suzuki reactions under the supervision of Prof. M. Beller until 1998. Then he joined the Leibniz-Institut für Organische Katalyse in Rostock, where he became the project leader of "Ar−X activation" in 1999. Pd-catalyzed coupling reactions of aryl chlorides and bromides are the subject of most of the projects, which are mainly worked on in cooperation with industry. Alexander has been a fellow of the Studienstiftung des deutschen Volkes and the Max-Buchner-Forschungsstiftung.

Matthias Beller, born 1962 in Gudensberg, Germany, studied chemistry at the University of Göttingen and obtained his doctorate in 1989 under the guidance of Prof. L. F. Tietze. After postdoctoral studies (1990) with Prof. K. B. Sharpless at Massachussetts Institute of Technology (USA) funded with a Liebig scholarship of the Verband der Chemischen Industrie, he became a research chemist in the Central Research of Hoechst AG in Frankfurt, Germany. In 1993 he became group leader of "Organometallic chemistry - catalysis" and in 1994 project leader of "Homogeneous catalysis" at Hoechst AG. From 1996 to 1998 he was Associate Professor for Inorganic Chemistry at the Technical University of Munich and since June 1998 he is Director of the Leibniz-Institut für Organische Katalyse (IfOK) aligned with a full professorship "Catalysis" at the University of Rostock. His research topics cover the development of a wide range of practical catalytic methodologies. Special attention is given to selective and environmentally benign transformations. More specifically he is interested in palladium-catalyzed coupling reactions, carbonylation reactions, catalytic amination of olefins and oxidations of olefins using air or molecular oxygen as the final oxidant. His scientific work has been published in more than 140 original publications and review articles. In addition 70 patent applications have been filed in the last decade. Together with Prof. Carsten Bolm he has edited a book on the use of "Transition Metals for Organic Synthesis". Matthias Beller is married since 1992 to Dr. Anja Fischer-Beller and they have two sons (Marc-Philipp and Jan-Niclas).

MICROREVIEWS: This feature introduces the readers to the author's research through a concise overview of the selected topic. Reference to important work from others in the field is included.

benzonitrile, which is available from 4-chloro(trifluoromethyl)benzene by nickel-catalyzed cyanation on ton-scale, serves as an intermediate.[1−3]

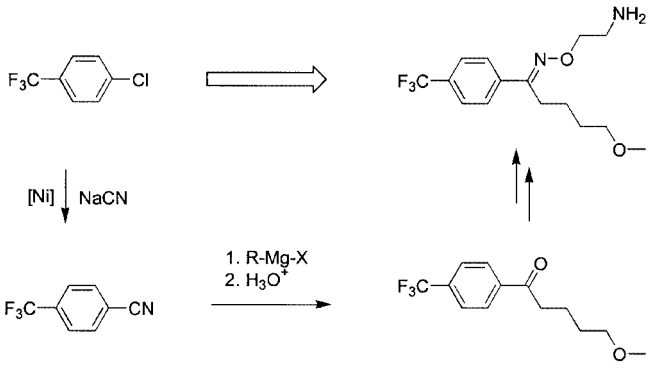

Scheme 1. 4-(Trifluoromethyl)benzonitrile, a key intermediate in the synthesis of Fluvoxamine

Benzonitriles themselves are also of significant interest, for example as substructures in biologically active agents. In Figure 1 selected examples of pharmaceuticals containing an aromatic nitrile as integral part of the molecule are shown along with their names, producers, and effects.[4] In the case of biologically active benzonitrile derivatives another aspect is worth noting. By applying transition-metal-catalyzed cyanation of aryl halides using $K^{11}CN$, $K^{13}CN$ or $K^{14}CN$ isotopically labeled compounds are easily accessible.[5−9] The resulting products are used in pharmacokinetic studies and investigations on the metabolism of pharmaceuticals.

Clearly, benzonitriles can be prepared in numerous ways.[10−14] Most often they are synthesized by the Rosenmund-von Braun reaction[15−19] from aryl halides or diazotization of anilines and subsequent Sandmeyer reaction[20−22] on a laboratory as well as on an industrial scale. On a ton-scale the method of choice in industry is ammoxidation, whereby the corresponding toluene derivatives are reacted with oxygen and ammonia at 300−550 °C in the presence of heterogeneous fixed-bed catalysts.[23−25]

A drawback of the Rosenmund-von Braun and the Sandmeyer reactions is the use of stoichiometric amounts of copper(I) cyanide as cyanating agent, which leads to equimolar amounts of heavy metal waste. Other disadvantages of the Rosenmund-von Braun reaction are the relatively high temperature (150−250 °C) and the low reactivity of aryl chlorides and bromides (in general the use of expensive aryl iodides is required). The ammoxidation is restricted to simpler substrates because of the high temperature, high pressure, and the large excess of ammonia required. Furthermore, only a limited number of toluene derivatives are available on a larger scale. Hence, this procedure is applied for products such as benzonitrile, terephthalodinitrile, and chlorobenzonitriles.[26,27]

A useful alternative for the preparation of substituted benzonitriles is the transition-metal-catalyzed cyanation of aryl−X compounds (X = Cl, Br, I, OTf etc.) with cheap and readily available cyanation agents like sodium or potassium cyanide (Scheme 2).[28−31] The order of reactivity of the aryl−X derivatives is opposite to the bond-dissociation energy of the C−X bond (reactivity: I ≈ OTf > Br > Cl).[32,33] Electron-withdrawing substituents on the aryl ring increase the reactivity, while electron-donating substituents decrease reactivity. Most common catalysts for coupling of aryl halides or triflates with cyanide are transition metal complexes of the platinum group, especially palladium or nickel complexes. Palladium catalysts tolerate a wider vari-

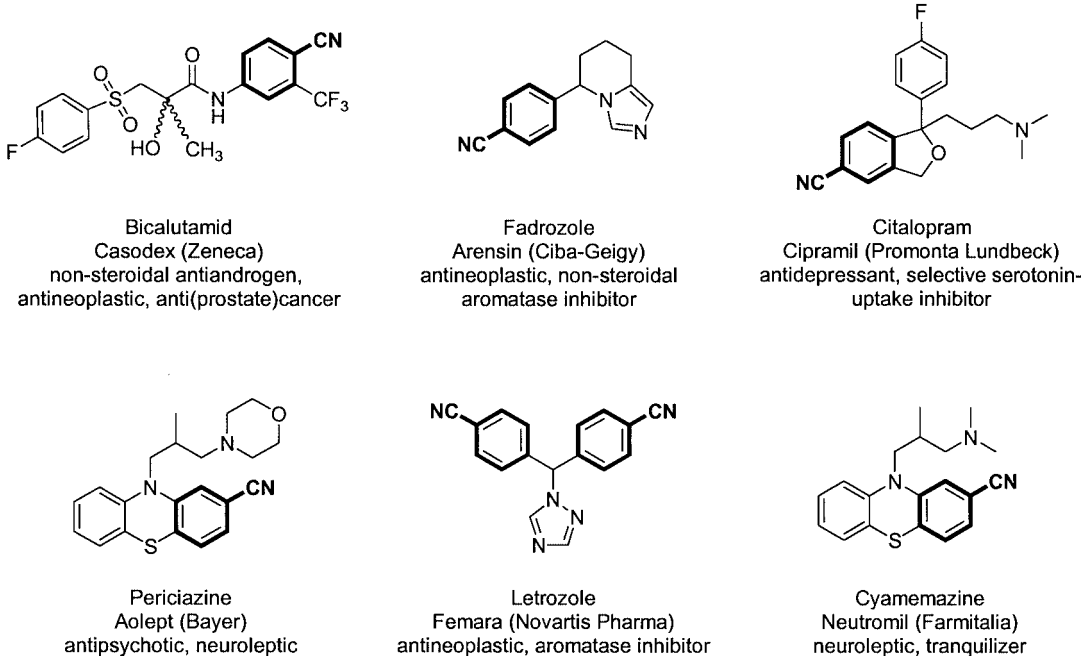

Figure 1. Examples of pharmaceutically active benzonitriles

 © 2003 Wiley-VCH Verlag GmbH & Co. KGaA, Weinheim

ety of functional groups and are less sensitive to air and humidity than nickel catalysts.

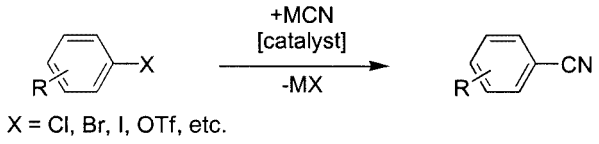

Scheme 2. Transition-metal-catalyzed cyanation of aryl halides

The first palladium-catalyzed cyanation of aryl−X derivatives has been introduced in 1973 by Takagi and co-workers using aryl bromides and iodides with potassium cyanide as the cyanating agent (Scheme 3).[34] Palladium(II) cyanide or palladium(II) acetate served as the catalyst without additional ligands present. Typical reaction conditions were DMF as solvent, 140−150 °C and 2−12 h reaction time.

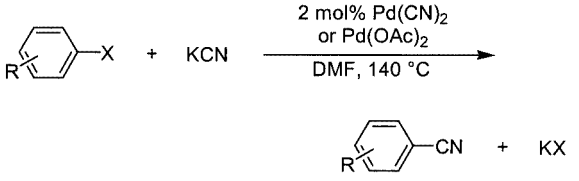

Scheme 3. First palladium-catalyzed cyanation of aryl bromides and iodides

Early mechanistic studies by Takagi and co-workers[35] led to the mechanistic proposal shown in Scheme 4. The mechanism consists of two cycles, one representing the typical cycle for a palladium-catalyzed cross-coupling reaction with oxidative addition and reductive elimination, and a second prior cycle, where palladium species act as cyanide carriers. It was pointed out that an excess of cyanide ions inhibits the catalytic cycle. This deactivation was explained by the reaction of cyanide with palladium(II) species, forming inactive palladium(II) cyano compounds, which cannot be reduced to catalytically active palladium(0) species.

Potassium tetracyanopalladate(II) and palladium(II) cyanide were shown to be almost inactive in the cyanation reaction, and a dramatic solvent effect was described which can be explained by the influence of the cyanide solubility in different reaction media. The higher the solubility of the cyanide salt, the lower the reaction outcome. Another finding of this work is the positive effect of co-catalysts like potassium hydroxide, sodium ethoxide, potassium carbonate, or sodium phenoxide, which facilitate the reduction of palladium(II) species.[36,37]

The reaction conditions have subsequently been optimized and the substrate scope of the method has been considerably enhanced by different groups. In Table 1 the different conditions of palladium-catalyzed cyanation reactions of aryl halides known prior to 1997 are summarized. In general the cyanation of aryl bromides and iodides has been performed in the presence of an excess of KCN in dipolar aprotic solvents. In addition, NaCN, Me_3SiCN, nBu_3SnCN and $Zn(CN)_2$ were employed in selected examples as cyanide sources. Apparently there is no difference in applying palladium(II) or palladium(0) pre-catalysts. In a few cases the cyanation of chloroarenes was also performed. However, in all these examples highly reactive heteroaryl chlorides have been used.

Table 1 demonstrates that the palladium-catalyzed cyanation of aryl bromides and iodides works with different palladium catalysts and cyanide sources. However, the described catalyst productivity was always quite low (turnover numbers (TON) are in general 10−50). Furthermore, many systems need additives or a special cyanide source to enable good product yields. In the last five years new approaches have been made by us and other groups which will be discussed below.

Results and Discussion

Recent Developments in the Palladium-Catalyzed Cyanation of Aryl Bromides and Iodides

Due to the low catalyst efficiency realized with KCN in the palladium-catalyzed cyanation of aryl halides, some recent publications focused on the development of alternative cyanation agents. A somewhat unusual cyanide source are alkyl nitriles, which represent common solvents. In this re-

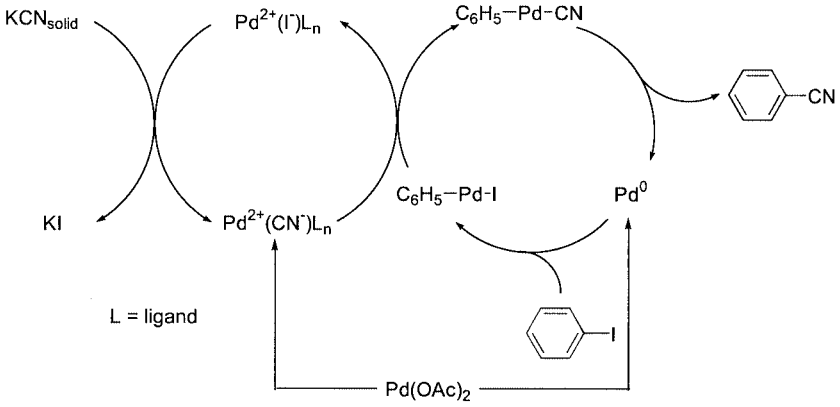

Scheme 4. Proposed mechanism of the palladium-catalyzed cyanation according to Takagi et al.

 © 2003 Wiley-VCH Verlag GmbH & Co. KGaA, Weinheim

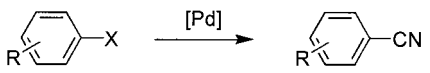

Scheme 5. Palladium-catalyzed cyanation of aryl halides

an overstoichiometric amount of zinc powder as additive (4 equiv.). Thus, this protocol might be a viable alternative only for a limited number of benzonitriles. The unusual reaction mechanism is, however, worth mentioning, as it is completely different from the general mechanism for the palladium-catalyzed cyanations. As shown in Scheme 6 the

Table 1. Evolution of the palladium-catalyzed cyanation of aryl halides

Entry	X	Catalyst (mol %)	Additive (mol %)	Cyanide (equiv.)	Solvent	T [°C]/t [h]	Ref.
1	I, Br	$Pd(OAc)_2$ (2)	–	KCN (2)	DMF	140/2–12	[34]
2	I	$[Pd(PPh_3)_4]$ (20)	–	KCN (1.5)	THF	reflux/8	[38]
3	I, Br	$Pd(OAc)_2$ (1.5)	KOH (0.05) KI (9)	KCN (2)	HMPT	60–90/2–9	[39]
4	I, Br	$[Pd(PPh_3)_4]$ (10)	–	NaCN on Al_2O_3 (5)[a]	Toluene	80–100/2–40	[40]
5	I, Br	$[Pd(PPh_3)_4]$ (10)	Al_2O_3	NaCN (5)	Toluene	80–100/2–40	[40]
6	Cl[b]	$[Pd(PPh_3)_4]$ (5)	–	KCN (1.5)	DMF	reflux/2.5	[41]
7	Br	$[Pd(PPh_3)_4]$ (20)	18-C-6 (40)	KCN (1)	Benzene	100/65	[42]
8	I	$[Pd(PPh_3)_4]$ (2)	–	Me_3SiCN (1.5)	Et_3N	reflux/0.17–0.5	[43]
9	Br[c]	$[Pd(PPh_3)_4]$ (1.5)	18-C-6 (7.5) CuI (250)	KCN (250)	DMF	reflux/2	[44]
10	I[d]	$[Pd(PPh_3)_4]$ (n.g.)[e]	–	nBu_3SnCN (n.g.)[e]	DMF	n.g.[e]	[45]
11	Cl[f]	$[PdCl_2(PPh_3)_2]$ (2)	–	KCN (2)	DMF	reflux/2	[46]
12	I	$[Pd_2(dba)_3(CHCl_3)]$·0.5dppf[g] (2)	–	KCN (2)	NMP	60–80/1–8	[47]
13	I, Br	$[Pd(PPh_3)_4]$ (2–6)	–	$Zn(CN)_2$ (0.6)	DMF	80/0.5–7	[48]
14	Cl[f]	$[Pd(PPh_3)_4]$ (7)	–	$Zn(CN)_2$ (0.6)	NMP	90/20	[49]

[a] 5 mmol NaCN per g Al_2O_3. [b] Only chloropyrazines. [c] Only bromopyrazines. [d] Only 2-iodoadenosine. [e] Not given. [f] Only chloropurines. [g] 1,1′-Bis(diphenylphosphanyl)ferrocene.

gard it is interesting to note that Luo et al. have shown that a transfer of the nitrile function from acetonitrile to aryl halides is possible at high temperature (160 °C).[50] Table 2 presents a summary of the obtained results. In contrast to most other cyanation protocols good yields of 2-substituted benzonitriles and even 2,6-disubstituted benzonitriles are obtained.

Table 2. Acetonitrile as solvent and cyanide source

Entry	Substrate	Product[a]	Catalyst	Yield [%][b]
1	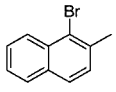	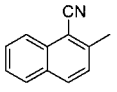	$[PdCl_2(PBu_3)_2]$	81
2			$[PdCl_2(PPh_3)_2]$/8 PPh_3	76 (69)[c]
3			$[PdCl_2(dppp)_2]$	90
4	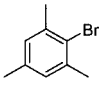	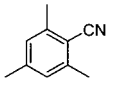	$[PdCl_2(PBu_3)_2]$	100
5			$[PdCl_2(PPh_3)_2]$/8 PPh_3	94 (76)[c]
6	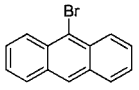	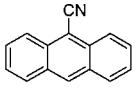	$[PdCl_2(PBu_3)_2]$	(70)[c]
7	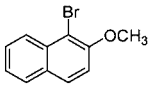	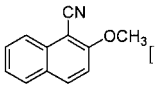	$[PdCl_2(PBu_3)_2]$	32
8			$[PdCl_2(PPh_3)_2]$/8 PPh_3	30 (28)[c]

[a] General conditions: 5 mmol aryl bromide, 10 mol % Pd-catalyst, 4 equiv. Zn-powder, 30 mL acetonitrile, 160 °C, 24 h.[b] Yields determined by ^1H NMR using $HCONEt_2$ as internal standard.[c] Isolated yield in parentheses.

Unfortunately, this transformation requires high catalyst concentration (10 mol %), high temperature (160 °C) and

oxidative addition product of the aryl halide and palladium(0) first gives the corresponding imine, which is then degraded by Lewis acid catalysis to the desired nitrile. Stoichiometric amounts of zinc(II) salts are formed during the reaction.

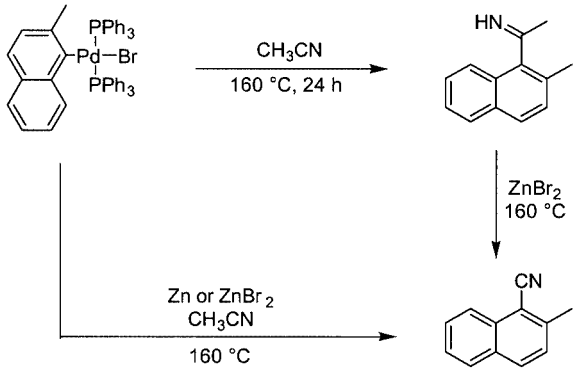

Scheme 6. Mechanism of the palladium-catalyzed cyanation using acetonitrile as cyanating agent

Surprisingly, copper(I) cyanide, the typical cyanating agent in the Rosenmund-von Braun and the Sandmeyer reaction, was not described as a cyanide source in palladium-catalyzed reactions of aryl halides until recently. Hence, the first palladium-catalyzed Rosenmund-von Braun reaction was developed by Sakamoto and Ohsawa in 1999 (Scheme 7).[51]

This protocol is useful for the transformation of electron-rich and electron-poor aryl bromides. Also *N*-heteroaryl iodides and bromides [e.g., *N*-(phenylsulfonyl)indoles, pyrrols, quinolines] give the corresponding nitriles in good

 © 2003 Wiley-VCH Verlag GmbH & Co. KGaA, Weinheim

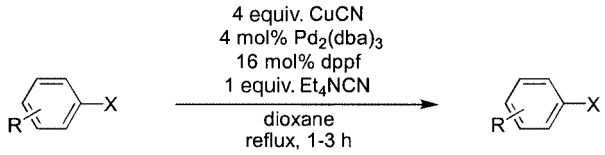

R	X = I	X = Br
4-OMe	82 %	91 %
4-CO_2Me	88 %	89 %
4-NO_2	65 %	56 %
2-OMe	94 %	76 %
2-CO_2Me	88 %	83 %
2-NO_2	67 %	23 %

Scheme 7. Palladium-catalyzed Rosenmund-von Braun reaction

yield. A comparison of the palladium-catalyzed variant and the noncatalytic reaction shows that the palladium catalyst leads to higher yields. Nevertheless, the use of copper(I) cyanide leads to no improvement of the palladium catalyst efficiency compared to other cyanating agents. A comparatively high catalyst concentration (8 mol % Pd), an overstoichiometric amount of copper(I) cyanide (4 equiv.) and a stoichiometric amount of an additive (Et_4NCN) are still required for successful reactions.

Based on the knowledge of the well-established palladium-catalyzed cross-coupling of aryl halides with organoboron compounds (Suzuki reaction), Jiang et al. used dialkyl cyanoboronates as the cyanide source.[52] Dialkyl cyanoboronates are easily prepared by the reaction of sodium cyanoborohydride and 1,2-diols (Scheme 8). As shown in Table 3, the cyanation of aryl bromides, iodides and strongly activated chlorides is possible under these conditions.

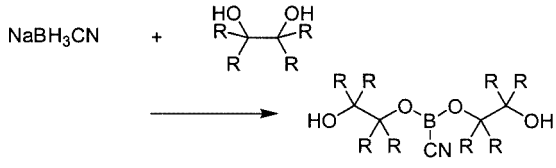

Scheme 8. Dialkyl cyanoboronates — new cyanating agents

Apart from variations of the cyanide source the optimization of co-catalysts and ligands was studied in order to improve the palladium-catalyzed cyanation of aryl halides in efficiency and scope. For example Okano et al. introduced a new class of phase-transfer-type phosphane ligands for this reaction. Here, the known positive effect of a phase-transfer catalyst (PTC) was introduced in the phosphane ligand in order to control the reactivity of the palladium catalyst. Several ligands, containing crown ether, sulfonic acid, carbonic acid or ammonium salts, or similar substructures were tested (Figure 2).[53,54] The best results were obtained in the presence of PPh_2(bc-5) and PPh_2(ms) as ligand (Table 4 and 5).

As shown in Table 4, when using PPh_2(bc-5) as ligand the cyanation of bromo- and iodoarenes is possible in the presence of a comparatively low catalyst concentration (0.33 mol %). Here, no further additives are necessary, but

Table 3. Dialkyl cyanoboronates in the palladium-catalyzed cyanation of aryl halides

Entry	Substrate	Product[a]	t [h]	Conversion (yield) [%][b]
1		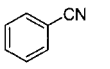	24	80 (78)
2	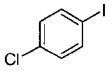	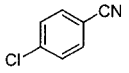	17	67 (37)
3	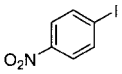	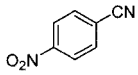	48	58 (50)
4			10	72 (69)
5		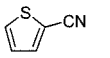	24	83 (75)
6	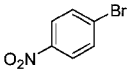	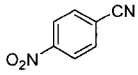	144	97 (89)
7			24	87 (72)
8	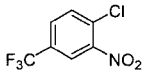	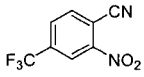	24	40 (19)
9	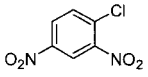	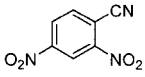	12	58 (50)

[a] General conditions: 0.5 mmol aryl bromide, 5 mol % $[Pd(PPh_3)_4]$, 1.2 equiv. cyanoboronate ester, 1.5 equiv. K_3PO_4, 5 mL THF, 50 °C. [b] Conversions determined by GC-MS, isolated yield in parentheses.

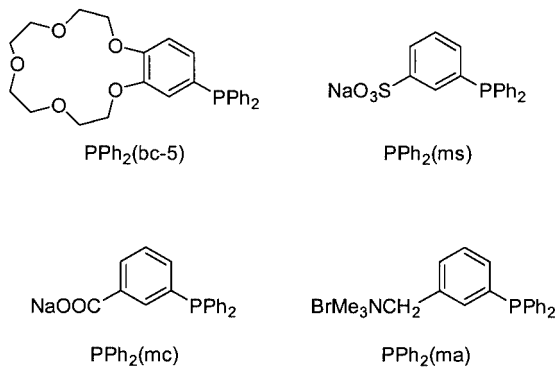

Figure 2. Ligands with phase-transfer catalyst properties

PPh_2(ms) as ligand requires the addition of $ZnCl_2$ and $NaBH_4$ in order to obtain satisfactory results (Table 5).

Unfortunately, using PPh_2(ms) as ligand just aryl iodides and electron-deficient aryl bromides can be cyanated in good yield, whereas bromobenzene is hardly converted. Without sodium borohydride, no catalytic activity at all is observed. The authors state that the hydride is needed for reduction of the catalyst precursor $[PdCl_2\{PPh_2(ms)\}_4]$,

 © 2003 Wiley-VCH Verlag GmbH & Co. KGaA, Weinheim

Table 4. PPh_2(bc-5) as new ligand in the palladium-catalyzed cyanation

Entry	Substrate	Product[a]	Yield [%][b]
1	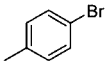	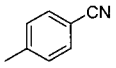	92 (77)
2	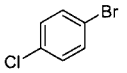	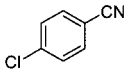	93 (81)
3	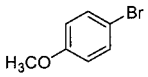	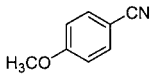	86
4			91
5	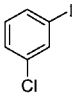	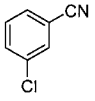	87

[a] General conditions: 7.5 mmol aryl bromide, 3 equiv. NaCN, 0.33 mol % *trans*-[PhPdBr{PPh_2(bc-5)$_2$}], 0.66 mol % PPh_2(bc-5), 5 mL dioxane, reflux, 20 h. [b] Yields determined by GC-MS, isolated yield in parentheses.

however the reduction of catalytically nonactive cyanopalladium species, which result from catalyst deactivation processes in the presence of an excess of cyanide ions, has to be considered, too.

Anderson et al. studied the influence of solvent, cyanide source, co-catalysts, and the palladium source on the palladium-catalyzed cyanation of aryl halides.[55] Depending on the reaction conditions, potassium and sodium cyanide both gave satisfactory results. The choice of the right cyanide source is mainly influenced by the solvent. While KCN gives better results in THF, NaCN is preferable in ethyl acetate or acetonitrile. Furthermore, the authors discovered that copper salts were effective additives for the cyanation of 1-iodonaphthalene (Scheme 9, Table 6). In addition, aryl bromides and triflates can be coupled to the corresponding nitriles in good to very good yields.

Another new procedure has been described by Maligres et al.[56] They combined the palladium catalyst system introduced by Takagi ($Pd_2(dba)_3$/dppf)[47] with the use of zinc(II) cyanide as the cyanating agent (introduced by Tschaen et al.)[48] to get an efficient system for the palladium-catalyzed cyanation of aryl bromides (Scheme 10). Besides dppf several other phosphane ligands have also been tested, but with little success.

Palladium-Catalyzed Cyanation of Aryl Chlorides

Regarding costs and availability aryl chlorides are favorable substrates for catalytic refinement of aryl−X derivatives.[57−60] Because of their low reactivity, the cyanation of chloroarenes has been known prior to 2000 only with nickel catalysts[29,61−68] or with palladium catalysts for activated (hetero)aryl chlorides (e.g., pyrazines,[44] purines[46,49]). In 2000, Jin and Confalone reported the first general method for the palladium-catalyzed cyanation of aryl chlorides (Scheme 11).[69]

Table 5. Palladium-catalyzed cyanation of aryl halides using PPh_2(ms) as ligand

Entry	Substrate	Product[a]	*t* [h]	Yield [%][b]
1	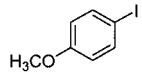	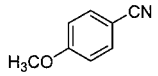	7	98
2	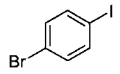	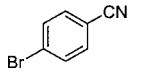	3	82[c]
3	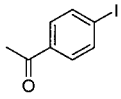	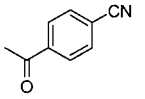	1	97 (91)
4	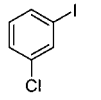	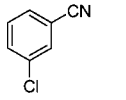	3	98
5	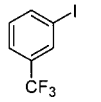	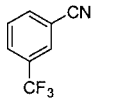	3	98 (93)
6	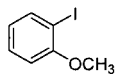	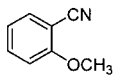	24	78
7	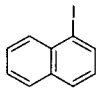	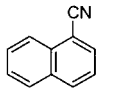	7	97 (89)
8	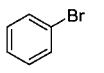	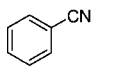	5	8
9	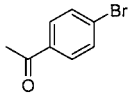	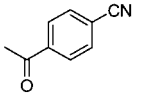	10	95

[a] General conditions: 10 mmol aryl halide, 1.3 equiv. NaCN, 1 mol % [$PdCl_2$[{Ph_2(ms)}$_4$], 50 mol % $ZnCl_2$, 20 mol % $NaBH_4$, 10 mL heptane, 10 mL water, reflux. [b] Yields determined by GC-MS, isolated yield in parentheses. [c] 13% Terephthalonitrile detected.

As shown in Table 7 the corresponding benzonitriles were obtained in good to very good yields by using 4 mol % of a palladium complex generated in situ from [tris(dibenzylideneacetone)dipalladium(0)] and [1,1′-bis(diphenylphosphanyl)ferrocene] (dppf). The use of zinc(II) cyanide as cyanide source and catalytic amounts of zinc powder to reduce palladium(II), which is formed to some extent in side reactions, is important for successful cyanation.

Despite its usefulness the procedure has some drawbacks such as the need for a comparatively high amount of catalyst (4 mol % palladium) and the use of zinc(II) cyanide as cyanide source, which leads to significant amounts of metal waste.

In a joint project with SKW Trostberg AG (now Degussa AG) we became interested in this topic in 1998. Based on our catalyst developments for Heck,[70−73] Suzuki[74−77] and amination[78,79] reactions of aryl chlorides, we were primarily attracted in finding more productive palladium catalyst

 © 2003 Wiley-VCH Verlag GmbH & Co. KGaA, Weinheim

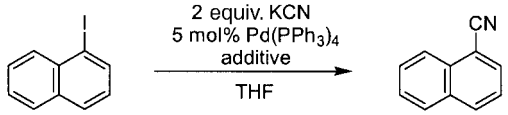

Scheme 9. Additive effects on the Pd-catalyzed cyanation of 1-iodonaphthalene

Table 6. Effect of additives on the palladium-catalyzed cyanation of 1-iodonaphthalene

Entry	Additive[a]	*t* [h]	Conversion [%][b]
1	–	6	7
2	5 mol % CuI	2	100
3	10 mol % CuCN	2	100
4	10 mol % CuOTf	4	94
5	10 mol % $Cu(OTf)_2$	3	57
6	10 mol % CuBr	3	100
7	10 mol % ZnI_2	2.5	100
8	10 mol % TMSCN	3.5	> 98
9	10 mol % BPh_3	2	100

[a] General conditions: 0.4 M 1-iodonaphthalene in THF, 2 equiv. KCN, 5 mol % $[Pd(PPh_3)_4]$. [b] Determined by HPLC.

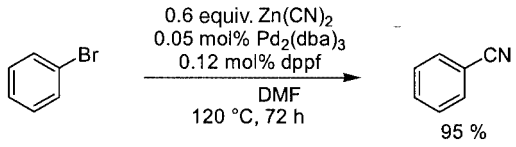

Scheme 10. Palladium-catalyzed cyanation of aryl bromides according to Maligres et al.

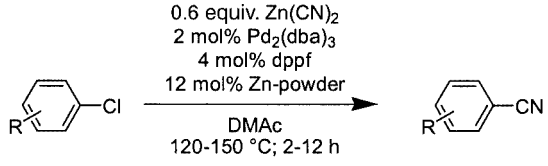

Scheme 11. Palladium-catalyzed cyanation of aryl chlorides according to Jin et al.

systems for the cyanation of aryl chlorides, which work in the presence of a cheap and readily available cyanide source (e.g., sodium or potassium cyanide). Initially, we studied the relation of various positive additives described for cyanations of aryl bromides using 4-chloro(trifluoromethyl)benzene as a model substrate. For example, we combined the known positive effect of crown ethers[53,54] with the use of inorganic bases like sodium carbonate or potassium hydroxide as co-catalysts.[39] Surprisingly, this combination of additives has never been tested before. As shown in Table 8 (Entries 1–3) a significant improvement of the product yield can be realized under these conditions.[80] Apart from additives the right choice of phosphane ligand is also important in order to obtain good results. Similar to carbonylation reactions of aryl chlorides,[81–85] the best results are observed in the presence of chelating phosphane ligands such as dppb and dpppe.

Table 7. Palladium-catalyzed cyanation of aryl chlorides by Jin and Confalone

Entry	Substrate	Product[a]	*T* [°C]	*t* [h]	Yield [%][b]
1[c]	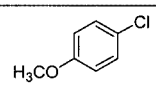	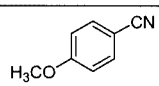	150	4	88
2	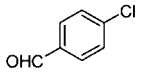	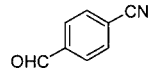	120	0.75	92
3	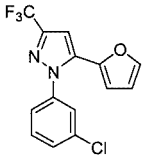	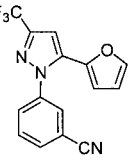	150	10	91
4	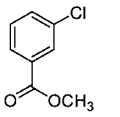	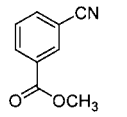	120	10	91
5	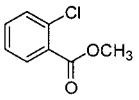	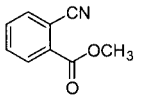	120	2	93
6	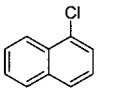	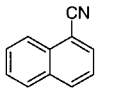	150	2	96

[a] General conditions: 3 mmol aryl chloride, 0.6 equiv. $Zn(CN)_2$, 2 mol % $[Pd_2(dba)_3]$, 4 mol % dppf, 12 mol % Zn, 6 mL DMAc. [b] Isolated yield. [c] 4 Mol % $[Pd_2(dba)_3]$, 8 mol % dppf, 24 mol % Zn.

Table 8. Palladium-catalyzed cyanation of 4-chloro(trifluoromethyl)benzene with different co-catalysts

Entry[a]	Na_2CO_3 [mol %]	18-Crown-6 [mol %]	TMEDA [mol %]	Conv. [%][b]	Yield [%][b]
1	–	–	–	15	13
2	20	–	–	37	18
3	20	2	–	63	58
4[c]	20	2	–	42	38
5	20	2	20	56	49
6	20	–	20	50	43
7	–	2	20	10	8
8	–	–	20	97	91

[a] General conditions: 2 mmol 4-chloro(trifluoromethyl)benzene, 1 equiv. potassium cyanide, 2 mol % palladium(II) acetate, 4 mol % 1,5-bis(diphenylphosphanyl)pentane, 2 mL toluene, 16 h, 160 °C. [b] Conversions and yields were determined by GC using an internal standard (diethylene glycol di-*n*-butyl ether). [c] Triphenylphosphane instead of 1,5-bis(diphenylphosphanyl)pentane.

As the combination of base and crown ether led to better results in the cyanation reaction, the question arose as to whether both properties could be combined into one single additive. *N*,*N*,*N*′,*N*′-Tetramethylethylenediamine (TMEDA) is a typical candidate for the desired type of substances. Therefore, we tried the cyanation reaction in the presence of various amounts of TMEDA. To our delight,

 © 2003 Wiley-VCH Verlag GmbH & Co. KGaA, Weinheim

the addition of 20 mol % of TMEDA as co-catalyst (Table 8, Entries 5−8) gave excellent yield (91%) and selectivity (94%) of 4-trifluoromethylbenzonitrile. Somewhat surprisingly, the combination of TMEDA with sodium carbonate and 18-crown-6 gave lower yields than with TMEDA alone. In the presence of TMEDA and 18-crown-6 a disappointingly low yield (8%) of the desired nitrile was observed. The dramatic influence of these additives on selectivity and yield of the desired benzonitrile is explained by their effect on the cyanide concentration in solution. While a high concentration of cyanide ions leads to immediate catalyst deactivation, a low concentration of CN^- retards the reductive coupling of the aryl group and cyanide ions (see mechanistic discussion below). The general applicability of the new protocol is shown in Table 9.

Table 9. Scope and limitations of the palladium-catalyzed cyanation of aryl and heteroaryl chlorides in the presence of TMEDA

Entry	Substrate	Product[a]	Conversion [%][b]	Yield [%][b]
1	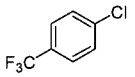	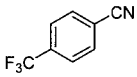	97	91
2	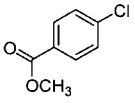	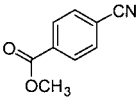	85	75
3			96	91
4	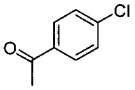	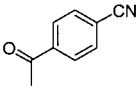	99	96
5[c]			33	33
6[c]			23	17
7			48	46
8	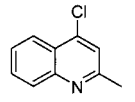	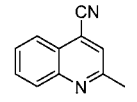	76	74 (67)[d]

[a] General conditions: 2 mmol aryl or heteroaryl chloride, 1 equiv. potassium cyanide, 2 mol % palladium(II) acetate, 4 mol % 1,5-bis(diphenylphosphanyl)pentane, 20 mol % TMEDA, 2 mL toluene, 16 h, 160 °C. [b] Conversions and yields were determined by GC using an internal standard (diethylene glycol di-*n*-butyl ether). [c] Reaction conditions: 2 mmol aryl chloride, 1 equiv. potassium cyanide, 3 mol % palladium(II) acetate, 6 mol % 1,5-bis(diphenylphosphanyl)pentane, 30 mol % TMEDA, 2 mL toluene, 16 h, 160 °C. [d] Isolated yield in parentheses.

The catalyst system is applicable to activated aryl chlorides, which react with KCN to give the corresponding benzonitriles in high yields. Also *N*-heteroaryl chlorides such as 3-chloropyridine and 4-chloroquinaldine give the desired product in moderate to good yield. Unfortunately, deactivated and nonactivated aryl chlorides like chlorobenzene and 3-chlorotoluene lead to poor results under these conditions (Table 9, Entries 5−6).

The beneficial effect of TMEDA as co-catalyst prompted us to investigate the influence of other amines in the palladium-catalyzed cyanation of nonactivated chloroarenes. Here, chlorobenzene was used as a more suitable model system, which does not react efficiently with KCN under standard conditions, i.e., benzonitrile is obtained only in 13% in the presence of 0.2 equiv. of TMEDA and 2 mol % palladium catalyst. Selected examples of successful co-catalysts are shown in Scheme 12.[86]

Clearly, the reaction outcome is significantly influenced by the added amine. Among the various amines tested the best results were obtained in the presence of sparteine, 1,1′-methylenedipiperidine (MDP), 2,2′-bipyridine, and 1-adamantylamine. A closer look at the catalysis results reveals that there is no obvious connection of catalytic activity and any structural property of the amine (e.g., basicity or sterics). Because of the promising results using MDP, the reaction of other nonactivated, deactivated, or sterically hindered aryl chlorides and *N*-heteroaryl chlorides was investigated with this additive (Table 10).

In most cases we observed considerably improved results with MDP as co-catalyst compared to TMEDA. Almost all problematic substrates are converted into the desired benzonitriles in good to very good yields. This procedure

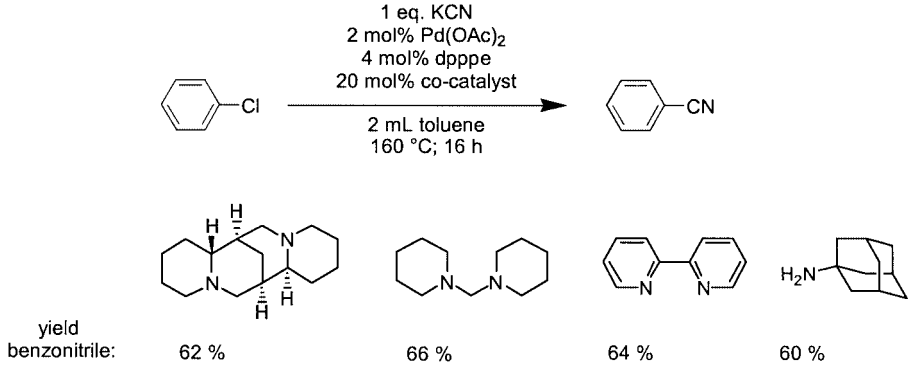

Scheme 12. Variation of the co-catalyst in the palladium-catalyzed cyanation of chlorobenzene

 © 2003 Wiley-VCH Verlag GmbH & Co. KGaA, Weinheim

Table 10. Catalytic cyanation of various aryl chlorides

Entry	Substrate	Product[a]	Conv. [%][b]	Yield [%][b]
1			67	66
2[c]			89	84
3	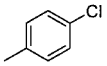	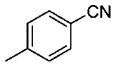	71	59
4	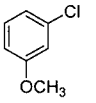	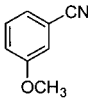	62	53
5	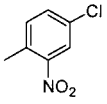	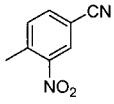	46	41
6[d]			66	55
7	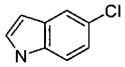	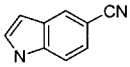	52	(22)[e]
8	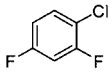	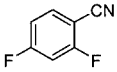	67	42
9	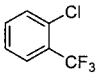	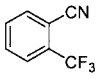	74	73
10	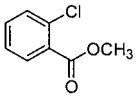	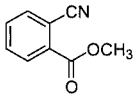	93	75 (71)[e]
11	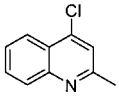	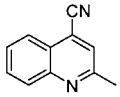	68	63 (58)[e]
12			87	80
13[c]			61	55
14	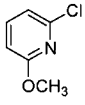	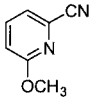	95	91

[a] General conditions: 2 mmol aryl or heteroaryl chloride, 1 equiv. potassium cyanide, 2 mol % palladium(II) acetate, 4 mol % 1,5-bis(diphenylphosphanyl)pentane, 20 mol % MDP, 2 mL toluene, 16 h, 160 °C. [b] Conversions and yields were determined by GC using an internal standard (diethylene glycol di-*n*-butyl ether). [c] 1,4-Bis(diphenylphosphanyl)butane instead of 1,5-bis(diphenylphosphanyl)pentane. [d] 4 Mol % palladium(II) acetate, 8 mol % 1,5-bis(diphenylphosphanyl)pentane. [e] Isolated yield in parentheses.

with either TMEDA or MDP as co-catalyst is until today the most efficient and widely applicable method for the palladium-catalyzed cyanation of aryl chlorides with readily available and cheap KCN.

Mechanistic Investigations into the Palladium-Catalyzed Cyanation of Aryl Halides

The catalysis results discussed above show that different amines have a positive effect on the palladium-catalyzed cyanation reaction. The question remains, however, which elementary steps are influenced by the addition of amine. Because of the high temperatures palladium colloids also have to be considered as potential catalysts. It is known that such colloids, or nanoparticles, are formed from unstable palladium phosphane complexes at high temperature and that they show catalytic activity in C−C coupling reactions.[87,88] However, the color of the reaction mixtures (typically pale yellow for palladium phosphane complexes) makes this unlikely.

In order to understand the effect of the organic co-catalyst in more detail, single steps of the generally accepted mechanism for such types of palladium-catalyzed C−C coupling reactions[89−92] were performed in the presence and absence of TMEDA. As shown in Scheme 13 the catalytic cycle starts with the oxidative addition of the aryl halide to a Pd^0 species. In case of aryl chlorides the activation of the C−X bond is more difficult than with aryl bromides, aryl iodides or aryl triflates.[93]

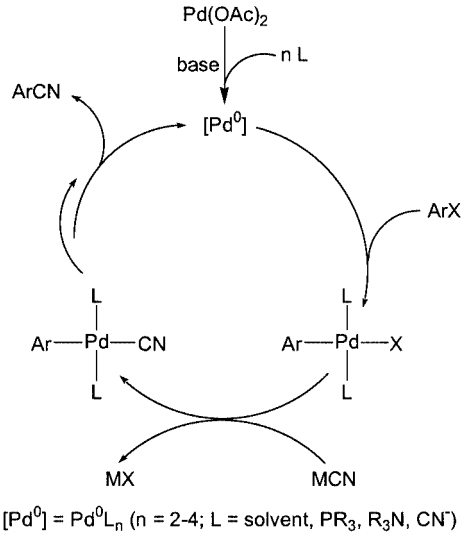

Scheme 13. Proposed mechanism of the palladium-catalyzed cyanation of aryl−X

Despite the simplicity and analogy to similar coupling reactions there should be some concern about the viability of the proposed mechanism, because so far there is no report known about the isolation of an arylpalladium(II) cyanide complex. Recent ^1H and ^{31}P NMR experiments concerning the oxidative addition of 4-bromo(trifluoromethyl)-benzene to $[Pd(PPh_3)_4]$ at different cyanide concentrations showed that excess cyanide ions not only deactivate palladium(II), but also turn off the activity of palladium(0) complexes.[86] It was suggested that only 1−2 equivalents of cyanide ions with respect to palladium are tolerated by the catalyst system.

In the presence of TMEDA deactivation of the palladium(0) complex is prevented, even in the presence of an overstoichiometric amount of cyanide (five equivalents). It was assumed that the amine is capable of substituting cyanide ions at the palladium center, thereby regenerating an active palladium catalyst. Interestingly, the in situ formed arylpalladium(II) halide complex reacts immediately with cyanide to give the corresponding benzonitrile and a pal-

 © 2003 Wiley-VCH Verlag GmbH & Co. KGaA, Weinheim

ladium(0) complex. Hence, the second and third elementary steps in the catalytic cycle — transmetalation and reductive elimination — must be much faster than the oxidative addition. In stoichiometric oxidative addition reactions of 4-bromo(trifluoromethyl)benzene and Pd^0 it has also been shown that TMEDA increases the stability of the phosphane ligand towards ligand degradation (aryl-aryl scrambling[94−96]).

Improved Efficiency by Dosage of the Cyanide Source as a Result of the Mechanistic Studies

As discussed above various palladium species [palladium(0) as well as palladium(II) species] are deactivated by cyanide ions in solution. To overcome this problem it is necessary to control the concentration of cyanide at a predefined low level, which allows the reductive coupling to proceed efficiently but prevents catalyst deactivation at the same time. In the past, this was done by careful selection of a solvent, in which the solubility of the cyanide is low and can be increased by means of a phase-transfer catalyst (crown ether, amine, etc.). However, it is clear that the CN^- concentration is difficult to control and that reproducibility problems might arise.

A more elegant and promising approach is the defined dosage of cyanide to the reaction mixture. Unfortunately, dosage of a solid cyanide source like potassium or sodium cyanide is difficult. However, the continuous addition of a liquid cyanide source using a syringe pump is easy. One of the simplest soluble cyanide sources for such reactions is acetone cyanohydrin, which is cheap and commercially available on a large scale (Scheme 14).[97−99]

Scheme 14. Acetone cyanohydrin, a useful HCN equivalent

As shown in Table 11, the cyanation of 4-bromo(trifluoromethyl)benzene with acetone cyanohydrin is possible in a very efficient manner.[100] The convenient reaction conditions, the excellent nitrile selectivity and the low catalyst concentration (Table 11, Entry 10) are remarkable. So far the highest turnover number for palladium-catalyzed cyanation of aryl halides known has been reported by applying acetone cyanohydrin as cyanating agent (TON 1900).

The generality of this approach is shown in Table 12. Activated, nonactivated, and deactivated aryl bromides give very good results in the cyanation, as do heteroaryl bromides. Electron-deficient aryl chlorides also react under these conditions (Table 12, Entries 13−15). However, conversion of *ortho*-substituted aryl halides to their corresponding benzonitriles is not satisfactory.

Another useful liquid cyanating agent is trimethylsilyl cyanide (TMSCN).[101] It has been described for the palladium-catalyzed cyanation of aryl iodides, whereas conversion of aryl bromides and chlorides was not possible in the past.[43] Apparently, catalyst deactivation takes place. Recently, we observed that *trans*-bromo[4-(trifluoromethyl)-phenyl]bis(triphenylphosphane)palladium(II) (**1**) reacts readily with TMSCN yielding the corresponding benzonitrile even at 0 °C (Scheme 15).[102]

So it was not surprising that continuous dosage of TMSCN works well for aryl bromides. By using the corresponding oxidative addition product with additional phosphane ligand as catalyst system the cyanation reactions exhibited excellent yield and selectivity (Scheme 16).[102]

As outlined in Table 13, a plethora of aryl bromides can easily be transformed into the corresponding benzonitriles. Less-reactive aryl chlorides can be coupled only with moderate success under these conditions (Table 13, Entry 14). However, utilization of an autoclave with dosage equipment, which allows to work at temperatures significantly above the boiling point of TMSCN and the solvent, should provide a possibility to overcome this problem.

Microwave-Assisted Palladium-Catalyzed Cyanation of Aryl Bromides

For many reactions it is possible to enhance the reaction rate by applying microwaves. This holds also true for the palladium-catalyzed cyanation of aryl halides. Alterman

Table 11. Acetone cyanohydrin as cyanating agent in the Pd-catalyzed cyanation of 4-bromo(trifluoromethyl)benzene

Entry[a]	$Pd(OAc)_2$ [mol %]	Pd:P	TMEDA [mol %]	Dosage rate [mmol/h]	*t* [h]	*T* [°C]	Conversion [%][b]	Yield [%][b]
1	2	1:4	20	0.1	21	120	100	≥ 99
2	2	1:4	20	0.1	21	100	100	≥ 99
3	2	1:4	20	0.1	21	80	100	≥ 99
4	2	1:4	20	0.1	21	60		1
5	1	1:4	20	0.1	21	100	100	≥ 99
6	0.5	1:4	10	0.1	21	100	100	≥ 99
7	0.1	1:4	10	0.1	21	120	0	0
8	0.1	1:8	10	0.05	42	120	81	80
9	0.1	1:8	–	0.05	42	120	8	0
10	0.05	1:16	10	0.05	42	140	97	95

[a] General conditions: 2 mmol 4-bromo(trifluoromethyl)benzene, 2.1 mL acetone cyanohydrin solution (1 M in DMAc), 1,5-bis(diphenylphosphanyl)pentane, 2.1 mmol sodium carbonate, 2 mL DMAc. [b] Conversions and yields were determined by GC using an internal standard (diethylene glycol di-*n*-butyl ether).

 © 2003 Wiley-VCH Verlag GmbH & Co. KGaA, Weinheim

Table 12. Scope of the palladium-catalyzed cyanation using acetone cyanohydrine

Entry	Substrate	Product[a]	T [°C]	Conversion [%][b]	Yield [%][b]
1	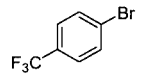	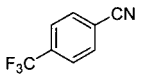	100	100	≥ 99
2	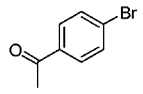	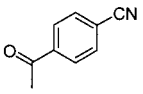	100	100	≥ 99
3	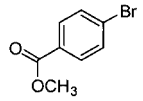	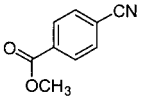	100	100	95
4	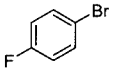	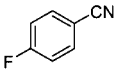	120	98	96
5	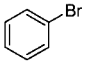	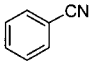	120	96	96
6	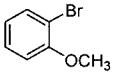	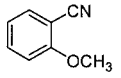	140	27	21
7	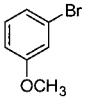	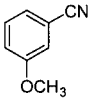	120	99	99
8	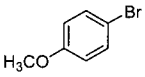	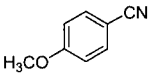	120	98	98
9	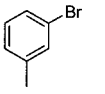	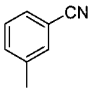	120	100	≥ 99
10	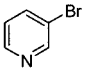	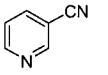	100	82	82
12	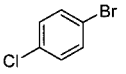	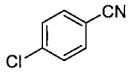	100	82	82
13[c]	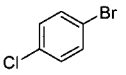	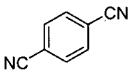	120	100	≥ 99
14[d]	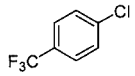	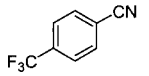	140	78	77
15[d]	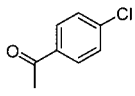	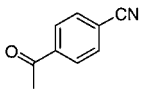	140	90	89

[a] General conditions: 2 mmol aryl or heteroaryl bromide, 2.1 mL acetone cyanohydrine solution (1 M), dosage rate 0.1 mL/h, 0.5 mol % palladium(II) acetate, 1 mol % 1,5-bis(diphenylphosphanyl)-pentane, 10 mol % TMEDA, 1.05 equiv. sodium carbonate, 2 mL DMAc, 21 h. [b] Conversions and yields were determined by GC using an internal standard (diethylene glycol di-*n*-butyl ether). [c] 4.2 mL acetone cyanohydrin solution (1 M), dosage rate 0.1 mL/h, 2.1 equiv. sodium carbonate, 42 h. [d] 1 mol % palladium(II) acetate, 2 mol % 1,5-bis(diphenylphosphanyl)pentane.

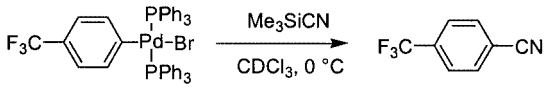

Scheme 15. Stoichiometric reaction of the oxidative addition product **1** with TMSCN

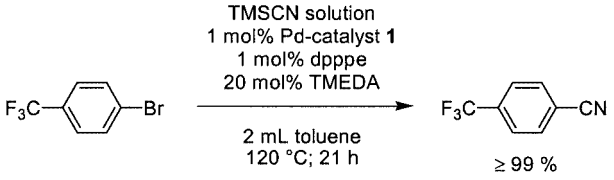

Scheme 16. Use of TMSCN in the palladium-catalyzed cyanation of 4-bromo(trifluoromethyl)benzene

and Halberg have shown that microwave irradiation accelerates the rate of cyanation considerably. Reaction times could be reduced from hours to a few minutes in the case of aryl bromides. The corresponding benzonitriles were obtained in high yield and selectivity. Some examples of this methodology are given in Table 14.[103]

Conclusion

Significant progress with regard to substrate compatibility and catalyst efficiency has been achieved in the palladium-catalyzed cyanation of aryl halides. Hence, industrial realizations of this methodology in the area of fine chemical syntheses seem to be feasible in the near future. Based on mechanistic investigations it became clear that catalyst deactivation by excess cyanide ions is one of the main reasons for the low productivity and activity of palladium catalysts in the cyanation reaction of aryl halides when compared to other C−C-coupling reactions.[104−113] Hence, an important factor for further development of this reaction is the control of the concentration of cyanide ions in solution. One way to achieve this is the continuous dosage of cyanide to the reaction mixture. Another possibility is to apply a two-phase system (liquid-liquid or liquid-solid) and to control the cyanide concentration by use of phase transfer catalysts or by adjusting the solubility by choosing an appropriate solvent.

Because of the relatively mild reaction conditions and the broad scope, the palladium-catalyzed cyanation of aryl halides has become an interesting tool for the total synthesis of natural products and pharmaceuticals. Since the first total synthesis using this methodology (the synthesis of (+)-estradiol[114]), numerous biologically active substances have been synthesized including a palladium-catalyzed cyanation step (Fadrozol, Robalzotan, etc.).[5−7,45,115−118] In addition to active agents, other more complicated organic products, for example special calixarenes,[119] have also been synthesized by palladium-catalyzed cyanations. Obviously, further catalyst improvements will increase the usage of this methodology in organic synthesis.

 © 2003 Wiley-VCH Verlag GmbH & Co. KGaA, Weinheim

Table 13. Scope of the palladium-catalyzed cyanation using TMSCN

Entry	Substrate	Product[a]	Catalyst	Conversion [%][b]	Yield [%][b]
1	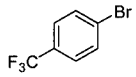	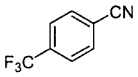	**1**[c]	100	≥ 99
2			**2**[d]	100	98
3	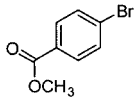	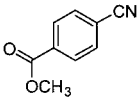	**2**	87	82
4	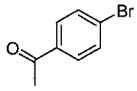	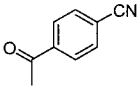	**2**	71	56
5	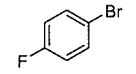	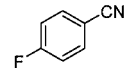	**2**	83	76
6	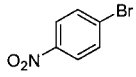	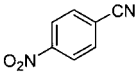	**2**	67	53
7	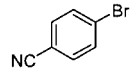	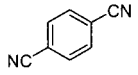	**2**	100	63
8	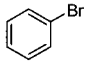	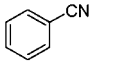	**2**	100	≥ 99
9[e]	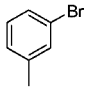	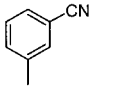	**2**	100	92
10	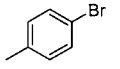	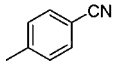	**2**	99	96
11	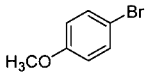	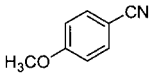	**2**	70	62
12	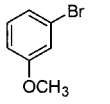	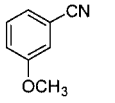	**2**	90	89
13	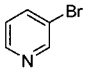	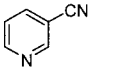	**2**	75	68
14[f]	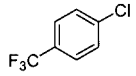	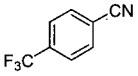	**1**	50	39

[a] General conditions: 2 mmol aryl or heteroaryl bromide, 2.1 mL trimethylsilyl cyanide solution (1 M in toluene), dosage rate 0.1 mL/h, 2 mol % palladium-catalyst, 2 mol % 1,5-bis(diphenylphosphanyl)pentane, 20 mol % TMEDA, 2 mL toluene, reflux, 21 h. [b] Conversions and yields were determined by GC using an internal standard (diethylene glycol di-*n*-butyl ether). [c] *trans*-Bromo[4-(trifluoromethyl)phenyl]bis(triphenylphosphane)palladium(II). [d] *trans*-Bromo[3-tolyl]bis(triphenylphosphane)palladium(II). [e] 1 Mol % palladium catalyst, 2 mol % 1,5-bis(diphenylphosphanyl)-pentane. [f] Xylene (mixture of isomers) instead of toluene, 140 °C.

Table 14. Palladium-catalyzed cyanation of aryl bromides promoted by microwave irradiation

Entry	Substrate	Product[a]	*t* [min]	Power [W]	Yield [%][b]
1	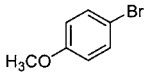	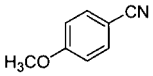	2	60	81
2	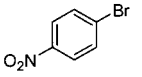	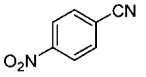	2	60	78
3	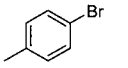	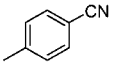	2	60	90
4	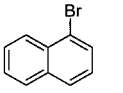	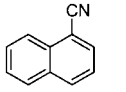	2	60	90
5	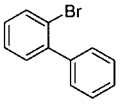	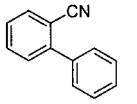	2	60	95
6	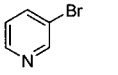	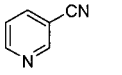	2	60	88
7	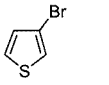	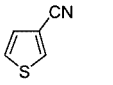	2.5	60	80

[a] General conditions: 0.2 mmol aryl or heteroaryl bromide, 0.2 mmol $Zn(CN)_2$, 3 mol % $Pd(PPh_3)_4$, 1 mL DMF. [b] Isolated yields.

Acknowledgments

The work presented from our side was supported by Degussa AG (formerly SKW Trostberg), the Fonds der Chemischen Industrie, the BMBF, and the state Mecklenburg-Western Pomerania. The authors thank OMG for gifts of palladium compounds. Dr. Stefan Weiss, Dr. Jürgen Sans and Dr. Mario Gómez Andreu (all Degussa AG) are thanked for general discussions and a successful cooperation. Dr. Wolfgang Baumann (IfOK) is thanked for NMR experiments regarding the mechanism. We also acknowledge the work of Dr. Anke Spannenberg (IfOK) on the X-ray analysis of complex **1** and Dr. Mutyala Sateesh on catalytic reactions using trimethylsilyl cyanide.

[1] H. Hugl (Bayer AG); Presentation at the conference "*50 Years of Catalysis Research in Rostock*", July 1st-3rd **2002**, Rostock.
[2] M.-H. Rock, A. Merhold (Bayer AG), *WO 98/37058*, **1998**.
[3] M.-H. Rock, A. Merhold (Bayer AG), *US 6,162,942*, **2000**.
[4] A. Kleemann, J. Engel, B. Kutscher, D. Reichert, *Pharmaceutical substances: syntheses, patents, applications*, 4th Ed., Georg Thieme Verlag, Stuttgart, New York, **2001**, 241−242, 488−489, 553, 825−826, 1154, 1598−1599.
[5] A. J. Allentoff, B. Markus, T. Duelfer, A. Wu, L. Jones, G. Ciszewska, T. Ray, *J. Labelled Compd. Radiopharm.* **2000**, *43*, 1075−1085.
[6] T. F. Werner, D. Sohn, R. Johansson, *J. Labelled Compd. Radiopharm.* **2000**, *43*, 437−447.
[7] K. M. Cable, G. N. Wells, D. R. Sutherland, *J. Labelled Compd. Radiopharm.* **2000**, *43*, 29−45.
[8] Y. Andersson, B. LÅngström, *J. Chem. Soc., Perkin. Trans. 1* **1994**, 1395−1400.
[9] R. M. Carr, K. M. Cable, G. N. Wells, D. R. Sutherland, *J. Labelled Compd. Radiopharm.* **1994**, *34*, 887−897.
[10] R. C. Larock, *Comprehensive Organic Transformations*, VCH, New York, **1989**, 819−995.

 © 2003 Wiley-VCH Verlag GmbH & Co. KGaA, Weinheim

[11] C. Grundmann, in *Houben-Weyl: Methoden der organischen Chemie, Vol. E5* (Ed.: J. Falbe), 4th Ed., Georg Thieme Verlag, Stuttgart, **1985**, 1313−1527.
[12] F. Hagedorn, H.-P. Gelbke, in *Ullmanns Encyklopädie der technischen Chemie, Vol. 17* (Eds.: E. Bartholomé, E. Biekert, H. Hellmann, H. Ley, W. M. Weigert, E. Weise), 4th Ed., Verlag Chemie, Weinheim, **1979**, 333−338.
[13] C. Ferri, *Reaktionen der organischen Chemie*, Georg Thieme Verlag, Stuttgart, **1978**, 571−581.
[14] P. Kurtz, in *Houben Weyl: Methoden der organischen Chemie, Vol. 8* (Ed.: E. Müller), 4th Ed., Georg Thieme Verlag, Stuttgart, **1952**, 265−345.
[15] J. Lindley, *Tetrahedron* **1984**, *40*, 1433−1456.
[16] R. G. R Bacon, H. A. O. Hill, *J. Chem. Soc.* **1964**, 1097−1107.
[17] J. von Braun, G. Manz, *Justus Liebigs Ann. Chem.* **1931**, *488*, 111−126.
[18] K. W. Rosenmund, E. Struck, *Ber. Dtsch. Chem. Ges.* **1919**, *52*, 1749−1756.
[19] Meister, Lucius, Brüning, *DE 271,790*, **1913**.
[20] T. Sandmeyer, *Ber. Dtsch. Chem. Ges.* **1885**, *18*, 1946−1948.
[21] T. Sandmeyer, *Ber. Dtsch. Chem. Ges.* **1885**, *18*, 1492−1496.
[22] T. Sandmeyer, *Ber. Dtsch. Chem. Ges.* **1884**, *17*, 2650−2653.
[23] A. C. Stevenson, *Ind. Eng. Chem.* **1949**, *41*, 1846−1851.
[24] W. I. Denton, R. B. Bishop, H. P. Caldwell, H. D. Chapman, *Ind. Eng. Chem.* **1950**, *42*, 796−800.
[25] A. Martin, N. V. Kalevaru, B. Lücke, J. Sans, *Green Chemistry* **2002**, *4*, 481−485.
[26] A. Martin, G. U. Wolf, U. Steinike, B. Lücke, *J. Chem. Soc., Faraday Trans.* **1998**, *94*, 2227−2233.
[27] A. Martin, B. Lücke, *Catal. Today* **1996**, *32*, 279−283.
[28] J. Tsuji, *Transition Metal Reagents and Catalysts − Innovations in Organic Synthesis*, John Wiley & Sons, Chichester, **2000**.
[29] L. Brandsma, S. F. Vasilevsky, H. D. Verkruijsse, *Application of Transition Metal Catalysts in Organic Synthesis*, Springer Verlag, Berlin, Heidelberg, **1999**, 149−177.
[30] G. P. Ellis, T. M. Romney-Alexander, *Chem. Rev.* **1987**, *87*, 779−794.
[31] R. F. Heck, *Palladium Reagents in Organic Syntheses*, Academic Press, London, **1985**.
[32] D. F. McMillen, D. M. Golden, *Annu. Rev. Phys. Chem.* **1982**, *33*, 493−532.
[33] J. D. Cox, G. Pilcher, *Thermochemistry of Organic and Organometallic Compounds*, Academic Press, London, **1970**.
[34] K. Takagi, T. Okamoto, Y. Sakakibara, S. Oka, *Chem. Lett.* **1973**, 471−474.
[35] K. Takagi, T. Okamoto, Y. Sakakibara, A. Ohno, S. Oka, N. Hayama, *Bull. Chem. Soc. Jpn.* **1976**, *49*, 3177−3180.
[36] J. Chatt, B. L. Shaw, *J. Chem. Soc.* **1962**, 5075−5084.
[37] L. Malatesta, *J. Chem. Soc.* **1955**, 3924−3926.
[38] A. Sekiya, N. Ishikawa, *Chem. Lett.* **1975**, 277−278.
[39] K. Takagi, T. Okamoto, Y. Sakakibara, A. Ohno, S. Oka, N. Hayama, *Bull. Chem. Soc. Jpn.* **1975**, *48*, 3298−3301.
[40] J. R. Dalton, S. L. Regen, *J. Org. Chem.* **1979**, *44*, 4443−4444.
[41] Y. Akita, M. Shimazaki, A. Ohta, *Synthesis* **1981**, 974−975.
[42] M. Procházka, M. Široký, *Coll. Czech. Chem. Commun.* **1983**, *48*, 1765−1773.
[43] N. Chatani, T. Hanafusa, *J. Org. Chem.* **1986**, *51*, 4714−4716.
[44] N. Sato, M. Suzuki, *J. Heterocycl. Chem.* **1987**, *24*, 1371−1372.
[45] V. Nair, D. F. Purdy, T. B. Sells, *J. Chem. Soc., Chem. Commun.* **1989**, 878−879.
[46] K. Tanji, T. Higashino, *Heterocycles* **1990**, *30*, 435−440.
[47] K. Takagi, K. Sasaki, Y. Sakakibara, *Bull. Chem. Soc. Jpn.* **1991**, *64*, 1118−1121.
[48] D. M. Tschaen, R. Desmond, A. O. King, M. C. Fortin, B. Pipik, S. King, T. R. Verhoeven, *Synth. Commun.* **1994**, *24*, 887−890.
[49] L. L. Gunderson, *Acta Chim. Scand.* **1996**, *50*, 58−63.
[50] F.-H. Luo, C.-I. Chu, C.-H. Cheng, *Organometallics* **1998**, *17*, 1025−1030.
[51] T. Sakamoto, K. Ohsawa, *J. Chem. Soc., Perkin Trans. 1* **1999**, 2323−2326.
[52] B. Jiang, Y. Kann, A. Zangh, *Tetrahedron* **2001**, *57*, 1581−1584.
[53] T. Okano, M. Iwahara, J. Kiji, *Synlett* **1998**, 243−244.
[54] T. Okano, J. Kiji, Y. Toyooka, *Chem. Lett.* **1998**, 425−426.
[55] B. A. Anderson, E. C. Bell, F. O. Ginah, N. K. Harn, L. M. Pagh, J. P. Wepsiec, *J. Org. Chem.* **1998**, *63*, 8224−8228.
[56] P. E. Maligres, M. S. Waters, F. Fleitz, D. Askin, *Tetrahedron Lett.* **1999**, *40*, 8193−8195.
[57] For an excellent review on refinement reactions of aryl chlorides see: A. F. Littke, G. C. Fu, *Angew. Chem.* **2002**, *114*, 4350−4386; *Angew. Chem. Int. Ed.* **2002**, *41*, 4176−4211.
[58] A. Zapf, M. Beller, *Top. Catal.* **2002**, *19*, 101−109.
[59] M. Beller, A. Zapf, W. Mägerlein, *Chem. Eng. Techn.* **2001**, *24*, 575−582.
[60] I. Beletskaya, A. V. Cheprakov, *Chem. Rev.* **2000**, *100*, 3009−3066.
[61] J. van Soolingen, *PhD thesis*, University of Groningen, **1999**.
[62] Y. Sakakibara, Y. Ido, K. Sasaki, M. Sakai, N. Uchino, *Bull. Chem. Soc. Jpn.* **1993**, *66*, 2776−2778.
[63] K. Takagi, Y. Sakakibara, *Chem. Lett.* **1989**, 1957−1958.
[64] M. R. I. Chambers, D. A. Widdowson, *J. Chem. Soc., Perkin Trans. 1* **1989**, 1365−1366.
[65] Y. Sakakibara, F. Okuda, A. Shimobayashi, K. Kirino, M. Sakai, N. Uchino, K. Takagi, *Bull. Chem. Soc. Jpn.* **1988**, *61*, 1985−1990.
[66] L. Cassar, M. Foá, F. Montanari, G. P. Marinelli, *J. Organomet. Chem.* **1979**, *173*, 335−339.
[67] L. Cassar, S. Ferrara, M. Foá, *Adv. Chem. Ser.* **1974**, *132*, 252−273.
[68] L. Cassar, *J. Organomet. Chem.* **1973**, *54*, C57−C58.
[69] F. Jin, P. N. Confalone, *Tetrahedron Lett.* **2000**, *41*, 3271−3273.
[70] A. Zapf, M. Beller, *Chem. Eur. J.* **2001**, *7*, 2908−2915.
[71] A. Ehrentraut, A. Zapf, M. Beller, *Synlett* **2000**, 1589−1592.
[72] M. Beller, A. Zapf, *Synlett* **1998**, 792−793.
[73] W. A. Herrmann, C. Broßmer, C.-P. Reisinger, K. Öfele, M. Beller, T. H. Riermeier, *Chem. Eur. J.* **1997**, *3*, 1357−1364.
[74] M. Gómez Andreu, A. Zapf, M. Beller, *Chem. Commun.* **2000**, 2475−2476.
[75] A. Zapf, A. Ehrentraut, M. Beller, *Angew. Chem.* **2000**, *112*, 4315−4317; *Angew. Chem. Int. Ed.* **2000**, *39*, 4153−4155.
[76] M. Beller, H. Fischer, W. A. Herrmann, K. Öfele, C. Broßmer, *Angew. Chem.* **1995**, *107*, 1992−1993; *Angew. Chem. Int. Ed. Engl.* **1995**, *34*, 1848−1849.
[77] M. Beller, J. G. E. Krauter, A. Zapf, *Angew. Chem.* **1997**, *109*, 793−795; *Angew. Chem. Int. Ed. Engl.* **1997**, *36*, 772−774.
[78] A. Ehrentraut, A. Zapf, M. Beller, *J. Mol. Cat.* **2002**, *182−183*, 515−523.
[79] M. Beller, T. H. Riermeier, C.-P. Reisinger, W. A. Herrmann, *Tetrahedron Lett.* **1997**, *38*, 2073−2076.
[80] M. Sundermeier, A. Zapf, M. Beller, J. Sans, *Tetrahedron Lett.* **2001**, *42*, 6707−6710.
[81] W. Mägerlein, A. F. Indolese, M. Beller, *Angew. Chem.* **2001**, *113*, 2940−2943; *Angew. Chem. Int. Ed.* **2001**, *40*, 2856−2859.
[82] M. Beller, W. Mägerlein, A. F. Indolese, C. Fischer, *Synthesis* **2001**, 1098−1109.
[83] M. Beller, A. F. Indolese, *Chimia* **2001**, *55*, 684−687.
[84] W. Mägerlein, A. F. Indolese, M. Beller, *J. Organomet. Chem.* **2002**, *641*, 30−40.
[85] Y. Ben-David, M. Portnoy, D. Milstein, *J. Am. Chem. Soc.* **1989**, *111*, 8742−8744.
[86] M. Sundermeier, A. Zapf, S. Mutyala, W. Baumann, S. Sans, S. Weiss, M. Beller, *Chem. Eur. J.* **2003**, *9*, 1828−1836.
[87] M. Beller, H. Fischer, K. Kühlein, C.-P. Reisinger, W. A. Herrmann, *J. Organomet. Chem.* **1996**, *520*, 257−259.
[88] M. T. Reetz, E. Westermann, *Angew. Chem.* **2000**, *112*, 170−173; *Angew. Chem. Int. Ed.* **2000**, *39*, 165−168.
[89] J. F. Hartwig, *Angew. Chem.* **1998**, *110*, 2154−2177; *Angew. Chem. Int. Ed.* **1998**, *37*, 2046−2067.
[90] C. Amatore, A. Jutand, *Acc. Chem. Res.* **2000**, *33*, 314−321.
[91] C. Amatore, A. Jutand, A. Thuilliez, *Organometallics* **2001**, *20*, 3241−3249.

 © 2003 Wiley-VCH Verlag GmbH & Co. KGaA, Weinheim

[92] E. Galardon, S. Ramdeehul, J. M. Brown, A. Cowley, K. K. M. Hii, A. Jutand, *Angew. Chem.* **2002**, *114*, 1838−1841; *Angew. Chem. Int. Ed.* **2002**, *41*, 1760−1763.
[93] V. V. Grushin, H. Alper, in *Topics in Organometallic Chemistry − Activation of Unreactive Bonds and Organic Synthesis*, (Ed.: S. Murai), Springer-Verlag, Berlin, **1999**, 193−226.
[94] V. V. Grushin, *Organometallics* **2000**, *19*, 1888−1900.
[95] W. A. Herrmann, C. Broßmer, K. Öfele, M. Beller, H. Fischer, *J. Organomet. Chem.* **1995**, *491*, C1−C4.
[96] K.-C. Kong, C.-H. Cheng, *J. Am. Chem. Soc.* **1991**, *113*, 6313−6315.
[97] A. Mori, S. Inoue, in *Comprehensive Asymmetric Catalysis, Vol. 2* (Eds.: E. N. Jacobsen, A. Pfaltz, H. Yamamoto), Springer-Verlag, Berlin, Heidelberg, **1999**, 983−994.
[98] R. J. H. Gregory, *Chem. Rev.* **1999**, *99*, 3649−3682.
[99] G. Tennant, in *Comprehensive Organic Chemistry, Vol. 2* (Eds.: D. Barton, W. D. Ollis, E. Haslam, D. Neville Jones, P. G. Sammes, J. F. Stoddart, I. O. Sutherland, C. J. Drayton), Pergamon Press Ltd., Oxford, **1979**, 528−539.
[100] M. Sundermeier, A. Zapf, M. Beller, *Angew. Chem.* **2003**, *115*, 1700−1703; *Angew. Chem. Int. Ed.* **2003**, *42*, 1661−1664.
[101] R. M Coates, S. E. Denmark, *Handbook of Reagents for Organic Synthesis − Reagents, Auxiliaries and Catalysts for C−C bonds*, John Wiley & Sons, Chichester, **1999**, 236−238.
[102] M. Sundermeier, S. Mutyala, A. Zapf, A. Spannenberg, M. Beller, *J. Organomet. Chem.* **2003**, in press.
[103] M. Alterman, A. Halberg, *J. Org. Chem.* **2000**, *65*, 7984−7989.
[104] R. B. Bedford, C. S. J. Cazin, S. L. Hazelwood, nee Welch, *Angew. Chem.* **2002**, *114*, 4294−4296; *Angew. Chem. Int. Ed.* **2002**, *41*, 4120−4122.
[105] R. Jackstell, M. Gómez Andreu, A. Frisch, H. Klein, K. Selvakumar, A. Zapf, A. Spannenberg, D. Röttger, O. Briel, R. Karch, M. Beller, *Angew. Chem.* **2002**, *114*, 1028−1031; *Angew. Chem. Int. Ed.* **2002**, *41*, 986−989.
[106] R. Jackstell, A. Frisch, M. Beller, D. Röttger, M. Malaun, B. Bildstein, *J. Mol. Catal.* **2002**, *185*, 105−112.
[107] J. A. Loch, M. Albrecht, E. Peris, J. Mata, J. W. Faller, R. H. Crabtree, *Organometallics* **2002**, *21*, 700−706.
[108] M. Feuerstein, H. Doucet, M. Santelli, *Tetrahedron Lett.* **2001**, *42*, 6667−6670.
[109] A. F. Littke, C. Dai, G. C. Fu, *J. Am. Chem. Soc.* **2000**, *122*, 4020−4028.
[110] R. B. Bedford, S. M. Draper, P. N. Scully, S. L. Welch, *New J. Chem.* **2000**, *24*, 745−747.
[111] V. P. W. Böhm, W. A. Herrmann, *Chem. Eur. J.* **2000**, *6*, 1017−1025.
[112] J. M. Fox, X. Huang, A. Chieffi, S. L. Buchwald, *J. Am. Chem. Soc.* **2000**, *122*, 1360−1370.
[113] M. Kawatsura, J. F. Hartwig, *J. Am. Chem. Soc.* **1999**, *121*, 1473−1478.
[114] W. Oppolzer, D. A. Roberts, *Helv. Chim. Acta* **1980**, *63*, 1703−1705.
[115] R. Rezaie, B. Joseph, J. B. Bremner, G. Guillaument, *Heterocycles* **1998**, *48*, 2079−2088.
[116] B. A. Anderson, L. M. Becke, R. N. Booher, M. E. Flaugh, N. K. Ham, T. J. Kress, D. L. Varie, J. P. Wepsiec, *J. Org. Chem.* **1997**, *62*, 8634−8639.
[117] C. Kehr, R. Neidlein, R. A. Engh, H. Brandstetter, R. Kucznierz, H. Leinert, K. Marzenell, K. Strein, W. v. d. Saal, *Helv. Chim. Acta* **1997**, *80*, 892−896.
[118] G. A. Kraus, H. Maeda, *Tetrahedron Lett.* **1994**, *35*, 9189−9190.
[119] H. Hioki, R. Nakaoka, A. Maruyama, M. Kodama, *J. Chem. Soc., Perkin Trans. 1* **2001**, 3265−3268.

Received March 27, 2003
Early View Article
Published Online September 12, 2003

 © 2003 Wiley-VCH Verlag GmbH & Co. KGaA, Weinheim

Synthesis and Structural Elucidation of a "Free" Phosphinoamide Anion

Zhaofu Fei,[a] Rosario Scopelliti,[a] and Paul J. Dyson*[a]

Keywords: N,P ligands / Potassium / Crown ether / X-ray structure

The reaction of the aminophosphane C_6H_4(*o*-CN)$NHPPh_2$ with elemental potassium in the presence of 18-crown-6 affords the phosphinoamide-containing complex [C_6H_4(*o*-CN)N-PPh_2(THF)(18-Crown-6)K] which has been fully characterised in solution and the solid state. The potassium cation interacts with the nitrile substituent group and crown, but does not interact with the P–N bond. The anion appears to be considerably more reactive than related anions in which the cation interacts with the P-N unit, as demonstrated by the reaction with O_2/H_2O which affords [Ph_2P(:O)OK(18-Crown-6)] and C_6H_4(*o*-CN)NH_2. A co-crystal containing these two products was obtained and the structure has been elucidated by single-crystal X-ray diffraction analysis.

(© Wiley-VCH Verlag GmbH & Co. KGaA, 69451 Weinheim, Germany, 2003)

Introduction

The chemistry of aminophosphanes and their anionic derivatives (phosphinoamide anions) has been intensively explored over the years.[1] Phosphinoamide anions are frequently used as precursors in synthesis, including, for example, for the synthesis of compounds containing P−P bonds.[2] Detailed structural studies on these anions were first reported by Ashby in 1992,[3] and there are now numerous papers describing the synthesis, structure[4] and reactivity[5] of phosphinoamide anions. Much effort has been directed towards rationalising the nature of the P−N bond in these anions and various theoretical studies have been made.[6] The short P−N distance implies that the bond has mostly double-bond character with the negative charge located on the nitrogen centre; however, their reactivity often leads to different conclusions. For example, in [$Ph_2PNLiPh\cdot(Et_2O)]_2$, while there are both P−Li and N−Li interactions, reaction with Ph_2PCl quantitatively gives $(Ph_2P)_2NPh$. In contrast, the anion of the functionalised aminophosphane [$Ph_2PNLiC_6H_4$(*o*-CN)·(THF)]$_2$, which shows only a N−Li interaction in the solid state, reacts with Ph_2PCl to afford Ph_2P-PPh_2=NC_6H_4(*o*-CN) as the only product.[7]

As far as we are aware, there are no examples of phosphinoamide anions in which the P−N bond does not interact in some way with the cation. Free anions of other types of compounds have been isolated by incorporation of a crown ether during their synthesis which serves to separate the cation from the anion.[8] This strategy has also been used with phosphinoamide-type anions, but weak interactions with the P- and N-centres and the cation remain.[9] However, we proposed that it might be possible to isolate a free anion by combining the crown ether strategy with the use of an appropriate functional group attached to the aminophosphane precursor and we report on our findings in this communication.

Results and Discussion

The reaction of the aminophosphane C_6H_4(*o*-CN)-$NHPPh_2$ (**1**) with elemental potassium in the presence of 18-crown-6 gave the anion **2**. The reaction proceeds smoothly in toluene under ambient conditions. Tetrahydrofuran or diethyl ether can also be used in place of toluene, but the yield of **2** is somewhat lower, with side-products being formed in significant quantities. The ^{31}P NMR spectrum of the reaction mixture in THF exhibits a singlet at δ = 26.5 ppm as the main signal. A signal at δ = −19.1 ppm with low relative intensity (less than 5%) is also observed. Although many phosphinoamide anions have been reported in the last years, supporting ^{31}P and ^{7}Li NMR spectroscopic data are rare. In our experience, under inert conditions, these anions give sharp signals in THF. However, traces of moisture may cause the signals to broaden, sometimes to an extent that the signal is so broad it cannot be observed. The signal at δ = 26.5 ppm in the ^{31}P NMR spectrum of **2** is at slightly lower frequency than that of the parent aminophosphane **1** (δ = 28.5 ppm). In general, phosphinoamide anions give rise to signals at higher frequency than their precursor aminophosphanes.[4,7]

Compound **2** is stable in the solid state or in dry solution under an inert atmosphere and can be stored for weeks without any appreciable decomposition. Crystallisation of **2** from a solution of THF and diethyl ether yielded crystals that were analysed by single-crystal X-ray diffraction. The

[a] Institut de Chimie Moléculaire et Biologique, Ecole Polytechnique Fédérale de Lausanne, EPFL − BCH
1015 Lausanne, Switzerland
Fax: (internat.) + 41-21/6939885
E-mail: paul.dyson@epfl.ch

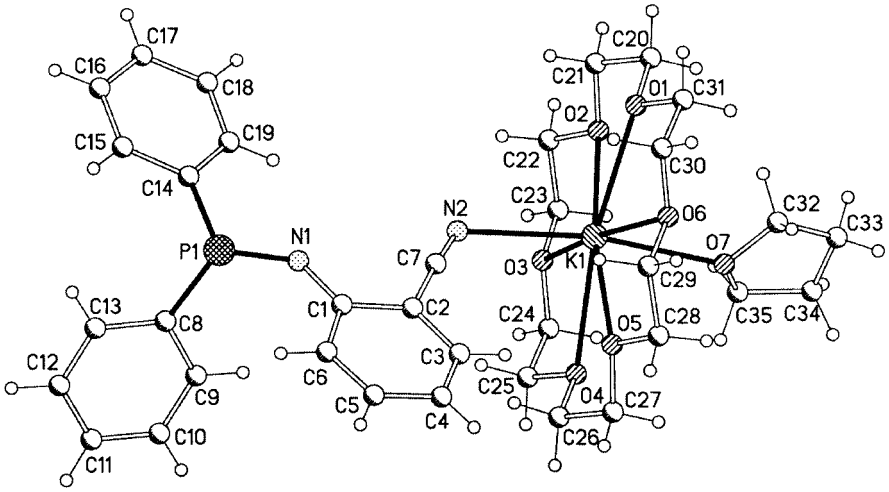

Figure 1. The molecular structure of **2** in the solid state (external THF has been omitted for clarity); key bond lengths (Å) and angles (°) include: P1−N1 1.675(5), N1−C1 1.353(7), N2−C7 1.145(7), K1−N2 2.862(5), N1−P1−C14 100.7(3), N1−P1−C8 106.0(3), C14−P1−C8 101.7(2), C1−N1−P1 118.3(4), C7−N2−K1 126.1(5)

molecular structure of **2** is shown in Figure 1 and key bond parameters are given in the caption. Compound **2** is monomeric, with both the crown ether and the nitrile functional group involved in coordinating to the potassium cation, leaving the P−N unit free. The P−N bond length is 1.675(5) Å, which is somewhat shorter than in the precursor C_6H_4(*o*-CN)NHPPh_2 **1** [1.7155(14) Å]; the N1−C1 bond is considerably shorter [1.353(7) vs. 1.393(2) Å].[7] The bond lengths associated with the P, N and the aromatic ring substituent show delocalization of the negative charge along the ring and, to some extent, towards the P centre.

In keeping with the distinct structural data in both solution and the solid state, the chemical behaviours of **2** differs from that of other phosphinoamide anions. Reaction of **2** with oxygen and water does not lead to the formation of the parent aminophosphane **1**, but results in cleavage of the P−N bond with the formation of [Ph_2P(:O)OK(18-crown-6)] (**3**) and C_6H_4(*o*-CN)NH_2.[10] Previously, re-protonation of phosphinoamide anions has been used to help establish their structure;[2c,2d] reformation of the aminophosphane takes place such that the P−N bond remains intact. For example, [Ph_2PNLiPh·(Et_2O)]$_2$ and [C_6H_4(*o*-CN)PNLiPh·(THF)]$_2$[7] react with O_2/H_2O to give the neutral aminophosphanes, as evidenced by ^{31}P NMR spectroscopy.[11]

The reaction of **2** with O_2/H_2O immediately gave two signals in the ^{31}P NMR spectrum at δ = 82.5 and 12.3 ppm, in approximately equal intensity, corresponding to Ph_2P−O−K[12] and **3**, respectively. After 48 hours, the signal at δ = 82.5 ppm disappears completely, and only the signal at δ = 12.3 ppm remains. There is no evidence for the formation of the original aminophosphane **1** or its oxide. The identity of **3** was confirmed by single-crystal X-ray diffraction analysis. The molecular structure of **3** is shown in Figure 2 and key bond parameters are given in the caption. The structure shows a heptacoordinate potassium cation coordinated to the crown ether and the Ph_2P(:O)O anion, similar structures to this latter unit are known.[13] The C_6H_4(*o*-CN)NH_2 by-product co-crystallises with **3** and interacts via hydrogen bonds with both O atoms of the anion [N1···O1, 3.072(10) Å; N1···O2, 3.270(11) Å] and with one oxygen of the crown ether [N1···O7, 3.195(13) Å].

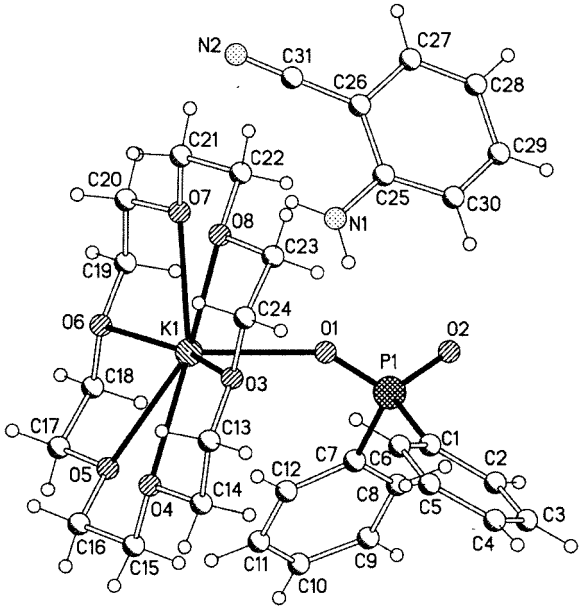

Figure 2. The molecular structure of **3**·C_6H_4(*o*-CN)NH_2 in the solid state; key bond lengths (Å) and angles (°) include: K1−O1 2.578(6), P1−O1 1.504(6), P1−O2 1.495(6), N1−C25 1.39(2), N2−C31 1.11(4), O2−P1−O1 119.7(4), P1−O1−K1, 148.2(3)

In conclusion, we have provided the first experimental example of a "free" phosphinoamide anion. The reactivity of the anion is also markedly different from that of lithium-coordinated anions, being considerably more reactive, although one cannot assume that the solution structure is the same as that observed in the solid state. However, this methodology, in which a crown ether and functional group are utilised in the synthesis of such anions, could lead to new phosphinoamide anion chemistry.

 © 2003 Wiley-VCH Verlag GmbH & Co. KGaA, Weinheim

Experimental Section

The compound C_6H_4(*o*-CN)NHPPh_2 (**1**) was prepared by the literature method[7] and all other reagents were purchased from Aldrich and used as received. Solvents were dried using the appropriate reagents and distilled prior to use. NMR spectra were obtained at 20 °C on a Bruker DMX 200 instrument using $SiMe_4$ (for ^1H) and 85% H_3PO_4 (for ^{31}P) as external standards. ESI-MS spectra were recorded on a ThermoFinnigan LCQ Deca XP Plus quadrupole ion trap instrument using literature methods[14] with samples infused directly into the source at 5 μL min^{-1} using a syringe pump. Elemental analysis was carried out by the Institute of Molecular and Biological Chemistry (EPFL).

Synthesis of 2: Elemental potassium (0.078 g, 2.0 mmol) and dry toluene (10 mL) were heated to 100 °C for 5 min with stirring until the potassium was distributed as a fine suspension. After cooling to room temp. the suspension was transferred to a solution of **1** (0.604 g, 2.0 mmol) and 18-crown-6 (0.530 g, 2.0 mmol) in toluene (5 mL). After 5 h stirring at room temp. (heating should be avoided) the evolution of hydrogen gas was complete and all the potassium had disappeared completely. The solvent was removed under vacuum and the resulting solid was recrystallised from THF and diethyl ether. Yield: 1.150 g (81%). ^1H NMR ([D_8]THF): δ = 6.70−8.40 (m, aromatic H), 3.62 (m, OCH_2 of THF), 3.60 (s, OCH_2 of the crown), 1.75 (m, CH_2 of THF) ppm. ^{31}P NMR ([D_8]THF): δ = 26.5 (s) ppm. Positive ion ESI-MS: *m*/*z* = 303 $[C_{12}H_{24}O_6K]^+$. Negative ion ESI-MS: *m*/*z* = 301 $[(C_6H_5)_2PNC_6H_4(o\text{-}CN)]^-$.

Synthesis of 3: A solution of **2** (0.709 g, 1.0 mmol) in THF (10 mL) was exposed to moisture at room temp. for 48 h. The solvent was removed under vacuum and the resulting solid was crystallised from THF and diethyl ether to give the product as colourless crystals. Yield: 0.562 g; 88%. M.p: 101 °C. ^1H NMR ([D_8]THF): δ = 6.60−8.20 (m, aromatic H), 5.95 (broad signal, NH_2), 3.60 (s, OCH_2 of crown) ppm. ^{31}P NMR ([D_8]THF): 12.3 (s) ppm. Positive ion ESI-MS: *m*/*z* = 303 $[C_{12}H_{24}O_6K]^+$. Negative ion ESI-MS: *m*/*z* = 217 $[(C_6H_5)_2P(O)O]^-$. $C_{31}H_{40}KN_2O_8P$ (638.7): C 58.29, H 6.31, N 4.39; found C 58.43, H 6.46, N 4.33.

Crystal Data for 2: $C_{39}H_{54}KN_2O_8P$, *M* = 748.91, monoclinic, space group $P2_1/c$, *a* = 9.5723(6), *b* = 14.3422(12), *c* = 28.928(3) Å, β = 95.072(6)°, *V* = 3955.9(5) $Å^3$, *T* = 140(2) K, *Z* = 4, μ = 0.227 mm^{-1}, λ = 0.71073 Å, 22845 measured reflections, 6367 independent reflections, R_{int} = 0.0771, R_1 [$I > 2\sigma(I)$] = 0.0627, wR_2 (all data) = 0.1771.

Crystal Data for 3: C_6H_4(*o*-CN)NH_2: $C_{31}H_{40}KN_2O_8P$, *M* = 638.72, monoclinic, space group $P2_1/n$, *a* = 9.7036(13), *b* = 14.6000(19), *c* = 23.287(3) Å, β = 93.277(11)°, *V* = 3293.8(7) $Å^3$, *T* = 140(2) K, *Z* = 4, μ = 0.260 mm^{-1}, λ = 0.71073 Å, 19252 measured reflections, 5506 independent reflections, R_{int} = 0.1238, R_1 [$I > 2\sigma(I)$] = 0.0806, wR_2 (all data) = 0.2041.

CCDC-203628 (**2**) and -203629 (**3**) contain the supplementary crystallographic data for this paper. These data can be obtained free of charge at www.ccdc.cam.ac.uk/conts/retrieving.html [or from the Cambridge Crystallographic Data Centre, 12, Union Road, Cambridge CB2 1EZ, UK; Fax: (internat.) +44-1223/336-033; E-mail: deposit@ccdc.cam.ac.uk].

Acknowledgments

We thank the EPFL and Swiss National Science Foundation for financial support.

[1] See, for example: [1a] F. R. Hartley, *The Chemistry of Organophosphorus Compounds*, Vol. 1, John Wiley & Sons, Chichester, **1990**. [1b] O. J. Scherer, *Multiple Bonds and Low Coordination in Phosphorus Chemistry*, Georg Thieme Verlag, Stuttgart, **1990**.

[2] [2a] O. Scherer, W. M. Janssen, *J. Organomet. Chem.* **1969**, *20*, 111. [2b] A. Schmidtpeter, G. Burget, *Angew. Chem. Int. Ed. Engl.* **1985**, *24*, 580. [2c] A. H. Cowley, R. A. Kemp, *J. Chem. Soc., Chem. Commun.* **1982**, 319. [2d] A. H. Cowley, R. A. Kemp, *Inorg. Chem.* **1983**, *22*, 547.

[3] M. T. Ashby, Z. Li, *Inorg. Chem.* **1992**, *31*, 1321.

[4] [4a] N. Poetschke, M. Nieger, M. A. Khan, E. Niecke, M. T. Ashby, *Inorg. Chem.* **1997**, *36*, 4087. [4b] I. Schranz, L. Stahl, R. J. Staples, *Inorg. Chem.* **1998**, *37*, 1493. [4c] B. Eichhorn, H. Nöth, T. Seifert, *Eur. J. Inorg. Chem.* **1999**, *12*, 2355.

[5] [5a] D. Fenske, B. Maczek, K. Maczek, *Z. Anorg. Allg. Chem.* **1997**, *623*, 1113. [5b] T. G. Wetzel, S. Dehnen, P. W. Roesky, *Angew. Chem. Int. Ed.* **1999**, *38*, 1086.

[6] [6a] A. H. Cowley, M. W. Taylor, M.-H. Whangbo, S. Wolfe, *J. Chem. Soc., Chem. Commun.* **1976**, 838. [6b] G. Tringuier, M. T. Ashby, *Inorg. Chem.* **1994**, *33*, 1306. [6c] T. Kremer, F. Hampel, F. A. Knoch, W. Bauer, A. Schmidt, P. Gabold, M. Schütz, J. Ellermann, P. v. R. Schleyer, *Organometallics* **1996**, *15*, 4776.

[7] Z. Fei, R. Scopelliti, P. J. Dyson, *Inorg. Chem.* **2003**, *42*, 2125.

[8] P. P. Power, *Acc. Chem. Res.* **1988**, *21*, 147.

[9] J. Ellermann, W. Bauer, M. Schütz, F. W. Heinemann, M. Moll, *Monatsh. Chem.* **1998**, *129*, 547.

[10] In order to assess the influence of the CN group and the crown moiety, two more reactions were carried out: (1) The reaction of the unfunctionalised aminophosphane Ph_2PNHPh with elemental potassium in the presence of 18-crown-6 in a 1:1:1 ratio in THF under the same conditions gave an orange powder that was highly soluble in THF. Recrystallisation from THF and diethyl ether gave orange crystals, but not of sufficient quality for X-ray diffraction analysis. The ^{31}P NMR spectrum ([D_8]THF) of the orange compound displays a singlet at δ = 32.8 ppm. The ESI-MS (positive ion mode) exhibits a peak at *m*/*z* = 303 indicative of $[C_{12}H_{24}O_6K]^+$ (18-crown-6-K)$^+$, indicating that the potassium ion is coordinated to the crown moiety. The ESI-MS (negative ion mode) gives a low intensity peak corresponding to the anion at 276, with the main peak at 292, which is the oxidised product. Based on these data, we are not sure if the potassium is coordinated to the N. Reprotonation of this compound gave signals at δ = 81.3 (Ph_2P-O-K), 27 ($Ph_2P-NHPh$), −71 and −77 ppm (Ph_2P-K?) as the main signals. (2) The reaction of C_6H_4(*o*-CN)NHPPh_2 (**1**) and elemental potassium in a 1:1 ratio without 18-crown-6 gave a yellow powder with a chemical shift of δ = 32.7 ppm in the ^{31}P NMR spectrum. Re-protonation of this compound gave **1** in quantitative yield as indicated by a singlet at δ = 30.7 ppm in the ^{31}P NMR spectrum and a broad signal centred at δ = 5.5 ppm in the ^1H NMR spectrum.

[11] W. Wiegräbe, H. Boch, *Chem. Ber.* **1968**, *101*, 1414.

[12] K. Issleib, B. Walter, E. Fluck, *Z. Chem.* **1968**, *8*, 67.

[13] S. Wingerter, M. Pfeiffer, F. Baier, T. Stey, D. Stalke, *Z. Anorg. Allg. Chem.* **2000**, *626*, 1121.

[14] W. Henderson, J. S. McIndoe, B. K. Nicholson, P. J. Dyson, *J. Chem. Soc., Dalton Trans.* **1998**, 519.

Received May 1, 2003
Early View Article
Published Online September 12, 2003

 © 2003 Wiley-VCH Verlag GmbH & Co. KGaA, Weinheim

The Water-Exchange Rate in Neutral Heptadentate DO3A-Like Gd^{III} Complexes: Effect of the Basicity at the Macrocyclic Nitrogen Site

Enzo Terreno,[a] Patrizia Boniforte,[a] Mauro Botta,[b] Franco Fedeli,[c] Luciano Milone,[a] Armando Mortillaro,[c] and Silvio Aime*[a]

Keywords: Gadolinium / Water exchange / Imaging agents / Kinetics

The rate of exchange of the two water molecules coordinated to a Gd^{III} centre in neutral complexes with heptadentate DO3A derivatives is modulated by the basicity of the macrocyclic nitrogen bearing the pendant group: a lower basicity results in a slower water-exchange rate.

(© Wiley-VCH Verlag GmbH & Co. KGaA, 69451 Weinheim, Germany, 2003)

Introduction

The exchange rate (k_{ex}) of the metal-coordinated water protons in lanthanide(III) complexes plays a fundamental role in determining their efficiency as contrast agents (CA) for Magnetic Resonance Imaging (MRI) applications.[1] In the case of Gd^{III}-based agents the attainment of high relaxivity values is strongly dependent on k_{ex}. In fact, the paramagnetic relaxation of the water protons for a given Gd^{III} chelate reaches the maximum efficiency when k_{ex} is significantly larger than the longitudinal relaxation rate of the water protons bound to the Gd^{III} ion, i.e. $k_{ex} >> R_{1M}$. To this regard, it has been calculated that a k_{ex} value of about 5×10^7 s^{-1} at 298 K allows the attainment of the highest relaxivity (at 0.47 T) for a large-sized Gd^{III}-based system.[2] Conversely, a novel class of paramagnetic CAs based on saturation transfer, the so-called CEST (Chemical Exchange Saturation Transfer) agents, require much lower k_{ex} values.[3,4] In these Ln^{III} chelates (with Ln ≠ Gd) the contrast in the MR image arises from the decrease of the NMR signal intensity of the bulk water protons following the irradiation of the water protons coordinated to the Ln^{III} ion. Here, the condition $\Delta\omega > k_{ex}$ has to be fulfilled ($\Delta\omega$ is the chemical shift separation, in rad·Hz, between the free and metal-bound water protons) and, therefore, k_{ex} values of about two orders of magnitude smaller than the optimal values required for Gd^{III}-based agents are necessary for ensuring an efficient saturation transfer.

It is worth remembering that k_{ex} refers to the exchange of the water protons coordinated to the metal centre and not to the exchange of the whole water molecule ($k_{ex\text{-}w}$). Nevertheless, at pH values around neutrality the proton exchange is extremely slow (about 10^3 s^{-1}) when compared with the typical $k_{ex\text{-}w}$ values measured for Ln^{III} chelates. Thus, it is reasonable to assume that at physiological pH values k_{ex} corresponds to $k_{ex\text{-}w}$.

In the case of nine-coordinate Gd^{III} complexes, it has been established that the water-exchange process occurs through a dissociative pathway in which the transition state is represented by an eight-coordinate species.[5] Thus, the exchange rate is related to the free-energy difference, $\Delta G^{\#}$, between the transition and the ground states. Several factors contribute to the $\Delta G^{\#}$ value. $\Delta G^{\#}$ is usually dominated by the enthalpic term, $\Delta H^{\#}$, which mainly depends on the strength of the $Ln-O_{(water)}$ bond. The highly electrostatic nature of this bond accounts for the marked dependence of the water-exchange rate on the overall electric charge in isostructural Ln^{III} chelates. In fact, relatively fast and exceedingly slow exchange rates have been observed for anionic and cationic Gd^{III} complexes, respectively.[1] Moreover, the $\Delta H^{\#}$ term may be affected either by the steric crowding at the water coordination site or by the structural properties of the second hydration sphere of the metal ion.[6–8] The large number of parameters that contribute to determine the water-exchange process renders the assessment of the relative role played by each single contribution quite difficult. For this reason, the evaluation of the k_{ex} values for Gd^{III} complexes differing in only one main struc-

[a] Dipartimento di Chimica I.F.M., Università di Torino
Via P. Giuria 7, 10125 Torino, Italy
Fax: (internat.) +39-011/670-7855
E-mail: silvio.aime@unito.it
[b] Dipartimento di Scienze e Tecnologie Avanzate, Università del Piemonte Orientale "Amedeo Avogadro"
Corso Borsalino 54, 15100 Alessandria, Italy
Fax: (internat.) +39-0131/287-431
E-mail: mauro.botta@unipmn.it
[c] Laboratorio Integrato di Metodologie Avanzate, Bioindustry Park del Canavese
Via Ribes 5, Colleretto Giacosa (TO), Italy
Fax: (internat.) +39-0125/538-346

tural or electronic feature may be particularly useful. On this basis, it was deemed of interest to investigate the dependence of the water-exchange rate on the basicity of the macrocyclic nitrogen bearing the non-coordinating substituent in two neutral heptadentate DO3A-like Gd^{III} chelates. To this purpose, the ligands reported below, and their corresponding Eu^{III}, Gd^{III} and Yb^{III} complexes, have been synthesised. In spite of a very similar structure, the two Ln^{III} chelates have a noticeable difference in the electronic availability at the macrocyclic nitrogen bearing the phenyl group [$\sigma_{para}(NO_2) = 0.78$, $\sigma_{para}(NH_2) = -0.66$].

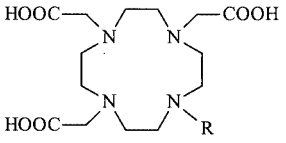

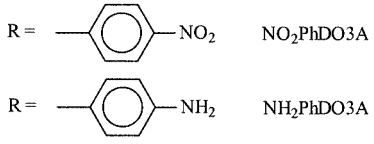

Results and Discussion

The synthesis of the ligands (see Exp. Sect.) was carried out by reacting 1,4,7,10-tetraazacyclododecane (TAZA) with *p*-nitrofluorobenzene (molar ratio 3:1) in acetonitrile. The purified mono-alkylated TAZA derivative was then exhaustively carboxymethylated with bromoacetic acid at pH 10. The NH_2PhDO3A ligand (pale brown) was obtained upon hydrogenation (Pd/C) of the nitro derivative. The synthesis of the Ln^{III} complexes was carried out in water at pH 7 by mixing equimolar amounts of the ligand and the corresponding Ln^{III} chloride.

Figure 1 shows the pH dependence of the relaxivity, r_1, for the two Gd^{III} complexes at 0.235 *T* (corresponding to a proton Larmor frequency of 10 MHz) and 298 K.

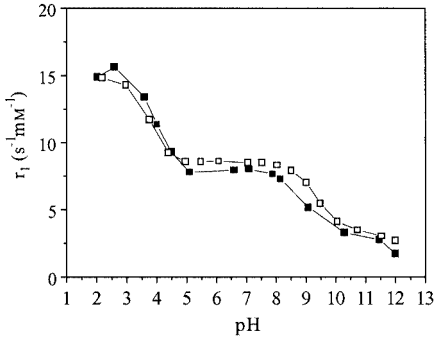

Figure 1. pH dependence of relaxivity for [Gd(NO_2PhDO3A] (■) and [Gd(NH_2PhDO3A] (□) at 298 K and 10 MHz

Qualitatively, both chelates behave similarly to other neutral heptadentate DO3A-like complexes.[9] r_1 is constant in the pH interval 5 and 8; at lower pH values r_1 increases owing to the acid-catalysed demetallation process, whereas at higher pH values the relaxivity decreases owing to the formation of ternary adducts with anionic species like carbonate (from dissolved CO_2) and hydroxide anions which displace the metal-bound water molecule(s). This behaviour, coupled with the relatively high r_1 values {8.0 and 8.5 $s^{-1}\cdot mM^{-1}$ at 298 *K* and pH = 7 for [Gd(NO_2PhDO3A)] and [Gd(NH_2PhDO3A)], respectively} provides a strong indication that the hydration sphere of the two complexes is closely analogous to that of the parent [Gd(DO3A)] complex,[10] i.e. characterised by the presence of two water molecules coordinated to the metal ion. Nevertheless, it is likely that the complexes are present in solution as a mixture of species which may differ in the conformation of the donor atoms wrapped around the metal centre (Δ/Λ and δδδδ/λλλλ isomerism)[11] or in the hydration state of the metal ion (equilibrium between nine- and eight-coordinate isomers).[10,12]

In principle, each species may have a different k_{ex} value[13] and thus the isomeric population of the two complexes has to be checked.

Figure 2 shows a comparison of the ^1H NMR high resolution spectra of the Eu^{III} chelates. In spite of the complexity of the spectra, it is evident that they are very similar in terms of chemical shift range and number and relative intensity of the resonances. Analogous conclusions can be drawn by analysing the ^1H NMR spectra of the corresponding Yb^{III} complexes.

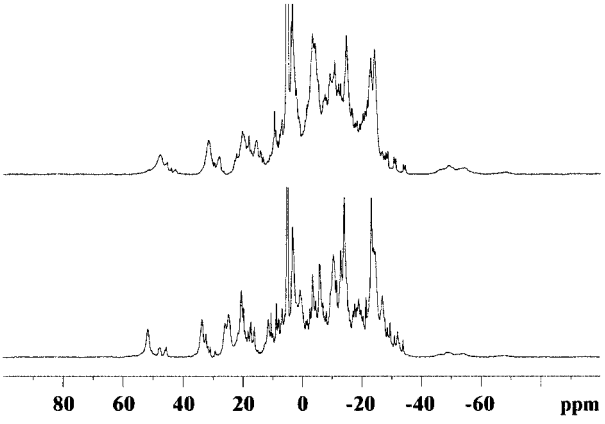

Figure 2. ^1H NMR spectra at 7.05 T, pH 7 and 275 K in D_2O of [Eu(NH_2PhDO3A)] (top) and [Eu(NO_2PhDO3A)] (bottom)

Further confirmation that the isostructurality between the two Ln^{III} chelates is retained for the Gd^{III} complexes was gained by the analysis of their NMRD (Nuclear Magnetic Relaxation Dispersion) profiles (Figure 3). Again, the two complexes display a very similar magnetic-field dependence of their r_1 values (measured at pH 7 and 298 K) even if the relaxivity of the *p*-nitro derivative is slightly lower over the entire range of magnetic-field strengths investigated.

Finally, the exchange rate of the water molecules coordinated to Gd^{III} has been determined through the well-established NMR method based on the analysis of the tempera-

 © 2003 Wiley-VCH Verlag GmbH & Co. KGaA, Weinheim

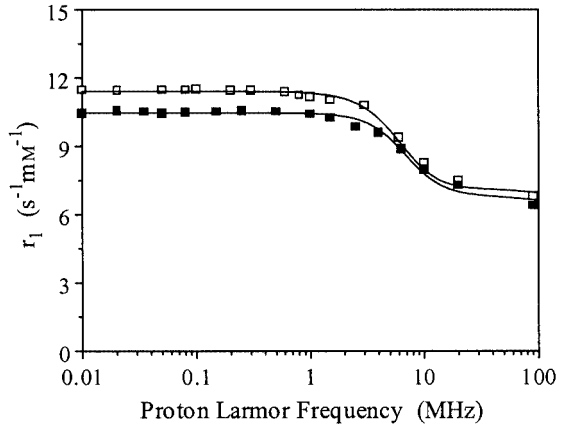

Figure 3. ^{1}H NMRD profiles for [Gd(NO_2PhDO3A)] (■) and [Gd(NH_2PhDO3A)] (□) at pH 7 and 298 K

ture dependence of the paramagnetic contribution to the transverse relaxation rate of the ^{17}O-water nuclei. Figure 4 reports the data obtained for the two complexes.

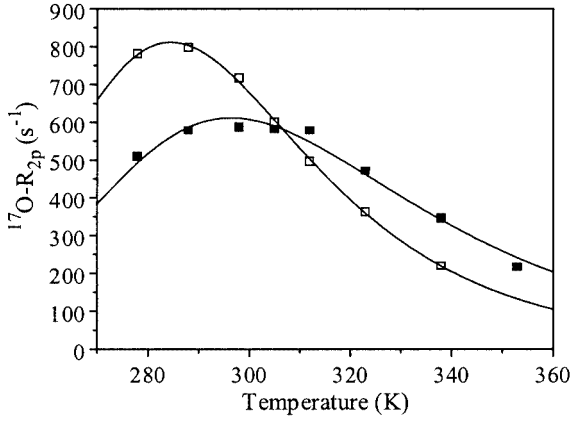

Figure 4. Temperature dependence of ^{17}O-R_{2p} for [Gd(NO_2PhDO3A)] (■) and [Gd(NH_2PhDO3A)] (□) at pH 7 and 7.05 T ([GdL] = 10 mM)

The profiles appear rather different, with the top of the bell-shaped curve shifted to lower temperature for the *p*-amino derivative. This behaviour suggests that k_{ex} is significantly influenced by the nature of the substituent at the macrocyclic nitrogen.

A quantitative analysis of the ^{17}O NMR spectroscopic data, according to the available theory,[5] confirms this effect. The result of the best-fitting procedure, on the assumption that the two labile water molecules have the same exchange rate, is reported in Table 1, along with the results obtained from the analysis of the NMRD profiles carried out according to the usual inner- and outer-sphere model.[1]

No relevant differences were obtained, within the same experimental data set, for the parameters controlling the electronic relaxation times Δ^2 and τ_V, which represent the mean energy of the transient zero-field splitting (ZFS) and its time modulation, respectively. Nevertheless, different Δ^2 and τ_V values were obtained depending on the experimental technique. It is likely that this discrepancy is due to the

Table 1. Best-fit parameters (at 298 K) obtained from the analysis of ^{17}O-R_{2p} versus T profiles and NMRD profiles of [Gd(NO_2PhDO3A)] and [Gd(NH_2PhDO3A)] at pH 7

	[Gd(NO_2PhDO3A)]		[Gd(NH_2PhDO3A)]	
	NMRD[a]	^{17}O-R_{2p} [b]	NMRD	^{17}O-R_{2p}
k_{ex} ($\times 10^6 s^{-1}$)	[c]	7.4 ± 1.2	[c]	17.6 ± 3.8
ΔH_M (kJ·mol^{-1})	[d]	33.8 ± 1.6	[d]	36.2 ± 2.8
Δ^2 ($\times 10^{19}$ s^{-2})	5.8 ± 0.5	11.6 ± 0.8	5.7 ± 0.4	9.8 ± 0.4
τ_V ($\times 10^{-12}$ s)	22.0 ± 0.3	13.0 ± 0.6	20.3 ± 0.7	15.0 ± 0.7
τ_R ($\times 10^{-12}$ s)	77.0 ± 0.4	[d]	81.1 ± 0.3	[d]

[a] The fitting of the NMRD profiles has been carried out by keeping fixed the following parameters: r = 3.1 Å, q = 2, a = 3.8 Å, $D = 2.25 \times 10^{-5}$ cm^2·s^{-1}. [b] The fitting of the temperature dependence of ^{17}O-R_{2p} has been performed by keeping fixed the following parameters: ΔH_v = 5.0 kJ·mol^{-1}, (A/ħ) = -3.8×10^6, q = 2. [c] This parameter has been fixed to the value obtained by the fitting of the data obtained with the other experimental technique. [d] This parameter cannot be obtained from the fitting.

limitations of the currently available theory for describing adequately the magnetic-field dependence of the electronic relaxation times, but, fortunately, this concern has only a small effect on the estimation of k_{ex}. Therefore, the relaxometric analysis indicates that the water exchange for the *p*-amino derivative occurs faster than the *p*-nitro complex.

It seems reasonable that such a difference could be accounted for in terms of the different electronic properties of the two *p*-substituents on the aromatic ring. The strong electron-withdrawing character of the *p*-nitro group makes the Gd−N bond much more polarised, thus increasing the positive charge at the metal centre. This effect results in a stabilisation of the nine-coordinate ground state of the complex, thus slowing down the rate of exchange of the coordinated water molecules. The opposite electronic effect of the *p*-amino group leads to a destabilisation of the $Gd^{III}-O_{(water)}$ bond and to a faster exchange rate.

Interestingly, the water-exchange regime reported for [Gd(DO3A)] (11.0×10^6 s^{-1})[10] is intermediate as expected on the ground of the basicity of the secondary amino group.

The results reported here might also help to rationalise the fast water-exchange rates (ca. 5.0×10^7 s^{-1} at 298 K) reported in the literature for several *N*-benzyl-DO3A derivatives[14] and support the hypothesis forwarded for explaining the relatively fast exchange rate observed in a cationic *N*-methyl DO3A derivative.[15] In fact, in these complexes a destabilisation of the $Gd^{III}-O_{(water)}$ bond is expected on the basis of the inductive effect (−I) of the alkyl group on the macrocyclic nitrogen.

Conclusion

In conclusion, the experimental evidence reported in this communication supports the view that the exchange rate of the water molecules coordinated to the Gd^{III} ion in a nine-coordinate DO3A-like arrangement may be successfully modulated through a proper choice of the electronic properties of the substituent on the macrocyclic nitrogen.

 © 2003 Wiley-VCH Verlag GmbH & Co. KGaA, Weinheim

However, whether the two water molecules exchange at the same rate and/or the substituent effect described herein affects the dissociation rate at the two coordination sites to a different extent still remain undefined.

Experimental Section

Synthesis of NO_2PhDO3A: This ligand was synthesised in two steps. First, a suspension of 1,4,7,10-tetraazacyclododecane, TAZA, (35.05 g, 0.2035 mol) in acetonitrile (500 mL) was dissolved whilst stirring at 60 °C by adding 50 mL of water. To this solution was then added dropwise 50 mL of a solution of acetonitrile containing 1-fluoro-4-nitrobenzene (9.57 g, 0.0678 mol). After 8 h at 60 °C the suspension was cooled down and filtered. The crude solid was dissolved in 1 L of boiling water and the resulting solution (obtained by filtration) was first diluted 1:1 with water, loaded onto a chromatographic column (Amberlite® XAD 1600) and then eluted with water in order to separate the unchanged TAZA. The 1-(4-nitrophenyl)-1,4,7,10-tetraazacyclododecane ligand (14.08 g; 0.048 mol, 70.8% yield) was obtained by eluting the column with methanol and subsequent evaporation of the solvent.

In the second step, 2-bromoacetic acid (22.23 g, 0.16 mol) was added whilst stirring to an aqueous solution of 1-(4-nitrophenyl)-1,4,7,10-tetraazaciclododecane (11.73 g, 0.04 mol in 50 mL of water). The pH of the solution was brought to 10 by adding 2 N NaOH. The solution was heated at 50 °C for 6 h by keeping the pH constant. The reaction mixture was cooled down, filtered and the filtrate was acidified at pH 3 with HCl. This solution was loaded onto a chromatographic column (Amberlite® XAD 1600) and then eluted first with water, in order to separate the bromide ions, and then with methanol. After evaporation of the solvent the NO_2PhDO3A ligand was obtained in the acid form as a yellow solid (16.38 g, 0.035 mol, 87.6% yield). ^{1}H NMR (D_2O, *t*BuOH as internal reference, 298 K): δ = 8.0 (d, 2 H), 6.65 (d, 2 H), 3.7 (s, 4 H), 3.45 (s, 4 H), 3.35 (s, 2 H), 3−3.2 (m, 12 H) ppm. $^{13}C\{^1H\}$ NMR (D_2O, *t*BuOH as internal reference, 298 K): δ = 173.2, 169.2, 153.9, 142.7, 124.2, 122.3, 55.1, 51.6, 50.9, 50.0, 47.7, 46.9 ppm. MS (MALDI-TOF): calcd. for $C_{20}H_{29}N_5O_8$ 467.47 uma; found 468.4 [MH^+].

Synthesis of NH_2PhDO3A: Ammonia solution (26%) was added to a suspension of NO_2PhDO3A in water (7.70 g; 0.02 mol in 50 mL of water) until the ligand dissolution was complete. Then, 0.7 g of 10% Pd/C, previously treated with 5 mL of water, was added to the solution and the catalytic hydrogenation was carried out at room temperature and pressure with hydrogen (1180 mL, 0.05 mol) produced electrochemically (Hydrogen generator HG 600; CLAIND). After 4 h the suspension was filtered in order to remove the catalyst. The filtrate (brown colour) was lyophilised and then redissolved in water acidified (pH 2.3) with HCl. 0.5 g of Carbopuron was then added in order to partially decolourise and stabilise the product. After filtration, the solution was re-lyophilised and the NH_2PhDO3A ligand was obtained in the acid form as a dark-brown solid (8.16 g; 0.016 mol, 80% yield). ^{1}H NMR (D_2O, *t*BuOH as internal reference, 298 K): δ = 7.15 (d, 2 H), 6.7 (d, 2 H), 3.6 (s, 4 H), 3.4 (s, 4 H), 3.3 (s, 2 H), 3.27 (s, 8 H), 3.1 (s, 4 H) ppm. $^{13}C\{^1H\}$ NMR (D_2O, *t*BuOH as internal reference, 298 K): δ = 176.8, 169.1, 143.6, 138.9, 124.8, 116.0, 55.7, 54.2, 51.0, 50.2, 49.5, 47.9 ppm. MS (MALDI-TOF): calcd. for $C_{20}H_{31}N_5O_6$ 437.5 uma; found 438.3 [MH^+].

Synthesis of the Ln^{III} Complexes: The Ln^{III} complexes (Ln = Gd, Eu and Yb) were synthesised in water at room temperature by adding an equimolar amount of $LnCl_3$ to the selected ligand. The pH was monitored during the synthesis in order to keep it in the 6−8 range. The final concentration of the metal chelates was checked by Evans' method.[16]

NMR Measurements: The high resolution NMR spectra and the ^{17}O-R_{2p} measurements were performed on a Bruker Avance 300 spectrometer (Karlsruhe, Germany) operating at 7.05 T (proton Larmor frequency of 300 MHz).

The water-proton longitudinal relaxation rates at 0.235 T (proton Larmor frequency of 10 MHz) as well as the NMRD profiles in the 0.000235−0.235 T range (0.01−10 MHz) were obtained from a Stelar Fast Field Cycling Relaxometer (Mede (Pv), Italy). The temperature was controlled with a Stelar VTC-91 air-flow heater equipped with a copper-constantan thermocouple (uncertainty of ±0.1 °C). The NMRD profile was completed with data obtained at 20 MHz and 90 MHz by using a Stelar Spinmaster and a JEOL EX-90 NMR spectrometer, respectively.

Acknowledgments

Financial support from MIUR and Bracco Imaging S.p.A (Milano, Italy) is gratefully acknowledged. This work was carried out under the framework of the COST-D18 action. A. M. is recipient of a Research Fellowship from the Fondazione Internazionale di Ricerca in Medicina Sperimentale, Torino, Italy.

[1] *The Chemistry of Contrast Agents in Medical Magnetic Resonance Imaging* (Eds.: A. E. Merbach; E. Toth), 2001, John Wiley & Sons, Chichester (UK), Chapters 2 and 5.
[2] S. Aime, M. Botta, M. Fasano, E. Terreno, *Chem. Soc. Rev.* **1998**, *27*, 19−29.
[3] S. Zhang, P. Winter, K. Wu, A. D. Sherry, *J. Am. Chem. Soc.* **2001**, *123*, 1517−1518.
[4] S. Aime, D. Delli Castelli, E. Terreno, *Angew. Chem. Int. Ed.* **2002**, *41*, 4334−4336.
[5] H. D. Powell, O. M. Ni Dhubhghaill, D. Pubanz, L. Helm, Y. Lebedev, W. Schlaepfer, A. E. Merbach, *J. Am. Chem. Soc.* **1996**, *118*, 9333−9346.
[6] D. Pubanz, G. Gonzalez, D. H. Powell, A. E. Merbach, *Inorg. Chem.* **1995**, *34*, 4447−4453.
[7] S. Aime, M. Botta, S. Geninatti Crich, G. B. Giovenzana, R. Pagliarin, M. Piccinini, M. Sisti, E. Terreno, *J. Biol. Inorg. Chem.* **1997**, *2*, 470−479.
[8] M. Botta, *Eur. J. Inorg. Chem.* **2000**, 399−407.
[9] S. Aime, M. Botta, S. Geninatti Crich, G. Giovenzana, R. Pagliarin, M. Sisti, E. Terreno, *Magn. Res. Chem.* **1998**, *36*, S200−S208.
[10] E. Toth, O. M. Ni Dhubhghaill, G. Besson, L. Helm, A. E. Merbach, *Magn. Res. Chem.* **1999**, *37*, 701−708.
[11] P. Caravan, J. J. Ellison, T. J. McMurry, R. B. Lauffer, *Chem. Rev.* **1999**, *99*, 2293−2352.
[12] F. A. Dunand, S. Aime, S. G. Crich, G. B. Giovenzana, A. E. Merbach, *Magn. Res. Chem.* **2002**, *40*, 87−92.
[13] S. Aime, A. Barge, M. Botta, D. Parker, A. S. De Sousa, *Angew. Chem. Int. Ed.* **1998**, *37*, 2673−2675.
[14] S. Aime, E. Gianolio, E. Terreno, G. B. Giovenzana, R. Pagliarin, M. Sisti, G. Palmisano, M. Botta, M. P. Lowe, D. Parker, *J. Biol. Inorg. Chem.* **2000**, *5*, 488−497.
[15] M. Botta, S. Aime, A. Barge, G. Bobba, R. S. Dickins, D. Parker, E. Terreno, *Chem. Eur. J.* **2003**, *9*, 2102−2109.
[16] D. M. Corsi, C. Platas-Iglesias, H. van Bekkum, J. A. Peters, *Magn. Reson. Chem.* **2001**, *39*, 723−726.

Received June 9, 2003
Early View Article
Published Online August 14, 2003

 © 2003 Wiley-VCH Verlag GmbH & Co. KGaA, Weinheim

A Template-Interface Co-Reduction Synthesis of Hollow Sphere-like Carbides

Cun Li,[a,b] Xiaogang Yang,[a] Baojun Yang,[a] Yan Yan,[a] and Yitai Qian*[a]

Keywords: Nanostructures / Carbides / Titanium / Vanadium / Synthesis design

Hollow sphere-like carbides MC (M = Ti, V) with diameters of between 70 and 170 nm were synthesized via a template-interface co-reduction (TICR) route, in which MCl_4 and hexachlorobuta-1,3-diene (C_4Cl_6) were reacted with metallic sodium at 500 °C for 24 h. X-ray powder diffraction (XRD) patterns indicated the samples were single-phase NaCl-type carbides. Transmission electron microscopy (TEM) photographs showed the hollow spheres consisted of nanocrystalline carbides. The possible formation mechanism of hollow sphere-like carbides is discussed.
(© Wiley-VCH Verlag GmbH & Co. KGaA, 69451 Weinheim, Germany, 2003)

Introduction

The transition-metal carbides of groups IV and V possess unusual properties that make them desirable and useful engineering materials in industry.[1] Nanosized TiC and VC powders have promising applications in mechanical and tribological fields.[2] Recent research work has proved that some transition metal carbides have similar catalytic properties to those of the platinum-group metals. For instance, vanadium carbide is an active NH_3 decomposition catalyst.[3]

Hollow spheres consisting of nanoparticles are useful as fillers, coatings, catalysts, and encapsulating agents because of their low density, large specific surface area, and interesting optical properties.[4] Various hollow spheres including carbon,[5] polymers,[6] metals,[7] and inorganic oxides[8] have been synthesized by using spherical templates such as polystyrene beads or silica sol.[9] Several other methods have also been developed to fabricate hollow spheres, such as coaxial nozzle techniques,[10] microemulsion and reverse microemulsion methods,[11] exchange-resin methods,[12] self-organization,[13] and template-interface reactions.[14] Hollow sphere carbides may be promising materials in mechanical and catalyst fields. However, to the best of our knowledge, there are few reports on these compounds.[15]

Generally, transition metal carbides, including TiC and VC, are prepared by either direct element reaction,[16] carbothermal reduction,[17] self-propagating high-temperature synthesis (SHS)[18] or solid-state metathesis (SSM) [19] at elevated temperatures. Previously, we have developed a co-reduction method to synthesize nanocrystalline carbides by allowing CCl_4 and MCl_4 to react with metallic sodium at relatively low temperatures.[20]

Herein, we report a template-interface co-reduction (TICR) route to synthesize TiC and VC hollow spheres, using $TiCl_4$ or VCl_4 as the titanium or vanadium source, C_4Cl_6 as the carbon source and Na as reductant. $TiCl_4$ or VCl_4 and C_4Cl_6 are co-reduced by metallic Na at 500 °C. Metallic Na droplets generated in the co-reduction process may play a role as a template in the formation process of hollow sphere carbides. The formation of carbides can be expressed as shown in Equation (1):

$$4MCl_4 + C_4Cl_6 + 22Na \xrightarrow{500^\circ C} 4MC + 22NaCl\ (M = Ti, V) \quad (1) \qquad (1)$$

Results and Discussion

Figure 1 shows the XRD patterns of as-prepared samples. All the diffraction peaks in the XRD patterns can

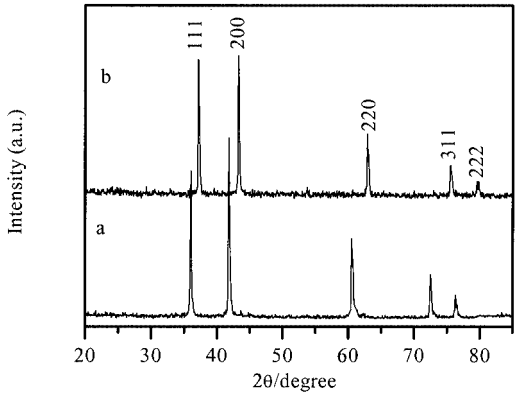

Figure 1. XRD patterns of as-prepared samples of (a) TiC and (b) VC

[a] Structure Research Laboratory and Department of Chemistry, University of Science and Technology of China, Hefei, Anhui 230026, China
Fax: (internat.) +86-551/363-1760
E-mail: ytqian@ustc.edu.cn
[b] Department of Chemistry, Anhui University, Hefei, Anhui 230039, China
Fax: (internat.) +86-551/510-7342
E-mail: licun@mail.ustc.edu.cn

 © 2003 Wiley-VCH Verlag GmbH & Co. KGaA, Weinheim DOI: 10.1002/ejic.200300183

be indexed as face-centered cubic (fcc) carbides. The shifts of the peak positions correspond to the different lattice constants of these two samples, due to the different ionic radii of Ti and V. The lattice parameters obtained from as-prepared products are $a = 4.322$ Å for TiC and $a = 4.169$ Å for VC, in good agreement with the values in the literature.[21]

The size and morphology of the carbides was studied by TEM. The TEM photographs and selected area electron diffraction (SAED) patterns of as-prepared carbides are shown in Figure 2a−d. From the TEM photographs it can be seen that there is an obvious contrast between the dark edge and the pale center of the samples, revealing that the core is hollow.[22] The hollow nature of the spheres is also supported by the observation of a TiC sphere with a broken shell [Figure 2a (inset)]. The as-prepared carbide spheres have diameters ranging from 70 to 120 nm; the thickness of the shell is about 10−20 nm for carbides. The SAED patterns of a single sphere of both samples show three clear ring patterns corresponding to the (111), (200) and (220) reflections of cubic TiC (Figure 2b) and VC (Figure 2d). The cell constants calculated from the radii of the diffraction rings confirm the results from the XRD patterns. No diffuse rings of amorphous carbon are observable. These results indicate that the hollow spheres are mainly composed of polycrystalline carbides. From the HRTEM photographs (Figure 2e and 2f), it can be seen that the shells of the carbide spheres are composed of nanoparticles of between 2 and 5 nm. FESEM micrographs of both carbides are shown in Figure 3. Besides some irregular particles, the portion of spheres with sizes of about 70−170 nm in the products is above 60%. It can be seen that a big sphere is usually found with a broken shell (indicated by an arrow in Figure 3a).

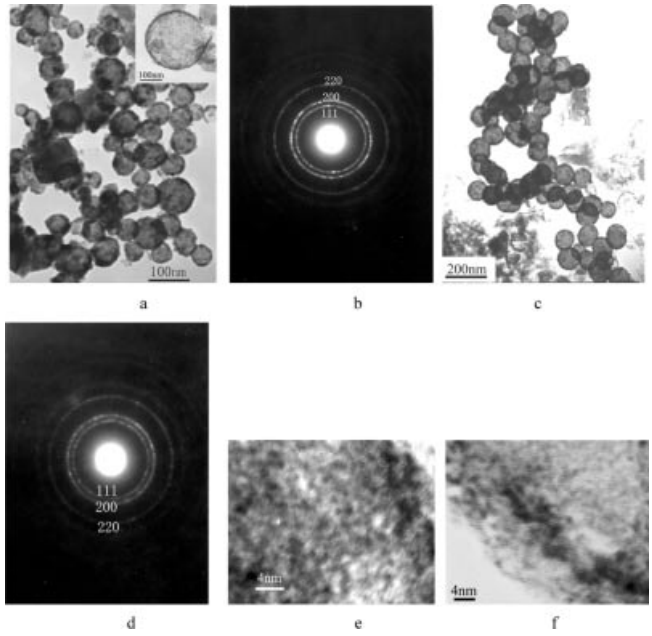

Figure 2. (a) (b) TEM micrograph and SAED pattern of TiC [(inset in a) single TiC hollow sphere with broken shell]; (c) (d) TEM micrograph and SAED pattern of VC; (e) HRTEM micrograph of the sphere shell of TiC; (f) HRTEM micrograph of the sphere shell of VC

Based on our previous experiment results,[20] the overall reaction [Equation (1)] might occur via a co-reduction route, which could be described by Equations (2)−(4):

$$C_4Cl_6 + 6Na \rightarrow 4C + 6NaCl \quad (2)$$

$$MCl_4 + 4Na \rightarrow M + 4NaCl\ (M = Ti, V) \quad (3)$$

$$M + C \rightarrow MC\ (M = Ti, V) \quad (4)$$

Similar to the reaction between CCl_4 and Na, C_4Cl_6 could be reduced by Na to generate carbon [Equation (2)], which should be a thermodynamically spontaneous and exothermic process concluded from the very high Gibbs energy of formation and enthalpy of NaCl ($\Delta_fG^o = -384.1$ kJ·mol^{-1}, $\Delta_fH^o = -411.2$ kJ·mol^{-1}).[23] The reaction in Equation (3) is highly exothermic ($\Delta H^o = -881.6$ kJ·mol^{-1} using $TiCl_4$ as reactant; $\Delta H^o = -1075.4$ kJ·mol^{-1} using VCl_4 as reactant).[23] The reaction in Equation (4), which produces TiC ($\Delta H^o = -92$ kJ·mol^{-1}) or VC ($\Delta H^o = -51$ kJ·mol^{-1}),[24] is also exothermic. Hence, the overall reaction in Equation (1) is highly exothermic.

In this synthetic system, metallic sodium may form droplets owing to reaction heat generated from the exothermic reactions, and these metallic Na droplets may act as templates in the formation process of hollow sphere carbides. This possible formation process is illustrated in Figure 4 and is similar to the mechanism of formation of CdS hollow spheres via a template-interface reaction.[14] In our experiment, upon increasing the reaction temperature to 500 °C C_4Cl_6 (b.p. 215 °C), $TiCl_4$ (b.p. 136.4 °C) and VCl_4 (b.p. 148 °C) begin to vaporize.[23] Strongly exothermic reactions then take place on the surface of the fused sodium (m.p. 97.82 °C),[23] raising the local temperature near the surface

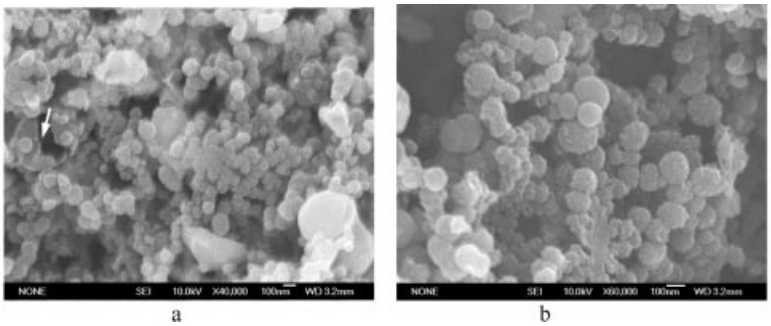

Figure 3. (a) FESEM micrographs of TiC; the arrow indicates a broken sphere; (b) FESEM micrographs of VC

 © 2003 Wiley-VCH Verlag GmbH & Co. KGaA, Weinheim

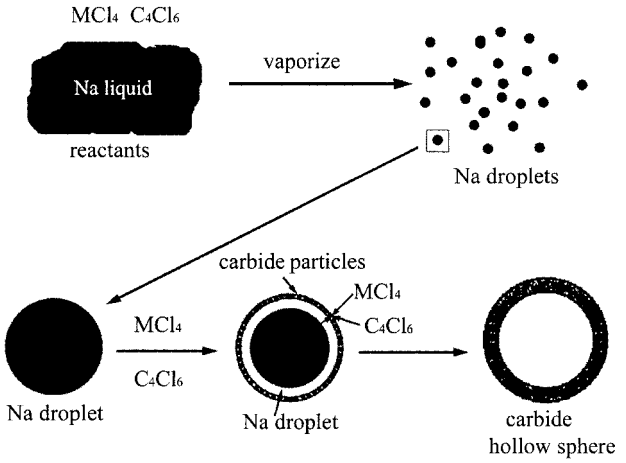

Figure 4. The formation mechanism of hollow carbide spheres

and hence causing the sodium to vaporize (b.p. 881.4 °C).[23] This sodium vapor could form many small droplets in the autoclave. Subsequently, the co-reduction reactions could occur on the surface of the Na droplets in the atmosphere of C_4Cl_6 and MCl_4, which may result in the formation of a carbide shell around the Na core. This is an important step in the formation of hollow spheres. Analogous to the synthesis of hollow spheres using emulsion droplets as templates,[25] the produced carbide shell could stabilize the sodium droplets, thus preserving the spherical shape. As the reaction continues the amount of sodium becomes depleted and the shell gradually thickens, resulting finally in hollow spheres with a polycrystalline carbide shell. In this co-reduction procedure the sodium droplets may serve as a template with the carbide shells being formed near the liquid-gas interface. We have therefore called it a template-interface co-reduction (TICR) route. We have not observed sodium encapsulated in carbides by TEM directly due to the high reactivity and air sensitivity of sodium. However, the formation of broken spheres may be ascribed to the presence of unconsumed sodium in the hollow sphere, which could react with water to blow out the hollow spheres due to gas evolution. This may be a supportive evidence for the proposed mechanism. In order to understand the formation process of hollow sphere carbides, further extensive studies are underway.

Conclusion

We have successfully prepared TiC and VC hollow spheres via a template-interface co-reduction (TICR) route. The TiC and VC hollow spheres have potential applications in catalysis and mechanical fields. A possible template-interface reaction mechanism for the formation of carbide spheres has been proposed. This TICR route may be applied to produce other carbide hollow spheres.

Experimental Section

All manipulations were carried out in a dry glovebox under N_2. In a typical synthetic procedure for TiC, 0.02 mol of $TiCl_4$ and 0.005 mol of C_4Cl_6 were syringed into a stainless steel autoclave of 50 mL capacity, and 0.12 mol of granular metallic Na was added. The autoclave was sealed and maintained at 500 °C for 24 h, then allowed to cool slowly to room temperature. The product was collected and washed successively with absolute ethanol, 1 M hydrochloric acid and distilled water. After drying in vacuo at 60 °C for 4 h, 0.98 g of black powder was obtained. Substitution of VCl_4 for $TiCl_4$ gave VC.

The samples were characterized by X-ray powder diffraction (XRD) on a Japan Rigaku Dmax-γA X-ray diffractometer with graphite-monochromated Cu-K_α radiation (λ = 1.54178 Å). Transmission electron microscopy (TEM) photographs and selected area electron diffraction (SAED) patterns were taken with a Hitachi Model H-800 transmission electron microscope. High resolution transmission electron microscopy (HRTEM) was carried out using a JEOL-2010 transmission electron microscope. Field-emission scanning electron microscopy (FESEM) images were taken with a JEOL JSM-6700F scanning electron microscope.

Acknowledgments

The authors thank Prof. Shuyuan Zhang for his help with the HRTEM and Prof. Fanqing Li for his help with the FESEM measurements. Financial support from the National Natural Science Funds and the 973 Projects of China is gratefully acknowledged.

[1] L. E. Toth, *Transition Metal Nitrides and Carbides*, Academic press, New York, **1971**.
[2] S. Lee, O. El-bjeirami, S. S. Perry, S. V. Didziulis, P. Frantz, G. Radhakrishnan, *J. Vac. Sci. Technol., B* **2000**, *18*, 69−75.
[3] J. G. Choi, *J. Catal.* **1999**, *182*, 104−116.
[4] [4a] Y. D. Yin, Y. Lu, B. Gates, Y. N. Xia, *Chem. Mater.* **2001**, *13*, 1146−1148. [4b] M. Ohmori, E. Matijevic, *J. Colloid Interface Sci.* **1992**, *150*, 594−598.
[5] [5a] J. Lee, K. Sohn, T. Hyeon, *J. Am. Chem. Soc.* **2001**, *123*, 5146−5147. [5b] S. B. Yoon, K. Sohn, J. Y. Kim, C. H. Shin, J. S. Yu, T. Hyeon, *Adv. Mater.* **2002**, *14*, 19−21.
[6] [6a] E. Donath, G. B. Sukhorukov, F. Caruso, S. A. Davis, H. Mohwald, *Angew. Chem. Int. Ed.* **1998**, *37*, 2202−2205. [6b] T. K. Mandal, M. S. Fleming, D. R. Walt, *Chem. Mater.* **2000**, *12*, 3481−3487. [6c] S. B. Han, X. Y. Shi, F. M. Zhou, *Nano Lett.* **2002**, *2*, 97−100.
[7] [7a] G. L. Egan, J. S. Yu, C. H. Kim, S. J. Lee, R. E. Schaak, T. E. Mallouk, *Adv. Mater.* **2000**, *12*, 1040−1042. [7b] C. Graf, A. Blaaderen, *Langmuir* **2002**, *18*, 524−534. [7c] N. Kawahashi, H. Shiho, *J. Mater. Chem.* **2000**, *10*, 2294−2297. [7d] O. Andersen, U. Waag, L. Schneider, G. Stephani, B. Kieback, *Adv. Eng. Mater.* **2000**, *2*, 192−195.
[8] [8a] F. Caruso, R. A. Caruso, H. Mohwald, *Science* **1998**, *282*, 1111−1114. [8b] A. Imhof, *Langmuir* **2001**, *17*, 3579−3585. [8c] F. Caruso, X. Shi, R. A. Caruso, A. Susha, *Adv. Mater.* **2001**, *13*, 740−744. [8d] Z. B. Lei, J. M. Li, Y. X. Ke, Y. G. Zhang, H. C. Zhang, F. Q. Li, J. Y. Xing, *J. Mater. Chem.* **2001**, *11*, 2930−2933.
[9] [9a] D. Wang, R. A. Caruso, F. Caruso, *Chem. Mater.* **2001**, *13*, 364−371. [9b] K. M. Kulinowski, V. Harsha, V. L. Colvin, *Adv. Mater.* **2000**, *12*, 833−830. [9c] S. Han, K. Sohn, T. Hyeon, *Chem. Mater.* **2001**, *12*, 3337−3341.
[10] R. Meyer, H. Weitzing, Q. Xu, Q. Zhang, R. E. Newnham, J. K. Cochran, *J. Am. Ceram. Soc.* **1994**, *77*, 1669−1672.
[11] [11a] M. Jafelicci, M. R. Davolos, F. J. Santos, S. J. Andrade, *J.*

 © 2003 Wiley-VCH Verlag GmbH & Co. KGaA, Weinheim

Non-Cryst. Solids **1999**, *247*, 98−102. [11b] W. Wang, X. A. Fu, J. A. Tang, L. Jiang, *Colloids Surf. A* **1993**, *81*, 177−180.
[12] A. Bourlinos, N. Boukos, D. Petridis, *Adv. Mater.* **2002**, *14*, 21−24.
[13] [13a] S. Varghese, A. K. Lee, D. Srinivas, M. Sastry, R. A. Mashelkar, *Adv. Mater.* **2001**, *13*, 1544−1548. [13b] G. Hu, D. Ma, M. Cheng, L. Liu, X. Bao, *Chem. Commun.* **2002**, 1948−1949.
[14] J. X. Huang, Y. Xie, B. Li, Y. Liu, Y. T. Qian, S. Y. Zhang, *Adv. Mater.* **2000**, *12*, 808−811.
[15] K. B. Tang, G. Z. Shen, D. Chen, C. H. An, C. R. Wang, Y. T. Qian, *Chem. Lett.* **2002**, *32*, 116−117.
[16] P. Schwarzkopf, P. Kieffer, *Refractory Hard Metals*, MacMillan, New York, **1953**.
[17] [17a] H. Preiss, D. Schultze, K. Szulzewsky, *J. Eur. Ceram. Soc.* **1999**, *19*, 187−194. [17b] H. Preiss, L. M. Berger, D. Schultze, *J. Eur. Ceram. Soc.* **1999**, *19*, 195−206. [17c] R. Kapoor, S. T. Oyama, *J. Solid State Chem.* **1995**, *120*, 320−326.
[18] [18a] K. S. Vecchio, J. C. LaSalvia, M. A. Meyers, G. T. Gray, *Metall. Mater. Trans. A* **1992**, *23*, 87−97. [18b] Z. A. Munir, W. Lai, *Combust. Sci. Technol.* **1993**, *88*, 201−209.
[19] [19a] A. M. Nartowski, I. P. Parkin, M. MacKenzie, A. J. Craven, *J. Mater. Chem.* **2001**, *11*, 3116−3119. [19b] A. M. Nartowski, I. P. Parkin, M. MacKenzie, A. J. Craven, I. MacLeod, *J. Mater. Chem.* **1999**, *9*, 1275−1281.
[20] [20a] Q. Y. Lu, J. Q. Hu, K. B. Tang, B. Deng, Y. T. Qian, G. E. Zhou, X. M. Liu, *Chem. Phys. Lett.* **1999**, *314*, 37−39. [20b] C. Li, X. G. Yang, Z. Y. Zhao, Y. T. Qian, *Chem. Lett.* **2002**, *11*, 1088−1089. [20c] J. Q. Hu, Q. Y. Lu, K. B. Tang, B. Deng, R. R. Jiang, Y. T. Qian, W. C. Yu, G. E. Zhou, X. M. Liu, J. X. Wu, *J. Phys. Chem. B* **2000**, *104*, 5251−5254.
[21] JCPDS File, 73−472 (TiC) and No. 73−476 (VC).
[22] P. V. Braun, S. I. Stupp, *Mater. Res. Bull.* **1999**, *34*, 463.
[23] J. A. Dean, *Lange's Handbook of Chemistry*, 15th Edition, McGraw-Hill, New York, **1999**.
[24] S. A. Meschel, O. J. Kleppa, *J. Alloys Comp.* **1997**, *257*, 227−233.
[25] O. D. Velev, K. Furusawa, K. Nagayama, *Langmuir* **1996**, *12*, 2374−2384.

Received April 2, 2003

 © 2003 Wiley-VCH Verlag GmbH & Co. KGaA, Weinheim

Synthesis of Chiral Cationic (Diimino- and diaminodiphosphane)ruthenium Complexes and Their Applications in Catalytic Oxidation − Crystal Structures of *cis*-[RuCl(py){κ^4-$Ph_2PC_6H_4CH{=}NC_6H_{10}N{=}CHC_6H_4PPh_2$}]$BF_4$ and *cis*-[RuCl(py){κ^4-$Ph_2PC_6H_4CH{=}NC_6H_{10}N(H)CH_2C_6H_4PPh_2$}]$BF_4$

Wai-Kwok Wong,*[a] Xiao-Ping Chen,[a] Tat-Wai Chik,[a] Wai-Yeung Wong,[a] Jian-Ping Guo,[a] and Fu-Wa Lee[a]

Keywords: Catalysis / Chiral complexes / Oxidation / N,P ligands / Ruthenium

Halide abstraction of *trans*-[$RuCl_2${κ^4-(1*R*,2*R*)-PNNP}] {(1*R*,2*R*)-PNNP = (1*R*,2*R*)-*N*,*N*′-bis[2-(diphenylphosphanyl)-benzylidene]-1,2-diiminocyclohexane} and *trans*-[$RuCl_2${κ^4-(1*R*,2*R*)-P(NH)(NH)P}] {(1*R*,2*R*)-P(NH)(NH)P = (1*R*,2*R*)-*N*,*N*′-bis[2-(diphenylphosphanyl)benzylidene]-1,2-diaminocyclohexane} with $AgBF_4$ in acetonitrile at ambient temperature gave *cis*-[RuCl(CH_3CN){κ^4-(1*R*,2*R*)-PNNP}][BF_4] (**1**) and *cis*-[RuCl(CH_3CN){κ^4-(1*R*,2*R*)-P(NH)(NH)P}][BF_4] (**2**), respectively. When **1** was refluxed in pyridine (py), the coordinated CH_3CN was replaced by pyridine to form *cis*-[RuCl(py){κ^4-(1*R*,2*R*)-PNNP}][BF_4] (**3**). However, when **2** was refluxed in pyridine, one of the amino moieties (–CH_2–NH–)was oxidized to an imino moiety (–CH=N–) with concomitant displacement of the coordinated CH_3CN by pyridine to produce *cis*-[RuCl(py){κ^4-(1*R*,2*R*)-P(N)(NH)P}][BF_4] (**4**). The structures of **3** and **4** were ascertained by X-ray crystallography. Compounds **1**–**4** are effective catalysts for the epoxidation of various olefins with air. A turnover frequency of up to 733 h^{-1} and an enantiomeric excess of up to 24% were obtained for the epoxidation of styrene catalysed by **2**. Compound **2** can also catalyse the epoxidation, dehydrogenation and C–H activation of various olefins, alcohols and alkanes by *tert*-butyl hydroperoxide with high chemical selectivity.

(© Wiley-VCH Verlag GmbH & Co. KGaA, 69451 Weinheim, Germany, 2003)

Introduction

Diamino-, diimino- and diamidodiphosphanes are very versatile ligands. Their transition metal complexes are effective catalysts for asymmetric hydrogenation,[1] epoxidation,[2] cyclopropanation,[3] and allylic alkylation.[4,5] Thus, the synthesis of chiral diamino-, diimino- and diamidodiphosphane ligands and their applications as auxiliaries for the preparation of chiral catalysts have aroused considerable interest. We have investigated the preparation and chemistry of such phosphanes,[5−10] and reported the synthesis of (1*R*,2*R*)-*N*,*N*′-bis[2-(diphenylphosphanyl)benzylidene]-1,2-diiminocyclohexane [(1*R*,2*R*)-PNNP], (1*R*,2*R*)-*N*,*N*′-bis[2-(diphenylphosphanyl)benzylidene]-1,2-diaminocyclohexane [(1*R*,2*R*)-P(NH)(NH)P], and their Ru^{II},[8] Cu^{I} and Ag^{I} [9] complexes. Recently, we reported the synthesis, structure and catalytic activity of *trans*-[$RuCl_2${κ^3-(1*R*,2*R*)-P(NH)(NH)P}(PPh_3)][11] and its nonchiral analogue *trans*-[$RuCl_2${κ^3-P(NH)(NH)P}(PPh_3)] {P(NH)(NH)P = *N*,*N*′-bis[2-(diphenylphosphanyl)benzylidene]-1,2-diaminoethane}.[12] Here we describe the synthesis of *cis*-[RuCl(CH_3CN){κ^4-(1*R*,2*R*)-PNNP}][BF_4] (**1**), *cis*-[RuCl(CH_3CN)-{κ^4-(1*R*,2*R*)-P(NH)(NH)P}][BF_4] (**2**), *cis*-[RuCl(py){κ^4-(1*R*,2*R*)-PNNP}][BF_4] (**3**) and *cis*-[RuCl(py){κ^4-(1*R*,2*R*)-P(NH)NP}][BF_4] (**4**), and their applications in catalytic oxidation. The crystal structures of **3** and **4** are also presented.

[a] Department of Chemistry, Hong Kong Baptist University
Waterloo Road, Kowloon Tong, Hong Kong
Fax: (internat.) + 852/3411-5862
E-mail: wkwong@hkbu.edu.hk

Results and Discussion

Synthesis and Characterisation of the Complexes

Scheme 1 summarises the reactions leading to complexes **1**−**4**. One chloride ion from *trans*-[$RuCl_2${κ^4-(1*R*,2*R*)-PNNP}] or *trans*-[$RuCl_2${κ^4-(1*R*,2*R*)-P(NH)(NH)P}] was abstracted by $AgBF_4$ in CH_3CN at ambient temperature to afford the solvent-coordinated complex *cis*-[RuCl(CH_3CN){κ^4-(1*R*,2*R*)-PNNP}][BF_4] (**1**) or *cis*-[RuCl(CH_3CN){κ^4-(1*R*,2*R*)-P(NH)(NH)P}][BF_4] (**2**), respectively. The coordination of CH_3CN in **1** and **2** was revealed by their FAB MS, ^{1}H NMR and IR data. The $^{31}P\{^1H\}$ NMR spectra of both **1** and **2** exhibit two doublets [δ = 44.0 ($^2J_{P,P}$ = 24.3 Hz) and 49.8 ppm ($^2J_{P,P}$ = 24.3 Hz) for **1**; δ = 37.3 ($^2J_{P,P}$ = 24.5 Hz) and 44.1 ppm ($^2J_{P,P}$ = 24.5 Hz) for **2**], implying a *cis*-[RuCl(CH_3CN)] arrangement, which is further supported by the X-ray structures of the pyridine derivatives of **1** and **2** (vide infra).

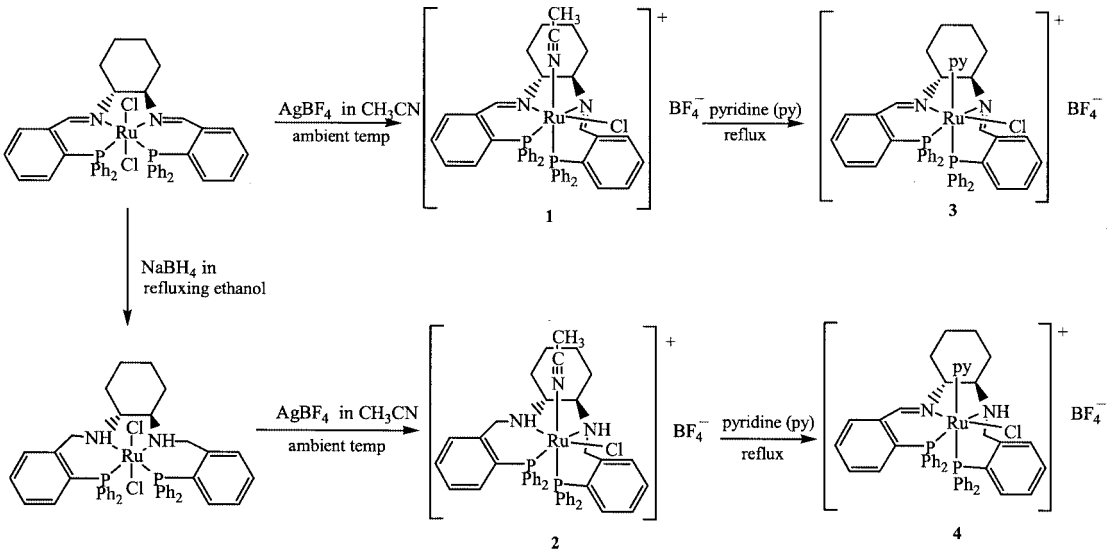

Scheme 1

When **1** was heated under reflux in pyridine the coordinated CH_3CN molecule was substituted by pyridine to give *cis*-[RuCl(py){κ⁴-(1*R*,2*R*)-PNNP}][BF_4] (**3**). The presence of the pyridine ligand was confirmed by FAB MS and ^1H NMR spectroscopic data. The $^{31}P\{^1H\}$ NMR spectrum of **3** exhibited two doublets at δ = 45.1 ($^2J_{P,P}$ = 29.5 Hz) and 46.7 ppm ($^2J_{P,P}$ = 29.5 Hz), suggesting two non-equivalent phosphorus atoms. The structure of **3** was ascertained by X-ray crystallography. A perspective drawing of the cation of **3** is shown in Figure 1. Selected bond lengths and angles are given in Table 1. The Ru atom adopts a distorted octahedral geometry with the chloro and pyridine ligands in a *cis* arrangement and the (1*R*,2*R*)-PNNP ligand behaving as a chelating tetradentate ligand. The chloro ligand is *trans* to the imino group N(1), whereas the pyridine group is

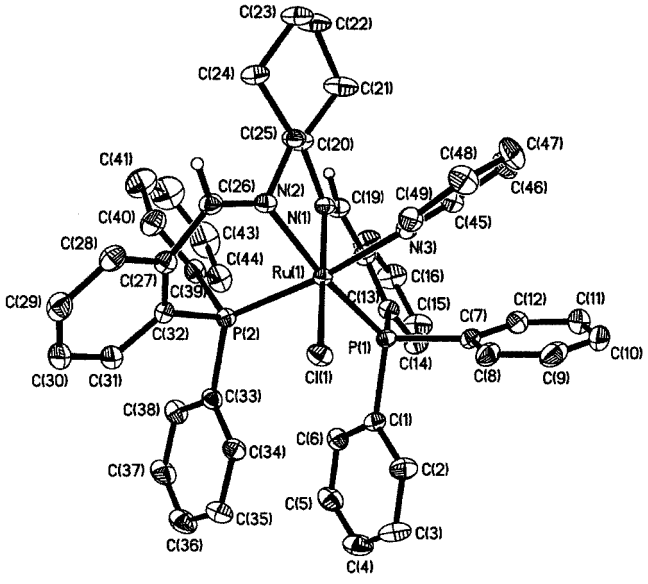

Figure 1. A perspective drawing of the cation of **3**, with the atoms shown at the 30% probability level; hydrogen atoms of the cyclohexyl, pyridine and phenyl rings are omitted for clarity

Table 1. Selected bond lengths [Å] and bond angles [°] for **3** and **4**

Complex **3**			
Ru(1)−N(1)	2.0436(19)	Ru(1)−N(2)	2.1251(17)
Ru(1)−N(3)	2.1799(17)	Ru(1)−P(1)	2.2946(5)
Ru(1)−P(2)	2.3104(5)	Ru(1)−Cl(1)	2.4326(6)
N(1)−C(19)	1.283(3)	N(2)−C(26)	1.260(3)
N(2)−C(25)	1.482(3)	N(1)−C(20)	1.528(3)
N(1)−Ru(1)−N(2)	78.58(7)	P(1)−Ru(1)−P(2)	100.00(2)
N(3)−Ru(1)−Cl(1)	88.18(5)	P(1)−Ru(1)−Cl(1)	94.16(2)
N(2)−Ru(1)−Cl(1)	94.38(6)	N(1)−Ru(1)−Cl(1)	171.54(5)
C(26)−N(2)−C(25)	118.67(17)	C(19)−N(1)−C(20)	113.50(19)
N(1)−Ru(1)−N(3)	86.63(7)	N(3)−Ru(1)−P(2)	168.17(5)
Complex **4**			
Ru(1)−N(1)	2.022(4)	Ru(1)−N(2)	2.162(3)
Ru(1)−N(3)	2.192(4)	Ru(1)−P(1)	2.2835(11)
Ru(1)−P(2)	2.3339(11)	Ru(1)−Cl(1)	2.4364(12)
N(1)−C(19)	1.296(6)	N(2)−C(31)	1.480(6)
N(1)−C(25)	1.527(5)	N(2)−C(30)	1.485(6)
N(1)−Ru(1)−N(2)	81.49(14)	N(1)−Ru(1)−N(3)	86.28(14)
N(2)−Ru(1)−N(3)	82.57(13)	N(1)−Ru(1)−P(1)	93.80(10)
N(1)−Ru(1)−Cl(1)	172.67(10)	N(3)−Ru(1)−Cl(1)	89.64(11)
P(1)−Ru(1)−Cl(1)	92.32(4)	P(1)−Ru(1)−P(2)	99.98(4)
N(1)−C(19)−C(12)	129.7(4)	N(2)−C(31)−C(32)	116.3(4)

trans to the diphenylphosphanyl group P(2). The Ru−P, Ru−Cl and Ru−N distances are in the ranges expected for similar (diamino- and diaminodiphosphane)ruthenium complexes.[1,8,11−13] The relatively short Ru(1)−N(1) bond [2.0436(19) Å] is a reflection of the *trans* influence. The difference between Ru(1)−N(2) [2.1251(17) Å] and Ru(1)−N(3) [2.1799(17) Å] may be attributed to the chelating effect of the tetradentate diiminodiphosphane ligand. The N(1)−C(19) [1.283(3) Å] and N(2)−C(26) [1.260(3) Å] distances fall in the normal range observed for carbon−nitrogen double bonds.[11,12]

When **2** was heated under reflux in pyridine one of the two amino moieties (−CH_2−NH−) of the tetradentate diaminodiphosphane ligand was oxidized to an imino moiety

 © 2003 Wiley-VCH Verlag GmbH & Co. KGaA, Weinheim

(−CH=N−) with concomitant displacement of the coordinated CH_3CN by pyridine to give *cis*-[RuCl(py){κ⁴-(1*R*,2*R*)-P(NH)NP}][BF_4] (**4**), whose structure was established by X-ray crystallography. A perspective drawing of the cation of **4** is shown in Figure 2 and selected bond lengths and bond angles are listed in Table 1. Structural analysis revealed that the κ⁴-(1*R*,2*R*)-P(NH)(NH)P ligand had been oxidized to a κ⁴-(1*R*,2*R*)-P(NH)NP ligand with the amino group *trans* to the chloride ion oxidized to an imino group. The N(1)−C(19) and N(2)−C(31) distances [1.296(6) and 1.480(6) Å] lie in the normal ranges observed for carbon−nitrogen double and single bonds, respectively. The Ru atom adopts a slightly distorted octahedral geometry with a *cis* arrangement of the chloro and pyridine ligands. The Ru−P, Ru−Cl and Ru−N distances are similar to those of **3**. The Ru−P bond [Ru(1)−P(1) 2.2835(11) Å] *trans* to the amino group N(2) is shorter than that [Ru(1)−P(2) 2.3133(11) Å] *trans* to the pyridine group N(3) due to the *trans* influence. The difference in Ru−N distances [Ru−N(1) 2.022(4) Å vs. Ru(1)−N(2) 2.162(3) Å] implies that the imino nitrogen atom, N(1), is more tightly bound to the Ru centre than the amino nitrogen atom, N(2), presumably due to dπ−pπ back donation to the imino group. The N(1)−Ru(1)−Cl(1) angle of 172.67(10)° indicates that the chloro ligand is *trans* to the imino nitrogen atom. This configuration is favoured over the alternative with *trans*-Cl−Ru−N(amine) as an imino nitrogen atom is a better π-acceptor than an amino nitrogen atom. The solid-state structure of **4** is consistent with its $^{31}P\{^1H\}$ and ^1H NMR, IR and FAB MS data. The $^{31}P\{^1H\}$ NMR spectrum shows two doublets at δ = 42.7 ($^2J_{P,P}$ = 28.8 Hz) and 52.7 ppm ($^2J_{P,P}$ = 28.8 Hz), which can be assigned to P(1) and P(2), respectively (Figure 2). The presence of the imino group is further supported by the ^1H NMR spectrum, which shows a broad singlet at δ = 9.42 ppm for the −C*H*=N− proton. The IR spectrum also shows the *ν*(C=N) absorption at 1657 cm^{-1}. Oxidation of the coordinated amino moiety to a coordinated imino moiety has been reported recently for related (diaminodiphosphane)ruthenium complexes. At room temperature, *trans*-[$RuCl_2${κ³-(1*R*,2*R*)-P(NH)(NH)P}(PPh_3)] was slowly oxidized by air to *trans*-[$RuCl_2${κ³-(1*R*,2*R*)-P(NH)NP}(PPh_3)],[11] and *trans*-[$RuCl_2${κ³-P(NH)(NH)P(O)}(PPh_3)] by H_2O_2 to *trans*-[$RuCl_2${κ³-P(NH)NP(O)}(PPh_3)].[12] In both cases one of the two coordinated amino moieties was oxidized to a coordinated imino moiety.

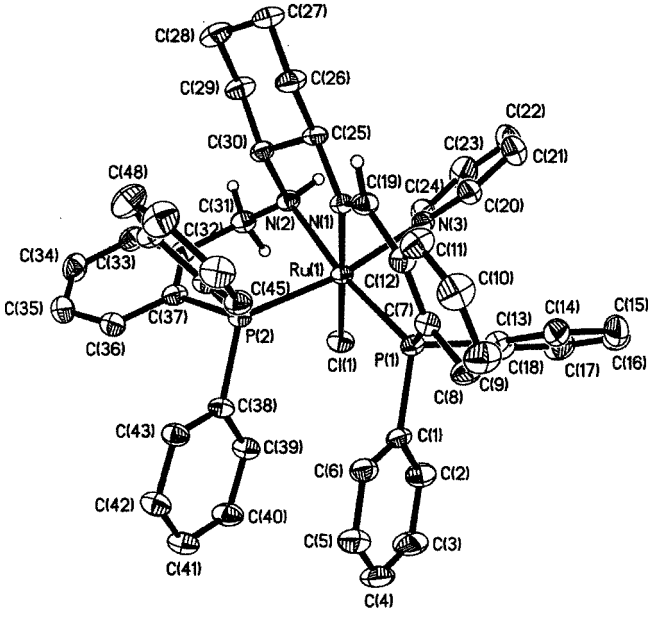

Figure 2. A perspective drawing of the cation of **4**, with the atoms shown at the 30% probability level; hydrogen atoms of the cyclohexyl, pyridine and phenyl rings are omitted for clarity

Catalytic Oxidation

Ruthenium-catalysed oxidation of alkenes with various oxidants has drawn considerable interest recently, but there are very few studies on aerobic oxidation.[11,12,14,15] In this work, air was chosen as one of the oxidants. Furthermore, complexes **1**−**4** were employed as the catalysts for the asymmetric oxidation of olefins. Styrene, the first substrate we used, gave three main products, namely styrene oxide, benzaldehyde and phenylacetaldehyde (Table 2). Nevertheless, with **4** as the catalyst, styrene was converted into styrene oxide with exceptionally high selectivity (80%). Presumably, epoxidation prevails over the oxidative cleavage of the C=C double bond. In addition, the enantioselectivity of all these catalytic epoxidation reactions is comparatively low. However, the highest TOF (733 h^{-1}) and the highest enantiomeric excess (*ee*) (24%) were obtained with **2**. Therefore, complex **2** was chosen to study the catalytic asymmetric oxidation of various olefins with air (Table 3). Although conversions of sterically crowded *cis*- and *trans*-stilbene were expected, and found, to be very low, those of α-methylstyrene and 1,2-dihydronaphthalene were as good as that of styrene. It is noteworthy that the catalytic oxidation of α-methylstyrene and 1,2-dihydronaphthalene with air using **2** selectively gave acetophenone and 1,2-dihydronaphthalene epoxide, respectively. Unfortunately, only a moderate *ee* was obtained from α-methylstyrene, which is attributed to the formation of a planar intermediate. In addition, the dependence of the asymmetric oxidation of styrene using **2** on various oxidants was investigated (Table 4). *tert*-Butyl hydroperoxide (TBHP) clearly gave the highest TOF and the highest selectivity for styrene oxide but only with poor enantioselectivity. The catalytic oxidation probably proceeds via a planar species, without the involvement of a chiral metal centre as an active intermediate. Investigation on the mechanism of the autoxidation of olefins is in progress.

The catalytic activity of **2** towards the oxidation of organic substrates with TBHP has also been studied (Table 5). In control experiments, no oxidized product was detected in the absence of either **2** or TBHP. Complex **2** catalysed the oxidation of styrene (Entry 1), with TBHP giving styrene oxide as the major product along with benzylaldehyde, possibly by C=C cleavage, and phenylacetaldehyde; α-methylstyrene (Entry 2) mainly afforded phenylacetalde-

 © 2003 Wiley-VCH Verlag GmbH & Co. KGaA, Weinheim

Table 2. Asymmetric oxidation of styrene with air using **1**−**4** as catalysts

Catalyst	TOF [h^{-1}][a]	Selectivity (%)[b] Styrene oxide (*ee* in %)[c]	Benzaldehyde	Phenylacetaldehyde
1	704	47 (11)	44	9
2	733	43 (24)	53	3
3	451	33 (23)	43	16
4	352	80 (18)	18	2

[a] Determined by GC analysis based on the starting substrate using an internal standard. [b] Identified by GC-MS. [c] Determined by GC analysis with a chiral column based on an internal standard.

Table 3. Asymmetric oxidation of olefins with air using **2** as catalyst

Substrate	Conv. (%)[a]	Selectivity (%)[b] Epoxide (*ee* in %) [c]	Benzaldehyde
Styrene	52	43 (24)	53
α-Methylstyrene	32	7.5 (23.4)	89[d]
1,2-Dihydronaphthalene	64	96 (0)	0
cis-Stilbene	9	53 (0)	19
trans-Stilbene	2	28 (0)	39

[a] Determined by GC analysis based on the starting substrate using an internal standard. [b] Identified by GC-MS. [c] Determined by GC analysis with a chiral column based on an internal standard. [d] Acetophenone was obtained.

Table 4. Asymmetric oxidation of styrene with various oxidants using **2** as catalyst

Oxidant	TOF [h^{-1}][a]	Selectivity (%)[b] Styrene oxide (*ee* in %) [c]	Benzaldehyde	Phenylacetaldehyde
TBHP	305	53 (2.3)	31	12
H_2O_2	55	11 (7.8)	84	5.5
$NaIO_4$	61	45 (23.7)	37	15
NaOCl	38	0 (0)	87	13

[a] Determined by GC analysis based on the starting substrate using an internal standard. [b] Identified by GC-MS. [c] Determined by GC analysis with a chiral column based on an internal standard.

hyde. Notably, *cis*- and *trans*-stilbene (Entries 3 and 4) were selectively oxidized to 2,3-diphenyloxirane whereas oxidation of 1,2-dihydronaphthalene (Entry 5) gave only naphthalene; we believe that the formation of a highly conjugated system provides the necessary driving force for the conversion. It is interesting that the oxidation of *cis*-cyclooctene (Entry 6) and of norbornene (Entry 7) produced predominantly 9-oxabicyclo[6.1.0]nonane and 2,3-epoxynorbornane, respectively, whereas oxidation of cyclohexene (Entry 8) afforded 2-cyclohexen-1-one as the major product. The oxidation of cyclohexene (Entry 9) was notably suppressed when 2,6-di-*tert*-butyl-4-methylphenol was added to the reaction mixture, which suggests a substantial radical character in the active intermediate.[16] When the terminal oxidant was changed from TBHP to cumene hydroperoxide (CHP), the product profile (Entry 10) is dominated by cumene, acetophenone and 2-phenyl-2-propanol, which are presumably generated by β-scission of cumyloxy radicals. The oxidation of cyclohexene by TBHP might involve abstraction of the allylic hydrogen atom from the relatively flexible six-membered ring to give an allylic free radical intermediate that can be stabilized by the π-system of the double bond; this is unlikely to occur with *cis*-cyclooctene and norbornene due to inefficient allylic stabilisation in the more rigid and nonplanar norbornenyl and cyclooctenyl radicals. Conversely, the epoxidation of norbornene and *cis*-cyclooctene could result from the homolytic addition of the *t*BuOO$^{\cdot}$ species to the more strained double bond, followed by homolytic cyclisation.[17−20] The homolytic mechanism accords with the absence of epoxidation with cyclohexene, which is less prone to addition of peroxy radicals. Indeed, the predominance of peroxy substitution follows from the ease with which H-atom abstraction occurs from the allylic position of cyclohexene.

Moreover, complex **2** would also be an efficient catalyst for the oxidation of alcohol with TBHP. In the presence of 2 equiv. of TBHP in benzene, complex **2** catalysed the oxidation of primary alcohols (Entries 11 and 12, Table 5) to the corresponding acid and/or ester, of secondary alcohols (Entries 13 and 14) to the corresponding ketones, and of phenol (Entries 15 and 16) to *p*-benzoquinone. Minisci and co-workers have reported (porphyrin)Fe^{III}-catalysed oxidation of phenol to *p*-benzoquinone by TBHP by a free

 © 2003 Wiley-VCH Verlag GmbH & Co. KGaA, Weinheim

Table 5. Catalytic oxidation of organic compounds with TBHP using **2** as catalyst

Entry	Substrate	Conv. (%)[a]	Product[b]	Selectivity (%)[c]
1	styrene	86	benzylaldehyde	31
			styrene oxide	53
			phenylacetaldehyde	12
2	α-methylstyrene	88	phenylacetaldehyde	96
3	*trans*-stilbene	70	benzaldehyde	15
			benzoic acid	17
			2,3-diphenyloxirane	58
4	*cis*-stilbene	15	benzaldehyde	19
			benzoic acid	3.5
			2,3-diphenyloxirane	71
5	1,2-dihydronaphthalene	85	naphthalene	97
6	*cis*-cyclooctene	39	9-oxabicyclo[6.1.0]nonane	95
7	norbornene	27	2,3-epoxynorbornane	96
8	cyclohexene	17	2-cyclohexen-1-ol	2
			2-cyclohexen-1-one	95
9	cyclohexene[d]	1.1	2-cyclohexen-1-one	96
10	cyclohexene[e]	1.1	2-cyclohexen-1-ol	1
			2-cyclohexen-1-one	1
			cumene	11
			acetophenone	29
			2-phenyl-2-propanol	29
11	benzyl alcohol	75	benzoic acid	75
			benzyl benzoate	20
12	3-methyl-1-butanol	58	3-methylbutyl 3-methylbutanoate	94
13	2-nonanol	77	2-nonanone	99
14	cyclohexanol	59	cyclohexanone	98
15	phenol	49	*p*-benzoquinone	95
16	phenol[f]	80	*p*-benzoquinone	96
17	*n*-octane	4	2-octanone	33
			4-octanone	61
18	cyclohexane	1	cyclohexanol	22
			cyclohexanone	77
19	cyclohexane[g]	1	cyclohexanol	37
			cyclohexanone	39
			cyclohexyl chloride	18
20	cyclohexane[h]	2	cyclohexanol	1
			cyclohexanone	1.1
			cumene	9
			acetophenone	27
			2-phenyl-2-propanol	29
21	adamantane	30	adamantan-1-ol	59
			2-adamantanone	35
22	*n*-propylbenzene	17	1-phenyl-1-propanone	98
23	ethylbenzene	36	acetophenone	96
24	diphenylmethane	73	benzophenone	99
25	cumene	40	2-phenyl-2-propanol	85
			acetophenone	8
26	1,3-diisopropylbenzene	58	2,4-diisopropylphenol	94

[a] Determined by GC analysis based on the starting substrate using an internal standard. [b] Identified by GC-MS. [c] Selectivity: determined by GC analysis based on the amount of converted substrate using an internal standard. [d] 2,6-Di-*tert*-butyl-4-methylphenol (0.35 g, 1.60 mmol) was also added to the reaction mixture. [e] Cumene hydroperoxide was used as the oxidant. [f] Triethylamine (0.09 mmol) was also added to the reaction mixture. [g] Benzene/CCl_4 (9:1, v/v) as solvent. [h] Cumene hydroperoxide was used as the oxidant.

radical mechanism.[21] They found that addition of a nitrogen-containing base such as pyridine enhanced the production of *p*-benzoquinone by catalyzing the decomposition of the alkylperoxy intermediate. We used a similar strategy to test the involvement of reactive free radical species during catalysis and found that the rate of *p*-benzoquinone formation was enhanced by the addition of triethylamine, which is consistent with the formation of a *tert*-butylperoxy intermediate.[21]

Furthermore, complex **2** can catalyse the oxidation of unactivated saturated C−H bonds with TBHP. Alkanes (Table 5, Entries 17, 18 and 21) were oxidized to their corresponding ketones, alcohols or a mixture of both. In the presence of 2 equiv. of TBHP and a catalytic amount of **2**, *n*-octane was oxidized to a mixture of 2-octanone and 4-octanone, cyclohexane to a mixture of cyclohexanol and cyclohexanone, and adamantane to adamantan-1-ol and 2-adamantone. The results revealed that oxidation of *n*-

 © 2003 Wiley-VCH Verlag GmbH & Co. KGaA, Weinheim

octane proceeded by secondary C−H bond activation exclusively with no detectable products from primary C−H bond activation, and that adamantane preferentially gave a tertiary alcohol. Presumably, alkane oxidation proceeded by an H-atom abstraction pathway to give a relatively stable free radical intermediate. This is supported by the formation of cyclohexyl chloride (Entry 19) along with cyclohexanone and cyclohexanol upon catalytic oxidation of cyclohexane by TBHP in the presence of CCl_4. Moreover, copious formation of cumene, acetophenone and 2-phenyl-2-propanol (Entry 20) from cumene hydroperoxide also implies an alkylperoxy radical as the transient intermediate.[22] A similar mechanism has been proposed for the ruthenium-catalysed oxidation of alkanes with TBHP.[23] Under similar conditions, *n*-propylbenzene (Entry 22) was oxidized to 1-phenyl-1-propanone, ethylbenzene (Entry 23) to acetophenone, diphenylmethane (Entry 24) to benzophenone, cumene (Entry 25) to a mixture of 2-phenyl-2-propanol and acetophenone, and 1,3-diisopropylbenzene (Entry 26) to 2,4-diisopropylphenol. It is obvious that the activity of arylalkanes towards oxidation by **2** is higher than those of nonarylalkanes and it is consistent with the relative stability of the radicals generated by H-atom abstraction, i.e. aryl-substituted radicals are more stable than unsubstituted radicals. Experimental evidence suggests that free radicals are probably involved in the catalytic oxidation of various organic substrates. In general, the oxidation of a series of organic substrates with TBHP by complex **2** involves a free radical mechanism.

Conclusion

We have described the synthesis, characterisation and structural studies of a series of new chiral cationic (diimino- and diaminodiphosphane)ruthenium complexes. Detailed investigations of their catalytic properties in the asymmetric oxidations of various organic molecules show that these chiral complexes effectively catalyse the epoxidation of a range of alkenes with air; the data are compared to those using other oxidants. Experimental evidence suggests that free radicals are probably involved in the catalytic oxidation processes associated with these chiral complexes.

Experimental Section

General Remarks: Unless otherwise stated, all experiments were conducted under dry nitrogen. Solvents were dried by standard procedures, distilled and deaerated before use. Reagent grade chemicals were used and, where appropriate, degassed before use. All organic substrates were purified by literature methods, and their purities verified by GC or ^{1}H NMR analysis. Melting points were taken in sealed capillaries and are uncorrected. The compounds *trans*-[$RuCl_2${κ^4-(1*R*,2*R*)-PNNP}][8] and *trans*-[$RuCl_2${κ^4-(1*R*,2*R*)-P(NH)(NH)P}][11] were prepared according to literature methods. IR spectra (KBr pellets) were recorded with a Nicolet Nagna-IR 550 spectrometer and NMR spectra with a JEOL EX270 spectrometer. Chemical shifts of ^{1}H NMR spectra were referenced to internal deuterated solvents and then recalculated to TMS (δ = 0.00 ppm) and those of ^{31}P{^{1}H} NMR spectra were referenced to external 85% H_3PO_4. Low-resolution mass spectra were obtained with Finnigan MAT SSQ-710 and MAT 95 spectrometers in positive FAB mode and are reported as *m*/*z*. Gas chromatograms were obtained with an HP 5890 GC system equipped with an FID detector or an HP 6890−5972 GC-MSD system. An HP 5890 GC equipped with a WCOT fused silica capillary column (25 × 0.25 mm, 0.25-μm film, Varian) was used for chiral analyses. Microanalyses were performed by the Shanghai Institute of Organic Chemistry, Chinese Academy of Sciences. The progress of all reactions was monitored by ^{31}P{^{1}H} NMR spectroscopy.

***cis*-[RuCl(CH_3CN){κ^4-(1*R*,2*R*)-PNNP}][BF_4] (1):** A red solution of *trans*-[$RuCl_2${κ^4-(1*R*,2*R*)-PNNP}] (0.260 g, 0.313 mmol) in acetonitrile (10 mL) was added dropwise to a solution of $AgBF_4$ (0.062 g, 0.318 mmol) in acetonitrile (10 mL). The mixture was then stirred at ambient temperature for 24 h to give an orange solution with a white precipitate. The solution was filtered and the solvents evaporated to dryness. The resultant orange residue was redissolved in CH_2Cl_2 and filtered. Diethyl ether was added and the mixture was then cooled to 0 °C to give an orange solid that was filtered off, washed with diethyl ether and *n*-hexane, and dried in vacuo. Yield: 0.220 g, 76%; m.p. 180−182 °C (dec). IR (KBr): $\tilde{\nu}$ = 3059 s, 2932 m, 2858 m, 1964 m, 1642 s, 1434 s, 1085 br, 749 s, 702 s, 527 s cm^{-1}. ^{1}H NMR ($CDCl_3$): δ = 1.20−2.31 (m, 8 H, CH_2CH_2), 2.53 (s, 3 H, CH_3CN), 3.71 (m, 2 H, NC*H*−C*H*N), 6.37−7.76 (m, 28 H, aryl *H*), 8.77 (d, $^3J_{P-H}$ = 10.0 Hz, 1 H, −C*H*=N−), 8.97 (d, $^3J_{P-H}$ = 8.6 Hz, 1 H, −C*H*=N−) ppm. ^{31}P{^{1}H} NMR ($CDCl_3$): δ = 44.0 (d, $^2J_{P,P}$ = 24.3 Hz), 49.8 (d, $^2J_{P,P}$ = 24.3 Hz) ppm. FAB MS: *m*/*z* = 836 [M − BF_4]$^+$, 795 [M − CH_3CN − BF_4]$^+$. $C_{46}H_{43}BClF_4N_3P_2Ru\cdot1.5CH_2Cl_2\cdot H_2O$ (1068.56): calcd. C 53.38, H 4.54, N 3.93; found C 53.01; H 4.62; N 4.11. $[\alpha]_D^{20}$ = −91.56 (*c* = 0.5, CH_2Cl_2).

***cis*-[RuCl(CH_3CN){κ^4-(1*R*,2*R*)-P(NH)(NH)P}][BF_4] (2):** *trans*-[$RuCl_2${κ^4-(1*R*,2*R*)-P(NH)(NH)P}] (0.400 g, 0.480 mmol) and $AgBF_4$ (0.100 g, 0.513 mmol) were dissolved in acetonitrile (40 mL) and the mixture stirred at ambient temperature for 24 h. A yellow solution with a white precipitate was obtained. The solution was filtered and the solvents evaporated to dryness in vacuo. The resultant yellow residue was then redissolved in CH_2Cl_2 and *n*-hexane was added to initiate the crystallisation of the product as a yellow solid. Yield: 0.400 g, 90%; m.p. 189−190 °C (dec). IR (KBr): $\tilde{\nu}$ = 3431 s, 3053 m, 2934 m, 1963 m, 1476 m, 1439 s, 1077 vs, 746 s, 700 s, 519 s cm^{-1}. ^{1}H NMR ($CDCl_3$): δ = 1.58−2.04 (m, 8 H, CH_2CH_2), 2.62 (s, 3 H, CH_3CN), 2.81−3.01 (m, 4 H, CH_2N), 3.65 (m, 2 H, NC*H*−C*H*N), 4.21 (m, 2 H, N*H*), 6.71−8.00 (m, 28 H, aryl *H*) ppm. ^{31}P{^{1}H} NMR ($CDCl_3$): δ = 37.3 (d, $^2J_{P,P}$ = 24.5 Hz), 44.1 (d, $^2J_{P,P}$ = 24.5 Hz) ppm. FAB MS: *m*/*z* = 840 [M − BF_4]$^+$, 799 [M − CH_3CN − BF_4]$^+$. $C_{46}H_{47}BClF_4N_3P_2Ru\cdot CH_2Cl_2\cdot 2H_2O$ (1048.14): calcd. C 53.81, H 5.06, N 4.01; found C 53.71, H 5.16, N 3.92. $[\alpha]_D^{20}$ = 72.80 (*c* = 0.5, CH_2Cl_2).

***cis*-[RuCl(py){κ^4-(1*R*,2*R*)-PNNP}][BF_4] (3):** Complex **1** (0.100 g, 0.108 mmol) was dissolved in pyridine (20 mL) and the mixture was heated under reflux for 30 min in air and then all volatile components were removed in vacuo. The resultant residue was washed with diethyl ether and recrystallised from CH_2Cl_2/*n*-hexane to give red crystals. Yield: 0.085 g, 82%; m.p. 197−198 °C (dec). IR (KBr): $\tilde{\nu}$ = 3058 m, 2924 m, 1636 m, 1486 m, 1439 s, 1310 m, 1088 vs, 752 m, 700 m, 524 s cm^{-1}. ^{1}H NMR ($CDCl_3$): δ = 0.90−1.82 (m, 8 H, CH_2CH_2), 2.49 (m, 1 H, NCH−C*H*N), 2.78 (m, 1 H, NC*H*−CHN), 6.58−7.90 (m, 28 H, aryl *H*), 8.30 (d, $^3J_{P-H}$ = 8.7 Hz, 1 H, −C*H*=N−), 8.41 (m, 3 H, pyridyl *H*s), 8.72 (d,

 © 2003 Wiley-VCH Verlag GmbH & Co. KGaA, Weinheim

$^3J_{P-H}$ = 8.7 Hz, 1 H, −C*H*=N−), 9.03 (m, 2 H, pyridyl *H*) ppm. $^{31}P\{^1H\}$ NMR ($CDCl_3$): δ = 45.1 (d, $^2J_{P,P}$ = 29.5 Hz), 46.7 (d, $^2J_{P,P}$ = 29.5 Hz) ppm. FAB MS: *m*/*z* = 874 $[M - BF_4]^+$, 795 $[M - py - BF_4]^+$. $C_{49}H_{45}BClF_4N_3P_2Ru{\cdot}CH_2Cl_2{\cdot}2H_2O$ (1082.15): calcd. C 55.49, H 4.76, N 3.88; found C 55.73, H 4.95, N 3.87. $[\alpha]_D^{20}$ = −45.85 (*c* = 0.5, CH_2Cl_2).

***cis*-[RuCl(py){κ⁴-(1*R*,2*R*)-P(NH)NP}][BF₄] (4):** Complex **2** (0.100 g, 0.108 mmol) was added to pyridine (20 mL) and the mixture heated under reflux for 6 h in air. All volatiles were then removed in vacuo and the residue was washed, with *n*-hexane and toluene, and then recrystallised from CH_2Cl_2/toluene to give an orange solid. Yield: 0.070 g, 67%; m.p. 185−186 °C. IR (KBr): ν̃ = 3058 m, 2955 m, 1657 m, 1558 m, 1481 m, 1429 s, 1258 s, 1083 vs, 803 s, 746 m, 695 s, 524 s cm^{-1}. ^1H NMR ($CDCl_3$): δ = 1.69−2.01 (m, 8 H, C*H*$_2$C*H*$_2$), 2.51 (m, 1 H, CH*H*N), 2.76 (m, 1 H, C*H*HN), 3.67 (m, 1 H, −NCH−C*H*N−), 4.45 (m, 2 H, N*H* and −NC*H*−CHN−), 6.24−8.59 (m, 33 H, aryl and pyridyl *H*), 9.42 (br. s, 1 H, −C*H*=N−) ppm. $^{31}P\{^1H\}$ NMR ($CDCl_3$): δ = 42.69 (d, $^2J_{P,P}$ = 28.8 Hz), 52.71 (d, $^2J_{P,P}$ = 28.8 Hz) ppm. FAB MS: *m*/*z* = 876 $[M - BF_4]^+$, 797 $[M - py - BF_4]^+$. $C_{49}H_{47}BClF_4N_3P_2Ru{\cdot}C_7H_8$ (1055.35): calcd. C 63.72, H 5.26, N 3.98; found C 63.58, H 5.37, N 3.90. $[\alpha]_D^{20}$ = 81.31 (*c* = 0.5, CH_2Cl_2).

General Procedure for Catalytic Oxidation by Air: A reaction mixture of organic substrate (3.0 g) and catalyst (0.001 mmol) was stirred in open air at 80 °C for 16 h. The resultant solution was analysed by GC, and the identity of the analytes verified by GC-MS and standard compounds (Tables 2 and 3). Control experiments were performed in the absence of catalyst under identical conditions.

General Procedure for Catalytic Oxidation by TBHP: A solution of organic substrate (1.5 mmol), TBHP (80% in di-*tert*-butyl peroxide, 3.2 mmol) and **2** (1.0 mg, 0.001 mmol) in benzene (3 mL) was stirred under nitrogen at ambient temperature for 16 h. The reaction mixture was then poured slowly into a 10% aqueous Na_2SO_3 solution (5 mL) to destroy any remaining TBHP and the resultant solution was extracted with dichloromethane (2 × 5 mL). The organic layer was separated, dried with anhydrous Na_2SO_4 and analysed by GC (Tables 4 and 5). The identity of the analytes was verified by GC-MS and standard compounds. Control experiments without either the catalyst or TBHP were performed under identical conditions.

General Procedure for Catalytic Oxidation by H_2O_2: Styrene (0.16 g, 1.5 mmol) and **2** (2.0 mg, 0.002 mmol) were dissolved in acetone (3 mL). Aqueous hydrogen peroxide [0.29 g, 35% (w/w), 3.0 mmol] was then added as one portion and the reaction mixture was stirred under nitrogen at ambient temperature for 16 h, and then slowly poured into a 10% aqueous Na_2SO_3 solution (5 mL) to destroy any remaining H_2O_2. The resultant solution was extracted with dichloromethane (2 × 5 mL) and the organic layer was separated, dried with anhydrous Na_2SO_4 and analysed by GC (Table 4). Control experiments without either the catalyst or H_2O_2 were performed under identical conditions.

General Procedure for Catalytic Oxidation by $NaIO_4$: Styrene (0.16 g, 1.5 mmol) and **2** (2.0 mg, 0.002 mmol) were dissolved in acetone (3 mL). $NaIO_4$ (0.64 g, 3.0 mmol) was then added as one portion and the reaction mixture was stirred under nitrogen at ambient temperature for 16 h. The resultant solution was analysed by GC (Table 4). Control experiments in the absence of either the catalyst or $NaIO_4$ were performed under identical conditions.

General Procedure for Catalytic Oxidation by NaOCl: Styrene (0.16 g, 1.5 mmol) and **2** (2.0 mg, 0.002 mmol) were dissolved in acetone (3 mL). An excess of aqueous NaOCl was added as one portion and the reaction mixture was stirred under nitrogen at ambient temperature for 16 h. The resultant solution was analysed by GC (Table 4). Control experiments in the absence of either the catalyst or NaOCl were performed under identical conditions.

X-ray Crystallographic Studies: Pertinent crystallographic data and other experimental details are summarised in Table 6. Crystals of **3**·1.5CH_2Cl_2 and **4**·1.5CH_2Cl_2 suitable for X-ray diffraction studies

Table 6. Crystallographic data for complexes **3** and **4**

	3·1.5CH_2Cl_2	**4**·1.5CH_2Cl_2
Empirical formula	$C_{49}H_{45}BClF_4N_3P_2Ru{\cdot}1.5CH_2Cl_2$	$C_{49}H_{47}BClF_4N_3P_2Ru{\cdot}1.5CH_2Cl_2$
Formula mass	1088.53	1090.55
Crystal size [mm]	0.20 × 0.15 × 0.10	0.20 × 0.15 × 0.12
Crystal system	monoclinic	monoclinic
Space group	*C*2	*C*2
a [Å]	35.122(2)	35.0430(19)
b [Å]	10.4480(7)	10.4501(6)
c [Å]	13.0196(8)	13.4397(7)
α [°]	90	90
β [°]	91.143(2)	93.8820(10)
γ [°]	90	90
V [Å^3]	4776.7(5)	4910.4(5)
Z	4	4
T [K]	293	293
μ(Mo-K_α) [mm^{-1}]	0.674	0.656
F(000)	2208	2216
θ range [°]	1.93−27.51	1.52−27.51
Reflections collected	14010	14609
Independent reflections (R_{int})	8351 (0.0168)	7466 (0.0272)
Observed reflections	7267	6535
Goodness-of-fit on F^2	1.060	1.029
*R*1, *wR*2 [$I > 2\sigma(I)$]	0.0348, 0.0987	0.0358, 0.0896
*R*1, *wR*2 (all data)	0.0361, 0.0999	0.0440, 0.0981

 © 2003 Wiley-VCH Verlag GmbH & Co. KGaA, Weinheim

were grown by slow concentration of solutions of **3** and **4** in CH_2Cl_2/*n*-hexane. The crystals were wrapped in epoxy glue, to prevent solvent loss, and mounted on a thin glass fibre. No decay in intensity was encountered during the data collection. Intensity data were collected at 293 K with a Bruker Axs SMART 1000 CCD area-detector diffractometer using graphite-monochromated Mo-K_α radiation. The collected frames were processed with the software SAINT[24] and an absorption correction was applied (SADABS)[25] to the collected reflections. The structures were solved by direct methods (SHELXTL™)[26] and refined against F^2 by full-matrix least-squares analysis. All non-hydrogen atoms were refined anisotropically. Except for the hydrogen atoms of the solvent molecules in **3** and **4**, which were not located, all other hydrogen atoms were generated in their idealised positions and allowed to ride on their respective parent carbon atoms. CCDC-204329 and -204330 contain the supplementary crystallographic data for this paper. These data can be obtained free of charge at www.ccdc.cam.ac.uk/conts/retrieving.html [or from the Cambridge Crystallographic Data Centre, 12 Union Road, Cambridge CB2 1EZ, UK; Fax: (internat.) + 44-1223/336-033; E-mail: deposit@ccdc.cam.ac.uk].

Acknowledgments

W. K. W. thanks the Hong Kong Baptist University and the Hong Kong Research Grants Council (HKBU 2053/97P) for financial support.

[1] J. X. Gao, T. Ikariya, R. Noyori, *Organometallics* **1996**, *15*, 1087−1089.
[2] R. M. Stoop, A. Mezzetti, *Green Chem.* **1999**, *1*, 39−41.
[3] B. M. Trost, *Acc. Chem. Res.* **1996**, *29*, 355−364.
[4] C. P Butts, J. Crosby, G. C. Lloyd-Jones, S. C. Stephen, *Chem. Commun.* **1999**, 1707−1708.
[5] J. H. Song, D. J. Cho, S. J. Jeon, Y. H. Kim, T. J. Kim, J. H. Jeong, *Inorg. Chem.* **1999**, *38*, 893−896.
[6] W. K. Wong, J. X. Gao, Z. Y. Zhou, T. C. W. Mak, *Polyhedron* **1993**, *12*, 1415−1417.
[7] J. X. Gao, H. L. Wan, W. K. Wong, M. C. Tse, W. T. Wong, *Polyhedron* **1996**, *15*, 1241−1251.
[8] W. K. Wong, T. W. Chik, X. Feng, T. C. W. Mak, *Polyhedron* **1996**, *15*, 3905−3907.
[9] W. K. Wong, T. W. Chik, K. N. Hui, I. Williams, X. Feng, T. C. W. Mak, C. M. Che, *Polyhedron* **1996**, *15*, 4447−4460.
[10] W. K. Wong, J. X. Gao, W. T. Wong, C. M. Che, *Polydedron* **1993**, *12*, 2063−2066.
[11] W. K. Wong, X. P. Chen, W. X. Pan, J. P. Guo, W. Y. Wong, *Eur. J. Inorg. Chem.* **2002**, 231−237.
[12] W. K. Wong, X. P. Chen, J. P. Guo, Y. G. Chi, W. X. Pan, W. Y. Wong, *J. Chem. Soc., Dalton Trans.* **2002**, 1139−1146.
[13] R. M. Stoops, S. Bachmann, M. Valentini, A. Mezzetti, *Organometallics* **2000**, *19*, 4117−4126.
[14] A. S. Goldstein, R. H. Beer, R. S. Drago, *J. Am. Chem. Soc.* **1994**, *116*, 2424−2429.
[15] C. A. Bessel, R. A. Leising, K. J. Takeuchi, *J. Chem. Soc., Chem. Commun.* **1991**, 833−835.
[16] T. Kojima, H. Matsuo, Y. Matsuda, *Inorg. Chim. Acta* **2000**, *300*, 661−667.
[17] J. Koola, D. Kochi, K. Jay, *J. Org. Chem.* **1987**, *52*, 4545−4553.
[18] D. E. V. Sickle, F. R. Mayo, R. M. Arluck, *J. Am. Chem. Soc.* **1965**, *87*, 4824−4832.
[19] A. Bottcher, M. W. Grinstaff, J. A. Labinger, H. B. Gray, *J. Mol. Catal. A: Chem.* **1996**, *113*, 191−200.
[20] K. Sato, M. Aoki, M. Ogawa, T. Hashimoto, D. Panyella, R. Noyori, *Bull. Chem. Soc. Jpn.* **1997**, *70*, 905−915.
[21] A. Brovo, F. Fontana, F. Minisci, *Chem. Lett.* **1996**, 401−402.
[22] D. W. Snelgrove, P. A. Macfaul, K. U. Ingold, M. D. D. Wayner, *Tetrahedron Lett.* **1996**, *37*, 823−826.
[23] C. M. Che, K. W. Cheng, M. C. W. Chan, T. C. Lau, C. K. Mak, *J. Org. Chem.* **2000**, *65*, 7996−8000.
[24] *SAINT, Reference manual*, Siemens Energy and Automation, Madison, WI, **1994−1996**.
[25] G. M. Sheldrick, *SADABS, Empirical Absorption Correction Program*, University of Göttingen, Germany, **1997**.
[26] G. M. Sheldrick, *SHELXTL™ Reference manual*, version 5.1, Siemens, Madison, WI, **1997**.

Received April 25, 2003

 © 2003 Wiley-VCH Verlag GmbH & Co. KGaA, Weinheim

The Preparation and Study of Bis(2-quinolyl) and Bis(2-[1,8]naphthyridyl) Derivatives of Pyrimidine and Pyrazine as Bridging Ligands for Ru^{II}

Darren Brown,[a] Seema Muranjan,[a] and Randolph P. Thummel*[a]

Keywords: Bridging ligands / Ruthenium / N ligands

The 2:1 Friedländer condensation of 2-aminobenzaldehyde or 2-aminonicotinaldehyde with either 4,6-diacetylpyrimidine or 2,5-diacetylpyrazine leads to a family of four new bis(bidentate) bridging ligands. Subsequent complexation of these ligands with $[RuCl_2(bpy)_2]$ (bpy = 2,2′-bipyridine) leads to the corresponding mononuclear and dinuclear mixed-ligand Ru^{II} complexes. Analysis of the ^1H NMR spectra of these systems affords some insight into their conformational properties. Electronic spectra of the complexes evidence two long-wavelength absorption bands which correspond to typical metal-to-ligand charge transfer states. The energies of these states may be explained by electronegativities of the pendant rings on the bridging ligand as well as the substitution pattern on the central ring. For the dinuclear complexes the lowest energy absorption shows components associated with coordination to the pendant and the central rings. The appearance of two metal-based oxidations gives good evidence for strong intermetalic interaction and Koopman's theorem is obeyed for all systems.

(© Wiley-VCH Verlag GmbH & Co. KGaA, 69451 Weinheim, Germany, 2003)

Introduction

One recurrent theme in the burgeoning field of supramolecular chemistry is the construction of organized assemblies through the judicious juxtaposition of appropriate ligands and metals. These systems take advantage of complementarity effects in the ligands as well as the principle of maximum occupation of sites to allow for the formation of a wide variety of multimetallic networks having interesting and often useful shapes. The bridging ligands used for this construction often have two equivalent bidentate chelating sites which allow the formation of linear assemblies as well as multidirectional dendritic structures.[1] Two such building blocks which have found considerable utility are 4,6-bis(2′-pyridyl)pyrimidine (**1**)[2] and 2,5-bis(2′-pyridyl)pyrazine (**2**).[3] Tris(complexation) of either ligand around a single Ru^{II} center leaves three equivalent bidentate sites available for further elaboration. If these sites are occupied by $[Ru(L)_2]^{2+}$ fragments where L = **1** or **2**, further branching is possible and polynuclear dendritic structures result. One reason for the strong interest in such systems is their potential to act as antennae where metal-based chromophores on the periphery could gather light energy and funnel it to a central, often different, metallic core.

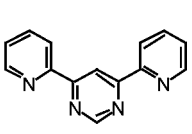

1

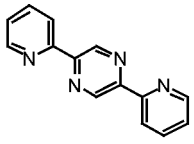

2

There are several problems associated with these multimetallic dendritic systems. Firstly, the asymmetric chelating sites of the bridging ligands lead to metal-based stereocenters, Δ or Λ, so that the number of stereoisomers increases with the number of metal atoms in the system. The problems associated with separating and evaluating individual stereoisomers have been largely ignored since the photochemical properties of these very similar stereoisomers does not appear to differ substantially.[4] Nevertheless, impressive progress has been made in the construction of stereochemically discrete systems.[5] The other issue of concern is the directionality of energy or electron transfer. Photoexcitation of such dendritic systems often involves a metal-to-ligand charge transfer (MLCT) state in which the photoexcited electron is promoted from the metal atom to the most electronegative ligand.[6] Although **1** and **2** are more electronegative than 2,2′-bipyridine (bpy), their π*-states are not that much lower than that of bpy and it occurred to us that more electronegative analogues of these ligands might enhance the directionality of energy transfer.

In earlier work we have used the Friedländer condensation of 8-aminoquinoline-7-carbaldehyde with diacetyl derivatives of pyrimidine and pyrazine to afford bis([1,10]-phenanthrolinyl)diazines and we have examined the be-

[a] Department of Chemistry, 136 Fleming Building, University of Houston,
Houston, Texas 77204-5003, USA

havior of these ligands as bis(tridentate) chelators.[7] In this work we will utilize a similar Friedländer approach to prepare the 2-quinolyl and 2-[1,8]naphthyridyl derivatives of these same diazines (**3**−**6**) and examine the properties of their mono- and dinuclear Ru^{II} complexes.

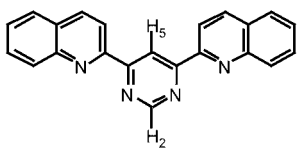

3

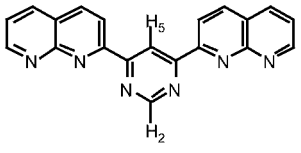

4

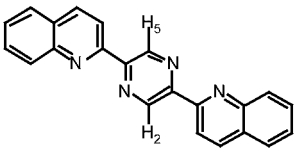

5

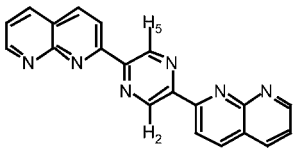

6

Results and Discussion

The ligands were synthesized by a Friedländer reaction[8] between 2 equiv. of 2-aminobenzaldehyde (**9**) or 2-aminonicotinaldehyde (**10**) and either 4,6-diacetylpyrimidine (**7**)[9] or 2,5-diacetylpyrazine (**8**).[10] The reactions proceed smoothly in refluxing ethanol to provide the ligands **3**−**6** in yields of 40−98%. The ligands were characterized by their ^1H NMR spectra which were readily assigned due to high symmetry. The quinoline and naphthyridine rings give characteristic and similar patterns with little variation between the pyrimidine and pyrazine systems. The central pyrimidine ring shows two singlets with 2-H appearing at δ = 9.48−9.51 ppm. The singlet of 5-H (being closer to the substituent rings) shows more variation appearing at δ = 9.78 ppm for the quinoline and at δ = 10.09 ppm for the naphthyridine derivatives. The central pyrazine ring shows only one singlet at δ = 9.95 ppm for **5** and at δ = 10.51 ppm for the more deshielded **6**.

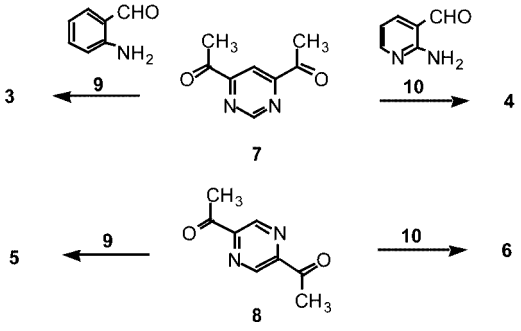

Ru^{II} complexes were prepared by treating the ligands **3**−**6** with either 1 or 2 equiv. of $[Ru(bpy)_2Cl_2]$ in refluxing aqueous ethanol. The complexes were precipitated as their hexafluorophosphate salts and purified by chromatography on alumina (CH_3CN/toluene) or silica gel (CH_3CN/H_2O/satd. KNO_3, 5:4:1). Due to stereochemical complexities, only the ^1H singlets on the central diazine ring of the complexes could be confidently assigned.

The mononuclear complexes of **3** and **4** display two singlets, δ = 8.45 (2-H) and 9.81 (5-H) for **3** and δ = 8.63 (2-H) and 9.86 (5-H) for **4**. The coordination of $[Ru(bpy)_2]^{2+}$ disrupts the symmetry of **5** and **6** so that their mononuclear complexes also exhibit two singlets, δ = 8.86 (2-H) and 9.86 (5-H) for **5** and δ = 9.09 (2-H) and 9.93 (5-H) for **6.**

The dinuclear complexes of **3**−**6** possess two chiral octahedral centers and therefore exist as both *rac* (ΔΔ and ΛΛ) and *meso* (ΔΛ) diastereomers (Figure 1). The existence of two diastereomers, each having 22−24 unique protons, gives rise to rather complex ^1H NMR spectra. However, the protons on the central rings appear as singlets making them easier to identify and assign. For the dinuclear complex of **3**, two singlets are observed at δ = 7.53 and 9.54 ppm, which can be assigned, respectively, to 2-H and 5-H of the major diastereomer. The singlet assigned to 2-H is shifted upfield with respect to the mononuclear complex because this proton is now shielded by two pyridine rings. We assign the singlet at δ = 9.63 to 5-H of the minor diastereomer and thus integration of the two 5-H signals gives a diastereomeric ratio of 7:3. The dinuclear complex of **4** also shows two singlets at δ = 7.91 and 9.67 ppm which are assigned to 2-H and 5-H, respectively, of the major diastereomer. The two singlets at δ = 7.84 and 9.72 ppm are assigned to the minor diastereomer and a diastereomeric ratio of 4:1 was determined. For the dinuclear complexes involving pyrazine ligands **5** and **6**, 2-H and 5-H are equivalent so that only one singlet is observed for these protons, appearing at δ = 8.47 and 8.53 ppm for the major and minor diastereomers of $[(bpy)_2Ru(\mathbf{5})Ru(bpy)_2]^{4+}$ and at δ = 8.66 and 8.73 ppm for the major and minor diastereomers of $[(bpy)_2Ru(\mathbf{6})Ru(bpy)_2]^{4+}$. Due to the complexity of the spectra, clear diastereomeric ratios could not be determined.

The electronic absorption and luminescence spectra of the ligands **3**−**6** and their Ru^{II} complexes were determined in acetonitrile solution and the data are collected in Table 1. The ligands show low energy absorption bands in the range of 316−355 nm and several interesting correlations can be made involving the energies of these absorptions and structure. First, the ligands involving naphthyridine, **4** and **6**, absorb at longer wavelengths (324 and 355 nm) than their quinoline counterparts (316 and 340 nm) which agrees with increased electronegativity due to two additional nitrogen atoms. However, for the two isomeric quinoline systems, the one involving a central pyrazine ring (**5**) absorbs at 24 nm longer wavelength than the one involving a central pyrimidine ring (**3**). For the two isomeric naphthyridine systems the difference is 31 nm. This difference can be explained by considering the planar conformations available to the ligands. From a chelation point of view it is convenient to view them in their *syn*,*syn* conformation. However, this conformation involves unfavorable N−N lone pair interactions as well as some H−H congestion which can be relieved in the *anti*,*anti* conformation. For **3** and **4** the *anti*,*anti* form provides a less extended structure while for the pyrazine

 © 2003 Wiley-VCH Verlag GmbH & Co. KGaA, Weinheim

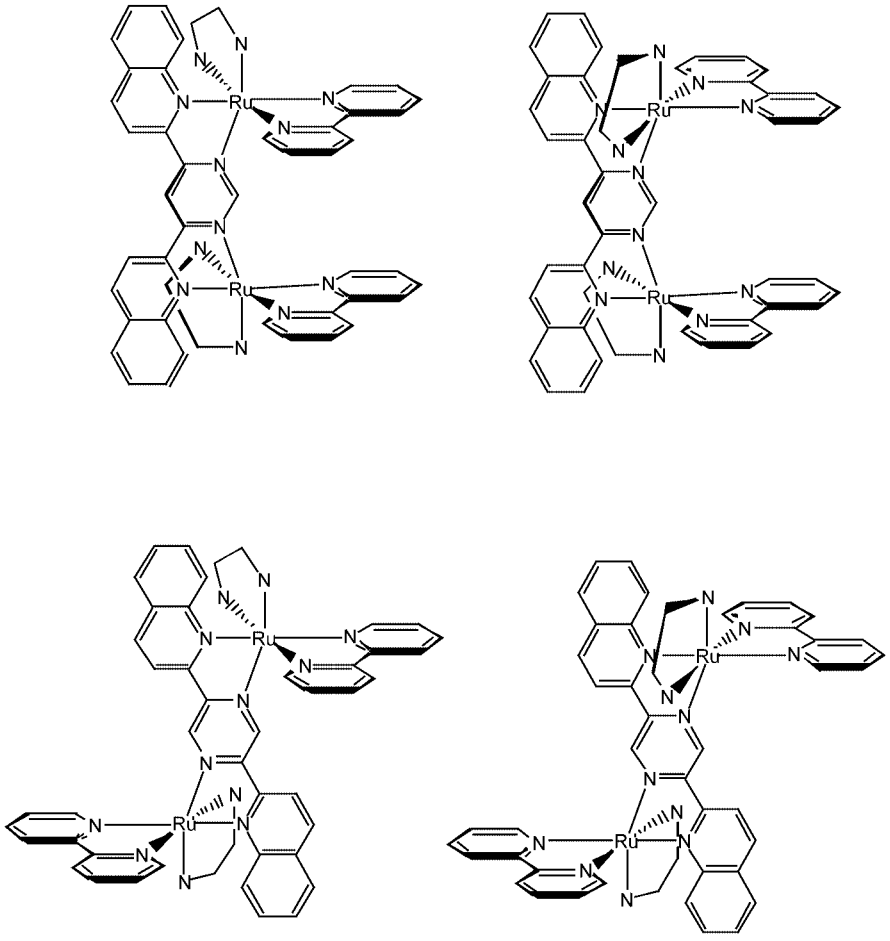

Figure 1. Stereochemical representation of the diastereomeric forms of $[(bpy)_2Ru(\mathbf{3})Ru(bpy)_2]^{4+}$ (top) and $[(bpy)_2Ru(\mathbf{5})Ru(bpy)_2]^{4+}$ (bottom)

systems **5** and **6** both conformations have a similar longitudinal arrangement, explaining the lower energy absorption. It is intriguing to speculate that a bulky C-2 substituent on either **3** or **4** would inhibit the normal bidentate coordination and one might expect to see some cyclometalation through the potential tridentate *anti*,*anti* conformation.

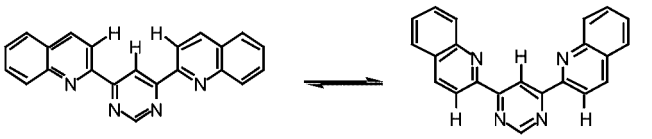

3 (syn, syn) **3** (anti, anti)

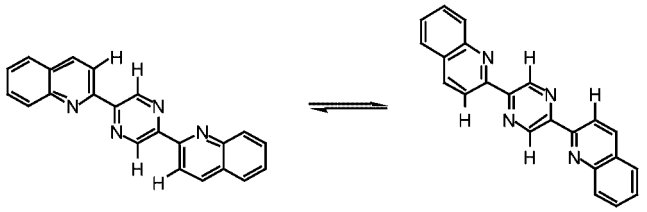

5 (syn, syn) **5** (anti, anti)

Table 1. Photophysical data for free ligands

Ligand	Absorption[a] λ_{max} [nm] (ε [$M^{-1}cm^{-1}$])	Emission[a] λ_{em} [nm] (rel. int.)
3	316 (24934), 250 (58052), 206 (53344)	406 (m)
4	324 (26776), 231 (43578)	430 (m)
5	340 (28140), 262 (26964), 207 (41490)	435 (s)
6	355 (27946), 253 (18544)	440 (m)

[a] 5×10^{-5} M in CH_3CN at 25 °C; s = strong, m = medium.

The absorption properties of the mononuclear complexes $[Ru(\mathbf{3}-\mathbf{6})(bpy)_2]^{2+}$ are well behaved and consistent with structure. Each complex shows two long-wavelength absorption bands which are associated with a metal-to-ligand charge transfer (MLCT) wherein a photoexcited electron is promoted from a metal d-orbital to the π*-orbital of a ligand (Figures 2 and 3). The longer wavelength band in the region of 510−559 nm correlates with MLCT to the more electronegative bridging ligand while the shorter wavelength band, in the much narrower range of 427−431 nm, correlates with MLCT to the auxiliary bpy ligand. The more

 © 2003 Wiley-VCH Verlag GmbH & Co. KGaA, Weinheim

electronegative naphthyridine ligands have lower energy π*-states and thus absorb at lower energy with a difference from the corresponding quinoline ligands of 32 nm when the central ring is pyrimidine and 33 nm when the central ring is pyrazine.

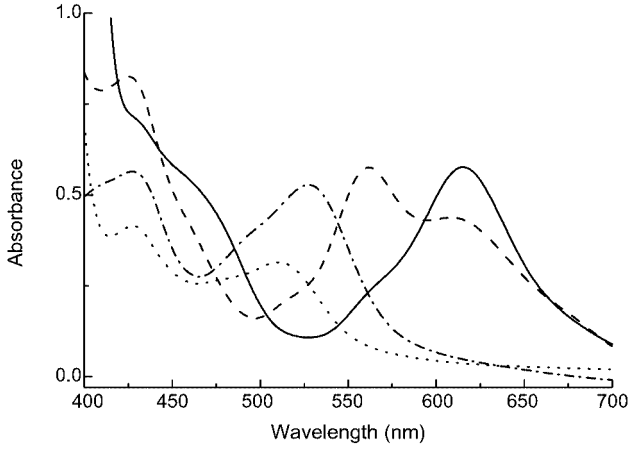

Figure 2. Long-wavelength portion of the electronic absorption spectra of the quinoline-containing systems $[Ru(\mathbf{3})(bpy)_2]^{2+}$ (dash-dot), $[Ru(\mathbf{5})(bpy)_2]^{2+}$ (dot), $[(bpy)_2Ru(\mathbf{3})Ru(bpy)_2]^{4+}$ (dash), and $[(bpy)_2Ru(\mathbf{5})Ru(bpy)_2]^{4+}$ (solid)

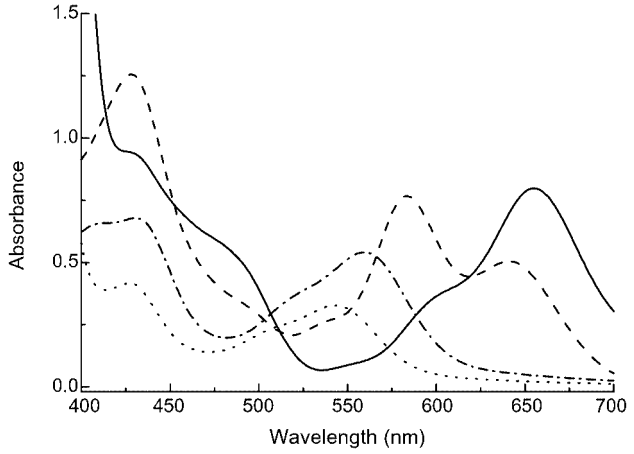

Figure 3. Long-wavelength portion of the electronic absorption spectra of the 1,8-naphthyridine-containing systems $[Ru(\mathbf{4})(bpy)_2]^{2+}$ (dash-dot), $[Ru(\mathbf{6})(bpy)_2]^{2+}$ (dot), $[(bpy)_2Ru(\mathbf{4})Ru(bpy)_2]^{4+}$ (dash), and $[(bpy)_2Ru(\mathbf{6})Ru(bpy)_2]^{4+}$ (solid)

It is especially interesting that the MLCT bands for the pyrimidine and pyrazine systems are reversed in energy when compared to the free ligands, with the pyrimidine complexes showing lower energy absorptions. The conformational effects cited for the free ligands are less important for the complexes. Rather the pendant, uncomplexed quinoline or naphthyridine may be considered as a substituent on the diazine portion of the bidentate chelator. For the pyrimidine systems this substituent is located in the 4-position where it will have a stronger resonance interaction with the coordinated metal atom. For the pyrazine systems, the substituent is in the 3-position and the delocalizing effect is weaker.

The absorption properties of the dinuclear complexes $[(bpy)_2Ru(\mathbf{3}-\mathbf{6})Ru(bpy)_2]^{4+}$ are somewhat unusual. Once again, there are long- and short-wavelength components to the MLCT absorption bands. All four systems show bands at 425−428 nm which correspond to charge transfer to the less electronegative bpy ligands. However, the long-wavelength component consists of two bands. For the naphthyridine systems these bands appear at longer wavelengths than for the quinoline systems. Charge transfer to the bridging ligands may involve either the pendant quinoline or naphthyridine moiety as the receptor or the central diazine ring as the receptor with the latter species being lower in energy. Thus, we observe that the long-wavelength contribution is more intense for the pyrazine systems where the *para* disposition of the metal centers on the pyrazine ring provides better communication and consequent delocalization than for the *meta*-substituted pyrimidine rings where charge transfer to the pendant groups is preferred.

The luminescence properties of the complexes were measured at room temperature in acetonitrile solution. As expected, the mononuclear complexes showed modest emission while the dinuclear complexes were less intense and completely quenched in the cases of $[(bpy)_2Ru(\mathbf{4}, \mathbf{6})Ru(bpy)_2]^{4+}$.

The half-wave redox potentials of the complexes were measured in acetonitrile and the data are collected in Table 2. For systems of this type, oxidations are typically associated with the removal of an electron from a metal d-orbital while reduction involves the addition of an electron to the π*-orbital of a coordinated ligand. In this regard the mononuclear complexes are well behaved. Metal-based $Ru^{II,III}$ oxidation occurs at +1.34−1.46 V. Pyrimidine is more basic than pyrazine and thus better able to stabilize a positive charge, which explains the lower oxidation potential of the complexes of **3** and **4**. Three reduction waves are observed for the mononuclear complexes, which can be associated with the addition of an electron to the π*-orbital of each of the three ligands around the metal atom. The first reduction for each system involves the ligands **3**−**6** and is more positive for the more electronegative ligands containing the naphthyridine ring. Plotting the lowest energy absorptions against the energy gap between the frontier redox couples gives a good linear relationship with a slope of 0.75 and a correlation coefficient of 0.9952 demonstrating good agreement with Koopman's theorem.

The dinuclear complexes show strong interaction between the two complexed metal centers as evidenced by two well-separated oxidation waves. Analogous with the mononuclear complexes, the naphthyridine-containing systems oxidize more readily, at less positive potentials, than the quinoline-containing systems. The separation between the two oxidations is greater for the pyrazines (+0.23 V) than for the pyrimidines (+0.14 to +0.15 V). Comproportionation constants may be calculated for all four complexes and fall in the range of 230−7730, in good agreement with previously reported systems involving **1** and **2**.[11]

 © 2003 Wiley-VCH Verlag GmbH & Co. KGaA, Weinheim

Table 2. Photophysical and electrochemical data for mono- and dinuclear Ru^{II} complexes

Complex	Absorption[a] λ_{max} [nm] (ε [$M^{-1}cm^{-1}$])	Emission[b] λ_{em} [nm] (rel. int)	$E_{1/2}$ [V][a] OX	RED
$[Ru(\mathbf{3})(bpy)_2]^{2+}$	527 (10556), 427 (11286)	762 (m)	+1.38	−0.76, −1.29, −1.60
$[Ru(\mathbf{4})(bpy)_2]^{2+}$	559 (10816), 431 (13580)	817 (w)	+1.34	−0.62, −1.12, −1.57
$[Ru(\mathbf{5})(bpy)_2]^{2+}$	510 (6292), 427 (8294)	745 (m)	+1.46	−0.76, −1.26, −1.57
$[Ru(\mathbf{6})(bpy)_2]^{2+}$	543 (6546), 427 (8340)	807 (w)	+1.40	−0.63, −1.06, −1.59
$[(bpy)_2Ru(\mathbf{3})Ru(bpy)_2]^{4+}$	613 (8704), 562 (11512), 461 (8188), 425 (16514)	838 (w)	+1.49, +1.64	−0.34, −0.83, −1.49, −1.73
$[(bpy)_2Ru(\mathbf{4})Ru(bpy)_2]^{4+}$	640 (10062), 584 (15332), 489 (6900), 428 (25120)	no emission	+1.37, +1.51	−0.30, −0.76, −1.49
$[(bpy)_2Ru(\mathbf{5})Ru(bpy)_2]^{4+}$	615 (14016), 573 (5702), 457 (11098), 428 (14276)	829 (w)	+1.45, +1.68	−0.36, −0.79, −1.43, −1.74
$[(bpy)_2Ru(\mathbf{6})Ru(bpy)_2]^{4+}$	615 (14016), 573 (5702), 457 (11098), 428 (14276)	no emission	+1.34, +1.57	−0.31, −0.67, −1.49

[a] Solutions were 0.1 M TBAP in CH_3CN; the sweep rate was 200 mV/s. [b] 5×10^{-5} M in CH_3CN at 25 °C; m = medium, w = weak.

The dinuclear complexes exhibit 3−4 reduction waves with the first reductions falling in the range of −0.30 to −0.36 V and the second reductions in the range of −0.67 to −0.83 V. Both of these reductions are associated with the bridging ligand while the third reduction at −1.43 to −1.49 V is associated with one of the bpy ligands. The bridging ligand reductions are consistent with structure in that the naphthyridine-containing ligands reduce more readily than the quinoline containing ones.

Summary

Four bis(bidenate) bridging ligands have been prepared containing a central pyrimidine or pyrazine ring symmetrically substituted with either two 2-quinolyl or two 2-[1,8]naphthyridyl moieties. Mixed-ligand complexes of these ligands have been prepared by incorporating either one or two $[Ru(bpy)_2]^{2+}$ centers into the available bidentate sites. The resulting complexes possess one stereocenter at each metal atom resulting in an inseparable mixture of diastereomers for the dinuclear systems as evidenced by characteristic ^1H NMR singlets for protons on the central diazine ring. MLCT absorptions are observed for charge transfer to the bridging ligand in the range of 510−559 nm for the mononuclear complexes. For the dinuclear complexes this band splits into two components, at 562−612 and 613−655 nm, which are tentatively associated with the central and pendant rings on the bridging ligand. Charge transfer to the auxiliary bpy remains fairly constant for all complexes in the range of 425−431 nm. Clear splitting of the metal-based oxidation potential indicates interaction between two bound metal atoms with the pyrazine system showing the stronger coupling. Reduction potentials correlate well with electronegativities of the bridging ligand.

Experimental Section

General: Nuclear magnetic resonance spectra were recorded at 300 MHz for ^1H and at 75 MHz for $^{13}C\{^1H\}$ referenced to TMS in $CDCl_3$ and to the solvent peak in all other solvents (CD_3CN). Electronic spectra were obtained with a Perkin−Elmer Lambda 3B spectrophotometer. Emission spectra were obtained with a Perkin−Elmer LS-50 luminescence spectrometer. Cyclic voltammetry (CV) was carried out in a conventional three-electrode cell with a BAS-27 voltammeter and a Houston Instruments model 100 X-Y recorder according to a previously described procedure.[12] Mass spectra were obtained with an Applied Biosystems Voyager System 4160 MALDI-TOF spectrometer. Melting points were measured with a Hoover capillary melting point apparatus and are not corrected. Elemental analyses were performed by Quantitative Technologies Inc., P. O. Box 470, Whitehouse, NJ 08888, USA. 2,5-Diacetylpyrazine,[10] 4,6-diacetylpyrimidine,[9] 2-aminobenzaldehyde,[13] 2-aminonicotinaldehyde,[14] and $[Ru(bpy)_2Cl_2]$[15] were prepared according to published procedures.

4,6-Bis(2′-quinolinyl)pyrimidine (3): 50% ethanolic KOH (2 mL) was added to a stirred solution of 4,6-diacetylpyrimidine (50 mg, 0.30 mmol) and 2-aminobenzaldehyde (73 mg, 0.60 mmol) in EtOH (10 mL). The solution was allowed to reflux overnight. After cooling to room temperature, the precipitate was filtered and rinsed with EtOH. The product was purified by chromatography (silica gel, hexanes/EtOAc, 1:1) to give **3** (91 mg, 91%) as a white solid; m.p. 230−233 °C. ^1H NMR ($CDCl_3$): δ = 9.80 (s, 1 H), 9.49 (s, 1 H), 8.66 (d, J = 8.7 Hz, 2 H), 8.37 (d, J = 8.7 Hz, 2 H), 8.36 (d, J = 8.4 Hz, 2 H), 7.92 (d, J = 8.1 Hz, 2 H), 7.82 (t, J = 7.2 Hz, 2 H), 7.63 (t, J = 7.2 Hz, 2 H). ^{13}C NMR ($CDCl_3$): δ = 164.1, 158.6, 154.1, 148.1, 137.1, 130.3, 129.9, 128.9, 127.64, 127.61, 118.9, 115.0. MS: m/z = 334 [M^+]. $C_{22}H_{14}N_4 \cdot 0.5H_2O$ (343): calcd. C 76.97, H 4.37, N 16.32; found C 76.58, H 3.71, N 16.16.

4,6-Bis(2′-[1′,8′]naphthyridyl)pyrimidine (4): 50% ethanolic KOH (2 mL) was added to a stirred solution of 4,6-diacetylpyrimidine (100 mg, 0.61 mmol) and 2-aminonicotinaldehyde (164 mg, 1.34 mmol) in EtOH (10 mL). The solution was allowed to reflux overnight. After cooling to room temperature, the solvent was evaporated and the resulting solids were dissolved in $CHCl_3$ (50 mL). The organic phase was washed with water (50 mL), and brine (50 mL), dried ($MgSO_4$) and concentrated. The solid residue was purified by washing with cold EtOH until the washings ran clear to give **4** (84 mg, 41%) as a gray solid; m.p. > 280 °C. ^1H NMR ($CDCl_3$): δ = 10.07 (s, 1 H), 9.51 (s, 1 H), 9.24 (dd, J = 4.2, 1.8 Hz, 2 H), 8.78 (d, J = 8.4 Hz, 2 H), 8.42 (d, J = 8.7 Hz, 2 H), 8.22 (dd, J = 8.1, 1.8 Hz, 2 H), 7.57 (dd, J = 8.1, 4.2 Hz, 2 H). ^{13}C NMR ($CDCl_3$): δ = 163.8, 158.4, 157.1, 155.4, 154.2, 138.5, 137.2,

 © 2003 Wiley-VCH Verlag GmbH & Co. KGaA, Weinheim

123.7, 123.0, 120.1, 116.5. MS: m/z = 336 [M^+]. $C_{20}H_{12}N_6 \cdot 0.5H_2O$ (345): calcd. C 69.57, H 3.77, N 24.34; found C 69.59, H 3.26, N 24.39.

2,5-Bis(2′-quinolinyl)pyrazine (5): 50% ethanolic KOH (2 mL) was added to a stirred solution of 2,5-diacetylpyrazine (100 mg, 0.61 mmol) and 2-aminobenzaldehyde (155 mg, 1.27 mmol) in EtOH (20 mL). The solution was allowed to reflux overnight. After cooling to room temperature, the precipitate was filtered and rinsed with EtOH. The solid product was recrystallized from EtOH to give **5** (81 mg, 40%) as a light brown solid; m.p. 262−264 °C. ^{1}H NMR ($CDCl_3$): δ = 10.03 (s, 2 H), 8.64 (d, J = 8.7 Hz, 2 H), 8.2−8.5 (m, 4 H), 7.91 (d, J = 8.1 Hz, 2 H), 7.82 (t, J = 8.1 Hz, 2 H), 7.63 (t, J = 7.5 Hz, 2 H). ^{13}C NMR ($CDCl_3$): δ = 152.9, 149.3, 146.3, 142.0, 136.6, 129.3, 128.5, 127.5, 126.7, 126.6, 118.3. MS: m/z = 334 [M^+]. $C_{22}H_{14}N_4 \cdot 0.25CHCl_3$ (364): calcd. C 73.39, H 3.92, N 15.39; found C 73.25, H 3.33, N 15.33.

2,5-Bis(2′-[1′,8′]naphthyridyl)pyrazine (6): Solid KOH (200 mg) was added to a stirred solution of 2,5-diacetylpyrazine (400 mg, 2.44 mmol) and 2-aminonicotinaldehyde (625 mg, 5.12 mmol) in EtOH (10 mL). The solution was allowed to reflux for 5 h after which it was cooled to room temperature and the solids were collected by vacuum filtration. The solid product was purified by washing with cold EtOH until the washings ran clear to give **6** (820 mg, 98%) as a gray solid; m.p. > 280 °C. ^{1}H NMR ($CDCl_3$): δ = 10.15 (s, 2 H), 9.22 (dd, J = 3.9, 1.8 Hz, 2 H), 8.83 (d, J = 8.4 Hz, 2 H), 8.41 (d, J = 8.7 Hz, 2 H), 8.30 (dd, J = 8.1, 2.1 Hz, 2 H), 7.57 (dd, J = 8.1, 4.2 Hz, 2 H). ^{13}C NMR ($CDCl_3$): δ = 157.5, 155.8, 154.2, 150.4, 143.2, 138.2, 137.1, 123.3, 122.6, 120.5. MS: m/z = 336 [M^+]. $C_{20}H_{12}N_6 \cdot 0.25H_2O$ (341): calcd. C 70.48, H 3.67, N 24.67; found C, 70.24, H 3.36, N 24.27.

[Ru(3)(bpy)$_2$](PF$_6$)$_2$: A stirred suspension of **3** (20 mg, 0.06 mmol) and [Ru(bpy)$_2$Cl$_2$] (62 mg, 0.12 mmol) in EtOH/H_2O (3:1, 12 mL) was heated at reflux overnight after which the solution was cooled to room temperature, and filtered. NH_4PF_6 (20 mg) was added and the solution was concentrated. The product was purified by chromatography (silica gel, CH_3CN/H_2O/sat. KNO_3, 5:4:1) and the counterion was exchanged with satd. NH_4PF_6 to give [Ru(**3**)(bpy)$_2$](PF$_6$)$_2$ (38 mg, 66%) as a red solid. ^{1}H NMR (CD_3CN): δ = 9.81 (s, 1 H), 8.95 (d, J = 8.7 Hz, 1 H), 8.72 (d, J = 8.7 Hz, 1 H), 8.63 (d, J = 8.7 Hz, 2 H), 8.58 (d, J = 6.9 Hz, 2 H), 8.46 (s, 1 H), 8.39 (d, J = 8.1 Hz, 1 H), 8.32 (m, 2 H), 8.0−8.2 (m, 6 H), 7.9−8.0 (m, 3 H), 7.77 (t, J = 6.9 Hz, 2 H), 7.69 (t, J = 7.5 Hz, 2 H), 7.50 (m, 2 H), 7.2−7.4 (m, 4 H). MS: m/z = 893 [$M^+ - PF_6$], 748 [$M^+ - 2\ PF_6$].[16]

[(bpy)$_2$Ru(3)Ru(bpy)$_2$](PF$_6$)$_4$: A stirred suspension of **3** (34 mg, 0.033 mmol) and [Ru(bpy)$_2$Cl$_2$] (66 mg, 0.066 mmol) in EtOH/H_2O (3:1, 12 mL) was heated at reflux overnight after which the solution was cooled to room temperature, filtered, NH_4PF_6 (20 mg) was added and the solution was concentrated. The product was purified by chromatography (silica gel, CH_3CN/H_2O/satd. KNO_3, 5:4:1) and the counterion was exchanged with satd. NH_4PF_6 to give [(bpy)$_2$Ru(**3**)Ru(bpy)$_2$](PF$_6$)$_4$ (16 mg, 28%) as a green solid. The dinuclear complex exists as a mixture of diastereomers which were not further separated: ^{1}H NMR (CD_3CN): δ = 9.63 (s, 1 H), 9.54 (s, 1 H), 9.00 (2 overlapping d, J = 8.7 Hz), 9.73 (2 overlapping d, J = 9.0 Hz), 8.55 (d, J = 8.1 Hz), 8.41 (t, J = 7.5 Hz), 8.26 (t, J = 7.8 Hz), 7.8−8.3 (m), 7.6−7.8 (m), 7.1−7.6 (m), 7.00 (t, J = 7.2 Hz). MS: m/z = 1594 [$M^+ - PF_6$], 1452 [$M^+ - 2\ PF_6$], 1306 [$M^+ - 3\ PF_6$].[16]

[Ru(4)(bpy)$_2$](PF$_6$)$_2$: A stirred suspension of **4** (17 mg, 0.051 mmol) and [Ru(bpy)$_2$Cl$_2$] (27 mg, 0.051 mmol) in EtOH/H_2O (3:1, 12 mL) was heated at reflux overnight after which the solution was cooled to room temperature, and filtered. NH_4PF_6 (17 mg) was added and the solution was concentrated. The product was purified by chromatography (alumina, CH_3CN/toluene, 1:1) followed by recrystallization (CH_3CN/toluene, 1:1) to give [Ru(**4**)Ru(bpy)$_2$](PF$_6$)$_2$ (30 mg, 47%) as red crystals. ^{1}H NMR (CD_3CN): δ = 9.86 (d, J = 0.9 Hz, 1 H), 9.24 (dd, J = 4.2, 1.8 Hz, 1 H), 9.06 (d, J = 8.7 Hz, 1 H), 8.74 (d, J = 8.7 Hz, 1 H), 8.68 (d, J = 8.4 Hz, 1 H), 8.60−8.65 (m, 2 H), 8.55 (dd, J = 8.1, 4.8 Hz, 1 H), 8.49 (d, J = 8.1 Hz, 1 H), 8.37 (t, J = 6.9 Hz, 2 H), 8.16 (dd, J = 4.2, 1.8 Hz, 1 H), 8.12 (dd, J = 7.8, 1.8 Hz, 1 H), 8.0−8.1 (m, 2 H), 7.95 (td, J = 7.8, 1.5 Hz, 1 H), 7.80 (t, J = 4.8 Hz, 2 H), 7.67−7.77 (m, 3 H), 7.59 (dd, J = 8.4, 4.2 Hz, 1 H), 7.2−7.5 (m, 4 H). MS: m/z = 895 [$M^+ - PF_6$], 750 [$M^+ - 2\ PF_6$]. $C_{40}H_{28}F_{12}N_{10}P_2Ru \cdot 0.3PhCH_3 \cdot 1.0H_2O$ (1085): calcd. C 46.58, H 2.98, N 12.91; found C, 46.87, H 2.67, N 12.90.

[(bpy)$_2$Ru(4)Ru(bpy)$_2$](PF$_6$)$_4$: A stirred solution of **4** (30 mg, 0.089 mmol) and [Ru(bpy)Cl$_2$] (100 mg, 0.191 mmol) in EtOH/H_2O (3:1, 12 mL) was refluxed under argon overnight. The dark green solution was cooled, NH_4PF_6 (50 mg) was added and the solvent was evaporated to give a black solid. The material was purified by chromatography (silica gel, CH_3CN/H_2O/satd. KNO_3, 5:4:1) and the counterion was exchanged with saturated NH_4PF_6 to give [(bpy)$_2$Ru(**4**)Ru(bpy)$_2$](PF$_6$)$_4$ (90 mg, 58%) as a green solid: ^{1}H NMR (CD_3CN): δ = 9.66 (s), 9.13 (d, J = 8.7 Hz), 8.80 (d, J = 8.7 Hz), 8.2−8.6 (m), 7.9−8.2 (m), 7.0−7.7 (m). MS: m/z = 1596 [$M^+ - PF_6$], 1451 [$M^+ - 2\ PF_6$], 1306 [$M^+ - 3\ PF_6$], 1161 [$M^+ - 4\ PF_6$]. $C_{60}H_{44}F_{24}N_{14}P_4Ru_2 \cdot 0.5H_2O$ (1752): calcd. C 41.12, H 2.57, N 11.19; found C 40.79, H 2.52, N 10.96.

[Ru(5)(bpy)$_2$](PF$_6$)$_2$: A stirred suspension of **5** (30 mg, 0.08 mmol) and [Ru(bpy)$_2$Cl$_2$] (94 mg, 0.18 mmol) in EtOH/H_2O (3:1, 20 mL) was heated at reflux overnight after which the solution was cooled to room temperature, filtered, NH_4PF_6 (60 mg) was added and the solution was concentrated. Chromatography (silica gel, CH_2Cl_2/CH_3CN, 3:2) gave [Ru(**5**)(bpy)$_2$](PF$_6$)$_2$ (35 mg, 37%) as a red solid. ^{1}H NMR (CD_3CN): δ = 9.86 (s, 1 H), 8.86 (s, 1 H), 8.4−8.8 (m), 8.34 (m), 7.9−8.2 (m), 7.6−7.9 (m), 7.54 (AB pattern, J = 6.9 Hz), 7.48 (d, J = 8.4 Hz), 7.2−7.4 (m). MS: m/z = 893 [$M^+ - PF_6$], 748 [$M^+ - 2\ PF_6$]. $C_{42}H_{30}F_{12}N_8P_2Ru \cdot CHCl_3$ (1156): calcd. C 44.71, H 2.68, N 9.70; found C 44.86, H 2.16, N 9.64.

[(bpy)$_2$Ru(5)Ru(bpy)$_2$](PF$_6$)$_4$: A stirred solution of **5** (30 mg, 0.08 mmol) and [Ru(bpy)Cl$_2$] (94 mg, 0.18 mmol) in EtOH/H_2O (3:1, 20 mL) was refluxed under Ar overnight. The dark green solution was cooled, NH_4PF_6 (60 mg) was added and the solvent was evaporated to give a black solid. The material was purified by chromatography (silica gel, CH_2Cl_2/CH_3CN, 65:35) and the counterion was exchanged with satd. NH_4PF_6 to give [(bpy)$_2$Ru(**5**)Ru(bpy)$_2$](PF$_6$)$_4$ (35 mg, 22%) as a green solid. The dinuclear complex exists as a mixture of diastereomers which were not further separated. ^{1}H NMR (CD_3CN): δ = 8.73 (t, J = 7.8 Hz), 8.66 (t, J = 9.0 Hz), 8.52 (s) 8.4−8.5 (m) 8.2−8.4 (m), 8.11 (t, J = 7.8 Hz), 7.8−8.1 (m), 7.6−7.7 (m), 7.4−7.6 (m) 7.2−7.4 (m), 7.06 (t, J = 7.5 Hz). MS: m/z = 1594 [$M^+ - PF_6$], 1304 [$M^+ - 3\ PF_6$]. $C_{60}H_{44}F_{24}N_{14}P_4Ru_2 \cdot 0.1KPF_6$ (1754): calcd. C 39.28, H 2.47, N 8.26; found C 38.70, H 2.39, N 8.73.

[Ru(6)(bpy)$_2$](PF$_6$)$_2$: A stirred suspension of **6** (50 mg, 0.15 mmol) and [Ru(bpy)$_2$Cl$_2$] (79 mg, 0.15 mmol) in EtOH/H_2O (3:1, 12 mL) was heated at reflux overnight after which the solution was cooled to room temperature, filtered, NH_4PF_6 (49 mg) was added and the solution was concentrated. Chromatography (alumina, CH_3CN/toluene, 1:1) gave [Ru(**6**)(bpy)$_2$](PF$_6$)$_2$ (86 mg, 55%) as a red solid. ^{1}H NMR (CD_3CN): δ = 9.93 (s, 1 H), 9.0−9.2 (m, 2 H), 8.83 (d,

 © 2003 Wiley-VCH Verlag GmbH & Co. KGaA, Weinheim

J = 8.7 Hz, 1 H), 8.6−8.8 (2 overlapping doublets, 2 H), 8.57(d, J = 8.4 Hz, 1 H), 8.46 (dd, J = 8.1, 1.8 Hz, 1 H), 8.41 (dd, J = 8.1, 1.8 Hz, 1 H), 8.13 (dd, J = 4.2, 2.1 Hz, 1 H), 7.63 (dd, J = 8.1, 4.2 Hz, 1 H), 7.57 (dd, J = 8.1, 4.2 Hz, 1 H). MS: m/z = 895 [$M^+ - PF_6$], 750 [$M^+ - 2\ PF_6$]. $C_{40}H_{28}F_{12}N_{10}P_2Ru$ (1039): calcd. C 46.20, H 2.69, N 13.47; found C 46.58, H 2.61, N 13.06.

[(bpy)$_2$Ru(6)Ru(bpy)$_2$](PF$_6$)$_4$: A stirred solution of **6** (30 mg, 0.09 mmol) and [Ru(bpy)Cl_2] (100 mg, 0.19 mmol) in EtOH/H_2O (3:1, 12 mL) was refluxed under Ar overnight. The dark green solution was cooled, NH_4PF_6 (58 mg) was added and the solvent was evaporated to give a black solid. The material was purified by chromatography (silica gel, CH_3CN/H_2O/sat. KNO_3, 5:4:1) and the counterion was exchanged with satd. NH_4PF_6 to give [(bpy)$_2$Ru(**6**)-Ru(bpy)$_2$](PF$_6$)$_4$ (100 mg, 65%) as a green solid: ^{1}H NMR (CD_3CN): δ = 8.75 (s), 8.6−8.7 (m), 8.53 (t, J = 8.1 Hz), 8.3−8.5 (m), 7.8- 8.3 (m), 7.65−7.8 (m), 7.55−7.65 (m), 7.3−7.5 (m), 7.18 (m), 7.52 (m) ppm. $C_{60}H_{44}F_{24}N_{14}P_4Ru_2$ (1743): calcd. C 41.33, H 2.53, N 11.25; found C 41.46, H 2.74, N 11.51.

Acknowledgments

We would like to thank the Robert A. Welch Foundation (E-621) and the Division of Chemical Sciences, Office of Basic Energy Sciences, U. S. Department of Energy (Contract No. DE-FG03-02ER15334) for financial support of this work.

[1] [1a] G. R. Newkome, E. He, C. N. Moorefield, *Chem. Rev.* **1999**, *99*, 1689−1746. [1b] G. F. Swiegers, T. J. Malefetse, *Chem. Rev.* **2000**, *100*, 3483−3537. [1c] E. C. Constable, *Chem. Commun.* **1997**, 1073−1080. [1d] G. Denti, S. Campagna, L. Sabatino, S. Serroni, M. Ciano, *Inorg. Chem.* **1990**, *29*, 4750−4758. [1e] S. Campagna, G. Denti, S. Serroni, M. Ciano, V. Balzani, *Inorg. Chem.* **1991**, *30*, 3728−3732.

[2] [2a] S. Takagi, T. Sahashi, K. Sako, K. Mizuno, M. Kurihara, H. Nishihara, *Chem. Lett.* **2002**, 628−629. [2b] T. Ishida, T. Kawakami, S. Mitsubori, T. Nogami, K. Yamaguchi, H. Iwamura, *J. Chem. Soc., Dalton Trans.* **2002**, 3177−3186. [2c] L. Kovbasyuk, M. Hoppe, H. Pritzkow, R. Krämer, *Eur. J. Inorg. Chem.* **2001**, 1353−1360. [2d] R. Krämer, I. O. Fritsky, *Eur. J. Inorg. Chem.* **2000**, 3505−3510. [2e] I. O. Fritsky, R. Ott, R. Krämer, *Angew. Chem. Int. Ed.* **2000**, *39*, 3255−3258.

[3] [3a] S. Campagna, G. Denti, G. De Rosa, L. Sabatino, M. Ciano, V. Balzani, *Inorg. Chem.* **1989**, *28*, 2565−2570. [3b] A. Neels, H. Stoeckli-Evans, *Inorg. Chem.* **1999**, *38*, 6164−6170. [3c] R. R. Ruminski, J. O. Johnson, *Inorg. Chem.* **1987**, *26*, 210−212. [3d] J. A. Baiano, W. R. Murphy, Jr., *Inorg. Chem.* **1991**, *30*, 4594−4598. [3e] F. R. Heirtzler, *Synlett* **1999**, 1203−1206. [3f] A. Neels, H. Stoeckli-Evans, A. Escuer, R. Vincente, *Inorg. Chem.* **1995**, *34*, 1946−1949. [3g] A. Neels, B. M. Neels, H. Stoeckli-Evans, A. Clearfield, D. M. Poojary, *Inorg. Chem.* **1997**, *36*, 3402−3409. [3h] S. Serroni, G. Denti, *Inorg. Chem.* **1992**, *31*, 4251−4255. [3i] K. J. Brewer, W. R. Murphy, Jr., S. R. Spurlin, J. D. Peterson, *Inorg. Chem.* **1986**, *25*, 882−884.

[4] S. Campagna, S. Serroni, S. Bodige, F. M. MacDonnell, *Inorg. Chem.* **1999**, *38*, 692−701.

[5] [5a] X. Hua, A. von Zelewsky, *Inorg. Chem.* **1995**, *34*, 5791−5797. [5b] F. M. MacDonnell, M.-J. Kim, S. Bodige, *Coord. Chem. Rev.* **1999**, *185−186*, 535−549. [5c] J. Chen, F. M. MacDonnell, *Chem. Commun.* **1999**, 2529−2530. [5d] M.-J. Kim, F. M. MacDonnell, M. E. Gimon-Kinsel, T. Du Bois, N. Asgharian, J. C. Griener, *Angew. Chem. Int. Ed.* **2000**, *39*, 615−619. [5e] S. Bodige, A. S. Torres, D. J. Maloney, D. Tate, G. R. Kinsel, A. K. Walker, F. M. MacDonnell, *J. Am. Chem. Soc.* **1997**, *119*, 10364−10369.

[6] D. M. Roundhill, *Photochemistry and Photophysics of Metal Complexes*, Plenum, New York, **1994**, chapter 5.

[7] D. Brown, S. Muranjan, Y. Jang, R. P. Thummel, *Org. Lett.* **2002**, *4*, 1253−1256.

[8] [8a] R. P. Thummel, *Synlett* **1992**, 1−12. [8b] P. Caluwe, *Tetrahedron* **1980**, *36*, 2359−2407. [8c] R. P. Thummel, *Tetrahedron* **1991**, *47*, 6851−6886. [8d] C.-C. Cheng, S.-J. Yan, *Org. React.* **1982**, *28*, 37−201.

[9] [9a] J.-M. Lehn, D. M. Bessani, *Bull. Soc. Chim. Fr.* **1997**, *134*, 897−906. [9b] R. C. Gadwood, M. R. Rubino, S. C. Nagarajan, S. T. Michel, *J. Org. Chem.* **1985**, *50*, 3255−3260. [9c] A. J. Majeed, O. Antonses, T. Benneche, K. Undheim, *Tetrahedron* **1989**, *45*, 993−1006.

[10] T. Caronna, G. Fronza, F. Minsci, O. Porta, *J. Chem. Soc., Perkin Trans. 2* **1972**, 2035−2038.

[11] [11a] S. Ernst, V. Kasack, W. Kaim, *Inorg. Chem.* **1988**, *27*, 1146−1148. [11b] I. G. Phillips, P. J. Steel, *Aust. J. Chem.* **1998**, *51*, 371−382.

[12] V. Goulle, R. P. Thummel, *Inorg. Chem.* **1990**, *29*, 1767−1772.

[13] L. I. Smith, J. W. Opie, *Org. Syn. Coll. Vol. III* **1955**, 56−58.

[14] T. G. Majewicz, P. Caluwe, *J. Org. Chem.* **1974**, *39*, 720−721.

[15] J. V. Caspar, J. K. Nagle, T. J. Meyer, *J. Am. Chem. Soc.* **1982**, *104*, 4803−4810.

[16] Insufficient sample for combustion analysis.

Received April 4, 2003

 © 2003 Wiley-VCH Verlag GmbH & Co. KGaA, Weinheim

Study of the D→Sb (D = O, S) Transannular Interaction in Sb-Monohalogenated Dibenzostibocines − An Experimental and Theoretical Study

José G. Alvarado-Rodríguez,*[a] Noemí Andrade-López,[a] Simplicio González-Montiel,[a] Gabriel Merino,[b] and Alberto Vela[b]

Keywords: Antimony / Density functional calculations / Halogens / Hypervalent compounds / Structure elucidation

In order to gain a greater insight in the nature of the D→Sb transannular interaction in dibenzostibocines, a series of $D(C_6H_4S)_2SbHal$ complexes (D = S; Hal = Cl **1**, Br **2**, I **3**; D = O, Hal = Cl **4**) has been synthesised. X-ray structure determinations of complexes **1**–**4** reveal that the antimony atom is in a distorted ψ-bipyramidal geometry, acting as an acceptor atom. The eight-membered ring conformation in **1**, **2** and **4** can be described as a twist-boat, while in **3** it is approaching C_s symmetry. DFT calculations were carried out on **1** and **4**. Topological analysis of the electron density in **1** and **4** showed the presence of critical points in the D→Sb direction (D = O, S). The electron localisation function showed the presence of a lone pair located in an equatorial position on the antimony, and a lone pair of the donor along the D→Sb direction, confirming the presence of a dative bond in the system.
(© Wiley-VCH Verlag GmbH & Co. KGaA, 69451 Weinheim, Germany, 2003)

Introduction

The coordinating capabilities of ligands such as **I** (unsubstituted or benzene ring-substituted) have been extensively studied, particularly in the formation of dibenzoheterocycles **II** (Scheme 1). These studies have focused mainly on the synthesis of heterodinuclear compounds containing nickel and iron for modelling of active sites of [NiFe] hydrogenases,[1,2] and also on structural investigations devoted to understanding of the factors involved in the valence expansion of the acceptor atom A through formation of intramolecular transannular bonds with D and its relation with the adopted conformation of the central eight-membered ring.[3,4]

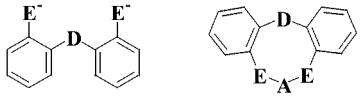

I **II**

A Lewis acid
D Lewis base
E O, S

Scheme 1

The coordination mode of **I** can mainly be di- or tridentate. In the first case, the lack of interactions results in atoms without valence expansion. The chemistry of the ligands with D = S and E = O is so far the most widely investigated. Metal complexes with *d*-block elements (Ti,[5] Zr,[6] V,[7] Co,[8] Cu,[9] W[10]) and light *p*-block elements, mainly phosphorus[11−13] and silicon,[4] acting as acceptor atoms A have been studied. Two spirocyclic germanium(IV) compounds containing ligands of type **I** (D = S, Se; E = O) have been crystallographically characterised. These compounds show the capabilities of **I** to expand the normal valence of the acceptor atom A.[14,15] In both cases, the germanium displays a distorted octahedral geometry with two transannular interactions D→Ge significantly shorter than the corresponding sums of the van der Waals radii.

For metal complexes **II** with D = S, and E = S, on the other hand, the chemistry is completely dominated by the *d*-block metals Fe,[16,17] Ni,[18−21] Pd[18−20] and Pt.[18,19] It is worth noting that, in the molecular structures determined in the solid state, the metal-sulfur (thioether) distance is always shorter than the metal-sulfur (thiolate) distance.

To the best of our knowledge, there are no reports of **II** complexes with heavier *p*-block elements, in particular complexes with antimony, in spite of the numerous studies carried out with similar stibocanes in which the presence of transannular D→A interactions and a large number of conformations of the eight-membered ring have been

[a] Centro de Investigaciones Químicas, Universidad Autónoma del Estado de Hidalgo,
Km. 4.5 Carretera Pachuca-Tulancingo, Pachuca, Hidalgo, México. C. P. 42076
Fax: (internat.) + 52-771/717-2000 ext. 6502
E-mail: galvarad@uaeh.reduaeh.mx
[b] Departamento de Química, Centro de Investigación y de Estudios Avanzados, I.P.N.
A. P. 14-740, México
Fax: (internat.) +52-55/5747-7113

 © 2003 Wiley-VCH Verlag GmbH & Co. KGaA, Weinheim **DOI: 10.1002/ejic.200300199**

observed.[22−26] Here we report an experimental and theoretical study of type **II** complexes with antimony as acceptor atom. These compounds are good models for further understanding of the nature of the D→Sb interaction. After the description of the synthesis of stibocine Sb-halogen complexes, NMR and X-ray crystallographic data are presented and discussed. Finally, density functional theory (DFT) calculations on the chloro complexes are discussed, together with an analysis of the bonding based on some molecular scalar fields.

Results and Discussion

Synthesis of $D(C_6H_4S)_2SbHal$ (D = O, S; Hal = Cl, Br, I)

The $S(C_6H_4SH)_2$ compound was obtained in a four-step, one-pot reaction by the method reported by Sellmann.[19] The $O(C_6H_4SH)_2$ compound was obtained in a similar way (see Exp. Sect. for details). Treatment of $S(C_6H_4SH)_2$ and $O(C_6H_4SH)_2$ with $SbCl_3$ in benzene yielded $S(C_6H_4S)_2SbCl$ (**1**) and $O(C_6H_4S)_2SbCl$ (**4**), respectively (see Scheme 2).

1 D = S
4 D = O

Scheme 2

Both complexes are air-stable, soluble in benzene and chloroform, and insoluble in pentane, hexane and 2-propanol. $S(C_6H_4S)_2SbI$ (**3**) was obtained from a halogen-exchange reaction between **1** and two equivalents of KI in hot toluene, yielding pale-yellow crystals. However, $S(C_6H_4S)_2SbBr$ (**2**) could not be obtained in a similar way. More drastic conditions were tested, and compound **2** was synthesized from **1** by treatment with two equivalents of KBr in a refluxing HBr/toluene mixture, giving **2** as colourless crystals.

Mass Spectra

The FAB mass spectra of all the compounds each exhibit a low intensity ion with the appropriate isotopic ratio representing the molecular ion; in all cases the $M^+ - Hal$ peak is assigned to the $D(C_6H_4S)_2Sb$ tricyclic moiety, confirming the binding of antimony to sulfur atoms. No more peaks could be assigned.

NMR Spectroscopy

NMR spectroscopic data are given in Table 1. At 25 °C, the ^1H NMR spectra of **1** and **3** in $CDCl_3$ and the ^1H spectrum of **2** in C_6D_6 each show four signals in an ABCD pattern, typical of *ortho*-substituted benzene rings. In **4**, the ^1H NMR spectrum in $CDCl_3$ at the same temperature shows two signals at δ = 7.55 and 7.13 ppm for protons H-4 and H-2, respectively, and one more at δ = 7.18 ppm for H-1 and H-3 (see Scheme 3). In solution, the two C_6H_4S halves are equivalent. In all complexes, protons H-2 and H-4 are shifted to higher frequencies with respect to the free neutral ligand.

Table 1. ^1H NMR chemical shifts (δ values, ppm) for **1−4**

Compound	D	Hal	H-1	H-2	H-3	H-4
1[a]	S	Cl	7.51	7.27	7.16	7.60
2[b]	S	Br	7.01	6.61	6.54	7.21
3[a]	S	I	7.44	7.27	7.17	7.60
4[a]	O	Cl	7.18	7.13	7.18	7.55

[a] In $CDCl_3$. [b] In C_6D_6.

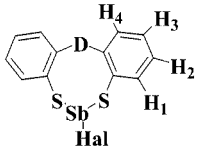

Scheme 3

The ^{13}C spectra of **1** and **3** in $CDCl_3$ at 25 °C each show the *ipso* carbons 1a (see Table 2, Scheme 4) at higher frequencies and the *ipso* carbons 4a at lower frequencies. An interesting observation in **3** is that the *ipso* carbon 1a is the most strongly shifted to lower frequencies. In **4**, the ^{13}C NMR spectrum in $CDCl_3$ at the same temperature shows C-1a and C-3 at 127.4 ppm; an APT experiment confirmed the previous result. The unequivocal assignment in **1** and **4** were performed by HETCOR and HMBC experiments.

Table 2. ^{13}C NMR chemical shifts (δ values, ppm) for **1−4**

Compound	D	Hal	C-1	C-1a	C-2	C-3	C-4	C-4a
1[a]	S	Cl	134.3	143.2	130.1	127.2	132.6	132.0
2[b]	S	Br	134.1	143.6	129.5	126.4	132.3	132.4
3[a]	S	I	134.8	141.9	129.9	127.2	132.2	132.1
4[a]	O	Cl	126.4	127.4	120.7	127.4	133.3	153.4

[a] In $CDCl_3$. [b] In C_6D_6.

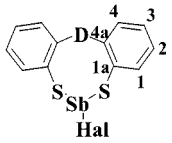

Scheme 4

The ^1H and ^{13}C NMR spectra of **1** in $CDCl_3$ at −65 °C show only a very small displacement to higher frequencies (less than 0.1 and 0.5 ppm in ^1H and ^{13}C NMR, respectively), showing that any conformational equilibrium is too fast to be determined.

 © 2003 Wiley-VCH Verlag GmbH & Co. KGaA, Weinheim

X-ray Structures of Compounds 1−4

The solid-state structures of **1**−**4** were determined by single-crystal X-ray diffraction analyses. The structures are depicted in Figure 1. The unit cell of **3** has two crystallographically independent molecules (**3a** and **3b**). Compounds **1** and **2** co-crystallised with benzene and toluene, respectively. Selected bond lengths and angles are given in Table 3.

If the covalent bonds are taken into consideration, the structure determination of all complexes reveals tricoordinate pyramidal antimony atoms. The Sb−S distances are in good agreement with those reported in other eight-membered heterocycles containing antimony-sulfur bonds.[22−26] The Sb−Hal distances (Hal = Cl, Br, I) are 1−5% longer than the corresponding sums of the covalent radii [Σ_{rcov} (Sb,Cl) = 2.39 Å; Σ_{rcov} (Sb,Br) = 2.54 Å; Σ_{rcov} (Sb,I) = 2.73 Å][27,28] and compare well with other distances found in similar eight-membered heterocycles. In addition to the expected bonding of the two sulfurs (thiolate) and the halogen ligands to the antimony atom, a short distance of the transannular D atoms to Sb is observed (D = S in **1**, **2** and **3**; D = O in **4**). These distances are longer than the corresponding sums of covalent radii but shorter than the sums of the corresponding van der Waals radii, and can be described as secondary interactions.[29] Moreover, the S···Sb distance in the complexes **1**−**3** decreases in the order of *trans* substituents, with the shortest distance in the iodo complex **3**.

If the secondary interactions are taken into account, the geometry of the coordination sphere of the antimony atom can be described as ψ-trigonal bipyramidal (TBP), in which the halogen and thioether-like sulfur atoms are in the axial positions, the two thiolate-like sulfur atoms occupy two equatorial positions and, in terms of the VSEPR model, we are tempted to envisage a stereochemical activity of the lone pair of the antimony(III) atom in the fifth position. Furthermore, the degree of TBP coordination can be determined by

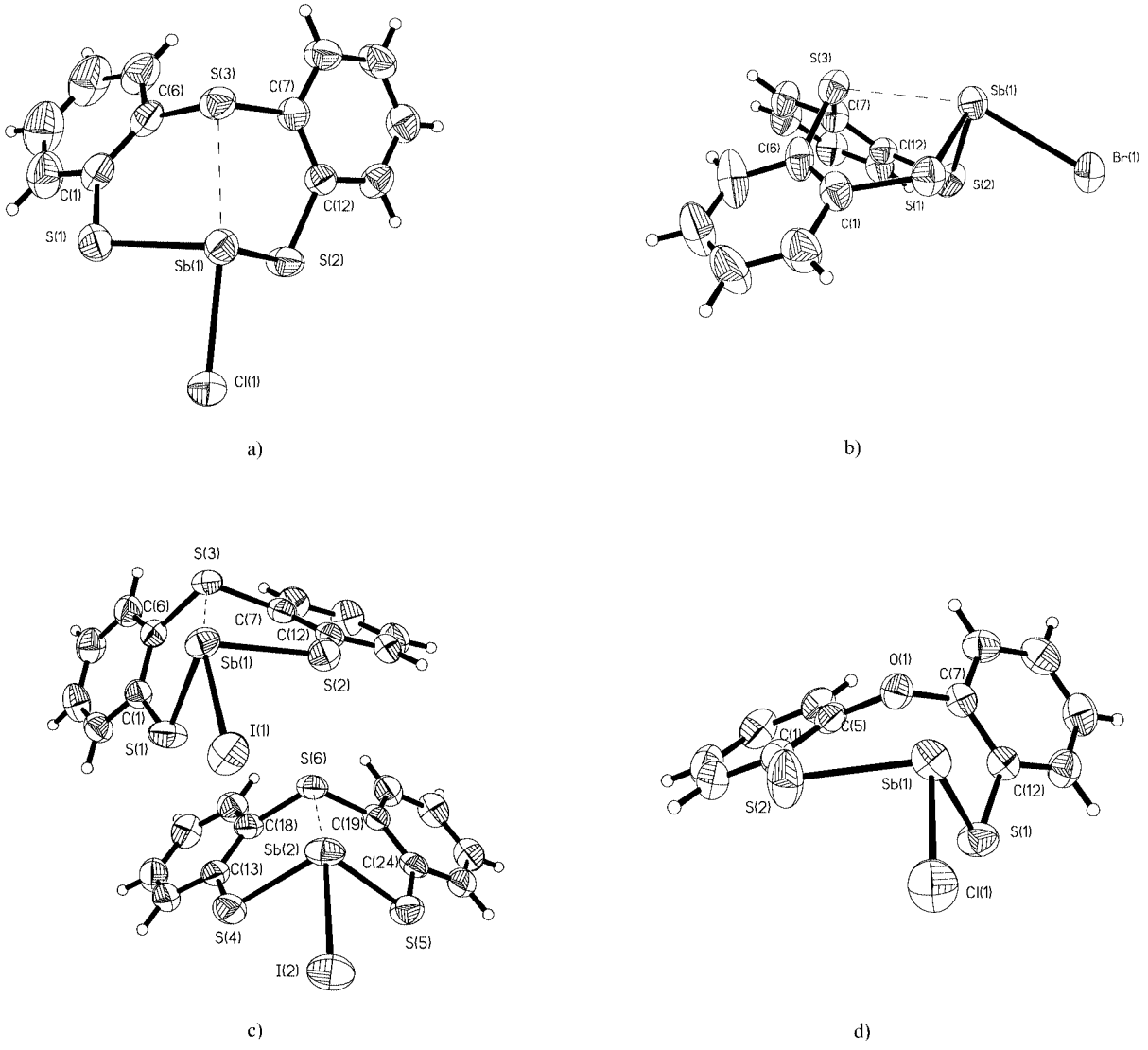

Figure 1. ORTEP diagrams of: a) $S(C_6H_4S)_2SbCl{\cdot}0.5C_6H_6$ (**1**·$0.5C_6H_6$), b) $S(C_6H_4S)_2SbBr{\cdot}0.5C_6H_5CH_3$ (**2**·$0.5C_6H_5CH_3$), and c) $S(C_6H_4S)_2SbI$ (**3**) and $O(C_6H_4S)_2SbCl$ (**4**) (50% probability ellipsoids, solvent molecules omitted)

 © 2003 Wiley-VCH Verlag GmbH & Co. KGaA, Weinheim

Table 3. Selected bond lengths [Å] and bond angles [°] of $D(C_6H_4S)_2SbHal$

Compound	**1**·0.5C_6H_6	**2**·0.5$C_6H_5CH_3$	**3a**	**3b**	**4**
D	S	S	S	S	O
Hal	Cl	Br	I	I	Cl
Sb−Hal	2.4807(6)	2.6373(6)	2.8603(6)	2.8747(6)	2.4066(9)
Sb···D	2.8187(6)	2.8047(13)	2.7839(15)	2.7710(16)	2.596(2)
Sb−S(1)	2.4569(6)	2.4575(14)	2.4602(17)	–	2.4295(9)
Sb−S(2)	2.4640(6)	2.4637(14)	2.4445(15)	–	2.4280(10)
Sb−S(4)	–	–	–	2.4585(18)	–
Sb−S(5)	–	–	–	2.4639(17)	–
Hal−Sb···D	155.24(2)	155.86(4)	158.62(4)	158.61(4)	153.22(5)
S(1)−Sb−S(2)	98.39(2)	98.66(5)	95.71(6)	–	100.15(4)
S(4)−Sb−S(5)	–	–	–	96.38(6)	–
C(6)−D−C(7)	103.33(11)	103.3(3)	103.1(3)	–	116.2(2)
C(18)−D−C(19)	–	–	–	103.7(3)	–
C(1)−C(6)−D−C(7)	121.4(2)	122.5(5)	82.4(5)	–	139.6(3)
C(12)−C(7)−D−(C6)	−84.3(2)	−84.9(5)	−119.2(5)	–	−91.9(3)
C(1)−S(1)−Sb(1)−S(2)	−57.9(2)	−61.4(2)	−103.0(2)	–	−51.9(1)
C(12)−S(2)−Sb(1)−S(1)	104.3(8)	102.8(2)	65.8(2)	–	106.9(1)
C(13)−C(18)−D−C(19)	–	–	–	107.4(5)	–
C(24)−C(19)−D−C(18)	–	–	–	−98.4(5)	–
C(13)−S(4)−Sb(2)−S(5)	–	–	–	−80.5(2)	–
C(24)−S(5)−Sb(2)−S(4)	–	–	–	90.4(2)	–

a method used to describe structural displacements between pyramidal and trigonal bipyramidal idealised geometries.[30−32] In this method the degree of displacement from a lower (pyramidal) toward higher coordination geometry (TBP) is simply evaluated from the acceptor-donor atom distance and by how far this distance is displaced from the sum of the van der Waals radii (0% displacement) to the sum of covalent radii (100% displacement) of the acceptor-donor atoms. The results are presented in Table 4.

Table 4. Comparison of D···Sb−Hal geometrical bond parameters in **1−4** complexes; bond lengths in Å and bond angles in degrees

Compound	D	Hal	Sb···D	% TBP	D···Sb−Hal
1	S	Cl	2.8187(6)	73	155.24(2)
2	S	Br	2.8047(13)	74	155.86(4)
3a	S	I	2.7839(15)	76	158.62(4)
3b	S	I	2.7710(16)	77	158.61(4)
4	O	Cl	2.5960(2)	69	153.22(5)

The eight-membered ring conformations of compounds **1**, **2** and **4** can be described as twist-boat (C_1 symmetry).[15] This description is based on the non-equivalence of the torsional angles, mainly those formed by the torsion of the carbon-sulfur (thioether) bond and the antimony-sulfur (thiolate) bond (Table 3). The ring conformation of compound **3** deserves some comments. In the **3a** molecule the conformation can also be described as twist-boat, but in **3b** the conformation could better described as boat-boat (C_s symmetry). This proposal is supported by the closer similitude between the torsion angles of the C−C−D−C and C−S−Sb−S atoms (ca. 10°).

DFT Calculation on Compounds 1 and 4

In order to analyse the bonding situation in the different molecules we performed a set of DFT calculations. The systems were fully optimised, and the nature of the chemical bonding was analysed in terms of the topology of the electronic density [$\rho(\mathbf{r})$[33]] and the electron localisation function [ELF($\mathbf{r}$)[34,35]].

All calculations were performed with the aid of Gaussian 98,[36] by use of the hybrid functional BHandHLYP. The selection of this hybrid functional was made for one reason. The half-and-half mixing of exact exchange and density-dependent exchange is justified by approximating the adiabatic connection formula.[37] For the geometry optimization, the 6-31++G(d,p) basis set was employed for all atoms, except for the antimony, for which a relativistic effective core potential (RECP) was used.[38] We denote these calculations as BHandHLYP/6-31++G(d,p) + RECP(Sb). All stationary points were characterised on the potential energy surface by a harmonic frequency analysis. For the generation of the molecular scalar fields, a double-ζ basis set with one polarisation function in all atoms (DZVP) was used.[39] The contractions of the DZVP basis set are (41/1*) for hydrogen, (621/41/1*) for carbon and oxygen, (6321/521/1*) for sulfur and chlorine, and (633321/53321/531*) for antimony. These calculations are denoted as BHandHLYP/DZVP. The Kohn−Shan orbitals were determined by BHandHLYP/DZVP//BHandHLYP/6-31++G(d,p) + RECP(Sb). The analysis of the electron density and the ELF were performed with the aid of the AIM2000[40] and the TopMod[41] programs, respectively.

A set of selected bond lengths and angles of the optimised structures are reported in Table 5. The calculated geometrical parameters are in good agreement with the crystallographic data. In relation to the initial structure in

 © 2003 Wiley-VCH Verlag GmbH & Co. KGaA, Weinheim

Table 5. Selected experimentally measured and theoretical bond lengths and bond angles of $D(C_6H_4S)_2SbCl$ (D = S, O); bond lengths are in Å and bond angles are in degrees; dipole moments are in Debyes

	1[a]	**1**[b]	**1′**[b]	**4**[a]	**4**[b]	**4′**[b]
Sb−Cl	2.4807(6)	2.415	2.425	2.4066(9)	2.393	2.394
Sb···D	2.8187(6)	3.002	2.902	2.596(2)	2.697	2.614
Sb−S(1)	2.4569(6)	2.469	2.463	2.4295(9)	2.455	2.446
Sb−S(2)	2.4640(6)	2.460	–	2.4280(10)	2.461	–
S(1)−C(1)	1.773(2)	1.776	1.772	1.766(3)	1.772	1.773
S(2)−C(12)	1.771(2)	1.776	–	1.769(3)	1.777	–
C(6)−D	1.791(3)	1.786	1.787	1.412(4)	1.388	1.393
C(7)−D	1.790(2)	1.781	–	1.414(3)	1.385	–
Cl−Sb···D	155.24(2)	158.8	160.7	153.22(5)	155.4	156.9
Cl−Sb−S(1)	85.66(2)	93.2	88.1	90.09(3)	93.3	90.3
Cl−Sb−S(2)	84.38(2)	91.1	–	88.64(3)	94.4	–
C(1)−S(1)−Sb	107.39(9)	104.9	109.5	104.30(11)	104.0	102.6
C(12)−S(2)−Sb	105.28(7)	102.8	–	97.00(10)	95.9	–
C(6)−D−Sb	99.46(8)	94.4	100.4	113.04(16)	111.5	113.1
C(7)−D−Sb	98.63(8)	93.0	–	104.58(16)	102.0	–
D···Sb−S(1)	79.32(2)	73.7	79.5	72.88(5)	71.7	74.7
D···Sb−S(2)	78.538(18)	75.2	–	74.69(5)	70.7	–
S(1)−Sb−S(2)	98.39(2)	99.5	99.6	100.15(4)	101.6	97.3
C(6)−D−C(7)	103.33(11)	103.2	105.4	116.2(2)	117.9	123.9
Dipole	–	6.27	7.1	–	5.87	6.45

[a] Experimental data. [b] Theoretical data.

the solid, the largest deviations are found in the D→Sb (D = O, S) and Sb−Cl bonds. The Sb−D bond length in the solid state is shorter than calculated for the gas phase. This behaviour is very common in donor-acceptor molecules and it is a consequence of the electrostatic dipole-dipole interactions (μ = 6.27 and 5.87 D in **1** and **4**, respectively).[42,43]

Of the possible isomers, the C_s structures (denoted as **1′** and **4′**, respectively) were considered, and their geometrical parameters are summarised in Table 5. These structures are transition states on the corresponding potential energy surface. Harmonic analysis shows one small imaginary frequency (−33 and −52 cm^{-1} in **1′** and **4′**, respectively). The relative energies of isomers **1′** and **4′** with respect to the unsymmetrical structures are ΔE = 3.2 and 4.2 kcal/mol, respectively. On the other hand, the Sb···D distances are smaller in the C_s structures than in unsymmetrical isomers. The largest bond length difference between the C_s and C_1 structures is the Sb···D distance (≈0.1 Å in **1** and ≈0.08 Å in **4**). It is worth noting that the Sb···D distances in the C_s structures are closer to the solid-state data and they have the largest dipole moment. This is in line with the model suggesting that donor-acceptor complex systems are stabilized by the dipole-dipole interactions.

To analyse the bonding in molecules **1** and **4**, the critical points of the electron density (CPs) and the gradient paths were determined. Here we focus the analysis mainly on the (3,-1) saddle points. Results of topological analysis of the electron density (TAED) are presented in Table 6, and the molecular graphs of **1** and **4** are depicted in Figure 2. All systems show bond critical points along the Sb···D directions, even though these distances are longer than the Sb−S(1) and Sb−S(2) bond lengths. The values of ρ_c(D···Sb) are smallest (≈0.027 a.u.) and $\nabla^2\rho_c$ are positive.

Table 6. Topological analysis of the electronic density; ρ, L and ε are the density, Laplacian ($-1/4\nabla^2\rho$) and ellipticity at the critical points, respectively; all quantities are in atomic units

	D = S			D = O		
	ρ	L	ε	ρ	L	ε
Sb−Cl	0.074	−0.032	0.027	0.077	−0.034	0.029
Sb···D	0.029	−0.014	0.053	0.026	−0.022	0.113
Sb−S(1)	0.079	−0.015	0.134	0.081	−0.015	0.162
Sb−S(2)	0.079	−0.015	0.139	0.080	−0.015	0.146
S(1)−C(1)	0.192	0.089	0.119	0.192	0.090	0.132
S(2)−C(12)	0.192	0.090	0.120	0.192	0.089	0.110
C(6)−D	0.192	0.090	0.099	0.260	0.061	0.019
C(7)−D	0.194	0.092	0.077	0.263	0.064	0.034

It is important to note that the L values of all bond critical points connecting Sb with its neighbours are negative, three interactions are stronger than the dative bond and have a very important ionic contribution.

The distribution of the lone pairs in the complexes is therefore a crucial question. In this sense, the electron localisation function is a good molecular scalar field with which to study this situation. The local maxima of this function define attractors corresponding to core, bonding and non-bonding electron pairs. The analysis of the ELF for molecules **1** and **4** are presented in Figure 3. The first important feature to note is the presence of a lone pair located on the antimony atom. At the same time, there are two basins around the equatorial sulfur atoms, which are related to the lone pairs on these atoms. However, the situation of the possible donor atom is special. In this case, the D atom has two basins, but one of them is found along the D→Sb interaction. On the other hand, one of lone pairs of the D atom is oriented towards antimony.

 © 2003 Wiley-VCH Verlag GmbH & Co. KGaA, Weinheim

Figure 2. Molecular graphs of **1** and **4**; the small black and light grey spheres are the bond and ring critical points, respectively

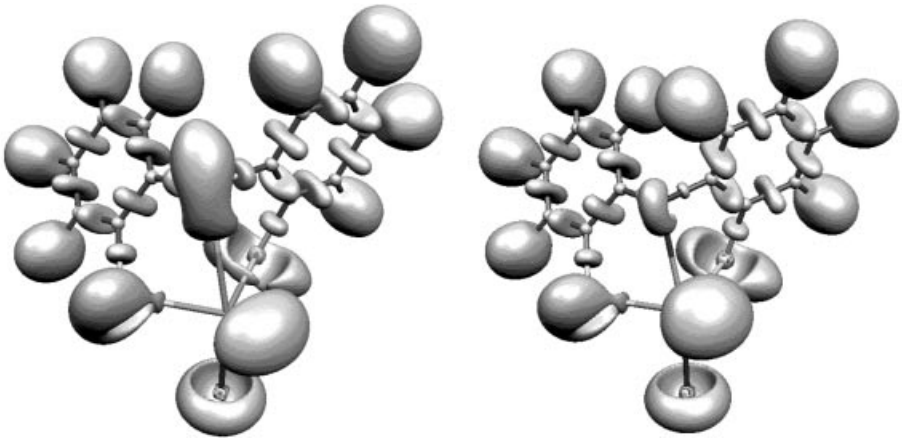

Figure 3. ELF isosurfaces [ELF(**r**) = 0.85] for **1** and **4**

The analyses presented above allow us to classify these molecules as intramolecular donor-acceptor complexes, in which Sb acts as an acceptor and the D atom as a donor.

Concluding Discussion

In the quest for good models with which to understand the nature of the D→Sb interactions, the complexes $D(C_6H_4S)_2SbHal$ **1**−**4** have been synthesised, structurally characterised and theoretically studied. All compounds display a distorted ψ-bipyramidal trigonal geometry of the antimony atom.

The X-ray analysis of the transannular Sb···S distances in the complexes **1**−**3** are 16.5−4.5% longer than the corresponding sums of the covalent radii and they indicate secondary bonding. This situation is different from that in *d*-block metals complexes in which the metal-sulfur (thioether) distance is shorter than the metal-sulfur (thiolate) distance. The Sb···S distance decreases as the electronegativity of the halogen ligand decreases. Moreover, there is a correlation between the symmetry of the eight-membered ring and the transannular distance: the higher the symmetry of the ring, the shorter the Sb···S distance, reflecting the flexibility of the $[S(C_6H_4S)_2]^{2-}$ ligand. In the chloro stibocine derivatives, the sulfur atom is a better donor that the oxygen atom. This is also consistent with the larger % TBP displacement determined in **1**.

The theoretical calculations predict a Sb···D bond length longer than in the solid state. This is a typical effect when a donor-acceptor complex is formed. On the other hand, the relative energies of the symmetrical isomers (**1′** and **4′**) with respect to unsymmetrical structures are ΔE = 3.2 and 4.2 kcal/mol, respectively, in agreement with the NMR results in which the conformational equilibria are too fast to be determined. Molecules **1** and **4** show bond critical points along the Sb···D directions. The topological descriptors allow us to classify the Sb···S interaction as a weak interaction. The ELF for the molecules **1** and **4** indicates the presence of a lone pair located on the antimony atom at the equatorial position. The D atoms (D = S, O in **1** and **4**, respectively) have two basins, one of them being found

 © 2003 Wiley-VCH Verlag GmbH & Co. KGaA, Weinheim

along the D→Sb direction. These experimental and theoretical results allow us to classify these compounds as intramolecular donor-acceptor complexes in which the antimony atom acts as acceptor atom.

Experimental Section

General Methods: Unless noted otherwise, all reactions and operations were carried out under argon at room temperature with use of standard Schlenk techniques. Solvents were dried and distilled before use. Melting points were determined on a Melt-Temp II instrument and are uncorrected. Spectra were recorded with the following instruments. Mass spectra: for EI, a Hewlett Packard 5989A mass spectrometer was used. FAB+ mass spectra were recorded on a JEOL JMS-AX505HA by using a Xe beam at 6 keV, with nitrobenzyl alcohol (NBA) as matrix. Elemental analysis: Perkin-Elmer Series II CHNS/O Analyzer. The IR spectra were record in the 4000−400 cm^{-1} range on a Perkin−Elmer System 2000 FT-IR spectrometer, as KBr pellets or in CsI cuvettes. NMR: Jeol Eclipse 400 spectrometer; with the residual protio-solvent signal used as referenced for ^1H NMR spectra. $^{13}C\{^1H\}$ NMR spectra were referred through the solvent peaks. Chemical shifts are quoted on the δ scale (downfield shifts are positive) relative to tetramethylsilane (^1H, $^{13}C\{^1H\}$). Spectra were recorded at 25 °C. ^1H; 399.78 MHz, $^{13}C\{^1H\}$; 100.53 MHz. $S(C_6H_5)_2$, $O(C_6H_5)_2$, *n*BuLi (1.6 M, in hexanes), KI, KBr and HBr were purchased from Aldrich and Fluka. $SbCl_3$ was sublimed prior to use. The $S(C_6H_4SH)_2$ compound was prepared as reported.[19]

$O(C_6H_4SH)_2$: TMEDA (12.20 mL, 81.15 mmol), a solution of *n*BuLi in hexanes (1.6 M, 50 mL, 80 mmol) and diphenyl ether (6 mL, 37.85 mmol) were successively added at room temperature to 60 mL of hexanes. The solution was stirred for 24 h, in the course of which a beige solid precipitated. Elemental sulfur (3.46 g, 108.00 mmol) was added with vigorous stirring, and the resulting yellow suspension was stirred for 48 h and concentrated to dryness. The yellow residue was dissolved in THF (60 mL) and immersed in an ice bath, and $LiAlH_4$ (3.02 g, 84.85 mmol) was added in small portions. ***Caution: A vigorous reaction takes place and the reaction suspension starts to foam.*** Subsequently, the reddish-brown suspension was heated at reflux for 5 h, in the course of which the colour turned to light yellow green. The resulting mixture was cautiously added in small portions to a mixture of crushed ice (60 g) and concentrated hydrochloric acid (60 mL) immersed in an ice-bath. ***Caution: Vigorous evolution of H_2 and H_2S occurs, and this reaction must be carried out in a well ventilated fumehood.*** After the vigorous reaction had ceased, further concentrated hydrochloric acid (20 mL) was added, and the resulting suspension was extracted with CH_2Cl_2 (3 × 60 mL). The combined organic phases were washed with dilute HCl and passed through a column of Celite and Na_2SO_4, and evaporation of the solvent yielded a yellow oil. Yield: 3.0 g (34%) $O(C_6H_4SH)_2$. MS (EI, CH_2Cl_2): *m*/*z* = 234 [$M^{\cdot+}$ peak base], 200 [$M^{\cdot+}$ − H_2S]. ^1H NMR ($CDCl_3$): δ = 3.90 (s, 2 H, SH), 6.82 (dd, 2 H, C_6H_4), 7.04 (dt, 2 H, C_6H_4), 7.09 (dt, H, C_6H_4), 7.36 (dd, 2 H, C_6H_4) ppm. $^{13}C\{^1H\}$ NMR ($CDCl_3$): δ = 118.6, 123.7, 124.5, 126.7, 130.2, 152.1 ppm. IR (CsI): $\tilde{\nu}$ = 3052, 2555 (SH), 1582, 1446, 1426, 1036, 747 cm^{-1}. The neutral ligand was used further without purification.

$S(C_6H_4S)_2SbCl$ (1): A solution of freshly sublimed $SbCl_3$ (1.62 g, 7.10 mmol) in benzene (25 mL) was added dropwise to a solution of $S(C_6H_6SH)_2$ (1.76 g, 7.03 mmol) in benzene (25 mL). The yellow solution was stirred for 30 min, upon which a green solution resulted, and this was heated at reflux for 5 h. The solution was allowed to cool to room temperature. The resulting colourless crystals of **1**, as a benzene solvate, were separated by suction filtration and washed with *i*PrOH (40 mL). Yield: 2.40 g (84%) based on $S(C_6H_4S)_2SbCl$ free compound. FAB+: *m*/*z* (%) = 404 (4) [$M^{\cdot+}$], 369 (17) [$M^{\cdot+}$ − Cl]. M.p. 183−189 °C. $S(C_6H_4S)_2SbCl{\cdot}0.5C_6H_6$ (444.66): calcd. C 40.52, H 2.49; found C 39.29, H 2.36. ^1H NMR ($CDCl_3$): δ = 7.16 (ddd, 2 H, C_6H_4), 7.27 (ddd, 2 H, C_6H_4), 7.51 (dd, 2 H, C_6H_4), 7.60 (dd, 2 H, C_6H_4) ppm. $^{13}C\{^1H\}$ NMR ($CDCl_3$): δ = 127.17, 130.1, 132.0, 132.6, 134.3, 143.2 ppm. IR (KBr): $\tilde{\nu}$ = 3048, 1568, 1444, 1421, 1035, 744 cm^{-1}.

$S(C_6H_4S)_2SbBr$ (2): $S(C_6H_4S)_2SbCl{\cdot}0.5C_6H_6$·(**1**·$0.5C_6H_6$, 160 mg, 0.36 mmol), KBr (86 mg, 0.72 mmol) and HBr 48% (2 mL) were suspended in toluene (25 mL) and heated at reflux for 16 h. The water was removed from the resulting colourless solution by means of a Dean−Stark trap. The yellow solution obtained was dried by passage through a column of Celite and Na_2SO_4. The solution was left under an argon flow to provide yellow crystals of **2** as a toluene solvate, which were washed with hexanes (40 mL) and filtered by suction. Yield: 100 mg (62% based on free compound **2**). FAB+: *m*/*z* (%) = 448 (5) $[M]^+$, 369 (74) $[M - Br]^+$. M.p. 193−194 °C. $S(C_6H_4S)_2SbBr\ 0.5C_6H_5CH_3$ (496.13): calcd. C 37.52, H 2.44; found C 37.61, H 2.26. ^1H NMR (C_6D_6): δ = 6.54 (td, 2 H, C_6H_4), 6.62 (td, 2 H, C_6H_4), 7.01 (dd, 2 H, C_6H_4), 7.21 (dd, 2 H, C_6H_4) ppm. $^{13}C\{^1H\}$ NMR (C_6D_6): δ = 126.4, 129.5, 132.3, 132.4, 134.1, 143.6 ppm. IR (KBr): $\tilde{\nu}$ = 3046, 1568, 1443, 1420, 1245, 1036, 745 cm^{-1}.

$S(C_6H_4S)_2SbI$ (3): $S(C_6H_4S)_2SbCl\ 0.5C_6H_6$·(**1**·$0.5C_6H_6$, 160 mg, 0.36 mmol) and KI (120 mg, 0.72 mmol) were suspended in dry toluene (25 mL) and heated at reflux for 16 h. The yellow solution was dried by passage through a column of Celite and Na_2SO_4 whilst still warm, and was then allowed to cool to room temperature. On cooling, yellow crystals separated, and these were washed with *n*-hexanes (40 mL) and filtered by suction. Yield: 71 mg (40%). FAB+: *m*/*z* (%) = 496 (2) $[M]^+$, 369 (5) $[M - I]^+$. m.p. 200−204 °C. $S(C_6H_4S)_2SbI$ (497.05): calcd. C 29.00, H 1.62; found C 28.98, H 1.55. ^1H NMR ($CDCl_3$): δ = 7.17 (ddd, 2 H, C_6H_4), 7.27 (ddd, 2 H, C_6H_4), 7.44 (dd, 2 H, C_6H_4), 7.60 (dd, 2 H, C_6H_4) ppm. $^{13}C\{^1H\}$ NMR ($CDCl_3$): δ = 127.2, 129.9, 132.1, 132.2, 134.8, 141.9 ppm. IR (KBr): $\tilde{\nu}$ = 3045, 1569, 1447, 1415, 1247, 1034, 742 cm^{-1}.

$O(C_6H_4S)_2SbCl$ (4): A solution of $O(C_6H_6SH)_2$ (2.0 g, 8.54 mmol) in benzene (25 mL) was added to a solution of $SbCl_3$ (1.95 g, 8.54 mmol) in benzene (25 mL). The yellow solution was stirred for 30 min and was heated to reflux for 5 h. The solution was allowed to cool to room temperature. On cooling, colourless crystals separated, and these were washed with *i*PrOH (40 mL) and filtered by suction. Yield: 1.76 g (53%). FAB+: *m*/*z* (%) = 388 (2) $[M]^+$, 353 (5) $[M - Cl]^+$. m.p. 164−5 °C. $O(C_6H_4S)_2SbCl$ (389.54): calcd. C 37.00, H 2.07; found C 36.65. H 2.12. ^1H NMR ($CDCl_3$): δ = 7.11−7.20 (m, 6 H, C_6H_4), 7.53−7.58 m, 2 H, C_6H_4) ppm. $^{13}C\{^1H\}$ NMR ($CDCl_3$): δ = 120.7, 126.4, 127.4, 133.3, 153.41 ppm. IR (KBr): $\tilde{\nu}$ = 3055, 1584, 1458, 1435, 1054, 752 cm^{-1}.

X-ray Structure Analysis of $S(C_6H_4S)_2SbCl{\cdot}0.5C_6H_6$ (1·0.5C_6H_6), $S(C_6H_4S)_2SbBr{\cdot}0.5CH_3C_6H_5$ (2·0.5 $CH_3C_6H_5$), $S(C_6H_4S)_2SbI$ (3) and $O(C_6H_4S)_2SbCl$ (4)

Suitable single crystals of **1** were grown by slow evaporation of the solvent from a benzene solution, and crystals of **2** and **3** were grown similarly from toluene solutions. Single crystals of **4** were grown by slow diffusion of pentane into a **4**/toluene solution in a 5:1 solvent ratio

 © 2003 Wiley-VCH Verlag GmbH & Co. KGaA, Weinheim

Table 7. Selected crystallographic data for complexes **1**−**4**

Compound	**1**	**2**	**3**	**4**
Empirical formula	$C_{15}H_{11}ClS_3Sb$	$C_{15.53}H_{12}BrS_3Sb$	$C_{12}H_8IS_3Sb$	$C_{12}H_8ClOS_2Sb$
M_r [g/mol]	444.62	496.50	497.01	389.50
Crystal size [mm]	0.50 × 0.21 × 0.10	0.13 × 0.19 × 0.20	0.15 × 0.23 × 0.25	0.08 × 0.10 × 0.28
F(000)	1736	1914	928	752
Crystal system	Monoclinic	Monoclinic	Triclinic	Monoclinic
Space group	$C2/c$	$C2/c$	$P\bar{1}$	$P2_1/c$
a (Å)	23.3503(9)	23.4224(9)	9.3319(6)	4.6860(3)
b (Å)	8.1526(3)	8.3738(3)	11.6186(7)	15.6037(10)
c (Å)	18.3156(8)	18.3659(7)	13.8542(9)	17.8196(10)
α [°]	90	90	103.0640(10)	90
β [°]	109.525(1)	110.193(1)	92.518(2)	91.303(2)
γ [°]	90	90	104.584(2)	90
V (Å^3)	3286.2(2)	3380.8(2)	1407.97(15)	1302.61(14)
Z	8	8	4	4
$\rho_{calcd.}$ [Mg/m^3]	1.797	1.951	2.345	1.986
μ [mm^{-1}]	2.209	4.355	4.571	2.622
Temperature [K]	293(2)	293(2)	294(2)	294(2)
θ range [°]	1.85 to 26.52	1.85 to 26.00	1.52 to 26.00	1.73 to 26.57
Reflections collected	10991	10884	9554	9004
Unique. reflections	3420	3328	5514	2713
R_{int}	0.0358	0.0614	0.0516	0.0605
Solution method	Direct	Patterson	Patterson	Direct
$R1$; $wR2$ [$I > 2\sigma(I)$]	0.0248, 0.0588	0.0342, 0.0830	0.0352, 0.0778	0.0287, 0.0518
$R1$; $wR2$ [all data]	0.0291, 0.0610	0.0501, 0.1003	0.0548, 0.0900	0.0431, 0.0560
Largest residuals [e·Å^{-3}]	0.472/−0.560	0.709/−0.932	0.752/−1.270	0.432/−0.765

Suitable crystals were glued and mounted on fibre glass with the aid of epoxy resin. Intensity data were collected at room temperature on a CCD Smart 6000 diffractometer through the use of Mo-K_α radiation (λ = 0.71073 Å, graphite monochromator). Empirical absorption correction was applied for all complexes. The structures were solved by direct (**1**, **4**) or heavy atom (**2**, **3**) methods, and full-matrix, least-squares refinement was carried out on F^2 (SHELXTL NT 5.10).[44] All non-hydrogen atoms were refined anisotropically. The positions of the hydrogen atoms were kept fixed with a common isotropic displacement parameter. Selected crystallographic data are given in Table 7.[45]

Acknowledgments

JGAR gratefully acknowledges the CONACyT (Project J27919-E) for financial support for these investigations. We wish to thank Dra. Verónica García Montalvo (UNAM) for the recording of FAB+ Mass Spectra.

[1] D. Sellmann, F. Geipel, F. W. Heinemann, *Chem. Eur. J.* **2002**, *8*, 958.
[2] D. Sellmann, F. Geipel, F. Laudebach, F. W. Heinemann, *Angew. Chem. Int. Ed.* **2002**, *41*, 632.
[3] A. J. Arduengo, C. A. Stewart, *Chem. Rev.* **1994**, *94*, 1215−1237.
[4] R. R. Holmes, *Chem. Rev.* **1996**, *96*, 927−950, and references therein cited.
[5] F. Amor, S. Fokken, T. Kleinhenn, T. P. Spaniol, J. Okuda, *J. Organomet. Chem.* **2001**, *621*, 3−9.
[6] L. Porri, A. Ripa, P. Colombo, E. Miano, S. Capelli, S. V Meille, *J. Organomet. Chem.* **1996**, *514*, 213−217.
[7] C. R. Cornman, K.M. Geiser-Bush, J. W. Kampf, *Inorg. Chem.* **1999**, *38*, 4303.
[8] H. Muller, A. Holzmann, W. Hinrichs, G. Klar, *Z. Naturforsch., Teil B* **1982**, *37*, 341.
[9] P. Chaudhuri, M. Hess, U. Florke, K. Wieghardt, *Angew. Chem. Int. Ed.* **1998**, *37*, 2217.
[10] Y. Nakayama, H. Saito, N. Ueyama, A. Nakamura, *Organometallics* **1999**, *18*, 3149.
[11] R. R. Holmes, *Acc. Chem. Res.* **1998**, *31*, 535−542, and references therein cited.
[12] R. R. Holmes, A. Chandrasekaran, P. Sood, R. O. Day, *Inorg. Chem.* **1999**, *38*, 3369−3376.
[13] R. R. Holmes, A. Chandrasekaran, R. O. Day, P. Sood, N. V. Timosheva, D. J. Sherlock, *Phosphorus, Sulfur and Silicon* **2000**, *160*, 1−27.
[14] S. D. Pastor, V. Huang, D. Nabi-Rahni, S. A. Koch, H.-F. Hsu, *Inorg. Chem.* **1997**, *36*, 5966.
[15] T. Thompson, S. D.Pastor, G.Rihs, *Inorg. Chem.* **1999**, *38*, 4163.
[16] D. Sellmann, F. Geipel, F. W. Heinemann, *Chemistry A European Journal* **2002**, *8*, 958.
[17] D. Sellmann, F. Geipel, F. Lauderbach, F. W. Heinemann, *Angew. Chem. Int. Ed.* **2002**, *41*, 632.
[18] D. Sellmann, F. Geipel, F. W. Heinemann, *Eur. J. Inorg. Chem.* **2000**, 59.
[19] D. Sellmann, D. Haussinger, *Eur. J. Inorg. Chem.* **1999**, 1715.
[20] D. Sellmann, F. Geipel, F. W. Heinemann, *Eur. J. Inorg. Chem.* **2000**, 4279.
[21] D. Sellmann, F. Geipel, F. W. Heinemann, *Eur. J. Inorg. Chem.* **2000**, 271.
[22] M. Draeger, R. Engler, *Z. Anorg. Allg. Chem.* **1974**, *405*, 183−192.
[23] M. Draeger, *Z. Anorg. Allg. Chem.* **1976**, *424*, 183−189.
[24] H. M. Hoffmann, M. Draeger, *J. Organomet. Chem.* **1985**, *295*, 33−46.
[25] H. M. Hoffmann, M. Draeger, *J. Organomet. Chem.* **1987**, *320*, 273−281.
[26] M. A. Muñoz Hernández, R. Cea Olivares, S. Hernández Ortega, *Z. Anorg. Allg. Chem.* **1996**, *622*, 1392−1398.
[27] r_{cov}(Sb) = 1.40, r_{cov} (O) = 0.73, r_{cov} (S) = 1.02, r_{cov} (Cl) = 0.99, r_{cov} (Br) = 1.14, r_{cov} (I) = 1.33, = 1.40, r_{vdW} (O) = 1.52,

 © 2003 Wiley-VCH Verlag GmbH & Co. KGaA, Weinheim

r_{vdw} (S) = 1.80, r_{vdW} (Cl) = 1.75, r_{vdW} (Br) = 1.85, r_{vdw} (I) = 1.96 Å, from W. W. Porterfield, *Inorganic Chemistry: A Unified Approach*, 2nd ed., Academic Press, Inc. USA **1993**, p. 214.
[28] r_{vdW} (Sb) = 2.12 Å, in A. Bondi, *J. Phys. Chem.* **1964**, *68*, 441−451.
[29] N. W. Alcock, *Adv. Inorg. Chem. Radiochem.* **1972**, *15*, 1−50.
[30] A. Chandrasekaran, P. Sood, R. O. Day, R. R. Holmes, *Inorg. Chem.* **1999**, *38*, 3369−3376.
[31] N. V. Timosheva, A. Chandrasekaran, R. O. Day, R. R. Holmes, *Inorg. Chem.* **1998**, *37*, 3862−3867.
[32] D. J. Sherlock, A. Chandrasekaran, R. O. Day, R. R. Holmes, *Inorg. Chem.* **1997**, *36*, 5082−5089.
[33] R. F. Bader, *Atoms in Molecules: A Quantum Theory*; Oxford University Press: Oxford, U. K., **1994**.
[34] A. D. Becke, K. E. Edgecombe, *J. Chem. Phys.* **1990**, *92*, 5397−5403.
[35] B. Silvi, A. Savin, *Nature* **1994**, *371*, 683−686.
[36] *Gaussian 98, Revision A.7*, M. J. Frisch, G. W. Trucks, H. B. Schlegel, G. E. Scuseria, M. A. Obb, J. R. Cheeseman, V. G. Zakrzewski, J. A. Montgomery, Jr., R. E. Stratmann, J. C. Burant, S. Dapprich, J. M. Millam, A. D. Daniels, K. N. Kudin, M. C. Strain, O. Farkas, J. Tomasi, V. Barone, M. Cossi, R. Cammi, B. Mennucci, C. Pomelli, C. Adamo, S. Clifford, J. Ochterski, G. A. Petersson, P. Y. Ayala, Q. Cui, K. Morokuma, D. K. Malick, A. D. Rabuck, K. Raghavachari, J. B. Foresman, J. Cioslowski, J. V. Ortiz, A. G. Baboul, B. B. Stefanov, G. Liu, A. Liashenko, P. Piskorz, I. Komaromi, R. Gomperts, R. L. Martin, D. J. Fox, T. Keith, M. A. Al-Laham, C. Y. Peng, A. Nanayakkara, M. Challacombe, P. M. W. Gill, B. Johnson, W. Chen, M. W. Wong, J. L. Andres, C. Gonzalez, M. Head-Gordon, E. S. Replogle, J. A. Pople, Gaussian, Inc., Pittsburgh, PA, **1998**.
[37] J. Harris, *Phys. Rev.* **1984**, *A29*, 1648−1659.
[38] C. E. Check, T. O. Faust, J. M. Bailey, B. J. Wright, T. M. Gilbert, L. S. Sunderlin, *J. Phys. Chem. A* **2001**, *105*, 8111−8116.
[39] N. Godbout, D. R. Salahub, J. Andzelm, E. Wimmer, *Can. J. Chem.* **1992**, *70*, 560−571.
[40] *AIM2000*, version 1.0, Biegler-Köning, University of Applied Sciences, Bielefeld, Germany, **2000**.
[41] *ToPMoD package*, S. Noury, X. Krokidis, F. Fuster, B. Silvi, B.; Universite Pierre et Marie Curie, Paris, France, **1997**.
[42] G. Merino, V. I. Bakhmutov, A. Vela, *J. Phys. Chem.* **2002**, *106*, 8491−8494.
[43] A. Haaland, *Angew. Chem. Int. Ed. Engl.* **1989**, *28*, 992−1007.
[44] *SHELXTL 5.10 Bruker AXS*, Inc., Madison, WI, USA 1998.
[45] CCDC-207115 (**1**·0.5C_6H_6), -207117 (**2**·$C_6H_5CH_3$), -207118 (**3**) and -207116 (**4**) contain the supplementary crystallographic data for this paper. These data can be obtained free of charge at www.ccdc.cam.ac.uk/conts/retrieving.html [or from the Cambridge Crystallographic Data Centre, 12, Union Road, Cambridge CB2 1EZ, UK; Fax: (internat.) + 44-1223/336-033; E-mail: deposit@ccdc.cam.ac.uk].

Received April 8, 2003
Early View Article
Published Online August 14, 2003

 © 2003 Wiley-VCH Verlag GmbH & Co. KGaA, Weinheim

Synthesis, Structure, and Reactivity of Novel Intramolecularly Coordinated Organolead(II) Compounds[‡]

Klaus Jurkschat,*[a] Katja Peveling,[a] and Markus Schürmann[a]

Dedicated to Professor Jaroslaw Holeček on the occasion of his 70th birthday

Keywords: Lead / Chain structures / Carbene homologues / Phosphorus / Hypervalent compounds

The intramolecularly coordinated heteroleptic organolead(II) compounds {4-*t*Bu-2,6-[P(O)(OEt)$_2$]$_2$C$_6$H$_2$}PbX (**2**, X = Cl; **3**, X = SPh) have been synthesized. Single-crystal X-ray analyses reveal that both compounds adopt polymeric chain structures by intermolecular Pb–X···Pb bridges, a structural motif previously unknown for organolead(II) derivatives. Compound **2** reacts with lithium diisopropylamide, *i*Pr$_2$NLi, and lithium bis(trimethylsilyl)methane, (Me$_3$Si)$_2$CHLi, respectively, to provide in situ the corresponding organolead(II) compounds {4-*t*Bu-2,6-[P(O)(OEt)$_2$]$_2$C$_6$H$_2$}PbX (**4**, X = *i*Pr$_2$N; **5**, X = (Me$_3$Si)$_2$CH], which were identified by NMR spectroscopy but could not be obtained as analytically pure substances. Attempts to isolate the intramolecularly coordinated organolead(II) hexafluorophosphate {4-*t*Bu-2,6-[P(O)(OEt)$_2$]$_2$C$_6$H$_2$}Pb$^+$PF$_6^-$ from the reaction of **2** with TlPF$_6$ also failed. Instead, the unprecedented salt [{5-*t*Bu-1,3-[P(O)(OEt)$_2$]$_2$C$_6$H$_3$}$_4$·(Pb$_2$F)] [PF$_6$]$_3$·4THF (**6**) was obtained, in which the [(Pb–F–Pb)]$^{3+}$ cation is stabilized by eight intermolecular P=O→Pb interactions. Compound **6** was characterized by single-crystal X-ray analysis and electrospray mass spectrometry.

(© Wiley-VCH Verlag GmbH & Co. KGaA, 69451 Weinheim, Germany, 2003)

Introduction

Most of the extensive research on the chemistry of the heavier group-14 element carbene analogues ER$_2$ (E = Si, Ge, Sn, Pb; R = alkyl, aryl, alkoxide, thiolate, diorganoamide)[1] has focused on divalent tin[1] and germanium[1] compounds, with fewer studies on low-valent silicon[2–7] and organolead compounds.[1,4,8,9] Of the latter, compounds containing π-bonded ligands[10–17] and Pb–C σ-bonds have been investigated. Divalent lead compounds can be stabilized by bulky[18–33] intramolecularly coordinating substituents.[33–43] Unlike diorganolead compounds[18–31,34–41] there are few examples of RPbX heteroleptic plumbylenes {R = 2,6-[2,4,6-(*i*Pr)$_3$C$_6$H$_2$]$_2$C$_6$H$_3$, C(SiMe$_3$)$_3$, C(SiMe$_3$)$_2$(SiMe$_2$OMe), N(SiMe$_3$)C(Ph)C(SiMe$_3$)$_2$, C(SiMe$_3$)$_2$(SiMe$_2$C$_5$H$_4$N-2), C(SiMe$_2$Ph)$_3$, X = Br, Cl},[31–33,42,43] which are particularly interesting as they allow further derivatizations at the Pb–X function.

Recently, we reported the arylbis(phosphonic) esters 5-*t*Bu-1,3-[P(O)(OR)$_2$]$_2$C$_6$H$_3$ (**A**, R = Et; **B**, R = *i*Pr) and the application of their deprotonated monoanions to the synthesis of intramolecularly coordinated organosilicon(IV),[44–46] organotin(IV),[47–49] and organolead(IV)[50] compounds, and of intramolecularly coordinated heteroleptic stannylenes.[51] The latter, owing to intramolecular P=O→Sn coordination, show notably enhanced stability towards oxidation and thermal decomposition. We present here the synthesis and structure of the corresponding heteroleptic plumbylene and describe its reactivity towards nucleophiles.

Results and Discussion

The organolithium compound {4-*t*Bu-2,6-[P(O)(OEt)$_2$]$_2$C$_6$H$_2$}Li (**1**)[47] reacts with PbCl$_2$ to give the heteroleptic plumbylene {4-*t*Bu-2,6-[P(O)(OEt)$_2$]$_2$C$_6$H$_2$}PbCl (**2**) as colorless crystals in good yield [Equation (1)].

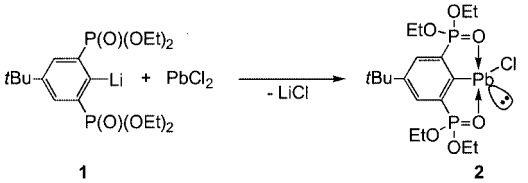

1 2 (1)

[‡] Some of these results were first presented at the 10th International Conference on the Coordination and Organometallic Chemistry of Germanium, Tin and Lead, ICCOC-GTL-10, 8–12 July 2001, Bordeaux, France (Book of Abstracts 2P26). This work includes parts of the intended PhD thesis of K. Peveling.

[a] Lehrstuhl für Anorganische Chemie II der Universität Dortmund,
44221 Dortmund, Germany
Fax: (internat.) + 49-231/7555048
E-mail: kjur@platon.chemie.uni-dortmund.de

Supporting information for this article is available on the WWW under http://www.eurjic.org or from the author.

On contact with air and moisture, it slowly decomposes to give the protonated ligand **A** ($\delta^{31}P$ = 18.5 ppm) and unidentified products (10% decomposition after 4 d, 99% decomposition after 41 d). Under inert conditions and dissolved in C_6D_6, **2** is rather stable. No decomposition was observed after storage at 65 °C for 41 d.

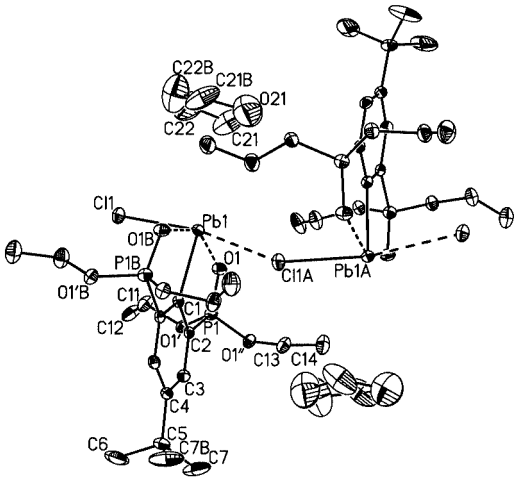

Figure 1. General view (SHELXTL) of two molecular units of **2**·THF showing 30% probability displacement ellipsoids and the atom numbering (symmetry transformations used to generate equivalent atoms: $a = -0.5 + x, y, -0.5 - z$; $b = x, 0.5 - y, z$; $c = 0.5 + x, y, -0.5 - z$)

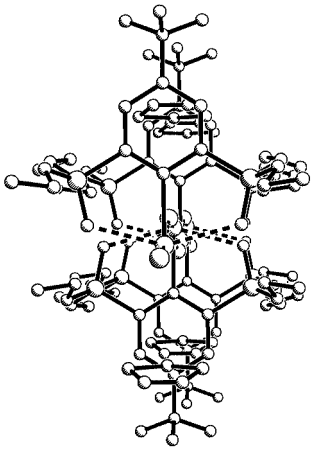

Figure 2. View along the Pb−Cl axis of **2**·THF

The molecular structure of **2**·THF (Figures 1 and 2), selected geometrical data (Table 1) and relevant crystallographic parameters (Table 2) are given here.

Unlike related heteroleptic plumbylenes $[C(SiMe_3)_2(SiMe_2C_5H_4N\text{-}2]PbCl$,[43] $[\{2,6\text{-}[2,4,6\text{-}(i\text{Pr})_3C_6H_2]_2C_6H_3\}PbBr]_2$,[31] $[(PhMe_2Si)_3CPbCl]_2$,[32,33] $\{[C(SiMe_3)_2(SiMe_2OMe)]PbCl\}_2$,[33] $\{[N(SiMe_3)C(Ph)C(SiMe_3)_2]PbCl\}_2$,[42] and $[(Me_3Si)_3CPbCl]_3$[33] being monomers, dimers and trimers, respectively, in the solid state, compound **2** forms an infinite zigzag chain via intermolecular, almost symmetrical Pb−Cl−Pb bridges (ΔPb−Cl 0.106 Å, Pb(1)−Cl(1)−Pb(1A) 155.96(6)°]. The Pb(1)−Cl(1) and Pb(1)···Cl(1A) distances of 2.795(1) and 2.901(1) Å, respectively, are in the range found in other monoorganoplumbylenes such as $[(PhMe_2Si)_3CPbCl]_2$ [Pb−Cl = 2.729(3) Å, Pb···Cl′ = 2.962(3) Å],[32,33] $[(Me_3Si)_3CPbCl]_3$ [Pb−Cl = 2.71(2) Å, 2.73(1) Å, 2.74(1) Å],[33] $\{[C(SiMe_3)_2(SiMe_2OMe)]PbCl\}_2$ [Pb−Cl = 2.680(5) Å, Pb···Cl′ = 2.868(5) Å],[33] $\{[N(SiMe_3)C(Ph)C(SiMe_3)_2]PbCl\}_2$ [Pb−Cl = 2.609(3) Å, Pb···Cl′ = 3.276(3) Å],[42] and $[C(SiMe_3)_2(SiMe_2C_5H_4N\text{-}2]PbCl$ [Pb−Cl = 2.647(3) Å].[43] The organic substituents at adjacent lead atoms in the heteroleptic plumbylene **2** are staggered with C(1)−Pb(1)···Pb(1A)−C(1A) = 180.0°.

Table 1. Selected bond lengths [Å], bond angles [°], and torsion angles [°] for **2**·THF and **3**

	2·THF	**3**
Pb(1)−C(1)	2.305(5)	2.327(3)
Pb(1)−O(1)	2.518(2)	2.671(2)
Pb(1)−O(2)		2.520(2)
Pb(1)−Cl(1)	2.795(1)	
Pb(1)−Cl(1A)	2.901(1)	
Pb(1)−S(1)		2.7090(9)
Pb(1)−S(1A)		3.2958(9)
S(1)−C(21)		1.755(4)
P(1)−O(1)	1.480(2)	1.483(2)
P(1)−O(1′)	1.577(2)	1.570(2)
P(1)−O(1′′)	1.574(2)	1.584(2)
P(2)−O(2)		1.488(2)
P(2)−O(2′)		1.578(2)
P(2)−O(2′′)		1.563(2)
P(1)−C(2)	1.788(3)	1.755(3)
P(2)−C(6)		1.783(3)
O(1)−Pb(1)−C(1)	74.78(5)	72.5(1)
O(2)−Pb(1)−C(1)		76.2(1)
O(1)−Pb(1)−O(2)		148.70(6)
O(1)−Pb(1)−O(1B)	149.5(1)	
O(1)−P(1)−C(2)	110.0(1)	111.5(1)
O(2)−P(2)−C(6)		111.8(1)
P(1)−O(1)−Pb(1)	116.4(1)	114.1(1)
P(2)−O(2)−Pb(1)		113.7(1)
P(1)−C(2)−C(3)	121.3(2)	122.6(3)
P(2)−C(6)−C(5)		119.2(3)
C(2)−C(1)−Pb(1)	121.5(2)	124.1(2)
C(6)−C(1)−Pb(1)		119.6(2)
Pb(1A)−Cl(1A)−Pb(1)	155.96(6)	
Cl(1)−Pb(1)−Cl(1A)	169.60(1)	
C(1)−Pb(1)−Cl(1)	89.1(1)	
C(1)−Pb(1)−Cl(1A)	80.5(1)	
O(1)−Pb(1)−Cl(1)	89.23(5)	
O(1)−Pb(1)−Cl(1A)	88.04(5)	
Pb(1)−S(1)−Pb(1A)		18.72(1)
S(1)−Pb(1)−S(1A)		158.533(8)
C(1)−Pb(1)−S(1)		84.96(8)
O(1)−Pb(1)−S(1)		91.44(5)
Pb(1)−S(1)−C(21)		104.2(1)
Pb(1)−C(1)−C(2)−C(3)	169.3(2)	172.0(2)
P(1)−C(2)−C(3)−C(4)	177.5(3)	−177.8(3)
O(1)−P(1)−C(2)−C(3)	−170.9(2)	−170.2(3)
C(1)−Pb(1)−Cl(1)−Pb(1C)	0.0	
O(1)−Pb(1)−Cl(1)−Pb(1A)	74.79(5)	
Cl(1A)−Pb(1)−Cl(1)−Pb(1C)	0.0	
C(1)−Pb(1)−S(1)−C(21)		−149.6(1)
C(1)−Pb(1)−S(1)−Pb(1A)		−114.00(9)
O(1)−Pb(1)−S(1)−Pb(1A)		173.68(6)
S(1)−Pb(1)−S(1a)−Pb(1A)		101.18(6)

 © 2003 Wiley-VCH Verlag GmbH & Co. KGaA, Weinheim

Table 2. Crystallographic data for **2**·THF, **3**, and **6**·THF

	2·THF	**3**	**6**
Empirical formula	$C_{22}H_{39}ClO_7P_2Pb$	$C_{24}H_{36}O_6P_2PbS$	$C_{88}H_{160}F_{19}O_{28}P_{11}Pb_2$
Formula mass	720.11	721.72	2782.21
Crystal system	orthorhombic	monoclinic	monoclinic
Crystal size [mm]	0.17 × 0.15 × 0.15	0.15 × 0.15 × 0.13	0.15 × 0.15 × 0.13
Space group	*Pnma*	$P2_1/n$	$C2/c$
a [Å]	11.0907(2)	14.0353(3)	36.1419(5)
b [Å]	16.3289(4)	10.5415(2)	18.3134(3)
c, [Å]	15.6283(4)	19.6993(5)	26.1390(5)
β [°]	90	99.9054(8)	127.2822(7)
V [Å^3]	2830.3(1)	2871.1(1)	13765.7(4)
Z	4	4	4
$\rho_{calcd.}$ [g/m^3]	1.690	1.670	1.342
ρ_{found} [g/cm^3]	1.620 ± 0.05	1.518 ± 0.003	not measured
μ [mm^{-1}]	6.205	6.095	2.653
F(000)	1424	1424	5648
θ range [°]	3.19 to 27.47	2.95 to 27.45	2.96 to 27.46
Index ranges	$-14 \le h \le 14$	$-18 \le h \le 18$	$-46 \le h \le 46$
	$-21 \le k \le 21$	$-13 \le k \le 13$	$-23 \le k \le 23$
	$-20 \le l \le 20$	$-25 \le l \le 25$	$-33 \le l \le 26$
No. of reflns. collected	21665	27814	55752
Completeness to θ_{max}	99.8%	99.6%	98.6%
No. of independent reflns./R_{int}	3349/0.042	6531/0.053	15542/0.043
No. of reflns. obsd. with [$I > 2\sigma(I)$]	1996	3517	6078
No. of refined parameters	160	316	704
GooF (F^2)	0.915	0.598	0.812
$R1$ (F) [$I > 2\sigma(I)$]	0.0232	0.0248	0.0489
$wR2$ (F^2) (all data)	0.0455	0.0353	0.1273
$(\Delta/\sigma)_{max}$	0.001	0.001	0.001
Largest diff. peak/hole [e/Å^3]	0.830/−0.966	0.862/−0.971	0.731/−0.488

The lead atom exhibits a ψ-octahedral configuration with O(1), O(1B), Cl(1) and Cl(1A) occupying the equatorial positions and C(1) being almost perpendicular to these atoms and *trans* to the lone pair. The stereochemical influence of the lone pair is mainly manifested by the Cl(1)−Pb(1)−Cl(1A), C(1)−Pb(1)−Cl(1), and C(1)−Pb(1)−Cl(1A) angles of 169.60(1), 89.1(1), and 80.5(1)°, respectively. The O(1)−Pb(1)−O(1B) angle of 149.5(1)° is close to the corresponding angle in the related heteroleptic stannylene {4-*t*Bu-2,6-[P(O)(O*i*Pr)$_2$]$_2$-C$_6$H$_2$}SnCl [O(1)−Sn(1)−O(2) 152.00(5)°][52] but much bigger than the O(1)−Pb(1)−O(2) of 119.36(5)° in the intramolecularly [4+2]-coordinated tetraorganolead(IV) derivative {4-*t*Bu-2,6-[P(O)(OEt)$_2$]$_2$C$_6$H$_2$}PbPh$_3$.[50] In contrast to related organosilicon(IV),[44−46] organotin(IV),[47−49] and organolead(IV)[50] compounds containing the O,C,O-coordinating ligand {4-*t*Bu-2,6-[P(O)(OR)$_2$]$_2$C$_6$H$_2$}$^-$ (R = Et, *i*Pr), in the organoplumbylene **2** the P(O)(OEt)$_2$ groups and the lead atom are slightly displaced in the same direction from the plane defined by the aromatic ring [P(1)−C(2)−C(3)−C(4) = 177.5(3)°, Pb(1)−C(1)−C(2)−C(3) = 169.3(2)°]. The intramolecular Pb(1)−O(1) and Pb(1)−O(1B) distances of 2.518(2) Å are close to the intramolecular Pb−O [2.52(2) Å] reported for {2-[Ph$_2$P(O)CH$_2$]C$_6$H$_4$S}$_2$Pb.[53] The IR spectrum of **2** shows a band at $\tilde{\nu}$(P=O) = 1201 cm^{-1} which is similar to that for the related stannylene {4-*t*Bu-2,6-[P(O)(OEt)$_2$]$_2$C$_6$H$_2$}SnCl [$\tilde{\nu}$(P=O) = 1192 cm^{-1}].[51]

The singlet at δ = 52.0 [J(^{207}Pb−^{31}P) = 127 Hz] ppm in the ^{31}P NMR (C$_6$D$_6$) spectrum of organolead(II) chloride **2** is at a higher frequency than for the corresponding organotin(II) compound {4-*t*Bu-2,6-[P(O)(OEt)$_2$]$_2$C$_6$H$_2$}SnCl (in [D$_8$]toluene: δ = 39.1 ppm).[51] The solid-state ^{31}P NMR spectrum shows a broad resonance at δ = 54.5 ppm. No ^{207}Pb NMR chemical shift could be obtained, which accords with reported problems in recording ^{207}Pb NMR spectra of [(PhMe$_2$Si)$_3$CPbCl]$_2$,[32,33] [(Me$_3$Si)$_3$CPbCl]$_3$,[33] [{2,6-[2,4,6-(*i*Pr)$_3$C$_6$H$_2$]$_2$C$_6$H$_3$}PbBr]$_2$,[31] and [{2,6-[2,4,6-(*i*Pr)$_3$C$_6$H$_2$]$_2$C$_6$H$_3$}PbBr·py].[31]

Compound **2** reacts with sodium thiophenolate under nucleophilic substitution at the Pb−Cl function to give the corresponding organolead(II) thiophenolate **3** as a colorless crystalline solid that is stable at 20 °C under aerobic conditions for several days (Scheme 1).

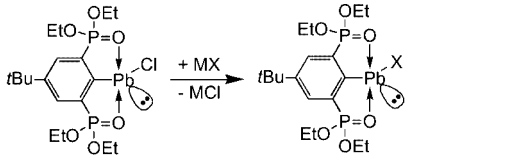

2

3, X = SPh, M = Na
4(*in situ*), X = N(*i*Pr)$_2$, M = Li
5(*in situ*), X = CH(SiMe$_3$)$_2$, M = Li

Scheme 1

The molecular structure of compound **3** (Figures 3 and 4), selected geometrical data (Table 1), and relevant crystal-

 © 2003 Wiley-VCH Verlag GmbH & Co. KGaA, Weinheim

lographic parameters (Table 2) are detailed here. As with organolead(II) chloride **2**, the organolead(II) thiophenolate **3** forms a polymeric zigzag chain with, however, a less symmetric intermolecular Pb−S···Pb bridge [ΔPb−S 0.5868 Å, Pb(1)−S(1)−Pb(1A) 18.72(1)°]. The torsion angle C(1)−Pb(1)···Pb(1a)−C(1a) is 170.9(1)°. The related organolead(II) thiophenolate derivative {2,4,6-$[(Me_3Si)_2CH]_3C_6H_2$}Pb{2,4,6-$[(Me_3Si)_2CH]_3C_6H_2S$},[54,55] however, is a monomer. As with compound **2**, the lead atom in the organolead(II) thiophenolate **3** shows a distorted ψ-octahedral configuration with O(1), O(2), S(1) and S(1A) occupying the equatorial positions and C(1) being almost perpendicular to these atoms. The stereochemical influence of the lone pair is shown by the S(1)−Pb(1)−S(1A) angle of 158.533(8)°. In contrast to the related organolead(II) chloride **2**, in **3** the intramolecular Pb(1)−O(1) and Pb(1)−O(2) distances differ [2.671(2) and 2.520(2) Å, respectively]. The non-equivalence of the two phosphorus atoms is also shown in the solid-state ^{31}P NMR spectrum by two resonances at δ = 50.4 and 45.0 ppm. The IR spectrum, however, is not sensitive enough to distinguish the two phosphonyl groups and shows only one band at $\tilde{\nu}$(P=O) = 1208 cm^{-1}. The O(1)−Pb(1)−O(2) angle of 148.70(6)° is again rather similar to the 152.48(7)° found in the related stannylene {4-*t*Bu-2,6-$[P(O)(OiPr)_2]_2C_6H_2$}SnSPh.[52] The Pb(1)−S(1) distance of 2.7090(9) Å lies in the range of Pb−S distances found in $([\{2,6\text{-}(iPr)_2C_6H_2\}S]_2Pb)_3$ [Pb−S = 2.554(4)−2.896(3) Å].[56] The Pb(1)···S(1A) distance [3.2958(9) Å] is in the range of lead−sulfur secondary bond lengths found in $_\infty[(S_2PPh_2)_2Pb]$ (Pb···S = 3.270−3.448 Å).[57] Compounds **2** and **3** appear to be the first organolead(II) derivatives to exhibit polymeric chain structures.

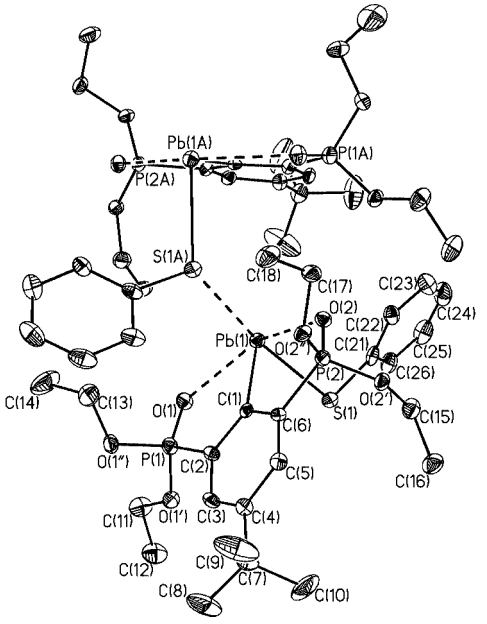

Figure 3. General view (SHELXTL) of two molecular units of **3** showing 30% probability displacement ellipsoids and the atom numbering (symmetry transformations used to generate equivalent atoms: $a = -0.5 - x, -0.5 + y, 0.5 - z$)

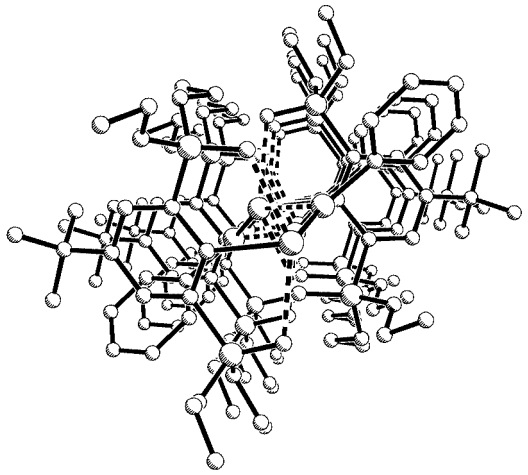

Figure 4. View along the Pb−S axis of **3**

Osmometric molecular weight determinations in THF showed that plumbylenes **2** and **3** are monomeric in solution.

Compound **2** also reacts with lithium diisopropylamide and lithium bis(trimethylsilyl)methane by nucleophilic substitution at the Pb−Cl function to give, in situ, moderate yields of the heteroleptic plumbylenes {4-*t*Bu-2,6-$[P(O)(OEt)_2]_2C_6H_2$}PbN*i*Pr_2 (**4**) and {4-*t*Bu-2,6-$[P(O)(OEt)_2]_2C_6H_2$}$PbCH(SiMe_3)_2$ (**5**) (Scheme 1). Neither **4** nor **5** could be obtained analytically pure but their identity was confirmed by NMR spectroscopy (see Exp. Sect. and Supporting Information). Remarkably, the ^{207}Pb NMR chemical shift of **5** could be determined {δ = 6874 [$J(^{207}Pb$-$^{31}P)$ = 129 Hz] ppm}.

The reactions shown in Scheme 1 are always accompanied by Pb−C bond cleavage. No reaction between **2** and sulfur was observed even at 60 °C.

In an attempt to prepare the intramolecularly coordinated organolead(II) hexafluorophosphate [{4-*t*Bu-2,6-$[P(O)(OEt)_2]_2C_6H_2$}Pb]$^+$ PF_6^- (**6a**), compound **2** was treated with $TlPF_6$ in THF at −78 °C (Scheme 2). The ^{31}P

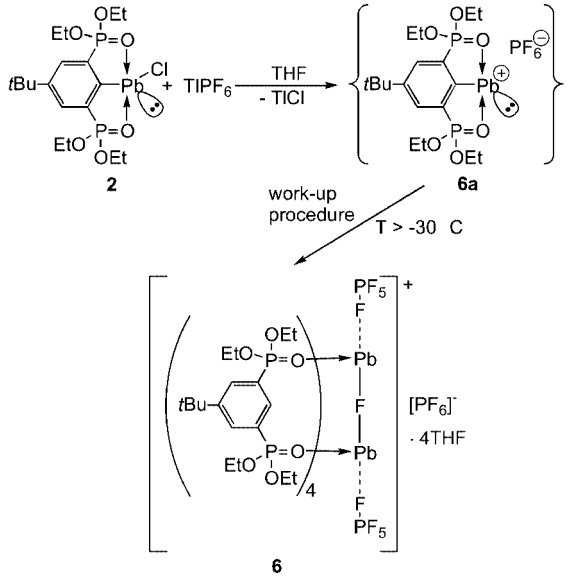

Scheme 2

NMR spectrum of the crude reaction mixture showed signals (a) at δ = 18.0 (integral 27%, assigned to 5-*t*Bu-1,3-$[P(O)(OEt)_2]_2C_6H_3$) ppm and (b) at δ = 54.1 [$J(^{31}P$-$^{207}Pb)$ = 150 Hz, integral 73%] ppm. The latter signal is assigned with caution to the phosphonyl phosphorus atom in the salt **6a**.

After filtration under inert conditions through a diatomaceous earth filter, in the filtrate, the ratio of the ^{31}P NMR signals (a) to (b) changed to 88:12. From this filtrate, air- and moisture-sensitive single crystals of [{5-*t*Bu-1,3-$[P(O)(OEt)_2]_2C_6H_3\}_4$·$(Pb_2F)$] $[PF_6]_3$·4THF (**6**) were obtained.

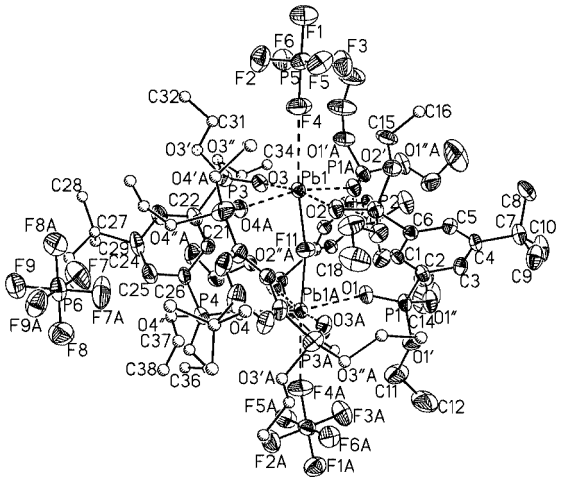

Figure 5. General view (SHELXTL) of a molecule of **6** showing 30% probability displacement ellipsoids and the atom numbering (symmetry transformations used to generate equivalent atoms: $-x$, y, $0.5 - z$)

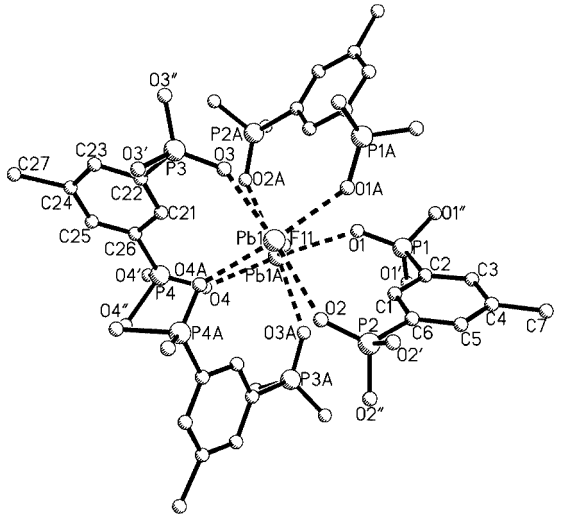

Figure 6. View along the Pb−F−Pb axis of **6**; methyl and ethyl groups, as well as THF and PF_6^-, are omitted for clarity

The molecular structure of **6** (Figures 5 and 6), selected geometrical data (Table 3), and relevant crystallographic parameters (Table 2) are given below.

The salt **6** consists of a $[(Pb-F-Pb)]^{3+}$ cation stabilized by eight intermolecular P=O→Pb coordinations of four 5-*t*Bu-1,3-$[P(O)(OEt)_2]_2C_6H_3$ molecules, three $[PF_6]^-$ anions, and four THF molecules. The cationic part of the structure has an axis of improper rotation. The three $[PF_6]^-$ anions are crystallographically non-equivalent. Two symmetry-related ones (P5/P5A) show a Pb(1)···F(4) distance of 3.075(5) Å whereas the third one (P6) is far from the lead atoms [Pb(1)···F(7) 8.437(6) Å]. The Pb(1)−F(11) distance of 2.2762(7) Å is rather short compared with Pb−F in α-PbF_2 [2.418(2), 2.439(8) Å][58] and β-PbF_2 (2.573 Å).[59] Lead−fluorine distances of 3.04(6) and 3.30 Å have been

Table 3. Selected bond lengths [Å], bond angles [°], and torsion angles [°] of **6**

	6
Pb(1)−F(11)	2.2762(7)
Pb(1A)−F(11)	2.2762(7)
Pb(1)−O(2)	2.536(4)
Pb(1)−O(3)	2.479(4)
Pb(1)−O(1A)	2.550(4)
Pb(1)−O(4A)	2.426(4)
Pb(1)−F(4)	3.075(5)
Pb(1A)−O(1)	2.550(4)
P(5)−F(5)	1.601(5)
P(5)−F(4)	1.578(5)
P(5)−F(2)	1.574(5)
P(1)−O(1)	1.479(4)
P(1)−O(1′)	1.547(5)
P(1)−O(1″)	1.529(5)
P(2)−O(2)	1.485(4)
P(2)−O(2′)	1.559(5)
P(2)−O(2″)	1.559(5)
P(1)−C(2)	1.786(6)
P(2)−C(6)	1.789(6)
Pb(1)−F(11)−Pb(1A)	167.4(3)
F(4)−Pb(1)−F(11)	172.8(2)
O(1A)−Pb(1)−O(2)	95.6(1)
O(1A)−Pb(1)−O(3)	87.7(1)
O(3)−Pb(1)−O(4A)	84.4(1)
O(4A)−Pb(1)−O(2)	90.1(1)
O(2)−Pb(1)−O(3)	170.2(1)
O(1A)−Pb(1)−O(4A)	163.3(1)
P(1)−O(1)−Pb(1A)	140.2(3)
P(2)−O(2)−Pb(1)	146.1(3)
P(4)−O(4)−Pb(1A)	137.0(3)
F(11)−Pb(1)−O(2)	85.6(1)
F(11)−Pb(1)−O(3)	86.2(1)
F(11)−Pb(1)−O(1A)	76.5(2)
P(1)−C(2)−C(3)−C(4)	−177.9(5)
O(1)−P(1)−C(2)−C(3)	−155.5(5)
F(11)−Pb(1)−O(4A)	88.3(2)
O(4A)−Pb(1)−F(4)	97.8(2)
O(1)−P(1)−O(1′)	115.7(3)
O(1)−P(1)−O(1″)	113.6(3)
O(1′)−P(1)−O(2″)	102.0(3)
C(6)−P(2)−O(2)	112.7(3)
C(2)−P(1)−O(1)	112.3(3)
C(1)−C(6)−P(2)	118.2(5)
C(1)−C(2)−P(1)	118.5(5)
C(3)−C(4)−C(7)	122.4(6)
C(2)−C(3)−C(4)	120.8(6)
C(4)−C(5)−C(6)	121.1(6)
F(4)−P(5)−F(6)	88.9(3)
F(2)−P(5)−F(4)	91.5(3)
C(6)−C(2)−Pb(1A)−Pb(1)	37.5(2)
C(4)−C(5)−C(6)−P(2)	−177.7(5)
O(2)−P(2)−C(6)−C(5)	159.6(5)

 © 2003 Wiley-VCH Verlag GmbH & Co. KGaA, Weinheim

reported for $Pb(dhfa)_2$ [Hdhfa = 1,5-bis(undecafluorocyclohexyl)pentane-2,4-dione][60] and bis(2,2-dimethyl-6,6,7,7,8,8,8-heptafluorooctane-3,5-dionato)lead,[61] respectively. The lead atom exhibits a distorted octahedral configuration with four P=O oxygen atoms equatorial and F(4), F(11) in axial positions. Distortion from the ideal geometry is manifested by F(4)−Pb(1)−F(11), O(2)−Pb(1)−O(3), and O(1A)−Pb(1)−O(4A) angles of 172.8(2), 170.2(1), and 163.3(1)°, respectively. The Pb−O distances lie between 2.426(4) [Pb(1)−O(4A)] and 2.550(4) Å [Pb(1)−O(1A)]. They are up to 0.245 Å shorter than the Pb−O distance in the intramolecularly coordinated organolead(II) chloride and thiophenolate **2** and **3**, respectively. The Pb(1)−F(11)−Pb(1A) angle amounts to 167.4(3)°. The electrospray mass spectrum of **6** in CH_3CN shows a cluster pattern at m/z = 1039, which is assigned to $\{(Pb + F + 2\ (5\text{-}t\text{Bu-}1,3\text{-}[P(O)(OEt)_2]_2C_6H_3)\}^+$. The IR spectrum (KBr pellet) of **6** shows a band at $\tilde{\nu}$(P=O) = 1197 cm^{-1}, indicating strong P=O→Pb coordination. The ^1H and ^{31}P NMR spectra of **6** exclusively show signals corresponding to the protonated ligand 5-*t*Bu-1,3-$[P(O)(OEt)_2]_2C_6H_3$ (**A**), THF, and PF_6^- anion.

Conclusion

We have demonstrated the capacity of the phosphorus-containing O,C,O-coordinating ligand 4-*t*Bu-2,6-$[P(O)(OEt)_2]_2C_6H_2^-$ for the synthesis of stable heteroleptic organolead(II) compounds. This ligand or a modified version (replacement of ethyl groups by more bulky substituents) is also, probably, suitable to stabilize the corresponding germanium(II) and silicon(II) compounds. Although no rational synthesis for compound **6** has been developed yet, its serendipitous formation might help in developing concepts for the stabilization of di- and oligonuclear metal cations. Notably, Mews et al. have isolated and structurally characterized a compound that contains an $[(Sn-F-Sn)\cdot 4Ph_3PO]^{3+}$ cation.[62]

Experimental Section

General Remarks: All solvents were dried and purified by standard procedures. All reactions were carried out under argon using Schlenk techniques. Bruker DPX-300 and DRX-400 spectrometers were used to obtain ^1H, ^{13}C, ^{31}P, and ^{207}Pb NMR spectra. ^{31}P MAS NMR spectra were recorded with a Bruker MSL 400 spectrometer using cross-polarisation and high-energy proton decoupling. Two rotation frequencies (6000−9000 Hz) have been used to identify the isotropic shift. A repetition delay of 4.0 s and a 90.0° pulse of 5.0 μs were employed. ^1H, ^{13}C, ^{31}P, and ^{207}Pb NMR chemical shifts (δ) are given in ppm and referenced to Me_4Si, H_3PO_4 (85%), and $PbNO_3$ (saturated in D_2O) as appropriate. NMR spectra were recorded at room temperature unless otherwise stated. IR spectra were recorded with a Bruker IFS 28 spectrometer. UV measurements were performed with a Varian Cary 100. Elemental analyses were obtained with a LECO-CHNS-932 analyser. Molecular weight determinations were performed with a Knauer Osmometer K7000 in freshly distilled solvent and were referenced against benzil. Electrospray mass spectra were recorded in the positive mode with a Thermoquest-Finnigan instrument using CH_3CN as the mobile phase. The relevant compound was dissolved in CH_3CN to give an approximate solution concentration of $1\cdot10^{-4}$ mol·L^{-1}. The sample was then introduced via a syringe pump operating at 10 μL min^{-1}. The capillary voltage was varied between 7.0 and 8.7 V, while the cone-skimmer voltage was varied between 33.7 and 83.5 V. Identification of the inspected ions was assisted by comparison of experimental and calculated isotope distribution patterns. The m/z values reported correspond to the most intense peaks in the corresponding isotope pattern. {4-*t*Bu-2,6-$[P(O)(OEt)_2]_2C_6H_2$}Li (**1**) was prepared as previously reported.[47]

[4-*tert*-Butyl-2,6-bis(diethoxyphosphonyl)phenyl]chloroplumbylene (2): $PbCl_2$ (3.32 g, 11.94 mmol) was added portionwise, at −78 °C, to a solution of [4-*tert*-butyl-2,6-bis(diethoxyphosphonyl)phenyl]lithium (**1**) (3.12 g, 7.57 mmol) in THF (150 mL). The reaction mixture was then stirred for 16 h (−78 °C to room temperature) and, after filtration, the solvent (50 mL) was evaporated. Crystallization at −6 °C afforded 4.42 g (81%) of **2**·THF as colorless crystals, m.p. 185 °C. After removal of THF by reduced pressure (11 Torr), **2** was characterized. ^1H NMR (400.13 MHz, C_6D_6): δ = 1.08 (t, 12 H, CH_3), 1.13 (s, 9 H, CH_3), 4.02−4.17 ($\nu_{1/2}$ = 32 Hz, 4 H, CH_2), 4.17−4.33 ($\nu_{1/2}$ = 36 Hz, 4 H, CH_2), 8.29 (complex pattern, 2 H, aromatics) ppm. $^{13}C\{^1H\}$ NMR (100.61 MHz, C_6D_6): δ = 16.4 (d, $^3J_{C,P}$ = 6 Hz, 4 C, CH_3), 31.0 (s, 3 C, CH_3), 34.9 (s, 1 C, C), 63.3 ($\nu_{1/2}$ = 23 Hz, 4 C, CH_2), 135.1 (dd, $^1J_{C,P}$ = 196, $^3J_{C,P}$ = 24 Hz, 2 C, C-2,6), 135.7 (dd, $^2J_{C,P}$ = 16, $^4J_{C,P}$ = 5 Hz, 2 C, C-3,5), 150.1 (t, $^3J_{C,P}$ = 12 Hz, 1 C, C-4), 250.7 (t, $^2J_{C,P}$ = 35 Hz, 1 C, C-1) ppm. $^{31}P\{^1H\}$ NMR (161.98 MHz, C_6D_6): δ = 52.0 (s, $J_{P,Pb}$ = 127, $^1J_{C,P}$ = 196 Hz ppm. $^{31}P\{^1H\}$ MAS NMR (161.98 MHz): δ = 54.6 ppm. IR (KBr): $\tilde{\nu}$(P=O) = 1201, 1179 cm^{-1}. UV/Vis (CH_3CN): λ = 217 nm, ε = 25309 L·mol^{-1}·cm^{-1}; λ = 279 nm, ε = 3122 L·mol^{-1}·cm^{-1}; λ = 286 nm, ε = 3039 L·mol^{-1}·cm^{-1}. Molecular weight determination (THF, 28 °C, c = 0.0147 mol·L^{-1}): 602.0 g mol^{-1}. $C_{18}H_{31}ClO_6P_2Pb$ (648.0): calcd. C 33.4, H 4.8; found C 33.4, H 4.8. MS: m/z (%) = 647 (45) [M − H], 612 (88) [M − Cl − H], 539 (52) [M − Cl − OEt − Et].

Investigations on the Stability of [4-*tert*-Butyl-2,6-bis(diethoxyphosphonyl)phenyl]chloroplumbylene (2). A: [4-*tert*-Butyl-2,6-bis(diethoxyphosphonyl)phenyl]chloroplumbylene (**2**) was exposed to light and atmospheric moisture on a watch glass. After t_1 = 4 d and t_2 = 41 d, respectively, representative portions were dissolved in C_6D_6 and analysed by NMR spectroscopy. $^{31}P\{^1H\}$ NMR (161.98 MHz, C_6D_6, t_1): δ = 19.0 [s, 1-*tert*-butyl-3,5-bis(diethoxyphosphonyl)benzene, 10%], 52.5 (s, $J_{P,Pb}$ = 128 Hz, **2**, 90%) ppm; $^{31}P\{^1H\}$ NMR (161.98 MHz, C_6D_6, t_2): δ = 19.0 [s, 1-*tert*-butyl-3,5-bis(diethoxyphosphonyl)benzene, 99%], 52.5 (s, $J_{P,Pb}$ = 128 Hz, **2**, 1%) ppm. **B:** [4-*tert*-Butyl-2,6-bis(diethoxyphosphonyl)phenyl]chloroplumbylene (**2**) (10 mg, $1.5\cdot10^{-5}$ mol) in C_6D_6 (0.4 mL) was sealed under inert conditions in an NMR tube at 65 °C for t_3 = 41 d. $^{31}P\{^1H\}$ NMR (161.98 MHz, C_6D_6, t_3): δ = 19.0 [s, 1-*tert*-butyl-3,5-bis(diethoxyphosphonyl)benzene, 6%], 52.5 (s, $J_{P,Pb}$ = 128 Hz, **2**, 94%) ppm.

[4-*tert*-Butyl-2,6-bis(diethoxyphosphonyl)phenyl]thiophenolatoplumbylene (3): $NaSC_6H_5$ (0.16 g, 1.21 mmol) was added portionwise, at −78 °C, to a suspension of [4-*tert*-butyl-2,6-bis(diethoxyphosphonyl)phenyl]chloroplumbylene (**2**) (0.41 g, 0.63 mmol) in THF (100 mL). After the reaction mixture had been stirred for 16 h (−78 °C to room temperature), it was decanted from an insoluble residue. The solution was then kept at −6 °C to afford **3** [0.15 g (33%)] as colorless crystals, m.p. 86 °C. ^1H NMR (400.13 MHz, $[D_8]$thf): δ = 1.26 (t, 6 H, CH_3), 1.31 (t, 6 H, CH_3), 1.36 (s, 9 H,

 © 2003 Wiley-VCH Verlag GmbH & Co. KGaA, Weinheim

CH_3), 4.02−4.23 (complex pattern, 6 H, CH_2), 4.28−4.40 (complex pattern, 2 H, CH_2), 6.86 (t, 1 H, aromatics), 7.04 (t, 2 H, aromatics), 7.33 (d, 2 H, aromatics), 8.05 (complex pattern, 2 H, aromatics) ppm. $^{13}C\{^1H\}$ NMR (100.61 MHz, [D$_8$]thf): δ = 17.7 (d, $^3J_{C,P}$ = 6 Hz, 2 C, CH_3), 17.8 (d, $^3J_{C,P}$ = 6 Hz, 2 C, CH_3), 32.4 (s, 3 C, CH_3), 36.6 (s, 1 C, C), 63.9 (d, $^2J_{C,P}$ = 6 Hz, 2 C, CH_2), 65.0 (d, $^2J_{C,P}$ = 4 Hz, 2 C, CH_2), 124.8 (s, 2 C, C_p), 129.2 (s, 2 C, C_m), 135.2 (s, 2 C, C_o), 136.9 (dd, $^2J_{C,P}$ = 17, $^4J_{C,P}$ = 4 Hz, 2 C, C-3,5), 137.2 (dd, $^1J_{C,P}$ = 195, $^3J_{C,P}$ = 25 Hz, 2 C, C-2,6), 145.3 (s, 1 C, C_i), 151.4 (t, $^3J_{C,P}$ = 13 Hz, 1 C, C-4), 239.4 (t, $^2J_{C,P}$ = 35 Hz, 1 C, C-1) ppm. $^{31}P\{^1H\}$ NMR (161.98 MHz, [D$_8$]thf): δ = 47.8 (s, $J_{P,Pb}$ = 123 Hz) ppm. $^{31}P\{^1H\}$ MAS NMR (161.98 MHz): δ = 45.5, 50.4 ppm. IR (KBr): $\tilde{\nu}$(P=O) = 1208, 1183 cm^{-1}. UV/Vis (CH_3CN): λ = 215 nm, ε = 28695 L·mol^{-1}·cm^{-1}; λ = 259 nm, ε = 13211 L·mol^{-1}·cm^{-1}. Molecular weight determination (THF, 28 °C, c = 0.0069 mol·L^{-1}): 727.7 g mol^{-1}. $C_{24}H_{36}O_6P_2PbS$ (721.8): calcd. C 39.9, H 5.0; found C 40.0, H 5.1. MS: m/z (%) = 613 (100) [M − SPh], 391 (65) [M − SPh −3 OEt − Et − tBu], FAB-MS: m/z (%) = 613 (100) [M − SPh].

[4-*tert*-Butyl-2,6-bis(diethoxyphosphonyl)phenyl](diisopropylamino)-plumbylene (4). Method A: A solution of iPr$_2$NLi in hexane/diethyl ether (3:1) (37 mL, 0.75 M) was added, at −78 °C, to a solution of 1-*tert*-butyl-3,5-bis(diethoxyphosphonyl)benzene (7.5 g, 18.5 mmol) in THF (120 mL) and the reaction mixture was stirred at this temperature for 5 h. $PbCl_2$ (3.85 g, 13.8 mmol) was added portionwise and the suspension stirred for 16 h (−78 to −30 °C). After filtration some of the solvent (75 mL) was evaporated. Crystallization at −6 °C afforded **2**·THF [1.98 g (20%)]. The solvent was then evaporated, and the residue dissolved in hexane (50 mL). After decantation from insoluble **2** and 1-*tert*-butyl-3,5-bis(diethoxyphosphonyl)benzene, the solvent was removed in vacuo to give 4.18 g of a yellow oil containing **4** (yield 45%, purity 83%) and residues of **2** (δ^{31}P = 52.0 ppm, 5%) and 1-*tert*-butyl-3,5-bis(diethoxyphosphonyl)benzene (δ^{31}P = 18.4 ppm, 12%). ^1H NMR (400.13 MHz, C_6D_6): δ = 0.98 (t, 6 H, CH_3), 1.13 (s, 9 H, CH_3), 1.22 (t, 6 H, CH_3), 1.53 [s, 6 H, C(H)(CH_3)$_2$], 1.55 [s, 6 H, C(H)(CH_3)$_2$], 3.68−3.79 (complex pattern, 2 H, CH_2), 3.86−3.97 (complex pattern, 2 H, CH_2), 4.17−4.34 (complex pattern, 4 H, CH_2), 5.12−5.28 (sept, 2 H, CH), 8.20 (complex pattern, 2 H, aromatics) ppm. $^{13}C\{^1H\}$ NMR (100.61 MHz, C_6D_6): δ = 16.4 (complex pattern, $^3J_{C,P}$ = 7 Hz, 4 C, CH_3), 30.1 [s, 3 C, C(CH_3)$_3$], 31.0 [s, 4 C, C(H)(CH_3)$_2$], 34.7 (s, 1 C, C), 53.7 (s, 2 C, CH), 62.1 (d, 2 C, $^2J_{C,P}$ = 5 Hz, CH_2), 62.3 (d, 2 C, $^2J_{C,P}$ = 6 Hz, CH_2), 134.8 (dd, $^2J_{C,P}$ = 17, $^4J_{C,P}$ = 4 Hz, 2 C, C-3,5), 136.1 (dd, $^1J_{C,P}$ = 197, $^3J_{C,P}$ = 26 Hz, 2 C, C-2,6), 148.9 (t, $^3J_{C,P}$ = 13 Hz, 1 C, C-4), 236.8 (t, $^2J_{C,P}$ = 38 Hz, 1 C, C-1) ppm. $^{31}P\{^1H\}$ NMR (161.98 MHz, C_6D_6): δ = 41.7 (s, $J_{P,Pb}$ = 116 Hz) ppm. IR (KBr): $\tilde{\nu}$(P=O) = 1203 cm^{-1}. **Method B:** A solution of LDA in hexane/diethyl ether (3:1) (0.4 mL, 0.75 M) was added, at −78 °C, to a suspension of [4-*tert*-butyl-2,6-bis(diethoxyphosphonyl)phenyl]chloroplumbylene (**2**) (0.187 g, 0.289 mmol) in THF (15 mL). After the reaction mixture had been stirred for 4 h at this temperature, it was characterized by ^{31}P NMR spectroscopy. $^{31}P\{^1H\}$ NMR (81.02 MHz, D_2O capillary): δ = 18.4 [s, 1-*tert*-butyl-3,5-bis(diethoxyphosphonyl)benzene, 5%], 41.7 (s, $J_{P,Pb}$ = 122 Hz, **4**, 83%), 52.0 (s, **2**, 12%).

[4-*tert*-Butyl-2,6-bis(diethoxyphosphonyl)phenyl]{[bis(trimethylsilyl)]methyl}plumbylene (5): LiCH(SiMe$_3$)$_2$ (0.181 g, 1.09 mmol) was added portionwise, at −78 °C, to a suspension of [4-*tert*-butyl-2,6-bis(diethoxyphosphonyl)phenyl]chloroplumbylene (**2**) (0.679 g, 1.05 mmol) in THF (50 mL). After the reaction mixture had been stirred for 16 h (−78 to −30 °C), it was filtered. Evaporation of the solvent then afforded 0.20 g (25%) of **5** as a pale yellow oil. ^1H NMR (400.13 MHz, C_6D_6): δ = −0.60 [s, 1 H, CH(SiMe$_3$)$_2$], 0.39 (s, 18 H, SiMe$_3$), 0.95 (t, 6 H, CH_3), 1.16 (s, 9 H, CH_3), 1.20 (t, 6 H, CH_3), 3.66−3.76 (complex pattern, 2 H, CH_2), 3.83−3.93 (complex pattern, 2 H, CH_2), 4.07−4.24 (complex pattern, 4 H, CH_2), 8.10 (complex pattern, 2 H, aromatics) ppm. $^{13}C\{^1H\}$ NMR (100.61 MHz, C_6D_6): δ = 5.4 (s, 6 C, SiMe$_3$), 16.3 (complex pattern, 2 C, CH_3), 16.5 (complex pattern, 2 C, CH_3), 31.1 (s, 3 C, CH_3), 34.7 (s, 1 C, C), 62.3 (complex pattern, CH_2), 62.9 [s, 1 C, C(H)(SiMe$_3$)$_2$], 134.4 (dd, $^2J_{C,P}$ = 17, $^4J_{C,P}$ = 5 Hz, 2 C, C-3,5), 135.8 (dd, $^1J_{C,P}$ = 198, $^3J_{C,P}$ = 25 Hz, 2 C, C-2,6), 149.0 (t, $^3J_{C,P}$ = 13 Hz, 1 C, C-4), 231.8 (t, $^2J_{C,P}$ = 37 Hz, 1 C, C-1) ppm. $^{31}P\{^1H\}$ NMR (161.98 MHz, C_6D_6): δ = 42.1 (s, $J_{P,Pb}$ = 125 Hz) ppm. $^{207}Pb\{^1H\}$ NMR (83.72 MHz, C_6D_6): δ = 6874 (t, $J_{P,Pb}$ = 129 Hz) ppm. IR (KBr): $\tilde{\nu}$(P=O) = 1208 cm^{-1}. MS: m/z (%) = 613 (48) [M − C(H)(SiMe$_3$)$_2$], 406 (39) [M − C(H)(SiMe$_3$)$_2$ − Pb].

[{5-*t*Bu-1,3-[P(O)(OEt)$_2$]$_2$C$_6$H$_3$}$_4$·(Pb$_2$F)] [PF$_6$]$_3$·4THF (6): [4-*tert*-Butyl-2,6-bis(diethoxyphosphonyl)phenyl]chloroplumbylene (**2**) (0.107 g, 0.165 mmol) was added portionwise, at −78 °C, to a solution of $TlPF_6$ (0.055 g, 0.157 mmol) in THF (20 mL). The reaction mixture was then stirred at −78 °C under exclusion of light for 140 min. After storage at −35 °C for 5 d, the suspension was characterized by ^{31}P NMR spectroscopy. $^{31}P\{^1H\}$ NMR (81.02 MHz, D_2O capillary): δ = 18.0 [s, 1-*tert*-butyl-3,5-bis(diethoxyphosphonyl)benzene, 27%], 54.1 (s, 73%). After the suspension had been filtered through a diatomaceous earth filter, the solution was once more characterized by ^{31}P NMR spectroscopy. $^{31}P\{^1H\}$ NMR (161.98 MHz, D_2O capillary): δ = 17.9 [s, 1-*tert*-butyl-3,5-bis(diethoxyphosphonyl)benzene, 88%], 54.0 (s, 12%). Crystallization at −35 °C afforded 0.13 g (29%) of **6** as colorless crystals. ^1H NMR (400.13 MHz, C_6D_6): δ = 1.14 (s, 9 H, CH_3), 1.17 (t, 12 H, CH_3), 1.45 (m, 4 H, THF), 3.61 (m, 4 H, THF), 4.10−4.26 (complex pattern, 8 H, CH_2), 8.20 (d, 2 H, aromatics), 8.81 (t, 1 H, aromatics) ppm. $^{31}P\{^1H\}$ NMR (161.98 MHz, C_6D_6): δ = 18.8 [s, 1-*tert*-butyl-3,5-bis(diethoxyphosphonyl)benzene], −142.3 (PF_6^-) ppm. IR (KBr, inert): $\tilde{\nu}$(P=O) = 1197 cm^{-1}, $\tilde{\nu}$(OH) not observed. ESMS: m/z = 1039 [Pb + F + 2 1-*tert*-butyl-3,5-bis(diethoxyphosphonyl)benzene]$^+$; 713 [Pb + 3 1-*tert*-butyl-3,5-bis(diethoxyphosphonyl)benzene]$^{2+}$; 510 [2 Pb + 4 1-*tert*-butyl-3,5-bis(diethoxyphosphonyl)benzene]$^{4+}$; 407 [1-*tert*-butyl-3,5-bis(diethoxyphosphonyl)benzene + H]$^+$. Elemental analysis and the melting point of **6** were obtained after THF had been removed under reduced pressure (11 Torr). $C_{72}H_{128}F_{19}O_{24}P_{11}Pb_2$ (2493.9): calcd. C 34.6, H 5.2; found C 34.2, H 5.0.

The ^1H, ^{13}C, and ^{31}P NMR spectra of compound **4** and the ^1H, ^{13}C, ^{31}P, and ^{207}Pb NMR spectra of compound **5** are available.[2]

X-ray Crystallographic Study: Intensity data for the colorless crystals were collected with a Nonius KappaCCD diffractometer with graphite-monochromated Mo-K_α (0.71073 Å) radiation at 173(1) K. The data collection covered almost the whole sphere of the reciprocal space with 3 collections at different k angles with 244 (**2**), 305 (**3**), and 260 (**6**) frames via w rotation (Δ/ω = 1°) at two times 15 s (**2**), 20 s (**3**), and 30 s (**6**) per frame. The crystal-to-detector distance was 3.4 cm. Crystal decay was monitored by repeating the initial frames at the end of the data collection. Analysis of the duplicate reflections revealed no indication of any decay. The structure was solved by direct methods SHELXS-97[63] and successive difference Fourier syntheses. Refinement was applied with full-matrix least-squares methods SHELXL-97.[64] H atoms were placed in geometrically calculated positions using a riding model with U_{iso} constrained at 1.2 for non-methyl and at 1.5 for methyl groups times U_{eq} of the carrier C atom. In **3** a disordered ethoxy group was found with occupancies of 0.6 [C(14)] and 0.4 [C(14′)]. In **6**

 © 2003 Wiley-VCH Verlag GmbH & Co. KGaA, Weinheim

the *tert*-butyl and the ethoxy groups are disordered over two sites with occupancies of 0.4 [C(27′), C(28′), C(29′)], 0.5 [O(3′), O(3′′), O(4′), O(4′′), C(34), C(35), C(36), C(37), C(38), O(3′A), O(3′′A), O(4′A), O(4′′A), C(34′), C(35′), C(36′), C(37′), C(38′)] and 0.6 [C(27), C(28), C(29)]. The disordered groups, one solvent molecule [O(71) to C(75)], C(16), C(30), C(31), C(32) and C(33) were refined isotropically whereas C(73), C(74), C(73′), C(73′) are disordered over two positions with an occupancy of 0.5. All solvent molecules were refined with an occupancy of 0.5 except for the disordered atoms. Atomic scattering factors for neutral atoms and real and imaginary dispersion terms were taken from the International Tables for X-ray Crystallography.[65] The figures were created by SHELXTL.[66] Crystallographic data are given in Table 2, selected bond lengths and angles for **2** and **3** in Table 1, and for **6** in Table 3. CCDC-205058 (**2**), -205059 (**3**), and -205060 (**6**) contain the supplementary crystallographic data for this paper. These data can be obtained free of charge at www.ccdc.cam.ac.uk/conts/-retrieving.html [or from the Cambridge Crystallographic Data Centre, 12 Union Road, Cambridge CB2 1EZ, UK; Fax: (internat.) + 44-1223/336-033; E-mail: deposit@ccdc.cam.ac.uk].

Acknowledgments

We thank the Deutsche Forschungsgemeinschaft and the Fonds der Chemischen Industrie for financial support.

[1] K. W. Klinkhammer, in *The Chemistry of Organic Germanium, Tin and Lead Compounds* (Ed.: Z. Rappoport), John Wiley & Sons Ltd., Chichester **2002**, vol. 2, part 1, p. 283−357.
[2] M. Weidenbruch, *Coord. Chem. Rev.* **1994**, *130*, 275−300.
[3] J. Belzner, H. Ihmels, *Adv. Organomet. Chem.* **1998**, *43*, 1−42.
[4] M. Weidenbruch, *Eur. J. Inorg. Chem.* **1999**, 373−381.
[5] M. Haaf, T. A. Schmedake, R. West, *Acc. Chem. Res.* **2000**, *33*, 704−714.
[6] M. Kira, T. Iwamoto, *J. Organomet. Chem.* **2000**, *611*, 236−247.
[7] R. West, *Polyhedron* **2002**, *21*, 467−472.
[8] M. Driess, H. Grützmacher, *Angew. Chem.* **1996**, *108*, 900−929; *Angew. Chem. Int. Ed. Engl.* **1996**, *35*, 828−856.
[9] M. F. Lappert, *Main Group Met. Chem.* **1994**, *17*, 183−207.
[10] E. O. Fischer, H. Grubert, *Z. Anorg. Allg. Chem.* **1956**, *286*, 237−242.
[11] A. K. Holliday, P. H. Makin, R. J. Puddephatt, *J. Chem. Soc., Dalton Trans.* **1976**, 435−438.
[12] P. Jutzi, R. Dickbreder, H. Nöth, *Chem. Ber.* **1989**, *122*, 865−870.
[13] N. Kuhn, G. Henkel, S. Stubenrauch, *Angew. Chem.* **1992**, *104*, 766−768; *Angew. Chem. Int. Ed. Engl.* **1992**, *31*, 778−779.
[14] L. Pu, P. P. Power, I. Boltes, R. Herbst-Irmer, *Organometallics* **2000**, *19*, 352−356.
[15] D. J. Burkey, T. P. Hanusa, J. C. Huffman, *Inorg. Chem.* **2000**, *39*, 153−155.
[16] S. P. Constantine, H. Cox, P. B. Hitchcock, G. A. Lawless, *Organometallics* **2000**, *19*, 317−326.
[17] X. Zheng, G. E. Herberich, *Eur. J. Inorg. Chem.* **2001**, 3013−3019.
[18] P. J. Davidson, M. F. Lappert, *Chem. Commun.* **1973**, 317.
[19] P. J. Davidson, D. H. Harris, M. F. Lappert, *J. Chem. Soc., Dalton Trans.* **1976**, 2268−2274.
[20] S. Brooker, J.-K. Buijink, F. T. Edelmann, *Organometallics* **1991**, *10*, 25−26.
[21] K. W. Klinkhammer, W. Schwarz, *Angew. Chem.* **1995**, *107*, 1448−1451; *Angew. Chem. Int. Ed. Engl.* **1995**, *34*, 1334−1337.
[22] R. S. Simons, L. Pu, M. M. Olmstead, P. P. Power, *Organometallics* **1997**, *16*, 1920−1925.
[23] C. Eaborn, T. Ganicz, P. B. Hitchcock, J. D. Smith, S. E. Sözerli, *Organometallics* **1997**, *16*, 5621−5622.
[24] K. W. Klinkhammer, T. F. Fässler, H. Grützmacher, *Angew. Chem.* **1998**, *110*, 114−116; *Angew. Chem. Int. Ed.* **1998**, *37*, 124−126.
[25] M. Stürmann, M. Weidenbruch, K. W. Klinkhammer, F. Lissner, H. Marsmann, *Organometallics* **1998**, *17*, 4425−4428.
[26] M. Stürmann, W. Saak, M. Weidenbruch, K. W. Klinkhammer, *Eur. J. Inorg. Chem.* **1999**, 579−582.
[27] M. Stürmann, W. Saak, H. Marsmann, M. Weidenbruch, *Angew. Chem.* **1999**, *11*, 145−147; *Angew. Chem. Int. Ed.* **1999**, *38*, 187−198.
[28] N. Kano, K. Shibata, N. Tokitoh, R. Okazaki, *Organometallics* **1999**, *18*, 2999−3007.
[29] J. Klett, K. W. Klinkhammer, M. Niemeyer, *Chem. Eur. J.* **1999**, *5*, 2531−2536.
[30] G. L. Wegner, R. J. F. Berger, A. Schier, H. Schmidbaur, *Z. Naturforsch., Teil B* **2000**, *55*, 995−999.
[31] L. Pu, B. Twamley, P. P. Power, *Organometallics* **2000**, *19*, 2874−2881.
[32] C. Eaborn, K. Izod, P. B. Hitchcock, S. E. Sözerli, J. D. Smith, *Chem. Commun.* **1995**, 1829.
[33] C. Eaborn, P. B. Hitchcock, J. D. Smith, S. E. Sözerli, *Organometallics* **1997**, *16*, 5653−5658.
[34] P. P. de Wit, H. O. van der Kooi, J. Wolters, *J. Organomet. Chem.* **1981**, *216*, C9−C11.
[35] P. B. Hitchcock, M. F. Lappert, Z.-X. Wang, *Chem. Commun.* **1997**, 1113−1114.
[36] C. Drost, P. B. Hitchcock, M. F. Lappert, L. J.-M. Pierssens, *Chem. Commun.* **1997**, 1141−1142.
[37] W.-P. Leung, W.-H. Kwok, L.-H. Weng, L. T. C. Law, Z. Y. Zhou, T. C. W. Mak, *J. Chem. Soc., Dalton Trans.* **1997**, 4301−4305.
[38] N. Seidel, K. Jacob, A. A. H. van der Zeijden, H. Menge, K. Merzweiler, C. Wagner, *Organometallics* **2000**, *19*, 1438−1441.
[39] S. Wingerter, H. Gornitzka, R. Bertermann, S. K. Pandey, J. Rocha, D. Stalke, *Organometallics* **2000**, *19*, 3890−3894.
[40] W.-P. Leung, Z.-X. Wang, H.-W. Li, T. C. W. Mak, *Angew. Chem.* **2001**, *113*, 2569−2571; *Angew. Chem. Int. Ed.* **2001**, *40*, 2501−2503.
[41] W.-P. Leung, Z.-X. Wang, H.-W. Li, Q.-C. Yang, T. C. W. Mak, *J. Am. Chem. Soc.* **2001**, *123*, 8123−8124.
[42] P. B. Hitchcock, M. F. Lappert, M. Layh, *Inorg. Chim. Acta* **1998**, *269*, 181−190.
[43] S. S. Al-Juaid, A. G. Avent, C. Eaborn, M. S. Hill, P. B. Hitchcock, D. J. Patel, J. D. Smith, *Organometallics* **2001**, *20*, 1223−1229.
[44] M. Mehring, K. Jurkschat, M. Schürmann, *Main Group Met. Chem.* **1998**, *21*, 635−641.
[45] K. Peveling, M. Schürmann, K. Jurkschat, *Main Group Met. Chem.* **2001**, *24*, 251−252.
[46] K. Peveling, M. Schürmann, R. Ludwig, K. Jurkschat, *Organometallics* **2001**, *20*, 4654−4663.
[47] M. Mehring, M. Schürmann, K. Jurkschat, *Organometallics* **1998**, *17*, 1227−1236.
[48] M. Mehring, C. Löw, M. Schürmann, K. Jurkschat, *Eur. J. Inorg. Chem.* **1999**, 887−898.
[49] M. Mehring, I. Vrasidas, D. Horn, M. Schürmann, K. Jurkschat, *Organometallics* **2001**, *20*, 4647−4653.
[50] K. Peveling, M. Schürmann, K. Jurkschat, *Z. Anorg. Allg. Chem.* **2002**, *628*, 2435−2442.
[51] M. Mehring, C. Löw, M. Schürmann, F. Uhlig, K. Jurkschat, B. Mahieu, *Organometallics* **2000**, *19*, 4613−4623.
[52] M. Henn, M. Schürmann, K. Jurkschat, unpublished results.
[53] P. Pérez-Lourido, J. Romero, J. A. Garcia-Vázquez, A. Sousa, Y. Zheng, J. R. Dilworth, J. Zubieta, *J. Chem. Soc., Dalton Trans.* **2000**, 769−774.
[54] N. Kano, N. Tokitoh, R. Okazaki, *Organometallics* **1997**, *16*, 4237−4239.

 © 2003 Wiley-VCH Verlag GmbH & Co. KGaA, Weinheim

[55] N. Kano, N. Tokitoh, R. Okazaki, *Phosphorus, Sulfur, Silicon Relat. Elemen.* **1997**, *124 & 125*, 517−520.
[56] P. B. Hitchcock, M. F. Lappert, B. J. Samways, E. L. Weinberg, *Chem. Commun.* **1983**, 1492−1494.
[57] K. H. Ebert, H. J. Breunig, C. Silvestru, I. Stefan, I. Haiduc, *Inorg. Chem.* **1994**, *33*, 1695−1699.
[58] P. Boldrini, B. O. Loopstra, *Acta Crystallogr.* **1967**, *22*, 744−745.
[59] K. Koto, H. Schulz, R. A. Huggins, *Solid State Ionics* **1980**, *1*, 355−365.
[60] V. V. Krisyuk, I. A. Baidina, I. K. Igumenov, *Main Group Met. Chem.* **1998**, *21*, 199−206.
[61] M. A. Malik, P. O′Brien, M. Motevalli, A. C. Jones, T. Leedham, *Polyhedron* **1999**, *18*, 1641−1646.
[62] E. Lork, R. Kapoor, R. Mews, B. Zemva, unpublished results.
[63] G. M. Sheldrick, *Acta Crystallogr., Sect. A* **1990**, *46*, 467−473.
[64] G. M. Sheldrick, *SHELXL-97*, Universität Göttingen, **1993**.
[65] *International Tables for Crystallography*, Kluwer Academic Publishers, Dortrecht **1992**, vol. C.
[66] G. M. Sheldrick *SHELXTL, Release 5.1, Software Reference Manual*, Bruker AXS, Inc., Madison, Wisconsin, USA, **1997**.

Received March 13, 2003
Early View Article
Published Online August 14, 2003

 © 2003 Wiley-VCH Verlag GmbH & Co. KGaA, Weinheim

First Examples of Ternary Lanthanide 2,2′-Diphenyldicarboxylate Complexes: Hydrothermal Syntheses and Structures of Lanthanide Coordination Polymers of 2,2′-Diphenyldicarboxylic Acid and 1,10-Phenanthroline

Yibo Wang,[a] Xiangjun Zheng,[a] Wenjuan Zhuang,[a] and Linpei Jin*[a]

Keywords: Complexes / Hydrothermal synthesis / Lanthanides / Hydrogen bonds / X-ray diffraction

In the four new lanthanide coordination polymers $\{[La_2(2,2'\text{-dpdc})_3(phen)(H_2O)]\cdot 2H_2O\}_n$ (**1**), $[Eu_2(2,2'\text{-dpdc})_3(phen)(H_2O)_2]_n$ (**2**), $\{[Ln_2(2,2'\text{-dpdc})_3(phen)_2(H_2O)_2]\cdot 4H_2O\}_n$ [Ln = Tb (**3**), Yb (**4**)] (2,2′-dpdc = 2,2′-diphenyldicarboxylate, phen = 1,10-phenanthroline), prepared by hydrothermal synthesis, the 2,2′-dpdc dianion affords tetradentate, pentadentate, and hexadentate coordination modes. Complex **1** is a two-dimensional network of infinite 1-D chains assembled through π–π interactions, with nine- and ten-coordinate La^{3+}, and arranged in wave-like layers. In **2**, Eu^{3+} possesses nine- and ten-coordinate geometries bridged by 2,2′-dpdc ligands to give a 3-D structure. The isomorphous complexes **3** and **4**, in which Tb^{3+} and Yb^{3+} ions are both nine-coordinate, have two-dimensional structures of 1-D zigzag chains stacked via hydrogen bonds and π–π interactions of phen molecules. The high-resolution emission spectrum of **2** shows two Eu^{3+} ion sites, which is consistent with the results of the X-ray crystal structure analysis.
(© Wiley-VCH Verlag GmbH & Co. KGaA, 69451 Weinheim, Germany, 2003)

Introduction

The design and syntheses of one-, two-, three-dimensional coordination polymers is an attractive area of research due to their structural characteristics, such as diverse coordination modes, intriguing architecture, and porosity, and also to their tremendous potential as catalysts,[1,2] luminescent materials,[3−6] in reversible guest exchange,[7−10] and magnetism.[11−14] Coordination polymers are built by the rational selection of metal ions and the use of structurally interesting ligands with specific functionality to construct metal-organic frameworks. The synthesis of coordination polymers with fascinating structures requires careful selection of the organic ligands.

Hydrogen bonds are well suited for the design of polymeric arrangement and crystal engineering because of their important directional interactions, and because they can interlink 1-D, or 2-D structures into higher-dimensionality systems.[15,16] Ligands with aromatic rings may be assembled into a supramolecular structure via π−π interactions. As a building block to construct coordination polymers, 2,2′-diphenyldicarboxylic acid (2,2′-H_2dpdc) is considered because (1) it affords various coordination modes due to its multifunctional carboxylate groups, and it can bridge metal atoms; (2) as a flexible ligand it allows the formation of multi-dimensional structures constructed from different directions; (3) it displays high reactivity to d and f elements, especially lanthanides since the carboxyl group has a strong affinity for Ln^{3+}. A few transition metal coordination polymers using 2,2′-dpdc as bridging ligand have been reported.[17,18] The coordination modes of 2,2′-dpdc ligands in these polymeric complexes are shown in Scheme 1 (a). Lanthanide ions have larger radii and higher coordination numbers than transition metals, as well as luminescent properties for fluorescent probes, and so their introduction into metal-organic frameworks may generate polymers with a distinctive molecular structure and unusual properties. In addition, phen groups can enhance the luminescent properties of lanthanide complexes. However, to the best of our knowledge, there have been no systematic studies on lanthanide supramolecular coordination polymers with the 2,2′-dpdc ligand.

The hydrothermal method is effective for the crystal growth of many coordination polymers.[19,20] Under hydrothermal conditions, the properties of the reactants and the interactions between organic and inorganic partners are quite different from those under conventional conditions in water. Therefore, various simple precursors and metastable compounds may be produced by hydrothermal reactions, and it facilitates crystal growth from solution.[21,22] Thus, we chose the 2,2′-dpdc ligand as a reactant to build multidimensional architectures by a hydrothermal reaction. Our current focus on rational synthetic strategies for lanthanide coordination polymers, using the hydrothermal method, has yielded some fascinating crystal structures with luminescent properties.[23−25] Herein, we report the syntheses and struc-

[a] Department of Chemistry, Beijing Normal University, Beijing 100875, People's Republic of China
Fax: (internat.) + 86-10/62200567
E-mail: lpjin@bnu.edu.cn

 © 2003 Wiley-VCH Verlag GmbH & Co. KGaA, Weinheim **DOI: 10.1002/ejic.200300121**

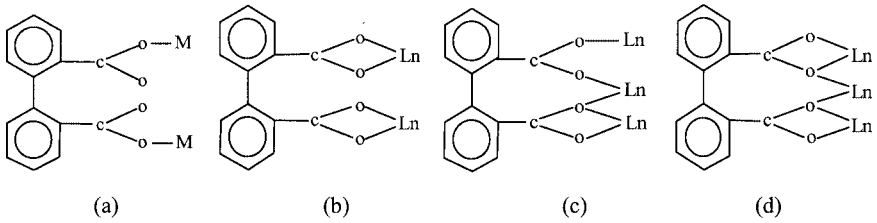

Scheme 1. Coordination modes of 2,2′-dpdc in transition metal 2,2′-dpdc complexes and complexes **1**−**4**

tures of four lanthanide complexes with 2,2′-dpdc ligand and phen ligand.

Results and Discussion

Crystal data of the title complexes (Table 1) and selected bond lengths and angles of **1**−**4** (Tables 2−4) are given here. The 2,2′-dpdc ligands are all completely deprotonated and afford three types of coordination modes (Scheme 1, b, c and d). The crystallographic analyses reveal a two-dimensional network (**1**, **3** and **4**) or a three-dimensional structure (**2**) made up of infinite 1-D chains, and that complexes **3** and **4** are isomorphous.

Crystal Structure of $\{[La_2(2,2'\text{-dpdc})_3(phen)(H_2O)]\cdot 2H_2O\}_n$ (1)

In the crystal structure of **1**, $[La_2(2,2'\text{-dpdc})_3(phen)(H_2O)]\cdot 2H_2O$, the 2,2′-dpdc ligands exhibit penta- and hexadentate coordination modes (Scheme 1, c and d). In an asymmetric unit, there are two types of environment for La^{3+} centers (Figure 1). La(1) is coordinated to ten atoms: eight carboxylate oxygen atoms (O1, O2, O1A, O4A, O5A, O6A, O11A, O12A) of three pentadentate 2,2′-dpdc ligands and one hexadentate 2,2′-dpdc ligand, and two nitrogen atoms (N1, N2) of one phen ligand. The mean La(1)−O(carboxylate) distance is 2.670 Å. La(2) is coordinated by eight carboxylate oxygen atoms (O3, O5, O7, O9, O10, O8B, O10B, O11B) of three pentadentate 2,2′-dpdc ligands and two hexadentate 2,2′-dpdc ligands, and one oxygen atom (O13) provided by a water molecule. The mean La(2)−O(carboxylate) distance is 2.568 Å. La(1) and La(2) are linked by a pentadentate 2,2′-dpdc ligand with an interatomic distance of 7.990 Å. Clearly, the steric hindrance around La(1) is greater than that around La(2) − La(1)−O(carboxylate) bonds are longer than La(2)−O(carboxylate) bonds. Influenced by the steric hindrance and coordination modes of the 2,2′-dpdc ligand and phen, the carboxylate planes of the pentadentate 2,2′-dpdc ligand connecting La(1) and La(2) deflect their aromatic rings with similar dihedral angles, 38.1° and 39.0°.

The one-dimensional chain of **1** (Figure 2) can be viewed as composed of an $\{[La_2(2,2'\text{-dpdc})_3(phen)(H_2O)]\cdot 2H_2O\}_2$ building block. In Figure 2, La1A and La1C (or La1B and La1D) are associated by two chelating-bridging carboxylate groups of two pentadentate 2,2′-dpdc ligands and are 4.487Å apart; La2C and La1A (La2D and La1B, La1C and La2A, or La1D and La2B) are linked by three carboxylate groups of two pentadentate 2,2′-dpdc ligands and one hexa-

Table 1. Crystal data for **1**−**4**

	1	**2**	**3**	**4**
Empirical formula	$C_{54}H_{38}La_2N_2O_{15}$	$C_{54}Eu_2H_{36}N_2O_{14}$	$C_{33}H_{26}N_2O_9Tb$	$C_{33}H_{26}N_2O_9Yb$
FW	1232.68	1240.77	753.54	767.58
Crystal system	triclinic	monoclinic	monoclinic	monoclinic
Space group	$P\bar{1}$	$P2_1/n$	$C2/c$	$C2/c$
a [Å]	12.390(3)	14.378(6)	24.480(8)	24.412(10)
b [Å]	15.419(3)	20.933(9)	12.104(4)	12.129(4)
c [Å]	15.951(3)	15.457(6)	22.940(7)	22.580(8)
α [°]	117.53(3)	90(3)	90	90
β [°]	95.18(3)	95.757(7)	115.571(5)	115.167(10)
γ [°]	107.28(3)	90	90	90
Z	2	4	8	8
V [Å^3]	2485.4(9)	4629(3)	6131(3)	6051(4)
$\rho_{calcd.}$ [g·cm^{-3}]	1.647	1.781	1.613	1.696
T [K]	293(2)	293(2)	293(2)	293(2)
μ [mm^{-1}]	1.768	2.760	2.363	3.150
Reflections collected:				
total, independent	14108, 9956	18917, 8168	12234, 5311	12678, 5542
R_{int}	0.0442	0.0376	0.0407	0.0374
λ (Mo-K$_\alpha$) [Å]	0.71073	0.71073	0.71073	0.71073
R_1, wR_2 [$I > 2\sigma(I)$]	0.0517, 0.1033	0.0290, 0.0548	0.0320, 0.0729	0.0378, 0.0833

 © 2003 Wiley-VCH Verlag GmbH & Co. KGaA, Weinheim

Table 2. Selected bond lengths [Å] and bond angles [°] for **1**; symmetry operations: #1: $-x+1, -y+1, -z$; #2: $x, y, z-1$; #3: $-x+1, -y+1, -z+1$

La(1)−O(1)	2.667(5)	La(2)−O(3)	2.481(5)
La(1)−O(1)#1	2.676(5)	La(2)−O(5)	2.609(5)
La(1)−O(2)	2.683(6)	La(2)−O(7)	2.470(6)
La(1)−O(4)#1	2.500(5)	La(2)−O(8)#3	2.610(6)
La(1)−O(5)#1	2.684(5)	La(2)−O(9)	2.648(5)
La(1)−O(6)#1	2.732(5)	La(2)−O(10)	2.633(5)
La(1)−O(11)#2	2.912(5)	La(2)−O(10)#3	2.511(5)
La(1)−O(12)#2	2.508(5)	La(2)−O(11)#3	2.581(5)
La(1)−N(1)	2.782(6)	La(2)−O(13)	2.726(8)
La(1)−N(2)	2.754(7)	O(11)#2−La(1)−N(1)	110.84(17)
O(1)−La(1)−O(2)	49.42(16)	O(11)#2−La(1)−N(2)	71.33(17)
O(1)−La(1)−O(1)#1	65.78(19)	O(12)#2−La(1)−N(1)	71.97(17)
O(1)−La(1)−O(4)#1	99.24(17)	O(12)#2−La(1)−N(2)	73.16(19)
O(1)−La(1)−O(5)#1	81.43(15)	N(1)−La(1)−N(2)	60.2(2)
O(1)−La(1)−O(6)#1	71.20(16)	O(3)−La(2)−O(5)	73.88(17)
O(1)−La(1)−O(11)#2	139.77(15)	O(3)−La(2)−O(7)	140.96(18)
O(1)−La(1)−O(12)#2	130.34(18)	O(3)−La(2)−O(9)	82.37(19)
O(1)−La(1)−N(1)	102.42(18)	O(3)−La(2)−O(10)	119.31(17)
O(1)−La(1)−N(2)	147.85(17)	O(3)−La(2)−O(13)	68.4(2)
O(1)#1−La(1)−O(4)#1	69.26(16)	O(3)−La(2)−O(8)#3	78.75(18)
O(1)#1−La(1)−O(5)#1	117.92(15)	O(3)−La(2)−O(10)#3	148.51(19)
O(1)#1−La(1)−O(6)#1	136.71(16)	O(3)−La(2)−O(11)#3	94.65(17)
O(1)#1−La(1)−O(11)#2	146.87(16)	O(5)−La(2)−O(7)	69.16(16)
O(1)#1−La(1)−O(12)#2	141.74(16)	O(5)−La(2)−O(9)	76.06(16)
O(1)#1−La(1)−N(1)	70.41(17)	O(5)−La(2)−O(10)	116.58(16)
O(1)#1−La(1)−N(2)	82.40(17)	O(5)−La(2)−O(13)	117.8(2)
O(2)−La(1)−O(1)#1	91.18(16)	O(5)−La(2)−O(8)#3	150.75(17)
O(2)−La(1)−O(4)#1	148.52(17)	O(5)−La(2)−O(10)#3	130.72(17)
O(2)−La(1)−O(5)#1	105.86(16)	O(5)−La(2)−O(11)#3	68.63(16)
O(2)−La(1)−O(6)#1	63.24(16)	O(7)−La(2)−O(9)	77.06(19)
O(2)−La(1)−O(11)#2	121.26(16)	O(7)−La(2)−O(10)	69.20(18)
O(2)−La(1)−O(12)#2	83.79(17)	O(7)−La(2)−O(13)	141.8(2)
O(2)−La(1)−N(1)	72.10(19)	O(7)−La(2)−O(8)#3	133.52(17)
O(2)−La(1)−N(2)	131.32(17)	O(7)−La(2)−O(10)#3	69.86(18)
O(4)#1−La(1)−O(5)#1	65.95(16)	O(7)−La(2)−O(11)#3	83.48(19)
O(4)#1−La(1)−O(6)#1	114.49(16)	O(8)#3−La(2)−O(10)#3	78.52(18)
O(4)#1−La(1)−O(11)#2	83.39(16)	O(8)#3−La(2)−O(11)#3	124.5(2)
O(4)#1−La(1)−O(12)#2	126.89(18)	O(9)−La(2)−O(10)	49.47(15)
O(4)#1−La(1)−N(1)	120.11(18)	O(9)−La(2)−O(13)	140.5(2)
O(4)#1−La(1)−N(2)	72.12(18)	O(9)−La(2)−O(8)#3	90.4(2)
O(5)#1−La(1)−O(6)#1	48.62(16)	O(9)−La(2)−O(10)#3	119.24(16)
O(5)#1−La(1)−O(11)#2	62.89(15)	O(9)−La(2)−O(11)#3	143.89(18)
O(5)#1−La(1)−O(12)#2	99.84(16)	O(10)−La(2)−O(13)	124.7(2)
O(5)#1−La(1)−N(1)	171.63(16)	O(10)−La(2)−O(8)#3	68.86(19)
O(5)#1−La(1)−N(2)	119.78(18)	O(10)−La(2)−O(10)#3	71.29(18)
O(6)#1−La(1)−O(11)#2	71.32(16)	O(10)−La(2)−O(11)#3	145.99(16)
O(6)#1−La(1)−O(12)#2	73.30(17)	O(10)#3−La(2)−O(11)#3	80.69(16)
O(6)#1−La(1)−N(1)	125.29(18)	O(13)−La(2)−O(8)#3	59.0(2)
O(6)#1−La(1)−N(2)	140.84(18)	O(13)−La(2)−O(10)#3	81.2(2)
O(11)#2−La(1)−O(12)#2	47.73(15)	O(13)−La(2)−O(11)#3	67.3(2)

dentate 2,2′-dpdc ligand through bridging or chelating-bridging coordination modes, and are 4.398 Å apart. La2A and La2D of two neighboring building blocks are connected by two bridging carboxylate groups of two pentadentate 2,2′-dpdc ligands and by two chelating-bridging carboxylate groups of two hexadentate 2,2′-dpdc ligands. Thus, the number of 2,2′-dpdc ligands linking two La^{3+} ions (4 for La2A and La2D, 3 for La2C and La1A, 2 for La1A and La1C, and 1 for La1A and La2A) increases with the decreasing distances between the two La^{3+} ions in the 1-D chain structure; the difference in La···La distances in **1** may be due to the different coordination modes and spatial arrangement of the 2,2′-dpdc ligands. In the chain of **1**, the lattice water molecules form strong hydrogen bonds with the carboxylate oxygen atoms of 2,2′-dpdc ligands and the coordinated water molecules simultaneously (Figure 2). The oxygen atoms of the carboxylate groups and coordinated water behave as H-bond acceptors. Thus, three types of hydrogen-bond interactions are observed (Figure 2): (1) between coordinated water (O13A) and lattice water (O15A), $O_w\cdots O_w$ (3.066 Å); (2) between lattice water (O15A) and carboxylate oxygen (O3A and O8BA), $O_w\cdots$O(carboxylate)

 © 2003 Wiley-VCH Verlag GmbH & Co. KGaA, Weinheim

Table 3. Selected bond lengths [Å] and bond angles [°] for **2**;symmetry operations: #1: $-x, -y + 2, -z + 2$; #2: $-x + 1, -y + 2, -z + 2$

Eu(1)−O(2)	2.464(3)	Eu(2)−O(1)	2.820(3)
Eu(1)−O(3)	2.350(3)	Eu(2)−O(2)	2.567(3)
Eu(1)−O(3)#2	2.534(3)	Eu(2)−O(7)	2.496(3)
Eu(1)−O(4)#2	2.505(3)	Eu(2)−O(8)	2.671(3)
Eu(1)−O(5)	2.573(3)	Eu(2)−O(9)	2.431(3)
Eu(1)−O(6)	2.414(3)	Eu(2)−O(10)	2.465(3)
Eu(1)−O(7)	2.459(3)	Eu(2)−O(13)	2.497(3)
Eu(1)−O(11)#1	2.490(3)	Eu(2)−O(14)	2.435(3)
Eu(1)−O(12)#1	2.397(3)	Eu(2)−N(1)	2.657(4)
O(2)−Eu(1)−O(3)	90.54(10)	Eu(2)−N(2)	2.582(4)
O(2)−Eu(1)−O(3)#2	157.12(9)	O(1)−Eu(2)−O(13)	101.51(10)
O(2)−Eu(1)−O(4)#2	145.17(10)	O(1)−Eu(2)−O(14)	64.08(10)
O(2)−Eu(1)−O(5)	73.53(10)	O(1)−Eu(2)−N(1)	127.96(11)
O(2)−Eu(1)−O(6)	121.06(10)	O(1)−Eu(2)−N(2)	135.66(11)
O(2)−Eu(1)−O(7)	67.07(10)	O(2)−Eu(2)−O(7)	64.97(9)
O(2)−Eu(1)−O(11)#1	74.25(10)	O(2)−Eu(2)−O(8)	105.42(10)
O(2)−Eu(1)−O(12)#1	96.64(11)	O(2)−Eu(2)−O(9)	84.43(10)
O(3)−Eu(1)−O(5)	81.43(10)	O(2)−Eu(2)−O(10)	113.07(10)
O(3)−Eu(1)−O(6)	100.51(10)	O(2)−Eu(2)−O(13)	69.97(10)
O(3)−Eu(1)−O(7)	150.85(10)	O(2)−Eu(2)−O(14)	80.21(10)
O(3)−Eu(1)−O(3)#2	67.58(12)	O(2)−Eu(2)−N(1)	146.41(11)
O(3)−Eu(1)−O(4)#2	117.11(10)	O(2)−Eu(2)−N(2)	147.99(12)
O(3)−Eu(1)−O(11)#1	121.01(11)	O(7)−Eu(2)−O(8)	49.79(9)
O(3)−Eu(1)−O(12)#1	73.44(11)	O(7)−Eu(2)−O(9)	144.53(10)
O(3)#2−Eu(1)−O(5)	108.05(10)	O(7)−Eu(2)−O(10)	154.76(10)
O(3)#2−Eu(1)−O(11)#1	110.54(10)	O(7)−Eu(2)−O(13)	85.35(10)
O(3)#2−Eu(1)−O(12)#1	71.46(10)	O(7)−Eu(2)−O(14)	71.40(10)
O(4)#2−Eu(1)−O(5)	128.26(10)	O(7)−Eu(2)−N(1)	88.11(11)
O(4)#2−Eu(1)−O(3)#2	51.64(9)	O(7)−Eu(2)−N(2)	121.70(11)
O(4)#2−Eu(1)−O(11)#1	73.34(10)	O(8)−Eu(2)−O(9)	131.65(11)
O(4)#2−Eu(1)−O(12)#1	73.68(11)	O(8)−Eu(2)−O(10)	141.45(10)
O(5)−Eu(1)−O(6)	51.92(10)	O(8)−Eu(2)−O(13)	72.63(11)
O(5)−Eu(1)−O(7)	74.59(10)	O(8)−Eu(2)−O(14)	105.70(11)
O(5)−Eu(1)−O(11)#1	140.54(10)	O(8)−Eu(2)−N(1)	65.93(11)
O(5)−Eu(1)−O(12)#1	153.00(11)	O(8)−Eu(2)−N(2)	71.98(11)
O(6)−Eu(1)−O(7)	77.56(10)	O(9)−Eu(2)−O(10)	53.33(10)
O(6)−Eu(1)−O(3)#2	71.77(10)	O(9)−Eu(2)−O(13)	66.73(11)
O(6)−Eu(1)−O(4)#2	76.63(11)	O(9)−Eu(2)−O(14)	122.64(11)
O(6)−Eu(1)−O(11)#1	136.46(11)	O(9)−Eu(2)−N(1)	126.43(12)
O(6)−Eu(1)−O(12)#1	142.11(11)	O(9)−Eu(2)−N(2)	75.62(12)
O(7)−Eu(1)−O(3)#2	135.78(10)	O(10)−Eu(2)−O(13)	118.44(11)
O(7)−Eu(1)−O(4)#2	91.03(10)	O(10)−Eu(2)−O(14)	83.40(10)
O(7)−Eu(1)−O(11)#1	72.26(10)	O(10)−Eu(2)−N(1)	82.50(11)
O(7)−Eu(1)−O(12)#1	125.49(10)	O(10)−Eu(2)−N(2)	74.31(11)
O(11)#1−Eu(1)−O(12)#1	53.25(10)	O(13)−Eu(2)−O(14)	148.01(10)
O(1)−Eu(2)−O(2)	47.94(9)	O(13)−Eu(2)−N(1)	130.30(12)
O(1)−Eu(2)−O(7)	102.38(9)	O(13)−Eu(2)−N(2)	79.15(12)
O(1)−Eu(2)−O(8)	151.27(9)	O(14)−Eu(2)−N(1)	71.98(11)
O(1)−Eu(2)−O(9)	64.78(10)	O(14)−Eu(2)−N(2)	131.69(12)
O(1)−Eu(2)−O(10)	66.53(10)	N(1)−Eu(2)−N(2)	63.12(13)

(3.003 Å), (3) another between lattice water (O14A) and carboxylate oxygen (O2B), $O_w\cdots O$(carboxylate) (3.033 Å). The phen molecules in a chain of **1** are parallel, but no π−π stacking interactions are found. However, the phen molecules of neighboring chains, which are stacked along the *a* axis, are parallel and 3.48 Å apart. Therefore, the chains packing in the *a* direction interdigitate to assemble into an extended network through π−π stacking interactions of phen molecules. The La^{3+} ions are arranged in a ruffled sheet parallel to the *ac* plane in waving pattern and the 2,2′-dpdc ligands and phen molecules run through the whole sheet.

Crystal Structure of $[Eu_2$ (2, 2′-dpdc)$_3$(phen)·$(H_2O)_2]_n$ (2)

Complex **2** is a 3-D structure of $[Eu_2$ (2,2′-dpdc)$_3$(phen)·$(H_2O)_2]_n$. Unlike **1**, the 2,2′-dpdc ligands in **2** present not only pentadentate and hexadentate coordination modes, but also a tetradentate one (Scheme 1, b, c, and d). The asymmetric unit of **2** also contains two crystallographically independent Eu^{3+} ions (Figure 3). Eu(1) is coordinated by three oxygen atoms (O5, O6 and O7) of two carboxylate groups of a pentadentate 2,2′-dpdc ligand, two oxygen atoms (O2, O3) of two carboxylate groups of one

 © 2003 Wiley-VCH Verlag GmbH & Co. KGaA, Weinheim

Table 4. Selected bond lengths [Å] and bond angles [°] for **3** and **4**; symmetry operation: #1 $-x, -y + 1, -z$

3		**4**	
Tb(1)−O(1)	2.423(3)	Yb(1)−O(1)	2.358(4)
Tb(1)−O(2)	2.379(3)	Yb(1)−O(2)	2.320(4)
Tb(1)−O(3)#1	2.400(3)	Yb(1)−O(3)#1	2.299(5)
Tb(1)−O(4)#1	2.509(3)	Yb(1)−O(4)#1	2.607(6)
Tb(1)−O(5)	2.405(3)	Yb(1)−O(5)	2.316(4)
Tb(1)−O(6)	2.564(3)	Yb(1)−O(6)	2.558(4)
Tb(1)−O(7)	2.443(3)	Yb(1)−O(7)	2.362(4)
Tb(1)−N(1)	2.532(3)	Yb(1)−N(1)	2.466(5)
Tb(1)−N(2)	2.548(3)	Yb(1)−N(2)	2.489(5)
O(1)−Tb(1)−O(2)	54.04(10)	O(1)−Yb(1)−O(2)	55.56(14)
O(1)−Tb(1)−O(5)	84.48(10)	O(1)−Yb(1)−O(5)	82.86(15)
O(1)−Tb(1)−O(6)	76.80(10)	O(1)−Yb(1)−O(6)	76.53(15)
O(1)−Tb(1)−O(7)	128.15(10)	O(1)−Yb(1)−O(7)	128.79(15)
O(1)−Tb(1)−O(3)#1	87.55(11)	O(1)−Yb(1)−O(3)#1	85.12(16)
O(1)−Tb(1)−O(4)#1	77.29(10)	O(1)−Yb(1)−O(4)#1	75.57(15)
O(1)−Tb(1)−N(1)	156.48(11)	O(1)−Yb(1)−N(1)	153.79(16)
O(1)−Tb(1)−N(2)	128.32(10)	O(1)−Yb(1)−N(2)	129.27(15)
O(2)−Tb(1)−O(5)	133.66(10)	O(2)−Yb(1)−O(5)	133.18(15)
O(2)−Tb(1)−O(6)	74.20(10)	O(2)−Yb(1)−O(6)	74.18(15)
O(2)−Tb(1)−O(7)	106.12(10)	O(2)−Yb(1)−O(7)	105.47(15)
O(2)−Tb(1)−O(3)#1	81.46(10)	O(2)−Yb(1)−O(3)#1	82.58(17)
O(2)−Tb(1)−O(4)#1	114.68(10)	O(2)−Yb(1)−O(4)#1	116.14(15)
O(2)−Tb(1)−N(1)	141.17(10)	O(2)−Yb(1)−N(1)	142.61(16)
O(2)−Tb(1)−N(2)	76.40(10)	O(2)−Yb(1)−N(2)	76.31(15)
O(3)#1−Tb(1)−O(4)#1	53.04(10)	O(3)#1−Yb(1)−O(4)#1	52.40(17)
O(3)#1−Tb(1)−N(1)	79.72(11)	O(3)#1−Yb(1)−N(1)	80.86(17)
O(3)#1−Tb(1)−N(2)	69.93(11)	O(3)#1−Yb(1)−N(2)	72.78(17)
O(4)#1−Tb(1)−N(1)	79.26(11)	O(4)#1−Yb(1)−N(1)	78.33(16)
O(4)#1−Tb(1)−N(2)	116.97(10)	O(4)#1−Yb(1)−N(2)	118.64(16)
O(5)−Tb(1)−O(6)	77.14(11)	O(5)−Yb(1)−O(6)	76.10(16)
O(5)−Tb(1)−O(7)	82.25(10)	O(5)−Yb(1)−O(7)	83.04(15)
O(5)−Tb(1)−O(3)#1	120.36(10)	O(5)−Yb(1)−O(3)#1	117.37(18)
O(5)−Tb(1)−O(4)#1	67.57(10)	O(5)−Yb(1)−O(4)#1	65.07(16)
O(5)−Tb(1)−N(1)	85.03(11)	O(5)−Yb(1)−N(1)	84.11(16)
O(5)−Tb(1)−N(2)	147.11(11)	O(5)−Yb(1)−N(2)	147.85(15)
O(6)−Tb(1)−O(7)	51.41(9)	O(6)−Yb(1)−O(7)	52.30(14)
O(6)−Tb(1)−O(3)#1	155.59(11)	O(6)−Yb(1)−O(3)#1	155.87(16)
O(6)−Tb(1)−O(4)#1	137.69(10)	O(6)−Yb(1)−O(4)#1	134.26(16)
O(6)−Tb(1)−N(1)	121.02(10)	O(6)−Yb(1)−N(1)	121.91(15)
O(6)−Tb(1)−N(2)	105.34(11)	O(6)−Yb(1)−N(2)	107.09(16)
O(7)−Tb(1)−O(3)#1	141.25(10)	O(7)−Yb(1)−O(3)#1	143.96(16)
O(7)−Tb(1)−O(4)#1	139.05(10)	O(7)−Yb(1)−O(4)#1	138.04(15)
O(7)−Tb(1)−N(1)	70.87(10)	O(7)−Yb(1)−N(1)	71.62(15)
O(7)−Tb(1)−N(2)	75.04(10)	O(7)−Yb(1)−N(2)	75.18(15)
N(1)−Tb(1)−N(2)	65.31(11)	N(1)−Yb(1)−N(2)	66.83(16)

hexadentate 2,2′-dpdc ligand in bridging mode, two oxygen atoms (O3A, O4A) of one carboxylate group of another hexadentate 2,2′-dpdc ligand in chelating mode, and two oxygen atoms (O11A, O12A) of a carboxylate group of a tetradentate 2,2′-dpdc ligand. The coordination sphere of Eu(2) differs from that of Eu(1) and is ten-coordinate. Around Eu(2), one tetradentate 2,2′-dpdc ligand chelates to Eu(2) through O9 and O10, one hexadentate 2,2′-dpdc ligand is simultaneously coordinated to Eu(1) and Eu(2) through O1 and O2 in chelating-bridging mode, and the pentadentate 2,2′-dpdc ligand is coordinated to Eu(1) and Eu(2) through O7 and O8 in the same mode. Of these oxygen atoms, O2 and O7 act as μ_2-oxygen atoms, connecting Eu(1) and Eu(2) with an Eu(1)···Eu(2) distance of 4.185 Å. Besides these six oxygen atoms, there are two nitrogen atoms (N1, N2) of one phen molecule and two oxygen atoms (O13, O14) of two coordinated water molecules to complete the ten-coordinate geometry of Eu(2). The mean Eu(2)−O(carboxylate) distance (2.575Å) is longer than Eu(1)−O(carboxylate) (2.465 Å), possibly because Eu(2) has a larger coordination number than Eu(1) [Eu(1) is nine-coordinate], resulting in a larger steric effect in the Eu(2) environment.

Unlike **1**, in the 1-D chain of **2**, every four Eu^{3+} (Eu2B, Eu1B, Eu1D, Eu2D), two tetradentate 2,2′-dpdc ligands, two pentadentate 2,2′-dpdc ligands and two hexadentate 2,2′-dpdc ligands fabricate one $\{[Eu_2(2,2'\text{-dpdc})_3(phen)]\cdot(H_2O)_2\}_2$ building block along the *a* axis (Figure 4). In each building block, two carboxylate groups of the hexadentate 2,2′-dpdc ligand are coordinated to

 © 2003 Wiley-VCH Verlag GmbH & Co. KGaA, Weinheim

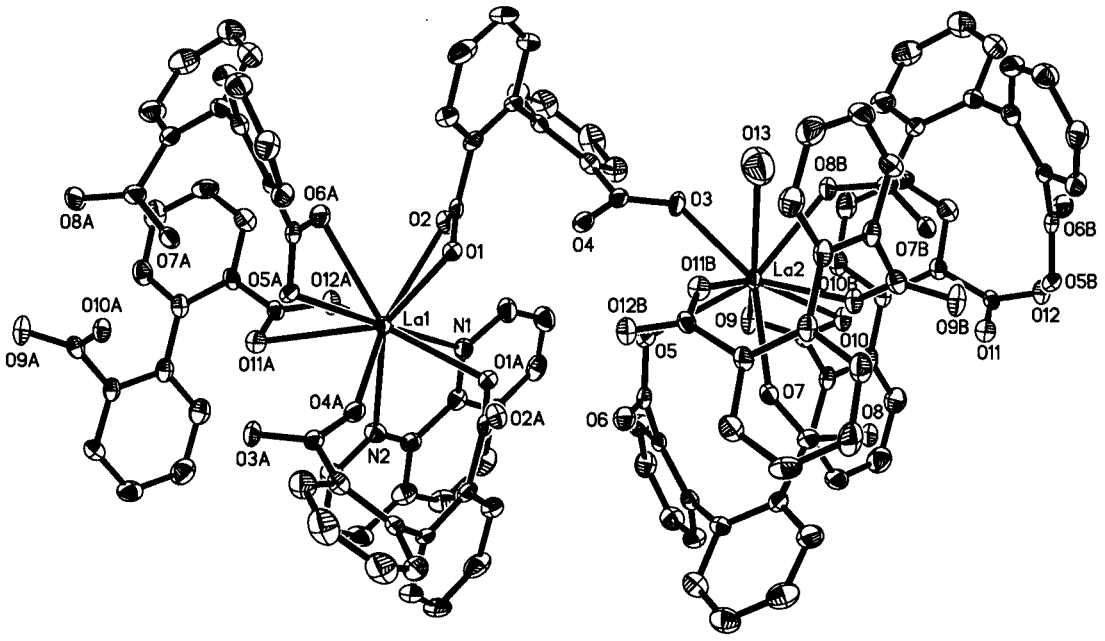

Figure 1. Coordination environment of the two La^{III} ions in **1** with thermal ellipsoids at 30% probability; all hydrogen atoms are omitted for clarity

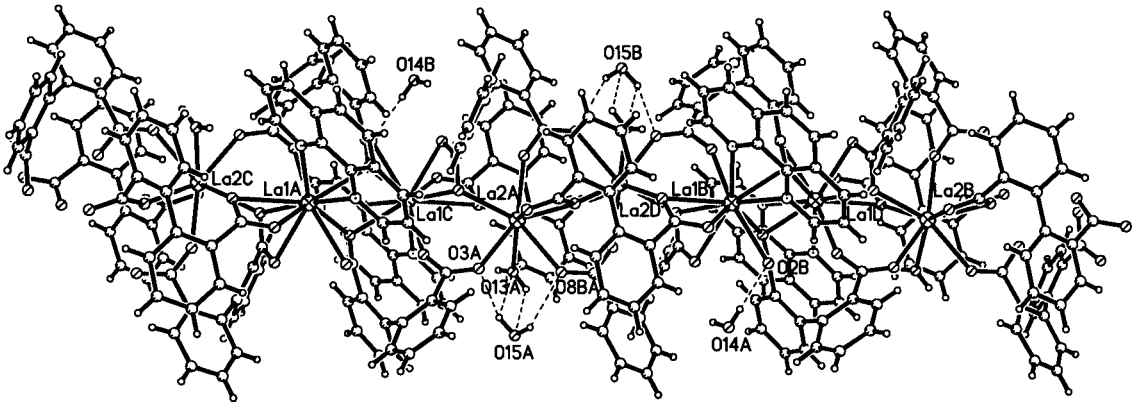

Figure 2. 1-D chain of **1** viewed along the *a* axis; hydrogen bonds containing lattice water are shown as dotted lines

three Eu^{3+} ions in chelating-bridging coordination mode. Each pentadentate 2,2′-dpdc ligand only links two Eu^{3+} ions belonging to the same asymmetric unit. Two pentadentate and two hexadentate 2,2′-dpdc ligands construct one building block through bridging four Eu^{3+} ions, while two carboxylate groups of each tetradentate 2,2′-dpdc ligand coordinate with two Eu^{3+} ions of two adjacent building blocks in chelating-bridging mode. Thus, it is tetradentate 2,2′-dpdc ligands that connect two adjacent building blocks, forming a 1-D infinite chain along the *a* axis. The phen molecules of adjacent chains are parallel and stacked next to each other (3.47 Å apart). The carbon atoms of these parallel phen molecules are also involved in weak C−H···O hydrogen bonds with the carboxylate oxygen atoms of 2,2′-dpdc ligands, and the C···O(carboxylate) distances are all 3.198 Å (Figure 5). Consequently, a three-dimensional supramolecular polymer is generated not only by coordination bonds but also by intermolecular hydrogen bonds and interchain π−π interactions.

Crystal Structure of $\{[Ln_2(2,2'\text{-dpdc})_3(phen)_2(H_2O)_2]\cdot 4H_2O\}_n$ [Ln=Tb (3), Yb (4)]

Since complexes **3** and **4** are isomorphous we will only describe the crystal structure of **3**. In **3**, each 2,2′-dpdc ligand shows the tetradentate coordination mode only (Scheme 1, b). Each Tb^{3+} is nine-coordinate and the coordination geometry is roughly a tricapped trigonal prism. Around each Tb center are two nitrogen atoms (N1, N2) of one phen, six carboxylate oxygen atoms (O1, O2, O3A, O4A, O6, O7) of three chelating carboxylate groups of three tetradentate bridging 2,2′-dpdc ligands, and one oxygen atom (O5) of coordinated water (Figure 6). The mean Tb−O(carboxylate) distance (2.453 Å) is longer than those in $[Tb_2(BDC)_3(H_2O)_4]_n$ [3] and $[Tb_2(oba)_3(2,2'\text{-bpy})_2]_n$,[27]

 © 2003 Wiley-VCH Verlag GmbH & Co. KGaA, Weinheim

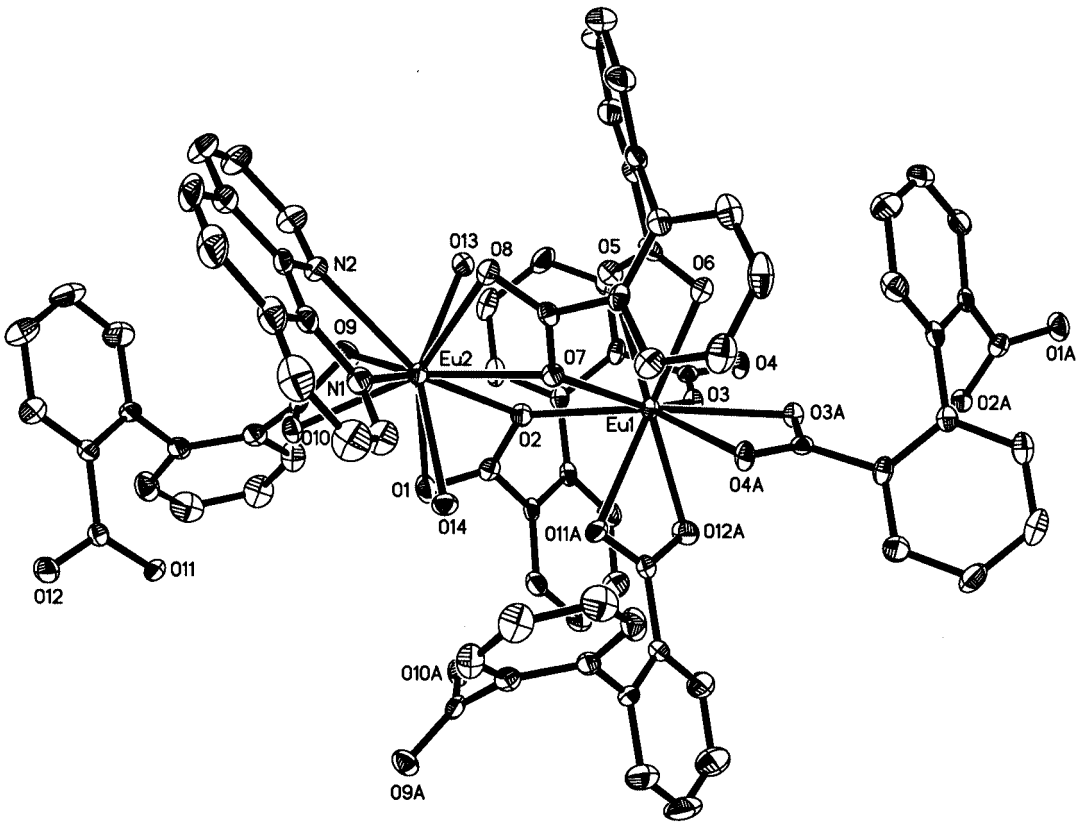

Figure 3. Coordination environment of the two Eu^{III} ions in **2** with thermal ellipsoids at 30% probability; all hydrogen atoms are omitted for clarity

which may be due to the larger steric hindrance of 2,2′-dpdc ligands and phen molecules. The coordination environment shows that there are three tetradentate 2,2′-dpdc ligands to chelate each Tb^{3+}, which is fewer than the 2,2′-dpdc ligands coordinated with La^{3+}. In addition, the 2,2′-dpdc ligand presents a tetradentate coordination mode to furnish the nine-coordinate coordination geometry in **3** and **4** because of the smaller radii of Tb^{3+} and Yb^{3+} ions.

In **3**, the dinuclear species $[Tb_2(2,2'\text{-dpdc})_3(phen)_2(H_2O)_2]\cdot 4H_2O$ is centrosymmetric, and these units are linked through 2,2′-dpdc ligands; a 1-D infinite zigzag chain is then constructed through coordination bonds. In each dinuclear motif, there are three chelating-bridging tetradentate 2,2′-dpdc ligands and two phen molecules coordinated to two Tb^{3+} ions. Two Tb^{3+} ions are linked by two chelating-bridging tetradentate 2,2′-dpdc ligands with a $Tb^{3+}\cdots Tb^{3+}$ distance of 6.992 Å. Two neighboring $[Tb_2(2,2'\text{-dpdc})_3(phen)_2(H_2O)_2]\cdot 4H_2O$ dinuclear motifs are connected by the third 2,2′-dpdc ligand by four $Tb^{3+}-O$(carboxylate) bonds. Two adjacent Tb^{3+} ions of two different dinuclear motifs are 6.317 Å apart.

In the 2-D network of **3**, there are hydrogen bonds between a coordination carboxylate atom (O7AD) and the C−H of a phen molecule (C8FC) of a neighboring chain, C···O(carboxylate) (3.313 Å). At the same time, the adjacent chains are stacked in a staggered fashion along the *b* axis through π−π interactions between phen molecules of two neighboring chains (3.434 Å apart). Hence, phen is crucial to the formation and stabilization of the structure of **3** because of its simultaneous participation in formation of the hydrogen bonds and π−π interactions. Thus, a two-dimensional layered supramolecular array parallel to the *bc* plane is constructed with the chains pulled together by a series of interchain hydrogen bonds and π−π interactions along the *b* axis (Figure 7). The Tb^{3+} ions are distributed on the layer in an undulating way and the Tb···Tb distance of neighboring chains is 12.104 Å. The 2,2′-dpdc ligands and phen interdigitate the whole undulating plane.

In terms of the structural characteristics and the formation of the supramolecular architecture of the title complexes, several parallels can be obtained: (1) Each complex has one or two coordinated water molecules to meet the high coordination number of Ln^{III} ions. (2) Much lattice water is held within the 1-D chains of **1**, **3** and **4**, therefore extensive intramolecular hydrogen bonds are formed among lattice water molecules, coordinated water molecules and carboxylate groups, which further stabilize the 1-D chain structure. Therefore, water molecules not only act as a reaction medium in the formation of these supramolecular structures, but also contribute positively to the interaction with 2,2′-dpdc ligands by hydrogen bonds. (3) The 2-D network (for **1**, **3** and **4**) and the 3-D structure (for **2**) are all constructed by 1-D chains linked through hydrogen bonds and packed by π−π interactions between phen molecules of adjacent chains (for **1**, **2**, **3**, and **4**). However, the title complexes also exhibit considerable differences with regard to

 © 2003 Wiley-VCH Verlag GmbH & Co. KGaA, Weinheim

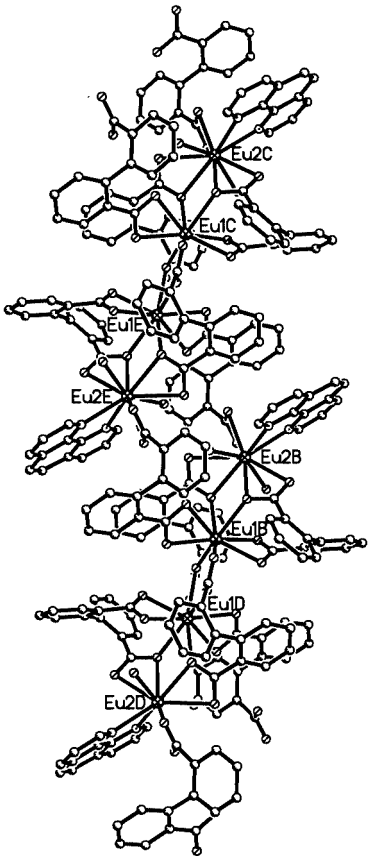

Figure 4. 1-D chain of **2** viewed along the *b* axis; all hydrogen atoms are omitted for clarity

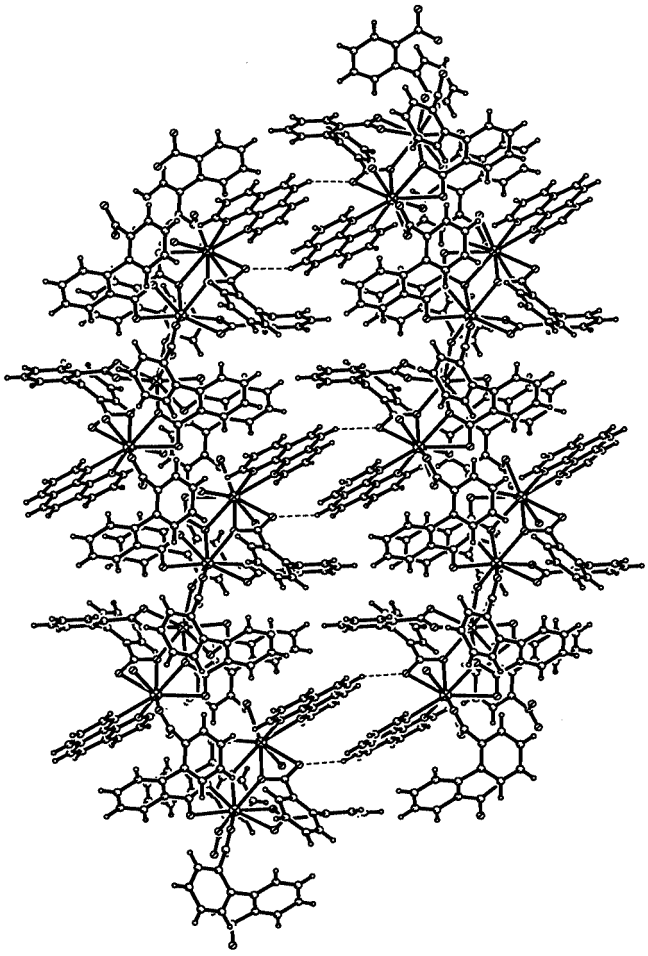

Figure 5. 2-D structure of **2** viewed along the *a* axis; hydrogen bonds are shown as dotted lines

the lattice water, hydrogen bonds, and π−π interactions. One difference is the absence of lattice water within the structure of **2** and, correspondingly, no O···H−O hydrogen bonds are observed. In addition, a 3-D network of **2** is formed by O···C−H (phen) hydrogen bonds and π−π interactions of phen from different orientations.

Lanthanide contraction clearly effects the formation and crystal structure of the title compounds. First, the Ln−O bond lengths decrease with increasing lanthanide atomic number: the mean Ln−O(carboxylate) distance follows the order La−O(carboxylate) > Eu−O(carboxylate) > Tb−O(carboxylate) > Yb−O(carboxylate); the mean Ln−O_w distances are 2.736, 2.466, 2.403, and 2.316 Å for La, Eu, Tb, and Yb, respectively. Similarly, the mean Ln−N distances are 2.768, 2.620, 2.540, and 2.478 Å for La, Eu, Tb, and Yb, respectively. Secondly, the coordination number and the number of 2,2′-dpdc ligands around Ln^{3+} all decrease with decreasing ionic radii of the lanthanides. Thirdly, the variations in coordination modes of 2,2′-dpdc ligands in these complexes are connected with the decreasing ionic radii of the La^{3+}, Eu^{3+}, Tb^{3+} and Yb^{3+} ions. As La^{3+} has the largest ionic radius in **1**−**4** the 2,2′-dpdc ligands adopt pentadentate and hexadentate coordination modes in **1** (Scheme 1, c and d). The tetradentate and pentadentate coordination modes of 2,2′-dpdc ligands in **2** (Scheme 1, b and c) and the tetradentate coordination modes of 2,2′-dpdc ligands in **3** and **4** reflect the decreasing

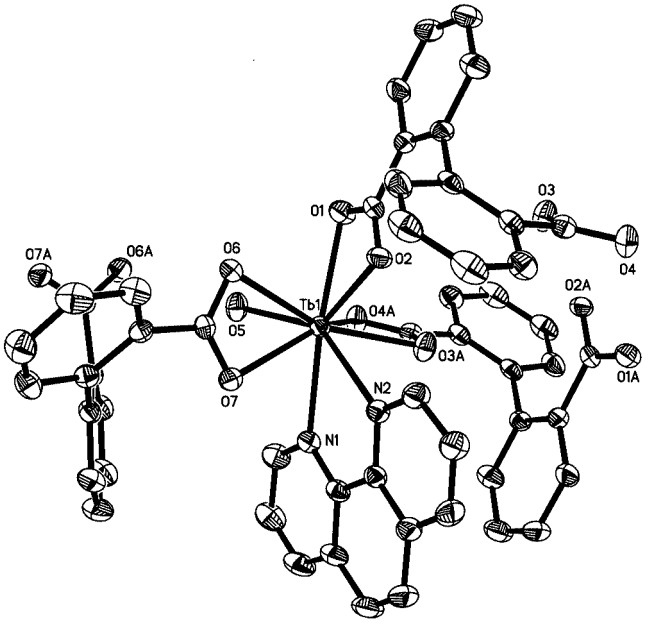

Figure 6. Coordination environment of the Tb^{III} ion in **3** with thermal ellipsoids at 30% probability; all hydrogen atoms are omitted for clarity

 © 2003 Wiley-VCH Verlag GmbH & Co. KGaA, Weinheim

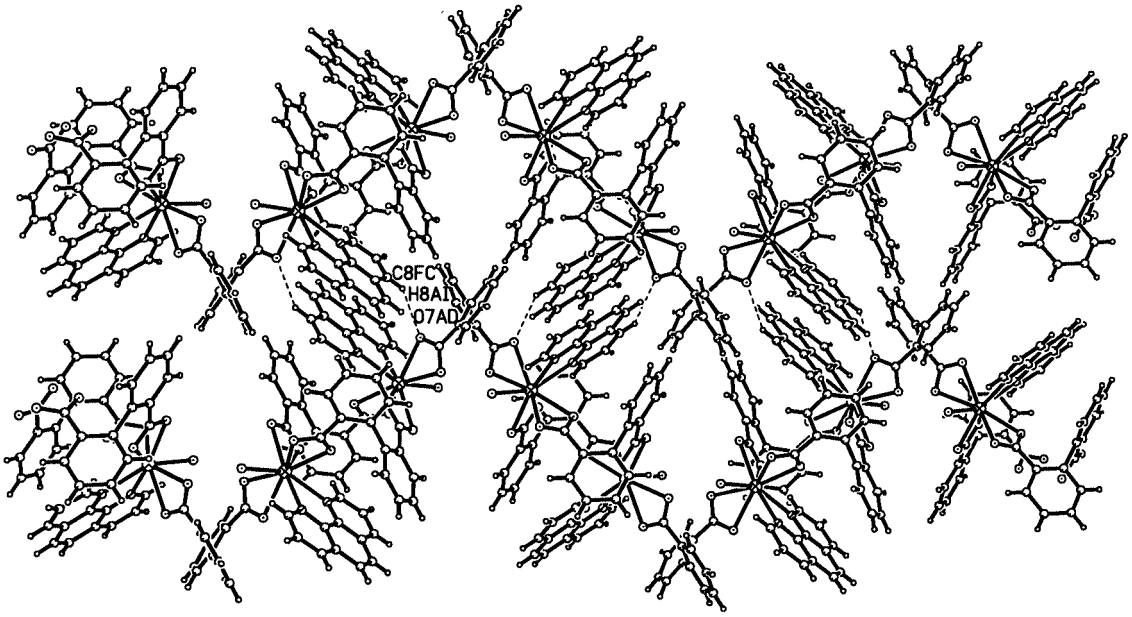

Figure 7. 2-D network of **3** viewed along the *a* axis

ionic radii of the respective lanthanides with increasing atomic number. These results are all in line with lanthanide contraction.

Contrasting the title complexes with binary lanthanide 2,2′-diphenyldicarboxylate complexes,[25] the mean Ln−O(carboxylate) distances for La, Eu and Tb in the title complexes are all longer than those in the binary complexes. Obviously, this is due to the steric hindrance of phen molecules. Similarly, because of the participation of phen molecules, the title complexes exhibit 2-D (**1**, **3** and **4**) or 3-D (**2**) supramolecular architectures constructed by 1-D chains through hydrogen bonds of neighbouring chains, while the binary complexes show 1-D chain structures. As regards 2,2′-dpdc ligands, there is a hexadentate coordination mode in the title complexes that is not present in the binary lanthanide complexes (Scheme 1, d). In addition, the tetradentate coordination mode of 2,2′-dpdc ligands in the binary complexes is quite different from that in the title complexes.

Photophysical Properties of 2

Eu^{3+} complexes can undergo characteristic Eu^{3+} ion emission when excited, and Eu^{3+} is usually regarded as a structural probe to determine the local ion sites based on its unique nondegenerate lowest emission level of $^5D_0$. In the asymmetric unit of the coordination polymer **2**, the two Eu^{3+} ions have obviously different coordination environments: one is coordinated by phen, while the other is not, which led us to probe its local structure in detail.

Figure 8 illustrates the emission spectrum of **2** corresponding to $^5D_0 \rightarrow {}^7F_J$ ($J = 0-4$) transitions in the range of 13900−17300 cm^{-1} at 77 K, in which the $^5D_0 \rightarrow {}^7F_3$ transition is too weak to be observed. The apparent four peaks corresponding to the $^5D_0 \rightarrow {}^7F_1$ transition and the

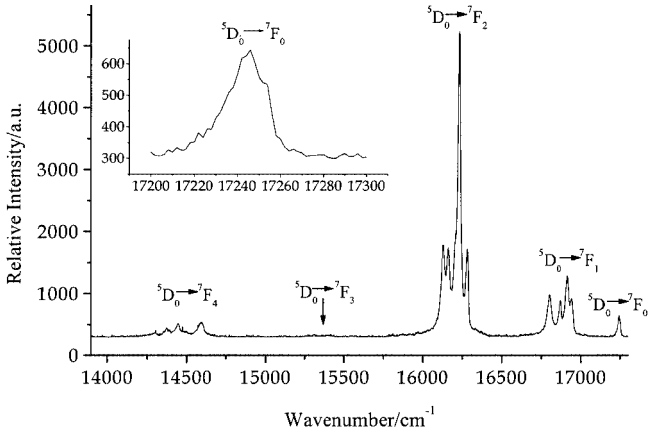

Figure 8. Emission spectrum of **2** corresponding to $^5D_0 \rightarrow {}^7F_J$ ($J = 0-4$) transitions at 77 K, $\lambda_{exc} = 355$ nm

shoulder at the peak (Figure 8, insert) corresponding to the $^5D_0 \rightarrow {}^7F_0$ transition both imply that there is more than one Eu^{3+} ion site in **2**. To further investigate the Eu^{3+} ion sites in the coordination polymer, selective excitation technology was applied. The excitation spectra (Figure 9, a and b) at 77 K were obtained by setting 16235 and 16204 cm^{-1} as the analyzing wavenumbers. Scanning in the range of 578.0−581.0 nm revealed two sharp excitation peaks, which show that there are two Eu^{3+} ion sites,[28] located at 579.58 nm and 579.84 nm, respectively, which is in good agreement with the results of X-ray diffraction.

Conclusion

Complexes **1**−**4** exhibit 2-D (**1**, **3**, and **4**) and 3-D (**2**) structures, and **3** and **4** are isomorphous. The 2,2′-dpdc li-

 © 2003 Wiley-VCH Verlag GmbH & Co. KGaA, Weinheim

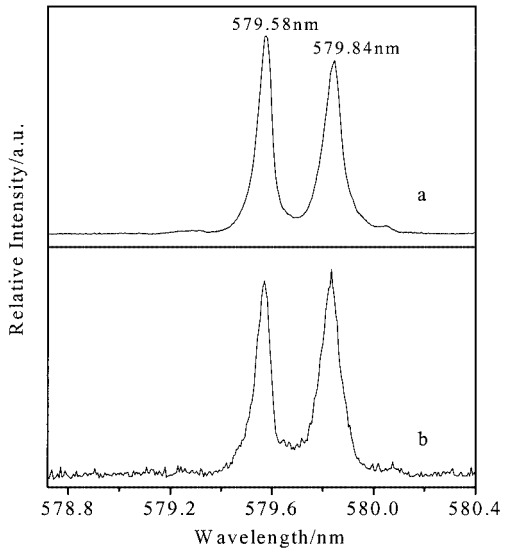

Figure 9. Excitation spectra of **2** at 77 K, analyzing wavenumber: (a) 16235 and (b) 16204 cm^{-1}

gands in these complexes adopt tetradentate, pentadentate and hexadentate coordination modes. The components of the building blocks for the title complexes, the coordination mode of the carboxylate groups, Ln−O and Ln−N distances, and the coordination number all clearly indicate the effect of lanthanide contraction on the formation and structure of the ternary lanthanide 2,2′-diphenyldicarboxylate complexes with 1,10-phenanthroline. Utilizing the characteristic emission of Eu^{3+} ions as a conformation probe, we confirm that there are two Eu^{3+} ion sites in **2**. Finally, the phen molecule clearly contributes to the formation of 2-D and 3-D structures in the title complexes.

Experimental Section

General: Materials: $LaCl_3·7H_2O$, $EuCl_3·6H_2O$, $TbCl_3·6H_2O$, and $YbCl_3·6H_2O$ were prepared by dissolving their respective oxides in hydrochloric acid followed by drying. 2,2′-Diphenyldicarboxylic acid was purchased from Aldrich and used without further purification. All the other reagents were commercially available and used as received. Instrumentation: Elemental analyses were performed with an Elementar Vario EL analyzer. The IR spectra were recorded with a Nicolet Avatar 360 FT-IR spectrometer as KBr pellets. For the emission studies, the excitation light source was a YAG-Nd laser that emits at 1.064 μm, and the excitation wavelength was 355 nm. The sample was placed in a Dewar, cooled with liquid nitrogen, and the fluorescence was collected at right angles through a Spex 1403 monochromator with a photomultiplier tube, then averaged by Boxcar integrator and, finally, the data were transferred to a computer.

X-ray Crystallographic Study: X-ray single-crystal data collection for complexes **1**, **2**, **3** and **4** was performed with a Bruker Smart 1000 CCD diffractometer, using graphite-monochromated Mo-K_α radiation (λ = 0.71073Å). Semiempirical absorption corrections were applied using the SADABS program. The structures were solved by direct methods and refined by full-matrix least-squares on $|F|^2$ using the SHELXTL-97 program.[26] All non-hydrogen atoms were refined anisotropically. The hydrogen atoms were generated geometrically and treated by a mixture of independent and constrained refinement. CCDC-201295 to -201298 contain the supplementary crystallographic data for this paper. These data can be obtained free of charge at www.ccdc.cam.ac.uk/conts/retrieving.html [or from the Cambridge Crystallographic Data Centre, 12 Union Road, Cambridge CB2 1EZ, UK; Fax: (internat.) + 44-1223/336-033; E-mail: deposit@ccdc.cam.ac.uk].

Syntheses

$\{[La_2(2,2'\text{-dpdc})_3(phen)(H_2O)]·2H_2O\}_n$ (1): A mixture of $LaCl_3·7H_2O$(0.111 g, 0.3 mmol), 2,2′-diphenyldicarboxylic acid (0.109 g, 0.45 mmol), phen·H_2O (0.059 g, 0.3 mmol), H_2O (10 mL), and an aqueous solution of NaOH (0.625 mL, 0.4 mmol) was heated in a stainless-steel reactor (23-mL capacity) with a Teflon liner at 170 °C for 3 d and then slowly cooled to room temperature by air cooling. The yellowish crystals so obtained were collected by filtration, washed with ethanol, and then air-dried to give a 57.9% yield (0.107 g). $C_{54}H_{38}La_2N_2O_{15}$ (1232.68): calcd. C 52.62, H 3.11, N 2.27; found C 52.85, H 2.68, N 2.09. IR (KBr pellet): $\tilde{\nu}$ = 3436 (m), 1600 (s), 1577 (s), 1544 (s), 1442 (s), 1406 (s), 756 (m), 730 (m) cm^{-1}.

$[Eu_2(2,2'\text{-dpdc})_3(phen)·(H_2O)_2]_n$ (2): A mixture of $EuCl_3·6H_2O$-(0.11 g, 0.3 mmol), 2,2′-diphenyldicarboxylic acid (0.109 g, 0.45 mmol), phen·H_2O (0.059 g, 0.3 mmol), H_2O (10 mL), and aqueous solution of NaOH (0.56 mL, 0.366 mmol) was heated in a stainless-steel reactor (23-mL capacity) with Teflon liner at 190 °C for 3 d and then slowly cooled to room temperature by air-cooling. The resultant flesh-colored crystals were collected by filtration, washed with ethanol, and then air-dried; 62.3% yield (0.116 g). $C_{54}H_{36}Eu_2N_2O_{14}$ (1240.77): calcd. C 52.27, H 2.93, N 2.26; found C 52.78, H 2.58, N 2.04. IR (KBr pellet): $\tilde{\nu}$ = 3551 (m), 1621 (s), 1552 (s), 1525 (s), 1442 (s), 1407 (s), 772 (m), 762 (m) cm^{-1}.

$\{[Ln(2,2'\text{-dpdc})_{1.5}(phen)(H_2O)]·2H_2O\}_n$ [Ln = Tb (3), Yb (4)]: The syntheses of complexes **3** and **4** followed the same procedure as for **2.** Colorless and pale yellow crystals of **3** and **4**, respectively, were obtained by filtration and washed with ethanol, then air-dried to give yields of 53.1% (0.061 g) and 58.3% (0.067 g), respectively. $C_{33}H_{26}N_2O_9Tb$ (**3**) (753.54): calcd. C 52.57, H 3.48, N 3.723; found C 52.54, H 3.01, N 3.43. IR (KBr pellet): $\tilde{\nu}$ = 3423 (m), 1600 (s), 1576 (s), 1544 (s), 1477 (s), 1408 (s), 766 (m), 728 (m) cm^{-1}. $C_{33}H_{26}N_2O_9Yb$ (**4**) (767.58): calcd. C 51.61, H 3.42, N 3.65; found C 51.46, H 3.24, N 3.60. IR (KBr pellet): $\tilde{\nu}$ = 3422 (m), 1600 (s), 1577 (s), 1546 (s), 1479 (s), 1412 (s), 766 (m), 726 (m) cm^{-1}.

Acknowledgments

This work is supported by the State Key Program of Fundamental Research (G1998061308) and the Natural Science Foundation of China (29971005).

[1] J. S. Seo, D. Whang, H. Lee, S. I. Jun, J. Oh, Y. J. Jeon, K. Kim, *Nature* **2000**, *404*, 982−983.
[2] B. Gomez-Lor, E. Gutiérrez-Puebla, M. Iglesias, M. A. Monge, C. Ruiz-Valero, N. Snejko, *Inorg. Chem.* **2002**, *41*, 2429−2432.
[3] T. M. Reineke, M. Eddaoudi, M. Fehr, D. Kelley, O. M. Yaghi, *J. Am. Chem. Soc.* **1999**, *121*, 1651−1657.
[4] C. Reinhard, H. U. Güdel, *Inorg. Chem.* **2002**, *41*, 1048−1055.
[5] S.-L. Zheng, M.-L. Tong, S.-D. Tan, Y. Wang, J.-X. Shi, Y.-X. Tong, H. K. Lee, X.-M. Chen, *Organometallics* **2001**, *20*, 5319−5325.
[6] L. Ma, O. R. Evans, B. M. Foxman, W. Lin, *Inorg. Chem.* **1999**, *38*, 5837−5840.

 © 2003 Wiley-VCH Verlag GmbH & Co. KGaA, Weinheim

[7] T. M. Reineke, M. Eddaoudi, M. O'Keeffe, O. M. Yaghi, *Angew. Chem. Int. Ed.* **1999**, *38*, 2590−2594, *Angew. Chem.* **1999**, *111*, 2712−2716.
[8] S. Noro, S. Kitagawa, M. Kondo, K. Seki, *Angew. Chem. Int. Ed.* **2000**, *39*, 2082−2084, *Angew. Chem.* **2000**, *112*, 2162−2164.
[9] K. Endo, T. Koike, T. Sawaki, O. Hayashida, H. Masuda, Y. Aoyama, *J. Am. Chem. Soc.* **1997**, *119*, 4117−4122.
[10] P. Brunet, M. Simard, J. D. Wuest, *J. Am. Chem. Soc.* **1997**, *119*, 2737−2738.
[11] K. P. Mörtl, J.-P. Sutter, S. Golhen, L. Ouahab, O. Kahn, *Inorg. Chem.* **2000**, *39*, 1626−1627.
[12] Z.-L. Huang, M. Drillon, N. Masciocchi, A. Sironi, J.-T. Zhao, P. Rabu, P. Panissod, *Chem. Mater.* **2000**, *12*, 2805−2812.
[13] M. Riou-Cavellec, C. Albinet, J.-M. Grenèche, G. Férey, *J. Mater. Chem.* **2001**, *11*, 3166−3171.
[14] J. Guilhem, L. Tchertanov, K. Nakatani, *J. Am. Chem. Soc.* **2000**, *122*, 9444−9454.
[15] J. C. MacDonald, G. M. Whitesides, *Chem. Rev.* **1994**, *94*, 2383−2420.
[16] C. B. Aakeröy, K. R. Seddon, *Chem. Soc. Rev.* **1993**, *22*, 397−407.
[17] H. Kumagai, K. Inoue, M. Kurmoo, *Bull. Chem. Soc. Jpn.* **2002**, *75*, 1283−1289.
[18] J. M. Rueff, S. Pillet, N. Claiser, G. Bonaventure, M. Souhassou, P. Rabu, *Eur. J. Inorg. Chem.* **2002**, 895−900.
[19] O. M. Yaghi, H. Li, T. L. Groy, *J. Am. Chem. Soc.* **1996**, *118*, 9096−9101.
[20] S. O. H. Gutschke, M. Molinier, A. K. Powell, R. E. P. Winpenny, P. T. Wood, *Chem. Commun.* **1996**, 823−824.
[21] A. Rabenau, *Angew. Chem. Int. Ed. Engl.* **1985**, *24*, 1026−1040, *Angew. Chem.* **1985**, *97*, 1017.
[22] J. Gopalakrishnan, *Chem. Mater.* **1995**, *7*, 1265−1275.
[23] Y. Wan, L. Jin, K. Wang, L. Zhang, X. Zheng, S. Lu, *New J. Chem.* **2002**, *26*, 1590−1596.
[24] X. Zheng, L. Jin, S. Lu, *Eur. J. Inorg. Chem.* **2002**, 3356−3363.
[25] Y. Wang, X. Zheng, W. Zhuang, L. Jin, *Eur. J. Inorg. Chem.*, **2003**, 1355−1360.
[26] G. M. Sheldrick, *SHELX-97*, PC-version, University of Göttingen, Germany, **1997**.
[27] G.-F. Liu, Z.-P. Qiao, H.-Z. Wang, X.-M. Chen, G. Yang, *New J. Chem.* **2002**, *26*, 791−795.
[28] J.-C. G. Bünzli, in *Lanthanide Probes in Life, Chemical and Earth Sciences. Theory and Practice* (Eds.: J.-C. G. Bünzli, G. R. Choppin), Elsevier Scientific Publishers, Amsterdam, **1989**, chapter 7.

Received March 5, 2003
Early View Article
Published Online August 14, 2003

 © 2003 Wiley-VCH Verlag GmbH & Co. KGaA, Weinheim

Organic Functional Group Transformations in the Periphery of a Group-4 Metallocene Complex: 2*H*-Pyrrole Formation at a Pendant Boron Lewis Acid

Michael Hill,[a] Gerald Kehr,[a] Roland Fröhlich,[a][‡] and Gerhard Erker*[a]

Keywords: Boron / Hydroboration / Lewis acids / Tautomerism / Zirconium

The allyl-substituted *ansa*-zirconocene dichloride [$Me_2Si(C_5H_4)(C_5H_3CH_2CH{=}CH_2)ZrCl_2$] (**1**) cleanly adds the borane 9-BBN to the allyl C=C double bond to yield the corresponding hydroboration product **2**. The borane $HB(C_6F_5)_2$ (**3**) is also added regioselectively to **1** to yield [$Me_2Si(C_5H_4)\{C_5H_3(CH_2)_3B(C_6F_5)_2\}ZrCl_2$] (**4**). The strongly electrophilic boron Lewis acid in **4** adds 2-methyl-4,5-dihydrooxazole to yield **6**. Treatment of **4** with pyrrole results in the formation of the respective borane adduct **7** of the pyrrole tautomer 2*H*-pyrrole. The 2*H*-pyrrole ligand in **7** is deprotonated at C-2 upon treatment with pyridine, followed by proton transfer and replacement of pyrrole with formation of the corresponding pyridine adduct **12**. The complexes **1**, **4** and **7** were characterized by X-ray diffraction.
(© Wiley-VCH Verlag GmbH & Co. KGaA, 69451 Weinheim, Germany, 2003)

Introduction

There are numerous examples showing that typical organic functional group chemistry can be carried out at the Cp ligands of many transition metals from the middle and the right-hand side of the Periodic Table.[1] This is much more difficult to achieve in the case of the Group-4 metallocenes (and the corresponding complexes of the oxophilic f-block elements). Functional group chemistry here is usually carried out at the stage of the free ligand. Usually the functionalized Cp ligands are then subsequently attached to the respective metal centre.[2,3] Introduction of functional groups at the Cp rings of Cp_2ZrCl_2, for example, or conversion of functional groups at the zirconocene Cp rings is much more difficult, and consequently only a limited number of examples of such chemistry has so far been described in the literature. Noteworthy examples include Mannich-type enamine coupling reactions[4] and photochemical [2+2] cycloadditions,[5] both producing novel variants of *ansa*-metallocenes. The olefin metathesis reaction has been used for intra- and intermolecular carbon coupling reactions at bent metallocenes.[6] Moreover, various types of borylation[7] and hydroboration reactions[8] have been shown to be compatible with the general chemical features of many Group-4 metallocene complexes and related systems. We have now used such a reaction to attach a highly electrophilic borane at a Cp side chain of an *ansa*-metallocene and to carry out Lewis acid promoted reactions at the boron centre in the direct vicinity of the mildly electrophilic Group-4 metal centre. A first example is described in this article. We hope that our findings may contribute to the eventual development of novel bifunctional transition metal/main group element systems well suited for selective organic reactions, that may otherwise be hard to achieve, within such specific frameworks.

Results and Discussion

We had previously shown that [(allyl-C_5H_4)Cp] zirconium dichloride complexes can be cleanly hydroborated at the pendant allyl group.[8] Piers recently showed that similar $HB(C_6F_5)_2$[9] additions at such systems were feasible.[10] Such hydroboration reactions at open, unbridged Group-4 metallocenes (and at some related "constrained geometry" Zr complexes[10]) provided the synthetic basis for this work. We have now extended these reactions to the allyl-substituted rigid *ansa*-metallocene dichloride complex **1**. In contrast to the previously employed unbridged bent metallocenes,[8,10] the system **1** is no longer conformationally flexible but has its pendant functional group oriented towards the (chemically active) front side of the bent metallocene wedge.

Complex **1** was prepared as recently described by us[11] by adaptation of established literature procedures.[12] The X-ray crystal structure analysis of **1** was carried out and described previously.[11]

Treatment of **1** with 9-BBN was carried out in toluene at room temperature. The reaction was rather slow and required overnight stirring to go to completion. The hydroborated product **2** was isolated as a solid in almost quantitative yield. Complex **2** contains a chiral *ansa*-metallocene backbone, and therefore shows a total of seven ^1H NMR

[a] Organisch-Chemisches Institut der Universität Münster, Corrensstr. 40, 48149 Münster, Germany
[‡] X-ray crystal structure analyses
Supporting information for this article is available on the WWW under http://www.eurjoc.org or from the author.

methine signals of the two substituted Cp-type ligands [δ = 6.61, 5.91, 5.54 (C_5H_3), 7.02, 6.92, 5.98, 5.82 (C_5H_4) ppm] and a 1:1 intensity pair of Si−CH_3 signals (δ = 0.72, 0.69 ppm). It also shows three distinct ^{1}H NMR multiplets for the connecting trimethylene bridging unit (δ = 2.69, 1.75, 1.40 ppm) and the signals of the BBN residue.

Single crystals suitable for the X-ray crystal structure determination of **2** were obtained from a dichloromethane solution at −30 °C. In the solid state, complex **2** has a rigid *ansa*-metallocene framework. Because of the geometric constraints in such a system the Zr−C(Cp) bond lengths vary from 2.443(3) to 2.596(3) Å inside the C_5H_3 unit and from 2.471(3) to 2.535(3) Å inside the Zr(C_5H_4) moiety. The smaller values are found at the narrow backside of the bent metallocene wedge oriented toward the $SiMe_2$ unit. The C1−Si and C8−Si bond lengths are 1.866(3) and 1.862(3) Å, respectively. These (sp^2)C−Si bonds are slightly longer than the adjacent (sp^3)C−Si linkages [C6−Si 1.846(4) Å, C7−Si 1.849(4) Å], which is an additional indication that the *ansa*-metallocene framework is strained. The C1−Si−C8 angle is found at 93.6(1)° and the Cp(centroid)−Zr−Cp(centroid) angle in **2** is 126.0°. The Cl1−Zr−Cl2 angle is in the normal range at 99.60(4)°.

The attached −$(CH_2)_3$−BBN side chain is pointing toward the open front side of the bent metallocene wedge [C11−C13 1.499(5) Å] and is arranged at a maximum extension such as to bring the bulky −BBN group away from the $ZrCl_2$ unit (see Figure 1). This extended conformational arrangement is characterized by the corresponding dihedral angles C12−C11−C13−C14 −85.0(4)°, C11−C13−C14−C15 −179.2(3)°, and C13−C14−C15−B −172.3(4)°.

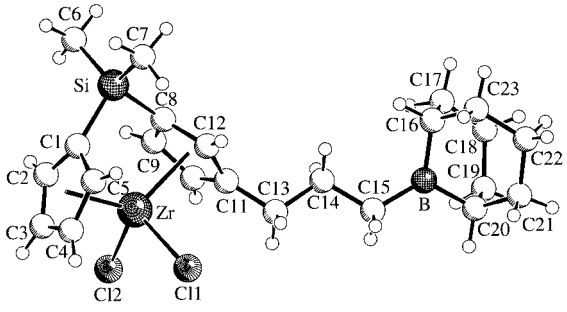

Figure 1. A view of the molecular geometry of complex **2**; selected bond lengths [Å] and angles (°): Zr−Cl1 2.431(1), Zr−Cl2 2.431(1), Si−C1 1.866(3), Si−C8 1.862(3), Si−C6 1.846(4), Si−C7 1.849(4), C11−C13 1.499(5), C13−C14 1.526(5), C14−C15 1.517(5), C15−B 1.555(6), B−C16 1.569(6), B−C20 1.566(6); Cl1−Zr−Cl2 99.60(4), C1−Si−C8 93.6(1), C1−Si−C6 112.6(2), C1−Si−C7 110.8(2), C8−Si−C6 112.7(2), C8−Si−C7 110.4(2), C6−Si−C7 114.8(2), C11−C13−C14 111.5(3), C13−C14−C15 113.6(3), C14−C15−B 118.3(3), C15−B−C16 126.3(4), C15−B−C20 122.5(4), C16−B−C20 111.1(4)

From its monomer/dimer equilibrium[9] the borane $HB(C_6F_5)_2$ (**3**) reacts much more rapidly with **1**. The hydroboration reaction was complete after ca. 30 min at room temperature in toluene solution, and the product **4** was isolated in a close to quantitative yield. It shows NMR spectroscopic features very similar to those of **2**, which let us assume that both complexes have similar structures. The chiral metallocene core shows a total of seven ^{1}H NMR methane signals, at δ = 6.56, 5.87, 5.47 (C_5H_3) and 7.00, 6.92, 5.96, 5.80 (C_5H_4) ppm. The ^{1}H NMR resonances of the trimethylene side chain of **4** occur at δ = 2.72, 1.96 and 1.80 ppm, with corresponding ^{13}C NMR features at δ = 32.3, 30.9 and 25.5 ppm. As would be expected, the pair of C_6F_5 groups at the boron atom behaves in symmetry-equivalent fashion in solution, producing a single set of *o*-, *p*- and *m*-^{19}F resonances at δ = −130.2, −148.6 and −160.8 ppm, respectively. The strongly electrophilic boron centre does not interact with the $ZrCl_2$ moiety in **4**. The ^{11}B NMR chemical shift of δ = 75.6 ppm ($\nu_{1/2} \approx 190$ Hz) indicates the presence of a coordinatively unsaturated tricoordinate boron centre [similarly to $B(C_6F_5)_3$:[13] δ(^{11}B) = 60.0 ($\nu_{1/2} \approx 400$ Hz); in contrast the dimeric $[HB(C_6F_5)_2]_2$ reagent features δ(^{11}B{^{1}H}) = 19.5 ($\nu_{1/2} \approx$ 320 Hz), as would be expected for a dimeric doubly H-bridged structure with two tetracoordinate boron atoms present].

Complex **4** reacts rapidly with a variety of two-electron donor ligands.[14] A typical product is the 2-methyl-4,5-dihydrooxazole adduct **6**, the molecular structure of which is depicted in Figure 2. Complex **6** was formed readily by treatment of **4** with the heterocyclic donor ligand in toluene solution at room temperature (see the Exp. Sect. for details). The attached trimethylene chain again adopts a fully extended "zigzag" conformation featuring a series of antiperiplanar conformational arrays [dihedral angles C11−C13−C14−C15 −175.4(2)°, C13−C14−C15−B −176.6(2)°]. This arrangement resembles the conformation of the side chain in **4** (see above and Figure 1), except that its torsional orientation relative to the adjacent Cp ring is quite different. In **4** (see above), the substituent chain is rotated *away* from the Cp plane, whereas in **6** it is rotated almost by 90° so that the w-shaped carbon skeleton of the side chain is now lying almost coplanar with its adjacent C8−C11 η^5-C_5H_4 ring [dihedral angle C10−C11−C13−C14 −25.8(3)°]. This brings the boron centre in the adduct **6** much closer to the zirconium atom (B···Zr separation in **6**: 6.395Å, in **2**: 7.621Å) and it brings the attached heterocycle almost in a direct opposition to the $ZrCl_2$ unit at the front side of the bent metallocene unit. The corresponding dihedral angles are −77.5(3)° (C14−C15−B−N1) and −2.8(4)° (C15−B−N1−C18). The bonding features of the dihydrooxazole heterocycle have not changed much upon complexation to the boron atom [N1−C16 1.277(3) Å, C16−O1 1.323(3) Å, N1−C18 1.507(4) Å].[15] The N1−B bond length is 1.626(4) Å, which is similar to the adjacent B−C bond lengths [B−C(aryl) 1.651(4) and 1.664(4) Å; B−C15 1.636(4) Å]. The N−B−C15 bond angle was found to be 110.1(2)°. The remaining bond angles at the boron atom were found to lie in a range between 105.0(2)° (N1−B−C31) and 114.0(2)° (C21−B−C31). With regard to their conformational orientation, the B−N vector is oriented almost coplanar with the C21−C26 aryl plane [dihedral angle C22−C21−B−N1 14.3(3)°] whereas it adopts a gauche orientation with the C31−C36 aryl ring [C32−C31−B−N1 −69.5(3)°].

 © 2003 Wiley-VCH Verlag GmbH & Co. KGaA, Weinheim

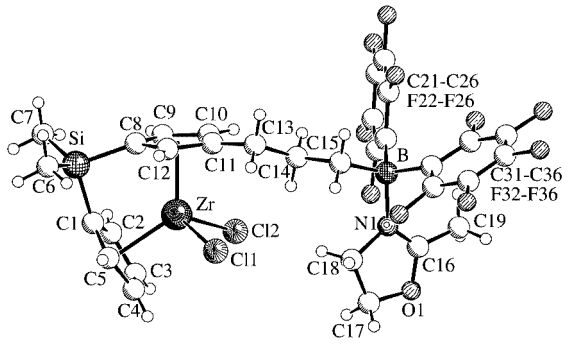

Figure 2. Molecular structure of the adduct **6**; selected bond lengths [Å] and angles [°]: Zr−Cl1 2.440(1), Zr−Cl2 2.445(1), Si−C1 1.868(2), Si−C8 1.877(2), Si−C6 1.847(3), Si−C7 1.846(3), C11−C13 1.501(3), C13−C14 1.527(3), C14−C15 1.528(3), C15−B 1.636(4), B−N1 1.626(4), B−C21 1.651(4), B−C31 1.664(4), N1−C16 1.277(3), N1−C18 1.507(4), C16−O1 1.323(3), C16−C19 1.467(4), O1−C17 1.451(4), C17−C18 1.491(4); Cl1−Zr−Cl2 95.56(3), C1−Si−C8 93.8(1), C1−Si−C6 110.9(1), C1−Si−C7 112.6(1), C8−Si−C6 112.7(1), C8−Si−C7 111.7(1), C6−Si−C7 113.5(1), C11−C13−C14 113.3(2), C13−C14−C15 114.1(2), C14−C15−B 115.8(2), C15−B−N1 110.1(2), C15−B−C21 106.4(2), C15−B−C31 110.1(2), N1−B−C21 111.2(2), N1−B−C31 105.0(2), C21−B−C31 114.0(2), B−N1−C16 128.9(2), B−N1−C18 123.4(2), C16−N1−C18 107.7(2), N1−C16−O1 116.5(3), N1−C16−C19 127.6(3), C19−C16−O1 115.9(2), C16−O1−C17 107.6(2), O1−C17−C18 105.3(2), C17−C18−N1 102.9(2)

We had previously shown that unstable tautomers of a variety of aromatic and heteroaromatic compounds can be formed and stabilized by coordination to the strong organometallic Lewis acid $B(C_6F_5)_3$. The first examples included the α-naphthol/benzocyclohexadienone tautomerism (see Scheme 1).[16] We have also formed the 2*H*-pyrrole tautomer from its parent hetarene in the $B(C_6F_5)_3$ coordination sphere by a three-step procedure involving deprotonation at the nitrogen atom, attachment at the boron atom, and then protonation at the carbon atom to yield the 2*H*-pyrrole/$B(C_6F_5)_3$ adduct **10**.[17] Resconi has recently found a direct route yielding examples of the compound type **10** by treatment of pyrrole derivatives with $B(C_6F_5)_3$.[18]

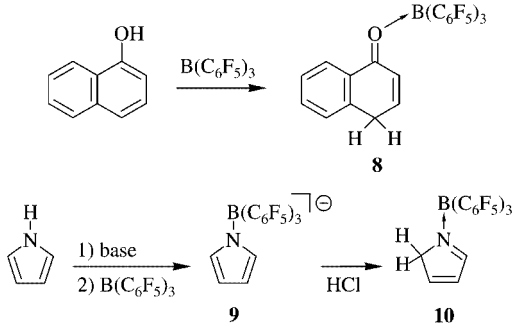

Scheme 1

We were able to carry out such a pyrrole/2*H*-pyrrole tautomerism reaction at the *ansa*-zirconocene−trimethylene−$B(C_6F_5)_2$ complex **7**. A mixture of **4** and pyrrole was stirred in toluene/diethyl ether solution at room temperature for 18 h. During this time a close to quantitative conversion of the hetarene took place, with formation of the 2*H*-pyrrole adduct **7**. The coordination of the "isopyrrole tautomer" to the boron atom was apparent from the characteristic NMR spectra. The 2*H*-pyrrole moiety gave rise to a set of three methine ^{1}H NMR signals, one at rather low field (δ = 7.65 ppm, −N=C*H*−), the other two at δ = 6.42 ppm (10-H, see Scheme 2) and 5.61 (11-H) [corresponding ^{13}C NMR signals at δ = 169.3 (−N=*C*H−), 127.1 (C-11), 154.2 ppm (C-10)]. The remaining $N-CH_2$ group gives rise to a characteristic AB pattern at δ = 3.72 and 3.68 ppm ($^2J_{H,H}$ = 27 Hz, ^{13}C signal at δ = 65.0 ppm). The diastereotopic splitting of the 9-H/H′ ^{1}H NMR resonance of the 2*H*-pyrrole moiety is due to the chirality of the metal complex backbone. This also becomes evident in **7** in the partial splitting of the 7-H/H′ (δ = 1.52/1.36) and 8-H/H′ (δ = 1.36/1.21) signals of the bridging trimethylene unit (6-H/H′ ^{1}H NMR resonance at δ = 2.83 ppm). As would be expected, a 1:1 intensity pair of $SiMe_2$ ^{1}H NMR methyl resonances is observed for **7** (δ = 0.14 and 0.08 ppm). The diastereotopic splitting is even extended into the $B(C_6F_5)_2$ unit. The two pentafluorophenyl groups at the tetravalent boron centre [δ(^{11}B) = 4.7, $\nu_{1/2} \approx 414$ Hz)] have become diastereotopic. Consequently, we observed equal intensity pairs of ^{19}F NMR signals of the *ortho*- (δ = −158.1 and −158.2 ppm) and *para*-C_6F_5 signals (δ = −132.6 and −132.9 ppm). The *meta*-C_6F_5 resonances of the two diastereotopic C_6F_5 ligands are isochronous (δ = −163.3 ppm).

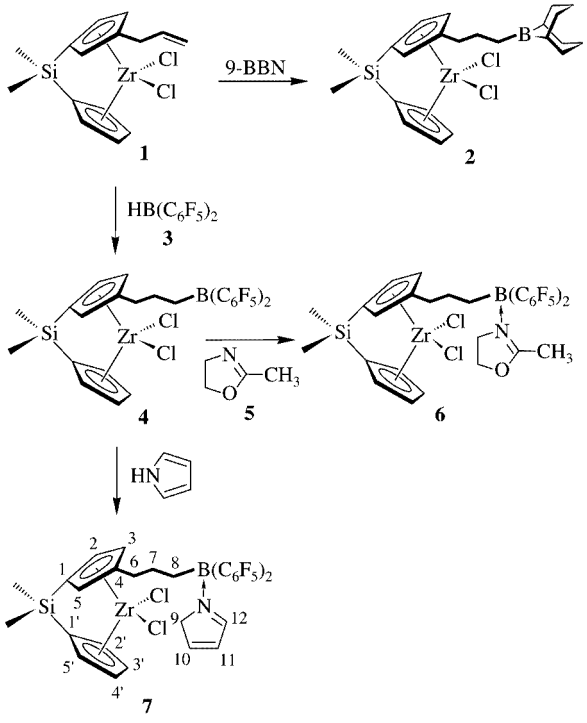

Scheme 2

Single crystals of **7** were obtained from a concentrated toluene solution at room temperature. The X-ray crystal

 © 2003 Wiley-VCH Verlag GmbH & Co. KGaA, Weinheim

structure analysis confirms the formation of the 2*H*-pyrrole unit. The C_4H_5N moiety shows a short N=C bond inside the heterocyclic ring system [see Figure 3, N1−C16 1.294(4) Å], whereas the adjacent N1−C19 linkage [1.462(4) Å] denotes the presence of a single bond. The remaining framework of the five-membered nitrogen heterocycle exhibits a typical bond alternation [C16−C17 1.443(5) Å, C17−C18 1.326(5) Å, C18−C19 1.474(4) Å]. The N1−B bond length amounts to 1.612(4) Å, and the N1−B−C15 bond angle is found at 107.9(2)°. The remaining bond angles at the boron atom are within a range of 103.3(2) to 116.1(2)°.

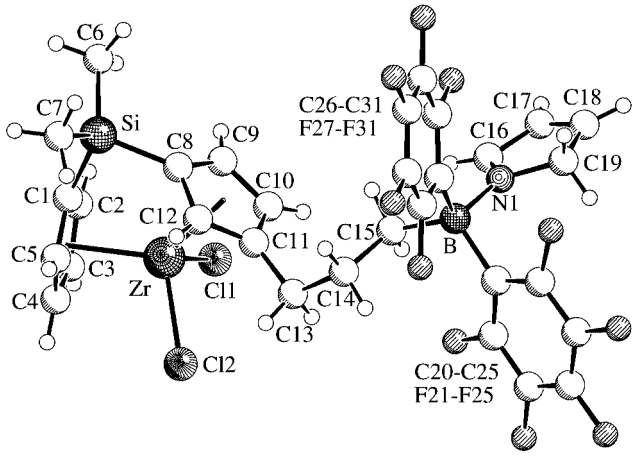

Figure 3. A projection of the molecular geometry of the 2*H*-pyrrole addition product **7**; selected bond lengths [Å] and angles [°]: Zr−Cl1 2.448(1), Zr−Cl2 2.414(1), Si−C1 1.877(3), Si−C8 1.875(3), Si−C6 1.845(4), Si−C7 1.857(4), C11−C13 1.506(4), C13−C14 1.541(4), C14−C15 1.531(4), C15−B 1.631(4), B−N1 1.612(4), B−C20 1.653(5), B−C26 1.651(4), N1−C16 1.294(4), N1−C19 1.462(4), C16−C17 1.443(5), C17−C18 1.326(5), C18−C19 1.474(4); Cl1−Zr−Cl2 98.76(4), C1−Si−C8 94.8(1), C1−Si−C6 112.5(2), C1−Si−C7 110.7(2), C8−Si−C6 110.6(2), C8−Si−C7 112.1(2), C6−Si−C7 114.5(2), C11−C13−C14 113.8(3), C13−C14−C15 113.1(3), C14−C15−B 115.9(2), C15−B−N1 107.9(2), C15−B−C20 116.1(2), C15−B−C26 108.4(2), N1−B−C20 103.3(2), N1−B−C26 108.8(2), C20−B−C26 112.0(2), B−N1−C16 126.9(3), B−N1−C19 125.3(2), C16−N1−C19 107.8(3), N1−C16−C17 111.8(3), C16−C17−C18 107.3(3), C17−C18−C19 108.7(3), C18−C19−N1 104.3(3)

The 2*H*-pyrrole unit is oriented in plane with the B1−C15 vector [dihedral angle C16−N1−B−C15 2.5(4)°]. The connecting trimethylene chain between the *ansa*-metallocene framework and the borate section of **7** adopts a conformation different from those of the two complexes **2** and **6** (see above). As can be seen from the projection of **7**, depicted in Figure 3, the $-(CH_2)_3-$ chain in **7** contains an additional gauche conformation [C11−C13−C14−C15 −63.0(4)°]. The C13−C14−C15−B1 arrangement is antiperiplanar [θ = −165.9(3)°] and the C10−C11−C13−C14 dihedral angle [84.1(4)°] removes the borate end away from the centre of the metallocene unit. Consequently, the Zr···B separation in **7** (6.837Å) is smaller than in **2** (7.621Å) but larger than in **6** (6.395Å).

The methylene hydrogen atoms of the previously prepared and studied 2*H*-pyrrole/$B(C_6F_5)_3$ adduct **10** are rather acidic. The system **10** has been used as a Brønsted acid activator component for generating homogeneous Ziegler−Natta catalyst systems.[17] The 2*H*-pyrrole methylene hydrogen atoms are also acidic. Treatment with pyridine as a base removed one of these hydrogen atoms. We assume that salt **11** may be formed as an intermediate, and may then have reacted further in an acid/base reaction to yield the stable adduct **12** and free pyrrole (see Scheme 3).

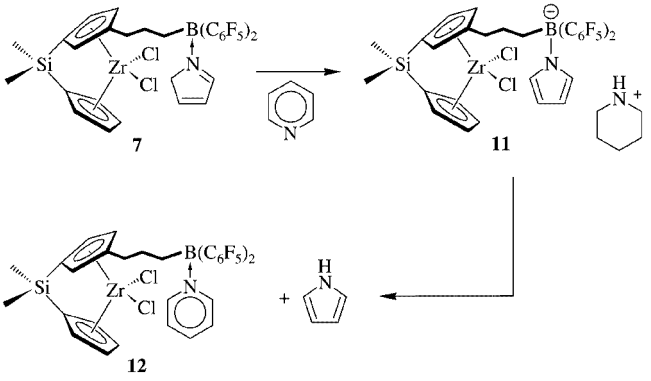

Scheme 3

We next intend to try to make use of the specific coordinative features of such main group element/transition metal combinations and to investigate whether the zirconocene units in adducts such as **6** or **7** can be activated to undergo, for example, C−H or C−C activation reactions with substrates attached at their neighbouring electrophilic borane centre.

Experimental Section

General: All reactions were carried out under dry argon in Schlenk-type glassware or in a glove-box. Solvents, including deuterated solvents used for NMR spectroscopy, were dried and distilled prior to use. For additional general conditions, including a list of instruments used for a physical characterization of the compounds see ref.[6] Most NMR assignments were secured by carrying out a variety of 2D NMR experiments.[19]

X-ray Crystal Structure Analyses: Data sets were collected with a Nonius KappaCCD diffractometer, equipped with a Nonius FR591 rotating anode generator. Programs used: data collection COLLECT (Nonius B.V., **1998**), data reduction Denzo-SMN,[20] absorption correction SORTAV,[21] structure solution SHELXS-97,[22] structure refinement SHELXL-97,[23] graphics SCHAKAL.[24] CCDC-202081 to -202083 contain the supplementary crystallographic data for this paper. These data can be obtained free of charge at www.ccdc.cam.ac.uk/conts/retrieving.html [or from the Cambridge Crystallographic Data Centre, 12 Union Road, Cambridge CB2 1EZ, UK; Fax: (internat.) + 44-1223/336-033; E-mail: deposit@ccdc.cam.ac.uk].

Preparation of the *ansa*-Zirconocene Dichloride Complex 1: Chilled toluene (250 mL, −78 °C) was added to a solid mixture of the reagent $[Me_2Si(3\text{-}C_5H_3CH_2CH{=}CH_2)(C_5H_4)Li_2]$ (3.47 g, 14.5 mmol) and $ZrCl_4$ (3.37 g, 14.5 mmol). The suspension immediately became yellow. It was allowed to warm to room temperature with stirring. After stirring overnight, the yellow suspension was filtered through Celite. Removal of the volatiles in vacuo pro-

vided the product (3.23 g, 57%) as a yellow solid. M.p. 104 °C. ^{1}H NMR ($CDCl_3$, 600 MHz): δ = 7.03 (m, 1 H, 4′-H), 6.93 (m, 1 H, 3′-H), 6.60 (m, 1 H, 3-H), 5.98 (m, 1 H, 2′-H), 5.92 (m, 3 H, 2-H, 7-H), 5.82 (m, 1 H, 5′-H), 5.54 (m, 1 H, 5-H), 5.06, 5.04 (each m, each 1 H, 8-H, 8-H′), 3.47, 3.38 (each m, each 1 H, 6-H, 6-H′), 0.72, 0.69 [each s, each 3 H, $Si(CH_3)_2$] ppm. $^{13}C\{^1H\}$ NMR ($CDCl_3$, 150 MHz): δ = 141.0 (C-4), 135.9 (C-7), 128.0 (C-3), 127.8 (C-3′), 127.7 (C-4′), 116.7 (C-8), 115.3 (C-2), 114.1 (C-2′), 113.6 (C-5′), 113.5 (C-5), 107.9 (C-1), 107.8 (C-1′), 34.3 (C-6), −5.1, −5.3 [$Si(CH_3)_2$] ppm. $C_{15}H_{18}Cl_2SiZr$ (388.5): calcd. C 46.37, H 4.67; found C 46.26, H 4.70.

Treatment of Complex 1 with 9-BBN; Preparation of Complex 2: 9-BBN (95 mg, 78.0 mmol) and **1** (302 mg, 78.0 mmol) were combined in a flask, and toluene (20 mL) was added at room temperature. The reaction mixture was stirred for 12 h. The solvent was removed in vacuo, which provided the product (381 mg, 97%) as a light yellow solid. Crystals suitable for an X-ray crystal structure analysis were obtained from a concentrated solution in dichloromethane at −30 °C. M.p. 155 °C. ^{1}H NMR ($CDCl_3$, 600 MHz): δ = 7.02 (m, 1 H, 4′-H), 6.92 (m, 1 H, 3′-H), 6.61 (m, 1 H, 3-H), 5.98 (m, 1 H, 2′-H), 5.91 (m, 1 H, 2-H), 5.82 (m, 1 H, 5′-H), 5.54 (m, 1 H, 5-H), 2.69 (m, 2 H, 6-H), 1.81, 1.64 (each m, each 4 H, 10-H), 1.81, 1.18 (each m, each 2 H, 11-H), 1.75 (m, 2 H, 7-H), 1.64 (m, 2 H, 9-H), 1.40 (t, $^3J_{H,H}$ = 7.8 Hz, 2 H, 8-H), 0.72, 0.69 [each s, each 3 H, $Si(CH_3)_2$] ppm. $^{13}C\{^1H\}$ NMR ($CDCl_3$, 150 MHz): δ = 143.9 (C-4), 127.9 (C-3), 127.7 (C-3′), 127.5 (C-4′), 115.2 (C-2), 113.9 (C-2′), 113.7 (C-5), 113.6 (C-5′), 107.6 (C-1), 107.5 (C-1′), 33.1 (C-6), 33.1 (C-10), 31.0 (br., C-9), 27.9 (br., C-8), 25.4 (C-7), 23.2 (C-11), −5.1, −5.2 [$Si(CH_3)_2$] ppm. $^{11}B\{^1H\}$ NMR ($CDCl_3$, 64 MHz): δ = 86.8 ($\nu_{1/2}$ = 320 Hz) ppm. $C_{23}H_{33}BCl_2SiZr$ (510.5): calcd. C 54.11, H 6.52; found C 53.09, H 6.54.

X-ray Crystal Structure Analysis of 2: Empirical formula $C_{23}H_{33}BCl_2SiZr$, M = 510.51, colourless crystal 0.40 × 0.25 × 0.05 mm, a = 8.175(1), b = 26.251(1), c = 11.251(1) Å, β = 98.13(1)°, V = 2390.2(4) Å^3, $\rho_{calcd.}$ = 1.419 g cm^{-3}, μ = 7.41 cm^{-1}, empirical absorption correction (0.756 ≤ T ≤ 0.964), Z = 4, monoclinic, space group $P2_1/n$ (no. 14), λ = 0.71073 Å, T = 198 K, ω and φ scans, 9625 reflections collected (±h, ±k, ±l), [(sinθ)/λ] = 0.65 Å^{-1}, 5428 independent (R_{int} = 0.028) and 4617 observed reflections [$I \geq 2\ \sigma(I)$], 255 refined parameters, R = 0.045, wR^2 = 0.105, max. residual electron density 1.27 (−0.68) e·Å^{-3} close to the $ZrCl_2$ core, hydrogen atoms calculated and refined as riding atoms.

Treatment of Complex 1 with $HB(C_6F_5)_2$ (3); Preparation of Complex 4: Bis(pentafluorophenyl)borane (254 mg, 73.0 mmol) and **1** (285 mg, 73.0 mmol) were combined in a flask, and toluene (50 mL) was transferred into the flask at 0 °C. The reaction mixture was stirred while being allowed to warm to room temperature, and the volatiles were removed in vacuo, resulting in the product (524 mg, 97%) as a light yellow solid. M.p. 142 °C. ^{1}H NMR ($CDCl_3$, 600 MHz): δ = 7.00 (m, 1 H, 4′-H), 6.92 (m, 1 H, 3′-H), 6.56 (m, 1 H, 3-H), 5.96 (m, 1 H, 2′-H), 5.87 (m, 1 H, 2-H), 5.80 (m, 1 H, 5′-H), 5.47 (m, 1 H, 5-H), 2.72 (m, 2 H, 6-H), 1.96 (m, 2 H, 7-H), 1.80 (m, 2 H, 8-H), 0.72, 0.66 [each s, each 3 H, $Si(CH_3)_2$] ppm. $^{13}C\{^1H\}$ NMR ($CDCl_3$, 150 MHz): δ = 146.8 (dm, $^1J_{C,F}$ = 246.1 Hz), 143.4 (dm, $^1J_{C,F}$ = 249.7 Hz), 137.4 (dm, $^1J_{C,F}$ = 258.0 Hz) (*o*-, *p*-, *m*-C_6F_5), 142.1 (C-4), 128.2 (C-3′), 127.8 (C-3), 126.9 (C-4′), 114.9 (C-2), 114.3 (C-5′), 113.8 (C-2′), 113.6 (C-5), 107.7 (C-1), 107.6 (C-1′), 32.3 (C-6), 30.9 (C-7), 25.5 (C-8), −5.6, −5.7 [$Si(CH_3)_2$] ppm. $^{11}B\{^1H\}$ NMR ($CDCl_3$, 64 MHz): δ = 75.6 ($\nu_{1/2}$ = 190 Hz). ^{19}F NMR ($CDCl_3$, 564 MHz): δ = −130.2 (m, *o*-C_6F_5), −148.6 (m, *p*-C_6F_5), −160.8 (m, *m*-C_6F_5) ppm. $C_{27}H_{19}BCl_2F_{10}SiZr$ (734.5): calcd. C 44.15, H 2.61; found C 43.23, H 2.56.

Treatment of 4 with 2-Methyl-4,5-dihydrooxazole; Formation of the Dihydrooxazole Adduct 6: A solution of 2-methyl-4,5-dihydrooxazole (9 mg, 104.8 mmol) in toluene (20 mL) was added at room temperature to a light yellow solution of **4** (77 mg, 104.8 mmol) in toluene (20 mL) and the mixture was stirred for 0.5 h. Removal of the volatiles in vacuo provided the product (85 mg, 99%) as a light yellow solid. Crystals suitable for an X-ray crystal structure analysis were obtained from a concentrated solution in benzene at room temperature. ^{1}H NMR (C_7D_8, 600 MHz): δ = 6.68 (m, 1 H, 4′-H), 6.67 (m, 1 H, 3′-H), 6.50 (m, 1 H, 3-H), 5.38 (m, 1 H, 2′-H), 5.37 (m, 1 H, 2-H), 5.33 (m, 1 H, 5′-H), 5.15 (m, 1 H, 5-H), 3.45/3.39 (each m, each 1 H, dihydrooxazole-CH_2), 3.38/3.26 (each m, each 1 H, dihydrooxazole-CH_2), 2.80/2.75 (each m, each 1 H, 6-H, 6-H′), 1.43/1.29 (each m, each 1 H, 7-H, 7-H′), 1.37/1.12 (each m, each 1 H, 8-H, 8-H′), 1.36 (s, 3 H, dihydrooxazole-CH_3), 0.13/0.06 [each s, each 3 H, $Si(CH_3)_2$] ppm. $^{13}C\{^1H\}$ NMR (C_7D_8, 150 MHz): δ = 174.4 (dihydrooxazole-C), 142.5 (C-4), 129.2 (C-3′), 128.4 (C-3), 125.8 (C-4′), 114.7 (C-5′), 114.6 (C-5), 113.6 (C-2), 112.4 (C-2′), 107.8 (C-1′), 107.2 (C-1), 67.9/51.3 (dihydrooxazole-CH_2), 33.1 (C-6), 26.9 (C-7), 22.9 (C-8), 13.1 (dihydrooxazole-CH_3), −5.7, −6.4 [$Si(CH_3)_2$]; 148.5 ($^1J_{C,F}$ = 239.7 Hz), 139.7 ($^1J_{C,F}$ = 240.6 Hz), 137.6 ($^1J_{C,F}$ = 253.9 Hz), 120.6 (*o*-, *p*-, *m*-, *ipso*-C_6F_5) ppm. $^{11}B\{^1H\}$ NMR (C_7D_8, 64 MHz): δ = −5.0 ($\nu_{1/2}$ = 290 Hz) ppm. ^{19}F NMR (C_7D_8, 564 MHz): δ = −133.2/−133.7 (each m, each 2 F, *o*-C_6F_5), −158.1/−158.4 (each t, each 1 F, $^3J_{FF}$ = 20.6/20.8 Hz, *p*-C_6F_5), −163.4/−163.5 (each m, each 2 F, *m*-C_6F_5) ppm. $C_{31}H_{26}BCl_2F_{10}NOSiZr$ (819.6): calcd. C 45.43, H 3.20, N 1.71; found C 45.15, H 3.05, N 1.65.

X-ray Crystal Structure Analysis of 6: Empirical formula $C_{31}H_{26}BCl_2F_{10}NOSiZr{\cdot}1/2C_6H_6$, M = 858.60, colourless crystal 0.30 × 0.15 × 0.10 mm, a = 8.017(1), b = 11.120(1), c = 20.434(1) Å, α = 87.13(1), β = 84.78(1), γ = 81.23(1)°, V = 1791.7(3) Å^3, $\rho_{calcd.}$ = 1.592 g cm^{-3}, μ = 5.71 cm^{-1}, empirical absorption correction (0.847 ≤ T ≤ 0.945), Z = 2, triclinic, space group $P\bar{1}$ (no. 2), λ = 0.71073 Å, T = 198 K, ω and φ scans, 10918 reflections collected (±h, ±k, ±l), [(sinθ)/λ] = 0.65 Å^{-1}, 7958 independent (R_{int} = 0.017) and 6149 observed reflections [$I \geq 2\ \sigma(I)$], 463 refined parameters, R = 0.037, wR^2 = 0.083, max. residual electron density 0.38 (−0.40) e·Å^{-3}, hydrogen atoms calculated and refined as riding atoms.

Treatment of 4 with Pyrrole; Formation of the 2*H*-Pyrrole Adduct 7: A solution of pyrrole (37 mg, 0.54 mmol) in toluene (10 mL) was added at room temperature to a light yellow solution of **4** (406 mg, 0.51 mmol) in toluene/diethyl ether (10:1, 20 mL), and the mixture was stirred for 18 h. Removal of the volatiles in vacuo provided the product (407 mg, 99%) as a light yellow solid. Crystals suitable for an X-ray crystal structure analysis were obtained from a concentrated solution in toluene at room temperature. ^{1}H NMR (C_7D_8, 600 MHz): δ = 7.65 (br. s, 1 H, 12-H), 6.72 (m, 1 H, 4′-H), 6.66 (m, 1 H, 3′-H), 6.48 (m, 1 H, 3-H), 6.42 (dq, $^3J_{10\text{-}H,11\text{-}H}$ = 5.5, $^4J_{10\text{-}H,12\text{-}H}$ = 0.9 Hz, 1 H, 10-H), 5.61 (dq, $^3J_{10\text{-}H,11\text{-}H}$ = 5.5, $^3J_{11\text{-}H,12\text{-}H}$ = 1.1, $^4J_{9\text{-}H,11\text{-}H}$ = 1.3 Hz, 1 H, 11-H), 5.43 (m, 1 H, 2′-H), 5.38 (m, 1 H, 2-H), 5.32 (m, 1 H, 5′-H), 5.17 (m, 1 H, 5-H), 3.72/3.68 (AB, $^2J_{H,H}$ = 26.7 Hz, each 1 H, 9-H, 9-H′), 2.83 (m, 2 H, 6-H, 6-H′), 1.52/1.36 (each m, each 1 H, 7-H, 7-H′), 1.36/1.21 (each m, each 1 H, 8-H, 8-H′), 0.14/0.08 [each s, each 3 H, $Si(CH_3)_2$] ppm. $^{13}C\{^1H\}$ NMR (C_7D_8, 150 MHz): δ = 169.3 (C-12), 154.2 (C-10), 143.1 (C-4), 128.7 (C-3′), 128.6 (C-3), 127.1 (C-11), 125.6 (C-4′), 114.2 (C-2), 114.0 (C-5), 114.0 (C-5′), 113.1 (C-

 © 2003 Wiley-VCH Verlag GmbH & Co. KGaA, Weinheim

2′), 107.8 (C-1′), 107.4 (C-1), 65.0 (C-9), 33.4 (C-6), 27.0 (C-7), 24.2 (C-8), −6.8, −5.9 [Si(CH_3)$_2$]; 148.4 ($^1J_{C,F}$ = 240.0 Hz), 139.8 ($^1J_{C,F}$ = 248.6 Hz), 137.6 ($^1J_{C,F}$ = 250.3 Hz), 121.4 (*o*-, *p*-, *m*-, *ipso*-C_6F_5) ppm. $^{11}B\{^1H\}$ NMR (C_7D_8, 64 MHz): δ = 4.7 ($\nu_{1/2}$ = 415 Hz) ppm. ^{19}F NMR (C_7D_8, 564 MHz): δ = −132.6/−132.9 (each m, each 2 F, *o*-C_6F_5), −158.1/−158.2 (each t, each 1 F, $^3J_{FF}$ = 21.0/20.6 Hz, *p*-C_6F_5), −163.3 (m, 4 F, *m*-C_6F_5) ppm. $C_{31}H_{24}BCl_2F_{10}NSiZr$ (801.5): calcd. C 46.45, H 3.02, N 1.75; found C 46.84, H 3.30, N 1.40.

X-ray Crystal Structure Analysis of 7: Empirical formula $C_{31}H_{24}BCl_2F_{10}NSiZr{\cdot}C_7H_8$, M = 893.67, light yellow crystal 0.30 × 0.20 × 0.20 mm, a = 10.371(1), b = 14.683(1), c = 15.239(1) Å, α = 115.75(1), β = 96.40(1), γ = 107.10(1)°, V = 1919.0(3) Å^3, $\rho_{calcd.}$ = 1.547 g cm^{-3}, μ = 5.35 cm^{-1}, empirical absorption correction (0.856 ≤ T ≤ 0.901), Z = 2, triclinic, space group $P\bar{1}$ (no. 2), λ = 0.71073 Å, T = 198 K, ω and φ scans, 21470 reflections collected (±h, ±k, ±l), [(sinθ)/λ] = 0.66 Å^{-1}, 9013 independent (R_{int} = 0.039) and 7127 observed reflections [$I \geq 2\,\sigma(I)$], 490 refined parameters, R = 0.048, wR^2 = 0.109, max. residual electron density 1.38 (−0.70) e·Å^{-3} close to the solvate molecule, hydrogen atoms calculated and refined as riding atoms.

Treatment of 7 with Pyridine; Formation of the Pyridine Adduct 12: A solution of pyridine (7.6 mg, 96 mmol) in toluene (20 mL) was added at room temperature to a light yellow solution of **7** (77 mg, 96 mmol) in toluene (20 mL), and the mixture was stirred for 2 h. Removal of the volatiles in vacuo provided the product (77 mg, 99%) as a light yellow solid. ^1H NMR (C_7D_8, 600 MHz): δ = 8.13 (d, $^3J_{H,H}$ = 5.8 Hz, 2 H, 9-H), 6.73 (m, 1 H, 11-H), 6.72 (m, 1 H, 4′-H), 6.66 (m, 1 H, 3′-H), 6.45 (m, 2 H, 10-H), 6.44 (m, 1 H, 3-H), 5.42 (m, 1 H, 2′-H), 5.38 (m, 1 H, 2-H), 5.32 (m, 1 H, 5′-H), 5.16 (m, 1 H, 5-H), 2.84 (t, $^3J_{H,H}$ = 5.8 Hz, 2 H, 6-H, 6-H′), 1.62/1.42 (each m, each 1 H, 8-H, 8-H′), 1.50/1.26 (each m, each 1 H, 7-H, 7-H′), 0.12/0.08 [each s, each 3 H, Si(CH_3)$_2$] ppm. $^{13}C\{^1H\}$ NMR (C_7D_8, 150 MHz): δ = 145.4 (C-9), 143.0 (C-4), 140.5 (C-11), 128.2 (C-3′), 128.1 (C-3), 126.5 (C-4′), 125.3 (C-10), 114.3 (C-2), 113.8 (C-5), 113.7 (C-5′), 113.0 (C-2′), 107.7 (C-1′), 107.3 (C-1), 33.7 (C-6), 27.1 (C-7), 24.2 (C-8), −5.8, −6.3 [Si(CH_3)$_2$]; 148.6 ($^1J_{C,F}$ = 241.4 Hz), 140.0 ($^1J_{C,F}$ = 249.6 Hz), 137.7 ($^1J_{C,F}$ = 249.7 Hz), 120.9 (*o*-, *p*-, *m*-, *ipso*-C_6F_5) ppm. $^{11}B\{^1H\}$ NMR (C_7D_8, 64 MHz): δ = −0.6 ($\nu_{1/2}$ = 335 Hz) ppm. ^{19}F NMR (C_7D_8, 564 MHz): δ = −131.6 (m, 4 F, *o*-C_6F_5), −157.5/−157.7 (each t, each 1 F, $^3J_{FF}$ = 20.5/20.6 Hz, *p*-C_6F_5), −163.1/−163.3 (each m, each 2 F, *m*-C_6F_5) ppm. $C_{32}H_{24}NBCl_2F_{10}SiZr$ (813.6): calcd. C 47.24, H 2.97, N 1.72; found C 46.88, H 2.88, N 1.62.

Supporting Information: See footnote on the first page of this article. Details of the NMR spectroscopic characterization of the compounds **1**, **2**, **4**, **6**, **7** and **12**.

Acknowledgments

Financial support from the Fonds der Chemischen Industrie and the Deutsche Forschungsgemeinschaft (SPP 1118) is gratefully acknowledged.

[1] M. Rosenblum, R. B. Woodward, *J. Am. Chem. Soc.* **1958**, *80*, 5443−5449; S. G. Davies, M. L. H. Green, D. M. P. Mingos, *Tetrahedron* **1978**, *34*, 3047−3077; A. Togni, T. Hayashi (Eds.), *Ferrocenes: Homogeneous Catalysis, Organic Synthesis, Materials Science*, VCH, Weinheim, **1995**.

[2] K. Hafner, G. Schulz, K. Wagner, *Justus Liebigs Ann. Chem.* **1964**, *678*, 39−53; M. F. Lappert, C. J. Pickett, P. I. Riley, P. I. W. Yarrow, *J. Chem. Soc., Dalton Trans.* **1981**, 805−813; W. P. Hart, D. Shihua, M. D. Rausch, *J. Organomet. Chem.* **1985**, *282*, 111−121; M. D. Rausch, J. F Lewison, W. P. Hart, *J. Organomet. Chem.* **1988**, *358*, 161−168; S. S. Jones, M. D. Rausch, T. E. Bitterwolf, *J. Organomet. Chem.* **1990**, *396*, 279−287; M. Ogasa, D. T. Malin, D. W. Macomber, M. D. Rausch, R. D. Rogers, A. N. Rollins, *J. Organomet. Chem.* **1991**, *405*, 41−52; S. S. Jones, M. D. Rausch, R. Bitterwolf, *J. Organomet. Chem.* **1993**, *450*, 27−31; C. Müller, P. Jutzi, *Synthesis* **2000**, *3*, 389−394; C. Müller, D. Lilge, M. O. Kristen, P. Jutzi, *Angew. Chem.* **2000**, *112*, 800−803; *Angew. Chem. Int. Ed.* **2000**, *39*, 789−792.

[3] M. Bochmann, S. J. Lancaster, O. B. Robinson, *J. Chem. Soc., Chem. Commun.* **1995**, 2081−2082; R. Duchateau, S. J. Lancaster, M. Thornton-Pett, M. Bochmann, *Organometallics* **1997**, *16*, 4995−5005; S. J. Lancaster, M. Thornton-Pett, D. M. Dawson, M. Bochmann, *Organometallics* **1998**, *17*, 3829−3831; D. Hüerländer, R. Fröhlich, G. Erker, *J. Chem. Soc., Dalton Trans.* **2002**, 1513−1520.

[4] S. Knüppel, G. Erker, R. Fröhlich, *Angew. Chem.* **1999**, *111*, 2048−2051; *Angew. Chem. Int. Ed.* **1999**, *38*, 1923−1926; S. D. Bai, X. H. Wei, J. P. Guo, D. S. Liu, Z. Y. Zhou, *Angew. Chem.* **1999**, *111*, 2051−2054; *Angew. Chem. Int. Ed.* **1999**, *38*, 1926−1928; P. Liptau, S. Knüppel, G. Kehr, O. Kataeva, R. Fröhlich, G. Erker, *J. Organomet. Chem.* **2001**, *637−639*, 621−630.

[5] G. Erker, S. Wilker, C. Krüger, R. Goddard, *J. Am. Chem. Soc.* **1992**, *114*, 10983−10984; G. Erker, S. Wilker, C. Krüger, M. Nolte, *Organometallics* **1993**, *12*, 2140−2151.

[6] D. Hüerländer, N. Kleigrewe, G. Kehr, G. Erker, R. Fröhlich, *Eur. J. Inorg. Chem.* **2002**, 2633−2642; M. Ogasawara, T. Nagano, T. Hayashi, *J. Am. Chem. Soc.* **2002**, *124*, 9068−9069.

[7] J. Ruwwe, G. Erker, R. Fröhlich, *Angew. Chem.* **1996**, *108*, 108−110; *Angew. Chem. Int. Ed. Engl.* **1996**, *35*, 80−82; H. Braunschweig, C. von Koblinski, U. Englert, *Chem. Commun.* **2000**, *12*, 1049−1050.

[8] G. Erker, R. Aul, *Chem. Ber.* **1991**, *124*, 1301−1310.

[9] D. J. Parks, R. E. v. H. Spence, W. E. Piers, *Angew. Chem.* **1995**, *107*, 895−897; *Angew. Chem. Int. Ed. Engl.* **1995**, *34*, 809−811; R. E. v. H. Spence, D. J. Parks, W. E. Piers, M. A. MacDonald, M. J. Zaworotko, S. J. Rettig, *Angew. Chem.* **1995**, *107*, 1337−1340; *Angew. Chem. Int. Ed. Engl.* **1995**, *34*, 1230−1233; Y. Sun, W. E. Piers, S. J. Rettig, *Organometallics* **1996**, *15*, 4110−4112; Y. Sun, R. E. v. H. Spence, W. E. Piers, M. Parvez, G. P. A. Yap, *J. Am. Chem. Soc.* **1997**, *119*, 5132−5143; W. E. Piers, T. Chivers, *Chem. Soc., Rev.* **1997**, *26*, 345−354; D. J. Parks, W. E. Piers, G. P. A. Yap, *Organometallics* **1998**, *17*, 5492−5503; L. W. M. Lawrence, W. E. Piers, M. Parvez, S. J. Rettig, V. G. A. Young Jr., *Organometallics* **1999**, *18*, 3904−3912.

[10] R. E. v. H. Spence, W. E. Piers, *Organometallics* **1995**, *14*, 4617−4624.

[11] J. Cano Sierra, D. Hüerländer, M. Hill, G. Kehr, G. Erker, R. Fröhlich, *Chem. Eur. J.*, in press.

[12] G. M. Diamond, R. F. Jordan, J. L. Petersen, *Organometallics* **1996**, *15*, 4045−4053; and references cited therein.

[13] A. G. Massey, A. J. Park, F. G. A. Stone, *Proc. Chem. Soc., London* **1963**, 212; A. G. Massey, A. J. Park, *J. Organomet. Chem.* **1964**, *2*, 245−248; A. G. Massey, A. J. Park, in *Organometallic Synthesis*, vol. 3 (Eds: R. B. King, J. J. Eisch), Elsevier, New York, **1986**, p. 461.

[14] D. J. Parks, W. E. Piers, M. Parvez, R. Atencio, M. J. Zaworotko, *Organometallics* **1998**, *17*, 1369−1377; S. Döring, G. Erker, R. Fröhlich, O. Meyer, K. Bergander, *Organometallics* **1998**, *17*, 2183−2187; H. Jacobsen, H. Berke, S. Döring, G. Kehr, G. Erker, R. Fröhlich, O. Meyer, *Organometallics* **1999**,

 © 2003 Wiley-VCH Verlag GmbH & Co. KGaA, Weinheim

18, 1724−1735; J. M. Blackwell, W. E. Piers, M. Parvez, R. McDonald, *Organometallics* **2002**, *21*, 1400−1407.
[15] F. H. Allen, O. Kennard, D. G. Watson, L. Brammer, A. G. Orpen, R. Taylor, *J. Chem. Soc., Perkin Trans. 2* **1987**, S1−S19.
[16] D. Vagedes, R. Fröhlich, G. Erker, *Angew. Chem.* **1999**, *111*, 3561−3565; *Angew. Chem. Int. Ed.* **1999**, *38*, 3362−3365.
[17] G. Kehr, R. Fröhlich, B. Wibbeling, G. Erker, *Chem. Eur. J.* **2000**, *6*, 258−266.
[18] L. Resconi, personal communication.
[19] S. Braun, H. O. Kalinowski, S. Berger, *150 and More Basic NMR Experiments*, VCH, Weinheim, **1995**, and references cited therein.
[20] Z. Otwinowski, W. Minor, *Methods Enzymol.* **1997**, *276*, 307−326.
[21] R. H. Blessing, *Acta Crystallogr., Sect. A* **1995**, *51*, 33−37; R. H. Blessing, *J. Appl. Crystallogr.* **1997**, *30*, 421−426.
[22] G. M. Sheldrick, *Acta Crystallogr., Sect. A* **1990**, *46*, 467−473.
[23] G. M. Sheldrick, Universität Göttingen, **1997**.
[24] E. Keller, Universität Freiburg, **1997**.

Received January 30, 2003
Early View Article
Published Online August 14, 2003

 © 2003 Wiley-VCH Verlag GmbH & Co. KGaA, Weinheim

Preparation of Optically Active α-Amino[3]ferrocenophanes − Building Blocks for Chelate Ligands in Asymmetric Catalysis

Patrick Liptau,[a] Ludger Tebben,[a] Gerald Kehr,[a] Birgit Wibbeling,[a][‡] Roland Fröhlich,[a][‡] and Gerhard Erker*[a]

Keywords: Ferrocenes / Ferrocenophanes / Chelate ligands

Treatment of 1,1′-diacetylferrocene (**4**) with dimethylamine and $TiCl_4$ yielded the unsaturated dimethylamino-substituted [3]ferrocenophane product **5**. Its catalytic hydrogenation gave the corresponding saturated [3]ferrocenophane system **6** (*trans*/*cis* ≈ 7:1). The *rac*-[3]ferrocenophane amine **6** was partially resolved (to ca. 80% *ee*) by means of L- or D-*O*,*O*′-dibenzoyltartrate salt formation. Treatment of **4** with the pure (*R*)- or (*S*)-methyl(1-phenylethyl)amine (**8**)/$TiCl_4$ gave the corresponding optically active unsaturated [3]ferrocenophane amines (*R*)-(+)-**9** and (*S*)-(−)-**9**, respectively. Their catalytic hydrogenation again proceeded *trans*-selectively, giving the corresponding saturated diastereomeric [3]ferrocenophane amines (1*R*,3*R*,5*R*)-**10a** and (1*S*,3*S*,5*R*)-**10b** [starting from (*R*)-**9**], their enantiomers *ent*-**10a** and *ent*-**10b** were obtained from (*S*)-**9**, but with a poor asymmetric induction (**10a**/**10b** < 2:1). Quaternization of **6** (CH_3I) followed by amine exchange using (*R*)- or (*S*)-methyl(1-phenylethyl)-amine (**8**), respectively, proceeded with overall retention. Subsequent chromatographic separation gave the pure diastereoisomers (1*R*,3*R*,5*R*)-**10a** and (1*S*,3*S*,5*R*)-**10b** [from (*R*)-**8**, *ent*-**10a** and *ent*-**10b** from (*S*)-**8**] in > 60% yield. Subsequently, the benzylic (1-phenylethyl) auxiliary was removed from the nitrogen atom by catalytic hydrogenolysis to yield the enantiomerically pure (> 98%) ([3]ferrocenophanyl)-methylamines (1*R*,3*R*)-**11** and (1*S*,3*S*)-**11**, respectively, which were converted into the corresponding dimethylamino-substituted [3]ferrocenophanes (1*R*,3*R*)-**6** and (1*S*,3*S*)-**6**. Each enantiomer from the following enantiomeric pairs was isolated in its pure form and characterized by X-ray diffraction: (*R*)-**9**/(*S*)-**9**; (1*R*,3*R*,5*R*)-**10a**/(1*S*,3*S*,5*S*)-**10a**; (1*R*,3*R*,5*S*)-**10b**/(1*S*,3*S*,5*R*)-**10b**; (1*R*,3*R*)-**11**/(1*S*,3*S*)-**11**.

(© Wiley-VCH Verlag GmbH & Co. KGaA, 69451 Weinheim, Germany, 2003)

Introduction

Ferrocene-derived chelate ligands have found significant use in asymmetric catalysis.[1] A prime example is the "*Josiphos*" ligand (**1**) which has served as a very useful ligand especially in asymmetric hydrogenation.[2] Many variations of this ligand type have become known. Among them the [3]ferrocenophane systems may eventually find some specific use because of their very rigid framework. Based on early work by the Dijon group,[3] Weissensteiner et al. have developed synthetic pathways to optically active chelate bis(phosphanyl)[3]ferrocenophanes, such as **2**.[4,5] We had recently found an interesting complementary synthetic entry into such functionalized [3]ferrocenophane ligand systems that was based on the very readily available 1,1′-diacetylferrocene[6] (**4**) starting material. Treatment of **4** with e.g. dimethylamine in the presence of titanium tetrachloride probably gave the corresponding enamine[7] that was, however, not stable under the applied reaction conditions. It underwent an intramolecular Mannich-type condensation reaction to yield the unsaturated [3]ferrocenophane system **5**[8,9] (see Scheme 1). Subsequent (heterogeneous) catalytic hydrogenation in the presence of Pd/C gave a ca. 7:1 mixture of *trans*-**6**/*cis*-**6**. The major product of this surprisingly high *trans*-selective reduction (*trans*-**5**) was obtained in its pure

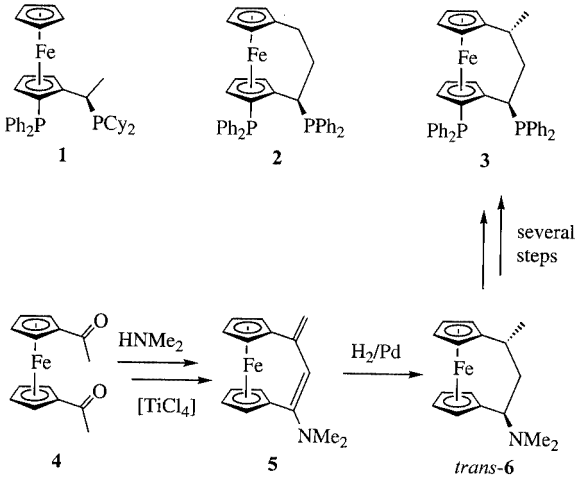

Scheme 1

[‡] X-ray crystal structure analyses.
[a] Organisch-Chemisches Institut der Universität Münster, Corrensstrasse 40, 48149 Münster, Germany
Supporting information for this article is available on the WWW under http://www.eurjic.org or from the author.

 © 2003 Wiley-VCH Verlag GmbH & Co. KGaA, Weinheim **DOI: 10.1002/ejic.200300152**

form after recrystallization.[10] The product *rac-trans*-**6** was then converted into a series of chelate ligands, especially to the bis(phosphanyl)[3]ferrocenophane *rac*-**3**, which was used to generate a very active Pd-based catalyst for the alternating CO/ethene copolymerization.[11,12]

So far our chemistry leading to **3** and a number of related compounds was carried out at the stage of the racemic compounds which were also used in the first catalytic test reactions.[11] We have now developed a viable synthetic entry to the amino-substituted [3]ferrocenophane enantiomers (1*R*,3*R*)-**6** and (1*S*,3*S*)-**6** and related systems that will eventually allow us to prepare both enantiomers of the chelate ligand **3** and other related [3]ferrocenophane-derived chelate systems. Several possible pathways were tested that will briefly be described in this account before the rather simple route was successfully established that led to the practically optically pure α-amino[3]ferrocenophanes. The essential products along this pathway had their structural assignments secured by X-ray diffraction.

Results and Discussion

Attempted Asymmetric Enamine Hydrogenation

The observation that the catalytic hydrogenation of the doubly unsaturated enamine **5** in the presence of palladium on charcoal proceeded predominantly with an overall *trans* stereochemistry[10] indicated a stepwise hydrogenation pathway with an active involvement of the amino group at the surface of the catalyst. Therefore, it needed to be tested whether the attachment of a chiral amino auxiliary would lead to a considerable asymmetric induction. For this reason we selected the secondary amine methyl(1-phenylethyl)-amine [(*R*)-**8**, (*S*)-**8**] as the amine component in the enamine formation/Mannich condensation sequence. The respective enantiomers of **8** were prepared starting from the optically active (1-phenylethyl)amine by $LiAlH_4$ reduction of their methyl carbamates (**7**).[13]

Right from the beginning the chosen reaction sequence proceeded unsatisfactorily. The Mannich coupling required a ca. 16 fold excess of the expensive amino component [(*R*)-**8** or (*S*)-**8**] to produce the corresponding [3]ferrocenophane derivatives [(*R*)-**9**, (*S*)-**9**], but even under these forced conditions the optically active aminoferrocenophane derivatives were only isolated in less than 20% yield. The enantiomers are characterized by an optical rotation of $[\alpha]_D^{20} = +44$ [(*R*)-**9**]. Figure 1 shows the CD spectrum of (*R*)-**9**, featuring a negative Cotton effect at the short wavelength edge of the spectrum [$\Delta\varepsilon$ (λ_{max}) = −0.37 (348), +0.11 (444)].

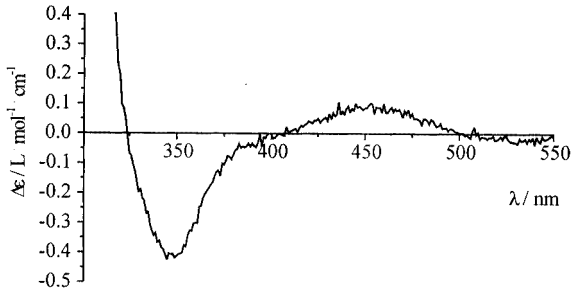

Figure 1. CD spectrum of the [3]ferrocenophane derivative (*R*)-**9** (8×10^{-4} g mL^{-1}) in CH_3CN

Single crystals that were suitable for characterization by X-ray diffraction were obtained for both enantiomers (*R*)-**9** and (*S*)-**9**. Figure 2 provides a view of the structures of the pair of enantiomers in the crystal. Since the solved structures are enantiomeric, only some of the data from enantiomer (*R*)-**9** will be given. The ferrocene framework of

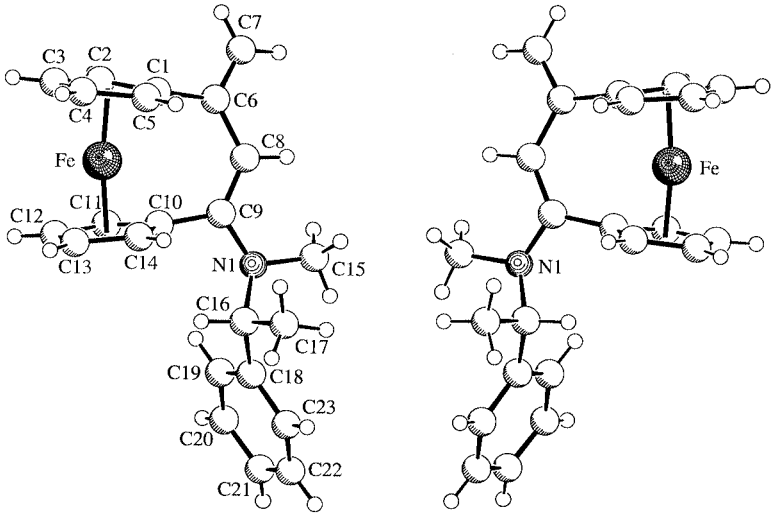

Figure 2. A view of the molecular geometries of the pair of the enantiomers (*R*)-(+)-**9** (left) and (*S*)-(−)-**9** (right) (with unsystematical atom numbering scheme), originating from different enantiomorphic crystals; selected bond lengths [Å] and angles [°] [values are from (*R*)-(+)-**9**]: C1−C6 1.491(5), C6−C7 1.333(5), C6−C8 1.471(5), C8−C9 1.362(4), C9−C10 1.477(5), C9−N1 1.408(4), N1−C15 1.455(4), N1−C16 1.481(4), C16−C17 1.526(5), C16−C18 1.525(5); C1−C6−C7 117.2(3), C1−C6−C8 122.3(3), C7−C6−C8 120.5(3), C6−C8−C9 129.0(3), C8−C9−C10 124.1(3), C8−C9−N1 121.4(3), C10−C9−N1 114.2(3), C9−N1−C15 117.9(3), C9−N1−C16 119.6(3), C15−N1−C16 114.1(3), N1−C16−C17 111.1(3), N1−C16−C18 109.3(3), C17−C16−C18 115.2(3)

 © 2003 Wiley-VCH Verlag GmbH & Co. KGaA, Weinheim

(*R*)-**9** is almost undistorted. The Cp(centroid)−Fe−Cp(centroid) angle amounts to 171.9°. Both Fe−C1/C10 [*ipso*-C(Cp)] linkages [2.001(4), 1.995(3) Å] are slightly shorter than the adjacent proximal Fe−CH(Cp) distances [ranging between 2.017(3) and 2.037(3) Å], which are in turn slightly shorter than the distal Fe−C(Cp) bonds [range: 2.045(3) Å for Fe−C4 to 2.062(4) Å for Fe−C12]. The substituted 1-aminobutadienediyl unit that bridges between the pair of Cp ligands in (*R*)-**9** is planar and features the expected bond alternation sequence[14] [C1−C6 1.491(5) Å, C6−C7 1.333(5) Å, C6−C8 1.471(5) Å, C8−C9 1.362(4) Å, C9−C10 1.477(5) Å, see Figure 2]. The bond angles inside the [3]ferrocenophane bridge amount to 122.3(3)° (C1−C6−C8), 129.0(3)° (C6−C8−C9), and 124.1(3)° (C8−C9−C10), which indicates a rather unstrained situation. The connecting C9−N bond is found at 1.408(4) Å, and the sum of the bonding angles at the nitrogen atom is 351.6°.[15]

The ^{1}H NMR spectrum of compound **9** shows the expected split signals of the butadienediyl $=CH_2$ terminus (δ = 4.99, 4.62 ppm; $^2J_{H,H}$ = 2.5 Hz) and a singlet of the corresponding central =CH− butadienediyl methine-H (δ = 5.52 ppm). The attached chiral amino substituents make the C_5H_4 methine CH groups pairwise diastereotopic. This is clearly resolved for the 2-H/5-H (δ = 4.30/4.29 ppm) and 2′-H/5′-H (δ = 4.35/4.32 ppm) pairs but not for their adjacent "distal" CH moieties.

The catalytic hydrogenation of (*R*)-(+)-**9** was carried out in THF at room temperature and an atmospheric pressure of hydrogen in the presence of a heterogeneous Pd/C catalyst (Scheme 2). Workup after a typical reaction time of 2 h gave a complicated mixture of products. Since we had prepared the expected hydrogenation products separately as pure isomers (see below) it was possible to positively identify the major components of the mixture as the two saturated [3]ferrocenophane derivatives (1*R*,3*R*,5*R*)-**10a** and (1*S*,3*S*,5*R*)-**10b** (both of the *trans* series) and the product *trans*-**11**, which was derived from the *trans*-**10** compounds by hydrogenolytic removal of the benzylic-type "protective" group at the nitrogen atom.[16] In addition, there were several other [3]ferrocenophane products, probably the corresponding *cis* isomers or compounds derived from them. Most significantly, the ratio of the major products (1*R*,3*R*,5*R*)-**10a**/(1*S*,3*S*,5*R*)-**10b** was found as < 2:1. This meant that a significant enrichment had not been achieved in either of the expected diastereomers. Therefore, we decided to pursue other ways of preparing the diastereomerically and enantiomerically pure [3]ferrocenophanylamines.

Resolution of the trans-6 Enantiomers by Dibenzoyltartrate Salt Formation

The separation of the enantiomers of chiral (aminoalkyl)ferrocenes had previously been achieved by resolution via L- or D-*O*,*O*′-dibenzoyltartrate salt formation.[17] We therefore treated the racemate of the dimethylamino-substituted [3]ferrocenophane *trans*-**6** with L(−)-*O*,*O*′-dibenzoyltartaric acid. Salt formation in refluxing methanol followed by crystallization gave two fractions, a solid enriched in the dibenzoyltartrate of (1*R*,3*R*)-**6**, and a mother liquor that contained an excess of the respective salt of (1*S*,3*S*)-**6** (see Scheme 3). The resolution procedure was repeated once. The combined fractions of the respective enriched diastereomeric salts were then treated with excess triethylamine to liberate the free bases of **6**. The enantiomerically enriched compounds were obtained in almost equal amounts (total yield: 46%) and they are equally enriched as judged from their optical rotations {found: enriched (1*R*,3*R*)-**6**: $[\alpha]_D^{20}$ = +71; enriched (1*S*,3*S*)-**6**: $[\alpha]_D^{20}$ = −72}. The enantiomeric excess that was actually achieved by the dibenzoyltartrate resolution procedure was determined by converting samples of the enriched (1*R*,3*R*)-**6** material to their diastereomeric amine derivatives (1*R*,3*R*,5*R*)-**10** and (1*S*,3*S*,5*R*)-**10**, respectively, by an amine exchange reaction with (*R*)-methyl(1-phenylethyl)amine, subsequent to quat-

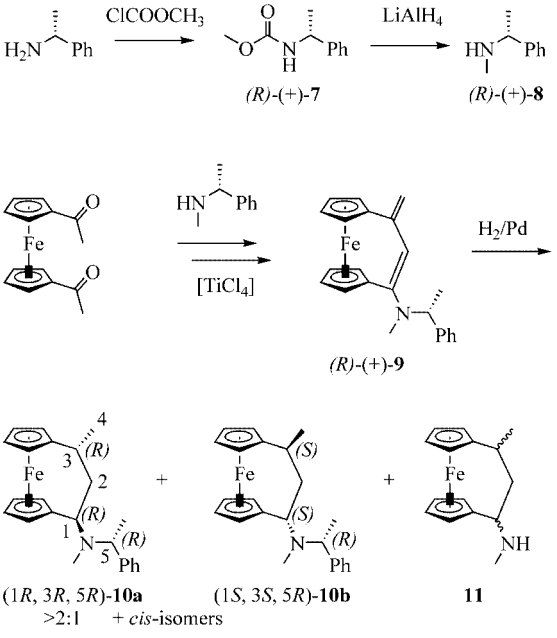

Scheme 2

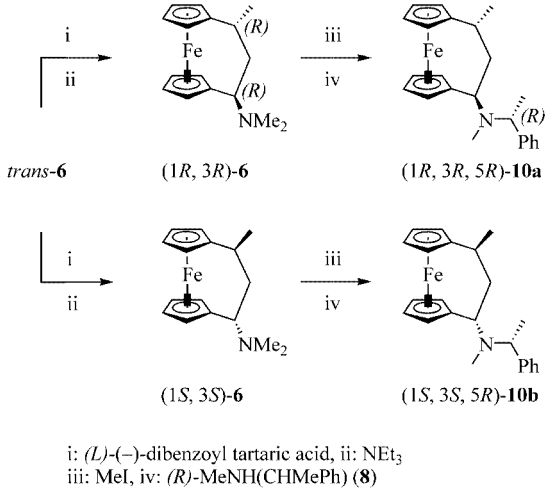

Scheme 3

 © 2003 Wiley-VCH Verlag GmbH & Co. KGaA, Weinheim

ernization with methyl iodide.[18] The ^{1}H NMR spectroscopic analysis showed the presence of a ca. 9:1 ratio of the (1*R*,3*R*,5*R*)-**10**/(1*S*,3*S*,5*R*)-**10** diastereoisomers in the resulting reaction mixture. The isolated product featured an optical rotation of $[\alpha]_D^{20} = +108$. We will see later that the pure (1*R*,3*R*,5*R*)-**10a** isomer has an optical rotation of $[\alpha]_D^{20} = +129$. Thus, from these measurements we must conclude that the resolution of *trans*-**6** via L(−)-*O*,*O*′-dibenzoyltartrate salt formation has resulted in a ca. 80% *ee* of (1*R*,3*R*)-**6** and (1*S*,3*S*)-**6**, respectively.

To achieve an independent absolute stereochemical assignment the partially resolved isolated complex (1*R*,3*R*)-**6** was treated with L-tartaric acid to form the respective salt **12** [i.e. L-tartrate·(1*R*,3*R*)-**6**], and the corresponding ca. 80% enantiomerically enriched (1*S*,3*S*)-**6** sample was treated with D-tartaric acid to give the salt *ent*-**12** [i.e. D-tartrate·(1*S*,3*S*)-**6**]. Single crystals of each of these independently prepared salts were obtained from methanol into which diethyl ether vapor was allowed to diffuse. The X-ray crystal structure analyses of the two sets of crystals confirmed the structural assignments to be correct (see Figure 3).

Inside the [L-tartrate·(1*R*,3*R*)-**6**] salt (**12**), the substituted symmetry-equivalent [3]ferrocenophane units attain a very typical conformation. The C8 methylene group is characteristically placed outside the C1−C6/C9−C13 plane, so that the substituents at the saturated C3 bridge [C1−C6 1.515(3), C6−C8 1.546(4), C8−C9 1.537(3), C9−C10 1.502(3) Å; C1−C6−C8 112.6(2), C6−C8−C9 112.5(2), C8−C9−C10 113.9(2)°] have become oriented pseudo-axially (CH_3 at C6) or pseudo-equatorially (NMe_2 at C9).[10] The corresponding dihedral angles of the [3]ferrocenophane framework amount to 63.8(3)° (C1−C6−C8−C9) and −79.0(2)° (C6−C8−C9−C10). The respective substituent positions at this framework are characterized by dihedral angles of −63.6(3)° (C7−C6−C8−C9) and 153.1(2)° (C6−C8−C9−N1). The C9−N1 bond length is 1.515(3) Å. The sum of C−N−C bonding angles at N1 is only 336.0°, which indicates that the amino nitrogen atom is protonated and connected to the tartrate oxygen O20 in the crystal by means of a hydrogen bond (N1−O20 distance 2.707Å). The tartrate dianion is bridging between a pair of protonated enantiomeric (dimethylamino)[3]ferrocenophane units. The tartrate conformation is as expected with the $-CO_2-$ groups arranged *antiperiplanar* (C18−C21−C21*−C18* −157.8(3)°] and the −OH substituents *gauche* (θ O22−C21−C21*−O22* −53.2(3)°].

Resolution of the Amino[3]ferrocenophanes by Separation of Covalent Diastereomeric Derivatives

It is well established that amine exchange by a suitable nucleophile at the α-carbon position at the ferrocene proceeds in a sequential two-step pathway with a neighboring group participation of the Fe metal center to result in overall stereochemical retention.[18,19] Early work by the Dijon group[3] supported by recent work e.g. by Weissensteiner et al.[4] has shown that this double inversion pathway also governs the stereochemical outcome of the respective substitution reactions at the [3]ferrocenophane framework.[11] We have therefore quaternized the (dimethylamino)[3]ferrocenophane system **6** by treating it with methyl iodide and then with a slight excess of the secondary amine (*R*)-methyl(1-phenylethyl)amine [(*R*)-**8**].[13] The amine exchange reaction was complete after 40 h of refluxing in acetonitrile in the presence of potassium carbonate. The mixture of the diastereomeric products (1*R*,3*R*,5*R*)-**10a** and (1*S*,3*S*,5*R*)-**10b**

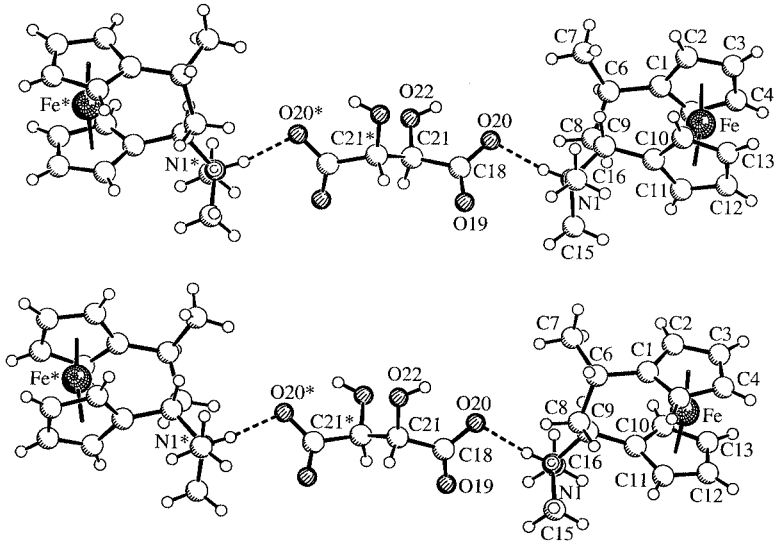

Figure 3. Views of the molecular structures of the independently prepared enantiomeric L-tartrate salt of (1*R*,3*R*)-**6** (**12**, top) and the D-tartrate salt of (1*S*,3*S*)-**6** (*ent*-**12**, bottom); selected bond lengths [Å] and angles [°] of the L-tartrate-derived enantiomer **12**: C1−C6 1.515(3), C6−C7 1.526(4), C6−C8 1.546(4), C8−C9 1.537(3), C9−C10 1.503(3), C9−N1 1.515(3), N1−C15 1.486(3), N1−C16 1.490(3), C18−O19 1.242(4), C18−O20 1.264(3), C18−C21 1.528(3), C21−C21* 1.524(5), C21−O22 1.412(3); C1−C6−C7 112.3(3), C1−C6−C8 112.6(2), C7−C6−C8 111.5(2), C6−C8−C9 112.5(2), C8−C9−C10 113.9(2), C8−C9−N1 110.6(2), C10−C9−N1 112.5(2), C9−N1−C15 114.8(2), C9−N1−C16 111.1(2), C15−N1−C16 110.1(2), O19−C18−O20 126.3(3), O19−C18−C21 117.6(3), O20−C18−C21 116.0(2), C18−C21−C21* 111.7(3), C18−C21−O22 113.0(2), O22−C21−C21* 111.7(2)

 © 2003 Wiley-VCH Verlag GmbH & Co. KGaA, Weinheim

was obtained in a near to quantitative yield. Chromatographic separation of the diastereoisomers was achieved by column chromatography on silica gel using a mixture of cyclohexane, THF, and ethyl acetate in a ratio of 34:5:1 as an eluent. The two *trans* isomers [R_f = 0.83 for (1*S*,3*S*,5*R*)-**10a**;R_f = 0.74 for (1*R*,3*R*,5*R*)-**10b**] were clearly separated from each other and from residual reagent [(*R*)-**8**: R_f = 0.30]. The respective minor *cis* isomers were apparently lost during the separation and workup procedure; they could not be recovered. Subsequent recrystallization from diethyl ether gave the pure (1*R*,3*R*,5*R*)-**10a** and (1*S*,3*S*,5*R*)-**10b** isomers each in almost equal quantities (ca. 2 g, 66% yield). Their respective enantiomers were prepared analogously by amine exchange from **6** and the enantiomeric amine reagent (*S*)-**8** and the diastereoisomers *ent*-**10a** (1*S*,3*S*,5*S*) and *ent*-**10b** (1*R*,3*R*,5*S*) were separated accordingly. The (1*R*,3*R*,5*R*)-**10a** diastereomer is characterized by an optical rotation of $[\alpha]_D^{20}$ = +129 ($c = 4 \times 10^{-3}$ g mL^{-1}, CH_3CN), the (1*S*,3*S*,5*R*)-**10b** diastereomer by $[\alpha]_D^{20}$ = −49 ($c = 4 \times 10^{-3}$ g mL^{-1}, CH_3CN). Figure 4 shows the CD curves of the enantiomeric pair of the complexes **10b** (1*S*,3*S*,5*R*) and *ent*-**10b** (1*R*,3*R*,5*S*).

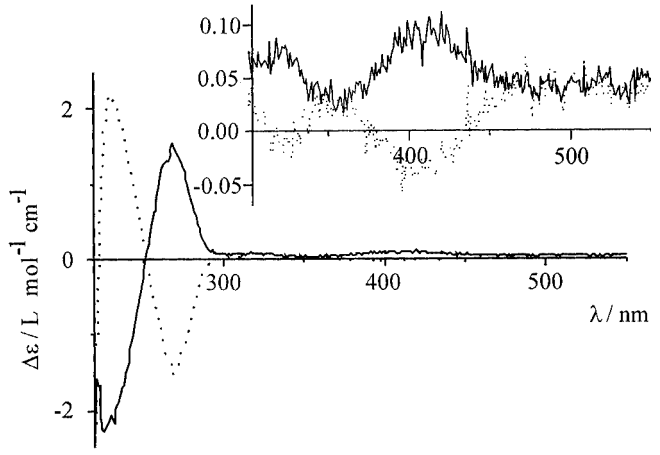

Figure 4. CD spectra of the enantiomeric pair of the complexes **10b** (solid line, 8×10^{-5} g mL^{-1}) and *ent*-**10b** (dotted line, 8×10^{-5} g mL^{-1}) in CH_3CN

The overall pattern of the NMR spectra of **10a** and **10b** are similar although distinctly different in detail. The ^{1}H NMR spectroscopic features of the 3-CH_3 group occur at δ = 0.91 (**10a**) and 1.16 (**10b**) ppm, respectively [corresponding ^{13}C NMR signals at δ = 16.8 (**10a**) and 17.3 (**10b**) ppm]. The 1-H, 2-H/H′ and 3-H signals of **10a** were found at δ = 3.39 (^{13}C: δ = 52.8 ppm), 2.55, 1.92 (^{13}C: δ = 47.9 ppm), and 2.65 ppm, whereas the corresponding **10b** NMR resonances were observed at δ = 3.57 (^{13}C: δ = 52.4 ppm), 2.42, 2.11 (^{13}C: δ = 45.6 ppm), and 2.76 ppm. Also, the NCH_3 (**10a**: δ = 2.25/33.8 ppm; **10b**: δ = 2.14/34.5 ppm) and the 5-CH_3 resonances inside the amino substituent (**10a**: δ = 1.24 ppm; **10b**: δ = 1.30 ppm) are sufficiently different to allow for an easy determination of the diastereomeric purity of the obtained samples. Within the limits of the 600 MHz ^{1}H NMR spectroscopic detection the isolated **10a** and **10b** diastereoisomers were > 99% isomerically pure. A close to complete isomeric separation was thus achieved (see Figure 5 for an illustration).

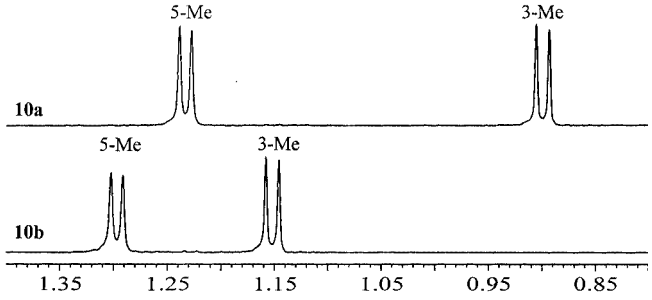

Figure 5. A comparison of the 3-CH_3 and 5-CH_3 ^{1}H NMR region of the (1*R*,3*R*,5*R*)-**10a** and (1*S*,3*S*,5*R*)-**10b** diastereoisomers isolated after chromatographic separation and recrystallization from diethyl ether

The absolute stereochemical assignment was again secured by X-ray diffraction. Single crystals were obtained from all stereoisomers (i.e. **10a**, *ent*-**10a**, **10b**, and *ent*-**10b**). Figure 6 shows the molecular structures of the enantiomeric pairs of both diastereoisomers.

The structural features of the two diastereomers are very similar. This may be illustrated by a comparison of some typical structural parameters of the [3]ferrocenophane frameworks of the complexes **10a** and *ent*-**10b** (values in parentheses), that both contain an (*R*)-configurated methyl(1-phenylethyl)amino substituent. The complexes feature almost identical bond lengths and angles of the central core, e.g. C1−C6 1.511(2) [1.508(2) Å], C6−C8 1.543(2) [1.549(2) Å], C8−C9 1.538(3) [1.545(2) Å], C9−N1 1.486(2) [1.487(2) Å], C9−C10 1.523(2) Å [1.511(2) Å]; C1−C6−C8 112.6(2) [112.8(1)°], C1−C6−C7 112.4(2) [112.2(1)°], C7−C6−C8 111.9(2) [112.1(1)°], C6−C8−C9 115.1(2) [114.3(1)°], N1−C9−C10 115.7(1) [115.8(1)°], N1−C9−C8 109.2(1)° [109.5(1)°]. However, there are a few conformational differences between the diastereomers with regard to the orientation of the methyl(1-phenylethyl)amino substituent. In **10a**, the phenyl group is rotated away from the central [3]ferrocenophane framework, whereas in *ent*-**10b** it is the adjacent methyl substituent that is rotated away. Typically this can be expressed by the characteristic differences in the C15−N1−C16−C17 dihedral angles of **10a** [−43.9(2)°] and *ent*-**10b** [179.6(2)°]. The remaining dihedral angles around the substituted nitrogen atom are again quite similar in both complexes, e.g. C10−C9−N1−C16 74.4(2) (**10a**), −65.7(2) (*ent*-**10b**); C9−N1−C16−C18: 67.7(2) (**10a**), −173.4(1) (*ent*-**10b**); C10−C9−N1−C15: −55.1(2) (**10a**), 59.3(2)° (*ent*-**10b**).

Conversion of the Enantiomerically Pure [3]Ferrocenophanes 10: Removal of the Chiral Auxiliary

We anticipated that the optically active systems **10** could be directly employed in the synthesis of chiral chelate ligands such as **3** in the enantiomerically pure form.[2a,11,20] However, it turned out that the specific systems **10** proved to be rather unreactive. Directed *ortho*-metalation[2,18] of

 © 2003 Wiley-VCH Verlag GmbH & Co. KGaA, Weinheim

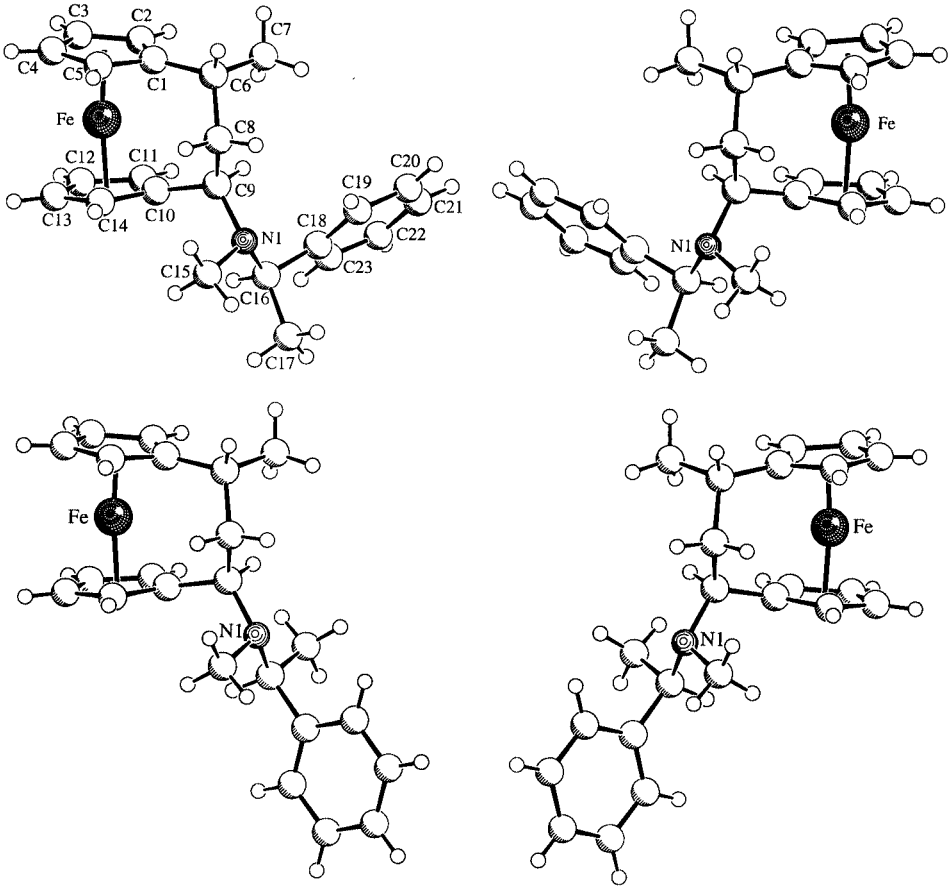

Figure 6. A comparison of the molecular geometries of the enantiomeric pairs (**10**/*ent*-**10**) of the diastereomers **10a** and **10b** [top left: **10a** (1*R*,3*R*,5*R*); top right: *ent*-**10a** (1*S*,3*S*,5*S*); bottom left: **10b** (1*R*,3*R*,5*S*); bottom right: *ent*-**10b** (1*S*,3*S*,5*R*)] (with unsystematical atom numbering scheme)

the adjacent Cp ring was unsuccessful. Moreover, the compounds **10** turned out to be unsuited for amine versus external nucleophile exchange, at least under the various conditions that we tried.

We therefore had to take a short detour to convert the complexes **10** into established building blocks for the synthesis of chiral [3]ferrocenophane-based chelate ligand systems. This was achieved by catalytic hydrogenolysis (see Scheme 4). The methyl(1-phenylethyl)amino substituent in this respect behaved as a typical benzylic amine.[16] Catalytic hydrogenolysis at ambient conditions in methanol (90 min) selectively removed the −CHMePh substituent from the nitrogen atom to yield the product **11** (isolated in ca. 90% yield). It shows the typical ^{1}H NMR spectroscopic features of the *trans*-1,3-disubstituted [3]ferrocenophane system with the framework hydrogen resonances appearing at δ = 3.28 (1-H), 2.00 (2-H$_{exo}$), 2.20 (2-H$_{endo}$) and 2.50 (3-H) ppm. The observed set of coupling constants [^3J(1-H,2-H$_{exo}$) = 3.0, ^3J(1-H,2-H$_{endo}$) = 8.0, ^3J(2H$_{exo}$,3-H) = 7.5, ^3J(2-H$_{endo}$,3-H) = 3.1, ^2J(2-H$_{exo}$,2-H$_{endo}$) = 13.6 Hz] shows that the 3-CH$_3$ group [δ = 1.21 ppm; $^3J_{H,H}$ = 7.3 Hz] attains a pseudo-axial orientation, whereas the NHCH$_3$ substituent is placed pseudo-equatorially at the non-planar saturated [3]ferrocenophane framework.

This was confirmed by X-ray diffraction. Single crystals of each of the enantiomers (1*R*,3*R*)-**11** and (1*S*,3*S*)-**11** were obtained from diethyl ether. Figure 7 shows a view of both structures. They feature the typical arrangement of the non-planar three-carbon containing bridge with the 3-CH$_3$ and 1-NH(CH$_3$) substituents in a *trans* position to one another. In the crystal the NHCH$_3$ group adopts a conformation that leads to maximum extension of the C6−C7−C8−N9−C16 chain (see Figure 7). The carbon−nitrogen bond lengths were found at 1.475(3) (C9−N1) and 1.462(3) Å (N1−C15); the C15−N1−C9 angle amounts to 113.3(2)°.

Each of the enantiomers of **11** was then subsequently *N*-methylated by treatment with formaldehyde/NaBH$_4$ (see Scheme 4) to yield the enantiomers (1*R*,3*R*)-**6** {$[\alpha]_D^{20}$ = +86 (c = 2 × 10^{-3} g mL^{-1}, CH$_3$CN)} and (1*S*,3*S*)-**6** {$[\alpha]_D^{20}$ = −85 (c = 2 × 10^{-3} g mL^{-1}, CH$_3$CN)} almost quantitatively. Their CD spectra are shown in Figure 8. The enantiomers (1*R*,3*R*)-*trans*-**6** and (1*S*,3*S*)-*trans*-**6** were thus prepared in a 5-step synthesis (plus one chromatographic separation), starting from 1,1′-diacetylferrocene and obtained in an overall yield of ca. 23% (out of a possible 50%). We will now use these compounds as building blocks for the preparation of optically active [3]ferrocenophane-derived

 © 2003 Wiley-VCH Verlag GmbH & Co. KGaA, Weinheim

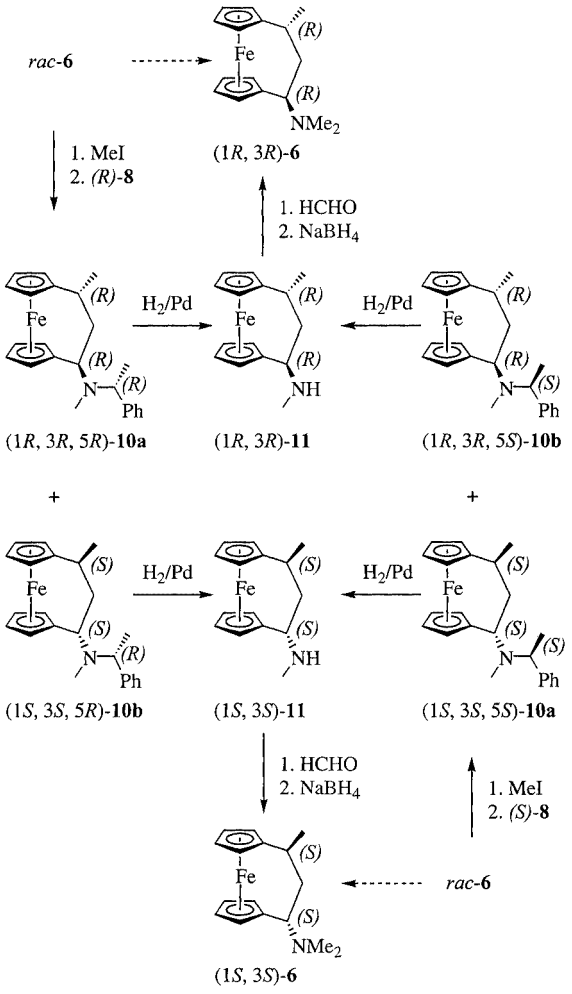

Scheme 4

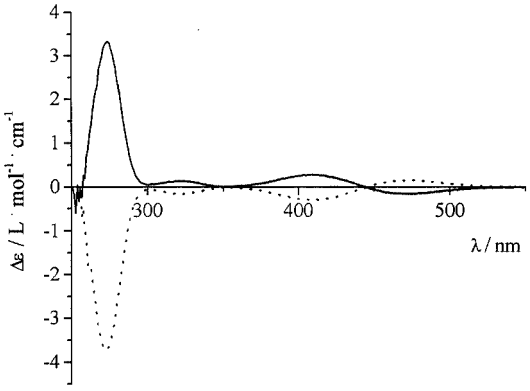

Figure 8. CD spectra of (1*R*,3*R*)-**6** (solid line, 4×10^{-4} g mL^{-1}) and (1*S*,3*S*)-**6** (dotted line, 4×10^{-4} g mL^{-1}) in CH_3CN

chelate ligands to study their potential for asymmetric catalysis.[11,21]

Experimental Section

General Methods: All reactions were carried out under dry argon in Schlenk-type glassware or in a glove-box. Solvents were dried and distilled prior to use. NMR spectra were recorded with a Varian UNITY*plus* 600 (^{1}H: 599.9 MHz; ^{13}C: 150.8 MHz) spectrometer. The atom numbering scheme used for the description of the NMR spectra in the Exp. Sect. deviates from the IUPAC nomenclature used in the text − it is equivalent as depicted in Figures 2, 3, 6, and 7. Most assignments were confirmed by 2D NMR spectra,[22] for details see the Supporting Information. The following instruments were used for additional physical characterization: IR spectroscopy: Nicolet 5DXC FT-IR spectrometer; melting points: DSC 2010 (TA instruments); elemental analyses: Foss Heraeus CHN-O-Rapid; optical rotation: Perkin−Elmer polarimeter 351; circular dichroism: Jobin Yvon-Spex CD-6 dichro-

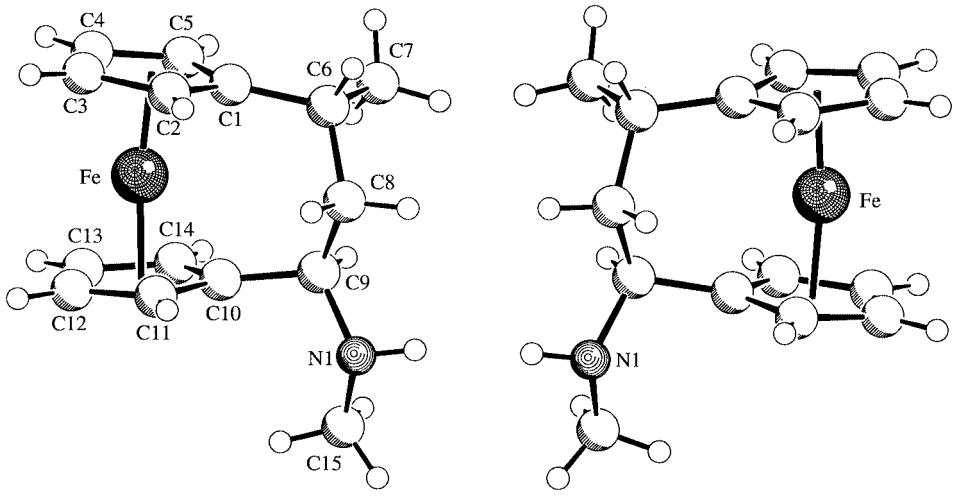

Figure 7. Molecular geometries of the isolated enantiomers (1*R*,3*R*)-**11** (left) and (1*S*,3*S*)-**11** (right) (with unsystematical atom numbering scheme); selected bond lengths [Å] and angles [°] [from the solution of the (1*R*,3*R*)-**11** structure]: C1−C6 1.523(3), C6−C7 1.527(4), C6−C8 1.537(3), C8−C9 1.530(3), C9−C10 1.514(2), C9−N1 1.475(3), N1−C15 1.462(3); C1−C6−C7 112.1(2), C1−C6−C8 112.1(2), C7−C6−C8 112.1(2), C6−C8−C9 116.4(2), C8−C9−C10 113.4(2), C8−C9−N1 108.4(2), C10−C9−N1 110.3(2), C9−N1−C15 113.3(2)

 © 2003 Wiley-VCH Verlag GmbH & Co. KGaA, Weinheim

graph. The following starting materials were prepared according to literature procedures: 1,1′-diacetylferrocene (**4**),[6] ferrocenophane **6**,[9] carbamate **7**,[13] methyl(1-phenylethyl)amine (**8**).[13]

X-ray Diffraction: Data sets were collected with a Nonius KappaCCD diffractometer, equipped with a rotating anode generator Nonius FR591. Programs used: data collection COLLECT (Nonius B.V., **1998**), data reduction Denzo-SMN,[23] absorption correction SORTAV[24], structure solution SHELXS-97,[25] structure refinement SHELXL-97,[26] graphics SCHAKAL.[27] CCDC-205072 to -205081 contain the supplementary crystallographic data for this paper. These data can be obtained free of charge at www.ccdc.cam.ac.uk/conts/retrieving.html [or from the Cambridge Crystallographic Data Centre, 12 Union Road, Cambridge CB2 1EZ, UK; Fax: (internat.) + 44-1223/336-033; E-mail: deposit@ccdc.cam.ac.uk].

Preparation of 6 (from 11): A solution of (1*S*,3*S*)-**11** (100 mg, 0.37 mmol) in MeOH (4 mL) was cooled to 4 °C and treated with formaldehyde solution (4 mL, 37% in MeOH). After stirring at this temperature for 10 min, $NaBH_4$ (233 mg, 6.2 mmol) was added in small portions. The reaction mixture was stirred at room temperature for 1 h and then heated to 75 °C for 18 h. After removal of the solvent under reduced pressure, the residue was extracted with water/CH_2Cl_2. The organic phases were washed with water and brine and dried with $MgSO_4$. Evaporation of the solvent yielded (1*S*,3*S*)-**6** as a yellow solid (104 mg, 97%). $[\alpha]_D^{20} = -85$ ($c = 2 \times 10^{-3}$ g mL^{-1}, CH_3CN). CD: $\Delta\varepsilon$ (λ_{max}) = −3.70 (274), −0.15 (326), −0.28 (412), +0.15 (476) ($c = 4 \times 10^{-4}$ g mL^{-1}, CH_3CN). $C_{16}H_{21}FeN$ (283.20): calcd. C 67.86, H 7.47, N 4.95; found C 67.78, H 7.32, N 4.84. (1*R*,3*R*)-**6** was prepared analogously starting from (1*R*,3*R*)-**11** (443 mg, 1.65 mmol), yield: 453 mg (97%). $[\alpha]_D^{20} = +86$ ($c = 2 \times 10^{-3}$ g mL^{-1}, CH_3CN). CD: $\Delta\varepsilon$ (λ_{max}) = +3.33 (274), +0.14 (326), +0.28 (412), −0.15 (476) ($c = 4 \times 10^{-4}$ g mL^{-1}, CH_3CN). $C_{16}H_{21}FeN$ (283.20): calcd. C 67.86, H 7.47, N 4.95; found C 67.62, H 7.25, N 4.93.

Synthesis of 9: A suspension of 1,1′-diacetylferrocene (**4**) (4.0 g, 14.8 mmol) and either (*S*)- or (*R*)-**8** (35 mL, 240 mmol) in pentane (200 mL) was cooled to 4 °C. Over a period of 20 min a solution of $TiCl_4$ (2.0 mL, 18.2 mmol) in pentane (90 mL) was added dropwise. Afterwards, the reaction mixture was stirred at room temperature overnight. The resulting deep red suspension was filtered through Celite and the solvent removed in vacuo. Unchanged amine **8** could be regained by vacuum condensation of the product at 72 °C. The enantiomers (*S*)-**9** and (*R*)-**9** were each obtained as red to brown solids [(*S*)-**9**: 1.08 g, 20%; (*R*)-**9**: 1.03 g, 19%], m.p. 75 °C (DSC). IR (KBr): $\tilde{\nu}$ = 3855 (m), 3757 (m), 3085 (m), 2980 (s), 2868 (w), 2796 (w), 2380 (w), 1598 (vs), 1479 (vs), 1275 (vs), 1098 (vs), 1019 (vs), 907 (s), 802 (vs), 696 (vs) cm^{-1}. Crystals suitable for X-ray structure analysis were grown by slow diffusion of pentane into an Et_2O solution. ^{1}H NMR (599.9 MHz, CD_2Cl_2, 25 °C): δ = 1.35 [d, $^3J_{H,H}$ = 6.9 Hz, 3 H, C(17)−H], 2.47 [s, 3 H, C(15)−H], 4.13 [m, 2 H, C(2−4)−H], 4.21 [m, 2 H, C(11−14)−H], 4.28 [m, 1 H, C(2−4)−H], 4.29 [m, 1 H, C(2−4)−H], 4.31 [m, 1 H, C(11−14)−H], 4.34 [m, 1 H, C(11−14)−H], 4.64 [d, $^2J_{H,H}$ = 2.5 Hz, 1 H, C(7)−H$_{exo}$], 4.82 [q, $^3J_{H,H}$ = 6.9 Hz, 1 H, C(16)−H], 4.98 [d, $^2J_{H,H}$ = 2.5 Hz, 1 H, C(7)−H$_{endo}$], 5.50 [s, 1 H, C(8)−H], 7.21 (m, 1 H, Ph$_{para}$), 7.23 (m, 2 H, Ph$_{ortho}$), 7.30 (m, 2 H, Ph$_{meta}$) ppm. ^{13}C{^{1}H} NMR (150.8 MHz, CD_2Cl_2, 25 °C): δ = 15.6 [C(17)], 32.1 [C(15)], 56.4 [C(16)], 70.0 [C(2−4)], 70.1 [C(2−4)], 70.3 [C(11−14)], 70.4 [C(2−4)], 70.6 [C(2−4)], 71.8 [C(11−14)], 71.9 [C(11−14)], 84.2 [C(10)], 90.5 [C(1)], 109.0 [C(7)], 109.2 [C(8)], 127.0 (Ph$_{para}$), 127.3 (Ph$_{ortho}$), 128.4 (Ph$_{meta}$), 142.8 [C(6/9)], 142.9 (Ph$_{ipso}$), 146.2 [C(6/9)] ppm. (*S*)-**9**: $[\alpha]_D^{20} = -43$ ($c = 2 \times 10^{-3}$ g mL^{-1}, $CHCl_3$); (*R*)-**9**: $[\alpha]_D^{20} = +44$ ($c = 2 \times 10^{-3}$ g mL^{-1}, $CHCl_3$). CD: (*S*)-**9**: $\Delta\varepsilon$ (λ_{max}) = −4.56 (284), +0.30 (348), −0.09 (444) ($c = 8 \times 10^{-5}$ g mL^{-1}, CH_3CN); (*R*)-**9**: $\Delta\varepsilon$ (λ_{max}) = +6.37 (284), −0.37 (348), +0.11 (444) ($c = 8 \times 10^{-5}$ g mL^{-1}, CH_3CN). $C_{23}H_{23}FeN$ (369.29): calcd. C 74.81, H 6.28, N 3.79; (*S*)-**9**: found C 74.32, H 6.50, N 3.79; (*R*)-**9**: found C 74.41, H 6.26, N 3.71.

X-ray Crystal Structure Analysis of (*R*)-(+)-9: Empirical formula $C_{23}H_{23}FeN$, M = 369.29, red crystal, 0.50 × 0.20 × 0.10 mm, a = 6.216(1), b = 12.121(1), c = 23.536(1) Å, V = 1773.3(3) Å^3, $\rho_{calcd.}$ = 1.383 g cm^{-3}, μ = 8.55 cm^{-1}, empirical absorption correction (0.675 ≤ T ≤ 0.919), Z = 4, orthorhombic, space group $P2_12_12_1$ (no. 19), λ = 0.71073 Å, T = 198 K, ω and φ scans, 8928 reflections collected (±h, ±k, ±l), [(sinθ)/λ] = 0.68 Å^{-1}, 4355 independent (R_{int} = 0.055) and 3156 observed reflections [$I \geq 2\sigma(I)$], 228 refined parameters, R = 0.049, wR^2 = 0.092, Flack parameter 0.01(2), max. residual electron density 0.44 (−0.43) e·Å^{-3}, hydrogen atoms calculated and refined as riding atoms.

X-ray Crystal Structure Analysis of (*S*)-(−)-9: Empirical formula $C_{23}H_{23}FeN$, M = 369.29, yellow crystal, 0.30 × 0.07 × 0.03 mm, a = 6.201(1), b = 12.119(1), c = 23.604(1) Å, V = 1773.8(3) Å^3, $\rho_{calcd.}$ = 1.383 g cm^{-3}, μ = 8.54 cm^{-1}, empirical absorption correction (0.784 ≤ T ≤ 0.975), Z = 4, orthorhombic, space group $P2_12_12_1$ (no. 19), λ = 0.71073 Å, T = 198 K, ω and φ scans, 12989 reflections collected (±h, ±k, ±l), [(sinθ)/λ] = 0.66 Å^{-1}, 4168 independent (R_{int} = 0.063) and 3222 observed reflections [$I \geq 2\sigma(I)$], 228 refined parameters, R = 0.051, wR^2 = 0.080, Flack parameter 0.02(2), max. residual electron density 0.51 (−0.26) e·Å^{-3}, hydrogen atoms calculated and refined as riding atoms.

Preparation of 10. a) By Hydrogenation: The Pd/C catalyst (10 mg, 10% Pd) was added to a solution of (*R*)-**9** (200.0 mg, 0.54 mmol) in THF (40 mL). Hydrogenation was carried out at ambient pressure under vigorous stirring for 2 h. The reaction mixture was filtered through Celite and the solvent removed in vacuo. An orange oil (179.0 mg) was obtained which was identified to be a complex mixture of all possible isomers of **10** and **11**. **b) By Amine Exchange:** A solution of *rac-trans*-**6** (6.00 g, 21.2 mmol) in CH_3CN (120 mL) was treated with CH_3I (84 mL) and stirred at room temperature for 1 h. Excess CH_3I was then removed in vacuo. K_2CO_3 (6.44 g, 46 mmol), (*R*)-**8** (3.8 mL, 26 mmol) and CH_3CN (300 mL) were added to the obtained trimethylammonium salt. The mixture was heated to reflux for 40 h. After removal of the solvent in vacuo, the residue was suspended in pentane (100 mL). Filtration through Celite and concentration of the filtrate yielded the crude product as a mixture of diastereomers (6.90 g, 87%). Purification was achieved by column chromatography (SiO_2; cyclohexane/THF/ethyl acetate, 34:5:1). (1*R*,3*R*,5*R*)-**10a**: R_f = 0.74; (1*S*,3*S*,5*R*)-**10b**: R_f = 0.83. Furthermore, the products were recrystallized from Et_2O.

(1*R*,3*R*,5*R*)-10a: orange solid, 2.01 g (34%) isolated from 6.0 g of crude product; m.p. 87 °C (DSC). IR (KBr): $\tilde{\nu}$ = 3855 (m), 3750 (m), 3085 (m), 3019 (w), 2973 (s), 2927 (s), 2881 (s), 2855 (s), 2796 (s), 2361 (w), 1664 (m), 1558 (m), 1460 (vs), 1032 (vs), 815 (vs), 769 (vs), 696 (vs) cm^{-1}. Crystals suitable for X-ray structure analysis were grown from an Et_2O solution at −18 °C. ^{1}H NMR (599.9 MHz, CD_2Cl_2, 25 °C): δ = 0.91 [d, $^3J_{H,H}$ = 7.3 Hz, 3 H, C(7)−H], 1.24 [d, $^3J_{H,H}$ = 6.7 Hz, 3 H, C(17)−H], 1.92 [ddd, $^3J_{H,H}$ = 3.7, $^3J_{H,H}$ = 2.0, $^2J_{H,H}$ = 12.9 Hz, 1 H, C(8)−H$_{exo}$], 2.25 [s, 3 H, C(15)−H], 2.55 [ddd, $^3J_{H,H}$ = 11.4, $^3J_{H,H}$ = 4.0, $^2J_{H,H}$ = 12.9 Hz, 1 H, C(8)−H$_{endo}$], 2.65 [m, 1 H, C(6)−H], 3.39 [dd, $^3J_{H,H}$ = 11.4, $^3J_{H,H}$ = 1.8 Hz, 1 H, C(9)−H], 3.48 [q, $^3J_{H,H}$ = 6.7 Hz, 1 H, C(16)−H], 3.80 [m, 1 H, C(11−14)−H], 3.86 [m, 1 H,

 © 2003 Wiley-VCH Verlag GmbH & Co. KGaA, Weinheim

C(2−5)−H], 3.97 [m, 1 H, C(2−5)−H], 4.00 [m, 1 H, C(11−14)−H], 4.02 [m, 1 H, C(2−5)−H], 4.09 [m, 1 H, C(2−5)−H], 4.11 [m, 1 H, C(11−14)−H], 4.25 [m, 1 H, C(11−14)−H], 7.25 (m, 1 H, Ph_{para}), 7.35 (m, 2 H, Ph_{meta}), 7.37 (m, 2 H, Ph_{ortho}) ppm. $^{13}C\{^1H\}$ NMR (150.8 MHz, CD_2Cl_2, 25 °C): δ = 16.8 [C(7)], 21.9 [C(17)], 28.2 [C(6)], 33.8 [C(15)], 47.9 [C(8)], 52.8 [C(9)], 62.5 [C(16)], 66.9 [C(2−5)], 68.2 [C(11−14)], 68.3 [C(11−14)], 68.4 [C(2−5)], 68.5 [C(2−5)], 69.1 [C(2−5)], 69.4 [C(11−14)], 72.1 [C(11−14)], 79.1 [C(10)], 93.3 [C(1)], 126.9 (Ph_{para}), 127.8 (Ph_{ortho}), 128.5 (Ph_{meta}), 146.8 (Ph_{ipso}) ppm. $[\alpha]_D^{20}$ = +129 ($c = 4 \times 10^{-3}$ g mL^{-1}, CH_3CN). CD: Δε (λ_{max}) = +1.19 (273), +0.12 (320), +0.21 (456) ($c = 8 \times 10^{-5}$ g mL^{-1}, CH_3CN). $C_{23}H_{27}FeN$ (373.32): calcd. C 74.00, H 7.29, N 3.75; found C 74.01, H 7.24, N 3.83.

(1*S*,3*S*,5*S*)-10a (= *ent*-10a): In an analogous procedure, starting from *rac-trans*-**6** (5.9 g, 20.8 mmol) in CH_3CN (120 mL), CH_3I (75 mL) followed by (*S*)-**8** (3.8 mL, 25 mmol) and K_2CO_3 (6.44 g, 46 mmol) in CH_3CN (200 mL), 1.28 g (16%) of an orange solid were isolated.

X-ray Crystal Structure Analysis of 10a: Empirical formula $C_{23}H_{27}FeN$, M = 373.32, yellow-orange crystal, 0.40 × 0.40 × 0.05 mm, a = 10.826(1), b = 8.042(1), c = 10.934(1) Å, β = 98.09(1)°, V = 942.5(2) Å^3, $\rho_{calcd.}$ = 1.315 g cm^{-3}, μ = 8.04 cm^{-1}, empirical absorption correction ($0.739 \le T \le 0.924$), Z = 2, monoclinic, space group $P2_1$ (no. 4), λ = 0.71073 Å, T = 198 K, ω and φ scans, 5778 reflections collected (±h, ±k, ±l), [(sinθ)/λ] = 0.66 Å^{-1}, 3776 independent (R_{int} = 0.030) and 3629 observed reflections [$I \ge 2\sigma(I)$], 229 refined parameters, R = 0.026, wR^2 = 0.065, Flack parameter −0.02(1), max. residual electron density 0.23 (−0.27) e·Å^{-3}, hydrogen atoms calculated and refined as riding atoms.

X-ray Crystal Structure Analysis of *ent*-10a: Empirical formula $C_{23}H_{27}FeN$, M = 373.32, yellow crystal, 0.30 × 0.20 × 0.05 mm, a = 10.827(1), b = 8.029(1), c = 10.938(1) Å, β = 98.07(1)°, V = 941.4(2) Å^3, $\rho_{calcd.}$ = 1.317 g cm^{-3}, μ = 8.05 cm^{-1}, empirical absorption correction ($0.794 \le T \le 0.961$), Z = 2, monoclinic, space group $P2_1$ (no. 4), λ = 0.71073 Å, T = 198 K, ω and φ scans, 8282 reflections collected (±h, ±k, ±l), [(sinθ)/λ] = 0.67 Å^{-1}, 4038 independent (R_{int} = 0.029) and 3544 observed reflections [$I \ge 2\sigma(I)$], 229 refined parameters, R = 0.039, wR^2 = 0.075, Flack parameter −0.04(2), max. residual electron density 0.26 (−0.26) e·Å^{-3}, hydrogen atoms calculated and refined as riding atoms.

(1*S*,3*S*,5*R*)-10b: Orange solid, 1.97 g (33%) isolated from 6.0 g of crude product; m.p. 88 °C (DSC). IR (KBr): ṽ = 3432 (w), 3086 (m), 2979 (vs), 2955 (s), 2842 (s), 2796 (s), 1975 (w), 1886 (w), 1820 (w), 1657 (w), 1599 (s), 1473 (vs), 1374 (s), 1242 (s), 1150 (s), 1080 (vs), 1032 (vs), 947 (s), 815 (vs), 703 (vs) cm^{-1}. Crystals suitable for X-ray structure analysis were grown from an Et_2O solution at −18 °C. ^1H NMR (599.9 MHz, CD_2Cl_2, 25 °C): δ = 1.16 [d, $^3J_{H,H}$ = 7.3 Hz, 3 H, C(7)−H], 1.30 [d, $^3J_{H,H}$ = 6.6 Hz, 3 H, C(17)−H], 2.11 [ddd, $^3J_{H,H}$ = 3.9, $^3J_{H,H}$ = 2.0, $^2J_{H,H}$ = 13.1 Hz, 1 H, C(8)−H_{exo}], 2.14 [s, 3 H, C(15)−H], 2.42 [ddd, $^3J_{H,H}$ = 11.3, $^3J_{H,H}$ = 3.8, $^2J_{H,H}$ = 13.1 Hz, 1 H, C(8)−H_{endo}], 2.76 [m, 1 H, C(6)−H], 3.57 [dd, $^3J_{H,H}$ = 11.3, $^3J_{H,H}$ = 2.0 Hz, 1 H, C(9)−H], 3.68 [q, $^3J_{H,H}$ = 6.6 Hz, 1 H, C(16)−H], 3.94 [m, 1 H, C(2−5)−H], 4.01 [m, 1 H, C(11−14)−H], 4.03 [m, 1 H, C(11−14)−H), 4.05 [m, 1 H, C(2−5)−H], 4.11 [m, 1 H, C(11−14)−H], 4.13 [m, 1 H, C(2−5)−H], 4.14 [m, 1 H, C(2−5)−H], 4.32 [m, 1 H, C(11−14)−H], 7.22 (m, 1 H, Ph_{para}), 7.31 (m, 2 H, Ph_{meta}), 7.36 (m, 2 H, Ph_{ortho}) ppm. $^{13}C\{^1H\}$ NMR (150.8 MHz, CD_2Cl_2, 25 °C): δ = 17.3 [C(7)], 18.0 [C(17)], 28.2 [C(6)], 34.5 [C(15)], 45.6 [C(8)], 52.4 [C(9)], 61.2 [C(16)], 67.2 [C(2−5)], 67.8 [C(11−14)], 68.2 [C(11−14)], 68.6 [C(2−5)], 68.6 [C(2−5)], 69.2 [C(2−5)], 69.4 [C(11−14)], 71.3 [C(11−14)], 82.7 [C(10)], 93.0 [C(1)], 126.8 (Ph_{para}), 127.8 (Ph_{ortho}), 128.4 (Ph_{meta}), 146.6 (Ph_{ipso}) ppm. $[\alpha]_D^{20}$ = −49 ($c = 4 \times 10^{-3}$ g mL^{-1}, CH_3CN). CD: Δε (λ_{max}) = +2.16 (228), −1.52 (269), −0.03 (320), −0.05 (408) ($c = 8 \times 10^{-5}$ g mL^{-1}, CH_3CN). $C_{23}H_{27}FeN$ (373.32): calcd. C 74.00, H 7.29, N 3.75; found C 73.97, H 7.37, N 3.78.

(1*R*,3*R*,5*S*)-10b (= *ent*-10b): In an analogous procedure, starting from *rac-trans*-**6** (5.9 g, 20.8 mmol) in CH_3CN (120 mL), CH_3I (75 mL) followed by (*S*)-**8** (3.8 mL, 25 mmol) and K_2CO_3 (6.44 g, 46 mmol) in CH_3CN (200 mL), 2.78 g (34%) of an orange solid were isolated.

X-ray Crystal Structure Analysis of 10b: Empirical formula $C_{23}H_{27}FeN$, M = 373.32, yellow crystal, 0.30 × 0.25 × 0.20 mm, a = 9.739(1), b = 8.135(1), c = 12.652(1) Å, β = 109.59(1)°, V = 944.4(2) Å^3, $\rho_{calcd.}$ = 1.313 g cm^{-3}, μ = 8.03 cm^{-1}, empirical absorption correction ($0.795 \le T \le 0.856$), Z = 2, monoclinic, space group $P2_1$ (no. 4), λ = 0.71073 Å, T = 198 K, ω and φ scans, 5835 reflections collected (±h, ±k, ±l), [(sinθ)/λ] = 0.68 Å^{-1}, 4060 independent (R_{int} = 0.042) and 3663 observed reflections [$I \ge 2\sigma(I)$], 229 refined parameters, R = 0.036, wR^2 = 0.083, Flack parameter 0.04(2), max. residual electron density 0.24 (−0.34) e·Å^{-3}, hydrogen atoms calculated and refined as riding atoms.

X-ray Crystal Structure Analysis of *ent*-10b: Empirical formula $C_{23}H_{27}FeN$, M = 373.32, yellow crystal, 0.35 × 0.25 × 0.20 mm, a = 9.737(1), b = 8.135(1), c = 12.634(1) Å, β = 109.59(1)°, V = 942.8(2) Å^3, $\rho_{calcd.}$ = 1.315 g cm^{-3}, μ = 8.04 cm^{-1}, empirical absorption correction ($0.766 \le T \le 0.856$), Z = 2, monoclinic, space group $P2_1$ (no. 4), λ = 0.71073 Å, T = 198 K, ω and φ scans, 8847 reflections collected (±h, ±k, ±l), [(sinθ)/λ] = 0.67 Å^{-1}, 4119 independent (R_{int} = 0.030) and 3969 observed reflections [$I \ge 2\sigma(I)$], 229 refined parameters, R = 0.023, wR^2 = 0.057, Flack parameter −0.02(1), max. residual electron density 0.18 (−0.41) e·Å^{-3}, hydrogen atoms calculated and refined as riding atoms.

Synthesis of 11: A suspension of (1*R*,3*R*,5*R*)-**10a** (245 mg, 0.65 mmol) and Pd/C catalyst (25 mg, 10% Pd) in MeOH (12.5 mL) was hydrogenated at 0.75 bar under vigorous stirring for 90 min. The reaction mixture was filtered through Celite and the solvent removed in vacuo to yield (1*R*,3*R*)-**11** as a yellow solid (161 mg, 91%), m.p. 99 °C (DSC). IR (KBr): ṽ = 3552 (sh), 3493 (sh), 3420 (s), 3236 (sh), 2972 (m), 1657 (m), 1617 (m), 1137 (m), 801 (m) cm^{-1}. Crystals suitable for the X-ray structure analysis were grown by slow evaporation of an Et_2O solution. ^1H NMR (599.9 MHz, $CDCl_3$, 25 °C): δ = 1.21 [d, $^3J_{H,H}$ = 7.3 Hz, 3 H, C(7)−H], 2.00 [ddd, $^3J_{H,H}$ = 3.0, $^3J_{H,H}$ = 7.5, $^2J_{H,H}$ = 13.6 Hz, 1 H, C(8)−H_{exo}], 2.20 [ddd, $^3J_{H,H}$ = 3.1, $^3J_{H,H}$ = 8.0, $^2J_{H,H}$ = 13.6 Hz, 1 H, C(8)−H_{endo}], 2.39 [s, 3 H, C(15)−H], 2.50 [ddd, $^3J_{H,H}$ = 3.1, $^3J_{H,H}$ = 7.3, $^3J_{H,H}$ = 7.5 Hz, 1 H, C(6)−H], 3.28 [dd, $^3J_{H,H}$ = 3.0, $^3J_{H,H}$ = 8.0 Hz, 1 H, C(9)−H], 3.99 [m, 2 H, C(2−5)−H, C(11−14)−H], 4.00 [m, 1 H, C(2−5)−H], 4.03 [m, 2 H, C(11−14)−H], 4.06 [m, 1 H, C(2−5)−H], 4.07 [m, 1 H, C(2−5)−H], 4.20 [m, 1 H, C(11−14)−H] ppm. $^{13}C\{^1H\}$ NMR (150.8 MHz, $CDCl_3$, 25 °C): δ = 19.4 [C(7)], 25.5 [C(6)], 35.0 [C(15)], 49.9 [C(8)], 53.0 [C(9)], 66.5 [C(11−14)], 66.9 [C(2−5)], 67.8 [C(2−5)/C(11−14)], 68.1 [C(11−14)], 68.2 [C(11−14)], 68.3 [C(2−5)], 69.0 [C(2−5)/C(11−14)], 69.2 [C(2−5)], 87.9 [C(10)], 91.5 [C(1)] ppm. (1*R*,3*R*)-**11**: $[\alpha]_D^{20}$ = +105 ($c = 2 \times 10^{-3}$ g mL^{-1}, CH_3CN). CD: Δε (λ_{max}) = +0.87 (275), −0.07 (334), +0.39 (416), −0.09 (483) ($c = 4 \times 10^{-4}$ g mL^{-1}, CH_3CN). $C_{15}H_{19}FeN$ (269.17): calcd. C 66.93, H 7.11, N 5.20; found C 66.75, H 6.97, N 5.13. The complex (1*S*,3*S*)-**11** was prepared analogously starting from

 © 2003 Wiley-VCH Verlag GmbH & Co. KGaA, Weinheim

(793 mg, 1.12 mmol) of (1*S*,3*S*,5*R*)-**10b**, 720 mg (90%) isolated. $[\alpha]_D^{20} = -104$ ($c = 2 \times 10^{-3}$ g mL^{-1}, CH_3CN). CD: $\Delta\varepsilon$ (λ_{max}) = −0.86 (275), +0.09 (334), −0.38 (416), +0.09 (483) ($c = 4 \times 10^{-4}$ g mL^{-1}, CH_3CN). $C_{15}H_{19}FeN$ (269.17): calcd. C 66.93, H 7.11, N 5.20; found C 66.74, H 6.90, N 5.13.

X-ray Crystal Structure Analysis of (1*R*,3*R*)-11: Empirical formula $C_{15}H_{19}FeN$, $M = 269.17$, yellow crystal, 0.25 × 0.15 × 0.10 mm, $a = 7.420(1)$, $b = 10.017(1)$, $c = 8.255(1)$ Å, $\beta = 99.29(1)°$, $V = 605.5(1)$ Å^3, $\rho_{calcd.} = 1.476$ g cm^{-3}, $\mu = 12.20$ cm^{-1}, empirical absorption correction ($0.750 \le T \le 0.888$), $Z = 2$, monoclinic, space group $P2_1$ (no. 4), $\lambda = 0.71073$ Å, $T = 198$ K, ω and φ scans, 4068 reflections collected ($\pm h$, $\pm k$, $\pm l$), [(sinθ)/λ] = 0.66 Å^{-1}, 2503 independent ($R_{int} = 0.028$) and 2385 observed reflections [$I \ge 2\sigma(I)$], 159 refined parameters, $R = 0.026$, $wR^2 = 0.065$, Flack parameter 0.02(2), max. residual electron density 0.33 (−0.33) e·Å^{-3}, hydrogen atom at N1 from difference map, others calculated and all refined as riding atoms.

X-ray Crystal Structure Analysis of (1*S*,3*S*)-11: Empirical formula $C_{15}H_{19}NFe$, $M = 269.17$, yellow crystal, 0.30 × 0.30 × 0.20 mm, $a = 7.415(1)$, $b = 10.009(1)$, $c = 8.250(1)$ Å, $\beta = 99.26(1)°$, $V = 604.3(1)$ Å^3, $\rho_{calcd.} = 1.479$ g cm^{-3}, $\mu = 12.23$ cm^{-1}, empirical absorption correction ($0.711 \le T \le 0.792$), $Z = 2$, monoclinic, space group $P2_1$ (no. 4), $\lambda = 0.71073$ Å, $T = 198$ K, ω and φ scans, 3352 reflections collected ($\pm h$, $\pm k$, $\pm l$), [(sinθ)/λ] = 0.68 Å^{-1}, 2467 independent ($R_{int} = 0.030$) and 2349 observed reflections [$I \ge 2\sigma(I)$], 159 refined parameters, $R = 0.033$, $wR^2 = 0.088$, Flack parameter 0.00(2), max. residual electron density 0.50 (−0.62) e·Å^{-3}, hydrogen atom at N1 from difference map, others calculated and all refined as riding atoms.

(1*R*,3*R*)-11: The complex (1*R*,3*R*)-**11** was prepared analogously starting from (1*R*,3*R*,5*S*)-**10b** (1.00 g, 2.68 mmol), 0.65 g (91%) were isolated.

(1*S*,3*S*)-11: The complex (1*S*,3*S*)-**11** was prepared analogously starting from (1*S*,3*S*,5*S*)-**10a** (250 mg, 0.67 mmol), 175 mg (97%) were isolated.

Synthesis of 12: A solution of L-(−)-*O*,*O*′-dibenzoyltartaric acid (3.94 g, 11.0 mmol) in MeOH (21 mL) was heated to 60 °C and added to a solution of *rac*-*trans*-**6** (3.12 g, 11.0 mmol) in MeOH (11 mL) at this temperature. The mixture was heated to reflux for 1 h. Next, it was allowed to gradually cool to room temperature over the course of 4 h. After storage at 4 °C overnight, a yellow precipitate was collected and washed with cold MeOH. The mother liquor and the filtrates were combined and freed from solvent in vacuo. The precipitate and the residue were individually converted into the free bases by treatment with NEt_3 (1.6 mL, 11.5 mmol) and extraction with water/Et_2O. The organic phases were washed with water and brine and dried with $MgSO_4$. After removal of the solvent, the yield was 0.98 g (3.46 mmol) from the former precipitate and 1.01 g (3.57 mmol) from the former mother liquor. In a second resolution step, the free base from the former precipitate was again treated with L-(−)-*O*,*O*′-dibenzoyltartaric acid (1.24 g, 3.46 mmol) in MeOH (10.4 mL) under reflux (1 h) and processed as described above. Optically enriched (1*R*,3*R*)-**6** was obtained as a yellow solid (0.720 g, 2.55 mmol, 23%). $[\alpha]_D^{20} = +71$ ($c = 4 \times 10^{-3}$ g mL^{-1}, CH_3CN). Crystals of the L-tartrate salt (**12**) suitable for X-ray structure analysis were grown by reaction of a solution of optically enriched (1*R*,3*R*)-**6** (50 mg, 0.18 mmol) in MeOH (1 mL) with a solution of L-tartaric acid (26 mg, 0.18 mmol) in MeOH (1 mL). The reaction mixture was heated to 70 °C and slowly cooled to room temperature. The precipitate was collected, redissolved in MeOH (0.5 mL) and Et_2O was allowed to slowly diffuse into this solution. The free base from the former mother liquor was treated with D-(+)-*O*,*O*′-dibenzoyltartaric acid (1.28 g, 3.57 mmol) in MeOH (10.7 mL) under reflux (1 h) and processed as described above. Optically enriched (1*S*,3*S*)-**6** was obtained as a yellow solid (0.72 g, 2.55 mmol, 23%). $[\alpha]_D^{20} = +72$ ($c = 4 \times 10^{-3}$ g mL^{-1}, CH_3CN). Crystals of the D-tartrate salt (*ent*-**12**) suitable for X-ray structure analysis were grown by reaction of a solution of optically enriched (1*S*,3*S*)-**6** (50 mg, 0.18 mmol) in MeOH (1 mL) with a solution of D-tartaric acid (26 mg, 0.18 mmol) in MeOH (1 mL). The reaction mixture was heated to 70 °C and slowly cooled to room temperature. The precipitate was collected, redissolved in MeOH (0.5 mL) and Et_2O was allowed to slowly diffuse into this solution. Amine exchange with (*R*)-**8** (see **10**) followed by integration of suitable signals in the ^{1}H NMR spectrum showed an enantiomeric excess of 78% after the tartrate resolution.

X-ray Crystal Structure Analysis of (1*R*,3*R*)-12: Empirical formula $C_{16}H_{22}FeN{\cdot}0.5\ C_4H_4O_6$, $M = 358.23$, yellow crystal, 0.30 × 0.15 × 0.07 mm, $a = 16.234(1)$, $b = 8.513(1)$, $c = 12.723(1)$ Å, $\beta = 109.84(1)°$, $V = 1654.0(3)$ Å^3, $\rho_{calcd.} = 1.439$ g cm^{-3}, $\mu = 9.26$ cm^{-1}, empirical absorption correction ($0.769 \le T \le 0.938$), $Z = 4$, monoclinic, space group $C2$ (no. 5), $\lambda = 0.71073$ Å, $T = 293$ K, ω and φ scans, 5331 reflections collected ($\pm h$, $\pm k$, $\pm l$), [(sinθ)/λ] = 0.66 Å^{-1}, 3401 independent ($R_{int} = 0.027$) and 3154 observed reflections [$I \ge 2\sigma(I)$], 215 refined parameters, $R = 0.031$, $wR^2 = 0.068$, Flack parameter −0.01(2), max. residual electron density 0.32 (−0.42) e·Å^{-3}, hydrogen atom at N1 from difference map, others calculated and all refined as riding atoms.

X-ray Crystal Structure Analysis of (1*S*,3*S*)-12: Empirical formula $C_{16}H_{22}FeN{\cdot}0.5\ C_4H_4O_6$, $M = 358.23$, yellow crystal, 0.35 × 0.20 × 0.05 mm, $a = 16.168(1)$, $b = 8.457(1)$, $c = 12.715(1)$ Å, $\beta = 110.15(1)°$, $V = 1632.1(3)$ Å^3, $\rho_{calcd.} = 1.458$ g cm^{-3}, $\mu = 9.38$ cm^{-1}, empirical absorption correction ($0.735 \le T \le 0.955$), $Z = 4$, monoclinic, space group $C2$ (no. 5), $\lambda = 0.71073$ Å, $T = 198$ K, ω and φ scans, 5402 reflections collected ($\pm h$, $\pm k$, $\pm l$), [(sinθ)/λ] = 0.66 Å^{-1}, 3475 independent ($R_{int} = 0.029$) and 3324 observed reflections [$I \ge 2\sigma(I)$], 215 refined parameters, $R = 0.027$, $wR^2 = 0.061$, Flack parameter −0.01(1), max. residual electron density 0.29 (−0.28) e·Å^{-3}, hydrogen atom at N1 from difference map, others calculated and all refined as riding atoms.

Acknowledgments

Financial support from the Fonds der Chemischen Industrie and the Deutsche Forschungsgemeinschaft is gratefully acknowledged.

[1] A. Togni, T. Hayashi (Eds.), *Ferrocenes: Homogenous Catalysis, Organic Synthesis, Materials Science*, VCH, Weinheim, **1995**.
[2] [2a] Josiphos: A. Togni, C. Breutel, A. Schnyder, F. Spindler, H. Landert, A. Tijani, *J. Am. Chem. Soc.* **1994**, *116*, 4062−4066. [2b] Walphos: T. Sturm, W. Weissensteiner, F. Spindler, *Adv. Synth. Catal.* **2003**, *345*, 160−164.
[3] [3a] G. Tainturier, K. Chhor y Sok, B. Gautheron, *C. R. Acad. Sci. Paris C* **1973**, 1269−1270. [3b] K. Chhor y Sok, G. Tainturier, B. Gautheron, *Tetrahedron Lett.* **1974**, *25*, 2207−2208. [3c] K. Chhor y Sok, G. Tainturier, B. Gautheron, *J. Organomet. Chem.* **1977**, *132*, 173−189.
[4] [4a] A. Mernyi, C. Kratky, W. Weissensteiner, M. Widhalm, *J. Organomet. Chem.* **1996**, *508*, 209−218. [4b] F. Gómez-de la Torre, F. A. Jalón, A. López-Agenjo, B. R. Manzano, A. Rodríguez, T. Sturm, W. Weissensteiner, M. Martínez-Ripoll, *Organometallics* **1998**, *17*, 4634−4644. [4c] F. A. Jalón, A. López-Agenjo, B. R. Manzano, M. Moreno-Lara, A. Rodríguez, T. Sturm, W. Weissensteiner, *J. Chem. Soc., Dalton Trans.* **1999**, 4031−4039. [4d] T. Sturm, W. Weissensteiner, K. Mereiter, T.

 © 2003 Wiley-VCH Verlag GmbH & Co. KGaA, Weinheim

Kégl, G. Jeges, G. Petölz, L. Kollár, *J. Organomet. Chem.* **2000**, *595*, 93−101. [4e] E. M. Caynela, L. Xiao, T. Sturm, B. R. Manzano, F. A. Jalón, W. Weissensteiner, *Tetrahedron: Asymmetry* **2000**, *11*, 861−869. [4f] B. R. Manzano, F. A. Jalón, F. Gómez-de la Torre, A. M. López-Agenjo, A. M. Rodríguez, K. Mereiter, W. Weissensteiner, T. Sturm, *Organometallics* **2002**, *21*, 789−802. [4g] T. Sturm, W. Weissensteiner, F. Spindler, K. Mereiter, A. M. López-Agenjo, B. R. Manzano, F. A. Jalón, *Organometallics* **2002**, *21*, 1766−1774.

[5] M. Weißenbach, T. Sturm, K. Kalchhauser, C. Kratky, W. Weissensteiner, *Monatsh. Chem.* **2002**, *133*, 991−1009.

[6] [6a] M. Rosenblum, R. B. Woodward, *J. Am. Chem. Soc.* **1958**, *80*, 5443−5449. [6b] A. N. Nesmeyanov, E. V. Leonova, N. S. Kochetkova, A. I. Malkova, *J. Organomet. Chem.* **1975**, *96*, 271−274.

[7] W. A. White, H. Weingarten, *J. Org. Chem.* **1967**, *32*, 213−214.

[8] [8a] S. Knüppel, R. Fröhlich, G. Erker, *J. Organomet. Chem.* **1999**, *586*, 218−222. [8b] S. Knüppel, R. Fröhlich, G. Erker, *J. Organomet. Chem.* **2000**, *595*, 308−312.

[9] [9a] S. Knüppel, G. Erker, R. Fröhlich, *Angew. Chem.* **1999**, *111*, 2048−2051; *Angew. Chem. Int. Ed.* **1999**, *38*, 1923−1926. [9b] S.-D.Bai, X.-H. Wei, J.-P. Guo, D.-S. Liu, Z.-Y. Zhou, *Angew. Chem.* **1999**, *111*, 2051−2054; *Angew. Chem. Int. Ed.* **1999**, *38*, 1926−1928.

[10] P. Liptau, S. Knüppel, G. Kehr, O. Kataeva, R. Fröhlich, G. Erker, *J. Organomet. Chem.* **2001**, *637*, 621−630.

[11] P. Liptau, T. Seki, G. Kehr, A. Abele, R. Fröhlich, G. Erker, S. Grimme, *Organometallics* **2003**, *22*, 2226−2232.

[12] [12a] E. Drent, P. H. M. Budzelaar, *Chem. Rev.* **1996**, *96*, 663−681. [12b] C. Bianchini, A. Meli, *Coord. Chem. Rev.* **2002**, *225*, 35−66.

[13] L. A. Paquette, J. Tae, *J. Org. Chem.* **1998**, *63*, 2022−2030.

[14] K. L. Brown, L. Damm, J. Dunitz, A. Eschenmoser, R. Hobi, C. Kratky, *Helv. Chim. Acta* **1978**, *61*, 3108−3135.

[15] F. H. Allen, O. Kennard, D. G. Watson, L. Brammer, A. G. Open, *J. Chem. Soc., Perkin Trans. 2.* **1987**, S1−S19.

[16] [16a] M. Reetz, M. W. Drewes, A. Schmitz, *Angew. Chem.* **1987**, *99*, 1186−1187; *Angew. Chem. Int. Ed. Engl.* **1987**, *26*, 1141. [16b] W. H. Hartung, R. Simonoff, *Org. React.* **1953**, *7*, 263. [16c] J.-L. Vasse, V. Levacher, J. Bourguignon, G. Dupas, *Tetrahedron: Asymmetry* **2002**, *13*, 227−232.

[17] K. Schlögl, M. Fried, *Monatsh. Chem.* **1964**, *95*, 558−575.

[18] [18a] D. Marquarding, H. Klusacek, G. Gokel, P. Hoffmann, I. Ugi, *J. Am. Chem. Soc.* **1970**, *92*, 5389−5393. [18b] G. Gokel, D. Marquarding, I. Ugi, *J. Org. Chem.* **1972**, *37*, 3052−3058. [18c] T. Hayashi, T. Mise, M. Fukushima, M. Kagotani, N. Nagashima, Y. Hamada, A. Matsumoto, S. Kawakami, M. Konishi, K. Yamamoto, M. Kumada, *Bull. Chem. Soc. Jpn.* **1980**, *53*, 1138−1151. [18d] C. Ganter, T. Wagner, *Chem. Ber.* **1995**, *128*, 1157−1161.

[19] [19a] For related (fulvene)metal-type structures, see e.g.: M. Watanabe, I. Motoyama, T. Takayama, *J. Organomet. Chem.* **1996**, *524*, 9−18. [19b] See also: V. Kupfer, U. Thewalt, I. Tišlerová, P. Štepnicka, R. Gyepes, J. Kubišta, M. Horácek, K. Mach, *J. Organomet. Chem.* **2001**, *620*, 39−50.

[20] [20a] A. Togni, R. Häusle, *Synlett* **1990**, 633−535. [20b] A. Togni, G. Rihs, R. E. Blumer, *Organometallics* **1992**, *11*, 613−621.

[21] [21a] C. Gambs, S. Chaloupka, G. Consiglio, A. Togni, *Angew. Chem.* **2000**, *112*, 2602−2604; *Angew. Chem. Int. Ed.* **2000**, *39*, 2486−2488. [21b] C. Gambs, G. Consiglio, A. Togni, *Helv. Chim. Acta* **2001**, *84*, 3105−3126.

[22] S. Braun, H.-O. Kalinowski, S. Berger, *150 and More Basic NMR Experiments*, Wiley-VCH, Weinheim, **1995**.

[23] Z. Otwinowski, W. Minor, *Methods Enzymol.* **1997**, *276*, 307−326.

[24] R. H. Blessing, *Acta Crystallogr., Sect. A* **1995**, *51*, 33−37; R. H. Blessing, *J. Appl. Crystallogr.* **1997**, *30*, 421−426

[25] SHELXS-97: G. M. Sheldrick, *Acta Crystallogr., Sect. A* **1990**, *46*, 467−473

[26] SHELXL-97: G. M. Sheldrick, Universität Göttingen, **1997**.

[27] SCHAKAL: E. Keller, Universität Freiburg, **1997**.

Received March 19, 2003

 © 2003 Wiley-VCH Verlag GmbH & Co. KGaA, Weinheim

Synthesis, Equilibrium and Kinetic Properties of Gd^{3+} Complexes of Three DTPA-Bis(Amide) Derivatives Containing Stable Nitroxide Free Radical Substituents

Zoltán Jászberényi,[a] Ernő Brücher,*[a] József Jekő,[b] Kálmán Hideg,[c] Tamás Kálai,[c] and Róbert Király[a]

Keywords: Chelates / Imaging agents / Kinetics / Lanthanides / Radicals

Two new DTPA-bis(amide) derivatives containing stable nitroxide free radicals, H_3L^2 and H_3L^3, were synthesized. The complexation properties of L^2 and L^3 with Gd^{3+} were compared with those of H_3L^1, synthesized earlier. The sums of the protonation constants $\Sigma\log K_i^H$ of the DTPA-bis(amide) derivative ligands with stable nitroxide free radicals are somewhat higher than that for DTPA-bis(methylamide) (H_3L^4). The ligands L^1, L^2, and L^3 form complexes with a metal-to-ligand ratio of 1:1 with Gd^{3+} (GdL), while the species formed with Zn^{2+} are ZnL, ZnHL, ZnH_2L, and Zn_2L. The formation of the dinuclear complex Zn_2L results in a lower selectivity of the ligands for Gd^{3+} over Zn^{2+} than was assumed for L^4. The relaxivities of the complexes GdL^1, GdL^2, and GdL^3 are close to the sums of the relaxivities of the complex GdL^4 and of the free ligands L^1, L^2, and L^3. The relaxivities of GdL^1, GdL^2, and GdL^3 are practically independent of temperature in the 7–30 °C range, which is probably a result of the relatively long lifetime of the water molecules in the inner spheres of the [$GdL(H_2O)$] complexes. The kinetic stabilities of the Gd^{3+} complexes were characterized by the rates of the exchange reactions taking place between the complexes GdL and Lu^{3+} or Zn^{2+}. The reactions occur through the proton-assisted dissociation of the complexes, with the formation of a protonated intermediate. Another pathway is the direct reaction between the Gd^{3+} complex and Lu^{3+} or Zn^{2+}, which occurs with the formation of a dinuclear intermediate, GdLM. The exchange reactions proceed about five times more rapidly with Zn^{2+} than with Lu^{3+}, indicating the importance of the formation of an intermediate containing an N–Zn^{2+} bond, which is stronger than the N–Lu^{3+} bond in an intermediate with similar structure. The exchange reactions of the complex GdL^3 formed with the disubstituted ligand L^3 are significantly slower than those of the complexes of the monosubstituted ligands L^1 and L^2.
(© Wiley-VCH Verlag GmbH & Co. KGaA, 69451 Weinheim, Germany, 2003)

Introduction

The Gd^{3+} complex of diethylenetriamine-*N*,*N*,*N*′,*N*′′,*N*′′-pentaacetic acid (H_5DTPA) is a clinically used contrast agent in magnetic resonance imaging (MRI). The negative charges on $Gd(DTPA)^{2-}$ are neutralized with methylglucosamine cations, so the osmotic pressure in the body fluids after intravenous administration of the contrast agent is relatively high.[1a−1c] Nonionic Gd^{3+} complexes are formed with the ligands obtained by replacement of two terminal carboxylates of DTPA with uncharged functional groups.[2] Of the uncharged functionalities investigated, the amide group has proven to be most suitable because it forms the strongest bonds with lanthanide(III) ions (Ln^{3+}).[3,4] The nonionic complexes [Gd(DTPA-BMA)] and [Gd(DTPA-BMEA)] are clinically used MRI contrast agents (H_3DTPA-BMA = H_3L^4 and H_3DTPA-BMEA = H_3L^5, see Scheme 1).[2,5−7] The stability constants of the Gd^{3+} complexes formed with the DTPA-bis(amide) derivative ligands are significantly lower than that of $[Gd(DTPA)]^{2-}$.[3,5−7] However, the selectivity of DTPA-BMA for Gd^{3+} over the endogenous Zn^{2+} was found to be significantly higher than that of DTPA, and as a consequence of the favorable selectivity, [Gd(DTPA-BMA)] is a safe contrast agent.[5]

The results of NMR spectroscopic and X-ray structural studies revealed that the octadentate DTPA-bis(amide) derivative ligands coordinate to Ln^{3+} through three amine nitrogen atoms, and three carboxylate and two amide oxygen atoms.[6−11] The ninth coordination site is occupied by an H_2O molecule, as found by fluorescence-lifetime measurements on the complexes of Eu^{3+}.[6,12] The rate of exchange of the H_2O molecule between the nonionic complexes [$Gd(DTPA\text{-}BMA)(H_2O)$] or [$Gd(DTPA\text{-}BMEA)(H_2O)$]

[a] University of Debrecen, Department of Inorganic and Analytical Chemistry,
4010 Debrecen, Hungary
Fax: (internat.) +36-52/489-667
E-mail: ebrucher@delfin.klte.hu
[b] ICN Hungary LTD,
4440 Tiszavasvári, Hungary
[c] University of Pécs, Institute of Organic and Medicinal Chemistry,
7643 Pécs, Hungary

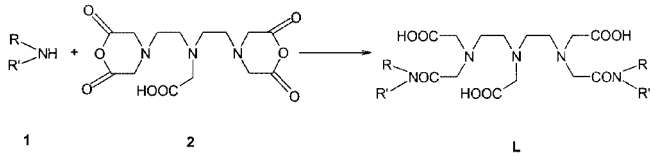

R	H	H		H	CH_3
R'			CH_3	$CH_2CH_2OCH_3$	
1	a	b	c		
Ligand	L^1	L^2	L^3	L^4	L^5

Scheme 1

and bulk water, as studied by ^{17}O NMR spectroscopy, was found to be about 10 times lower than that for $[Gd(DTPA)(H_2O)]^{2-}$.[10,13,14]

The successful use of [Gd(DTPA-BMA)] as a nonionic contrast agent has resulted in growing interest in the synthesis and study of new DTPA-bis(amide) derivative ligands and their Gd^{3+} complexes. Through the use of different alkyl- and arylamines, a number of new ligands have been synthesized.[15−22] The structures and relaxation properties of the Gd^{3+} complexes formed with these ligands are similar to those of [Gd(DTPA-BMA)] and [Gd(DTPA-BMEA)].

Besides the paramagnetic metal complexes, nitroxide-stable free radicals are also known to increase the relaxation rates of water protons. The relaxation properties of several five-membered pyrrolidine and six-membered piperidine derived free radicals have been studied as potential contrast agents.[23−27] In order to increase the relaxation effect of Gd^{3+} complexes, Sosnovsky et al. synthesized a DTPA-bis(amide) derivative ligand (L^1 in Scheme 1) labeled with two piperidine-*N*-oxyl free radicals.[28] The increase in the relaxation effect of the complex GdL^1 was not significant, but attachment of GdL^1 to bovine serum albumin resulted in a spin-labeled macromolecule with high relaxivity.[29] As far as we know, however, the complexation properties of the ligands with stable nitroxide free radicals, the stability constants, and the kinetic stability of the Gd^{3+} complex have not yet been studied.

We recently synthesized two new DTPA-bis(amide) derivatives containing stable nitroxide free radical moieties (L^2 and L^3 in Scheme 1) and compared their complexation properties and their selectivities for Gd^{3+} over Zn^{2+} with those of L^1. The kinetic stabilities of the Gd^{3+} complexes were also studied by investigation of the rates of the exchange reactions between the Gd^{3+} complexes and Lu^{3+} or Zn^{2+}. We set out to obtain information on how the presence of bulky free radicals affects the equilibria and kinetic properties of the complexes.

Results and Discussion

Protonation and Stability Constants

The titration curves of L^1, L^2, and L^3 reveal two different buffer regions, in the pH ranges about 4−7 and 8−10. Typical titration curves of L^1 in the absence and in the presence of equivalent amounts of Gd^{3+} or Zn^{2+} are shown in Figure 1. The number of titration data points used to calculate the protonation constants of L^1, L^2, and L^3 were 213, 180, and 279, respectively. The protonation constants (K_i^H) are defined as described in Equation (1), where i = 1, 2, ... 5.

$$K_i^H = [H_iL]/\{[H_{i-1}L][H^+]\} \quad (1)$$

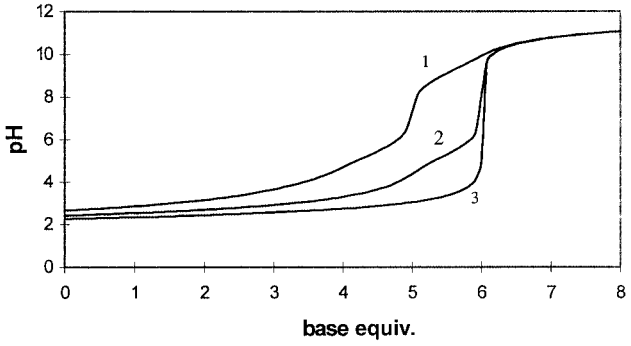

Figure 1. Titration curves of the ligand L^1 (1) alone or in the presence of Zn^{2+} (2) or Gd^{3+} (3), $[L^1] = [Zn^{2+}] = [Gd^{3+}] = 1 \times 10^{-3}$ M

The calculated protonation constants are presented in Table 1, which also gives the known protonation constants for L^4 and L^5 for comparison.

Table 1. Protonation constants of the ligands L^1, L^2, L^3 (25 °C, 0.1 M KCl), L^4 and L^5 (25 °C, 0.1 M $NaClO_4$)

	L^1	L^2	L^3	L^4 [a]	L^5[b]
$\log K_1^H$	9.13 (0.07)	8.99 (0.03)	9.46 (0.05)	9.37	9.40
$\log K_2^H$	5.40 (0.09)	5.07 (0.04)	5.82 (0.07)	4.38	6.22
$\log K_3^H$	3.87 (0.09)	3.81 (0.04)	4.21 (0.07)	3.31	3.99
$\log K_4^H$	2.90 (0.08)	2.57 (0.05)	3.01 (0.07)	1.43	2.26
$\log K_i^H$	21.30	20.44	22.50	18.49	21.87

[a] Ref.[6] [b] Ref.[7]

The first protonation constants of the different DTPA-bis(amide) derivative ligands are quite similar. The second protonation constants are somewhat lower for L^1 and L^2, containing two monosubstituted -C(O)NHR amide groups, than for L^3, containing two disubstituted -C(O)NR_2 amide groups. Similar results were found for L^4 and L^5, so the amide group does not decrease the $\log K_2^H$ value of the DTPA derivative so significantly if both amide hydrogens

 © 2003 Wiley-VCH Verlag GmbH & Co. KGaA, Weinheim

are replaced with alkyl (or aryl) groups.[7] This result was explained by the assumption of the formation of more hydrogen bonds in the ligands containing amide [-C(O)NHR] hydrogen atoms.[7]

The titration curves of the ligands obtained in the presence of equivalent amounts of Zn^{2+} (Figure 1) could be fitted with lower values of the standard deviations and fitting parameters (the difference between the experimentally ascertained and the calculated volumes of base needed to attain a given pH value) if formation of the species ZnL, ZnHL and ZnH_2L was assumed. The stability constants are defined as described in Equation (2), where $i = 0$, 1 or 2.

$$K_{MH,L} = [MH_iL]/\{[M][H_iL]\} \quad (2)$$

The stability constants, calculated by use of 214, 202, and 220 data points for L^1, L^2, and L^3, respectively, are presented in Table 2. The formation of mono- and diprotonated complexes is probably a consequence of the presence of more basic donor atoms in the ligands than the number of Zn^{2+} coordination sites. The complexes with Zn^{2+} are mainly formed in the pH range from 3−6, whereas the formation of Gd^{3+} complexes starts at pH values lower than 1.7 (the extent of complex formation at pH = 1.7 is about 50−60%) and it is completed at pH values around 3. Through the use of the titration data obtained in the pH range from 1.7−3 it was possible to calculate reliable stability constants, as indicated by the relatively low values of the standard deviations and fitting parameters. Similarly to the other DTPA−bis(amides) L^4 and L^5, the ligands L^1, L^2, and L^3 form only the species GdL, since the coordination number of Gd^{3+} practically agrees with the number of ligand donor atoms. This is probably the reason why the complexes GdL do not form dinuclear complexes in the presence of excess Gd^{3+}. In the ZnL^--Zn^{2+} systems, however, the formation of dinuclear complexes Zn_2L is possible because of the existence of free functional groups of the coordinated ligands. The differences between the titration curves obtained in the absence and the presence of excess Zn^{2+} clearly indicate the competition between H^+ and Zn^{2+} for the ZnL complexes. The stability constants of the dinuclear complexes Zn_2L [Equation (3)] were calculated from the titration data (42, 61 and 100 data points for the systems ZnL^1-Zn^{2+}, ZnL^2-Zn^{2+}, and ZnL^3-Zn^{2+}, respectively), and the $\log K_{M_2L}$ values are presented in Table 2.

$$K_{M_2L} = [M_2L]/\{[ML][M]\} \quad (3)$$

The formation of the dinuclear complexes Zn_2L results in more successful competition of Zn^{2+} with Gd^{3+} for the ligand, as found experimentally by Puttagunta et al.[30] These findings also mean that the selectivity of the DTPA-bis(amide) derivative ligands for Gd^{3+} over Zn^{2+} is lower than calculated by Cacheris et al.,[5] who assumed the formation only of the complexes ZnL and ZnHL.

The stability constants of the complexes of L^1, L^2, and L^3 with Gd^{3+} and Zn^{2+} are higher than those of the complexes with L^4 and L^5. This result can at least in part be interpreted in terms of the different media. In 0.1 M $NaClO_4$, Na^+ forms complexes with L^4 and L^5 more stable than those of K^+ with L^1, L^2, and L^3. The stronger competition of Na^+ with Gd^{3+} or Zn^{2+} for the ligand may result in some decrease in the stability constants in relation to the equilibrium constants observed in KCl solution.[31] Further, the basicity of L^1, L^2, and L^3 is higher than that of L^4 and L^5, as expressed in the values of the protonation constants.

Table 2. Stability constants ($\log K$) of the complexes Gd^{3+} and Zn^{2+} formed with the ligands L^1, L^2, L^3 (25 °C, 0.1 M KCl), L^4 and L^5 (25 °C, 0.1 M $NaClO_4$)

	L^1	L^2	L^3	L^4[a]	L^5[b]
GdL	18.51 (0.05)	17.80 (0.07)	19.87 (0.05)	16.38	17.68
ZnL	14.06 (0.03)	13.63 (0.03)	15.18 (0.02)	12.04	–
ZnHL	10.20 (0.02)	9.05 (0.01)	10.64 (0.01)	6.66	–
ZnH_2L	8.00 (0.02)	6.36 (0.06)	7.67 (0.01)	–	–
Zn_2L	3.97 (0.09)	3.57 (0.06)	3.30 (0.02)	–	–

[a] Ref.[6] [b] Ref.[7]

Relaxivities of the Ligands and Complexes

The relaxivities of the ligands with stable nitroxide free radicals, measured at 9 MHz, are significantly lower than those of their Gd^{3+} complexes. For L^1, L^2, and L^3, the relaxivities were found to be 0.68, 0.57, and 0.88 $mM^{-1}\cdot s^{-1}$, respectively. The relaxivities of the five- and six-membered nitroxide stable free radicals are around 0.26 $mM^{-1}\cdot s^{-1}$ (25 °C, 9 MHz). Comparison of these values indicates that the relaxivities of L^1 and L^2 are a little higher than the sums of the relaxivities of the free radicals attached to the DTPA-bis(amide), while that of L^3 is somewhat lower (the error in the measurement of the relaxivities is ≤ 5%). On the basis of EPR studies, Sosnowsky et al. assumed a weak exchange interaction between the free radicals attached to EDTA or DTPA.[28]

The relaxivities of the complexes GdL^1, GdL^2, and GdL^3 are 7.46, 6.11, and 6.60 $mM^{-1}\cdot s^{-1}$, respectively. Since the relaxivity of [Gd-DTPA-BMA] is about 5.5 $mM^{-1}\cdot s^{-1}$ (25 °C, 9 MHz), the attachment of the nitroxide free radicals to the Gd-DTPA-bis(amide) complexes resulted in a weak increase in relaxivity. The interaction between the unpaired electron of the free radicals and Gd^{3+} must be negligible because the free radicals are not coordinated in the inner sphere of Gd^{3+} and some magnetic interaction is possible only if the free radical is in the inner sphere.[32]

The relaxivities of L^1, L^2, and L^3 decrease with increasing temperature. The temperature dependence of the relaxivity of the complex $[Gd(DTPA)]^{2-}$ is similar: the relaxivity decreases with increasing temperature (Figure 2). The relaxation effect of free radicals (and partly the Gd^{3+} complexes) arises from the translational diffusion of the water molecules near the paramagnetic centers, which results in the so-called outer-sphere contribution. An increase in temperature increases the rates of diffusion, which results in a decrease in the relaxivity values.[1a,1b] The exchange between the water molecule(s) coordinated in the inner sphere

 © 2003 Wiley-VCH Verlag GmbH & Co. KGaA, Weinheim

of Gd^{3+} complexes and the bulk water also produces an increase in the relaxivities. The contribution of the inner sphere effect is determined predominantly by the rotation correlation time of the complex at suitable rates of water exchange {e.g. for $[Gd(DTPA)]^{2-}$}. Increasing temperatures bring about decreases in the rotation correlation times and in relaxivities, as observed for $[Gd(DTPA)]^{2-}$.[1a,1b,10] However, the relaxivities of the complexes GdL^1, GdL^2, and GdL^3 in the 7−30 °C range exhibit practically no change with increasing temperature (Figure 2). Similarly, the relaxivities of GdL^4 were found to be practically independent of temperature.[10] An increasing temperature also results in decreases in the rotation correlation times for the Gd^{3+} complexes of the DTPA-bis(amide) derivatives. However, the rates of water exchange on the complexes of the DTPA-bis(amide) derivatives are about 10 times lower at 25 °C than those for $[Gd(DTPA)]^{2-}$, and the slower water exchange results in lower relaxivity values.[10,13,19,33] Increasing temperature causes an increase in the rate of water exchange, which would result in an increase of the relaxivity but this increase is compensated by the decrease in the relaxivity due to the shortening of the rotation correlation time. These results indicate that the Gd^{3+} complexes formed with the DTPA-bis(amide) derivatives containing stable nitroxide free radicals behave similarly to the complexes of the other DTPA-bis(amide)derivatives, which regularly display inner-sphere lifetimes of the water molecules longer than those seen for the ionic Gd^{3+} complexes such as $[Gd(DTPA)]^{2-}$ and $[Gd(DOTA)]^{-}$.[10,13,19,33]

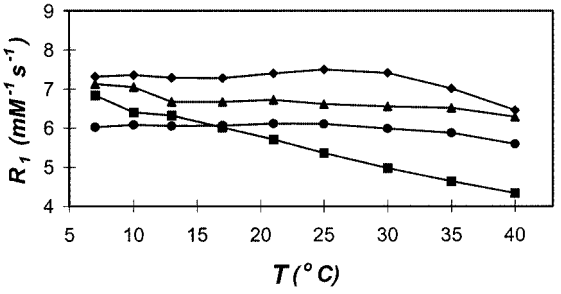

Figure 2. Temperature dependence of the relaxivities of the Gd^{3+} complexes (pH = 5, [GdL] = 1 × 10^{-3} M, 9 MHz) (◆ GdL^1, ● GdL^2, ▲ GdL^3, ■ $GdDTPA^{2-}$)

Kinetic Stabilities of Gd^{3+} Complexes

As far as the clinical use of Gd^{3+} complexes as MRI contrast agents is concerned, high kinetic stability is an important requirement. Since both Gd^{3+} and the aminopolycarboxylate ligand are toxic, the extent of dissociation of the complexes in the body has to be practically negligible. It has been proposed that the kinetic stabilities, measured in 0.1 M HCl (or $HClO_4$) are characterized by the rates of dissociation of the complexes.[34,35] In 0.1 M acid, the dissociation occurs predominantly through the proton-assisted dissociation of the complexes, and the role of direct reactions taking place through direct attack of the endogenous ions (e.g., Cu^{2+} or Zn^{2+}) on the complexes is neglected. In the dissociation of the DTPA and DTPA derivative complexes of Gd^{3+}, however, the direct reactions can be important, particularly at physiological pH values.[36,37]

The significance of the proton- and metal ion-assisted dissociation of complexes can be directly compared by study of the rates of the exchange reactions taking place between the Gd^{3+} complexes and some other Ln^{3+}, Cu^{2+} and Zn^{2+} species.[36,38] As the exchanging ion in this study we used Lu^{3+}, which forms more stable complexes than Gd^{3+} with L^1, L^2, and L^3, as indicated by the results of our preliminary experiments. Cu^{2+} could not be used as the exchanging ion because of its redox reactions with the free radicals. Of the endogenous ions, Zn^{2+} was used; this is present in the body fluids as an exchangeable species at relatively high concentrations.[39]

The rates of the exchange reactions were studied [in Equation (4), L = L^1, L^2 or L^3, and M = Lu^{3+} or Zn^{2+}].

$$GdL + M^{z+} \rightarrow ML^{(z-3)+} + Gd^{3+} \quad (4)$$

In the kinetic studies, the concentrations of the exchanging ions Lu^{3+} and Zn^{2+} were 20−60 times higher than the concentrations of the Gd^{3+} complexes. Under such conditions, the reactions can be regarded as pseudo-first order and the rates of the reactions can be expressed as in Equation (5), where k_p is a pseudo-first order rate constant, and $[GdL]_t$ is the total concentration of the Gd^{3+} complex.

$$-d[GdL]_t/dt = k_p [GdL]_t \quad (5)$$

The rates of the exchange reactions were studied at different concentrations of the exchanging Lu^{3+} and Zn^{2+} and at different pH values in the 4−5.2 range.

As can be seen in Table 2, the stability constants of the complexes ZnL formed with L^1, L^2, and L^3 are significantly lower than those of the respective Gd^{3+} complexes. Were only the complexes with a metal to ligand ratio of 1:1 formed, the extent of formation of Zn^{2+} complexes would be low. However, the relaxivities of the samples indicate that at equilibrium the Gd^{3+} is mostly present in the form of Gd^{3+}·aq species, which is possible only if some other Zn^{2+}-containing species is also formed besides the complexes ZnL, ZnHL, and ZnH_2L. This species is the dinuclear complex Zn_2L, as found in the equilibrium studies. In order to obtain reliable pseudo-first order rate constants, the rate data were used until about 60% conversion in the exchange reactions, and the k_p values were calculated by use of Equation (12). The relaxivities of the complexes GdL and the Gd^{3+}·aq ion were measured in separate experiments. The relaxivities of the complexes are presented above, while that of Gd^{3+}·aq is R_{Gd} = 16.9 mM^{-1}·s^{-1}. The pseudo-first order rate constants obtained are presented in Figure 3 and 4. The k_p values determined at different Lu^{3+} and Zn^{2+} concentrations are plotted against the H^+ concentration. As shown in Figure 3, the rates of the exchange reactions between the Gd^{3+} complexes and Lu^{3+} increase with rising H^+ concentration. The dependence can be expressed by a

 © 2003 Wiley-VCH Verlag GmbH & Co. KGaA, Weinheim

second degree equation for the H^+ concentration. However, the k_p values increase very slightly with increasing Lu^{3+} concentration. For the reactions with Zn^{2+} (Figure 4) the k_p values are directly proportional to the H^+ concentration and increase with increasing Zn^{2+} concentration.

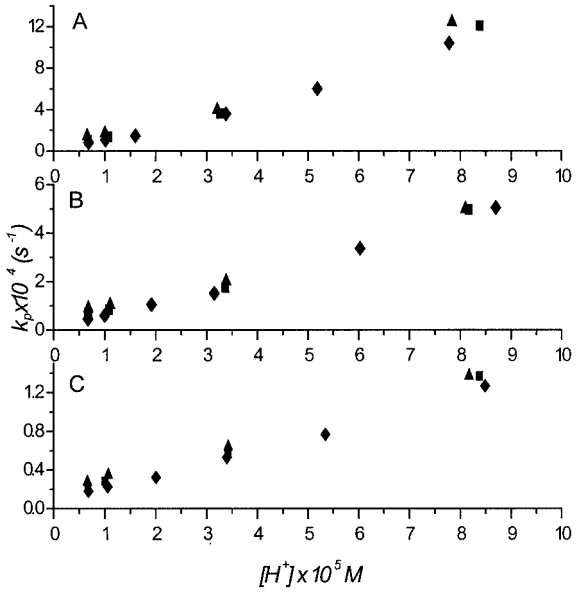

Figure 3. Rates of exchange reactions between Gd^{3+} complexes (5×10^{-4} M) and Lu^{3+}; $[Lu^{3+}] = 0.01$ M (◆), 0.02 M (■), and 0.03 M (▲) A: GdL^1; B: GdL^2, C: GdL^3 (25 °C, 1.0 M KCl)

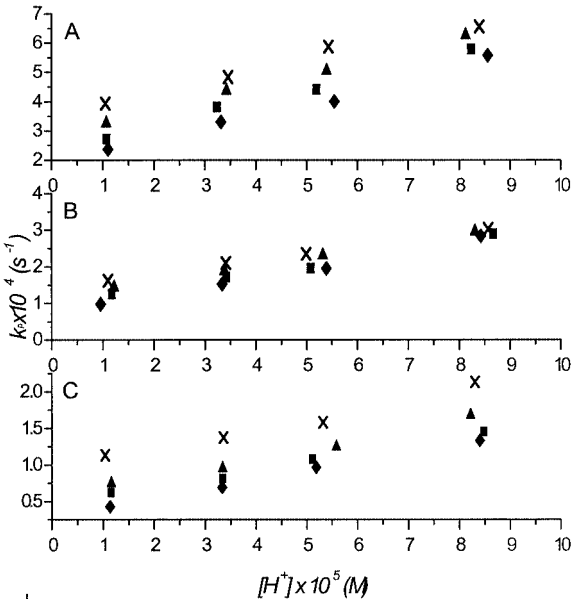

Figure 4. Rates of exchange reactions between Gd^{3+} complexes (5×10^{-4} M) and Zn^{2+}; $[Zn^{2+}] = 0.01$ M (◆), 0.015 M (■), 0.02 M (▲), and 0.03 M (×) A: GdL^1; B: GdL^2, C: GdL^3 (25 °C, 1.0 M KCl)

These findings are similar to those obtained for the exchange reactions of the DTPA and DTPA-mono(amide) complexes of Gd^{3+}.[36–38] The increases in the rates of the exchange reactions with increasing H^+ concentration can be interpreted in terms of the relatively slow, proton-assisted dissociation of Gd^{3+} complexes, which is followed by the fast reaction between the free ligand and the exchanging Lu^{3+} or Zn^{2+}. It can be assumed that H^+ protonates a carboxylate group of the ligand, which may be followed by the transfer of proton to a N atom when a glycinate functionality of the ligand becomes free, and the dissociation of the ligand can take place step by step.

The formation and dissociation of protonated complexes can be expressed as follows:

$$GdL + H^+ \overset{K_{GdHL}}{\rightleftharpoons} GdHL^+ \xrightarrow{k_{GdHL}} Gd^{3+} + HL^{2-} \quad (6)$$

The dissociation may occur more rapidly if a second proton is attached to the monoprotonated complex:

$$GdHL + H^+ \xrightarrow{k^H_{GdHL}} Gd^{3+} + H_2L^- \quad (7)$$

The increase in the exchange rate with increasing Lu^{3+} or Zn^{2+} concentration can be explained in terms of the direct attack of the exchanging metal ion on the complex, in which a dinuclear complex, GdLM, is formed, the ligand being transferred slowly, step by step, to the attacking ion:[36]

$$GdL + M^{z+} \overset{K_{GdLM}}{\rightleftharpoons} GdLM \xrightarrow{k_{GdLM}} ML + Gd^{3+} \quad (8)$$

From consideration of the reaction pathways [Equations (6)–(8)], the rates of the exchange reactions can be expressed as in Equation (9):

$$-d[GdL]_t/dt = k_{GdHL}[GdHL] + k^H_{GdHL}[GdHL][H^+] + k_{GdLM}[GdLM] \quad (9)$$

The pseudo-first order rate constant k_p can be expressed from Equations (5) and (9). By use of the expression for the total concentration of the complex, $[GdL]_t = [GdL] + [GdHL] + [GdLM]$, the equations defining the protonation constant $\{K_{GdHL} = [GdHL]/[GdL][H^+]\}$ and the stability constant of dinuclear complex $\{K_{GdLM} = [GdLM]/[GdL][M]\}$, k_p can be expressed as in Equation (10), where the rate constants $k_1 = k_{GdHL}K_{GdHL}$ and $k_2 = k^H_{GdHL}K_{GdHL}$ characterize the rates of the proton-assisted dissociation of the complexes, and $k_3 = k_{GdLM}K_{GdLM}$ is characteristic for the rates of exchange occurring through the direct attack of Lu^{3+} or Zn^{2+} on the complex:

$$k_p = \{k_1[H^+] + k_2[H^+]^2 + k_3[M]\}/\{1 + K_{GdLM}[M] + K_{GdHL}[H^+] \quad (10)$$

In the denominator of Equation (10), the term $K_{GdHL}[H^+]$ can be neglected since the protonation con-

 © 2003 Wiley-VCH Verlag GmbH & Co. KGaA, Weinheim

stants of the Gd^{3+} complexes are very low (the formation of protonated complexes cannot be detected by pH potentiometry.)

The rate constants k_1, k_2, and k_3 and the stability constants K_{GdLM} were calculated by fitting the k_p values, obtained at different H^+ and exchanging metal concentrations, to Equation (10), and are given in Table 3. The K_{GdLM} values are relatively low and so could not be calculated for all the exchange reactions. Because of the low K_{GdLM} value in the denominator of Equation (10), $K_{GdLM}[M] << 1$ when the error in the calculated K_{GdLM} is high (in some cases the error was higher than the constant itself).

Table 3. Rate constants k_1 ($M^{-1}\cdot s^{-1}$), k_2 ($M^{-2}\cdot s^{-1}$) and k_3 ($M^{-1}\cdot s^{-1}$) characterizing the exchange reactions between the complexes GdL and Lu^{3+} or Zn^{2+} (25 °C, 1.0 M KCl)

Complex	Lu^{3+}	Zn^{2+}
GdL^1	$k_1 = 6.1\pm0.4$, $k_2=(9.6\pm0.7)\times10^4$, $k_3 = (3.3\pm0.2)\times10^{-3}$	$k_1 = 5.6\pm0.2$, $k_3 = (2.1\pm0.1)\times10^{-2}$, $K_{GdLZn} = 22\pm3$
GdL^2	$k_1 = 3.4\pm0.2$, $k_2=(2.9\pm0.4)\times10^4$, $k_3 = (2.4\pm0.2)\times10^{-3}$, $K_{GdLLu} = 3.0\pm1.8$	$k_1 = 3.1\pm0.1$, $k_3 = (9.2\pm0.4)\times10^{-3}$, $K_{GdLZn} = 27\pm3$
GdL^3	$k_1 = 1.4\pm0.1$, $k_3=(6.6\pm0.4)\times10^{-4}$	$k_1 = 1.2\pm0.1$, $k_3 = (3.1\pm0.1)\times10^{-3}$
$Gd(DTPA)^{2-}$[a]	$k_1 = 0.58$, $k_2 = 9.7\times10^4$, $k_3 = 4.9\times10^{-4}$, $K_{GdLEu}=20$	$k_3 = 5.6\times10^{-2}$
GdL^4 [a]		$k_1 = 12.7$, $k_3 = 7.8\times10^{-3}$

[a] Ref.[42]

The rate constants k_1 obtained for a given complex GdL in the reactions with Lu^{3+} and Zn^{2+} are practically equal, because the rates of the proton-assisted dissociation of the complexes are independent of the nature of the exchanging ion.

The exchange reactions occur more rapidly with Zn^{2+} than with Lu^{3+}. This is a result of the higher value of k_3, which is about five times greater for the reactions with Zn^{2+} than for Lu^{3+}. Zn^{2+} is more active than Lu^{3+} in the direct reaction because a $N-Zn^{2+}$ bond, which is stronger than the $N-Lu^{3+}$ bond, is formed in the dinuclear intermediate before the rate-determining step, and transfer of the other donor atoms from the Gd^{3+} to the Zn^{2+} is more probable.

Comparison of the values of k_1 and k_3 for the complexes GdL^1, GdL^2, GdL^3, and GdL^4 shows that the attachment of the free radicals to the DTPA-bis(amide) generally has only a slight effect on k_3. However, the k_1 values characteristic for the proton-assisted dissociation decrease by a factor of about 10 in the sequence GdL^4, GdL^1, GdL^2, and GdL^3. This sequence means that the kinetic stabilities are higher for the DTPA-bis(amide) derivative complexes containing free radicals.

The equilibrium and kinetic properties of the Gd^{3+} complexes indicate that the number of substituted amide hydrogens influences both the thermodynamic and kinetic stabilities. The stability constants of the Gd^{3+} complexes formed with the ligand L^3, containing two disubstituted amide groups, are higher than those of GdL^2, in which the ligand contains two monosubstituted amide groups. The trend in the kinetic stabilities is similar. The rate of proton-assisted dissociation is higher for GdL^2 than for GdL^3, so the complex formed with the disubstituted amide has the higher kinetic stability.

Experimental Section

Synthesis of the Ligands

DTPA dianhydride **2** (Scheme 1) was treated with paramagnetic amines RNHR′ **1** for L^1, L^2 and L^3 according to published procedures.[28,29,40,41] Since five-membered nitroxides are more stable than six-membered ones,[42] the syntheses were carried out with the five-membered ring nitroxide radical **1b** to give the biradical L^2. Since the preliminary results were promising, we tried to increase the number of the paramagnetic centers by treatment of DTPA dianhydride **2** with the biradical **1c** to yield the tetraradical L^3 (Scheme 1). For comparison, the ligand L^1 was synthesized by means of the reaction between **1a** and **2**, as carried out by Sosnowsky et al.[28]

A solution of the corresponding amine **1a**, **1b**, or **1c** (4.0 mmol) in dry DMF (30 mL) was added dropwise at 40 °C to a stirred solution of DTPA dianhydride **2** (758 mg, 2.2 mmol) in dry dimethylformamide (DMF, 60 mL), and the resulting mixture was stirred further at this temperature for 2 h. The mixture was left stand overnight and then filtered, and the filtrate was evaporated to dryness in vacuo. The residue was suspended in acetone (100 mL) and left stand at room temperature for 2 h. The turbid solution was then decanted from the residue, was again suspended in acetone (100 mL), and the mixture was left stand at 4 °C for 2 h. The resulting gummy material was filtered off and left stand over P_2O_5 in a vacuum desiccator overnight. The glassy semisolid was purified by flash column chromatography with $CHCl_3$/MeOH, 3:1, followed by $CHCl_3$/MeOH, 1:1 and $CHCl_3$/MeOH, 1:3. The effluents gathered with $CHCl_3$/MeOH, 1:1 and $CHCl_3$/MeOH, 1:3 were pooled and the solvents were evaporated to dryness. The crystalline residue was taken up in Et_2O (20 mL) and filtered, and the filter cake was washed with acetone (30 mL), then with a 1:1 mixture of acetone/Et_2O (30 mL), and air-dried.

DTPA-Bis(amide) H_3L^2: A yellow solid, 532 mg (38%); m.p. 130−133 °C; $R_f = 0.28$ (MeOH). IR (Nujol): $\tilde{\nu}$ = 3270, 1710, 1640, 1530 cm^{-1}. $C_{32}H_{53}N_7O_{10}$ (695.81): calcd. C 55.24, H 7.68, N 14.09; found C 55.05, H 7.86, N 14.00.

DTPA-Bis(amide) H_3L^3: Et_2O was used instead of acetone during the workup. A yellow solid, 800 mg (40%); m.p. 140−142 °C; R_f = 0.37 (MeOH). IR (Nujol): $\tilde{\nu}$ = 3400, 1710, 1650 cm^{-1}. $C_{50}H_{81}N_9O_{12}$ (1000.25): calcd. C 60.04, H 8.16, N 12.60; found C 60.19, H 8.14, N 12.74.

Melting points were determined with a Boetius micro melting point apparatus and are uncorrected. Elemental analyses (C, H, N, S) were performed with a Fisons EA 1110 CHNS elemental analyzer. The IR (Specord 75) spectra were in each case consistent with the assigned structure. Flash column chromatography was performed on Merck Kieselgel 60 (0.040−0.063 mm). Qualitative TLC was carried out on commercially prepared plates (20 × 20 × 0.02 cm)

 © 2003 Wiley-VCH Verlag GmbH & Co. KGaA, Weinheim

coated with Merck Kieselgel GF_{254}. DTPA dianhydride **2** was purchased from Aldrich. Compounds **1b** and **1c** were prepared as published earlier.[43,44]

Equilibrium Measurements

For the preparation of $GdCl_3$ and $LuCl_3$ stock solutions, Gd_2O_3 and Lu_2O_3 (99.9%, Fluka) were dissolved in 1:1 HCl and the excess of acid was evaporated off. $ZnCl_2$ solution was prepared by dissolving $ZnCl_2$ in doubly distilled water. The concentrations of the metal chloride solutions were determined by complexometry with standardized K_2H_2edta, with xylenol orange as indicator (H_4edta = ethylenediaminetetraacetic acid).

The concentrations of the ligands L^1, L^2, and L^3 were determined by pH-potentiometry, on the basis of the titration curves obtained in the presence and absence of an excess of $CaCl_2$ ($c_{Ca}/cL \approx 40$, when all the dissociable protons of the ligands dissociate).

The protonation constants of the ligands were determined by pH-potentiometric titrations with a Radiometer PHM 93 Reference pH-meter, an ABU 80 autoburette, and PHG 211 glass and K 401 calomel electrodes. The titration vessel was thermostatted at 25 °C. The titrated solutions (15 mL, 1 mM) were stirred and N_2 was bubbled through them. The titrations were carried out in the pH range 1.7−11.5. For the calibration of the pH-meter, KH phthalate (pH = 4.008) and borax (pH = 9.180) buffers were used. The titrations were performed in 0.1 M KCl solutions with standardized KOH solution. To obtain H^+ concentrations from the measured pH values, the method proposed by Irving et al. was used.[45] A 0.01 M HCl solution (0.1 M for KCl) was titrated with standardized KOH solution. The differences between the measured and calculated pH values were used to calculate the H^+ concentrations from the pH values obtained in the titration experiments.

The stability constants of the complexes GdL and ZnL were determined by pH-potentiometry. The titrations were performed at metal to ligand ratios of 1:1 in 1.0 mM solutions (0.1 M KCl) in the pH range 1.7−11.5.

The formation equilibria of the dinuclear complexes Zn_2L were studied by pH-potentiometry. The solutions of ligands (1.5×10^{-3} M) were titrated with 0.2 M KOH in the presence of an excess of Zn^{2+} (3.1×10^{-3} M). In the knowledge of the stability constants of the complexes ZnL, ZnHL, and ZnH_2L and on the basis of the competition of H^+ and Zn^{2+} for ZnL, the stability constants of the complexes Zn_2L were determined.

The protonation and stability constants of the complexes were calculated with the program PSEQUAD.[46]

Measurement of Relaxation Times

The relaxation times of the water protons were measured at 9 MHz with an MS-4 NMR spectrometer. The temperature of the sample holder was controlled with a thermostatted air stream. The longitudinal relaxation times (T_1) were measured by the inversion recovery method (180°-τ-90°), with five to nine measurements at six to eight different τ values at 25 °C. In the study of the temperature dependence (7−40 °C) of the relaxation times, the concentration of the complexes GdL^1, GdL^2, and GdL^3 was 1.0 mM, while the concentration of the free radical ligands L^1, L^2, and L^3 was 10.0 mM. In the preparation of the solutions of complexes, a slight ligand excess was used. The pH of the solutions was around 5. To characterize the relaxation behavior of the free ligands and the complexes GdL, the water proton relaxation rates ($1/T_1$) were used as in Equation (11), where T_{1m} and T_{1w} are the relaxation times, measured in the presence and absence of the paramagnetic compound:

$$1/T_1 = 1/T_{1m} - 1/T_{1w} \quad (11)$$

The relaxivity (R_1) of the solutions is the increase in the relaxation rates observed on an increase in the concentration of the paramagnetic species (c_p) by 1.0 mM (i.e., $R_1 = (1/T_1) \times (1/c_p)$ $mM^{-1} \cdot s^{-1}$).

Kinetic Studies

The kinetic stabilities of the complexes (GdL) were characterized by the rates of the exchange reactions occurring between the paramagnetic complex and the diamagnetic Lu^{3+} or Zn^{2+}. The progress of the exchange reactions was followed by measurement of the relaxation rates, since the relaxivities of the complexes GdL and the ion Gd^{3+}.aq formed in the exchange reactions differ considerably. The exchanging metal ions were used in large excess in order to guarantee pseudo-first order conditions. The ionic strength of the solutions was kept constant (1.0 M for KCl). The exchange rates were studied in the pH range about 4−5.2. In the reactions with Zn^{2+} or Lu^{3+}, boric acid (0.01 M) − mannitol (0.04 M) or *N*-methylpiperazine (0.01 M) buffers were used, respectively. The pseudo-first order rate constants (k_p) were calculated by fitting the relaxation rate data to the Equation (12), where R_t is the relaxivity at time t, and R_0 and R_p are the relaxivities at the start of the reaction and at equilibrium, respectively.

$$R_t = (R_0 - R_p) \exp(-k_p t) + R_p \quad (12)$$

Acknowledgments

This work was supported by grants from the Hungarian National Research Foundation (OTKA T34307, OTKA T25462 and OTKA T38364) and Schering AG (Berlin).

[1a] B. Lauffer, *Chem. Rev.* **1987**, *87*, 901. [1b] P. Caravan, J. J. Ellison, T. J. McMurry, R. B. Lauffer, *Chem. Rev.* **1999**, *99*, 2293. [1c] *The Chemistry of Contrast Agents in Medical Magnetic Resonance Imaging* (Eds.: A. E. Merbach, E. Toth); John Wiley & Sons, LTD, New York **2001**.
[2] S. C. Quay, *Diamine-DTPA Paramagnetic Constant Agents for MR Imaging*, U.S. Patent No. 4, **1987**, 687.
[3] A. D. Sherry, W. P. Cacheris, K.-T. Kuan, *Magn. Reson. Med.* **1988**, *8*, 191.
[4] C. Paul-Roth, K. N. Raymond, *Inorg. Chem.* **1995**, *34*, 1408.
[5] W. P. Cacheris, S. C. Quay, S. M. Rocklage, *Magn. Reson. Imag.* **1990**, *8*, 467.
[6] E. N. Rizkalla, G. R. Choppin, W. P. Cacheris, *Inorg. Chem.* **1993**, *32*, 582.
[7] H. Imura, G. R. Choppin, W. P. Cacheris, L. A. LeLearie, T. J. Dumn, D. H. White, *Inorg. Chim. Acta* **1997**, *258*, 227.
[8] C. F. G. C. Geraldes, A. M. Urbano, M. C. Alpoim, M. A. Hoefnagel, J. A. Peters, *J. Chem. Soc., Chem. Commun.* **1991**, 656.
[9] C. F. G. C. Geraldes, A. M. Urbano, M. A. Hoefnagel, J. A. Peters, *Inorg. Chem.* **1993**, *32*, 2426.
[10] S. Aime, M. Botta, M. Fasano, S. Paoletti, P. L. Anelli, F. Uggeri, M. Virtuani, *Inorg. Chem.* **1994**, *33* 4707.
[11] L. Ehnebom, B. F. Pedersen, *Acta Chem. Scand.* **1992**, *46*, 126.
[12] C. F. G. C. Geraldes, A. D. Sherry, W. P. Cacheris, K.-T. Kuan, R. D. Brown, III, S. Koenig, M. Spiller, *Magn. Reson. Med.* **1988**, *8*, 191.
[13] G. Gonzalez, D. H. Powell, U. Tissierez, A. E. Merbach, *J. Phys. Chem.* **1994**, *98*, 53.

 © 2003 Wiley-VCH Verlag GmbH & Co. KGaA, Weinheim

[14] E. Toth, L. Helm, A. E. Merbach, R. Heidinger, K. Hegetschweiler, A. Janossy, *Inorg. Chem.* **1998**, *37*, 4104.
[15] S. W. A. Bligh, A. H. M. S. Chowdhury, M. McPartlin, I. J. Scowen, R. A. Bulman, *Polyhedron* **1995**, *14*, 567.
[16] S. W. A. Bligh, A. H. M. S. Chowdhury, D. Kennedy, C. Luchinat, G. Parigi, *Magn. Reson. Med.* **1999**, *41*, 767.
[17] C. Geze, C. Mouro, F. Hindre, M. Le Plouzennec, C. Moinet, R. Rolland, L. Aldereghi, A. Vacca, G. Simonneaux, *Bull. Soc. Chim. Fr.* **1996**, *133*, 267.
[18] H. Lammers, F. Maton, D. Pubanz, M. W. van Laren, H. van Bekkum, A. E. Merbach, R. N. Muller, J. A. Peters, *Inorg. Chem.* **1997**, *36*, 2527.
[19] S. Aime, F. Benetollo, G. Bombieri, S. Colla, M. Fasano, S. Paoletti, *Inorg. Chim. Acta* **1997**, *254*, 63.
[20] H. Lammers, A. M. van der Heijden, H. van Bekkum, C. F. G. C. Geraldes, J. A. Peters, *Inorg. Chim. Acta* **1998**, *268*, 249.
[21] X. Zhao, R. Zhuo, Z. Lu, W. Liu, *Polyhedron* **1997**, *16*, 2755.
[22] Y.-M. Wang, Y.-J. Wang, R.-S. Sheu, G.-C. Liu, W.-C. Liu, J.-H. Liao, *Polyhedron* **1999**, *18*, 1147.
[23] H. F. Bennett, R. D. Brown, III, S. H. Koenig, H. M. Swartz, *Magn. Reson. Med.* **1987**, *4*, 93.
[24] H. F. Bennett, R. D. Brown, III, J. F. W. Keana, S. H. Koenig, H. M. Swartz, *Magn. Reson. Med.* **1990**, *14*, 40.
[25] E. G. Janzen, R. A. Towner, *Aminoxyl Radicals as MRI Contrast Agents, in Bioactive Spin Labels* (Ed.: R. I. Zhadorov), Springer Verlag, Berlin, **1999**, p. 573.
[26] P. Vallet, Y. Van Haverbeke, P. A. Bonnet, G. Subra, J.-P. Chapat, R. N. Muller, *Magn. Reson. Med.* **1994**, *32*, 11.
[27] R. A. Carvalho, J. A. Peters, C. F. G. C. Geraldes, *Inorg. Chim. Acta* **1997**, *262*, 167.
[28] G. Sosnovsky, S. W. Li, U. M. Rao, R. C. Brasch, *Z. Naturforsch., Teil B* **1985**, *40*, 1558.
[29] G. Sosnovsky, N. U. M. Rao, J. Lukszo, R. C. Brasch, *Z. Naturforsch., Teil B* **1986**, *41*, 1170.
[30] N. R. Puttagunta, W. A. Gibby, V. L Puttagunta, *Invest. Radiol.* **1996**, *31*, 619.
[31] H. Maumela, R. D. Hancock, L. Carlton, J. H. Reibenspies, K. P. Wainwright, *J. Am. Chem. Soc.* **1995**, *117*, 6698.
[32] C. Lescop, E. Belorizky, D. Luneau, P. Ray, *Inorg. Chem.* **2002**, *41*, 3375.
[33] F. Botteman, G. M. Nicole, L. V. Elst, S. Laurent, A. E. Merbach, R. N. Muller, *Eur. J. Inorg. Chem.* **2002**, 2686.
[34] P. Wedeking, K. Kumar, M. F. Tweedle, *Magn. Reson. Imaging* **1992**, *10*, 641.
[35] K. P. Pulukkody, T. J. Norman, D. Parker, L. Royle, C. J. Brown, *J. Chem. Soc., Perkin Trans.* **1993**, *2*, 605.
[36] L. Sarka, L. Burai, E. Brücher, *Chem. Eur. J.* **2000**, *6*, 719.
[37] E. Brücher, *Top. Curr. Chem.* **2002**, *221*, 103.
[38] G. L. Rothermel, Jr., E. N Riskalla, G. R. Choppin, *Inorg. Chim. Acta* **1997**, *262*, 133.
[39] P. M. May, P. W. Linder, D. R. Williams, *J. Chem. Soc., Dalton Trans.* **1977**, 588.
[40] G. C. F. G. C. Geraldes, R. Delgado, A. M. Urbano, J. Costa, F. Jasanada, F. Nepveu, *J. Chem. Soc., Dalton Trans.* **1995**, 327.
[41] F. Jasanada, F. Nepveu, *Tetrahedron Lett.* **1992**, *33*, 5745.
[42] R. C. Brasch, M. T. McNamara, R. L. Ehman, W. R. Couet, T. N. Tozer, G. Sosnovsky, N. U. Maheswara Rao, I. Prakash, *Eur. J. Med. Chem.* **1989**, *24*, 335.
[43] H. O. Hankovszky, K. Hideg, L. Lex, *Synthesis* **1981**, 147.
[44] K. Hideg, H. O. Hankovszky, L. Lex, Gy. Kulcsár, *Synthesis* **1980**, 911.
[45] H. M. Irving, M. G. Miles, L. Pettit, *Anal. Chim. Acta* **1967**, *28*, 475.
[46] L. Zekany, I. Nagypal, in *Computational Methods for Determination of Formation Constants* (Ed.: D. J. Legett), Plenum, New York, **1985**, p. 291.

Received February 3, 2003

 © 2003 Wiley-VCH Verlag GmbH & Co. KGaA, Weinheim

Lanthanide Complexes of 2,6-Dihydroxybenzoic Acid: Synthesis, Crystal Structures and Luminescent Properties of $[n\mathrm{Bu_4N}]_2[\mathrm{Ln(2,6\text{-}dhb)_5(H_2O)_2}]$ (Ln = Sm and Tb)

Paula C. R. Soares-Santos,[a] Helena I. S. Nogueira,[a] Filipe A. Almeida Paz,[c] Rute A. Sá Ferreira,[b] Luís D. Carlos,[b] Jacek Klinowski,[c] and Tito Trindade*[a]

Keywords: Lanthanides / O ligands / Luminescence / Triboluminescence

Lanthanide complexes of 2,6-dihydroxybenzoic acid (2,6-Hdhb), namely $[n\mathrm{Bu_4N}]_2[\mathrm{Ln(2,6\text{-}dhb)_5(H_2O)_2}]$ [Ln = Sm (**1**) and Tb (**2**)], were synthesized and their crystal structures determined by single-crystal X-ray diffraction studies. The 2,6-$\mathrm{dhb^-}$ ligand coordinates to the lanthanide cations through the carboxylate group in a monodentate or bidentate chelating coordination mode. The compounds were further characterised using IR, Raman, ^{1}H and ^{13}C NMR spectroscopy and elemental analysis. Photoluminescence measurements were performed on both compounds. In particular, the terbium complex **2** shows intense photoluminescence both in the solid state and in ethanolic solution. Compound **2** also exhibits triboluminescence.

(© Wiley-VCH Verlag GmbH & Co. KGaA, 69451 Weinheim, Germany, 2003)

Introduction

Interest in the photophysical properties of lanthanide ion complexes has grown considerably in the last few years[1−3] since Lehn proposed that such complexes could be used as light conversion molecular device units (LCMDs).[4] Appropriate organic ligands can act as light collectors (antenna) and transfer absorbed energy to the coordinated lanthanide ion (emitter). These highly luminescent lanthanide complexes can act as functional units for the creation of luminescent devices on the nanoscale or molecular scale. We have been interested in the synthesis and characterisation of such complexes and in particular, lanthanide compounds containing aromatic ambidentate ligands in the first coordination shell.[5]

Complexes of Y^{3+}, La^{3+}, Pr^{3+}, Nd^{3+}, Sm^{3+} and Gd^{3+} with 2,6-dihydroxybenzoic acid (2,6-Hdhb) have been reported, along with their IR and UV/Vis spectra in ethanolic solutions, but their molecular formulae were not determined.[6] Brzyska et al. investigated the IR spectra and the thermal behaviour of 2,6-Hdhb complexes for a series of lanthanides including those of Y^{3+}, the series La^{3+} to Eu^{3+}[7] and Gd^{3+} to Lu^{3+},[8] with general formulae being proposed as $[\mathrm{Ln(C_7H_5O_4)_3}]\cdot n\mathrm{H_2O}$, where $n = 4$ for Ln = La^{3+} to Sm^{3+}, $n = 6$ for Eu^{3+}; $[\mathrm{Ln(C_7H_5O_4)_3(H_2O)_4}]\cdot 2\mathrm{H_2O}$ for Ln = Y^{3+} and Gd^{3+} to Lu^{3+}.[8] Glowiak et al. reported the crystal structures of the Tb^{3+} and Ho^{3+} complexes of 2,6-Hdhb,[9] confirming their molecular formula. 2,6-Hdhb complexes of the d-block metals have also been reported, namely those of Mo^{VI}, Os^{VI},[10] Re^{V},[10,11] Cu^{II} [12] and Ag^{I}.[13]

Here we report the synthesis and structural characterisation of new Sm^{3+} and Tb^{3+} complexes of 2,6-Hdhb. The 2,6-Hdhb ligand shows different coordination modes, either using both the carboxylate group and an adjacent hydroxy group in a salicylato-type chelate,[11] or utilising only the carboxylate group in a monodentate[12] or bidentate fashion.[9,14] The crystal structures of the complexes $[n\mathrm{Bu_4N}]_2[\mathrm{Ln(2,6\text{-}dhb)_5(H_2O)_2}]$ [Ln = Sm (**1**) and Tb (**2**)], were determined by single-crystal X-ray diffraction studies.

In complexes **1** and **2** the 2,6-$\mathrm{dhb^-}$ ligand coordinates both in a monodentate or chelating bidentate manner which is in contrast to that seen in similar compounds reported in the literature.[9] The photoluminescent behaviour of the complexes was investigated and the photophysical properties of the Tb^{3+} complex **2** were studied both in the solid state and in ethanolic solution. It was found that when compound **2** was subjected to mechanical force, luminescence was observed. This phenomenon is known as triboluminescence and the corresponding spectrum for compound **2** is presented and discussed. The compound $[\mathrm{Tb(2,6\text{-}dhb)_3(H_2O)_4}]\cdot 2\mathrm{H_2O}$ (**3**), previously reported by

[a] Department of Chemistry, University of Aveiro, CICECO, 3810-193 Aveiro, Portugal
E-mail: ttrindade@dq.ua.pt
[b] Department of Physics, University of Aveiro, CICECO, 3810-193 Aveiro, Portugal
E-mail: lcarlos@fis.ua.pt
[c] Department of Chemistry, University of Cambridge, Lensfield Road, Cambridge CB2 1EW, U.K.
E-mail: jk18@cam.ac.uk

Brzyska et al.,[8] was also synthesized by us in order to perform comparative photoluminescence studies with our new compounds.

Results and Discussion

Crystal Structures of $[n\mathrm{Bu_4N}]_2[\mathrm{Ln(2,6\text{-}dhb)_5(H_2O)_2}]$ Complexes

Single-crystal X-ray diffraction studies revealed similar crystal structures for the Sm^{3+} and Tb^{3+} complexes, which crystallise in the chiral and non-centrosymmetric $P2_1$ space group. The molecular formulae were calculated as $[n\mathrm{Bu_4N}]_2[\mathrm{Ln(2,6\text{-}dhb)_5(H_2O)_2}]$ [where Ln = Sm^{3+} (**1**) and Tb^{3+} (**2**)] (Table 1). Phase purity and homogeneity of the bulk samples were confirmed by elemental analyses and X-ray powder diffraction experiments. The crystal structures contain only one crystallographically unique metal centre coordinated to five 2,6-dhb$^-$ organic ligands and two water molecules, in a geometry which is best described as a distorted tricapped trigonal prism (Figures 1 and 2, Tables 2 and 3). The $[\mathrm{Ln(2,6\text{-}dhb)_5(H_2O)_2}]^{2-}$ complex anions (Ln = Sm^{3+} and Tb^{3+}) are chiral and the average Ln−O distance for the coordinated solvent molecules is 2.45 and 2.41 Å (for compounds **1** and **2**, respectively), in good agreement with reported results for other Ln complexes.[15] 2,6-dhb$^-$ appears as an *exo*-monodenate ligand forming two coordinative η^3-*syn*,*syn*-chelates and three *syn*-unidentate bonds to the lanthanide centres. All the carboxylate groups maintain the equivalence of the C−O bonds, with the distances being in the 1.26−1.28 Å range (Table 2). This is particularly unexpected for the unidentate groups, and can be explained by the presence of strong hydrogen bonds with the water molecules (Table 4).[16] The average O−C−O angles for the carboxylate groups (121.5 and 121.4° for **1** and **2**, respectively) are also close to the expected values.[16] An interesting feature of the crystal is the medium-intensity hydrogen bond between the O2 water molecule and the O14 hydroxy group of the neighbouring $[\mathrm{Ln(2,6\text{-}dhb)_5(H_2O)_2}]^{2-}$ complex ($O2\cdots O14^{i} \approx 2.9$ Å; symmetry code i: $x-1, y, z$), leading to the formation of a hydrogen-bonded metal chain which runs along the *a* direction of the unit cell (Figures 2 and 3, Table 4). Each hydroxy group of the 2,6-dhb$^-$ ligands is also involved in strong hydrogen bonding with the nearest oxygen atoms (Table 4).

Vibrational and NMR Spectra

Selected IR and Raman spectroscopic data for the free ligand 2,6-Hdhb, the tetrabutylammonium salt of the 2,6-dhb$^-$ ligand, $[n\mathrm{Bu_4N}]$[2,6-dhb], and the lanthanide complexes are shown in Table 5. Tentative assignments are based on those found in the literature for other 2,6-Hdhb complexes.[10,11] The IR spectra of the 2,6-dhb$^-$ tetrabutylammonium salt and of the lanthanide complexes both exhibit a broad band with a maximum in the region 3453−3419 cm^{-1} which can be assigned to the phenolic ν(O−H) stretch (3478 cm^{-1} in the free ligand) and to the coordinated water molecules. The corresponding δ(OH) bend is observed at 1351 cm^{-1} in the ligand, at 1345 cm^{-1} in the 2,6-dhb$^-$ tetrabutylammonium salt and at 1355 cm^{-1} in the complexes. The IR and Raman spectra of the free ligand both show a very strong band which may be assigned to the ν(C=O) at 1681 and 1674 cm^{-1}, respectively. In the

Table 1. Crystal data and structure refinement information for **1** and **2**

	1	**2**
Empirical formula	$C_{67}H_{101}N_2O_{22}Sm$	$C_{67}H_{101}N_2O_{22}Tb$
Formula mass	1436.85	1445.42
Crystal system	monoclinic	monoclinic
Space group	$P2_1$	$P2_1$
a [Å]	11.089(2)	11.061(2)
b [Å]	23.395(5)	23.371(5)
c [Å]	14.632(3)	14.598(3)
β [°]	109.87(3)	109.72(3)
Volume [Å^3]	3569.8(12)	3552.6(12)
Z	2	2
$D_{calcd.}$ [g cm^{-3}]	1.337	1.351
μ(Mo-K_α) [mm^{-1}]	0.896	1.069
Crystal size [mm]	0.23 × 0.16 × 0.12	0.16 × 0.10 × 0.05
Crystal type	colourless blocks	orange blocks
θ range [°]	3.68−27.48	3.79−27.41
Index ranges	$-14 \le h \le 14$ $-30 \le k \le 28$ $-18 \le l \le 19$	$-14 \le h \le 13$ $-30 \le k \le 26$ $-18 \le l \le 18$
Reflections collected	26761	32607
Independent reflections	14390 (R_{int} = 0.0336)	13984 (R_{int} = 0.0572)
Absolute structure parameter	−0.017(7)	−0.021(7)
Final *R* indices [$I > 2\sigma(I)$]	$R1$ = 0.0340, $wR2$ = 0.0880	$R1$ = 0.0411, $wR2$ = 0.0828
Final *R* indices (all data)	$R1$ = 0.0388, $wR2$ = 0.0936	$R1$ = 0.0584, $wR2$ = 0.0889
Largest diff. peak and hole [e Å^{-3}]	0.917 and −0.840	0.913 and −0.677

 © 2003 Wiley-VCH Verlag GmbH & Co. KGaA, Weinheim

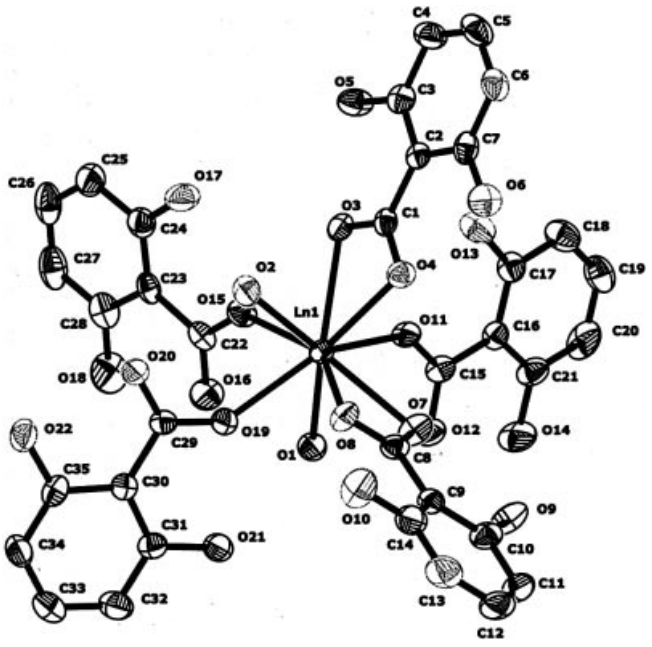

Figure 1. Chiral complex anion, $[Ln(2,6\text{-dhb})_5(H_2O)_2]^{2-}$, present in the crystal structures of **1** and **2**, showing the distorted tricapped trigonal-prismatic $\{LnO_9\}$ coordination environment for the crystallographically unique metal centres (Ln = Sm^{3+} or Tb^{3+}); hydrogen atoms are omitted for clarity; thermal displacement ellipsoids are drawn at the 50% probability level

Table 2. Selected bond lengths [Å] for **1** and **2**

	1	**2**
Ln1−O1	2.464(3)	2.419(3)
Ln1−O2	2.446(3)	2.407(3)
Ln1−O3	2.531(4)	2.506(4)
Ln1−O4	2.526(3)	2.486(3)
Ln1−O7	2.473(3)	2.448(3)
Ln1−O8	2.552(4)	2.515(5)
Ln1−O11	2.455(3)	2.422(3)
Ln1−O15	2.377(3)	2.326(3)
Ln1−O19	2.433(3)	2.401(3)
C1−O3	1.265(5)	1.287(5)
C1−O4	1.271(5)	1.271(6)
C8−O7	1.279(5)	1.276(6)
C8−O8	1.267(5)	1.269(6)
C15−O11	1.280(4)	1.271(5)
C15−O12	1.272(5)	1.280(6)
C22−O15	1.282(5)	1.283(5)
C22−O16	1.258(5)	1.251(6)
C29−O19	1.270(5)	1.267(5)
C29−O20	1.265(5)	1.263(5)

Table 3. Selected bond angles [°] for **1** and **2**

	1	**2**
O1−Ln1−O2	135.60(10)	136.17(11)
O1−Ln1−O3	131.52(11)	131.88(13)
O1−Ln1−O4	145.48(10)	145.33(10)
O1−Ln1−O7	70.86(10)	71.00(12)
O1−Ln1−O8	98.33(12)	97.98(14)
O1−Ln1−O11	73.11(10)	73.60(11)
O1−Ln1−O15	77.32(10)	77.78(12)
O1−Ln1−O19	66.57(10)	66.60(11)
O2−Ln1−O3	73.47(12)	73.13(14)
O2−Ln1−O4	78.53(10)	77.87(11)
O2−Ln1−O7	132.45(11)	131.99(13)
O2−Ln1−O8	82.01(12)	81.28(15)
O2−Ln1−O11	142.95(11)	142.37(13)
O2−Ln1−O15	79.90(11)	80.33(13)
O2−Ln1−O19	71.47(11)	71.62(12)
O11−Ln1−O3	69.50(10)	69.25(12)
O11−Ln1−O4	79.40(9)	79.73(11)
O11−Ln1−O7	71.98(10)	71.99(12)
O11−Ln1−O8	122.04(11)	122.83(12)
O11−Ln1−O15	87.29(11)	87.15(12)
O11−Ln1−O19	138.98(9)	139.26(11)
O15−Ln1−O3	71.26(10)	70.98(12)
O15−Ln1−O4	122.28(9)	123.02(11)
O15−Ln1−O7	145.81(10)	146.16(12)
O15−Ln1−O8	148.20(11)	147.67(13)
O15−Ln1−O19	77.07(11)	76.55(12)
O19−Ln1−O3	135.97(10)	135.17(12)
O19−Ln1−O4	140.68(9)	140.17(11)
O19−Ln1−O7	100.75(11)	101.93(13)
O19−Ln1−O8	72.45(11)	72.50(13)

spectra of the complexes, the assymetric $\nu_{as}(CO_2)$ is shifted to a higher wavenumber by up to 11 cm^{-1} upon coordination, when compared with the tetrabutylammonium salt of the 2,6-dhb^- ligand (1633 cm^{-1}). The symmetric mode $\nu_s(CO_2)$ also shows shifts to a higher wavenumber upon coordination (1292 cm^{-1} in the complexes) when compared with the tetrabutylammonium salt of the ligand (1286 cm^{-1}). The band at 1241 cm^{-1} in the spectrum of the tetrabutylammonium salt of the ligand, assigned to the $\nu(C-O)_h$ stretch (at 1236 cm^{-1} in the free ligand) of the phenolic groups, shifts to 1228 cm^{-1} on coordination, possibly due to hydrogen bonding.

^1H and ^{13}C NMR spectroscopic data for the free ligand and its lanthanide complexes in deuterated dimethyl sulfoxide solution are given in Table 6 (see Scheme 1 for labelling and Table 6 for tentative assignments). In the ^1H NMR spectra, the line arising from H^3 and H^5 appears as a doublet, and the line arising from H^4 as a triplet, with relative intensities of 2:1, respectively, either in the free ligand or in the complexes. The resonances of these protons shift to higher field on coordination. The resonances due to the protons of the counterion can also be observed in the spectra of the complexes. The resonances of the aromatic protons in **2** show higher shifts when compared with the values obtained for **1**, which may be induced by the Tb^{III} ion. In the spectra of **1** and **2** we can also observe resonances due to the phenolic protons as a broad signal (at δ = 14.5 and 14.0 ppm), with relative intensities of 2:1 when compared with the line assigned to H^4.

^{13}C NMR spectroscopy shows the resonances of all the carbon atoms, both of the ligand and the counterion. The most relevant shifts are observed in the signal of the carboxylate atom C^7, which shifts to lower-field on coordination, showing that the ligand is bound to the lanthanide atom through the carboxylate oxygen atoms.

 © 2003 Wiley-VCH Verlag GmbH & Co. KGaA, Weinheim

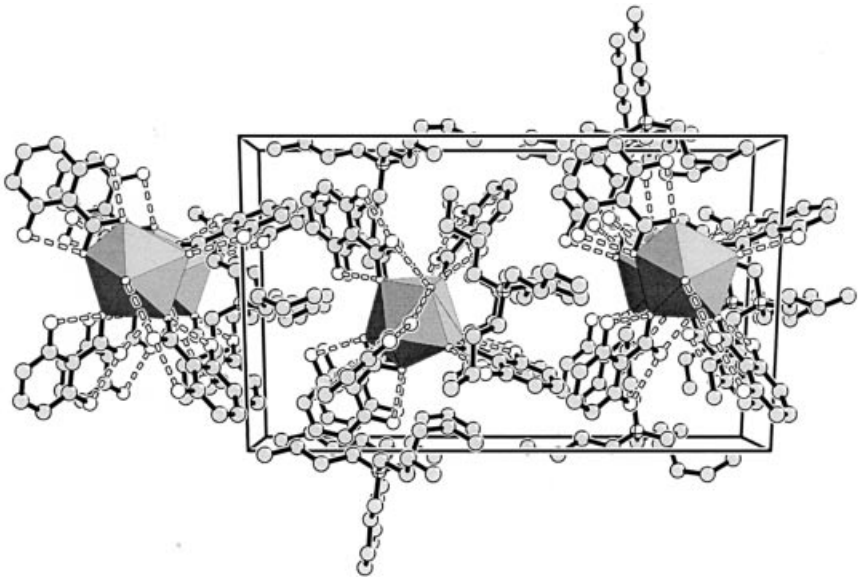

Figure 2. Perspective along the *a* axis of $[n\mathrm{Bu_4N}]_2[\mathrm{Ln(2,6\text{-}dhb)_5(H_2O)_2}]$; lanthanide centres are represented as polyhedra and hydrogen bonds (see Table 4) as white-filled dashed lines

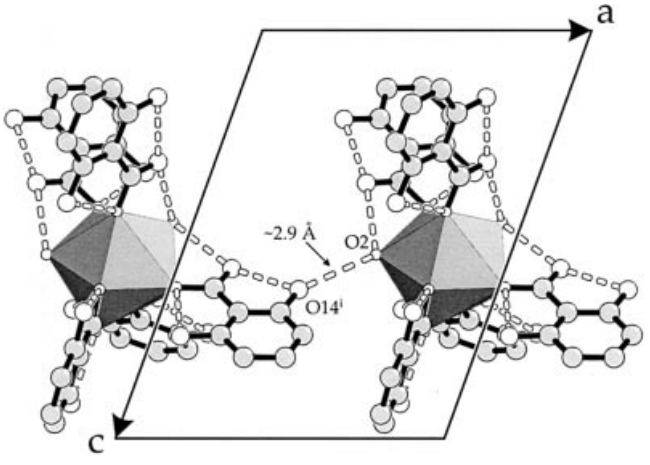

Figure 3. View along the *b* axis showing the hydrogen bond linking neighbouring $[\mathrm{Ln(2,6\text{-}dhb)_5(H_2O)_2}]^{2-}$ complexes; lanthanide centres are represented as polyhedra and hydrogen bonds (see Table 4) as dashed lines; symmetry code i: $x - 1, y, z$

Table 4. Distances [Å] and angles [°] between donors (D) and acceptors (A) for the D−H···A hydrogen bonds present in the crystal structures of **1** and **2**; symmetry code i: $x - 1, y, z$

	1		**2**	
D···A	*d*(D···A)	<(D−H···A)	*d*(D···A)	<(D−H···A)
O1···O12	2.644(4)	159(5)	2.642(5)	161(5)
O1···O16	2.725(5)	157(5)	2.713(5)	165(5)
O2···O20	2.726(4)	155(5)	2.712(5)	159(5)
O2···O14^{i}	2.907(4)	155(4)	2.954(5)	162(4)
O5···O3	2.553(5)	147(5)	2.553(6)	148(5)
O6···O4	2.591(4)	147(5)	2.594(4)	148(5)
O9···O7	2.552(5)	148(5)	2.540(5)	148(5)
O10···O8	2.573(5)	146(5)	2.561(7)	148(5)
O13···O11	2.572(4)	146(5)	2.569(5)	146(5)
O14···O12	2.510(4)	149(5)	2.517(5)	149(5)
O17···O15	2.547(4)	147(5)	2.563(5)	146(5)
O18···O16	2.512(5)	148(5)	2.522(5)	148(5)
O21···O19	2.584(4)	146(5)	2.594(5)	146(5)
O22···O20	2.528(4)	148(5)	2.534(5)	148(5)

Luminescence Spectra

Figures 4 and 5 show the room-temp. photoluminescence (PL) features of compounds **1**, **2** and **3**, excited at 350, 344 and 342 nm, respectively. The emission spectrum of the Sm^{3+} complex (Figure 4) is composed of a large broad band between 380 and 500 nm and a series of straight lines assigned to intra-4f^5 transitions between the $^4G(4)_{5/2}$ and the $^6H_{5/2,7/2,9/2,11/2}$ levels. Apart from a red shift (2000 cm^{-1}), the large broad band was already observed in the emission spectrum of 2,6-Hdhb, as shown in the inset of Figure 4. In the emission spectra of the Tb^{3+} compounds **2** and **3** only the intra-4f^8 lines, corresponding to transitions between the $^5D_4$ and $^7F_{6-0}$ levels, could be detected (Figure 5). The fact that the ligand's broad band could not be observed, clearly indicates a more efficient energy transfer between the Tb^{3+} ions and the 2,6-dhb ligand than that involving the Sm^{3+} cations.

The Tb^{3+} emission of compound **2** was compared with that of compound **3** and with the emission arising from compound **2** in a 1.4 mM alcoholic solution (Figure 5). All the spectra display the typical Tb^{3+} lines resulting from $^5D_4 \rightarrow {}^7F_{6-0}$ transitions. The emission lines of the Tb^{3+} alcoholic solution are almost identical to the ones observed for the powdered compound **2** in terms of energy and full width at half maximum. However, the Tb^{3+} transitions in compound **3** are more structured, providing evidence for a higher number of Stark components. In order to evaluate accurately the PL differences between the two Tb^{3+} solid samples, the respective emission spectra were measured at 10 K (Figure 6, A and B).

 © 2003 Wiley-VCH Verlag GmbH & Co. KGaA, Weinheim

Table 5. Analytical and vibrational data for 2,6-dihydroxybenzoic acid and the Sm^{III} and Tb^{III} complexes

Compound	Analysis[a] C	N	H	Ln	Vibrational spectra[b] [cm^{-1}] $\nu_{as}(CO_2)$	$\delta(OH)$	$\nu_s(CO_2)$	$\nu(C-O)_h$
2,6-dihydroxybenzoic acid					1681 vs	1351 m	1294 m	1236 s
					1674(7)	1353(1)	1308(5)	1226(4)
[nBu$_4$N][2,6-dhb]					1633 vs	1345 m	1286 s	1241 vs
					1628(1)	1356(1)	1285(2)	1236(1)
[nBu$_4$N]$_2$[Sm(2,6-dhb)$_5$(H$_2$O)$_2$] (**1**)	55.08	1.96	7.14	10.53	1643 vs	1355 s	1292 s	1228 vs
	(56.00)	(1.95)	(7.09)	(10.45)	1649(2)	1355(1)	1298(10)	1231(1)
[nBu$_4$N]$_2$[Tb(2,6-dhb)$_5$(H$_2$O)$_2$] (**2**)	55.20	1.98	7.06	10.12	1644 vs	1355 s	1292 s	1228 vs
	(55.67)	(1.94)	(7.04)	(11.01)	1649(2)	1355(1)	1292(10)	1231(1)

[a] Calcd. values in parentheses. [b] Infrared and Raman (in italics) data; vs − very strong, s − strong, m − medium.

Table 6. ^1H and $^{13}C\{^1H\}$ NMR spectroscopic data for 2,6-dihydroxybenzoic acid and the Sm^{III} and Tb^{III} complexes

	Chemical shift [ppm][a] H^3	H^4	H^5	C^1	C^2	C^3	C^4	C^5	C^6	C^7
2,6-Dihydroxybenzoic acid	6.32 d	7.20 t	6.32 d	102.6	160.7	106.7	134.3	106.7	160.7	172.6
[nBu$_4$N]$_2$[Sm(2,6-dhb)$_5$(H$_2$O)$_2$] (**1**)	6.05 d	6.95 t	6.05 d	104.5	162.4	105.0	131.9	105.0	162.4	175.5
[nBu$_4$N]$_2$[Tb(2,6-dhb)$_5$(H$_2$O)$_2$] (**2**)	5.82 d	6.77 t	5.82 d	95.9	161.9	104.3	131.8	104.3	161.9	176.9

[a] Spectra in DMSO solution; d − doublet, t − triplet.

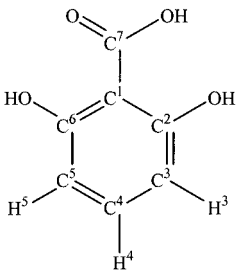

Scheme 1

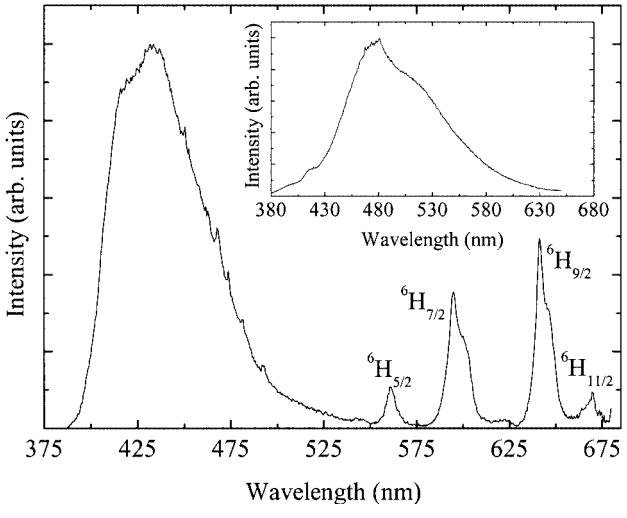

Figure 4. Room-temp. PL spectrum of [nBu$_4$N]$_2$[Sm(2,6-dhb)$_5$(H$_2$O)$_2$]; the inset shows the room-temp. PL spectrum of the 2,6-Hdhb ligand excited at 341 nm

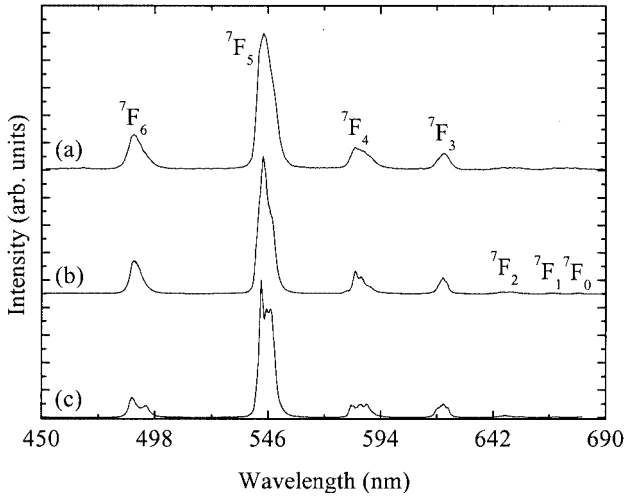

Figure 5. Room-temp. PL spectra of (a) 1.4 mM ethanolic solution of **2**, (b) compound **2** and (c) compound **3**

The most evident change with the decrease in temperature is related to the increase in the number of identified Stark components. For instance, in the most intense transition namely $^5D_4 \rightarrow {}^7F_5$, we can clearly distinguish 22 Stark components in both samples (Figure 6). Focusing our attention in the region of the $^5D_4 \rightarrow {}^7F_0$ transition, at least two lines, separated by 36 cm^{-1}, are undoubtedly discernable in the emission spectrum of **3**. For compound **2** the $^5D_4 \rightarrow {}^7F_0$ transition has a large value of 46 cm^{-1} for its full width at half maximum, suggesting the presence of more than one emission line. Since the Tb^{3+} ions lie in the same average local symmetry site (in agreement with the XRD data) and the $^7F_0$ is a non-degenerated level, the de-

 © 2003 Wiley-VCH Verlag GmbH & Co. KGaA, Weinheim

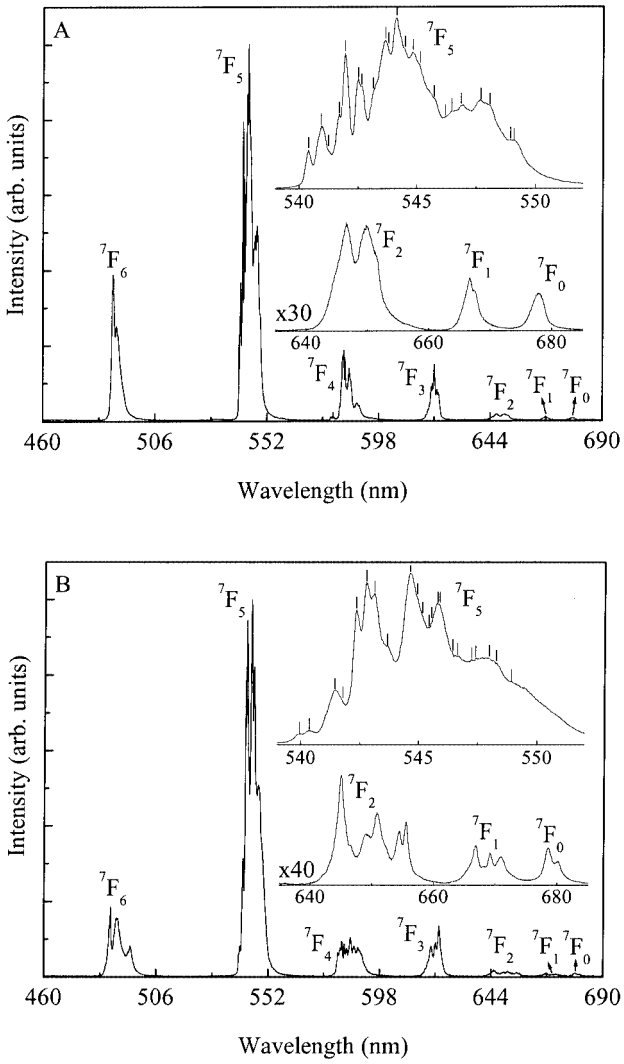

Figure 6. PL spectra, recorded at 10 K under 344 nm excitation wavelength of compound **2** (A) and compound **3** (B)

tection of more than one component in the $^5D_4 \rightarrow {}^7F_0$ region points to the thermal population of the upper $^5D_4$ levels. Even at 10 K, the emission from such levels, usually termed as hot lines, is not quenched making the emission spectra quite intricate.[17] These hot lines are responsible for the higher number of components perceived in the remaining transitions (Figure 6, A and B) and, thus, the observed local-field splitting of the $^5D_4 \rightarrow {}^7F_{1-6}$ transitions are in agreement with the point site symmetry group identified by XRD.

The differences observed between compounds **2** and **3** clearly indicate that the synthetic procedure results in different local coordination sites for the Tb^{3+} ions. On the contrary, dissolving the former compound in ethanol did not produce significant changes in the PL properties of the Tb^{3+}. This result suggests that the lanthanide ions are well shielded by the ligands from the incorporation of solvent molecules in the first coordination sphere which would contribute to the quenching of the emission intensity.

Figure 7 shows the room-temp. excitation (PLE) spectrum of the Sm^{3+} complex monitored around the cation's more intense line at 641 nm. The spectrum displays a large broad band between 250 and 420 nm, centred around 330 nm, and a series of sharp lines characteristic of the Sm^{3+} energy levels.

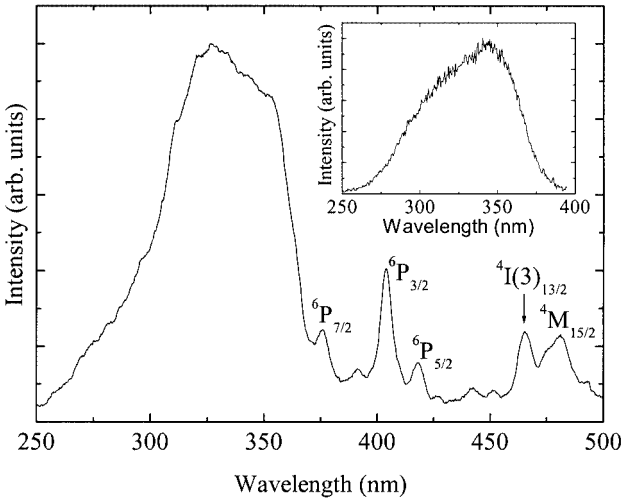

Figure 7. Room-temp. PLE spectrum of compound **1**; the inset shows the room-temp. PLE spectrum of the 2,6-Hdhb ligand detected around 480 nm

Figure 8 shows the PLE spectra of compounds **2** and **3** and of a 1.4 mM alcoholic solution of **2**. All the spectra exhibit a large broad band in the same spectral region of that observed in the PLE spectrum of the Sm^{3+}-based complex. The excited levels were only detected in the PLE spectrum of the Tb^{3+} solution. The large broad band is centred around 344, 342 and 327 nm, for **2**, **3** and the alcoholic solution, respectively. This band may be related to the ligand's excited states, since the PLE spectrum of the 2,6-

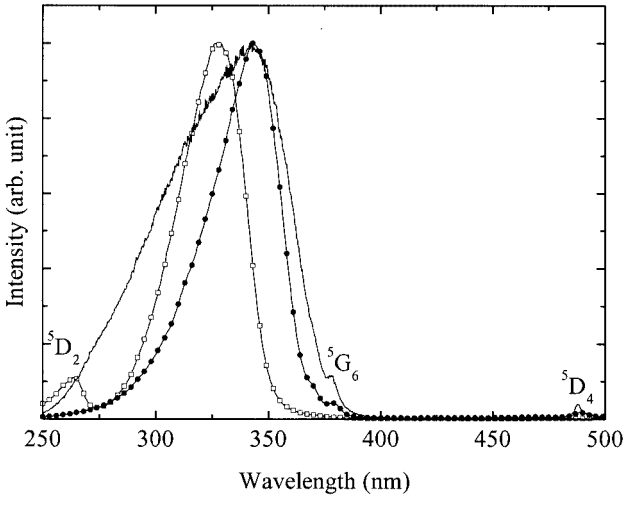

Figure 8. Room-temp. PLE spectra of compound **2** (solid line with solid circles), compound **3** (solid line) and a 1.4 mM ethanolic solution of **2** (solid line with open squares)

 © 2003 Wiley-VCH Verlag GmbH & Co. KGaA, Weinheim

Hdhb ligand is characterized by a similar large broad band with peaks around 341 nm (inset of Figure 7).

The lifetimes of the $^5D_4$ Tb^{3+} excited levels were measured at room temperature under the excitation wavelength that maximizes their luminescent intensity for the two powdered complexes and for the ethanolic solution. The monitoring wavelength was set around the more intense emission line (544 nm). The lifetime of the $^4G(4)_{5/2}$ Sm^{3+} excited level could not be recorded since it lies in a time scale below our lower experimental detection limit (10^{-5} s). Figure 9 depicts the experimental data in a logarithmic scale for the three Tb^{3+}-based samples. All the data were well fitted by a single exponential function, confirming that all lanthanide ions occupy the same average local environment within each complex.

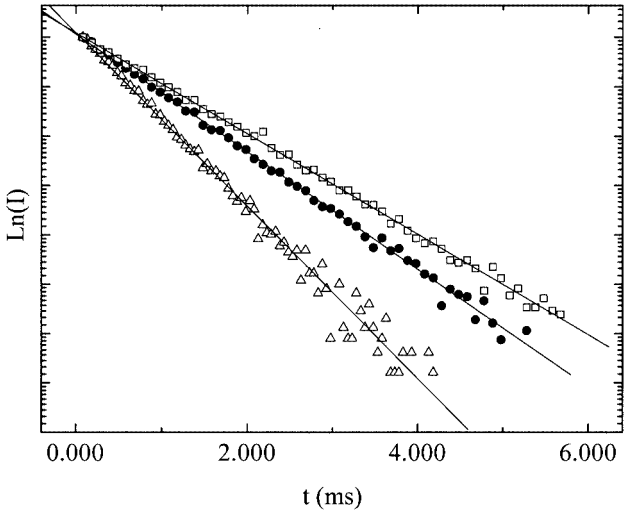

Figure 9. Room-temp. decay curves for compound **2** (solid circles), compound **3** (open triangles) and a 1.4 mM ethanolic solution of **2** (open squares); the solid lines represent the data best fits, assuming a single-exponential function ($r > 0.99$)

The $^5D_4$ lifetimes of **2** and the corresponding 1.4 mM ethanolic solution are 0.876 ±0.012 and 0.983 ±0.007 ms, respectively. Both values are similar, confirming the previous suggestion that solvation did not induce significant changes on the Tb^{3+} local environment, meaning that the ligands are efficiently shielding the lanthanide ions. The $^5D_4$ lifetime for **3** is smaller than the previous two values, being 0.562 ±0.001 ms. This decrease indicates that non-radiative pathways are more important in the latter complex. In fact, if we recall the local Tb^{3+} structure in both complexes, the lanthanide's first coordination sphere in **2** and **3** differs in the number of water molecules by two and four, respectively. It is well known that the presence of OH oscillators in the lanthanide first coordination sphere provides an efficient non-radiative path, so we can suggest that the observed decrease in the lifetime of the $^5D_4$ level is mainly related to an increase in non-raditive transitions due to the increase in the number of OH oscillators in the Tb^{3+} first coordination shell, which is in perfect agreement with the proposed structural results.

When ground by hand in daylight, single crystals of **2** exhibit green luminescence detectable by the naked-eye (Figure 10). The spectrum exactly matches that observed by excitation using UV light, indicating that triboluminescence (TL) involves the same Tb^{3+} excited-state deactivation as that observed in PL. The mechanisms behind TL are not well understood and predictions of this behaviour for a specific compound cannot be made. While TL behaviour of some compounds has been attributed to the piezoelectric properties of non-centrosymmetric crystals, many TL centrosymmetric crystals have also been reported.[18] Compound **2** is a non-centrosymmetric ionic complex and it has been suggested[18,19] that TL arises from charge separation by partial fracture along oppositely charged planes. Further work is under way to clarify the nature of the TL mechanism in this compound.

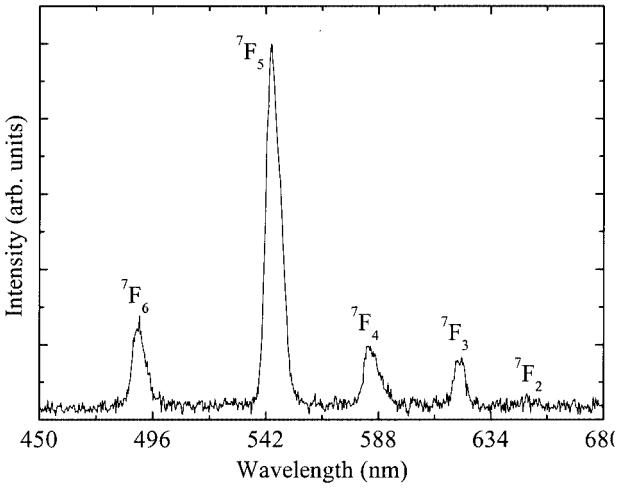

Figure 10. Room-temp. TL spectrum of compound **2**

Conclusion

New samarium and terbium complexes of 2,6-dihydroxybenzoic acid, each containing five 2,6-dhb$^-$ ligands coordinated to the metal centres and two tetrabutylammonium cations, have been synthesized and structurally characterized. The X-ray crystal structures show the carboxylate groups acting both as monodentate or bidentate chelating ligands; two water molecules complete the first coordination shell with a coordination number of nine. The luminescent properties of the Tb^{3+} complex with the 2,6-dhb$^-$ ligand are described here for the first time. The Tb^{3+} complex shows very high luminescence, even in an ethanolic solution. These particular luminescent properties may be explored in order to develop solution methods based on new luminescent materials in which this molecular unit could act as the active centre. Given its triboluminescent behaviour, the terbium compound is a potential candidate for the development of optical sensors.

 © 2003 Wiley-VCH Verlag GmbH & Co. KGaA, Weinheim

Experimental Section

General: All chemicals were supplied by Aldrich and used without further purification. The terbium complex [Tb(2,6-dhb)$_3$(H$_2$O)$_4$]·2H$_2$O (**3**) was synthesized as described by Brzyska et al.[8]

Preparation of [*n*Bu$_4$N]$_2$[Ln(2,6-dhb)$_5$(H$_2$O)$_2$] [Ln = Sm (1) and Tb (2)]: The lanthanide complexes were prepared by adding an aqueous solution (ca. 20 mL) of the lanthanide salt Ln(NO$_3$)$_3$·5H$_2$O (Ln = Sm^{3+}, Tb^{3+}; 0.889 g, 2.00 mmol and 0.872 g, 2.00 mmol, respectively) to an aqueous solution (ca. 40 mL, pH = 3.0±0.1) containing 2,6-dihydroxybenzoic acid (1.23 g, 8.00 mmol) and KOH (0.448 g, 8.00 mmol). After stirring the mixture for 1 h, an aqueous solution (5 mL) containing tetrabutylammonium chloride hydrate (*n*Bu$_4$NCl·*n*H$_2$O, 1.11 g, 4.00 mmol) was added and a flocculant white solid was immediately formed. The supernant solution was decanted and the precipitate collected and washed with distilled water. Crystals of [*n*Bu$_4$N]$_2$[Ln(2,6-dhb)$_5$(H$_2$O)$_2$] [Ln = Sm^{3+} (**1**) and Tb^{3+} (**2**), respectively], suitable for single-crystal X-ray diffraction were obtained from the filtrate after 1 d.

Preparation of [*n*Bu$_4$N][2,6-dhb]: The 2,6-dhb$^-$ tetrabutylammonium salt, [*n*Bu$_4$N][2,6-dhb], was prepared by adding an aqueous solution (ca. 5 mL) of *n*Bu$_4$NCl·*n*H$_2$O (0.556 g, 2.00 mmol) to an aqueous solution (ca. 10 mL) containing 2,6-dihydroxybenzoic acid (0.308 g, 2.00 mmol) and KOH (0.112 g, 2.00 mmol). After stirring the mixture for 1 h, the white precipitate formed was filtered and washed with distilled water.

Characterisation: IR spectra were measured using KBr disks with a Mattson 7000 FT instrument. Raman spectra were recorded using a Bruker RFS100/S FT-Raman spectrometer (Nd:YAG laser, 1064 nm excitation). ^{1}H spectra were obtained using a Bruker AMX-300 spectrometer (^{1}H, 300 MHz; ^{13}C, 75.4 MHz) referenced to Si(CH$_3$)$_4$ or the solvent. Elemental analyses for carbon, nitrogen and hydrogen were performed with an Exeter Analytical CE-440 Elemental Analyser. The sample was combusted under oxygen at 975 °C for 1 min, with He as the purge gas. The lanthanide content in the complexes was measured by ICP (Analytical Laboratories, University of Aveiro). Powder X-ray diffraction patterns (PXRD) were recorded at ambient temperature using a Philips X'Pert instrument, operating with a monochromated Cu-K_α radiation source at 40 kV/50 mA. Data were collected using the step-counting method (step 0.01°, 7 s per step) in the $2° \leq 2\theta \leq 60°$ range. Theoretical PXRD calculations were performed using the STOE Win XPOW software package.[20] Photoluminescence (PL) spectra, measured between 10 K and room temp. were recorded using a Jobin Yvon-Spex spectrometer (HR, 460) coupled to an R928 Hamamatsu photomultiplier. An Xe arc lamp (150 mW) coupled to a Jobin Yvon monochromator (TRIAX 180) was used as the excitation source. All the spectra were corrected for the response of the detector. The lifetime measurements were carried out using a pulsed Xe arc lamp (5 mJ/pulse, 3 μs bandwidth) coupled to a Kratos GM-252 monochromator and a Spex 1934 C phosphorimeter. The room-temp. triboluminescence (TL) spectra were recorded with a plug-in high-sensitivity fibreoptic UV/Vis shortwave master spectrometer, fitted with a grating blazed at 500 nm with 600 grooves per mm, with a 2048-element linear CCD-array detector (PC, 2000, Ocean Optics, Inc.). A PC 2000 was mounted on a 1 MHz ISA-bus A/D card fitted directly into a desktop PC. The single-crystals of **2** were ground by hand using the plug-in high sensitivity fibre optic.

X-ray Crystallographic Studies: Suitable single crystals of **1** and **2** were mounted on glass fibres using perfluoropolyether oil.[21] Data were collected with a Nonius Kappa CCD diffractometer with Mo-K_α graphite-monochromated radiation (λ = 0.7107 Å). The structures were solved by direct methods and refined by full-matrix least squares on F^2 with anisotropic displacement parameters for all non-hydrogen atoms.[22,23] Multi-scan absorption corrections were also applied.[24] All hydrogen atoms were placed in calculated positions, and refined using a riding model with an isotropic displacement parameter fixed at x times U_{eq} for the atom to which they are bound (x = 1.5 for all the O−H and −CH$_3$ groups, and x = 1.2 for the remaining hydrogen atoms). Bond-length restraints were not applied, except for H atoms associated with the water molecules, for which the O−H and H−O−H distances were restrained to ensure a chemically reasonable geometry for the water molecule. Information concerning crystallographic data collection and structure refinement for **1** and **2** is summarised in Table 1, while selected bond lengths and angles are given in Tables 2 and 3, respectively. CCDC-201808 and -201809 contain supplementary crystallographic data for this paper. These data can be obtained free of charge at www.ccdc.cam.ac.uk/conts/retrieving.html [or from the Cambridge Crystallographic Data Centre,12 Union Road, Cambridge CB2 2EZ, U.K.; Fax: (internat.) + 44-1223/336033; E-mail: deposit@ccdc.cam.ac.uk)].

Acknowledgments

We are grateful to J. Soares for assistance in the triboluminescence measurements, to the University of Aveiro for a PhD research grant (P. C. R. S. S.), and to Fundação para a Ciência e a Tecnologia (Portugal), for financial support through the SFRH/BD/3024/2000 (F. A. A. P.) and SFRH/BPD/11480/2002 (R. A. S. F.), PhD and post-doc scholarships, respectively. We are also grateful for additional financial support from the FCT (grant contract: POCTI/35378/QUI/2000 and POCTI/33653/CTM/2000) supported by FEDER.

[1] N. Arnaud, E. Vaquer, J. Georges, *Analyst* **1998**, *123*, 261−265.
[2] G. F. Sá, O. L. Malta, C. M. Donegá, A. M. Simas, R. L. Longo, P. A. Santa-Cruz, E. F. Silva, Jr., *Coord. Chem. Rev.* **2000**, *196*, 165−195.
[3] G. Vicentini, L. B. Zinner, J. Zukerman-Schpector, K. Zinner, *Coord. Chem. Rev.* **2000**, *196*, 353−382.
[4] J. M. Lehn, *Angew. Chem. Int. Ed. Engl.* **1990**, *29*, 1304−1319.
[5] P. C. R. Soares-Santos, H. I. S. Nogueira, V. Félix, M. G. B. Drew, R. A. Sá Ferreira, L. D. Carlos, T. Trindade, *Chem. Mater.* **2003**, *15*, 100−108.
[6] S. F. M. Ali, V. R. Rao, *J. Inorg. Nucl. Chem.* **1975**, *37*, 1041−1042.
[7] W. Brzyska, Z. Rzaczyńska, A. Kula, M. Jaroniec, *Pol. J. Chem.* **1998**, *72*, 2087−2092.
[8] W. Brzyska, A. Kula, Z. Rzaczyńska, M. Jaroniec, *Pol. J. Chem.* **1998**, *72*, 2524−2530.
[9] T. Glowiak, W. Brzyska, A. Kula, Z. Rzaczyńska, M. Jaroniec, *J. Coord. Chem.* **1999**, *48*, 477−486.
[10] W. P. Griffith, H. I. S. Nogueira, B. C. Parkin, R. N. Sheppard, A. J. P. White, D. J. Williams, *J. Chem. Soc., Dalton Trans.* **1995**, 1775−1781.
[11] G. Bandoli, A. Dolmella, T. I. A. Gerber, J. Perils, J. G. H. Preez, *Inorg. Chim. Acta* **1999**, *294*, 114−118.
[12] F. Cariati, L. Erre, G. Micera, A. Panzanelli, *Inorg. Chim. Acta* **1983**, *80*, 57−65.
[13] G. Smith, C. H. L. Kennard, T. C. W. Mak, *Z. Kristallogr.* **1988**, *184*, 275−280.
[14] T. Glowiack, H. Kozlowski, L. S. Erre, G. Micera, B. Gulinati, *Inorg. Chim. Acta* **1992**, *202*, 43−48.

 © 2003 Wiley-VCH Verlag GmbH & Co. KGaA, Weinheim

[15] See, for example: G. A. van Albada, S. Gorter, J. Reedijk, *Polyhedron* **1999**, *18*, 1821; W. Lu, Y. Cheng, N. Dong, C. Xu, C. Chen, *Acta Crystallogr. Sect. C* **1995**, *51*, 1756; J.-G. Mao, H.-J. Zhang, J.-Z. Ni, S.-B. Wang, T. C. W. Mak, *Polyhedron* **1999**, *18*, 1519; J.-F. Ma, Z.-S. Jin, J.-Z. Ni, *Acta Crystallogr. Sect. C* **1994**, *50*, 1008.
[16] C. Oldham, in *Comprehensive Coordination Chemistry*, 1st ed. (Ed.: S. G. Wilkinson), Pergamon Press, Oxford, **1987**, vol. 2, p. 435−459.
[17] M. D. Faucher, R. Morlotti, O. K. Moune, *J. Lumin.* **2002**, *96*, 37−49.
[18] X. Chen, X. Zhu, Y. Xu, S. S. S. Raj, S. Öztürk, H. Fun, J. Ma, X. You, *J. Mater. Chem.* **1999**, *9*, 2919−2922.
[19] A. L. Rheingold, W. King, *Inorg. Chem.* **1989**, *28*, 1715−1719.
[20] STOE, Cie GmbH, *Win XPOW THEO*, Version 1.15, **1999**.
[21] T. Kottke, D. Stalke, *J. Appl. Crystallogr.* **1993**, *26*, 615.
[22] G. M. Sheldrick, *SHELXL 97, Program for Crystal Structure Refinement*, University of Göttingen, **1997**.
[23] G. M. Sheldrick, *SHELXS 97, Program for Crystal Structure Solution*, University of Göttingen, **1997**.
[24] R. H. Blessing, *Acta Crystallogr., Sect. A* **1995**, *51*, 33.

Received February 12, 2003
Early View Article
Published Online August 14, 2003

 © 2003 Wiley-VCH Verlag GmbH & Co. KGaA, Weinheim

A Novel Mixed-Valence Cu^{I}/Cu^{II} Coordination Polymer: Solvothermal Synthesis, Crystal Structure, and Magnetic Properties of $Cu^{I}Cu^{II}$(2-Pyrazinecarboxylate)$_2$(H_2O)(ClO_4)

Cai-Ming Liu,*[a] De-Qing Zhang,*[a] Jian-Lin Luo,[b] Nan-Lin Wang,[b] Huai-Ming Hu,[a] and Dao-Ben Zhu*[a]

Keywords: Copper / Magnetic properties / N ligands / Solvothermal synthesis

The solvothermal reaction between $Cu(ClO_4)_2 \cdot 6H_2O$ and 2-pyrazinecarboxylic acid in methanol yields a novel mixed-valence Cu^{I}/Cu^{II} coordination polymer, $Cu^{I}Cu^{II}$(2-pyrazinecarboxylate)$_2$(H_2O)(ClO_4) (**1**), in which a three-dimensional supramolecular array with square channels (9.3 × 9.3 Å) is formed through crisscross arrangement of the one-dimensional $Cu^{I}Cu^{II}$(2-pyrazinecarboxylate)$_2$(H_2O)$^+$ coordination polymer cation chains in the adjacent layers. Complex **1** exhibits weak ferromagnetic interactions.

(© Wiley-VCH Verlag GmbH & Co. KGaA, 69451 Weinheim, Germany, 2003)

Introduction

Crystal engineering of coordination polymers has been one of the most rapidly developing areas in the past decade, due mainly both to theoretical aspects related to the topologies of novel frameworks and to the interesting physical and chemical properties of these rationally designed functional solids.[1] Their potential applications have been demonstrated in, for example, nonlinear optical,[2] electrical,[3] and magnetism materials.[4] Furthermore, because specific pore size, type, and functions of cavity have become designable, their implications in molecular recognition and host-guest chemistry,[5] and also as zeolite mimics,[6] are particularly attractive. Generally, treatment of transition metal ions with rigid or flexible polyfunctional ligands by self-assembly processes is one basic strategy to afford varied polymers with such features as diamondoid, honeycomb grid, square grid, ladder, brick wall, and octahedral frameworks.[3−7] Hydro(solvo)thermal techniques have also been developed for the preparation of a series of coordination polymers.[2,6d,6e,8] Here we present the solvothermal synthesis, crystal structure, and magnetic properties of a novel mixed-valence Cu^{I}/Cu^{II} coordination polymer: $Cu^{I}Cu^{II}$(2-pyrazinecarboxylate)$_2$(H_2O)(ClO_4) (**1**), in which the $Cu^{I}Cu^{II}$(2-pyrazinecarboxylate)$_2$(H_2O)$^+$ coordination polymer cation chains in adjacent layers are arranged in a cross-like fashion to generate a three-dimensional supramolecular array with square channels. In addition, the coordination polymer chain in complex **1** adopts an unusual *cis* configuration

[a] Center for Molecular Science, Institute of Chemistry, Organic Solids Laboratory, Chinese Academy of Sciences, Beijing 100080, P. R. China
E-mail: cmliu@iccas.ac.cn
[b] Institute of Physics, Chinese Academy of Sciences, Beijing 100080, P. R. China

Results and Discussion

Synthesis

Complex **1** was obtained as black blocks in 60% yield through a solvothermal reaction. A mixture of 2-pyrazinecarboxylic acid (0.4 mmol) and $Cu(ClO_4)_2 \cdot 6H_2O$ (0.4 mmol) in methanol (1 mL) was placed in a sealed thick Pyrex tube (ca. 20 cm long), which was kept at 80 °C under autogenous pressure for 2 d. The formation of Cu^{I} in **1** suggests that the methanol solvent and the 2-pyrazinecarboxylic acid may serve as effective reducing agents for Cu^{II} to Cu^{I} even under very mild solvothermal conditions. Similar trends have also been observed in the hydro(solvo)thermal syntheses of mixed-valence Cu^{I}/Cu^{II} tetranuclear complexes $[Cu_4(obpy)_4(tp)]$[9a] and $[Cu_4(ophen)_4(tp)]$[9a] (Hophen = 2-hydroxy-1,10-phenanthroline, Hobpy = 6-hydroxy-2,2′-bipyridine, tp = terephthalate) and mixed-valence Cu^{I}/Cu^{II} coordination polymers $[Cu_4\{1,4\text{-}C_6H_4(COO)_2\}_3(4,4'\text{-bipy})_2]_n$,[8a] $[Cu_2(ipO)(4,4'\text{-bpy})]$(ipOH = 2-hydroxyisophthalate),[9b] $Cu^{I}_2Cu^{II}(hedpH_2)_2(4,4'\text{-bpy})_2 \cdot 2H_2O$ (hedp = 1-hydroxyethylidenediphosphonate),[9c] but higher temperatures were required.

Crystal Structure

As shown in Figure 1 (top), the crystal structure of **1** consists of one-dimensional $Cu^{I}Cu^{II}$(2-pyrazinecarboxylate)$_2$(H_2O) cations and discrete perchlorate anions. Each Cu^{II}

 © 2003 Wiley-VCH Verlag GmbH & Co. KGaA, Weinheim DOI: 10.1002/ejic.200300227

atom is situated in a distorted square-pyramidal environment, with the two oxygen atoms and the two nitrogen atoms from two chelating 2-pyrazinecarboxylate ligands at the equatorial positions, and a coordinated water molecule at the apical position. The coordination environment of Cu^{II} in complex **1** is similar to that in [Cu(2-methylpyrazine-5-carboxylate)$_2$(H_2O)]·3H_2O,[10] but quite different from that in Cu(2-pyrazinecarboxylate)$_2$(H_2O)$_2$,[11] which has a disordered octahedral coordination sphere. The Cu^{II} centers in linear Cu(2-pyrazinecarboxylate)$_2$[11] and three-dimensional [Cu(pyzca)$_2$]$_2$$Cd_4I_8$]$_n$[12] (pyzca = 2-pyrazinecarboxylate) also have octahedral configurations. The Cu−Ow bond length of 2.228(9) Å (see Table 1) is similar to that in [Cu(2-methylpyrazine-5-carboxylate)$_2$(H_2O)]·3H_2O [2.257(2) Å],[9] but shorter than that in Cu(2-pyrazinecarboxylate)$_2$(H_2O)$_2$ (2.39 Å).[11]

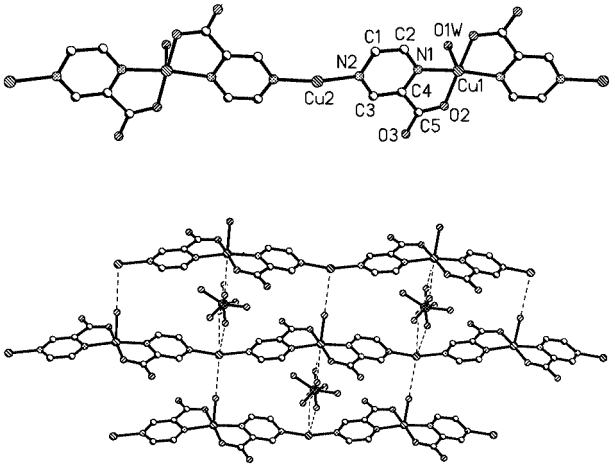

Figure 1. ORTEP figure of the cation chain in complex **1** at the 50% probability level showing the numbering scheme; all hydrogen atoms are omitted for clarity (top); illustration of the two-dimensional network layer formed by the mixed-valence Cu^{I}/Cu^{II} coordination polymer chains with Cu···$O_{perchlorate}$ short contacts (bottom)

Table 1. Selected distances [Å] and angles [°] for complex **1**; symmetry code: #1 $y-1, x+1, -z$; #2 $y, x, -z$

Cu(1)−N(1)	1.971(5)	Cu(1)−O(2)	1.941(3)
Cu(1)−O(2)#1	1.941(3)	Cu(1)−N(1)#1	1.971(5)
Cu(1)−O(1 W)	2.228(9)	Cu(2)−N(2)	1.949(5)
Cu(2)−N(2)#2	1.949(5)		
O(2)#1−Cu(1)−O(2)	176.0(3)	O(2)#1−Cu(1)−N(1)	96.39(16)
O(2)−Cu(1)−N(1)	83.18(16)	O(2)−Cu(1)−N(1)#1	96.39(16)
N(1)−Cu(1)−N(1)#1	167.7(4)	O(2)−Cu(1)−O(1 W)	92.02(13)
N(1)−Cu(1)−O(1 W)	96.2(2)	N(1)#1−Cu(1)−O(1 W)	96.2(2)
N(2)−Cu(2)−N(2)#2	161.2(3)		

The coordination sphere of the Cu^{I} site in complex **1** is defined by two crystallographically equivalent nitrogen donors from two Cu^{II}(2-pyrazinecarboxylate)$_2$(H_2O) molecules, with a Cu2−N2 distance of 1.949(5) Å. This coordination mode is quite similar to those of the Ag^{I} centers in Ag[Cu(2-methylpyrazine-5-carboxylate)$_2$(H_2O)$_2$]·(BF_4)[10] and Ag[Cu(2-methylpyrazine-5-carboxylate)$_2$(H_2O)$_2$]·(NO_3).[10] The N2−Cu2−N2^{i} (^{i} $y, x, -z$) bond angle of 161.2(3)° is a little smaller than the N2−Ag−N2 angle [165.7(2)°] in Ag[Cu(2-methylpyrazine-5-carboxylate)$_2$(H_2O)$_2$]·(BF_4),[10] but much larger than the N2−Ag−N2 angle [153.31(18)°] in Ag[Cu(2-methylpyrazine-5-carboxylate)$_2$(H_2O)$_2$]·(NO_3).[10]

The one-dimensional mixed-valence Cu^{I}/Cu^{II} cation chain is made up of alternating Cu^{I} centers and Cu^{II}(2-pyrazinecarboxylate)$_2$(H_2O) fragments. The intrachain Cu^{I}···Cu^{I}, Cu^{I}···Cu^{II}, and Cu^{II}···Cu^{II} distances are 13.203, 6.663, and 13.203 Å, respectively. Interestingly, all coordination water molecules in the same cation chain are arranged in a *cis* orientation. It is noteworthy that **1** is the first coordination polymer derived from 2-pyrazinecarboxylate known to adopt a *cis* configuration. Only a few examples of *cis* configurations in complexes of other carboxylate-substituted pyrazine derivatives are known, among them the two-dimensional {Cu_2(pzdc)$_2$(pyz)}$_n$ (pzdc = 2,3-pyrazinedicarboxylate, pyz = pyrazine),[13a] the one-dimensional {Co[pyz(COO)COOH]$_2$(H_2O)$_2$},[13b] and the mononuclear [NiL_2(H_2O)$_2$] (L = 1,4-dihydropyrazine-2,3-dione-5,6-dicarboxylate).[13c]

The disordered ClO_4^- anions are located between a Cu^{I} center and a Cu^{II} center of adjacent mixed-valence Cu^{I}/Cu^{II} cation chains (the related interchain Cu^{II}···Cu^{I} distance is 7.508 Å), with the shortest Cu^{I}···$O_{perchlorate}$ contact 2.684 Å and the shortest Cu^{II}···$O_{perchlorate}$ contact 2.865 Å (Figure 1, bottom). The chlorine atom of the ClO_4^- anion is a little closer to the Cu^{II} center than to the Cu^{I} center (the Cu···Cl contacts are 3.669 and 3.838 Å for Cu^{II} and Cu^{I}, respectively). The mixed-valence Cu^{I}/Cu^{II} coordination polymer chains are therefore bound to each other through ClO_4^- anions to generate a two-dimensional network layer parallel to the *ab* plane with the shortest interchain Cu^{II}···Cu^{I} distance 5.695 Å.

Within a layer, all mixed-valence Cu^{I}/Cu^{II} coordination polymer chains show the same orientation (along one of two diagonal lines of the *ab* plane). However, chains from each pair of adjacent layers are always crisscrossed through the Cu^{I}···$O_{carboxylate}$ short contacts of 2.464 Å and the Ow···$O_{carboxylate}$ hydrogen bond of 2.720 Å (Figure 2), resulting in a three-dimensional supramolecular array with square channels (9.3 × 9.3 Å) running along the *c* axis (Figure 3). This structure is quite different from those of the Ag[Cu(2-methylpyrazine-5-carboxylate)$_2$(H_2O)$_2$]·(BF_4)[10] and Ag[Cu(2-methylpyrazine-5-carboxylate)$_2$(H_2O)$_2$]·(NO_3),[10] in which all the Cu^{II}/Ag^{I} mixed-metal coordination polymer chains run in one direction, so square cavities cannot be generated. To the best of our knowledge, the only reported example of chains in adjacent layers being arranged in a cross-like fashion to generate a three-dimensional supramolecular array with channels is [Cu(4,4′-bipy)(H_2O)$_3$(SO_4)]·2H_2O,[14] in which the adjacent chains of Cu(4,4′-bipy)(H_2O)$_3$(SO_4) are arranged in a cross-like fashion at the midpoints of the 4,4′-bipy ligands, and so rhombic channels (11.12 × 11.12 Å) are formed.

 © 2003 Wiley-VCH Verlag GmbH & Co. KGaA, Weinheim

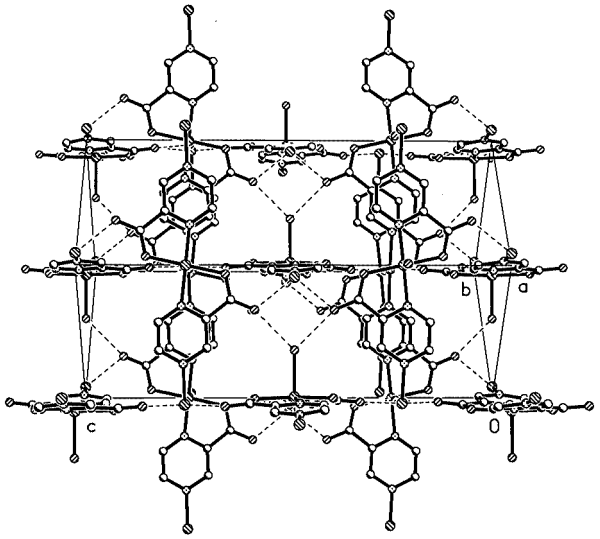

Figure 2. Perspective view showing some hydrogen bonds and short contacts between mixed-valence Cu^{I}/Cu^{II} coordination polymer chains from the same network layer and/or from neighboring network layers; all disordered perchlorate ions and hydrogen atoms are omitted for clarity

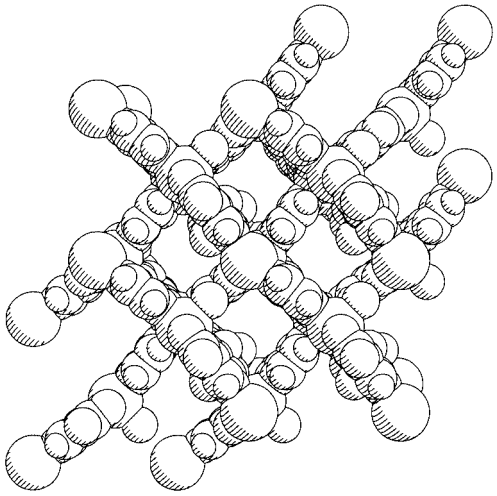

Figure 3. Space-filling model of complex **1**, viewed down the *c* axis

Magnetic Properties

The variation in the molar magnetic susceptibilities χ was investigated for complex **1** in the 5−300 K temperature range in a 10 kG applied field. The inset of Figure 4 shows that the χT value continuously increases with cooling while going from 250 to 9 K, and then drops down to 5 K, indicating the presence of a ferromagnetic exchange interaction. The room-temperature χT value of 0.375 emu·K·mol^{-1} is in good agreement with that of **1**, uncoupled $S = 1/2$ spins of Cu^{2+} atom (≈ 0.375 emu·K·mol^{-1}; supposed $g = 2.0$ for Cu^{2+}), confirming that only half of the Cu atoms in complex **1** are Cu^{II} atoms. It was surprising to find that there is ferromagnetic exchange interaction between two Cu^{II} atoms 13.203 Å apart. Perhaps the uncoupled electron of the Cu^{II} atom is delocalized to some degree over the Cu^{II} and Cu^{I} centers. A quite recently reported mixed-oxidation-state Cu^{I}/Cu^{II} cluster complex $[(PAH)_4Cu^{II}_4Cu^{I}_2Br_{10}]$ (PAH = picolinamide hydrazone) also exhibited weak ferromagnetic exchange.[15] The temperature dependence of χ is interpreted in terms of a one-dimensional ferromagnetic chain,[16] by use of Equation (1) with $K = J/(2K_BT)$. The theoretical best fitting to the experimental data is obtained with $J/K_B = 1.80$ K and $C = 0.375$ emu·K·mol^{-1}. The deviation factor defined by $R = [(\chi_{obsd.} - \chi_{calcd.})^2/\chi_{obsd.}^2]^{1/2}$ is equal to 0.04437.

$$\chi = (C/T)[(1 + 5.7979916\,K + 16.902653\,K^2 + 29.376885\,K^3 + 29.832959\,K^4 + 14.036981\,K^5)/(1 + 1.27979916\,K + 7.0086780\,K^2 + 8.6538644\,K^3 + 4.5743114\,K^4)]^{2/3} \quad (1)$$

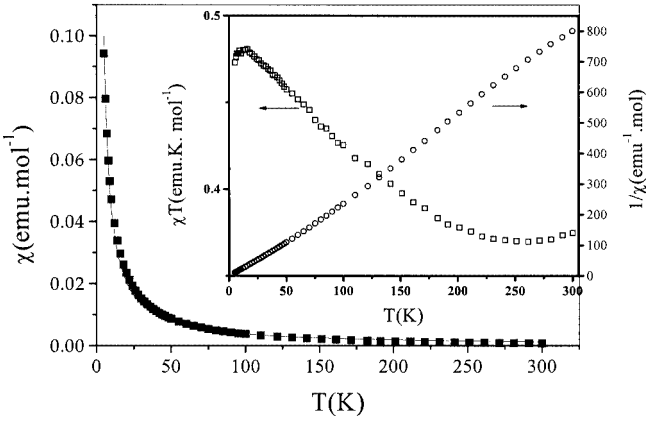

Figure 4. Temperature dependence of magnetic susceptibility of **1**: χ vs. T plots; inset, χT and/or χ^{-1} vs. T plots

IR and XPD Spectra

The strong and broad peak around 3454 cm^{-1} in the IR spectrum of complex **1** is mainly attributable to the presence of coordinated water molecules. The strong band at 1649 cm^{-1} is assignable to the antisymmetric C=O stretching vibration of the coordinated carboxylate group, while the strong band at 1120 cm^{-1} is typical of the uncoordinated perchlorate.

The powder XRD pattern of the complex and the pattern simulated on the basis of the single-crystal structure are presented in Figure 5. The diffraction peaks in both patterns correspond well in position, indicating the phase purity of the sample as synthesized.

In summary, this study illustrates that a three-dimensional supramolecular array with channels as exemplified by **1** can be achieved through crisscross arrangement of one-dimensional chains from parallel layers, and that solvothermal (or hydrothermal) synthesis is an effective method by which to obtain mixed-valence Cu^{I}/Cu^{II} coordination polymers.

 © 2003 Wiley-VCH Verlag GmbH & Co. KGaA, Weinheim

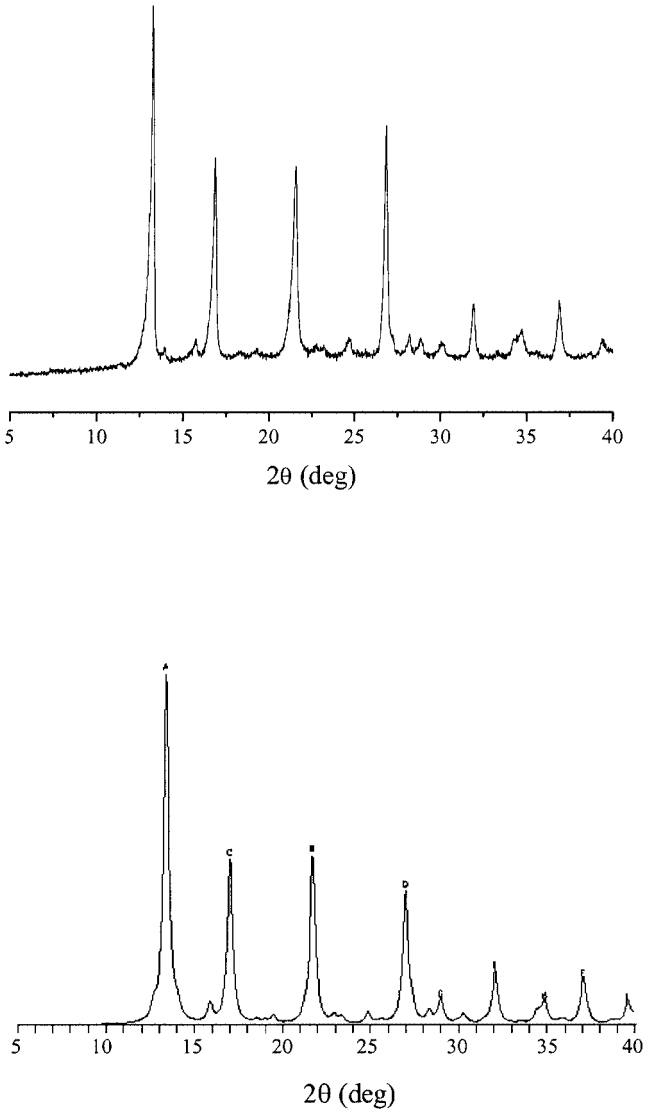

Figure 5. Experimental powder X-ray diffraction pattern of complex **1** (top) and the pattern calculated from the single-crystal data for complex **1** (bottom)

Experimental Section

General: All chemicals purchased were of reagent grade and were used without further purification. Elemental analyses (C, H and N) were performed with a Heraeus CHN-Rapid elemental analyzer. IR spectra were recorded with a Perkin−Elmer 2000 spectrophotometer on pressed KBr pellets. UV/Vis spectra were run with a U-3010 spectrophotometer. Powder X-ray diffraction (XRD) data were obtained with a Rigaku D/max-2500 X-ray diffractometer with Cu-K_α radiation (λ = 1.5406 Å). Variable-temperature magnetic susceptibility data were collected with a crystalline sample (11.75 mg) from 5 to 300 K in a magnetic field of 10 kG after zero-field cooling with a SQUID magnetometer. Diamagnetic corrections were estimated from Pascal's constants.

Synthesis of 1: A mixture of 2-pyrazinecarboxylic acid (0.4 mmol) and $Cu(ClO_4)_2{\cdot}6H_2O$ (0.4 mmol) in methanol (1 mL) was placed in a thick Pyrex tube (ca. 20 cm long), and the tube was frozen with liquid N_2, evacuated under vacuum, and sealed with a torch. The tube was then heated at 80 °C under autogenous pressure for 2 d to give dark crystals of **1** in 60% yield. An unidentified blue polycrystalline material was formed as a by-product. $C_{10}H_6ClCu_2N_4O_9$ (488.72): calcd. C 24.58, H 1.24, N 11.46; found C 24.49, H 1.32, N 11.40. UV (1×10^{-4} M, DMF): λ_{max} = 273 nm (ε = 4.46×10^4 $M^{-1}cm^{-1}$), 691 nm (very broad peak, ε = 729 $M^{-1}cm^{-1}$).

Caution: *$Cu(ClO_4)_2{\cdot}6H_2O$ is potentially explosive and should be handled with care!*

X-Ray Crystallography Analysis: The data were collected with a Rigaku RAXIS RAPID IP imaging plate system by use of Mo-K_α radiation (λ = 0.71073 Å). The structure was solved by the Patterson method and refined by a full-matrix, least-squares technique based on F^2 by use of the SHELXL 97 program. All non-hydrogen atoms except for the oxygen atoms of the perchlorate anion were refined anisotropically, and all hydrogen atoms other than those in coordinated hydrate molecule were allowed for as riding atoms. Crystal data for **1**: $C_{10}H_6ClCu_2N_4O_9$, tetragonal, space group $P4_12_12$, M = 488.72, $a = b$ = 9.3358(13), c = 20.835(4) Å, V = 1815.9(5) $Å^3$, Z = 4, $D_{calcd.}$ = 1.788 gcm^{-3}, T = 293(2)K, μ = 2.539 mm^{-1}, R_1 = 0.0494, wR_2 = 0.0863 for 1031 observed reflections[$I > 2\sigma(I)$] from 2071 independent reflections, GOF = 0.907. CCDC-187295 contains the supplementary crystallographic data for this paper. These data can be obtained free of charge at www.ccdc.cam.ac.uk/conts/retrieving.html [or from the Cambridge Crystallographic Data Centre, 12 Union Road, Cambridge CB2 1EZ, UK; Fax: (internat.) + 44-1223/336-033; E-mail: deposit@ccdc.cam.ac.uk].

Acknowledgments

This work was supported by the National Natural Science Foundation of China (no. 20201012, 90101025), the Major State Basic Research Development Program of the P. R. China (G2000077500 and 2001CB610507) and the Chinese Academy of Sciences. The authors also thank the referees for their excellent suggestions for improving the manuscript.

[1] [1a] S. R. Batten, R. Robson, *Angew. Chem. Int. Ed.* **1998**, *37*, 1460−1494. [1b] R. Robson, B. F. Abrahams, S. R. Batten, R. W. Gable, B. F. Hoskins, J. Liu, *Supramolecular Architecture*, American Chemical Society, Washington DC, **1992**, chapter 19. [1c] R. Robson in *Comprehensive Supramolecular Chemistry*, vol. 6 (Eds.: J. L. Atwood, J. E. D. Davies, D. D. MacNicol, F. Vögtle, F. Toda, R. Bishop), Pergamon, Oxford, **1996**, pp. 733−755.

[2] [2a] O. R. Evans, R-G. Xiong, Z. Wang, G. W. Wong, W. Lin, *Angew. Chem. Int. Ed.* **1999**, *38*, 536−538. [2b] W. Lin, Z. Wang, L. Ma, *J. Am. Chem. Soc.* **1999**, *121*, 11249−11250. [2c] W. Lin, O. R. Evans, R.-G. Xiong, Z. Wang, *J. Am. Chem. Soc.* **1998**, *120*, 13272−13273. [2d] R.-G. Xiong, J.-L. Zuo, X.-Z. You, B. F. Abrahams, Z.-P. Bai, C.-M. Che, H.-K. Fun, *Chem. Commun.* **2000**, 2061−2062. [2e] X. Xue, X.-S. Wang, R.-G. Xiong, X.-Z. You, B. F. Abrahams, C.-M. Che, H.-X. Ju, *Angew. Chem. Int. Ed.* **2002**, *41*, 2944−2946.

[3] [3a] M. Munakata, T. Kuroda-Sowa, M. Maekawa, A. Hirota, S. Kitagawa, *Inorg. Chem.* **1995**, *34*, 2705−2710. [3b] C. Jia, D. Zhang, C.-M. Liu, W. Xu, H. Hu, D. Zhu, *New J. Chem.* **2002**, *26*, 490−494.

[4] [4a] R. Cortes, L. Lezama, J. L. Pizarro, M. I. Arriortua, T. Rojo, *Angew. Chem. Int. Ed. Engl.* **1996**, *35*, 1810−1812. [4b] G. De Munno, M. Julve, G. Viau, F. Lloret, J. Faus, D. Viterbo, *Angew. Chem. Int. Ed. Engl.* **1996**, *35*, 1807−1810. [4c] C.-M. Liu, Z. Yu, R.-G. Xiong, K. Liu, X.-Z. You, *Inorg. Chem. Commun.* **1999**, *2*, 31−34.

 © 2003 Wiley-VCH Verlag GmbH & Co. KGaA, Weinheim

[5] [5a] S. Subramanian, M. J. Zaworotko, *Angew. Chem. Int. Ed. Engl.* **1995**, *34*, 2127−2129. [5b] K. Biradha, Y. Hongo, M. Fujita, *Angew. Chem. Int. Ed.* **2000**, *39*, 3843−3845. [5c] R.-G. Xiong, C.-M. Liu, J.-L. Zuo, X.-Z. You, *Inorg. Chem. Commun.* **1999**, *2*, 292−297. [5d] C.-M. Liu, R.-G. Xiong, X.-Z. You, W. Chen, *Acta Chem. Scand.* **1998**, *52*, 1353−1358.

[6] [6a] M. Fujita, Y. J. Kwon, S. Washizu, K. Ogura, *J. Am. Chem. Soc.* **1997**, *119*, 3929−3934. [6b] M. Kondo, T. Yoshitomi, K. Seki, H. Matsuzaka, S. Kitagawa, *Angew. Chem. Int. Ed. Engl.* **1997**, *36*, 1725−1727. [6c] Y. Diskin-Posner, S. Dahal, I. Goldberg, *Angew. Chem. Int. Ed.* **2000**, *112*, 1288−1292. [6d] Y.-Q. Tian, C.-X. Cai, Y. Ji, X.-Z. You, S.-M. Peng, G.-H. Lee, *Angew. Chem. Int. Ed.* **2002**, *41*, 1384−1386. [6e] R.-G. Xiong, X.-Z. You, B. F. Abrahams, Z. Xue, C.-M. Che, *Angew. Chem. Int. Ed.* **2001**, *40*, 4422−4425.

[7] [7a] T. M. Reineke, M. Eddaoudi, D. Moler, M. O'Keeffe, O. M. Yaghi, *J. Am. Chem. Soc.* **2000**, *122*, 4843−4844. [7b] M. J. Zaworotko, P. Losier, *Angew. Chem. Int. Ed. Engl.* **1996**, *35*, 2779−2782. [7c] M. J. Zaworotko, *Angew. Chem. Int. Ed.* **1998**, *37*, 1211−1213. [7d] M. Fujita, Y. J. Kwon, O. Sasaki, K. Yamaguchi, K. Ogura, *J. Am. Chem. Soc.* **1995**, *117*, 7287−7288. [7e] H. Gudbjartson, K. Biradha, K. M. Poiruer, M. J. Zaworotko, *J. Am. Chem. Soc.* **1999**, *121*, 2599−2600. [7f] S. Ferlay, S. Koenig, M. W. Hosseini, J. Pansanel, A. D. Cian, N. Kyritsakas, *Chem. Commun.* **2002**, 218−219. [7g] D.-L. Long, A. J. Blake, N. R. Champness, C. Wilson, M. Schröder, *Angew. Chem. Int. Ed.* **2001**, *40*, 2444−2447.

[8] [8a] S. M-F. Lo, S. S-Y. Chui, L.-Y. Shek, Z. Lin, X. X. Zhang, G.-H. Wen, I. D. Williams, *J. Am. Chem. Soc.* **2000**, *122*, 6293−6294. [8b] J. Y. Lu, B. R. Cabrera, R.-J. Wang, J. Li, *Inorg. Chem.* **1999**, *38*, 4608−4611.

[9] [9a] X.-M. Zhang, M.-L. Tong, X.-M. Chen, *Angew. Chem. Int. Ed.* **2002**, *41*, 1029−1031. [9b] J. Tao, Y. Zhang, M.-L. Tong, X.-M. Chen, T. Yuen, C. L. Lin, X. Huang, J. Li, *Chem. Commun.* **2002**, 1342−1343. [9c] L.-M. Zheng, P. Yin, X.-Q. Xin, *Inorg. Chem.* **2002**, *41*, 4084−4086.

[10] Y.-B. Dong, M. D. Smith, H.-C. zur Loye, *Inorg. Chem.* **2000**, *39*, 1943−1949.

[11] C. L. Klein, R. J. Majeste, L. M. Trefonas, C. J. O'Connor, *Inorg. Chem.* **1982**, *21*, 1891−1897.

[12] D. M. Ciurtin, M. D. Smith, H.-C. zur Loye, *Chem. Commun.* **2002**, 74−75.

[13] [13a] M. Kondo, T. Okubo, A. Asami, S. Noro, T. Yoshitomi, S. Kitagawa, T. Ishii, H. Matsuzaka, K. Seki, *Angew. Chem. Int. Ed.* **1999**, *38*, 140−143. [13b] J.-M. Rueff, N. Masciocchi, P. Rabu, A. Sironi, A. Skoulios, *Eur. J. Inorg. Chem.* **2001**, 2843−2848. [13c] C.-M. Liu, D.-Q. Zhang, A.-J. Qin, C. Ye, H.-M. Hu, D.-B. Zhu, *Eur. J. Inorg. Chem.* **2002**, 1595−1598.

[14] M.-L. Tong, X.-M. Chen, *CrystEngComm.* **2000**, 1−5.

[15] Z. Xu, L. K. Thompson, D. O. Miller, E. Ruiz, S. Alvarez, *Inorg. Chem.* **2003**, *42*, 1107−1111.

[16] D. D. Swank, C. P. Landee, R. D. Willett, *Phys. Rev. B.* **1979**, *20*, 2154−2166.

Received April 21, 2003

 © 2003 Wiley-VCH Verlag GmbH & Co. KGaA, Weinheim

Self-Assembly of Three Cd^{II}- and Cu^{II}-Containing Coordination Polymers from 4,4′-Dipyridyl Disulfide

Junhua Luo,[a] Maochun Hong,*[a] Ruihu Wang,[a] Daqiang Yuan,[a] Rong Cao,[a] Lei Han,[a] Yanqing Xu,[a] and Zhengzhong Lin[a]

Keywords: Cadmium / Coordination polymers / Copper / Fluorescence / Magnetic properties / N ligands

Three new organic/inorganic coordination polymers, $[\{Cu(4\text{-}DPDS)_2(H_2O)\}\cdot 2NO_3\cdot 3H_2O]_n$ (**1**), $[\{Cu(4\text{-}DPDS)_2(SO_4)\}\cdot 1.5H_2O\cdot CH_3OH]_n$ (**2**), and $[Cd(4\text{-}DPDS)_2Cl_2]_n$ (**3**), have been synthesized by using the flexible ligand 4,4′-dipyridyl disulfide (4-DPDS). Complex **1** crystallized in the *Ibca* space group: a = 10.5275(6), b = 20.2670(1), c = 27.235(1) Å, V = 5811.5(6) Å^3, Z = 16. Complex **2** crystallized in the *Pnna* space group: a = 10.547(2), b = 14.201(2), c = 19.667(3) Å, V = 2945.8(8) Å^3, Z = 8. Complex **3** crystallized in the $P2_1/c$ space group: a = 7.6146(3), b = 18.2606(8), c = 9.3203(2) Å, β = 100.26(1)°, V = 1275.24(8) Å^3, Z = 4. The three coordination polymers display a variety of structural architectures, ranging from double-stranded chains (**1**) to two-dimensional channels (**2**) and two-dimensional, puckered, grid-like arrays (**3**). Magnetic characterizations show that complex **1** exhibits antiferromagnetic interactions while **2** is ferromagnetic. Solid-state fluorescence results reveal that **3** exhibits fluorescence emissions at 418 and 575 nm (λ_{ex} = 314 nm).
(© Wiley-VCH Verlag GmbH & Co. KGaA, 69451 Weinheim, Germany, 2003)

Introduction

Self-assembly of organic ligands and inorganic metal ions is one of the most efficient and widely used approaches for the construction of supramolecular architectures. Owing to their potential as new functional solid materials, interest in self-assembled coordination polymers with interesting physical properties has grown rapidly.[1,2] An extensive amount of literature exists on networks crystallized from different dipyridyl ligands. A variety of architectures have been obtained over the past few years using the most simple of these ligands, i.e., 4,4′-bipyridyl.[3,4] The use of longer bis(pyridyl) spacers has afforded very interesting structural motifs, such as double helices,[5] multiple sheets,[6] interpenetrated ladders,[7] interpenetrated diamondoid nets,[8] and other noteworthy species.[9] Many of the architectures reported to date, however, are based upon rigid, linear, linker ligands, with only recent efforts being focused on the use of ligands showing conformational flexibility.[5,6,10,11] In addition, the design of coordination polymers from flexible ligands is highly influenced by factors such as the nature of coordination of the metal ion, the structural characteristics of the polydentate organic ligand, the metal:ligand ratio, and the possible influences of the counteranion and solvent. Thus, there is still a long way to go to rationalize the design of compounds with well-defined structures and useful functions by developing new architectures of coordination polymers using flexible spacers ligands.

In this report, we focus on 4,4′-dipyridyl disulfide (4-DPDS), in which the two pyridyl rings are bridged by the −S−S− group. Two enantiomeric conformers exist[12] (Scheme 1) with idealized dihedral angles (C−S−S−C) of 90° and the compound may assume a twisted conformation because of the flexible −S−S− group. Additionally, the bridging S atom has coordinating ability, which may lead to unique network structures because of its bonding ability to soft metal ions.[13] Several coordination polymers have been reported recently from the reaction of 4-DPDS with CuI,[14] $M(hfac)_2$ (M = Cu, Mn; hfac = 1,1,1,5,5,5-hexafluoroacetylacetone),[15] $Cd(NO_3)_2$,[16] platinum(II) subunits,[17] and various silver salts.[18] In this report, we describe the syntheses, structures, and properties of three new Cd^{II}- and Cu^{II}-containing coordination polymers, $[\{Cu(4\text{-}DPDS)_2(H_2O)\}\cdot 2NO_3\cdot 3H_2O]_n$ (**1**), $[\{Cu(4\text{-}DPDS)_2(SO_4)\}\cdot 1.5H_2O\cdot CH_3OH]_n$ (**2**), and $[Cd(4\text{-}DPDS)_2Cl_2]_n$ (**3**).

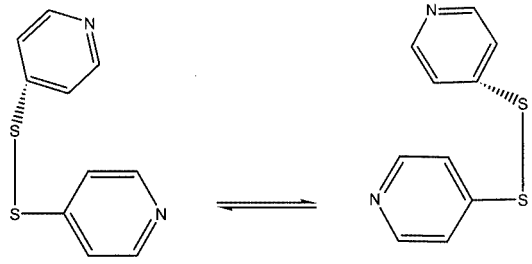

Scheme 1. The two enantiomeric conformers of 4-DPDS

[a] State Key Laboratory of Structural Chemistry, Fujian Institute of Research on the Structure of Matter, Chinese Academy of Sciences,
Fuzhou, Fujian, 350002, China
Fax: (internat.) + 86-591/371-4946
E-mail: hmc@ms.fjirsm.ac.cn

Results and Discussion

Crystal Structures

The energy-dispersive X-ray analyses confirm the presence of copper atoms in **1** and **2**, and cadmium atoms in **3**. On the basis of the results of single-crystal X-ray diffraction and elemental analyses, compounds **1**, **2**, and **3** are characterized as having the formulas $[\{Cu(4\text{-}DPDS)_2(H_2O)\}\cdot 2NO_3\cdot 3H_2O]_n$, $[\{Cu(4\text{-}DPDS)_2(SO_4)\}\cdot 1.5H_2O\cdot CH_3OH]_n$, and $[Cd(4\text{-}DPDS)_2Cl_2]_n$, respectively.

$[\{Cu(DPDS)_2(H_2O)\}\cdot 2NO_3\cdot 3H_2O]_n$ (1)

Figure 1 shows the ORTEP drawing of the copper center of **1**, with a numbering scheme, where the metal sites are in the crystallographic inversion center. The copper atom has a distorted square-pyramidal environment, which is surrounded by four nitrogen atoms from four 4-DPDS ligands in the base plane, and one oxygen atom from a water molecule occupying the axial position. The Cu−N(4-DPDS) bond lengths are 2.032(1) and 2.061(1) Å, and the Cu−O(water) distance is 2.305(1) Å. The *trans* N−Cu−N bond angles are 167.29(6) and 176.9(6)°, and the *cis* N−Cu−N and O−Cu−N bond angles range from 88.5(3) to 96.4(3)°, indicating the distorted square-pyramidal coordination environment of Cu center.

Each copper center is bridged by four 4-DPDS ligands to form a double-stranded chain (Figure 2). As in other double-stranded chain complexes,[20,21] two copper atoms and two 4-DPDS ligands in **1** form a metallacycle in which the non-bonded distance between the two copper atoms is ca. 10.528 Å. The two pyridyl rings of the 4-DPDS ligand are almost perpendicular, with a dihedral angle of 98.6°. The dimensions of the distorted square cavity are ca. 5 × 5 Å. The molecular box in **1** is twisted to make the enclosed cavity a small one, resulting from the flexibility of 4-DPDS and the pentacoordinate geometry of the Cu^{II} ion, and no solvent molecules are clathrated in the cavities.

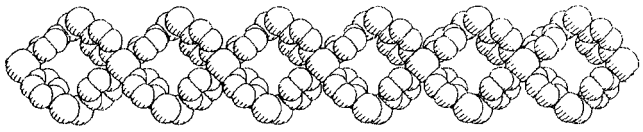

Figure 2. Space-filling representation of the double-stranded chain in **1**

It is interesting to note that in **1** the copper(II) ion has a pentacoordinate geometry and the water molecule occupies the axial position, and that all the axially coordinated water molecules are directed in the same direction. Two such chains lie reversibly and are linked into a ladder structure through hydrogen bonds between the axially coordinated water molecules and lattice water molecules (O1···O1W$^{\#1}$, 2.770 Å; O1···O1W$^{\#2}$, 2.770 Å; O1W···O1W$^{\#3}$, 2.785 Å; O1W···O2W$^{\#4}$, 2.769 Å; symmetry codes #1: $-x$, $-y$, $1-z$; #2: x, $y-1/2$, $1-z$; #3: $1/2-x$, y, $1-z$; #4: $1/2+$

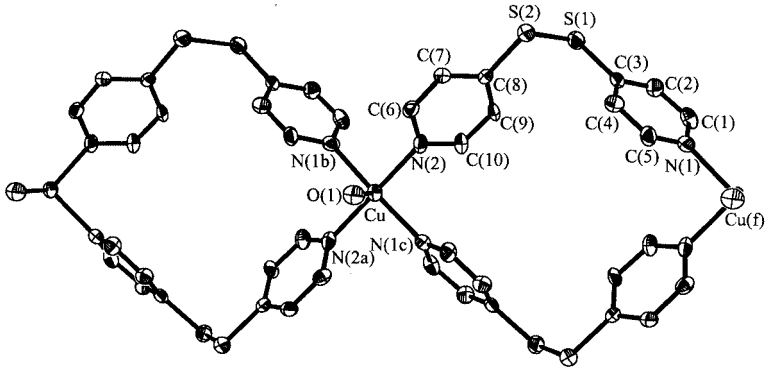

Figure 1. Drawing of the Cu^{II} ion coordination environment in **1**, and the atom numbering scheme

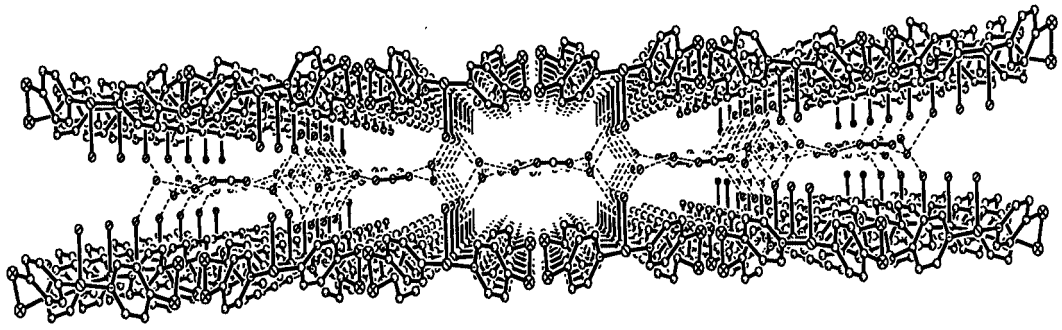

Figure 3. View of the double layer formed by hydrogen bond-mediated linking of the double-stranded chains in 1

 © 2003 Wiley-VCH Verlag GmbH & Co. KGaA, Weinheim

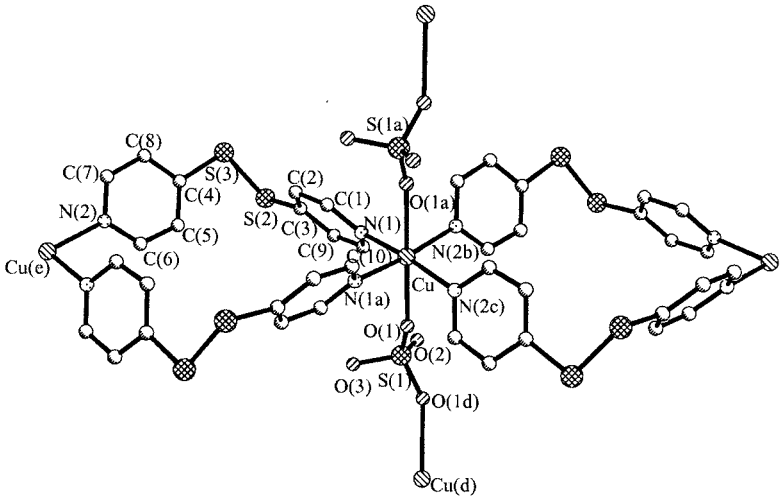

Figure 4. Drawing of the coordination environment of the Cu^{II} ion in **2**, and the atom numbering scheme

x, y, $1 - z$) and, furthermore, the ladders are linked into a bilayer through hydrogen bonds between free NO_3^- anions and the lattice water molecules (O1W···O5$^{\#1}$, 2.720 Å; O2W···O4$^{\#2}$, 2.893 Å; O2W···O4$^{\#3}$, 2.893 Å; symmetry codes #1: $1/2 + x$, y, $1 - z$; #2: $x - 1/2$, $1/2 - y$, $1 - z$; #3: $-x - 3/2$, $-y$, $z - 1/2$), as depicted in Figure 3.

$[\{Cu(DPDS)_2(SO_4)\}\cdot 1.5H_2O\cdot CH_3OH]_n$ (2)

Single-crystal X-ray crystallographic analysis of **2** revealed a two-dimensional assembly of Cu^{II} ions, wherein each Cu^{II} center is bonded to four different molecules of 4,4′-dipyridinedisulfide and two sulfate anions in a six-coordinate manner (Figure 4). Four nitrogen atoms from four 4-DPDS ligands coordinate to the copper(II) center in the base plane, and two oxygen atoms from two sulfate anions are located in the axial positions of the distorted octahedral geometry of the copper(II) center. The Cu−N(4-DPDS) bond lengths are 2.037(8) and 2.040(7) Å, which are similar to those of **1** and the 1D helical compound [4-DPDS·Cu(hfac)$_2$].[15] The *cis* N−Cu−N and O−Cu−N bond angles vary from 84.5(2) to 91.1(4)°, and the *trans* O(SO_4^{2-})−Cu−O(SO_4^{2-}) bond angle is 179.4(1)°.

Each copper ion is bridged by four 4-DPDS ligands to form a double-stranded chain. The sulfate anions take part in coordination and connect the double-stranded chains into a 2D sheet, as shown in Figure 5(a). The axial Cu−O(SO_4^{2-}) distance is 2.459(5) Å, which is similar to that found in other copper sulfate complexes,[22] and it is longer than the Cu−O(aqu) distance in **1**. The Cu···Cu separation through the sulfate anion is 7.118 Å, which is much shorter than the Cu···Cu separation through the bridge ligand 4-DPDS, which has a distance of 10.547 Å. Viewed along the *b* axis [Figure 5(b)], there are many one-dimensional channels in the 2D structure that are formed by the metallacycles $[Cu_2(4\text{-DPDS})_2]^{2+}$ linked by the sulfate anions, and these 1D channels are connected through the copper(II) centers to form the ultimate 2D sheets of **2**.

$[Cd(DPDS)_2Cl_2]_n$ (3)

The crystallographic analysis reveals that each cadmium(II) ion in **3** is coordinated by four nitrogen atoms from four 4-DPDS ligands and two chloride ions in a slightly distorted octahedral geometry (Figure 6). The four nitrogen atoms form the equatorial plane with the Cd center located in the plane, with the deviation of the Cd ion from the mean plane of [N(1b)N(1c)N(2a)] being 0.008(2) Å, and two Cl^- ions occupy the axial positions with a Cl−Cd−Cl(c) angle of just 180°.

Each 4-DPDS ligand acts as a single bridge to link two cadmium(II) ions through its two pyridine nitrogen atoms, and each cadmium(II) ion connects four 4-DPDS ligands to form an infinite two-dimensional structure with (4,4) topology, as shown in Figure 7. The cadmium(II) atoms, all of which are equivalent, serve as nodes and the ligands (L = 4-DPDS) as rods. Thus, the network is based upon squares $(CdL)_4$ formed by four 4-DPDS ligands and four quadruply connected cadmium(II) ions, forming 44-membered metallacyclic rings. Each of the four $(CdL)_4$ grids are joined together through sharing the cadmium apices to give the final two-dimensional layer structure consisting of puckered rhombus grids with dimensions of 12.265 × 12.265 Å based on the Cd···Cd distances. The most intriguing feature of the structure is that the basic grid is puckered (Figure 8), which is a different arrangement from that observed in previous grid-like structure in which the basic grids are usually coplanar or quasi-coplanar.[23] The puckered shape of the basic grid in **3** is understandable because the 4-DPDS unit may assume a twisted conformation because of the flexible -S−S- bridging group, which generates the non-linear grid sides and the puckered grids. The C−S−S angles of the 4-DPDS ligand are 105.1(2) and 106.3(2)°, the C−S−S−C torsion angle is 95.1°, and the two pyridine rings in each 4-DPDS ligand are almost perpendicular to one another with a dihedral angle of 81.9°. These data clearly depict the non-linear configuration of 4-DPDS in **3**. We note that the ulti-

 © 2003 Wiley-VCH Verlag GmbH & Co. KGaA, Weinheim

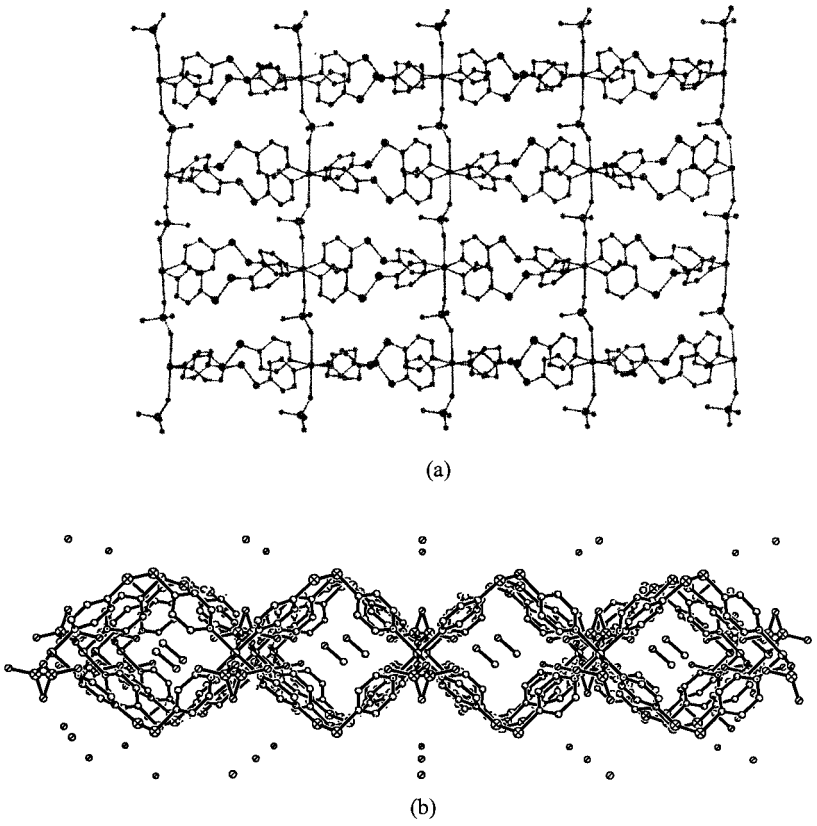

Figure 5. View of the 2D layer of **2** (a) along *a* axis and (b) along *b* axis

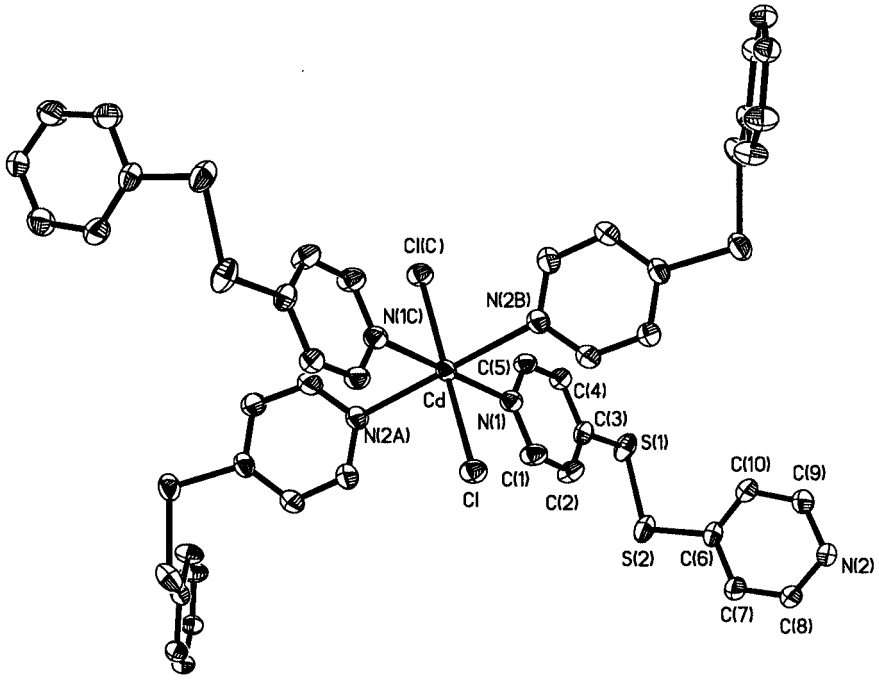

Figure 6. Drawing of the coordination environment of the Cd^{II} ion in **3**, and the atom numbering scheme

mate structure of the 2D layer is wave-like with a tightly puckered structure lacking any guest molecules.

The S−S bond length, the C−S−S−C torsion angles, and the dihedral angles of the two pyridyl rings in 4-DPDS in the three complexes **1**, **2**, and **3** are listed in Table 1. The S−S bond lengths are all ca. 2 Å, the C−S−S−C torsion angles are ca. 90° and the dihedral angles of the two pyridyl rings all show slight deviation from 90°. From these values

 © 2003 Wiley-VCH Verlag GmbH & Co. KGaA, Weinheim

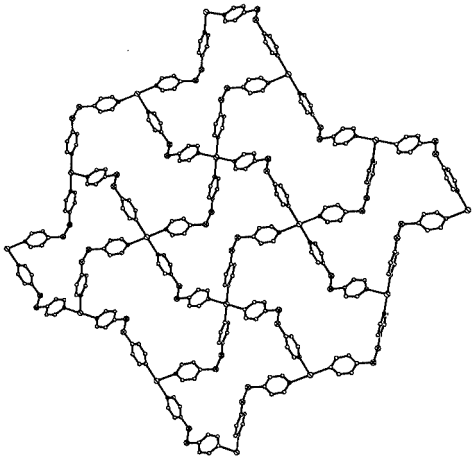

Figure 7. View of the 2D sheets of **3**

we see that the 4-DPDS ligand maintains its characteristic conformation despite the differences in the coordination schemes, but some notable differences exist between them. For the same metal ions, the M···M distances through the single 4-DPDS bridge are longer than those through the double 4-DPDS bridge (e.g., the Cd···Cd distance is 12.265 Å in **3**, but only 11.1 Å in the 1D structure $[Cd(4\text{-}DPDS)_2(H_2O)]\cdot 2NO_3\cdot 2EtOH\cdot 2H_2O$,[16] and the Cu···Cu separation is 11.26 Å in the single-helical chain complex $[4\text{-}DPDS\cdot Cu(hfac)_2]$,[15] while it is 10.528 Å in the double-stranded chain compound **1** and 10.547 Å in **2**). The most interesting differences in the present complexes are that the torsion angles of M−(4-DPDS)−M change from 15.1° in **1** and 15.0° in **2** to 37.9° in **3**, which we ascribed to the different coordination schemes of 4-DPDS. The 4-DPDS units in **1** and **2** link the metal ions to form double-stranded chains, but the 4-DPDS ligands in **3** connect the metal ions into a 2D grid-like sheet; the 4-DPDS ligand is more constrained in the double-stranded chains and more twisted in the 2D sheet because of steric factors.

Electronic Spectra

The reflectance spectra of the complexes in the solid state were recorded in the range 200−1100 nm. The visible reflectance spectra for **1** contain bands at $13.8\cdot10^3$ cm^{-1} with a shoulder $9.72\cdot10^3$ cm^{-1}, characteristic of a copper(II) $d_{xz},d_{yz} \rightarrow d_{x^2-y^2}$ transition[24] via ($^2B_1 \rightarrow {}^2E$) in a tetragonal ligand field, in which the copper(II) atom has a distorted square-based pyramidal coordination environment. The absorption of **2** at $14.97\cdot10^3$ cm^{-1} without a shoulder is assigned to copper(II) $d_{xz},d_{yz} \rightarrow d_{x^2-y^2}$ transitions[25] via ($^2B_{1g} \rightarrow {}^2E_g$) in a square-planar geometry (or elongated octahedron, due to the bridging sulfate anions), with the unpaired electron mainly located in the $d_{x^2-y^2}$ orbital. The d−d transition energy of complex **1** is lower than that of **2**, which is consistent with the crystal field splitting energy of the tetragonal ligand field when compared with that of the square planar ligand field in cases when there are similar or the same ligand field strengths of the donor ligands. The information obtained from the electronic spectra about the coordination configurations of the copper(II) ions in the two complexes is in agreement with that given by the structural data.

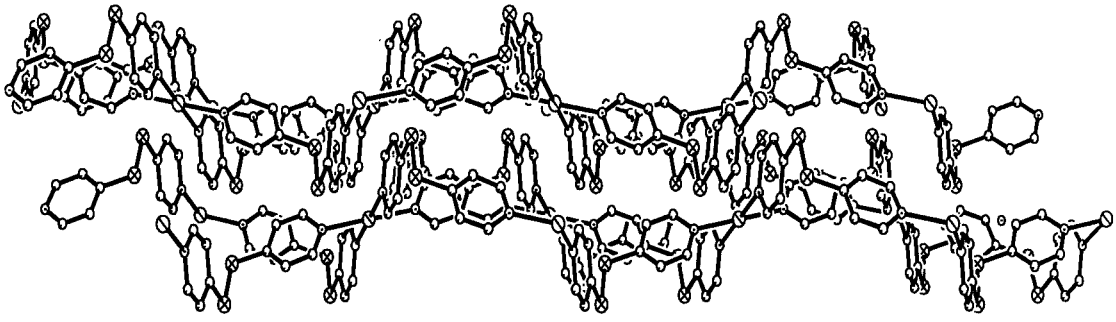

Figure 8. The tightly packed structure of **3**; only two layers are shown for clarity

Table 1. S−S bond lengths [Å] and C−S−S−C torsion angles [°], the dihedral angles of the two pyridyl rings [°] in the 4-DPDS ligands, and the M−[4-DPDS]−M torsion angles (°), for **1**, **2**, and **3**

Complexes	S−S distance (Å)	C−S−S−C torsion angle (°)	M···M separation through 4-DPDS (Å)	Dihedral angle of the two pyridyl rings (°)	M−(4-DPDS)−M torsion angle (°)
1	2.027(5)	89.8	10.528 (Cu···Cu)	98.6	15.1
2	2.033(5)	88.4	10.547 (Cu···Cu)	83.5	15.0
3	2.022(3)	95.1	12.265 (Cd···Cd)	81.9	37.9

 © 2003 Wiley-VCH Verlag GmbH & Co. KGaA, Weinheim

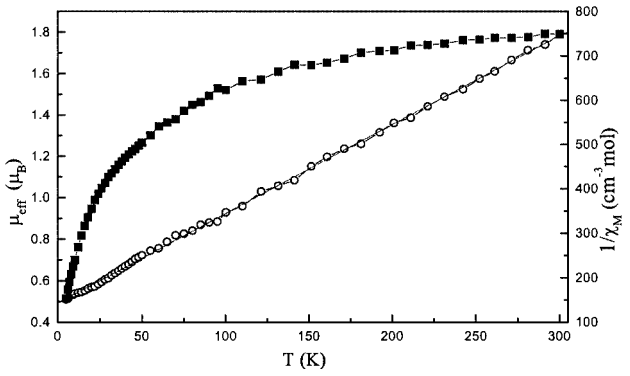

Figure 9. The plots for **1** of the effective magnetic moment μ_{eff} vs. T and $1/\chi_M$ vs. T

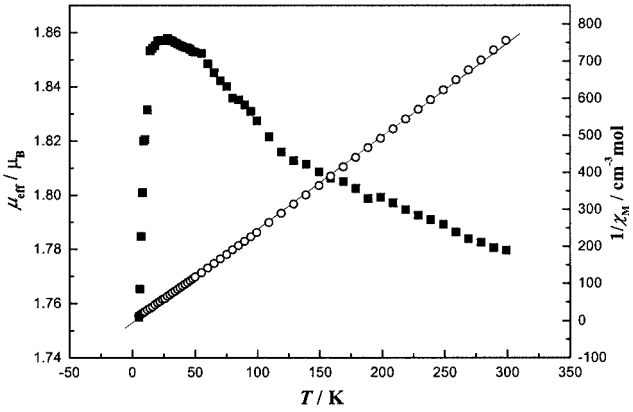

Figure 10. The plots for **2** of the effective magnetic moment μ_{eff} vs. T and $1/\chi_M$ vs. T

Magnetic Properties

Temperature-dependent magnetic susceptibility measurements for **1** and **2** were performed on the polycrystalline samples. The temperature dependence of $1/\chi_M$ and μ_{eff} [χ_M being magnetic susceptibility for one Cu^{II} ion, and $\mu_{eff} = (8\chi_M T)^{1/2}$] are shown in Figures 9 and 10, respectively. The value of μ_{eff} for **1** is 1.79 μ_B at room temperature, which is slightly larger than the spin-only value for an uncoupled Cu^{II} ion (g = 2.0, μ_{eff} = 1.73 μ_B). As the temperature decreases, the value of μ_{eff} decreases continuously and reaches 0.52 μ_B at 4 K, which indicates the occurrence of an antiferromagnetic interaction between the Cu^{II} ions in the double-stranded chain of **1**. A nonlinear fit of $\chi_M = C/(T - \Theta)$ to the data reveals a Curie−Weiss behavior, with the Weiss constant $\Theta = -2.27$ K. Taking into account the one-dimensional character of **1**, the magnetic susceptibility data were simulated by the Bonner−Fisher model[26] using the following polynomial expression:

$$\chi_M{}^J = \frac{N\beta^2 g^2 S(S+1)}{3kT}\frac{1+u}{1-u} \quad \left(u = \coth\left[\frac{JS(S+1)}{kT}\right] - \left[\frac{kT}{JS(S+1)}\right]\right) \qquad (1)$$

In this expression, $\chi = |J|/kT$ ($2J$ is the singlet−triplet splitting energy or the exchange integral in the spin Hamiltonian $H = -2J_{S1S2}$) and other symbols have their usual meanings. A satisfactory least-squares fitting of the observed data at 4−300 K led to g = 2.13 and $J/k = -2.5$ K. The small negative coupling constant imply the existence of a weak antiferromagnetic interaction between the copper(II) centers in the chain of **1**.

The value of μ_{eff} for **2** is 1.78 μ_B at room temperature, which is slightly larger than the spin-only value for an uncoupled Cu^{II} ion (g = 2.0, μ_{eff} = 1.73 μ_B). As the temperature decreases, the value of μ_{eff} increases gradually to 1.86 μ_B at 24 K, and then sharply decreases to 1.76 μ_B at 4 K, which implies the presence of ferromagnetic interactions between Cu^{II} ions in the 2D sheets of **2**. The nonlinear fit of $\chi_M = C/(T - \Theta)$ to the data reveals a Curie−Weiss behavior, with the Weiss constant Θ = 2.58 K. According to the structural data, the polymer may exhibit two types of Cu^{II}−Cu^{II} magnetic exchange interactions: type one is through a long double bridge, via 4-DPDS between copper centers in the double-stranded chain $[Cu(4\text{-}DPDS)_2]_n^{2n+}$, which is considered as the intrachain interaction; and type two is through a short bridge, via the sulfate groups between the adjacent chains, which is treated as the interchain interaction. The χ_M data are well interpreted based on the following expression:

A satisfactory least-squares fitting of the observed data at 4−300 K led to g = 2.10, $J/k = -2.3$ K, zJ'/k = 4.2 K. The value of J may be assigned to type one and that of zJ' to type two. The small negative J and small positive zJ'/k imply the existence of a weak intrachain antiferromagnetic interaction and a weak interchain ferromagnetic interaction. The interchain ferromagnetic interaction is stronger than the intrachain antiferromagnetic interaction, and **2** shows a overall weak ferromagnetic interaction between the copper(II) ions.

$$\chi_M{}^{J+J'} = \frac{\chi_M{}^J}{1-(2zJ'\times\chi_M{}^J/Ng^2\beta^2)}$$

$$\left(\chi_M{}^J = \frac{N\beta^2 g^2 S(S+1)}{3kT}\frac{1+u}{1-u};\ u = \coth\left[\frac{JS(S+1)}{kT}\right] - \left[\frac{kT}{JS(S+1)}\right]\right) \qquad (2)$$

The ESR spectra of **1** and **2** have been obtained at room temperature and 77 K, respectively; these spectra are almost the same. For **1** and **2**, both spectra exhibit the typical pattern, with the $d_{x^2-y^2}$ ground state [g (2.36) > $g_\perp$ (2.03) > 2.00 for **1**; g (2.14) > $g_\perp$ (2.06) > 2.00 for **2**], indicating the occupation of the unpaired d electron in the $d_{x^2-y^2}$ state.

Fluorescence Characterization

The diffuse reflectance UV/Vis spectra for 4-DPDS and the as-synthesized polymer of **3** (Figure 11) show different absorption features. There are two bands for the 4-DPDS ligand, with the longer- (332 nm) and shorter-wavelength (220 nm) absorptions corresponding to the intraligand n→π* and π→π* transitions, respectively. In comparison with the two bands for 4-DPDS, the shorter-wavelength

 © 2003 Wiley-VCH Verlag GmbH & Co. KGaA, Weinheim

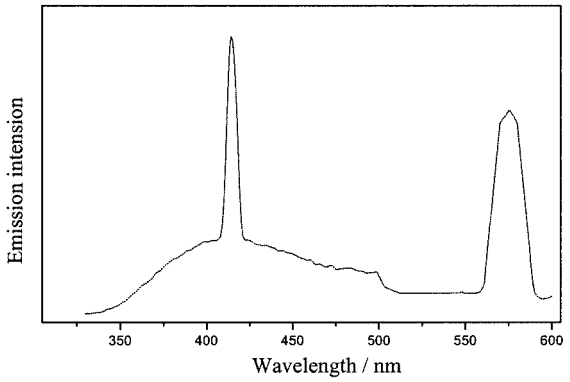

Figure 11. Solid-state emission spectra of **3** at room temperature

band for polymer **3** has the same energy, whereas the longer-wavelength band shifts to higher energy at 282 nm. This hypsochromic shift must be related to the coordination of Cd^{2+} to the 4-DPDS ligand, and it may arise from the same n→π* transitions. We note that the absorption intensity of **3** is markedly higher than that of the ligand. We attribute this increase in absorption intensity to the involvement of charge-transfer transitions from the N atoms of the ligands to the Cd^{2+} centers. The emission spectra of **3** show a broad emission band centered at 418 nm and a middle-intensity emission band occurring at 575 nm (λ_{ex} = 314 nm). The former may be assigned to the interligand transfer,[27] because the same emission appears also for the ligand 4-DPDS, and the latter may be due to the ligand-to-metal charge-transfer (LMCT) transition.[28]

Thermogravimetric Analysis

Thermogravimetric analysis (TGA) were performed to investigate the thermal stability of compounds **1**−**3**. All samples were heated under an N_2 atmosphere at a rate of 10 °C/min to 700 °C. The results show that **1** is stable up to 264 °C, although the first weight loss of 7.54% (calculated: 7.71), which corresponds to the loss of three lattice water molecules, occurred over the temperature range 65−128 °C. Complex **2** first lost one and a half water molecules and one CH_3OH molecule (obsd.: 8.68%; calcd.: 8.95%) and then gradually decomposed when the temperature reached 285 °C. Complex **3** is stable up to 302 °C, and above this temperature it decomposes.

Conclusions

Through the diffusion method, using different solvent systems, we acquired three coordination polymers (**1**, **2**, and **3**) derived from the flexible ligand 4-DPDS. The flexible ligand shows different coordination modes in the three complexes. In **1** and **2**, the 4-DPDS unit bridges the metal ions into double-stranded chains, but the 4-DPDS unit in **3** bridges the metal ions into a puckered (4,4) net sheet. The significant role of the anion is manifested in the dimension-

Table 2. Crystallographic data for the compounds **1**, **2**, and **3**

	1	**2**	**3**
Molecular formula	$C_{10}H_{12}Cu_{0.5}N_3O_5S_2$	$C_{10.5}H_{11.5}Cu_{0.5}N_2O_{3.25}S_{2.5}$	$C_{10}H_8Cd_{0.5}ClN_2S_2$
Molecular mass	350.12	329.64	311.95
T [K]	293(2)	293(2)	293(2)
Wavelength [Å]	0.71073	0.71073	0.71073
Crystal system	Orthorhombic	Orthorhombic	Monoclinic
Space group	*Ibca*	*Pnna*	$P2_1/c$
a [Å]	10.5275(6)	10.547(2)	7.6146(3)
b [Å]	20.270(1)	14.201(2)	18.2606(8)
c [Å]	27.235(1)	19.667(3)	9.3203(2)
α [°]	90	90	90
β [°]	90	90	100.26(1)
γ [°]	90	90	90
V [Å^3]	5811.5(6)	2945.8(8)	1275.24(8)
Z	16	8	4
$D_{calcd.}$ [Mg·m^{-3}]	1.601	1.487	1.625
Absorption coefficient [mm^{-1}]	1.101	1.139	1.409
F(000)	2872	1352	620
Crystal size [mm]	0.20 × 0.28 × 0.18	0.21 × 0.28 × 0.23	0.35 × 0.28 × 0.25
θ range for data collection [°]	1.50−25.00	1.77−25.00	2.23−25.05
Index ranges	$10 \le h \le 10$ $-19 \le k \le 17$ $-20 \le l \le 26$	$-10 \le h \le 10$ $-13 \le k \le 13$ $-18 \le l \le 18$	$-9 \le h \le 9$ $-18 \le k \le 21$ $-11 \le l \le 5$
Reflections collected	5746	9421	4067
Independent reflections	1356 (R_{int} = 0.047)	1380 (R_{int} = 0.0415)	2235 (R_{int} = 0.0306)
Refinement method	Full-matrix least-squares on F^2	Full-matrix least-squares on F^2	Full-matrix least-squares on F^2
Parameters	219	197	142
Goodness-of-fit on F^2	1.102	1.194	1.202
R_1 indices [$I > 2\sigma(I)$]	0.0527	0.0543	0.0532
wR_2 indices (all data)	0.1300	0.1478	0.1066

 © 2003 Wiley-VCH Verlag GmbH & Co. KGaA, Weinheim

alities of the phases isolated, as well as the detailed coordination geometries about the copper(II) center in **1** and **2**. The configuration of the Cu^{II} atoms is a square-based pyramid in **1** and an elongated-octahedron in **2**. The anions in **1** are non-coordinated, but the anions in **2** act as bridges between the double-stranded chains and link the double-stranded chains into a 2D channel-type sheet. The UV-Vis reflectance spectra and ESR spectra are consistent with the crystal structures. Magnetic characterizations of **1** and **2** show that complex **1** exhibits antiferromagnetic interactions while **2** is ferromagnetic. Complex **3** displays an emission band at 575 nm that is due to ligand-to-metal charge transfer.

Experimental Section

General: $Cu(NO_3)_2{\cdot}3H_2O$, $CuSO_4{\cdot}5H_2O$, and $CdCl_2{\cdot}2.5H_2O$ were purchased commercially and used without further purification. 4,4′-Dipyridyl disulfide was purchased from Fluka. Elemental analyses of C, H, and N were determined on a Perkin−Elmer 240C analyzer. IR spectra were measured as KBr pellets on a Nicolet Magna 750 FT-IR spectrometer in the range 200−4000 cm^{-1}. Thermogravimetric analyses were performed on a NETSCHZ STA-449C thermoanalyzer under N_2 (over a 26−750 °C range) at a heating rate of 10°/min. Electronic reflectance spectra were recorded on a Lambda 35 spectrometer. ESR spectra were recorded on powdered samples at an X-band frequency of ca. 9.77 GHz at room temperature or liquid nitrogen temperature (77 K) using a Bruker ER420 automatic spectrometer. Variable-temperature magnetic susceptibilities were determined in the temperature range 5−300 K on a Quantum Design MPMS SQUID magnetometer at 10 T. Corrections were applied for diamagnetism calculated from Pascal constants. Effective magnetic moments were calculated by the equation $\mu_{eff} = 2.828(\chi_M T)^{1/2}$, where χ_M is the magnetic susceptibility per formula unit. Fluorescence characterization was performed on an Edinburgh F900 analytical instrument in Fuzhou University.

$[\{Cu(4\text{-}DPDS)_2(H_2O)\}{\cdot}2NO_3{\cdot}3H_2O]_n$ (1): A solution of $Cu(NO_3)_2{\cdot}3H_2O$ (0.12 g, 0.5 mmol) in a methanol/water mixture (5:1, 5 mL) was slowly added to a solution of 4,4′-dipyridyl disulfide (0.22 g, 1 mmol) in dichloromethane (4 mL). After 4 days, blue crystals (0.25 g, 72% yield based on copper nitrate) grew at the bottom of the test tube. $C_{20}H_{24}CuN_6O_{10}S_4$ (700.24): calcd. C 34.27, H 3.43, N 12.00; found C, 34.36, H 3.46, N 12.07%. IR (KBr): $\tilde{\nu}$ = 3408 cm^{-1} (br), 1589 (s), 1543 (m), 1477 (m), 1414 (s), 1385 (s), 1308 (w), 1213 (m), 1099 (m), 1057 (m), 798 (s), 715 (s), 499 (s) cm^{-1}.

$[\{Cu(4\text{-}DPDS)_2(SO_4)\}{\cdot}1.5H_2O{\cdot}CH_3OH]_n$ (2): A solution of $CuSO_4{\cdot}5H_2O$ (0.125 g, 0.5 mmol) in a methanol/water mixture(5:1, 5 mL) was allowed to diffuse slowly into a solution of 4,4′-dipyridyl disulfide (0.22 g, 1 mmol) in chloroform (5 mL). Immediately, a blue precipitate formed at the interface of the two layers. Blue single crystals (0.21 g, 64% base on the copper sulfate) were formed after 3 days. $C_{21}H_{23}CuN_4O_{6.5}S_5$ (659.28): calcd. C 38.22, H 3.49, N 8.49; found C, 38.31, H 3.52, N 8.57%. IR (KBr): $\tilde{\nu}$ = 3412 (br), 1596 (s), 1548 (m), 1481 (s), 1417 (s), 1245 (w), 1218 (m), 1071 (m), 1035 (m), 815 (s), 802 (s), 713 (s), 494 (s) cm^{-1}.

$[Cd(4\text{-}DPDS)_2Cl_2]_n$ (3): A colorless solution of $CdCl_2{\cdot}2.5H_2O$ (0.114 g, 0.5 mmol) in methanol/water (5:1, 5 mL) was carefully layered onto a solution of 4,4′-dipyridyl disulfide (0.22 g, 1 mmol) in acetonitrile (5 mL). Diffusion between the two phases over a period of 5 days produced light-yellow crystals (0.26 g, 84% yield based on cadmium chloride). $C_{20}H_{16}CdN_4Cl_2S_4$ (623.9): calcd. C 38.47, H 2.56, N 8.98; found C, 38.52, H 2.59, N 9.05%. IR (KBr): $\tilde{\nu}$ = 1585 (s), 1543 (m), 1479 (s), 1414 (s), 1321 (w), 1223 (m), 1063 (m), 1009 (m), 820 (s), 808 (s), 708 (s), 496 (s) cm^{-1}.

X-ray Crystallography: Suitable single crystals of **1**, **2**, and **3** were selected for X-ray diffraction studies. The unit cell parameters and intensities were collected at 299 K on a Siemens SMART CCD diffractometer with graphite-monochromated Mo-K_α (λ = 0.71073Å) radiation. Measurements were made by using the ω scan mode in the range $1.50° < \theta < 20°$ for **1**, $1.77° < \theta < 20°$ for **2**, and $2.23° < \theta < 25.05°$ for **3** The structures were solved by direct methods and refined on F^2 by full-matrix least-squares procedures using SHELXTL software.[19] All non-hydrogen atoms were anisotropically refined. All H atoms were located theoretically and not refined. A summary of the crystallographic data of **1**, **2**, and **3** are presented in Table 2, and the selected bond lengths and bond angles are in Table 3.

Table 3. Selected bond lengths [Å] and angles [°] for **1**, **2**, and **3**

Complex **1**[a]			
Cu−N(2)	2.032(1)	Cu−N(1b)	2.061(1)
Cu−O(1)	2.305(1)	S(1)−S(2)	2.027(5)
S(1)−C(3)	1.792(2)	S(2)−C(8)	1.754(2)
N(2)−Cu−N(1b)	88.5(4)	N(2)−Cu−N(1c)	91.8(4)
N(2)−Cu−O(1)	88.5(3)	N(1b)−Cu−O(1)	96.4(3)
C(3)−S(1)−S(2)	105.2(4)	C(8)−S(2)−S(1)	104.9(4)
Complex **2**[b]			
Cu−N(1)	2.037(8)	Cu−N(2b)	2.040(7)
Cu−O(1)	2.459(5)	S(2)−S(3)	2.033(5)
S(2)−C(3)	1.785(9)	S(3)−C(4)	1.775(9)
O(6)−C(11)	1.45(9)		
N(1a)−Cu−N(1)	91.4(4)	N(1)−Cu−N(2b)	89.2(3)
N(2b)−Cu−N(2c)	91.3(4)	O(1)−Cu−O(1a)	179.4(1)
O(1)−Cu−N(1a)	87.7(1)	O(1)−Cu−N(2b)	84.5(2)
C(3)−S(2)−S(3)	105.0(4)	C(4)−S(3)−S(2)	105.0(4)
Complex **3**[c]			
Cd−N(2a)	2.410(5)	Cd−N(1)	2.418(5)
Cd−Cl	2.571(2)	S(1)−S(2)	2.022(3)
S(1)−C(3)	1.780(6)	S(2)−C(6)	1.775(6)
N(2A)−Cd−N(1)	96.20(2)	N(2a)−Cd−Cl	90.06(3)
N(2B)−Cd−N(1)	83.80(2)	N(2b)−Cd−Cl	89.94(3)
N(1)−Cd−Cl(c)	90.81(1)	N(1)−Cd−Cl	89.19(2)
C(6)−S(2)−S(1)	106.3(2)	C(3)−S(1)−S(2)	105.1(2)

[a] Symmetry codes: (a) $-x, -y - 1/2, z$; (b) $x + 1, y, z$; (c) $-x - 1, -y - 1/2, z$. [b] Symmetry codes: (a) $x, -y + 1/2, -z + 1/2$; (b) $x - 1, y, z$; (c) $x - 1, -y + 1/2, -z + 1/2$. [c] Symmetry codes: (a) $-x + 1, y + 1/2, -z + 1/2$; (b) $x - 1, -y + 1/2, z - 1/2$; (c) $-x, -y + 1, -z$.

CCDC-192657 (**1**), -192656 (**2**), and -192655 (**3**) contain the supplementary crystallographic data for this paper. These data can be obtained free of charge at www.ccdc.cam.ac.uk/conts/retrieving.html [or from the Cambridge Crystallographic Data Centre, 12, Union Road, Cambridge CB2 1EZ, UK; Fax: (internat.) + 44-1223/336-033; E-mail: deposit@ccdc.cam.ac.uk].

 © 2003 Wiley-VCH Verlag GmbH & Co. KGaA, Weinheim

Acknowledgments

We thank NNSFC, the Natural Foundation of Fujian Province, and the key project of CAS for financial support.

[1] [1a] B. Moulton, M. J. Zaworotko, *Chem. Rev.* **2001**, *101*, 1629−1658. [1b] K. Kim, *Chem. Soc. Rev.* **2002**, *31*, 96−107. [1c] O. R. Evans, W. Lin, *Acc. Chem. Res.* **2002**, *35*, 511−522. [1d] B. F. Abrahams, B. F. Hoskins, R. Robson, *J. Am. Chem. Soc.* **1991**, *113*, 3606−3607. [1e] M. Eddaoudi, D. B. Moler, H. Li, B. Chen, T. M. Reineke, M. O'Keeffe, O. M. Yaghi, *Acc. Chem. Res.* **2001**, *34*, 319−330. [1f] W. B. Lin, L. Ma, O. R. Evans, *Chem. Commun.* **2000**, 2263−2264. [1g] Q. Wang, X. Wu, W. Zhang, T. Sheng, P. Lin, J. Li, *Inorg. Chem.* **1999**, *38*, 2223−2226. [1h] M. Hong, Y. Zhao, W. Su, R. Cao, Z. Zhou, A. S. C. Chan, *Angew. Chem. Int. Ed.* **2000**, *39*, 2468−2470. [1i] M. Hong, Y. Zhao, W. Su, R. Cao, M. Fujita, Z. Zhou, A. S. C. Chan, *J. Am. Chem. Soc.* **2000**, *122*, 4819−4820. [1j] O. M. Yaghi, G. Li, *Angew. Chem. Int. Ed. Engl.* **1995**, *34*, 207−209. [1k] O. M. Yaghi, H. Li, C. Davis, D. Richardson, T. L. Groy, *Acc. Chem. Res.* **1998**, *31*, 474−484.

[2] [2a] M. P. Byrm, C. J. Curits, Y. Hsiou, S. I. Khan, P. A. Sawin, A. Terzis, C. E. Strouse, *Comprehensive Supramolecular Chemistry*, Vol. 6, *Solid State Supramolecular Chemistry: Crystal Engineering* (Eds.: D. D. MacNicol, F. Toda, R. Bishop), Elsevier, Oxford, UK, **1996**. [2b]M. Eddaoudi, H. Li, O. M. Yaghi, *J. Am. Chem. Soc.* **2000**, *122*, 1391−1397. [2c] O. Kahn, *Acc. Chem. Res.* **2000**, *33*, 647−657 and references therein. [2d] X. H. Bu, W. Chen, S. L. Lu, R. H. Zhang, D. Z. Liao, M. Shionoya, F. Brisse, J. Ribas, *Angew. Chem. Int. Ed.* **2001**, *40*, 3201−3203.

[3] [3a] P. Losier, M. J. Zaworotko, *Angew. Chem. Int. Ed. Engl.* **1996**, *35*, 2779−2782. [3b] M. Fujita, Y. J. Kwon, S. Washizu, K. Ogura, *J. Am. Chem. Soc.* **1994**, *116*, 1151−1152. [3c] R. W. Gable, B. F. Hoskings, R. Robson, *J. Chem. Soc., Chem. Commun.* **1990**, 1677−1678. [3d] M. L. Tong, H. J. Chen, X. M. Chen, *Inorg. Chem.* **2000**, *39*, 2235−2238. [3e] O. M. Yaghi, H. Li, *J. Am. Chem. Soc.* **1995**, *117*, 10401−10402. [3f] L. R. MacGillivray, S. Subramanian, M. J. Zaworotko, *J. Chem. Soc., Chem. Commun.* **1994**, 1325−1326. [3g] L. Carlucci, G. Ciani, D. M. Proserpio, A. Sironi, *J. Chem. Soc., Chem. Commun.* **1994**, 2755−2756. [3h] C. V. K. Sharma, G. A. Broker, J. G. Huddleston, J. W. Baldwin, R. D. Metzger, R. F. Rogers, *J. Am. Chem. Soc.* **1999**, *121*, 1137−1144.

[4] [4a] M. Fujita, D. Oguro, M. Miyazawa, H. Oka, K. Yamaguchi, K. Ogura, *Nature* **1995**, *378*, 469−471. [4b] A. J. Blake, N. R. Champness, P. Hubberstey, W. S. Li, M. A. Wilthersby, M. Schröder, *Coord. Chem. Rev.* **1999**, *183*, 117−138. [4c] S. Leiniger, B. Olenyuk, P. J. Stang, *Chem. Rev.* **2000**, *100*, 853−908. [4d] M. L. Tong, B. H. Ye, J. W. Cai, X. M. Chen, S. W. Ng, *Inorg. Chem.* **1998**, *37*, 2645−2650. [4e] K. Briadha, C. Seward, M. J. Zaworotko, *Angew. Chem. Int. Ed.* **1999**, *38*, 492−495.

[5] L. Carlucci, G. Ciani, D. W. v. Gudenberg, D. M. Proserpio, *Inorg. Chem.* **1997**, *36*, 3812−3813.

[6] [6a] T. Hennigar, D. C. MacQuarrie, P. Loiser, R. D. Rogers, M. J. Zaworotko, *Angew. Chem. Int. Ed. Engl.* **1997**, *36*, 972−973. [6b] L. Carlucci, G. Ciani, D. M. Proserpio, S. Rizzato, *Chem. Commun.* **2000**, 1319−1320.

[7] [7a] A. J. Blake Champness, A. Khlobystov, D. A. Lemenovskii, W.-S. Li, M. Schröder, *Chem. Commun.* **1997**, 2027−2028. [7b] M. Fujita, O. Sasaki, K.-y. Watanabe, K. Ougra, K. Yamaguchi, *New J. Chem.* **1998**, *22*, 189−192. [7c] L. Carlucci, G. Ciani, D. M. Proserpio, *J. Chem. Soc., Dalton Trans.* **1999**, 1799−1804.

[8] [8a] A. J. Blake, N. R. Champness, S. S. M. Chung, W.-S. Li, M. Schröder, *Chem. Commun.* **1997**, 1005−1006. [8b] M. A. Withersby, A. J. Blake, N. R. Champness, P. A. Cooke, P. Hubberstey, A. L. Realf, S. J. Teat, M. Schröder, *J. Chem. Soc., Dalton Trans.* **2000**, 3261−3268. [8c] C. He, B.-G. Zhang, C. Duan, J. Li, Q.-J. Meng, *Eur. J. Inorg. Chem.* **2000**, 2549−2554. [8d] S. R. Batten, J. C. Jeffery, M. D. Ward, *Inorg. Chim. Acta* **1999**, *292*, 231−237.

[9] [9a] L. Carlucci, G. Ciani, M. Moret, D. M. Proserpio, S. Rizzato, *Angew. Chem. Int. Ed.* **2000**, *39*, 1506−1507. [9b] L. Carlucci, G. Ciani, D. M. Proserpio, *Chem. Commun.* **1999**, 449−450. [9c] M. J. Plater, M. R. St. J. Foreman, T. Gelbrich, M. B. Hursthouse, *Cryst. Eng.* **2001**, *4*, 319−328.

[10] [10a] M. B. Zaman, M. D. Smith, H.-C. z. Loye, *Chem. Commun.* **2001**, 2256−2257. [10b] B. Moulton, E. B. Rather, M. J. Zaworotko, *Cryst. Eng.* **2001**, *4*, 309−317. [10c] M. Du, X.-H. Bu, Y.-M. Guo, H. Liu, S. R. Batten, J. Ribas, T. C. W. Mak, *Inorg. Chem.* **2002**, *41*, 4904−4908. [10d] M.-L. Tong, Y.-M. Wu, J. Ru, X.-M. Chen, H.-C. Chang, S. Kitagawa, *Inorg. Chem.* **2002**, *41*, 4846−4848. [10e] Z.-Y. Fu, X.-T. Wu, J.-C. Dai, S.-M. Hu, W.-X. Du, *New J. Chem.* **2002**, *26*, 978−980. [10f] M. J. Plater, M. R. St. J. Foreman, T. Gelbrich, M. B. Hursthouse, *J. Chem. Soc., Dalton Trans.* **2000**, 1995−2000.

[11] [11a] M. J. Plater, M. R. St. J. Foreman, T. Gelbrich, S. J. Coles, M. B. Hursthouse, *J. Chem. Soc., Dalton Trans.* **2000**, 3065−3073. [11b] M. Fujita, Y. J. Kwon, M. Miyazawa, K. Ogure, *J. Chem. Soc., Chem. Commun.* **1994**, 1977−1978. [11c] M. Fujita, Y. J. Kwon, O. Sasaki, K. Yamaguchi, K. Ogura, *J. Am. Chem. Soc.* **1995**, *117*, 7287−7288. [11d] X.-C. Su, S.-R. Zhu, H.-K. Lin, X.-B. Leng, Y.-T. Chen, *J. Chem. Soc., Dalton Trans.* **2001**, 3163−3168.

[12] [12a] H. Kessler, W. Rundel, *Chem. Ber.* **1968**, *101*, 3350−3359. [12b] R. R. Fraser, G. Boussard, J. K. Saunder, J. B. Lambert, C. E. Mixan, *J. Am. Chem. Soc.* **1971**, *93*, 3822−3823. [12c] H. Kessler, A. Rleker, W. Rundel, *J. Chem. Soc., Chem. Commun.* **1968**, 475−476. [12d] F. Seel, W. Gombler, R. Bundez, *Justus Liebigs Ann. Chem.* **1970**, *735*, 1−7.

[13] M. Hong, W. Su, R. Cao, M. Fujita, J. Lu, *Chem. Eur. J.* **2000**, *3*, 427−431.

[14] A. J. Blake, N. R. Brooks, N. R. Champness, M. Crew, A. Deveson, D. Fenske, D. H. Gregory, L. R. Hanton, P. Hubberstey, M. Schröder, *Chem. Commun.* **2001**, 1432−1433.

[15] R. Horikoshi, T. Mochida, H. Moriyama, *Inorg. Chem.* **2001**, *40*, 2430−2433.

[16] M. Kondo, M. Shimamura, S. Noro, Y. Kimura, K. Uemura, S. Kitagawa, *J. Solid State Chem.* **2000**, *152*, 113−119.

[17] F. M. Tabellion, S. R. Seidel, A. M. Arif, P. J. Stang, *J. Am. Chem. Soc.* **2001**, *123*, 7740−7741.

[18] R. Horikoshi, T. Mochida, N. Maki, S. Yamada, H. Moriyama, *J. Chem. Soc., Dalton Trans.* **2002**, 28−33.

[19] G. M. Sheldrick, SHELXTL NT Version 5.1. *Program for Solution, Refinement of Crystal Structures*, University of Göttingen, Göttingen, Germany, **1997**.

[20] [20a] M. L. Hernández, M. G. Barandika, M. K. Urtiaga, R. Cortés, L. Lezama, M. I. Arriortua, T. Rojo, *J. Chem. Soc., Dalton Trans.* **1999**, 1401−1406. [20b] M. J. Plater, M. R. St. J. Foreman, J. M. S. Snakle, *Cryst. Eng.* **2001**, *4*, 293−308.

[21] [21a] O. S. Jung, S. H. Park, D. C. Kim, K. M. Kim, *Inorg. Chem.* **1998**, *37*, 610−611. [21b] M. T. Bujaci, X. Wang, S. Li, C. Zheng, *Inorg. Chim. Acta* **2002**, *333*, 152−154.

[22] [22a] D. Hagrman, R. P. Hammond, R. Haushalter, J. Zubieta, *Chem. Mater.* **1998**, *10*, 2091−2100. [22b] X.-M. Chen, T. C. W. Mak, *Struct. Chem.* **1992**, *3*, 369−374.

[23] [23a] K. Biradha, M. Fujita, *J. Chem. Soc., Dalton Trans.* **2000**, 3805−3811. [23b] K. Biradha, M. Fujita, *Chem. Commun.* **2001**, 15−16. [23c] K. Biradha, Y. Hongo, M. Fujita, *Angew. Chem. Int. Ed.* **2000**, *39*, 3843−3845.

[24] M. Melnik, *Coord. Chem. Rev.* **1981**, *36*, 287−301.

[25] L. Araya, J. Vargas, J. Costamagna, *Trans. Met. Chem.* **1986**, *11*, 321−326.

[26] J. C. Bonner, M. E. Fisher, *Phys. Rev.* **1964**, *A135*, 640−658.

[27] [27a] N. W. Alcock, P. R. Barker, J. M. Haider, M. J. Hannon, C. L. Painting, Z. Pikramenou, E. A. Plummer, K. Rissanen, P. Saarenketo, *J. Chem. Soc., Dalton Trans.* **2000**, 1447−1462. [27b] K.-Y. Ho, W.-Y. Yu, K.-K. Cheung, C.-M. Che, *J. Chem. Soc., Dalton Trans.* **1999**, 1581−1586.

 © 2003 Wiley-VCH Verlag GmbH & Co. KGaA, Weinheim

[28] [28a] A. Meijerink, G. Blasse, M. Glasbeek, *J. Phys. Condense. Matter* **1990**, *2*, 6303−6313. [28b] R. Bertoncello, M. Bettinelli, M. Casarin, A. Gulino, E. Tondello, A. Vittadini, *Inorg. Chem.* **1992**, *31*, 1558−1565. [28c] J. Tao, M. L. Tong, J. X. Shi, X. M. Chen, S. W. Ng, *Chem. Commun.* **2000**, 2043−2044. [28d] Z. Y. Fu, X. T. Wu, J. C. Dai, L. M. Wu, C. C. Cui, S. M. Hu, *Chem. Commun.* **2001**, 1856−1857. [28e] W. Chen, J.-Y. Wang, C. Chen, Q. Yi, H.-M. Yuan, J.-S. Chen, S.-N. Wang, *Inorg. Chem.* **2003**, *42*, 944−946.

Received March 19, 2003
Early View Article
Published Online August 14, 2003

 © 2003 Wiley-VCH Verlag GmbH & Co. KGaA, Weinheim

Synthesis, Characterization, and DNA Binding Studies of a Chromium(III) Complex Containing a Tridentate Ligand

Vaidyanathan Ganesan Vaidyanathan[a] and Balachandran Unni Nair*[a]

Keywords: Chromium / Tridentate ligands / DNA cleavage / Radicals

[Cr(bzimpy)$_2$]Cl, where bzimpy is 2,6-bis(benzimidazol-2-yl)-pyridine, has been synthesized and characterized by ESI-MS, UV/Visible, and fluorescence spectra. Absorption titration and thermal denaturation experiments indicate that the complex binds to DNA with moderate strength, while viscosity measurements show that it may undergo surface binding. The fluorescence intensity of the complex increases with increasing DNA concentration, in contrast to [Cr(phen)$_3$]$^{3+}$ and [Cr(bpy)$_3$]$^{3+}$. The complex cleaves pBR322 DNA in the presence of H_2O_2.
(© Wiley-VCH Verlag GmbH & Co. KGaA, 69451 Weinheim, Germany, 2003)

The interaction of metal complexes with biomolecules has been extensively studied in recent decades.[1−13] Several metal complexes, which bind to DNA through different modes, have been used as probes for DNA structure in solution, as agents for mediation of strand scission of duplex DNA and as chemotherapeutic agents.[14−16] [M(LL)$_3$]$^{n+}$ metal complexes, where LL is 1,10-phenanthroline (phen) or a modified phenanthroline ligand, are particularly attractive species to recognize and cleave DNA.[17−22] Some transition metal complexes that bind covalently to DNA function as anti-tumor agents.

There has been renewed interest in biological aspects of chromium, and its extensive use in the tanning and electroplating industries has aroused much environmental concern over effluents bearing Cr^{VI} and Cr^{III}. Epidemiological and animal studies have firmly established hexavalent chromium compounds as potent carcinogens.[23−25] Chromate can form several DNA lesions, including DNA, DNA−protein, and DNA−amino acid crosslinks, strand breaks and alkali labile sites, which are responsible for its mutagenic and carcinogenic effects.[26,27] The carcinogenic activity of Cr^{VI} is due to its reduction by intracellular reductants to generate Cr^{V} and Cr^{IV} intermediates and finally Cr^{III}. The chromium(V/IV) intermediates are proposed to cause DNA damage that leads ultimately to tumor development.[28−32] Chromium(III) is believed to be non-toxic and is an essential trace element for glucose and lipid metabolism.[33] While chromium(III) picolinate complex is a therapeutic in the treatment of adult-onset diabetes,[34−35] Wetterhahn and coworkers have demonstrated that Cr(pic)$_3$ causes chromosomal damage in Chinese hamster ovary cells (CHO).[36] Chromium(III) not only affects DNA replication but also inhibits enzymatic activity in the biosynthesis of nucleotide pools, which in turn is responsible for mutations in cells.[37−38] We have demonstrated that a chromium(III) complex of a Schiff base having a donor−acceptor group exhibits nuclease activity, while [Cr(salen)(H$_2$O)$_2$]$^+$ can cleave DNA only in the presence of peroxide.[39−40] Furthermore, Sudgen et al. showed that Cr^{III} aromatic bidentate amines that can enter cells are mutagenic agents in the Ames test, as such complexes can generate a Cr^{III}/Cr^{II} active redox center.[41] These observations indicate that modification of the ligand environment would alter the binding affinities and DNA cleaving properties of the metal complex. Our present study focuses on the interaction of DNA with chromium(III) complex **1** which has a pyridine-type tridentate ligand, bzimpy.

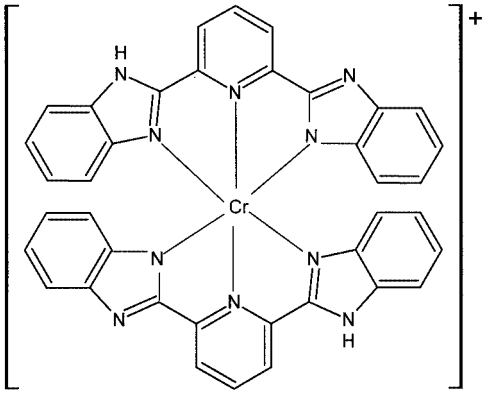

1

Results and Discussion

Compound **1** was synthesized in good yield by reaction of the ligand bzimpy with [Cr(dmso)$_6$]$^{3+}$ generated in situ.

[a] Chemical Laboratory, Central Leather Research Institute, Adyar, Chennai 600 020, India
Fax: (internat.) +91-44-24911589
E-mail: bcunchem@rediffmail.com

The ESI mass spectrum shows the base peak at m/z = 672 due to $[Cr(bzimpy)]^+$. The ESI spectrum thus confirms the authenticity of the complex. It is noteworthy that the ligand behaves like a monoanion (through the loss of a proton from a −NH group). Similar behaviour has been observed in Mn^{II} complex of this ligand.[42] However, with $[Ru(bzimpy)_2]^{2+}$ the ligand coordinates as a neutral tridentate ligand without such a loss of a proton.[43] Despite our best efforts we could not grow diffraction quality crystals. However, the Mn^{II} complex of the same ligand has been crystallographically characterized and found to have a regular octahedral geometry.[42] The Cr^{III} complex reported here is expected to have a similar geometry. The cyclic voltammogram of the complex shows a reduction of Cr^{III} to Cr^{II} at a cathodic peak potential, E_{pc}, of −1.05 V versus SCE. Reoxidation of the Cr^{II} species occurred at −0.81 V upon reversal of the scan (Figure 1). The separation of anodic and cathodic peak potentials, ΔE_p = 240 mV for $[Cr(bzimpy)_2]^+$, indicates a quasi-reversible redox process. Such behavior is typical of many Cr^{III}/Cr^{II} couples because of the Jahn−Teller distortion expected for the Cr^{II} ion.

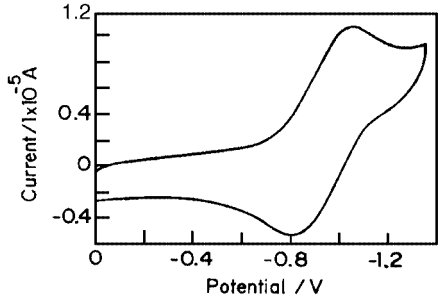

Figure 1. Cyclic voltammogram of $[Cr(bzimpy)_2]^+$

Absorption Titration

Absorption titration can monitor the interaction of a metal complex and DNA. In general, hypochromism and redshift are associated with the intercalative binding of the complex to the helix, due to strong stacking interactions between the aromatic chromophore of the complex and the base pairs of DNA. The chromium complex **1** shows an absorbance at 317 nm due to the intraligand (π−π*) transition of the ligand bzimpy. Binding of chromium(III) with DNA is expected to change markedly its electronic spectrum. Upon addition of CT DNA, the chromium(III) complex absorbance increases, and is accompanied by a small shift of 3 nm in λ_{max}, from 317 to 320 nm (Figure 2), that is consistent with groove binding, leading to small perturbations. Such a small increase in λ_{max} and hyperchromicity occurs with some porphyrin and copper complexes on their interaction with DNA.[44] This hyperchromism can be attributed to external contact (surface binding) with the duplex. The absorption data were analyzed to evaluate the intrinsic binding constant K_b, which can be determined from Equation (1), where ε_A corresponds to A_{obsd}/[Cr] and ε_F, and ε_B are the molar absorption coefficients for the free chromium complex and the chromium complex in the fully bound form, respectively.

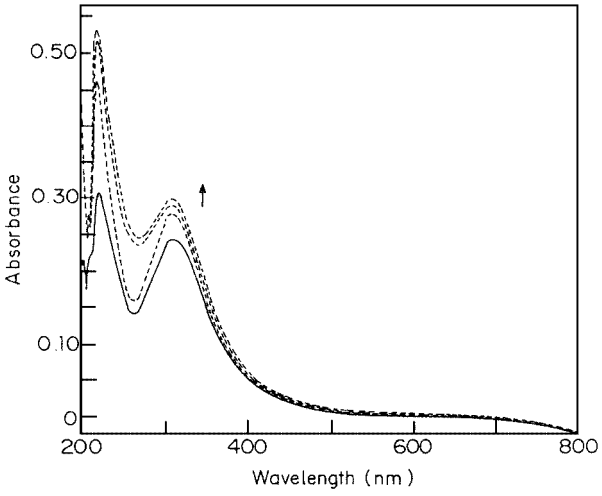

Figure 2. Electronic spectra of $[Cr(bzimpy)_2]^+$ in Hepes buffer upon addition of calf thymus DNA, [Cr] = 10 μM (—), [DNA] = 20−150 μM (- - -)

$$[DNA]/(\varepsilon_A - \varepsilon_F) = [DNA]/(\varepsilon_B - \varepsilon_F) + 1/K_b(\varepsilon_A - \varepsilon_F) \quad (1)$$

A plot of $[DNA]/(\varepsilon_A - \varepsilon_F)$ versus [DNA] revealed a moderate intrinsic binding constant K_b of $1.013 \pm 0.03 \times 10^4$ M^{-1}, which is similar to those observed for many other chromium and ruthenium complexes ($1-4 \times 10^4$ M^{-1}),[40,45] and is more in keeping with groove binding than intercalative binding. Further, since the complex is octahedral, and upon coordination the planarity of the ligand is lost, intercalative binding to DNA is highly unlikely.

Thermal Denaturation Studies

DNA melting is observed when double-stranded DNA molecules are heated and separate into two single strands; it occurs due to disruption in intermolecular forces such as π stacking and hydrogen bonding interactions between DNA base pairs. Here, a DNA melting experiment revealed that T_m of calf thymus DNA was 65±0.2 °C and 68±0.2 °C in the absence and presence of the complex, respectively. However, for the ligand alone, there is no change in DNA melting temperature. The ΔT_m of 3 °C indicates that the binding cannot be intercalative. Such a small ΔT_m is generally associated with surface binding of the metal complex. Generally one would expect a much larger increase in T_m for classical intercalators.[46−49] A small ΔT_m also indicates weak binding of the complex to DNA. This is also reflected in the binding constant.

Viscosity Measurement

Optical photophysical probes generally provide support for a binding model. Hydrodynamic measurements that are sensitive to length change are, in the absence of crystallographic data, regarded as the most critical tests of a binding model in solution. Intercalating agents are expected to destack the base pairs to accommodate the ligands, causing

 © 2003 Wiley-VCH Verlag GmbH & Co. KGaA, Weinheim

elongation of the double helix and an increase in the viscosity of the DNA. However, some complexes, which bind through non-intercalative modes, decrease the viscosity initially and then increase it at higher concentrations. With chromium complex **1**, the viscosity of DNA showed a complicated dependence on complex concentration. The change in viscosity with the addition of the complex to DNA is shown in Figure 3. The viscometric data rules out classical intercalation. Similar behaviour has been observed on the addition of $[Cu(bcp)_2]^+$ to ST DNA.[50] The viscometric results could be explained in terms of a bridged structure to promote the extension of duplexes. Here the binding may involve inner-sphere complex formation via phosphate oxygen, indicating that the binding of Cr^{III} complex with DNA could be surface binding or by forming bridged adducts. Adducts formed by bridging duplexes are stabilized by hydrophobic interaction or coulombic interaction, as with $[Cu(bcp)_2]^+$ and $[Cu(dpsmp)_2(H_2O)]$.[51–53]

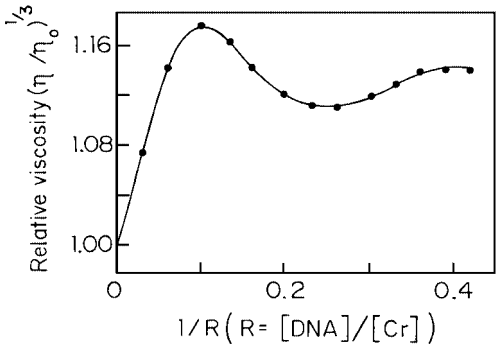

Figure 3. Effect of increasing amounts of $[Cr(bzimpy)_2]^+$ (–•–) on the relative viscosity of DNA

Fluorescence Spectroscopic Study

The emission spectra of $[Cr(bzimpy)_2]^+$ in the absence and the presence of CT DNA is shown in Figure 4. The luminescence spectrum of complex **1** shows an emission band at 717 nm when excited at 320 nm. The band at 717 nm is attributable to the $^2E_g \rightarrow {}^4A_{2g}$ transition of $[Cr(bzimpy)_2]^+$. Addition of DNA causes a gradual increase in the fluorescence intensity and the emission maximum also shifts by 2 nm to a longer wavelength. This is because, in the presence of DNA, the metal complex is bound in a relatively non-polar environment compared to water. Such an increase in fluorescence intensity has been reported for certain intercalators upon their binding to DNA. The increase observed here, however, is less than that observed for classical intercalators. In contrast, $[Cr(bpy)_3]^{2+}$ and $[Cr(phen)_3]^{2+}$ show a decrease in luminescence intensity in the presence of DNA, indicating that the excited state of these complexes are strong oxidizing agents that could oxidize guanine base.[54–55] The excited state potential for complex **1** was calculated as 0.92 V from Equation (2), where $E_{0-0}(Cr^{3+}/{}^*Cr^{3+})$ is the one-electron potential corresponding to the zero-zero spectroscopic energy of the excited state.

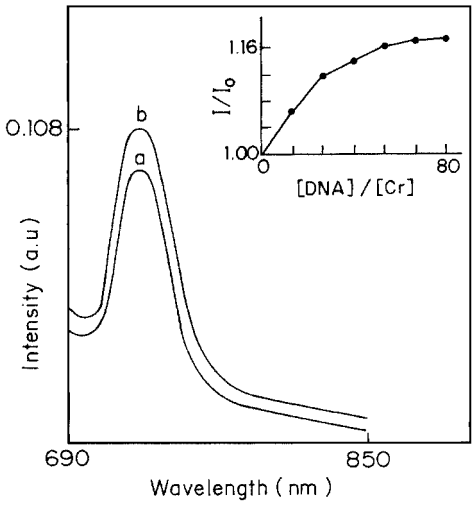

Figure 4. Emission spectra of $[Cr(bzimpy)_2]^+$ in aqueous solution in a) absence and b) presence of DNA. [Cr] = 10 mM, [DNA] = 200–800 mM. Inset: Relative emission intensity of $[Cr(bzimpy)_2]^+$ versus [DNA]/[Cr]

$$E^0({}^*Cr^{3+}/Cr^{2+}) = E^0(Cr^{3+}/Cr^{2+}) - E_{0-0}(Cr^{3+}/{}^*Cr^{3+}) \quad (2)$$

The reported excited state potentials of $[Cr(bpy)_3]^{3+}$ and $[Cr(phen)_3]^{3+}$ are 1.44 and 1.42 V, which are much greater than the 0.92 V in the present case. Hence, compared to $^*[Cr(bpy)_3]^{3+}$ and $^*[Cr(phen)_3]^{3+}$, the excited state of $[Cr(bzimpy)_2]^+$ is not a good oxidizing agent to oxidize the guanine base; as the excited state potential is low compared to that of guanine base.

DNA Cleavage by $Cr(bzimpy)_2^+$

The ability of $[Cr(bzimpy)_2]^+$ to serve as a metallonuclease has been examined. The reaction of $[Cr(bzimpy)_2]^+$ with pBR322 DNA was monitored by observing the conversion of supercoiled plasmid DNA (fastest migrating species) into the circular, nicked form (slowest migrating species). All reactions were evaluated by comparing the amount of circular plasmid to the amount present in plasmid controls. Neither relaxation nor nicking is observed in control reactions of DNA alone or with DNA and either $[Cr(bzimpy)_2]^+$ or hydrogen peroxide (Figure 5. lanes 1–3). However, with hy-

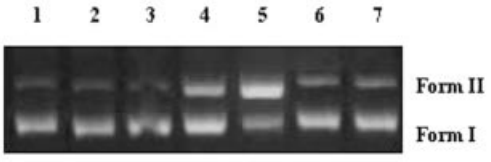

Figure 5. Nicking of pBR322 DNA by $[Cr(bzimpy)_2]^+$ over time. Lane 1, control DNA alone; lane 2, DNA + complex **1**; lane 3, DNA + H_2O_2; lanes 4 and 5, DNA + complex **1** + H_2O_2 incubated for 30 and 60 min, respectively. Lane 6, DNA + complex **1** + H_2O_2 + EtOH (1 M); lane 7, DNA + complex **1** + D-mannitol (500 mM)

 © 2003 Wiley-VCH Verlag GmbH & Co. KGaA, Weinheim

drogen peroxide, $[Cr(bzimpy)_2]^+$ relaxes supercoiled pBR322 DNA in a time-dependent manner (lanes 4,5). At longer times, the supercoiled form is completely converted into the open circular form (form II) in the presence of Cr^{III} complex. The time dependence of the reaction suggests that $[Cr(bzimpy)_2]^+$ acts as a catalyst. In the presence of Cr^{III} complex, H_2O_2 produces radical species, which cause the DNA cleavage. The addition of radical traps (1 M EtOH or D-mannitol) to reaction mixtures containing complex and H_2O_2 inhibited the cleavage of DNA (lanes 6 and 7 of Figure 6). Gel electrophoresis of similar DNA-cleaving experiments with CT DNA showed that complex **1** cleaved the CT DNA in a non-specific manner, in the presence of H_2O_2. The presence of hydroxyl radicals has been shown to lead to hydrolysis of *p*-nitrophenyl phosphate ester.[56] Treatment of p-nitrophenyl phosphate with complex **1** and H_2O_2 generates *p*-nitrophenol, which has an absorption at 404 nm (Figure 6). This confirms the formation of hydroxyl radicals from hydrogen peroxide in the presence of complex **1**.

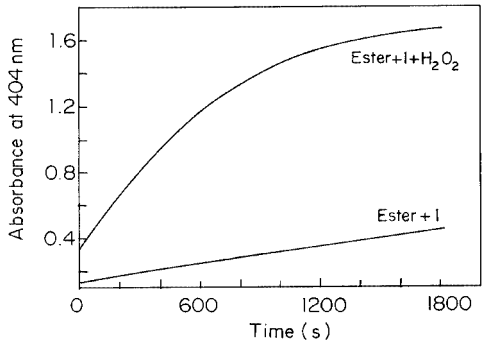

Figure 6. Kinetics of phosphate ester hydrolysis of *p*-nitrophenylphosphate by complex **1** in the presence of hydrogen peroxide

Conclusions

Chromium complexes having a tridentate ligand can bind DNA with moderate strength. Spectroscopic and viscosity measurements show that the Cr^{III} complex interacts with the DNA surface. A fluorescence study shows that the emission intensity of the complex increases on addition of DNA as the environment around the complex is more hydrophobic in the presence of DNA. The emission of both $[Cr(phen)_3]^{3+}$ and $[Cr(bpy)_3]^{3+}$ is quenched on binding to DNA. The emission of $[Cr(bzimpy)]^{2+}$, however, is not quenched by DNA as it has a lower excited state potential than that for guanine base. Gel electrophoresis shows that $[Cr(bzimpy)_2]^+$ nicks DNA in the presence of H_2O_2. The amount of nicked DNA formed increases with increasing incubation time of the Cr^{III} complex and H_2O_2 with DNA. The nicking of DNA is inhibited by radical scavengers such as ethanol and D-mannitol.

Experimental Section

Materials: *o*-Phenylenediamine, 2,6-pyridinedicarboxylic acid, and calf thymus DNA were obtained from Sigma chemicals, USA. Tris, Hepes, agarose, and pBR322 DNA were obtained from Bangalore Genei, Bangalore. All solvents were obtained from Ranbaxy, India. Milli Q water was used for preparing buffers.

Synthesis of $[Cr(bzimpy)_2]Cl$ (1): 2,6-Bis(benzimidazo-2-yl)pyridine was synthesized according to the published procedure.[57] An excess of DMSO was added to chromium(III) chloride salt (1 mmol, 0.267 g) and boiled under reflux for 1 h. The ligand bzimpy (2 mmol, 0.622 g) was then added to the resulting mixture, and refluxing was continued for a further hour. The volume of solvent was then minimised by rotary evaporation and a reddish orange precipitate was obtained on addition of diethyl ether. The precipitate was filtered off and dried in vacuo. The compound was then recrystallised from acetonitrile (yield 0.66 g, 75%); found C 64.33, H 3.34, N 19.80, Cr 7.32% calcd. for $C_{38}H_{24}ClCrN_{10}$ (M.wt. 707.5): C 64.43, H 3.41, N 19.78, Cr 7.34%. IR (KBr pellet): 3401 (N−H), 3057 (C−H), and 1615 (C=N) cm^{-1}.

Physical Measurements: UV/Visible spectra of the complex and DNA binding studies were recorded on a Perkin−Elmer Lambda 35 spectrophotometer at 25 °C. Elemental analysis was performed using a Heraeus-CHN-Rapid Analyzer at RSIC, IIT, Madras. The emission spectra were recorded on a Hitachi 650−40 spectrofluorimeter. The electrospray ionization (ESI) mass spectrum of the complex was recorded with a Hewlett−Packard 1100 mass spectrometer equipped with an electron spray source. The infrared spectrum of the complex was recorded on a Perkin-Elmer FT-IR spectrometer. Cyclic voltammetry was performed on an EG and G PAR 173 potentiostat/Galvanostat analyzer. Tetrabutylammonium perchlorate (TBAP) was used as supporting electrolyte. The sample in dried DMSO was purged with nitrogen prior to measurement. A standard three-electrode system consisted of a glassy carbon working electrode, platinum auxiliary electrode and a saturated calomel reference electrode (SCE).

DNA Binding Experiments: All experiments involving the interaction of the complex with DNA were carried out in Hepes buffer (10 mM, pH 7.5). A solution of calf thymus DNA in the buffer gave a ratio of UV absorbance at 260 and 280 nm of about 1.8−1.9:1, indicating that the DNA was sufficiently free from protein.[58] The DNA concentration per nucleotide was determined by absorption spectroscopy using the molar absorption coefficient (6600 $M^{-1}cm^{-1}$) at 260 nm.[59]

The electronic spectra of the Cr^{III} complex were monitored in both the presence and absence of DNA. The binding constant for the interaction of Cr^{III} complex **1** with DNA was obtained from absorption titration data. A fixed concentration of complex **1** (10 μM) was titrated with increasing amounts of DNA over the range 20−150 μM.

During measurement of the absorption spectra, an equal amount of DNA solution was added in both complex solution and reference solution to eliminate the absorbance of DNA itself.

Thermal denaturation studies were conducted in a Perkin−Elmer Lambda 35 spectrophotometer supplied with thermostatted cell holder. The temperature was controlled by a Peltier system (±0.1 °C). The absorbance at 260 nm was monitored for DNA (100 μM) in the absence and presence of the complex (10 μM).

Viscosity measurement was carried out on an Ostwald viscometer, immersed in a thermostatted water bath maintained at 28±0.1 °C.

 © 2003 Wiley-VCH Verlag GmbH & Co. KGaA, Weinheim

The DNA concentration was kept constant (150 μM) and that of the metal complex was varied from 5 to 75 μM. The flow time was measured with a stop-watch operated manually, and each sample was measured five times and an average flow time calculated. Data are presented as $(\eta/\eta_o)^{1/3}$ versus [Cr]/[DNA], where η is the viscosity of DNA in the presence of complex, and η_o is the viscosity of DNA alone. Viscosity values were calculated from the observed flow time of DNA-containing solutions corrected for the flow time of buffer alone (t_o), $\eta = t - t_o$.[60]

In steady state fluorescence experiments, the complex concentration (10 μM) was fixed while that of DNA was varied (200−800 μM). The chromium(III) complex in the presence of DNA was excited at 320 nm and the fluorescence spectra were recorded between 650 and 850 nm.

Phosphate ester hydrolysis was monitored on a Perkin−Elmer Lambda 35 spectrophotometer at 25 °C by measuring the production of p-nitrophenol at 404 nm. The background reaction was carried out with the peroxide and ester alone. A reaction mixture containing Cr^{III} complex **1** (0.025 mM), peroxide (0.1 mM, freshly prepared) and *p*-nitrophenylphosphate (1 mM) in Hepes (10 mM, pH 7.0) was used to determine the rate of *p*-nitrophenol formation at 404 nm.

For gel electrophoresis experiments, supercoiled pBR322 DNA (800 ng) was treated with Cr^{III} complex (100 μM) in Tris-EDTA buffer (10 mM, pH 8.0) and the solution was incubated for 16 h at room temperature. H_2O_2 (500 μM) was then added and a timed assay was carried out. The reactions were quenched at various times by adding loading buffer. The samples were analyzed by electrophoresis for 4 h at 50 V on a 0.8% agarose gel in Tris−boric acid−EDTA buffer. The gel was stained with 0.5 μg/mL ethidium bromide and photographed under UV light.

Acknowledgments

V. G. V thanks the CSIR for a research fellowship.

[1] S. M. Hecht, *Acc. Chem. Res.* **1986**, *19*, 383−391.
[2] T. D. Tullius, B. A. Dombroski, *Science* **1985**, *235*, 679−681.
[3] A. M. Burkoff, T. D. Tullius, *Nature* **1988**, *331*, 455−457.
[4] A. M. Burkoff, T. D. Tullius, *Cell* **1987**, *48*, 935−943.
[5] W. K. Pogozelski, T. K. Tullius, *Chem. Rev.* **1998**, *98*, 1089−1108.
[6] C. J. Burrows, J. G. Muller, *Chem. Rev.* **1998**, *98*, 1109−1152.
[7] A. E. Friedman, J. K. Barton, *J. Am. Chem. Soc.* **1990**, *112*, 4960−4962.
[8] R. M. Hartshorn, J. K. Barton, *J. Am. Chem. Soc.* **1992**, *114*, 5919−5925.
[9] C. J. Murphy, J. K. Barton, *Methods Enzymol.* **1993**, *226*, 576−594.
[10] Y. Jenkins, A. E. Friedman, N. J. Turro, J. K. Barton, *Biochemistry* **1992**, *31*, 10809−10816.
[11] C. Turro, S. H. Bossmann, Y. Jenkins, J. K. Barton, N. J. Turro, *J. Am. Chem. Soc.* **1995**, *117*, 9026−9032.
[12] N. Gupta, N. Grover, G. A. Neyhart, W. Liang, P. Singh, H. H. Thorpe, *Angew. Chem. Int. Ed. Engl.* **1992**, *31*, 1048−1050.
[13] X.-H. Zou, B.-H. Ye, H. Li, Q.-L. Zhang, H. Chao, J.-G. Liu, L.-N. Ji, *J. Biol. Inorg. Chem.* **2001**, *6*, 143−150.
[14] C. J. Burrows, S. E. Rokita, *Acc. Chem. Res.* **1994**, *27*, 295−301.
[15] T. D. Tullius, Metal-DNA chemistry, ACS Symposium Series 402, American Chemical Society, Washington DC, **1989**, pp. 1−23.
[16] A. R. Banerjee, J. A. Jaeger, D. H. Turner, *Biochemistry* **1993**, *32*, 153−163.
[17] D. S. Sigman, *Acc. Chem. Res.* **1986**, *19*, 180−186.
[18] A. M. Pyle, J. K. Barton, *Prog. Inorg. Chem.* **1990**, *38*, 413−475.
[19] S. Sigman, A. Mazumdar, D. M. Perrin, *Chem. Rev.* **1993**, *93*, 2295−2316.
[20] K. Naing, M. Takashani, M. Taniguchi, A. Yamagishi, *Inorg. Chem.* **1995**, *34*, 350−356.
[21] F. L. Liu, K. A. Meadows, D. R. Millin, *J. Am. Chem. Soc.* **1993**, *115*, 6699−6704.
[22] Y. Xiong, X.-F. He, X.-H. Zou, J.-Z. Wu, X.-M. Chen, L.-N. Ji, R.-H. Li, J.-Y. Zhou, K.-B. Yu, *J. Chem. Soc., Dalton Trans.* **1999**, 19−24.
[23] *IARC*, **1990**, *49*, 49−256.
[24] U. Glaser, D. Hochrainer, H. Kloppel, H. Oldiges, *Toxicology* **1986**, *42*, 219−232.
[25] A. Leonard, R. R. Lauwreys, *Mutat. Res.* **1980**, *76*, 227−239.
[26] S. De Flora, M. Bagnasco, D. Serra, P. Zanacchi, *Mutat. Res.* **1990**, *238*, 99−172.
[27] J.-L. Yang, Y.-C. Hsieh, C.-W. Wu, T.-C. Lee, *Carcinogenesis* **1992**, *12*, 2053−2057.
[28] S. Kawanishi, S. Inoue, S. Sano, *J. Biol. Chem.* **1986**, *261*, 5952−5958.
[29] X. Shi, N. S. Dalal, *Environ. Health. Perspect.* **1994**, *102*, 231−236.
[30] A. Kortenkamp, G. Oetken, D. Beyersmann, *Mutat. Res.* **1990**, *232*, 155−161.
[31] A. Mikalsen, J. Alexander, H. Wallin, M. I. Sundberg, R. A. Andersen, *Carcinogenesis* **1991**, *12*, 825−831.
[32] M. Sugiyama, K. Tsuzuki, R. Ogura, *J. Biol. Chem.* **1991**, *266*, 3383−3386.
[33] R. A. Anderson, *Biol. Trace Element Res.* **1992**, *32*, 19−24.
[34] R. A. Anderson, N. Cheng, N. A. Bryden, M. M. Polansky, N. Cheng, J. Chi, J. Feng, *Diabetes* **1997**, *46*, 1786−1791.
[35] A. Ravina, L. Slezack, *Harefuah* **1993**, *125*, 142−145.
[36] D. M. Stearns, J. P. Wise, S. R. Patierno, K. E. Wetterhahn, *FASEB J.* **1995**, *9*, 1643−1648.
[37] S. E. Kohlami, M. Gattke, E. M. McIntosh, B. A. Kunz, *J. Mol. Biol.* **1991**, *220*, 933−946.
[38] J. Singh, E. T. Snow, *Biochemistry* **1998**, *37*, 9371−9378.
[39] R. Vijayalakshmi, M. Kanthimathi, V. Subramanian, B. U. Nair, *Biochem. Biophys. Res. Commun.* **2000**, *271*, 731−734.
[40] R. Vijayalakshmi, M. Kanthimathi, V. Subramanian, B. U. Nair, *Biochim. Biophys. Acta* **2000**, *1475*, 157−162.
[41] K. D. Sugden, R. D. Geer, S. J. Rogers, *Biochemistry* **1992**, *31*, 11626−11631.
[42] R. Rajan, R. Rajaram, B. U. Nair, T. Ramasami, S. K. Mandal, *Dalton Trans.* **1996**, 2019−2020.
[43] V. G. Vaidyanathan, B. U. Nair, *J. Inorg. Biochem.* **2002**, *91*, 405−412.
[44] R. F. Pasternack, E. J. Gibbs, J. J. Villafranca, *Biochemistry* **1983**, *22*, 2406−2414.
[45] M. Erikkson, M. Leijon, G. Hiort, B. Norden, A. Graslund, *J. Am. Chem. Soc.* **1992**, *114*, 4933−4934.
[46] M. Cory, D. D. McKee, J. Kagan, D. W. Henry, J. A. Miller, *J. Am. Chem. Soc.* **1985**, *107*, 2528−2536.
[47] M. J. Waring, *J. Mol. Biol.* **1965**, *13*, 269−282.
[48] J. M. Kelly, A. B. Tossi, D. J. McConell, C. OhUigin, *Nucleic Acids Res.* **1985**, *13*, 6017−6034.
[49] G. A. Neyhart, N. Grover, S. R. Smith, W. A. Kalsbeck, T. A. Fairley, M. Cory, H. H. Thorp, *J. Am. Chem. Soc.* **1993**, *115*, 4423−4428.
[50] F. Liu, K. A. Meadows, D. R. McMillin, *J. Am. Chem. Soc.* **1993**, *115*, 6699−6704.
[51] P. G. Schultz, J. S. Taylor, P. B. Dervan, *J. Am. Chem. Soc.* **1982**, *104*, 6861−6863.
[52] S. Mahadevan, M. Palaniandavar, *Inorg. Chem.* **1998**, *37*, 693−700.
[53] G. Yang, F. Z. Wu, L. Wang, L. NianFi, X. Tina, *J. Inorg. Biochem.* **1997**, *66*, 141−144.

 © 2003 Wiley-VCH Verlag GmbH & Co. KGaA, Weinheim

[54] M. A. Jamieson, N. Serpone, M. Z. Hoffman, *Coord. Chem. Rev.* **1981**, *39*, 121−179.
[55] R. T. Watson, N. Desai, J. Wildsmith, J. F. Wheeler, N. A. P. Kane-Maguire, *Inorg. Chem.* **1999**, *38*, 2683−2687.
[56] A. Parand, A. C. Royer, T. L. Cantrell, M. Weitzel, N. Memon, J. B. Vincent, M. W. Crowder, *Inorg. Chim. Acta* **1998**, *268*, 211−219.
[57] A. W. Addison, P. J. Burke, *J. Heterocycl. Chem.* **1981**, *18*, 803−805.
[58] J. Marmur, *J. Mol. Biol.* **1961**, *3*, 208−218.
[59] M. F. Reichmann, S. A. Rice, C. A. Thomas, P. Doty, *J. Am. Chem. Soc.* **1954**, *76*, 3047−3053.
[60] G. Cohen, H. Eisenberg, *Biopolymers* **1969**, *8*, 45−55.
Received March 29, 2003

 © 2003 Wiley-VCH Verlag GmbH & Co. KGaA, Weinheim

Synthesis and Structural Characterization of Potassium Salts of Phosphane-Substituted (Cyclopentadienyl)iron Dicyanides, and Their Use as Bridging Ligands for Copper(I) Phosphane Derivatives

Donald J. Darensbourg,*[a] M. Jason Adams,[a] Jason C. Yarbrough,[a] and Andrea L. Phelps[a]

Dedicated to the memory of Professor Dieter Sellmann, a good friend and brilliant chemist

Keywords: Cyanides / Heterometallic complexes / Bridging ligands / Iron / Copper / Potassium

Phosphane-substituted $CpFe(CN)_2$ anions have been synthesized by photochemical decarbonylation of $KCpFe(CN)_2CO$ in the presence of various mono- and diphosphanes. The synthesis and characterization of uniquely bridged diphosphane derivatives, $[KCpFe(CN)_2]_2$-μ-$(Ph_2P)_2$–$(CH_2)_n$ (n = 2–4), are particularly noteworthy. These phosphane-substituted $CpFe(CN)_2^-$ units have afforded stable mixed-metal complexes upon reaction with Cu^I in the presence of tricyclohexylphosphane in acetonitrile solution. X-ray crystallography shows these derivatives to display two-dimensional diamond-shaped structures with copper(I) of the form $[Fe(CN)_2Cu]_2$, where the Cu^I centers exhibit both trigonal and tetrahedral geometries. Infrared data reveal that the withdrawal of electron density from the iron centers in these mixed metal cyanides via the cyanide ligands is enhanced upon replacing CO in $CpFe(CN)_2CO^-$ with phosphanes.
(© Wiley-VCH Verlag GmbH & Co. KGaA, 69451 Weinheim, Germany, 2003)

Introduction

The use of substitutionally inert organometallic cyanides as ligands to other metal ions has received much interest due to their ability to simplify studies utilizing cyanide as a bridging group.[1] Although, metal hexacyanide salts have long been known to complex other metal ions through bridging cyanide ligands, the resulting derivatives are often highly insoluble aggregates which are difficult to definitively characterize.[2] Organometallic derivatives having the three facial coordination sites occupied by an ancillary ligand, e.g., the cyclopentadienyl moiety, have been used to limit the degree of aggregation.[3] Substitution of the metal center by an additional strongly bonded ligand, such as a tertiary phosphane, further limits bridging in a multidimensional fashion. In addition to promoting solubility, phosphane adducts of these organometallic cyanides provide a convenient ^{31}P NMR probe for studying these complexes. Despite these advantages, relatively few studies have involved these simple metallocyanides.[4]

Vahrenkamp and co-workers have investigated neutral iron monocyanide complexes of the type CpFe(dppe)CN, where dppe = 1,2-bis(diphenylphosphanyl)ethane, as bridging ligands to other metal complexes.[5] The use of metal monocyanide derivatives is particularly beneficial at restricting the bridging capacity of the complex, and thus uncomplicating the study of the cyanide ligand as an electronic linkage between two metal centers. The chelated phosphane ligand serves to block any sites on the iron ion that a more labile ligand might leave open for substitution. Furthermore, the bulkiness of the phosphane ligand often aids in crystallization of the resulting multinuclear metal complexes. Indeed, this simple metallocyanide has allowed Vahrenkamp to examine in detail the redox chemistry of cyanide-bridged trimetallic complexes using cyclic voltammetry. One such study involved the effect of linear vs. bent bridging motifs in the Fe−CN−Pt−NC−Fe metallocyanide unit on electronic communication between the metal centers.[5,6]

A long standing focus in our research efforts involves the design of homogeneous catalysts for the copolymerization of epoxides and carbon dioxide to provide polycarbonates.[7] Relevant to this subject double metal cyanide derivatives, especially those of Fe(II and III) or Co^{III} and Zn^{II}, have received attention as heterogeneous catalysts for this process in the patent literature.[8] In our efforts to synthesize novel mixed-metal cyanides as models for these catalysts, a series of metal complex salts of the general formula $[K][CpFe(CN)_2PR_3]$ have been prepared and characterized both in solution and in the solid state. In addition, the employment of traditionally chelating phosphane ligands have extended the range of these salts to include diiron deriva-

[a] Department of Chemistry, Texas A&M University, College Station, Texas 77843, USA
Fax: (internat.) + 1-979/845-0158
E-mail: djdarens@mail.chem.tamu.edu

tives of the type $[K]_2[CpFe(CN)_2PR_2(CH_2)_nPR_2(CN)_2FeCp]$, where $n = 2-4$ and R = Ph, thereby affording unique bridging ligands with specific bite angles. Importantly, the electronic character of the cyanide ligands can be tailored by choosing phosphanes of the appropriate basicity. Examples of the viability of these anionic metallocyanide derivatives of iron as ligands towards copper(I) are demonstrated with the isolation and crystallographic characterization of the mixed-metal complexes $[CpFe(PPh_3)(\mu\text{-}CN)_2Cu(PCy_3)]_2$ and $Cu(PCy_3)[CpFe(\mu\text{-}CN)_2]_2Cu(PCy_3)_2$-μ-dppp [dppp = 1,2-bis(diphenylphosphanyl)propane].

Results and Discussion

A series of phosphane (= L) substituted salts of $[K][CpFe(CN)_2L]$ has been prepared through photolytic decarbonylation of the parent $[K][CpFe(CN)_2CO]$ compound (Scheme 1). The impetus for these studies comes from our desire to synthesize well-defined double-metal cyanide (DMC) complexes to serve as soluble structural and reactivity models for those employed as heterogeneous catalysts for the polymerization of epoxides to polyols or epoxides and CO_2 to polycarbonates/cyclic carbonates. Relevant to these studies we have previously noted that upon treating analogous DMC complexes derived from the $CpFe(CN)_2CO^-$ anion with excess PCy_3, the reaction according to Equation (1) occurred over an extended reaction time. That is, the metal aggregate was disrupted to afford a trigonal copper(I) center and PCy_3 had displaced CO at the iron center (**A**).[9] Hence, an obvious concern is whether dimer disruption is a necessary structural prerequisite upon substitution of the CO ligand at the iron center with a sterically demanding phosphane ligand.

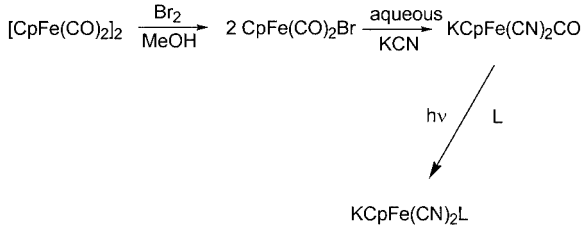

Scheme 1

$$[CpFe(CO)(\mu\text{-}CN)_2Cu(PCy_3)_2]_2 + 2\,PCy_3 \rightarrow 2\,CpFe(PCy_3)(CN)(\mu\text{-}CN)Cu(PCy_3)_2 + 2\,CO \quad (1)$$

In order to tailor the electronic and structural properties of the ancillary metal center we have photochemically substituted the CO ligand in the $KCpFe(CN)_2CO$ salt with various phosphane and diphosphane ligands. A mixture of methanol and acetonitrile was utilized to solubilize both the parent salt and in this instance PPh_3, respectively. Solubility of the reagents, especially the $KCpFe(CN)_2CO$ derivative, is

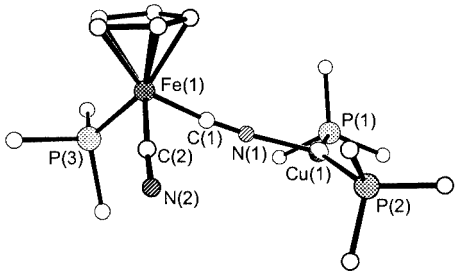

A

essential for complete conversion into product. This complex has alternatively been prepared thermally from $CpFe(CO)(PPh_3)I$ and KCN in refluxing ethanol by Reger.[4] The product, $KCpFe(CN)_2PPh_3$ (**1**), exhibited ν(CN) frequencies at 2055 vs, 2040 s, and 2028 sh cm^{-1} in methanol, which are shifted to lower wavenumbers when compared to the parent compound (see Table 1). This shift to lower frequencies is expected as the result of replacing the carbonyl ligand by primarily a donor phosphane ligand, thereby allowing the cyanide groups to be involved in greater π-backbonding with the iron center. The ^{31}P NMR spectrum of **1** displays a downfield chemical shift from that of the free ligand to δ = 86.9 ppm. The more basic methyldiphenylphosphane ligand was incorporated at the iron center for comparison with the PPh_3 analog, where the only other variance arises from its slightly reduced cone angle of 136 vs. 145° for PPh_3.[10–12] In this instance it was not necessary to employ a mixed-solvent system for the photolytic reaction since both the $KCpFe(CN)_2CO$ salt and PPh_2Me are soluble in methanol. As expected, the increased basicity of the monomethylated phosphane causes the ν(CN) vibrations in $KCpFe(CN)_2PPh_2Me$ (**2**) to shift to lower wavenumbers at 2050, 2034, and 2025 cm^{-1}. The ^{31}P NMR chemical shift in complex **2** appears at δ = 71.3 ppm. Interestingly, in an attempt to improve reaction yields, photolysis of the carbonyl salt with a fourfold excess of PPh_2Me afforded the bis(phosphane) neutral complex $CpFe(CN)(PPh_2Me)_2$ (**3**).

Table 1. Infrared and ^{31}P NMR spectroscopic data (all spectra were determined in methanol solution except for those of compound **3** which were determined in THF)

Compound	ν(CN) [cm^{-1}]	δ [ppm]
$KCpFe(CN)_2(CO)$	2095, 2084	N/A
$KCpFe(CN)_2(PPh_3)$ (**1**)	2055 vs, 2040 s, 2028 sh	86.9
$KCpFe(CN)_2(PPh_2Me)$ (**2**)	2050 vs, 2034 s, 2025 sh	71.3
$CpFe(CN)(PPh_2Me)_2$ (**3**)	2069	57.2
$[KCpFe(CN)_2]_2$ μ-dppe (**4**)	2050, 2032, 2025 sh	78.2
$[KCpFe(CN)_2]_2$ μ-dppp (**5**)	2050, 2032, 2025 sh	77.0
$[KCpFe(CN)_2]_2$ μ-dppb (**6**)	2050 vs, 2034 s, 2026 sh	76.5
$[KCpFe(CN)_2]_2$ μ-dppa (**7**)	2057 s, 2050 vs, 2032 sh	64.9

A number of bidentate phosphanes have been utilized as bridging ligands between two $CpFe(CN)_2$ anionic units. These derivatives were synthesized by photolysis of the parent salt $KCpFe(CN)_2CO$ in the presence of 0.5 equiv. of the

 © 2003 Wiley-VCH Verlag GmbH & Co. KGaA, Weinheim

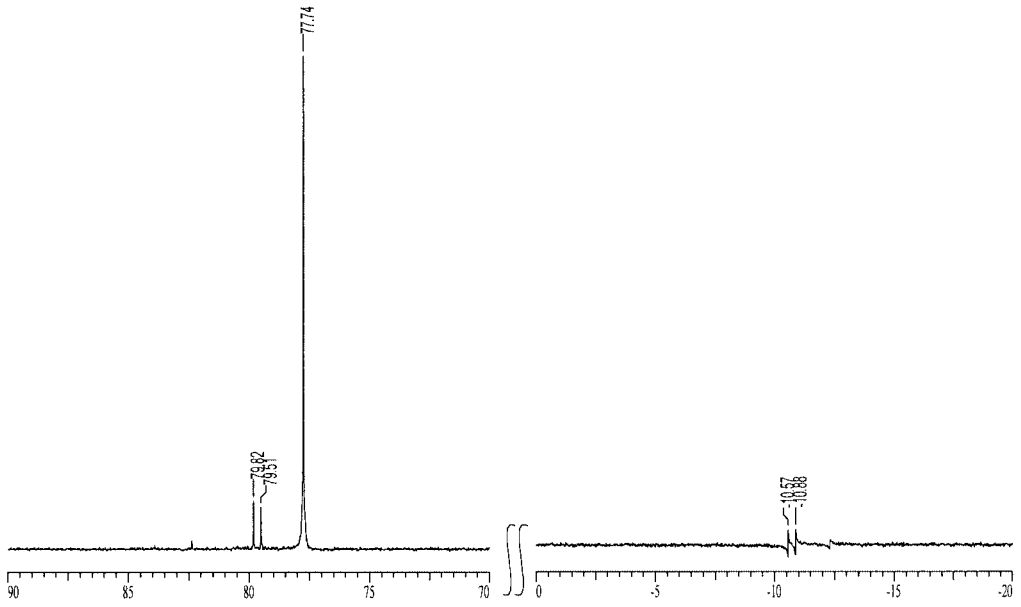

Figure 1. ^{31}P NMR spectrum of the crude product from the synthesis of $[KCpFe(CN)_2]_2$-μ-dppe (**4**) with baseline omitted from 0 to 70 ppm

corresponding diphosphane in a 1:1 mixture of acetonitrile/methanol. A small impurity of the singly bonded phosphorus derivative, such as $KCpFe(CN)_2$dppe, often accompanies these syntheses. Figure 1 depicts the ^{31}P NMR spectrum of the crude product resulting from the reaction of $KCpFe(CN)_2(CO)$ with 0.5 equiv. of dppe, where in addition to the desired product **4** ($\delta^{31}_P = 78.2$ ppm) two weak ^{31}P signals at $\delta = 79.7$ and -10.8 ppm with ^{31}P coupling constants of 38.3 Hz are observed corresponding to bound and free phosphane, respectively. Varying the number of $-CH_2-$ units linking the phosphorus donors from 2 to 4 allows for control of the orientation of the cyanide ligands with respect to one another (vide infra). As anticipated, the ν(CN) vibrational modes in complexes **4**, **5**, and **6** are virtually identical (see Table 1) since all of the bridging phosphane ligands are of similar basicity.

A more contrasting example of a bridging phosphane can be seen in the bis(diphenylphosphanyl)acetylene case, complex **7**. This short-chain bridging phosphane is comprised of a linear alkylene backbone, with diminished electron-donating ability compared to its dppe counterpart, **4**. The decrease in basicity is readily apparent in the ν(CN) values in complex **7** which are on average 10 cm^{-1} higher than those of complex **4**. Furthermore, the linear nature of the phosphane prohibits the cyanide ligands of the bis(iron) complex from interacting at the same metal center. One might imagine this bis(cyanometalate) behaving as a strut which links metal centers to form chain-like structures.

The solid-state structures of representative examples of these phosphane-substituted (cyclopentadienyl)iron dicyanide salts have been examined by X-ray crystallography. Single crystals of compounds **1** and **4** were grown from a concentrated methanol solution by slow concentration over several weeks at ambient temperature. Compound **6** was crystallized from THF/hexane at 10 °C, whereas single crystals of **3** were obtained by slow concentration of a hexane solution at room temperature. Selected bond lengths and angles of compounds **1**, **3**, **4**, and **6** are listed in Table 2.

Table 2. Selected bond lengths [Å] and angles [°] for compounds **1**, **3**, **4**, and **6**

	1	**3**	**4**	**6**
Fe(1)−C(6A)	1.880(8)	1.889(3)	1.871(12)	1.847(9)
Fe(1)−P(1)	2.175(2)	2.2025(8)	2.180(3)	2.183(2)
C(6A)−N(1A)	1.166(8)	1.156(3)	1.178(13)	1.163(10)
N(1A)−K(1)	2.847(5)	–	2.980(9)	2.982(8)
N(2A)−K(1)	–	–	3.086(10)	3.138(7)
N(2B)−K(2)	–	–	2.971(9)	–
N(1B)−K(1)	–	–	2.828(9)	–
N(2B)−K(1)	–	–	–	2.781(9)
N(1B)−K(2)	–	–	2.999(9)	2.744(7)
C(6A)−Fe(1)−C(7A)	89.3(3)	–	91.7(5)	91.6(3)
C(6A)−Fe(1)−P(1)	93.9(2)	87.73(8)	89.7(3)	88.8(3)
C(6A)−N(1A)−K(1)	136.8(4)	–	87.5(7)	85.9(6)
P(1)−Fe(1)−P(2)	–	98.42(3)	–	–

The effect of replacing the carbonyl group with a phosphane donor can be seen in the metric data for the iron cyanide unit. Specifically, the iron−carbon(cyanide) distances in compounds **1**, **4**, and **6** are shorter than those seen in $KCpFe(CN)_2CO$, where an average Fe−CN distance of 1.911(8) Å was observed.[13,14] This subtle yet statistically relevant bond-length change is the result of replacing the good π-acceptor, CO, with a good donor ligand, phosphane. Concomitantly, the increase in bond order to the Fe−CN bond causes a decrease in the C−N triple-bond

 © 2003 Wiley-VCH Verlag GmbH & Co. KGaA, Weinheim

character, where the C(6A)−N(1A) bond lengths in compounds **1**, **4**, and **6** are all longer than that determined in the CO analog [1.143(10) Å]. Although this is compelling crystallographic evidence, the decrease in the cyanide triple-bond order is more evident by observing the ν(CN) vibrational modes shift to lower frequencies as previously noted. As expected, the Fe−P bond lengths in compounds **1**, **4**, and **6** are quite similar, spanning the narrow range from 2.175(2) in **1** to 2.183(2) Å in **6**. In the diphosphane neutral derivative, **3**, there is a slight lengthening of the Fe−P bond where a distance of 2.2025(8) Å is observed. Although it is tempting to attribute the bond lengthening to an electronic effect, it might also be due to enhanced steric congestion about the iron center. Support for this latter explanation comes from the metric parameters obtained for the chelated CpFe(CN)(dppe) derivative. CpFe(CN)(dppe) was prepared by the method of Vahrenkamp and co-workers[5] and its solid-state structure defined by X-ray crystallography.[15] The average Fe−P bond length in this instance was found to be 2.1788(14) Å, which is indistinguishable from those seen in the anionic compounds **1**, **4**, and **6**. The thermal ellipsoid representations of these closely related neutral iron monocyanide derivatives, **3** and CpFe(CN)(dppe), are provided in Figure 2 and Figure 3. These drawings clearly illustrate the difference observed in the solid state of the orientation of the phenyl substituents of the phosphane ligands in **3** as compared with their imposed, sterically less demanding orientation seen in CpFe(CN)(dppe).

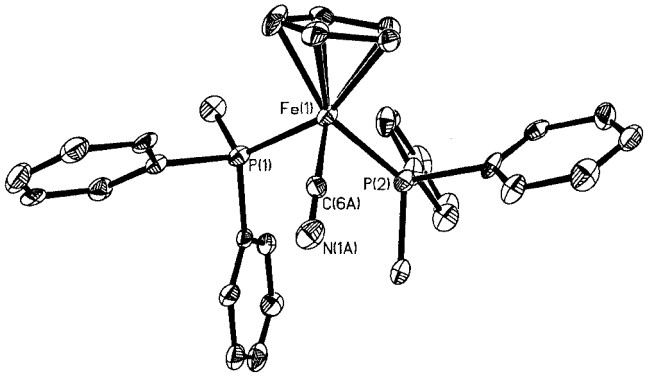

Figure 2. Thermal ellipsoid representation of CpFe(CN)-$(PPh_2Me)_2$ (**3**)

As noted in the thermal ellipsoid drawings in Figure 4, Figure 5 and Figure 6 of the salts, **1**, **4**, and **6**, in all instances the compounds pack in the crystal lattice so as to orient in such a manner as to maximize the number of cyanide−potassium interactions. These −CN−K interactions are either bridging or terminal in nature, with the two not being mutually exclusive. An instance of terminal interaction can be seen in Figure 4 between N(1A) and K(1), with an average distance of 2.847 Å. Potassium ions that bridge cyanide ligands on the same iron center, such as K(1) seen in Figure 5, display a stronger interaction with one of the cyanide nitrogen atoms. This is evidenced by a 0.1 Å

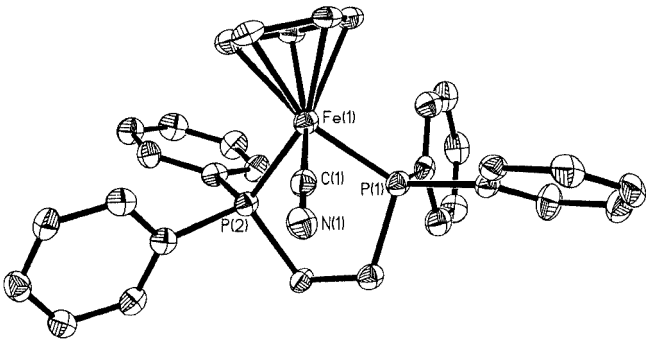

Figure 3. Thermal ellipsoid drawing of CpFe(CN)(dppe); selected bond lengths [A] and angles [°]: Fe(1)−P(2) 2.1747(14), Fe(1)−P(1) 2.1828(15), Fe(1)−C(1) 1.898(5), N(1)−C(1) 1.154(6); P(2)−Fe(1)−P(1) 84.76(6), C(1)−Fe(1)−P(2) 89.02(14), C(1)−Fe(1)−P(1) 88.43(14)

shorter interaction distance between N(1A) and K(1) as compared to that of N(2A)−K(1). In order to utilize these latter anionic metallocyanides as ligands towards other metal centers, the bridging diphosphane ligand must be flexible. That is, the orientation of the iron centers with respect to one another is controlled by the length of the chain between the Ph_2P- units. As is readily seen in Figure 5 of compound **4** the dppe bridge between the iron centers (n = 2) is sufficiently short so as to render it impossible for the four cyanide ligands on the two iron centers to become coplanar. The coplanarity of these four cyanide ligands is a requirement for providing mixed-metal diamond-shaped structures (vide infra). Upon lengthening the chain from n = 2 to n = 3 (**5**) or 4 (**6**) allows greater flexibility in the phosphane bridge, thereby, permitting the cyanide ligands to become coplanar in their chelation towards other metal centers (vide infra).

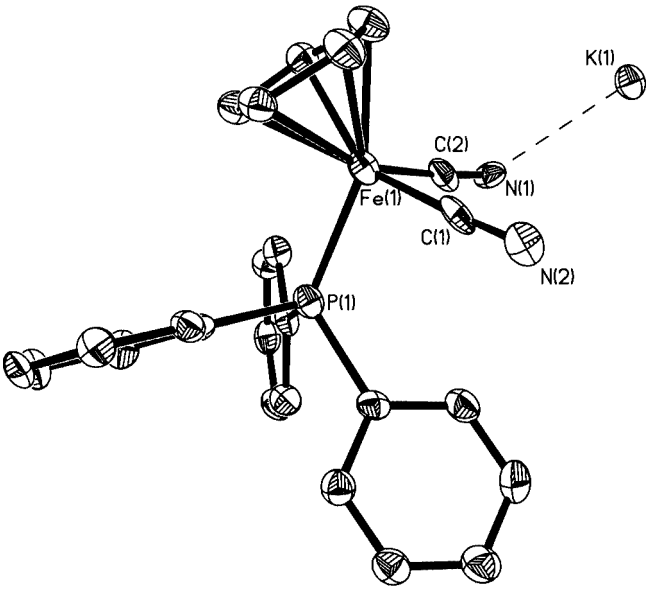

Figure 4. Thermal ellipsoid drawing of $KCpFe(CN)_2(PPh_3)$ (**1**) with solvent molecules and hydrogen atoms removed for clarity

Presently, we report studies involving the use of the $CpFe(CN)_2$ units with bound phosphanes as anionic li-

 © 2003 Wiley-VCH Verlag GmbH & Co. KGaA, Weinheim

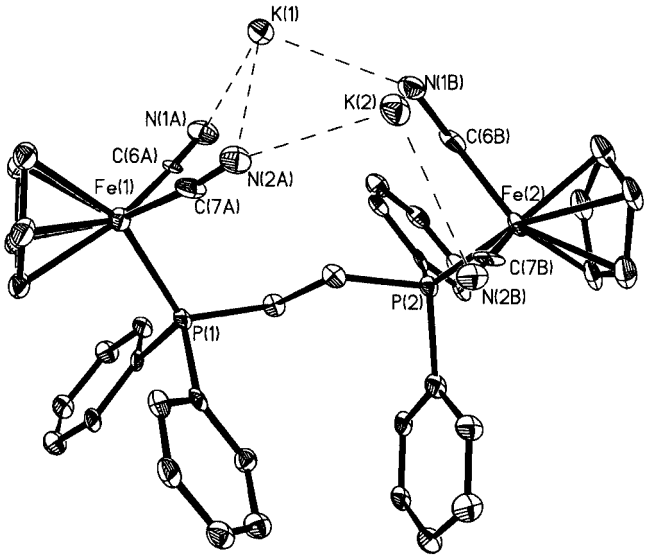

Figure 5. Thermal ellipsoid drawing of $[KCpFe(CN)_2]_2$-μ-dppe (**4**) with solvent molecules and hydrogen atoms removed for clarity

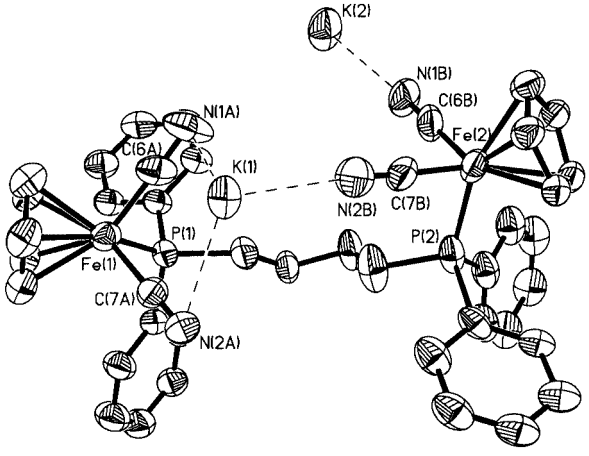

Figure 6. Thermal ellipsoid drawing of $[KCpFe(CN)_2]_2$-μ-dppb (**6**) with solvent molecules and hydrogen atoms removed for clarity

gands for the formation of double-metal cyanides. Specifically, the reaction of $KCpFe(CN)_2PPh_3$ with $Cu(CH_3CN)_4(BF_4)$ was carried out in acetonitrile to yield a fine yellow powder. This material was insoluble in all common organic solvents, which is in sharp contrast to its carbonylated analog.[16] In an effort to provide a soluble complex, a similar reaction was performed where an equivalent of PCy_3 was added to the copper(I) reagent prior to its addition to the iron dicyanide salt. This procedure led to the formation of a soluble double-metal cyanide derivative, complex **9**. Following the removal of acetonitrile, complex **9** was separated from the by-product KBF_4 salt by dissolution in dichloromethane. As anticipated for bridging cyanide ligands, the ν(CN) vibrational modes in complex **9** were shifted to higher frequencies compared to the corresponding values in the parent salt (see Table 1 and Table 3). Single crystals of **9** suitable for X-ray diffraction were grown by vapor diffusion of a CH_2Cl_2/hexane solution at 10 °C over a period of one week. A thermal-ellipsoid drawing of complex **9** is depicted in Figure 7, whereas selected bond lengths and angles are provided in Table 4.

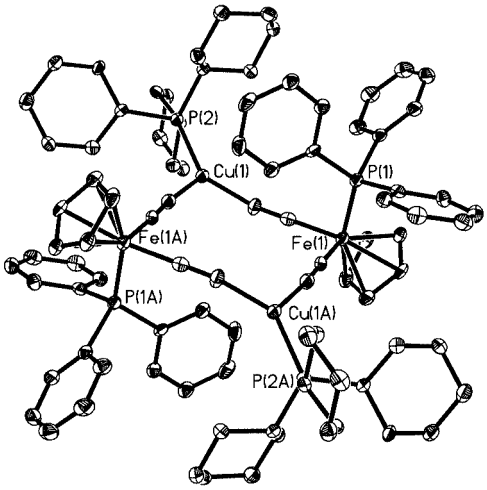

Figure 7. Thermal ellipsoid representation of $[CpFe(PPh_3)(\mu\text{-}CN)_2CuPCy_3]_2$ (**9**) with hydrogen atoms removed for clarity

The solid-state structure of complex **9** is similar to that seen for its $CpFe(CN)_2CO^-$-derived analog, $[\eta^5\text{-}C_5H_5Fe(CO)(\mu\text{-}CN)_2CuPCy_3]_2$.[16] That is, complex **9** exhibits a diamond-shaped motif composed of two $CpFe(PPh_3)$ fragments, two copper(I) centers, and four bridging CN^- ligands. The copper(I) centers display trigonal geometry as defined by the phosphorus and nitrogen donor groups. The iron-bound phosphane ligands lie on opposite sides of the metallacycle plane of the four metal atoms. The inversion center present in the structure of **9** demonstrates the metallacycle's high symmetry. Figure 8 illustrates the channels formed by the packing of complex **9** in the solid state, which

Table 3. Infrared [ν(CN)] and ^{31}P NMR spectral data for complexes **8**−**12**

Complex	Solvent	ν(CN) [cm^{-1}]	δ [ppm]
$[CpFe(PPh_3)(\mu\text{-}CN)_2Cu(CH_3CN)_2]_2$ [a] (**8**)	pyridine	2081, 2070	–
$[CpFe(PPh_3)(\mu\text{-}CN)_2Cu(PCy_3)]_2$ (**9**)	CH_2Cl_2	2085, 2078	84.7, 11.5
$[CpFe(\mu\text{-}CN)_2Cu(CH_3CN)_2]_2$-μ-dppp[a] (**10**)	pyridine	2075, 2065	–
$Cu(PCy_3)[CpFe(\mu\text{-}CN)_2]_2Cu(PCy_3)_2$-μ-dppp (**11**)	CH_2Cl_2	2089, 2083, 2077	74.2, 14.1, 11.2
$Cu(PCy_3)[CpFe(\mu\text{-}CN)_2]_2Cu(PCy_3)_2$-μ-dppb (**12**)	CH_2Cl_2	2082, 2077	74.3, 13.5, 10.7

[a] Complexes were only soluble in pyridine under which conditions the acetonitrile ligands on copper(I) are most likely displaced by pyridine.

 © 2003 Wiley-VCH Verlag GmbH & Co. KGaA, Weinheim

Table 4. Selected bond lengths [Å] and bond angles [°] in complexes **9** and **11**

Complex **9**			
Fe(1)−C(1)	1.868(7)	Cu(1)−N(2)	1.949(7)
Fe(1)−C(2)	1.865(8)	Cu(1)−P(2)	2.1865(19)
Fe(1)−P(1)	2.173(2)	C(1)−N(1)	1.169(8)
Cu(1)−N(1)	1.917(6)	C(2)−N(2A)	1.168(8)
C(1)−Fe(1)−P(1)	92.4(2)	C(1)−N(1)−Cu(1)	153.6(6)
C(2)−Fe(1)−P(1)	87.0(2)	C(2)−N(2A)−Cu(1A)	171.8(6)
N(1)−C(1)−Fe(1)	178.6(6)	N(1A)−Cu(1A)−N(2A)	109.2(3)
N(2A)−C(2)−Fe(1)	178.0(6)	P(2)−Cu(1)−N(1)	133.0(2)
Complex **11**			
Fe(1)−C(1)	1.96(2)	Cu(1)−P(3)	2.324(7)
Fe(1)−C(2)	1.87(2)	Cu(1)−P(4)	2.287(7)
Fe(2)−C(3)	1.92(2)	Cu(2)−P(5)	2.206(8)
Fe(2)−C(4)	2.03(2)	C(1)−N(1)	1.18(2)
Fe(1)−P(1)	2.174(6)	C(2)−N(2)	1.19(2)
Fe(2)−P(2)	2.177(7)	C(3)−N(3)	1.13(2)
Cu(1)−N(1)	1.986(18)	C(4)−N(4)	1.07(2)
Cu(1)−N(3)	2.062(19)		
Cu(2)−N(2)	1.949(18)		
Cu(2)−N(4)	1.901(17)		
C(1)−Fe(1)−P(1)	90.9(6)	C(3)−N(3)−Cu(1)	175.0(19)
N(1)−C(1)−Fe(1)	178(2)	C(4)−N(4)−Cu(2)	164(2)
N(2)−C(2)−Fe(1)	173.9(18)	N(1)−Cu(1)−N(3)	100.4(7)
N(3)−C(3)−Fe(2)	177(2)	N(2)−Cu(2)−N(4)	105.0(8)
N(4)−C(4)−Fe(2)	177(2)	N(2)−Cu(2)−P(5)	123.3(5)
C(1)−N(1)−Cu(1)	159.3(18)	N(1)−Cu(1)−P(3)	100.8(5)
C(2)−N(2)−Cu(2)	163.9(16)	P(3)−Cu(1)−P(4)	127.3(3)

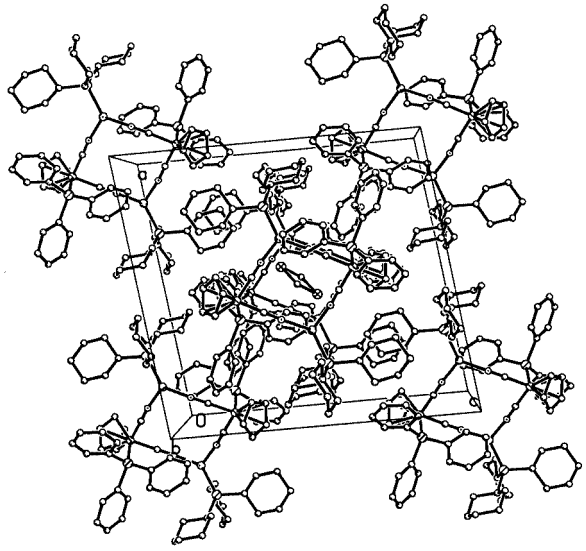

Figure 8. Crystal packing diagram of $[CpFe(PPh_3)(\mu\text{-}CN)_2CuPCy_3]_2$ (**9**), where the dichloromethane molecule is disordered

results in the inclusion of dichloromethane solvent molecules.

Utilization of two anionic $CpFe(CN)_2$ units bridged by diphosphanes containing three or four methylene linkers should afford particularly stable metallacycle derivatives with a second metal center as a result of the chelate effect. In a similar manner to the procedure employed in the synthesis of complex **9**, the iron cyanide salts (complexes **5** and **6**) were treated with $Cu(CH_3CN)_4(BF_4)$ in the presence of 2 equiv. of Cy_3P. The resulting mixed-metal cyanides **11** (dppp) and **12** (dppb) are soluble in dichloromethane, and as expected for bridging CN ligands, exhibit ν(CN) vibrational modes shifted to higher frequencies compared to the parent salts (see Table 1 and Table 3). The ^{31}P NMR spectra of both **11** and **12** display two broadened PCy_3 peaks indicative of two different phosphorus environments, with a single sharp signal for the iron-bound phosphorus atoms. The broadened phosphorus resonances for the PCy_3 ligands bound to Cu^I result from quadrupolar broadening i.e., for ^{63}Cu and ^{65}Cu, $I = 3/2$. Hence, spectroscopic data (IR and ^{13}P NMR) suggest the derivatives have similar structures.

Single crystals of **11** were grown by slow concentration of a concentrated hexanes solution of **11** over several days at ambient temperature, and were subjected to X-ray diffraction analysis. A thermal ellipsoid representation of complex **11** is shown in Figure 9, with selected bond lengths and angles given in Table 4. The crystal structure of **11** shows the familiar diamond-shaped motif with the bound phosphanes bridging the iron(II) centers. This phosphane-bridged form of the mixed-metal dimer forces both iron-bound phosphane ligands to be positioned on the same face

 © 2003 Wiley-VCH Verlag GmbH & Co. KGaA, Weinheim

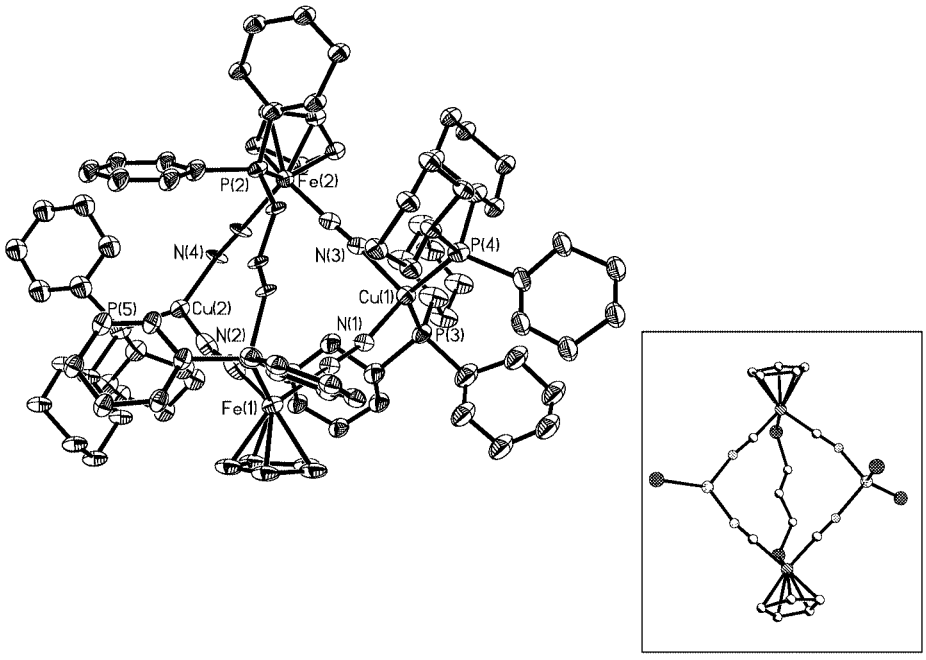

Figure 9. Thermal ellipsoid representation (drawn with 30% probability) of $Cu(PCy_3)[CpFe(\mu\text{-}CN)_2]_2Cu(PCy_3)_2$-μ-dppp (**11**); insert illustrates a ball-and-stick drawing of **11** where the substituents on the phosphane ligands are removed for clarity

of the metallacycle, with the two Fe−P distances being statistically equivalent at 2.174(6) and 2.177(7) Å. Interestingly, the basket shaped complex **11** crystallized with two PCy_3 ligands bonded to one Cu^I center, and one PCy_3 ligand attached to the other Cu^I center. This results in tetrahedral and trigonal-planar coordination geometries for the two copper centers, respectively. In addition to the differences in coordination geometries, the CN−Cu distances are shorter for Cu(2) as compared with Cu(1), i.e., the average CN−Cu(2) distance is 1.925(17) Å vs. the average CN−Cu(1) distance of 2.024(18) Å. This can be explained based on the higher Lewis acidity of Cu(2) resulting from fewer electron-donating PCy_3 ligands occupying its coordination sphere. The same effect is noted in the shorter Cu(2)−P(5) bond of 2.206(8) Å, as compared to the average Cu(1)−P bond length of 2.306(7)Å.

Unlike the $[Fe_2(CN)_4Cu_2]$ derivative containing a monodentate phosphane ligand bound to iron(II), as in complex **9**, complex **11** possesses *no* void channels for encompassing solvent molecules. This is best illustrated in their respective space-filling models depicted in Figure 10.

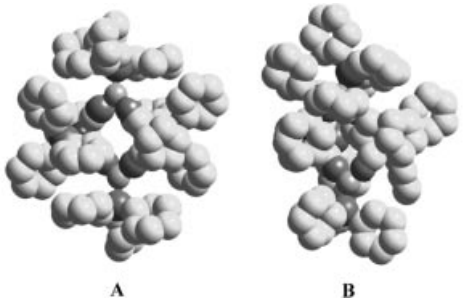

Figure 10. Space-filling model of: (A) $[CpFe(PPh_3)(\mu\text{-}CN)_2Cu(PCy_3)]_2$ (**9**) and (B) $Cu(PCy_3)[CpFe(\mu\text{-}CN)_2]_2Cu(PCy_3)_2$-μ-dppp (**11**)

Concluding Remarks

In summary, we have reported the syntheses and structures of several phosphane-substituted $CpFe(CN)_2$ salts obtained by photochemical decarbonylation of $KCpFe(CN)_2CO$ in methanol. The anions of these salts, which offer the opportunity for variation in steric and electronic modifications, were shown to serve as uninegative bridging ligands towards copper(I) centers. Unique among these derivatives was the preparation and characterization of the diphosphane-bridged iron species, $CpFe(CN)_2PPh_2-(CH_2)_n-PPh_2Fe(CN)_2Cp^{2-}$ ($n = 2-4$). These latter anions were shown to act as pincers to encapsulate (phosphane)copper(I) complexes, thereby leading to very stable diamond-shaped, two-dimensional $[Fe_2(CN)_4Cu_2]$, mixed-metal derivatives. These bridged (phosphane)metal anions may also serve to bind a variety of $M^{II}X^+$ or $M^{III}X_2^+$ ions in an analogous manner.[17]

Experimental Section

Methods and Materials: All manipulations were carried out using standard Schlenk techniques under argon unless otherwise stated. THF and hexane were dried by refluxing in the presence of sodium/benzophenone and distillation prior to use. Methanol was dried by distillation from magnesium turnings and iodine. Acetonitrile was dried by successive distillation from CaH_2 and P_2O_5. 1-Propanol was dried with molecular sieves and degassed by argon purge prior to use. All phosphanes were purchased from Strem Chemicals, ex-

 © 2003 Wiley-VCH Verlag GmbH & Co. KGaA, Weinheim

cept for triphenylphosphane, which was purchased from Aldrich. Copper(I) oxide and nitrosyl tetrafluoroborate were obtained from Aldrich and Lancaster, respectively. $KCpFe(CN)_2(CO)$ was prepared by applying published procedures.[13,18] Unless otherwise stated, all photolysis reactions were performed using a mercury-arc 450-W UV immersion lamp purchased from Hanovia. The 200-mL water-cooled photolysis vessel was purchased from Ace Glass. CpFe(dppe)CN was synthesized according to the procedure described by Vahrenkamp and co-workers.[5] Copper tetrafluoroborate was prepared as described previously.[19]

Physical Measurements: All vibrational studies were carried out with a Mattson 6021 FTIR spectrometer, using a 0.1-mm CaF_2 sealed cell. ^1H and ^{31}P NMR were recorded with a 300-MHz Varian Unity Plus spectrometer (121.4 MHz, ^{31}P), with methanol as the solvent unless otherwise stated. Deuterated water was used as the lock solvent, and all spectra were referenced to an 85% phosphoric acid solution.

Synthesis of $KCpFe(CN)_2(PPh_3)$ (1): 100 mL of a 1:1 mixture of acetonitrile/methanol was added to $KCpFe(CN)_2(CO)$ (4.2 mmol, 1.0 g) and PPh_3 (4.2 mmol, 1.1 g) in a photolysis vessel. An argon purge was bubbled through the reaction slurry and the mixture was photolyzed for 2 h while monitoring the infrared spectra in the ν(CN) region at 30-min intervals to ensure complete replacement of CO. The crude orange product precipitated from the solution and the solvent was removed under vacuum. The isolated product was dissolved in 1-propanol and filtered through a frit containing Celite. The solvent was once again removed under vacuum, and the solid washed with pentane to give **1** in 88% yield (1.7 g). Single crystals of **1** were obtained by slow concentration of a methanol solution of **1** at room temperature over several days. $C_{25}H_{20}FeKN_2P{\cdot}CH_3CN$ (515.3): calcd. C 62.92, H 4.50, N 8.15; found C 62.54, H 4.67, N 8.03.

Synthesis of $KCpFe(CN)_2(PPh_2Me)$ (2): 100 mL of methanol was added to $KCpFe(CN)_2(CO)$ (1.0 mmol, 0.25 g) and PPh_2Me (1.0 mmol, 0.21 g) in a photolysis vessel and the solution was photolyzed with IR monitoring as described for the preparation of **1**. The reaction solution was concentrated to dryness under vacuum to yield an orange powder. The solid product was washed repeatedly with hexane and dried to provide **2** in a 70% yield (0.31 g). $C_{20}H_{18}FeKN_2P{\cdot}CH_3OH$ (444.3): calcd. C 56.77, H 4.99, N 6.30; found C 55.97, H 5.08, N 6.52.

Synthesis of $CpFe(CN)(PPh_2Me)_2$ (3): Photolysis of $KCpFe(CN)_2CO$ (1.8 mmol, 0.45 g) and PPh_2Me (7.4 mmol, 1.5 g) in 100 mL of methanol was carried out in a photolysis vessel under argon. Upon reaction completion, ca. 30 min as revealed by infrared spectroscopy in the ν(CO) region, the solution was concentrated to dryness under vacuum and the product was dissolved in hexane. The solution was filtered through a glass frit containing Celite to remove any remaining impurities and the product, complex **3**, was isolated upon removing the solvent under vacuum in a yield of 56% (0.52 g). Single crystals of **3** were grown by slow concentration of a hexane solution at ambient temperature. $C_{32}H_{31}FeNP$ (516.4): calcd. C 70.21, H 5.71; found C 69.92, H 5.86.

Synthesis of $[KCpFe(CN)_2]_2$-μ-$[Ph_2P-(CH_2)_n-PPh_2]$ [n = 2 (4), n = 3 (5), n = 4 (6), C≡C instead $(CH_2)_n$ (7)]: These four derivatives were prepared in a similar manner by photolysis of $KCpFe(CN)_2CO$ and the diphosphanes in a 1:1 mixture of acetonitrile/methanol over a 60-min reaction period in a photolysis vessel. After the photolysis, the reaction solution was concentrated to dryness under vacuum to produce an orange solid product. The crude product was dissolved in 1-propanol and filtered through a frit containing Celite. Subsequent to removal of solvent, the product was washed repeatedly with hexane and dried under vacuum. Specifics of reactions: $KCpFe(CN)_2CO$ (4.2 mmol, 1.0 g) and dppe (1.0 mmol, 0.40 g) provided **4** in an 85% yield (0.70 g). X-ray quality crystals were grown by slow concentration of a solution of **4** in methanol at ambient temperature over several weeks. $C_{40}H_{34}Fe_2K_2N_4P_2{\cdot}6CH_3OH$ (1014.5): calcd. C 54.44, H 5.76; found C 55.01, H 5.52. $KCpFe(CN)_2CO$ (4.6 mmol, 1.1 g) and dppp (1.6 mmol, 0.64 g) provided **5** in an 81% yield (1.08 g). Single crystals of **5** were grown as described for compound **4**. $C_{41}H_{36}Fe_2K_2N_4P_2{\cdot}6CH_3OH$ (1028.5): calcd. C 54.87, H 5.88, N 5.45; found C 55.10, H 5.55, N 5.70. $KCpFe(CN)_2(CO)$ (1.6 mmol, 0.40 g) and dppb (0.70 mmol, 0.30 g)provided **6** in a 61% yield (0.36 g). Single crystals of **6** were grown by vapor diffusion of hexane into a THF solution of **6** maintained at 10° for approximately one week. $C_{42}H_{38}Fe_2K_2N_4P_2{\cdot}2THF{\cdot}2H_2O{\cdot}CH_3OH$ (1062.6): calcd. C 58.51, H 5.97; found C 58.97, H 5.62. $KCpFe(CN)_2CO$ (3.1 mmol, 0.75 g) and dppa (1.0 mmol, 0.41 g) provided **7** in an 82% yield (0.67 g).

Synthesis of $[CpFe(PPh_3)(\mu\text{-}CN)_2Cu(CH_3CN)_2]_2$ (8): A solution of $Cu(CH_3CN)_4(BF_4)$ (0.08 g, 0.25 mmol) in 15 mL of CH_3CN was transferred via cannula to a Schlenk flask containing $KCpFe(CN)_2PPh_3$ (0.12 g, 0.25 mmol) in 10 mL of CH_3CN. The reaction mixture was stirred at ambient temperature for 1 h to afford a yellow precipitate. Upon removal of the solvent under vacuum a fine yellow powder was isolated. Among common organic solvents, only pyridine was found to solubilize the yellow solid product.

Synthesis of $[CpFe(PPh_3)(\mu\text{-}CN)_2Cu(PCy_3)]_2$ (9): $Cu(CH_3CN)_4(BF_4)$ (0.06 g, 0.19 mmol) in 15 mL of CH_3CN was transferred via cannula to a Schlenk flask containing 0.054 g (0.19 mmol) of PCy_3 in 10 mL of CH_3CN, and the solution was stirred at ambient temperature for 1 h prior to adding 0.091 g (0.19 mmol) of $KCpFe(CN)_2PPh_3$ in CH_3CN. The reaction mixture was stirred for an additional hour during which time a turbid yellow solution was observed. The solvent was removed under vacuum and the product was redissolved in dichloromethane, leaving behind a white precipitate of KBF_4 which was removed by filtration through a frit containing Celite. Evaporation of the solvent from the filtrate yielded a fine yellow powder in a yield of 62% (0.092 g). Single crystals of **9** were grown by vapor diffusion of CH_2Cl_2/hexane at 10 °C over a period of one week. $C_{86}H_{106}Cu_2Fe_2N_4P_4{\cdot}CH_2Cl_2$ (1651.1): calcd. C 63.58, H 6.62, N 3.41; found C 62.98, H 6.54, N 3.29.

Synthesis of $[CpFe(\mu\text{-}CN)_2Cu(CH_3CN)_2]_2$-μ-dppp (10): A solution of 0.1 g (0.32 mmol) of $Cu(CH_3CN)_4(BF_4)$ in 15 mL of CH_3CN was transferred via a cannula to a flask containing 0.133 g (0.16 mmol) of $[KCpFe(CN)_2]_2$-μ-dppp in 10 mL of CH_3CN. The solution was stirred at room temperature for 1.5 h to yield a yellow precipitate. The solvent was evaporated under vacuum to give a fine yellow powder. Among common organic solvents, only pyridine was found to solubilize the precipitate.

Synthesis of $Cu(PCy_3)[CpFe(\mu\text{-}CN)_2]_2Cu(PCy_3)_2$-μ-dppp (11): $Cu(CH_3CN)_4(BF_4)$ (0.03 g, 0.1 mmol) in acetonitrile (15 mL) was added via cannula to a Schlenk flask containing PCy_3 (0.054 g, 0.2 mmol). The solution was stirred at room temperature for 1 h. The mixture was transferred via cannula to a second flask containing $[KCpFe(CN)_2]_2$-μ-dppp (0.04 g, 0.05 mmol) in CH_3CN (10 mL), and the reaction mixture was stirred at room temperature for 1.5 h to afford a turbid yellow solution. The solvent was removed under vacuum and the product dissolved in dichlorometh-

 © 2003 Wiley-VCH Verlag GmbH & Co. KGaA, Weinheim

Table 5. X-ray crystallographic data for $KCpFe(CN)_2(PPh_3)$ (**1**), $CpFe(PPh_2Me)_2(CN)$ (**3**), $[KCpFe(CN)_2]_2\mu$-dppe (**4**), $[KCpFe(CN)_2]_2\mu$-dppb (**6**), $[CpFe(PPh_3)(\mu\text{-}CN)_2Cu(PCy_3)]_2$ (**9**), and $Cu(PCy_3)[CpFe(\mu\text{-}CN)_2]_2Cu(PCy_3)_2$-μ-dppp (**11**)

	1	**3**	**4**	**6**	**9**	**11**
Empirical formula	$C_{25}H_{20}FeKN_2P\cdot CH_3CN$	$C_{32}H_{31}FeNP_2\cdot H_2O$	$C_{40}H_{34}Fe_2K_2N_4P_2\cdot 6CH_3OH$	$C_{42}H_{38}Fe_2K_2N_4P_2\cdot 2THF\cdot 2H_2O\cdot CH_3OH$	$C_{86}H_{106}Cu_2Fe_2N_4P_4\cdot CH_2Cl_2$	$C_{105}H_{159}Cu_2Fe_2N_4P_5$
Formula mass [g/mol]	515.40	563.37	1002.71	1061.88	1643.4	1870.99
Crystal system	triclinic	monoclinic	triclinic	monoclinic	monoclinic	triclinic
Space group	$P\bar{1}$	$P2_1/c$	$P\bar{1}$	$P2_1/c$	$P2_1/n$	$P\bar{1}$
Z·	2	4	2	4	4	2
a [Å]	7.962(2)	9.959(2)	12.302(3)	14.4418(9)	17.248(3)	12.925(13)
b [Å]	9.180(2)	14.458(3)	13.550(3)	34.147(2)	12.686(2)	17.871(18)
c [Å]	17.425(4)	19.892(4)	16.119(3)	10.2584(6)	18.556(4)	23.75(2)
α [°]	92.230(4)	90	92.873(4)	90	90	98.23(2)
β [°]	97.864(4)	102.344(4)	94.038(4)	94.7500(10)	96.929(4)	101.62(2)
γ [°]	113.721(4)	90	115.227(4)	90	90	104.79(2)
Volume [Å^3]	1148.8(5)	2798.0(10)	2415.0(9)	5041.5(5)	4030.7(14)	5086(9)
$d_{calcd.}$ [g/cm^3]	1.490	1.337	1.379	1.399	1.354	1.222
Temperature [K]	110(2)	110(2)	110(2)	110(2)	110(2)	110(2)
Wavelength [Å]	0.71073	0.71073	0.71073	0.71073	0.71073	0.71073
Abs. coeff. [mm^{-1}]	0.929	0.679	–	0.854	1.066	0.817
Goodness of fit on F^2	0.867	0.801	0.757	0.899	0.599	0.662
R[a] (%)	6.28	4.59	8.60	7.18	6.69	10.37
(%)						
R_w[b] (%)	16.46	10.01	19.25	18.47	18.66	50.41

[a] $R = \Sigma|F_o| - |F_c|/\Sigma|F_o|$. [b] $Rw = \{[\Sigma w(F_o^2 - F_c^2)^2]/[\Sigma w(F_o^2)^2]\}^{1/2}$.

ane. The salt by-product was removed by filtration through Celite, and the solvent evaporated to give a yellow powder of **11** in a yield of 54% (0.050 g). Crystals suitable for X-ray diffraction studies were obtained from hexanes by slow concentration at ambient temperature over several days. $C_{105}H_{159}Cu_2Fe_2N_4P_5$ (1871.2): calcd. C 67.40, H 8.57, N 2.99; found C 66.92, H 8.43, N 3.05.

Synthesis of $Cu(PCy_3)[CpFe(\mu\text{-}CN)_2]_2Cu(PCy_3)_2$-μ-dppb (12): $Cu(CH_3CN)_4(BF_4)$ (0.022 g, 0.07 mmol) in 15 mL of CH_3CN was transferred via cannula to a Schlenk flask containing PCy_3 (0.04 g, 0.14 mmol) in 10 mL of CH_3CN. The reaction mixture was stirred at room temperature for 1 h and transferred to a second flask containing 0.03 g (0.035 mmol) of $[KCpFe(CN)_2]_2$-μ-dppb in 10 mL of CH_3CN. The solution was stirred for 1.5 h to give a turbid yellow solution. Upon removal of the CH_3CN solvent under vacuum, the product was redissolved in dichloromethane and filtered through Celite to remove KBF_4. A yellow product of **12** was obtained in a yield of 39% (0.026 g) following the evaporation of solvent and was recrystallized from hexanes by slow concentration at ambient temperature. $C_{106}H_{161}Cu_2Fe_2N_4P_5$ (1885.2): calcd. C 67.54, H 8.61; found C 68.05, H 8.48.

X-ray Crystallography: Orange single crystals of compounds **1**, **3**, **4**, **6**, and CpFe(CN)(dppe), and yellow crystals of **9** and **11** were coated with paratone and mounted on a glass fiber using apiezon grease at ambient temperature. The crystals were placed on a Bruker SMART 1000 diffractometer equipped with a CCD detector. The crystals were placed in a nitrogen cold stream maintained at 110 K. More than a hemisphere of data was collected on each crystal over three batches of exposures using Mo-K_α radiation (λ = 0.71073 Å). A fourth set of data was measured and compared to the initial set to monitor and correct for decay, which was negligible in all cases. Details of crystal data for all compounds examined are found in Table 5. Systematic absences and intensity statistics were used in space-group determination. All structures were solved by direct methods. Anisotropic structure refinements were achieved using full-matrix least-squares techniques on all non-hydrogen atoms. All hydrogen atoms were placed in idealized positions based on hybridization, with isotropic thermal parameters fixed at 1.2 or 1.5 times the value of the attached atom. All atom scattering factors were obtained from the *International Tables for X-ray Crystallography*, vol. C. For all compounds, data collection and cell refinement, SMART;[20] data reduction, SAINTPLUS (Bruker[21]); programs used to solve structures, SHELXS-86 (Sheldrick[22]); programs used to refine structures, SHELXL-97 (Sheldrick[23]); molecular graphics and to prepare material for publication, SHLXTL-Plus version 5.0 (Bruker[24]). CCDC-211280 (**1**), -211281 (**3**), -211282 (**4**), -211283 (**6**), -211284 (**9**), -211285 (**11**) and -213786 [CpFe(CN)dppe] contain the supplementary crystallographic data for this paper. These data can be obtained free of charge at www.ccdc.cam.ac.uk/conts/retrieving.html [or from the Cambridge Crystallographic Data Centre, 12 Union Road, Cambridge CB2 1EZ, UK; Fax: (internat.) + 44-1223/336-033; E-mail: deposit@ccdc.cam.ac.uk].

Acknowledgments

Financial support from the National Science Foundation (CHE 99-10342 and CHE 02-34860), and CHE 98-07975 for purchase of X-ray equipment, the Robert A. Welch Foundation, and by the Texas Advanced Research Technology Program (Grant No. 0390-1999) is greatly appreciated.

[1] K. R. Dunbar, R. A. Heitz, *Prog. Inorg. Chem.* **1997**, *45*, 283–391.
[2] A. M. Golub, H. Kohler, V. V. Skopenko (Eds.), *Chemistry of Pseudohalides*, Elsevier, New York, **1986**, pp. 142–160.
[3] K. K. Klausmeyer, T. B. Rauchfuss, S. R. Wilson, *Angew. Chem. Int. Ed.* **1998**, *37*, 1694–1696.
[4] D. L. Reger, *Inorg. Chem.* **1975**, *14*, 660–664.

 © 2003 Wiley-VCH Verlag GmbH & Co. KGaA, Weinheim

[5] G. N. Richardson, U. Brand, H. Vahrenkamp, *Inorg. Chem.* **1999**, *38*, 3070−3079.
[6] G. N. Richardson, H. Vahrenkamp, *J. Organomet. Chem.* **2000**, *597*, 38−41.
[7] See: D. J. Darensbourg, J. C. Yarbrough, C. Ortiz, C. C. Fang, *J. Am. Chem. Soc.* **2003**, *125*, 7586−7591 and references cited therein.
[8] W. J. Kruper, Jr., D. J. Swart, U. S. Patent 4,500,704, **1985**.
[9] D. J. Darensbourg, W.-Z. Lee, M. J. Adams, J. C. Yarbrough, *Eur. J. Inorg. Chem.* **2001**, 2811−2822.
[10] C. A. Tolman, *Chem. Rev.* **1977**, *77*, 313−348.
[11] M. M. Rahman, H. Y. Liu, A. Prock, W. P. Giering, *Organometallics* **1987**, *6*, 650−658.
[12] T. L. Brown, *Inorg. Chem.* **1992**, *31*, 1286−1294.
[13] C.-H. Lai, W.-Z. Lee, M. L. Miller, J. H. Reibenspies, D. J. Darensbourg, M. Y. Darensbourg, *J. Am. Chem. Soc.* **1998**, *120*, 10103−10114.
[14] D. J. Darensbourg, J. H. Reibenspies, C.-H. Lai, W.-Z. Lee, M. Y. Darensbourg, *J. Am. Chem. Soc.* **1997**, *119*, 7903−7904.
[15] Crystal for CpFe(CN)(dppe)·CH_2Cl_2: $C_{33}H_{31}C_{12}FeNP_2$ (630.28), monoclinic, $P2_1/n$, a = 12.842(2), b = 8.8075(16), c = 25.732(5) Å, β = 90.824(4)°, V = 2910.2(9) Å^3, Z = 4, $\rho_{calcd.}$ = 1.439 Mg/m^3, Mo-K_α radiation, λ = 0.71073 Å, T = 293(2) K, 17540 measured reflections, 6613 unique, μ = 0.836 mm^{-1}, $R1$ [$I > 2\sigma(I)$] = 0.0623, $wR2$ = 0.1341, GOF = 0.882, no. of parameters = 352.
[16] D. J. Darensbourg, W.-Z. Lee, M. J. Adams, D. L. Larkins, J. H. Reibenspies, *Inorg. Chem.* **1999**, *38*, 1378−1379.
[17] D. J. Darensbourg, M. J. Adams, J. C. Yarbrough, *Inorg. Chem.* **2001**, *40*, 6543−6544.
[18] C. E. Coffey, *J. Inorg. Nucl. Chem.* **1963**, *25*, 179−185.
[19] G. J. Kubas, *Inorg. Synth.* **1979**, *19*, 90−92.
[20] *SMART 1000 CCD*, Bruker Analytical X-ray Systems, Madison, WI, USA, **1999**.
[21] *SAINT-Plus*, version 6.02, Bruker, Madison, WI, USA, **1999**.
[22] G. Sheldrick, *SHELXS-86, Program for Crystal Structure Solution*, Institut für Anorganische Chemie der Universität, Göttingen, Germany, **1986**.
[23] G. Sheldrick, *SHELXL-97, Program for Crystal Structure Refinement*, Institut für Anorganische Chemie der Universität, Göttingen, Germany, **1997**.
[24] *SHELXTL*, version 5.0, Bruker, Madison, WI, USA, **1999**.

Received May 21, 2003

 © 2003 Wiley-VCH Verlag GmbH & Co. KGaA, Weinheim

Self-Organization of Dipolar 4,4′-Disubstituted 2,2′-Bipyridine Metal Complexes into Luminescent Lamellar Liquid Crystals

Daniela Pucci,*[a] Giovanna Barberio,[a] Alessandra Crispini,[a] Oriano Francescangeli,[b] Mauro Ghedini,[a] and Massimo La Deda[a]

Keywords: N ligands / Platinum / Zinc / Nickel / Metallomesogens

Mononuclear *cis*-dichloro complexes, [L^nMCl_2], with different metal centres (Pt^{II}, Ni^{II}, and Zn^{II}) and a series of palladium and platinum derivatives, [L^2MX_2], in which chloride groups are replaced with iodide, bromide, and azide ligands, have been synthesized from 4,4′-disubstituted-2,2′-bipyridines. Upon complexation of these non-mesogenic ligands, the peculiar structural arrangement, characterized by intermolecular associations of the new derivatives, induces mesomorphism in most [L^2MX_2] complexes, confirming the importance of coordination chemistry in metal-mediated formation of liquid crystals. Single crystal X-ray structures have been determined for dihexadecyl 2,2′-bipyridyl-4,4′-dicarboxylatopalladium and -zinc dichloride derivatives. Both the metal centres and the ancillary ligands have been varied to use dipole coupling as a tool to control molecular architecture: thermal, as well as spectroscopic properties, depend strongly upon molecular dipolar interactions. Tunable red and blue emitters based on Pd^{II} and Pt^{II}, both in solution and in the solid state, have been obtained.

(© Wiley-VCH Verlag GmbH & Co. KGaA, 69451 Weinheim, Germany, 2003)

Introduction

"Unconventional" metallomesogens form a new class of liquid crystals that exhibit novel structural and physical properties and numerous strategies have recently been developed for their design. Coordination chemistry has received increasing attention as a metal ion can induce mesomorphism in non-mesomorphic ligands.[1,2]

This phenomenon can be achieved through changes of molecular conformation, shape and structure induced both by complexation[3−6] and association phenomena of different natures, giving rise to supramolecular assemblies.[7−9] We are particularly interested in the so-called complementary shape approach, which is usually adopted to promote columnar mesophases, and we have looked at obtaining novel superstructures in calamitic mesophases by utilising attractive dimeric associations of small molecules with a large central dipole moment. 2,2′-Bipyridines are very attractive ligands because of their extensive coordination chemistry and their versatility: their spectroscopic and chemical properties can be tuned by the choice of metal centre and substituents.[10−14]

We recently reported the synthesis of a new family of non-mesomorphic dialkyl-2,2′-bipyridine-4,4′-dicarboxylates, L^n; the induction of a dipole moment, upon coordination with a $PdCl_2$ moiety, resulted in self-assembling dimers of metallomesogenic [L^nPdCl_2] species **I**−**III**, confirming the role of coordination chemistry in the metal-mediated formation of liquid crystals.[15]

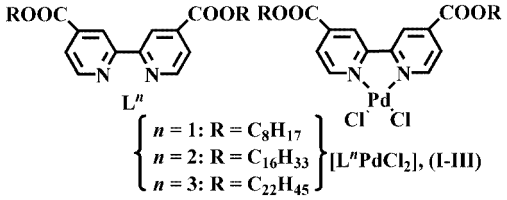

Here we report the crystal structure characterization of the [L^2PdCl_2] (**II**) derivative. The head-to-tail arrangement of the single molecules of this class of complexes is confirmed and the packing and Pd···Pd intermolecular separation within the dimer and between dimers is discussed.

Liquid crystal displays (LCDs), which currently dominate flat panel technology, have severe limitations in brightness and energy efficiency due to the use of absorbing polarizers and color filters which convert a major amount (more than 80%) of the incident light into thermal energy.[16] Photoluminescent materials that act as "active" color filters and, therefore, might enhance the visual performance of LCDs.[17] Although luminescent platinum(II) complexes have attracted much attention recently as possible sen-

[a] LASCAMM, Unità INSTM della Calabria, Dipartimento di Chimica, Università della Calabria, 87030 Arcavacata (CS), Italy
[b] Dipartimento di Fisica e Ingegneria dei Materiali e del Territorio and Istituto Nazionale per la Fisica della Materia, Università di Ancona, Via Brecce Bianche, 60131 Ancona, Italy

sors,[18] photochemical and electroluminescent devices,[19] there are few examples of emitters based on Pd^{II}.[20] Therefore, absorption and fluorescence measurements, in solution and in the condensed state, have been performed on the L^n ligands and the corresponding **I**−**III** palladium complexes. Moreover, to study systematically the effect of structural changes on the dipole moments, intermolecular stacking interactions and supramolecular arrangements, two new classes of the dialkyl 2,2′-bipyridine-4,4′-dicarboxylates metal derivatives have been prepared (**1**−**15**). This paper reports the synthesis and thermal and spectroscopic characterization of a family of *cis*-dichloro complexes $[L^nMCl_2]$ where M is Pt^{II}, Ni^{II}, and Zn^{II}. The crystal structure determination of $[L^2ZnCl_2]$ is also reported. In addition, a series of dihexadecyl 2,2′-bipyridyl-4,4′-dicarboxylate palladium and platinum derivatives $[L^2MX_2]$, in which the chlorine groups are replaced with iodide, bromide, and azide ligands, have also been prepared. Several novel complexes with potential applications as blue and red metallomesogens emitters have been obtained and the correlations between the self-assembling properties of these complexes and their photophysical properties are discussed.

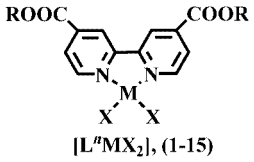

$[L^nMX_2]$, (1-15)

Results and Discussion

Single-Crystal X-ray Diffraction for $[L^2PdCl_2]$ (II·2CHCl$_3$) and $[L^2ZnCl_2]$ (8) Complexes

The structure of **II**·2CHCl$_3$ is shown in Figure 1 and the bond lengths and angles are listed in Table 1.

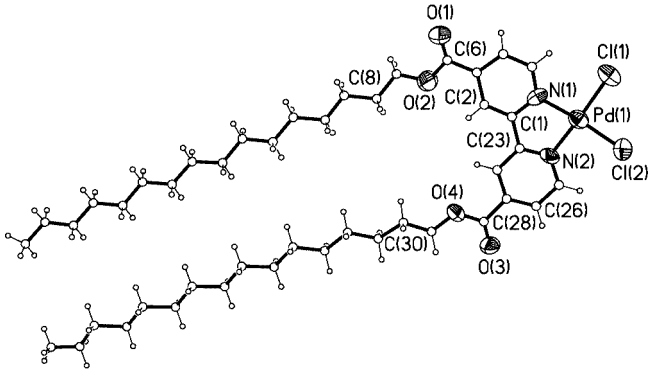

Figure 1. Molecular structure and atomic labeling scheme (50% probability thermal ellipsoids) of complex **II**·2CHCl$_3$

There are two cocrystallized chloroform molecules per complex molecule in the asymmetric unit. The Pd atom has a distorted square-planar geometry with a bite angle N(1)−Pd−N(2) of 81.6(4)°. The bond lengths and angles within the five-membered chelate ring agree well with those reported for other dichlorine palladium(II) species and various substituted 2,2′-bipyridine complexes.[21]

Table 1. Selected bond lengths [Å] and angles [°] for complex **II**·2CHCl$_3$

Pd(1)−N(1)	2.016(10)	Pd(1)−N(2)	2.041(10)
Pd(1)−Cl(1)	2.291(4)	Pd(1)−Cl(2)	2.281(4)
N(1)−Pd(1)−N(2)	81.6(4)	Cl(1)−Pd(1)−Cl(2)	90.7(2)
N(1)−Pd(1)−Cl(1)	95.3(4)	N(1)−Pd(1)−Cl(2)	86.4(2)
N(2)−Pd(1)−Cl(1)	176.8(4)	N(2)−Pd(1)−Cl(2)	92.4(4)

The five-membered chelate ring is essentially planar with a maximum deviation from planarity of 0.03(1) Å [C(1)]. The carboxylic oxygen atoms O(1) and O(3) of the dihexadecyl 2,2′-bipyridine-4,4′-dicarboxylate ligands point in opposite directions, with torsion angles C(2)−C(3)−C(6)−O(1) and C(24)−C(25)−C(28)−O(3) of 165 and 168°, respectively. Hence, the two carboxylic hydrocarbon chains are straight and parallel, and they both have a regular *anti* conformation, with mean torsion angles of 177(2) and 178(2)°, respectively.

The shortest Pd···Pd intermolecular separation of 3.487(2) Å was found between centrosymmetrically related molecules arranged in a head-to-tail fashion, which was approximately superimposed along the *a* axis (Figure 2, a).

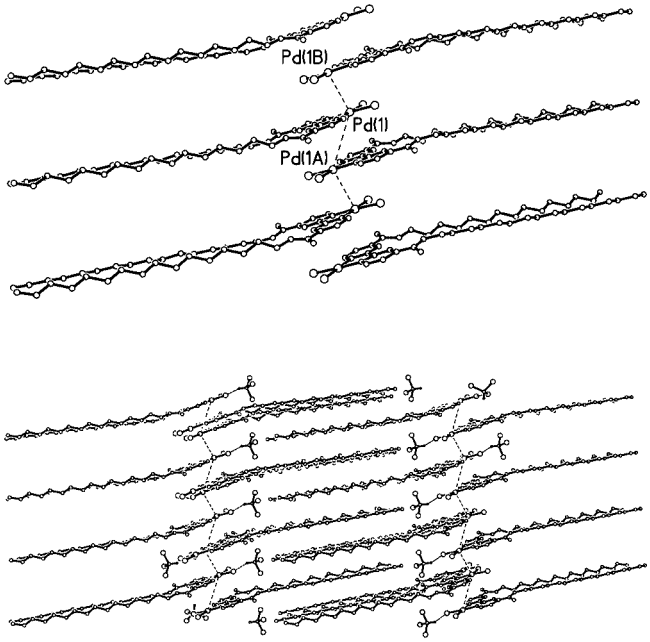

Figure 2. Ball and stick representation of the crystal packing of complex **II**·2CHCl$_3$ (b), viewed along the *b*-axis. Separate view (a) shows the alternating short and long Pd···Pd intermolecular contacts

This distance is similar to a polymorph of the (2,2′-bipyridine)dichloropalladium(II) complex (3.46 Å)[22] and is shorter than other similar complexes containing substituted 2,2′-bipyridine (found in the Cambridge Structural Database, CSD). Within the dimer the Pd···Pd vector deviates slightly from orthogonality to the coordination plane (9° angle with the plane normal), suggesting a very weak at-

 © 2003 Wiley-VCH Verlag GmbH & Co. KGaA, Weinheim

tractive character for the Pd···Pd interaction. The coordinated portions of the bipyridine ligands are oriented in opposing directions and thus no significant aromatic π−π stacking within the dimer was observed. In fact, the pyridine rings have interplanar and centroid-centroid distances of 3.44 and 5.91 Å, respectively, and interplanar and displacement angles of 0.4 and 126°, respectively, and a horizontal slip of 4.81 Å.

A second rather longer Pd···Pd separation of 4.778 Å was found between the dimers. The Pd···Pd contacts alternate along a zig-zag chain with an off-set of 1.78 Å [Pd(a)−Pd−Pd(b) 127.5(2)°]. The 3D-space complex **II**·2$CHCl_3$ gives rise to a layered structure (Figure 2, b), where the planar cores (representing the polar, or at least polarizable, part of the molecule), superimposed along one direction, alternate with non-polar chains, confined to a non-polar region. The degree of interdigitation within the paraffinic sublayer is not as high as expected from the segregation effects of the alkyl chains, due to the chloroform molecules that fill the holes between the two sublayers. The resultant calculated interlayer spacing is 31.9 Å.

The overall structure of the analogous complex containing Zn^{II}, **8**, is completely different from the palladium one (Figure 3). As with [Zn(bipy)Cl_2][23] and [Zn(phen)Cl_2],[24] complex **8** is tetrahedral. Bond lengths and angles are listed in Table 2. The neutral complex has a C_2 symmetry axis passing through the zinc ion and the midpoint of the bipyridine ligand.

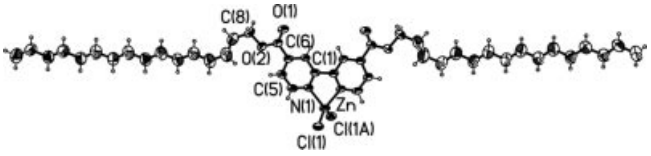

Figure 3. Molecular structure and atomic labeling scheme (50% probability thermal ellipsoids) of complex **8**

Table 2. Selected bond lengths [Å] and angles [°] for complex **8**

Zn−N(1)	2.064(3)	Zn−Cl(1)	2.211(1)
N(1)−Zn−N(1a)	79.5(2)	Cl(1)−Zn−Cl(1a)	123.1(1)
N(1)−Zn−Cl(1)	111.7(1)	N(1a)−Zn−Cl(1)	111.2(1)

The bond lengths and angles are similar to those for [Zn(bipy)Cl_2][23] and other Zn^{II} substituted 2,2′-bipyridine derivatives,[25] and [Zn(phen)Cl_2].[24] Because the zinc is tetrahedral, the $ZnCl_2$ moiety is not coplanar with the mean plane passing through the five-membered chelate ring. The dihedral angles Cl(1)−Zn−N(1)−C(1) and Cl(1a)−Zn−N(1)−C(1) are 107.9(3) and −110.3(3)°, respectively. The two carboxylic oxygen atoms O(1) and O(1a) point towards the internal part of the bipyridine ligand [torsion angle C(2)−C(3)−C(6)−O(1) 6.5(7)°].

Moreover, since O(2)−C(6)−C(7)−C(8) and C(8)−C(9)−C(10)−C(11) torsion angles are in a *gauche* conformation [54.6(7) and −85.2(8)°, respectively), the two carboxylic hydrocarbon chains run in opposite directions.

The dihedral geometry of the zinc ion prevented the formation of dimers in the crystal packing, as observed in the analogous complex **II**, and favour strong intermolecular contacts involving the bipyridine hydrogen atoms that are *ortho* and *meta* with respect to the $ZnCl_2$ moiety.

In fact, while H(4) participates in H···Cl contacts that are shorter than the sum of the van der Waals radii of hydrogen and chlorine atoms [Cl(1)···H(4b) = 2.863(1) Å, C(4b)−H(4b)···Cl(1) = 143.5(3)°, C(4b)···Cl(1) = 3.668(5) Å, b = x, 1 − y, z − 1/2), H(5) showed an hydrogen bond interaction with the carboxylic oxygen atom O(1) [O(1)···H(5c) = 2.424(3) Å, C(5c)−H(5c)···Cl(1) = 158.6(3)°, C(5c)···O(1) = 3.307(5) Å, c = x, 1 + y, z) (Figure 4, a).

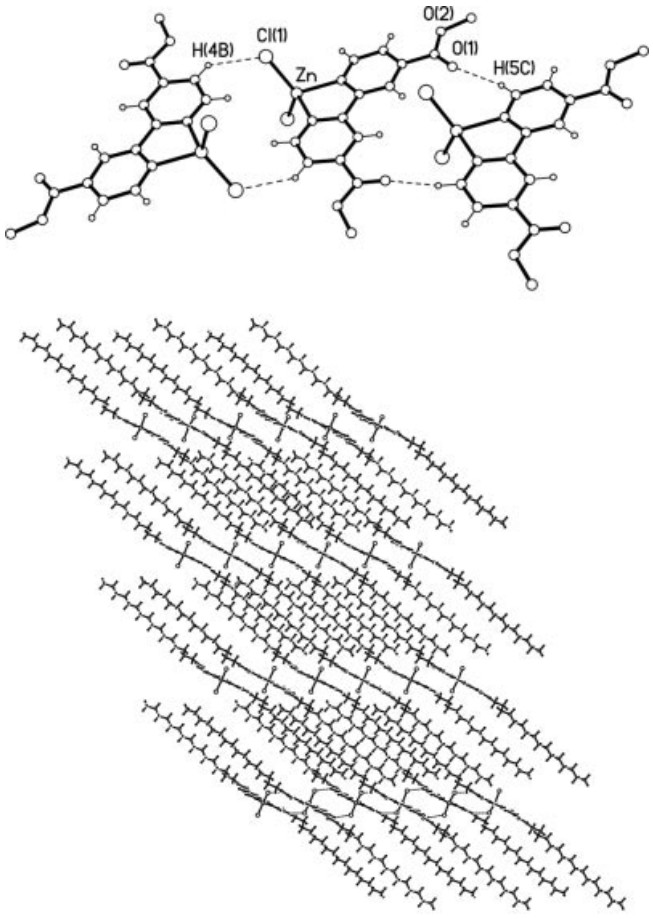

Figure 4. Ball and stick representation of the crystal packing of complex **8** (b), viewed along the *b* axis. Separate view (a) shows the C−H···X (X = Cl, O) intermolecular contacts within the *ac* plane

The crystal packing of **8** is characterized by a layered structure with a calculated interlayer spacing of 19.8 Å (Figure 4, b). Each carboxylic chain of a molecule of **8** is part of each paraffinic sub-layer, in which the segregation effects of the alkyl chains cause a high degree of interdigitation. The long molecular axis is tilted with respect to the layer normal by 56°.

 © 2003 Wiley-VCH Verlag GmbH & Co. KGaA, Weinheim

Synthesis

The [L^nMCl_2] complexes **1**−**9** were prepared by the reaction of an equimolar amount of the appropriate L^n ligands with [$Pt(PhCN)_2Cl_2$] (in toluene, under reflux), $NiCl_2$ (in ethanol, under reflux) or $ZnCl_2$ (in dichloromethane, at room temperature) (Scheme 1).

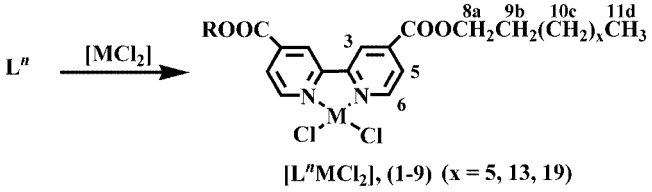

Scheme 1. Synthetic route to [L^nMCl_2] complexes **1**−**9** and related proton numbering scheme. *Reagents and conditions*: *i)* [MCl_2] = [$Pt(PhCN)_2Cl_2$], toluene, ΔT; *ii)* [MCl_2] = $NiCl_2$, ethanol, ΔT; *iii)* [MCl_2] = $ZnCl_2$, dichloromethane, room temp.

The dihexadecyl 2,2′-bipyridyl-4,4′-dicarboxylate palladium and platinum *cis*-dichloro complexes were transformed into the corresponding [L^2MX_2] derivatives by metathetical reactions with potassium iodide (**10**, **11**), potassium bromide (**12**, **13**), and sodium azide (**14**, **15**) (Scheme 2).

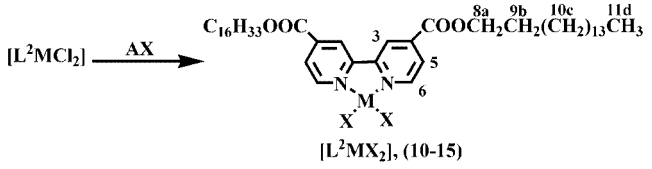

Scheme 2. Synthetic route to [L^2MX_2] complexes **10**−**15** and related proton numbering scheme. *Reagents and conditions*: *i)* AX = KI, acetone, room temp.; *ii)* AX = KBr, DMF, room temp.; *iii)* AX = NaN_3, acetone, room temp.

The structure and purity of all the compounds were confirmed using elemental analyses, IR and ^1H NMR spectroscopy, as reported in the Exp. Sect. For all of the investigated complexes, IR spectra showed ν(COO) absorptions for the carbonyls groups at higher wavenumbers (ca. 20 cm^{-1}) than for the free ligands. Moreover, the azide compounds **14** and **15** showed a strong band at 2043 and 2063 cm^{-1} respectively, due to the asymmetric N_3 stretching vibration, suggesting coordination of the ligand to the metal centre.[26] In the ^1H NMR spectra of the platinum and zinc [L^nMCl_2] complexes the resonance attributable to the $H^{6,6'}$ protons is low-field shifted by about 1 ppm with respect to the organic precursors. These observations confirm the coordination of bipyridines to the metal fragment. In the ^1H NMR spectra of the Ni^{II} complexes the signals are very broad, confirming the assumed distorted square-planar structure induced by the 4,4′ substituents of the bipyridine ligand. The few examples of crystal structures of dihalo disubstituted Ni^{II} complexes show a strong substituent effect on the geometry around the metal ion, with the promotion of distorted square-planar coordinations.[27−29]

Upon exposure to air, **4** and **5** are not stable as solids but gradually adsorbed water, as evidenced by the change from pale green to deep green, IR spectroscopy and elemental analysis.

The ^1H NMR resonance frequencies of the $H^{6,6'}$ protons of the palladium and platinum [L^2MX_2] complexes are very sensitive to the nature of the metal-bonded ancillary groups. This electronic effect of the ligand is seen for **10**−**13** where the $H^{6,6'}$ signal progressively moved downfield (Δδ of ca. 0.3 and 0.6 ppm for the bromo and iodo derivatives, respectively) as the electron-withdrawing power of the X-bridging ligand decreases. For complexes **14** and **15** the $H^{6,6'}$ proton resonances shifted upfield by ca. 0.7 ppm with respect to the homologous signals of the corresponding chloro precursors, as observed in related azido complexes of diimines.[14]

Liquid Crystalline Properties

[L^nMCl_2] Complexes

Although free 2,2′-bipyridine-4,4′-dicarboxylates (L^n) are not liquid crystals, most of their metal complexes [L^nMCl_2] show mesomorphism (investigated by polarized optical microscope and XRD); the phase diagram is shown in Figure 5. Thermal data, obtained using differential scanning calorimetry (DSC), are summarized in Table 3.

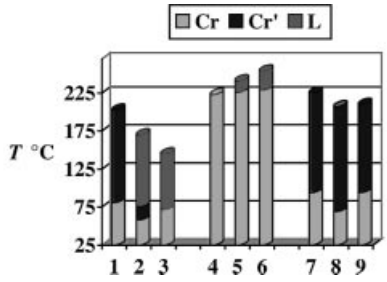

Figure 5. Bar graph showing the mesomorphic behaviour of [L^nMCl_2] (**1**−**9**) complexes

The *cis*-dichloro complexes with the shortest tail (R = C_8H_{16}) melted directly into an isotropic liquid at temperatures higher than for the corresponding free ligand, irrespective of the metal atoms.

The higher homologues of platinum, **2** and **3**, showed a mesophase with a mosaic-like texture (Figure 6), as observed in analogous palladium derivatives.[15]

As expected, the melting and clearing points decreased with aliphatic chain length, ranging from 16 to 22 carbon atoms, and, thus, complex **3** showed a more stable mesomorphism.

The X-ray diffraction (XRD) patterns of platinum complexes **2** and **3** in the mesophase were very similar to those of the analogous palladium complexes **II** and **III**.[15] The XRD pattern of **2** exhibits sharp inner reflections and diffuse outer halos that are consistent with a layered structure (Figure 7).

 © 2003 Wiley-VCH Verlag GmbH & Co. KGaA, Weinheim

Table 3. Optical and thermal properties of the [L^{n}MCl$_2$] (**1**−**9**) complexes

Complex	Transition[a]	T[°C]	ΔH[kJ·mol^{-1}]	d[Å]
	Cr − Cr′	80.9	3.8	22.3 (Cr)
1	Cr′ − I	202.35	11.4	23.3 (Cr′)
	I − Cr	201.7	11.0	
	Cr − Cr′	57.8	8.9	31.3 (Cr)
	Cr′ − L	76.0	5.4	34.3 (Cr′)
2	L − I	170.1	13.0	36.5 (L)
	I − L	172.0	12.9	
	L − Cr	59.4	5.3	
	Cr − Cr′	33.8	26.4	
	Cr − L	71.6	41.3	37.3 (Cr)
3	L − I	144.7	5.3	44.0 (L)
	I − L	138.5	5.8	
	L − Cr	64.9	39.8	
4	Cr − I	223.3 dec	11.3	
5	Cr − L	225.6	14.0	
	L − I	233.5	1.9	
6	Cr − L	229.3	15.4	
	L − I	251.4 dec	15.1	
	Cr − Cr′	94.0	4.4	
7	Cr′ − I	224.6	44.9	
	I − Cr	204.2	27.9	
	Cr − Cr′	68.9	37.4	
8	Cr′ − I	207.2	27.9	
	I − Cr′	195.8	36.2	
	Cr′ − Cr	64.4	37.1	
	Cr − Cr′	93.7	91.0	
9	Cr′ − I	210.0	12.7	
	I − Cr′	198.4	26.8	
	Cr′ − Cr	68.3	45.4	

[a] Cr: crystal; L: lamellar; I: isotropic liquid.

Figure 6. Polarized optical micrograph of the mosaic texture for complex **2** at 150 °C.

In fact, the inner reflections consist of a set of *00n* peaks centred at $q = 2\pi n/d$ ($q = 2\pi\sin\theta/\lambda$ is the modulus of the scattering vector, 2θ is the scattering angle), where n is an integer ($n = 1-4$) and $d = 36.7$ Å is the layer spacing. The wide diffuse outer halo centred about $q = 1.3$ Å^{-1} is associated with the short-range liquid-like positional ordering of the hydrocarbon chains. Moreover, two additional peaks appeared, corresponding to $d_1 = 10.5$ Å and $d_2 = 3.4$ Å, which arise from Pt−Pt in-plane correlations along mutually-orthogonal directions which are parallel and orthogonal, respectively, to the long side of the molecular core (i.e. the axis of the benzene rings). This type of XRD pattern is consistent with an ordered smectic phase with one-dimensional ordering of the molecules within the layers as well as a lamello-columnar mesophase without positional correlation between the layers. Because the spacing of the layers in this compound is larger than the calculated molecular length in the fully extended configuration ($L \approx 28$ Å), but smaller than $2L$ ($d/L \approx 1.3$), if we assume that the arrangement is of a smectic type, the molecules are not arranged in single molecular layers but organized in semi-bilayers that are partially interdigitated, giving rise to a bilayered SmA$_d$ phase.[30] Here the semi-bilayer ordering is caused by dipole−dipole interactions and antiparallel correlations of nearest neighbour molecules, characterised by short intermetallic M···M distances (Figure 8).

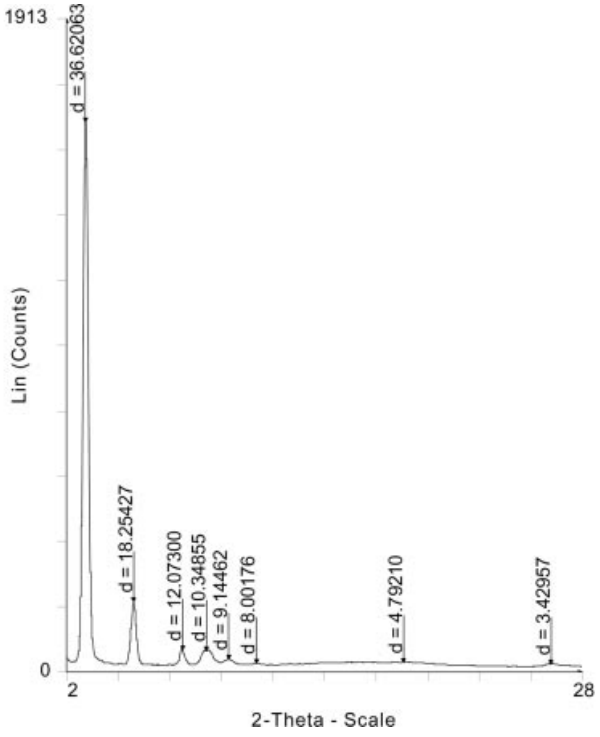

Figure 7. XRD pattern of the smectic phase of complex **2** recorded at $T = 140$ °C

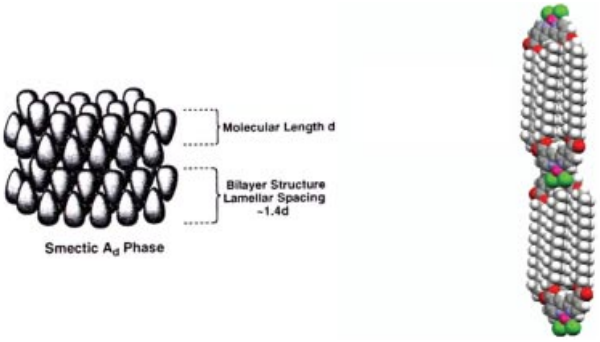

Figure 8. Idealized molecular arrangement for complex **2** in the SmAd phase

 © 2003 Wiley-VCH Verlag GmbH & Co. KGaA, Weinheim

However, a very similar XRD pattern has been reported for *ortho*-palladated 5,5′-dialkyl-2,2′-bipyridines, where it was concluded that the mesophase, although showing a schlieren texture, was a lamello-columnar phase, with aromatic cores stacked in columns and in close contact with one another to form defined layers.[31]

Therefore, even for our complexes, the lamellar structure in the mesophase could be described as columnar. In this case the flat molecular cores of each molecule would be stacked along the *a* direction to form columns that would be in close contact with one another to form layers. The repetition of these layers (separated by the disordered aliphatic chains) along the *c* direction would give rise to a periodic structure (Figure 9).

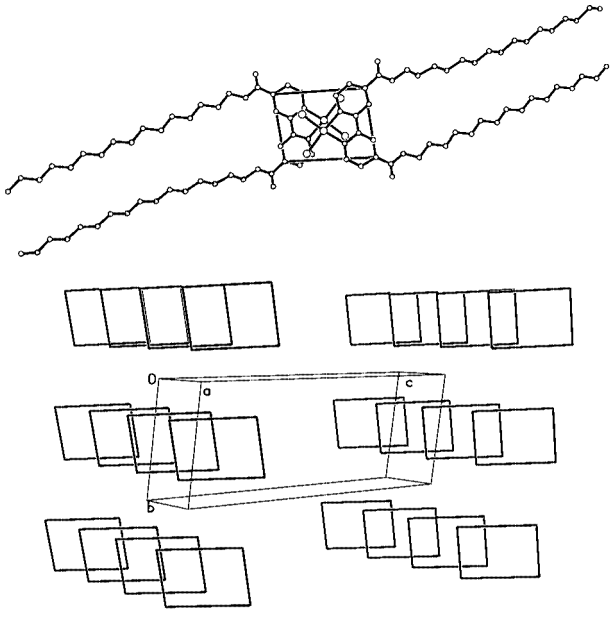

Figure 9. Schematic view of the molecular packing of complex **2** showing the stacking of the aromatic cores

In summary, since the XRD patterns of complexes **2** and **3** agree with both assignments (SmAd or lamello-columnar) and because the literature lacks a typical texture for the SmAd mesophase, while different textures are associated with a lamello-columnar phase,[31−33] we shall refer to this phase as L.

Ni^{II} compounds **5** and **6** showed a layered mesophase whose high transition temperatures prevented a complete identification by optical microscopy and X-ray powdered diffraction. Thermal analysis of Ni^{II} complexes on fresh samples and on samples stored in air for some days confirmed the addition of molecules of water. None of the zinc complexes were mesomorphic: after a crystal-to-crystal transition they melted into the isotropic liquid at temperatures much higher than the corresponding organic precursor. For **8** and **9** the total loss of liquid crystalline properties was ascribed to the tetrahedral coordination, which promoted strong intermolecular interactions in the crystal packing other than the metal−metal ones observed in the square-planar derivatives.

Both melting and clearing points, as expected, depended mostly on the aliphatic chains but were also very sensitive to the metal atom and the core interactions. Comparison of the thermal properties of complexes **1**−**6** with those reported for palladium(II)[15] shows that the melting temperatures, in each series, decreased in the order Pt < Pd < Ni whereas for the clearing points the trend was Pd < Pt < Ni, illustrating that the platinum derivatives have the largest mesomorphic range.

$[L^2MX_2]$ Complexes

All the dihexadecyl 2,2′-bipyridyl-4,4′-dicarboxylate palladium and platinum derivatives $[L^2MX_2]$ displayed enantiotropic liquid crystalline behaviour and were investigated by polarized optical microscope and XRD. The phase diagram is shown in Figure 10. The thermal data of $[L^2MX_2]$ complexes, as measured using DSC, are summarized in Table 4.

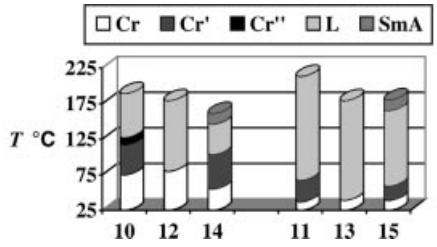

Figure 10. Bar graph showing the mesomorphic behaviour of $[L^2MX_2]$ (**10**−**15**) complexes

The phase sequence is notably dependent on the ancillary ligands overcoming the effect of the different metal atoms, which directly influence the thermal ranges. In particular, the iodo complexes **10** and **11**, after a crystal-to-crystal transition, gave rise to an L phase with the same mosaic texture as the chloro precursors. The thermotropic behaviour of the bromo derivatives **12** and **13** was also characterized as an L phase whose texture is retained, on cooling, in the solid state. The substitution of chloro for bromo atoms did not lead to crystal-to-crystal transitions. The mesomorphic properties were slightly changed when azide groups replaced the chloride ligands. When heated, complexes **14** and **15** gave, in addition to the crystal-to-crystal and the crystal-to-L transitions, an L-SmA transition phase, as confirmed by XRD analysis. For the chloro, iodo, and bromo complexes the layer thickness in the L phase increases with temperature due to an increase in molecular mobility and a progressive decrease in the degree of orientational order. This behaviour was magnified in the azide complexes. Indeed, in the high-temperature SmA phase the peaks corresponding to $d_1 \approx 10.5$ Å disappeared. These results suggest that, in this mesophase, thermal disorder within the layer weakened the intermolecular dipole interactions. In complexes **14** and **15**, on cooling the isotropic liquid, the SmA phase was observed, *via batonnets*, turning into a focal-conic texture and then homeotropic. On further cooling the L phase is restored, with a schlieren texture, which remained until solidification.

 © 2003 Wiley-VCH Verlag GmbH & Co. KGaA, Weinheim

Table 4. Optical and thermal properties of the [L^2MX_2] (**10**−**15**) complexes

Complex	Transition[a]	T [°C]	ΔH [kJ·mol^{-1}]	d [Å]
	Cr − Cr′	75.1	55.6	30.1 (Cr)
	Cr′ − Cr′′	116.7	0.5	34.2 (Cr′′)
	Cr′′ − L	123.6	2.3	36.5 (L)
10	L − I	186.1	19.0	
	I − L	184.2	18.6	
	L − Cr′	116.6	2.8	
	Cr′ − Cr	62.4	50.5	
	Cr − Cr′	36.8	8.4	30.0 (Cr)
	Cr′ − L	67.3	38.8	35.9 (L)
11	L − I	212.2	19.6	
	I − L	211.8	20.3	
	L − Cr	51.5	35.7	
	Cr − Cr′	38.8	5.5	
	Cr − L	79.6	53.0	36.5 (L)
12	L − I	178.5	13.6	
	I − L	178.0	12.5	
	L − Cr	41.9	24.8	
	Cr − L	39.2	15.0	32.5 (Cr)
13	L − I	179.0	1.8	36.0 (L)
	I − L	178.0	3.0	
	L − Cr	37.3	9.4	
	Cr − Cr′	55.2	24.5	36.7 (Cr)
	Cr′ − L	103.2	17.1	37.1 (Cr′)
	L − SmA	145.6	2.4	37.3 (L)
14	SmA − I	159.3	9.3	34.1 (SmA)
	I − SmA	154.2	7.6	
	SmA − L	144.2[b]	//	
	L − Cr	26.9	39.0	35.7 (L)
				37.7 (Cr)
	Cr − Cr′	39.1	20.1	34.0 (Cr)
	Cr′ − L	58.5	1.2	37.7 (L)
	L − SmA	164.7	1.5	
15	SmA − I	169.5	2.7	
	I − SmA	160.9	2.1	
	SmA − L	150.0[b]	//	
	L − Cr	35.2	2.7	

[a] Cr: crystal; L: lamellar; Sm: smectic; I: isotropic liquid. [b] Data by optical observation.

For all palladium and platinum complexes **10**−**15** the mesomorphic behaviour depends on the size of X and on the dipole moment associated with the M−X bond, irrespective of the metal atom. Indeed, the mesophase appeared at increasing temperatures in the order Br < I < Cl while the sequence for the clearing points was Cl < Br < I. However, with respect to the halo-compounds, the azide group promoted a lowering of both transition temperatures.

Finally, regardless of the X group, compared to the corresponding palladium compounds, the platinum complexes formed more stable mesophases, exhibiting, on average, much lower melting points and higher clearing temperatures.

Photophysical Studies − Absorption and Emission Spectroscopy

Uncomplexed Bipyridine Ligands

The absorption spectra of L^n ligands, in solution, were unaffected by their chain length, all showing a strong band at 300 nm with a shoulder at about 315 nm, attributed to a spin-allowed π→π* transitions involving the aromatic rings. At longer wavelengths a weakly absorbing tail at about 340 nm was assigned to an n→π* transition, probably involving pyridine nitrogens and ester fragments (Table 5). With respect to the unsubstituted bipyridine, the electron-withdrawing carboxylate groups induced a red-shift of the absorption bands, as determined by the LUMO stabilization.[34] The electronic spectra recorded from microcrystalline samples of L^n were identical to those in solution, indicating the absence of any relevant interactions in the solid state that can modify the energy states.

Table 5. Absorption data; MLCT bands are typed in bold

Compound	Solution (CH_2Cl_2) Abs., λ_{max}/nm (ε/M^{-1}·cm^{-1})	Solid (KBr pellet) Abs., λ_{max}/nm
L^2	300 (6700), 315 (sh), 340 (sh)	300
II	320 (sh), 330 (18700), **355 (2900)**	335
2	300 (15100), 320 (sh), 340 (6350), 360 (sh), 400 (sh), **422 (4400)**, 450 (sh)	300, **433**
5	314 (13500), 324 (14000)	322
8	314 (16700), 324 (19500)	322
10	320 (18000), 334 (17400), 350 (sh), **394 (4000)**, 496 (2600)	320, 500
11	316 (21400), 330 (sh), 360 (sh), **460 (5800)**, 525 (sh)	300, **480**
12	320 (sh), 332 (17300), **360 (3100)**	340
13	305 (14700), 340 (sh), 360 (sh), **432 (3300)**, 470 (sh)	310, **440**
14	304 (21400), 315 (sh), 332 (13700), **377 (4100)**	300, **390**
15	312 (20050), 330 (sh), 350 (sh), 440 (sh), **455 (4550)**, 500 (sh)	300, **460**

The ligand L^2 exhibited UV luminescence (Table 6) when excited on the π→π* absorption band (quantum yield of L^2 7.5%). Because of the energy and quantum yield, the emission was assigned to the singlet π→π* excited state.

Table 6. Photophysical data (Em. = Emission)

Compound	Solution (CH_2Cl_2) Em., λ_{max}/nm	Φ (%)	Solid (KBr pellet) Em., λ_{max}/nm
L^2	350	7.5	300
II	n.o.	−	456
2	482	$< 10^{-2}$	640
15	640	0.65	n.o.

[L^2MCl_2] Complexes

Preliminary investigation of the [L^nMCl_2] complexes revealed that the photophysical characteristics remained constant despite variation in the chain length of the ligands. Consequently, only the L^2 complexes will be discussed.

 © 2003 Wiley-VCH Verlag GmbH & Co. KGaA, Weinheim

The absorption spectrum of **2** in solution (Figure 11 and Table 5) clearly showed two well-defined bands, centred at 300 and 422 nm, and a series of shoulders.

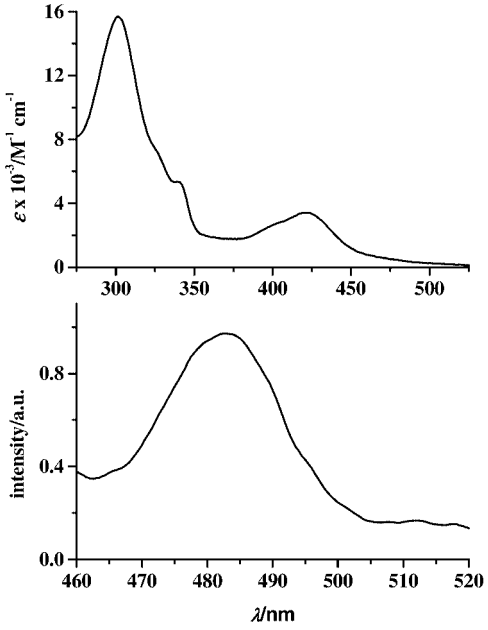

Figure 11. Absorption (top) and emission (down) spectra of complex **2** in dichloromethane solution

In accord with the literature,[35−37] the intense band at 300 nm, with a shoulder at about 320 nm, was attributed to spin-allowed ligand-centred transitions (^{1}LC). The band at 422 nm and its shoulder at about 430 nm could be attributed to ^{1}MLCT and ^{3}MLCT transitions, respectively.[38] A metal-perturbed LC transition could be give the band at 340 nm, while spin-allowed ligand field transitions (LF) produce weak shoulders at about 360 nm.[39]

The electronic spectrum of microcrystalline samples of **2** (Table 5) is not well resolved, due to the reflecting properties of the KBr support, which reduced signal intensity; it is possible to distinguish the principal maxima at 300 and 433 nm, with the first due to an ^{1}LC transition and the second to a ^{1}MLCT. The red-shift of this band was attributed to the environment sensitivity of this type of transition on passing from solution to the solid state.

As expected, the absorption spectrum of **II** (Table 5) did not show a MLCT band in the visible region, since the palladium(II) centre is more difficult to oxidize than the platinum(II) centre. Therefore, the observed UV-band at 355 nm could be assigned to a MLCT transition. The absorption spectrum of complex **II**, recorded from the KBr pellet, showed a 335 nm band corresponding to LC excitation.

The absorption spectra of **5** and **8** are very similar: in the near-UV region both exhibit two maxima at 314 and 324 nm in dichloromethane solution with a single peak at 322 nm in the solid state (Table 5). These features are assigned to the metal-perturbed ligand centred transition, showing two vibronic components in solution.

Complex **2** in dichloromethane solution has an emission band centred at 482 nm (Figure 11 and Table 6), as confirmed by the excitation spectrum.

This band can be attributed to a low-yield ($\Phi < 10^{-2}$ %) radiative deactivation from an ^{1}LF excited state. As expected, the analogous palladium complex **II**, in solution, did not emit, due to low-lying metal-centred excited states (MC), which can be populated easily by thermal activation and provide fast deactivation pathways via molecular distortion.[40]

The solid-state luminescence behaviours of **2** and **II** show interesting differences (Figure 12 and Table 6).

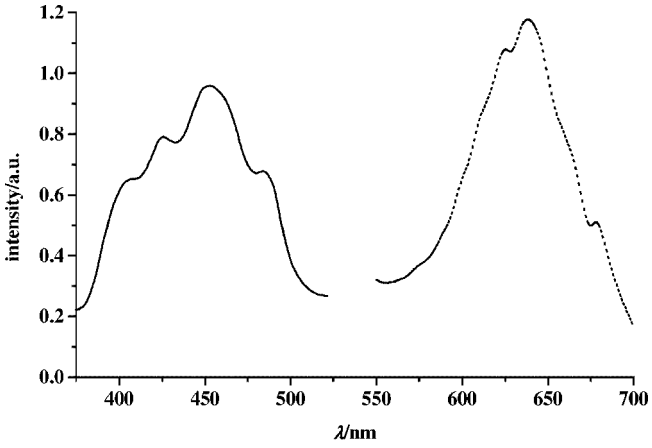

Figure 12. Emission spectra of complex **2** (dotted line) and complex **II** (solid line) in microcrystalline samples

Comparing the emission maximum of **2** in the solid state to that in solution, it is evident that d_z^2(Pt) orbital interactions in the stacked complexes in the microcrystalline sample are strong enough to affect the photophysical properties of the molecules. Therefore a Pt−Pt distance similar to the yellow form of (2,2′-bipyridine)dichloroplatinum(II) can be assumed.[41−43] The structured emission band at about 456 nm in the microcrystalline emission spectrum of **II** seems to indicate that the bipyridyl ligand is involved in the formation of the state responsible for the luminescence.[42] Moreover, the shortest Pd···Pd intermolecular separation of 3.487(2) Å, observed in the X-ray crystal structure determination, does not seem to be strong enough to affect the photophysical properties of the "isolated" molecules. This accounts for a small contribution of the metal in the electronic transition, in which LC character could be mixed with LF transitions. Further studies are necessary to clarify this crucial point.

[L^{n}MX$_2$] Complexes

The origin and position of the bands in the electronic spectra of [L^{2}MX$_2$] can be accounted for in the same way as for the [L^{2}MCl$_2$] spectra, irrespective of X. However, by modifying the donor character of X the MLCT state energy can be adjusted and, consequently, MLCT bands fall in the ranges 355−394 nm and 422−460 nm for the palladium and platinum derivatives, respectively. As discussed above,

 © 2003 Wiley-VCH Verlag GmbH & Co. KGaA, Weinheim

the weak fluorescence of **2** in solution is due to the emission from a ^{1}LF state, while the ^{1}MLCT state was deactivated by intersystem crossing (i.s.c.) to the ^{3}MLCT state. For **11** and **13** no luminescence was observed in solution at room temperature. This may be ascribable to the heavy atom effect which, favouring i.s.c. to the ^{3}MLCT state, quenched the fluorescence more efficiently than in **2**. With the complex bearing the azide ligands, **15**, an interesting emission at 640 nm was recorded. This complex did not undergo i.s.c, and a spin-allowed emission from the ^{1}MLCT state was now observed, whereby the photoluminescence quantum yield is higher than that of the ^{1}LF emission (0.65 vs. 0.02 %, respectively).

Although emission was expected in microcrystalline **11**, by analogy with that reported for [(bipy)PtI_2] luminescence,[42] it was not possible to detect it as scattered light fell in the observed spectral range. Likewise, it was difficult to record a clear emission spectrum from the microcrystalline **15** sample, in which emission could be self-quenched by dimeric interactions.

Finally, it was very difficult to assign the low-energy band in the electronic spectrum of **10**, which showed a peak at 496 nm that probably resulted from a mixed triplet−singlet state, favouring spin−orbit coupling.[37] As expected, no emission was detected from solution and microcrystalline samples of palladium complexes **10**, **12**, **14** with X = Br, N_3, I, respectively.

Conclusions

We have further characterized a recently reported[15] series of non-mesogenic dialkyl 2,2′-bipyridine-4,4′-dicarboxylates, L^n, and their *cis*-dichloro palladium liquid crystalline derivatives. Preliminary XRD experiments on the mesophase of the [L^n$PdCl_2$] complexes led us to propose a model in which the promotion of a dipole moment upon complexation induces self-assembling in dimers with antiparallel disposition. The aggregation of each pair of molecules into a layered structure affords a lamellar L phase.[15] This arrangement in the crystalline state has been confirmed by single-crystal X-ray diffraction analysis of the [L^2$PdCl_2$] derivative, **II**. A relatively short Pd···Pd intermolecular separation of 3.487(2) Å is found between centrosymmetrically related molecules arranged in a head-to-tail fashion. Pd···Pd contacts of 4.778 Å between dimers, alternating along a zig-zag chain, give rise to a layered structure. The solid-state luminescence at room temperature of complex **II** is shifted to the violet region with respect to the corresponding ligand.

The synthesis and characterization of two new series of complexes are also described: the *cis*-dichloro compounds [L^nMCl_2], where the palladium is replaced with Pt, Ni, and Zn, and the dihexadecyl 2,2′-bipyridyl-4,4′-dicarboxylate palladium and platinum derivatives, [L^2MX_2], in which the chloride groups are replaced with iodide, bromide, and azide ligands. Careful choice of the molecular building blocks with suitable shapes and geometries enable control of the supramolecular structure, and prediction of the nature of the induced thermal behaviour. Most of the [L^nMX_2] complexes retained the enantiotropic lamellar L phase of the chloro palladium derivatives, while the thermal and spectroscopic behaviour depend on molecular assemblies and thus on electronic and steric factors. In particular, the appearance of mesomorphism is related to the length of the alkyl chains, with long chains (n = 12, 16) producing the global rod-like shape responsible for the liquid crystalline behaviour. Comparing the *cis*-dichloro derivatives containing the same aliphatic tails, their mesomorphic behaviour is directly related to the nature of the metal centre. A single-crystal X-ray structure has been determined for the dihexadecyl 2,2′-bipyridyl-4,4′-dicarboxylate zinc derivative **8**: the tetrahedral geometry prevented dimer formation in the crystal packing and favoured intermolecular contacts that are too strong to induce mesomorphic behaviour. Conversely, the distorted square-planar nickel complexes displayed a lamellar phase at temperatures higher than for the palladium and platinum homologous. For all square-planar complexes the ancillary ligands were varied to use dipole coupling as a tool of molecular architecture. All complexes exhibited the same L phase, but both thermal and spectroscopic properties appeared to depend strongly upon the molecular dipolar interactions.

New photoluminescent metallomesogens have been obtained that display highly desirable optical properties such as a good degree of tunability. The band due to the ^{1}MLCT transition red-shifts, increasing the π-donor capacity of the X ligands, and most of these compounds, including the palladium derivatives, exhibit excellent luminescence properties. Interestingly, the platinum compound bearing chloride ligands is a blue emitter in solution but a red emitter in the solid state. With the azide group, however, the platinum complex is a red emitter in solution but is not an emitter at all in the solid state.

Experimental Section

Materials and Methods: All chemical, reagents and solvents were used as received from commercial sources without further purification. Ligands (L^n) were synthesized as previously reported.[15]

Infrared spectra were recorded on a Perkin-Elmer FT 2000 spectrophotometer and the ^{1}H NMR spectra were recorded on a Bruker WH-300 spectrometer in $CDCl_3$ solution, with TMS as internal standard. Elemental analyses were performed with a Perkin−Elmer 2400 analyzer. The textures of the mesophases were studied with a Zeiss Axioscope polarizing microscope equipped with a Linkam CO 600 heating stage. The transition temperatures and enthalpies were measured on a Perkin−Elmer Pyris 1 Differential Scanning Calorimeter with a heating and cooling rate of 10 °C/min. The apparatus was calibrated with indium. Two or more heating/cooling cycles were performed on each sample.

Spectrofluorimetric grade solvent (Acros Organics) was used for the photophysical investigations in solution at room temperature. Solid-state spectra were obtained from microcrystalline samples on KBr pellets. Absorption spectra were recorded with a Perkin−Elmer Lambda 900 spectrophotometer; uncorrected emis-

 © 2003 Wiley-VCH Verlag GmbH & Co. KGaA, Weinheim

sion spectra were obtained with a Perkin-Elmer LS-50B spectrofluorimeter. Fluorescence quantum yields in solution were measured by the method described by Demas and Crosby[44] using [Ru(bipy)$_3$]Cl$_2$ (bipy = 2,2′-bipyridine, $\Phi = 0.028$ in aerated water)[45] as standard. The experimental uncertainty on the band maximum for absorption and luminescence spectra is 2 nm; that on the luminescence intensity is 20% and that on the molar absorption coefficient is 10%. The free ligand and its metal complexes are fairly stable in CH_2Cl_2, as demonstrated by the constancy of their absorption spectra over a week.

The X-ray powder diffraction patterns were obtained using a Bruker AXS General Area Detector Diffraction System (D8 Discover with GADDS). Monochromatized Cu-$K\alpha$ radiation (λ = 1.54 Å) impinged on the about 1 mm thick sample, the temperature of which was controlled to ±0.1° by a hot stage containing electrical resistors.

Crystal Structure Studies: Pale yellow needles of [L^{2}PdCl$_2$] (**II**) with a relatively poor crystal habit were crystallized at room temperature from a chloroform/ethanol mixture. Different crystallization conditions gave no better results. A needle of suitable dimensions was mounted in a fiber glass capillary to avoid solvent evaporation during data collection. Crystal data of [L^{2}ZnCl$_2$] (**8**) were collected on a white, thin plate crystal obtained from a chloroform/ethanol mixture. In both cases diffraction measurements were carried out at room temperature on a Siemens *R3m/V* automated four-circle diffractometer equipped with graphite-monochromated Mo-K_α radiation (λ = 0.71073 Å). The data were corrected for Lorentz, polarization and X-ray absorption effects. For **8** an empirical absorption correction was applied using a method based upon azimuthal (Ψ) scan data.[46] With **II**·2CHCl$_3$ a slow loss of cocrystallized solvent prevented this type of data correction. Therefore the data were corrected for X-ray absorption effects using the *XABS2* program.[47] Details of the crystal data collections are listed in Table 7.

Both structure solutions (Patterson method) and full-matrix least-squares refinements based on F^2 were performed with *SHELXS*/*L* programs of the *SHELXTL-NT* software package (Version 5.10).[48]

For **II**·2CHCl$_3$, only palladium, chlorine (excluding the chlorine atoms of the two co-crystallized chloroform molecules), nitrogen and oxygen atoms were refined anisotropically, for **8**, however, all non-hydrogen atoms were refined anisotropically. In both cases hydrogen atoms were included as idealized atoms riding on the respective carbon atom hybridisation. The bipyridine hydrogen atoms of **8** were included in the refinement in their observed positions.

Synthesis of [L^{n}PtCl$_2$] Complexes 1−3: The [L^{n}PtCl$_2$] derivatives were prepared by the procedure described for the analogous palladium complexes,[15] starting from the suitable ligand and varying the solvent and reaction time for more energetic reaction conditions. The synthesis of [L^{1}PtCl$_2$] (**1**) is detailed below; all other homologues were prepared in a similar fashion and only yields, solvents, ^{1}H NMR, IR, and analytical data are reported.

(Dioctyl 2,2′-Bipyridyl-4,4′-dicarboxylate)platinum(II) Chloride ([L^{1}PtCl$_2$], 1): A solution of [Pt(PhCN)$_2$Cl$_2$] (0.1 g, 0.213 mmol) and dioctyl 2,2′-bipyridine-4,4′-dicarboxylate, L^1, (0.1 g, 0.213 mmol) in toluene (12 mL) was heated at reflux for 24 h. The solvent was then evaporated and the residue recrystallized from dichloromethane/methanol to give a yellow solid complex (0.092 g, 59%). Thermotropic behaviour: Table 3. ^{1}H NMR (300 MHz, CDCl$_3$, 25 °C, ppm): δ = 0.82 (m, 6 H, H$^{11d,11d'}$), 1.23 (m, 20 H, H$^{10c,10c'}$), 1.78 (m, 4 H, H$^{9b,9b'}$), 4.40 (t, ^3J = 6.8 Hz, 4 H, H$^{8a,8a'}$), 8.02 (dd, $^3J_{H,H}$ = 6.2, $^4J_{H,H}$ = 1.7 Hz, 2 H, H$^{5,5'}$), 8.54 (s, 2 H, H$^{3,3'}$), 9.77 (d, $^3J_{H,H}$ = 6.2 Hz, 2 H, H$^{6,6'}$). FTIR (KBr, cm^{-1}):

Table 7. Crystal and structure refinements for complexes **II**·2CHCl$_3$ and **8**

Empirical formula	$C_{44}H_{72}Cl_2N_2O_4Pd.2CHCl_3$ (**II**·2CHCl$_3$)	$C_{44}H_{72}Cl_2N_2O_4Zn$ (**8**)
Molecular mass	1109.1	829.3
Temperature [K]	298	298
Wavelength [Å]	0.71073	0.71073
Crystal system	triclinic	monoclinic
Space group	$P\bar{1}$	$C2/c$
a [Å]	7.436(2)	41.228(8)
b [Å]	11.917(3)	7.937(2)
c [Å]	31.869(13)	14.689(3)
α [°]	92.28(3)	90
β [°]	92.78(3)	107.71(3)
γ [°]	96.72(2)	90
V [Å^3]	2798(1)	4579(2)
Z	2	4
Density [Mg/m^{-3}]	1.316	1.203
Absorption Coefficient [mm^{-1}]	0.752	0.693
F(000)	1156	1784
No. indep. refl.	5966 [R(int) = 0.071]	4058 [R(int) = 0.032]
No. obs. refl.	2012	2107
Data / restraints / parameters	5966 / 0 / 157	4058 / 0 / 240
R_1[a] [$I > 2\sigma(I)$]	0.0779	0.0552
wR_2[b]	0.1133	0.1294
Goodness-of-fit on F^2	0.976	0.870
Largest diff. peak and hole [e·Å^{-3}]	0.457 and −0.575	0.472 and −0.536

[a] $R1 = \Sigma(|F_o| - |F_c|)/\Sigma|F_o|$. [b] $wR2 = \{\Sigma[w(F_o^2 - F_c^2)^2]/\Sigma[w(F_o^2)^2]\}^{1/2}$.

 © 2003 Wiley-VCH Verlag GmbH & Co. KGaA, Weinheim

ν(C=O) 1730. $C_{28}H_{40}Cl_2N_2O_4Pt$ (734.62): calcd. C 45.78, H 5.49, N 3.81; found C 45.25, H 5.61, N 3.30.

(Dihexadecyl 2,2′-Bipyridyl-4,4′-dicarboxylate)platinum(II) Chloride ([L²PtCl₂], 2): Yield: 0.076 g, 55%. Recrystallized from dichloromethane/light petroleum; thermotropic behaviour: Table 3. ^{1}H NMR (300 MHz, $CDCl_3$, 25 °C, ppm): δ = 0.88 (t, $^3J_{H,H}$ = 6.7 Hz, 6 H, $H^{11d,11d'}$), 1.26 (m, 52 H, $H^{10c,10c'}$), 1.86 (m, 4 H, $H^{9b,9b'}$), 4.47 (t, $^3J_{H,H}$ = 6.8 Hz, 4 H, $H^{8a,8a'}$), 8.10 (d, $^3J_{H,H}$ = 6.1 Hz, 2 H, $H^{5,5'}$), 8.61 (d, $^4J_{H,H}$ = 1.7 Hz, 2 H, $H^{3,3'}$), 9.88 (d, $^3J_{H,H}$ = 6.1 Hz, 2 H, $H^{6,6'}$). FTIR (KBr, cm^{-1}): ν(C=O) 1730. $C_{44}H_{72}Cl_2N_2O_4Pt$ (959.05): calcd. C 55.10, H 7.57, N 2.92; found C 54.82, H 7.57, N 3.01.

(Didocosyl 2,2′-Bipyridyl-4,4′-dicarboxylate)platinum(II) Chloride ([L³PtCl₂], 3): Yield: 0.076 g, 58%. Recrystallized from dichloromethane/diethyl ether; thermotropic behaviour: Table 3. ^{1}H NMR (300 MHz, $CDCl_3$, 25 °C, ppm): δ = 0.88 (t, $^3J_{H,H}$ = 6.5 Hz, 6 H, $H^{11d,11d'}$), 1.27 (m, 76 H, $H^{10c,10c'}$), 1.86 (m, 4 H, $H^{9b,9b'}$), 4.47 (t, $^3J_{H,H}$ = 6.5 Hz, 4 H, $H^{8a,8a'}$), 8.11 (d, $^3J_{H,H}$ = 6.3 Hz, 2 H, $H^{5,5'}$), 8.61 (s, 2 H, $H^{3,3'}$), 9.94 (d, $^3J_{H,H}$ = 6.3 Hz, 2 H, $H^{6,6'}$). FTIR (KBr, cm^{-1}): ν(C=O) 1733. $C_{56}H_{96}Cl_2N_2O_4Pt$ (1127.37): calcd. C 59.66, H 8.58, N 2.48; found C 59.24, H 9.02, N 2.68.

Synthesis of [L″NiCl₂] Complexes 4−6: The preparation of [L^1NiCl$_2$] (**4**) complex is detailed below; all other homologues were prepared in a similar fashion and only yields, solvents, ^{1}H NMR, IR, and analytical data are reported.

(Dioctyl 2,2′-Bipyridyl-4,4′-dicarboxylate)nickel(II) Chloride ([L¹NiCl₂], 4): A solution of $NiCl_2$ (0.041 g, 0.32 mmol) and dioctyl 2,2′-bipyridine-4,4′-dicarboxylate, L^1, (0.150 g, 0.32 mmol) in ethanol (25 mL) was heated at reflux for 48 h. The solvent was evaporated and the residue recrystallized from dichloromethane/diethyl ether to give a green solid (0.179 g, 94%). Thermotropic behaviour: Table 3. FTIR (KBr, cm^{-1}): ν(C=O) 1729. $C_{28}H_{40}Cl_2N_2NiO_4$ (598.24): calcd. C 56.22, H 6.74, N 4.68; found C 56.83, H 6.44, N 5.02.

(Dihexadecyl 2,2′-Bipyridyl-4,4′-dicarboxylate)nickel(II) Chloride ([L²NiCl₂], 5): 24 h. Yield: 0.159 g, 89%. Thermotropic behaviour: Table 3. FTIR (KBr, cm^{-1}): ν(C=O) 1725. $C_{44}H_{72}Cl_2N_2NiO_4$ (822.67): calcd. C 64.24, H 8.82, N 3.41; found C 64.34, H 8.94, N, 3.77.

(Didocosyl 2,2′-Bipyridyl-4,4′-dicarboxylate)nickel(II) Chloride ([L³NiCl₂], 6): 24 h. Yield: 0.130 g, 75%. Thermotropic behaviour: Table 3. FTIR (KBr, cm^{-1}): ν(C=O) 1725. $C_{56}H_{96}Cl_2N_2NiO_4$ (990.99): calcd. C 67.87, H 9.76, N 2.83; found C 67.77, H 9.09, N 2.90.

Synthesis of [L″ZnCl₂] Complexes 7−9: Compound [L^1ZnCl$_2$] (**7**) was prepared as detailed below; all other homologues were prepared in a similar fashion and only yields, solvents, ^{1}H NMR, IR, and analytical data are reported.

(Dioctyl 2,2′-Bipyridyl-4,4′-dicarboxylate)zinc Chloride ([L¹ZnCl₂], 7): Zinc chloride (0.02 g, 0.171 mmol) was added to a solution of dioctyl 2,2′-bipyridine-4,4′-dicarboxylate, L^1, (0.08 g, 0.171 mmol) in dichloromethane (10 mL). The resultant suspension was stirred at room temperature for 4 days. The solvent was then evaporated and the residue recrystallized from dichloromethane/diethyl ether to give a white solid (0.080 g, 78%). Thermotropic behaviour: Table 3. ^{1}H NMR (300 MHz, $CDCl_3$, 25 °C, ppm): δ = 0.89 (t, ^3J = 6.6 Hz, 6 H, $H^{11d,11d'}$), 1.30 (m, 20 H, $H^{10c,10c'}$), 1.85 (m, 4 H, $H^{9b,9b'}$), 4.49 (t, ^3J = 6.6 Hz, 4 H, $H^{8a,8a'}$), 8.30 (d, ^3J = 4.7 Hz, 2 H, $H^{5,5'}$), 8.89 (s, 2 H, $H^{3,3'}$), 9.05 (d, ^3J = 4.7 Hz, 2 H, $H^{6,6'}$). FTIR (KBr, cm^{-1}): ν(C=O) 1732. $C_{28}H_{40}Cl_2N_2O_4Zn$ (604.92): calcd. C 55.40, H 6.66, N 4.63; found C 55.60, H 6.51, N 4.60.

(Dihexadecyl 2,2′-Bipyridyl-4,4′-dicarboxylate)zinc Chloride ([L²ZnCl₂], 8): Yield: 0.060 g, 72%. Thermotropic behaviour: Table 3. ^{1}H NMR (300 MHz, $CDCl_3$, 25 °C, ppm): δ = 0.88 (t, $^3J_{H,H}$ = 6.8 Hz, 6 H, $H^{11d,11d'}$), 1.26 (m, 52 H, $H^{10c,10c'}$), 1.85 (m, 4 H, $H^{9b,9b'}$), 4.49 (t, $^3J_{H,H}$ = 6.8 Hz, 4 H, $H^{8a,8a'}$), 8.30 (dd, $^3J_{H,H}$ = 5.1, $^4J_{H,H}$ = 1.2 Hz, 2 H, $H^{5,5'}$), 8.89 (s, 2 H, $H^{3,3'}$), 9.04 (d, $^3J_{H,H}$ = 5.1 Hz, 2 H, $H^{6,6'}$). FTIR (KBr, cm^{-1}): ν(C=O) 1733. $C_{44}H_{72}Cl_2N_2O_4Zn$ (829.35): calcd. C 63.72, H 8.75, N 3.38; found C 63.15, H 8.48, N 3.11.

(Didocosyl 2,2′-Bipyridyl-4,4′-dicarboxylate)zinc Chloride ([L³ZnCl₂], 9): Yield: 0.084 g, 72%. Thermotropic behaviour: Table 3. ^{1}H NMR (300 MHz, $CDCl_3$, 25 °C, ppm): δ = 0.88 (t, $^3J_{H,H}$ = 6.7 Hz, 6 H, $H^{11d,11d'}$), 1.25 (m, 76 H, $H^{10c,10c'}$), 1.85 (m, 4 H, $H^{9b,9b'}$), 4.49 (t, $^3J_{H,H}$ = 6.7 Hz, 4 H, $H^{8a,8a'}$), 8.30 (d, $^3J_{H,H}$ = 5.3 Hz, 2 H, $H^{5,5'}$), 8.89 (s, 2 H, $H^{3,3'}$), 9.04 (d, $^3J_{H,H}$ = 5.3 Hz, 2 H, $H^{6,6'}$). FTIR (KBr, cm^{-1}): ν(C=O) 1732. $C_{56}H_{96}Cl_2N_2O_4Zn$ (997.68): calcd. C 67.42, H 9.70, N 2.81; found C 67.32, H 9.41, N 2.79.

Synthesis of [L²MX₂] Complexes 10−15: The [L^2MX_2] complexes, starting from suitable precursors [L^2MCl_2] (M = Pd, Pt), were prepared by metathetical reactions with appropriate salts AX (X = I, Br, N_3). The synthesis of the [L^2PdI_2] (**10**) complex is described in detail; all other complexes were prepared in a similar fashion and only reagents, yields, solvents, ^{1}H NMR, IR, and analytical data are reported.

(Dihexadecyl 2,2′-Bipyridyl-4,4′-dicarboxylate)palladium(II) Iodide ([L²PdI₂], 10): KI (0.096 g, 0.58 mmol) was added to a yellow solution of [L^2PdCl_2], (**II**) (0.05 g, 0.058 mmol) in acetone (10 mL). The resultant suspension was then stirred at room temperature for 24 h. The so-obtained brown solid was filtered off and purified by recrystallization from chloroform/acetone to give the pure dark red product as a solid (0.050 g, 82%). Thermotropic behaviour: Table 4. ^{1}H NMR (300 MHz, $CDCl_3$, 25 °C, ppm): δ = 0.88 (m, 6 H, $H^{11d,11d'}$), 1.26 (m, 52 H, $H^{10c,10c'}$), 1.86 (m, 4 H, $H^{9b,9b'}$), 4.48 (t, $^3J_{H,H}$ = 6.8 Hz, 4 H, $H^{8a,8a'}$), 8.14 (d, $^3J_{H,H}$ = 5.9 Hz, 2 H, $H^{5,5'}$), 8.70 (s, 2 H, $H^{3,3'}$), 10.18 (d, $^3J_{H,H}$ = 5.9 Hz, 2 H, $H^{6,6'}$). FTIR (KBr, cm^{-1}): ν(C=O) 1729. $C_{44}H_{72}I_2N_2O_4Pd$ (1053.30): calcd. C 50.17, H 6.89, N 2.66; found C 50.50, H 7.51, N 3.25.

(Dihexadecyl 2,2′-Bipyridyl-4,4′-dicarboxylate)platinum(II) Iodide ([L²PtI₂], 11): 10 equiv. of KI; three days. Red product obtained from chloroform/methanol (0.082 g, 86%). Thermotropic behaviour: Table 4. ^{1}H NMR (300 MHz, $CDCl_3$, 25 °C, ppm): δ = 0.88 (t, $^3J_{H,H}$ = 6.9 Hz, 6 H, $H^{11d,11d'}$), 1.26 (m, 52 H, $H^{10c,10c'}$), 1.86 (m, 4 H, $H^{9b9b'}$), 4.48 (t, $^3J_{H,H}$ = 6.9 Hz, 4 H, $H^{8a,8a'}$), 8.12 (d, $^3J_{H,H}$ = 6.05 Hz, 2 H, $H^{5,5'}$), 8.63 (s, 2 H, $H^{3,3'}$), 10.51 (d, $^3J_{H,H}$ = 6.05 Hz, 2 H, $H^{6,6'}$). FTIR (KBr, cm^{-1}): ν(C=O) 1720. $C_{44}H_{72}I_2N_2O_4Pt$ (1141.96): calcd. C 46.28, H 6.36, N 2.45; found C 46.60, H 6.24, N 2.56.

(Dihexadecyl 2,2′-Bipyridyl-4,4′-dicarboxylate)palladium(II) Bromide ([L²PdBr₂], 12): 20 equiv. of KBr; DMF; three days. Yellow product obtained from chloroform/methanol (0.054 g, 80%). Thermotropic behaviour: Table 4. ^{1}H NMR (300 MHz, $CDCl_3$, 25 °C, ppm): δ = 0.88 (t, $^3J_{H,H}$ = 6.7 Hz, 6 H, $H^{11d,11d'}$), 1.26 (m, 52 H, $H^{10c,10c'}$), 1.85 (m, 4 H, $H^{9b,9b'}$), 4.48 (t, $^3J_{H,H}$ = 6.7 Hz, 4 H, $H^{8a,8a'}$), 8.11 (d, $^3J_{H,H}$ = 6.1 Hz, 2 H, $H^{5,5'}$), 8.66 (s, 2 H, $H^{3,3'}$), 9.85 (d, $^3J_{H,H}$ = 6.1 Hz, 2 H, $H^{6,6'}$). FTIR (KBr, cm^{-1}): ν(C=O) 1722. $C_{44}H_{72}Br_2N_2O_4Pd$ (959.29): calcd. C 55.09, H 7.57, N 2.92; found C 54.79, H 7.11, N 2.43.

 © 2003 Wiley-VCH Verlag GmbH & Co. KGaA, Weinheim

(Dihexadecyl 2,2′-Bipyridyl-4,4′-dicarboxylate)platinum(II) Bromide ([L^{2}PtBr$_2$], 13): 20 equiv. of KBr; DMF; four days. Yellow product obtained from chloroform/methanol (0.066 g, 76%). Thermotropic behaviour: Table 4. ^{1}H NMR (300 MHz, $CDCl_3$, 25 °C, ppm): δ = 0.88 (t, $^3J_{H,H}$ = 6.6 Hz, 6 H, H$^{11d,11d'}$), 1.26 (m, 52 H, H$^{10c,10c'}$), 1.86 (m, 4 H, H$^{9b,9b'}$), 4.47 (t, $^3J_{H,H}$ = 6.6 Hz, 4 H, H$^{8a,8a'}$), 8.11 (d, $^3J_{H,H}$ = 5.8 Hz, 2 H, H$^{5,5'}$), 8.60 (s, 2 H, H$^{3,3'}$), 10.23 (d, $^3J_{H,H}$ = 5.8 Hz, 2 H, H$^{6,6'}$). FTIR (KBr, cm^{-1}): ν(C=O) 1730. $C_{44}H_{72}Br_2N_2O_4Pt$ (1047.95): calcd. C 50.43, H 6.93, N 2.67; found C 50.14, H 6.75, N 2.32.

(Dihexadecyl 2,2′-Bipyridyl-4,4′-dicarboxylate)palladium(II) Azide ([L^{2}Pd(N$_3$)$_2$], 14): 10 equiv. of NaN_3; 24 h. Yellow product obtained from chloroform/acetone (0.033 g, 65%). Thermotropic behaviour: Table 4. ^{1}H NMR (300 MHz, $CDCl_3$, 25 °C, ppm): δ = 0.88 (t, $^3J_{H,H}$ = 6.5 Hz, 6 H, H$^{11d,11d'}$), 1.26 (m, 52 H, H$^{10c,10c'}$), 1.86 (m, 4 H, H$^{9b,9b'}$), 4.47 (t, $^3J_{H,H}$ = 6.5 Hz, 4 H, H$^{8a,8a'}$), 8.145 (d, $^3J_{H,H}$ = 5.5 Hz, 2 H, H$^{5,5'}$), 8.67 (s, 2 H, H$^{3,3'}$), 8.81 (d, $^3J_{H,H}$ = 5.5 Hz, 2 H, H$^{6,6'}$). FTIR (KBr, cm^{-1}): ν(C=O) 1728, ν(N_3) 2043. $C_{44}H_{72}N_8O_4Pd$ (883.53): calcd. C 59.82, H 8.21, N 12.68; found C 60.01, H 8.69, N 12.32.

(Dihexadecyl 2,2′-Bipyridyl-4,4′-dicarboxylate)platinum(II) Azide ([L^{2}Pt(N$_3$)$_2$], 15): 10 equiv. of NaN_3; 48 h. Orange product obtained from chloroform/methanol (0.036 g, 45%). Thermotropic behaviour: Table 4. ^{1}H NMR (300 MHz, $CDCl_3$, 25 °C, ppm): δ = 0.88 (t, $^3J_{H,H}$ = 6.6 Hz, 6 H, H$^{11d,11d'}$), 1.26 (m, 52 H, H$^{10c,10c'}$), 1.86 (m, 4 H, H$^{9b,9b'}$), 4.47 (t, $^3J_{H,H}$ = 6.6 Hz, 4 H, H$^{8a,8a'}$), 8.10 (d, $^3J_{H,H}$ = 5.9 Hz, 2 H, H$^{5,5'}$), 8.63 (s, 2 H, H$^{3,3'}$), 9.14 (d, $^3J_{H,H}$ = 5.9 Hz, 2 H, H$^{6,6'}$). FTIR (KBr, cm^{-1}): ν(C=O) 1728, ν(N_3) 2063. $C_{44}H_{72}N_8O_4Pt$ (972.19): calcd. C 54.36, H 7.46, N 11.53; found C 54.04, H 7.20, N 11.40.

CCDC-208739 and CCDC-208740 contain the supplementary crystallographic data for this paper. These data can be obtained free of charge at www.ccdc.cam.ac.uk/conts/retrieving.html [or from the Cambridge Crystallographic Data Centre, 12 Union Road, Cambridge CB2 1EZ, UK; Fax: (internat.) +44−1223/336-033; E-mail: deposit@ccdc.cam.ac.uk].

Acknowledgments

This work was partly supported by CIPE grants (Clusters 14 and 26) from the Ministero dell'Istruzione, dell'Università e della Ricerca.

[1] J. L. Serrano, *Metallomesogens*, VCH, Weinheim, **1996**.
[2] B. Donnio, D. W. Bruce, *Structure and Bonding*, (Ed.: D. M. P. Mingos, Vol. 95, Liquid Crystals II. Metallomesogens, Springer, **1999**.
[3] H. Richtzenhain, A. J. Blake, D. W. Bruce, I. A. Fallis, W. Li, M. Schroder, *Chem. Commun.* **2001**, 2580−2581.
[4] I. Aiello, M. Ghedini, M. La Deda, D. Pucci, O. Francescangeli, *Eur. J. Inorg. Chem.* **1999**, 1367−1372.
[5] T. Hegmann, F. Peidis, S. Diele, C. Tschierske, *Liq. Cryst.* **2000**, *27*, 1261−1265.
[6] M. Benouazzane, S. Coco, P. Espinet, J. Barbera, *J. Mater. Chem.* **2001**, *11*, 1740−1744.
[7] S. T. Trzaska, T. M. Swager, *Chem. Mater.* **1998**, *10*, 438−443.
[8] S. Coco, F. Diez-Exposito, P. Espinet, C. Fernandez-Mayordomo, J. M. Martin-Alvarez, A. M. Levelut, *Chem. Mater.* **1998**, *10*, 3666−3671.
[9] C. Yang, Y. Pang, C. K. Lai, *Liq. Cryst.* **2001**, *28*, 191−195.
[10] K. E. Rowe, D. W. Bruce, *Liq. Cryst.* **1996**, *20*, 183−193.
[11] C. Tschierske, *Angew. Chem. Int. Ed.* **2000**, *39*, 2454−2458.
[12] O. Maury, J.-P. Guégan, T. Renouard, A. Hilton, P. Dupau, N. Sandon, L. Toupet, H. Le Bozec, *New J. Chem.* **2001**, *25*, 1553−1566.
[13] R. Ziessel, *Coord. Chem. Rev.* **2001**, *216−217*, 195−223 and references therein.
[14] S. S. Kamath, V. Uma, T. S. Srivastava, *Inorg. Chim. Acta* **1989**, *161*, 49−56.
[15] D. Pucci, G. Barberio, A. Crispini, O. Francescangeli, M. Ghedini, *Mol. Cryst. Liq. Cryst.* **2003**, *395*, 325−335.
[16] T. J. Nelson, J. R. Wullert II, *Electronic Information Display Technologies*, World Scientific Publishing,Singapore, **1997**.
[17] [17a] H. J. Coles, *Liq. Cryst.* **1993**, *14*, 1039−1042. [17b] R. Yamaguchi, J. Kishida, S. Sato, *Jpn. J. Appl. Phys.* **2000**, *39*, 5235−5237.
[18] D. Song, Q. Wu, A. Hook, I. Kozin, S. Wang, *Organometallics* **2001**, *20*, 4683−4689.
[19] W. Lu, N. Zhu, C. Che, *Chem. Commun.* **2002**, 900−901.
[20] F. Neve, A. Crispini, C. Di Pietro, S. Campagna, *Organometallics* **2002**, *21*, 3511−3518 and references therein.
[21] [21a] G. R. Newkome, F. R. Fronczek, V. K. Gupta, W. E. Puckett, D. C. Pantaleo, G. E. Kiefer, *J. Am. Chem. Soc.* **1982**, *104*, 1782−1783. [21b] P. D. Beer, N. C. Fletcher, M. G. B. Drew, T. J. Wear, *Polyhedron* **1997**, *16*, 815−823.
[22] M. Maekawa, M. Munakata, S. Kitagawa, M. Nakamura, *Anal. Sci.* **1991**, *7*, 521−523.
[23] M. A. Khan, D. G. Tuck, *Acta Crystallogr., Sect. C* **1984**, *40*, 60−62.
[24] C. W. Reimann, S. Block, A. Perloff, *Inorg. Chem.* **1966**, *5*, 1185−1189.
[25] H.-L. Kwong, K.-M. Lau, W.-S. Lee, W.-T. Wong, *New. J. Chem.* **1999**, *23*, 629−632.
[26] K. Nakamoto, *Infrared and Raman Spectra of Inorganic and Coordination Compounds*, Wiley-Interscience, New York, 4th edn., pp. 231, 290−291, **1986**.
[27] J. Kaiser, J. Sieler, U. Braun, L. Golic, E. Dinjus, D. Walther, *J. Organomet. Chem.* **1982**, *224*, 81−87.
[28] D. W. Evans, G. R. Newkome, F. R. Fronczek, *Acta Crystallogr., Sect. C* **1990**, *46*, 490−491.
[29] T. J. Kinnunen, M. Haukka, T. T. Pakkanen, T. A. Pakkanen, *J. Organomet. Chem.* **2000**, *613*, 257−262.
[30] J. Goodby, in: *Phase Structures of Calamitic Liquid Crystals*, Vol. 2A. *Handbook of Liquid Crystals* (Eds.: D. Demus, J. Goodby, G. W. Gray, H.-W. Spiess, V. Vill); Weinheim: Wiley-VCH, **1998**.
[31] A. El-ghayoury, L. Douce, A. Skoulios, R. Ziessel, *Angew. Chem. Int. Ed.* **1998**, *37*, 1255−1258.
[32] D. Felder, B. Heinrich, D. Guillon, J.-F. Nicoude, J.-F. Nierengarten, *Chem. Eur. J.* **2000**, *6*, 3501−3507.
[33] S. Méry, D. Haristoy, J.-F. Nicoude, D. Guillon, S. Diele, H. Monobe, Y. Shimizu, *J. Mater. Chem.* **2002**, *12*, 37−41.
[34] E. J. L. McInnes, R. D. Farley, C. C. Rowlands, A. J. Welch, L. Rovatto, L. J. Yellowless, *J. Chem. Soc., Dalton Trans.* **1999**, 4203−4208.
[35] P. M. Gidney, R. D. Gillard, B. T. Haeton, *J. Chem. Soc., Dalton Trans.* **1973**, 132−134 and references therein.
[36] V. M. Houlding, V. M. Miskowski, *Coord. Chem. Rev.* **1991**, *111*, 145−152 and references therein.
[37] W. B. Connick, V. M. Miskowski, V. M. Houlding, H. B. Gray, *Inorg. Chem.* **2000**, *39*, 2585−2592 and references therein.
[38] V. M. Miskowski, V. H. Houlding, *Inorg. Chem.* **1989**, *28*, 1529−1533.
[39] V. Balzani, V. Carassiti, *Photochemistry of Coordination Compounds*, Academic Press, London, **1970**.
[40] [40a] M. Maestri, C. Deuschel-Cornioley, A. von Zelewsky, *Coord. Chem. Rev.* **1991**, *111*, 117−123. [40b] M. Maestri, V. Balzani, C. Deuschel-Cornioley, A. von Zelewsky, *Adv. Photochem.* **1992**, *17*, 1−68.
[41] [41a] V. M. Textor, H. R. Oswald, *Z. Anorg. Allg. Chem.* **1974**, *407*, 244−256. [41b] R. S. Osborn, D. Rogers, *J. Chem. Soc., Dalton Trans.* **1974**, 1002−10004.

 © 2003 Wiley-VCH Verlag GmbH & Co. KGaA, Weinheim

[42] V. M. Miskowski, V. H. Houlding, C-M. Che, Y. Wang, *Inorg. Chem.* **1993**, *32*, 2518−2524.
[43] W. B. Connick, L. M. Henling, R. E. Marsh, H. B. Gray, *Inorg. Chem.* **1996**, *35*, 6261−6265.
[44] J. N. Demas, G. A. Crosby, *J. Phys. Chem.* **1971**, *93*, 2841−2844.
[45] K. Nakamaru, *Bull. Soc. Chem. Jpn.* **1982**, *5*, 2697−2705.
[46] A. C. T. North, D. C. Phillips, F. S. Mathews, *Acta Crystallogr., Sect. A* **1968**, *24*, 351−359.
[47] S. Parkin, B. Moezzi, H. J. Hope, *Appl. Crystallogr.* **1995**, *28*, 53−56.
[48] *SHELXTL*/*NT* crystal structure analysis package, Bruker AXS, Inc.: Madison, WI, **1999**.

Received April 17, 2003

 © 2003 Wiley-VCH Verlag GmbH & Co. KGaA, Weinheim

Intercalates of Vanadyl Phosphate with Benzonitrile and Tolunitrile

Ludvík Beneš,*[a] Víztězslav Zima,[a] Klára Melánová,[a] Jiří Dybal,[b] Miroslava Trchová,[c] and Pavel Matějka[d]

Keywords: Intercalations / X-ray diffraction / Vibrational spectroscopy / Ab initio calculations / Semiempirical calculations

Intercalates of vanadyl phosphate with benzonitrile and *p*-tolunitrile were prepared and characterized by X-ray powder diffraction, TG analysis, IR and Raman spectroscopy. Both intercalates contain one nitrile molecule per formula unit. The intercalates prepared are moisture sensitive and guest molecules are easily replaced by water molecules. The nitrile molecules are anchored to the host layers by an N–V donor-acceptor bond. Local structures and interactions appearing in the intercalates were suggested on the base of quantum chemical calculations. These calculations support the results of the IR and Raman spectroscopy, indicating the formation of a C≡N→V bond in the intercalates. The calculated basal spacings (11.32 Å for the benzonitrile and 13.00 Å for the tolunitrile intercalates) are in good agreement with the experimental values (11.22 and 13.19 Å, respectively).

(© Wiley-VCH Verlag GmbH & Co. KGaA, 69451 Weinheim, Germany, 2003)

Introduction

Vanadyl phosphate is able to accommodate various types of organic compounds having Lewis base character.[1] Less attention has been paid to intercalations of carboxylic acids[2] and their derivatives.[3−6] Intercalates of vanadyl phosphate with nitriles (acetonitrile, propionitrile, butyronitrile, valeronitrile, hexanenitrile)[5] and dinitriles (malononitrile, succinonitrile, glutaronitrile, adiponitrile, pimelonitrile, suberonitrile)[6] were prepared. The nitrile intercalates (except for acetonitrile) contain one nitrile molecule per formula unit. The dinitrile content in the intercalates decreases with increasing chain length. In contrast to most $VOPO_4$ intercalates with guest molecules containing aliphatic chains where the basal spacing increases with increasing chain length,[2,7−11] the basal spacings of all the nitrile and the dinitrile intercalates prepared are practically the same. This demonstrates that the aliphatic part of the guest molecules must be parallel to the host layers.

In this paper we report on the intercalation of benzonitrile and *p*-tolunitrile into vanadyl phosphate to complete the picture on the intercalation ability of vanadyl phosphate towards different nitriles.

Results and Discussion

Similarly to aliphatic nitriles and dinitriles, the aromatic nitriles analysed cannot be intercalated directly into anhydrous vanadyl phosphate and also a replacement of the water molecules in $VOPO_4 \cdot 2H_2O$ does not lead to an intercalation. The benzonitrile and *p*-tolunitrile intercalates can be prepared by replacing 2-propanol or 1-propanol in the corresponding $VOPO_4$ intercalates. While the 2-propanol molecules are replaced very easily, the replacement of the 1-propanol molecules is very slow and intermediate phases are formed. Therefore, it is necessary to repeat the reaction with a new amount of the corresponding nitrile.

The intercalates prepared are greenish-yellow crystalline solids, indicating that only a small part of vanadium(V) has been reduced to vanadium(IV). The diffractogram of the benzonitrile intercalate shows sharp (00*l*) and weak (200 and 201) reflections (Figure 1a). Reflections at 201, 202 and 310 are present in the diffractogram of the *p*-tolunitrile intercalate (Figure 1b). The low intensity of a few (*hkl*) lines in the intercalates suggests a turbostratic structure where the original tetragonal layers of the host are retained, but are shifted in the directions of the *x* and/or *y* axes. The lattice parameters of the tetragonal structures are $a = 6.21$ Å, $c = 11.22$ Å and $a = 6.21$ Å, $c = 13.19$ Å for the benzonitrile and tolunitrile intercalates, respectively.

[a] Joint Laboratory of Solid State Chemistry of Institute of Macromolecular Chemistry of Academy of Sciences of the Czech Republic and University of Pardubice,
Studentská 84, 532 10 Pardubice, Czech Republic
Fax: (internat.) +420-46/6036011
E-mail: ludvik.benes@upce.cz
[b] Institute of Macromolecular Chemistry, Academy of Sciences of the Czech Republic,
Heyrovský Sq. 2, 162 06 Prague 6, Czech Republic
[c] Faculty of Mathematics and Physics, Charles University,
V Holešovickách 2, 180 00 Prague 2, Czech Republic
[d] Department of Analytical Chemistry, Institute of Chemical Technology,
Technická 5, 166 28 Prague, Czech Republic

 © 2003 Wiley-VCH Verlag GmbH & Co. KGaA, Weinheim **DOI: 10.1002/ejic.200300109**

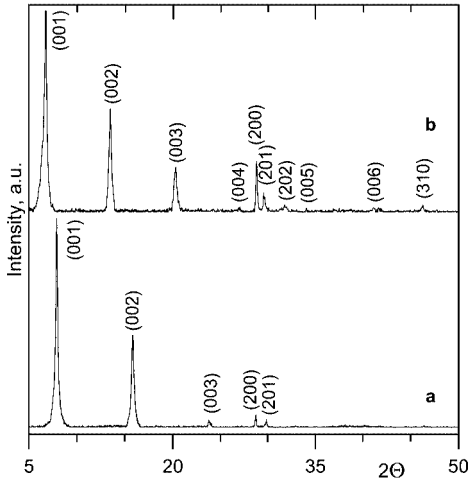

Figure 1. Diffractogram of benzonitrile (a) and *p*-tolunitrile (b) intercalated $VOPO_4$

The compositions of the intercalates were determined by thermogravimetric analysis (see Figure 2). During heating, nitriles are slowly released in two steps in the temperature range 100−550 °C. The second step is very slow and the DTA shows a broad exothermic peak probably due to the combustion of the nitriles. The product of the thermal decomposition is anhydrous vanadyl phosphate. Total weight losses correspond to the stoichiometric ratio $x = 1$, that is, one molecule of nitrile per formula unit (for the benzonitrile intercalate: calcd. 38.9%; found 38.1% and for the *p*-tolunitrile intercalate: calcd. 42.2%; found 40.9%).

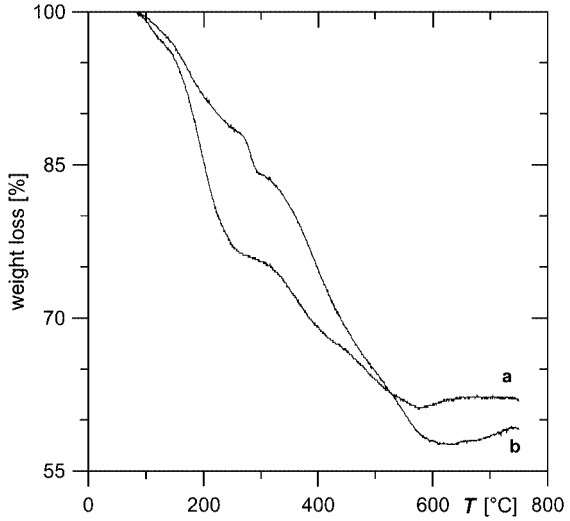

Figure 2. TG curves of the benzonitrile (a) and *p*-tolunitrile (b) intercalates

The benzonitrile and *p*-tolunitrile intercalates are more stable in air (at relative humidity 40−50%) than the nitrile intercalates[5] and less stable than the dinitrile intercalates.[6] The course of the hydration of both intercalates was followed by XRD. A small amount of dihydrate appeared after twenty minutes and the intercalates were completely decomposed after one day.

The character of the bonding between the guest and the host layers in the nitrile intercalates was studied by IR and Raman spectroscopy. From the point of view of the host-guest interaction, the most important position is that of the C≡N stretching vibration. The C≡N group can act either as a σ-donor, by donating nitrogen electrons to a metal, or as a π-donor, by donating electrons of a nitrile π-bond. The wavenumber of the C≡N stretching vibration is shifted to higher values in the case of σ-donation and to lower values in the case of π-donation.[12]

The IR spectra of pure benzonitrile and its $VOPO_4$ intercalate (KBr pellet and Nujol suspension), in the region from 2100 to 2400 cm^{-1}, are given in Figure 3. The strong C≡N stretching absorption band of pure benzonitrile is observed at 2228 cm^{-1}. In the spectrum of the benzonitrile intercalate, measured as a Nujol suspension, we observed two absorption bands at 2228 and at 2252 cm^{-1}. No shifted nitrile band was observed in the samples prepared as KBr pellets. The band with the same position as in the pure benzonitrile spectrum most probably corresponds to free benzonitrile molecules, which are present in the sample due to the instability of the intercalate in air. While preparing the KBr pellets the samples decomposed to free nitrile and vanadyl phosphate hydrate. In the case of the Nujol dispersion only a partial decomposition takes place. The shifted band observed at 2252 cm^{-1} in the IR spectrum of the Nujol suspension corresponds to coordinated benzonitrile. The observed shift indicates the formation of a C≡N→V bond in the intercalate.

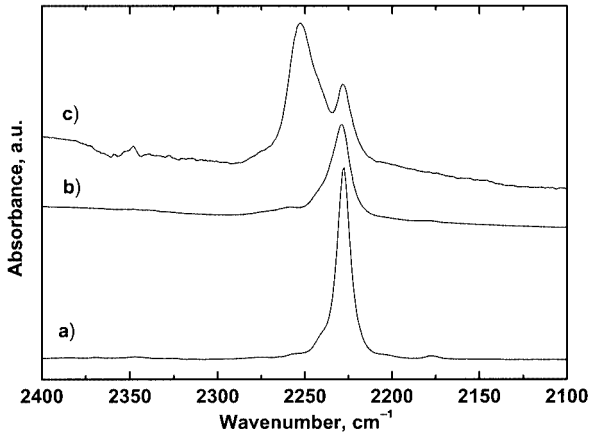

Figure 3. FTIR spectra of pure benzonitrile measured by the ATR technique (a) and of the benzonitrile intercalate measured as a KBr pellet (b) and as a Nujol suspension (c)

The Raman spectra of benzonitrile and its intercalate in the region from 400 to 4000 cm^{-1} are given in Figure 4. One can observe the intense band of the symmetric $\nu(PO_4)$ stretching vibration of a phosphate tetrahedron in the $(VOPO_4)_\infty$ layers. It is situated at about 941 cm^{-1} in the spectrum of the intercalate. Strong bands of aromatic vibrations at the same positions as in the spectrum of pure benzonitrile (1002, 1600 and 3078 cm^{-1}) are observed in the spectrum of the intercalate. The spectrum of the intercalate confirms that the structure of the original $VOPO_4$ layers

 © 2003 Wiley-VCH Verlag GmbH & Co. KGaA, Weinheim

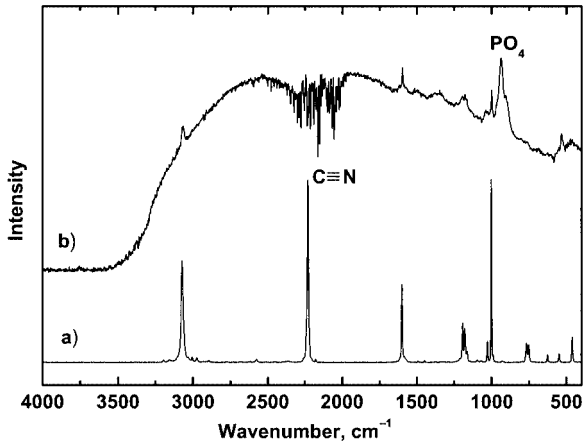

Figure 4. Raman spectra of liquid benzonitrile (a) and the benzonitrile intercalate (b)

remains unchanged and there are no significant changes in the guest molecules after intercalation. The vanadyl stretching band expected at about 1002 cm^{-1}, which appears to be especially sensitive to atoms coordinated to vanadium within an octahedral arrangement in the host-lattice structure, overlaps with one of the benzonitrile bands. The part of the Raman spectrum corresponding to the nitrile stretching vibration is strongly influenced by the baseline radiation. This is most probably due to the excitation of the benzonitrile molecules by the laser beam while the measurements were being performed.

The infrared spectra of pure tolunitrile and its intercalate in $VOPO_4$ (as a KBr pellet and as a Nujol suspension) in the region from 2100 to 2400 cm^{-1} are given in Figure 5. The strong C≡N stretching absorption band of pure tolunitrile is observed at 2228 cm^{-1}, exactly at the same position as for pure benzonitrile. There are three absorption bands at 2228, 2256 and 2269 cm^{-1} in the IR spectrum of the tolunitrile intercalate measured in the Nujol suspension. New shifted bands at 2256 and 2269 cm^{-1} correspond to two non-equivalent tolunitriles. From the fact that only one shifted nitrile band (2269 cm^{-1}) is observed in the IR spectrum of the tolunitrile intercalate dispersed in the KBr pellet, it follows that the bands at 2256 and 2269 cm^{-1} correspond to two (slightly different) arrangements of tolunitrile in the interlayer space.

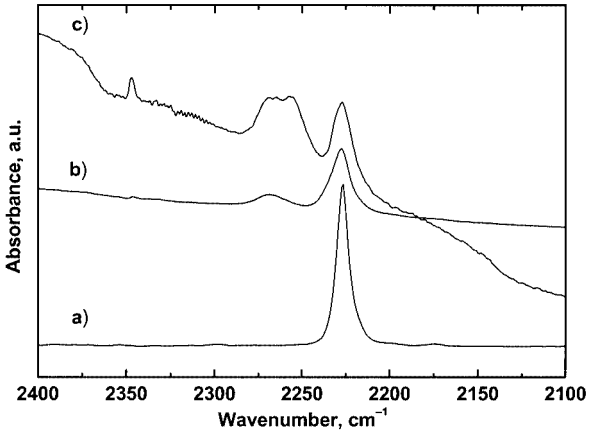

Figure 5. FTIR spectra of pure tolunitrile (a) and the tolunitrile intercalate measured as a KBr pellet (b) and as a Nujol suspension (c)

The Raman spectra of tolunitrile and its intercalate in the region from 400 to 4000 cm^{-1} are given in Figure 6. Only a part of the intercalate spectrum, including an intense band for the symmetric $\nu(PO_4)$ stretching vibration of the phosphate tetrahedron in the $(VOPO_4)_\infty$ layers situated at about 903 cm^{-1}, can be observed. The band for the aromatic vibration of tolunitrile is observed at about 1605 cm^{-1}. The part of the spectrum above 1800 cm^{-1} could not be measured due to the strong influence of the baseline radiation.

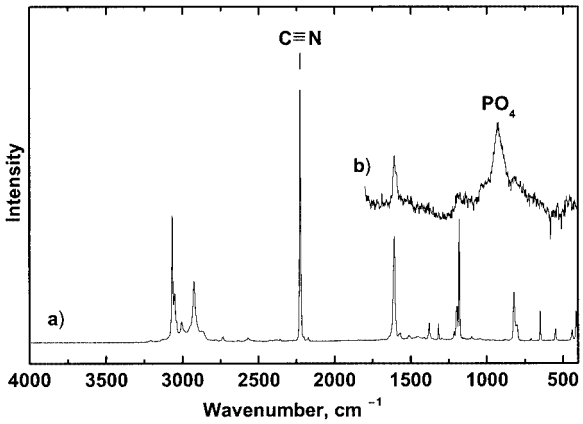

Figure 6. Raman spectra of liquid *p*-tolunitrile (a) and its intercalate (b)

The conclusions on the character of the bonding between the guest and the host layer in the nitrile intercalates are strongly supported by the results of quantum mechanical calculations and modeling. Figure 7 shows a DFT optimized structure of the molecular segment representing interactions of vanadyl phosphate with nitriles. In order to make the electronic structure in the segment close to the conditions appearing in the intercalates, free terminal oxygen atoms were substituted by OH groups and the total charge of the model compound was set to +3, the nitrile group being represented by acetonitrile. It was found that all the geometry optimizations, with various starting orientations for the acetonitrile with respect to the vanadyl group, lead to the structure displayed in Figure 7. Quantum chemical calculations thus support the results of the IR and Raman spectroscopy indicating the formation of the C≡N→V bond in the intercalates.

Because of the size and computational demand, the simulation of larger local intercalate structures, including two $VOPO_4$ layers, could only be done by using the semiempirical quantum-chemical method PM3. However, the model structure shown in Figure 7 was reoptimized with the PM3 method and only slight changes in optimized molecular parameters were found in comparison with a high precision DFT approach. This indicates that no serious artifacts are produced by the semiempirical PM3 method. The optimized geometries of the molecular segments, representing two

 © 2003 Wiley-VCH Verlag GmbH & Co. KGaA, Weinheim

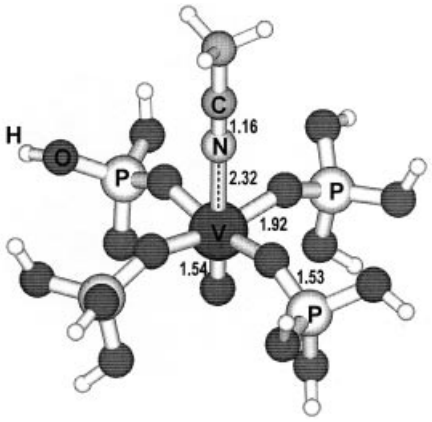

Figure 7. Optimized DFT structure of the molecular segment modeling the vanadyl phosphate-nitrile interaction, with indicated bond lengths (in Å)

layers of $VOPO_4$ and five molecules of benzonitrile and *p*-tolunitrile, intercalated between the two layers, are given in Figures 8 and 9, respectively. Free terminal oxygen atoms were substituted by OH groups and the total charge of the model compounds was set to −2. The coordination of the vanadium atoms to the nitriles in adjacent guest interlayer spaces was simulated by coordinating acetonitrile molecules, which are not shown in Figures 8 and 9. The initial geometrical parameters (bond lengths and angles) for the $VOPO_4$ layers were taken from the experimental X-ray diffraction data determined for $VOPO_4 \cdot 2H_2O$[13] and the initial basal spacings were set to the above given values of the lattice parameters c = 11.22 and 13.19 Å, determined by X-ray diffraction for the benzonitrile and *p*-tolunitrile intercalates, respectively. The first geometrical optimizations of the model structures were performed under various symmetry constraints and fixed parameters c. In the final energy minimization all the variables defining the positions of the atoms, both in the host and guest layers, were fully optimized, with the exception of the constraints arising from the symmetry conditions defining the polyhedra in the $VOPO_4$ layers and the relative orientations of four equivalent guest molecules in the interlayer space with respect to the $VOPO_4$ layer. The calculated basal spacings of 11.32 Å for benzonitrile and 13.00 Å for tolunitrile are in good agreement with the experimental values of 11.22 and 13.19 Å, respectively. The mutual position of the successive layers exhibits a shift that can be characterized by a vector with the components 0.12 and 0.14 Å for the benzonitrile and 0.08 and 0.06 Å for the tolunitrile intercalates.

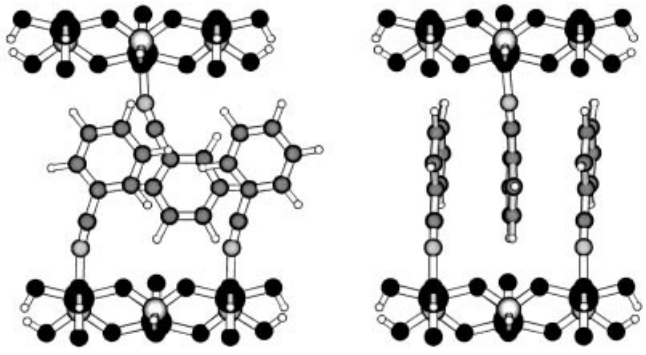

Figure 8. Side view of the PM3 optimized geometry of the molecular segment modeling the arrangement of benzonitrile molecules between the $VOPO_4$ layers

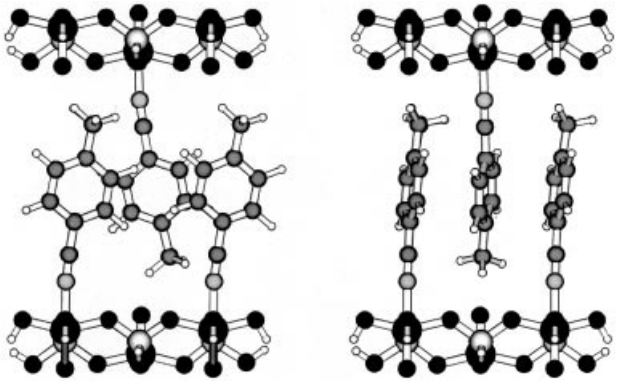

Figure 9. Side view of the PM3 optimized geometry of the molecular segment modeling the arrangement of *p*-tolunitrile molecules between the $VOPO_4$ layers

In the modeled structures one can observe cavities, which are larger for the tolunitrile intercalate than for the benzonitrile intercalate. The results of the model calculations indicate that water molecules, which are hydrogen-bonded to the oxygen atoms of the phosphate tetrahedron of the host layers, can be inserted into these cavities, in analogy with the second water molecules in vanadyl phosphate dihydrate.[14] Such water molecules can penetrate into the samples as soon as the latter are taken out of the ampoule. Amounts of incorporated water have been observed in the tolunitrile intercalate IR spectrum (as a Nujol suspension) at about 3500 and 3350 cm^{-1}, but they were not observed in the IR spectrum of the benzonitrile intercalate or of pure Nujol (see Figure 10). The overall (basic) crystalline structure of the intercalate is influenced by the presence of these water molecules only negligibly and thus the induced change is not observed in the diffractogram. However, the presence of the water molecules influences the coordination of the tolunitrile molecules in the vanadyl octahedron and

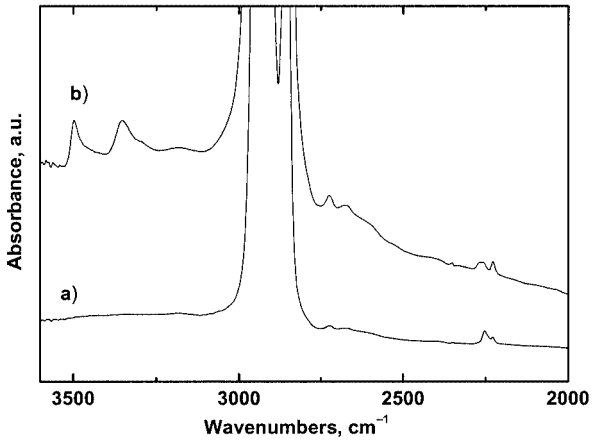

Figure 10. FTIR spectra of the benzonitrile (a) and tolunitrile (b) intercalates measured as a Nujol suspension

 © 2003 Wiley-VCH Verlag GmbH & Co. KGaA, Weinheim

in the spectrum of the sample prepared as a Nujol suspension. This fact is probably shown by the presence of the second nitrile band at 2256 cm^{-1}, while the band at 2269 cm^{-1} corresponds to the original anhydrous tolunitrile intercalate structure. In the case of the KBr pellets we observe only a weak band of coordinated nitrile molecules in the hydrous intercalate, due to the decomposition of the sample by hydration during milling.

Conclusion

In contrast to aliphatic nitriles, molecules of aromatic nitriles are oriented perpendicularly to the host layers. The guest molecules are arranged in the interlayer space in an interdigitated manner, with the planes of the aromatic rings being parallel. This arrangement forms cavities between the guest molecules, especially in the *p*-tolunitrile intercalate. These cavities facilitate the incorporation of water molecules into the intercalates and thus reduce their stability. The assumption of the perpendicular arrangement of the guest molecules is supported by the fact that the basal spacing of the *p*-tolunitrile intercalate is about 2 Å higher than that of the benzonitrile intercalate. Quantum chemical calculations support the results of the IR and Raman spectroscopy indicating the formation of the C≡N→V donor-acceptor bond in the intercalates.

Experimental Section

Preparation: The intercalation compounds were obtained by a displacement reaction. The solid 2-propanol intercalate[10] was prepared in advance and used as a starting material for the reaction with the corresponding aromatic nitrile. The 2-propanol intercalate (0.5 g) was suspended in 10 mL of benzonitrile or molten *p*-tolunitrile and heated in a microwave field for 10 min. The samples were washed with toluene, dried in vacuo, and stored in a sealed evacuated ampoule.

XRD: Powder data were obtained with a D8 Advance X-ray diffractometer (Bruker AXS, Germany) using Cu-K_α radiation with a graphite secondary monochromator. Diffraction angles were measured from 5 to 50° (2θ). The samples were kept under a protection foil during the measurements and the signal of this foil in the diffractograms was compensated.

Thermogravimetry: The TG analyses were performed using a Derivatograph C (MOM Budapest, Hungary). The measurements were carried out in air between 20 and 700°C at a heating rate of 5 $K \cdot min^{-1}$.

IR Spectral Measurements: IR spectra in the range 400−4000 cm^{-1} were measured with a fully computerized Nicolet IMPACT 400 FTIR spectrometer (300 scans per spectrum at 2 cm^{-1} resolution). Measurements were performed in the transmission mode on a KBr pellet and a Nujol suspension for the intercalates and by the ATR technique on a ZnSe crystal for pure liquid guest-molecules. The spectra were corrected for the H_2O and CO_2 content in the optical path.

Raman Spectral Measurements: FT Raman spectra were collected using a Fourier transform near-infrared (FT-NIR) spectrometer Equinox 55/S (Bruker) equipped with FT Raman module FRA 106/S (Bruker) (128 interferograms were co-added per spectrum in the range 4000 to −1000 cm^{-1} at 4 cm^{-1} resolution).

Modeling: The strategy of the modeling was based on the quantum chemical geometry optimization of model compounds representing local structures and interactions appearing in the intercalates of vanadyl phosphate with nitriles. Quantum chemical calculations were carried out at the ab initio and semiempirical levels of theory employing the Gaussian 98[15] and MOPAC 2002[16] program packages, respectively. Local interactions and structures in intercalates of vanadyl phosphate with the nitrile group were studied at the DFT level using the B3LYP functional and 6-31G(d) basis set, geometrical optimization of larger structures including two vanadyl phosphate layers and five benzonitrile or *p*-tolunitrile molecules were performed at the semiempirical level using the PM3 method.

Acknowledgments

The authors wish to thank the Grant Agency of the Czech Republic (grant No. 202/01/0520) for financial support. The help of the Ministry of Education, Youth and Sports of the Czech Republic (VZ, 113200002 and MSM 253100001) and the Academy of Sciences of the Czech Republic (Key project KSK 4050111 and grant AVOZ4050913) is also appreciated.

[1] J. Kalousová, J. Votinský, L. Beneš, K. Melánová, V. Zima, *Collect. Czech. Chem. Commun.* **1998**, *63*, 1−19.
[2] L. Beneš, J. Votinský, J. Kalousová, K. Handlíř, *Inorg. Chim. Acta* **1990**, *176*, 255−259.
[3] M. Martinez-Lara, L. Moreno-Real, A. Jimenez-Lopez, S. Bruque-Gamez, A. Rodriguez-Garcia, *Mater. Res. Bull.* **1986**, *21*, 13−23.
[4] V. Zima, L. Beneš, K. Melánová, *Solid State Ionics* **1998**, *106*, 285−290.
[5] L. Beneš, V. Zima, K. Melánová, M. Trchová, P. Matějka, *J. Inclusion Phenom.* **2002**, *43*, 95−99.
[6] L. Beneš, V. Zima, K. Melánová, M. Trchová, P. Matějka, *J. Inclusion Phenom.* **2003**, *45*, 235−239.
[7] K. Beneke, G. Lagaly, *Inorg. Chem.* **1983**, *22*, 1503−1507.
[8] L. Beneš, K. Melánová, V. Zima, J. Kalousová, J. Votinský, *Inorg. Chem.* **1997**, *36*, 2850−2853.
[9] J. W. Johnson, A. J. Jacobson, J. F. Brody, S. M. Rich, *Inorg. Chem.* **1982**, *21*, 3820−3825.
[10] L. Beneš, V. Zima, K. Melánová, *J. Inclusion Phenom.* **2001**, *40*, 131−138.
[11] L. Beneš, K. Melánová, V. Zima, M. Trchová, E. Uhlířová, P. Matějka, *Eur. J. Inorg. Chem.* **2001**, 713−719.
[12] K. Nakamoto, *Infrared and Raman Spectra of Inorganic and Coordination Compounds. Part B: Applications in Coordination, Organometallic, and Bioinorganic Chemistry*, John Wiley & Sons, New York, **1997**, pp. 113−115, 284.
[13] H. R. Tietze, *Aust. J. Chem.* **1981**, *34*, 2035−2038.
[14] M. Trchová, P. Čapková, P. Matějka, K. Melánová, L. Beneš, *J. Solid State Chem.* **1999**, *148*, 197−204.
[15] M. J. Frisch, G. W. Trucks, H. B. Schlegel, G. E. Scuseria, M. A. Robb, J. R. Cheeseman, V. G. Zakrzewski, J. A. Montgomery, Jr., R. E. Stratmann, J. C. Burant, S. Dapprich, J. M. Millam, A. D. Daniels, K. N. Kudin, M. C. Strain, O. Farkas, J. Tomasi, V. Barone, M. Cossi, R. Cammi, B. Mennucci, C. Pomelli, C. Adamo, S. Clifford, J. Ochterski, G. A. Petersson, P.

 © 2003 Wiley-VCH Verlag GmbH & Co. KGaA, Weinheim

Y. Ayala, Q. Cui, K. Morokuma, D. K. Malick, A. D. Rabuck, K. Raghavachari, J. B. Foresman, J. Cioslowski, J. V. Ortiz, A. G. Baboul, B. B. Stefanov, G. Liu, A. Liashenko, P. Piskorz, I. Komaromi, R. Gomperts, R. L. Martin, D. J. Fox, T. Keith, M. A. Al-Laham, C. Y. Peng, A. Nanayakkara, M. Challacombe, P. M. W. Gill, B. Johnson, W. Chen, M. W. Wong, J. L. Andres, C. Gonzalez, M. Head-Gordon, E. S. Replogle, J. A. Pople, *Gaussian 98, Revision A.9*, Gaussian, Inc., Pittsburgh PA, **1998**.

[16] J. J. P. Stewart, *MOPAC 2002*, Fujitsu Limited, Tokyo, Japan, **1999**.

Received February 21, 2003

 © 2003 Wiley-VCH Verlag GmbH & Co. KGaA, Weinheim

EurJIC
European Journal of Inorganic Chemistry

Issue 20/2003
Pages 3669–3832

Papers available ahead of print in Early View at www.interscience.wiley.com

Earliest available Table of Contents:
Automatically, free of charge by e-mail through
www.interscience.wiley.com/alerts

COVER PICTURE

The cover picture shows a chain of seven metal atoms parallel to a chain of Chinese friendship symbols (locks which people like to fix at high lookout points and then throw the keys down). The background photo was taken in the Chinese Huangshan mountains, but it relates to friendship grown in Fraiburg, Germany, and symbolizes a truly international scientific collaboration. As a result, the Chinese author of this paper has prepared the chainlike Fe–C–N–Ni–Ni–Ni–Ni–Ni–N–C–Fe complex, while the senior author is the godfather of his daughter, the energetic baby with the name Freia, pregnant with meaning. Details are discussed in the article by H. Vahrenkamp et al. on p. 3731 ff.

MICROREVIEW

Contents

3681 **M. Gómez**

(Alkyl)(monocyclopentadienyl)niobium and -tantalum Complexes in Insertion Processes

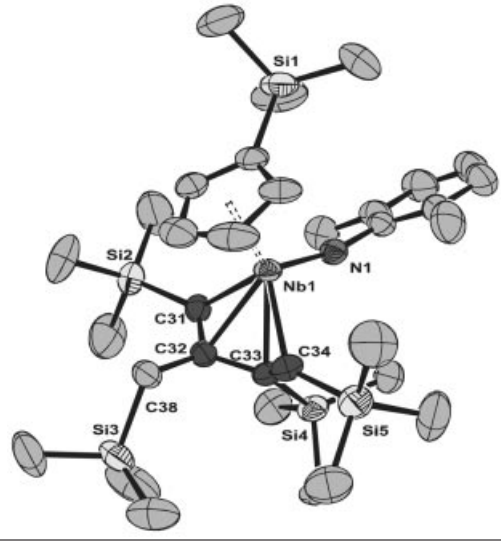

Keywords: Niobium / Tantalum / Cyclopentadienyl ligands / Insertions

 © 2003 Wiley-VCH Verlag GmbH & Co. KGaA, Weinheim

SHORT COMMUNICATIONS

3699 **B. Yang, C. Li, H. Hu, X. Yang, Q. Li, Y. Qian***

A Room-Temperature Route to Bismuth Nanotube Arrays

Keywords: Bismuth / Nanostructures / Nanotubes / Synthesis design

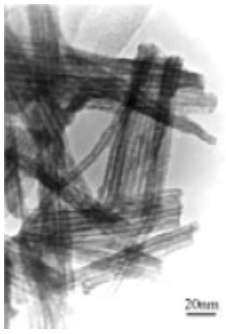

3703 **M. Fondo,* A. M. García-Deibe, J. Sanmartín, M. R. Bermejo, L. Lezama, T. Rojo**

A Binuclear Copper(II) Acetate Complex Showing a 3D Supramolecular Network with Hydrophilic Pockets: Its Unusual Magnetic Behaviour

Keywords: 3D network / Copper / Magnetic properties / Bridging ligands / Intermolecular interactions

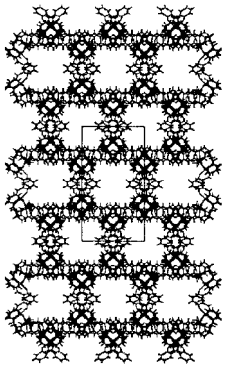

3707 **L. Vieille-Petit, B. Therrien, G. Süss-Fink***

Chiral Arene Ruthenium Complexes: Synthesis and Molecular Structure of the Enantiopure Cluster Cation (*S*)-$[H_3Ru_3\{C_6H_5[CH(CH_3)CH_2OH]\}(C_6Me_6)_2(O)]^+$

Keywords: Arene ligands / Chirality / Cluster compounds / Ruthenium

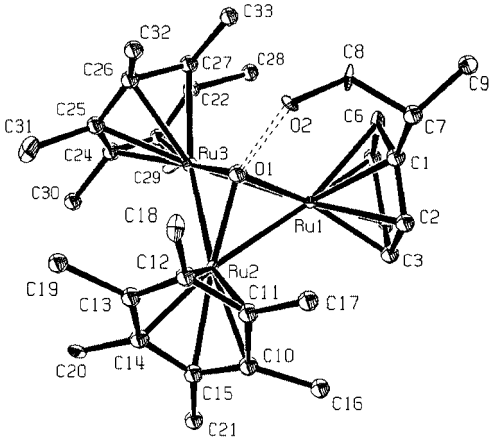

3712 **Y.-R. Xie, H. Zhao, X.-S. Wang, Z.-R. Qu, R.-G. Xiong,* X. Xue, Z. Xue, X.-Z. You**

2D Chiral Uranyl(VI) Coordination Polymers with Second-Harmonic Generation Response and Ferroelectric Properties

Keywords: Chirality / Polymers / Uranium / Crystal engineering / SHG properties

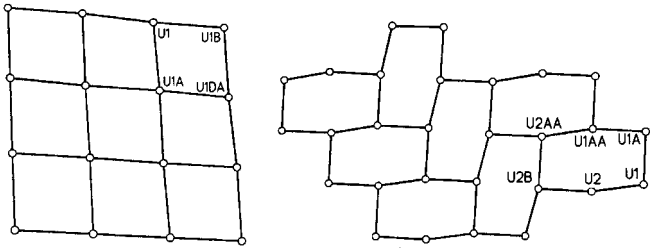

3716 **A. Ishii,* M. Murata, H. Oshida, K. Matsumoto, J. Nakayama***

Oxosulfido Complexes of Platinum − $(Ph_3P)_2Pt(S_2O)$ and $(Ph_3P)_4Pt_2(\mu\text{-}S)(\mu\text{-}SO)$ − Their Formation and Properties

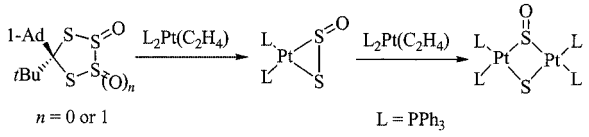

Keywords: Platinum / S ligands / Oxo ligands

FULL PAPERS

3723 **D. Badura, H. Vahrenkamp***

Pyrazolylboratozinc Complexes of Nucleosides and Nucleoside Analogues

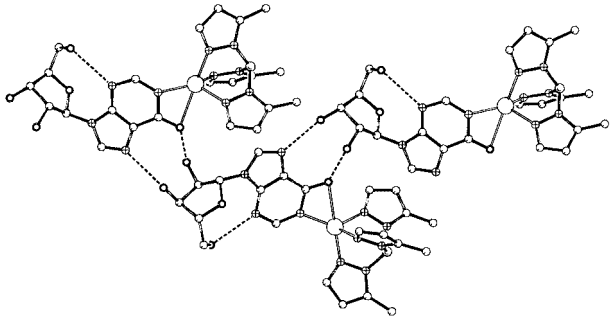

Keywords: Zinc / Nucleosides / Bioinorganic chemistry / N ligands

3731 **T. Sheng, R. Appelt, V. Comte, H. Vahrenkamp***

Chain-Like Tetra-, Penta- and Heptanuclear Cyanide-Bridged Complexes by Attachment of Organometallic Cyanides to M_2, M_3 and M_5 Units

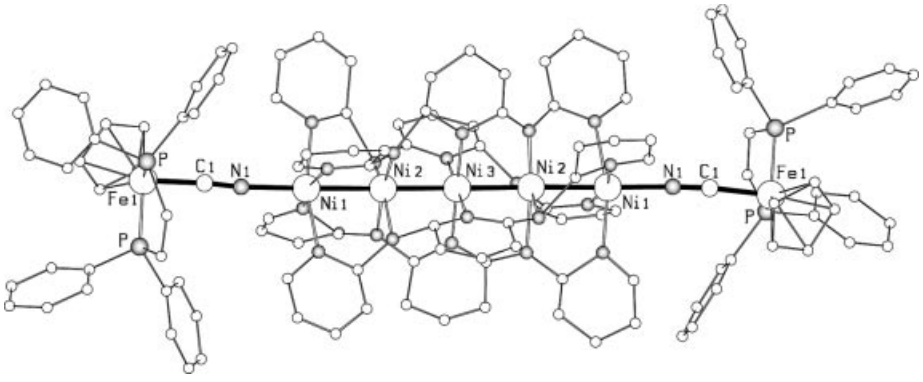

Keywords: Cyanides / Polynuclear complexes / Metal-metal interactions / Electrochemistry

3738 **B. M. Alzoubi, M. S. A. Hamza, A. Felluga, L. Randaccio, G. Tauzher, R. van Eldik***

Coenzyme B_{12} Model Studies − Kinetics of Axial Ligation of Alkylcobalt Complexes Containing a Tridentate Amino-Oximate Ligand

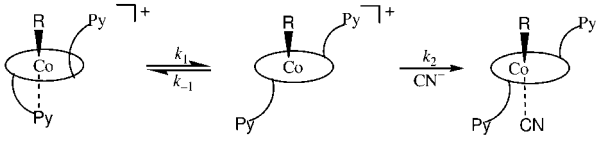

Keywords: Ligand substitution / Cobalt / Kinetics / Mechanism / Enzymes / High-pressure chemistry

 © 2003 Wiley-VCH Verlag GmbH & Co. KGaA, Weinheim

3745 **J. Schapp, K. Haas, K. Sünkel, W. Beck***

Cyclotetrapeptide Complexes of Nickel(II) and Palladium(II) by Template Synthesis from Dipeptide Esters with Functionalized Side Chains − Crystal Structure of [(*cyclo*-Gly-β-Ala-Gly-β-Ala-4H$^+$)Cu](PPN)$_2$

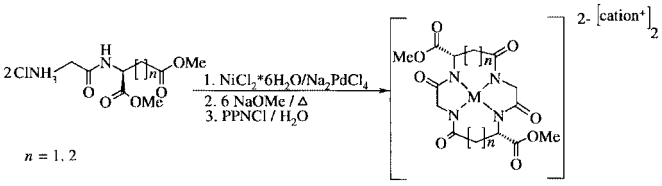

Keywords: Peptides / Nickel / Palladium / Copper

3752 **C. Goze, J.-C. Chambron, V. Heitz,* D. Pomeranc, X. J. Salom-Roig, J.-P. Sauvage,* A. F. Morales, F. Barigelletti***

Long-Lived MLCT Excited States-Ru^{II} Complexes with a Helical Bis-Phen Ligand

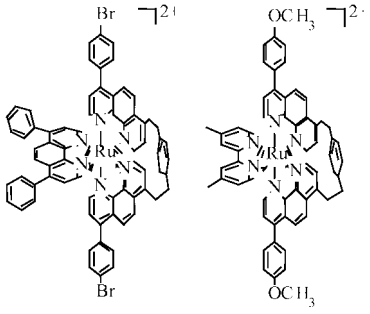

Keywords: Luminescence / N ligands / Photochemistry / Ruthenium

3759 **A. Tellenbach, M. Jansen***

$P_8O_{12}{\cdot}2BH_3$ − The Borane Adduct of a New Molecular Phosphorus Oxide

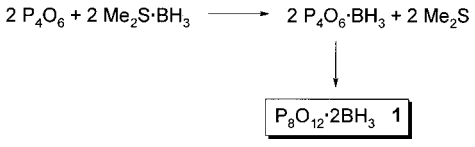

Keywords: Phosphorus / Phosphorus oxides / Boranes / Cage compounds / Dimerization

3767 **M. Heitzmann, J.-C. Moutet,* J. Pécaut, O. Reynes, G. Royal,* E. Saint-Aman, G. Serratrice**

Modulation of the Communication between Redox Centers in a Tris(ferrocene)-tren Ligand by Complexation of Lanthanide Ions

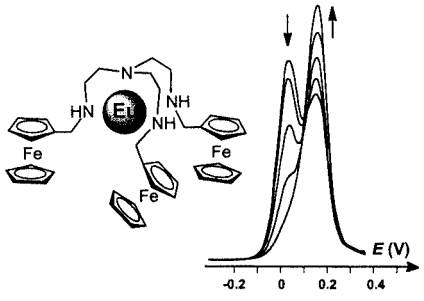

Keywords: Sandwich complexes / Electrostatic interactions / Electrochemistry / Lanthanides

3774 **D. Song, S. Wang***

Pd^{II}, Zn^{II} and Ag^{I} Complexes of Tetrakis-(*N*-7-azaindolyl)benzene: Variation of Bonding Modes, Extended Structures and Luminescence

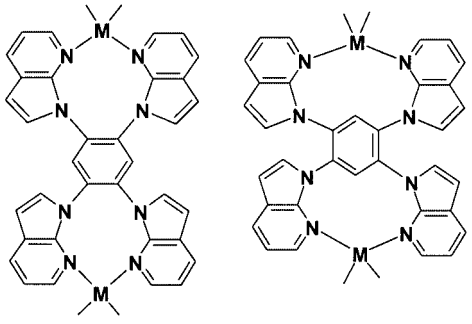

Keywords: N ligands / Coordination modes / Palladium / Zinc / Silver / Luminescence

 © 2003 Wiley-VCH Verlag GmbH & Co. KGaA, Weinheim

3783 **S.-Y. Wan, Y.-Z. Li, T. Okamura, J. Fan, W.-Y. Sun,* N. Ueyama**

Syntheses, Structures, and Properties of Two-Dimensional Honeycomb Networks from the Assembly of the Tripodal Ligand 2,4,6-Tris[4-(imidazol-1-ylmethyl)phenyl]-1,3,5-triazine with Metal Salts

Keywords: Tripodal ligands / Zinc / Nickel / Supramolecular chemistry / Organic-inorganic hybrid composites

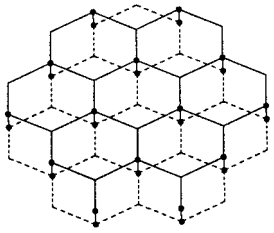

3790 **M. Sobczyk, A. Sawicka, P. Skurski***

Theoretical Search for Anions Possessing Large Electron Binding Energies

Keywords: Anions / Superhalogens / Electron-binding energy

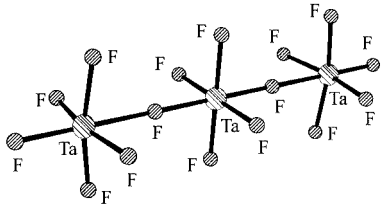

$Ta_3F_{16}^-$ (VDE = 12.63 eV)

3798 **Y. Steudel, R. Steudel***

Structures of the Octahedral Persulfuranes H_4SF_2, H_2SF_4, Me_2SH_4 and Me_2SF_4, and Activation Enthalpies for Their *cis*/*trans* Isomerization

Keywords: Hypercoordinate molecules / Ab initio calculations / Transition states / Isomerism / Sulfur / Fluorides

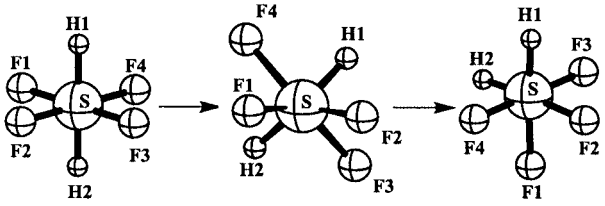

TS

3803 **F. De Proft, R. Vivas-Reyes, M. Biesemans, R. Willem, J. M. L. Martin, P. Geerlings***

Density Functional Study of the Complexation Reaction of $Sn(CH_3)_3X$ (X = F, Cl, Br and I) with Halide Anions

Keywords: Tin / Halides / HSAB / Density functional calculations / NMR spectroscopy

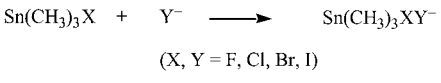

3811 **J. W. Sprengers, M. de Greef, M. A. Duin, C. J. Elsevier***

Stable Platinum(0) Catalysts for Catalytic Hydrosilylation of Styrene and Synthesis of [Pt(Ar-bian)(η^2-alkene)] Complexes

Keywords: Platinum / Hydrosilylations / N ligands / Homogeneous catalysis / Alkene ligands

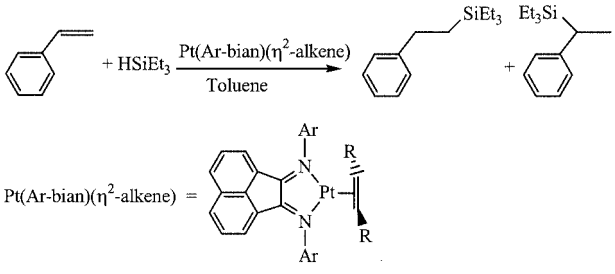

 © 2003 Wiley-VCH Verlag GmbH & Co. KGaA, Weinheim

3820 **S. Chakrabarti, S. K. Pati, M. A. Green, S. Natarajan***

Synthesis, Structure and Magnetic Properties of a New Iron Arsenate, $[C_{10}N_4H_{28}][\{FeF(OH)(HAsO_4)\}_4]$, with a Layer Structure

Keywords: Iron / Arsenic / Solvothermal synthesis / N ligands

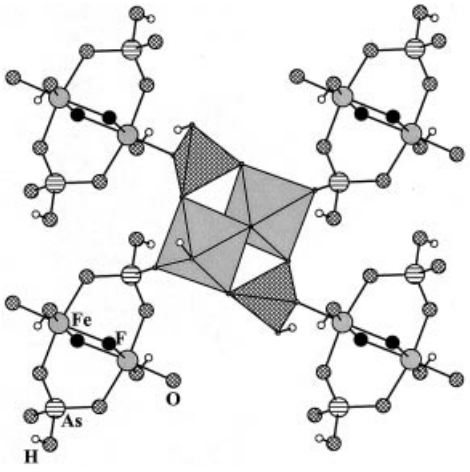

3826 **M. Papachristou, I. Pirmettis, T. Siatra-Papastaikoudi, M. Pelecanou, C. Tsoukalas, C. P. Raptopoulou, A. Terzis, E. Chiotellis, M. Papadopoulos***

Synthesis and Characterization of Oxorhenium and Oxotechnetium Complexes with a Novel Tetradentate N_3O Bifunctional Agent

Keywords: Rhenium / Technetium / N,O ligands / Radiopharmaceuticals

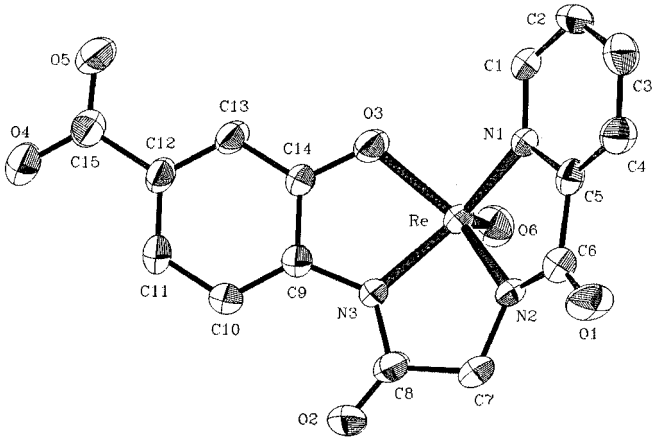

CORRECTION

3831 **Rosa M. Claramunt, Pilar Cornago, Mercedes Cano,* José V. Heras, M. Luz Gallego, Elena Pinilla, M. Rosario Torres**

New Tris(pyrazolyl)triazine and Pyrazolylpyridine Gold(I) and Palladium(II) Derivatives Based on the 3,5-Bis(4-butoxyphenyl)pyrazole Group − Architectures with Different Types of Bonding Interactions

Keywords: Gold / Hydrogen bonds / Palladium / Supramolecular Chemistry / Triazine

 © 2003 Wiley-VCH Verlag GmbH & Co. KGaA, Weinheim

(Alkyl)(monocyclopentadienyl)niobium and -tantalum Complexes in Insertion Processes

Manuel Gómez[a]

Dedicated to Professor Pascual Royo on the ocassion of his 65th birthday

Keywords: Niobium / Tantalum / Cyclopentadienyl ligands / Insertions

Alkyl high-valent early transition metal compounds are important organometallic species, particularly because their reactions with unsaturated molecules, such as carbon monoxide and organic isocyanides, are relevant to several industrial stoichiometric and catalytic processes. Recently, we have reported several studies concerning (alkyl)(monocyclopentadienyl) derivatives of group-5 metals, including both synthetic aspects and chemical behaviour in insertion reactions. This Microreview is an account of this work, covering syntheses, structure, spectroscopic, and reactivity details that have been reported by us together with the most significant contributions from other authors.
(© Wiley-VCH Verlag GmbH & Co. KGaA, 69451 Weinheim, Germany, 2003)

Introduction

The transfer of alkyl groups from transition metal atoms to coordinated unsaturated molecules,[1] such as carbon monoxide and isocyanides, is an important organometallic reaction that has been the subject of relevant synthetic, mechanistic and theoretical studies.[2] Further, the resulting η^2-acyl− and η^2-iminoacyl−metal functionalities constitute a powerful strategy for C−C bond formation under mild reaction conditions and are versatile reactive intermediates in many transition-metal-promoted stoichiometric and catalytic organometallic transformations.[3]

Compared with the η^2-acyl moiety, the reactivity of the η^2-iminoacyl group is even more versatile because it can be transformed into metallacyclic imines,[2d,2f,2h,2k] azaallyl complexes,[3i,3j,3k] and aminocarbyne derivatives[3f] or may participate in alkyne coupling processes[3g] and double[3e,3i,3j,3k] or multiple[3e,3i,3j,3k] isocyanide insertion reactions. It may also be transformed into azametallacyclopropane species, which give imido complexes[2e] by thermal decomposition. These reactions[2c,2d,2j,3g] are profoundly dependent on both the metal and the nature of its substituents, particularly on the number of metal-bound alkyl groups that can participate in the reaction. In this context, a systematic study[4] of isocyanide insertion reactions into methyl−tantalum bonds of different chloro(methyl)(pentamethylcyclopentadienyl) derivatives ($TaCp^*Cl_{4-x}Me_x$) led us to isolate a series of (η^2-iminoacyl)- ($x = 1$) and dichloroazatantalacyclopropane ($x = 2$) as well as chloro- and (methyl)(alkenylamido)(imido) ($x = 3, 4$) complexes.

This Microreview aims to systematically overview the synthetic methods of producing different alkyl(monocyclopentadienyl)niobium- and -tantalum(v) derivatives and also their behaviour in insertion reactions, as well as provid-

[a] Departamento de Química Inorgánica, Universidad de Alcalá de Henares, Campus Universitario,
28871 Alcalá de Henares, Spain
Fax: (internat.) + 34-91/885-4683
E-mail: manuel.gomez@uah.es

Manuel Gómez was born in Cieza (Murcia, Spain) in 1954. He received his Diploma in Chemistry at the University of Murcia in 1976 and his Ph.D. in 1981 from the University of Alcalá de Henares working in the field of coordination and organometallic chemistry with Professor Pascual Royo. He was a postdoctoral fellow at the University of Sheffield in 1982−1983 under the supervision of Professor Peter M. Maitlis. He subsequently joined the Inorganic Chemistry Department at the University of Alcalá de Henares where he is Professor of Inorganic Chemistry, a position he has held since 1985. His main research interests are in the field of organometallic chemistry, with an emphasis on synthesis, reactivity and applications of mono(cyclopentadienyl)niobium and -tantalum complexes.

MICROREVIEWS: This feature introduces the readers to the authors' research through a concise overview of the selected topic. Reference to important work from others in the field is included.

ing some data on intra- or intermolecular rearrangement processes of the insertion products.

Results and Discussion

Synthesis of Dichloro Complexes

The studies described here start with dichloro(imido)-, dialkyldichloro-, (alkyne)dichloro-, and (diazabutadiene)dichloro(monocyclopentadienyl)niobium and -tantalum complexes. Recent years have witnessed an extensive development of imido group-5 metal chemistry containing monofunctional,[5] tetradentate triamidoamine,[6] and cyclopentadienyl ligands in mono-[7] and dicyclopentadienyl-type[8] complexes. Protonated lithium amides[7b] have been extensively used to generate the imido ligand, but other synthetic strategies have been based on the deprotonation of cyclopentadiene by metal amides,[7e,8c] β-hydrogen elimination of amides and amines coordinated to metal(III) compounds[8a,8b] and oxidation of metal(III) complexes with azides.[8b] Related alkoxyimido and hydrazido(2−) derivatives have been reported[9] more recently.

Pseudo-tetrahedral dichloro(imido) compounds **$MCpCl_2(NR^1)$** (M = Nb,[10] Cp = η^5-$C_5H_4SiMe_3$ = Cp′, R^1 = 2,6-$Me_2C_6H_3$, **1**; 2,6-*i*$Pr_2C_6H_3$, **2**; $SiMe_3$, **3**; M = Ta, Cp = η^5-C_5Me_5 = Cp*, R^1 = C_6H_5, **4**;[11] 2,6-$Me_2C_6H_3$, **5**[4]) can be easily obtained from the corresponding tetrachloro derivative $MCpCl_4$ (Scheme 1). Complex **5** was prepared by reacting $TaCp^*Cl_2Me_2$[12] with 2 equiv. of 2,6-$Me_2C_6H_3NC$ in toluene as described previously.[4c]

Dialkyldichloro complexes **$MCp^*Cl_2R_2$** (M = Nb, R = Me, **6**;[13c] M = Ta, R = CH_2SiMe_3, **7**;[13d] CH_2CMe_2Ph **8**;[13d] CH_2CMe_3, **9**;[13a,13b] CH_2Ph, **10**[13a,13b]) have been obtained by treating *n*-hexane suspensions of the MCp^*Cl_4 complex with stoichiometric amounts of the Grignard reagents MgClR (R = Me, CH_2SiMe_3, CH_2CMe_2Ph, CH_2Ph) or $Mg(CH_2CMe_3)_2(THF)_2$ under rigorously anhydrous conditions at room temperature (Scheme 1).

The (alkyne)dichloro complex **$NbCp'Cl_2(Me_3SiCCSiMe_3)$**, **11**[14] has been synthesized in high yield by treating $NbCp'Cl_4$ with an excess of aluminium powder and mercury(II) chloride in the presence of 1 equiv. of bis(trimethylsilyl)acetylene. Additionally, the reaction of **11** with 2,3-dimethyl-1,4-diphenyl-1,4-diazabuta-1,3-diene (Me,Ph-DAD) in hexane leads to the (diazabutadiene)dichloro complex **$NbCp'Cl_2$(Me,Ph-DAD)**, **12**[15] with elimination of $C_2(SiMe_3)_2$ (Scheme 1). Related DAD complexes[16] have been, essentially, isolated by treatment of the corresponding half-sandwich complexes $NbCpCl_4$ (Cp = η^5-C_5H_5, η^5-C_5Me_5) with a dilithium salt of the different DAD ligands.

Synthesis of Alkyl Complexes

Although the imido ligand has been employed as an ancillary group to support high-oxidation state metal centres,[17] these complexes can be made highly reactive in terms of synthesizing coordinatively unsaturated derivatives containing multiple π-bonded ligands. Further, an increasing number of complexes having reactive imido ligands have been shown to participate in C−H activation[18] and cycloaddition reactions.[19] Conversely, reactions based on carbon−carbon bond formation have led to many important synthetic applications of organo group-5 metal complexes by migration of methyl substituents to unsaturated isocyanide[4,20] and carbonyl[20a] ligands through the intermediate formation of (iminoacyl)- and (acyl)metal compounds, respectively. Whereas the chemistry of (cyclopentadienyl)(halo)(imido)niobium and -tantalum complexes is well defined, the alkyl derivatives are less well known although a great number of related amido and alkoxide complexes have been reported recently. Following our preliminary work on the dichloro- and chloro(methyl)(imido) derivatives[4b,20a] we reported a systematic study on the reactivity of (arylimido)(monocyclopentadienyl)niobium and -tantalum complexes towards alkylating reagents.

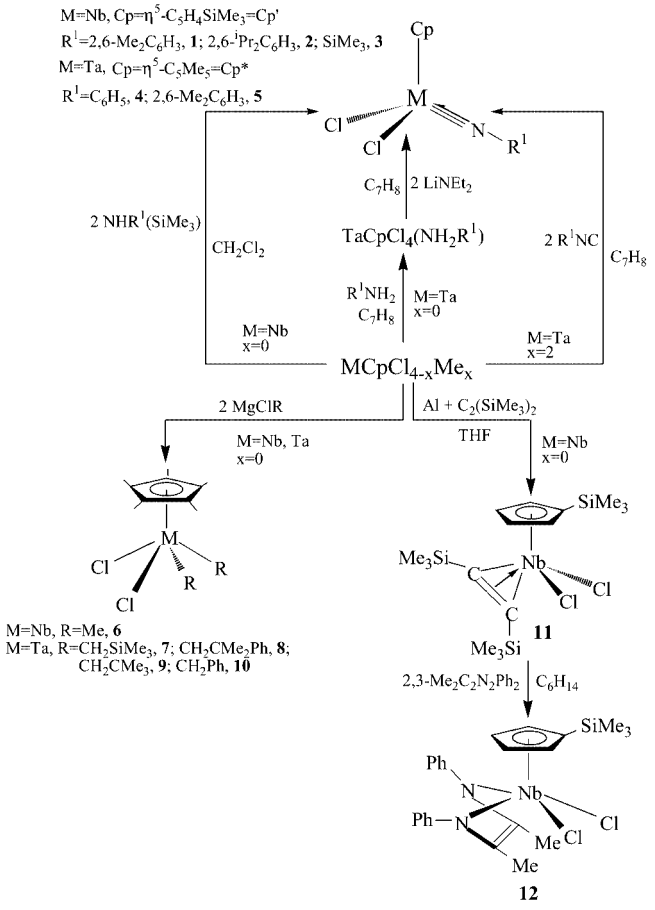

Scheme 1. Synthesis of dichloro complexes

Thus, the reactions of the dichloro complexes **1** and **5** with a stoichiometric amount of the alkylating reagent gave solutions from which the alkyl(chloro)imido complexes **$MCpClR(NR^1)$** [R^1 = 2,6-$Me_2C_6H_3$; M = Nb,[10] Cp = Cp′, R = Cp*, **13**; Me, **14**; M = Ta, Cp = Cp*, R = Me, **15**;[10] CH_2SiMe_3, **16**;[21] CH_2CMe_2Ph, **17**;[21] CH_2CMe_3, **18**;[21] $CH_2C_6H_5$, **19**;[21] 2-$(CH_2NMe_2)C_6H_4$, **20**;[21] Cp′,

 © 2003 Wiley-VCH Verlag GmbH & Co. KGaA, Weinheim

21;[21] NMe_2, **22**;[10] O*t*Bu, **23**[10]] and dialkyl(imido) complexes **$MCpR_2(NR^1)$** [R^1 = 2,6-$Me_2C_6H_3$; M = Nb,[10] Cp = Cp′, R = Me, **24**; CH_2SiMe_3, **25**; CH_2CMe_3, **26**; NMe_2, **27**; $CH_2C_6H_5$, **28**; M = Ta, Cp = Cp*, R = CH_2SiMe_3, **29**;[21] CH_2CMe_2Ph, **30**;[21] C_6H_5, **31**;[21] $CH_2C_6H_5$, **32**;[21] CH_2CMe_3, **33**;[21] *o*-$(NSiMe_3)_2C_6H_4$, **34**;[10] Me, **35**[20a]] were isolated. Alternatively, the chloro(methyl)(imido)tantalum derivative **15** can be prepared[21] by treating the (alkenylamido)imido(methyl) complex [TaCp*Me(NR^1){η^1-NR^1-C(Me)=CMe_2}] (R^1 = 2,6-$Me_2C_6H_3$)[4c] with HCl or by a redistribution[21] reaction between the corresponding dichloro- (**5**)[4c] and dimethyl- (**35**)[20a] (imido)tantalum derivatives (Scheme 2).

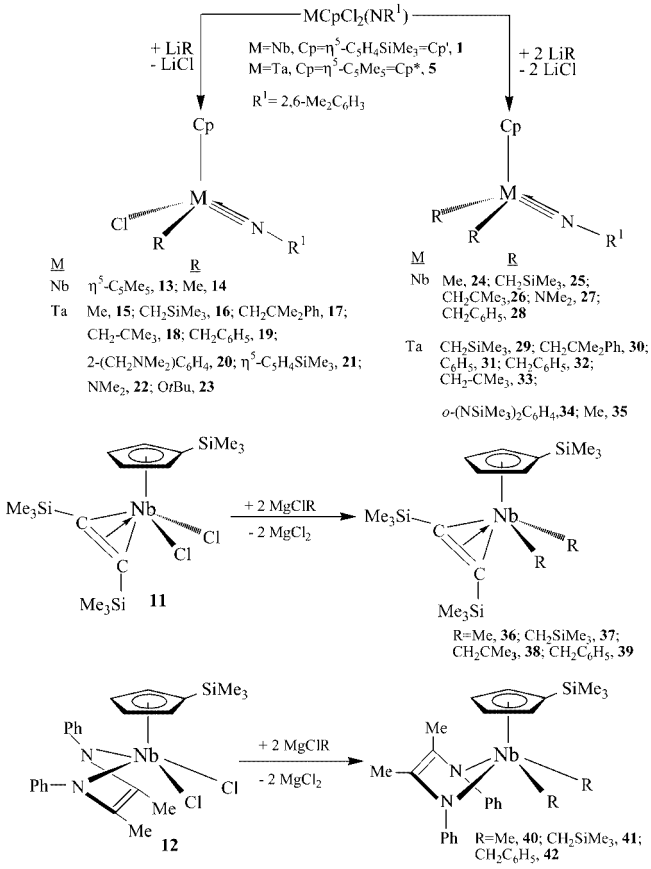

Scheme 2. Synthesis of alkyl(chloro) and dialkyl complexes

Conversely, dialkyl(alkyne) derivative **$NbCp'R_2(Me_3Si$-$CCSiMe_3)$**[14] (R = Me, **36**; CH_2SiMe_3, **37**; CH_2CMe_3, **38**; $CH_2C_6H_5$, **39**) and dialkyl(diazabutadiene) derivative **$NbCp'R_2(\eta^2$-$Ph_2N_2C_2Me_2$-2,3)**[15] (R = Me, **40**; CH_2SiMe_3, **41**; $CH_2C_6H_5$, **42**) were, respectively, isolated in good yields by alkylation of the dichloro complexes **11** and **12** with Grignard reagents in a 1:2 molar ratio (Scheme 2).

As shown in Scheme 3, the mixed alkylated imido compounds **MCpRMe(NR^1)** [R^1 = 2,6-$Me_2C_6H_3$; M = Nb,[10] Cp = Cp′, R = CH_2SiMe_3, **43**; NMe_2, **44**; M = Ta, Cp = Cp*, R = CH_2SiMe_3, **45**,[21] CH_2CMe_2Ph, **46**;[21] CH_2CMe_3, **47**;[21] C_6H_5, **48**;[21] 2-$(CH_2NMe_2)C_6H_4$, **49**;[21] $CH_2C_6H_5$, **50**;[21] Cp′, **51**;[21] NMe_2, **52**;[10] N*i*Pr_2, **53**;[10] NH*t*Bu, **54**;[10] 2,6-$Me_2C_6H_3O$, **55**[10]] were obtained from the starting chloro(methyl)imido complexes **14** and **15** by reactions with the corresponding alkylating reagent, except for the methyl(imido) phenoxide complex **55** which was synthesized by treating the alkenylamido(imido)methyltantalum derivative [TaCp*Me(NR^1){η^1-NR^1-C(Me)=CMe_2}] (R^1 = 2,6-$Me_2C_6H_3$)[4c] with 2,6-$Me_2C_6H_3$(OH). Related alkyl, amido, and imido alkoxide derivatives of different stoichiometries such as *monoalkyl compounds* MCpClR(NR^1) [M = Nb, Cp = η^5-C_5H_5, R = Me, R^1 = *t*Bu;[7c] 2,6-$Me_2C_6H_3$;[22d] 2,6-*i*$Pr_2C_6H_3$;[7c,22d] R = CH_2Ph, NH*t*Bu, R^1 = 2,6-*i*$Pr_2C_6H_3$;[22a,22d] R = NHR^1,[22d] R^1 = *t*Bu; 2,6-$Me_2C_6H_3$; R = NEt_2, R^1 = *t*Bu;[22d] R = $CH_2CH=CH_2$, $CH_2C(Me)=CH_2$, R^1 = *t*Bu;[22b] Cp = η^5-$C_5H_4SiClMe_2$;[7h,22c] η^5-$C_5H_4SiClMePh$,[7c] R = CH_2Ph, R^1 = *t*Bu; Cp = η^5-$C_5H_4SiMe_2NH$*t*Bu,[7h] R = CH_2Ph, NH*t*Bu, R^1 = *t*Bu; M = Ta,[22f] Cp = η^5-C_5Me_5, R = Me, NH*t*Bu, R^1 = *t*Bu], *dialkyl compounds* $MCpR_2(NR^1)$ (M = Nb, Cp = η^5-C_5H_5, R = NHR^1, R^1 = 2,6-$Me_2C_6H_3$;[22e] R = Ph, R^1 = 2,6-*i*$Pr_2C_6H_3$;[22a] R = *t*BuO; 2,6-Me_2-C_6H_3O, R^1 = Me;[7a] R = 2,6-*i*$Pr_2C_6H_3O$; 2,6-$Ph_2C_6H_3O$, R^1 = *t*Bu;[7a] Cp = η^5-C_5Me_5, R = Me,[7c] CH_2Ph,[22a] R^1 = 2,6-*i*$Pr_2C_6H_3$; Cp = η^5-$C_5H_4CMe_2C_9H_7$, R = NEt_2, R^1 = 2,6-*i*$Pr_2C_6H_3$;[22e] Cp = η^5-$C_5H_4SiMeXY$, X = Cl, CH_2Ph, Y = Me,Ph; X = Me, Y = NH*t*Bu; R = CH_2Ph, R^1 = *t*Bu;[7h] M = Ta, Cp = η^5-C_5Me_5, R^1 = *t*Bu;[2d] 2,6-*i*$Pr_2C_6H_3$[7c]) and *mixed alkyl* compounds $MCpRR'(NR^1)$ [M = Nb, Cp = η^5-C_5H_5, R = Me, R′ = NH*t*Bu, R^1 = 2,6-*i*$Pr_2C_6H_3$;[22d] R = NH*t*Bu, R′ = *n*Bu, NEt_2, σ-C_5H_5, R^1 = *t*Bu;[22d] R = Me, R′ = NHR^1, R^1 = 2,6-Me_2-C_6H_3;[22e] M = Ta, Cp = η^5-C_5Me_5, R = Me, R′ = NMe_2, NHMe, $OOCNMe_2$, OOCNH*t*Bu, R^1 = *t*Bu;[22g] R = Me, R′ = OMe, O*t*Bu, NH*t*Bu, R^1 = *t*Bu;[22f] R = Me, R′ = NPh_2, $N(SiMe_3)_2$ [22h]] have been reported.

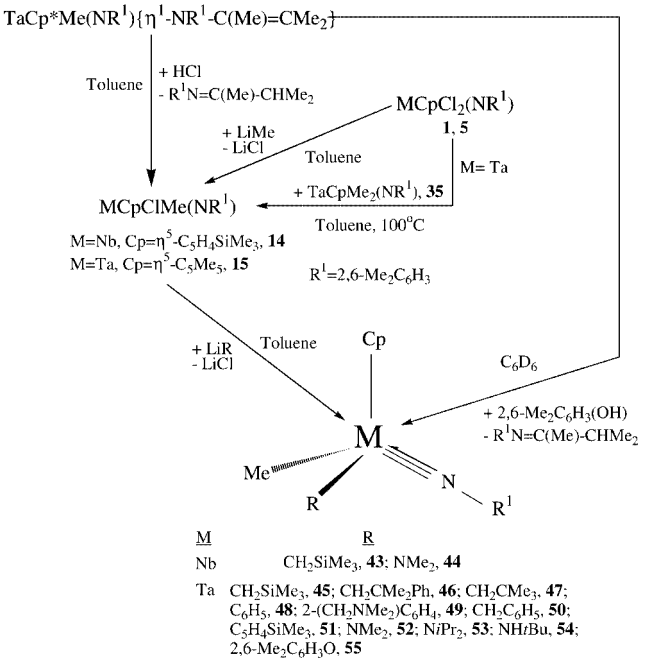

Scheme 3. Synthesis of alkyl(methyl)imido complexes

 © 2003 Wiley-VCH Verlag GmbH & Co. KGaA, Weinheim

Complexes **1**−**55** are air- and moisture-sensitive and soluble in most organic solvents, including saturated hydrocarbons, except that dichloro(diazabutadiene) complex **12** is insoluble in hexane.

Imido complexes **1**−**5**, **13**−**35**, and **43**−**55** are monomers, pseudotetrahedral, and isostructural with other half-sandwich imido group-5 metal derivatives.[7a,23] The formulation as dichloro- **1**−**5**, (alkyl)chloro- **13**−**23**, dialkyl- **24**−**35**, and alkyl(methyl)- **43**−**55** -(imido) complexes is supported by analytical and spectroscopic data (IR, and ^{1}H and ^{13}C{^{1}H} NMR) that show the expected behaviour for such prochiral, chiral, prochiral and chiral species, respectively. Further, the molecular structure of **21** (Figure 1) shows a typical bent-metallocene moiety with the chlorine atom and the imido group lying in the equatorial plane. Although the two Cp rings differ, the distance from the tantalum atom to both centroids is the same, the angles between the equatorial plane and the mean Cp planes are also equivalent, and the bonding of both Cp rings to the metal centre is very similar. The Ta1−N1 distance of 1.803(4) Å is very similar to those of the closely related complexes [TaCp*$_2$X(NPh)] [X = Cl: 1.799(4) Å;[8a] X = H: 1.831(10) Å[9c]] and the Ta1−N1−C41 angle, 174.6(3)°, is almost linear. These data are consistent with a Ta−N bond order of about 2, in an 18-electron configuration at the metal centre,[24] and an sp nitrogen atom with a lone pair of electrons involved in bonding with the phenyl substituent centred on it.

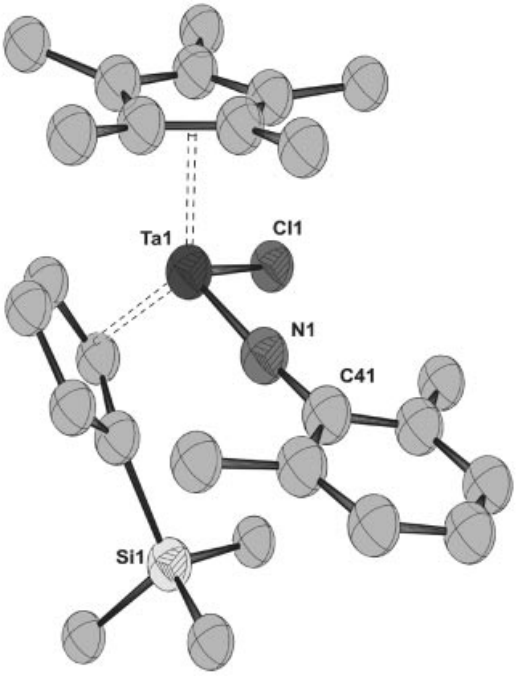

Figure 1. Molecular structure and atom labelling scheme for **[TaCp*Cp′Cl(NR^1)]** (Cp* = η^5-C_5Me_5; Cp′ = η^5-$C_5H_4SiMe_3$; R^1 = 2,6-$Me_2C_6H_3$, **21**)

The dichloro- **11** and dialkyl- **36**−**39** -(alkyne) complexes are monomers with a C_s symmetry and spectroscopic properties that are basically similar to those reported for metallacyclopropene derivatives[25,26] in which the alkyne ligand acts as a four-electron donor. The IR spectra show an absorption band for the stretching vibration $\nu_{(C=C)}$ ($\tilde{\nu} \approx$ 1582 cm^{-1}) in accordance with the hybridization change of the carbon atoms in the alkyne ligand,[26,27] whereas ^{13}C{^{1}H} NMR chemical shifts for the acetylenic carbon atoms appear to be $\delta \approx 244$.[28] Complex **37** (Figure 2) can be described as a monomer with a typical three-legged piano-stool environment for the niobium atom, assuming that the centroid of the alkyne ligand occupies a single coordination site. Notable are the perpendicular disposition of the alkyne ligand with respect to the $C_5H_4SiMe_3$ ring and the plane formed by the alkyl substituents at the niobium centre. The average Nb−C_{alkyne} distance is 2.090(6) Å and C41−C51 is 1.323(7) Å, values just within the range expected for a four-electron-donor alkyne ligand,[26,29] in which the C−C bond order is less than 3. Conversely, the DFT theoretical data[14] corresponding to the dichloro- and dimethyl(acetylene) compounds $NbCpR_2(HCCH)$ (R = Cl, Me) agree with a preferential disposition of the alkyne ligand lying perpendicular to the Cp plane, such as that observed for complex **37**.

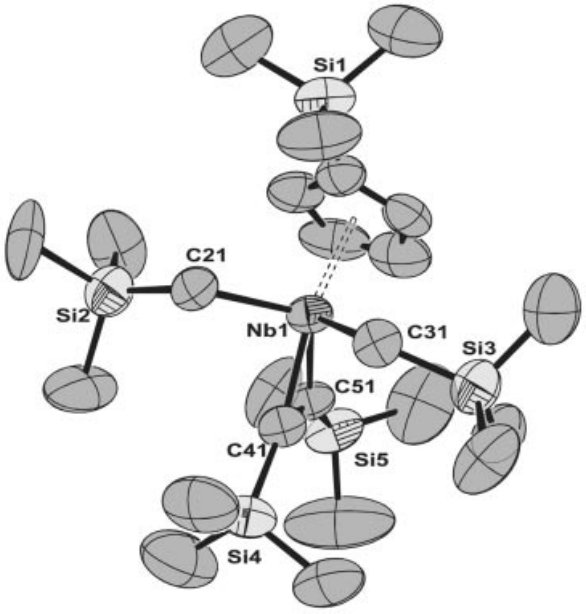

Figure 2. Molecular structure and atom labelling scheme for **[NbCp′R$_2$(Me$_3$SiCCSiMe$_3$]** (Cp′ = η^5-$C_5H_4SiMe_3$; R = CH_2SiMe_3, **37**)

The NMR spectroscopic data of complex **12** suggest that the (ene)diamido ligand adopts a *supine* conformation with respect to the (trimethylsilyl)cyclopentadienyl ring (Scheme 2), which accords with studies by Mashima et al.[30] on the geometric preferences of 1,4-diazadiene ligands in half-sandwich metallocene complexes of early transition metals. Furthermore, detailed DFT analysis of the fragment orbital interactions in the model complex $NbCpCl_2(HNCHCHNH)$ provides no evidence for positive overlap between the niobium centre and the inner carbon atoms of the DAD ligand.[15] The ^{1}H NMR spectrum of **40**

 © 2003 Wiley-VCH Verlag GmbH & Co. KGaA, Weinheim

displays a singlet at δ = 0.15 due to the Nb−Me, and shows an AB spin system for the diastereotopic α-CH_2 protons of alkyl groups in complexes **41** and **42**. The singlet δ = 1.75 due to the methyl substituents of the (ene)diamido ligand is at higher field than the δ = 1.84 ppm of the starting dichloro complex **12**. The ^{13}C resonances of the inner carbon atoms also show a high field displacement. These data, along with the preferential orientation discussed by Mashima et al.[30] in related complexes, suggest that the alkylation reactions of the dichloro complex involve an orientation change in the (ene)diamido ligand from the *supine* conformation in **12** to the *prone* form in the dialkyl derivatives **40**−**42**.[16d]

Insertion Processes

Reactions with Carbon Monoxide

Dimethyl(imido) complex **35** reacts with carbon monoxide (1 atm) at room temperature in toluene to give the dinuclear μ-enediolate complex **[{TaCp*Me(NR^1)}$_2${μ-η^2-OC(Me)=C(Me)O}]** (R^1 = 2,6-$Me_2C_6H_3$, **58**)[20a] in good yield. This takes place by intermolecular coupling between two acyl carbon atoms of the intermediate η^2-acyl(methyl)imido derivative **[TaCp*Me(NR^1){η^2-C(Me)=O}]** (R^1 = 2,6-$Me_2C_6H_3$, **57**),[20a] (Scheme 4) whose formation can be observed in situ by NMR spectroscopy[31] at low temperatures. Complex **57** is quantitatively transformed into the enediolate species **58** on heating to room temperature, preventing its isolation as a solid.

With the chloro(methyl)imido complex **15** as starting material the expected η^2-acyl(imido) derivative was not obtained, since it was spontaneously converted into the chloro(η^2-methyliminoacyl)oxo complex **[TaCp*Cl(O){η^2-C(Me)=NR^1}]** (R^1 = 2,6-$Me_2C_6H_3$, **59**).[20a] The formation of **59** can be explained (Scheme 4) by assuming the initial coordination of CO, followed by migration of the methyl group bonded to the metal atom to the electrophilic carbonyl carbon atom to give the scarcely stable intermediate η^2-acyl(chloro)imido complex **[TaCp*Cl(NR^1){η^2-C(Me)=O}]** (R^1 = 2,6-$Me_2C_6H_3$, **56**),[20a] which was identified in solution by NMR spectroscopy[31] at −40 °C. Nucleophilic attack of the imido nitrogen atom at the electrophilic acyl carbon atom leads to an unidentified intermediate species that spontaneously rearranges, breaking the C−O bond with simultaneous formation of M−C single and M=O double bonds to give the final chloro(η^2-methyliminoacyl)oxo compound **59**. Complex **59** is chiral and its structure (Figure 3) shows the tantalum centre in a three-legged piano-stool environment, assuming that the centroid of the Cp* ring and the centroid of the iminoacyl group is taken as occupying a single coordination site. The η^2-iminoacyl group is coordinated in a similar mode to that in related complexes[4c] with Ta−C1 and Ta−N1 distances of 2.133(9) and 2.132(7) Å, respectively, corresponding to single bonds, and a C1−N1 distance of 1.276(11) Å, which implies double-bond character. The oxygen ligand−tantalum atom bond of 1.731(7) Å is in the range reported for Ta=O double bonds.[32]

As well as alkyl (methyl) groups, the alkyl(chloro)- (**17**, **18**, **22**), dialkyl- (**29**−**33**), and alkyl(methyl)- (**46**, **47**, **49**) -imidotantalum complexes [TaCp*XR(NR^1)] (R^1 = 2,6-$Me_2C_6H_3$) also react with carbon monoxide (1 atm) at

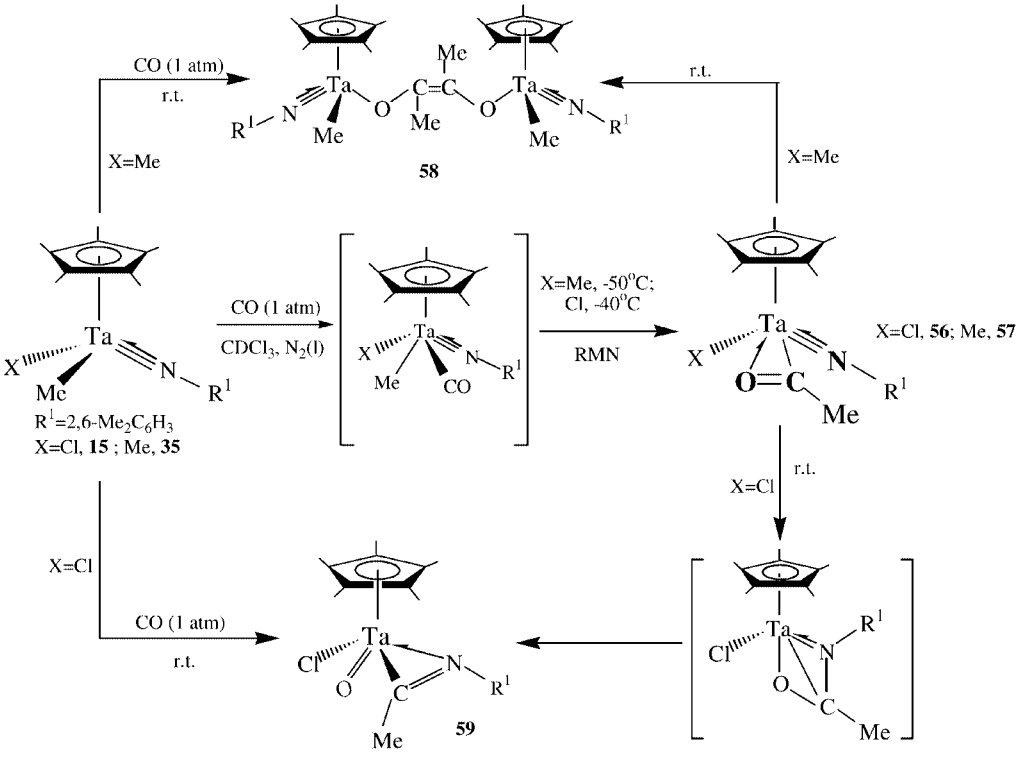

Scheme 4. Insertion reactions of carbon monoxide

 © 2003 Wiley-VCH Verlag GmbH & Co. KGaA, Weinheim

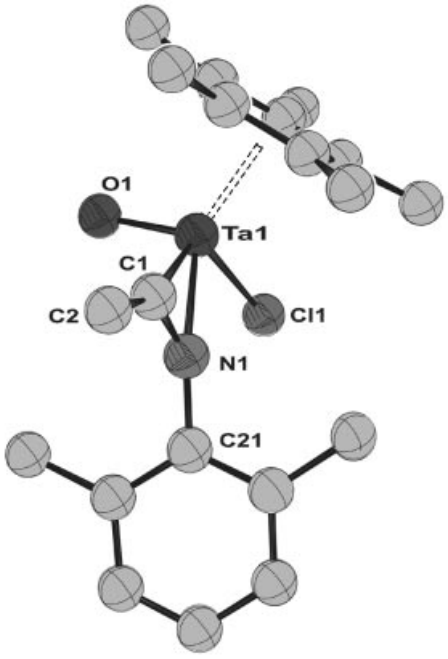

Figure 3. Molecular structure and atom labelling scheme for **[TaCp*Cl(O){η²-C(Me)=NR¹}]** (Cp′ = η⁵-C_5Me_5; R^1 = 2,6-$Me_2C_6H_3$, **59**)

room temperature in hexane or [D_6]benzene (NMR tube scale) to give η²-acyl(chloro)- (X = Cl, R = CH_2CMe_2Ph, **60**), (η²-carbamoyl)chloro- (X = Cl, R = NMe_2, **61**), (η²-acyl)alkyl- (X = R = CH_2SiMe_3, **62**; CH_2CMe_2Ph, **63**; CH_2CMe_3, **64**; CH_2Ph, **65**), and (η²-acyl)methyl- (X = Me, R = CH_2CMe_2Ph, **66**; CH_2CMe_3, **67**) -imido complexes **[TaCp*X(NR¹){η²-C(R)=O}]** (**60**−**67**)[33] (Scheme 5), as result of migration of the alkyl group bonded to the metal atom to the electrophilic carbonyl atom of the previously coordinated CO ligand. The regioselective synthesis of the (η²-acyl)methyl complexes **66** and **67** reflects the preferential migration of CH_2CMe_2Ph and CH_2CMe_3 groups with respect to the methyl group, which accords with the sequence established for the isocyanide insertion process.[33]

When X = Cl, R = CH_2CMe_3 (**18**) and X = Me, R = 2-(CH_2NMe_2)C_6H_4 (**49**) the η²-acyl derivatives can neither be isolated nor detected by ^{1}H NMR spectroscopy due to their very low stability; however, the dinuclear μ-enediolate complexes **[{TaCp*X(NR¹)}₂{μ-η²-OC(R)=C(R)O}]** [R^1 = 2,6-$Me_2C_6H_3$; X = Cl, R = CH_2CMe_3, **68**; X = Me, R = 2-(CH_2NMe_2)C_6H_4, **69**] are easily obtained when the corresponding chloro- or methyl(alkyl)imido complex reacts with CO under the same conditions (Scheme 5), probably by intermolecular coupling between two acyl carbon atoms of the unstable intermediate η²-acyl complexes "[TaCp*X(NAr){η²-C(R)=O}]", which could not be observed in situ by ^{1}H NMR spectroscopy.[20a] The same reaction with CO but using [TaCp*XR(NR^1)] (R^1 = 2,6-$Me_2C_6H_3$; X = Cl, R = CH_2CMe_3, **18**; X = R = Ph, **31**) as starting materials failed to give the expected (η²-acyl)imido derivatives as they were spontaneously converted into the (η²-iminoacyl)oxo complexes **[TaCp*X(O){η²-C(R)=NR¹}]** after 35 d (X = Cl, R = CH_2CMe_3, **70**) and 12 h (X = R = Ph, **71**), respectively (Scheme 5); the formation of these products can be explained as with the analogous chloro(methyl)imidotantalum derivatives.[20a]

When X = Cl and R = CH_2SiMe_3, **16**; CH_2Ph, **19**; and X = Me and R = CH_2SiMe_3, **45**; Ph, **48**; CH_2Ph, **50** the reaction with CO leads to an unidentified mixture of products, whereas for X = Cl, R = 2-(CH_2NMe_2)C_6H_4, **20** there is no reaction, even on heating at 100 °C.

The dimethyl complexes [TaCp*Cl_2Me_2] (**72**)[12] and [NbCp′Me_2(Me,Ph-DAD)] (**40**) react with carbon monoxide (1 atm) at room temperature in [D_6]benzene and toluene

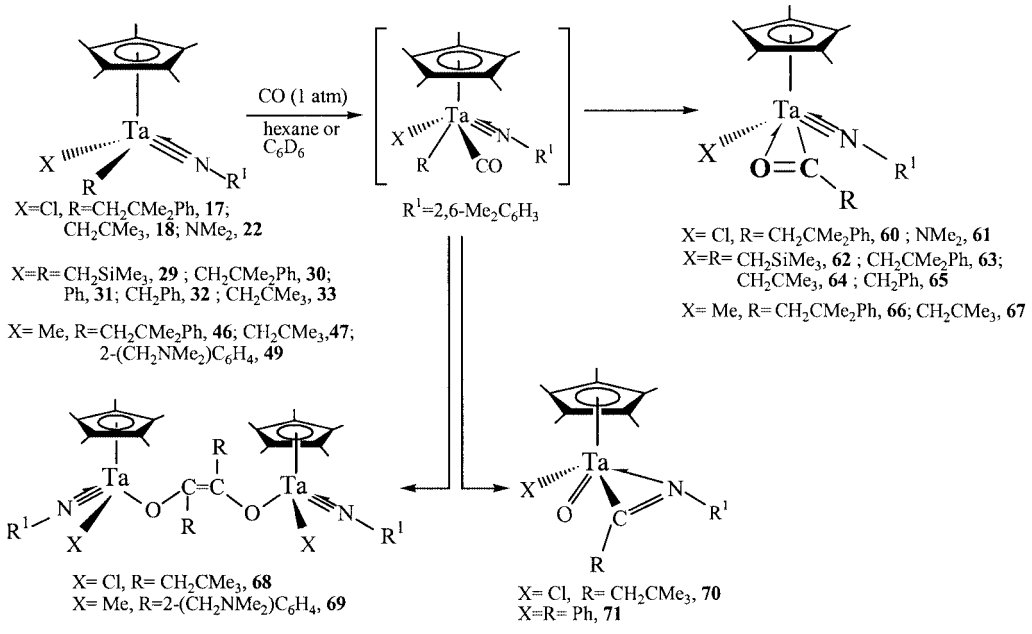

Scheme 5. Insertion reactions of carbon monoxide

 © 2003 Wiley-VCH Verlag GmbH & Co. KGaA, Weinheim

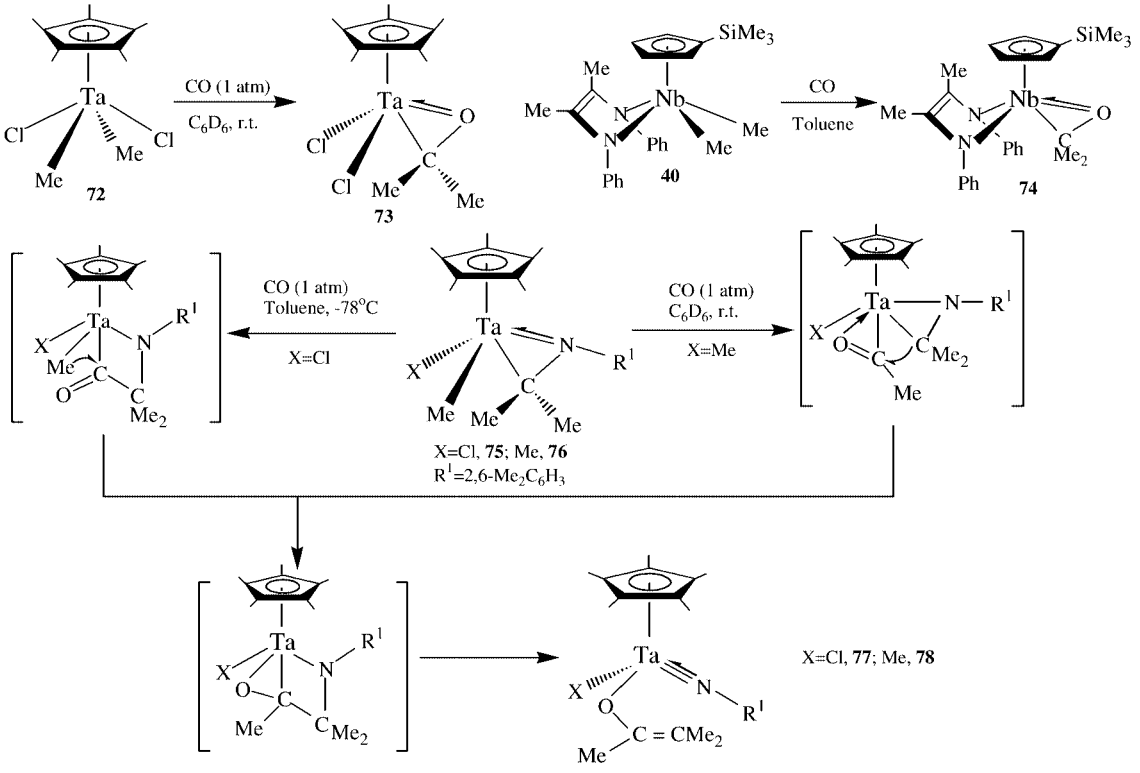

Scheme 6. Insertion reactions of carbon monoxide

to give the oxametallacyclopropane complexes **[TaCp*Cl_2(η^2-CMe_2-O)]** (**73**)[20a] and **[NbCp′(η^2-CMe_2-O)(Me,Ph-DAD)]** (**74**),[15] respectively, by double migration of two methyl groups, first to the electrophilic carbon atom of the coordinated CO ligand and then to the related η^2-acyl intermediate, which could not be detected (Scheme 6). The oxametallacyclopropane moiety, which is not further transformed, is analogous to that reported for the (acetone)tantalum complex [TaCp*Me_2(η^2-CMe_2-O)].[2d,34]

Conversely, the azatantalacyclopropane complexes [TaCp*XMe(η^2-CMe_2NR^1)] (R^1 = 2,6-$Me_2C_6H_3$; X = Cl, **75**; Me, **76**)[4b] react with 1 equiv. of CO, leading to the pseudotetrahedral enolate derivatives **[TaCp*X(NR^1){η^1-OC(Me)=CMe_2}]** (X = Cl, **77**; Me, **78**)[20a] (Scheme 6), probably by formation of intermediate species that could not be detected in situ by ^{1}H NMR spectroscopy.

All spectroscopic data for compounds **56**−**78** are consistent with their formulation. The (η^2-acyl)imido complexes **56**, **57** and **60**−**67** show $\nu_{Ta=N}$[7a,35] and $\nu_{C(R)=O}$[1d,36] at $\tilde{\nu} \approx$ 1327 and 1589 cm^{-1}, respectively. The C=O stretching vibration in η^2-acyl compounds ranges from 1453 to 1625 cm^{-1} and the lowest stretching frequencies occur for η^2-acyl complexes containing high-valent metal atoms (as we also found). This has been attributed to the participation of a "carbene-like" resonance form[37] or to the contribution of a "carbenium-ion-like" acceptor orbital on the undistorted η^2-acyl structure.[38] The η^2-acyl[39] and η^2-carbamoyl[40] (**61**) carbon resonances appear at $\delta \approx$ 317 and 228 ppm, respectively, in the typical ranges for both types of complexes. The η^2-acyl(methyl)imido complex **66** (Figure 4) is a monomer with a chiral tantalum atom in a typical four-legged piano-stool environment. The imido ligand is bonded to the metal centre in an almost linear disposition[4a,20a] with a Ta1−N1 bond length and a Ta1−N1−C21 bond angle of 1.815(11) Å and 172.2(10)°, respectively. The bonding system between the η^2-acyl moiety and the metal centre is similar to that of the trichloro derivative [TaCp*Cl_3\{η^2-C(CH_2CMe_3)=O\}],[41] but in our case the Ta1−C31 [2.126(14) Å] and Ta1−O1 [2.214(11) Å] bond lengths are slightly longer due to the different donor capacities and the *trans* influence of the chloride and imido ligands.

The μ-enediolates **58**, **68**−**69**, the (η^2-iminoacyl)oxo compounds **59**, **70**−**71**, the oxametallacyclopropanes **73** and **74**, and the enolate complexes **77** and **78** show the expected structural behaviour according to IR and NMR spectroscopy.

Reactions with 2,6-Dimethylphenyl Isocyanide

Several years ago we reported a systematic study[4] on the insertion of isocyanides into Ta−C(methyl) bonds of various chloro methyl derivatives, TaCp*$Cl_{4-x}Me_x$. When x = 2 azatantalacyclopropane species are formed in which the imine linkage typically binds strongly to the metal centre in an η^2-CN fashion.[2,42] These complexes have been postulated as intermediates in organometallic transformations[2a,2g,2i,20a] but few have been isolated and fully characterized.[4b,13d,43] Because of such high reactivity,[2b,4,42a,42d,44] we decided to extend our study to bulky alkyltantalum derivatives.

 © 2003 Wiley-VCH Verlag GmbH & Co. KGaA, Weinheim

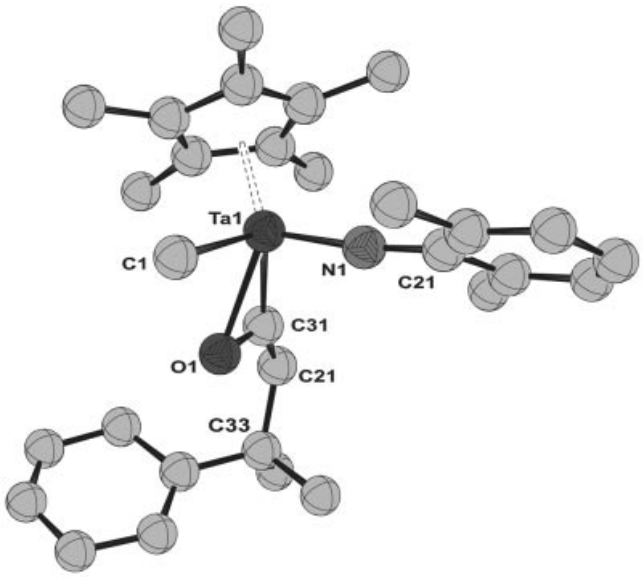

Figure 4. Molecular structure and atom labelling scheme for **[TaCp*Me(NR^1){η^2-C(CH$_2$CMe$_2$Ph)=O}]** (Cp′ = η^5-C$_5$Me$_5$; R^1 = 2,6-Me$_2$C$_6$H$_3$, **66**)

The complexes TaCp*Cl$_2$R$_2$ (R = CH$_2$SiMe$_3$, **7**;[13d] CH$_2$CMe$_2$Ph **8**;[13d] CH$_2$CMe$_3$, **9**;[13a,13b] CH$_2$Ph, **10**[13a,13b]) react with 1 equiv. of 2,6-Me$_2$C$_6$H$_3$NC in hexane under a rigorously dry inert gas to give reddish solutions, from which, after workup, the alkyldichloro(η^2-iminoacyl)tantalum complexes **[TaCp*Cl$_2$R{η^2-C(R)=NR^1}]** (R^1 = 2,6-Me$_2$C$_6$H$_3$; R = CH$_2$SiMe$_3$, **79**; CH$_2$CMe$_2$Ph, **80**; CH$_2$CMe$_3$, **81**; CH$_2$Ph, **82**)[13d] could be recovered (Scheme 7). This behaviour contrasts with that observed[4b] for the [TaCp*Cl$_2$Me$_2$] derivative, which with 1 equiv. of isocyanide gives a dichloroazatantalacyclopropane complex by a migration of the second methyl group to the electrophilic iminoacyl carbon atom of the dichloro(methyl)(η^2-iminoacyl) intermediate. In the present case, the remaining bulkier alkyl substituent does not migrate. Furthermore, the same η^2-iminoacyl complexes (**79**−**82**) are obtained by treating [D$_6$]benzene solutions of the starting dialkyldichloro compounds with 2 equiv. of isocyanide at room temperature, and no bis(η^2-iminoacyl) species are formed.

On the other hand, the η^2-iminoacyl complexes **79**−**82** slowly decompose at room temperature in [D$_6$]benzene or hexane solutions to give the dichloro(imido)tantalum compound **TaCp*Cl$_2$(NR^1)** (R^1 = 2,6-Me$_2$C$_6$H$_3$, **5**) together with a mixture of *cis* and *trans* olefins **R′-CH$_2$-CH=CH-R′** (R′ = SiMe$_3$, **79**o; CMe$_2$Ph, **80**o; CMe$_3$, **81**o; Ph, **82**o),[13d] probably via intermediate dialkylazatantalacyclopropane complexes (Scheme 7), which cannot be detected in situ by ^{1}H NMR spectroscopy. However, the azatantalacyclopropane structure favours agostic interactions between the β-hydrogen atoms of the alkyl groups and the tantalum atom, leading to concerted four-centre transition states **A** and **B**. Subsequent 2,1-migration of the hydrogen atom and back-rearrangements give the imido complex with elimination of the corresponding olefins.

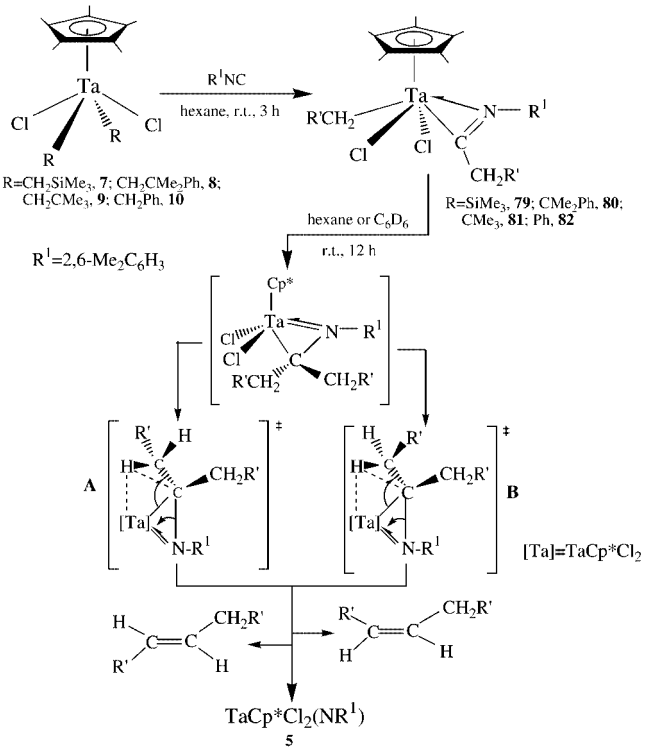

R′	trans%	Olefin
SiMe$_3$	90	1,3-bistrimethylsilyl-propene, **79**o
CMe$_2$Ph	80	2,6-dimethyl-2,6-diphenyl-3-heptene, **80**o
CMe$_3$	66	2,2,6,6-tetramethyl-3-heptene, **81**o
Ph	100	1,2-diphenyl-propene, **82**o

Scheme 7. Insertion reactions of isocyanide

The spectroscopic data (IR and ^{1}H and ^{13}C{^{1}H} NMR) are consistent with the expected pseudooctahedral geometries of these η^2-iminoacyl complexes. Compound **80** (Figure 5) has a tantalum atom in a pseudooctahedral environment, with the centroid of the Cp* ring and the carbon atom of the iminoacyl ligand occupying the axial positions. The tantalum atom is 0.61(1) Å above the plane

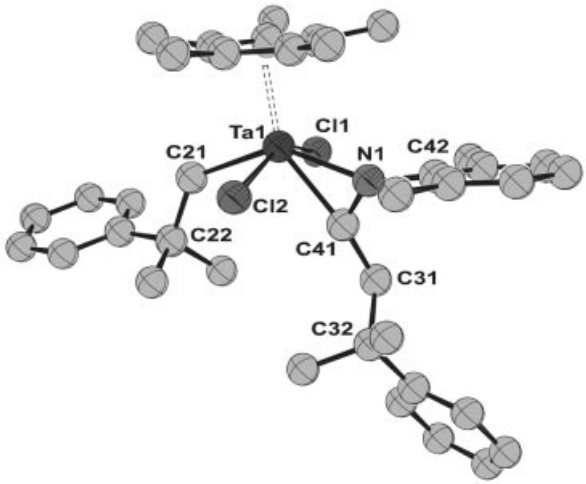

Figure 5. Molecular structure and atom labelling scheme for **[TaCp*Cl$_2$R{η^2-C(R)=NR^1}]** (Cp′ = η^5-C$_5$Me$_5$; R = CH$_2$CMe$_2$Ph; R^1 = 2,6-Me$_2$C$_6$H$_3$, **80**)

 © 2003 Wiley-VCH Verlag GmbH & Co. KGaA, Weinheim

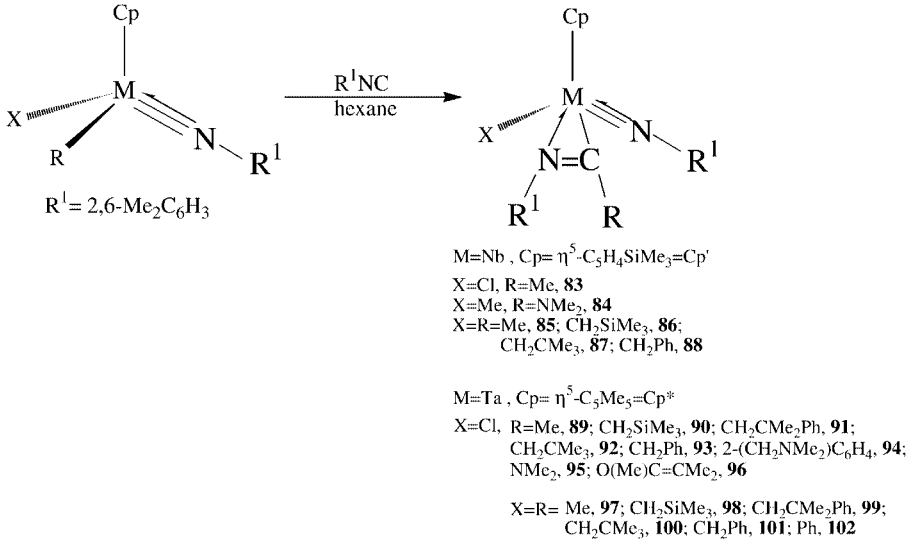

Scheme 8. Insertion reactions of isocyanide

formed by C21, Cl1, Cl2, and N1[45] and the C=N bond of the iminoacyl group is almost perpendicular to this plane.

When R^1NC is added to hexane solutions of the alkyl(chloro)- or dialkyl(imido) complexes $MCpXR(NR^1)$ (R^1 = 2,6-$Me_2C_6H_3$; M = Nb, Cp = η^5-$C_5H_4SiMe_3$=Cp′; M = Ta, Cp = η^5-C_5Me_5 = Cp*) in a 1:1 molar ratio an instantaneous insertion reaction gives the stable 18-electron chloro imido(η^2-iminoacyl) [M = Nb, Cp = Cp′, X = Cl, R = Me, **83**;[33] M = Ta, Cp = Cp*, X = Cl, R = Me, **89**;[20a] CH_2SiMe_3, **90**;[33] CH_2CMe_2Ph, **91**;[33] CH_2CMe_3, **92**;[33] $CH_2C_6H_5$, **93**;[33] 2-$(CH_2NMe_2)C_6H_4$, **94**;[33] O(Me)C=CMe_2, **96**[20]], alkyl(imido)η^2-iminoacyl (M = Nb, Cp = Cp′, X = R = Me, **85**;[33] CH_2SiMe_3, **86**;[33] CH_2CMe_3, **87**;[33] CH_2Ph, **88**;[33] M = Ta, Cp = Cp*, X = R = Me, **97**;[20a] CH_2SiMe_3, **98**;[33] CH_2CMe_2Ph, **99**;[33] CH_2CMe_3, **100**;[33] $CH_2C_6H_5$, **101**;[33] C_6H_5, **102**[33]], methyl- and chloro(imido)(η^2-iminocarbamoyl) (M = Nb, Cp = Cp′, X = Me, R = NMe_2, **84**;[33] M = Ta, Cp = Cp*, X = Cl, R = NMe_2, **95**[33]) derivatives **[MCpX(NR¹){η²-C(R)=NR¹}]** (R^1 = 2,6-$Me_2C_6H_3$, **83**−**102**) (Scheme 8).

For dialkyl derivatives (X = R = alkyl) the migration of the second alkyl group observed for $[TaCp^*Cl_2Me_2]$[4b] does not occur and an excess of isocyanide does not produce a second insertion reaction in the M−C(alkyl) or M−C(iminoacyl) bonds.[1d,3d,3i,3j] However, when X = OC(Me)=CMe_2 and R = Me the methyl group bound to

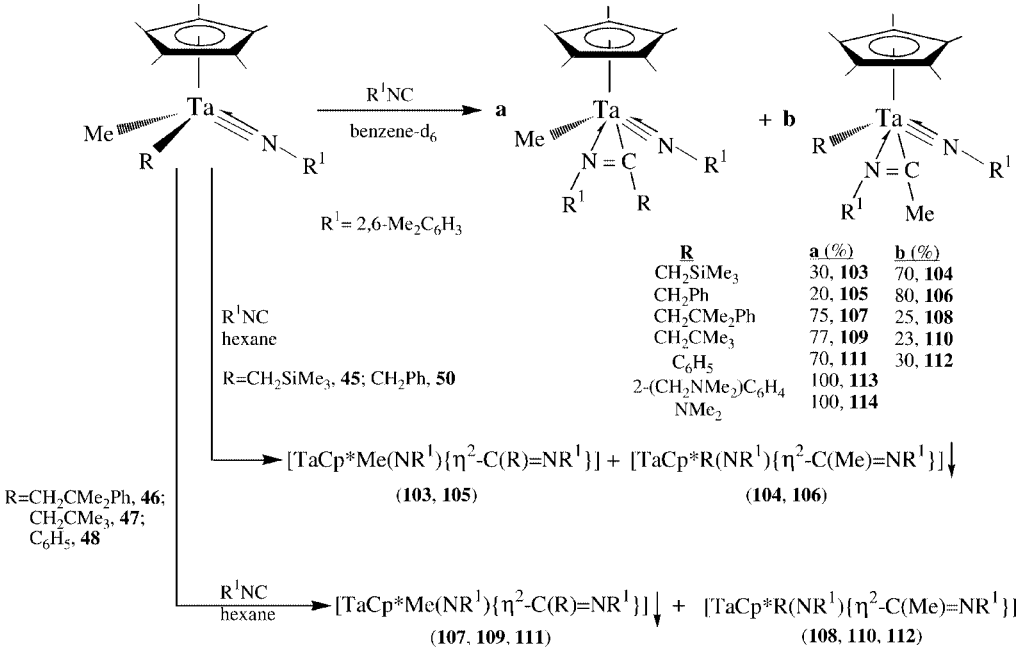

Scheme 9. Insertion reactions of isocyanide

 © 2003 Wiley-VCH Verlag GmbH & Co. KGaA, Weinheim

the tantalum atom migrates to the electrophilic carbon atom of the isocyanide ligand, which does not attack the terminal olefinic carbon atom of the enolate ligand, in contrast to when (alkenylamido)imido complexes[4c] are used.

The addition of 1 equiv. of 2,6-$Me_2C_6H_3NC$ to [D_6]benzene solutions of the alkyl(methyl)imido complexes [TaCp* RMe(NR^1)] under rigorously anhydrous conditions gives a mixture of (η^2-alkyliminoacyl)imido(methyl) **[TaCp* Me(NR^1){η^2-C(R)=NR^1}]** (R^1 = 2,6-$Me_2C_6H_3$; R = CH_2SiMe_3, **103**; CH_2Ph, **105**; CH_2CMe_2Ph, **107**; CH_2CMe_3, **109**; C_6H_5, **111**; 2-(CH_2NMe_2)C_6H_4, **113**; NMe_2, **114**)[33] and alkyl(η^2-methyliminoacyl)imido **[TaCp* R(NR^1){η^2-C(Me)=NR^1}]** (R^1 = 2,6-$Me_2C_6H_3$; R = CH_2SiMe_3, **104**; CH_2Ph, **106**; CH_2CMe_2Ph, **108**; CH_2CMe_3, **110**; C_6H_5, **112**)[33] complexes, in ratios determined from ^{1}H NMR spectra (Scheme 9).

The same reaction at room temperature using *n*-hexane as solvent in a dry box affords the insoluble microcrystalline (alkyl)imido(η^2-methyliminoacyl) (R = CH_2SiMe_3, **104**; CH_2Ph, **106**) and (η^2-alkyliminoacyl)methyl(imido) (R = CH_2CMe_2Ph, **107**; CH_2CMe_3, **109**. C_6H_5, **111**) complexes as solids, which are major components in the above-mentioned mixture. Further, when the resulting suspension of the above experiment is concentrated to dryness, the ^{1}H NMR spectrum in [D_6]benzene of the crude residue gave the same result. The yields reflect the relative ease of migration[46] of the various alkyl groups, such as 2-(CH_2NMe_2)C_6H_4 ≈ NMe_2 > CH_2CMe_2Ph ≈ CH_2CMe_3 > C_6H_5 > ***Me*** > CH_2SiMe_3 > CH_2Ph as compared with the methyl group. Our particular contribution also establishes the regioselective migration of the 2-[(dimethylamino)methyl]phenyl (**113**) and dimethylamido groups (**114**). The preferential migration of the NMe_2 moiety, for starting amido(methyl)niobium and -tantalum derivatives that give (η^2-iminocarbamoyl)methyl complexes **84** and **114**, is quite unusual because in similar alkyl- or methyl(amido)titanium,[47] -zirconium,[48] -tungsten[49] and -uranium[50] complexes the insertion occurs preferentially at the M−C_{alkyl} bond. More recent reports[22h] found similar behaviour in an almost instantaneous reaction of the amido(imido)methyl complexes [TaCp*MeX(N*t*Bu)] (X = NMe_2, NHMe) with 1 equiv. of R^1NC to give the corresponding η^2-iminocarbamoyl compounds [TaCp*Me(N*t*Bu){η^2-C(X)=NR^1}] (R^1 = 2,6-$Me_2C_6H_3$; X = NMe_2, NHMe). The authors justify, by DFT calculations, that coordination of the isocyanide ligand followed by nucleophilic attack initiates the insertion reaction, neither into Ta−NR_2 nor Ta−Me bonds, and is governed by kinetic factors. However, insertion into the Ta−Me bond is preferred for amido(imido)methyl [TaCp* Me(NR_2)(N*t*Bu)] (R = Ph, $SiMe_3$) complexes to give (amido)imido(η^1-iminoacyl) derivatives [TaCp*(NR_2)(N*t*Bu)-{η^1-C(Me)=NR^1}], whereas stereoselective insertion into the Ta−NR_2 bond occurs for related amido(methyl) derivatives, leading to (methyl)imido(η^2-iminocarbamoyl) complexes [TaCp*Me(N*t*Bu){η^2-C(X)=NR^1}] (X = NMe_2, NHMe).

The reaction of the starting mixed alkyl(imido)methyl derivatives with 2 equiv. of the isocyanide ligand in [D_6]benzene solutions at room temperature affords the same η^2-iminoacyl complexes **103**−**114**, and bis(η^2-iminoacyl) derivatives cannot be detected by ^{1}H NMR spectroscopy.

Structural studies[33] of the imido(η^2-iminoacyl) (**83**, **85**−**113**) and imido(η^2-iminocarbamoyl) (**84**, **95**, **114**) complexes agree with the expected pseudo-square-pyramidal geometry found for similar chiral niobium and tantalum derivatives.[20]

Early transition metal complexes[2f,42a,51] constitute a powerful component in carbon−carbon bond formation strategies in organic synthesis[52] and catalytic polymerization.[53] In particular, (alkyne)niobium and -tantalum complexes have provided convenient routes to carbonylic derivatives[54] and nitrile[55] coupling reactions via metallacyclic intermediates. Furthermore, (alkyne)niobium- and -tantalum(III) derivatives react with nitriles to give azatantalacyclopentene complexes that may participate in an intermolecular tautomerization process to enamines,[42c] and are also efficient catalysts for the oligomerization and polymerization of internal alkynes.[53]

In accord with this background, we recently reported a novel study[14] of the chemical behaviour of the (alkyl)alkyne[(trimethylsilyl)cyclopentadienyl]niobium complexes [NbCp′R_2($Me_3SiCCSiMe_3$)][14] (Cp′ = η^5-$C_5H_4SiMe_3$; R = Me, **36**; CH_2SiMe_3, **37**; CH_2CMe_3, **38**; $CH_2C_6H_5$, **39**) in insertion processes. Thus, when 1 equiv. of the isocyanide 2,6-$Me_2C_6H_3NC$ was added to [D_6]benzene solutions of the dialkyl(alkyne) derivatives **36**−**39**, under a rigorously dry inert gas in a sealed NMR tube, reddish solutions corresponding to (alkyl)alkyne(η^2-iminoacyl) complexes **[NbCp′R{η^2-C(R)=NR^1}($Me_3SiCCSiMe_3$)]**[14] (Cp′ = η^5-$C_5H_4SiMe_3$; R^1 = 2,6-$Me_2C_6H_3$; R = Me, **115**; CH_2SiMe_3, **116**; CH_2CMe_3, **117**) as the unique reaction products were obtained (Scheme 10). The insertion process is instantaneous and after coordination of the isocyanide ligand the migration of one alkyl group to the electrophilic isocyanide carbon atom produces an η^2-iminoacyl complex. With (alkyne)dibenzyl complex **39** the reaction takes place but, probably, the η^2-iminoacyl derivative is very unstable and decomposes to an unidentified product mixture. In the same reactions carried out in a Schlenk tube using hexane as solvent, only complex **116**, as a crystalline red solid, could be isolated. Both **115** and **117** are unstable at room temperature, and while **115** is partially transformed into an imidoniobacyclopent-3-ene complex (**118**) the alkyne(η^2-iminoacyl)neopentyl derivative **117** decomposes into an unidentified products mixture.

Alternatively, the imidoniobacyclopent-3-ene complex **[NbCp′(NR^1){η^4-CH($SiMe_3$)-C($SiMe_3$)=C(Me)-CH_2}]**[14] (Cp′ = η^5-$C_5H_4SiMe_3$; R^1 = 2,6-$Me_2C_6H_3$, **118**) can be prepared when the (alkyne)dimethyl derivative **36** is treated with 1 equiv. of isocyanide in hexane at 40−50 °C for 12 h (Scheme 11). Conversely, if the alkyne(trimethylsilylmethyl)-(η^2-iminoacyl) complex **116** is heated to 80 °C in hexane for 12 h it can be isolated as an imido(vinyl)niobacyclopropane derivative **[NbCp′(NR^1){η^4-CH($SiMe_3$)C($SiMe_3$)-C(CH_2SiMe_3)=CH($SiMe_3$)}]**[14] (Cp′ = η^5-$C_5H_4SiMe_3$; R^1 = 2,6-$Me_2C_6H_3$, **119**), a crystalline red solid, the struc-

 © 2003 Wiley-VCH Verlag GmbH & Co. KGaA, Weinheim

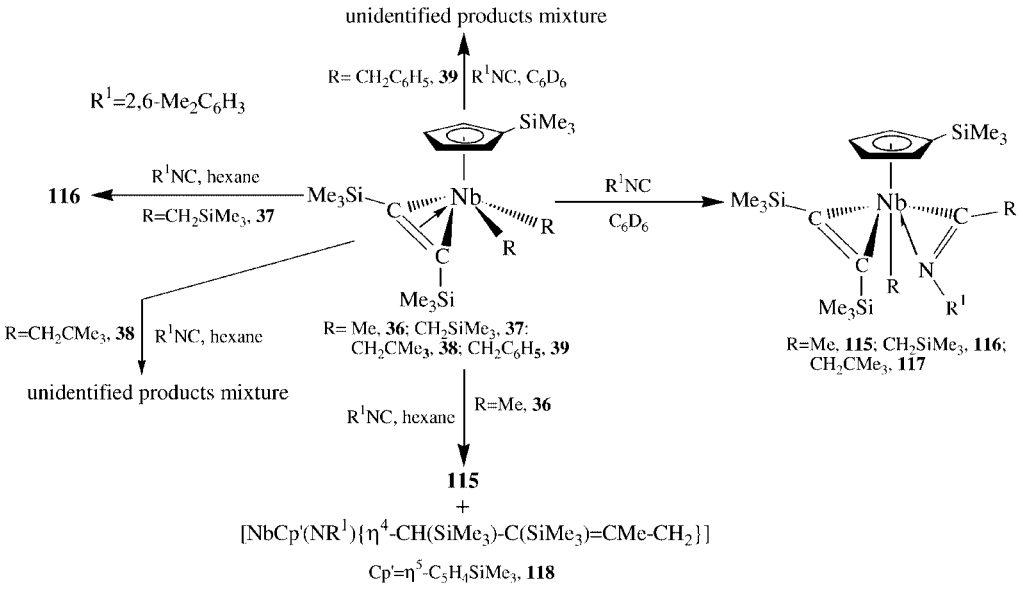

Scheme 10. Insertion reactions of isocyanide

ture of which was determined by X-ray diffraction methods. Identical results are obtained by thermally treating a mixture of **37** and 2,6-$Me_2C_6H_3NC$ (1:1 molar ratio). In contrast, the reaction between the (alkyne)bis(neopentyl) complex **39** and 2,6-$Me_2C_6H_3NC$ leads, in a first step, to an alkyne(η^2-iminoacyl)neopentyl complex (**117**) that is gradually transformed into the imidoniobacyclohept-2-ene complex **[NbCp′(NR¹){η²-$CH_2CMe_2CH_2CH(CH_2CMe_3)$C-($SiMe_3$)=C($SiMe_3$)}]**[14] (Cp′ = η^5-$C_5H_4SiMe_3$; R^1 = 2,6-$Me_2C_6H_3$, **120**), the structure of which may be proposed on the basis of NMR spectroscopic data.

On monitoring the formation processes of complexes **118**−**120** by ^{1}H NMR spectroscopy, only complex **118** was found to give an intermediate (alkyne)azaniobacyclopropane derivative, **[NbCp′{η²-C(CH_2R'')-NR¹}(Me_3SiCC-$SiMe_3$)]**[14] (Cp′ = η^5-$C_5H_4SiMe_3$; R^1 = 2,6-$Me_2C_6H_3$; R′′ = $SiMe_3$, **115i**). This transformation can be rationalized by migration of the second metal-bonded methyl group to the iminoacyl carbon center to give the intermediate **115i** (Scheme 12). Similar azametallacyclopropane species have been proposed and isolated by us in the reactions of dichlorodimethyl(pentamethylcyclopentadienyl)niobium[13d] and

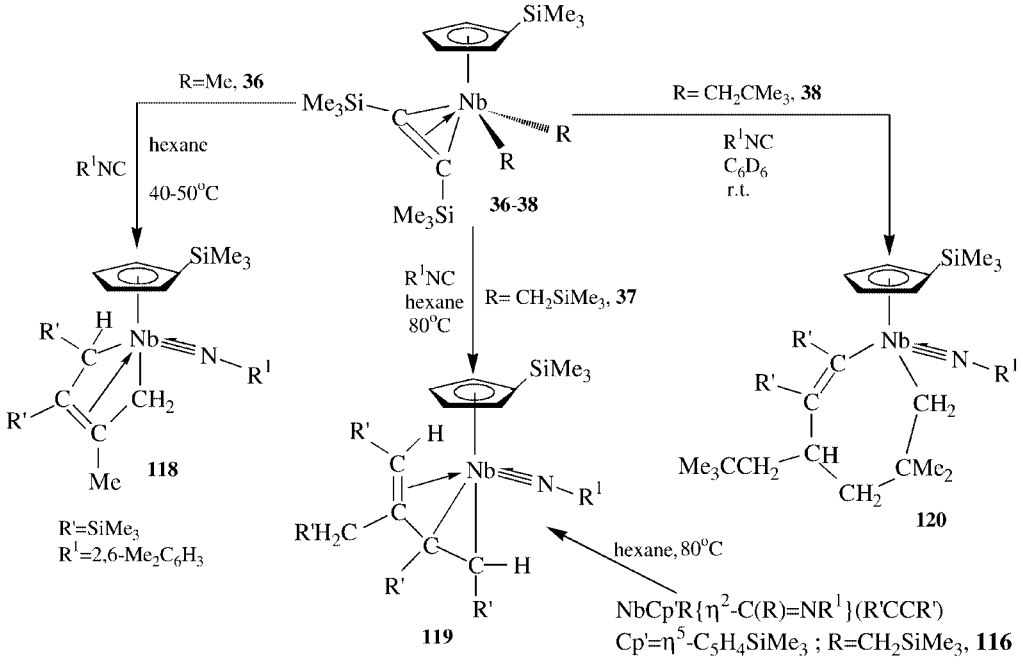

Scheme 11. Insertion reactions of isocyanide

 © 2003 Wiley-VCH Verlag GmbH & Co. KGaA, Weinheim

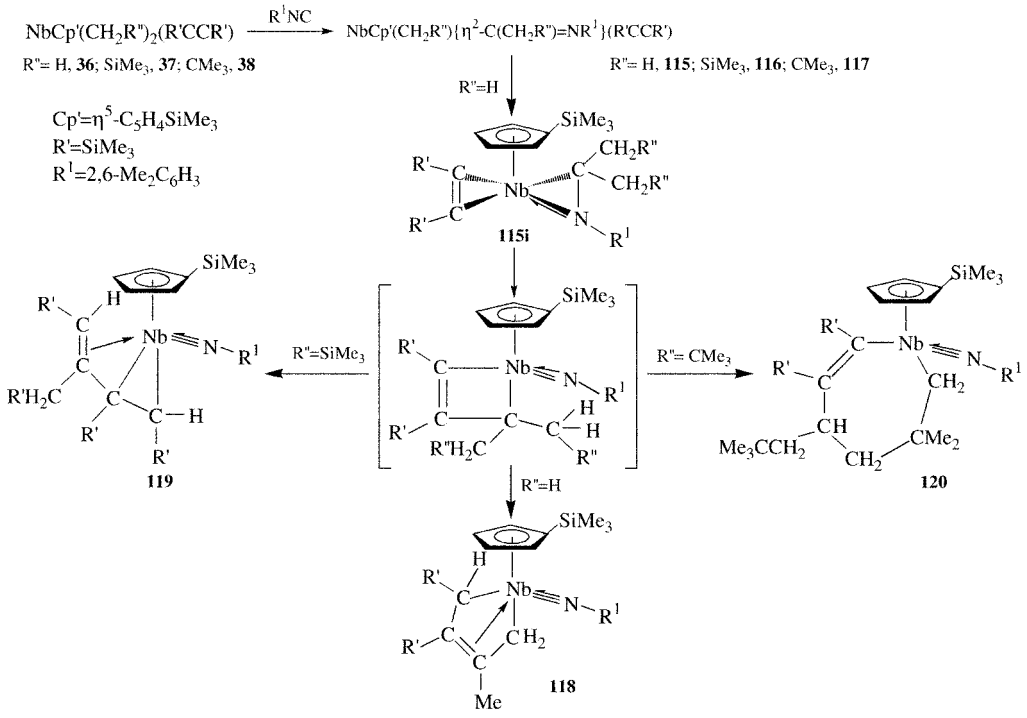

Scheme 12. Insertion reactions of isocyanide

-tantalum[4b] complexes and isocyanides and their structures confirmed by X-ray diffraction methods. Rearrangement of the intermediate **115i** is followed by migration of the hydrogen atom, and back-rearrangement gives the imidoniobacyclopent-3-ene complex **118**. Complexes **119** and **120** could be formed via imidoniobacyclobutene intermediates; when R′′ = $SiMe_3$, migration of the hydrogen atom and subsequent rearrangement leads to **119**, which is a niobacyclopropane complex with an η^2-coordinated vinyl substituent at the metal center. However, a different pathway may be proposed by the formation of azaniobacyclopentatriene species[3b,3g,56] as result of the intramolecular coupling between both alkyne and iminoacyl ligands. When R′′ = CMe_3, C−H activation of a methyl group of the *tert*-butyl fragment and back-rearrangement leads to the imidoniobacyclohept-2-ene complex **120**. This is probably due to the steric and electronic differences between $SiMe_3$ and CMe_3 groups. Thus, the lesser steric hindrance of the *tert*-butyl group permits a closer approach to the metal atom and the activation of a C−H bond gives the complex **120**.

Structural studies (IR, ^1H and $^{13}C\{^1H\}$ NMR)[14] of complexes **115**−**120** agree with the proposed structures. The pseudooctahedral complexes **115**−**117**, due to the chiral character of the metal center, show in their ^1H and $^{13}C\{^1H\}$ NMR spectra an ABCD spin system and five resonances, respectively, for the $C_5H_4SiMe_3$ moiety and, also, two inequivalent methyl groups for the 2,6-$Me_2C_6H_3$ ring, in accordance with the slow rotation of the aryl substituent around the N−C_{ipso}(aryl) bond. Complex **118** exhibits NMR behaviour that is consistent with a diene ligand in an *s-cis* conformation, as has been observed in other diene group-5 metal derivatives.[57] The unusual conformation of the diene ligand in complex **119** was deduced from detailed analysis of the NMR spectroscopic and X-ray diffraction data, which strongly suggest that the diene ligand is bonded

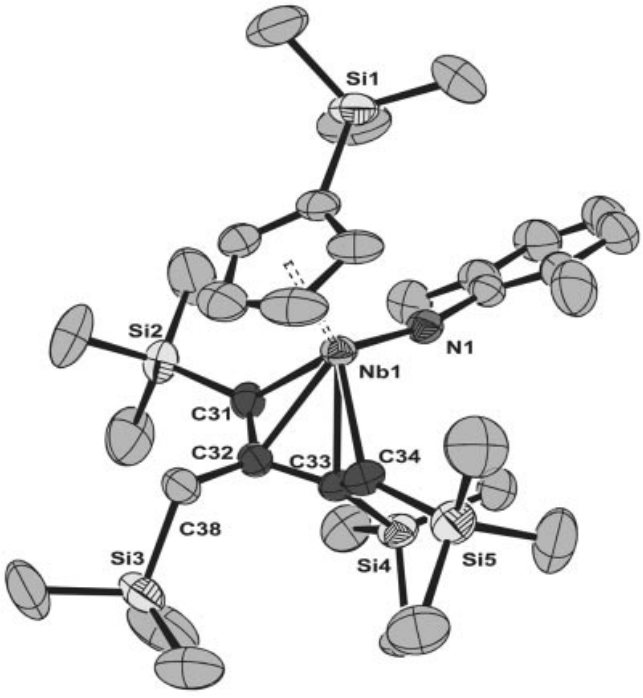

Figure 6. Molecular structure and atom labelling scheme for **[NbCp′(NR1){η4-CH(SiMe3)C(SiMe3)C(CH2SiMe3)=CH(SiMe3)}]** (Cp′ = η^5-$C_5H_4SiMe_3$; R^1 = 2,6-$Me_2C_6H_3$, **119**)

 © 2003 Wiley-VCH Verlag GmbH & Co. KGaA, Weinheim

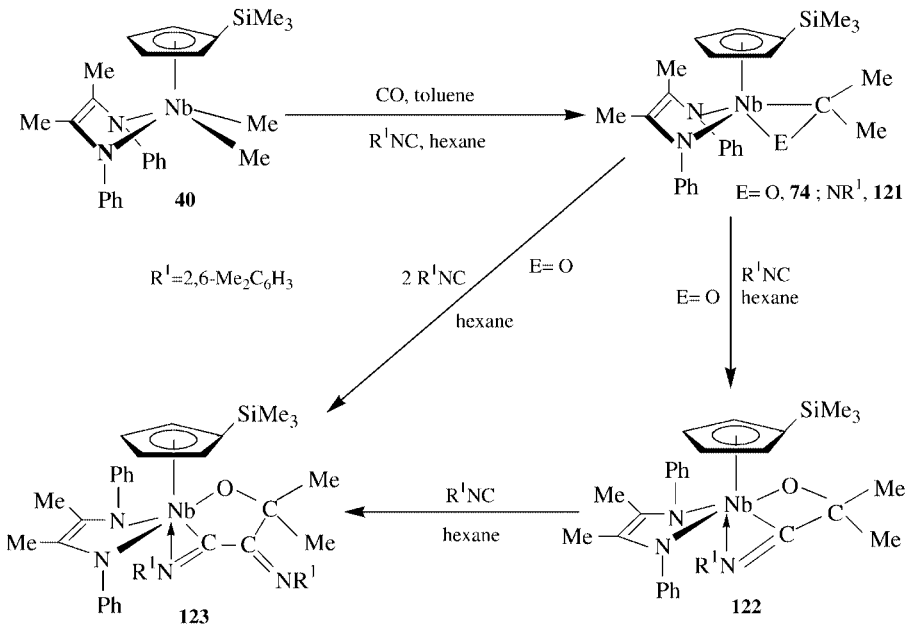

Scheme 13. Insertion reactions of carbon monoxide and isocyanide

in an η^2-niobacyclopropane fashion with a vinyl substituent η^2-coordinated to the metal center. This is the most relevant detail of the molecular structure (Figure 6) because, frequently, in diene mono(cyclopentadienyl)niobium and -tantalum complexes[57a,57d,58] the diene ligand forms a metallacyclopent-3-ene system with a preferred *supino* conformation, although there are examples with a *prono* conformation. Furthermore, the diene ligand can adopt an *s-trans* conformation, as observed in bis(cyclopentadienyl)zirconium,[59] mono(cyclopentadienyl)tantalum[60] and cationic bis(cyclopentadienyl)tantalum[61] complexes. In our case, the crystallographic data do not correspond to the same bonding system and, therefore, we propose a moiety consisting of a "diene" C31−C32−C33−C34 fragment linked to the metal atom through the C33−C34 atoms, forming a niobacyclopropane ring, and the donor vinyl substituent C31−C32.

Finally, when 2,6-$Me_2C_6H_3NC$ (1 equiv.) is added to a hexane solution of the dimethyl complex $NbCp'Me_2$(Me,Ph-DAD) (Cp′ = η^5-$C_5H_4SiMe_3$, **40**) under rigorously anhydrous conditions an orange solution is obtained, which after evaporation of the solvent produces the azaniobacyclopropane complex **[NbCp′(η²-CMe₂NR¹)(Me,Ph-DAD)]** (R^1 = 2,6-$Me_2C_6H_3$, **121**),[15] as the result of two consecutive steps (Scheme 13). The first step involves migration of one methyl group to the electrophilic isocyanide carbon atom to form an η^2-iminoacyl intermediate,[1d,2f,2h,2i,2j,2k,62] which could not be detected by ^1H NMR spectroscopy. Subsequent migration of the second methyl group to the iminoacyl carbon centre yields an azaniobacyclopropane.[2b,2c,4b,13d,63]

Dialkyl complexes **41** (R = CH_2SiMe_3) and **42** (R = $CH_2C_6H_5$) do not react with isocyanide at room temperature; when the solution is heated the reaction probably takes place simultaneously with the decomposition of the organometallic complex formed, leading to an unidentified product mixture. When **40** is treated with 2 equiv. of isocyanide the result is the same, in contrast to the behaviour of the azatantalacyclopropane derivatives [$TaCp^*Cl_2(\eta^2$-$CMe_2NR^1)$][4b] (R^1 = 2,6-$Me_2C_6H_3$; 2,4,6-$Me_3C_6H_2$), which in the presence of isocyanides give the corresponding dichloro(imido) complex [$TaCp^*Cl_2(NR^1)$] with elimination of the arylimine ketene $ArN{=}C{=}CMe_2$. However, the oxaniobacyclopropane [$NbCp'Cl_2(\eta^2$-CMe_2-O)(Me,Ph-DAD)] (**74**),[15] reacts with 1 or 2 equiv. of 2,6-$Me_2C_6H_3NC$ to give the expected insertion products **[NbCp′Cl₂{η²-OCMe₂(CNR¹)ₓ}(Me,Ph-DAD)]** (R^1 = 2,6-$Me_2C_6H_3$; x = 1, **122**; x = 2, **123**).[15] Complex **122** can be transformed into **123** by a simple isocyanide insertion reaction.

Conclusions

The review shows that direct alkylation of the corresponding chloro derivatives can afford dialkyldichloro [$MCp^*Cl_2R_2$] (**6**−**10**), alkyl(chloro)imido [$MCpClR(NR^1)$] (**13**−**23**), dialkyl(imido) [$MCpR_2(NR^1)$] (**24**−**35**), alkyl(methyl)imido [$MCpRMe(NR^1)$] (**43**−**55**), dialkyl(alkyne) [$NbCp'R_2(Me_3SiCCSiMe_3)$] (**36**−**39**), and dialkyl(diazabutadiene) complexes [$NbCp'R_2$(Me,Ph-DAD)] (**40**−**42**), whose reactivity has been studied in carbon monoxide and isocyanide insertion processes.

Imido(methyl) complexes [$TaCp^*MeX(NR^1)$] (R^1 = 2,6-$Me_2C_6H_3$; X = Cl, **15**; Me, **25**) react with carbon monoxide via the expected η^2-acyl derivatives [$TaCp^*X(NR^1)\{\eta^2$-C(Me)=O}] (X = Cl, **56**; Me, **57**) but lead to different products that depend on X. The higher carbenoid character of the η^2-acyl ligand when X = Me affords dinuclear μ-enedi-

 © 2003 Wiley-VCH Verlag GmbH & Co. KGaA, Weinheim

olate complex **58**, whereas imido nitrogen attack at the more electrophilic acyl carbon atom when X = Cl gives the chloro (η^2-iminoacyl)oxo complex **59**.

Alkyl groups, other than methyl, as in alkyl(chloro)- (**17**, **18**, **22**) dialkyl- (**29**−**33**) and alkyl(methyl)- (**46**, **47**, **49**) -imidotantalum complexes react with CO (1 atm) to give (η^2-acyl)chloro (X = Cl, R = CH_2CMe_2Ph, **60**), (η^2-carbamoyl)chloro (X = Cl, R = NMe_2, **61**), (η^2-acyl)alkyl (X = R = CH_2SiMe_3, **62**; CH_2CMe_2Ph, **63**; CH_2CMe_3, **64**; $CH_2C_6H_5$, **65**), and (η^2-acyl)methyl (X = Me, R = CH_2CMe_2Ph, **66**; CH_2CMe_3, **67**) -imido derivatives [TaCp*X(NR^1){η^2-C(R)=O}] (R^1 = 2,6-$Me_2C_6H_3$) as result of a simple insertion process. The preferential migration of neophyl and neopentyl groups with respect to the methyl group determines the regioselective synthesis of complexes **66** and **67**, but when X = Cl, R = CH_2CMe_3 (**18**) and X = Me, R = 2-$(CH_2NMe_2)C_6H_4$ (**49**) the dinuclear μ-enediolate complexes **68** and **69** are formed through intermolecular coupling between two acyl carbon atoms of the unstable intermediate η^2-acyl complexes. For **18** and X = R = Ph (**31**) insertion of CO furnishes (η^2-iminoacyl)oxo complexes **70** and **71** by a mechanism similar to that proposed for the chloro(methyl)imidotantalum derivative **15**. However, the related dichlorodimethyl complex TaCp*Cl_2Me_2 (**72**) reacts with CO to give the oxametallacyclopropane derivative TaCp*Cl_2(η^2-CMe_2-O) (**73**) as result of a double migration of both methyl groups, whereas the azatantalacyclopropane complexes [TaCp*XMe(η^2-CMe_2NR^1)] (X = Cl, **75**; Me, **76**) lead to the pseudotetrahedral enolate derivatives [TaCp*X(NR^1){η^1-OC(Me)=CMe_2}] (R^1 = 2,6-$Me_2C_6H_3$; X = Cl, **77**; Me, **78**) by formation of unidentified intermediate species.

Dialkyldichloro complexes **7**−**10** react with R^1NC (1 equiv.) to give (alkyl)dichloro(η^2-iminoacyl) derivatives [TaCp*Cl_2R{η^2-C(R)=NR^1}] (R^1 = 2,6-$Me_2C_6H_3$; R = CH_2SiMe_3, **79**; CH_2CMe_2Ph, **80**; CH_2CMe_3, **81**; $CH_2C_6H_5$, **82**) in contrast to the related dichlorodimethyl compounds (M = Nb, **6**: Ta, **72**) which, under the same conditions, give a dichloroazametallacyclopropane system by migration of the second methyl substituent to the electrophilic iminoacyl carbon atom of the dichloro(η^2-iminoacyl)methyl intermediate species. Here, the remaining bulkier alkyl group does not migrate and no bis(η^2-iminoacyl) complexes are formed by treating the starting dialkyldichloro compounds with 2 equiv. of isocyanide. The η^2-iminoacyl complexes **79**−**82** slowly decompose at room temperature in [D_6]benzene solutions to give [TaCp*Cl_2(NR^1)] and a mixture of *cis*/*trans* olefins R′CH_2CH=CHR′ (**79**o−**82**o), probably via unidentified intermediate azatantalacyclopropane species.

Stable 18-electron η^2-iminoacyl derivatives, [MCpX(NR^1){η^2-C(R)=NR^1}] (**83**−**102**), are obtained by inserting 1 equiv. of R^1NC into the M−C(alkyl) bonds of alkyl(chloro) or dialkyl(imido) complexes. In contrast, alkyl(methyl)imidotantalum complexes react by migration of alkyl or methyl substituent to give a mixture of (η^2-alkyliminoacyl)methyl(imido) [TaCpMe(NR^1){η^2-C(R)=NR^1}] (**103**, **105**, **107**, **109**, **111**, **113**, **114**) and (alkyl)imido(η^2-methyliminoacyl) derivatives [TaCpR(NR^1){η^2-C(Me)=NR^1}] (**104**, **106**, **108**, **110**, **112**), respectively. When starting with {2-[(dimethylamino)methyl]phenyl}methyl and (dimethylamido)imido(methyl) complexes, insertion takes place with regioselective migration of 2-[(dimethylamino)-methyl]phenyl and dimethylamido groups.

The reaction of dialkyl(alkyne) derivatives **36**−**38** with 2,6-$Me_2C_6H_3NC$ (1 equiv.) occurs through initial formation of the (alkyl)alkyne(η^2-iminoacyl) compounds [NbCp′R-{η^2-C(R)=NR^1}($Me_3SiCCSiMe_3$)] (R^1 = 2,6-$Me_2C_6H_3$; R = Me, **115**; CH_2SiMe_3, **116**; CH_2CMe_3, **117**) but leads to different coupling products depending on R. When hexane solutions of **36** or **37** were treated with isocyanide (1 equiv.) at 40−50 °C (**36**) and 80 °C (**37**), respectively, imidoniobacyclopent-3-ene [NbCp′(NR^1){η^4-$CH(SiMe_3)C(SiMe_3)$=$C(Me)CH_2$}] (**118**) and imido(vinyl)niobacyclopropane [NbCp′(NR^1){η^4-$CH(SiMe_3)C(SiMe_3)C(CH_2SiMe_3)$=CH-$(SiMe_3)$}] (**119**) complexes are obtained, probably via azaniobacyclopropane intermediates. If R = CH_2CMe_3, after the initial formation of a non-stable η^2-iminoacyl complex (**117**), spontaneous conversion into the imidoniobacylohept-2-ene complex [NbCp′(NR^1){η^2-$CH_2CMe_2CH_2CH$-$(CH_2CMe_3)C(SiMe_3)$=$C(SiMe_3)$}] (**120**) occurs, but the intermediate species could not be observed by ^1H NMR spectroscopy. The NMR spectroscopic data of the coupling products confirmed an *s*-*cis* conformation for the diene ligand in complex **118**, while in complex **119** such a ligand presents an unusual coordination mode and forms, with the metal center, a niobacylopropane system with an η^2-vinyl substituent.

The dimethyl(diazabutadiene) complex **40** reacts with carbon monoxide and isocyanide to give oxa- and azaniobacyclopropane derivatives [NbCp′(η^2-CMe_2E)(Me,Ph-DAD)] (E = O, **74**; NR^1, **121**) due to migration of both methyl groups and, probably, via undetected η^2-acyl and η^2-iminoacyl intermediates. Successive isocyanide insertion reactions into the Nb−C bond take place in the oxaniobacyclopropane complex **74**, leading to insertion products **122** and **123**.

Acknowledgments

I am grateful to DGICYT (Project. No. PB 97-0761), to MCYT (Project No. BQU2002-03754) and to Universidad de Alcalá (Projects No. E009/98 and 2002-018) for financial support for this research. I also acknowledge P. Gómez-Sal and A. Martín for their help with X-ray studies, and A. Galindo and D. del Rio for DFT studies, and M. V. Galakhov for D NMR experiments and useful discussions. A. Castro, F. Sánchez, and P. Velasco as Ph.D. students carried out the experimental work.

[1] [1a] E. J. Kuhlmann, J. J. Alexander, *Coord. Chem. Rev.* **1980**, *33*, 195−225. [1b] M. J. Wax, R. G. Bergman, *J. Am. Chem. Soc.* **1981**, *103*, 7028−7030. [1c] J. J. Alexander, *The Chemistry of the Metal-Carbon Bond* (Ed.: F. R. Hartley), Wiley, New York, **1985**, vol. 2. [1d] L. D. Durfee, I. P. Rothwell, *Chem. Rev.* **1988**, *88*, 1059−1079.

[2] [2a] P. T. Wolczanski, J. E. Bercaw, *Acc. Chem. Res.* **1980**, *13*, 121−127. [2b] K. W. Chiu, R. A. Jones, G. Wilkinson, A. M. R. Galas, M. B. Hursthouse, *J. Am. Chem. Soc.* **1980**, *102*, 7978−7979. [2c] K. W. Chiu, R. A. Jones, G. Wilkinson, A. M.

 © 2003 Wiley-VCH Verlag GmbH & Co. KGaA, Weinheim

R. Galas, M. B. Hursthouse, *J. Chem. Soc., Dalton Trans.* **1981**, 2088−2097. [2d] J. M. Mayer, C. J. Curtis, J. E. Bercaw, *J. Am. Chem. Soc.* **1983**, *105*, 2651−2660. [2e] W. A. Nugent, D. W. Overall, S. J. Holmes, *Organometallics* **1983**, *2*, 161−162. [2f] L. R. Chamberlain, I. P. Rothwell, J. C. Huffman, *J. Chem. Soc., Chem. Commun.* **1986**, 1203−1205. [2g] T. Sielisch, U. Behrens, *J. Organomet. Chem.* **1986**, *310*, 179−187. [2h] H. Brunner, J. Wachter, J. Schmidbauer, *Organometallics* **1986**, *5*, 2212−2219. [2i] L. D. Durfee, P. E. Fanwick, I. P. Rothwell, K. Folting, J. C. Huffman, *J. Am. Chem. Soc.* **1987**, *109*, 4720−4722. [2j] L. R. Chamberlain, B. D. Steffey, I. P. Rothwell, J. D. Huffman, *Polyhedron* **1989**, *8*, 341−349. [2k] L. D. Durfee, J. E. Hill, P. E. Fanwick, I. P. Rothwell, *Organometallics* **1990**, *9*, 75−80.

[3] [3a] W. J. Evans, J. H. Meadows, W. E. Hunter, J. L. Atwood, *Organometallics* **1983**, *2*, 1252−1254. [3b] M. D. Curtis, J. Real, *J. Am. Chem. Soc.* **1986**, *108*, 4668−4669. [3c] S. M. Beshouri, P. E. Fanwick, I. P. Rothwell, J. C. Huffman, *Organometallics* **1987**, *6*, 891−893. [3d] E. Carmona, J. M. Marín, P. Palma, M. L. Poveda, *J. Organomet. Chem.* **1989**, *377*, 157−169. [3e] A. C. Filippou, E. O. Fischer, W. Grünleitner, *J. Organomet. Chem.* **1990**, *386*, 333−347. [3f] A. C. Filippou, W. Grünleitner, *J. Organomet. Chem.* **1990**, *398*, 99−115. [3g] M. D. Curtis, J. Real, W. Hirpo, W. M. Butler, *Organometallics* **1990**, *9*, 66−74. [3h] A. C. Filippou, W. Grünleitner, E. O. Fischer, W. Imhof, G. Huttner, *J. Organomet. Chem.* **1991**, *413*, 165−179. [3i] A. C. Filippou, W. Grünleitner, C. Völkl, P. Kiprof, *J. Organomet. Chem.* **1991**, *413*, 181−203. [3j] A. C. Filippou, C. Völkl, P. Kiprof, *J. Organomet. Chem.* **1991**, *415*, 375−394. [3k] A. Martin, M. Mena, M. A. Pellinghelli, P. Royo, R. Serrano, A. Tiripicchio, *J. Chem. Soc., Dalton Trans.* **1993**, 2117−2122.

[4] [4a] M. V. Galakhov, M. Gómez, G. Jiménez, M. A. Pellinghelli, P. Royo, A. Tiripicchio, *Organometallics* **1994**, *13*, 1564−1566. [4b] M. V. Galakhov, M. Gómez, G. Jiménez, P. Royo, M. A. Pellinghelli, A. Tiripicchio, *Organometallics* **1995**, *14*, 1901−1910. [4c] M. V. Galakhov, M. Gómez, G. Jiménez, P. Royo, M. A. Pellinghelli, A. Tiripicchio, *Organometallics* **1995**, *14*, 2843−2854.

[5] [5a] S. G. Bott, D. M. Hoffman, S. P. Rangarajan, *Inorg. Chem.* **1995**, *34*, 4305−4310. [5b] P. J. Stewart, A. J. Blake, P. Mountford, *Inorg. Chem.* **1997**, *36*, 1982−1986.

[6] [6a] J. S. Freundlich, R. R. Schrock, C. C. Cummins, W. M. Davis, *J. Am. Chem. Soc.* **1994**, *116*, 6476−6477. [6b] J. S. Freundlich, R. R. Schrock, W. M. Davis, *J. Am. Chem. Soc.* **1996**, *118*, 3643−3655.

[7] [7a] D. N. Williams, J. P. Mitchell, A. D. Poole, U. Siemeling, W. Clegg, D. C. R. Hockless, P. A. O'Neil, V. C. Gibson, *J. Chem. Soc., Dalton Trans.* **1992**, 739−751. [7b] T. C. Baldwin, S. R. Huber, M. A. Bruck, D. E. Wigley, *Inorg. Chem.* **1993**, *32*, 5682−5686. [7c] V. C. Gibson, A. D. Poole, U. Siemeling, D. N. Williams, W. Clegg, D. C. R. Hockless, *J. Organomet. Chem.* **1993**, *462*, C12−C14. [7d] S. Schmidt, J. Sundermeyer, *J. Organomet. Chem.* **1994**, *472*, 127−138. [7e] V. C. Gibson, A. D. Poole, *J. Chem. Soc., Chem. Commun.* **1995**, 2261−2262. [7f] W. A. Herrmann, W. Baratta, *J. Organomet. Chem.* **1996**, *506*, 357−361. [7g] L. Djakovitch, W. A. Herrmann, *J. Organomet. Chem.* **1998**, *562*, 71−78. [7h] M. I. Alcalde, P. Gómez-Sal, A. Martín, P. Royo, *Organometallics* **1998**, *17*, 1144−1150. [7i] A. Antiñolo, M. Fajardo, C. Huertas, A. Otero, S. Prashar, A. M. Rodriguez, *J. Organomet. Chem.* **1999**, *585*, 154−161. [7j] A. Schorm, J. Sundermeyer, *Eur. J. Inorg. Chem.* **2001**, 2947−2955.

[8] [8a] D. M. Antonelli, W. P. Schaefer, G. Parkin, J. E. Bercaw, *J. Organomet. Chem.* **1993**, *462*, 213−220. [8b] A. Antiñolo, P. Espinosa, M. Fajardo, P. Gómez-Sal, C. López-Mardomingo, A. Martín, A. Otero, *J. Chem. Soc., Dalton Trans.* **1995**, 1007−1013. [8c] W. A. Herrmann, W. Baratta, E. Herdtweck, *Angew. Chem. Int. Ed. Engl.* **1996**, *35*, 1951−1953. [8d] G. Proulx, R. G. Bergman, *Organometallics* **1996**, *15*, 684−692.

[9] [9a] M. L. H. Green, J. T. James, J. F. Saunders, *Chem. Commun.* **1996**, 1343−1344. [9b] M. L. H. Green, J. T. James, J. F. Saunders, J. Souter, *J. Chem. Soc., Dalton Trans.* **1997**, 1281−1288. [9c] M. L. H. Green, J. T. James, A. N. Chernega, *J. Chem. Soc., Dalton Trans.* **1997**, 1719−1726.

[10] A. Castro, M. V. Galakhov, M. Gómez, F. Sánchez, *J. Organomet. Chem.* **1999**, *580*, 161−168.

[11] M. Gómez, P. Gómez-Sal, M. P. Nicolás, P. Royo, *J. Organomet. Chem.* **1995**, *491*, 121−125.

[12] M. Gómez, G. Jimenez, P. Royo, J. M. Selas, P. R. Raithby, *J. Organomet. Chem.* **1992**, *439*, 147−154.

[13] [13a] S. J. McLain, R. R. Schrock, P. R. Sharp, M. R. Churchill, W. Youngs, *J. Am. Chem. Soc.* **1979**, *101*, 263−265. [13b] L. W. Messerle, P. Jennische, R. R. Schrock, G. Stucky, *J. Am. Chem. Soc.* **1980**, *102*, 6744−6752. [13c] P. A. Belmonte, F. G. N. Cloke, K. H. Theopold, R. R. Schrock, *Inorg. Chem.* **1984**, *23*, 2365−2367. [13d] A. Castro, M. V. Galakhov, M. Gómez, P. Gómez-Sal, A. Martín, F. Sánchez, P. Velasco, *Eur. J. Inorg. Chem.* **2000**, 2047−2054.

[14] A. Galindo, M. Gómez, P. Gómez-Sal, A. Martín, D. del Rio, F. Sánchez, *Organometallics* **2002**, *21*, 293−304.

[15] A. Galindo, M. Gómez, D. del Rio, F. Sánchez, *Eur. J. Inorg. Chem.* **2002**, 1326−1335.

[16] [16a] K. Aoyagi, P. K. Gantzel, T. D. Tilley, *Polyhedron* **1996**, *15*, 4299−4302. [16b] K. Mashima, Y. Matsuo, K. Tani, *Chem. Lett.* **1997**, 767−768. [16c] G. Jimenez Pindado, M. Thornton-Pett, M. Bochmann, *J. Chem. Soc., Dalton Trans.* **1998**, 393−400. [16d] K. Mashima, Y. Matsuo, K. Tani, *Organometallics* **1999**, *18*, 1471−1481.

[17] [17a] W. A. Nugent, *Inorg. Chem.* **1983**, *22*, 965−969. [17b] W. A. Nugent, J. M. Mayer, *Metal-Ligand Multiple Bonds*, John Wiley&Sons, New York, **1988**. [17c]D. E. Wigley, *Prog. Inorg. Chem.* **1994**, *42*, 239−482.

[18] [18a] P. J. Walsh, F. J. Hollander, R. G. Bergman, *J. Am. Chem. Soc.* **1988**, *110*, 8729−8731. [18b] C. C. Cummins, S. M. Baxter, P. T. Wolczanski, *J. Am. Chem. Soc.* **1988**, *110*, 8731−8733. [18c] D. S. Glueck, J. Wu, F. J. Hollander, R. G. Bergman, *J. Am. Chem. Soc.* **1991**, *113*, 2041−2054. [18d] C. C. Cummins, C. P. Schaller, G. D. Van Duyne, P. T. Wolczanski, A. W. E. Chan, R. Hoffman, *J. Am. Chem. Soc.* **1991**, *113*, 2985−2994. [18e] P. J. Walsh, A. M. Baranger, R. G. Bergman, *J. Am. Chem. Soc.* **1992**, *114*, 1708−1719. [18f] T. R. Cundari, *J. Am. Chem. Soc.* **1992**, *114*, 10557−10563. [18g] J. de With, A. D. Horton, *Angew. Chem. Int. Ed. Engl.* **1993**, *32*, 903−905. [18h] C. P. Schaller, P. T. Wolczanski, *Inorg. Chem.* **1993**, *32*, 131−144. [18i] J. L. Bennett, P. T. Wolczanski, *J. Am. Chem. Soc.* **1994**, *116*, 2179−2180.

[19] [19a] D. S. Glueck, F. J. Hollander, R. G. Bergman, *J. Am. Chem. Soc.* **1989**, *111*, 2719−2721. [19b] M. H. Schofield, T. P. Kee, J. T. Anhaus, R. R. Schrock, K. H. Johnson, W. M. Davis, *Inorg. Chem.* **1991**, *30*, 3595−3604. [19c] R. I. Michelman, R. A. Anderson, R. G. Bergman, *J. Am. Chem. Soc.* **1991**, *113*, 5100−5102.

[20] [20a] M. Gómez, P. Gómez-Sal, G. Jimenez, A. Martín, P. Royo, J. Sánchez-Nieves, *Organometallics* **1996**, *15*, 3579−3587. [20b] P. Royo, J. Sánchez-Nieves, M. A. Pellinghelli, A. Tiripicchio, *J. Organomet. Chem.* **1998**, *563*, 15−21. [20c] M. I. Alcalde, P. Gómez-Sal, P. Royo, *Organometallics* **2001**, *20*, 4623−4631.

[21] A. Castro, M. V. Galakhov, M. Gómez, P. Gómez-Sal, A. Martín, P. Royo, *J. Organomet. Chem.* **1998**, *554*, 185−194.

[22] [22a] M. C. W. Chan, J. M. Cole, V. C. Gibson, J. A. K. Howard, C. Lehmann, A. D. Poole, U. Siemeling, *J. Chem. Soc., Dalton Trans.* **1998**, 103−111. [22b] A. Antiñolo, C. Huertas, I. del Hierro, M. F. Lappert, A. Otero, S. Prashar, A. N. Rodriguez, E. Villaseñor, *Organometallics* **1998**, *17*, 5874−5879. [22c] M. I. Alcalde, P. Gómez-Sal, P. Royo, *Organometallics* **1999**, *18*, 546−554. [22d] M. J. Humphries, M. L. Green, M. A. Leech, V. C. Gibson, M. Jolly, D. N. Williams, M. R. J. Elsegood, W. Clegg, *J. Chem. Soc., Dalton Trans.* **2000**, 4044−4051. [22e] M. J. Humphries, M. L. Green, R. E. Douthwaite, L. H. Rees, *J. Chem. Soc., Dalton Trans.* **2000**, 4555−4562. [22f] J. Sánchez-Nieves, P. Royo, M. A. Pellinghelli, A. Tiripicchio, *Organometallics* **2000**, *19*, 3161−3169. [22g] J. Sánchez-Nieves, P. Royo, *J.*

 © 2003 Wiley-VCH Verlag GmbH & Co. KGaA, Weinheim

Organomet. Chem. **2001**, *621*, 299−303. [22h] F. Amor, J. Sánchez-Nieves, P. Royo, H. Jacobsen, O. Blacque, H. Berke, M. Lanfranchi, M. A. Pellinghelli, A. Tiripicchio, *Eur. J. Inorg. Chem.* **2002**, 2810−2817.
[23] J.-K. F. Buijink, A. Meetsma, J. H. Teuben, H. Kooijman, A. L. Speck, *J. Organomet. Chem.* **1995**, *497*, 161−170.
[24] K. A. Jorgensen, *Inorg. Chem.* **1993**, *32*, 1521−1522.
[25] M. D. Curtis, J. Real, *Organometallics* **1985**, *4*, 940−942.
[26] G. Smith, R. R. Schrock, M. R. Churchill, W. J. Youngs, *Inorg. Chem.* **1981**, *20*, 387−393.
[27] [27a] P. A. Bianconi, I. D. Williams, M. P. Engeler, S. J. Lippard, *J. Am. Chem. Soc.* **1986**, *108*, 311−313. [27b] P. A. Bianconi, R. N. Vrtis, C. P. Rao, I. D. Williams, M. P. Engeler, S. J. Lippard, *Organometallics* **1987**, *6*, 1968−1977. [27c] M. J. McGeary, A. S. Gamble, J. L. Templeton, *Organometallics* **1988**, *7*, 271−279.
[28] J. L. Templeton, B. C. Ward, *J. Am. Chem. Soc.* **1980**, *102*, 1532−1538; **1980**, *102*, 3288−3290.
[29] [29a] S. A. Cohen, J. E. Bercaw, *Organometallics* **1985**, *4*, 1006−1014. [29b] D. Kwon, J. Real, M. D. Curtis, A. Rheingold, B. S. Haggerty, *Organometallics* **1991**, *10*, 143−148. [29c] M. I. Alcalde, J. de la Mata, M. Gómez, P. Royo, M. A. Pellinghelli, A. Tiripicchio, *Organometallics* **1994**, *13*, 462−467.
[30] A. Nakamura, K. Mashima, *J. Organomet. Chem.* **2001**, *621*, 224−230.
[31] NMR spectroscopic data for the fragment η^2-C(Me)=O in the complexes **56** and **57**: **56**: ^{1}H NMR ($CDCl_3$, −40 °C): δ = 3.12 [s, 3 H, C(*Me*)=O]. $^{13}C\{^1H\}$ NMR ($CDCl_3$, −40 °C): δ = 316.1 [s, *C*(Me)=O]. **57**: ^{1}H NMR ($CDCl_3$, −50 °C): δ = 3.13 [s, 3 H, C(*Me*)=O]. $^{13}C\{^1H\}$ NMR ($CDCl_3$, −50 °C): δ = 320 [s, *C*(Me)=O].
[32] G. Parkin, A. Van Asselt, D. J. Leahy, L.-R. Whinnery, N. H. Hua, R. W. Quan, L. M. Henling, W. P. Schaefer, B. D. Santarsiero, J. E. Bercaw, *Inorg. Chem.* **1992**, *31*, 82−85.
[33] A. Castro, M. V. Galakhov, M. Gómez, P. Gómez-Sal, A. Martín, F. Sánchez, *J. Organomet. Chem.* **2000**, *595*, 36−53.
[34] C. D. Wood, R. R. Schrock, *J. Am. Chem. Soc.* **1979**, *101*, 5421−5422.
[35] D. C. Bradley, M. B. Hursthouse, A. J. Howes, A. N. de M. Jelfs, J. D. Runnacles, M. Thornton-Pett, *J. Chem. Soc., Dalton Trans.* **1991**, 841−847.
[36] [36a] J. A. McCleverty, G. Wilkinson, *J. Chem. Soc.* **1963**, 4096. [36b] H. G. Alt, *J. Organomet. Chem.* **1977**, *127*, 349−356.
[37] J. Teuben, in: *Fundamental and Technological Aspects of Organo-f-Element Chemistry* (Eds.: T. J. Marks, I. L. Fragala); Dordrecht, Holland, **1986**.
[38] K. Tatsumi, A. Nakamura, P. Hofmann, P. Stauffert, R. Hoffmann, *J. Am. Chem. Soc.* **1985**, *107*, 4440−4451.
[39] K. G. Moloy, T. J. Marks, *J. Am. Chem. Soc.* **1984**, *106*, 7051−7064.
[40] D. C. Sonnenberger, E. A. Mintz, T. J. Marks, *J. Am. Chem. Soc.* **1984**, *106*, 3484−3491.
[41] T. Y. Meyer, L. R. Garner, N. C. Baenzinger, L. W. Messerle, *Inorg. Chem.* **1990**, *29*, 4045−4050.
[42] [42a] E. J. Roskamp, S. F. Pedersen, *J. Am. Chem. Soc.* **1987**, *109*, 6551−6553. [42b] S. L. Buchwald, B. T. Watson, M. W. Wannamaker, J. C. Dewan, *J. Am. Chem. Soc.* **1989**, *111*, 4486−4494. [42c] J. R. Strickler, D. E. Wigley, *Organometallics* **1990**, *9*, 1665−1669. [42d] N. Coles, M. C. J. Harris, R. J. Whitby, J. Blagg, *Organometallics* **1994**, *13*, 190−199. [42e] B. Richter, J. Scholz, J. Sieler, K.-H. Thiele, *Angew. Chem. Int. Ed. Engl.* **1995**, *34*, 2649−2651. [42f] D. A. Gately, J. R. Norton, P. A. Goodson, *J. Am. Chem. Soc.* **1995**, *117*, 986−996. [42g] P. Legzdins, P. J. Lundmark, S. J. Rettig, *Organometallics* **1996**, *15*, 2988−2993. [42h] Y. Makioka, Y. Taniguchi, Y. Fujiwara, K. Takaki, Z. Hou, Y. Wakatsuki, *Organometallics* **1996**, *15*, 5476−5478. [42i] M. J. Scott, S. J. Lippard, *Organometallics* **1997**, *16*, 5857−5868. [42j] K. Takai, T. Ishiyama, H. Yasue, T. Nobunaka, M. Itoh, T. Oshiki, K. Mashima, K. Tani, *Organometallics* **1998**, *17*, 5128−5132.
[43] [43a] D. R. Neithamer, L. Párkányi, J. F. Mitchell, P. T. Wolczanski, *J. Am. Chem. Soc.* **1988**, *110*, 4421−4423. [43b] J. R. Strickler, M. A. Bruck, D. E. Wigley, *J. Am. Chem. Soc.* **1990**, *112*, 2814−2816. [43c] D. P. Smith, J. R. Strickler, S. D. Gray, M. A. Bruck, R. S. Holmes, D. E. Wigley, *Organometallics* **1992**, *11*, 1275−1288. [43d] J. M. Boncella, M. L. Cajigal, K. A. Abboud, *Organometallics* **1996**, *15*, 1905−1912. [43e] J. R. Clark, P. E. Fanwick, I. P. Rothwell, *Organometallics* **1996**, *15*, 3232−3237.
[44] [44a] M. Jensen, T. Livinghouse, *J. Am. Chem. Soc.* **1989**, *111*, 4495−4496. [44b] E. J. Roskamp, P. S. Dragovich, J. B. Hartung Jr., S. F. Pedersen, *J. Org. Chem.* **1989**, *54*, 4736−4737. [44c] T. Imamoto, S. Nishimura, *Chem. Lett.* **1990**, 1141−1142. [44d] H. Ito, T. Taguchi, Y. Hanzawa, *Tetrahedron Lett.* **1992**, *33*, 4469−4472. [44e] T. Honda, S.-I. Satoh, M. Mori, *Organometallics* **1995**, *14*, 1548−1550. [44f] Y. Gao, Y. Yoshida, F. Sato, *Synlett* **1997**, 1353−1354.
[45] PARST: [45a] M. Nardelli, *Comput. Chem.* **1983**, *7*, 95−98. [45b] M. Nardelli, *J. Appl. Crystallogr.* **1995**, *28*, 659.
[46] [46a] K. B. Sharpless, R. C. Michaelson, *J. Am. Chem. Soc.* **1973**, *95*, 6136−6137. [46b] S. Tanaka, H. Yamamoto, H. Nozaki, K. B. Sharpless, R. C. Michaelson, J. D. Cutting, *J. Am. Chem. Soc.* **1974**, *96*, 5254−5255. [46c] K. B. Sharpless, T. R. Verhoeven, *Aldrichim. Acta* **1979**, *12*, 63. [46d] K. Suzuki, E. Katayama, G. Tsuchihashi, *Tetrahedron Lett.* **1983**, *24*, 4997−5000. [46e] B. Rickborn, *Comprehensive Organic Synthesis* (Eds.: B. M. Trock, I. Fleming), Pergamon Press, New York, **1991**, vol. 3, pp. 721−732. [46f]C. M. Marson, A. J. Walker, J. Pickering, A. D. Hobson, R. Wrigglesworth, S. J. Edge, *J. Org. Chem.* **1993**, *58*, 5994−5999.
[47] [47a] L. Kloppenburg, J. L. Petersen, *Organometallics* **1997**, *16*, 3548−3556. [47b] M. A. Putzer, B. Neumüller, K. Dehnicke, *Z. Anorg. Allg. Chem.* **1998**, *624*, 57.
[48] R. P. Planalp, R. A. Andersen, *Organometallics* **1983**, *2*, 1675−1680.
[49] R. L. Huff, S.-Y. Wang, K. Abboud, J. M. Boncella, *Organometallics* **1997**, *16*, 1779−1785.
[50] P. Zanella, N. Brianese, U. Castellato, F. Ossala, M. Porchin, G. Rossetto, R. Graziani, *J. Chem. Soc., Dalton Trans.* **1987**, 2039−2043.
[51] [51a] A. K. McMullen, I. P. Rothwell, J. C. Huffman, *J. Am. Chem. Soc.* **1985**, *107*, 1072−1073. [51b] E. Negishi, S. J. Holmes, J. M. Tour, J. A. Miller, *J. Am. Chem. Soc.* **1985**, *107*, 2568−2569. [51c] S. L. Buchwald, B. T. Watson, J. C. Huffman, *J. Am. Chem. Soc.* **1986**, *108*, 7411−7413. [51d] S. L. Buchwald, R. T. Lum, J. C. Dewan, *J. Am. Chem. Soc.* **1986**, *108*, 7441−7442. [51e] S. L. Buchwald, B. T. Watson, J. C. Huffman, *J. Am. Chem. Soc.* **1987**, *109*, 2544−2546. [51f] W. A. Nugent, D. L. Thorn, R. L. Harlow, *J. Am. Chem. Soc.* **1987**, *109*, 2788−2796. [51g] L. R. Chamberlain, L. D. Durfee, P. E. Fanwick, L. M. Kobriger, S. L. Latesky, A. K. McMullen, B. D. Steffey, I. P. Rothwell, K. Folting, J. C. Huffman, *J. Am. Chem. Soc.* **1987**, *109*, 6068−6076. [51h] E. Negishi, D. R. Swanson, F. E. Cederbaum, T. Takahashi, *Tetrahedron Lett.* **1987**, *28*, 917−920. [51i] S. L. Buchwald, R. B. Nielsen, *J. Am. Chem. Soc.* **1989**, *111*, 2870−2874. [51j] J. H. Freudenberger, A. W. Konradi, S. F. Pedersen, *J. Am. Chem. Soc.* **1989**, *111*, 8014−8016.
[52] [52a] S. L. Buchwald, R. B. Nielsen, *Chem. Rev.* **1988**, *88*, 1047−1058. [52b] J. E. McMurry, *Chem. Rev.* **1989**, *89*, 1513−1524. [52c] J. B. Hartung Jr., S. F. Pedersen, *J. Am. Chem. Soc.* **1989**, *111*, 5468−5469. [52d] A. C. Williams, P. Sheffels, D. Sheehan, T. Livinghouse, *Organometallics* **1989**, *8*, 1566−1567.
[53] [53a] T. Masuda, E. Isobe, T. Higashimura, K. Takada, *J. Am. Chem. Soc.* **1983**, *105*, 7473−7474. [53b] F. A. Cotton, W. J. Roth, *Inorg. Chim. Acta* **1984**, *85*, 17−21. [53c] T. Masuda, A. Niki, E. Isobe, T. Higashimura, *Macromolecules* **1985**, *18*, 2109−2113.
[54] J. R. Strickler, M. A. Bruck, P. A. Wexler, D. E. Wigley, *Organometallics* **1990**, *9*, 266−273.
[55] [55a] E. J. Roskamp, S. F. Pedersen, *J. Am. Chem. Soc.* **1987**, *109*, 3152−3154. [55b] S. L. Buchwald, B. T. Watson, R. T. Lum, W. A. Nugent, *J. Am. Chem. Soc.* **1987**, *109*, 7137−7141.
[56] [56a] W. Hirpo, M. D. Curtis, *J. Am. Chem. Soc.* **1988**, *110*,

 © 2003 Wiley-VCH Verlag GmbH & Co. KGaA, Weinheim

5218−5219. [56b] J. L. Kerschner, P. E. Fanwick, I. P. Rothwell, *J. Am. Chem. Soc.* **1988**, *110*, 8235−8238. [56c] B. Hessen, J. H. Teuben, *J. Organomet. Chem.* **1989**, *367*, C18−C20. [56d] B. Hessen, A. Meetsma, F. V. Bolhuis, J. H. Teuben, *Organometallics* **1990**, *9*, 1925−1936. [56e] C. E. Kriley, J. L. Kerschner, P. E. Fanwick, I. P. Rothwell, *Organometallics* **1993**, *12*, 2051−2058. [56f] W. Hirpo, M. D. Curtis, *Organometallics* **1994**, *13*, 2706−2712.

[57] [57a] H. Yasuda, K. Tatsumi, T. Okamoto, K. Mashima, K. Lee, A. Nakamura, Y. Kai, N. Kanehisa, N. Kasai, *J. Am. Chem. Soc.* **1985**, *107*, 2410−2422. [57b] T. Okamoto, H. Yasuda, A. Nakamura, Y. Kai, N. Kanehisa, N. Kasai, *J. Am. Chem. Soc.* **1988**, *110*, 5008−5017. [57c] K. Mashima, M. Kaidzu, Y. Nakayama, A. Nakamura, *Organometallics* **1997**, *16*, 1345−1348. [57d] K. Mashima, M. Kaidzu, Y. Tanaka, Y. Nakayama, A. Nakamura, J. G. Hamilton, J. J. Rooney, *Organometallics* **1998**, *17*, 4183−4195. [57e] H. C. Strauch, B. Wibbeling, R. Fröhlich, G. Erker, H. Jacobsen, H. Berke, *Organometallics* **1999**, *18*, 3802−3812.

[58] K. Mashima, S. Fujikawa, Y. Tanaka, Y. Urata, T. Oshiki, E. Tanaka, A. Nakamura, *Organometallics* **1995**, *14*, 2633−2640.

[59] Y. Kai, N. Kanehisa, K. Miki, N. Kasai, K. Mashima, K. Nagasuna, H. Yasuda, A. Nakamura, *J. Chem. Soc., Chem. Commun.* **1982**, 191−192.

[60] A. D. Hunter, P. Legzdins, C. R. Nurse, F. W. B. Einstein, A. C. Willis, *J. Am. Chem. Soc.* **1985**, *107*, 1791−1792.

[61] H. C. Strauch, G. Erker, R. Fröhlich, *Organometallics* **1998**, *17*, 5746−5757.

[62] L. R. Chamberlain, L. D. Durfee, P. E. Fanwick, L. Kobriger, S. L. Latesky, A. K. McMullen, I. P. Rothwell, K. Folting, J. C. Huffman, W. E. Streib, R. Wang, *J. Am. Chem. Soc.* **1987**, *109*, 390−402.

[63] A. S. Guram, D. C. Swenson, R. F. Jordan, *J. Am. Chem. Soc.* **1992**, *114*, 8991−8996.

Received April 10, 2003

 © 2003 Wiley-VCH Verlag GmbH & Co. KGaA, Weinheim

A Room-Temperature Route to Bismuth Nanotube Arrays

Baojun Yang,[a,b] Cun Li,[a] Hanmei Hu,[a] Xiaogang Yang,[a] Qiaowei Li,[a] and Yitai Qian*[a]

Keywords: Bismuth / Nanostructures / Nanotubes / Synthesis design

A room-temperature aqueous-chemical route has been developed to synthesize a high proportion (above 80%) of bamboo-raft-like bismuth nanotube arrays using bismuth chloride and metallic zinc powder as reagents. The prepared Bi nanotubes have uniform diameters of approximately 3–5 nm and lengths from several hundred nanometers to several micrometers. HRTEM observations show that the axial direction of the prepared nanotubes is along the normal direction of the (012) lattice planes of the rhombohedral bismuth. The possible formation mechanism is discussed.
(© Wiley-VCH Verlag GmbH & Co. KGaA, 69451 Weinheim, Germany, 2003)

Introduction

The discovery of carbon nanotubes[1] has initiated enormous interest in one-dimensional (1D) nanostructured materials, such as nanorods, nanowires, nanobelts and nanotubes, due to both their interesting physical properties and the wide range of their potential applications.[2] Over the past several years, various nanotubular materials, including oxides,[3] sulfides,[4] BN,[5] $NiCl_2$,[6] Te,[7] Au,[8] Ni,[9] Pt,[10] and Bi[11] have been successfully synthesized.

Bismuth (Bi) is a semimetal with a quasi-layered structure formally like that of rhombohedral graphite and black phosphorus.[12] The distances between one Bi atom and its three close neighbors in the same layer and the neighboring layers are 3.072 and 3.529 Å, respectively. Bismuth has unusual electronic properties that result from its highly anisotropic Fermi surface, low carrier concentration, small effective mass and long mean free path of the carriers.[13] These properties make Bi a good candidate to study quantum-confinement effects in 1D systems and very promising materials for thermoelectric applications. However, due to the relatively low melting point of Bi (273.1 °C), most of the existing high-temperature approaches, such as laser ablation, plasma-arc, or CVD (chemical vapor deposition) are inappropriate to synthesize 1D Bi nanomaterials. Hence, a low-temperature chemical approach may provide a more rational technique to prepare 1D Bi nanomaterials. Recently, Bi nanowires[14] (with a proportion of about 20%) have been solvothermally synthesized at 160 °C, using bismuth nitrate [$Bi(NO_3)_3{\cdot}5H_2O$] and ethylenediamine as starting materials. Bi nanotubes[11a] (with a proportion of about 30%) have been hydrothermally synthesized at 120 °C, using bismuth nitrate and aqueous hydrazine [$N_2H_4{\cdot}H_2O$] as starting materials. Bi nanotube arrays[11b] have been solvothermally synthesized at 200 °C, using bismuth oxide (Bi_2O_3) and ethylene glycol as starting materials.

Herein, we report a novel room-temperature aqueous-chemical route that has been developed in our synthesis of a high proportion (above 80%) of bamboo-raft-like bismuth nanotube arrays through the reduction of bismuth chloride by metallic zinc powder. The prepared bismuth nanotubes are arrayed side by side along the axial direction with uniform diameters of approximately 3−5 nm and lengths from several hundred nanometers to several micrometers. This method requires no complex apparatus or technique, and requires no catalyst or template.

Results and Discussion

Figure 1 shows a typical XRD pattern of a prepared sample. All of the sharp peaks can be indexed to a pure rhombohedral phase [space group: $R\bar{3}m$ (166)] of crystalline Bi. The calculated cell constants are a = 4.544 Å and c = 11.85 Å, which are in good agreement with the literature values of a = 4.547Å and c = 11.86 Å (JC,PDS 44-1246). This XRD pattern indicates that the reduction of Bi^{3+} to elemental Bi is complete and pure phase crystalline Bi products can be obtained under current synthetic conditions.

The morphologies and the size of the prepared Bi samples were characterized by TEM. As shown in Figure 2A and 2B, a high proportion (above 80%) of the

[a] Structure Research Laboratory and Department of Chemistry, University of Science and Technology of China,
Hefei, Anhui 230026, P. R. China.
Fax: (internat.) + 86-551/360-7402
E-mail: ytqian@ustc.edu.cn
[b] The School of Chemical Engineering, Hefei University of Technology,
Hefei, Anhui 230009, P. R. China.
Fax: (internat.) + 86-551/290-2956
E-mail: lhmybigy@mail.ustc.edu.cn
Supporting information for this article is available on the WWW under http://www.eurjic.org or from the author.

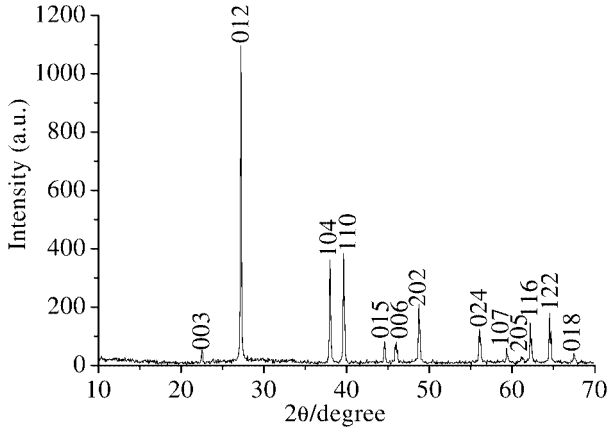

Figure 1. Typical XRD pattern of the prepared bismuth samples

sample dispersed on the TEM copper grids exhibits a nanotubular morphology. Small amounts of flake-like Bi were also observed. Interestingly, except for a small amount of individual Bi nanotubes (marked by the arrow in Figure 2A), almost all these bismuth nanotubes are arrayed like bamboo rafts. Each "bamboo raft" is comprised of several parallel straight bismuth nanotubes lying side by side along the axial direction. It can be seen that these Bi nanotubes have uniform diameters of approximately 3−5 nm and lengths from several hundred nanometers to several micrometers. Energy-dispersive X-ray spectrum (EDS) analysis (Figure 2D) shows that the prepared sample is pure bismuth. This result is consistent with the XRD pattern presented above, in which no impurity phase is observed.

The prepared samples are highly sensitive to electron beam irradiation during the TEM examination due to the relatively low melting point of Bi (273.1 °C), which makes it much more difficult to get clear HRTEM images. The TEM image of a prepared sample after several seconds of

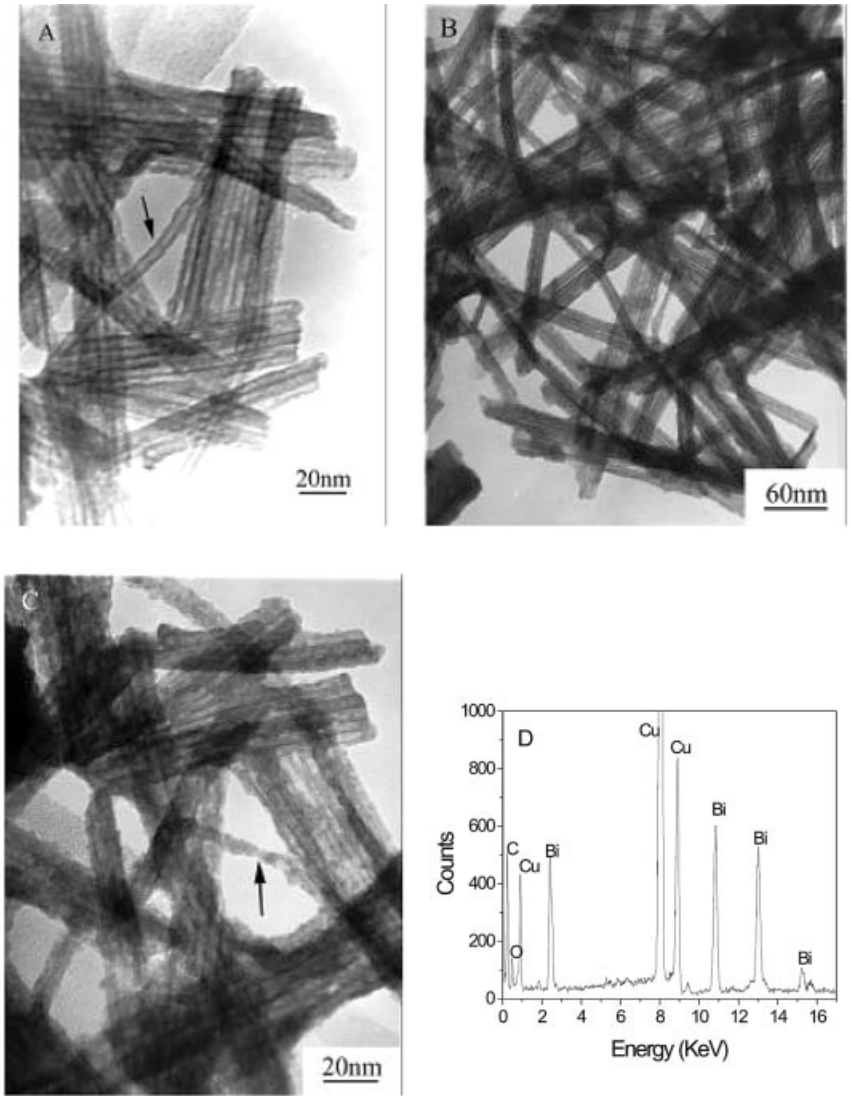

Figure 2. Typical TEM images (A-C) and EDS spectrum (D) of the prepared bismuth nanotubes

 © 2003 Wiley-VCH Verlag GmbH & Co. KGaA, Weinheim

intensive electron beam irradiation is shown in Figure 2C. It can be seen that the morphologies of the bismuth nanotubes have become blurry, some individual Bi nanotubes have melted (marked by the arrow in Figure 2C) and transformed into polycrystalline nanowires. A similar phenomenon was also reported previously.[11a,15] However, some distinguishable HRTEM images have been obtained in our experiments. A representative HRTEM image of one section of a "bamboo raft" is shown in Figure 3. It can be seen that there are four Bi nanotubes which are lying side by side in the image. The discriminable lattice fringes, which are perpendicular to the axial direction of the nanotubes, illustrate that the prepared Bi nanotubes are single crystals in the area shown. The fringe spacing is about 3.2 Å, which is close to the interplanar spacing of the (012) lattice planes of the rhombohedral bismuth. This means that the axial direction of the prepared nanotubes is along the normal direction of the (012) lattice planes of the rhombohedral bismuth.

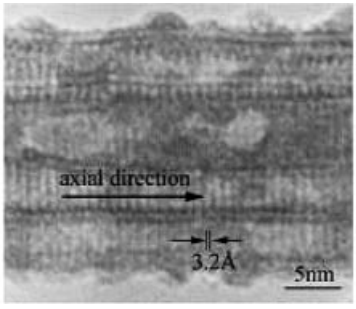

Figure 3. HRTEM image of a "bamboo raft" comprised of four parallel nanotubes

The overall reaction in our system can be simply formulated as shown in Equation (1):

$$2BiCl_3 + 3Zn \rightarrow 2Bi + 3ZnCl_2 \quad (1)$$

The reaction above includes two following steps formulated as Equations (2) and (3):

$$BiCl_3 + H_2O \rightarrow BiOCl + 2HCl \quad (2)$$

$$2BiOCl + 3Zn + 4HCl \rightarrow 2Bi + 2H_2O + 3ZnCl_2 \quad (3)$$

First, $BiCl_3$ hydrolyzes in water to form BiOCl, a white precipitate [Equation (2)], which is then reduced by metallic zinc powder to form metallic Bi. The reduction reaction [Equation (3)] is comprised of two half reactions [Equations (4) and (5)]:

$$BiOCl + 2H^+ + 3e^- \rightarrow Bi + H_2O + Cl^- \ (E^\circ = 0.170\ V) \quad (4)$$

$$Zn^{2+} + 2e^- \rightarrow Zn \ (E^\circ = -0.7626\ V) \quad (5)$$

According to the standard of the formal potential of half reactions (4) and (5), it can be seen that there is a strong tendency for reduction reaction (3) to the formation of metallic Bi. According to the added quantity of $BiCl_3$, the yield of metallic Bi is above 90% by weight.

The specific formation mechanism of the Bi nanotubes is not yet clear and warrants further investigation. Concerning the formation mechanisms for nanotubes, several models have been suggested. For instance, curving followed by seaming of molecular layers (CSML) has been proposed to be responsible for the tube-formation process of materials with layered structure.[16] Direct growth through concentration depletion at the surfaces of cylindrical seeds has been suggested to explain the formation process of Te nanotubes containing chain-like building blocks,[7a] and helical nanobelt-twist-join-growth has been suggested for the formation of Te nanotubes.[7b] Li and co-workers[11a] have described that the formation of metallic Bi nanotubes may be associated with the quasi-layered structure of metallic Bi. Similarly, the observation of tubular and flake-like structures of Bi strongly induce us to speculate that the formation of Bi nanotubes under our experimental conditions is closer to the CSML model, though further investigation about a reliable model for the structure and growth of nanotubes is necessary. As regards the formation of the "bamboo raft", we hypothesize that it might be due to the well-known surface effects of nanostructured materials. The small diameters and the high aspect ratios cause the surface of the newly formed bismuth nanotubes to have large numbers of surface atoms, a lack of atomic coordination and high surface energy. These may lead to a strong tendency of the newly formed bismuth nanotubes to get close to each other and then arrange side by side along the 1D direction (the axial direction), thus forming the bamboo-raft-like nanostructure. The observations that almost all of these nanotubes exhibit a bamboo-raft-like nanostructure, and only a small amount of tubes exist as individual nanotubes, may indirectly confirm the hypothesis described above. However, the intermediate process of the formation of the bamboo-raft-like Bi nanostructure is not yet clear.

The proper reducing agent is crucial for the formation of bismuth nanotubes. Further investigation shows that similar bamboo-raft-like bismuth nanotubes can also be obtained in alkaline solution at room temperature, using tin chloride dihydrate ($SnCl_2 \cdot 2H_2O$) as reducing agent (see Supporting Information). But we failed to get Bi nanotubes at room temperature by using sodium borohydride or aqueous hydrazine as reducing agent. The specific reasons for these observations are unknown.

Conclusion

In summary, we have described a room-temperature aqueous-chemical route to obtain a high proportion (above 80%) of bamboo-raft-like bismuth nanotubes, which are comprised of several parallel straight bismuth nanotubes lying side by side along the axial direction. HRTEM observations show that the axial direction of the prepared nanotubes is along the normal direction of the (012) lattice planes of the rhombohedral bismuth. The present study

 © 2003 Wiley-VCH Verlag GmbH & Co. KGaA, Weinheim

may be advantageous over most of the previously reported approaches in terms of no requirement of complex apparatus or techniques, and the possibility of production on a large scale. In addition, as a tubular sacrificing template, the prepared Bi nanotubes might also be potentially converted into 1D nanostructures of many technologically important materials, such as Bi_2S_3, Bi_2Se_3, Bi_2Te_3, and so forth.

Experimental Section

All reagents used in our experiments were analytical pure grade, purchased from Shanghai Chemicals Co. (China), and were used without further purification. In a typical procedure, 2 mmol of $BiCl_3$ was added to 50 mL of distilled water whilst stirring with a magnetic stirrer to yield a white precipitate. Then, 4 mmol of metallic zinc powder (about 200 mesh) was added to the above system, and the mixture was continuously stirred at room temperature for 2−4 h. The obtained mixture was added to dilute hydrochloric acid (1 M) and left to react for several minutes to remove the excess metal zinc and by-products. The mixture was then filtered, washed with distilled water several times, and the resulting black powder was finally dried in a vacuum at 60 °C for 4 h.

The samples were characterized by X-ray powder diffraction data (XRD), which were recorded on a Japan Rigaku Dmax-γA X-ray powder diffractometer with graphite monochromated Cu-K_α radiation (λ = 1.54178 Å). Transmission electron microscopy (TEM) images and high-resolution transmission electron microscopy (HRTEM) images, accompanied by Energy-dispersive X-ray spectrum (EDS), were obtained with a JEOL-2010 transmission electron microscope, employing an accelerating voltage of 200 kV.

Acknowledgments

Financial support from the National Natural Science Funds and the 973 Projects of China is gratefully acknowledged. The author would like to thank Prof. Shuyuan Zhang for HRTEM observations and Dr. Maosong Mo for helpful discussions.

[1] S. Iijima, *Nature* **1991**, *354*, 56−58.
[2] J. T. Hu, T. W. Odom, C. M. Lieber, *Acc. Chem. Res.* **1999**, *32*, 435−445.
[3] [3a] A. Dobley, K. Ngala, S. F. Yang, P. Y. Zavalij, M. S. Whittingham, *Chem. Mater.* **2001**, *13*, 4382−4386. [3b] B. D. Yao, Y. F. Chan, X. Y. Zhang, W. F. Zhang, Z. Y. Yang, Z. Wang, *Appl. Phys. Lett.* **2003**, *82*, 281−283.
[4] [4a] R. Tenne, L. Margulis, M. Genut, G. Hodes, *Nature* **1992**, *360*, 444−446. [4b] M. Hershfinkel, L. A. Gheber, V. Volterra, J. L. Hutchison, L. Margulis, R. Tenne, *J. Am. Chem. Soc.* **1994**, *116*, 1914−1917. [4c] Y. Q. Zhu, T. Sekine, K. S. Brigatti, S. Firth, R. Tenne, R. Rosentsveig, H. W. Kroto, D. M. R. Walton, *J. Am. Chem. Soc.* **2003**, *125*, 1329−1333. [4d] M. Nath, C. N. R. Rao, *J. Am. Chem. Soc.* **2001**, *123*, 4841−4842.
[5] N. G. Chopra, R. J. Luyken, K. Cherrey, V. H. Crespi, M. L. Cohen, S. G. Louie, A. Zettl, *Science* **1995**, *269*, 966−967.
[6] Y. R. Hacohen, E. Grunbaum, R. Tenne, J. Sloan, J. L. Hutchison, *Nature* **1998**, *395*, 336−337.
[7] [7a] B. Mayers, Y. N. Xia, *Adv. Mater.* **2002**, *14*, 279−282. [7b] M. S. Mo, J. H. Zeng, X. M. Liu, W. C. Yu, S. Y. Zhang, Y. T. Qian, *Adv. Mater.* **2002**, *14*, 1658−1662.
[8] C. R. Martin, M. Nishizawa, K. Jirage, M. Kang, *J. Phys. Chem. B* **2001**, *105*, 1925−1934.
[9] [9a] J. C. Bao, C. Y. Tie, Z. Xu, Q. F. Zhou, D. Shen, Q. Ma, *Adv. Mater.* **2001**, *13*, 1631−1633. [9b] J. C. Bao, K. Y. Wang, Z. Xu, H. Zhang, Z. H. Lu, *Chem. Commun.* **2003**, 208−209.
[10] Y. Oshima, H. Koizumi, K. Mouri, H. Hirayama, K. Takayanagi, Y. Kondo, *Phys. Rev. B* **2002**, *65*, 121401−1-4.
[11] [11a] Y. D. Li, J. W. Wang, Z. X. Deng, Y. Y. Wu, X. M. Sun, D. P. Yu, P. D. Yang, *J. Am. Chem. Soc.* **2001**, *123*, 9904−9905. [11b] X. Y. Liu, J. H. Zeng, S. Y. Zhang, R. B. Zheng, X. M. Liu, Y. T. Qian, *Chem. Phys. Lett.* **2003**, *374*, 348−352.
[12] R. W. G. Wyckoff. *Crystal Structures*; 2nd. Ed.; Interscience: New York, **1973**; Vol. 1, p 32.
[13] [13a] F. Y. Yang, K. Liu, K. M. Hong, D. H. Reich, P. C. Searson, C. L. Chien, *Science* **1999**, *284*, 1335−1337. [13b] X. Sun, Z. Zhang, M. S. Dresselhaus, *Appl. Phys. Lett.* **1999**, *74*, 4005−4007.
[14] Y. H. Gao, H. L. Niu, C. Zeng, Q. W. Chen, *Chem. Phys. Lett.* **2003**, *367*, 141−144.
[15] Z. B. Zhang, D. Gekhtman, M. S. Dresselhaus, J. Y. Ying, *Chem. Mater.* **1999**, *11*, 1659−1665.
[16] C. H. Ye, G. W. Meng, Z. Jiang, Y. H. Wang, G. Z. Wang, L. D. Zhang, *J. Am. Chem. Soc.* **2002**, *124*, 15180−15181.

Received June 6, 2003

 © 2003 Wiley-VCH Verlag GmbH & Co. KGaA, Weinheim

A Binuclear Copper(II) Acetate Complex Showing a 3D Supramolecular Network with Hydrophilic Pockets: Its Unusual Magnetic Behaviour

Matilde Fondo,*[a] Ana M. García-Deibe,[a] Jesús Sanmartín,[a] Manuel R. Bermejo,[a] Luis Lezama,[b] and Teófilo Rojo[b]

Keywords: 3D network / Copper / Magnetic properties / Bridging ligands / Intermolecular interactions

The binuclear complex $[Cu_2L(OAc)]\cdot 6H_2O$ (**1**) {H_3L = 2-(2-hydroxyphenyl)-1,3-bis[4-(2-hydroxyphenyl)-3-azabut-3-enyl]-1,3-imidazolidine} which shows an unusual magnetic superexchange behaviour, acts as a building block for a novel three-dimensional metal-organic framework, with hydrophilic pockets.
(© Wiley-VCH Verlag GmbH & Co. KGaA, 69451 Weinheim, Germany, 2003)

Introduction

Coordination complexes that define unusual network topologies have attracted special interest not only because of their intriguing architectures, but also of their tremendous potential applications in a wide number of fields.[1−7] However, the assembly of inorganic materials from organic ligands and metal-ion building blocks to generate new supramolecular architectures is still a challenge. Supramolecular inorganic/organic hybrid materials have so far been constructed through two principal design philosophies. The most common approach is the assembly of transition metal complexes into coordination polymers using coordinative covalent bonds.[2−6,8−11] The second method makes use of weaker intermolecular forces (particularly π-π interactions and hydrogen bonding)[7,12−15] for connecting building blocks into a wide variety of extended networks.

In this work, a novel case of "one-pot" self-assembled 3D networks, by combination of coordinative and intermolecular interactions, with brick-wall shaped channels, is described (Figure 1). This topology has not been previously reported to the best of our knowledge. The binuclear copper complex, which acts as building block, shows an unfamiliar superexchange pathway, with a net ferromagnetic behaviour.

Results and Discussion

The reaction of 2-(2-hydroxyphenyl)-1,3-bis[4-(2-hydroxyphenyl)-3-azabut-3-enyl]-1,3-imidazolidine (H_3L)[16] with copper(II) acetate dihydrate in methanol/acetonitrile yields a deep green solution in air. Its slow evaporation leads to the isolation of crystals of $[Cu_2L(OAc)]\cdot 6H_2O$ (**1**), suitable for X-ray diffraction studies.

The crystal structure shows that **1** consists of binuclear $[Cu_2L(OAc)]$ units (Figure 2) with water molecules as solvates. The isolated units contain both copper atoms doubly bridged by a phenolate oxygen atom [O(103)] of the central ligand arm and by an oxygen atom from an acetate ligand [O(11)]. This gives rise to an intramolecular Cu(11)···Cu(12) separation of 3.1450(19) Å. The Cu−O distances [Cu(11)−O(103) and Cu(12)−O(103); Cu(11)−O(11) and Cu(12)−O(11)] reflect the asymmetry of both endogenous and exogenous bridges. The Cu(11)−O(103)−Cu(12) and Cu(11)−O(11)−Cu(12) bridging angles are 102.5(2)° and 91.8(2)° respectively. The geometry around both copper atoms can be described as highly distorted square pyramidal (τ = 0.43 and 0.35 for Cu(11) and Cu(12) respectively), with O(11) at the apex of both pyramids. As a result, the complex consists of two distorted square pyramids sharing one base-to-apex edge (Scheme 1, Type I). The distorted basal planes form an angle of 133.9°. Two other types of arrangements are described in the literature for square-pyramidal complexes containing a Cu_2O_2 core: a) square pyramids sharing one base-to-apex edge but with parallel basal planes (Scheme 1, Type II); b) square pyramids sharing one basal edge with coplanar basal planes (Scheme 1, Type III). To the best of our knowledge, the situation Type I has not been previously reported for this kind of complex. In addition, the nearly perpendicular orientation of the Cu−Oph−Cu ideal plane and the central phenyl ring (90.6°) is remarkable.

The $[Cu_2L(OAc)]$ units form an extended array by a combination of π···π, CH···π and C−H···O hydrogen bonds,[17] leading to the formation of a 3D network with hydrophilic channels along the (001) direction of ca. 11 × 7 Å^2 (Fig-

[a] Departamento de Química Inorgánica, Facultade de Química, Universidade de Santiago de Compostela, 15706 Santiago de Compostela, Spain
E-mail: qimatf69@usc.es
[b] Departamento de Química Inorgánica, Facultad de Ciencias, Universidad del Pais Vasco, 48080 Bilbao, Spain

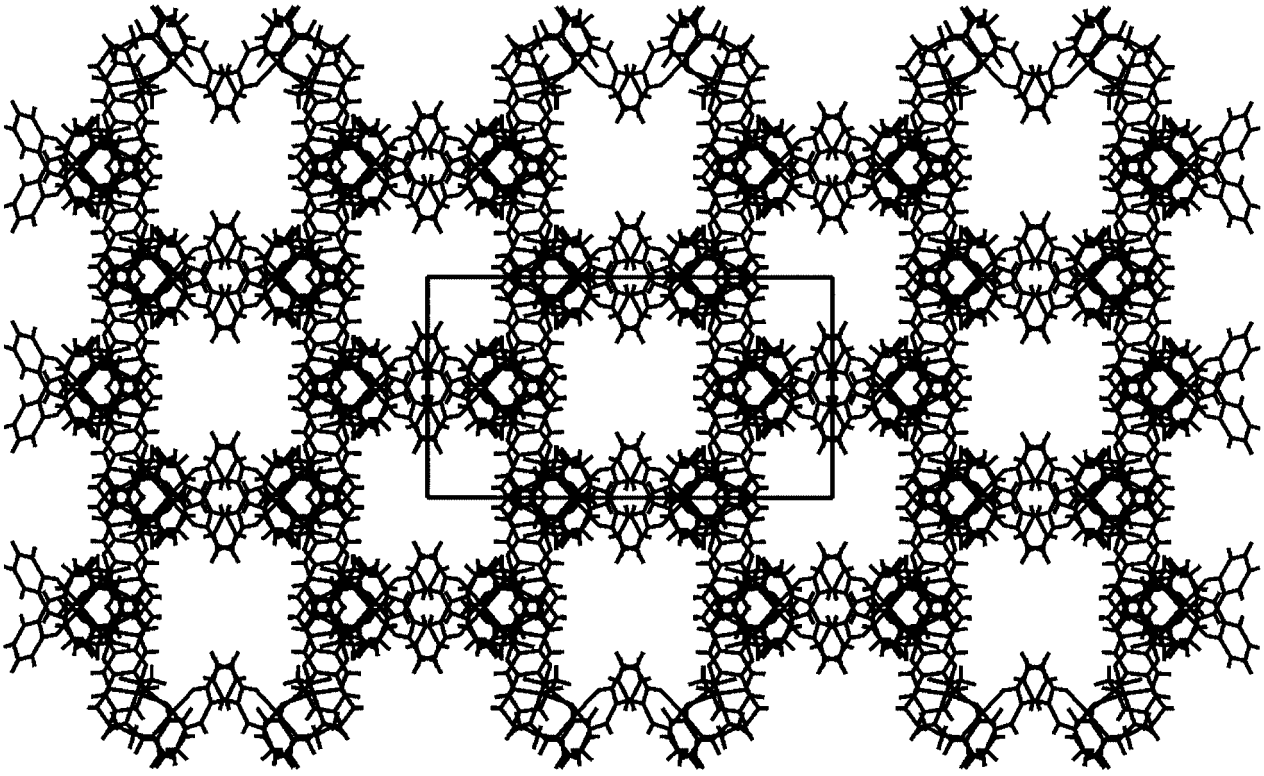

Figure 1. View of the packing of **1** along the (001) direction; guest water molecules are omitted for clarity

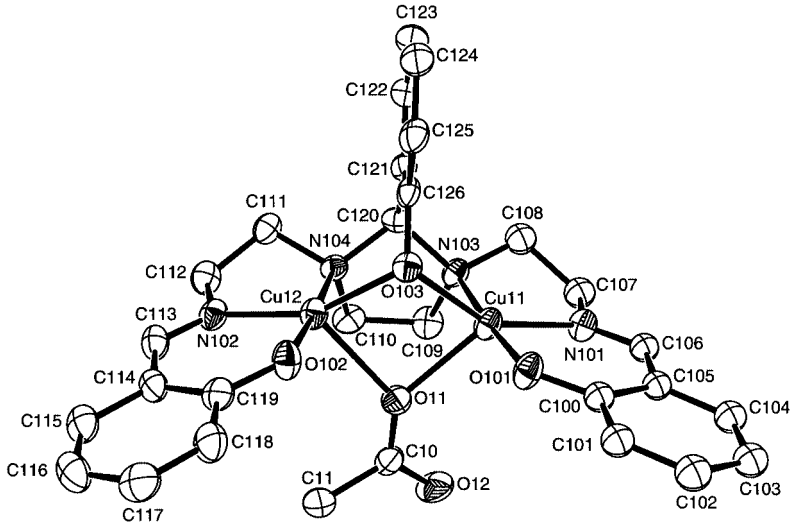

Figure 2. An ORTEP view of **1** showing 30% probability thermal ellipsoids (water molecules and hydrogen atoms are omitted for clarity); selected bond lengths and angles: Cu(11)−O(101) 1.909(6), Cu(11)−N(101) 1.950(7), Cu(11)−O(103) 2.042(6), Cu(11)−N(103) 2.076(7), Cu(11)−O(11) 2.171(6), Cu(12)−O(102) 1.919(6), Cu(12)−N(102) 1.931(7), Cu(12)−O(103) 1.991(5), Cu(12)−N(104) 2.076(7), Cu(12)−O(11) 2.208(6); O(101)−Cu(11)−N(103) 175.4(3), N(101)−Cu(11)−O(103) 149.5(3), N(101)−Cu(11)−O(11) 130.4(3), O(103)−Cu(11)−O(11) 79.5(2), O(102)−Cu(12)−N(104) 176.3(3), N(102)−Cu(12)−O(103) 155.2(3), N(102)−Cu(12)−O(11) 124.2(3), O(103)−Cu(12)−O(11) 79.7(2)

ure 1). Thus, the total void space, neglecting the solvent molecules, represents 34.2% of the cell volume. The water molecules occupy most of the void space and form an intricate hydrogen bond scheme. According to the structural data, they can be roughly assigned as: a) tightly bonded molecules, anchored to the network by one or more hydrogen bonds involving the phenol oxygen atoms or the uncoordinated acetate oxygen atom (O1w, O2w, O4w, O5w); b) loosely bonded molecules showing only contacts with other water molecules (the remaining solvent molecules).

ESR spectra for the title compound were recorded on powdered samples in the temperature ranges 4.2−300 K and 100−300 K operating at X- and Q-bands, respectively. Despite the extremely large observed signals, the spectrum

 © 2003 Wiley-VCH Verlag GmbH & Co. KGaA, Weinheim

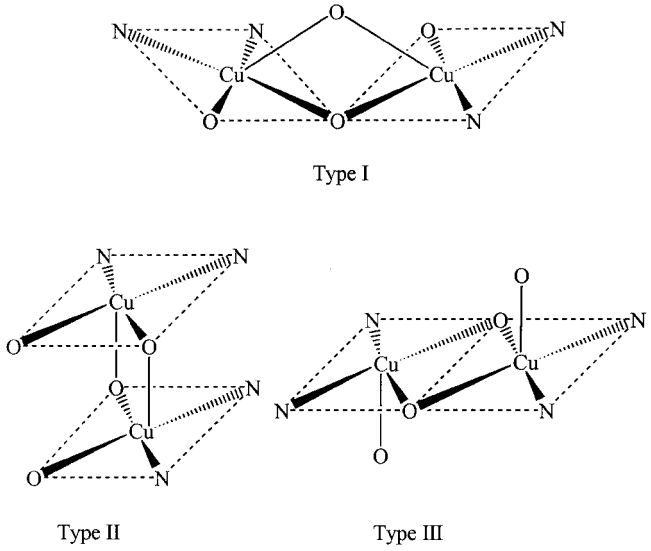

Scheme 1. Square pyramidal arrangements for Cu_2O_2 containing complexes

obviously corresponds to an $S = 1$ triplet state, as expected for an isolated binuclear Cu^{II} complex, with important zero-field splitting. The existence of a triplet state is confirmed by the presence of a "half-field" signal ($\Delta M_s = \pm 2$) in both X- and Q-band spectra. Unfortunately, the poor resolution of the spectra has precluded any unambiguous determination of the main components of the g and D tensors.

Magnetic susceptibility measurements have been performed between 5 and 300 K. Figure 3 shows the thermal evolution of the magnetic molar susceptibility, together with a plot of $\chi_m T$ vs T ($\chi_m T = \mu_{eff}^2/8$). Above 100 K, the data are well described by a Curie−Weiss law ($\chi_m = C_m/T-\theta$), with $C_m = 0.86$ cm^3 K/mol and $\theta = +12.6$ K. The positive θ value, as well as the overall appearance of the $\chi_m T$ vs. T curve, are indicative of the predominance of ferromagnetic interactions in this compound. The $\chi_m T$ product increases from 0.89 cm^{3}K/mol at room temperature to 1.13 cm^{3}K/mol at 5 K.

Taking into account the crystal structure of this compound, the susceptibility data have been fitted to the Bleaney−Bowers equation[18] derived from the Heisenberg spin Hamiltonian ($H = -2JS_1S_2$) for two coupled $S = 1/2$ ions:

$$\chi_m = \frac{2Ng^2\beta^2}{kT}\left[\frac{1}{3+\exp(-2J/kT)}\right] \quad (1)$$

The best least-squares fit (solid lines in Figure 3) is obtained with the parameter $2J = +49.2$ cm^{-1} ($J/k = +35.4$ K) and $g = 2.13$. Attempts to evaluate the possible interbinuclear interactions by means of a J' parameter treated in the molecular field approximation, led to extremely low values without any significant improvement of the fit.

As the geometry around both copper atoms is distorted square pyramidal, the $d_{x^2-y^2}$ magnetic orbitals (containing the unpaired electron) point towards the bridging phenolate oxygen atom. Therefore, the structure of complex **1** suggests that O(103) provides the likely pathway for coupling. The bridging acetate oxygen atom is at the common apical position of the square pyramidal chromophores, indicating that O(11) does not participate or shows negligible contribution to the superexchange pathway. Therefore, the magnetic behaviour of this complex is rather unusual. The main superexchange pathway is a phenolate oxygen atom, and binuclear copper complexes that share just one basal phenolate oxygen atom are usually antiferromagnetic.[19−23] In fact, just one binuclear copper of this type, which shows a square pyramidal arrangement of Type II, is described to be weakly ferromagnetic.[24] Besides, doubly bridged phenolate copper complexes usually show strong antiferromagnetic coupling.[25−29] The ferromagnetic behaviour of complex **1** can be attributed to its unusual structural features, detailed above.

In summary, this study reports the first complex containing a Cu_2O_2 core with a Type I arrangement, which shows an unfamiliar magnetic behaviour. Complex **1** acts as a building block to produce a 3D framework via weak intermolecular interactions. The network shows brick-wall shaped hydrophilic channels with unprecedented topology.

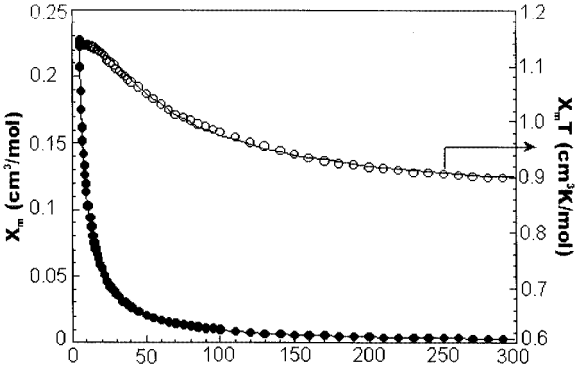

Figure 3. Magnetic data for **1** at 5−300 K

Experimental Section

General: Elemental analysis was performed on a Carlo Erba EA 1108 analyser. Infrared spectrum was recorded as KBr pellets on a Bio-Rad FTS 175 spectrophotometer in the range 4000−600 cm^{-1}. Electrospray mass spectrum was obtained on a Hewlett−Packard LC/MS spectrometer with methanol as solvent.

Synthesis of 1: A solution of copper acetate dihydrate (0.25 g, 1.25 mmol) in methanol (30 mL) was mixed with a solution of H_3L (0.287 g, 6.23 mmol) in acetonitrile (30 mL). The resultant green solution was stirred at room temperature for 4 h. Slow evaporation of the solution yielded crystals of **1** (Yield: 0.35 g, 74.6%). $C_{29}H_{42}Cu_2N_4O_{11}$ (749.75): calcd. C 46.5, H 5.6, N 7.5; found C 46.9, H 5.7, N 7.2. (KBr): ν(C=N) = 1634 cm^{-1} (s). ES-MS: $m/z = 581.1$ [Cu_2L^+].

X-ray Crystallography: Prism-shaped green crystals of **1** were grown as detailed above. Data were collected on a Smart-CCD-

 © 2003 Wiley-VCH Verlag GmbH & Co. KGaA, Weinheim

1000 BRUKER diffractometer, using graphite monochromated Mo-K_α radiation (λ = 0.71073 Å), operating at room temperature. The structure was solved by direct methods and refined by full-matrix least-squares based on F^2 using the SHELX-97 program package.[30] Absorption correction was carried out semi-empirically from equivalents using the SADABS program.[31] Crystal data: $C_{29}H_{42}Cu_2N_4O_{11}$, M_r = 749.75 g·mol^{-1}, monoclinic, space group $C2/c$, a = 31.831(11), b = 13.968(5), c = 20.754(7) Å, β = 126.359(19)°, V = 7431(4) Å^3, Z = 8, D_c = 1.340 Mg·m^{-3}, $F(000)$ = 3120, μ(Mo-K_α) = 1.201 mm^{-1}. 5367 Unique reflections were measured. Final $R1$ = 0.1480 on all data, conventional $R1$ = 0.0661 on [$I > 2\sigma(I)$].

CCDC-205980 contains the supplementary crystallographic data for this paper. These data can be obtained free of charge at www.ccdc.cam.ac.uk/conts/retrieving.html [or from the Cambridge Crystallographic Data Centre, 12, Union Road, Cambridge CB2 1EZ, UK; Fax: (internat.) +44-1223/336-033; E-mail: deposit@ccdc.cam.ac.uk].

EPR and Magnetic Measurements: A Bruker ESP300 spectrometer, operating at X- and Q-bands and equipped with standard Oxford low temperature devices, was used to record the ESR powder spectra of **1** at different temperatures. The magnetic field was calibrated by an NMR probe and the frequency inside the cavities was determined with a Hewlett−Packard 5352B microwave frequency counter. Magnetic susceptibility measurements were performed on powdered samples between 5 and 300 K with a Quantum Design MPMS-7 SQUID magnetometer. The magnetic field used in the experiments was 0.1 T, a value at which the magnetisation versus magnetic field curve was still linear at 5 K. Experimental susceptibility values were corrected for diamagnetic contributions and for temperature-independent paramagnetism.

[1] V. A. Russell, C. C. Evans, W. Li, M. D. Ward, *Science* **1997**, *276*, 575−579.
[2] S. R. Batten, R. Robson, *Angew. Chem. Int. Ed.* **1998**, *37*, 1461−1494.
[3] D. M. L. Goodgame, D. A. Grachvogel, D. J. Williams, *Angew. Chem. Int. Ed.* **1999**, *38*, 153−156.
[4] N. Matsumoto, Y. Sunatsuki, H. Miyasaka, Y. Hashimoto, D. Luneau, J-P. Tuchages, *Angew. Chem. Int. Ed.* **1999**, *38*, 171−173.
[5] H. Li, A. Laine, M. O′Keefe, O. M. Yaghi, *Science* **1999**, *283*, 1145−1147.
[6] A. J. Blake, N. R. Champness, P. A. Cooke, J. E. B. Nicolson, *Chem. Commun.* **2000**, 665−666.
[7] D. V. Soldatov, J. A. Ripmeester, *Chem. Eur. J.* **2001**, *7*, 2979−2994.
[8] L. Carlucci, G. Ciani, M. Moret, D. M. Proserpio, S. Rizzato, *Angew. Chem. Int. Ed.* **2000**, *39*, 1506−1510.
[9] A. N. Khlobystov, A. J. Blake, N. R. Champness, D. A. Lemenovskii, A. G. Majouga, N. V. Zyk, M. Schröder, *Coord. Chem. Rev.* **2001**, *222*, 155−192.
[10] J. Tercero, C. Diaz, J. Ribas, E. Ruiz, J. Mahia, M. Maestro, *Inorg. Chem.* **2002**, *41*, 6780−2789.
[11] T. J. Prior, D. Bradshaw, S. J. Teat, M. J. Rosseinsky, *Chem. Commun.* **2003**, 500−501.
[12] C-Y. Su, X-P. Yang, B-S. Kang, T. C. W. Mak, *Angew. Chem. Int. Ed.* **2001**, *40*, 1725−1728.
[13] P. J. Nichols, C. L. Raston, J. W. Steed, *Chem. Commun.* **2001**, 1062−1063.
[14] T. P. Vaid, O. L. Sydora, R. E. Douthwaite, P. T. Wolczanski, E. B. Lobkovsky, *Chem. Commun.* **2001**, 1300−1301.
[15] V. G. Albano, M. C. Aragoni, M. Arca, C. Castellari, F. Demartin, F. A. Devillanova, F. Isaia, V. Lippolis, L. Loddo, G. Verani, *Chem. Commun.* **2002**, 1170−1171.
[16] l-W. Yang, S. Liu, E. Wong, S. J. Rettig, C. Orvig, *Inorg. Chem.* **1995**, *34*, 2164−2178.
[17] W. Grochala, A. Jagielska, K. Wozniak, A. Wiekowska, R. Bilewicz, B. Korybut-Daszkiewicz, J. Bukowska, L. Piela, *J. Phys. Org. Chem.* **2001**, *14*, 63−73.
[18] B. Bleaney, K. D. Bowers, *Proc. R. Soc., London, Ser. A* **1952**, *214*, 451−465.
[19] Y. Nishida, T. Tokii, Y. Mori, *J. Chem. Soc., Chem. Commun.* **1988**, 675−676.
[20] [20a] K. Bertoncello, G. D. Fallon, J. H. Hodgkin, K. S. Murray, *Inorg. Chem.* **1988**, *27*, 4750−4758. [20b] P. Dalgaard, A. Hazell, C. J. Mckenzie, B. Moubaraki, K. S. Murray, *Polyhedron* **2000**, *19*, 1909−1915.
[21] R. C. Holz, J. M. Bradshaw, B. Bennett, *Inorg. Chem.* **1998**, *37*, 1219−1225.
[22] T. M. Rajendiran, R. Kannappan, R. Venkatesan, P. S. Rao, M. Kandaswamy, *Polyhedron* **1999**, *18*, 3085−3091.
[23] K. J. Oberhausen, J. F. Richardson, R. M. Buchanan, J. K. McCusker, D. N. Hendrickson, J-M. Latour, *Inorg. Chem.* **1991**, *30*, 1357−1365.
[24] H. P. Berends, D. W. Stephan, *Inorg. Chem.* **1987**, *26*, 749−754.
[25] J. Loroesch, U. Quotschalla, W. Haase, *Inorg. Chim. Acta* **1987**, *131*, 229−236.
[26] L. K. Thompson, S. K. Mandal, S. S. Tandon, J. N. Brisdon, M. K. Park, *Inorg. Chem.* **1996**, *35*, 3117−3125.
[27] [27a] Y. Sunatsuki, M. Nakamura, N. Matsumoto, F. Kai, *Bull. Chem. Soc. Jpn.* **1997**, *70*, 1851−1858. [27b] H. Saimiya, Y. Sunatsuki, M. Kojima, S. Kashino, T. Kambe, M. Hirotsu, H. Akashi, K. Nakajima, T. Tokii, *J. Chem. Soc., Dalton Trans.* **2002**, 3737−3742.
[28] [28a] N. R. Sangeetha, K. Baradi, R. Gupta, C. K. Pal, V. Manivannan, S. Pal, *Polyhedron* **1999**, *18*, 1425−1429. [28b] R. Gupta, S. Mukherjee, R. Mukherjee, *J. Chem. Soc., Dalton Trans.* **1999**, 4025−4030.
[29] X. Wang, J. Ding, J. D. Ranford, J. J. Vitall, *J. Appl. Phys.* **2003**, *93*, 7819−7821.
[30] G. M. Sheldrick, SHELX-97 (SHELXS 97 and SHELXL 97), Programs for Crystal Structure Analyses, University of Göttingen, Germany, **1998**.
[31] SADABS, Area-Detector Absorption Correction. Siemens Industrial Automation Inc., Madison, WI, **1996**.

Received July 18, 2003

 © 2003 Wiley-VCH Verlag GmbH & Co. KGaA, Weinheim

Chiral Arene Ruthenium Complexes: Synthesis and Molecular Structure of the Enantiopure Cluster Cation (*S*)-$[H_3Ru_3\{C_6H_5[CH(CH_3)CH_2OH]\}(C_6Me_6)_2(O)]^+$

Ludovic Vieille-Petit,[a] Bruno Therrien,[a] and Georg Süss-Fink*[a]

Keywords: Arene ligands / Chirality / Cluster compounds / Ruthenium

The reaction of enantiopure (*R*)-(2-cyclohexa-1,4-dienyl)propan-1-ol with ruthenium chloride hydrate yields, without racemisation of the chiral ligand, the chloro-bridged dinuclear complex (*S*,*S*)-$[RuCl_2\{C_6H_5[CH(CH_3)CH_2OH]\}]_2$ (**1**). The dimer **1** reacts with triphenylphosphane to give the mononuclear complex (*S*)-$[RuCl_2\{C_6H_5[CH(CH_3)CH_2OH]\}(PPh_3)]$ (**2**). A single-crystal X-ray structure analysis of **2** reveals the absolute configuration of the asymmetric carbon atom to have remained, the change from (*R*) to (*S*) being due to the priority change caused by coordination; in the solid state, one-dimensional hydrogen-bonded chains are formed between the hydroxy functions and chloro ligands of neighbouring molecules. The mononuclear cationic complex (*S*)-$[Ru\{C_6H_5[CH(CH_3)CH_2OH]\}(H_2O)_3]^{2+}$, formed in situ from **1** in aqueous solution, reacts with the dinuclear complex $[H_3Ru_2(C_6Me_6)_2]^+$ to give a chiral trinuclear arene-ruthenium cluster, the cation (*S*)-$[H_3Ru_3\{C_6H_5[CH(CH_3)CH_2OH]\}(C_6Me_6)_2(O)]^+$ (**3**). This enantiopure cation has been isolated and characterised as its tetrafluoroborate salt. The single-crystal X-ray structure analysis of (*S*)-[**3**][BF_4] shows a strong intramolecular hydrogen bond between the μ_3-oxo cap and the hydroxy function, which also persists in acetone solvent, as demonstrated by NMR spectroscopy.

(© Wiley-VCH Verlag GmbH & Co. KGaA, 69451 Weinheim, Germany, 2003)

Introduction

Recently, we found the water-soluble cluster cation $[H_3Ru_3(C_6H_6)(C_6Me_6)_2(O)]^+$ to efficiently catalyse the hydrogenation of benzene to give cyclohexane under biphasic conditions.[1,2] On the other hand, much attention has been given to the development of chiral arene-ruthenium complexes for the catalytic transfer hydrogenation of ketones[3−6] and for asymmetric Diels−Alder reactions.[7] Therefore, trinuclear ruthenium cluster cations with functional substituents at the η^6-moiety could give rise to homogeneous catalysts which display special solubility properties or can be immobilised on resins.[8]

Herein we report the synthesis and characterisation of a new chloro-bridged arene-ruthenium dimer, (*S*,*S*)-$[RuCl_2\{C_6H_5[CH(CH_3)CH_2OH]\}]_2$ (**1**), in which the η^6-arene ligand possesses a side-arm substituent incorporating an asymmetric carbon. The dimeric species is used to synthesise an enantiopure mononuclear complex, (*S*)-$[RuCl_2\{C_6H_5[CH(CH_3)CH_2OH]\}(PPh_3)]$ (**2**), as well as an enantiopure trinuclear cluster cation, (*S*)-$[H_3Ru_3\{C_6H_5[CH(CH_3)CH_2OH]\}(C_6Me_6)_2(O)]^+$ (**3**). NMR spectroscopy as well as single-crystal X-ray analyses show that the chiral centre is stable under various reaction conditions.[9]

[a] Institut de Chimie, Université de Neuchâtel,
Case postale 2, CH-2007 Neuchâtel, Switzerland
E-mail: georg.suess-fink@unine.ch

Results and Discussion

The reaction of (*R*)-(2-cyclohexa-1,4-dienyl)propan-1-ol, accessible from the Birch reduction[10] of commercially available (*R*)-(2-phenyl)propan-1-ol, with ruthenium(III) chloride hydrate, in refluxing ethanol, gives the new chiral chloro-bridged dimer (*S*,*S*)-$[RuCl_2\{C_6H_5[CH(CH_3)CH_2OH]\}]_2$ (**1**), which can be isolated quantitatively as an orange powder (Scheme 1). From enantiopure (2-cyclohexa-1,4-dienyl)propan-1-ol only the (*S*,*S*)-isomer is formed. There is no change in the absolute configuration of the asymmetric carbon atom, the change from (*R*) to (*S*) in the denomination is only due to the change in the priority (Cahn−Ingold−Prelog rules) by the coordination of the phenyl group to a ruthenium atom.

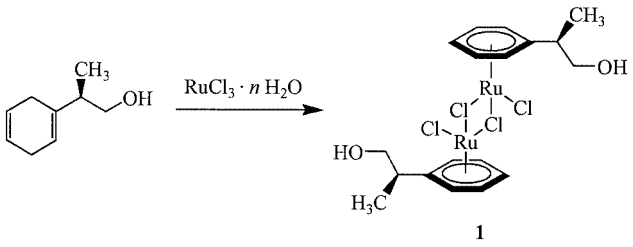

1

Scheme 1

Despite the strong acidic conditions during the dehydrogenation reaction, there is no evidence for racemisation of the (*R*)-(2-phenyl)propanol ligands. The ^1H and $^{13}C\{^1H\}$ NMR spectra of **1** show only one set of signals, the $^{13}C\{^1H\}$

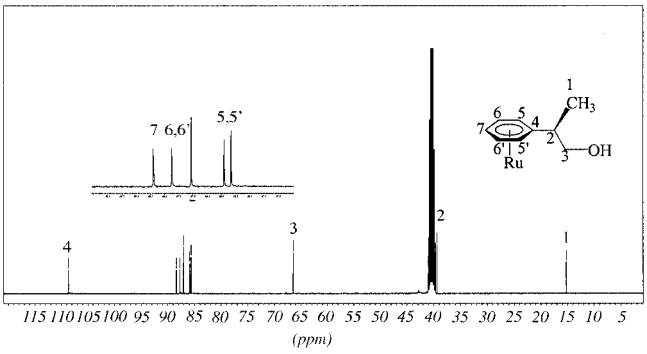

Figure 1. $^{13}C\{^1H\}$ NMR spectrum of **1** in $[D_6]$DMSO (400 MHz)

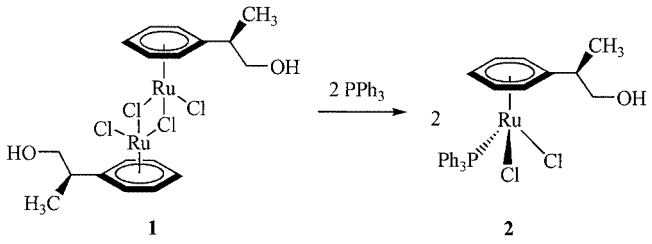

Scheme 2

NMR spectrum in $[D_6]$DMSO is presented in Figure 1. Except for the distinction between the two carbons at the *ortho* positions as well as the two carbons at the *meta* positions of the η^6-arene moiety, all diastereotopic carbons can be assigned unambiguously.

Cleavage of the chloro bridges of the dinuclear complex **1** with two equivalents of triphenylphosphane in CH_2Cl_2 gives the mononuclear complex (*S*)-$[RuCl_2\{C_6H_5$-$[CH(CH_3)CH_2OH]\}(PPh_3)]$ (**2**) in good yield (Scheme 2). The formation of **2** is conveniently monitored by $^{31}P\{^1H\}$ NMR spectroscopy, the $^{31}P\{^1H\}$ NMR signal being shifted downfield by 33.2 ppm (as compared to uncoordinated triphenylphosphane).

The orange air-stable compound was crystallised from a slow diffusion of hexane into a chloroform solution containing **2**. A single-crystal X-ray analysis was performed, confirming the molecular structure of **2** (Figure 2).

The ruthenium atom possesses a pseudo-octahedral geometry, and the metrical parameters around the metallic core compare well with those of similar three-legged pianostool $[RuCl_2(\eta^6$-arene$)(PPh_3)]$ complexes.[11−14] A distortion at the arene ligand is present, the Ru−C bond length *trans* to the phosphorous atom, Ru(1)−C(1) 2.274(4) Å, is elongated as compared to the other Ru−C bonds [ranging between 2.187(4) and 2.244(3) Å]. In the solid state, a series of hydrogen bonds between hydroxy functions and chloride

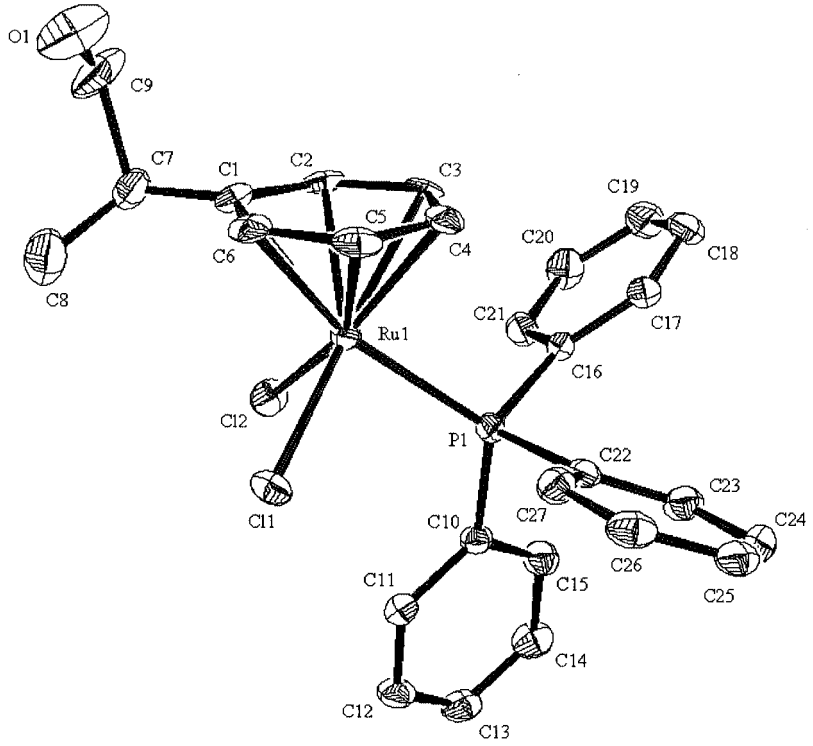

Figure 2. ORTEP view of **2**; displacement ellipsoids are drawn at the 50% probability level; hydrogen atoms and chloroform molecule are omitted for clarity; selected bond lengths (Å) and angles (°): Ru(1)−P(1) 2.3530(10), Ru(1)−Cl(1) 2.4134(9), Ru(1)−Cl(2) 2.3995(10), Ru(1)−C(1) 2.274(4), Ru(1)−C(2) 2.187(4), Ru(1)−C(3) 2.205(4), Ru(1)−C(4) 2.195(4), Ru(1)−C(5) 2.187(4), Ru(1)−C(6) 2.244(3); P(1)−Ru(1)−Cl(1) 91.81(3), P(1)−Ru(1)−Cl(2) 86.34(4), Cl(1)−Ru(1)−Cl(2) 86.62(4)

 © 2003 Wiley-VCH Verlag GmbH & Co. KGaA, Weinheim

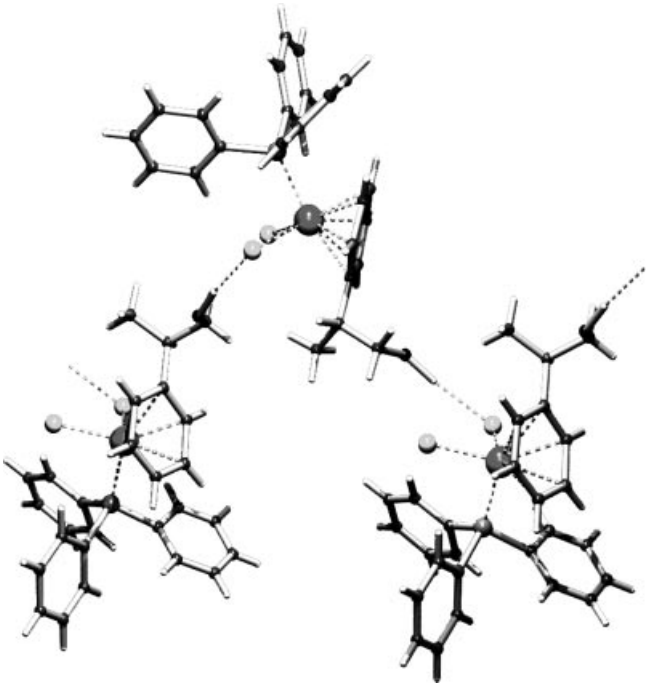

Figure 3. One-dimensional hydrogen bonded chains in the crystalline form of **2**

ligands of neighbouring molecules forms one dimensional chains through the crystal (Figure 3).

In aqueous solution, the dinuclear complex **1** forms the mononuclear complex $[Ru\{C_6H_5[CH(CH_3)CH_2OH]\}(H_2O)_3]^{2+}$, an analogue of the known cation $[(C_6H_6)Ru(H_2O)_3]^{2+}$,[15] which reacts in situ with the dinuclear complex $[H_3Ru_2(C_6Me_6)_2]^+$ [16,17] to give the chiral cluster cation (*S*)-$[H_3Ru_3\{C_6H_5[CH(CH_3)CH_2OH]\}(C_6Me_6)_2(O)]^+$ (**3**; Scheme 3).

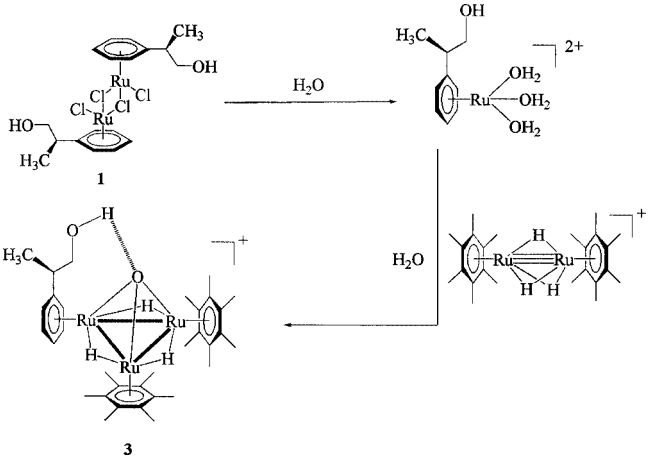

Scheme 3

The enantiopure cation (*S*)-[**3**] has been isolated and characterised as its tetrafluoroborate salt. Whereas the known trinuclear ruthenium cluster cation analogues $[H_3Ru_3(\eta^6\text{-arene})(\eta^6\text{-arene'})_2(O)]^+$ [1,14,18,19] give rise to two hydride signals, a triplet and a doublet integrating for one and two protons, respectively, in the ^1H NMR spectra. The three hydrido ligands in **3** are all inequivalent and give rise to three independent signals. The ^1H NMR spectrum of **3** in [D_6]acetone shows three multiplets at high field centered at $\delta = -19.86$, -19.43 and -19.23 ppm, due to the presence of the asymmetric α-carbon on the side arm. In order to ascertain the retention of the chirality during the synthesis of **3**, a single crystal structure analysis of [**3**][BF_4] was performed.

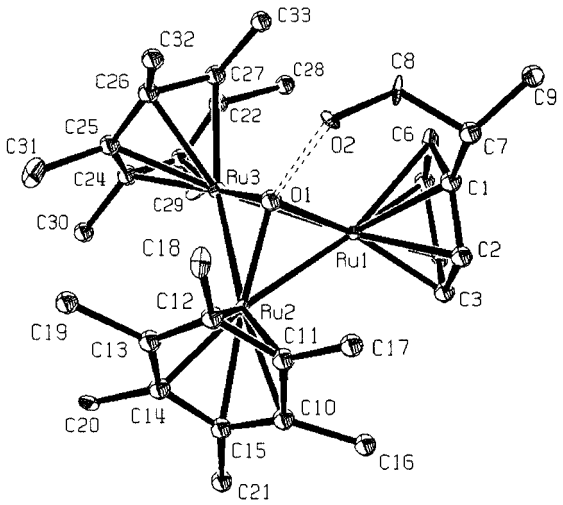

Figure 4. ORTEP view of [**3**]$^+$; displacement ellipsoids are drawn at the 35% probability level, hydrogen atoms, solvent, and the anion are omitted for clarity; selected bond lengths (A) and angles (°): Ru(1)−Ru(2) 2.751(3), Ru(1)−Ru(3) 2.749(3), Ru(2)−Ru(3) 2.785(2), Ru(1)−O(1) 2.058(16), Ru(2)−O(1) 1.935(18), Ru(3)−O(1) 1.971(16); Ru(1)−Ru(2)−Ru(3) 59.54(7), Ru(2)−Ru(3)−Ru(1) 59.62(7), Ru(3)−Ru(1)−Ru(2) 60.84(6), Ru(1)−O(1)−Ru(2) 87.0(6), Ru(1)−O(1)−Ru(3) 86.0(6), Ru(2)−O(1)−Ru(3) 90.9(5)

Poor quality crystals of [**3**][BF_4] were obtained by slow diffusion of benzene into an acetone solution of the salt. The asymmetric unit comprises two independent molecules of **3**, two BF_4 anions, and half a molecule of a disordered benzene. Only one molecule of **3** is shown in Figure 4. The two independent molecules show identical symmetrical data.

The metal core consists of three ruthenium atoms, the three Ru−Ru distances being in accordance with a metal-metal single bond. The three ruthenium atoms are capped by a μ_3-oxo ligand which is almost symmetrically coordinated. As shown by its molecular structure, the presence of the $CH(CH_3)CH_2OH$ side-arm allows **3** to form a strong intramolecular hydrogen bond with the μ_3-oxo cap. The distances between the two oxygen atoms involved in the intramolecular hydrogen bonds are 2.69(3) Å for molecule 1 and 2.66(2) Å for molecule 2.

The strong intramolecular hydrogen bond in **3**, found in the solid state, seems to persist also in acetone solution. The ^1H NMR spectrum of **3** in [D_6]acetone shows a well defined doublet of doublets centered at $\delta = 6.67$ ppm attributed to the proton of the OH group coupled to the two diastereotopic protons of the neighbouring CH_2 group.

 © 2003 Wiley-VCH Verlag GmbH & Co. KGaA, Weinheim

Conclusion

The chiral chloro-bridged η^6-(*S*)-(2-phenyl)propan-1-ol ruthenium complex (*S*,*S*)-**1** can be synthesised by dehydrogenation of (*R*)-(2-cyclohexa-1,4-dienyl)propan-1-ol without racemisation. Cleavage of the chloro bridges with triphenylphosphane gives the enantiopure mononuclear complex (*S*)-**2** in good yield. The first water-soluble trinuclear arene-ruthenium cluster cation containing an asymmetric carbon atom tethered to an arene ligand was isolated as the tetrafluoroborate salt (*S*)-[**3**][BF_4]. NMR spectroscopy and X-ray analyses show that no racemisation is observed during the different steps of synthesis. The absolute configuration at the asymmetric α-carbon remains unchanged under the different reaction conditions: acidic conditions during the dehydrogenation to form **1**, basic conditions during the cleavage of the chloro bridges of **2** with triphenylphosphane, and aqueous conditions during the formation of **3**.

Experimental Section

General Remarks: All manipulations were carried out by routine methods under a nitrogen atmosphere. De-ionised water and organic solvents were degassed and saturated with nitrogen prior to use. NMR spectra were recorded using a Varian Gemini 200 BB spectrometer and a Bruker 400 MHz spectrometer. Microanalyses were carried out by the Laboratory of Pharmaceutical Chemistry, University of Geneva (Switzerland). Electro-spray mass spectra were obtained in positive-ion mode with an LCQ Finnigan mass spectrometer. The starting dinuclear dichloro complex [$RuCl_2(C_6Me_6)]_2$ was prepared according to known literature methods.[20] (*R*)-(2-Cyclohexa-1,4-dienyl)propan-1-ol was synthesised by sodium reduction of (*R*)-(2-phenyl)propan-1-ol in liquid ammonia.[21]

Complex 1: (*R*)-(2-Cyclohexa-1,4-dienyl)propan-1-ol (2.5 g, 18.1 mmol) was added to a solution of ruthenium trichloride hydrate (1.0 g, 3.8 mmol) in ethanol (70 mL), and the mixture was refluxed overnight. After cooling to room temperature, half of the solvent was evaporated. The orange precipitate was filtered, washed with diethyl ether, and dried under vacuum to give pure [$RuCl_2${C_6H_5[$CH(CH_3)CH_2OH$]}]$_2$. Yield: 1.90 g (81%). ^{1}H NMR (400 MHz, [D$_6$]DMSO): δ = 1.17 (d, ^3J = 6.92 Hz, 6 H, CH_3), 2.73 [m, 2 H, C*H*(CH_3)CH_2OH], 3.44 [dd, ^2J = 10.63, ^3J = 6.01 Hz, 2 H, $CH(CH_3)CH_2$OH], 3.55 [dd, ^2J = 10.63 Hz, ^3J = 5.38 Hz, 2 H, $CH(CH_3)CH_2$OH], 4.06 [br., 2 H, $CH(CH_3)CH_2O$*H*], 5.75 (m, 6 H, H_{arom}), 5.87 (m, 4 H, H_{arom}) ppm. ^{13}C{^{1}H} (100 MHz, [D$_6$]DMSO): δ = 15.24 (CH_3), 39.37 [*C*H(CH_3)CH_2OH], 66.43 [$CH(CH_3)$*C*H_2OH], 85.67, 85.90, 87.06, 87.75, 88.40, 108.63 (C_{arom}) ppm. MS (ESI, positive mode, dmso): *m*/*z* = 580.5 [M − Cl]$^+$ $C_{18}H_{24}Cl_4O_2Ru_2$ (616.3): calcd. C 35.08, H 3.92; found C 34.96, H 4.01.

Complex 2: Two equivalents of triphenylphosphane (170 mg, 0.6 mmol) was added to a suspension of **1** (200 mg, 0.3 mmol) in 30 mL of CH_2Cl_2. The mixture was stirred at room temperature during 2 hours and then filtered through celite to eliminate insoluble degradation materials. The product was purified on a silica gel column, eluting CH_2Cl_2/acetone (10:2) to give **2** as an orange-brown powder. Yield: 295 mg (80%). Orange crystals suitable for X-ray analysis were obtained by recrystallisation from $CHCl_3$/*n*-hexane. ^{1}H NMR (400 MHz, $CDCl_3$): δ = 1.39 (d, ^3J = 5.98 Hz, 3 H, CH_3), 2.36 [m, 1 H, C*H*(CH_3)CH_2OH], 3.19 [br., 1 H, $CH(CH_3)CH_2O$*H*], 3.99 [m, 1 H, $CH(CH_3)$C*H*$_2$OH], 4.14 [m, 1 H, $CH(CH_3)$C*H*$_2$OH], 4.74 to 4.89 (m, 3 H, Ru-C_6H_5), 5.70 to 5.86 (m, 2 H, Ru-C_6H_5), 7.42 (m, 9 H, P-C_6H_5), 7.76 (m, 6 H, P-C_6H_5) ppm. ^{13}C{^{1}H} (50 MHz, $CDCl_3$): δ = 17.49 (CH_3), 39.06 [*C*H(CH_3)CH_2OH], 66.51 [$CH(CH_3)$*C*H_2OH], 84.10, 84.19, 84.37, 91.78, 92.99, 113.51 (Ru-C_6H_5), 128.48, 130.79, 133.54, 134.45 (P-C_6H_5) ppm. ^{31}P{^{1}H} (80 MHz, $CDCl_3$): δ = 28.93 ppm. MS (ESI, positive mode, CH_3OH): *m*/*z* = 535 [M − Cl]$^+$. $C_{27}H_{27}Cl_2OPRu$ (570.5): calcd. C 56.85, H 4.77; found C 57.02, H 4.71.

Complex 3: A mixture of [$RuCl_2(C_6Me_6)]_2$ (400 mg, 0.6 mmol) and Ag_2SO_4 (376 mg, 1.2 mmol) in water (40 mL) was stirred in the dark for 1 h. During this period the mixture was treated several times with ultrasound, until the orange solid was completely dissolved. The white precipitate (AgCl) was removed by filtration from the yellow solution containing [$Ru(C_6Me_6)(H_2O)_3]^{2+}$. An aqueous solution containing $NaBH_4$ (100 mg, 2.6 mmol, 10 mL H_2O) was then added dropwise to this yellow solution. The solution turned dark-red due to the formation of [$Ru_2(C_6Me_6)_2(\mu_2$-H)$_3]^+$. After filtration, solid [$RuCl_2${C_6H_5[$CH(CH_3)CH_2OH$]}]$_2$ (345 mg, 0.56 mmol) was added. The mixture was heated to 60 °C for 50 hours in a closed pressure Schlenk tube. The resulting red solution was filtered, and a large excess of $NaBF_4$ was added to precipitate [**2**][BF_4]. The precipitate was centrifuged, dissolved in CH_2Cl_2, filtered through celite to eliminate excess $NaBF_4$ and purified on silica-gel plates (eluent: CH_2Cl_2/acetone 2:1). Yield: 210 mg (40%). ^{1}H NMR (400 MHz, [D$_6$]acetone): δ = −19.86 (m, 1 H, hydride), −19.43 (m, 1 H, hydride), −19.23 (m, 1 H, hydride), 1.21 [d, ^3J = 7.03 Hz, 3 H, $CH(CH_3)CH_2OH$], 2.49 [m, 1 H, C*H*(CH_3)CH_2OH], 2.77 [s, 18 H, $C_6(CH_3)_6$], 2.78 [s, 18 H, $C_6(CH_3)_6$], 3.63 [m, 1 H, $CH(CH_3)CH_2OH$], 3.90 [m, 1 H, $CH(CH_3)CH_2OH$], 5.39 (m, 2 H, H_{arom}), 5.56 (m, 1 H, H_{arom}), 6.01 (m, 1 H, H_{arom}), 6.10 (m, 1 H, H_{arom}), 6.67 [dd, ^3J = 3.63, ^3J = 11.09 Hz, 1 H, $CH(CH_3)CH_2O$*H*] ppm. ^{13}C{^{1}H} (100 MHz, [D$_6$]acetone): δ = 17.46 [$CH(CH_3)CH_2OH$], 17.51 [$C_6(CH_3)_6$], 42.07 [*C*H(CH_3)CH_2OH], 66.77 [$CH(CH_3)$*C*H_2OH], 74.42, 76.72, 81.57, 84.59, 87.67, 95.29, 113.66 (C_{arom}) ppm. MS (ESI positive mode, acetone): *m*/*z* = 783 [M + H]$^+$. $C_{33}H_{51}BF_4O_2Ru_3$ (869.8): calcd. C 45.57, H 5.91; found C 45.41, H 6.07.

X-ray Crystallographic Study

X-ray Data for (*S*)-[2]·$CHCl_3$: $C_{28}H_{28}Cl_5OPRu$, *M* = 689.79 gmol^{-1}, monoclinic, *P*2$_1$ (no. 4), *a* = 9.6386(9), *b* = 13.5325(11), *c* = 11.4019(12) Å, β = 105.096(11)°, *U* = 1435.9(2) Å^3, *T* = 153 K, *Z* = 2, μ(Mo-K_α) = 1.088 mm^{-1}, 10215 reflections measured, 4654 unique (R_{int} = 0.0317) which were used in all calculations. The final wR_2 (F^2) was 0.0620 (all data).

X-ray Data for (*S*)-[3][BF_4]·C_6H_6: $C_{72}H_{108}B_2F_8O_4Ru_6$, *M* = 1817.62 gmol^{-1}, monoclinic, *P*2$_1$ (no. 4), *a* = 8.8158(9), *b* = 20.2561(14), *c* = 23.352(2) Å, β = 91.870(12)°, *U* = 4167.6(7) Å^3, *T* = 153 K, *Z* = 2, μ(Mo-K_α) = 1.118 mm^{-1}, 15789 reflections measured, 13603 unique (R_{int} = 0.0920) which were used in all calculations. The final wR_2 (F^2) was 0.3828 (all data).

The data were measured using a Stoe Image Plate Diffraction system equipped with a φ circle, using Mo-K_α graphite monochromated radiation (λ = 0.71073 Å) with φ range 0−200°, increment of respectively 1.6 and 1.0°, 2θ range from 2.0−26°, D_{max}-D_{min} = 12.45−0.81 Å. The structures were solved by direct methods using the program SHELXS-97.[22] The refinement and all further calculations were carried out using SHELXL-97.[23] The H-atoms were included in calculated positions and treated as riding atoms using the SHELXL default parameters. The non-H atoms were refined

 © 2003 Wiley-VCH Verlag GmbH & Co. KGaA, Weinheim

anisotropically, using weighted full-matrix least-square on F^2. Figure 2 and 4 were drawn with ORTEP [24] and Figure 3 with POV-Ray.[25]

CCDC-213712 (**2**) and -213713 (*S*)-**3**[BF_4] contain the supplementary crystallographic data for this paper. These data can be obtained free of charge at www.ccdc.cam.ac.uk/conts/retrieving.html [or from the Cambridge Crystallographic Data Centre, 12, Union Road, Cambridge CB2 1EZ, UK; Fax: (internat.) +44-1223/336-033; E-mail: deposit@ccdc.cam.ac.uk].

Acknowledgments

The authors are grateful to the Fonds National Suisse de la Recherche Scientifique for financial support. A generous loan of ruthenium chloride hydrate from the Johnson Matthey Technology Centre is gratefully acknowledged.

[1] M. Faure, M. Jahncke, A. Neels, H. Stoeckli-Evans, G. Süss-Fink, *Polyhedron* **1999**, *18*, 2679−2685.
[2] G. Süss-Fink, M. Faure, T. R. Ward, *Angew. Chem.* **2002**, *114*, 105−107; *Angew. Chem. Int. Ed.* **2002**, *41*, 99−101.
[3] Á. Kathó, D. Carmona, F. Viguri, C. D. Remacha, J. Kovács, F. Joó, L. A. Oro, *J. Organomet. Chem.* **2000**, *593−594*, 299−306.
[4] M. Yamakawa, H. Ito, R. Noyori, *J. Am. Chem. Soc.* **2000**, *122*, 1466−1478.
[5] K. Polborn, K. Severin, *Chem. Commun.* **1999**, *24*, 2481−2482.
[6] D. A. Alonso, P. Brandt, S. J. M. Nordin, P. G. Andersson, *J. Am. Chem. Soc.* **1999**, *121*, 9580−9588.
[7] D. L. Davies, J. Fawcett, S. A. Garratt, D. R. Russell, *Chem. Commun.* **1997**, *15*, 1351−1352.
[8] S. B. Wendicke, E. Burri, R. Scopelliti, K. Severin, *Organometallics* **2003**, *22*, 1894−1897.
[9] H. Dialer, P. Mayer, K. Polborn, W. Beck, *Eur. J. Inorg. Chem.* **2001**, 1051−1055.
[10] A. J. Birch, *J. Chem. Soc.* **1950**, 1951.
[11] M. R. J. Elsegood, D. A. Tocher, *Polyhedron* **1995**, *14*, 3147−3156.
[12] A. Hafner, A. Mühlebach, P. A. van der Schaaf, *Angew. Chem.* **1997**, *109*, 2213−2216; *Angew. Chem. Int. Ed. Engl.* **1997**, *36*, 2121.
[13] H. D. Hansen, J. H. Nelson, *Organometallics* **2000**, *19*, 4740−4755.
[14] L. Vieille-Petit, S. Unternährer, B. Therrien, G. Süss-Fink, *Inorg. Chim. Acta*, in press.
[15] M. Stebler-Röthlisberger, W. Hummel, P. A. Pittet, H.-B. Bürgi, A. Ludi, A. E. Merbach, *Inorg. Chem.* **1988**, *27*, 1358−1363.
[16] M. A. Bennett, J. P. Ennett, K. I. Gell, *J. Organomet. Chem.* **1982**, *233*, C17; M. A. Bennett, J. P. Ennett, *Inorg. Chim. Acta* **1992**, *198−200*, 583−592.
[17] M. Jahncke, G. Meister, G. Rheinwald, H. Stoeckli-Evans, G. Süss-Fink, *Organometallics* **1997**, *16*, 1137−1143.
[18] L. Vieille-Petit, B. Therrien, G. Süss-Fink, *Inorg. Chim. Acta*, in press.
[19] L. Vieille-Petit, B. Therrien, G. Süss-Fink, T. R. Ward, *J. Organomet. Chem.*, in press.
[20] M. A. Bennett, T.-N. Huang, T. W. Matheson, A. K. Smith, *Inorg. Synth.* **1982**, *21*, 74−78.
[21] M. E. Kuehne, B. F. Lambert, *Org. Synth.* **1973**, *5*, 400−403.
[22] G. M. Sheldrick, *Acta Crystallogr., Sect. A* **1990**, *46*, 467.
[23] G. M. Sheldrick, *SHELXL-97*, University of Göttingen, Göttingen, Germany, **1999**.
[24] L. J. Farrugia, *J. Appl. Crystallogr.* **1997**, *30*, 565.
[25] S. Anger, D. Bayer, C. Cason, C. Dayley, S. Demlow, A. Enzmann, D. Farmer, T. Wegner, C. Young, POV-Ray software version 3.1, Indianapolis, USA, **1991**.

Received June 27, 2003

 © 2003 Wiley-VCH Verlag GmbH & Co. KGaA, Weinheim

2D Chiral Uranyl(VI) Coordination Polymers with Second-Harmonic Generation Response and Ferroelectric Properties

Yong-Rong Xie,[a] Hong Zhao,[a] Xi-Sen Wang,[a] Zhi-Rong Qu,[a] Ren-Gen Xiong,*[b] Xiang Xue,[a] Ziling Xue,[c] and Xiao-Zeng You[a]

Keywords: Chirality / Polymers / Uranium / Crystal engineering / SHG properties

The in situ hydrothermal reactions of $UO_2(NO_3)_2$ with 1-oxo-4-cyanopyridine (ocpy) and ethyl (*S*)-lactate (e-la) afforded two unprecedented chiral 2D neutral luminescent square grids, uranyl-bis(1-oxo-4-pyridylcarboxylate) $UO_2(opyca)_2$ (**1**) and homochiral uranyl-bis[(*S*)-lactate] (**2**). Their solid-state structures, preliminary optical and photoluminescent properties are reported.
(© Wiley-VCH Verlag GmbH & Co. KGaA, 69451 Weinheim, Germany, 2003)

Introduction

The crystal engineering strategy has provided many advantages to construct chiral or polar supramolecular motifs with many useful physical properties, especially the nonlinear optical properties [second harmonic generation (SHG) response].[1,2] Enantiopure or homochiral metal-organic coordination polymers have found some applications in selective enantio-separation and asymmetric catalysis.[3] Apart from those achievements, however, as Ward et al. pointed out,[1a] the prediction of crystal structures based solely on the structure of their molecular components still remains unexplored and crystal engineering has not developed to the stage where a desired structure (or crystal symmetry) can be ensured. One of the foremost challenges not only in organic solid-state chemistry, but also in supramolecular materials design with SHG properties, essentially requires crystallization in noncentrosymmetric space groups (those lacking inversion symmetry). Moreover, a noncentrosymmetric polar packing arrangement is a requirement for a number of macro-physical properties, such as piezoelectricity, pyroelectricity, and ferroelectricity as well as SHG, which describes the capacity of a material to double the frequency of incident light. A ferroelectric material is one which can be switched rapidly between different states by means of an external electric field. Such materials may be useful in a variety of new technologies, such as electric-optical devices, information storage, switchable NLO (nonlinear optical) devices and light modulators. Recently, some polar and chiral metal-organic coordination polymers have been used as SHG materials with metal ions such as Zn^{2+}, Cd^{2+}, and Ag^{+}.[2] To this end, chiral or enantiopure organic-inorganic hybrid coordination polymers containing the uranium(VI) ion, to the best of our knowledge, remain unexplored and unknown, although there has been much current interest in multi-dimensional U^{VI} coordination polymers which have widespread properties such as fluorescence and zeolite-likeness.[4−6] To our surprise, the in situ hydrothermal reactions of $UO_2(NO_3)_2$ with 1-oxo-4-cyanopyridine (ocpy) and ethyl (s)-lactate(e-la) afford two unprecedented chiral 2D neutral luminescent square grids, uranyl-bis(1-oxo-4-pyridylcarboxylate) $UO_2(opyca)_2$ (**1**) and homochiral uranyl-bis[(*S*)-lactate] (**2**). Herein, we report their synthesis, solid state structures, fluorescent and optical properties (1).

Results and Discussion

The hydrolysis reaction of $UO_2(NO_3)_2$ with ocpy under hydrothermal reaction conditions gave **1**, as shown by the absence of the cyano group peak (ca. 2200 cm^{-1}) and appearance of a strong carboxylate peak at 1600 cm^{-1} in its IR spectrum. The hydrolysis reaction of $UO_2(NO_3)_2$ with e-la under hydrothermal reaction conditions yielded **2**, as confirmed by the appearance of the carboxylate peak (ca. 1600 cm^{-1}).

[a] Coordination Chemistry Institute, The State Key Laboratory of Coordination Chemistry, Nanjing University,
210093 Nanjing, P. R. China,
Fax: (internat.) +86-25/331-4502
(internat.) +86-25/331-7761
E-mail: xiongrg@netra.nju.edu.cn
[b] The State Key Lab of Rare Earth Materials Chemistry and Application, Chemistry Department,
Beijing University, 100871, P. R. China
[c] Department of Chemistry, University of Tennessee,
Knoxville, Tennessee 37996, USA
Supporting information for this article is available on the WWW under http://www.eurjic.org or from the author.

 © 2003 Wiley-VCH Verlag GmbH & Co. KGaA, Weinheim **DOI: 10.1002/ejic.200300483**

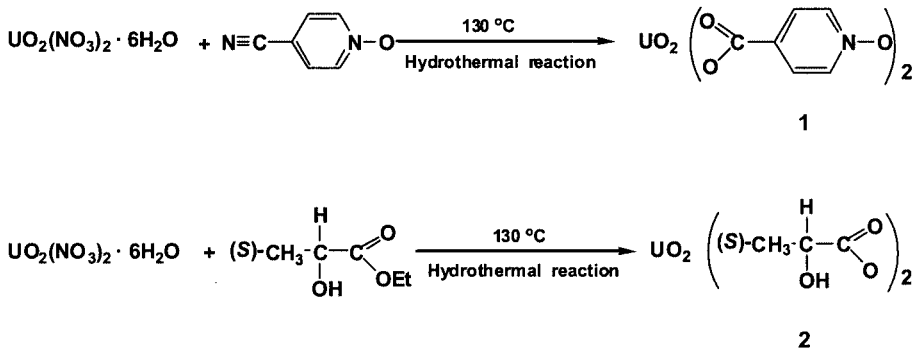

Scheme 1

These in situ hydrolysis reactions or in situ ligand syntheses provide an excellent route to novel metal-organic coordination polymer construction for chemists.[7]

The solid-state structure of **1** (Figure 1a) has a slightly distorted pentagonal bipyramid as the local coordination geometry around each U atom center, defined by seven oxygen atoms from two carboxylate groups, two N-oxide and two oxo groups. Thus, there are two kinds of opyca ligands, one serves as a tridentate spacer, and the other acts as a bidentate linker. Overall each opyca ligand bridges two U atom centers, resulting in the formation of a 2D square grid network with dimensions of 10.07 × 10.04 Å (Figure 1b). The relationship between two layers in the packing diagram in **1** should be an ABAB-type stack, as observed (Supporting Information). No interpenetration was observed in **1**. To the best of our knowledge, this is the first example of neutral square networks containing an U atom as the connecting node.[8]

Like **1**, the local coordination geometry around each U atom center in **2** can best be described as a distorted pentagonal bipyramid. However, there are two crystallographically different U centers (Figure 2a). There are also three kinds of lactate ligands: One serves as a bidentate ligand to chelate one U atom using two oxygens from one carboxylate and one hydroxy group; the second lactate ligand acts as a bidentate bridge to link two U atoms using one carboxylate group; the third lactate ligand is a monodentate terminal group with coordination of its carboxylate to one U atom. Such coordination results in the formation of a 2D brick-wall type grid network with approximate dimensions of 3 × 6.04 Å (Figure 2b). The relationship between two layers is also an ABAB-type stack (Supporting Information). No interpenetration was found in **2**.

Compounds **1** and **2** crystallize in the chiral space groups $P2_12_12_1$ and $P2_1$ respectively. These two space groups belong to the crystal classes 222 and 2, respectively, where their optical activity can occur as a specific physical effect. Preliminary experimental results show that **1** and **2** display powder SHG efficiencies ca. 0.4 and 0.1 times that of urea. Due to **2** having a polar point group (C_2) which theoretically can display potential ferroelectric property. However **1**, with a point group of D_2, fails to do that in principle.

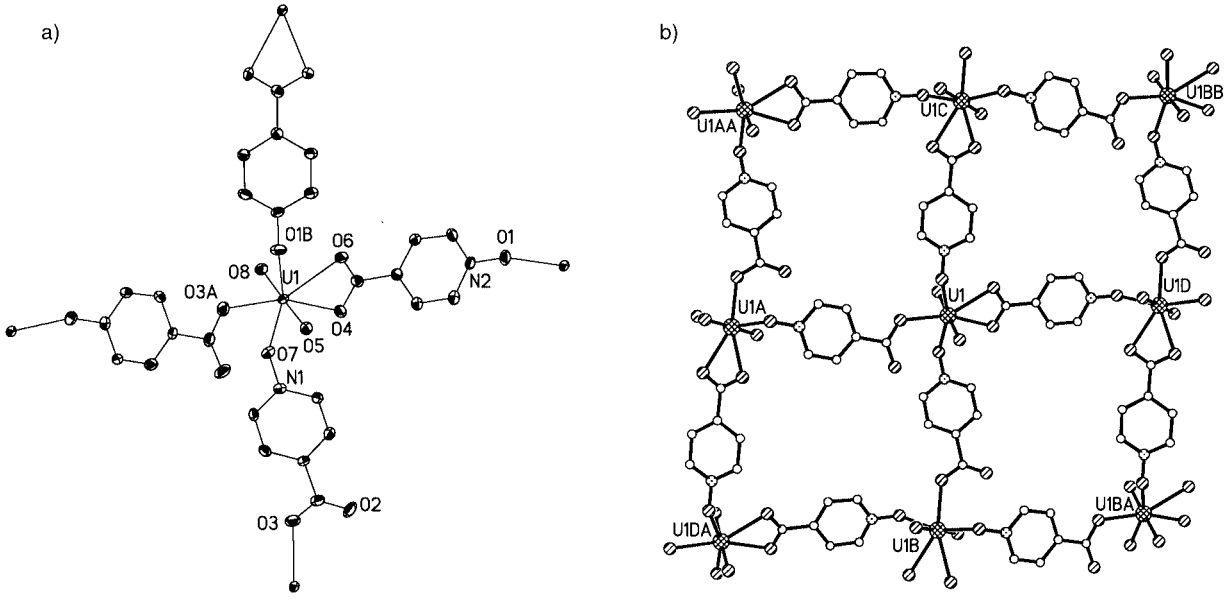

Figure 1. (a) An asymmetric unit of **1** in which thermal ellipsoids are drawn at the 30% probability level; (b) a 2D square grid representation of **1**

 © 2003 Wiley-VCH Verlag GmbH & Co. KGaA, Weinheim

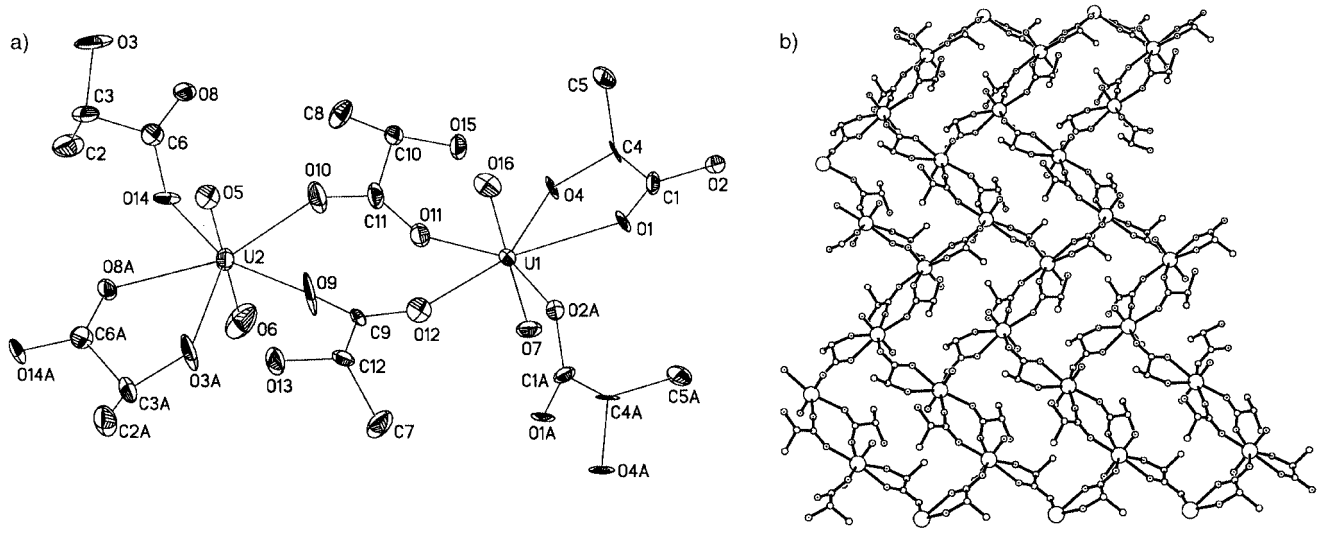

Figure 2. (a) An asymmetric unit of **2** in which thermal ellipsoids are drawn at 30% probability level; (b) a 2D brick-wall representation of **2**

Experimental results indicate that **2** exhibits a low ferroelectric behavior (Figure 3), while **1** does not [Figure 4 shows that there is a weak electric hysteresis loop which is a ferroelectric feature with a remanent polarization (Pr) of 0.12 $\mu C \cdot cm^{-2}$ and coercive field (Ec) of 5 $kVcm^{-1}$. The saturation spontaneous polarization (Ps) of **2** was not observed, probably due to current leakage]. Maybe H-bonds and the layered structure are responsible for **2**'s ferroelectric behavior.[9] Furthermore, **1** and **2** are thermally stable up to 250 and 300 °C, respectively, and are insoluble in common solvents. On the other hand, both **1** and **2** exhibit strong green fluorescent emission at room temperature (Figure 4), which is typical for the uranyl fluorescent spectrum. Thus, **1** represents the first neutral luminescent molecular box with uranyl.[10]

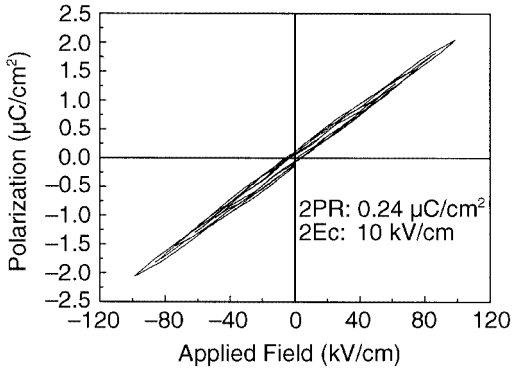

Figure 3. An electric hysteresis loop of **2** was observed by Virtual Ground Mode in a powdered sample in the form of a pellet using an RT6000 ferroelectric tester at room temperature while the sample was immerged in insulating oil; the measurement was performed using ac-pulse

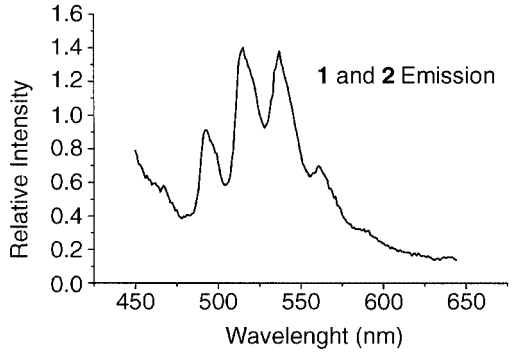

Figure 4. Fluorescent emission spectra of **1** and **2** in the solid state at room temperature

The synthesis of chiral or homchiral novel UO_2-coordination polymer self-assembled through in situ ligand hydrolysis is an extension of a crystal engineering strategy, which is very useful for functional materials design, while the properties of **1** and **2** perhaps make them potential candidates for fluorescent and opto-electronic information storage materials.

Experimental Section

Caution: Compounds containing UO_2^{2+} should be handled with great care (no skin contact or respiration).

Preparation of 1: Hydrothermal treatment of $U(NO_3)_2 \cdot 6H_2O$ (1.0 mmol, 0.502 g), 1-oxo-4-cyanopyridine (2.0 mmol, 0.240 g) and H_2O (2 mL) over 4 days at 130 °C yielded yellowish block crystals of **1** (0.355 g, only one pure phase) in 65% yield based on 1-oxo-4-cyanopyridine. $C_{12}H_8N_2O_8U$ (546.23): calcd. C 26.45, H 1.53, N 5.60; found C 26.36, H 1.47, N 5.13. IR spectrum (KBr): $\tilde{\nu}$ = 3449 cm^{-1} (w), 3112 (w), 3039 (w), 1644 (s), 1617 (w), 1583 (w), 1562 (w), 1540 (m), 1491 (w), 1425 (s), 1352 (s), 1226 (m), 1210 (s), 1177 (m), 1150 (w), 924 (m), 916 (s), 876 (m), 784 (m), 683 (w), 642 (m), 559 (w), 467 (w).

Preparation of 2: Hydrothermal treatment of $U(NO_3)_2 \cdot 6H_2O$ (1.0 mmol, 0.502 g) and ethyl (*S*)-lactate (2.0 mL, 17.6 mmol, 2.084 g) over 4 days at ca. 80−100 °C yielded yellowish block crystals of **2** (0.202 g, only one pure phase) in 45% yield based on $U(NO_3)_2 \cdot 6H_2O$. $C_6H_{10}O_8U$ (448.17): calcd. C 16.07, H 2.23; found

 © 2003 Wiley-VCH Verlag GmbH & Co. KGaA, Weinheim

C 16.12, H 2.31. IR spectrum (KBr): $\tilde{\nu}$ = 3449 cm^{-1} (br., w), 2989 (w), 1620 (m), 1562 (br.,s), 1471 (m), 1432 (w), 1372 (w), 1314 (w), 1261 (m), 1118 (m), 1048 (m), 940 (s), 865 (w), 787 (w), 767 (w), 557 (m), 477 (w).

Crystal Data for 1: $C_{12}H_8N_2O_8U$, M_r = 546.23 g·mol^{-1}, orthorhombic, $P2_12_12_1$, a = 7.1116(5), b = 13.4060(10), c = 14.9176(11) Å, α = β = γ = 90.00°, V = 1422.22(18) $Å^3$, Z = 4, D_c = 2.551 Mg·m^{-3}, R_1 = 0.0240, wR_2 = 0.0659, T = 293 K, μ = 11.459 mm^{-1}, S = 0.518. The crystal was twinned.
Crystal Data for 2: $C_6H_{10}O_8U$, M_r = 448.17 g·mol^{-1}, monoclinic, $P2_1$, a = 8.2854(5), b = 8.1836(5), c = 15.1707(9) Å, α = γ =90°, β = 92.9830(10)°, V = 1027.25(1) $Å^3$, Z = 4, D_c = 2.898 Mg·m^{-3}, R_1 = 0.0660, wR_2 = 0.1732, T = 293 K, μ = 15.823 mm^{-1}, S = 1.333, Flack χ = 0.04(3).
The structures were solved by Direct methods using the program SHELXTL (Sheldrick, 1997).[11] All the non-hydrogen atoms were located from the trial structure and then refined anisotropically with SHELXTL using a full-matrix least-squares procedure. The hydrogen atom positions were fixed geometrically at calculated distances and allowed to ride on the parent carbon atoms. The final difference Fourier map was found to be featureless. CCDC-215386−215387 (**1** and **2** respectively) contains the supplementary crystallographic data for this paper. These data can be obtained free of charge at www.ccdc.cam.ac.uk/conts/retrieving.html [or from the Cambridge Crystallographic Data Centre, 12, Union Road, Cambridge CB2 1EZ, UK; Fax: (internat.) +44-1223/336-033; E-mail: deposit@ccdc.cam.ac.uk].

Acknowledgments

This work was funded by The Major State Basic Research Development Program (Grant No. G2000077500), National Natural Science Foundation of China, Distinguished Young Scholar Fund to X. R. G. and L. Z. from NSFC (No. 2025103 and No. 20028101), BK2003204, Camille Dreyfus Teacher-Scholar Program, and National Science Foundation of the U.S.A. (CHE-9904338).

[1] [1a] K. T. Holman, A. M. Pivovar, M. D. Ward, *Science* **2001**, *294*, 1907. [1b] V. R. Thalladi, S. Brasselet, H. C. Weiss, D. Blaser, A. K. Katz, H. L. Carrell, R. Boese, J. Zyss, A. Nangia, G. R. Desiraju, *J. Am. Chem. Soc.* **1998**, *120*, 2563. [1c] M. Muthurman, R. Masse, J. F. Nicoud, G. R. Desiraju, *Chem. Mater.* **2001**, *13*, 1473. [1d] H. Zhang, X. M. Wang, K. C. Zhang, B. K. Teo, *Coord. Chem. Rev.* **1999**, *183*, 157 and references cited therein. [1e] M. S. Wong, C. Bosshard, P. Gunter, *Adv. Mater.* **1997**, *9*, 837. [1f] C. Janiak, *Dalton Trans.* **2003**, 2781.

[2] [2a] W. Lin, O. R. Evans, R.-G. Xiong, Z. Wang, *J. Am. Chem. Soc.* **1998**, *120*, 13272. [2b] O. R. Evans, R.-G. Xiong, Z. Wang, G. K. Wong, W. Lin, *Angew. Chem. Int. Ed.* **1999**, *38*, 536. [2c] O. R. Evans, W. Lin, *Chem. Mater.* **2001**, *13*, 3009. [2d] O. R. Evans, W. Lin, *Chem. Mater.* **2001**, *13*, 2705. [2e] W. Lin, L. M. O. R. Evans, *Chem. Commun.* **2000**, 2263. [2f] W. Lin, Z. Wang, L. Ma, *J. Am. Chem. Soc.* **1999**, *121*, 11249. [2g] C. Janiak, T. G. Scharmann, P. Albrecht, F. Marlow, R. Macdonald, *J. Am. Chem. Soc.* **1996**, *118*, 6307.

[3] [3a] T. E. Mallouk, J. A. Gavin, *Acc. Chem. Res.* **1998**, *31*, 209 and references cited therein. [3b] G. Cao, M. E. Garcia, M. L. Alcala, F. Burgess, T. E. Mallouk, *J. Am. Chem. Soc.* **1992**, *114*, 7574. [3c] J. S. Seo, D. Whang, H. Lee, S. I. Jun, J. Oh, Y. J. Jeon, K. Kim, *Nature* **2000**, *404*, 982. [3d] R.-G. Xiong, X.-Z. You, B. F. Abrahams, Z. Xue, C.-M. Che, *Angew. Chem. Int. Ed.* **2001**, *40*, 4422. [3e] O. R. Evans, H. L. Ngo, W. Lin, *J. Am. Chem. Soc.* **2001**, *123*, 10395. [3f] C. J. Kepert, T. J. Prior, M. J. Rosseinsky, *J. Am. Chem. Soc.* **2000**, *122*, 5158.

[4] [4a] D. Grohol, A. Clearfield, *J. Am. Chem. Soc.* **1997**, *119*, 4662. [4b] Y. P. Li, C. L. Cahill, P. C. Burns, *Chem. Mater.* **2001**, *13*, 4026. [4c] C. L. Cahill, P. C. Burns, *Inorg. Chem.* **2001**, *40*, 1347. [4d] J. A. Danis, W. H. Runde, B. Scott, J. Fettinger, B. Eichhorn, *Chem. Commun.* **2001**, 2378.

[5] [5a] B. Eichhorn, *Chem. Commun.* **2001**, 2378. [5b] A. C. Bean, C. F. Campana, O. Kwon, T. E. Albrecht-Schmitt, *J. Am. Chem. Soc.* **2001**, *123*, 8806. [5c] A. C. Bean, S. M. Peper, T. E. Albrecht-Schmitt, *Chem. Mater.* **2001**, *13*, 1266. [5d] P. M. Almond, L. Deakin, M. J. Porter, A. Mar, T. E. Albrecht-Schmitt, *Chem. Mater.* **2000**, *12*, 3208. [5e] P. M. Almond, L. Deakin, A. Mar, T. E. Albrecht-Schmitt, *Inorg. Chem.* **2001**, *40*, 886. [5f] P. M. Almond, C. E. Talley, A. C. Bean, S. M. Peper, T. E. Albrecht-Schmitt, *J. Solid State Chem.* **2000**, *154*, 635.

[6] [6a] S. M. Walker, P. S. Halasyamani, S. Allen, D. O'Hare, *J. Am. Chem. Soc.* **1999**, *121*, 10513. [6b] P. S. Halasyamani, S. M. Walker, D. O'Hare, *J. Am. Chem. Soc.* **1999**, *121*, 7415. [6c] R. J. Francis, P. S. Halasyamani, J. S. Bee, D. O'Hare, *J. Am. Chem. Soc.* **1999**, *121*, 1609. [6d] R. J. Francis, P. S. Halasyamani, D. O'Hare, *Chem. Mater.* **1998**, *10*, 3131. [6e] R. J. Francis, P. S. Halasyamani, D. O'Hare, *Angew. Chem. Int. Ed.* **1998**, *37*, 2214.

[7] [7a] O. R. Evans, W. Lin, *Acc. Chem. Res.* **2002**, *35*, 511 and references cited therein. [7b] R.-G. Xiong, X. Xue, H. Zhao, X.-Z. You, B. F. Abrahams, Z. Xue, *Angew. Chem. Int. Ed.* **2002**, *41*, 3800. [7c] N. F. Zheng, X. Bu, P. Feng, *J. Am. Chem. Soc.* **2002**, *124*, 9688.

[8] [8a] S. Leininger, B. Olenyuk, P. J. Stang, *Chem. Rev.* **2000**, *100*, 853 and references cited therein. [8b] M. Eddaoudi, D. B. Moler, H. Li, B. Chen, T. M. Reineke, M. O'Keeffe, O. M. Yaghi, *Acc. Chem. Res.* **2001**, *34*, 319 and references cited therein. [8c] B. Moulton, M. J. Zaworotko, *Chem. Rev.* **2001**, *101*, 1629 and references cited therein. [8d] P. J. Hagrman, D. Hagrman, J. Zubieta, *Angew. Chem. Int. Ed.* **1999**, *38*, 2639 and references cited therein. [8e] L. R. MacGillivray, J. L. Atwood, *Angew. Chem. Int. Ed.* **1999**, *38*, 1019. [8f] K. A. Hirsch, S. R. Wilson, J. S. Moore, *J. Am. Chem. Soc.* **1997**, *119*, 10401 and references cited therein. [8g] D. M. Ciurtin, N. G. Pschirer, M. D. Smith, U. H. F. Bunz, H. C. zur Loye, *Chem. Mater.* **2001**, *13*, 2743. [8h] Y. Cui, H. L. Ngo, W. Lin, *Inorg. Chem.* **2002**, *41*, 1033. [8i] L. M. Zheng, T. Whitefield, X. Q. Wang, A. J. Jacobson, *Angew. Chem. Int. Ed.* **2000**, *39*, 4528. [8j] S. R. Batten, R. Robson, *Angew. Chem. Int. Ed.* **1998**, *37*, 1460 and references cited therein. [8k] M. Fujita, *Chem. Soc. Rev.* **1998**, *27*, 417. [8l] C. J. Jones, *Chem. Soc. Rev.* **1998**, *27*, 281. [8m] D. L. Caulder, K. N. Raymond, *Acc. Chem. Res.* **1999**, *32*, 975. [8n] L. Carlucci, G. Ciani, D. M. Proserpio, S. Rizzato, *Chem. Eur. J.* **2002**, *8*, 1520.

[9] [9a] M. Szafranski, A. Katrusiak, G. J. McIntyre, *Phys. Rev. Lett.* **2002**, *89*, 215507. [9b] A. Katrusiak, M. Szafranski, *Phys. Rev. Lett.* **1999**, *82*, 576. [9c] R. P. Lemieux, *Acc. Chem. Res.* **2001**, *34*, 845. [9d] K. E. Maly, M. D. Wand, R. P. Lemieux, *J. Am. Chem. Soc.* **2002**, *124*, 7898. [9e] W. H. Baur, *Acta Crystallogr., Sect. B* **1982**, *24*, 1968. [9f] B. C. Frazer, R. Peninsky, *Acta Crystallogr.* **1967**, *1*, 1948. [9g] S. Endo, T. Chino, S. Tsuboi, K. Koto, *Nature* **1989**, *340*, 452.

[10] [10a] R. G. Denning, *Struct. Bonding.* **1992**, *79*, 215. [10b] V. C. Williams, M. Muller, M. A. Leech, R. G. Denning, M. L. H. Green, *Inorg. Chem.* **2000**, *39*, 2538. [10c] M. P. Wilkerson, C. J. Burns, D. E. Morris, R. T. Paine, B. L. Scott, *Inorg. Chem.* **2002**, *41*, 3110. [10d] C. K. Jorgensen, R. Reisfeild, *Struct. Bonding.* **1982**, *50*, 121.

[11] G. M. Sheldrick, (1997). SHELXTL V5.1 Software Reference Manual, Bruker AXS, Inc., Madison, Wisconsin, USA

Received July 21, 2003

 © 2003 Wiley-VCH Verlag GmbH & Co. KGaA, Weinheim

Oxosulfido Complexes of Platinum — $(Ph_3P)_2Pt(S_2O)$ and $(Ph_3P)_4Pt_2(\mu\text{-}S)(\mu\text{-}SO)$ — Their Formation and Properties

Akihiko Ishii,*[a] Masami Murata,[a] Hideaki Oshida,[a] Kimiyo Matsumoto,[a] and Juzo Nakayama*[a]

Keywords: Platinum / S ligands / Oxo ligands

The platinum S_2O complex $[(Ph_3P)_2Pt(S_2O)]$ (**10**) was obtained by S_2O transfer reactions from tetrathiolane 2-oxide (**8**), tetrathiolane 2,3-dioxide (**5**), and pentathiane 3-oxide (**6**) to $[(C_2H_4)Pt(PPh_3)_2]$ (**4**). The S_2O complex **10** further reacts with **4** to give a novel binuclear platinum complex **16**, which is found to be a source of several platinum S_nO_m complexes. (© Wiley-VCH Verlag GmbH & Co. KGaA, 69451 Weinheim, Germany, 2003)

The coordination chemistry of organotransition metal compounds of sulfur oxides has been attracting considerable attention.[1−4] Among them, disulfur monoxide (S_2O) complexes **1** of several transition metals (Nb,[5] Mo,[6] Mn,[7−11] Re,[8] Rh,[2] Os,[12] Ir,[2,5,9,10,12,13] and Pt[14]) are known, in which platinum−S_2O complexes **2** (E = S, E′ = SO) were reported very recently by Tokitoh and co-workers.[14] They synthesized the platinum−S_2O and −Se_2O complexes, **2** by oxidation of the respective S_2 and Se_2 complexes,[15] which were prepared for the first time by taking advantage of bulky phosphane ligands ($TbtMe_2P$ and $BbtMe_2P$). Similarly, most of the other S_2O complexes were synthesized by oxidation of the corresponding S_2 complexes, and a few were prepared by S_2O transfer reactions from 4,5-diphenyl-3,6-dihydro-1,2-dithiin 1-oxide[6,9,10] or reaction with $S_2O(THF)_x$.[2] On the other hand, the chemistry of sulfido complexes of platinum bearing the Pt_2S_2 core (**3**) has also been drawing considerable interest.[16] Another recent topic in this field is oxidative additions of Pt^0 complex **4** to a thiosulfinate [−S−S(O)−] moiety in cyclic sulfur compounds.[17−21] We have been studying the synthesis and reactivities of cyclic polysulfides, and have reported on the chemistry of tetrathiolane 2,3-dioxide (**5**),[22,23] pentathiane 3-oxide (**6**),[24,25] and S_8O,[26] all of which act as S_2O transfer reagents.[27−30] Recently we also reported the reaction of dithiirane 1-oxides **7** with **4**.[31] Here, we report the reaction of **5**, **6**, and tetrathiolane 2-oxide (**8**)[23] with **4**, where an S_2O transfer took place giving rise to $[(Ph_3P)_2Pt(S_2O)]$ which further reacted with **4** to yield the binuclear platinum complex $[(Ph_3P)_4Pt_2(\mu\text{-}S)(\mu\text{-}SO)]$.

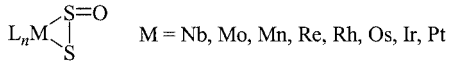

1

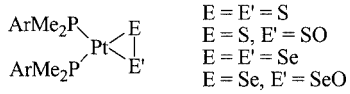

2

Ar = 2,4,6-$[(Me_3Si)_2CH]_3C_6H_2$ (Tbt) or
2,6-$[(Me_3Si)_2CH]_2$-4-$[(Me_3Si)_3C]C_6H_2$ (Bbt)

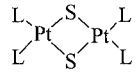

3

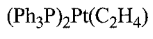

4

L = phosphine ligands

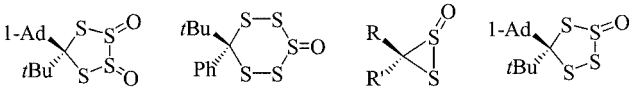

5 **6** **7** **8**

1-Ad = 1-adamantyl

Tetrathiolane 2-oxide (**8**), prepared in situ by oxidation of tetrathiolane (**9**) with dimethyldioxirane (DMD)[32,33] at −20 °C,[23] was allowed to react with two molar equivalents of **4** in toluene at −20 °C to produce $[(Ph_3P)_2Pt(S_2O)]$ (**10**; 0.80 molar equiv.), $[(Ph_3P)_2Pt(S_3O)]$ (**11**; 0.19 molar equiv.),[34] the dithiolato complex **12** (0.09 molar equiv.), $[(Ph_3P)_2Pt\{(1\text{-}Ad)(t\text{Bu})C{=}S\}]$ (**13**; 0.31 molar equiv.),[31] and (1-Ad)(*t*Bu)C=S (**14**; 0.47 molar equiv.) [Equation (1)].

[a] Department of Chemistry, Faculty of Science,
Saitama University,
Sakura-ku, Saitama 338−8570, Japan
Fax: (internat.) +81-48/858-3700
E-mail: ishiiaki@chem.saitama-u.ac.jp

Supporting information for this article is available on the WWW under http://www.eurjic.org or from the author.

 © 2003 Wiley-VCH Verlag GmbH & Co. KGaA, Weinheim **DOI: 10.1002/ejic.200300348**

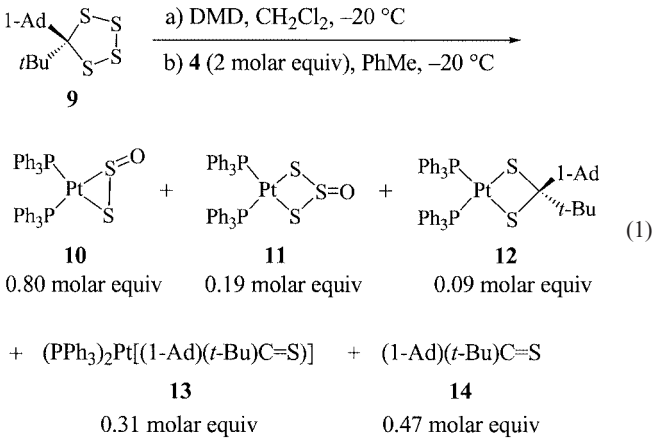

The structure of the S_2O complex **10** was determined by X-ray crystallography (Figure 1).[35] The crystal contained one molecule of benzene — the recrystallization solvent — per two molecules of **10**, and the $Pt(S_2O)$ moiety was disordered as shown in Figure 1a: the occupancies of the set A [Pt(1A)S(1A)S(2A)O(1A)] and the set B [Pt(1B)S(1B)S(2B)O(1B)] were almost equivalent (0.515 and 0.485, respectively). Figure 1b shows the whole of the molecule

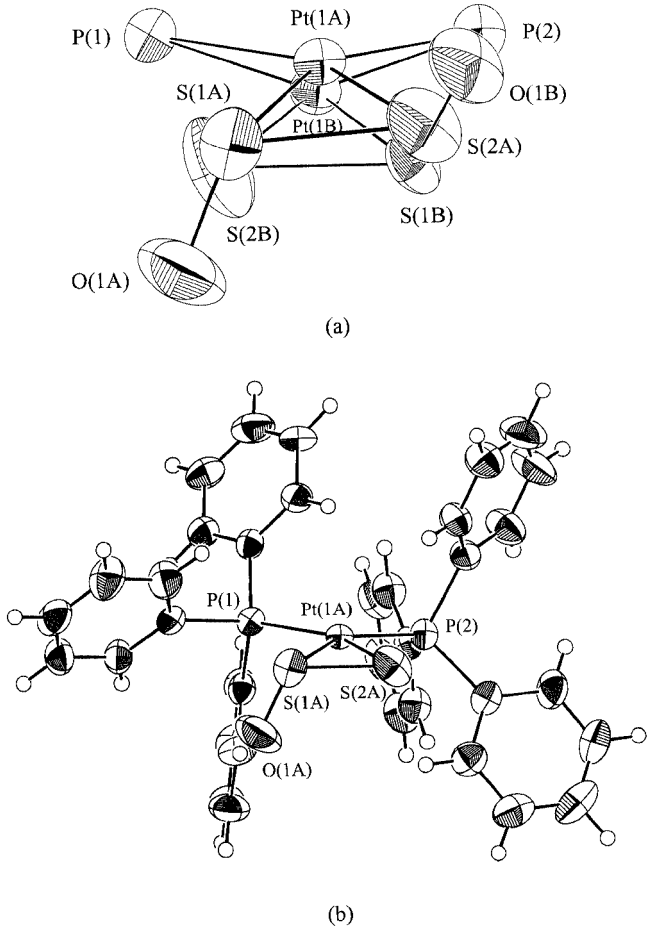

Figure 1. ORTEP drawings of $(Ph_3P)_2Pt(S_2O)$ (**10**) (50% ellipsoidal probability): (a) disorder of the $Pt(S_2O)$ moiety (phenyl groups are omitted for clarity), set A (0.515 occupancy) Pt(1A)S(1A)S(2A)O(1A), set B (0.485 occupancy) Pt(1B)S(1B)S(2B)O(1B); (b) the whole of **10** drawn with the set A

with only the set A. In the ^{31}P NMR spectrum, two doublets appear at $\delta = 18.2$ and 18.4 [$^2J_{P,P} = 7$ Hz] with satellite signals due to the ^{195}Pt nucleus [$^1J_{Pt,P} = 4364$ and 3410 Hz in $CDCl_3$, respectively]. These coupling constant values are quite similar to those of the S_2O complex **2** (Ar = Bbt, E = S, E′ = SO) [$^2J_{P,P} = 8$, $^1J_{Pt,P} = 4263$ and 3254 Hz].[14] Shaver reported that the S_3O complex **11** can be obtained by reaction of $[(PPh_3)_2Pt(SH)_2]$ with SO_2,[34] while we found that the reaction of S_8O with **4** yields **11** in good yield.[36]

The reaction of tetrathiolane 2,3-dioxide (**5**) with an equimolar amount of **4** yielded the S_2O complex **10** (0.62 molar equiv.) along with (1*R**,3*S**)- and (1*R**,3*R**)-dithiirane 1-oxides (**15**)[22,23] (0.24 and 0.25 molar equiv., respectively) and thioketone **14** (0.21 molar equiv.) [Equation (2)]. Interestingly, when two molar equivalents of **4** were employed, binuclear platinum complex **16** was obtained. Indeed, the isolated S_2O complex **10** reacted with **4** very quickly to give **16** in high yield [Equation (3)]. Insertion reactions of **4** into the S−S bond of cyclic oligosulfide oxides[17−21] and $Fe_2(\mu\text{-}S_2)(CO)_6$[37] have been reported. The properties of complex **16** will be described later in this paper.

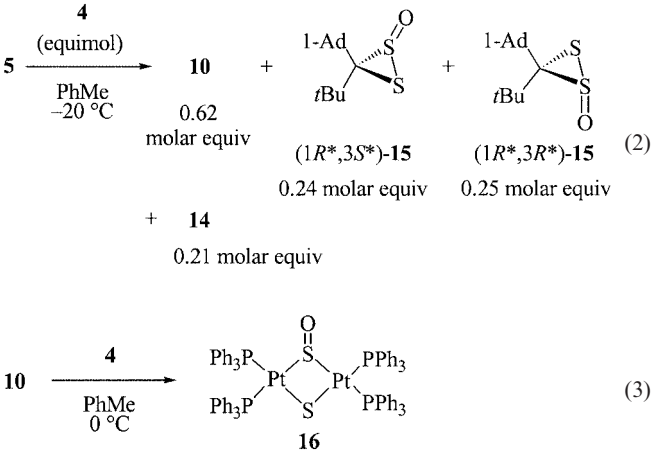

Similarly, pentathiane 3-oxide (**6**) was treated with **4** (2 molar equiv.) to furnish the S_2O complex **10** and the dithiolato-thiolato complex **17** in 0.70 and 0.85 molar equiv., respectively [Equation (4)]. The structure of **17** was determined by X-ray crystallography (Figure 2).[35]

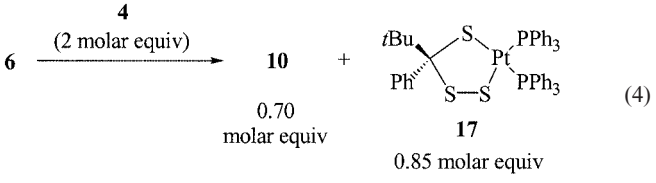

Interestingly, complex **17** decomposes in $CDCl_3$ at 65 °C (2 h) to give an alternative complex **18** (0.23 molar equiv.) and *t*Bu(Ph)C=S (0.23 molar equiv.) [Equation (5)]. Complex **18** exhibits a singlet at $\delta = 22.7$ ($^1J_{Pt,P} = 3939$ Hz) in the ^{31}P NMR spectrum of the mixture, and this $^1J_{Pt,P}$ value is quite similar to that of **2** (Ar = Bbt, E = E′ = S) ($\delta = -32.2$ ppm, $^1J_{Pt,P} = 3909$ Hz).[15] Thus, we tentatively as-

 © 2003 Wiley-VCH Verlag GmbH & Co. KGaA, Weinheim

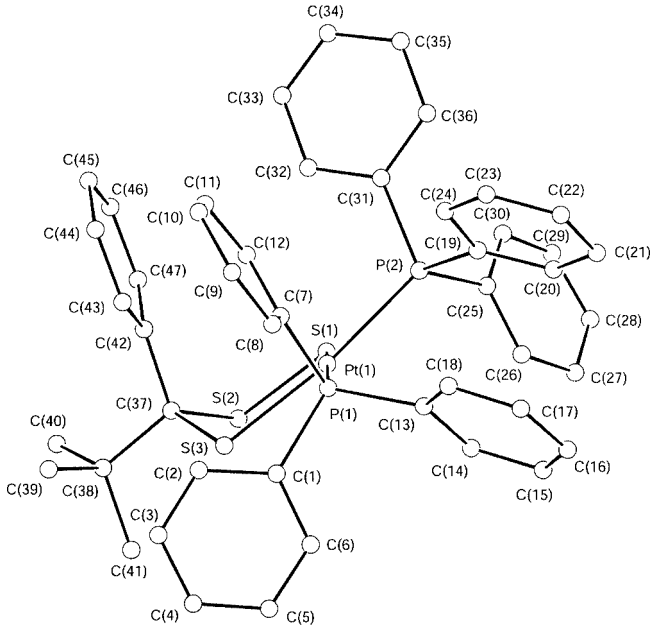

Figure 2. Molecular structure of $[(t\text{Bu})(\text{Ph})\text{CS}_3]\text{Pt}(\text{PPh}_3)_2$ (**17**); hydrogen atoms are omitted for clarity; selected bond lengths [A] and angles [deg]: Pt(1)−P(1) 2.2854(19), Pt(1)−P(2) 2.297(3), Pt(1)−S(3) 2.307(2), Pt(1)−S(1) 2.3350(18), S(1)−S(2) 2.061(4), S(2)−C(37) 1.837(9), S(3)−C(37) 1.837(8); P(1)−Pt(1)−P(2) 99.39(8), P(1)−Pt(1)−S(3) 86.99(8), P(2)−Pt(1)−S(3) 171.29(8), P(1)−Pt(1)−S(1) 174.65(9), P(2)−Pt(1)−S(1) 84.32(8), S(3)−Pt(1)−S(1) 89.74(8), S(2)−S(1)−Pt(1) 106.27(12), C(37)−S(2)−S(1) 100.5(3), C(37)−S(3)−Pt(1) 103.6(3), C(7)−P(1)−Pt(1) 114.7(3), C(13)−P(1)−Pt(1) 111.5(3), C(1)−P(1)−Pt(1) 115.4(3), C(31)−P(2)−Pt(1) 112.7(4), C(25)−P(2)−Pt(1) 112.4(3), C(19)−P(2)−Pt(1) 120.3(3), S(2)−C(37)−S(3) 105.3(5), C(42)−C(37)−C(38) 112.1(8)

signed the S_2 complex structure **18** to this compound. However, the complex was not stable enough to be isolated; prolonged heating of the mixture or even allowing it to stand at room temperature for several hours led to complete disappearance of the signal. We also examined the reaction of tetrathiolane **9** with **4**. The reaction yielded mainly the dithiolato complex **12** and the thioketone complex **13**. In addition, ^{31}P NMR spectroscopy showed a small signal due to **18** [Equation (6)]. The dithiolato complex **12** was also formed by the reaction of dithiirane **19** with **4** in benzene.[38]

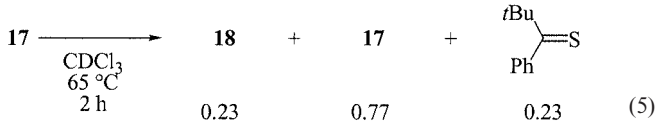

(5)

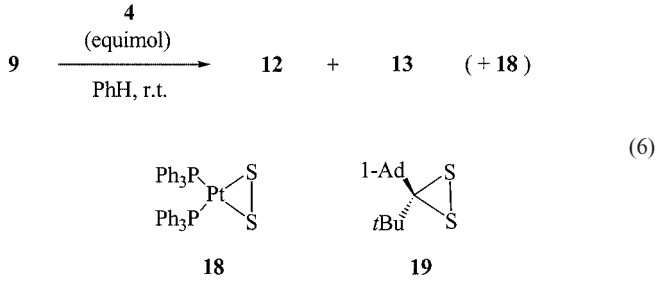

(6)

We tried to prepare the binuclear platinum complex **16** by oxidation of $[(\text{Ph}_3\text{P})_2\text{Pt}]_2(\mu\text{-S})_2$ (**3**: L = PPh_3).[39] It has been reported that oxidation of a binuclear platinum complex bridged by S gives the μ-SO complex.[40] However, **16** was not obtained because of the insolubility of $[(\text{Ph}_3\text{P})_2\text{Pt}]_2(\mu\text{-S})_2$ in the usual organic solvents. Complex **16** decomposes upon heating at 50 °C in CDCl_3 to yield the S_2O complex **10**, the S_2O_2 complex **20**,[41] and $[(\text{PPh}_3)_2\text{PtCl}_2]$ [Equation (7)]. The identification of the S_2O_2 complex **20** was done by comparison of the ^{31}P NMR spectrum of an authentic sample prepared by the reported method.[41] The decomposition in the presence of (1-Ad)(*t*Bu)C=S (**14**) in PhH yielded the thioketone complex **13** and the S_2O complex **10** as the main products in 0.66 and 0.61 molar equiv., respectively, along with the S_2O_2 complex **20** and recovered thioketone **14**. The formation of the thioketone complex **13** indicates the intervention of $(\text{PPh}_3)_2\text{Pt}$.

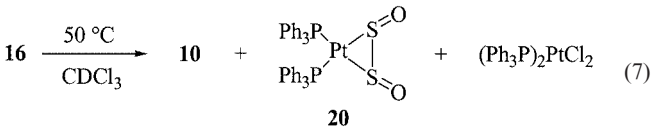

(7)

A plausible mechanism for the thermal decomposition of **16** is depicted in Scheme 1. Initially, **16** decomposes via two pathways: in Path A, it extrudes $(\text{PPh}_3)_2\text{Pt}$, which is trapped by thioketone **14** to yield **13**, to give the S_2O complex **10**; in Path B, **16** splits into the SO complex **21** and $[(\text{PPh}_3)_2\text{Pt(S)}]$. Lorenz and Kull have reported that an attempt to prepare the SO complex **21** by thermolysis of the episulfoxide complex **22** results in the formation of the S_2O_2 complex **20**.[41] We propose that the SO complex **21** dimerizes to give another binuclear platinum complex **23** that readily extrudes $(\text{PPh}_3)_2\text{Pt}$ to furnish the S_2O_2 complex **20**. This proposal is strongly supported by the fact that oxidation of **16** with

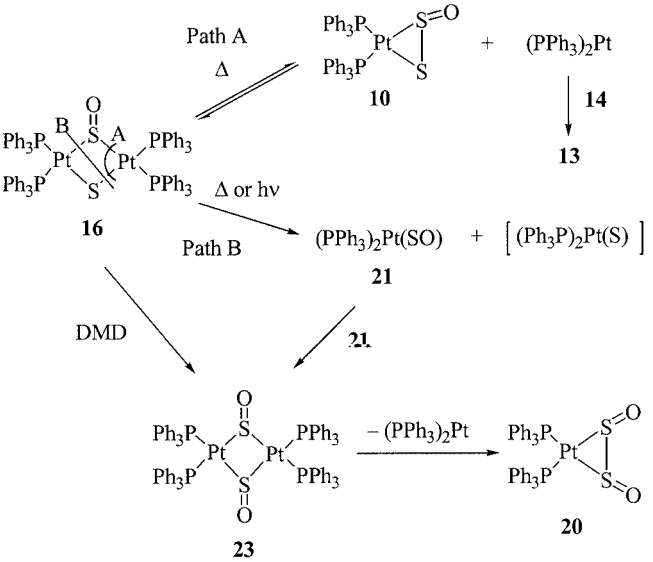

Scheme 1. Plausible mechanism for reactions of the platinum dinuclear complex **16**

 © 2003 Wiley-VCH Verlag GmbH & Co. KGaA, Weinheim

DMD yields the S_2O_2 complex **20** in high yield, probably via **23**. The fate of $[(PPh_3)_2Pt(S)]$ is unclear, but the formation of $[(PPh_3)_2PtCl_2]$ upon thermolysis in $CDCl_3$ implies the formation of $[(Ph_3P)_2Pt]_2(\mu\text{-}S)_2$ (**3**: L = PPh_3), which reportedly reacts with CH_2Cl_2 to give $[(PPh_3)_2PtCl_2]$.[16] Irradiation of **16** with light in $CDCl_3$ gave the S_2O_2 complex **20**, $[PtCl_2(PPh_3)_2]$, and $Ph_3P{=}X$ (X = O, S) indicating that Path B is dominant in the photolysis.

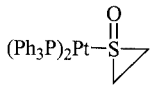

22

In summary, the platinum S_2O complex **10** was obtained by S_2O transfer reactions from tetrathiolane 2-oxide (**8**), tetrathiolane 2,3-dioxide (**5**) and pentathiane 3-oxide (**6**) to $[(PPh_3)_2Pt(C_2H_4)]$ (**4**). The S_2O complex **10** further reacts with **4** to give a novel binuclear platinum complex **16**, which is found to be a source of several platinum$-S_nO_m$ complexes.

Experimental Section

Reaction of Tetrathiolane 2-Oxide (8) with 4: An acetone solution of DMD (0.106 M, 0.30 mL, 0.032 mmol) was added to a solution of tetrathiolane **9** (10 mg, 0.031 mmol) in CH_2Cl_2 (2 mL) at −20 °C under argon. The mixture was stirred for 1 h at this temperature and then the solvent was removed in vacuo below −20 °C. The residue was dissolved in toluene (1 mL) at −20 °C and then treated with a solution of $[(PPh_3)_2Pt(C_2H_4)]$ (**4**; 48 mg, 0.062 mmol) in toluene (2 mL). After stirring for 10 min, the solvent was evaporated to dryness and the residue was subjected to column chromatography (silica gel, CH_2Cl_2/Et_2O, 5:1) to elute first a mixture of 1-adamantyl *tert*-butyl thioketone (**14**), the dithiolato complex (**12**), and $[(PPh_3)_2Pt\{(1\text{-Ad})(t\text{Bu})C{=}S\}]$ (**13**) and then $[(PPh_3)_2Pt(S_3O)]$ (**11**; 4.9 mg, 0.19 molar equiv.) and $[(PPh_3)_2Pt(S_2O)]$ (**10**; 19.7 mg, 0.80 molar equiv.) in this order. The mixture of **12**, **13**, and **14** was further subjected to gel permeation chromatography (GPC) with $CHCl_3$ as solvent to give a mixture (12.8 mg) of **12** (0.09 molar equiv.) and **13** (0.31 molar equiv.), and 1-adamantyl *tert*-butyl thioketone (**14**; 3.5 mg, 0.47 molar equiv.). The yields of **12** and **13** were estimated on the basis of the ^1H NMR integral ratio. The crude S_2O complex **10** was precipitated from a mixed solvent of dichloromethane and hexane, and the collected powder was washed with benzene several times to give the analytical sample. When the reaction was conducted using four molar equivalents of **4**, the thioketone complex **13** was not formed and the dithiolato complex **12** was isolated in nearly pure form after chromatographic purification. The crude dithiolato complex **12** was washed with ethanol several times to give the analytical sample.

10: Yellow powder, m.p. 200 °C (dec.). ^1H NMR (400 MHz, $CDCl_3$): δ = 7.15−7.23 (m, 12 H), 7.28−7.36 (m, 18 H) ppm. ^{31}P NMR (162 MHz, $CDCl_3$): δ = 18.2 (d, $^2J_{P,P}$ = 7, $^1J_{Pt,P}$ = 4364 Hz), 18.4 (d, $^2J_{P,P}$ = 7, $^1J_{Pt,P}$ = 3409 Hz) ppm. FAB MS (*m*-nitrobenzyl alcohol): *m*/*z* = 800 [M^+ + 1], 719. $C_{36}H_{30}OP_2PtS_2$ (799.78): calcd. C 54.06, H 3.78; found C 53.58, H, 3.54.

12: Off-white powder, m.p. 225−226 °C (dec.). ^1H NMR (400 MHz, $CDCl_3$): δ = 1.20−1.40 (m, 9 H), 1.52−1.68 (m, 6 H), 1.94 (br. s, 3 H), 2.21 (br. s, 6 H), 7.14 (t, *J* = 7.0 Hz, 12 H), 7.23 (t, *J* = 7.0 Hz, 6 H), 7.44−7.49 (m, 12 H) ppm. ^{31}P NMR (162 MHz,$CDCl_3$): δ = 22.9 (s, $^1J_{Pt,P}$ = 2925 Hz) ppm. FAB MS (*m*-nitrobenzyl alcohol): *m*/*z* = 989 [M^+ + 1], 931, 853. $C_{51}H_{54}P_2PtS_2$ (988.14): calcd. C 61.99, H, 5.51; found C 62.00, H 5.62.

Reaction of Tetrathiolane 2,3-Dioxide 5 with 4

Equimolar Amount of 4: Compound **4** (20.7 mg, 0.0277 mmol) was added to a solution of **5** (10.1 mg, 0.0277 mmol) in toluene (1 mL) at −20 °C under argon. The mixture was stirred for 1 h at this temperature and the solvent was then evaporated to dryness. The residue was subjected to column chromatography (silica gel, CH_2Cl_2/Et_2O, 5:1) to give a mixture of thioketone **14** and the (1*R**,3*R**)- and (1*R**,3*S**)-dithiirane 1-oxides **15**, and the S_2O complex **10** (13.8 mg, 0.62 molar equiv.). The mixture of **14** and **15** was further subjected to HPLC (silica gel, CH_2Cl_2/hexane 1:1) to give the thioketone **14** (1.4 mg, 0.21 molar equiv.), (1*R**,3*R**)-dithiirane 1-oxide [**(1*R**,3*R**)-15**; 1.9 mg, 0.24 molar equiv.], and (1*R**,3*S**)-dithiirane 1-oxide [**(1*R**,3*S**)-15**; 2.0 mg, 0.25 molar equiv.].

Two Molar Equivalents of 4: Tetrathiolane **9** (10 mg, 0.031 mmol) was oxidized with four molar equivalents of DMD (0.102 M, 1.2 mL, 0.123 mmol) in dichloromethane (1.5 mL) for 1 h at −20 °C. The solvent was removed under reduced pressure below −20 °C, and the resulting tetrathiolane 2,3-dioxide **5** was used without further purification. The 2,3-dioxide **5** was dissolved in toluene (2 mL) at −20 °C, and the solution was treated with a solution of **4** (45 mg, 0.060 mmol) in toluene (2 mL) at this temperature. The solution turned immediately from colorless to deep yellow and was stirred for 10 min at −20 °C. Removal of the solvent under reduced pressure gave an orange residue, the ^{31}P NMR integral ratio of which indicated the formation of the thioketone complex **13**, $[(PPh_3)_4Pt_2(\mu\text{-}S)(\mu\text{-}SO)]$ (**16**), the S_2O complex **10**, and the *S*-oxides of **12**[31] in the molar ratio of 26:13:29:32, along with $Ph_3P{=}O$ and $Ph_3P{=}S$. The molar ratio was obtained based on the ^{31}P NMR integral ratio. The *S*-oxides of **12** are considered to be formed by reactions of dithiirane 1-oxides **15** with **4**.[31] The binuclear platinum complex **16** could not isolated in this experiment because it was not eluted from the silica-gel column.

Reaction of the S_2O Complex 10 with 4: A solution of **4** (21.7 mg, 0.029 mmol) in toluene (1.5 mL) was added at 0 °C to a solution of **10** (23.2 mg, 0.029 mmol) in toluene (1.5 mL) under argon. The mixture was stirred for 1 h at 0 °C, and the solution was concentrated to ca. one-fourth of its original volume under reduced pressure. Diethyl ether was added to precipitate the product, and the resulting precipitates were collected by filtration to give 47.7 mg (0.71 molar equiv.) of $[(PPh_3)_4Pt_2(\mu\text{-}S)(\mu\text{-}SO)]$ (**16**).

16: Yellow powder, m.p. 179 °C (dec.). ^1H NMR (400 MHz, $CDCl_3$): δ = 6.97−7.02 (m, 24 H), 7.11−7.18 (m, 12 H), 7.29−7.34 (m, 12 H), 7.47−7.52 (m, 12 H) ppm. ^{31}P NMR ($CDCl_3$, 162 MHz): δ = 21.0 (m, $^1J_{Pt,P}$ = 3394 Hz), 21.8 (m, $^1J_{Pt,P}$ = 2427 Hz) ppm. IR (KBr): $\tilde{\nu}$ = 1095 cm^{-1}. ESI MS: *m*/*z* = 1519.2 [M^+ + 1]. $C_{72}H_{60}OP_4Pt_2S_2$ (1519.44): calcd. C 56.91, H 3.98; found C 56.13, H 3.94.

Reaction of Pentathiane 3-Oxide 6 with 4: A solution of **4** (84 mg, 0.113 mmol) in toluene (12 mL) was added over 15 min to a solution of **6** (18 mg, 0.056 mmol) in toluene (2 mL) at −15 °C. The solvent was removed under reduced pressure, and the residue was subjected to column chromatography (silica gel, $CHCl_3$ and then CH_2Cl_2/Et_2O 4:1) to give $[(t\text{Bu})(\text{Ph})CS_3]Pt(PPh_3)_2$ (**17**; 46 mg, 0.85 molar equiv.) and the S_2O complex **10** (31.3 mg, 0.70 molar equiv.).

17: Yellow crystals, m.p. 143−147 °C (dec.) ($CHCl_3$/EtOH). ^1H NMR ($CDCl_3$, 400 MHz): δ = 1.11 (s, 9 H), 6.95−7.01 (m, 6 H),

 © 2003 Wiley-VCH Verlag GmbH & Co. KGaA, Weinheim

7.03−7.09 (m, 6 H), 7.14−7.19 (m, 8 H), 7.26−7.38 (m, 7 H), 7.48−7.54 (m, 6 H), 8.08−8.11 (m, 2 H) ppm. ^{31}P NMR (162 MHz, $CDCl_3$): δ = 18.5 (d, $^2J_{P,P}$ = 23, $^1J_{Pt,P}$ = 2754 Hz), 22.9 (d, $^2J_{P,P}$ = 23, $^1J_{Pt,P}$ = 3057 Hz) ppm. $C_{47}H_{44}P_2PtS_3{\cdot}2CHCl_3$ ($C_{49}H_{46}Cl_6P_2PtS_3$; 1200.80): calcd. C 49.01, H 3.86; found C 49.06, H 3.75.

Reaction of Tetrathiolane 9 with 4: Compound **4** (6.1 mg, 0.0081 mmol) was added at room temperature to a solution of **9** (2.7 mg, 0.0081 mmol) in benzene (2 mL). The yellow mixture was stirred for 15 min at room temperature, and the solvent was removed under reduced pressure. The ^{31}P NMR spectrum of the residue indicated the formation of the dithiolato complex **12**, the thioketone complex **13**, and a compound assigned tentatively to the S_2 complex **18** (δ = 22.7 ppm, $^1J_{Pt,P}$ = 3939 Hz) in the molar ratio of 32:57:11.

Thermal Decomposition of 16. In $CDCl_3$: A solution of **16** (10 mg, 0.0065 mmol) in $CDCl_3$ (4 mL) under argon was heated at 50 °C for 1.5 h. The ^{31}P NMR spectrum of an aliquot taken from the mixture indicated the formation of the S_2O complex **10**, the S_2O_2 complex **20** (δ = 6.4, $^1J_{Pt,P}$ = 4019 Hz), [$(PPh_3)_2PtCl_2$] (δ = 14.9, $^1J_{Pt,P}$ = 3672 Hz), **16**, $Ph_3P{=}S$ (δ = 44.0 ppm), and $Ph_3P{=}O$ (δ = 29.8 ppm) in the molar ratio of 33:11:21:11:14:11.

In Benzene in the Presence of Thioketone 14: A solution of **16** (23 mg, 0.015 mmol) and **14** (3.6 mg, 0.015 mmol) in benzene (4.5 mL) was heated at 50 °C for 4 h under argon, and then the solvent was removed under reduced pressure. The ^{31}P NMR spectrum of the residue indicated the formation of the thioketone complex **13**, the S_2O complex **10**, and the S_2O_2 complex **20** in the molar ratio of 50:43:7. The residue was subjected to column chromatography (silica gel, CH_2Cl_2/Et_2O, 5:1) to give a mixture of **14** and **13** (14 mg), and **10** (7.4 mg, 0.61 molar equiv.). The S_2O_2 complex **20** was not eluted from the silica-gel column. The molar ratio of **14** and **13** was 31:69, giving calculated yields of 0.0042 mmol (0.28 molar equiv.) and 0.010 mmol (0.66 molar equiv.), respectively.

When a solution of **16** (10 mg, 0.0065 mmol) in benzene (1.5 mL) was heated at 50 °C, 1.0 mg of unidentifiable precipitates (ESI-MS: $m/2z$ = 999.5) were collected by filtration.

Photolysis of 16: A solution of **16** in $CDCl_3$ in an NMR tube was irradiated with a high-pressure Hg lamp through a Pylex filter in an ice-water bath for 1 h. The ^{31}P NMR spectrum showed the formation of the S_2O_2 complex **20**, [$(PPh_3)_2PtCl_2$], $Ph_3P{=}O$, and $Ph_3P{=}S$ in the molar ratio of 19:24:40:16. The signals due to the S_2O complex **10** were not observed (it was verified by a controlled experiment that **10** barely decomposed under the conditions).

Acknowledgments

We are grateful to Dr. Hideki Saito (Saitama University) for kind discussion on the X-ray analysis of **10**. This work was supported by a Grant-in-Aid for Scientific Research (No. 12440174) from the Ministry of Education, Culture, Sports, Science and Technology, Japan.

[1] W. A. Schenk, *Angew. Chem.* **1987**, *99*, 101−112; *Angew. Chem. Int. Ed. Engl.* **1987**, *26*, 98−109.
[2] K. K. Pandey, *Prog. Inorg. Chem.* **1992**, *40*, 445−502.
[3] A. F. Hill, *Adv. Organomet. Chem.* **1994**, *36*, 159−227.
[4] A. Müller, W. Jaegermann, J. H. Enemark, *Coord. Chem. Rev.* **1982**, *46*, 245−280.
[5] J. E. Hoots, D. A. Lesch, T. B. Rauchfuss, *Inorg. Chem.* **1984**, *23*, 3130−3136.
[6] D. S. Brown, C. F. Owens, B. G. Wilson, M. E. Welker, *Organometallics* **1991**, *10*, 871−875.
[7] M. Herberhold, B. Schmidkonz, M. L. Ziegler, T. Zahn, *Angew. Chem.* **1985**, *97*, 517−518; *Angew. Chem. Int. Ed. Engl.* **1985**, *24*, 515−516.
[8] M. Herberhold, B. Schmidkonz, *J. Organomet. Chem.* **1986**, *308*, 35−45.
[9] G. A. Urove, M. E. Welker, *Organometallics* **1988**, *7*, 1013−1014.
[10] G. A. Urove, M. E. Welker, *J. Organomet. Chem.* **1990**, *384*, 105−114.
[11] K. K. Pandey, *J. Mol. Struct. (Theochem)* **1999**, *491*, 231−235.
[12] M. Herberhold, A. F. Hill, *J. Chem. Soc., Dalton Trans.* **1988**, 2027−2031.
[13] G. Schmid, G. Ritter, T. Debaerdemaeker, *Chem. Ber.* **1975**, *108*, 3008−3013.
[14] K. Nagata, N. Takeda, N. Tokitoh, *Chem. Lett.* **2003**, *32*, 170−171.
[15] K. Nagata, N. Takeda, N. Tokitoh, *Angew. Chem.* **2002**, *114*, 144−146; *Angew. Chem. Int. Ed.* **2002**, *41*, 136−138.
[16] S.-W. A. Fong, T. S. A. Hor, *J. Chem. Soc., Dalton Trans.* **1999**, 639−651.
[17] W. Weigand, R. Wünsch, *Chem. Ber.* **1996**, *129*, 1409−1419.
[18] W. Weigand, R. Wünsch, K. Polborn, G. Mloston, *Z. Anorg. Allg. Chem.* **2001**, *627*, 1518−1522.
[19] W. Weigand, R. Wünsch, C. Robl, G. Mloston, H. Nöth, M. Schmidt, *Z. Naturforsch., Teil B* **2000**, *55*, 453−458.
[20] R. Wünsch, W. Weigand, G. Nuspl, *J. Prakt. Chem.* **1999**, *341*, 768−772.
[21] W. Weigand, R. Wünsch, K. Polborn, *Inorg. Chim. Acta* **1998**, *273*, 106−110.
[22] A. Ishii, M. Nakabayashi, J. Nakayama, *J. Am. Chem. Soc.* **1999**, *121*, 7959−7960.
[23] A. Ishii, M. Nakabayashi, Y.-N. Jin, J. Nakayama, *J. Organomet. Chem.* **2000**, *611*, 127−135.
[24] A. Ishii, H. Oshida, J. Nakayama, *Tetrahedron Lett.* **2001**, *42*, 3117−3119.
[25] A. Ishii, H. Oshida, J. Nakayama, *Bull. Chem. Soc. Jpn.* **2002**, *75*, 319−328.
[26] A. Ishii, T. Kawai, K. Tekura, H. Oshida, J. Nakayama, *Angew. Chem.* **2001**, *113*, 1978−1980; *Angew. Chem. Int. Ed.* **2001**, *40*, 1924−1926.
[27] P. W. Schenk, R. Steudel, *Angew. Chem.* **1965**, *77*, 437−445; *Angew. Chem. Int. Ed. Engl.* **1965**, *4*, 402−409.
[28] P. W. Schenk, R. Steudel, in *Inorganic Sulfur Chemistry* (Ed.: G. Nickless), Elsevier, Amsterdam, 1968, p. 367.
[29] R. Steudel, in *Gmelin Handbuch der Anorganischen Chemie, Schwefel, Ergänzungsband 3*, Springer, Berlin, 1980, p. 1−69.
[30] A. R. V. Murthy, T. R. N. Kutty, D. K. Sharma, *Int. J. Sulfur Chem. B* **1971**, *6*, 161−175.
[31] A. Ishii, M. Saitoh, M. Murata, J. Nakayama, *Eur. J. Org. Chem.* **2002**, 979−982.
[32] W. Adam, J. Bialas, L. Hadjiarapoglou, *Chem. Ber.* **1991**, *124*, 2377.
[33] W. Adam, L. Hadjiarapoglou, A. Smerz, *Chem. Ber.* **1991**, *124*, 227−232.
[34] A. Shaver, M. El-khateeb, A.-M. Lebuis, *Angew. Chem.* **1996**, *108*, 2510−2512; *Angew. Chem. Int. Ed. Engl.* **1996**, *35*, 2362−2363.
[35] Crystal data for **10**: $C_{36}H_{30}OP_2PtS_2{\cdot}0.5C_6H_6$ ($C_{39}H_{33}OP_2PtS_2$), M_w = 838.858, yellow plate, 0.30 × 0.16 × 0.06 mm^3, monoclinic, space group $P2_1/c$, a = 9.6861(6), b = 21.5760(10), c = 20.540(2) Å, β = 126.779(9)°, V = 3438.1(4) Å^3, Z = 4, $\rho_{calcd.}$ = 1.621 g cm^{-3}, μ(Mo-K_α) = 4.326 mm^{-1}. Intensity data of 7920 independent reflections were collected in the range of $-12 \le h \le 12$, $0 \le k \le 28$, $-26 \le l \le 12$ with a Mac Science MXC18 diffractometer using graphite-monochromated Mo-K_α radiation (λ = 0.71073 Å) at 298 K. The structure was solved by direct methods using SIR[42] and refined with full-matrix least-squares (SHELXL-97[43]) using all the independent reflec-

 © 2003 Wiley-VCH Verlag GmbH & Co. KGaA, Weinheim

tions for 442 parameters. Absorption corrections were done by a psi-scan method. The non-hydrogen atoms were refined anisotropically, and hydrogen atoms were placed at calculated positions. Final $R1 = 0.0608$ [$I > 2\sigma(I)$, 6880 reflections], $wR2 = 0.1465$ (for all), GOF = 1.315; max/min residual density = 1.584/−2.129 e·Å^{-3}. Selected bond lengths [Å] and angles [deg]: Pt(1A)−S(1A) 2.34(2), Pt(1A)−S(2A) 2.362(18), Pt(1A)−P(1) 2.286(6), Pt(1A)−P(2) 2.267(6), S(1A)−O(1A) 1.50(3), S(1A)−S(2A) 2.09(3), S(1A)−Pt(1A)−S(2A) 52.7(6), P(1)−Pt(1A)−S(1A) 102.0(5), P(2)−Pt(1A)−S(2A) 102.5(5), P(1)−Pt(1A)−P(2) 102.0(2), P(2)−Pt(1A)−S(1A) 153.4(5), P(1)−Pt(1A)−S(2A) 154.6(5), Pt(1B)−S(1B) 2.292(17), Pt(1B)−S(2B) 2.30(3), Pt(1B)−P(1) 2.270(7), Pt(1B)−P(2) 2.320(6), S(1B)−O(1B) 1.456(17), S(1B)−S(2B) 2.09(3), S(1B)−Pt(1B)−S(2B) 54.1(7), P(1)−Pt(1B)−S(1B) 155.2(4), P(2)−Pt(1B)−S(2B) 157.9(7), P(1)−Pt(1B)−P(2) 100.9(3), P(2)−Pt(1B)−S(1B) 103.8(4), P(1)−Pt(1B)−S(2B) 101.2(7).

Crystal data for **17**: $C_{47}H_{44}P_2PtS_3 \cdot 2CHCl_3$ ($C_{49}H_{46}Cl_6P_2PtS_3$), $M_w = 1200.855$, yellow plate, 0.18 × 0.12 × 0.06 mm^3, monoclinic, space group $P2_1/n$, $a = 15.0340(9)$, $b = 20.890(2)$, $c = 16.1150(10)$ Å, $\beta = 98.270(3)°$, $V = 5008.5(6)$ Å^3, $Z = 4$, $\rho_{calcd.} = 1.593$ g cm^{-3}, μ(Mo-K_α) = 3.344 mm^{-1}. 9865 independent reflections were collected in the range of $-19 \leq h \leq 16$, $0 \leq k \leq 26$, $0 \leq l \leq 20$ with a Mac Science DIP3000 diffractometer using graphite-monochromated Mo-K_α radiation ($\lambda = 0.71073$ Å) at 298 K. Absorption corrections were done by a multi-scan method (SORTAV[44]). 581 parameters, $R1 = 0.0606$ [$I > 2\sigma(I)$, 4874 reflections], $wR2 = 0.1212$ (for all), GOF = 0.888; max/min residual density = 0.807/−0.708 e·Å^{-3}.

CCDC-212018 (**10**) and CCDC-212019 (**17**) contain the supplementary crystallographic data for this paper. These data can be obtained free of charge via www.ccdc.cam.ac.uk/conts/retrieving.html (or from the Cambridge Crystallographic Data Centre, 12, Union Road, Cambridge CB21EZ, UK; fax: (internat.) +44-1223/336-033; or deposit@ccdc.cam.ac.uk).

[36] A. Ishii, T. Kawai, J. Nakayama, unpublished results.
[37] V. W. Day, D. A. Lesch, T. B. Rauchfuss, *J. Am. Chem. Soc.* **1982**, *104*, 1290−1295.
[38] We reported in a previous paper[31] that the dithiirane **19** decomposes to thioketone **14** upon treatment with **4** in dichloromethane.
[39] R. Ugo, G. L. Monica, S. Cenini, F. Conti, *J. Chem. Soc., (A)* **1971**, 522−528.
[40] R. Huang, I. A. Guzei, J. H. Espenson, *Organometallics* **1999**, *18*, 5420−5422.
[41] I.-P. Lorenz, J. Kull, *Angew. Chem.* **1986**, *98*, 276−278; *Angew. Chem. Int. Ed. Engl.* **1986**, *25*, 261−262.
[42] A. Altomare, G. Cascarano, C. Giacovazzo, A. Guagliardi, *J. Appl. Crystallogr.* **1993**, *26*, 343−350.
[43] G. M. Sheldrick, SHELXL-97, *Program for Crystal Structure Refinement*, Göttingen University, Germany, 1997.
[44] R. H. Blessing, *Acta Crystallogr., Sect. A* **1995**, *51*, 33−38.

Received June 6, 2003

 © 2003 Wiley-VCH Verlag GmbH & Co. KGaA, Weinheim

Pyrazolylboratozinc Complexes of Nucleosides and Nucleoside Analogues[‡]

Dirk Badura[a] and Heinrich Vahrenkamp*[a]

Keywords: Zinc / Nucleosides / Bioinorganic chemistry / N ligands

Attachment of deprotonated nucleosides or of alkylated nucleobases, as their analogues, to zinc was achieved by condensation reactions between TpZn-OH complexes and nucleobase derivatives. Pyrazolylboratozinc complexes with derivatives of uracil, thymine, guanine, xanthine and hypoxanthine were obtained and characterized by structure determination. In the uracil, thymine, guanine and hypoxanthine derivatives, zinc is bound to the nitrogen atom which bears the proton in the nucleoside. In the xanthine derivatives all three possible bonding modes are realized.
(© Wiley-VCH Verlag GmbH & Co. KGaA, 69451 Weinheim, Germany, 2003)

Introduction

The success of cisplatin as a drug has triggered a plethora of studies on the interactions of metal ions with nucleic acids, nucleotides and their constituents.[2−4] Among these, the number of those related to zinc is relatively small. Yet it is known that zinc affects the various structures of DNA,[5] of chromatin[6] and of ribosomes,[7] as well as impeding the melting of DNA[8,9] and facilitating the recombination of the double helix.[10] Furthermore zinc ions have structural and functional roles in nucleic acid-binding retroviruses,[11] in t-RNA, DNA, and RNA polymerases,[3,11] endonucleases,[13] cytidine and adenosine deaminases,[13] aspartate transcarbamoylase,[11] and dihydroorotase.[14]

The small-molecule chemistry of zinc related to nucleotides, nucleobases and models thereof has evolved in recent years. Lippert[15] and Dubler[16] pioneered the studies of zinc-nucleobase interactions. Sigel[3,17] and Marzilli[18,19] made the leading contributions to zinc-nucleotide chemistry. Our own contributions to this field describe the interactions of nucleic acid constituents and analogues thereof with pyrazolylboratozinc units.[1,20,21]

The basis of the work reported here are our observations with nucleobases[1,21] and with drug substances, some of which are derivatives of the nucleobases.[22−26] All the substances investigated are nitrogen heterocycles with rather acidic NH functions. This was favourable as it facilitated the synthesis of pyrazolylboratozinc substrate (TpZn-X) complexes by a condensation reaction between TpZn-OH and the NH heterocycle HX. It was, however, unfavourable in terms of modelling zinc-nucleotide interactions, as the most acidic NH functions in the nucleobases are often those whose nitrogen is attached to the sugar moiety in the nucleotides. Due to this the nucleobases were attached to the TpZn unit by that nitrogen atom which is not available for attachment in DNA, RNA and their constituents.

To overcome this disadvantage we resorted to nucleobases which are alkylated at the nitrogen atom to which the sugar moiety would be attached. This paper describes the pyrazolylboratozinc complexes derived from such nucleoside analogues. The alkylated nucleobases represent uridine, thymidine, guanosine and xanthosine. A genuine nucleoside inosine (i.e. glycosylated hypoxanthine) was included in order to complement our previous studies with uridine and xanthosine.[21] The nucleobases were reacted with the pyrazolylborate-Zn-OH complexes **1a** and **1b**.

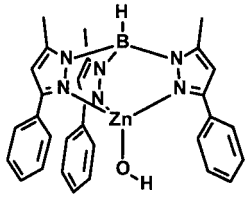

1a

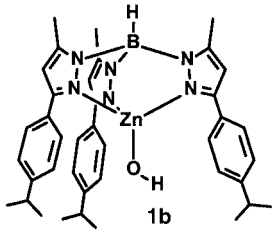

1b

Results and Discussion

Uracil and Thymine

1-Methyluracil and 1-methylthymine were chosen as the simplest nucleoside analogues. Although their NH functions, flanked by two carbonyl groups, are quite acidic, their reactions with TpZn-OH were not straightforward. It turned out that the reaction products **2** and **3** are very moisture sensitive, easily reverting to the starting materials. Pure **2** and **3** were finally obtained after removing water

[‡] Pyrazolylboratozinc-Nucleobase Complexes, 4. Part 3: Ref. [1]

[a] Institut für Anorganische und Analytische Chemie der Universität Freiburg
Albertstr. 21, 79104 Freiburg, Germany
Fax: (internat.) +49-761/203-6001
E-mail: vahrenka@uni-freiburg.de

from the reaction mixture by running the reactions in a Soxhlet extractor filled with molecular sieves.

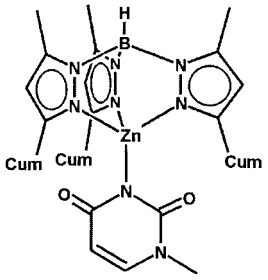

2

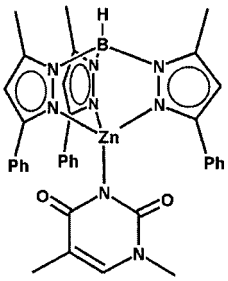

3

The structural assignment of **2** and **3** rests on the structure determination of **2** (see below). The spectroscopic data support the statement that all zinc complexes of 1-alkylated uracil and thymine derivatives have the nucleobase attached to zinc in the same way, i.e. via the N3 atom. The main feature is the position of the highest energy ν(CO) band in the IR spectrum. It is observed in the 1640−1670 cm^{-1} range here as well as in N_3O-tripod[27] and [12]ane-N_4 zinc complexes.[28] Its position is higher than that of the anionic 1-alkylated nucleobases, thereby excluding coordination via the oxygen atom, as this would lower the ν(CO) value. The structure determination of **2** and the similarity of all the spectroscopic data also confirm our previous structural assignment of the uridine $Tp^{Cum,Me}$Zn-Urd complex.[21]

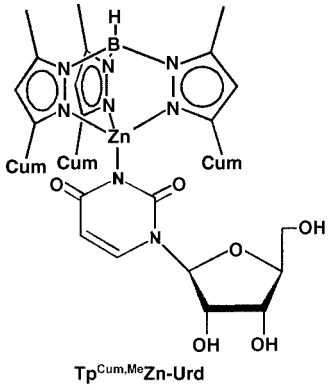

$Tp^{Cum,Me}$Zn-Urd

Figure 1 shows the molecular structure of **2**. Notable features are the complete embedding of the nucleobase in the $Tp^{Cum,Me}$ ligand-pocket, the typically short[1,20,21] Zn−N3 bond, the non-existence of Zn−O interactions and the 10° angle between the Zn−N3 bond and the least-squares plane of the heterocycle. Unlike most other TpZn-nucleobase complexes[1,20,21] this one does not dimerize in the solid state via hydrogen bonding, as it does not contain NH or OH units.

Cytosine and Adenine

N1-alkylated cytosine and N9-alkylated adenine derivatives were found to be unsuitable for reactions with TpZn-OH. We had already observed that cytosine itself is not acidic enough for such a reaction while adenine is.[20] 9-Alkylated adenine has no additional heterocyclic (i.e. acidic) NH functions.

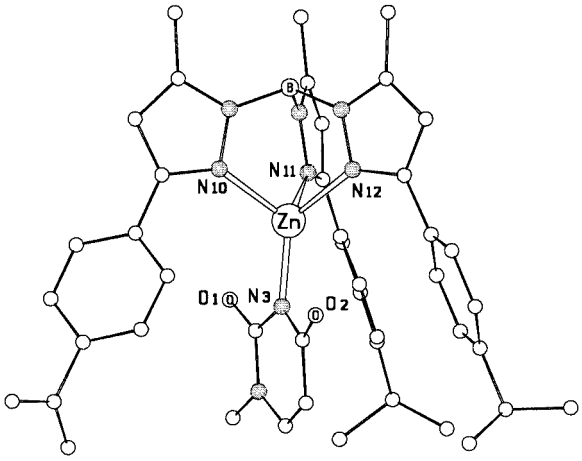

Figure 1. Molecular structure of **2**; relevant atomic distances (Å): Zn−N3 1.930(3), Zn−N10 2.034(3), Zn−N11 2.100(3), Zn−N12 2.049(3), Zn···O1 2.914(5), Zn···O2 3.086(5)

Guanine

The coordination chemistry of guanine is not well developed, and like others we have not been able to prepare zinc-guanine complexes.[20] Guanosine and 9-alkylated guanine derivatives, however, bind to zinc via N7 as uncharged molecules.[29−32] We tried to prepare a TpZn complex of anionic guanosine by reacting guanosine with **1a** and **1b** or the corresponding TpZn-H complexes. We failed, however, to separate the resulting product mixtures.

These problems did not exist when resorting to 9-isobutylguanine as a guanosine analogue. By reaction with $Tp^{Ph,Me}$Zn-H the expected complex **4** was obtained. Compound **4** seems to exist as two isomers **4′** and **4′′**. Precipitation from benzene by addition of heptane yielded **4′** as very thin needles which are not suitable for structure determination. Slow recrystallization of raw **4** or of **4′** from benzene/heptane yielded **4′′** as well-shaped crystals which were used for X-ray analysis. Based on this and on the spectroscopic evidence (see below) we assign the two isomers as follows:

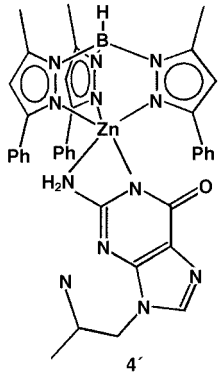

4′

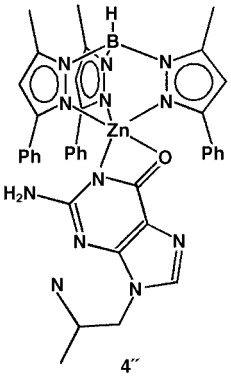

4′′

 © 2003 Wiley-VCH Verlag GmbH & Co. KGaA, Weinheim

The molecular structure of **4′′** is shown in Figure 2. The nucleobase is attached to zinc as a bidentate ligand via N1 and the adjacent carbonyl oxygen, forming a four-membered chelate ring. Such a bonding mode is very rare for metal-nucleobase interactions. It has not been observed before with zinc, but it occurs in zinc complexes of α-pyridone,[33,34] and we have described related N,S chelate complexes of 6-methylthiouracil and 6-mercaptopurine.[21] The Zn−O and Zn−N1 bond lengths show that both interactions are strong, i.e. zinc is genuinely five-coordinate. However, the coordination geometry of zinc cannot be described as the transition from trigonal bipyramidal to square pyramidal.[35] It seems more appropriate to assume that N1 and O1 share the single coordination position of a ligand X in the TpZn-X complexes, like the two oxygen atoms of a symmetrically bidentate carboxylate ligand in TpM-carboxylate complexes.[35] Apart from this peculiar situation, the nitrogen atom which bonds to zinc (N1), is a typical, yet not the only possible, donor atom in other metal complexes of anionic guanosine derivatives.

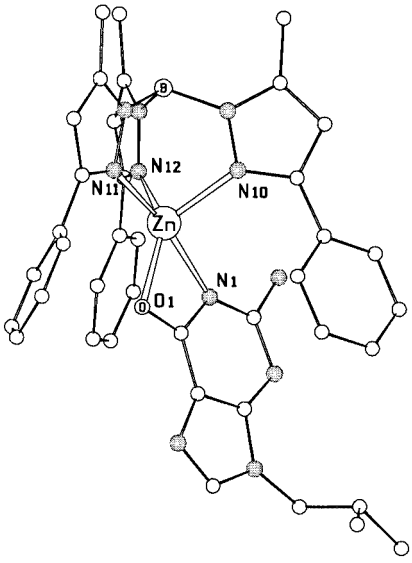

Figure 2. Molecular structure of **4′′**; relevant bond lengths (Å) and angles (°): Zn−O1 2.061(2), Zn−N1 2.182(3), Zn−N10 2.097(3), Zn−N11 2.103(3), Zn−N12 2.084(3), O1−Zn−N1 62.96(9)

In the solid state, complex **4′′** forms dimers across an inversion center by two symmetrically equivalent hydrogen bonds between the NH_2 group and N3. This is different from all other such dimer structures of TpZn-nucleobase complexes,[1,20,21] but it is the common type of self-association for guanosine and its derivatives.[40]

The solution NMR spectra of **4′** and **4′′** are identical, indicating a rapid equilibrium between their two structures or possibly a third structure, e.g. one with a monodentate attachment of the nucleobase via N1. The IR spectra of **4′** and **4′′** in KBr show small, yet significant, differences. These concern the vibrational modes of the C=O and NH_2 units. In free 9-isobutyguanine ν(CO) and δ(NH_2) appear as strong bands at 1688 and 1631 cm^{-1}, respectively. Zinc complexes of uncharged 9-alkylguanines show very little shifts for these two band positions. Complex **4′** has its ν(CO)band at 1692 cm^{-1} (i.e. unshifted) and its δ(NH_2) band at 1611 cm^{-1} (i.e. shifted to lower wavenumbers). Complex **4′′** shows no typical ν(CO) band and its δ(NH_2) band at 1638 cm^{-1} (i.e. unshifted). This indicates that in **4′′** the CO function is involved in the zinc bonding , as proved by the structure determination. Likewise in **4′** the NH_2 group seems to act as a donor. Taking into account that N1 is most probably the main donor for zinc in both isomers, this leads to the structural assignment given above for **4′**, again with a four-membered chelate ring.

Xanthine

The xanthine-derived nucleoside xanthosine has already been incorporated in a TpZn complex, the structure of which (with zinc attachment at N7) was assigned as follows:[21]

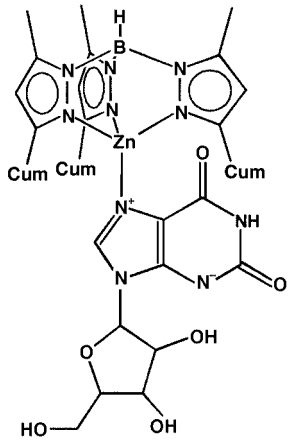

$Tp^{Cum,Me}$Zn-Xao

The nucleobase xanthine with three NH functions permits various N-alkylations, allowing us to probe the variation of its metal binding properties. The simplest xanthosine analogue is 9-methylxanthine, while some of the other methylated xanthines are well-known purine alkaloids. For example, caffeine (1,3,7-trimethylxanthine), theophylline (1,3-dimethylxanthine) and theobromine (3,7-dimethylxanthine) are the stimulating ingredients of coffee, tea, and cocoa, respectively. Amongst these, 9-methylxanthine, theophylline and theobromine were chosen for this investigation.

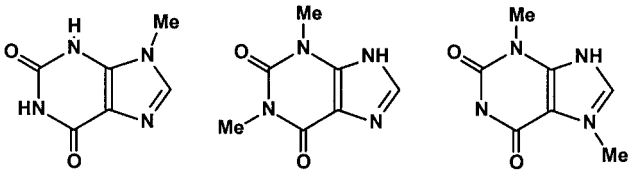

9-methylxanthine theophylline theobromine

9-Methylxanthine and **1a** yielded **5**. The NMR spectrum of **5** indicates that the attachment of the nucleobase to the zinc is different from that in the xanthosinate complex (see

 © 2003 Wiley-VCH Verlag GmbH & Co. KGaA, Weinheim

above). The strongest indicator is the C8-H signal at δ = 6.92 ppm, representing an upfield shift of ca. 1 ppm relative to free 9-methylxanthine. However, in all TpZn complexes of purine bases which are coordinated to zinc via N7 or N9, the C8-H resonance experiences an upfield shift of ca. 2 ppm due to the location of C8-H inside the pocket between the three phenyl groups of the Tp ligand.[1,20,21] Thus, while the C8-H proton resonance excludes N7 coordination, the N9-methyl resonance speaks against N1 coordination and favours N3 coordination. The upfield shift for this resonance, relative to that of free 9-methylxanthine, is ca. 1 ppm, which is typical for methyl groups in the Tp ligand pocket, while for N1 coordination the methyl group would point away from the Tp ligand and experience only little shielding from it. Thus the most likely structure for **5** is the following:

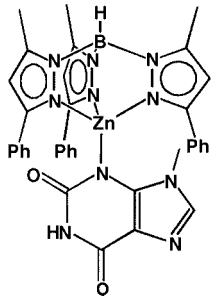

5

Anionic theophylline has been well-investigated as a ligand, showing a pronounced preference to coordinate via N7.[41,42] This was reproduced here with the complex, **6**, resulting from **1b** and theophylline. Again, NMR spectroscopic data allow a reliable structural assignment. While the 2 ppm upfield shift of the C8-H resonance indicates coordination via N7 or N9, the proton resonances of the two methyl groups make the assignment clear: the N3-methyl resonance is shifted upfield by 0.3 ppm and that of the N1-methyl group by 0.9 ppm. This places the N1-methyl group deeper into the Tp ligand pocket, which calls for attachment of theophylline to zinc via N7. Confirmation of this structural assignment also comes from the structure determination of the related $Tp^{Ph,Me}$Zn complex of 1-methyl-3-isobutylxanthine.[43]

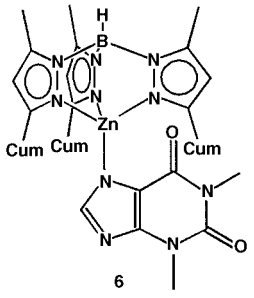

6

In anionic theobromine N1 and N9 are available for coordination to zinc. This was tested by the formation of **7** from **1a** and theobromine. In the NMR spectrum of **7** the C8-H resonance is shifted upfield by only 0.3 ppm relative to free theobromine. Thus a coordination via N9 is unlikely, but the 0.5 ppm upfield shifts for both N-methyl resonances favour coordination via N1.

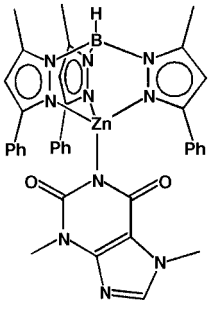

7

The assignment was confirmed by the structure determination of **7** (Figure 3). There are two independent molecules of **7** in the asymmetric unit, differing in the orientation of the purine base in the $Tp^{Ph,Me}$ ligand-pocket, but not in the relevant intramolecular bonding distances and angles. The theobrominate ligand is monodentate, and the two carbonyl functions flanking N1 are not within bonding range of the zinc ion. Correspondingly the Zn−N1 bond is quite short. As two of the three nitrogen atoms of theobromine pointing outward from the TpZn unit are methylated, there exists no possibility for the dimerization of **7** by means of hydrogen bonds. In all these respects complex **7** is unique, as no metal complex with N1-bound theobromine has been reported so far.

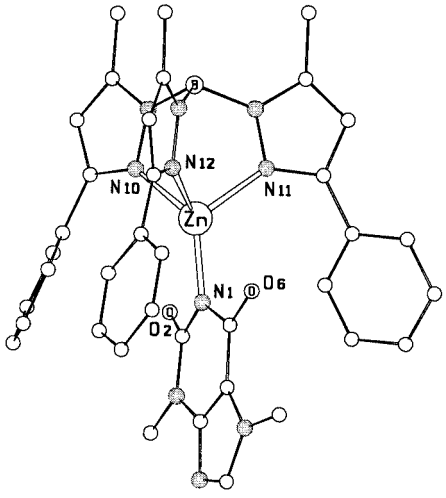

Figure 3. Molecular structure of **7** (one of the two independent molecules in the asymmetric unit); relevant atomic distances (average values, Å): Zn−N1 1.905(3), Zn−N10 2.065(4), Zn−N11 2.030(4), Zn−N12 2.010(4), Zn···O2 2.913(5), Zn···O6 2.943(5)

In all the zinc complexes of xanthine derivatives described here, the nucleobase has two or three nitrogen atoms available for zinc coordination (four in free xanthine). Xanthine, xanthosine and theophylline use N7, 9-methylxanthine uses N3, and theobromine uses N1. We see no consistent interpretation of this in the steric or electronic environment of the xanthine derivatives themselves. There-

 © 2003 Wiley-VCH Verlag GmbH & Co. KGaA, Weinheim

fore we think that secondary interactions like base pairing or π-stacking favour the observed constitutions.

Hypoxanthine

The nucleoside of hypoxanthine is inosine. It reacted cleanly with **1a** and **1b**, producing complexes **8a** and **8b** of which **8a** could be subjected to a structure determination. Having achieved this, it was no longer necessary to resort to alkylated hypoxanthine derivatives as inosine analogues.

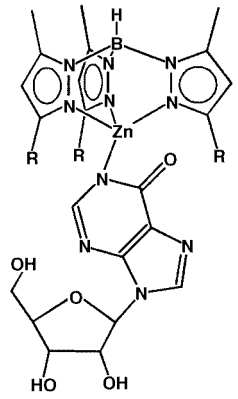

8a: R = Ph, **8b:** R = Cum

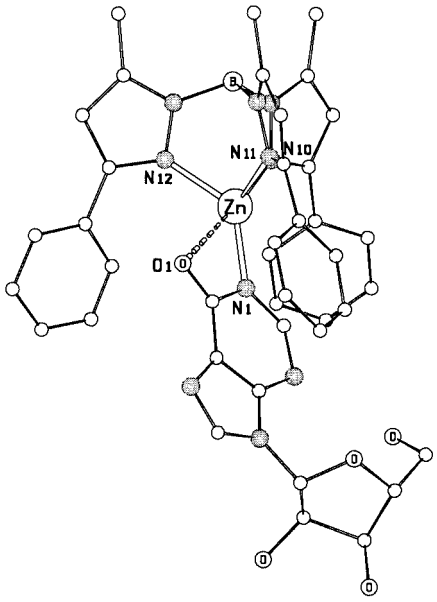

Figure 4. Molecular structure of **8a** (conformer **8a.4**); relevant bond lengths (average values, Å): Zn−N1 1.968(8), Zn−O1 2.528(8), Zn−N10 2.059(8), Zn−N11 2.031(8), Zn−N12 2.019(8)

The structure determination of **8a** was plagued by the fact that the asymmetric unit contains four independent complex units, i.e. the conformational freedom of the molecules is displayed even in the solid state. Even though enantiomerically pure D-inosine is present, its orientation in the Tp ligand-pocket yields two conformers, each of which is obtained with two different conformations of the sugar moiety. Although this generates a large amount of structural data, the essential part of the structures, i.e. the interaction between the zinc ion and the anionic nucleobase, varies very little.

In **8a** the nucleobase binds to zinc via N1, which is the nitrogen bearing the proton in neutral inosine. The negative charge in anionic inosine is presumed to rest on N1, N3 and mostly O6.[41,44] This makes O6 a potential donor atom, as is observed in the structure of **8a** by clearly noticeable Zn···O interactions (2.53−2.76 Å), creating a four-membered chelate ring. These Zn···O interactions are intermediate between the very weak ones in **2** and the very strong ones in **4′′**. Accordingly the ν(CO) IR bands for the coordinating carbonyl functions appear at 1670 cm^{-1} for **2** and at 1632 cm^{-1} for **8a**, but are absent from the IR spectrum of **4′′**. For this reason it is not appropriate to consider zinc as five-coordinate in **2** and **8a**, which is also reflected by the fact that the Zn−N1 bond in **8a** is close to the trigonal axis of the TpZn unit. There seems to be a relation, however, between the strengths of the Zn−N(nucleobase) and the Zn−O(nucleobase) interactions: in **2** and **7**, where the the Zn−O interactions are very weak, Zn−N is very short; in **8a**, where the Zn−O interactions are intermediate, it is elongated; and in **4′′**, where the Zn−O interactions are strong, Zn−N is unusually long.

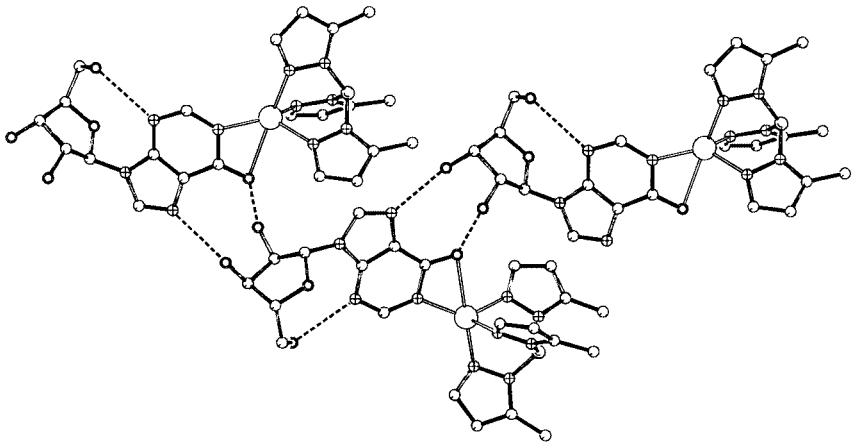

Figure 5. Hydrogen-bonding network for the conformer **4** of complex **8a**

 © 2003 Wiley-VCH Verlag GmbH & Co. KGaA, Weinheim

We are not aware of any other zinc complexes of anionic hypoxanthine or inosine. There is a bis(methylmercury) complex of inosinate which has mercury attached at N1 and N7.[45] Inosinemonophosphate also coordinates to zinc via N7.[46]

Like in the other compounds described here, the zinc ion in **8a** is not necessarily attached to the point of highest electron density in the nucleobase. One factor supporting the observed zinc-nucleobase interaction is certainly the additional bonding interaction with the carbonyl oxygen. In addition, like many other of these zinc complexes **8a** displays various kinds of hydrogen bonding which may contribute significantly to the overall stability. Each of the four individual conformers of **8a** is linked to its symmetry-related neighbours by one or two hydrogen bonds such that infinite chains result. Figure 5 displays this for the conformer **8a.4**, for which the linking consists of hydrogen bonds between the 2′-OH group and the carbonyl oxygen as well as between the 3′-OH group and N7.

Conclusions

This study brings our investigation on pyrazolylboratozinc complexes of nucleobases, nucleosides and analogues thereof to completion. Of the nine nucleobases applied[20] only guanine evaded zinc complexation. Of the four nucleosides used, three (uridine, xanthosine, inosine) could be attached to zinc. The alkylated nucleobases filled the gaps. In addition, a small number of nucleotide analogues[21] and of sugar phosphates[47] were included.

In all cases the advantage of encapsulating pyrazolylborate ligands, i.e. the limitation of the coordination space at the zinc ion, could be exploited. In all but a few cases the nucleobase-derived substrates are attached to zinc in a monodentate fashion, thereby showing their preferred donor site which is always located at a nitrogen atom. The other advantage of the Tp ligands, i.e. the preference for monoanionic coligands, which results in the formation of uncharged (and hence easily isolable) zinc complexes, could also be put to use.

The latter aspect requires, however, all the nucleobase-derived coligands to be anionic. This limits their selection to those which have at least one NH or OH function in their uncharged forms. It also means that the nitrogen atom that binds to zinc is not necessarily the one which was deprotonated. Moreover, it also means that in the free nucleobases "unnatural" coordination to zinc can occur via that nitrogen atom which bears the sugar moiety in the nucleosides; we found that this is actually the preferred bonding mode.

In the nucleosides and nucleoside analogues which are the subject of this paper "natural" binding to zinc must occur. In the pyrimidine-derived nucleobases (substituted uracil and thymine) there is only one possible donor atom, N3, which is used. In all the other (purine-derived) nucleobase derivatives there are three or more possible nitrogen donors. We have observed that the choice of the actual donor site cannot be predicted from the acid/base, electron density, or from the geometrical properties of the substrates. Instead additional bonding interactions seem to control the zinc-substrate connectivity. Thus in **4** and **8** the coordination of a carbonyl oxygen to zinc, in other cases hydrogen-bonding patterns, and possibly in all cases, π-stacking between the nucleobases of adjacent molecules or between the nucleobases and the phenyl substituents of the Tp ligands offer major contributions to the overall stability and hence to the choice of the zinc-binding nitrogen donor.

Conversely, according to the specific modes of attachment, the zinc ions can exert different kinds of influence on the electronic nature and hence the reactivity of the bound substrates. This in turn might be of use for an understanding of the modes of action of the various zinc enzymes along the metabolic pathways of the nucleobases, the nucleosides and the nucleotides.

Experimental Section

General: Reactions were performed under a nitrogen atmosphere in anhydrous solvents. The TpZn-OH complexes were prepared as described.[48,49] All other starting materials were obtained commercially. The analytical equipment was as described previously.[50]

Complex 2: A solution of **1b** (207 mg, 0.30 mmol) and 1-methyluracil (45 mg, 0.36 mmol) in 160 mL of benzene was refluxed for 3 days in a Soxhlet extractor filled with 4 Å molecular sieves. After reducing in vacuo to 40 mL and cooling to 4 °C a precipitate of unused starting materials was formed. After filtration the solution was evaporated to dryness. The residue was dissolved in a minimum amount of benzene which was layered with heptane. Within one week 128 mg (53%) of **2** had separated as colourless crystals. M.p. 211 °C. $C_{44}H_{51}BN_8O_2Zn$ (800.14): calcd. C 66.05, H 6.42, N 14.00; found C 66.11, H 6.16, N 13.70. IR (KBr): $\tilde{\nu}$ = 2547 cm^{-1} (m, BH), 1646 (vs, CO). ^1H NMR ($CDCl_3$): δ = 1.19 [d, *J* = 6.9 Hz, 18 H, Me(*i*Pr)], 2.51 [s, 9 H, Me(pz)], 2.57 (s, 3 H, MeN), 2.84 [sept, *J* = 6.9 Hz, 3 H, CH(*i*Pr)], 5.04 (d, *J* = 7.5 Hz, 1 H, C5H), 6.12 [s, 3 H, CH(pz)], 6.52 (d, *J* = 7.5 Hz, 1 H, C6H), 7.06 (d, *J* = 8.1 Hz, 6 H, Ph), 7.45 (d, *J* = 8.1 Hz, 6 H, Ph) ppm.

Complex 3: Like **2**, from **1a** (400 mg, 0.73 mmol) and 1-methylthymine (102 mg, 0.73 mmol). Yield: 386 mg (77%) of **3** as colourless crystals; m.p. 257 °C (dec.). $C_{36}H_{35}BN_8O_2Zn$ (687.93): calcd. C 62.86, H 5.13, N 16.29; found C 62.65, H 5.28, N 16.35. IR (KBr): $\tilde{\nu}$ = 2544 cm^{-1} (w, BH), 1655 (vs, CO). ^1H NMR ($CDCl_3$): δ = 1.41 (d, *J* = 1.1 Hz, 3 H, C5-Me), 2.53 [s, 9 H, Me(pz)], 2.63 (s, 3 H, NMe), 6.16 [s, 3 H, H(pz)], 6.43 (d, *J* = 1.1 Hz, 1 H, C6H), 7.16 (m, 9 H, Ph), 7.55 (m, 6 H, Ph) ppm.

Complex 4: $Tp^{Ph,Me}$Zn-H (133 mg, 0.24 mmol) and 9-isobutylguanine (50 mg, 0.24 mmol) in 30 mL of dichloromethane were stirred for 24 h. The solvent was removed in vacuo, the residue dissolved in 15 mL of benzene, filtered and layered with heptane. Within a short time a fluffy precipitate was formed, followed slowly by the growth of small evenly shaped crystals. After 2 days the heterogeneous mixture was separated by vigorous stirring and decanting of the solution in which the fluffy precipitate was suspended. The remaining crystals were washed with a small amount of heptane and dried in vacuo. 95 mg (45%) of **4′′·1.5C$_6$H$_6$** remained as colourless crystals. M.p. 203 °C. $C_{39}H_{40}BN_{11}OZn{\cdot}1.5C_6H_6$ (755.02 + 117.17): calcd. C 66.10, H 5.66, N 17.67; found C 65.53, H 5.68, N 17.77. IR (KBr): $\tilde{\nu}$ = 3471 cm^{-1} (s, NH), 2533 (m, BH), 1638

 © 2003 Wiley-VCH Verlag GmbH & Co. KGaA, Weinheim

Table 1. Crystallographic data

	2	**4"**	**7**	**8a**
Empirical formula	$C_{44}H_{51}BN_8O_2Zn$	$C_{39}H_{40}BN_{11}OZn{\cdot}1.5\ C_6H_6$	$C_{37}H_{35}BN_{10}O_2Zn$	$C_{40}H_{39}BN_{10}O_5Zn$
Molecular mass	800.14	755.02 +117.17	727.95	816.01
Crystal size [mm]	0.5 × 0.3 × 0.2	0.2 × 0.2 × 0.55	0.15 × 0.2 × 0.3	0.15 × 0.35 × 0.55
Space group	$P2_1/n$	$C2/c$	$P2_1/c$	$P2_1$
Z	4	8	8	8
a [Å]	17.664(4)	29.879(7)	20.271(5)	21.572(9)
b [Å]	12.824(3)	18.191(4)	13.907(3)	16.128(7)
c [Å]	18.882(4)	19.470(5)	24.912(6)	22.806(10)
α [°]	90	90	90	90
β [°]	98.64(3)	118.834(4)	91.657(5)	103.658(10)
γ [°]	90	90	90	90
V [Å^3]	4228.7(16)	9271(4)	7020(3)	7710(1)
D(calc) [gcm^{-3}]	1.26	1.25	1.38	1.41
μ(Mo-K_α) [mm^{-1}]	0.63	0.58	0.75	0.70
hkl range	*h:* 0 to 21	*h:* −39 to 38	*h:* −27 to 25	*h:* −23 to 23
	k: −15 to 0	*k:* −24 to 24	*k:* −18 to 16	*k:* −17 to 17
	l: −23 to 23	*l:* −25 to 25	*l:* −32 to 32	*l:* −25 to 25
Measured reflections	8566	69233	62688	54436
Independent reflections	8294	11199	17031	22152
Observed refl. [$I>2\sigma(I)$]	5541	6414	6107	14627
Parameters	505	578	927	2053
Refined reflections	8294	11199	17031	22152
R_1 (obs.refl.)	0.049	0.055	0.070	0.062
wR_2 (all refl.)	0.155	0.176	0.178	0.157
Residual electron density [e/Å^3]	+0.6/-0.4	+0.5/-0.8	+0.7/-1.1	+0.5/-0.4

(s, CO). ^{1}H NMR ($CDCl_3$): δ = 0.87 [d, J = 6.8 Hz, 6 H, Me(*i*Bu)], 2.05 [m, 1 H, CH(*i*Bu)], 2.56 [s, 9 H, Me(pz)], 3.31 (s, 2 H, NH_2), 3.60 [d, J = 7.2 Hz, 2 H, CH_2(*i*Bu)], 6.21 [s, 3 H, H(pz)], 6.99−7.17 (m, 9 H, Ph), 7.30 (s, 1 H, C8H), 7.34 (s, 9 H, C_6H_6), 7.60 (d, J = 6.8 Hz, 6 H, Ph) ppm.

The decanted suspension was filtered and the precipitate dried in vacuo, leaving behind 33 mg (18%) of **4′** as colourless needles. M.p. 216 °C. $C_{39}H_{40}BN_{11}OZn$ (755.02): calcd. C 62.04, H 5.34, N 20.41; found C 61.87, H 5.64, N 20.27. IR (KBr): $\tilde{\nu}$ = 3414 cm^{-1} (m, NH_2), 2548 (w, BH), 1692 (s, CO). ^{1}H NMR ($CDCl_3$): identical to the spectrum of **4′′**.

Complex 5: Complex **1a** (28.5 mg, 0.05 mmol) and 9-methylxanthine (8.4 mg, 0.05 mmol) in 10 mL of dichloromethane were stirred for 2 days. The solvent was removed in vacuo and the residue dissolved in 8 mL of benzene and 2 mL of dichloromethane. Slow evaporation yielded 18 mg (50%) of **5** which, after drying in vacuo, was isolated as a colourless powder. M.p. 158 °C. $C_{36}H_{33}BN_{10}O_2Zn$ (713.92): calcd. C 60.57, H 4.66, N 19.62; found C 60.17, H 5.01, N 18.50. IR (KBr): $\tilde{\nu}$ = 2550 cm^{-1} (m, BH), 1673 (vs, CO). ^{1}H NMR ($CDCl_3$): δ = 2.54 (s, 3 H, NMe), 2.58 [s, 9 H, Me(pz)], 6.23 [s, 3 H, H(pz)], 6.92 (s, 1 H, C8H), 7.12 (m, 9 H, Ph), 7.46 (m, 6 H, Ph), 7.71 (s, 1 H, N3H) ppm.

Complex 6: Complex **1b** (200 mg, 0.29 mmol) and theophylline·H_2O (58 mg, 0.29 mmol) in 50 mL of dichloromethane were stirred for 36 h. After filtration the volume was reduced to 10 mL in vacuo. Cooling to 4 °C yielded colourless crystals. The solvent was decanted and the crystals dried in vacuo, leaving behind 125 mg (50%) of **6** as a colourless powder. M.p. 241 °C. $C_{46}H_{53}BN_{10}O_2Zn$ (854.19): calcd. C 64.68, H 6.25, N 16.40; found C 64.48, H 6.24, N 16.29. IR (KBr): $\tilde{\nu}$ = 2540 cm^{-1} (m, BH), 1698 (s, CO). ^{1}H NMR ($CDCl_3$): δ = 1.12 [d, J = 7.0 Hz, 18 H, Me(-*i*Pr)], 2.55 [s, 9 H, Me(pz)], 2.63 (s, 3 H, NMe), 2.75 [sept, J = 7.0 Hz, 3 H, CH(*i*Pr)], 3.37 (s, 3 H, NMe), 6.04 (s, 1 H, C8H), 6.14 [s, 3, H(pz)], 6.91 (d, J = 8.0 Hz, 6 H, Ph), 7.20 (d, J = 8.0 Hz, 6 H, Ph) ppm.

Complex 7: A solution of **1a** (213 mg, 0.38 mmol) in 20 mL of dichloromethane was added to a suspension of theobromine·3H_2O (86 mg, 0.37 mmol) in 30 mL of methanol. After stirring for 12 h and filtration, the solution was evaporated to 30 mL. Upon cooling to 4 °C a fine precipitate of impure product was formed. This was filtered off and the filtrate evaporated to 10 mL. Further cooling to 4 °C yielded 156 mg (58%) of **7** as colourless crystals. M.p. 244 °C. $C_{37}H_{35}BN_{10}O_2Zn$ (727.95): calcd. C 61.05, H 4.85, N 19.24; found C 60.93, H 5.07, N 18.98. IR (KBr): $\tilde{\nu}$ = 2547 cm^{-1} (m, BH), 1655s, 1632 (vs, CO). ^{1}H NMR ($CDCl_3$): δ = 2.54 [s, 9 H, Me(pz)], 3.00 (s, 3 H, NMe), 3.52 (s, 3 H, NMe), 6.17 [s, 3 H, H(pz)], 7.10 (m, 9 H, Ph), 7.22 (s, 1 H, C8H), 7.56 (m, 6 H, Ph) ppm.

Complex 8a: A suspension of inosine (150 mg, 0.56 mmol) in 30 mL of methanol was treated with a solution of **1a** (316 mg, 0.56 mmol) in 40 mL of dichloromethane. After stirring for 12 h and filtration, the solution was evaporated to 20 mL. Cooling to 4 °C yielded colourless crystals. The solution was decanted and the residue dried in vacuo, leaving behind 325 mg (71%) of **8a** as colourless crystals. M.p. 320 °C (dec.). $C_{40}H_{39}BN_{10}O_5Zn$ (816.01): calcd. C 58.88, H 4.82, N 17.16; found C 58.66, H 4.81, N 17.28. IR (KBr): $\tilde{\nu}$ = 3274 cm^{-1} (broad OH), 2546 (m, BH), 1632 (vs, CO). ^{1}H NMR ([D_6]DMSO, assignments by COSY): δ = 2.58 [s, 9 H, Me(pz)], 3.49−3.72 (m, 2 H, C5′H_2), 3.95 (m, 1 H, C4′H), 4.11 (m, 1 H, C3′H), 4.45 (m, 1 H, C2′H), 5.16 (d, J = 4.8 Hz, 1 H, O3′H), 5.21 (d, J = 6.1 Hz, 1 H, O5′H), 5.36 (d, J = 6.4 Hz, 1 H, O2′H), 5.74 (d, J = 6.0 Hz, 1 H, C1′H), 6.09 (s, 1 H, C2H), 6.44 [s, 3 H, H(pz)], 7.11 (m, 9 H, Ph), 7.41 (m, 6 H, Ph), 7.96 (s, 1 H, C8H) ppm.

Complex 8b: Like **8a**, from inosine (32 mg, 0.31 mmol) and **1b** (212 mg, 0.31 mmol). Yield: 240 mg (83%) of **8b** as colourless needles. M.p. 206 °C. $C_{49}H_{57}BN_{10}O_5Zn$ (942.25): calcd. C 62.46, H

 © 2003 Wiley-VCH Verlag GmbH & Co. KGaA, Weinheim

6.10, N 14.87; found C 61.90, H 6.01, N 14.49. IR (KBr): $\tilde{\nu}$ = 3430 cm^{-1} (broad, OH), 2542 (m, BH), 1639 (vs, CO). ^1H NMR ([D_6]DMSO, assignments by COSY): δ = 1.02 [d, J = 6.9 Hz, 18 H, Me(*i*Pr)], 2.56 [s, 9 H, Me(pz)], 2.69 [sept, J = 6.9 Hz, 3 H, CH(*i*Pr)], 3.46−3.70 (m, 2 H, C5′H_2), 3.90 (m, 1 H, C4′H), 4.09 (m, 1 H, C3′H), 4.37 (m, 1 H, C2′H), 5.13 (m, 2 H, O3′H and O5′H), 5.25 (d, J = 6.1 Hz, 1 H, O2′H), 5.68 (d, J = 5.0 Hz, 1 H, C1′H), 6.12 (s, 1 H, C2H), 6.39 [s, 3 H, H(pz)], 6.94 (d, J = 8.1 Hz, 6 H, Ph), 7.33 (d, J = 8.1 Hz, 6 H, Ph), 7.97 (s, 1 H, C8H) ppm.

Structure Determinations:[51] Crystals were obtained as described in the Exp. Sect.. Diffraction data were recorded at 180 K (**7**) and at room temp. (**2, 4′′, 8a**) on a Nonius CAD4 (**2**) or a Bruker Smart CCD diffractometer (**4′′, 7, 8a**). Empirical absorption corrections were applied for **4′′, 7** and **8a**. The structures were solved with direct methods and refined anisotropically with the SHELX program suite.[52] Hydrogen atoms were included with fixed distances and isotropic temperature factors 1.5 times those of their attached atoms. Parameters were refined against F^2. The R values are defined as $R_1 = \Sigma|F_0 - F_c|/\Sigma F_o$ and $wR_2 = [\Sigma[w(F_0^2 - F_c^2)^2]-\Sigma[w(F_0^2)^2]]^{1/2}$. Drawings were produced with SCHAKAL.[53] Table 1 lists the crystallographic data.

Acknowledgments

This work was supported by the Fonds der Chemischen Industrie.

[1] Previous communication: D. Badura, H. Vahrenkamp, *Inorg. Chem.* **2002**, *41*, 6020−6027.
[2] W. Saenger, *Principles of Nucleic Acid Structure*, Springer, New York, **1984**.
[3] *Interactions of Metal Ions with Nucleotides, Nucleic Acids and their Constituents* (Ed.: H. Sigel), Metal Ions in Biological Systems, Vol. 32, Mercel Dekker, New York, **1996**.
[4] B. Lippert, *Prog. Inorg. Chem.* **1989**, *37*, 1−97.
[5] A. Martinez Balbaz, F. Azorin, *Nucleic Acid Res.* **1993**, *21*, 2557−2562.
[6] T. V. O′Halloran, *Science* **1993**, *261*, 715−725.
[7] G. L. Eichhorn, in *Inorganic Biochemistry* (Ed.: G. L. Eichhorn), Elsevier, Amsterdam, **1973**, Vol. 2, pp 1210−1243.
[8] Y. A. Shin, G. L. Eichhorn, *Biochemistry* **1968**, *7*, 1026−1032.
[9] E. Kimura, T. Ikeda, S. Aoki, M. Shionoya, *J. Biol. Inorg. Chem.* **1998**, *3*, 259−267.
[10] G. L. Eichhorn, Y. A. Shin, *J. Am. Chem. Soc.* **1968**, *90*, 7323−7328.
[11] J. E. Coleman, *Annu. Rev. Biochem.* **1992**, *61*, 897−946.
[12] M. Czupryn, K. H. Falchuk, A. Stankiewicz, B. L. Vallee, *Biochemistry* **1993**, *32*, 1204−1211.
[13] K. D. Wilson, F. A. Quiocho, *Nat. Struct. Biol.* **1994**, *1*, 691−694.
[14] D. C. Brown, K. D. Collins, *J. Biol. Chem.* **1991**, *266*, 1597−1604.
[15] E. Fusch, B. Lippert, *J. Am. Chem. Soc.* **1994**, *116*, 7204−7209.
[16] E. Dubler in ref. 3, pp 301−338.
[17] H. Sigel, *Chem. Soc. Rev.* **1993**, *22*, 255−267; H. Sigel, R. B. Martin, *Chem. Soc. Rev.* **1994**, *23*, 83−91.
[18] L. G. Marzilli, T. G. Kistenmacher, G. L. Eichhorn, in *Nucleic Acid Metal Interactions* (Ed.: T. G. Spiro), Wiley, New York, **1980**, Vol. 1, pp 179−250.
[19] S. K. Miller, L. G. Marzilli, S. Dörre, P. Kollat, R. D. Stigler, *Inorg. Chem.* **1986**, *25*, 4272−4277.
[20] D. Badura, H. Vahrenkamp, *Inorg. Chem.* **2002**, *41*, 6013−6019.
[21] M. Ruf, K. Weis, H. Vahrenkamp, *Inorg. Chem.* **1997**, *36*, 2130−2137.
[22] U. Hartmann, H. Vahrenkamp, *Inorg. Chem.* **1991**, *30*, 4676−4677.
[23] U. Hartmann, H. Vahrenkamp, *Z. Naturforsch., Teil B* **1994**, *49*, 1725−1730.
[24] U. Hartmann, R. Gregorzik, H. Vahrenkamp, *Chem. Ber.* **1994**, *127*, 2123−2127.
[25] U. Hartmann, H. Vahrenkamp, *Chem. Ber.* **1994**, *127*, 2381−2385.
[26] A. Koppenhöfer, U. Hartmann, H. Vahrenkamp, *Chem. Ber.* **1995**, *128*, 779−785.
[27] A. Trösch, H. Vahrenkamp, *Inorg. Chem.* **2001**, *40*, 2305−2311.
[28] T. Koike, T. Gotoh, S. Aoki, E. Kimura, M. Shiro, *Inorg. Chim. Acta* **1998**, *270*, 424−432, and references cited therein.
[29] S. K. Miller, D. G. Van Derveer, L. G. Marzilli, *J. Am. Chem. Soc.* **1985**, *107*, 1048−1055.
[30] M. R. Taylor, M. J. McCall, *Acta Crystallogr. Sect. A.* **1975**, *31*, S42.
[31] A. Garcia-Raso, J. J. Fiol, F. Badenas, R. Cons, A. Terron, M. Quiros, *J. Chem. Soc., Dalton Trans.* **1999**, 167−173.
[32] M. Shionoya, T. Ikeda, E. Kimura, M. Shiro, *J. Am. Chem. Soc.* **1994**, *116*, 3848−3859.
[33] C. G. Mowat, S. Parsons, G. A. Solan, R. E. P. Winpenny, *Acta Crystallogr., Sect. C* **1997**, *53*, 282−283.
[34] C. Bazzicalupi, A. Bencini, A. Bianchi, V. Fusi, L. Mazzanti, P. Paoletti, B. Valtancoli, *Inorg. Chem.* **1995**, *34*, 3003−3010.
[35] For a comprehensive discussion of five-coordinate TpZn(X,Y) complexes, see: M. Rombach, C. Maurer, K. Weis, E. Keller, H. Vahrenkamp, *Chem. Eur. J.* **1999**, *5*, 1013−1027.
[36] G. Frommer, H. Schöllhorn, U. Thewalt, B. Lippert, *Inorg. Chem.* **1990**, *29*, 1417−1422.
[37] G. Schröder, B. Lippert, M. Sabat, C. J. L. Lock, R. Faggiani, B. Song, H. Sigel, *J. Chem. Soc., Dalton Trans.* **1995**, 3667−3775.
[38] W. S. Sheldrick, P. Gross, *Inorg. Chim. Acta* **1988**, *153*, 247−254.
[39] G. Frommer, I. Mutikainen, F. J. Pesch, E. C. Hillgeris, H. Preut, B. Lippert, *Inorg. Chem.* **1992**, *31*, 2429−2434.
[40] D. Voet, A. Rich, *Prog. Nucleic Acid Res. Mol. Biol.* **1970**, *10*, 183−265.
[41] D. J. Hodgson, *Prog. Inorg. Chem.* **1977**, *23*211−254.
[42] L. G. Marzilli, T. G. Kistenmacher, *Acc. Chem. Res.* **1977**, *10*, 146−152.
[43] D. Badura, H. Vahrenkamp, unpublished.
[44] A. Psoda, D. Shugar, *Biochim. Biophys. Acta* **1971**, *247*, 507−513.
[45] F. Belanger-Garipy, A. L. Beauchamp, *Cryst. Struct. Commun.* **1982**, *11*, 991−993.
[46] P. DeMeester, D. M. L. Goodgame, T. J. Jones, A. C. Skapski, *Biochim. Biophys. Acta* **1974**, *353*, 392−398.
[47] K. Weis, M. Rombach, H. Vahrenkamp, *Inorg. Chem.* **1998**, *37*, 2470−2475.
[48] M. Ruf, H. Vahrenkamp, *Inorg. Chem.* **1996**, *35*, 6571−6578.
[49] M. Ruf, R. Burth, K. Weis, H. Vahrenkamp, *Chem. Ber.* **1996**, *129*, 1251−1257.
[50] M. Gelinsky, H. Vahrenkamp, *Eur. J. Inorg. Chem.* **2002**, 2458−2462.
[51] CCDC-209510 (**2**), CCDC-209511 (**4"**), CCDC-209512 (**7**) and CCDC-209513 (**8**a), contain the supplementary crystallographic data for this paper. These data can be obtained free of charge at www.ccdc.cam.ac.uk/conts/retrieving.html [or from the Cambridge Crystallographic Data Centre, 12, Union Road, Cambridge CB2 1EZ, UK; Fax: (internat.) +44-1223/336-033; E-mail: deposit@ccdc.cam.ac.uk].
[52] G. M. Sheldrick, *SHELX-86 and SHELXL-93, Programs for Crystal Structure Determination*, Univeristät Göttingen, **1986** and **1993**.
[53] E. Keller, *SCHAKAL for Windows*, Universität Freiburg, **2001**.
Received May 8, 2003

 © 2003 Wiley-VCH Verlag GmbH & Co. KGaA, Weinheim

Chain-Like Tetra-, Penta- and Heptanuclear Cyanide-Bridged Complexes by Attachment of Organometallic Cyanides to M_2, M_3 and M_5 Units

Tianlu Sheng,[a] Ralf Appelt,[a] Virginie Comte,[a] and Heinrich Vahrenkamp*[a]

Keywords: Cyanides / Polynuclear complexes / Metal-metal interactions / Electrochemistry

Attachment of the "ligands" [Cp(dppe)Fe-CN], [Cp(PPh_3)$_2$-Ru-CN], [Cp(CO)$_2$Fe-CN] and [(CO)$_5$M-CN]$^-$, (where M = Cr, Mo, W) to the polymetallic centres [$Ru_2(OAc)_4$]$^+$, [$Co_3(dpa)_4$]$^{2+}$ and [$Ni_5(tdpa)_4$]$^{2+}$ yielded two tetra-, three penta- and five heptanuclear complexes with chain-like linear arrangements of the metal ions and the bridging cyanide ligands, as proved by the structure determination of [$Ni_5(tdpa)_4${Cp(dppe)$_2$Fe-CN}$_2$](PF_6)$_2$. IR and CV data show that the Ru_2, Co_3 and Ni_5 centres of these complexes withdraw electron density from the external organometallic units. This prevents electronic interactions between the two terminal metal ions, yet allows multistep one- and two-electron redox processes.

(© Wiley-VCH Verlag GmbH & Co. KGaA, 69451 Weinheim, Germany, 2003)

Introduction

Molecular wires, comprised of arrays of metal atoms surrounded by ligands as insulators, are attractive as conducting leads in nanoscale devices, with possible applications ranging from electrical connections to light harvesting antennas.[1−3] One approach to the design of such wires is the lining up of metals and bridging ligands up to infinite arrays, as was successfully applied to metal-cyanide combinations.[3−5] The other approach is direct linking of the metal atoms along the chain, as applied successfully in the Krogmann salts.[6]

Well-defined molecular species of this kind, with nanoscale dimensions, have not been prepared yet. The longest (M-CN)$_x$ chain which has been crystallographically characterised contains seven manganese atoms.[7] Likewise, the longest chain-like array with metal-metal bonds is formed from seven chromium atoms.[8] Like others,[5] we are involved in attempts to stretch these limits.

Our contributions to this field have so far consisted in the synthesis and investigation of (M-CN)$_x$ arrays.[9−14] We were able to show that there exist electronic interactions between terminal metals as far as 12 Å apart[9] and that a 90° angle in a chain interrupts such interactions.[11] We also observed the drawback that with increasing length the (M-CN)$_x$ chains become fragile, showing a tendency for dismutation with formation of shorter fragments.

Following on from here, it seemed favourable to us to combine the advantages of the cyanometal building blocks (i.e. a large variability) with those of the metal-metal bonded chains (i.e. rigidity due to their rigid ligand environment). This paper reports on some combinations of Ru_2, Co_3 and Ni_5 chains with terminal organometallic cyanides. Other than us[15] only the group of Kühn has prepared related complexes based on [$Re_2(OAc)_4$][16] and [$Mo_2(OAc)_4$] units.[17]

Results and Discussion

Derivatives of [$Ru_2(OAc)_4$]$^+$

The [$Ru_2(OAc)_4$]$^+$ unit is a mixed-valence species containing Ru^{II} and Ru^{III}. This is promising in terms of redox chemistry, particularly when combined with the redox chemistry of cyanide-linked metal complex units. We therefore attached the organometallic cyanides [Cp(dppe)Fe-CN] and [Cp(PPh_3)$_2$Ru-CN] to this core by reacting them with [$Ru_2(OAc)_4(THF)_2$]BF_4. The complex cations **1a** and **1b** were obtained as tetrafluoroborate salts.

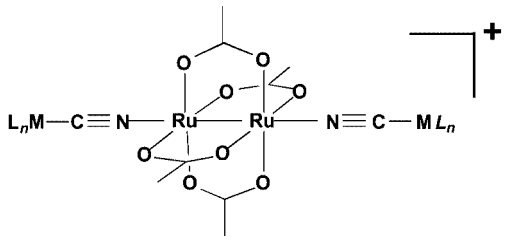

1a: L_nM = Cp(dppe)Fe **1b:** L_nM = Cp(PPh_3)$_2$Ru

Confirmation of the identity of complexes **1a** and **1b** was obtained independently by an X-ray analysis of **1b** as a hexafluoroantimonate salt.[15] Information on their electronic nature can be drawn from the ν(CN) values in their

[a] Institut für Anorganische und Analytische Chemie der Universität Freiburg
Albertstr. 21, 79104 Freiburg, Germany
Fax: (internat.) +49-761/203-6001
E-mail: vahrenka@uni-freiburg.de

IR spectra. The corresponding bands (2059 cm^{-1} for **1a** and 2061 cm^{-1} for **1b**) are lower by 3 and 10 cm^{-1}, respectively, than those in the free L_nM-CN "ligands". Previously, we observed that ν(CN) is raised in similar situations, reflecting the kinematic effect, i.e. the increased energy for the CN vibration due to the attachment of CN^- to two metal centres.[11−13] However, for dinuclear CN-bridged complexes we had also observed that ν(CN) can be lowered when the metal centre attached at the N terminus is strongly electron-withdrawing.[18] In those cases the electron withdrawal is compensated by increased M→C π-back-donation from the other metal centre, which populates antibonding orbitals and lowers the strength of the C−N bond. Complexes **1** seem to represent an intermediate situation, where the kinematic effect and the back-bonding effect are virtually identical. The important conclusion from this is that the Ru_2 core is an electron sink which may impede electronic interactions between the two terminal metal centres.

This is also evident from the electrochemical investigation of **1a** and **1b**. The electrochemical response of the Ru_2 core of these complexes is poor, as is that of the parent complexes $[Ru_2Cl(RCOO)_4]$,[19] showing only an irreversible reduction around −0.4 V (in CH_2Cl_2 vs. Ag/AgCl). The oxidative waves assigned to the organometallic cyanides occur at +0.67 V for **1a** and +1.02 V for **1b**. Both these values are 0.2 V higher than those of the free organometallic cyanides. This confirms the electron withdrawal by the Ru_2 core, which, by means of the π-back-donation, extends to the terminal metal centres. The electrochemical waves have the characteristics of reversible one-electron transfers. Together with the notion that there is no splitting of the redox waves, this indicates that there is no electronic interaction between the two terminal iron or ruthenium atoms. The same observation was made by Kühn for the related complexes with Re_2 and Mo_2 cores.[16,17]

Derivatives of $[Co_3(dpa)_4]^{2+}$

Complexes with metal chains stabilized by sawtooth-like pyridylamide ligands were introduced by Peng.[8,20,21] To start with we chose the best-investigated example with the shortest chain length, i.e. the cobalt(II) complex.[22,23] The reactions between $[Co_3(dpa)_4]Cl_2$ and the cyanometal complexes [Cp(dppe)Fe-CN], $[Cp(PPh_3)_2Ru$-CN] and Na-$[(CO)_5Cr$-CN] were straightforward and yielded the pentanuclear complexes **2a**−**c**. Complexes **2a** and **2b** are dications and were isolated as hexafluoroantimonate salts. Complex **2c** is neutral.

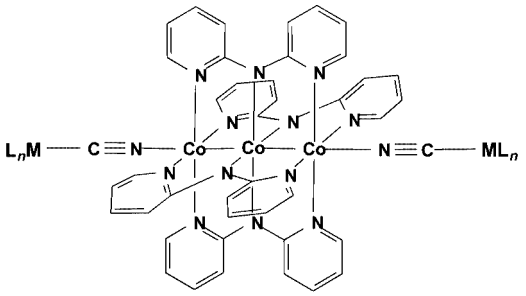

2a: L_nM = Cp(dppe)Fe **2b:** L_nM = $Cp(PPh_3)_2Ru$ **2c:** L_nM = $(CO)_5Cr$

Complexes **2a**−**c** could not be obtained in the form of crystals suitable for X-ray analysis, yet their identity is evident from their spectra and their redox behaviour. The ν(CN) band-positions of **2a** and **2b** (2055 and 2057 cm^{-1}) are virtually identical to those of **1a** and **1b**. The slight lowering of the ν(CN) values relative to those of the free organometallic cyanides leads to the same conclusions as above: the $[Co_3(dpa)_4]^{2+}$ core, just like the $[Ru_2(OAc)_4]^+$ core, seems to be a rather strong electron acceptor. The fact that the ν(CN) band of **2c** (2120 cm^{-1}) is raised by 17 cm^{-1} with respect to that of free $[(CO)_5Cr$-$CN]^-$ is not in contradiction with this conclusion: upon formation of the pentanuclear complex the negative charge of $[(CO)_5Cr$-$CN]^-$ disappears, hence the strong Cr→C π-back-donation is diminished and this results in a strengthening of the C−N bond.

The electrochemical behaviour of complexes **2** underlines the strong electron-acceptor properties of their $[Co_3(dpa)_4]^{2+}$ cores (see Table 1 and Figure 1). The first oxidative wave corresponds to a one-electron oxidation of the Co_3 unit. The second wave represents the transfer of two electrons, one each from the two terminal metal atoms. Relative to free $[Co_3(dpa)_4(CH_3CN)_2]^{2+}$ the Co_3 core in complexes **2** is easier to oxidize by 0.1−0.2 V, reflecting the electron donation from the organometallic cyanides, typically strongest from the anionic $[(CO)_5Cr$-$CN]^-$. In turn, the terminal metal units are more difficult to oxidize by roughly 0.4 V, in comparison to the free organometallic cyanides. This is about twice as much as in complexes **1**, indicating that the Co_3 unit is a stronger electron acceptor than the Ru_2 unit. As above, the redox wave for the organometallic cyanides is not split into two components, again indicat-

Table 1. Cyclovoltammetric data (in CH_2Cl_2, potentials in V vs. Ag/AgCl) of complexes **2** and their reference compounds

	$E_{1/2}(1)$	$E_{1/2}(2)$
[Cp(dppe)Fe-CN]		0.48
$[Cp(PPh_3)_2Ru$-CN]		0.79
$[(CO)_5Cr$-$CN]^-$		0.58
$[Co_3(dpa)_4(CH_3CN)_2]^{2+}$	0.60	
2a	0.46	0.83
2b	0.51	1.25(irr)
2c	0.40	0.93

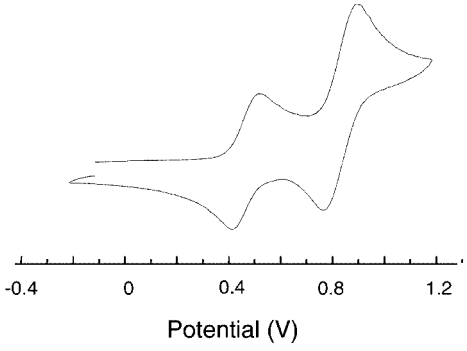

Figure 1. Cyclic voltammogram of **2a** (in CH_2Cl_2, potentials vs. Ag/AgCl)

 © 2003 Wiley-VCH Verlag GmbH & Co. KGaA, Weinheim

ing that the central polymetallic unit interrupts electronic communication between the two terminal metal atoms.

The electronic spectra of complexes **2** (for details see Exp. Sect.) are very similar to those of the Co_3 parent compounds $[Co_3(dpa)_4]Cl_2$ and $[Co_3(dpa)_4(CH_3CN)_2](PF_6)_2$.[22,23] Very strong absorptions in the near UV and one strong absorption in the visible range can be assigned to π-π* and MLCT transitions, and very weak absorptions in the NIR to d-d transitions of the Co^{II} ions. Complexes **2** show no additional features other than a slight intensification of the NIR bands. The positions of the NIR bands of **2a** and **2b** make it clear that they are not MMCT bands representing electron transfer from the outer metal centres to the Co_3 core: the prominent band for the Ru complex **2b** at 1248 nm occurs at lower energy by 26 nm than the corresponding band for the Fe complex **2a** at 1222 nm. Yet $[Cp(PPh_3)_2Ru\text{-}CN]$ is much more difficult to oxidize than [Cp(dppe)Fe-CN] (see Table 1). Hence these band positions only reflect the influence of the terminal organometallic units on the electronic structure of the Co_3 core.

The reversible redox steps in the cyclic voltammograms indicate that complexes **2** should be suitable for chemical oxidations. This was probed for **2a**. Addition of one equivalent of magic blue $[(4\text{-}Br\text{-}C_6H_4)_3N^+$ as the SbF_6 salt, $E_{1/2} = +1.0$ V[24]] produced a change of colour and spectra, addition of two further equivalents produced another. The resulting complex cations which we assign as **2a′** and **2a′′** were stable enough to be investigated in solution, but we failed to isolate them as pure complex salts.

$[Cp(dppe)Fe\text{-}CN\text{-}Co_3(dpa)_4\text{-}NC\text{-}Fe(dppe)Cp]^y$

2a: $y = 2+$, **2a′**: $y = 3+$, **2a"**: $y = 5+$

The ν(CN) bands in the IR spectra of **2a**, **2a′** and **2a′′** occur at 2057, 2047 and 2134 cm^{-1}, respectively, in CH_2Cl_2 solution. The changes are in agreement with the structural and electronic assignments given above. The decrease from **2a** to **2a′** reflects the increased charge on the Co_3 core and hence its increased electron withdrawal. The sharp rise from **2a′** to **2a′′** reflects the positive charges on the two terminal Cp(dppe)Fe units, which dramatically reduces their ability for M→C π-back-donation. In the electronic spectrum of **2a′** (for details see Exp. Sect.) two new bands of medium intensity occur in the far visible and near IR range. In the electronic spectrum of **2a′′** these two new bands are shifted to lower energies. New bands of similar position and intensity were also observed upon one-electron oxidation of $[Co_3(dpa)_4]Cl_2$.[25] The simplest interpretation is that they are due to MMCT transitions within the $Co^{II}_2Co^{III}$ core. There is no obvious relation in terms of MMCT with the terminal [FeCp(dppe)] units, other than the band shift upon changing their oxidation state. Thus, similar to the situation with the $[Ru_2(OAc)_4]$-derived complexes, neither the electrochemical behaviour nor the electronic spectroscopy of complexes **2** indicate any electron transfer behaviour, be it between the two terminal metal units or between one of these units and the trimetal core.

Derivatives of $[Ni_5(tpda)_4]^{2+}$

The starting material for our heptanuclear complexes, $[Ni_5Cl_2(tpda)_4]$, was also described for the first time by Peng.[20] After conversion to its more reactive form, $[Ni_5(tpda)_4(CH_3CN)_2]^{2+}$, by reaction with $AgBF_4$ in acetonitrile,[26] it could be reacted with [Cp(dppe)Fe-CN], $[Cp(PPh_3)_2Ru\text{-}CN]$, $[Cp(CO)_2Fe\text{-}CN]$, $Na[(CO)_5Mo\text{-}CN]$ and $Na[(CO)_5W\text{-}CN]$. Complexes **3a**−**e** resulted in moderate yields. They were isolated as deeply coloured crystalline hexafluorophosphate salts (**3a**, **3b**, **3c**) or neutral complexes (**3d**, **3e**).

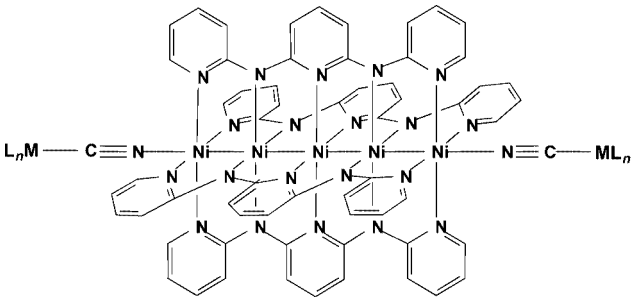

3a: $L_nM = Cp(dppe)Fe$ **3b:** $L_nM = Cp(PPh_3)_2Ru$ **3c:** $L_nM = Cp(CO)_2Fe$

3d: $L_nM = (CO)_5Mo$ **3e:** $L_nM = (CO)_5W$

Crystals of **3a** were chosen for a representative structure determination (see Figure 2). The complex cation has internal symmetry, with the central nickel atom being located on a twofold axis. The central molecular axis of **3a** which is comprised of 11 atoms (5 Ni, 2 Fe, 2 CN) is almost perfectly linear, with the strongest bending occurring typically at the nitrogen atom of the bridging cyanide (172°). The helical nature of the $[Ni_5(tdpa)_4]$ core, due to the wrapping of the tdpa ligands, and the uneven distribution of Ni−Ni distances along the Ni_5 chain closely correspond to those in the parent complexes, $[Ni_5Cl_2(tpda)_4]$[20] and $[Ni_5(tpda)_4(CH_3CN)_2](PF_6)_2$.[26] The geometry of the [Cp(dppe)Fe-CN] "ligands" compares well with that in related di- and trinuclear complexes.[9−14,18] Neither the Fe−C nor the C−N distances in all the cyanide-bridged complexes derived from [Cp(dppe)Fe-CN] vary so much as to draw reliable conclusions on the amount of Fe→C π-back-donation. Thus, the structural data of such oligometallic complexes yield no information about the net electron withdrawal from the terminal organometallic cyanides to the central M_2, M_3 or M_5 core. The two iron atoms in **3a** are 19.4 Å apart, which is the longest distance between such terminal redox centres in cyanide-bridged complexes observed so far.

As for complexes **1** and **2**, the IR data of complexes **3** yield unambiguous information on the net electron withdrawal from the terminal organometallic cyanides into the Ni_5 core. Table 2 shows that this is the same as in **1** and **2** for **3a** and **3b** [slight lowering of ν(CN)] as well as for **3d** and **3e** [slight increase of ν(CN)]. Complex **3c** shows a large increase in ν(CN) as compared to free $[Cp(CO)_2Fe\text{-}CN]$. This clearly supports the notion that in all the other complexes described here, it is the M→C π-back-donation

 © 2003 Wiley-VCH Verlag GmbH & Co. KGaA, Weinheim

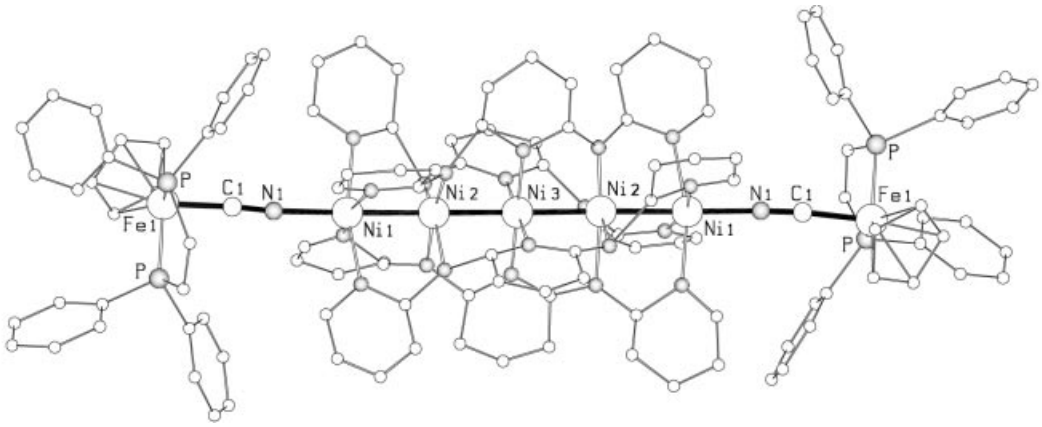

Figure 2. Molecular structure of the complex cation of **3a**; relevant bond lengths (Å) and angles (°): Ni1−Ni2 2.384(1), Ni2−Ni3 2.306(1), Ni1−N1 2.021(6), N1−C1 1.14(1), C1−Fe1 1.882(7); Fe1−C1−N1 175.4(2), C1−N1−Ni1 172.3(1), N1−Ni1−Ni2 178.7(1), Ni1−Ni2−Ni3 178.8(1), Ni2−Ni3−Ni2′ 180

Table 2. ν(CN) Data of complexes **3** and reference compounds

	Complex	Free L_nM-CN
3a	2062	2062
3b	2067	2072
3c	2141	2106
3d	2116	2107
3e	2120	2111

which provides the electron flow from the terminal metal units to the M_n complex cores: $[Cp(CO)_2Fe\text{-}CN]$ is quite electron-poor compared to [Cp(dppe)Fe-CN] (its redox potential is more than 1 V higher), and hence it can provide much less electron density for π-back-donation. Thus, the kinematic effect is the decisive influence on ν(CN) of **3c**, resulting in a rather high ν(CN) value.

The redox behaviour of complexes **3a**−**c** is mostly that of their Ni_5 core (see Table 3). The reference complex $[Ni_5(tdpa)_4]^{2+}$ undergoes a reversible one-electron oxidation and can be isolated in the form of $[Ni_5(tdpa)_4]^{3+}$ compounds.[27] As we found for $[Ni_5(tdpa)_4(CH_3CN)_2]^{2+}$, there are two further irreversible oxidation steps. Complexes **3a**−**c** also show these three redox steps, albeit in ill-resolved, yet reversible, cyclic voltammograms. Figure 3 shows this in the case of **3a**, which is the only complex **3** that also displays the redox wave for the organometallic cyanide.

In the cyclic voltammogram of **3a** the redox wave assigned as $E_{1/2}(2)$ is twice as high and hence must be associated with the oxidation of the two [FeCp(dppe)] units present. If this is so, then **3a** compares favourably with **2a**: in both cases the redox potential of the organometallic cyanide is raised by 0.2−0.3 V while that of the Co_3 or Ni_5 core is lowered by ca. 0.2 V. This clearly reproduces the conclusions on the net flow of electron density drawn from the IR data. Complexes **3b** and **3c** do not give such a clear indication of the electronic situation. Their organometallic cyanides are more difficult to oxidize. This results in a lesser effect on the first redox potential of the Ni_5 unit and hides their redox waves in the cyclic voltammograms. Again, as before for **1a** and **2a**, there is no splitting of the redox wave due to the [FeCp(dppe)] unit in **3a**. Furthermore, attempts at chemical one-electron oxidation of **3a** (which was shown to be possible for the parent Ni_5 complex[27]) were not successful.

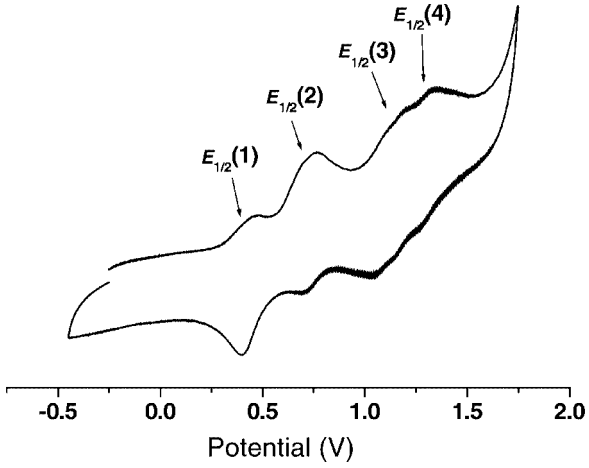

Figure 3. Cyclic voltammogram of **3a** (in CH_2Cl_2, potentials vs. Ag/AgCl)

Table 3. Cyclovoltammetric data (in CH_2Cl_2, potentials in V vs. Ag/AgCl) for complexes **3** and the Ni_5 reference compound

	$E_{1/2}(1)$	$E_{1/2}(2)$	$E_{1/2}(3)$	$E_{1/2}(4)$
3a	0.44	0.72	1.11	1.31
3b	---	0.67	1.10	1.28
3c	---	0.68	1.08	1.26
$[Ni_5(tpda)_4(CH_3CN)_2](PF_6)_2$		0.68	0.94(irr)	1.29(irr)

The UV/Vis spectra of complexes **3** (for details see Exp. Sect.) only show the features of their Ni_5 core. The absorptions due to the organometallic cyanides are completely hidden. There are intense π-π* and MLCT transitions up to about 400 nm and weak d-d bands in the 500−700 nm range.[26] Upon one-electron oxidation of $[Ni_5Cl_2(tpda)_4]$

 © 2003 Wiley-VCH Verlag GmbH & Co. KGaA, Weinheim

MMCT bands show up in the NIR.[27] The spectra of complexes **3** show no features of this kind which might be attributed to a MMCT from the electron-rich organometllic units to the electron-poor Ni_5 core. Actually the spectrum of **3a**, which, due to its easily oxidizable [FeCp(dppe)] constituents, should be most suitable for such a MMCT, is virtually superimposable to that of $[Ni_5(tpda)_4Cl_2]$.

Conclusions

The concept of constructing cyanide-bridged extended arrays of metal ions by linking organometallic cyanides to chain-like polymetallic units was applied successfully. Tetra-, penta- and heptanuclear complexes based on Ru_2, Co_3 and Ni_5 cores were obtained. The pronounced electron-acceptor properties of the core units result in a stable attachment of the terminal cyanometal constituents. The structure determination of **3a** with an almost perfectly linear Fe-CN-Ni_5-NC-Fe array and an Fe−Fe distance of 19.4 Å has confirmed the longest distance between two such Cp(dppe)Fe-CN units yet.

The spectroscopic data of the new complexes have shown uniformly that their Ru_2, Co_3 and Ni_5 cores are electron sinks. They withdraw electron density from the terminal organometallic units via the CN bridges, yet not to an extent that optically induced MMCT occurs. For all three complex types the first oxidative process converts one of the metal ions in the core from the M^{II} to the M^{III} state. This further increases the electron-sink properties of the core units. As a result any possible MMCT between the two terminal organometallic units is interrupted, and MMCT occurs either within the core units or from one of the terminal units into the core.

One goal of this work, i.e. finding electronic communication between the terminal units in complexes with longer chain lengths, could not be achieved. Both the electron-sink properties of the core units and the failure to observe split redox waves for [FeCp(dppe)] and related units prevented this. It has been achieved in much longer chains with electronically more balanced (e.g. polyacetylide) chains,[28] leaving the challenge to find similarly suitable chains in cyanide-bridged systems.

Experimental Section

General: The general experimental and measuring techniques are given in ref.[11]. $[Ru_2(OAc)_4(THF)_2]BF_4$,[29] $[Co_3(dpa)_4]Cl_2$,[22] $[Ni_5(tpda)_4(CH_3CN)_2](BF_4)_2$,[26] [Cp(dppe)Fe-CN],[30] $[Cp(PPh_3)_2$-Ru-CN],[30] $[Cp(CO)_2$Fe-CN][31] and Na[$(CO)_5$M-CN] with M = Cr, Mo, W[32] were prepared according to the published procedures.

1a: [Cp(dppe)Fe-CN] (30 mg, 0.06 mmol) was added with stirring to a solution of $[Ru_2(OAc)_4(THF)_2]BF_4$ (20 mg, 0.03 mmol) in 10 mL of THF. After 2 h the solvent was removed in vacuo and the residue dissolved in 10 mL of dichloromethane. Layering with hexane led, within a few days, to the separation of 25 mg (50%) of **1a** as blue-green crystals. M.p. 330 °C (dec.). $C_{72}H_{70}BF_4Fe_2N_2O_8P_4Ru_2$ (1615.89): calcd. C 53.52, H 4.37, N 1.73; found C 52.91, H 4.28, N 1.64.

1b: Like **1a** from $[Cp(PPh_3)_2$Ru-CN] (170 mg, 0.20 mmol) and $[Ru_2(OAc)_4(THF)_2]BF_4$ (80 mg, 0.10 mmol). Yield 100 mg (50%) of **1b** as red-brown crystals. M.p. 174 °C. $C_{92}H_{82}BF_4N_2O_8P_4Ru_4 \cdot 2CH_2Cl_2$ (1958.65 + 169.87): calcd. C 53.04, H 4.07, N 1.32; found C 52.81, H 4.04, N 1.13.

2a: A mixture of $[Co_3(dpa)_4]Cl_2$ (102 mg, 0.09 mmol) and [Cp(dppe)Fe-CN] (101 mg, 0.19 mmol) in 40 mL of ethanol and 20 mL of dichloromethane was treated with $NaSbF_6$ (48 mg, 0.19 mmol) and stirred for 1 h. After filtration the solvents were removed in vacuo. The residue was extracted with 20 mL of dichloromethane and the extract layered with 60 mL of hexane. Within a few days 135 mg (60%) of **2a** had separated as brown crystals. M.p. 223 °C. $C_{104}H_{90}Co_3F_{12}Fe_2N_{14}P_4Sb_2$ (2419.81): calcd. C 51.62, H 3.75, N 8.10; found C 51.07, H 3.57, N 7.93. UV/Vis (CH_2Cl_2): λ (ε) = 404sh (19000), 430sh (10500), 460sh (2100), 560 (3600), 1222 nm (240).

2b: Like **2a** from $[Co_3(dpa)_4]Cl_2$ (85 mg, 0.08 mmol), $[Cp(PPh_3)_2$Ru-CN] (114 mg, 0.16 mmol) and $NaSbF_6$ (41 mg, 0.16 mmol). Yield 92 mg (43%) of **2b** as brown crystals. M.p. 240 °C. $C_{124}H_{102}Co_3F_{12}N_{14}P_4Ru_2Sb_2$ (2762.57): calcd. C 53.91, H 3.72, N 7.10; found C 53.93, H 2.78, N 7.20. UV/Vis (CH_2Cl_2): λ (ε) = 396sh (17000), 452sh (5800), 512sh (1500), 526 (2800), 1248 nm (190).

2c: Like **2a** from $[Co_3(dpa)_4]Cl_2$ (79 mg, 0.07 mmol) and Na-[$(CO)_5$Cr-CN] (35 mg, 0.15 mmol) in 50 mL of ethanol. Yield 50 mg (57%) of **2c** as a red powder. M.p. 184 °C. $C_{52}H_{32}Co_3Cr_2N_{14}O_{10}$ (1293.70): calcd. C 48.28, H 2.49, N 15.16; found C 48.05, H 2.43, N 14.10. UV/Vis (CH_2Cl_2): λ (ε) = 394 (13500), 458sh (5200), 510sh (1550), 558 (2830), 1194 nm (300).

Chemical Oxidation of 2a: A 0.1 M solution of $[(4\text{-Br-}C_6H_4)_3N]$-$SbF_6$ [24] in CH_2Cl_2 was added dropwise with stirring to a 0.1 M solution of **2a** in CH_2Cl_2. IR spectroscopy indicated the formation of **2a′** after addition of one molar equivalent and the formation of **2a′′** after the addition of two further molar equivalents, as evident from their ν(CN) bands at 2047 and 2134 cm^{-1}, respectively. UV/Vis data: **2a′**: λ (ε) = 424 (8300), 582sh (3050), 712 (6900), 1096 (2300); **2a′′**: λ(ε) = 432 (10300), 546 (3200), 714 (3400), 1180 (1800), 1420 nm (1300).

3a: A solution of $[Ni_5Cl_2(tpda)_4]$ (42 mg, 0.03 mmol) and $AgBF_4$ (12 mg, 0.06 mmol) in 20 mL of dichloromethane and 4 mL of acetonitrile was stirred for 1 h. After removal of the solvents in vacuo the residue was extracted with 10 mL of dichloromethane and the extract filtered off. [Cp(dppe)Fe-CN] (33 mg, 0.06 mmol) was added to this solution. After 4 h of stirring, NH_4PF_6 (12 mg, 0.07 mmol) and 1 mL of methanol were added. After 10 min of stirring the solution was filtered off. Slow diffusion of diethyl ether into this solution yielded, within one week, 48 mg (63%) of **3a** as black crystals. M.p. 340 °C (dec.). These crystals, containing dichloromethane and methanol, were taken as such for the structure determination. Pumping in vacuo converted them into a solvent-free powder. $C_{124}H_{102}F_{12}Fe_2N_{22}Ni_5P_6$ (2719.28): calcd. C 54.77, H 3.78, N 11.33; found C 54.23, H 4.07, N 11.04. UV/Vis (CH_2Cl_2): λ (ε) = 368 (9400), 472 (640), 596 nm (880).

3b: Like **3a** from $[Ni_5(tpda)_4Cl_2]$ (56 mg, 0.04 mmol), $AgBF_4$ (16 mg, 0.08 mmol), $[Cp(PPh_3)_2$Ru-CN] (57 mg, 0.08 mmol) and NH_4PF_6 (15 mg, 0.09 mmol). Yield 32 mg (25%) of **3b** as black crystals. M.p. 320 °C (dec.). $C_{144}H_{114}F_{12}N_{22}Ni_5P_6Ru_2 \cdot CH_2Cl_2$

 © 2003 Wiley-VCH Verlag GmbH & Co. KGaA, Weinheim

(3070.11 + 84.93): calcd. C 55.34, H 3.72, N 9.79; found C 55.41, H 4.25, N 9.79. UV/Vis (CH_2Cl_2): λ (ε) = 364 (6800), 388 (6000), 482 (680), 536 (790), 600 nm (980).

3c: Like **3b** with [Cp(CO)$_2$Fe-CN] (16 mg, 0.08 mmol). Yield 31 mg (38%) of **3c** as black crystals. M.p. 340 °C (dec.). $C_{76}H_{54}F_{12}Fe_2N_{22}Ni_5O_4P_2$ (2034.48): calcd. C 44.87, H 2.68, N 15.15; found C 44.77, H 2.58, N 15.04. UV/Vis (CH_2Cl_2): λ (ε) = 360 (5100), 388 (4300), 492 (700), 548 (760), 606 nm (820).

3d: Like **3a** from [$Ni_5(tpda)_4Cl_2$] (56 mg, 0.04 mmol), $AgBF_4$ (16 mg, 0.08 mmol) and Na[(CO)$_5$Mo-CN] (23 mg, 0.08 mmol), without addition of NH_4PF_6. Yield 15 mg (20%) of **3d** as black crystals. M.p. 340 °C (dec.). $C_{72}H_{44}Mo_2N_{22}Ni_5O_{10}\cdot 0.5CH_2Cl_2$ (1870.64 +42.47): calcd. C 45.71, H 2.38, N 16.18; found C 45.53, H 2.49, N 15.53. UV/Vis (CH_2Cl_2): λ (ε) = 366 (2500), 376 (2300), 470 (170), 536 (200), 588 nm (250).

3e: Like **3d** with Na[(CO)$_5$W-CN] (30 mg, 0.08 mmol). Yield 11 mg (12%) of **3e** as black crystals. M.p. 340 °C (dec.). $C_{72}H_{44}N_{22}Ni_5O_{10}W_2\cdot 2CH_2Cl_2$ (2038.43 + 169.87): calcd. C 40.25, H 2.19, N 13.95; found C 40.56, H 2.32, N 13.80. UV/Vis (CH_2Cl_2): λ (ε) = 356 (10700), 394 (8700), 474 (1900), 534 (2400), 590 nm (2900).

Structure Determination:[33] The crystal of **3a** was taken directly from the reaction solution. Diffraction data were recorded at room temperature on a Bruker Smart CCD diffractometer and subjected to an empirical absorption correction. The structure was solved with direct methods and refined anisotropically with the SHELX program suite.[34] Hydrogen atoms were included with fixed distances and isotropic temperature factors 1.5 times those of their attached atoms. Parameters were refined against F^2. The R values are defined as $R_1 = \Sigma|F_o - F_c|/\Sigma F_o$ and $wR_2 = \{\Sigma[w(F_o^2 - F_c^2)^2]\Sigma[w(F_o^2)^2]\}^{1/2}$. Drawings were produced with SCHAKAL.[35] Table 4 lists the crystallographic data.

Table 4. Crystallographic data for complex **3a**

Empirical formula	$C_{127}H_{112}Cl_2F_{12}Fe_2N_{22}Ni_5O_2P_6$
Molecular mass	2868.36
Crystal size (mm)	0.25 × 0.25 × 0.10
Space group	*C*2
Z	2
a (Å)	20.852(7)
b (Å)	18.706(6)
c (Å)	18.727(6)
α (°)	90
β (°)	90.817(6)
γ (°)	90
V (Å^3)	7303(4)
D(calc) (gcm^{-3})	1.30
μ(Mo-K_α) (mm^{-1})	0.99
hkl range	*h:* −27 to 19
	k: −23 to 25
	l: −25 to 24
Measured reflections	22385
Independent reflections	14607
Observed refl. [$I > 2\sigma(I)$]	6545
Parameters	776
Refined reflections	14607
R_1 (obs.refl.)	0.090
wR_2 (all refl.)	0.320
Residual electron density (e/Å^3)	+1.2/-0.6

Acknowledgments

This work was supported by the Deutsche Forschungsgemeinschaft (Graduiertenkolleg "Ungepaarte Elektronen").

[1] J. M. Lehn, *Supramolecular Chemistry*, VCH, Weinheim, **1995**.
[2] F. Paul, C. Lapinte, *Coord. Chem. Rev.* **1998**, *178–180*, 431–509.
[3] C. A. Bignozzi, J. R. Schoonover, F. Scandola, *Prog. Inorg. Chem.* **1997**, *44*, 1–95.
[4] K. R. Dunbar, R. A. Heintz, *Prog. Inorg. Chem.* **1997**, *45*, 283–391.
[5] H. Vahrenkamp, A. Geiss, G. N. Richardson, *J. Chem. Soc., Dalton Trans.* **1997**, 3643–3651.
[6] J. S. Miller, A. J. Epstein, *Prog. Inorg. Chem.* **1976**, *20*, 1–151.
[7] S. Decurtins, private communication.
[8] Y.-H. Chen, C.-C. Lee, C.-C. Wang, G.-H. Lee, S.-Y. Lai, F.-Y. Li, C.-Y. Mou, S.-M. Peng, *Chem. Commun.* **1999**, 1667–1668.
[9] A. Geiß, M. Keller, H. Vahrenkamp, *J. Organomet. Chem.* **1997**, *541*, 441–443.
[10] N. Zhu, H. Vahrenkamp, *J. Organomet. Chem.* **1999**, *573*, 67–72.
[11] G. N. Richardson, U. Brand, H. Vahrenkamp, *Inorg. Chem.* **1999**, *38*, 3070–3079.
[12] G. N. Richardson, H. Vahrenkamp, *J. Organomet. Chem.* **2000**, *593–594*, 44–48.
[13] A. Geiß, M. J. Kolm, C. Janiak, H. Vahrenkamp, *Inorg. Chem.* **2000**, *39*, 4037–4043.
[14] R. Appelt, H. Vahrenkamp, *Inorg. Chim. Acta* **2003**, *350*, 387–398.
[15] A few of the results reported here were reproduced by Z. N. Chen, who at the time of their emergence worked as a postdoctoral follow in Freiburg: L.-Y. Zhang, J.-L. Chen, L.-X. Shi, Z.-N. Chen, *Organometallics* **2000**, *21*, 5919–5925.
[16] F. E. Kühn, I. S. Goncalves, A. D. Lopes, J. P. Lopes, C. C. Romao, W. Wachter, J. Mink, L. Hajba, A. J. Parola, F. Pina, J. Sotomayor, *Eur. J. Inorg. Chem.* **1999**, 295–301.
[17] W.-M. Xue, F. E. Kühn, G.-F. Zhang, E. Herdtweck, G. Raudaschl-Sieber, *J. Chem. Soc., Dalton Trans.* **1999**, 4103–4110.
[18] N. Zhu, H. Vahrenkamp, *Chem. Ber./Recueil* **1997**, *130*, 1241–1252.
[19] F. A. Cotton, E. Pedersen, *Inorg. Chem.* **1975**, *14*, 388–391.
[20] S. J. Shie, C. C. Chou, H. G. Lee, C. C. Wang, S. M. Peng, *Angew. Chem.* **1997**, *109*, 57–59; *Angew. Chem. Int. Ed. Engl.* **1997**, *36*, 56–58.
[21] S. Y. Lai, T. W. Lin, Y. H. Chen, C. C. Wang, G. H. Lee, M. H. Yang, M. K. Leung, S. M. Peng, *J. Am. Chem. Soc.* **1999**, *121*, 250–251.
[22] E. C. Yang, M. C. Cheng, M. S. Tsai, S. M. Peng, *J. Chem. Soc., Chem. Commun.* **1994**, 2377–2378; F. A. Cotton, L. M. Daniels, G. T. Jordan, *Chem. Commun.* **1997**, 421–422.
[23] R. Clerac, F. A. Cotton, K. R. Dunbar, T. Lu, C. A. Murillo, X. Wang, *Inorg. Chem.* **2000**, *39*, 3065–3070.
[24] P. Coggan, A. T. McPhail, F. E. Mabbs, A. Richards, A. S. Thornley, *J. Chem. Soc. (A)* **1970**, 3296–3303.
[25] R. Clerac, F. A. Cotton, K. R. Dunbar, T. Lu, C. A. Murillo, X. Wang, *J. Am. Chem. Soc.* **2000**, *122*, 2272–2278.
[26] C. C. Wang, W. C. Lo, C. C. Chou, G. H. Lee, G. M. Chen, S. M. Peng, *Inorg. Chem.* **1998**, *37*, 4059–4065.
[27] C. Y. Yeh, Y. L. Chiang, G. H. Lee, S. M. Peng, *Inorg. Chem.* **2002**, *41*, 4096–4098.
[28] T. Bartik, B. Bartik, M. Brady, R. Dembinski, J. A. Galdysz, *Angew. Chem.* **1996**, *108*, 467–469; *Angew. Chem. Int. Ed. Engl.* **1996**, *35*, 414–417.
[29] R. W. Mitchell, A. Spencer, G. Wilkinson, *J. Chem. Soc., Dalton Trans.* **1973**, 846–854.
[30] G. J. Baird, S. G. Davis, *J. Organomet. Chem.* **1984**, *262*, 215–221.
[31] B. D. Dombek, R. J. Angelici, *Inorg. Chim. Acta* **1973**, *7*, 345–347.

 © 2003 Wiley-VCH Verlag GmbH & Co. KGaA, Weinheim

[32] R. B. King, *Inorg. Chem.* **1967**, *6*, 25−29.
[33] CCDC-209740 (**3a**) contains the supplementary crystallographic data for this paper. These data can be obtained free of charge at www.ccdc.cam.ac.uk/conts/retrieving.html [or from the Cambridge Crystallographic Data Centre, 12, Union Road, Cambridge CB2 1EZ, UK; Fax: (internat.) +44-1223/336-033; E-mail: deposit@ccdc.cam.ac.uk].
[34] *SHELX* program package for the Bruker Smart CCD diffractometer, version 5.1, 2002.
[35] E. Keller, *SCHAKAL for Windows*, Universität Freiburg, **2001**.
Received May 8, 2003

 © 2003 Wiley-VCH Verlag GmbH & Co. KGaA, Weinheim

Coenzyme B_{12} Model Studies − Kinetics of Axial Ligation of Alkylcobalt Complexes Containing a Tridentate Amino-Oximate Ligand

Basam M. Alzoubi,[a] Mohamed S. A. Hamza,[a] Alessandro Felluga,[c] Lucio Randaccio,[c] Giovanni Tauzher,[c] and Rudi van Eldik*[a]

Keywords: Ligand substitution / Cobalt / Kinetics / Mechanism / Enzymes / High-pressure chemistry

The ligand-substitution reaction of $[RCo(LNHpy)(HLNHpy)]^+$ by cyanide was studied in methanol as a solvent, where R = Et (**1**), Me (**2**), CF_3CH_2 (**3**), and bridging CH_2 (**4**), HLNHpy = 2-(2-pyridylethyl)amino-3-butanone oxime and $LNHpy^-$ is its conjugate base. The second-order rate constants for the substitution of the 2-pyridylethyl moiety in $[RCo(LNHpy)(HLNHpy)]^+$ by cyanide were found to be 19.1, 0.25, $2.2\cdot10^{-2}$, and $1.7\cdot10^{-2}$ $M^{-1}\cdot s^{-1}$ for R = Et, Me, CF_3CH_2, and bridging CH_2, respectively. From the temperature- and pressure-dependence studies of the substitution reaction, the activation parameters ($\Delta H^{\ddagger}$, $\Delta S^{\ddagger}$, $\Delta V^{\ddagger}$) for the reaction of $[RCo(LNHpy)(HLNHpy)]^+$ with cyanide in methanol were found to be, for R = Et: 69±2 kJ·mol^{-1}, +11±7 J·K^{-1} mol^{-1}, +9.6±0.3 cm^3·mol^{-1}; R = Me: 86±4 kJ·mol^{-1}, +31±15 J·K^{-1}·mol^{-1}, +4.3±0.2 cm^3·mol^{-1}; R = CF_3CH_2: 73±3 kJ·mol^{-1}, −33±10 J·K^{-1}·mol^{-1}, +8.7±0.2 cm^3·mol^{-1}; R = bridging CH_2: 80±1 kJ·mol^{-1}, −13±3 J·K^{-1}·mol^{-1}, +5.4±0.1 cm^3·mol^{-1}, respectively. Based on the reported rate and activation parameters, the mechanism of the ligand-substitution reaction varies between a limiting dissociative and a dissociative interchange type of mechanism depending on the σ-donor and steric effects of the alkyl group.
(© Wiley-VCH Verlag GmbH & Co. KGaA, 69451 Weinheim, Germany, 2003)

Introduction

The discovery of coenzyme B_{12} and the increasing amount of information on its biochemical role[1,2] has led to great efforts in the synthesis and study of model organocobalt complexes with a coordination sphere as similar as possible to that of the corrin ring. Much work has been carried out on organocobalt B_{12} model complexes to achieve a deeper understanding of the behaviour of coenzyme B_{12} by studying *cis* and *trans* effects which significantly influence the physical and chemical properties of vitamin B_{12} and its chemical models.[3−6] The nature of the alkyl group in the axial position has an effect on the Co−C and $Co-N_{(axial)}$ bond lengths, where the latter increase with increasing donor properties of the σ-donor ligand and are significantly influenced by the nature of the equatorial ligand.[7−9] The reaction of cyanide with different alkylcobalamines (RCb1, where R = CF_3, CF_3CH_2, CF_2H, Me, and CH_2Br) showed that the nature of the alkyl group has an influence on the thermodynamic stability constants, as well as on the rate constants of the substitution reactions of the axial ligand *trans* to the alkyl group.[10]

In order to obtain further insight into these reactions, a class of organocobalt complexes *trans*-$[(R)Co(LNHpy)(HLNHpy)]ClO_4$, where HLNHpy is the tridentate ligand 2-(2-pyridyethyl)amino-3-butanone oxime and LNHpy is its conjugated base, were synthesized.[5,11] The alkyl group R was Me, Et, CF_3CH_2, or the intramolecular bridging CH_2 group as shown in Figure 1. The geometry of these compounds is reminiscent of the lariat-type ligands previously reported,[3,12] since they contain a potentially quinquedentate ligand forming an equatorial chelating system bearing a pendant pyridyl group axially coordinated to the cobalt atom. The structural features of these complexes allow better modeling of the displacement of 5,6-dimethylbenzimidazole in coenzyme B_{12} than any other model so far studied. It is further of interest that the geometry of the N−Co−C unit in the Me derivative [Co−C = 1.971(7) Å, Co−N = 2.159(5) Å] is much closer to that of MeCbl [Co−C = 1.979(4) Å, Co−N = 2.162(4) Å] than of any other previously proposed B_{12} model complex.[5]

Ligand-substitution reactions of vitamin B_{12} and its model complexes in general follow a dissociative (I_d or D) type of mechanism.[13−15] In the case of the coenzyme, however, evidence was originally reported for an associative substitution mode, which was later corrected to result from the combination of a rapid substitution of dimethylbenzimi-

[a] Institute for Inorganic Chemistry, University of Erlangen-Nürnberg
Egerlandstr. 1, 91058 Erlangen, Germany
[b] Department of Chemistry, Faculty of Science, Ain Shams University, Cairo, Egypt
[c] Dipartimento di Scienze Chimiche, Università degli Studi di Trieste, 34127 Trieste, Italy

 © 2003 Wiley-VCH Verlag GmbH & Co. KGaA, Weinheim **DOI: 10.1002/ejic.200300206**

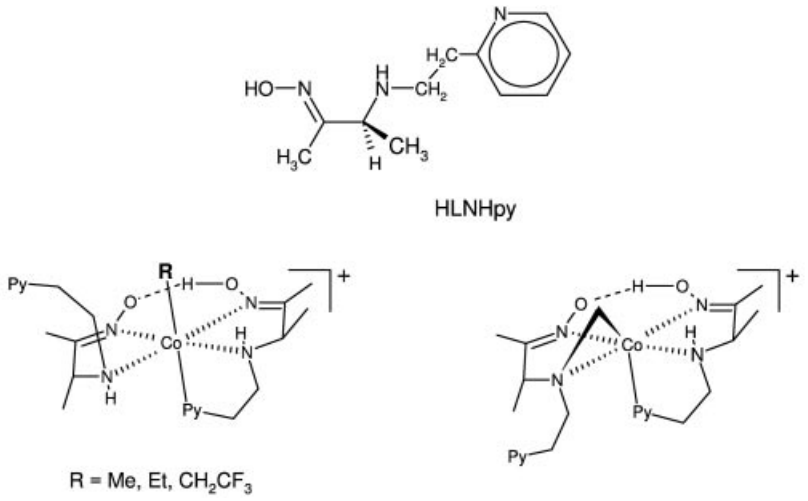

Figure 1. Structures of HLNHpy, which is the tridentate ligand 2-(2-pyridyethyl)amino-3-butanone oxime, and of *trans*-[(R)Co(LNHpy)(HLNHpy)]$^+$, where R = Et, Me, CF_3CH_2, and bridging CH_2

dazole and subsequent water-assisted heterolysis of the cobalt−carbon (adenosyl) bond.[16,17] Ligand-substitution reactions of different cobalamins (R = CF_3, CN^-, $NCCH_2$) with cyanide have been studied,[10,18] and it was found that CN^- substitutes the 5,6-dimethylbenzimidazole (DMBz) moiety in all cases. The activation parameters were interpreted in terms of a limiting D mechanism.

Kinetic and mechanistic studies on the substitution behaviour of alkyl derivatives of bis(dimethylglyoximate)-cobalt(III) complexes have been performed extensively.[19−33] Most of these studies have been aimed to asses the role of the σ-bonded alkyl group to Co^{III} in affecting the axial substitution rates in the *trans* position. Typical reactions that have been studied can be represented by Equations (1) and (2), where DH represents the monoanion of dimethylglyoxime, R is an alkyl group, and L and L^I are neutral bases.

$$\textit{trans}\text{-}[RCo(DH)_2H_2O] + L \rightarrow \textit{trans}\text{-}[RCo(DH)_2L] + H_2O \quad (1)$$

$$\textit{trans}\text{-}[RCo(DH)_2L] + L^I \rightarrow \textit{trans}\text{-}[RCo(DH)_2L^I] + L \quad (2)$$

In the present study, we investigated the ligand-substitution reactions of *trans*-[(R)Co^{III}(LNHpy)(HLNHpy)]$^+$, where R = Et, Me, CF_3CH_2, and bridging CH_2. These reactions were studied as a function of entering nucleophile concentration, temperature, and pressure in order to elucidate the reasons for the observed lability and the intimate mechanisms of these reactions.

Results and Discussion

The kinetics of the reaction of complexes of the type *trans*-[(R)Co(LNHpy)(HLNHpy)]$^+$, R = Et (**1**), Me (**2**) and CF_3CH_2 (**3**), with CN^- were studied in methanol. Cyanide was used as the entering nucleophile, since other less-strong nucleophiles are known to be incapable of replacing any of the axial ligands in these complexes. The reaction of the complex[11] *trans*-[(CH_2)Co(LNHpy)(HLNpy)]$^+$ (**4**) with CN^- was also studied. Complex **4** was characterized to involve a $-CH_2-$ group that forms a three-membered metallacycle,[34,35] in which the other two members are the Co atom and the equatorial nitrogen donor. Complexes containing this type of metallacycle are quite rare[34,35] and scarcely studied. In view of the unusual geometry of this complex, it seemed to be of interest to examine its kinetic properties with reference to the reactivity of the *trans* position with respect to the bridging $-CH_2-$ fragment.

Reaction of *trans*-[(R)Co(LNHpy)(HLNHpy)]$^+$ with Cyanide

R = Et

The UV/Vis spectrum of *trans*-[(Et)Co(LNHpy)-(HLNHpy)]$^+$ shows two bands at 368 and 464 nm (376 and 207 $M^{-1}\cdot cm^{-1}$, respectively) in methanol at 25.0 °C. The substitution reaction of *trans*-[(Et)Co(LNHpy)-(HLNHpy)]$^+$ occurs by displacement of the axial 2-pyridylethyl ligand by cyanide, which is positioned *trans* to the ethyl group. The product is light-sensitive, suggesting the presence of the alkyl group in the axial position. The product spectrum has a single band at 452 nm (137 $M^{-1}\cdot cm^{-1}$) with a shoulder at 338 nm (441 $M^{-1}\cdot cm^{-1}$); good isosbestic points at 334 and 360 nm were observed during the reaction.

Figure 2 presents a plot of k_{obs} versus [CN^-] for the reaction of $2.5\cdot10^{-3}$ M *trans*-[(Et)Co(LNHpy)(HLNHpy)]$^+$ with cyanide (0.025−0.20 M) at I = 0.5 M (CF_3SO_3Li) in methanol at 25.0 °C. The linear plot has a negligible intercept, indicating that the back reaction does not contribute significantly and that no parallel reaction takes place. The second-order rate constant for the substitution of 2-pyridylethyl by

 © 2003 Wiley-VCH Verlag GmbH & Co. KGaA, Weinheim

CN^- was found to be 19.1±0.2 $M^{-1}s^{-1}$ at 25.0 °C. This behaviour can be expressed by the rate law given in Equation (3).

$$k_{obs} = k_a [CN^-] \quad (3)$$

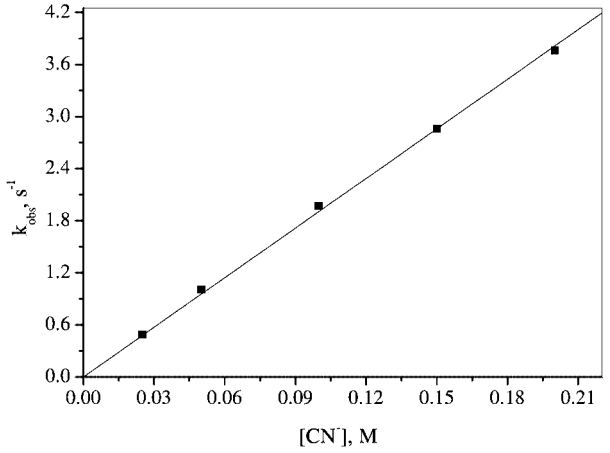

Figure 2. Plot of k_{obs} versus [CN^-] for the reaction of *trans*-[(Et)Co(LNHpy)(HLNHpy)]$^+$ with cyanide in methanol; experimental conditions: [Co^{III}] = $1\cdot10^{-3}$ M, I = 0.5 M, T = 25.0 °C

The reaction was also studied as a function of temperature and pressure, for which the results are reported in Tables 1 and 2. A plot of ln k_a versus pressure gives a good linear relationship as shown in Figure 3. The activation parameters ($\Delta H^{\ddagger}$, $\Delta S^{\ddagger}$, $\Delta V^{\ddagger}$) were found to be 69±2 kJ·mol^{-1}, 11±7 J K^{-1}·mol^{-1} and 9.6±0.3 cm^3·mol^{-1}, respectively. Based on the reported rate and activation parameters, the ligand-substitution reaction of the complex *trans*-[(Et)Co(LNHpy)(HLNHpy)]$^+$ with cyanide follows a dissociative mechanism as presented in reaction [Equation (4)].

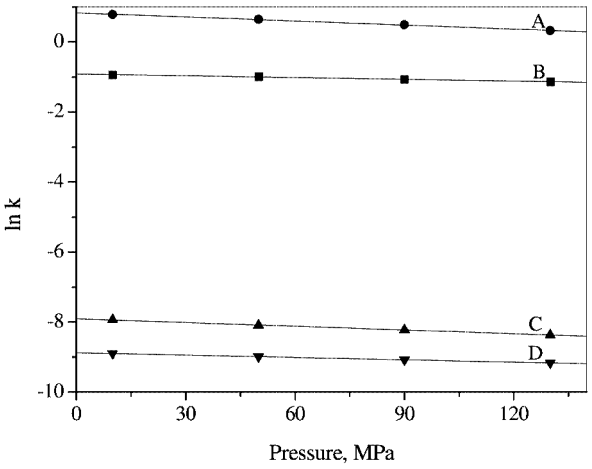

Figure 3. Plots of ln$k$ versus pressure for the reaction of *trans*-[(R)Co(LNHpy)(HLNHpy)]$^+$ with cyanide in methanol; experimental conditions: A) R = Et, [Co^{III}] = $2.5\cdot10^{-3}$ M, [CN^-] = 0.1 M, I = 0.5, T = 25.0 °C; B) R = Me, [Co^{III}] = $2.5\cdot10^{-3}$ M, [CN^-] = 0.2 M, I = 0.5 M, T= 35.0 °C; C) R = CF_3CH_2, [Co^{III}] = $1\cdot10^{-3}$ M, [CN^-] = 0.025 M, I = 0.5 M, T = 20.0 °C; D) R = CH_2, [Co^{III}] = $1\cdot10^{-3}$ M, [CN^-] = 0.025 M, I = 0.5 M, T = 15.0 °C

Table 1. Kinetic data for the reaction of *trans*-[(R)Co(LNHpy)(HLNHpy)]$^+$ with cyanide in methanol as a function of temperature

Temp. [°C]	k_a [$M^{-1}s^{-1}$]			
	R = Et[a]	R = Me[b]	R = CF_3CH_2[c]	R = CH_2[d]
5.0	2.5±0.1	–	–	–
10.0	4.4±0.1	(3.25±0.27)·10^{-2}	–	–
15.0	8.4±0.1	(7.60±0.33)·10^{-2}	(7.70±0.30)·10^{-3}	(4.80±0.08)·10^{-3}
20.0	12.7±0.2	(1.25±0.04)·10^{-1}	(1.43±0.06)·10^{-2}	(8.48±0.26)·10^{-3}
25.0	20.7±0.4	(2.50±0.07)·10^{-1}	(2.32±0.09)·10^{-2}	(1.56±0.09)·10^{-2}
30.0	31.7±0.7	(3.94±0.05)·10^{-1}	(4.06±0.12)·10^{-2}	(2.62±0.09)·10^{-2}
35.0	–	–	(5.80±0.20)·10^{-2}	(4.40±0.08)·10^{-2}
$\Delta H^{\ddagger}$ [kJ·mol^{-1}]	69±2	86±4	73±3	80±1
$\Delta S^{\ddagger}$, [J·K^{-1}·mol^{-1}]	+11±7	+31±15	−33±10	−13±3

[a] *trans*-[(Et)Co(LNHpy)(HLNHpy)]$^+$ = $1\cdot10^{-3}$ M, [CN^-] = 0.1 M and I = 0.5 M. [b] *trans*-[(Me)Co(LNHpy)(HLNHpy)]$^+$ = $2.5\cdot10^{-4}$ M, [CN^-] = 0.2 M and I = 0.5 M. [c] *trans*-[(CF_3CH_2)Co(LNHpy)(HLNHpy)]$^+$ = $1.0\cdot10^{-3}$ M, [CN^-] = 0.05 M and I = 0.5 M. [d] *trans*-[(CH_2)Co(LNHpy)(HLNHpy)]$^+$ = $2.5\cdot10^{-3}$ M, [CN^-] = 0.025 M and I = 0.5 M.

Table 2. Kinetic data for the reaction of *trans*-[(R)Co(LNHpy)(HLNHpy)]$^+$ with cyanide in methanol as a function of pressure

Presssure [MPa]	k_{obs} [s^{-1}]			
	R = Et[a]	R = Me[b]	R = CF_3CH_2[c]	R = CH_2[d]
10	2.19±0.01	0.39±0.01	(3.57±0.03)·10^{-4}	(1.36±0.08)·10^{-4}
50	1.91±0.02	0.37±0.01	(3.05±0.04)·10^{-4}	(1.25±0.02)·10^{-4}
90	1.63±0.05	0.34±0.01	(2.68±0.03)·10^{-4}	(1.14±0.02)·10^{-4}
130	1.38±0.3	0.32±0.01	(2.32±0.02)·10^{-4}	(1.04±0.02)·10^{-4}
$\Delta V^{\ddagger}$ [cm^3·mol^{-1}]	+9.6±0.3	+4.3±0.2	+8.7±0.2	+5.4±0.1

[a] *trans*-[(Et)Co(LNHpy)(HLNHpy)]$^+$ = $2.5\cdot10^{-3}$ M, [CN^-] = 0.1 M, T = 25.0 °C and I = 0.5 M. [b] *trans*-[(Me)Co(LNHpy)(HLNHpy)]$^+$ = $2.5\cdot10^{-3}$ M, [CN^-] = 0.2 M, T = 35.0 °C and I = 0.5 M. [c] *trans*-[(CF_3CH_2)Co(LNHpy)(HLNHpy)]$^+$ = $1.0\cdot10^{-3}$ M, [CN^-] = 0.025 M, T = 20.0 °C and I = 0.5 M. [d] *trans*-[(CH_2)Co(LNHpy)(HLNHpy)]$^+$ = $1.0\cdot10^{-3}$ M, [CN^-] = 0.025 M, T = 15.0 °C and I = 0.5 M.

 © 2003 Wiley-VCH Verlag GmbH & Co. KGaA, Weinheim

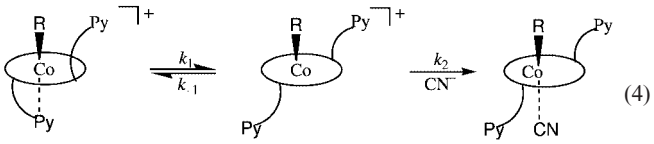

(4)

R = Me, CF_3CH_2, and Bridging CH_2

The UV/Vis spectra of *trans*-[(R)Co(LNHpy)-(HLNHpy)]$^+$ show two bands at 362 and 452 nm (466 and 330 $M^{-1}\cdot cm^{-1}$, respectively) for R = Me, one band at 462 nm (187 $M^{-1}\cdot cm^{-1}$) with a shoulder at 364 nm (256 $M^{-1}\cdot cm^{-1}$) for R = CF_3CH_2, and a single band at 400 nm (509 $M^{-1}\cdot cm^{-1}$) with a shoulder at 472 nm (303 $M^{-1}\cdot cm^{-1}$) for R = bridging CH_2 in methanol at 25.0 °C. The ligand-substitution reactions of *trans*-[(R)Co(LNHpy)-(HLNHpy)]$^+$ occurrs by displacement of the axial 2-pyridylethyl ligand, which is located *trans* to the alkyl group, by cyanide. Good isosbestic points at 361 and 328 nm for R = Me, at 364 nm for R = CF_3CH_2, and at 362 and 398 nm for R = bridging CH_2, were obtained upon mixing the complex with cyanide. The UV/Vis spectra of the products show a band at 450 nm (274 $M^{-1}\cdot cm^{-1}$) with a shoulder at 340 nm (554 $M^{-1}\cdot cm^{-1}$) for R = Me, one band at 452 nm (132 $M^{-1}\cdot cm^{-1}$) for R = CF_3CH_2, and one band at 476 nm (233 $M^{-1}\cdot cm^{-1}$) with a shoulder at 372 nm (692 $M^{-1}\cdot cm^{-1}$) for R = bridging CH_2.

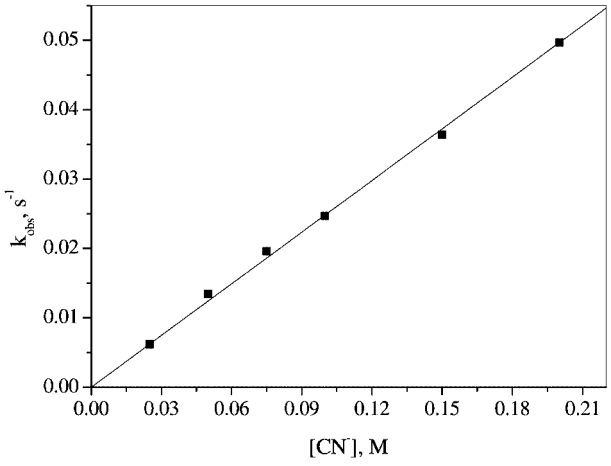

Figure 4. Plot of k_{obs} versus [CN^-] for the reaction of *trans*-[(Me)Co(LNHpy)(HLNHpy)]$^+$ with cyanide in methanol; experimental conditions: [Co^{III}] = $2.5\cdot10^{-4}$ M, I = 0.5 M, T = 25.0 °C

Figures 4, 5, and 6 report plots of k_{obs} versus [CN^-] for the reaction of *trans*-[(R)Co(LNHpy)(HLNHpy)]$^+$ with cyanide (0.025−0.20 M) at I = 0.5 M (CF_3SO_3Li) in methanol at 25.0 °C. The linear plots have negligible intercepts, indicating that the back reaction does not contribute significantly and that no parallel reaction takes place. The second-order rate constants for the substitution of 2-pyridylethyl by CN^- were found to be 0.25±0.01, $(2.3\pm0.1)\cdot10^{-2}$, and $(1.6\pm0.1)\cdot10^{-2}$ $M^{-1}\cdot s^{-1}$ for R = Me, CH_2CF_3 and bridging CH_2, respectively, at 25.0 °C. This behaviour can be expressed by a rate law similar to that given in Equation (3).

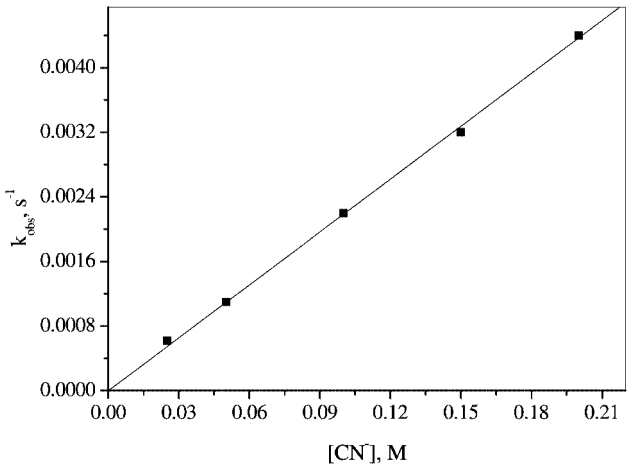

Figure 5. Plot of k_{obs} versus [CN^-] for the reaction of *trans*-[(CF_3CH_2)Co-(LNHpy)(HLNHpy)]$^+$ with cyanide in methanol; experimental conditions: [Co^{III}] = $1\cdot10^{-3}$ M, I = 0.5 M, T = 25.0 °C

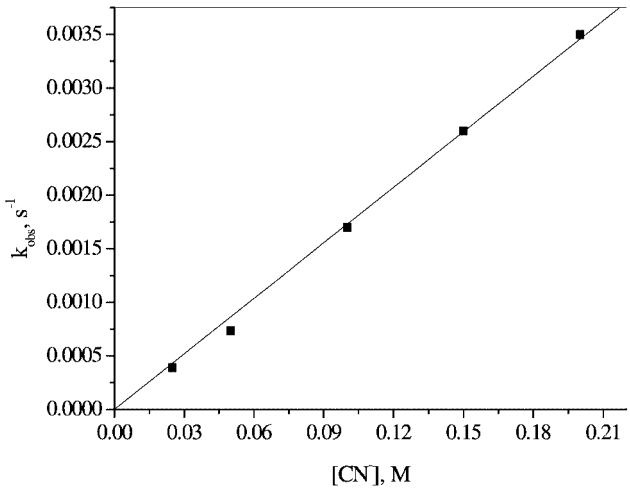

Figure 6. Plot of k_{obs} versus [CN^-] for the reaction of *trans*-[(CH_2)Co(LNHpy)(HLNHpy)]$^+$ with cyanide in methanol; experimental conditions: [Co^{III}] = $2.5\cdot10^{-3}$ M, I = 0.5 M, T = 25.0 °C

The reactions were studied as a function of temperature and pressure, for which the results are reported in Tables 1 and 2. Plots of lnk_a versus pressure gave good linear relationships as shown in Figure 3. The activation parameters ($\Delta H^{\ddagger}$, $\Delta S^{\ddagger}$, $\Delta V^{\ddagger}$) were found to be 86±4 kJ·mol^{-1}, +31±15 J·K^{-1}·mol^{-1}, and +4.3±0.2 cm^3·mol^{-1} for R = Me; 73±3 kJ·mol^{-1}, −33±10 J·K^{-1}·mol^{-1}, and +8.7±0.2 cm^3·mol^{-1} for R = CF_3CH_2; and 80±1 kJ·mol^{-1}, −13±3 J·K^{-1}·mol^{-1}, and +5.4±0.1 cm^3·mol^{-1} for R = bridging CH_2, respectively. Based on the reported rate and activation parameters, it is reasonable to suggest that ligand substitution in the complexes *trans*-[(R)Co(LNHpy)(HLNHpy)]$^+$ proceeds by a dissociative interchange (I_d) mechanism.

Overall Mechanistic Comparison

It is interesting to compare the structural and solution properties of complexes **1**−**3** with those of the corresponding alkylcobaloximes. It has been shown that in the latter

 © 2003 Wiley-VCH Verlag GmbH & Co. KGaA, Weinheim

series, the $Co-N_{(axial)}$ distance increases with the σ-donor property of R. Thus, the order of increasing $Co-N_{(axial)}$ distance is: CF_3CH_2 (2.041 Å) < Me (2.068 Å) < Et (2.081 Å).[36] There is also a defined trend in the rate constant of the axial ligation for a given incoming base. In all the studied cases, it was found that the rate constants increase on increasing the σ-donor strength of the R alkyl group.[19−33,37] By way of example, some data for the axial ligation of a series of alkyl(aqua)cobaloximes by the neutral dimethoxyethylamine base are summarized in Table 3. These data show that the ground-state *trans* influence of a given R group parallels the kinetic *trans* effect of the same group, both effects being controlled by the electronic properties of R. Similarly to that observed in the alkylcobaloximes, it has been shown that the electronic properties of the R group affect the $Co-N_{(axial)}$ bond lengths and control the *trans* influence and *trans* effect in some other complexes with tetradentate chelating systems such as the alkyl derivatives[33,36] of the type $[RCo(DO)(DOH)pnH_2O]^+$ {where (DO)(DOH)pn = N^2,$N^{2\prime}$-propanediylbis(2,3-butanedione) 2-imine 3-oxime} and alkylrhodoximes.[38,39]

Table 3. Second-order rate constants for the reaction *trans*-$[(R)Co(DH)_2H_2O]$ + DEA → *trans*-$[(R)Co(DH)_2DEA]$ + H_2O

R[21]	σ*	*k* at 25 °C, $M^{-1}\cdot s^{-1}$
Et	−0.10	81±6
Me	0.00	5.1±0.2
CF_3CH_2	+0.99	$(2.7\pm0.1)\cdot10^{-2}$

Contrary to the cobaloximes, there is no definite trend in the observed $Co-N_{(axial)}$ distances along the series **1**−**3**. In this series the distances are 2.160(6), 2.158(5), and 2.168(5) Å for the CF_3CH_2, Me (mean value of two structurally independent molecules) and Et derivatives, respectively.[5] The difference in the $Co-N_{(axial)}$ distances between the Me and Et derivatives, although smaller than that found in the corresponding alkylcobaloximes, is in agreement with the donating properties of the R groups. However, a shorter $Co-N_{(axial)}$ distance with respect to that observed would be expected for **3**, due to the poorer donor ability of CF_3CH_2. This apparent anomaly can be explained on the basis of the structural features of complexes **1**−**3**, and of the different steric properties of the R groups considered. In particular, it is observed that the flexibility of the ethylene chain bearing the coordinated pyridyl group allows the axial pyridyl residue to rotate around the $Co-N_{(pyridyl)}$ bond. There is clear evidence that the orientation of the pyridyl moiety appreciably influences the length of the $Co-N_{(axial)}$ bond, so that by varying the R group, the trend in the *trans* influence is modified with respect to that expected on the basis of the donating properties of R.

These conformational changes have been observed not only in complexes **1**−**3**, but also in some other alkylcobalt chelates.[3,12,40,41] Hence the $Co-N_{(axial)}$ distances found in complexes **1**−**3** are a result of a compromise between the energies involved either in the torsion or in the stretching of the $Co-N_{(axial)}$ bond.[5] This leads to the conclusion that for compounds **1**−**3** any attempt to correlate the electronic properties of the R group with the ground state *trans* influence, has to be considered as of little use.

The second-order rate constants for substitution of 2-pyridylethyl by cyanide were found to be 19.1, 0.25, $2.2\cdot10^{-2}$, and $1.7\cdot10^{-2}$ $M^{-1}\cdot s^{-1}$ at 25 °C for the series of complexes *trans*-$[(R)Co(LNHpy)(HLNHpy)]^+$, where R = Et, Me, CF_3CH_2, and CH_2, respectively. It seems that this trend reflects the σ-donor properties of R. However, significant differences are observed in the transmission of effects of R when the series **1**−**3** are compared with the corresponding cobaloximes. A comparison of the rate constant ratios Et/Me and CF_3CH_2/Me for cobaloximes and for the series **1**−**3** can illustrate these differences. From the data for the second-order rate constants of complexes **1**−**3** and the data reported in Table 3, these ratios are 15.9 and $5.3\cdot10^{-3}$ for cobaloximes and 76.4 and $88.0\cdot10^{-3}$ for complexes **1**−**3**. From this it follows that in reference to the Me derivatives, the ligation rates in both Et and CF_3CH_2 derivatives are greatly enhanced in **2** and **3** with respect to the corresponding cobaloximes. By assuming that in the latter compounds the effect of R is mainly an electronic one, it can be deduced that steric effects play an important role in affecting the reaction rates also for **1**−**3**. Structural data show that, according to the bending angle (a) values,[42−45] bending away from the neutral base L between the two DH units is significantly smaller than that of the Schiff-base complexes and range between 0 and 3°; the bending angles in complexes **1**−**3**[5] range between 8 and 16°. This is probably due to the higher flexibility of the equatorial system in complexes **1**−**3** with respect to the $Co(DH)_2$ moiety. The increased level of flexibility in the latter compounds can be ascribed to the presence of only one O−H···O bridge (vs. two present in cobaloximes) and to the less-extensive electronic delocalization over the equatorial plane (two conjugated C=N bond vs. four conjugated C=N bond in cobaloximes). Based on the above argument it may be inferred that in approaching the transition state, the bending of the equatorial ligand toward the pyridyl group is permissible and that this contributes to the extension of the $Co-N_{(pyridyl)}$ bond. It is reasonable to expect that these steric effects will be more pronounced in complexes having relatively bulky R groups such as Et and CF_3CH_2.

The activation volume data reported in Table 2 suggest an increasing dissociative character of the ligand-substitution process on going along the series Me < CF_3CH_2 < Et. This order does not reflect the donating properties of R. As suggested above, this order has to be largely ascribed to steric effects. Probably in the case of the large value found for the Et derivative, both electronic and steric effects contribute. By way of comparison, we reported $\Delta V^{\ddagger}$ values for the ligation of cysteine to *trans*-$[(R)Co(DH)_2H_2O]$, where DH = dimethylglyoximate anion for R = CF_3CH_2, Ph, and CH_2Ph, of 0±1, +4.9±0.3, and +5.9±0.4 $cm^3\cdot mol^{-1}$, respectively.[46] The sequence CF_3CH_2 < Ph < CH_2Ph is as expected and corresponds to an increase in the dissociative character of the process with increasing donor properties of R.

 © 2003 Wiley-VCH Verlag GmbH & Co. KGaA, Weinheim

The reaction of cyanide with different alkycobalamines (RCbl, where R = CF_3, CF_3CH_2, CF_2H, Me, and CH_2Br) was studied, and it was found that the nature of the alkyl group has a strong influence on the thermodynamic stability constants as well as the rate constants for the substitution reactions of the axial ligand *trans* to the alkyl group.[10] It was found that Co−N and Co−C bond lengths increase in the RCbl series in the order $H_2O < CN < CF_3 < CF_2H <$ Me < adenosyl.[47−50] The second-order rate constants for RCbl with CN^- were found to be 1.1 (25 °C), 217 (10 °C), 483 (5 °C), and $1{\cdot}10^3$ $M^{-1}{\cdot}s^{-1}$ (5 °C), for X= CN^-, CF_3, $NCCH_2$, and CF_2H, respectively.[18] The kinetic *trans* effect was found to decrease in the order *n*Pr ≥ adenosyl ≥ Me ≥ $CF_3CH_2 > CF_2H > NCCH_2 > CF_3 > CN^-$.

The relatively slow reaction rate of complex **4** is consistent with the short $Co-N_{(pyridyl)}$ bond[11] [2.118(3) Å], and the $\Delta V^{\ddagger}$ value suggests an $Co-N_{(pyridyl)}$ bond extension in the transition state similar to that of the Me derivative. Therefore, this complex exhibits no special kinetic properties. Perhaps the only relevant point is the presence of the $-CH_2-$ arm, which imparts a greater rigidity to the system, so that in this case the steric effects become less important.

On the basis of the activation parameters presented in Tables 1 and 2, it is reasonable to conclude that the ligand-substitution reactions of *trans*-$[(R)Co(LNHpy)(HLNHpy)]^+$ with cyanide, where R = Et, Me, CF_3CH_2, and bridging CH_2, follow a dissociative mechanism whose nature can vary from limiting dissociative to a dissociative interchange (I_d) mechanism, depending on the σ-donor and steric properties of the alkyl group, as discussed in detail above. It may be concluded, that the complexes studied here are more suitable than the cobaloximes to examine the influence of steric effects, which have up to now been disregarded in the study of model compounds for coenzyme B_{12}.

Experimental Section

Materials: All chemicals were of analytical reagent grade and used as received. Sodium cyanide was purchased from Merck and lithium trifluoromethanesulfonate from Aldrich. *trans*-$[(R)Co(LNHpy)(HLNHpy)]ClO_4$ (R = Me, Et, CF_3CH_2) were prepared by reduction of *trans*-$[Co(LNHpy)(HLNHpy)](ClO_4)_2$ by $NaBH_4$ and addition of alkyl iodide under nitrogen. The remaining complex *trans*-$[(CH_2)Co(LNHpy)(HLNHpy)]ClO_4$ was prepared by treating *trans*-$[(ClCH_2)Co(LNHpy)(HLNHpy)]ClO_4$ with NaOH. The complexes were characterised by elemental analysis and NMR spectroscopy, and the results were in agreement with those reported in the literatures.[5,11] All preparations and measurements were carried out in the dark since alkylcobaloximes are light-sensitive.

Instrumentation: UV/Vis spectra were recorded with Shimadzu UV-2101 and Hewlett Packard 8452A spectrophotometers. Kinetic measurements were carried out with the Shimadzu instrument. Measurements at elevated pressures (up to 150 MPa) were carried out using the Shimadzu spectrophotometer equipped with a home-made high-pressure unit for slow reactions,[51] and a high-pressure stopped-flow unit for fast reactions.[52] Kinetic data were analyzed with the OLIS KINFIT program. The standard deviations reported for the experimental data were estimated using the ORIGIN program. All instruments were thermostatted to the desired temperature (±0.1 °C). Kinetic measurements were carried out under pseudo-first-order conditions, i.e. the ligand concentration was in at least a 10-fold excess.

Acknowledgments

The authors gratefully acknowledge financial support from CNR (Rome), MIUR (Rome), PRIN No. MMO3185591, the Alexander von Humboldt Foundation (M. S. A. H.), and the Deutsche Forschungsgemeinschaft (R. v. E.).

[1] J. Halpern, *Science* **1985**, *227*, 869.
[2] R. Banerjee, *Chemistry and Biochemistry of B_{12}, Wiley & Sons, New York,* **1999**.
[3] A. Gerli, M. Sabat, L. G. Marzilli, *J. Am. Chem. Soc.* **1992**, *114*, 6711.
[4] P. G. Yohannes, N. Bresciani-Pahor, L. Randaccio, E. Zangrando, *Inorg. Chem.* **1988**, *27*, 4738.
[5] R. Dreos, A. Felluga, G. Nardin, L. Randaccio, P. Siega, G. Tauzher, *Eur. J. Inorg. Chem.* **2001**, 267.
[6] B. M. Alzoubi, M. S. A. Hamza, C. Dücker-Benefer, R. van Eldik, *Eur. J. Inorg. Chem.* **2002**, 968.
[7] L. M. Hansen, P. N. V. Paven Kumar, D. S. Marynick, *Inorg. Chem.* **1994**, *33*, 728.
[8] S. J. Moore, A. Kutikev, R. J. Lachicotte, L. G. Marzilli, *Inorg. Chem.* **1999**, *38*, 768.
[9] F. Asaro, R. Dreos, S. Geremia, G. Nardin, G. Pellizer, L. Randaccio, G. Tauzher, S. Vuano, *J. Organomet. Chem.* **1997**, *548*, 211.
[10] M. S. A. Hamza, X. Zou, K. L. Brown, R. van Eldik, *Inorg. Chem.* **2001**, *40*, 5440.
[11] R. Dreos, A. Felluga, G. Nardin, L. Randaccio, P. Siega, G. Tauzher, *Inorg. Chem.* **2001**, *40*, 5541.
[12] L. G. Marzilli, A. Gerli, A. M. Calafat, *Inorg. Chem.* **1992**, *31*, 4617.
[13] [13a] G. Stochel, R. van Eldik, *Inorg. Chem.* **1990**, *29*, 2075. [13b] F. F. Prinsloo, M. Meier, R. van Eldik, *Inorg. Chem.* **1994**, *33*, 900. [13c] M. Meier, R. van Eldik, *Inorg. Chem.* **1993**, *32*, 2635. [13d] F. F. Prinsloo, E. L. J. Breet, R. van Eldik, *J. Chem. Soc., Dalton Trans.* **1995**, 685. [13e] A. G. Gergan, N. E. Brasch, R. van Eldik, *Inorg. Chem.* **2001**, *40*, 1430. [13f] M. S. A. Hamza, C. Dücker-Benfer, R. van Eldik, *Inorg. Chem.* **2000**, *39*, 3777. [13g] B. M. Alzoubi, M. S. A. Hamza, C. Dücker-Benfer, R. van Eldik, *Eur. J. Inorg. Chem.* **2002**, 968.
[14] [14a] H. M. Marques, *J. Chem. Soc., Dalton Trans.* **1991**, 339. [14b] H. M. Marques, J. C. Bradley, L. A. Campbell, *J. Chem. Soc., Dalton Trans.* **1992**, 2019. [14c] H. M. Marques, J. C. Bradley, K. L. Brown, H. Brooks, *J. Chem. Soc., Dalton Trans.* **1993**, 3475. [14d] H. M. Marques, O. Q. Munro, B. M. Cumming, C. de Nysschen, *J. Chem. Soc., Dalton Trans.* **1994**, 297.
[15] [15a] D. Thusius, *J. Am. Chem. Soc.* **1971**, *93*, 2629. [15b] F. Nome, J. H. Fendler, *J. Chem. Soc., Dalton Trans.* **1976**, 1212. [15c] W. C. Randall, R. A. Alberty, *Biochemistry* **1967**, *6*, 1520. [15d] W. W. Reenstra, W. P. Jencks, *J. Am. Chem. Soc.* **1979**, *101*, 5780.
[16] N. E. Brasch, M. S. A. Hamza, R. van Eldik, *Inorg. Chem.* **1997**, *36*, 3216.
[17] M. S. A. Hamza, A. G. Cregan, N. Brasch, R. van Eldik, *Dalton Trans.* **2003**, 596.
[18] M. S. A. Hamza, X. Zou, K. L. Brown, R. van Eldik, *J. Chem. Soc., Dalton Trans.* **2002**, 3832.
[19] A. L. Crumbliss, W. K. Wilmarth, *J. Am. Chem. Soc.* **1970**, *92*, 2593.
[20] K. L. Brown, D. Cernoff, D. J. Keljo, R. G. Kallen, *J. Am. Chem. Soc.* **1975**, *97*, 7338.

 © 2003 Wiley-VCH Verlag GmbH & Co. KGaA, Weinheim

[21] K. L. Brown, D. Lyles, N. Pencovici, R. G. Kallen, *J. Am. Chem. Soc.* **1972**, *94*, 6697.
[22] K. L. Brown, A. W. Awtrey, *Inorg. Chem.* **1978**, *17*, 111.
[23] N. Bresciani-Pahor, L. Randaccio, A. C. Sandercock, L. G. Marzilli, *J. Chem. Soc., Dalton Trans.* **1982**, 129.
[24] M. F. Summers, P. J. Toscano, N. Bresciani-Pahor, G. Nardin, L. Randaccio, L. G. Marzilli, *J. Am. Chem. Soc.* **1983**, *105*, 6259.
[25] W. C. Trogler, R. C. Stewart, L. G. Marzilli, *J. Am. Chem. Soc.* **1974**, *96*, 3697.
[26] R. C. Stewart, L. G. Marzilli, *J. Am. Chem. Soc.* **1978**, *100*, 817.
[27] K. L. Brown, R. G. Kallen, *J. Am. Chem. Soc.* **1972**, *94*, 1894.
[28] J. K. Espenson, R. Russell, *Inorg. Chem.* **1974**, *13*, 7.
[29] R. Dreos Garlatti, G. Tauzher, G. Costa, *Inorg. Chim. Acta* **1983**, *70*, 83.
[30] R. Dreos Garlatti, G. Tauzher, G. Costa, *Inorg. Chim. Acta* **1983**, *71*, 9.
[31] R. Dreos Garlatti, G. Tauzher, G. Costa, *Inorg. Chim. Acta* **1981**, *50*, 95.
[32] R. Dreos Garlatti, G. Tauzher, G. Costa, *Inorg. Chim. Acta* **1986**, *121*, 27.
[33] R. Dreos Garlatti, G. Tauzher, G. Costa, *Inorg. Chim. Acta* **1984**, *82*, 197.
[34] S. M. Polson, L. Hansen, L. G. Marzilli, *J. Am. Chem. Soc.* **1996**, *118*, 4804.
[35] L. G. Marzilli, S. M. Polson, L. Hansen, S. G. Moore, *Inorg. Chem.* **1997**, *36*, 3854.
[36] N. Bresciani-Pahor, M. Forcolin, L. G. Marzilli, L. Randaccio, M. F. Summers, P. J. Toscano, *Coord. Chem. Rev.* **1985**, *63*, 1.
[37] F. Mancia, N. H. Keep, A. Nakagawa, P. F. Leadlay, S. McSweeney, B. Rasmussen, P. Boske, O. Diat, P. R. Evans, *Structure* **1996**, 339.
[38] C. Dücker-Benfer, R. Dreos, R. van Eldik, *Angew. Chem. Int. Ed. Engl.* **1995**, *34*, 2245.
[39] L. Randaccio, S. Geremia, R. Dreos-Garlatti, G. Tauzher, F. Asaro, G. Pellizer, *Inorg. Chim. Acta* **1992**, *194*, 1.
[40] R. Cini, S. J. Moore, L. G. Marzilli, *Inorg. Chem.* **1998**, *37*, 6890.
[41] S. Kirota, S. M. Polson, J. M. Puskett, S. J. Moore, M. B. Mitchell, L. G. Marzilli, *Inorg. Chem.* **1996**, *35*, 5645.
[42] A. Clearfield, R. Gopal, R. J. Kline, M. Spiski, O. L. Urban, *J. Coord. Chem.* **1978**, *7*, 163.
[43] M. Calligaris, G. Nardin, L. Randaccio, *Inorg. Nucl. Chem. Lett.* **1972**, *8*, 477.
[44] M. Calligaris, G. Nardin, L. Randaccio, *J. Chem. Soc. A* **1972**, 1433.
[45] M. F. Summers, L. G. Marzilli, N. Bresciani-Pahor, L. Randaccio, *J. Am. Chem. Soc.* **1984**, *106*, 4478.
[46] M. S. A. Hamza, A. Felluga, L. Randaccio, G. Tauzher, R. van Eldik, *Dalton Trans.*, submitted for publication.
[47] L. Randaccio, M. Furlan, S. Geremia, M. Slouf, I. Srnova, D. Toffoli, *Inorg. Chem.* **2000**, *39*, 3403.
[48] T. Wagner, C. E. Afshar, H. L. Cavrell, J. P. Glusker, U. Englert, H. P. C. Hogenkamp, *Inorg. Chem.* **1999**, *38*, 1785.
[49] X. Zou, K. L. Brown, *Inorg. Chim. Acta* **1997**, *267*, 305.
[50] [50a] C. Kratky, G. Färber, K. Gruber, K. Wilson, Z. Dauter, H-F. Nolting, R. Konrat, B. Kraütler, *J. Am. Chem. Soc.* **1995**, *117*, 4654. [50b] M. Rossi, J. P. Glusker, L. Randaccio, M. F. Summers, P. J. Toscano, L. G. Marzilli, *J. Am. Chem. Soc.* **1985**, *107*, 1729.
[51] M. Spitzer, F. Gartig, R. van Eldik, *Rev. Sci. Instrument* **1988**, *59*, 2092−2093.
[52] R. van Eldik, W. Gaede, S. Wieland, J. Kraft, M. Spitzer, D. A. Palmer, *Rev. Sci. Instrument.* **1993**, *64*, 1355−1357.

Received April 10, 2003
Early View Article
Published Online August 14, 2003

 © 2003 Wiley-VCH Verlag GmbH & Co. KGaA, Weinheim

Cyclotetrapeptide Complexes of Nickel(II) and Palladium(II) by Template Synthesis from Dipeptide Esters with Functionalized Side Chains − Crystal Structure of [(*cyclo*-Gly-β-Ala-Gly-β-Ala-4H$^+$)Cu](PPN)$_2$[‡]

Jan Schapp,[a] Katharina Haas,[a] Karlheinz Sünkel,[a] and Wolfgang Beck*[a]

Dedicated to Professor Dieter Seebach on the occasion of his 65th birthday

Keywords: Peptides / Nickel / Palladium / Copper

The cyclocondensations of dipeptide esters [Gly-L-Asp(OMe)$_2$, Gly-L-Glu(OMe)$_2$, L-AspOMe-β-AlaOMe, β-Ala-L-Lys(ω-*N*-Boc,OMe), β-Ala-L-Orn(ω-*N*-Boc,OMe)] at nickel(II), palladium(II), and copper(II) templates give dianionic square-planar complexes of deprotonated cyclotetrapeptides that contain functional groups in the side chains. The complexes with 14- or 16-membered rings were isolated as [Ph$_3$PNPPh$_3$]$^+$ salts. Hydrolysis of {[*cyclo*-Gly-Asp(OMe)-Gly-Asp(OMe)-4H$^+$]Pd}$^{2-}$ affords the tetraanionic complex [{*cyclo*-Gly-Asp(O$^-$)-Gly-Asp(O$^-$)-4H$^+$}Pd]$^{4-}$(Li$^+$)$_2$(PNP$^+$)$_2$. The crystal structure of [(*cyclo*-Gly-β-Ala-Gly-β-Ala-4H$^+$)Cu](PPN)$_2$ is also reported.
(© Wiley-VCH Verlag GmbH & Co. KGaA, 69451 Weinheim, Germany, 2003)

Introduction

Biologically active natural cyclic tetrapeptides[2] are promising candidates for new anticancer agents.[3] Seebach et al. have pioneered studies on the synthesis, structure, and biological activity of *cyclo*-β-tetrapeptides.[2,4] Although some cyclotetrapeptides are difficult to synthesize,[2,4,5,6] our facile route from non-activated peptide esters on metal centres[7,8] involves the cyclocondensation of dipeptide esters at metal templates (Cu^{2+}, Ni^{2+}, Pd^{2+}) and requires neither a protecting nor an activating group or a coupling agent. Also, high dilution of the reaction mixture is not necessary. With half sandwich tripeptide ester ruthenium complexes cyclization to cyclotripeptides has been observed.[9] Current interest in the metal complexes of cyclic peptides includes the functionalization of biomolecules,[10] complexes with marine natural products,[11] their structure,[12] in "molecular engineering",[13] as selective ligands,[14] as models for metal enzymes,[8,11,12,15] and as precursors for polyazamacrocyclic complexes.[1,16] Cyclopeptide complexes may be suitable diagnostic and therapeutic tools.[17] For example, linear peptides have been cyclized using conventional methods and their metal complexes may find use for scintigraphy and radiotherapy.[18] These applications seem to require water-soluble complexes and, therefore, we aimed to synthesize cyclotetrapeptide complexes that contain functional groups in the ligands. Seebach and co-workers have reported a series of linear and cyclic β-oligopeptides with functionalized polar side chains derived from serine, aspartic and glutamic acids.[19] We also report here the crystal structure of [Cu(*cyclo*-Gly-β-Ala-Gly-β-Ala-4H$^+$)](PPN)$_2$.

Results and Discussion

1. Cyclotetrapeptide Complexes with Aspartic and Glutamic Acid Units

The hydrochlorides of dipeptide dimethyl esters from aspartic acid and glycine react with Na_2PdCl_4 and $NiCl_2$ in the presence of NaOMe to give the dianionic complexes **1** and **2**, which have been isolated as their PPN$^+$ salts (**1a**, **2**) [PPN$^+$ = bis(triphenylphosphoranylidene)ammonium] in good yields. Similarly, [Gly-L-Glu(OMe)$_2$] and Na_2PdCl_4 gave the cyclotetrapeptide complex **3**. The dipeptide of β-alanine and aspartic acid affords complexes **4** and **5**.

Condensation of [Gly-L-Asp(OMe)$_2$] and [L-Asp(OMe)-β-AlaOMe] at the metal centre could lead to either 12- or 14-membered chelate rings. The less strained C_2-symmetric 14-membered ring is probably formed; a 12-membered chelate from Gly-L-AlaOMe was obtained only in low yield.[7] Recently it was demonstrated that 13-membered cyclic tetrapeptides are easier to synthesize from linear tetrapeptides, and are more stable and conformationally more homogeneous, than are 14-membered rings, which have unfavorable strain.[20]

[‡] Metal Complexes of Biologically Important Ligands, CLIII. Part CLII: Ref.[1]

[a] Department Chemie der Ludwig-Maximilians-Universität, Butenandtstr. 5−13, 81377 München, Germany
E-mail: wbe@cup.uni-muenchen.de

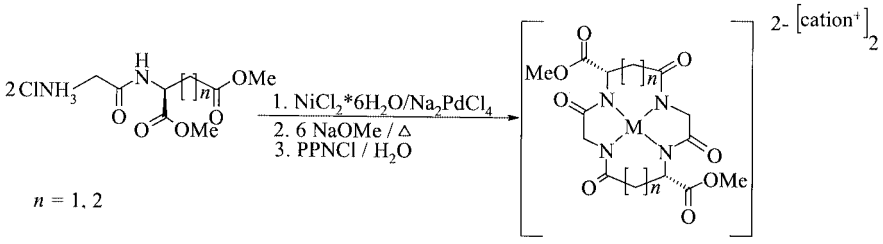

1a: $n = 1$, M = Pd^{2+}, cation = PPN^+
1b: $n = 1$, M = Pd^{2+}, cation = Na^+
2: $n = 1$, M = Ni^{2+}, cation = PPN^+
3: $n = 2$, M = Pd^{2+}, cation = PPN^+

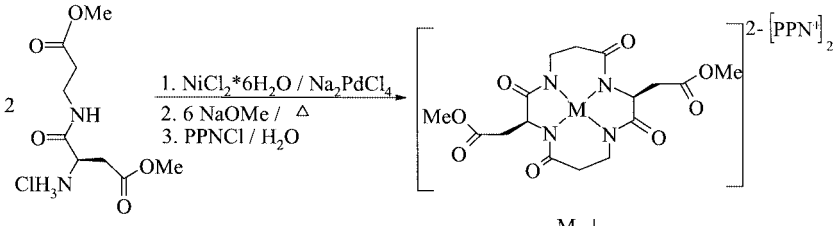

M	
Ni^{2+}	**4**
Pd^{2+}	**5**

The ester groups of complex **1** were hydrolyzed to give the tetraanionic palladium complex in **6**. For possible use in diagnostics and radiotherapy [17,18] the water-soluble sodium salts **1b** and **7** were prepared by the addition of water to a mixture of H-Gly-Asp(OMe)$_2$, NaOMe, and metal salt. The structures of complexes **1b** and **7** were verified by 2D NMR techniques. In one preparation of **7** the sodium compound $Na(OH_2)_4[O_2CCH_2CHC(O)NHCH_2C(O)NH]_2$ was obtained, as a by-product containing the (3,6-dioxopiperazine-2-yl)acetate anion, from [Gly-L-Asp(OMe)$_2$] by cyclocondensation of the amino group of the glycine component and the α-CO_2Me group of the aspartic acid component in the dipeptide. This product was characterized by X-ray crystallography [21] after recrystallization from water.

The mass spectra (FAB) show peaks for [M^{2-} + H^+] (m/z = 475 (**1**), 427 (**2**), 455 (**4**), 503 (**3**, **5**). An ESI spectrum of **6** exhibits peaks, among others, at m/z = 447 [M^{4-} + $3H^+$], 984 [M^{4-} + PPN^+ + $2H^+$] and 453 [M^{4-} + Li^+ + $2H^+$].

In the IR spectra characteristic signals appear for the ester groups (**1**: 1735 cm^{-1}; **4**, **5**: 1725 cm^{-1}) and for the carboxylate group in **6** at 1677 and 1665 cm^{-1}.

Two amide I absorptions of **1**−**5** appear at 1590 and 1570 cm^{-1}.

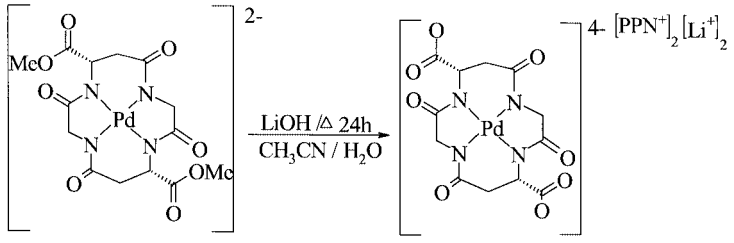

1 **6**

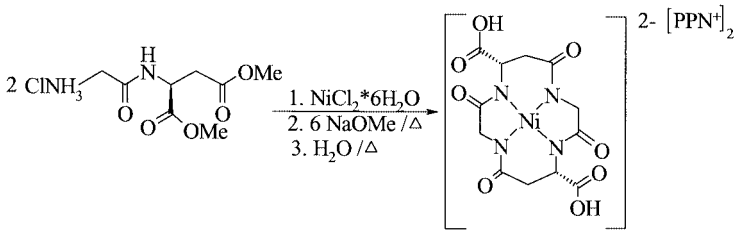

7

 © 2003 Wiley-VCH Verlag GmbH & Co. KGaA, Weinheim

The nickel complex **2** undergoes stepwise and selective hydroxylation at the α-carbon atom of the glycine units with oxygen in air.[8] This reaction is related to the copper enzyme peptidylglycine α-hydroxylating monooxygenase (PHM), which catalyzes the stereospecific hydroxylation of the α-C atom of the terminal glycine unit of a peptide.[22]

The ^{1}H NMR spectra (Tables 1 and 2) of compound **1** show only one signal for the two COOMe groups of the cyclotetrapeptide, while for **2**−**5** there are two singlets in a 1:1 ratio. Concomitantly, the glycine-containing complexes **2** and **3** show two AB sets for the glycine CH_2 protons, whereas **1**, and the hydrolyzed carboxylate derivatives **6** and **7**, have only one such set. Therefore compounds **1**, **6**, and **7** have a C_2 symmetry, while **2**−**5** have only C_1 symmetry, but for all compounds there exsists only one conformation of the cyclotetrapeptide unit. [Some weaker signals (< 10% intensities compared with the main signals) in all spectra indicate other, minor, cyclopeptide conformations.] Careful analysis of the AB parts of the glycine moieties of **1**−**3** and **6**, **7** (using the program WinDNMR) shows that the two CH_2 protons generally have quite different environments ($\Delta\delta > 0.20$ ppm), except for both glycine chelates in **3** and one in **2** (Table 1).

Table 1. ^{1}H NMR data (glycyl protons) of **1**−**3**, **6**, **7**

Compound	δ ($H_{A/B}$) [ppm]	J_{AB} [Hz]	Δδ (H_A/H_B)
1a	4.085/ 3.837	−19	0.248
2	3.725/ 3.477	−19	0.248
	3.588/ 3.534	−19	0.054
3	3.961/ 3.873	−19	0.088
	3.890/ 3.741	−19	0.149
6	4.120/ 3.863	−18	0.257
7	4.052/ 3.835	−18	0.217

Table 2. ^{1}H NMR data (aspartyl protons) of **1**, **2**, **6**, **7**

Compound	δ (H_A)	δ (H_B)	δ (H_X)	J_{AB}	J_{AX}	J_{BX}
1a	2.692	2.528	4.427	−15.7	4.7	4.6
2	2.696	2.639	4.014	−14	6	6
	2.454	2.489	4.122	−16.3	6	3
6	2.730	2.507	4.359	−15	4	4
7	2.673	2.692	4.136	−17	10.3	1.7

The ^{13}C NMR spectra of all compounds confirm the given interpretations, although good-quality spectra could not always be obtained.

2. Cyclopeptide Complexes with Lysine and Ornithine Units

The dipeptide esters β-Ala-L-Lys(ω-NBoc)OMe and β-Ala-L-Orn(ω-NBoc)OMe afforded, with Na_2PdCl_4 or $NiCl_2$, compounds **8**−**10**. Treatment of **9** with a solution of hydrogen chloride in methanol furnished the free cyclopeptide **11**, which was easily separated due to its low solubility in methanol. Finally, the Boc protecting group can be cleaved by trifluoroacetic acid.

3. Crystal and Molecular Structure of [(*cyclo*-Gly-β-Ala-Gly-β-Ala-4H$^+$)Cu(PPN)$_2$ (12)

The crystal structure of the palladium complex [Pd(*cyclo*-Gly-β-Ala-Gly-β-Ala-4H$^+$)](PPN)$_2$ has been reported.[7] Crystals of the copper complex **12**, formed from Gly-β-Ala-OMe at the Cu^{2+} ion,[7] were obtained from acetonitrile solution, but as they quickly became opaque when taken out of the mother liquor the structure was determined at 266 K. Even so, the crystals decayed slowly, approximately 12% over the course of the measurement. The structure refinement yielded an average composition of the crystal as **12**·MeOH·2MeCN·6H_2O, with the methanol solvent disordered over two positions and two of the water molecules disordered over three positions.

The program VOID revealed that without the solvents the crystal structure contains large voids, making up for nearly 25% of the cell volume. The structure can be described as a sheet structure with alternating cation and anion layers parallel to the *ab* plane. Within the anion sheets, the anions are connected to a one-dimensional polymer in the (0 1 0) direction via a complex system of hydrogen bonds involving the amide oxygens and the water and methanol OH functions. A side view of the undulating sheets thus formed is given in Figure 1. The acetonitrile molecules are situated between the PPN cations, with their molecular axes almost parallel to the *z*-direction and their methyl groups pointing towards the neighbouring anion layers, excluding any hydrogen bond interactions of the nitrile nitrogens with the anion H-bond system.

The molecular structure (Figure 2) requires only a few comments on the complex anion. Due to crystal decomposition and other common difficulties in describing structures containing so many water molecules, the geometrical parameters have rather high standard deviations. Nonetheless, the copper ion clearly has a square-planar coordination with the four deprotonated amide nitrogens [the σ(plane)

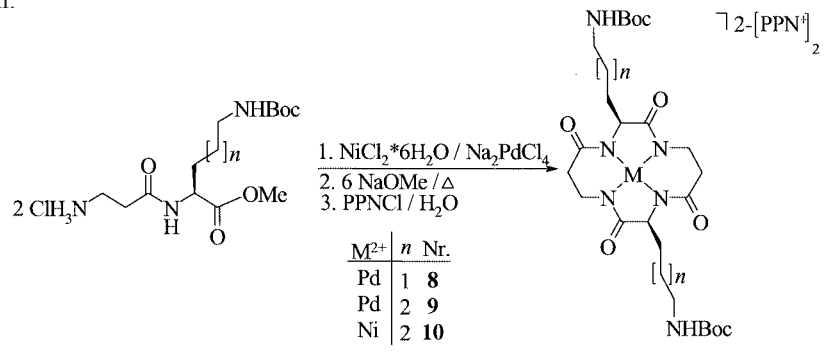

 © 2003 Wiley-VCH Verlag GmbH & Co. KGaA, Weinheim

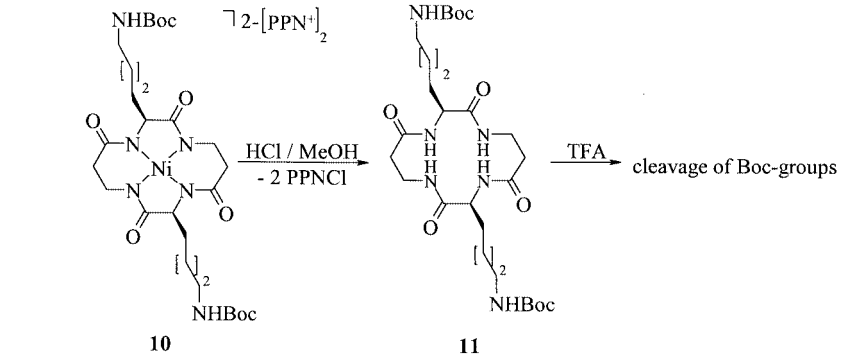

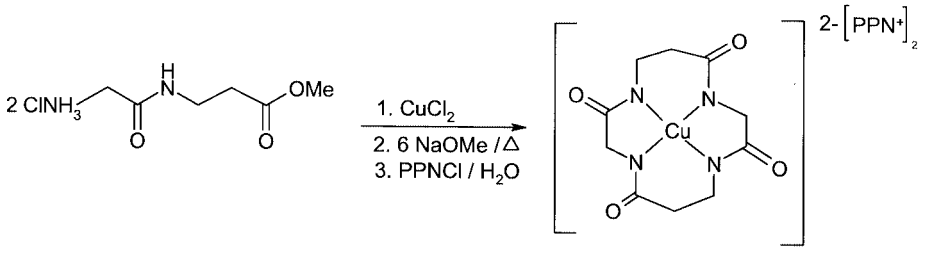

12

parameter is 0.123 Å, with Cu1 0.032(6) Å out of that plane]. There are no further ligands attached to the copper, and no intermolecular contacts within 4.0 Å of the copper. The average copper−nitrogen distance of 1.928 Å is normal for a deprotonated amide nitrogen, and the long C−O and short C−N distances of the amide group suggest a strong contribution of the O−C=N form. Table 3 gives the important geometrical parameters of **12** along with those of other copper complexes of 1,4,8,11-tetraazacyclotetradecanes with 0, 1, and 2 oxo groups in the ligand backbone and the corresponding parameters of the Pd^{II} analogue of **12**.[7]

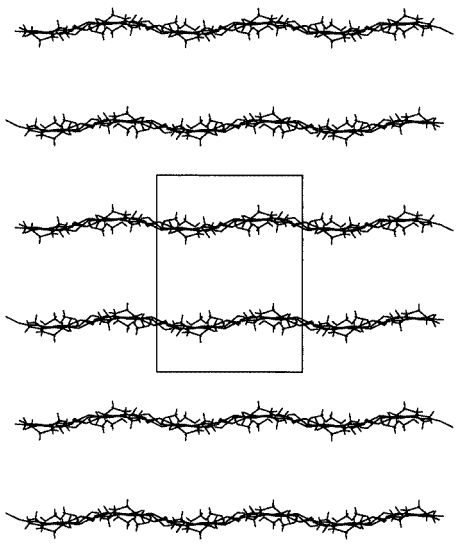

Figure 1. Packing of the anion sheets in the crystal of **12**

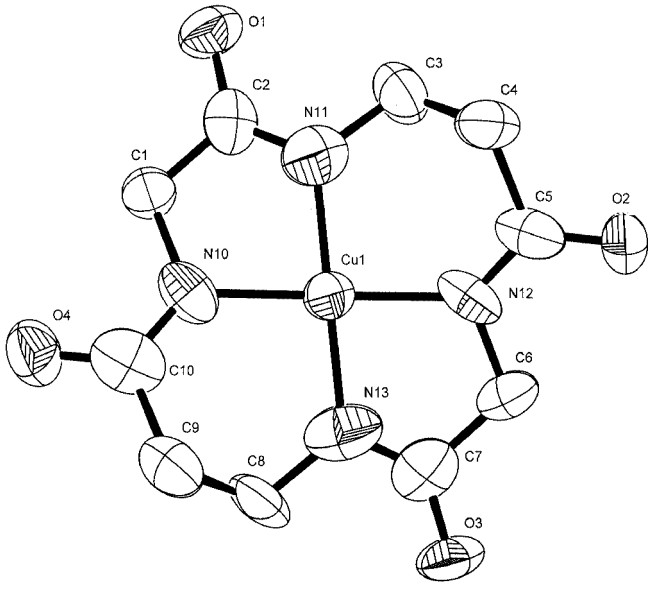

Figure 2. Molecular structures of the dianion of **12** in the crystal

Conclusion

Cyclotetrapeptides containing functional groups are accessible from the corresponding dipeptide esters by template synthesis at nickel(II) and palladium(II) centres. This is a very facile method in comparison to conventional procedures.

 © 2003 Wiley-VCH Verlag GmbH & Co. KGaA, Weinheim

Table 3. Geometrical parameters of tetraazacyclotetradecanes

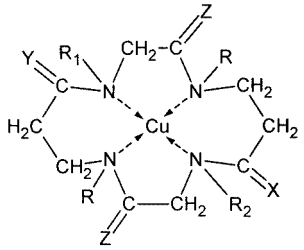

	R	R^1	R^2	X	Y	Z	Cu−NR[a]	Cu−N⁻	α, γ[a]	β, δ	C−O	C−N
[A]	H	H	H	H_2	H_2	H_2	2.012	–	85.7	94.3	–	1.49
[B]	H	H	⊖	O	H_2	H_2	2.017	1.960	85.6	94.2	1.286	1.299
[C]	CH_2py	⊖	⊖	O	O	H_2	2.054	1.962	84.6	95.5	1.280	1.314
12	⊖	⊖	⊖	O	O	O	–	1.93	83.5	96.6	1.294	1.252
[D]	⊖	⊖	⊖	O	O	O	–	–	83.0	97.0	1.280	1.291

[a] The angles α and γ correspond to the five-membered chelate rings, while β and δ are the bite angles in the six-membered chelates. The distances [Å] and angles [°] are average values. A: M. Studer, A. Riesen, T. A. Kaden, *Helv. Chim. Acta* **1984**, *72*, 1253. B: L. Siegfried, M. Neuburger, M. Zehnder, T. A. Kaden, *Chem. Commun.* **1994**, 951. C: A. E. Goeta, J. A. K. Howard, D. Maffeo, H. Paschmann, J. A. G. Williams, D. S. Yufit, *J. Chem. Soc.*, *Dalton Trans.* **2000**, 1873. D: Ref.[7]

Experimental Section

General Method for the Preparation of 1−10 (except for 1b, 6, 7): A methanolic sodium methoxide solution (6 mmol) was added dropwise to a mixture of the dipeptide ester hydrochloride (2 mmol) and metal salt (Na_2PdCl_4 or $NiCl_2{\cdot}6H_2O$, 1 mmol) dissolved in methanol (40 mL). The resultant solution was then heated to 65 °C for 24 h, after which [PPN]Cl (2 mmol) was added. Upon addition of water, the products **1−9** were obtained as crystalline solids.

{*cyclo*-[(Gly-L-Asp(OMe)-Gly-L-Asp(OMe)-4H$^+$]Pd}(PPN)$_2$ (1a): Colorless crystalline needles, yield: 1004 mg (58%). $C_{86}H_{76}N_6O_8P_4Pd{\cdot}10H_2O$ (1730.42): calcd. C 59.64, H 6.47, N 4.85; found C 59.61, H 5.54, N 4.76. ^{1}H NMR (CD_3OD, 400 MHz, ppm): δ = 3.634 (OCH_3). ^{13}C NMR (CD_3OD, 100 MHz, ppm): δ = 44.0, 52.4, 55.7, 57.9, 170.8, 174.3, 181.0. MS (FAB−): *m*/*z* = 475 [M^{2-} + H^+], 1012 [M^{2-} + PPN^+], 415 [M^{2-} + H^+ − ($HCOOCH_3$)]. IR (KBr): ν(OH) 3436 vs (H_2O), ν(C=O) 1735 s (COOMe), 1578vs, 1557 vs (amide-I).

{*cyclo*-[(Gly-L-Asp(OMe)-Gly-L-Asp(OMe)-4H$^+$]Pd}Na$_2$ (1b): A solution of NaOMe (6 mmol) in methanol (1.5 mL) was added dropwise to a solution of H-Gly-Asp(OMe)$_2$ (508 mg, 2 mmol) and Na_2PdCl_4 (284 mg, 0.97 mmol) in methanol (40 mL) − whereby the light yellow solution became colorless. The reaction mixture was then boiled under reflux for 48 h (60 °C). After removal of the solvent in vacuo the residue was dissolved in water (5 mL) and purified by HPLC (stationary C-18 reversed phase, mobile phase 100% of water). Colorless needles, yield: 402 mg (66%). $C_{14}H_{16}N_4Na_2O_8Pd{\cdot}6H_2O$ (628.52): calcd. C 26.73, H 4.46, N 8.91; found C 26.38, H 4.33, N 8.83. IR (KBr, cm^{-1}): ν(OH) 3436 vs (H_2O), ν(C=O), 1726 s (COOMe), 1598 vs, 1552 vs (amide-I). ^{1}H NMR (CD_3OD, 400 MHz, ppm): δ = 3.694 (OCH_3). ^{13}C NMR (100 MHz, CD_3OD, ppm): δ = 43.1, 52.6, 55.8, 57.7, 171.1, 174.7, 181.4. MS (FAB−/mNBA): *m*/*z* = 475 [M^{2-} + H^+], 497 [M^{2-} + Na^+].

{*cyclo*-[Gly-L-Asp(OMe)-Gly-L-Asp(OMe)-4H$^+$]Ni}(PPN)$_2$ (2): Yellow crystalline needles, yield: 950 mg (59%). $C_{86}H_{76}N_6NiO_8P_4{\cdot}6H_2O$ (1610.71): calcd. C 64.07, H 5.46, N 5.22; found C 63.91, H 5.49, N 5.15. ICP-AES (Ni, 231.60) calcd. Ni 3.64; Ni 4.16. ^{1}H NMR (CD_3OD; 400 MHz, ppm): δ = 3.667, 3.663 (OCH_3). ^{13}C NMR (CD_3OD, 100 MHz, ppm): δ = 38.7, 42.1, 52.0, 52.4, 53.0, 54.5, 57.5, 61.3, 171.7, 173.4, 174.7, 178.9; 180.1, 181.9. MS (FAB−): *m*/*z* = 427 [M^{2-} + H^+], 964 [M^{2-} + PPN^+], 367 [M^{2-} + H^+ − (HCOOMe)]. IR (KBr, cm^{-1}): ν(OH) 3428 vs (H_2O), ν(C=O) 1730s (COOMe), 1592 vs, 1581 vs, 1567 vs (amide-I).

{*cyclo*-[Gly-L-Glu(OMe)-Gly-L-Glu(OMe)-4H$^+$]Pd}(PPN)$_2$ (3): Colorless crystalline needles, yield: 1073 mg (61%). $C_{88}H_{80}N_6O_8P_4Pd{\cdot}10H_2O$ (1758.42): calcd. C 60.05, H 5.69, N 4.78; found C 60.18, H 5.69, N 4.74. ICP-AES (Pd, 340.46) calcd. Pd 6.05; Pd 6.24. ^{1}H NMR (CD_3OD, 400 MHz, ppm): δ = 3.613, 3.597 (OCH_3); δ (glutamyl res.) = 4.14 m/4.04 m (2 × H_X), 2.64 m/2.47 m/ 2.30 m/ 2.14 m/ 2.00 m/ 1.86 m (2 × H_{ABCD}). ^{13}C NMR (CD_3OD, 100 MHz, ppm): δ = 28.0, 30.0, 31.5, 34.3, 51.8, 51.9, 53.1, 59.4, 60.9, 65.3, 175.9, 176.4, 179.3, 179.8, 181.6, 184.4. MS (FAB−): *m*/*z* = 503 [M^{2-} + H^+], 443 [M^{2-} + H^+ − HCOOMe]. IR (KBr, cm^{-1}): ν(OH) 3436 vs (H_2O), ν(C=O) 1726 s (COOMe), 1590 vs, 1568 vs, 1557 vs (amide-I).

{*cyclo*-[β-Ala-L-Asp(OMe)-β-Ala-L-Asp(OMe)-4H$^+$]Ni}(PPN)$_2$ (4): Yellow crystalline needles, yield: 1193 mg (72%). $C_{88}H_{80}N_6NiO_8P_4{\cdot}7H_2O$ (1656.69): calcd. C 63.74, H 5.67, N 5.07; found C 64.08, H 5.57, N 4.43. ^{1}H NMR (CD_3OD, 400 MHz, ppm): δ = 3.814, 3.785; (OCH_3) 4.20 m, 3.25−3.15 m, 2.80−2.60 m, 2.43−2.07 m, 1.98−1.92m (2 × H_{ABX} + 2 × H_{ABCD}). ^{13}C NMR (CD_3OD, 100 MHz, ppm): δ = 39.3, 39.4, 39.5, 39.8, 40.0, 40.4, 51.9, 52.0, 62.4, 62.5, 173.96, 174.00, 176.2, 176.3, 180.0, 180.6. MS (FAB−): *m*/*z* = 455 [M^{2-} + H^+]; 381 [M^{2-} + H^+ − (CH_3COOCH_3)]. IR (KBr, cm^{-1}): ν(OH) 3429 vs (H_2O), ν(C=O) 1727 s (COOMe), 1580vs, 1548 vs (amide-I).

{*cyclo*-[β-Ala-L-Asp(OMe)-β-Ala-L-Asp(OMe)-4H$^+$]Pd}(PPN)$_2$ (5): Colorless crystalline needles, yield: 1091 mg (64%). $C_{88}H_{80}N_6O_8P_4Pd{\cdot}7H_2O$ (1704.42): calcd. C 61.96, H 5.52, N 3.29; found C 62.39, H 5.80, N 4.15. ^{1}H NMR (CD_3OD, 400 MHz,

 © 2003 Wiley-VCH Verlag GmbH & Co. KGaA, Weinheim

ppm): δ = 3.701, 3.687 (OCH_3); 5.12 m, 4.97 m, 4.57−4.47 m, 3.65 m, 3.54−3.47 m, 2.92−2.45 m, 2.42−2.07 m. MS (FAB−): *m*/*z* = 503 [$M^{2-} + H^+$], 429 [$M^{2-} + H^+ - (CH_3COOCH_3)$], 1040 [$M^{2-} + PPN^+$]. IR (KBr, cm^{-1}): (OH) 3414 vs (H_2O), ν(C=O) 1723 s (COOMe), 1590 vs, 1568 vs, (amide-I).

{*cyclo*-[Gly-L-Asp-Gly-L-Asp-6H$^+$]Pd}Li$_2$(PPN)$_2$ (6): A mixture of **1a** (173 mg, 0.1 mmol) and LiOH (10 mg, 0.4 mmol) were dissolved in CH_3CN (10 mL). After the addition of H_2O (2 mL) the mixture was heated to 65 °C for 24 h. Colorless crystalline needles of **6** were then obtained following the addition of water. Yield: 115 mg (67%). $C_{84}H_{70}Li_2N_4O_8PdP_4 \cdot 10H_2O$ (1714.42): MS (ESI−): *m*/*z* = 447 [$M^{4-} + 3H^+$], 453 [$M^{4-} + Li^+ + 2H^+$], 984 [$M^{4-} + PPN^+ + 2H^+$], 1074 [$M^{4-} + PPN^+ + 5\ H_2O + 2H^+$], 1521 [$M^{4-} + 2\ PPN^+ + H^+$], 1611 [$M^{4-} + 5\ H_2O + 2\ PPN^+ + H^+$], 1701 [$M^{4-} + 10\ H_2O + 2\ PPN^+ + H^+$]. IR (KBr, cm^{-1}): ν(OH) 3377 vs (H_2O), ν(C=O) 1677 s, 1665 s (COOLi), 1570 vs (amide-I), 1438 s, 1415 cm^{-1} (COOLi).

{*cyclo*-[Gly-L-Asp-Gly-L-Asp-4H$^+$]Ni}Na$_2$ (7): A solution of NaOMe (6 mmol) in methanol (1.5 mL) was added dropwise to a solution of H-Gly-Asp(OMe)$_2$ (508 mg, 2 mmol) and $NiCl_2 \cdot 6H_2O$ (238 mg, 1 mmol) in methanol (40 mL), whereupon the light yellow solution became colorless. The reaction mixture was then boiled under reflux (60 °C) for 48 h. After removal of the solvent the residue was dissolved in water (5 mL) and purified by HPLC (stationary C-18 reversed phase, mobile phase 100% of water). Yellow needles, yield: 287 mg (60%). $C_{12}H_{12}N_4Na_2NiO_8 \cdot 2H_2O$ (478.69): calcd. C 30.08, H 3.34, N 11.70; found C 30.56, H 4.21, N 11.20. IR (KBr): ν(OH) 3429 vs (H_2O), ν(C=O), 1687 s, 1661 s (COOH), 1597 vs (amide-I), 1463 s, 1421 cm^{-1} (COOH). ^{13}C NMR (CD_3OD, 67 MHz, ppm): δ = 41.5, 45.6, 54.2, 168.6, 171.1, 177.3. MS (ESI−): *m*/*z* = 365 [$M^{2-} - 2CO_2 + 2H_2O + H^+$].

{*cyclo*-[β-Ala-L-Orn(ω-NHBoc)-β-Ala-L-Orn(ω-NHBoc)-4H$^+$]Pd}-(PPN)$_2$ (8): MS (FAB−): *m*/*z* = 673 [$M^{2-} + H^+$], 691 [$M^{2-} + H^+ + H_2O$], 709 [$M^{2-} + H^+ + 2H_2O$], 1097 [$M^{2-} + PPN^+ - 2\cdot(CH_3)_3C$].

{*cyclo*-[β-Ala-L-Lys(ω-NHBoc)-β-Ala-L-Lys(ω-NHBoc)-4H$^+$]Pd}-(PPN)$_2$ (9): Colorless powder, yield: 1150 mg (61%). $C_{100}H_{106}N_8O_8P_4Pd \cdot 6H_2O$ (1884.42): calcd. C 63.68, H 6.26, N 5.94; found C 63.26, H 6.09, N 6.17. MS (FAB−): *m*/*z* = 701 [$M^{2-} + H^+$]. IR (KBr): ν(OH) 3414 vs (H_2O), ν(C=O) 1699 s (amide-I), 1588 vs (amide-I), 1567 vs (amide-I), 1548 vs (amide-I), ν(NH) 1628 s (amide-II).

{*cyclo*-[β-Ala-L-Lys(ω-NHBoc)-β-Ala-L-Lys(ω-NHBoc)-4H$^+$]Ni}-(PPN)$_2$ (10): Yellow powder, yield: 1131 mg (62%). $C_{100}H_{106}N_8NiO_8P_4 \cdot 3CH_3OH$ (1824.72): calcd. C 65.76, H 5.81, N 6.13; found C 68.70, H 6.13, N 5.13. ^{13}C NMR (CD_3OD, ppm): δ = 20.0, 28.6, 30.7, 26.0, 36.8, 37.5, 38.8, 61.5, 155.5, 172.1, 178.5. MS (FAB−): *m*/*z* = 653 [$M^{2-} + H^+$].

***cyclo*-[β-Ala-L-Lys(ω-NHBoc)-β-Ala-L-Lys(ω-NHBoc)] (11):** Colorless powder, yield: 270 mg (90%). $C_{28}H_{50}N_6O_8$ (598.74): calcd. C 56.12, H 8.35, N 14.03; found C 55.77, H 8.43, N 13.94. MS (FAB+): *m*/*z* = 600 [$M + H^+$]; 500 [$M + 2H^+ - (COO\mathit{t}Bu^+)$], 400 [$M + 3H^+ - 2\cdot(COO\mathit{t}Bu^+)$]. IR (KBr, cm^{-1}): ν(OH) 3318 vs (H_2O), ν(C=O) 1689 s (amide-I), 1648 vs (amide-I), ν(NH) 1538 s (amide-II).

[*cyclo*-(Gly-β-Ala-Gly-β-Ala-4H$^+$)Cu](PPN)$_2$ (12): A solution of MeONa (6 mmol) in methanol was added dropwise to a mixture of Gly-β-AlaOMe·HCl (425 mg, 2 mmol) and $CuCl_2 \cdot 2H_2O$ (170 mg, 1 mmol) in methanol (40 mL), whereupon the initial green solution turned deep blue and NaCl was precipitated. The reaction mixture was then boiled under reflux for 24 h, filtered and the filtrate concentrated to 5 mL in vacuo. [Ph_3PNPPh_3]Cl (2 mmol) was then added. After the addition of water (100 mL), bronze-like plates of the cyclopeptide copper complexes were obtained, recrystallized from MeOH/H_2O, and dried in vacuo. Yield: 535 mg (37%). IR (KBr): $\tilde{\nu}$ = 1575, 1542 cm^{-1}. MS (FAB−, mNBA): *m*/*z* (%) = 316 (100) [$M^{2-} + H^+$], 853 (3) [$M^{2-}PPN^+$]. $C_{82}H_{72}CuN_6O_4P_4 \cdot 3H_2O$ (1447.0): calcd. C 68.00, H 5.39, N 5.81; found C 68.04, H 5.40, N 5.09.

Crystal Structure Determination of 12: An orange-brown block crystal was grown from acetonitrile solution and placed with a small amount of mother liquor inside a glass capillary that was sealed and transferred to a SYNTEX R3/Siemens P4 diffractometer equipped with a low-temperature measurement device, LT-1. The temperature was adjusted to −7 °C. As the LT-1 prevented the measurement of a psi-scan, no semi-empirical absorption correction could be applied. The data were processed with the Siemens XSCANS software, and the structure was solved with SHELXS-86 and refined with SHELXL-97.[23]

The refinement for the PPN cations and the complex anion as well as for the two acetonitrile and four of the water solvent molecules presented no difficulties, but that of the disordered methanol and two water molecules was less straightforward. The methanol was refined with a fixed C−O distance of 1.38 Å and common isotropic thermal parameters for each of the disordered carbon and oxygen positions and the sum of the s.o.f.s was fixed to 1.0. Three relatively weak peaks were found in the difference Fourier synthesis and assigned to the oxygen atoms of disordered water molecules. First, a common "reasonable" isotropic thermal parameter U of 0.09 was assigned to these atoms and the site occupancies were refined. This procedure led to approximate s.o.f.s of 0.7, 0.75 and 0.55, which were fixed afterwards on these values, since they added, reasonably, to an integer (2). With these fixed s.o.f.s the thermal parameters of the three oxygen atoms were refined freely isotropic. Geometrical analyses were performed with the program package WinGX v.1.64.04, the graphics were produced by the programs PLUTO and ORTEP3 for Windows, which are part of the WinGX suite.[24] CCDC-191607 contains the supplementary crystallographic data for this paper. These data can be obtained free of charge at www.ccdc.cam.ac.uk/conts/retrieving.html [or from the Cambridge Crystallographic Data Centre, 12 Union Road, Cambridge CB2 1EZ, UK; fax: (internat.) + 44-1223/336-033; E-mail: deposit@ccdc.cam.ac.uk].

Acknowledgments

We thank the Deutsche Forschungsgemeinschaft, Fonds der Chemischen Industrie and Wacker-Chemie, München, for generous support.

[1] M. A. Lang, W. Beck, *Z. Naturforsch., Teil B* **2003**, *58*, 447−450.
[2] S. A. Miller, S. I. Griffiths, D. Seebach, *Helv. Chim. Acta* **1993**, *76*, 563−595; H. Kessler, Angew. Chem. **1982**, *94*, 509−520; *Angew. Chem. Int. Ed. Engl.* **1982**, *21*, 512−523; U. Schmidt, *Nachr. Chem. Tech. Lab.* **1989**, *37*, 1034−1043; D. Seebach, O. Bezencon, B. Jaun, T. Pietzonka, J. L. Matthews, F. N. M. Kühnle, W. B. Schweizer, *Helv. Chim. Acta* **1996**, *79*, 588−608; R. E. Shute, M. Kawai, D. H. Rich, *Tetrahedron* **1988**, *44*, 685−695; U. Schmidt, *Pure Appl. Chem.* **1986**, *58*, 295−304; U. Schmidt, J. Langner, *J. Peptide Res.* **1997**, *49*, 67, zit. ref.; K. Gademann, D. Seebach, *Helv. Chim. Acta* **1999**, *82*,

 © 2003 Wiley-VCH Verlag GmbH & Co. KGaA, Weinheim

957−962; T. Shimizu, Y. Tanaka, K. Tsuda, *Bull. Chem. Soc., Jpn.* **1982**, *55*, 3817−3823.

[3] M. Jung, *Current Medicinal Chem.* **2001**, *8*, 1505−1511.

[4] D. Seebach, M. Brenner, M. Rueping, B. Jaun, *Chem. Eur. J.* **2002**, *8*, 573−578; K. Gademann, D. Seebach, *Helv. Chim. Acta* **2001**, *84*, 2924−2937; K. Gademann, M. Ernst, D. Seebach, D. Hoyer, *Helv. Chim. Acta* **2000**, *83*, 16−33; K. Gademann, M. Ernst, D. Hoyer, D. Seebach, *Angew. Chem.* **1999**, *111*, 1302−1303; *Angew. Chem. Int. Ed.* **1999**, *38*, 1223−1226; D. Seebach, J. L. Matthews, A. Meden, T. Wessels, C. Baerlocher, L. B. McCusker, *Helv. Chim. Acta* **1997**, *80*, 173−182.

[5] K. D. Kopple, *J. Pharm. Sci.* **1972**, *61*, 9; C. M. Deber, V. Madison, I. R. Blout, *Acc. Chem. Res.* **1976**, *9*, 106; M. Rothe, K. D. Steffen, I. Rothe, *Angew. Chem.* **1965**, *22*, 347; *Angew. Chem. Int. Ed. Engl.* **1965**, *4*, 356; M. Rothe, J. Haas, in: *Peptides* (Eds.: E. Giralt and D. Andreu), **1990**, ESCOM Science Publishers B. V., Leiden, **1991**, p. 212.

[6] J. N. Lambert, J. P. Mitchell, K. D. Roberts, *J. Chem. Soc., Perkin Trans. 1* **2001**, 471−484.

[7] K. Haas, W. Ponikwar, H. Nöth, W. Beck, *Angew. Chem.* **1998**, *110*, 1200−1203; *Angew. Chem. Int. Ed.* **1998**, *37*, 1086−1089; K. Haas, E.-M. Ehrenstorfer-Schäfers, K. Polborn, W. Beck, *Eur. J. Inorg. Chem.* **1999**, 465−469.

[8] K. Haas, H. Dialer, H. Piotrowski, J. Schapp, W. Beck, *Angew. Chem.* **2002**, *114*, 1969−1972; *Angew. Chem. Int. Ed.* **2002**, *41*, 1879−1881.

[9] K. Haas, W. Beck, *Z. Anorg. Allg. Chem.* **2002**, *628*, 788−796.

[10] M. Shionoya, K. Tanaka, *Bull. Chem. Soc., Jpn.* **2000**, *73*, 1945−1954; for other cyclooligomerizations of linear peptides and amino acids at metal templates see ref. [6] and: M. North, G. Pattenden, *Tetrahedron* **1990**, *46*, 8267−8290; A. J. Blake, J. S. Hannam, K. A. Joliffe, G. Pattenden, *Synlett* **2000**, 1515−1518; J. N. Lambert, J. P. Mitchell, K. D. Roberts, *J. Chem. Soc., Perkin Trans.* 2 **2001**, *1*, 471−484; N. Sokolenko, G. Abbenannte, M. J. Scanlon, A. Jones, L. R. Gahan, G. R. Hanson, D. P. Fairlie, *J. Am. Chem. Soc.* **1999**, *121*, 2603−2604; L. Zhang, J. P. Tam, *Tetrahedron Lett.* **1997**, *38*, 4375; H. Gerlach, A. Thalmann, *Helv. Chim. Acta* **1974**, *57* 2661; S. Masamune, S. Kamata, W. Schilling, *J. Am. Chem. Soc.* **1975**, *97*, 3515.

[11] J. P. Michael, G. Pattenden, *Angew. Chem.* **1993**, *105*, 1−136; *Angew. Chem. Int. Ed. Engl.* **1993**, *32*, 1; D. J. Freeman, G. Pattenden, A. F. Drake, G. Siligardi, *J. Chem. Soc., Perkin Trans. 2* **1998**, *1*, 129−136; K. Kustin, G. C. McLeod. *Top. Curr. Chem.* **1977**, *69*, 1.

[12] A. L. Nivorozhkin, B. M. Segal, K. B. Musgrave, S. A. Kates, B. Hedman, K. O. Hodgson, R. H. Holm, *Inorg. Chem.* **2000**, *39*, 2306−2313; V. Pavone, E. Benedetti, B. Di Blasio, A. Lombardi, C. Pedone, L. Tomasich, G. P. Lorenzi, *Biopolymers* **1989**, *28*, 215; *Chem. Abstr.* **1989**, *111*, 195383; Z.-Q. Tian, P. A. Bartlett, *J. Am. Chem. Soc.* **1996**, *118*, 943−949; P. Comba, R. Cusack, D. P. Fairlie, L. R. Gahan, G. R. Hanson, U. Kazmaier, A. Ramlow, *Inorg. Chem.* **1998**, *37*, 6721−6727; P. Xie, M. Diem, *J. Am. Chem. Soc.* **1995**, *117*, 429−437; A. L. van den Brenk, K. A. Byriel, D. P. Fairlie, L. R. Gahan, G. R. Hanson, C. J. Hawkins. A. Jones, C. H. L. Kennard, B. Moubaraki, K. S. Murray, *Inorg. Chem.* **1994**, *33*, 3549−3557; P. Xie, M. Diem, *J. Am. Chem. Soc.* **1995**, *117*, 429; E. Benedetti, B. Di Blasio, C. Pedone, M. Scalone, C. Toniolo, *Proc. Am. Pept. Symp.* **1979**, *6*, 141−144; R. EtTorre, V. Guantieri, A. M. Tamburro, L. De Nardo, *Inorg. Chim. Acta* **1979**, *32*, L39−L41.

[13] A. J. Blake, J. S. Hannam, K. A. Joliffe, G. Pattenden, *Synlett* **2000**, *10*, 1515; S. Wakita, Osaka Kogyo Gijutsu Shikensho Hokoku **1992**, *387*, 51 *Chem. Abstr.* **1993**, *119*, 250398; K. Tanaka, M. Shionoya, K. Shigemori, *Chem. Commun.* **1999**, 2475; E. Ozeki, S. Kimura, Y. Imanishi, *Int. J. Pept. Protein Res.* **1989**, *84*, 14; *Chem. Abstr.* **1989**, *112*, 179821; T. Yamamura, JP 89−88561, *Chem. Abstr.* **1990**, *114*, 186079; D. Ranganathan, *Acc. Chem. Res.* **2001**, *34*, 919−930.

[14] St. Kubik, *J. Am. Chem. Soc.* **1999**, *121*, 5846−5855; C. Garcia-Echeverria, F. Albericio, E. Giralt, M. Pons, *J. Am. Chem. Soc.* **1993**, *115*, 11663−11670; H. Miyake, N. Kato, Y. Kojima, A. Sugihara, *Inorg. Chim. Acta* **1994**, *223*, 121; Y. Imanishi, *Chem. Abstr.* **1982**, *99*, 158832; Y. Fusaoka, E. Ozeki, S. Kimura, Y. Imanishi, *Int. J. Pept. Protein Res.* **1984**, *84*, 104; *Chem. Abstr.* **1989**, *112*, 134663; T. Shimizu, Y. Tanaka, JP − 84182965, *Chem. Abstr.* **1986**, *105*, 227317; C. M. Deber, E. R. Blout, *Isr. J. Chem.* **1974**, *12*, 15−29; T. Shimizu, K. Ueno, Y. Tanaka, K. Tsuda, *Chem. Abstr.* **1982**, *96*, 104753; P. Wipf, P. C. Fritch, S. J. Gieb, A. M. Sefler, *J. Am. Chem. Soc.* **1998**, *120*, 4105−4112; L. Scheibler, P. Dumy, D. Stamou, C. Duschl, H. Vogel, M. Mutter, *Polym. Bull. (Berlin)* **1998**, *40*, 151−157.

[15] A. Mori, Kagaku to Kogyo, **1993**, *46*, 202−205; *Chem. Abstr.* **1993**, *118*, 220544; G. Arena, G. Impellizzeri, G. Maccarrone, G. Pappalardo, E. Rizzarelli, *J. Chem. Soc., Dalton Trans.* **1994**, 1227−1230; R. Fattorusso, G. Morelli, A. Lombardi, F. Nastri, O. Maglio, G. D'Auria, C. Pedone, V. Pavone, *Biopolymers* **1995**, *37*, 401−410; V. Pavone, E. Benedetti, B. Di Blasio, A. Lombardi, C. Pedone, L. Tomasich, G. P. Lorenzi, *Biopolymers* **1989**, *28*, 215−223; R. P. Bonomo, G. Impellizzeri, G. Pappalardo, R. Purrello, E. Rizzarelli, G. Tabbi, *J. Chem. Soc., Dalton Trans.* **1998**, 3851−3857; G. Arena, R. P. Bonomo, G. Impellizzeri, R. M. Izatt, J. D. Lamb, E. Rizzarelli, *Inorg. Chem.* **1987**, *26*, 795−800; G. R. Brubaker, N. Y. Sakkab, *Bioinorg. Chem.* **1974**, *3*, 243−260.

[16] K. W. Aston, S. L. Henke, A. S. Modak, D. P. Riley, K. R. Sample, R. H. Weiss, W. L. Neumann, *Tetrahedron Lett.* **1994**, *35*, 3687−3690; M. Lang, Dissertation, Universität München **2001**.

[17] J. C. Alexander, P. J. Lennon, A. S. Modak, W. L. Neumann, D. P. Riley, R. H. Weiss, *PCT Int. Appl.* **1995**, US 94−231599, *Chem. Abstr.* **1996**, *124*, 202319; R. T. Dean, US 5433815, *Chem. Abstr.* **1998**, *129*, 136495; D. S. Edwards, S. Liu, *PCT Int. Appl.* **1996**, WO 96 31243, *Chem. Abstr.* **1996**, *126*, 3911; G. R. Bower, A. M. Forster, A. L. M. Riley, A. E. Storey, *PCT Int. Appl.* **1995**, WO 95-GB 42 19950111; *Chem. Abstr.* **1995**, *123*, 279961; A. Kuranari, A. Somoto, H. Kawagishi, JP 92−31006, *Chem. Abstr.* **1994**, *120*, 132445; W. F. DeGrado, S. A. Mousa, M. Sworin, J. A. Barrett, D. S. Edwards, T. D. Harris, M. Rajopadhye, S. Liu, WO 94 22494; *Chem. Abstr.* **1995**, *123*, 199405; US 94−218861; *Chem. Abstr.* **1999**, *130*, 237883; M. Rajopadhye, D. S. Edwards, T. D. Harris, S. J. Heminway, S. Liu, R. P. Prahlad, *PCT Int. Appl.* WO 99-US6826, *Chem. Abstr.* **1999**, *131*, 351678.

[18] W.-R. Press, M. Bauer, H. Randow, W. Krause, *Ger. Offen.* **1996**, DE 94−4433572, *Chem. Abstr.* **1996**, *124.* 336873.

[19] J. L. Matthews, K. Gademann, B. Jaun, D. Seebach, *J. Chem. Soc., Perkin Trans. 1* **1998**, 3331−3340; K. Gademann, D. Seebach, *Helv. Chim. Acta* **1999**, *82*, 957−962; see also: Y. Fusaoka, S. Kimura, Y. Imanishi, *Kyoto Jpn, Pept. Chem.* **1982**, *19*, 191−194; Y, Imanishi, *Dep. Polymer Chem.* **1982**, *41*, 279−287; Y. Fusaoka, E. Ozeki, S. Kimura, Y. Imanishi, Kyoto Jpn., *Int. J. Pept. Protein Res.* **1989**, *34*, 104−110, *Chem. Abstr.* **1990**, *112*, 134663; H. Kiniwa, Y. Imanishi, T. Higashimura, *Kyoto, Jpn, Polym. Commun.* **1983**, *24*, 188−191.

[20] M. P. Glenn, M. J. Keiso, J. D. A. Tyndall, D. P. Fairlie, *J. Am. Chem. Soc.* **2003**, ASAP.

[21] P. Mayer, J. Schapp, W. Beck, *Z. Kristallogr. NCS*, **2003**, *218*, 113−114.

[22] S. T. Prigge, R. E. Mains, B. A. Eipper, L. M. Amzel, *Cell. Mol. Life Sci.* **2000**, *57*, 1236−1259.

[23] SHELXL-97: G. M. Sheldrick, SHELX-97. Programs for Crystal Structure Analysis (Release 97−2). University of Göttingen, **1997**, Germany.

[24] WinGX: L. J. Farrugia, *J. Appl. Cryst.* **1999**, *32*, 837.

Received February 6, 2003

 © 2003 Wiley-VCH Verlag GmbH & Co. KGaA, Weinheim

Long-Lived MLCT Excited States-Ru^{II} Complexes with a Helical Bis-Phen Ligand

Christine Goze,[a] Jean-Claude Chambron,[a][‡] Valérie Heitz,*[a] Didier Pomeranc,[a] Xavier J. Salom-Roig,[a] Jean-Pierre Sauvage,*[a] Angeles Farrán Morales,[b] and Francesco Barigelletti*[b]

Keywords: Luminescence / N ligands / Photochemistry / Ruthenium

The synthesis of a new Ru^{II} complex [Ru(**L$_1$**)(4,7-dpphen)]$^{2+}$, bearing a tetradentate bis-1,10-phenanthroline ligand **L$_1$**, is described. X-ray crystal structure analysis shows that the tetradentate ligand **L$_1$** coils around the metal and occupies both axial and two of the equatorial positions of the complex. ^{1}H NMR studies clearly indicate that the complex has C_2 symmetry in solution. The room temperature luminescence properties of [Ru(**L$_1$**)(4,7-dpphen)]$^{2+}$ have been studied, as have those of the related complex [Ru(**L$_2$**)(4,4′-dmbp)]$^{2+}$. For both complexes, the luminescence quantum yields and lifetimes are three to ten times higher than those of [Ru(bpy)$_3$]$^{2+}$. These unusual results are explained by the geometrical constraints imposed by the tetradentate ligands **L$_1$** and **L$_2$** in their respective complexes, resulting in an effective decoupling between the ^{3}MLCT and ^{3}MC excited states.

(© Wiley-VCH Verlag GmbH & Co. KGaA, 69451 Weinheim, Germany, 2003)

Introduction

[Ru(bipy)$_3$]$^{2+}$ (bipy = 2,2′-bipyridine) continues to be the most popular transition metal complex in the field of photochemistry and electron transfer.[1] A huge number of derivatives have been prepared and studied by numerous groups with the improvement of the photochemical properties of Ru-polypyridine complexes in mind, in view of their utilisation in, for instance, molecular photovoltaics and the chemical conversion of light energy.[2,3] In fact, the photochemical stability, the thermal stability of the reduced and oxidized states, the energy levels of the singlet and triplet MLCT states, the emission quantum yield, the ^{3}MLCT excited state lifetime, and the redox properties of the ground and excited states are important parameters that can, to a large extent, be controlled by the structural features of the chelates.[1,4] We now report that, through the use of tetradentate bis-1,10-phenanthroline ligands, which impose a helical geometry to the system in a strictly controlled fashion, the obtained ruthenium(II) complexes display unusually long-lived excited states. This behaviour is probably due to a cage-like effect for the employed tetradentate ligands rather than to electronic delocalisation in their frame systems.

Results and Discussion

The synthesis of [Ru**L$_1$**(4,7-dpphen)](PF$_6$)$_2$ is described in Figure 1 (4,7-dpphen represents 4,7-diphenyl-1,10-phenanthroline, as shown in Figure 2). This complex contains the 1,4-phenylenebis(7-bromo-1,10-phenanthroline) ligand **L$_1$**, which was synthesized from 7-*p*-bromophenyl-4-methyl-1,10-phenanthroline (**1**). At first, **1** was obtained through a Skraup reaction between 4-methyl-8-aminoquinoline[5,6] and *p*-bromophenyl β-chloroethyl ketone[7] in sulfuric acid in the presence of arsenic pentoxide, in 71% yield.[8] Subsequent treatment of **1** with LDA at −70 °C, followed by addition of α,α′-dibromo-*p*-xylene at −40 °C, afforded **L$_1$** in 7% yield, which is quite low in comparison with a similar reaction producing **L$_2$** in 88% yield.[5,6] This may be due to lower stability of the carbanion of **1**.

Coordination of ligand **L$_1$** on the ruthenium centre was achieved under high-dilution conditions in refluxing dichloroethane with use of [Ru(CH$_3$CN)$_4$Cl$_2$] as precursor complex, as described by von Zelewsky and co-workers.[9] The intermediate complex, [Ru**L$_1$**Cl$_2$], formed during the reaction, was treated directly with 4,7-dpphen in a refluxing mixture of water and ethanol. After anion exchange with an aqueous solution of KPF$_6$ and separation by column chromatography, the complex [Ru**L$_1$**(4,7-dpphen)](PF$_6$)$_2$

[‡] Present address: Université de Bourgogne, Faculté des Sciences Gabriel, LIMSAG, UMR5633 du CNRS; 6, Boulevard Gabriel; 21100 Dijon, France
[a] Laboratoire de Chimie Organo-Minérale, UMR 7513 du CNRS, Université Louis Pasteur, Faculté de Chimie, 4, rue Blaise Pascal, 67070 Strasbourg Cedex, France
[b] Istituto ISOF-CNR, Via P. Gobetti 101, 40129 Bologna, Italy

 © 2003 Wiley-VCH Verlag GmbH & Co. KGaA, Weinheim **DOI: 10.1002/ejic.200300161**

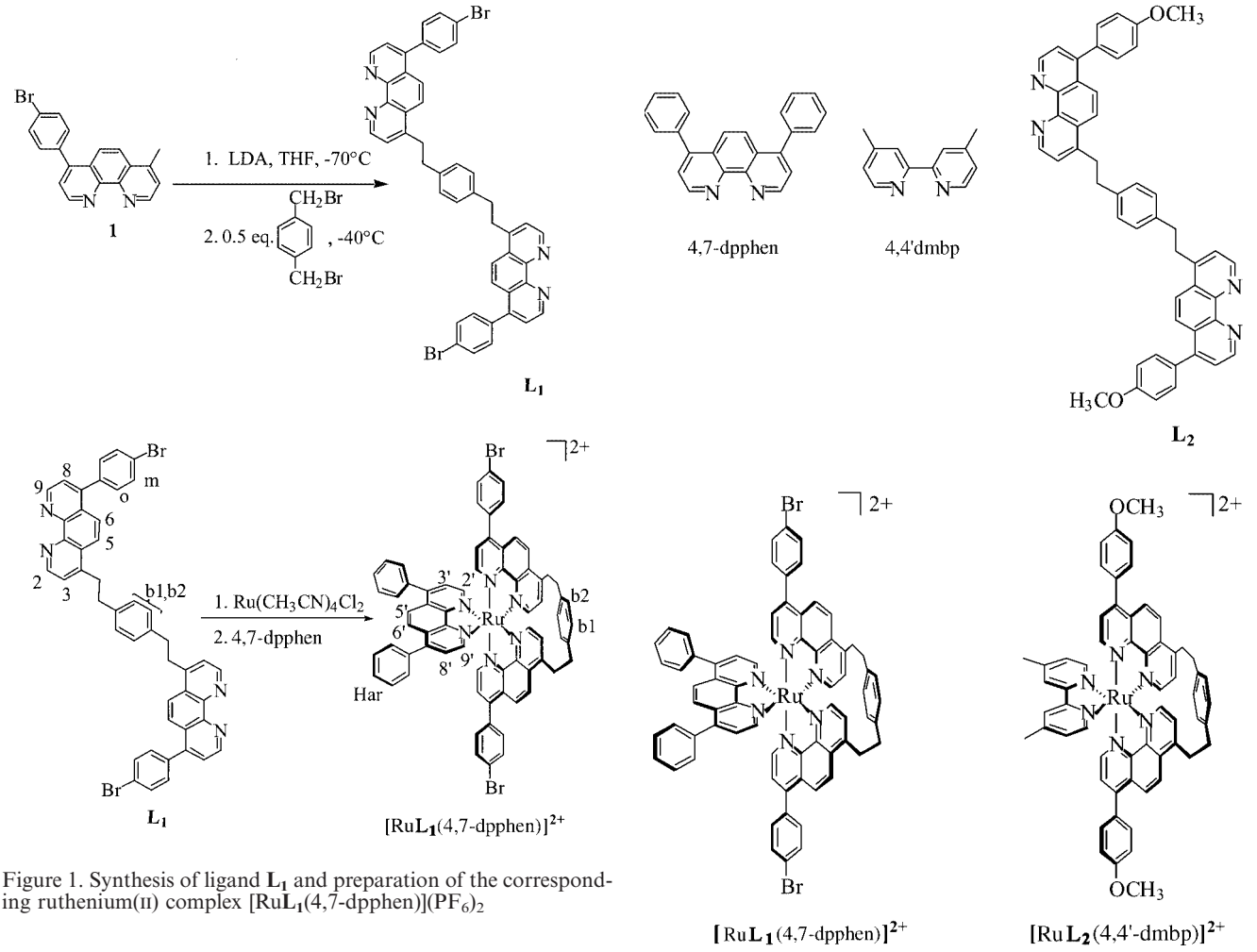

Figure 1. Synthesis of ligand $\mathbf{L_1}$ and preparation of the corresponding ruthenium(II) complex [Ru$\mathbf{L_1}$(4,7-dpphen)](PF$_6$)$_2$

Figure 2. Chemical formulae of the ligands and the complexes studied

was isolated in 44% yield. The C_2 symmetry of the complex in solution is clearly shown by analysis of its ^{1}H NMR spectrum (Figure 3). Protons H^2 and H^9 and protons H^{b1} and H^{b2} of ligand $\mathbf{L_1}$ are particularly sensitive to geometric and electronic changes on going from the free ligand $\mathbf{L_1}$ to the Ru-coordinated ligand $\mathbf{L_1}$ in [Ru$\mathbf{L_1}$(4,7-dpphen)](PF$_6$)$_2$, as shown in Figure 3. Protons H^{b1} and H^{b2}, homotopic in $\mathbf{L_1}$ (singlet at δ = 7.13 ppm), become diastereotopic in the C_2 symmetric complex [Ru$\mathbf{L_1}$(4,7-dpphen)](PF$_6$)$_2$, appearing as a pair of doublets [δ(H^{b1}) = 6.67 ppm, δ(H^{b2}) = 6.32 ppm]). In the non-coordinated ligand $\mathbf{L_1}$, protons H^2 and H^9 have low-field chemical shifts typical of protons located α to the nitrogen atom of a free 1,10-phenanthroline [δ(H^2) = 9.04 ppm and δ(H^9) = 9.19 ppm]. These protons are shifted upfield in the complex [δ(H^2) = 7.39 ppm and δ(H^9) = 7.99 ppm], since coiling of the ligand around the ruthenium centre places H^2 in the shielding field of the other phenanthroline of $\mathbf{L_1}$ and H^9 in that of the ancillary ligand 4,7-dpphen.

The X-ray crystal structure of the complex [Ru$\mathbf{L_1}$(4,7-dpphen)](PF$_6$)$_2$ was solved (Figure 4).[10] The complex crystallises in the monoclinic $P12/n1$ space group, with two molecules in the unit cell. The structure clearly shows that the axial and two equatorial positions are occupied by the nitrogen atoms of the ligand $\mathbf{L_1}$ and that the remaining equatorial positions are occupied by the 4,7-dpphen ligand. The Ru−N distances range between 2.057(9) Å and 2.076(9) Å. This structure is close to that of the complex [Ru$\mathbf{L_2}$(4,4′-dmbp)](PF$_6$)$_2$,[5] but with less distortion from linearity. The angle Br(1)−Ru−Br(2) is 174.6(9)°, as compared with 169.9(7)° for O−Ru−O. The distance Br(1)···Br(2) is 21.86(8) Å.

The synthesis of the ruthenium complex [Ru$\mathbf{L_2}$(4,4′-dmbp)](PF$_6$)$_2$ has been described previously.[5,6] This complex contains a bis-1,10-phenanthroline ligand $\mathbf{L_2}$, functionalized with a *p*-anisyl group on each position 7 of the phenanthroline unit (Figure 2), and differs from the former mainly in the nature of the ancillary ligand [4,4′-dimethyl-2,2′-bipyridine (4,4′-dmbp)].

Figure 5 shows the absorption spectra ($1\cdot10^{-5}$ M, acetonitrile) of the investigated complexes containing the tetradentate ligands $\mathbf{L_1}$ and $\mathbf{L_2}$; for purposes of comparison, the spectrum of [Ru(bpy)$_3$](PF$_6$)$_2$ is also shown.

For the [Ru$\mathbf{L_2}$(4,4′-dmbp)](PF$_6$)$_2$ and [Ru$\mathbf{L_1}$(4,7-dpphen)](PF$_6$)$_2$ complexes, the lowest-lying ^{1}MLCT band maxima fall at slightly lower energies − 458 and 460 nm, respectively − than that of the reference complex [Ru-

 © 2003 Wiley-VCH Verlag GmbH & Co. KGaA, Weinheim

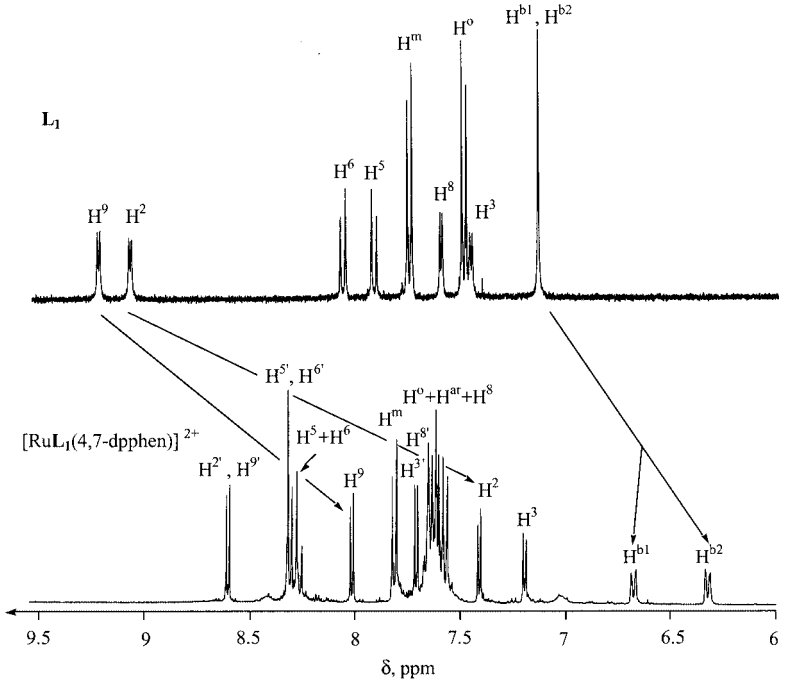

Figure 3. 400 MHz ^{1}H NMR spectra (low field region, CD_2Cl_2) of ligand $\mathbf{L_1}$ and complex [Ru$\mathbf{L_1}$(4,7-dpphen)]$(PF_6)_2$

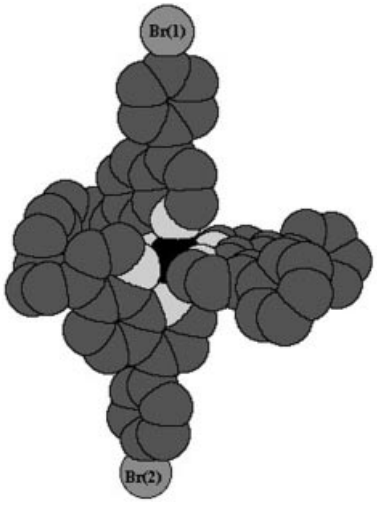

Figure 4. X-ray crystal structure of [Ru$\mathbf{L_1}$(4,7-dpphen)]$(PF_6)_2$

$(bpy)_3](PF_6)_2$ (452 nm). The absorption intensities at the MLCT band maxima are $\varepsilon = 20300$ and 20600 $M^{-1}\cdot cm^{-1}$, respectively, and hence about 40% higher than that of the reference complex ($\varepsilon = 14300$ $M^{-1}\cdot cm^{-1}$). This is an effect due to the "transfer term" for the promoted electron,[11−13] the average displacement of which during the MLCT transition is larger than that occurring in the case of $[Ru(bpy)_3]^{2+}$. The MLCT absorption features for [Ru$\mathbf{L_2}$(4,4′-dmbp)]$(PF_6)_2$ and [Ru$\mathbf{L_1}$(4,7-dpphen)]$(PF_6)_2$ thus suggest that the MLCT transitions in the visible region probably involve the extended frames of the $\mathbf{L_2}$ and $\mathbf{L_1}$ ligands, respectively {and also of the ligand 4,7-dpphen in the case of [Ru$\mathbf{L_1}$(4,7-dpphen)]$(PF_6)_2$}.

An observation of interest relates to the presence of intense absorption bands appearing at 310−320 nm for [Ru$\mathbf{L_2}$(4,4′-dmbp)]$(PF_6)_2$ and [Ru$\mathbf{L_1}$(4,7-dpphen)]$(PF_6)_2$, but not exhibited by $[Ru(bpy)_3](PF_6)_2$ (see Figure 5). This is a spectral region in which ^{1}MC (d-d) transitions are expected for Ru^{II}-polypyridine complexes.[1] This type of transition is Laporte-forbidden, and its extinction coefficient is estimated $\varepsilon \approx 10^2$ $M^{-1}\cdot cm^{-1}$ for $[Ru(bpy)_3]^{2+}$.[14] The fact that for [Ru$\mathbf{L_1}$(4,7-dpphen)]$(PF_6)_2$ and − even more so − for [Ru$\mathbf{L_2}$(4,4′-dmbp)]$(PF_6)_2$, the forbidden nature of the transition appears to be substantially lifted may be associated with permanent or transient distortions of the octahedral environment around the metal centre; the X-ray results (see above) are consistent with this interpretation. Finally, the absorption features in the 280−290 nm spectral portion are ^{1}LC in nature and are probably attributable to the ligand subunits directly coordinated to the metal centre,[1] as shown by the fact that their intensities are similar; see Figure 5.

Room temperature luminescence properties of [Ru$\mathbf{L_2}$(4,4′-dmbp)]$(PF_6)_2$ and [Ru$\mathbf{L_1}$(4,7-dpphen)]$(PF_6)_2$, obtained in degassed acetonitrile, are illustrated in Table 1; for purposes of comparison, luminescence results for $[Ru(bpy)_3](PF_6)_2$ are also listed.

The room temperature luminescence profiles (shown in the inset of Figure 5), the band peaks and the lifetime values are consistent with a ^{3}MLCT nature for the lowest-lying level of the investigated Ru-polypyridine luminophores. The band maxima of [Ru$\mathbf{L_2}$(4,4′-dmbp)]$(PF_6)_2$ and [Ru$\mathbf{L_1}$(4,7-dpphen)]$(PF_6)_2$ are slightly lower in energy than that of $[Ru(bpy)_3](PF_6)_2$, consistently with the absorption results. The relevant observation here is that, for the two complexes containing the tetradentate ligands $\mathbf{L_1}$ and $\mathbf{L_2}$, the lumi-

 © 2003 Wiley-VCH Verlag GmbH & Co. KGaA, Weinheim

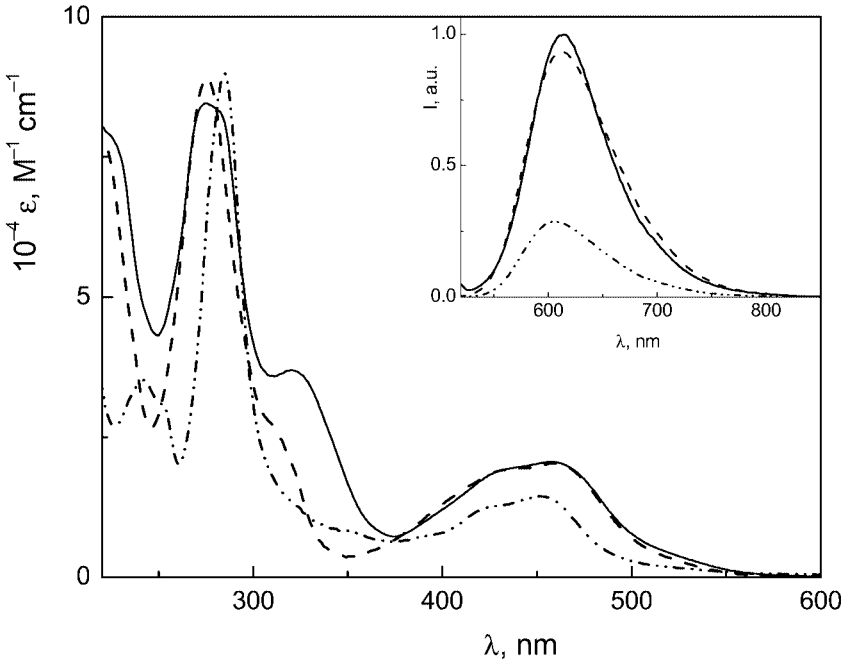

Figure 5. Ground state absorption spectra in acetonitrile for [Ru$\mathbf{L_2}$(4,4′-dmbp)]$(PF_6)_2$ (full line), [Ru$\mathbf{L_1}$(4,7-dpphen)]$(PF_6)_2$ (dash), and [Ru(bpy)$_3$]$(PF_6)_2$ (dash-dot-dot); the inset shows luminescence spectra obtained from excitation of isoabsorbing solutions at 450 nm

Table 1. Luminescence properties (O_2-free acetonitrile solvent, excitation at 450 or 337 nm)

	298 K					77 K	
	λ_{max}, nm	φ	τ, μs	$k_r \times 10^4$, s^{-1}[a]	$k_{nr} \times 10^5$, s^{-1}[b]	λ_{max}, nm	τ, μs
[Ru$\mathbf{L_2}$(4,4′-dmbp)]$(PF_6)_2$	614	0.30	4.0	7.5	1.8	608	10.5
[Ru$\mathbf{L_1}$(4,7-dpphen)]$(PF_6)_2$	612	0.28	8.6	3.3	0.83	610	11.2
[Ru(bpy)$_3$]$(PF_6)_2$	608	0.086	0.90	9.6	10.2	585	4.9

[a] $k_r = \varphi / \tau$. [b] $k_{nr} = (1 - \varphi)/\tau$.

nescence quantum yields (Φ) and lifetimes (τ) are three to ten times larger than those for [Ru(bpy)$_3$]$(PF_6)_2$. In these complexes, this happens because the non-radiative transitions (as quantified by the appropriate rate constant k_{nr}; see Table 1), known to govern the luminescence properties in the Ru-polypyridine complexes,[1,4] appear to be substantially depressed. Below we briefly discuss possible reasons for this behaviour.

With regard to the nature of the non-radiative processes deactivating the ^{3}MLCT luminescent level in Ru-polypyridine complexes, three main issues can be considered. These are: (i) the effect of the electronic delocalisation in the ligand system,[13,15,16] (ii) the effect of the energy gap law (regarding the direct ^{3}MLCT-to-GS transition),[17,18] and (iii) the thermal accessibility from the luminescent ^{3}MLCT level of a higher-lying ^{3}MC state, an effective doorway both to photochemistry (ligand release) and to fast, non-radiative deactivation (because of the strong ^{3}MC-GS coupling).[1] Given the extended ligand systems of $\mathbf{L_1}$ and $\mathbf{L_2}$, and also of 4,7-dpphen, we have addressed the role of electronic delocalisation, point (i), in detail. The extent of delocalisation is related to the displacement of the potential energy curve for the luminescent MLCT excited state with respect to the curve for the ground state (GS) (i.e., a high degree of delocalisation is accompanied by a small displacement). Analysis of the luminescence profiles affords the displacement parameter, the Huang−Rys electron-vibrational coupling constants pertinent to average frequencies (S_M) of ligand origin, $\hbar\omega_M = 1350$ cm^{-1}, corresponding to the vibrational progression exhibited by the low-temperature luminescence spectra.[15,16] The results of the vibronic analysis on the corrected luminescence profiles (on an energy scale, spectra obtained in frozen solvent at 77 K) are illustrated in Figure 6 and summarized in Table 2.

While for complexes containing highly delocalised ligand systems, such as dipyrido-phenazine,[19] pyrimidine-substituted terpyridine (tpy)[20] or back-to-back bis-tpy,[13] this type of vibronic analysis provides S_M values of between 0.2 and 0.5, for [Ru$\mathbf{L_2}$(4,4′-dmbp)]$(PF_6)_2$ and [Ru$\mathbf{L_1}$(4,7-dpphen)]$(PF_6)_2$ we find $S_M = 0.75$ and 0.78 (Table 2). These values are not greatly different from that for [Ru(bpy)$_3$]$(PF_6)_2$ ($S_M = 0.92$) taken as a prototype of a complex in which the ligand system is not greatly delocalised. The vibronic analysis does not therefore support delocalisation

 © 2003 Wiley-VCH Verlag GmbH & Co. KGaA, Weinheim

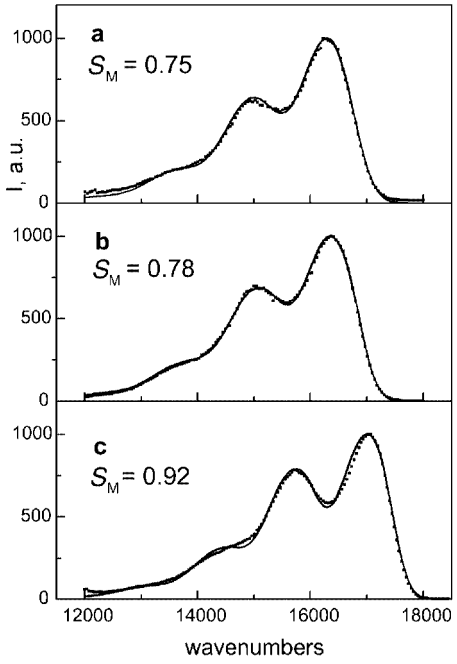

Figure 6. Vibronic analysis of the luminescence profiles for [Ru$\mathbf{L_1}$(4,7-dpphen)]$(PF_6)_2$ (**a**), [Ru$\mathbf{L_2}$(4,4′-dmbp)]$(PF_6)_2$ (**b**), and [Ru(bpy)$_3$]$(PF_6)_2$ (**c**), obtained at 77 K, acetonitrile, excitation at 450 nm; see text for further details

Table 2. Parameters from vibronic analysis (from fitting of the 77 K luminescence profiles, Equation (2) of text)

	E_{00}, cm^{-1} [a]	S_M [b]
[Ru$\mathbf{L_2}$(4,4′-dmbp)]$(PF_6)_2$	16680	0.78
[Ru$\mathbf{L_1}$(4,7-dpphen)]$(PF_6)_2$	16540	0.75
[Ru(bpy)$_3$]$(PF_6)_2$	17250	0.92

[a] Energy of the luminescent level (0−0 transition). [b] Huang−Rys factor for frequencies of ligand origin, $\hbar\omega_M$ = 1350 cm^{-1}.

in the ligands as a crucial factor for explaining the quite different luminescence features of [Ru$\mathbf{L_2}$(4,4′-dmbp)]$(PF_6)_2$ and [Ru$\mathbf{L_1}$(4,7-dpphen)]$(PF_6)_2$, in comparison with the case of [Ru(bpy)$_3$]$(PF_6)_2$. Effects related to point (ii) above (energy-gap law)[17,18] would also be expected to be of limited importance, given that the luminescent levels are not too apart from one another in energy (Table 2). In conclusion, we point to the fact that the tetradentate $\mathbf{L_1}$ and $\mathbf{L_2}$ ligands contain two bidentate subunits linked together. Literature examples exist in which constraints against elongation of the Ru−N bonds (inhibiting ligand release as a consequence of extreme elongation) can result in a sort of cage-like effect; this type of restrictions can originate from physical interactions, as found within zeolite frameworks, for instance,[21] or can be imposed at the molecular level by linking the coordinating bpy units together, thus yielding caged or hemi-caged complexes.[22] For the luminescent levels of both the [Ru$\mathbf{L_2}$(4,4′-dmbp)]$(PF_6)_2$ and the [Ru$\mathbf{L_1}$(4,7-dpphen)]$(PF_6)_2$ complexes, the reduced role of the non-radiative relaxation is probably related to such a cage-type effect, due to coordination of the tetradentate $\mathbf{L_1}$ and $\mathbf{L_2}$ ligands.

In conclusion, we have been able to show that the use of a bis-phen ligand, displaying geometrically constraining properties with respect to the coordination sphere of the complexed ruthenium(II) centre, produces effective decoupling between the ^{3}MLCT and the ^{3}MC excited states. This effect results in remarkably long-lived ^{3}MLCT excited states for the corresponding ruthenium(II)-tris(diimine) complexes.

Experimental Section

Materials: Starting materials were from commercial sources and were used as received. THF was distilled from sodium/benzophenone prior to use. Reactions performed under an atmosphere of argon used standard Schlenk techniques. [Ru$(CH_3CN)_4Cl_2$] was prepared according to the literature procedure.[9]

Physical Measurements: ^{1}H NMR: Bruker WP200SY (2OOMHz) and Bruker AM (400 MHz) instruments; the reported chemical shifts are referenced to Me_4Si as an internal standard. Mass spectroscopic data were obtained on a ZAB-HF (FAB) spectrometer with a nitrobenzyl alcohol matrix.

7-(*p*-Bromophenyl)-4-methyl-1,10-phenanthroline (1): A mixture of 4-methylquinolin-8-ylamine (1.5 g, 9.5 mmol), arsenic acid (5.65 g, 13.3 mmol), and phosphoric acid (15 mL) was heated at 100 °C. *p*-Bromophenyl-β-chloroethylketone[7] (3.28 g, 13.3 mmol) was added over a period of 1 h at such a rate that the temperature did not exceed 120 °C. After the addition the temperature was raised to 140 °C for 2 hours. After cooling, the mixture was poured onto ice and the resulting solution was neutralised with aqueous sodium hydroxide (30%), resulting in the precipitation of a brown solid. The mixture was left at 0 °C overnight. The precipitate was extracted several times with boiling toluene, the combined solutions were dried with $MgSO_4$, and the solvent was evaporated. The crude product was chromatographed on silica, eluted with hexane/ethyl acetate (50:50), with a gradient to ethyl acetate/methanol (99:1), yielding **1** as a pale brown solid (2.34 g, 71%). ^{1}H NMR (200 MHz, $CDCl_3$): δ = 2.78 (s, 3 H, CH_3), 7.42 (d, ^3J = 8.12 Hz, 2 H, H^m), 7.49 (d, ^3J = 4.42 Hz, 1 H, H^3), 7.53 (d, ^3J = 4.42 Hz, 1 H, H^8), 7.70 (d, ^3J = 8.12 Hz, 2 H, H^o), 7.86 (d, ^3J = 9.34 Hz, 1 H, H^5), 7.97 (d, ^3J = 9.36 Hz, 1 H, H^6), 9.07 (d, ^3J = 4.42 Hz, 1 H, H^2), 9.22 (d, ^3J = 4.42 Hz, 1 H, H^9) ppm. FAB-MS: *m*/*z* = 349.4 [M + H]$^+$.

$\mathbf{L_1}$: Diisopropylamine (0.162 mL, 1.15 mmol) was dissolved in THF (4 mL) under argon. *n*-Butyllithium (1.5 M, 0.764 mL) was added at 0 °C, and the mixture was stirred at 0 °C for 1 h. Compound **1** (400 mg, 1.15 mmol) was dissolved in THF (10 mL) under argon and transferred by cannula at −40 °C to the freshly prepared LDA solution. The solution instantly turned dark red and was stirred for 1 hour at −70 °C and for 1/2 h at −40 °C. α,α′-Dibromo-*p*-xylene (151.2 mg, 0.057 mmol) was dissolved in THF (5 mL) under argon and transferred to the reaction mixture at −40 °C by cannula. The mixture was stirred at room temperature overnight, during which the dark red solution turned pale brown. The solution was poured into water and extracted with dichloromethane. The combined organic phases were washed with ethanol in order to remove the oligomers and chromatographed on alumina, eluted with dichloromethane with a gradient to dichloromethane/methanol (98:2), to yield $\mathbf{L_1}$ as a brown solid (32 mg, 7%). ^{1}H

 © 2003 Wiley-VCH Verlag GmbH & Co. KGaA, Weinheim

NMR (400 MHz, CD_2Cl_2): δ = 3.09 (m, 4 H, CH_2), 3.42 (m, 4 H, CH_2), 7.13 (s, 4 H, H^{b1}+H^{b2}), 7.44 (d, ^3J = 4.20 Hz, 2 H, H^3), 7.47 (d, ^3J = 8.25 Hz, 4 H, H^o), 7.58 (d, ^3J = 4.39 Hz, 2 H, H^8), 7.73 (d, ^3J = 8.22 Hz, 4 H, H^m), 7.90 (d, ^3J = 9.37 Hz, 2 H, H^5), 8.05 (d, ^3J = 9.43 Hz, 2 H, H^6), 9.04 (d, ^3J = 4.32 Hz, 2 H, H^2), 9.19 (d, ^3J = 4.35 Hz, 2 H, H^9) ppm. FAB MS: *m*/*z* = 801 [M + H]$^+$.

[RuL_1(4,7-dpphen)]$(PF_6)_2$: Compound $\mathbf{L_1}$ (50 mg, 0.062 mmol) was dissolved in 1,2-dichloroethane (15 mL) under argon. Freshly prepared [Ru$(CH_3CN)_4Cl_2$] (21 mg, 0.062 mmol) was dissolved in 1,2-dichloroethane (15 mL) under argon. The two solutions were simultaneously added dropwise to refluxing 1,2-dichloroethane (800 mL) at a rate of 5 mL/h. After completion of the addition, the dark violet mixture was heated at reflux for two more hours, and allowed to cool overnight. The solvent was evaporated, and the resulting dark violet solid was dissolved in a mixture of ethanol/water (8 mL/1 mL) under argon. 4,7-Diphenylphenanthroline (4,7-dpphen, 20.6 mg, 0.062 mmol) was then added, and the reaction mixture was heated for 4 h, during which the solution turned orange-red. After the mixture had cooled, the ethanol was evaporated and the product was precipitated with a saturated aqueous solution of potassium hexafluorophosphate. The resulting precipitate was filtered under vacuum and chromatographed on silica, eluting with a gradient of dichloromethane/methanol, from 100:0 to 90:10. The complex [Ru$\mathbf{L_1}$(4,7-dpphen)]$(PF_6)_2$ was obtained as an orange solid (41 mg, 44%). TLC: one spot, R_f = 0.62 (CH_2Cl_2/MeOH, 8:2). ^{1}H NMR (400 MHz, CD_2Cl_2): δ = 3.11 (m, 2 H, CH_2), 3.28 (m, 2 H, CH_2), 3.42 (m, 2 H, CH_2), 3.94 (m, 2 H, CH_2), 6.32 (dd, ^3J = 7.95, ^4J = 1.6 Hz, 2 H, H^{b2}), 6.67 (dd, ^3J = 8.07, ^4J = 1.72 Hz, 2 H, H^{b1}), 7.18 (d, ^3J = 5.36 Hz, 2 H, H^3), 7.39 (d, ^3J = 5.4 Hz, 2 H, H^2), 7.55 (d, ^3J = 8.52 Hz, 4 H, H^o), 7.59 (d, ^3J = 5.5 Hz, 2 H, H^8), 7.61 (m, 10 H, H^{ar}), 7.68 (d, ^3J = 5.52 Hz, 2 H, $H^{3',8'}$), 7.79 (d, ^3J = 8.52 Hz, 4 H, H^m), 7.99 (d, ^3J = 5.4 Hz, 2 H, H^9), 8.24 (d, ^3J = 9.32 Hz, 2 H, H^5), 8.28 (d, ^3J = 9.2 Hz, 2 H, H^6), 8.29 (s, 2 H, $H^{5',6'}$), 8.57 (d, ^3J = 5.52 Hz, 2 H, $H^{2',9'}$) ppm. FAB MS: *m*/*z* = 1379.1 [M − PF_6^-]$^+$, 1234.2 [M − 2PF_6^- + e$^-$]$^+$, 617.6 [M − 2PF_6^-]$^{2+}$/2.

Optical Spectroscopy: Absorption spectra were recorded with a Perkin−Elmer Lambda 9 spectrophotometer in dilute (10^{-5} M) acetonitrile solutions. Luminescence experiments were performed in pump-freeze-thaw degassed acetonitrile at room temperature and at 77 K (liquid nitrogen temperature, samples were in capillary tubes immersed in a quartz finger Dewar).

Luminescence spectra were obtained with a Spex Fluorolog II spectrofluorimeter equipped with a Hamamatsu R928 phototube. Uncorrected luminescence band maxima are used throughout the text unless otherwise stated; in order to determine luminescence quantum yields and to perform the vibronic analyses (see below) of luminescence intensity profiles, we employed corrected luminescence spectra on an energy scale (cm^{-1}). The corrected spectra were obtained either by use of a correction curve provided by the supplier or by employment of a calibrated 45-W quartz-halogen tungsten filament lamp (Optronic Laboratories) as a standard for the correction of the phototube response. Luminescence quantum yields Φ_s were obtained according to Equation (1),[23] where *s* and *r* stand for sample and reference standard, respectively, A is the absorbance (taken ≤ 0.1) at the selected excitation wavelength, and n is the refractive index of the solvent. [Ru$(bpy)_3$]Cl_2 was chosen as a reference standard ($\Phi = 2.8\cdot10^{-2}$ in air-equilibrated water).[24] The experimental uncertainty in the band maximum for absorption and luminescence spectra is 2 nm; that for luminescence quantum yield is 20%. Luminescence lifetimes were obtained with an IBH single-photon-counting apparatus (N_2 lamp, excitation at 337 nm). The uncertainty in the evaluated lifetimes is 8%.

$$\frac{\Phi_s}{\Phi_r} = \frac{A_r n_s^2 (area)_s}{A_s n_r^2 (area)_r} \quad (1)$$

Vibronic band intensities of the luminescence spectra on an energy scale (cm^{-1}) were analysed according to a fitting procedure proposed by Meyer and co-workers.[25,26] For the luminescence spectra obtained at 77 K we used a two-mode analysis according to the following expression [Equation (2)]:

$$I(\bar{\nu}) = \sum_{v_M=0}^{\infty}\sum_{v_L=0}^{\infty}\left(\frac{\bar{\nu}_{00} - v_M\bar{\nu} - v_L\bar{\nu}}{\bar{\nu}_{00}}\right)^3\left(\frac{S_M^{v_M}}{v_M!}\right)\times \left(\frac{S_L^{v_L}}{v_M!}\right)\exp\left[-(4\ln 2)\left(\frac{\bar{\nu} - \bar{\nu}_{00} - v_M\bar{\nu} - v_L\bar{\nu}}{\bar{\nu}_{1/2}}\right)^2\right] \quad (2)$$

where $I(\bar{\nu})$ is the luminescence intensity profile, $\bar{\nu}_\infty$ is the energy of the 0−0 transition (hereafter indicated as E_∞), *v* are vibrational quantum numbers, *M* and *L* are labels for average and low frequency modes, taken as $\hbar\omega_M$ = 1350 cm^{-1} and $\hbar\omega_M$ = 400 cm^{-1}, respectively, S_M and S_L are displacement parameters along the indicated vibrational modes, and $\bar{\nu}_{1/2}$ is the bandwidth at half maximum (fwhm) of the vibronic line.

Acknowledgments

Thanks are due to the EU for financial support (A. F. M., TMR contract CT98-0226), and to Prof. T. J. Meyer and D. J. P. Claude for kindly providing the software for the vibronic analysis. X. J. S. R. thanks the Rectorat de l'Université Louis Pasteur for financial support. D. P. thanks the French Ministry of education for a fellowship.

[1] A. Juris, V. Balzani, F. Barigelletti, S. Campagna, P. Belser, A. von Zelewsky, *Coord. Chem. Rev.* **1988**, *84*, 85−277.
[2] C. A. Bignozzi, J. R. Schoonover, F. Scandola, *Molecular Level Artificial Photosynthetic Materials* **1997**, *44*, 1−95.
[3] J. K. McCusker, *Science* **2001**, *293*, 1599−1601.
[4] J.-P. Sauvage, J.-P. Collin, J.-C. Chambron, S. Guillerez, C. Coudret, V. Balzani, F. Barigelletti, L. De Cola, L. Flamigni, *Chem. Rev.* **1994**, *94*, 993−1019.
[5] D. Pomeranc, V. Heitz, J.-C. Chambron, J.-P. Sauvage, *J. Am. Chem. Soc.* **2001**, *123*, 12215−12221.
[6] D. Pomeranc, J.-C. Chambron, V. Heitz, J.-P. Sauvage, *Comptes Rendus Acad. Sci. Ser. II C* **2001**, *4*, 197−200.
[7] F. G. Bordwell, W. T. Brannen, Jr., *J. Am. Chem. Soc.* **1964**, *86*, 4645−4650.
[8] F. H. Case, *J. Chem. Soci.* **1951**, 1541−1545.
[9] P. Hayoz, A. von Zelewsky, H. Stoeckli-Evans, *J. Am. Chem. Soc.* **1993**, *115*, 5111−5114.
[10] Summary of data: formula: $C_{78}H_{60}Br_2F_{12}N_{10}P_2Ru_1$. Unit cell parameters: *a:* 13.0677(1), *b:* 15.3308(3), *c:* 20.3461(3) Å; beta: 100.641(5)°. Space group *P2/n.* CCDC-201524 contains the supplementary crystallographic data for this paper. These data can be obtained free of charge at www.ccdc.cam.ac.uk/conts/retrieving.html [or from the Cambridge Crystallographic Data

 © 2003 Wiley-VCH Verlag GmbH & Co. KGaA, Weinheim

Centre, 12, Union Road, Cambridge CB2 1EZ, UK; Fax: (internat.) +44-1223/336-033; E-mail: deposit@ccdc.cam.ac.uk].
[11] P. Day, N. Sanders, *J. Chem. Soc., A* **1967**, 1536.
[12] L. De Cola, F. Barigelletti, *Inorg. Chim. Acta* **1989**, *159*, 169.
[13] L. Hammarström, F. Barigelletti, L. Flamigni, M. T. Indelli, N. Armaroli, G. Calogero, M. Guardigli, A. Sour, J.-P. Collin, J.-P. Sauvage, *J. Phys. Chem. A* **1997**, *101*, 9061−9069.
[14] D. M. Roundhill, *Photochemistry and Photophysics of Metal Complexes*, Plenum Press, New York, **1994**, Ch. 5.
[15] J. A. Treadway, B. Loeb, R. Lopez, P. A. Anderson, F. R. Keene, T. J. Meyer, *Inorg. Chem.* **1996**, *35*, 2242−2246.
[16] G. F. Strouse, J. R. Schoonover, R. Duesing, S. Boyde, W. E. Jones, T. J. Meyer, *Inorg. Chem.* **1995**, *34*, 473−487.
[17] J. V. Caspar, E. M. Kober, B. P. Sullivan, T. J. Meyer, *J. Am. Chem. Soc.* **1982**, *104*, 630.
[18] R. Englman, J. Jortner, *Mol. Phys.* **1970**, *18*, 145.
[19] J. A. Treadway, G. F. Strouse, R. R. Ruminski, T. J. Meyer, *Inorg. Chem.* **2001**, *40*, 4508−4509.
[20] Y. Q. Fang, N. J. Taylor, G. S. Hanan, F. Loiseau, R. Passalacqua, S. Campagna, H. Nierengarten, A. Van Dorsselaer, *J. Am. Chem. Soc.* **2002**, *124*, 7912−7913.
[21] K. Maruszewski, J. R. Kincaid, *Inorg. Chem.* **1995**, *34*, 2002−2006.
[22] F. Barigelletti, L. De Cola, V. Balzani, P. Belser, A. von Zelewsky, F. Vögtle, F. Ebmeyer, S. Grammenudi, *J. Am. Chem. Soc.* **1989**, *111*, 4662−4668.
[23] J. N. Demas, G. A. Crosby, *J. Phys. Chem.* **1971**, *75*, 991.
[24] K. Nakamaru, *Bull. Chem. Soc., Jpn.* **1982**, *55*, 2967.
[25] J. P. Claude, T. J. Meyer, *J. Phys. Chem.* **1995**, *99*, 51−54.
[26] K. R. Barqawi, Z. Murtaza, T. J. Meyer, *J. Phys. Chem.* **1991**, *95*, 47−50.

Received March 27, 2003

 © 2003 Wiley-VCH Verlag GmbH & Co. KGaA, Weinheim

$P_8O_{12}\cdot 2BH_3$ – The Borane Adduct of a New Molecular Phosphorus Oxide

Akbar Tellenbach,[a] and M. Jansen*[a]

Keywords: Phosphorus / Phosphorus oxides / Boranes / Cage compounds / Dimerization

$P_4O_6\cdot BH_3$, which readily forms from P_4O_6 and $Me_2S\cdot BH_3$ in a stoichiometric reaction, dimerizes spontaneously at –30 °C in a concentrated toluene solution resulting in the crystallization of $P_8O_{12}\cdot 2BH_3$ (**1**). The synthesis of **1** represents the first selective interconnection of molecular phosphorus chalcogenides leading to the formation of a new, flexible P_8O_{12} cage. The thermodynamic driving force for the dimerization reaction results from a gain of enthalpy due to enhanced P–O double-bond contributions and a relief of angular strain. In terms of kinetics, the behavior of $P_4O_6\cdot BH_3$, differing from that of other P_4O_6 derivatives, is caused by the low π-donor ability of BH_3 provoking a Michaelis–Arbuzov-like reactivity at the adjacent phosphorus atom and thus inducing cage opening. **1** was characterized by means of X-ray diffractometry (powder, single crystal), NMR spectroscopy (solution, solid), IR spectroscopy, Raman spectroscopy, and mass spectrometry. Mass spectrometric investigations suggest considerable BH_3 abstraction as well as an enhanced stability of $P_8O_{12}\cdot BH_3$ and P_8O_{12}, compared to **1**.

(© Wiley-VCH Verlag GmbH & Co. KGaA, 69451 Weinheim, Germany, 2003)

Introduction

The chemical behavior of P_4O_6, a molecular phosphorus oxide having an adamantane-like birdcage structure, seems to be rather ambivalent. On the one hand P_4O_6 reacts readily with electrophilic compounds resulting in the attachment of terminal atoms or groups to phosphorus atoms of the cage. The electrophilic addition gives rise to the formation of chalcogen derivatives P_4O_n ($n = 7-10$),[1−6] $P_4O_6S_n$ ($n = 1-4$),[7−10] $P_4O_6Se_n$ ($n = 1-4$),[11−14] and transition metal complexes like $P_4O_6[Ni(CO)_3]_n$ ($n = 1-4$),[15,16] $P_4O_6[Fe(CO)_4]_n$ ($n = 1-4$),[17,18] and $P_4O_6[M(CO)_5]$ (M = Cr, Mo, W).[19] On the other hand, ring-opening reactions are much more difficult to control and normally lead to complete degradation of the framework.[20−22] Among the few selective cage-opening reactions, known so far, there is the formation of P_4O_6NR (R = organic groups) by nitrene insertion and rearrangement of the cage structure, resulting in an adamantane-like P_4O_5N unit.[23−25] Although quantum chemical calculations for P_4O_6X (X = O, S, H^+, F^+, Cl^+, N^-)[26] indicate a strong dependence of the P−O cage bond lengths on the electronegativity of terminal atoms attached to the phosphorus atom, very similar geometrical parameters have been found for the P_4O_6 cages of P_4O_7,[2,3] P_4O_6S,[7] P_4O_6Se,[11] and $P_4O_6Fe(CO)_4$.[18] Up to now, this observation and the different behavior of P_4O_6NR in comparison with P_4O_6X (e.g. X = O, S, Se, etc.) are not completely understood.

In contrast to chalcogen atoms, the electrophilic addition of BH_3 is expected to affect the cage bonds in a different manner due to the reduced π-donor abilities of boron. For this reason we have tried to synthesize and characterize borane complexes of P_4O_6, the constitutions of which were previously studied by ^{31}P NMR spectra of solutions.[27−29] Thus far, a detailed investigation of these compounds in a pure state failed because of their high sensitivity and instability. During our recent attempts in crystallizing dissolved $P_4O_6\cdot BH_3$, we have achieved the first selective dimerization of phosphorus chalcogenides. The obtained product, $P_8O_{12}\cdot 2BH_3$ (**1**), is the bis(borane) adduct of a new molecular phosphorus oxide P_8O_{12}.[30]

Results and Discussion

Synthesis and Thermal Properties

Depending on the relative quantities, P_4O_6 readily forms $P_4O_6\cdot nBH_3$ ($n = 1-3$) when reacting with gaseous diborane in organic solvents at room temperature.[28,29] The reaction takes place in a sequential manner with the successive coordination of one, two, and three BH_3 groups. The chemical shifts, coupling constants, and splitting patterns, observed in ^{31}P NMR spectra, clearly indicate boron atoms being attached to phosphorus atoms.[28,29] If pure liquid P_4O_6 is used, electrophilic addition stops at the stage of $P_4O_6\cdot 2BH_3$ due to crystallization.[27] For practical reasons, we have chosen $Me_2S\cdot BH_3$ as a reagent. The first equivalent of $Me_2S\cdot BH_3$ reacts completely within an hour, giving mainly $P_4O_6\cdot BH_3$ with small amounts of $P_4O_6\cdot 2BH_3$, P_4O_7, P_4, and some residual P_4O_6. $Me_2S\cdot BH_3$ is less effective than B_2H_6. Thus, $P_4O_6\cdot BH_3$ and $P_4O_6\cdot 2BH_3$ are generated in a 1:2.5

[a] Max Planck Institute for Solid State Research
Heisenbergstr. 1, 70569 Stuttgart, Germany
Fax: (internat.) + 49-711/689-1502
E-Mail: m.jansen@fkf.mpg.de

ratio without any $P_4O_6 \cdot 3BH_3$, even if 4 equiv. of $Me_2S \cdot BH_3$ are applied. The NMR spectroscopic data of these compounds (see Exp. Sect.) are in good agreement with those described earlier.[28] After removing Me_2S and storing a highly concentrated solution of $P_4O_6 \cdot BH_3$ in toluene at −30 °C for a period of three months, cuboid crystals were recovered. Crystal structure determination, ^{31}P NMR spectroscopy, and mass spectrometry (see below) demonstrate that the crystallization product does not consist of the expected $P_4O_6 \cdot BH_3$, but of the corresponding dimer $P_8O_{12} \cdot 2BH_3$, (Scheme 1).

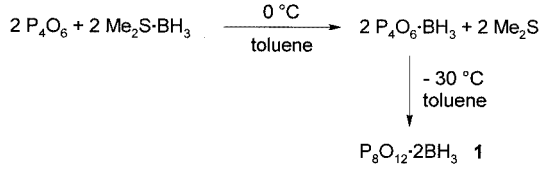

Scheme 1. Reaction scheme of the formation of **1**

Under standard conditions, **1** forms a colorless solid, which is extremely sensitive to humidity as well as to nucleophilic or protic reagents. Furthermore, **1** is highly explosive, when exposed to any kind of pressure, traces of pure water or ethanol. Upon heating the solid above 70 °C for some hours, decomposition occurs, with the color turning yellow, orange, and finally red. According to the results of temperature-dependent powder diffractometry (Guinier−Simon technique), crystalline BPO_4 (tetragonal) is generated above 230 °C. As is to be expected, the thermal decomposition is irreversible. Apart from a slight mass loss of about 4%, thermal analyses by DTA and TGA do not show any well-defined effect below 250 °C. In solution (toluene, xylene, CH_2Cl_2) **1** slowly decomposes furnishing a mixture of **1**, $P_4O_6 \cdot BH_3$, P_4O_6, and some P_4O_7. At room temperature the monomer/dimer ratio climbs to 1:1 within 18 h. Furthermore, the solution mainly contains entire molecules of **1**, even on heating at 70 °C for 2 h. On the other hand, $P_8O_{12} \cdot 2BH_3$ is stable at −30 °C both, as a solid and in solution.

Crystal Structure Determination

The powder diffraction pattern of **1** (Figure 1; Table 1) has been indexed based on an orthorhombic unit cell (Table 2). The crystal structure has been determined and refined using single-crystal X-ray methods. The crystal data are summarized in Table 2. A powder diffraction pattern, which has been calculated on the basis of the single-crystal data, is in good agreement with the observed one (Figure 1).

The crystal structure consists of $P_8O_{12} \cdot 2BH_3$ molecular units. As shown in Figure 2, two bicyclic $P_4O_5 \cdot BH_3$ subunits are connected by O1 and O7 in a way, such that the BH_3 groups are pointing in opposite directions (head−tail linkage). Thus, $P_8O_{12} \cdot 2BH_3$ represents the bis(borane) complex of a new molecular phosphorus oxide P_8O_{12}, which is the dimer of the well-known P_4O_6. In recent investigations concerning the dimerization tendency of molecular phosphorus oxides, we have been able to confirm the existence of ligand-free P_8O_{12} by means of ^{31}P NMR spectroscopy (P_8O_{12} has been mentioned before by Meisel and co-workers,[31] but neither experimental evidence nor analytical data were presented). Due to packing effects the point symmetry C_{2h}, expected for free $P_8O_{12} \cdot 2BH_3$ molecules, is reduced to C_1 in the crystalline solid. As a consequence, the two bicyclic $P_4O_5 \cdot BH_3$ units are folded and slightly twisted against each other (folding along the O1−O7 axis with torsion angles of 151° for P1−O1−O7−P5 and 164° for P4−O7−O1−P8; twisting along the O4−O10 axis; see Figure 2).

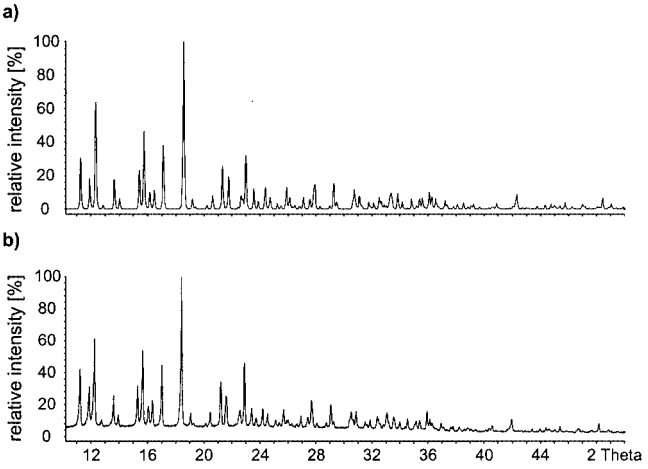

Figure 1. Powder diffraction pattern of **1**; calculated from single-crystal data (a) and observed (b)

Table 1. The 25 most intense reflections of the powder diffraction pattern of **1**; zero-point correction on the basis of silicon as external standard (a = 5.43088 Å[62])

$h\ k\ l$	2θ [°]	d [Å]	I_{rel} [%]
0 2 0	11.309	7.8178	41.7
0 2 1	11.948	7.4010	30.8
1 1 1	12.335	7.1697	61.1
0 2 2	13.688	6.4639	24.8
0 0 4	15.405	5.7471	32.0
1 2 1	15.772	5.6142	53.1
0 2 3	16.184	5.4722	18.2
1 1 3	16.473	5.3768	22.4
1 2 2	17.134	5.1709	43.7
1 0 4	18.543	4.7810	100.0
2 0 0	20.599	4.3082	14.9
1 3 2	21.355	4.1574	34.1
2 1 1	21.726	4.0872	24.2
1 2 4	21.772	4.0787	24.3
2 1 2	22.746	3.9062	16.4
1 3 3	23.057	3.8542	45.4
2 2 0	23.559	3.7732	17.4
2 1 3	24.356	3.6515	17.1
1 2 5	24.707	3.6004	14.1
0 2 6	25.876	3.4403	17.1
1 3 5	27.848	3.2010	22.0
2 3 3	29.289	3.0467	19.9
1 3 6	30.741	2.9061	15.1
2 3 4	31.080	2.8751	15.1
1 6 1	36.195	2.4797	15.4

 © 2003 Wiley-VCH Verlag GmbH & Co. KGaA, Weinheim

Table 2. Crystallographic data for **1**

Empirical formula	$H_6B_2O_{12}P_8$
Formula mass	467.43
Crystal size	0.7 × 0.7 × 0.7 mm
Temperature	−90(1) °C
Wavelength	λ(Mo-K_α) = 0.71073 Å
Detector distance	3 cm
Exposure time	10 s
Scan type, width	ω, 0.3°
Exposures taken	1800
$2\theta_{max}$	65°
Crystal system	orthorhombic
Lattice parameters:	
Single crystal[a]	a = 8.606(3) Å
	b = 15.686(6) Å
	c = 22.960(9) Å
	V = 3099(2) Å^3
Powder[b]	a = 8.6163(2) Å
	b = 15.6350(3) Å
	c = 22.9882(5) Å
	V = 3096.8(1) Å^3
Space group	*Pbca* (no. 61)
Z	8
hkl range	h: −13 to 13; k: −23 to 23; l: −34 to 34
F(000)	1856
Density (calculated)	2.003 g cm^{-3}
Linear absorption coefficient	μ = 0.952 mm^{-1}
Transmission factors	0.3898 and 0.4991
Reflections collected	49064
Independent reflections	5604
Reflections observed [$I > 2\ \sigma(I)$]	4704
Parameters refined	224
Absorption correction	semiempirical (see text)
R_{int}	0.0465
R_1 (observed reflections)	0.0364
wR_2 (observed reflections)	0.0938
GOOF	1.072
Largest diff. peak and hole	0.762 and −0.318 e·Å^{-3}

[a] At −90 °C. [b] At 25 °C, refined.

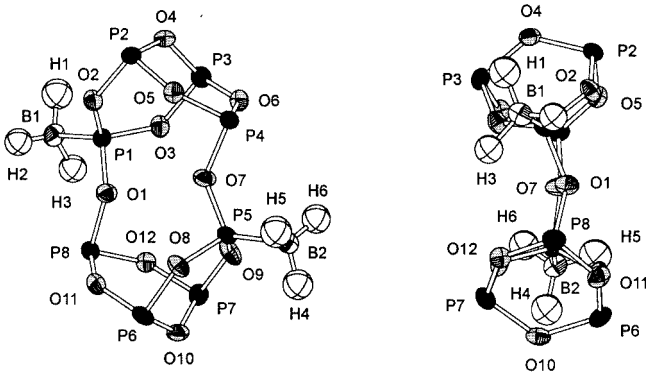

Figure 2. Molecular structure of **1** (two views; ellipsoids for 50% probability)

As there are no other phosphorus compounds known that have a similar structure, we are restricted to comparing the geometric parameters of **1** with those of P_4O_6X (X = O, S, Se) and $(RO)_3P{\cdot}BH_3$ (R = organic groups). The P−O bond lengths, varying between 157.8 and 167.1 pm, indicate pronounced P−O double-bond contributions [P−O (calculated): 176 pm;[32] P=O: 145.0 pm in P_4O_7,[3] 145.5 pm in P_4O_8 [4]] and may be subdivided into three types: P(B)−O_P^{III}, P^{III}−$O_{P(B)}$, and P^{III}−O_P^{III}, with P(B) and P^{III} being phosphorus atoms in the unit O_3PB and O_3P, respectively. The corresponding bond lengths reflect a characteristic distortion of the phosphorus−oxygen framework, which is already known from P_4O_6X (Table 3; X = O, S, Se) and is apparently induced by the electrophilic addition to the P_4O_6 cage. Thus, starting from the respective four-fold-coordinated phosphorus atom, the P−O bonds display an alternating contraction and elongation compared to the corresponding length in P_4O_6 (P−O: 165.3 pm[33]). But in the case of **1**, the distorting effect spreads out from two centers (P1 and P5) across a larger network. As mentioned in the introduction, the degree of this distortion so far seems to be rather independent of the nature of the terminal atom attached to the phosphorus atom. In this regard, the significant contraction of all P−O bonds by about 1 or 2 pm, as determined for **1**, is remarkable (Table 3). According to quantum chemical calculations,[26] the P(X)−O_P^{III} bonds are elongated, as the positive polarization of P(X) decreases, which on its part depends on the electron-withdrawing character of the attached element X. In contrast to these findings, boron generates significantly shorter P−O bonds than the more electronegative elements oxygen, sulfur, and selenium. A possible explanation for this observation may be seen in the fact that, contrary to chalcogen atoms, BH_3 groups are σ-acceptors with strongly reduced π-donor capabilities. A small degree of π-back donation by BH_3 was postulated very early in the investigations of the bonding in $PF_3{\cdot}BH_3$ [34,35] and $CO{\cdot}BH_3$.[34,36] More recent theoretical studies including natural energy decomposition analyses seem to confirm the effect of hyperconjugation for $CO{\cdot}BH_3$ [37,38] and $PF_3{\cdot}BH_3$.[39,40] On the other hand, it has to be stated that hyperconjugation is not mentioned in some of the respective treatments[41] and experimental evidence for it can hardly be provided. Anyway, the efficiency of π-back donation should be smaller for BH_3 than for chalcogen atoms leading, in the case of **1**, to an enhanced positive polarization of P(X). Another special feature of **1** arises from the head−tail linkage in combination with the alternation of contracted and stretched P−O bonds. As a result, both $P_4O_5{\cdot}BH_3$ units are connected by extremely asym-

Table 3. Mean bond lengths [pm] and mean bond angles [°] for **1**, P_4O_7, P_4O_6S, and P_4O_6Se; X = B, O, S, Se; P(X) = P in unit O_3PX; P^{III} = P in unit O_3P

	$P_8O_{12}{\cdot}2BH_3$	P_4O_7 [a]	P_4O_6S [b]	P_4O_6Se [c]
P(X)−O_P^{III}	158.3	159.4	159.6	160.2
P^{III}−$O_{P(X)}$	166.3	168.4	167.8	167.3
P^{III}−O_P^{III}	162.9	164.6	163.7	163.6
X−P(X)−O	115.2	114.9	115.3	115.8
O−P(X)−O	103.2	103.5	103.1	102.5
O−P^{III}−O	99.2	98.9	98.9	99.0
P(X)−O−P^{III}	132.7	123.9	124.2	124.6
P^{III}−O−P^{III}	132.9	128.1	128.1	128.0

[a] Refs.[2,3] [b] Ref.[7] [c] Ref.[11]

 © 2003 Wiley-VCH Verlag GmbH & Co. KGaA, Weinheim

metrical P−O−P bridges, containing the longest and the two shortest P−O bonds in the molecule (167.1, 158.0, and 157.8 pm, respectively). These bridges are arranged in a way that favors a symmetrical cleavage of the molecule. In fact, this is what we have observed in both, solution (^{31}P NMR spectra) and gas phase (mass spectra).

The O−P−O bond angles ranging from 95.3 to 104.7° tend to be about 4° smaller at the P^{III} than at the P(X) atom (Table 3). The mean bond angles for O−P−O and X−P−O are nearly identical to those in P_4O_6X (Table 3), whereas the mean values for P−O−P are substantially larger [about 5° for P^{III}−O−P^{III} and about 9° for P(X)−O−P^{III}]. Both, contraction of P−O bonds and widening of P−O−P bond angles, are consistent with assuming an increased double-bond character. These π-interactions are promoted by a reduction of ring strain upon dimerization, and balance the positive polarization of the P(B) atom at the same time.

The geometric parameters within the $O_3P{\cdot}BH_3$ unit of **1** correspond quite well with the values obtained for borane complexes of organic phosphites $(RO)_3P{\cdot}BH_3$.[42−45] The P−B mean bond length of 187.0 pm, especially, is in line with assuming a pure single bond. Due to the difficulties in accurately localizing hydrogen positions by X-ray diffraction methods, the B−H bond lengths and bond angles vary significantly (mean values for B−H: 109.8 pm; P−B−H: 103.5°). However, the H−B−H mean bond angle of 114.7° is exactly the average value of 109.4 and 120°, encountered for tetrahedral and trigonal-planar coordination of the boron center, respectively. The intermolecular atomic distances are in the range as expected for van der Waals interactions.

NMR Spectroscopy

In our previous investigations on phosphorus oxides and their derivatives, NMR spectroscopy turned out to be a useful tool, sometimes providing essential insights otherwise not accessible.[46−48] For **1** the isotropic signals of nearly all eight crystallographically independent phosphorus atoms can be resolved in the ^{31}P MAS NMR spectrum (Figure 3).

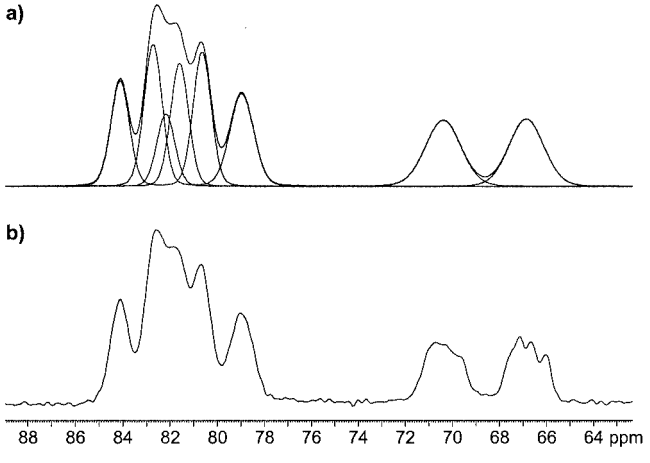

Figure 3. Isotropic signals of the ^{31}P MAS NMR spectrum of **1**; simulated with deconvolution (a; see Table 4) and observed (b)

Table 4. Simulation parameters for the isotropic ^{31}P MAS NMR signals of **1** (see Figure 3)

δ [ppm]	Amplitude	Line width [Hz]	Intensity [%]
66.9	73.5	279.6	13.4
70.4	72.1	286.2	13.5
79.0	101.0	190.4	12.6
80.7	146.9	145.8	14.0
81.6	134.6	145.4	12.9
82.2	79.0	145.8	7.6
82.8	155.2	145.8	14.9
84.2	115.1	145.7	11.1

A simulation using the individual chemical shifts given in Table 4 is in good agreement with the observed spectrum (Figure 3). By means of cross polarization from ^{1}H onto ^{31}P spins the signals at δ = 66.9 and 70.4 ppm could be assigned to the BH_3-bearing phosphorus atoms P1 and P5. This is in accordance with additional broadening and splitting of these signals due to coupling with ^{11}B nuclei having a quadrupole moment. Thus, the other six signals can be attributed to the P2, P3, P4, P6, P7, and P8 atoms. A further assignment to individual atoms has not been attempted. An explanation for the low signal intensity at δ = 82.2 ppm cannot be given. The isotropic chemical shifts of the BH_3 groups of **1**, observed in ^{1}H and ^{11}B MAS NMR spectra, are δ = 0.88 and −39.6 ppm, respectively, and match quite well with the values of $P_4O_6{\cdot}BH_3$ (δ = 0.6 and −40 ppm[29]).

The NMR spectra of **1**, in solution, are in accordance with molecules exhibiting C_{2h} symmetry. This observation might be understood by assuming a flexible P_8O_{12} framework allowing fast internal motion in solution, and adaptation to packing requirements in the solid phase. In the case of fluctuations being faster than the time-scale of the NMR spectroscopic experiments, a time-averaged state of the molecule is recorded instead of an individual conformer. As a consequence, the P1 and P5 atoms appear as chemically equivalent, but magnetically inequivalent nuclei. The same holds for P4 and P8 and for P2, P3, P6, and P7, respectively giving an AA′BB′B′′B′′′XX′ spin system. Therefore, a set of three signals is obtained in the ^{31}P NMR spectrum (Figure 4). P1 and P5 give rise to a signal appearing as a diffuse hump at δ = 71.5 ppm due to the quadrupole moment of the boron atom and complicated spin-spin coupling with hydrogen, boron, and trivalent phosphorus

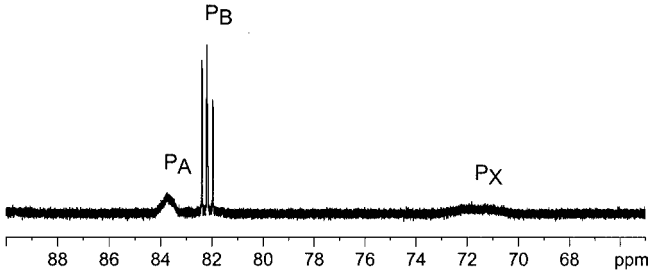

Figure 4. ^{31}P NMR spectrum of dissolved **1** at 23 °C

 © 2003 Wiley-VCH Verlag GmbH & Co. KGaA, Weinheim

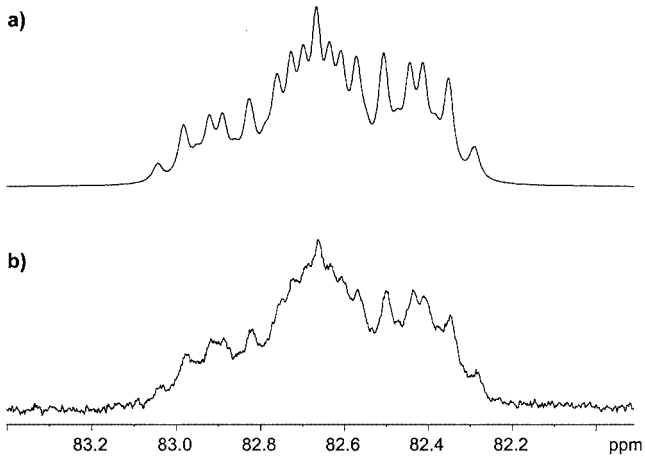

Figure 5. Splitting pattern for P_A in the ^{31}P NMR spectrum of dissolved **1**; simulated (a; see Table 5) and observed at −20 °C (b)

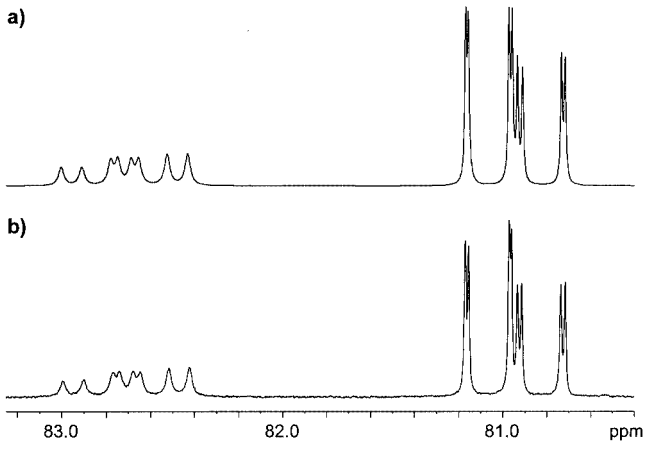

Figure 6. Splitting patterns for P_A and P_B in the $^{31}P\{^1H\}$ NMR spectrum of dissolved **1**; simulated (a; see Table 5) and observed at −20 °C (b)

atoms. The best resolution for the splitting pattern of the broad signal at δ = 83.7 ppm has been obtained at −20 °C for the temperature-dependent measurements (Figure 5; the displacement of the signal is caused by the general temperature dependence of chemical shifts). The corresponding $^{31}P\{^1H\}$ NMR signal (Figure 6) indicates pronounced ^{31}P-^1H coupling, whereas the other signals remain unchanged. The splitting patterns for both NMR spectra can be explained and simulated in full detail using the parameters summarized in Table 5 (Figures 5 and 6). The assignments are consistent with homonuclear decoupling experiments and an intensity ratio of 1:2:1 for the signals of P_A, P_B, and P_X, respectively.

In line with increased P−O double-bond contributions as discussed above, a considerable upfield shift is to be expected for the ^{31}P NMR signals of **1** in comparison with its monomeric counterpart $P_4O_6{\cdot}BH_3$ (the upfield shifts for the BH_3-bearing and for the trivalent phosphorus atoms are about 20 and 40 ppm, respectively; see Exp. Sect.). Among molecular phosphorus oxides and their derivatives only the trivalent phosphorus atoms of $P_4O_6X_3$ (X = O, S, Se; also mixed) exhibit chemical shifts in this region. Surprisingly, the coupling constants are nearly unaffected by the change in bonding situation. Thus, the coupling constants within the bicyclic $P_4O_5{\cdot}BH_3$ unit ($^2J_{AB}$ = 29.2; $^2J_{BX}$ = 24.0 Hz) are of the same order as the $^2J_{P,P}$ values, found for $P_4O_6{\cdot}BH_3$ (27.7 Hz) and $P_4O_6{\cdot}2BH_3$ (24.5 Hz). The weak coupling across P1−O1−P8 and P4−O7−P5 ($^2J_{AX}$ = 11.4 Hz) reflects the flexible linkage between the $P_4O_5{\cdot}BH_3$ subunits. The additional quadruplet splitting of the P_A signal, observed in the ^{31}P NMR spectrum (Figure 5), may be considered as either $^4J_{AH}$ or $^6J_{AH}$. Having the flexible linkages in mind, coupling along the rigid $P_4O_5{\cdot}BH_3$ units ($^6J_{AH}$) seems to be more favorable.

Vibrational Spectroscopy

On dimerization, the molecular symmetry of $P_4O_6{\cdot}BH_3$ (C_{3v}) is reduced to at least C_{2h}, leading to the splitting of vibrational modes of the *E* representation. Moreover, the distortion of the P_8O_{12} cage in the crystalline solid provokes a further symmetry reduction to C_1, which is confirmed by the violation of the mutual exclusion rule normally holding for centrosymmetric molecules. Thus, absorptions at 431, 655, 666, 757, 1119, 2343, and 2363 cm^{-1} are observed in both, IR and Raman spectra (Figure 7; Table 6). As expected, the spectra are very similar to those of P_4O_6 [49] and P_4O_7,[3] for which strong bands around 950 cm^{-1} in the IR spectrum (broad) and around 620 cm^{-1} in the Raman spectrum (sharp) are quite characteristic. The vibrational frequencies of **1** are shifted by up to 20 cm^{-1} compared to

Table 5. Simulation parameters for the ^{31}P NMR spectrum of dissolved **1** (see Figures 5 and 6)

Molecular symmetry	C_{2h}		
Spin system	AA′BB′B′′B′′′XX′		
Spectrometer type	300 MHz		
Frequency	121.5008 MHz		
Nuclei	δ [ppm]		Line width [Hz]
P_A: P4, P8	82.65		3.5
P_B: P2, P3, P6, P7	80.95		1.2
P_X: P1, P5	70.5		1.2
H	0.8		0.3
Coupling constants [Hz]			
$^2J_{AB}$: J_{24}, J_{34}, J_{68}, J_{78}	29.2	$^2J_{BX}$: J_{12}, J_{13}, J_{56}, J_{57}	24.0
$^2J_{AX}$: J_{18}, J_{45}	11.4	J_{AH}: J_{4H}, J_{8H}	7.5

 © 2003 Wiley-VCH Verlag GmbH & Co. KGaA, Weinheim

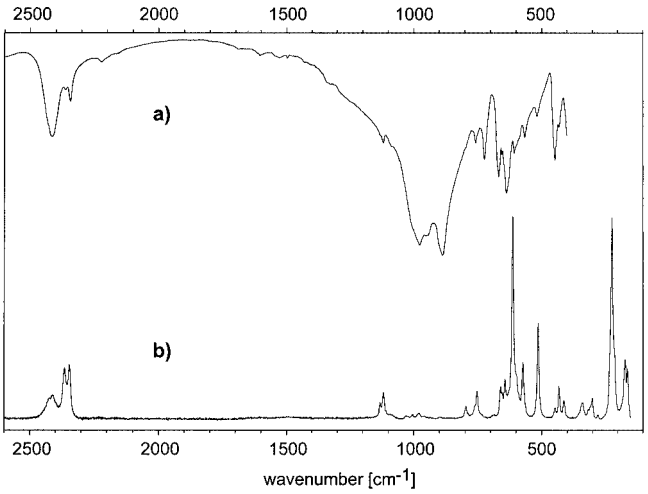

Figure 7. IR (a) and Raman (b) spectrum of solid **1**

those of P_4O_6 and P_4O_7 (Table 6). As cage vibrations are always mixed with motions of the terminally bonded groups, which is different for P_4O_7 and **1**, reliable conclusions concerning the nature of the P−O cage bonds cannot be drawn from the comparison of individual frequencies at a first glance. The four absorptions ranging from 2340 to 2430 cm^{-1} may be attributed to symmetric and antisymmetric B−H stretching modes and agree with data of compounds containing similar P−BH_3 groups.[42,50] The region in which ν(P−B) modes are observed for $R_3P{\cdot}BH_3$ (R = H, Me, Cl),[50] is between 560 and 585 cm^{-1}. Pronounced bands at 565 and 574 cm^{-1} are obtained in the IR and Raman spectra of **1** and are not significant in the spectra of P_4O_6 and P_4O_7. Therefore, assigning them as ν(P−B) seems to be reasonable.

Table 6. Vibrational frequencies [cm^{-1}] observed in the IR and Raman spectra of solid **1** (see Figure 7), P_4O_7, and P_4O_6

$P_8O_{12}{\cdot}2BH_3$		P_4O_7 [a]		P_4O_6 [b]	
IR	Raman	IR	Raman	IR	Raman
	162 m				
	171 m				
	215 s,sh				
	224 vs				
	279 vw	266 m	269 m		285 vw
	301 m	299 m	306 m	302 vw	302 m
	310 w, sh	314 w			
	317 w, sh	323 w	333 w		
	342 m	353 vw			
	413 m	392 vw	392 m	407 vs	407 m
431 m, sh	433 m	427 m	429 m		
446 s	448 w				
518 w	515 s	532 m	534 m		
		554 vw			570 w
565 m, P−B	574 m, P−B				
607 m	600 m, sh				
	614 vs	615 m	625 vs		614 vs
636 s	644 m	635 sh		644 vs	644 s
655 m	655 m, sh	653 w	657 m		
666 s	661 m	667 sh			
		674 w			673 w
		695 vw			
723 s		711 m	708 vw		
757 m	753 m				
	762 w, sh				
	797 w	781 w			
886 vs, br					
947 vs, sh		930 sh	935 vw	921 vs	921 vw
975 vs, br	981 vw	965 vs, br	960 vw		
	1005 vw				
1119 m, sh	1120 m				
	1133 w				
		1345 s	1333 m		
1496 vw					
1530 vw					
1604 vw					
1687 vw					
2224 w					
2343 m, B−H	2346 m, B−H				
2363 m, B−H	2366 m, B−H				
2417 s, B−H	2412 w, B−H				
	2426 w, sh, B−H				

[a] Ref.[3] [b] Refs.[49,3]

Mass Spectrometry

Some instructive conclusions can be drawn about the nature of the P_8O_{12} cage from mass spectrometry. The corresponding data for **1** are given in the Exp. Sect. Boron-containing species are easily identified by their characteristic isotope patterns, which are modified by consecutive hydrogen abstraction from BH_3 groups. In contrast to the molecular ions almost not being detected at all, peaks with intensities around 13% are observed in the EI mass spectrum at 100 °C arising from P_8O_{12} and $P_8O_{12}{\cdot}BH_3$. MS/MS experiments could not be used to decide whether the corresponding BH_3 abstraction occurs before ionization or afterwards, due to the low intensity of the molecular ion peak. Nevertheless, the differing peak intensities for P_8O_{12}-containing species suggest an enhanced stability for P_8O_{12} and $P_8O_{12}{\cdot}BH_3$ ions. In addition, the three P_8O_{12}-containing species show different fragmentation behaviors. Thus, the P_8O_{12} cage of **1** is cleaved symmetrically yielding mainly P_4O_6 and $P_4O_6{\cdot}BH_3$ [MS (EI, 40 °C): *m/z* = 220 and 233, respectively; Exp. Sect.), whereas for $P_8O_{12}{\cdot}BH_3$ the cleavage takes place asymmetrically (MS of $P_8O_{12}{\cdot}BH_3^+$; Exp. Sect.), resulting in an enhanced formation of $P_4O_7{\cdot}BH_2^+$ in the EI mass spectrum of **1** at 100 °C (*m/z* = 249; Exp. Sect.). For $P_8O_{12}^+$ both, symmetrical and asymmetrical cleavage, occur to the same extent generating $P_4O_5^+$ and $P_4O_6^+$ (MS of $P_8O_{12}^+$; Exp. Sect.). The increased stability of P_8O_{12} and $P_8O_{12}{\cdot}BH_3$ compared to **1** is supported by further observations. Because Chemical Ionization (CI) is less destructive than Electron Impact (EI), the cleavage of $P_8O_{12}{\cdot}BH_3$ is drastically reduced, whereas that of **1** is boosted (cf. peak intensity ratio of *m/z* = 233 and 249 for MS (EI, 100 °C) and MS (CI, 100 °C); Exp. Sect.). In the absence of collision gas no cleavage is detected at all for $P_8O_{12}^+$, even at 100 °C. Both, the different stabilities and fragmentation patterns may be fully understood from the results of the crystal structure determination. Due to the formation of asymmetrical P1−O−P8 and P4−O−P5

 © 2003 Wiley-VCH Verlag GmbH & Co. KGaA, Weinheim

bridges, the complexation of borane groups at P1 and P5 destabilizes the P_8O_{12} cage of **1** and induces symmetrical cleavage. On the other hand, in P_8O_{12} the two bicyclic P_4O_5 units are connected by symmetrical P−O−P bridges stabilizing the framework and permitting symmetrical as well as asymmetrical cleavage, at the same time. Finally, $P_8O_{12}{\cdot}BH_3$ is destabilized by only one asymmetrical P−O−P linkage. These results encourage further investigations aiming at the synthesis of dimeric phosphorus oxides. Selective BH_3 abstraction cannot be accomplished by thermal degradation, for example by heating solid **1** for some days at 90 °C. The decomposition product thus obtained is an amorphous orange solid, which is insoluble in toluene.

Conclusion

The thermodynamic driving force of the dimerization of $P_4O_6{\cdot}BH_3$ consists in a gain of enthalpy due to additional P−O double-bond contributions within the P_8O_{12} cage. These are promoted by a relief of angular strain and are in line with contracted P−O bonds (about 20 pm per P_4O_6 unit), enlarged P−O−P bond angles, and enhanced electronic shielding of phosphorus nuclei in **1**. At low temperatures, the benefit in enthalpy compensates for the loss in entropy, associated with dimerization. As the solubility of dimeric species is lower than that of $P_4O_6{\cdot}BH_3$, **1** is continuously removed from the solution through crystallization. As a result, the solved $P_4O_6{\cdot}BH_3$ dimerizes selectively in a kinetically controlled reaction in the absence of nucleophilic reagents. The poor π-donor property of BH_3 is responsible for the different reactivity of $P_4O_6{\cdot}BH_3$, compared to other P_4O_6 derivatives. The additional double-bond contributions within P(B)−O, balancing the positive polarization at the fourfold-coordinated phosphorus atom P(B) at the expense of the adjacent $P^{III}-O_{P(B)}$ bonds, strongly favor the fission of one of the destabilized $P^{III}-O_{P(B)}$ bonds. In this respect, the behavior of the $H_3B-P(OP)_3$ group would be very similar to that of alkylated phosphites $[R'-P(OR)_3]^+$, which are immediately cleaved in the well-known Michaelis−Arbuzov reaction[51−53] yielding organic phosphonates $R'-PO(OR)_2$. If the resulting polarities are taken into account, intermolecular recombination of the dangling P−O bonds create molecules having exactly the constitution observed for **1** (head−tail linkage). But, of course, a concerted mechanism via a four-membered P−O−P−O ring including two intact $P_4O_6{\cdot}BH_3$ units is also a reasonable alternative. This type of ring-opening reaction is considered as one possible pathway for the cationic polymerization of cyclosiloxanes.[54] In any case, the electrophilic addition of BH_3 seems to be associated with kinetic activation of the P_4O_6 cage.

Experimental Section

General: Synthesis of **1** as well as all sample preparations were carried out under inert conditions (argon) either in a glass apparatus or in a glove box. P_4O_6 (Hoechst) was purified by distillation at 50 °C under reduced pressure into a cooling trap. Toluene was heated under reflux over P_4O_{10} and freshly distilled prior to use. $Me_2S{\cdot}BH_3$ was commercially available (Strem Chemicals; about 5% excess of Me_2S).

Synthesis: $Me_2S{\cdot}BH_3$ (0.47 mL, 0.38 g, 4.96 mmol) was added dropwise to a solution of P_4O_6 (1.2 g, 5.46 mmol) in toluene (1.0 mL) at 0 °C while stirring. The clear colorless solution was stirred at 0 °C for a further 2 h and Me_2S was subsequently removed in vacuo at −10 °C over 4 min. At this stage the solution contained mainly $P_4O_6{\cdot}BH_3$ with small amounts of P_4O_6, $P_4O_6{\cdot}2BH_3$, P_4O_7, and P_4. After storage for three months at −30 °C the almost solidified solution was warmed up to room temperature. Clear colorless crystals of **1**, which were up to 1 mm in size and cuboid in shape, initially remained undissolved. The crystals were separated from the mother liquor at 0 °C and dried in vacuo at room temperature for 5 h giving pure **1** (yield: ca. 0.38 g, 0.82 mmol, 30%). The reproducibility of the crystallization strongly depends on temperature and concentration. The best results were obtained for concentrations ranging from 1.25 to 1.43 mg of P_4O_6 per mL of toluene (after removal of Me_2S and some solvent in vacuo).

Caution: Solid $P_8O_{12}{\cdot}2BH_3$ is highly explosive when exposed to any kind of mechanical stress, even under inert conditions at −80 °C (friction- and shock-sensitive). Contact with pure water or ethanol causes violent decomposition. We recommend that the solid should be neither handled in sealed glass vessels nor in large amounts (maximum 1.5 g). Under argon, loose crumbs can be ground without danger, if portions less than 100 mg are used. For disposal, **1** is covered with aromatic solvents and carefully decomposed by adding ethanol in small portions (formation of H_2).

Crystal Structure Analysis: A cuboid crystal with dimensions given in Table 2 was picked up by a mounted CryoLoop (Hampton Research) using an inert immersion oil (Hampton Research) and then measured at −90 °C using a SMART 1000 diffractometer with CCD detector and graphite monochromator (Bruker AXS). Absorption corrections based on symmetry-equivalent and redundant reflections (SADABS); structure solution by direct methods (SHELXS-97[55]); structure refinement according to full-matrix least-squares procedures against F^2 (SHELXL-97[56]); hydrogen atoms refined freely (isotropic); display of molecular structure by DIAMOND.[57] Further details of the crystal structure investigation may be obtained from Table 2 and from the Fachinformationszentrum Karlsruhe, 76344 Eggenstein-Leopoldshafen, Germany [Fax: (internat.) + 49-7247/808-666; E-mail: crysdata@fiz-karlsruhe.de], on quoting the depository number CSD-411904 and the names of the authors.

Powder Diffractometry: Stadi P diffractometer (Stoe & Cie); Debye−Scherrer geometry; Ge single crystal (111) as monochromator; $\lambda(\text{Cu-}K_{\alpha 1}) = 154.0598$ pm; **1** was ground in a glove box and sealed in a capillary (Hilgenberg) with 0.2 mm in diameter; after zero point correction on the basis of silicon as external standard and baseline correction profile fitting was performed by FULLPROF98[58] using least-squares procedures; refinement results are given in Table 1 (reflection positions) and Table 2 (lattice parameters).

NMR Spectroscopy: Solutions: 300 MHz spectrometer (Avance DPX 300 SB; Bruker); 121.50 MHz (^{31}P), 96.29 MHz (^{11}B); in toluene; [D_6]benzene or [D_8]toluene as lock solvents; glass tubes (Wilmad) were sealed; simulation by WINDAISY.[59] Solid: 400 MHz spectrometer (Avance DSX 400 WB; Bruker); 2.5 mm CP MAS

 © 2003 Wiley-VCH Verlag GmbH & Co. KGaA, Weinheim

probe; 161.98 (^{31}P), 128.38 (^{11}B), 400.12 MHz (^{1}H); simulation by WINFIT;[60] 85% phosphoric acid, tetramethylsilane, and $(C_2H_5)_2O{\cdot}BF_3$ as external standards with upfield being negative; display of spectra by WINNMR.[61] **$P_4O_6{\cdot}BH_3$:** $^{11}B\{^1H\}$ NMR: $\delta = -39.6$ [d, $^1J_{PB} = 57$ Hz, 1 B, P*B*H$_3$] ppm. ^{31}P NMR: $\delta = 90.0$ [broad, 1 P, O$_3$*P*B], 117.1 [dq, $^2J_{P,P} = 27.7$, $^4J_{PH} = 0.7$ Hz, 3 P, O$_3$*P*] ppm. **$P_4O_6{\cdot}2BH_3$:** $^{11}B\{^1H\}$ NMR: $\delta = -40.2$ [d, $^1J_{PB} = 53$ Hz, 2 B, P*B*H$_3$] ppm. ^{31}P NMR: $\delta = 98.4$ [broad, 2 P, O$_3$*P*B], 117.4 [t, $^2J_{P,P} = 24.5$ Hz, 2 P, O$_3$*P*] ppm.

IR and Raman Spectroscopy: FT-IR spectrometer IFS 113v (Bruker); Genzel interferometer; KBr pellet (decomposition within CsI). FT-Raman spectrometer LabRam system (Jobin Yvon); He-Ne LASER (632.817 nm); sample sealed in a silica capillary.

Mass Spectrometry: Triple-quadrupole mass spectrometer TSQ 700 (Finnigan MAT); direct inlet; heatable sample holder; ionization at 150 °C. MS (EI, 70 eV, 40 °C): *m/z* (%) = 47 (48) $[PO]^+$, 95 (13) $[P_2O_2H]^+$, 123 (16) $[P_2O_3{\cdot}BH_2]^+$, 157 (81) $[P_3O_4]^+$, 173 (13) $[P_3O_5]^+$, 185 (7) $[P_4O_3{\cdot}BH_2]^+$, 204 (67) $[P_4O_5]^+$, 220 (100) $[P_4O_6]^+$, 233 (33) $[P_4O_6{\cdot}BH_2]^+$, 249 (8) $[P_4O_7{\cdot}BH_2]^+$, 440 (< 1) $[M - 2\,BH_3]^+$, 452 (1) $[M - BH_3 - H_2]^+$. MS (EI, 70 eV, 100 °C): *m/z* (%) = 47 (86) $[PO]^+$, 94 (20) $[P_2O_2]^+$, 123 (16) $[P_2O_3{\cdot}BH_2]^+$, 141 (13) $[P_3O_3]^+$, 157 (100) $[P_3O_4]^+$, 173 (24) $[P_3O_5]^+$, 185 (20) $[P_4O_3{\cdot}BH_2]^+$, 204 (82) $[P_4O_5]^+$, 220 (85) $[P_4O_6]^+$, 233 (29) $[P_4O_6{\cdot}BH_2]^+$, 249 (94) $[P_4O_7{\cdot}BH_2]^+$, 267 (83) $[P_5O_7]^+$, 283 (37) $[P_5O_8]^+$, 311 (12) $[P_5O_9{\cdot}BH]^+$, 359 (9) $[P_7O_8{\cdot}BH_3]^+$, 440 (13) $[M - 2\,BH_3]^+$, 452 (13) $[M - BH_3 - H_2]^+$, 464 (< 1) $[M - 2\,H_2]^+$. MS (CI, methane, 3−9 Torr, 100 °C): *m/z* (%) = 92 (13) $[P_2O{\cdot}BH_3]^+$, 111 (10) $[P_2O_3H]^+$, 125 (23) $[P_3O_2]^+$, 157 (76) $[P_3O_4]^+$, 173 (13) $[P_3O_5]^+$, 205 (54) $[P_4O_5H]^+$, 220 (72) $[P_4O_6]^+$, 233 (100) $[P_4O_6{\cdot}BH_2]^+$, 249 (31) $[P_4O_7{\cdot}BH_2]^+$, 267 (15) $[P_5O_7]^+$, 285 (8) $[P_4O_{10}H]^+$, 441 (4) $[M + H - 2\,BH_3]^+$, 453 (26) $[M + H - BH_3 - H_2]^+$. MS of $P_8O_{12}{\cdot}BH_3^+$ (**1** as source compound at 80 °C): *m/z* (%) = 249 (90) $[P_4O_7{\cdot}BH_2]^+$, 454 (100) $[P_8O_{12}{\cdot}BH_3]^+$. MS of $P_8O_{12}^+$ (**1** as source compound at 100 °C, argon as collision gas): *m/z* (%) = 204 (20) $[P_4O_5]^+$, 220 (20) $[P_4O_6]^+$, 440 (100) $[P_8O_{12}]^+$ (without collision gas no fragmentation was observed).

Acknowledgments

We are grateful to Hoechst AG (Knapsack, Germany) for the generous supply of P_4O_6.

[1] K. H. Jost, M. Schneider, *Acta Crystallogr., Sect. B* **1981**, *37*, 222.
[2] M. Jansen, M. Voss, *Angew. Chem.* **1981**, *93*, 120, *Angew. Chem. Int. Ed. Engl.* **1981**, *20*, 100.
[3] M. Möbs, M. Jansen, *Z. Anorg. Allg. Chem.* **1984**, *514*, 39.
[4] S. Strojek, M. Jansen, *Z. Naturforsch., Teil B* **1997**, *52*, 906.
[5] B. Lüer, M. Jansen, *Z. Kristallogr.* **1991**, *197*, 247.
[6] M. Jansen, B. Lüer, *Z. Kristallogr.* **1986**, *177*, 149.
[7] F. Frick, M. Jansen, P. J. Bruna, S. D. Peyerimhoff, *Chem. Ber.* **1991**, *124*, 1711.
[8] F. Frick, M. Jansen, *Z. Anorg. Allg. Chem.* **1993**, *619*, 281.
[9] F. Frick, M. Jansen, *Z. Kristallgr.* **1994**, *209*, 985.
[10] F. Frick, PhD Thesis, Univ. Bonn, **1993**.
[11] J. Clade, M. Jansen, B. Engels, C. M. Marian, *Z. Anorg. Allg. Chem.* **1995**, *621*, 2065.
[12] M. Jansen, A. Tellenbach, *Z. Anorg. Allg. Chem.* **1998**, *624*, 1267.
[13] J. Clade, M. Jansen, *Z. Anorg. Allg. Chem.* **1996**, *622*, 1630.
[14] J. Clade, PhD Thesis, Univ. Bonn, **1996**.
[15] J. G. Riess, J. R. Van Wazer, *J. Am. Chem. Soc.* **1966**, *88*, 2166.
[16] E. D. Pierron, P. J. Wheatley, J. G. Riess, *Acta Crystallogr.* **1966**, *21*, 288.
[17] M. L. Walker, J. L. Mills, *Inorg. Chem.* **1975**, *14*, 2438.
[18] M. Jansen, J. Clade, *Acta Crystallogr., Sect. C* **1996**, *52*, 2650.
[19] M. L. Walker, J. L. Mills, *J. Organomet. Chem.* **1976**, *120*, 355.
[20] J. G. Riess, J. R. Van Wazer, *Inorg. Chem.* **1966**, *5*, 178.
[21] M. Loeper, U. Schülke, *Z. Anorg. Allg. Chem.* **1983**, *500*, 40.
[22] U. Schülke, *Phosphorus, Sulfur Silicon* **1990**, *51/52*, 153.
[23] M. Jansen, S. Strojek, *J. Chem. Soc., Chem. Commun.* **1995**, 1509.
[24] S. Strojek, M. Jansen, *Chem. Ber.* **1996**, *129*, 121.
[25] S. Strojek, PhD Thesis, Univ. Bonn, **1998**.
[26] M. Mühlhäuser, B. Engels, C. M. Marian, S. D. Peyerimhoff, P. J. Bruna, M. Jansen, *Angew. Chem.* **1994**, *106*, 578; *Angew. Chem. Int. Ed. Engl.* **1994**, *33*, 563.
[27] G. Kodama, H. Kondo, *J. Am. Chem. Soc.* **1966**, *88*, 2045.
[28] J. G. Riess, J. R. Van Wazer, *J. Am. Chem. Soc.* **1966**, *88*, 2339.
[29] J. G. Riess, J. R. Van Wazer, *J. Am. Chem. Soc.* **1967**, *89*, 851.
[30] A. Tellenbach, M. Jansen, *Angew. Chem.* **2001**, *113*, 4838; *Angew. Chem. Int. Ed.* **2001**, *40*, 4691.
[31] W. Eiserbeck, P. Neumann, U. Schülke, M. Meisel, *Phosphorus, Sulfur Silicon* **1994**, *93/94*, 373.
[32] L. Pauling, *The Nature of the Chemical Bond*, Cornell University Press, Ithaca − New York, **1948**, p. 160−167.
[33] M. Jansen, M. Möbs, *Inorg. Chem.* **1984**, *23*, 4486.
[34] K. F. Purcell, *Inorg. Chem.* **1972**, *11*, 891.
[35] I. H. Hillier, J. C. Marriott, V. R. Saunders, M. J. Ware, D. R. Lloyd, N. Lynaugh, *J. Chem. Soc., Chem. Commun.* **1970**, 1586.
[36] D. R. Lloyd, N. Lynaugh, *J. Chem. Soc., Chem. Commun.* **1970**, 1545.
[37] E. D. Glendening, A. Streitwieser, *J. Chem. Phys.* **1994**, *100*, 2900.
[38] C. W. Bauschlicher, A. Ricca, *Chem. Phys. Lett.* **1995**, *237*, 14.
[39] H. Anane, A. Jarid, A. Boutalib, I. Nebot-Gil, F. Tomás, *Chem. Phys. Lett.* **2000**, *324*, 156.
[40] C. Loschen, K. Voigt, J. Frunzke, A. Diefenbach, M. Diedenhofen, G. Frenking, *Z. Anorg. Allg. Chem.* **2002**, *628*, 1294.
[41] I. Røeggen, *Chem. Phys.* **1992**, *162*, 271.
[42] J. C. Clardy, D. S. Milbrath, J. G. Verkade, *Inorg. Chem.* **1977**, *16*, 2135.
[43] S. Cserepi-Szucs, I. Toth, L. Parkanyi, J. Bakos, *Tetrahedron* **1998**, 3135.
[44] Y. Yamanoi, T. Imamoto, *J. Org. Chem.* **1997**, *62*, 8560.
[45] T. Imamoto, E. Nagato, Y. Wada, H. Masuda, K. Yamaguchi, T. Uchimaru, *J. Am. Chem. Soc.* **1997**, *119*, 9925.
[46] W. Hoffbauer, S. Wefing, G. Klösters, F. Frick, M. Jansen, *Solid State Nucl. Magn. Reson.* **1999**, *14*, 211.
[47] G. Jeschke, W. Hoffbauer, M. Jansen, *Chem. Eur. J.* **1998**, *4*, 1755.
[48] U. Fleischer, F. Frick, A. R. Grimmer, W. Hoffbauer, M. Jansen, W. Kutzelnigg, *Z. Anorg. Allg. Chem.* **1995**, *621*, 2012.
[49] A. R. S. Valentim, B. Engels, S. D. Peyerimhoff, J. Clade, M. Jansen, *J. Phys. Chem.* **1998**, *A102*, 3690.
[50] J. Weidlein, U. Müller, K. Dehnicke, *Schwingungsfrequenzen I − Hauptgruppenelemente*, Georg Thieme, Stuttgart − New York, **1981**.
[51] B. A. Arbuzov, *Pure Appl. Chem.* **1964**, *9*, 307.
[52] R. G. Harvey, E. R. De Sombre, *Top. Phosphorus Chem.* **1964**, *1*, 61.
[53] R. F. Hudson, *Structure and Mechanism in Organophosphorus Chemistry*, Academic Press, London, **1965**.
[54] R. Bischoff, P. Sigwalt, *Polym. Int.* **1996**, *40*, 99.
[55] G. M. Sheldrick, *SHELXS-97*, Univ. Göttingen, Germany, **1997**.
[56] G. M. Sheldrick, *SHELXL-97*, Univ. Göttingen, Germany, **1997**.
[57] K. Brandenburg, *DIAMOND*, version 2.1a, Bonn, Germany, **1999**.
[58] J. Rodriguez-Carvajal, *FULLPROF98*, version 0.2, Laboratoire Leon Brillouin, France, **1998**.
[59] *WINDAISY*, version 4.05, Bruker-Franzen Analytik GmbH, Germany.
[60] *WINFIT*, Bruker-Franzen Analytik, Germany.
[61] *WINNMR*, version 6.1, Bruker Daltonik, Germany, **1999**.
[62] Natl. Bur. Stand. (U. S.), Monogr. **1976**, *25*, 35.

Received April 15, 2003

 © 2003 Wiley-VCH Verlag GmbH & Co. KGaA, Weinheim

Modulation of the Communication between Redox Centers in a Tris(ferrocene)-tren Ligand by Complexation of Lanthanide Ions

Marie Heitzmann,[a,d] Jean-Claude Moutet,*[a,d] Jacques Pécaut,[b,d] Olivier Reynes,[a,d] Guy Royal,*[a,d] Eric Saint-Aman,[a,d] and Guy Serratrice[c,d]

Keywords: Sandwich complexes / Electrostatic interactions / Electrochemistry / Lanthanides

The tripodal ligand L built on the tren platform and bearing three chemically equivalent ferrocene units was prepared and characterized. Electrochemical investigations indicate that electrostatic communication occurs between the three ferrocene groups in L, which leads to the observation of two distinct voltammetric waves. The electrochemical communication between the three ferrocene moieties is disrupted in 1:1 ($L:M^{3+}$) type complexes formed between L and Y^{3+} or Eu^{3+} metal cations and their electrochemical response tends towards that of a single three-independent-electrons oxidation wave. Modulation of the electrochemical properties of L in the presence of lanthanide ions might be exploited with a view to their electrochemical sensing in organic and aqueous media.
(© Wiley-VCH Verlag GmbH & Co. KGaA, 69451 Weinheim, Germany, 2003)

Introduction

Macromolecular systems containing multiple redox active centers have been the subject of numerous studies due to their intriguing electrical and redox properties, and their potential use as functional nanostructured materials.[1−3] In particular, structures such as linked metallocenes,[3−7] metallodendrimers,[6,8,9] or polymers containing metallocenes[2,10,11] may present remarkable intramolecular electrostatic communication throughout the redox active sites due to their spatial proximity. An interesting feature of the multi-redox systems is that the extent of communication between the redox centers can be controlled and modulated in several ways, including protonation or alkylation of the compounds,[4−7,12] or changes in solvent polarity[5,13] and supporting electrolyte composition.[14] Here, we report how the degree of electrostatic communication between three chemically equivalent redox centers in the tren-based tris(ferrocene) ligand L is deeply changed upon complexation of the secondary nitrogen bridging atoms by Eu^{3+} and Y^{3+} ions.

Moreover, important applications in sensors are envisaged for multi-redox molecules and macromolecular systems, with the opportunity of coupling the interactions of analyte-redox material into transducible responses.[15−17] We demonstrate that the very simple redox receptor L might be used for the electrochemical detection and titration of lanthanide ions (Eu^{3+} and Y^{3+} which is considered as a pseudo lanthanide), through the modification of the interactions between the redox active groups that occurs in the presence of these guests metal cations.

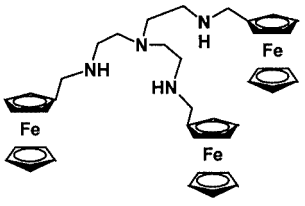

L

Results and Discussion

The homotrimetallic ligand L used in this study is based on the tripodal tetramine tren, namely the tris(2-aminoethyl)amine, which is a well-known ligand for metal cations[18] and an excellent platform on which to build sensing devices. For example, a redox-responsive receptor[19] for

[a] Laboratoire d'Electrochimie Organique et de Photochimie Rédox, UMR CNRS 5630,
Université Joseph Fourier Grenoble 1, BP 53,
38041 Grenoble Cédex 9, France
Fax: (internat.) +33-4-76514267
E-mail: Jean-Claude.Moutet@ujf-grenoble.fr
Guy.Royal@ujf-grenoble.fr
[b] CEA-Grenoble, DRFMC/SCIB/3MC,
38041 Grenoble, France
[c] Laboratoire de Chimie Biomimétique, LEDSS, UMR CNRS 5616, Université Joseph Fourier Grenoble 1,
BP 53, 38041 Grenoble Cédex 9, France
[d] Institut de Chimie Moléculaire de Grenoble, ICMG, FR CNRS 2607,
38041 Grenoble, France

halide anions and fluorescent sensors[20−22] for the recognition of anions, transition metals or protons have been developed by linking cobaltocenium[19] and photoactive fragments[20−22] to the tren unit.

Synthesis and Characterization of L

The tripodal receptor L was readily synthesized in a two-step procedure. Reaction of the tris(2-aminoethyl)amine with three equivalents of ferrocenecarboxaldehyde in biphasic media (water/diethyl ether) allows the precipitation of the trisimine intermediate, which is further reduced with sodium borohydride to produce L as an oily solid. Crystals of the protonated form of L could be obtained from a solution containing L along with ten equivalents of HCl_{aq}. It has to be noted that the solid state of the hydrochloride form of L is highly unstable and fuses rapidly when manipulated at room temperature. This results in a poor quality crystal. However, the data collection (Table 3) undoubtedly reveals a triply-protonated molecular structure, LH_3^{3+}, $3Cl^-$, depicted in Figure 1.

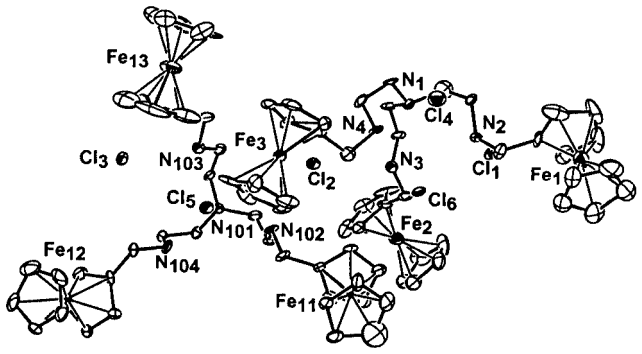

Figure 1. X-ray structure of the two entities of LH_3^{3+}, $3Cl^-$. Hydrogen atoms and solvent molecules are omitted for clarity. Hydrogen bonds lengths [Å]: Cl(1)···H−N(2), 2.31; Cl(6)···H−N(2), 2.26; Cl(2)···H−N(3), 2.27; Cl(6)···H−N(3), 2.27; Cl(4)···H−N(4), 2.20; Cl(6)···H−N(4), 2.27; Cl(2)···H−N(102), 2.20; Cl(5)···H−N(102), 2.24; Cl(3)···H−N(103), 2.21; Cl(5)···H−N(103), 2.22; Cl(1)#···H−N(104), 2.24; Cl(5)···H−N(104), 2.23 [symmetry transformation: # $-x+1$, $y-1/2$, $-z+3/2$; d(N−H) = 0.92 Å]

The X-ray structure determination shows that LH_3^{3+}, $3Cl^-$ crystallizes in the $P2_12_12_1$ space group of the orthorhombic system, revealing two independent molecular entities. These two entities display very close crystallographic data. The molecular structure, formulated as $[C_{39}H_{51}Fe_3N_4]Cl_3{\cdot}2CH_3CN{\cdot}C_2H_5CO_2CH_3{\cdot}H_2O$, consists of a tricationic LH_3^{3+}, three Cl^- counterions and four disordered solvent molecules (two acetonitrile molecules, one ethyl acetate, and one water molecule). The three metallocene units are located on the same side of the bridging nitrogen atom; the three iron centers in L are separated by ca. 11 Å and the distance between the iron center of a metallocene unit and its bridging secondary nitrogen is ca. 4.4 Å. The three chloride anions are closer to the secondary nitrogen atoms [N(2−4)···Cl distances of ca. 3.1 Å) than to the tertiary nitrogen, N(1)···Cl ranging between 3.73 and 4.43 Å. Cl(5) and Cl(6) are located inside the tren cavities, defined by N(101−104) and N(1−4), respectively, suggesting that these chloride anions are complexed by L via three convergent N−H···Cl hydrogen bonds (the distances between Cl(6) and N(2−4) are close to 3.1 Å). On the contrary, Cl(3) and Cl(4) interact only with HN(103) and HN(4), respectively. Finally, when referring to the two entities, Cl(1) bridges HN(2) and HN(104) (from an entity in a symmetrical position) and Cl(2) bridges HN(3) and HN(102).

Complexation Studies

Potentiometric titration studies and electrospray-mass spectra (ES-MS) experiments were first used to investigate the complexation of L by lanthanide ions.

Potentiometric Titration

The protonation constants of L and the stability constants of the corresponding Eu^{3+} and Y^{3+} complexes were calculated using the HYPERQUAD program,[23,24] from potentiometric titration curves obtained in a CH_3OH/H_2O solution (3:1, v:v) containing 0.1 M tetra-*n*-butylammonium perchlorate (TBAP). Three pK_a values (9.37, 8.13, and 6.47 at 25 °C) were measured for L. The species LH_4^{4+} could not be reached, its pK_a being too low to be observed. In agreement with the results of Fabbrizzi et al.,[21] based on other tren derivatives, the three protons in LH_3^{3+} are bound to the secondary amino groups. Protonation of the sole secondary amino groups is corroborated by the crystallographic data of the hydrochloride form of L showing that *(i)* LH_3^{3+}, $3Cl^-$ was obtained in the presence of a large excess of HCl and *(ii)* the Cl^- ions are closer to the secondary amino groups than to the apical nitrogen atom. As already observed for alkylated-tren derivatives, the pK_a's are lower than those of the tren parent.[25,26] Stability constants of the complexes formed between L and the Y^{3+} or Eu^{3+} cations were then determined at a molar ratio of 1:1 (L/M^{3+}). Measurements were made in the 2.5 to 7 pH range, the precipitation of hydroxylated species being observed above pH 7−8. The best fit of the data was obtained by considering only the 1:1 species (LM) and $[LM(OH)_2]$ and yielded log$K$(LM) = 9.17(0.05) and 9.48(0.05) with $K(LM) = [LM]/[M][L]$, log$K$(LM{OH}$_2$) = 13.50(0.05) and 13.00(0.05) with $K(LM\{OH\}_2) = [LM]/[LM(OH)_2][H^+]^2$, for the LEu and LY complexes, respectively. Coordination numbers for lanthanide or yttrium (which is often treated as a "pseudo-lanthanide") trivalent cations are typically between seven and ten,[27] and only four coordination sites can be afforded by the amino groups in L. It can thus be assumed that counterions and/or solvent molecules are also coordinated to the metal center in LEu and LY complexes.

ES-MS Qualitative Speciation

The binding of the Eu^{3+}, Y^{3+}, La^{3+}, and Sm^{3+} cations by L was studied by electrospray-mass spectrometry. Solutions of complexes were prepared by mixing equimolar solutions (1 mg·mL^{-1}) of L and the nitrate salt of a given metal cation in acetonitrile:water (1:1, v:v). In all cases, only one kind of complex was detected (Figure 2 and Table 1).

 © 2003 Wiley-VCH Verlag GmbH & Co. KGaA, Weinheim

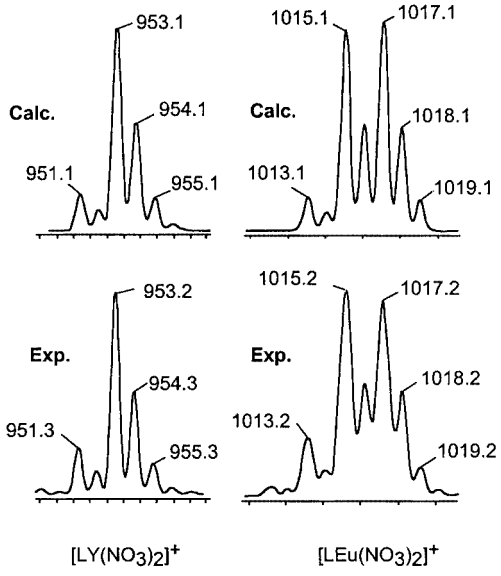

Figure 2. Calculated and experimental ES-MS spectra of $[LY(NO_3)_2]^+$ and $[LEu(NO_3)_2]^+$

Table 1. Electrospray-mass spectroscopic data (*m*/*z*) for L + M^{3+} 1:1 complexes (M = Eu, Y, Sm, La)

Species	Eu^{3+}	Y^{3+}	Sm^{3+}	La^{3+}
$[LM(NO_3)_2]^+$	1017.2	953.2	1016.2	1003.3
$[LM(NO_3)_3]^+$	1079.2	1015.2	1078.3	1065.3

All the isotopic peaks are separated by 1.0 *m*/*z* unit, revealing a charge state of +1 for the corresponding ions. Calculated spectra (Figure 2) show unambiguously that these signals correspond to the $[LM(NO_3)_2]^+$complexes, i.e. a 1:1 (L/M^{3+}) stoichiometry is observed, two nitrate anions being coordinated to the metal center. Interestingly, a second and smaller signal {10% in intensity compared with the signal of $[LM(NO_3)_2]^+$} corresponding to the complex $[LM(NO_3)_3]^+$ was also observed from the mass spectra. It can be assumed that the positive charge of this last species is provided by oxidation of one ferrocene unit of the complex under our experimental conditions. Spectra showing the same features were also obtained starting from isolated LY and LEu complexes.

Electrochemical Results

Electrochemical Behavior of Free L

The electrochemical behavior of the free receptor L was investigated by cyclic voltammetry (CV) and differential pulse voltammetry (DPV) in methanol containing 0.1 M tetrabutylammonium perchlorate (TBAP) as the supporting electrolyte. In weakly polar solvents such as CH_2Cl_2, the poor solubility of the electrogenerated compounds was responsible for adsorption phenomena and led to the observation of complex voltammograms. CV experiments revealed the presence of two partially overlapping waves at $E_{1/2}$ = +25 mV and +135 mV, with ΔE_p = 90 mV in both cases. Two peaks at +30 mV and +140 mV were observed by DPV (Table 2). The three ferrocene groups in L being chemically equivalent, this behavior (observation of two distinguishable signals) can be attributed to interactions occurring between the three redox centers. Indeed, a separation $\Delta E°$ of $(RT/F)\ln 2^3$, i.e. 57 mV, between the first and third electron transfer is expected in a molecule with three completely non-interacting equivalent redox centers,[28,29] leading to the observation of a voltammetric curve with the shape of a single-electron transfer reaction (one CV wave with $\Delta E_p \approx 60$ mV, and a single peak by differential pulse voltammetry). In contrast, significant electronic or electrostatic communication between these three redox centers should lead to larger $\Delta E°$ values and, therefore, to the observation of multiple CV waves.[29,30] The degree of communication between the three ferrocene groups in L was evaluated via the determination of the three formal potentials $E°^1$, $E°^2$, and $E°^3$, corresponding to the successive oxidations of the three ferrocene subunits (Scheme 1).

Table 2. Electrochemical data for free L, LH_3^{3+}, LEu, and LY complexes

	Experimental CV data[a]				Formal potentials[b]		DPV data
	E_{pa}, V[c]	E_{pc}, V[c]	ΔE_p, mV[c]	$E_{1/2}$, V[d]	$E°$, V	$\Delta E°$, mV[e]	Ep, V[f]
Free L	0.070	−0.020	90	0.025	0.001 ($E°^1$)	67 ($\Delta E°^{2-1}$)	0.030
	0.180	0.090	90	0.135	0.068 ($E°^2$)	71 ($\Delta E°^{3-2}$)	0.140
					0.139 ($E°^3$)	138 ($\Delta E°^{3-1}$)	
LEu	0.190	0.098	92	0.144	0.112 ($E°^1$)	33 ($\Delta E°^{2-1}$)	0.140
					0.145 ($E°^2$)	26 ($\Delta E°^{3-2}$)	
					0.171 ($E°^3$)	59 ($\Delta E°^{3-1}$)	
LY	0.199	0.097	102	0.148	0.122 ($E°^1$)	33 ($\Delta E°^{2-1}$)	0.150
					0.155 ($E°^2$)	26 ($\Delta E°^{3-2}$)	
					0.181 ($E°^3$)	59 ($\Delta E°^{3-1}$)	
LH_3^{3+} [g]	0.270	0.130	140	0.180	[h]	[h]	0.175

[a] All potentials are referred to the regular Fc/Fc^+ couple. [b] Calculated by fitting simulated voltammograms to experimental data. [c] E_{pa} and E_{pc} are the anodic and cathodic peak potentials. ΔE_p states for the peak-to-peak potential splitting ($E_{pa}-E_{pc}$). [d] $E_{1/2}$ is the apparent half-wave potential [(E_{pa} + E_{pc})/2]. [e] $\Delta E°$ represents the difference between the calculated redox potentials. [f] DPV peak potential. [g] L in the presence of five equivalents of H^+. [h] Not determined (see the text).

 © 2003 Wiley-VCH Verlag GmbH & Co. KGaA, Weinheim

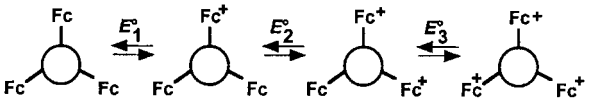

Scheme 1. Schematic representation of the three oxidation steps of L

The experimental voltammograms were fitted to digitally simulated voltammograms using the ESP software.[31] Results are depicted in Figure 3(A) and the three formal potentials evaluated from the optimization of the fitting analysis are given in Table 2. ΔE° values of ca. 70 mV between two consecutive redox systems (i.e. $E^{\circ 2} - E^{\circ 1}$ and $E^{\circ 3} - E^{\circ 2}$) were found. These results are in accordance with those already reported for bis[5] and tris[13] ferrocenyl compounds that showed significant communication between the redox centers and were characterized by two distinguishable voltammetric waves.

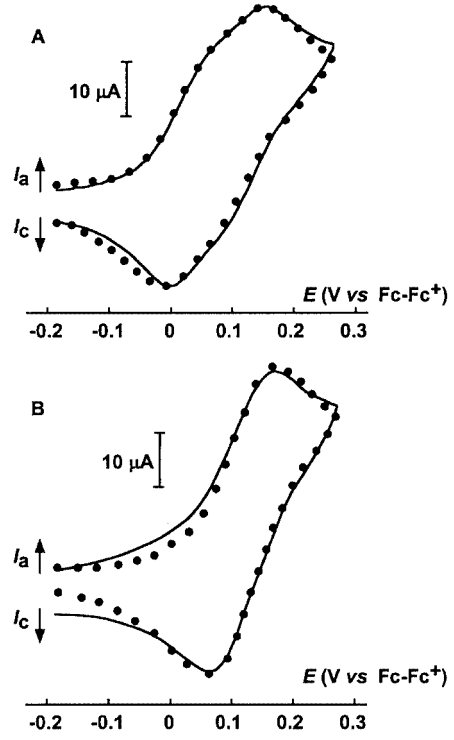

Figure 3. Experimental (continuous line) and best-fit simulated (dotted line) cyclic voltammograms of (A) 1 mM free L and (B) 1 mM LEu complex in CH_3OH containing 0.1 M TBAP; sweep rate 0.1 $V \cdot s^{-1}$

Since the three ferrocene groups in L are relatively far one from one another and separated by simple bonds, electronic communication through the bonds could not be invoked. Thus, it is reasonable to deduce that there are electrostatic interactions occurring between the electrogenerated positive charge of the first ferricinium group and the lone pair of a nitrogen atom connected to a second ferrocene group, the latter being more difficult to oxidize. In the same way, the third ferrocene group is oxidized at a higher potential than the second one. This hypothesis will be further discussed in the following paragraph.

Electrochemical Behavior of the Eu^{3+} and Y^{3+} Complexes of L

The same electrochemical experiments were conducted starting from chloride or nitrate salts of the isolated LEu and LY complexes. Results are summarized in Table 2. Both complexes exhibit one quasi-reversible CV wave [see for example Figure 3(B), for LEu] at $E_{1/2}$ = 144 (ΔE_p = 92 mV) and 148 mV (ΔE_p = 102 mV), and one DPV peak at E_p = 140 and 150 mV for LEu and LY complexes, respectively. These observations reveal a strong decrease in the communication between the three redox active units. The metallocene moieties of the complexed L therefore exhibit a more independent electrochemical behavior and the shape of the resulting voltammograms tends towards that of a single three-independent-electrons oxidation wave.

As mentioned previously, the determination of the three formal potentials E° corresponding to the three successive oxidations of the ferrocene groups in the complexes was performed by fitting simulated voltammograms to experimental CV curves. The data are summarized in Table 2. Firstly, due to electrostatic repulsion effects arising between the bound metal cation and the positive charge on the electrooxidized ferrocenyl unit, these potentials are logically shifted to more positive values as compared to those measured for the free receptor. Moreover, the three successive oxidations in both complexes are separated by ca. 30 mV and the separation between the first and the third redox events ($E^{\circ 3} - E^{\circ 1}$) is 59 mV, showing that the communication between the three ferrocene units is almost fully cancelled upon metallation of the receptor. The strong decrease in the interactions is thus a direct consequence of the complexation of L by metal ions through the secondary nitrogen atoms, and this result confirms that the lone pairs of the secondary amines are involved in the communication between the ferrocene groups in L.

In order to further confirm the above hypothesis, CV and DPV experiments were conducted on L in acidic media. Addition of $HClO_4$ in a solution of L led to the emergence of a single DPV peak at E_p = 175 mV and of a unique CV wave at $E_{1/2}$ = 180 mV (ΔE_p = 140 mV). These observations clearly indicate a strong decrease in the interactions between the three iron centers upon protonation of L, in accordance with that already observed with others nitrogen-bridged polyferrocenes.[4−7,12] Moreover, as in the metallic complexes, the average apparent potential for the first oxidation of the ferrocene centers is shifted to more positive values upon protonation of L. The potential shift is due to the electron-withdrawing effect induced by the introduction of positive charges on the bridging nitrogen atoms. Unfortunately, owing to complex voltammograms due to adsorption phenomena the potentials for the three electron transfers in LH_3^{3+} could not be accurately evaluated using electrochemical simulation. However, the potential shift for the first oxidation of L ($E^{\circ 1}$) induced by its protonation can be roughly evaluated to ca. +160 mV. This value is in agree-

 © 2003 Wiley-VCH Verlag GmbH & Co. KGaA, Weinheim

ment with the results of Plenio et al.[32] who studied a number of ferrocene-nitrogen compounds and their protonated forms. They found a linear relationship between the inverse Fe−N distance (provided by X-ray data) and the shift of the potential of the ferrocene-ferricinium couple observed upon protonation of the neutral compounds. In particular, a shift of +190 mV was found for an iron-ammonium distance equal to 4.56 Å,[32] that is similar to the 4.4 Å Fe−N distance in LH_3^{3+} (Figure 1).

Electrochemical Behavior of L_1 after Addition of Increasing Amounts of Eu^{3+} or Y^{3+} Cations

We took advantage of the disruption of the communication in L upon complexation to investigate the sensing properties of this redox receptor towards lanthanide cations. Electrochemical experiments were carried out by DPV in CH_3OH solution containing 0.1 M TBAP. Results are illustrated in Figure 4. The addition of increasing amounts of Eu^{3+} or Y^{3+} cations (as nitrate or chloride salts) in a solution of L causes the linear growth of the intensity of the second DPV peak, along with the decrease of that for the first one. It must be pointed out that such evolution is observed because the electrochemical signal due to the lanthanide complex (140 and 150 mV for LEu and LY respectively) is very close to the second redox event in free L (E_{p2} = 140 mV). The first peak disappears and the second one reaches full development when one molar equivalent of metal salt has been added. This result is in keeping with ES-MS and potentiometric titration experiments and confirms the 1:1 binding mode between L and Eu^{3+} or Y^{3+} ions. Moreover, it has to be noted that a very slight precipitate was observed in the solution following the addition of a small amount of metal cation (ca. 0.1 molar equivalent), accompanied by a slight decrease in the intensity of the electrochemical signals. This precipitate disappeared when more metal cation was added. The intermediate formation of an insoluble complex, most likely an oligomeric assembly, at a low M^{3+}-to-L ratio could explained these observations.

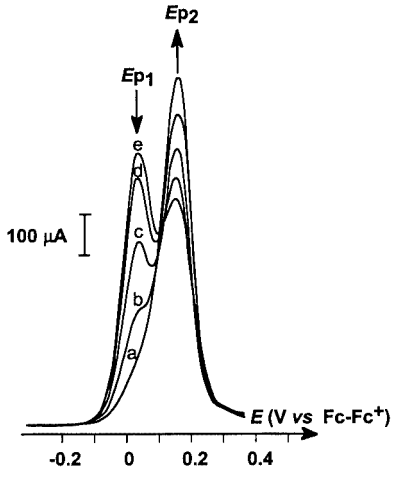

Figure 4. DPV curves for L (1 mM in CH_3OH +0.1 M TBAP) in the presence of increasing amounts of Eu^{3+} cations: Eu^{3+}/L = 0.1 (a), 0.25 (b), 0.5 (c), 0.75 (d) and 1 (e); sweep rate 0.01 $V{\cdot}s^{-1}$; pulse height 25 mV; step time 0.2 s

Analysis of the intensities of the two DPV peaks allowed us to draw amperometric titration curves (Figure 5), which clearly show the linear growth above 0.2 equivalent of the second DPV peak and the linear decrease of the first one upon addition of increasing amounts of trivalent cation. The same experiments were conducted in a CH_3OH/H_2O mixture (3:1, v:v) containing 0.1 M TBAP or $LiClO_4$. No major changes were observed, i.e. the same amperometric calibration curves were obtained, indicating that the electrochemical response of L towards lanthanide ions is not affected by the presence of water.

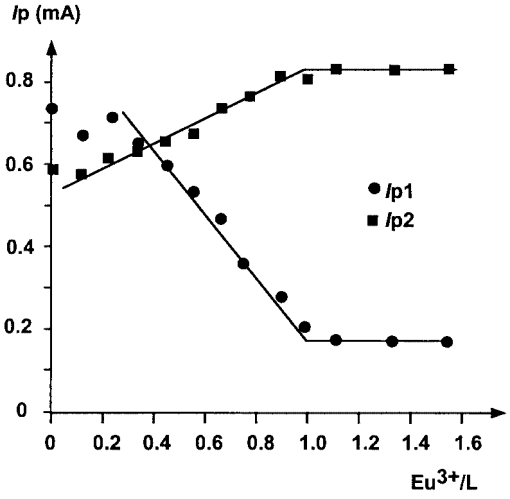

Figure 5. Amperometric titration curves: evolution of the DPV peak currents as a function of the Eu^{3+}-to-L ratio (see Figure 4)

Conclusion

The three chemically equivalent ferrocene subunits in L show a significant degree of electrostatic communication, which is responsible for the observation of two distinct electrochemical signals. These interactions are severely disrupted upon complexation of this tren-based ligand by lanthanide ions to form 1:1 (L:M) complexes. This leads to the observation of a unique voltammetric wave. Changes in the redox features of L in the presence of lanthanide ions can thus be exploited to detect and sense these guest species. Although a number of redox-active receptors able to electrochemically sense metal cations have been described previously,[33−35] to the best of our knowledge, L is the first example of a multi-redox ligand allowing an amperometric titration of metal cations in organic and aqueous media, via a large decrease in the communication between the redox active sites upon complexation.

Experimental Section

General Remarks: Hydrated metal ions (chloride or nitrate salts) were obtained from Aldrich. All compounds were of reagent grade and were used without further purification. Methanol (SDS, 99%,

 © 2003 Wiley-VCH Verlag GmbH & Co. KGaA, Weinheim

purex analytical grade) was used as received. Tetra-*n*-butylammonium perchlorate (TBAP) was purchased from Fluka and dried under vacuum at 80 °C for 3 days. ^{1}H and ^{13}C NMR spectroscopic experiments were conducted at 22 °C on a Bruker AC250 spectrometer using the solvent deuterium signal as internal reference. FAB (positive mode) mass spectra were recorded with an AEI Kratos MS 50 spectrometer fitted with an Ion Tech Ltd. gun and using *m*-nitrobenzyl alcohol as a matrix. ES-MS spectra were recorded on a Micromass Quattro mass spectrometer, equipped with an electrospray source. The temperature was set at 80 °C. The electrospray probe (capillary) voltage was optimized in the range 3.5−5 kV for positive ion electrospray. The sample cone voltage was set within the range 40−200 V. Complexes in solution [1 mg·mL^{-1} in CH_3CN/H_2O (3:1, v:v)] were infused in CH_3CN containing 0.01% HCOOH, through a fused silica tubing, using a syringe pump at a flow rate in the range 5−10 μL·min^{-1}. Potentiometric titrations were performed at 25 °C and the solutions were prepared in CH_3OH/H_2O (3:1, v:v). The ionic strength was fixed at I = 0.1 M with TBAP. An automatic titrator system (DMS, 716 Titrino Metrohm) equipped with a combined glass electrode and connected to an IBM Aptiva microcomputer was used. The electrodes were calibrated to read pH according to the classical method.[36] The ligand and its metal(III) complex of ca. 0.001 M were titrated with standardized 0.025 M NaOH at 25 °C. Argon was bubbled through the solutions to exclude CO_2 and O_2. A NaOH solution was standardized against potassium hydrogenphtalate. Carbonate content was checked by Gran's method. The titration data were refined by the non-linear least-squares refinement program HYPERQUAD[23,24] to determine the stability constants. The values of the stability constants are the mean values calculated from three titrations.

Electrochemical Studies: Experiments were conducted in a conventional three-electrode cell using an EGG PAR model 273 potentiostat, at 20 °C under an argon atmosphere. The Ag|10 mM $AgNO_3$ + 0.1 M TBAP in CH_3CN was used as a reference electrode. The potential of the regular Fc/Fc^+ redox couple used as an internal standard was 0.130 V under our experimental conditions. The working electrode consisted of a platinum disk (5 mm diameter) polished with 2 μm diamond paste. DPV curves were recorded at a 10 mV·s^{-1} scan rate with pulse height of 25 mV and a step time of 0.2 s. Electrochemical simulations and best fitting of experimental data were performed by the Electrochemical Simulations Package [ESP software, version 2.4, by Dr. Carlo Nervi (nervi@lem.ch.unito.it)]. The common approximation, which considers that formal potentials and half-wave potentials are identical, was applied.[30] The electrochemical parameters used for the digital simulation are: α = 0.5, k^0 = 0.02 cm·s^{-1}, and D = 10^{-5} cm^2·s^{-1}, α and k^0 being respectively the transfer coefficients and the heterogeneous transfer constant of the corresponding electrochemical reactions and D being the diffusion coefficient of the species. These values were assumed to be constant for all the systems studied since a slight modification of these parameters does not significantly affect the results.

Synthesis of L: Tris(2-aminoethyl)amine (0.5 g, 3.42 mmol) were dissolved in water (15 mL). A solution of ferrocenecarboxaldehyde (2.2 g; 3 × 3.42 mmol) in diethyl ether (15 mL) was then added and the biphasic solution was stirred vigorously in a sealed vessel for 12 hours. The orange precipitate was then filtered off, washed with diethyl ether (5 × 10 mL), and dried under vacuum. The trisimine intermediate was obtained in 95% yield (2.44 g). ^{1}H NMR (250 MHz, CD_3OD): δ = 2.73 (t, 6 H, N-CH_2CH$_2$-), 3.18 (t, 6 H, N-CH$_2$CH_2-), 4.07 (s, 15 H, Fc), 4.32 (m, 6 H, Fc), 4.51 (m, 6 H, Fc), 8.01 (s, 3 H, *H*C=N) ppm. ^{13}C NMR (250 MHz, CD_3OD): δ = 57.98, 61.58, 71.51, 71.90, 73.56, 82.16, 167.44 ppm. FAB-MS, *m/z*: 735 [M + H]$^+$. UV/vis, λ_{max} (ε/M^{-1}·cm^{-1}): 326 (6700), 455 nm (1300). $C_{39}H_{42}Fe_3N_4$, H_2O (752.32): calcd. C 62.26, H 5.89, N 7.45; found C 62.37, H 5.87, N 7.71.

Trisimine (500 mg) was dissolved in CH_3OH (50 mL) after which $NaBH_4$ (100 mg) was slowly added. The solution was then stirred for 4 hours. CH_3OH was removed by distillation, the residue was dissolved in H_2O (100 mL) and extracted with CH_2Cl_2 (3 × 30 mL). The organic phases were washed with water (2 × 10 mL), dried with $MgSO_4$, and the solvents evaporated to give the expected compound as a brown oil. Yield 93%. (470 mg). ^{1}H NMR (250 MHz, $CDCl_3$): δ = 1.90 (br. s, 3H N*H*), 2.50 (t, 6 H, N-CH_2CH$_2$-), 2.61 (t, 6 H, N-CH$_2$CH_2-), 3.45 (s, 6 H, Fc-CH_2) 4.08−4.16 (m, 27 H, Fc) ppm. ^{13}C NMR (250 MHz, $CDCl_3$): δ = 47.17, 49.05, 54.32, 67.79, 68.40, 68.62, 86.42 ppm. FAB-MS, *m/z*: 741 [M + H]$^+$. UV/Vis λ_{max} (ε/M^{-1}·cm^{-1}): 323 (440), 436 nm (370). $C_{39}H_{48}Fe_3N_4$ (740.36): calcd. C 63.27, H 6.53, N 7.57; found C 62.55, H 6.64, N 7.53.

LEu and LY Complexes: The LEu and LY complexes were isolated by mixing L and one equivalent of metal cation (as chloride or nitrate salts) in CH_3OH. The solution was stirred for one hour and the complexes were precipitated as a yellow powder upon addition of diethyl ether. Complexes were characterized by ES-MS measurements (see the text). No reproducible elemental analysis could be obtained and crystals suitable for X-ray studies could not be grown, due to hygroscopic properties

X-ray Crystallographic Study: Crystals of the hydrochloride form of L (LH_3^{3+}, 3Cl$^-$) were obtained by slow diffusion of diethyl ether into a solution of L with ten equivalents of HCl_{aq} in ethyl acetate/acetonitrile. Due to its instability, the crystal was mounted on the X-ray diffractometer and its structure determined at low temperature (143 K). Diffraction data (Table 3) were collected with a SMART CCD diffractometer (Mo-K_α radiation, graphite-monochromator, λ = 0.71073 Å). Intensity data were corrected for Lorentz polarization effects and absorption. Structure solution and refinement were performed with the SHELXTL package. Hydrogen

Table 3. Summary of crystallographic data for LH_3^{3+}, 3Cl$^-$

Formula	$C_{39}H_{51}Cl_3Fe_3N_4$ ·2CH_3CN·$C_2H_5CO_2CH_3$·H_2O
M	1037.97
Cryst. Syst.	orthorhombic
Space Group	$P2_12_12_1$
a [Å]	19.274(4)
b [Å]	22.753(5)
c [Å]	23.361(5)
V [Å^3] / Z	10245(4) / 8
D_x [g cm^{-3}]	1.346
λ [Å]	0.71073
T, K	143(2)
Size [mm]	0.2 × 0.2 × 0.2
Color	brown
μ [mm^{-1}]	1.039
F(000)	4352
No. of reflns. collected	18436
θ range [°]	1.64−28.97
Data/restraints/parameters	16889/0/996
Goodness on fit S	1.242
$\Delta\rho_{min}$/ $\Delta\rho_{max}$ [e·Å^{-3}]	1.956/-1.029
R {$I>2\sigma(I)$}[a]	0.1008

[a] $R = \Sigma||F_o| - |F_c||/\Sigma|F_o|$.

 © 2003 Wiley-VCH Verlag GmbH & Co. KGaA, Weinheim

atoms were included in calculated positions with isotropic thermal coefficients. CCDC-194179 contains the supplementary crystallographic data for this paper. These data can be obtained free of charge at www.ccdc.cam.ac.uk/conts/retrieving.html [or from the Cambridge Crystallographic Data Centre, 12, Union Road, Cambridge CB2 1EZ, UK; fax: (internat.) +44−1223/336-033; E-mail: deposit@ccdc.cam.ac.uk].

Acknowledgments

The authors wish to thank Dr. Brasme and M. Lefêvre (CRSSA, La Tronche, France) for their invaluable help for the collection of ES-MS data.

[1] A. E. Kaifer, M. Gomez-Kaifer, *Supramolecular Electrochemistry* **1999**, Wiley-VCH, Weinheim, Germany.
[2] P. Nguyen, P. Gómez-Elipe, I. Manners, *Chem. Rev.* **1999**, *99*, 1515−1548.
[3] S. Barlow, D. O′Hare, *Chem. Rev.* **1997**, *97*, 637−669.
[4] J. Alvarez, A. E. Kaifer, *Organometallics* **1999**, *18*, 5733−5734.
[5] J. Alvarez, Y. Ni, T. Ren, A. E. Kaifer, *J. Supramol. Chem.* **2001**, *1*, 7−16.
[6] J. Alvarez, T. Ren, A. E. Kaifer, *Organometallics* **2001**, *20*, 3543−3549.
[7] A. Tarraga, P. Molina, D. Curiel, M. D. Velasco, *Organometallics* **2001**, *20*, 2145−2152.
[8] I. Cuadrado, C. M. Casado, B. Alonso, M. Moran, J. Losada, V. Belsky, *J. Am. Chem. Soc.* **1997**, *119*, 7613−7614.
[9] G. R. Newkome, E. F. He, C. N. Moorefield, *Chem. Rev.* **1999**, *99*, 1689−1746.
[10] G. E. Southard, M. D. Curtis, *Organometallics* **2001**, *20*, 508−522.
[11] R. Rulkens, A. J. Lough, I. Manners, S. R. Lovelace, C. Grant, W. E. Geiger, *J. Am. Chem. Soc.* **1996**, *118*, 12683−12695.
[12] A. Tarraga, P. Molina, D. Curiel, M. D. Velasco, *Tetrahedron* **2001**, *57*, 6765−6774.
[13] P. D. Beer, Z. Chen, M. G. B. Drew, P. A. Gale, *J. Chem. Soc., Chem. Commun.* **1995**, 1851−1852.
[14] F. Barriere, N. Camire, W. E. Geiger, U. T. Mueller-Westerhoff, R. Sanders, *J. Am. Chem. Soc.* **2002**, *124*, 7262−7263.
[15] P. D. Beer, P. A. Gale, G. Z. Chen, *J. Chem. Soc., Dalton Trans.* **1999**, 1897−1910.
[16] D. T. McQuade, A. E. Pullen, T. M. Swager, *Chem. Rev.* **2000**, *100*, 2537−2574.
[17] P. G. Pickup, *J. Mater. Chem.* **1999**, *9*, 1641−1653.
[18] M. Ciampolini, *Struct. Bonding* **1969**, *6*, 52.
[19] P. D. Beer, C. Hazlewood, D. Hesek, J. Hodacova, S. E. Stokes, *J. Chem. Soc., Dalton Trans.* **1993**, 1327−1332.
[20] L. Fabbrizzi, M. Licchelli, L. Parodi, A. Poggi, A. Taglietti, *Eur. J. Inorg. Chem.* **1999**, 35−39.
[21] L. Fabbrizzi, M. Licchelli, A. Perotti, A. Poggi, G. Rabaioli, D. Sacchi, A. Taglietti, *J. Chem. Soc., Perkin Trans. 2* **2001**, *2*, 2108−2113.
[22] L. Fabbrizzi, I. Faravelli, *Chem. Commun.* **1998**, 971−972.
[23] L. Alderighi, P. Gans, A. Ienco, D. Peters, A. Sabatini, A. Vacca, *Coord. Chem. Rev.* **1999**, *184*, 311−318.
[24] P. Gans, A. Sabatini, A. Vacca, *Talanta* **1996**, *43*, 1739−1753.
[25] F. Thaler, C. D. Hubbard, F. W. Heinemann, R. Van Eldik, S. Schindler, I. Fabian, A. M. Dittler-Klingemann, F. E. Hahn, C. Orvig, *Inorg. Chem.* **1998**, *37*, 4022−4029.
[26] G. Anderegg, V. Gramlich, *Helv. Chim. Acta* **1994**, *77*, 685−690.
[27] S. Liu, D. S. Edwards, *Bioconjugate Chemistry* **2001**, *12*, 7−34.
[28] F. Ammar, J.-M. Savéant, *Electroanal. Chem.* **1973**, *47*, 215−221.
[29] J. B. Flanagan, S. Margel, A. J. Bard, F. Anson, *J. Am. Chem. Soc.* **1978**, *100*, 4248−4253.
[30] A. J. Bard, L. R. Faulkner, *Electrochemical Methods: Fundamentals and Applications*; **1980**, Wiley: New York, 232−235.
[31] D. K. Gosser, F. Zhang, *Talanta* **1991**, *38*, 715.
[32] H. Plenio, J. Yang, R. Diodone, J. Heinze, *Inorg. Chem.* **1994**, *33*, 4098−4104.
[33] C. D. Hall, N. W. Sharpe, I. P. Danks, Y. P. Sang, *J. Chem. Soc., Chem. Commun.* **1989**, 419−421.
[34] C. D. Hall, S. Y. F. Chu, *J. Org. Chem.* **1995**, 221−228.
[35] G. D. Brindley, O. D. Fox, P. D. Beer, *J. Chem. Soc., Dalton Trans.* **2000**, 4354−4359.
[36] A. E. Martell, R. J. Motekaitis, *Determination and use of Stability Constants*, **1992**, 2nd ed., VCH Publishers, New York.

Received February 10, 2003

 © 2003 Wiley-VCH Verlag GmbH & Co. KGaA, Weinheim

Pd^{II}, Zn^{II} and Ag^{I} Complexes of Tetrakis(*N*-7-azaindolyl)benzene: Variation of Bonding Modes, Extended Structures and Luminescence

Datong Song[a] and Suning Wang*[a]

Keywords: N ligands / Coordination modes / Palladium / Zinc / Silver / Luminescence

Pd^{II}, Ag^{I} and Zn^{II} complexes of tetrakis(7-azaindolyl)benzene (ttab), $[(PdCl_2)_2(ttab)]$ (**1**), $[(ZnCl_2)_2(ttab)]$ (**2**), $[Ag(NO_3)]_2$-(ttab) (**3a**) and $[Ag(NO_3)(DMSO)]_2(ttab)$ (**3b**) were synthesized and fully characterized by NMR spectroscopy, single-crystal X-ray diffraction and elemental analyses. The ttab ligand in these complexes displays two different bonding modes. In the Pd^{II} and Zn^{II} complexes, the ttab ligand chelates to the metal center via two *ortho* 7-azaindolyl groups (the *ortho* mode). In contrast, in the Ag^{I} complex, it chelates to the Ag^{I} ion via two *meta* 7-azaindolyl groups (the *meta* mode). In the solid state, molecules of **1** and **2** form grid-like extended structures that host solvent molecules such as DMSO and CH_2Cl_2. Compound **3a** appears to be a coordination polymer and can be converted into compound **3b** when dissolved in DMSO. A hydrogen bonded complex $[Zn(O_2CCF_3)_2(H_2O)_2](ttab)$ (**4**), which displays an unusual hydrogen bonded helical chain structure in the solid state, was also characterized. Except for compound **1**, these new compounds all emit blue light when irradiated by UV radiation.

(© Wiley-VCH Verlag GmbH & Co. KGaA, 69451 Weinheim, Germany, 2003)

Introduction

Luminescent transition metal complexes are of great interest because of their potential application in chemical optical sensors, photosensitization and electroluminescent devices.[1,2] We have previously demonstrated that Pt^{II} and Pd^{II} complexes of 7-azaindole based organic ligands can emit green and orange light, either in frozen solutions or in the solid state, when irradiated by UV light.[2f,3a] In addition to luminescent properties, the coordination chemistry displayed by transition metal complexes of the 7-azaindole-based ligands is also interesting. As we reported previously, the coordination mode displayed by ligands involving 7-azaindolyl groups varies drastically according to the geometry of the ligand. For example, as shown in Scheme 1, the 1,3-bis(7-azaindolyl)benzene ligand has been found to bind to Pd^{II} or Pt^{II} centers as a tridentate NCN-type ligand through cyclometallation[3] (bonding mode **A**). In contrast, the 1,2-bis(7-azaindolyl)benzene ligand usually acts as a bidentate chelate ligand through the two 7-azaindolyl groups (bonding mode **B** in Scheme 1).[3b] The 1,3,5-tris(7-azaindolyl)benzene ligand, on the other hand, uses two of the 7-azaindolyl groups to chelate to the metal center with the NCN type of binding similar to that in **A**, and uses the remaining 7-azaindolyl group as a bridging ligand to form a trinuclear complex (**C**).[2f] Recently we reported the synthesis of the new ligand 1,2,4,5-tetrakis(7-azaindolyl)benzene (ttab),[4] which is a bright blue luminescent emitter. The organoplatinum complexes of ttab have been found to display unusual structural features and chemical reactivity.[4] In the previously reported organoplatinum complexes, the ttab ligand chelates to the Pt^{II} center in the *ortho* bonding mode (**D**) as shown in Scheme 1. Further investigation revealed that the ttab ligand also displays a second bonding mode (**E**), the *meta* mode. The third bonding mode (**F**), the cyclometallation mode, was not observed for the ttab ligand.

The metal ion and the ligands surrounding the metal ion appear to play a key role in the bonding mode of the ttab ligand. We report herein the results of our investigation on Pd^{II}, Ag^{I} and Zn^{II} complexes of the ttab ligand.

Results and Discussion

Syntheses of Complexes

The ttab ligand reacts readily with K_2PdCl_4 and $ZnCl_2$ in solution to afford complexes $[(PdCl_2)_2(ttab)]$ (**1**) and $[(ZnCl_2)_2(ttab)]$ (**2**), respectively, in nearly quantitative yields. When ttab was reacted with $AgNO_3$, we obtained a white solid of **3a**, which displays blue luminescence at ambient temperature and is insoluble in most organic solvents. Based on elemental analysis results, **3a** has the formula $[Ag(NO_3)]_2(ttab)$. Compound **3a** can be dissolved in DMSO under sonication to form a dinuclear complex $[Ag(NO_3)(DMSO)]_2(ttab)$ (**3b**), in which the DMSO molecules coordinate to the Ag^{I} center through the oxygen atom, as

[a] Department of Chemistry, Queen's University, Kingston, Ontario, Canada, K7 L 3N6
E-mail: wangs@chem.queensu.ca

Supporting information for this article is available on the WWW under http://www.eurjic.org or from the author.

 © 2003 Wiley-VCH Verlag GmbH & Co. KGaA, Weinheim **DOI: 10.1002/ejic.200300249**

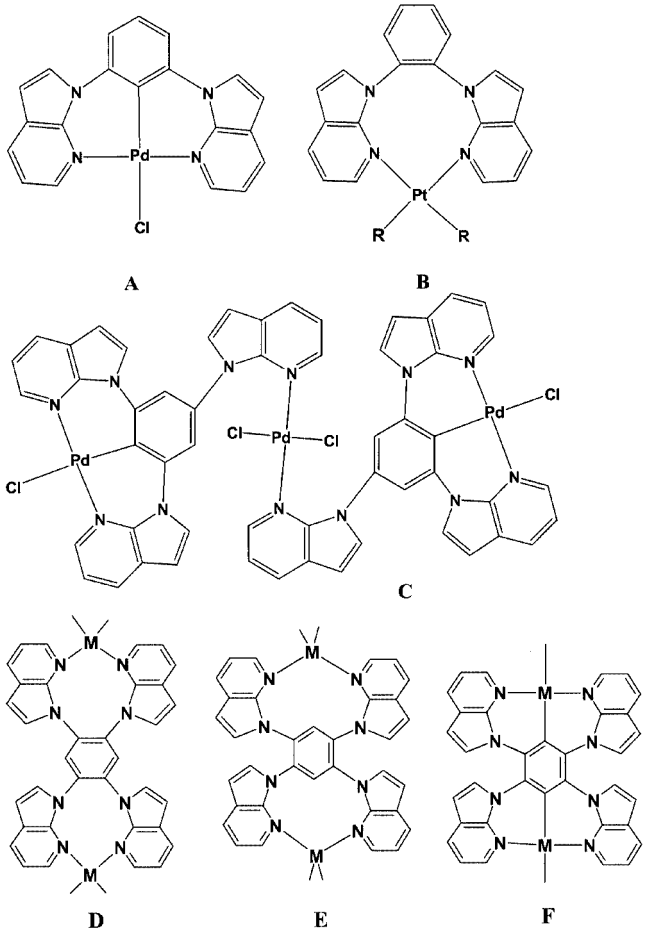

Scheme 1

confirmed by X-ray diffraction analysis. Anhydrous $ZnCl_2$ reacts with ttab in a THF solution, resulting in a blue luminescent white solid of **2**. Attempts to synthesize the complex $[Zn(O_2CCF_3)_2]_2$(ttab) by reacting $Zn(O_2CCF_3)_2$ hydrate with ttab were unsuccessful. Every attempt led to the isolation of crystals of $[Zn(O_2CCF_3)_2(H_2O)_2]$(ttab) (**4**), where the $Zn(O_2CCF_3)_2(H_2O)_2$ molecule is not coordinated to the ttab ligand but hydrogen bonded with the ttab ligand in the crystal lattice as confirmed by the X-ray diffraction study. The structures of ttab, **1**, **2**, **3b** and **4** were determined by X-ray diffraction analyses. Selected bond lengths and angles for **1**, **2**, **3b** and **4** are provided in Table 1.

Table 1. Selected bond lengths [Å] and angles [°]

		1	
Pd(1)−N(2)	2.022(4)	N(2)−Pd(1)−N(4)	87.25(15)
Pd(1)−N(4)	2.032(4)	N(2)−Pd(1)−Cl(2)	176.34(13)
Pd(1)−Cl(2)	2.2852(15)	N(4)−Pd(1)−Cl(2)	90.46(11)
Pd(1)−Cl(1)	2.2900(14)	N(2)−Pd(1)−Cl(1)	90.51(12)
		N(4)−Pd(1)−Cl(1)	177.76(11)
		Cl(2)−Pd(1)−Cl(1)	91.78(6)
		C(7)−N(2)−Pd(1)	123.7(4)
		C(14)−N(4)−Pd(1)	124.0(3)
		2	
Zn(1)−N(2)	2.053(10)	N(2)−Zn(1)−N(4)	97.2(3)
Zn(1)−N(4)	2.068(9)	N(2)−Zn(1)−Cl(1)	116.7(2)
Zn(1)−Cl(1)	2.196(3)	N(4)−Zn(1)−Cl(1)	123.9(3)
Zn(1)−Cl(2)	2.246(3)	N(2)−Zn(1)−Cl(2)	105.6(3)
		N(4)−Zn(1)−Cl(2)	104.6(3)
		Cl(1)−Zn(1)−Cl(2)	107.05(12)
		C(7)−N(2)−Zn(1)	131.1(8)
		C(14)−N(4)−Zn(1)	129.4(7)
		3b	
Ag(1)−N(1)	2.300(7)	N(1)−Ag(1)−N(3)	136.3(2)
Ag(1)−N(3)	2.335(9)	N(1)−Ag(1)−O(1)	128.9(3)
Ag(1)−O(1)	2.403(7)	N(3)−Ag(1)−O(1)	88.3(3)
Ag(1)−O(3A)	2.53(3)	N(1)−Ag(1)−O(3A)	106.4(13)
		N(3)−Ag(1)−O(3A)	80.9(8)
		O(1)−Ag(1)−O(3A)	103.8(15)
		4	
Zn(1)−O(6)	1.930(12)	O(6)−Zn(1)−O(5)	103.0(4)
Zn(1)−O(5)	1.943(10)	O(6)−Zn(1)−O(3)	98.9(6)
Zn(1)−O(3)	2.04(2)	O(5)−Zn(1)−O(3)	135.7(7)
Zn(1)−O(1)	2.066(17)	O(6)−Zn(1)−O(1)	96.0(6)
Zn(1)−O(4)	2.467(16)	O(5)−Zn(1)−O(1)	101.1(6)
Zn(1)−O(2)	2.557(16)	O(3)−Zn(1)−O(1)	114.4(9)

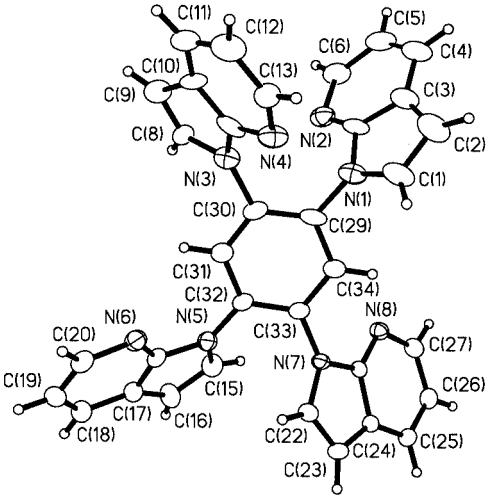

Figure 1. A diagram showing the structure of one of the independent ttab molecules in the crystal lattice with labeling schemes

Structures of ttab and of the Complexes

There are 1.5 independent molecules in each asymmetric unit of the crystal lattice of ttab, with one of the ttab molecules being located at the inversion center of symmetry. The structure of one of the independent molecules in the crystal lattice of ttab is shown in Figure 1. The ttab ligand has a non-planar structure. The 7-azaindolyl groups do not have significant conjugation with the central benzene ring as indicated by the dihedral angle between the central benzene plane and the 7-azaindolyl plane that ranges from 46.6° to 76.7°. Unlike 1,2-bis(7-azaindolyl)benzene or 1,3-bis(7-azaindolyl)benzene, which have only one way of chelating to the metal center, ttab has four nitrogen donor atoms available, which can chelate to the metal center either with two *ortho* 7-azaindole moieties (*ortho* fashion, **D**) or with two *meta* 7-azaindole moieties (*meta* fashion, **E**). In addition, it is conceivable that the ttab ligand could also form cyclometallated complexes (**F**), especially with the Pd^{II}

 © 2003 Wiley-VCH Verlag GmbH & Co. KGaA, Weinheim

and Pt^{II} centers, in the same manner as 1,3-bis(7-azaindolyl)benzene and 1,3,5-tris(7-azaindolyl)benzene, as shown in Scheme 1. However, despite our repeated attempts to react Pd^{II} and Pt^{II} ions with ttab under various conditions, no cyclometallated products were obtained. For the Pd^{II} ion, the *ortho* chelated complex **1** was isolated, instead.

The structure of **1**, as shown in Figure 2, has a crystallographically imposed inversion center of symmetry. Each Pd^{II} ion in **1** is chelated by two *ortho* 7-azaindolyl groups via the nitrogen atoms, resulting in a dinuclear complex. Each Pd^{II} center adopts a typical square-planar geometry, with the two nitrogen donor atoms *cis* to each other and two chloride ligands *trans* to each nitrogen atom. The Pd−N and Pd−Cl bonds in **1** show typical bond lengths with averages of 2.027(4) Å and 2.2876(14) Å, respectively, which are close to those reported previously.[2f,3a] The four 7-azaindolyl planes are nearly perpendicular to the central benzene ring as indicated by the dihedral angles between the 7-azaindolyl plane and the benzene ring (100.2° and 102.6°, respectively). The central benzene ring of the ttab ligand is "sandwiched" midway between the two $PdCl_2N_2$ planes. The $PdCl_2N_2$ plane is approximately parallel to the central benzene plane as indicated by the dihedral angle of 25.5° between these two planes. The separation distance between the two Pd^{II} centers in **1** is 6.660(2) Å. As a result, the distance between the center of the benzene ring and the Pd atom is 3.33(1) Å. The shortest contact distances between the Pd atom and the carbon atoms of the benzene ring are 2.99(1) Å [Pd(1)−C(16)] and 3.01(1) Å [Pd(1)−C(15)]. These distances are considerably shorter than the sum (≈3.22 Å) of the van der Waals radii of Pd and C, indicating the presence of some interactions between the Pd atom and the benzene ring. The structure of **1** resembles that of $[(PtR_2)_2(ttab)]$, where R equals methyl or

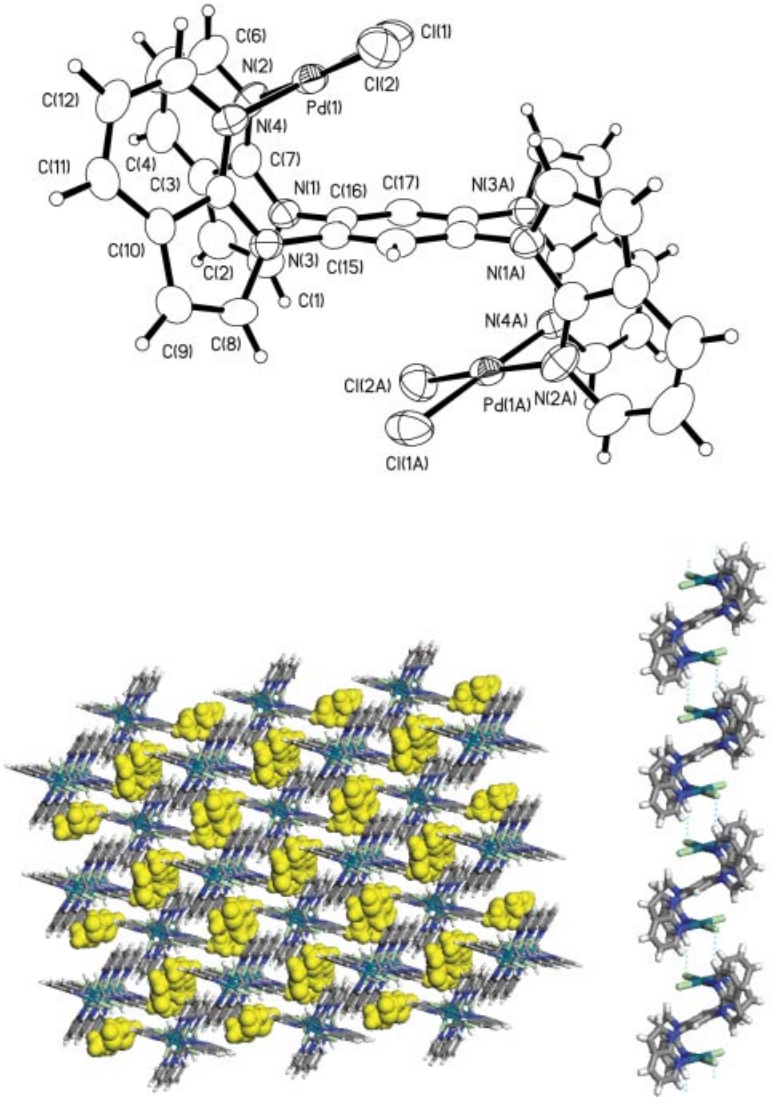

Figure 2. Top: a diagram showing the structure of **1** with labeling schemes; bottom, right: the hydrogen bond-linked 1D column; left: unit cell packing diagram viewed down the 1D column, the DMSO solvent molecules are shown using space-filling models

 © 2003 Wiley-VCH Verlag GmbH & Co. KGaA, Weinheim

phenyl, reported previously, where substantial interactions between the Pt atom and the central benzene ring were also observed.[4]

Molecules of **1** stack along the *b* axis as shown in Figure 2. There are weak intermolecular hydrogen bonding interactions between the chloride ligands and the protons on the 7-azaindole rings of the neighboring molecules [Cl(1)···C(13) = 3.62 Å, Cl(2)···C(6) = 3.70 Å], leading to the formation of a 1D column. The shortest intermolecular Pd···Pd distance along the 1D column is 4.800(2) Å. The void space between the 1D columns forms extended channels in the crystal lattice. DMSO solvent molecules are located in these channels, as shown in Figure 2. There are hydrogen bonding interactions between the oxygen atom of the DMSO molecule and a proton on the central phenyl ring of the ttab ligand as indicated by the O···C distance of 3.10 Å. Crystals of **1** are stable at ambient temperature and no loss of DMSO solvent molecules was observed, as evident by the elemental analysis results.

Earlier we postulated that a "sandwich" structure similar to **1** is only possible for metal ions that have a square-planar geometry,[4] based on the assumption that if the metal ion has a tetrahedral geometry, it would bring the ligands bound to the metal center into close contact with the central benzene ring of the ttab ligand and as a result, the *ortho* coordination mode would not be possible. To prove this postulation, we examined the structure of **2**. As shown in Figure 3, the molecule of **2** has a crystallographically imposed inversion center. One surprising finding is that the ttab ligand adopts the *ortho* coordination mode with the Zn^{II} ion in the same manner as that observed in **1**. The common coordination geometry for a four-coordinate Zn^{II} ion is tetrahedral. The *ortho* bonding mode displayed by the ttab ligand in **2** is therefore totally unexpected. Each Zn^{II} center in **2** has a distorted tetrahedral geometry, with two nitrogen donor atoms from the ttab ligand occupying two coordination sites and two chloride ligands occupying the other two sites. The bond angles of N(2)−Zn(1)−N(4), N(2)−Zn(1)−Cl(1), and N(4)−Zn(1)−Cl(1), which are 97.2(3)°, 116.7(2) °, and 123.9(3) °, respectively, deviate significantly from a typical tetrahedral geometry. To minimize steric interactions between the chloride ligand Cl(1) and the central phenyl ring of the ttab ligand, the Zn(1)−Cl(1) bond is almost parallel to the central phenyl ring of ttab. The Zn(1)−Zn(1A) separation distance is 7.538(2) Å, much longer than the Pd(1)−Pd(1A) distance in **1**. The distance between Cl(1) and the center of the central phenyl ring of ttab is 3.19 Å. The distances between the Cl(1) atom and C(15), C(16), C(17) atoms of the phenyl ring are in the range of 3.42 to 3.50 Å, much shorter than the corresponding Cl−C separation distances in **1** [the shortest Cl−C distance in **1**, 3.76 Å, is between Cl(1) and C(16)]. The Zn(1)−Cl(2) bond is considerably longer than the Zn(1)−Cl(1) bond (by 0.05 Å). The Zn−N and Zn−Cl bond lengths in **2** [av. 2.060(9) Å and 2.221(3)Å, respectively] are typical.[5] The orientation of the 7-azaindolyl groups in **2** is similar to their orientation in **1**, with the dihedral angles between the 7-azaindolyl planes and the central benzene plane being 82.7° and 82.4°, respectively. However, the bond angles of C(7)−N(2)−Zn(1) [131.1(8)°] and C(14)−N(4)−Zn(1) [129.4(7)°] are considerably larger than the corresponding ones in **1** [C(7)−N(2)−Pd(1) = 123.7(4)°, C(14)−N(4)−Pd(1) = 124.0(3)°]. The geometry distortion around the metal ions and the nitrogen donor atoms in **2** is clearly a consequence of steric interactions between the chloride ligands and the central phenyl group. Nonetheless, the structure of **2** demonstrates that the *ortho* bonding mode is possible and favorable for a tetrahedrally coordinated Zn^{II} ion. In solution, only one set of chemical shifts for the ttab ligand was observed in the ^1H NMR spectrum of **2**. Therefore, we believe that only one bonding mode, most likely the *ortho* mode, exists in solution for complex **2**. In coordinating solvents such as DMSO, the $ZnCl_2$ units appear to dissociate from the ttab ligand as indicated by the ^1H NMR spectrum of **2** in [D_6]DMSO, which is exactly identical to that of the free ttab ligand in [D_6]DMSO. We believe that the DMSO solvent molecules are coordinated to the $ZnCl_2$ unit in solution, replacing the nitrogen donor atoms of the ttab ligand and resulting in the dissociation of the complex **2**.

In the crystal lattice, molecules of **2** (Figure 3) form one-dimensional chains through intermolecular hydrogen bonding interactions between the chloride ligands of one molecule and the protons on the 7-azaindole rings of the neighboring molecules in a similar manner as observed in **1**. The intermolecular Cl(1)···C(2′) separation distance is 3.67 Å. An interesting feature is that the 1D columns of **2** are arranged in such a way that rhombohedral-shaped channels are formed. Disordered CH_2Cl_2 solvent molecules occupy these channels. The crystals of **2** lose the trapped solvent molecules rapidly at ambient temperature, causing the collapse of the crystal lattice. The structure of the dinuclear silver complex **3b** is shown in Figure 4. In contrast to the structures of **1** and **2**, the ttab ligand in **3b** adopts the *meta* bonding mode. The molecule of **3b** has a crystallographically imposed center of inversion symmetry. Each Ag^{I} ion is coordinated to two 7-azaindolyl groups at the 1,3 positions of the ttab ligand. The Ag^{I} center is also coordinated to two oxygen atoms, one from the DMSO molecule and the other from a disordered nitrate anion. Coordination to a metal center via the oxygen atom of the DMSO ligand has previously been observed.[6] The bond angles around the Ag(1) atom range from 80.9(8) to 136.3(2)°. The geometry of the Ag(1) center can therefore be best described as a highly distorted tetrahedron. The dihedral angles between the 7-azaindolyl plane and the central benzene ring are 123.7° and 115.9°, respectively, much greater than those of **1** and **2**. The preference for the "*meta*" bonding mode shown by the ttab ligand in **3b** could be attributed to the relative bulkiness of the DMSO and NO_3^- ligands compared to the chloride ligands. The *meta* mode appears to minimize the interactions between the oxygen donor ligands and the central phenyl ring as well as satisfy the geometric preference of the Ag(1) ion. The distance between the two Ag(1) centers in **3b** is 6.594(2) Å, similar to the Pd−Pd distance observed in **1**. The distances between the

 © 2003 Wiley-VCH Verlag GmbH & Co. KGaA, Weinheim

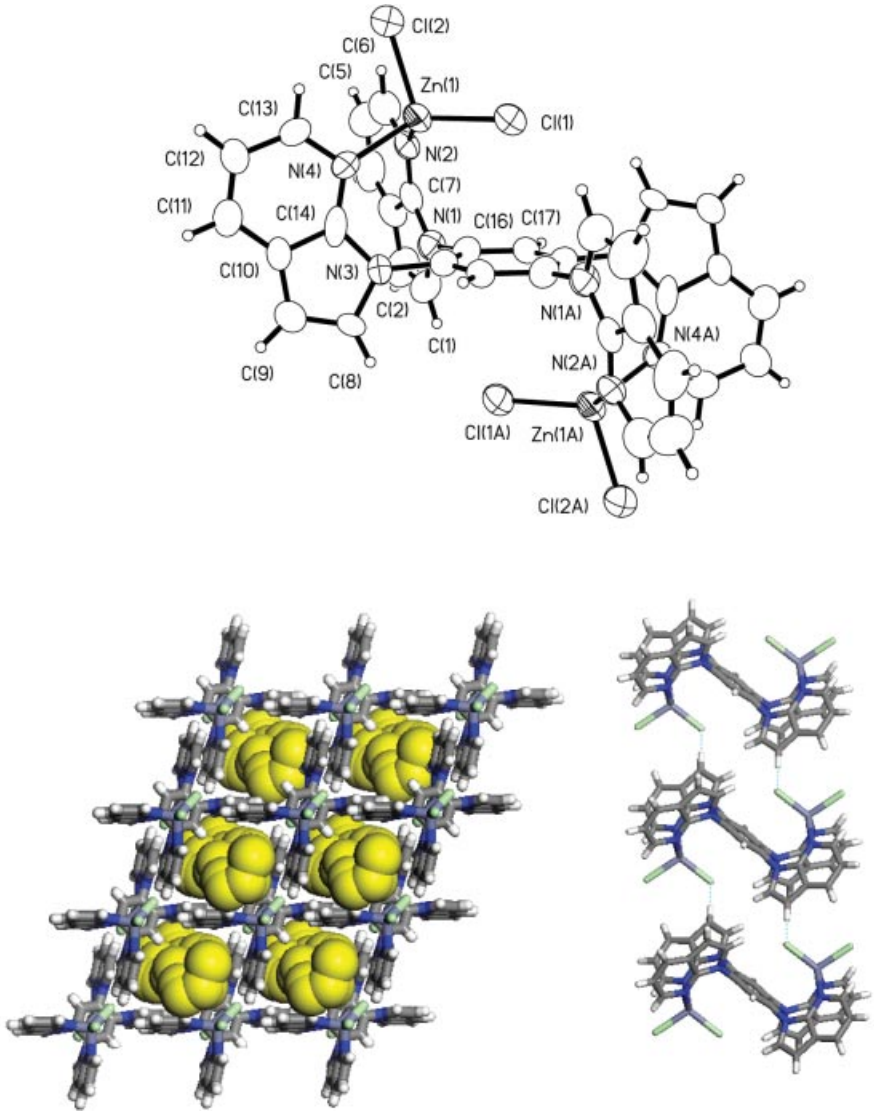

Figure 3. Top: a diagram showing the structure of **2** with labeling schemes; bottom, right: the hydrogen bond-linked 1D column; left: unit cell packing diagram viewed down from the 1D column, the disordered CH_2Cl_2 solvent molecules are shown using space-filling models

Ag(1) center and the carbon atoms C(15), C(16) and C(17) of the central phenyl ring, which are 3.20 Å, 2.72 Å and 3.17 Å, respectively, are either close to or less than the van der Waals contact distance of Ag−C (literature C−Ag bond length: ≈2.58 Å).[7b] Therefore, some weak bonding interactions between the Ag centers and the central phenyl ring appear to be present. The Ag(1)−O(1) and Ag(1)−O(3A) bond lengths are similar to those reported previously.[7]

The extended structure of **3b** is shown in Figure 4. Each molecule of **3b** is bonded to four neighboring molecules through hydrogen bonding between the oxygen atom of the nitrate ion and a proton (H14′) on the 7-azaindole ring of the neighboring molecule, as indicated by the O(4)···C(12′) distance of 3.33 Å, to form a two-dimensional layered network. In the crystal lattice, these layers stack on top of one another in an *ABAB* fashion, with toluene molecules filling the gaps. Compound **3b** slowly loses the DMSO ligands and reverts back to **3a** upon standing at ambient temperature. Due to the poor solubility of **3a**, NMR and X-ray diffraction experiments could not be carried out. Based on the poor solubility, the elemental analysis and the structure of **3b**, we believe that **3a** is likely to be a one-dimensional coordination polymer, where the nitrate anions function as bridging ligands, linking the dinuclear silver units together (in a similar way as that observed in **3b)** to form a coordination polymer chain.

Because the *meta* structure displayed by complex **3b** appears to be the consequence of the relatively large ligands DMSO and nitrate, we decided to examine the reaction of $Zn(O_2CCF_3)_2$ with the ttab ligand, anticipating a *meta* structure similar to that of **3b**. However, surprisingly, the product we isolated does not contain any coordination bonds between the Zn^{II} ion and the ttab ligand. Instead, the ttab ligand and the $Zn(O_2CCF_3)_2(H_2O)_2$ molecule located in the crystal lattice are linked together via hydrogen bonds, as shown in Figure 5. The H_2O ligands are from the starting material. Repeated efforts to synthesize the water-

 © 2003 Wiley-VCH Verlag GmbH & Co. KGaA, Weinheim

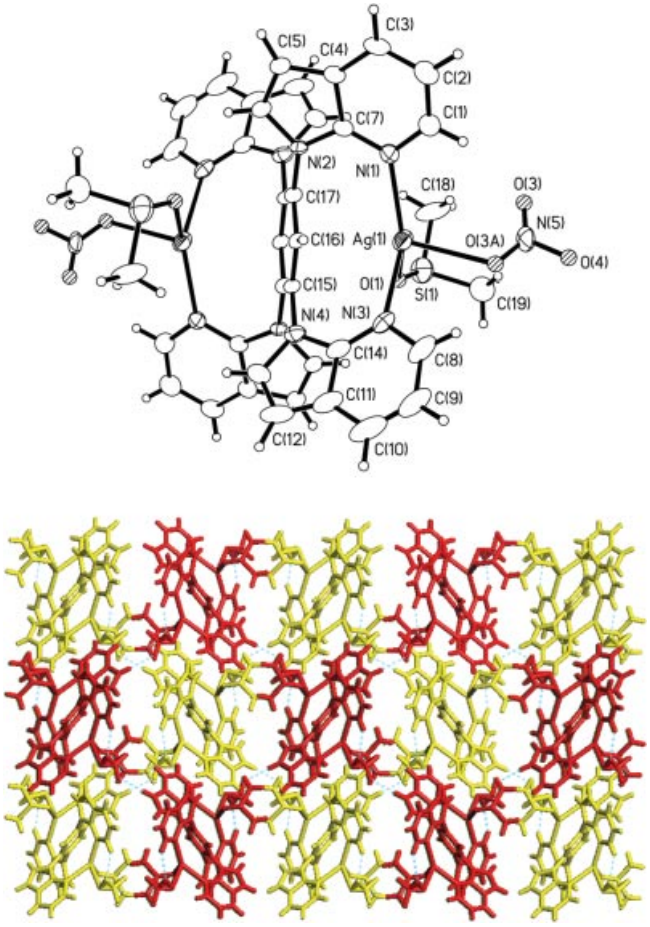

Figure 4. Top: a diagram showing the structure of **3b** with labeling schemes; for clarity, the oxygen atoms on DMSO and the NO_3^- are shown as ideal spheres; one of the disordered oxygen atoms [O(4A)] is not shown; bottom: unit cell diagram showing two layers (red and yellow) of hydrogen bond-linked 2D sheets

free complex $[Zn(O_2CCF_3)_2]_2$(ttab) were unsuccessful. Despite the poor quality of the crystal of **4**, the crystal data established unambiguously that the Zn^{II} ion is coordinated to two trifluoroacetate ligands and two H_2O ligands with an irregular geometry: four normal Zn−O bonds and two long Zn−O bonds [Zn(1)−O(2) = 2.557(16) Å, Zn(1)−O(4) = 2.467(16) Å]. The four non-coordinating nitrogen atoms of the ttab ligands form hydrogen bonds with the coordinated H_2O ligands. The N(8) and N(6) atoms are hydrogen-bonded to the O(6) atom while the N(2) and N(4) atoms are bonded to the O(5A) atom from a neighboring $Zn(O_2CCF_3)_2(H_2O)_2$ group, as indicated by the distances of O(5A)···N(2), 2.73(2) Å; O(5A)···N(4), 2.74(2) Å; O(6)···N(6), 2.70(2) Å; O(6)···N(8), 2.71(2) Å. The $[Zn(O_2CCF_3)_2(H_2O)_2]$ unit therefore functions as a linker for the ttab ligands through hydrogen bonds, leading to the formation of an unusual hydrogen-bond linked 1D chain (Figure 5). Extended structures involving metal complexes and organic molecules linked by hydrogen bonds have been reported previously.[8] One important feature of **4** is that the hydrogen-bonded 1D chains are helical and rotate in the same direction in the crystal lattice, resulting in the formation of a chiral lattice as shown in Figure 5. Interestingly, the hydrogen-bonding interactions between the zinc(II) complex and the ttab molecule are apparently retained in non-coordinating solvents such as CH_2Cl_2, as confirmed by the ^1H NMR study, which shows that the chemical shifts of the ttab molecule in **4** are drastically different from those of the free ttab molecule. In coordinating solvents such as DMSO, the NMR spectrum of **4** is identical to that of the free ttab ligand, indicating the Zn^{II} complex is no longer interacting with the ttab ligand through hydrogen bonds. It is very likely that the DMSO molecules coordinate to the Zn^{II} center and saturate the coordination sphere of the Zn^{II} ion, which may or may not lead to the replacement of the H_2O ligands at the zinc center. Due to the presence of an excess of DMSO molecules, the H_2O ligands are very likely to form hydrogen bonds with the DMSO solvent molecules instead of the ttab molecule, thus resulting in the free ligand-like behavior of the ttab molecule in DMSO. Toluene solvent molecules were also found in the lattice of **4** (one toluene per molecule of **4**), which do not escape from the crystal lattice at ambient temperature, as indicated by elemental analysis results.

Luminescent Properties

When irradiated by UV light, ttab emits a bright blue light both in solution and in the solid state. The emission maximum of ttab in a CH_2Cl_2 solution is at 377 nm when the concentration of the solution is approximately 10^{-4} M, while at high concentrations a significant red shift is observed (e.g. 0.10 M solution, emission maximum at approximately 463 nm), which can be attributed to intermolecular interactions or excimer emission. Compound **1** shows no detectable luminescence in solution or in the solid state, attributable to the quenching by the Pd^{II} ion. Compound **2** is blue luminescent in solution and in the solid state (λ_{max} = 380 nm). Compound **3a** is blue luminescent in the solid state with the emission maximum at 432 nm. The substantial red shift of the emission band of **3a**, compared to that of free ttab in solution, is clearly caused by intermolecular interactions in the solid state. Due to the insolubility of **3a** in most solvents, no spectrum was recorded in solution. Compound **3b** does not display any significant luminescence in the solid state, weak blue luminescence from **3b** in solution was observed (λ_{max} = 375 nm). The emission spectra of ttab, **2**, **3a**, **3b** and **4** are shown in Figure 6. The emission maximum of **2** (375 nm) in a CH_2Cl_2 solution (approx. 10^{-4} M) is essentially the same as that of the free ligand ttab. The emission bands of **2** and **3b** in solution at the same concentration resemble that of the free ttab ligand in solution, indicating that they are all ttab-based emissions. However, the intensity of the emission bands of **2** and **3b** is much weaker than that of the free ttab under the same conditions, indicating that the Zn^{II} ion and the Ag^{I} ion partially quench the emission from the ttab ligand. Compound **4** displays blue luminescence in solution. However, the emission spectrum of **4** recorded in CH_2Cl_2 is blue-shifted by about 20 nm, compared to that of the free ttab ligand recorded under the same conditions. Furthermore, the emis-

 © 2003 Wiley-VCH Verlag GmbH & Co. KGaA, Weinheim

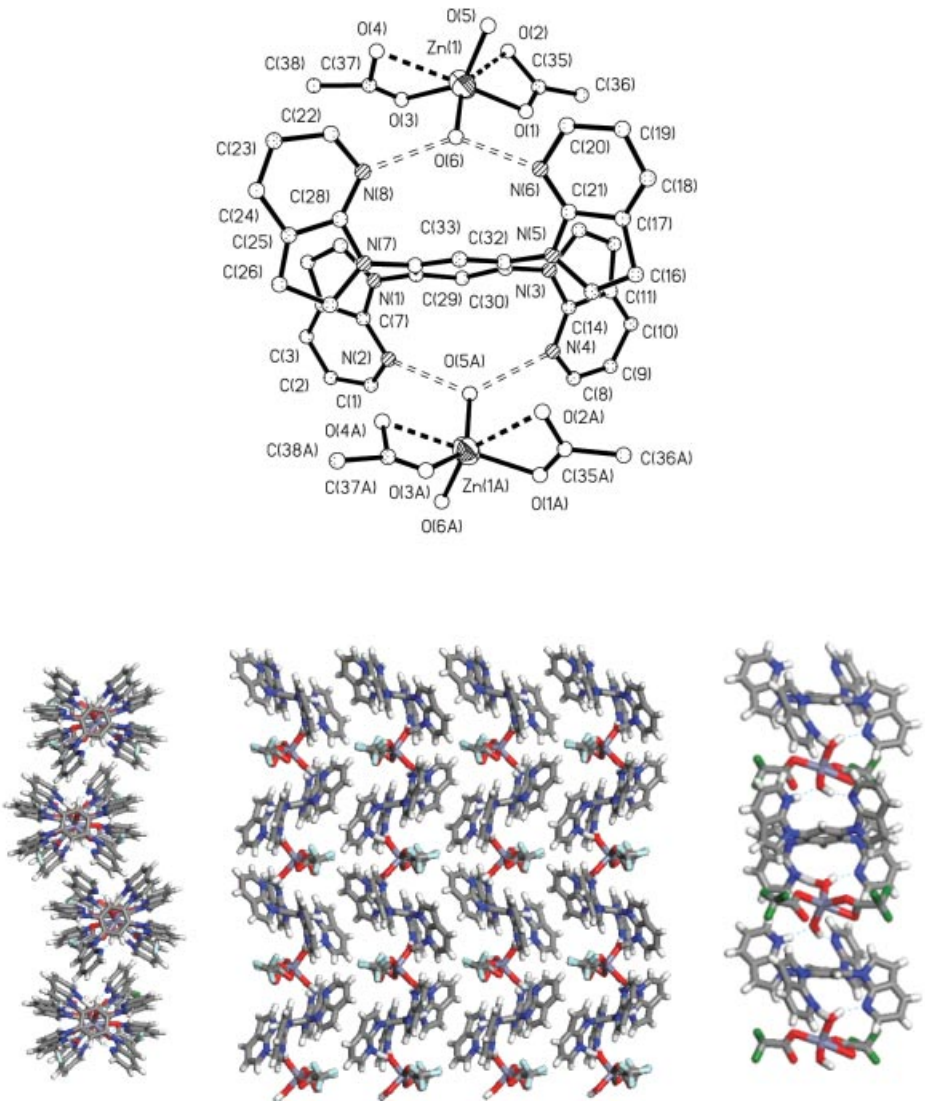

Figure 5. Top: a diagram showing the structure of **4** with labeling schemes (a second $[Zn(O_2CCF_3)_2(H_2O)_2]$ unit from a neighboring molecule is also shown to demonstrate the hydrogen bond pattern.); for clarity, the disordered fluorine atoms are omitted and all atoms except zinc are shown as ideal spheres; bottom, right: the hydrogen bond linked 1D chain; left: the view projected down the 1D chain; middle: the packing of the 1D chains in the lattice

sion intensity of **4** is about 1% of the intensity of the free ttab ligand. These experimental observations provide further support for the presence of hydrogen-bonding interactions between the $[Zn(O_2CCF_3)_2(H_2O)_2]$ group and the ttab ligand in solution. This appears to partially quench the emission of the ttab ligand.

In summary, both the *meta* and *ortho* coordination modes of the ttab ligand were established. The cyclometallated bonding mode was not observed for the ttab ligand. Both the coordination geometry of the metal ion and the nature of the surrounding ligands appear to influence the bonding mode of the ttab ligand. The unusual extended structures displayed by the complexes of the ttab ligand and its hydrogen-bonded compound were demonstrated. The fact that these extended structures have the tendency to host solvent molecules makes these compounds potentially useful for applications in host-guest chemistry. The Pd^{II} ion appears to be capable of completely quenching the lumi-

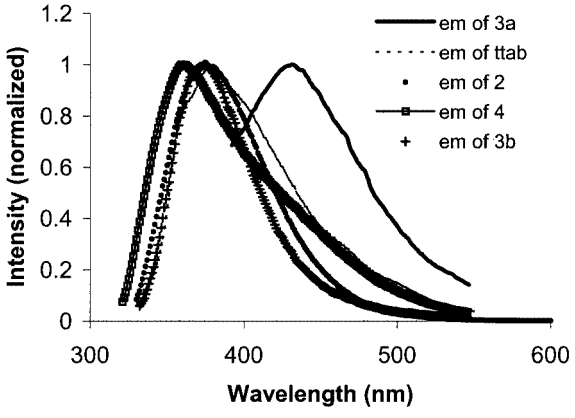

Figure 6. The emission spectra of ttab (1.0×10^{-4} M, CH_2Cl_2), **2** (1.0×10^{-4} M, CH_2Cl_2), **3a** (solid), **3b** (1.0×10^{-4} M, DMSO) and **4** (1.0×10^{-4} M, CH_2Cl_2)

 © 2003 Wiley-VCH Verlag GmbH & Co. KGaA, Weinheim

nescence of the ttab ligand while the Zn^{II} and Ag^{I} ions partially quench the emission of the ttab ligand. Hydrogen-bonding interactions also lead to the significant quenching of the ttab luminescence. The sensitivity of the ttab luminescence toward various metal ions and hydrogen-bonding interactions makes it potentially useful as a fluorescent sensor for certain metal ions and molecules, which are being investigated in our laboratory.

Experimental Section

All the starting materials were purchased from Aldrich Chemical Co. THF was dried by refluxing over sodium and was freshly distilled prior to use. All the other reagent-grade solvents were used without further purification. ^{1}H and ^{13}C NMR spectra were recorded on a Bruker Advance 300 or 500 MHz spectrometer. Excitation and emission spectra were recorded on a Photon Technologies International QuantaMaster Model 2 spectrometer. Elemental analyses were performed by Canadian Microanalytical Service, Ltd, Delta, British Columbia.

Synthesis of $[(PdCl_2)_2(ttab)]$ (1): A solution of ttab (0.20 mmol, 0.108 g) in 20 mL of CH_3CN was added to a solution of K_2PdCl_4 (0.40 mmol, 0.130 g) in a minimum amount of water. The mixture was stirred at room temperature for 0.5 h, and the yellow precipitate was collected by filtration and washed with CH_3OH and diethyl ether. Recrystallization of the crude product from DMSO yielded orange crystals of **1** (0.204 g 97%). ^{1}H NMR (500 MHz, [D$_6$]DMSO, 25 °C): δ = 8.93 (d, *J* = 5.0 Hz, 4 H, 7-aza), 8.17 (s, 2 H, phenyl), 8.14 (d, *J* = 7.0 Hz, 4 H, 7-aza), 7.70 (d, *J* = 3.5 Hz, 4 H, 7-aza), 7.29 (dd, *J* = 7.0, *J* = 5.0, 4 H, 7-aza), 6.76 (d, *J* = 3.5 Hz, 4 H, 7-aza) ppm. ^{13}C NMR: δ = 147.4, 145.6, 137.7, 136.7, 132.3, 131.3, 122.3, 117.7, 103.4 ppm. $C_{34}H_{22}Cl_4N_8Pd_2{\cdot}2DMSO$ (1053.52): calcd. C 43.32, H 3.25, N 10.64; found C 42.85, H 3.20, N 10.48.

Synthesis of $[(ZnCl_2)_2(ttab)]$ (2): Anhydrous $ZnCl_2$ (0.054 g, 0.4 mmol) and ttab (0.108 g, 0.2 mmol) were mixed in 20 mL of THF and stirred overnight under nitrogen. The white precipitate formed was collected by decanting the solution, it was washed with THF and dried under vacuum to afford a white powder of **2** (0.148 g, 91%). ^{1}H NMR (500 MHz, CD_2Cl_2, 25 °C): δ = 9.14 (dd, *J* = 5.5, *J* = 1.5 Hz, 4 H, 7-aza), 8.16 (dd, *J* = 8.0, *J* = 1.5 Hz, 4 H, 7-aza), 7.74 (d, *J* = 4.0 Hz, 4 H, 7-aza), 7.55 (s, 2 H, phenyl), 7.30 (dd, *J* = 8.0, *J* = 5.5 Hz, 4 H, 7-aza), 6.72 (d, *J* = 4.0 Hz, 4 H, 7-aza) ppm. ^{13}C NMR (CD_2Cl_2, 25 °C): δ = 147.9, 145.2, 139.3, 136.1, 134.3, 131.7, 124.7, 117.5, 104.1 ppm. $C_{34}H_{22}Cl_4N_8Zn_2{\cdot}0.5CH_2Cl_2$ (857.66): calcd. C 48.32, H 2.70, N 13.07; found C 48.56, H 2.73, N 13.02.

Synthesis of $[Ag_2(NO_3)_2(ttab)]_n$ (3a): A solution of $AgNO_3$ (0.50 mmol, 0.085 g) in 5 mL of H_2O was layered on top of a solution of ttab (0.10 mmol, 0.0542 g) in 5 mL of CH_2Cl_2. After 12 days standing at ambient temperature, the white precipitate formed was collected and washed with H_2O, ethanol and then CH_2Cl_2, and dried under vacuum to afford **3a** (0.064 g, 73%). Compound **3a** is not soluble in non-coordinating solvents. As a result, NMR spectra were not recorded. $C_{34}H_{22}Ag_2N_{10}O_6$ (882.32): calcd. C 46.28, H 2.51, N 15.87; found C 46.91, H 2.65, N 15.75.

Synthesis of $[Ag_2(NO_3)_2(ttab)(DMSO)_2]$ (3b): Upon dissolution in DMSO under sonication, **3a** was converted into **3b** quantitatively. ^{1}H NMR (300 MHz, DMSO, 25 °C): δ = 8.50 (s, 2 H, phenyl), 8.24 (d, *J* = 4.5 Hz, 4 H, 7-aza), 8.08 (d, *J* = 7.5 Hz, 4 H, 7-aza), 7.24 (dd, *J* = 7.8, *J* = 4.8 Hz, 4 H, 7-aza), 7.10 (d, *J* = 3.0 Hz, 4 H, 7-aza), 6.52 (d, *J* = 3.6 Hz, 4 H, 7-aza) ppm. ^{13}C NMR: δ = 146.6, 143.6, 132.4, 129.7, 128.6, 128.1, 121.3, 117.0, 102.2 ppm. The CHN analysis results for **3b** are identical to those of **3a**, due to the loss of DMSO ligands prior to the analysis.

Table 2. Crystallographic data

Compound	**1**	**2**	**3b**	**4**
Formula	$C_{34}H_{22}Cl_4N_8Pd_2{\cdot}2DMSO$	$C_{38}H_{34}N_8Zn_2Cl_4{\cdot}4CH_2Cl_2$	$C_{38}H_{34}Ag_2N_{10}O_8S_2{\cdot}2C_7H_8$	$C_{38}H_{24}N_8O_6F_6Zn{\cdot}C_7H_8$
FW	1053.45	1154.79	1222.88	962.13
Wavelength	0.71073 Å	0.71073 Å	0.71073 Å	0.71073 Å
Space group	$P2_1/n$	$P\bar{1}$	$P2_1/c$	$Pca2_1$
a, Å	12.072(3)	9.553(5)	10.032(4)	18.853(11)
b, Å	11.333(3)	9.753(5)	19.692(9)	12.279(7)
c, Å	15.538(4)	14.156(7)	13.866(6)	19.603(11)
α, °	90	85.300(13)	90	90
β, °	93.693(4)	89.561(11)	106.307(10)	90
γ, °	90	63.010(9)	90	90
V, Å^3	2121.4(8)	1170.8(11)	2628.9(19)	2628.9(19)
Z	2	1	2	4
$D_{calc.}$, g cm^{-3}	1.649	1.638	1.545	1.408
T, K	297	296	298	298
μ, cm^{-1}	12.42	17.48	8.88	6.22
2θ, max, °	56.66	56.80	56.70	56.80
Reflns measured	14855	8374	17597	29882
Reflns used	5043	5373	6286	8729
Parameters	253	265	317	559
Final *R* [$I > 2\theta(I)$]	R_1 [a] = 0.0459 wR_2 [b] = 0.0694	R_1 [a] = 0.0948 wR_2 [b] = 0.1961	R_1 [a] = 0.0625 wR_2 [b] = 0.1262	R_1 [a] = 0.0893 wR_2 [b] = 0.1871
R (all data)	R_1 = 0.1362 wR_2 = 0.0823	R_1 = 0.2833 wR_2 = 0.2458	R_1 = 0.2822 wR_2 = 0.1682	R_1 = 0.3045 wR_2 = 0.2440
Goodness-of-fit on F^2	0.769	0.745	0.685	0.777

[a] $R_1 = \Sigma|F_o| - |F_c|/\Sigma|F_o|$. [b] $wR_2 = [\Sigma w [(F_o^2 - F_c^2)^2]/\Sigma[w(F_o^2)^2]]^{1/2}$, $w = 1/[\sigma^2(F_o^2)+(0.075P)^2]$, where $P = [\mathrm{Max}(F_o^2,0)+2F_c^2]/3$.

 © 2003 Wiley-VCH Verlag GmbH & Co. KGaA, Weinheim

Synthesis of $[Zn(O_2CCF_3)_2(H_2O)_2]$(ttab) (4): $Zn(CF_3COO)_2 \cdot 3H_2O$ (0.079 g, 0.23 mmol) and ttab (0.070 g, 0.13 mmol) were dissolved in 20 mL of THF at ambient temperature. Slow diffusion of toluene into the solution afforded colorless crystals of **4**. (0.114 g, 91%). ^1H NMR (300 MHz, CD_2Cl_2, 25 °C): δ = 8.49 (br. s, 4 H, H_2O), 8.17 (s, 2 H, phenyl), 8.10 (d, J = 4.2 Hz, 4 H, 7-aza), 7.25 (m, 8 H, 7-aza), 7.11 (d, J = 3.6 Hz, 4 H, 7-aza), 6.56 (d, J = 3.6 Hz, 4 H, 7-aza) ppm. For comparison purposes, the ttab free ligand ^1H NMR spectroscopic data are also included here (CD_2Cl_2, 25 °C): δ = 8.25 (s, 2 H, phenyl), 8.16 (dd, ^3J = 5.0, ^4J = 1.5 Hz, 4 H, 7-aza), 7.85 (dd, ^3J = 7.5, ^4J = 1.5 Hz, 4 H, 7-aza), 7.05 (dd, $^3J_1$ = 7.5, $^3J_2$ = 5.0 Hz, 4 H, 7-aza), 6.98 (d, ^3J = 3.5 Hz, 4 H, 7-aza), 6.37 (d, ^3J = 3.5 Hz, 4 H, 7-aza) ppm. $C_{38}H_{26}F_6N_8O_6Zn \cdot C_7H_8$ (962.20): calcd. C 56.17, H 3.56, N 11.65; found C 55.94, H 3.44, N 11.98.

X-ray Crystallographic Analysis: Single crystals of ttab were obtained by slow diffusion of hexanes into a CH_2Cl_2 solution. Single crystals of **1** were obtained from a saturated DMSO solution. Single crystals of **2** were obtained from a CH_2Cl_2 solution. Single crystals of **3b** were obtained by slow diffusion of toluene and ethanol into a DMSO solution. Single crystals of **4** were obtained from a toluene/THF solution. All crystals were mounted on glass fibers. All data were collected on a Bruker P4 X-ray diffractometer with a SMART CCD 1000 detector, with monochromated Mo-K_α radiation, operating at 50 kV, 30 mA and ambient temperature. No significant decay was observed during the data collection. Data were processed on a Pentium PC using Bruker Axs Windows NT SHELXTL software package (version 5.10).[9] Neutral atom scattering factors were taken from Cromer and Waber.[10] Empirical absorption correction was applied to all crystals. The crystals of ttab and **2** belong to the triclinic space group $P\bar{1}$. The crystals of **1** and **3b** belong to the monoclinic space groups $P2_1/n$ and $P2_1/c$, respectively. The crystals of **4** belong to the orthorhombic space group $Pca2_1$. All structures were solved by direct methods. DMSO molecules were located in the lattice of **1** (2 DMSO per molecule of **1**). Disordered CH_2Cl_2 molecules were located in the lattice of **2** (4 CH_2Cl_2 per molecule of **2**). Toluene molecules were located in the lattice of **3b** and **4** (2 toluene per molecule of **3b**, 1 toluene per molecule of **4**). There are 1.5 independent molecules in the asymmetric unit of ttab. The disordered nitrate ions of **3b** and the CH_2Cl_2 molecules that co-crystallized with **2** were modeled successfully. All non-hydrogen atoms in **1**−**3b** were refined anisotropically except for the disordered nitrate ion, the co-crystallized toluene and CH_2Cl_2 molecules. The quality of the crystals of **4** is poor and partially twin. The CF_3 groups in **4** are all disordered. As a result, not all non-hydrogen atoms in **4** can be refined anisotropically. The positions of the hydrogen atoms were calculated and their contributions in structural factor calculations were included. The crystal data are summarized in Table 2. (The crystal data for the free ttab ligand are provided in the supporting information).

CCDC-213370 (**1**), -213371 (**3b**), -213372 (**4**), and -213374 (**2**) contain the supplementary crystallographic data for this paper. These data can be obtained free of charge at www.ccdc.cam.ac.uk/conts/retrieving.html [or from the Cambridge Crystallographic Data Centre, 12, Union Road, Cambridge CB2 1EZ, UK; Fax: (internat.) +44-1223/336-033; E-mail: deposit@ccdc.cam.ac.uk].

Supporting Information Available (see footnote on the first page of this article): A complete drawing of compound **3b** and the excitation and emission spectra.

Acknowledgments

We thank the National Sciences and Engineering Research Council of Canada for financial support.

[1] [1a] W. Paw, S. D. Cummings, M. A. Mansour, W. B. Connick, D. K. Geiger, R. Eisenberg, *Coord. Chem. Rev.* **1998**, *171*, 125. [1b] S. D. Cummings, R. Eisenberg, *J. Am. Chem. Soc.* **1996**, *118*, 1949. [1c] S. Huertas, M. Hissler, J. E. McGarrah, R. J. Lachicotte, R. Eisenberg, *Inorg. Chem.* **2001**, *40*, 1183. [1d] M. Hissler, W. B. Connick, D. K. Geiger, J. E. McGarrah, D. Lipa, R. J. Lachicotte, R. Eisenberg, *Inorg. Chem.* **2000**, *39*, 447. [1e] K. H. Wong, M. C. W. Chan, C. M. Che, *Chem. Eur. J.* **1999**, *5*, 2845. [1f] Y. Kunugi, K. R. Mann, L. L. Miller, C. L. Exstrom, *J. Am. Chem. Soc.* **1998**, *120*, 589. [1g] W. Y. Wong, K. H. Choi, K. W. Cheah, *J. Chem. Soc., Dalton Trans.* **2000**, 113. [1h] J. Pang, E. J. -P. Marcotte, C. Seward, R. S. Brown, S. Wang, *Angew. Chem. Int. Ed.* **2001**, *40*, 4042.

[2] [2a] M. A. Baldo, D. F. O′Brien, Y. You, A. Shoustikov, S. Sibley, M. E. Thompson, S. R. Forrest, *Nature* **1998**, *395*, 151. [2b] D. F. O′Brien, M. A. Baldo, M. E. Thompson, S. R. Forrest, *Appl. Phys. Lett.* **1999**, *74*, 442. [2c] R. C. Kwong, S. Sibley, T. Subovoy, M. Baldo, S. R. Forrest, M. E. Thompson, *Chem. Mater.* **1999**, *11*, 3709. [2d] R. C. Kwong, S. Laman, M. E. Thompson, *Adv. Mater.* **2000**, *12*, 1134. [2e] Q. Wu, J. A. Lavigne, Y. Tao, M. D′Iorio, S. Wang, *Chem. Mater.* **2001**, *13*, 71. [2f] Q. Wu, A. Hook, S. Wang, *Angew. Chem. Int. Ed.* **2000**, *39*, 3933.

[3] [3a] D. Song, Q. Wu, A. Hook, I. Kozin, S. Wang, *Organometallics* **2001**, *20*, 4683. [3b] D. Song, L. Thorne, S. Wang, manuscript in preparation.

[4] D. Song, K. Sliwowski, J. Pang, S. Wang, *Organometallics* **2002**, *21*, 4978.

[5] [5a] W. Yang, H. Schmider, Q. Wu, Y. Zhang, S. Wang, *Inorg. Chem.* **2000**, *39*, 2397. [5b] C. Seward, J. Pang, S. Wang, *Eur. J. Inorg. Chem.* **2002**, 1390.

[6] [6a] L. Ohrstrom, G. Svensson, *Inorg. Chim. Acta* **2000**, *305*, 157. [6b] F. T. Greenaway, E. Riviere, J. J. Girerd, X. Labouze, G. Morgant, B. Viossat, J. C. Daran, M. R. Arveiller, N. H. Dung, H. Gustaf, *J. Inorg. Biochem.* **1999**, *76*, 19. [6c] T. M. Reineke, M. Eddaoudi, D. Moler, M. O'Keeffe, O. M. Yaghi, *J. Am. Chem. Soc.* **2000**, *122*, 4843.

[7] [7a] W. Xu, R. J. Puddephatt, *Organometallics* **1994**, *13*, 3054. [7b] J. E. Gano, G. Subramaniam, R. Birnbaum, *J. Org. Chem.* **1990**, *55*, 4760. [7c] H. C. Kang, A. W. Hanson, B. Eaton, V. Beokelheide, *J. Am. Chem. Soc.* **1985**, *107*, 1979.

[8] J. L. Atwood, L. J. Barbour, S. Dalgarno, C. L. Raston, H. R. Webb, *J. Chem. Soc., Dalton Trans.* **2002**, 4351.

[9] SHELXTL NT Crystal Structure Analysis Package, Version 5.10; Bruker Axs, Analytical X-ray System, Madison, WI, 1999.

[10] D. T. Cromer, J. T. Waber, *International Tables for X-ray Crystallography*; Kynoch Press: Birmingham, Al., 1974; Vol. 4, Table 2.2A.

Received April 29, 2003

 © 2003 Wiley-VCH Verlag GmbH & Co. KGaA, Weinheim

Syntheses, Structures, and Properties of Two-Dimensional Honeycomb Networks from the Assembly of the Tripodal Ligand 2,4,6-Tris[4-(imidazol-1-ylmethyl)phenyl]-1,3,5-triazine with Metal Salts

Shuang-Yi Wan,[a] Yi-Zhi Li,[a] Taka-aki Okamura,[b] Jian Fan,[a] Wei-Yin Sun,*[a] and Norikazu Ueyama[b]

Keywords: Tripodal ligands / Zinc / Nickel / Supramolecular chemistry / Organic-inorganic hybrid composites

Two novel coordination networks, $[Zn_2(timpt)_2(\mu\text{-}OH)](NO_3)_3$ (**1**) and $[Ni_2(timpt)_2(H_2O)_2(SO_4)_2]\cdot 0.5H_2O$ (**2**) were obtained by assembly of 2,4,6-tris[4-(imidazol-1-ylmethyl)phenyl]-1,3,5-triazine (timpt) with the corresponding metal salts. The X-ray single-crystal diffraction analysis reveals that complex **1** possesses μ-OH-bridged dinuclear zinc(II) subunits (Zn_2OH) and each timpt ligand connects three metal atoms to form a two-dimensional (2D) honeycomb network structure, in which each independent sheet contains two sublayers. While in the case of complex **2**, the nickel(II) atom is coordinated by N atoms of timpt, O atoms of sulfate anions and water molecules to give a 2D honeycomb network. The luminescence properties of timpt, **1** and **2** in the solid state were investigated at room temperature. The maximum emission wavelength of **1** is red-shifted by 17 nm compared with that of timpt. While complex **2** showed an emission with remarkably reduced intensity under the same conditions. The results imply that the metal ions have great influence on the structure and properties of the complexes.

(© Wiley-VCH Verlag GmbH & Co. KGaA, 69451 Weinheim, Germany, 2003)

Introduction

Employing multidentate organic ligands and suitable metal salts to construct supramolecular architectures has been a major strategy in recent years.[1] Metal-organic frameworks (MOFs) with specific topologies such as cage-like structures, honeycomb and interpenetrating networks have been obtained by self-assembly of suitable metal salts with rigid or flexible tripodal ligands, for example 1,3,5-tricyanobenzene,[2] 1,3,5-tris(4-ethynylbenzonitrile)benzene,[3] 2,4,6-tris(4-pyridyl)-1,3,5-triazine,[4] 1,3,5-benzenetricarboxylate,[5] 1,3,5-benzenetribenzoate,[6] 1,3,5-tris(pyrazol-1-ylmethyl)-2,4,6-triethylbenzene,[7] 1,3,5-tris(4-pyridylmethyl)benzene,[8] 1,3,5-tris(benzimidazol-1-ylmethyl)-2,4,6-trimethylbenzene.[9] In contrast to the rigid tripodal ligands with little or no conformational changes when they interact with metal salts, the flexible tripodal ligands have much more possible coordination modes than the rigid ones due to their flexibility and low symmetry, since the flexible ligands can adopt different conformations according to the geometric needs of different metal ions. Accordingly, we designed and synthesized a series of flexible tripodal ligands with aromatic core rings as spacers and systematically investigated their assembly reactions with metal salts.[10] Most recently, we prepared a novel nanometer-sized tripodal ligand 2,4,6-tris[4-(imidazol-1-ylmethyl)phenyl]-1,3,5-triazine (timpt) which reacted with $Pb(NO_3)_2$ to give a two-dimensional (2D) 4.8^2 network with threefold interpenetrations.[11] We report herein two novel 2D honeycomb coordination polymers $[Zn_2(timpt)_2(\mu\text{-}OH)](NO_3)_3$ (**1**) and $[Ni(timpt)_2(H_2O)_2(SO_4)_2]\cdot 0.5H_2O$ (**2**) obtained by solvothermal reactions of timpt with $Zn(NO_3)_2\cdot 6H_2O$ and $Ni(SO_4)_2\cdot 7H_2O$, respectively.

Results and Discussion

Crystal Structure Description

The structures of complexes **1** and **2** were determined by X-ray crystallography. The crystal and data collection parameters are summarized in Table 3 and selected bond lengths and angles are listed in Table 1.

Crystal Structure of 1

The complex crystallizes in rhombohedral space group of $R\bar{3}c$ and all the zinc(II) atoms have a tetrahedral coordination geometry with an N_3O donor set as illustrated in Figure 1. The three N atoms are from the imidazole groups

[a] Coordination Chemistry Institute, State Key Laboratory of Coordination Chemistry, Nanjing University,
Nanjing 210093, China
Fax: (internat.) + 86-25/3314502 or 3317761
E-mail: sunwy@nju.edu.cn
[b] Department of Macromolecular Science, Graduate School of Science, Osaka University,
Toyonaka, Osaka 560-0043, Japan
Supporting information for this article is available on the WWW under http://www.eurjic.org or from the author.

Table 1. Selected bond lengths [Å] and angles [°] for **1** and **2**

$[Zn_2(timpt)_2(\mu\text{-}OH)](NO_3)_3$ (**1**)			
Zn(1)−O(1)	1.874(2)	Zn(1)−N(1)	2.001(3)
O(1)−Zn(1)−N(1)[a]	104.3(2)	N(1)−Zn(1)−N(1)[a]	106.95(11)
$[Ni(timpt)_2(H_2O)_2(SO_4)_2]\cdot 0.5H_2O$ (**2**)			
Ni(1)−N(12)	2.033(5)	Ni(1)−N(112)	2.038(4)
Ni(1)−N(22)	2.078(4)	Ni(1)−O(11)	2.049(4)
Ni(1)−O(1)	2.225(4)	Ni(1)−O(2)	2.152(4)
Ni(2)−N(32A)[b]	2.018(4)	Ni(2)−N(122)	1.978(5)
Ni(2)−N(132)	2.024(4)	Ni(2)−O(21)	2.058(4)
Ni(2)−O(22)	2.067(3)	N(112)−Ni(1)−O(11)	91.50(16)
N(12)−Ni(1)−N(112)	97.50(18)	N(112)−Ni(1)−N(22)	97.10(17)
N(12)−Ni(1)−O(11)	170.49(17)	N(12)−Ni(1)−O(2)	81.18(19)
N(12)−Ni(1)−N(22)	96.88(18)	O(11)−Ni(1)−O(2)	89.42(18)
O(11)−Ni(1)−N(22)	85.01(17)	N(12)−Ni(1)−O(1)	91.46(17)
N(112)−Ni(1)−O(2)	169.87(17)	O(11)−Ni(1)−O(1)	86.06(16)
N(22)−Ni(1)−O(2)	93.03(18)	O(2)−Ni(1)−O(1)	83.95(16)
N(112)−Ni(1)−O(1)	86.05(16)	N(122)−Ni(2)−N(132)	99.09(16)
N(22)−Ni(1)−O(1)	170.60(18)	N(122)−Ni(2)−O(21)	107.82(17)
N(122)−Ni(2)−N(32A)[b]	97.30(16)	N(132)−Ni(2)−O(21)	148.54(16)
N(32A)−Ni(2)−N(132)[b]	100.70(16)	N(32A)−Ni(2)−O(22)[b]	157.23(16)
N(32A)−Ni(2)−O(21)[b]	91.90(15)	N(132)−Ni(2)−O(22)	91.13(14)
N(122)−Ni(2)−O(22)	99.97(15)	O(21)−Ni(2)−O(22)	68.74(14)

[a] Equivalent atoms generated by $-x + y, -x + 1, z$. [b] Equivalent atoms generated by $x, y - 1, z - 1$.

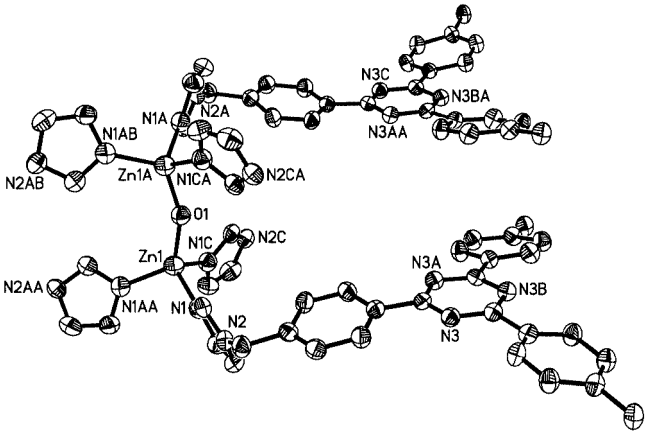

Figure 1. The coordination environment of Zn^{II} in **1**; thermal ellipsoids are drawn at 30% probability; the carbon atoms are unlabelled and hydrogen atoms are omitted for clarity

of three different timpt ligands with the Zn−N bond lengths of 2.001(3) Å. The fourth site was completed by an O atom from a hydroxy group which connects another zinc(II) atom to form a μ-hydroxy bridge. The Zn−O bond length is 1.874(2) Å which is slightly shorter than the Zn−O distances in the reported hydroxy-bridged zinc(II) complexes.[12] The Zn−O-Zn bond angle is 156.7° and the Zn···Zn distance is 3.67 Å, which are within the ranges of the reported Zn−O−Zn angles and Zn···Zn separations in the hydroxy-bridged zinc(II) complexes.[12] The N−Zn−N and N−Zn−O bond angles are ranging from 106.95(11) to 104.3(2)°, which are close to the ideal tetrahedral angle of 109.5°.

Each timpt ligand coordinated to three different zinc(II) atoms to form an equilateral triangle with an edge length (Zn···Zn separation) of 17.57 Å. Such units repeated along the *ab* plane to generate an infinite 2D honeycomb network as shown in Figure 2 (part a). It is noteworthy that two such networks are bridged by hydroxy groups through the Zn−O coordination bonds to form an independent layer (Figure 2, b). Namely, every independent 2D layer in complex **1** contains two sublayers which are connected by the hydroxy bridges. This is, to the best of our knowledge, the first example of 2D honeycomb networks in which each independent layer contains two sublayers linked by μ-hydroxy bridges through the M−O(H)−M (M represents the metal ion) bonds. Disordered nitrate anions are located between the two sublayers of an independent layer and held there by O(1B)−H(1AB)···O(3) (NO_3^-) with an O(1B)···O(3) distance of 3.269(12) Å and C−H···O (NO_3^-) hydrogen bonds with C···O distances of 3.381(15) and 3.398(11) Å (Figure 3, a). The 2D independent layers are closely stacked with each other and connected by the NO_3^- anions through the C−H···O hydrogen bond with C···O distance of 3.212(8) Å to produce a 3D framework as exhibited in Figure 3 (part b). The hydrogen-bonding data are summarized in Table 2.

In addition to the hydrogen bonds as mentioned above, there are weak π−π interactions between the benzene rings of the timpt ligands. The two benzene rings from two different ligands are nearly parallel with a dihedral angle of 2.2° and a centroid-to-centroid distance of 4.28 Å. The two tri-

 © 2003 Wiley-VCH Verlag GmbH & Co. KGaA, Weinheim

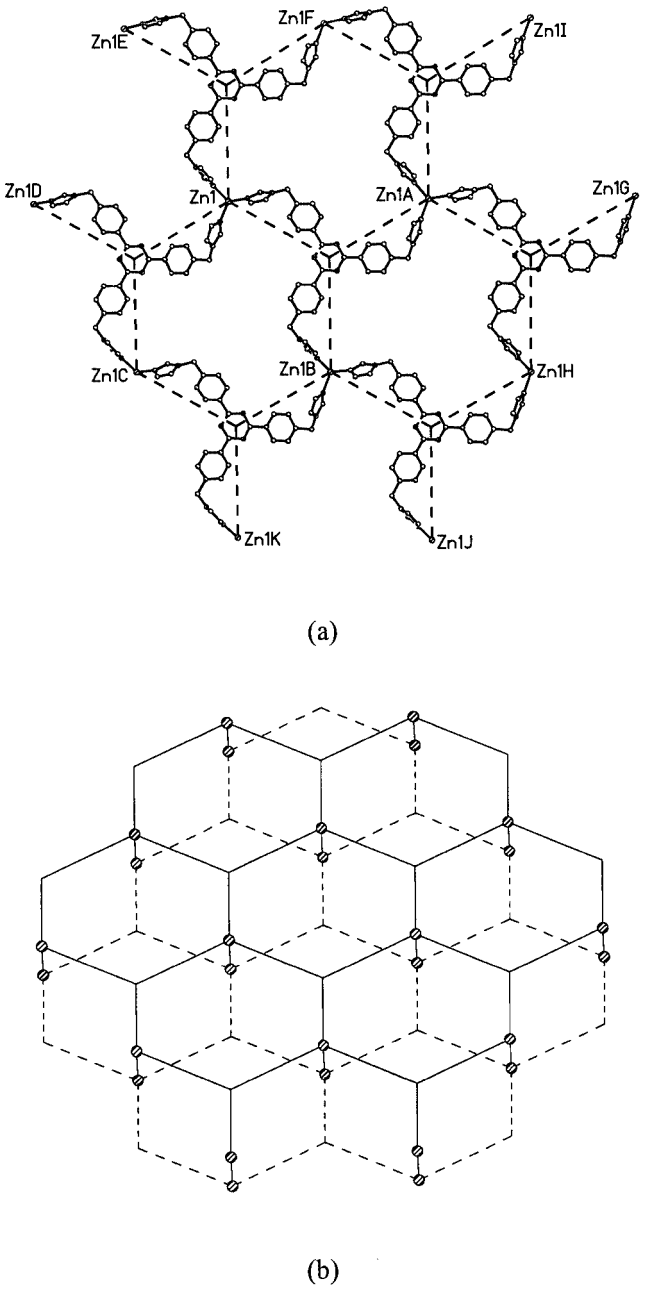

Figure 2. (a) The perspective view of the 2D cationic sublayer with the honeycomb structure (dashed lines) in the *ab* plane; (b) schematic drawing of 2D honeycomb network in which the timpt ligands are represented by three spokes radiating from a point and Zn centers by circles; the hydroxy bridges (Zn−O−Zn) are represented by solid lines; the solid and dashed lines refer to timpt ligands of each sublayer

azine rings of the two ligands of the neighboring sublayers of the two different layers adopt a face-to-face conformation and are strictly parallel to each other with a centroid-to-centroid distance of 3.44 Å, indicating the presence of π−π stacking interactions (Figure 4). The hydrogen bonding and π−π interactions as well as Zn−O−Zn bridges may play an important role in stabilizing the layered structures in the titled complex.

Crystal Structure of 2

In contrast to the tetrahedral coordination geometry of the zinc(II) atom in complex **1**, nickel(II) atoms usually adopt octahedral geometry when they interact with N-donor ligands. Thus, the reaction of timpt with nickel(II) sulfate was carried out and complex **2** was obtained. From the X-ray analysis, it is interesting that there are two kinds of Ni^{II} atoms with different coordination environments: the Ni(1) atom is six-coordinate with a distorted octahedral geometry while the Ni(2) atom is five-coordinate with a distorted trigonal-bipyramidal geometry as shown in Figure 5. The Ni1 atom lies in the plane defined by the O(1), O(2), N(22), and N(112) atoms since the deviation of Ni(1) from this plane is 0.08 Å. Three of the six sites of Ni(1) are coordinated by three N atoms of imidazole groups from three different timpt ligands with Ni−N bond lengths varying from 2.033(5) to 2.078(4) Å (Table 1), and the remaining three sites are occupied by O atoms from a monodentate sulfate anion and two water molecules. The Ni(2) atom lies above the plane of the O(21), N(122), and N(132) atoms by 0.23 Å. The three sites of Ni(2) are coordinated by three imidazole-group N atoms with Ni−N bond lengths ranging from 1.978(5) to 2.024(4) Å, while the additional two sites are completed by two O atoms of a sulfate anion in a bidentate mode.

An infinite 2D honeycomb network sheet of **2** is achieved by the coordination of the timpt ligands to Ni^{II} atoms as shown in Figure 6. The triangles formed by three Ni^{II} atoms connected by one timpt ligand are non-equilateral which are different from those observed in complex **1**. Furthermore, there are two kinds of triangles in **2**: one is formed by two five-coordinate Ni atoms and one six-coordinate Ni^{II} atom with the edge lengths of 19.85, 19.52, and 16.47 Å, respectively, e.g. Ni(2), Ni(2B), and Ni(1B) in Figure 6; another one is formed by one five-coordinate Ni^{II} atom and two six-coordinate Ni^{II} atoms [e.g. Ni(2B), Ni(1A), and Ni(1C) in Figure 6] with the edge lengths of 19.19, 19.11, and 16.47 Å, respectively. Disordered water molecules are located in the voids between the adjacent sheets through C−H···O hydrogen bonds (Table 2). The 2D honeycomb sheets are linked through the C−H···O (coordinated water molecules and sulfate anions) hydrogen-bonding interactions to form a 3D structure (Figure 7).

Face-to-face π−π interactions were found between the triazine rings of the two layers since the two triazine ring planes are strictly parallel to each other with a centroid-to-centroid distance of 3.86 Å. In addition, π−π interactions are also found between the triazine rings and the benzene rings of two adjacent layers. The dihedral angle between them is 11.8° and the centroid-to-centroid separation is 3.88 Å (Figure S1 in Supporting Information, see footnote on page 1 of this article).

Although both complexes **1** and **2** have the honeycomb network structures, there are distinct differences between these two complexes. First, they crystallize in different crystal systems with **1** in rhombohedral $R\bar{3}c$ and **2** in triclinic $P\bar{1}$. Another important difference is that each independent layer in **1** contains two sublayers which feature the honey-

 © 2003 Wiley-VCH Verlag GmbH & Co. KGaA, Weinheim

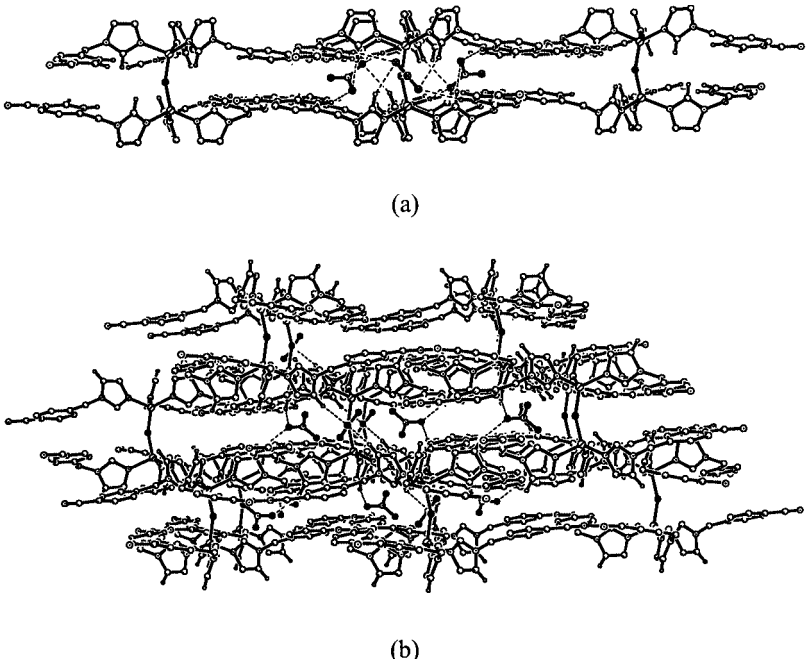

Figure 3. (a) View of an independent layer with nitrate anions located within the layer through hydrogen bonds (dashed lines); (b) crystal packing diagram of **1**; the two adjacent independent layers are connected by nitrate anions through hydrogen-bonding interactions

comb structures and are connected by hydroxy bridges, while **2** contains no sublayers. Furthermore, the conformations of the timpt ligand in **1** and **2** are obviously different. In complex **1**, the dihedral angle between the central triazine ring plane and the benzene ring plane is 12.6°. While the one between the terminal imidazole ring plane and the benzene ring plane is 109.4°, indicating a near perpendicular orientation of the imidazole ring plane to the benzene ring plane (Figure 2, a). The plane defined by three coordinated imidazolyl N atoms of one timpt ligand is parallel to the triazine ring plane with a separation of 1.35 Å. In the previously reported metal complexes of 1,3,5-tris(imidazol-1-ylmethyl)-2,4,6-trimethylbenzene (timtb) with *cis*,*cis*,*cis* conformation, the distance between the plane defined by three coordinated imidazolyl N atoms and the central benzene ring plane is ca. 3.1 Å.[10f,10g] Therefore, the conformation of timpt in **1** is a propeller-type rather than *cis*,*cis*,*cis* or *cis*,*trans*,*trans* as observed in complexes of timtb (Scheme 1).[10] In complex **2**, the three coordinated imidazolyl N atoms of the timpt ligand are at both sides of the central triazine ring plane and the dihedral angles between the plane defined by the three N atoms and the triazine ring plane are 16.9 and 19.8°, respectively, since there are two kinds of timpt ligand in **2** as mentioned above. This causes the backbone of complex **2** to be different from that of **1**. In addition, the vacancies between the two sublayers in **1** are occupied by nitrate anions, while in the case of **2**, the sulfate anions are coordinated with the Ni^{II} atoms and the voids between the 2D layers are filled with disordered lattice water molecules.

In the reported 2D coordination polymers with honeycomb structures, rigid tripodal ligands, e.g., 1,3,5-tricyanobenzene or 1,3,5-benzenetricarboxylate, enclosing an angle of 120° were used to link the linear metal centers.[2,5] In our previously reported honeycomb complexes, the flexible tripodal ligand timtb with the *cis*,*cis*,*cis* conformation, connected three six-coordinate metal centers to direct the formation of the 2D honeycomb network.[10f] However, in the present case, the metal atom in **1** is four-coordinate with three sites occupied by three N atoms from three ligands and the fourth site finished by a hydroxy O atom. If the Zn−O−Zn units are considered as one metal center M, then the metal center M is six-coordinate and the backbone of **1** is identical with those of the complexes with honeycomb structures reported previously.[10f] However, the backbone of **2** is different from **1** and other reported complexes with timtb ligand.[10f]

Luminescent Properties

The photoluminescence studies of timpt, **1** and **2** in the solid state under the same conditions showed that, although the maximum-excitation wavelengths of the complexes **1** and **2** are the same as that of the timpt ligand at 396 nm, the maximum emission wavelength of **1** is red-shifted by 17 nm from 443 to 460 nm compared with that of the ligand, accompanied by an increase of luminescent intensity (Figure 8). However, the maximum-emission wavelength of **2** is red-shifted by 25 nm from 443 to 468 nm relative to that of the ligand, accompanied by a greatly decreased luminescent intensity. The red shift of emission maxima

 © 2003 Wiley-VCH Verlag GmbH & Co. KGaA, Weinheim

Table 2. Hydrogen-bond data for complexes **1** and **2**

D−H···A	Distance of D···A [Å]	Angles of D−H−A [°]
$[Zn_2(timpt)_2(\mu\text{-}OH)](NO_3)_3$ (**1**)		
O(1B)−H(1AB)···O(3)[a]	3.269(12)	154
C(2)−H(2)···O(2)[b]	3.212(8)	155
C(3)−H(3)···O(3)	3.398(11)	156
C(6)−H(6)···O(3)[c]	3.381(15)	147
$[Ni_2(timpt)_2(H_2O)_2(SO_4)_2]\cdot 0.5H_2O$ (**2**)		
C(17)−H(5)···O(12)[d]	3.387(7)	158
C(17)−H(6)···O(2)[e]	3.373(7)	150
C(18)−H(7)···O(12)[e]	3.329(7)	150
C(27)−H(15)···O(14)[e]	3.307(7)	146
C(28)−H(16)···O(14)[e]	3.043(7)	141
C(33)−H(20)···O(23)[f]	3.339(8)	162
C(38)−H(25)···O(24)[f]	3.491(7)	172
C(115)−H(30)···O(14)[e]	3.343(7)	154
C(118)−H(34)···O(13)[e]	3.101(6)	142
C(127)−H(42)···O(22)[g]	3.463(8)	162
C(128)−H(43)···O(24)[h]	3.123(7)	154
C(133)−H(47)···O(22)[h]	3.412(6)	166
C(137)−H(50)···O(23)[h]	3.285(7)	139
C(138)−H(52)···O(23)[h]	3.027(6)	126
C(11D)−H(29A)···O(3)[i]	3.304(6)	130
C(11H)−H(32A)···O(3)[i]	3.106(7)	139

[a] Equivalent atoms generated by $x + 1/3, y + 5/3, z + 2/3$. [b] Equivalent atoms generated by $1/3 - x, 5/3 - y, 5/3 - z$. [c] Equivalent atoms generated by $2/3 + x - y, 4/3 - y, 1/6 - z$. [d] Equivalent atoms generated by $2 - x, 2 - y, 1 - z$. [e] Equivalent atoms generated by $-1 + x, y, z$. [f] Equivalent atoms generated by $1 + x, 1 + y, 1 + z$. [g] Equivalent atoms generated by $-1 - x, 1 - y, -z$. [h] Equivalent atoms generated by $1 + x, y, z$. [i] Equivalent atoms generated by $x, y - 1, z$.

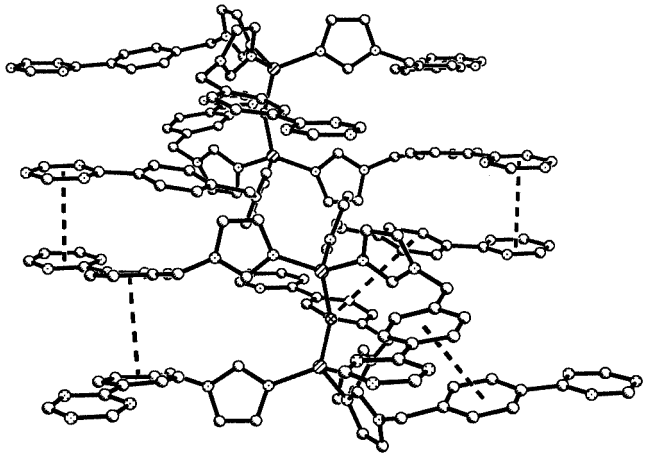

Figure 4. The π−π interactions in **1** indicated by dashed lines

may be a result of the above-mentioned multiple π−π interactions in **1** and **2**.[13] The results indicate that photoluminescent properties of timpt can be controlled by coordination of different metal salts.

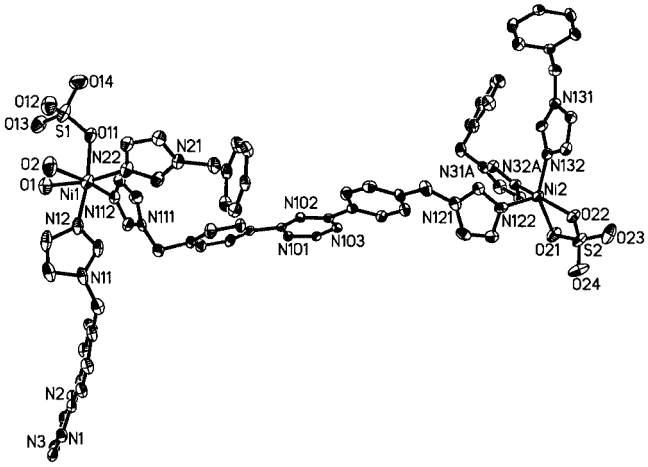

Figure 5. The coordination environment of Ni^{II} in **2**; thermal ellipsoids are drawn at 30% probability; the carbon atoms are unlabelled and hydrogen atoms are omitted for clarity

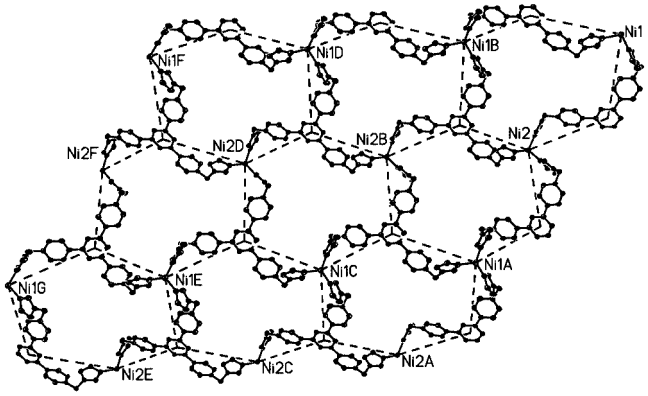

Figure 6. Perspective view of the 2D cationic sheet with the honeycomb structure (dashed lines) in the *bc* plane

Conclusion

The present study evidences that flexible tripodal ligands are efficient in constructing novel coordination networks with metal salts. The nanometer-sized flexible tripodal ligand timpt, using its imidazolyl N atoms, coordinates to metal atoms to form 2D coordination polymers with honeycomb network structures. In the zinc(II) complex **1**, each independent layer has two sublayers which are linked by hydroxy bridges through Zn−O coordination bonds. The emission maximum of timpt is red-shifted and the intensity is enhanced by coordination of timpt with zinc(II) nitrate. While in the case of the Ni^{II} complex of timpt (**2**), the luminescent intensity was remarkably reduced compared with that of timpt. The results show that the metal ions have great influence on the structure and properties of the timpt complexes.

 © 2003 Wiley-VCH Verlag GmbH & Co. KGaA, Weinheim

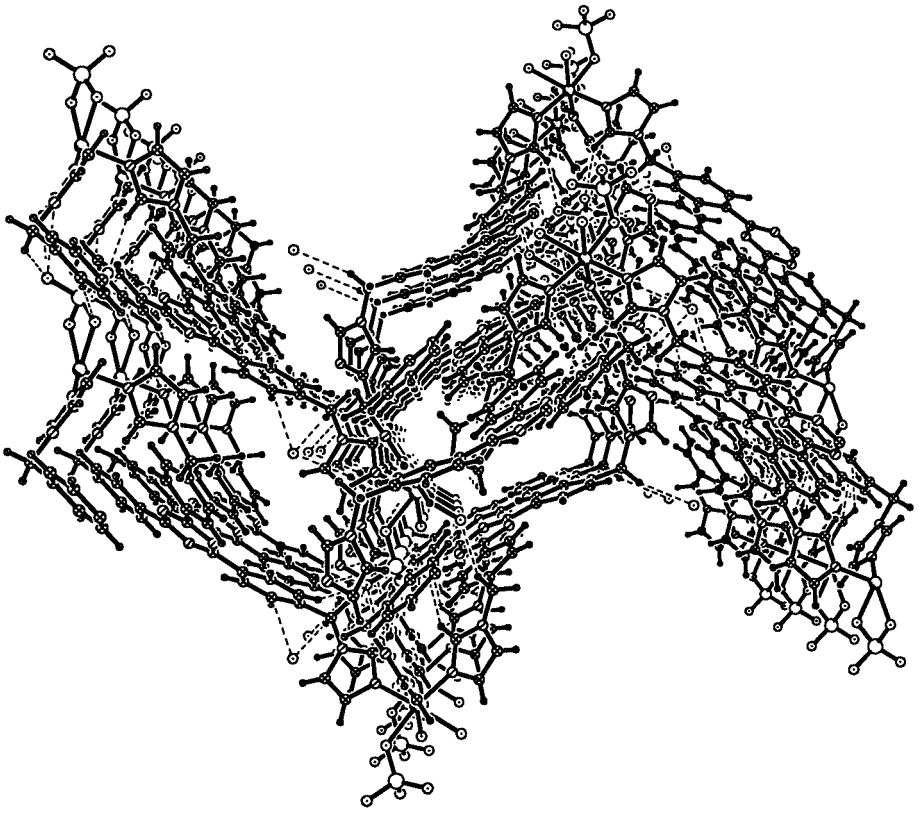

Figure 7. Crystal packing diagram of **2** with voids formed between two adjacent sheets and occupied by disordered water molecules; the hydrogen bonds are shown with dashed lines

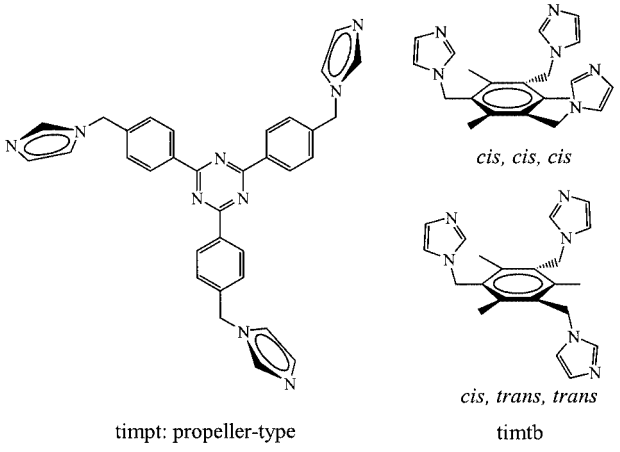

Scheme 1

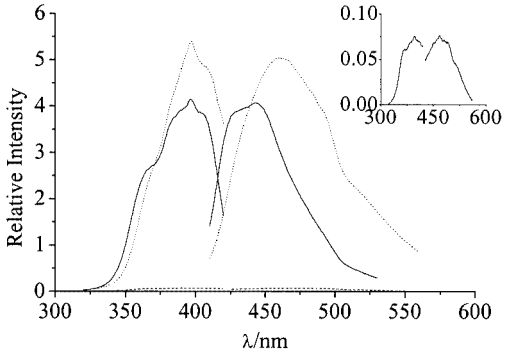

Figure 8. Excited (left) and emission (right) spectra of timpt (solid lines), **1** (dotted lines), and **2** (dashed lines) in the solid state at room temperature; the enlarged spectral picture of **2** is at top right corner

Experimental Section

General: The timpt ligand was synthesized as described previously.[11] All the chemicals were of reagent grade and used as received without further purification. C, H, and N analyses were carried out with a Perkin−Elmer 240C elemental analyzer at the analysis center of Nanjing University. Luminescence spectra for the solid samples were recorded with a Hitachi 850 fluorescence spectrophotometer at room temperature (25 °C). TGA measurement was performed with a simultaneous SDT 2960 thermal analyzer under nitrogen with a heating rate of 10 °C·min^{-1}.

Synthesis of $[Zn_2(timpt)_2(\mu\text{-}OH)](NO_3)_3$ (1): The complex was prepared by solvothermal reaction. The timpt ligand (61.9 mg, 0.11 mmol) was added to a water/ethanol (6:1, v/v) solution (14 mL) of $Zn(NO_3)_2{\cdot}6H_2O$ (46.0 mg, 0.15 mmol). After stirring at room temperature for ca. 15 min, the reaction mixture was transferred to an autoclave and kept at 150 °C for 3 d. Light yellow cubic crystals (50.2 mg) were obtained in 62% yield (based on ligand) after cooling the autoclave. $C_{66}H_{55}N_{21}O_{10}Zn_2$ (1433.05): calcd. C 55.32, H 3.87, N 20.52; found C 55.49, H 3.82, N 20.55.

Synthesis of $[Ni_2(timpt)_2(H_2O)_2(SO_4)_2]{\cdot}0.5H_2O$ (2): Complex **2** was synthesized in a similar manner to that of **1**. The timpt ligand (28.3 mg, 0.052 mmol) was added to a water/ethanol (6:1, v/v) solu-

 © 2003 Wiley-VCH Verlag GmbH & Co. KGaA, Weinheim

tion (14 mL) of $NiSO_4 \cdot 7H_2O$ (15.7 mg, 0.056 mmol). After stirring at room temperature for ca. 15 min, the reaction mixture was placed in an autoclave and kept at 150 °C for 1 d. Green plate crystals (23.0 mg) were obtained in 61% yield (based on ligand) after cooling the autoclave. $C_{66}H_{59}N_{18}Ni_2O_{10.5}S_2$ (1453.81): calcd. C 54.53, H 4.09 N 17.34; found C 54.57, H 4.17, N 17.31. TGA data of **2** show that the weight loss of 3.06% between 10 and 90 °C corresponds to the loss of 2.5 water molecules per molecule of **2** (calcd. 3.10%). No further weight loss was observed from 90 to 310 °C.

X-ray Crystal Structure Analysis for Complexes 1 and 2: Data collection for **1** (Table 3) was performed with a Smart Apex CCD diffractometer at 293 K, using graphite-monochromated Mo-K_α radiation ($\lambda = 0.71073$ Å). The structure was solved by direct methods with SHELXTL and refined by full-matrix least-squares calculations. All non-hydrogen atoms were refined anisotropically. Hydrogen atoms were generated geometrically. The O1 atom of the hydroxy ion is disordered in three positions [O(1), O(1A), and O(1B)], each assigned 1/3 site occupancy. The O(2) and O(3) atoms of the nitrate anion are disordered in two positions, each with 1/2 site occupancy. The intensity data for complex **2** (Table 3) were collected with a Rigaku RAXIS-RAPID Imaging Plate diffractometer at 200 K, using graphite-monochromated Mo-K_α radiation ($\lambda = 0.71069$ Å). The structure was solved by direct method with SIR92, and expanded with Fourier techniques. All data were refined anisotropically by full-matrix least-squares calculations for non-hydrogen atoms. The hydrogen atoms were generated geometrically except those of water molecules. CCDC-201837 (**1**) and -201838 (**2**) contain the supplementary crystallographic data for this paper. These data can be obtained free of charge at www.ccdc.cam.ac.uk/conts/retrieving.html [or from the Cambridge Crystallographic Data Centre, 12 Union Road, Cambridge CB2 1EZ, UK; Fax: (internat.) + 44-1223/336-033; E-mail: deposit@ccdc.cam.ac.uk].

Table 3. Crystallographic data for complexes **1** and **2**

Compound	**1**	**2**
Empirical formula	$C_{66}H_{55}N_{21}O_{10}Zn_2$	$C_{66}H_{59}N_{18}Ni_2O_{10.5}S_2$
Formula mass	1433.05	1453.81
Crystal system	rhombohedral	triclinic
Space group	$R\bar{3}c$	$P\bar{1}$
a [Å]	17.573(1)	8.3122(2)
b [Å]	17.573(1)	16.4661(5)
c [Å]	35.410(3)	23.2800(7)
α [°]	90	90.7639(4)
β [°]	90	90.7241(6)
γ [°]	90	94.6208(5)
V [Å^3]	9470.0(11)	3175.38(16)
Z	6	2
D_c [g·cm^{-3}]	1.508	1.530
μ [cm^{-1}]	0.839	0.738
Crystal habit, color	colorless block	green platelet
Crystal size [mm]	0.40×0.25×0.12	0.30×0.15×0.10
$2\theta_{max}$ [°]	50	55
Index ranges	$-17 \le h \le 0$	$-10 \le h \le 10$
	$0 \le k \le 20$	$-21 \le k \le 21$
	$0 \le l \le 40$	$-30 \le l \le 30$
Reflns. collected	14831	28186
Independent reflns.	1848	13964
R_{int}	0.0209	0.0608
Obsd. reflns.[$I > 2\sigma(I)$]	1089	6616
Parameters refined	149	893
R (obsd. data)	0.0484	0.0706
wR (obsd. data)	0.1397[a]	0.1639[b]
Goodness of fit	0.972	0.930
Residuals [e·Å^{-3}]	0.861; −0.529	1.045; −0.593

[a] $\omega = 1/[\sigma^2(F_o^2) + (0.0800P)^2 + 1.9900P]$, where $P = (F_o^2 + 2F_c^2)/3$. [b] $\omega = 1/[\sigma^2(F_o^2) + (0.1000P)^2]$, where $P = (F_o^2 + 2F_c^2)/3$.

Acknowledgments

This work was supported by National Natural Science Foundation of China (Grant No. 20231020).

[1] P. N. W. Baxter, in *Comprehensive Supramolecular Chemistry* (Ed.: J.-M. Lehn), Pergamon, Oxford, **1996**, vol. 9.
[2] G. B. Gardner, D. Venkataraman, J. S. Moore, S. Lee, *Nature* **1995**, *374*, 792−795.
[3] [3a] D Ventakaraman, S. Lee, J. S. Moore, P. Zhang, K. A. Hirsch, G. B. Gardner, A. C. Covey, C. L. Prentice, *Chem. Mater.* **1996**, *8*, 2030−2040. [3b] G. B. Gardner, Y.-H. Kiang, S. Lee, A. Asgaonkar and D Ventakaraman, *J. Am. Chem. Soc.* **1996**, *118*, 6946−6953.
[4] [4a] S. R. Batten, B. F. Hoskins, R. Robson, *J. Am. Chem. Soc.* **1995**, *117*, 5385−5386. [4b] B. F. Abrahams, S. R. Batten, H. Hamit, B. F. Hoskins, R. Robson, *Angew. Chem. Int. Ed. Engl.* **1996**, *35*, 1690−1692. [4c] B. F. Abrahams, S. R. Batten, M. J. Grannas, H. Hamit, B. F. Hoskins, R. Robson, *Angew. Chem. Int. Ed.* **1999**, *38*, 1475−1477. [4d] S. R. Batten, B. F. Hoskins, B. Moubaraki, K. S. Murray, R. Robson, *Chem. Commun.* **2000**, 1095−1096.
[5] H. J. Choi, M. P. Suh, *J. Am. Chem. Soc.* **1998**, *120*, 10622−10628.
[6] B. L. Chen, M. Eddaoudi, S. T. Hyde, M. O'Keeffe, O. M. Yaghi, *Science* **2001**, *291*, 1021−1023.
[7] C. M. Hartshorn, P. J. Steel, *Chem. Commun.* **1997**, 541−542.
[8] M. Fujita, S. Nagao, K. Ogura, *J. Am. Chem. Soc.* **1995**, *117*, 1649−1650.
[9] C.-Y. Su, Y.-P. Cai, C.-L. Chen, F. Lissner, B.-S. Kang, W. Kaim, *Angew. Chem. Int. Ed.* **2002**, *41*, 3371−3375.
[10] For examples: [10a] H.-K. Liu, W.-Y. Sun, W.-X. Tang, T. Yamamoto, N. Ueyama, *Inorg. Chem.* **1999**, *38*, 6313−6316. [10b] H.-K. Liu, W.-Y. Sun, D.-J. Ma, K.-B. Yu, W.-X. Tang, *Chem. Commun.* **2000**, 591−592. [10c] W.-Y. Sun, J. Xie, T.-a. Okamura, C.-K. Huang, N. Ueyama, *Chem. Commun.* **2000**, 1429−1430. [10d] W.-Y. Sun, J. Fan, T.-a. Okamura, J. Xie, K.-B. Yu, N. Ueyama, *Chem. Eur. J.* **2001**, *7*, 2557−2562. [10e] J. Fan, W.-Y. Sun, T.-a. Okamura, J. Xie, W.-X. Tang, N. Ueyama, *New J. Chem.* **2002**, *26*, 199−201. [10f] J. Fan, B. Sui, T.-a. Okamura, W.-Y. Sun, W.-X. Tang, N. Ueyama, *J. Chem. Soc., Dalton Trans.* **2002**, 3868−3873. [10g] J. Fan, H. F. Zhu, T.-a. Okamura, W.-Y. Sun, W.-X. Tang, N. Ueyama, *Inorg. Chem.* **2003**, *42*, 158−162.
[11] S.-Y. Wan, J. Fan, T.-a. Okamura, H.-F. Zhu, X.-M. Ouyang, W.-Y. Sun, N. Ueyama, *Chem. Commun.* **2002**, 2520−2521.
[12] [12a] P. Chaudhuri, C. Stockheim, K. Wieghardt, W. Deck, R. Gregorzik, H. Vahrenkamp, B. Nuber, J. Weiss, *Inorg. Chem.* **1992**, *31*, 1451−1457. [12b] A. Erxleben, *Inorg. Chem.* **2001**, *40*, 412−414, and references therein.
[13] C.-M. Che, C.-W. Wan, W.-Z. Lin, W.-Y. Yu, Z.-Y. Zhou, W.-Y. Lai, S.-Y. Lee, *Chem. Commun.* **2001**, 721−722.

Received February 19, 2003

 © 2003 Wiley-VCH Verlag GmbH & Co. KGaA, Weinheim

Theoretical Search for Anions Possessing Large Electron Binding Energies

Monika Sobczyk,[a] Agnieszka Sawicka,[a,b] and Piotr Skurski*[a,b]

Keywords: Anions / Superhalogens / Electron-binding energy

The vertical electron detachment energies (VDE) of several anions were calculated at the OVGF level with 6-311++G(d) basis sets. The negatively charged species studied were chosen based on the observation that the largest electron binding energies for such systems are expected to be found for the anions whose neutral parents are polynuclear superhalogens. The largest vertical electron binding energy of 12.63 eV was found for $Ta_3F_{16}^-$, and this is the largest excess electron binding energy of a molecular system reported in the literature thus far. Moreover, the VDEs of 12.63 and 12.20 eV calculated for $Ta_3F_{16}^-$ and $As_3F_{16}^-$, respectively, exceed the upper limit for the excess electron binding energy (thought to be 12 eV). Several other anions were also found [at the OVGF/6-311++G(d) level] to possess very large VDEs (i.e. $Al_2Br_7^-$: 7.08 eV, $Al_2Cl_7^-$: 7.75 eV, $Al_2F_7^-$: 11.16 eV, $P_2F_{11}^-$: 10.95 eV, $V_2F_{11}^-$: 10.98 eV, $As_2F_{11}^-$: 11.43 eV, and $Ta_2F_{11}^-$: 11.84 eV).

(© Wiley-VCH Verlag GmbH & Co. KGaA, 69451 Weinheim, Germany, 2003)

1. Introduction

The electron affinities of molecules are of interest not only in areas where gas-phase ions are encountered (e.g. negative-ion analytical mass spectrometry, gas-phase radiation chemistry, and electron capture detector gas chromatography), but also in the much wider field of condensed-phase chemistry.[1] Since molecular systems exhibiting extreme characteristics are of particular interest from both theoretical and practical points of view, the molecules possessing large electron affinities (EA) have been extensively studied in the past, primarily by Gutsev and Boldyrev.

It is well-known that halogen atoms possess the highest electron affinities among the elements (fluorine 3.40 eV, chlorine 3.62 eV).[2] However, the EA of a polyatomic system may exceed the 3.62 eV limit due to collective effects. Such species are of great importance in chemistry since they can be used for the oxidation of counterpart systems with relatively high ionisation potentials (such as O_2, Xe) and allow the synthesis of unusual chemical compounds (e.g. those involving noble gases atoms). In addition, molecules possessing high electron affinities are widely used in the production of organic super-conductors.[3,4]

Such species have been attracting the attention of chemists since the early 60's; however, the term *superhalogens* for these species was proposed by Gutsev and Boldyrev as late as 1981. Further, they introduced a simple formula for one class of these compounds, MX_{k+1}, where M is a main group or transition metal atom, X is a halogen atom, and k is the maximal formal valence of the atom M.[5] This work was of great importance since Gutsev and Boldyrev not only provided theoretically estimated electron binding energies of superhalogen-based anions, but they also explained the reason for the increase in the vertical electron detachment energy (VDE) of MX_{k+1}^- relative to X^-. These reasons include: (i) the delocalisation of the extra electron over $k+1$ halogen atoms instead of one only, (ii) the non-bonding character of the highest occupied molecular orbital (HOMO), (iii) the coordination of the X^- anion to the electropositive ion M^{k+} (electrostatic effect), and (iv) the stabilising electron relaxation and correlation effects.[5]

Since the early 80's many other theoretical studies have been undertaken to estimate the VDEs of various anions having superhalogens as their neutral parents (see refs.[6–9] and references cited therein). Major progress was made in 1999 in the investigations involving superhalogen systems due to the joined theoretical and experimental studies. This resulted in an excellent report comprising the first experimental photoelectron spectra of superhalogens (measured by Wang's group), together with theoretical interpretations provided by Boldyrev and Simons.[10] In particular, the photoelectron spectra of the anions MX_2^- (where M = Li, Na, and X = Cl, Br, I) have been obtained and assigned on the basis of ab initio outer valence Green function (OVGF) calculations. An excellent agreement between experimentally and theoretically estimated values of VDEs has been achieved, and all the anions have been proven to be superhalogen–based species since their electron binding energies were found to be greater than 3.62 eV (see ref.[10] for details).

Recently, Schaefer's group studied the electron affinities of arsenic fluorides AsF_n (n = 1–6), from which they deduced that the AsF_6^- anion has a very large vertical elec-

[a] Department of Chemistry, University of Gdańsk, Sobieskiego 18, 80-952 Gdańsk, Poland
E-mail: piotr@chem.univ.gda.pl
[b] Department of Chemistry, University of Utah, Salt Lake City, UT 84112, U.S.A.

 © 2003 Wiley-VCH Verlag GmbH & Co. KGaA, Weinheim **DOI: 10.1002/ejic.200300180**

tron detachment energy (VDE = 7.95−10.54 eV, depending on the density functional method used).[9]

It should be noted that although there are many theoretical results for superhalogen anions available, most were obtained in the 80's when computational resources limited the level of the calculations. In particular, early discrete−variational X_a-method (DV-X_a) calculations led to underestimated values of the VDEs of many superhalogen anions. However, it should be stated that the main goal of these investigations was to prove that such species indeed exhibit extremely large electron binding energies, rather than to provide precise vertical detachment energies.[5,6]

The problem of estimating the maximum possible electron binding energy for a molecular system was raised by Gutsev and Boldyrev in the 80's.[6] Naturally, these two authors began their theoretical search for the species possessing extremely large VDE values by investigating the superhalogen anions. From their experience in examining such negatively charged molecules, they concluded that the anion should contain the maximum possible number of fluorine atoms as ligands. This issue has also been discussed by Kalcher and Sax,[12] who investigated the relationship between the EA of a molecule M and the ionisation potential (IP) of the same molecule. On the basis of the observation that the IP of a given molecule always exceeds its own EA, and that the IPs of some molecules (such as fluorides like CF_4, SiF_4, SF_6, etc.) are found to be in the range 15−17 eV, they concluded that the EA value in that range (i.e. 15−17 eV) should be considered as the upper limit for the electron affinity characterising the neutral molecular system. However, Kalcher and Sax admitted that neither theoretical nor experimental evidence could be provided for such high values.[12] In fact, this idea had been proposed earlier by Gutsev and Boldyrev who based their analysis on the anionic daughters of the MF_6 superhalogens in which the extra electron resides in a nonbonding orbital which is delocalised over all F ligands.[6,13] These authors observed that the EAs of such systems depend primarily on the F_k ligand framework (rather than the nature of the transition metal centre), and estimated that the maximum EA (EA_{max}) for $k = 2$ is 5.5 eV, $EA_{max} = 6.5$ eV for $k = 6$, and that the limiting EA value (i.e. for $k = \infty$) is 10−12 eV.[13]

The estimate of the maximum value possible for the EA, made originally by Gutsev and Boldyrev, is of great importance for studying the properties of the chemical species in general, and for designing novel super-conductors in particular. However, it should be stressed that despite determining the 12 eV limit, there is no evidence that any of the known (reliable) EA values approaches this ultimate theoretical value. In particular, the early calculations (using discrete-variational X_a-method) performed on As_2F_{11} and P_2F_{11} resulted in an EA of 8.6 eV (for both cases).[6] To the best of our knowledge, the only known VDE that approaches the 12 eV limit is that estimated by Boldyrev and Simons[14] for TeF_7^- (11.9 eV); however, it corresponds to the result calculated at the Koopmans' Theorem (KT)[15] level, which is not very accurate.[16]

In this paper we present the results of our theoretical search for anions that possess extremely large (i.e. approaching the 12 eV limit or above) electron binding energies. While performing our search, we followed the very interesting and valuable suggestions on designing such species described by Gutsev and Boldyrev,[6] which, in fact, allowed us to find the anions that exhibit such large VDEs. In particular, we focused our studies on the various polynuclear superhalogen anions, for which we calculated VDE values that may possibly be accurate.

2. Methods

Since our main goal was to calculate the vertical electron detachment energies for several anions, we limited our geometry optimization calculations to the closed-shell anionic species for which we also obtained harmonic vibrational frequencies at their minimum energy structures. For this purpose we applied the Hartree−Fock Self-Consistent Field method (SCF). Since the SCF method does not include electron correlation effects, we decided to test if this affects the equilibrium geometries of the anions studied. Therefore, for two cases (i.e. $Al_2F_7^-$ and $Al_2Cl_7^-$) we performed geometry optimization calculations (followed by the calculations of harmonic vibrational frequencies) at the second-order Møller−Plesset (MP2) perturbational level. We concluded that the equilibrium structures obtained with the SCF method are very similar to those calculated at the MP2 level (the average differences in bond lengths and valence angles did not exceed 0.2 Å and 0.5 deg, respectively). Since the possible inaccuracies in our vertical electron detachment energies (caused by using the SCF rather than MP2 geometries) was considered to be most important, we verified that our best VDE estimates (i.e. calculated with the outer valence Green function method) for $Al_2F_7^-$ and $Al_2Cl_7^-$ differ by less than 0.05 eV (which corresponds to 1% of the total VDE value) when obtained using the SCF and MP2 equilibrium anionic structures. Therefore, we concluded that using the SCF rather than MP2 geometries does not cause any significant errors in the systems studied in this work.

In order to obtain reliable vertical electron detachment energies of the superhalogen anions, a more accurate treatment of the data is required, thus we decided to perform both *direct* and *indirect* calculations of the electron binding energies. A *direct* scheme was based on applying the outer valence Green function (OVGF) method,[17,18] while the latter (*indirect*) approach involved subtracting the anion energies from those of the neutral species (both calculated at the same level of theory). In the *indirect* approach, we used the MP2 perturbational method. The core electrons were frozen when treating the electron correlation.

We applied the 6-311++G(d) basis sets[19,20] for the calculations of the equilibrium geometries and harmonic frequencies, and for estimating the vertical electron detachment energies at various levels, since analogous basis sets have recently been used for the BeX_3^- superhalogen anions

 © 2003 Wiley-VCH Verlag GmbH & Co. KGaA, Weinheim

(X = F, Cl, Br), which have provided reliable VDEs for these species.[21] However, it is important to note that applying the OVGF method with the 6-311++G(3df) basis sets would most likely provide better vertical electron detachment energies [as described in ref.[10] for LiX_2^- and NaX_2^- (X = F, Cl, Br, I), and in ref.[21] for BeX_3^- (X = F, Cl, Br)], since the OVGF/6-311++G(3df) treatment was found to produce an excellent agreement between such calculated and experimentally measured VDEs. Since the species studied in this work are relatively large (i.e. containing up to 19 heavy atoms) we had to employ the 6-311++G(d) basis set rather than the 6-311++G(3df) basis set. On the basis of our previous results [obtained for the BeX_3^- superhalogen anions (X = F, Cl, Br)],[21] we expect our final VDEs to be underestimated by less than 0.2 eV (which corresponds to ca. 1−2% of the vertical electron detachment energies).

All calculations were performed with the GAUSSIAN98 program[22] on Intel Pentium IV computers and an SGI Origin2000 numerical server.

3. Results

The theoretical and experimental results involving the superhalogen anions available in the literature relate mostly to *mononuclear systems* (i.e. those involving one central atom and several halogen ligands).[5−14,21] As we stated in Section 1, the mononuclear anionic system most likely possessing the largest vertical electron detachment energy that has been found thus far is TeF_7^-, for which the VDE of 11.9 eV was estimated (at the KT level) by Boldyrev and Simons.[14] Since the VDE of the superhalogen anion increases with the number of halogen ligands involved, one could explore this route in order to search for systems that maximise the VDE. However, one should recall that the TeF_7^- anion contains seven halogen atoms, and it is clear that attempts to search for another mononuclear anion involving larger number of ligands would be extremely difficult due to central atom valence saturation and topological limitations. Moreover, it has been shown that mononuclear species containing larger number of ligands, such as MnF_8^- or TcF_8^-, possess VDEs that are actually *smaller* than those of the anions MX_6^- or MX_7^- (the VDE values for MnF_8^- and TcF_8^- were found to be 6.7 and 5.8 eV, respectively).[6] Therefore, it seemed natural to examine whether the polynuclear superhalogen anions could exist as (geometrically and electronically) stable species since this would provide more than one central atom and hence would greatly increase the maximum number of halogen atoms in the system. This idea had been originally investigated as early as in 1987 by Gutsev and Boldyrev.[6] They proposed a few polynuclear superhalogen anions and estimated their VDEs.

The polynuclear superhalogen anions proposed by Gutsev and Boldyrev involved phosphorus, aluminium, arsenic, and vanadium as the central atoms and fluorine atoms as the ligands. On the basis of the DV-X_a calculations, they estimated the following electron binding energies: 8.6 eV

Table 1. The SCF geometrical parameters and the MP2 and OVGF estimates of the vertical electron detachment energies (VDE) for dinuclear superhalogen anions studied in this work [calculated with the 6-311++G(d) basis sets]. Bond lengths (R) in Å, valence angles ($\angle$) in degrees, vertical electron detachment energies in eV

Species (symmetry)	VDE [eV] 6-311++G(d)	Geometry
$Al_2F_7^-$	MP2 9.84	R(Al−F) = 1.667 ∠(FAlF1) = 104.96 ∠(AlF1Al) = 180.0
(D_{3d})	OVGF **11.16**	R(Al−F1) = 1.779 ∠(FAlF) = 113.58
$Al_2Cl_7^-$	MP2 7.56	R(Al−Cl1) = 2.126 R(Al−Cl4) = 2.313 ∠(Cl3AlCl4) = 105.97
(C_2)	OVGF **7.75**	R(Al−Cl2) = 2.121 ∠(Cl1AlCl3) = 112.56 ∠(AlCl4Al) = 123.09
		R(Al−Cl3) = 2.133 ∠(Cl2AlCl3) = 114.44
$Al_2Br_7^-$	MP2 6.96	R(Al−Br1) = 2.298 R(Al−Br4) = 2.493 ∠(Br2AlBr3) = 114.29
(C_2)	OVGF **7.08**	R(Al−Br2) = 2.288 ∠(AlBr4Al) = 118.93 ∠(Br1AlBr3) = 112.39
		R(Al−Br3) = 2.305 ∠(Br3AlBr4) = 106.34
$P_2F_{11}^-$	MP2 9.66	R(P1F2) = 1.835 R(P3F13) = 1.571 ∠(F2P1F7) = 85.60
(C_1)	OVGF **10.95**	R(P1F4) = 1.569 R(P3F2) = 1.834 ∠(P1F2P3) = 168.19
		R(P1F6) = 1.571 R(P3F5) = 1.569 ∠(F5P3F10) = 94.05
		R(P3F10) = 1.573 R(P3F12) = 1.573 ∠(F2P3F13) = 86.23
		R(P1F7) = 1.572 ∠(F4P1F6) = 94.11 ∠(F2P3F12) = 85.27
		R(P1F8) = 1.571 ∠(F2P1F9) = 85.57 ∠(F2P3F11) = 86.27
		R(P1F9) = 1.572 ∠(F2P1F8) = 86.26 ∠(F2P3F10) = 85.58
		R(P3F11) = 1.571 ∠(F2P1F6) = 86.22
$V_2F_{11}^-$	MP2 8.67	R(V−F1) = 1.691 ∠(F1VF) = 94.03 ∠(VF2V) = 180.0
(D_{4h})	OVGF **10.98**	R(V−F) = 1.723 ∠(FVF2) = 85.96
		R(V−F2) = 1.950 ∠(FVF) = 89.72
$As_2F_{11}^-$	MP2 9.86	R(As−F1) = 1.695 ∠(F1AsF) = 93.84 ∠(AsF2As) = 180.0
(D_{4h})	OVGF **11.43**	R(As−F) = 1.696 ∠(FAsF2) = 86.16
		R(As−F2) = 1.903 ∠(FAsF) = 89.74
$Ta_2F_{11}^-$	MP2 9.79	R(Ta−F1) = 1.855 ∠(F1TaF) = 94.35 ∠(TaF2Ta) = 180.0
(D_{4h})	OVGF **11.84**	R(Ta−F) = 1.877 ∠(FTaF2) = 85.65
		R(Ta−F2) = 2.066 ∠(FTaF) = 89.67

 © 2003 Wiley-VCH Verlag GmbH & Co. KGaA, Weinheim

(for $P_2F_{11}^-$), 7.5 eV (for $Al_2F_7^-$), 8.6 eV (for $As_2F_{11}^-$), and 8.0 eV (for $V_2F_{11}^-$).[6] Moreover, Gutsev and Boldyrev concluded that exploring the polynuclear superhalogen species is a promising way of searching for systems with the maximum VDE value. Therefore, we decided to take a closer look at such species to examine whether VDE values that exceed the 12 eV limit (see Section 1) could be found.

3.1. Dinuclear Superhalogen Anions

We begin our discussion with the superhalogen anions that possess two central atoms and consider a few species that have been proposed earlier by Gutsev and Boldyrev (the VDEs of these species could not be estimated accurately in the past due to the rather limited computer resources available at the time).[6] In addition, we examine other ligands of $Al_2X_7^-$, such as chlorine and bromine, to verify (or confirm) whether F ligands indeed lead to the largest vertical electron detachment energies.

3.1.1. Equilibrium Geometries

The parameters defining the geometries corresponding to the minima on the potential energy surfaces for $Al_2F_7^-$, $Al_2Cl_7^-$, $Al_2Br_7^-$, $P_2F_{11}^-$, $V_2F_{11}^-$, $As_2F_{11}^-$, and $Ta_2F_{11}^-$ are presented in Table 1, and the equilibrium structures are depicted in Figure 1. In each case, the two central atoms (M) are linked via a halogen atom (X), and the M−X−M bond could be linear (as in $Al_2F_7^-$, $V_2F_{11}^-$, $As_2F_{11}^-$, and $Ta_2F_{11}^-$), quasi-linear (as in $P_2F_{11}^-$) or bent (as in $Al_2Cl_7^-$ and $Al_2Br_7^-$) (see Figure 1).

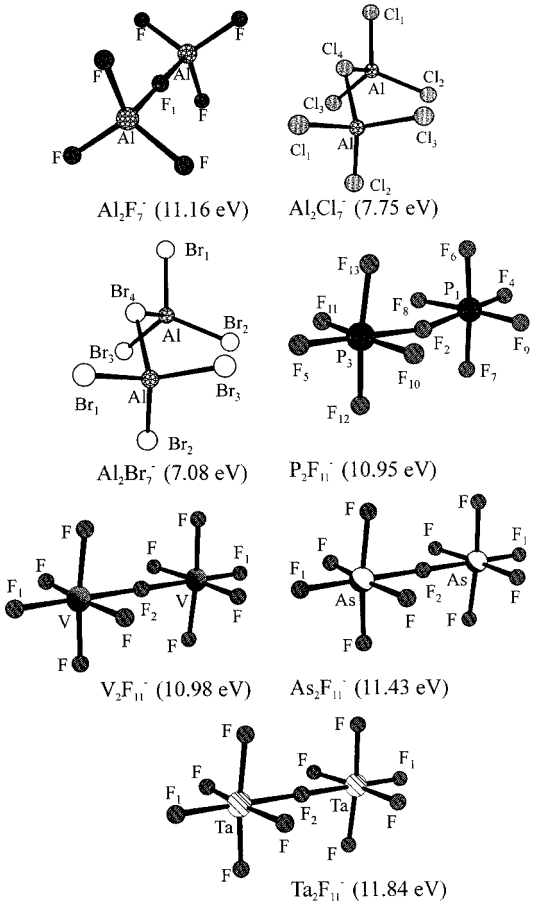

Figure 1. The SCF/6-311++G(d) equilibrium structures of the dinuclear superhalogen anions studied in this work. The corresponding OVGF/6-311++G(d) vertical electron detachment energies are given in parenthesis

The Al−F bond lengths in the $-AlF_3$ units in $Al_2F_7^-$ are shorter (by 0.1 Å) than the Al−F distances in the −Al−F−Al− fragment that serves as a bridge between the two subunits in this superhalogen anion. A similar observation can be made in the case of other dinuclear anions containing Al as the central atoms (see Table 1). Specifically, in the case of $Al_2Cl_7^-$ (and $Al_2Br_7^-$), the Al−Cl (Al−Br) bond lengths in the $-AlCl_3$ ($-AlBr_3$) units are shorter by ca. 0.2 Å than the Al−Cl (Al−Br) distances in the −Al−Cl−Al− (−Al−Br−Al−) fragment.

The P−F bonds in the $-PF_5$ subunits of the quasi-linear $P_2F_{11}^-$ structure are also shorter (by ca. 0.25 Å) than the P−F distances in the −P−F−P− fragment (see Table 1). An analogous situation can be observed in the case of all other dinuclear anions (i.e. $V_2F_{11}^-$, $As_2F_{11}^-$, and $Ta_2F_{11}^-$). The V−F bonds in the $-VF_5$ subunits of the $V_2F_{11}^-$ structure are shorter by ca. 0.2 Å than those in the −V−F−V− fragment connecting the two central atoms (see Table 1). A similar elongation (by ca. 0.2 Å) of the M−X distance is observed in $As_2F_{11}^-$ and $Ta_2F_{11}^-$ (see Table 1).

Since the corresponding harmonic vibrational frequencies for all the dinuclear superhalogen anions studied are positive (see Table 2), we conclude that each of these anionic structures is a true minimum on the potential energy surface, and this indicates the geometrical stability of such a system.

3.1.2. Vertical Electron Detachment Energies

The VDEs of all the dinuclear superhalogen anions studied in this work [calculated at the OVGF and MP2 levels with the 6-311++G(d) basis sets] are presented in Table 1. The second-order MP vertical electron detachment energies are usually smaller than those calculated at the OVGF level. This is consistent with the fact that the OVGF method approximately corresponds to the third-order perturbational treatment. Moreover, the largest discrepancies between MP2 and OVGF results were found for the superhalogens anion which had fluorine atoms as ligands.[21] This is also the case for the dinuclear superhalogen anions studied in this work (see Table 1). Therefore, we prefer to use the OVGF values in our discussion (given in this Section) since the OVGF treatment[23] has proven to produce a much better agreement between the calculated and experimentally determined electron binding energies of such species.[21]

Our results obtained for $Al_2X_7^-$ anions (X = F, Cl, Br) support the observation established earlier by others that species with fluorine ligands tend to have the largest VDE values (see Table 1). Indeed, the VDE calculated for $Al_2F_7^-$ is 11.16 eV, while those obtained for the analogous species with chlorine and bromine ligands are smaller (7.75 and 7.08 eV for $Al_2Cl_7^-$ and $Al_2Br_7^-$, respectively). To support this finding we calculated the vertical electron binding energies for mononuclear octahedral superhalogen anions hav-

 © 2003 Wiley-VCH Verlag GmbH & Co. KGaA, Weinheim

Table 2. The SCF harmonic vibrational frequencies (in cm^{-1}) for dinuclear superhalogen anions

Al_2F_7			Al_2Br_7			Al_2Cl_7			
ν_1 (a_{1u})	19	ν_1 (a)	12	ν_{15} (b)	213	ν_1 (b)	14	ν_{15} (b)	337
$\nu_{2,3}$ (e_u)	21	ν_2 (b)	12	ν_{16} (b)	286	ν_2 (a)	18	ν_{16} (b)	395
$\nu_{4,5}$ (e_g)	140	ν_3 (a)	27	ν_{17} (a)	347	ν_3 (a)	40	ν_{17} (a)	442
ν_6 (a_{1g})	171	ν_4 (a)	57	ν_{18} (b)	441	ν_4 (a)	91	ν_{18} (b)	550
$\nu_{7,8}$ (e_u)	201	ν_5 (b)	57	ν_{19} (a)	448	ν_5 (b)	91	ν_{19} (a)	554
$\nu_{9,10}$ (e_g)	258	ν_6 (a)	62	ν_{20} (b)	461	ν_6 (a)	99	ν_{20} (b)	570
ν_{11} (a_{2u})	298	ν_7 (b)	77	ν_{21} (a)	463	ν_7 (b)	125	ν_{21} (a)	570
$\nu_{12,13}$ (e_u)	304	ν_8 (a)	95			ν_8 (a)	151		
ν_{14} (a_{1g})	446	ν_9 (b)	104			ν_9 (b)	162		
ν_{15} (a_{2u})	651	ν_{10} (a)	108			ν_{10} (a)	167		
ν_{16} (a_{1g})	697	ν_{11} (b)	115			ν_{11} (b)	182		
ν_{17} (a_{2u})	703	ν_{12} (b)	131			ν_{12} (b)	196		
$\nu_{18,19}$ (e_g)	842	ν_{13} (a)	134			ν_{13} (a)	207		
$\nu_{20,21}$ (e_u)	852	ν_{14} (a)	202			ν_{14} (a)	312		
As_2F_{11}			Ta_2F_{11}		V_2F_{11}			P_2F_{11}	
ν_1 (a_{1u})	13	ν_1 (a_{1u})	13	ν_1 (a_{1u})	25	ν_1 (a)	9	ν_{25} (a)	656
$\nu_{2,3}$ (e_u)	33	$\nu_{2,3}$ (e_u)	43	$\nu_{2,3}$ (e_u)	39	ν_2 (a)	12	ν_{26}(a)	800
ν_4 (a_{1g})	152	$\nu_{4,5}$ (e_g)	102	ν_4 (b_{2u})	130	ν_3 (a)	26	ν_{27} (a)	812
$\nu_{5,6}$ (e_g)	165	ν_6 (b_{2u})	111	$\nu_{5,6}$ (e_g)	136	ν_4 (a)	135	ν_{28} (a)	881
ν_7 (b_{2u})	219	ν_7 (b_{1g})	119	ν_7 (b_{1g})	137	ν_5 (a)	167	ν_{29} (a)	944
ν_8 (b_{1g})	224	ν_8 (a_{1g})	123	ν_8 (a_{1g})	153	ν_6 (a)	216	ν_{30} (a)	1011
$\nu_{9,10}$ (e_u)	276	$\nu_{9,10}$ (e_u)	184	$\nu_{9,10}$ (e_u)	213	ν_7 (a)	222	ν_{31} (a)	1011
ν_{11} (a_{2u})	303	ν_{11} (a_{2u})	211	ν_{11} (a_{2u})	281	ν_8 (a)	287	ν_{32} (a)	1043
$\nu_{12,13}$ (e_g)	331	$\nu_{12,13}$ (e_g)	219	$\nu_{12,13}$ (e_g)	282	ν_9 (a)	292	ν_{33} (a)	1043
$\nu_{14,15}$ (e_u)	388	ν_{14} (a_{1g})	261	$\nu_{14,15}$ (e_u)	350	ν_{10} (a)	348		
$\nu_{16,17}$ (e_g)	415	$\nu_{15,16}$ (e_u)	262	$\nu_{16,17}$ (e_g)	352	ν_{11} (a)	351		
ν_{18} (b_{1u})	419	$\nu_{17,18}$ (e_g)	266	ν_{18} (a_{1g})	366	ν_{12} (a)	432		
ν_{19} (b_{2g})	420	ν_{19} (b_{1u})	308	ν_{19} (b_{1u})	380	ν_{13} (a)	432		
ν_{20} (a_{1g})	435	ν_{20} (b_{2g})	311	$\nu_{20,21}$ (e_u)	381	ν_{14} (a)	486		
$\nu_{21,22}$ (e_u)	441	$\nu_{21,22}$ (e_u)	337	ν_{22} (b_{2g})	382	ν_{15} (a)	488		
ν_{23} (a_{2u})	531	ν_{23} (a_{2u})	541	ν_{23} (a_{2u})	496	ν_{16}(a)	547		
ν_{24} (b_{2u})	635	ν_{24} (b_{2u})	634	ν_{24} (b_{2u})	610	ν_{17} (a)	547		
ν_{25} (b_{1g})	640	ν_{25} (b_{1g})	638	ν_{25} (b_{1g})	617	ν_{18} (a)	585		
ν_{26} (a_{1g})	722	$\nu_{26,27}$ (e_g)	648	ν_{26} (a_{2u})	728	ν_{19} (a)	585		
ν_{27} (a_{2u})	730	ν_{28} (a_{1g})	668	ν_{27} (a_{1g})	733	ν_{20} (a)	595		
ν_{28} (a_{2u})	757	$\nu_{29,30}$ (e_u)	670	$\nu_{28,29}$ (e_g)	751	ν_{21} (a)	600		
ν_{29} (a_{1g})	768	ν_{31} (a_{2u})	671	ν_{30} (a_{2u})	792	ν_{22} (a)	600		
$\nu_{30,31}$ (e_g)	795	ν_{32} (a_{1g})	760	$\nu_{31,32}$ (e_u)	795	ν_{23} (a)	625		
$\nu_{32,33}$ (e_u)	810	ν_{33} (a_{2u})	763	ν_{33} (a_{1g})	814	ν_{24} (a)	650		

ing phosphorus as a central atom. The results shown in Tables 3 and 4 indicate that the VDE of PF_6^- is relatively large (9.4 eV) and decreases when the F ligands are replaced with Cl or Br ligands. In addition, our earlier results obtained for BeX_3^- (X = F, Cl, Br),[21] as well as the results obtained by others,[5–7] support this conclusion. Hence, we decided not to calculate the electron binding energies for other species containing either Cl or Br ligands, since it can be predicted that such anions would have smaller VDEs than the corresponding species containing fluorine atoms as the ligands.

Table 3. The SCF geometrical parameters and the MP2 and OVGF estimates of the vertical electron detachment energies (VDE) for mononuclear superhalogen anions studied in this work [calculated with the 6-311++G(d) basis sets]. Bond lengths (R) in Å, vertical electron detachment energies in eV

Species (symmetry)	VDE [eV] 6-311++G(d)	Geometry
PF_6^-	MP2 8.49	R(P–F) = 1.603
(O_h)	OVGF **9.43**	
PCl_6^-	MP2 5.94	R(P–Cl) = 2.168
(O_h)	OVGF **7.55**	
PBr_6^-	MP2 5.30	R(P–Br) = 2.374
(O_h)	OVGF **6.66**	

Table 4. The SCF harmonic vibrational frequencies (in cm^{-1}) for mononuclear superhalogen anions

PBr_6		PCl_6		PF_6	
$\nu_{1,2,3}$ (t_{2u})	99	$\nu_{1,2,3}$ (t_{2u})	172	$\nu_{1,2,3}$ (t_{2u})	333
$\nu_{4,5,6}$ (t_{2g})	145	$\nu_{4,5,6}$ (t_{2g})	256	$\nu_{4,5,6}$ (t_{2g})	504
$\nu_{7,8}$ (e_g)	157	$\nu_{7,8}$ (e_g)	271	$\nu_{7,8,9}$ (t_{1u})	600
$\nu_{9,10,11}$ (t_{1u})	174	$\nu_{9,10,11}$ (t_{1u})	305	$\nu_{10,11}$ (e_g)	603
ν_{12} (a_{1g})	215	ν_{12} (a_{1g})	377	ν_{12} (a_{1g})	787
$\nu_{13,14,15}$(t_{1u})	387	$\nu_{13,14,15}$(t_{1u})	481	$\nu_{13,14,15}$(t_{1u})	943

 © 2003 Wiley-VCH Verlag GmbH & Co. KGaA, Weinheim

One should also notice that the VDE of $Al_2F_7^-$ calculated at the OVGF/6-311++G(d) level differs significantly from the electron binding energy determined by Gutsev and Boldyrev (7.5 eV).[6] We believe that our OVGF value of 11.16 eV, even if slightly overestimated, is much closer to the true vertical electron detachment energy of this anion. The VDE calculated for the $P_2F_{11}^-$ superhalogen anion (10.95 eV) is slightly smaller than that of $Al_2F_7^-$ (see Table 1). On the basis of the discussion given in the preceding paragraphs, we do not expect the VDE to increase when the fluorine atoms in $P_2F_{11}^-$ are replaced by other halogen atoms. However, we have verified that replacing the phosphorus atoms (the central atoms) by other elements, such as V, As, or Ta, may lead to larger electron binding energies. In particular, the VDE for the superhalogen anion $V_2F_{11}^-$ [calculated at the OVGF/6-311++G(d) level] approaches the value of 11 eV (10.98 eV, see Table 1), while the vertical electron detachment energy of $As_2F_{11}^-$ is even larger and equals to 11.43 eV. The largest VDE for a dinuclear superhalogen anion was found for $Ta_2F_{11}^-$ (11.84 eV). We considered this finding to be promising because the VDE of dinuclear $Ta_2F_{11}^-$ (11.84 eV) approaches the value of 12 eV (which is supposed to be the VDE limit according to the recent studies[6,12,13]), and one could expect the VDE to increase when a third central atom is added. Therefore, we now move on to the discussion of the vertical electron detachment energies of the superhalogen anions containing three central atoms.

3.2. Trinuclear Superhalogen Anions

3.2.1. Equilibrium Geometries

Although our original intention was to determine the vertical electron binding energies for four trinuclear superhalogen anions $M_3F_{16}^-$ (where M = P, V, As, Ta), the VDEs of only two trinuclear species were determined. In the case of the two species $P_3F_{16}^-$ and $V_3F_{16}^-$, whose geometrical stability we initially assumed, it was not possible to find any structures corresponding to local minima on the potential energy surface. Instead, the geometry optimisations led to fragmentation of these two systems. Therefore, we concluded that neither $P_3F_{16}^-$ nor $V_3F_{16}^-$ was geometrically stable, and hence decided to focus on two trinuclear species, $As_3F_{16}^-$ and $Ta_3F_{16}^-$.

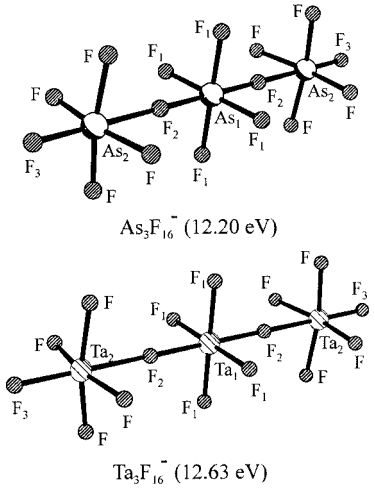

Figure 2. The SCF/6-311++G(d) equilibrium structures of the trinuclear superhalogen anions studied in this work. The corresponding OVGF/6-311++G(d) vertical electron detachment energies are given in parenthesis

The equilibrium structures of $As_3F_{16}^-$ and $Ta_3F_{16}^-$ are depicted in Figure 2 and the corresponding parameters defining these geometries are given in Table 5. Since the harmonic vibrational frequencies calculated for these structures are positive (see Table 6), we conclude that each of these trinuclear superhalogen anions is a true minimum on the potential energy surface. This indicates the geometrical stability of such a system.

In $As_3F_{16}^-$ and $Ta_3F_{16}^-$, the central atoms (M) are linked via fluorine atoms and the M−F−M bonds are linear (see Figure 2 and Table 5). The As−F bonds in the As−F−As−F−As linking fragment in $As_3F_{16}^-$ are longer (by ca. 0.1−0.3 Å) than those in which only two atoms (i.e. one As and one F atom) are involved. A similar situation can be observed in $Ta_3F_{16}^-$, where the Ta−F distances in the Ta−F−Ta−F−Ta linking fragment are longer (by ca. 0.1−0.3 Å) than those that involve only two atoms (see Table 5).

Both the $As_3F_{16}^-$ and $Ta_3F_{16}^-$ equilibrium structures possess relatively high symmetry (D_{4h}), and each of these

Table 5. The SCF geometrical parameters and the MP2 and OVGF estimates of the vertical electron detachment energies (VDE) for trinuclear superhalogen anions studied in this work [calculated with the 6-311++G(d) basis sets]. Bond lengths (R) in Å, valence angles (∠) in degrees, vertical electron detachment energies in eV

Species (symmetry)	VDE [eV] 6-311++G(d)	Geometry
$As_3F_{16}^-$ (D_{4h})	MP2 12.46 OVGF **12.20**	R(As1F1) = 1.686, R(As2F) = 1.689, ∠(FAs2F) = 89.38 R(As1F2) = 1.799, ∠(F1As1F2) = 90.0, ∠(FAs2F3) = 95.89 R(As2F2) = 2.029, ∠(F1As1F1) = 90.0, ∠(As2F2As1) = 180.0 R(As2F3) = 1.682 ∠(F2As2F) = 84.11
$Ta_3F_{16}^-$ (D_{4h})	MP2 10.45 OVGF **12.63**	R(Ta1F1) = 1.864, R(Ta2F) = 1.871, ∠(FTa2F) = 89.28 R(Ta1F2) = 1.983, ∠(F1Ta1F2) = 90.0, ∠(FTa2F3) = 96.44 R(Ta2F2) = 2.134, ∠(F1Ta1F1) = 90.0, ∠(Ta2F2Ta1) = 180.0 R(Ta2F3) = 1.842, ∠(F2Ta2F) = 83.55

 © 2003 Wiley-VCH Verlag GmbH & Co. KGaA, Weinheim

Table 6. The SCF harmonic vibrational frequencies (in cm^{-1}) for trinuclear superhalogen anions

As_3F_{16}				Ta_3F_{16}			
ν_1 (a_{1u})	12	ν_{30} (b_{2g})	426	ν_1 (a_{1u})	9	ν_{29} (b_{2g})	313
$\nu_{2,3}$ (e_u)	14	ν_{31} (b_{1u})	430	$\nu_{2,}$(a_{2g})	16	ν_{30} (b_{1u})	314
ν_4 (a_{2g})	21	ν_{32} (b_{2g})	431	$\nu_{3,4}$ (e_u)	17	ν_{31} (b_{2g})	317
$\nu_{5,6}$ (e_g)	33	$\nu_{33,34}$ (e_u)	442	$\nu_{5,6}$ (e_g)	46	$\nu_{32,33}$ (e_u)	323
ν_7 (a_{1g})	95	ν_{35} (a_{2u})	448	ν_7 (b_{2u})	73	$\nu_{34,35}$ (e_g)	336
ν_8 (a_{2u})	130	ν_{36} (a_{1g})	556	$\nu_{8,9}$ (e_u)	85	ν_{36} (a_{2u})	565
$\nu_{9,10}$ (e_u)	138	ν_{37} (a_{2u})	594	ν_{10} (a_{1g})	90	ν_{37} (a_{1g})	597
$\nu_{11,12}$ (e_g)	184	ν_{38} (b_{1g})	647	ν_{11} (b_{1g})	107	ν_{38} (b_{1g})	649
ν_{13} (b_{2u})	193	ν_{39} (b_{2u})	648	ν_{12} (b_{2u})	108	ν_{39} (b_{2u})	649
ν_{14} (b_{1g})	194	ν_{40} (b_{1g})	657	ν_{13} (a_{2u})	130	$\nu_{40,41}$ (e_u)	656
ν_{15} (b_{2u})	215	ν_{41} (a_{1g})	742	$\nu_{14,15}$ (e_g)	139	ν_{42} (b_{1g})	670
$\nu_{16,17}$ (e_u)	281	ν_{42} (a_{2u})	744	ν_{16} (a_{2u})	188	$\nu_{43,44}$ (e_g)	681
$\nu_{18,19}$ (e_g)	316	$\nu_{43,44}$ (a_{1g})	762	$\nu_{17,18}$ (e_u)	192	$\nu_{45,46}$ (e_u)	692
ν_{20} (a_{2u})	320	ν_{45} (a_{2u})	781	$\nu_{19,20}$ (e_g)	217	ν_{47} (a_{2u})	710
$\nu_{21,22}$ (e_u)	342	$\nu_{46,47}$ (e_u)	812	$\nu_{21,22}$ (e_u)	218	ν_{48} (a_{1g})	711
ν_{23} (a_{1g})	358	$\nu_{48,49}$ (e_g)	817	ν_{23} (a_{1g})	237	ν_{49} (a_{1g})	770
$\nu_{24,25}$ (e_g)	386	$\nu_{50,51}$ (e_u)	832	ν_{24} (a_{2u})	255	ν_{50} (a_{2u})	773
$\nu_{26,27}$ (e_u)	410			$\nu_{25,26}$ (e_u)	259	ν_{51} (a_{1g})	776
$\nu_{28,29}$ (e_g)	425			$\nu_{27,28}$ (e_g)	259		

species can be viewed as three quasi-octahedral MF_6 systems (M = As, Ta) linked together by two bridging fluorine atoms.

3.2.2. Vertical Electron Detachment Energies

The vertical electron detachment energies for the two trinuclear superhalogen anions studied in this work [calculated at the OVGF and MP2 levels with the 6-311++G(d) basis sets] are presented in Table 5. As in the preceding Section (related to dinuclear species), we use the OVGF values whilst discussing the VDEs of $As_3F_{16}^-$ and $Ta_3F_{16}^-$.

We expected the VDEs of the $As_3F_{16}^-$ and $Ta_3F_{16}^-$ anions to be larger than the VDEs calculated for the corresponding dinuclear species (i.e. $As_2F_{11}^-$ and $Ta_2F_{11}^-$) because the excess negative charge can be delocalized over a larger number of electronegative ligands in the trinuclear superhalogen anions. Indeed, the VDE calculated for $As_3F_{16}^-$ (12.20 eV) is larger by 0.77 eV than the VDE of $As_2F_{11}^-$, and the VDE obtained for $Ta_3F_{16}^-$ (12.63 eV) is greater (by 0.79 eV) than that of $Ta_2F_{11}^-$ (see Tables 1 and 5). Hence, in both cases, the VDE of the superhalogen anion increases by ca. 0.8 eV when another central atom (of the same type) and the proper number of fluorine ligands is added to the parent structure.

We believe that our VDE values that exceed the 12 eV limit by 0.2−0.6 eV, found for the two negatively charged systems $As_3F_{16}^-$ and $Ta_3F_{16}^-$ may be approaching the largest possible VDE values because: (i) the largest known vertical electron detachment energies described in the literature thus far are those calculated by Boldyrev and Simons for TeF_7^- (11.9 eV),[14] and those obtained (also theoretically) by Schaefer's group for AsF_6^- (10.5 eV),[11] and (ii) the limit for the maximum possible excess electron binding energy is thought to be about 12 eV.[12,13] Although the extremely large VDE (12.63 eV) calculated by us for $Ta_3F_{16}^-$ seems to be the largest excess electron binding energy reported in the literature thus far, we believe the maximum possible VDE value has not yet been achieved. In addition, we conclude that the upper limit for the electron affinity characterising the neutral molecular system is in fact higher than 12 eV, and it seems likely it might be larger than 13 eV, as suggested by Gutsev and Boldyrev in the 80′s.[24] Therefore, we believe that the negatively charged system that has the maximum vertical electron detachment energy is yet to be found and we consider such species (i.e. those possessing extremely large VDEs) as systems of great importance in chemistry.

4. Summary

The vertical electron detachment energies of several polynuclear superhalogen anions were calculated at the OVGF/6-311++G(d) level. The largest vertical electron binding energy of 12.63 eV was found for $Ta_3F_{16}^-$, and it is recognised as the largest excess electron binding energy of a molecular system reported in the literature thus far. Since the VDE of 12.63 eV (found for $Ta_3F_{16}^-$) exceeds the upper VDE limit that was thought to be 12 eV, it is proposed that the largest possible excess electron binding energy of a molecular system be reconsidered. Several other anions were also found [at the OVGF/6-311++G(d) level] to have very large VDEs (i.e. $Al_2Br_7^-$: 7.08 eV, $Al_2Cl_7^-$: 7.75 eV, $Al_2F_7^-$: 11.16 eV, $P_2F_{11}^-$: 10.95 eV, $V_2F_{11}^-$: 10.98 eV, $As_2F_{11}^-$: 11.43 eV, $Ta_2F_{11}^-$: 11.84 eV, and $As_3F_{16}^-$: 12.20 eV).

Acknowledgments

We would like to thank Prof. J. Rak for his valuable comments. This work was supported by the Polish State Committee for Scientific Research (KBN) Grant No. DS/8371-4-0137-3 and the NSF Grant 9982420. The computer time provided by the Academic Computer Center in Gdańsk (TASK) and the Center for High Performance Computing at the University of Utah is also gratefully acknowledged.

[1] P. Kebarle, S. Chowdhury, *Chem. Rev.* **1987**, *87*, 513−534.
[2] H. Hotop, W. C. Lineberger, *J. Phys. Chem. ref. Data* **1985**, *14*, 731−750.
[3] N. Bartlett, *Proc. Chem. Soc.* **1962**, 218.
[4] F. Wudl, *Acc. Chem. Res.* **1984**, *17*, 227−232.
[5] G. L. Gutsev, A. I. Boldyrev, *Chem. Phys.* **1981**, *56*, 277−283.
[6] G. L. Gutsev, A. I. Boldyrev, *Russian Chemical Reviews* **1987**, *56*, 519−531.
[7] G. L. Gutsev, R. J. Bartlett, A. I. Boldyrev, J. Simons, *J. Chem. Phys.* **1997**, *107*, 3867−3875.
[8] M. K. Scheller, L. S. Cederbaum, *J. Chem. Phys.* **1994**, *100*, 8934−8942.
[9] J. V. Ortiz, *Chem. Phys. Lett.* **1993**, *214*, 467−472.
[10] X.-B. Wang, C.-F. Ding, L.-S. Wang, A. I. Boldyrev, J. Simons, *J. Chem. Phys.* **1999**, *110*, 4763−4770.
[11] W. Xu, G. Li, G. Yu, Y. Zhao, Q. Li, Y. Xie, H. F. Schaefer III, *J. Phys. Chem. A* **2003**, *107*, 258−266.
[12] J. Kalcher, A. F. Sax, *Chem. Rev.* **1994**, *94*, 2291−2318.
[13] G. L. Gutsev, A. I. Boldyrev, *J. Phys. Chem.* **1990**, *94*, 2256−2259.
[14] A. I. Boldyrev, J. Simons, *J. Chem. Phys.* **1992**, *97*, 2826−2827.
[15] T. Koopmans, *Physica* **1934**, *1*, 104−113.

 © 2003 Wiley-VCH Verlag GmbH & Co. KGaA, Weinheim

[16] Koopmans' Theorem (KT) estimate of the vertical electron detachment energy of an anion is the negative of the energy of the relevant singly-occupied orbital obtained from a Hartree−Fock self-consistent-field calculation.
[17] J. V. Ortiz, *J. Chem. Phys.* **1988**, *89*, 6348−6352.
[18] L. S. Cederbaum, *J. Phys. B8* 1975, 290−303.
[19] A. D. McLean, G. S. Chandler, *J. Chem. Phys.* **1980**, *72*, 5639−5648.
[20] R. Krishnan, J. S. Binkley, R. Seeger, J. A. Pople, *J. Chem. Phys.* **1980**, *72*, 650−654.
[21] I. Anusiewicz, P. Skurski, *Chem. Phys. Lett.* **2002**, *358*, 426−434.
[22] *GAUSSIAN 98, Revision A.7*, M. J. Frisch, G. W. Trucks, H. B. Schlegel, G. E. Scuseria, M. A. Robb, J. R. Cheeseman, V. G. Zakrzewski, J. A. Montgomery, Jr., R. E. Stratmann, J. C. Burant, S. Dapprich, J. M. Millam, A. D. Daniels, K. N. Kudin, M. C. Strain, O. Farkas, J. Tomasi, V. Barone, M. Cossi, R. Cammi, B. Mennucci, C. Pomelli, C. Adamo, S. Clifford, J. Ochterski, G. A. Petersson, P. Y. Ayala, Q. Cui, K. Morokuma, D. K. Malick, A. D. Rabuck, K. Raghavachari, J. B. Foresman, J. Cioslowski, J. V. Ortiz, A. G. Baboul, B. B. Stefanov, G. Liu, A. Liashenko, P. Piskorz, I. Komaromi, R. Gomperts, R. L. Martin, D. J. Fox, T. Keith, M. A. Al-Laham, C. Y. Peng, A. Nanayakkara, C. Gonzalez, M. Challacombe, P. M. W. Gill, B. Johnson, W. Chen, M. W. Wong, J. L. Andres, C. Gonzalez, M. Head-Gordon, E. S. Replogle, and J. A. Pople, Gaussian, Inc., Pittsburgh PA, **1998**.
[23] The OVGF method corresponds approximately to the third-order MP perturbational treatment.
[24] G. L. Gutsev, A. I. Boldyrev, *Chem. Phys. Lett.* **1984**, *108*, 250−255.

Received April 1, 2003

 © 2003 Wiley-VCH Verlag GmbH & Co. KGaA, Weinheim

Structures of the Octahedral Persulfuranes H_4SF_2, H_2SF_4, Me_2SH_4 and Me_2SF_4, and Activation Enthalpies for Their *cis*/*trans* Isomerization[‡]

Yana Steudel[a] and Ralf Steudel*[a]

Keywords: Hypercoordinate molecules / Ab initio calculations / Transition states / Isomerism / Sulfur / Fluorides

Eight hypothetical persulfurane molecules of the type X_2SY_4 (X, Y = H, F, Me) have been studied by ab initio MO calculations at the G3(MP2) level of theory. Depending on the substituents either the *cis* or the *trans* isomers of these octahedral molecules are most stable. While H_4SF_2 is most stable as the *cis* isomer, the global minimum structures of H_2SF_4, Me_2SH_4, and Me_2SF_4 are the *trans* isomers. The enthalpy differences between the corresponding isomers are in the range 7–53 kJ·mol^{-1}. The transition states for the intramolecular *cis* ⇌ *trans* isomerization have been located in all cases. Starting from the global minimum geometries the activation enthalpies ($\Delta H^{\#}_{298}$) for this isomerization are in the range 199–263 kJ·mol^{-1}, indicating rather rigid structures. Therefore, it should be possible to isolate both isomers at low to moderate temperatures.

(© Wiley-VCH Verlag GmbH & Co. KGaA, 69451 Weinheim, Germany, 2003)

Introduction

The persulfurane SF_6 is not only an important industrial product[2] but also one of the most-investigated molecules as far as the bonding properties of so-called hypervalent or hypercoordinate molecules are concerned.[3] Numerous derivatives of the types RSF_5 and R_2SF_4 are known[4,5] but the most simple examples, HSF_5 and H_2SF_4, have never been prepared. While HSF_5 has been investigated by ab initio MO calculations,[6,7] the related molecules H_2SF_4 and H_4SF_2 have not yet been studied at all. We have used these species as model compounds to determine the activation energies for the mutual isomerization of the *cis* and *trans* isomers of octahedral persulfuranes for the first time. To further study the influence of the substituents on these energies the methyl-substituted species Me_2SH_4 and Me_2SF_4 were also included in this investigation. These molecules are also hypothetical species. A theoretical treatment of Me_2SF_4 (at the HF/3-21G* level of theory) has been published before,[8] but no structural data were given and only *trans*-Me_2SF_4 was considered. The formation of Me_2SF_4 from Me_2SF_2 and F_2 was shown to be exothermic.

Calculations

Standard ab initio MO calculations were performed using the Gaussian 98 series of programs.[9] The energies of various equilibrium structures and transition states were examined at the G3(MP2) level of theory.[10] In brief, the G3(MP2) method is a composite procedure which provides an accurate approximation, to a high level of theory, at QCISD(T)/GTMP2LARGE//MP2(full)/6-31G(d), with the incorporation of zero-point energy (ZPE) [calculated from HF/6-31G(d) vibrational wavenumbers, scaled by 0.8929] and higher level corrections. It has been shown before that this theoretical method is suitable for hypercoordinate molecules: The reaction enthalpy for the formation of SF_6 from F_2 and SF_4 was obtained as −439.1 kJ·mol^{-1} at 0 K,[1] whereas from the best available experimental enthalpies of formation of these compounds[11] the reaction enthalpy is calculated as −450±20 kJ·mol^{-1} at 0 K. In the case of the hypervalent SF_6 molecule the related G2(MP2) method − using the same geometry calculation as in G3(MP2) − reproduced the very accurately known experimental enthalpy of formation within 7.5 kJ·mol^{-1}.[11]

For all investigated molecules a charge-density analysis, at the MP2(full)/6-31G(d) level, was performed using the natural bond orbital (NBO) approach.[12] NBO atomic charges of small molecules have recently been demonstrated to agree well with experimental values obtained from X-ray diffraction data.[13] Unless otherwise noted, all relative energies reported in this publication are given as ΔH^{o}_{298} and correspond to the G3(MP2) level, while structural parameters were obtained at the MP2(full)/6-31G(d) level. Since *trans*-Me_2SF_4 (**4a**) does not represent a minimum at the HF/6-31G(d) level of theory, for the calculation of G3MP2 enthalpies and Gibbs energies of **4a**, **4b**, and **TS4** the ZPE and the entropy values obtained from the frequency calculation at the MP2(full)/6-31G(d) level of theory were used.

[‡] Sulfur Compounds, 228. Part 227: Y. Steudel, R. Steudel, *Eur. J. Inorg. Chem.* **2003**, 2149.

[a] Institut für Chemie, Technische Universität Berlin, Sekr. C2, 10623 Berlin, Germany
Fax: (internat.) +49-(0)30-31426519
E-mail: steudel@schwefel.chem.tu-berlin.de

 © 2003 Wiley-VCH Verlag GmbH & Co. KGaA, Weinheim **DOI: 10.1002/ejic.200300240**

The transition states obtained were characterized by one imaginary vibrational wavenumber whereas the wavenumbers of the structures of minimal energy were all real. The intrinsic reaction coordinates were calculated at the HF/6-31G* level.[14]

Results and Discussion

Sulfur Hydride Fluorides

The possible isomers of H_4SF_2 (**1**) and H_2SF_4 (**2**) are shown in Figure 1, which also gives the internuclear distances; bond angles are listed in Table 1. The two *trans* isomers are of D_{4h} symmetry with all bond angles either 90° or 180°. The *cis* isomers are of C_{2v} symmetry.

Unexpectedly, the *cis* isomer of H_4SF_2 (**1a**) and the *trans* isomer of H_2SF_4 (**2a**) represent the global minimum structures. The *trans* isomer of H_4SF_2 (**1b**) is 53 kJ·mol^{-1} and the *cis* isomer of H_2SF_4 (**2b**) is 37 kJ·mol^{-1} less stable than the most stable structures **1a** and **2a**, respectively. The origin of these differing stabilities is not evident from the molecular structures. The NBO charges of the sulfur atoms (in atomic units) are +1.29 in **1a**, +1.45 in **1b**, +2.12 in **2a** and +2.13 in **2b**. For comparison, for the octahedral SF_6 molecule we found a charge of +2.85 at the sulfur atom at the same level of theory. It appears that the higher the fluorine content the smaller is the NBO charge on the F atoms (**1a**: −0.62, **1b**: −0.60, **2a**: −0.55, **2b**: −0.53, SF_6: −0.475).

The SH and SF internuclear distances given in Figure 1 show an interesting pattern. As a reference value the SF

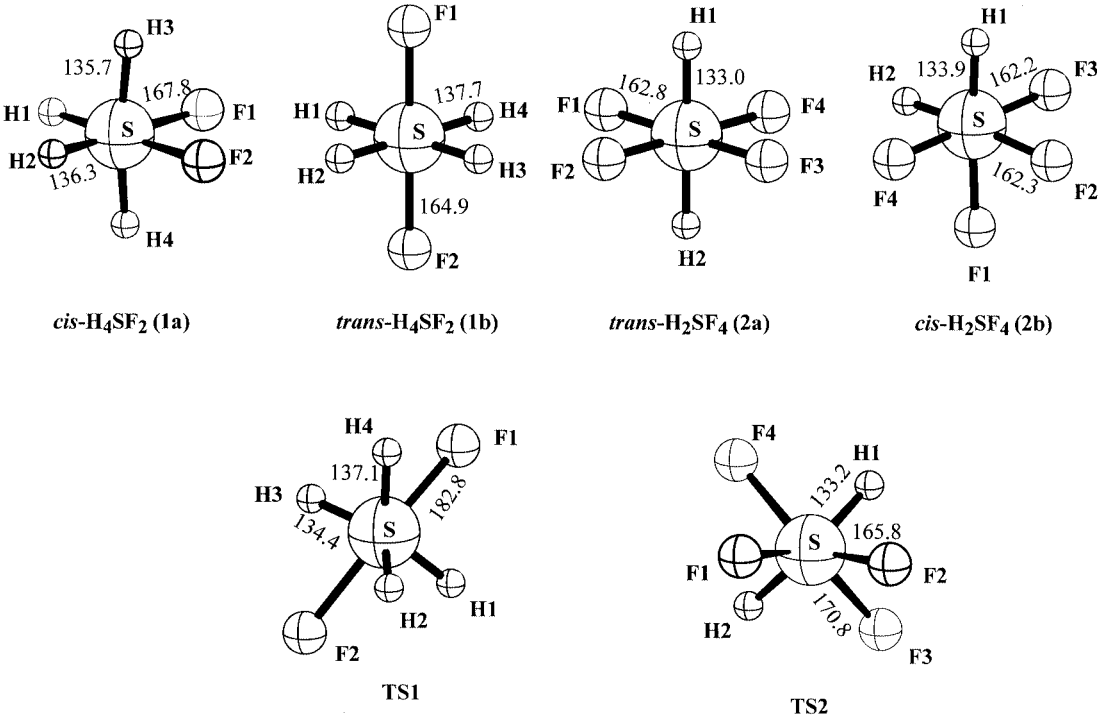

Figure 1. Molecular structures and bond lengths (pm) of the two persulfuranes H_4SF_2 (**1a**, **1b**) and H_2SF_4 (**2a**, **2b**), as well as of the transition states for the *cis* ⇌ *trans* isomerizations **1a** → **1b** (**TS1**) and **2a** → **2b** (**TS2**)

Table 1. Selected bond angles (degree) of the molecules H_4SF_2 and H_2SF_4 (two isomers each) and of the transition states **TS1** and **TS2** for the *cis* ⇌ *trans* isomerization of these species

Angle	*cis*-H_4SF_2 (**1a**)	*cis*-H_2SF_4 (**2b**)	TS1	TS2
F−S−F	89.4 (F1SF2)	87.0 (F1/F2)	140.6	79.9 (F1/F2)
		89.9 (F1/F3)		134.3 (F1/F3)
		179.7 (F3/F4)		83.1 (F1/F4)
				135.7 (F3/F4)
H−S−F	90.6 (H1/F1)	175.3 (H1/F1)	73.4 (H1/F1)	135.0 (H1/F1)
	86.9 (H3/F1)	90.1 (H1/F4)	138.6 (H2/F1)	85.5 (H1/F2)
	180.0 (H1/F2)	88.3 (H1/F2)	85.6 (H3/F1)	84.8 (H1/F3)
			74.4 (H4/F1)	77.4 (H1/F4)
H−S−H	93.1 (H1/H3)	96.4	94.1 (H1/H2)	131.6
	89.4 (H1/H2)		115.2 (H1/H3)	
			134.0 (H1/H4)	
			88.9 (H2/H4)	

 © 2003 Wiley-VCH Verlag GmbH & Co. KGaA, Weinheim

bond length of SF_6 was calculated as 159.3 pm, 3.6 pm (2.2%) longer than the experimental value of 155.7 pm.[15] In **1a** through **2b** the SF distances range from 162.3 to 167.8 pm. With decreasing fluorine content all bonds in the molecules shown in Figure 1 increase substantially in length. Comparing the two pairs of isomers of identical composition (**1a**/**1b** and **2a**/**2b**) one notices that the SH bonds are shortest and the SF bonds are longest in the global minimum structures but the sum of all bond lengths is practically identical in each pair of compounds.

Previous authors have discussed the possibility of so-called *cis*- and *trans*-effects in HSF_5 and related molecules.[6,7] Such effects can partly be seen in the structures investigated in this work as judged from the bond length variation. For the fluorine atoms of H_4SF_2 it is more favorable for them to be *cis* to each other, as in **1a**, while the hydrogen atoms do not show any preference for either *cis* or *trans* positions to each other or to the F atoms. However, the structure of the H_2SF_4 isomer **2b**, with practically identical SH and SF bonds (as judged by the internuclear distances), seemingly rules out any *trans* effect.

The structure of *cis*-H_4SF_2 (**1a**) demonstrates that the formal space requirement of the SH bonds is larger than that of the SF bonds, as expected from the much lower electronegativity of H compared to F. Thus, the H3−S−H4 angle is 171° and the two SH bonds are bent towards the fluorine atoms (see Figure 1). Of course, this effect can also be interpreted as a sign of attractive interactions between the two positively charged hydrogen atoms H3 and H4 (+0.015) and the negatively charged fluorine atoms (−0.62). The hydrogens *trans* to the fluorine atoms (H1 and H2) are slightly negatively charged (−0.04).

The transition states for the *cis*/*trans* isomerization, and vice versa, have been located on the potential energy hypersurfaces; their structures are also shown in Figure 1 (**TS1** and **TS2**). For the *cis* → *trans* isomerization **1a** → **1b** via **TS1** an activation enthalpy of 263 kJ·mol^{-1} is needed ($\Delta G^{\#}_{298}$ = 265 kJ·mol^{-1}). The *trans* → *cis* isomerization **2a** → **2b** via **TS2** requires an activation enthalpy of 199 kJ·mol^{-1} ($\Delta G^{\#}_{298}$ = 196 kJ·mol^{-1}). To the best of our knowledge, neither experimental nor theoretical activation energies for the *cis*/*trans* isomerization of octahedral persulfuranes have been published before, excepting our own recent work on $SF_4(CN)_2$.[1] The data obtained in the present investigation indicate that these molecules are rather rigid, in sharp contrast to the well-known fluxionality of sulfuranes of the type SX_4: in the case of SF_4 the barrier for pseudorotation is only $\Delta H^{\#}_{298}$ = 47 kJ·mol^{-1}.[16] In the case of the persulfurane **A** no *cis*/*trans* isomerization was observed within 254 h at 238 °C under basic conditions. However, the compound isomerized rapidly after addition of a catalytic amount of SbF_5, which cleaved one of the SF bonds, generating a cationic five-coordinate intermediate.[17]

The two transition states **TS1** and **TS2** are of C_2 symmetry and may be regarded as distorted trigonal-prismatic structures. During the isomerization of **1** the F−S−F bond

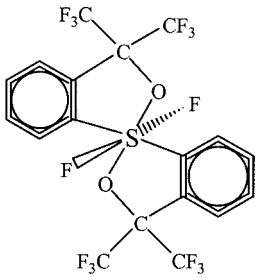

A

angle changes from 89.4° in **1a** via 140.6° in **TS1** to 180° in **1b**. Similarly, the H−S−H bond angle of **2** decreases from 180° in **2a** via 131.6° in **TS2** to 96.4° in **2b**. The latter value, together with the other bond angles of **2b**, demonstrates once more that the formal space requirement of the SH bonds is larger than that of the SF bonds in these molecules (in **2b** all F−S−F angles are smaller than 90°). This finding is in agreement with the expectations from the VSEPR model of molecular structures[18] but in contrast to the size of the atoms.

The bond length variations during the isomerization processes are most interesting. For example, the SF bond lengths of H_4SF_2 increase from 167.8 pm in **1a** to 182.8 pm in **TS1** and then decrease to 164.9 pm in **1b**. The SH bonds are much less affected: they change from 135.7/136.3 pm in **1a** via 134.4/137.1 pm in **TS1** to 137.7 pm in **1b**. The corresponding transformation **2a** → **2b** takes the SF bond lengths from 162.8 pm in **2a** via 165.8/170.8 pm in **TS2** to 162.2/162.3 pm in **2b** while the SH bonds change simultaneously only from 133.0 via 133.2 to 133.9 pm. The NBO charges on the sulfur atoms in these transition state structures are slightly lower than in the *cis* and *trans* isomers (**TS1**: +1.18; **TS2**: +2.07).

Dimethyl Sulfur Tetrahydride and Tetrafluoride

The *cis* and *trans* isomers of Me_2SH_4 and Me_2SF_4 are shown in Figure 2. The geometrical data are presented in Table 2 (bond lengths) and Table 3 (bond angles).

The *trans* isomer of Me_2SH_4 (**3a**) is of C_{2h} symmetry and is more stable than the *cis* form **3b**, which is of C_s symmetry, by 7 kJ·mol^{-1}. The transition state **TS3** for the *trans*→*cis* isomerization is also shown in Figure 2. The activation enthalpy of 236 kJ·mol^{-1} ($\Delta G^{\#}_{298}$ = 246 kJ·mol^{-1}) is of the same order of magnitude as in the case of the other octahedral molecules studied here and in our recent work on the isomers of $SF_4(CN)_2$.[1] The *trans* isomer of Me_2SF_4 (**4a**; C_{2v} symmetry) is 31 kJ·mol^{-1} more stable than the *cis* isomer **4b** ($\Delta G°_{298}$ =38 kJ·mol^{-1}); the transition state for this isomerization (**TS4**; see Figure 2) is 238 kJ·mol^{-1} higher in energy than the *trans* isomer ($\Delta G^{\#}_{298}$ = 252 kJ·mol^{-1}).

The geometry of *trans*-Me_2SH_4 (**3a**) is highly symmetrical (C_{2h}) and all bond angles at the sulfur atom are either 90° or 180°. The atomic charges of this molecule are as follows: S +0.90, C −0.69, H1−H4 −0.14, methyl-H +0.17. Although the electronegativities of sulfur and carbon are usually believed to be more or less identical,[19] and that of

 © 2003 Wiley-VCH Verlag GmbH & Co. KGaA, Weinheim

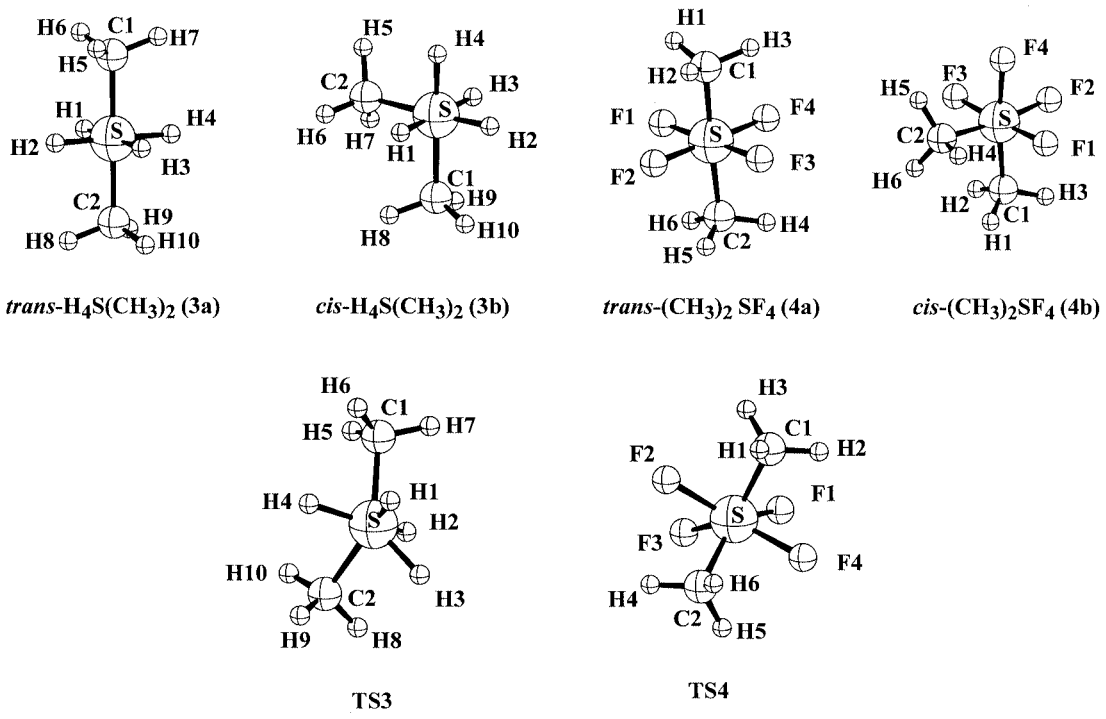

Figure 2. Molecular structures and bond lengths (pm) of the two persulfuranes Me_2SH_4 (**3a**, **3b**) and Me_2SF_4 (**4a**, **4b**), as well as of the transition states for the *cis* ⇌ *trans* isomerizations **3a** → **3b** (**TS3**) and **4a** → **4b** (**TS4**); Me: CH_3

Table 2. Internuclear distances (pm) of two isomers each of Me_2SH_4 and Me_2SF_4, as well as of the transition states for the *cis* ⇌ *trans* interconversion of these isomers, **TS3** and **TS4**

Bond	Me_2SH_4 (**3a**)	Me_2SH_4 (**3b**)	Me_2SF_4 (**4a**)	Me_2SF_4 (**4b**)	TS3	TS4
C−S:	185.9	187.5	180.7	181.1	187.8	181.1
S−H:	142.0	140.5/142.0	–	–	144.2/148.0	–
S−F:	–	–	165.9/166.2	164.8/165.1	–	168.3/177.1

Table 3. Selected valence angles (degree) of two isomers each of the sulfuranes Me_2SH_4 and Me_2SF_4 as well as of the transition states **TS3** and **TS4** for the *cis* ⇌ *trans* isomerization

Angle	Me_2SH_4 (**3a**)	Me_2SH_4 (**3b**)	Me_2SF_4 (**4a**)	Me_2SF_4 (**4b**)	TS3	TS4
C−S−C:	180.0	91.7	176.6	97.3	133.3	130.6
H(F)1−S−H(F)3:	180.0	178.8	180.0	175.4	83.2	77.8
H(F)2−S−H(F)4:	180.0	87.9	178.0	84.7	137.0	141.2
H(F)1−S−H(F)4:	90.0	89.8	89.0	87.8	79.7	79.8
H(F)1−S−H(F)2:	90.0	89.3	89.0	88.8	136.7	133.9

hydrogen considerably smaller, our calculated NBO charges show a different picture: The carbon atoms of **3a** are negative, sulfur and the methyl H atoms are positive and the four hydrogen atoms linked directly to the central atom are negatively charged. It has been noted before[19] that the electronegativity of hydrogen is not a constant value and, in general, most electronegativity data are derived from non-hypervalent molecules and may not apply to atoms in species of the type investigated in this work.

The geometry of *trans*-Me_2SF_4 (**4a**) is much less symmetrical (C_{2v}) than that of **3a** although the bond angles at the sulfur atom deviate from the ideal values of 90° and 180° by only 1.0−3.4° (Table 2). The atomic charges of **4a** are as follows: S +2.48, C −0.80, F −0.61, H +0.26. Surprisingly, both the sulfur atom in **4a** is more negative than in H_2SF_4 (**2a**: +2.12) and the two carbon atoms are more negative than in **3a** (−0.69), although one would expect the opposite from the well-known inductive effects of the four fluorine atoms and two methyl groups, respectively. Evidently, the electron-donating properties of methyl groups known from organic chemistry are not active in hypervalent sulfur compounds.

The methyl groups of **3a** and **4a** can be rotated separately about the C−S axis without much change in energy. Scans

 © 2003 Wiley-VCH Verlag GmbH & Co. KGaA, Weinheim

over 75° in steps of 5° with optimization of all other parameters resulted in absolute energies which differed by less than 0.02 kJ·mol^{-1}.

We now turn to the structures of the less stable isomers. The geometry of *cis*-Me_2SH_4 (**3b**) is of C_2 symmetry with a C−S−C bond angle of 91.7°. As far as possible, the methyl groups are staggered with respect to the hydrogen atoms of the SH_4 group. Thus, the pairwise equivalent torsion angles H8−C1−S−H1/H7−C2−S−H3 are 48.9°, H5−C2−S−H4/H10−C1−S−H2 are +19° and H9−C1−S−H3/H6−C2−S−H1 are −11°. The torsion angles H8−C1−S−C4/H7−C2−S−C1 are −43°. The geometry of *cis*-Me_2SF_4 (**4b**) is also of C_2 symmetry but the orientation of the methyl groups is different since there are evidently attractive non-bonding H···F interactions as a result of the opposite charges on these atoms (H atoms: +0.19−0.22; F atoms: −0.55±0.01). For example, the two pairs of symmetry-related distances H2···F3 and H4···F1 (235 pm) as well as H3···F2 and H5···F4 (233 pm) are shorter than the van der Waals distance of 260 pm between hydrogen and fluorine atoms. The corresponding torsion angles H2−C1−S−F3 and H4−C2−S−F1 are −1° and the C−S−C angle of **4b** is 97.3°.

The transition states **TS3** and **TS4** are of C_1 symmetry but both geometries are very close to C_2 symmetry, the small deviation from the higher symmetry being caused by the methyl groups. The C−S−C angles are 133.3° in **TS3** and 130.6° in **TS4**. The NBO charges of the sulfur atoms are +0.91 in **TS3** and +2.23 in **TS4**. As a result of these differing charges, the C−S bond lengths are considerably longer in **TS3** (187.8 pm) than in **TS4** (181.4 pm), a situation very similar to the one in the stable isomers **3a,b** and **4a,b**.

Summary

We have shown that the most stable structures of several persulfuranes of the type X_2SY_4 (X = H, Me, F; Y = H, F) are in agreement with the predictions made by the VSEPR model. All molecules are approximately octahedral, and the relative stability of the *cis* and *trans* isomers depends on the substituents. An unusual charge distribution has been discovered in these molecules by an NBO analysis. Starting from the most stable of the two isomers, the intramolecular *cis* ⇌ *trans* isomerization is possible only if an activation barrier of $\Delta H^{\#}_{298} \geq 200$ kJ·mol^{-1} can be overcome. Therefore, it should be possible to prepare both isomers separately. The geometries of the transition state structures are all very similar and correspond approximately to a distorted trigonal prism with the sulfur atom at the center.

Acknowledgments

This work was supported by the Deutsche Forschungsgemeinschaft and the Verband der Chemischen Industrie.

[1] Y. Steudel, R. Steudel, *Eur. J. Inorg. Chem.* **2003**, 2149.
[2] *Ullmann's Encyclopedia of Industrial Chemistry, Vol. A11*, VCH, Weinheim, **1988**, p. 337.
[3] A. E. Reed, F. Weinhold, *J. Am. Chem. Soc.* **1986**, *108*, 3586. A. E. Reed, P. von R. Schleyer, *J. Am. Chem. Soc.* **1990**, *112*, 1434. D. L. Cooper, T. P. Cunningham, J. Gerratt, P. B. Karadakov, M. Raimondi, *J. Am. Chem. Soc.* **1994**, *116*, 4414. R. Ponec, X. Gironés, *J. Phys. Chem. A* **2002**, *106*, 9506.
[4] R. D. Verma, R. L. Kirchmeier, J. M. Shreeve, *Adv. Inorg. Chem.* **1994**, *41*, 125.
[5] D. Lentz, K. Seppelt, in: *Chemistry of Hypervalent Compounds* (Ed.: K. Akiba), VCH-Wiley, New York, **1999**, p. 295.
[6] D. Christen, H. G. Mack, H. Oberhammer, *J. Chem. Phys.* **1987**, *87*, 2001.
[7] K. O. Christe, D. A. Dixon, W. W. Wilson, *J. Am. Chem. Soc.* **1994**, *116*, 7123.
[8] E. A. Innes, I. G. Csizmadia, Y. Kanada, *J. Mol. Struct. (Theochem)* **1989**, *186*, 1.
[9] M. J. Frisch, G. W. Trucks, H. B. Schlegel, G. E. Scuseria, M. A. Robb, J. R. Cheeseman, V. G. Zakrzewski, J. A. Montgomery, R. E. Stratmann, J. C. Burant, S. Dapprich, J. M. Millam, A. D. Daniels, K. N. Kudin, M. C. Strain, O. Farkas, J. Tomasi, V. Barone, M. Cossi, R. Cammi, B. Mennucci, C. Pomelli, C. Adamo, S. Clifford, J. Ochterski, G. A. Petersson, P. Y. Ayala, Q. Cui, K. Morokuma, D. K. Malick, A. D. Rabuck, K. Raghavachari, J. B. Foresman, J. Cioslowski, J. V. Ortiz, B. B. Stefanov, G. Liu, A. Liashenko, P. Piskorz, I. Komaromi, R. Gomperts, R. L. Martin, D. J. Fox, T. Keith, M. A. Al-Laham, C. Y. Peng, A. Nanayakkara, C. Gonzalez, M. Challacombe, P. M. W. Gill, B. G. Johnson, W. Chen, M. W. Wong, J. L. Andres, M. Head-Gordon, E. S. Replogle, J. A. Pople, *Gaussian 98, Revision A.6*, Gaussian, Inc., Pittsburgh PA, **1998**.
[10] L. A. Curtiss, P. C. Redfern, K. Raghavachari, V. Rassolov, J. A. Pople, *J. Chem. Phys.* **1999**, *110*, 4703.
[11] Y.-S. Cheung, Y.-J. Chen, C. Y. Ng, S.-W. Chiu, W.-K. Li, *J. Am. Chem. Soc.* **1995**, *117*, 9725, and references cited therein.
[12] A. E. Reed, L. A. Curtiss, F. Weinhold, *Chem. Rev.* **1988**, *88*, 899.
[13] M. Messerschmidt, A. Wagner, M. W. Wong, P. Luger, *J. Am. Chem. Soc.* **2002**, *124*, 732.
[14] K. Fukui, *Acc. Chem. Res.* **1981**, *14*, 363. C. Gonzales, H. B. Schlegel, *J. Phys. Chem.* **1989**, *90*, 2154.
[15] A. A. Ischenko, J. D. Ewbank, L. Schäfer, *J. Phys. Chem.* **1994**, *98*, 4287.
[16] A. N. Taha, N. S. True, C. B. LeMaster, C. L. LeMaster, S. M. Neugebauer-Crawford, *J. Phys. Chem. A* **2000**, *104*, 3341.
[17] R. S. Michalak, S. R. Wilson, J. C. Martin, *J. Am. Chem. Soc.* **1982**, *104*, 1683.
[18] R. J. Gillespie, I. Hargittai, *The VSEPR Model of Molecular Geometry*, Allyn and Bacon, Boston, **1991**.
[19] N. Matsunaga, D. W. Rogers, A. A. Zavitsas, *J. Org. Chem.* **2003**, *68*, 3158.

Received April 25, 2003

 © 2003 Wiley-VCH Verlag GmbH & Co. KGaA, Weinheim

Density Functional Study of the Complexation Reaction of $Sn(CH_3)_3X$ (X = F, Cl, Br and I) with Halide Anions

Frank De Proft,[a] Ricardo Vivas-Reyes,[a] Monique Biesemans,[b] Rudolph Willem,[b] Jan M. L. Martin,[c] and Paul Geerlings*[a]

Keywords: Tin / Halides / HSAB / Density functional calculations / NMR spectroscopy

The Lewis acid-base reaction between $Sn(CH_3)_3X$ and Y^- (with X, Y = F, Cl, Br and I) has been studied using quantum chemical calculations. Complexation energies were calculated at the Density Functional Theory (DFT) level and rationalized on the basis of a local application of the hard and soft acids and bases principle. It was observed that smaller differences in the local softness of the interacting sites in the Lewis acid and base correspond to stronger interactions. Moreover, the calculated sequences in complexation energies can be reproduced using equations containing chemical concepts introduced within the framework of conceptual density functional theory and rooted in the hard and soft acids and bases principle and referring only to the reactants. A method of treating the electronegativity and softness of the halide anions is presented based on a Taylor expansion of the electronegativity of the neutral halogens and the softness-polarizability proportionality. Experimental evidence for the calculated sequences was gathered from measured ^{117}Sn chemical shifts and ^1J (^{13}C-$^{119/117}Sn$) coupling constant changes upon complexation.
(© Wiley-VCH Verlag GmbH & Co. KGaA, 69451 Weinheim, Germany, 2003)

Introduction

It is well-known that four-coordinate Sn^{IV} compounds bearing electronegative groups react with nucleophiles to form pentacoordinate stannate complexes through expansion of the coordination sphere.[1] An example is the following Lewis acid-base reaction

$$Sn(CH_3)_3X + Y^- \rightarrow Sn(CH_3)_3XY^- \quad (a)$$

where both X and Y are halogens. A detailed and systematic theoretical and experimental analysis of this reaction has not yet been provided. Tudela and co-workers[2] performed experimental and theoretical studies on tri- and tetrahalodiorganostannate salts and studied, inter alia, their complexation reactions. In their studies, they considered the following reactions:

$$SnR_2X_2 + X^- \rightarrow SnR_2X_3^- \quad (b)$$

$$SnR_2X_3^- + X^- \rightarrow SnR_2X_4^{2-} \quad (c)$$

with R being an alkyl group (more specifically Me or Et) and X being F, Cl, Br or I. They concluded,[2] from computations at the Hartree−Fock level, that the formation of the pentacoordinate anions is an exothermic process, while the formation of the octahedral compounds is endothermic, these compounds thus being unstable in the gas phase. They also confirmed that the exothermicity of reaction (b) increased with the electronegativity of the halogen X.

In the present combined theoretical and experimental study, DFT calculations have been performed for the energetics of reaction (a), in order to gain insight into the nature of the tin atom in these interactions. As such, the resultant sequences were assessed on the basis of predictions resulting from the application of the hard and soft acids and bases principle,[3] using reactivity descriptors defined within the framework of conceptual density functional theory.[4] These descriptors, such as the chemical potential,[5] the electronegativity,[5,6] chemical hardness and softness,[7,8] Fukui functions,[9] local softness[8,10] and hardness[11] have been used quite exhaustively among others and by our group for the study of general Lewis acid-base reactions and have proven to be valuable in the interpretation of observed differences in reactivity.[4f,12]

High level ab-initio computational studies on tin compounds are still relatively scarce[13] as are the interpretations of observations in tin chemistry using the above mentioned reactivity indices.[14−16] Recently, our group has contributed significantly to this area, computing ^{119}Sn chemical shifts using Gauge-Including Atomic Orbitals and interpreting them via group electronegativities and hardness,[14] studying

[a] Eenheid Algemene Chemie (ALGC), Vrije Universiteit Brussel (VUB), Faculteit Wetenschappen,
Pleinlaan 2, 1050 Brussels, Belgium
[b] High resolution NMR centre, Vrije Universiteit Brussel,
Pleinlaan 2, 1050 Brussels, Belgium
[c] Department of Organic Chemistry, Weizmann Institute of Science,
Kimmelman Building, Room 262, 76100 Rehovot, Israel

the interaction of the tin nanocluster $[(RSn)_{12}O_{14}(OH)_6]^{2+}$ with negatively charged and neutral nucleophiles[15] and investigating the simultaneous complexation of a Sn containing crown ether compound with positive and negative ions.[16]

Experimentally, it is well-known that ^{117}Sn NMR spectroscopic data are useful for assessing the complexation of R_3SnX compounds with nucleophiles and halide anions, since this gives rise to low frequency changes in the $^{119(117)}$Sn chemical shifts as well as increasing the magnitude of the $^1J(^{13}C\text{-}^{119/117}Sn)$ coupling constants reflecting increases in the percentage of s character of the hybridized atomic orbitals of the tin upon change from four- to five-coordination.[17,18] For the sake of comparison of the calculations and in the context of our long standing interest in NMR studies on Sn compounds,[19] experimental ^{117}Sn chemical shifts δ as well as $^1J(^{13}C\text{-}^{117}Sn)$ coupling constants are provided for equilibrium mixtures of reaction (1) for X = Cl, Br and Y = F, Cl, Br and I. To the best of our knowledge, such a systematic and internally consistent NMR study of these systems has not yet been published.

The combined theoretical and experimental data provide insight into the Lewis acidity of tin compounds, place the tin element in the context matter of hard or soft character and provide, via a number of reactivity descriptors, the rationalization of its behavior in reaction (a).

Theory, Computational and Experimental Details

All molecular systems were optimized at the B3LYP level[20] using the cc-pVTZ basis set for C and H,[21] the aug-cc-pVTZ basis set for F, Cl and Br,[22] the SDB-cc-pVTZ for Sn and the aug-SDB-cc-pVTZ for I[23] using Gaussian 98.[24]

On the carbon and hydrogen atoms, the standard Dunning cc-pVTZ (correlation consistent polarized valence triple zeta[21]) basis set was used, while on the F, Cl, and Br halides, the diffuse-function augmented version of the same basis sets (aug-cc-pVTZ[22]) was employed. For the heavier tin and iodine atoms, we employed regular and diffuse-function augmented versions, respectively, of the SDB-cc-pVTZ basis set,[23] which is a valence basis set of cc-pVTZ quality optimized for use with a large-core (46-electron) Stuttgart−Dresden relativistic effective core potential.[25]

Since the 4d orbitals of free tin are energetically quite close to the valence s orbitals of the halides (particularly the 2s of fluorine), it could not be taken for granted that the large −core RECPs would be sufficient. In order to ascertain that this was indeed the case, we repeated our calculations for $Sn(CH_3)_3F$ and $Sn(CH_3)\ F^-$ with a small-core (28-electron) ECP on tin.[26] The accompanying basis set was developed for the purpose of this work as follows: (a) a 28s23p17d well-tempered basis set[27] was placed on Sn, the inner 28 electrons replaced by the RECP, and an SCF calculation carried out; (b) all primitives contributing less than 0.0001 to any atomic orbital were deleted, leaving an 18s15p11d basis set; (c) this "pruned' basis set was contracted based on the SCF orbitals; (d) the 2nd through 5th outermost s and p primitives were expanded, as were the four othermost d primitives; (e) additional d and f functions were optimized at the CISD level, correlating valence electrons only; (f) in order to accommodate angular correlation from the (4d) orbital, additional (2f1 g) functions were optimized for the difference between the valence+(4d) and valence CISD correlation energies. The use of this small core basis set yielded, for these two systems, only minor differences in geometry and complexation energy. When the small core ECP on Sn was used, the Sn−F distance in the $Sn(CH_3)_3F_2^-$ complex was 2.103 Å. Upon using the large core ECP this distance changes by less than 1 mÅ. The complexation energies using the large and small core Sn ECP amount to −52.1 and −50.7 kcal/mol respectively. As a result, the large core ECP on Sn was used throughout this study.

Anions of the type $Sn(CH_3)_3X_2^-$ show a trigonal-bipyramidal geometry with the methyl groups (average distance Sn−C = 2.17 Å) in the equatorial position. The average Sn−X bond lengths decrease in the order Sn−I (2.98 Å) > Sn−Br (2.77 Å) > Sn−Cl (2.61 Å) > Sn−F (2.09 Å). The Cartesian coordinates of all geometries are available in the supplementary material. All structures were confirmed to be minima by vibrational frequency calculations. DFT complexation energies, enthalpies and free energies were computed on this basis. In view of the extent of the basis set used and the conceptual difficulties arising from the use of effective core potentials, no correction for the basis set superposition error has been included.

In order to judge the effect of the solvent, the free energies of solvation of the Lewis acid-base complexes were estimated using the PCM model.[28]

As stated in the introduction, in addition to the generally accepted computational advantages of density functional theory, it has also been a source for the introduction of chemical concepts readily known by chemists but in most cases defined only on an empirical basis. Also several principles, such as Sanderson's principle of electronegativity equalization and Pearson's hard and soft acids and bases and maximum hardness principles have received theoretical justification. The complexation energy sequences of reaction (a) were rationalized using a local version of the hard and soft acids and bases principle. This principle, introduced by Pearson in the 1960s, states that hard acids prefer to bond to hard bases and soft acids to soft bases.[3] This principle and related chemical concepts have received theoretical justification within the framework of conceptual density functional theory. It can be adopted locally as follows: consider the interaction between a site k in a Lewis acid and a site l in the Lewis base. Application of the local HSAB principle would imply that the interaction between these sites will be favorable when the difference in their local softness is small, as was shown by Gazquez et al.[29] and elaborated among others by our group.[12,30] The local softness[10] can be obtained as described in Equation (1)

$$s(\mathbf{r}) = Sf(\mathbf{r}) \quad (1)$$

 © 2003 Wiley-VCH Verlag GmbH & Co. KGaA, Weinheim

where S is the global softness of the system[8] and $f(\boldsymbol{r})$ the so-called Fukui function,[9] a frontier MO reactivity index defined as the derivative of the electron density of the system with respect to the number of electrons at a constant external (i.e. due to the nuclei) potential:

$$f(\boldsymbol{r}) = \left(\frac{\partial \rho(\boldsymbol{r})}{\partial N}\right)_v \tag{2}$$

Due to the discontinuity of $\rho(\boldsymbol{r})$ with respect to N, left and right derivatives have to be associated with Equation (2):

$$f^-(\boldsymbol{r}) = \left(\frac{\partial \rho(\boldsymbol{r})}{\partial N}\right)^-_v \tag{3}$$

$$f^+(\boldsymbol{r}) = \left(\frac{\partial \rho(\boldsymbol{r})}{\partial N}\right)^+_v \tag{4}$$

corresponding to the cases of electrophilic and nucleophilic attacks, respectively. In the present contribution, the so-called condensed Fukui functions[31] were calculated as described in Equation (5) and (6), where $N_k(N + 1)$, $N_k(N)$ and $N_k(N - 1)$ are the number of electrons on atom k in the $N + 1$, N and N - 1 electron system.

$$f_k^-(\boldsymbol{r}) \approx N_k(N) - N_k(N-1) \tag{5}$$

$$f_k^+(\boldsymbol{r}) \approx N_k(N+1) - N_k(N) \tag{6}$$

The condensed local softnesses are then obtained by multiplying the appropriate Fukui function with the global softnesses, approximated as described in Equation (7), where IE and EA are the vertical ionization energies and electron affinities respectively.

$$S \approx \frac{1}{IE - EA} \tag{7}$$

In a final stage, the complexation energy was calculated using Equation (8) derived within the framework of the hard and soft acids and bases principle,[29] which was already applied successfully in the past.[32] This equation results from a decomposition of the interaction energy of two systems A and B into two terms: the first term, ΔE_v, representing the energy change at constant external potential and corresponding to the charge transfer process between A and B at constant external potential, and the second term, an energy change, equivalent to a reshuffling of the charge distribution at constant chemical potential ΔE_μ, :

$$(\Delta E_{int})_{AB} = -\frac{1}{2}\left(\frac{(\mu_A - \mu_B)^2}{S_A + S_B}\right)(S_A S_B) - \frac{1}{2}\left(\frac{\lambda}{S_A + S_B}\right) \tag{8}$$

In this expression μ is the chemical potential of A and B.

The chemical potential μ has been calculated using Equation (9).

$$\mu = \left(\frac{\partial E}{\partial N}\right)_v \approx \frac{IE + EA}{2} \tag{9}$$

The parameter λ has been shown to be proportional to an effective number of valence electrons involved in the interaction between A and B. Pal and co-workers have recently defined the parameter λ as the change in the electronic densities of the system before and after the interaction process.[32c,32d,32e] In this work however, the choice was made to set this parameter equal to 0.5, in accordance with previous studies by Gazquez and Mendez[29a] and our group.[32b] This methodology avoids the evaluation of λ using information about the electronic structure of the product and thus enhances the predictive ability of the method.

If the interaction on A is localized on an atomic site k, Equation (8) changes to Equation (10), where $f_{A,k}$ is the Fukui function value of the site k of system A.

$$(\Delta E_{int})_{Ak,B} = -\frac{1}{2}\left(\frac{(\mu_A - \mu_B)^2}{S_A f_{A,k} + S_B}\right)(S_A f_{A,k} S_B) - \frac{1}{2}\left(\frac{\lambda}{S_A f_{A,k} + S_B}\right) \tag{10}$$

In the evaluation of the condensed Fukui functions and local softnesses, NPA charges[33] were used showing less basis set dependence than the Mulliken[34] type charges[35] and avoiding certain difficulties associated with electrostatic potential based charges[36] for atoms buried withing the molecule.[37]

The trend in DFT complexation energies was compared with experimental data. It is well-known that the ^{119}Sn or ^{117}Sn resonance shifts to lower frequency when the tin nucleus extends its coordination.[17] Typically a difference of 150−200 ppm is noticed when going from coordination 4 to 5.[17] At the same time the $^1J(^{13}C\text{-}^{119/117}Sn)$ coupling constant increases by 100−150 Hz.[17,18] Both parameters are useful for detecting complexation in the reaction of $Sn(CH_3)_3X$ with halide anions. Thus standard 1D ^1H-decoupled ^{117}Sn spectra were recorded with a Bruker Avance 250 spectrometer. Solutions of $Sn(CH_3)_3Cl$ and $Sn(CH_3)_3Br$ in $CDCl_3$ were mixed with equimolar amounts of $(CH_3CH_2CH_2CH_2)_4NY$ (Y = F, Cl, Br, I). For two of the salts (Y = Br and I) more aliquots were added in order to perform a titration experiment from which the association constant K_{ass} for the complex formation could be determined by fitting the experimental chemical shift to Equation (18) (vide infra) using a two parameter ($K_{ass}^{-1} = K_{diss}$, δ_{bound}) non-linear regression as implemented with SigmaPlot 2000 software (Jandel Scientific).

Results and Discussion

The DFT reaction energies, enthalpies and free energies of reaction (1) for X or Y = F, Cl, Br and I can be found

 © 2003 Wiley-VCH Verlag GmbH & Co. KGaA, Weinheim

Table 1. Hybrid HF-DFT complexation energies ΔE, enthalpies ΔH (298.18 K) and free energies ΔG (298.15 K) for the reaction $Sn(CH_3)_3X + Y^- \rightarrow Sn(CH_3)_3XY^-$ with X, Y = F, Cl, Br and I. Also listed are the PCM free energies of solvation ΔG_s of the Lewis acid-base complexes $Sn(CH_3)_3XY^-$. All values are in kcal/mol

(X, Y)	ΔE	ΔH	ΔG	ΔG_s
(F,F)	−52.1	−52.3	−45.8	−35.0
(F,Cl)	−25.6	−25.6	−17.3	−31.8
(F,Br)	−20.6	−20.5	−12.9	−31.2
(F,I)	−15.6	−15.4	−7.6	−30.5
(Cl,F)	−57.5	−57.3	−49.0	−31.8
(Cl,Cl)	−28.9	−30.4	−19.3	−28.4
(Cl,Br)	−23.2	−23.0	−16.7	−27.9
(Cl,I)	−17.4	−17.7	−9.5	−26.3
(Br,F)	−59.8	−59.4	−51.7	−31.2
(Br,Cl)	−30.5	−30.2	−23.8	−27.9
(Br,Br)	−24.5	−25.3	−17.0	−27.4
(Br,I)	−18.3	−19.1	−10.2	−26.0
(I,F)	−62.6	−62.1	−53.9	−30.5
(I,Cl)	−32.5	−32.7	−24.2	−26.3
(I,Br)	−26.2	−27.0	−17.8	−26.0
(I,I)	−19.5	−19.7	−12.3	−24.9

in Table 1. Also given in this table are the free energies of solvation of the acid-base complexes estimated using the PCM model. As can be seen, the values of ΔE, ΔH and ΔG are all negative, implying that the formation of the products from the starting compounds is an energetically favourable process which is also exergonic in all cases. Moreover, one can make the following general conclusions: for a given halogen X in the Lewis acid, the complexation energies become less negative when going from F^- to I^-. For a given Lewis base Y^-, the complexation energies become more negative going from $Sn(CH_3)_3F$ to $Sn(CH_3)_3I$. As such, the complexation energy of $Sn(CH_3)_3I$ with F^- is the most negative. This indicates that the Sn atom in these Lewis acids preferably interacts with the hardest anion (F^-) in the series of nucleophiles and that a complexation with the softest anion (I^-) is always the least favourable. From the application of the HSAB principle, it can be concluded that the Sn atom is essentially hard in these compounds, in line with our previous work on the $[(RSn)_{12}O_{14}(OH)_6]^{2+}$ nanocluster and the Sn containing crown ether compounds.[15,16] The free energies of solvation become more negative with decreasing size of the Lewis acid-base complex, in line with a simple Born-type[38] model. The ΔG_s values follow the same trends as the ΔG values so that, although there is a very large contribution of ΔG_s to the energy of association in solution, the trends are almost identical as in the gas phase (vide infra).

In order to gain more insight into the trends of the gas-phase complexation energies, they were interpreted within the framework of the HSAB principle, using the method of "softness matching", introduced and applied in many of our previous papers.[30] As the interaction occurs between the electrophilic Sn atom in the trimethyltinhalides and the nucleophilic halide ion, the most favorable interaction should take place when the difference of the local softnesses on both of these atoms is the smallest.

The difficulty lies however in the determination of the softness, both global and local, of the halide anions. It has been suggested repeatedly[39] that in order to estimate the relative ordering of the hardness of anions, the hardness of the corresponding uncharged radicals can be used, that is, the hardnesses of F^-, Cl^-, Br^- and I^- should have the same ordering as those of F, Cl, Br and I. However, now absolute hardness values are needed, since these can now be compared with those of the Lewis acids for which the usual approach can be adopted. Furthermore, the values of the electronegativities of the halide anions are also unknown. However, they can in principle be estimated from a Taylor series expansion of the electronegativity with respect to the charge q on the atom.[4a] Indeed :

$$\chi(q) \approx \chi^0 + 2\eta^0 q \tag{11}$$

where χ^0 and η^0 are the electronegativity and hardness of the corresponding uncharged system. Since for an anion $q = -1$, this equation can be rewritten as shown in Equation (12), indicating that the electronegativity of the anion $[\chi(-1)]$ is the difference of the electronegativity χ^0 and twice the hardness η^0 of the corresponding neutral atom..

$$\chi(-1) \approx \chi^0 - 2\eta^0 \tag{12}$$

Table 2. Polarizabilities of Y [α (Y)] and Y^- [α (Y^-)] (au), together with their hardnesses η (Y) and η (Y^-) (eV). Also given are the condensed local softnesses s_{Y^-} of the bases Y^- (The condensed Fukui functions are all equal to 1) and the electronegativities of Y χ(Y) (eV)

Atom (Y)	α (Y)	α (Y^-)	η (Y)	η (Y^-)	s_{Y^-}	χ(Y)
F	3.57	8.85	7.11	2.86	4.75	10.64
Cl	14.82	28.78	4.70	2.42	5.62	8.38
Br	21.43	41.97	4.20	2.14	6.35	7.75
I	32.81	56.68	3.65	2.11	6.44	6.94

These values can also be found in Table 2. As can be seen, this leads in most cases to very small and even negative estimates of the electronegativity of the anion. As a result, the electronegativities of these anions were set equal to zero in this work.

The next problem consists of estimating the absolute hardness of the anions. In order to deal with this problem, the following approach was adopted. It has been proposed several times[40] that the global softness is proportional to the polarizability of the system. We then assumed that the ratio of the global softness values of the neutral halogen atom and the halide anion is equal to the ratio of their polarizabilities as described in Equation (13) so that an estimate of the global softness of Y^- can be obtained as demonstrated in Equation (14).

$$\frac{S_{Y^-}}{S_Y} \approx \frac{\alpha_{Y^-}}{\alpha_Y} \tag{13}$$

 © 2003 Wiley-VCH Verlag GmbH & Co. KGaA, Weinheim

$$S_{Y^-} \approx \frac{\alpha_{Y^-}}{\alpha_Y} S_Y \tag{14}$$

The hardness of the halide ions Y^- (= $1/(2S_{Y^-})$) obtained in this way which are, to the best of our knowledge, the first absolute, theoretically evaluated, numerical gas phase values, are given in Table 2, together with the polarizability and the hardness of the corresponding neutral halogens and the polarizabilities of the halide anions. As can be seen by comparison with the global hardness values of the Lewis acids $Sn(CH_3)_3X$ given in Table 3, these anions are all softer than the Lewis acids. Moreover, as stated many times in the literature,[39] the hardness sequence is $\eta(F^-) > \eta(Cl^-) > \eta(Br^-) > \eta(I^-)$.

Table 3. Chemical potential μ (eV), hardness η (eV) and polarizabilities α (au) of the Lewis acids considered in this work. Also given are the condensed Fukui functions, local softness and charges on the Sn atom, all in au

Lewis acid	μ	η	α	f^+_{Sn}	s^+_{Sn}	q_{Sn}
$Sn(CH_3)_3F$	−4.30	5.71	74.3	0.24	0.57	2.19
$Sn(CH_3)_3Cl$	−4.23	5.47	90.5	0.25	0.61	1.91
$Sn(CH_3)_3Br$	−4.22	5.24	99.7	0.29	0.75	1.82
$Sn(CH_3)_3I$	−4.13	4.93	114.9	0.36	1.00	1.71

The condensed local softnesses for the Lewis acids and bases are given in Table 2 and 3. As can be seen with the use of Figure 1, the principle of softness matching (i.e. looking for the smallest softness difference between the acceptor atom in the Lewis acid and the donor atom in the Lewis base) perfectly explains the two above mentioned sequences for the complexation energies. From Figure 1, it can be seen that all the Lewis acids are harder than the Lewis bases and since F^- is the hardest Lewis base, the smallest local softness difference always occurs with F^-. Furthermore, since the softness of the Sn atom in $Sn(CH_3)_3I$ is the highest, the complexation energies of this compound with the halide ions are more negative than for the other $Sn(CH_3)_3X$ compounds. In the next step, the complexation energies were correlated with the absolute value of the softness difference between the Sn atom and the Lewis base as shown in Equation (15).

$$\Delta s = \left| s^+_{Sn} - s^-_{Y^-} \right| \tag{15}$$

From the HSAB principle, it can be inferred that the smaller the value of this difference, the more negative the complexation energy should be. This can indeed be deduced from Figure 2, where the correlation is shown ($r^2 = 0.91$).

In a final step, the complexation energies, as determined from Equation (10) were correlated with the DFT values from Table 1. This correlation ($r^2 = 0.94$) is depicted in Figure 3. As stated in Section 2, the parameter λ, which is proportional to the effective number of valence electrons part-

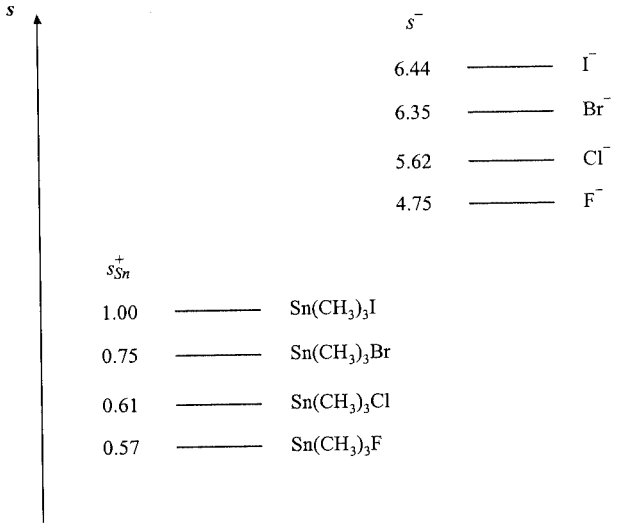

Figure 1. Relative ordering of the local softness of the Sn atom in the $Sn(CH_3)_3X$ compounds and the halide anions. All values are in au

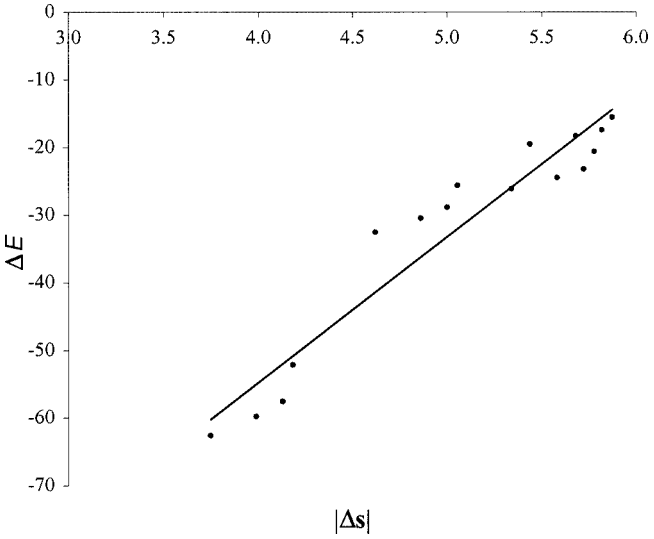

Figure 2. Correlation of the softness difference (au), defined in Equation (15) with the ab-initio complexation energies (kcal/mol)

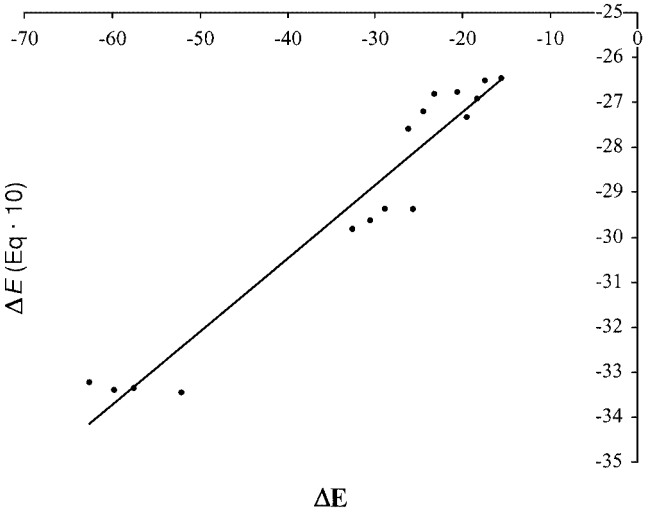

Figure 3. Correlation of the complexation energies (kcal/mol), as calculated from Equation (10) with the ab-initio complexation energies (kcal/mol).

 © 2003 Wiley-VCH Verlag GmbH & Co. KGaA, Weinheim

icipating in the interaction, was arbitrarily set to 0.5. With this value, the second term in Equation (10) is dominant and accounts for 77 (X,Y = I) to 88% (X,Y = F) of the total interaction energy. Moreover, the correlation coefficient r^2 does not drop below 0.9 when λ is varied between 0.3 and 1.0. This is again a fine example of the usefulness of the concepts introduced within the framework of conceptual DFT. The correct trends in complexation energies can be recovered from equations involving properties only associated with the reagents.

The Lewis acidities of the tin compounds have also been analyzed by considering the charge of the tin atoms in the different compounds, given in Table 3. Assuming that a more positive tin reflects a higher Lewis acidity, the charge sequence shown in Table 3 should also reflect the acidity sequence.

$Sn(CH_3)_3F > Sn(CH_3)_3Cl \approx Sn(CH_3)_3Br \approx Sn(CH_3)_3I$

This trend is however the reverse of that seen in the computed complexation energies. Moreover, it can be deduced from Table 3 that electronegativity differences apparently do not strongly affect the charge on the tin atom. This leads to the conclusion that the interaction of the tin halides with halide ions is essentially orbitally controlled and not charge controlled. Indeed, when using the concept of softness matching, one considers the reaction to be orbitally controlled, whereas in the case of hard-hard interactions, charge control is implied. It has been argued recently by Chattaraj[41] that the maximum Fukui function (or local softness) site is the best for the frontier-controlled soft-soft reactions whereas for the charge-controlled hard-hard interactions the preferred site is associated with the maximum net charge and not necessarily the minimum Fukui function.

Our results for the relative Lewis acidities of $Sn(CH_3)_3F$, $Sn(CH_3)_3Cl$, $Sn(CH_3)_3Br$ and $Sn(CH_3)_3I$ are in line with the findings of Frenking et al.[42] They have shown that for the Lewis acids BX_3 (with X = F, Cl, Br and I), the hydride affinity increases from BF_3 to BI_3, although the p(π) population is higher in BI_3 than in BF_3. Moreover, they demonstrated that the electronic structure of the Lewis acid alone is not sufficient to determine the affinity toward a nucleophile.

^{117}Sn chemical shifts and $^1J(^{13}C\text{-}^{117}Sn)$ coupling constants for $Sn(CH_3)_3Cl$ and $Sn(CH_3)_3Br$ mixed with an equimolar amount of $(CH_3CH_2CH_2CH_2)_4N^+X^-$ are summarized in Table 4. As the anion exchange is fast on the ^{117}Sn NMR timescale the experimental chemical shifts and $^1J(^{13}C\text{-}^{117}Sn)$ coupling constants are weighted averages of free and complexed species and as such reflect the amount of complexation or, indirectly, the association constant of the formed complex. The NMR measurements show, for a given halogen X, a difference in chemical shift and $^1J(^{13}C\text{-}^{117}Sn)$ coupling constant between the uncomplexed and complexed species that decreases along the series F > Cl > Br > I in accordance with the calculated complexation energies. Since however the difference in chemical shift is not only dependent on the strength of the formed complex but also influenced by the nature of the complexing halide,

Table 4. ^{117}Sn chemical shifts and $^1J(^{13}C\text{-}^{117}Sn)$ coupling constants for compounds $(CH_3)_3SnCl$ and $(CH_3)_3SnBr$ in $CDCl_3$ before and after addition of an equimolar amount of $(CH_3CH_2CH_2CH_2)_4NX$; Δδ refers to the difference in chemical shift between the complexed and uncomplexed species

X	$Sn(CH_3)_3Cl$ δ (ppm)	Δδ	$^1J(^{13}C\text{-}^{117}Sn)$ (Hz)	$Sn(CH_3)_3Br$ δ (ppm)	Δδ	$^1J(^{13}C\text{-}^{117}Sn)$ (Hz)
–	170.7	–	360	137.1	–	345
F	−41.4	212.1	530	−34.1	171.2	515
Cl	−24.0	194.7	496	−8.2	145.3	474
Br	−12.1	182.8	480	7.7	129.4	454
I	47.5	123.2	430	22.1	115.0	437

a more elaborate ^{117}Sn NMR titration experiment was performed for two of the salts, in order to determine the association constants in an independent way.[43] The dependence of the ^{117}Sn chemical shift on the concentration of complexed species is given by the Equation (16), where $\delta_{obsd.}$ is the ^{117}Sn chemical shift of the fast exchanging triorganotin compound observed for a given analytical concentration $[Y^-]_0$, whereas δ_{bound} and δ_{free} are the ^{117}Sn chemical shifts of the complexed and free R_3SnX respectively.

$$(\delta_{obs} - \delta_{free}) = \frac{[R_3SnXY^-]_e}{[R_3SnX]_0}(\delta_{bound} - \delta_{free}) \quad (16)$$

The actual equilibrium concentration of the adduct $[R_3SnXY^-]_e$ in solution obeys Equation (17) with $C = [R_3SnX]_0 + [Y^-]_0$, where, in both equations, $[R_3SnX]_0$ represents the analytical concentration of the trimethyltin halide under consideration.

$$[R_3SnXY^-]_e = \frac{1}{2}\left\{\left(C + K_{ass}^{-1}\right) - \sqrt{\left(C + K_{ass}^{-1}\right)^2 - 4[R_3SnX]_0[Y^-]_0}\right\} \quad (17)$$

Substituting Equation (17) into Equation (16) and solving $\delta_{obsd.}$ gives Equation (18)

$$\delta_{obs} = \delta_{free} + \frac{(\delta_{bound} - \delta_{free})\left\{\left(C + K_{ass}^{-1}\right) - \sqrt{\left(C + K_{ass}^{-1}\right)^2 - 4[R_3SnX]_0[Y^-]_0}\right\}}{2[R_3SnX]_0} \quad (18)$$

By fitting $\delta_{obsd.}$ to Equation (18) using a non-linear regression the parameters $K_{ass}^{-1} = K_{diss}$ and δ_{bound} were obtained. These data are summarized in Table 5. From this

Table 5. Dissociation constants of the complexes $(CH_3)_3SnClY^-$ and $(CH_3)_3SnBrY^-$ in $CDCl_3$ solution, obtained by fitting ^{117}Sn chemical shifts to Equation (18)

X	$Sn(CH_3)_3Cl$	$Sn(CH_3)_3Br$
I^-	$(8 \pm 2) \times 10^{-2}$	$(9 \pm 2) \times 10^{-2}$
Br^-	$(1.3 \pm 0.4) \times 10^{-2}$	$(3.1 \pm 0.1) \times 10^{-2}$

 © 2003 Wiley-VCH Verlag GmbH & Co. KGaA, Weinheim

table it is again clear that Br^- forms more stable complexes than I^- for a given $(CH_3)_3SnX$ in accordance with our earlier statement and the calculated complexation energies. Comparison of the dissociation constants of $(CH_3)_3SnCl$ for both complexing anions with those of $(CH_3)_3SnBr$ indicate that the first one has slightly higher association constants than the latter one, whereas the calculations predict the reverse order. However for both the calculated complexation energies and the experimentally obtained association constants the differences between the two are rather small. From the experimentally determined association constants, it can indeed be deduced that the difference in complexation free energy between $(CH_3)_3SnCl$ and $(CH_3)_3SnBr$ amounts to 0.51 and 0.07 kcal/mol upon complexation with Br^- or I^- respectively, which is well below what is considered to be chemically accurate in quantum chemical computations. Moreover, the computed free energy differences for these compounds are also below 1 kcal/mol. The addition of the free energies of solvation of the Lewis acid-base complexes, computed using the PCM model, to the gas phase free energies of complexation in the case of the reaction of $Sn(CH_3)_3Cl$ and $Sn(CH_3)_3Br$ with Br^- reverses the gas phase trend in agreement with the solution phase dissociation constants. In the case of the complexation of $Sn(CH_3)_3Cl$ and $Sn(CH_3)_3Br$ with I^- however, the reversal is not achieved. The difference between the gas phase and solution phase free energies however being reduced to around 0.4 kcal/mol.

The $^1J(^{13}C\text{-}^{117}Sn)$ coupling constants in Table 4, being weighted averages of those in the free and complexed species, reflect the geometry of the formed complexes. These data indeed depend on the percentage of s character in the Sn−C bond and thus the trigonal bipyramidal character of the resultant compound. Inspection of the data indicate that the highest values are found after complexation with F^-, followed by Cl^-, Br^- and finally I^-, again in accordance with the calculated complexation energies.

Conclusions

A combined theoretical and experimental NMR study of the complexation reaction between $Sn(CH_3)_3X$ and a halide ion Y^- (X, Y = F^-,Cl^-,Br^-, and I^-) has been carried out.

For a given Lewis acid, the ab-initio complexation energy becomes more negative upon going from F^- to I^-. For a given Lewis base, $Sn(CH_3)_3I$ is always found to give the most negative interaction energies. It was shown that complexation energies become more negative when the softness difference between the acceptor atom in the Lewis acid and the donor atom in the Lewis base becomes smaller, in agreement with the hard and soft acids and bases principle. Moreover, a quantitative agreement of the DFT complexation energies and an expression, derived within the framework of conceptual density functional theory, has been put forward. In this way, high level ab-initio computed complexation energies of medium sized tin compounds, combined with the first ab-initio evaluation of halide anion hardness, have provided insight into the ordering of the Lewis acidities of these compounds and in the interpretation of the strength of the Lewis acid-Lewis base interaction in terms of the HSAB principle in a parameter free context. Both experimentally measured ^{117}Sn chemical shifts and $^1J(^{13}C\text{-}^{119}Sn)$ coupling constants for the $Sn(CH_3)_3Cl$ and $Sn(CH_3)_3Br$ compounds confirm the computed complexation energy ordering $F^- > Cl^- > Br^- > I^-$. In addition, association constants of these two Lewis acids with Br^- and I^- have been calculated and lead to the same conclusion.

Acknowledgments

P. G. wishes to acknowledge the Free University of Brussels (VUB) and the Fund for Scientific Research Flanders (Belgium) (FWO) for continuous support to his group. R. W. and M. B. are indebted to the Fund for Scientific Research Flanders (Belgium) (FWO) for a research grant (G.0016.02). This work was partially supported by the Helen and Martin A. Kimmel Center for Molecular Design (JM). R. V. R wishes to thank the Colombian Institute for Science and Development, Colciencias, and the Universidad de Cartagena (Cartagena, Colombia) for a PhD fellowship.

[1] M. Suzuki, I. Son, R. Noyori, H. Masuda, *Organometallics* **1990**, *9*, 3043−3053.
[2] D. Tudela, M. Diaz, D. A. Alvaro, J. Ignacio, L. Seijo, V. K. Belsky, *Organometallics* **2001**, *20*, 654−662.
[3] [3a] R. G. Pearson, *J. Am. Chem. Soc.* **1963**, *85*, 3533−3539. [3b] R. G. Pearson, *Chemical Hardness*, John Wiley & Sons, **1997**.
[4] [4a] R. G. Parr, W. Yang, *Density Functional Theory of Atoms and Molecules*, Oxford University Press, New York, **1989**. [4b]R. G. Parr, W. Yang, *Ann. Rev. Phys. Chem.* **1995**, *46*, 701−728. [4c] W. Kohn, A. D. Becke, R. G. Parr, *J. Phys. Chem.* **1996**, *100*, 12974−12980. [4d] H. Chermette, *J. Comp. Chem.* **1999**, *20*, 129−154. [4e] P. Geerlings, F. De Proft, W. Langenaeker, *Adv. Quant. Chem.* **1999**, *33*, 303−328. [4f] P. Geerlings, F. De Proft, W. Langenaeker, *Chem. Rev.* **2003**, *105*, 1793−1873.
[5] R. G. Parr, R. A. Donnelly, M. Levy, W. E. Palke, *J. Chem. Phys.* **1978**, *68*, 3801−3807.
[6] For a detailed account on the different electronegativity scales introduced, see, for example J. Mullay in *Electronegativity, Structure and Bonding*, Vol. 66 (Eds.: K. D. Sen, C. K. Jørgenson), Springer-Verlag, Berlin, Heidelberg, **1987**, pp. 1−25.
[7] R. G. Parr, R. G. Pearson, *J. Am. Chem. Soc.* **1983**, *105*, 7512−7516.
[8] W. Yang, R. G. Parr, *Proc. Natl. Acad. Sci.* **1985**, *82*, 6723−6726.
[9] R. G. Parr, W. Yang, *J. Am. Chem. Soc.* **1984**, *106*, 4049−4050.
[10] C. Lee, W. Yang, R. G. Parr, *J. Mol. Struct. (Theochem)* **1988**, *163*, 305−313.
[11] [11a] M. Berkowitz, S. K. Ghosh, R. G. Parr, *J. Am. Chem. Soc.* **1985**, *107*, 6811−6814. [11b] M. K. Harbola, P. K. Chattaraj, R. G. Parr, *Isr. J. Chem.* **1991**, *31*, 395−402. [11c] W. Langenaeker, F. De Proft, P. Geerlings, *J. Phys. Chem.* **1995**, *99*, 6424−6431. [11d] F. De Proft, S. Liu, R. G. Parr, *J. Chem. Phys.* **1997**, *107*, 3000−3006.
[12] P. Geerlings, F. De Proft, *Int. J. Quant. Chem.* **2000**, *80*, 227−235.
[13] [13a] A. Marquez, G. G. Gonzalez, F. Fernandez-Sanz, *Chem. Phys.* **1989**, *138*, 99−104. [13b] M. A. Buntine, V. J. Hall, F. J. Kosovel, E. R. T. Tiekink, *J. Phys. Chem. A* **1998**, *102*, 2472−2482. [13c] J. Leszczynki, I. J. Yanov, *J. Phys. Chem. A.* **1999**, *103*, 396−401. [13d] G. Barone, M. C. Ramusino, R. Barbieri, G. Lamanna, *J. Mol. Struct. (Theochem).* **1999**, *469*, 143−149. [13e] M. Yasuda, K. Chiba, A. Baba, *J. Am. Chem. Soc.* **2000**, *122*, 7549−7555. [13f] D. Duca, G. Barone, G. La

 © 2003 Wiley-VCH Verlag GmbH & Co. KGaA, Weinheim

Manna, T. Fiore, C. Pellerito, R. Di Stefano, M. Scopello, L. Pellerito, *Appl. Organomet. Chem.* **2001**, *15*, 581−592.
[14] R. Vivas- Reyes, F. De Proft, M. Biesemans, R. Willem, P. Geerlings, *J. Phys. Chem. A* **2002**, *106*, 2753−2759.
[15] R. Vivas- Reyes, F. De Proft, M. Biesemans, R. Willem, F. Ribot, C. Sanchez, P. Geerlings, *New J. Chem.* **2002**, *26*, 1108−1117.
[16] R. Vivas- Reyes, F. De Proft, M. Biesemans, R. Willem, P. Geerlings, *Eur. J. Inorg. Chem.* **2003**, 1315−1324.
[17] [17a] B. Wrackmeyer, *Ann. Rep. NMR Spectrosc.* **1985**, *16*, 73−186. [17b] B. Wrackmeyer, *Ann. Rep. NMR Spectrosc.* **1999**, *38*, 203−264.
[18] B. Wrackmeyer in *Advanced Applications of NMR to Organometallic Chemistry*, (Eds.: M. Gielen, R. Willem, B. Wrackmeyer), John Wiley & Sons, Chichester, **1996**, pp. 87−122.
[19] J. C. Martins, M. Biesemans, R. Willem, *Progress in NMR Spectroscopy* **2000**, *36*, 271−322.
[20] [20a] A. D. Becke, *J. Chem. Phys.* **1993**, *98*, 5648−5652. [20b] C. Lee, W. Yang, R. G. Parr, *Phys. Rev. B* **1988**, *37*, 785−789.
[21] Hydrogen and 1st row: T. H. Dunning, *J. Chem. Phys.* **1989**, *90*, 1007−1023; 2nd row: D. E. Woon, T. H. Dunning, *J. Chem. Phys.* **1993**, *98*, 1358−1371; 3rd row: A. K. Wilson, D. E. Woon, K. A. Peterson, T. H. Dunning, *J. Chem. Phys.* **1999**, *110*, 7667−7676.
[22] Hydrogen and 1st-row: R. A. Kendall, T. H. Dunning, R. J. Harrison, *J. Chem. Phys.* **1992**, *96*, 6796−6806; 2nd row: D. E. Woon, T. H. Dunning, *J. Chem. Phys.* **1993**, *98*, 1358−1371; 3rd row: A. K. Wilson, D. E. Woon, K. A. Peterson, T. H. Dunning, *J. Chem. Phys.* **1999**, *110*, 7667−7676.
[23] J. M. L. Martin, A. Sunderman, *J. Chem. Phys.* **2001**, *114*, 3408−3420.
[24] M. J. Frisch, G. W. Trucks, H. B. Schlegel, G. E. Scuseria, M. A. Robb, J. R. Cheeseman, V. G. Zakrzewski, J. A. Montgomery, Jr., R. E. Stratmann, J. C. Burant, S. Dapprich, J. M. Millam, A. D. Daniels, K. N. Kudin, M. C. Strain, O. Farkas, J. Tomasi, V. Barone, M. Cossi, R. Cammi, B. Mennucci, C. Pomelli, C. Adamo, S. Clifford, J. Ochterski, G. A. Petersson, P. Y. Ayala, Q. Cui, K. Morokuma, D. K. Malick, A. D. Rabuck, K. Raghavachari, J. B. Foresman, J. Cioslowski, J. V. Ortiz, A. G. Baboul, B. B. Stefanov, G. Liu, A. Liashenko, P. Piskorz, I. Komaromi, R. Gomperts, R. L. Martin, D. J. Fox, T. Keith, M. A. Al-Laham, C. Y. Peng, A. Nanayakkara, M. Challacombe, P. M. W. Gill, B. Johnson, W. Chen, M. W. Wong, J. L. Andres, C. Gonzalez, M. Head-Gordon, E. S. Replogle, J. A. Pople, Gaussian 98, *Revision A.9*, Gaussian, Inc., Pittsburgh PA, **1998**.
[25] A. Bergner, M. Dolg, W. Kuechle, H. Stoll, H. Preuss, *Mol. Phys.* **1993**, *80*, 1431−1441.
[26] B. Metz, H. Stoll, M. Dolg, *J. Chem. Phys.* **2000**, *113*, 2563−2569.
[27] S. Huzinaga, M. Klobukowski, *Chem. Phys. Lett.* **1993**, *212*, 260−264.
[28] [28a] S. Miertus, E. Scrocco, J. Tomasi, *Chem. Phys.* **1981**, *55*, 117−129. [28b] R. Cammi, J. Tomasi, *J. Chem. Phys.* **1994**, *100*, 7495−7502. [28c] J. Tomasi, M. Perisco, *Chem. Rev.* **1994**, *94*, 2027−2094. [28d] V. Barone, M. Cossi, J. Tomasi, *J. Chem. Phys.* **1997**, *107*, 3210−3221.
[29] [29a] J. L. Gazquez, F. Méndez, *J. Am. Chem.* **1994**, *116*, 9298−9301. [29b] J. L. Gazquez, F. Méndez, *J. Phys. Chem.* **1994**, *98*, 4591−4593. [29c] J. L. Gazquez, in *Chemical Hardness*, Structure and Bonding, Vol. 80 (Ed.: K. D. Sen), Springer-Verlag, Berlin, Heidelberg, **1993**; pp. 27−43. [29d]R. G. Parr, J. L. Gazquez, *J. Phys. Chem.* **1993**, *97*, 3939−3940.
[30] [30a] S. Damoun, G. Van de Woude, F. Méndez, P. Geerlings, *J. Phys. Chem.* **1997**, *101*, 886−893. [30b] L. T. Nguyen, T. N. Le, F. De Proft, A. K. Chandra, W. Langenaeker, M. T. Nguyen, P. Geerlings, *J. Am. Chem. Soc.* **1999**, *121*, 5992−6001. [30c] T. N. Le, L. T. Nguyen, A. K. Chandra, F. De Proft, P. Geerlings, M. T. Nguyen, *J. Chem. Soc., Perkin Trans. 2* **1999**, 1249−1255.
[31] W. Yang, W. J. Mortier, *J. Am. Chem. Soc.* **1986**, *108*, 5708−5711.
[32] [32a] F. Méndez, J. Tamariz, P. Geerlings, *J. Phys. Chem.* A **1998**, *102*, 6292−6296. [32b]S. Damoun, G. Van de Woude, K. Choho, P. Geerlings, *J. Phys. Chem. A* **1999**, *103*, 7861−7866. [32c] S. Pal, K. R. S. Chandrakumar, *J. Am. Chem. Soc.* **2000**, *122*, 4145−4153. [32d] K. R. S. Chandrakumar, S. Pal, *J. Phys. Chem. B* **2001**, *105*, 4541−4544. [32e] K. R. S. Chandrakumar, S. Pal, *Int. J. Mol. Sci.* **2002**, *3*, 324−337.
[33] A. E. Reed, R. B. Weinstock, F. Weinhold, *J. Chem. Phys.* **1985**, *83*, 735−746.
[34] R. S. Mulliken, *J. Chem. Phys.* **1955**, *23*, 1833, 1841, 2338, 2343.
[35] [35a] S. M. Bachrach in *Reviews in Computational Chemistry*, Vol. 5 (Eds.: K. B. Lipkowitz, D. B. Boyd), VCH Publishers, New York, **1994**, pp. 171−227. [35b]F. De Proft, J. M. L. Martin, P. Geerlings, *Chem. Phys. Lett.* **1996**, *250*, 393−401.
[36] [36a] L. E. Chirlian, M. M. Francl, *J. Comput. Chem.* **1987**, *8*, 894−905. [36b] C. M. Breneman, K. B. Wiberg, *J. Comput. Chem.* **1990**, *11*, 361−373. [36c] B. H. Besler, K. M. Merz, P. A. Kollman, *J. Comput. Chem.* **1990**, *11*, 431−439.
[37] P. Bultinck, W. Langenaeker, P. Lahorte, F. De Proft, P. Geerlings, C. Van Alsenoy C, J. P. Tollenaere, *J. Phys. Chem. A* **2002**, *106*, 7895−7901.
[38] M. Born, H. S. Green, *Proc. Roy. Soc., (London)* **1946**, *A188*, 10−18.
[39] [39a] R. G. Pearson in *Theoretical Models of Chemical Bonding, Part 2: The Concept of the Chemical Bond* (Ed.: Z. B. Maksic), Springer-Verlag, Berlin, Heidelberg, **1990**, pp. 45−76. [39b]R. G. Pearson, *J. Org. Chem.* **1989**, *54*, 1423−1430. [39c] D. Datta, S. N. Singh, *J. Chem. Soc., Dalton Trans.* **1991**, 1541−1549.
[40] [40a] P. Politzer, *J. Chem. Phys.* **1987**, *86*, 1072−1073. [40b] A. Vela, J. L. Gazquez, *J. Am. Chem. Soc.* **1990**, *112*, 1490−1492.
[41] P. K. Chattaraj, *J. Phys. Chem. A* **2001**, *105*, 511−513.
[42] G. Frenking, S. Fau, C. M. Marchand, H. Gruetzmacher, *J. Am. Chem. Soc.* **1997**, *119*, 6648−6655.
[43] [43a] K. A. Connors in *Binding Constants, the Measurement of Molecular Complex Stability*, John Wiley & Sons, Chichester, **1987**, pp. 189. [43b]J. K. Tsagatakis, N. A. Chaniotakis, K. Jurkschat, S. Damoun, P. Geerlings, A. Bouhdid, M. Gielen, I. Verbruggen, M. Biesemans, J. C. Martins, R. Willem, *Helv. Chim. Acta* **1999**, *82*, 531−542.

Received January 17, 2003

 © 2003 Wiley-VCH Verlag GmbH & Co. KGaA, Weinheim

Stable Platinum(0) Catalysts for Catalytic Hydrosilylation of Styrene and Synthesis of [Pt(Ar-bian)(η^2-alkene)] Complexes

Jeroen W. Sprengers,[a] Michiel de Greef,[a] Marcel A. Duin,[a] and Cornelis J. Elsevier*[a]

Keywords: Platinum / Hydrosilylations / N ligands / Homogeneous catalysis / Alkene ligands

The use of alkenes and bidentate N-ligands in the platinum(0)-catalyzed hydrosilylation of styrene with triethylsilane has been evaluated. A number of bidentate N-ligands, phen, bpy, dafo, and phenyl-bian, were tested at various reaction temperatures using in situ formed catalysts with [Pt(nbe)$_3$] as a precursor. The main conclusions are: (i) ligands, such as phen, which form stable platinum(0) complexes, give lower catalytic activities compared to the ligands which form less stable complexes; (ii) a small ligand effect is observed with dafo and phenyl-bian compared to [Pt(nbe)$_3$], the precursor complex, displaying the lability of these ligands. The complex [Pt(nbe)$_3$], that only has labile alkene ligands, is an active catalyst at low temperatures. At higher temperatures, the catalyst is no longer stable and a decrease in yield is observed. Several novel complexes have been synthesized: [Pt(*m*,*m*-(CF$_3$)$_2$-C$_6$H$_3$-bian)(tcne)], [Pt(*m*,*m*-(CF$_3$)$_2$-C$_6$H$_3$-bian)(ma)], [Pt(*p*-MeO-C$_6$H$_4$-bian)(ma)], [Pt(*p*-MeO-C$_6$H$_4$-bian)(dmfu)] and [Pt(phenyl-bian)(dmfu)]. Whereas the two [Pt(Ar-bian)(ma)] complexes are intrinsically more active than the two [Pt(Ar-bian)(dmfu)] complexes, the latter are much more stable, i.e. the nature of the alkene in these complexes is an important factor in determining their catalytic behavior. Compared to [Pt(Me-nq)(nbe)$_2$], the two [Pt(Ar-bian)(dmfu)] complexes are much more stable resulting in significantly higher overall yields.

(© Wiley-VCH Verlag GmbH & Co. KGaA, 69451 Weinheim, Germany, 2003)

1. Introduction

The catalytic hydrosilylation of unsaturated compounds, such as alkenes, alkynes, ketones, and imines, is one of the most elegant methods for the synthesis of organosilicon compounds [Equation (1)].[1] The use of organosilicon compounds as reagents and synthons for the construction of natural products has become a powerful tool in synthesis. In addition to its use in laboratory syntheses, the hydrosilylation reaction is used in many ways in the industrial manufacture of silicon polymers, for example for the curing and modification of polyorganosiloxanes and the modification of unsaturated polymers.

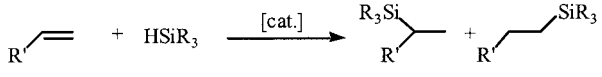

(1)

Since the first report on catalyzed hydrosilylation in 1947 by Sommer et al.,[2] many efforts have been made to develop optimized catalytic systems. By now, numerous transition metal based catalysts have been reported for hydrosilylation, including metals of groups 8, 9, and 10. Platinum catalysts, especially, are very active in the hydrosilylation of unsaturated carbon−carbon bonds. The Speier catalyst,[3] H_2PtCl_6 dissolved in 2-propanol, and the Karstedt catalyst,[4] H_2PtCl_6 dissolved in tetramethyldivinyldisiloxane [(CH$_2$=CHSiMe$_2$)$_2$O], are frequently used.

However, a problem associated with these platinum catalysts is their very limited stability when exposed to hydrosilylation conditions; rapid formation of platinum colloids, that are catalytically not active, takes place. The preparative scope of Speier's catalyst is further restricted by its long and variable induction period. The nature of the catalytically active species, homogeneous vs. heterogeneous, has been questioned in the literature for a long time.[5] Recently, it has become clear that the type of platinum compound that would generate the highest activity is one in which formation of a single platinum(0) atom and concomitant loss of ligands is facile.[5] It has been observed that the Karstedt catalyst contains preponderantly [Pt$_2$(CH$_2$=CHSiMe$_2$)$_2$O]$_3$, a platinum(0) complex containing one bridging tetramethyldivinyldisiloxane ligand.[6] A widely accepted mechanism for hydrosilylation of alkenes is the Chalk−Harrod mechanism which consists of oxidative addition of a hydrosilane, insertion of an alkene into the metal−hydride bond, and reductive coupling of the alkyl and silyl fragments.[7]

Osborn et al.[8] published a series of platinum(0) complexes with the general formula [Pt(η^2-alkene)(η^4-CH$_2$=CHSiMe$_2$)$_2$O]. When naphthoquinones were used as the co-

[a] Institute of Molecular Chemistry, Coordination and Organometallic Chemistry, Universiteit van Amsterdam, Nieuwe Achtergracht 166, 1018 WV Amsterdam, The Netherlands
Fax: (internat.) + 31-20/5256456
E-mail: elsevier@science.uva.nl

ordinating alkene, highly active catalysts were obtained. Markó et al.[9] used platinum(0) catalysts with N-heterocyclic carbenes as ligands. These catalysts were less active than the Karstedt catalyst, but side-reactions, such as isomerization and dehydrogenative silylation, were significantly suppressed. Also our group used some N-heterocyclic carbene ligands which yielded outstanding catalysts.[10]

Hydrosilylation of alkenes is often accompanied by side-reactions such as isomerization and dehydrogenative silylation. The latter can be of interest, because it produces vinylsilanes, which are very useful synthetic reagents in synthesis [Equation (2)].

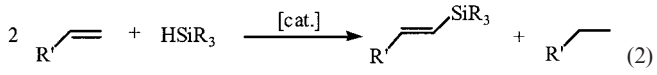

(2)

Of course, it would be desirable to have catalysts that are selective either to hydrosilylation or to dehydrogenative silylation. For instance, the catalysts $[Ru_3(CO)_{12}]$[11] and $[Fe_3(CO)_{12}]$[12] are known to be very selective towards dehydrogenative silylation of several alkenes, which is also true for rhodium(I)[13] and palladium(II) catalysts[14] when employing an excess of styrene relative to the hydrosilane or a more steric hydrosilane. Also platinum(0) catalysts can give rise to a certain extent of dehydrogenative silylation,[15,16] for which the Chalk−Harrod mechanism does not account. Therefore, other mechanisms have been proposed to explain this reaction. Characteristically, these mechanisms feature the formation of an olefin-hydride complex, arising from β-hydride elimination of a β-silylalkyl intermediate [Equation (3)]. Dissociation of the *trans*-vinylsilane yields a metal hydride complex, which is responsible for the hydrogenated product. This dissociation of the vinylsilane is favored by a high styrene concentration and by using more steric hydrosilanes.

As mentioned before, many of the known platinum(0) catalysts suffer from deactivation. For instance, Steffanut et al.[8] observed decomposition of [Pt(η^2-2-methylnaphthoquinone)(η^4-CH_2=$CHSiMe_2$)$_2$O] at temperatures higher than 20 °C. Moreover, alkene/hydrosilane ratios of two were used in their experiments, which contributes to a significantly higher catalyst stability. It would be desirable to use an alkene/hydrosilane ratio of one, but then more stable catalysts are definitely required. Thus, further manipulation of the coordination sphere of the metal center will be indispensable in order to obtain an active catalyst that is stable under the reaction conditions.

We have been interested in the use of bidentate N-ligands, especially bidentate N-ligands, for several catalytic and stoichiometric transition metal mediated carbon−element coupling reactions and for the stereoselective *cis*-hydrogenation of alkynes.[17−22] These ligands are known to stabilize platinum(0) compounds when coordinated in a bidentate manner,[23−24] yet readily give rise to free coordination sites due to their hemilability.[25−26]

An effective catalyst for hydrogenation or hydrosilylation requires a low coordination number and valence. Hence, hydrosilylation should proceed effectively for those late transition metal compounds that can readily vacate two or more coordination sites, in order to accommodate substrates, yet is able to stabilize the complex in its resting state by re-coordination of the hemilabile donor atom. In this respect, platinum based precatalysts combining a labile alkene with a hemilabile, bidentate N-ligand, specifically 1,10-phenanthroline (**1**) (phen), 2,2′-bipyridyl (**2**) (bpy), 4,5-diazafluoren-9-one (**3**) (dafo), and bis(arylimino)acenaphtene (**4**) (Ar-bian), seem to be very promising indeed for platinum(0)-catalyzed hydrosilylation.

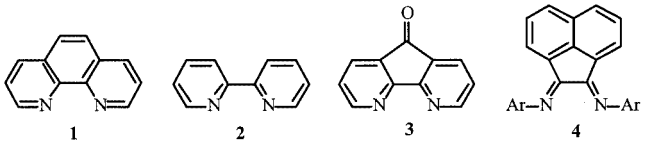

In this paper, the use of bidentate N-ligands, as ligands for Pt-catalyzed hydrosilylation of styrene with triethylsilane, is reported. The performance and stability of several in situ prepared systems, obtained from [Pt(2-norbornene)$_3$], [Pt(nbe)$_3$], with appropriate bidentate N-ligands, has been evaluated and compared with several novel [Pt(Ar-bian)(η^2-alkene)] complexes.

2. Results and Discussion

Bidentate N-Ligands as Ligands in the Hydrosilylation of Styrene by Triethylsilane

First, the platinum(0) complex [Pt(nbe)$_3$][27] was used as a precursor for the hydrosilylation of styrene with triethylsilane yielding products **I** and **II** (Scheme 1). The hydrosilylation of styrene is always accompanied by dehydrogenative silylation, yielding products **III** and **IV**. Throughout, ethylbenzene (**IV**) was always formed in the same amount as the unsaturated silyl product (**III**) by subsequent hydrogenation of styrene. Since the nbe ligands readily dissociate from platinum, active, coordinately unsaturated platinum(0) species are readily obtained.

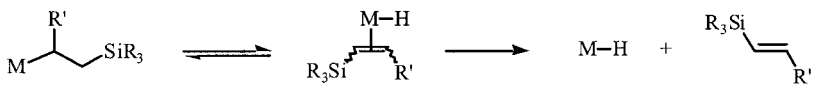

 © 2003 Wiley-VCH Verlag GmbH & Co. KGaA, Weinheim

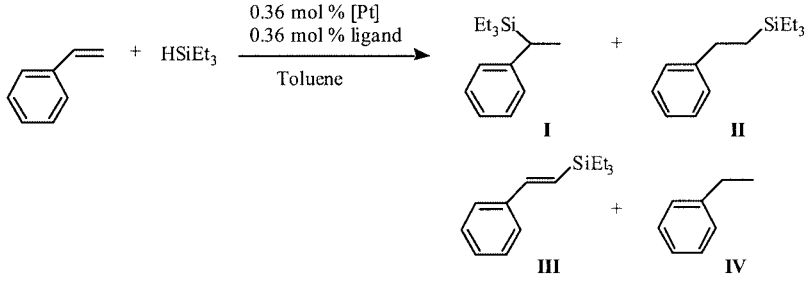

Scheme 1. Hydrosilylation and dehydrogenative silylation of styrene with triethylsilane

The bidentate N-ligands are expected to coordinate to platinum immediately upon their addition, prior to the start of catalysis. Thus influencing the activity and stability of the hydrosilylation reaction. Liedtke et al.[28] also used $[Pt(nbe)_3]$ as a precursor in their hydrosilylation reactions with certain phosphiranes as ligands. These experiments were performed at different temperatures and at a styrene/hydrosilane ratio of 2.8. For comparison, 2-methylnaphthoquinone (Me-nq), Osborn's ligand,[8] and bis(diphenylphosphanyl)ethane (dppe), a strongly coordinating ligand, which results in a platinum complex with low activity,[29] were also tested in this catalytic system. The results of these catalytic hydrosilylations have been collected in Table 1.

Table 1. Hydrosilylation of styrene with triethylsilane

Entry	Ligand[a]	Temp. [°C]	Yield [%][b]	Selectivity [%][c] **I/II/III**
1	–	30	91.9	2.0:67.0:31.0
		50	60.4	2.5:68.0:29.5
		100	19.7	2.7:67.6:29.7
2	Me-nq	30	92.5	2.0:66.9:31.1
		50	62.3	2.7:68.5:28.8
		100	20.7	3.0:66.0:31.0
3	phen	30	–	–
		50	–	–
		100	16.7	4.4:54.3:41.3
4	bpy	30	31.7	2.0:72.6:25.4
		50	81.7	2.6:63.9:33.5
		100	19.1	3.8:60.0:36.2
5	dafo	30	88.1	2.0:66.8:31.2
		50	69.6	2.6:65.2:32.2
		100	14.6	3.1:65.4:31.4
6	phenyl-bian	30	86.0	2.0:67.5:30.5
		50	66.0	2.6:67.8:29.6
		100	26.9	3.4:67.4:29.2
7	dppe	30	–	–
		50	–	–
		100	5.1	3.5:67.2:29.3

[a] 0.36 mol % of catalyst, styrene/triethylsilane ratio 2.8, toluene. [b] Combined GC yield, after 2 h, of products **I**, **II**, and **III** using *n*-decane as the internal standard. [c] Product **IV** was always observed in the same amount as product **III**, therefore the amount of **IV** has been omitted.

It is clear that the precursor complex $[Pt(nbe)_3]$ is an active catalyst at 30 °C, but that it progressively loses its activity at higher temperatures due to deactivation of the catalyst (Entry 1). Addition of 1 equiv. of Me-nq to $[Pt(nbe)_3]$ (Entry 2) gives results that are similar to those of $[Pt(nbe)_3]$: the same trend in deactivation at higher temperatures is observed and only a small increase in the yield of product **I** relative to the other products was observed. So, Me-nq is not able to act as a stabilizing ligand at higher temperatures.[8] Furthermore, the use of Me-nq does not lead to a higher yield at 30 °C compared to $[Pt(nbe)_3]$ itself, which generates highly active platinum species. This observation is in agreement with the common view that single unsaturated platinum(0) atoms are highly active hydrosilylation catalysts.[5,8]

A completely different catalytic behavior is observed when 1,10-phenanthroline (phen) is used as the ligand (Entry 3). In this case, hydrosilylation only takes place at a very slow rate at 100 °C. Apparently, phen forms a very stable platinum(0) complex. This idea is supported by the fact that no significant catalyst deactivation was observed, even when running this reaction at 100 °C for 24 h, which resulted in a total yield (**I** + **II** + **III**) of 81%. The relative amount of dehydrogenative silylation has increased using phen, which can be explained by invoking the strong bidentate coordination of phen to the Pt center, favoring the dissociation of the *trans*-vinylsilane.

When bpy is used in the hydrosilylation (Entry 4), the yield obtained increases when going from 30 to 50 °C due to the increased lability of bpy with temperature. The low yield observed at 100 °C is caused by the deactivation of the catalyst at this temperature. The selectivity (**I/II/III**) obtained with this ligand changes significantly with temperature and differs from the selectivity obtained in Entries 1 and 3. Furthermore, bpy shows an increased amount of dehydrogenative silylation compared to $[Pt(nbe)_3]$, but not to the same degree as phen. This can be understood from differences in the fluxional behavior of phen and bpy: by its rigidity, phen forms complexes more readily than bpy, but bpy is more flexible and can easily adapt to the η^1-coordinate structure.

The ligand dafo (Entry 5) shows a behavior completely different from phen and bpy. Only a very small decrease in yield and the same selectivity compared to $[Pt(nbe)_3]$ is observed. These results indicate that dafo coordinates relatively weakly, in a bidentate fashion, to the platinum(0) atom, which is most likely due to the larger bite angle of this ligand (about 82°) compared to phen and bpy (about 77°). Indeed, Klein et al.[26] have previously observed an enhanced aptitude for dissociation of one of the donor atoms of dafo in platinum(0) and palladium(0) complexes,

 © 2003 Wiley-VCH Verlag GmbH & Co. KGaA, Weinheim

due to the reduced overlap between relevant metal and ligand orbitals caused by the larger bite angle. Also dimeric palladium(II) complexes have already been synthesized with dafo as a bridging ligand.[30]

Although phenyl-bian (Entry 6) possesses a bite angle similar to phen and bpy (about 77°), the catalytic results obtained with this ligand differ completely from that of phen and bpy. In fact, almost the same yield and selectivity were obtained as observed for dafo. Similarly to dafo, phenyl-bian displays a significant lability. Although platinum(0) or palladium(0) complexes in which the Ar-bian ligands act as monodentate ligands are not known, several palladium(II) complexes containing monodentate Ar-bian ligands are known.[25,31] These studies have shown that rigid bidentate N-ligands are more prone to hemilabile behavior than the more flexible ones. Assuming partial dissociation of Ar-bian in such cases may explain the observed selectivity for phenyl-bian.

Results obtained for dppe (Entry 7) again demonstrate that this bidentate phosphane ligand forms a stable chelate with platinum(0), resulting in zero activity at 30 and 50 °C and only a very low activity at 100 °C. Triphenylphosphane was also tested once in the hydrosilylation at 30 °C. After 2 h, a total yield of only 8.5% was obtained with a selectivity of 3.0:73.0:24.0 (**I/II/III**).

As mentioned before, the selectivities of platinum catalysts depend strongly on the styrene/triethylsilane ratio. For example, applying a styrene/triethylsilane ratio of 0.5 using [Pt(nbe)$_3$] as the catalyst yielded a selectivity (**I/II/III**) of 2.0:90.0:8.0. However, when a styrene/triethylsilane ratio of 6.4 was used, an enormous increase in dehydrogenative silylation was observed: 37% of product **III** was obtained. This observation supports the idea[13,14] that the dissociation of the vinylsilane is favored by a higher styrene concentration [Equation (3)]. Comparing our selectivities obtained with already reported catalysts is not straightforward since the conditions applied can have a significant influence. For example, Skoda-Földes et al.[29] obtained 12.3% of **III** with $PtCl_2$ as a catalyst and using a styrene/triethylsilane ratio of 1.0 in the hydrosilylation of styrene with triethylsilane. Employing 2.8 equiv. of styrene, we obtained 31.0% of product **III** using [Pt(nbe)$_3$] as the catalyst. However, when using a styrene/triethylsilane ratio of 1.0 with this catalyst, product **III** was observed in only 11.0%, which is almost similar to the result obtained by Skoda-Földes et al. with $PtCl_2$. Also, Dötz et al.[15] and Caseri and Pregosin[16] obtained considerable amounts of product **III** in this reaction, using [Pt(η^2-2-methylnaphthoquinone)(η^4-CH_2=$CHSiMe_2$)$_2$O] and *trans*-[$PtCl_2$(PhCH=CH_2)$_2$] as the catalyst, respectively.

The activities of our catalysts are influenced by several reaction conditions; temperature was already discussed, but the styrene concentration also influences the reaction significantly. In general, a higher styrene concentration contributes to a higher stability of the catalyst. Consequently, when [Pt(nbe)$_3$] was used as a catalyst using a styrene/triethylsilane ratio of 1.0, a yield of only 32% was obtained after 2 h, which is rather low when compared to the 91.9% yield using a styrene/triethylsilane ratio of 2.8 (Table 1, Entry 1). However, when the reaction using a styrene/triethylsilane ratio of 1.0 was repeated, but now without 20 mL of toluene as the solvent, an increase in yield was also observed: from 32 to 88%. Caseri and Pregosin[16] reported that [Pt(styrene)$_3$] was more active than *trans*-[$PtCl_2$(PhCH=CH_2)$_2$] and that this complex did not show an induction period. From our results, we can say that [Pt(nbe)$_3$] also generates highly active platinum(0) species, probably similar to [Pt(styrene)$_3$][16] although we did not check if this complex is formed during catalysis.

The lability of the phenyl-bian ligand was studied in more detail by substituting the aryl groups of this ligand. Thus, ligands **4**−**9** were synthesized and tested in the catalytic hydrosilylation of styrene with triethylsilane at 30 °C. The results are collected in Table 2.

Table 2. Hydrosilylation of styrene with triethylsilane using Ar-bian ligands

Entry	Ligand[a]	Yield [%][b]	Selectivity [%][c] **I/II/III**
1	**4**	86.0	2.0:67.5:30.5
2	**5**	84.7	2.0:67.5:30.5
3	**6**	87.0	2.0:67.0:31.0
4	**7**	91.0	2.0:67.5:30.5
5	**8**	90.1	2.0:66.5:31.5
6	**9**	90.0	2.0:67.5:30.5

[a] 0.36 mol % of catalyst, styrene/triethylsilane ratio 2.8, toluene, 30 °C. [b] Combined GC yield, after 2 h, of products **I**, **II**, and **III** using *n*-decane as the internal standard. [c] Product **IV** was always observed in the same amount as product **III**, therefore the amount of **IV** has been omitted.

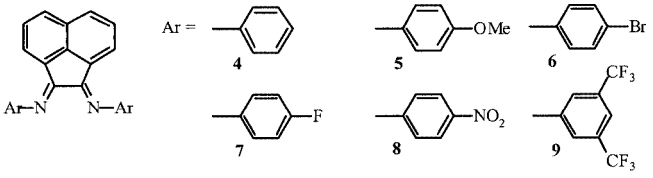

It is immediately evident from Table 2 that substitution of the Ar-bian ligands has no significant influence on the selectivity of the hydrosilylation. There seems to be a relation between the yield and the inductive effect of the *para* substituents on the aryl groups of the Ar-bian ligand, as increasing yields are observed with decreasing electron-donating ability. This can be explained by the fact that electron-donating substituents increase the basicity of the Ar-bian ligand, resulting in more stable platinum(0) complexes. As a consequence, the lowest yield is obtained for *p*-MeO-C_6H_4-bian (Entry 2), but the differences are small.

Synthesis of [Pt(Ar-bian)(η^2-alkene)] Complexes

When obtaining the catalysts in situ, there may be competition for the substrate, due to the relatively large amount (2−3 equiv.) of alkene liberated upon reaction of [Pt(nbe)$_3$] with the bidentate N-ligand (Scheme 2). On the other hand, the Ar-bian ligands are also labile. Therefore, we were inter-

 © 2003 Wiley-VCH Verlag GmbH & Co. KGaA, Weinheim

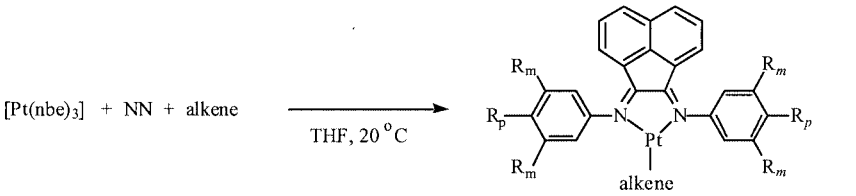

10; R_m = CF_3 ; R_p= H (*m*,*m*-$(CF_3)_2$-C_6H_3-bian)
11; R_m = H ; R_p= OMe (*p*-MeO-C_6H_4-bian)
12; R_m = H ; R_p= H (phenyl-bian)
alkene = ma (**a**), tcne (**b**), dmfu (**c**)

Scheme 2. Synthesis of [Pt(Ar-bian)(η^2-alkene)] complexes

ested in comparing our hitherto obtained results with experiments employing predefined [Pt(Ar-bian)(η^2-alkene)] complexes as catalyst precursors in the hydrosilylation of styrene with triethylsilane. The stability of these complexes will depend on the nature of the Ar-bian ligand as well as of the alkene. Electron-donating substituents on the Ar-bian ligand, concomitant with the use of electron-poor alkenes is expected to increase the stability of complexes of this type. Van Asselt et al.[24] already synthesized several [Pt(Ar-bian)(η^2-alkene)] complexes. By employing *p*-Me-C_6H_4-bian and *o*,*o*′-*i*Pr_2-bian with fumaronitrile (fn), maleic anhydride (ma), and tetracyanoethylene (tcne) as coordinating alkenes, stable complexes were obtained starting from [Pt$(dba)_2$]. However, complexes with the less electron-poor dimethyl fumarate (dmfu) could not be obtained by using this method, which includes heating in THF at 45 °C for 16 h. Since our aim was the synthesis of several new complexes with alkenes like dmfu, which at the same time have Ar-bian ligands containing electron-withdrawing substituents, such as *m*,*m*-$(CF_3)_2$-C_6H_3-bian, we selected [Pt$(nbe)_3$] instead of [Pt$(dba)_2$] as the precursor, allowing milder reaction conditions.[23,32,33] First, the synthesis of various platinum(0) complexes of type [Pt(*m*,*m*-$(CF_3)_2$-C_6H_3-bian)(η^2-alkene)] was addressed by treating [Pt$(nbe)_3$] with stoichiometric amounts of the ligands. Attempts to prepare [Pt(*m*,*m*-$(CF_3)_2$-C_6H_3-bian)(dmfu)] were not successful. Allowing equimolar amounts of [Pt$(nbe)_3$], *m*,*m*-$(CF_3)_2$-C_6H_3-bian, and dmfu to react in tetrahydrofuran at room temperature led to the formation of mixtures of starting materials and reaction products. Similar results were obtained when diethyl ether instead of tetrahydrofuran was used as a solvent. In both cases, purification of the reaction product was troublesome due to its complete solubility in most common organic solvents. ^{1}H NMR spectroscopy of the crude reaction product suggested that ligand substitution had not been complete: large amounts of uncomplexed *m*,*m*-$(CF_3)_2$-C_6H_3-bian were present. Using [Pt$(cod)_2$] as starting material, [Pt{*m*,*m*-$(CF_3)_2$-C_6H_3-bian}(dmfu)] could not be obtained either.

Initial attempts to prepare [Pt{*m*,*m*-$(CF_3)_2$-C_6H_3-bian}(ma)] by adding [Pt$(nbe)_3$] to a dilute solution of equimolar amounts of *m*,*m*-$(CF_3)_2$-C_6H_3-bian and maleic anhydride in tetrahydrofuran were in vain. Similar to the case of [Pt{*m*,*m*-$(CF_3)_2$-C_6H_3-bian}(dmfu)], purification of the reaction product was tedious and ^{1}H NMR spectroscopy suggested incomplete ligand substitution. Better results were obtained, when *m*,*m*-$(CF_3)_2$-C_6H_3-bian was added to an ice cold concentrated solution of ma and [Pt$(nbe)_3$]. After washing the crude reaction product with pentane, [Pt{*m*,*m*-$(CF_3)_2$-C_6H_3-bian}(ma)] readily precipitated from the combined organic extract and was obtained as a pure compound.

Similarly, the synthesis of [Pt{*m*,*m*-$(CF_3)_2$-C_6H_3-bian}(tcne)] was straightforward and proceeded as expected. In order to probe the influence of electronic effects on the synthesis of platinum(0) complexes of type [Pt{*m*,*m*-$(CF_3)_2$-C_6H_3-bian}(η^2-alkene)], it was attempted to use electron-rich instead of electron-deficient alkenes. Thus, synthesis of [Pt{*m*,*m*-$(CF_3)_2$-C_6H_3-bian}(trimethylvinylsilane)] was attempted by stirring equimolar amounts of [Pt$(nbe)_3$], *m*,*m*-$(CF_3)_2$-C_6H_3-bian, and trimethylvinylsilane in tetrahydrofuran. Although nearly all of the starting materials had reacted after 4 h of stirring at room temperature, at least six different reaction products were formed as was evident from TLC and no efforts were made to further purify the crude reaction product.

Next, in order to study the influence of electronic effects on the synthesis of platinum(0) complexes of type [Pt(Ar-bian)(η^2-alkene)] and also on their catalytic hydrosilylation behavior, the synthesis of various platinum(0) complexes of type [Pt(*p*-MeO-C_6H_4-bian)(η^2-alkene)] was addressed. As opposed to the synthesis of [Pt{*m*,*m*-$(CF_3)_2$-C_6H_3-bian}(dmfu)], the synthesis of [Pt(*p*-MeO-C_6H_4-bian)(dmfu)] was successful and yielded the desired reaction product in excellent yield. Likewise, the synthesis of [Pt(*p*-MeO-C_6H_4-bian)(ma)] was straightforward, but the synthesis of [Pt(*p*-MeO-C_6H_4-bian)(acrylonitrile)] was more troublesome. Although TLC revealed that all of the starting materials had reacted after 2 h of stirring at room temperature, it was not possible to unambiguously characterize the residue obtained after washing the crude reaction mixture with diethyl ether/pentane. Finally, the complex [Pt(phenyl-bian)(dmfu)] was also synthesized in good yield using the same procedure.

Synthesis of [Pt(dafo)(dmfu)], [Pt(dafo)(ma)], and [Pt(dafo)(tcne)] was also addressed, but these attempts were not successful. Adding dafo to a concentrated solution of [Pt$(nbe)_3$] and 1.20 equiv. of dmfu in tetrahydrofuran did not result in the formation of [Pt(dafo)(dmfu)] after overnight stirring at reflux. None of the starting dafo had re-

 © 2003 Wiley-VCH Verlag GmbH & Co. KGaA, Weinheim

acted, as was evident from ^{1}H NMR spectroscopy. Likewise, the synthesis of [Pt(dafo)(ma)] and [Pt(dafo)(tcne)] did not succeed. In the latter cases a slight amount of complexed dafo was observed by ^{1}H NMR spectroscopy, but the yields remained very low, in keeping with the weak ligating properties of dafo.

Hydrosilylation of Styrene by Triethylsilane Catalyzed by [Pt(Ar-bian)(η^2-alkene)] Complexes

In order to study the catalytic behavior of platinum(0) complexes of type [Pt(Ar-bian)(η^2-alkene)], [Pt{*m*,*m*-$(CF_3)_2$-C_6H_3-bian}(ma)], [Pt(*p*-MeO-C_6H_4-bian)(ma)], [Pt(*p*-MeO-C_6H_4-bian)(dmfu)], and [Pt(C_6H_5-bian)(dmfu)] were tested as catalysts in the hydrosilylation of styrene by triethylsilane, applying a styrene/triethylsilane ratio of only 1.0. The complex [Pt(Me-nq)$(nbe)_2$], an active hydrosilylation catalyst,[8] was also tested. The yields of the combined silyl products against time are shown in Figure 1.

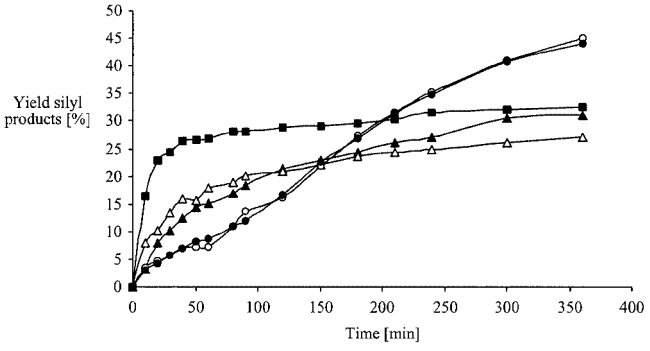

Figure 1. Hydrosilylation of styrene by triethylsilane catalyzed by [Pt(*m*,*m*-$(CF_3)_2$-C_6H_3-bian)(ma)] (open triangles), [Pt(*p*-MeO-C_6H_4-bian)(ma)] (filled triangles), [Pt(*p*-MeO-C_6H_4-bian)(dmfu)] (open circles), [Pt(C_6H_5-bian)(dmfu)] (filled circles), and [Pt(Me-nq)$(nbe)_2$] (filled squares); conditions: 0.36 mol % of catalyst, styrene/triethylsilane ratio 1.0, toluene, 30 °C; yield is the combined GC yield after 2 h of products **I**, **II**, and **III** using *n*-decane as the internal standard

From these results, it is obvious that the nature of the coordinated alkene determines the catalytic behavior of the complexes. [Pt(*p*-MeO-C_6H_4-bian)(dmfu)] and [Pt(C_6H_5-bian)(dmfu)] show an almost completely identical catalytic activity and stability. The complexes [Pt{*m*,*m*-$(CF_3)_2$-C_6H_3-bian}(ma)] and [Pt(*p*-MeO-C_6H_4-bian)(ma)] give different results compared to the two dmfu complexes: they show a higher initial activity, but decompose faster, resulting in a lower overall yield. From the synthetic experiments (see above), it is known that electron-donating substituents on the Ar-bian ligand increase the stability of the complex. However, for the two maleic anhydride complexes only a small difference in catalytic behavior is observed. In the beginning of the reaction, [Pt(*p*-MeO-C_6H_4-bian)(ma)] is slightly less active than [Pt{*m*,*m*-$(CF_3)_2$-C_6H_3-bian}(ma)], but is slightly more stable. [Pt(Me-nq)$(nbe)_2$] is a very active catalyst, but decomposition of the catalyst starts immediately after addition of triethylsilane. After 6 h, a yield of 32.5% was obtained with [Pt(Me-nq)$(nbe)_2$], which is almost similar to [Pt{*m*,*m*-$(CF_3)_2$-C_6H_3-bian}(ma)] (27.1%) and [Pt(*p*-MeO-C_6H_4-bian)(ma)] (31.1%). Although [Pt(*p*-MeO-C_6H_4-bian)(dmfu)] and [Pt(C_6H_5-bian)(dmfu)] are less active catalysts, there stability resulted in higher overall yields of 41.1% and 44.9%, respectively, after 6 h with the catalysts still being active after this time. After 24 h, a yield of 65% was obtained for [Pt(*p*-MeO-C_6H_4-bian)(dmfu)].

For all complexes, compound **II** was observed as the major product (85−87%) along with a minor amount of compound **I** (about 2%). The dehydrogenative silylation product **III** was observed in about 11−13% yield. The selectivities obtained with these catalysts were constant in time. The decreased amount of dehydrogenative silylation, compared to the reactions with in situ prepared catalysts, is caused by the lower styrene concentration compared to the other experiments, since a styrene/triethylsilane ratio of 1.0 instead of 2.8 was employed. As discussed before, the selectivities obtained are quite similar to those obtained using $PtCl_2$ as the catalyst.[29] $PtCl_2$, in fact every platinum(II) or platinum(IV) catalyst, is deemed to be reduced to a platinum(0) species. The reduction process, often of variable duration, causes the frequently observed induction periods for these catalysts.[3a] For example, using [$PtCl_2$(PhCH=$CH_2)_2$] as a catalyst, Caseri and Pregosin showed that the hydrosilylation of styrene proceeded by reduction of the Pt^{II} complex to [Pt(styrene)$_3$] with concomitant formation of 2 equiv. of R_3SiCl and 1 equiv. of ethylbenzene.[37] From Figure 1 it becomes quite obvious that our [Pt(Ar-bian)(η^2-alkene)] complexes do not suffer from an induction period; the hydrosilylation reactions start immediately after addition of the substrates. This behavior is in agreement with that observed for other platinum(0) catalysts.[8−10,16]

Since the palladium complexes [Pd(Ar-bian)(η^2-alkene)] are versatile catalysts for the selective hydrogenation of alkynes to (*Z*)-alkenes,[21] we also tested [Pd(*p*-MeO-C_6H_4-bian)(dmfu)] as a hydrosilylation catalyst and compared its catalytic behavior with its platinum analogue. However, it appears that this compound does not catalyze the hydrosilylation reaction at all: the complex immediately decomposed under hydrosilylation conditions in both THF and toluene at 30 °C.

Conclusion

In conclusion, several bidentate N-ligands have been evaluated in the hydrosilylation of styrene with triethylsilane at different temperatures, using in situ formed catalysts with [Pt(nbe)$_3$] as a precursor. In general, the ligands which form more stable platinum(0) complexes result in a lower catalytic activity and somewhat more dehydrogenative silylation compared to the ligands which form less stable complexes. Consequently, the precursor complex, [Pt(nbe)$_3$] itself, which has only labile alkene ligands, is an active catalyst at 30 °C and at a styrene to triethylsilane ratio of 2.8. At higher temperatures, the catalyst is no longer stable and

 © 2003 Wiley-VCH Verlag GmbH & Co. KGaA, Weinheim

a decrease in yield is observed when the temperature is increased. The complex [Pt(Me-nq)(nbe)$_2$], does not give significantly higher yields. Common bidentate ligands such as phen and dppe form stable complexes, resulting in no or very low hydrosilylation activity. However, for the ligands dafo and phenyl-bian, a small ligand effect is observed. Substituting the aryl groups of phenyl-bian ligand does not influence the catalysis significantly. By studying the behavior of various [Pt(Ar-bian)(alkene)] complexes, it has become clear that the nature of the alkene ligand in these complexes determines its catalytic behavior; the [Pt(Ar-bian)(ma)] complexes are intrinsically slightly more active than the two [Pt(Ar-bian)(dmfu)] complexes, however, the [Pt(Ar-bian)(dmfu)] complexes result in much more stable catalysts. The fact that the different Ar-bian ligands do not have a major influence on the catalytic behavior of the complexes demonstrates the lability of these bidentate ligands compared to several alkenes. Importantly, compared to [Pt(Me-nq)(nbe)$_2$], the two [Pt(Ar-bian)(dmfu)] complexes show an intrinsically lower activity, but are at the same time much more stable, resulting in significantly higher overall yields under similar conditions. We are at present investigating the use of alkenes as ligands in the platinum(0)-catalyzed hydrosilylation in more detail.

Experimental Section

General Remarks: All experiments were carried out by using standard Schlenk techniques under dry nitrogen. The solvents were dried according to standard procedures and distilled before use. Quantitative gas liquid chromatography (GLC) analyses were carried out with a Varian 3300 apparatus equipped with a semicapillary column (J&W, DB 5, 30 m × 1 μm) with *n*-decane as internal standard. Elemental analyses were carried out by Kolbe, Mikroanalytisches Laboratorium, Mülheim a. d. Ruhr, Germany. ^{1}H, ^{13}C, and ^{19}F NMR spectra were recorded at 300.1, 75.5, and 282.4 MHz, respectively, with a Varian Mercury 300 and with a Varian Inova 500 spectrometer at 499.8 and 125.7 MHz, respectively. Chemical shift values are in ppm relative to external TMS or Cl_3CF with high frequency shifts signed as positive. Abbreviations used are s = singlet, d = doublet, pst = peudotriplet, m = multiplet; multiplicity, number of protons and coupling constants (Hz) in parentheses. Triethylsilane (Acros), *n*-decane (Acros), dimethyl fumarate (Merck), tetracyanoethylene (Fluka), 1,10-phenanthroline (Aldrich), 2,2′-dipyridyl (Aldrich), triphenylphosphane (Aldrich), bis(diphenylphosphanyl)ethane (Strem), 2-methyl-2,4-naphthoquinone (Aldrich), acenaphthenequinone (Aldrich), and 4-fluoroaniline (Janssen Chimica) were used as received. Styrene (Acros) was purified by flash chromatography on alumina immediately prior to use. Maleic anhydride (EGA) was recrystallized from dichloromethane. [Pt(nbe)$_3$],[27] [Pd(*p*-MeO-C$_6$H$_4$-bian)(DMFU)],[24] phenyl-bian,[34] *p*-MeO-C$_6$H$_4$-bian,[34] *p*-Br-C$_6$H$_4$-bian,[34] *p*-NO$_2$-C$_6$H$_4$-bian,[35] and *m*,*m*-(CF$_3$)$_2$-C$_6$H$_3$-bian[35] were synthesized according to published procedures. 4.5-Diazafluoren-9-one[36] was synthesized according to the literature, but was additionally purified using column chromatography [silica, MeOH/dichloromethane (5:95)].

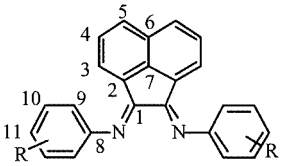

Bis(4-fluorophenylimino)acenaphthene (*p*-F-C$_6$H$_4$-bian, 7): The ligand was prepared analogous to the method described in the literature[36] for that of acenaphthenequinone and 4-fluoroaniline and was obtained as an orange solid. Yield: 1.81 g, 75%. ^{1}H NMR (300.1 MHz, $CDCl_3$): δ = 6.94 (d, ^3J = 7.14 Hz, 2 H, 3-H), 7.10 (m, 4 H, 9-H), 7.18 (m, 4 H, 10-H), 7.42 (pst, ^3J = 7.42 Hz, 2 H, 4-H), 7.93 (d, ^3J = 7.14 Hz, 2 H, 5-H) ppm. ^{13}C NMR (75.5 MHz, $CDCl_3$): δ = 116.52 (d, $^2J_{F,C}$ = 22.57 Hz, C-10), 119.95 (d, $^3J_{F,C}$ = 8.06 Hz, C-9), 124.10 (C-3), 127.91 (C-4), 128.48 (C-2), 129.46 (C-5), 131.47 (C-6), 142.03 (C-7), 147.71 (C-8), 160.28 (d, $^1J_{F,C}$ = 243.46 Hz, C-11), 162.00 (C-1) ppm. ^{19}F NMR (282.4 MHz, $CDCl_3$): δ = −119.31 ppm.

(σ-*N*,σ-*N*′-Bis{3,5-bis(trifluoromethyl)phenylimino}acenaphthene)-(η^{2}maleic anhydride)platinum(0) (10a): THF (2.5 mL) was added to maleic anhydride (127.0 mg, 275 μmol). The colorless solution was cooled to 0 °C, after which [Pt(nbe)$_3$] (119.5 mg, 250 μmol) was added. The solution was stirred at 0 °C for 15 min, after which *m*,*m*-(CF$_3$)$_2$-C$_6$H$_3$-bian (164.9 mg, 273 μmol) was added. Stirring was continued at 0 °C for 45 min, followed by the heating of the reaction mixture to room temperature. The orange solution was concentrated to dryness and the residue dissolved in 2 mL of dichloromethane. Pentane (20 mL) was added to the solution, after which a dark precipitate formed. The solvent was removed via a syringe and the solid was washed with pentane (4 × 20 mL) and dried in vacuo. The isolated dark purple powder was analyzed by NMR spectroscopy and appeared to be a mixture of reaction products. However, upon standing, a dark solid had precipitated from the combined organic extract. The precipitate was washed with pentane (8 × 10 mL) and dried in vacuo, after which **10a** was obtained as a dark purple powder. Yield: 96.5 mg, 43.0%. ^{1}H NMR (499.8 MHz, CD_2Cl_2): δ = 3.76 (s, $J_{Pt\text{-}H}$ = 89.84 Hz, 2 H, ma), 7.49 (d, ^3J = 7.32 Hz, 2 H, 3-H), 7.63 (pst, ^3J = 7.70 Hz, 2 H, 4-H), 8.10 (s, 2 H, 11-H), 8.21 (s, 4 H, 9-H), 8.38 (d, ^3J = 8.24 Hz, 2 H, 5-H) ppm. No ^{13}C NMR spectrum was recorded due to the low solubility and stability of the complex. ^{19}F NMR (282.4 MHz, CD_2Cl_2): δ = −63.35 ppm. $C_{32}H_{14}F_{12}N_2O_3Pt$ (897.52): calcd. C 42.82, H 1.57, N 3.12; found C 42.67, H 1.63, N 3.04.

(σ-*N*,σ-*N*′-Bis{3,5-bis(trifluoromethyl)phenylimino}acenaphthene)(η^2-tetracyanoethene)platinum(0) (10b): THF (20 mL) was added to *m*,*m*-(CF$_3$)$_2$-C$_6$H$_3$-bian (121 mg, 200 μmol), and tetracyanoethene (26.3 mg, 205 μmol). [Pt(nbe)$_3$] (92.1 mg, 193 μmol) was added to this mixture, and the solution changed color from bright orange to deep red. The mixture was stirred for 4 h at room temperature, after which the reaction was complete as was evident from TLC. The solvent was removed in vacuo and the residue washed with diethyl ether (3 × 2 mL) to afford **10b** as an orange solid. Yield: 151 mg, 81.6%. ^{1}H NMR (499.8 MHz, [D$_6$]acetone): δ = 7.80 (d, ^3J = 7.33 Hz, 2 H, 3-H), 7.85 (pst, ^3J = 7.81 Hz, 2 H, 4-H), 8.38 (s, 2 H, 11-H), 8.52 (s, 4 H, 9-H), 8.58 (d, ^3J = 8.06 Hz, 2 H, 5-H) ppm. ^{13}C NMR (125.7 MHz, [D$_6$]acetone): δ = 115.07 (CN), 123.92 (q, $^1J_{F,C}$ = 272.68 Hz, CF_3), 124.08 (C-9), 124.35 (C3), 125.84 (C-2), 126.78 (C-4), 130.77 (C-5), 133.18 (C-6), 134.44 (q, $^2J_{F,C}$ = 33.94 Hz, C-10), 134.45 (C-11), 149.69 (C-8), 150.07 (C-7), 176.67 (C-1) ppm. ^{19}F NMR (282.4 MHz, [D$_6$]acetone): δ = −63.57 ppm. $C_{34}H_{12}F_{12}N_6Pt$ (927.56): calcd. C 44.03, H 1.30, N 9.06; found C 44.11, H 1.36, N 9.13.

 © 2003 Wiley-VCH Verlag GmbH & Co. KGaA, Weinheim

(σ-*N*,σ-*N*′-Bis{4-methoxyphenylimino}acenaphthene)(η²-maleic anhydride)platinum(0) (11a): THF (3.5 mL) was added to *p*-MeO-C_6H_4-bian (107.3 mg, 273 μmol), and maleic anhydride (27.2 mg, 277 μmol). [Pt(nbe)$_3$] (120 mg, 251 μmol) was added to this solution after which the solution changed color from deep red to dark green. The mixture was stirred at room temperature for 60 min, and the solvent was removed in vacuo. The dark residue was washed with diethyl ether (3 × 3 mL), dried, dissolved in 5 mL of dichloromethane, and filtered through Celite Hyflo. Pentane (20 mL) was added to the filtrate followed by the formation of a dark precipitate. The solid was washed with pentane (4 × 10 mL) and dried in vacuo, after which **11a** was obtained as a brown red solid. Yield: 98.3 mg, 57.3%. ^{1}H NMR (499.8 MHz, CD_2Cl_2): δ = 3.55 (s, J_{Pt-H} = 84.46 Hz, 2 H, ma), 3.93 (s, 6 H, MeO), 7.09 (d, ^3J = 9.03 Hz, 4 H, 9-H), 7.48 (pst, ^3J = 7.81 Hz, 2 H, 4-H), 7.63−7.71 (m, 6 H, 3-H and 10-H), 8.17 (d, ^3J = 8.06 Hz, 2 H, 5-H) ppm. ^{13}C NMR (125.7 MHz, CD_2Cl_2): δ = 25.97 (ma), 55.81 (MeO), 114.45 (C-10), 123.39 (C-9), 124.97 (C-3), 127.30 (C-2), 128.94 (C-4), 130.41 (C-5), 132.19 (C-6), 141.26 (C-8), 145.50 (C-7), 160.47 (C-11), 168.64 (C-1), 174.51 (ma) ppm. $C_{30}H_{22}N_2O_5Pt$ (685.58): calcd. C 52.56, H 3.23, N 4.09; found C 52.48, H 3.20, N 3.99.

(σ-*N*,σ-*N*′-Bis{4-methoxyphenylimino}acenaphthene)(η²-dimethyl fumarate)platinum(0) (11c): THF (20 mL) was added to *p*-MeO-C_6H_4-bian (78 mg, 199 μmol) and dimethyl fumarate (31.0 mg, 215 μmol). The solution changed color from deep red to dark green upon addition of [Pt(nbe)$_3$] (120 mg, 251 μmol). The mixture was stirred at room temperature for 90 min, after which the reaction was complete as was evident from TLC. The solvent was removed in vacuo and the dark brown residue washed with diethyl ether (2 × 3 mL) and dissolved in 5 mL of dichloromethane. The dark brown solution was filtered through Celite Hyflo and the filtrate concentrated to dryness in vacuo. The desired reaction product **11c** was obtained as a dark brown solid. Yield: 137 mg; 94.0%. ^{1}H NMR (300.1 MHz, CD_2Cl_2): δ = 3.40 (s, 6 H, dmfu), 3.72 (s, J_{Pt-H} = 91.22 Hz, 2 H, dmfu), 3.98 (s, 6 H, MeO), 7.49 (d, ^3J = 7.42 Hz, 2 H, 3-H), 7.63 (pst, ^3J = 7.70 Hz, 2 H, 4-H), 8.10 (s, 2 H, 10-H), 8.21 (s, 4 H, 9-H), 8.14 (d, ^3J = 8.24 Hz, 2 H, 5-H) ppm. ^{13}C NMR (125.7 MHz, CD_2Cl_2): δ = 27.29 (dmfu), 50.57 (dmfu), 56.17 (MeO), 115.07 (C-10), 123.54 (C-9), 125.72 (C-3), 129.21 (C-2), 130.11 (C-4), 130.71 (C-5), 133.43 (C-6), 134.04 (C-8), 142.62 (C-7), 160.92 (C-11), 168.93 (C-1), 176.45 (dmfu) ppm. $C_{32}H_{28}N_2O_6Pt$ (731.65): calcd. C 52.53, H 3.86, N 3.83; found C 52.34, H 3.76, N 3.95.

(σ-*N*,σ-*N*′-Bis{phenylimino}acenaphthene)(η²-dimethyl fumarate)-platinum(0) (12c): [Pt(nbe)$_3$] (0.92 g, 1.93 mmol), C_6H_5-bian (0.70 g, 2.11 mmol) and dimethyl fumarate (0.31 g, 2.15 mmol) were dissolved in THF (20 mL). The color of the solution changed to dark green immediately. The mixture was stirred at room temperature for 60 min and the solution was filtered through Celite Hyflo. The filtrate was concentrated to dryness in vacuo and was washed with a 50-mL pentane/diethyl ether (1:1) mixture and 2 × 50 mL of pentane. The desired reaction product **12c** was obtained as a dark green solid. Yield: 1.04 g; 80.0%. ^{1}H NMR (300.1 MHz, CD_2Cl_2): δ = 3.33 (s, 6 H, dmfu), 3.71 (s, J_{Pt-H} = 93.15 Hz, 2 H, dmfu), 7.46−7.53 (m, 6 H, 3-H + 4-H + 11-H), 7.60 (m, 8 H, 9-H + 10-H), 8.21 (d, ^3J = 5.50 Hz, 1 H, 5-H), 8.23 (d, ^3J = 5.50 Hz, 1 H, 5-H) ppm. ^{13}C NMR (125.7 MHz, CD_2Cl_2): δ = 27.93 (dmfu), 50.96 (dmfu), 122.87 (C-9), 123.76 (C-3), 128.30 (C-2), 128.62 (C-4), 129.87 (C-11), 130.16 (C-10), 130.43 (C-5), 132.7 (C-6), 145.85 (C-7), 149.19 (C-8), 169.65 (C-1), 176.47 (dmfu) ppm. $C_{30}H_{24}N_2O_4Pt$ (671.60): calcd. C 53.65, H 3.60, N 4.17; found C 53.88, H 3.74, N 4.08.

General Procedure for the Hydrosilylation of Styrene with Triethylsilane: A two-necked Schlenk tube equipped with a septum, a reflux condenser and a stirring bar was charged with the appropriate platinum complex (0.022 mmol) and, in the case of the in situ prepared catalysts, 1 equiv. of ligand. The Schlenk tube was evacuated and filled with nitrogen three times. Then toluene (20 mL), styrene (6.16 mmol or 17.24 mmol), *n*-decane (3.08 mmol), and triethylsilane (6.16 mmol) were added, in this order, in quick succession from syringes through the septum. The reactor was immediately immersed in an oil bath, which was kept at the required reaction temperature. Samples were taken periodically for GC analyses. Products were characterized using NMR spectroscopy and GC-MS.

Acknowledgments

The research has been performed within the National Research School Combination Catalysis (project number: 2000-14), which is gratefully acknowledged for financial support. We thank M. W. van Laren for synthesizing [Pd(*p*-MeO-C_6H_4-bian)(dmfu)].

[1] B. Marciniec, *Comprehensive Handbook on Hydrosilylation*, Pergamon Press, London, **1992**.
[2] L. H. Sommer, E. W. Pietrusza, F. C. Whitmore, *J. Am. Chem. Soc.* **1947**, *69*, 188.
[3] [3a] J. L. Speier, J. A. Webster, G. H. Barnes, *J. Am. Chem. Soc.* **1957**, *79*, 974−979. [3b] J. L. Speier, *Adv. Organomet. Chem.* **1979**, 407−447.
[4] B. D. Karstedt (General Electric Co.), USP 226928, **1972**.
[5] J. Stein, L. N. Lewis, Y. Gao, R. A. Scott, *J. Am. Chem. Soc.* **1999**, *121*, 3693−3703.
[6] P. B. Hitchcock, M. F. Lappert, N. J. W. Warhurst, *Angew. Chem. Int. Ed. Engl.* **1991**, *30*, 438−440.
[7] A. J. Chalk, J. F. Harrod, *J. Am. Chem. Soc.* **1965**, *87*, 16.
[8] P. Steffanut, J. A. Osborn, A. DeCain, J. Fisher, *Chem. Eur. J.* **1998**, *4*, 2008−2017.
[9] I. E. Markó, S. Stérin, O. Buisine, G. Mignani, P. Branlard, B. Tinant, J.-P. Declercq, *Science* **2002**, *298*, 204−206.
[10] J. W. Sprengers, M. J. Mars, M. A. Duin, K. J. Cavell, C. J. Elsevier, *J. Organomet. Chem.* **2003**, *679*, 149−152.
[11] Y. Seki, K. Takeshita, K. Kawamoto, S. Murai, N. Sonoda, *J. Org. Chem.* **1986**, *51*, 3890−3895.
[12] F. Kakiuchi, Y. Tanaka, N. Chatani, S. Murai, *J. Organomet. Chem.* **1993**, *456*, 45−47.
[13] R. Takeuchi, H. Yasue, *Organometallics* **1996**, *15*, 2098−2102.
[14] A. M. LaPointe, F. C. Rix, M. Brookhart, *J. Am. Chem. Soc.* **1997**, *119*, 906−917.
[15] A. Hopf, K. H. Dötz, *J. Mol. Catal. A* **2000**, *164*, 191−194.
[16] W. Caseri, P. S. Pregosin, *J. Organomet. Chem.* **1988**, *356*, 259−269.
[17] R. van Asselt, C. J. Elsevier, *Organometallics* **1992**, *11*, 1999.
[18] R. van Belzen, H. Hoffmann, C. J. Elsevier, *Angew. Chem. Int. Ed. Engl.* **1997**, *36*, 1743−1745.
[19] R. van Belzen, R. A. Klein, H. Kooijman, N. Veldman, A. L. Spek, C. J. Elsevier, *Organometallics* **1998**, *17*, 1812.
[20] C. J. Elsevier, *Coord. Chem. Rev.* **1999**, *185−186*, 809−822.
[21] M. W. van Laren, C. J. Elsevier, *Angew. Chem. Int. Ed.* **1999**, *38*, 3715−3717.
[22] M. W. van Laren, M. A. Duin, C. Klerk, M. Naglia, D. Rogolino, P. Pelagatti, A. Bacchi, C. Pelizzi, C. J. Elsevier, *Organometallics* **2002**, *21*, 1546−1553.
[23] D. S. Tromp, M. A. Duin, A. M. Kluwer, C. J. Elsevier, *Inorg. Chim. Acta* **2002**, *327*, 90−97.
[24] R. van Asselt, C. J. Elsevier, W. J. J. Smeets, A. L. Spek, *Inorg. Chem.* **1994**, *33*, 1521−1531.
[25] J. H. Groen, C. J. Elsevier, K. Vrieze, W. J. J. Smeets, A. L. Spek, *Organometallics* **1996**, *15*, 3445−3455.

 © 2003 Wiley-VCH Verlag GmbH & Co. KGaA, Weinheim

[26] R. A. Klein, P. Witte, R. van Belzen, J. Fraanje, K. Goubitz, M. Numan, H. Schenk, J. M. Ernsting, C. J. Elsevier, *Eur. J. Inorg. Chem.* **1998**, *3*, 319−330.
[27] L. E. Crascall, J. L. Spencer, *Inorg. Synth.* **1990**, *28*, 126−132.
[28] J. Liedtke, S. Loss, G. Alcaraz, V. Gramlich, H. Grützmacher, *Angew. Chem. Int. Ed.* **1999**, *38*, 1623−1626.
[29] R. Skoda-Földes, L. Kollár, B. Heil, *J. Organomet. Chem.* **1989**, *399*, 275−279.
[30] R. A. Klein, PhD Dissertation, Univ. of Amsterdam, **1996**.
[31] J. H. Groen, B. J. de Jong, J. M. Ernsting, P. W. N. M. van Leeuwen, K. Vrieze, W. J. J. Smeets, A. L. Spek, *J. Organomet. Chem.* **1999**, *573*, 3−13.
[32] F. Ruffo, A. De Renzi, A. Panunzi, *Inorg. Synth.* **1998**, *32*, 158−162.
[33] A. Kundu, B. P. Buffin, *Organometallics* **2001**, *20*, 3635−3637.
[34] R. van Asselt, C. J. Elsevier, A. L. Spek, R. Benedix, *Recl. Trav. Chim. Pays-Bas* **1994**, *113*, 88−98.
[35] M. Gasperini, F. Ragaini, S. Cenini, *Organometallics* **2002**, *21*, 2950−2957.
[36] M. J. Plater, S. Kemp, E. Lattmann, *J. Chem. Soc., Perkin Trans. 1* **2000**, 971−979.
[37] W. Caseri, P. S. Pregosin, *Organometallics* **1988**, *7*, 1373−1380.
Received February 13, 2003

 © 2003 Wiley-VCH Verlag GmbH & Co. KGaA, Weinheim

Synthesis, Structure and Magnetic Properties of a New Iron Arsenate, $[C_{10}N_4H_{28}][\{FeF(OH)(HAsO_4)\}_4]$, with a Layer Structure

Sandip Chakrabarti,[a] Swapan K. Pati,[b] Mark A. Green,[c] and Srinivasan Natarajan*[a]

Keywords: Iron / Arsenic / Solvothermal synthesis / N ligands

The reaction of $FeCl_3 \cdot 6H_2O$, H_3AsO_4, HF and 1,4-bis(3-aminopropyl)piperazine under solvothermal conditions gives rise to a new iron arsenate, $[C_{10}N_4H_{28}][\{FeF(OH)(HAsO_4)\}_4]$ (**I**) with a layered structure. The cell parameters are monoclinic, space group = $P2_1/n$ (no.14), M = 1143.08, a = 9.6320(3), b = 8.3598(3), c = 10.7794(1) Å, β = 115.036(1)°, V = 786.42(4) Å^3, Z = 4, R_1 = 0.0492, wR_2 = 0.1227 [1114 observed reflections with $I > 2\sigma(I)$]. The connectivity between $FeO_3F_2(OH)$ octahedra and $HAsO_4$ tetrahedra forms a secondary building unit (SBU) of the type SBU-4. The SBU-4 units are linked together to form a layer structure with apertures formed by 8-T atoms (T = Fe, As). The amine molecules are disordered and occupy the inter-lamellar region. To the best of our knowledge, **I** is the first example of an iron arsenate structure formed from only one type of secondary building unit, SBU-4. A dimer model has been used to describe the magnetic behavior.

(© Wiley-VCH Verlag GmbH & Co. KGaA, 69451 Weinheim, Germany, 2003)

Introduction

The synthesis, structure and properties of metal phosphates prepared in the presence of organic amines has been intensely researched during the last two decades.[1] Of these, the transition metal phosphates are interesting due to the variations in the oxidation state and coordination preferences of the transition element. Thus, a large number of iron phosphates with novel structures have been prepared and characterized.[2,3] Most of these iron phosphates have been prepared by employing hydrothermal methods. In some cases HF was used as the mineralizer, which also becomes part of the structure by linking the metal centers.[2−4] It is interesting to note that the use of HF produced a number of novel phosphate frameworks that do not generally form in the fluoride-free medium.

Though arsenic belongs to the same group as phosphorous, little work has been carried out on arsenate-based framework structures. It is likely that the larger size of the As^{5+} cation (0.335 Å) compared to the P^{5+} cation (0.17 Å)[5] would lead to the formation of completely different structures. In addition, a comparison of the pK_a values of H_3PO_4 and H_3AsO_4 also gives an idea about the relative ease of removal of protons. Thus for H_3PO_4, pK_{a1}, pK_{a2} and pK_{a3} are 2.12, 7.21 and 12.32, respectively, while for H_3AsO_4, pK_{a1}, pK_{a2} and pK_{a3} are 2.3, 6.9 and 11.5, respectively. This probably indicates that arsonic acid is somewhat weaker than phosphoric acid. The research in arsenate-based framework compounds are beginning to emerge, but is limited possibly due to the toxicity associated with arsenic and its relative inability to form extended networks. The intense investigations by many researchers during the last decade or so have given rise to new arsenates of different compositions and structures. Thus, arsenates of aluminum,[6,7] gallium,[8−10] molybdenum,[11,12] vanadium,[13−18] iron[19−24] and zinc[25−27] have been prepared and their structures reported in the literature. In order to expand the family of known arsenate framework structures, we have been investigating the formation of iron arsenates in the presence of structure-directing organic amine molecules. In this paper, we report the hydrothermal synthesis, crystal structure and spectroscopic and magnetic properties of a new iron(III) arsenate prepared in the presence of 1,4-bis(3-aminopropyl)piperazine (AP-PIP) cations, $[C_{10}N_4H_{28}][\{FeF(OH)(HAsO_4)\}_4]$ (**I**). This compound possesses a layer structure formed entirely by the linking between only one type of secondary building units (SBU-4),[28,29] which to the best of our knowledge is the first example of an iron arsenate formed with organic cations.

[a] Framework Solids Laboratory, Chemistry and Physics of Materials Unit, Jawaharlal Nehru Centre for Advanced Scientific Research,
Jakkur P. O., Bangalore 560 064, India
Fax: (internat.) +91-80/846-2766, 856-6581
E-mail: raj@jncasr.ac.in
[b] Theoretical Sciences Unit, Jawaharlal Nehru Centre for Advanced Scientific Research,
Jakkur P. O., Bangalore 560 064, India
[c] Davy-Faraday Research Laboratory, The Royal Institution of Great Britain, 21
Albemarle Street, London W1S 4BS, UK

Results and Discussion

The structure consists of macroanionic layers of $[\{FeF(OH)(HAsO_4)\}_4]^{4-}$ formed by the linking of FeO_4-

 © 2003 Wiley-VCH Verlag GmbH & Co. KGaA, Weinheim DOI: 10.1002/ejic.200300237

F(OH) octahedra and $AsO_3(OH)$ tetrahedra. The AP-PIP cations are located in the inter-lamellar region. The asymmetric unit of the layer is shown in Figure 1. There is only one crystallographically distinct Fe and As atom in the asymmetric unit. The Fe atom is octahedrally coordinated by four O and two F atoms with Fe−O/F bond lengths in the range 1.884(6)−2.049(5) Å (av. 1.9842 Å). The octahedral O/F−Fe−O/F bond angles are in the range 77.6(2)−176.3(3)° (av. 106.3°). The iron atom is linked to the arsenic atom by three Fe−O−As bonds, two Fe−F−Fe bonds and one terminal -OH group. The As atom also has three As−O−Fe bonds and one terminal As−O bond. The As atom is tetrahedrally coordinated by oxygen atoms with an average As−O distance of 1.6873 Å and O−As−O bond angle of 109.4°. Using the Brown−Altermatt formalism[30] for the bond length/bond valence relationship for Fe−O and As−O, bond-order sums for the cations and anions were calculated (Table 1). The calculated bond-order sums for both cations and anions are in agreement with the formal oxidation states of +3, +5 and −2 for Fe, As and O atoms respectively.

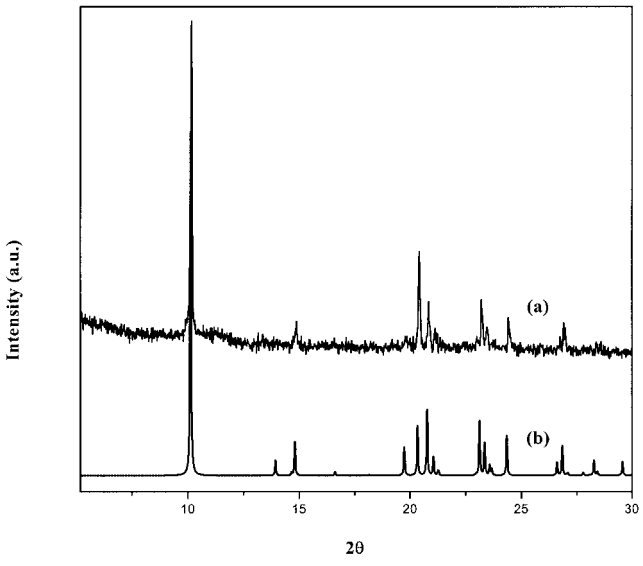

Figure 1. ORTEP diagram of $[C_{10}N_4H_{28}][\{FeF(OH)(HAsO_4)\}_4]$ showing the atoms that constitute the layer; thermal ellipsoids are given at 50% probability

The inset of Figure 2 shows the $\{FeF(OH)(HAsO_4)\}^-$ segment of the structure. As can be seen, two $FeO_3F_2(OH)$ distorted octahedra share a common edge. These dimeric units are connected by AsO_4 groups in a doubly bridging fashion. The AsO_4 units also act as a terminal ligand to the neighboring $FeO_3F_2(OH)$ octahedra. Thus, each AsO_4 unit is linked to three $FeO_3F_2(OH)$ octahedra, its fourth vertex being free and pointing into the inter-lamellar region. Similarly, each $FeO_3F_2(OH)$ octahedron links with three AsO_4 tetrahedra and connects to another Fe through the edge, with the remaining vertex, which is an -OH group, pointing into the interlayer region. The $(Fe_2F_2)^{4+}$ core and the two AsO_4 units linking it in a chelating fashion is identical to the secondary building unit SBU-4, formulated by Ferey.[28,29] Similar building units and connectivity have also been observed in A-frame compounds.[31] The SBU-4 units are linked through their corners forming an extended layered structure (Figure 2). The arrangement of layers in the *ab* plane is shown in Figure 3. As can be seen there are

Table 1. Selected bond lengths and angles for $[C_{10}N_4H_{28}][\{FeF(OH)(HAsO_4)\}_4]$ (**I**)[a]

Bond	Distance (Å)	Bond	Distance (Å)
As(1)−O(3)	1.668(6) [1.321]	Fe(1)−O(1)#1	1.928(6) [0.637]
As(1)−O(1)	1.678(6) [1.275]	Fe(1)−O(3)	1.999(6) [0.520]
As(1)−O(2)	1.689(6) 1.235]	Fe(1)−F(1)	2.011(5) [0.411]
As(1)−O(4)	1.713(6) [1.139]	Fe(1)−O(2)#2	2.028(6) [0.483]
Σ(As − O)	**[4.970]**	Fe(1)−F(1)#2	2.049(5) [0.366]
Fe(1)−O(5)	1.884(6) [0.700]	**Σ(Fe − O/F)**	**[3.117]**
Moiety	**Angle (°)**	**Moiety**	**Angle (°)**
O(3)−As(1)−O(1)	113.4(3)	O(1)#1−Fe(1)−O(2)#2	94.1(3)
O(3)−As(1)−O(2)	114.5(3)	O(3)−Fe(1)−O(2)#2	169.7(3)
O(1)−As(1)−O(2)	108.8(3)	F(1)−Fe(1)−O(2)#2	87.7(2)
O(3)−As(1)−O(4)	104.8(3)	O(5)−Fe(1)−F(1)#2	91.7(2)
O(1)−As(1)−O(4)	108.8(3)	O(1)#1−Fe(1)−F(1)#2	176.3(3)
O(2)−As(1)−O(4)	106.1(3)	O(3)−Fe(1)−F(1)#2	86.8(2)
O(5)−Fe(1)−O(1)#1	91.1(3)	F(1)−Fe(1)−F(1)#2	77.6(2)
O(5)−Fe(1)−O(3)	92.9(3)	O(2)#2−Fe(1)−F(1)#2	83.5(2)
O(1)#1−Fe(1)−O(3)	95.4(3)	As(1)−O(1)−Fe(1)#3	139.1(4)
O(5)−Fe(1)−F(1)	169.3(2)	As(1)−O(2)−Fe(1)#2	124.0(3)
O(1)#1−Fe(1)−F(1)	99.6(2)	As(1)−O(3)−Fe(1)	122.9(4)
O(3)−Fe(1)−F(1)	86.8(2)	Fe(1)−F(1)−Fe(1)#2	102.4(2)
O(5)−Fe(1)−O(2)#2	90.0(3)		

[a] Symmetry transformations used to generate equivalent atoms: #1 $-x+1, y+1/2, -z+1/2$; #2 $-x+1, -y+1, -z+1$; #3 $-x+1, y-1/2, -z+1/2$. Values in brackets are the bond valences. Their sum SVB appears in bold type at the end of the list of the distances around every cation.

 © 2003 Wiley-VCH Verlag GmbH & Co. KGaA, Weinheim

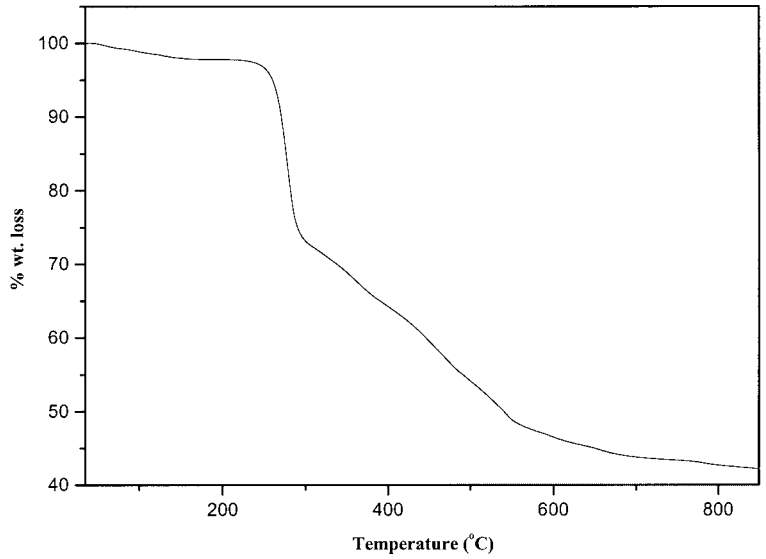

Figure 2. Polyhedral view of the structure of $[C_{10}N_4H_{28}][\{FeF(OH)(HAsO_4)\}_4]$ in the *bc* plane showing a single layer; the inset shows the SBU-4 units; the amine molecules are not shown

interactions between the layers through the terminal Fe−OH bonds.

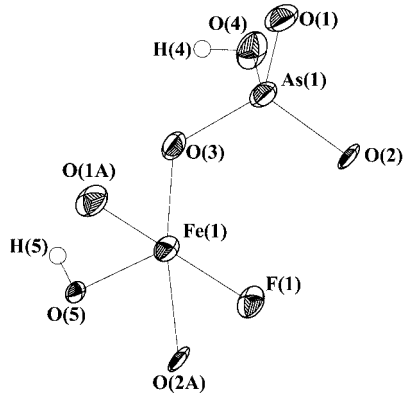

Figure 3. Polyhedral view of the structure of $[C_{10}N_4H_{28}][\{FeF(OH)(HAsO_4)\}_4]$ in the *ac* plane showing the arrangement of layers; the amine molecules are not shown for clarity; dotted lines represent possible hydrogen bond interactions

The concept of secondary building units for the description of framework structures is common in pure tetrahedral aluminosilicate and phosphate structures.[32] Recently, many secondary building units have been identified and proposed for the description of octahedral-tetrahedral frameworks.[28,29] Though many secondary building units have been identified to describe the structure of an octahedral-tetrahedral framework solid, the assembly of only one type of secondary building unit is rare. To the best of our knowledge, $[C_{10}N_4H_{28}][\{FeF(OH)(HAsO_4)\}_4]$ (**I**) is the first example possessing only the SBU-4 units, though similar layers formed by SBU-4 units are known for vanadium arsenate.[15] Similar building units of the type described here have also been observed earlier in a gallium phosphate, $[C_6N_2H_{14}][Ga_3(OH)F_3(PO_4)(HPO_4)_2]\cdot 0.5H_2O$.[33]

The variable-temperature magnetic susceptibility measurements of $[C_{10}N_4H_{28}][\{FeF(OH)(HAsO_4)\}_4]$ (**I**) were carried out on a powdered sample in the range from 4 to 300 K. Plots of the χ_m versus T is shown in Figure 4 and the inset shows the χ^{-1} versus temperature plot. The molar magnetic susceptibility increases with decreasing temperature and reaches a sharp maximum around 20 K. If T is reduced further, the susceptibility decreases very sharply. This sharp exponential decrease of magnetic susceptibility corresponds to a finite spin-gap in the system. In general, for a system with a spin-gap at low temperature, the susceptibility obeys a form given by χ (low-T) = $A\exp(-\Delta/T)/T^{\zeta}$, where A and ζ are constants and Δ represents the magnetic gap.[34,35] By fitting the experimental data at low temperature with this form of χ, we obtain a gap of about 8.1 K (with A = 2.5, and ζ = 0.6). On the other hand, the high temperature susceptibility data fits with the Curie−Weiss form χ(high-T) = C/(T-θ), with θ = −31 K and C = 16.424. High temperature χ of this form fits well with the experimental data (χ_m) up to a temperature of about 65 K.

A closer look at the magnetic lattice suggests that within the Fe_2F_2 dimers, the magnetic super-exchange is very strong, while the Fe_2F_2 dimers interact with the neighboring dimers through the AsO_4 bridges by weak super-exchange interactions. The Fe−F−Fe bond angle of 102.4° seems to favor ferromagnetic interactions, while those between the dimers through arsenate with the Fe−O−As bond angles of 128.67° favor anti-ferromagnetic interactions, according to the Goodenough rules.[36] Using the Heisenberg model for two S = 5/2 spins (dimer), the magnetic energy levels can be written as E_S = -J/2[$S(S + 1) - 35/2$] with S values 0,1,2,3,4 and 5. The magnetic susceptibility can be defined as $\chi = g^2\mu_B{}^2[\langle M^2\rangle - \langle M\rangle^2]/K_BT$, where $[\langle M\rangle^2 - \langle M\rangle^2]$ is the fluctuation in magnetization, M. For an antiferromagnet in the absence of magnetic field, the average

 © 2003 Wiley-VCH Verlag GmbH & Co. KGaA, Weinheim

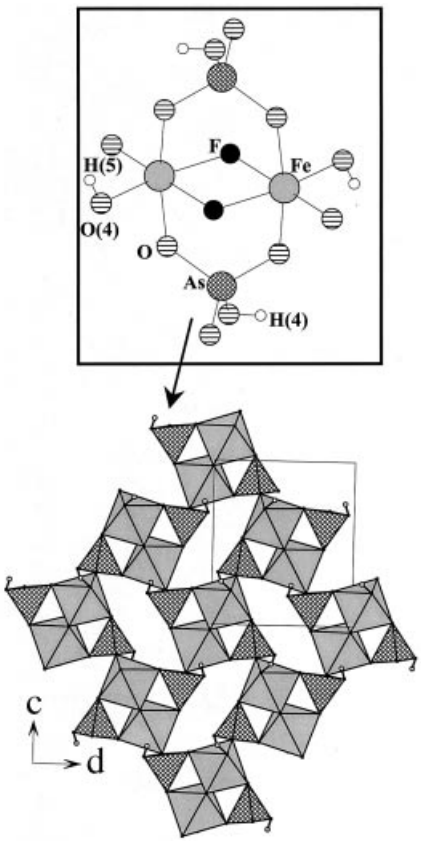

Figure 4. Thermal variation of the experimental magnetic susceptibility (χ) of $[C_{10}N_4H_{28}][\{FeF(OH)(HAsO_4)\}_4]$; the solid line is a fit using the exponential form (see text); the Inset shows the variation of inverse magnetic susceptibility (χ^{-1}) with temperature; the Curie−Weiss fit is shown as dotted lines

magnetization, <M>, vanishes. Thus the magnetic susceptibility for the dimer can be written as $\chi_{dimer} = g^2\mu_B{}^2/K_BT[\Sigma_S\{S(S+1)\exp(E_S/K_BT)\}/\Sigma_S\exp(E_S/K_BT)]$, $S = 0,1,2,3,4$ and 5. In Figure 5 we have fitted this dimer susceptibility with the experimental χ_mT, varying the exchange constant, J, and the Lande factor, g. The best fit is obtained with $g = 2.01$ and $J = -12$ K. The same $\chi_{dimer}T$ formula with fitted J and g values is used to calculate the effective magnetic moment. The effective magnetic moment (μ_{eff}) appears to compare well with the presence of iron in the +3 state. Note that the dimer model cannot adequately reproduce the experimental data over all the temperatures. The lowest magnetic gap is 12 K (−J) from the dimer model, while the fit of the low temperature χ_m gives a gap of about 8.1 K (Δ). This discrepancy can be attributed to the neglect of inter-dimer exchange interactions in the dimer model. More work is clearly necessary to understand the significance of inter-dimer exchange interactions in two-dimensional systems.

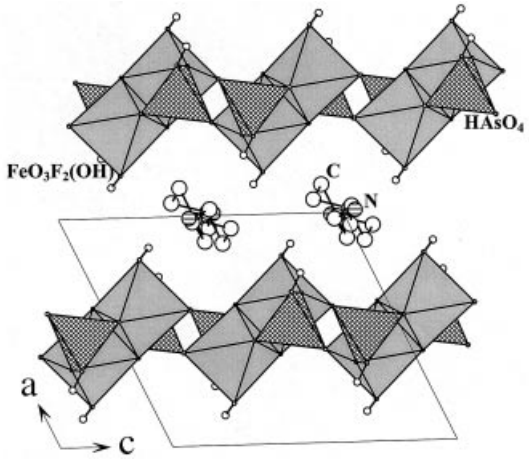

Figure 5. The variation of the χT as a function of temperature for $[C_{10}N_4H_{28}][\{FeF(OH)(HAsO_4)\}_4]$; the inset shows the variation of $\mu_{eff.}$ as a function of temperature; the solid line in both the cases shows the dimer-model fit to the experimental data

Conclusions

In conclusion, a new layered Fe^{III} arsenate, $[C_{10}N_4H_{28}][\{FeF(OH)(HAsO_4)\}_4]$, has been prepared in the presence of 1,4-bis(3-aminopropyl)piperazine by employing hydrothermal methods. The formation of the layered structure based purely on only one type of building unit (SBU-4) and its assembly through their corners are noteworthy structural features. Our continuing investigations clearly reveal that the chemistry of inorganic compounds possessing octahedral-tetrahedral building units is rich and many more novel structures are likely to be discovered. We are currently pursuing this theme.

Experimental Section

Synthesis and Initial Characterization

Solvothermal reactions were carried out under autogenous pressure in PTFE-lined stainless steel acid digestion bombs. For the preparation of $[C_{10}N_4H_{28}][\{FeF(OH)(HAsO_4)\}_4]$ (**I**) a mixture of iron chloride hexahydrate $[FeCl_3{\cdot}6H_2O]$ (0.1487 g), arsonic acid (0.6248 g), AP-PIP (0.441 g), HF (48%, 0.12 mL), water (4 mL) and *n*-hexanol (2 mL) were taken in the ratio 1:8:4:6:400:29. The mixture was homogenized at room temperature for 30 min and heated

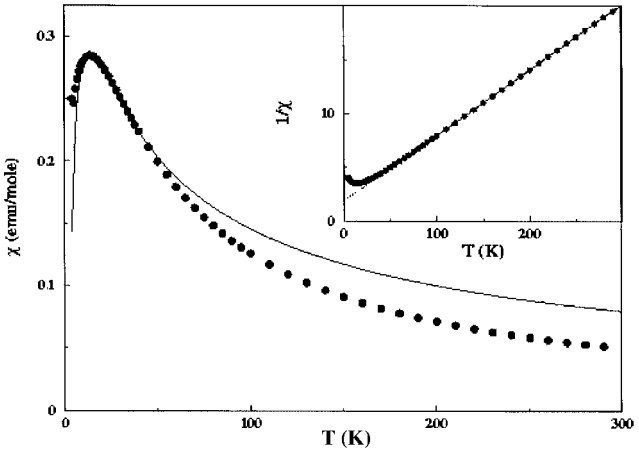

Figure 6. Powder XRD pattern of $[C_{10}N_4H_{28}]$-$[\{FeF(OH)(HAsO_4)\}_4]$ (a) experimental (Cu $K\alpha$) and (b) simulated

 © 2003 Wiley-VCH Verlag GmbH & Co. KGaA, Weinheim

at 150 °C for 72 h. The initial pH of the reaction mixture was about 2 and there was no appreciable change in the pH after the reaction. The resulting product, a crop of colorless plate-like crystals, was filtered, washed with water, and dried at room temperature [yield = 70% based on Fe]. A microanalysis of this phase by energy-dispersive X-ray fluorescence indicated the presence of As and Fe in a 1:1 ratio. $[C_{10}N_4H_{28}][\{FeF(OH)(HAsO_4)\}_4]$ (1131.07): calcd. C 10.6, H 3.18, N 4.95; found C 10.1, H 3.01, N 4.89. A chemical analysis also confirmed the presence of fluorine (calcd. 6.65%; found 6.5%).[37]

The product contained a single crystalline phase as judged by a comparison of the powder pattern with the pattern simulated from the atomic coordinates obtained from the single crystal structure analysis (Figure 6). A least-squares fit of the powder XRD (Cu *Kα* radiation) lines, using the *hkl* indices garnered from single-crystal data, gave the following cell: a = 9.5941(3), b = 8.3335(4), c = 10.7420(4) Å, β = 114.99(3)°. The cell parameters are in good agreement with those determined from the single crystal XRD.
Thermogravimetric analysis (TGA) of $[C_{10}N_4H_{28}][\{FeF(OH)(HAsO_4)\}_4]$ (**I**) was carried out under N_2 (flow rate = 50 mL/min) in the range between 25 and 700 °C (heating rate = 10 °C/min) (Figure 7). A small initial weight loss of about 2% observed in the region 25−200 °C, probably corresponds to the loss of some adsorbed water on the surface of the sample. Similar initial weight losses have been encountered in many solids with open-framework structures. The TGA shows a sharp weight loss in the region 250−300 °C followed by a tail up to 600 °C. The total weight loss of 57% corresponds very well with the loss of the amine, fluoride, the condensation of the -OH groups and the partial removal of As_2O_5 (calcd. 57.5%). The powder XRD showed the resulting decomposed powder to be amorphous.

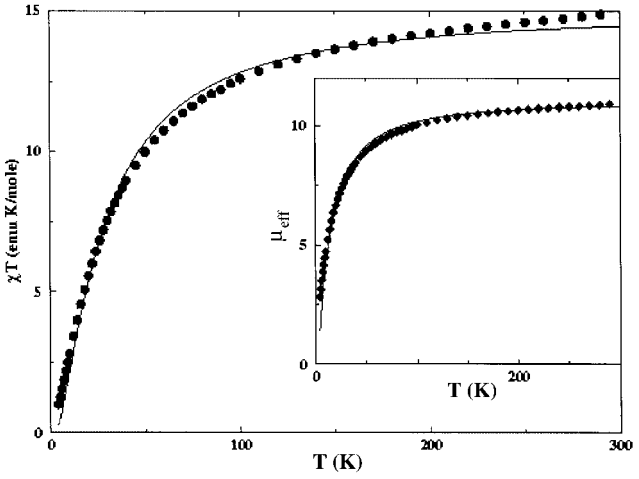

Figure 7. Thermogravimetric analysis (TGA) of $[C_{10}N_4H_{28}][\{FeF(OH)(HAsO_4)\}_4]$

Infrared (IR) spectra of $[C_{10}N_4H_{28}][\{FeF(OH)(HAsO_4)\}_4]$ (**I**) was recorded in the range 400−4000 cm^{-1} using the KBr pellet method. The IR spectra showed typical peaks with absorption bands for N−H, C−H and O−H bending and stretching vibrations: ν_s(OH) = 3426 cm^{-1} (vb), ν_s(NH) = 2873 (w), $\delta_s(NH_2)$ = 1619 cm^{-1} (s) and 1524 (s) cm^{-1}, $\delta(N^+\text{-}CH_2$ asym. drift) = 1480 cm^{-1} (m), ν_s(C−N) = 843 cm^{-1} (s), $\rho_r(CH_2)$ = 767 cm^{-1} (m), $\nu(NH_2^+)$ = 2373 cm^{-1} (m) and ν(C−C) = 1058 cm^{-1} (w).

Single-Crystal Structure Determination

A suitable colorless single crystal was carefully selected under a polarizing microscope and glued to a thin glass fiber with cyanoacrylate (superglue) adhesive. Crystal structure determination by X-ray diffraction was performed on a Siemens SMART-CCD diffractometer equipped with a normal focus, 2.4 kW sealed tube X-ray source (Mo-K_α radiation, λ = 0.71073Å) operating at 40 kV and 40 mA. A hemisphere of intensity data was collected at room temperature in 1321 frames with ω scans (width of 0.30° and exposure time of 20 s per frame) in the 2θ range 3 to 46.5°. Pertinent experimental details for the structure determination of $[C_{10}N_4H_{28}][\{FeF(OH)(HAsO_4)\}_4]$ (**I**) are presented in Table 2.

Table 2. Crystal data and structure refinement parameters for $[C_{10}N_4H_{28}][\{FeF(OH)(HAsO_4)\}_4]$ (**I**)

Empirical formula	$C_{10}N_4H_{36}Fe_4F_4As_4O_{20}$
Formula mass	1131.07
T (K)	293(2)
Space group	$P2_1/c$ (No. 14)
a (Å)	9.6320(3)
b (Å)	8.3598(3)
c (Å)	10.7794(1)
β (°)	115.036(1)
V (Å^3)	786.42(4)
Z	4
D_{calcd} (g cm^{-3})	2.378
μ (mm^{-1})	6.093
R indexes [$I > 2\sigma(I)$]	R_1 = 0.0497;[a] wR_2 = 0.1238[b]
R (all data)	R_1 = 0.0729; wR_2 = 0.1366

[a] $R_1 = \Sigma||F_0| - |F_c||/\Sigma|F_0|$. [b] $wR_2 = \{\Sigma[w(F_0^2 - F_c^2)^2]/\Sigma[w(F_0^2)^2]\}^{1/2}$. $w = 1/[\sigma^2(F_0)^2 + (aP)^2 + bP]$, $P = [\max.(F_0^2,0) + 2(F_c)^2]/3$, where a = 0.0738 and b = 0.0.

An absorption correction based on symmetry equivalent reflections was applied using the SADABS program (maximum and minimum effective transmission: 1.000000, 0.639708).[38] Other effects, such as absorption by the glass fiber, were simultaneously corrected. The structures were solved by direct methods and in each case, a sufficient fragment of the structure was revealed (As, Fe and O) to enable the remainder of the non-hydrogen atoms to be located from difference Fourier maps and the refinements to proceed to $R <$ 10%. Fluorine atoms, identified by chemical analysis, were localized after consideration of thermal motion parameters and bond valence calculations.[30] The amine molecule was disordered and a model was established based on the observed positions of the various peaks in the difference Fourier map, resulting in shorter C−C distances and angles. Geometric constraints on the bond lengths have been used to keep the molecule in position during the refinement cycles. The disorder of the amine molecule also precluded the anisotropic refinement of the C and N atoms. No hydrogen atoms corresponding to the amine molecules were found in the difference Fourier map and hence were not included. The hydrogen atoms attached to the oxygen atoms [O(4) and O(5)] were placed and held in the riding mode during the refinement cycles. The last cycles of refinement included atomic positions for all the atoms, anisotropic thermal parameters for all non-hydrogen framework atoms, isotropic thermal parameters for all the hydrogen atoms attached to the oxygen atoms. Full-matrix least-squares refinement against $|F^2|$ was carried out using the SHELXTL-PLUS[39] suite of programs. Details of the final refinement are given in Table 2. The selected bond lengths and angles are given in Table 1. CCDC-204836 contains the supplementary crystallographic data for this paper. These data can be obtained free of charge at www.ccdc.cam.ac.uk/conts/

 © 2003 Wiley-VCH Verlag GmbH & Co. KGaA, Weinheim

retrieving.html [or from the Cambridge Crystallographic Data Centre, 12, Union Road, Cambridge CB2 1EZ, UK; Fax: (internat.) +44-1223/336-033; E-mail: deposit@ccdc.cam.ac.uk].

Acknowledgments

The authors thank Prof. C.N.R. Rao, FRS for his support. SN thanks the Department of Science and Technology (DST), Government of India for the award of a research grant.

[1] A. K. Cheetham, T. Loiseau, G. Ferey, *Angew. Chem. Int. Ed.* **1999**, *38*, 3268 and references cited therein.
[2] M. Riou-Cavellec, D. Riou, G. Ferey, *Inorg. Chim. Acta* **1999**, *291*, 317 and references cited therein.
[3] K.-H. Lii, Y.-F. Huang, V. Zima, C.-Y. Huang, H.-M. Lin, Y.-C. Jiang, F.-L. Liao, S.-L. Wang, *Chem. Mater.* **1998**, *10*, 2599 and references cited therein.
[4] A. Choudhury, S. Natarajan, C. N. R. Rao, *Chem. Commun.* **1999**, 1305.
[5] R. D. Shannon, *Acta Crystallogr., Sect. A* **1976**, *32*, 751.
[6] W. T. A. Harrison, M. L. F. Phillips, A. V. Chavez, T. M. Nenoff, *J. Mater. Chem.* **1999**, *9*, 3087.
[7] P. Feng, T. Zhang, X. Bu, *J. Am. Chem. Soc.* **2001**, *123*, 8608.
[8] J. Chen, R. Xu,, *J. Solid State Chem.* **1989**, *80*, 149.
[9] J. Chen, L. Li, G. Yang, R. Xu, *J. Chem. Soc., Chem. Commun.* **1989**, 1217.
[10] X. Bu, P. Feng, T. E. Gier, G. D. Stucky, *J. Solid State Chem.* **1998**, *136*, 210.
[11] R. C. Haushalter, Z. Wang, L. M. Meyer, S. S. Dhingra, M. E. Thompson, J. Zubieta, *Chem. Mater.* **1994**, *6*, 1463.
[12] K.-F. Hsu, S.-L. Wang, *Chem. Mater.* **1999**, *11*, 1876.
[13] M.-Y. Lee, S.-L. Wang, *Chem. Mater.* **1999**, *11*, 3588.
[14] C. A. Bremner, W. T. A. Harrison, *Acta Crystallogr.* **2002**, *E58*, m319.
[15] F. Gagnard, C. Reisner, W. Tremel, *Inorg. Chem.* **1997**, *36*, 352.
[16] L.-H. Huang, H.-M. Kao, K.-H. Lii, *Inorg. Chem.* **2002**, *41*, 2936.
[17] S.-L. Wang, Y.-H. Lee, *Inorg. Chem.* **1994**, *33*, 3845.
[18] A.-H. Liu, S.-L. Wang, *Inorg. Chem.* **1998**, *37*, 3415.
[19] Y.-C. Liao, S.-H. Luo, S.-L. Wang, H.-M. Kao, K.-H. Lii, *J. Solid State Chem.* **2000**, *155*, 37.
[20] S.-H. Luo, Y.-C. Jiang, S.-L. Wang, H.-M. Kao, K.-H. Lii, *Inorg. Chem.* **2001**, *40*, 5381.
[21] B. Bazan, J. L. Mesa, J. L. Pizarro, L. Lezama, M. I. Arriortua, T. Rojo, *Inorg. Chem.* **2000**, *39*, 6056.
[22] S. Ekambaram, S. C Sevov, *Inorg. Chem.* **2000**, *39*, 2405.
[23] S. Chakrabarti, S. Natarajan, *Angew. Chem. Int. Ed.* **2002**, *41*, 1224.
[24] B. Bazan, J. L. Mesa, J. L. Pizarro, A. Goni, L. Lezama, M. I. Arriortua, T. Rojo, *Inorg. Chem.* **2001**, *40*, 5691.
[25] N.-Y. Fan, S.-L. Wang, *Inorg. Chem.* **1996**, *35*, 4708.
[26] S. Chakrabarti, S. Natarajan, *J. Chem. Soc., Dalton Trans.* **2002**, 3874.
[27] S. Chakrabarti, S. Natarajan, *J. Chem. Soc., Dalton Trans.* **2002**, 4156.
[28] G. Ferey, *J. Fluorine Chem.* **1995**, *72*, 187 and the references therein.
[29] G. Ferey, *Chem. Mater.* **2001**, *13*, 3084 and the references therein.
[30] I. D. Brown, D. Altermatt, *Acta Crystallogr., Sect. B* **1985**, *41*, 244.
[31] D. M. Hoffman, R. M. Fisel, R. H. Hoffman, *J. Am. Chem. Soc.* **1982**, *104*, 3859.
[32] *Atlas of Zeolite Framework Types* (Eds. Ch. Baerlocher, W. H. Meier and D. H. Olson), Elsevier, NY, 2001.
[33] T. Loiseau, G. Ferey, *J. Chem. Soc., Chem. Commun.* **1992**, 1197.
[34] J. W. Bray, L. V. Interrante, I. S. Jacobs and J. C. Bonnere, *Extended Linear Chain Compounds* (Ed. J. S. Miller), Plenum, New York, 1985, p.353.
[35] M. Troyer, H. Tsunetsugu, D. Wurtz, *Phys. Rev. B* **1994**, *50*, 13515.
[36] J. B. Goodenough, *Magnetism and the Chemical Bond*; Interscience; New York, 1963.
[37] *Vogel's Textbook of Quantitative Chemical Analysis*, Vth Edition, John Wiley & Sons Inc., New York, (1989).
[38] G. M. Sheldrick, *SADABS Siemens area detector absorption correction program*, University of Gottingen, Germany (1994).
[39] G. M. Sheldrick, *SHELX-97 A program for crystal structure solution and refinement*, University of Gottingen, Germany (1997).

Received April 25, 2003

 © 2003 Wiley-VCH Verlag GmbH & Co. KGaA, Weinheim

Synthesis and Characterization of Oxorhenium and Oxotechnetium Complexes with a Novel Tetradentate N_3O Bifunctional Agent

Maria Papachristou,[a] Ioannis Pirmettis,[a] Theodora Siatra-Papastaikoudi,[b] Maria Pelecanou,[c] Charalambos Tsoukalas,[a] Catherine P. Raptopoulou,[d] Aris Terzis,[d] Efstratios Chiotellis,[e] and Minas Papadopoulos*[a]

Keywords: Rhenium / Technetium / N,O ligands / Radiopharmaceuticals

The novel tetradentate N_3O bifunctional agent 3-hydroxy-4-[2-(2′-pyridinecarboxamido)acetylamino]benzoic acid (**1**), reacts with $[Bu_4N][ReOCl_4]$ or $[Bu_4N][^{99g}TcOCl_4]$ in EtOH resulting in neutral and stable oxorhenium **2** or oxotechnetium-99 g **3** complexes. Both complexes were characterized by elemental analysis, IR, ^1H and ^{13}C NMR spectroscopy. X-ray analysis of **2** showed that the rhenium atom is pentacoordinate presenting a distorted square-pyramidal coordination geometry. The analogous oxotechnetium-99m complex **4** was also prepared quantitatively by the reaction of ligand **1** with $Na^{99m}TcO_4$ in isotonic saline using tin chloride as reducing agent. Its identity was established by chromatographic comparison to the oxorhenium **2** and oxotechnetium **3** complexes.

(© Wiley-VCH Verlag GmbH & Co. KGaA, 69451 Weinheim, Germany, 2003)

Introduction

Technetium belongs to Group 7 of the Periodic Table and its chemistry has been explored extensively over the past years primarily because of the importance of the radioisotope ^{99m}Tc in the field of diagnostic nuclear medicine.[1,2] Rhenium, which also belongs to Group 7, exhibits similar chemical properties to technetium and is often used as a nonradioactive alternative to working with technetium radionuclides.[2] Furthermore, the β-emitting radionuclides ^{186}Re ($t_{1/2}$ = 90 h) and ^{188}Re ($t_{1/2}$ = 17 h) are of great interest to nuclear medicine as they possess physical and nuclear properties favourable for use in systemic radiotherapy.[3] In fact, ^{99m}Tc and $^{186/188}Re$ can be considered to be a matched pair for imaging and therapy.

The bifunctional strategy for the development of technetium and rhenium radiopharmaceuticals has become the most widely used method for producing well-defined technetium- and rhenium-labelled receptor ligands capable of highly specific in vivo localization in target tissues.[4] In this strategy a bifunctional coupling agent (BFCA) is used for the chelation of the radionuclide (^{99m}Tc or ^{188}Re) and the conjugation of the receptor ligand. An ideal BFCA is one which is able to form stable and inert ^{99m}Tc or ^{188}Re complexes in high yield at low concentration without the formation of isomers.

In this work, we report the synthesis and characterization of the new BFCA 3-hydroxy-4-[2-(2′-pyridinecarboxamido)acetylamino]benzoic acid and of the corresponding oxorhenium(v) and oxotechnetium(v) complexes. Studies at tracer level using ^{99m}Tc are also reported. This ligand is designed with the purpose of chelating to oxorhenium and oxotechnetium with an N_3O donor system involving the pyridine nitrogen, the amide nitrogens and the phenolate oxygen. For coupling to the target molecule, the carboxyl group is selected since many biomolecules contain amino groups available for formation of amide bonds. Furthermore, this ligand system does not lead to formation of *syn-anti* isomers.

Results and Discussion

Condensation of ethyl 4-amino-3-hydroxybenzoate, N-Boc-glycine and 2-carboxypyridine in the presence of DCC resulted in the novel tetradentate ligand 3-hydroxy-4-[2-(2′-pyridinecarboxamido)acetylamino]benzoic acid (**1**; Scheme 1).[5] The product was purified by flash column chromatography and characterized by elemental analysis, ^1H and ^{13}C NMR spectroscopy (Table 1 and Figure 1).

[a] Institutes of Radioisotopes-Radiodiagnostic Products, NCSR "Demokritos",
Ag. Paraskevi, Athens, Greece
Fax: (internat.) +30-210/652-4480
E-mail: mspap@rrp.demokritos.gr
[b] Department of Pharmaceutical Chemistry, University of Athens,
Athens, Greece
[c] Institutes of Biology, NCSR "Demokritos",
Ag. Paraskevi, Athens, Greece
[d] Institutes of Materials Science, NCSR "Demokritos",
Ag. Paraskevi, Athens, Greece
[e] School of Pharmacy, Aristotelian University of Thessaloniki, Thessaloniki, Greece

 © 2003 Wiley-VCH Verlag GmbH & Co. KGaA, Weinheim **DOI: 10.1002/ejic.200300298**

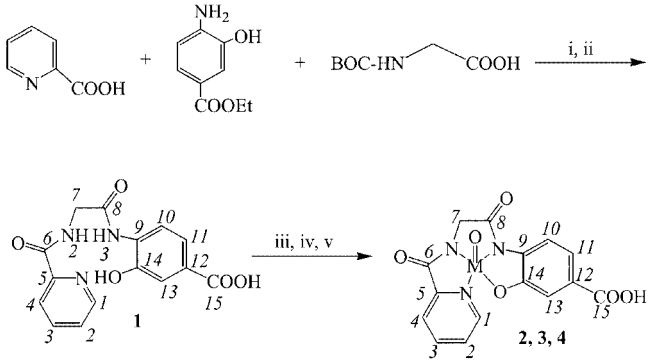

Scheme 1. Synthesis of ligand and complexes studied: (i) DCC, THF, 25 °C, 4 h; (ii) $NaHCO_3$, CH_3COOH (yield 42%); (iii) M= Re, $[Bu_4N][ReOCl_4]$ for **2**; (iv) M=^{99g}Tc, $[Bu_4N][^{99g}TcOCl_4]$ for **3**; (v) M=^{99m}Tc, $Na^{99m}TcO_4$, $SnCl_2$ for **4**

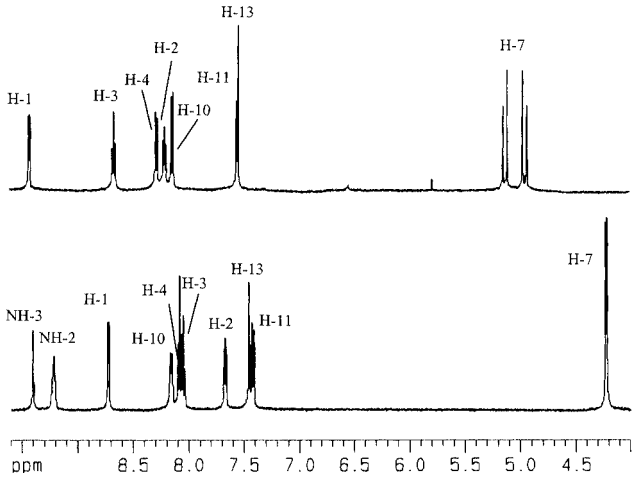

Figure 1. ^{1}H NMR spectra of ligand **1** (bottom) and complex **3** (top) in $[D_6]$DMSO (range 9.60−4.00 ppm) at 25 °C

The oxorhenium complex **2** was prepared by reacting ligand **1** with the $[Bu_4N][ReOCl_4]$ precursor in EtOH (Scheme 1). A similar reaction was employed for the preparation of the oxotechnetium complex **3** using $[Bu_4N][^{99g}TcOCl_4]$ as a precursor. Complexes **2** and **3** were characterized by elemental analysis, IR, UV/Vis, ^{1}H and ^{13}C NMR spectroscopy (Table 1 and Figure 1). Complex **2** was also characterized by X-ray crystallography. Both complexes are soluble in DMSO, slightly soluble in dichloromethane, methanol and ethanol and insoluble in water. They are stable in the solid state as well as in organic solvents (for a period of months), as shown by HPLC and NMR spectroscopy. Their stability is not affected by the presence of air or moisture.

The IR spectra of the complexes show characteristic peaks at 981 cm^{-1} and 972 cm^{-1} that can be attributed to oxorhenium and oxotechnetium bond stretches respectively.[6] The Re=O stretch in **2** is higher than the Tc=O stretch in **3**. This shift to higher frequencies of the Re=O compared to Tc=O complex has been attributed to the greater orbital overlap of the 5d orbitals of rhenium as compared to the 4d orbitals of technetium.[7] The electronic absorption spectra of the oxorhenium and oxotechnetium complexes were determined upon HPLC analysis by using a photodiode array detector. The UV/Vis spectrum of complex **2** is characterized by an intense band at 380 nm, while the UV/Vis spectra of the oxotechnetium complex **3** is characterized by an intense band at 480 nm.

An ORTEP diagram of complex **2** is given in Figure 2. Selected distances and angles are listed in Table 2. The coordination geometry about the metal is distorted square pyramidal with the pyridine nitrogen, the two amide nitrogens and the phenolate oxygen of the tetradendate ligand occupying the equatorial plane and the oxo group directed in the apical position. The carboxylate group of the tetradentate ligand remains uncoordinated. Rhenium lies 0.76 Å out of the equatorial plane toward the oxo group. The angles between the opposite atoms of the equatorial plane severely deviate from the ideal value of 180° [N(1)−Re−N(3) = 135.3(3)°, N(2)−Re−O(3) = 134.7(3)°]. Inspection of the shape-determining angles about the metal

Table 1. ^{1}H and ^{13}C NMR chemical shifts (ppm) for ligand **1** and complexes **2** and **3** in $[D_6]$DMSO at 25 °C; the numbering used is shown in Scheme 1 and is according to the crystallographic structure of Figure 2

	1	**2**	**3**		**1**	**2**	**3**
H-1	8.72	9.55	9.42	C-1	148.64	159.40	151.69
H-2	7.67	8.31	8.21	C-2	126.97	128.63	129.22
H-3	8.05	8.56	8.66	C-3	138.00	144.34	146.02
H-4	8.09	8.15	8.28	C-4	121.98	124.86	125.05
H-7	4.23	5.24,	5.13,	C-5	149.29	152.68	151.87
		4.83 (^2J = 18.3 Hz)	4.95 (^2J = 18.0 Hz)	C-6	163.59	179.05	170.74
				C-7	43.58	59.88	58.22
H-10	8.16	8.29	8.14	C-8	168.01	184.05	181.07
H-11	7.42	7.45	7.56	C-9	146.13	147.56	145.14
H-13	7.45	7.54	7.54	C-10	119.72	116.89	116.90
NH-2	9.22	–	–	C-11	120.96	120.64	121.57
NH-3	9.40	–	–	C-12	125.83	126.01	126.62
OH	10.35	–	–	C-13	115.44	116.04	115.09
COOH	12.69	12.73	12.74	C-14	146.03	173.35	165.12
				C-15	166.62	167.75	166.63

 © 2003 Wiley-VCH Verlag GmbH & Co. KGaA, Weinheim

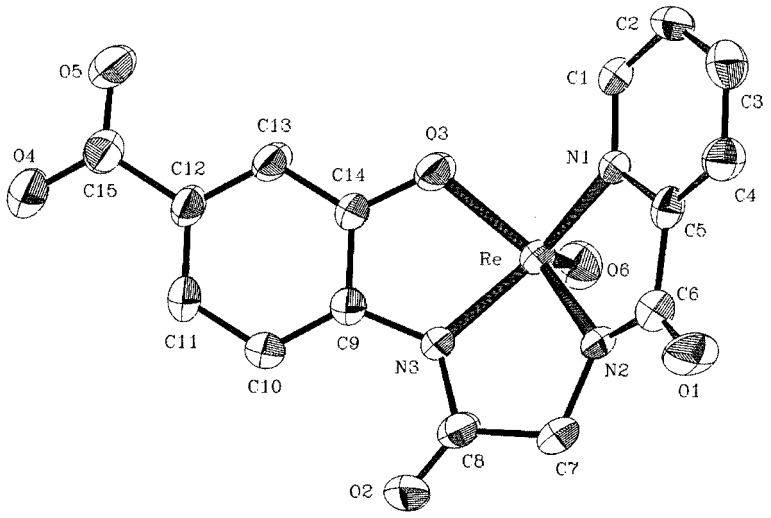

Figure 2. ORTEP diagram of **2** with 50% probability thermal ellipsoids showing the atomic labelling scheme

according to the analysis of Addison et al.[8] gives a value of 0.01 for the trigonality index, τ. The Re−N_{amide} bond lengths are 1.965(6) Å while the Re−$N_{pyridine}$ bond length is slightly longer at 2.076(6) Å. The Re−O_{oxo} and the Re−$O_{phenolate}$ bond lengths are 1.685(6) and 1.962(5) Å respectively. These values are in agreement with those found in analogous pentacoordinate oxorhenium complexes.[9] However, the Re−$N_{pyridine}$ and the Re−$O_{phenolate}$ bond lengths are shorter than heptacoordinated oxorhenium complexes with similar donor centers.[10] The two five-membered rings in the coordination sphere, i.e. those defined by Re−N2−C7−C8−N3 and Re−N3−C9−C14−O3 adopt the stable envelope configuration, with the metal being 0.53 and 0.35 Å, respectively, out of the mean plane of the remaining four atoms. On the contrary, the five-membered ring defined by Re−N1−C5−C6−N2 is planar, with C5 having the largest displacement of 0.028 Å out of the best mean plane.

Table 2. Selected bond lengths (Å) and angles (°) for complex **2**

Distances (Å)			
Re−O(6)	1.685(6)	Re−N(2)	1.965(6)
Re−O(3)	1.962(5)	Re−N(3)	1.965(6)
Re−N(1)	2.076(6)		
Angles (°)			
O(6)−Re−O(3)	112.9(3)	N(3)−Re−N(2)	79.1(3)
O(6)−Re−N(3)	113.1(3)	O(6)−Re−N(1)	111.3(3)
O(3)−Re−N(3)	80.4(2)	O(3)−Re−N(1)	87.8(2)
O(6)−Re−N(2)	112.2(3)	N(3)−Re−N(1)	135.3(3)
O(3)−Re−N(2)	134.7(3)	N(2)−Re−N(1)	79.4(2)

The two amide functions of the tetradentate ligand are planar, as indicated by the values of the ω_1 (C-C-*N*-C), ω_2 (O-C-*N*-M) and ω_3 (O-C-*N*-C) torsion angles and the values of the parameters τ [$(\omega_1 + \omega_2)/2(|\omega_1 - \omega_2| < \pi)$], χ_N [$(\omega_2 - \omega_3 + \pi)$mod2π] and χ_C [$(\omega_1 - \omega_3 + \pi)$mod2π], where τ is the approximate measure of the angles between the nitrogen and carbonyl carbon π orbitals and χ_N and χ_C describe the out-of-plane bending at the amide nitrogen and at the amide carbon respectively.[11] The torsion angles for the one amide group are: ω_1 = C5−C6−N2−C7 = −165.47°, ω_2 = O1−C6−N2−Re = 173.14° and ω_3 = O1−C6−N2−C7 = 11.32° thus, the calculated parameters are τ = 3.84°, χ_N = −18.18° and χ_C = 3.21°. For the second amide function these angles are: ω_1 = C7−C8−N3−C9 = −158.85°, ω_2 = O2−C8−N3−Re = −167.91° and ω_3 = O2−C8−N3−C9 = 22.33° thus, the calculated parameters are τ = −163.38°, χ_N = −10.24° and χ_C = −1.18°.

The short interatomic distance between the carboxylate oxygens O(4)···O(5′) (1 − *x*, 1 − *y*, −*z*) = 2.603 Å belonging to adjacent molecules is probably indicative of a hydrogen bonding interaction, although the hydrogen atom was not located in the difference map.

The synthesis of the complex was successfully transferred at tracer level (^{99m}Tc). Ligand **1** reacted with $Na^{99m}TcO_4$ in isotonic saline using tin chloride as reducing agent (Scheme 1) to give the oxotechnetium-99m complex **4**. The radiochemical purity of the reaction mixture was checked by HPLC and the radioactivity of the major peak was more than 85%, while the recovery of radioactivity from the column was quantitative. The characterization of complex **4** was accomplished by chromatographic comparison (HPLC) to the analogous oxorhenium (**2**) and oxotechnetium-99 g (**3**) complexes adopting parallel radiometric and photometric detection. Thus, by co-injection of the respective ^{99m}Tc and Re/^{99g}Tc complexes, identical retention times were obtained revealing the structural analogy of the three complexes (Figure 3).

In conclusion, the novel tetradentate ligand 3-hydroxy-4-[2-(2′-pyridinecarboxamido)acetylamino]benzoic acid (**1**) was synthesized and successfully used for the synthesis of stable and neutral complexes with rhenium and technetium at carrier (Re/^{99g}Tc) and at tracer level (^{99m}Tc). The carboxyl group does not coordinate to the metal and thus it

 © 2003 Wiley-VCH Verlag GmbH & Co. KGaA, Weinheim

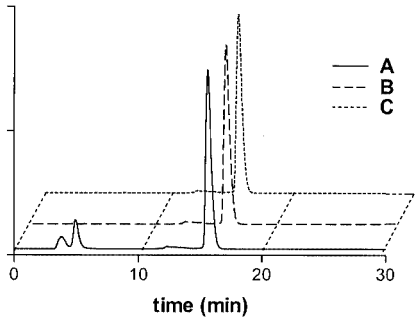

Figure 3. Comparative reverse-phase HPLC chromatograms: **A** (radiometric detection): reaction mixture from the preparation at tracer level (^{99m}Tc), complex **4** (t_R: 15.58 min, 85%); **B** (UV recording at 254 nm): complex **2** (t_R: 15.04 min); **C** (UV recording at 254 nm): complex **3** (t_R: 15.34 min)

could be used for the conjugation of the receptor ligand to develop target-specific radiopharmaceuticals for diagnosis and therapy.

Experimental Section

Caution!!! Technetium-99 g is a weak β-emitter (0.292 MeV) with a half life of 2.12×10^5 years. All manipulations of solutions and solids were carried out in a laboratory approved for the handling of low-level radioisotopes. Normal safety procedures were followed at all times to prevent contamination.

IR spectra were recorded as KBr pellets in the range 4000−500 cm^{-1} on a Perkin−Elmer 1600 FT-IR spectrophotometer. NMR spectra were recorded in [D_6]DMSO, at 25 °C on a Bruker 500 MHz Avance DRX spectrometer using TMS as internal standard. Chemical shift assignments were based on a series of 2D homo- and heteronuclear correlation spectra. Elemental analyses were performed on a Perkin−Elmer 2400/II automated analyser. ^{99g}Tc was purchased as ammonium pertechnetate from the Oak Ridge National Laboratory. The impure black solid was purified prior to use by overnight treatment with hydrogen peroxide and ammonium hydroxide in methanol. Evaporation of the solvent gave ammonium pertechnetate as a white powder. $Na^{99m}TcO_4$ was obtained in isotonic saline as commercial ^{99}Mo/^{99m}Tc generator eluate (Cis International). The precursors [Bu_4N][$ReOCl_4$] and [Bu_4N][$^{99g}TcOCl_4$] were synthesized by literature methods.[12,13] Ethyl 4-amino-3-hydroxybenzoate was prepared by refluxing 4-amino-3-hydroxybenzoic acid in EtOH in the presence of HCl. All laboratory chemicals were reagent grade.

High performance liquid chromatography (HPLC) analysis was performed on a Waters 600E Chromatography System coupled to both a Waters 991 photodiode array detector (UV trace for ^{99g}Tc, Re and ligands) and a GABI gamma detector from Raytest (γ trace for ^{99m}Tc). Separations were achieved on a Techsil C18 (10 μm, 250 mm × 4 mm) column eluted with a binary gradient system at a 1.0 mL/min flow rate. Mobile phase A was water containing 0.1% trifluoroacetic acid while mobile phase B was methanol. The elution profile was: 0 min 5% B followed by a linear gradient to 70% in 8 min; this composition was held for another 12 min. Prior to each injection the column was washed with 95% B for 5 min and re-equilibrated by applying the initial conditions (5% B) for 15 min.

NMR spectroscopic data for **1**, **2** and **3** are given in Table 1.

Synthesis of Ligand 1: A solution in THF (40 mL) of ethyl 4-amino-3-hydroxybenzoate (1.81 g, 0.01 mol), N-Boc-glycine (1.75 g, 0.01 mol), 2-carboxypyridine (1.23 g, 0.01 mol) and *N*,*N*′-dicyclohexylcarbodiimide (2.48 g, 0.012 mol) was stirred at room temperature for 4 hours. The insoluble urea was removed by filtration, the solvent was replaced by ethyl acetate and the solution was washed with dilute acetic acid and aqueous sodium hydrogencarbonate. The solvent was removed and the product was purified by flash column chromatography (silica gel 60, $CHCl_3$/MeOH/CH_3COOH, 77:15:8). Yield 42%. $C_{15}H_{13}N_3O_5$ (315.28): calcd. C 57.14, H 4.16, N 13.33; found C 57.07, H 4.22, N 13.17.

Synthesis of Oxorhenium Complex 2: A solution of ligand **1** (40 mg, 0.1 mmol) in MeOH (3 mL) was added to a solution of [Bu_4N][$ReOCl_4$] (58.6 mg, 0.1 mmol) in MeOH (15 mL). The reaction mixture was refluxed for 1 h. After cooling to room temperature the reaction mixture was diluted with CH_2Cl_2 and then washed with water. The organic layer was collected and dried over $MgSO_4$. The volume of the solution was reduced and then 5 mL of MeOH was added. Slow evaporation of the solvents at room temperature afforded the product as red crystals. Recrystallization from CH_2Cl_2/MeOH afforded crystals of **2** suitable for X-ray crystallography. Yield: 50%; R_f (SiO_2, CH_2Cl_2): 0.5; HPLC retention time: 15.04 min. FT-IR (KBr): $\tilde{\nu}$ = 981 cm^{-1} (Re=O). UV/Vis: λ_{max} = 229 nm, 271, 380. $C_{15}H_{10}N_3O_6Re$ (514.46): calcd. C 35.02, H 1.96, N 8.17; found C 34.95, H 1.94, N 8.04.

Synthesis of Oxotechnetium-99g Complex 3: A solution of **1** (40 mg, 0.1 mmol) in MeOH (2 mL) was added to a solution of [Bu_4N][$^{99g}TcOCl_4$] (50 mg, 0.1 mmol) in MeOH (10 mL) and the mixture was stirred at room temperature for 1 h. Upon standing, a brown solid precipitated that was collected and washed with Et_2O. Yield: 40%; R_f (SiO_2,CH_2Cl_2): 0.5; HPLC retention time: 15.34 min. FT-IR (KBr): $\tilde{\nu}$ = 972 cm^{-1} (Tc=O). UV/Vis: λ_{max} = 229 nm, 265, 480. $C_{15}H_{10}N_3O_6Tc$ (427.16): calcd. C 42.18, H 2.36, N 9.84; found C 42.08, H 2.29, N 9.73.

Synthesis of Oxotechnetium-99m Complex 4: Ligand **1** (0.5 mg in 100 μL saline solution) and $Na^{99m}TcO_4$ (40 mCi in 600 μL saline solution) were added to a vial containing a 0.1 M solution of sodium citrate (100 μL). A fresh solution of $SnCl_2$ in EtOH (20 μg, 20 μL) was subsequently added and the mixture was left to react at room temperature for 15 min. The pH was then brought to 7.0 and the reaction was analysed by HPLC. HPLC retention time: 15.58 min. Labelling yield >85%. The identity of the ^{99m}Tc complex was established by comparative HPLC studies using samples of the well-characterized corresponding oxorhenium and oxotechnetium complexes as references.

X-ray Crystal Structure Determination: A red crystal of **2** with approximate dimensions 0.04 × 0.20 × 0.40 mm was mounted in air. Diffraction measurements were made on a Crystal Logic Dual Goniometer diffractometer using graphite monochromated Mo-K_α radiation. Complete crystal data and parameters for data collection and refinement are listed in Table 3. Unit cell dimensions were determined and refined by using the angular settings of 25 automatically centered reflections in the range $11 < 2\theta < 23°$.

Intensity data were recorded using the θ-2θ scan method. Three standard reflections monitored every 97 reflections showed less than 3% variation and no decay. Lorentz, polarization and ψ-scan absorption corrections were applied using the Crystal Logic software.

 © 2003 Wiley-VCH Verlag GmbH & Co. KGaA, Weinheim

Table 3. Summary of crystal data for complex **2**

Parameter	**2**
Empirical formula	$C_{15}H_{10}N_3O_6Re$
Mol. wt.	514.46
Crystal system	Monoclinic
Space group	$P2_1/n$
a (Å)	9.836(6)
b (Å)	21.60(1)
c (Å)	7.606(5)
β (°)	111.99(2)
V (Å^3)	1498(2)
Z	4
ρ (Mg·m^{-3})	2.281
T (°C)	25
λ (Mo-K_α) (Å)	0.71073
μ (mm^{-1})	8.151
F(000)	976
$2\theta_{max}$ (°)	50
Index ranges	$-11 \le h \le 8$, $-25 \le k \le 0$, $0 \le l \le 9$
No. of reflections collected	2682
No. of indep. refls./ Rint	2519/0.0303
Data with $I > 2\sigma(I)$	2184
$(\Delta/\sigma)_{max}$	0.041
GOF (on F^2)	1.089
$R1$[a]	0.0376
$wR2$[b]	0.0947
Residuals (e·Å^{-3})	0.798/−0.403

[a] $R1 = \Sigma(|F_o| - |F_c|)/\Sigma(|F_o|)$. [b] $wR2 = \{\Sigma[w[(F_o^2 - F_c^2)^2]/\Sigma[w(F_o^2)^2]\}^{1/2}$.

The structure was solved by direct methods using SHELXS-86[14] and refined by full-matrix least-squares techniques on F^2 with SHELXL-93.[15] All hydrogen atoms (except that of the carboxylate group which was not included in the refinement) were located by difference maps and their positions were refined isotropically. All non-hydrogen atoms were refined anisotropically.

CCDC-208922 contains the supplementary crystallographic data for this paper. These data can be obtained free of charge at www.ccdc.cam.ac.uk/conts/retrieving.html [or from the Cambridge Crystallographic Data Centre, 12, Union Road, Cambridge CB2 1EZ, UK; Fax: (internat.) +44-1223/336-033; E-mail: deposit@ccdc.cam.ac.uk].

[1] S. Jurisson, J. D. Lydon, *Chem. Rev.* **1999**, *99*, 2205−2218.
[2] S. Jurisson, D. B. Berning, W. Jia, D. Ma, *Chem. Rev.* **1993**, *93*, 1137−1156.
[3] J. Dilworth, S. Parrot, *Chem. Soc. Rev.* **1998**, *27*, 43−55.
[4] S. Liu, D. S. Edwards, *Chem. Rev.* **1999**, *99*, 2235−2268.
[5] J. Sheehan, G. Hess, *J. Am. Chem. Soc.* **1955**, *77*, 1067−1068.
[6] [6a] U. Mazzi, *Polyhedron* **1989**, *8*, 1683−1688. [6b] T. N. Rao, D. Adhikesavalu, A. Camerman, A. R. Fritzberg, *J. Am. Chem. Soc.* **1990**, *112*, 5798−5804. [6c] J. O'Neil, S. Wilson, J. Katzenellenbogen, *Inorg. Chem.* **1994**, *33*, 319−325. [6d] M. Pelecanou, I. Pirmettis, M. Papadopoulos, C. P. Raptopoulou, A. Terzis, E. Chiotellis, C. I. Stassinopoulou, *Inorg. Chim. Acta* **1999**, *287*, 142−151.
[7] A. Davison, C. Orving, H. S. Trop, M. Sohn, B. V. DePamphilis, A. G. Jones, *Inorg. Chem.* **1980**, *19*, 1988−1992.
[8] A. W. Addison, T. N. Rao, J. Reedijk, G. C. Verschoor, *J. Chem. Soc., Dalton Trans.* **1984**, 1349−1356.
[9] M. Papadopoulos, B. Nock, T. Maina, I. Pirmettis, C. Raptopoulou, A. Tasiopoulos, A. Troganis, T. Kabanos, A. Terzis, E. Chiotellis, *J. Biol. Inorg. Chem.* **2001**, *6*, 159−165.
[10] L. Xu, I. Setyawati, J. Pierreroy, M. Pink, V. Young Jr, B. Patrick, S. Rettig, C. Orvig, *Inorg. Chem.* **2000**, *39*, 5958−5963.
[11] F. C. Anson, T. J. Collins, S. L. Gipson, J. T. Keech, T. E. Kraft, G. T. Peake, *J. Am. Chem. Soc.* **1986**, *108*, 6593−6605.
[12] R. Alberto, R. Schibli, A. Egli, A. Schubiger, W. A. Herrmann, G. Artus, U. Abram, T. Kaden, *J. Organomet. Chem.* **1995**, *492*, 217−224.
[13] A. Davison, H. S. Trop, B. V. DePamphilis, A. G. Jones, *Inorg. Synth.* **1982**, *21*, 160−162.
[14] G. M. Sheldrick, *SHELXS-86, Program for the Solution of Crystal Structures*, University of Göttingen, Germany, **1986**.
[15] G. M. Sheldrick, *SHELXL-93, Program for the Refinement of Crystal Structures*, University of Göttingen, Germany, **1993**.

Received May 19, 2003

 © 2003 Wiley-VCH Verlag GmbH & Co. KGaA, Weinheim

New Tris(pyrazolyl)triazine and Pyrazolylpyridine Gold(I) and Palladium(II) Derivatives Based on the 3,5-Bis(4-butoxyphenyl)pyrazole Group – Architectures with Different Types of Bonding Interactions

Rosa M. Claramunt, Pilar Cornago, Mercedes Cano,* José V. Heras, M. Luz Gallego, Elena Pinilla, M. Rosario Torres

Keywords: Gold / Hydrogen bonds / Palladium / Supramolecular Chemistry / Triazine

In the original article[1] the footnotes of Tables 1 and 2 on pages 2694 and 2695 are erroneous. The correct version is given below.

Table 1. Selected bond lengths [Å] and angles [°] for **4** with e.s.d.s. in parentheses, including the hydrogen bond geometries

	A	B	C	
Pd−N1	2.10(2)	2.12(1)	2.12(1)	
Pd−N3	2.11(1)	2.12(1)	2.10(1)	
Pd−C9	2.10(1)	2.10(1)	2.10(1)	
Pd−C10	2.13(2)	2.10(1)	2.10(1)	
Pd−C11	2.15(2)	2.12(2)	2.12(2)	
C9−C10	1.382(5)	1.384(5)	1.384(5)	
C10−C11	1.377(5)	1.384(5)	1.386(5)	
N1−Pd−N3	91.1(3)	93.4(4)	93.3(4)	
N1−Pd−C9	98.8(6)	97.9(4)	100.0(4)	
N1−Pd−C10	132.8(6)	130.3(4)	131.1(4)	
N1−Pd−C11	167.1(6)	167.2(4)	169.3(4)	
N3−Pd−C11	100.8(6)	99.3(4)	97.1(4)	
N3−Pd−C9	170.0(6)	168.3(3)	166.1(4)	
N3−Pd−C10	132.9(6)	132.7(4)	131.2(4)	
C9−Pd−C10	38.2(3)	38.3(2)	38.7(2)	
C9−Pd−C11	69.3(5)	69.3(3)	69.8(3)	
C10−Pd−C11	37.6(3)	38.3(2)	38.4(2)	
Hydrogen bond geometries				
D−H···A	D···A	D−H	H···A	D−H···A
N2A−H2A···F9′ [a]	2.81(2)	0.86	1.97	167.9
N4A−H4A···F2	2.89(1)	0.86	2.06	162.9
N2B−H2B···F7	3.02(1)	0.86	2.19	161.7
N4B−H4B···F1	2.81(1)	0.86	1.99	174.0
N2C−H2C···F11	2.81(1)	0.86	1.91	163.8
N4C−H4C···F5	2.81(1)	0.86	2.01	175.1

[a] $x, y, z + 1$.

Table 2. Selected bond lengths [Å] and angles [°] for **5** with e.s.d.s. in parentheses, including the hydrogen bond geometries

N3−O5	1.236(9)			
N3−O3	1.245(8)			
N3−O4	1.213(8)			
Au1−N1	2.077(5)			
Au1−P1	2.239(2)			
P1−C32	1.800(8)			
P1−C26	1.826(8)			
P1−C38	1.822(7)			
Au1···O1′ [a]	3.540(6)			
N1−Au1−P1	178.1(2)			
O5−N3−O3	117.9(8)			
O5−N3−O4	121.0(8)			
O3−N3−O4	121.2(7)			
Hydrogen bond geometries				
D−H···A	D···A	D−H	H···A	D−H···A
N2−H2···O3	2.764(9)	0.95(6)	1.82(7)	171(6)
C4−H4A···O4′′[b]	3.382(9)	0.93	2.63	137.3
C40−H40A···O5′′′[c]	3.31(1)	0.93	2.88	115.1

[b] $-x + 1, -y + 1, -z + 1$. [b] $-x, -y + 1, -z + 1$. [c] $-x, -y + 1, -z$.

[1] R. M. Claramunt, P. Cornago, M. Cano, J. V. Heras, M. L. Gallego, E. Pinilla, M. R. Torres, *Eur. J. Inorg. Chem.*, **2003**, 2693−2704.

Received September 24, 2003
The Editors

 DOI: 10.1002/ejic.200300663 © 2003 Wiley-VCH Verlag GmbH & Co. KGaA, Weinheim

EurJIC
European Journal of Inorganic Chemistry

Issue 21/2003

Pages 3833–3974

Papers available ahead of print in Early View at www.interscience.wiley.com

Earliest available Table of Contents:
Automatically, free of charge by e-mail through
www.interscience.wiley.com/alerts

COVER PICTURE

The cover picture shows the crystal structure of lithium bis[benzoyl-$W(CO)_5$][μ_2-hydrogen] (orange: tungsten; red: oxygen; blue: lithium; grey: carbon), a new class of hydrogen-bridged organometallic complexes exhibiting strong, charge-assisted hydrogen bonds between anionic metal–acyl moieties in Fischer-type carbene precursors. The novel cation-exchange procedure used here could find application in future organometallic crystal engineering studies involving carbonylmetal fragments. Details are discussed in the article by H. G. Raubenheimer et al. on p. 3861 ff. *Dedicated to E. O. Fischer on the occasion of his 85th birthday*

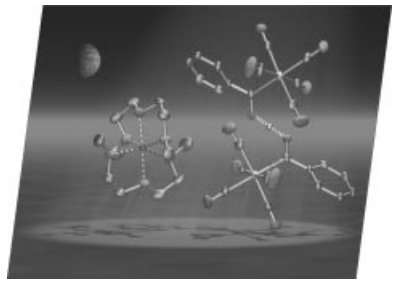

MICROREVIEW

Contents

3843 **C. Den Auwer,* E. Simoni, C. Conradson, C. Madic**

Investigating Actinyl Oxo Cations by X-ray Absorption Spectroscopy

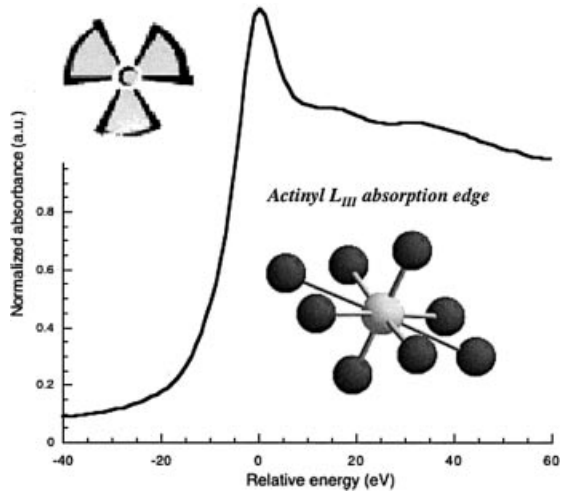

Keywords: Actinides / Oxo ligands / XANES / EXAFS

 © 2003 Wiley-VCH Verlag GmbH & Co. KGaA, Weinheim

FULL PAPERS

3861 **M. W. Esterhuysen, H. G. Raubenheimer***

Lithium [Bis{benzoyl-W(CO)$_5$}(μ_2-hydrogen)] − A Charge-Assisted H$^+$-Bridged Organometallic Complex Prepared by Selective Li$^+$ Ion Replacement

Keywords: Lithium / Tungsten / Hydrogen bonds / Crystal engineering / Carbene complexes / Self-assembly

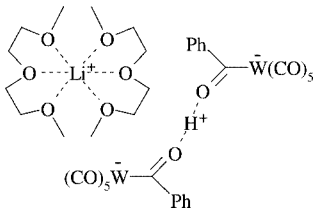

3870 **C. D. Nunes, M. Pillinger, A. A. Valente, J. Rocha, A. D. Lopes, I. S. Gonçalves***

Dioxomolybdenum(VI)-Modified Mesoporous MCM-41 and MCM-48 Materials for the Catalytic Epoxidation of Olefins

Keywords: Molybdenum / N ligands / Mesoporous materials / Supported catalysts / Epoxidations

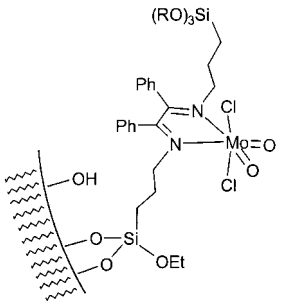

3878 **M. Doux, N. Mézailles, L. Ricard, P. Le Floch***

Group 10 Metal Complexes of SPS-Based Pincer Ligands: Syntheses, X-ray Structures, and DFT Calculations

Keywords: Phosphorus / S ligands / Donor-acceptor systems / Density functional calculations / Group 10 elements

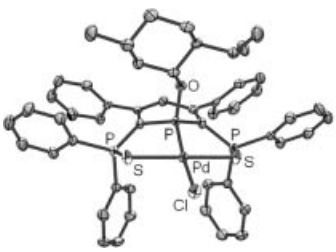

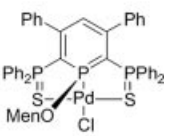

3895 **M. H. Garcia,* S. Royer, M. P. Robalo,* A. R. Dias, J.-P. Tranchier, R. Chavignon, D. Prim, A. Auffrant, F. Rose-Munch, E. Rose,* J. Vaissermann, A. Persoons, I. Asselberghs**

Synthesis, Characterisation of (Arene)tricarbonylchromium Complexes Linked to Cationic Fe and Ru Derivatives and Studies of First Hyperpolarisabilities by Hyper-Rayleigh Scattering

Keywords: Chromium / Iron / Ruthenium / Non-linear optics / Arene ligands / Carbonyl ligands / Hyperpolarisability

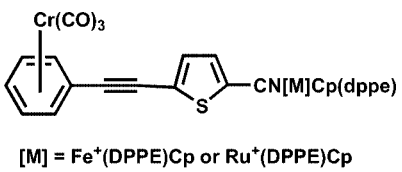

3905 **J. Sanmartín,* A. M. García-Deibe, M. R. Bermejo, F. Novio, D. Navarro, M. Fondo**

Mono- and Dinuclear Complexes of a Flexible Schiff Base Ligand − Crystal Structures of a Bishelicate and Two Acentric Monohelicates

Keywords: Helical structures / N ligands / Schiff bases / Supramolecular chemistry / Transition metals

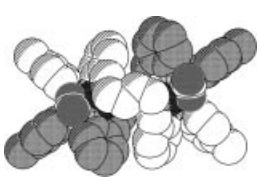

 © 2003 Wiley-VCH Verlag GmbH & Co. KGaA, Weinheim

3914 **A. L. Litvinov, D. V. Konarev, A. Y. Kovalevsky, A. N. Lapshin, E. I. Yudanova, N. V. Drichko, P. Coppens, R. N. Lyubovskaya***

Synthesis, Crystal Structure, and Optical Properties of a New Molecular Complex of C_{60} with a Covalently Linked $(Fe^{III}TPP)_2O$ Dimer

Keywords: Fullerenes / Porphyrinoids / Crystal engineering / Solid-state structures / UV/Vis spectroscopy

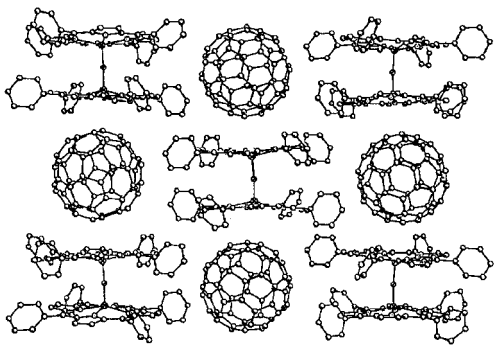

3918 **K. Heinze,* V. Jacob**

Stepwise Assembly of Mixed Metal Dinuclear Carbonyl Complexes

Keywords: Heterometallic complexes / Isocyanide ligands / Bridging ligands / Isomers / Group 6 elements

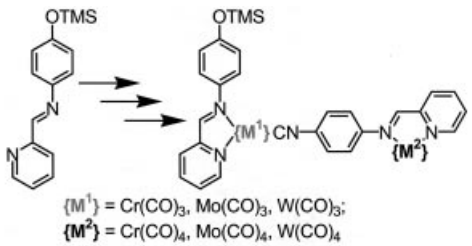

3924 **I. M. Mbomekalle, B. Keita, L. Nadjo,* W. A. Neiwert, L. Zhang, K. I. Hardcastle, C. L. Hill, T. M. Anderson**

Lacunary Wells–Dawson Sandwich Complexes – Synthesis, Characterization, and Stability Studies of Multi-Iron Species

Keywords: Polyoxometalates / Sandwich complexes / Iron / Manganese

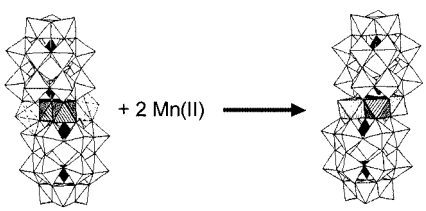

3929 **D. Ghoshal, H. Bialas, A. Escuer, M. Font-Bardía, T. K. Maji, J. Ribas, X. Solans, R. Vicente,* E. Zangrando, N. R. Chaudhuri**

Syntheses, Structure and Magnetic Properties of the First $\mu_{1,5}$-Dicyanamido-Bridged Dinuclear Compounds $[Ni(\mu_{1,5}\text{-dca})(dca)(dpt)]_2$ and $[Ni(\mu_{1,5}\text{-dca})(dca)(medpt)]_2$

Keywords: N ligands / Bridging ligands / Nickel / Magnetic properties

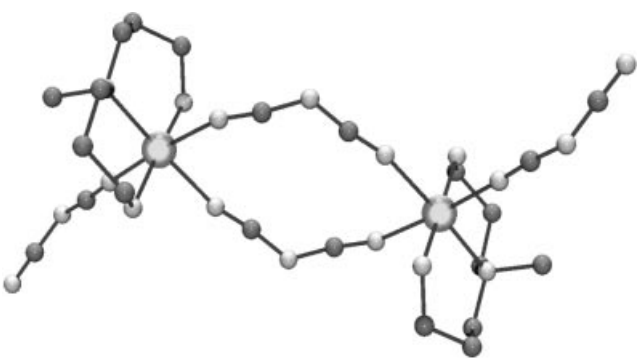

3934 **M. C. Mimmi, M. Gullotti,* L. Santagostini, R. Pagliarin, L. De Gioia, E. Monzani, L. Casella**

Synthesis and Conformational Studies of a Chiral Octadentate Ligand Derived from (*R*)-1,1′-Binaphthyl-2,2′-diamine and its Dinuclear Zinc(II) and Nickel(II) Complexes

Keywords: N ligands / Zinc / Chirality / Conformational analysis / Nickel

 © 2003 Wiley-VCH Verlag GmbH & Co. KGaA, Weinheim

3945 **P. C. Kunz, G. J. Reiß, W. Frank, W. Kläui***

A Novel Water-Soluble Tripodal Imidazolyl Ligand as a Model for the Tris(histidine) Motif of Zinc Enzymes: Nickel, Cobalt and Zinc Complexes and a Comparison with Metal Binding in Carbonic Anhydrase

Keywords: Bioinorganic chemistry / Cobalt / Enzyme models / N ligands / Nickel / Tripodal ligands / Zinc

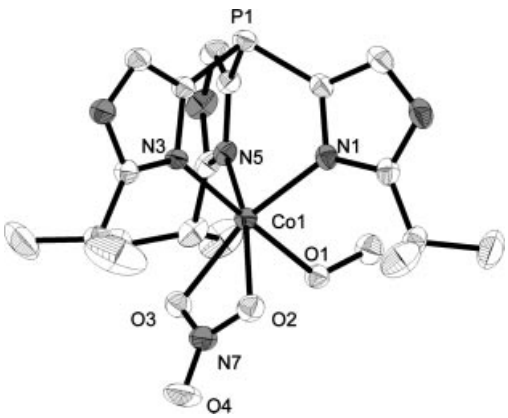

3952 **J. García-Antón, J. Pons,* X. Solans, M. Font-Bardia, J. Ros***

Synthesis of New Pd^{II} Complexes Containing a Thioether-Pyrazole Hemilabile Ligand − Structural Analysis by ^{1}H, ^{13}C NMR Spectroscopy and Crystal Structure of $[PdCl(bdtp)]BF_4$ [bdtp = 1,5-Bis(3,5-dimethyl-1-pyrazolyl)-3-thiapentane]

Keywords: Palladium / N,S ligands / Hemilabile ligands

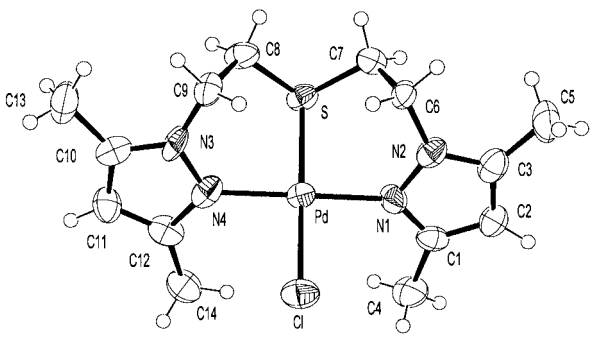

3958 **A. L. Bandini,* G. Banditelli, M. Manassero,* A. Albinati,* D. Colognesi, J. Eckert**

Binuclear Hydridoplatinum(II): One-Pot Synthesis, INS Spectra and X-ray Crystal Structure of $[Pt_2(dcype)_2(H)_3][BPh_4]$ {dcype = 1,2-Bis(dicyclohexylphosphanyl)ethane}

Keywords: Hydride ligands / INS spectroscopy / Phosphane ligands / Platinum / X-ray diffraction

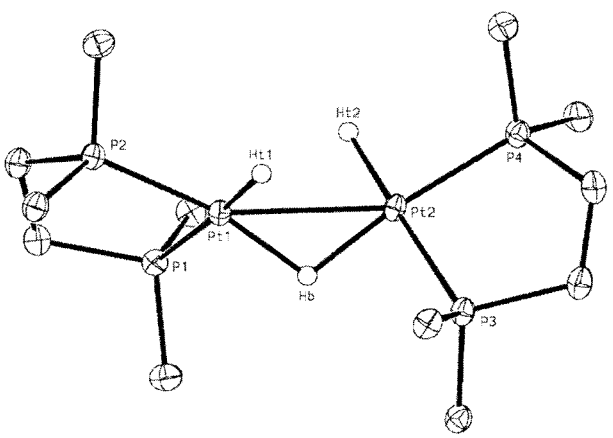

3968 **J. A. W. Verhagen, M. Lutz, A. L. Spek, E. Bouwman***

Synthesis and Characterisation of New Nickel-Iron Complexes with an S_4 Coordination Environment around the Nickel Centre

Keywords: Nickel / Iron / S ligands / Electronic structure / Electrochemistry

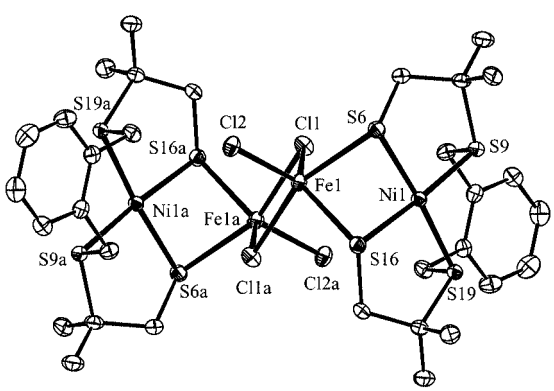

 © 2003 Wiley-VCH Verlag GmbH & Co. KGaA, Weinheim

Investigating Actinyl Oxo Cations by X-ray Absorption Spectroscopy

Christophe Den Auwer,*[a] Eric Simoni,[b] Steven Conradson,[c] and Charles Madic[d]

Keywords: Actinides / Oxo ligands / XANES / EXAFS

Early actinide elements (from U to Am) have the ability to form linear *trans*-dioxo complexes with formal valence of the actinide being equal to (V) or (VI). For instance, the ubiquity of the uranyl cation in uranium aqueous chemistry is the basis for its very important industrial and environmental concerns. As a result, the physical chemistry of the actinyl moieties has been the subject of constantly growing investigations. Among all the spectroscopic probes, X-ray absorption spectroscopy is a particularly useful element and energy-selective technique. This article reviews the investigation of molecular actinyl complexes using both XANES and EXAFS tools. The absorption edge features have long been used to characterize the frontier orbitals of the absorbing atom. In the case of actinide cations, the L_{III} edge, located in the hard X-ray region, provides a useful fingerprint of the cation polyhedron. Tentatively, simple molecular orbital considerations together with full multiple scattering simulation codes have provided significant interpretations of the edge features. Various examples involving a distortion of the actinyl coordination sphere, starting from the aqueous species are given. Complementary structural data can be obtained in the EXAFS region of the absorption spectrum. In the literature, such molecular systems have been well documented from uranyl aqueous chemistry to neptunyl or plutonyl coordination complexes with oxygen donor ligands. Furthermore, complexation mechanisms upon absorption onto mineral surfaces have been increasingly investigated over the past few years. Overall, contribution of the XAS technique to a better understanding of the actinide bonding is demonstrated from various examples of the literature and the authors' data. Importance of the simulation codes in order to better describe the absorption features is also strongly underlined.
(© Wiley-VCH Verlag GmbH & Co. KGaA, 69451 Weinheim, Germany, 2003)

1. Introduction

Due to their incomplete 5f and 6d electronic subshells, the actinide elements present some unusual physical and chemical properties. Moreover, the very large atomic numbers of the actinides are also responsible for very important relativistic effects, among which the scalar effect is at the origin of the so-called lanthanidic and actinidic contraction. As a consequence, the elements from the first half of the actinide series exhibit a large number of stable or metastable formal oxidation states ranking from (III) to (VII), de

[a] CEA Marcoule, DEN/DRCP/Service de Chimie des Procédés et de Séparation,
30207 Bagnols sur Cèze Cédex, France
E-mail: christophe.denauwer@cea.fr
[b] Institut de Physique Nucléaire Orsay
91405 Orsay Cedex, France
E-mail: simoni@ipno.in2p3.fr
[c] Los Alamos National Laboratory
MST-8, Los Alamos, NM 87545, USA
E-mail: conradson@lanl.gov
[d] CEA Saclay, DEN
91191 Gif sur Yvette Cedex, France
E-mail: madic@amandine.cea.fr

Dr. Christophe Den Auwer (top, left) has completed his PhD in 1996 at the chemistry department of McGill University (Canada) and the LURE synchrotron center of Paris XI University (France). He his now a staff scientist at CEA Marcoule in charge of synchrotron radiation studies and molecular radiochemistry. Since 1997, he has been involved in the synchrotron radiation studies of a joint CNRS/CEA/EDF/ANDRA research cluster about the investigation of the physical-chemical properties of actinide elements in solution. His research interests include the electronic and structural investigation of molecular actinide and transition metal species. He has particularly focused on the use of X-ray absorption techniques using synchrotron radiation in order to probe the metal−ligand bond.

Prof. Eric Simoni (top, right) is in charge of the radiochemistry graduate studies at Paris XI University/IPN. He has completed his PhD in the Institute of Nuclear Physics of Paris XI University in 1988. He has been working in the field of the electronic structure of actinides in condensed matter and specialized in optical spectroscopy. He is now involved in the mechanistic understanding of radionuclide transport in the environment related to nuclear waste disposal and environmental contamination, using several spectroscopic techniques such as photoelectron spectroscopy (XPS), time resolved laser induced fluorescence (TRLIF) and X-ray absorption spectroscopy (XAS).

Dr. Steven Conradson (bottom, left) is a project leader in the Materials Science and Technology Division at Los Alamos National Laboratory. Beginning in 1988, he has led a major program in synchrotron X-ray studies of actinides including both X-ray absorption and scatteringmethods, determining speciation in studies of both the environmental and fundamental chemistry of actinides as well as characterizing the local structure in actinide-containing solids. His current interests beyond these include the extension of local structure and lattice distortions into the origins, attributes, and implications of nanoscale heterogeneity in crystalline materials.

Prof. Charles Madic (bottom, right) presented his PhD in 1975 at the Paris VI University, France. His PhD, concerning the solvent extraction of transuranium elements from nitric acid solutions by synergistic mixture of extractants was prepared at the Fontenay-aux-Roses Nuclear Research Center of the CEA and Paris VI University. He became a Professor at the National Institute for Training Nuclear Techniques in 1988 and Director of research at the CEA in 1995. At the beginning of the 1990s, he was nominated as French delegate at the Nuclear Science Committee of the NEA (OECD). His field of interest in research concerns the chemistry of actinide elements in relation with the reprocessing of nuclear spent fuels and the treatment of nuclear wastes. Since the beginning of the 1990s, he is in charge of research programs in these fields financed by the European Commission.

MICROREVIEWS: This feature introduces the readers to the author's research through a concise overview of the selected topic. Reference to important work from others in the field is included.

pending on the atomic number. The question of delocalized vs. localized behavior of the 5f electrons still remains a critical issue to be addressed from both experimental and theoretical points of view. For that purpose, comparisons between the properties of actinides and lanthanides or even transition metals is often a common way to study these elements, although the radial extension of the 5f wavefunctions is larger than those of the 4f wavefunctions. Consequently, the actinides behave either as itinerant d transition-like systems or as localized lanthanide-like systems.[1] Indeed, americium ($5f^7 7s^2$) is considered the first actinide in the series to exhibit rare-earth-like behavior. From the structural point of view and due to their sizeable ionic radii, the actinides exhibit a wide variety of coordination numbers and therefore, both the molecular and solid-state chemistry of these elements have been extensively investigated. According to the relatively large ionic radii, these coordination numbers are rather high (6 to 12).

From both electronic and structural points of view, investigations of actinide compounds have been performed using several different techniques such as X-ray or neutron scattering, optical and vibrational spectroscopy, NMR and Mössbauer spectroscopy. Most of this work, originating from the early 1940s has dealt with condensed matter. As one of the numerous fields of investigation, the actinide electronic structure exemplifies the specificity of the 5f orbitals. In this framework, fluorescence emission lifetime, oscillator strength measurements and Zeeman effects have been widely studied and compared with corresponding lanthanide data such as those of Nd^{3+}, Eu^{3+} and Er^{3+} in the same host material.[2−5] These studies have dealt mainly with the crystal-field parameters, the wavefunctions and the associated 5f-5f transition probabilities,[6,7] the 5f-6d energy gap[8−17] (experimental values compared to ab initio DV-Xα calculations) and the energy transfers between lanthanide and actinide ions.[18] The delocalization of the 5f electrons has mainly been investigated by Mössbauer spectroscopy (mainly on the Np element), which is an efficient tool for measuring hyperfine interactions and thus to study the electronic configuration of actinides bound in solids.[19−30] many of the actinide intermetallic compounds (monopnictides and monochalcogenides) present 5f-electron behavior analogous to the 4f electrons (NpSb, NpAs, ...) but could show itinerant behavior as for the 3d electrons ($NpCo_2Si_2$, Usb, UP, ...).[31−39]

Since the mid 1970s, X-ray absorption spectroscopy (XAS) has become widely recognized as an element-specific and non-destructive structure and electronic probe. It is of particular interest when the system under investigation is lacking crystallographic order (as in glasses, solutions or gases) and precludes the use of X-ray or neutron diffraction as the preferred structural probe. NMR and Mössbauer spectroscopy are also restricted to the use of adequate nuclei. Although the applications of XAS to material or biological sciences, for instance, have been extensive since the 1980s, its use for actinide systems is relatively recent. This is mainly due to three reasons as pointed out by Karim and co-workers in 1980:[40] the need for high-energy X-ray beams as a result of the high atomic numbers of the actinides, the lack of either reliable computed electronic parameters or model compounds and the safety requirements associated with high radioactivity of most of these elements. Despite these difficulties, XAS has now been largely applied to the structural and electronic understanding of actinide materials, as summarized by P. G. Allen or S. D. Conradson in their 1997[41] and 1998[42] reviews. See also refs.[43,44] and references herein for a larger discussion on the use of XAS in coordination or environmental chemistry.

In this article, we report on the use of the XAS technique to investigate the coordination chemistry of actinyl cations. Indeed, this technique has revealed itself as one of the unique tools for addressing the characterization of the heavy cation coordination sphere in solution or in amorphous materials. We do not intend to fully describe the theory and practice of XAS as well as the physical-chemical properties of the actinyl adducts as many books and review articles have dealt with the subject extensively.[45−49] Only a brief overview is given.

XAS is a spectroscopic technique based on the informative modulations of the X-ray absorption cross section. The electronic transitions driving the absorption cross section obey the Fermi−Golden rule in its dipolar approximation, where $i>$ is the initial state wave function of eigenvalue E_i, $|f>$ is the final state wave function of eigenvalue E_f, $\varepsilon \cdot r$ is the interaction hamiltonian in the dipolar approximation and $h\omega$ is the energy of the incoming photon [Equation (1)].

$$\mu \propto \sum_f \left|\langle i|\varepsilon . r|f\rangle\right|^2 \delta\left(E_i + \hbar\omega - E_f\right) \quad (1)$$

Because of the δ function, no quantum transition can occur before the incident photon energy $h\omega$ is at least equal to the energy of the LUMO or partially vacant authorized orbital. The dipolar transition operator results in the following transition rules for the absorption process: $\Delta L = \pm 1$; $\Delta J = 0, \pm 1$ (where L is the angular momentum term and J is the LS coupling term).

It is then convenient to divide the absorption process into two parts, depending on the incident photon energy. Above the threshold (X-ray absorption near edge structure, XANES), the photoelectron is trapped inside the absorber potential barrier and it is promoted to vacant or partially vacant bound states. As the kinetic energy of the photoelectron increases, transitions outside the potential barrier can occur towards the continuum states of the system. From ca. 100 eV above the absorption edge to ca. 1000 eV (extended X-ray absorption fine structure, EXAFS), modulations of the absorption coefficient are driven by the interference between the outgoing wave function associated with the photoelectron and the backscattered ones. The EXAFS signal χ is given as the ratio between the absorption cross section μ and the atomic absorption function μ_0 [Equation (2)].

$$\mu = \mu_0(1 + \chi) \quad (2)$$

 © 2003 Wiley-VCH Verlag GmbH & Co. KGaA, Weinheim

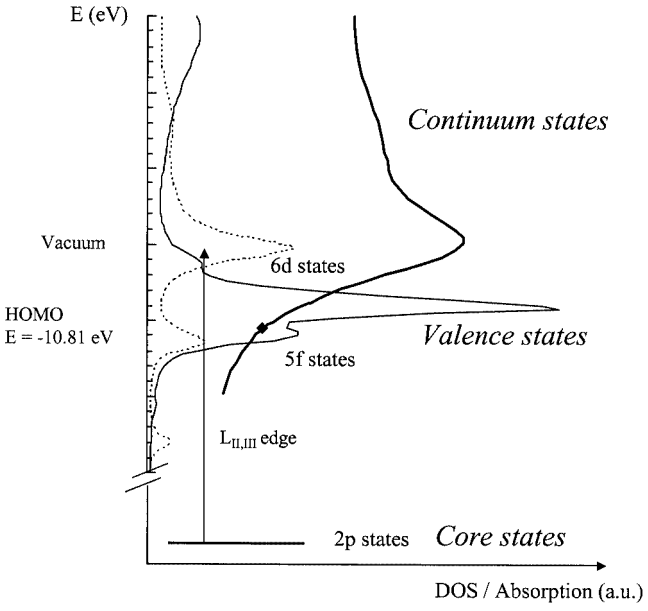

Figure 1. Schematic transitions involved in the L_{III} edge of uranyl moiety; both density of states (DOS) and absorption edge have been calculated with Feff8.1 code[50]

Figure 1 shows a schematic representation of the absorption process in the case of the L_{III} edge of UO_2^{2+}. In the primary channel picture, the $L_{II,III}$ edge corresponds to a $2p^6_{1/2,3/2}$-$nd^m \rightarrow 2p^5_{1/2,3/2}$-$nd^{m+1}$ transition (for the actinides, the first partially available d orbital is the 6d one). The threshold energy, the d and f Density of States (DOS) and the absorption spectrum have been calculated using Feff8.1 code.[50] Above the threshold, transitions occur towards the first allowed empty orbitals (6d) of uranium. Above the ionization potential (vacuum level), transitions occur towards the continuum states of the molecule.

Because most of the actinide complexes (from uranium to americium) with oxidation states higher than (IV) contain the actinyl AnO_2^{n+} ($n = 1, 2$) moieties, they are of technological and environmental importance.[41,43,51–53] Furthermore, the ubiquity of the uranyl cation in the geosphere, due to its remarkable stability, makes it one of the most extensively investigated cations within the actinide family.

The major characteristic of actinyl cations is the occurrence of quasi-linear O–An–O units with a short An–O multiple bond and a bond length ranging from 1.7 to 1.9 Å depending on the cation. This characteristic is also specific to the actinide family as only one analogue (the osmyl cation OsO_2^{2+}) is known in the d block.[54] This is good evidence of the bonding particularity that involves significant participation of the 5f orbitals in the HOMO of the AnO_2^{n+} unit. As a matter of fact, the bent structure of molecular ThO_2 versus the linear one has been the subject of numerous theoretical works questioning the extent of the 5f and 6d participation in the bonding molecular orbitals involving the two oxygen atoms.[55–59] This discussion is, however, beyond the scope of this paper as the authors would like to emphasize the role of XAS in understanding the physicochemical properties of actinyl cations.

2. Working with Actinide Elements

Although one of the major advantages of XAS is the ability to tune the absorption edge for a given element, most of the actinyl studies have dealt with L_{III} and more rarely L_I edges. Reasons for this limitation are mainly technical, as explained in the following.

The high specific radioactivity of most of the actinide elements impinges strong experimental limitations in order to comply with the safety regulations. Although dedicated research nuclear laboratories possess the experimental specific setup, this is often not the case of traditional beam line hutches at the synchrotron. Therefore, either the sample holder itself must be adequately shielded or the beam line hutch must be specifically designed. Lately, the design of dedicated beam lines at the synchrotron with appropriate shielding and/or radiation equipment has been a major improvement in the acquisition of data on actinide elements.[60–63] However, when available, the use of a specific low active radioisotope such as the uranium-238 natural isotope (^{238}U has a specific activity of $3.4 \cdot 10^{-7}$ $Ci \cdot g^{-1}$ that does not require any specific shielding) is always the preferred method. Because the X-ray beam must be transmitted through the shielding barriers, the most conveniently accessible absorption edges of the actinide series are the L edges located in the hard X-ray region from ca. 17000 to 25000 eV from U to Cf. This energy range allows successive shielding of the sample with negligible absorption of the photon beam (typically, layers of polymer or beryllium windows are used to confine the sample). Among the L edges, the L_{III} edge is very sensitive to the polyhedron structure because of the presence of strong multiple scattering contributions, as will be developed in the course of the next sections. The edge resolution is, however, limited by the short core hole life-time (giving a width of typically 7 eV at the L_{III} edge of uranium[64]). Lower energy studies at the M, N or O edges present a better edge resolution because of the larger core hole life-time and allows the 5f orbitals to be probed through the allowed dipolar transition. However, to date, these studies are scarce, given the technical difficulties in shielding the sample in the soft X-ray region. General considerations related to the manipulation of radionuclides at the synchrotron sources have been summarized in the Proceeding of the 2nd Euroconference and NEA Workhop on Speciation, Techniques and Facilities for Radioactive Materials at Synchrotron Light Sources.[61]

Another crucial issue of XAS analysis is obtaining reliable electronic model parameters [phase $\Phi(\theta, k, R) = 2kR + \varphi$, amplitude $f(\theta, k, R)$, electron mean free path $\lambda(k)$ and inelastic losses S_0^2]. Two ways of evaluating the electronic parameters are either to calculate it or to extract it from a model compound that is of known structure (i.e. the absorber to neighbor distance R and the number of neighbors

 © 2003 Wiley-VCH Verlag GmbH & Co. KGaA, Weinheim

N are known) and chemically close to the material under study. On the one hand the use of experimental model compounds is the preferred method in order to obtain reliable electronic parameters. However, the difficulty in obtaining three-dimensional structures from single crystals of actinide elements is responsible for the scarcity of adequate model compounds. This statement should be tempered in the case of thorium and uranium adducts since many crystallographic data are available for these two elements. On the other hand, XAS simulation codes have become accessible for 5f elements and can be used to calculate the electronic parameters on the basis of assumed atomic coordinates.[50] In that case, several methods have been used: extrapolation from known uranium or thorium structures;[65] extrapolation from corresponding isostructural lanthanide compounds;[66] comparison with simple molecular clusters based on either quantum chemical or molecular dynamics considerations.[67] Over the past few years, the Feff code (versions 7 and 8) has been extensively tested for the actinide elements as will be reported on in the following sections. In the field of absorption edge simulation, major developments have included the implementation of self-consistent fully relativistic potential calculations based on Dirac−Hara atomic calculations and full multiple scattering treatment of the photoelectron.[68,69]

3. Actinide XANES and Electronic Structure

Near-edge spectroscopy has long been used as a fingerprint of the absorbing atom coordination geometry and electronic state. Because at low kinetic energy the photoelectron mean free path increases dramatically, the structural component of XANES can be viewed as an extension of the EXAFS energy region, given that high-order multiple scattering paths are dominant. Many works have aimed at simulating and better understanding the information included in the edge features. Depending on the relative proportion of delocalization in the valence states or electronic correlation within the final state, so-called multiple scattering or multiplet approaches have been developed.[70] Such quantitative approaches in the hard X-ray region have long been applied to spin state or local symmetry studies of transition or lanthanide metal series. On the other hand, a limited number of studies have been devoted to actinide elements, most of which deal with oxide, halide or intermetallic solid-state materials.[68,69,71−76] At the molecular level, only a few papers have addressed the simulation of actinide L edges with a multiple scattering approach.[77,78] In that framework, Ankudinov et al.[68,69] have published an extensive comparison between the series of Pu hydrates and simulations with the Feff code. Other studies have addressed this issue using both phenomenological and computational approaches.[77,78] There is still some controversy as to whether the edge features, depending on their energy (or position in the XANES spectrum) must be interpreted in terms of transitions to bound, semi-bound or continuum states. Within the absorber potential barrier, the electron is trapped above the energy threshold and both multiple scattering or molecular orbital pictures can be used as they should reflect the same underlying phenomena when electronic correlations are negligible.[79] Whether or not part of the edge features must be considered as transitions to bound states or to continuum states depends on the work function of the system. It is well known for instance that pre-edge features of the transition metal K edges can be treated as transitions to bound states made up of the hybridized unoccupied or partially occupied d states.[80−82] In the case of the L_{III} edges of the actinide elements, it has been suggested that the multiple scattering picture is more suitable to explain the edge features[69] since mixed bound-continuum states are believed to dominate the white line (WL) shape and intensity. In contrast, the L_{III} edges of the lanthanide ions exhibit a very sharp, intense and often featureless WL.[71] In the one-electron picture, this high WL ratio reflects the transition to the narrow 5d states compared to the more diffused 6d states. Additional broadening by the core hole life-time must also be taken into account as it increases with atomic number *Z*.[64,72,74] In Figure 2, the broad and intense WL, A, is typical for the actinyl L_{III} edge, from uranium to americium. Figure 2 compares the full multiple scattering (FMS) simulation of the uranyl L_{III} edge to the atomic absorption spectrum (absorption edge calculated as if the absorption atom was isolated) using the Feff-8.1 code (simulation parameters are described in ref.[83]). Calculations have been carried out on a pentagonal bipyramid cluster using self-consistency methods and muffin tin potentials, but without taking into account any sol-

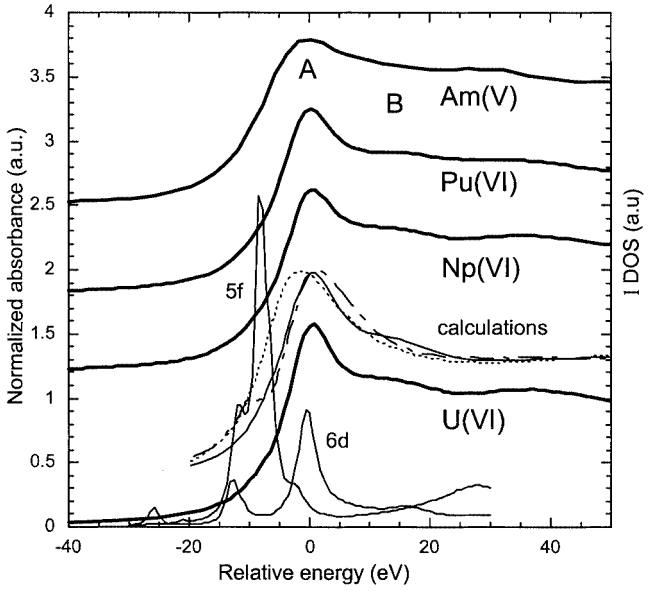

Figure 2. Experimental L_{III} edges of UO_2^{2+} (solution in perchloric acid[84]), NpO_2^{2+} (solution in perchloric acid), PuO_2^{2+} [solution of $PuO_2(NO_3)_2TBP_2$ in TBP[85]] and AmO_2^{+} [solid $K_3AmO_2(CO_3)_2$ [86]] (—); calculations (Feff-8.1) are compared to the experimental uranium edge: FMS (—), single scattering (− −) and atomic absorption (----); the $l = 2$ and $l = 3$ projected DOS is also displayed on the same relative energy scale; all the experimental spectra have been shifted in energy with respect to the calculated uranium pentagonal bipyramid edge maximum

 © 2003 Wiley-VCH Verlag GmbH & Co. KGaA, Weinheim

vent effects. In addition, the *l* projected density of states (DOS) calculated with the same potentials but with no core hole, for $l = 2$ and 3, are shown on the same relative energy scale. The interpretation of A originating from a 2p to mixed 6d-continuum state transition (as the primary channel $\Delta l = +1$ of the Golden Rule) is in agreement with the 6d DOS. The similarity between the experimental WL and the atomic absorption background confirms the partial atomic character of the WL. Note that in the molecular picture, the 6d state should split under the crystal field energy (D_{5h} symmetry) but this splitting is not observed here. At about 15 eV above the WL maximum, feature B is clearly reproduced by the FMS calculation but not by the atomic absorption spectrum. A similar calculation using a single scattering approach does not account for B either. The identification of the multiple scattering (MS) paths in the FMS calculation shows that B originates from the multiple scattering paths along the *trans*-dioxo cation for both AnO_2^+ and AnO_2^{2+} moieties. This attribution of B in terms of MS contributions was previously demonstrated by Templeton[87] and Petiau[72] using polarized XAS.

Relative position of the edge is also informative as an increase in the central atom partial charge leads to a stabilization of the electronic core levels (because of the decrease in the screening effect) and a destabilization of the valence levels. If the WL is mainly of atomic-like character (as the L_{III} edge of the lanthanide for instance), the net result, everything else being equal, is a shift of the absorption edge towards higher energies as the central atom partial charge increases. Although the partial charge is often correlated to the formal oxidation state, this simplification can be misleading when different ligands yield different charge transfers between the ligands and the metal cation for a given oxidation state. This interpretation can be partially used for instance to explain the breakdown of the linear increase in edge energy (taken at the inflexion point) from An^{IV} to An^{V} [88] as a diminution in the difference of the An charge associated with the presence of covalent bonding within the *trans*-dioxo unit. More often, the absorption edge is not of pure atomic character and this leads to a mixing of both electronic and geometrical effects. This is a common ambiguity in XANES analysis as a change in the central atom oxidation state is often correlated to a change in coordination sphere. The following two examples illustrate this difficulty.

Firstly, we consider the series of Ba_2ZnAnO_6 perovskite solid-state compounds (An = U, Np, Pu) in which the actinide formal oxidation state is (VI) as in the actinyl hydrate. In these compounds, the actinide cation has been shown to be mainly ionic with an octahedral environment of 6 oxygen atoms at 2.09 Å,[89] in contrast with the rod-like structure of the actinyl cation. XANES spectra exhibit both an edge energy shift and a shape modification compared to the aqua species.[83,90] Although the edge feature can be explained in terms of transitions to the t_{2g} and e_g 6d states in an O_h symmetry, multiple scattering interpretation has also been used successfully.[83,91] In Figure 3, the *l* projected DOS calculations (Feff-8.1) of the 6d orbital matches the XANES

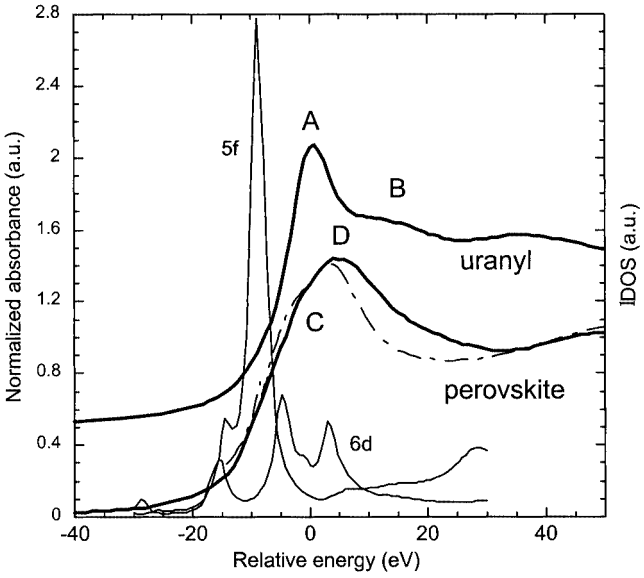

Figure 3. Experimental L_{III} edges of U^{VI} in perchloric acid and solid-state Ba_2ZnUO_6 (—) compared to FMS calculation (Feff-8.1[83]) of Ba_2ZnUO_6 (– – –); both experimental spectra have been shifted in the same relative energy scale with respect to the calculated uranium

features in terms of $t_{2g}-e_g$ splitting. The splitting energy (8 eV) is in relative agreement with previous calculations on UO_8^{13-}, AmO_8^{13-} and CmO_8^{13-} clusters (ca. 5 eV).[92] However, attribution of C and D to transitions to bound 6d states depends on the position of the ionization potential. The present calculation places the vacuum level just above C feature, meaning that D would be better described as a mixed bound−continuum state. In the MS picture, path analysis at the edge energy reveals that the low energy shoulder can be attributed to constructive interference from triangular paths within the octahedron. The high energy shift of the edge maxima from UO_2^{2+} (A) to Ba_2ZnUO_6 (D) (ca. 5 eV) would be in agreement with an increase of the uranium partial charge from uranyl to perovskite. However, attribution of D as the formal WL maximum is doubtful and the symmetry change from D_{5h} to O_h makes difficult the energy comparison with respect to the edge maximum. Also, there is a low energy shift of the inflexion point of ca. 2 eV from uranyl to perovskite, in contradiction with the above explanation. These simplistic interpretations lack a quantitative evaluation of the symmetry effect compared to the electronic effect, both effects being highly related. The energy threshold calculated by Feff-8.1 in both cases shows an increase of 1.14 eV from uranyl to perovskite and places the position of the threshold at the bottom of the absorption edge. Although this increase seems small compared to the calculation accuracy (1−2 eV [68]) it is in agreement with a significant decrease of the charge transfer (from 0.69 for uranyl to 0.35 for perovskite) calculated with the same code. At the M_v edge (3d−5f dipolar transition), the very intense WL ratio of Figure 4 reflects the more localized character of the 5f orbitals compared to the 6d ones, as well has the magnitude of the core hole attraction.[72] MS contributions

 © 2003 Wiley-VCH Verlag GmbH & Co. KGaA, Weinheim

are therefore expected to be relatively weak and comparison of the WL full width at half maximum (FWHM) should reflect the trend in the 5f relative localization. Although small, the reduction of the FWHM from uranyl to perovskite (from 9.1 to 6.9 eV) agrees with the previous interpretations accounting for an increase of the uranium ionic character. Simulation of the M_V edge using a cluster based on the crystallographic structure of $UO_2(NO_3)_2{\cdot}6H_2O$ also suggests that the WL, E, is mainly driven by the final state density. Features F and G have been described in the literature [72,74] as a satellite peak (F), as an MS *trans*-dioxo contribution (G). Other authors have also observed these features in U^{VI} complexes but did not attribute it.[93] The absence of feature F in the simulation backs the interpretation of this shoulder as a multielectronic process that cannot be reproduced by the MS-based simulation code. Also, path analysis shows that G is driven by the presence of the *trans*-dioxo group and H originates from the contributions of the equatorial atoms.

As a second example, we consider the $Np^{VI}O_2^{2+}$ cation in basic and acidic solutions. In the first case, the Np atom is surrounded by 2 axial oxygen atoms at 1.82 Å and 4 equatorial oxygen atoms at 2.21 Å [94] and in the second case by 2 axial oxygen atoms at 1.75 Å and 5 equatorial oxygen atoms at 2.41 Å.[60] Both L_{III} edge spectra are compared in Figure 5 (a). From acidic to basic, they exhibit in one hand a broadening of WL A and on the other hand a shift to lower energy (-1 ± 0.5 eV for the inflexion point; -0.7 ± 0.2 eV for the WL maximum). In order to quantify the experimental changes in the edge shape and position, two series of simulations with Feff-8.1 code have been undertaken using similar parameters as those used in the case of aqueous uranyl.[84] Starting from a pentagonal bipyramid structure with the structural parameters in acidic solution, the coordination sphere has been distorted towards the structural parameters of the basic solution. Note that the symmetry is frozen at the D_{5h} point group and that neither the hydrogen atoms nor the solvent water molecules have been included in the cluster. In process I, the axial bonds have been elongated from 1.75 to 1.82 Å, the equatorial bonds being kept fixed at 2.41 Å; in process II, the equatorial bonds have been shortened from 2.41 to 2.21 Å, the axial bonds being kept fixed at 1.82 Å. The L_{III} edge simulations are compared to the experimental spectra in Figure 5 (a). The broadening of the WL from acidic to basic medium is qualitatively reproduced by the simulation. Figure 5 (b) presents the second derivative spectra calculated from the edges. Figure 5 (c) reports the first and second derivative zero points as well as the position of B shoulder. In process I, the elongation of the axial bond results in a shift of B towards A, in agreement with the relation $\Delta E{\cdot}R^2 = \text{cst}$,[72,95,96] as shown in Figure 5 (c). At the same time, both inflexion point and A are shifted to lower energy, demonstrating the sensitivity of the edge position to the coordination sphere distortion. In process II, the shortening of the equatorial distances interferes very little with the position of B, while the inflexion point and A are shifted similarly as in process I. The net result at the end of process II is an energy shift between the simulation and the experimental spectrum relative to the basic medium (Figure 5, a,b). The lower energy position of the experimental spectrum could be explained as a charge effect as the negative charge of the hydroxy ions have not been taken into account in the simulation. A higher electronic density around the neptunium atom is in agreement with a low energy shift, as observed here.

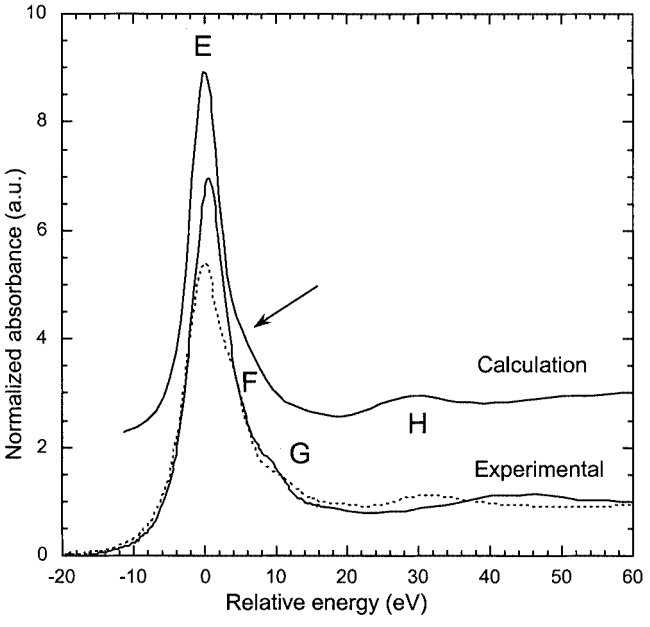

Figure 4. Experimental M_V edges of Ba_2ZnUO_6 (----) and $UO_2(NO_3)_2{\cdot}6H_2O$ (—) compared to the simulated M_V edge of $UO_2(NO_3)_2{\cdot}6H_2O$ (—);[83] all spectra have been shifted in the same relative energy scale with respect to the calculated uranium $UO_2(NO_3)_2{\cdot}6H_2O$ edge maximum

4. XAS, a Probe for Actinyl Complexes

4.1. Aqueous Actinyl Cations

The speciation of the actinyl cations in aqueous electrolytes shows a strong pH dependence and can also be affected by the presence of complexing ligands.

Although many studies have concentrated on the redox equilibrium behavior of the actinyl ions, fewer are reported on the actinide coordination sphere characterization. Lately, these data have also been complemented by quantum chemical calculations as to support the experimental results [67,97–100]. Generally speaking and in noncomplexing electrolytes, the hydrated cations can be written as $AnO_2^{n+}{\cdot}mH_2O$ (n = 1, 2) below the pH of hydrolysis and $AnO_2(OH)_{m'}^{2-m'}$ in alkaline solution. The coordination polyhedron of the actinide atom can be described as a bipyramid with the axial *trans*-dioxo atoms in the apical position and equatorial coordination geometry from trigonal to hexagonal. In acidic media, both formal oxidation states (V) and (VI) have been reported with U, Np, Pu and Am cations. As an example, the L_{III} edges of UO_2^{2+}/aq.,[84] NpO_2^{2+}/aq., PuO_2^{2+} [101] and AmO_2^{+} [86] are compared in Figure 2. All spectra are similar with a strong white line (A)

 © 2003 Wiley-VCH Verlag GmbH & Co. KGaA, Weinheim

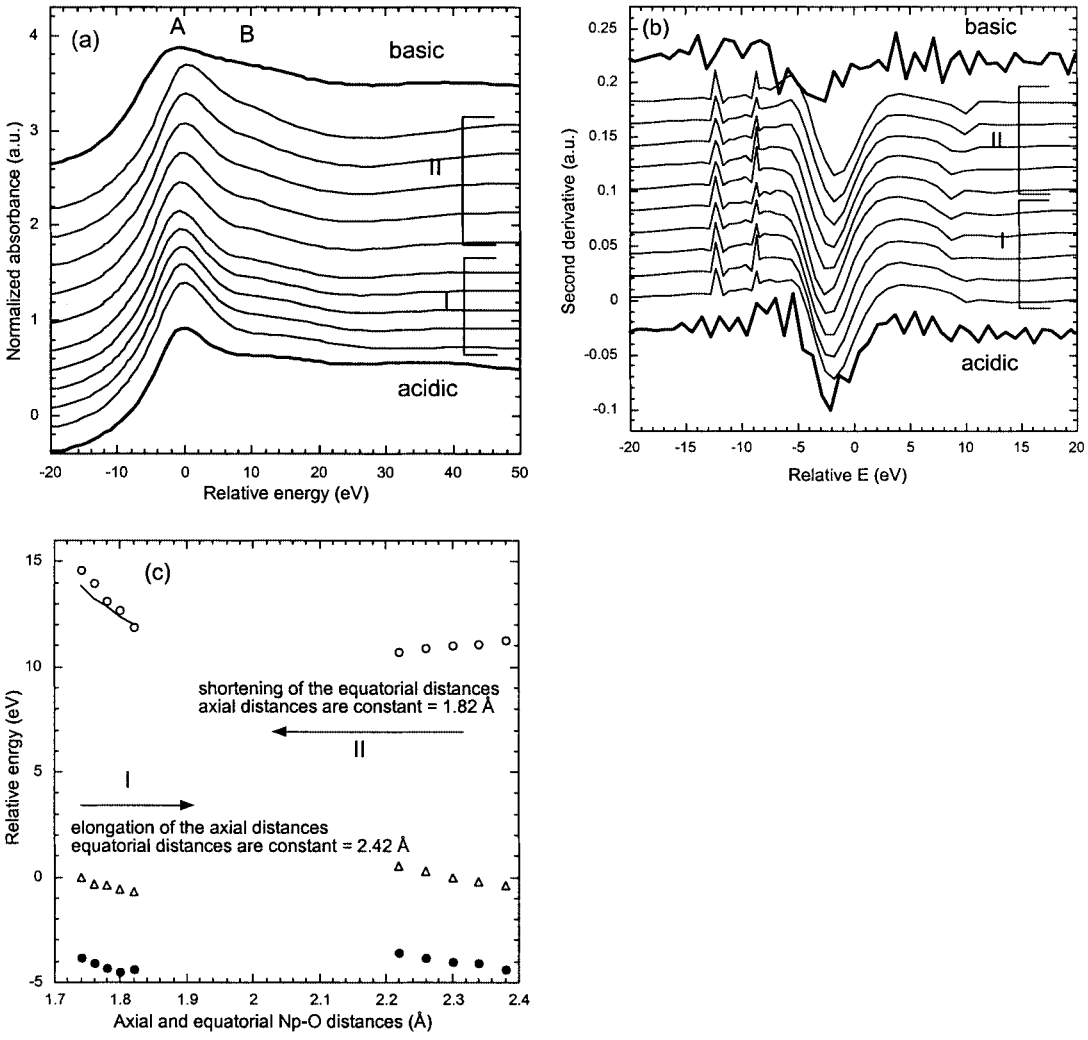

Figure 5. (a) Experimental (—) and simulated (—) L_{III} edges of $Np^{VI}O_2^{2+}$ in basic (TMA-OH) and acidic ($HClO_4$) solutions; simulations (Feff-8.1) have been carried out starting from the acidic structural parameters by successive elongation of the two apical oxygen atoms by 0.02-Å steps (process I) and by further successive shortening of the five equatorial oxygen atoms by 0.02-Å steps (process II); (b) second derivatives of the experimental (—) and simulated (—) edges; in (a) and (b) experimental and simulated spectra have been shifted in the same relative energy scale with respect to the edge maximum of the experimental acidic spectrum; (c) energy position of the simulated edge inflexion point (filled circles), maximum (triangles) and shoulder (empty circles) as a function of the axial and equatorial distances (process I and process II); the straight line (—) represents the correlation $\Delta E \cdot R^2$ = cst

and a shoulder (B) at about 15 eV above the WL maximum. Note that the relative smaller intensity of the WL in the case of the Am compound is due to the lower resolution of the beam line used to record the spectrum.

In order to address the structure of the aqueous ions, EXAFS data on aqueous actinyl ions have been well documented in the literature. Figure 6 (a,b,c) present an overview of the published data for U, Np and Pu, including the author's results. Agreement within the axial (not shown) and equatorial distances is usually satisfactory. On the contrary, it is well known that one of the major limitation of the XAS technique is the accurate determination of all the amplitude terms because they are significantly correlated. Many of the structural determinations reported in Figure 6 have used a fixed number of neighbors for the equatorial coordination shell. When floating, the parameter uncertainty is close to 20% due to amplitude transferability and experimental accuracy. This means in the case of actinyl ions that the equatorial shell is defined within plus or minus one oxygen atom.

Np and Pu are notable among the actinides for having the largest number of accessible valences, up to valence (VII). The valence (VII) state was first reported in the Russian literature[112−114] under alkaline conditions although detailed studies about the precise coordination sphere remain scarce. Due to its greatest stability for the (VII) state within the actinide family, neptunium has been the subject of most of the investigations. Recently, a few groups have provided a much more complete characterization of Np^{VII} complexes, both in the solid state and alkaline solution.[91,94,115−117] In the solid state, current XAFS[91] and single-crystal diffraction studies support the original Russian results, finding the tetraoxo configuration in the highly alkaline solutions (> 4 M OH^-) that stabilize this

 © 2003 Wiley-VCH Verlag GmbH & Co. KGaA, Weinheim

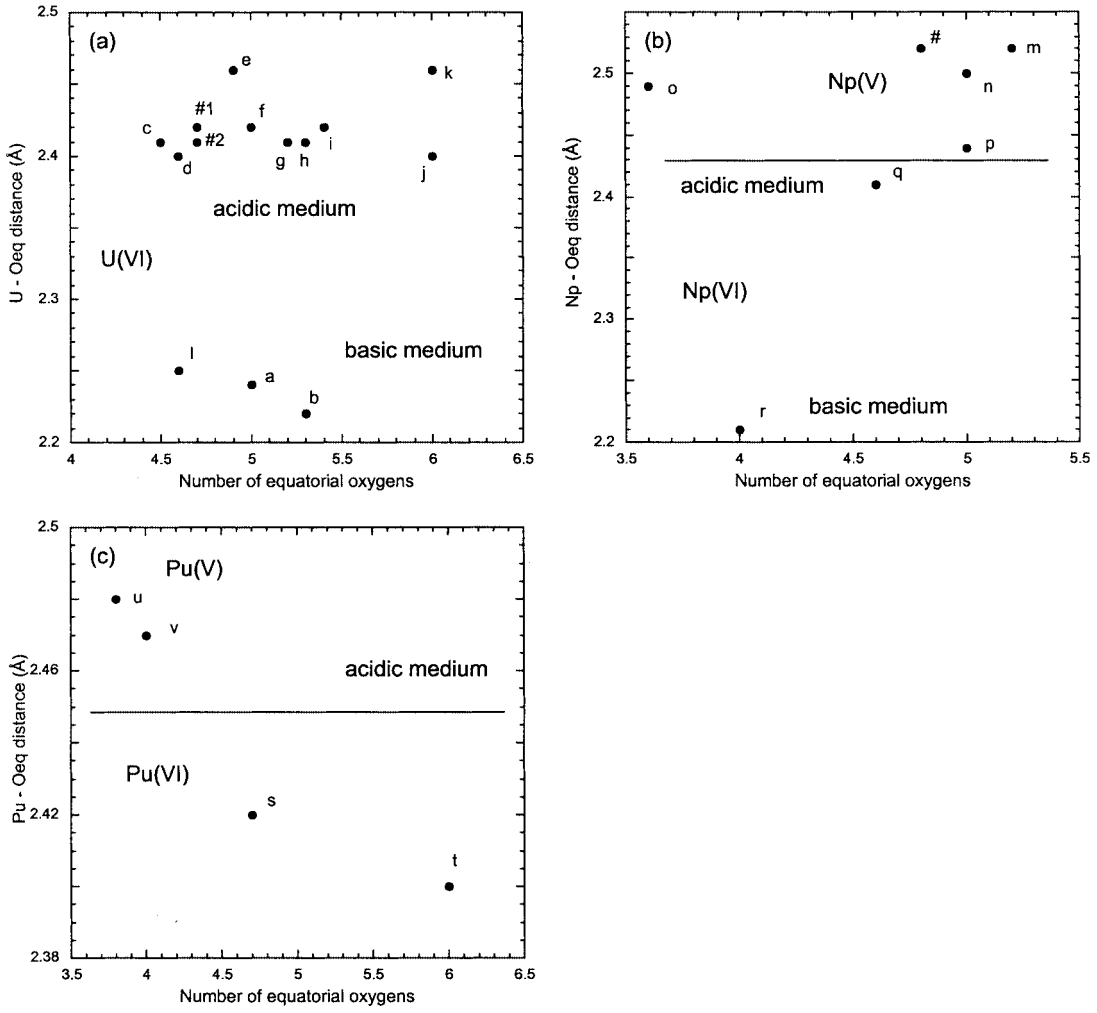

Figure 6. Actinide−oxygen equatorial distances [Å] and number of neighbors as reported from the literature: (a) uranium: a[100] − b,c[102] − d[99] − e,i[103] − f[104] − g[67] − h[105] − j[106] − k[107] − l[108] − # this work (#1 in 0.1 M $HClO_4$; #2 in 0.1 M HNO_3); (b) neptunium: the horizontal line represents the border between the Np^V/Np^{VI} domains: m[109] − n[105] − o,q[60] − p[110] − r[94] − # this work (0.01 M in $HClO_4$); (c) plutonium: the horizontal line represents the border between the Pu^V/Pu^{VI} domains; s,u[111] − t,v[42]

high oxidation state and in crystals of $Co(NH_3)_6NpO_4(OH)_2{\cdot}2H_2O$ grown from this medium. In this compound, the four Np=O oxo bonds expand to 1.85−1.90 Å, ca. 0.05 Å longer than in dioxo compounds, and the pair of *trans*-hydroxo ligands are also found at a longer 2.35−2.40 Å distance. This radical change in geometry produces a comparable change in the XANES, as shown in Figure 7. In these tetraoxo complexes the inverted ratio of short to long An−O bonds results in a shift in the relative amplitudes of the two principal features typical of the XANES of $An^{V,VI}$ with their two different An−O distances. The lower energy peak, A, corresponding to the white line in the spectra of $An^{V,VI}$ complexes decreases in intensity slightly while the higher energy feature, B, that typically occurs as a shoulder on this peak increases by a larger amount. This results in a spectrum with two resolved peaks of comparable amplitude. The separation between these features by ca. 10 eV is quite close to the energy between the peak and shoulder in the spectra of dioxo materials. This result corroborates the importance of the nearest neighbor distances as the primary origin and determinant of these two spectral features. Relative to Np^{VI} complexes, an increase in the edge energy of 1−2 eV (smaller relative to carbonato complexes, larger for hydroxo) occurs, consistent with a higher charge on the Np but also demonstrating that the incremental charge is, as expected, less than found in the oxidation from (V) to (VI). As a possible explanation, the combination of high oxidation state and OH^- donor properties promotes a higher degree of covalency and a lower charge on the central Np.

This scenario is complicated in solution, however, as observation of both dioxo and tetraoxo complexes under conditions identical to those used to prepare the tetraoxo crystals have been reported [94,115,116] by using the XAS technique. Although the Np−O distances are similar to those in Np^{VI} hydroxo complexes, the energies of the absorption edges of these samples are higher than those of Np^{VI} and close to those of the Np^{VII} tetraoxo compounds, consistent with Np^{VII} (Figure 7). However, both close inspection and curve-fits of the EXAFS indicate the presence of a small

 © 2003 Wiley-VCH Verlag GmbH & Co. KGaA, Weinheim

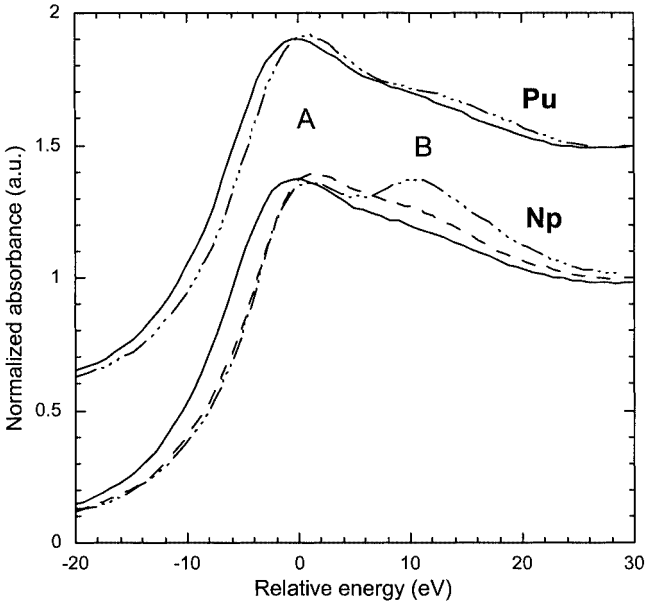

Figure 7. Experimental L_{III} edges showing both dioxo (VI) and (VII) and tetraoxo (VII) signatures of Np and Pu cations;[118] plain line spectra (—) represent the Np, Pu cations at oxidation state (VI) (in concentrated sodium hydroxide); dotted line spectra represent the Np, Pu cations at oxidation state (VII): dioxo Np^{VII} (– –) (in concentrated sodium hydroxide), tetraoxo Np^{VII} (–···–···) [in $Co(NH_3)_6NpO_4(OH)_2{\cdot}2H_2O$] and dioxo Pu^{VII} (–···–···) (in concentrated sodium hydroxide); spectra have been shifted in ordinates and energy calibrated with respect to the edge maximum of the Np^{VI} spectrum

amount of CO_3^{2-} in addition to the OH^-, so that these actually exhibit mixed hydroxy/carbonato coordination. Curve-fits show a larger number of O at the shorter Np–OH distance, which suggests an increase in number of equatorial ligands to five. The presence of strongly bound carbonate would be expected to disrupt the formation of the tetraoxo complex, resulting in the more typical dioxo geometry. This result, therefore, also demonstrates that the balance between the two geometries is delicate so that Np^{VII} is stable in both conformations, even while displaying a slight preference for the tetraoxo configuration. As would be expected from the correlation between the geometry and XANES features, the shape of the XANES of these compounds are quite similar to those of the Np^{VI} hydroxide materials, with a single peak broadened on the high energy side as the separation between the peak and shoulder decrease. The only unique signature of the Np^{VII} state is thus the somewhat higher energy of the edge. A full discussion about this issue is to be published in ref.[118] Recently, these findings have been corroborated to the Pu^{VII} system. The reversible, electrochemical production of soluble Pu^{VII} in highly alkaline media results in a dioxo complex with very slightly contracted bond lengths (0.01–0.02 Å) relative to the original Pu^{VI} starting material and a 1 eV increase in the energy of the absorption edge. At least under the conditions used in this experiment,[118] the number or order of the equatorial ligands was shown by the EXAFS to be altered in the Pu^{VII} product. No sign of CO_3^{2-} ligation is seen in the EXAFS, but only of OH^- ligation, showing that the fine balance between tetra- and dioxo configurations tips toward the latter for Pu. The Pu–O distances are also very similar between the (VI) starting material and oxidized (VII) state. Therefore, the principal effect of the higher valence on the XANES is, similarly, a 1-eV increase in the edge energy.

Studies including a variation of the electrolyte have shown that the counterion may enter the equatorial coordination sphere. Although it is usually accepted that perchlorate ions never coordinate the cation in aqueous solutions,[99] other counterions like F^-, Cl^-, CO_3^{2-} or SO_4^{2-} may form inner-sphere complexes, depending on the anion ionic strength. In the case of Cl^-/NpO_2^+ or UO_2^{2+}, it leads to a decrease of the hydration number and an increase in the Np,U–O equatorial distances as a maximum of 1.0 Cl^- (Np) or 2.6 Cl^- (U) enter the coordination sphere.[105] Similar behavior has been reported for PuO_2^{2+} with replacement of hydration water molecules with chloride ligands.[119] In the case of F^-/UO_2^{2+}, a combined EXAFS and quantum chemistry study[67] has shown that $UO_2F_n(H_2O)_{5-n}^{2-n}$ ($n = 3-5$) complexes can form within a pentagonal bipyramid geometry. Because of its ubiquity in ground water systems, carbonate ions have been extensively studied, revealing complex equilibria in solution.[120–125] Sulfate ions in binary or ternary systems have also been investigated.[126]

4.2. Coordination of Actinyl Cations with Oxygen Donor Ligands

Both steric and electronic ability of the actinide oxo cations to accept donor ligands in the equatorial plane has been at the origin of numerous coordination chemistry species.[49] As mentioned in the introduction of this article, both environmental and nuclear fuel applications of actinyl coordination chemistry have yielded a significant quantity of literature data. Most of it illustrates the use of XAS for the study of short range interactions in the solvent phase or as a complementary technique to X-ray diffraction measurements. Among the coordinating ligands of interest, oxygen donor (mono-, bi- or polydentate) ligands have been predominantly investigated. Hydroxy, carboxylate, phosphate or ether functions are often the functional groups used as donor agent in the actinyl equatorial plane.

For instance, various liquid alkyl phosphate ligands have been the subject of structural variation studies within the actinyl series from uranyl to plutonyl.[85,127] In comparison, the humic acids contain several of the above functional oxygen groups and are indeed among the most complex natural systems. Donor sites are therefore difficult to identify and alternate strategies as complexation by synthetic identified functional groups as xylose, phenylalanine or glycine are needed in order to understand the complex formation.[128] Comparison between the natural and synthetic humic acids has revealed no severe discrepancies, showing that the carboxylate groups act predominantly as monodentate ligands.[127,129] Similarly, natural wood-degradation processes lead to possible complexation by either hydroxybenzoic acids or phenols.[130] Under acidic conditions, the carboxylic

 © 2003 Wiley-VCH Verlag GmbH & Co. KGaA, Weinheim

group coordinates in a bidentate mode to the uranyl cation, where under basic conditions the phenolic OH functions are the coordinating ones. Biological systems as cells have also been investigated recently. For instance, complexation of uranyl[131] and plutonyl[111] by *Bacillus sphaericus* has shown that the actinyl ion is coordinated to organophosphate groups.

Because of the relatively large atomic number of the phosphorus atom compared to C, N and H and because of the pseudo linear binding mode of the M−O=P group (M = metal), alkyl phosphates can be easily identified using EXAFS spectroscopy. Figure 8 shows the experimental and calculated EXAFS spectra and corresponding FT of solid-state compound $UO_2(NO_3)_2(TiBP)_2$ (TiBP = triisobutyl phosphate). Calculated spectra have been carried out with Feff-7 code based on the crystal structure of the compound at 77 K.[132] In this structure, the uranyl equatorial plane is filled with two bidentate nitrate ions and two monodentate phosphate ligands, the uranium atom being located on a center of symmetry. Deconvolution of the FT modulus in *n* moduli corresponding to *n* backscattering paths can be misleading if no phase is taken into account. Overall, assignment of the FT peaks in terms of backscatters is helpful, although it should be kept in mind that doing so, constructive and destructive interference are neglected. In Figure 8, the 11 paths represent the most intense backscattering process of the photoelectron. Path description is provided below with relative amplitude with respect to the one of the most intense path (a).

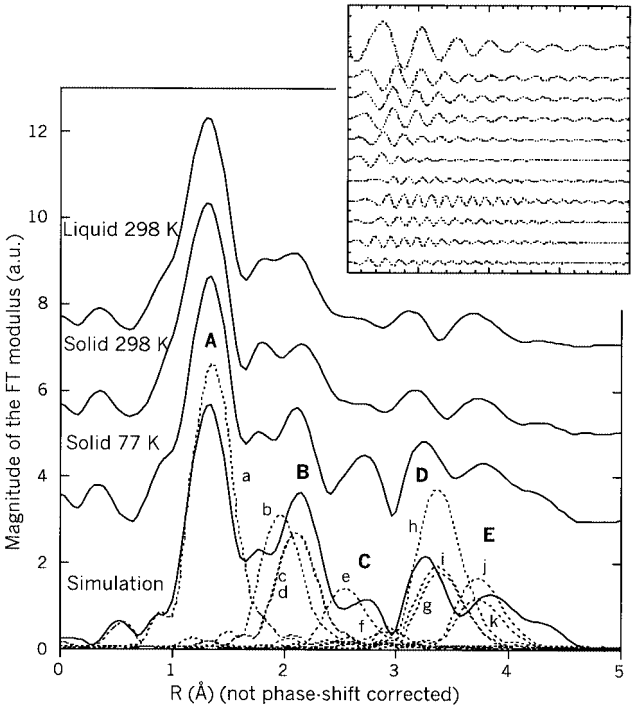

Figure 8. FT (moduli) of the EXAFS spectra of $UO_2(NO_3)_2(TBP)_2$ in TBP solution, solid-state $UO_2(NO_3)_2(TiBP)_2$ (298 K) and $UO_2(NO_3)_2(TiBP)_2$ (77 K);[85] calculated spectrum (Feff-7) of $UO_2(NO_3)_2(TiBP)_2$ is compared with moduli of each back-scattering path a to k; insert: EXAFS oscillations of each back-scattering path

Some of these paths are out of phase within each other as shown in the EXAFS spectra, leading to complex structures in the FT modulus between 2.5 and 4.5 Å (not phase-shift-corrected). For instance, peaks C and D can be mainly attributed to the two nitrogen atoms of the nitrate groups and to the phosphorus atoms of the equatorial ligands. In reality, paths e, f, g, h and i interfere. Peak E originates in a simpler way from the centrifugal oxygen atoms of the two nitrate groups. On the basis of such a path analysis, modifications of the multiple scattering amplitude factors can be used to trace deviations from linear tricenter atomic arrangements. This is the case here with the quasi linear U−O=P bonds. The quadratic dumping of the 4-leg multiple scattering path amplitude as well as the phase shift when the bond angle decreases can be used to extract bond angle information.[85]

On Figure 8, comparison is made with the FT of both solid-state $UO_2(NO_3)_2(TiBP)_2$ at 298 K and $UO_2(NO_3)_2(TBP)_2$ (TBP = tributyl phosphate) in TBP solution at 298 K. Both liquid and solid-state complexes analyzed at room temperature exhibit the same FT, in particular in the multiple-scattering 2.5−4.5-Å region. However, discrepancies with the same solid-state complex analyzed at 77 K indicate that the conformation of the uranyl coordination sphere is temperature-dependent. Decrease of the Debye−Waller factors upon temperature drop may also account for differences on the FT although data fitting has not shown any significant trend in this particular case.[85] The best fit results exhibit a nonsignificant expansion (+ 0.01 Å) of the equatorial U−O bond lengths from 77 to 298 K. At the same temperature, the solid-state and solution complexes are similar from the EXAFS point of view with 2 axial O at 1.77 Å, 2 equatorial O(phosphate) at 2.40

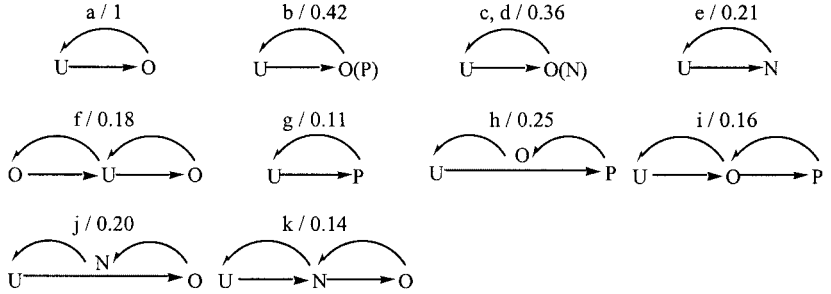

 © 2003 Wiley-VCH Verlag GmbH & Co. KGaA, Weinheim

Å and 4 equatorial O(nitrate) at 2.54 Å. From U to Pu, no significant evolution of the coordination sphere can be observed. The slight coordination sphere contraction of ca. 0.03 Å upon atomic number increase can be attributed to the actinidic contraction, a direct effect of the relativistic character of the 5f electrons.[101]

Monoamide and Malonamides are also oxygen donor monodentate ligands and bind in a similar way to the uranyl equatorial plane. Few solid-state crystal structures have been published[133,134] with nitrate ligands. In Figure 9 (a,b), comparison between solid-state $UO_2(NO_3)_2(TiBP)_2$ [85] and $UO_2(NO_3)_2(DBDMBA)_2$ (*N*,*N*-dibutyl-dimethylbutaramide)[135] complexes shows minor differences. In the multiple scattering regime, peaks C, D and E are present with modulations compared to $UO_2(NO_3)_2(TiBP)_2$ because of differences in backscattering phases and amplitudes. The coordinating carboxy group plays an equivalent role as the phosphorus one, and paths g, h and i apply to peak D with a carbon atom replacing the phosphate one. Similarly with phosphate coordination, comparison between solid state and solution, both at room temperature, shows no significant difference. However, at high acidity (above ca. 5 M), protonation of the malonamide occurs and direct binding to the uranyl is inhibited.[136] Such complexes are known as ion-pairs in which outer-sphere interactions between the actinyl and the malonamide occur. Such structural modification causes dramatic changes in the EXAFS spectra as shown in Figure 9 (a,b). Symmetrization of the equatorial plane by introducing 3 bidentate nitrate ions causes a large increase in peak B of the FT. Peak D decreases in amplitude and is shifted toward smaller distances. In the absence of any U−O=C MS paths, it originates exclusively from axial oxygen atoms (path f). Overall, the U−O(nitrate) distances decrease from 2.52 Å in the inner-sphere complex to 2.48 Å in the outer-sphere complex and this contraction is explained in terms of reduced steric hindrance in the outer-sphere complex. The U−O(axial) distance is unchanged at 1.77 Å.

4.3. Actinyl Uptake from Mineral Surfaces

Actinyl interactions with mineral surfaces is of very important environmental impact, as stressed in the introduction of this article. Among the questions that XAS has addressed are inner- versus outer-sphere complexation, formation of polynuclear precipitates, and mono- vs. polydentate surface binding modes. Such data are the prerequisite to further model the interactions between the heavy metal ions and the mineral surfaces in aqueous medium. Although one of the drawbacks of the technique is to average the signal over all the possible species, tentative site-by-site data analysis has been successfully undertaken. Some of the more recent studies[84,137−140] exemplify this method, considering a topological approach between the cation coordination sphere and the surface. Such data have to be compared to the coordination processes to natural substances as humic acids, as described in the previous paragraph. The uranium cation has been the most extensively studied because of its ubiquity in the geosphere and the absence of radiological concerns[106,140−152]. However, recent work has also been devoted to thorium[138] or neptunium.[109,139] Many mineral substrates have been use, based on their occurrence in the geosphere: goethite (FeOOH), muscovite $[KAl_2(AlSi_3O_{10})(F,OH)_2]$, mackinawite (FeS),[139,144] hematite (Fe_2O_3),[137,141] ferrihydrite ($Fe_2O_3H_2O$),[150] montmorillonite $[(Na,Ca)(Al,Mg)_6(Si_4O_{10})_3(OH)_6n(H_2O)]$,[107,153] zircon ($ZrSiO_4$),[154] zirconium diphosphate (ZrP_2O_7),[142] titania (TiO_2),[84] silica,[151,155] alumina (Al_2O_3)[140] etc. In most cases, intricate binary or ternary complexes are formed between the oxo cation, the surface and the solution counterions or water molecules. Note that for all these systems the species involved in the interface chemical reactions are difficult to measure due to their low

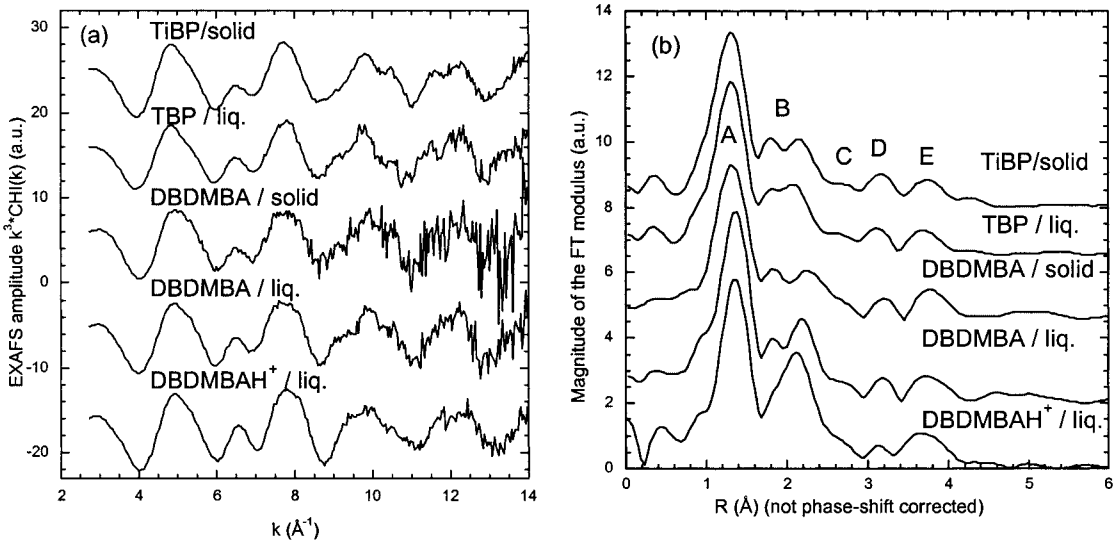

Figure 9. EXAFS spectra of solid-state compound $UO_2(NO_3)_2(TiBP)_2$, $UO_2(NO_3)_2(TBP)_2$ in TBP solution,[85] solid-state $UO_2(NO_3)_2(DBDMBA)_2$, $UO_2(NO_3)_2(DBDMBA)_2$ and $UO_2(NO_3)_3^-DBDMBAH^+$ in DBDMBA;.[135] all spectra were recorded at 298 K; (a) raw EXAFS oscillations and (b) corresponding modulus of the Fourier transform

 © 2003 Wiley-VCH Verlag GmbH & Co. KGaA, Weinheim

concentration on the solid surface. Participation of the counterion to the surface complex depends on its chelating ability under the sorption conditions.

The redox chemistry of uranium in aqueous solution is predominantly governed by the +VI oxidation state (the +VI/+IV potential with respect to the standard electrode is equal to 0.27 V). As a consequence, no reduction to the +IV oxidation state is expected upon sorption under atmospheric conditions as confirmed by the invariance of the uranium L_{III} edges observed in most of the above references. Similarly, the +V oxidation state is conserved when NpO_2^+ is sorbed onto goethite (FeOOH).[109] Conversely, when mackinawite (FeS) is used as a substrate, reduction of Np^V to Np^{IV} has been observed.[139] The authors have observed a similar behavior when PuO_2^{2+} is sorbed onto thorine (ThO_2): reduction of the plutonium oxidation state from +VI to +IV occurs. This phenomenon is not explained to date. Indeed, no redox reaction can occur between the plutonium species and the tetravalent thorium as it appears with iron substrates. The physico-chemical parameters at the solid/solution interface such as pH, redox potential, structure of the water molecules, may be different than those in the bulk solution, which could change drastically the radionuclide's chemical properties at the interface. Therefore, careful investigation of the microscopic properties of this interface should be carried out. In Figure 10, examples of EXAFS spectra of UO_2^{2+}/H_2O/substrate (substrate = $LaPO_4$, ZrP_2O_7 and TiO_2)/surface complexes are presented. Table 1 summarizes the structural parameters (the first uranium coordination sphere) of surface complexes published in the literature. Confirming the XANES results, the uranyl entity is conserved in all cases. When complexing counterions are present, such as carbonate anions, ternary inner-sphere complexes can be formed with the surface and the counterion.[137,141,151] The final stoichiometry often depends on the sorption conditions (pH, concentration in the solution). In presence of perchlorate ions, no inner-sphere complex with the counterion has been published to date. On the average, the equatorial uranium coordination number ranges from 5 to 6 as in aqueous uranyl. When a two-shell fit of the equatorial oxygen atoms is performed, a shorter bond length is observed between the uranium atom and the surface than between the uranium atom and the outer oxygen atoms (carbonate oxygen atoms,[137] water oxygen atoms[84,142,151,154–156]). For example, the Fourier transform of the EXAFS spectrum, corresponding to the U^{VI}/ZrP_2O_7 system, exhibits two equatorial oxygen atoms contributions and another one arising from the phosphorus atoms. The $U-O_{surf.}$ (2.33 Å) and U–P (3.60 Å) distances and the $O_{surf.}-P-O_{surf.}$ (110°) and P–O–P (150°) angles indicate clearly that the two oxygen atoms on the surface (associated to the shorter bond length) cannot belong to only one P_2O_7 surface group, but to two different ones.[142] A similar structural investigation has been carried out with the same metal ion on the $LaPO_4$ substrate. One phosphorus atom has been found at 2.74 Å. In that case, according to the bond lengths $U-O_{surf.}$ (2.31 Å) and P–O (at 1.50 Å in the PO_4 group), the $U-O_{surf.}-P$ angle is around 90°. Consequently, if the two oxygen atoms ($U-O_{surf.}$ at 2.31 Å) belong to the same PO_4 surface group, the $O_{surf.}-P-O_{surf.}$ angle should be around 114°, which is a reasonable value for the PO_4 tetrahedron. Therefore, it is assumed that the uranyl ion is complexed with only one PO_4 surface group. Moreover, as the phosphorus atom is at only 2.74 Å from the uranium atom, this indicates that there is no water molecule layer between the sorbed uranyl ion and the surface and thus that this ion is sorbed as an inner-sphere complex.[156] Nevertheless, the data from Waite et al.[150] seem to contradict this kind of interpretation with a reverse order of the distances. EXAFS studies have been performed on totally different substrates such as montmorillonite clay as well. By comparing the EXAFS data for uranyl ions in solution and sorbed onto this clay, it has been possible to distinguish different sorption mechanisms depending on the pH value of the suspension. For instance, for a pH value equal to 5, the EXAFS spectrum of loaded uranyl is identical to the one corresponding to the uranyl ions in solution, which demonstrates that these ions are sorbed as an outer-sphere complex onto the ion-exchange interlayer site of the clay.[106]

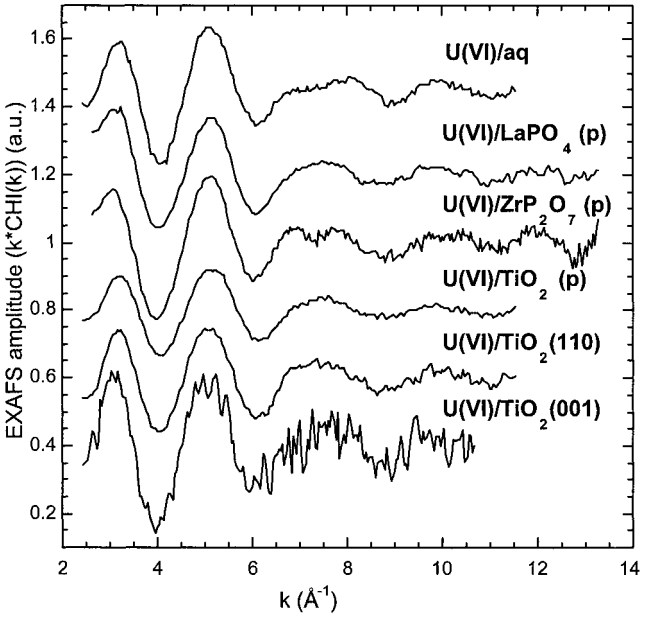

Figure 10. Raw EXAFS spectra of uranyl uptake from polycrystalline $LaPO_4$, ZrP_2O_7, TiO_2 powders[84,142,156] and single crystal of the (110) and (001) planes of TiO_2;[84] the spectrum of starting uranyl solution in perchloric acid is also displayed

As demonstrated by the growing number of sorption/XAS references, the use of polycrystalline substrates is essential to pin down the sorption mechanisms. Site-by-site interpretation of the sorption sites has even been attempted.[137,157] However, in order to better describe these surface sites, the use of crystallographic plane substrates allows a real site-by-site investigation of the surface complexes.[147,148] In the case of the uranyl oxo cation, advantage of the linear polarization of the synchrotron light has been taken in order to seek the uranyl rod orientation on the surface. Such experiment is known as Grazing Incidence

 © 2003 Wiley-VCH Verlag GmbH & Co. KGaA, Weinheim

Table 1. Uranium−oxygen bond lengths [Å] in various uranyl−surface complexes as given in the literature; only binary UO_2^{2+}/H_2O/substrate complexes are summarized

Sample[a]	Axial	Equatorial (out)[b]	Equatorial (surface)	Ref.
U^{VI}/aq.	*2.0(−)*[c] O−1.77(1)	4.7(3) O −2.42(1)		[84]
U^{VI}/LaPO4	2.1(4) O−1.77(1)	1.8(4) O −2.47(2)	2.4(5) O −2.31(2)	[156]
$U^{VI}/ZrSiO_4$	2.3(4) O−1.81(2)	1.9(4) O −2.54(2)	3.1(6) O −2.36(2)	[154]
U^{VI}/ZrP_2O_7	*2.0(−)* O−1.76(2)	3.0(5) O −2.46(2)	2.1(5) O −2.33(2)	[142]
U^{VI}/rutile	*2.0(−)* O−1.79(1)	3.1(1) O −2.49(3)	2.5(4) O −2.33(2)	[84]
U^{VI}/TiO_2(110)	*2.0(−)* O −1.78(1)	2.9(2) O −2.46(1)	2.1(2) O −2.31(1)	[84]
U^{VI}/TiO_2(001)[d]	*2.0(−)* O −1.77(1)	5.5(14) O −2.43(2)		[84]
U^{VI}/goethite	2.0(10) O −1.80(2)	5.0(10) O −2.40(2)		[144]
U^{VI}/lepidocrocite	2.0(10) O −1.80(2)	4.0(10) O −2.40(2)		[144]
U^{VI}/muscovite	2.0(10) O −1.80(2)	4.0(10) O −2.35(2)		[144]
U^{VI}/mackinawite	2.0(10) O −1.81(2)	4.0(10) O −2.40(2)		[144]
U^{VI}/montmorillonite[d]	*2.0(−)* O −1.79(2)	4.6(−) O −2.44(2)		[107]
U^{VI}/ferrihydrite	*2.0(−)* O −1.80(2)	3.0(−) O −2.35(2)	2.0(−) O −2.52(2)	[131]
U^{VI}/FeOOH	*2.0(−)* O −1.79(2)	5.0(10) O −2.35(2)		[152]
U^{VI}/montmorillonite[d]	*2.0(−)* O −1.79(1)	5.4(8) O −2.43(1)		[155]
U^{VI}/silica	*2.0(−)* O −1.78(1)	3.0(9) O −2.46(3)	2.1(6) O −2.28(2)	[155]

[a] Details about sorption conditions are given in the corresponding reference. In case of varying parameters such as pH or stock solution concentration, only one result is reported in the Table. [b] Distinction between surface-bonded and outer oxygen atoms is provided when a two-shell fit is provided. [c] Numbers in *italic* correspond to fixed or linked variables. [d] Outer-sphere complex.

XAS (GXAS) and its application to actinide chemistry is relatively new.[84,143] In a general sense, GXAS is based on the variation of the apparent number of neighbors with the angle between the electric field and the chemical bond.[158] Figure 11 shows the calculated effect of polarization on the sorption orientation of UO_2^{2+} onto the (011) plane of rutile. The modulations of feature B associated with the *trans*-dioxo unit are monitored by the angle between the O=U=O bond vector and the electric field vector: maximum intensity when both vectors are collinear, minimum intensity when both vectors are normal to each other. In comparison with the calculation, the parallel and perpendicular experimental measurements exhibit a slight decrease of feature B.[84] The small difference between the two measurements suggests that the uranyl rod sorbs quasi parallel to the surface, deviation from ideality being attributed to surface defects.[159]

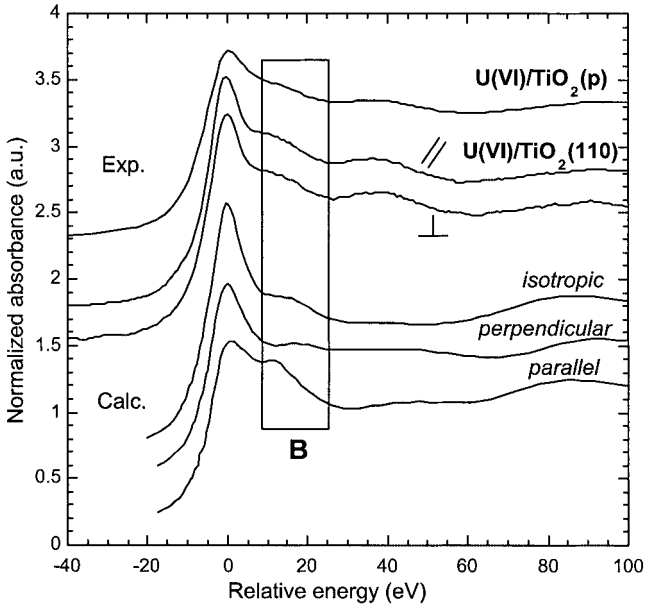

Figure 11. Uranium L_{III} edge experimental spectra of U^{VI}/TiO_2(p) and U^{VI}/TiO_2(110); U^{VI}/TiO_2(p) corresponds to an isotropic measurement; U^{VI}/TiO_2(110) has been measured with the electric field vector ε parallel (∥) and perpendicular (⊥) to the (110) surface;[84] comparison with uranium L_{III} edge simulated spectra (Feff-8.1) of $UO_2(O)_5^{2+}$ and $UO_2(O)_5$ cluster onto the TiO_2 (110) surface in the parallel and perpendicular configuration of the oxo cation bond vector with respect to ε ; for clarity, spectra have been shifted in ordinates and energy calibrated with respect to the edge maximum

EXAFS data analysis of the uranyl sorbed onto the (110) plane shows a splitting of the equatorial U−O bond lengths between U−O(surface) and U−O(out). Two possible sorption sites are available for bidentate complexation on the (110) surface: shared-edge distorted TiO_6 polyhedra and shared-summit polyhedra. Both sites are present in the surface complexes in proportions that are unknown from data analysis. Figure 12 shows a schematic representation of the surface complex in the case of the shared-edge sorption site of the (110) surface. The structural parameters are similar to the one obtained from uranyl sorption on polycrystalline

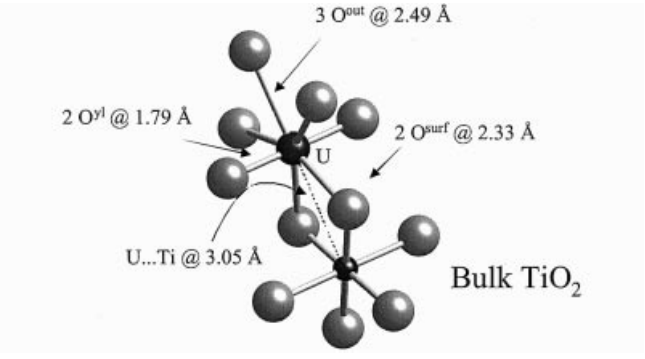

Figure 12. From EXAFS data analysis, schematic representation of the uranyl surface complex on the (110) surface of TiO_2; only the shared-edge site is represented[84]

 © 2003 Wiley-VCH Verlag GmbH & Co. KGaA, Weinheim

rutile (Table 1). The shortening of the U−O equatorial bond from 2.42 Å for aqueous uranyl to 2.32 Å for U−O(surface) suggests an increase in covalency of the U−O(surface) bond. This would not be surprising, taking into account the lack of coordination for the rutile surface oxygen atoms and the possibility of charge delocalization along the surface.

5. Summary

This overview on structural and electronic aspects of actinide molecular chemistry, although limited, has hopefully demonstrated the advantages of XAS for such chemical systems. Since the actinide elements are electron-rich cations from high atomic numbers, they bear remarkable chemical properties, from the availability of many stable oxidation states to the formation of large coordination polyhedra. Such properties demonstrate the richness of the actinyl chemistry; they also underline the intricacy of working with actinide cations.

Two major issues have been schematically addressed in this article. The first one deals with acute understanding of the actinyl electronic properties. Clearly the XAS probe by itself will not fully describe the electronic valence states of the molecule and a palette of complementary techniques and calculations must be employed. Coupling simulation codes to experimental results is also essential. In that sense, the selection of various transition channels from core spectroscopy to higher primary quantum numbers is a unique tool based on the tinability of the synchrotron radiation. Photoelectron or photoemission spectroscopy are examples of electronic probes based also on the interaction of a photon with the electronic cloud. In all cases, the key approximations that must be made for simulation purposes are driven by the final state. Although the relative qualitative evolution of the features driven by the absorption processes in homogeneous series of complexes is most often understood, absolute qualitative values are much more difficult to obtain. One of the major difficulties lies in the evaluation of the structural and electronic contributions to the absorption edge, both being highly related. In that sense, increased accuracy in the calculation results, such as Fermi levels, should be particularly helpful. The development of full multiple scattering codes can be considered as one of the major milestones in the field, although progresses must be carried out in the definition of the scattering potentials.

The second issue deals with the high energy part of the absorption process, where modulations of the absorption coefficient is related to the spatial arrangement around the absorbing atom. Although the single backscattering processes describe adequately the first coordination sphere, they are of limited information beyond this shell and multiple scattering processes must be taken into account. Accurate geometrical information can also be drawn from the multiple scattering paths as their phases and amplitudes are affected by the relative bond angles and distances. Finally, coupling with quantum chemistry is essential in order to validate or favor one of the geometrical models deduced from the EXAFS data. One of the major difficulties to be pointed out occurs when several species or conformations are present. This is a common case in solution coordination chemistry when either labile complexes or low equilibrium constants are encountered. As a result, the data analysis accuracy is limited by an increasing number of fitting parameters.

From speciation to simulation, XAS has proven to be one of the useful probes for actinyl chemistry. As suggested in this article, limitation of XAS data analysis to phenomenological aspects is often restrictive and coupling with calculation codes should help to quantify the links between absorption processes and electronic properties.

Acknowledgments

This research was mainly carried out at the Laboratoire d'Utilisation du Rayonnement Electromagnétique (Orsay, France) a national user facility operated by CEA/CNRS/MR and the Stanford Synchrotron Radiation Laboratory (Stanford, USA), a national user facility operated by Stanford University on behalf of the U.S. Department of Energy, Office of Basic Energy Sciences. The authors are particularly grateful to the beam line scientists and health physicists of LURE for their constant help, support and advice. They would like also to acknowledge the beam line scientists of SSRL and health physicists supported by the Seaborg Institute at LANL. Many fruitful discussions with J. J. Rehr, A. Ankudinov and C. Cartier dit Moulin played an important part in this work and the authors would like to thank them for their help. This work has been financially supported by CEA/DEN, PRACTIS (France) and by DOE OBES Division of Chemical Sciences under Contract W-7405 (USA).

[1] A. J. Freeman, J. B. Darby, Jr., *The Actinides: Electronic structure and related properties*, Academic Press, New York, **1974**, vols. I, II.
[2] M. Karboviak, J. Drozdzynski, S. Hubert, E. Simoni, W. STREK, *J. Chem. Phys.* **1998**, 108−124, 10181−10188.
[3] P. A. Tanner, *J. Mol. Struct.* **1995**, *355*, 299−306.
[4] M. Karboviak, E. Simoni, J. Drozdzynski, S. Hubert, *Acta Phys. Pol.* **1996**, *A90*, 367−370.
[5] M. Karboviak, J. Drozdzynski, K. M. Murdoch, N. M. Edelstein, S. Hubert, *J. Chem. Phys.* **1997**, *106*, 3067−3075.
[6] E. Simoni, M. Louis, S. Hubert, M. F. Reid, *J. Phys. II* **1995**, *5*, 755−764.
[7] J. C. Krupa, E. Simoni, J. Systma, N. M. Edelstein, *J. Alloys Compd.* **1994**, *213*, 471−474.
[8] E. Simoni, M. Louis, S. Hubert, S. Xia, *Opt. Mater. (N. Y.)* **1995**, *4*, 641−650.
[9] Y. Tahri, H. Chermette, N. El Khatib, J. C. Krupa, E. Simoni, *J. Less-Common Met.* **1990**, *158*, 105−116.
[10] L. J. Nugent, R. D. Baybartz, J. L. Burnett, J. L. Ryan, *J. Inorg. Nucl. Chem.* **1971**, *33*, 2503−2530.
[11] L. J. Nugent, R. D. Baybartz, J. L. Burnett, J. L. Ryan, *J. Phys. Chem.* **1973**, *77*, 1528−1538.
[12] W. T. Carnall, H. M. Crosswhite, J. Crosswhite, J. Hessler, N. M. Edelstein, J. C. Conway, G. V. Shalimoff, R. Sarup, *J. Chem. Phys.* **1980**, *72*, 5089−5096.
[13] R. Mcdiarmid, *J. Chem. Phys.* **1976**, *65*, 168−173.
[14] D. D. Koelling, D. E. Ellis, R. J. Barlett, *J. Chem. Phys.* **1976**, *65*, 3331−3340.
[15] D. E. Ellis, A. Rosen, V. A. Gubanov, *J. Chem. Phys.* **1982**, *77*, 4051−4060.

 © 2003 Wiley-VCH Verlag GmbH & Co. KGaA, Weinheim

[16] K. Pierloot, A. Renders, G. L. Goodman, D. Devoghel, C. Gorller-Walrand, L. G. Vanquickenborne, *J. Chem. Phys.* **1991**, *94*, 2928−2939.
[17] P. J. Hay, W. R. Wadt, L. R. Kahn, R. C. Raffenetti, D. H. Phillips, *J. Chem. Phys.* **1979**, *71*, 1767−1779.
[18] M. Louis, S. Hubert, E. Simoni, J. Y. Gesland, *Opt. Mater. (N.Y.)* **1996**, *6*, 121−127.
[19] J. Gal, M. Kroup, Z. Hadari, I. Nowik, *Phys. Rev. B* **1977**, *16*, 3913−3920.
[20] J. Gal, S. Fredo, Z. Hadari, J. L. Buevoz, C. de Novion, *J. Magn. Magn. Mater.* **1979**, *10*, 100−108.
[21] J. Gal, C. Musikas, J. Jové, M. Pagès, I. Nowik, *Phys. Rev. B* **1981**, *23*, 4324−4330.
[22] B. D. Dunlap, G. M. Kalvius, *J. Phys., Colloq. C4* **1979**, *40*, 192−200.
[23] B. D. Dunlap, G. H. Lander, *Phys. Rev. Lett.* **1974**, *33*, 1046−1050.
[24] H. Abazli, A. Cousson, J. Jové, M. Pagès, M. Gaspérin, *J. Less-Common Met.* **1984**, *96*, 23−31.
[25] H. Abazli, A. Cousson, J. Jové, M. Pagès, *J. Fluorine* **1980**, *16*, 647−651.
[26] T. Thévenin, J. Jové, M. Pagès, D. Damien, *Sol. State Commun.* **1981**, *40*, 1065−1072.
[27] D. G. Karraker, J. A. Stone, *Inorg. Chem.* **1979**, *70*, 2041−2050.
[28] D. G. Karraker, J. A. Stone, *Inorg. Chem.* **1980**, *19*, 3545−3552.
[29] D. G. Karraker, J. A. Stone, *Phys. Rev. B* **1980**, *22*, 111−120.
[30] D. D. Bodé, J. F. Wild, E. K. Hulet, *J. Inorg. Nucl. Chem.* **1976**, *38*, 1291−1299.
[31] D. Damien, A. Wojakowski, W. Müller, *Inorg. Nucl. Chem. Lett.* **1976**, *12*, 441−450.
[32] D. Damien, R. G. Haire, J. R. Peterson, *J. Phys. Colloq. C4* **1979**, *40*, 95−100.
[33] J. P. Charvillat, D. Damien, A. Wojakowski, *Rev. Chim. Miner.* **1977**, *14*, 178−189.
[34] A. Wojakowski, D. Damien, *J. Less-Common Met.* **1982**, *83*, 263−271.
[35] G. Calestani, J. C. Spirlet, J. Rebizant, W. Müller, *J. Less-Common Met.* **1979**, *68*, 207−212.
[36] T. Thévenin, M. Pagès, A. Wojakowski, *J. Less-Common Met.* **1982**, *84*, 133−140.
[37] A. Blaise, D. Damien, J. Mulak, *Phys. Status Solidi* **1982**, *72*, K145−K150.
[38] T. Thévenin, J. Jové, M. Pagès, *Hyperfine Interact.* **1984**, *20*, 173−179.
[39] Y. Héry, D. Damien, J. P. Charvillat, *Radiochem. Radioanal. Lett.* **1979**, *37*, 17−23.
[40] D. P. Karim, P. Georgopoulos, *Nucl. Tech.* **1980**, *51*, 162−168.
[41] P. G. Allen, J. J. Bucher, M. A. Denecke, N. M. Edelstein, N. Kaltsoyannis, H. Nitsche, T. Reich, D. K. Shuh, *Synchrotron Radiation Techniques in Industrial, Chemical and Material Sciences* (Ed.: D'Amico), Plenum Press, **1996**, p. 169−185.
[42] S. D. Conradson, *Appl. Spectrosc.* **1998**, *52*, 252−279.
[43] R. J. Silva, H. Nitsche, *Radiochim. Acta* **1995**, *70/71*, 377−396.
[44] J. E. Penner-Hahn, *Coord. Chem. Rev.* **1999**, *190/192*, 1101−1123.
[45] B. K. Teo, *Basic Principles and Data Analysis*, Springer Verlag, Berlin, **1986**.
[46] A. Bianconi, L. Incoccia, S. Stipcich, *EXAFS and Near Edge Structure, Proceedings of the International Conference, Frascati, Italy 1982*, Springer Verlag, New York, **1983**.
[47] J. Stöhr, *NEXAFS Spectroscopy*, Springer Verlag, New York, **1992**.
[48] J. J. Rehr, R. C. Albers, *Rev. Mod. Phys.* **2000**, *72*, 621−654.
[49] K. W. Bagnall, *Comprehensive Coordination Chemistry* (Ed.: G. Wilkinson), Pergamon Press, **1987**, vol. 7, chapter 40.
[50] J. J. Rehr, A. L. Ankudinov, *J. Electron Spectrosc. Relat. Phenom.* **2001**, *114−116*, 1115−1121 and references herein.
[51] C. Hennig, T. Reich, H. Funke, A. Roβberg, M. Rutsch, G. Bernhard, *J. Synchrotron Radiat.* **2001**, *8*, 695−697.
[52] W. W. Schulz, L. L. Burger, J. D. Navratil, *Science and Technology of Tributylphosphate*, CRC-Press Inc., Boca-Raton, Florida, USA, **1990**, vol. III.
[53] M. Viala, M. Salvatores, *Proceedings of the GLOBAL'95 Conference*, Versailles, France, **1995**, vol. I, p. 11−14.
[54] N. Kaltsoyannis, P. Scott, *The f elements*, Oxford Science Publisher, Zeneca, **1999**.
[55] L. Gagliardi, B. O. Roos, P-A. Malmqvist, J. M. Dyke, *J. Phys. Chem. A* **2001**, *105*, 10602−10606.
[56] P. J. Hay, R. L. Martin, G. Schreckenbach, *J. Phys. Chem. A* **2000**, *104*, 6259−6270.
[57] P. Pyykkö, L. J. Laakkonen, K. Tatsumi, *Inorg. Chem.* **1989**, *28*, 1801−1805.
[58] M. Pepper, B. Bursten, *Chem. Rev.* **1991**, *91*, 719−741.
[59] R. G. Denning, *Struct. Bonding* **1992**, *79*, 217−276.
[60] T. Reich, G. Bernhard, G. Geipel, H. Funke, C. Heining, A. Roβberg, W. Matz, N. Schell, H. Nitsche, *Radiochim. Acta* **2000**, *88*, 633−637.
[61] *Proceedings of the Workshop on Speciation, Techniques and facilities for Radioactive Materials at Sunchrotron Light Sources*, OECD − NEA, 4−6 October **1998**, Grenoble, France and *Proceedings of the 2nd Euroconference and NEA Workshop on Speciation, Techniques and Facilities for Radioactive Materials at Synchrotron Light Sources* **2001**, Grenoble, France.
[62] H. Konishi, A. Yokoya, H. Shiwaku, H. Motohashi, T. Makita, Y. Kashihara, S. Hashimoto, T. Harami, T. Sasaki, H. Maeta, H. Ohno, H. Maezawa, S. Asaoka, N. Kanaya, K. Ito, N. Usami, K. Kobayashi, *Nucl. Instrum. Methods Phys. Res.* **1996**, *372*, 322−332.
[63] T. Nakatani, Y. Saitoh, Y. Teraoka, T. Okane, A. Yokoya, *J. Synchrotron Radiat.* **1998**, *5*, 536−538.
[64] M. O. Kraus, J. H. Oliver, *J. Phys. Chem. Ref. Data* **1979**, *8*, 329−338.
[65] R. Revel, C. Den Auwer, C. Madic, F. David, B. Fourest, S. Hubert, J. F. Le Du, L. R. Morss, *Inorg. Chem.* **1999**, *38*, 4139−4141.
[66] C. Den Auwer, M. C. Charbonnel, M. G. B. Drew, M. Grigoriev, M. J. Hudson, P. B. Iveson, C. Madic, M. Nierlich, M. T. Presson, R. Revel, M. L. Russel, P. Thuéry, *Inorg. Chem.* **2000**, *39*, 1487−1495.
[67] V. Vallet, U. Wahlgren, B. Schimmelpfennig, H. Moll, Z. Szabo, I. Grenthe, *Inorg. Chem.* **2001**, *40*, 3516−3525.
[68] A. L. Ankudinov, B. Ravel, J. J. Rehr, S. D. Conradson, *Phys. Rev. B* **1998**, *58*, 7565−7576.
[69] A. L. Ankudinov, S. D. Conradson, J. Mustre de Leon, J. J. Rehr, *Phys. Rev. B* **1998**, *57*, 7518−7525.
[70] F. de Groot, *Chem. Rev.* **2001**, *101*, 1779−1808.
[71] J. M. Lawrence, M. L. den Boer, R. D. Parks, J. L. Smith, *Phys. Rev. B* **1984**, *29*, 568−575.
[72] J. Petiau, G. Calas, D. Petitmaire, A. Bianconi, M. Benfatto, A. Marcelli, *Phys. Rev. B* **1986**, *34*, 7350−7361.
[73] G. Kalkowski, G. Kaindl, S. Bertram, G. Schmiester, J. Rebizant, J. C. Spirlet, O. Vogt, *Solid State Commun.* **1987**, *64*, 193−196.
[74] G. Kalkowski, G. Kaindl, W. D. Brewer, W. Krone, *Phys. Rev. B* **1987**, *35*, 2667−2677.
[75] J. Guo, D. E. Ellis, E. L. Soderholm, G. K. Shenoy, *Phys. Rev. B* **1989**, *39*, 6125−6139.
[76] F. Jollet, T. Petit, S. Gota, N. Thromat, M. Gautier-Soyer, A. Pasturel, *J. Phys.: Condens. Matter* **1997**, *9*, 9393−9401.
[77] E. A. Hudson, J. J. Rehr, J. J. Bucher, *Phys. Rev. B* **1995**, *52*, 13815−13826.
[78] E. A. Hudson, P. G. Allen, L. J. Terminello, M. A. Denecke, T. Reich, *Phys. Rev. B* **1996**, *54*, 156−165.
[79] A. L. Ankudinov, A. I. Nesvizhskii, J. J. Rehr, *J. Synchrotron Radiat.* **2001**, *8*, 92−95.
[80] S. E. Shadle, B. Hedman, K. O. Hodgson, E. I. Solomon, *J. Am. Chem. Soc.* **1995**, *117*, 2259−2272.
[81] V. Briois, C. Cartier dit Moulin, P. Sainctavit, C. Brouder, A. M. Flank, *J. Am. Chem. Soc.* **1995**, *117*, 1019−1026.
[82] V. Briois, P. Sainctavit, G. J. Long, F. Grandjean, *Inorg. Chem.* **2001**, *40*, 912−918.

 © 2003 Wiley-VCH Verlag GmbH & Co. KGaA, Weinheim

[83] C. Den Auwer, E. Simoni, S. D. Conradson, J. Mustre de Leon, P. Moisy, A. Bérès, *C. R. Acad. Sci., Ser. IIc: Chim.* **2000**, *3*, 327−333.
[84] C. Den Auwer, E. Simoni, R. Drot, M. Gailhanou, S. D. Conradson, J. Mustre de Leon, *New J. Chem.* **2003**, *27*, 648−655.
[85] C. Den Auwer, C. Lecouteux, M. C. Charbonnel, C. Madic, R. Guillaumont, *Polyhedron* **1997**, *16*, 2233−2238; C. Den Auwer, M. C. Charbonnel, M. T. Presson, C. Madic, R. Guillaumont, *Polyhedron* **1998**, *17*, 4507−4517.
[86] D. Meyer, S. Fouchard, E. Simoni, C. Den Auwer, *Radiochim. Acta* **2002**, *90*, 253−258.
[87] D. H. Templeton, L. K. Templeton, *Acta Crystallogr., Sect. A* **1982**, *38*, 62−67.
[88] S. D. Conradson, I. Al Mahamid, D. L. Clark, N. J. Hess, E. A. Hudson, M. P. Neu, P. D. Palmer, W. H. Runde, C. Drew Tait, *Polyhedron* **1998**, *17*, 599−601.
[89] E. Simoni, H. Abazli, A. Cousson, M. Pagès, *Radiochem. Radioanal. Lett.* **1981**, *49*, 37−40.
[90] J. Rakovan, R. J. Reeder, E. J. Elzinga, D. J. Cherniak, C. Drew Tait, D. E. Morris, *Environ. Sci. Technol.* **2002**, *36*, 3114−3117.
[91] J. Mustre de Leon, S. D. Conradson, D. L. Clark, C. Den Auwer, N. Hess, D. W. Keogh, P. D. Palmer, E. Simoni, D. Blanchard, to be submitted.
[92] E. Simoni, M. Louis, S. Hubert, S. Xia, *Opt. Mater.* **1995**, *4*, 641 −650.
[93] A. J. Francis, C. J. Dodge, F. Lu, G. P. Halada, C. R. Clayton, *Environ. Sci. Technol.* **1994**, *28*, 636−639.
[94] C. W. Williams, J-P. Blaudeau, J. C. Sullivan, M. R. Antonio, B. Bursten, L. Soderholm, *J. Am. Chem. Soc.* **2001**, *123*, 4346−4347.
[95] P. Jolivet, C. Den Auwer, E. Simoni, *J. Nucl. Mater.* **2002**, *301*, 142−152.
[96] M. A. Denecke, *Proceedings of the Workshop on Speciation, Techniques and Facilities for Radioactive Materials at Sunchrotron Light Sources*, OECD − NEA, 4−6 October **1998**, Grenoble, France.
[97] S. Spencer, L. Gagliardi, N. C. Handy, A. G. Ioannou, C-K. Skylaris, A. Willetts, A. M. Simper, *J. Phys. Chem. A* **1999**, *103*, 1831−1837.
[98] L. Gagliardi, B. O. Roos, *Inorg. Chem.* **2002**, *41*, 1315−1319.
[99] L. Sémon, C. Boehme, I. Billard, C. Hennig, K. Lützenkirchen, T. Reich, A. Roβberg, I. Rossini, G. Wipff, *ChemPhysChem* **2001**, *2*, 591−598.
[100] U. Wahlgren, H. Moll, I. Grenthe, B. Schimmelpfennig, L. Maron, V. Vallet, O. Gropen, *J. Phys. Chem. A* **1999**, *103*, 8257−8264.
[101] C. Den Auwer, R. Revel, M. C. Charbonnel, M. T. Presson, S. D. Conradson, E. Simoni, J. F. Le Du, C. Madic, *J. Synchrotron Rad.* **1999**, *6*, 101−104.
[102] D. L. Clark, S. D. Conradson, R. J. Donohoe, D. W. Keogh, D. E. Morris, P. D. Palmer, R. D. Rogers, C. Drew Tait, *Inorg. Chem.* **1999**, *38*, 1456−1466.
[103] P. Charpin, A. Dejean, G. Folcher, P. Rigny, P. Navaza, *J. Chim. Phys. (Paris)* **1985**, *82*, 925−932.
[104] H. A. Thompson, G. E. Brown, Jr., G. A. Parks, *Am. Mineral.* **1997**, *82*, 483−496.
[105] P. G. Allen, J. J. Bucher, D. K. Shuh, N. M. Edelstein, T. Reich, *Inorg. Chem.* **1997**, *36*, 4676−4683.
[106] A. J. Dent, J. D. Ramsay, S. W. Swanton, *J. Colloid Interface Sci.* **1992**, *150*, 45−60.
[107] C. Chisholm-Brause, S. D. Conradson, C. T. Buscher, P. G. Eller, D. E. Morris, *Geochim. Cosmoschim. Acta* **1994**, *58*, 3625−3631.
[108] H. Moll, T. Reich, Z. Szabo, *Radiochim. Acta* **2000**, *88*, 411−415.
[109] J-M Combes, C. J. Chisholm-Brause, G. E. Brown, Jr., G. A. Parks, S. Conradson, P. G. Eller, I. R. Triay, D. E. Hobart, A. Meijer, *Environ. Sci. Technol.* **1992**, *26*, 376−382.
[110] M. R. Antonio, L. Soderholm, C. W. Williams, J-P. Blaudeau, B. E. Bursten, *Radiochim. Acta* **2001**, *89*, 17−25.
[111] P. J. Panak, C. H. Booth, D. L. Caulder, J. J. Bucher, D. K. Shuh, H. Nitsche, *Radiochim. Acta* **2002**, *90*, 315−321.
[112] N. N. Krot, A. D. Gelman, *Dokl. Akad. Nauk SSSR* **1967**, *177*, 124.
[113] M. S. Grigoriev, B. F. Gulev, N. N. Krot, *Radiochemistry* **1986**, *28*, 630−634.
[114] V. P. Shilov, *Radiochemistry* **1998**, *40*, 11−16.
[115] D. L. Clark, S. D. Conradson, M. P. Neu, P. D. Palmer, W. Runde, C. Drew Tait, *J. Am. Chem. Soc.* **1997**, *119*, 5259−5260.
[116] H. Bolvin, U. Wahlgren, H. Moll, T. Reich, G. Geipel, T. Fanghänel, I. Grenthe, *J. Phys. Chem. A* **2001**, *105*, 11441−11445.
[117] L. Soderholm, M. R. Antonio, C. W. Williams, J. C. Sullivan, S. R. Wasserman, J-P. Blaudeau, *Second Euroconference and NEA Workshop on Speciation, Techniques and Facilities for Radioactive Materials at Synchrotron Light Source*, September 10−12, **2000**, Grenoble, France.
[118] S. D. Conradson, R. J. Donohoe, D. W. Keogh, D. E. Morris, P. D. Palmer, B. L. Scott, C. Drew Tait, manuscript in preparation; D. L. Clark, S. D. Conradson, R. J. Donohoe, D. W. Keogh, D. E. Morris, P. D. Palmer, B. L. Scott, C. Drew Tait, manuscript in preparation.
[119] W. Runde, M. P. Neu, S. D. Conradson, D. L. Clark, P. D. Palmer, S. D. Reilly, B. L. Scott, C. D. Tait, *Mat. Res. Soc. Symp. Proc.* **1997**, *465*, 693−703.
[120] P. G. Allen, J. J. Bucher, D. L. Clark, N. M. Edelstein, S. A. Ekberg, J. W. Gohdes, E. A. Hudson, N. Kaltsoyannis, W. W. Lukens, M. P. Neu, P. D. Palmer, T. Reich, D. K. Shuh, C. D. Tait, B. D. Zwick, *Inorg. Chem.* **1995**, *34*, 4797−4807.
[121] T. I. Docrat, J. F. W. Mosselmans, J. M. Charnock, M. W. Whiteley, D. Collison, F. R. Livens, C. Jones, M. J. Edmiston, *Inorg. Chem.* **1999**, *38*, 1879−1882.
[122] G. Bernhard, G. Geipel, T. Reich, V. Brendler, S. Amayri, H. Nitsche, *Radiochim. Acta* **2001**, *89*, 511−518.
[123] D. L. Clark, S. D. Conradson, S. A. Ekberg, N. J. Hess, D. R. Janecky, M. P. Neu, P. D. Palmer, C. Drew Tait, *New J. Chem.* **1996**, *20*, 211−220.
[124] D. L. Clark, S. D. Conradson, S. A. Ekberg, N. J. Hess, M. P. Neu, P. D. Palmer, W. Runde, C. Drew Tait, *J. Am. Chem. Soc.* **1996**, *118*, 2089−2090.
[125] D. L. Clark, D. E. Hobart, M. P. Neu, *Chem. Rev.* **1995**, *95*, 25−48.
[126] H. Moll, T. Reich, C. Henning, A. Roβberg, Z. Szabo, I. Grenthe, *Radiochim. Acta* **2000**, *88*, 559−566.
[127] M. A. Denecke, S. Pompe, T. Reich, H. Moll, M. Bubner, K. H. Heise, R. Nicolai, H. Nitsche, *Radiochim. Acta* **1997**, *79*, 151−159.
[128] S. Pompe, M. Bubner, M. A. Denecke, T. Reich, A. Brachmann, G. Geipel, R. Nicolai, K. H. Heise, H. Nitsche, *Radiochim. Acta* **1996**, *74*, 135−140.
[129] M. A. Denecke, T. Reich, S. Pompe, M. Bubner, K. H. Heise, H. Nitsche, P. G. Allen, J. J. Bucher, N. M. Edelstein, D. K. Shuh, K. R. Czerwinski, *Radiochim. Acta* **1998**, *82*, 103−108.
[130] A. Roβberg, L. Baraniak, T. Reich, C. Hennig, G. Bernhard, H. Nitsche, *Radiochim. Acta* **2000**, *88*, 593−597.
[131] C. Hennig, P. J. Panak, T. Reich, A. Roβberg, J. Raff, S. Selenska-Pobell, W. Matz, J. J. Bucher, G. Bernhard, H. Nitsche, *Radiochim. Acta* **2001**, *89*, 625−631.
[132] J. H. Burns, G. M. Brown, R. R. Ryan, *Acta Crystallogr., Sect. C* **1985**, *41*, 1446−1448.
[133] P. Charpin, M. Lance, M. Nierlich, D. Vigner, *Acta Crystallogr., Sect. C* **1986**, *42*, 560−563.
[134] P. Charpin, M. Lance, M. Nierlich, D. Vigner, *Acta Crystallogr., Sect. C* **1987**, *43*, 231−233.
[135] C. Den Auwer, M. C. Charbonnel, M. T. Presson, unpublished data.
[136] N. Condamines, C. Musikas, *Solvent Extr. Ion Exch.* **1992**, *10*, 69−100.
[137] J. R. Bargar, R. Reitmeyer, J. J. Lenhart, J. A. Davis, *Geochim. Cosmoschim. Acta* **2000**, *64*, 2737−2749.
[138] P. Dähn, A. M. Scheidegger, A. Manceau, E. Curti, B. Baeyens,

M. H. Bradbury, D. Chateigner, *J. Colloid Interface Sci.* **2002**, *249*, 8−21.
[139] L. N. Moyes, M. J. Jones, W. A. Reed, F. R. Livens, J. M. Charnock, J. F. W. Mosselmans, C. Hennig, D. J. Vaughan, R. A. D. Pattrick, *Environ. Sci. Technol.* **2002**, *36*, 179−183.
[140] M. A. Denecke, J. Rothe, K. Dardenne, P. Lindqvist-Reis, *Phys. Chem. Chem. Phys.* **2003**, *5*, 939−946.
[141] J. R. Bargar, R. Reitmeyer, J. A. Davis, *Environ. Sci. Technol.* **1999**, *33*, 2481−2484.
[142] R. Drot, E. Simoni, C. Den Auwer, *C. R. Acad. Sci., Ser. IIc: Chim.* **1999**, *2*, 111−117.
[143] G. N. Greaves, N. T. Barrett, G. M. Antonini, F. R. Thornley, B. T. M. Willis, A. Steel, *J. Am. Chem. Soc.* **1989**, *111*, 4313−4324.
[144] L. N. Moyes, R. H. Parkman, J. M. Charnock, D. J. Vaughan, F. R. Livens, C. R. Hugues, A. Braithwaite, *Environ. Sci. Technol.* **2000**, *34*, 1062−1068.
[145] R. J. Reeder, M. Nugent, G. M. Lamble, C. D. Tait, D. E. Morris, *Environ. Sci. Technol.* **2000**, *34*, 638−644.
[146] A. M. Scheidegger, G. M. Lamble, D. L. Sparks, *J. Colloid Interface Sci.* **1997**, *186*, 118−128.
[147] S. N. Towle, G. E. Brown, Jr., G. A. Parks, *J. Colloid Interface Sci.* **1999**, *217*, 299−311.
[148] S. N. Towle, J. R. Bargar, G. E. Brown, Jr., G. A. Parks, *J. Colloid Interface Sci.* **1999**, *217*, 312−321.
[149] T. P. Trainor, J. P. Fitts, A. S. Templeton, D. Grolimund, G. E. Brown, Jr., *J. Colloid Interface Sci.* **2001**, *244*, 239−244.
[150] T. D. Waite, J. A. Davis, T. E. Payne, G. A. Waychunas, N. Xu, *Geochim. Cosmochim. Acta* **1994**, *58*, 5465−5478.
[151] T. Reich, H. Moll, T. Arnold, M. A. Denecke, C. Hennig, G. Geipel, G. Bernhard, H. Nitsche, P. G. Allen, J. J. Bucher, N. M. Edelstein, D. K. Shuh, *J. Electron Spectrosc. Relat. Phenom.* **1998**, *96*, 237−243.
[152] A. Manceau, L. Charlet, M. C. Boisset, B. Didier, L. Spadini, *Appl. Clay Sci.* **1992**, *7*, 201−223.
[153] C. Hennig, T. Reich, R. Dähn, A. M. Scheidegger, *Radiochim. Acta* **2002**, *90*, 653−657.
[154] C. Lomenech, E. Simoni, R. Drot, J.-J. Ehrardt, J. Mielczarski, *J. Colloid Interface Sci.* **2003**, *261/262*, 221−232.
[155] E. R. Sylwester, E. A. Hudson, P. G. Allen, *Geochim. Cosmochim. Acta* **2000**, *64*, 2431−2438.
[156] E. Ordoñez-Regil, R. Drot, E. Simoni, J-J. Ehrhardt, *Langmuir* **2002**, *18*, 7977−7984.
[157] J. R. Bargar, G. E. Brown Jr., G. A. Parks, *Geochim. Cosmochim. Acta* **1998**, *62*, 193−207.
[158] P. H. Citrin, *Phys. Rev. B* **1985**, *31*, 700−721.
[159] G. E. Brown, Jr., V. E. Henrich, W. H. Casey, D. L. Clark, C. Eggleston, A. Felmy, D. W. Goodman, M. Grätzel, G. Maciel, M. I. McCarthy, K. H. Nealson, D. A. Sverjensky, M. F. Toney, J. M. Zachara, *Chem. Rev.* **1999**, *99*, 77−174.

Received February 17, 2003

 © 2003 Wiley-VCH Verlag GmbH & Co. KGaA, Weinheim

Lithium [Bis{benzoyl-$W(CO)_5$}(μ_2-hydrogen)] − A Charge-Assisted H^+-Bridged Organometallic Complex Prepared by Selective Li^+ Ion Replacement

Matthias W. Esterhuysen[a] and Helgard G. Raubenheimer*[a]

Dedicated to E. O. Fischer on the occasion of his 85th birthday

Keywords: Lithium / Tungsten / Hydrogen bonds / Crystal engineering / Carbene complexes / Self-assembly

Efficient syntheses and isolation procedures of two closely related benzoyl–$W(CO)_5$ compounds, [{Li(diglyme)}{Ph(O)-$CW(CO)_5$}] (**1**) and [$Li(diglyme)_2$][(μ_2-H){Ph(O)$CW(CO)_5$}$_2$] (**2**) are reported. The empirical formulae of **1** and **2** differ only in that the latter contains half the number of Li^+ ions, with the balance of cations replaced by protons through an acidic silica gel filtration procedure. X-ray structural investigations of both compounds revealed a self-assembled polymeric Li^+-bridged structure for **1**, and a strikingly dissimilar H^+-bridged structure for **2**, thereby emphasising the important influences of strong, charge-assisted hydrogen bonds on solid-state structures. Possible implications of this novel route to charge-assisted hydrogen bonds for crystal engineering are discussed.
(© Wiley-VCH Verlag GmbH & Co. KGaA, 69451 Weinheim, Germany, 2003)

Introduction

Hydrogen bonding effects are essential in crystal engineering.[1] Recent advances in organometallic crystal engineering, especially by the group of Braga and Grepioni, have exhibited the versatility of hydrogen bonds in the "construction" of extended organometallic structures.[2] Variation of the non-covalently bonded ligand components in the crystals may then ultimately enable chemists to "tune" the crystal so that aspects of transition metal coordination chemistry (e.g. variable valence, oxidation, and spin states of the metal atoms) are incorporated in the crystals.[2] Organometallic crystal engineering studies are presently focused mainly on the use of functionalised ferrocenes, and other sandwich compounds, in forming crystals with extended structures.[2] Carboxylic acid and 1,3-cyclohexanedione functionalities in these compounds are, furthermore, the preferred vehicles for introducing hydrogen bonds, which ultimately produce the extended structures of molecules in the crystals.[2] Strong, charge-assisted O−H···O^- hydrogen bonds − valuable tools for crystal engineers − are generally obtained by partial deprotonation of acidic moieties (typically carboxylic acids) in the crystals and significantly strengthen the extended structures.[3] These short hydrogen bonds, as they occur in homonuclear molecule−ion associates, AHA^- (A = anion base, e.g. carboxylate anion), have been subject to intensive theoretical and experimental investigations and, also, much debate.[4]

Transition metal−acyl complexes are an extremely important class of organometallic compounds; they feature in many homogeneous catalytic processes, especially ones involving carbon monoxide,[5] and have hence been the subject of many reactivity and theoretical studies.[6] Transition metal−acyl complexes are also useful models for key catalytic intermediates in heterogeneous catalytic processes,[7] such as the Fischer−Tropsch process, where Fe-surface alkyl and acyl species play an important role in the formation of oxygenates (mainly formates, alcohols, and ketones).[8] Anionic transition metal−acyl complexes are, furthermore, important water-soluble intermediates in many synthetic routes to useful organometallic compounds, including Fischer's classical, and Semmelhack's more recent, methods to prepare carbene complexes.[9] Both routes involve the formation of anionic metal−acyl species that, upon oxygen alkylation/protonation, yield a wide variety of carbene complexes. Even though hydrogen bonding and cation coordination to metallo-acyl oxygen atoms in hydroxycarbene[10] and metal−acyl[11] complexes is well known, no examples of such complexes with extended solid state structures have been described.

We report here the isolation and structural characterisation of the widely employed organometallic reaction intermediate [Li(diglyme){Ph(O)$CW(CO)_5$}] (**1**), as a diglyme stabilised Li^+ salt, and the closely related H^+-bridged organometallic compound [$Li(diglyme)_2$][(μ_2-H){Ph(O)-$CW(CO)_5$}$_2$] (**2**) − both prepared from identical reaction mixtures. In the solid state, complex **1** exhibits a linear polymeric structure of Li^+-ion-bridged Ph(O)$CW(CO)_5^-$ ions

[a] Department of Chemistry, University of Stellenbosch, Private Bag X1, 7602 Matieland, South Africa
E-mail: hgr@sun.ac.za

in which the Li^+ ions coordinate to the acyl oxygen atom and a carbonyl oxygen atom of a neighbouring $Ph(O)CW(CO)_5^-$ ion. A strong, charge-assisted hydrogen bond in **2** bridges two $Ph(O)CW(CO)_5^-$ ions in the solid state structure. The remaining positive charge in **2** is provided by a Li^+ ion, indicating that only one Li^+ ion was selectively replaced during the filtration/protonation procedure executed on the common reaction mixture. In both compounds 1 mol equiv. of diglyme (diethylene glycol dimethyl ether) is incorporated to stabilise the Li^+ ion and it is, furthermore, thought to be imperative to the efficient selective protonation that affords **2**.

Results and Discussion

Synthesis and Isolation of Benzoyl−$W(CO)_5$ Complexes, Their Crystal Structures, IR Spectra, and NMR Spectra

The anionic benzoyl−$W(CO)_5$ complexes, **1** and **2**, were synthesized in the same manner as the first step of the synthesis of the Fischer-type carbene complex [Ph(OR)C=$W(CO)_5$], i.e. by dropwise addition of 1.2 mol equiv. PhLi to a suspension of $W(CO)_6$ in Et_2O at room temperature.[9a] However, instead of alkylating the so-formed Li[Ph(O)-$CW(CO)_5$], **1** and **2** were prepared using slightly modified procedures (Scheme 1). Complex **1** was isolated in high yield [78%, based on $W(CO)_6$] as bright-red crystals, suitable for X-ray crystallographic analysis, by the addition of 1 mol equiv. diglyme to the reaction mixture and subsequent crystallisation from a diethyl ether/*n*-pentane mixture. Complex **2** was prepared similarly, except that the red reaction mixture was carefully filtered through cooled (0 °C) acidic silica gel (10−15 cm, Ø 4 cm) before crystallisation from a diethyl ether/*n*-pentane mixture to afford bright-red crystals of **2**, suitable for X-ray crystallographic analysis, in moderate yields [69%, based on $W(CO)_6$]. Et_2O was used to elute the mixture from which **2** crystallised as a slow-moving red band from the silica gel. This procedure is closely related to the synthesis of hydroxycarbene complexes, as originally reported by Fischer et al.[12]

Removal of half the Li^+ ions from the reaction mixture by proton exchange upon filtration through silica gel, so that **2** may crystallise, is closely linked to the amount of diglyme present in the reaction mixture. The Li^+ ions in the reaction mixture have to be strongly solvated to pass through the silica gel during the filtration procedure. As only one mol equivalent of diglyme is added to the reaction mixture, and two diglyme molecules are required to solvate each Li^+ ion (as in the crystal structure of **2**, Figure 3), exactly half the Li^+ ions remain in solution after chromatography. The other half are immobilised on the silica gel and, to balance the charge, are replaced by mobile protons. Et_2O solvent molecules do not solvate Li^+ ions strongly enough to facilitate their efficient mobilisation through silica gel.

Low-temperature crystal and molecular structures of **1** (173 K) and **2** (173 K) (Figure 1 and Figure 3) were determined by X-ray diffraction. The structure of **1** clearly shows a $Ph(O)CW(CO)_5^-$ ion interacting with a Li^+ ion through its acyl moiety. Li^+-coordination to the oxygen atom of the CO ligand *trans* to the benzoyl group [O(3)] in neighbouring anions results in infinite zig-zag chains of alternating $Ph(O)CW(CO)_5^-$ and Li^+ ions along the *a* axis of the unit cell of **1** (Figure 2). The remaining coordination positions on the Li^+ ion are occupied by a diglyme molecule, coordinating to the cation through all three of its ether oxygen atoms. The coordination mode of the five-coordinate Li^+ ion is best described as distorted square pyramidal, with O(3) at the apex. O(5) lies on the underside of the square pyramid, beyond bonding distance [O(5)−Li = 3.506(4) Å],

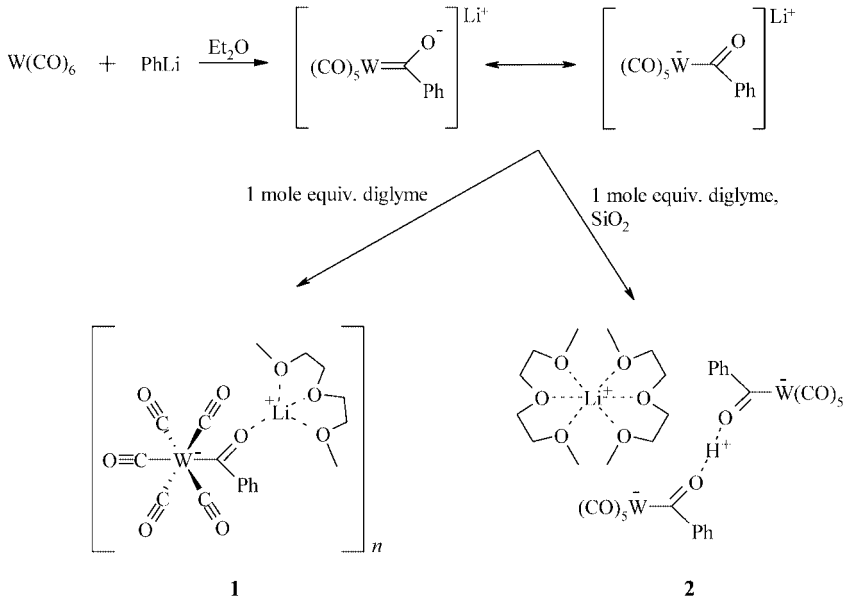

1 **2**

Scheme 1

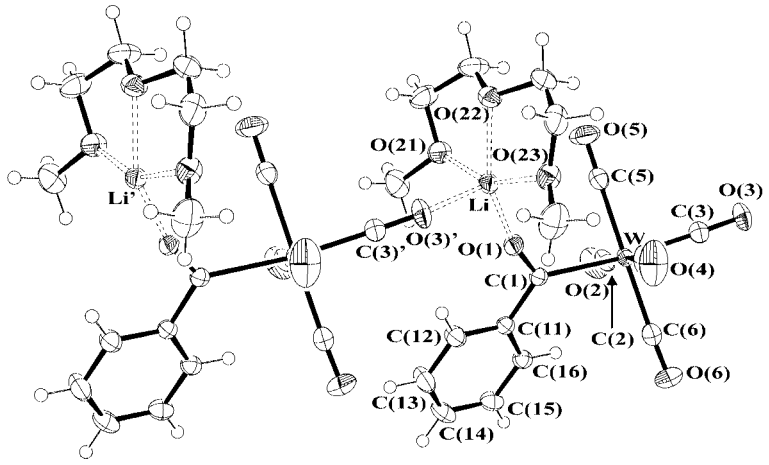

Figure 1. ORTEP[13] plot of **1** (two asymmetric units, 50% probability ellipsoids), showing the atomic numbering scheme and the polymeric structure observed in the crystal; selected bond lengths [Å] and angles [°]: W−C(1) 2.283(2), O(1)−C(1) 1.239(2), C(1)−C(11) 1.523(3), O(1)−Li 1.875(4), O(3)−Li 2.071(4), O(5)−Li 3.506(4), O(21)−Li 2.095(4), O(22)−Li 2.083(4), O(23)−Li 2.070(4), W−C(2) 2.026(2), W−C(3) 1.981(2), W−C(4) 2.047(2), W−C(5) 2.048(2), W−C(6) 2.024(3), C(2)−O(2) 1.150(3), C(3)−O(3) 1.164(3), C(4)−O(4) 1.136(3), C(5)−O(5) 1.137(3), C(6)−O(6) 1.143(3), C(1)−W−C(3) 171.8(1), C(2)−W−C(4) 175.0(1), C(5)−W−C(6) 179.5(1), W−C(1)−O(1) 119.9(2), W−C(1)−C(11) 126.6(1), O(1)−C(1)−C(11) 113.5(2), O(1)−Li−O(3)′ 105.2(2), O(1)−Li−O(21) 95.8(2), O(1)−Li−O(22) 150.5(2), O(1)−Li−O(23) 102.4(2), O(21)−Li−O(23) 154.1(2), O(3)′−Li−O(21) 95.6(2), O(3)′−Li−O(22) 104.1(2), O(3)′−Li−O(23) 97.3(2), W−C(2)−O(2) 178.8(2), W−C(3)−O(3) 178.3(2), W−C(4)−O(4) 178.0(3), W−C(5)−O(5) 179.2(2), W−C(6)−O(6) 177.5(2), O(1)−C(1)−C(11)−C(12) 8.9(3), C(5)−W−C(1)−O(1) 34.7(2)

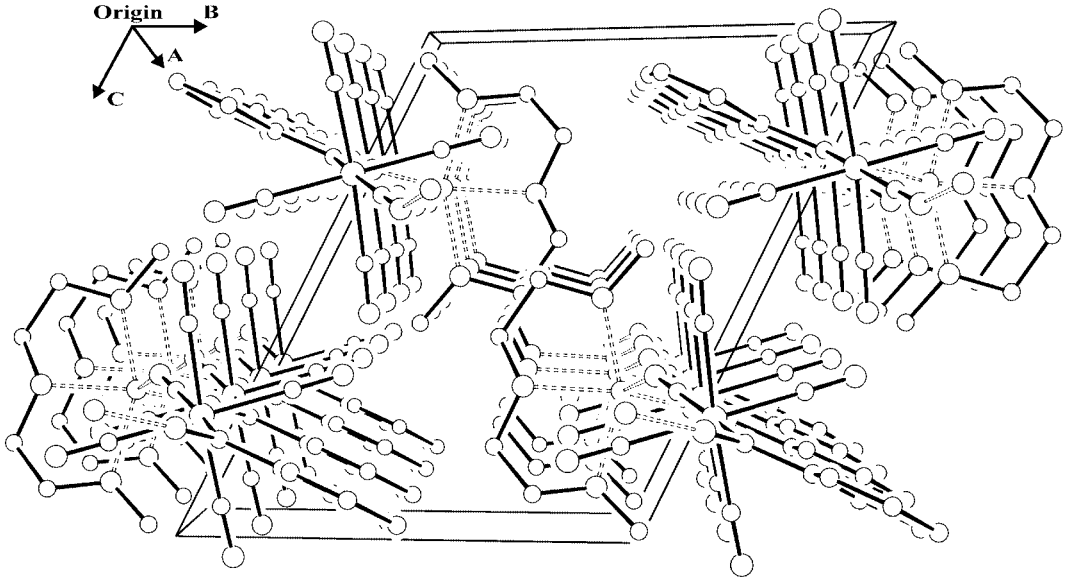

Figure 2. Packing diagram of **1**, viewed along the *a* axis, showing the extended structure of linked molecules (hydrogen atoms are omitted for clarity)

but sterically preventing the diglyme molecule from assuming a coordination mode that is closer to trigonal bipyramidal.

Interestingly the Li−O separations in the structure of **1** vary: Li to the diglyme oxygen atoms and to the CO ligand, O(3) are slightly shorter than in comparable five-coordinate Li[diglyme] structures [average of these four Li−O separations = 2.080(4) Å],[14] but the Li−acyl oxygen separation is still ca. 0.2 Å shorter than this [Li−O(1) = 1.875(4) Å]. In the absence of any obvious steric reasons, this difference within **1** indicates a much stronger electronic interaction between the Li^+ ion and O(1) than with other oxygen atoms.

The W−C(1) and C(1)−O(1) bond lengths [2.283(2) and 1.239(2) Å] in **1** are consistent with a small amount of charge delocalisation from the tungsten to the oxygen atom, due to Li^+-acyl coordination. Pure zero-valent tungsten W−C(sp^2) single bonds are usually slightly longer [≈ 2.31 Å][15] whereas uncoordinated acyl C=O double bonds are usually slightly shorter [≈ 1.21 Å].[16] An O(1)−C(1)−C(11)−C(12) torsion angle of 8.9(3)° describes the orientation of the phenyl ring toward the acyl moiety. The sp^2 hybridisation of C(1) is confirmed by its, within experimental error, flat bonding geometry [the greatest deviation from the least-squares plane through W, C(1), O(1),

 © 2003 Wiley-VCH Verlag GmbH & Co. KGaA, Weinheim

and C(11) is 0.004(2) Å for C(1)]. A C(5)−W−C(1)−O(1) torsion angle of 34.7(2)° describes how the benzoyl ligand is rotated relative to the $W(CO)_4$ coordination plane. Distortion of the $W(CO)_4$ coordination plane from planarity, due to bonding of the benzoyl ligand, is described by deviations from planarity from the least-squares plane through W, C(2), C(4), C(5) and C(6) of −0.0253(9), 0.0477(11), −0.0472(11), −0.0334(11), and −0.0362(12) Å respectively, and, furthermore, concurs with the relatively intense and infrared active B_1 absorption mode in the carbonyl region of the IR spectrum of **1** (see below).

In the crystal, asymmetric units of **1** pack in infinite polymeric chains, as described above, along the *a* axis of the unit cell in the triclinic centrosymmetric space group, $P\bar{1}$ (Figure 2). No significant intermolecular interactions, other than the intramolecular Li^+-bridges, are observed in the crystal structure of **1**. The highly ordered polymeric chain structure found for **1** might be partly responsible for the low crystal mosaicity [0.464(1)°] in the crystal selected for the X-ray diffraction study. It is noteworthy that this crystal yielded excellent diffraction data and that hence a very well-determined crystal structure was obtained for **1** [$R_1(I > 2\sigma I) = 1.38\%$].

Although lithium alkyl/aryl pentacarbonyl chromates/molybdates/tungstates are common organometallic intermediates in the synthesis of many alkyl/aryl alkoxy Fischer-type carbene complexes, the crystal structure of **1** appears to be the first example of this commonly employed organometallic Li^+-salt. The structure of a complicated lithium−(μ^2-benzoyl)-1,10-bis(diphenylphosphanyl)-(1,4,7,10-tetraoxadecane)$Mo(CO)_3$ complex, specifically designed to trap this Li^+ metallo−acyl species, has, however, been reported.[11a]

The crystal and molecular structure of **2** (Figure 3), although possessing a very similar empirical formula to **1** and containing the same metal carbonyl moieties, exhibits a completely different molecular arrangement. The structure of **2**, which is formally also a rare example of a hydrogen bond stabilised Fischer-type hydroxycarbene complex, clearly shows a Li^+ ion coordinated to two diglyme molecules, and two $Ph(O)CW(CO)_5^-$ ions linked via a strong, negative charge-assisted hydrogen bond between their acyl oxygen atoms. The striking difference in structure between **1** and **2** is down to the different interaction patterns of the cations. Protons, unlike Li^+ ions, are sufficiently stabilised in a two-coordinate hydrogen-bonded system while Li^+ ions can easily accommodate up to eight oxygen donor species and are rarely stabilised by less than four neutral oxygen donor atoms in the solid state.[17] Replacing half the Li^+ ions in solution thus allows the Li^+ ion to very efficiently coordinate to two diglyme molecules, whereas the strongly hydrogen-bonded proton in **2** is situated between two acyl groups of separate $Ph(O)CW(CO)_5^-$ ions.

The W−C(1) bond in **2** is slightly shorter than in **1** [W−C(1) = 2.238(5) Å in **2** vs. 2.284(2) Å in **1**] while the C(1)−O(1) bond in **2** is slightly longer [C(1)−O(1) = 1.276(6) Å in **2** vs. 1.239(2) Å in **1**]. These changes indicate a slight shift in electron density from the $W(CO)_5$ fragment

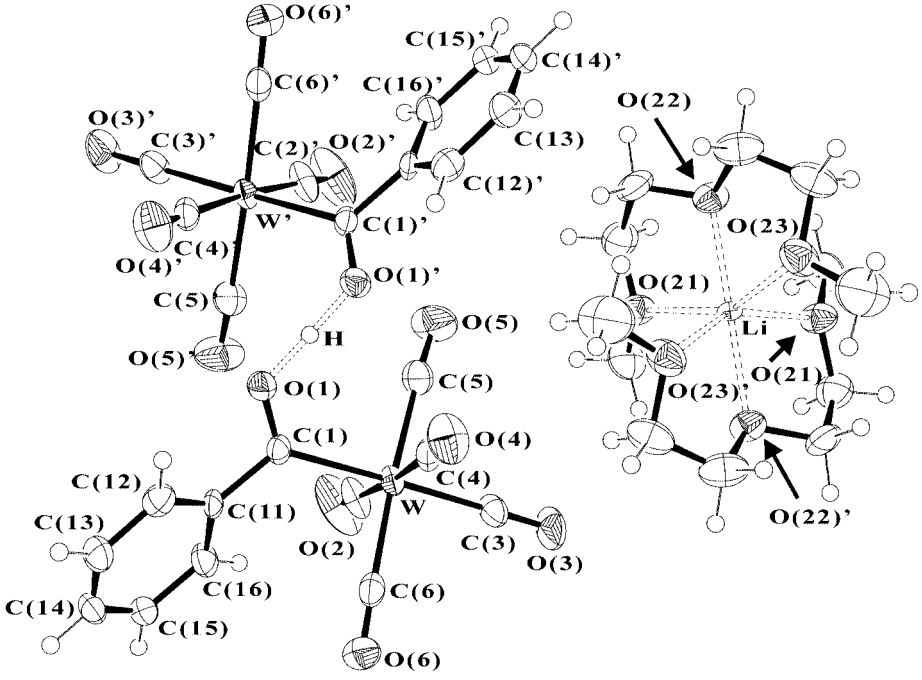

Figure 3. ORTEP[13] plot of **2** (two asymmetric units, 50% probability) showing the numbering scheme and charge-assisted hydrogen-bonding interactions observed in the crystal; selected bond lengths [A] and angles[°]: W−C(1) 2.237(5), O(1)−H 1.233(12), O(1)−C(1) 1.277(6), C(1)−C(11) 1.505(7), O(1)−O(1)′ 2.442(6), W−C(2) 2.015(7), W−C(3) 1.996(6), W−C(4) 2.025(6), W−C(5) 2.044(6), W−C(6) 2.028(6), O(21)−Li 2.170(8), O(22)−Li 2.075(3), O(23)−Li 2.169(9), O(2)−C(2) 1.152(8), O(3)−C(3) 1.147(6), O(4)−C(4) 1.136(7), O(5)−C(5) 1.149(6), O(6)−C(6) 1.155(6), O(1)−H−O(1)′ 164.5(3), C(1)−W−C(3) 173.9(2), C(2)−W−C(4) 176.1(3), C(5)−W−C(6) 174.7(2), W−C(1)−O(1) 125.1(3), W−C(1)−C(11) 123.9(3), O(1)−C(1)−C(11) 110.7(4), W−C(2)−O(2) 176.4(5), W−C(3)−O(3) 178.5(6), W−C(4)−O(4) 178.5(5), W−C(5)−O(5) 175.2(5), W−C(6)−O(6) 177.4(5), O(21)−Li−O(23) 150.7(2), O(22)−Li−O(22)′ 167.8(6), C(5)−W−C(1)−O(1) 35.9(5), O(1)−C(1)−C(11)−C(12) 29.2(6)

 © 2003 Wiley-VCH Verlag GmbH & Co. KGaA, Weinheim

to the acyl oxygen atom from **1** to **2** and suggest a stronger bonding interaction between the proton and the acyl oxygen atoms in **2** than between the Li^+ ion and the acyl oxygen atom in **1**. The O···O separation in **2** is very short [2.442(6) Å], showing that the hydrogen bond is indeed strong.[2] The position of the proton could be reliably determined and refined from the difference Fourier map and is, as expected in a hydrogen-bonding situation that involves identical anionic moieties, evenly spaced between the metallo-acyl oxygen atoms [O(1)−H = 1.232(11) Å].[18] The bridging hydrogen atom is, furthermore, situated on a crystallographic twofold rotation axis that lies parallel to the *c* axis of the unit cell and relates the anions in the formula unit to one another. Braga suggests that strong inter-anionic hydrogen bonds could be the result of a residual negative charge residing on the oxygen donor atoms.[2] In **2** this is clearly not the case. The bulk of the negative charge in anionic metallo-acyl metal carbonyl species is expected to be on the strongly electron-withdrawing $M(CO)_n$ fragments, as the W−C(1) and C(1)−O(1) bond orders and IR data, discussed below, of **1** and **2** reflect. Although some increase in the W−C(1) bond order and reduction of the C(1)−O(1) bond is seen upon hydrogen bonding in **2** (compared to **1**), the observed bond lengths and $\tilde{\nu}$(CO) absorption bands of **2** still suggest large amounts of negative charge delocalised onto the $W(CO)_5$ fragment. In [$(CO)_5$W=C(OEt)Ph], in which some delocalisation of negative charge to the $W(CO)_5$ fragment is also present, these separations are 2.195 and 1.299 Å.[19] These observations suggest that the hydrogen bonding interactions observed in **2** are the result of classical hydrogen bonds and do not involve residual negative charge on the oxygen atom.[4d,20]

The Li^+ ion in **2** also resides on the twofold rotation axis in this space group, indicating that the Li(diglyme)$_2$ coordination possesses twofold symmetry. The crystallographic asymmetric unit of **2** thus consists of a single $Ph(O)CW(CO)_5^-$ ion hydrogen-bonded to a bridging proton, and one diglyme molecule coordinated to a shared Li^+ ion. Interestingly the hydrogen-bonded proton does not lie linearly between the metallo-acyl oxygen atoms [O(1)−H−O(1)′ = 164.5(3)°]; this measurement is not biased by the proton's crystallographically special position. The O(1)−H−O(1)′ angle depends on the unique coordinate of the proton along the *c* axis of the unit cell, which is free to change during the structure refinement. The reason for this kink in the hydrogen bond is not entirely clear. Similar kinks in hydrogen bonding interactions have, however, been reported between other anionic organometallic fragments and have been linked to weakening of the hydrogen bonding interaction, especially once the O−H−O angle exceeds 165°.[18,20]

An O(1)−C(1)−C(11)−C(12) torsion angle of 29.2(6)° describes the orientation of the phenyl ring toward the acyl moiety. Curiously, the sp^2 hybridisation of C(1) is somewhat more distorted from trigonal planar geometry than in **1**, possibly due to steric considerations [the respective deviations from the least-squares plane through W, C(1), O(1), and C(11) are 0.012(1), −0.044(4), 0.018(2), and 0.015(1) Å]. A C(5)−W−C(1)−O(1) torsion angle of 35.9(5)° is similar to that in **1**, and describes how the benzoyl ligand is rotated on the $W(CO)_4$ coordination plane. Distortion of the $W(CO)_4$ coordination plane from planarity, due to bonding of the benzoyl ligand, is also more than in **1**, and is described by deviations from planarity from the least-squares plane through W, C(2), C(4), C(5), and C(6) of −0.013(2), −0.057(3), −0.054(3), −0.063(3), and −0.061(3) Å, respectively. Coordination of the Li^+ ion to the six ether oxygen atoms of the two diglyme molecules in **2** is best described as a distorted, yet symmetrical, octa-

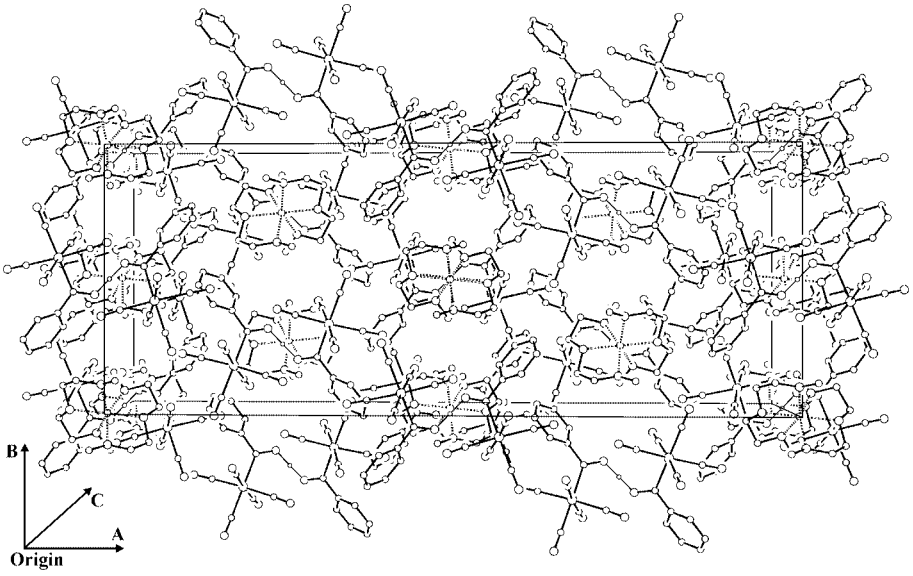

Figure 4. Packing diagram of **2**, viewed along the *c* axis of the unit cell, showing the packing arrangement of the dimeric H^+-bridged units in the crystal (all H atoms, except the bridging proton, have been omitted for clarity)

 © 2003 Wiley-VCH Verlag GmbH & Co. KGaA, Weinheim

hedron with O(22) and its symmetry equivalent, O(22)′ occupying the axial positions. The Li−O separations in this arrangement are normal.[21]

In the crystal, **2** packs in the unusual orthorhombic and non-centrosymmetric face-centred space group, *Fdd*2. A view along the *c* axis of the unit cell (Figure 4) shows how eight hydrogen-bonded molecules (16 asymmetric units) pack in the unit cell with the bridging protons and Li^+ ions situated on the eight twofold rotation axes parallel to the *c* axis in this space group. No other significant intermolecular interactions were observed for **2**.

The crystal structures of hydroxycarbene complexes exhibit characteristic hydrogen bonding interactions involving the hydroxyl hydrogen atom. Of the 20 reported structures in the Cambridge Crystallographic Database[22] that can formally be regarded as hydroxycarbene complexes, 17 exhibit intramolecular hydrogen bonds [10c,23] while the remaining three exhibit intermolecular hydrogen bonds (two with $CF_3SO_3^-$ ions and one with an acetonitrile solvent molecule).[10a,10b,24] Consequently, the OH hydrogen atoms in hydroxycarbene complexes, without consideration of their spectroscopic or thermodynamic characteristics, are weakly linked to what is a pseudo metallo-acyl oxygen atom, and require further stabilisation through hydrogen bonding interactions. This interpretation is supported by the significant double bond character of the C(carb)−O bond in hydroxycarbene complexes (average C−O separation = 1.290 Å). The only neutron diffraction study of a hydroxycarbene complex, furthermore, reports a long O−H separation [1.142 Å].[10c] Hydroxycarbene complexes would therefore perhaps be better described as ion-paired [metallo−acyl][H] complexes, exhibiting hydrogen bonding interactions between acyl-oxygen atoms and a second donor atom, rather than complexes with a formal oxygen−hydrogen bond.

This approach enables a more accurate description of the hydrogen bonding interactions found in **2** as no classical donor−acceptor definitions are applicable. The hydrogen-bonded structure in **2** can thus be described as an anionic homonuclear molecule−ion associate of two $Ph(O)CW(CO)_5^-$ ions interacting with a proton, thus forming the strong, charge-assisted hydrogen-bonded complex found in the crystal (Scheme 2). Similar centred O···H···O hydrogen bonds have been described as quasi-covalent.[4d] Comparable μ_2-hydrogen-bonded structures have been reported for anionic organometallic cyanide complexes $[(CO)_5Cr\{C{\equiv}N{\cdots}H{\cdots}N{\equiv}C\}Cr(CO)_5]^-$ and

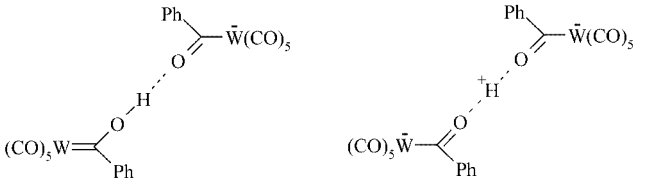

Classical donor-acceptor H-bond model of **2**

Homonuclear molecule-ion associates H-bond model of **2**

Scheme 2

$[(CO)_5Cr\{C{\equiv}N{\cdots}H{\cdots}N{\equiv}C\}FeCp(dppe)]$ [18] as well as for several carboxylate-functionalised sandwich compounds,[2,3] but not for complexes with metallo-acyl ligands.

Furthermore, of the 17 crystal structures of hydroxycarbene complexes that exhibit intramolecular hydrogen bonds, all but three [23j,23k,23l] contain two metallo-acyl moieties on a single metal atom involved in the hydrogen bonding interaction. This arrangement, forming six-membered metallacyclic rings (Scheme 3), is thus particularly favoured.

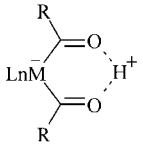

Scheme 3

The hydrogen bonding arrangement found in the crystal structure of **2** is similar to those described above (between two metallo-acyl groups), except that the metallo-acyl moieties involved in the hydrogen bonding interaction are on separate metal centres and, therefore, form a pseudo-linear hydrogen bonding arrangement. The structure of **2**, although novel, is thus not completely unexpected. Moreover, the structural characteristics of anionic metal−acyl complexes exhibited in the current structures, together with their general physical properties (e.g. stability, water solubility), firmly places them in the realm of suitable candidates for building blocks in organometallic crystal engineering. The selective introduction of a strong, charge-assisted hydrogen bonding interaction by selective Li^+ ion replacement in complex **2** may, furthermore, be a valuable tool to crystal engineers.

The infrared (IR) spectra of **1** and **2** were recorded as KBr pellets. The $\tilde{\nu}$(CO) absorption peaks for the CO ligands in both complexes exhibit the typical pattern of $A_1^{(1)}$, $A_1^{(2)}$, B_1, and E vibrational modes for molecules of the type $[M(CO)_5L]$ and are practically identical. The only clear deduction from the CO ligand stretching frequencies of **1** and **2** is that the metal atoms in these compounds are electron rich relative to other reported $[W(CO)_5L]$ complexes.[25] Comparison of the acyl C=O stretching frequencies [1517 cm^{-1} (**1**) and 1510 cm^{-1} (**2**)] is more fruitful. The 7 cm^{-1} lower C=O stretching frequency in **2** indicates that this bond is slightly more reduced in **2**, suggesting better interaction of the metallo-acyl anions with the proton in **2** than with the Li^+ ion in **1**, and corresponds to the results described by the crystal structures. The $\tilde{\nu}$(OH) frequency in **2** could, unfortunately, not be assigned reliably.

The IR spectrum of **1** was measured in CH_2Cl_2 solution. Dissolution of **1** causes a large change in the stretching frequency of the acyl vibrational mode (89 cm^{-1} "blue shift"). The $A_1^{(2)}$ vibration, assigned to the stretching frequency of the CO ligand trans to the metallo-acyl moiety, is unfortunately barely observable as a narrow shoulder on the intense E absorption peak in the solution IR spectrum of **1**, but is nevertheless shifted to higher energy (≈ 10−15 cm^{-1}).

 © 2003 Wiley-VCH Verlag GmbH & Co. KGaA, Weinheim

These shifts strongly suggest that the clear interactions in the solid state of the Li^+ ions with the metallo acyl group, as well as with the CO ligand *trans* to the metallo acyl bond on a neighbouring anion, do not persist in dichloromethane solution. No interaction with Li^+ ions translates to less loss of electrons from the oxygen atoms in the groups that interact with the cation in the solid state and translates to stronger C≡O and C=O bonds in these groups.

The solution IR spectrum of **2** (CH_2Cl_2) is dominated by an extremely broad, intense and unresolved absorption band at ca. 1900 cm^{-1}. This is probably because, upon dissolution, **2** reverts, according to NMR spectroscopic data (discussed below), to a 50/50 mixture of Li[Ph(O)CW(CO)$_5$] and [Ph(OH)C=W(CO)$_5$] from whence it crystallised, and thus gives an IR spectrum for both compounds with broad, overlapping absorption bands. The ν(CO) for the acyl groups in this mixture as well as the ν(OH) absorption could, unfortunately, not be assigned reliably.

The ^1H and $^{13}C\{^1H\}$ NMR spectra of **1** are identical to the reported values,[12b] whereas the spectra of **2** contain partly overlapping resonances of both **1** and [Ph(OH)C=W(CO)$_5$]. For both compounds additional NMR resonances, representing 1 mol equiv. of diglyme, were also present. These resonances appear as a singlet at δ = 3.42 (6 H, OCH_3) and two triplet signals at δ = 3.77 and 3.66 ppm ($^3J_{H,H} \approx 5$ Hz, 4 H each), representing two sets of unique CH_2 groups in the diglyme molecule. In the $^{13}C\{^1H\}$ NMR spectra of **1** and **2** the resonances corresponding to diglyme appear at δ = 59.0, 70.7, and 72.2.

Experimental Section

General: All reactions and manipulations were carried out under a dry argon atmosphere using standard Schlenk and vacuum-line techniques. Et_2O was dried and purified by conventional methods and was freshly distilled under argon shortly before use. Melting points were measured with a Büchi 535 melting point determination apparatus and are uncorrected. NMR spectra were recorded on a Varian INOVA 600 spectrometer (^1H, 600 MHz; $^{13}C\{^1H\}$, 151 MHz; $^{31}P\{^1H\}$, 243 MHz) at 25 °C. NMR chemical shifts are reported in ppm relative to the ^1H and ^{13}C residue of the deuterated solvents. IR spectra were recorded on a Perkin−Elmer 1600 Series FTIR spectrometer. Elemental analyses were performed on a Fisons CHNS elemental analyser 1108. PhLi was prepared and standardised according to standard procedures. Diglyme and $W(CO)_6$ were purchased from Aldrich and used without purification.

Preparation of 1 and 2: PhLi (1.2 equiv., 0.6 mL, 1.6 M solution in Et_2O) was added dropwise to a suspension of $W(CO)_6$ (282 mg, 0.8 mmol) suspended in dry, degassed Et_2O (30 mL) over 30 min, and the resultant red reaction mixture was stirred for a further 1 h. Diglyme (1 equiv., 110 mg) was then added. To prepare crystals of **1** the volume of this mixture was reduced in vacuo to ca. 15 mL, carefully layered with an equal amount of *n*-pentane and cooled to −20 °C. $C_{18}H_{19}LiO_9W$ (570.13): calcd. C 37.9, H 3.36, O 25.3;

Table 1. Crystal data and structure refinement

Compound	**1**	**2**
Empirical formula	$C_{18}H_{19}O_9LiW$	$C_{36}H_{39}LiO_{18}W_2$
Formula mass [g/mol]	570.12	1134.29
Crystal system	Triclinic	Orthorhombic
Space group	$P\bar{1}$	*F*dd2
a [Å]	8.8289(1)	37.8020(7)
b [Å]	11.1285(1)	14.8039(2)
c [Å]	12.9991(2)	15.1227(3)
α [°]	113.709(1)	90
β [°]	95.826(1)	90
γ [°]	108.179(1)	90
V [Å^3]	1072.55(2)	8462.9(3)
Z	2	8
$d_{calcd.}$ [g/cm^3]	1.765	1.781
T [K]	173(2)	173(2)
$\mu_{Mo\text{-}K\alpha}$ [cm^{-1}]	5.429	5.504
$2\theta_{max}$ [°]	26.00	26.00
Radiation	Mo-*Kα*, graphite-monochromated	Mo-*Kα*, graphite-monochromated
Crystal size [mm]	0.17 × 0.20 × 0.25	0.20 × 0.30 × 0.40
Index range	$-10 \le h \le 10$ $-13 \le k \le 13$ $-16 \le l \le 16$	$-46 \le h \le 36$ $-18 \le k \le 13$ $-17 \le l \le 18$
No. of reflections collected	8195	9371
No of independent reflections (R_{int})	4203 (0.0151)	3936 (0.0335)
Data/parameters	4203/264	3936/261
Refinement	Full matrix on F^2 (SHELXL)	Full matrix on F^2 (SHELXL)
Final *R* indices ($I > 2\sigma I$)	$R_1 = 0.0138$, $wR_2 = 0.0317$	$R_1 = 0.0249$, $wR_2 = 0.0487$
R indices (all data)	$R_1 = 0.0151$, $wR_2 = 0.0321$	$R_1 = 0.0304$, $wR_2 = 0.0501$
Largest diff peak and hole [e$^-$/Å^3]	0.476, −0.733	0.602, −0.907

 © 2003 Wiley-VCH Verlag GmbH & Co. KGaA, Weinheim

found C 37.8, H 3.40, O 25.4. m.p. 76 °C. IR (KBr): ν(CO) = 2049 cm^{-1} (m, $A_1^{(1)}$), 1968 cm^{-1} (w, B_1), 1895 cm^{-1} (vs, E), 1885 cm^{-1} (m, sh, $A_1^{(2)}$), 1517 cm^{-1} (m, C=O). IR (CH_2Cl_2): ν(CO) = 2050 cm^{-1} (m, $A_1^{(1)}$), 1975 cm^{-1} (w, B_1), 1908 cm^{-1} (vs, E), ≈ 1895−1900 cm^{-1} (m, sh, $A_1^{(2)}$), 1606 cm^{-1} (m, C=O).

Crystals of **2** were prepared by filtering the red reaction mixture through acidic silica gel (10−15 cm, Ø 4 cm), using additional Et_2O to elute the red complex from the column. The volume of the elute was then reduced in vacuo to ≈ 15 mL, which was then carefully layered with an equal amount of *n*-pentane and cooled to −20 °C. $C_{36}H_{39}LiO_{18}W_2$ (1134.32): calcd. C 38.1, H 3.47, O 25.4; found C 38.0, H 3.40, O 25.5. m.p. 68 °C (decomp.). IR (KBr): ν(CO) 2049 cm^{-1} (m, $A_1^{(1)}$), 1968 cm^{-1} (w, B_1), 1904 cm^{-1} (vs, E), 1885 cm^{-1} (m, sh, $A_1^{(2)}$), 1510 cm^{-1} (m, C=O).

X-ray Crystallographic Analysis of 1 and 2: Suitable crystals of **1** and **2** were selected and mounted on glass fibres. Low temperature (173 K) diffraction data were collected for both crystals on a Nonius−Kappa CCD diffractometer,[26] equipped with an Oxford Cryostream cooling apparatus, using graphite monochromated Mo-K_α radiation (λ = 0.71073 Å). A summary of the diffraction data is given in Table 1. Data sets for both crystals were scaled, reduced and corrected for Lorenz and polarisation effects using DENZO-SMN.[27] Both structures were solved by the interpretation of Patterson syntheses (SHELX-97),[28] which produced the positions of the metal atoms. The structures were completed by full-matrix least-squares calculations (SHELXL-97)[28] on F^2 and anisotropic thermal motion was allowed for all the non-hydrogen atoms during the final cycles of refinement. The space group in **2** is non-centrosymmetric; the Flack test[29] suggested the presence of a racemic twin and subsequent refinement revealed a racemic twin ratio of 0.886:0.114. Although the positions of most of the hydrogen atoms in **1** and **2** could be located from the difference Fourier map, all the hydrogen atoms situated on the phenyl rings were placed in idealised positions with their thermal parameters fixed at 1.2 times the equivalent isotropic displacement parameters of their parent atoms. The position of the bridging hydrogen atom in **2** could be reliably located from the difference Fourier map and refined isotropically. CCDC-211587 (**1**) and -211588 (**2**) contain the supplementary crystallographic data for this paper. These data can be obtained free of charge at www.ccdc.cam.ac.uk/conts/retrieving.html or from the Cambridge Crystallographic Data Centre, 12 Union Road, Cambridge CB2 1EZ, UK [Fax: (internat.) +44-1223/336-033; E-mail: deposit@ccdc.cam.ac.uk].

Acknowledgments

We thank Dr. John Bacsa for the collection of the X-ray data.

[1] [1a] G. R. Desiraju, *Crystal Engineering: The Design of Organic Solids*, Elsevier, Amsterdam, **1989**. [1b] D. Braga, F. Grepioni, *J. Chem. Soc., Dalton Trans.* **1999**, 1−8.
[2] D. Braga, L. Maini, M. Polito, L. Scaccianoce, G. Cojazzi, F. Grepioni, *Coord. Chem. Rev.* **2001**, *216−217*, 225−248.
[3] D. Braga, F. Grepioni, *Coord. Chem. Rev.* **1999**, *183*, 19−41.
[4] [4a] J. Emsley, *New Scientist* **1981**, *91*, 291−293. [4b] B. S. Ault, *Acc. Chem. Res.* **1982**, *15*, 103−109. [4c] D. Mootz, K. Bartmann, *Angew. Chem. Int. Ed. Engl.* **1988**, *27*, 391−392. [4d] T. Steiner, *Chem. Commun.* **1999**, 2299−2300.
[5] [5a] G. E. Coates, M. L. H. Green, K. Wade, *Organometallic Compounds*, Methuen, London, **1968**, *vol. 2*, pp. 257−263. [5b]A. Wojcicki, *Adv. Organomet. Chem.* **1973**, *11*, 87−145. [5c] F. Calderazzo, *Angew. Chem. Int. Ed. Engl.* **1977**, *16*, 299−311. [5d] E. J. Kuhlman, J. J. Alexander, *Coord. Chem. Rev.* **1980**, *33*, 195−225.
[6] [6a] L. D. Durfee, I. P. Rithwell, *Chem. Rev.* **1988**, *88*, 1059−1079. [6b] A. R. Cutler, P. K. Hanna, J. C. Vites, *Chem. Rev.* **1988**, *88*, 1363−1403. [6c] T. Kinnunen, K. Laason, *Theochem.* **2001**, *542*, 273−288.
[7] J. R. Moss, *J. Mol. Catal. A: Chem.* **1996**, *107*, 169−174.
[8] M. E. Dry, *Catal. Today* **1990**, *6*, 183−206.
[9] [9a] E. O. Fischer, A. Maasböl, *Angew. Chem. Int. Ed. Engl.* **1964**, *3*, 580. [9b] M. F. Semmelhack, G. R. Lee, *Organometallics* **1987**, *6*, 1839−1844.
[10] [10a] R. J. Klingler, J. C. Huffman, J. K. Kochi, *Inorg. Chem.* **1981**, *20*, 34−40. [10b] P. L. Motz, D. M. Ho, M. Orchin, *J. Organomet. Chem.* **1991**, *407*, 259−269. [10c] A. J. Schultz, K. Srinivasan, R. G. Teller, J. M. Williams, C. M. Lukehart, *J. Am. Chem. Soc.* **1984**, *106*, 999−1003.
[11] [11a] J. Powell, A. Kuksis, C. J. May, S. C. Nyburg, S. J. Smith, *J. Am. Chem. Soc.* **1981**, *103*, 5941−5943. [11b] A. Wacker, H. Pritzkow, W. Siebert, *Eur. J. Inorg. Chem.* **1998**, 843−849.
[12] [12a] E. O. Fischer, G. Kreis, F. R. Kreissl, *J. Organomet. Chem.* **1973**, *56*, C37−C40. [12b] K. Weiss, E. O. Fischer, *Chem. Ber.* **1976**, *109*, 1120−1127.
[13] L. J. Farrugia, *J. Appl. Cryst.* **1997**, *30*, 565.
[14] [14a] C. Hilf, F. Bosold, K. Harms, M. Marsch, G. Boche, *Chem. Ber./Recueil* **1997**, *130*, 1213−1221. [14b] H.-J. Gais, J. Vollhardt, G. Hellmann, H. Paulus, H. J. Lindner, *Tetrahedron Lett.* **1988**, *29*, 1259−1262. [14c] H.-J. Gais, M. van Gumpel, G. Raabe, J. Muller, S. Braun, H. J. Lindner, S. Rohs, J. Runsink, *Eur. J. Org. Chem.* **1999**, 1627−1651.
[15] C. P. Casey, S. W. Polichnowski, H. E. Tuinstra, L. D. Albin, J. C. Calabrese, *Inorg. Chem.* **1978**, *17*, 3045−3049.
[16] [16a] F. Y. Petillon, J.-L. Quere, F. le Floch-Perennou, J.-E. Guerchias, M.-B. Gomes de Lima, L. Manojlovic-Muir, K. W. Muir, D. W. A. Sharp, *J. Organomet. Chem.* **1983**, *255*, 231−244. [16b] M. F. McGuiggan, D. H. Doughty, L. H. Pignolet, *J. Organomet. Chem.* **1980**, *185*, 241−249.
[17] [17a] A. Purath, R. Koppe, H. Schnöckel, *Chem. Commun.* **1999**, 1933−1934. [17b] C. Emmerich, G. Huttner, *J. Organomet. Chem.* **1993**, *447*, 81−89. [17c] W. Palitzsch, U. Bohme, G. Roewer, *Chem. Commun.* **1997**, 803−804.
[18] E. Bär, J. Fuchs, D. Rieger, F. Aguilar-Parrilla, H.-H. Limbach, W. P. Fehlhammer, *Angew. Chem. Int. Ed. Engl.* **1991**, *30*, 88−90.
[19] R. J. Staples, D. M. Potts, J. C. Joder, *Z. Kristallogr.* **1995**, *210*, 381−382.
[20] P. Gilli, V. Bertolasi, V. Ferretti, G. Gilli, *J. Am. Chem. Soc.* **1994**, *116*, 909−915.
[21] G. Guillemot, E. Solari, C. Floriani, N. Re, C. Rizolli, *Organometallics* **2000**, *19*, 5218−5230.
[22] F. H. Allen, O. Kennard, R. Taylor, *Acc. Chem. Res.* **1983**, *16*, 146−153.
[23] [23a] M. Gerisch, F. W. Heinemann, C. Bruhn, J. Scholz, D. Steinborn, *Organometallics* **1999**, *18*, 564−572. [23b] F. W. Heinemann, M. Gerisch, D. Steinborn, *Z. Kristallogr. New Crystal Structures* **1997**, *212*, 181. [23c] C. Jones, J. W. Steed, R. C. Thomas, *J. Chem. Soc., Dalton Trans.* **1999**, 1541−1542. [23d] D. Steinborn, M. Gerisch, C. Bruhn, J. A. Davies, *Inorg. Chem.* **1999**, *38*, 680−683. [23e] D. Steinborn, M. Gerisch, T. Hoffmann, C. Bruhn, G. Israel, F. W. Muller, *J. Organomet. Chem.* **2000**, *598*, 286−291. [23f] D. Steinborn, M. Gerisch, F. W. Heinemann, C. Bruhn, *Chem. Commun.* **1997**, 843−844. [23g] M. Gerisch, C. Bruhn, A. Porzel, D. Steinborn, *Eur. J. Inorg. Chem.* **1998**, 1655−1659. [23h] M. Gerisch, C. Bruhn, D. Steinborn, *Polyhedron* **1999**, *18*, 1953−1956. [23i] D. Steinborn, M. Gerisch, K. Merzweiler, K. Schenzel, K. Pelz, H. Bogel, J. Magull, *Organometallics* **1996**, *15*, 2454−2457. [23j] J. R. Knox, C. K. Prout, *Acta Crystallogr., Sect. B* **1969**, *25*, 1952−1958. [23k] J. Powell, D. H. Farrar, S. J. Smith, *Inorg. Chim. Acta* **1984**, *85*, L23−L25. [23l] K. A. Johnson, M. D. Vashon, B. Moasser, B. K. Warmka, W. L. Gladfelter, *Organometallics* **1995**, *14*, 461−470.

 © 2003 Wiley-VCH Verlag GmbH & Co. KGaA, Weinheim

[24] Y. Ishii, K.-I. Ogio, M. Nishio, M. Retboll, S. Kuwata, H. Matsuzaka, M. Hidai, *J. Organomet. Chem.* **2000**, *599*, 221−231.
[25] H. G. Raubenheimer, M. W. Esterhuysen, A. Timoshkin, Y. Chen, G. Frenking, *Organometallics* **2002**, *21*, 3173−3181.
[26] B. V. Nonius, *COLLECT, Data collection software* Delft, The Netherlands, **1999**.
[27] Z. Otwinowski, W. Minor, *Methods Enzymol.* **1997**, *276*, 307.
[28] G. M. Sheldrick, *SHELX-97, Program for X-ray Crystal Structure Solution and Refinement*, University of Göttingen, Göttingen, Germany, **1997**.
[29] H. D. Flack, *Acta Crystallogr., Sect. A* **1983**, *39*, 876−881.
Received June 2, 2003

 © 2003 Wiley-VCH Verlag GmbH & Co. KGaA, Weinheim

Dioxomolybdenum(VI)-Modified Mesoporous MCM-41 and MCM-48 Materials for the Catalytic Epoxidation of Olefins

Carla D. Nunes,[a] Martyn Pillinger,[a] Anabela A. Valente,[a] João Rocha,[a] André D. Lopes,[b] and Isabel S. Gonçalves*[a]

Keywords: Molybdenum / N ligands / Mesoporous materials / Supported catalysts / Epoxidations

The dioxomolybdenum(VI) complex $[MoO_2Cl_2(L\text{-}L)]$, containing the bidentate 1,4-diazabutadiene ligand RN=C(Ph)–C(Ph)=NR [R = $(CH_2)_3Si(OEt)_3$], was immobilised in the ordered mesoporous silica MCM-41 by carrying out a grafting reaction in dichloromethane. The grafted material (3.3 wt.-% Mo) was tested as a catalyst for the epoxidation of cyclooctene with *tert*-butyl hydroperoxide (TBHP) at 55 °C. Selectivity to the epoxide was very high and the observed kinetic profile was similar to that of the complex $[MoO_2Cl_2(L\text{-}L)]$ in the homogeneous phase. On recycling several times, some activity was lost from the first to second runs, but thereafter stabilised. Tethered complexes of this type were also prepared by a stepwise approach. The mesoporous silicas MCM-41 and MCM-48 were first treated with a toluene solution of the ligand L-L under reflux. Before isolating the grafted materials, the silylating agent Me_3SiCl was added to remove the residual Si–OH groups on the surface of the mesoporous materials. Oxomolybdenum species were subsequently introduced into the ligand-silicas by pore volume impregnation of a solution of the complex $[MoO_2Cl_2(THF)_2]$ in CH_2Cl_2 at room temperature. The modified materials have been characterised by powder X-ray diffraction, N_2 adsorption, and solid-state MAS NMR (^{13}C, ^{29}Si). Despite having lower metal loadings (1 wt.-% Mo), the materials exhibited similar catalytic activities for the epoxidation of cyclooctene to that of the modified MCM-41 with 3.3 wt.-% of Mo. However, selectivities to the epoxide were lower. The MCM supported catalysts have also been tested for the epoxidation of cyclododecene and α-pinene with TBHP.

(© Wiley-VCH Verlag GmbH & Co. KGaA, 69451 Weinheim, Germany, 2003)

Introduction

High-valent d^0 transition metal complexes, such as Mo^{VI}, V^V, and Ti^{IV}, are effective catalysts for the selective epoxidation of olefins by alkyl hydroperoxides (ROOH).[1] In particular, Mo^{VI} complexes of the type $[MoO(O_2)_2(L^1)(L^2)]$ and $[MoO_2X_2(L^1)(L^2)]$ (X = Cl, Br, CH_3), with different combinations of base ligands L^1 and L^2, have been experimentally characterised and tested as catalysts for epoxidation reactions, usually employing *tert*-butyl hydroperoxide (TBHP) as the mono-oxygen source.[2,3] It is ever more accepted that alkyl peroxides activate these complexes by an intermediate η^2-coordination of the peroxidic agent to the Lewis acidic metal centre.[4] Important properties, such as the solubility of the complex and the Lewis acidity of the metal centre, can be fine-tuned by variation of either X or L.

Despite the good results obtained for oxomolybdenum(VI) complexes in homogeneous catalysis, increasing attention is being paid to heterogeneous catalysts since these can be easily separated from a reaction mixture and recycled, which is of significant industrial interest. The immobilisation of transition metal catalysts, for example on an inorganic support,[5] may also eliminate other problems associated with homogeneous catalysis, such as dimerisation of the active complex or auto-oxidation. One approach is to use support materials modified with Lewis base ligands. Sherrington and co-workers reported that polymer-supported molybdenum(VI) complexes are active and recyclable catalysts for olefin epoxidation with TBHP.[6] For inorganic supports, a general strategy is to use functional alkoxy silanes. Corma et al. have prepared dioxomolybdenum(VI) complexes with chiral ligands derived from (2*S*,4*R*)-4-hydroxyproline.[7] The complexes bearing a $Si(OEt)_3$ group were heterogenised to a modified USY-zeolite by covalent bonding.

Micelle-templated silicas as catalyst supports for transition metal catalysts have been extensively studied over the last decade,[5] and are often more effective than amorphous silica.[8] This is probably due to the unique combination of a high surface area, allowing a good dispersion of active sites, with an ordered mesoporous structure, allowing selective catalysis in a constrained environment. Jia and Thiel modified the ordered mesoporous silica MCM-41 with a bidentate pyrazolylpyridine ligand and prepared a coval-

[a] Department of Chemistry, CICECO, University of Aveiro, Campus de Santiago, 3810-193 Aveiro, Portugal
Fax: (internat.) +351-234-370084
E-mail: igoncalves@dq.ua.pt
[b] Faculty of Science and Technology, Department of Chemistry and Biochemistry, University of the Algarve, Campus de Gambelas, 8000-062 Faro, Portugal

 © 2003 Wiley-VCH Verlag GmbH & Co. KGaA, Weinheim **DOI: 10.1002/ejic.200300278**

ently anchored complex of the type $[MoO(O_2)_2(L\text{-}L)]$.[9] The hybrid system was highly active and truly heterogeneous for liquid-phase epoxidation of cyclooctene with TBHP as the oxygen source. The molybdenum(VI) complexes $[MoO_2Cl_2(L^1)(L^2)]$ have also been immobilised in MCM-41 derivatised with monodentate nitrile and bidentate bipyridyl ligands.[10] Unfortunately, they are unstable towards molybdenum leaching, which accounts for their nearly complete loss of activity in a second reaction cycle. The high molybdenum loadings resulted in weakly adsorbed Mo dimeric species that were easily extracted during the oxidative transformations.

In the present work, we have attempted to prepare more stable heterogeneous olefin epoxidation catalysts by immobilisation of dioxomolybdenum(VI) complexes in the ordered mesoporous silicas MCM-41 and MCM-48 functionalised with a bidentate 1,4-diazabutadiene ligand.

Results and Discussion

The supported catalysts were prepared from MCM-41 and MCM-48 materials (Scheme 1). First, the triethoxysilyl ligand RN=C(Ph)−C(Ph)=NR (**1**) [R = $(CH_2)_3Si(OEt)_3$] was prepared by the reaction of benzil $[C_6H_5(CO)(CO)C_6H_5]$ with two equivalents of (3-aminopropyl)triethoxysilane. Treatment of the solvent adduct $[MoO_2Cl_2(THF)_2]$ with one equivalent of the ligand **1** gave the complex $[MoO_2Cl_2(L\text{-}L)]$ (**2**) in good yield. Such complexes, with bidentate substituted 1,4-diazabutadiene ligands L-L (RN=CR′−CR′=NR), are active, stable homogeneous catalysts for the epoxidation of olefins using TBHP.[3b] Treatment of MCM-41 with a solution of complex **2** in dichloromethane gave a modified material **3** containing approximately 3.3 wt.-% Mo (0.34 mmol·g^{-1}). The solid-state ^{13}C CP MAS NMR spectrum of **3** was similar to that of **2** except for less intense peaks corresponding to the OEt groups (δ = 58.4 and 18.3), due to the grafting on MCM-41. Tethered complexes of this type were also prepared by an alternative stepwise approach. MCM-41 and MCM-48 were first treated with a toluene solution of **1** under reflux. Before isolating the grafted materials, the silylating agent Me_3SiCl was added to remove the residual Si−OH groups on the surface of the mesoporous materials, which could be unfavourable for the catalytic reaction.[9] Trimethylsilylation may also render the surface more hydrophobic and improve stability against moisture and mechanical compression. Oxomolybdenum species were subsequently introduced into the ligand-silicas **4** (MCM-41) and **6** (MCM-48) by pore volume impregnation of a solution of the dioxomolybdenum(VI) complex $[MoO_2Cl_2(THF)_2]$ in CH_2Cl_2 at room temperature. Elemental analysis indicated metal loadings of 1.0 wt.-% (0.10 mmol·g^{-1}) for **5** (MCM-41) and 1.4 wt.-% (0.14 mmol·g^{-1}) for **7** (MCM-48).

The solid-state ^{13}C CP MAS NMR spectra of the ligand-silicas **4** and **6**, and the derivatised materials **5** and **7**, were similar to those of the grafted material **3**, confirming the presence of surface-bound 1,4-diazabutadiene groups. An

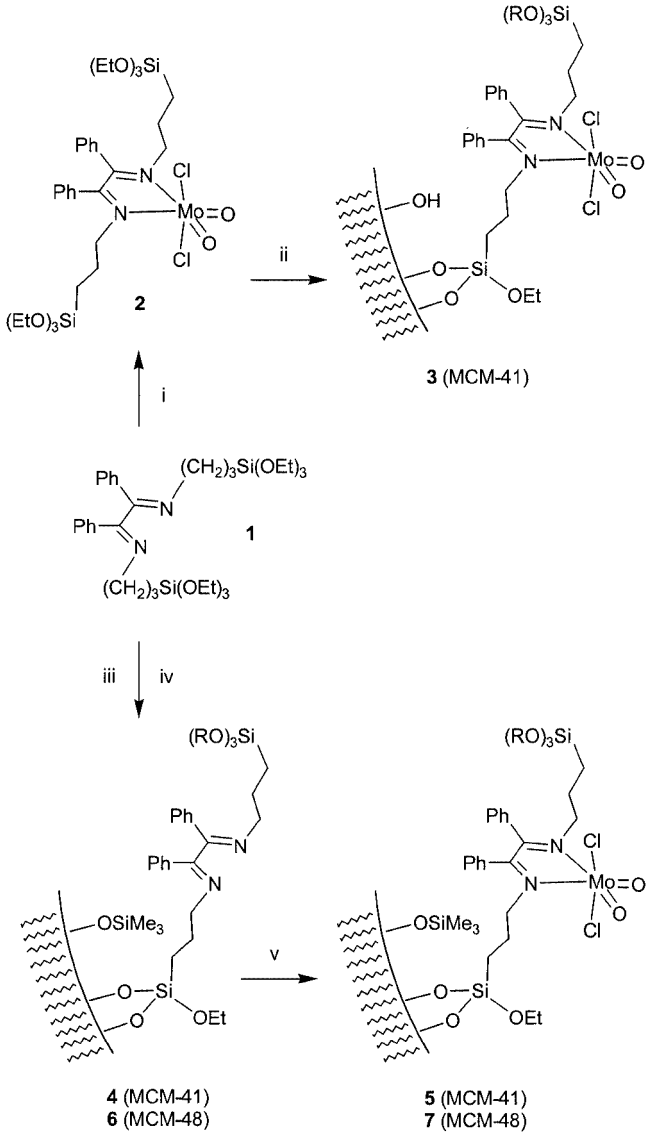

Scheme 1. Reagents: i, THF, $[MoO_2Cl_2(THF)_2]$; ii, CH_2Cl_2, MCM-41; iii, toluene, MCM-41 or MCM-48; iv, Me_3SiCl; v, CH_2Cl_2, $[MoO_2Cl_2(THF)_2]$

additional peak at about δ = −0.5 was attributed to $(-O)_3Si-O-SiMe_3$ species. The solid-state ^{29}Si MAS NMR spectra of the grafted materials **3**−**7** provide direct evidence for the incorporation of the covalently anchored organic system. Figure 1 shows the ^{29}Si MAS and CP MAS NMR spectra for pristine calcined MCM-41, the ligand-silica **4**, and the derivatised material **5**. Similar results were obtained for the corresponding MCM-48 materials. Unmodified MCM-41 displays two broad convoluted resonances in the ^{29}Si CP MAS NMR spectrum at δ = −110.7 and −100.9, assigned to Q^4 and Q^3 species of the silica framework, respectively [$Q^n = Si(OSi)_n(OH)_{4-n}$]. A weak shoulder is also observed at δ = −91.0 for the Q^2 species. The Q^3 sites are associated with the single silanols Si−OH (including hydrogen-bonded silanols), and the Q^2 sites correspond to the geminal silanols. Grafting of the triethoxysilane ligand **1** and Me_3SiCl into MCM-41 reduces

 © 2003 Wiley-VCH Verlag GmbH & Co. KGaA, Weinheim

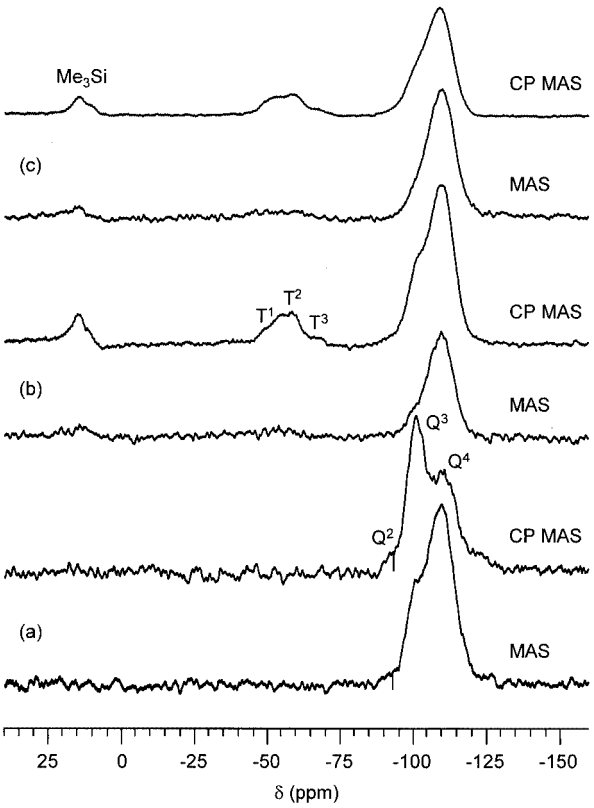

Figure 1. ^{29}Si MAS and CP MAS NMR spectra of (a) MCM-41, (b) MCM-41-L/Me_3SiCl (**4**), and (c) MCM-41-L/Me_3SiCl/MoO_2Cl_2 (**5**)

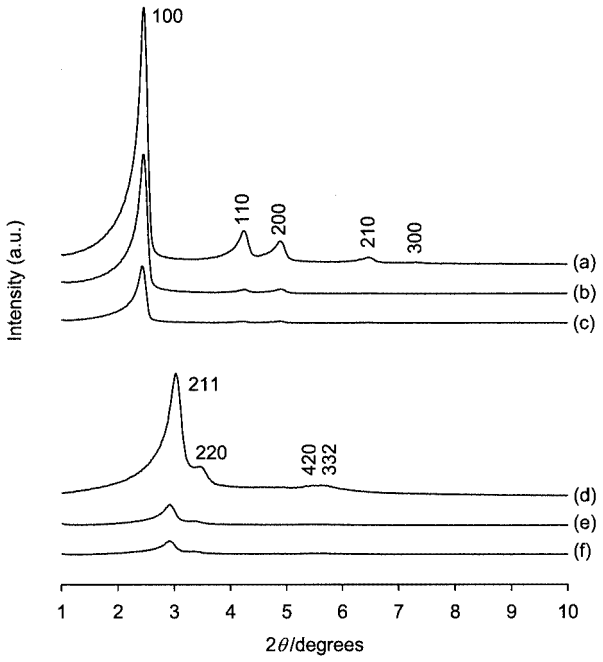

Figure 2. Powder XRD patterns of (a) MCM-41, (b) MCM-41-L/Me_3SiCl (**4**), (c) MCM-41-L/Me_3SiCl/MoO_2Cl_2 (**5**), (d) MCM-48, (e) MCM-48-L/Me_3SiCl (**6**), and (f) MCM-48-L/Me_3SiCl/MoO_2Cl_2 (**7**)

the Q^3 and Q^2 resonances and, concomitantly, increases the Q^4 resonance. This is consistent with esterification of the isolated silanol groups by nucleophilic substitution at the silicon atom in the organic compounds. The ^{29}Si CP MAS NMR spectrum of **4** reveals unchanged Q^3 silicon atoms. These might be hydrogen-bonded surface silanols, $(SiO)_3Si-OH-OH-Si(SiO)_3$, which are unreactive to silylating agents.[11] The ^{29}Si CP MAS NMR spectra of **4** and **6** also display two signals at $\delta = -50.0$ and -58.5, assigned to T^1 and T^2 organosilica species, respectively [$T^m = R.Si(OSi)_m(OEt)_{3-m}$]. A weak, broad signal at $\delta = -67.5$ is assigned to a T^3 environment, and a sharp peak at about $\delta = 14.0$ to the silicon nuclei of the Me_3Si groups. Reaction of the ligand-silicas **4** and **6** with the complex $[MoO_2Cl_2(THF)_2]$ does not measurably change the ^{29}Si MAS and CP MAS NMR spectra (Figure 1).

The powder XRD patterns of the pristine calcined MCM-41 and MCM-48 starting materials agree with reported patterns, indicating well-ordered materials (Figure 2).[12,13] Several distinct Bragg peaks are observed in the range $2\theta = 2-8°$, which can be indexed to different *hkl* reflections. MCM-41 is indexed on a hexagonal unit cell (using the strongest reflection, d_{100}, $a = 2d_{100}/\sqrt{3} = 41.4$ Å) and MCM-48 on a cubic unit cell (using the strongest reflection, d_{211}, $a = d_{211}\sqrt{6} = 71.5$ Å). Upon grafting with the triethoxysilyl ligand **1** and Me_3SiCl, several distinct Bragg peaks are still observed, indicating retention of the long-range hexagonal and cubic symmetries (Figure 2). A significant attenuation of the XRD peak intensities is not interpreted as a loss of order, but to a likely reduction in the X-ray scattering contrast between the silica walls and pore-filling material.[14] Reaction of the ligand-silicas **4** and **6** with the complex $[MoO_2Cl_2(THF)_2]$ does not change the powder XRD patterns significantly. There is a further slight reduction of peak intensities, for the reason outlined above. A similar result was obtained after reaction of the complex $[MoO_2Cl_2(THF)_2]$ with MCM-41 functionalised with bipyridyl groups.[10b]

The pristine MCM solids show reversible type IV N_2 adsorption−desorption isotherms, typical of mesoporous solids (pore width between 2 and 50 nm, according to IUPAC).[15] The step corresponding to capillary condensation in the primary mesopores appears in the relative pressure ranges 0.3−0.4 and 0.15−0.27 for unmodified MCM-41 and MCM-48, respectively, and is less pronounced for the latter (Figure 3). The specific surface area and total pore volume of the pristine MCM materials are greater than 940 $m^2 \cdot g^{-1}$ and 0.7 $cm^3 \cdot g^{-1}$, respectively (Table 1). The isotherms of the functionalised MCM samples show a lower N_2 uptake, pointing to a decrease in the specific surface area and pore volume. This effect is more pronounced for the trimethylsilylated samples **5** and **7**, for which S_{BET} decreased more than 33% and V_p decreased more than 56%. The height of the capillary condensation step and the p/p_0 coordinate of the inflection point decreases significantly, indicating changes in pore size distribution due to grafting of the internal silica surface with the molybdenum species and, for **5** and **7**, with Me_3SiCl.[10b,16,17] This is confirmed by comparing the pore size distributions (PSD) of the pristine and modified MCM materials (Figure 3). Upon surface

 © 2003 Wiley-VCH Verlag GmbH & Co. KGaA, Weinheim

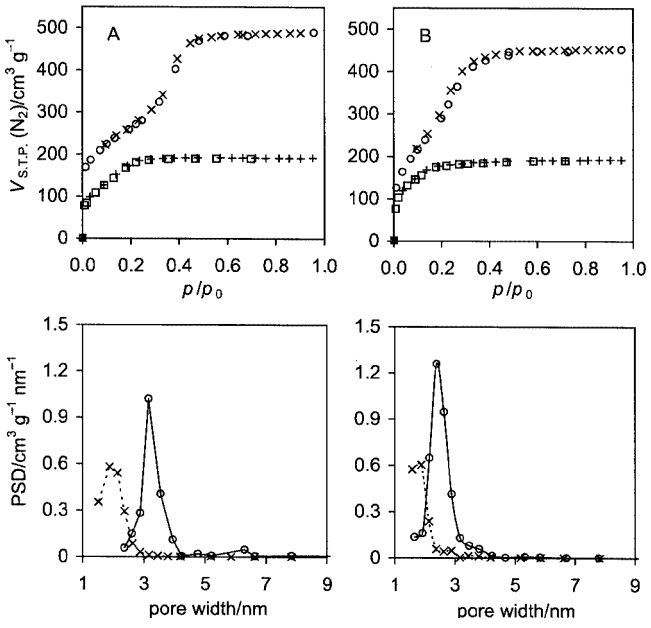

Figure 3. Nitrogen isotherms at 77 K of pristine MCM-41 (A) and MCM-48 (B) [(O) adsorption; (×) desorption], and surface-grafted **5** (A) and **7** (B) [(□) adsorption; (+) desorption]. Pore size distribution curves are also shown for the pristine (—) and surface-grafted materials (- - -)

grafting, the PSDs shift towards smaller pore sizes and the peaks become lower, indicating decreased uniformity of the pores.

The catalytic performance of complex **2** was studied for the epoxidation of cyclooctene with TBHP at 55 °C (1% molar ratio of complex/cyclooctene). After one hour the turnover frequency (TOF) was 18 mmol g^{-1}_{cat} h^{-1} and after 24 h the selectivity to cyclooctene oxide was 96% at 56% conversion (Table 2). The activity of **2** is similar to that reported under identical reaction conditions for other (dichloro)dioxomolybdenum(VI) catalysts bearing 1,4-diazabutadiene ligands without aromatic substituents.[3b] Despite using excess of oxidant with respect to the substrate, cyclooctene conversion at 24 h is still far from quantitative. In these catalysts the molybdenum centre acts as a Lewis acid, thereby decreasing the electron density in the coordinated TBHP molecule and promoting nucleophilic attack of the olefin on the O−O bond.[4b] The formation of *tert*-butyl alcohol during epoxidation may contribute to the decay in the reaction rate since it may act as a competitive inhibitor for the attack of TBHP at the Mo centre.[4b,10a,18] Conversely, although the complex bears relatively stable chelating nitrogen ligands,[3b,3c] the pendant triethoxysilyl groups may furnish less reactive dimers/oligomers, thus accounting for catalyst deactivation during epoxidation.

As described above, complex **2** was grafted onto the surface of MCM-41 to give the supported catalyst **3** at a metal loading of approximately 3.3 wt.-% Mo. The catalytic results obtained in the presence of **3** are similar to those obtained in homogeneous phase for complex **2** (Table 2, Figure 4). The corresponding kinetic curves are alike, suggesting a similar reaction mechanism. The reaction rate decreases after 7 h reaching a maximum conversion of 65% after 24 h (Table 2). Such retardation may result from the competitive reaction of the active Mo complex with *tert*-butyl alcohol, as in the homogeneous phase, and/or catalyst deactivation. The stability of catalyst **3** was studied by reusing the recovered solid in three consecutive reaction cycles. Before each reuse the solid was separated from the reaction solution, thoroughly washed with dichloromethane and dried at 60 °C. The catalytic activity decreased from the first to the second run, but afterwards tended to remain constant (Table 2, Figure 4). Probably, weakly adsorbed molybdenum complexes that were not efficiently solvent extracted after the grafting reaction were leached to the reaction solution. The catalyst stability was further investigated by reusing **3** in a fourth reaction cycle. After 2 h, the catalyst was separated at the reaction temperature and the solution was stirred for another 4 h. Cyclooctene conversion remained practically unchanged and molybdenum was not detected in the reaction solution by ICP-AES. Furthermore, the FTIR spectra of the solids recorded before and after catalysis showed no major changes. These results suggest that catalyst **3** is fairly stable and that catalysis is, in principle, heterogeneous.

The modified materials **5** and **7** were also tested as catalysts for the epoxidation of cyclooctene with TBHP at 55 °C. Considering the initial activities, the epoxidation of cyclooctene in the presence of **5** is slightly faster than for **7** (TOF = 6.7 and 5.9 mmol·g^{-1}_{cat}·h^{-1}, respectively), despite the lower molybdenum content of the former. However, at 24 h, both catalysts give approximately 63% conversion (Table 2). Overall, the kinetic profiles for **5** and **7** are similar (Figure 5). The difference in initial activities may be due, in part, to different internal diffusion rates during the initial unsteady operation as a result of the different channel structures of the mesoporous hosts. MCM-41 consists of an

Table 1. Texture parameters of MCM samples taken from nitrogen adsorption data

Sample	S_{BET} [$m^2 \cdot g^{-1}$]	ΔS_{BET} (%)[a]	V_P [$cm^3 \cdot g^{-1}$]	ΔV_P (%)[b]	d_p [nm]
MCM-41−1	1033	−	0.78	−	3.5
3	803	−22	0.56	−28	3.2
MCM-41−2	948	−	0.76	−	3.2
5	630	−34	0.30	−61	1.9
MCM-48−1	1161	−	0.70	−	2.4
7	672	−42	0.30	−57	1.9

[a] Variation of surface area in relation to parent MCM material. [b] Variation of total pore volume in relation to parent MCM material.

 © 2003 Wiley-VCH Verlag GmbH & Co. KGaA, Weinheim

Table 2. Catalytic results of cyclooctene epoxidation with catalysts **2**, **3**, **5**, or **7**, at 55 °C

Catalyst	TOF [mmol·g$^{-1}_{cat}$·h^{-1}][a]	Conversion (%)[b]	Selectivity to cyclooctene oxide (%)[c]
2	18	56	96
3 (run, 1)	4.5	65	100
3 (run, 2)	0.7	50	98
3 (run, 3)	0.4	48	98
5 (run, 1)	6.7	62	81
5 (run, 2)	1.1	55	89
5 (run, 3)	0.7	50	92
7 (run, 1)	5.9	63	94
7 (run, 2)	0.8	58	94
7 (run, 3)	0.5	55	95

[a] Calculated for ca. 1 hour reaction. [b] Cyclooctene conversion after 24 h. [c] 1,2-Cyclooctanediol was formed.

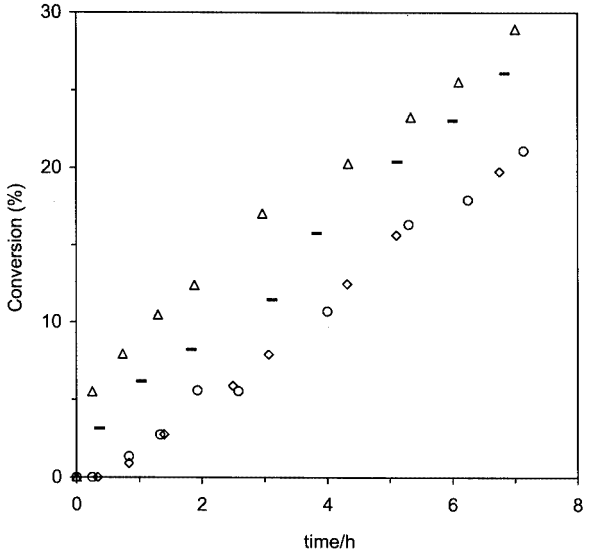

Figure 4. Kinetic profiles of cyclooctene epoxidation in the presence of **2** (−) and **3** [(Δ) − run 1; (O) − run 2; (◇) − run 3]

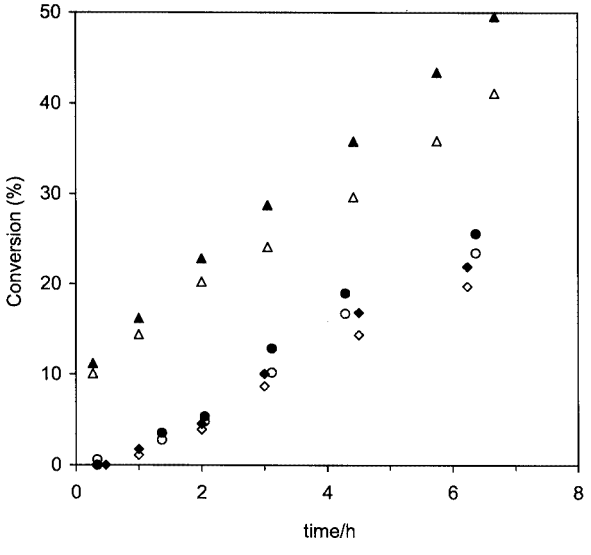

Figure 5. Kinetic profiles of cyclooctene epoxidation in the presence of **5** [(▲) − run 1; (●) − run 2; (◆) − run 3] and **7** [(Δ) − run 1; (O) − run 2; (◇) − run 3]

hexagonal arrangement of cylindrical pores, whereas MCM-48 possesses a three-dimensional gyroid-type pore structure. Despite the lower Mo loadings of catalysts **5** and **7** in comparison to **3**, they are more active initially (Table 2). Trimethylsilyation of MCM-41 and MCM-48 makes the surface more hydrophobic, thereby enhancing the adsorption of the olefin, and concomitantly reducing the adsorption of polar *tert*-butyl alcohol, making the Mo centres more available for the attack of TBHP. For catalysts **5** and **7** the selectivity to cyclooctene oxide is lower than for **3** and the complex **2**. This is unexpected since the adsorption of the polar epoxide should be less favourable on a more hydrophobic surface. Probably, trace amounts of HCl, which remained inside the MCM materials after silylation, are responsible for the ring opening reaction. In fact, selectivity to 1,2-cyclooctanediol decreases in recycling runs (Table 2). The stability of **5** and **7** was studied in a similar fashion to that of **3**. The Mo loading after three reaction cycles is at least 99% of the original value, as ascertained by ICP-AES. The main loss of catalytic activity is observed from the first to the second run, but the activity then tends to remain constant, similar to that observed for **3** (Table 2, Figure 4). The leaching of some weakly adsorbed molybdenum complexes present in the fresh catalyst may account for the initial loss of activity.

The MCM catalysts **3**, **5**, and **7** were also tested for the epoxidation of cyclododecene and α-pinene with TBHP at 55 °C (Figure 6). For each catalyst, olefin conversion at 24 h decreases in the order: cyclooctene (Cy8=) > cyclododecene (Cy12=) > α-pinene. Cyclododecene oxidation yields exclusively the corresponding epoxide (Cy12 oxide). A higher conversion is achieved with **3** (60% at 24 h) than with **5** and **7**, which may be due to the faster diffusion of the bulky substrate molecules inside the wider pores of **3**. For α-pinene oxidation, less than 2.5% α-pinene oxide is yielded at 24 h. The main reaction product is campholenic aldehyde (< 6% yield), which is an intermediate for sandalwood fragrance santalol and may be formed by the Lewis acid catalysed rearrangement of α-pinene oxide.[18,19]

Conclusions

The prepared supported catalysts reported here are active for the epoxidation of olefins using TBHP as the oxidant.

 © 2003 Wiley-VCH Verlag GmbH & Co. KGaA, Weinheim

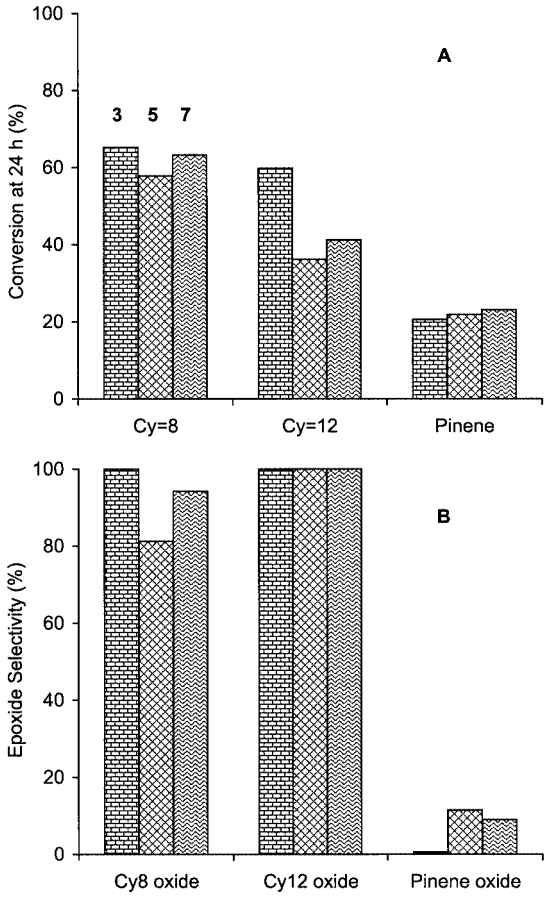

Figure 6. Conversion of cyclooctene (Cy8=), cyclododecene (Cy12=) and α-pinene (A) and selectivity towards the epoxide (B) observed for **3** (bricks), **5** (diamonds) or **7** (waves), at 24 h

Some activity is lost from the first to second runs, but thereafter the solids can be recycled without significant loss of activity. Tests indicate that the recycled solids operate as true heterogeneous catalysts. Previously, 2,2′-bipyridine was covalently grafted to MCM-41 and the resulting MoO_2Cl_2 supported material used as an epoxidation catalyst.[10b] However, most of the observed activity was due to leached molybdenum species in solution. Better results have been obtained here by using the 1,4-diazabutadiene ligand bearing triethoxysilyl groups. Future studies will centre on the use of this chelating ligand to immobilise other transition metal homogeneous catalysts.

Experimental Section

Material and Methods: Starting materials were obtained from commercial sources and used as received. All preparations and manipulations were carried out using standard Schlenk techniques under nitrogen. Solvents were dried by standard procedures (THF, hexane, and diethyl ether with Na/benzophenone ketyl; CH_2Cl_2 with CaH_2), distilled under nitrogen and kept over 4 Å molecular sieves. The solvent adduct $[MoO_2Cl_2(THF)_2]$ was prepared as described previously.[20]

Microanalyses were performed at the University of Aveiro. Powder XRD data were collected on a Phillips X'pert diffractometer using Cu-K_α radiation filtered by Ni. Nitrogen adsorption−desorption isotherms were measured at 77 K, using a gravimetric adsorption apparatus equipped with a CI electronic MK2−M5 microbalance and an Edwards Barocel pressure sensor. Before the measurements the MCM silicas were outgassed at 450 °C and the modified materials at 140 °C (to minimise destruction of the functionalities) and maintained at that temperature overnight to a residual pressure of ca. 10^{-4} mbar. The texture parameters, BET specific surface area (S_{BET}) and specific total pore volume (micropore plus mesopore, V_P), were estimated from the adsorption isotherm data. The pore size distribution curves (PSD − differential volume adsorbed with respect to the differential pore size per unit mass vs. pore width) were computed from the desorption branch of the experimental isotherms, using a method based on the area of the pore walls.[15,21] Assuming open cylindrical pores with radius r_p and zero contact angle and correcting for the thickness of the layer already adsorbed, r_p can be calculated by summing the Kelvin radius and the statistical average thickness (t, calculated using the Halsey equation) of the adsorbed layer.

IR spectra in transmission mode were measured with a Mattson Mod 7000 FTIR spectrometer using KBr pellets. Raman spectra were recorded on a Bruker RFS 100/S FT Raman spectrometer using a 1064 nm excitation of the Nd/YAG laser. ^1H and ^{13}C solution NMR spectra were obtained with a Bruker AMX-300 spectrometer. ^{29}Si and ^{13}C solid-state NMR spectra were recorded at 79.49 and 100.62 MHz, respectively, on a (9.4 T) Bruker Avance 400P spectrometer. ^{29}Si MAS NMR spectra were recorded with 40° pulses, spinning rates 5.0−5.5 kHz, and 60 s recycle delays. ^{29}Si CP MAS NMR spectra were recorded with 5.5 μs ^1H 90° pulses, 8 ms contact time, a spinning rate of 4.5 kHz, and 4 s recycle delays. ^{13}C CP MAS NMR spectra were recorded with a 4.5 μs ^1H 90° pulse, 2 ms contact time, a spinning rate of 8 kHz, and 4 s recycle delays. Chemical shifts are quoted in ppm from TMS. ^{13}C spectra were also recorded in the solid state at 125.76 MHz on a Bruker Avance 500 spectrometer.

MCM-41 and MCM-48: Purely siliceous MCM-41 was synthesised as described previously using $[(C_{14}H_{29})N(CH_3)_3]Br$ ($C_{14}TMABr$) as the templating agent.[10b] MCM-48 was crystallised from a gel with the molar composition SiO_2:0.26Na_2O:60H_2O:0.8$C_{16}TMABr$. Specifically, a solution of tetraethyl orthosilicate (17.36 g, 0.083 mol) in H_2O (30 mL) was added slowly to a vigorously stirred solution of $[(C_{16}H_{33})N(CH_3)_3]Br$ (24.05 g, 0.066 mol) in H_2O (40 mL). A solution of NaOH (1.76 g, 0.044 mol) in water (20 mL) was then added and the resulting mixture was stirred for 30 min and then autoclaved at 110 °C for 2 days in Teflon-lined stainless steel reaction vessels. The solid product was recovered by filtration, washed with hot water and air-dried at 30 °C. Calcination at 540 °C for 6 h then removed the surfactant template. Before the grafting experiments with MCM-41 and MCM-48, physisorbed water was removed from the calcined materials by heating at 180 °C in vacuo (10^{-2} Pa) for 2 h.

Ph-DAB-$(CH_2)_3Si(OEt)_3$ (1): A solution of (3-aminopropyl)triethoxysilane (2.85 g, 12.9 mmol) in THF (10 mL) was added to a solution of benzil (1.35 g, 6.4 mmol) in THF, followed by 4 Å molecular sieves (1.6 mm pellets, 0.6 g) and a catalytic amount of $ZnCl_2$. After 12 h at 50 °C the solution was filtered , and the resultant residue rinsed with THF and the filtrate evaporated in vacuo to give the product as a pale yellow oil (3.98 g) in 84.7% yield. IR (KBr): $\tilde{\nu}$ = 3062 (m), 2973 (vs), 2926 (vs), 2885 (vs), 1674 (vs), 1626 (s), 1595 (s), 1579 (s), 1448 (s), 1390 (s), 1318 (m), 1294 (m), 1281 (m), 1220 (s), 1166 (vs), 1102 (vs), 1062 (vs), 957 (vs), 792 (s), 776 (s), 724 (m), 696 (s), 623 (m) cm^{-1}. ^1H NMR (300.13 MHz,

 © 2003 Wiley-VCH Verlag GmbH & Co. KGaA, Weinheim

$CDCl_3$, 25 °C, TMS): δ = 0.60−0.68 (m, 4 H, $SiCH_2$), 1.15−1.24 (m, 18 H, OCH_2CH_3), 1.76−1.86 (m, 4 H, $CH_2CH_2CH_2$), 3.40−3.44 (t, 4 H, NCH_2), 3.73−3.84 (m, 12 H, OCH_2CH_3), 7.32−7.50 (m, 5 H, Ph), 7.57−7.75 (m, 3 H, Ph), 7.88−7.93 (m, 2 H, Ph) ppm. $^{13}C\{^1H\}$ NMR (75.47 MHz, $CDCl_3$, 25 °C, TMS): δ = 8.0 ($SiCH_2$), 18.3 (OCH_2CH_3), 24.3 ($CH_2CH_2CH_2$), 56.4 (CH_2N=C), 58.1 (OCH_2CH_3), 127.2, 128.6, 129.1 (Ph), 166.3 (CH_2N=*C*) ppm. ^{29}Si NMR (59.62 MHz, $CDCl_3$, 25 °C, TMS): δ = −52.90 ppm. $C_{32}H_{52}N_2O_6Si_2$ (616.99): calcd. C 62.30, H 8.50, N 4.54; found C 62.00, H 8.41, N 4.28.

MoO_2Cl_2[Ph-DAB-$(CH_2)_3Si(OEt)_3$] (2): A solution of $MoO_2Cl_2(THF)_2$ (0.25 g, 0.75 mmol) in THF (10 mL) was treated with 1 equivalent of the ligand **1** in THF (5 mL). The resulting turbid solution was stirred for a further 30 min at room temperature. The solvent was then evaporated, and the resultant solid product washed with hexane and dried in vacuo. Yield: 0.47 g, 76%. IR (KBr): $\tilde{\nu}$ = 2973 (s), 1681 (s), 1674 (vs), 1594 (s), 1491 (m), 1449 (s), 1306 (m), 1230 (m), 1077 (vs), 1047 (vs), 984 (s), 943 (vs), 915 (vs), 879 (s), 774 (m), 703 (m), 684 (m), 643 (m) cm^{-1}. ^{13}C CP MAS NMR: δ = 9.6 ($SiCH_2$), 18.3 (OCH_2CH_3), 21.7 ($CH_2CH_2CH_2$), 55.0 (CH_2N=C), 58.4 (OCH_2CH_3), 128.8 (Ph), 167.5 (CH_2N=*C*) ppm. ^{29}Si MAS NMR: δ = −54.4 ppm. $C_{32}H_{52}Cl_2MoN_2O_8Si_2$ (816.90): calcd. C 46.99, H 6.65, N 3.42; found C 46.56, H 6.29, N 3.38.

MCM-41/MoO_2Cl_2[Ph-DAB-$(CH_2)_3Si(OEt)_3$] (3): A solution of **2** (0.40 g, 0.49 mmol) in CH_2Cl_2 (10 mL) was added to a suspension of MCM-41 (1.0 g) in CH_2Cl_2 (15 mL) and the mixture stirred at room temperature for 24 h. The solution was then filtered and the so-obtained pale blue powder washed repeatedly with CH_2Cl_2 (4 × 20 mL), before drying in vacuo at room temperature for several hours. IR (KBr): $\tilde{\nu}$ = 1633 (m), 1596 (w), 1450 (m), 1384 (w), 1230 (sh), 1078 (vs), 954 (m), 914 (sh), 798 (m), 568 (m), 455 (s) cm^{-1}. ^{13}C CP MAS NMR: δ = 8.7, 15.6, 21.1, 53.2, 58.8, 128.7, 131.7, 136.6, 137.9 ppm. ^{29}Si MAS NMR: δ = −50.4, −56.2, −102.6 (Q^3), −108.0 (Q^4) ppm. Elemental analysis found C 8.50, N 0.49, H 0.90, Mo 3.3.

MCM-41-L/Me_3SiCl (4): A solution of the ligand **1** (0.66 g, 1.07 mmol) in toluene (5 mL) was added to a suspension of MCM-41 (1.0 g) in toluene (10 mL) and the mixture heated at 100 °C for 9 h. After cooling to ambient temperature, Me_3SiCl (5 mL) was added and the mixture stirred at room temperature for a further 24 h. The resultant solid was then filtered off and washed twice with acetone (2 × 20 mL), twice with CH_2Cl_2 (2 × 15 mL), and dried in vacuo at 100 °C for 3 h. Selected FT Raman: $\tilde{\nu}$ = 3069 (m), 2961 (m), 2904 (s), 1600 (s), 1552 (w), 1452 (m), 1415 (w), 1028 (w), 1001 (s), 617 (m) cm^{-1}. ^{13}C CP MAS NMR: δ = −0.5 (Me_3SiO−), 8.4 ($SiCH_2$), 16.4, 20.8, 24.9, 57.8, 127.6 (phenyl-C) ppm. ^{29}Si MAS NMR: δ = 14.5 (bd), −53.8 (bd), −109.5 ppm. ^{29}Si CP MAS NMR: δ = 13.8 (Me_3SiO−), −54.0 (T^1), −58.5 (T^2), −67.5 (T^3), −102.0 (sh, Q^3), −108.8 (sh, Q^4) ppm. Elemental analysis found C 16.24, N 1.34, H 2.33.

MCM-41-L/Me_3SiCl/MoO_2Cl_2 (5): A solution of $MoO_2Cl_2(THF)_2$ (0.52 g, 1.5 mmol) in CH_2Cl_2 (5 mL) was added to a suspension of the ligand-silica **4** (1.0 g) in CH_2Cl_2 (10 mL) and the mixture stirred overnight at room temperature. The resultant solid was then filtered off and washed with CH_2Cl_2 (4 × 20 mL), and dried in vacuo at room temperature for 3 h. Selected FT Raman: $\tilde{\nu}$ = 3069 (m), 2962 (m), 2904 (s), 1602 (m), 1001 (m) cm^{-1}. ^{13}C CP MAS NMR: δ = −0.3 (Me_3SiO−), 9.3 ($SiCH_2$), 20.8, 25.0, 57.9, 128.5 (phenyl-C). ^{29}Si MAS NMR: δ = 14.6, −55.0 (bd), −110.0 ppm. ^{29}Si CP MAS NMR: δ = 14.4 (Me_3SiO−), −54.0 (T^1), −58.0 (T^2), −67.5 (T^3), −108.9 (sh, Q^4) ppm. Elemental analysis found C 10.94, N 1.25, H 2.63, Mo 1.0.

MCM-48-L/Me_3SiCl (6): A solution of the ligand **1** (0.71 g, 1.15 mmol) in toluene (5 mL) was added to a suspension of MCM-48 (1.15 g) in toluene (10 mL) and the mixture heated at 100 °C for 9 h. After cooling to ambient temperature, Me_3SiCl (5 mL) was added and the mixture stirred at room temperature for a further 24 h. The so-obtained solid was then filtered off and washed twice with acetone (2 × 20 mL), twice with CH_2Cl_2 (2 × 15 mL), and dried in vacuo at 100 °C for 3 h. Selected FT Raman: $\tilde{\nu}$ = 3068 (s), 2971 (m), 2932 (s), 2901 (s), 1599 (s), 1550 (w), 1452 (m), 1414 (w), 1028 (w), 1001 (s), 617 (m) cm^{-1}. ^{13}C CP MAS NMR: δ = −0.3 (Me_3SiO−), 9.3 ($SiCH_2$), 17.0, 20.8, 58.9, 128.2 (phenyl-C) ppm. ^{29}Si MAS NMR: δ = −109.6 ppm. ^{29}Si CP MAS NMR: δ = 13.9 (Me_3SiO−), −50.0 (T^1), −58.4 (T^2), −67.5 (T^3), −101.9 (Q^3), −109.4 (Q^4) ppm. Elemental analysis found C 13.38, N 1.30, H 2.33.

MCM-48-L/Me_3SiCl/MoO_2Cl_2 (7): A solution of $MoO_2Cl_2(THF)_2$ (0.52 g, 1.5 mmol) in CH_2Cl_2 (5 mL) was added to a suspension of the ligand-silica **6** (1.0 g) in CH_2Cl_2 (10 mL) and the mixture stirred overnight at room temperature. The resultant solid was then filtered off and washed with CH_2Cl_2 (4 × 20 mL), and dried in vacuo at room temperature for 3 h. Selected FT Raman: $\tilde{\nu}$ = 3066 (m), 2962 (m), 2903 (s), 1598 (m), 1001 (m) cm^{-1}. ^{13}C CP MAS NMR: δ = 0.7 (Me_3SiO−), 8.7 ($SiCH_2$), 17.5, 20.7, 58.9, 128.7 (phenyl-C), 184.4 ppm. ^{29}Si MAS NMR: δ = 14.8, −55.0 (bd), −108.7 ppm. ^{29}Si CP MAS NMR: δ = 14.7 (Me_3SiO−), −54.7 (T^1), −59.4 (T^2), −67.5 (T^3), −108.7 (Q^4) ppm. Elemental analysis found C 10.94, N 1.30, H 2.63, Mo 1.4.

Catalysis: The liquid-phase epoxidation of cyclooctene was carried out at 55 °C under air in a micro reaction vessel equipped with a magnetic stirrer, which was loaded with complex (0.073 mmol) or MCM-catalyst (175 mg), olefin (7.3 mmol) and TBHP (11 mmol, 5.5 M in decane). Samples were withdrawn periodically and analysed using a gas chromatograph (Varian 3800) equipped with a capillary column (SPB-5, 20 m × 0.25 mm × 0.25 μm) and a flame ionisation detector. Undecane was used as internal standard added after the reaction.

Acknowledgments

The authors are grateful to FCT, POCTI, and FEDER for financial support (Project PCTI/1999/QUI/32889). CN thanks the University of Aveiro and the FCT for research grants. Paula Brandão and Cláudia Morais are acknowledged for assistance with the NMR experiments.

[1] [1a] K. A. Jörgensen, *Chem. Rev.* **1989**, *89*, 431−458. [1b] M. H. Dickman, M. T. Pope, *Chem. Rev.* **1994**, *94*, 569−584. [1c] C. C. Romão, F. E. Kühn, W. A. Herrmann, *Chem. Rev.* **1997**, *97*, 3197−3246. [1d] A. Corma, H. García, *Chem. Rev.* **2002**, *102*, 3837−3892.

[2] [2a] W. R. Thiel, M. Angstl, T. Priermeier, *Chem. Ber.* **1994**, *127*, 2373−2379. [2b] W. R. Thiel, M. Angstl, N. Hansen, *J. Mol. Catal. A: Chem.* **1995**, *103*, 5−10. [2c] W. R. Thiel, T. Priermeier, *Angew. Chem. Int. Ed. Engl.* **1995**, *34*, 1737−1738. [2d] W. R. Thiel, J. Eppinger, *Chem. Eur. J.* **1997**, *3*, 696−705.

[3] [3a] F. E. Kühn, E. Herdtweck, J. J. Haider, W. A. Herrmann, I. S. Gonçalves, A. D. Lopes, C. C. Romão, *J. Organomet. Chem.* **1999**, *583*, 3−10. [3b] F. E. Kühn, A. D. Lopes, A. M. Santos, E. Herdtweck, J. J. Haider, C. C. Romão, A. G. Santos, *J. Mol. Catal. A: Chem.* **2000**, *151*, 147−160. [3c] F. E. Kühn,

 © 2003 Wiley-VCH Verlag GmbH & Co. KGaA, Weinheim

A. M. Santos, A. D. Lopes, I. S. Gonçalves, E. Herdtweck, C. C. Romão, *J. Mol. Catal. A: Chem.* **2000**, *164*, 25−38.

[4] [4a] A. Hroch, G. Gemmecker, W. R. Thiel, *Eur. J. Inorg. Chem.* **2000**, 1107−1114, and references cited therein. [4b] F. E. Kühn, M. Groarke, É. Bencze, E. Herdtweck, A. Prazeres, A. M. Santos, M. J. Calhorda, C. C. Romão, I. S. Gonçalves, A. D. Lopes, M. Pillinger, *Chem. Eur. J.* **2002**, *8*, 2370−2383, and references cited therein.

[5] D. E. De Vos, M. Dams, B. F. Sels, P. A. Jacobs, *Chem. Rev.* **2002**, *102*, 3615−3640.

[6] [6a] D. C. Sherrington, *Catal. Today* **2000**, *57*, 87−104. [6b] S. Leinonen, D. C. Sherrington, A. Sneddon, D. McLoughlin, J. Corker, C. Canevali, F. Morazzoni, J. Reedijk, S. B. D. Spratt, *J. Catal.* **1999**, *183*, 251−266. [6c] M. M. Miller, D. C. Sherrington, *J. Catal.* **1995**, *152*, 368−376. [6d] M. M. Miller, D. C. Sherrington, *J. Catal.* **1995**, *152*, 377−383.

[7] A. Corma, A. Fuerte, M. Iglesias, F. Sánchez, *J. Mol. Catal. A: Chem.* **1996**, *107*, 225−234.

[8] [8a] J. Jarupatrakorn, J. D. Tilley, *J. Am. Chem. Soc.* **2002**, *124*, 8380−8388. [8b] R. D. Oldroyd, G. Sankar, J. M. Thomas, D. Ozkaya, *J. Phys. Chem. B* **1998**, *102*, 1849−1855. [8c] A. Maldotti, A. Molinari, G. Varani, M. Lenarda, L. Storaro, F. Bigi, R. Maggi, A. Mazzacani, G. Sartori, *J. Catal.* **2002**, *209*, 210−216.

[9] [9a] M. Jia, W. R. Thiel, *Chem. Commun.* **2002**, 2392−2393. [9b] M. Jia, A. Seifert, W. R. Thiel, *Chem. Mater.* **2003**, *15*, 2174−2180.

[10] [10a] P. Ferreira, I. S. Gonçalves, F. E. Kühn, A. D. Lopes, M. A. Martins, M. Pillinger, A. Pina, J. Rocha, C. C. Romão, A. M. Santos, T. M. Santos, A. A. Valente, *Eur. J. Inorg. Chem.* **2000**, 2263−2270. [10b] C. D. Nunes, A. A. Valente, M. Pillinger, A. C. Fernandes, C. C. Romão, J. Rocha, I. S. Gonçalves, *J. Mater. Chem.* **2002**, *12*, 1735−1742.

[11] X. S. Zhao, G. Q. Lu, A. K. Whittaker, G. J. Miller, H. Y. Zhu, *J. Phys. Chem. B* **1997**, *101*, 6525−6531.

[12] [12a] C. T. Kresge, M. E. Leonowicz, W. J. Roth, J. C. Vartuli, J. S. Beck, *Nature* **1992**, *359*, 710−712. [12b] J. S. Beck, J. C. Vartuli, W. J. Roth, M. E. Leonowicz, C. T. Kresge, K. D. Schmitt, C. T. -W. Chu, D. H. Olson, E. W. Sheppard, S. B. McCullen, J. B. Higgins, J. L. Schlenker, *J. Am. Chem. Soc.* **1992**, *114*, 10834−10843.

[13] [13a] A. A. Romero, M. D. Alba, W. Zhou, J. Klinowski, *J. Phys. Chem. B* **1997**, *101*, 5294−5300. [13b] J. Xu, Z. Luan, H. He, W. Zhou, L. Kevan, *Chem. Mater.* **1998**, *10*, 3690−3698.

[14] [14a] B. Marler, U. Oberhagemann, S. Vortmann, H. Gies, *Microporous Mater.* **1996**, *6*, 375−383. [14b] W. Hammond, E. Prouzet, S. D. Mahanti, T. J. Pinnavaia, *Micropor. Mesopor. Mater.* **1999**, *27*, 19−25.

[15] S. J. Gregg, K. S. W. Sing, *Adsorption, Surface Area and Porosity*, 2nd ed., Academic Press, London, **1982**.

[16] M. Pillinger, C. D. Nunes, P. D. Vaz, A. A. Valente, I. S. Gonçalves, P. J. A. Ribeiro-Claro, J. Rocha, L. D. Carlos, F. E. Kühn, *Phys. Chem. Chem. Phys.* **2002**, *4*, 3098−3105.

[17] D. Brunel, A. Cauvel, F. Fajula, F. DiRenzo, *Zeolites: A Refined Tool for Designing Catalytic Sites* (Eds.: L. Bonneviot et al.), Elsevier Science B. V., **1995**, p. 173.

[18] A. A. Valente, I. S. Gonçalves, A. D. Lopes, J. E. Rodríguez-Borges, M. Pillinger, C. C. Romão, J. Rocha, X. García-Mera, *New J. Chem.* **2001**, *25*, 959−963.

[19] P. J. Kunkeler, J. C. Van der Waal, J. Bremmer, B. J. Zuurdeeg, R. S. Dowing, H. Van Bekkum, *Catal. Lett.* **1998**, *53*, 135−138.

[20] W. M. Carmichael, D. A. Edwards, G. W. A. Fowles, P. R. Marshall, *Inorg. Chim. Acta* **1964**, *1*, 93−96.

[21] J. M. Thomas, W. J. Thomas, *Principles and Practices of Heterogeneous Catalysis*, VCH, Weinheim, **1997**.

Received May 9, 2003

 © 2003 Wiley-VCH Verlag GmbH & Co. KGaA, Weinheim

Group 10 Metal Complexes of SPS-Based Pincer Ligands: Syntheses, X-ray Structures, and DFT Calculations

Marjolaine Doux,[a] Nicolas Mézailles,[a] Louis Ricard,[a] and Pascal Le Floch*[a]

Keywords: Phosphorus / S ligands / Donor-acceptor systems / Density functional calculations / Group 10 elements

The 2,6-bis(diphenylphosphanylsulfide)phosphinine (**1**) reacts with water to afford a 1,2-dihydrophosphinine oxide **5** featuring a P–H bond. Reaction of **5** with one equivalent of $[Pd(COD)Cl_2]$ yields the SPS pincer-based complex **6** with a P(OH) λ^5-phosphinine central ligand. Complex **6** has been structurally characterized. Two possible mechanisms account for the formation of **5**: an intramolecular P–H to P–Pd metathesis or one based on the P=O to POH equilibrium. Methanol, ethanol or diethylamine also react with **1** to afford the corresponding P(H)(OMe) **7**, P(H)(OEt) **8**, and P(H)(NEt_2) **9** λ^5-phosphinines. No definitive mechanism for the formation of **7**–**9** can be proposed since no intermediates were detected in situ by ^{31}P NMR spectroscopy. However, DFT calculations (at the B3LYP 6-311+G(d,p) level of theory) suggest that the conversion of 1,2-dihydrophosphinines into λ^5-phosphinines is not viable because it involves a high activation energy. Like **5**, λ^5-phosphinines **7** and **8** react with $[Pd(COD)Cl_2]$ to afford the expected palladium complexes **10** and **11**. An alternative method relies on the reactivity of nucleophiles with a SPS pincer-based complex **2** featuring a P–Cl bond. (–)-Menthol and lithium diethylamide react with **2** to yield the expected P-OMen **13** and P-NEt_2 **14** complexes. Both complexes have been structurally characterized. Bromonickel **18** and chloroplatinum **19** complexes of the SPS ligand, featuring a P–Br or P–Cl bond, have also been prepared by reacting **1** with $[NiBr_2(DME)]$ and $[Pt(COD)Cl_2]$, respectively. Like their palladium congener, both species react with ethanol to afford the corresponding P–OEt derivatives **20** [M = Ni] and **21** [M = Pt]. *n*Butyl derivatives of these SPS ligands also bind to Ni–Br (complex **22**) and Pt–Cl (complex **23**) fragments. Both complexes were straightforwardly prepared by reacting anion **3**, resulting from the reaction of *n*BuLi with **1**, with the $[NiBr_2(DME)]$ and $[Pt(COD)Cl_2]$ precursors. The chloride ligand is readily substituted by acetonitrile in complexes **4**, **11**, **20**, and **21** upon treatment with $AgBF_4$ in dichloromethane. Reaction of AgOTf with the palladium complex **4** affords complex **28** via substitution of the chloride ligand by TfO^-. The X-ray crystal structures of the dimethyl-λ^5 derivative **29** of **1**, and that of its P-OMe anion **30**, have been recorded. Anion **30** can be regarded as a phosphanyl-substituted pentadienyl anion. DFT calculations and a charge decomposition analysis (CDA) show that the phosphorus atom in these SPS-pincer structures is a classical tertiary phosphane ligand in terms of donation and acceptance.
(© Wiley-VCH Verlag GmbH & Co. KGaA, 69451 Weinheim, Germany, 2003)

Introduction

The last decade has seen considerable interest in the synthesis and use of pincer ligands in coordination chemistry and catalysis, largely due to their particular backbone that allows not only the meridional encapsulation of transition metals but also the fine tuning of their coordination behavior and electronic capacity by varying the central or ancillary ligands. This area, pioneered by Shaw,[1] has been thoroughly reviewed recently.[2−4] Though early studies mainly focused on the ubiquitous PCP systems, polyheteroatomic-based pincer ligands featuring N, O, P, and S atoms have attracted increasing attention because multiple combinations can be used to build mixed systems.[5−7] Sulfur-based ligands are particularly appealing since they can also be employed in the elaboration of synthetic models of enzymes.[8] Mainly, four types of sulfur ligands are used: classical thioethers,[9−12] thiolates,[13,14] sulfoxides,[15] in which coordination occurs through the remaining lone pair at sulfur, and phosphane sulfides.[16,17] The latter, though not yet employed in pincer type structures, have found an interesting application in the rhodium-catalyzed carbonylation of methanol when incorporated in a mixed P−P=S bidentate ligand.[18,19]

Conversely, phosphane derivatives (probably the most studied ligands) have essentially been used as peripheral binding sites in pincer systems. This clearly results from their tetrahedral geometry that precludes the elaboration of planar rigid-backbones when the phosphorus atom is the central ligand. Therefore, the building of pincer systems incorporating a planar phosphorus atom as central binding site is an interesting challenge. Besides their structural interest, such systems exhibit very peculiar electronic properties that markedly differ from those of classical phosphanes and

[a] Laboratoire "Hétéroéléments et Coordination", UMR CNRS 7653 (DCPH), Département de Chimie, Ecole Polytechnique, 92128 Palaiseau Cédex, France
Fax: (internat.) +33-1-69333990
E-mail: lefloch@poly.polytechnique.fr
Supporting information for this article is available on the WWW under http://www.eurjic.org or from the author.

 © 2003 Wiley-VCH Verlag GmbH & Co. KGaA, Weinheim DOI: 10.1002/ejic.200300303

nitrogen analogs. Indeed, phosphorus in multiple bonds essentially behaves as a relatively poor σ-donor ligand but displays a powerful π-accepting capacity.[20] Very different systems, incorporating phosphaalkene (P analogs of alkenes) or heterocycles, can be anticipated but, in practice, only aromatic phosphorus heterocycles are sufficiently stable.

We thus recently launched a program aimed at incorporating phosphinines (phosphorus analogs of pyridines) in pincer-type structures. Our initial work focused on the synthesis of mixed S-P-S ligands featuring a phosphinine as central unit and two phosphane sulfides as ancillary ligands. Such systems proved to be easily available in large amounts by sulfurization of the corresponding 2,6-bis(diphenylphosphanyl)-λ^3-phosphinines. However, the highly electropositive phosphorus atoms are particularly reactive towards nucleophilic attack. Thus the reaction of ligand **1** with [Pd(COD)Cl_2] afforded a complex **2** featuring a central (λ^5-σ^4) pentavalent tetracoordinate phosphorus atom.[21] This new type of palladium complex, which can be derivatized by nucleophilic displacement of the chlorine atom at phosphorus, is particularly stable. Recently, we devised a much more rational approach to these complexes through the reaction of 1-*R*-1-*P*-phosphahexadienyl anions with [Pd(COD)Cl_2]. Thus, anion **3**, which is readily obtained by reacting *n*BuLi with phosphinine **1**, reacted with [Pd(COD)Cl_2] to afford complex **4** (Scheme 1). The latter proved to be particularly active (TON up to 10000) in the Miyaura-catalyzed cross-coupling process that allows the synthesis of aromatic boronic esters from halo aromatic and dialkoxyboranes.[22]

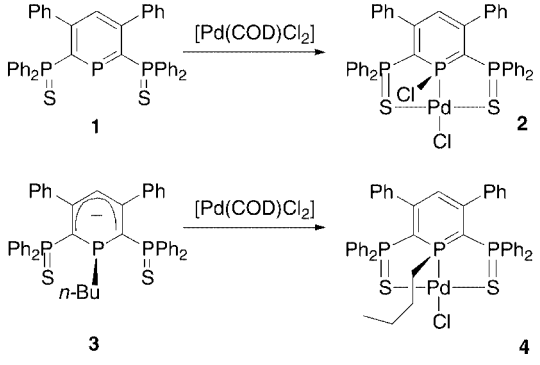

Scheme 1

As this chemistry might be extended to other metal centers, we aimed to expand the synthesis of this new type of phosphorus ligand and their applications in coordination chemistry and catalysis. We report here the synthesis of group 10 metal complexes. Different synthetic methodologies, the X-ray structures of some complexes as well as a preliminary theoretical study of their electronic properties are reported.

Results and Discussion

Two routes that exploit the high electrophilicity of the phosphorus atom in **1** have already been designed for the synthesis of these SPS palladium complexes. In exploring the reactivity of **1** toward nucleophiles, we found that reaction with water readily afforded the 1,2-dihydrophosphinine oxide **5** (Scheme 2). This is a common transformation for non-kinetically stabilized phosphaalkenes, but not, usually, for λ^3 -phosphinines in which the P=C double bond is thermodynamically stabilized.[23,24] However, the presence of strong acceptor groups at the α position of phosphorus (C2 and C6) sometimes provokes a significant dearomatization of the ring.[25] Interestingly, only one diastereomer of **5** was formed. The mechanism leading to **5** is discussed below.

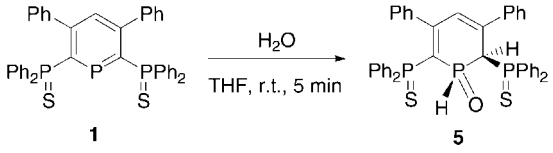

Scheme 2

The structure of **5**, fully characterized by NMR spectroscopy and elemental analysis, was confirmed by an X-ray crystal structure study. It shows no particular features and is not presented here.[26] Interestingly, **5** could also be used as a source of [Pd(SPSOH)Cl] (**6**) [SPS = $C_5H(Ph_2PS)_2P$] upon reaction with [Pd(COD)Cl_2] (Scheme 3).

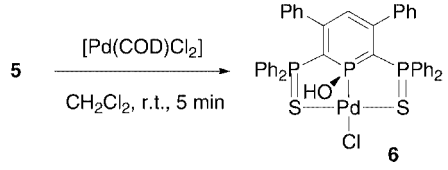

Scheme 3

Complex **6** was characterized by ^{31}P and ^{1}H NMR as well as by elemental data but was too insoluble to be characterized by ^{13}C NMR spectroscopy. Fortunately, suitable crystals for an X-ray crystal analysis could be grown by diffusing hexanes into a chloroform solution of the complex. A view of one molecule of **6** and the most significant metric parameters (Figure 1), and crystal data and structural refinement details (Table 6), are presented here. Complex **6** adopts a distorted planar geometry around the palladium atom and the two sulfides act as ancillary ligands. The most interesting data are the internal metric parameters within the SPS ligand. As previously noted for the *n*Bu derivative **4**, the phosphorus atom and the C3 carbon atom escape from the plane defined by the C1−C2−C4 and C5 atoms by 19.0° and 4.8°, respectively, to yield a boat-like conformation. Though the pyramidality of the phosphorus atom (316.5°) compares with that of classical tertiary phosphanes, the P−C1 [1.757(4) Å] and P−C5 [1.767(4) Å] bond lengths are very short. At first sight, these data suggest that the ylidic character of the λ^5-phosphinine has been pre-

 © 2003 Wiley-VCH Verlag GmbH & Co. KGaA, Weinheim

served upon coordination. Another intriguing piece of data is the bond lengths within the two ancillary P=S ligands. Indeed, whereas the two external P−C bond lengths [e.g. P3−C5 = 1.776(4) Å] are also very short compared to classical P−C single bonds, the two P=S bonds are lengthened [e.g. P2−S1 = 2.039(2) Å] compared with classical uncoordinated and coordinated phosphane sulfides. For example, in [Pd(R_3P=S)] complexes the P=S bond length usually falls between 1.9823(17), 2.0089(18) and 2.0237(9) Å.[27−29] The concomitant lengthening of this P−S bond with the shortening of the external P−C bond suggests there is delocalization within the unsaturated ligand backbone. Theoretical calculations to clarify this point will be presented below. The structure of **6** shows no other particular features.

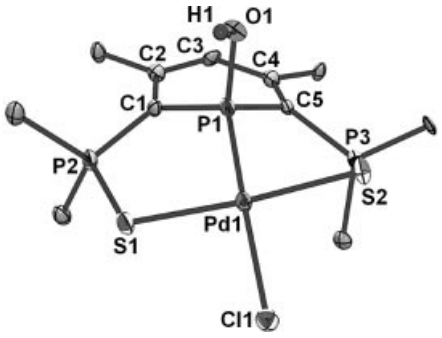

Figure 1. ORTEP view of complex **6**. Atoms are drawn as 50% thermal ellipsoids. Phenyl groups are omitted for clarity. The numbering is arbitrary and different from that used in the NMR spectroscopic data. Selected bond lengths [Å]: P1−C1 1.757(4), C1−C2 1.420(5), C2−C3 1.391(5), C3−C4 1.407(5), C4−C5 1.384(5), C5−P1 1.767(4), P1−O1.597(4), P2−C1, 1.759(4), P2−S1 2.039(2), P3−C5 1.776(4), P3−S2 2.1018(2), P1−Pd1 2.186(1), S1−Pd1 2.310(1), S2−Pd1 2.353(1), Pd1−Cl1 2.405(1); selected bond and dihedral angles [°]: C1−P1−C5 102.7(2), P1−C1−C2 117.5(3), C1−C2−C3 122.2(4), C2−C3−C4 125.2(4), C3−C4−C5 122.6(4), C4−C5−P1 119.3(3), P1−Pd1−Cl1 174.66(4), S1−Pd1−S2 174.67(4), (mean plane C1−C2−C4−C5)−P1 19.0, (mean plane C1−C2−C4−C5)−C3 4.8. Σangles at P1 316.5

It is relatively difficult to propose a definitive mechanism to account for the formation of **6** from **5**. Indeed, ^{31}P NMR monitoring of the reaction revealed only signals corresponding to **5** and **6**. Two possible mechanisms leading to **6** can be proposed, both of which are promoted by the initial displacement of the COD ligand by the two ancillary phosphane sulfide groups to yield an intermediary $PdCl_2$ complex. In the first mechanism, the close proximity of the P−H and Pd−Cl bond leads to dehydrochlorination to yield HCl and a metallated 1,2-dihydrophosphinine oxide; the last step can be regarded as a (1,3) shift of hydrogen from the C2 carbon atom to the P=O bond (Scheme 4). The second mechanism relies on the phosphane oxide−hydroxyphosphane tautomerism. Thus, displacement of one chloride ligand by the phosphorus atom lone pair would yield a cationic complex that could further undergo a dehydrochlorination. Such metal-promoted P=O to POH or P=S to P−SH rearrangements have been used to prepare palladium-phosphinous or palladium phosphinothious acid complexes, and in C−P coupling.[30−32]

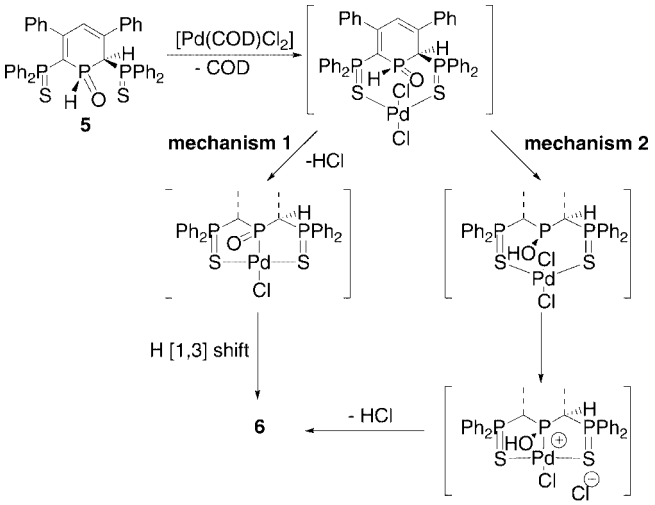

Scheme 4

Compound **1** also reacted with primary alcohols and secondary amines to afford the corresponding λ^5-phosphinines that formally result from the insertion of the phosphorus atom lone pair into the A−H bond (A = RO or R_2N). Whereas the reactions with methanol and ethanol to give **7** and **8** are rather slow and need excess ROH to go to completion, diethylamine readily reacts with **1** to form compound **9**. These derivatives are the first examples of λ^5-phosphinines featuring a P−H bond.[22,33] Both compounds were fully characterized by NMR and mass spectroscopy, as well as by elemental analysis for **7** (Scheme 5). Only primary alcohols react with **1** and additional experiments with menthol and phenol led to the recovery of **1**, even under forcing conditions (heating, high concentration of reagents). In ^{31}P NMR, the formation of **7**, **8**, and **9** was evidenced by the presence of two magnetically equivalent PPh_2S groups. The presence of a P−H bond was definitively established in the ^{1}H NMR spectrum by a strong ^1J(P-H) coupling constant (619.0 Hz in **7**, 613.0 Hz in **8** and 545.0 Hz in **9**).

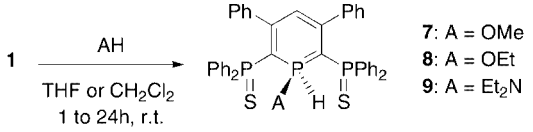

Scheme 5

The formation of λ^5-phosphinines by the direct condensation of alcohols and amines with phosphinines is unprecedented and emphasizes the reactivity of **1**. In most of the several synthetic approaches towards λ^5-phosphinines they are obtained directly by trapping the 1-R-1-*P*-phosphahexadienyl anions with electrophiles. Indeed, these anions are ambident and display two sites of attack, the lone pair at phosphorus and the Cα and Cγ carbon atoms of the carbocyclic backbone. "Soft electrophiles" (MeI for example) react at the phosphorus atom whereas "hard electro-

 © 2003 Wiley-VCH Verlag GmbH & Co. KGaA, Weinheim

philes'' (such as H^+) tend to react at the anionic part of the ring to afford 1,2-dihydrophosphinines.[34−36] This is probably why λ^5-phosphinines featuring a PH bond have never been synthesized before (Scheme 6).

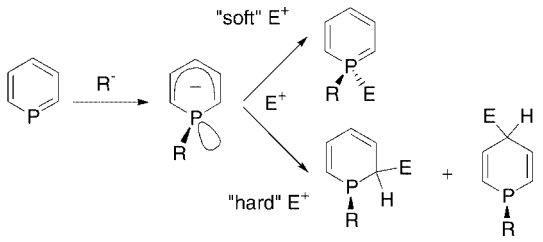

Scheme 6

However, λ^5-phosphinines are supposed intermediates in the thermolysis of 1,2-dihydrophosphinines to produce phosphinines. This transformation, which involves a (1,2) shift of the R group from the Cα carbon atom to phosphorus (Scheme 7) followed by an elimination of AH, usually occurs at high temperature and is well documented.[34,37]

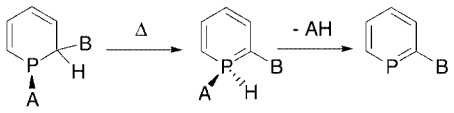

Scheme 7

Though no intermediates could be detected during our experiments, we first supposed that the reaction of MeOH and Et_2NH initially produces transient 1,2-dihydrophosphinines that can further isomerize to yield the corresponding λ^5 derivatives. No theoretical data are available on this isomerization. To clarify this point, DFT calculations were carried out using the combination of the B3LYP functional with the 6-311+G(d,p) basis set. We first focused on the rearrangement of Cα-unsubstituted compounds derived from the parent phosphinine (compounds **Ia**, **b**, **c**, **d**). The relative energies show that the 1,2-dihydro derivative are the most stable isomers (Table 1). Substitution of alkyl groups by OMe or NH_2 groups tends to reduce the energetic difference. This is in good agreement with previous theoretical calculations, which showed that the introduction of an electronegative atom on phosphorus slightly increases the aromaticity of the ring by negative hyperconjugation.[38] However, whatever the substituent at phosphorus, conversions of the 1,2-dihydrophosphinines into the corresponding λ^5-compounds (**IIa**, **b**, **c**, **d**) require a high activation energy (E_A) (from 50.442 kcal/mol for R = OMe to 66.393 kcal/mol for R = H) (Scheme 8). To assess the influence of the substitution pattern of the ring, calculations were performed on a model compound featuring two PPH_2S at the α-positions and a methoxy group at phosphorus. However, as in Cα-unsubstituted derivatives, a high activation barrier (44.848 kcal/mol) is required to form the corresponding λ^5-phosphinine (Scheme 9).

Table 1. Relative energies (ZPE corrected) in kcal/mol of model compounds **I**, **II**, and their corresponding **TS**

I		TS		II	
Ia	0	TSa	+66.393	IIa	+18.235
Ib	0	TSb	+62.475	IIb	+11.790
Ic	0	TSc	+50.442	IIc	+1.892
Id	0	TSd	+57.760	IId	+6.874
Ie	0	TSe	+44.848	IIe	+0.245

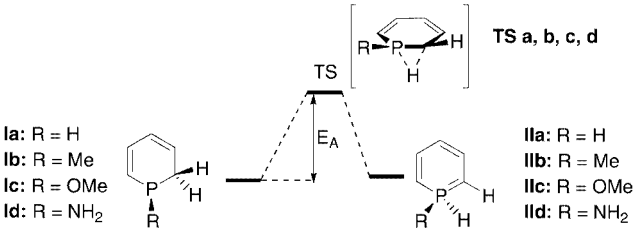

Scheme 8

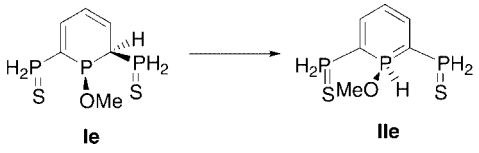

Scheme 9

This short theoretical investigation clearly shows that the introduction of two diphosphanylsulfide groups at the Cα position of phosphorus does not significantly modify the reaction pathway. Therefore, at this stage, no definitive mechanism can be proposed. However, we believe that this transformation is promoted by an initial attack of the oxygen or nitrogen atom at the phosphorus, the two ancillary PPh_2S groups assisting, in a second step, the transfer of H^+ to phosphorus (Scheme 10). Further calculations to localize a possible transition state as well as a complete study on the transformation of λ^5 and dihydrophosphinines into phosphinines are currently underway and will be reported in due course. Very probably, a similar mechanism takes place between **1** and H_2O in the formation of **5** via a transient λ^5-phosphinine. Indeed, λ^5-phosphinines featuring a P−OH group rapidly isomerize to the corresponding 1,2-dihydrophosphinine oxide derivatives.[39]

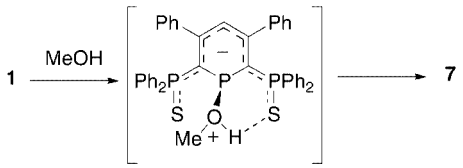

Scheme 10

Interestingly, compounds **7**, **8** can also be used as precursors for the synthesis of P-alkoxy-substituted PdCl complexes. Thus when **7**, **8** were treated with $[Pd(COD)Cl_2]$ in THF at room temperature, complexes **10** and **11** were cle-

 © 2003 Wiley-VCH Verlag GmbH & Co. KGaA, Weinheim

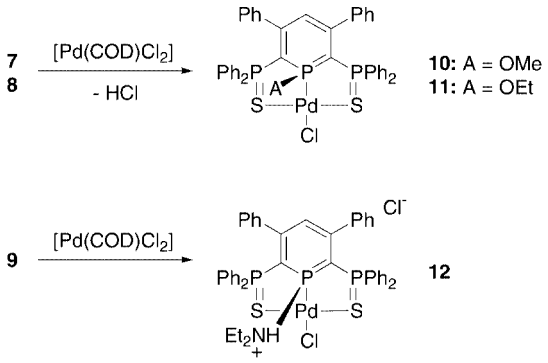

Scheme 11

anly formed in good yields (Scheme 11). Complex **10** has previously been obtained by a nucleophilic substitution of the P−Cl complex. Complex **10** and **11** were identified by NMR techniques and elemental analyses.

The synthesis of an amino derivative proved to be much more difficult to handle because of the concomitant release of HCl. For example, reaction of **9** with $[Pd(COD)Cl_2]$ in THF at room temperature afforded the poorly soluble salt **12**. The formulation of **12** was established on the basis of its ^1H NMR spectrum, which reveals an acidic proton at $\delta(CD_3COCD_3) = 9.25$ ppm, and elemental analyses. The formation of **12** could not be prevented even in the presence of a large excess of diethylamine as HCl scavenger.

Since no intermediates could be detected in ^{31}P NMR spectroscopy during the synthesis of **10** and **11**, no definitive mechanism can be proposed. However, a mechanism close to that proposed for the synthesis of complex **6** seems plausible. In a first step, the COD ligand is displaced from palladium by the two ancillary sulfide ligands and an elimination of HCl takes place to form the P−Pd bond (Scheme 12).

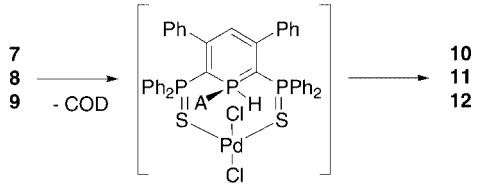

Scheme 12

Alkoxy complexes can also be obtained by the classical route that relies on the displacement of the Cl atom from phosphorus by ROH in complex **2**. Thus, complex **13** was easily obtained by treating (−)-menthol with **2** in dichloromethane at room temperature. The formation of **13** was evidenced by an ABC spin system pattern in ^{31}P NMR spectrum − a result of the chiral group introduced at phosphorus, which renders the two ancillary PPh_2S substituents magnetically non-equivalent (see Exp. Sect.). The formulation of **13** was confirmed by an X-ray structural study. A view of one molecule of **13** and the most significant metric

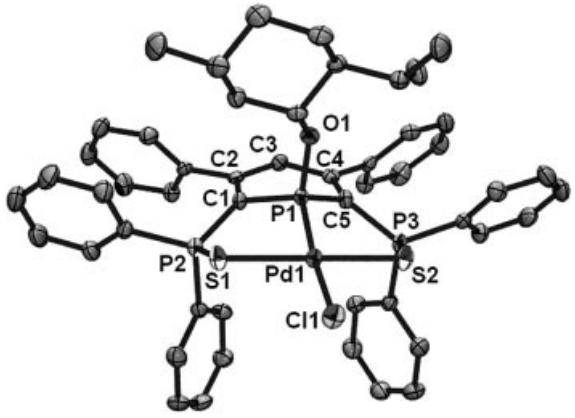

Figure 2. ORTEP view of complex **13**. Atoms are drawn as 50% thermal ellipsoids. The numbering is arbitrary and different from that used in the NMR spectroscopic data; selected bond lengths [Å]: P1−C1 1.761(3), C1−C2 1.408(4), C2−C3 1.389(4), C3−C4 1.409(4), C4−C5 1.407(4), C5−P1 1.751(3), P1−Pd1 2.188(1), C1−P2 1.778(3), P2−S1 2.033(2), C5−P3 1.774(3), P3−S2 2.033(2), P1−O1 1.600(2), S1−Pd1 2.328(1), S2−Pd1 2.313(1), Pd1−Cl1 2.396(1). Selected angles and dihedral angles [°]: P1−C1−C2 118.2(2), C1−C2−C3 122.0(3), C2−C3−C4 125.7(3), C3−C4−C5 121.2(3), C4−C5−P1 118.6(2), P1−Pd1−Cl1 170.11(3), S1−Pd1−S2 172.98(3). C4−C2−C1−P1 20.0, C1−C5−C4−C3 5.2, (mean plane C1−C2−C4−C5)−P1 20.9, (mean plane C1−C2−C4−C5)−C3 5.5. Σangles at P1 313.3

parameters (Figure 2), and crystal data and structural refinement details (Table 6), are given. This route was also efficient for the synthesis of the amino derivative **14**. Reaction of Et_2NLi with **2** in THF at low temperature cleanly afforded **14** which was recovered as a yellow solid in nearly quantitative yield (Scheme 13).

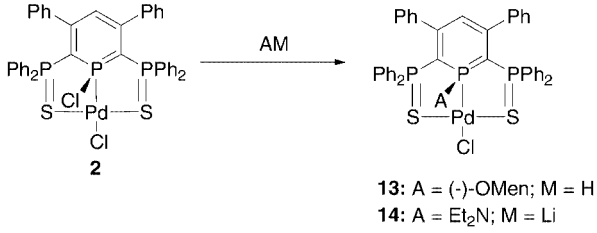

Scheme 13

The structure of **14** was confirmed by an X-ray analysis. An ORTEP view of one molecule of **14** (Figure 3), and crystal data and structural refinement details (Table 7), are given. The structure of **14** does not significantly differ from that of **5**. The two internal P−C bond lengths [P1−C1 1.756(2) Å and P1−C5 1.763(2) Å] as well as the external ones [C1−P2 1.766(2) Å and C5−P3 1.762(2) Å] are also short, and the two P−S bond lengths [P2−S1 2.029(1) Å and P3−S2 2.033(1) Å] are long.

Our investigations on potential precursors of these palladium(II) complexes have yielded another approach to P-alkyl derivatives. Reaction of anion **15** with C_2Cl_6 afforded the λ^5-phosphinine **16** featuring a P−Cl bond (Scheme 14). This compound, isolated as a moisture-sensitive solid, was successfully characterized by NMR and mass spectroscopy.

 © 2003 Wiley-VCH Verlag GmbH & Co. KGaA, Weinheim

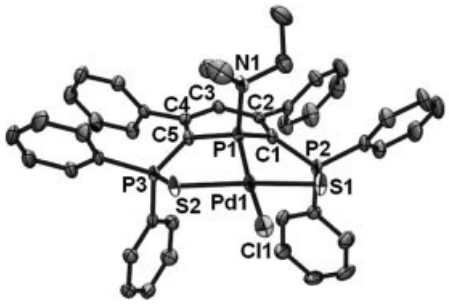

Figure 3. ORTEP view of complex **14**. Atoms are drawn as 50% thermal ellipsoids. The numbering is arbitrary and different from that used in the NMR spectroscopic data; selected bond lengths [Å]: P1−C1 1.756(2), C1−C2 1.409(3), C2−C3 1.408(3), C3−C4 1.400(3), C4−C5 1.411(3), C5−P1 1.763(2), P1−N1 1.681(2), P2−C1 1.766(2), P2−S1 2.029(1), C5−P3 1.762(2), P3−S2 2.033(1), P1−Pd1 2.186(1), S1−Pd 2.3250(8), S2−Pd 2.3275(8), Pd1−Cl1 2.404(1). Selected angles and dihedral angles [°]: C1−P1−C5 103.3(1), P1−C1−C2 117.0(2), C1−C2−C3 122.3(2), C2−C3−C4 125.3(2), C3−C4−C5 122.2(2), C4−C5−P1 117.3(2), P1−Pd1−Cl1 167.07(2), S1−Pd−S2 171.42(2), (mean plane C1−C2−C4−C5)−P1 20.6, (mean plane C1−C2−C4−C5)−C3 5.75. Σangles at P1 314.1

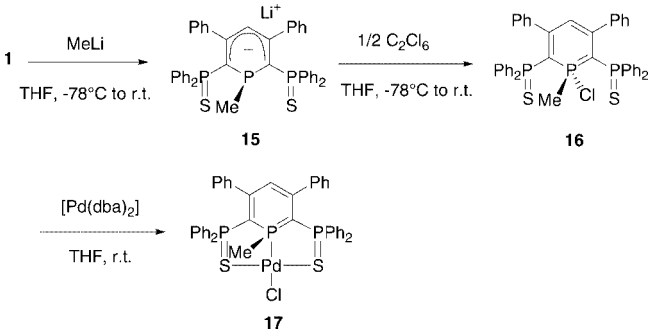

Scheme 14

Interestingly, **16** reacts with the [Pd(dba)$_2$] complex to form complex **17** (Scheme 14), which can be rationalized following a classical mechanism that involves the insertion of palladium into the P−Cl bond of **16**. Practically, this route is probably less straightforward than the direct reaction of anion **15** with [Pd(COD)Cl$_2$]. (Scheme 1) However, it shows that zerovalent metal centers can readily be inserted into the P−Cl bond of λ^5-phosphinines. This strategy could be particularly useful when divalent metal precursors are not available.

We wished to extend our several methods devised to introduce any substituent at the phosphorus to nickel and platinum(II) derivatives. All the approaches developed with palladium complexes have not yet been systematically explored. The original method involving the displacement of a chloride atom from the metal to the phosphorus atom could be duplicated with nickel and platinum using [NiBr$_2$(DME)] (DME = dimethoxyethane) and [Pt(COD)Cl$_2$] as starting precursors. Both reactions took place in dichloromethane at room temperature to afford

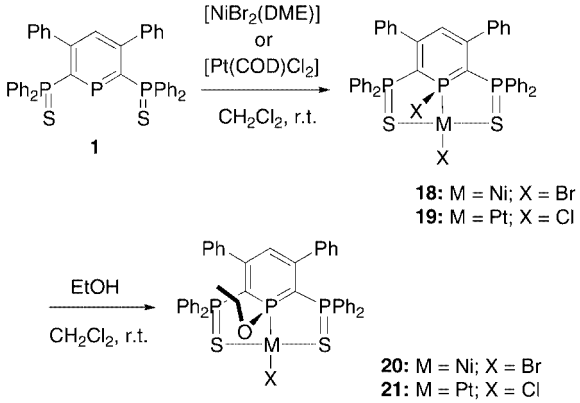

Scheme 15

complexes **18** and **19** respectively (Scheme 15). The P−Br **18** and P−Cl **19** derivatives, which are moisture sensitive, were characterized by ^{31}P NMR spectroscopy and by X-ray diffraction studies. However their structures, which are similar to that of the Pd−Cl complex **2**, are not reported here. As with the palladium derivative the P−Br and P−Cl bonds are sufficiently reactive to undergo nucleophilic substitution. Thus, reaction of EtOH with **18** and **19** cleanly afforded complexes **20** and **21**, respectively, which were fully characterized by NMR and mass spectroscopy as well by elemental analysis. Under standard conditions, intermediates **18** and **19** need not be isolated (Scheme 15).

Nickel and platinum complexes of alkyl derivatives were also prepared using the anionic approach. Phosphinine **1** reacted with *n*BuLi in THF at low temperature to produce anion **3** which was subsequently treated with [NiBr$_2$(DME)] and [Pt(COD)Cl$_2$] to yield complexes **22** and **23**, respectively (Scheme 16). The NMR spectroscopic data of **22** and **23** are comparable to those of their palladium analog **4**.

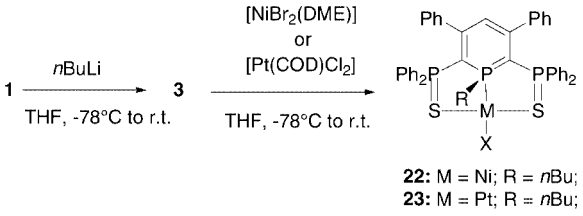

Scheme 16

Complex **22** was structurally characterized. An ORTEP view of one molecule of **22** and the most significant metric parameters (Figure 4), and crystal data and structural refinement details (Table 7), are presented here. These data reveal that replacement of palladium by nickel does not significantly modify the λ^5-phosphinine backbone, and the same trends are observed. The P−C bonds (external and internal) are short and the P−S bonds are slightly lengthened. The two angles between the C1−C2−C4−C5 plane and the phosphorus atom (21.05°) and the C3 carbon (4.7°)

 © 2003 Wiley-VCH Verlag GmbH & Co. KGaA, Weinheim

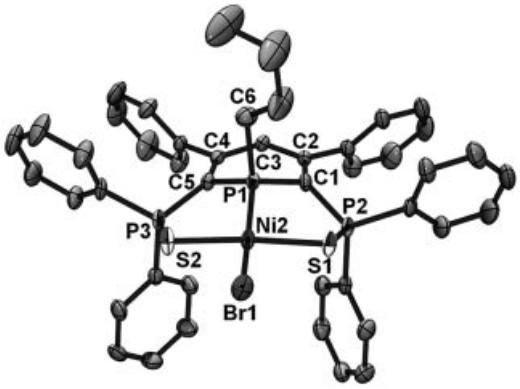

Figure 4. ORTEP view of complex **22**. Atoms are drawn as 50% thermal ellipsoids. The numbering is arbitrary and different from that used in the NMR spectroscopic data; selected bond lengths [Å]: P1−C1 1.776(3), C1−C2 1.384(5), C2−C3 1.412(4), C3−C4 1.412(4), C4−C5 1.390(5), C5−P1 1.778(3), P1−Ni2 2.111(1), C1−P2 1.768(3), P1−C6 1.829(4), P2−S1 2.039(2), C5−P3 1.761(3), P3−S2 2.045(2), P1−C6 1.829(4), S1−Ni2 2.185(1), S2−Ni2 2.194(1), Ni2−Br1 2.363(1). Selected angles [°]: P1−C1−C2 129.4(2), C1−C2−C3 121.8(3), C2−C3−C4 124.9(3), C3−C4−C5 122.8(3), C4−C5−P1 118.0(2), P1−Ni2−Br1 163.89(3), S1−Ni2−S2 172.57(4). (mean plane C1−C2−C4−C5)−P1 21.05, (mean plane C1−C2−C4−C5)−C3 4.7. Σangles at P1 315.3

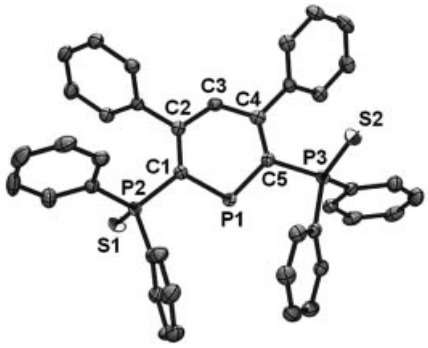

Figure 5. ORTEP view of phosphinine **1**. Ellipsoids are 50% thermal ellipsoids. The numbering is arbitrary and different from that used in the NMR spectroscopic data; selected bond lengths [Å]: P1−C1 1.742(2), P1−C5 1.745(2), C1−C2 1.409(3), C2−C3 1.399(3), C3−C4 1.399(3), C4−C5 1.417(3), P2−C1 1.826(2), S1−P2 1.956(1), P3−C5 1.835(2), S2−P3 1.9532(8). Selected angles [°]: C1−P1−C5 103.9(1), P1−C1−C2 123.2(2), C1−C2−C3 121.0(2), C2−C3−C4 127.9(2), C3−C4−C5 120.4(2), C4−C5−P1 123.3(2), P1−C1−P2 111.8(1), P1−C5−P3 112.9(1), C1−P2−S1 112.73(7), C5−P3−S2 112.54(8), (mean plane C1−C2−C4−C5)−P1 4.1, (mean plane C1−C2−C4−C5)−C3 3.7

atom also compare with those of **5**, **13** and **14** as well as the pyramidality of the phosphorus atom.

Finally, a preliminary study of the reactivity of the halogen ligand in these complexes showed that the chloride (Pd and Pt) or bromide ligand (Ni) is easily abstracted upon reaction with $AgBF_4$ in dichloromethane at room temperature in the presence of acetonitrile (Scheme 17). Four cationic complexes **24**−**27** were thus obtained and fully characterized by NMR techniques and elemental analyses. Interestingly, reaction of the palladium complex **4** with AgOTf furnished the neutral complex **28**. Its formulation was unambiguously established on the basis of NMR spectroscopic data and elemental analysis.

Having developed several new synthetic pathways to these d^8 metal complexes, we turned our attention to the electronic structure of the SPS pincer ligands. As noted earlier, some X-ray structural data suggest that electronic delocalization occurs within the ligand. To establish a significant structural comparison, three compounds were crystallized and submitted to X-ray crystal structure analysis, the phosphinine precursor **1**, the free anionic ligand **15** and the λ^5-dimethylphosphinine **29**. Phosphinine **1** was easily crystallized by diffusion of hexanes into a solution of **1** in CH_2Cl_2. An ORTEP view of one molecule of **1** and the most relevant metric parameters (Figure 5), and crystal data and structural refinement details (Table 5), are presented.

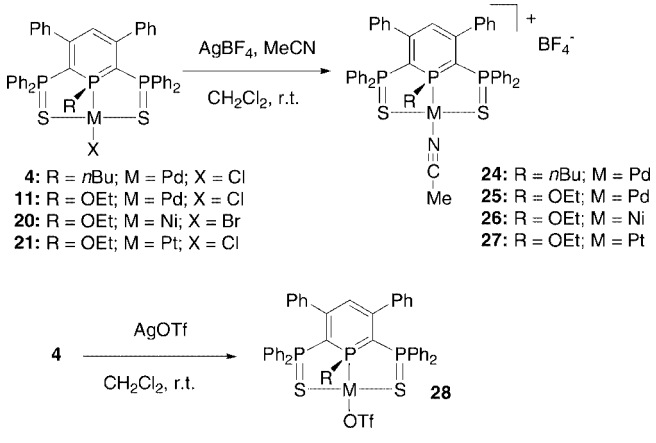

Scheme 17

Compound **29** was prepared conventionally with the subsequent trapping of anion **15** with methyl iodide. As explained above, in good agreement with literature data, the alkylation takes place exclusively at the phosphorus atom lone pair to yield **29** in very good yields (Scheme 18). The formulation of **29** was easily established on the basis of NMR spectroscopic data and combustion analysis. Suitable crystals were obtained by diffusion of hexanes into a solution of **29** in $CDCl_3$. An ORTEP view of one molecule of **29** and the most significant metric parameters (Figure 6), and crystal data and structural refinement details (Table 5), are given.

The crystallization of an anionic derivative of **1** proved to be much more difficult. To draw a precise comparison with the dimethyl-λ^5-phosphinine **29**, the crystallization of anion **15** was attempted. However, whatever the experimental conditions used (solvent, temperature, presence or absence of cryptand) no suitable crystals could be grown. However, crystallization of the methoxy-substituted species **30** gave more satisfying results. Anion **30** was readily prepared by reacting 3 equivalents of MeONa with **1** in THF at room temperature (Scheme 19). Suitable crystals of this anion were obtained upon crystallization with the (2.2.2) cryptand. An ORTEP view of one molecule of **30** and the most relevant bond lengths and bond angles (Figure 7), and crystal data and structural refinement details (Table 5), are presented.

 © 2003 Wiley-VCH Verlag GmbH & Co. KGaA, Weinheim

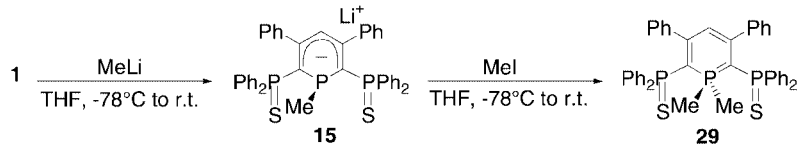

Scheme 18

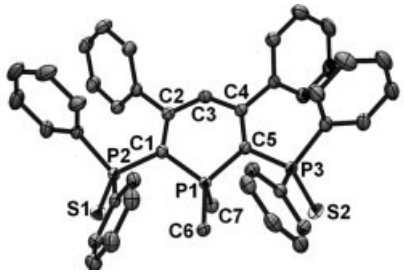

Figure 6. ORTEP view of phosphinine **29**. Ellipsoids are 50% thermal ellipsoids. The numbering is arbitrary and different from that used in the NMR spectroscopic data; selected bond lengths [Å]: P1−C1 1.767(2), P1−C5 1.768(2), C1−C2 1.410(2), 1.410(2), C2−C3 1.402(2), C3−C4 1.411(2), C4−C5 1.404(2), P1−C6 1.799(2), P2−C1 1.789(2), S1−P2 1.9675(8). Selected angles [°]: C1−P1−C5 106.25(8), P1−C1−C2 112.3(1), C1−C2−C3 123.1(2), C2−C3−C4 126.6(2), C3−C4−C5 122.7(2), C4−C5−P1 113.0(1), P1−C1−P2 120.9(1), P1−C5−P3 119.2(1), C1−P2−S1 114.24(7), C4−P3−S2 113.36(7), (mean plane C1−C2−C4−C5)−P1 37.0, (mean plane C1−C2−C4−C5)−C3 17.0

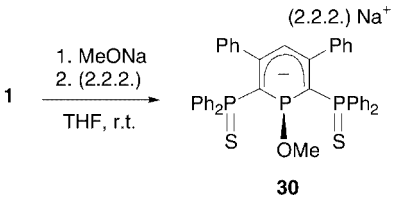

Scheme 19

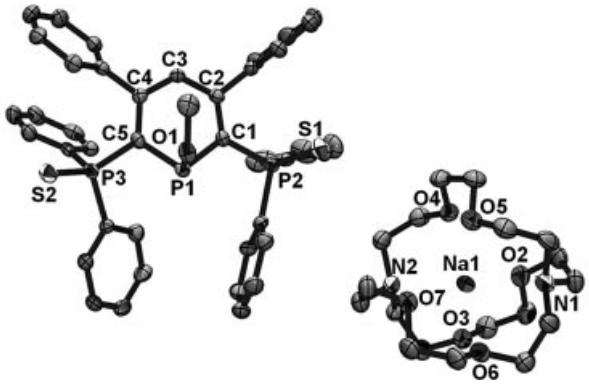

Figure 7. ORTEP view of anion **30**. Ellipsoids are 50% thermal ellipsoids. The numbering is arbitrary and different from that used in the NMR spectroscopic data; selected bond lengths [Å]: P1−C1 1.802(4), C1−C2 1.390(7), C2−C3 1.408(7), C3−C4 1.393(6), C5−C5 1.406(7), C5−P1 1.791(5), C5−P1 1.791(5), C1−P2 1.794(5), C5−P3 1.770(4), P3−S2 1.974(2), P2−S1 1.968(2), P1−O1 1.661(4). Selected angles and dihedral angles [°]: C5−P1−C1 105.0(2), P1−C1−C2 121.5(3), C1−C2−C3 122.6(4), C2−C3−C4 125.4(4), C3−C4−C5 121.4(4), C4−C5−P1 122.2(3), P1−C5−P3 116.4(3), P1−C1−P2 115.9(3), (mean plane C1−C2−C4−C5)−P1 21.0, (mean plane C1−C2−C4−C5)−C3 6.0

The structural data of **1**, **29**, and **30** provide interesting information. The structure of ligand **1** is relatively classical and compares with those of other λ^3-phosphinines. The two internal P=C bond lengths and the C−C bond lengths within the ring fall in the usual range and the ring is planar. The two sulfide groups point towards the back of the molecule to minimize the electronic repulsion between the lone pair at phosphorus and that of sulfur atoms (Figure 5). Of most interest is the external P−C bond lengths [C1−P2 1.826(2) Å and C5−P3 1.835(2) Å], which compare with those of classical P−C single bonds. Moreover, the P=S bond lengths [P2−S1 1.956(1) Å and P3−S2 1.953(1) Å] are normal. Transformation of **1** into **29** obviously induces important distortions and the phosphorus atom now escapes, by 23.15°, from the C1−C2−C4 and C5 plane. While the ylidic structure of the ring is evidenced by a small lengthening of the internal P−C bonds, the two external ones are slightly shortened [1.789(2) Å and 1.792(2) Å], suggesting that a delocalization occurs. However, this delocalization is probably weak and does not extend to the two P=S bonds due to the orientation of the two phosphane-sulfides groups, which are not coplanar with the unsaturated part of the ring. This effect is also apparent in **30**, which consists of two discrete units of the anionic ligand and [Na(2.2.2)]. Though the substituent at phosphorus is different (Me in **29**, OMe in **30**), the introduction of the charge significantly modifies the hybridization state of the phosphorus atom. Thus, in **30** the two internal P−C bond lengths [1.802(4) Å and 1.791(5) Å] have lost their ylidic character and this anion can be considered as a simple phosphanyl-substituted pentadienyl anion.[40] Note also that, as in **29**, the two external P−C bond lengths [1.794(5) Å and 1.770(4) Å] are also quite short.

These data do not obviously compare with those of the Pd and Ni complexes, and it is relatively difficult to establish whether the ligand behaves as an anionic λ^4-phosphinine (form A) or as a classical tertiary phosphane (form B). The short internal P−C bond lengths suggest that the ylidic structure of the phosphinine has been restored upon complexation but, conversely, the relatively long P−S bonds and short external P−C connections point to delocalization within the unsaturated part of the ligand (form B) (Scheme 20).

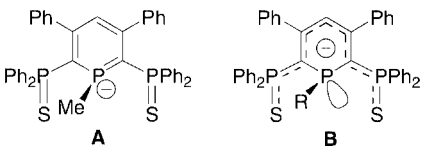

Scheme 20

 © 2003 Wiley-VCH Verlag GmbH & Co. KGaA, Weinheim

Reasonably, one may propose that both forms can contribute to the bonding, the respective contributions being determined by the nature of the metal centre and its formal oxidation state. Lacking a wide range of complexes and X-ray structures, it seems premature to propose a definitive model to rationalize the bonding in these complexes. A preliminary theoretical study aimed at evaluating the electronic capacity of the ligand in these group 10 complexes was thus undertaken. Optimizations were carried out on the two model complexes **IIIa**, **b** featuring a methyl group and a methoxy group at phosphorus, respectively (Scheme 21). The ligand substitution scheme was simplified to save computation time, and phenyl groups of the phosphane sulfide substituents, as well as those located on the phosphinine ring, were replaced by hydrogen atoms (Scheme 21).

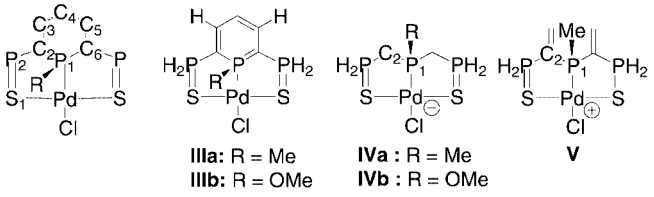

Scheme 21

Various functional and basis sets were tested. The best compromise, in terms of computation time and accuracy of structural data, was a combination of the B3LYP functional with a mixed basis set composed of the 6-31G* basis set for C, H, O, P, S and Cl atoms and the effective core potentials (ECP) of Hay and Wadt for Pd. The most significant bond lengths and bond angles of **IIIa**, **b** (Table 2) show an acceptable fit between theoretical and experimental parameters. Thus, the same trend is seen for P−C (internal and external) and P−S bond lengths. For example in **IIIa**, the internal P−C bonds (1.796 Å) are close to that in the *n*Bu derivative [1.762(7) Å] whose structure was previously reported. In **IIIb**, the external P−C bonds are shortened (1.774 Å *vs* 1.778(3) Å in **13**) and the P−S bonds are lengthened (2.049 Å vs. 2.033(2) Å in **13**). The only discrepancies arise from the P−Pd and S−Pd bond lengths and from the dihedral angle measuring the out-of-plane distortion of the phosphorus atom. Indeed, P−Pd and S−Pd bond lengths are overestimated and the out-of-plane distortion is underestimated in the theoretical structures. However, modification of the basis set for Pd (all electron-basis sets, other ECP, diffuse functions) or phosphorus and sulfur (diffuse functions) did not significantly improve data.

An analysis of natural charge (NBO method) reveals that, in **IIIa**, **b**, the phosphorus atom bears a significant positive charge and that the α (C2 and C6) and γ (C4) carbon atoms are negatively charged (Table 3). Conversely, the β (C3 and C5) carbon atoms are positively charged. This charge distribution is relatively equivalent to that observed in λ^5-phosphinines (see for example data for **IIe**). However, a relatively similar charge distribution is observed in the phosphane-based complexes **IVa**, **b** and **V**. These data also suggest that the P−Pd bond is slightly more polarized in **IIIa**, **b** than in **IVa**, **b** and **V**, but these differences are not very significant. Care must be taken in drawing rapid conclusion from charge distributions, especially in transition metal complexes.

Table 2. Most significant geometrical data for calculated structures **IIIa**, **b**, **IVa**, **b**, and **V**. Distances [Å] and angles [°]

	IIIa	IIIb	IVa	IVb	V
P1−C2	1.796	1.780	1.881	1.882	1.843
C2−C3	1.395	1.397			
C3−C4	1.404	1.403			
C2-P2	1.768	1.774	1.856	1.859	1.829
P2−S1	2.050	2.049			
P1−R	1.846	1.650	1.834	1.612	1.836
P1−Pd	2.258	2.243	2.300	2.275	2.302
Pd1−Cl	2.377	2.377	2.322	2.323	2.324
C6−P1−C2	101.7	101.5	107.4	106.6	108.0

Table 3. Calculated NBO charge distribution for ligands **IIe**, **f**, and complexes **IIIa**, **b** and **V**

	IIe	IIIa	IIIb	IVa	IVb	V
P1	1.662	1.170	1.420	1.038	1.375	1.060
C2	−0.950	−0.922	−0.942	−1.123	−1.156	−0.744
C3	−0.136	−0.139	−0.151			
C4	−0.326	−0.350	−0.334			
P2	0.880	0.921	0.917	0.850	0.846	0.856
S	−0.563	−0.457	−0.398	−0.302	−0.293	−0.308
Pd		0.351	0.367	0.313	0.310	0.323
Cl		−0.576	−0.560	−0.433	−0.437	−0.440

To determine which form (A or B) is preponderant in the bonding to the metal, a charge decomposition analysis was carried out using the CDA program developed by Frenking and coll. Such analysis has proved to be very useful in estimating the ratio between donation and back-donation for ligands following the classical Dewar−Chatt−Duncansson (DCD) model. Further explanations about the method, the terms used in these calculations and their relevance are given in the theoretical section. Complexes **IIIa**, **b** were compared to the virtual cationic complexes **IVa**, **b**, and **V** featuring a tertiary phosphane as central ligand and two peripheral phosphane sulfide groups. Complex **V** only differs from **IVa** by the presence of two exocyclic CH_2 groups which mimic the unsaturated backbone of the phosphinine ring.

The results of the CDA analysis are presented in Table 4. A first important remark concerns the residual term (Δ) which allows one to consider the interaction in terms of donor−acceptor behavior. All of the complexes exhibit a low (Δ) value, indicating that their bonding to Pd can be described following the DCD model. The second interesting point concerns the $b/(d+b)$ value which reflects the percentage of π-acceptance. The similarity of these values clearly indicates that the central phosphorus atom in **IIIa**, **b** (15.19 and 19.23%) exhibits electronic properties that are close to

 © 2003 Wiley-VCH Verlag GmbH & Co. KGaA, Weinheim

Table 4. Charge decomposition analysis of complexes **IIIa**, **b**, **IVa**, **b**, and **V**

	IIIa	IIIb	IVa	IVb	V
d[a]	1.089	0.844	0.855	0.935	0.863
b[b]	0.195	0.201	0.171	0.160	0.147
d/b	5.58	4.20	5.00	5.843	5.87
$b/(d+b)$	15.19	19.23	16.66	14.62	14.55
r[c]	−0.397	−0.076	0.069	−0.092	−0.093
Δ	−0.008	−0.005	−0.001	0.025	0.004

those of classical tertiary phosphane complexes **IV** and **V** (between 14.55 and 16.66%). Note that the exocyclic double bonds in **V** do not significantly modify the electronic capacity of the ligand. Overall, we therefore propose that, at least in the case of d^8 palladium complexes, the delocalized form B is probably preponderant.

Conclusion

We have presented several unusual routes towards λ^5-phosphinines derivatives of the 2,6-bis(diphenylphosphanyl)phosphinine. Easy access towards previously unknown P−H derivatives and a straightforward preparation of a P−Cl derivative have also been devised. Additionally, new synthetic approaches towards SPS-λ^5 phosphinine group 10 metal complexes have been developed using either these P−H, P−Cl derivatives or a 1,2-dihydrophosphinine oxide. Most of these routes should be operative with other metal halides. Structural data as well as a preliminary theoretical investigation suggests that a delocalization takes place within the carbocyclic part of the ligand but that the central phosphorus atom behaves as a classical tertiary phosphane. Further studies will now focus on the catalytic properties of the group 10 complexes and on a systematic investigation of the coordinative properties of SPS based-ligands. A detailed theoretical study of their electronic properties will be reported elsewhere.

Experimental Section

General Remarks: All reactions were routinely performed under an inert atmosphere of argon or nitrogen using Schlenk and glove-box techniques and dry deoxygenated solvents. Dry THF and hexanes were obtained by distillation from Na/benzophenone and dry diethyl ether from $CaCl_2$ and then NaH and dry CH_2Cl_2 from P_2O_5. Acetonitrile (99.5% purity) was purchased from SDS and used without further purification. $CDCl_3$ was dried over P_2O_5, and stored on 4Å Linde molecular sieves. CD_2Cl_2, [D_8]THF, and [D_6]acetone were used as purchased and stored in the glove-box. Nuclear magnetic resonance spectra were recorded on a Bruker AC-200 SY spectrometer operating at 300.0 MHz for ^{1}H, 75.5 MHz for ^{13}C and 121.5 MHz for ^{31}P. Solvent peaks were used as internal reference relative to Me_4Si for ^{1}H and ^{13}C chemical shifts (ppm); ^{31}P chemical shifts are relative to an 85% H_3PO_4 external reference. Coupling constants are given in Hertz. The following abbreviations are used: s, singlet; d, doublet; t, triplet; q, quadruplet; p, pentuplet; m, multiplet; v, virtual; b, broad. Mass spectra were obtained at 70 eV with a HP 5989B spectrometer coupled to a HP 5980 chromatograph by the direct inlet method. Elemental analyses were performed by the "Service d′analyse du CNRS", at Gif sur Yvette, France. Phosphinine **1** and complex **2**,[21] anion **3** and complex **4**,[22] [Ni(dme)Br_2],[41] [Pd(COD)Cl_2],[42] [Pd(dba)$_2$],[43] and [Pt(COD)Cl_2][44] were prepared according to reported procedures.

Phosphinine 1: Suitable crystals for X-ray structure analysis were grown by diffusion of hexanes into a solution of **1** in CH_2Cl_2.

Phosphane Oxide 5: Water (0.1 ml) was added to a solution of **1** (370 mg, 0.54 mmol) in THF (20 mL). The reaction was then stirred for 5 min at room temperature and the solvent was removed under vacuum. The solid was washed with diethyl ether (2 × 5 mL) and, after drying, **5** was recovered as a yellow powder. Suitable crystals for X-ray structure analysis were grown from a diffusion of hexanes into a solution of **5** in CH_2Cl_2.Yield: 97%, 366 mg. ^{1}H NMR (300 MHz, $CDCl_3$, 298 K): δ = 5.05 [ABB′X, td, ^2J(H-P_A) = ^2J(H-P_B) = 16.6, ^3J(H−H) = 2.1, 1 H, H^2], 6.55 (ABB′X, m, ΣJ= 9, 1 H, H^4), 6.74 [dd, ^1J(H-P_A) = 580, ^3J(H−H) = 2.7, 1 H, PH], 6.82−8.20 (m, 30 H, CH of Ph) ppm. ^{13}C NMR (75.5 MHz, $CDCl_3$, 298 K): δ = 43.5 (m, C^2H), 119.9 (m, C^6), 127.7−133.4 (m, C^4H, CH and C of Ph), 137.4 (ABB′X, m, ΣJ= 20, $C^{5\ or\ 3}$), 140.5 (ABB′X, m, ΣJ= 21, $C^{3\ or\ 5}$), 163.4 [d, ^3J(C-P_A) = 3.7, C of Ph] ppm. ^{31}P NMR (121.5 MHz, $CDCl_3$, 298 K): δ = 4.22 [ABB′, dd, ^2J(P_A-P_B) = 35.3, ^2J(P_A-$P_{B'}$) = 17.0, P_AH], 36.47 [ABB′, d, ^2J(P_A-P_B) = 35.3, P_BPh$_2$], 38.92 [ABB′, d, ^2J(P_A-$P_{B'}$) = 17.0, $P_{B'}$Ph$_2$] ppm. MS (EI): m/z = 682 [M^+ − (H_2O)]. $C_{41}H_{33}OP_3S_2$ (698.75): calcd. C 70.47, H 4.76; found C 70.03, H 4.34.

Complex 6: A solution of [Pd(COD)Cl_2] (155 mg, 0.54 mmol) and **5** (380 mg, 0.54 mmol) in CH_2Cl_2 (10 mL) was stirred for 2 h at room temperature. After removing the solvent under vacuum, the resultant yellow solid was washed with hexanes (3 × 5 mL) and dried. Suitable crystals for an X-ray structure analysis were grown from a diffusion of hexanes into a solution of $CDCl_3$. Yield: 83%, 376 mg. ^{1}H NMR (300 MHz, $CDCl_3$, 298 K): δ = 5.83 (m, 1 H, H^4), 6.60−7.60 (m, 30 H, CH of Ph) ppm. ^{31}P NMR (121.5 MHz, $CDCl_3$, 298 K): δ = 54.36 [AB_2, d, ^2J(P_A-P_B) = 105.7, P_BPh$_2$], 90.10 [AB_2, t, ^2J(P_A-P_B) = 105.7, P_A] ppm. Complex **6** was too insoluble to a give a satisfactory ^{13}C NMR spectrum. $C_{41}H_{32}ClOP_3PdS_2$ (839.62): calcd. C 58.65, H 3.84; found C 58.28, H 3.47.

λ^5-Phosphinine 7: A solution of **1** (100 mg, 0.15 mmol) and methanol (200 μL, 4.9 mmol) in THF (5 mL) was stirred for 24 h at 40 °C. After removing the solvent under vacuum, the resultant yellow solid was washed first with hexanes (3 × 2 mL) and then with diethyl ether (3 × 2 mL). After drying, **7** was recovered as a yellow powder in 73% (78 mg) yield. ^{1}H NMR (300 MHz, CD_2Cl_2, 298 K): δ = 3.38 (d, $^3J_{H-P}$ = 13.8, 3 H, CH_3), 5.7 [td, ^4J(H-P_B) = 3.8, ^4J(H-P_A) = 1.7, 1 H, H^4], 7.56 [dt, ^1J(H-P_A) = 619.0, ^3J(H-P_B) = 1.9, 1 H, PH], 6.80−7.76 (m, 30 H, CH of Ph) ppm. ^{13}C NMR (75.5 MHz, CD_2Cl_2, 298 K): δ = 49.5 (br. s, CH_3), 80.7 (m, $C^{2,6}$), 116.3 (m, C^4H), 125.8−133.5 (m, CH and C of Ph), 140.5 [m, ΣJ(C-P) = 20.7, $C^{3,5}$], 156.4 (s, C of Ph) ppm. ^{31}P NMR (121.5 MHz, CD_2Cl_2, 298 K): δ = 27.57 [AB_2, t, ^2J(P_A-P_B) = 43.7, P_A], 39.46 [AB_2, d, ^2J(P_A-P_B) = 43.7, P_B] ppm. MS (EI): m/z = 682 [M^+ − (MeOH)]. $C_{42}H_{35}OP_3S_2$ (712.78): calcd. C 70.77, H 4.95; found C 70.31, H 4.44.

λ^5-Phosphinine 8: A solution of **1** (550 mg, 0.8 mmol) and ethanol (200 μL, 3.4 mmol) in THF (5 mL) was stirred for 24 h at 40 °C. After removing the solvent under vacuum, the resultant solid was

 © 2003 Wiley-VCH Verlag GmbH & Co. KGaA, Weinheim

washed first with hexanes (3 × 2 mL) and then with diethyl ether (3 × 2 mL). After drying, **8** was recovered as a yellow powder in 78% (433 mg) yield. ^{1}H NMR (300 MHz, CD_2Cl_2, 298 K): δ = 1.26 [t, ^3J(H−H) = 7.2, 3 H, CH_3], 3.90 [dq, ^3J(H−H) = ^3J(H-P_A) = 7.2, 2 H, CH_2], 5.72 [t, ^4J(H-P_B) = 7.2, 1 H, H^4], 6.84−7.76 (m, 30 H, CH of Ph), 7.73 [d, ^1J(H-P_A) = 613.0, 1 H, PH] ppm. ^{13}C NMR (75.5 MHz, CD_2Cl_2, 298 K): δ = 15.1 [d, ^3J(C-P_A) = 16.0, CH_3], 63.3 [d, ^2J(C-P_A) = 6.9, CH_2O], 81.7 [ddd, ^1J(C-P_A) = 101.2, ^1J(C-P_B) = 80.5, ^3J(C-$P_{B'}$) = 4.6, $C^{2,6}$], 117.2 (m, C^4H), 127.1−132.2 (m, CH of Ph), 133.5 [dd, ^1J(C-P_B) = 11.5, ^3J(C-P_A) = 3.5, C of Ph], 134.7 [dd, ^1J(C-P_B) = 13.8, ^3J(C-P_A) = 3.4, of Ph], 141.5 [dt, ^2J(C-P_A) = 11.5, ^2J(C-P_B) = ^4J(C-$P_{B'}$) = 3.4, $C^{3,5}$], 156.3 (s, C of Ph) ppm. ^{31}P NMR (121.5 MHz, CD_2Cl_2, 298 K): δ = 25.87 [AB_2X, t, ^2J(P_A-P_B) = 43.1, P_A], 39.46 [AB_2, d, ^2J(P_A-P_B) = 43.1, P_B] ppm. MS (EI): *m*/*z* = 682 [M^+ − (EtOH)]. $C_{43}H_{37}OP_3S_2$ (726.81): calcd. C 71.06, H 5.13; found C 70.67, H 4.82.

λ^5-Phosphinine 9: A solution of **1** (100 mg, 0.15 mmol) and diethylamine (200 μL, 1.9 mmol) in CH_2Cl_2 (5 mL) was stirred for 15 min at room temperature. After removing the solvent under vacuum, the so-obtained yellow solid was washed first with hexanes (3 × 2 mL) and then with diethyl ether (3 × 2 mL). After drying, **9** (98 mg) was recovered as a yellow powder in 87% yield. ^{1}H NMR (300 MHz, $CDCl_3$, 298 K): δ = 1.14 [t, ^3J(H−H) = 6.9, 6 H, CH_3], 2.92 [q, ^3J(H−H) = 6.9, 4 H, CH_2], 5.59 [t, ^3J(H-P_B) = 4.6, 1 H, H^4], 7.29 [dt, ^1J(H-P_A) = 545.0, ^1J(H-P_B) = 2.0, 1 H, PH], 6.76−7.72 (m, 30 H, CH of Ph) ppm. ^{13}C NMR (75.5 MHz, $CDCl_3$, 298 K): δ = 10.9 (s, CH_3), 41.5 [d, ^2J(C-P_A) = 19.6, CH_2], 87.6 (m, $C^{2,6}$), 113.9 [d, ^4J(C-P_A) = 13.6, C^4H], 122.6−131.1 (m, CH of Ph), 134.5 [d, ^1J(C-P_B) = 84.1, C of Ph], 135.2 [d, ^1J(C-P_B) = 86.8, C of Ph], 141.4 (m, $C^{3,5}$), 155.5 (m, Cq de C_6H_5) ppm. ^{31}P NMR (121.5 MHz, $CDCl_3$, 298 K): δ = −0.31 [AB_2, t, ^2J(P_A-P_B) = 50.6, P_A], 37.36 [AB_2, d, ^2J(P_A-P_B) = 50.6, P_B] ppm. MS (EI): *m*/*z* = 682 [M^+ − ($NHEt_2$)]. $C_{45}H_{42}NP_3S_2$ (753.88): calcd. C 71.69, H 5.62; found C 41.26, H 5.17.

Complex 10: A mixture of [Pd(COD)Cl_2] (28 mg, 0.1 mmol) and **7** (71 mg, 0.1 mmol) in THF (10 mL) was stirred for 1 h at room temperature. After removing the solvent under vacuum, the resultant solid was washed first with hexanes (3 × 2 mL) then with diethyl ether (3 × 2 mL). After drying, **10** (78 mg) was recovered as a yellow solid in 92% yield. For characterization see ref.[21]

Complex 11: A mixture of [Pd(COD)Cl_2] (28 mg, 0.1 mmol) and **8** (71 mg, 0.1 mmol) in THF (10 mL) was stirred for 1 h at room temperature. After removing the solvent under vacuum, the so-obtained solid was washed first with hexanes (3 × 2 mL) and then with diethyl ether (3 × 2 mL). After drying, **11** (76 mg) was recovered as a yellow powder in 78% yield. ^{1}H NMR (300 MHz, CD_2Cl_2, 298 K): δ = 1.20 [t, ^3J(H−H) = 7.0, 3 H, CH_3], 4.30 [dq, ^2J(H-P_A) = 9, ^4J(H−H) = 7, 2 H, CH_2], 5.47 [t, ^3J(H-P_B) = 7.0, 1 H, H^4], 6.68−7.89 (m, 30 H, CH of Ph) ppm. ^{13}C NMR (75.5 MHz, CD_2Cl_2, 298 K): δ = 17.6 (m, CH_3), 66.0 [d, ^2J(C-P_A) = 4.6, CH_2], 95.9 [ddd, ^1J(C-P_A) = 91, ^1J(C-P_B) = 66.3, ^3J(C-$P_{B'}$) = 7.7, $C^{2,6}$], 116.1 [q, ^4J(C-P_A) = ^4J(C-P_B) = 12.2, C^4H], 128.8−129.9 (m, CH of Ph), 131.7 [dd, ^1J(C-P_B) = 84.3, ^3J(C-P_A) = 8.5, C of Ph], 132.8 [dd, ^1J(C-P_B) = 37.2, ^3J(C-P_A) = 3.8, C of Ph], 133.2−133.8 (m, CH of Ph), 141.5 [dt, ^2J(C-P_A) = 9.2, ^2J(C-P_B) = ^4J(C-$P_{B'}$) = 3.5, $C^{3,5}$], 155.5 [d, ^3J(C-P_A) = 2.3, C of Ph] ppm. ^{31}P NMR (121.5 MHz, CD_2Cl_2, 298 K): δ = 52.20 [AB_2, d, ^2J(P_A-P_B) = 103.0, P_B], 96.24 [AB_2, t, ^2J(P_A-P_B) = 103.0, P_A] ppm. $C_{43}H_{36}ClOP_3PdS_2$ (867.67): calcd. C 59.52, H 4.18; found C 59.14, H 3.79.

Pd Complex 12: A mixture of [Pd(COD)Cl_2] (37.9 mg, 0.13 mmol) and λ^5-phosphinine **9** (100 mg, 0.13 mmol) in CH_2Cl_2 (5 mL) was stirred for 30 min at room temperature. The so-obtained yellow precipitate was washed first with hexanes (3 × 2 mL) and then with diethyl ether (3 × 2 mL). After drying, complex **12** (114 mg) was recovered as a yellow solid in 90% yield . ^{1}H NMR (300 MHz, [D_6]acetone, 298 K): δ = 1.27 [t, $^3J_{H,H}$ = 6.3, 6 H, CH_3], 2.95 [dq, ^3J(H-P_A) = ^3J(H−H) = 6.3, 4 H, CH_2], 5.84 [dt, ^3J(H-P_A) = ^3J(H-P_B) = 3.5, 1 H, H^4], 6.66−7.70 (m, 30 H, CH of Ph), 9.25 (br. s, 1 H, NH) ppm. ^{31}P NMR (121.5 MHz, CH_2Cl_2, 298 K): δ = 49.32 [AB_2, d, ^2J(P_A-P_B) = 100.1, P_BPh_2], 82.18 [AB_2, t, ^2J(P_A-P_B) = 100.1, P_A]. **12** was too insoluble to give a satisfactory ^{13}C NMR spectrum. $C_{45}H_{42}Cl_2NP_3PdS_2$ (931.20): calcd. C 58.04, H 4.55; found C 57.91, H 4.37.

Pd Complex 13: A mixture of **1** (300 mg, 0.44 mmol) and [Pd(COD)Cl_2] (125 mg, 0.44 mmol) in CH_2Cl_2 (10 mL) was stirred for 15 min at room temperature. Menthol (6.9 mg, 0.44 mmol) was then added to the solution, which was stirred for a further hour at room temperature and then filtered through celite. After evaporation of the solvent, the resultant solid was washed first with hexanes (3 × 2 mL) and then with diethyl ether (3 × 2 mL). After drying, complex **13** was recovered as a yellow solid. Suitable crystals for X-ray structure analysis were grown by diffusion of hexanes into a solution of **13** in CH_2Cl_2. Yield 94%, 404 mg. ^{1}H NMR (300 MHz, CD_2Cl_2, 298 K): δ = 0.75 [d, ^3J(H−H) = 7.1, 3 H, CH_3], 0.87 [d, ^3J(H−H) = 6.2, 3 H, CH_3], 0.95 [d, ^3J(H−H) = 6.8, 3 H, CH_3], 1.08−1.75 (m, 8 H, CH and CH_2), 2.57 [d, ^2J(H−H) = 13.4, 1 H, CH_2], 4.78−4.87 (m, 1 H, OMen), 5.65 [t, ^4J(H-P_B) = 4.3, 1 H, H^4], 6.64−7.60 (m, 30 H, CH of Ph) ppm. ^{13}C NMR (75.5 MHz, CD_2Cl_2, 298 K): δ = 16.7 (s, CH_3), 20.4 (s, CH_3), 21.2 (s, CH_3), 22.4 (s, CH_2), 24.4 (s, CH), 31.3 (s, CH), 33.6 (s, CH_2), 44.2 (s, CH_2), 48.9 [d, ^3J(C-P_A) = 6.6, O−CH−CH], 77.2 [d, ^1J(C-P_A) = 6.4, O-CH], 116.6 [AB_2X, q, ^4J(C-P_A) = ^4J(C-P_B) = 10.7, C^4H], 127.0−128.2 (m, CH of Ph), 130.1 [dd, ^1J(C-P_B) = 83.3, ^3J(C-P_A) = 7.6, C of Ph], 130.4 [dd, ^1J(C-P_B) = 84.3, ^3J(C-P_A) = 7.2, C of Ph], 131.2−132.1 (m, CH of Ph), 139.2 (m, $C^{3,5}$), 155.8 (br. s, C of Ph), 156.4 (br. s, C of Ph). C^2 and C^6 not observed. ^{31}P NMR (121.5 MHz, CD_2Cl_2, 298 K): δ = 47.67 [ABB′, d, ^2J(P_A-P_B) = 111.3, P_B], 49.89 [ABB′, d, ^2J(P_A-$P_{B'}$) = 104.1, $P_{B'}$], 88.24 [ABB′, dd, ^2J(P_A-P_B) = 111.3, ^2J(P_A-$P_{B'}$) = 104.1, P_A] ppm. $C_{51}H_{50}ClONP_3PdS_2$ (977.87): calcd. C 62.64, H 5.15; found C 62.19, H 4.84.

Pd Complex 14: A mixture of **1** (100 mg, 0.15 mmol) and [Pd(COD)Cl_2] (42 mg, 0.15 mmol) in THF (5 mL) was stirred for 15 min at room temperature. In a glove-box, Et_2NLi (15 mg, 0.19 mmol) was added to the solution which was then stirred for 30 min at room temperature. The solvent was subsequently removed under vacuum and the resultant solid washed first with hexanes (3 × 2 mL) and then with diethyl ether (3 × 2 mL). After evaporation of the solvent, the resulting solid was dissolved in CH_2Cl_2 and filtered through celite. After drying, complex **14** was recovered as a yellow solid. Suitable crystals for X-ray structure analysis were grown by diffusion of hexanes into a solution of CH_2Cl_2. Yield: 89%, 132 mg. ^{1}H NMR (300 MHz, CD_2Cl_2, 298 K): δ = 1.14 [t, ^3J(H−H) = 7.1, 6 H, CH_3], 4.30 [dq, ^3J(H-P_A) = 11.3, ^4J(H−H) = 7.1, 4 H, CH_2], 5.45 [t, ^4J(H-P_B) = 4.9, H^4], 6.71−7.52 (m, 30 H, CH of Ph) ppm. ^{13}C NMR (75.5 MHz, CD_2Cl_2, 298 K): δ = 11.1 (s, CH_3), 42.1 (m, CH_2), 89.1 [ddd, ^1J(C-P_A) = 89.0, ^1J(C-P_B) = 64.3, ^3J(C-$P_{B'}$) = 7.6, $C^{2,6}$], 115.0 [td, ^4J(C-P_B) = 10.3, ^4J(C-P_A) = 2.9, C^4H], 127.6−128.8 (m, CH of Ph), 131.6 [dd, ^1J(C-P_B) = 78.9, ^3J(C-P_A) = 5.4, C of Ph], 132.4 [dd, ^1J(C-P_B) = 84.3, ^3J(C-P_A) = 5.7, C of Ph], 132.1−132.7 (m, C of Ph), 141.5 [m,

 © 2003 Wiley-VCH Verlag GmbH & Co. KGaA, Weinheim

Σ^2J(C-P) = 14.8, $C^{3,5}$], 155.5 (m, C of Ph) ppm. ^{31}P NMR (121.5 MHz, CH_2Cl_2, 298 K): δ = 51.77 [AB_2, d, $^2J(P_A\text{-}P_B)$ = 100.0, P_B], 66.46 [AB_2, t, $^2J(P_A\text{-}P_B)$ = 100.0, P_A] ppm. $C_{45}H_{41}ClNP_3PdS_2$ (894.74): calcd. C 60.41, H 4.62; found C 59.96, H 4.13.

Anion 15: A solution of MeLi in Et_2O (1.8 mL, C = 0.16 M, 0.29 mmol) was added by syringe into a solution of **1** (200 mg, 0.29 mmol) in THF (10 mL) at −78 °C. The solution was then warmed to room temperature and stirred for 20 min. After drying, **15** (206 mg) was recovered as a red solid in 100% yield. ^{1}H NMR (300 MHz, [D$_8$]THF, 298 K): δ = 0.99 [d, $^2J(H\text{-}P_A)$ = 3.4, 3 H, CH_3], 5.13 [t, $^4J(H\text{-}P_B)$ = 4.8, 1 H, H^4], 6.53−7.57 (m, 30 H, CH of Ph) ppm. ^{31}P NMR (121.5 MHz, [D$_8$]THF, 298 K): δ = 45.87 [AB_2, d, $^2J(P_A\text{-}P_B)$ = 155.5, P_B], −65.70 [AB_2, t, $^2J(P_A\text{-}P_B)$ = 155.5, P_AMe].

λ^5-Phosphinine 16: A solution of MeLi in Et_2O (1.8 mL, C = 0.16 M, 0.29 mmol) was added by syringe into a solution of **1** (200 mg, 0.29 mmol) in THF (10 mL) at −78 °C. The solution was then warmed to room temperature and stirred for 20 min. Complete formation of **15** was checked by ^{31}P NMR spectroscopy. After cooling at −78 °C, C_2Cl_6 (69 mg, 0.29 mmol) was added and the resultant solution was warmed to room temperature and stirred for a further 20 min. After removing the solvent, the solid was washed first with hexanes (3 × 2 mL) and then with diethyl ether (3 × 2 mL). The so-obtained solid was then dissolved in CH_2Cl_2 and filtered through celite. After drying, **16** (201 mg) was recovered as a yellow solid in 95% yield. ^{1}H NMR (300 MHz, [D$_8$]THF, 298 K): δ = 2.04 [d, $^2J(H\text{-}P_A)$ = 15.1, 3 H, CH_3], 6.16 [vq, $^4J(H\text{-}P_B)$ = $^4J(H\text{-}P_B)$ = 4.1, 1 H, H^4], 6.97−8.15 (m, 30 H, CH of Ph) ppm. ^{13}C NMR (75.5 MHz, [D$_8$]THF, 298 K): δ = 18.6 [d, $^1J(C\text{-}P_A)$ = 67.3, CH_3], 83.8 [dd, $^1J(C\text{-}P_A)$ = 90.9, $^1J(C\text{-}P_B)$ = 83.1, $^3J(C\text{-}P_{B'})$ = 3.2, $C^{2,6}$], 117.7 [dt, $^3J(C\text{-}P_A)$ = 27.8, $^3J(C\text{-}P_B)$ = 9.0, C^4H], 128.5−138.7 (m, C and CH of Ph), 143.5 [m, ΣJ(C-P) = 18.3, $C^{3,5}$], 157.6 [d, ^3J(C-P) = 5.3, C of Ph] ppm. ^{31}P NMR (121.5 MHz, [D$_8$]THF, 298 K): δ = 65.62 [AB_2, t, $^2J(P_A\text{-}P_B)$ = 42.5, P_A], 35.16 [AB_2, d, $^2J(P_A\text{-}P_B)$ = 42.5, P_B] ppm. MS (EI): m/z = 732 [M$^+$]. **16** was too moisture sensitive to give satisfactory elemental data.

Pd Complex 17: A mixture of [Pd(dba)$_2$] (79 mg, 0.14 mmol) and **16** (100 mg, 0.14 mmol) in CH_2Cl_2 (5 mL) was stirred for 30 min at room temperature. After evaporation of the solvent, the resultant solid was washed first with hexanes (3 × 2 mL) and then with diethyl ether (3 × 2 mL). After drying, **17** (108 mg) was recovered as a brown powder in 92% yield. ^{1}H NMR (300 MHz, CD_2Cl_2, 298 K): δ = 1.88 [d, $^2J(H\text{-}P_A)$ = 9.6, 3 H, CH_3], 5.42 [t, $^4J(H\text{-}P_B)$ = 4.4, 1 H, H^4], 6.61−7.47 (m, 30 H, CH of Ph) ppm. ^{13}C NMR (75.5 MHz, CD_2Cl_2, 298 K): δ = 24.3 (m, CH_3), 74.2 [dd, $^1J(C\text{-}P_A)$ = 97.4, $^1J(C\text{-}P_B)$ = 53.0, $C^{2,6}$], 117.7 [m, ΣJ(C-P) = 36.5, C^4H], 127.6−132.5 (m, C and CH of Ph), 141.5 [m, ΣJ(C-P) = 23.1, $C^{3,5}$], 158.9 (s, C of Ph) ppm. ^{31}P NMR (121.5 MHz, CD_2Cl_2, 298 K): δ = 49.44 [AB_2, m, $^2J(P_A\text{-}P_B)$ = 35.0, P_A], 50.44 [AB_2, m, $^2J(P_A\text{-}P_B)$ = 35.0, P_B] ppm. $C_{42}H_{34}ClP_3PdS_2$ (837.65): calcd. C 60.22, H 4.09; found C 59.83, H 3.86.

Ni Complex 18: A mixture of [Ni(dme)Br$_2$] (136 mg, 0.44 mmol) and **1** (300 mg, 0.44 mmol) in CH_2Cl_2 (10 mL) was stirred for 1 h at 40 °C. After evaporation of the solvent, the resulting solid was washed with hexanes (3 × 2 mL) and, after drying, complex **18** (384 mg) was then recovered as a brown powder in 97% yield. ^{31}P NMR (121.5 MHz, CD_2Cl_2, 298 K): δ = 55.92 [AB_2, d, $^2J(P_A\text{-}P_B)$ = 137.4, P_BPh_2], 98.52 [AB_2, t, $^2J(P_A\text{-}P_B)$ = 137.4, P_A]. Complex **18** was too moisture sensitive to give satisfactory elemental data.

Pt Complex 19: A mixture of [Pt(COD)Cl$_2$] (165 mg, 0.44 mmol) and **1** (300 mg, 0.44 mmol) in CH_2Cl_2 (10 mL) was stirred for 15 min at room temperature. After evaporation of the solvent, the resulting solid was washed with hexanes (3 × 2 mL) and then dried to afford complex **19** (400 mg) as a yellow powder in 96% yield. ^{31}P NMR (121.5 MHz, CD_2Cl_2, 298 K): δ = 47.99 [AB_2, d, $^2J(P_A\text{-}P_B)$ = 109.1, P_B], 67.10 [AB_2M, td, $^1J(P_A\text{-Pt})$ = 3860.3, $^2J(P_A\text{-}P_B)$ = 109.1, P_A].

Ni Complex 20: A solution of [Ni(dme)Br$_2$] (136 mg, 0.44 mmol) and **1** (300 mg, 0.44 mmol) in CH_2Cl_2 (10 mL) was stirred for 30 min at room temperature and then ethanol (200 μL, 3.4 mmol) was added. After stirring for 15 min at room temperature, the solvent was removed under vacuum and the resulting solid was washed first with hexanes (3 × 2 mL) and then with diethyl ether (3 × 2 mL). After drying, complex **20** (365 mg) was recovered as a brown powder in 96% yield. ^{1}H NMR (300 MHz, CD_2Cl_2, 298 K): δ = 1.27 [d, $^3J(H\text{−}H)$ = 7.0, CH_3], 4.52 [AB_2X, dq, $^3J(H\text{−}H)$ = $^3J(H\text{-}P_A)$ = 7.2, 2 H, CH_2], 6.73−7.82 (m, 31 H, H^4 and CH of Ph) ppm. ^{13}C NMR (75.5 MHz, CD_2Cl_2, 298 K): δ = 16.4 [d, $^3J(C\text{-}P_A)$ = 8.0, CH_3], 65.4 [d, $^2J(C\text{-}P_A)$ = 4.0, CH_2], 95.9 [m, ΣJ(C-P) = 158.1, $C^{2,6}$], 114.8 [q, $^3J(C\text{-}P_A)$ = $^3J(C\text{-}P_B)$ = 10.1, C^4H], 127.6−132.5 (m, C and CH of Ph), 140.9 [p, $^2J(C\text{-}P_A)$ = $^2J(C\text{-}P_B)$ = $^4J(C\text{-}P_{B'})$ = 3.4, $C^{3,5}$], 154.4 (s, C of Ph) ppm. ^{31}P NMR (121.5 MHz, CD_2Cl_2, 298 K): δ = 58.26 [AB_2, d, $^2J(P_A\text{-}P_B)$ = 123.9, P_B], 104.57 [AB_2, t, $^2J(P_A\text{-}P_B)$ = 123.9, P_A] ppm. $C_{43}H_{36}BrNiOP_3S_2$ (864.40): calcd. C 59.75, H 4.20; found C 59.29, H 3.80.

Pt Complex 21: A solution of [Pt(COD)Cl$_2$] (165 mg, 0.44 mmol) and **1** (300 mg, 0.44 mmol) in CH_2Cl_2 (10 mL) was stirred for 15 min at room temperature and ethanol (200 μL, 3.4 mmol) was then added. After stirring for a further 15 min at room temperature, the solvent was removed under vacuum and the resulting solid was washed first with hexanes (3 × 2 mL) and then with diethyl ether (3 × 2 mL). After drying, complex **21** (400 mg) was recovered as a yellow powder in 95% yield. ^{1}H NMR (300 MHz, CD_2Cl_2, 298 K): δ = 1.38 [d, $^3J(H\text{−}H)$ = 7.0, CH_3], 4.31 [dq, $^3J(H\text{-}P_A)$ = 9.0, $^3J(H\text{−}H)$ = 7.0, 2 H, CH_2], 5.66 [dt, $^4J(H\text{-}P_B)$ = 4.8, $^4J(H\text{-}P_A)$ = 0.8, 1 H, H^4], 6.69−7.67 (m, 30 H, CH of Ph) ppm. ^{13}C NMR (75.5 MHz, CD_2Cl_2, 298 K): δ = 16.6 [d, $^3J(C\text{-}P_A)$ = 7.3, CH_3], 62.7 [d, $^2J(C\text{-}P_A)$ = 5.0, CH_2], 88.8 [ddd, $^1J(C\text{-}P_A)$ = 92.6, $^1J(C\text{-}P_B)$ = 80.0, $^3J(C\text{-}P_{B'})$ = 5.0, $C^{2,6}$], 116.3 [q, $^4J(C\text{-}P_A)$ = $^4J(C\text{-}P_B)$ = 12.8, C^4H], 127.6−128.8 (m, CH of Ph), 130.7 [dd, $^1J(C\text{-}P_B)$ = 83.9, $^3J(C\text{-}P_A)$ = 5.7, C of Ph], 131.5 [dd, $^1J(C\text{-}P_B)$ = 86.6, $^3J(C\text{-}P_A)$ = 3.4, C of Ph], 132−132.8 (m, C of Ph), 140.5 [dt, $^2J(C\text{-}P_A)$ = 8.3, $^2J(C\text{-}P_B)$ = $^4J(C\text{-}P_{B'})$ = 2.9, $C^{3,5}$], 155.5 (s, C of Ph) ppm. ^{31}P NMR (121.5 MHz, CD_2Cl_2, 298 K): δ = 48.86 [AB_2M, d, $^2J(P_A\text{-}P_B)$ = 98.5, P_B], 65.47 [AB_2M, t, $^1J(P_A\text{-Pt})$ = 3640.0, $^2J(P_A\text{-}P_B)$ = 98.5, P_A] ppm. $C_{43}H_{36}ClOP_3PtS_2$ (956.33): calcd. C 54.00, H 3.79; found C 53.64, H 3.48.

Ni Complex 22: A solution of *n*BuLi in hexanes (0.275 mL, C = 1.6 M, 0.44 mmol) was added by syringe into a solution of **1** (300 mg, 0.44 mmol) in THF (10 mL) at −78 °C. The resultant solution was then warmed to room temperature and stirred for 20 min. Complete formation of **3** was checked by ^{31}P NMR (121.5 MHz, THF, 298 K): δ = 45.80 [AB_2, d, ^2J(P-P) = 156.0, P_BPh_2], −66.20 [AB_2, t, $^2J(P_A\text{-}P_B)$ = 156.0, P_A-*n*Bu]. After cooling at −78 °C, [Ni(dme)Br$_2$] (136 mg, 0.44 mmol) was added and the solution was warmed to room temperature and stirred for 15 min. The solvent was then removed and the resulting solid was dissolved in CH_2Cl_2 (8 mL) and filtered through celite. After evaporating the solvent under vacuum, the solid was washed several times with hexanes (3 × 2 mL) and diethyl ether (3 × 2 mL). After drying, **22** was recovered as a

 © 2003 Wiley-VCH Verlag GmbH & Co. KGaA, Weinheim

brown solid. Suitable crystals for X-ray structure analysis were grown from a diffusion of hexanes into a solution of CH_2Cl_2. Yield: 91%, 350 mg. ^{1}H NMR (300 MHz, CD_2Cl_2, 298 K): δ = 0.97 [t, ^3J(H-H) = 7.2, 3 H, CH_3], 1.53 (m, 2 H, CH_2), 2.00 (br. s, 4 H, CH_2), 5.38 [t, ^4J(H-P_B) = 4.2, 1 H, H^4], 6.62−7.44 (m, 30 H, CH of Ph) ppm. ^{13}C NMR (75.5 MHz, CD_2Cl_2, 298 K): δ = 12.8 (s, CH_3), 23.2 [d, ^3J(C-P_A) = 13.7, CH_2], 25.2 (s, CH_2), 38.9 [d, ^1J(C-P_A) = 25.7, CH_2], 72.5 (m, $C^{2,6}$), 118.6 (m, C^4H), 126.7−132.0 (m, CH and C of C_6H_5), 139.4 [d, ^2J(C-P_A) = 6.8, $C^{3,5}$], 158.1 (s, C of C_6H_5) ppm. ^{31}P NMR (121.5 MHz, THF, 298 K): δ = 57.34−63.09 (m, AB_2) ppm. $C_{45}H_{40}BrNiP_3S_2$ (876.45): calcd. C 61.67, H 4.60; found C 61.31, H 4.24.

Pt Complex 23: A solution of *n*BuLi in hexanes (0.275 mL, C = 1.6 M, 0.44 mmol) was added by syringe into a solution of **1** (300 mg, 0.44 mmol) in THF (10 mL) at −78 °C. The resultant solution was then warmed to room temperature and stirred for 20 min. Complete formation of **3** was checked by ^{31}P NMR spectroscopy. After cooling at −78 °C, [Pt(COD)Cl_2] (165 mg, 0.44 mmol) was added and the solution was warmed to room temperature and stirred for 15 min. The solvent was then evaporated and the resulting solid was dissolved in CH_2Cl_2 (8 mL) and filtered through celite. After removing the solvent under vacuum, the solid was washed several times with hexanes (3 × 2 mL) and diethyl ether (3 × 2 mL), and, after drying, **23** (392 mg) was recovered as a yellow solid in 92% yield. ^{1}H NMR (300 MHz, CD_2Cl_2, 298 K): δ = 1.1−2.22 (m, 9 H, CH_3 and CH_2), 5.60 [br. d, ^4J(H-P_A) = 2.4, 1 H, H^4], 6.70−7.70 (m, 30 H, CH of C_6H_5) ppm. ^{31}P NMR (121.5 MHz, THF, 298 K): δ = 21.52 [AB_2M, td, ^2J(P_A-Pt) = 3030.6, ^2J(P_A-P_B) = 81.0, P_A], 46.95 [AB_2M, d, ^2J(P_A-P_B) = 87.0, P_B]. **24** was too insoluble in common solvents to give a satisfactory ^{13}C NMR spectrum. $C_{45}H_{40}ClP_3PtS_2$ (968.38): calcd. C 55.81, H 4.16; found C 55.43, H 3.75.

Pd Complex 24: Acetonitrile (50 μL, 0.96 mmol) was added to a mixture of **4** (150 mg, 0.17 mmol) and $AgBF_4$ (37 mg, 0.19 mmol) in CH_2Cl_2 (5 mL). The resultant solution was stirred for 15 min at room temperature and was then filtered through celite. After drying, **24** (140 mg) was recovered as an orange powder in 85% yield. ^{1}H NMR (300 MHz, CD_2Cl_2, 298 K): δ = 1.05 [t, ^3J(H−H) = 7.3, 3 H, CH_3 of *n*Bu], 1.62 [qt, ^3J(H−H) = 14.6, ^3J(H−H) = 7.3, CH_2], 2.03 (m, 2 H, CH_2), 2.26 (m, 2 H, CH_2), 2.23 (s, 3 H, CH_3 of CH_3CN), 2.44 (m, 2 H, CH_2), 5.60 [t, ^4J(H-P_B) = 5.1, 1 H, H^4], 6.69−7.89 (m, 30 H, CH of Ph) ppm. ^{13}C NMR (75.5 MHz, CD_2Cl_2, 298 K): δ = 8.6 (s, CH_3 of CH_3CN), 13.4 (s, CH_3 of *n*Bu), 23.5 [d, ^3J(C-P_A) = 17.2, CH_2], 25.7 [d, ^2J(C-P_A) = 15.7, CH_2], 45.2 [d, ^1J(C-P_A) = 38.2, CH_2], 71.5 (m, $C^{2,6}$), 119.3 (m, C^4H), 126.2 [d, ^2J(C-P_A) = 25.5, C of CH_3CN], 125.2−134.5 (m, CH and C of Ph), 138.4 [ABB′X, dt, ^2J(C-P_A) = ^2J(C-P_B) = 9.0, ^4J(C-$P_{B'}$) = 3.1, $C^{3,6}$], 163 (m, C of Ph) ppm. ^{31}P NMR (121.5 MHz, THF, 298 K): δ = 49.72 [AB_2, d, ^2J(P_A-P_B) = 69.6, P_BPh_2], 64.61 [AB_2, t, ^2J(P_A-P_B) = 69.6, P_A] ppm. $C_{47}H_{43}BF_4NP_3PdS_2$ (972.13): calcd. C 58.07, H 4.46; found C 57.67, H 4.02.

Pd Complex 25: Acetonitrile (50 μL, 0.96 mmol) was added to a mixture of **11** (148 mg, 0.17 mmol) and $AgBF_4$ (37 mg, 0.19 mmol) in CH_2Cl_2 (5 mL). After stirring for 15 min at room temperature, the solution was filtered through celite. After drying, **25** (155 mg) was recovered as an orange powder in 95% yield. ^{1}H NMR (300 MHz, CD_2Cl_2, 298 K): δ = 1.35 [t, ^3J(H−H) = 7.0, 3 H, CH_3 of EtO], 2.20 (s, 3 H, CH_3 of CH_3CN), 4.22 [dq, ^3J(H-P_A) = 1.2, ^3J(H−H) = 7.0, 2 H, CH_2], 5.71 [t, ^4J(H-P_B) = 4.9, 1 H, H^4], 6.69−7.79 (m, 30 H, CH of Ph) ppm. ^{13}C NMR (75.5 MHz, CD_2Cl_2, 298 K): δ = 2.3 (s, CH_3), 16.2 [d, ^3J(C-P_A) = 8.6, CH_3], 66.9 [d, ^2J(C-P_A) = 8.1, CH_2], 91.6 [ddd, ^1J(C-P_A) = 93.2, ^1J(C-P_B) = 71.0, ^3J(C-$P_{B'}$) = 7.7, $C^{2,6}$], 117.1 [q, ^4J(C-P_A) = ^4J(C-P_B) = 12.2, C^4H], 121.2 (br. s, C of CH_3CN), 127.8 [dd, ^1J(C-P_B) = 84.7, ^3J(C-P_A) = 7.4, C of Ph], 128.1 [ABX, d, ^1J(C-P_B) = 86.6, C of Ph], 128.1−134.8 (m, CH of Ph), 139.0 [dt, ^2J(C-P_A) = 9.1, ^2J(C-P_B) = ^4J(C-$P_{B'}$) = 3.5, $C^{3,5}$], 160.5 (s, C of Ph) ppm. ^{31}P NMR (121.5 MHz, THF, 298 K): δ = 49.03 [AB_2, d, ^2J(P_A-P_B) = 85.5, P_B], 87.81 [AB_2, t, ^2J(P_A-P_B) = 85.5, P_A] ppm. $C_{45}H_{39}BF_4NOP_3PdS_2$ (960.08): calcd. C 56.30, H 4.09; found C 55.84, H 3.75.

Ni Complex 26: Acetonitrile (50 μL, 0.96 mmol) was added to a mixture of **20** (138 mg, 0.16 mmol) and $AgBF_4$ (37 mg, 0.19 mmol) in CH_2Cl_2 (5 mL), and the resultant solution was stirred for 15 min at room temperature. The solution was then filtered through celite and, after drying, **26** was recovered as a brown powder (yield: 92%, 134 mg). ^{1}H NMR (300 MHz, CD_2Cl_2, 298 K): δ = 1.20 (br. s, 3 H, CH_3 of Et), 2.30 (br. s, 3 H, CH_3 of CH_3CN), 4.15 (br. s, 2 H, CH_2), 5.60 (br. s, 1 H, H^4), 6.40−7.80 (m, 30 H, CH of Ph) ppm. ^{13}C NMR (75.5 MHz, CD_2Cl_2, 298 K): δ = 7.8 (s, CH_3 of CH_3CN), 15.7 [s, ^3J(C-P_A) = 8, CH_3 of Et], 64.6 [d, ^2J(C-P_A) = 6.9, CH_2], 91.9 (m, $C^{2,6}$), 115.1 [q, ^4J(C-P_A) = ^4J(C-P_B) = 9.8, C^4H], 127.19−132.4 (m, CH and C of Ph and C of CH_3CN), 139.0 [dt, ^4J(C-P_B) = 8, ^2J(C-P_A) = ^2J(C-P_B) = 4, $C^{3,5}$], 156.5 (s, C of Ph) ppm. ^{31}P NMR (121.5 MHz, THF, 298 K): δ = 55.22 [AB_2, d, ^2J(P_A-P_B) = 106.3, P_B], 88.79 [AB_2, t, ^2J(P_A-P_B) = 106.3, P_A] ppm. $C_{45}H_{39}BF_4NNiOP_3S_2$ (912.35): calcd. C 59.24, H 4.31; found C 58.79, H 3.92.

Pt Complex 27: Acetonitrile (50 μL, 0.96 mmol) was added to a mixture of **21** (153 mg, 0.16 mmol) and $AgBF_4$ (37 mg, 0.19 mmol) in CH_2Cl_2 (5 mL). After stirring for 15 min at room temperature, the solution was filtered through celite. After drying, **27** was recovered as a yellow powder (yield: 93%, 156 mg). ^{1}H NMR (300 MHz, CD_2Cl_2, 298 K): δ = 1.49 [t, ^3J(H−H) = 7.0, 3 H, CH_3 of Et], 2.37 (s, 3 H, CH_3 of CH_3CN), 4.15 [p, ^3J(H-P_B) = ^3J(H−H) = 7.0, 2 H, CH_2], 5.97 [t, ^4J(H-P_B) = 5.1, 1 H, H^4], 6.75−7.82 (m, 30 H, CH of Ph) ppm. ^{13}C NMR (75.5 MHz, CD_2Cl_2, 298 K): δ = 3.5 (s, CH_3), 16.5 [d, ^3J(C-P_A) = 7.5, CH_3], 65 [d, ^2J(C-P_A) = 9.8, CH_2], 84.5 [ddd, ^1J(C-P_A) = 96.8, ^1J(C-P_B) = 87.2, ^3J(C-$P_{B'}$) = 5.6, $C^{2,6}$], 118.5 [q, ^4J(C-P_A) = ^4J(C-P_B) = 2.1, C^4H], 125.0 [d, ^2J(C-P_A) = 21.4, C of CH_3CN], 127 [dd, ^1J(C-P_B) = 91.0, ^3J(C-P_A) = 4.1, C of Ph], 128 [dd, ^1J(C-P_B) = 95.7, ^3J(C-P_A) = 3.7, C of Ph], 128.1−134.8 (m, CH of Ph), 139 (m, $C^{3,5}$), 160.5 (s, C of Ph) ppm. ^{31}P NMR (121.5 MHz, THF, 298 K): δ = 48.92 [AB_2M, d, ^2J(P_A-P_B) = 80.4, P_B], 54.60 [AB_2M, ptt, ^1J(P_A-Pt) = 3592.9, ^2J(P_A-P_B) = 75.2, P_A] ppm. $C_{45}H_{39}BF_4NOP_3PtS_2$ (1048.73): calcd. C 51.54, H 3.75; found C 51.29, H 3.24.

Pd Complex 28: A mixture of **4** (97 mg, 0.11 mmol) and AgOTf (37 mg, 0.19 mmol) was stirred in CH_2Cl_2 (3 mL) for 15 min at room temperature and filtered through celite. After drying, **28** was recovered as a red powder (yield: 87%, 95 mg). ^{1}H NMR (300 MHz, CD_2Cl_2, 298 K): δ = 1.05 [t, ^3J(H−H) = 6.9, 3 H, CH_3], 1.62 [qt, ^3J(H−H) = 6.9, ^3J(H−H) = 13.8, CH_2], 1.92−2.06 (m, 2 H, CH_2), 2.19−2.31 (m, 2 H, CH_2), 5.50 [t, ^4J(H-P_B) = 4.7, 1 H, H^4], 6.68−7.56 (m, 30 H, CH of Ph) ppm. ^{13}C NMR (75.5 MHz, CD_2Cl_2, 298 K): δ = 13.9 (s, CH_3 of *n*Bu), 23.5 [d, ^3J(C-P_A) = 2.6, CH_2], 25.5 [d, ^2J(C-P_A) = 2.6, CH_2], 38.3 (m, CH_2), 71.6 (m, $C^{2,6}$), 118.6 [q, ^4J(C-P_A) = ^4J(C-P_B) = 10.6, C^4H], 127.7−128.8 (m, CH of Ph), 131.1 [dd, ^1J(C-P_B) = 83.8, ^3J(C-P_A) = 8.3, C of Ph], 131.9−133.0 (m, CH of Ph), 139.6 (m, $C^{3,5}$), 159.5 ppm (m, C of Ph), CF_3 not observed. ^{31}P NMR (121.5 MHz, THF, 298 K): δ = 49.47 [AB_2, d, ^2J(P_A-P_B) = 84.4, P_B], 56.05 [AB_2,

 © 2003 Wiley-VCH Verlag GmbH & Co. KGaA, Weinheim

t, $^2J(P_A\text{-}P_B)$ = 84.4, P_A] ppm. $C_{46}H_{40}F_3O_3P_3PdS_3$ (993.34): calcd. C 55.62, H 4.06; found C 55.43, H 3.86.

λ⁵-Dimethylphosphinine 29: A solution of MeLi in hexanes (275 μL, *C* = 1.6 M, 0.44 mmol) was added by syringe into a solution of **1** (300 mg, 0.44 mmol) in THF (10 mL) at −78 °C. The resultant solution was then warmed to room temperature and stirred for 20 min. Complete formation of **15** was checked by ^{31}P NMR (121.5 MHz, THF, 298 K): δ = 44.83 [AB_2, d, $^2J(P_A\text{-}P_B)$ = 156.7, P_B], −66.52 [AB_2, t, $^2J(P_A\text{-}P_B)$ = 156.7, P_A]. After cooling at −78 °C, MeI (50 μL, 0.80 mmol) was added and the solution was warmed to room temperature and stirred for 15 min. The solvent was then evaporated and the resulting solid was dissolved in CH_2Cl_2 (8 mL) and filtered through celite. After removing the solvent under vacuum, the solid was washed several times with hexanes (3 × 2 mL) and then diethyl ether (3 × 2 mL). After drying, **29** was recovered as an orange powder. Suitable crystals for X-ray structure analysis were grown by diffusion of hexanes into a solution of $CDCl_3$.Yield: 89%, 278 mg. ^1H NMR (300 MHz, $CDCl_3$, 298 K): δ = 1.64 [d, $^2J(P_A-H)$ = 13.4, 6 H, CH_3], 5.34 [t, $^4J(H\text{-}P_B)$ = 4.8, 1 H, H^4], 6.71−7.81 (m, 30 H, CH of Ph) ppm. ^{13}C NMR (75.5 MHz, $CDCl_3$, 298 K): δ = 12.2 [d, $^1J(C\text{-}P_A)$ = 58.4, CH_3], 67.0 [ddd, $^1J(C\text{-}P_A)$ = 88.8, $^1J(C\text{-}P_B)$ = 76.9, $^3J(C\text{-}P_{B'})$ = 2.9, $C^{2,6}$], 118.5 [m, ΣJ(C-P) = 42.8, C^4H], 127.6−131.9 (m, CH of Ph), 136.5 [dd, $^1J(C\text{-}P_B)$ = 85.4, $^3J(C\text{-}P_A)$ = 2.5, C of Ph], 142.8 [ddd, $^2J(C\text{-}P_A)$ = 10.9, $^2J(C\text{-}P_B)$ = 6.9, $^4J(C\text{-}P_{B'})$ = 3.3,$C^{3,5}$], 157.8 (s, C of Ph) ppm. ^{31}P NMR (121.5 MHz, THF, 298 K): δ = 20.77 [AB_2, t, $^2J(P_A\text{-}P_B)$ = 41.1, P_A], 37.44 [AB_2, d, $^2J(P_A\text{-}P_B)$ = 41.1, P_B] ppm. MS (EI): *m*/*z* = 712 [M^+]. $C_{43}H_{37}P_3S_3$ (710.81): calcd. C 72.66 H, 5.25; found C 72.28 H, 4.91.

Anion 30: In a glove-box, a mixture of **1** (150 mg, 0.22 mmol) and MeONa (36 mg, 0.66 mmol) in THF (5 mL) was stirred for 15 min. After drying, **30** was recovered as a yellow powder. Suitable crystals for X-ray structure analysis were grown from a diffusion of hexanes into a solution of THF. ^{31}P NMR (121.5 MHz, THF, 298 K): δ = 44.60 [AB_2, d, $^2J(P_A\text{-}P_B)$ = 153.2, P_B], 66.55 [AB_2, dd, $^2J(P_A\text{-}P_B)$ = 148.4, P_A] ppm. **30** was too moisture sensitive to give satisfactory elemental data.

X-ray Crystallographic Study: Crystals of compounds **1** (Table 5), **5**, **6**, **13** (Table 6), **14**, **22** (Table 7), **29** and **30** (Table 5) suitable for X-ray diffraction were obtained by slow diffusion of hexanes into a CH_2Cl_2 solution for **1**, **5**, **13**, **14**, **22**, into a $CDCl_3$ solution for **6**, **29**, and into a THF solution for **30**. Data were collected at 150.0(1) K on a Nonius Kappa CCD diffractometer using a Mo-*K*α (λ = 0.71070 Å) X-ray source and a graphite monochromator. All data were measured using phi and omega scans. Experimental details are described in tables 1, 3 and 4. The crystal structures were solved using SIR 97[45] and Shelxl-97.[46] ORTEP drawings were made using ORTEP III for Windows.[47] CCDC-210894 to 210900 and 210982 contain the supplementary crystallographic data for this paper. These data can be obtained free of charge at www.ccdc.cam.ac.uk/conts/retrieving.html [or from the Cambridge Crystallographic Data Centre, 12 Union Road, Cambridge CB2 1EZ, UK; fax: (internat.) +44−1223/336-033; E-mail: deposit@ccdc.cam.ac.uk].

Theoretical Methods: The calculations were performed with the GAUSSIAN 98 series of programs.[48] The geometries of compounds I and II were optimized using the gradient-corrected

Table 5. Crystal data and structural refinement details for **1**, **29**, **30**

	1	**29**	**30**
Empirical formula	$C_{41}H_{31}P_3S_2{\cdot}CH_2Cl_2$	$C_{43}H_{37}P_3S_2{\cdot}CHCl_3$	$C_{42}H_{34}OP_3S_2{\cdot}C_{18}H_{36}N_2O_6Na$
M_r	765.61	830.12	1111.20
T [K]	150.0(1)	150.0(1)	150.0(1)
Crystal system	monoclinic	monoclinic	triclinic
Space group	$P2_1/n$	$P2_1/n$	$P\bar{1}$
a [Å]	9.4560(10)	9.225(5)	9.127(1)
b [Å]	28.7580(10)	17.593(5)	17.624(1)
c [Å]	13.5950(10)	24.926(5)	17.900(1)
α [°]	90	90	94.980(1)
β [°]	95.5600(10)	92.167(5)	98.650(1)
γ [°]	90	90	96.410(1)
V [Å^3]	3679.6(5)	4042(3)	2813.0(4)
Z	4	4	2
ρ [g cm^{-3}]	1.382	1.364	1.312
μ [cm^{-1}]	0.452	0.481	0.242
Crystal size [mm]	0.22 × 0.09 × 0.09	0.18 × 0.18 × 0.12	0.20 × 0.16 × 0.10
F(000)	1584	1720	1176
Index ranges	$-11 \le h \le 11$; $35 \le k \le 34$; $-16 \le l \le 16$	$-12 \le h \le 12$; $21 \le k \le 23$; $-31 \le l \le 33$	$-9 \le h \le 10$; $-19 \le k \le 19$; $19 \le l \le 19$
Scan type	phi and omega	phi	phi and omega
$2\Theta_{max}$ [°]/criterion	26.37/>2σ*I*	28.70/>2σ*I*	22.98/>2σ*I*
Param. refined; data/param.	442; 12	471; 16	677; 8
Reflections collected	13188	17199	13666
Independent reflections	7483	10430	7760
Reflections used	5431	7671	5963
*wR*2	0.1168	0.1098	0.2142
*R*1	0.0437	0.0415	0.0784
Goodness of fit	1.040	1.048	1.054
Largest diff. peak / hole [e·Å^{-3}]	0.352(0.067) / −0.616(0.067)	0.335(0.064) / −0.571(0.064)	0.688(0.093) / −0.475(0.093)

 © 2003 Wiley-VCH Verlag GmbH & Co. KGaA, Weinheim

Table 6. Crystal data and structural refinement details for **6**, **13**

	6	**13**
Empirical formula	$C_{41}H_{32}ClOP_3PdS_2 \cdot CH_2Cl_2$	$C_{51}H_{50}Cl_3OP_3PdS_2 \cdot CH_2Cl_2$
M_r	924.47	1062.72
T [K]	150.0(1)	150.0(1)
Crystal system	monoclinic	orthorhombic
Space group	$P2_1/n$	$P2_12_12_1$
a [Å]	15.644(5)	9.597(5)
b [Å]	12.229(5)	18.767(5)
c [Å]	21.024(5)	26.834(5)
β [°]	96.100(5)	
V [Å^3]	3999(2)	4833(3)
Z	4	4
ρ [g cm^{-3}]	1.535	1.461
μ [cm^{-1}]	0.923	0.774
Crystal size [mm]	0.18 × 0.04 × 0.03	0.20 × 0.20 × 0.20
F(000)	1872	2184
Index ranges	$-18 \le h \le 18$; $-13 \le k \le 14$; $-25 \le l \le 25$	$-13 \le h \le 13$; $-26 \le k \le 26$; $-37 \le l \le 37$
Scan type	phi and omega	phi
$2\Theta_{max}$ [°]/criterion	25.35/>2σI	30.03/>2σI
Param. refined; data/param.	470; 10	562; 19
Reflections collected	12483	13591
Independent reflections	7319	13591
Reflections used	4986	11109
$wR2$	0.0925	0.1036
$R1$	0.0482	0.0428
Flack parameter		−0.042(18)
Goodness of fit	1.000	1.022
Largest diff. peak / hole [e·Å^{-3}]	1.212(.104) / −1.067(.104)	0.486(0.096) / −0.844(0.096)

Table 7. Crystal data and structural refinement details for **14**, **22**

	14	**22**
Empirical formula	$C_{45}H_{41}ClNP_3PdS_2 \cdot CH_2Cl_2$	$C_{45}H_{40}BrNiP_3S_2 \cdot CH_2Cl_2$
M_r	979.59	961.34
T [K]	150.0(1)	150.0(1)
Crystal system	monoclinic	orthorhombic
Space group	$P2_1/n$	$Pna2_1$
a [Å]	9.507(5)	19.445(5)
b [Å]	19.410(5)	23.835(5)
c [Å]	24.136(5)	9.475(5)
β [°]	90.290(5)	
V [Å^3]	4454(3)	4391(3)
Z	4	4
ρ [g·cm^{-3}]	1.461	1.454
μ [cm^{-1}]	0.832	1.710
Crystal size [mm]	0.20 × 0.20 × 0.20	0.18 × 0.12 × 0.04
F(000)	2000	1968
Index ranges	$-13 \le h \le 13$; $-27 \le k \le 24$; $-33 \le l \le 33$	$-26 \le h \le 26$; $-32 \le k \le 32$; $-12 \le l \le 12$
Scan type	phi	phi and omega scans
$2\Theta_{max}$ [°]/criterion	30.03/>2σI	28.70/>2σI
Param. refined; data/param.	480;18	541;17
Reflections collected	21883	11058
Independent reflections	12955	11058
Reflections used	8989	9596
$wR2$	0.1166	0.0945
$R1$	0.0414	0.0399
Flack parameter		0.511(7)
Goodness of fit	1.008	1.009
Largest diff. peak / hole [e·Å^{-3}]	0.356(0.090) / 0.874(0.090)	0.200(0.037) / 0.192(0.037)

 © 2003 Wiley-VCH Verlag GmbH & Co. KGaA, Weinheim

density functional theory (DFT) utilizing Becke's three-parameter hybrid method B3LYP.[49,50] The standard 6-311+G(d,p) basis set was used for all atoms (C, H, P, O, N, and S). Harmonic frequencies were calculated at the same level of theory to characterize the stationary points and to determine the zero-point energies (ZPE). Intrinsic reaction coordinates calculations (IRC) were performed to ensure that the transition states found for the (1,2) hydrogen-shift actually connect the two products. Final energies were optimized, including ZPE energies scaled by the empirical factor of 0.9806. All optimized structures reported here have only positive eigenvalues of the Hessian matrix, i.e. they are minima on the potential energy surface. Optimizations of complexes **III**, **IV**, and **V** were also carried out with the hybrid B3LYP functional. The basis set is identical to that used by Frenking and co-workers in many studies.[51] The basis set, which is known as "Basis set II", incorporates the Hay−Wadt small-core relativistic effective core potential[52] and double-ζ valence basis set (441/2111/31) in conjunction with the all-electron 6-31G(d) basis sets for the main-group elements, H, C, O, P, S, Cl.

Inspection of ligand-to-metal donor−acceptor interactions were performed by charge-decomposition analysis (CDA).[53] In the CDA method the (canonical, natural, or Kohn Sham) molecular orbitals of the complex are expressed in terms of MOs of appropriately chosen fragments. In the cases studied the Kohn−Shan orbitals of the B3LYP/II calculations are formed in the CDA procedure as a linear combination of the MOs of the SPS anionic ligand and those of the remaining cationic fragment $[PdCl]^+$ for complexes **IIIa**, **b**. The same method was used to analyze complexes **IVa**, **b**, and **V**, but the two fragments are the neutral ligand $[RP(CH_2PH_2S)_2]$, and the cationic fragment $[PdCl]^+$. In both cases, the ligands and the metal fragments were computed in the geometry of the complex. The orbital contributions are divided into four parts: (i) the mixing of the occupied MOs of the ligand and the unoccupied MOs of the metal fragment. This value (denoted *d*) represents the donation ligand → [metal fragment]; (ii) the mixing of the unoccupied MOs of the ligand and the occupied MOs of the metal fragment. This value (denoted *b*) accounts for the back donation [metal fragment] → ligand; (iii) the mixing of the occupied MOs of the ligand and the occupied MOs of the metal fragment. This term (denoted *r*), which describes the repulsive polarization ligand ⇄ [metal fragment], is negative because electronic charge is removed from the overlapping area of the occupied orbitals; (iv) the residual term (Δ) which results from the mixing of the unoccupied MOs of the two respective fragments. Usually this term is very close to zero for closed-shell interactions. This value constitutes an important probe to determine whether the bonding studied can be really classified as a donor−acceptor interaction following the Dewar−Chatt−Duncansson model. Important deviations from $\Delta = 0$ imply that the bond studied is more conventionally described as a normal covalent bond between two open shell fragments. A more detailed presentation of the CDA method and the interpretation of the results can be found in the literature.[53] CDA calculations were performed with the program CDA version 2.1.[54] These calculations were also performed with the Gaussian-98 program. The charge distributions in the optimized structures were calculated with the NBO partitioning scheme.[55]

Supporting Information Available: ORTEP drawing of compound **5** and geometrical parameters of theoretical structure of **Ia-Ie**, **TSa-TSd**, **IIa−IIe**, **IIIa**, **IIIb**, **IVa**, **IVb**, and **V**.

Acknowledgments

This work was supported by the CNRS, the Ecole Polytechnique and the DGA. M. D. thanks the DGA for financial support. The authors thank IDRIS (Paris XI Orsay University) for the allowance of computer time.

[1] C. J. Moulton, B. L. Shaw, *J. Chem. Soc., Dalton Trans.* **1976**, 1020−1024.
[2] M. Albrecht, G. Van Koten, *Angew. Chem.* **2001**, *113*, 3866−3878; *Angew. Chem. Int. Ed.* **2001**, *40*, 3750−3781.
[3] J. T. Singleton, *Tetrahedron Lett.* **2003**, *59*, 1837−1857.
[4] M. E. van der Boom, D. Milstein, *Chemical Reviews* **2003**, *103*, 1759−1792.
[5] S. Grundemann, M. Albrecht, J. A. Loch, J. W. Faller, R. H. Crabtree, *Organometallics* **2001**, *20*, 5485−5488.
[6] P. Kapoor, A. Pathak, R. Kapoor, P. Venugopalan, M. Corbella, M. Rodriguez, J. Robles, A. Llobet, *Inorg. Chem.* **2002**, *41*, 6153−6160.
[7] A. S. Ionkin, W. J. Marshall, *Heteroatom Chem.* **2002**, *13*, 662−666.
[8] See for example: J. D. Niemoth-Anderson, K. A. Clark, T. A. George, C. R. Ross, *J. Am. Chem. Soc.* **2000**, *122*, 3977−3978.
[9] M. Tschoerner, G. Trabesinger, A. Albinati, P. S. Pregosin, *Organometallics* **1997**, *16*, 3447−3453.
[10] D. A. Evans, K. R. Campos, J. S. Tedrow, F. E. Michael, M. R. Gagne, *J. Am. Chem. Soc.* **2000**, *122*, 7905−7920.
[11] D. R. Evans, M. Huang, W. M. Seganish, E. W. Chege, Y. F. Lam, J. C. Fettinger, T. L. Williams, *Inorg. Chem.* **2002**, *41*, 2633−2641.
[12] X. Verdaguer, M. A. Pericàs, A. Riera, M. J. Maestro, *Organometallics* **2003**, *22*, 1868−1877.
[13] N. Brugat, A. Polo, A. Alvarez-Larena, J. F. Piniella, J. Real, *Inorg. Chem.* **1999**, *38*, 4829−4837.
[14] K. Ortner, L. Hilditch, Y. F. Zheng, J. R. Dilworth, U. Abram, *Inorg. Chem.* **2000**, *39*, 2801−2806.
[15] D. R. Evans, M. S. Huang, W. M. Seganish, J. C. Fettinger, T. L. Williams, *Organometallics* **2002**, *21*, 893−900.
[16] H. Brunner, H. J. Lautenschlager, W. A. König, R. Krebber, *Chem. Ber.* **1990**, *123*, 847−853.
[17] S. M. Aucott, A. M. Z. Slawin, J. D. Woolins, *Eur. J. Inorg. Chem.* **2002**, 2408−2418.
[18] M. J. Baker, M. F. Giles, A. G. Orpen, M. J. Taylor, R. J. Watt, *J. Chem. Soc., Chem. Commun.* **1995**, 197−198.
[19] L. Gonsalvi, H. Adams, G. J. Sunley, E. Ditzel, A. Haynes, *J. Am. Chem. Soc.* **2002**, *124*, 13597−13612.
[20] K. B. Dillon, F. Mathey, J. F. Nixon, *Phosphorus: The Carbon Copy*, John Wiley & Sons, Chichester, **1998**.
[21] M. Doux, C. Bouet, N. Mézailles, L. Ricard, P. Le Floch, *Organometallics* **2002**, *21*, 2785−2788.
[22] M. Doux, N. Mézailles, M. Melaimi, L. Ricard, P. Le Floch, *Chem. Commun.* **2002**, 1566−1567.
[23] P. Le Floch, in *Phosphorus-Carbon Heterocyclic Chemistry: The Rise of a New Domain* (Ed.: F. Mathey), Pergamon, **2001**, pp. 485−533.
[24] N. Mézailles, P. Le Floch, F. Mathey, in: *Progress in Inorganic Chemistry, Vol. 49* (Ed.: K. D. Karlin), John Wiley & Sons, Inc., **2001**, pp. 455−550.
[25] P. Le Floch, D. Carmichael, F. Mathey, *Organometallics* **1991**, *10*, 2432−2436.
[26] See supplementary material available.
[27] See for example: R. Broussier, E. Bentabet, M. Laly, P. Richard, L. G. Kuz′mina, P. Serp, N. Wheatley, P. Kalck, B. Gautheron, *J. Organomet. Chem.* **2000**, *613*, 77−85.
[28] See for example: T. S. Lobana, R. Verma, A. Singh, M. Shikha, A. Castineiras, *Polyhedron* **2002**, *21*, 205−209.
[29] See for example: K. V. Katti, P. R. Singh, C. L. Barnes, *Inorg. Chem.* **1992**, *31*, 4588−4593.
[30] G. Y. Li, *Angew. Chem.* **2001**, *113*, 1561−1564; *Angew. Chem. Int. Ed.* **2001**, *40*, 1513−1515.
[31] N. K. Gusarova, A. M. Reutskaya, N. I. Ivanova, A. S. Medvedeva, M. M. Demina, P. S. Novopashin, A. V. Afonin, A. I. Albanov, B. A. Trofimov, *J. Organomet. Chem.* **2002**, *659*, 172−175.

 © 2003 Wiley-VCH Verlag GmbH & Co. KGaA, Weinheim

[32] G. Y. Li, W. J. Marshall, *Organometallics* **2002**, *21*, 590−591.
[33] K. Dimroth, *Acc. Chem. Res.* **1982**, *15*, 58−64.
[34] G. Märkl, A. Merz, *Tetrahedron Lett.* **1971**, *17*, 1215−1218.
[35] A. J. Ashe III, T. W. Smith, *J. Am. Chem. Soc.* **1976**, *98*, 7861−7862.
[36] A. J. Ashe III, T. W. Smith, *Tetrahedron Lett.* **1977**, *5*, 407−410.
[37] G. Märkl, K.-H. Heier, *Angew. Chem.* **1972**, *84*, 1066−1067; *Angew. Chem. Int. Ed. Engl.* **1972**, *11*, 1016−1017.
[38] Z. X. Wang, P. v. Ragué Schleyer, *Helv. Chim. Acta* **2001**, *84*, 1578−1600.
[39] K. Dimroth, A. Hettche, H. Kanter, W. Städe, *Tetrahedron Lett.* **1972**, *9*, 835−838.
[40] A. Moores, L. Ricard, P. Le Floch, N. Mézailles, *Organometallics* **2003**, *22*, 1960−1966.
[41] R. B. King, in *Organometallic Syntheses Academic, Vol. 1*, New York, **1965**, p. 71.
[42] D. Drew, J. R. Doyle, in: *Inorganic Syntheses, Vol. 28* (Ed.: R. J. Angelici), **1990**, pp. 348−349.
[43] M. F. Rettig, P. M. Maitlis, in: *Inorganic Syntheses, Vol. 28* (Ed.: R. J. Angelici), **1990**, pp. 110−111.
[44] J. X. McDermott, J. F. White, J. F. Whitesides, *J. Am. Chem. Soc.* **1976**, *98*, 6521−6528.
[45] A. Altomare, M. C. Burla, M. Camalli, G. Cascarano, C. Giacovazzo, A. Guagliardi, A. G. G. Moliterni, G. Polidori, R. Spagna, *SIR97, an integrated package of computer programs for the solution and refinement of crystal structures using single crystal data*.
[46] G. M. Sheldrick, *SHELXL-97*, Universität Göttingen, Göttingen, Germany, **1997**.
[47] L. J. Farrugia, *ORTEP-3*, Department of Chemistry, University of Glasgow.
[48] M. J. Frisch, G. W. Trucks, H. B. Schlegel, G. E. Scuseria, M. A. Robb, J. R. Cheeseman, V. G. Zakrzewski, J. J. A. Montgomery, R. E. Stratmann, J. C. Burant, S. Dapprich, J. M. Millam, A. D. Daniels, K. N. Kudin, M. C. Strain, O. Farkas, J. Tomasi, V. Barone, M. Cossi, R. Cammi, B. Mennucci, C. Pomelli, C. Adamo, S. Clifford, J. Ochterski, G. A. Petersson, P. Y. Ayala, Q. Cui, K. Morokuma, D. K. Malick, A. D. Rabuck, K. Raghavachari, J. B. Foresman, J. Cioslowski, J. V. Ortiz, A. G. Baboul, B. B. Stefanov, G. Liu, A. Liashenko, P. Piskorz, I. Komaromi, R. Gomperts, R. L. Martin, D. J. Fox, T. Keith, M. A. Al-Laham, C. Y. Peng, A. Nanayakkara, M. Challacombe, P. M. W. Gill, B. Johnson, W. Chen, M. W. Wong, J. L. Andres, C. Gonzalez, M. Head-Gordon, E. S. Replogle, J. A. Pople, *Gaussian Revision A-11 ed.,* Gaussian, Inc., Pittsburgh PA, **1998**.
[49] J. P. Perdew, *Phys. Rev. B.* **1986**, *33*, 8822−8832.
[50] A. D. Becke, *Phys. Rev. A* **1988**, *38*, 3098−3108.
[51] G. Frenking, N. Fröhlich, *Chem. Rev.* **2000**, *100*, 717 −774.
[52] P. J. Hay, W. R. Wadt, *J. Chem. Phys.* **1995**, *82*, 299−310.
[53] G. Frenking, *J. Phys. Chem.* **1995**, *99*, 9352−9362.
[54] S. Dapprich, G. Frenking, CDA 2.1. The program is available online: ftp://chemie. uni-marburg.de (/pub/cda), Marburg, **1995**.
[55] A. E. Reed, L. A. Curtiss, F. Weinhold, *Chem. Rev.* **1988**, *88*, 899−926.

Received May 21, 2003

 © 2003 Wiley-VCH Verlag GmbH & Co. KGaA, Weinheim

Synthesis, Characterisation of (Arene)tricarbonylchromium Complexes Linked to Cationic Fe and Ru Derivatives and Studies of First Hyperpolarisabilities by Hyper-Rayleigh Scattering

Maria Helena Garcia,*[a,b] Sophie Royer,[b] Maria Paula Robalo,*[b,c] Alberto Romão Dias,[b] Jean-Philippe Tranchier,[d] René Chavignon,[d] Damien Prim,[d] Audrey Auffrant,[d] Françoise Rose-Munch,[d] Eric Rose,*[d] Jacqueline Vaissermann,[e] André Persoons,[f] and Inge Asselberghs[f]

Keywords: Chromium / Iron / Ruthenium / Non-linear optics / Arene ligands / Carbonyl ligands / Hyperpolarisability

In order to investigate the non-linear optical properties, in particular second-order effects of binuclear organometallic complexes, a series of new cationic binuclear [MCp(DPPE)N≡C–(spacer)–C≡C–$C_6H_5Cr(CO)_3$]$^+$[PF_6]$^-$ compounds and mononuclear precursors [N≡C–(spacer)–C≡C–$C_6H_5Cr(CO)_3$] have been synthesised [where M = Fe^{II} or Ru^{II}; Cp = η^5-C_5H_5 and spacer = phenyl ring (C_6H_4), thiophene, (C_4H_2S), or bithiophene ($C_4H_2S)_2$]. The Fe or Ru organometallic π-donor fragments were linked by an extended π system to the acceptor $Cr(CO)_3$ fragment. The effect of π back-donation involving the second Fe or Ru metal centre and the π* orbitals of the N≡C-coordinated group, was probed by the $\nu_{(N\equiv C)}$ stretching bands on the IR spectra and also by NMR spectroscopic data. The planarity, largely due to the π-electron resonance, found on the solid state structure of the mononuclear complex [N≡C–C_6H_5–C≡C–(η^6-C_6H_5)$Cr(CO)_3$] (**1Cr**) determined by X-ray diffraction [monoclinic system, $P2_1/c$ space group, with a = 10.326(2) Å, b = 13.209(5) Å, c = 11.799(2) Å and Z = 4] emphasises the electronic effect of this building block. The significant values of first hyperpolarisability β determined by hyper-Rayleigh scattering (HRS) indicate that the Fe containing compounds were more efficient on second-order non-linear optical properties than the ruthenium analogues and the parent mononuclear chromium compounds.

(© Wiley-VCH Verlag GmbH & Co. KGaA, 69451 Weinheim, Germany, 2003)

Introduction

Over the past decade a pattern has emerged for the design of organometallic materials with large second-order optical non-linearities, in which the molecules have important changes of dipole moments between ground and excited states and large transition dipole moments.[1] Using this molecular criteria, organometallic and coordination chemists have synthesised compounds possessing very intense metal-to-ligand and ligand-to-metal charge transfer bands in the UV/Visible spectrum, which showed very large molecular hyperpolarisabilities.[2] The use of organometallic polarising groups in dipole structures has been of growing interest in the search for new molecular materials for non-linear optics, and various binuclear compounds have been published in the literature presenting significant values of first hyperpolarisabilities β. Representative examples are the ferrocenyl derivatives where the best reported β values are found for bimetallic compounds possessing an (η^5-thiophene)$Mn(CO)_3$,[3] a group 6 pentacarbonyl,[4] or an η^7-cycloheptatrienyltricarbonylchromium[5] as the acceptor moieties. Also indenyl or cyclopentadienylruthenium(II) donor moieties and group 6 pentacarbonyl or pentaminaruthenium(III) acceptor partners have been used successfully as building blocks for the synthesis of bimetallic non-linear optical (NLO) active systems.[6]

Our approach to the synthesis of bimetallic molecules for NLO purposes, was based on the use of the fragment

[a] Faculdade de Ciências da Universidade de Lisboa, Ed. C8, Campo Grande, 1749-016 Lisboa, Portugal
[b] Centro de Química Estrutural, Instituto Superior Técnico, Av. Rovisco Pais 1049-001 Lisboa codex, Portugal
Fax: (internat.) + 351-21/8464455
E-mail: lena.garcia@ist.utl.pt
[c] Departamento de Engenharia Química, Instituto Superior de Engenharia de Lisboa, Rua Conselheiro Emídio Navarro, 1, 1949-014 Lisboa, Portugal
[d] Laboratoire de Synthèse Organique et Organometallique, UMR CNRS 7611, Tour 44-4, Place Jussieu, 75252 Paris, Cedex 05, France
E-mail: rose@ccr.jussieu.fr
[e] Laboratoire de Chimie Inorganique et Matériaux Moléculaires, UMR CNRS 7071 Leuven, Belgium
[f] Laboratory of Chemical and Biological Dynamics, Center for Research on Molecular Electronics and Photonics, University of Leuven, Leuven, Belgium

$[M(\eta^5\text{-}C_5H_5)(P\text{-}P)]^+$ (M = Fe^{II} or Ru^{II} and P-P = diphosphane) as a π-donor building block, bridged through a π-delocalised system to the auxochrome $[\eta^6\text{-}(benzene)\text{-}Cr(CO)_3]$. The amphoteric nature has been studied in monometallic compounds.[7] The π-donor ability of the Ru^{II}/Fe^{II} fragments and the high values found for the quadratic hyperpolarisabilities of some monometallic molecules based on these moieties, have been explained on the basis of π back-donation towards the π* empty orbitals of −N≡C− and −C≡C− functional groups.[8,9]

The interest surrounding the use of these $[M(\eta^5\text{-}C_5H_5)(P\text{-}P)]^+$ fragments as building blocks also comes from their cationic nature, where the contribution for the alignment of the chromophores in the solid state can be of potential interest for macroscopic NLO properties, as found for $[Fe(\eta^5\text{-}C_5H_5)\{(R)\text{-prophos}\}(p\text{-}NCC_6H_4NO_2)][PF_6]$ ($\beta = 545\cdot10^{-30}$ esu)[10].

In the present work based on donor−spacer−acceptor structures, besides the exploitation of two donor fragments based on Ru^{II} and Fe^{II} centres, we have studied different spacers, using conjugated π systems containing the benzene ring and alternatively one or two thiophene rings.

Results and Discussion

Preparation of the Mononuclear Chromium $[\{N\equiv C-(spacer)-C\equiv C-\eta^6\text{-}C_6H_5\}Cr(CO)_3]$ Complexes 1Cr, 2Cr, and 3Cr

Mononuclear chromium complexes of the general formula $[\{N\equiv C-(spacer)-C\equiv C-\eta^6\text{-}C_6H_5\}Cr(CO)_3]$, where the spacer is a phenyl ring $-C_6H_4$ (**1Cr**), a thiophene ring $-C_4H_2S$ (**2Cr**) or two thiophene rings $(C_4H_2S)_2$ (**3Cr**) were obtained[11] by a Sonogashira palladium-catalysed cross-coupling reaction[12] between the (η^6-phenyl)ethynyltricarbonylchromium complex and various bromo, iodo arenes substituted by a nitrile group, **1-CN**, **2-CN**, and **3-CN** as depicted in Scheme 1. The free ligands **1**−**3** were synthesised analogously by the palladium copper catalysed coupling of iodonitrile aromatics **1-CN**, **2-CN**, and **3-CN** and phenylacetylene, see Experim. Section.

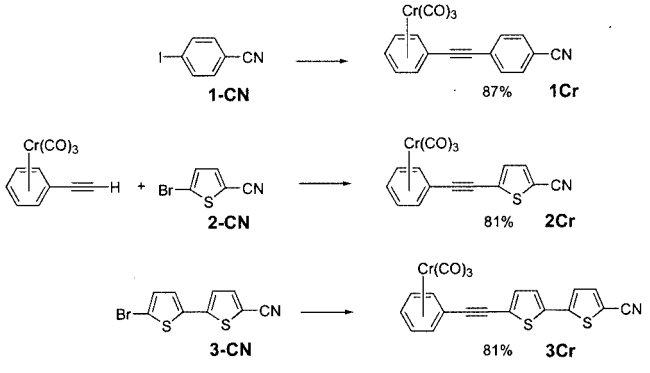

Scheme 1. Sonogashira-coupling reactions

Preparation of the Bimetallic Iron/Chromium and Ruthenium/Chromium Derivatives

$[FeCp(DPPE)\{N\equiv C-(spacer)-C\equiv C-\eta^6\text{-}C_6H_5\}Cr(CO)_3][PF_6]$ [Cp = $\eta^5\text{-}C_5H_5$; spacer = C_6H_4: **1FeCr**, C_4H_2S (thiophene): **2FeCr**, and $(C_4H_2S)_2$ (bithiophene): **3FeCr**] were prepared following the general procedure of iodide abstraction of the parent compound [FeCp(DPPE)I] by the use of $TlPF_6$, in the presence of a slight excess of the corresponding chromophores,[13] which in the present case were the mononuclear chromium complexes **1Cr**, **2Cr**, and **3Cr** described above. The reactions were carried out in dichloromethane by stirring at room temperature for several hours, and were followed by thin layer chromatography (TLC). After workup, orange reddish crystalline compounds were obtained in a yield of ca. 90%.

$[RuCp(DPPE)\{N\equiv C-(spacer)-C\equiv C-\eta^6\text{-}C_6H_5\}Cr(CO)_3][PF_6]$ [DPPE = 1,2-diphenylphosphanyl ethane; with the spacer as C_6H_4: **1RuCr**, C_4H_2S (thiophene): **2RuCr**, and $(C_4H_2S)_2$ (bithiophene): **3RuCr**], were prepared following the same general procedure of halide abstraction, by precipitation of TlCl from the parent compound [RuCp(DPPE)Cl], with $TlPF_6$ in the presence of a slight excess of the corresponding chromophores $[\{N\equiv C-(spacer)-C\equiv C-\eta^6\text{-}C_6H_5\}Cr(CO)_3]$ (compounds **1Cr**, **2Cr**, and **3Cr**) in dichloromethane.[14] Depending on the chromium derivative, the reactions were carried out at room temperature or refluxed for several hours. The evolution of the reactions was followed by TLC, as in the case of the iron analogues. After workup orange crystalline compounds were obtained in a yield of ca. 70%.

Characterisation of the New Mono 1Cr, 2Cr, and 3Cr and Binuclear 1FeCr−3FeCr and 1RuCr−3RuCr Compounds

All the new compounds are fairly stable towards oxidation in air and to moisture, but the ruthenium bithiophene derivative $[RuCp(DPPE)\{N\equiv C-2\text{-}(5\text{-}C_4H_2S)_2-C\equiv C-\eta^6\text{-}C_6H_5\}Cr(CO)_3][PF_6]$ (**3RuCr**) turned out to be light-sensitive. Analytical data, IR spectroscopy, and ^1H, ^{31}P, and ^{13}C NMR spectroscopy support the formulations. For the cationic binuclear complexes, the molar conductivities of 10^{-3} M solutions in acetone, in the range 101−115 $\Omega^{-1}\cdot cm^2\cdot mol^{-1}$, are consistent with values reported for 1:1 electrolytes.[15]

IR Spectroscopic Studies

Two well resolved CO stretching modes in accordance with the symmetry C_{3v} are observed from IR measurements on solutions of chromium tricarbonyl arene complexes. The wavenumber of the CO modes is known to reflect the effect of a substituent on the coordinated aromatic ring. For example the complex of anisole presents two bands at 1978.9 and 1908.9 in isooctane whereas the complex of methylbenzoate shows two bands at 1992.5 and 1929.2, which have to be compared with the values of 1984.3 and 1916.5 for $[C_6H_6Cr(CO)_3]$.[16a] Thus an electron donating group significantly decreases the IR resonance. The two bands relative to the ν(C≡O) are in the range 1985−1898 cm^{-1} for the

 © 2003 Wiley-VCH Verlag GmbH & Co. KGaA, Weinheim

mononuclear complexes and in the range 1969−1888 cm^{-1} for the dinuclear complexes. Coordination of **1Cr** with Fe and Ru give the dinuclear complexes **1FeCr** and **1RuCr** which present resonances at lower frequencies: up to −17 cm^{-1} is in good agreement with π back-bonding from the other metal. This effect is also observed for complexes **2FeCr** and **2RuCr**. As for complexes **3FeCr** and **3RuCr**, the spectra exhibit a small decrease of the E mode but an unexpected although small increase of the A1 mode, Table 1.

Table 1. Selected IR data (KBr)

	ν CN (cm^{-1})	ν CO (cm^{-1})
1	2218	–
1Cr	2222	1985−1902
1FeCr	2216	1969−1900
1RuCr	2227	1968−1890
2	2220	–
2Cr	2214	1972−1915
2FeCr	2197	1969−1890
2RuCr	2216	1969−1892
3	2220	–
3Cr	2212	1957−1898
3FeCr	2197	1965−1888
3RuCr	2212	1966−1889

The ν(N≡C) IR analysis of mononuclear complexes **1Cr**, **2Cr**, **3Cr** shows the presence of the characteristic nitrile band in the range 2212 to 2222 cm^{-1}. For the binuclear derivatives, typical IR bands confirm the presence of the cyclopentadienyl ligand (≈ 3060 cm^{-1}), the $[PF_6]^-$ anion (840 and 545 cm^{-1}), the characteristic band of the coordinated nitrile ν(N≡C) in the range 2197 to 2227 cm^{-1}. Comparison of ν(N≡C) upon coordination of the chromium mononuclear complexes to iron or ruthenium centres, reveals a negative shift −6 to −17 cm^{-1} for the iron binuclear compounds indicating the existence of π back-bonding from the metal to the N≡C group, Table 1. The unexpected slight positive shifts, +5 cm^{-1} for **1RuCr**, +2 cm^{-1} for **2RuCr**, and no shift for **3RuCr**, observed for the corresponding ruthenium atom which are less effective π donors than the iron derivatives, can also be correlated with a weaker π back-donation effect, since normal σ coordination leads to significant positive shifts on ν(N≡C) (up to +80 cm^{-1}). The present results for terminal nitrile coordination are in good agreement with our earlier reports dealing with iron and ruthenium related monometallic compounds.[13,14]

NMR Spectroscopic Studies

^1H NMR spectroscopic data of arenetricarbonylchromium complexes **1Cr**, **2Cr**, **3Cr** are presented together with the corresponding data for the free aromatic ligands and the binuclear iron **1FeCr**−**3FeCr** and ruthenium **1RuCr**−**3RuCr** complexes in Tables 2, 3, and 4. The complexation of the benzene ring to the chromiumtricarbonyl moiety in complexes **1Cr**, **2Cr**, **3Cr** was easily identified due to the characteristic upfield shift to the region 5.3−5.6 ppm.[16b] The protons of the free arene give rise to different sets of signals and multiplicity in the region 7.2−7.5 ppm. We took into account that in the case of diphenyl acetylene, the protons H^2 and H^6 resonated at the highest frequency and the protons H^3, H^5, and H^4 resonated almost at the same frequency (increment H_{ortho} = +0.19, increment H_{meta} = +0.02 and increment H_{para} = +0.00). It is worth noting that in the case of tricarbonylchromiumarene complexes, the differences in the chemical shifts between the *meta* and the *ortho* protons: $\delta(H^3) - \delta(H^2)$ can give an idea as to the effect of the substituent and about the conformation of the tripod in solution with respect to the arene ring.[17a−17g] By using the classical equation $\delta(H^3) - \delta(H^2) = (2x - 1)\cdot\Delta\delta_{max}$[17g] we calculated the percentage of the conformation eclipsing the substituted

Table 2. ^1H NMR spectroscopic data of ligand **1** derivatives

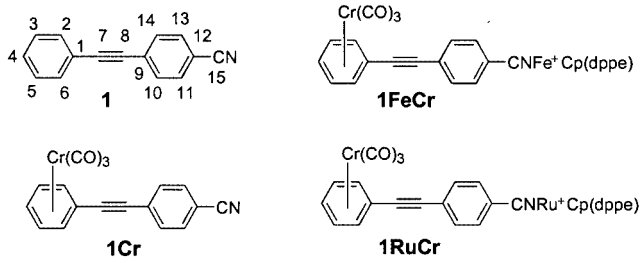

	$H^{2,6}$	$H^{3,5}$	H^4	$H^{10,14}$	$H^{11,13}$	C_5H_5	$\delta(H_3) - \delta(H_2)$	*x* %
1	7.45	7.28	7.28	7.52	7.49	–	−0.17	–
1Cr	5.55	5.34	5.34	7.57	7.63	–	−0.21	38
1FeCr	5.49	5.34	5.34	7.62	6.45[a]	4.48	−0.15	41
1RuCr	5.49	5.33	5.33	7.53	6.52[b]	4.83	−0.16	41

[a] $\delta_{1Cr} - \delta_{1FeCr}$ = 1.18 ppm. [b] $\delta_{1Cr} - \delta_{1RuCr}$ = 1.11 ppm.

Table 3. ^1H NMR spectroscopic data of ligand **2** derivatives

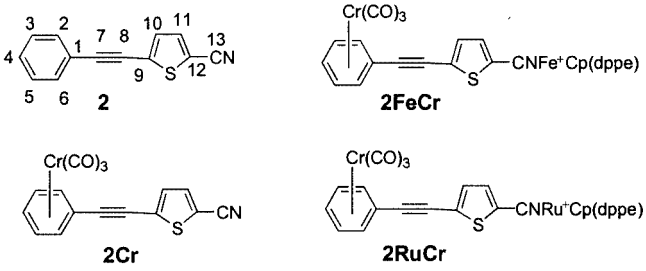

	$H^{2,6}$	$H^{3,5}$	H^4	H^{10}	H^{11}	C_5H_5	$\delta(H_3) - \delta(H_2)$	*x* %
2	7.44	7.30	7.30	7.10	7.40	–	−0.14	–
2Cr	5.52	5.34	5.34	7.23	7.51	–	−0.18	40
2FeCr	5.48	5.32	5.32	6.94[a]	6.65[b]	4.46	−0.16	41
2 RuCr	5.51	5.35	5.35	7.00[c]	6.79[d]	4.84	−0.16	41

[a] $\delta_{2Cr} - \delta_{2FeCr}$ = 0.29 ppm. [b] $\delta_{2Cr} - \delta_{2FeCr}$ = 0.86 ppm. [c] $\delta_{2Cr} - \delta_{2RuCr}$ = 0.23 ppm. [d] $\delta_{2Cr} - \delta_{2RuCr}$ = 0.72 ppm.

 © 2003 Wiley-VCH Verlag GmbH & Co. KGaA, Weinheim

Table 4. ^{1}H NMR spectroscopic data of ligand **3** derivatives

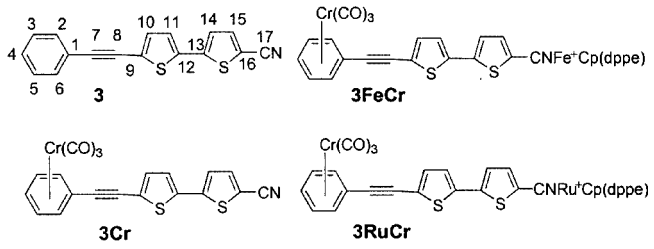

	$H^{2,6}$	$H^{3,5}$	H^4	H^{10}	H^{11}	H^{14}	H^{15}	C_5H_5	$\delta(H_3)-\delta(H_2)$	x %
3	7.40	7.28	7.28	7.08	7.11	7.05	7.43	–	−0.12	–
3Cr	5.53	5.28	5.28	7.16	7.16	7.22	7.52	–	−0.25	36
3FeCr	5.50	5.31	5.31	7.15	7.01	6.87[a]	6.65[b]	4.45	−0.19	39
3RuCr	5.51	5.32	5.32	7.20	7.03	6.90[c]	6.75[d]	4.80	−0.19	39

[a] $\delta_{3Cr} - \delta_{3FeCr} = 0.35$ ppm. [b] $\delta_{3Cr} - \delta_{3FeCr} = 0.87$ ppm. [c] $\delta_{3Cr} - \delta_{3RuCr} = 0.32$ ppm. [d] $\delta_{3Cr} - \delta_{3RuCr} = 0.77$ ppm.

aromatic carbons. Thus we obtained populations x of 38, 40, and 36% for complexes **1Cr**, **2Cr**, and **3Cr** respectively, Tables 2−4, in good agreement with the almost staggered conformation found in the solid state, Figure 1.

Analysis of the ^{1}H NMR spectroscopic data of the iron binuclear complex [FeCp(DPPE)(N≡C−C_6H_4−C≡C−η^6-C_6H_5)Cr(CO)$_3$][PF_6] (**1FeCr**), and its ruthenium analogue [RuCp(DPPE)(N≡C−C_6H_4−C≡C−η^6-C_6H_5)Cr(CO)$_3$][PF_6] (**1RuCr**), Table 2, shows a shielding $\delta_{1Cr} - \delta_{1FeCr} = 1.18$ and $\delta_{1Cr} - \delta_{1RuCr} = 1.11$ ppm, respectively, for protons $H_{11,13}$, placed at the *ortho* position relative to the N≡C functional group with respect to the mononuclear complex **1Cr**. Such shielding could be in good agreement with the π back-donation from the other metal already suggested by the $\Delta\nu_{(N\equiv C)}$ found for both compounds, and also with the results earlier reported for other monocyclopentadienylruthenium/iron mononuclear compounds containing benzonitrile ligands as chromophores.[13,14] This is better proved by the fact that the $H_{2,6}$ protons even farther from the Fe and the Ru residues resonate at slightly lower frequencies for **1FeCr**−**3FeCr** and **1RuCr**−**3RuCr** with respect to the mononuclear complex **1Cr**−**3Cr**, the anisotropy of the Cp and the phenyl groups of the phosphane ligand being unable to interfere at this distance. This indicated a weak electron donating ability of the −CC−C_6H_4−CNFeCp(DPPE) residue; indeed, it is well reported that the protons of C_6H_5R−Cr(CO)$_3$ (R = electron donating group) resonate at lower frequencies than the protons of C_6H_6−Cr(CO)$_3$.[16b]

In a similar manner the analysis of Tables 3 and 4, for compounds containing one and two thiophene units, reveals a shielding of 0.86 ppm ($\delta_{2Cr} - \delta_{2FeCr}$) and 0.72 ppm ($\delta_{2Cr} - \delta_{2RuCr}$) for protons H^{11} (*ortho* to the NC group) with respect to the mononuclear complex **2Cr** and smaller shieldings for the adjacent H^{10} protons. Similar shielding values were also found for the equivalent protons H^{14} and H^{15} of the bithiophene containing compounds. Nevertheless this shift effect is barely felt on the H^{11} proton of the second thiophene ring where only the small shielding values of ca. 0.15 ppm were observed for H^{11}. The chemical shifts of the $H^{2,6}$ protons of complexes **2FeCr**,**3FeCr** and **2RuCr**,**3RuCr** resonate at lower frequencies with respect to the mononuclear complexes **2Cr**,**3Cr** but the shielding is small.

Selected ^{13}C NMR spectroscopic data of mononuclear complexes are reported in Table 5. The carbon resonances of the C^1 to C^4 atoms (complexed phenyl rings of **1Cr**, **2Cr**,

Table 5. Selected ^{13}C NMR spectroscopic data of complexes 1, 2, 3-Cr: and complexing chemical shifts (CCS)

	C^1 [a]	C^2	C^3	C^4	C^7	C^8
1	121.1	130.7	127.5	128.1	92.7	86.7
1Cr	88.3	95.0	91.3	91.3	89.6	87.6
CCS[b]	32.9	35.7	36.2	36.8	3.1	−0.9
2	120.5	130.6	127.5	128.4	95.7	79.5
2Cr	87.3	95.1	91.1	91.6	91.9	80.5
CCS[b]	33.2	35.5	36.4	36.8	3.8	−1.0
3	121.3	130.4	127.5	127.9	94.5	81.1
3Cr	88.8	94.7	91.0	91.2	90.5	82.0
CCS[b]	32.5	35.7	36.5	36.7	.0	−0.9

[a] $CDCl_3$. [b] CCS = Complexing Chemical Shift.

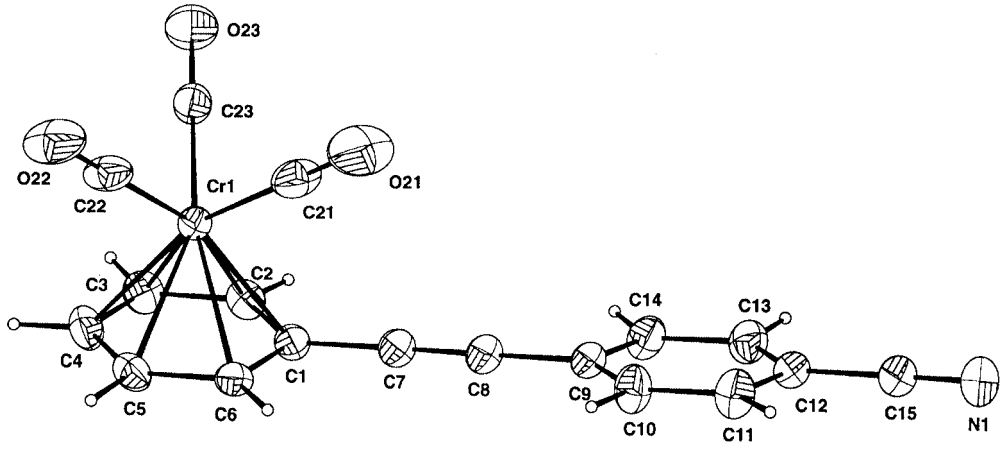

Figure 1. ORTEP diagram and atomic numbering scheme of the molecular structure of complex **1Cr** including a view along the Cr-ring axis. Thermal ellipsoids are presented at the 30% probability level

 © 2003 Wiley-VCH Verlag GmbH & Co. KGaA, Weinheim

3Cr) are assigned by CH correlation spectroscopy. They are shifted to lower frequency in the region 88−96 ppm. It is worth calculating the complexing chemical shifts (CCS)[18,19] of these carbons. Indeed the shifts due to the complexation are characteristic of each carbon, this is also true for the resonances of the alkyne carbon atoms C^7 and C^8. Thus the quaternary carbon C^1 is shifted by 32.8±0.4 ppm, the carbons C^2, C^3, and C^4 are shielded by 35.6±0.1, 36.3±0.3, and 36.7±0.1 ppm, respectively. The carbon C^7 is shielded by 3.5±0.5 ppm whereas the carbon C^8 is deshielded by 1.0±0.1 ppm. The carbonyl carbon resonances of complexes **1Cr**, **2Cr**, and **3Cr** appeared almost at the same frequency δ = 231.8 ppm for **1Cr** and **2Cr**, δ = 231.9 ppm for **3Cr**.

The ^{13}C NMR spectra of the binuclear compounds reveal a deshielding of up to ca. 7.5 ppm of the carbon atom of the NC group, as expected. The ^{31}P NMR spectra of the Fe/Cr and Ru/Cr binuclear compounds display one singlet relative to the dppe coligand at δ ≈ 97 ppm for the Fe derivatives and at δ ≈ 79 ppm for the Ru analogues, at about the same chemical shifts found for other related compounds.[14] The signal relative to the PF_6^- counterion is placed for all the compounds at δ ≈ −143 ppm as a septet.

X-ray Structural Determination of [(N≡C−C_6H_4−C≡C−η^6-C_6H_5)Cr(CO)$_3$]

Information on [(N≡C−C_6H_4−C≡C−η^6-C_6H_5)Cr(CO)$_3$] (**1Cr**) and conformation of the solid state could be obtained from the X-ray crystal analysis, Table 6. Suitable crystals were obtained by crystallisation of complex **1Cr** in a mixture of diethyl ether and petroleum ether. The structure represented in Figure 1 shows an almost staggered conformation of the Cr(CO)$_3$ tripod with respect to the carbon atoms of the aromatic ring, with the Cr−C^{21} bond rotating 23° away from the alkynyl substituent.

The C^7≡C^8 triple bond: 1.196(3) Å is slightly longer than those observed in two relevant examples in the literature

Table 6. Selected interatomic distances (Å) for **1Cr**

1Cr	
C1−C2	1.398(4)
C2−C3	1.406(3)
C3−C4	1.391(4)
C4−C5	1.407(4)
C5−C6	1.397(3)
C6−C1	1.427(3)
C7−C8	1.196(3)
C1−C7	1.431(3)
C8−C9	1.430(3)
C15−N	1.133(4)
C12−C15	1.447(4)
Cr−C1	2.216(2)
Cr−C2	2.220(2)
Cr−C3	2.211(2)
Cr−C4	2.215(2)
Cr−C5	2.220(2)
Cr−C6	2.216(2)

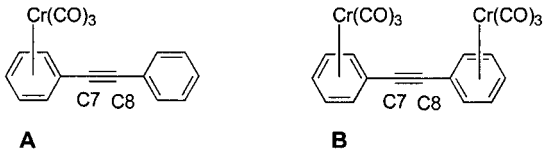

Figure 2. Complexes **A**[18] and **B**[19]

shown in Figure 2. 1.167 Å for C^7≡C^8 in complex **A**,[18] 1.188(5) Å for complex **B**.[19] The slight elongation observed for the C^7≡C^8 triple bond in our compound [(N≡C−C_6H_4−C≡C−η^6-C_6H_5)Cr(CO)$_3$] when compared with complex **B** [with two Cr(CO)$_3$ tripods attached to the phenyl rings] shows that the effect of the N≡C group can be compared with the effect of the Cr(CO)$_3$ acceptor group.

The C^{15}−N bond length of 1.113 Å in **1Cr** should be compared with a similar value of 1.114 Å described in the case of a nitrile coordinated to a cationic Ru(Cp)(PPh$_3$)$_2$ fragment: [CpFeC_5H_4−CH=CH−*p*-C_6H_4−CN−Ru(Cp)(PPh$_3$)$_2$].[2c] These values seem similar but with the nature of the phosphanes being different it is hard to compare the back-donation of the metal in these mono and dinuclear complexes.

The deviation from co-planarity of the complexed and uncomplexed phenyl rings in **1Cr** is small (10°) whereas the corresponding dihedral angle in complex **A** is 50.9° (in complex **B** this deviation is small: 3°). It would be interesting to evaluate the preservation of the planarity in the spacer in the binuclear compounds. Nevertheless, attempts of growing suitable single crystals for this purpose have been unsuccessful so far.

UV/Visible Studies

The UV/Vis electronic spectra of the aromatic free ligands **1**−**3**, the new monometallic **1Cr**−**3Cr** and the bimetallic **1FeCr**−**3FeCr** and **1RuCr**−**3RuCr** compounds were studied in acetone and chloroform solutions, in order to characterise the absorption bands and to obtain some idea of their hyperpolarisabilities, Table 7.

The spectra of the aromatic free ligands **1**−**3** displayed one intense π-π* intraligand absorption band (ILCT) in the region 317 to 370 nm.

The spectra of the monometallic complexes **1Cr**−**3Cr** in chloroform solutions, were characterised by two bands, one at ca. 425 nm and the other one in the region 300−360 nm. The first band was assigned to a metal-to-ligand charge transfer (MLCT) transition originating due to the charge transition from the chromium centre to the π- and σ-bound ligands. Although spectroscopic and theoretical studies[20,21] predict the existence of two bands for the dominant excitations d_π-to-2π*(CO) and d_π-to-π*(arene) in [(η^6-C_6H_6)Cr(CO)$_3$] related compounds, only one band was clearly observed in the present studies. A similar situation was also reported by other authors for related complexes, namely alkynyl and the alkenyltricarbonylchromium derivative.[7c] The second and more intense absorption band, predicted for the π-π* intraligand transitions (ILCT),[20] was

 © 2003 Wiley-VCH Verlag GmbH & Co. KGaA, Weinheim

Table 7. UV/Vis spectroscopic data for compounds [MCp-(DPPE)N≡C(arene)C≡CC_6H_4Cr $(CO)_3$][PF_6] measured in solutions ≈10^{-4} M of acetone and chloroform (M = Fe^{II} and Ru^{II}.

Compound[a]	Acetone		Chloroform	
	λ_{max} (nm)	ε_{max} ($mol^{-1}\cdot L\cdot cm^{-1}$)	λ_{max} (nm)	ε_{max}) ($mol^{-1}\cdot L\cdot cm^{-1}$)
1FeCr	–[b]	–	317	19500
	366	13500	348	14750
	430	13850	429	12000
2FeCr	–[b]	–	307	30120
	385[c]	–	374	12820
	443	15920	444	12690
3FeCr	365	29760	398[d]	26840
	392	27920		
1RuCr	–[b]	–	317	30690
	338(sh)	≈ 26540	–	–
	376(sh)	≈ 12530	–	–
2RuCr	352	20990	330	38070
	414	11150	414	16420
3RuCr	362	31980	364	32130
	426	16650	426	17110
1Cr	–[b]	–	325	13090
	416	4550	422	4720
2Cr	–[b]	–	305	27110
	424	5290	430	5490
3Cr	351	28860	355	29640
	424	8070	424	9010
1	–	–	317	17680
2	–	–	349	7170
3	–	–	370	10010

[a] [Fe] = FeCp(DPPE)–, [Ru] = RuCp(DPPE)–, [Cr] = Cr(η^6-C_6H_5)$(CO)_3$. [b] Obscured by the solvent signal. [c] Broad band. [d] Very broad and intense band.

found in the range 300–360 nm, in agreement with the electronic spectra of the aromatic free ligands **1**–**3**.

The spectra of the bimetallic compounds (chloroform solution) showed the expected MLCT (at ca. 430 nm) and ILCT (in the range 320–400 nm) bands attributed to the monometallic parent [{N≡C–(spacer)–C≡C–η^6-C_6H}-$Cr(CO)_3$] complexes. The MLCT band was found to be insensitive to the polarity of the solvent, when chloroform was replaced by acetone, suggesting that there is no significant variation of polarity between the fundamental and the excited states, while the ILCT band showed some solvochromicity. In addition to these bands, a third band emerged in the electronic spectra of some of the binuclear complexes, namely **1FeCr** (348 nm) and **2FeCr** (374 nm), and it was attributed to a new metal-to-ligand charge transfer band involving the iron centre. The characterisation of this new band as a MLCT transition centred at the iron fragment, was supported by our previous studies in other related mononuclear iron compounds and explained by π back-donation involving d_π-π*(N≡C) orbitals.[8,22]

In Figure 3, the electronic spectrum of the binuclear compound **2FeCr** is compared with the spectrum of the parent mononuclear compound **2Cr** in chloroform. The arrow in the figure points indicates this new Fe centred MLCT band, clearly absent in the spectrum of the mononuclear parent compound.

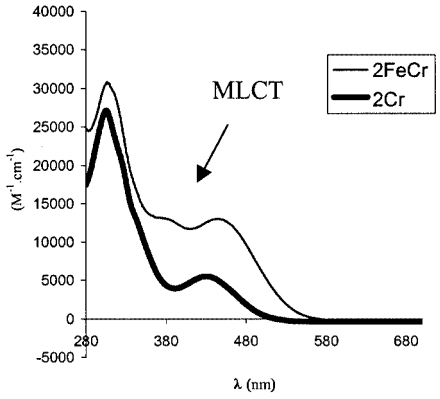

Figure 3. UV/Vis. Electronic spectra of **2FeCr**, showing a weak MLCT band, and **2Cr**

Interestingly, the **3FeCr** showed only one very broad and intense band (chloroform solution), centred at 398 nm, with the shape suggesting the overlap of the observed bands for **1FeCr** and **2FeCr**. The complexity of this band was corroborated by the optical spectrum of this compound in acetone, where two peaks seem to emerge clearly from that broad band.

The general characteristic of the electronic spectra of the studied set of binuclear complexes was a comparative increase of the intensity of the MLCT (Cr centred) and ILCT absorption to the corresponding mononuclear chromium derivatives. This effect was more pronounced on the ILCT band and particularly for ruthenium derivatives. In addition, the existence of a new MLCT, centred on the second metal, clearly observed in the binuclear iron derivatives and located in the same direction of the strengthened ILCT transition, might be the origin of the higher hyperpolarisabilities found for the binuclear derivatives, discussed below.

Nonlinear Optical Studies

The dynamic first hyperpolarisabilities β of the new complexes were measured in chloroform using the HRS technique[23–25] with a 1064 nm Nd:YAG laser fundamental. Results are presented in Table 8. The applicability of the two-level model to these types of chromium tricarbonyl arene derivatives has been questioned.[20] For the push-pull extended organic π-system chromophores func-

Table 8. Experimental first hyperpolarisability β determined by hyper-Rayleigh scattering of mono Cr complexes and the corresponding Fe and Ru binuclear derivatives

Compound	β(10^{-30}esu)
1FeCr	94
2FeCr	170
3FeCr	197
1RuCr	42
2RuCr	83
3RuCr	143
1Cr	28
2Cr	59
3Cr	88

 © 2003 Wiley-VCH Verlag GmbH & Co. KGaA, Weinheim

tionalised with the $Cr(CO)_3$ group, this model has been applied based on the assumption that the major contribution to the hyperpolarisabilities arises from the ILCT transition occurring along the chromophore molecular axis.[7c] The additional MLCT band centred at the second metal (Fe^{II} or Ru^{II}) fragment due to an enhanced back-donation to the π* nitrile group, found clearly for the iron binuclear derivatives, and the evidence found in the IR and ^1H NMR spectroscopic data, for its existence in the ruthenium analogues, strongly suggests that the two-level approximation should not be applied in this case and therefore the corresponding static hyperpolarisabilities β_0 were not calculated. Moreover, the similarity in the positions of the charge-transfer bands would result in approximately identical resonance enhancement for all the complexes.

The β values found for compounds [{N≡C−(spacer)−C≡C−η⁶-C_6H_5}$Cr(CO)_3$] (28−88 $\times 10^{-30}$ esu), where N≡C− is an acceptor group, are similar to those reported in the literature for compounds of the same general formula, namely [$Cr(\eta^6$-$C_6H_5R)(CO)_3$] with R= −C≡C−C_6H_4R' or −C(H)=C(H)−C_6H_4R' (R′ = NMe_2, NO_2), corroborating that the chromium tricarbonyl arene fragment is amphoteric with respect to its electronic behaviour.[7] Indeed, electron donating or electron withdrawing behaviour in NLO chromophores depends on the electronic nature of the far end group of the chromophore.[7c] In addition, the substitution of the phenyl spacer **1Cr** by a thiophene spacer **2Cr** causes a twofold increase in the β value, probably due to the reduced aromaticity of the thiophene. The introduction of the second thiophene unity **3Cr** also enhances the hyperpolarisability, as expected due to the increase of the conjugation length.

The experimental β values measured for all the binuclear compounds studied (Table 8) showed that the best values of β were obtained for the Fe binuclear derivatives **2FeCr** and **3FeCr**, 170 and 197 $\times 10^{-30}$ esu, respectively. These values are relatively higher than those of the precursor mononuclear compounds **2Cr** ($59 \cdot 10^{-30}$ esu) and **3Cr** ($88 \cdot 10^{-30}$ esu). The ruthenium series **1RuCr**, **2RuCr**, and **3RuCr** showed lower β values relative to the iron series, as would be expected from our previous studies on similar systems[8] and in accordance with the better donor role of the iron fragment. Comparison of the different spacers follow the same trend observed for the corresponding mononuclear chromium complexes. The β values obtained can be compared with other β values of organometallic congeners described in the literature[1b,2i,5,7c] and with the $31 \cdot 10^{-30}$ esu β value in the case of the prototypical "push-pull" chromophore (*Z*)-1-ferrocenyl-2-(4-nitrophenyl)ethylene complex[2m] which has an SHG efficiency 62 times that of urea.

The comparison of the β values of mono and binuclear compounds studied in the present work show relatively higher values for the binuclear derivatives. These results might be expected by the higher intensity of the ILCT transitions observed in the optical spectra of the binuclear compounds and the existence of a second MLCT band (iron/ruthenium centred) in the axis of the chromophore, due to d_π-π*(N≡C) π back-donation. It is important to note that the direction of the ILCT transition is reversed when the binuclear compounds are formed. In fact, the N≡C ending group, in the chromium mononuclear compounds [{N≡C−(spacer)−C≡C−η⁶-C_6H}$Cr(CO)_3$], plays the role of acceptor while the chromiumtricarbonylarene fragment acts as the donor group (see Figure 4, a). However, the coordination of this N≡C group to a second metal (Fe/Ru) makes it behave as a π* acceptor relatively to this new metal centre. Thus, in the binuclear complexes, the new ending group [MCp(DPPE)(N≡C)−]$^+$ acts as a π donor while the chromiumtricarbonyl fragment now behaves as an acceptor (see Figure 4, b). These results are in good agreement with the electronically amphoteric character reported for the chromium tricarbonyl arene fragment in analogous compounds of general structure [{R−(spacer)−C≡C−η⁶-C_6H}$Cr(CO)_3$] where R is the donor NMe_2 or the acceptor NO_2.[7c]

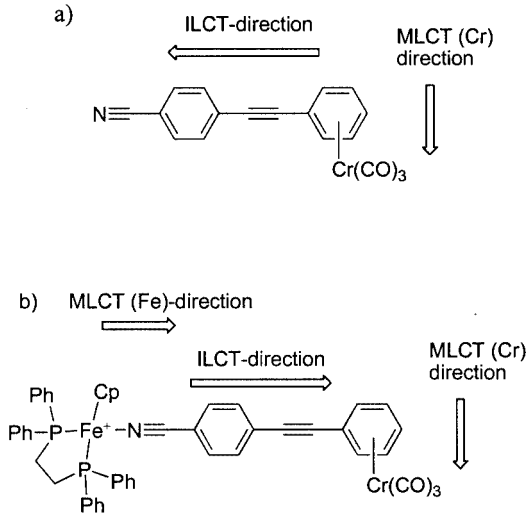

Figure 4. Ground state dipole vectors of chromium mononuclear complexes compared with the corresponding binuclear complexes. The direction of the ILCT contribution in the binuclear complexes is reversed, due to the role of the new ending group [MCp(DPPE)(N≡C−)]$^+$

Conclusion

The synthesis of nitrile ligands linked to tricarbonyl (η⁶-arene)chromium complexes [{N≡C−(spacer)−C≡C−η⁶-C_6H_5}$Cr(CO)_3$] by conjugated spacers is performed by reacting aromatic bromo or iodo nitrile derivatives with tricarbonyl chromium complexed phenylacetylene using the Sonogashira-coupling reaction. Characterisation of these mononuclear complexes obtained and the corresponding dinuclear [M{N≡C−(spacer)−C≡C−η⁶-C_6H_5}$Cr(CO)_3$] complexes M = Fe(dppe)Cp, Ru(dppe)Cp has been studied using ^1H, ^{13}C, IR, and UV/Vis spectroscopy and in the case of one of them by X-ray crystallography. Measurements of the dynamic first hyperpolarisabilities (β) by HRS, showed significant higher values for the binuclear derivatives when

 © 2003 Wiley-VCH Verlag GmbH & Co. KGaA, Weinheim

compared with the corresponding monometallic parent compounds. This enhancement of β observed upon coordination of the [{N≡C−(spacer)−C≡C−η^6-C_6H_5}Cr(CO)$_3$] ligand complex to a second iron(II) or ruthenium(II) metal centre can be explained by the significant enhancement observed for the molar absorptivity of the ILCT band relative to the nitrile chromophore and the synergic effect of a new MLCT band originating due to π back-bonding from the second metal towards the nitrile functional group.

Experimental Section

General Procedures: All the experiments were carried out under vacuum or nitrogen atmosphere using standard Schlenk techniques, and solvents were dried following published methods.[26] [Cr(η^6-C_6H_5−C≡CH)(CO)$_3$] was easily prepared as reported recently.[18] Chlorobenzene tricarbonylchromium complex was prepared according to literature procedures.[27] The halo nitrile aromatics **1-CN**−**3-CN** are commercially available or prepared using standard literature procedures.[28] The synthesis of some new chromium derivatives was recently published in a preliminary communication.[11] Fe(η^5-C_5H_5)(dppe)(I)][22] and [Ru(η^5-C_5H_5)(dppe)(Cl)][29,30] were prepared according to the procedures described in the literature. IR spectra were recorded in KBr pellets on a Perkin−Elmer 683 spectrophotometer; only significant bands are cited. ^{1}H, ^{13}C, and ^{31}P NMR spectra were recorded in $CDCl_3$ on a Varian Unity 300 spectrometer at probe temperature. The UV/Vis spectra were taken on a Perkin−Elmer λ9 UV/Vis/Nir spectrophotometer. Elemental analysis of mononuclear compounds were performed by "le service de Microanalyses" (Université Pierre et Marie Curie). Binuclear compounds were analysed at Laboratório de Análises, Instituto Superior Técnico, using a Fisons Instruments EA1108 system. Data acquisition, integration, and handling were performed using a PC with the software package Eager-200 (Carlo Erba Instruments). Melting points were obtained on a Reichert Thermovar. The molar condutivities of 10^{-3} mol·L^{-1} solutions of the complexes in acetone were recorded with a Schott CGB55 Konduktometer. The ^{1}H ([D]chloroform) and ^{13}C ([D]chloroform) chemical shifts are reported in parts per million downfield from internal Me_4Si and the ^{31}P NMR spectra are reported downfield from external 85% H_3PO_4 ([D]chloroform). Spectral assignments follow the numbering scheme shown in Tables 2−4.

Synthesis of the Free Ligands 1, 2, and 3: The free ligands were synthesised in a similar manner to the chromium complexes (see below) by the palladium copper catalysed coupling of the aromatic iodonitriles **1-CN**, **2-CN**, and **3-CN** and phenylacetylene.

N≡C−(C_6H_4)−C≡C−C_6H_5 (1): 54% yield. IR: see Table 1. ^{1}H NMR: see Table 2. ^{13}C NMR: see Table 5 and 127.2 (C^9), 131.0 (C^{10},C^{14}), 131.0 (C^{11},C^{13}), 110.4 (C^{12}), 117.5 (C^{15}), (UV/Vis, see Table 7).

N≡C−2-(5-C_4H_2S)−C≡C−C_6H_5 (2): 49% yield. IR: see Table 1. ^{1}H NMR: see Table 3. ^{13}C NMR: see Table 5 and 129.7 (C^9), 130.4 (C^{10}), 136.2 (C^{11}), 108.8 (C^{12}), 112.6 (C^{13}).

N≡C−2-(5-C_4H_2S)$_2$−C≡C−C_6H_5 (3): 33% yield. IR: see Table 1. ^{1}H NMR: see Table 4. ^{13}C NMR: see Table 5 and 134.7 (C^9), 124.8 (C^{10}), 131.8 (C^{11}), 149.7 (C^{12}), 123.8 (C^{13}), 123.8 (C^{14}), 137.3 (C^{15}), 109.7 (C^{16}), 113.0 (C^{17}).

General Procedure for the Synthesis of Chromium Mononuclear Complexes

[{N≡C−(C_6H_4)−C≡C−η^6-C_6H_5}Cr(CO)$_3$] (1Cr): (η^6-Phenyl)-ethynyltricarbonylchromium complex (171 mg, 0.71 mmol), [$PdCl_2(PPh_3)_2$] (25 mg, 0.035 mmol), CuI (7 mg, 0.035 mmol), and *p*-iodobenzonitrile (158 mg, 0.69 mmol) were placed in a bicol under unit atmosphere and dried in vacuo for 30 min. NEt_3 (5 mL) and anhydrous THF (10 mL) were then added and the mixture was immediately heated to reflux for 3 h. After cooling at room temperature, the suspension was filtered, washed with Et_2O (3 × 20 mL) and the solvents were removed under reduced pressure. The residue was chromatographed on silica gel (diethyl ether/ petroleum ether 96:4 to 80:20) to afford **1Cr** (210 mg) in 87% yield as an orange solid. m.p. 168 °C (dec). IR: see Table 1. ^{1}H NMR: see Table 2. ^{13}C NMR: see Table 5 and 126.8 (C^9), 132.2 (C^{10},C^{14}), 132.5 (C^{11},C^{13}), 112.4 (C^{12}), 118.4 (C^{15}), 231.6 (CO) ppm. $C_{18}H_9CrNO_3$ (339.3): calcd. C 63.72, H 2.65, N 4.13; found C 63.13, H 2.84, N 3.96.

[{N≡C−2-(5-C_4H_2S)−C≡C−η^6-C_6H_5}Cr(CO)$_3$] (2Cr): (η^6-Phenyl)ethynyltricarbonylchromium complex (119 mg, 5 mmol), [$PdCl_2(PPh_3)_2$] (175 mg, 0.25 mmol), 2-bromocyanothiophene (6.05 g, 25 mmol), and NEt_3 (30 mL) were added together in a bicol under N_2. The mixture was heated for 3 h. By using the same procedures complex **2Cr** was obtained in 81% (1.38 g) as an orange solid. m.p. 140 °C (dec). IR (KBr): see Table 1. ^{1}H NMR: see Table 3. ^{13}C NMR: see Table 5 and 129.2 (C^9), 132.9 (C^{10}), 137.4 (C^{11}), 111.1 (C^{12}), 113.6 (C^{13}), 231.8 (CO) ppm. $C_{16}H_7CrNO_3S$: calcd. C 55.65, H 2.02, N 4.05; found C 55.43, H 2.21, N 3.92.

[{N≡C−2-(5-C_4H_2S)$_2$−C≡C−η^6-C_6H_5}Cr(CO)$_3$] (3Cr):[11] 81% yield; m.p. 141 °C (dec). IR: see Table 1. ^{1}H NMR: see Table 4. ^{13}C NMR: see Table 5, and 134.2 (C^9), 125.9 (C^{10}), 132.7 (C^{11}), 143.4 (C^{12}), 123.1 (C^{13}), 124.2 (C^{14}), 138.4 (C^{15}), 112.2 (C^{16}), 114.2 (C^{17}), 231.9 (CO) ppm.

General Procedure for the Synthesis of the Bimetallic Iron/Chromium Derivatives

[FeCp(dppe){N≡C−(spacer)−C≡C−C_6H_5}Cr(CO)$_3$][PF_6]: A slight excess of the adequate amount of chromium chromophore [{N≡C−(arene)−C≡C−C_6H_5}Cr(CO)$_3$] (1.1 mmol) and $TlPF_6$ (1.1 mmol) was added to a solution of the [CpFe(dppe)(I)] (1 mmol) in dichloromethane (25 ml) followed by stirring, at room temperature, for 3 h in the case of [{N≡C−(C_6H_4)−C≡C−η^6-C_6H_5}Cr(CO)$_3$] and 18 h for the thiophene derivatives. The evolution of these reactions was followed by TLC (thin layer chromatography). A colour change was observed from brown to red with simultaneous precipitation of thallium iodide.

After filtration, the solution was evaporated under vacuum to dryness and washed several times with diethyl ether to remove the excess of chromium [{N≡C−(arene)−C≡C−C_6H_5}Cr(CO)$_3$] starting material. The residue was recrystallised from dichloromethane/ diethyl ether.

[FeCp(dppe)(N≡C−C_6H_4−C≡C−C_6H_5)Cr(CO)$_3$][PF_6] (1FeCr): 90% yield, red-orange, m.p. 128−130 °C. IR: see Table 1. ^{1}H NMR: see Table 2. ^{13}C NMR: δ = 79.8 (η^5-C_5H_5), 88.3 (C^1), 95.1 (C^2,C^6), 91.3 (C^3,C^4,C^5), 90.1 (C^7), 87.6 (C^8), 126.5 (C^9), 132.7 (C^{10},C^{14}), 131.6 (C^{11},C^{13}), 112.0 (C^{12}), 110.9 (C^{15}), 231.9 (CO) ppm. ^{31}P NMR: δ = 97.59 (s, dppe), −143.69 (hept, PF_6) ppm. $C_{49}H_{38}CrF_6FeNO_3P_3$·1/2($C_2H_5)_2$O: calcd. C 58.64, H 3.80, N 1.39; found C 59.8, H 3.70, N 1.47. Molar conductance: 113.7 cm^{-1}·mol^{-1}·Ω^{-1}.

[FeCp(dppe){N≡C−2-(5-C_4H_2S)−C≡C−C_6H_5}Cr(CO)$_3$][PF_6] (2FeCr): 86% yield, red, m.p. 130−132 °C. IR: see Table 1. ^{1}H

 © 2003 Wiley-VCH Verlag GmbH & Co. KGaA, Weinheim

NMR: see Table 3. ^{13}C NMR: δ = 80.2 (η^5-C_5H_5), 87.0 (C^1), 95.0 (C^2,C^6), 91.0 (C^3,C^4,C^5), 91.4 (C^7), 80.8 (C^8), 129.3 (C^9), 132.6 (C^{10}), 138.6 (C^{11}), 110.4 (C^{12}), 108.8 (C^{13}), 231.6 (CO) ppm. ^{31}P NMR: δ = 97.43 (s, dppe), −143.53 (hept, PF_6) ppm. $C_{47}H_{36}CrF_6FeNO_3P_3S$: calcd. C 55.90, H 3.57, N 1.38, S 3.18; found C 55.8, H 3.52, N 1.31, S 3.0. Molar conductance: 109.4 $cm^{-1}\cdot mol^{-1}\cdot\Omega^{-1}$.

[CpFe(dppe){N≡C−2-(5-C_4H_2S)$_2$−C≡C−C_6H_5}Cr(CO)$_3$][PF_6] (3FeCr): 91% yield, orange reddish, m.p. 127−129 °C. IR: see Table 1. ^1H NMR: see Table 4. ^{13}C NMR: δ = 80.0 (η^5-C_5H_5), 88.9 (C^1), 94.8 (C^2, C^6), 91.3 (C^3, C^4, C^5), 91.1 (C^7), 82.0 (C^8), 134.3 (C^9), 132.6 (C^{10}), 131.1 (C^{11}), 143.2 (C^{12}), 122.9 (C^{13}), 130.7 (C^{14}), 139.6 (C^{15}), 124.2 (C^{16}), 106.9 (C^{17}); 231.9 (CO) ppm. ^{31}P NMR: δ = 97.48 (s, dppe), −143.63 (hept, PF_6) ppm. $C_{51}H_{38}CrF_6FeNO_3P_3S_2\cdot 2(CH_3CH_2)_2O$: calcd. C 57.14, H 4.70, N 1.10, S 5.17; found C 57.13, H 4.73, N 0.90, S 5.14. Molar conductance: 101.2 $cm^{-1}\cdot mol^{-1}\cdot\Omega^{-1}$.

General Procedure for the Synthesis of the Bimetallic Ruthenium/Chromium Derivatives

[RuCp(DPPE){N≡C−(spacer)−C≡C−C_6H_5}Cr(CO)$_3$][PF_6] (1RuCr−3RuCr): The corresponding chromium complex [(N≡C−(arene)−C≡CC_6H_5)Cr(CO)$_3$] (1.1 mmol) was added to a solution of the [RuCp(dppe)Cl] (1 mmol) in dichloromethane (25 mL) followed by addition of $TlPF_6$ (1.1 mmol) at room temperature. The mixture was refluxed for 12 h in the case of [(NC−C_6H_4−CC−C_6H_5)Cr(CO)$_3$] and 48 h for [{N≡C−2-(5-C_4H_2S)−C≡C−C_6H_5}Cr(CO)$_3$]. In the case of the bithiophene derivative the reaction was carried out at room temperature for 14 h. The evolution of these reactions was followed by TLC. A colour change was observed from red to orange with the simultaneous precipitation of thallium chloride. After filtration, the solution was evaporated under vacuum to dryness and washed several times with diethyl ether to remove the excess of the chromium chromophores [{N≡C−(arene)−C≡C−C_6H_5}Cr(CO)$_3$]. The residue was recrystallised from dichloromethane/diethyl ether.

[CpRu(dppe)(N≡C−C_6H_4−C≡C−C_6H_5)Cr(CO)$_3$][PF_6] (1RuCr): 70% yield, red-orange, m.p. 125−128 °C. IR: see Table 1. ^1H NMR:see Table 2. ^{13}C NMR: δ = ^{13}C NMR: δ = 82.2 (η^5-C_5H_5), 88.3 (C^1), 95.1 (C^2,C^6), 91.3 (C^3,C^4,C^5), 90.1 (C^7), 87.7 (C^8), 126.7 (C^9), 133.0 (C^{10},C^{14}), 131.7 (C^{11},C^{13}), 112.0 (C^{12}), 110.4 (C^{15}), 231.8 (CO) ppm. ^{31}P NMR: δ = 79.85 (s, dppe), −143.73 (hept, PF_6) ppm. $C_{49}H_{38}CrF_6NO_3P_3Ru\cdot 2(CH_3CH_2)_2O$: calcd. C 57.19, H 4.8, N 1.20; found: C 57.10, H 4.10, N 1.29. Molar conductance: 114.8 $cm^{-1}\cdot mol^{-1}\cdot\Omega^{-1}$.

[RuCp(dppe)(N≡C−2-(5-C_4H_2S)−C≡C−C_6H_5)Cr(CO)$_3$][PF_6] (2RuCr): 71% yield, orange, m.p. 133−135 °C. IR: see Table 1. ^1H NMR: see Table 3. ^{13}C NMR: δ = 82.5 (η^5-C_5H_5), 87.0(C^1), 95.0 (C^2, C^6), 91.1 (C^3, C^4, C^5), 91.6(C^7), 80.2 (C^8), 129.3 (C^9), 132.9 (C^{10}), 138.9 (C^{11}), 109.0 (C^{12}), 108.0 (C^{13}), 231.7 (CO) ppm. ^{31}P NMR: δ = 79.59 (s, dppe), −143.71 (hept, PF_6) ppm. $C_{47}H_{36}CrF_6NO_3P_3RuS$: calcd. C 53.51, H 3.42, N 1.32, S 3.04; found: C 53.50, H 3.41, N 1.33, S 2.90. Molar conductance: 115.2 $cm^{-1}\cdot mol^{-1}\cdot\Omega^{-1}$.

[RuCp(dppe){N≡C−2-(5-C_4H_2S)$_2$−C≡C−C_6H_5}Cr(CO)$_3$][PF_6] (3RuCr): Light-sensitivity prevented complete characterisation by elemental analysis. NMR samples were prepared in the dark. 70% yield; orange-brownish; m.p. 94−97 °C. IR: see Table 1. ^1H NMR: see Table 4. ^{13}C NMR: δ = 82.5 (η^5-C_5H_5), 89.2 (C^1), 94.7 (C^2, C^6), 91.1 (C^3, C^4, C^5), 82.0 (C^8), 134.8 (C^9), 133.1 (C^{10}), 131.5 (C^{11}), 130.7 (C^{14}), 138.3 (C^{15}), 124.1 (C^{16}), 106.7 (C^{17}); 231.8 (CO) ppm. ^{31}P NMR: δ = 79.66 (s, dppe), −143.61 (hept, PF_6) ppm. * Located under a broad signal.

Crystal Structure of 1Cr: [(CO)$_3$Cr($C_{15}H_9N$)], M = 339.27, μ = 0.735 mm^{-1}, ρ = 1.46 $g\cdot cm^{-3}$, monoclinic, $P2_1/c$, Z = 4, a = 10.326(2), b = 13.209(5), c = 11.799(2) Å, β = 106.61(2)°, V = 1542.3(7) $Å^3$, from 25 reflections (27.6°< 2θ < 28.4°). Cell dimensions and intensities were measured at 295 K on a Nonius CAD4 diffractometer with graphite-monochromated Mo-K_α radiation (λ = 0.71069 Å). ω/2θ scans, two standard reflections measured every hour showed no significant variation.1° < θ < 28° (0 < h < 13, 0 < k < 17, −15 < l < 14), 4085 measured reflections, 3715 unique reflections of which 2590 were observed [$F_o^2 > 3\sigma(F_o^2)$]; R_{int}= 0.03 for equivalent reflections. Data were corrected for Lorentz and polarisation effects. The structure was solved by direct methods using SHELXS,[31] all other calculations used CRYSTALS.[32] Atomic scattering factors and anomalous dispersion terms were taken from the literature.[33] Full-matrix least-squares refinement based on F and a Chebychev weighting scheme gave final values R = 0.0399, wR= 0.0508, and s = 1.05 for 209 variables and 2590 contributing reflections. The maximum shift/esd on the last cycle was 1.75. Non-hydrogen atoms were anisotropically refined. Hydrogen atoms were located on a difference Fourier map; they were allocated an overall isotropic thermal parameter. The final difference electron density map showed a maximum of 0.42 and a minimum of −0.30 $e\cdot Å^{-3}$.

Hyper-Rayleigh Scattering: Details of the HRS experiment have been discussed previously.[20] A Q-switched Nd: YAG laser emitting at 1064 nm was used to obtain the incident light. A reference value of $23\cdot 10^{-30}$ esu[23] for 4-nitroaniline in chloroform was used to calculate the hyperpolarisability of the compounds by the external reference method. Solutions for measurements until 10^{-4} M depending on the nature of the complex under study, the low concentration being necessary to minimise absorptive losses. One-dimensional hyperpolarisability is assumed, i.e. $\beta_{1064} = \beta_{333}$, and a relative error of ±10% is estimated.

Supplementary Material: Crystallographic data for the structural analysis of compound [Cr(η^6-C_6H_5−C≡C−C_6H_4C≡N)(CO)$_3$] (excluding structure factors) have been deposited in the Cambridge data base. CCDC-147256 contains the supplementary crystallographic data for this paper. These data can be obtained free of charge at www.ccdc.cam.ac.uk/conts/retrieving.html [or from the Cambridge Crystallographic Data Centre, 12, Union Road, Cambridge CB2 1EZ, UK; Fax: (internat.) +44-1223-336-033; E-mail: deposit@ccdc.cam.ac.uk].

Acknowledgments

Financial support for this work was provided by the TMR "Organometallic dipoles with NLO properties" contract ERBFMRXCTCT980166, by COST D14 and partly by Fundação para a Ciência e Tecnologia PRAXIS PCEX/C/QUI/96/96 and CNRS.

[1] [1a] T. MeyerFriedrichsen, H. Wong, M. H. Prosenc, J. Heck, *Eur. J. Inorg. Chem.* **2003**, *5*, 936−946. [1b] E. Goovaerts, W. E. Wenseleers, M. H. Garcia and G. H. Cross, *Handbook of Advanced Electronic and Photonic Materials* (Ed. H. S. Nalwa), Vol. 9, Ch. 3, p. 127−191, **2001** and references cited therein. [1c]J. A. Mata, E. Peris, R. Llusar, S. Uriel, M. P. Cifuentes, M. G. Humphrey, M. Samoc, B. LutherDavies, *Eur. J. Inorg. Chem.* **2001**, 2113−2122. [1d] J. A. Mata, E. Peris, I. Asselberghs, R. Van Boxel, A. Persoons, *New J. Chem.* **2001**,

 © 2003 Wiley-VCH Verlag GmbH & Co. KGaA, Weinheim

1043−1046. [1e] K. D. Demadis, C. M. Hartshorn, T. J. Meyer, *Chem. Rev.* **2001**, *101*, 2655−2685. [1f] H. Le Bozec, T. Renouzard, *Eur. J. Inorg. Chem.* **2000**, 229−239. [1g] I. R. Whittall, A. M. McDonagh, M. G. Humphrey, M. Samoc, *Adv. Organomet. Chem.* **1998**, *42*, 291 and references cited therein.

[2] [2a] S. Fukuzumi, K. Okamoto, Y. Yoshida, H. Imahori, Y. Araki, O. Ito, *J. Am. Chem. Soc.* **2003**, *125*, 1007−1013. [2b] I. Ratera, D. RuizMolina, F. Renz, J. Ensling, K. Wurst, C. Rovira, P. Gütlich, J. Veciana, *J. Am. Chem. Soc.* **2003**, *125*, 1462−1463. [2c] J. A. Mata, E. Peris, S. Uriel, R. Llusar, I. Asselberghs, A. Persoons, *Polyhedron* **2001**, *20*, 2083−2088. [2d] T. Farrell, T. MeyerFriedrichsen, J. Heck, A. R. Manning, *Organometallics* **2000**, *19*, 3410. [2e] J. A. Mata, E. Falomir, R. Llusar, E. Peris, *J. Organomet. Chem.* **2000**, *616*, 80. [2f] H. Wong, T. MeyerFriedrichsen, T. Farrel, C. Mecker, J. Heck, *Eur. J. Inorg. Chem.* **2000**, 631−646. [2g] V. Cadierno, S. Conejero, M. Pilar Gamasa, J. Gimeno, I. Asselberghs, S. Houbrechts, K. Clays, A. Persoons, J. Borge, S. GarciaGranda, *Organometallics* **1999**, *18*, 582−597. [2h] I. S. Lee, H. Seo, Y. K. Chung, *Organometallics* **1999**, *18*, 1091. [2i] G. G. A. Balavoine, J. C. Daran, G. Iftime, P. G. Lacroix, E. Manoury, J. A. Delaire, I. MalteyFanton, K. Nakatani, S. Di Bella, *Organometallics* **1999**, *18*, 21−29. [2j] R. H. Naulty, A. M. McDonagh, I. R. Whittall, M. P. Cifuentes, M. G. Humphrey, S. Houbrechts, J. Maes, A. Persoons, G. A. Heath, D. C. R. Hockless, *J. Organomet. Chem.* **1998**, *563*, 137−146. [2k] T. Le Bouder, P. Massiot, H. Le Bozec, *Tetrahedron Lett.* **1998**, *39*, 6869−6872. [2l] I. R. Whittall, M. G. Humphrey, A. Persoons, S. Houbrechts, *Organometallics* **1996**, *15*, 1935−1941. [2m] M. L. H. Green, S. R. Marder, M. E. Thomson, J. A. Bandy, D. Bloor, P. V. Kolinsky, R. J. Jones, *Nature* **1987**, *330*, 360−362.

[3] I. S. Lee, H. Seo, Y. K. Chung, *Organometallics* **1999**, *18*, 1091−1096.

[4] P. C. Jayprakash, R. I. Matsuoka, M. M. Bhadbhade, V. G. Puranik, P. K. Das, H. Nishihara, A. Sarkar, *Organometallics* **1999**, *18*, 3851−3858.

[5] J. Heck, S. Dabeck, T. MeyerFriedrichsen, H. Wong, *Coord. Chem. Rev.* **1999**, *190−192*, 1217−1254.

[6] [6a] W. M. Laidlaw, R. G. Denning, T. Verbiest, E. Chauchard, A. Persoons, *Proc. SPIE* **1994**, *2143*, 14−19. [6b] W. M. Laidlaw, R. G. Denning, T. Verbiest, E. Chauchard, A. Persoons, *Nature (London)* **1993**, *363*, 58−60.

[7] [7a] C. A. Merlic, M. M. Miller, B. N. Hietbunk, K. N. Houk, *J. Am. Chem. Soc.* **2001**, *123*, 4904−4918. [7b] C. A. Merlic, J. C. Walsh, D. J. Tantillo, K. N. Houk, *J. Am. Chem. Soc.* **1999**, *121*, 3596−3606. [7c] T. J. J. Müller, A. Netz, M. Ansorge, E. Schmälzlin, C. Bräuchle, K. Meerholz, *Organometallics* **1999**, *18*, 5066−5074.

[8] W. Wenseleers, A. W. Gerbrandij, E. Goovaerts, M. H. Garcia, M. P. Robalo, P. J. Mendes, J. C. Rodrigues, A. R. Dias, *J. Mater. Chem.* **1998**, *8*, 925−930.

[9] M. H. Garcia, M. P. Robalo, A. R. Dias, M. T. Duarte, W. Wenseleers, G. Aerts, E. Goovaerts, M. P. Cifuentes, S. Hurst, M. G. Humphrey, M. Samoc, B. LutherDavies, *Organometallics* **2002**, *21*, 2107−2118.

[10] E. Goovaerts, W. Wenseleers, P. Hepp, M. H. Garcia, M. P. Robalo, A. R. Dias, M. F. M. Piedade, M. T. Duarte, *Chem. Phys. Letters* **2003**, *367*, 390−397.

[11] J. P. Tranchier, R. Chavignon, D. Prim, A. Auffrant, Z. Plyta, F. RoseMunch, E. Rose, *Tetrahedron Lett.* **2000**, *41*, 2607−2611.

[12] K. Sonogashira, *Comprehensive Organic Chemistry* (Ed.: B. M. Trost), Pergamon, Oxford, **1991**, *3*, 521−549.

[13] A. R. Dias, M. H. Garcia, M. P. Robalo, M. L. H. Green, K. K. Lai, A. J. Pulham, S. M. Kuebler, G. Balavoine, *J. Organomet. Chem.* **1993**, *453*, 241−247.

[14] A. R. Dias, M. H. Garcia, J. C. Rodrigues, M. L. H. Green, S. M. Kuebler, *J. Organomet. Chem.* **1994**, *475*, 241−245.

[15] W. J. Geary, *Coord. Chem. Rev.* **1977**, *7*, 81−122.

[16] [16a] F. Van Meurs, J. M. A. Baas, H. van Bekkum, *J. Organomet. Chem.* **1976**, *113*, 353−259. [16b] F. Van Meurs, J. M. van der Toorn, H. van Bekkum, *J. Organomet. Chem.* **1976**, *113*, 341−251.

[17] [17a] G. Loire, S. Schouteeten, B. Andrioletti, D. Prim, J. P. Tranchier, F. RoseMunch,E. Rose, A. Persoons, *Comptes Rendus Chimie* **2003**, 223−230. [17b] F. RoseMunch, E. Rose, *Modern Arene Chemistry* **2002**, chapter 11, p. 368 (D. Astruc, Ed.), Wiley-VCH, Weinheim, Germany. [17c] F. RoseMunch, E. Rose, *Eur. J. Inorg. Chem.* **2002**, *6*, 1269−1283. [17d] F. RoseMunch, E. Rose, J. P. Djukic, J. Vaisserman, *Eur. J. Inorg. Chem.* **2000**, *5*, 1295−1306. [17e] F. RoseMunch, V. Gagliardini, C. Renard, E. Rose, *Coord. Chem. Rev.* **1998**, *178−180*, 249−268. [17f] F. RoseMunch, K. Aniss, E. Rose, J. Vaisserman, *J. Organomet. Chem.* **1991**, *415*, 223−255. [17g] A. Solladié-Cavallo, J. Suffert, *Org. Magn. Res.* **1980**, *14*, 426−430.

[18] T. J. J. Müller, M. Ansorge, H. J. Lindnes, *Chem. Ber.* **1996**, *129*, 1433−1440.

[19] T. J. J. Müller, H. J. Lindnes, *Chem. Ber.* **1996**, *129*, 607−613.

[20] D. R. Kanis, M. A. Ratner, T. J. Marks, *J. Am. Chem. Soc.* **1992**, *114*, 10338−10357.

[21] [21a] D. G. Carroll, S. P. McGlynn, *Inorg. Chem.* **1968**, *7*, 1285−1290. [21b] R. T. Lundquist, M. J. Cais, *J. Org. Chem.* **1962**, *27*, 1167−1170.

[22] M. H. Garcia, M. P. Robalo, A. R. Dias, M. F. M. Piedade, A. Galvão, W. Wenseleers, E. Goovaerts, *J. Organomet. Chem.* **2001**, *619*, 252−264.

[23] [23a] K. Clays, A. Persoons, *Phys. Rev. Lett.* **1991**, *66*, 2980. [23b] K. Clays, A. Persoons, *Rev. Sci. Instrum.* **1992**, *63*, 3285−3289.

[24] E. Hendrickx, K. Clays, A. Persoons, C. Dehu, J. L. Brédas, *J. Am. Chem. Soc.* **1995**, *117*, 3547−3555.

[25] S. Houbrechts, K. Clays, A. Persoons, Z. Pikramenou, J.M. Lehn, *Chem. Phys. Lett.* **1996**, *258*, 485−489.

[26] D. D. Perrin, W. L. F. Amarego, D. R. Perrin, *Purification of Laboratory Chemicals*, 2nd ed., Pergamon, New York, **1969**.

[27] C. A. L. Mahaffy, P. L. Pauson, *Inorg. Syntheses* **1990**, *28*, 136−140.

[28] [28a] C. Dell'Erba, D. Spinelli, *Tetrahedron* **1965**, *21*, 1061−1066. [28b] P. Reynaud, R. Delaby, *Bull. Soc. Chem. Fr.* **1955**, 1614−1615. [28c] P. Hapiot, F. Demanzane, A. Yassar, F. Garnier, *J. Phys. Chem.* **1996**, *100*, 8397−8401. [28d] D. Prim, G. Kirsh, *J. Chem. Soc., Perkin Trans. 1* **1994**, 2603−2606.

[29] G. Balavoine, M. L. H. Green, J. P. Sauvage, *J. Organomet. Chem.* **1977**, *128*, 247−252.

[30] G. S. Ashby, M. I. Bruce, I. B. Tomkins, R. C. Walli, *Aust. J. Chem.* **1979**, *32*, 1003−1016.

[31] G. M. Sheldrick, *SHELXS86, Program for Crystal Structure Solution*, University of Göttingen, **1986**.

[32] D. J. Watkin, C. K. Prout, J. R. Carruthers, P. W. Betteridge, *Crystals*, issue 10, Chemical Crystallography Laboratory, University of Oxford, U. K. **1996**.

[33] D. T. Cromer, *International Tables for Xray Crystallography*, vol. IV, Kynoch Press, Birmingham, U. K., **1974**.

Received April 3, 2003

 © 2003 Wiley-VCH Verlag GmbH & Co. KGaA, Weinheim

Mono- and Dinuclear Complexes of a Flexible Schiff Base Ligand − Crystal Structures of a Bishelicate and Two Acentric Monohelicates

Jesús Sanmartín,*[a] Ana M. García-Deibe,[a] Manuel R. Bermejo,[a] Fernando Novio,[a] Debora Navarro,[a] and Matilde Fondo[a]

Keywords: Helical structures / N ligands / Schiff bases / Supramolecular chemistry / Transition metals

Neutral Ni^{II}, Pd^{II}, Cu^{II}, Ag^{I}, Zn^{II}, Cd^{II}, and Pb^{II} complexes of *N*,*N*′-bis(2-tosylaminobenzylidene)-1,4-diaminobutane (H_2SB) have been prepared. The Schiff base seems to exist in a helically coiled state around nickel, copper and zinc ions, but not in $Pd(SB)\cdot 3H_2O\cdot MeCN$, $Ag_2(SB)\cdot 2H_2O$, $Cd(SB)\cdot 3H_2O$, and $Pb(SB)\cdot 3H_2O$, the metal ions of which seem to show planar geometries. The determination of the absolute structures of $Cu(SB)\cdot MeCN$ and $Zn(SB)\cdot 2MeCN$, which crystallise as non-centrosymmetric racemic compounds, shows that these metal(II) ions assume distorted tetrahedral coordination geometries involving the four N atoms of the dianionic ligand. X-ray structural characterisation also shows that this ligand behaves as a $N_2{+}N_2$ donor in the [4+4] bishelicate $Ni_2(SB)_2\cdot 5MeCN$. Secondary interactions between metal centres and one of the O atoms of each tosyl group are detected in these three crystal structures, being especially intense in the dimeric one.

(© Wiley-VCH Verlag GmbH & Co. KGaA, 69451 Weinheim, Germany, 2003)

Introduction

Among other reasons, helical metal complexes[1−4] have attracted physicists' and chemists' attention due to their potential optical activity.[5] As achiral ligands are unable to induce predetermined chirality, helicates crystallise as racemic compounds or as mechanical mixtures of enantiopure crystals (racemic mixtures or conglomerates).[6−7] Of these two types of crystalline racemates, conglomerates are far easier to resolve, but much rarer.

The obtaining of non-centrosymmetric inorganic materials with nonlinear optical properties is undoubtedly a challenge in chemistry.[8] Since the inverse of a left-handed helix is a right-handed one, a helical compound may crystallise with an inversion centre if both types of handedness appear in a crystal. Thus, with achiral ligands, the heterochiral interaction required to form racemic compounds takes place in centrosymmetric space groups, the overwhelming majority, whereas the minority homochiral crystallisation required to obtain conglomerates exclusively occurs in non-centrosymmetric space groups.

We have recently reported the crystal structures of the two compounds $Zn_2(SB^1)_2\cdot 1.5H_2O\cdot MeCN$[9] (a typical racemic compound) and Λ-$Zn(SB^2)\cdot H_2O$,[10] which homochirally crystallises as a conglomerate. Despite the intrinsic similarities between these two symmetric *N*-tosyl-substituted Schiff bases, which contain $(CH_2)_3$ and $CH_2CH(OH)CH_2$ groups, respectively, as spacers (Scheme 1), their behaviour in their corresponding helical Zn^{II} complexes is either binucleating ($N_2{+}N_2$ donor) or mononucleating (N_4 donor), respectively. Another ligand with a three-membered spacer, although a more rigid one, in the form of H_2SB^3 (Scheme 1), only yielded racemic monohelicates.[11]

In an effort to understand the behaviour of this type of helical thread, we wished to explore how the higher flexibility of a $(CH_2)_4$ spacer might influence the coordination behaviour and spatial arrangement of the potential helicand H_2SB ("S" arranged, for a classic bisbidentate conduct, in Scheme 1) in several main group and transition (first and second row) metal complexes.

Results and Discussion

Mass and IR Spectroscopic Data

The mass spectra of these complexes exhibit medium- to high-intensity signals, with satisfactory isotopic profiles, attributable to $[M(SB) + H]^+$ species, as expected for mononuclear and monomeric compounds. This kind of species is more in accordance with a solvated nature than with coordinating behaviour of the water molecules present in these complexes. With respect to the ESI MS spectrum of the Ag^{I} complex, a group of peaks assignable to $[Ag_2(SB) + H]^+$ species could be notable, since it seems to corroborate the $Ag_2(SB)\cdot 2H_2O$ formula found by elemental analysis.

[a] Dpto. de Química Inorgánica, Facultade de Química, Universidade de Santiago de Compostela, Campus Sur, Santiago de Compostela, 15782 Spain
Fax: (internat.) +34-(0)981-597525
E-mail: qisuso@usc.es

Supporting information for this article is available on the WWW under http://www.eurjic.org or from the author.

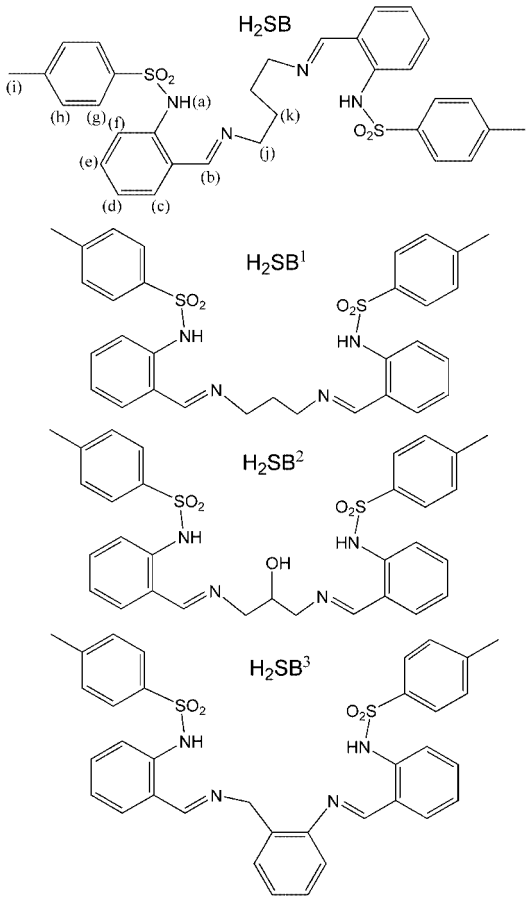

Scheme 1. Schematic representation of the *N*-tosyl-substituted Schiff bases H_2SB^1, H_2SB^2, H_2SB^3, and H_2SB (with labelling scheme for ^1H NMR studies)

It may also be worth mentioning that no peaks with intensities higher than 4% can be detected in the spectra of these complexes in those regions in which dimeric species could appear, even in the case of the dimeric Ni^{II} complex. This prevents the use of the ESI-MS technique to determine whether these complexes are of the type M(SB) or $M_2(SB)_2$.

The IR spectra of these complexes contain absorptions consistent with the presence of the N_4 donor ligand. The CN stretching frequencies show shifts to lower wavenumber values with respect to those observed for the free ligand.[12] The slight shifts of the ν(C=N) bands to lower wavenumber (in the 1−15 cm^{-1} range) contrasts with the substantial shifts observed for the ν(C−N) stretching frequencies (30−45 cm^{-1}). These facts, together with the absence of the ν(N−H) band, are in agreement with double deprotonation of the ligand, as well as with the participation of both the amide and imine N atoms in the coordination to the metal centres.[9−12]

Other bands attributable to $\nu_{as}(SO_2)$ and $\nu_s(SO_2)$ vibration modes also experience significant decreases in their frequencies. This behaviour could be a sign of interaction between the metal centre and the O atoms belonging to the tosyl groups.

Single-Crystal X-ray Diffraction Studies

Cu(SB)·MeCN and Zn(SB)·2MeCN

Slow evaporation of saturated acetonitrile solutions of $Cu(SB)\cdot 4H_2O$ and $Zn(SB)\cdot H_2O$ yielded brown and yellow X-ray-quality crystals of Cu(SB)·MeCN and Zn(SB)·2MeCN, respectively. The crystallographic analyses reveal that in both asymmetric units, a solvated acetonitrile molecule (with 0.5 and 1 occupancy sites, respectively) coexists with half a molecule of the symmetric helical complex M(SB) (M= Cu or Zn), the metal ion of which is situated on a twofold axis positioned along *z*. The whole complex molecules can be generated by the same symmetry operation (−*x*, −*y*, *z*). All the atoms so generated have been labelled with $^{\#1}$.

Although both helical enantiomers (Λ and Δ) are present in the unit cell, only the molecular structure of the single-stranded helix corresponding to Λ-Cu(SB) is represented in Figure 1, whereas Δ-Zn(SB) is shown in Figure 2, with the atom labelling schemes used in Table 1. This table lists the most significant bond lengths and angles.

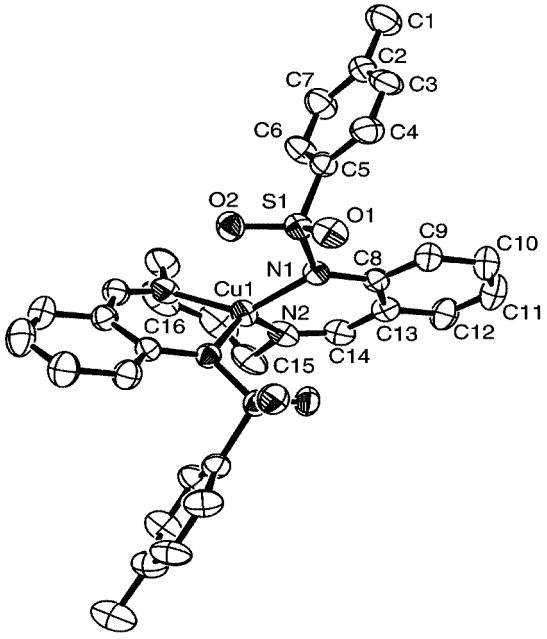

Figure 1. ORTEP view of Λ-Cu(SB), contained in the Cu(SB)·MeCN unit cell; symmetry transformations used to generate equivalent atoms: $^{\#1}$ −*x*, −*y*, *z*

The ions in both complexes are symmetrically tetra-coordinated to the four N atoms of the Schiff base, with bond lengths in the ranges typical for this sort of complex. Both coordination environments can be regarded as distorted tetrahedra, especially that corresponding to the Cu^{II} ion, in that the dihedral angles between the two N−M−N terminal planes (θ) are 65.79(14)° and 73.31(7)° for the Cu^{II} and Zn^{II} complexes, respectively. Moreover, one of the O atoms of each tosyl group [O(2) and $O(2)^{\#1}$] is weakly interacting with the Cu^{II} and Zn^{II} ions, although these M···O distances (ca. 2.8 Å) are too long to be viewed as true coordinated bonds. The $S(1)\cdots S(1)^{\#1}$ distance (about

 © 2003 Wiley-VCH Verlag GmbH & Co. KGaA, Weinheim

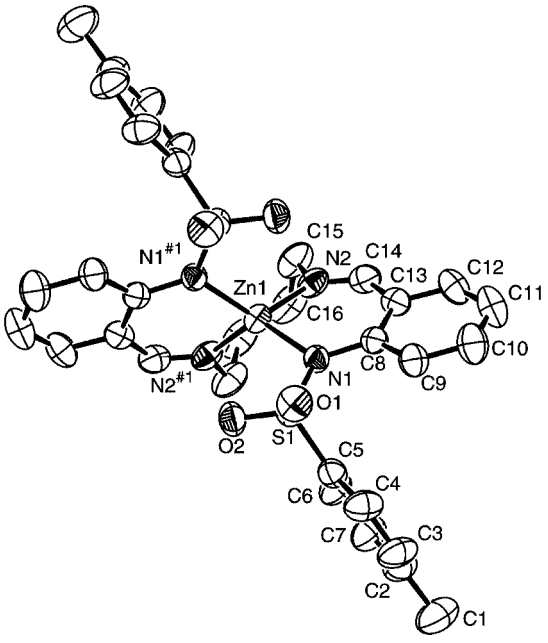

Figure 2. ORTEP view of Δ-Zn(SB), contained in the Zn(SB)·2MeCN unit cell; symmetry transformations used to generate equivalent atoms: #1 $-x, -y, z$

4.34 and 4.62 Å for the copper and zinc complex, respectively) could in both cases be regarded as a rough estimate of the pitch.[3] As also occurs in other related monohelicates,[9−12] if we consider the whole ligand, the wrapping angle would exceed 360°.

The chemical species concerned here, Cu(SB)·MeCN and Zn(SB)·2MeCN, are intrinsically chiral due to their helicity, crystallising in the non-centrosymmetric space group *Fdd*2 of the orthorhombic system, belonging to the *mm*2 crystal class. Although this class is not qualified as chiral or enantiomorphic, it does present a polar axis direction (z),[13] which means that the unit-cell origin may be arbitrarily placed along this axis. In these cases, the values found for the Flack parameter[14] [0.03(19) and 0.021(11) for the Cu^{II} and Zn^{II} complexes, respectively] determine a correct absolute structure, as well as a closely coincident orientation of the structure with respect to the polar axis, more than the enantiopurity or racemic twinning evaluation related with homochiral crystals.

Both crystal packings, which we can see in Figure 3 for Zn(SB)·2MeCN, are based on feeble C−H···O, C−H/π and π-π stacking interactions. They clearly show both types of helical molecules, with right- and left-handedness (Δ and Λ enantiomers, respectively) arranged on infinite sheets parallel to their C faces, indicative of their non-linearity. This heterochiral crystallisation satisfactorily explains the lack of global optical activity exhibited by crystalline samples of these racemic compounds in acetonitrile solution.

$Ni_2(SB)_2$·5MeCN

This crystal structure shows the double helical assembly of this neutral dinuclear Ni^{II} complex (Figure 4), in which the ligand assumes a N_2+N_2 bisbidentate coordinating behaviour. As is the case for many other homotopic double-stranded helicates, this one crystallises as a racemate in the most frequently occurring space group for metallohelicates: the centrosymmetric $C2/c$.[3] The X-ray structural characterisation reveals that its asymmetric unit contains half the bishelicate, with a crystallographically imposed twofold symmetry, which allows the other half molecule to be generated by use of the symmetry operation $-x, y, -z + 1/2$. All the atoms related in this way have been denoted with #1. Additionally, two and a half molecules of solvated acetonitrile are also present, with some disorder, in the asymmetric unit.

Table 1. Selected bond lengths and angles for $Ni_2(SB)_2$·5MeCN, Cu(SB)·MeCN, and Zn(SB)·2MeCN

$Ni_2(SB)_2$·5MeCN[a]		Cu(SB)·MeCN[b]		Zn(SB)·2MeCN[b]	
Bond lengths					
Ni(1)−N(21)	1.965(6)	Cu(1)−N(1)	1.965(3)	Zn(1)−N(1)	1.978(2)
Ni(1)−N(11)	1.973(8)	Cu(1)−N(1)#1b	1.965(3)	Zn(1)−N(1)#1b	1.978(2)
Ni(1)−N(12)	1.987(6)	Cu(1)−N(2)	1.961(4)	Zn(1)−N(2)	2.009(2)
Ni(1)−N(22)	2.030(5)	Cu(1)−N(2)#1b	1.961(4)	Zn(1)−N(2)#1b	2.009(2)
N(11)−C(108)	1.418(11)	N(1)−C(8)	1.393(5)	N(1)−C(8)	1.405(3)
N(11)−S(1)	1.588(9)	N(1)−S(1)	1.612(3)	N(1)−S(1)	1.605(2)
N(12)−C(114)	1.316(9)	N(2)−C(14)	1.273(6)	N(2)−C(14)	1.274(4)
N(21)−S(2)	1.605(5)	N(2)−C(15)	1.455(6)	N(2)−C(15)	1.475(4)
N(21)−C(208)	1.408(9)	S(1)−O(1)	1.436(3)	S(1)−O(1)	1.444(2)
N(22)−C(214)	1.267(9)	S(1)−O(2)	1.447(3)	S(1)−O(2)	1.444(2)
Bond angles					
N(11)−Ni(1)−N(22)	104.0(3)	N(1)−Cu(1)−N(1)#1b	108.2(2)	N(1)−Zn(1)−N(1)#1b	119.02(13)
N(11)−Ni(1)−N(12)	91.3(3)	N(1)−Cu(1)−N(2)	93.90(14)	N(1)−Zn(1)−N(2)	94.47(9)
N(11)−Ni(1)−N(21)	151.9(3)	N(1)−Cu(1)−N(2)#1b	132.99(14)	N(1)−Zn(1)−N(2)#1b	124.55(9)
N(12)−Ni(1)−N(21)	107.0(2)	N(2)−Cu(1)−N(2)#1b	100.5(2)	N(2)−Zn(1)−N(2)#1b	101.07(15)
Torsion angles					
N(12)−C(115)−C(116)−C(16)#1a	45.7(6)	N(2)−C(15)−C(16)−C(16)#1b	−77.8(7)	N(2)−C(15)−C(16)−C(16)#1b	−78.3(4)
N(22)−C(215)−C(216)−C(216)#1a	75.7(6)				

[a] Symmetry transformations used to generate equivalent atoms: #1a: $-x, y, -z + 1/2$. [b] #1b: $-x, -y, z$.

 © 2003 Wiley-VCH Verlag GmbH & Co. KGaA, Weinheim

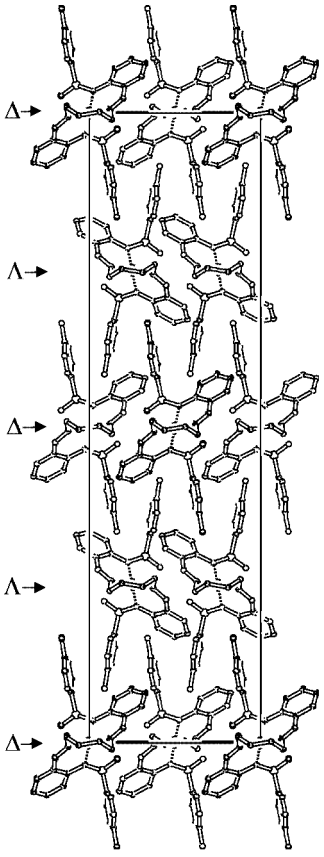

Figure 3. View normal to the *C* face of the crystal packing of Zn(SB)·2MeCN, showing the lamination of both types of helical enantiomers (Δ and Λ); acetonitrile molecules have been omitted for clarity

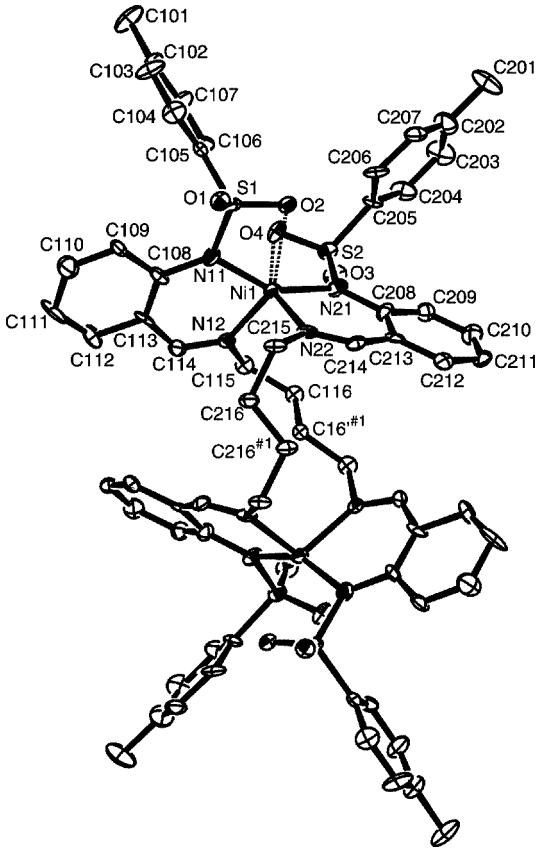

Figure 4. ORTEP view of Δ,Δ-$Ni_2(SB)_2$ contained in the $Ni_2(SB)_2$·5MeCN unit cell, with the secondary Ni···O interactions shown as dotted lines; symmetry transformations used to generate equivalent atoms: $^{\#1}$ $-x, y, -z + 1/2$

The [4 +4] bishelical nature of $Ni_2(SB)_2$·5MeCN is not common for dinuclear Ni^{II} complexes with bisbidentate ligands, which mostly give rise to [6 + 6] triple-stranded helicates.[3−4,15] However, so far the X-ray evidence available indicates, this sort of *N*-tosyl-substituted ligand only yields four coordinate complexes, both in double-stranded helicates[9,16] and monohelicates.[9−12] This even occurs with metal ions that characteristically display pseudooctahedral geometries, such as Mn^{II} or Fe^{II}, in that they exhibit unfamiliar tetrahedral geometries with H_2SB^3.[11]

The explanation for this low coordination number may lie in the bulky tosyl groups. On one hand, they appear to exert such substantial steric hindrance as apparently to avoid the presence of exogenous coordinating groups, solvent molecules or additional ligand units suitable for achieving an actual hexa-coordination. On the other hand, this uncommon tetra-coordination of the Ni^{II} ions may be easier to understand if we also consider that significant secondary Ni···O interactions (ca. 2.5 Å) exist between the Ni^{II} ion and an O atom of each adjacent tosyl group [O(2) and O(4)]. As a result, each N_4 pseudotetrahedral Ni^{II} environment (Figure 4) suffers a substantial seesaw-shaped distortion that the value of θ (ca. 80.15°) does not reveal at first sight, but the N−Ni−N angles do (Table 1). Although these minor M···O contacts are typical of metal complexes containing this type of *N*-tosyl-substituted Schiff-base ligand,[9−12,16] it could be worthy of mention that these interactions seem to be significantly shorter when the ligand behaves as N_2+N_2-bisbidentate (about 2.5 Å),[9,16] than as merely N_4-tetradentate (usually about 2.8 Å),[9−12] as in the preceding Cu^{II} and Zn^{II} complexes (vide supra).

The bishelical arrangement of $Ni_2(SB)_2$·5MeCN with metal coordination environments that could be also regarded as severely distorted N_4O_2 pseudooctahedral (Figure 4), therefore seems to be more appropriate than simple mononucleating N_4 donor behaviour for satisfying the stereochemical requirements of Ni^{II} (preferably octahedral). This tendency of Ni^{II} to achieve a pseudooctahedral coordination through secondary Ni···O contacts had also been indicated for some mesohelicates containing bisbidentate ligands designed to provide tetrahedral coordination environments.[17] Something similar also occurred in the case of $Ni_2(SB^1)_2$·MeCN,[16] whereas the rigid H_2SB^3 (Scheme 1), designed to be N_4-mononucleating, is able to impose a distorted tetrahedral geometry, though also exhibiting Ni···O interactions (2.5 and 2.8 Å).[11] In contrast, a simple N_4-compartment can adequately fulfil the tetrahedral coordination preferences of Cu^{II} ions. Unlike Cu^{II} and Ni^{II}, the spherical Zn^{II} ions (d^{10}) allow both monohelicates to be obtained, with H_2SB, H_2SB^2 [10] or H_2SB^3, and also a bishelicate,[9] when interacting with H_2SB^1 (Scheme 1). Hence, while the spacer length has a significant influence on the

 © 2003 Wiley-VCH Verlag GmbH & Co. KGaA, Weinheim

stereochemistry of some types of helicates,[18] it does not appear to be a crucial factor for providing single- or double-stranded helicates with *N*-tosyl-substituted Schiff bases.

Ideally, homotopic helicates should give rise to palindromic helices; this means with constant pitch,[3] as occurs in $Ni_2(SB^1)_2$·MeCN,[16] in which both $(SB^1)^{2-}$ threads are similarly arranged, the centroids of their benzylidene groups being at about 10 Å. In principle, the ligand array in $Ni_2(SB)_2$·5MeCN could appear similar to that, even also showing a minor and a major groove. However, a thorough inspection allows it to be established that the higher flexibility of SB^{2-} seems to tolerate a clear disparity of both helical strands, with substantially different arrangements (Figure 5). Thus, we can see that the C101−C101$^{\#1}$ ligand strand (shaded in Figure 5) seems more stretched than the C201−C201$^{\#1}$ one, which shows a pronounced folding. Hence, the theoretical pitch must be longer for the first one. In fact, the distances between their benzylidene centroids are about 10.9 and 8.6 Å, respectively. Although the two coilings are fairly different, their assembly, lacking significant intra- or intermolecular π-π or C−H/π interactions, produces a symmetric, even crystallographically, homotopic double-helix.[3] Consequently, their also different wrapping angles could compensate for their differences, and result in an intramolecular Ni···Ni distance of about 6.8 Å. This is only slightly longer than that reported for $Ni_2(SB^1)_2$·MeCN (6.2 Å).[16] Similitude in the intramolecular M···M distances with $(CH_2)_2$ and $(CH_2)_3$ bridging groups has also been observed for some [6+6] Fe^{II} bishelicates.[19]

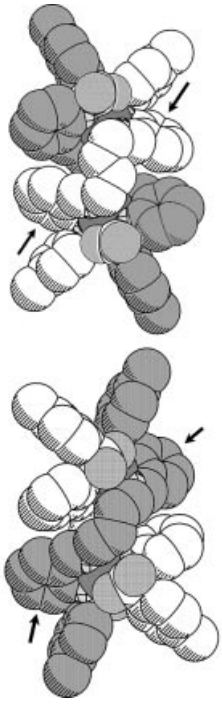

Figure 5. Two opposite views of a compact ball scheme for $Ni_2(SB)_2$·5MeCN with the helical axis parallel to left margin; the more stretched ligand strand (C101−C101$^{\#1}$) is shaded; the intramolecular distances between those ring centroids signed by arrows are: 8.6 Å (top) and 10.9 Å (bottom)

Finally, the C−N distances found confirm those observed in the IR spectroscopy section. Thus, the $C{=}N_{imine}$ and $C\text{-}N_{imine}$ distances show values similar to those reported for the free ligand,[12] whereas the $C\text{-}N_{amide}$ distances are significantly longer. The M−N distances (Table 1) are in the usual range reported for Ni^{II}, Cu^{II}, and Zn^{II} complexes containing N_{amide} and N_{imine} donor atoms.[9−12,16,20] As was also suggested by the IR techniques, M···O interactions seem to affect the S−O bonds, since these are slightly longer than those found for the free ligand.[12]

^{1}H NMR Studies

Zn(SB)·H$_2$O

In order to investigate the solution behaviour of Zn(SB)·H_2O, we have studied its ^{1}H NMR spectra in $CDCl_3$ at temperatures ranging between 323 and 218 K (deposited as Electronic Supporting Information, see footnote on the first page of this article). From these results, and in view of the ligand symmetry, the observation of two signals each for H_j and H_k (Scheme 1), must be a consequence of the diastereotopic natures of the geminal protons of each methylene group. This is consistent with a helical arrangement,[21] as also occurred in the solid state. Since both methylene protons are non-equivalent even at 323 K, Zn(SB)·H_2O seems to preserve its helical conformation in chloroform solution on the NMR timescale, which is also indicative of a strong coordination of the N atoms to the metal centre. On the basis of the kinetic stability of this complex, the results obtained at room temperature can be used as a diagnostic probe for helicity.

Both COSY and NOESY experiments at room temperature in chloroform, acetonitrile or dimethyl sulfoxide solutions allow a full assignment of the ^{1}H NMR signals (see Experim. Section). They clearly show AB spin behaviour of the methylene protons on the NMR timescale, since those protons situated near to equatorial positions with respect to the C(15)N(2)C(14) or C(15$^{\#1}$)N(2$^{\#1}$)C(14$^{\#1}$) planes, H_{jeq} and H_{keq}, are observed at higher field than those situated close to axial positions (H_{jax} and H_{kax}).

A NOESY experiment (Figure 6) shows coupling of H_b with H_c and H_{jeq} (but not with H_{jax}), as well as between H_g and H_f. Consequently, these intramolecular H···H distances should be lower than ca. 3.1 Å in solution. The X-ray crystal studies determined that the H_b···H_c, H_b···H_{jeq} and H_g···H_f distances in the solid state are in the 2.2−2.7 Å range, whereas H_b···H_{jax} is higher (3.1 Å). These facts seem to indicate that the spatial arrangement of the helical ligand in the zinc complex is analogous, both in the solid state and in solution (even in a coordinating solvent such as dmso).

Pb(SB)·3H$_2$O

A NOESY experiment was a key element in the full assignment of the proton signals (deposited as Electronic Supporting Information). Since the H_b and H_i signals are two clear references in the spectrum, the H_i-H_h, H_b-H_c and H_b-H_j couplings allow the unequivocal identification

 © 2003 Wiley-VCH Verlag GmbH & Co. KGaA, Weinheim

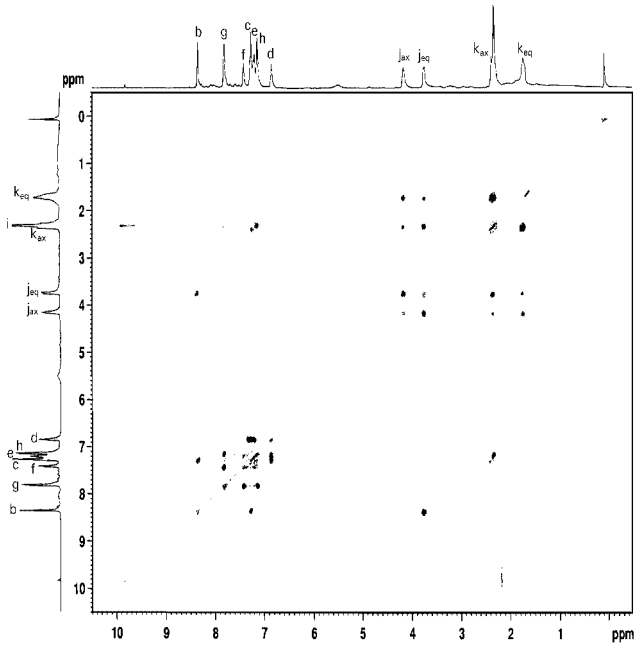

Figure 6. NOESY experiment for $Zn(SB)\cdot H_2O$ in $CDCl_3$ at 300 K

of H_h, H_c, and H_j, respectively. Similarly, the H_c-H_d, H_d-H_e, and H_e-H_f couplings provide evidence of the H_d, H_e, H_f, and H_g positions, whilst the absence of coupling between H_g and H_f seems to indicate that the spatial arrangement of the tosyl groups, with respect to benzylidene rings, is not equivalent to that observed in $Zn(SB)\cdot H_2O$.

The experiment mentioned also shows the enantiotopic nature of the geminal protons in each methylene group on the NMR timescale at room temperature. This could rule out a helical arrangement of SB^{2-} in this complex. Although the observation of one signal each for H_j and H_k (in $[D_6]$DMSO or Cl_3CD at room temperature) could be due to a fast exchange between helical and non-helical arrangements of SB^{2-} in the Pb^{II} complex, a series of ^1H NMR spectra in the 323−218 K range reveals the kinetic stability of this complex in chloroform solution, even at high temperatures.

Pd(SB)·3H₂O·MeCN, Ag₂(SB)·2H₂O and Cd(SB)·3H₂O

The diamagnetism of the Pd^{II} complex attests to the electronic pairing in the d_{xz}, d_{yz}, d_z^2, and d_{xy} orbitals, which is consistent with a square planar symmetry for a d^8 ion. Both the spectra of the Pd^{II} and Cd^{II} complexes display only one signal each for H_j and H_k, as would be expected for a planar arrangement of SB^{2-}. NOESY experiments in $[D_6]$DMSO at room temperature allow a rigorous assignment of the ^1H NMR signals for these complexes (see Experim. Section).

The diamagnetism shown by $Ag_2(SB)\cdot 2H_2O$ attests to the presence of Ag^I ions and consequently the inability of the ligand to stabilise Ag^{II} even under strongly oxidising conditions (10 V). As in previous cases, the observation of only one signal each for H_j and H_k at room temperature (Electronic Supplementary Material) is indicative of a non-helical arrangement of SB^{2-} in this complex. Its anomalous stoichiometry and the ligand versatility allows the postulation that the ligand could behave as bisbinucleating, so it could act as a bridge between the two Ag^I ions.

Diffuse Reflectance and Magnetism

The diffuse reflectance spectrum of $Ni_2(SB)_2\cdot 2H_2O$ is characterised by a medium intensity broad band around 680 nm, which is attributed to a *d-d* transition expected for d^8 ions in tetrahedral fields.[22] In the spectrum of $Cu(SB)\cdot 4H_2O$, the only absorption attributable to a *d-d* transition is observed at about 460 nm, which is also consistent with a tetrahedral geometry.[23]

The magnetic moment for the Ni^{II} dimer at room temperature (3.0 BM per mol of Ni^{2+}) is quite low for a tetrahedral compound. This could be caused by a considerable distortion from the ideal geometry, resulting in a fall in the orbital contribution to this value.[24] In fact, we have found a similar value (3.3 BM per mol of Ni^{2+}) for $Ni_2(SB^1)_2\cdot MeCN$,[16] in which the ligand, helical arrangement and the Ni···Ni distance (ca. 6.2 Å) are not very different from those observed for $Ni_2(SB)_2\cdot 2H_2O$. No coupling interactions between the two Ni^{2+} ions are to be expected, because these are quite far apart (ca. 6.8 Å) and the ligands seem incapable of transmitting any interaction. Finally, a μ value at room temperature (2.1 BM) in the narrow range expected for a magnetically dilute tetrahedral compound arises from the magnetic susceptibility measurements for $Cu(SB)\cdot 4H_2O$.

Conclusions

The studied N_4 donor ligand displays a helical arrangement around those ions corresponding to the fourth period − Ni^{II}, Cu^{II}, and Zn^{II} − but it appears planar around Pd^{II}, Ag^I, Cd^{II}, and Pb^{II} ions, belonging to the fifth and sixth periods. Ionic radii thus seem to play a relevant role in the stereochemistry. Similarly, and in view of the secondary M···O interactions, a predilection for pseudooctahedral rather than distorted tetrahedral environments could be responsible for the obtaining of double-stranded Ni^{II} helicates, instead of monohelicates, with *N*-tosyl-substituted Schiff bases containing a pure alkyl chain of three or four members as spacer. Both Cu^{II} and Zn^{II} ions assume distorted tetrahedral coordination geometries involving the four N atoms of the dianionic ligand in their monohelicates, whereas the ligand behaves as a N_2+N_2 donor in $Ag_2(SB)\cdot 2H_2O$ and $Ni_2(SB)_2\cdot 5MeCN$.

The studied $(CH_2)_4$ spacer between the two 2-tosylaminobenzylidene units has not given rise to homochiral crystals of $Ni_2(SB)_2\cdot 5MeCN$, $Cu(SB)\cdot MeCN$, or $Zn(SB)\cdot 2MeCN$. However the last two crystallise in an acentric space group with a polar axis, forming alternative sheets of the two helical enantiomers (Λ and Δ), which is unusual for helical racemic compounds.

 © 2003 Wiley-VCH Verlag GmbH & Co. KGaA, Weinheim

Experimental Section

General: Elemental analyses were performed on a Carlo−Erba EA 1108 analyser. NMR spectra were recorded on a Bruker DRX 500 spectrometer in $CDCl_3$, CD_3CN, or [D_6]DMSO as solvents. Infrared spectra were recorded as KBr pellets on a Bio-Rad FTS 135 spectrophotometer in the 4000−600 cm^{-1} range. Electrospray mass spectra were recorded on a LC/MSD Hewlett−Packard 1100 spectrometer with DMSO and methanol with formic acid (2%) as solvent. The FAB mass spectrum was recorded on a Micromass Autospec spectrometer, with *m*-nitrobenzyl alcohol as matrix. Diffuse reflectance spectra were recorded on a Perkin−Elmer Lambda 9 spectrophotometer. Magnetic susceptibility measurements were performed on pulverised samples at room temperature with a Sherwood Scientific magnetic susceptibility balance.

Syntheses: Chemicals of the highest commercial grade available (Aldrich) were used as received. *N*,*N*′-Bis(2-tosylaminobenzylidene)-1,4-diaminobutane (H_2SB) was prepared[12] by condensation of 2-(tosylamino)benzaldehyde[25] with 1,4-diaminobutane. Complexes, except for Pd(SB)·3H_2O·MeCN, were obtained by an electrochemical method,[9−12,22] in which a metal anode was oxidised in an acetonitrile solution of H_2SB. The preparation of Zn(SB)·H_2O is outlined below. The cell can be summarised as:
$Zn_{(+)}|H_2SB + NMe_4ClO_{4(MeCN)}|Pt_{(-)}$.

Caution: *Although no problem has been encountered in this work, all perchlorate compounds are potentially explosive, and should be handled in small quantities and with great care!*

An acetonitrile solution (80 cm^3) of H_2SB (100 mg, 0.166 mmol), containing about 30 mg of tetramethylammonium perchlorate, was electrolysed for 1 h 45′, with use of a 5 mA current intensity and an initial voltage of 16 V. Filtration and concentration of the resulting solution yielded a solid that was washed with diethyl ether and dried in vacuo. The ligand amount, current intensity and electrolysis time were identical for all the complexes. Initial voltages were in the 8−16 V range.

Pd(SB)·3H_2O·MeCN was obtained by heating of a methanol solution containing H_2SB, NaOH, and $Pd(AcO)_2$ in 1:2:1 molar ratio at reflux for 6 hours. Filtration of the resulting suspension yielded a solid that was washed with diethyl ether and dried in vacuo. The reaction end was determined by TLC.

$Ni_2(SB)_2$·2H_2O: Green solid. Yield 81%. M.p. > 320 °C. $C_{64}H_{68}N_8Ni_2O_{10}S_4$ (1354.91): calcd. C 56.7, H 5.1, N 8.3, S, 9.5; found C 56.7, H 5.3, N 8.5, S 9.2. IR (KBr): $\tilde{\nu}$ = 3440 (br., O−H), 1626 (s, C=N), 1301 (s, C−N), 1260, 1134 (s, SO_2) cm^{-1}. FAB-MS: *m*/*z* (%) = 659.0 (55%) [Ni(SB) + H]$^+$; μ (300 K): 6.0 B.M. UV/Vis (solid): λ_{max} (nm) = 680 [m, $^3T_1(P)\leftarrow{}^3T_1(F)$].

Pd(SB)·3H_2O·MeCN: Brown solid. Yield 82%. M.p. 260 °C. $C_{34}H_{41}N_5O_7PdS_2$ (802.27): calcd. C 51.9, H 4.9, N 7.5, S 8.6; found C 51.6, H 4.7, N 7.7, S 8.3. IR (KBr): $\tilde{\nu}$= 3441 (br., O−H), 1632 (s, C=N), 1294 (s, C−N), 1242, 1143 (s, SO_2) cm^{-1}. ESI-MS (100 V): *m*/*z* (%) = 707.0 (100) [Pb(SB) + H]$^+$. ^{1}H NMR (500 MHz, [D_6]DMSO): δ = 1.58 (m, 4 H, H_k), 1.88 (m, 4 H, H_j), 2.07 (s, 6 H, H_i), 7.10 (m, 14 H, H_c+H_d+H_e+H_g+H_h), 7.20 (d, 2 H, H_f), 7.65 (s, 2 H, H_b) ppm.

Cu(SB)·4H_2O: Brown solid. Yield 87%. M.p. 250 °C. $C_{32}H_{40}CuN_4O_8S_2$ (736.36): calcd. C 52.2, H 5.5, N 7.6, S, 8.7; found C 52.7, H 5.3, N 7.8, S 8.7. IR (KBr): $\tilde{\nu}$ = 3442 (br., O−H), 1621 (s, C=N), 1295 (s, C−N), 1263, 1138 (s, SO_2) cm^{-1}. FAB-MS: *m*/*z* (%) = 664.0 (60) [Cu(SB) +H]$^+$. μ (293 K): 2.1 B.M. UV/Vis (solid) λ_{max} (nm) = 460 (m, $^2E\leftarrow{}^2T$).

$Ag_2(SB)$·2H_2O: Grey solid. Yield 76%. M.p. 250 °C. $C_{32}H_{36}Ag_2N_4O_6S_2$ (852.52): calcd. C 45.1, H 4.3, N 6.6, S 7.5; found C 45.2, H 4.1, N 7.0, S 7.3. IR (KBr): $\tilde{\nu}$ = 3453 (br., O−H), 1633 (s, C=N), 1293 (s, C−N), 1261, 1126 (s, SO_2) cm^{-1}. ESI-MS (150 V): *m*/*z* (%) = 603.3 (100) [H_2SB + H]$^+$, 711.2 (25) [Ag(HSB) + H]$^+$, 817.0 (5) [$Ag_2(SB)$ + H]$^+$. ^{1}H NMR (500 MHz, [D_6]DMSO): δ = 1.85 (m, 4 H, H_k), 2.29 (s, 6 H, H_i), 3.62 (m, 4 H, H_j), 6.70 (t, 2 H, H_d), 7.05 (t, 2 H, H_e), 7.16 (d, 4 H, H_h), 7.22 (d, 2 H, H_c), 7.33 (d, 2 H, H_f), 7.67 (d, 4 H, H_g), 8.47 (s, 2 H, H_b) ppm.

Zn(SB)·H_2O: Beige solid. Yield 70%. M.p. 210 °C. $C_{32}H_{34}N_4O_5S_2Zn$ (684.15): calcd. C 56.2, H 5.0, N 8.2, S 9.4; found C 56.8, H 5.0, N 8.6, S 8.9. IR (KBr): $\tilde{\nu}$ = 3442 (br., O−H), 1634 (s, C=N), 1299 (s, C−N), 1261, 1140 (s, SO_2) cm^{-1}. FAB-MS: *m*/*z* (%) = 665.3 (72) [Zn(SB) + H]$^+$. ^{1}H NMR (500 MHz, Cl_3CD): δ = 1.76 (m, 2 H, H_{keq}), 2.35 (s, 6 H, H_i), 2.39 (m, 2 H, H_{kax}), 3.76 (m, 2 H, H_{jeq}), 4.19 (m, 2 H, H_{jax}), 6.82 (t, 2 H, H_d), 7.12 (d, 4 H, H_h), 7.18 (t, 2 H, H_e), 7.25 (d, 2 H, H_c), 7.40 (d, 2 H, H_f), 7.75 (d, 4 H, H_g), 8.32 (s, 2 H, H_b) ppm.

Cd(SB)·3H_2O: White solid. Yield 70%. M.p. 24 5 °C. $C_{32}H_{38}CdN_4O_7S_2$ (767.21): calcd. C 50.1, H 5.0, N 4.9, S 8.3; found C 49.6, H 5.4, N 4.7, S 8.0. IR (KBr): $\tilde{\nu}$ = 3443 (br., O−H), 1628 (s, C=N), 1293(s, C−N), 1261, 1128 (s, SO_2) cm^{-1}. ESI-MS (150 V): *m*/*z* (%) = 715.1 (24) [Cd(SB) +H]$^+$. ^{1}H NMR (500 MHz, [D_6]DMSO): δ = 2.27 (m, 4 H, H_k), 2.31 (s, 6 H, H_i), 3.80 (m, 4 H, H_j), 6.84 (t, 2 H, H_d), 7.20 (m, 4 H, H_e+H_c), 7.24 (d, 4 H, H_h), 7.37 (d, 2 H, H_f), 7.75 (d, 4 H, H_g), 8.56 (s, 2 H, H_b) ppm.

Pb(SB)·3H_2O: White solid. Yield 80%. M.p. 320 °C. $C_{32}H_{38}N_4O_7PbS_2$ (862.00): calcd. C 40.8, H 4.1, N 5.6, S 6.8; found C 41.7, H 4.9, N 5.6, S 6.8. IR (KBr): $\tilde{\nu}$ = 3442 (br., O−H), 1635 (s, C=N), 1283(s, C−N), 1259, 1131 (s, SO_2) cm^{-1}. ESI-MS (150 V): *m*/*z* (%) = 809.2 (15) [Pb(SB) +H]$^+$. ^{1}H NMR (500 MHz, Cl_3CD) δ = 1.92 (m, 4 H, H_k) 7.69 (d, 4 H, H_g), 7.60 (d, 2 H, H_f), 7.25 (m, 4 H, H_e+H_c), 7.07 (d, 4 H, H_h), 7.00 (t, 2 H, H_d), 3.75 (m, 4 H, H_j), 2.20 (s, 6 H, H_i), 8.31 (s, 2 H, H_b) ppm.

Single-Crystal X-ray Diffraction Studies

Cu(SB)·MeCN and Zn(SB)·2MeCN: Diffraction intensity data were collected at room temperature on a Bruker SMART CCD-1000 diffractometer with use of graphite-monochromatised Mo-K_α radiation (λ = 0.71073 Å). Absorption correction was carried out from equivalents with the aid of the SADABS program.[26] The structures were solved by direct methods and refined by full-matrix, least-squares based on F^2, with the aid of SHELX-97 software.[27] All non-hydrogen atoms were anisotropically refined. Hydrogen atoms were included at geometrically calculated positions with thermal parameters derived from the parent atoms. Table 2 provides a summary of crystal data, data collection and refinement parameters. Molecular graphics are represented by Ortep-3 for Windows, RasWin, and Platon.[28]

$Ni_2(SB)_2$·5MeCN: Several green needle crystals from different recrystallisation attempts of $Ni_2(SB)_2$·2H_2O were measured at 120 K, showing poor diffracting behaviour. This could be the result of extensive solvation and disorder,[3] as several low-quality refinements indicated. For the best data set that could be obtained, the measured crystal proved to be a two-component twin [twin ratio: 0.719(5)], arising from a rotation of −179.94° around the vector normal to (1 0 0) in the reciprocal space. The twin law was used to process the data with the aid of the GEMINI program.[29] The structure was solved with the help of DIRDIF[30] and then treated as in the two previous cases. The C atoms of one of the methylene

 © 2003 Wiley-VCH Verlag GmbH & Co. KGaA, Weinheim

Table 2. Crystal and structure refinement data for $Ni_2(SB)_2$·5MeCN, Cu(SB)·MeCN, and Zn(SB)·2MeCN

	$Ni_2(SB)_2$·5MeCN	Cu(SB)·MeCN	Zn(SB)·2MeCN
Empirical formula	$C_{74}H_{79}N_{13}Ni_2O_8S_4$	$C_{34}H_{35}CuN_5O_4S_2$	$C_{36}H_{38}N_6O_4S_2Zn$
M	1524.16	705.33	748.21
Crystal system	monoclinic	orthorhombic	orthorhombic
Space group	*C*2/*c* (No. 15)	*Fdd*2 (No. 43)	*Fdd*2 (No. 43)
a [Å]	34.212(12)	47.029(11)	12.3928(15)
b [Å]	12.443(4)	12.258(3)	47.606(6)
c [Å]	18.114(6)	12.297(3)	12.1526(15)
β [°]	93.234(7)	90	90
U [Å^3]	7699(5)	7089(3	7169.7(15)
T [K]	120(2)	293(2)	298(2)
Z	4	8	8
μ(Mo-K_α) [mm^{-1}]	0.659	0.777	0.849
No. ref. col./ no. ref. ind./R_{int}	12223/12228/0.00	8095/3112/0.0257	3732/3531/0.00
Data/restraints/parameters	12228/6/456	3112/1/223	3531/1/224
*R*1, *wR*2 [$I > 2\sigma(I)$]	0.0831, 0.1987	0.0397, 0.1073	0.0304, 0.0690
*R*1, *wR*2 (all data)	0.1241, 0.2199	0.0565, 0.1167	0.0423, 0.0747
Abs. struct. Flack parameter		0.034(19)	0.021(11)
Residuals [e·Å^{-3}]	0.769, −0.590	0.409, −0.300	0.241, −0.214

chains could be located in two disordered positions [C(115)−C(116) and C(15′)−C16′) with 51.6 and 48.4% occupation sites, respectively], and they were isotropically treated. Some of the solvent molecules also show some disorder, and they were isotropically treated and some restraints applied.

CCDC-189324, -197776, and -197777 contain the supplementary crystallographic data for this paper. These data can be obtained free of charge at www.ccdc.cam.ac.uk/conts/retrieving.html [or from the Cambridge Crystallographic Data Centre, 12, Union Road, Cambridge CB2 1EZ, UK; Fax: (internat.) +44-1223-336-033; E-mail: deposit@ccdc.cam.ac.uk].

[1] J. M. Lehn, *Supramolecular Chemistry: Concepts and Perspectives*, VCH, Weinheim, Germany, **1995**.
[2] E. C. Constable, in: *Comprehensive Supramolecular Chemistry, Vol. 9* (Eds.: J. P. Sauvage, M. W. Hosseini), Pergamon, Oxford, **1996**, pp. 213−252.
[3] C. Piguet, G. Bernardinelli, G. Hopfgartner, *Chem. Rev.* **1997**, *97*, 2005−2062.
[4] M. Albrecht, *Chem. Rev.* **2001**, *101*, 3457−3497.
[5] A. von Zelewsky, O. Mamula, *J. Chem. Soc., Dalton Trans.* **2000**, 219−231.
[6] [6a] A. Collet, M.-J. Brienne, J. Jacques, *Chem. Rev.* **1980**, *80*, 215−230. [6b] J. J. Jacques, A. Collet, S. H. Wilen, *Enantiomers, Racemates and Resolutions*, John Wiley & Sons, New York, **1981**.
[7] I. Katsuki, Y. Motoda, Y. Sunatsuki, N. Matsumoto, T. Nakashima, M. Kojima, *J. Am. Chem. Soc.* **2002**, *124*, 629−640.
[8] [8a] S. R. Marder, J. E. Sohn, G. D. Stucky, *Materials for Nonlinear Optics: Chemical Perspectives*, ACS Symposium Series 455, American Chemical Society, Washington DC, **1991**. [8b] P. A. Maggard, C. L. Stern, K. R. Poeppelmeier, *J. Am. Chem. Soc.* **2001**, *123*, 7742−7743.
[9] M. Vázquez, M. R. Bermejo, M. Fondo, A. M. García-Deibe, A. M. González, R. Pedrido, *Eur. J. Inorg. Chem.* **2002**, 465−472.
[10] M. R. Bermejo, M. Vázquez, J. Sanmartín, A. M. García-Deibe, M. Fondo, C. Lodeiro, *New J. Chem.* **2002**, 1365−1370.
[11] M. Vázquez, M. R. Bermejo, M. Fondo, A. M. García-Deibe, J. Sanmartín, M. Fondo, *Eur. J. Inorg. Chem.* **2003**, 1128−1135.
[12] M. R. Bermejo, J. Sanmartín, A. M. García-Deibe, M. Fondo, F. Novio, D. Navarro, *Inorg. Chim. Acta* **2003**, *347*, 53−60.
[13] P. G. Jones, *Acta Crystallogr., Sect. A* **1986**, *42*, 57.
[14] H. D. Flack, *Acta Crystallogr., Sect. A* **1983**, *39*, 876−881.
[15] [15a] M. J. Hannon, C. L. Painting, A. Jackson, J. Hamblin, W. Errington, *Chem. Commun.* **1997**, 1807−1808. [15b] H. Cheng, D. Chun-Ying, F. Chen-Jie, M. Qing-Jin, *J. Chem. Soc., Dalton Trans.* **2000**, 2419−2424.
[16] M. Vázquez, M. R. Bermejo, M. Fondo, A. M. González, J. Mahía, L. Sorace, D. Gatteschi, *Eur. J. Inorg. Chem.* **2001**, 1863−1868.
[17] [17a] A. Bilyk, M. M. Harding, P. Turner, T. W. Hambley, *J. Chem. Soc., Dalton Trans.* **1994**, 2783−2790. [17b] A. Bilyk, M. M. Harding, P. Turner, T. W. Hambley, *J. Chem. Soc., Dalton Trans.* **1995**, 2549−2553.
[18] [18a] M. J. Hannon, S. Bunce, A. J. Clark, N. W. Alcock, *Angew. Chem. Int. Ed.* **1999**, *38*, 1277−1278. [18b] M. Albrecht, *Chem. Eur. J.* **2000**, *6*, 3485−3489 and references cited therein.
[19] [19a] S. L. Larson, S. M. Hendrickson, S. Ferrere, D. L. Derr, C. M. Elliott, *J. Am. Chem. Soc.* **1995**, *117*, 5881−5882. [19b] B. R. Serr, K. A. Anderson, C. M. Elliott, O. P. Anderson, *Inorg. Chem.* **1988**, *27*, 4499−4504.
[20] [20a] T. Koike, E. Kimura, I. Nakamura, Y. Hashimoto, M. Shiro, *J. Am. Chem. Soc.* **1992**, *114*, 7338−7345. [20b] A. Jäntti, K. Rissanen, J. Valkonen, *Acta Chem. Scand.* **1998**, *52*, 1010−1016.
[21] [21a] T. Adatia, N. Beynek, B. P. Murphy, *Polyhedron* **1995**, *14*, 335−338. [21b] D. Zurita, P. Baret, J.-L. Pierre, *New. J. Chem.* **1994**, *18*, 1143−1146. [21c] G. Mugesh, H. B. Singh, R. P. Patel, R. J. Butcher, *Inorg. Chem.* **1998**, *37*, 2663−2669. [21d] G. Mugesh, H. B. Singh, R. J. Butcher, *Eur. J. Inorg. Chem.* **1999**, 1229−1236.
[22] J. Sanmartín, M. R. Bermejo, A. M. García-Deibe, M. Maneiro, C. Lage, A. J. Costa-Filho, *Polyhedron* **2000**, *19*, 185−192.
[23] [23a] N. Yoshida, H. Oshio, T. Ito, *J. Chem. Soc., Perkin Trans. 2* **1999**, 975−983. [23b] N. Yoshida, H. Oshio, T. Ito, *J. Chem. Soc., Perkin Trans. 2* **2001**, 1674−1678.
[24] [24a] A. Bencini, F. Mani, L. Sacconi, in: *Comprehensive Coordination Chemistry, Vol. 5* (Eds.: G. Wilkinson, R. D. Gillard and J. McCleverty), Pergamon Press, Oxford, **1987**. [24b] M. Gerloch, D. A. Cruse, *J. Chem. Soc., Dalton Trans.* **1977**, 152−159. [24c] M. Gerloch, D. A. Cruse, *J. Chem. Soc., Dalton Trans.* **1977**, 1613−1617.

 © 2003 Wiley-VCH Verlag GmbH & Co. KGaA, Weinheim

[25] J. Mahía, M. Maestro, M. Vázquez, M. R. Bermejo, A. M. González, M. Maneiro, *Acta Crystallogr., Sect. C* **1999**, *55*, 2158−2160.
[26] *Area-Detector Absorption Correction.* Siemens Industrial Automation Inc., Madison, WI, **1996**.
[27] G. M. Sheldrick, *SHELX-97* (*SHELXS 97* and *SHELXL 97*), Programs for Crystal Structure Analyses, University of Göttingen, Germany, **1998**.
[28] [28a] L. J. Farrugia, *J. Appl. Cryst.* **1997**, *30*, 565. [28b] R. Sayle, *RasWin Molecular Graphics*, Windows version 2.6-ucb, **1995**. [28c] A. L. Spek, *PLATON*, A Multipurpose Crystallographic Tool, Utrecht University, Utrecht, The Netherlands, **1998**.
[29] R. Sparks, *GEMINI*, Bruker-AXS Inc., Madison, WI, **1999**.
[30] P. T. Beurskens, G. Beurskens, R. de Gelder, S. Garcia-Granda, R. O. Gould, R. Israel, J. M. M. Smits, *DIRDIF 99.2 for Windows.* Programs for Crystal Structure Determination, Crystallography Laboratory, University of Nijmegen, The Netherlands, **1999**.

Received April 29, 2003

 © 2003 Wiley-VCH Verlag GmbH & Co. KGaA, Weinheim

Synthesis, Crystal Structure, and Optical Properties of a New Molecular Complex of C_{60} with a Covalently Linked $(Fe^{III}TPP)_2O$ Dimer

Aleksey L. Litvinov,[a] Dmitri V. Konarev,[a] Andrey Yu. Kovalevsky,[b] Alexander N. Lapshin,[a] Evgeniya I. Yudanova,[a] Natalia V. Drichko,[c] Philip Coppens,[b] and Rimma N. Lyubovskaya*[a]

Keywords: Fullerenes / Porphyrinoids / Crystal engineering / Solid-state structures / UV/Vis spectroscopy

A new molecular complex of C_{60} with covalently linked μ-oxo dimer $(Fe^{III}TPP)_2O$ are (TPP = tetraphenylporphyrin) was obtained. The complex has a neutral ground state and is formed mainly by van der Waals forces. The X-ray analysis of the crystal structure of the complex showed it to have isolated packing of fullerenes in which each fullerene molecule is embraced in a pocket built by porphyrins. Optical properties and EPR behavior of the complex are described.
(© Wiley-VCH Verlag GmbH & Co. KGaA, 69451 Weinheim, Germany, 2003)

Introduction

Fullerenes form complexes with aromatic hydrocarbons, amines, substituted tetrathiafulvalenes, metallocenes, porphyrins, and metalloporphyrins.[1−6] The latter family of complexes is of great interest because of their promising photoactive properties.[7] Metalloporphyrins can be used to develop neutral and ionic multi-component systems[8,9] and to determine the molecular structure of endohedral[10] and chemically modified fullerenes.[6] Different chemically modified porphyrins in which two porphyrin moieties bonded by one (''jaw'' porphyrins[11]) or two bridged chains (cyclic dimers[12]) have been used to prepare complexes with fullerenes. These molecules have a high affinity for fullerenes.[11,12]

Additionally to monomeric and chemically modified porphyrins, covalently linked dimers of metal-containing porphyrins with different bridging atoms (O,[13] N,[14] and C[15]) are also promising components for the development of photoactive complexes with fullerenes. It has been shown that, on photoexcitation with a 441.6 nm laser, $(Fe^{III}TPP)_2O$ undergoes photodisproportionation to the oxoferryl species Fe^{IV}=O(TPP) and five-coordinate, high-spin Fe^{II}-TPP(L).[16]

The present work reports for the first time the synthesis, crystal structure, and optical properties of the C_{60} complex, $(Fe^{III}TPP)_2O{\cdot}C_{60}$ (**1**), with a covalently linked μ-oxo-bis[5,10,15,20-tetraphenylporphyrinatoiron(III)] dimer.

Results and Discussion

X-ray diffraction[17] shows that **1** has a 1:1 solid-state stoichiometry $[(Fe^{III}TPP)_2O{:}C_{60}]$. The crystal is a racemic twin with two equal components [the Flack parameter[18] is 0.50(2)].

In the crystal, the $(Fe^{III}TPP)_2O$ and C_{60} molecules alternate in chains along the crystallographic *c* axis (Figure 1, a). The chains are positioned so that each C_{60} molecule is surrounded only by $(Fe^{III}TPP)_2O$ moieties; their are no inter-fullerene contacts. Because of this, $(Fe^{III}TPP)_2O$ forms a three-dimensional supramolecular network (Figure 1, b) through shortened H(Ph)···H′(Ph) (2.20−2.28 Å) and H(Ph)···C′(Ph) (2.72−2.86 Å) contacts. Each fullerene molecule is found in a pocket built by two porphyrin moieties from one chain and the phenyl substituents of four porphyrins from the adjacent chains. The phenyl substituents form short van der Waals contacts with fullerenes, with C(Ph)···C(C_{60}) distances in the 3.235−3.358 Å range.

The bond lengths and angles of $(Fe^{III}TPP)_2O$ in **1** are similar to those of the parent compound[13] (Table 1). The Fe−O−Fe moiety is bent, with an Fe1−O−Fe2 bond angle of 173.7(2)°. Four nitrogen atoms form an almost perfect plane. The Fe1 and Fe2 atoms are displaced from their planes by 0.46 and 0.47 Å, respectively, in the direction of the μ-oxo group. The porphyrin rings are strongly distorted and have a saddle-like conformation. Moreover, the por-

[a] Institute of Problems of Chemical Physics RAS,
Chernogolovka, Moscow region 142432, Russia
Fax: (internat.) +7-096-5155420
E-mail: lyurn@icp.ac.ru
[b] Department of Chemistry, State University of New York at Buffalo,
Buffalo, New York, 14214, USA
Fax: (internat.) +1-716-6456948
E-mail: ayk@buffalo.edu
[c] A.F. Ioffe Physical-Technical Institute,
St.-Petersburg, 194021, Russia,
Fax: (internat.) +7-0812-5156747
E-mail: natalia.drichko@mail.ioffe.ru
Supporting information for this article is available on the WWW under http://www.eurjic.org or from the author.

 © 2003 Wiley-VCH Verlag GmbH & Co. KGaA, Weinheim **DOI: 10.1002/ejic.200300256**

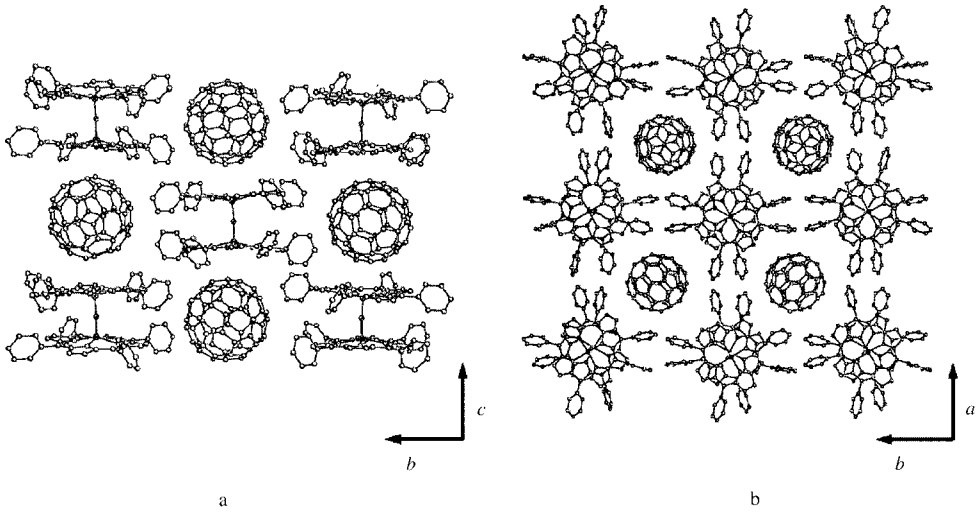

Figure 1. Projections of the crystal structure of **1** along the *bc* (a) and *ab* (b) planes

Table 1. Bond lengths and angles for parent $(Fe^{III}TPP)_2O$ and for the $(Fe^{III}TPP)_2O$ moieties in **1**

Compound	Fe1−O	Fe2−O	Fe1−Fe2	Fe1−Ct	Fe2−Ct	Fe1−O−Fe2	Torsion angle N−Fe−Fe′−N′
$[Fe^{III}TPP]_2O$[13]	1.763	1.763	3.522	0.54	0.54	174.5(1)°	35.4°
$[Fe^{III}TPP]_2O{\cdot}C_{60}$	1.745	1.771	3.511	0.47	0.46	173.7(2)°	29.7°

phyrin rings are rotated about the Fe−O−Fe moiety (the least torsion angle N−Fe1−Fe2−N′ is 29.7°).

The iron atoms of $(Fe^{III}TPP)_2O$ are located on the other side of the porphyrin macrocycle from the fullerene. Because of this the Fe···C(C_{60}) contacts of 3.239−3.513 Å are rather long compared to those in fullerene complexes with other metal-containing porphyrins (2.57−3.12 Å[5,6,8,19]). In addition to the Fe···C_{60} contacts (Figure 2), the porphyrins form shortened contacts with fullerenes through nitrogen [the N(TPP)···C(C_{60}) contacts are 3.081−3.186 Å] and carbon atoms [the C(TPP)···C(C_{60}) contacts are 3.244−3.425 Å]. For comparison, the sum of the van der Waals radii of two C atoms is 3.42 Å and that of a C and an N atom is 3.21 Å.[20]

Two complexes of C_{60} with Fe^{III} porphyrinates have been structurally characterized (Table 2). Provided the absence of an axial ligand at $Fe^{III}TPP$, a shortened Fe···C(C_{60}) contact of 2.56 Å is observed in $Fe^{III}TPP{\cdot}[B(C_6F_5)_4]{\cdot}C_{60}{\cdot}2.5C_6H_4Cl_2$ ($C_6H_4Cl_2$ = 1,2-dichlorobenzene),[19] while because of the presence of chlorine in octaethylporphyrinatoiron(III) chloride ($Fe^{III}ClOEP$), these contacts are much longer (3.20 Å[6]) in $Fe^{III}ClOEP{\cdot}C_{60}{\cdot}CHCl_3$. In **1** the Fe···$C_{60}$ contacts are close to those in the C_{60} complex with $Fe^{III}ClOEP$. The van der Waals N(TPP)···C(C_{60}) and C(TPP)···C(C_{60}) contacts have similar values in all three complexes (Table 2). It should be noted that the C_{60} molecules in **1** and in the C_{60} complex with $Fe^{III}TPP{\cdot}[B(C_6F_5)_4]$[19] are isolated, while in the C_{60} complex with $Fe^{III}ClOEP$ one observes one-dimensional zig-zag chains from C_{60}.[6]

The IR spectrum of **1** is a superposition of those of the individual components, namely C_{60} and $(Fe^{III}TPP)_2O$. The band for the $F_{1u}(4)$ vibration of C_{60}, which is most sensitive to charge transfer to the C_{60} molecule, is observed at 1427

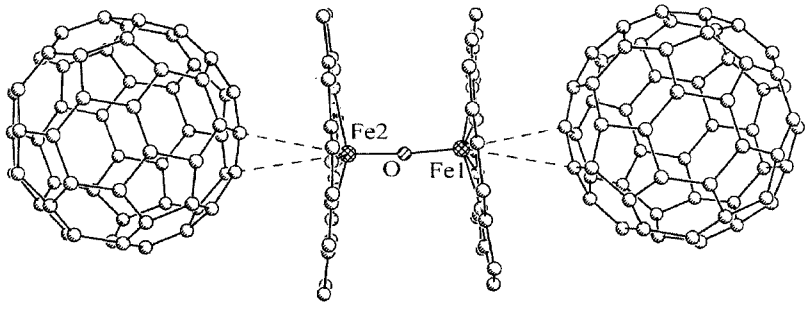

Figure 2. Mutual arrangement of $(Fe^{III}TPP)_2O$ and C_{60} molecules in **1**; phenyl substituents of $(Fe^{III}TPP)_2O$ are not shown

 © 2003 Wiley-VCH Verlag GmbH & Co. KGaA, Weinheim

Table 2. Structural data for C_{60} complexes with Fe^{III}-containing porphyrins

Complex	C_{60} order	$C_{60}\cdots C_{60}$ centre to center	Fe···Fe	Fe···C(C_{60})	N···C(C_{60})	C(porphyrin)···C(C_{60})
$Fe^{III}ClOEP\cdot C_{60}\cdot CHCl_3$[6]	–	9.94	8.079	3.204–3.371	3.020–3.208	3.237–3.336
$Fe^{III}TPP\cdot[B(C_6F_5)_4]\cdot C_{60}\cdot 2.5C_6H_4Cl_2$[19]	–	14.43	11.684	2.570–3.413	3.018–3.448	3.263–3.421
$(Fe^{III}TPP)_2O\cdot C_{60}$	+	14.20	3.511	3.239–3.513	3.090–3.247	3.245

cm^{-1} in **1**, and is similar to that in the parent fullerene (1429 cm^{-1}), indicating no noticeable charge transfer. The absorption bands of $(Fe^{III}TPP)_2O$ are slightly shifted in **1** (up to 4 cm^{-1}) relative to the parent porphyrin.

The Vis-NIR reflectance spectra of a single crystal of **1** were measured in two perpendicular polarizations with maximal anisotropy of reflectivity from the most developed face of the crystal ($E\|c$ and $E\perp c$). The corresponding absorption spectra in both polarizations (Figure 3) show strong bands attributed to the dipole-allowed electronic transitions in the fullerene: $h_u\rightarrow h_g$ and $g_g,h_g\rightarrow t_{1u}$ at 270 and 343 nm for $E\perp c$, and 272 and 335 nm for $E\|c$. The $E\perp c$ spectrum also shows strong bands attributed to the absorption of $(Fe^{III}TPP)_2O$, at 417 and 579 nm, with a shoulder at 615 nm. These bands are red shifted (up to 10 nm) relative to the parent metalloporphyrin indicating a slight change in its initial geometry. In the structure of **1** the $(Fe^{II}TPP)_2O$ and fullerene molecules alternate in the stacks directed parallel to the crystallographic *c* axis, the planes of the porphyrin macrocycles of $(Fe^{III}TPP)_2O$ being perpendicular to the *c* axis. Consequently, with polarization perpendicular to the porphyrin planes ($E\|c$), the absorption bands of $(Fe^{III}TPP)_2O$ are absent. A similar anisotropy was observed in the spectrum of $Co^{II}TPP\cdot C_{60}\cdot 0.5CS_2$.[5] Thus, the absorption spectrum of the complex is a superposition of those of the parent molecules, indicating a neutral ground state in **1**.

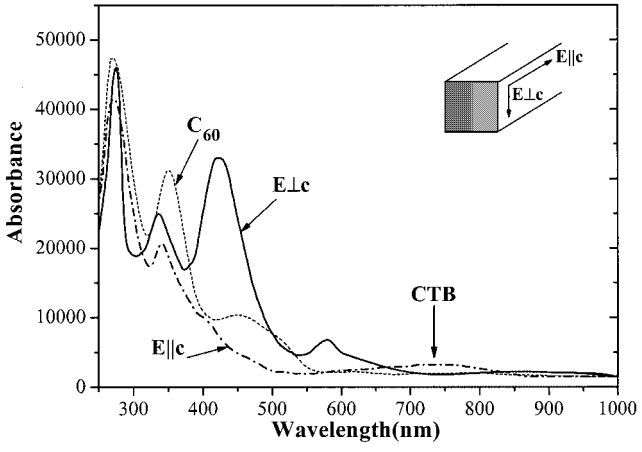

Figure 3. The UV/Visible absorption spectra of a single crystal of **1** for two polarizations of light ($E\|c$ and $E\perp c$)

It should be noted that the bands of dipole-allowed transitions of the fullerene ($h_u\rightarrow h_g$ and $g_g,h_g\rightarrow t_{1u}$) in the spectrum of the complex are narrower than those in the spectrum of a pure fullerene crystal and are shifted to higher frequencies. In $E\|c$ polarization, the position of the band $g_g,h_g\rightarrow t_{1u}$ is close to that of the parent C_{60} molecule (335 nm). The absorption band of C_{60} at 450 nm is also absent in the spectrum of the complex (Figure 3). Previously,[21] this band was attributed to intermolecular electron transfer between the adjacent C_{60} molecules. Indeed, the isolation of fullerene molecules from each other by the $(Fe^{III}TPP)_2O$ ones in **1** results in the absence of the band at 450 nm.

An additional weak absorption is observed in the visible range with a maximum at 720 nm in $E\perp c$ polarization. This band is also present in the isotropic spectrum of **1** in a KBr matrix and could be evidence of photoinduced charge transfer from $(Fe^{III}TPP)_2O$ to C_{60}. The position of this band is close to that in C_{60} complexes with (tetraphenylporphyrin)cobalt(II): $Co^{II}TPP\cdot C_{60}\cdot 0.5CS_2$ (750 nm)[5] and tetrakis(*p*-methoxyphenyl)porphyrincobalt(II): $Co^{II}TMPP\cdot(C_{60})_2\cdot 3C_7H_8$ (820 nm).[8] The position of a charge-transfer band (CTB) in a series of complexes with one acceptor is dependent on the ionization potentials of the donors. The ionization potential of $(Fe^{III}TPP)_2O$ is not known. However, metal-containing tetraphenylporphyrins have similar ionization potentials ($Fe^{III}TPPCl$: 6.1±0.2 eV; $Co^{II}TPP$: 6.1±0.2 eV; $Cu^{II}TPP$: 6.2±0.2 eV; $Mn^{III}TPP$: 6.0±0.2 eV[22]) that can be evidence of a close position of CTB in the complexes with C_{60}.

The EPR behavior of **1** is close to that of parent $(Fe^{III}TPP)_2O$. EPR signals were not observed at room temperature, whereas upon lowering the temperature down to 77 K, EPR signals with $g = 5.7$ and $\Delta H_{pp} = 200$ G appeared in both compounds. The *g* factor of the signal is characteristic of a square-planar complex of Fe^{III} with a high-spin $3d^5$ configuration. A strong exchange interaction between Fe^{III} in the dimer results in the absence of EPR signals at room temperature. However, the temperature decrease seems to cause a freezing of the state with the dihedral N–Fe–Fe′–N angle differing slightly from 180° between the porphyrin planes and results in the appearance of a weak EPR signal.[23] The similarity of the EPR spectra of **1** and $(Fe^{III}TPP)_2O$ indicates the absence of Fe^{III} coordination to fullerene and the changes in $(Fe^{III}TPP)_2O$ geometry in the complex with C_{60}, in agreement with the data of the X-ray analysis. A similar phenomenon was observed earlier for a C_{60} complex of $Fe^{III}ClTPP$, which also has an EPR spectrum similar to that of starting $Fe^{III}ClTPP$.[5] It seems that Fe^{III} is shifted from the porphyrin plane to oxygen in **1** as well as to chlorine in $Fe^{III}ClTPP$ that hinders the Fe^{III} coordination to C_{60}.

 © 2003 Wiley-VCH Verlag GmbH & Co. KGaA, Weinheim

Conclusion

A new complex of C_{60} with $(Fe^{III}TPP)_2O$ has been synthesized. The complex has a neutral ground state and is formed mainly by van der Waals forces. The neutral ground state and the occurrence of a charge-transfer band in **1** provides for possible photoinduced charge transfer in the complex.

Experimental Section

General Remarks: The IR spectra of the powdered samples pressed in KBr pellets (1:400) were registered with a Perkin−Elmer 1725X spectrophotometer in the 400−7000 cm^{-1} range. Electronic absorption spectra were registered with a Perkin−Elmer Lambda 19 UV/Vis-NIR spectrophotometer in the 220−3000 nm range (KBr pellet, 1:2000). Polarized reflectance spectra of the single crystals were recorded with a microspectroreflectometer equipped with a UV/Vis microscope in the 260−1000 nm range at room temperature. The spectra were measured from one crystal face in two orthogonal directions with the maximal reflectance anisotropy, their orientation relative to the crystal axis was done based on the positions of the polarized absorption bands of the $(Fe^{III}TPP)_2O$ molecule. The absorption spectra were derived from the reflectance ones by the Kramers−Kronig transformation. EPR spectra were registered with a Radiopan SE/X 2547 spectrometer.

$(Fe^{III}TPP)_2O·C_{60}$ (1): Crystals of **1** were obtained by slow evaporation of the solvent from a toluene solution containing 20 mg of C_{60} and 38 mg of $(Fe^{III}TPP)_2O$[24] (1:1 molar ratio) under argon during a week (yield 18 mg, 90%). The composition of the complex was determined by X-ray diffraction on a single crystal.

X-ray Crystallographic Study: X-ray diffraction data for **1**[17] were collected at 90(1) K using a Bruker SMART1000 CCD diffractometer with a rotating anode source (Mo-K_α radiation, λ = 0.71073 Å), and equipped with an Oxford Cryosystems nitrogen gas-flow apparatus. The data were collected by the rotation method with a 0.3° frame-width (ω scan) and 40 sec exposure time per frame. Four sets of data (600 frames in each set) were collected, nominally covering half of the reciprocal space. The data were integrated, scaled, sorted and averaged using the SMART software package.[25] The structure was solved by the Patterson method using SHELXTL NT Version 5.10.[26] The structure was refined by full-matrix least-squares against F^2.

Non-hydrogen atoms were refined in the anisotropic approximation. Anisotropic thermal parameters of several carbon atoms were restrained to behave isotropically. Positions of hydrogen atoms were refined using the "riding" model with $U_{iso} = 1.2U_{eq}$.

Acknowledgments

The work was supported by the Russian Program "Fullerenes and Atomic Clusters" and the RFFR grant N 03-03-32699.

[1] D. V. Konarev, R. N. Lyubovskaya, N. V. Drichko, E. I. Yudanova, Yu. M. Shul′ga, A. L. Litvinov, V. N. Semkin, B. P. Tarasov, *J. Mater. Chem.* **2000**, 803−818.
[2] A. L. Balch, M. M. Olmstead, *Chem. Rev.* **1998**, *98*, 2123−2166.
[3] D. V. Konarev, R. N. Lyubovskaya, *Russ. Chem. Rev.* **1999**, *68,* 19−38.
[4] P. D. W. Boyd, M. C. Hodgson, C. E. F. Rickard, A. G. Oliver, L. Chaker, P. J. Brothers, R. D. Bolskar, F. S. Tham, C. A. Reed, *J. Am. Chem. Soc.* **1999**, *121*, 10487−10495.
[5] D. V. Konarev, I. S. Neretin, Yu. L. Slovokhotov, E. I. Yudanova, N. V. Drichko, Yu. M. Shul′ga, B. P. Tarasov, L. L. Gumanov, A. S. Batsanov, J. A. K. Howard, R. N. Lyubovskaya, *Chem. Eur. J.* **2001**, *7*, 2605−2616.
[6] M. M. Olmstead, D. A. Costa, K. Maitra, B. C. Noll, S. L. Phillips, P. M. Van Calcar, A. L. Balch, *J. Am. Chem. Soc.* **1999**, *121*, 7090−7097.
[7] F. D′Souza, N. P. Rath, G. R. Deviprasad, M. E. Zandler, *Chem. Commun.* **2001**, 267−268.
[8] D. V. Konarev, A. Yu. Kovalevsky, X. Li, I. S. Neretin, A. L. Litvinov, N. V. Drichko, Yu. L. Slovokhotov, P. Coppens, R. N. Lyubovskaya, *Inorg. Chem.* **2002**, *41*, 3638−3646.
[9] D. V. Konarev, S. S. Khasanov, A. Otsuka, Y. Yoshida, G. Saito, *J. Am. Chem. Soc.* **2002**, *124*, 7648−7649.
[10] S. Stevenson, G. Rice, T. Glass, K. Harich, F. Cromer, M. R. Jordan, J. Craft, E. Hadju, R. Bible, M. M. Olmstead, K. Maitra, A. J. Fisher, A. L. Balch, H. C. Dorn, *Nature* **1999**, *401*, 55−57.
[11] D. Sun, F. S. Tham, C. A. Reed, L. Chaker, P. D. W. Boyd, *J. Am. Chem. Soc.* **2002**, *124*, 6604−6612.
[12] J.-Y. Zheng, K. Tashiro, Y. Hirabayashi, K. Kinbara, K. Saigo, T. Aida, S. Sakamoto, K. Yamaguchi, *Angew. Chem. Int. Ed.* **2001**, *40*, 1857−1861.
[13] A. B. Hoffman, D. M. Collins, V. W. Day, E. B. Fleischer, T. S. Srivastava, J. L. Hoard, *J. Am. Chem. Soc.* **1972**, *94*, 3620−3626.
[14] W. R. Scheidt, D. A. Summerville, I. A. Cohen, *J. Am. Chem. Soc.* **1976**, *98*, 6623−6628.
[15] V. L. Goedken, M. R. Deakin, L. A. Bottomley, *J. Chem. Soc., Chem. Commun.* **1982**, 607−608.
[16] P. K. Shantha, A. L. Verma, *Inorg. Chem.* **1996**, *35*, 2723−2725.
[17] Crystallographic data for **1**: $C_{148}H_{56}Fe_2N_8O$, M_r = 2073.71 g·mol^{-1}, black parallelepipeds, tetragonal, $P\text{-}42_1c$, a = 33.1647(9), b = 33.1647(9), c = 16.8998(7) Å, γ = 90°, V = 18588(1) $Å^3$, Z = 8, $\rho_{calcd.}$ = 1.482 g·cm^{-3}, μ = 0.383 mm^{-1}, T = 90(1) K, max. 2θ = 49.7°, R_{int} = 15033 (0.102), Reflections $I > 2\sigma(I)$ = 10476, $R[I > 2\sigma(I)]$ = 0.052, wR_2 = 0.162, G.O.F. = 1.095. CCDC-209328 contains the supplementary crystallographic data for this paper. These data can be obtained free of charge at www.ccdc.cam.ac.uk/conts/retrieving.html [or from the Cambridge Crystallographic Data Centre, 12, Union Road, Cambridge CB2 1EZ, UK; fax: (internat.) +44-1223/336-033; E-mail: deposit@ccdc.cam.ac.uk].
[18] H. D. Flack, *Acta Crystallogr., Sect. A* **1983**, *39*, 876−881.
[19] D. R. Evans, N. L. P. Fackler, Z. Xie, C. E. F. Rickard, P. D. W. Boyd, C. A. Reed, *J. Am. Chem. Soc.* **1999**, *121*, 8466−8474.
[20] Yu. V. Zefirov, P. M. Zorkii, *Russ. Chem. Rev.* **1989**, *58*, 713.
[21] H. J. Byrne, in: *Progress in Fullerene Research.* (Eds.: H. Kuzmany, J. Fink, M. Mehring, S. Roth), World Scientific, Singapore, **1995**, p. 183.
[22] Y. Nakato, K. Abe, H. Tsubomura, *Chem. Phys. Lett.* **1976**, *39*, 358−360.
[23] S. H. Strauss, M. J. Pawlik, J. Skowyra, J. R. Kennedy, O. P. Anderson, K. Spartalian, J. L. Dye, *Inorg. Chem.* **1987**, *26*, 724−730.
[24] C.-C. Guo, *J. Catal.* **1998**, *178*, 182−187.
[25] *SMART* and *SAINTPLUS*, Area detector control and integration software, version 6.01. Bruker Analytical X-ray Systems, Madison, Wisconsin, U. S. A, **1999**.
[26] *SHELXTL*, An integrated system for solving, refining and displaying crystal structures from diffraction data, version 5.10. Bruker Analytical X-ray Systems, Madison, Wisconsin, U. S. A, **1997**.

Received May 1, 2003

 © 2003 Wiley-VCH Verlag GmbH & Co. KGaA, Weinheim

Stepwise Assembly of Mixed Metal Dinuclear Carbonyl Complexes

Katja Heinze*[a] and Volker Jacob[a]

Keywords: Heterometallic complexes / Isocyanide ligands / Bridging ligands / Isomers / Group 6 elements

The one-pot/three-step solution synthesis of a library of nine directional, dinuclear mixed-metal complexes composed of different metal-carbonyl units (M = Cr, Mo, W) and a bifunctional bridging isocyanide Schiff-base ligand is described. The well-defined metal sequence in these complexes with Cr, Mo, and W in two positions can be determined post-synthesis by a combination of spectroscopic methods.

(© Wiley-VCH Verlag GmbH & Co. KGaA, 69451 Weinheim, Germany, 2003)

Introduction

One-dimensional materials are interesting with respect to their exceptional physical and chemical,[1−3] such as photophysical or electrochemical properties.[4] However, the synthesis of metal-containing chain complexes with defined chain lengths is difficult to achieve. An elegant approach to overcome the problem of obtaining mixtures of complexes with different chain lengths is the design and synthesis of special ligands which allow for only one definite chain length. This approach has been used, for example, in the synthesis of oligo-α-pyridylamino ligands which form string complexes with two, three, four, five, and seven metal centres depending on the length of the ligand.[5−8] The problem is thus transferred to organic synthesis of the ligand while metal incorporation is subject to self-organisation processes. A particular drawback of this approach is the need to synthesise special ligands for each chain length and the limited control over the metal sequence within the chain, as usually only homometallic complexes are obtained.

The construction of oligonuclear metal complexes may also be achieved by the stepwise connection of stable metal complexes through covalent bonds using a protection/deprotection strategy which has been successfully applied, for example, to defined ferrocene oligomers[9,10] and oligo-porphyrin systems.[11−14]

A similar, albeit more difficult, approach is the controlled stepwise assembly of building blocks through coordinative bonds. Such a procedure should allow the synthesis of complexes with any desired chain length controlled by the number of repetition cycles. Repeated complex activation and subsequent addition of a metal-bridging ligand fragment to a starting complex has been employed for the synthesis of oligonuclear ruthenium−pyrazine complexes.[15] Sequential protection/deprotection of a potential coordination site of a coordinated ligand has allowed a step-by-step synthesis of oligonuclear ruthenium and osmium polypyridine complexes.[16] Redox activation has been used to construct oligomeric iron/platinum complexes by a stepwise procedure.[17]

The repeated alternate addition of metal complex fragments and bridging ligands would be a procedure which allows full control over chain length, metal, and ligand sequence within the backbone. An important prerequisite for this method is the kinetic stability of the metal−ligand bonds within the chain so that undesired self-organisation processes, which would ultimately lead to the thermodynamically most stable species (e.g. scrambled metals, oligomer mixtures, or polymers), are suppressed.

The stepwise solution synthesis and characterisation of nine dinuclear chain complexes composed of different metal−carbonyl units (M = Cr, Mo, W) and a bifunctional bridging isocyanide Schiff-base ligand is the subject of this contribution.

Results and Discussion

Inert metal−ligand bonds are required for the stepwise controlled synthesis of multinuclear metal chain complexes. The coordinative bond between isocyanides and M^0 carbonyl complexes (M = Cr, Mo, W) is kinetically stable so that ligand-exchange processes are prevented.[18−20] Consequently, a suitable bridging ligand with an isocyano group is used in the assembly of dinuclear metal complexes.

The bridging Schiff-base ligand (4-isocyanophenyl)pyridine-2-ylmethylenamine C≡N−(N∩N′) is accessible by a two-step procedure starting from 1,4-diaminobenzene (Scheme 1). Transformation of one amino group into the desired isocyano group gives 4-isocyanophenylamine in rather poor yields according to the literature.[21] Optimis-

[a] Anorganisch-Chemisches Institut der Universität Heidelberg, Im Neuenheimer Feld 270, 69120 Heidelberg, Germany
Fax.: (internat.) +49-(0)6221-545707
E-mail: katja.heinze@urz.uni-heidelberg.de

 © 2003 Wiley-VCH Verlag GmbH & Co. KGaA, Weinheim **DOI: 10.1002/ejic.200300272**

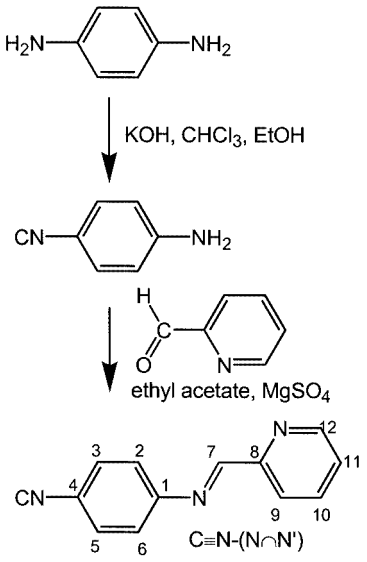

Scheme 1

ation of the purification increased the yield to 45% (see Exp. Sect.). Schiff-base condensation of the remaining amino group with pyridine-2-carbaldehyde affords the desired ligand C≡N−(N∩N′) (Scheme 1). C≡N−(N∩N′) can act as bridging ligand between two M^0-carbonyl units through i) the chelating Schiff-base moiety, and ii) the isocyano group.

The trimethylsilyloxy-substituted analogous Schiff-base ligand TMSO−(N∩N′)[18] was used as the starting point for the synthesis of dinuclear complexes. TMSO−(N∩N′) reacts with one equivalent of $[(CH_3CN)_3M^1(CO)_3]$ (M^1 = Cr, Mo, W) in THF at ambient temperature to give the reactive intermediate complexes [TMSO−(N∩N′)-$M^1(CO)_3$thf] (Scheme 2).[18] The labile solvent molecule can be displaced by the isocyanide ligand C≡N−(N∩N′) to afford green stable intermediate isocyanide complexes [TMSO−(N∩N′)$M^1(CO)_3$C≡N−(N∩N′)] (Scheme 2). The potentially chelating Schiff-base site of the coordinated C≡N−(N∩N′) ligand is finally coordinated to an $M^2(CO)_4$ fragment by reaction with $[(CH_3CN)_2M^2(CO)_4]$ (M^1 = Cr, Mo, W) yielding the dinuclear complexes [TMSO−(N∩N′)$M^1(CO)_3$C≡N−(N∩N′)$M^2(CO)_4$] **1**−**9** with the metals Cr, Mo, and W in defined positions of M^1 and M^2 (Scheme 2). This reaction sequence may be performed as a one-pot procedure — isolation of the intermediate complexes is unnecessary — provided that exact stoichiometric conditions are fulfilled. Otherwise, side products such as [X−(N∩N′)$M^{1,2}(CO)_4$], [X−(N∩N′)$M^{1,2}(CO)_3$C≡N−(N∩N′)V (X = OTMS, CN) are obtained in larger amounts which have to be removed by chromatography. The reactions can easily be monitored by IR spectroscopy due to the characteristic IR absorption bands of the intermediate complexes (Table 1).

Formation of the intermediate complexes [TMSO−(N∩N′)$M^1(CO)_3$thf] is shown by the appearance of two absorption bands in the ν_{CO} region (Table 1). Coordination of the isocyanide ligand C≡N−(N∩N′) replaces

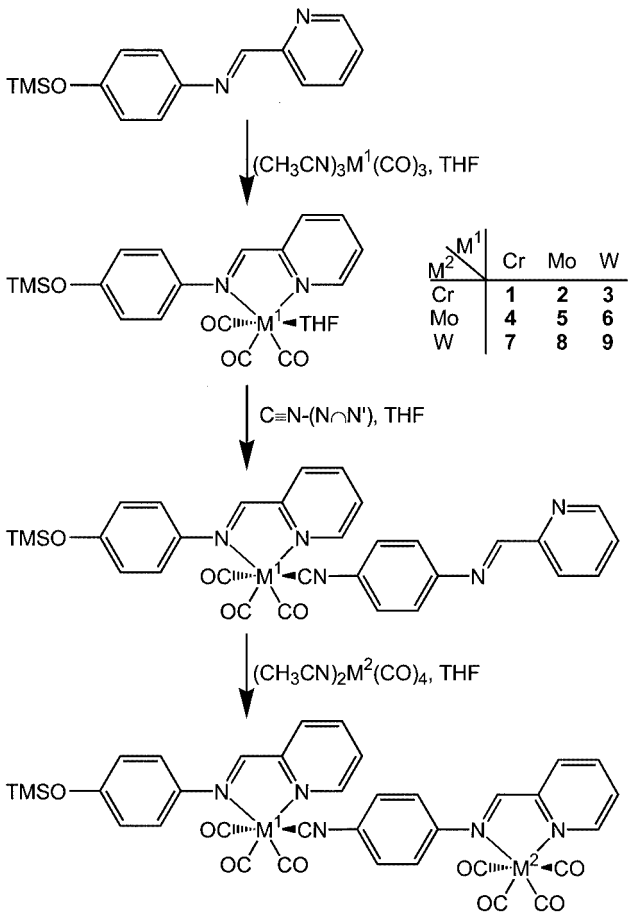

Scheme 2

Table 1. IR and UV/Vis spectroscopic data of intermediate complexes [TMSO−(N∩N′)$M(CO)_3$L] in THF ($\tilde{\nu}$ in cm^{-1}; λ_{max} in nm)

L	Cr	Mo	W	Assignment
$\tilde{\nu}$ THF	1805	1802	1808	CO
	1906	1910	1907	CO
$\tilde{\nu}$ C≡N−(N∩N′)	1826	1827	1827	CO
	1860	1855	1849	CO
	1915	1919	1915	CO
	2074	2076	2072	CN
λ_{max} THF	766	685	705	
λ_{max} C≡N−(N∩N′)	660	618	628	

these two bands with a new set of three ν_{CO} bands plus one ν_{CN} band (Table 1, cf.[18,19,20]). A further proof for isocyanide coordination is the shift of the ν_{CN} signal by about 50 cm^{-1} to lower energy than the signal of the free ligand C≡N−(N∩N′) (ν_{CN} = 2127 cm^{-1}). This shift is also observed in the IR spectra of the dinuclear complexes **1**−**9** (Table 2). Introduction of the $M^2(CO)_4$ fragment causes additional ν_{CO} bands to appear (Table 2) so that the IR spectra of the dinuclear complexes **1**−**9** can be described as a superposition of the IR spectra of the corresponding mononuclear isocyanide tricarbonyl complex [TMSO−(N∩N′)$M^1(CO)_3$C≡N−(N∩N′)] and the tetra-

 © 2003 Wiley-VCH Verlag GmbH & Co. KGaA, Weinheim

carbonyl complex [HO-(N∩N′)$M^2(CO)_4$][18,19,20] as shown in Figure 1 for the Cr-W complex **7**.

Table 2. IR spectroscopic data of complexes **1**−**9** in THF ($\tilde{\nu}$ in cm^{-1})

M^2 / M^1	Cr	Mo	W
Cr	1829	1827	1829
	1850	1850	1849
	1906	1906	1911 br
	1913	1918	
	2006	2007	2006
	2073	2075	2072
Mo	1829	1828	1827
	1849	1850	1849
	1907	1909	1907
	1913 sh	1917	1911 sh
	2013	2012	2013
	2069	2079	2068
W	1830	1827	1829
	1849	1849	1849
	1896	1897	1896
	1915	1914	1913
	2006	2008	2006
	2072	2079	2073

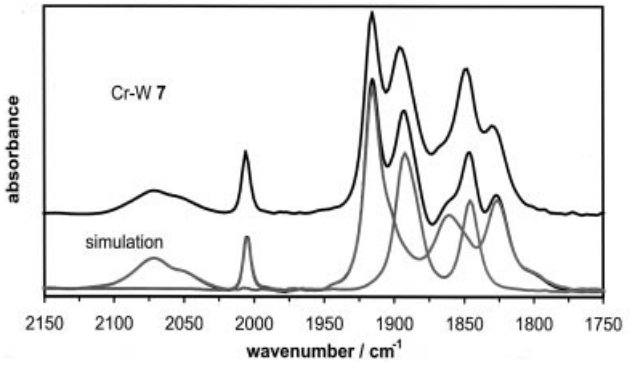

Figure 1. IR spectrum of dinuclear complex **7** and spectra of the corresponding mononuclear complexes [HO-(N∩N′)$W(CO)_4$][20] and [TMSO−(N∩N′)$Cr(CO)_3$C≡N−(N∩N′)] in THF

The ^{1}H NMR spectra of the complexes **1**−**9** show broad and overlapping multiplets in the aromatic region (see Exp. Section) and are thus not particularly informative. Only the signals for the imine protons (chemical shift range δ = 8.4−8.9 ppm) are clearly assignable (Table 3). A closer inspection reveals that imine protons of the tungsten complexes resonate at δ ≥ 8.84 ppm while imine protons of the chromium and molybdenum complexes resonate at higher fields with δ ≤ 8.62 ppm in THF. ^{13}C NMR spectra could not be obtained due to the low solubility of the complexes.

Table 3. ^{1}H NMR chemical shifts of imine protons of complexes **1**−**9** in CD_2Cl_2

M^2 / M^1	Cr	Mo	W
Cr	8.48	8.62	8.90
	8.54	8.49	8.48
Mo	8.42	8.61	8.83
	8.47	8.58	8.51
W	8.54	8.51	8.90
	8.87	8.84	8.87

In the UV/Vis spectra of complexes **1**−**9** one or two MLCT absorption bands are observed in the range 524−666 nm (Table 4). The low-energy absorption is due to the (N∩N′)$M^1(CO)_3$ chromophore, while the high-energy absorption arises from the (N∩N′)$M^2(CO)_4$ chromophore.[18−20,22−24] Like the IR spectra the UV/Vis spectra can be interpreted as a superposition of spectra of the individual chromophores, as shown for the ditungsten complex **9** in Figure 2. These observations demonstrate that, in each case, the two metal fragments of the dinuclear system behave as mechanically (IR) and electronically (UV/Vis) independent units, which appears reasonable in view of the large metal−metal distance of around 10 Å (estimated on model calculations) and the flexible orientation of the $M^2(CO)_4$ fragment with respect to the $M^1(CO)_3$ moiety.

Table 4. UV/Vis spectroscopic data of complexes **1**−**9** in THF (λ_{max} in nm; ε in $M^{-1}cm^{-1}$)

M^2 / M^1	Cr	Mo	W
Cr	598 (15200)	594 (9730)	608 (11900)
Mo	557 (8210)	524 (9000)	556 (12210)
	666 (5780, sh)	615 (7250, sh)	609 (11650)
W	570 (6030)	562 (9180)	570 (8170)
	640 (4390, sh)	613 (8600, sh)	600 (7760, sh)

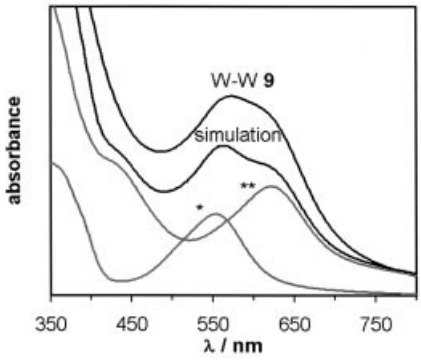

Figure 2. UV/Vis spectrum of the dinuclear complex **9** and spectra of the corresponding mononuclear complexes [HO−(N∩N′)-$W(CO)_4$] (*)[20] and [TMSO−(N∩N′)$W(CO)_3$C≡N−(N∩N′)] (**) in THF

As additional proof for the dinuclear nature of the complexes in solution, and to exclude a simple mixture of mononuclear complexes, the molecular masses of complexes **1**−**9** have been determined by osmometry (see Exp. Sect.). In all cases the results agree with the expected mass within experimental error. This also shows that the complexes remain stable in solution without dissociation, i.e. the metal−isocyanide bond remains intact.

The dinuclear species were further characterised by FAB mass spectroscopy (see Exp. Sect.). Peaks corresponding to

 © 2003 Wiley-VCH Verlag GmbH & Co. KGaA, Weinheim

ions of the dinuclear complexes and to fragments with loss of one to seven carbon monoxide ligands but with an intact {TMSO−(N∩N′)M^1C≡N−(N∩N′)M^2} backbone substantiate the above findings.

The cyclic voltammograms of complexes **1**−**9** in CH_2Cl_2/($n$$Bu_4N$)($PF_6$) show only irreversible and quasireversible oxidation waves, probably due to the loss of carbon monoxide upon oxidation. This behaviour has already been observed for the corresponding mononuclear complexes.[18−20]

With all these spectroscopic data at hand we tried to answer the following question: Is it possible to determine ("read") the metal sequence in these dinuclear complexes without any prior knowledge of the synthetic protocol used? In other words, can these nine complexes be distinguished with respect to their spectral properties? A closer inspection of the IR, ^{1}H NMR, and UV/Vis spectra of the complexes **1**−**9** reveals distinct differences between the individual complexes (Tables 2−4).

The IR spectra give three criteria:

(i) $\tilde{\nu}_{CN} \geq 2075$ cm^{-1} indicates M^1 = Mo (complex **2** or **8**)

(ii) $\tilde{\nu}_{CO,tetra} \geq 2012$ cm^{-1} indicates M^2 = Mo (complex **4** or **6**)

(iii) both (i) and (ii) indicates M^1 = M^2 = Mo (complex **5**)

The ^{1}H NMR spectra give two criteria:

(iv) one $\delta_{H(Imin)} \geq 8.84$ indicates M^1 = W or M^2 = W (**3**, **6**, **7**, or **8**)

(v) two $\delta_{H(Imin)} \geq 8.84$ indicates M^1 = M^2 = W (complex **9**)

Criteria (iii) and (v) completely assign complexes **5** and **9**. Taking (i), (ii), and (iv) together complexes **2**, **8**, **4**, and **6** can be unambiguously assigned. For example, (i) and (iv) together indicates complex **8**. Combining IR and ^{1}H NMR spectroscopy all complexes except the isomeric pair **3**/**7** can be unambiguously assigned.

The Cr/W isomers **3** and **7** can be distinguished on the basis of their UV/Vis spectra: the difference of λ_{max} for the MLCT absorption maxima of the individual chromophores in the dinuclear species is almost twice as large for complex **7** as for complex **3** (estimated on the basis of the absorption bands of corresponding mononuclear complexes[18−20]) so that for complex **7** a broad absorption with a low-energy shoulder is observed while complex **3** displays only one comparatively sharp band (Figure 3).

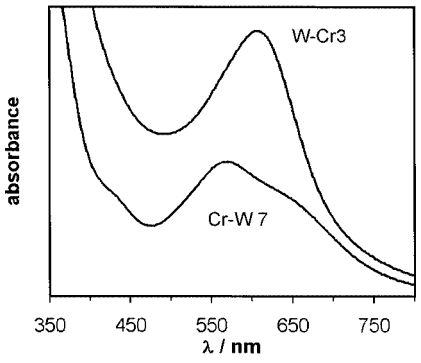

Figure 3. UV/Vis spectra of the dinuclear Cr/W complexes **3** and **7**

On the basis of IR (determination of molybdenum content and position), NMR (determination of tungsten content), and UV/Vis (discrimination between **3** and **7**) spectroscopy the metal positions in all nine dinuclear complexes **1**−**9** can be unambiguously determined.

Conclusion

Dinuclear directional complexes with well-defined metal sequences have been prepared in solution and characterised. However, low yields and lengthy purification renders this solution synthesis unsuitable for trinuclear and higher chain complexes which could be obtained by repeated chain growth cycles with [$(CH_3CN)_3M(CO)_3$] and C≡N−(N∩N′). Currently a new method for the stepwise assembly of tri- and oligonuclear complexes on a solid phase is being developed.[18,25,26]

The metal sequence of nine dinuclear complexes with Cr, Mo, and W in two possible positions can be determined using a combination of standard spectroscopic techniques. It should be possible to extend the sequence determination to "sequencing" or "readout" of oligonuclear complexes if the simulation technique based on spectra of mononuclear complexes is used in combination with chemometric methods such as, for example, principal component analysis (PCA) or partial least-squares (PLS).[29] As the spectroscopic determination of the chromium content is rather indirect a two letter code with molybdenum and tungsten as the basis might be advisable in larger chain complexes. The preparation and characterisation of oligonuclear complexes built from molybdenum and tungsten fragments is currently underway.[26]

Experimental Section

Unless noted otherwise, all manipulations were carried out under argon by means of standard Schlenk techniques. All solvents were dried by standard methods and distilled under argon prior to use. All other reagents were used as received from commercial sources. NMR: Bruker Avance DPX 200 at 200.15 MHz (^{1}H), 50.323 MHz (^{13}C) at 303 K; chemical shifts (δ) in ppm with respect to residual solvent peaks as internal standards: $CDCl_3$ (^{1}H: δ = 7.24; ^{13}C: δ = 77.0 ppm), [D_8]THF (^{1}H: δ = 1.73, 3.58; ^{13}C: δ = 25.5, 67.7), CD_2Cl_2 (^{1}H: δ = 5.32; ^{13}C: δ = 53.8 ppm). IR spectra were recorded on a BioRad Excalibur FTS 3000 spectrometer using CaF_2 cells or CsI disks. UV/Vis/NIR spectra were recorded on a Perkin−Elmer Lambda 19, 0.2 cm cells (Hellma, suprasil). Mass spectra were recorded on a Finnigan MAT 8400 spectrometer. Elemental analyses were performed by the microanalytical laboratory of the Organic Chemistry Department, University of Heidelberg. Molecular weight determinations in THF: Knauer vapour-pressure osmometer No. 7311100000, calibration with benzil.

The ligand TMSO−(N∩N′) was prepared according to the literature procedure.[18] The acetonitrile complexes were prepared from [(cycloheptatriene)$M(CO)_3$] and [(norbonadiene)$M(CO)_4$],[27,28] respectively, by reaction with CH_3CN (M = Cr, Mo, W).

4-Isocyanophenylamine:[21] 1,4-Diaminobenzene (0.28 mol, 30 g) was suspended in ethanol (120 mL) and chloroform (400 mL). A

 © 2003 Wiley-VCH Verlag GmbH & Co. KGaA, Weinheim

solution of KOH (200 g) in water (800 mL) was carefully added and the mixture was refluxed for 2.5 h. The organic layer was separated and the residue was extracted twice with dichloromethane. The combined organic phases were washed with water and dried with $MgSO_4$. After evaporation of the solvent the residue was purified by flash chromatography (Alox, diethyl ether, $R_f = 0.5$) giving the product as yellow needles. Yield: 15 g (0.13 mol, 45%). $C_7H_6N_2$ (118.1): calcd. C 71.17, H 5.12, N 23.71; found C 71.11, H 5.12, N 23.52. MS (EI): *m/z* (intensity [%], fragment) = 118 (100) [M^+], 91 (33) [M^+ − HCN]. IR ($CHCl_3$): $\tilde{\nu}$ = 2129 (s, CN), 3410 cm^{-1} (br., NH). IR (CsI): $\tilde{\nu}$ = 2129 (s, CN), 3460 cm^{-1} (s, NH). ^1H NMR ($CDCl_3$): δ = 3.79 (br., 2 H, NH_2), 6.62 (d, 2 H, $H^{2,6}$, $^3J_{H,H}$ = 8.5 Hz), 7.17 (d, 2 H, $H^{3,5}$, $^3J_{H,H}$ = 8.5 Hz) ppm. ^{13}C NMR ($CDCl_3$): δ = 115.2 (s, $C^{2,6}$), 128.0 (s, $C^{3,5}$), 147.8 (s, C^1), C^4 and *C*N not observed ppm.

(4-Isocyanophenyl)pyridine-2-ylmethyleneamine C≡N−(N∩N′): A mixture of 4-Isocyanophenylamine (34.6 mmol, 4.08 g), pyridine-2-carbaldehyde (52.3 mmol, 5 mL), $MgSO_4$ (5 g), and ethyl acetate (80 mL) was heated under reflux for 6 h. The resulting brown suspension was filtered and the orange solution was evaporated to dryness. After recrystallisation from acetone/diethyl ether the brown solid was dried in vacuo for 4 days. Yield 5.5 g (26.5 mmol, 77%). $C_{13}H_9N_3$ (20.7.2)·0.25 H_2O: calcd. C 73.74, H 4.52, N 19.85; found C 73.89, H 4.49, N 19.62. m.p. 84−85 °C. MS(EI): *m/z* (intensity [%], fragment) = 207 (31) [M^+], 179 (M^+ − HCN, − H), 79 (100) [$C_5H_5N^+$]. HR-MS(EI): Calcd. for $C_{13}H_9N_3$: 207.07965; found 207.07663. IR (CH_2Cl_2): $\tilde{\nu}$ = 2127 cm^{-1} (s, CN). IR (CsI): $\tilde{\nu}$ = 2131 cm^{-1} (s, CN). ^1H NMR ([D$_8$]THF): δ = 7.39 (d, 2 H, $H^{2,6}$, $^3J_{H,H}$ = 8.6 Hz), 7.45−7.49 (m, 1 H, H^{11}), 7.55 (d, 2 H, $H^{3,5}$, $^3J_{H,H}$ = 8.6 Hz), 7.90 (dvt, 1 H, H^{10}, *J* = 7.8, *J* = 1.2 Hz), 8.26 (d, 1 H, H^9, *J* = 7.8 Hz), 8.62 (s, 1 H, H^7), 8.72 (d, 1 H, H^{12}, *J* = 4.8 Hz) ppm. ^{13}C NMR ([D$_8$]THF): δ = 121.5 (s, C^9), 122.5 (s, $C^{2,6}$), 125.8 (s, C^{11}), 127.7 (s, $C^{3,5}$), 136.7 (s, C^{10}), 150.0 (s, C^1), 150.2 (s, C^{12}), 152.4 (s, C^4), 155.1 (s, C^8), 163.2 ppm (s, C^7), *C*N not observed. All signals were assigned on the basis of DEPT, CH-COSY, and NOESY experiments. The conformation in solution is *transoid* as no cross peak between H^7 and H^9 is observed in the NOESY spectrum.

Complexes 1−9: All glassware was passivated with $(CH_3)_3SiCl$ before use. [$(CH_3CN)_3M^1(CO)_3$] (1 mmol) was treated with TMSO−(N∩N′) (270 mg, 1 mmol) in 40 mL of THF and the solution was stirred until IR control (see Table 1) indicated complete formation of [TMSO−(N∩N′)M(CO)$_3$thf] (at least 15 min). C≡N−(N∩N′) (207 mg, 1 mmol) was added as a solid and the solution turned green immediately. IR control indicated complete formation of [TMSO−(N∩N′)M^1(CO)$_3$C≡N−(N∩N′)] after 10 min (see Table 1). A solution of [$(CH_3CN)_2M^2(CO)_4$] (1 mmol) in THF (10 mL) was then added. The reaction mixture turned black and was stirred for 30 min. Celite was added and the solution was evaporated to dryness. The dark residue was chromatographed on silica gel (*T* = 0 °C; Et_2O, purple fraction; THF, dark-blue fraction, product complex). The THF fraction was concentrated and layered with petroleum ether (40/60). The black precipitate was collected and dried in vacuo. Yields: 20−55% (0.2−0.55 mmol).

[TMSO−(N∩N′)Cr(CO)$_3$C≡N−(N∩N′)Cr(CO)$_4$] (1): $C_{35}H_{27}Cr_2N_5O_8Si$ (777.7): calcd. C 54.05, H 3.50, N 9.01; found C 53.22, H 3.62, N 9.58. Molecular mass found: 765. MS(FAB): *m/z* (intensity [%], fragment) = 777 (17) [M^+], 693 (100) [M^+ − 3CO], 581 (94) [M^+ − 7CO]. ^1H NMR (CD_2Cl_2): δ = 0.38 (s, 9 H, SiCH_3), 7.0 (br. s, 2 H), 7.2−7.6 (m, 8 H), 7.9 (br. s, 4 H), 8.48 (s, 1 H), 8.54 (s, 1 H), 9.29 (br. s, 1 H), 9.39 (br. s, 1 H) ppm. IR (CsI): $\tilde{\nu}$ = 1832, 1908, 2009 (CO), 2082 (CN) cm^{-1}.

[TMSO−(N∩N′)Mo(CO)$_3$C≡N−(N∩N′)Cr(CO)$_4$] (2): $C_{35}H_{27}CrMoN_5O_8Si$ (821.7): calcd. C 51.16, H 3.31, N 8.52; found C 50.74, H 3.38, N 8.97. Molecular mass found: 846. MS(FAB): *m/z* (intensity [%], fragment) = 823 (15) [M^+], 711 (100) [M^+ − 4CO], 683 (58) [M^+ − 5CO], 627 (40) [M^+ −5 CO]. ^1H NMR (CD_2Cl_2): δ = 0.38 (s, 9 H, SiCH_3), 7.02 (d, *J* = 8.0 Hz, 2 H), 7.2−7.6 (m, 8 H), 7.8−8.0 (m, 4 H), 8.49 (s, 1 H), 8.62 (s, 1 H), 9.2−9.4 (br. s, 2 H) ppm. IR (CsI): $\tilde{\nu}$ = 1832, 1911, 2010 (CO), 2084 (CN) cm^{-1}.

[TMSO−(N∩N′)W(CO)$_3$C≡N−(N∩N′)Cr(CO)$_4$] (3): $C_{35}H_{27}CrN_5O_8SiW$ (909.6): calcd. C 46.22, H 2.99, N 7.70; found C 46.32, H 3.47, N 8.02. Molecular mass found: 917. MS(FAB): *m/z* (intensity [%], fragment) = 908 (100) [M^+], 797 (66) [M^+ − 4CO]. ^1H NMR (CD_2Cl_2): δ = 0.38 (s, 9 H, SiCH_3), 7.0 (m, 2 H), 7.3−7.5 (m, 8 H), 7.93 (br. s, 4 H), 8.48 (s, 1 H), 8.90 (s, 1 H), 9.27 (br. s, 1 H), 9.38 (br. s, 1 H) ppm. IR (CsI): $\tilde{\nu}$ = 1828, 1907, 2008 (CO), 2080 (CN) cm^{-1}.

[TMSO−(N∩N′)Cr(CO)$_3$C≡N−(N∩N′)Mo(CO)$_4$] (4): $C_{35}H_{27}CrMoN_5O_8Si$ (821.7): calcd. C 51.16, H 3.31, N 8.52; found C 50.73, H 3.40, N 8.68. Molecular mass found: 806. MS(FAB): *m/z* (intensity [%], fragment) = 739 (36) [M^+ − 3CO], 711 (94) [M^+ − 4CO]. ^1H NMR (CD_2Cl_2): δ = 0.31 (s, 9 H, SiCH_3), 6.94 (d, *J* = 8.0 Hz, 2 H), 7.3−7.6 (m, 8 H), 7.9−8.0 (m, 4 H), 8.42 (s, 1 H), 8.47 (s, 1 H), 9.1−9.3 (m, 2 H) ppm. IR (CsI): $\tilde{\nu}$ = 1837, 1912, 2012 (CO), 2082 (CN) cm^{-1}.

[TMSO−(N∩N′)Mo(CO)$_3$C≡N−(N∩N′)Mo(CO)$_4$] (5): $C_{35}H_{27}Mo_2N_5O_8Si$ (865.6): calcd. C 48.57, H 3.14, N 8.09; found C 48.31, H 3.28, N 8.91. Molecular mass found: 841. MS(FAB): *m/z* (intensity [%], fragment) = 866 (67) [M^+], 782 (67) [M^+ − 3CO], 670 (100) [M^+ − 7CO]. ^1H NMR (CD_2Cl_2): δ = 0.38 (s, 9 H, SiCH_3), 7.0 (d, *J* = 8.4 Hz, 2 H), 7.34 (d, *J* = 8.4 Hz, 2 H), 7.5−7.7 (m, 6 H), 7.9−8.0 (m, 4 H), 8.58 (s, 1 H), 8.61 (s, 1 H), 9.22 (d, *J* = 3.7 Hz, 1 H), 9.28 (br. s, 1 H) ppm. IR (CsI): $\tilde{\nu}$ = 1830, 1911, 2016 (CO), 2084 (CN) cm^{-1}.

[TMSO−(N∩N′)W(CO)$_3$C≡N−(N∩N′)Mo(CO)$_4$] (6): $C_{35}H_{27}MoN_5O_8SiW$ (953.5): calcd. C 44.09, H 2.85, N 7.35; found C 43.34, H 3.22, N 8.01. Molecular mass found: 967. MS(FAB): *m/z* (intensity [%], fragment) = 955 (17) [M^+], 927 (71) [M^+ − CO], 915 (100) [M^+ − 5CO]. ^1H NMR (CD_2Cl_2): δ = 0.31 (s, 9 H, SiCH_3), 6.95 (d, *J* = 8.0 Hz, 2 H), 7.22 (d, *J* = 8.0 Hz, 2 H), 7.5−7.7 (m, 6 H), 7.9−8.0 (m, 4 H), 8.51 (s, 1 H), 8.83 (s, 1 H), 9.12 (br. s, 1 H), 9.31 (br. s, 1 H) ppm. IR (CsI): $\tilde{\nu}$ = 1829, 1907, 2016 (CO), 2077 (CN) cm^{-1}.

[TMSO−(N∩N′)Cr(CO)$_3$C≡N−(N∩N′)W(CO)$_4$] (7): $C_{35}H_{27}CrN_5O_8SiW$ (909.6): calcd. C 46.22, H 2.99, N 7.70; found C 45.41, H 3.29, N 7.88. Molecular mass found: 937. MS(FAB): *m/z* (intensity [%], fragment) = 909 (33) [M^+], 825 (100) [M^+ − 3CO], 797 (91) [M^+ − 4CO]. ^1H NMR (CD_2Cl_2): δ = 0.37 (s, 9 H, SiCH_3), 6.99 (m, 2 H), 7.4−7.6 (m, 8 H), 7.9−8.0 (m, 4 H), 8.54 (s, 1 H), 8.87 (s, 1 H), 9.30 (br. s, 1 H), 9.39 (br. s, 1 H) ppm. IR (CsI): $\tilde{\nu}$ = 1830, 1907, 2008 (CO), 2080 (CN) cm^{-1}.

[TMSO−(N∩N′)Mo(CO)$_3$C≡N−(N∩N′)W(CO)$_4$] (8): $C_{35}H_{27}MoN_5O_8SiW$ (953.5): calcd. C 44.09, H 2.85, N 7.35; found C 43.64, H 2.63, N 7.80. Molecular mass found: 945. MS(FAB): *m/z* (intensity [%], fragment) = 955 (50) [M^+], 927 (100) [M^+ − CO], 870 (50) [M^+ − 3CO], 759 (86) [M^+ − 7CO]. ^1H NMR (CD_2Cl_2): δ = 0.31 (s, 9 H, SiCH_3), 6.94 (d, *J* = 8.2 Hz, 2 H), 7.3−7.5 (m, 8 H), 7.9−8.0 (m, 4 H), 8.51 (s, 1 H), 8.84 (s, 1 H), 9.2−9.3 (br. s, 2 H) ppm. IR (CsI): $\tilde{\nu}$ = 1823, 1912, 2010 (CO), 2083 (CN) cm^{-1}.

 © 2003 Wiley-VCH Verlag GmbH & Co. KGaA, Weinheim

[TMSO−(N∩N′)W(CO)$_3$C≡N−(N∩N′)W(CO)$_4$] (9): $C_{35}H_{27}N_5O_8SiW_2$ (1041.4): calcd. C 40.37, H 2.61, N 6.73; found C 40.71, H 2.99, N 7.56. Molecular mass found: 1017. MS(FAB): *m/z* (intensity [%], fragment) = 1041 (100) [M^+], 845 (78) [M^+ − 7CO]. ^{1}H NMR (CD_2Cl_2): δ = 0.38 (s, 9 H, SiCH_3), 7.02 (d, *J* = 8.0 Hz, 2 H), 7.3−7.6 (m, 8 H), 7.9−8.0 (m, 4 H), 8.87 (s, 1 H), 8.90 (s, 1 H), 9.25−9.50 (m, 2 H) ppm. IR (CsI): $\tilde{\nu}$ = 1829, 1903, 2008 (CO), 2081 (CN) cm^{-1}.

Acknowledgments

This work was supported by the Deutsche Forschungsgemeinschaft and the Fonds der Chemischen Industrie. The permanent, generous support from Prof. Dr. G. Huttner is gratefully acknowledged. We thank Yasmin Nisar for preparative assistance.

[1] K. Müllen, G. Wegner, *Electronic Materials: The Oligomer Approach*, Wiley-VCH Weinheim, **1998**.
[2] J. K. Bera, K. R. Dunbar, *Angew. Chem.* **2002**, *114*, 4633−4637; *Angew. Chem. Int. Ed.* **2002**, *41*, 0000−0000.
[3] P. Nguyen, P. Gómez-Elipe, I. Manners, *Chem. Rev.* **1999**, *99*, 1515−1548.
[4] V. Balzani, A. Juris, M. Venturi, *Chem. Rev.* **1996**, *96*, 759−833.
[5] H.-C. Chang, J.-T. Li, C.-C. Wang, T.-W. Lin, H.-C. Lee, G.-H. Lee, S.-M. Peng, *Eur. J. Inorg. Chem.* **1999**, 1243−1251.
[6] S.-Y. Lai, T.-W. Lin, Y.-H. Chen, C.-C. Wang, G.-H. Lee, M.-H. Yang, M.-K. Leung, S.-M. Peng, *J. Am. Chem. Soc.* **1999**, *121*, 250−251.
[7] C.-C. Wang, W.-C. Lo, C.-C. Chou, G.-H. Lee, J.-M. Chen, S.-M. Peng, *Inorg. Chem.* **1998**, *37*, 4059−4065.
[8] S.-J. Shieh, C.-C. Chou, G.-H. Lee, C.-C. Wang, S.-M. Peng, *Angew. Chem.* **1997**, *109*, 57−59, *Angew. Chem. Int. Ed. Engl.* **1997**, *36*, 56−59.
[9] H. Plenio, J. Hermann, J. Leukel, *Eur. J. Inorg. Chem.* **1998**, 2063−2069.
[10] H. Plenio, J. Hermann, A. Sehring, *Chem. Eur. J.* **2000**, *6*, 1820−1828.
[11] R. W. Wagner, T. E. Johnson, J. S. Lindsey, *J. Am. Chem. Soc.* **1996**, *118*, 11166−11180.
[12] C. Clausen, D. T. Gryko, A. A. Yasseri, J. R. Diers, D. F. Bocian, W. G. Kuhr, J. S. Lindsey, *J. Org. Chem.* **2000**, *65*, 7371−7378.
[13] C. Clausen, D. T. Gryko, R. B. Dabka, N. Dontha, D. F. Bocia, W. G. Kuhr, J. S. Lindsey, *J. Org. Chem.* **2000**, *65*, 7363−7370.
[14] P. N. Taylor, J. Huuskonen, G. Rumbles, R. T. Aplin, E. Williams, H. L. Anderson, *Chem. Commun.* **1998**, 909−910.
[15] S. A. Adeyemi, E. C. Johnson, F. J. Miller, T. J. Meyer, *Inorg. Chem.* **1973**, *12*, 2371−2374.
[16] S. Serroni, G. Denti, *Inorg. Chem.* **1992**, *31*, 4251−4255.
[17] C. Chang, D. Ludwig, A. Bocarsly, *Inorg. Chem.* **1998**, *37*, 5467−5473.
[18] K. Heinze, *Chem. Eur. J.* **2001**, *7*, 2922−2932.
[19] K. Heinze, *J. Chem. Soc., Dalton Trans.* **2002**, 540−547.
[20] K. Heinze, V. Jacob, *J. Chem. Soc., Dalton Trans.* **2002**, 2379−2385.
[21] R. G. A. New, L. E. Sutton, *J. Chem. Soc.* **1932**, 1415−1422.
[22] H. Behrends, E. Lindner, G. Lehnert, *J. Organomet. Chem.* **1970**, *22*, 439−448.
[23] H. Brunner, W. A. Herrmann, *Chem. Ber.* **1972**, *105*, 770−783.
[24] A. Bell, R. A. Walton, *Polyhedron* **1986**, *5*, 951−958.
[25] K. Heinze, U. Winterhalter, T. Jannack, *Chem. Eur. J.* **2000**, *6*, 4203−4210.
[26] K. Heinze, J. D. Bueno Toro, *Angew. Chem.* accepted.
[27] M. A. Bennett, L. Pratt, G. Wilkinson, *J. Chem. Soc.* **1961**, 2037−2044.
[28] E. W. Abel, M. A. Bennett, R. Burton, G. Wilkinson, *J. Chem. Soc.* **1958**, 4559−4563.
[29] B. Yan, H. Yan, *J. Comb. Chem.* **2001**, *3*, 78−84.

Received May 7, 2003

 © 2003 Wiley-VCH Verlag GmbH & Co. KGaA, Weinheim

Lacunary Wells−Dawson Sandwich Complexes − Synthesis, Characterization, and Stability Studies of Multi-Iron Species

Israel Martyr Mbomekalle,[a] Bineta Keita,[a] Louis Nadjo,*[a] Wade A. Neiwert,[b] Lei Zhang,[b] Kenneth I. Hardcastle,[b] Craig L. Hill,[b] and Travis M. Anderson[b]

Keywords: Polyoxometalates / Sandwich complexes / Iron / Manganese

Reaction of α-$Na_{12}(As_2W_{15}O_{56})$ with Fe^{II} in 1 M NaCl solution followed by air oxidation yields αααα-$H_2Na_{14}[(NaOH_2)_2Fe^{III}_2(As_2W_{15}O_{56})_2]$ (Na**2**), the arsenic analogue of the divacant lacunary sandwich, αααα-$H_2Na_{14}[(NaOH_2)_2Fe^{III}_2(P_2W_{15}O_{56})_2]$ (Na**1**). This complex (Na**2**) consists of a Na_2Fe_2 central unit sandwiched between two B-α-$As_2W_{15}O_{56}^{12-}$ moieties. Both Na**1** and Na**2** react with one equivalent of Fe^{III} to give ααβα-$Na_{14}[(NaOH_2)(Fe^{III}OH_2)(Fe^{III})_2(X_2W_{15}O_{56})_2]$, where X = P (Na**3**) or As (Na**4**), or two equivalents of Mn^{II} to give αββα-$Na_{14}[(Mn^{II}OH_2)_2(Fe^{III})_2(X_2W_{15}O_{56})_2]$, where X = P (Na**5**) or As (Na**6**). A single-crystal X-ray diffraction analysis of Na**5** has been carried out [a = 13.5387(8) Å, b = 13.9327(9) Å, c = 21.3347(13) Å, α = 92.921(1) °, β = 94.367(1) °, γ = 118.154(1) °, triclinic, $P\bar{1}$, $R1$ = 5.49%, based on 24662 independent reflections], which revealed a Mn_2Fe_2 central unit sandwiched between two B-α-$P_2W_{15}O_{56}^{12-}$ units. All of the new complexes have been characterized by FTIR spectroscopy, UV/Visible spectroscopy, elemental analyses, and cyclic voltammetry, and they are all stable for at least 24 h over a wide pH range (0–7), except for Na**4**, which is unstable below pH 2.

(© Wiley-VCH Verlag GmbH & Co. KGaA, 69451 Weinheim, Germany, 2003)

Introduction

Polyoxometalates (POMs for convenience) and their transition metal substituted derivatives (TMSPs) are a versatile and robust group of metal−oxygen anionic clusters with applications in catalysis, medicine, and materials science.[1−3] Among known POM structural types, sandwich complexes are the largest class of TMSPs. There are five major families of sandwich POMs (Figure 1), four of which are derived from trivacant Keggin structures ($XW_9O_{34}^{n-}$ or $XW_9O_{33}^{n-}$, where X = Fe^{III}, Co^{II}, Cu^{II}, Zn^{II}, Si^{IV}, P^{V}, As^{III}, As^{V}, Sb^{III}, Bi^{III}, Se^{IV}, or Te^{IV}),[4−8] and the fifth consists of the Wells−Dawson-derived structures.[8−21] These complexes are composed of a central M_4O_{16} unit encapsulated by two B-α-$X_2W_{15}O_{56}^{12-}$ (X = P^{V} or As^{V}) trivacant POMs. The structural properties of sandwich compounds derived from B-α-$P_2W_{15}O_{56}^{12-}$ are among the most well known because they are more amenable to NMR studies (such as ^{31}P NMR) than are the analogous Keggin (i.e. B-α-$XW_9O_{34}^{n-}$) and arsenic-containing Wells−Dawson species (i.e. B-α-$As_2W_{15}O_{56}^{12-}$).[8,16,18]

Recently we reported the new sandwich complex αααα-$H_2Na_{14}[(NaOH_2)_2(Fe^{III})_2(P_2W_{15}O_{56})_2]$ (Na**1**), which differs from conventional B-type Keggin and Wells−Dawson species;[14] X-ray structure analysis reveals only two d-electron metals reside in the central unit,[22] and the other positions are occupied by two weakly bound and labile seven-coordinate Na^+ ions that can readily exchange with a number

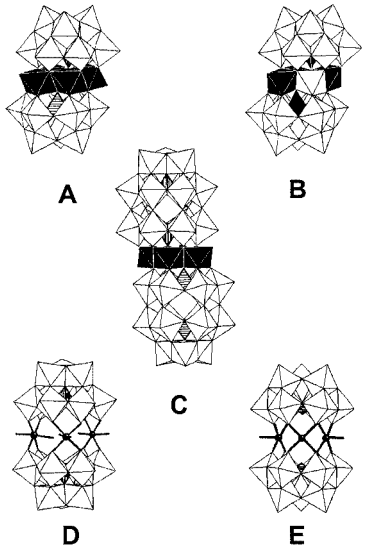

Figure 1. Polyhedral representations of the five major families of sandwich-type polyoxometalates. **A:** Conventional B-type Keggin sandwich **B:** Tourné B-type Keggin sandwich (transition metal heteroatoms) **C:** Wells−Dawson sandwich **D:** Conventional A-type Keggin Sandwich **E:** B-type Keggin sandwich with pyramidal heteroatoms

[a] Laboratoire de Chimie Physique, UMR 8000, CNRS, Université Paris-Sud,
Bâtiment 420, 91405 Orsay Cedex, France
[b] Department of Chemistry, Emory University, Atlanta, Georgia 30322, USA

 © 2003 Wiley-VCH Verlag GmbH & Co. KGaA, Weinheim **DOI: 10.1002/ejic.200300345**

of d-electron-containing metals, including Fe^{III}, Co^{II}, Cu^{II}, and Ni^{II}.[23]

We now report the first arsenic analogue of Na**1**, αααα-$Na_{16}[(NaOH_2)_2(Fe^{III})_2(As_2W_{15}O_{56})_2]$ (Na**2**), which is of considerable interest because the replacement of P with As in other sandwich-type complexes can greatly enhance catalytic activity for the H_2O_2-based epoxidation of alkenes without adversely affecting selectivity.[21,24] Both Na**1** and Na**2** react with a single equivalent of Fe^{III} to produce ααβα-$Na_{14}[(NaOH_2)(Fe^{III}OH_2)(Fe^{III})_2(X_2W_{15}O_{56})_2]$, where X = P (Na**3**)[16] or As (Na**4**), respectively.[25] Na**1** and Na**2** also react with two equivalents of Mn^{II} to yield new mixed-metal sandwich complexes, αββα-$Na_{14}[(Mn^{II}OH_2)_2(Fe^{III})_2(X_2W_{15}O_{56})_2]$, where X = P (Na**5**) or As (Na**6**). The four new complexes reported here (Na**2**, Na**4**, Na**5**, and Na**6**) have all been characterized by FTIR spectroscopy, UV/Visible spectroscopy, elemental analyses, and cyclic voltammetry. Complexes Na**2**, Na**4**, and Na**5** have also been characterized by X-ray crystallography.

Results and Discussion

Syntheses: The reaction of α-$Na_{12}(As_2W_{15}O_{56})$ with Fe^{II} in 1 M NaCl solution followed by air oxidation yields αααα-$H_2Na_{14}[(NaOH_2)_2Fe^{III}_2(As_2W_{15}O_{56})_2]$ (Na**2**), the arsenic analogue of the divacant lacunary sandwich, αααα-$H_2Na_{14}[(NaOH_2)_2Fe^{III}_2(P_2W_{15}O_{56})_2]$ (Na**1**). The synthesis of Na**2** is similar to Na**1** with two important exceptions.[14] First, the trivacant precursor α-$Na_{12}(As_2W_{15}O_{56})$ was used instead of α-$Na_{12}(P_2W_{15}O_{56})$. Second, the metastable dark green complex $Na_{16}[(Fe^{II}OH_2)_2Fe^{II}_2(As_2W_{15}O_{56})_2]$ was crystallized at 4 °C rather than at 10 °C.

Both Na**1** and Na**2** react with a single equivalent of Fe^{III} in water or in dilute NaCl to produce ααβα-$Na_{14}[(NaOH_2)(Fe^{III}OH_2)(Fe^{III})_2(X_2W_{15}O_{56})_2]$, where X = P (Na**3**)[16] or As (Na**4**), respectively.[26] Complexes Na**3** and Na**4** may also be isolated via fractional crystallization (≈ 48−70% yield for Na**4** and Na**3**, respectively) as byproducts in the synthesis of Na**1** and Na**2** {via the air-sensitive $Na_{16}[(Fe^{II}OH_2)_2Fe^{II}_2(X_2W_{15}O_{56})_2]$, where X = P^V or As^V, precursor}. Na**1** and Na**2** may also react with other d-electron-containing metals to yield mixed-metal sandwich complexes. Specifically, Na**1** and Na**2** react with 2.0 equivalents of Mn^{II} to yield αββα-$Na_{14}[(Mn^{II}OH_2)_2(Fe^{III})_2(X_2W_{15}O_{56})_2]$, where X = P (Na**5**) or As (Na**6**). ^{31}P NMR analysis of Na**5** suggests the reaction proceeds to 100% product (one peak for the symmetry-equivalent distal P atoms at δ = −11.9 ppm), although isolated yields of the arsenic analogue, Na**6**, were significantly higher than for the phosphorus analogue, Na**5** (84% versus 10% for Na**6** and Na**5**, respectively).

Crystallographic Studies: The X-ray structure of Na**2** reveals that only two Fe^{III} atoms are present in the innermost positions of the central tetrameric unit (Figure 2, A). The other two positions are occupied by two weakly-bound six-coordinate Na atoms. Each Na atom is coordinated to three oxygen atoms from one B-α-$As_2W_{15}O_{56}^{12-}$ moiety, two oxygen atoms from the other B-α-$As_2W_{15}O_{56}^{12-}$ moiety, and by a weakly-bound terminal water molecule. This complex is nearly isostructural to Na**1**, except that the As−O bond lengths in Na**2** are slightly longer than the analogous P−O bond lengths in Na**1**.[14] Disorder in the W_3O_{13} triad containing W1, W2, and W3 (rotation by 60 °) and of the Na counter cations and solvent water molecules prevented anisotropic refinement of all atoms (for details see data deposited in the crystal data base).

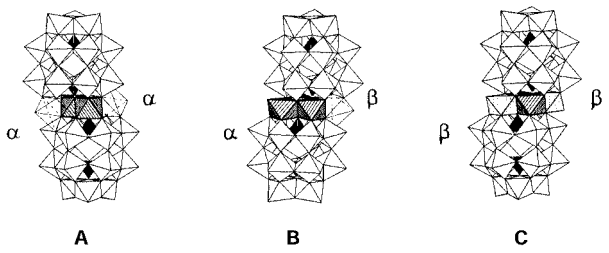

Figure 2. Polyhedral representations of the new Wells−Dawson sandwich complexes. **A:** Na**1** or Na**2** (W atoms are white, P or As atoms are black, Fe atoms are striped) **B:** Na**3** or Na**4** **C:** Na**5** or Na**6** (Mn atoms are gray). The central junctions are labeled α or β, and the central hexacoordinate Na atoms are shown for clarity.

An X-ray crystallographic analysis was also performed on the triferric arsenic complex, Na**4** (Figure 2, B). However, the crystals of this complex were of poorer quality than the analogous phosphorus complex, Na**3**.[16] While the structure of Na**4** was well determined and isostructural with the phosphorus complex, Na**3**, a poor refinement arose from the significant disorder of both a 60 ° rotation of the two W_3O_{13} triads containing W1, W2, and W3 and W28, W29, and W30 and the external Na1 and Fe1 positions in the $NaFe_3$ central unit (see crystal data base for additional details).[27]

An X-ray crystallographic analysis of the new mixed-metal sandwich POM, Na**5** (Table 1, Figure 2, C) shows that two Mn^{II} atoms have replaced the two Na^+ atoms of the

Table 1. Crystal Data and Structure Refinement for Na**5**

Empirical formula	$H_{66}Fe_2Mn_2Na_{14}O_{145}P_4W_{30}$
Formula mass	8569.35
Crystal system	triclinic
Space group	$P\bar{1}$
Unit cell	a = 13.5387(8) Å
	b = 13.9327(9) Å
	c = 21.3347(13) Å
	α = 92.921(1)°
	β = 94.367(1)°
	γ = 118.154(1)°
V	3520.6(4) Å^3
Z/density (calcd.)	1/4.042 Mg/m^3
Absorption coefficient	24.968 mm^{-1}
Reflns. collected	62359
Independent reflns.	24662 [R(int) = 0.0608]
GOF on F^2	1.025
Final R indices [$I > 2\sigma(I)$]	$R1$[a] = 0.0549
	$wR2$[b] = 0.1325

[a] $R1 = \Sigma||F_o| - |F_c||/\Sigma|F_o|$. [b] $wR2 = \{\Sigma[w(F_o^2 - F_c^2)^2/\Sigma[w(F_o^2)^2]\}^{0.5}$

 © 2003 Wiley-VCH Verlag GmbH & Co. KGaA, Weinheim

central unit of Na**1**. Each Mn^{II} atom is ligated by three oxygen atoms from one B-α-$P_2W_{15}O_{56}^{12-}$ unit, two oxygen atoms from the other B-α-$P_2W_{15}O_{56}^{12-}$ unit, and a terminal water ligand. Bond valence sum calculations from the X-ray crystal structure of Na**5** give an average oxidation state of 2.07 ± 0.02 for the two Mn atoms and 2.94 ± 0.02 for the two Fe atoms.[28] Crystals suitable for a complete X-ray crystallographic analysis could not be grown for the arsenic analogue (Na**6**).[29]

Stability Measurements: Unlike the Keggin-derived complexes which show a well-defined peak in their spectra, the UV/Visible spectra of the Wells−Dawson-derived species are usually more complex (with several broad absorptions). The complexes studied here exhibit spectra with different extinction coefficients and different peak wavelengths. Specifically, for a given pH, the spectra for Na**1**, Na**3**, and Na**5** show two main absorption bands around 220−250 nm and 340−360 nm, respectively. The same trends were observed for the As derivatives, Na**2**, Na**4**, and Na**6**. Thus, the stability of the oxidized forms of the complexes (Na**2**, Na**4**, Na**5**, and Na**6**), as a function of pH (0−7) and time (1 to 24 h), can be monitored by their UV/Visible spectra. Each experiment lasted 24 h, which is longer than necessary for complete electrochemical characterization of the complexes, but is relevant for long-lasting or preparative scale catalytic and electrocatalytic processes. All of the reported complexes (Na**2**, Na**4**, Na**5**, and Na**6**) are stable from pH 0 to 7 over a 24 hour period except for Na**4**, which is unstable below pH 2.

In additional stability tests on the reduced forms of the complexes, which are of interest for both catalytic and electrocatalytic processes, the Fe^{III} centers were exhaustively reduced to Fe^{II} by controlled potential coulometry and then reoxidized to the ferric state. The stability was monitored by cyclic voltammetry, recorded before and after the forward and backward electrolysis reaction. The data suggest that the Fe^{II} state within the complexes is stabilized by the two Mn^{II} centers (Na**5** and Na**6**). In contrast, electrolyses in pH < 4 media show that the Fe^{II} forms are unstable within Na**1** and Na**2** in the absence of Mn^{II}.

Electrochemistry: Cyclic voltammetry of the sandwich complexes, in a pH 3 sulfate medium (0.5 M Na_2SO_4 and H_2SO_4), afforded voltammograms of the arsenic complexes Na**2** and Na**4** that are similar to their corresponding phosphorus analogues.[15,20] However, the waves of the arsenic-containing species (Na**2** and Na**4**) are at slightly more positive potentials than for phosphorus-containing complexes (Na**1** and Na**3**).[24] Table 2 compares specifically the peak potential locations for the Fe waves and for the Mn waves (the Fe centers are arbitrarily numbered 1, 2, and 3 for clarity). The representative cyclic voltammograms in Figure 3 show in superposition the patterns for Na**1** and Na**5** (Figure 3, A) as well as Na**2** and Na**6** (Figure 3, B). As expected, only Na**5** and Na**6** show an oxidation process attributable to the overall four-electron oxidation of the Mn centers. The associated reduction patterns are composite and partially feature the characteristic shape of surface adsorbed species.

Table 2. Peak potential (V vs. SCE) for Fe waves E_{pc} (reduction) and the Mn wave (oxidation) determined by cyclic voltammetry at pH 3.00 (0.5 M Na_2SO_4 + H_2SO_4) for the new complexes. Scan rate: 10 $mV \cdot s^{-1}$, working electrode: glassy carbon

Compound	E_{pa} (V vs. SCE) **Mn**	$-E_{pc}$ (V vs. SCE) **Fe1**	**Fe2**	**Fe3**
Na1	–	0.132	0.238	
Na5	1.156	0.116	0.228	
Na2	–	0.118	0.208	
Na6	1.152	0.106	0.208	
Na4	–	−0.056	0.106	0.202

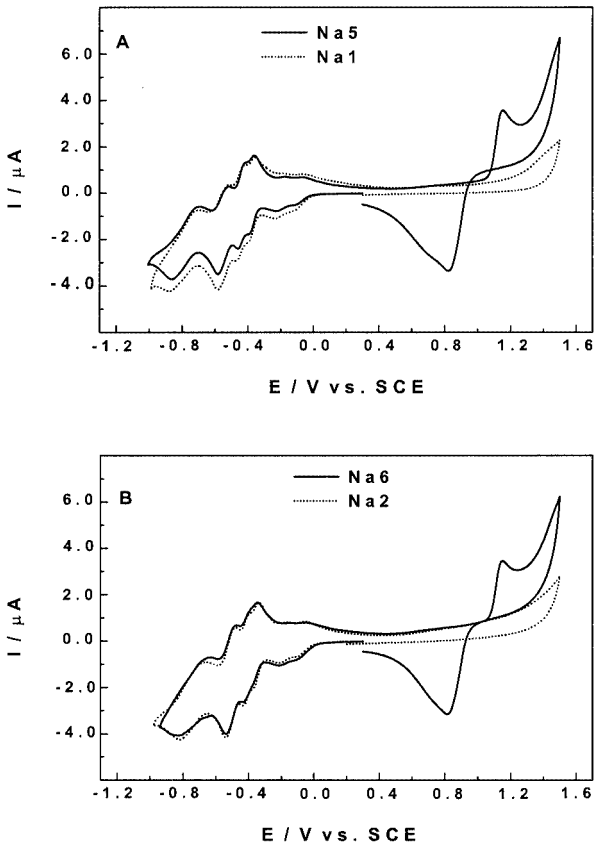

Figure 3. Cyclic voltammograms of Na**1**, Na**2**, Na**5**, and Na**6** in a pH 3 media (0.5 M Na_2SO_4 + H_2SO_4). Heteropolyanion concentration: 2×10^{-4} M; scan rate: 10 $mV \cdot s^{-1}$; working electrode: glassy carbon; reference electrode: SCE **A:** Comparison of the cyclic voltammograms of Na**1** and Na**5** **B:** Comparison of the cyclic voltammograms of Na**2** and Na**6**

The Fe and W waves are well separated in all of these complexes and the number of Fe waves observed for each complex corresponds exactly to that known from the stoichiometry of the relevant molecules.[15] Similar behavior has been observed for αββα-$Na_{12}[(Fe^{III}OH_2)_2(Fe^{III})_2(As_2W_{15}O_{56})_2]$.[20] Here again, controlled potential coulometry confirms that the exhaustive reduction of each Fe center consumes one electron per molecule. Also noteworthy is the observation that the first Fe wave of Na**4** is at a more positive potential than all other Fe waves present

 © 2003 Wiley-VCH Verlag GmbH & Co. KGaA, Weinheim

in the series (Table 2). The Mn^{II} in Na**5** and Na**6** also modifies the characteristics of the Fe waves, which are at slightly more positive potentials than for the divacant lacunary precursors Na**1** and Na**2**. Tentatively, and with the assumption of minimal variation in other electronic properties between the two complexes, this change might be attributable to differences in the overall negative charge of the complexes, which decreases from 16 (in Na**1** and Na**2**) to 14 (in Na**5** and Na**6**), thus rendering the Mn-containing complexes easier to reduce than their precursors. The magnitude of this difference, however, might be modulated by the acid−base properties of the reduced forms of these complexes. In short, as expected, Na**5** and Na**6** behave much like saturated sandwich-type derivatives while Na**1** and Na**2** are more lacunary. These observations are similar to those described by Pope and Chorghade for Sn-substituted monovacant POM complexes.[30] Sn^{II} is too large for the octahedral vacancy and the corresponding substituted derivatives behave much like the lacunary precursor complexes. In contrast, Sn^{IV} fits in the vacancy much better, and its derivatives behave very similarly to the saturated complexes.

Conclusions

The new divacant, lacunary arsenic-containing sandwich-type complex, Na**2**, synthesized here is isostructural with its phosphorus analogue, Na**1**. Both complexes react with one equivalent of Fe^{III} to yield triferric sandwich-type complexes, $\alpha\alpha\beta\alpha$-$Na_{14}[(NaOH_2)(Fe^{III}OH_2)(Fe^{III})_2(X_2W_{15}O_{56})_2]$, where X = P (Na**3**) or As (Na**4**). Na**1** and Na**2** also react with two equivalents of Mn^{II} to produce new mixed-metal sandwich-type complexes. All of the new complexes are stable for at least 24 h over the wide pH range 0−7, except for Na**4**, which is not stable below pH 2. This stability is remarkable and in sharp contrast with many other TMSPs. Typically within the Wells−Dawson family, the saturated compounds (formula $X_2W_{18}O_{62}^{6-}$, where X = P^V or As^V) are stable in mostly acidic media while their monosubstituted derivatives (formula $X_2MW_{17}O_{61}^{n-}$, where X = P^V or As^V and M = first row transition metal cation) require a higher pH. The wide stability seen here is an important prerequisite for substantial catalytic and electrocatalytic processes and may be a key parameter in preparing new effective catalysts.

Experimental Section

General Methods and Materials: α-$Na_{12}(As_2W_{15}O_{56})$, α-$Na_{12}(P_2W_{15}O_{56})$, Na**1**, and Na**3** were obtained by published procedures, and their purity was confirmed by IR, cyclic voltammetry, and ^{31}P NMR [except α-$Na_{12}(As_2W_{15}O_{56})$].[14,16−18,31] Elemental analyses of As, Fe, Mn, Na, P, and W were performed by Kanti Labs (Mississauga, Canada). Infrared spectra were recorded with a Perkin−Elmer Spectrum One and Nicolet 510 FT-IR instruments. All electrochemical measurements were performed with an EG and G 273A apparatus under computer control (M270 software). Potentials are quoted against a saturated calomel electrode (SCE). ^{31}P NMR measurements were made with a Varian INOVA 400 MHz spectrometer, and peaks were referenced to 85% H_3PO_4. Thermal analyses were performed with an ISI TGA 1000 and used to confirm the number of water molecules per POM.

X-ray Crystallography: Suitable crystals of Na**2**, Na**4**, and Na**5** were coated with Paratone N oil, suspended on a small fiber loop and placed in a cooled nitrogen stream at 100 K on a Bruker D8 SMART APEX CCD sealed tube diffractometer with graphite-monochromated Mo-K_α (0.71073 Å) radiation. A sphere of data was measured using a series of combinations of φ and ω scans with 10 s frame exposures and 0.3° frame widths. Data collection, indexing, and initial cell refinements were handled using SMART software.[32] Frame integration and final cell refinements were carried out using SAINT software.[33] The final cell parameters were determined from least-squares refinement. The SADABS program was used for absorption corrections.[34] The structures were solved by Direct Methods and difference Fourier techniques.[35] All atoms were refined anisotropically, except where noted (see data deposited in the crystal structure data base). The scattering factors and anomalous dispersion corrections were taken from the International Tables for X-ray Crystallography.[36] Additional details for Na**5** (Table 1) and polyhedral representations of Na**2**, Na**4**, and Na**5** (Figure 2) are given here (see crystallographic details for Na**2** and Na**4** and additional refinement information for Na**2**, Na**4**, and Na**5** deposited in the data base). Further details of the crystal structure investigations may be obtained from the Fachinformationzentrum Karlsruhe, 76344 Eggenstein-Leopoldshafen, Germany on quoting depository numbers CSD-380223 (Na**2**), -380224 (Na**4**), and -380225 (Na**5**).

Synthesis of $\alpha\alpha\alpha\alpha$-$H_2Na_{14}[(NaOH_2)_2Fe_2^{III}(As_2W_{15}O_{56})_2]\cdot 54H_2O$ (Na2) and $\alpha\alpha\beta\alpha$-$Na_{14}(NaOH_2)(Fe^{III}OH_2)Fe_2^{III}(As_2W_{15}O_{56})_2]\cdot 55H_2O$ (Na4): α-$Na_{12}(As_2W_{15}O_{56})$ (22.3 g, 5 mmol) was slowly added, with stirring, to a solution of $FeCl_2\cdot 4H_2O$ (1.96 g, 9.86 mmol) dissolved in NaCl solution (120 mL, 1 M). The resulting dark green solution was heated to 65 °C for 15 min, filtered hot, and cooled to 4 °C overnight. The crystals that formed were redissolved in deionized water (120 mL) and oxidized in air for one week at ambient temperature. A yellow-brown precipitate of Fe_2O_3 (determined by elemental analysis) was removed daily by filtration. NaCl (6 g) was then added, and the resultant additional yellow-brown precipitate was again filtered off. After 2−3 days, 2.56 g (yield 11%) of large, light-yellow crystals were collected and recrystallized from 0.5 M NaCl. IR (2% KBr pellet, 1000−400 cm^{-1}): $\tilde{\nu}$ = 947 (s), 871 (s), 831 (m), 724 (s), 519 (m), and 494 (w). $H_{114}As_4Fe_2Na_{16}O_{168}W_{30}$ (9097.5): calcd. Na 4.04, As 3.29, Fe 1.23, W 60.63; found Na 4.23, As 3.36, Fe 1.31, W 60.00. The filtrate was concentrated to approximately 70% of its original volume, and, after 2 days, 11 g (yield 48%) of a light yellow precipitate was collected by filtration. The precipitate was redissolved in 0.5 M NaCl to give diffraction-quality crystals. IR (2% KBr pellet, 1000−400 cm^{-1}): $\tilde{\nu}$ = 953 (s), 871 (s), 836 (m), 730 (s), 523 (m), and 494 (w). $H_{114}As_4Fe_3Na_{14}W_{30}O_{169}$ (9123.4): calcd. As 3.28, Fe 1.84, Na 3.53, W 60.45; found As 3.34, Fe 2.10, Na 3.85, W 59.60.

Synthesis of $\alpha\beta\beta\alpha$-$Na_{14}[(Mn^{II}OH_2)_2Fe_2^{III}(P_2W_{15}O_{56})_2]\cdot 8H_2O$ (Na5): $MnCl_2\cdot 4H_2O$ (1.38 g, 7 mmol) was slowly added to Na**1** (6.4 g, 0.7 mmol)[18] dissolved in a minimal amount of 0.5 M NaCl (pH adjusted to about 2 by 1 M NaOH). The initial light yellow-green solution turned dark red, and was then heated to 60 °C for 10 min. After 7−8 days, brown crystals formed (0.56 g, yield 10%). IR (2% KBr pellet, 1300−400 cm^{-1}): $\tilde{\nu}$ = 1085 (s), 1060 (w, sh), 1014 (w, sh), 941 (s), 918 (w), 890 (m), 816 (m), 776 (m), 734 (w) and 522

 © 2003 Wiley-VCH Verlag GmbH & Co. KGaA, Weinheim

(m). ^{31}P NMR (in D_2O): $\delta = -11.96$ ppm, $\Delta\nu_{1/2} = 100$ Hz. $H_{20}Fe_2Mn_2Na_{14}O_{122}P_4W_{30}$ (8154.9): calcd. Fe 1.37, Mn 1.35, Na 3.95, P 1.52, W 67.63; found Fe 1.47, Mn 1.62, Na 4.10, P 1.43, W 67.6.

Synthesis of αββα-$Na_{14}[(Mn^{II}OH_2)_2Fe_2^{III}(As_2W_{15}O_{56})_2]\cdot 29H_2O$ (Na6): Na**2** (1.9 g, 0.207 mmol) was added, with stirring and heating to 65 °C for about 5 min, to $MnCl_2\cdot 4H_2O$ (0.1 g, 0.5 mmol) dissolved in 1 M NaCl solution (10 mL). The resultant dark brown solution was filtered hot and, after approximately 7 days, 1.5 g (yield 84%) of a brown precipitate formed that was recrystallized from 0.5 M NaCl. IR (2% KBr pellet, 1000−400 cm^{-1}): $\tilde{\nu}$ = 949 (s), 871 (s), 823 (m), 712 (s), 523 (m), and 492 (m). $H_{62}As_4Fe_2Mn_2Na_{14}W_{30}O_{143}$ (8709.0): calcd. As 3.44, Fe 1.28, Mn 1.26, Na 3.70, W 63.33; found As 3.30, Fe 1.30, Mn 1.26, Na 3.58, W 62.3.

Acknowledgments

This work was supported in part by the University Paris XI and the CNRS (UMR, 8000). We also thank the NSF Grant CHE-0236686 for the research, and Grant CHE-9974864 for funding the D8 X-ray instrument.

[1] M. T. Pope, *Heteropoly and Isopoly Oxometalates*; Springer-Verlag: Berlin, **1983**.
[2] C. L. Hill, *Chem. Rev.* **1998**, *98*, 1−389.
[3] R. Contant, G. Hervé, *Rev. Inorg. Chem.* **2002**, *22*, 63−111.
[4] Representative papers on conventional B-type Keggin sandwich complexes include: [4a] T. J. R. Weakley, H. T. Evans, Jr., J. S. Showell, G. F. Tourné, C. M. Tourné, *J. Chem. Soc., Chem. Commun.* **1973**, *4*, 139−140. [4b] R. G. Finke, M. W. Droege, J. R. Hutchinson, O. Gansow, *J. Am. Chem. Soc.* **1981**, *103*, 1587−1589. [4c] J. M. Clemente, E. Coronado, J. R. Galán-Mascarós, C. J. Gómez-García, *Inorg. Chem.* **1999**, *38*, 55−63.
[5] Representative papers on conventional A-type Keggin sandwich complexes include: [5a] W. H. Knoth, P. J. Domaille, R. D. Farlee, *Organometallics* **1985**, *4*, 62−68. [5b] W. H. Knoth, P. J. Domaille, R. L. Harlow, *Inorg. Chem.* **1986**, *25*, 1577−1584. [5c] N. M. Okun, T. M. Anderson, C. L. Hill, *J. Am. Chem. Soc.* **2003**, *125*, 3194−3195.
[6] Representative papers on Tourné B-type Keggin sandwich complexes (i.e. those with transition metal heteroatoms) include: [6a] S. H. Wasfi, A. L. Rheingold, G. F. Kokoszka; A. S. Goldstein, *Inorg. Chem.* **1987**, *26*, 2934−2939. [6b] C. M. Tourné, G. F. Tourné, F. Zonnevijlle, *J. Chem. Soc., Dalton Trans.* **1991**, 143−155. [6c] E. M. Limanski, M. Piepenbrink, E. Droste, K. Burgemeister, B. Krebs, *J. Cluster Science* **2002**, *13*, 369−379.
[7] Representative papers on B-type Keggin sandwich complexes with pyramidal heteroatoms include: [7a] P. Mialane, J. Marrot, E. Rivière, J. Nebout, G. Hervé, *Inorg. Chem.* **2001**, *40*, 44−48. [7b] U. Kortz, N. K. Al-Kassem, M. G. Savelieff, N. A. Al Kadi, M. Sadakane, *Inorg. Chem.* **2001**, *40*, 4742−4749.
[8] R. G. Finke, M. W. Droege, P. J. Domaille, *Inorg. Chem.* **1987**, *26*, 3886−3896.
[9] R. G. Finke, M. W. Droege, *Inorg. Chem.* **1983**, *22*, 1006−1008.
[10] T. J. R. Weakley, R. G. Finke, *Inorg. Chem.* **1990**, *29*, 1235−1241.
[11] R. G. Finke, T. J. R. Weakley, *J. Chem. Crystallogr.* **1994**, *24*, 123−128.
[12] C. J. Gómez-García, J. J. Borrás-Almenar, E. Coronado, L. Ouahab, *Inorg. Chem.* **1994**, *33*, 4016−4022.
[13] X. Zhang, Q. Chen, D. C. Duncan, C. Campana, C. L. Hill, *Inorg. Chem.* **1997**, *36*, 4208−4215.
[14] X. Zhang, T. M. Anderson, Q. Chen, C. L. Hill, *Inorg. Chem.* **2001**, *40*, 418−419.
[15] T. M. Anderson, K. I. Hardcastle, N. Okun, C. L. Hill, *Inorg. Chem.* **2001**, *40*, 6418−6425.
[16] T. M. Anderson, X. Zhang, K. I. Hardcastle, C. L. Hill, *Inorg. Chem.* **2002**, *41*, 2477−2488.
[17] L. H. Bi, E.-B. Wang, J. Peng, R. D. Huang, L. Xu, C. W. Hu, *Inorg. Chem.* **2000**, *39*, 671−679.
[18] L. Ruhlmann, L. Nadjo, J. Canny, R. Contant, R. Thouvenot, *Eur. J. Inorg. Chem.* **2002**, 975−986.
[19] L. Ruhlmann, J. Canny, R. Contant, R. Thouvenot, *Inorg. Chem.* **2002**, *41*, 3811−3819.
[20] I. M. Mbomekalle, B. Keita, L. Nadjo, P. Berthet, K. I. Hardcastle, C. L. Hill, T. M. Anderson, *Inorg. Chem.* **2003**, *42*, 1163−1169.
[21] I. M. Mbomekalle, B. Keita, L. Nadjo, P. Berthet, W. A. Neiwert, C. L. Hill, M. D. Ritorto, T. M. Anderson, *Dalton Trans.* **2003**, 2646−2650.
[22] αααα is used in the Wells−Dawson sandwich-type structural formulas to indicate the connectivity for the first cap-belt junction, the first and second belt-central M_4 junctions, and the second belt-cap junctions, respectively.
[23] In addition, the junctions between each trivacant POM and the central tetrameric unit in Na**1** (and Na**2**) differ from those in all previously known sandwich-type POMs derived from Wells−Dawson and B-Keggin units. For more information on α- and β-junctions in Wells−Dawson sandwich-type structures, see ref.[16]
[24] B. Keita, I. M. Mbomekalle, L. Nadjo, R. Contant, *Eur. J. Inorg. Chem.* **2002**, 473−479.
[25] It is unclear whether Na**3** and Na**4** can be considered monovacant lacunary species. Studies are now underway to react these complexes with other d-electron-containing metals (such as Cu^{II}, Mn^{II}, and Co^{II}) and will be reported in due course.
[26] Complexes Na**3** and Na**4** may be isolated during the synthesis of Na**1** and Na**2** via metastable tetraferrous intermediates and separated via fractional crystallization. Na**3** and Na**4** are also formed by adding one equivalent of Fe^{III} to a solution of Na**1** or Na**2**, respectively [$FeCl_3\cdot 6H_2O$ (0.049 g) was dissolved in water (10 mL) and added dropwise to Na**1** or Na**2** (20 mL 9 mM) with stirring and heating to 55 °C for about 15 min]. The former method is preferable due to higher yields.
[27] Bond valence sum calculations from the X-ray structures of Na**2** and Na**4** yield average Fe oxidation states of 3.00 ± 0.02 and 3.04 ± 0.02, respectively.[28]
[28] I. D. Brown, D. Altermatt, *Acta Crystallogr., Sect. B* **1985**, *41*, 244−247.
[29] Crystals of Na**6** are very fragile. Even under a cooled nitrogen stream they shatter before a complete data set can be obtained.
[30] G. S. Chorghade, M. T. Pope, *J. Am. Chem. Soc.* **1987**, *109*, 5134−5138.
[31] B. J. Hornstein, R. G. Finke, *Inorg. Chem.* **2002**, *41*, 2720−2730.
[32] *SMART*, version 5.624, Bruker AXS, Inc., Madison, WI, **2002**.
[33] *SAINT*, version 6.36A, Bruker AXS, Inc., Madison, WI, **2002**.
[34] G. Sheldrick, *SADABS*, version 2.03, University of Göttingen: Göttingen, Germany, **2001**.
[35] *SHELXTL*, version 6.12, Bruker AXS, Inc.: Madison, WI, **2002**.
[36] *International Tables for X-ray Crystallography*, Kynoch Academic Publishers: Dordrecht, Netherlands, **1992**, Vol. C.

Received June 5, 2003

 © 2003 Wiley-VCH Verlag GmbH & Co. KGaA, Weinheim

Syntheses, Structure and Magnetic Properties of the First $\mu_{1,5}$-Dicyanamido-Bridged Dinuclear Compounds $[Ni(\mu_{1,5}\text{-dca})(dca)(dpt)]_2$ and $[Ni(\mu_{1,5}\text{-dca})(dca)(medpt)]_2$

Debajyoti Ghoshal,[a] Hanna Bialas,[b] Albert Escuer,[b] Mercé Font-Bardía,[c] Tapas Kumar Maji,[a] Joan Ribas,[b] Xavier Solans,[c] Ramon Vicente,*[b] Ennio Zangrando,[d] and Nirmalendu Ray Chaudhuri[a]

Keywords: N ligands / Bridging ligands / Nickel / Magnetic properties

The first structural determination of dinuclear compounds with $\mu_{1,5}$-dicyanamide [dca, $N(CN)_2^-$] as bridging ligand has been achieved with the products of formula $[Ni(\mu_{1,5}\text{-dca})(dca)(dpt)]_2$ (**1**) and $[Ni(\mu_{1,5}\text{-dca})(dca)(medpt)]_2$ (**2**) [dpt = bis(3-aminopropyl)amine and medpt = bis(3-aminopropyl)methylamine]. The X-ray diffraction analysis reveals dinuclear compounds with double $\mu_{1,5}$-dicyanamide bridges. The nickel atoms are hexacoordinate. The small differences in the terminal ligand (dpt or medpt) create a drastic change in the magnetic behaviour: the susceptibility measurements of **1** show weak antiferromagnetic coupling ($J = -1.2$ cm^{-1}, $g = 2.29$) whereas those of **2** show ferromagnetic coupling ($J = 0.7$ cm^{-1}, $g = 2.17$). The related compound (μ-terephthalato)$[Ni(dca)(dpt)(H_2O)]_2$ (**3**) is also described. The X-ray diffraction analysis reveals a dinuclear terephthalato-bridged Ni^{II} compound with terminal dca ligands. The susceptibility measurements of **3** indicate weak antiferromagnetic coupling: $J = -0.3$ cm^{-1}, $g = 2.13$.
(© Wiley-VCH Verlag GmbH & Co. KGaA, 69451 Weinheim, Germany, 2003)

Introduction

The dicyanamide ligand [dca, $N(CN)_2^-$] has been extensively used during the last few years to generate a wide variety of polynuclear compounds of different topologies and magnetic properties: 3-D compounds of general formula $[M(dca)_2]$ which order magnetically as weak ferro- or antiferromagnets[1−5] and low-dimensional systems (2D or 1D) with general formula $[M(L)_x(dca)_2]_n$ showing weak antiferromagnetic coupling have been obtained.[5−14] Another way of synthesising 3D systems with general formula $[M(L)(dca)_2]$ is by using ancillary ligands such as pyrazine, 4,4′-bipyridine, pyrimidine and 2,2′-bipyrimidine in addition to the dicyanamido ligand.[15−21] The $[M(L)(dca)_2]$ (L = pyrazine) compound exhibits long-range magnetic-ordering below 2.53(2) K.[19] Surprisingly, structurally described dinuclear dca compounds are rare: as far as we know, no dinuclear compounds with $\mu_{1,5}$-dicyanamide bridging ligands have been reported to date. Following our work in this field, we report in this paper the synthesis and magnetostructural characterisation of the first dinuclear $\mu_{1,5}$-dca derivatives with formula $[Ni(\mu_{1,5}\text{-dca})(dca)(dpt)]_2$ (**1**) and $[Ni(\mu_{1,5}\text{-dca})(dca)(medpt)]_2$ (**2**) with double dca bridges.

Alternating chains can be obtained by using two different bridging ligands. We have used this strategy successfully with azido and oxalate.[22,23] Similar attempts using dca and oxalate were unsuccessful, but in an attempt to obtain a mixed dca-terephthalato Ni^{II} chain the dinuclear compound (μ-terephthalato)$[Ni(dca)(dpt)(H_2O)]_2$ (**3**) was obtained. Here the terephthalato anion acts as a bridging ligand between two nickel atoms, whereas the dca anions act as terminal ligands. Susceptibility measurements indicate weak antiferromagnetic coupling for **1** and **3**, while for **2** weak ferromagnetic coupling is shown. The ferromagnetic coupling in low dimensional polynuclear compounds with $\mu_{1,5}$-dicyanamide bridging ligands is rare: it has been found in the sheet-like polymer of formula $[Cu(\mu_{1,5}\text{-dca})_2(phen)]_n$ and has been attributed to a case of accidental orthogonality between the magnetic orbitals.[24]

[a] Department of Inorganic Chemistry, Indian Association for the Cultivation of Science,
Kolkata 700032, India
[b] Departament de Química Inorgànica, Universitat de Barcelona,
Martí i Franquès 1−11, 08028 Barcelona, Spain
Fax: (internat.) + 34-934907725
E-mail: ramon.vicente@qi.ub.es
[c] Departament de Cristallografia i Mineralogia, Universitat de Barcelona,
Martí Franqués s/n, 08028 Barcelona, Spain
[d] Dipartimento di Scienze Chimiche, University of Trieste,
34127 Trieste, Italy

Results and Discussion

Crystal Structures

$[Ni(\mu_{1,5}\text{-dca})(dca)(dpt)]_2$ (1)

A labelled ORTEP plot of the structure of $[Ni(\mu_{1,5}\text{-dca})(dca)(dpt)]_2$ (**1**) is shown in Figure 1. Selected bond lengths and angles are reported in Table 1. The structure of the compound consists of dinuclear units of nickel atoms bridged by means of double end-to-end dicyanamide bridges. Each nickel atom is hexacoordinate, with a coordination polyhedron close to octahedral. Hexacoordination is achieved by means of three N atoms belonging to the dpt ligand in a *mer* disposition, two N atoms from the bridging dicyanamide ligands, and one N atom from the terminal dicyanamide ligand. The Ni−N distances are in the range 2.082(5) −2.217(3) Å. Bond angles related to the dicyanamide bridging ligands are Ni(1)−N(7)−C(9) and Ni(1)−N(9)−C(10) of 157.4(3)° and 155.3(3)°, respectively, with a central C(10)−N(8)−C(9) angle of 117.0(3)°. The intradimer Ni−Ni distance is 7.270(3) Å.

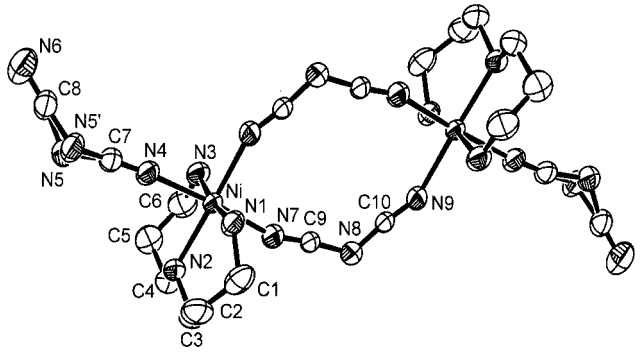

Figure 1. ORTEP drawing of $[Ni(\mu_{1,5}\text{-dca})(dca)(dpt)]_2$ (**1**)

Table 1. Selected bond lengths (Å) and angles (°) for $[Ni(\mu_{1,5}\text{-dca})(dca)(dpt)]_2$ (**1**)
Symmetry transformations used to generate equivalent atoms: #1 $-x, -y, -z$

Ni−N(3)	2.082(5)	Ni−N(1)	2.087(4)
Ni−N(4)	2.130(4)	Ni−N(7)	2.146(4)
Ni−N(2)	2.208(3)	Ni−N(9)#1	2.217(3)
N(4)−C(7)	1.149(4)	N(5)−C(7)	1.326(14)
N(5)−C(8)	1.367(16)	N(6)−C(8)	1.160(5)
N(7)−C(9)	1.127(4)	N(8)−C(9)	1.316(5)
N(8)−C(10)	1.343(4)	N(9)−C(10)	1.156(4)
N(9)−Ni#1	2.217(3)	N(3)−Ni−N(1)	171.44(14)
N(3)−Ni−N(4)	90.24(15)	N(1)−Ni−N(4)	88.93(15)
N(3)−Ni−N(7)	87.89(16)	N(1)−Ni−N(7)	93.56(15)
N(4)−Ni−N(7)	175.29(13)	N(3)−Ni−N(2)	85.83(15)
N(1)−Ni−N(2)	102.67(15)	N(4)−Ni−N(2)	88.84(12)
N(7)−Ni−N(2)	86.72(12)	N(3)−Ni−N(9)#1	94.38(15)
N(1)−Ni−N(9)#1	77.09(14)	N(4)−Ni−N(9)#1	89.11(13)
N(7)−Ni−N(9)#1	95.34(13)	N(2)−Ni−N(9)#1	177.94(12)
C(7)−N(5)−C(8)	118.0(10)	C(7)−N(5′)−C(8)	119.4(10)
C(9)−N(7)−Ni	157.4(3)	C(9)−N(8)−C(10)	117.0(3)
C(10)−N(9)−Ni#1	155.3(3)	N(4)−C(7)−N(5′)	164.1(6)
N(4)−C(7)−N(5)	160.8(7)	N(6)−C(8)−N(5′)	161.6(7)
N(6)−C(8)−N(5)	164.5(6)	N(7)−C(9)−N(8)	173.5(4)
N(9)−C(10)−N(8)	172.5(4)		

$[Ni(\mu_{1,5}\text{-dca})(dca)(medpt)]_2$ (2)

A labelled ORTEP plot of the structure of $[Ni(\mu_{1,5}\text{-dca})(dca)(medpt)]_2$ (**2**) is shown in Figure 2. Selected bond lengths and angles are reported in Table 2. The crystal structure of complex **2** is similar to **1**: dinuclear units of nickel atoms bridged by means of double end-to-end dicyanamide bridges. The Ni−N distances are in the range 2.071(3)−2.176(3) Å. Bond angles related to the dicyanamide bridging ligands are Ni−N(4)−C(8) and Ni−N(5)−C(9) of 165.1(3)° and 151.2(3)°, respectively, with a central C(8)−N(8)−C(9) angle of 122.2(4)°. The Ni−Ni intradimer distance is 7.520(3) Å. The same Ni−Ni intradimer distance is 0.25 Å shorter in **1** due to a lower central NCN(dicyanamide) angle [117.0(3)°]. For comparative purposes, the intermetallic separation inside the dinuclear unit in **2** is about 0.2 Å longer than the values detected in polymeric networks. In fact, in three topologically different structures the distance between Ni ions bridged by two dca ligands ranges from 7.310 to 7.364 Å, as documented in a layered framework, in a ladder-like 1D polymer,[25] and in a molecular tube-like structure.[26]

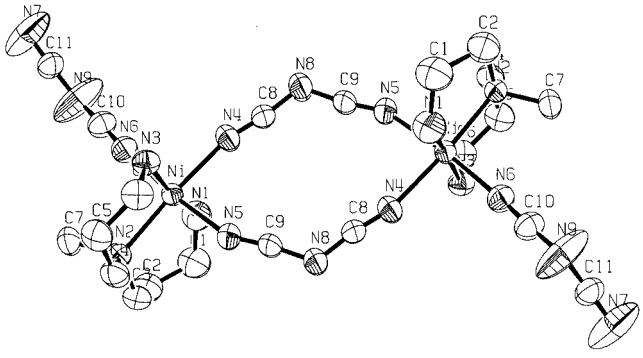

Figure 2. ORTEP drawing of $[Ni(\mu_{1,5}\text{-dca})(dca)(medpt)]_2$ (**2**)

Table 2. Selected bond lengths (Å) and angles (°) for complex $[Ni(\mu_{1,5}\text{-dca})(dca)(medpt)]_2$ (**2**)

Ni−N(1)	2.082(4)	Ni−N(4)	2.158(3)
Ni−N(2)	2.176(3)	Ni−N(5)	2.117(3)
Ni−N(3)	2.071(3)	Ni−N(6)	2.092(3)
N(5)−C(9)	1.136(5)	N(8)−C(9)	1.296(6)
N(8)−C(8)	1.297(7)	N(4)−C(8)	1.136(5)
N(1)−Ni−N(2)	94.8(1)	N(3)−Ni−N(4)	87.9(1)
N(1)−Ni−N(3)	172.4(1)	N(3)−Ni−N(5)	94.0(1)
N(1)−Ni−N(4)	87.1(1)	N(3)−Ni−N(6)	88.2(1)
N(1)−Ni−N(5)	91.2(1)	N(4)−Ni−N(5)	84.3(1)
N(1)−Ni−N(6)	86.0(1)	N(4)−Ni−N(6)	89.7(1)
N(2)−Ni−N(3)	90.7(1)	N(5)−Ni−N(6)	173.4(1)
N(2)−Ni−N(4)	174.4(1)	C(8)−N(4)−Ni	165.1(3)
N(2)−Ni−N(5)	90.4(1)	C(9)−N(5)−Ni	151.2(3)
N(2)−Ni−N(6)	95.7(1)	C(10)−N(6)−Ni	176.0(3)
C(8)−N(8)−C(9)	122.2(4)		

 © 2003 Wiley-VCH Verlag GmbH & Co. KGaA, Weinheim

(μ-terephthalato)[Ni(dca)(dpt)(H_2O)]$_2$ (3)

A labelled ORTEP plot of the structure of (μ-terephthalato)[Ni(dca)(dpt)(H_2O)]$_2$ is shown in Figure 3. The structure of the compound consists of dinuclear units in which the nickel atoms are bridged by the terephthalato ligand. Each nickel atom is hexacoordinate, with a coordination polyhedron close to octahedral. Hexacoordination is achieved by means of three N atoms belonging to the dpt ligand, one oxygen atom from the monodentate carboxylato ligand, one oxygen atom from the water molecule and, finally, one N atom from the terminal dicyanamido ligand. The bond lengths to the nickel atom are in the range 2.062(7)−2.097(6) Å except the relatively long Ni−O(water) of 2.186(5) Å. The bond angles related to the dicyanamido ligand are in the normal range for this ligand [Ni−N(4)−C(7) = 168.3(10)°], with a central C(7)−N(5)−C(8) angle of 121.4(10)°. The Ni···Ni intradinuclear distance is 11.379(10) Å (Table 3).

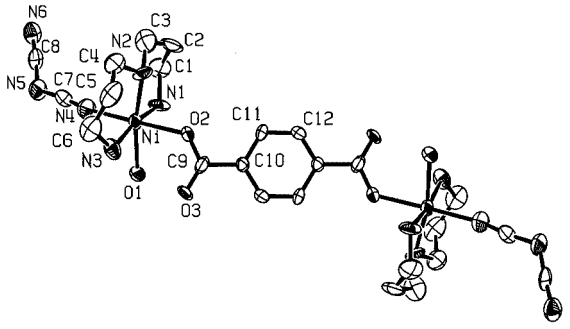

Figure 3. ORTEP drawing of (μ-terephthalato)[Ni(dca)(dpt)(H_2O)]$_2$ (**3**)

Table 3. Selected bond lengths (Å) and angles (°) for (μ-terephthalato)[Ni(dca)(dpt)(H_2O)]$_2$ (**3**)
Symmetry transformations used to generate equivalent atoms: #1 $-x-1, -y+2, -z+1$.

Ni−N(4)	2.062(7)	Ni−N(1)	2.075(7)
Ni−O(2)	2.081(5)	Ni−N(2)	2.083(7)
Ni−N(3)	2.097(6)	Ni−O(1)	2.186(5)
O(2)−C(9)	1.280(8)	O(3)−C(9)	1.215(9)
N(4)−C(7)	1.117(9)	C(7)−N(5)	1.280(9)
N(5)−C(8)	1.292(11)	C(8)−N(6)	1.165(10)
N(4)−Ni−O(2)	174.2(3)	N(1)−Ni−N(3)	169.4(2)
N(2)−Ni−O(1)	169.4(2)	Ni−O(2)−C(9)	130.1(5)
Ni−N(4)−C(7)	168.3(10)	N(4)−C(7)−N(5)	173.3(12)
N(6)−C(8)−N(5)	175.3(10)	C(7)−N(5)−C(8)	121.4(10)

Magnetic Properties

A plot of $\chi_M \cdot T$ vs. T for **1** in the temperature range 245−2 K is shown in Figure 4. The overall behaviour of **1** corresponds to an antiferromagnetically coupled system. $\chi_M \cdot T$ has a practically constant value of 2.59 $cm^3 \cdot K \cdot mol^{-1}$ in the range 245−60 K. In the 60 −2 K range, $\chi_M \cdot T$ decreases quickly, reaching 1.19 $cm^3 \cdot K \cdot mol^{-1}$ at 2 K. The magnetic data of **1**, in agreement with its dinuclear structure, were analysed by means of an analytical expression based on the Hamiltonian $H = -J S_1 S_2$ for local spin values $S = 1$. The best fit parameters were $J = -1.2(1)$ cm^{-1} and $g = 2.29(1)$ (Figure 4). Alternatively, the magnetic data of **1** were analysed by considering a non-coupled Ni^{II} mononuclear compound by using an equation[27] that considers only non-interacting $S = 1$ ions in the presence of a single ion anisotropy. The best fit is given by the parameters $D = -10.9(1)$ cm^{-1} and $g = 2.16(1)$. The reliability factors are similar in both cases: 1.5×10^{-4} and 9.8×10^{-4}, respectively. Compound **1** can be considered, according to these data, as a practically non-coupled Ni^{II} compound.

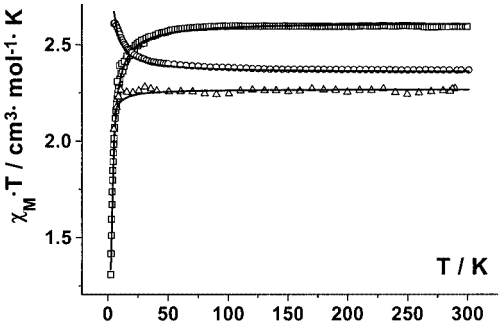

Figure 4. Plot of $\chi_M \cdot T$ vs. T for compounds [Ni($\mu_{1,5}$-dca)(dca)(dpt)]$_2$ (**1**) (open squares), [Ni($\mu_{1,5}$-dca)(dca)(Medpt)]$_2$ (**2**) (open circles) and (μ-terephthalato)[Ni(dca)(dpt)(H_2O)]$_2$ (**3**) (open up triangles); the solid line shows the best fit of the data (see text)

A plot of $\chi_M \cdot T$ vs. T for **2** in the temperature range 300−5 K is shown in Figure 4. The overall behaviour of **2** corresponds to a ferromagnetically coupled system. $\chi_M \cdot T$ has a value of 2.37 $cm^3 \cdot K \cdot mol^{-1}$ at room temperature and increases as the temperature decreases, reaching 2.61 $cm^3 \cdot K \cdot mol^{-1}$ at 5 K. The increase of the $\chi_M \cdot T$ product when T decreases is a clear evidence of a positive J value more important than the ZFS contribution. The magnetic data of **2**, in accordance with its dinuclear structure, were analysed by means of an analytical expression based on the Hamiltonian $H = -J S_1 S_2$ for local spin values $S = 1$. The best fit parameters were $J = 0.7(1)$ cm^{-1} and $g = 2.17(1)$ (Figure 4). In a previous work[10] we concluded from extended Hückel MO calculations that the dicyanamide $\mu_{1,5}$ bridge possesses two superexchange pathways: t_{2g}-π_y-t_{2g} and e_g-σ-e_g. The t_{2g}-π_y-t_{2g} pathway leads always to weak antiferromagnetically coupled systems, but in cases where this pathway is not active (d^8 and d^9 ions) there exists the possibility of accidental orthogonality via the e_g-σ-e_g pathway for M−N−C(dicyanamide) angles around 160°. The positive J value found in **2** is the first experimental evidence of the above proposal in a dinuclear compound.

A plot of $\chi_M \cdot T$ vs. T for **3** in the temperature range 300−5 K is shown in Figure 4. The overall behaviour of **3** corresponds to an antiferromagnetically coupled system. χ_M·T has a practically constant value of 2.26 $cm^3 \cdot K \cdot mol^{-1}$ in the range 300−15 K. In the 15−5 K range, $\chi_M \cdot T$ decreases, reaching 2.06 $cm^3 \cdot K \cdot mol^{-1}$ at 5 K. The magnetic

 © 2003 Wiley-VCH Verlag GmbH & Co. KGaA, Weinheim

data of **3**, in accordance with its dinuclear structure, were analysed by means of an analytical expression based on the Hamiltonian $H = -J S_1 S_2$ for local spin values $S = 1$. The best-fit parameters were $J = -0.3(1)$ cm^{-1} and $g = 2.13(1)$ (Figure 4). The very weak J value for **3** is in accordance with the previously published experimental data and MO calculations which conclude that the terephthalate bridge is not a suitable bridging unit to mediate significant exchange coupling.[28]

Experimental Section

[Ni(μ$_{1,5}$-dca)(dca)(dpt)]$_2$ (1): Na[N(CN)$_2$] (13.6 mmol in 30 mL of water), $(C_2H_5)_4NCl\cdot H_2O$ (13.6 mmol in 30 mL of water) and, drop by drop, dpt (6.8 mmol in 10 mL of water) were added successively to a stirred solution of $Ni(NO_3)_2\cdot 6H_2O$ (6.8 mmol in 50 mL of water). Finally a mixture of isophthalic acid (6.8 mmol in 30 mL of water) and NaOH (13.6 mmol in 15 mL of water) was added. The resulting blue solution was left to stand in the air. Blue crystals of **1** suitable for X-ray determination were formed over two weeks. $C_{20}H_{34}N_{18}Ni_2$ (644.0): calcd. C 37.3, H 5.3, N 39.1; found C 37.4, H 5.5, N 39.5.

[Ni(μ$_{1,5}$-dca)(dca)(medpt)]$_2$ (2): Bis(3-aminopropyl)methylamine (Medpt; 1 mmol) was added dropwise to an aqueous solution (10 mL) of $Ni(ClO_4)_2\cdot 6H_2O$ (1 mmol) with constant stirring. A solution of Na[N(CN)$_2$] (2 mmol of) in water (10 mL) was added and a bluish-violet precipitate formed immediately. The reaction mixture was stirred for 30 min and then filtered. After a few days deep bluish-violet single crystals of complex 2 suitable for X-ray diffraction were obtained from the filtrate. $C_{22}H_{38}N_{18}Ni_2$ (672.1): calcd. C 38.28, H 5.66, N 37.49; found C 38.42, H 5.37, N 37.91.

(μ-Terephthalato)[Ni(dca)(dpt)(H$_2$O)]$_2$ (3): Sodium terephthalate (0.723 g, 3.4 mmol in 20 mL of water), Na[N(CN)$_2$] (0.612 g in 20 mL of water), $(C_2H_5)_4NCl\cdot H_2O$ (1.262 g, 6.9 mmol in 20 mL of water) and dpt (0.451 g in 10 mL of water) were added successively to a stirred solution of $Ni(NO_3)_2\cdot 6H_2O$ (1 g, 3.4 mmol) in 30 mL of water. The resulting blue solution was left to stand in the air. Blue crystals of **4** suitable for X-ray determination were formed over ten days. $C_{10}H_{18}N_{10}Ni$ (337.0): calcd. C 34.2, H 5.1, N 23.8; found C 33.9, H 5.3, N 23.7.

Spectral and Magnetic Measurements: Magnetic susceptibility measurements were carried out for **1** and **2** on polycrystalline samples with a SQUID apparatus working in the range 2−300 K for **1** and 5−300 K for **2** in a magnetic field of 0.5 T. Magnetic susceptibility measurements in the temperature range 4−300 K were carried out for **3** on polycrystalline samples with a pendulum-type magnetometer (MANICS DSM8) equipped with a helium continuous-flow cryostat and a Bruker B E15 electromagnet. The magnetic field was approx. 1.5 T. Diamagnetic corrections were estimated from Pascal tables.

Crystal-Structure Determination: The X-ray single-crystal data for **1** and [**3**] were collected on an Enraf−Nonius CAD4 four-circle diffractometer. Crystal size: 0.1 × 0.1 × 0.2 [0.1 × 0.1 × 0.2] mm. The crystallographic data, conditions used for the intensity data collection, and some features of the structure refinement are listed in Table 4. Graphite-monochromated Mo-K_α radiation (λ = 0.71069 Å) with the ω/2θ technique was used to collect the data sets for **1** and **3**. The accurate unit-cell parameters were determined from automatic centring of 25 reflections, $12 < \theta < 21°$, [25 reflections, $12 < \theta < 21°$] and refined by least-squares methods. 4147 [4740] Reflections were collected in the range $2.67° < \theta < 31.96$ [$2.16° < \theta < 30.15°$]. 1878 [1758] reflections were assumed as observed applying the condition $I > 2\sigma(I)$. Corrections were applied for Lorentz-polarization effects, and for intensity decay during data reduction processing. The structures were solved by direct methods, using the SHELXS[29] computer program, and refined by full-matrix least-squares methods with the SHELXL-97[30] computer program using 4147 [4740] reflections (very negative intensities were not assumed). The function minimised was $\Sigma w| |F_o|^2 - |F_c|^2|^2$, where $w = |\sigma^2(I) + (0.0196\ P)^2|^{-1}$ and $P = (|F_o|^2 + 2|F_c|^2)/3$ for **1** and $w = |\sigma^2(I)|^{-1}$ for **3**. $P = (|F_o|^2 + 2|F_c|^2)/3$. f, f' and f'' were taken from the International Tables of X-ray Crystallography.[31]

For compound **1** sixteen hydrogen atoms were computed and refined, by using a riding model, with an isotropic temperature factor equal to 1.2-times the equivalent temperature factor of the atom to which they are linked. For **3** all H atoms were computed and refined, using a riding model, with an isotropic temperature factor equal to 1.2-times the equivalent temperature factor of the atom to which are linked. Number of refined parameters: 202 [199]. Maximum and minimum peaks in the final difference synthesis: 0.537 and −0.500 e·Å^{-3} [0.536 and −0.497 e·Å^{-3}]. Significant bond parameters are given in Tables 1 and 3, respectively. For compound **2** data collection was carried at 293(3) K using Mo-K_α radiation (λ = 0.71073 Å) on a Nonius DIP-1030H system (30 frames exposure time of 15 min with a rotation of 6° about , detector being at a distance of 90 mm from the crystal). Crystal size 0.35 × 0.35 × 0.40 mm. Cell refinement, indexing and scaling of the data set were carried out using Mosflm and Scala.[32] 191 Parameters and 4746 reflections, 2880 unique of which 2545 with $I > 2\sigma(I)$. The structure was solved by Patterson and Fourier analyses and refined by the full-matrix least-squares method based on F^2 with all observed reflections.[33] All the calculations were performed using the WinGX System, Ver 1.64.[34] Maximum and minimum peaks in the final difference synthesis: 0.543 and −0.511 e·Å^{-3}. Selected bond parameters are given in Table 2.

Table 4. Crystal data and structure refinement for [Ni(μ$_{1,5}$-dca)(dca)(dpt)]$_2$ (**1**), [Ni(μ$_{1,5}$-dca)(dca)(medpt)]$_2$ (**2**), and (μ-terephthalato)[Ni(dca)(dpt)(H$_2$O)]$_2$ (**3**)

	1	**2**	**3**
Empirical formula	$C_{20}H_{34}N_{18}Ni_2$	$C_{22}H_{38}N_{18}Ni_2$	$C_{24}H_{36}N_{12}Ni_2O_6$
Molecular mass	644.07	336.06	706.03
Crystal system	triclinic	triclinic	orthorhombic
Space group	$P\bar{1}$	*P*-1 (n°2)	*Pbca ba-c* (n° 61)
a [Å]	8.424(7)	7.677(3)	9.096(1)
b [Å]	9.368(11)	8.380(2)	13.229(1)
c [Å]	10.589(5)	12.238(3)	26.824(1)
α [°]	84.15(7)	80.24(2)	90.0
β [°]	79.83(5)	78.63(2)	90.0
γ [°]	66.33(9)	82.98(3)	90.0
V [Å^3]	752.9(11)	757.5(4)	3227.8(4)
Z	1	2	4
T [K]	293(2)	293(3)	293
λ(Mo-*Kα*) [Å]	0.71069	0.71073	0.71069
$d_{calcd.}$ [Mg·m^{-3}]	1.421	1.473	1.453
μ(Mo-*Kα*) [mm^{-1}]	1.294	1.290	1.223
R[a]	0.0422	0.0482	0.0458
$R^2\omega$[b]	0.0742	0.1263	0.1106

[a] $R(F_o) = \Sigma F_o - F_c/\Sigma F_o$ [b] $R\omega(F_o)^2 = \{\Sigma\{\omega[(F_o)^2 - (F_c)^2\}^2]/\Sigma\{\omega[(F_o)^2]^2\}^{1/2}$

 © 2003 Wiley-VCH Verlag GmbH & Co. KGaA, Weinheim

CCDC-200891 (**1**), -200892 (**2**), and -200894 (**3**) contain the supplementary crystallographic data for this paper. These data can be obtained free of charge at www.ccdc.cam.ac.uk/conts/retrieving.html [or from the Cambridge Crystallographic Data Centre, 12, Union Road, Cambridge CB2 1EZ, UK; Fax: (internat.) +44-1223/336-033; E-mail: deposit@ccdc.cam.ac.uk].

Acknowledgments

This research was partially supported by CICYT (Grant BQU2000/0791) and the Council of Scientific and Industrial Research, New Delhi, India (Granted to NRC).

[1] S. R. Batten, P. Jensen, B. Moubaraki, K. S. Murray, R. Robson, *Chem. Commun.* **1998**, 439.
[2] M. Kurmoo, C. J. Kepert, *New. J. Chem.* **1998**, 1515.
[3] J. L. Manson, C. R. Kmety, Q. Huang, J. W. Lynn, G. M. Bendele, S. Pagola, P. W. Stephens, L. M. Liable-Sands, A. L. Rheingold, A. J. Epstein, J. S. Miller, *Chem. Mater.* **1998**, *10*, 2552.
[4] J. L. Manson, C. R. Kmety, A. J. Epstein, J. S. Miller, *Inorg. Chem.* **1999**, *38*, 2552.
[5] S. R. Batten, P. Jensen, C. J. Kepert, M. Kurmoo, B. Moubaraki, K. S. Murray, D. J. Price, *J. Chem. Soc., Dalton Trans.* **1999**, 2987.
[6] P. Jensen, S. R. Batten, G. D. Fallon, D. C. R. Hockless, B. Moubaraki, K. S. Murray, R. Robson, *J. Solid State Chem.* **1999**, *145*, 387.
[7] J. L. Manson, D. W. Lee, A. L. Rheingold, J. S. Miller, *Inorg. Chem.* **1998**, *37*, 5966.
[8] J. L. Manson, C. D. Incarvito, A. L. Rheingold, J. S. Miller, *J. Chem. Soc., Dalton Trans.* **1998**, 3705.
[9] J. L. Manson, A. M. Arif, J. S. Miller, *J. Mater. Chem.* **1999**, *9*, 979.
[10] A. Escuer, F. A. Mautner, N. Sanz, R. Vicente, *Inorg. Chem.* **2000**, *39*, 1668.
[11] J. L. Manson, A. M. Arif, C. D. Incarvito, L. M. Liable-Sands, A. L. Rheingold, J. S. Miller, *J. Solid State Chem.* **1999**, *145*, 369.
[12] A. Claramunt, A. Escuer, F. A. Mautner, N. Sanz, R. Vicente, *J. Chem. Soc., Dalton Trans.* **2000**, 2627.
[13] J. Carranza, C. Brennan, J. Sletten, F. Lloret, M. Julve, *J. Chem. Soc., Dalton Trans.* **2002**, 3164.
[14] A. Escuer, F. A. Mautner, N. Sanz, R. Vicente, *Inorg. Chim. Acta* **2002**, *340*, 163.
[15] S. R. Marshall, C. D. Incarvito, J. L. Manson, A. L Rheingold, J. S. Miller, *Inorg. Chem.* **2000**, *39*, 1969.
[16] B.-W. Sun, S. Gao, B.-Q. Ma, Z.-M. Wang, *New J. Chem.* **2000**, *24*, 953.
[17] I. Riggio, G. A. van Albada, D. D. Ellis, A. L. Spek, J. Reedijk, *Inorg. Chim. Acta* **2001**, *313*, 120.
[18] S. Martín, M. G. Barandika, J. I. Ruiz de Larramendi, R. Cortés, M. Font-Bardía, L. Lezama, Z. E. Serna, X. Solans, T. Rojo, *Inorg. Chem.* **2001**, *40*, 3687.
[19] J. L. Manson, Q.-Z. Huang, J. W. Lynn, H.-J. Koo, M.-H. Whangbo, R. Bateman, T. Otsuka, N. Wada, D. N. Argyriou, J. S. Miller, *J. Am. Chem. Soc.* **2001**, *123*, 162.
[20] P. Jensen, S. R. Batten, B. Moubaraki, K. S. Murray, *J. Solid State Chem.* **2001**, *159*, 352.
[21] P. Jensen, S. R. Batten, B. Moubaraki, K. S. Murray, *J. Chem. Soc., Dalton Trans.* **2002**, 3712.
[22] A. Escuer, R. Vicente, X. Solans, M. Font-Bardía, *Inorganic Chemistry* **1994**, *33*, 6007.
[23] R. Vicente, A. Escuer, J. Ferretjans, H. Stoeckli-Evans, X. Solans, M. Font-Bardía, *J. Chem. Soc., Dalton Trans.* **1997**, 167.
[24] B. Vangdal, J. Carranza, F. Lloret, M. Julve, J. Sleten, *J. Chem. Soc., Dalton Trans.* **2002**, 566.
[25] P. M. van der Werff, S. R. Batten, P. Jensen, B. Moubaraki, K. S. Murray, E. H.-K. Tan, *Polyhedron* **2001**, *20*, 1129.
[26] P. Jensen, S. R. Batten, B. Moubaraki, K. S. Murray, *Chem. Commun.* **2000**, 793.
[27] C. P. Landee, D. M. Mudgett, B. M. Foxman, *Inorg. Chim. Acta* **1991**, *186*, 45.
[28] J. Cano, G. De Munno, J. L. Sanz, R. Ruiz, J. Faus, F. Lloret, M. Julve, A. Caneschi, *J. Chem. Soc., Dalton Trans.* **1997**, 1915.
[29] G. M. Sheldrick, SHELXS, Program for the Solution of Crystal Structure. University of Gottingen, Germany, **1997**.
[30] G. M. Sheldrick, SHELXL-97, Program for the Refinement of Crystal Structure. University of Gottingen, Germany, **1997**.
[31] International Tables of X-ray Crystallography, **1974**. Ed. Kynoch press, vol. IV, pp 99−100 and 149.
[32] Collaborative Computational Project, Number 4. *Acta Crystallogr., Sect. D* **1994**, *50*, 760.
[33] G. M. Sheldrick, SHELX-97: *Programs for Crystal Structure Analysis (Release 97−2)*. University of Göttingen, Germany, **1998**.
[34] WinGX: A Windows Program for Crystal Structure Analysis., L. J. Farrugia, University of Glasgow, Glasgow, **1998**.

Received January 16, 2003

 © 2003 Wiley-VCH Verlag GmbH & Co. KGaA, Weinheim

Synthesis and Conformational Studies of a Chiral Octadentate Ligand Derived from (*R*)-1,1′-Binaphthyl-2,2′-diamine and its Dinuclear Zinc(II) and Nickel(II) Complexes

Maria Chiara Mimmi,[a] Michele Gullotti,*[a] Laura Santagostini,[a] Roberto Pagliarin,[b] Luca De Gioia,[c] Enrico Monzani,[d] and Luigi Casella[d]

Keywords: N ligands / Zinc / Chirality / Conformational analysis / Nickel

The synthesis of the octadentate ligand (*R*)-(–)-*N*,*N*′-dimethyl-*N*,*N*′-bis{3-[bis(1-methyl-2-benzimidazolylmethyl)]-aminopropyl}-1,1′-binaphthyl-2,2′-diamine (**L**), containing a central 1,1′-binaphthalenediamine core connected to two aminobis(benzimidazole) arms by flexible trimethylene carbon chains, and its dinuclear complexes $[Zn_2\mathbf{L}](ClO_4)_4$ and $[Ni_2\mathbf{L}](ClO_4)_4$ is reported. The structural features of the free ligand and the metal complexes have been investigated by NMR, UV/Visible, CD, and computational methods, including simulated annealing-molecular mechanics and semiempirical PM3 calculations. The preferred conformation of the free ligand is characterized by a relatively small dihedral angle of about 75° between the two naphthyl rings, which is imposed by favorable stacking interactions between benzimidazole rings from different arms. In the dinuclear zinc(II) complex each metal ion is pseudotetrahedral and bound to three N donors of one aminobis(benzimidazole) arm and one N donor of the binaphthalenediamine residue. Coordination of the benzimidazole groups to the metal ions prevents the stacking interactions seen in the free ligand and, consequently, the dihedral angle between the naphthyl groups increases to the more usual ca. 90°. In the dinuclear nickel(II) complex, the ligand still provides four nitrogen donors to each metal centers, but the stereochemical preference of the nickel(II) ions imposes a ligand field of tetragonal symmetry, with pseudo-octahedral metal centers, and this occurs with pronounced flattening of the dihedral angle between the naphthyl groups. The change in conformation, from **L** to $[Zn_2\mathbf{L}]^{4+}$ to $[Ni_2\mathbf{L}]^{4+}$, of the critical 1,1′-binaphthalenediamine residue is clearly indicated by CD spectra.
(© Wiley-VCH Verlag GmbH & Co. KGaA, 69451 Weinheim, Germany, 2003)

Introduction

Polydentate ligands carrying nitrogen donor atoms have been extensively used in the biomimetic chemistry of metal enzymes, particularly those depending on copper and associated with oxidative processes, which typically contain dinuclear or trinuclear metal centers.[1] Surprisingly, though, few of the various ligands studied contain chiral centers. This is partly because of the difficulties encountered in synthesizing such polyfunctional molecules, as illustrated by our attempt to prepare biomimetic ligands containing L-histidine residues.[2] Nonetheless, chiral centers add a new dimension and open up interesting perspectives for synthetic active site analogues of metal enzymes, such as the possibility to perform asymmetric transformations.

We have, in particular, studied various copper complexes with polyamino-polybenzimidazole ligands to simulate structural and functional properties of dioxygen-activating copper enzymes.[3] Suitable dinucleating ligands usually contain a set of six nitrogen donors to be evenly distributed between the metal ions, whereas for trinuclear complexes the ligand must bind the metal ions with a total of eight nitrogen donors. A simple way to introduce a chiral moiety into the ligand scaffold is to use the 1,1′-binaphthalene residue. Chiral complexes of 1,1′-binaphthyl ligands have been extensively used in asymmetric catalysis; the complexes of 1,1′-bis(2-naphthol) (BINOL) and 2,2′-bis(diphenylphosphanyl)-1,1′-binaphthalene (BINAP)[4,5] are recent examples. In addition, the chiroptical properties and the conformations of 2,2′-homosubstituted 1,1′-binaphthyl derivatives have been studied in detail,[6,7] and useful correlations between CD spectra and solution conformation for these C_2-symmetric chromophores are available. We therefore designed the new chiral ligand **L**, in which an (*R*)-(+)-1,1′-

[a] Dipartimento di Chimica Inorganica, Metallorganica e Analitica, Università di Milano, Istituto ISTM-CNR,
Via Venezian 21, 20133 Milano, Italy
Fax: (internat.) +39-02-50314405
E-mail: michele.gullotti@unimi.it
[b] Dipartimento di Chimica Organica e Industriale, Università di Milano,
Via Venezian 21, 20133 Milano, Italy
[c] Dipartimento di Biotecnologie e Bioscienze, Università di Milano-Bicocca,
Piazza della Scienza 2, 20100 Milano, Italy
[d] Dipartimento di Chimica Generale, Università di Pavia,
Via Taramelli 12, 27100 Pavia, Italy

 © 2003 Wiley-VCH Verlag GmbH & Co. KGaA, Weinheim **DOI: 10.1002/ejic.200300103**

binaphthyl-2,2′-diamine residue acts as the spacer between two chelating arms containing tridentate aminobis(benzimidazole) donors (Scheme 1), and recently reported briefly that dinuclear and trinuclear copper(II) complexes derived from this ligand perform stereoselective catalytic oxidation of optically active diphenolic substrates.[8] We report here full synthetic details for the preparation of **L** and the conformational characterization of this new ligand and the corresponding dinuclear zinc(II) and nickel(II) complexes.

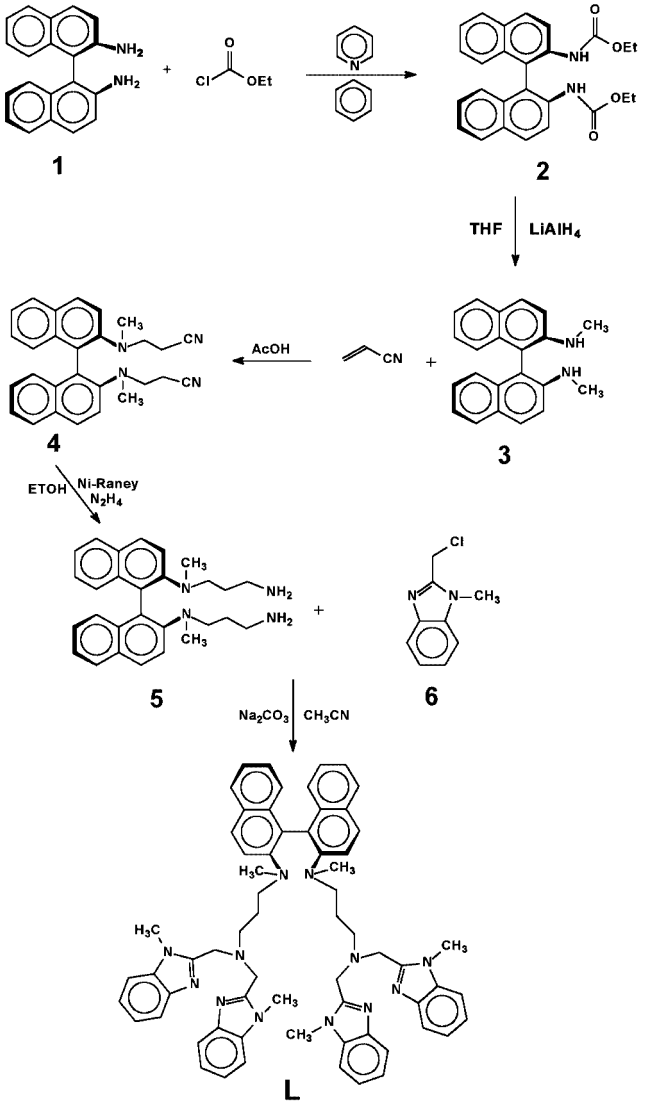

Scheme 1. Synthetic route for the preparation of ligand **L**

Results and Discussion

Synthesis

A particular challenge in the synthetic route to octadentate ligand **L** (Scheme 1) is to maintain an intact chiral moiety throughout the various reactions. To obtain a symmetric ligand containing a single arm attached to each nitrogen atom of the (*R*)-1,1′-binaphthyl-2,2′-diamine residue, compound **1** was initially derivatized with a double Benson-type monomethylation,[9] which gave the corresponding dicarbamate **2** in excellent yield (> 95%). The subsequent reduction using lithium aluminium hydride in anhydrous THF was also highly effective, since the *N*,*N*′-dimethyldiamine derivative **3** was isolated in high overall yield (> 70%). The diamine was then subjected to a Michael-type alkylation with acrylonitrile. This reaction was investigated under several conditions to avoid monoalkylation and/or oligomerization of the reagent. A good yield of the dialkylated compound proved difficult, but operating under nitrogen, and using acrylonitrile as solvent and a large excess of glacial acetic acid,[10] we obtained the dialkylated product **4** in > 80% yield. The pure compound was obtained by flash chromatography in 52% yield. The dicyano functionalities were reduced successfully to primary amines by reaction with Raney nickel and hydrazine hydrate in ethanol solution, and the resulting compound **5** was obtained in good yield (> 70%). Other reducing agents such as lithium aluminium hydride or sodium borohydride gave much poorer yields and formed by-products. Finally, the ligand **L** was obtained by condensation of an excess 2-(chloromethyl)-1-methylbenzimidazole, **6**,[11] with the diamine **5**. The use of *N*-methylated benzimidazoles increased the chemical stability of the resulting metal complexes in the oxidative reactions studied by us.[8]

The distribution of nitrogen donors of the ligand may allow one to obtain trinuclear metal complexes containing two equivalent metal coordination sites (**A**) within the tridentate units consisting of the aminobis(benzimidazole) residues and a third metal site at the binaphthalenediamine residue (**B**) (Scheme 2). This arrangement is adopted by the complex $[Cu_3\mathbf{L}]^{6+}$,[8] and reproduces the type of donor atom distribution among the metal centers in the trinuclear cluster of multicopper oxidases.[12] When the ligand **L** is used in a dinuclear complex several possibilities exist, according to the characteristics and stereochemical preferences of the metal ions, and the two sites may even result in non-equivalent coordination types. Since copper(II) is stereochemically flexible and a pair of Cu^{II} ions in close proximity can undergo electronic coupling interactions, unraveling the coordination environment of the two copper ions in $[Cu_2\mathbf{L}]^{4+}$ in solution[8] is difficult. The simplest situation occurs when the eight donor atoms of **L** are evenly distributed within the two metal ions (Scheme 3); a favored situation when the metal centers can adopt a tetrahedral geometry. Therefore, we anticipate that this structural ar-

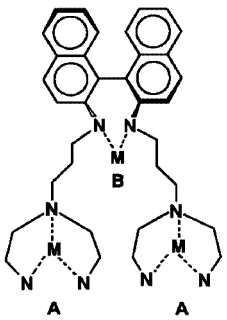

Scheme 2. Proposed structure for the trinuclear complexes of **L**

 © 2003 Wiley-VCH Verlag GmbH & Co. KGaA, Weinheim

rangement will be present in the dinuclear zinc(II) complex $[Zn_2L]^{4+}$; the diamagnetism of this metal ion is also useful since it enables a thorough investigation in solution by NMR spectroscopy. Only the dinuclear complex was isolated when we attempted to obtain a trinuclear zinc(II) complex, even upon reacting **L** with a large excess of Zn^{2+} at such high temperatures as boiling DMF, indicating that zinc(II) behaves differently from copper(II) in binding to **L**. This suggests that the binaphthalene-diamine nitrogen donors in the dinuclear complex $[Zn_2L]^{4+}$ cannot be made available for binding a third metal ion. The investigation has been extended to the dinuclear nickel(II) complex $[Ni_2L]^{4+}$, since the structural preferences of nickel(II) differ from those of zinc(II) and, in general, are relatively easy to assess on spectroscopic grounds. To this end, the spectral characteristics of $[Ni_2L]^{4+}$ were compared with those of the mononuclear nickel(II) complex with the ligand *N*,*N*-bis[(2-*N*-methylbenzimidazol-2-yl)ethyl]benzylamine (**BzB**),[13] which essentially reproduces the tridentate donor set provided by the aminobis(benzimidazole) units present in each arm of **L**.

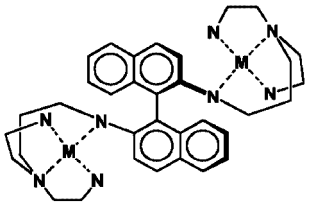

Scheme 3. Proposed structure for dinuclear complexes of **L** with metal ions in a tetrahedral geometry

Table 1. ^1H and ^{13}C NMR chemical shift assignments for ligand **L** in $[D_6]$acetone solution

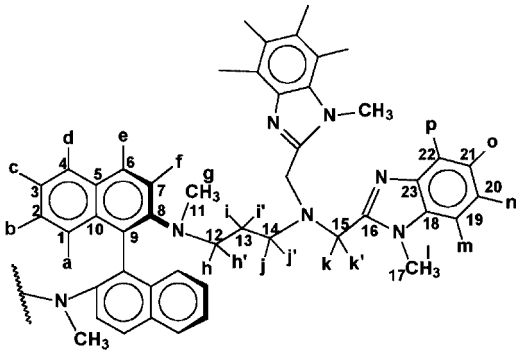

^1H	δ	^1H	δ	^1H	δ
a	6.87	h	2.23	k	3.72
b	6.93	h′	2.33	l	3.64
c	7.07	i	1.13	m	7.47
d	7.72	i′	1.23	n	7.26
e	7.79	j	1.55	o	7.20
f	7.26	j′	1.62	p	7.58
g	2.28				

^{13}C	δ	^{13}C	δ	^{13}C	δ
1	126.0	9	129.0	17	29.0
2	126.0	10	134.4	18	136.9
3	124.0	11	39.3	19	109.9
4	128.1	12	55.5	20	122.4
5	130.4	13	23.3	21	121.5
6	128.7	14	51.2	22	119.6
7	121.7	15	51.0	23	143.1
8	150.8	16	151.9		

NMR Experiments

Deuterated acetone was chosen as solvent for comparative NMR experiments between **L** and the zinc(II) complex because both compounds are sufficiently soluble in it, and the best peak resolution was obtained. The assignment of the ^1H and ^{13}C signals of **L** (Table 1) was based on the expected chemical shifts and *J*-coupling patterns, and was confirmed by two-dimensional NMR experiments (Figure 1). An unambiguous assignment of the particularly challenging aromatic resonances of the binaphthyl and benzimidazole residues was obtained from the combination of ^1H-^{13}C HMQC, ^1H-^1H COSY, DEPT135, and ^1H-^{13}C HMBC spectra. With an ^1H-^{13}C HMQC experiment all the direct connections between protons and carbons could be detected. Long-range correlation with the known methyl protons **g** allowed the assignment of the quaternary carbon **8** resonance; then proton **e** could be recognized by correlations with carbons **8** and **10**. Signals belonging to the benzimidazole residues could be assigned from the long-range correlation between carbon **16** and protons **k** and **l**. Similarly, long-range correlations among protons and quaternary carbons, combined with the ^1H-^1H COSY spectrum, led to the identification of all the aromatic signals.

The assignment of protons **g**, **k**, and **l**, respectively, correlated with carbons **11**, **15**, and **17**, is consistent with the signal intensities and with the analysis of the DEPT135 spectrum. Due to the chirality of the compound, the three pairs of geminal protons **h**, **h′**, **i**, **i′**, **j**, **j′** give rise to three pairs of multiplets. Despite the overlap of signals **g** and **h′**, the analysis of the ^1H-^{13}C HMQC spectrum clearly showed the correlation of protons **h** and **h′** to the same carbon. The diastereotopic proton pairs **i**, **i′**, **j**, **j′** are connected in the same fashion to carbons **13** and **14**. Interestingly, the geminal protons **k** exhibit a singlet peak.

The NMR spectra of **L** are strongly affected by the coordination of Zn^{2+} ions. When Zn^{2+} is added to the solution of **L** in a 1:1 stoichiometry, several isomeric species are formed, because the metal ion can bind in different coordination modes, and this gives a proton NMR spectrum dominated by broad, poorly defined envelopes as the result of many superimposed resonances. The addition of Zn^{2+} to the ligand in a 2:1 stoichiometry removes the coordinative vacancies and gives the dinuclear complex $[Zn_2L]^{4+}$ consisting of a single species. In the ^1H NMR spectrum, the broad envelopes are replaced by well-resolved peaks. Compared with the spectrum of the ligand, several signals undergo apparent splittings and many of them are shifted either downfield or upfield. Thus, the full assignment of the signals required the combination of one- and two-dimensional spectra (Figure 2). For the ^1H and ^{13}C NMR spectra

 © 2003 Wiley-VCH Verlag GmbH & Co. KGaA, Weinheim

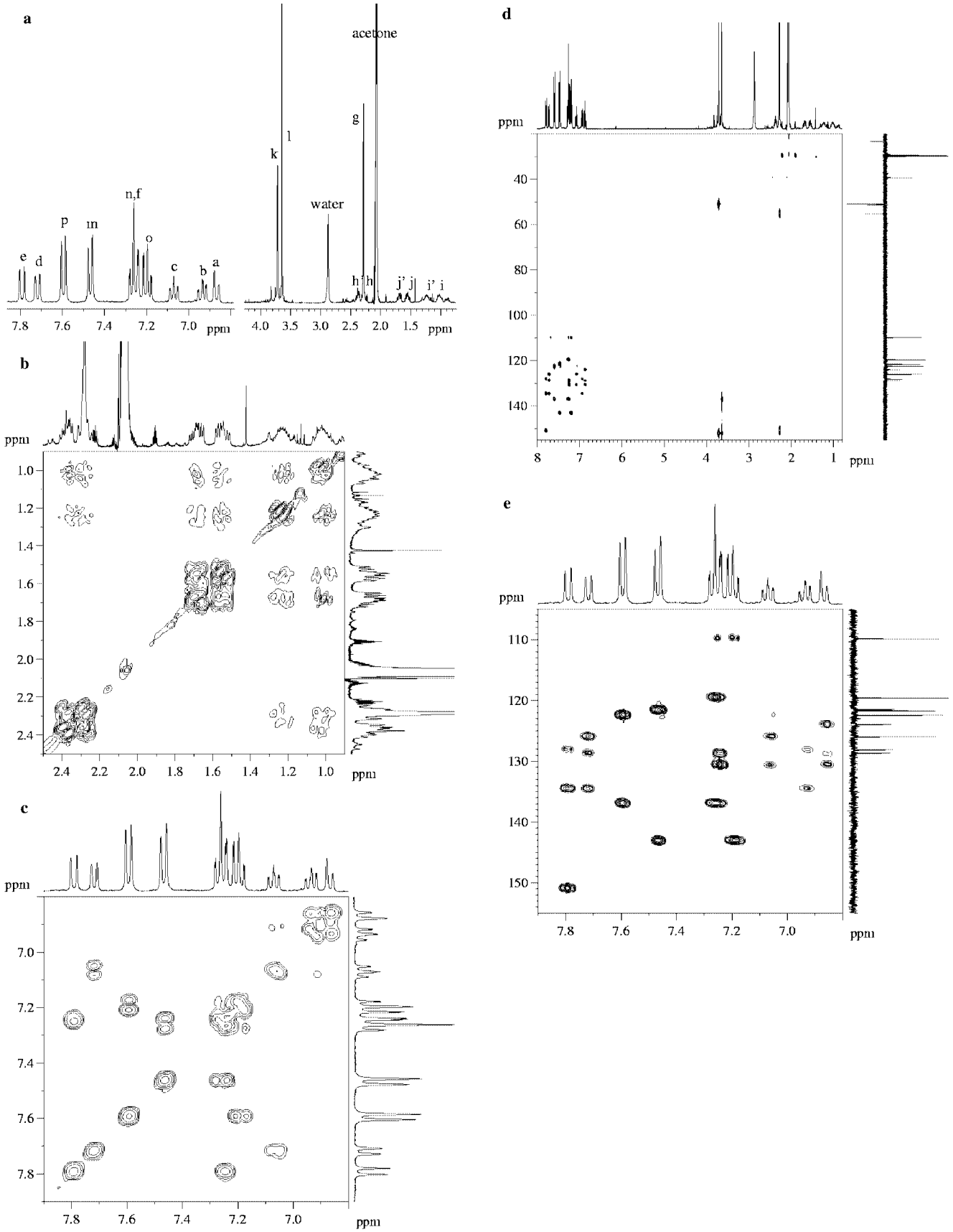

Figure 1. NMR spectroscopic data for **L** in [D_6]acetone solution: (a) proton NMR spectrum; (b) expanded plot of the aliphatic portion of the ^{1}H-^{1}H COSY spectrum; ^{1}H NMR spectrum of **L** at the right-hand edge and top of the map; (c) expanded plot of the aromatic portion of the spectrum of **L**; (d) long-range H-C correlated spectrum, with the ^{1}H NMR spectrum at the top edge and DEPT135 ^{13}C NMR at the right edge; (e) expanded plot of the aromatic portion of (d)

 © 2003 Wiley-VCH Verlag GmbH & Co. KGaA, Weinheim

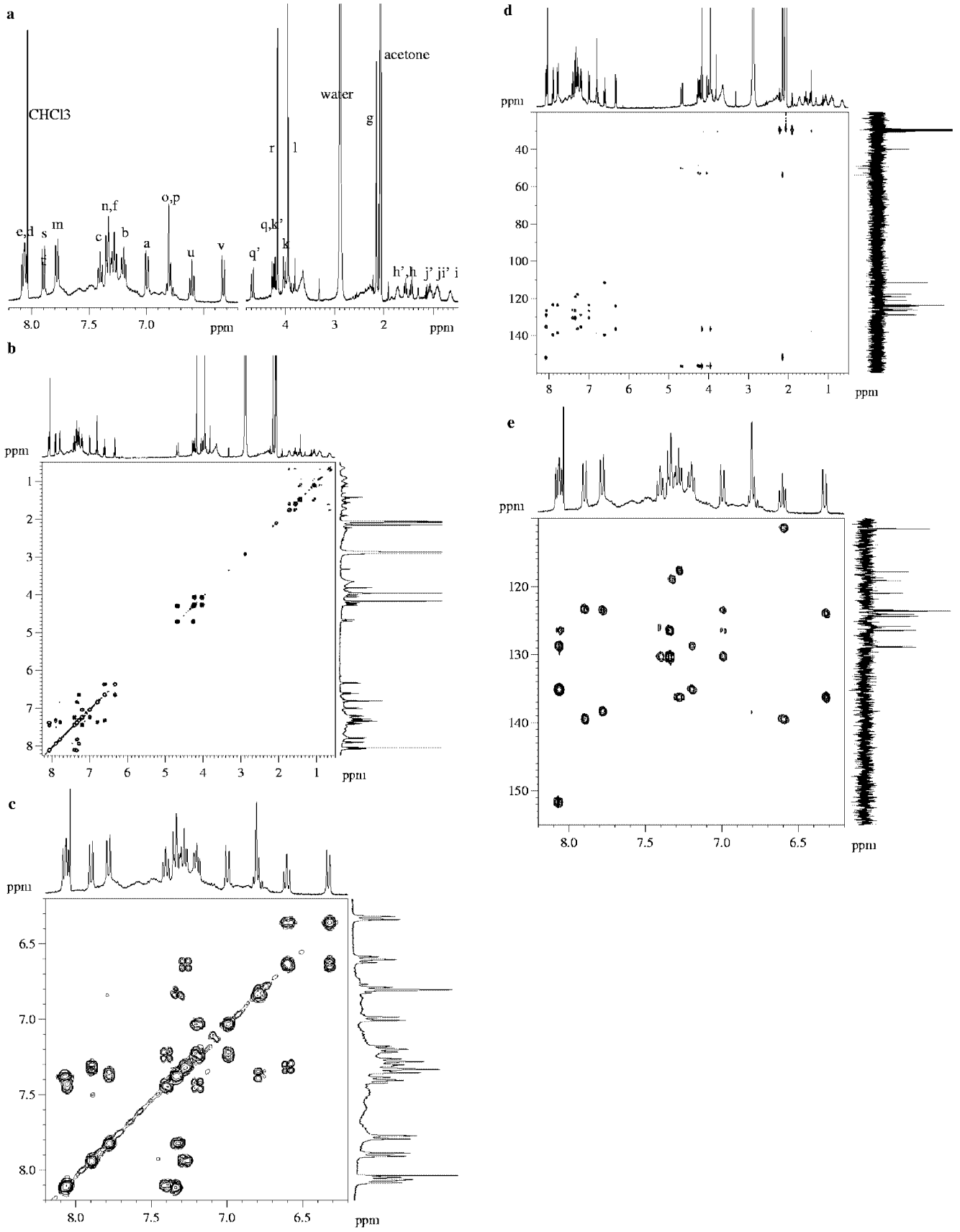

Figure 2. NMR spectroscopic data for $[Zn_2\mathbf{L}]^{4+}$ in $[D_6]$acetone solution: (a) proton NMR spectrum; (b) ^{1}H-^{1}H COSY spectrum; ^{1}H NMR spectrum of $[Zn_2\mathbf{L}]^{4+}$ at the right-hand edge and at the top; (c) expanded plot of the aromatic portion of the spectrum of $[Zn_2\mathbf{L}]^{4+}$; (d) long-range H-C correlated spectrum, with the ^{1}H NMR spectrum at the top edge and DEPT135 ^{13}C NMR at the right-hand edge; (e) expanded plot of the aromatic portion of (d)

 © 2003 Wiley-VCH Verlag GmbH & Co. KGaA, Weinheim

Table 2. ^1H and ^{13}C NMR chemical shift assignments for the $[Zn_2L]^{4+}$ complex in $[D_6]$acetone solution

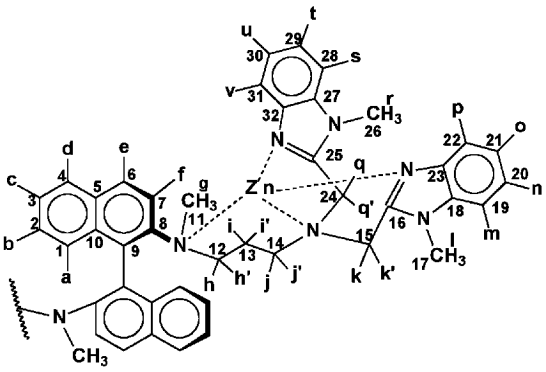

^1H	δ	^1H	δ	^1H	δ
a	7.00	i	0.66	o	6.80
b	7.20	i′	0.90	p	6.80
c	7.40	j	0.90	q	4.20
d	8.06	j′	1.06	q′	4.70
e	8.07	k	4.00	r	4.10
f	7.35	k′	4.15	s	7.90
g	2.10	l	3.90	t	7.29
h	1.57	m	7.78	u	6.60
h′	1.72	n	7.35	v	6.37

^{13}C	δ	^{13}C	δ	^{13}C	δ
1	125.5	12	52.0	23	138.5
2	126.0	13	23.0	24	48.0
3	123.5	14	53.0	25	157.0
4	128.5	15	50.0	26	29.0
5	130.5	16	157.0	27	137.0
6	128.5	17	29.0	28	111.2
7	121.0	18	137.0	29	124.0
8	152.0	19	111.0	30	123.3
9	130.8	20	124.0	31	117.2
10	135.1	21	123.5	32	139.5
11	38.0	22	119.0		

of the zinc complex (Table 2), as with **L**, the long-range correlations among protons and quaternary carbons combined with the $^1H-^1H$ COSY spectrum led to the identification of the signals of binaphthyl and benzimidazole residues. Analysis of the spectra of the cation $[Zn_2L]^{4+}$ gave many clues about the coordination mode of the Zn^{2+} ions, which is consistent with the computed structure of the complex (see below).

In general, the coordination of metal ions makes the ligand more rigid: consequently, in the complex $[Zn_2L]^{4+}$ there is no rapid exchange of nuclei and the signals of the methyl-benzimidazoles residues are split into two sets of resonances. As reported by Quiroz-Castro et al.,[14] the shift to higher frequencies of the **k** and **q** methylene groups indicates that the tertiary amine nitrogen atom is bonded to the metal center. The coordination of each Zn^{2+} ion with two benzimidazole *N*-donors is consistent with the downfield shift of the resonances of protons **m**, **n**, (at δ = 7.78, 7.35 ppm) and **s**, **t**, (7.90, 7.29) when compared with the corresponding protons **m** and **n** of the free ligand (at δ = 7.47, 7.26 ppm). Conversely, protons **o**, **p**, **u**, **v** undergo highfield shifts that can be explained by considering the computed structure of the complex. In fact, coordination of Zn^{2+} brings the aromatic protons **m**, **n**, **s**, **t** to an outer position with respect to the core of the molecule, while protons **o**, **p**, **u**, **v** occupy an inner position, where they are shielded by the aromatic binaphthyl residue.

The coordination of each Zn^{2+} ion to one naphthylamino nitrogen donor is shown by the downfield shift of all the ^1H signals of the naphthyl residue, with the strongest effect on proton **d** ($\Delta\delta = +0.34$, with respect to the free ligand), and on carbon **8** ($\Delta\delta = +1.2$). Interestingly, the two naphthylamine fragments still give a unique set of signals as for the free ligand: probably, the mobility of the molecule averages the signals in the dinuclear complex. Finally, the aliphatic chain with the carbon skeleton indicated as **12**, **13**, **14** undergoes some important modifications: strong positive shielding effects are observed on carbon **12** ($\Delta\delta = -3.5$ ppm) and on **h** and **h′** multiplets ($\Delta\delta = -0.66$ and -0.61 ppm, respectively), as well as on **j** and **j′** multiplets (-0.65 and -0.56, respectively), while a slight positive shielding effect occurs on carbon **13** ($\Delta\delta = -0.3$ ppm) and on **i** and **i′** multiplets (-0.47 and -0.33, respectively), and a deshielding effect is observed on carbon **14** ($+2.8$). The Δδ between geminal protons of these groups increases; the strongest effect is for the **i**, **i′** multiplets (Δδ of $+0.33$). The reported values arise from the opposing effects of coordination to a metal ion and interaction with the positive shielding zone of the binaphthalene and benzimidazole rings.

The proton NMR spectra of both $[Ni_2L]^{4+}$ and $[Ni(\mathbf{BzB})]^{2+}$ exhibit paramagnetically shifted resonances up to about 90 ppm (Figure 3). This precludes the metal centers having a four-coordinate, square-planar coordination environment as this would result in a diamagnetic species. The broad peaks downfield indicate an orbitally nondegenerate ground state, with excited states well separated in energy, for both complexes. This can occur with six-coordinate (pseudo-octahedral) or five-coordinate (both TBP and SP) nickel(II) complexes. By contrast, pseudo-tetrahedral nickel(II) complexes exhibit sharper NMR resonances due to fast electronic relaxation caused by the low energy excited states originating from the orbitally degenerate $^3T_1$ ground state of a pure tetrahedral symmetry.[15] Furthermore, in pseudo-tetrahedral nickel(II) complexes, the dipolar and spin polarization contributions to the paramagnetic shift generates both downfield and upfield shifts in the NMR resonances. The spectrum of $[Ni(\mathbf{BzB})]^{2+}$ exhibits sharper NMR lines than that of $[Ni_2L]^{4+}$, and also some upfield signals. The whole spectrum resembles those of five-coordinate, trigonal bipyramidal, nickel(II) complexes,[16] in which an unpaired electron in the equatorial plane accounts for the moderately intense spin-polarization and dipolar contributions. The donor groups for nickel(II) in $[Ni(\mathbf{BzB})]^{2+}$ are the two benzimidazoles, the central amine and two solvent molecules, as in structurally characterized copper(II) complexes with related aminobis(benzimidazole) ligands.[17] On the other hand, the NMR spectrum of

 © 2003 Wiley-VCH Verlag GmbH & Co. KGaA, Weinheim

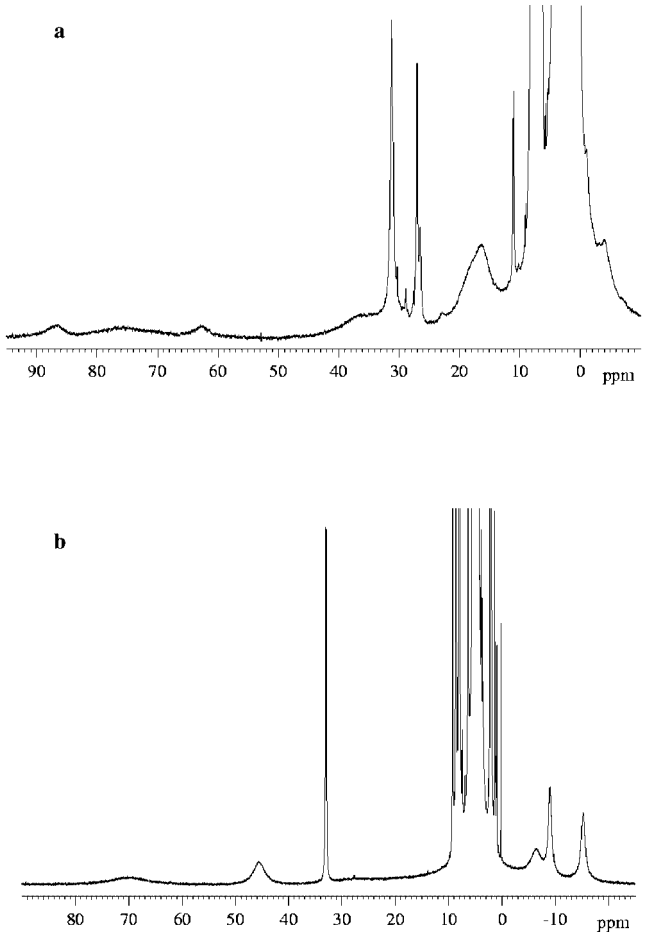

Figure 3. Paramagnetic NMR spectra recorded in [D_6]acetone solution at 25 °C of (a) $[Ni_2\mathbf{L}]^{4+}$ and (b) $[Ni(\mathbf{BzB})]^{2+}$ complexes

$[Ni_2\mathbf{L}]^{4+}$ shows essentially downfield shifts, indicating that the Fermi-contact is the predominant contribution to the paramagnetic NMR shifts. This situation is characteristic for electron configurations with a nondegenerate ground state, with unpaired electrons in σ-type d orbitals, as it occurs in six-coordinate, pseudo-octahedral or tetragonally distorted nickel(II) complexes.[15] The difference in metal coordination environment observed for $[Ni_2\mathbf{L}]^{4+}$ with respect to $[Ni(\mathbf{BzB})]^{2+}$ clearly arises from the additional binding of the binaphthalenediamine nitrogen donors in the former complex, which provide the tetragonal equatorial field for each metal ion.

Optical and CD Spectroscopy

The electronic spectrum of **L** consists of transitions associated with both the 1,1′-binaphthyl and the benzimidazole chromophores. The former is mostly responsible for the absorptions at 305 and 258 nm, and the latter for the multicomponent bands at 286, 278, and 271 nm, while both chromophores contribute to the band at 352 nm and the intense absorption at highest energy.[7a,11] The CD spectrum of **L** is dominated by the features of the (*R*)-1,1′-binaphthyl moiety (Figure 4), and from a comparison with the pattern of CD bands of (*R*)-*N*,*N*,*N*′,*N*′-tetramethyl-[1,1′-binaphthalene]-2,2′-diamine[7a] the replacement of a methyl group of each NMe_2 residue of the latter compound with the methylene chain carrying the aminobis(benzimidazole) arm in **L** clearly maintains the *cisoid* conformation (M helicity) of the naphthalene rings. This arrangement is determined by the steric hindrance between the amino substituents and the naphthyl group, which prevents their coplanar disposition maximizing conjugation of the nitrogen lone pair with the naphthalene ring.[7a]

In addition to the CD bands attributable to the binaphthyl chromophore, the CD spectrum of **L** displays a clearly defined positive peak at 248 nm (inset of Figure 4). This corresponds to a distinctive CD feature detected, or deduced from the CD lineshape, at 240 nm in the spectra of chain-bridged (*R*)-1,1′-binaphthyl derivatives.[7b] The latter feature, attributed to an inter-naphthalenic CT transition, witnesses that the dihedral angle between the naphthalene rings of the chromophore reduces to significantly below 90°.[7b] This unexpected arrangement for **L** is confirmed by the minimum energy conformation of the ligand resulting from the computations described below.

The CD spectrum of $[Zn_2\mathbf{L}]^{4+}$ is qualitatively similar to, though appreciably less intense than, that of the free ligand (Figure 4). Clearly, the M chirality of the (*R*)-1,1′-binaphthyl chromophore is maintained in the complex, but the spectrum lacks the distinctive positive CD peak at 248 nm which is present in the spectrum of **L**. This suggests that in the complex the dihedral angle between the naphthalene rings must increase to around 90°, which typically characterizes the conformation of unstrained 1,1′-binaphthyl chromophores.[7b] The decrease in intensity of the CD couplet, from **L** to $[Zn_2\mathbf{L}]^{4+}$, agrees with the increase in dihedral angle between the naphthalene rings.[6] The change in conformation undergone by the ligand on metal binding must be associated with the fact that the amino groups linked to the naphthalene rings are now involved in the coordination to the metal centers.

The reduction in CD amplitude of the exciton coupled binaphthalene transitions in the 210−230 nm range becomes drastic for the $[Ni_2\mathbf{L}]^{4+}$complex (Figure 4). Here, the ligand conformation must meet the coordination requirements of the metal ions, which tend to arrange the four nitrogen donor atoms in a nearly coplanar disposition. This apparently imposes a marked flattening of the dihedral angle between the naphthalene planes, as indicated by the much weaker intensity of the CD couplet.[6,7b] Also for $[Ni_2\mathbf{L}]^{4+}$ the CD spectrum has a positive peak in the 245 nm range, but the assignment to an intraligand transition is less certain, because LMCT transitions involving the Ni^{II} ions may occur in the same wavelength range. The optical and CD spectra of the $[Ni_2\mathbf{L}]^{4+}$complex exhibit additional weak absorptions in the visible region, which can be assigned to LF transitions. The reduced molar absorptivity observed in this range excludes pseudo-tetrahedral coordination, in agreement with the NMR spectrum of the complex. The LF spectrum (λ_{max} at 566 and 980 nm) is con-

 © 2003 Wiley-VCH Verlag GmbH & Co. KGaA, Weinheim

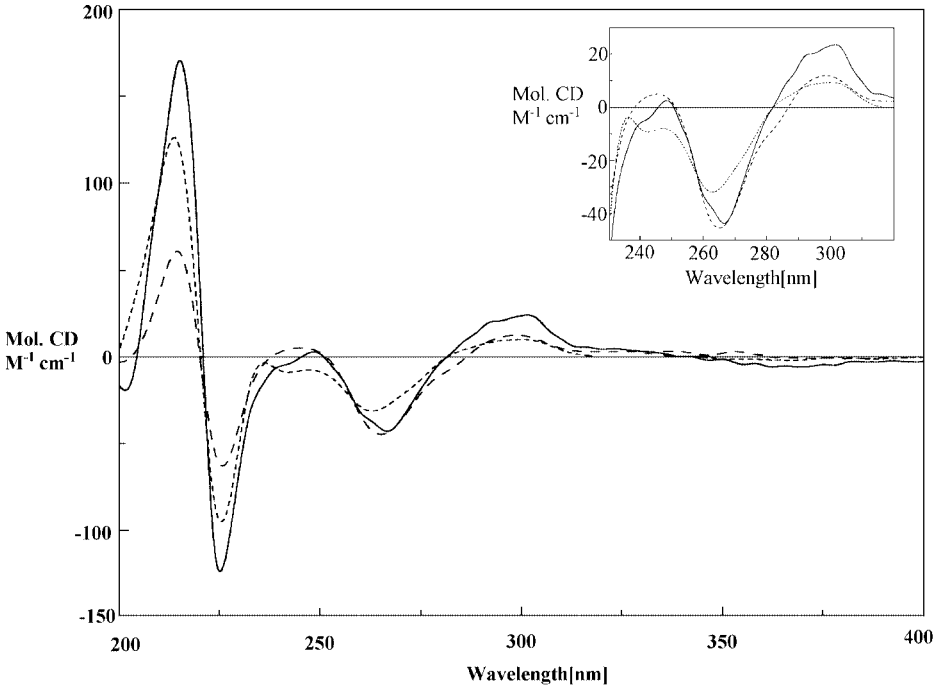

Figure 4. Circular dichroism spectra in CH_3CN solution of (—) **L**, (- - - -) $[Zn_2L]^{4+}$, and (– – –) $[Ni_2L]^{4+}$

sistent with six-coordinate, pseudo-octahedral metal centers,[18] which generally exhibit three absorption bands in the range 300−1200 nm. In the present case, the LF band at highest energy is clearly buried under the strong intraligand bands of **L**. The LF spectrum of $[Ni(\mathbf{BzB})]^{2+}$ contains absorptions of low intensity at 605, 920 and 1020 nm, which are consistent with a five-coordinate species and agree with the characteristics of the NMR spectrum. However, the optical spectrum cannot distinguish between trigonal bipyramidal and square-pyramidal configuration, due to the relatively high number of energy terms of the nickel(II) ion produced by even small geometric distortions from regular geometries.[19]

Computational Studies

Being unable to obtain crystals suitable for X-ray investigations, the structures of the ligand **L** and the binuclear complex $[Zn_2L]^{4+}$, for which the conformational preferences deduced from CD are more reliable, were investigated by simulated annealing (SA) molecular mechanics (MM) and semiempirical calculations (see Exp. Sect.). The best structures obtained are shown in Figure 5. In **L** the benzimidazole rings from different arms are involved in favorable stacking interactions and this forces the dihedral angle θ defining the conformation of the 1,1′-binaphthyl group to close to 75° (Figure 5, a). A very similar arrangement is observed in all the most stable **L** structures obtained by the computational procedure (θ = 77±4°). In the binuclear complex $[Zn_2L]^{4+}$ the benzimidazole rings are involved in Zn coordination. Both metal ions are in a slightly distorted tetrahedral environment, characterized by bond lengths ranging from 2.02 (Zn-*N*-benzimidazole) to 2.16 Å (Zn-*N*-binaphthyl). As a consequence of metal coordination, the benzimidazole rings fold around the two metal ions (Figure 5, b), which does not allow the stacking interactions observed in **L**, and relaxes the dihedral angle defining the conformation of the 1,1′-binaphthyl group to close to 90° (θ = 91±3°). In addition, the steric constraints imposed by the nitrogen ligand result in a distorted tetrahedral coordination geometry, suggesting that an extra ligand could bind to the metal forming a trigonal bipyramidal complex. To investigate this possibility we added a water molecule to the metal coordination environment and optimized the structure using semiempirical calculations. It turns out that a water molecule can bind (albeit weakly) to the metal center without affecting significantly the spatial disposition of the nitrogen ligands (data not shown). However, the slightly unfavourable reaction energy associated with its binding (0.2 kcal mol^{-1}) and the relatively long computed Zn−O distance (2.43 Å) indicate that it is more appropriate to consider the water molecule as only solvating the metal ion. Computed models of the $[Ni_2L]^{4+}$complex could not be investigated because the electronic structure of the metal ion

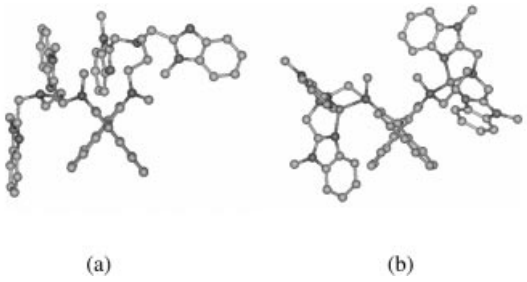

Figure 5. Best structures for **L** (a) and $[Zn_2L]^{4+}$ (b) as obtained by the combined SA-MM + PM3 procedure. Hydrogen atoms not shown for clarity

 © 2003 Wiley-VCH Verlag GmbH & Co. KGaA, Weinheim

precluded reliable results with MM and semiempirical methods.

Conclusion

We have shown that (*R*)-1,1′-binaphthyl-2,2′-diamine provides a useful starting point for the synthesis of polyfunctional chiral ligands. The conformational features of the octadentate ligand **L** markedly change when it folds around the metal ions in the dinuclear zinc(II) and nickel(II) complexes. The spectroscopic and CD features of these complexes are consistent with the adoption of pseudo-tetrahedral structures for the zinc(II) centers and pseudo-octahedral structures for the nickel(II) centers. The stereochemical arrangement of the critical binaphthalenediamine portion of the molecule carrying the chiral unit can be clearly assessed on the basis of the CD spectra.

Experimental Section

Materials and Physical Methods: All reagents and solvents were obtained from commercial sources and used without further purification. The ligand *N*,*N*-bis[(2-*N*-methylbenzimidazol-2-yl)ethyl]-benzylamine (**BzB**) was synthesized according to a published procedure,[13] while the corresponding nickel(II) complex was prepared in situ by mixing equimolar amounts of the ligand and nickel(II) salt. Tetrahydrofuran was dried by refluxing and distilling from metallic sodium. Elemental analyses were performed at the microanalytical laboratory of the Chemistry Department in Milan. Optical rotations were obtained from a Perkin−Elmer 241 polarimeter at 25 °C using a quartz cell of 10 cm path length. Optical spectra were obtained with HP 8452A and 8453 diode array spectrophotometers. MS spectra were obtained from a VG 7070 EQ spectrometer. Circular dichroism (CD) spectra were recorded with Jasco J-500 or J-710 spectropolarimeters, using quartz cells of 0.01−2 cm path length. ^{1}H and ^{13}C NMR spectra were recorded with Bruker AC 300 or Bruker AVANCE 400 spectrometers operating at 7.03 and 9.37 T, respectively. For solubility reasons, comparative NMR studies of **L** and $[Zn_2\mathbf{L}](ClO_4)_4$ were performed on CD_3COCD_3 solutions. A concentrated solution of the complex was obtained by mixing solutions of the ligand **L** and $Zn(ClO_4)_2{\cdot}7H_2O$ in [D_6]acetone and stirring for a few min in the NMR tube. The paramagnetic NMR spectra of $[Ni_2\mathbf{L}]^{4+}$ and $[Ni(\mathbf{BzB})]^{2+}$ complexes were recorded in the same solvent at 25 °C; the spectral width was increased to 50000 Hz and the pulse length reduced to 3 μs.

Ligand Synthesis. (*R*)-(+)-*N*,*N*′-(Ethoxycarbonyl)-1,1′-binaphthyl-2,2′-diamine (2): Compound **2** was prepared in accordance with Benson et al.[9] Commercial (*R*)-(+)-1,1′-binaphthyl-2,2′-diamine, **1**, (2.0 g, 7.19 mmol) was dissolved in benzene (25 mL) and pyridine (5 mL, 62.14 mmol) under N_2 and cooled to 0 °C. A solution of ethyl chloroformate (1.8 mL, 18.89 mmol) in benzene (5 mL) was then added dropwise during 15 min. The mixture was subsequently warmed to room temperature and stirred for 2 h. The reaction, followed by TLC (silica gel) using light petroleum/ethyl acetate (8:2, v:v) as eluent, was then quenched by the addition of 2 N KOH (40 mL); the organic layer was separated, and the aqueous layer was extracted with benzene (3 × 20 mL). The organic layers were dried with Na_2SO_4 and the solvent was removed by rotary evaporation. After drying, a slightly pink powder was obtained, with sufficient purity for the subsequent reaction (yield 97%). $[\alpha]_D^{20}$ = +86.68 ($c = 4.28{\cdot}10^{-3}$, $CHCl_3$). ^{1}H NMR (300 MHz, $CDCl_3$, 25 °C, TMS): δ = 1.18 (t, $J_{H,H}$ = 7.1 Hz, 6 H, CH_3), 4.1 (q, $J_{H,H}$ = 7.1 Hz, 4 H, CH_2), 6.28 (br., 2 H, NH), 6.98 (d, $J_{H,H}$ = 8.5 Hz, 2 H, CH), 7.24−7.30 (m, 2 H, CH), 7.41−7.46 (m, 2 H, CH), 7.94 (d, $J_{H,H}$ = 8.1 Hz, 2 H, CH), 8.08 (d, $J_{H,H}$ = 9.1 Hz, 2 H, CH), 8.57 (d, $J_{H,H}$ = 9.1 Hz, 2 H, CH) ppm.^{13}C NMR (75.5 MHz, $CDCl_3$, 25 °C, TMS): δ = 14.7, 61.8, 117.8, 119.7, 125.2, 125.5, 127.7, 128.7, 130.7, 131.0, 132.9, 135.7, 154.0 ppm.

(*R*)-(+)-*N*,*N*′-Dimethyl-1,1′-binaphthyl-2,2′-diamine (3): $LiAlH_4$ (2.65 g, 69.83 mmol) was suspended in dry THF (40 mL) under N_2, and cooled to 0 °C. The dicarbamate **2** (2.71 g, 6.33 mmol) dissolved in dry THF (15 mL) was then slowly added via addition funnel, and the mixture was warmed and then refluxed for 24 h. The reaction was followed by TLC (silica gel) using light petroleum/ethyl acetate (8:2, v:v) as eluent. After cooling to room temperature, excess $LiAlH_4$ was quenched with MeOH (2 mL), NaOH 15% (2 mL), and finally water (2 mL). The resultant gray precipitate was filtered off through Celite and washed with diethyl ether. The filtrate and washings were combined and the solvent was removed by rotary evaporation under vacuum, giving a pale yellow solid. The crude compound was purified by silica gel flash chromatography using light petroleum/ethyl acetate (8:2, v:v) as eluent, furnishing a white compound in 72% yield. $[\alpha]_D^{20}$ = +182.82 ($c = 4.08{\cdot}10^{-3}$, $CHCl_3$). ^{1}H NMR (300 MHz, $CDCl_3$, 25 °C, TMS): δ = 2.84 (s, 6 H, CH_3), 6.96−7.00 (m, 2 H, CH), 7.14−7.23 (m, 4 H, CH), 7.27 (d, $J_{H,H}$ = 8.9 Hz, 2 H, CH), 7.79−7.84 (m, 2 H, CH), 7.93 (d, $J_{H,H}$ = 8.9 Hz, 2 H, CH) ppm. ^{13}C NMR (75.5 MHz, $CDCl_3$, 25 °C, TMS): δ = 32.1, 113.1, 114.5, 122.8, 124.4, 127.5, 128.6, 130.5, 134.3, 145.6 ppm. MS (70 eV, EI): *m*/*z* (%) = 312 (100) $[M]^+$.

(*R*)-(−)-*N*,*N*′-Dimethyl-*N*,*N*′-[bis(2-cyanoethyl)]-1,1′-binaphthyl-2,2′-diamine (4): Glacial acetic acid (7 mL, 12.24 mmol) was added to compound **3** (1.5 g, 4.80 mmol) dissolved in acrylonitrile (35 mL). The resulting mixture was then heated to reflux whilst stirring in a nitrogen atmosphere for 72 h. Some signs of polymerization were evident on heating, and the initial yellow solution turned brown. The reaction was followed by TLC (silica gel) using light petroleum/ethyl acetate (8:2, v:v) as eluent. Excess acrylonitrile was removed by rotary evaporation and the remaining residue was extracted with aqueous Na_2CO_3 and CH_2Cl_2. The organic layer was anhydrified with Na_2SO_4. After filtration, the solvent was removed by rotary evaporation to give a brown, oily product. Silica gel flash chromatography using light petroleum/ethyl acetate (8:2, v:v) as eluent afforded a light yellow product in 52% yield. $[\alpha]_D^{20}$ = −173.48 ($c = 6.60{\cdot}10^{-3}$, $CHCl_3$). ^{1}H NMR (300 MHz, $CDCl_3$, 25 °C, TMS): δ = 1.46−1.70 (m, 4 H, CN-CH_2-CH_2-N), 2.80 (s, 6 H, CH_3), 2.80−2.89 (m, 4 H, CN-CH_2-CH_2-N), 7.12 (d, $J_{H,H}$ = 8.5 Hz, 2 H, CH), 7.23−7.29 (m, 2 H, CH), 7.38−7.43 (m, 2 H, CH), 7.55 (d, $J_{H,H}$ = 8.9 Hz, 2 H, CH), 7.90 (d, $J_{H,H}$ = 8.1 Hz, 2 H, CH), 7.98 (d, $J_{H,H}$ = 8.9 Hz, 2 H, CH) ppm. ^{13}C (75.5 MHz, $CDCl_3$, 25 °C, TMS) δ = 16.6, 41.2, 53.1, 118.9, 121.6, 125.4, 126.1, 127.6, 128.6, 129.9, 130.1, 131.2, 134.7, 148.9 ppm. MS (70 eV, EI): *m*/*z* (%) = 418 (100) $[M]^+$.

(*R*)-(−)-*N*,*N*′-Dimethyl-*N*,*N*′-bis[(3-aminopropyl)]-1,1′-binaphthyl-2,2′-diamine (5): Compound **4** (600 mg, 1.43 mmol) was dissolved in EtOH (30 mL) by heating to 60 °C. A water suspension of Ni-Raney (12 g) and $N_2H_4{\cdot}H_2O$ (8 mL, 257 mmol) was added and the mixture maintained at 60 °C. After 3 h, complete nitrile consumption was evident by TLC (silica gel); excess Ni-Raney was removed by filtration through Celite and the solvent distilled off under vacuum. The remaining residue was purified by silica gel flash chromatography eluting with CH_2Cl_2/*i*PrOH (60:40, v:v) and an increasing

 © 2003 Wiley-VCH Verlag GmbH & Co. KGaA, Weinheim

amount of concentrated NH_3 (0 to 7%). A light yellow oil was obtained in > 70% yield. $[\alpha]_D^{20} = -95.11$ ($c = 1.00 \cdot 10^{-2}$, $CHCl_3$). ^1H NMR (300 MHz, $CDCl_3$, 25 °C, TMS) δ = 0.85−0.95 (m, 2 H, CH_2-CH_2-CH_2), 1.16−1.27 (m, 2 H, CH_2-CH_2-CH_2), 1.82−1.94 (m, 4 H, CH_2), 2.52−2.64 (m, 4 H, CH_2), 2.64 (s, 6 H, CH_3), 7.09−7.22 (m, 4 H, CH), 7.26−7.36 (m, 2 H, CH), 7.53 (d, $J_{H,H}$ = 8.3 Hz, 2 H, CH), 7.83−7.93 (m, 4 H, CH) ppm. ^{13}C NMR (75.5 MHz, [$CDCl_3$, 25 °C, TMS): δ = 32.0, 40.4, 40.8, 56.0, 121.9, 124.6, 126.6, 126.9, 128.5, 129.1, 131.0, 135.1, 151.2 ppm. MS (FAB): *m*/*z* (%) = 428 (100) $[M+1]^+$.

(*R*)-(−)-*N*,*N*′-Dimethyl-*N*,*N*′-bis{3-[bis(1-methyl-2-benzimidazolylmethyl)]aminopropyl}-1,1′-binaphthyl-2,2′-diamine (L): (*R*)-(−)-*N*,*N*′-Dimethyl-*N*,*N*′-bis[(3-aminopropyl)]-1,1′-binaphthyl-2,2′-diamine (**5**, 332.5 mg, 0.78 mmol) was dissolved in anhydrous acetonitrile (40 mL). 2-(Chloromethyl)-1-methylbenzimidazole (**6**)[11] (365.7 mg, 3.45 mmol) and dry sodium carbonate were then added and the stirred mixture was boiled under reflux for 6 h under N_2. The reaction was followed by TLC (silica gel) using CH_2Cl_2/MeOH (9:1, v:v), as eluent. The mixture was then cooled to room temperature and the so-obtained precipitate filtered off; it consisted of product and inorganic salts and thus was treated with $CHCl_3$ and filtered again. The combined filtrates were finally dried under vacuum to afford a yellow powder in 65% yield. $C_{64}H_{66}N_{12}\cdot 1.5CHCl_3$ (1182.34): calcd. (%) C 66.53, H 5.80, N 14.22; found C 66.41, H 5.90, N 14.21. $[\alpha]_D^{20} = -87.40$ ($c = 5.00 \cdot 10^{-3}$, $CHCl_3$). ^1H NMR (300 MHz, $CDCl_3$, 25 °C, TMS): δ = 0.70−0.90 (m, 2 H, CH_2-CH_2-CH_2-N), 1.00−1.30 (m, 2 H, CH_2-CH_2-CH_2-N), 1.45−1.65 (m, 4 H, CH_2-CH_2-CH_2), 2.10−2.37 (m, 4 H, CH_2-*N*-binaphthyl), 2.37 (s, 6 H, CH_3-*N*-binaphthyl), 3.45 (s, 12 H, CH_3-*N*-benzimidazole), 3.51−3.64 (d, 8 H, CH_2-benzimidazole), 6.98−7.13 (m, 4 H, CH), 7.20−7.26 (m, 16 H, CH), 7.65−7.72 (m, 8 H, CH) ppm. ^{13}C NMR (75.5 MHz, $CDCl_3$, 25 °C, TMS): δ = 24.1, 30.1, 40.1, 51.2, 52.2, 55.5, 109.4, 113.7, 120.0, 121.4, 122.4, 123.1, 124.3, 126.4, 126.5, 128.0, 128.6, 129.1, 129.6, 130.5, 134.6, 136.4, 142.4, 150.7, 151.7 ppm. MS (FAB): *m*/*z* (%) = 1003 (100) $[M+1]^+$. UV/Vis (CH_3CN): λ_{max} (ε) = 208 (239000), 258 (71000), 271 sh (54400), 278 sh (43500), 286 (32400), 305 sh (11900), 352 nm (6300 $mol^{-1}\cdot dm^3\cdot cm^{-1}$). CD ($CH_3CN$): λ_{max} (Δε) = 214 (+169.8), 225 (−124.5), 240 sh (−3.8), 248 (+2.7), 260 sh (−36.1), 266 (−44.7), 301 (+23.2), 368 nm (−5.9 $mol^{-1}\cdot dm^3\cdot cm^{-1}$).

Caution! *1,1′-Binaphthyl-2,2′-diamine derivatives are not stable in solution; after a few hours a deeper color orange is observed. These compounds should be kept dry and protected from light.*

Synthesis of the Metal Complexes. $[Zn_2L](ClO_4)_4$: A methanolic solution of $Zn(ClO_4)_2\cdot 7H_2O$ (0.038 mmol) (4 mL) was added dropwise to a solution of the ligand **L** (0.019 mmol) in $CHCl_3$/MeOH (1:5, v:v) (20 mL). The mixture was stirred for 3 h at room temperature, and then the solvent was removed by rotary evaporation. The residue was washed with a little water, filtered, and dried under vacuum. Elemental analysis for $C_{64}H_{66}Cl_4N_{12}O_{16}Zn_2$ (1530.14): calcd. (%) C 50.20, H 4.31, N 10.98; found C 50.33, H 4.41, N 10.95. UV/Vis (CH_3CN): λ_{max} (ε) = 220 sh (99000), 254 (46300), 264 (44400), 272 (43000), 280 (37200), 300 sh (10500), 350 nm (3000 $mol^{-1}\cdot dm^3\cdot cm^{-1}$). CD ($CH_3CN$): λ_{max} (Δε) = 213 (+122.5), 225 (−95.1), 240 sh (−8.2), 263 (−31.9), 298 (+9.3), 365 nm (−2.8 $mol^{-1}\cdot dm^3\cdot cm^{-1}$).

$[Ni_2L](ClO_4)_4\cdot 2H_2O$: This compound was prepared in a similar way as for the zinc complex, but using $Ni(ClO_4)_2\cdot 6H_2O$ as metal salt. A pale green precipitate was obtained after addition of the metal salt to the ligand solution. The complex was separated by centrifugation, washed several times with MeOH, and dried under vacuum. Elemental analysis for $C_{64}H_{66}Cl_4N_{12}Ni_2O_{16}\cdot 2H_2O$ (1552.77): calcd. (%) C 49.50, H 4.54, N 10.83; found C 49.22, H 4.63, N 10.78. UV/Vis (CH_3CN): λ_{max} (ε) = 222 sh (97800), 260 (67500), 272 (56800), 282 (42600), 304 (15300), 356 (5400), 566 (8), 980 nm (2 $mol^{-1}\cdot dm^3\cdot cm^{-1}$). CD ($CH_3CN$): λ_{max} (Δε) = 214 (+61.0), 225 (−63.2), 245 (+4.72), 265 (−45.8), 278 sh (−13.0), 298 (+11.7), 331 sh (+1.9), 373 (−2.6), 583 nm (−0.1 $mol^{-1}\cdot dm^3\cdot cm^{-1}$).

Caution! *Perchlorate complexes with organic ligands are potentially explosive and should be handled with great care. Only small amounts of material should be prepared. We had no problems working with the small amounts of perchlorate complex described here.*

Molecular Modelling: The structures of the ligand and the corresponding dinuclear zinc(II) complex were derived as follows. Starting structures were submitted to SA calculations carried out in vacuo over 200 ps, starting from 10 K, heating the system to 500 K in 80 ps, and then cooling it to 10 K in 110 ps. The time step was set to 1 fs. The final structures were optimized by MM calculations, using the conjugate gradient algorithm and requiring that the residual gradient of energy did not exceed 0.01 $kcal\cdot mol^{-1}\cdot Å^{-1}$. SA and MM calculations were carried out using the Universal Force Field.[20] This cycle was repeated 50 times both for the ligand and the dinuclear zinc(II) complex. The families of structures generated were clustered according to RMSD and ranked by relative energies. The conformers within 10 $kJ\cdot mol^{-1}$ above the computed global minimum conformation were further optimized by semiempirical calculations using the PM3 method.[21] All calculations were performed on a Silicon Graphics Indigo workstation using the software packages InsightII and Cerius2 [Biosym/MSI 9685, Scranton Road, San Diego, CA, USA].

Acknowledgments

The authors thank the University of Milano for support through the FIRST, the University of Pavia for support through the FAR, and the C. I. R. C. S. M. B.

[1] [1a] A. G. Blackman, W. B. Tolman, *Struct. Bonding* **2000**, *97*, 179−211. [1b] K. D. Karlin, A. D. Zuberbuhler, in: *Bioinorganic Catalysis (2nd Edition, Revised and Expanded)* (Eds.: J. Reedijk, E. Bouwman), Dekker, New Jork, **1999**, pp. 469−534. [1c] P. Gamez, P. G. Aubel, W. L. Driessen, J. Reedijk, *Chem. Soc. Rev.* **2001**, *30*, 376−385. [1d] H.-C. Liang, M. Dahan, K. D. Karlin, *Curr. Opin. Chem. Biol.* **1999**, *3*, 168−175.

[2] L. Santagostini, M. Gullotti, R. Pagliarin, E. Bianchi, L. Casella, E. Monzani, *Tetrahedron: Asymmetry* **1999**, *10*, 281−295.

[3] [3a] L. Casella, E. Monzani, M. Gullotti, D. Cavagnino, G. Cerina, L. Santagostini, R. Ugo, *Inorg. Chem.* **1996**, *35*, 7516−7525. [3b] E. Monzani, L. Quinti, A. Perotti, L. Casella, M. Gullotti, L. Randaccio, S. Geremia, G. Nardin, P. Faleschini, G. Tabbì, *Inorg. Chem.* **1998**, *37*, 553−562. [3c] E. Monzani, G. Battaini, A. Perotti, L. Casella, M. Gullotti, L. Santagostini, G. Nardin, L. Randaccio, S. Geremia, P. Zanello, G. Opromolla, *Inorg. Chem.* **1999**, *38*, 5359−5369. [3d] L. Santagostini, M. Gullotti, E. Monzani, L. Casella, R. Dillinger, F. Tuczek, *Chem. Eur. J.* **2000**, *6*, 519−522. [3e] E. Monzani, L. Casella, G. Zoppellaro, M. Gullotti, R. Pagliarin, R. P. Bonomo, G. Tabbì, G. Nardin, L. Randaccio, *Inorg. Chim. Acta* **1998**, *282*, 180−192.

[4] [4a] S. Kobayashi, M. Kawamura, *J. Am. Chem. Soc.* **1998**, *120*, 5840−5841. [4b] M. Shibasaki, H. Sasai, T. Arai, *Angew. Chem. Int. Ed. Engl.* **1997**, *36*, 1237−1256.

[5] [5a] E. Hagiwara, A. Fujii, M. Sodeoka, *J. Am. Chem. Soc.* **1998**, *120*, 2474−2475. [5b] A. Yanagisawa, H. Nakashima, A.

 © 2003 Wiley-VCH Verlag GmbH & Co. KGaA, Weinheim

Ishiba, H. Yamamoto, *J. Am. Chem. Soc.* **1996**, *118*, 4723−4724. [5c] D. Ferraris, B. Young, T. Dudding, T. Lectka, *J. Am. Chem. Soc.* **1998**, *120*, 4548−4549.
[6] S. F. Mason, *Molecular Optical Activity & the Chiral Discriminations*, Cambridge University Press, Cambridge, U.K., **1982**, chapter 6.
[7] [7a] C. Rosini, L. Branzini, P. Salvadori, G. P. Spada, *J. Org. Chem.* **1992**, *57*, 6820−6824. [7b] L. Di Bari, G. Pescitelli, P. Salvadori, *J. Am. Chem. Soc.* **1999**, *121*, 7998−8004.
[8] M. C. Mimmi, M. Gullotti, L. Santagostini, A. Saladino, L. Casella, E. Monzani, R. Pagliarin, *J. Mol. Cat. A: Chem.* **2003**, *204−205*, 381−389.
[9] S. C. Benson, P. Cai, M. Colon, M. A. Haiza, M. Tokles, J. K. Snyder, *J. Org. Chem.* **1988**, *53*, 5335−5341.
[10] M. L. Turonek, P. Moore, H. J. Clase, N. W. Alcock, *J. Chem. Soc., Dalton Trans.* **1995**, 3659−3666.
[11] L. Casella, O. Carugo, M. Gullotti, S. Garofani, P. Zanello, *Inorg. Chem.* **1993**, *32*, 2056−2067.
[12] [12a] A. Messerschmidt, R. Ladenstein, R. Huber, M. Bolognesi, L. Avigliano, R. Petruzzelli, A. Rossi, A. Finazzi-Agrò, *J. Mol. Biol.* **1992**, *224*, 179−205. [12b] T. Bertrand, C. Jolivalt, P. Briozzo, E. Caminade, N. Joly, C. Madzak, C. Mougin, *Biochemistry* **2002**, *41*, 7325−7333. [12c] N. Hakulinen, L.-L. Kiiskinen, K. Kruus, M. Saloheimo, A. Paananen, A. Koivula, J. Rouvinen, *Nature Struct. Biol.* **2002**, *9*, 601−605. [12d] V. N. Zaitsev, I. Zaitseva, M. Papiz, P. F. Lindley, *J. Biol. Inorg. Chem.* **1999**, *4*, 579−587.
[13] [13a] S. Mandal, D. Macikenas, J. D. Protasiewicz, L. M. Sayre, *J. Org. Chem.* **2000**, *65*, 4804−4809. [13b] G. Battaini, M. De Carolis, E. Monzani, F. Tuczek, L. Casella, *Chem. Commun.* **2003**, 726−727.
[14] E. Quiroz-Castro, S. Bernès, N. Barba-Behrens, R. Tapia-Benavides, R. Contreras, H. Nöth, *Polyhedron* **2000**, *19*, 1479−1484.
[15] I. Bertini, C. Luchinat, *NMR of Paramagnetic Molecules in Biological Systems*, The Benjamin/Cummings Publishing Co., Menlo Park, CA, **1986**, chapter 9.
[16] G. La Mar, L. Sacconi, *J. Am. Chem. Soc.* **1967**, *89*, 2282−2291.
[17] L. Casella, O. Carugo, M. Gullotti, S. Doldi, M. Frassoni, *Inorg. Chem.* **1996**, *35*, 1101−1113.
[18] A. B. P. Lever, *Inorganic Electronic Spectroscopy*, Elsevier, Amsterdam, **1984**.
[19] R. S. Drago, *Physical Methods for Chemists, Second Edition*, Saunders, Ft. Worth, Mexico, **1992**, chapter 10.
[20] A. K. Rappe′, K. S. Colwell, C. J. Casewit, *Inorg. Chem.* **1993**, *32*, 3438−3450.
[21] J. J. P. Stewart, *Int. J. Quant. Chem.* **1996**, *58*, 133−146.

Received February 17, 2003

 © 2003 Wiley-VCH Verlag GmbH & Co. KGaA, Weinheim

A Novel Water-Soluble Tripodal Imidazolyl Ligand as a Model for the Tris(histidine) Motif of Zinc Enzymes: Nickel, Cobalt and Zinc Complexes and a Comparison with Metal Binding in Carbonic Anhydrase

Peter C. Kunz,[a] Guido J. Reiß,[a] Walter Frank,[a] and Wolfgang Kläui*[a]

Dedicated to Professor Bernt Krebs on the occasion of his 65th birthday

Keywords: Bioinorganic chemistry / Cobalt / Enzyme models / N ligands / Nickel / Tripodal ligands / Zinc

Tris[2-isopropylimidazol-4(5)-yl]phosphane (4-TIP^{iPr}), a novel model ligand for the tris(histidine) motif of many zinc enzymes, has been prepared. 4-TIP^{iPr} is hydrolytically stable and soluble in protic solvents. It readily forms chloro- and nitratocobalt, -nickel and -zinc complexes in aqueous methanol. The crystal structures of the solvates [(4-TIP^{iPr})Co(MeOH)(NO$_3$)]NO$_3$·2Et$_2$O (**3**·2Et$_2$O), [(4-TIP^{iPr})Ni(MeOH)(NO$_3$)]NO$_3$·Et$_2$O·MeOH (**4**·Et$_2$O·MeOH), [(4-TIP^{iPr})CoCl]Cl·MeOH·2.5H$_2$O (**5**·MeOH·2.5H$_2$O), and [(4-TIP^{iPr})ZnCl]Cl·MeOH·2.5H$_2$O (**6**·MeOH·2.5H$_2$O) have been determined. The complex **3** shows striking structural similarities to the hydrogencarbonate complex of cobalt-substituted human carbonic anhydrase II (HCA II).

(© Wiley-VCH Verlag GmbH & Co. KGaA, 69451 Weinheim, Germany, 2003)

Introduction

In mammalian carbonic anhydrases (CAs) and many other metalloenzymes, the metal-binding site is formed by histidine imidazole rings.[1] In HCA II the three histidine residues His-94, His-96, and His-119 complete a tetrahedral coordination geometry around a Zn−X moiety.

The hydrotris(pyrazolyl)borates (Tp$^{R,R'}$) are the best known of the structural model ligands (Figure 1).[2−4] Their complexes have many of the structural and spectroscopic properties of the active sites of metalloenzymes, though these compounds have been studied mainly in nonprotic solvents, due to the vulnerability of the Tp ligands towards hydrolysis. Attempts to substitute the B−N bonds, to yield more stable ligands, have been made. We have recently re-

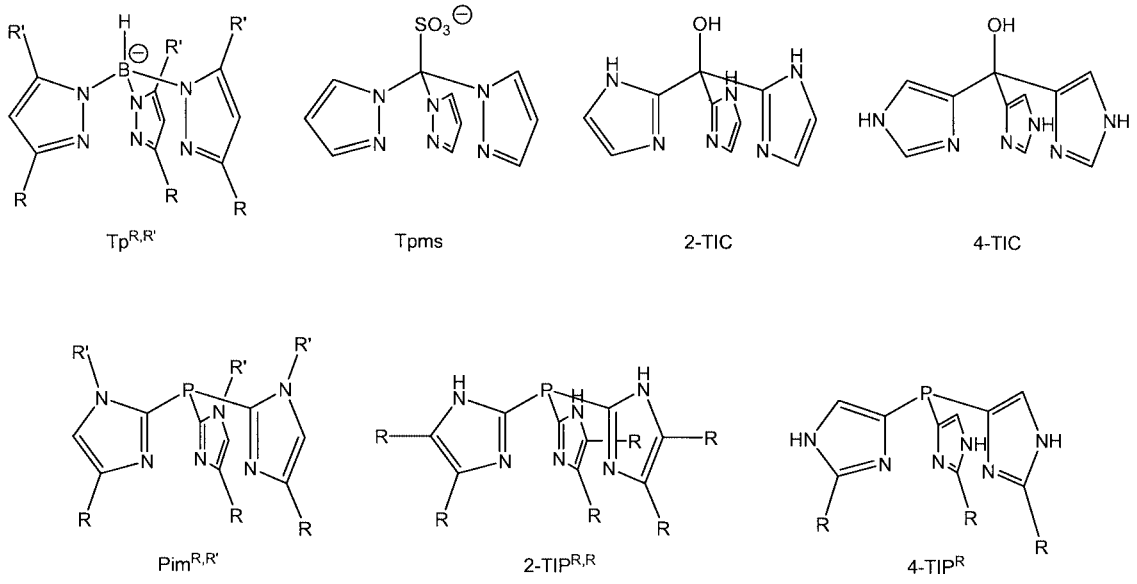

Figure 1. Schematic structures of the novel model ligand 4-TIP^{R} and of related tripodal nitrogen ligands based on pyrazoles and imidazoles

[a] Institut für Anorganische Chemie und Strukturchemie der Heinrich-Heine-Universität Düsseldorf,
Universitätsstr. 1, 40225 Düsseldorf, Germany
Fax: (internat.) + 49-211/8112287
E-mail: klaeui@uni-duesseldorf.de

ported on tris(pyrazolyl)methanesulfonate (Tpms) as a water-soluble Tp-like ligand.[5]

Imidazole ligands should model the actual binding site even better than pyrazole ligands. Attachment of imidazole rings at the 2-position to a molecular framework by the use of 2-lithioimidazoles is relatively simple. In nature, though, the imidazole ring is attached to the histidine side chain through the 4(5)-position. In the early 1980s, Breslow and co-workers synthesized a number of tripodal ligands bearing imidazolyl groups. Tris(imidazol-2-yl)carbinol (2-TIC) and tris(imidazol-4-yl)carbinol (4-TIC), together with M^{2+} complexes (M = Zn, Co) of these ligands, were synthesized as models for the zinc binding site of carbonic anhydrase and alkaline phosphatase.[6,7] Because of the small steric demand of these ligands, however, bis(ligand) formation could not be prevented. Attempts to introduce bulky substituents in the 2-position of 4-TIC resulted in the formation of fulvene-like dehydration products.[7,8]

From Carbinol to Phosphane

Tris(imidazolyl)phosphanes seem to be suitable *N*,*N*,*N*-ligands as models for the active site of the facial His triad in zinc-containing enzymes.[9] Substitution of the central carbinol unit by a phosphorus atom circumvents the dehydration reaction. We have recently reported on tris([2-(1-methyl-4-tolylimidazolyl)]phosphane ($Pim^{Me,pTol}$) and its zinc complexes as structural models of the active site of carbonic anhydrase.[10] The aromatic substituents of this ligand form a hydrophobic cavity around the metal centre and, unlike in the larger substituents, such as the tris(4-*tert*-butyl-1-isopropylimidazol-2-yl)phosphane ($Pim^{iPr,tBu}$),[9] the smaller methyl group in the 1-position provides better solubility in polar solvents.

By this concept, the next step would be not to have any substituent in the 1-position. However, the resulting tris[4(5)-organylimidazol-2-yl]phosphane would undergo prototropic shift reactions. All of the resulting tautomeric forms, after rotation around the phosphorus−carbon bonds, could act as tripodal nitrogen ligands, but with different orientations of the substituents R (Scheme 1).

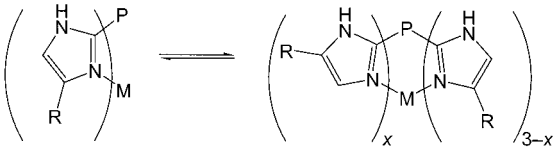

Scheme 1. The different tautomeric forms of tris[4(5)-organylimidazol-2-yl]phosphane; x = 0, 1, 2

This problem can be circumvented by symmetric disubstitution in the 4- and 5-positions of the imidazolyl rings (2-$TIP^{R,R}$),[11] but the introduction of three additional bulky substituents makes these ligands insoluble in protic solvents. To solve this problem we designed an isomeric ligand type, the tris[2-organylimidazol-4(5)yl]phosphanes (4-TIP^{R}s).[12] Here, the prototropic equilibrium and the rotation around the phosphorus−carbon bonds also creates a series of ligands with different binding modes, but only one can now act as a tripodal ligand and here all three substituents R form the desired hydrophobic cavity around the metal ion (Scheme 2).

Below we report on the synthesis of the first member of this class of ligands and of its coordination chemistry toward cobalt, nickel and zinc ions.

Results and Discussion

Synthesis and Spectroscopic Characterisation

2-Isopropylimidazole was protected with an easily removable diethoxymethyl group. In the following step the protected imidazole **1** was lithiated in the 5-position and was then treated with PCl_3 in diethyl ether at −78 °C. Tris[2-isopropylimidazol-4(5)-yl]phosphane (4-TIP^{iPr}, **2**) was isolated as a colourless solid after removal of the protective group (Scheme 3).

The ^{1}H NMR spectrum of **2** in [D_4]methanol shows the expected C_{3v} symmetry of the ligand. The isopropyl groups show a doublet at δ = 1.32 ppm and a septuplet at δ = 3.09 ppm, the signal at δ = 7.00 ppm being assigned to the protons of the imidazolyl rings. In the ^{31}P{^{1}H} NMR spectrum the ^{31}P signal appears as a singlet at δ = −80 ppm. The EI mass spectrum of **2** shows the peak for the molecular ion at the expected *m*/*z* value, together with a characteristic fragmentation pattern.

Cobalt, nickel, and zinc complexes were prepared in high yield by stirring the ligand **2** with the corresponding metal salts in wet methanol at ambient temperature (Scheme 4). The nitrato complexes [(4-TIP^{iPr})M(MeOH)(NO_3)]NO_3 form as violet (**3**) (M = Co) and as grass-green (**4**) (M = Ni) needles, while the chloro complexes [(4-TIP^{iPr})MCl]Cl form as deep blue rhombic (**5**) (M = Co) and colourless crystals (**6**) (M = Zn) by diffusion-controlled crystallisation from diethyl ether in methanolic solutions of the complexes.

The ^{1}H NMR spectrum of **6** has a doublet at δ = 1.39 ppm and a septuplet at δ = 3.62 ppm for the isopropyl groups and a doublet at δ = 7.55 with a $^1J_{PH}$ coupling constant of 2 Hz for the imidazolyl ring protons. The signals of the methyl protons of the isopropyl group show no

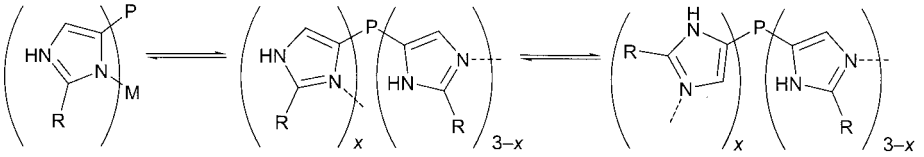

Scheme 2. Of all tris(2-organylimidazol-4(5)yl)phosphanes (4-TIP^{R}s), only one form can act as a tripodal ligand

 © 2003 Wiley-VCH Verlag GmbH & Co. KGaA, Weinheim

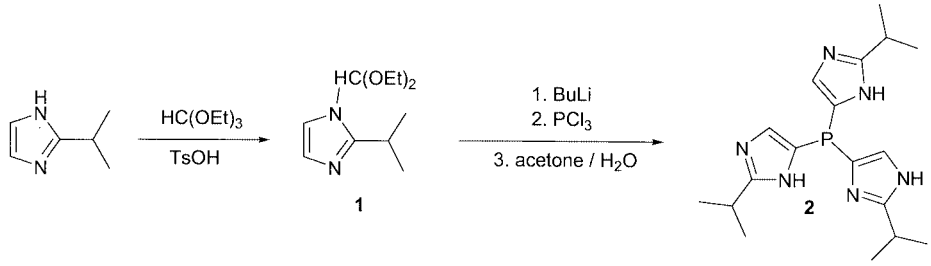

Scheme 3. Synthesis of tris[2-isopropylimidazol-4(5)-yl]phosphane (4-TIP^{iPr}, **2**) from 2-isopropylimidazole

Scheme 4. Synthesis of the nitrato (**3**, **4**) and chloro complexes (**5**, **6**)

significant shift upon coordination, whereas the methine proton of the isopropyl groups and the imidazolyl protons are shifted by about 0.5 ppm to lower field. Upon coordination the ^{31}P NMR signal of the Zn complex **6** is shifted to higher field ($\delta = -106$ ppm), whereas the ^{31}P NMR signals of the cobalt and nickel complexes are shifted to lower field (**3**: $\delta = +27$ ppm; **4**: $\delta = -40$ ppm; **5**: $\delta = -54$ ppm). The NMR spectra of the Co^{II} and Ni complexes show paramagnetic broadening. The FAB mass spectra of all complexes exhibit the peaks for the molecular ions at the expected *m*/*z* values, together with characteristic fragmentation patterns.

The IR spectra of the complexes in nujol and in fluorolube show the characteristic bands of the ligand. Upon preparation of the KBr pellet, the colour of the pellet of the Co^{II} complex turned from violet to deep blue and that of the Ni^{II} complex from green to red. This phenomenon is interpreted in terms of ligand exchange of NO_3^- with Br^- and a simultaneous change in coordination number from 6 to 4 [Equation (1)].

$$[(4\text{-TIP}^{iPr})M(MeOH)(NO_3)]^+ + KBr \rightarrow [(4\text{-TIP}^{iPr})MBr]^+ \quad (1)$$

This interpretation was confirmed by UV/Vis spectra of 1 mM methanolic solutions of **3** saturated with NaX (X = F^-, Cl^-, Br^-, I^-, N_3^-, OAc^-) (Figure 2). The spectrum of $[(4\text{-TIP}^{iPr})Co]^{2+}$ is markedly dependent upon the presence of added anions, indicating association of monovalent anions with the metal ion.

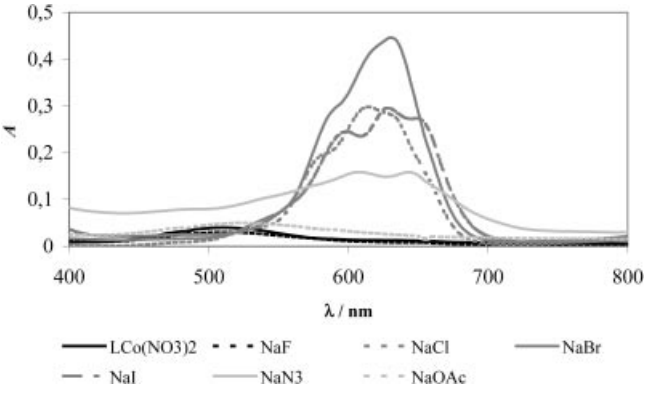

Figure 2. UV/Vis spectra of 1 mM methanolic solutions of **3** saturated with NaX (X = F^-, Cl^-, Br^-, I^-, N_3^-, OAc^-)

Solid-State Structures

The solid state structures of **3**, **4**, **5**, and **6** were determined by crystal structure analysis. The complexes crystallise from wet methanol/diethyl ether. The nitrato complex **3**·2Et_2O crystallises in the triclinic space group $P\bar{1}$, **4**·Et_2O·MeOH in the monoclinic space group $P2_1/c$. The central metal ions in the nitrato complexes are each coordinated facially by three N donor atoms of the 4-TIP^{iPr} li-

 © 2003 Wiley-VCH Verlag GmbH & Co. KGaA, Weinheim

gand, in bidentate fashion by the nitrato ligand, and by a methanol molecule to complete the distorted octahedral coordination geometry. Interestingly, the crystal structures each show the expected hydrogen bonds of the imidazolyl N−H protons to solvent molecules. Figure 3 shows an ORTEP plot of **3**·2Et_2O. Selected bond lengths and angles are summarised in Tables 1 and 2.

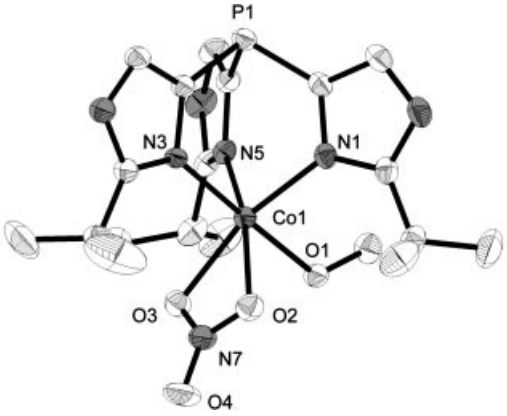

Figure 3. Structure of the cation [(4-TIP^{iPr})Co(HOMe)(NO_3)]$^+$ in **3**·2Et_2O; displacement ellipsoids are shown at the 20% probability level and H atoms are omitted for clarity

Table 1. Selected bond lengths [Å] and angles [°] for [(4-TIP^{iPr})Co(MeOH)(NO_3)]NO_3·2Et_2O (**3**·2Et_2O)

Co1−N1	2.092(3)	Co1−O1	2.167(2)
Co1−N3	2.140(3)	Co1−O2	2.168(3)
Co1−N5	2.096(3)	Co1−O3	2.149(3)
N7−O2	1.271(4)	N7−O3	1.273(4)
N7−O4	1.211(4)		
N1−Co1−N3	88.69(10)	N1−Co1−N5	92.47(12)
N3−Co1−N5	88.50(10)	N1−Co1−O1	90.29(10)
N1−Co1−O2	103.57(12)	N1−Co1−O3	162.76(12)
N3−Co1−O1	178.22(10)	N3−Co1−O2	97.56(10)
N3−Co1−O3	97.29(10)	N5−Co1−O1	90.09(10)
N5−Co1−O2	162.92(12)	N5−Co1−O3	103.79(11)
O1−Co1−O2	84.09(10)	O1−Co1−O3	84.10(10)
O2−Co1−O3	59.70(11)	O2−N7−O3	115.3(3)
O2−N7−O4	122.0(4)	O3−N7−O4	122.8(4)
N7−O2−Co1	92.1(2)	N7−O3−Co1	92.9(2)

The tripodal ligand is bound facially with non-equivalent M−N bond lengths. The M−N bond *trans* to methanol is slightly longer than the M−N bond *trans* to the nitrato ligand [**3**: *d*(Co−N) *trans* to NO_3 ≈ 2.10 Å, *d*(Co−N) *trans* to MeOH = 2.140(3) Å; **4**: *d*(Ni−N) *trans* to NO_3 ≈ 2.04 Å, *d*(Ni−N) *trans* to MeOH ≈ 2.101(3) Å]. Similar behaviour is observed for the M−O bond lengths. The differences in M−O bond lengths and dihedral angles of the NO_3 ligand indicate a bidentate coordination mode ($\Delta d \approx 0.02$ Å; $\Delta\theta$(N−O−M) ≈ 1°).[13]

The chloro complexes **5**·MeOH·2.5H_2O and **6**·MeOH·2.5H_2O crystallise in the monoclinic space group *C2/m*. Figure 4 shows an ORTEP plot of **5**·MeOH·2.5H_2O. Selected bond lengths and angles are summarised in Tables 3 and 4.

Table 2. Selected bond lengths [Å] and angles [°] for [(4-TIP^{iPr})Ni(MeOH)(NO_3)]NO_3·Et_2O·MeOH (**4**·Et_2O·MeOH)

Ni1−N1	2.037(3)	Ni1−O1	2.149(2)
Ni1−N3	2.034(3)	Ni1−O2	2.125(3)
Ni1−N5	2.104(3)	Ni1−O3	2.127(3)
N7−O2	1.264(4)	N7−O3	1.276(4)
N7−O4	1.212(4)		
N1−Ni1−N3	96.23(11)	N1−Ni1−N5	88.41(11)
N3−Ni1−N5	89.48(11)	N1−Ni1−O1	87.69(10)
N1−Ni1−O2	101.92(11)	N1−Ni1−O3	162.03(11)
N3−Ni1−O1	85.74(10)	N3−Ni1−O2	160.42(11)
N3−Ni1−O3	100.68(11)	N5−Ni1−O1	173.47(10)
N5−Ni1−O2	98.23(11)	N5−Ni1−O3	97.73(11)
O1−Ni1−O2	87.70(10)	O1−Ni1−O3	87.54(10)
O2−Ni1−O3	60.58(10)	O2−N7−O3	115.3(3)
O2−N7−O4	123.3(4)	O3−N7−O4	121.5(4)
N7−O2−Ni1	92.3(2)	N7−O3−Ni1	91.8(2)

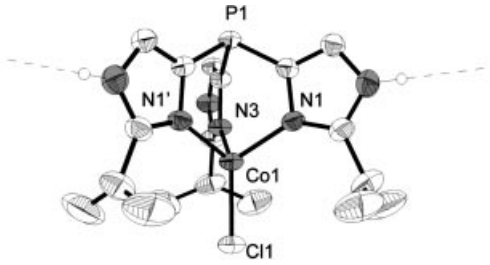

Figure 4. Structure of [(4-TIP^{iPr})CoCl]$^+$ in **5**·MeOH·2.5H_2O; displacement ellipsoids are shown at the 20% level; only the NH hydrogen atoms are shown, others are omitted for clarity; dashed lines indicate the NH−Cl hydrogen bond to the counter-ions in the solid

Table 3. Selected bond lengths [Å] and angles [°] for [(4-TIP^{iPr})CoCl]Cl·MeOH·2.5H_2O (**5**·MeOH·2.5H_2O)

Co1−N1	1.994(4)	Co1−N3	2.013(5)
Co1−Cl1	2.1870(15)		
N1−Co1−N1′	96.0(2)	N1−Co1−Cl1	121.67(9)
N1−Co1−N3	96.21(12)	N3−Co1−Cl1	119.00(13)

Table 4. Selected bond lengths [Å] and angles [°] for [(4-TIP^{iPr})ZnCl]Cl·MeOH·2.5H_2O (**6**·MeOH·2.5H_2O)

Zn1−N1	2.003(4)	Zn1−N3	1.994(6)
Zn1−Cl1	2.160(2)		
N1−Zn1−N1′	92.9(3)	N1−Zn1−Cl1	123.40(13)
N1−Zn1−N3	94.49(16)	N3−Zn1−Cl1	120.47(17)

In the chloro complexes **5**·MeOH·2.5H_2O and **6**·MeOH·2.5H_2O the central metal ion is coordinated tetrahedrally by the 4-TIP^{iPr} ligand and by one of the chloride ions. The angles around the central metal ion deviate significantly from tetrahedral angles; the N−M−Cl angles are larger (119−123°) and the N−M−N angles are smaller (93−96°). In the crystal of **5**·MeOH·2.5H_2O and **6**·MeOH·2.5H_2O, the imidazolyl N−H atoms of the cations

 © 2003 Wiley-VCH Verlag GmbH & Co. KGaA, Weinheim

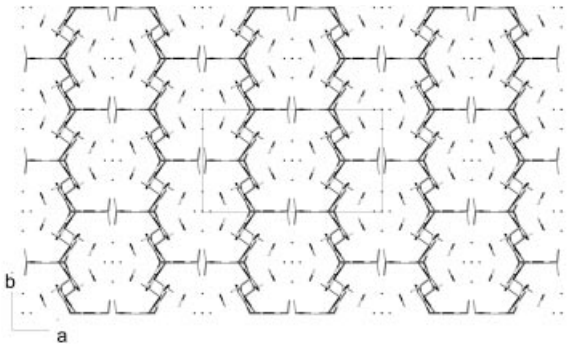

Figure 5. Molecular packing diagram of **5**·MeOH·2.5H_2O; view along the *c* axis; positions of the methanol and water molecules are represented by sticks and single balls; some are partially occupied

form hydrogen bonds to the chloride counter-ion. This results in the formation of hexagonal tubular structures (see Figure 5), filled with solvent molecules showing substantial disorder.

The bond lengths and angles of **6** do not differ significantly from those observed in the X-ray structure of dichloro[tris(4,5-diisopropylimidazol-2-yl)phosphane]zinc(II) bis(*N*,*N*-dimethylformamide).[11b]

The isopropyl groups in all complexes take up a conformation in which the methyl groups point away form the metal centre and the methine protons are oriented towards the metal centre. If this is also the favoured conformation in solution, this would explain the shift of the methine protons in the ^{1}H NMR spectrum of the zinc complex **6**.

Conclusion

We have synthesized the new tris(imidazolyl)phosphane ligand 4-TIP$^{i\mathrm{Pr}}$, which to the best of our knowledge is the first representative of tris[imidazol-4(5)-yl]phosphane ligands. These ligands possess all the minimum features a CA model compound should have: (i) large substituents around the metal centre to suppress bis(ligand) formation and model a hydrophobic cavity, (ii) sufficient solubility in aqueous solvents, and (iii) stability towards hydrolysis.

In 1992, Håkansson and Wehnert reported on the structure of cobalt carbonic anhydrase bearing a hydrogencarbonate ligand.[14] They found that the Co^{II} ion is coordinated by three histidyl ligands of the enzyme, one water molecule and two oxygen atoms of hydrogencarbonate. The structure of **3** shows exactly this motif: Co^{II} is coordinated in a distorted octahedral fashion by the three imidazolyl groups, methanol and two oxygen atoms of nitrate. In **3** we therefore observe a structure in which the coordinated water ligand of the active site of Co^{II}-CA is substituted by methanol and hydrogencarbonate is replaced by the isoelectronic nitrate.

Experimental Section

General: The preparation of the ligand **2** was carried out in Schlenk tubes under dry nitrogen with use of anhydrous solvents purified by standard procedures. The metal complexes were prepared with use of wet solvents. Crystals suitable for X-ray structure analysis were prepared by slow diffusion of diethyl ether into solutions of the complexes in wet methanol. All chemicals were used as purchased. ^{1}H and ^{31}P NMR spectra were recorded with a Bruker DRX 200 spectrometer. The ^{1}H and ^{13}C{^{1}H} NMR spectra were calibrated against the residual proton signals and the carbon signals of the solvents as internal references ([D_1]chloroform: δ_H = 7.30 ppm and δ_C = 77.0 ppm; [D_4]methanol: δ_H = 5.84 ppm and δ_C = 49.1 ppm), while the ^{31}P{^{1}H} NMR spectra were referenced to external 85% H_3PO_4. The EI mass spectra were recorded with a double focussing mass spectrometer, model 311 A Varian MAT, ionisation energy 70 eV. The FAB mass spectra were recorded with a Finnigan mass spectrometer, model MAT 8200, in an NBA matrix. Infrared spectra were recorded with a Bruker IFS 66 FT-IR spectrometer.

Synthesis of *N*-(Diethoxymethyl)-2-isopropylimidazole (1): 2-Isopropylimidazole (22 g, 0.2 mol), triethyl orthoformate (120 g, 0.8 mol), and *p*-toluenesulfonic acid (1 g) were heated at 130 °C for 24 h. Ethanol and excess orthoformate were removed in vacuo, solid Na_2CO_3 (1 g) was added, and the residue was fractionally distilled to yield a colourless oil (26 g, 62%). b.p. 65 °C ($2\cdot10^{-2}$ mbar). ^{1}H NMR ($CDCl_3$, 200 MHz, ppm): δ = 1.13 (t, *J* = 6.8 Hz, 6 H, CH_2CH_3), 1.24 [d, *J* = 6.8 Hz, 6 H, $CH(CH_3)_2$], 3.03 [sept, *J* = 6.8 Hz, 1 H, $CH(CH_3)_2$], 3.3−3.6 (m, 4 H, CH_2CH_3), 5.94 [s, 1 H, $CH(OEt)_2$], 6.83 (d, *J* = 1.3 Hz, 1 H, 4-*H* im), 6.98 (d, *J* = 1.3 Hz, 1 H, 5-*H* im). ^{13}C NMR ($CDCl_3$, 500 MHz, ppm): δ = 15.2 (CH_3CH_2), 22.4 [$(CH_3)_2CH$], 27.0 [$(CH_3)_2CH$], 62.0 (CH_3CH_2), 101.2 [$CH(OEt)_2$], 116.3 (C5 im), 127.2 (C4 im), 153.1 (C2 im). EI MS (70 eV, 30 °C): *m*/*z* (%) = 212 (3) $[M]^+$, 167 (11) $[M - OEt]^+$, 103 (99) $[HC(OEt)_2]^+$.

Synthesis of Tris[2-isopropylimidazol-4(5)-yl]phosphane (4-TIP$^{i\mathrm{Pr}}$) (2): *n*-Butyllithium in hexane (1.6 M, 33 mL, 53 mmol) was added at −78 °C to a solution of **1** (10.6 g, 50.0 mmol) in diethyl ether (300 mL). The solution was stirred at −78 °C for 30 min and additionally at room temperature for 30 min. After the mixture had been cooled to −78 °C, PCl_3 (1.49 mL, 16.7 mmol) in diethyl ether (10 mL) was added. The white suspension was stirred at room temperature overnight, concd. aqueous ammonia (75 mL) was added, and the organic layer was separated, washed with water, and dried with $MgSO_4$. After removal of the solvent, the oily residue was redissolved in acetone/water (10:1, 100 mL) and heated to reflux for 12 h. The resulting white precipitate was collected and recrystallized from methanol/acetone. Yield: 2.1 g (35%). ^{1}H NMR (200 MHz, [D_4]methanol, ppm): δ = 1.32 [d, *J* = 7 Hz, 6 H, $CH(CH_3)_2$], 3.09 [sept, 1 H, *J* = 7 Hz, $CH(CH_3)_2$], 7.00 (s, 1 H, H_{im}). ^{31}P{^{1}H} NMR (200 MHz, [D_4]methanol, ppm): δ = −80. EI MS (70 eV, 250 °C): *m*/*z* (%) = 358 (30) $[M]^+$, 249 (38) $[M - im^iPr]^+$. $C_{18}H_{27}N_6P_3\cdot H_2O$ (374.42): calcd. C 57.4, H 7.7, N 22.3; found C 58.5, H 7.4, N 22.4.

Synthesis of [(4-TIP$^{i\mathrm{Pr}}$)Co(NO_3)(MeOH)](NO_3) (3): A methanolic solution of **2** (180 mg, 50.0 μmol) and $Co(NO_3)_2\cdot6H_2O$ (145 mg, 50.0 μmol) was stirred for 2 h, diethyl ether was added, and the violet precipitate was washed with additional diethyl ether and dried in vacuo. Yield: 0.23 g (85%). ^{31}P{^{1}H} NMR (200 MHz, [D_4]methanol, ppm): δ = 27 ($h_{1/2}$ = 49 Hz). FAB^+ MS (NBA matrix): *m*/*z* (%) = 479 (100) $[(4\text{-}TIP^{i\mathrm{Pr}})Co(NO_3)]^+$, 416 (46) $[(4\text{-}TIP^{i\mathrm{Pr}})Co - H]^+$. $C_{19}H_{30}CoN_8O_7P_3\cdot H_2O$ (591.43): calcd. C 38.6, H 5.6, N 18.9; found C 38.3, H 5.5, N 18.3.

Synthesis of [(4-TIP$^{i\mathrm{Pr}}$)Ni(NO_3)](NO_3) (4): A methanolic solution of **2** (180 mg, 50.0 μmol) and $Ni(NO_3)_2\cdot6H_2O$ (145 mg, 50.0 μmol)

 © 2003 Wiley-VCH Verlag GmbH & Co. KGaA, Weinheim

was stirred for 2 h, diethyl ether was added, and the green precipitate was washed with additional diethyl ether and dried in vacuo. Yield: 0.22 g (65%). $^{31}P\{^1H\}$ NMR (200 MHz, [D$_4$]methanol, ppm): δ = −40 (HWB = 138 Hz). FAB$^+$ MS (NBA-matrix): *m*/*z* (%) = 478 (100) [(4-TIP^{iPr})Ni(NO$_3$)]$^+$. $C_{19}H_{30}N_8NiO_7P_3$·3MeOH (669.30): calcd. C 39.5, H 6.5, N 16.7; found C 41.2, H 6.1, N 16.5.

[(4-TIP^{iPr})CoCl]Cl (5): A methanolic solution of **2** (180 mg, 50.0 μmol) and $CoCl_2$ (65 mg, 50.0 μmol) was stirred for 2 h, diethyl ether was added, and the violet precipitate was washed with additional diethyl ether and dried in vacuo. Yield: 0.18 g (65%). $^{31}P\{^1H\}$ NMR (200 MHz, [D$_4$]methanol, ppm): δ = −54 ($h_{1/2}$ = 91 Hz). FAB$^+$ MS (NBA matrix): *m*/*z* (%) = 479 (100) [(4-TIP^{iPr})CoCl]$^+$, 416 (8) [(4-TIP^{iPr})Co − H]$^+$. $C_{18}H_{27}Cl_2CoN_6P_3$·MeOH·H$_2$O (538.32): calcd. C 45.3, H 6.5, N 15.1; found C 45.4, H 6.2, N 14.6.

[(4-TIP^{iPr})ZnCl]Cl (6): A methanolic solution of **2** (180 mg, 50.0 μmol) and $ZnCl_2$ (68 mg, 50.0 μmol) was stirred for 2 h, diethyl ether was added, and the colourless precipitate was washed with additional diethyl ether and dried in vacuo. Yield: 0.10 g (40%). ^1H NMR (200 MHz, [D$_4$]methanol, ppm): δ = 1.39 [d, *J* = 7 Hz, 6 H, CH(C*H*$_3$)$_2$], 3.62 [sept, *J* = 7 Hz, 1 H, C*H*(CH$_3$)$_2$], 7.55 (d, J_{PH} = 2 Hz, 1 H, H$_{im}$). $^{13}C\{^1H\}$ NMR (500 MHz, [D$_4$]methanol, ppm): δ = 21.7 [CH(*C*H$_3$)$_2$], 29.3 [*C*H(CH$_3$)$_2$], 104.3, 125.6 (d, *J* = 56 Hz), 133.3, 159.9 (*C*2$_{im}$). $^{31}P\{^1H\}$ NMR (200 MHz, [D$_4$]methanol, ppm): δ = −106 ($h_{1/2}$ = 3 Hz). FAB$^+$ MS (NBA matrix): *m*/*z* (%) = 457 (100) [(4-TIP^{iPr})ZnCl]$^+$. $C_{18}H_{27}Cl_2ZnN_6P$·MeOH (526.76): calcd. C 43.5, H 5.9, N 16.0; found C 43.1, H 5.7, N 16.4.

X-ray Crystallographic Study: Crystal structure determinations of compounds **3**·2Et$_2$O, **4**·Et$_2$O·MeOH, **5**·MeOH·2.5H$_2$O, and **6**·MeOH·2.5H$_2$O: Crystals suitable for X-ray study were selected by use of a polarisation microscope and investigated with area detector diffractometers by use of graphite-monochromatized Mo-K_α radiation (λ = 0.71073 Å). Unit cell parameters were determined by least-squares refinements on the positions of 6449, 3557, 8000, and 8000 reflections in the range 4° < θ < 25.1°, 4° < θ < 25.5°, 2° < θ < 22.9°, and 2° < θ < 25.8°, respectively. For **3**·2Et$_2$O, $P\bar{1}$ was confirmed to be the correct one of the two triclinic space groups in the course of refinement. Space group type no. 14 was uniquely determined in the case of **4**·Et$_2$O·MeOH. For the isotypical compounds **5**·MeOH·2.5H$_2$O and **6**·MeOH·2.5H$_2$O, systematic extinctions were consistent with space group types *I*2, *Im*, and *I*2/*m*. In accordance with E-statistics, significantly better results were

Table 5. Crystal data for **3**·2*E*t$_2$O, **4**·Et$_2$O·MeOH, **5**·MeOH·2.5H$_2$O, and **6**·MeOH·2.5H$_2$O

	3·2Et$_2$O	**4**·Et$_2$O·MeOH	**5**·MeOH·2.5H$_2$O	**6**·MeOH·2.5H$_2$O
Empirical formula	$C_{27}H_{51}CoN_8O_9P$	$C_{24}H_{45}N_8NiO_9P$	$C_{19}H_{36}Cl_2CoN_6O_{3.5}P$	$C_{19}H_{36}Cl_2N_6O_{3.5}PZn$
M_r	721.66	679.36	565.34	571.78
Crystal system	triclinic	monoclinic	monoclinic	monoclinic
Space group	$P\bar{1}$	$P2_1/c$	*C*2/*m*	*C*2/*m*
Z	2	4	4	4
Temperature [K]	293	293	293	293
Unit cell dimensions				
a [Å]	10.1416(10)	16.738(3)	20.8949(19)	20.962(4)
b [Å]	12.4194(11)	12.3251(15)	11.5197(13)	11.4751(19)
c [Å]	15.5836(16)	17.523(3)	15.1453(14)	15.056(3)
α [°]	91.649(8)	90	90	90
β [°]	100.255(8)	106.020(14)	103.825(11)	103.82(2)
γ [°]	94.649(8)	90	90	90
Volume [Å^3]	1923.2(3)	3474.6(8)	3539.9(6)	3516.7(11)
$D_{calcd.}$	1.246	1.299	1.061	1.080
Absorption coefficient	0.542	0.660	0.706	0.921
F(000)	766	1440	1184	1196
Crystal size [mm]	0.4 × 0.35 × 0.3	0.45 × 0.4 × 0.3	0.35 × 0.35 × 0.35	0.32 × 0.35 × 0.35
Crystal colour	violet	green	blue	colourless
Diffractometer type	Stoe-CCD	Stoe-CCD	Stoe-IPDS	Stoe-IPDS
Crystal−detector distance [mm]	80	80	70	70
Scan mode	ω (21 runs)	ω (21 runs)		
Θ range for data collection [°]	4.08−25.05	4.09−25.50	2.15−24.99	2.15−24.99
Limiting indices	$-12 < h < 12$	$-20 < h < 20$	$-24 < h < 24$	$-23 < h < 24$
	$-14 < k < 14$	$-14 < k < 14$	$-13 < k < 13$	$-13 < k < 13$
	$-18 < l < 18$	$-21 < l < 21$	$-18 < l < 18$	$-17 < l < 17$
Reflections collected	26584	47473	22973	12328
Reflections unique	6765	6420	3263	3201
Reflections observed	5417	5097	2341	1426
Criterion for observation	$I > 2\sigma(I)$	$I > 2\sigma(I)$	$I > 2\sigma(I)$	$I > 2\sigma(I)$
Completeness	0.994	0.995	0.992	0.978
Refined parameters	425	397	183	183
R_1[a], observed	0.0614	0.0633	0.0533	0.0574
wR_2[b], all data	0.1268	0.1158	0.1298	0.1398
Goodness-of-fit, *S*[c]	1.018	1.037	1.097	1.087
Largest diff. peak/hole	0.75/−0.43	0.61/−0.32	0.32/−0.23	0.57/−0.40
CCDC identifier	208101	208102	208099	208100

[a] $R_1 = ||F_o| - |F_c||/|F_o|$. [b] $wR_2 = \{w(F_o^2 - F_c^2)^2/w(F_o^2)^2]^{1/2}\}$, where $w = 1/[\sigma^2(F_o^2) + (aP^2)]$ and $P = (F_o^2 + 2F_c^2)/3$. [c] $S = [w(F_o^2 - F_c^2)^2/(n - p)]^{1/2}$.

 © 2003 Wiley-VCH Verlag GmbH & Co. KGaA, Weinheim

observed for disordered models in the centrosymmetric type *I*2/*m*. All data sets were corrected for Lorentz and polarization effects. The structures were solved by direct methods[15] and subsequent ΔF-syntheses. Approximate positions of the hydrogen atoms of all the complex cations were found in different stages of the refinements by full-matrix, least-squares calculations on F^2.[16] The hydrogen atom positions of the uncoordinated solvent molecules needed to be calculated with account being taken of plausible hydrogen bonding. In all cases refinements suffered from the high mobility of the incorporated solvent molecules, and appropriate distance and displacement parameter restraints and constraints had to be applied in order to achieve convergence. Anisotropic displacement parameters were refined for all atoms heavier than hydrogen, with the exception of the carbon and oxygen atoms of the highly mobile solvent molecules of **5**·MeOH·2.5H_2O and **6**·MeOH·2.5H_2O. For the OH group of the methanol molecule of **3**·2Et_2O a weak O−H bond length restraint was applied and the isotropic displacement parameter of the H atom were refined. With idealised bond lengths and angles assumed for the CH_3, CH_2, CH, NH groups of all the compounds, as well as for the methanol and water molecules of **4**·Et_2O·MeOH, **5**·MeOH·2.5H_2O, and **6**·MeOH·2.5H_2O, the riding model was applied for the H atoms. In addition, the H atoms of the CH_3 groups of **3**·2Et_2O and **4**·Et_2O·MeOH were allowed to move collectively around the neighbouring C−C axis. In the case of **4**·Et_2O·MeOH the H atoms of the OH groups of the methanol molecules were also given allowance for rotation around the neighbouring O−C axis. Isotropic displacement parameters of H atoms were kept equal to 120% of the equivalent isotropic displacement parameters of the parent O, N, and C atoms for the NH, CH, and CH_2 groups and equal to 150% for the CH_3 groups, the water molecules and the OH group of the methanol molecule in **4**·Et_2O·2MeOH. Scattering factors, dispersion corrections and absorption coefficients were taken from International Tables for Crystallography (1992, vol. C, Tables 6.114, 4.268, and 4.2.4.2). Details are listed in Table 5. CCDC-208099 to -208102 contain the supplementary crystallographic data for this paper. These data can be obtained free of charge at www.ccdc.cam.ac.uk/conts/retrieving.html [or from the Cambridge Crystallographic Data Centre, 12 Union Road, Cambridge CB2 1EZ, UK; Fax: (internat.) + 44-1223/336-033; E-mail: deposit@ccdc.cam.ac.uk].

Acknowledgments

We thank the Deutsche Forschungsgemeinschaft (DFG) and the Fonds der Chemischen Industrie for financial support.

[1] D. W. Christianson, C. A. Fierke, *Acc. Chem. Res.* **1996**, *29*, 331−339; S. Lindskog, *Pharmacol. Ther.* **1997**, *74*, 1−20.
[2] S. Trofimenko, *Scorpionates − The Coordination Chemistry of Polypyrazolylborate Ligands*, Imperial College Press, London, **1999** and references therein.
[3] G. Parkin, *Chem. Commun.* **2000**, 1971−1985.
[4] H. Vahrenkamp, *Acc. Chem. Res.* **1999**, *32*, 589−596.
[5] [5a] W. Kläui, M. Berghahn, G. Rheinwald, H. Lang, *Angew. Chem.* **2000**, *112*, 2590−2592; *Angew. Chem. Int. Ed.* **2000**, *39*, 2464−2466. [5b] W. Kläui, M. Berghahn, W. Frank, G. J. Reiß, T. Schönherr, G. Rheinwald, H. Lang, *Eur. J. Inorg. Chem.* **2003**, *10*, 2059−2070.
[6] C. C. Tang, D. Davalian, P. Huang, R. Breslow, *J. Am. Chem. Soc.* **1978**, *100*, 3918−3922.
[7] R. Breslow, J. T. Hunt, R. Smiley, T. Tarnowski, *J. Am. Chem. Soc.* **1983**, *105*, 5337−5342.
[8] Similar problems have been observed in the attempted preparation of 4,5-disubstituted tris(imidazol-2-yl)carbinols: R. S. Brown, J. Huguet, *Can. J. Chem.* **1980**, *58*, 889−901.
[9] [9a] C. Kimblin, W. E. Allen, G. Parkin, *Chem. Commun.* **1995**, 1813−1815. [9b] C. Kimblin, V. J. Murphy, G. Parkin, *Chem. Commun.* **1996**, 235−236. [9c] C. Kimblin, B. M. Bridgewater, D. G. Churchill, G. Parkin, *J. Chem. Soc., Dalton Trans.* **2000**, 2191−2194. [9d] C. Kimblin, V. J. Murphy, T. Hascall, B. M. Bridgewater, J. B. Bonanno, G. Parkin, *Inorg. Chem.* **2000**, *39*, 967−974.
[10] W. Kläui, C. Piefer, G. Rheinwald, H. Lang, *Eur. J. Inorg. Chem.* **2000**, *7*, 1549−1555.
[11] [11a] J. Huguet, R. S. Brown, *J. Am. Chem. Soc.* **1980**, *102*, 7572−7574. [11b] R. J. Read, M. N. G. James, *J. Am. Chem. Soc.* **1981**, *103*, 6947−6952. [11c] R. S. Brown, N. J. Curtis, J. Huguet, *J. Am. Chem. Soc.* **1981**, 6953−6959. [11d] R. S. Brown, D. Salmon, N. J. Curtis, S. Kusuma, *J. Am. Chem. Soc.* **1982**, *104*, 3188−3194. [11e] R. S. Brown, M. Zamkani, J. L. Cocho, *J. Am. Chem. Soc.* **1984**, *106*, 5222−5228. [11f] R. G. Ball, R. S. Brown, J. L. Cocho, *Inorg. Chem.* **1984**, *23*, 2315−2318.
[12] We use the acronyms 4-TIP^R and 2-TIP^{R,R} here in analogy to 4-TIC and 2-TIC, an abbreviation introduced by Breslow.[6]
[13] G. J. Kleywegt, W. G. R. Wiesmeijer, G. J. Van Driel, W. L. Driessen, J. Reedijk, J. H. Noordik, *J. Chem. Soc., Dalton Trans.* **1985**, 2177−2184.
[14] K. Håkansson, A. Wehnert, *J. Mol. Biol.* **1992**, *228*, 1212−1218.
[15] G. M. Sheldrick, *SHELXS-97, Program for the Solution of Crystal Structures*, University of Göttingen, Germany, **1990**.
[16] G. M. Sheldrick, *SHELXL-97, Program for the Refinement of Crystal Structures*, University of Göttingen, Germany, **1997**.

Received April 22, 2003

 © 2003 Wiley-VCH Verlag GmbH & Co. KGaA, Weinheim

Synthesis of New Pd^{II} Complexes Containing a Thioether-Pyrazole Hemilabile Ligand − Structural Analysis by ^1H, ^{13}C NMR Spectroscopy and Crystal Structure of $[PdCl(bdtp)]BF_4$ [bdtp = 1,5-Bis(3,5-dimethyl-1-pyrazolyl)-3-thiapentane]

Jordi García-Antón,[a] Josefina Pons,*[a] Xavier Solans,[b] Mercè Font-Bardia,[b] and Josep Ros*[a]

Keywords: Palladium / N,S ligands / Hemilabile ligands

Treatment of the ligand 1,5-bis(3,5-dimethyl-1-pyrazolyl)-3-thiapentane (bdtp) with $[PdCl_2(CH_3CN)_2]$ led to a $[PdCl_2(bdtp)]$ complex. Subsequent treatment of this complex with $AgBF_4$ gave $[PdCl(bdtp)](BF_4)$. These Pd^{II} complexes were characterised by elemental analysis, conductivity measurements, IR spectroscopy, and ^1H and ^{13}C NMR spectroscopy. Complex $[PdCl_2(bdtp)]$ was again obtained when the complex $[PdCl(bdtp)](BF_4)$ was heated under reflux in a solution of NEt_4Cl in CH_2Cl_2/MeOH (1:1). Ligand bdtp in complexes **1** and **2** exhibited a hemilabile character. The X-ray structure of the complex $[PdCl(bdtp)](BF_4)$ was determined. The metal atom is tricoordinated by the two azine nitrogen atoms and one thioether sulfur atom of the thioether-pyrazole ligand, its coordination (distorted square planar) being completed with one chloride ion.

(© Wiley-VCH Verlag GmbH & Co. KGaA, 69451 Weinheim, Germany, 2003)

Introduction

The chemistry of hemilabile ligands in coordination and organometallic chemistry has been widely studied in recent years due to their potential application in catalysis. In particular, bidentate ligands containing two donor centres of different strengths with respect to substitution (labile Y and inert D) have been reviewed in recent reports and articles.[1] According to the review by P. Braunstein and F. Naud[1a] there are three types of hemilability. In type I hemilability, the labile donor group coordinates and decoordinates from the metal centre spontaneously. In type II, there is intramolecular competition between donor groups of the same ligand (a) or between donor groups of two identical ligands (b). Finally, in type III, the hemilabile character is due to the presence of an external reagent (Scheme 1 shows these types of hemilability for mononuclear complexes).

In recent years, we have studied and reported on the properties of hemilabile ligands based on the pyrazolyl group and on some other groups containing N,[2] P[3] or O[4] atoms. This paper continues the study of the potential hemilability of ligands containing pyrazolyl and thioether groups.[5]

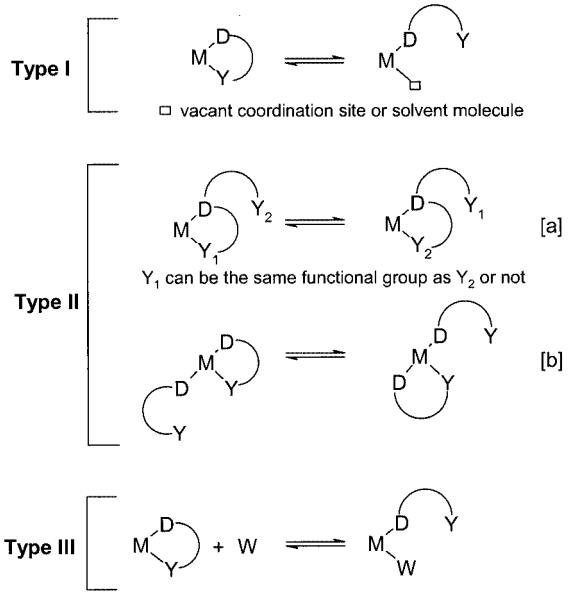

Scheme 1

The bonding properties of this family of ligands are also well documented,[6] especially the synthesis and structural characterisation of complexes of Co^{II},[7] Zn^{II},[8] Cd^{II},[8] Cu^{I} [7,9] and Ag^{I} [7] with 1,5-bis(3,5-dimethylpyrazol-1-yl)-3-

[a] Departament de Química, Facultat de Ciències, Universitat Autònoma de Barcelona,
08193 Bellaterra, Cerdanyola, Barcelona, Spain
Fax: (internat.) +34-935-813101
E-mail: Josefina.Pons@uab.es
[b] Cristallografia, Mineralogia i Dipòsits Minerals, Universitat de Barcelona,
Martí i Franquès s/n, 08028 Barcelona, Spain

Supporting information for this article is available on the WWW under http://www.eurjic.org or from the author.

 © 2003 Wiley-VCH Verlag GmbH & Co. KGaA, Weinheim **DOI: 10.1002/ejic.200300235**

thiapentane (bdtp). The ligand acts in a tridentate manner (NSN) in all these complexes except [$ZnCl_2$(bdtp)], in which it behaves in a bidentate fashion (NN).

In this paper, we report on the study of the coordination of the ligand bdtp[10] with Pd^{II}, and the isolation of the complex [$PdCl_2$(bdtp)] (**1**). Treatment of this complex with $AgBF_4$ gives [PdCl(bdtp)](BF_4) (**2**; Scheme 2). NMR spectroscopic studies and the X-ray crystal structure of **2** are also presented.

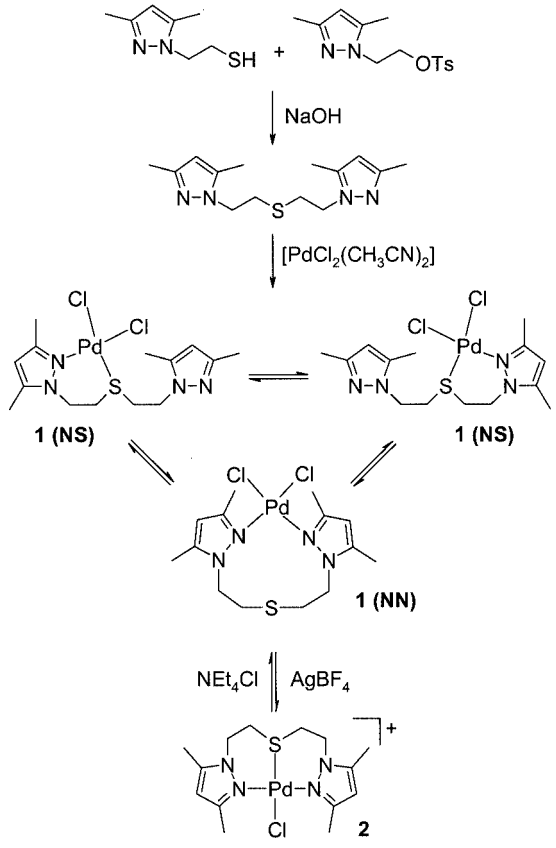

Scheme 2

Results and Discussion

Although 1,5-bis(3,5-dimethylpyrazol-1-yl)-3-thiapentane (bdtp) has previously been reported in the literature,[10] in this paper we describe an alternative synthetic route. Treatment of 1-(2-mercaptoethyl)-3,5-dimethylpyrazole and 1-[2-(*p*-tolylsulfonyloxy)ethyl]-3,5-dimethylpyrazole in the presence of sodium hydroxide in water gave the desired product (Scheme 2). The ligand bdtp was characterised by elemental analysis, mass spectrometry, IR spectroscopy, and ^1H and ^{13}C NMR spectroscopy.

[$PdCl_2$(bdtp)] (**1**) was obtained by treatment of the ligand with [$PdCl_2(CH_3CN)_2$] in a 1:1 M/L ratio. Treatment of **1** with one equivalent of $AgBF_4$ gave a compound of formula [PdCl(bdtp)](BF_4) (**2**). Both products are yellow and gave satisfactory C, H, N and S elemental analyses. When complex **2** was heated under reflux in a solution of Et_4NCl in CH_2Cl_2/MeOH (1:1) for 24 hours, complex **1** was again obtained.

Conductivity data in acetonitrile are in agreement with a non-electrolyte nature for compound **1** (37 Ω^{-1} cm^2mol^{-1}) and 1:1 electrolyte for compound **2** (123 Ω^{-1} cm^2mol^{-1}). The reported values for 10^{-3} M solutions of non-electrolyte compounds are lower than 120 $\Omega^{-1}cm^2mol^{-1}$ and between 120−160 Ω^{-1} cm^2mol^{-1} for 1:1 electrolyte compounds in acetonitrile.[11]

According to IR data for compound **1**, the Pd atom is coordinated to nitrogen atoms [ν(Pd−N) 456 cm^{-1}], two chlorine atoms in a *cis* arrangement [two bands are observed, ν(Pd−Cl) 367 and 336 cm^{-1}] and to sulfur atoms [ν(Pd−S) 280 cm^{-1}]. In compound **2** only one band for ν(Pd−Cl) (334 cm^{-1}) was observed as well as ν(Pd−N) (450 cm^{-1}) and ν(Pd−S) (256 cm^{-1}) bands.[12]

NMR Experiments

^1H and ^{13}C NMR spectra of compounds **1** and **2** were recorded in $CDCl_3$ and CD_2Cl_2, respectively, and show the signals of the coordinated ligands. NMR spectroscopic data are reported in the Exp. Sect.

The ^1H NMR spectrum of **1** in solution at 298 K shows sharp resonances for the CH and CH_3 groups of the pyrazolyl cycles, but poorly defined broad bands for the N−CH_2−CH_2−S chain. This suggests a fluxional process occurring in solution, which was studied carrying out a variable temperature ^1H NMR study in $CDCl_3$ (Figure 1). Lowering of the temperature induces a progressive broadening and splitting of the signal corresponding to the CH group of the pyrazolyl rings until 233 K, where three well-defined signals are observed at δ = 5.90, 5.82 and 5.77 ppm. The two signals at lower δ integrate for one H atom each, while the signal at δ = 5.90 ppm integrates for two H atoms. This suggests that at 298 K there is a fluxional process in which the thioether-pyrazole ligand alternates between the *N*,*N* and *N*,*S* bidentate coordinations (in the ratio of approximately 1:1). At 233 K, where both species can be observed, the *N*,*N* coordination shows only one signal for the CH group of the pyrazolyl rings,[5a] whereas in the *N*,*S* coordination mode the pyrazolyl groups are not equivalent

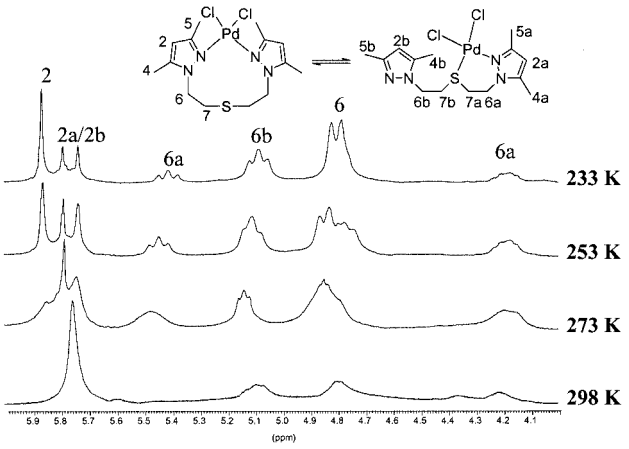

Figure 1. Numbering of complex [$PdCl_2$(bdtp)] and 400 MHz ^1H NMR variable temperature experiments for 2-H and 6-H

 © 2003 Wiley-VCH Verlag GmbH & Co. KGaA, Weinheim

(coordinated and free pyrazolyl groups) and there is one signal for each.

Ill defined broad bands corresponding to the methylenic groups of the $N-CH_2-CH_2-S$ chain at 298 K become assignable signals at 233 K. Thus, if we focus on 6-H (7-H is superimposed with other signals) at 233 K, four groups of signals can be attributed to the methylene functionalities directly linked to the pyrazolyl group in the NN and NS isomers. One of them (at $\delta = 4.84$ ppm) can be attributed to the CH_2 of the NN isomer (6-H, Figure 1), as it integrates for four H atoms. The signal at $\delta = 5.12$ ppm can be assigned to the CH_2 of the open arm of the NS isomer (6b-H). It integrates for two H atoms and resembles a triplet. Finally, signals at $\delta = 4.21$ and 5.45 ppm can be assigned to the CH_2 group in the chelating arm of the NS isomer (6a-H), as they integrate for one H atom each. The rigid conformation of this arm in this isomer leads to the two hydrogens of this CH_2 group becoming diastereotopic, and therefore they have different chemical displacements. Although they are not completely defined, these signals resemble those observed for complexes found in the literature with similar $Pd-N-N-C-C-S$ rings.[5]

The ^{13}C NMR spectrum, at room temperature, of complex **1** also shows broad bands. This is consistent with the fluxional process explained for the ^1H NMR spectra.

From the structure of complex **2** it can be seen that the two protons of each CH_2 moiety in the $S-CH_2-CH_2-N$ chains are diastereotopic, thus leading to four groups of signals which can be associated to a single hydrogen atom in each chain. This happens because of the rigid conformation of the ligand when complexed. Thus, each group of signals can be assigned as doublets of doublets of doublets (Figure 2). The HMQC spectrum allowed us to assign the two doublets of doublets of doublets of lower δ to 7-H and the ones at higher δ to 6-H.

Study of the $S-CH_2-CH_2-N$ fragment (in **2**) as an AA′XX′ system gave a set of coupling constants (Table 1). These constants were consistent with the simulated spectra obtained with the aid of the gNMR program.[13]

Table 1. ^1H NMR results: chemical shifts (ppm, CD_2Cl_2) and $^1H,^1H$ coupling constants (Hz) for **2**

δ H (6*S*)	4.92	^2J(6*R*,6*S*)	−15.9
δ H (6*R*)	5.20	^2J(7*R*,7*S*)	−14.8
δ H (7*R*)	2.97	^3J(7*R*,6*S*)	2.5
δ H (7*S*)	3.78	^3J(7*S*,6*S*)	3.2
		^3J(7*R*,6*R*)	12.1
		^3J(7*S*,6*R*)	1.6

In the NOESY spectrum it can be seen that the methyl group at $\delta = 2.40$ ppm shows an NOE interaction with the doublet of doublets of doublets at $\delta = 4.92$ ppm, but not with the one at $\delta = 5.20$ ppm. From the X-ray structure of **2** (Figure 3), it can be observed that the nearest proton to the $CH_3(5)$ moiety is 6S-H and therefore it should be the one with the NOE interaction. This information leads us to assign 6*S*-H to the doublet of doublets of doublets at $\delta = 4.92$ ppm and 6R-H to the signal at $\delta = 5.20$ ppm.

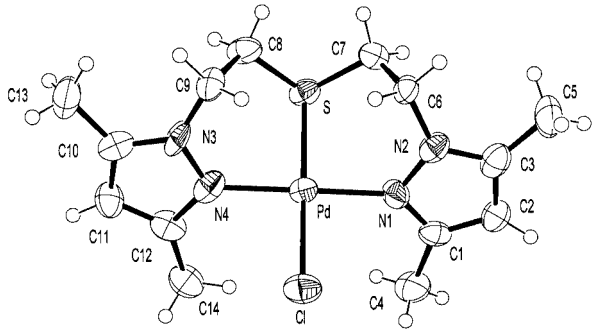

Figure 3. ORTEP drawing of $[PdCl(bdtp)]^+$ cation (293 K determination); 50% probability amplitude displacement ellipsoids are shown

The coupling constants enabled us to differentiate 7*R*-H and 7*S*-H. These coupling constants agree with the conformation of the $S-CH_2-CH_2-N$ chain as seen in Figure 2, which has been corroborated by an X-ray crystal study. Ge-

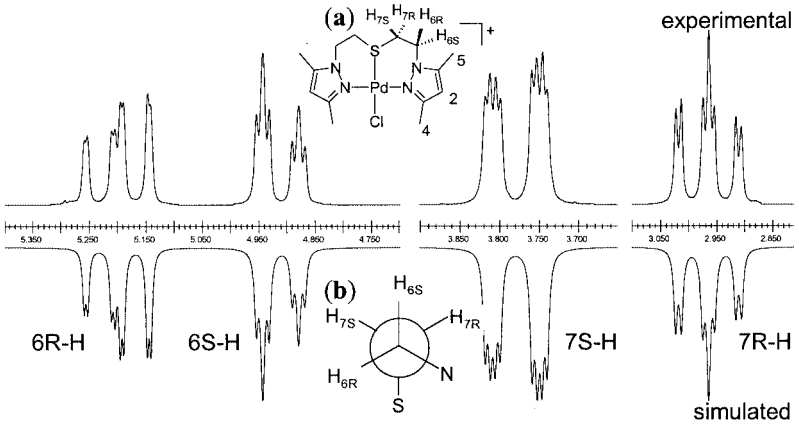

Figure 2. The 250 MHz ^1H NMR and the simulated gNMR spectrum for the NCH_2CH_2S fragment of $[PdCl(bdtp)](BF_4)$ including (a) the numbering and (b) the dihedral angles for the NCH_2CH_2S fragment

 © 2003 Wiley-VCH Verlag GmbH & Co. KGaA, Weinheim

minal ^2J and ca. 180° ^3J coupling constants have significantly higher values than ca. 30° and ca. 60° ^3J coupling constants .[14] Thus, 7*R*-H should correspond to the doublet of doublets of doublets at δ = 2.97 ppm and 7*S*-H to the one at δ = 3.78 ppm.

Crystal Structure of [PdCl(bdtp)](BF$_4$) (2)

The molecular structure of compound **2** consists of discrete $[PdCl(bdtp)]^+$ cations and BF_4^- anions (Figure 3), packed according to normal van der Waals forces.

The cation complex is mononuclear. The Pd^{II} ion is coordinated to the bdtp ligand by its three donors atoms via two pyrazole nitrogens and one thioether sulfur, along with one chlorine atom. The PdN_2SCl *core* (S thioether) is found in three complexes in the literature.[15] Some selected bond lengths and bond angles for this complex are listed in Table 2.

Table 2. Selected bond lengths (Å) and bond angles (°) for **2** with estimated standard deviations (e.s.d.s.) in parentheses

Pd−N1	2.004(7)
Pd−N4	2.040(7)
Pd−S	2.308(2)
Pd−Cl	2.291(2)
N1−Pd−S	90.5(2)
N4−Pd−S	88.5(2)
N1−Pd−N4	176.6(3)
N1−Pd−Cl	89.8(2)
N4−Pd−Cl	91.5(2)
S−Pd−Cl	175.18(8)

The Pd−N bond lengths [2.004(7) Å and 2.040(7) Å], the Pd−S bond length [2.308(2) Å] and the Pd−Cl bond length [2.291(2) Å] can be regarded as normal compared with the distances found in the literature.[16] The coordination geometry is square planar with a tetrahedral distortion, as can be deduced from the bond angles and the mean separation [0.0765 Å] of the atoms coordinated to the Pd atom in relation to the mean plane that contains these four atoms and the Pd atom. The dihedral angle between the planes N1−Pd−Cl and N4−Pd−S is 5.85°. Ligand bdtp acts as a tridentate chelate and forms two Pd−*N*−N−C−C−S six-membered rings with a boat conformation, sharing an edge (Pd−S). The boat distortions in the six-membered rings are $\Delta C_S[(S-C7)] = 12.4(6)°$ and $\Delta C_S[(N1-N2)] = 14.8(10)°$ for Pd−N1−N2−C6−C7−S and $\Delta C_S[(S-C8)] = 4.0(6)°$ and $\Delta C_S[(N3-N4)] = 5.2(9)°$ for Pd−N4−N3−C9−C8−S, respectively [see Equation (1)].

$$\Delta C_S = \sqrt{\frac{\sum_{i=1}^{m}(\phi_i + \phi_i')^2}{m}} \quad (1)$$

m = equivalent torsion angles

$\Phi_i+\Phi_i'$ = torsion angles related to the considered plane [17]

The nitrogen-thioether bite angles of the ligand are 90.5(2)° and 91.5(2)°, respectively, which are similar to the corresponding bite in the $[Co(NO_3)_2(bdtp)]$ and [CuBr(bdtp)] complexes.[7]

Conclusions

The thioether-pyrazole ligand bdtp can coordinate Pd^{II} centres in different ways. In this paper we describe all the possible polydentate coordinations in mononuclear complexes: two bidentate coordinations (NN and NS) and a tridentate coordination (NSN). Furthermore, we have demonstrated the hemilabile properties of this ligand when coordinated to Pd^{II}. In complex **1** the ligand alternates the NN and NS coordination types at room temperature, which would be type II hemilability.[1a]

Complex **2** (where ligand bdtp uses NSN coordination) is obtained from **1** by treatment with $AgBF_4$. When **2** is heated under reflux in a solution of Et_4NCl in CH_2Cl_2/MeOH (1:1), **1** is obtained once again. This could be considered as type III hemilability.

Experimental Section

Generals Remarks: Preparations were performed using usual vacuum line and Schlenk techniques. All reagents were commercial grade materials and were used without further purification. Acetonitrile and dichloromethane were dried and distilled by standard methods and previously deoxygenated in the vacuum line.

Samples of $[PdCl_2(CH_3CN)_2]$ were prepared as described in the literature.[18]

Analyses (C,N,H,S) were performed in our analytical laboratory on a Carlo Erba CHNS EA-1108 instrument. Conductivity measurements were performed at room temperature in ca. 10^{-3} M acetonitrile solutions employing a Crison, micro CM 2200 conductometer. Infrared spectra were recorded from KBr pellets or polyethylene mulls in the range 4000−100 cm^{-1} under a nitrogen atmosphere. The ^1H NMR, $^{13}C\{^1H\}$ NMR and HMQC spectra were obtained either on a Bruker 250 MHz or Bruker 400 MHz instrument. Chemical shifts (δ) were determined relative to internal TMS and are given in ppm. A mass spectrum was obtained with an Esquire 3000 ion trap mass spectrometer from Bruker Daltonics.

Synthesis of the Ligand 1,5-bis(3,5-dimethyl-1-pyrazolyl)-3-thiapentane (bdtp): Although the synthesis of the ligand bdtp has been previously reported in the literature,[10] here, we describe an alternative synthetic route. A solution of 1-(2-mercaptoethyl)-3,5-dimethylpyrazole (2.00 g, 12.8 mmol), 1-[2-(*p*-tolylsulfonyloxy)ethyl]-3,5-dimethylpyrazole (3.77 g, 12.8 mmol) and of sodium hydroxide (0.53 g, 12.9 mmol; 97%) of water (25 mL) was refluxed for five hours. After cooling to room temperature, the reaction mixture was extracted three times with $CHCl_3$ (15 mL). The collected organic layers were dried with anhydrous sodium sulfate and removed under vacuum to give a white solid. Yield: 2.17 g (61%). M.p. 80.3−80.9 °C. $C_{14}H_{22}N_4S$ (278.42): calcd. C 60.39, H 7.96, N 20.12, S 11.52; found C 60.20, H 7.73, N 20.41, S 11.23. IR (KBr, cm^{-1}): $\nu(C\text{-}H)_{al}$ = 2924, ν(C=C), ν(C=N) 1550, $\delta(CH_3)_{as}$ = 1481−1436, $\delta(CH_3)_s$ 1302, $\delta(C-H)_{oop}$ = 800−775. ^1H NMR (250 MHz, $CDCl_3$): δ = 2.22 (s, 6 H, Me), 2.27 (s, 6 H, Me), 2.84

 © 2003 Wiley-VCH Verlag GmbH & Co. KGaA, Weinheim

(t, ^3J = 6.9 Hz, 4 H, pz-CH_2−CH_2−S), 4.10 (t, ^3J = 6.9 Hz, 4 H, pz-CH_2−CH_2−S), 5.79 (s, 2 H, pz-CH). $^{13}C\{^1H\}$ NMR ($CDCl_3$, 63 MHz): δ = 11.4 (Me), 13.7 (Me), 32.5 (pz-CH_2−CH_2−S), 48.7 (pz-CH_2−CH_2−S), 105.3 (pz-CH), 139.5 (pz-C), 148.1 (pz-C) ppm. MS (ESI): *m*/*z* (%) = 279 (72) [M + H^+], 301 (100) [M + Na^+].

Synthesis of [$PdCl_2$(bdtp)] (1): A solution of [$PdCl_2(CH_3CN)_2$] (0.097 g, 0.374 mmol) in dichloromethane (15 mL) was added to a solution of bdtp (0.105 g, 0.378 mmol) in dichloromethane (10 mL). After the mixture had been stirred for 12 h, most of the solvent was removed under vacuum. Diethyl ether was then added to induce precipitation. The resulting precipitate was then filtered and washed with diethyl ether, yielding the desired compound. Yield: 0.157 g (92%). Conductivity ($\Omega^{-1}cm^2mol^{-1}$, $9.98\cdot10^{-4}$ M in acetonitrile): 37. $C_{14}H_{22}Cl_2N_4PdS$ (455.74): calcd. C 36.90, H 4.87, N 12.29, S 7.04; found C 36.58, H 4.92, N 12.11, S 6.93. IR (KBr, cm^{-1}): ν(C−H)$_{al}$ = 2920, ν(C=C), ν(C=N) 1557, δ$(CH_3)_{as}$ = 1467−1420, δ$(CH_3)_s$ = 1313, δ(C−H)$_{oop}$ = 788. IR (polyethylene, cm^{-1}): ν(Pd−N)$_{as}$ = 456, ν(Pd−Cl) = 336, 367, ν(Pd−S) = 280 cm^{-1}. ^1H NMR (400 MHz, $CDCl_3$, 233 K): (For simplicity we have used the numeration as in Figure 1; peaks from 2.20 ppm to 2.69 ppm are not integrated because they are superimposed with other signals, although these peaks all together integrate the expected 31 H atoms.) δ (isomer **N,N**) = 2.24, 2.55 [s, Me (4/5)], 2.69 [br., pz-CH_2−CH_2−S (7)], 4.84 [br., 4 H, pz-CH_2−CH_2−S (6)], 5.91 [s, pz-CH (2)]. δ (isomer **N,S**) = 2.25, 2.56 [s, Me (4a/b, 5a/b)], 2.20 [br., pz-CH_2−CH_2−S (7b)], 2.85 [br., 1 H, pz-CH_2−CHH−S (7a)], 3.37 [br., 1 H, pz-CH_2−CHH−S (7a)], 4.21 [br., 1 H, pz-CHH−CH_2−S (6a)], 5.12 [br., 2 H, pz-CH_2−CH_2−S (6b)], 5.45 [br., 1 H, pz-CHH−CH_2−S (6a)], 5.77, 5.83 [s, 1H each, pz-CH (2a/2b)]. $^{13}C\{^1H\}$ NMR ($CDCl_3$, 63 MHz, 298 K): δ = 12.3 (br., Me), 15.3 (br., Me), 29.9 (br., pz-CH_2−CH_2−S), 49.8 (br., pz-CH_2−CH_2−S), 108.2 (br., pz-CH), 143.6 (br., pz-C), 150.7 (br., pz-C).

Synthesis of [PdCl(bdtp)]BF_4 (2): A solution of $AgBF_4$ (0.063 g, 0.324 mmol) in methanol (2 mL) was added dropwise with vigorous stirring to a solution of **1** (0.149 g, 0.327 mmol) in dichloromethane (5 mL) and methanol (5 mL). The reaction was carried out in the dark to prevent reduction of Ag^I to Ag^0. After five minutes, stirring was stopped, and AgCl was filtered off through a pad of Celite. When the volume of the resultant solution had been reduced to roughly 5 mL, the product precipitated as a yellow solid. This solid was filtered and dried under vacuum. Yield: 0.146 g (89%). Conductivity ($\Omega^{-1}cm^2mol^{-1}$, $9.87\cdot10^{-4}$ M in acetonitrile): 123. $C_{14}H_{22}BClF_4N_4PdS$ (507.09): calcd. C 33.16, H 4.37, N 11.05, S 6.32; found C 33.45, H 4.40, N 10.93, S 6.12. IR (KBr, cm^{-1}): ν(C−H)$_{ar}$ = 3014, ν(C−H)$_{al}$ = 2967−2923, ν(C=C), ν(C=N) 1554, δ$(CH_3)_{as}$ = 1468−1423, δ$(CH_3)_s$ = 1319, ν(B−F) = 1049, δ(C−H)$_{oop}$ = 817. IR (polyethylene, cm^{-1}): ν(Pd−N)$_{as}$ = 450, ν(Pd−Cl) = 334, ν(Pd−S) = 256. ^1H NMR (250 MHz, CD_2Cl_2): δ = 2.40 (s, 6 H, Me), 2.70 (s, 6 H, Me), 2.97 (ddd, 2 H, pz-CH_2−CHH), 3.78 (ddd, 1 H, pz-CH_2−CHH), 4.92 (ddd, 1 H, pz-CHH−CH_2), 5.20 (ddd, 1 H, pz-CHH−CH_2), 6.08 (s, 2 H, pz-CH) ppm. $^{13}C\{^1H\}$ NMR (63 MHz, CD_2Cl_2): δ = 12.2 (Me), 15.7 (Me), 39.8 (S−CH_2−CH_2), 51.2 (pz-CH_2−CH_2), 109.3 (pz-CH), 145.1, 154.1 (pz-C).

Synthesis of [$PdCl_2$(bdtp)] (1) from [PdCl(bdtp)](BF_4): A solution of **2** (0.053 g, 0.104 mmol) and NEt_4Cl (0.033 g, 0.199 mmol) in a mixture (1:1) of dichloromethane and methanol (20 mL) was refluxed for 24 hours. After cooling to room temperature, the reaction mixture was extracted three times with 15 mL of $CHCl_3$. The collected organic layers were dried with anhydrous sodium sulfate and removed in vacuo to yield the desired product. Yield: 0.038 g (80%).

X-ray Crystallographic Study: Suitable crystals of compound **2** were obtained by crystallisation from CH_2Cl_2. Data were collected on an Enraf−Nonius CAD4 four-circle diffractometer, using the ω/2θ scan technique. The crystals were collected with graphite-monochromated Mo-K_α radiation. 2977 reflections were measured in the range $2.11° < \theta < 29.98$. 1529 reflections were assumed as observed applying the condition $I > 2\sigma(I)$. Three reflections were measured every two hours as orientation and intensity control and significant intensity decay was not observed. Lorentz-polarisation but no absorption corrections were performed. The structure was solved by direct methods using the SHELXS 97 computer program and refined by the full-matrix least-squares method with a SHELXL 97 computer program.[19] All hydrogen atoms were computed and refined with an overall isotropic temperature factor using a riding model. The final *R* (on *F*) factor and *wR* (on F^2) values, as well as the numbers of parameters refined and other details concerning the refinement of the crystal structure are presented in Table 3.

Table 3. Crystallographic data of **2**

Empirical formula	$C_{14}H_{22}BClF_4N_4PdS$
Molecular mass, g	507.08
Temperature, K	293(2)
Crystal system	monoclinic
Space group	C_C
Unit cell dimensions	
a, Å	5.138(8)
b, Å	30.957(6)
c, Å	12.355(3)
β, deg	92.87(7)
V, Å^3	1963(3)
Z	4
$D_{calcd.}$, g cm^{-3}	1.716
μ, mm^{-1}	1.230
F(000)	1016
Crystal size (mm)	0.1 × 0.1 × 0.2
θ range, deg	2.11 to 29.98
Reflections collected: total, independent, R_{int}	2977, 2977, 0.0134
Data/restraints/parameters	2977, 2, 235
a[a]	0.0095
Final *R*1, *wR*2	0.0337, 0.0492
*R*1 (all data), *wR*2	0.1430, 0.0656
Residual electron density, e·Å^{-3}	+0.774, −0.777

[a] The function minimized was $\Sigma w(|F_o|)^2 - |F_c|^2)^2$, where $w = [\sigma^2(I) + (aP)^2]^{-1}$, and $P = (|F_o|^2 + 2|F_c|^2)/3$.

CCDC-208981 contains the supplementary crystallographic data for this paper. These data can be obtained free of charge at www.ccdc.cam.ac.uk/conts/retrieving.html or from the Cambridge Crystallographic Data Centre, 12 Union Road, Cambridge CB2 1EZ, UK [Fax: (internat.) +44-1223-336-033; E-mail: deposit@ccdc.cam.ac.uk].

Acknowledgments

Support by the Spanish Ministerio de Educación y Cultura (Project BQU2000−0238 and a grant to J.G.) is gratefully acknowledged.

[1] [1a] P. Braunstein, F. Naud, *Angew. Chem. Int. Ed.* **2001**, *40*, 680. [1b] C. S. Slone, D. A. Weinberger, C. A. Mirkin, *Prog.*

Inorg. Chem. **1999**, *48*, 233. [1c] A. Bader, E. Lindner, *Coord. Chem. Rev.* **1991**, *108*, 27.

[2] [2a] R. Mathieu, G. Esquius, N. Lugan, J. Pons, J. Ros, *Eur. J. Inorg. Chem.* **2001**, 2683. [2b] G. Esquius, J. Pons, R. Yáñez, J. Ros, *J. Organomet. Chem.* **2001**, *619*, 14. [2c] G. Esquius, J. Pons, R. Yáñez, J. Ros, X. Solans, M. Font-Bardía, *J. Organomet. Chem.* **2000**, *605*, 226. [2d] G. Esquius, J. Pons, R. Yáñez, J. Ros, X. Solans, M. Font-Bardía, *Acta Crystallogr., Sect. C* **2002**, *58*, 133. [2e] G. Esquius, J. Pons, R. Yáñez, J. Ros, R. Mathieu, B. Donnadieu, N. Lugan, *Eur. J. Inorg. Chem.* **2002**, 2999.

[3] [3a] R. Tribó, J. Pons, R. Yáñez, J. F. Piniella, A. Álvarez-Larena, J. Ros, *Inorg. Chem. Commun.* **2000**, *3*, 545. [3b] G. Esquius, J. Pons, R. Yáñez, J. Ros, R. Mathieu, B. Donnadieu, N. Lugan, *J. Organomet. Chem.* **2003**, *667*, 126. [3c] R. Tribó, J. Ros, J. Pons, R. Yáñez, A. Álvarez-Larena, J. F. Piniella, *J. Organomet. Chem.* **2003**, *676*, 38.

[4] [4a] A. Boixassa, J. Pons, A. Virgili, X. Solans, M. Font-Bardía, J. Ros, *Inorg. Chim. Acta* **2002**, *340*, 49. [4b] A. Boixassa, J. Pons, X. Solans, M. Font-Bardía, J. Ros, *Inorg. Chim. Acta* **2003**, *346*, 151. [4c] A. Boixassa, J. Pons, X. Solans, M. Font-Bardía, J. Ros, *Inorg. Chim. Acta*, manuscript accepted.

[5] [5a] J. García-Antón, J. Pons, X. Solans, M. Font-Bardía, J. Ros, *Eur. J. Inorg. Chem.* **2002**, 3319. [5b] J. García-Antón, J. Pons, X. Solans, M. Font-Bardía, J. Ros, *Eur. J. Inorg. Chem.,* manuscript accepted.

[6] [6a] E. Bouwman, W. L. Driessen, J. Reedijk, *Coord. Chem. Rev.* **1990**, 143. [6b] M. Di Varia, F. Mani, *J. Chem. Soc., Dalton Trans.* **1985**, 2327. [6c] P. K. Byers, A. J. Canty, *Inorg. Chim. Acta* **1985**, *104*, L13. [6d] W. G. Haanstra, W. Van der Donk, W. L. Driessen, J. Reedijk, M. G. B. Drew, J. S. Wood, *Inorg. Chim. Acta* **1990**, *176*, 299. [6e] W. G. Haanstra, W. Van der Donk, A. J. W. Wilfred, W. L. Driessen, J. Reedijk, J. S. Wood, M. G. B. Drew, G. B. Michael, *J. Chem. Soc., Dalton, Trans.* **1990**, 3123. [6f] W. G. Haanstra, W. L. Driessen, R. A. G. De Graaff, J. Reedijk, Y. F. Wang, C. H. Stam, *Inorg. Chim. Acta* **1991**, *186*, 215. [6g] W. G. Haanstra, W. L. Driessen, J. Reedijk, *Acta Crystallogr., Sect. C* **1992**, *48*, 14. [6h] F. Meyer, A. Jacobi, L. Zsolnai, *Chem. Ber./Receuil* **1997**, 130, 1441. [6i] H. Cheng, J. K. Dutra, S. M. Sakya, *PCT Int. Appl.* **2001**, 93pp. [6j] U. Heinemann, B. W. Krueger, H. Gayer, F. Maurer, C. Boie, R. Ebbert, U. Wachendoff-Neumann, U. Mauler-Machnik, *Eur. Pat. Appl.* **2003**, 32pp.

[7] W. G. Haanstra, W. L. Driessen, M. van Roon, A. L. E. Stoffels, J. Reedijk, *Chem. Soc., J. Chem. Soc., Dalton Trans.* **1992**, 481.

[8] P. Ghosh, M. Wood, J. B. Bonanno, T. Hascall, G. Parkin, *Polyhedron* **1999**, *18*, 1107.

[9] A. L. E. Stoffels, W. G. Haanstra, W. L. Driessen, J. Reedijk, *Angew. Chem. Int. Ed. Engl.* **1990**, *29*, 1419.

[10] T. N. Sorrell, M. R. Malachowski, *Inorg. Chem.* **1983**, *22*, 1883.

[11] [11a] W. J. Geary, *Coord. Chem. Rev.* **1971**, *7*, 81. [11b] L. K. Thompson, F. L. Lee, E. J. Gabe, *Inorg. Chem.* **1988**, *27*, 39.

[12] [12a] R. J. H. Clark, G. Natile, U. Belluco, L. Cattalini, C. Filippin, *J. Chem. Soc.* **1970**, 659. [12b] K. Nakamoto, *Infrared and Raman Spectra of Inorganic and Coordination Compounds.* John Wiley & Sons, New York, **1986**.

[13] P. H. M. Budzelaar, *g NMR − version 4.0*, IvorySoft, Cherwell Scientific, Oxford, UK, **1997.**

[14] [14a] E. Pretsh, T. Clerc, J. Seibl, W. Simon, *Tables of Determination of Organic Compounds. ^{13}C NMR, ^{1}H NMR, IR, MS, UV/Vis, Chemical Laboratory Practice.* Springer-Verlag, Germany, **1989**. [14b] D. H. Williams, I. Fleming, *Spectroscopic Methods in Organic Chemistry.* McGraw-Hill, UK, **1995**.

[15] [15a] B. T. Khan, S. Shamsuddin, K. Venkatasubramanian, *Polyhedron* **1992**, *11*, 671. [15b] U. Heinzel, R. Mattes, *Inorg. Chim. Acta* **1992**, *194*, 157. [15c] B. Chak, A. McAuley, T. W. Whitcombe, *Inorg. Chim. Acta* **1996**, *246*, 349.

[16] [16a] D. B. Grotjahn, D. Combs, S. Van, G. Aguirre, F. Ortega, *Inorg. Chem.* **2000**, *39*, 2080. [16b] D. B. Grotjahn, S. Van, D. Combs, A. A. Lev, C. Schneider, C. D. Incarvito, K. Lam, G. Rossi, A. L. Rheingold, M. Rideout, C. Meyer, G. Hernandez, L. Mejorado, *Inorg. Chem.* **2003**, *42*, 3347.

[17] W. L. Drax, C. M. Weeks, D. C. Roher, *Topics in Sterechemistry* (Eds. E. L. Eliel, Allinger), John Wiley & Sons, New York, **1976**.

[18] S. Komiya, *Synthesis of Organometallic Compounds: A Practical Guide*, John Wiley & Sons, New York, **1997**.

[19] G. M. Sheldrick, *SHELXS 97*, *SHELXL 97*, *CIFTAB*-Program for Crystal Structure Analysis (Release 97−2), Institut fur Anorganische Chemie der Universität, Tammanstraβe 4, 3400 Göttingen, Germany, **1998.**

Received March 24, 2003

 © 2003 Wiley-VCH Verlag GmbH & Co. KGaA, Weinheim

Binuclear Hydridoplatinum(II): One-Pot Synthesis, INS Spectra and X-ray Crystal Structure of $[Pt_2(dcype)_2(H)_3][BPh_4]$ {dcype = 1,2-Bis(dicyclohexylphosphanyl)ethane}

Anna Laura Bandini,*[a] Guido Banditelli,[a] Mario Manassero,*[b] Alberto Albinati,*[b] Daniele Colognesi,[c] and Juergen Eckert[d,e]

Keywords: Hydride ligands / INS spectroscopy / Phosphane ligands / Platinum / X-ray diffraction

The binuclear platinum(II) hydride $[Pt_2(dcype)_2(H)_3][Cl]$ (**1b**) has been isolated in high yields by treatment of $Pt(dcype)Cl_2$ with $NaBH_4$ (molar ratio 1:2) in ethanol solution at room temperature. This one-pot synthesis is not straightforward when starting from diphenylphosphanylalkane complexes. The compounds $[Pt_2(dppp)_2(H)_3][OH]$ (**3b**) and $[Pt_2(dppb)_2(H)_3][OH]$ (**4**) were isolated by starting from the mononuclear hydrides {*cis*-$[Pt(P\text{-}P)(H)_2]$} while mixtures of both binuclear {$[Pt_2(dppe)_2(H)_3]^+$, **5**} and trinuclear {$[Pt_3(dppe)_3(H)_3]^+$, **6**} trihydrides were obtained with the dppe ligand. Various salts of the cation **1**, $[Pt_2(dcype)_2(H)_3][X]$ (X = BF_4, **1a**; OH, **1c**; BPh_4, **1d**), were isolated either from $[Pt(dcype)(\mu\text{-}OH)]_2[BF_4]_2$ (**2**) by a general procedure (**1a**), or by decomposition of the complex *cis*-$[Pt(dcype)(H)_2]$ in solution (**1c**), as well as by metathesis reactions (**1a**, **1c**, and **1d**). Compounds **1a**, **1b**, and **1d** react with CO under mild conditions to afford the corresponding Pt^I binuclear hydrides $[Pt_2(dcype)_2(\mu\text{-}CO)(\mu\text{-}H)][X]$ (X = Cl, **7a**; BF_4, **7b**; BPh_4, **7c**). The binuclear core of cation **1** is broken by KCN in methanol solution, yielding the mononuclear complex *cis*-$[Pt(dcype)(CN)(H)]$ (**8**). The complexes **1a–d**, **2**, **7a–c**, and **8** have been characterised by FAB MS, IR, and NMR (^1H, ^{31}P, and ^{195}Pt) spectroscopic techniques; the **1** and **7** cations show fluxional behaviour on the NMR timescale. The structure of compound **1d** was determined, at 200 K, by single-crystal X-ray diffraction. All the hydrido ligands were located. The Pt–Pt separation is 2.696(1) Å and the coordination geometry around each platinum centre can be regarded as distorted square planar. Incoherent Inelastic Neutron Scattering (INS) spectra were obtained for **1a** and $[Pt_2(dppe)_2(H)_3][BF_4]$ (**5a**); the spectra reflect the different geometries of the two "$P_4Pt_2(H)_3$" cores as found by single-crystal structure determinations.
(© Wiley-VCH Verlag GmbH & Co. KGaA, 69451 Weinheim, Germany, 2003)

Introduction

Since the first examples – $[Pt_2(PR_3)_2(H)_2(SiR_3)_2]$, reported by M. Green and co-workers[1] – binuclear platinum hydrides have been a topic of continuous interest. Besides complexes with monodentate tertiary phosphanes[2] or exobidentate (bridging) diphosphane,[3] a number of species with chelating diphosphanes (P-P) have also been described.[4–6] These complexes include 30-electron species, both neutral $[Pt(P\text{-}P)(H)]_2$[5] and cationic $[Pt_2(P\text{-}P)_2(H)_3]^+$,[4] as well as 28-electron $[Pt(P\text{-}P)(H)]_2^{2+}$ species.[6] The observed differences in their formation, spectroscopic properties and molecular structures seem to be largely dependent on the ancillary diphosphanyl ligand. Moreover, when chelating diphosphanes have been used, only a few examples of mononuclear *cis*-dihydrides {*cis*-$[Pt(P\text{-}P)(H)_2]$} have been described.[4d,5a,5c,7]

The trihydrido cations $\{[Pt_2(P\text{-}P)_2(H)_3]^+\}$ have been widely investigated. In solution they show fluxional behaviour on the NMR timescale over a wide temperature range, at least down to 183 K. Typically, only one resonance for the hydrides is observed in the ^1H NMR spectrum, coupled to four ^{31}P and two ^{195}Pt magnetically equivalent nuclei. In the solid state, however, two distinct types of structure have been observed, with either a $(H)Pt(\mu\text{-}H)_2Pt$ or a $(H)Pt(\mu\text{-}H)Pt(H)$ core. The former arrangement, with two bridging

[a] CNR-ISTM and Dipartimento di Chimica Inorganica, Metallorganica e Analitica, Università degli Studi di Milano, Via G. Venezian, 21 20133 Milano, Italy
E-mail: annalaura.bandini@unimi.it
[b] Dipartimento di Chimica Strutturale e Stereochimica Inorganica and INFM, UdR Milano, Università degli Studi di Milano
Via G. Venezian, 21 20133 Milano, Italy
E-mail: alberto.albinati@unimi.it
m.manassero@istm.cnr.it
[c] CNR Istituto di Fisica Applicata "Nello Carrara" 50127 Firenze, Italy
[d] LANSCE, Los Alamos National Laboratory, Los Alamos, NM 87545, USA
[e] Materials Research Laboratory, University of California Santa Barbara, Santa Barbara, CA 93106, USA.
Supporting information for this article is available on the WWW under http://www.eurjic.org or from the author.

 © 2003 Wiley-VCH Verlag GmbH & Co. KGaA, Weinheim **DOI: 10.1002/ejic.200300252**

and one terminal hydride, implies different environments for the two platinum atoms, as found in the structures of $[Pt_2\{Ph_2P(CH_2)_2PPh_2\}_2(H)_3]^+$ [4c,8] and $[Pt_2\{(Ph_2PC_5H_4)_2Fe\}_2(H)_3]^+$.[4f] On the other hand, the coordination geometries of the two platinum atoms in the structures of $[Pt_2(dtbpp)_2(H)_3]^+$ [4b] and $[Pt_2(butaphos)_2(H)_3]^+$ [4g] are approximately the same, and are consistent with the presence of two terminal and one bridging hydrides.

Different factors could be considered in order to explain the observed differences in the solid state, in particular: (i) the influence of the bite angle of the chelating ligands, and (ii) the steric demand of the substituents on the phosphorus atoms. Moreover, more subtle factors, such as crystal-packing forces, could also be responsible for the existence of different structures involving small energy differences.

In pursuit of our interest in platinum polynuclear hydrides, we report here the synthesis of the complexes $[Pt_2(dcype)_2(H)_3][X]$ (X= BF_4, **1a**; Cl **1b**; OH, **1c**; BPh_4, **1d**) and the X-ray crystal structure of the BPh_4 salt. In addition, the Incoherent Inelastic Neutron Spectra of complexes **1a** and $[Pt_2(dppe)_2(H)_3][BF_4]$ (**5a**) are also reported.

Complex **1b** can be obtained in good yields directly from $[Pt(dcype)Cl_2]$ by a one-pot reaction. This synthetic approach has also been used with less sterically demanding bis-diphenylphosphanylalkanes: satisfactory yields have been obtained in the case of dppp {$[Pt_2(dppp)_2(H)_3]^+$, **3**} and dppb {$[Pt_2(dppb)_2(H)_3]^+$, **4**} ligands, but the quantitative conversion of $Pt(P\text{-}P)Cl_2$ was only obtained when the corresponding mononuclear hydrides {*cis*-$[Pt(P\text{-}P)(H)_2]$} were isolated and then converted into the corresponding binuclear cations. With dppe mixtures, both binuclear {$[Pt_2(dppe)_2(H)_3]^+$, **5**} and trinuclear {$[Pt_3(dppe)_3(H)_3]^+$, **6**} trihydrides were obtained.

The $[Pt_2(dcype)_2(H)_3][X]$ species react with CO under mild conditions to give the binuclear p1atinum(I) hydrides $[Pt(dcype)_2(\mu\text{-}CO)(\mu\text{-}H)]^+$ (X = Cl, **7a**; BF_4, **7b**; BPh_4, **7c**).

The monuclear hydrido complex *cis*-[Pt(dcype)(CN)(H)] (**8**) has been obtained from the reaction between **1b** and KCN in methanol solution.

A preliminary report of this work has already appeared.[9]

Throughout this paper the chelating diphosphanyl ligands (P-P) are indicated as follows: dcype, 1,2-bis(dicyclohexylphosphanyl)ethane; dtbpe, 1,2-bis(di-*tert*-buthylphosphanyl)ethane; dppe, 1,2-bis(diphenylphosphanyl)ethane; dfepe, 1,2-bis[bis(perfluoroethyl)phosphanyl]ethane $(C_2F_5)_2PCH_2CH_2P(C_2F_5)$; dtbpp, 1,3-bis(di-*tert*-butylphosphanyl)propane; dippp, 1,3-bis(diisopropylphosphanyl)propane; dppp, 1,3-bis(diphenylphosphanyl)propane; butaphos, 1-(diphenylphosphinoxy)-2-[*N*-ethyl-*N*-(diphenylphosphanyl)amino]butane; dppb, 1,4-bis(diphenylphosphanyl)butane.

Results and Discussion

Our previously reported platinum binuclear trihydrides $[Pt_2(P\text{-}P)_2(H)_3]^+$ were synthesised from two different intermediates: cationic bis-pyrazole adducts (i) or μ-hydroxo binuclear cations (ii), as summarised in Scheme 1.

In the current case (P-P = dcype), attempts to operate according to path (i) were unsuccessful, owing to difficulties in isolating the pyrazolato precursor. Similarly, pathway (ii) was also unsatisfactory; compound $[Pt_2(dcype)_2(H)_3][BF_4]$ (**1a**) was isolated, but yields were erratic and often modest.[10] Analytical and NMR spectroscopic data suggested the formation of complex reaction mixtures in the first step: the synthesis of the binuclear μ-hydroxo complex $[Pt(dcype)(\mu\text{-}OH)]_2[BF_4]_2$ (**2**). The $^{31}P\{^1H\}$ NMR spectra of the crude products showed, besides the signals of compound **2**, a number of resonances in the 55−75 ppm range, probably due to other platinum species with oxygen donors. The values of the $^1J_{P,Pt}$ coupling constants, 3900−3400 Hz, suggest species with a *trans* P−Pt−O arrangement with anionic (OH or OR) rather than neutral (H_2O or CH_3OH) ligands (e.g. ref.[11b]). The chelating behaviour of dcype is confirmed by the large ^{31}P downfield shift with respect to the free ligand ($\Delta\delta$ = 50−70 ppm).

An analytical sample of the intermediate **2** was isolated from the crude product as a less soluble species in acetone. Its spectroscopic (IR, $^{3l}P\{^1H\}$ NMR, and FAB MS) properties (see Exp. Sect.) are highly reminiscent of those of homologous cations with various bis(diphenylphosphanyl)alkanes.[11]

The cation $[Pt_2(dcype)_2(H)_3]^+$ (**1**) had previously been detected in solution by multinuclear NMR spectra either as the final product of the decomposition of *cis*-$[Pt(dcype)(H)_2]$[7b] or as that of the protonation of the platinum(I) dihydride $[Pt(dcype)(H)]_2$,[5a] this compound also being reversibly obtained from *cis*-$[Pt(dcype)(H)_2]$[5a] (see Scheme 2).

It therefore seemed that cation **1** might be directly obtainable in a one-pot reaction, through the controlled decomposition of *cis*-$[Pt(dcype)(H)_2]$. Indeed, we were able to obtain the complex $[Pt_2(dcype)_2(H)_3][Cl]$ (**1b**) in high yields by treatment of a dichloromethane solution of $[Pt(dcype)Cl_2]$ with an ethanol solution of $NaBH_4$ (Pt/BH_4^- mo1ar ratio 1:2) at room temperature (under dinitrogen atmosphere). At lower reaction temperatures the yield was decreased and unchanged $[Pt(dcype)Cl_2]$ was recovered. Significant amounts of the mononuclear dihydride *cis*-$[Pt(dcype)(H)_2]$ have occasionally been detected in the crude products of synthesis reactions of compound **1b**; these could be converted into the compound $[Pt_2(dcype)_2(H)_3][OH]$ (**1c**) by treatment with wet methanol.

The corresponding tetrafluoroborate **1a** and the tetraphenylborate $[Pt_2(dcype)_2(H)_3][BPh_4]$ (**1d**) were easily obtained from **1b** through a metathesis reaction with a large excess of the sodium salt of the appropriate anion in methanol solution. Moreover, the more nucleophilic CN^- anion disrupts the binuclear core. Under analogous experimental conditions, complex **1b** and KCN react to give, in high yields, the mononuclear hydride *cis*-[Pt(dcype)(CN)(H)] (**8**), which in turn, in $CDCl_3$ solution, slowly decomposes to afford mixtures of *cis*-$[Pt(dcype)Cl_2]$ and *cis*-[Pt(dcype)(CN)(Cl)] (**9**). This decomposition path gave a clue for

 © 2003 Wiley-VCH Verlag GmbH & Co. KGaA, Weinheim

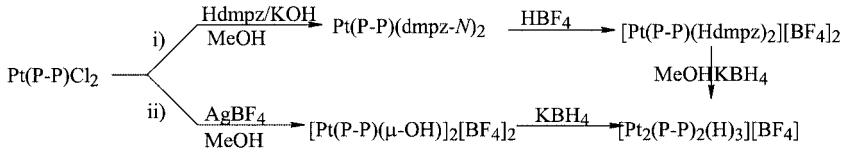

Hdmpz = 3,5-dimethylpyrazole

Scheme 1

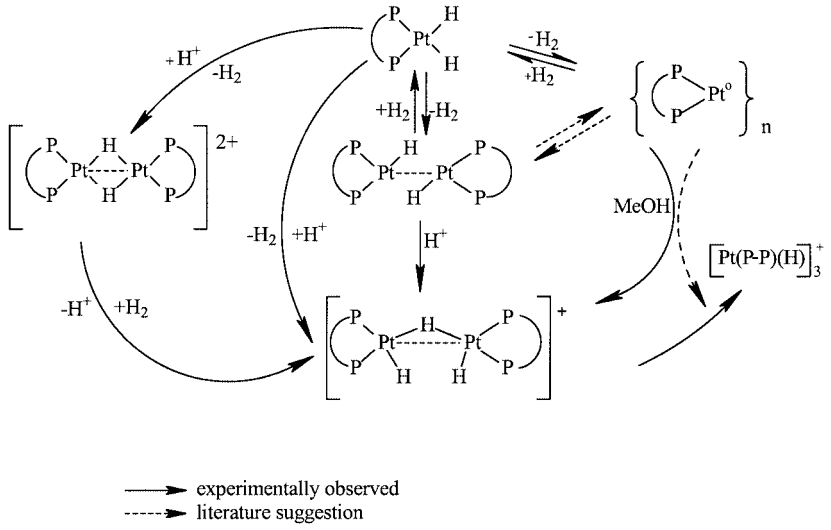

Scheme 2. For a detailed discussion of the steps summarised in this scheme see references [4−8]

reliable assignment of the NMR parameters of complex **8** (see Exp. Sect.), which indicate a larger *trans* influence from the terminal hydride [$^1J_{P(trans\text{-}H)\text{-}Pt}$ = 1714 Hz] than from the cyanide ligand [$^1J_{P(trans\text{-}CN)-Pt}$ = 2706 Hz].

A significant improvement was obtained on carrying out the synthesis of compound **1b** starting from [Pt(COD)Cl_2], the commonest precursor of Pt(P-P)Cl_2 species. Yields of **1b** close to 65% were obtained under the same experimental conditions by sequential addition of dcype ligand and $NaBH_4$ to a dichloromethane solution of [Pt(COD)Cl_2].

The role of the mononuclear *cis*-[Pt(P-P)$(H)_2$] complexes to give platinum polyhydrides is summarised in Scheme 2.

It is also worth notice that the neutral Pt^I and 28 e^- dihydrido species have been isolated only with aliphatic diphosphanes and that the complex *cis*-[Pt(dcype)$(H)_2$] seems to be the unique complex that acts as an effective precursor of all the known types of binuclear polyhydrides.

Thus, if the *cis*-[Pt(P-P)$(H)_2$] complexes are assumed to function as effective precursors in the formation of the binuclear trihydrides directly from [Pt(P-P)Cl_2], a dimerisation (see Scheme 2) aimed at a one-step synthesis could be envisaged under experimental conditions designed to enhance the lifetime of the mononuclear *cis*-dihydrides and avoid total dihydrogen loss (the most favoured reaction). We tested this approach to obtain complexes bearing bis(diphenylphosphanyl)alkane derivatives (dppe, dppp, and dppb) as ligands.

As far as we know, only two examples of *cis*-[Pt(P-P)$(H)_2$] compounds with (diphenylphosphanyl)alkane ligands (P-P = dppp, dppb) have been isolated and characterised; both are unstable in the absence of a dihydrogen atmosphere.[7c] In the dppe case, the mononuclear hydride was reported to be a source either of Pt^0 species[7a] or of various hydrides.[4d] Carmichael and co-workers inferred from a VT. NMR study (from 233 K to room temperature) that the hydride formation follows the sequence:[4d] *cis*-[Pt(dppe)$(H)_2$], [Pt(dppe)$(H)]_2$, [Pt_2(dppe)$_2(H)_3]^+$, and then [Pt_3-(dppe)$_3(H)_3]^+$.

We carried out a few attempts under different conditions (see Exp. Sect.) starting from the appropriate [Pt(P-P)Cl_2] precursor and obtained the binuclear hydrides [Pt_2(P-P)$_2(H)_3$][Cl] (P-P = dppp, **3a**; P-P = dppe, **5b**). However the one-pot reaction was unattractive, due to the unsatisfactory yields. With the dppe ligand, the major product was always the trinuclear cation [Pt_3(dppe)$_3(H)_3]^+$ (**6**),[4d,12] the product of a formal addition of a (P-P)Pt^0 fragment to the binuclear cation **5**.

However, compounds [Pt_2(P-P)$_2(H)_3$][OH] (P-P = dppp, **3b**; P-P = dppb, **4**) were obtained in nearly quantitative yields, provided that the corresponding mononuclear hy-

 © 2003 Wiley-VCH Verlag GmbH & Co. KGaA, Weinheim

drides were isolated. These were quickly converted into **3b** and **4**, respectively, after dissolution, under dinitrogen, in common organic solvents (e.g. chloroform).

The same conversion also occurs in the solid state: after two months, a not carefully stored sample of *cis*-[Pt(dppp)$(H)_2$] was found to have been fully converted into compound **3b**. Dimerisation reactions in the solid state are not unprecedented, but in the present case, in addition to a facile H_2 loss, the process requires a proton source, reasonably atmospheric moisture. In solution we cannot exclude different processes, as previously suggested for, for example, the formation of the cations $[Pt_2\{R_2P(CH_2)_nPR_2\}_2(H)_3]^+$ [R = *t*Bu, *n* = 2 (dtbpe), 3 (dtbpp)].[4b]

In the case of the dppe ligand, the one-pot reaction seems to be more profitable for synthesis of the trinuclear **6** species than of the binuclear **5**. The yield of compound **6**, calculated from the amounts of [Pt(dppe)Cl_2] consumed, reached 65%, a significant improvement with respect to the values obtained with other precursors {26% from the hydride **5** and from [Pt(dppe)(μ-OH)]$_2^{2+}$, and 30% from [Pt(dppe)$(Hdmpz)_2]^{2+}$},[12b] which in turn require at least two other synthetic steps from [Pt(dppe)Cl_2]. On the other hand, the isolation of the *cis*-[Pt(dppe)$(H)_2$] is ruled out by its well established instability, even though its formation during the one-pot reaction is suggested by the occasional presence in the ^{1}H NMR spectra of a complex multiplet [hydrido region in $(CD_3)_2CO$: δ ≈ −3.6, $^2J_{P-H}$ ≈ 168 and 10 Hz] with satellites (1:4:1; $^1J_{Pt-H}$ ≈ 880 Hz).

All the compounds **1**−**8** reported here have been identified by analytical and spectroscopic data, while the solid-state structure of complex **1d** has been established by single-crystal X-ray diffraction at 200 K.

The spectroscopic data for cation **1** are consistent with those reported for the analogous hydrides and are not significantly affected by the nature of the counter-ions.

The IR spectra show a strong and broad ν_{Pt-H} vibration at 1980 cm^{-1} (in CH_2Cl_2), not observed in the corresponding deuterides and thus attributable to terminal Pt−H bonds.

The ^{1}H, ^{31}P{^{1}H}, and ^{195}Pt NMR spectra confirm fluxional behaviour, not frozen at least down to 183 K. The hydrido resonance appears as a typical quintet with four satellites (intensity ratios: 1:8:18:8:1) indicating the magnetic equivalence of the four phosphorus and two platinum atoms.

Consistently, the ^{195}Pt{^{1}H} NMR spectra show the resonance of the most abundant isotopomer (^{195}Pt-Pt: 44.8%) as a triplet of triplets. In the ^{195}Pt{^{31}P} spectrum the central resonance is split into a quadruplet, giving unequivocal evidence for the number of hydrido ligands.

This determination is obviously a crucial point for the correct assignment of a new compound to the appropriate family of the different binuclear hydrides, namely the 30 e$^-$ species {[Pt(P-P)$(H)]_2$ or [Pt$_2$(P-P)$_2(H)_3]^+$} or the 28 e$^-$ derivatives {[Pt(P-P)$(H)]_2^{2+}$}. As these compounds are often formulated on the basis of spectroscopic data in solution, it is worth comparing their relevant IR and NMR spectroscopic properties (see Table 1).

In the IR spectra, the region of the terminal Pt−H stretching seems to be a diagnostic feature: the 28 e$^-$ species do not in fact show any vibration in this region, while one or two bands are observed in the case of 30 e$^-$ complexes (the Pt^{II} cations and the neutral Pt^I species, respectively).

In the NMR spectra the multiplicities of the main resonances, as well as the satellites' intensities, have no diagnostic value, owing to the fluxionality and identical nuclearity mentioned above. Significant differences between various NMR parameters are observed, however. Provided that the same diphosphanyl ligand is present, the following points can be used in order to distinguish the different binuclear hydrides: (i) greater $^1J_{H-Pt}$ values are associated with 28 e$^-$ species, (ii) shifts towards higher field of the hydrido resonances and smaller $^2J_{P,P}$ values are observed in the case of the 30 e$^-$ cations, and (iii) the neutral Pt^I complexes show the greatest $^2J_{P,Pt}$ values.

These observations allowed, inter alia, the proposal of a binuclear platinum(I) dihydride [Pt(dppp)$(H)]_2$ [^{1}H NMR in CD_2Cl_2 (hydrido region): δ = −1.5 (quintet with 1:8:18:8:1 satellites, $^1J_{Pt-H}$ = 529, $^2J_{P-H}$ = 39 Hz) ppm; ^{31}P{^{1}H} NMR (CD_2Cl_2): δ = 19.2, $^1J_{P,Pt}$ = 2420, $^2J_{P,Pt}$ = 318, J_{P-P} = 37 Hz] as a by-product in the crude mixtures isolated in the attempts to synthesise cation **3** directly from Pt(dppp)Cl_2.

Compounds **1a**, **1b**, or **1c** do not react with excess $NaBH_4$, unlike **5**, which gave rise to the trinuclear cation **6** $[Pt_3(dppe)_3(H)_3]^+$. We observe that these trinuclear hydrides are not known with diphosphanyl ligands that stabilise mononuclear *cis*-dihydrides in respect to Pt^0 species (i.e., with dppp, dppb, dtbpe, dtbpp, dippp, and dcype ligands).

Compounds **1a**, **1b**, and **1d** react with CO to give the corresponding μ-hydrido μ-carbonyl platinum(I) derivatives [Pt$_2$(dcype)$_2$(μ-H)(μ-CO)][X] (X = Cl, **7a**; BF_4, **7b**; BPh_4, **7c**), isolated as blue-green powders. The reactions, carried out as reported previously for the analogous species with various diphosphanyl ligands,[4e,13] seem to be dependent on the counter-ions: species **7b** and **7c** are in fact obtained nearly quantitatively, while the yields of **7a** are lower, due to the formation of minor by-products often including [Pt(dcype)Cl_2].

Their spectroscopic features (IR and NMR spectra) are reminiscent of those observed for the homologous complexes with different diphosphanes either of platinum[4e,13] or of palladium.[14] The IR spectra show the strong absorption due to the bridging carbonyl group at about 1710 cm^{-1}. Slight differences are observed with the different anions.

In the ^{1}H NMR spectra (300 MHz), the main resonance of the hydride (δ ≈ +0.7) and of the diphosphanyl ligand resonances overlap, so that only the two external satellites of the hydrido ligand ($^1J_{H-Pt}$ = 984 Hz) are observed. Their multiplicity (up to 323 K) is intermediate between the previously reported limiting spectra,[13] a quintet (fast exchange region) and a triplet of triplets (frozen), suggesting that the exchange process is slower in this case. Variable

 © 2003 Wiley-VCH Verlag GmbH & Co. KGaA, Weinheim

Table 1. Relevant IR and NMR data for selected diphosphanyl platinum hydrides

Compound	^1H[a] Hydrido region[b]			$^{31}P\{^1H\}$[a]					IR	Ref.
	δ	$^1J_{H-Pt}$	$^2J_{H-P}$	δ	$^1J_{P-Pt}$	$^2J_{P-Pt}$	$^3J_{P,P}$	J_{Pt-Pt}	ν_{Pt-H}	
$[Pt(P\text{-}P)H]_2$										
dcype[c] [d]	0.49	512	40	92.8	2180	420	44		1965, 1937	[5a]
dippe[c][e]	0.49	516	40	105.5	2210	410	45		1939, 1926	[5a]
dtbpe[c][f]	0.05	570	42	119.9	3112	362	47		1975, 1931	[5a]
dppe[g]	0.30[h]	564	42	70.9	2201	388	44	1902	not isolated	[4c]
$[Pt(P\text{-}P)H]_2^{2+}$ [i]										
dcype	n.r.[j]	n.r.[j]	n.r.[j]	96	2758	134	26		1644	[6]
dtbpe	1.72[k]	786	[k]	119	2880	139	35	1280	1631	[6]
dtbpp	0.12	767	31	61	2861	133	20[l]	1820	1629	[6]
$[Pt_2(P\text{-}P)_2(H)_3]^+$ [m]										
dcype	−2.77	480	38	84.0	2803	150	8.1	801	1980 s,br[n]	this work
dtbpe	−3.85	443	40	108.7	2946	161	7.9	815	2000, 1650	[4a]
dtbpp	−5.89	396	38	49.4	3039	168	6.8	840	2045, 1650	[4a]
dppe	−2.8	500	41	57.2	2925	171	9.8	793	2000 w,br	[4b]
dppp	−3.7	458	40	9.0	2913	172	7.3		2020 m,br	[4b]
$[Pt_3(dppe)_3(H)_3]^+$	−1.6	387	29	57.8	2837	108	17.7		2010 s	[12]

[a] At ambient temperature unless otherwise stated; *J* in Hz. [b] always observed as quintets with satellites. [c] In C_6D_6. [d] Frozen at 237 K. [e] Frozen at 219 K. [f] Fluxional at 183 K. [g] In $[D_8]$THF. [h] At 213 K. [i] In CD_2Cl_2. [j] Not reported. [k] Triplet of triplets: $^2J_{H-P}$*trans* = 73; $^2J_{H-P}$*cis* = 7. [l] Reported as mean value. [m] In $CDCl_3$. [n] In CH_2Cl_2.

temperature $^{31}P\{^1H\}$ NMR spectra (121.5 MHz) show a broad singlet with satellites at 323 K, which is split at room temperature. The dynamic behaviour of compounds **7a−c** seems to be frozen at ca. 223 K, allowing the full set of coupling constants for the hydrido resonance and for the two couples of equivalent P nuclei to be evaluated.

X-ray Crystal Structure of Compound 1d

The structure of compound **1d** consists of packing of $[Pt_2(dcype)_2(H)_3]^+$ cations and BPh_4^- anions in the molar ratio of 1:1 with normal van der Waals contacts. An ORTEP view of the cation is shown in Figure 1, while selected interatomic distances and angles are listed in Table 2. The cation consists of two five-membered rings, each made up of a Pt atom and a chelating dcype ligand, separated by a

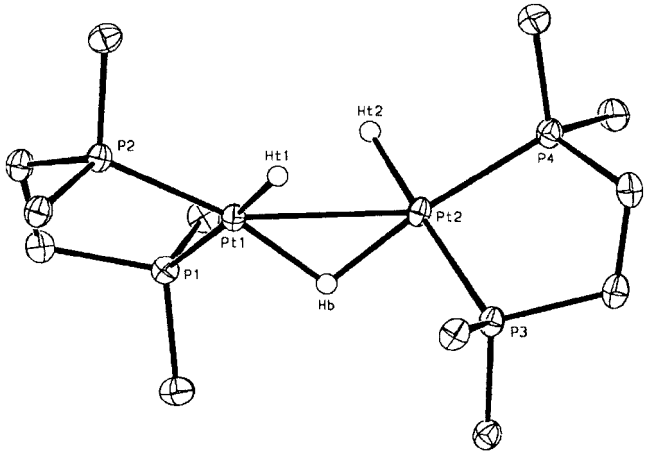

Figure 1. ORTEP view of the inner core of cation **1**, $[Pt_2(dcype)_2(H)_3]^+$; ellipsoids are drawn at 30% probability level

Table 2. Selected bond lengths [Å] and angles [°] for cation **1d** (e.s.d.s in parentheses)

Pt(1)−Pt(2)	2.696(1)	Pt(1)−P(l)	2.281(1)
Pt(1)−P(2)	2.223(1)	Pt(1)−Ht(1)	1.63(2)
Pt(1)−Hb	1.69(3)	Pt(2)−P(3)	2.277(1)
Pt(2)−P(4)	2.227(1)	Pt(2)−Ht(2)	1.61(2)
Pt(2)−Hb	1.75(2)		
P(2)−Pt(1)−P(1)	117.2(1)	Pt(2)−Pt(1)−P(2)	149.5(1)
P(1)−Pt(1)−P(2)	88.4(1)	P(1)−Pt(1)−Ht(1)	176.7(8)
P(1)−Pt(1)−Hb	91.5(9)	P(2)−Pt(1)−Ht(1)	88.5(8)
P(2)−Pt(1)−Hb	166.5(9)	Ht(1)−Pt(1)−Hb	92(1)
Pt(1)−Pt(2)−P(3)	116.3(1)	Pt(1)−Pt(2)−P(4)	149.7(1)
P(3)−Pt(2)−P(4)	88.2(1)	P(3)−Pt(2)−Ht(2)	177.6(9)
P(3)−Pt(2)−Hb	89.7(8)	P(4)−Pt(2)−Ht(2)	90.2(8)
P(4)−Pt(2)−Hb	171(1)	Ht(2) −Pt(2)−Hb	92(1)

Pt-Pt distance of 2.696(1) Å, which is the shortest value observed in these trihydrido cations but similar to that reported in the case of the doubly hydrido bridged 28e$^-$ species $[Pt(dcypp)(H)]_2^{2+}$ [Pt−Pt = 2.698(1) Å].[6] The two Pt atoms are also bonded to three hydride ligands, one bridging the Pt−Pt vector, and two terminally bonded, one for each metal atom.

The dihedral angle between the Pt1−P1−P2 and Pt2−P3−P4 planes is 82.74(1)°, in agreement with the "overall conformation" detected in homologous cations. At variance with this, the same dihedral angle ranges from "90° to 180° conformations" in the reported structures of the dihydrido platinum species,[5,6] either neutral Pt^I complexes $[Pt(P\text{-}P)(H)]_2$ or 28 e$^-$ platinum(II) cations $[Pt(P\text{-}P)(H)]_2^{2+}$, in which the geometry around each platinum centre was assumed to be square-planar as in cation **1**. The

 © 2003 Wiley-VCH Verlag GmbH & Co. KGaA, Weinheim

accommodation of the third hydride in the $Pt_2(P\text{-}P)_2(H)_2$ core may be responsible for the "90° conformation" which appears as a typical feature of these platinum(II) 30 e^- cations.

Bond lengths and angles involving the Pt atoms in the current cation can be compared with those found in cation $[Pt_2(butaphos)_2(H)_3]^+$ (**10**).[4g] Cation **10** differs from the present one only in the substitution of the two dcype ligands with two butaphos ones. In both cations the overall coordination around the Pt atom, if the Pt−Pt bond is neglected, can be described as distorted square planar, and the idealised symmetry of the two cations is C_2, with the two-fold axis passing through the bridging hydride ligand and the midpoint of the Pt−Pt vector. The Pt−P distances are of two kinds: two shorter [Pt1−P2 2.223(1) vs. 2.222(3) Å in **10**, and Pt2−P4 2.227(1) vs. 2.217(3) in **10**], and two longer [Pt1−P1 2.281(1) vs. 2.324(3) Å in **10**, and Pt2−P3 2.277(1) vs. 2.309(3) Å in **10**]. The longer bonds are approximately *trans* to the terminal hydrides, displaying the expected *trans* influence. We also note that the Pt1−P1 and Pt2−P3 bonds are significantly longer in **10**, possibly due to the different steric requirements of the butaphos and dcype ligands and the formation of seven vs. five-membered metallacycles, respectively.

Whereas in **10** only two hydride atoms had been detected in the final Fourier maps, and the third was placed in its position on the basis of symmetry considerations, in the current cation the three hydrides have been found in the final Fourier maps and included in the refinement with isotropic thermal parameters, thus confirming the stereochemistry suggested for **10**.[4g] The current structure is the first X-ray determination of a complex of the type $[Pt_2(P\text{-}P)_2(H)_x]^{n+}$ ($x = 2$, $n = 0, 2$; $x = 3$, $n = 1$) in which all the hydride ligands have been experimentally located, and the resulting bond parameters are consistent with those reported in the more precise neutron diffraction structure of the cation $[Pt_2(dppe)_2(H)_3]^+$.[8,15]

It was previously suggested that the geometry of the $Pt_2(P\text{-}P)_2(H)_3$ cores is controlled by the steric bulk of the phosphorus substituents,[4f] rather than by the bite angle of the chelating diphosphane. This view is supported by the current structure if comparison is made with the analogous cation with dppe: different structures are indeed observed with two diphosphanes with different steric bulk but similar bite angles. On the other hand, the same structure was reported for cations with diphosphanes displaying the same bite angle but different substituents (as in **10** or with dtbpp).[4b,4g] The available X-ray structure determinations therefore suggest that no conclusive statement can be made on this point, and that misleading conclusions may be drawn by use of comparison criteria focused only on these ligand features. As previously emphasised,[4c] the fluxional behaviour in solution suggests a very soft energy surface producing different core conformations, so that even apparently weak forces, such as crystal packing forces, could well be responsible for structural differences involving small energy changes. In this connection, it is worth noting the significant change, from a 90° to a 180° conformation, in the polymorphic platinum(I) hydride $[Pt(dfepe)H]_2$[5b] observed to occur at very low energy, also in the solid state.

Incoherent Inelastic Neutron Spectroscopy (INS) of 1a and 5a

As the structures of $[Pt_2(dcype)_2(H)_3][BF_4]$ (**1a**) and $[Pt_2(dppe)_2(H)_3][BF_4]$ (**5a**) have been shown by diffraction methods (X-ray and neutron for **1a** and **5a**,[4c,8] respectively) to be different, we have carried out an INS spectroscopic study of these complexes to obtain additional information on the nature of the Pt−H interactions.

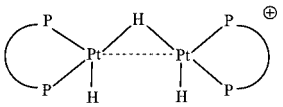

1a

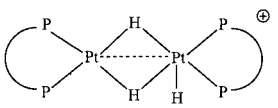

5a

While the vibrational modes of bridging hydrides can be investigated by optical spectroscopy,[16] this is in general rather difficult because of severe line broadening and interference from other modes. Instead, INS has the major advantage that the incoherent neutron scattering cross section for hydrogen is much larger than that for all other atomic species and that modes involving H atoms therefore dominate the INS spectra. To distinguish the vibrational modes of the hydrides from those of the hydrogens in the ligands unambiguously, however, a "sample difference"[17] technique has been used (see Exp. Sect.).

The INS difference spectra of **5a** and of **1a** are shown in Figures 2 and 3, respectively. As can be seen, the two spectra are quite different, reflecting the different coordination of the two "Pt_2H_3" moieties.

Although a complete assignment of the vibrational modes would require a normal coordinates analysis, a qualitative assignment of the main spectral features may still be carried out on the basis of published data for similar binuclear complexes[18] and other metal hydrides.[16,19] We note that the stretching frequency for a terminal "Pt−H" group is to be expected in the 1900−2100 cm^{-1} region,

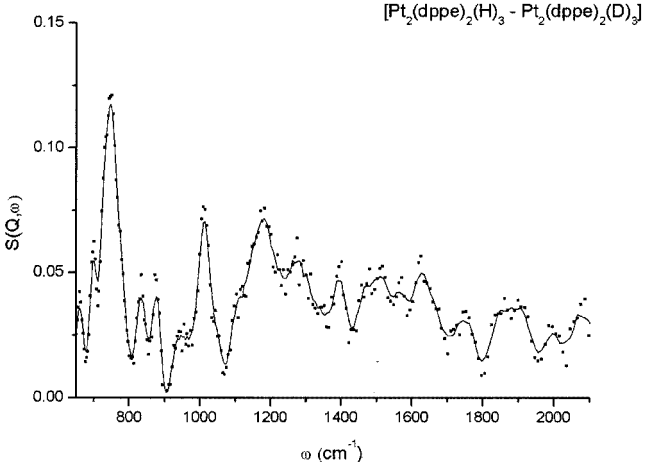

Figure 2. INS difference spectrum for compound **5a**; the line is drawn only as a guide for the eye

 © 2003 Wiley-VCH Verlag GmbH & Co. KGaA, Weinheim

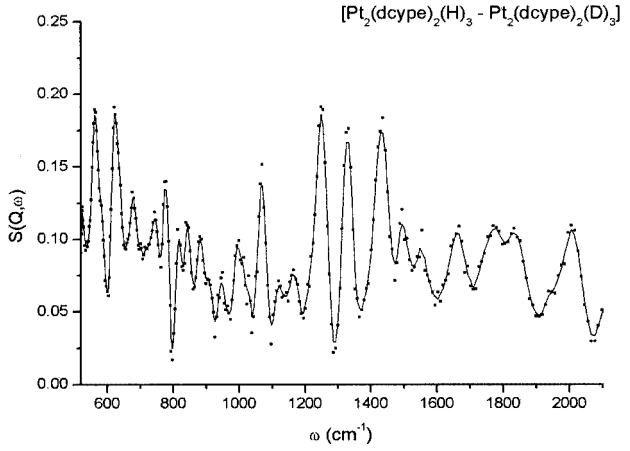

Figure 3. INS difference spectrum for compound **1a**; the line is drawn only as a guide for the eye

while the modes involving the μ-bridging H may be described in terms of a symmetric (ν_s) and anti-symmetric (ν_{as}) M−H−M stretching modes (1000−1400 cm^{-1}) as well as skeletal deformations and torsions (i.e., δ_{PMH} and δ_{MHM}) at lower frequencies.[18−20] As the intensities of the INS bands depend on the displacements of the H ligands, one would expect that the intensities of the deformation and torsional modes should be greater than those of the stretching modes, if coupling between the modes is small. These qualitative criteria allow for a relative straightforward assignment of the principal bands.

Thus, in the difference spectrum of **5a**, we assign the band at 2080 cm^{-1} to the Pt−H stretch (based on the correspondence with the IR broad band at ca. 2000 cm^{-1}), the 1170 cm^{-1} band to the ν_{as} and that at 1010 cm^{-1} to the ν_s mode of the "Pt(μ-H)Pt" moiety. The very intense bands at 750 cm^{-1} correspond to the δ_{MHM} mode of the same moiety.

It is worth noting that it is possible to obtain structural information on the M−H−M bridge from the ν_s/ν_{as} ratio. Howard and co-workers[21] have in fact shown that, if the metal framework may be regarded as rigid and the angle-bending force constant is small, then the following relation holds: $\nu_{as}/\nu_s = \tan(\theta/2)$, where θ is the M−H−M angle. We have also shown[18] that the above equation also holds accurately for compounds of the type [$PR_3LPt(\mu$-H)$PtLPR_3$] (L = Ph, H; PR_3 = PMe_3, PEt_3).

From the above assignment for **5a**, a value of θ = 98° is obtained from this relationship, in very good agreement with the average value of 97° for the Pt−H−Pt angle obtained from single-crystal neutron diffraction.[8]

The difference spectrum of **1a** clearly reflects a different disposition of the H ligands around the Pt centres, as found by X-ray diffraction. The Pt−H stretch is now at 2000 cm^{-1} [1970−1950 cm^{-1} in the IR (Nujol)], while the deformation modes are at lower frequencies (560−620 cm^{-1}), possibly reflecting the different electron densities at the metal centres due to the different basicity of the phosphanes.

A more complex pattern than in **5a** is found in the 1200−1600 cm^{-1} region. The ν_s mode is at 1080 cm^{-1}, while the ν_{as} bands are at 1240 cm^{-1} and 1340 cm^{-1}. These two bands are consistent with two slightly different environments around the two Pt atoms. Moreover, the new band at 1420 cm^{-1} may be connected with the presence of a single bridging hydride and thus a less rigid metal framework. To help with this assignment we have carried out a DFT calculation[22] on the model compound [$(PMe_3)_2HPt(\mu$-H)-$PtH(PMe_3)_2]^+$ and have found a mode at 1490 cm^{-1} corresponding to a combination of the $\nu_s(\mu$-H) and the out of plane bending of both terminal hydrides, a vibrational mode not possible when the platinum atoms are bridged by two hydrides.

These results, as also observed previously,[18] show that coupling between stretching and bending modes may be important in these bridging hydrides.

Experimental Section

Evaporation was always carried out under reduced pressure. The analytical samples were pumped to constant weight (room temperature, ca 0.1 Torr). Elemental analyses were performed by the Analytical Laboratory of the University of Milan and the Mikroanalytisches Labor Pascher (Remagen-Bandorf).

The infrared spectra were recorded on a Jasco FT/IR 420 spectrometer. NMR spectra were recorded at ambient temperature in $CDCl_3$ solutions unless otherwise stated, on a Bruker DRX 300 Avance spectrometer operating at 300 (^{1}H), 121.5 (^{31}P), and 64.5 MHz (^{195}Pt), respectively. The shift values are given in ppm from the usual standards; δ = ^{195}Pt is referred to $Na_2[PtCl_6]$ aqueous solution. Abbreviations used in the description of NMR spectroscopic data are as follows: br., broad; s., singlet; d., doublet; t., triplet; q., quintet; m., multiplet.

Solvents (RPE grade; Carlo Erba) were distilled prior to use. $NaBH_4$, $NaBD_4$ and KBH_4 were purchased from Merck, Aldrich and Fluka, respectively. The diphosphanyl ligands were obtained from Strem Chemicals and employed as received.

The [Pt(P-P)Cl_2][4d,23] from [Pt(COD)Cl_2] and the *cis*-[Pt(P-P)-$(H)_2$][7] complexes were synthesised by literature methods.

Synthesis and Characterisation. [Pt(dcype)(μ-OH)]$_2$[BF_4]$_2$ (2): The products isolated by previously reported procedures[11] were mixtures of different p1atinum species with O-donors; compound **2** was always the most abundant product (NMR). Starting from [Pt(dcype)Cl_2] (636 mg, 0.92 mmol) and $AgBF_4$ (360 mg, 1.9 mmol), the analytical sample was isolated as follows. After accurate elimination of the insoluble AgCl, the crude reaction product was crystallised from CH_2Cl_2/Et_2O. A first crop was precipitated by slow addition of diethyl ether to the dichloromethane solution; it was filtered off and then washed with acetone. Compound **2** was obtained as a residue (150 mg) slightly soluble in acetone. A second fraction (40 mg) of the same compound was obtained from the mother liquor by concentration in the presence of diethyl ether and of a few drops of MeOH. Yield 30%. IR (nujol, cm^{-1}): 3550 vbr. ν_{OH}, 1065 br. ν_{BF4}. $^{31}P\{^1H\}$ NMR: δ = 59.9 (s., $^1J_{P,Pt}$ = 3513 Hz) ppm. FAB MS (NBA): 1266 *m/z* $[M - 2H]^{+\cdot}$. M.p. 235 °C (dec). $C_{52}H_{98}B_2F_8O_2P_4Pt_2$ (1443.01): calcd. C 43.28, H 6.86, B 1.50, F 10.53, O 2.22, P 8.58, Pt 27.04; found C 43.32, H 7.10, F 9.93, P 8.4, Pt 26.7.

 © 2003 Wiley-VCH Verlag GmbH & Co. KGaA, Weinheim

$[Pt_2(dcype)_2(H)_3][X]$ (X: BF_4, 1a, Cl 1b; OH, 1c; BPh_4, 1d): The salts **1a**, **1b**, and **1c** were obtained from compound **2** (i), from $[Pt(dcype)Cl_2]$ (ii), or from *cis*-$[Pt(dcype)(H)_2]$[5a] (iii), respectively.

(i) $[Pt_2(dcype)_2(H)_3][BF_4]$ (1a): From $[Pt(dcype)(\mu\text{-}OH)]_2[BF_4]_2$ (**2**). A suspension of KBH_4 (7.5 mg. 0.14 mmol) in methanol (20 mL) was added under dinitrogen atmosphere to a stirred solution of compound **2** (172 mg, 0.12 mmol) in the same solvent (10 mL). After ten minutes the colourless solution was evaporated to dryness and the residue was extracted with CH_2Cl_2 (ca. 7 mL). The insoluble material was filtered off, and the white product (99 mg, yield 62%) was precipitated by addition of diethyl ether (ca. 20 mL) to the clear solution. IR (nujol, cm^{-1}): $\tilde{\nu}$ = 1970 s,br ν_{PtH}, 1050 s,br ν_{BF4}. FAB MS: 1237 *m/z* $[M]^+$. M.p. 218 °C (dec.). $C_{52}H_{99}BF_4P_4Pt_2$ (1325.22): calcd. C 47.14, H 7.54; found C 47.18, H 7.44.

(ii) $[Pt_2(dcype)_2(H)_3][Cl]$ (1b): From *cis*-$[Pt(dcype)Cl_2]$. A solution of $NaBH_4$ (120.0 mg, 3.17 mmol) in ethanol (50 mL) was added dropwise under dinitrogen atmosphere to a stirred solution of $[Pt(dcype)Cl_2]$ (1.00 g, 1.45 mmol) in dichloromethane (70 mL). After ten minutes, the turbid solution was evaporated to dryness and the white solid residue was extracted with few millilitres (ca. 5) of CH_2Cl_2. The crude product (830 mg) was precipitated by addition of diethyl ether to the clear, filtered solution. The analytical sample was obtained by crystallisation from CH_2Cl_2/Et_2O (790 mg; yield 85.6%). IR (nujol, cm^{-1}): 1970−1950 s,br (1980 s,br in CH_2Cl_2) ν_{PtH}. ^1H NMR (ppm): δ = 1.6−1.9 and 1.3−1.1 (m. unresolved, CH_2), δ = −2.77 (q. with satellites, H, $^1J_{H-Pt}$ = 480, $^2J_{H-P}$ = 38 Hz). $^{31}P\{^1H\}$ (ppm): δ = 84.0 (s., $^1J_{P,Pt}$ = 2803, $^2J_{P,Pt}$ = 150, $^3J_{P,P}$ = 8.1, $^1J_{Pt-Pt}$ = 801 Hz); $^{195}Pt\{^1H\}$ and $^{195}Pt\{^{31}P\}$ [$(CD_3)_2CO$, ppm]: δ = −5141 tt. ($^1J_{Pt-P}$ = 2795; $^2J_{Pt-P}$ = 148 Hz) or quadruplet ($^1J_{Pt-H} \approx$ 480 Hz), respectively. M.p. 185 °C (dec.). $C_{52}H_{99}ClP_4Pt_2$ (1273.87): calcd. C 49.04, H 7.85, Cl 2.79, P 9.74, Pt 30.65; found C 48.82, H 7.87, Cl 2.90, P 9.52, Pt 31.0.

[Depending on the $NaBH_4$ stock, indefinable salts of the binuclear cation (NMR data), possibly with B_xH_y type anions (IR suggestion), were isolated as white powders. By addition of a large excess (400%) of a methanolic solution of NH_4Cl to the reaction crude, it is converted to **1b** in few minutes (15′). This procedure is near quantitative (yield 80% after crystallisation). Take care that working with NaCl in acetone solution the major product was a yellow oily, in which 4-hydroxy-4-methyl-2-pentanone was identified by GC.MS and ^1H NMR data as the most abundant product.]

(iii) $[Pt_2(dcype)_2(H)_3][OH]$ (1c): From *cis*-$[Pt(dcype)(H)_2]$. A solution of *cis*-$[Pt(dcype)(H)_2]$ in methanol was stirred overnight under dinitrogen atmosphere, and was then evaporated to dryness. The white solid residue was dissolved in the minimum amount of CH_2Cl_2, and compound **1c** was precipitated by slow addition of diethyl ether (yield 95%). IR (nujol, cm^{-1}): 3400−3200 vs,br ν_{OH}, 1968 s,br ν_{PtH}. $C_{52}H_{100}OP_4Pt_2$ (1255.42): calcd. C 49.75, H 8.04; found C 49.31, H 7.90.

The tetraphenylborate salt **1d** was obtained variously from **1a**, **1b**, or **1c** by exchange reactions carried out in methanol solution with a large excess of $NaBPh_4$. The yields referred to analytical1y pure samples were: 80% from **1a**, 90% from **1b**, and 84% from **1c**. IR (nujol, cm^{-1}): $\tilde{\nu}$ = 1966br. s ν_{PtH}, 1580 m (BPh_4^-). M.p. 240 °C (dec). $C_{76}H_{119}BP_4Pt_2$ (1557.68): ca1cd. C 58.62, H 7.72; found C 58.71, H 7.68.

$[Pt_2(dcype)_2(D)_3][Cl]$ (1b-d_3): The deuteride was obtained by procedure (ii), but with use of $NaBD_4$ and deuterated solvents. The crude material was crystallised twice (yield 36%). $^{31}P\{^1H\}$ NMR (ppm): δ = 83.9 (br. s, $^1J_{P,Pt}$ = 2788, $^2J_{P,Pt}$ = 149, $^3J_{P,P}$ = not detectable, J_{Pt-Pt} = 802 Hz).

Reactions of $Pt(P\text{-}P)Cl_2$ (P-P = dppe, dppp, dppb) with BH_4^-: These reactions were attempted by procedure (ii) as reported above for **1b**, but under various experimental conditions [i.e., with or without H_2 atmosphere, with $NaBH_4$ or KBH_4, with use of different BH_4/Pt ratios (from 1:1 to 4:1), and at different temperatures (from −15 °C to room temperature]. Even though the formation of the $[Pt_2(P\text{-}P)_2(H)_3]^+$ cations was always observed, only the compounds $[Pt_2(dppp)_2(H)_3][Cl]$ (**3a**) and $[Pt_3(dppe)_3(H)_3][Cl]$ (**6**) were isolated as analytical samples.

The former product (**3a**) was isolated (yield 40%) by crystallisation from acetone/diethyl ether of reaction products obtained by procedure (ii), but with use of a BH_4/Pt ratio of 1:1.

With dppe ligand, under dihydrogen atmosphere but independently of temperature and BH_4/Pt ratio, the isolated powders were found to be mixtures of unchanged $Pt(dppe)Cl_2$ and variable amounts of the binuclear (**5**) and trinuclear (**6**) hydrides. Compound **6** was isolated as a pale yellow powder by slow addition of diethyl ether to clear solutions of these mixtures in a few millilitres (4−5) of dichloromethane. The best results (yield 63%) were obtained by carrying out the reactions in ethanol/dichloromethane mixtures (1:1), with use of a BH_4/Pt ratio of 4:1, either at −15 °C or at room temperature. The reaction times were 2 hours and 30 minutes, respectively.

Reaction of 1 with CO and KCN. $[Pt_2(dcype)_2(\mu\text{-}CO)(\mu\text{-}H)][X]$ (X: Cl, 7a; BF_4, 7b; BPh_4, 7c): The compounds were synthesised by bubbling CO through acetone solutions of the appropriate hydrido salt at room temperature. The colourless solutions quickly turned blue. The compounds were isolated by addition of diethyl ether to the concentrated solutions at different reaction times: 30 minutes (**7a**) or 4 hours (**7b** and **7c**). Compounds **7b** and **7c** were isolated as analytical samples (yields: 83% and 95%, respectively), while **7a** was crystallised from acetone/diethyl ether (yield 68%). IR (nujol, cm^{-1}): $\tilde{\nu}$ = 1710s ν_{CO} (1053 s,br, ν_{BF4}, **7b**; 1579 m, BPh_4, **7c**). $^{31}P\{^1H\}$ NMR [$(CD_3)_2CO$, under CO atmosphere, ppm]: δ = 64.3 (br, $^1J_{P,Pt}$ = 2260 Hz, $P_{trans\text{-}C}$), δ = 64.1 (br, $^1J_{P,Pt}$ = 4390, $^2J_{P,Pt}$ = 460 Hz, $P_{trans\text{-}H}$). ^1H NMR [$(CD_3)_2CO$, under CO atmosphere, at 243 K, ppm]: δ = +0.72 (hydrido resonance; external satellites observed as triplets of triplets: $^1J_{H-Pt}$ = 454, $J_{H-Ptrans}$ = 76, J_{H-Pcis} = 10 Hz). $^{31}P\{^1H\}$ NMR [$(CD_3)_2CO$, under CO atmosphere, at 223 K, ppm]: δ = 65.8 (d, $^1J_{P,Pt}$ = 2240, $^2J_{P,P}$ = 26 Hz, $P_{trans-C}$), δ = 65.0 (d, $^1J_{P,Pt}$ = 4370, $^2J_{P,Pt}$ = 470, $^2J_{P,P}$ = 26 Hz, $P_{trans-H}$). M.p. (dec) 200 °C, **7a**; 215 °C, **7b**; 190 °C, **7c**. $C_{53}H_{97}BF_4OP_4Pt_2$ (1351.21), **7b**: ca1cd. C 47.14, H 7.25, found C 47.42, H 7.22.

***cis*-Pt(dcype)(H)(CN) (8):** A suspension of KCN (100 mg; 1.54 mmol) in methanol (20 mL) was added to a vigorously stirred solution of **1b** (400 mg, 0.314 mmol) in the same solvent (25 mL). The solution immediately fizzed and a white precipitate was formed. After ten minutes the suspension was evaporated to dryness, the white residue was dissolved in CH_2Cl_2, and the insoluble material was filtered off; this was repeated twice. The analytical sample (300 mg; yield 75.3%) was obtained by addition of a large excess of diethyl ether to few millilitres of a dichloromethane solution of the crude product. IR (nujol, cm^{-1}) 2118 vs ν_{CN}, 1992 vs ν_{PtH}. ^1H NMR (hydrido region, ppm): δ = −2.01 (dd, $^2J_{H-Ptrans}$ = 178.4, $^2J_{H-Pcis}$ = 15; $^1J_{H-Pt}$ = 986 Hz). $^{31}P\{^1H\}$ NMR (ppm): δ = 71.8 (s, $^1J_{P(transCN)-Pt}$ = 2706 Hz), δ = 69.0 (s, $^1J_{P(transH)-Pt}$ = 1714 Hz). $^{195}Pt\{^1H\}$ NMR [$(CD_3)_2CO$, ppm]: δ = −5244 (dd). FAB MS (NBA): 644 *m/z* $[M]^{+\cdot}$. M.p.: 180 °C (dec). $C_{27}H_{49}NP_2Pt$ (644.72): calcd. C 50.30, H 7.68, N 2.17; found C 49.93, H 7.70,

 © 2003 Wiley-VCH Verlag GmbH & Co. KGaA, Weinheim

Table 3. Crystallographic data

Compound	**1d**
Formula	$C_{76}H_{119}BP_4Pt_2$
M	1557.68
Colour	Colourless
Crystal system	Monoclinic
Space group	$P2_1/n$ (no.14)
a [Å]	23.637(2)
b [Å]	13.328(1)
c [Å]	24.351(2)
α [°]	90
β [°]	109.17(1)
γ [°]	90
U [Å^3]	7246.0(11)
Z	4
F(000)	3184
Dc [g cm^{-3}]	1.43
T [K]	200
Crystal dimensions [mm]	0.25 × 0.25 × 0.40
μ (Mo-$K\alpha$) [cm^{-1}]	40.23
Min. and max. transmission factors	0.76−1.00
Scan mode	ω
Frame width [°]	0.30
Time per frame [s]	20
No. of frames	2450
Detector−sample distance [cm]	5.00
θ-range [°]	3−25
Reciprocal space explored	full sphere
No. of reflections (total; independent)	63529; 12751
R_{int}	0.038
Final R_2 and R_{2w} indices[a] (F^2, all reflections)	0.029, 0.043
Conventional R_1 index [$I > 2\sigma(I)$]	0.018
Reflections with $I > 2\sigma(I)$	10901
No. of variables	760
Goodness of fit[b]	0.93

[a] $R_2 = [\Sigma(F_o^2 - kF_c^2)/\Sigma F_o^2]$, $R_{2w} = [\Sigma w(F_o^2 - kF_c^2)^2/\Sigma w(F_o^2)^2]^{1/2}$. [b] $[\Sigma w(F_o^2 - kF_c^2)^2/(N_o - N_v)]^{1/2}$, where $w = 4F_o^2/\sigma\ (F_o^2)^2$, $\sigma(F_o^2) = [\sigma^2(F_o^2) + (0.02F_o^2)^2]^{1/2}$, N_o is the number of observations and N_v the number of variables.

N 2.16. During the $^{195}Pt\{^1H\}$ NMR spectrum ($CDCl_3$ solution) acquisition, compound **8** was converted into [Pt(dcype)Cl$_2$] and *cis*-[Pt(dcype)(Cl)(CN)] (**9**): $^{31}P\{^1H\}$ NMR (ppm): δ = 65.4 (s, $^1J_{P(trans\,Cl)-Pt}$ = 3337 Hz), δ = 63.0 (s, $^1J_{P(trans\,CN)-Pt}$ = 2568 Hz). $^{195}Pt\{^1H\}$ NMR (ppm): δ = −4839 (dd).

X-ray Data Collection and Structure Determination: Crystal data and other experimental details are summarised in Table 3. The diffraction experiment was carried out on a Bruker SMART CCD area-detector diffractometer at 200 K by use of Mo-$K\alpha$ radiation (λ = 0.71073 Å) with a graphite crystal monochromator in the incident beam. Cell parameters and orientation matrix were obtained from least-squares refinement of 123 reflections each measured in three different sets of 15 frames, in the range $3 < \theta < 23°$. At the end of data collection the first 50 frames, containing 235 reflections, were recollected to monitor crystal decay. No correction was necessary. The collected frames were processed with the SAINT software package,[24] and an absorption correction was applied (SADABS)[25] to the 63529 collected reflections, 12751 of which are unique with R_{int} = 0.0378 ($R_{int} = \Sigma|F_o^2 - F_{mean}^2|/\Sigma F_o^2$).

The calculations were performed on a Pentium III Pc by use of the Personal Structure Determination Package[26] and the physical constants tabulated therein. Scattering factors and anomalous dispersion corrections were taken from ref. 27. The structure was solved by direct methods (SHELXS 86)[28] and refined by full-matrix, least-squares, by using all reflections and minimising the function $\Sigma w(F_o^2 - kF_c^2)^2$. Anisotropic displacement factors were refined for all the non-hydrogen atoms. The three hydrides were found in the final Fourier maps and refined isotropically. The other hydrogen atoms were placed in their ideal positions (C−H = 0.97 Å, B 1.10 times that of the carbon atom to which they are attached) and not refined. In the final difference Fourier map the maximum residual was 1.06(14) Å^{-3} at 0.78 Å from Pt(2). CCDC-208551 contains the supplementary crystallographic data for this paper. These data can be obtained free of charge at www.ccdc.cam.uk/conts/retrieving.html or from the Cambridge Crystallographic Data Centre, 12 Union Road, Cambridge CB2 1EZ, UK; fax: (internat.) +44−1223/336-033; E-mail: deposit@ccdc.cam.ac.uk.

Inelastic Incoherent Neutron Scattering (INS) Measurements: The INS experiments were carried out on TOSCA-I, a crystal-analyser inverse-geometry spectrometer[29] operating at the ISIS pulsed-neutron source. The incident neutron beam spans a broad energy (E_0) range and energy selection is carried out on the secondary neutron flight-path by use of the (002) Bragg reflection of a graphite analyser placed in back-scattering position (≈ 136°). The resolving power of TOSCA-I is fairly good ($2\% < \Delta\hbar\omega/E_0 < 3.5\%$) in the accessible energy transfer range (24 cm^{-1} < ħω < 8065 cm^{-1}) making this instrument a neutron equivalent of a Raman optical spectrometer. All the intramolecular vibrations can in principle be easily observed by INS spectroscopy, but it should be also pointed out that, due to molecular recoil, the neutron-measured frequencies might be slightly different from those observed on a conventional Raman spectrometer.

The measurements were carried out on samples of [Pt$_2$(dppe)$_2$(H)$_3$][BF$_4$] (**5a**) and [Pt$_2$(dcype)$_2$(H)$_3$][BF$_4$] (**1b**) and their deuterium analogues (approximately 1 g each), all contained in individual thin Al-film bags. During the data collection, the samples were maintained at ca. 12 K and the spectra were recorded up to an integrated proton current of 1967 μA/h (roughly 10 hours of beam time).

In order to distinguish the M−H vibrational modes from all other vibrations involving hydrogen atoms of the ligands, a "sample difference" technique[17] was used. The method is based on the fact that the incoherent neutron scattering cross sections of hydrogen and deuterium are very different [79.91(4) and 2.94(3) barn, respectively),[30] making vibrational modes involving D atoms difficult to detect by INS in the presence of many hydrogen atoms. The difference between two experimental INS spectra (i.e., those containing the "Pt−D" and "Pt−H" moieties) should thus only leave the peaks involving the motion of the hydrides (bridging or terminal), provided that any possible coupling of the hydride modes to other molecular modes is negligible (on the scale of the resolution of the INS experiment). Therefore, as the contribution from the ligand modes is subtracted out, it is unnecessary to prepare samples with fully deuterated ligands.

Acknowledgments

A. A. and G. B. wish to thank the MIUR for financial support (PRIN 2002). We also wish to thank Mr. P. Illiano for assistance with the NMR experiments. Work at LANL was supported by the Office of Science, U. S. Department of Energy.

[1] M. Green, J. A. K. Howard, J. L. Spencer, F. G. A. Stone, C. A. Tsipis, *J. Chem. Soc., Chem. Commun.* **1976**, 671−672.
[2] e.g. [2a] L. M. Venanzi, *Coord. Chem. Rev.* **1982**, *43*, 251−274.

 © 2003 Wiley-VCH Verlag GmbH & Co. KGaA, Weinheim

[2b] F. Bachechi, *Acta Crystallogr., Sect. C* **1993**, *49*, 460−464, and references quoted therein.
[3] e.g. [3a] R. J. Puddephatt, *Chem. Soc. Rev.* **1983**, *12*, 99−127. [3b] C. Xu, G. K. Anderson, *Organometallics* **1996**, *15*, 1760−1764, and references cited therein.
[4] [4a] G. Minghetti, A. L. Bandini, G. Banditelli, *J. Organomet. Chem.* **1977**, *139*, C80−C82. [4b] T. H. Tulip, T. Yamagata, T. Yoshida, R. D. Wilson, J. A. Ibers, S. Otsuka, *Inorg. Chem.* **1979**, *18*, 2239−2250. [4c] C. B. Knobler, H. D. Kaesz, G. Minghetti, A. L. Bandini, G. Banditelli, F. Bonati, *Inorg. Chem.* **1983**, *22*, 2324−2331. [4d] D. Carmichael, P. B: Hitchcock, J. F. Nixon, A. P. Pidcock, *J. Chem. Soc., Chem. Commun.* **1988**, 1554−1556. [4e] A. L. Bandini, G. Banditelli, M. A. Cinellu, G. Sanna, G. Minghetti, F. Demartin, M. Manassero, *Inorg. Chem.* **1989**, *28*, 404−410. [4f] B. S. Haggerty, C. E. Housecroft, A. L. Rheingold, B. A. M. Shaykh, *J. Chem. Soc., Dalton Trans.* **1991**, 2175−2184. [4g] A. L. Bandini, G. Banditelli, E. Cesarotti, F. Demartin, M. Manassero, G. Minghetti, *Gazz. Chim. Ital.* **1994**, *124*, 43−50.
[5] [5a] D. J. Schwartz, R. A. Andersen, *J. Am. Chem. Soc.* **1995**, *117*, 4014−4025. [5b] B. L. Bennett, D. M. Roddick, *Inorg. Chem.* **1996**, *35*, 4703−4707. [5c] M. D. Fryzuk, G. K. B. Clentsmith, D. B. Leznoff, S. J. Rettig, S. J. Geib, *Inorg. Chim. Acta* **1997**, *265*, 169−177.
[6] L. Mole, J. L. Spencer, S. A. Litster, A. D. Redhouse, N. Carr, A. G. Orpen, *J. Chem. Soc., Dalton Trans.* **1996**, 2315−2321.
[7] [7a] T. Yoshida, T. Yamagata, T. H. Tulip, J. A. Ibers, S. Otsuka, *J. Am. Chem. Soc.* **1978**, *100*, 2063−2073. [7b] H. C. Clark, M. J. Hampden Smith, *J. Am. Chem. Soc.* **1986**, *108*, 3829−3830. [7c] A. Scrivanti, R. Campostrini, G. Carturan, *Inorg. Chim. Acta* **1988**, *142*, 187−189.
[8] M. Y. Chiang, R. Bau, G. Minghetti, A. L. Bandini, G. Banditelli, T. F. Koetzle, *Inorg. Chem.* **1984**, *23*, 122−124.
[9] A. L. Bandini, G. Banditelli, G. Minghetti, *XX Congresso Nazionale Società Chimica Italiana*, June **2000**, Rimini, INPO007.
[10] A. L. Bandini, G. Banditelli, G. Minghetti, *XXII Congresso Nazionale Chimica Inorganica* September **1993**, Villasimius, p. 386.
[11] e.g.: [11a] A. L. Bandini, G. Banditelli, E. Cesarotti, G. Minghetti, B. Bovio, *Inorg. Chem.* **1992**, *31*, 391−398. [11b] A. L. Bandini, G. Banditelli, F. Demartin, M. Manassero, G. Minghetti, *Gazz. Chim. Ital.* **1993**, *123*, 417−423. [11c] J. J. Li, P. R. Sharp, *Inorg. Chem.* **1996**, *35*, 604−613.
[12] [12a] G. Minghetti, A. L. Bandini, G. Banditelli, F. Bonati, *J. Organomet. Chem.* **1981**, *214*, C50−C52. [12b] S. Aime, R. Gobetto, G. Minghetti, A. L. Bandini, G. Banditelli, *J. Cluster Science* **1994**, *5*, 523−533.
[13] G. Minghetti, A. L. Bandini, G. Banditelli, F. Bonati, R. Szostak, C. E. Strouse, C. B. Knobler, H. D. Kaesz, *Inorg. Chem.* **1983**, *22*, 2332−2338.
[14] M. Portnoy, D. Milstein, *Organometallics* **1994**, *13*, 600−609.
[15] R. Bau, M. H. Drabnis, *Inorg. Chim. Acta* **1997**, *259*, 27−50.
[16] C. B. Cooper, D. F. Shriver, S. Onaka, *A. C. S. Adv. Chem. Series* **1978**, *167*, 232−247.
[17] J. Eckert, *Physica B* **1986**, *136*, 150−155.
[18] A. Albinati, S. Chaloupka, J. Eckert, L. M. Venanzi, M. K. Wolfer, *Inorg. Chimica Acta* **1997**, *259*, 305−316.
[19] J. Roziere, A. Potier, *Bull. Soc. Chim. Fr.* **1982**, I339−I346.
[20] I. J. Braid, J. Howard, J. Thomkinson, *J. Chem. Soc., Faraday Trans. 2* **1983**, *79*, 253−262.
[21] M. W. Howard, U. A. Jayasooriya, S. F. A. Kettle, D. B. Powell, N. Sheppard, *Chem. Commun.* **1979**, 18−20.
[22] The calculations were carried out by use of the TITAN programs suite (Wavefunction Inc., Irvine U. S. A. and Schroedinger Inc., Portland, U. S. A. **1999−2001**). A DFT/B3LYP method was used, employing the LACVP* pseudo-potential basis set.
[23] M. Hackett, G. M. Whitesides, *J. Am. Chem. Soc.* **1988**, *110*, 1449−1462.
[24] SAINT Reference manual, Siemens Energy and Automation, Madison, WI, **1994−1996**.
[25] G. M. Sheldrick, *SADABS*, Empirical Absorption Correction Program, University of Göttingen, **1997**.
[26] [26a] B. A. Frenz, *Comput. Phys.* **1988**, *2*, 42. [26b] *Crystallographic Computing* vol. 5, Oxford University Press: Oxford, U. K., **1991**; Chapter 11, p. 126.
[27] International *Tables for X-ray Crystallography*, Vol.4, Kynoch Press, Birmingham, **1974**.
[28] G. M. Sheldrick, *SHELXS-86*, Program for the solution of crystal structures, University of Göttingen, Germany, **1985**.
[29] Z. A. Bowden, M. Celli, F. Cilloco, D. Colognesi, R. J. Newport, S. F. Parker, F. P. Ricci, V. Rossi-Albertini, F. Sacchetti, J. Tomkinson, M. Zoppi, *Physica B* **2000**, *98*, 276−278.
[30] V. F. Sears, *Thermal Neutron Scattering Lengths and Cross-Sections for Condensed Matter Research.* Atomic Energy of Canada Ltd., Chalk River, Ont., Canada, **1984**.

Received April 30, 2003

 © 2003 Wiley-VCH Verlag GmbH & Co. KGaA, Weinheim

Synthesis and Characterisation of New Nickel-Iron Complexes with an S_4 Coordination Environment around the Nickel Centre

Johanna A. W. Verhagen,[a] Martin Lutz,[b] Anthony L. Spek,[b] and Elisabeth Bouwman*[a]

Keywords: Nickel / Iron / S ligands / Electronic structure / Electrochemistry

The nickel complex [Ni(xbsms)] [H_2xbsms is α,α′-bis(4-mercapto-3,3-dimethyl-2-thiabutyl)-*o*-xylene] was reacted with $FeCl_2$, $[Fe_2(CO)_9]$, $[Fe(CO)_2(NO)_2]$ and $[Fe(CO)_4I_2]$. The reaction with $FeCl_2$ gives the heterotetranuclear nickel–iron complex $[Ni(xbsms)FeCl_2]_2$. The complex was characterised by analytical, spectroscopic and electrochemical methods and by X-ray diffraction. $[Ni(xbsms)FeCl_2]_2$ crystallises in the monoclinic space group $P2_1/c$, with the dimer located on the inversion centre. The nickel ions are in a square-planar $S_2S'_2$ environment, comprised of two thioether and two thiolate sulfur atoms. The thiolate sulfur atoms form a bridge between the nickel ion and the iron centre. The iron ions are in a pseudo square-pyramidal S_2Cl_3 environment, with two chloride ions forming a bridge between the two iron centres. The Ni–Fe distance is 3.0403(3) Å. The reaction with $[Fe_2(CO)_9]$, $[Fe(CO)_2(NO)_2]$ or $[Fe(CO)_4I_2]$ gives the heterodinuclear complexes $[Ni(xbsms)Fe(CO)_4]$, $[Ni(xbsms)Fe(NO)_2]$ and $[Ni(xbsms)Fe(CO)_2I_2]$, respectively. These complexes were characterised by analytical, spectroscopic and electrochemical methods. In $[Ni(xbsms)Fe(CO)_4]$, one thiolate group bridges the Ni and Fe centres, whereas in $[Ni(xbsms)Fe(NO)_2]$ and $[Ni(xbsms)Fe(CO)_2I_2]$, two thiolate groups form a bridge between the centres. These newly synthesised nickel–iron complexes appear to be suitable complexes for new structural models for [NiFe]-hydrogenases.

(© Wiley-VCH Verlag GmbH & Co. KGaA, 69451 Weinheim, Germany, 2003)

Introduction

Hydrogenases are widespread among several classes of anaerobic and occasionally aerobic bacteria, and were first discovered in the 1930s.[1] These enzymes catalyse the reversible oxidation of dihydrogen, which allows the cell to generate or dispose of reducing equivalents during respiration. In vitro hydrogenases also catalyse H^+/D_2 exchange.[2] The reactivity of nickel enzymes in the generation or consumption of dihydrogen is interesting because of the fact that possible future energy problems may be solved using an hydrogen economy.[3] By studying the synthesis and characterisation of structural and functional models for the hydrogenases, we hope to contribute to the development of catalysts for, for example, fuel cells.

The hydrogenases have been divided into two main classes, based on their metal content, namely [NiFe]-hydrogenases and [Fe]-hydrogenases.[2] A subset of the first class has been shown to contain selenium, the [NiFeSe]-hydrogenases. Furthermore, a hydrogenase that does not contain any transition metal has been discovered.[4] Extensive studies and characterisations, including single-crystal X-ray diffraction, have revealed the structure of several [NiFe]-hydrogenases.[5,6] The X-ray studies have shown that the active sites of the [NiFe] enzymes isolated from *Desulfovibrio gigas*[5] and *Desulfovibrio vulgaris*[6] contain the heterodinuclear site $[(Cys\text{-}S)_2Ni^{II}(\mu\text{-}S\text{-}Cys)_2Fe^{II}(CN)_2(CO)]$, in which the nickel centre has an S_4 coordination environment. Two thiolate sulfur atoms form a bridge between the nickel and the iron centres. Furthermore, three diatomic molecules are coordinated to the iron centre, two CN molecules and one CO molecule. In the last few years, considerable interest has been shown in the structural modelling of the [NiFe]-hydrogenases.[7−12] However, most of the structural models have a mixed-donor environment around the nickel centres. A variety of square-planar nickel complexes have been synthesised with only sulfur donor atoms in the coordination environment,[13] and several nickel−iron complexes relevant for hydrogenase modelling have been synthesised.[2,14−18] However, so far only one heterodimetallic nickel−iron complex that has an S_4 coordination environment around the nickel centre has been reported.[19] In this paper, we describe the synthesis of new heterometallic nickel−iron complexes, starting from a nickel complex with an S_4 coordination environment.[20]

Results and Discussion

Syntheses: Four new nickel−iron complexes were synthesised by the reactions of [Ni(xbsms)] with the iron com-

[a] Leiden Institute of Chemistry, Gorlaeus Laboratories, Leiden University,
P. O. Box 9502, 2300 RA Leiden, The Netherlands
Fax: (internat.) + 31-71/527-4451
E-mail: bouwman@chem.leidenuniv.nl
[b] Bijvoet Center for Biomolecular Research, Crystal and Structural Chemistry, Utrecht University,
Padualaan 8, 3584 CH Utrecht, The Netherlands

 © 2003 Wiley-VCH Verlag GmbH & Co. KGaA, Weinheim **DOI: 10.1002/ejic.200300285**

plexes $FeCl_2$, $[Fe_2(CO)_9]$, $[Fe(CO)_2(NO)_2]$ and $[Fe(CO)_4I_2]$. The ligand H_2xbsms, α,α′-bis(4-mercapto-3,3-dimethyl-2-thiabutyl)-*o*-xylene, is a tetradentate ligand, which coordinates to the nickel centre through two thiolate groups that are forced in the *cis* positions. These thiolate groups provide a potential binding site for an iron centre.

The reaction of [Ni(xbsms)] with $FeCl_2$ produces the complex $[Ni(xbsms)FeCl_2]_2$ (**1**). In this synthesis either anhydrous $FeCl_2$ or $FeCl_2{\cdot}4H_2O$ can be used. Single crystals suitable for X-ray diffraction were obtained from the filtrate on standing at room temperature, after the removal of the initially formed precipitate.

The reaction of [Ni(xbsms)] with half an equivalent of $[Fe_2(CO)_9]$ gives the complex $[Ni(xbsms)Fe(CO)_4]$ (**2**), and that with $[Fe(CO)_2(NO)_2]$ the complex $[Ni(xbsms)Fe(NO)_2]$ (**3**).

The synthesis of $[Ni(xbsms)Fe(CO)_2I_2]$ (**4**) was performed in chloroform and the reaction mixture was cooled to 273 K in the absence of light. These conditions are necessary for the two CO molecules to remain coordinated to the iron centre. If the synthesis of **4** is carried out in acetonitrile, a compound is formed that lacks CO signals in its IR spectrum. This compound might have a structure that is similar to that of **1**; however, the exact nature of this product is still unknown.

All the complexes are moderately soluble in polar solvents. Furthermore, all the complexes decompose very rapidly in air and in solution. Complex **1** is the most stable, followed by complex **4**, and thereafter complexes **2** and **3**. Decomposition of complexes **2** and **3** leads to the regeneration of the parent nickel complex. Decomposition of **4** begins with the loss of the CO groups. The instability of complexes **2**, **3** and **4** is reflected in their NMR spectroscopic and magnetic susceptibility data. These complexes are diamagnetic as is confirmed by ^1H NMR spectroscopy; however, the μ_{eff} values are higher than expected as a result of decomposition to the paramagnetic species. The regenerated parent nickel complex can also be seen in the NMR spectra.

Structure of $[Ni(xbsms)FeCl_2]_2$ (1): A projection of the structure of the complex $[Ni(xbsms)FeCl_2]_2$ is shown in Figure 1. Crystal data are given in Table 1 and selected bond lengths and angles are given in Table 2.

$[Ni(xbsms)FeCl_2]_2$ crystallises in the space group $P2_1/c$ with two molecules in the unit cell. The complex is hetero-tetranuclear with two Ni^{II} centres in a square-planar $S_2S'_2$ environment and two Fe^{II} centres in a pseudo square-pyramidal S_2Cl_3 environment. The molecule is located around an inversion centre. The two thiolate groups of the ligand xbsms are forced in the *cis* positions, and form a bridge between one nickel and one iron centre. Furthermore, two thioether sulfur atoms are coordinated to the nickel centre. Two chloride ions form a bridge between the iron centres. The complex $[(BME\text{-}DACO)NiFeCl_2]_2$, reported by Darensbourg et al., has a similar hetero-tetranuclear structure, although, the nickel centre has an S_2N_2 coordination environment.[11]

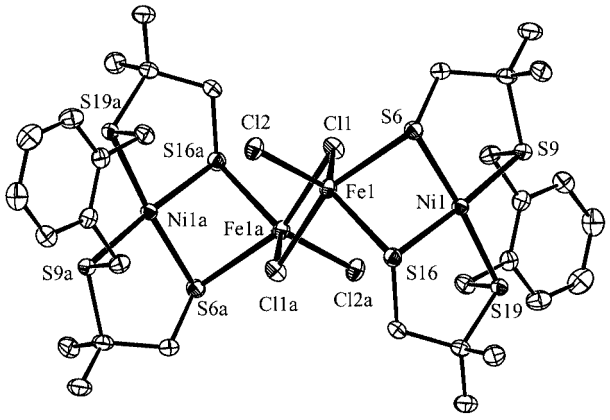

Figure 1. Displacement ellipsoid plot of $[Ni(xbsms)FeCl_2]_2$, drawn at the 50% probability level. Hydrogen atoms are omitted for clarity. Symmetry operation a: $1 - x, -y, 1 - z$

Table 1. Crystal and structure refinement data for the complex $[Ni(xbsms)FeCl_2]_2$

Empirical formula	$C_{32}H_{48}Cl_4Fe_2Ni_2S_8$
Molecular mass	1060.10
Crystal dimensions [mm]	0.06 × 0.20 × 0.20
Crystal system	Monoclinic
Space group	$P2_1/c$ (no. 14)
a (Å)	11.5980(1)
b (Å)	10.2036(1)
c (Å)	18.5642(2)
β [°]	104.4206(4)
V (Å^3)	2127.70(4)
Z	2
$D_{calcd.}$ [Mg·m^{-3}]	1.655
Absorption coefficient μ [mm^{-1}]	2.208
No. of measured reflections	30020
No. of independent reflections	4830
No. of observed reflections [$I > 2\sigma(I)$]	4235
R1 [a] [obsd. refl./all refl.]	0.0218/0.0283
wR2 [b] [obsd. refl./all refl.]	0.0511/ 0.0535
S [c]	1.038
No. of refined parameters	265

[a] $R1 = \Sigma(||F_o| - |F_c||)/\Sigma|F_o|$. [b] $wR2 = \{\Sigma[w(F_o^2 - F_c^2)^2]/\Sigma[w(F_o^2)^2]\}^{1/2}$. $S = \{\Sigma[w(F_o^2 - F_c^2)^2]/(n - p)\}^{1/2}$.

The coordination environment around the nickel ion has a small tetrahedral distortion, with an interplanar angle of 5.75(2)° between the planes S(6)−Ni(1)−S(9) and S(16)−Ni(1)−S(19).

The pseudo square-pyramidal environment of the iron centre is defined by the two thiolate sulfur atoms and two bridging chloride ions in the basal plane, and the terminal chloride ion Cl(2) in the apical position. The distortion towards a trigonal bipyramidal geometry is shown by S(6) and Cl(1a) in the apical positions and S(16), Cl(1) and Cl(2) in the trigonal plane. The two largest angles around the iron centre give a τ value of 0.45 (with τ = 0 for square-pyramidal and τ = 1 for trigonal bipyramidal geometries).[21] The distance between the two symmetry-related iron centres is 3.6947(5) Å, indicating that no metal-metal interaction is present. From the geometry around the iron centre, it can be concluded that the iron centre is in a high spin state. This

 © 2003 Wiley-VCH Verlag GmbH & Co. KGaA, Weinheim

Table 2. Selected bond lengths (Å) and angles (°) in $[Ni(xbsms)FeCl_2]_2$ (symmetry position a: $1-x, -y, 1-z$)

Ni(1)−S(6)	2.1781(4)	S(6)−Ni(1)−S(9)	92.01(16)	Cl(1)−Fe(1)−Cl(2)	112.144(17)
Ni(1)−S(9)	2.2016(4)	S(6)−Ni(1)−S(16)	85.040(17)	Cl(1)−Fe(1)−S(6)	94.950(15)
Ni(1)−S(16)	2.1776(4)	S(6)−Ni(1)−S(19)	174.675(18)	Cl(1)−Fe(1)−S(16)	130.767(17)
Ni(1)−S(19)	2.1958(4)	S(9)−Ni(1)−S(16)	175.287(18)	Cl(1)−Fe(1)−Cl(1a)	82.726(15)
Fe(1)−S(6)	2.5197(5)	S(9)−Ni(1)−S(19)	91.104(16)	Cl(2)−Fe(1)−S(6)	100.386(16)
Fe(1)−S(16)	2.4462(5)	S(16)−Ni(1)−S(19)	91.566(16)	Cl(2)−Fe(1)−S(16)	116.896(17)
Fe(1)−Cl(1)	2.3927(4)			Cl(2)−Fe(1)−Cl(1a)	100.914(17)
Fe(1)−Cl(2)	2.2657(5)	Ni(1)−S(6)−Fe(1)	80.301(14)	S(6)−Fe(1)−S(16)	72.695(14)
Fe(1)−Cl(1a)	2.5286(5)	Ni(1)−S(16)−Fe(1)	82.005(15)	S(6)−Fe(1)−Cl(1a)	157.808(17)
		Fe(1)−Cl(1)−Fe(1a)	97.273(15)	S(16)−Fe(1)−Cl(1a)	92.062(15)

observation has been confirmed by the room temperature magnetic susceptibility measurements, which give a μ_{eff} value of 5.35 μ_B per iron centre. This is consistent with a high spin Fe^{II} centre without any interaction between the two iron centres in the molecule.[22]

The Fe−S−Ni angles of 80.301(14) and 82.005(15)° lead to a Ni−Fe distance of 3.0403(3) Å. All distances and angles around the nickel centre are consistent with data of similar complexes in the literature.[2,13]

Proposed Structure of [Ni(xbsms)Fe(CO)$_4$] (2): A proposed structure based on elemental analysis and NMR spectroscopic studies is shown in Figure 2. This structure, containing a square-planar low spin Ni^{II} ion and a low spin Fe(0) moiety, is similar to that of [(BME-DACO)Ni-Fe(CO)$_4$].[16] In the IR spectrum of complex (2), three signals assigned to the CO groups are observed at 2009, 1945 and 1860 cm^{-1}. These are slightly different from those reported for a THF solution of [(BME-DACO)Ni-Fe(CO)$_4$];[16] however, they are in the same region as the CO absorption observed at 1943 cm^{-1} for [NiFe]-hydrogenase.[23] The ^{1}H NMR spectrum shows resonance signals for every proton and every methyl group, which is in agreement with the proposed asymmetric structure. Using NOESY and COSY NMR spectra, full assignments of all resonance signals could be made. The ^{1}H NMR spectrum, recorded at 253 K, is shown in Figure 3. The parent nickel complex can also be seen in the NMR spectrum, as a result of the decomposition of the [NiFe] complex. The ^{13}C NMR spectrum also reflects the asymmetry of the complex, all carbon atoms appear to be inequivalent. However, the CO resonance signals are not observed. This may be attributed to the low concentration and the instability of the complex, or to poor relaxation properties of the complex. The instability of the complex is confirmed by mass spectroscopy: $\{[Ni(xbsms)Fe(CO)_3]+H\}^+$ is observed as the main peak, indicating that one CO molecule is only loosely bound.

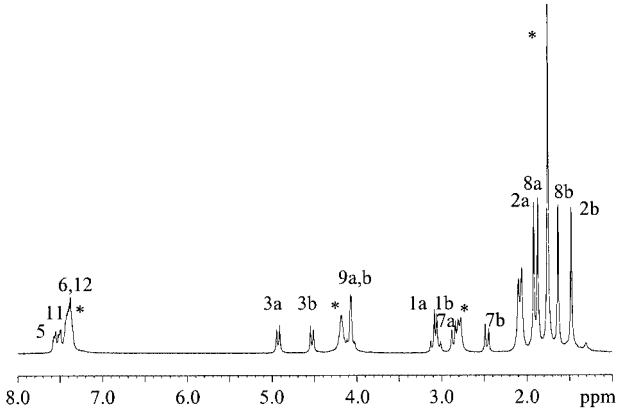

Figure 3. ^{1}H NMR spectrum of [Ni(xbsms)Fe(CO)$_4$] in [D$_6$]acetone at 253 K. Assignments in the figure correspond to numbers in Figure 2. The asterisks indicate signals from the decomposition product [Ni(xbsms)]

Proposed Structure of [Ni(xbsms)Fe(NO)$_2$] (3): A proposed structure based on elemental analysis and ^{1}H NMR spectroscopy is also shown in Figure 2. This structure, containing a square-planar low spin Ni^{II} ion and a low spin $[Fe(NO)_2]$ moiety, is similar to that of the Ni-Fe-nitrosyl complex reported by Osterloh et al.[15] In the IR spectrum, strong signals assigned to the NO groups are clearly observed at 1771 and 1733 cm^{-1}. These absorptions are at significantly higher energies compared with those in the reported complex (1663 and 1624 cm^{-1}),[15] and are also shifted relative to the starting Fe complex $[Fe(CO)_2(NO)_2]$ (1810 and 1766 cm^{-1}); however, they compare with those reported by Liaw et al. (1767 and 1725 cm^{-1}).[17] The NO stretches in the IR spectrum are in the range reported for linearly coordinated NO^+ molecules.[24] This indicates only a small increase in transfer of electron-density from Fe into

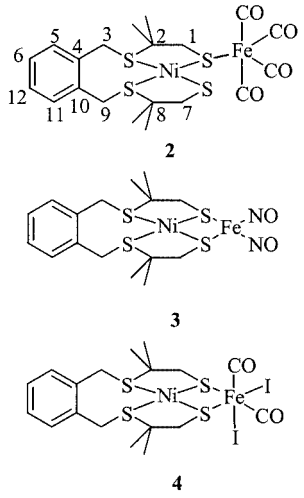

Figure 2. Schematic drawings of the postulated structure of [Ni(xbsms)Fe(CO)$_4$] (**2**), [Ni(xbsms)Fe(NO)$_2$] (**3**) and [Ni(xbsms)-Fe(CO)$_2$I$_2$] (**4**)

 © 2003 Wiley-VCH Verlag GmbH & Co. KGaA, Weinheim

the π* orbitals of the NO ligands, which is accompanied by the weakening of the NO triple bonds.

Proposed Structure of [Ni(xbsms)Fe(CO)$_2$I$_2$] (4): A proposed structure based on elemental analysis and mass spectrometry is also shown in Figure 2. The proposed structure is dinuclear with a square-planar low spin Ni^{II} ion, bridged via both thiolate sulfur atoms to the octahedral Fe^{II} ion. The IR spectrum of 4 is clearly different from that of 1, excluding a tetranuclear structure. Two signals which are assigned to CO vibrations are observed at 2048 and 2096 cm^{-1}. The mass spectra indicate that the iodide ions are coordinated to the iron centre.

UV/Visible-NIR Spectroscopy of the Complexes: The square-planar coordination environment of the nickel centres in all of the complexes is reflected in their ligand field spectra. The data are presented in Table 3. All complexes are brown solids and yield pale brown solutions in both chloroform and acetonitrile. Only small differences are observed between the UV/Visible-NIR spectra of the complexes in chloroform and in acetonitrile, indicating that in all cases solvent coordination does not take place and decomposition in solution is not within the timescale of the experiment.

Table 3. Electronic absorption maxima for the Ni^{II} complexes **1**−**4**

	$\tilde{\nu}$/cm^{-1} (ε/mol^{-1}·L·cm^{-1})		
	Solid state	Chloroform	Acetonitrile
[Ni(xbsms)$FeCl_2$]$_2$ (**1**)	16 600		
	19 200	19 200 (1017)	20 000 (1547)
	23 700	23 900 (2221)	23 500 (3535)
	30 200		31 000 (7843)
		34 900 (16135)	33 900 (9074)
[Ni(xbsms)Fe$(CO)_4$] (**2**)	14 400	15 000 (530)	15 000 (330)
	19 500	20 800 (2612)	
	23 900	25 300 (5241)	25 900 (3943)
	29 800	31 000 (6460)	30 600 (8167)
	36 700		35 500 (14142)
[Ni(xbsms)Fe$(NO)_2$] (**3**)	13 600		19 900 (sh)
	24 800	25 900 (sh)	25 000 (sh)
		30 200 (sh)	30 600 (6400)
		34 900 (16200)	34 900 (13800)
[Ni(xbsms)Fe$(CO)_2I_2$] (**4**)	10 800		
	14 300		
	19 300		20 000 (sh)
	23 400	22 500 (sh)	23 900 (4392)
		27 000 (4668)	27 900 (7719)
	34 900	34 400 (3108)	35 000 (36409)

The d−d transitions involving the nickel centre in the complex [Ni(xbsms)$FeCl_2$]$_2$ are at a higher energy than those in the complex [Ni(xbsms)], and the LMCT transitions are at a lower energy.[20] This can be explained by the fact that the iron centre in complex **1** has electron-donating chloride ions, and this results in a higher electron-density on the thiolate sulfur atoms. These thiolate sulfur atoms then donate more electron-density to the nickel centre, and as a result the nickel-thiolate distance is shorter. This observation is in agreement with the crystal structure. The shortening of this nickel−thiolate bond leads to longer thioether sulfur−nickel distances.

For **2** and **3**, the shift in energy is the opposite. As a result of the π back-donation from the iron centre to the CO ligands in **2** and NO ligands in **3**, the iron centre can accept electron-density from the thiolate sulfur atoms. Hence a lower ligand field splitting occurs, and the d-d absorption maxima are observed at lower energies relative to the parent nickel complex. The absorptions around 35 000 cm^{-1} in **2** can be explained by a d-d transition involving the iron centre.[25]

For **4**, which has electron-donating iodide ions and electron-withdrawing carbonyl molecules coordinated to the iron centre, both effects are observed. The d-d transitions are at a lower energy relative to [Ni(xbsms)], as is the case for **2**; however, the LMCT absorption maxima are also at a lower energy, as is the case for **1**. The latter observation also confirms the proposed structure with coordinated iodide ions.

Electrochemical Results: The electrochemical behaviour of the synthesised nickel−iron complexes was investigated using cyclic voltammetry. For complexes 1, 2 and 3 only quasi-reversible and irreversible redox couples were found, which cannot be interpreted unequivocally.

For complex **4**, the relevant data are presented in Table 4 and the cyclic voltammogram is shown in Figure 4. For comparison, the cyclic voltammograms of FeI_2 and NEt_4I have been recorded. In MeCN, with NBu_4PF_6 as the supporting electrolyte, FeI_2 shows two reversible waves at 232 mV (ΔE = 220 mV) and 654 mV (ΔE = 78 mV), and NEt_4I shows two reversible waves at 238 mV (ΔE = 191 mV) and 646 mV (ΔE = 92 mV). This indicates that the redox couples at around 250 and 640 mV most likely result from the iodide ions. The couple at around 250 mV appears to arise from a two-electron process, which might result from the oxidation of the iodide ions to I_2. The redox couple at 1246 mV could result from oxidation of the iron centre. Furthermore, **4** shows an irreversible reduction wave at around −500 mV.

The redox behaviour of **4** was also tested in dichloromethane. These data are included in Table 4. In CH_2Cl_2, the oxidation wave at 1206 mV is irreversible. The difference in the redox behaviour in both solvents is significant and probably due to the difference in solubility and ionisation of the complex, and of I^- and I_3^-.

Conclusions and Outlook

Four new nickel−iron complexes have been synthesised from the reactions of the nickel complex [Ni(xbsms)] with $FeCl_2$, [$Fe_2(CO)_9$], [$Fe(CO)_2(NO)_2$] and [$Fe(CO)_4I_2$].

The [NiFe] complexes with the ligand xbsms are generally less stable than other complexes with the ligands xbsms and bme-daco.[11,26] This might be as a result of the S_4 coordination environment around the nickel centre, instead of an S_2N_2 coordination environment. Furthermore, most of the [NiFe] complexes show quasi-reversible or irreversible oxidation waves when studied by cyclic voltammetry.

The synthesised compounds appear to be promising complexes for new structural models for the [NiFe]-hydro-

 © 2003 Wiley-VCH Verlag GmbH & Co. KGaA, Weinheim

Table 4. Electrochemical data for complexes **4**, compared with [Ni(xbsms)]

[a]	E_{pc} (mV)	E_{pa} (mV)	$E_{1/2}$ (mV)	ΔE (mV)	i_{pa}/i_{pc}
[Ni(xbsms)] (CH_3CN)[b]	−1572				
	−508				
		508			
		1406			
[Ni(xbsms)Fe(CO)$_2$I$_2$] (CH_3CN)	−469 (G)				
	195 (F)	308 (A)	252	113	0.7
	605 (E)	679 (B)	642	74	0.9
	1182 (D)	1309 (C)	1246	127	0.6
[Ni(xbsms)Fe(CO)$_2$I$_2$] (CH_2Cl_2)	−59	352	206	411	1.0
	513	645	579	132	1.0
		1191			

[a] 1 mM solutions containing 0.1 M NBu_4PF_6 at a scan rate of 0.2 V/s; Pt working electrode, Pt auxiliary electrode and an Ag/AgCl reference electrode. $E_{1/2}$ in mV vs. Ag/AgCl. The letter at the E value corresponds to the oxidative or reductive wave of the cyclic voltammogram, shown in Figure 4. [b] Taken from ref.[20]

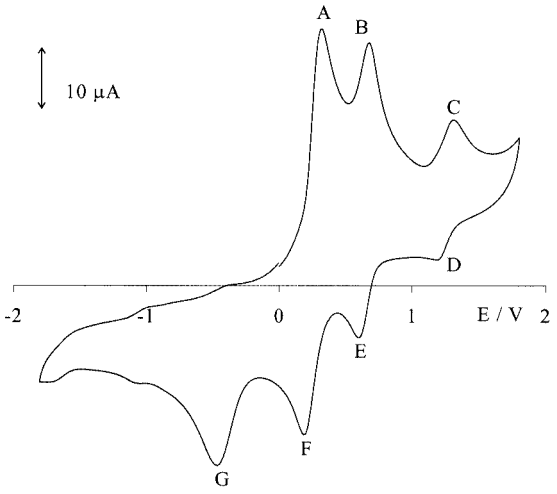

Figure 4. Cyclic voltammogram of [Ni(xbsms)Fe(CO)$_2$I$_2$] (**4**) at a scan rate of 0.2 V/s (1 mM solution in acetonitrile containing 0.1 M Bu_4NPF_6). E vs. Ag/AgCl

genases. An improved model for the hydrogenase active site may be achieved by exchanging the iodide ions in complex **4** for cyanide molecules, and this work is in progress.

In the near future, the complexes will be screened for hydrogenase activity by means of reaction with dihydrogen or protons.

Experimental Section

Chemicals: All preparations were carried out with reagent grade solvents. All chemicals used in the syntheses were obtained from Acros or Aldrich and were used without further purification, unless otherwise mentioned. The complexes were synthesised under argon using standard Schlenk techniques. Solvents were deoxygenated by bubbling a stream of argon through the solution, or by the freeze-pump-thaw method, and were dried with molecular sieves. The complexes [Ni(xbsms)],[20] [Fe(CO)$_2$(NO)$_2$][27] and [Fe(CO)$_4$I$_2$][28] were synthesised according to published methods.

Physical Measurements: The IR spectra were recorded with a Perkin−Elmer FT-IR Paragon 1000 spectrophotometer equipped with a golden gate ATR device, using the reflectance technique (4000−300 cm^{-1}, resolution 4 cm^{-1}). Elemental analyses were carried out with a Perkin−Elmer series II CHNS/O analyzer 2400. Metal analyses were performed with a Perkin−Elmer 3100 atomic absorption (AAS) and flame emission spectrometer using a linear calibration method. Ligand field spectra were recorded with a Perkin−Elmer Lambda 900 spectrophotometer. The diffuse reflectance technique, with MgO as a reference, was used for the solid compounds. Ligand field spectra of the solutions were obtained with the used solvent in the reference beam. NMR spectra were recorded with a Bruker WM 300 MHz spectrometer or on a Bruker AV 400 MHz spectrometer. Proton and carbon chemical shifts are indicated in ppm relative to tetramethylsilane (TMS). The electrochemical measurements were performed with an Autolab PGstat10 potentiostat controlled by GPES4 software. A three-electrode system was used, consisting of a platinum working electrode, a platinum auxiliary electrode and an Ag/AgCl reference electrode. The experiments were carried at room temperature under argon with tetrabutylammonium hexafluorophosphate (0.10 M) as the electrolyte. Under these conditions the ferrocenium-ferrocene couple is at +430 mV, with a peak separation of 59 mV. All potentials are reported relative to Ag/AgCl. Mass analyses were performed with a Finnigan MAT 900 equipped with an Electrospray interface (ESI). Spectra were collected by constant infusion of the sample dissolved in methanol/water containing 1% HOAc. Room temperature magnetic susceptibility measurements were performed using a magnetic susceptibility balance type MK1 or using the NMR method.[29]

[Ni(xbsms)FeCl$_2$]$_2$ (1): $FeCl_2 \cdot 4H_2O$ (0.049 g, 0.25 mmol) was added to a solution of [Ni(xbsms)] (0.100 g, 0.25 mmol) in acetonitrile (20 mL). After stirring for 2 h, the precipitate formed was collected by filtration. A brown product was obtained, with a yield of 0.082 g (62%). Single crystals suitable for X-ray diffraction were obtained from the filtrate on standing. IR: $\tilde{\nu}_{max}$ = 2975 w, 2947 w, 1486 w, 1440 m, 1380 m, 1362 m, 1300 w, 1256 m, 1223 m, 1192 m, 1135 s, 1075 s, 1007 w, 952 m, 890 m, 865 w, 772 s, 756 w, 730 m, 684 s, 608 s, 580 m, 544 m, 469 m, 418 w, 373 w, 310 s cm^{-1}. $C_{32}H_{48}Cl_4Fe_2Ni_2S_8$ (1060.1): calcd. C 36.25, H 4.56, S 24.19, Ni 11.08, Fe 10.54; found C 36.47, H 4.61, S 22.87, Ni 11.17, Fe 10.21.

[Ni(xbsms)Fe(CO)$_4$] (2): [$Fe_2(CO)_9$], (0.090 g, 0.25 mmol) was added to a solution of [Ni(xbsms)] (0.20 g, 0.50 mmol) in acetonitrile

 © 2003 Wiley-VCH Verlag GmbH & Co. KGaA, Weinheim

(30 mL). After stirring for 3 h, $[Fe_2(CO)_9]$ had completely dissolved. The acetonitrile was partly evaporated in vacuo until a precipitate was formed. The precipitate was collected by filtration, giving a brown product with a yield of 0.11 g (41%). ^{1}H NMR [300.13 MHz, CD_3CN, 298 K, see Figure 2 for numbering scheme): δ = 7.52 (m, 1 H, C^5-H), 7.46 (m, 1 H, C^{11}-H), 7.38 (m, 2 H, C^6-H, C^{12}-H), 4.76 (d, $^2J_{H,H}$ = 10.9 Hz, 1 H, C^3H*H*), 4.38 (d, $^2J_{H,H}$ = 10.9 Hz, 1 H, C^3*H*H), 4.01 (d, $^2J_{H,H}$ = 11.6 Hz, 1 H, C^9H*H*), 3.91 (d, $^2J_{H,H}$ = 11.6 Hz, 1 H, C^9*H*H), 3.05 (d, $^2J_{H,H}$ = 13.0 Hz, 1 H, C^1H*H*), 2.97 (d, $^2J_{H,H}$ = 13.0 Hz, 1 H, C^1*H*H), 2.81 (d, $^2J_{H,H}$ = 12.3 Hz, 1 H, C^7H*H*), 2.46 (d, $^2J_{H,H}$ = 12.3 Hz, 1 H, C^7*H*H), 1.82 (s, 3 H, C^2-Me), 1.71 (s, 3 H, C^8-Me), 1.60 (s, 3 H, C^8-Me), 1.43 (s, 3 H, C^2-Me) ppm. ^{13}C APT NMR [100.62 MHz, [D$_6$]acetone, 253 K]: δ = 135.37 (C^{10}), 134.20 (C^4), 133.41 (C^5), 131.63 (C^{11}), 129.38 (C^6), 129.11 (C^{12}), 67.19 (C^2), 62.41 (C^8), 48.01 (C^3), 40.63 (C^9), 35.29 (C^1), 34.92 (C^7), 27.04 (C^2-*C*H$_3$), 26.43 (C^2-*C*H$_3$), 25.20 (C^8-*C*H$_3$), 25.13 (C^8-*C*H$_3$) ppm. IR: $\tilde{\nu}_{max}$ = 2930 w, 2922 w, 2830 w, 2009 vs, 1944 vs, 1861 vs, 1456 m, 1435 m, 1380 m, 1260 m, 1234 w, 1212 w, 1188 w, 1165 w, 1133 m, 1070 m, 1002 w, 948 w, 892 m, 871 w, 781 s, 759 m, 706 m, 684 w, 616 s, 595 s, 571 s, 559 s, 490 m, 468 m, 436 m, 398 m, 368 s, 340 m cm^{-1}. $C_{20}H_{24}FeNiO_4S_4$ (571.2): calcd. C 42.06, H 4.23, S 22.45, Ni 10.28, Fe 9.78; found C 41.67, H 4.78, S 22.07, Ni 10.59, Fe 9.29. ESI-MS: *m*/*z* = 543 [M − "CO" + H]$^+$.

[Ni(xbsms)Fe(NO)$_2$] (3): A solution of $[Fe(CO)_2(NO)_2]$ (0.058 g, 0.34 mmol) in acetonitrile (3 mL) was added to a solution of [Ni(xbsms)] (0.137 g, 0.34 mmol) in acetonitrile (40 mL) at 273 K. Whilst stirring for 2 h, the evolution of a gas was observed, indicating the loss of CO. After the reaction was completed, the acetonitrile was partly evaporated until a precipitate was formed. This precipitate was collected by filtration to give a brown solid with a yield of 0.71 g (55%). ^{1}H NMR [300.13 MHz, $CDCl_3$, 300 K]: δ = 7.25 (m, 4 H, Ph-H), 3.98 (s, 4 H, Ph-C*H*$_2$−S−), 3.20 (s, 4 H, −C(CH$_3$)−C*H*−S−), 1.61 (s, 12 H, C*H*$_3$) ppm. IR: $\tilde{\nu}_{max}$ = 2934 w, 2928 w, 1809 w, 1771 s, 1733 vs, 1700 m, 1456 m, 1381 m, 1360 m, 1228 w, 1136 m, 1118 m, 1085 m, 957 m, 886 w, 786 m, 702 m, 554 w, 492 w, 469 m, 350 w, 302 m cm^{-1}. $C_{16}H_{24}FeN_2NiO_2S_4$·0.5 CH_3CN (539.8): calcd. C 37.83, H 4.76, N 6.49, S 23.76, Ni 10.81, Fe 10.35; found C 38.22, H 5.48, N 6.06, S 21.43, Ni 10.96, Fe 10.21.

[Ni(xbsms)Fe(CO)$_2$I$_2$] (4): $[Fe(CO)_4I_2]$ (0.105 g, 0.25 mmol) was added to a solution of [Ni(xbsms)] (0.101 g, 0.25 mmol) in chloroform (12 mL) at 273 K. After stirring for 1.5 h in the absence of light, the precipitate was collected by filtration. A brown product was obtained, with a yield of 0.050 g (24%). IR: $\tilde{\nu}_{max}$ = 2959 m, 2948 m, 2096s, 2048s, 1456s, 1417 m, 1389 m, 1372s, 1225 m, 1136s, 1081s, 955 m, 882 m, 772 vs, 694s, 606s, 570 m, 492s, 468s, 350s, 310m cm^{-1}. $C_{18}H_{24}FeI_2NiO_2S_4$ (769.0): calcd. C 28.11, H 3.15, S 16.68, Ni 7.64, Fe 7.26; found C 27.63, H 3.38, S 16.18, Ni 7.85, Fe 6.86. ESI-MS: *m*/*z* = 644 $[Ni(xbsms)Fe(CO)_2I]^+$, 616 $[Ni(xbsms)Fe(CO)I]^+$, 257 $[Ni(xbsms)Fe(CO)_2]^{2+}$, 243 $[Ni(xbsms)Fe(CO)]^{2+}$, 229 $[Ni(xbsms)Fe]^{2+}$.

Crystal Structure Determination of [Ni(xbsms)FeCl$_2$]$_2$: X-ray intensities were measured with a Nonius KappaCCD diffractometer with rotating anode (λ = 0.71073 Å) at a temperature of 150 K. The structure was solved with automated Patterson methods (DIRDIF97[30]) and refined with SHELXL-97[31] against F^2 for all reflections. Molecular illustration, structure checking and calculations were performed with the PLATON package.[32] The crystals were obtained as dark purple plates. The absorption correction was based on multiple measured reflections (program PLATON[32] routine MULABS, 0.79−0.89 transmission). Non-hydrogen atoms were refined freely with anisotropic displacement parameters. Hydrogen atoms were located in the difference Fourier map and refined freely with isotropic displacement parameters (methyl groups) or as rigid groups (all other H atoms). Further crystallographic details are given in Table 1.

CCDC-212533 contains the supplementary crystallographic data for this paper. These data can be obtained free of charge at www.ccdc.cam.ac.uk/conts/retrieving.html [or from the Cambridge Crystallographic Data Centre, 12, Union Road, Cambridge CB2 1EZ, UK; Fax: (internat.) +44-1223/336-033; E-mail: deposit@ccdc.cam.ac.uk].

Acknowledgments

Prof. Dr. Jan Reedijk is gratefully acknowledged for fruitful discussions. This work was supported in part (M.L., A.L.S.) by the Council for Chemical Sciences of the Netherlands Organization for Scientific Research (CW-NWO).

[1] M. W. W. Adams, E. I. Stiefel, *Science* **1998**, *282*, 1842−1843.
[2] A. C. Marr, D. J. E. Spencer, M. Schröder, *Coord. Chem. Rev.* **2001**, *219*, 1055−1074.
[3] J. Alper, *Science* **2003**, *299*, 1686−1687.
[4] R. K. Thauer, A. R. Klein, G. C. Hartmann, *Chem. Rev.* **1996**, *96*, 3031−3042.
[5] A. Volbeda, E. Garcia, C. Piras, A. L. de Lacey, V. M. Fernandez, E. C. Hatchikian, M. Frey, J. C. Fontecilla-Camps, *J. Am. Chem. Soc.* **1996**, *118*, 12989−12996.
[6] Y. Higuchi, T. Yagi, N. Yasuoka, *Structure* **1997**, *5*, 1671−1680.
[7] E. Bouwman, R. K. Henderson, A. L. Spek, J. Reedijk, *Eur. J. Inorg. Chem.* **1999**, 217.
[8] R. K. Henderson, E. Bouwman, A. L. Spek, J. Reedijk, *Inorg. Chem.* **1997**, *36*, 4616.
[9] V. E. Kaasjager, J. van den Broeke, R. K. Henderson, W. J. J. Smeets, A. L. Spek, W. L. Driessen, E. Bouwman, J. Reedijk, *Inorg. Chim. Acta* **2001**, *316*, 99−104.
[10] G. Musie, J. H. Reibenspies, M. Y. Darensbourg, *Inorg. Chem.* **1998**, *37*, 302−310.
[11] D. K. Mills, Y. M. Hsiao, P. J. Farmer, E. V. Atnip, J. H. Reibenspies, M. Y. Darensbourg, *J. Am. Chem. Soc.* **1991**, *113*, 1421−1423.
[12] V. E. Kaasjager, E. Bouwman, S. Gorter, J. Reedijk, C. A. Grapperhaus, J. H. Reibenspies, J. J. Smee, M. Y. Darensbourg, A. Derecskei-Kovacs, L. M. Thomson, *Inorg. Chem.* **2002**, *41*, 1837−1844.
[13] M. A. Halcrow, G. Christou, *Chem. Rev.* **1994**, *94*, 2421−2481.
[14] M. C. Smith, J. E. Barclay, S. P. Cramer, S. C. Davies, G. Wei-Wei, D. L. Hughes, S. Longhurst, D. J. Evans, *J. Chem. Soc., Dalton Trans.* **2002**, 2641−2647.
[15] F. Osterloh, W. Saak, D. Haase, S. Pohl, *Chem. Commun.* **1997**, 979−980.
[16] C. H. Lai, J. H. Reibenspies, M. Y. Darensbourg, *Angew. Chem. Int. Ed. Engl.* **1996**, *35*, 2390−2393.
[17] W. F. Liaw, C. Y. Chiang, G. H. Lee, S. M. Peng, C. H. Lai, M. Y. Darensbourg, *Inorganic Chemistry* **2000**, *39*, 480−484.
[18] M.-C. Chalbot, A. M. Mills, A. L. Spek, G. J. Long, E. Bouwman, *Eur. J. Inorg. Chem.* **2003**, 453−457.
[19] D. Sellmann, F. Geipel, F. Lauderbach, W. Heinemann, *Angew. Chem. Int. Ed.* **2002**, *41*, 632−634.
[20] J. A. W. Verhagen, D. D. Ellis, M. Lutz, A. L. Spek, E. Bouwman, *J. Chem. Soc., Dalton Trans.* **2002**, 1275−1280.

 © 2003 Wiley-VCH Verlag GmbH & Co. KGaA, Weinheim

[21] A. W. Addison, R. T. Nageswara, J. Reedijk, J. v. Rijn, G. C. Verschoor, *J. Chem. Soc., Dalton Trans.* **1984**, 1349.
[22] A. P. Ginsberg, M. E. Lines, K. D. Karlin, S. J. Lippard, F. J. DiSalvo, *J. Am. Chem. Soc.* **1976**, *98*, 6958.
[23] A. J. Pierik, W. Roseboom, R. P. Happe, K. A. Bagley, S. P. J. Albracht, *J. Biol. Chem.* **1999**, *274*, 3331−3337.
[24] K. Nakamoto, *Infrared and raman spectra of inorganic and coordination compounds*, John Wiley & Sons, New York, **1997**, ed. 5, p. 149−150.
[25] M. Dartiguenave, Y. Dartiguenave, H. B. Gray, *Bull. Soc. Chim. Fr.* **1969**, 4223.
[26] G. Musie, P. J. Farmer, T. Tuntulani, J. H. Reibenspies, M. Y. Darensbourg, *Inorg. Chem.* **1996**, *35*, 2176−2183.
[27] W. Hieber, H. Beutner, *Z. Anorg. Allg. Chemie* **1963**, *320*, 101−111.
[28] W. Hieber, G. Bader, *Ber. Dtsch. Chem. Ges.* **1928**, *61*, 558−563.
[29] D. F. Evans, *J. Chem. Soc.* **1959**, 2003−2005.
[30] P. T. Beurskens, G. Admiraal, G. Beurskens, W. P. Bosman, S. Garcia-Granda, R. O. Gould, J. M. M. Smits, C. Smykalla, *The DIRDIF97 program system, Technical Report of the Crystallography Laboratory*, University of Nijmegen, Nijmegen, **1997**.
[31] G. M. Sheldrick, *SHELXL-97. Program for crystal structure refinement*, University of Göttingen, Göttingen **1997**.
[32] A. L. Spek, *PLATON. A multipurpose crystallographic tool.,* Utrecht University, Utrecht **2000**.

Received May 14, 2003

 © 2003 Wiley-VCH Verlag GmbH & Co. KGaA, Weinheim

EurJIC
European Journal of Inorganic Chemistry

Issue 22/2003

Pages 3975–4122

Papers available ahead of print in Early View at www.interscience.wiley.com

Earliest available Table of Contents:
Automatically, free of charge by e-mail through
www.interscience.wiley.com/alerts

COVER PICTURE

The cover picture shows a typical bent-sandwich *commo*-metallacorborane product as well as its starting *nido*-carborane precursor of the smaller carborane cage system, together in a novel cluster. Details are discussed in the Microreview by N. S. Hosmane and J. A. Maguire on p. 3989 ff. The authors are indebted to their many students and coworkers who have borne the brunt of doing, and to the National Science Foundation, Alexander von Humboldt-Stiftung (to N. S. H.) and the R. A. Welch Foundation (to J. A. M.) for their generous support.

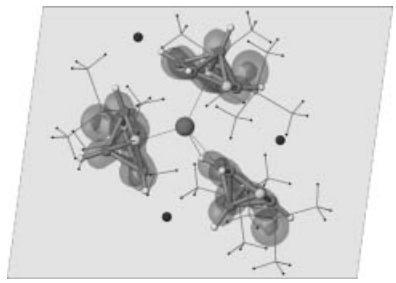

MICROREVIEW

Contents

3989 **N. S. Hosmane,* J. A. Maguire**

Recent Advances in the Chemistry of Metallacarboranes

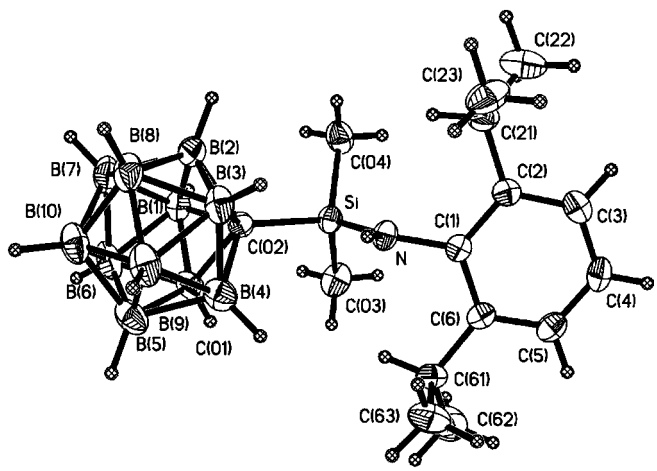

Keywords: Carboranes / Boranes / Lanthanides / *ansa* ligands / Sandwich complexes / Main group elements

 © 2003 Wiley-VCH Verlag GmbH & Co. KGaA, Weinheim

FULL PAPERS

4001 **V. Patroniak, P. N. W. Baxter, J.-M. Lehn,* M. Kubicki, M. Nissinen, K. Rissanen**

Self-Assembly and Characterisation of Grid-Type Iron(II), Cobalt(II) and Zinc(II) Complexes

Keywords: Grid-type complexes / Iron / Cobalt / Zinc / Supramolecular chemistry / Self-assembly

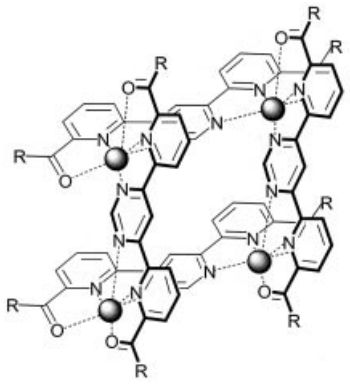

4010 **Y. Xie, Q. Liu,* H. Jiang, J. Ni**

Novel Complexes of Ligands Containing Phenol and Alcohol Groups: From Polynuclear Cluster, 1D Coordination Polymer to 2D Supramolecular Assemblies

Keywords: Copper / Cobalt / Silver / Coordination polymers / N,O ligands

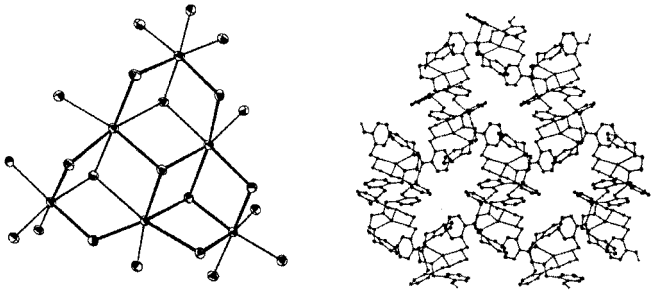

4017 **Y.-B. Dong,* X. Zhao, G.-X. Jin, R.-Q. Huang, M. D. Smith**

New Ag^{I} Organometallic Coordination Polymers and M^{II} (M = Cu^{II} and Co^{II}) Inorganic Supramolecular Complexes Generated from New Fulvene-Type Ligands

Keywords: Coordination polymers / Supramolecular chemistry / Silver / Cobalt / Copper

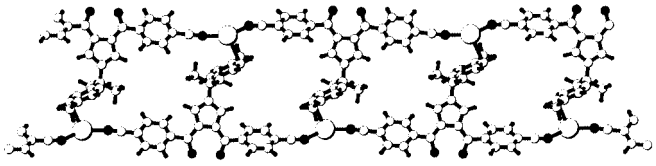

4025 **M. Gaspar, J. P. Telo, M. A. Santos***

A New Diazacyclooctane Dihydroxamate as a Siderophore Analogue. Synthesis and Equilibrium Studies of Iron(III) and Copper(II) Complexes

Keywords: Copper / Iron / Aminohydroxamates / Hydroxamic acids / Siderophores

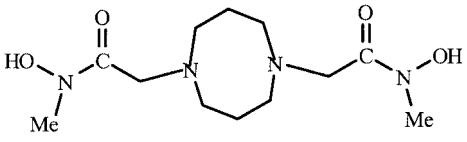

4035 **V. W.-W. Yam,* B. Li, Y. Yang, B. W.-K. Chu, K. M.-C. Wong, K.-K. Cheung**

Preparation, Photo-luminescence and Electro-Luminescence Behavior of Langmuir–Blodgett Films of Bipyridylrhenium(I) Surfactant Complexes

Keywords: Luminescence / Surfactants / Langmuir–Blodgett films / Rhenium

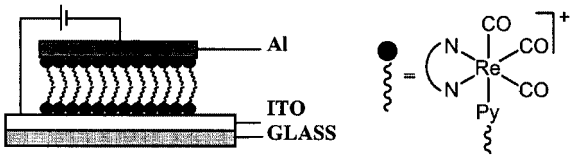

 © 2003 Wiley-VCH Verlag GmbH & Co. KGaA, Weinheim

4043 **A. Romaniewska, R. Jasztold-Howorko, A. Regiec, T. Lis, J. Kuduk-Jaworska***

Synthesis, Structure and Characterization of New Olivacine Derivatives and Their Platinum(II) Complexes

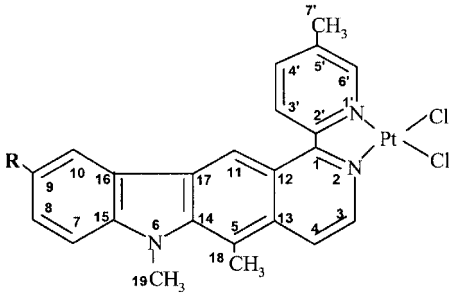

R = -O-C(20)H_3, -OH, -OOC(21)-C(20)H_3

Keywords: Antitumor agents / Template synthesis / Platinum / Structure elucidation / Conformational analysis

4055 **H. B. Ammar, J. Le Nôtre, M. Salem, M. T. Kaddachi, L. Toupet, J.-L. Renaud, C. Bruneau, P. H. Dixneuf**

New $[Ru_3(CO)_{12}]$-Based Catalysts with Imidazolinium Salt, Diimine, or Bis(oxazoline) Ligands and Ruthenium Bis(oxazoline) Complex for Tandem Isomerisation/Claisen Rearrangement of Dienyl Ethers − X-ray Structure of [RuCl{(*R*,*R*)-bis(isopropyloxazoline)}(*p*-cymene)]BF_4

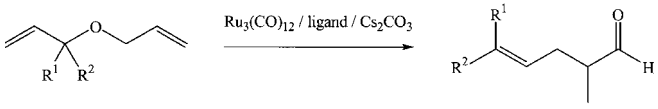

Keywords: Ruthenium / Isomerisation / Claisen reaction / Aldehydes / N ligands

4065 **G. Muller, C. L. Mauphin, J. P. Riehl, H. Birkedal, C. Piguet, J.-C. G. Bünzli***

Structural, Photophysical and Chiro-Optical Properties of Lanthanide Complexes with a Bis(benzimidazole)pyridine-Based Chiral Ligand

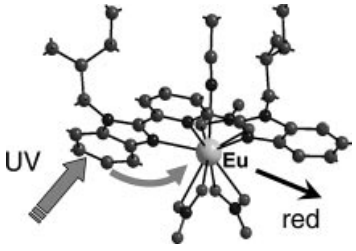

Keywords: Lanthanides / Luminescence / Chirality / Complexes / Terdentate ligand

4073 **Y. Song, P. Gamez, A. F. Stassen, M. Lutz, A. L. Spek, J. Reedijk***

Structure and Magnetism of a New Dodecanuclear Cu^{II} Complex with Acetato and Imidazolato Bridges, Formed by Oxidation of the Chelating Ligand 1,1,7,7-Tetrakis(imidazol-2-yl)-2,6-diazaheptane

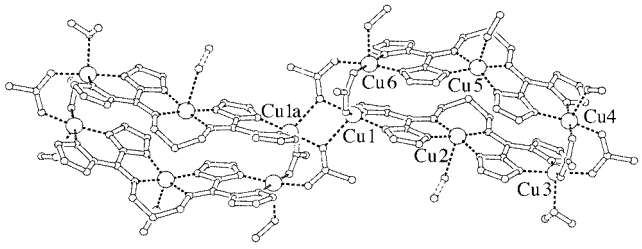

Keywords: Copper / Magnetic properties / N ligands / Chelates

 © 2003 Wiley-VCH Verlag GmbH & Co. KGaA, Weinheim

4078 **K. I. Nättinen, J. Linnanto, K. Rissanen***

Dimensionality Variation in Polymeric Metallo-Organic Frameworks

Keywords: Crystal engineering / X-ray diffraction / Self-assembly / Coordination polymers

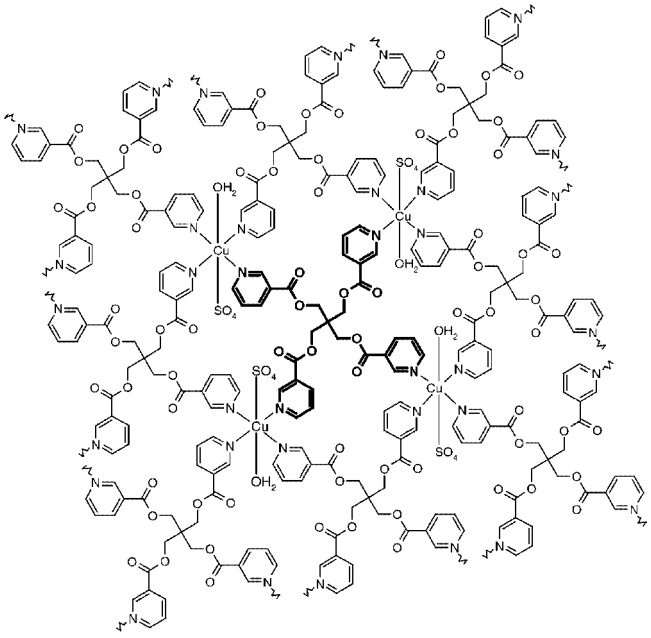

4087 **H.-J. Himmel***

H Activation by AlCl Monomers: Characterization of $HAl(Cl)CH_3$ as the Product of the Photoactivated Reaction Between AlCl and CH_4 in a Solid Ar Matrix at 12 K

Keywords: Aluminum / Hydrides / Matrix isolation / C−H activation / Reaction mechanisms / Photochemistry

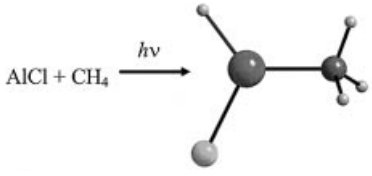

4093 **K. Kubo, M. Nakano, H. Tamura, G. Matsubayashi***

X-ray Crystal Structure and Electrical Conductivity of $[Au(ppy)(C_8H_4S_8)]_2[PF_6]$ [ppy^- = *C*-deprotonated 2-phenylpyridine(−); $C_8H_4S_8^{2-}$ = 2-{(4,5-ethylenedithio)-1,3-dithiol-2-ylidene}-1,3-dithiole-4,5-dithionate(2−)]

Keywords: Gold / S ligands / Oxidation / Sulfur / Electrochemistry

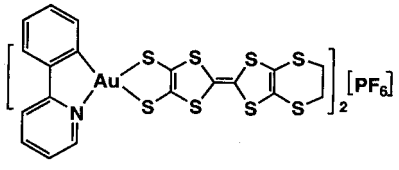

4099 **Y.-W. Zhang, Z.-G. Yan, L.-P. You, R. Si, C.-H. Yan***

General Synthesis and Characterization of Monocrystalline Lanthanide Orthophosphate Nanowires

Keywords: Nanostructures / Lanthanides / Orthophosphates / Solvothermal synthesis

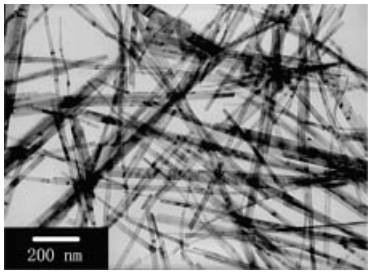

 © 2003 Wiley-VCH Verlag GmbH & Co. KGaA, Weinheim

4105 **E. Shandalov, I. Zilbermann, E. Maimon, Y. Nahmani, H. Cohen, E. Adar, D. Meyerstein***

Mechanism of Reduction of 2,2-Dibromomethyl-1,3-propanediol by Ni^{I}-Tetraazamacrocyclic Complexes in Aqueous Solution − A Pulse Radiolysis and Electrochemical Study

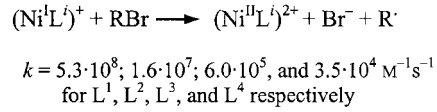

Keywords: Halogenated compounds / Pulse radiolysis / Reduction / Electrochemistry / Macrocycles

4110 **K. Belhamel, T. K. D. Nguyen, M. Benamor, R. Ludwig***

Design of Calixarene-Type Ligands for Second Sphere Complexation of Noble Metal Ions

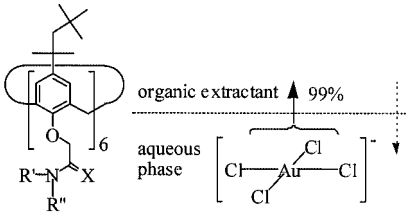

Keywords: Macrocyclic ligands / Host-guest systems / Calixarenes / Gold / Solvent extraction

4117 **S.-M. Park, Y. Kim, S.-J. Kim***

Synthesis and Structures of Fe^{III} Complexes Bridged by Cyanorhenium Clusters

Keywords: Cluster compounds / Nanostructures / Magnetic properties / Rhenium / Iron

 © 2003 Wiley-VCH Verlag GmbH & Co. KGaA, Weinheim

Recent Advances in the Chemistry of Metallacarboranes

Narayan S. Hosmane*[a] and John A. Maguire[b]

Keywords: Carboranes / Boranes / Lanthanides / *ansa* ligands / Sandwich complexes / Main group elements

Most carborane derivatives of the icosahedral (C_2B_{10}) or small cage (C_2B_4) systems are formed by varying the groups on the cage carbon atoms. This is usually accomplished in the original carborane synthesis by treating substituted acetylenes with either the decaborane(14) or pentaborane(9) precursors to give directly carboranes that have adjacent carbon atoms in the cage ("carbon atoms adjacent"). The larger cages are obtained as *closo*-icosahedra, while the small-cage C_2B_4 carboranes have *nido* structures as well as a cage geometry in which the carbon atoms are separated by a boron atom. Although these "carbon atoms apart" or *nido*-2,4-$(CR)_2B_4H_6$ carboranes are thermodynamically more stable and are more symmetric than the "carbon atoms adjacent" isomers, they have not been as well studied, mainly because they must be synthesized from their "carbon atoms adjacent" analogues through a sequential series of oxidative cage-closure/reductive cage-opening reactions. We have concentrated much of our recent research on the reactivity patterns of $C_{(cage)}$-appended alkyl- and silylamido, alkyloxo, alkylphosphido, and alkylthio derivatives of the "carbon atoms apart" carboranes. We have also sought to develop a safe, bench-scale preparation of small-cage carboranes that does not require isolating and handling dangerous and toxic carborane precursors such as pentaborane(9). This microreview discusses the latest developments towards such a process and the subsequent reaction chemistry of the "carbon atoms apart" carboranes.

((© Wiley-VCH Verlag GmbH & Co. KGaA, 69451 Weinheim, Germany, 2003)

Introduction

Extensive research has been reported on the chemical and structural properties of metallacarboranes in pentagonal-bipyramidal (MC_2B_4) and icosahedral (MC_2B_9) cage systems.[1] They are generally synthesized by the reaction of the mono- or dianions of their respective *nido*-C_2B_4 or C_2B_9

[a] Department of Chemistry and Biochemistry, Northern Illinois University,
DeKalb, Illinois 60115-2862, USA
E-mail: nhosmane@niu.edu
[b] Department of Chemistry, Southern Methodist University,
Dallas, Texas 75275-0314, USA
E-mail: jmaguire@mail.smu.edu

Narayan S. Hosmane was born in Gokarn, Southern India in 1948. He is a B.S. and MS graduate of Karnatak University, Karnataka State, India. He obtained a Ph.D. degree in Inorganic Chemistry in 1974 from the University of Edinburgh, Scotland, under the supervision of Professor Evelyn Ebsworth. After brief postdoctoral research training in Professor Frank Glockling's laboratory at the Queen's University of Belfast, he joined the Lambeg Research Institute in Northern Ireland, and then moved to the USA to study carboranes and metallacarboranes. After postdoctoral work with Professors W. E. Hill and F. A. Johnson at Auburn University and Russell Grimes at the University of Virginia, in 1979 he joined the faculty at the Virginia Polytechnic Institute and State University. In 1982 he joined the faculty at the Southern Methodist University, where he became Professor of Chemistry in 1989. In 1998, he moved to Northern Illinois University and is currently a Presidential Research Professor of Chemistry and Biochemistry. He was the founder of Boron in the Americas (formerly known as BUSA) and hosted the organization's first meeting in Dallas in April 1988. He has published over 200 papers in leading scientific journals. Later this year he will serve as the Jawaharlal Nehru Distinguished Chair of Chemistry for five weeks, at the University of Hyderabad, India, and in 2001 he received the Humboldt Research Prize for Senior US Scientists from the Alexander von Humboldt-Stiftung, and also received the University's Presidential Research Professorship. He has previously received a Camille and Henry Dreyfus Scholar Award, and has been honored with the Mother India International Award and the Boron in the USA Award for his distinguished achievements in boron science. In 1987 he was given the Sigma Xi Outstanding Research Award. A fellow of the Royal Society of Chemistry and the American Institute of Chemists, he has been listed in Who's Who in the World. His research interests are in main-group organometallic chemistry including the synthesis and structure of carboranes, metallacarboranes and organosilicon compounds, with particular emphasis on the Ziegler−Natta catalysis, and also bioboron chemistry and its applications in cancer treatment.

John Maguire is Professor of Chemistry at Southern Methodist University. He was born in Alabama in 1936, received his B.S. Degree in Chemistry from Birmingham Southern College in 1958 and his PhD Degree in Physical Chemistry in 1963 from Northwestern University under the direction of Ralph G. Pearson. He joined the faculty of Southern Methodist University as an Assistant Professor of Chemistry and is now Professor of Chemistry. From 1976 to 1979 he was Associate Dean of University College at SMU and from 1979 to 1981 he was Dean of University College and General Education at SMU. His research interests are in the structure and properties of intercalation compounds and in the bonding, structure and reactivity in carborane cage compounds. He has received several awards including the "M" Award for service to the University in 1979, the outstanding professor award for teaching in both 1975 and 1995, and the Perrine Prize for research. He has published over 120 scientific peer-reviewed papers and reviews and has been listed in the ISI's 10858 most cited chemists (1981−1997) in the world. In 2002 he was appointed University Distinguished Teaching Professor.

MICROREVIEWS: This feature introduces the readers to the authors' research through a concise overview of the selected topic. Reference to important work from others in the field is included.

carboranes with suitable metal reagents. Much of the interest in them stems from the fact that three primary metal-binding carborane π-type molecular orbitals that are localized on the C_2B_3 open pentagonal faces, which are quite similar to those in cyclopentadienide $[C_5R_5]^-$ ligands. Our research has involved synthetic, structural, reactivity and theoretical studies on the full- and half-sandwich metallacarboranes derived from the interactions of [*nido*-2-($SiMe_3$)-*n*-(*R*)-2,*n*-$C_2B_4H_4]^{2-}$ (n = 3, 4; R = $SiMe_3$, *n*Bu, *t*Bu, Me, H) with main-group,[2] d-group,[3] and f-group metals.[4] Originally, pentaborane(9) (B_5H_9), which reacts with various alkynes to furnish small-cage C_2B_4 carboranes, could be obtained from an extensive US-government surplus. However, at present, that source is no longer available, and no commercial source has taken its place.[5] Thus, a new, convenient and safe method of producing pentaborane(9) is needed − ideally a one-pot method from a readily available starting material so that the pentaborane(9) can then further react with the appropriate alkyne to generate, in situ, the corresponding small-cage carborane; such a method is described herein. With a steady source of starting materials available, we have extended our studies of the "carbon atoms apart" metallacarboranes. We have also embarked on the construction of $C_{(cage)}$-appended alkyl- and silylamido and alkyloxo derivatives of the larger C_2B_9 cage systems and have investigated their reactivity toward group-4 and -14 metals so as to prepare metallacarboranes with new geometries that could function as precursors to catalysts or possibly exhibit intrinsic catalytic activity. We hope that the reader will realize that there is still a wealth of fascinating research to be explored in this area.

1. Synthesis of Boron-10 Enriched Pentaborane(9) from Boric Acid and Its Conversion into *nido*-$^{10}B_{10}H_{14}$ and *anti*-$^{10}B_{18}H_{22}$

Pentaborane(9) is an important synthon for several higher polyhedral borane cages, including $[B_9H_{14}]^-$,[6] $[B_{11}H_{14}]^-$,[7] $[B_{12}H_{12}]^{2-}$ as well as other cage-expanded borane anions,[8] and the neutral decaborane, $B_{10}H_{14}$.[9] The corresponding ^{10}B-enriched species could function as precursors for several boron-based drugs for use in boron neutron capture therapy (BNCT). With the exception of the expensive $^{10}B_{10}H_{14}$,[10] there is no commercial supplier for any of these boranes. Therefore, a convenient synthesis for ^{10}B-enriched pentaborane(9) has an obvious appeal. It was this incentive that led us to explore alternative routes to ^{10}B-enriched polyhedral boranes, starting from the readily available ^{10}B-enriched boric acid, $H_3{}^{10}BO_3$. Specifically, $H_3{}^{10}BO_3$, was converted into the corresponding sodium borohydride, $Na^{10}BH_4$, in essentially quantitative yields, by using a slightly modified literature method, involving the formation of butyl borate, $(n\text{BuO})_3{}^{10}B$, and then treating it with NaH in mineral oil at 250 °C.[11,12] Subsequent oxidation of $Na^{10}BH_4$ with I_2 in diglyme, followed by the addition of dioxane during the purification step, gave the dioxane-complexed sodium salt of octahydrotriborate(−1), $Na[^{10}B_3H_8]{\cdot}3C_4H_8O_2$, in almost quantitative yields [Equation (1)].[13]

$$3\ Na^{10}BH_4 + I_2\ (\text{in diglyme/dioxane}) \rightarrow 2\ H_2 + 2\ NaI + Na[^{10}B_3H_8]{\cdot}3C_4H_8O_2 \quad (1)$$

Treatment of $Na[^{10}B_3H_8]{\cdot}3C_4H_8O_2$ with $NiCl_2$ in anhydrous benzene or heavy mineral oil at 110 °C [Equation (2)] gave the corresponding $^{10}B_5H_9$ as the first isolated ^{10}B-enriched pentaborane(9) in a laboratory environment.[14]

$$2\ Na[^{10}B_3H_8]{\cdot}3C_4H_8O_2 + NiCl_2 \xrightarrow[\text{heavy mineral oil}\ 110^{\circ}C/12\ h]{\text{Benzene or}} {}^{10}B_5H_9 + 2\ H_2 + C_4H_8O_2{\cdot}{}^{10}BH_3 \quad (2)$$
$$\text{– } 2\ NaCl/\text{– } Ni^0 \text{ – } 2\ C_4H_8O_2$$

Of the various reported methods of preparing natural B_5H_9,[15,16] that in Equation (2) is by far the most convenient and straightforward. Since the ^{10}B-enriched pentaborane is the only borane product of high volatility, its safe production, easy isolation and storage in heavy mineral oil make this method most attractive, to both those who work with small-cage (C_2B_4) carboranes and to researchers who did not have previous access to these materials. Boron-10 enriched decaborane, $^{10}B_{10}H_{14}$, is the key chemical in preparing almost all of the $C_{(cage)}$-substituted bio-boron molecules that are currently undergoing clinical trials as boron drugs for BNCT.[17] We therefore devised an alternative synthesis that started with the $^{10}B_5H_9$ prepared as described previously to afford, with slight modifications, using different oxidizing agents and reaction temperatures, either $^{10}B_{10}H_{14}$ or *anti*-$^{10}B_{18}H_{22}$ (Scheme 1).[18a] The conversion of natural pentaborane(9) to decaborane(14) has been previously demonstrated by Brewer and Grimes using the iron(II) and iron(III) chloride mediated cage fusion reactions.[18b]

This procedure constitutes the first systematic synthetic approach to pentaborane(9) and decaborane(14) of both natural and ^{10}B-enriched analogues and to their cage-expanded neutral and anionic borane species.[14,18]

2. Reductive Cage-Opening Process with Concomitant Metalation of the Resulting Carborane Ligand: A Novel Route to Metallacarborane Synthesis

The two-electron reductive cage-opening of the *closo*-carboranes has been well-documented.[19−21] In a series of papers Stone and co-workers reported the simultaneous cage reduction and metalation of *closo*-carboranes in the C_2B_n (n = 6, 8, 9) cage systems, using a number of zero-valent nickel, platinum, and palladium complexes.[22] The monocarbon carbaborane [*closo*-$CB_{10}H_{11}]^-$ reacts in a similar manner,[23] and the icosahedral *closo*-$(RC)_2B_{10}H_{10}$ cage has been opened by reaction with a group-1 metal, in both the

 © 2003 Wiley-VCH Verlag GmbH & Co. KGaA, Weinheim

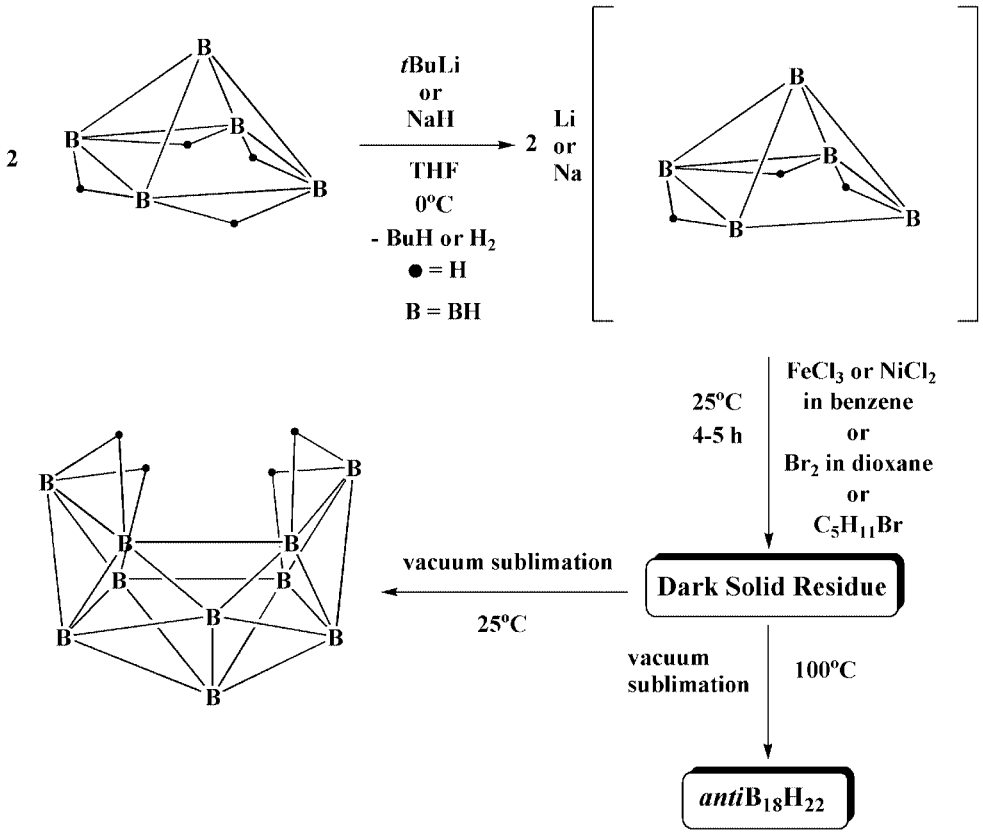

Scheme 1. Synthesis of *nido*-$^{10}B_{10}H_{14}$ and *anti*-$^{10}B_{18}H_{22}$ from $^{10}B_5H_9$

presence and absence of catalysts, to give the corresponding *nido*-carboranes.[24,25] In addition, Mg (group 2) reacts with *closo*-1,2-$C_2B_{10}H_{12}$ in the presence of catalytic amounts of 1,2-dibromomethane.[26] Conversely, Xie and co-workers have reported a noncatalyzed reduction of Na[1-$Me_2C(C_5H_5)$-*closo*-1,2-$C_2B_{10}H_{11}$] by Na metal to give the *ansa*-ligand Na_3[1-$Me_2C(C_5H_5)$-*nido*-1,2-$C_2B_{10}H_{11}$], in which a Cp^- group is tethered to a dianionic *nido*-$C_2B_{10}H_{11}$ moiety via an Me_2C bridge; metal complexes of this ligand were also described.[27] All such reductive cage opening processes yield *nido*-carborane products with a "carbon atoms apart" geometry in which the two cage carbon atoms are separated by at least one boron atom on the open faces of the carboranes. When the two-cage carbon atoms are bridged, by either an organic group or a metal complex, cage reduction produced the "carbon atoms adjacent" *nido*-C_2B_{10} cage, which seems to be susceptible to further reduction to give the respective *arachno*-carboranes.[28] There are a number of catalyzed and noncatalyzed approaches to cage reduction/opening processes for large-cage *closo*-carboranes, but only a few for small C_2B_4 cage systems. Despite some very interesting, but isolated, reports of reductive cage openings of *closo*-$C_2B_4H_6$ by Lewis bases, such as $(CH_3)_3N$,[29] and low-valent metal compounds,[30] the only general, high-yield method of transforming either *closo*-1,6-$(CR)_2B_4H_4$ (R = H or a cage carbon substituent) or its 1,2-isomer to the corresponding [*nido*-2,4-$(CR)_2B_4H_4]^{2-}$ species is by naphthalene-catalyzed group-1 metal reduction.[20]

The use of naphthalene in these traditional two-electron reductive cage-opening reactions has several disadvantages. It introduces an additional reagent that must be removed from the reaction mixture before the *nido*-carborane products can be treated further. In addition, naphthalene also has a tendency to co-crystallize with any product or to substitute for a terminal B−H hydrogen atom, which often interferes with the reactivity of these dianionic ligands. The subsequent metalations of these ligands, in the conventional synthetic procedure (Scheme 2) produce metallacarboranes of different geometries depending on the ratios of reactants involved.[31−40] The structures of some recently reported representative compounds are depicted in Figures 1 and 2.[39,40]

The seeming inability of the *closo*-carboranes to undergo reduction in the absence of naphthalene led us to question whether such carboranes could be reductively opened by the in situ generation of reactive metal atoms whose cations are good coordinators of the carborane. To explore this possibility, anhydrous $ErCl_3$ was treated with 4 equiv. of freshly cut potassium metal, under refluxing conditions in THF, to produce what we believe to be an active erbium metal alloy of the form of Er/K* (Scheme 3).

The alloy was immediately treated with the *closo*-carborane 1,2-$(SiMe_3)_2$-1,2-$C_2B_4H_4$ which, after refluxing overnight with constant stirring, produced a light-orange crystalline solid, identified as the "carbon atoms apart" erbacarborane sandwich, 2,2′,4,4′-$(SiMe_3)_4$-3,6′-[$(\mu$-$H)_2K(THF)_2$]-1,1′-*commo*-Er(η^5-2,4-$C_2B_4H_4)_2$, in 82%

 © 2003 Wiley-VCH Verlag GmbH & Co. KGaA, Weinheim

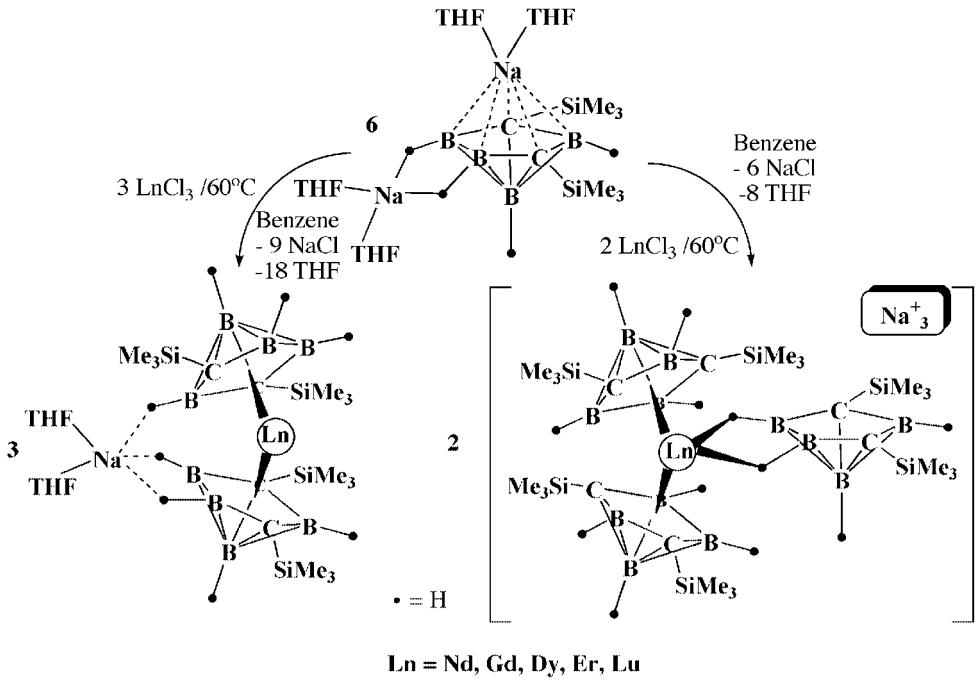

Ln = Nd, Gd, Dy, Er, Lu

Scheme 2. Conventional synthetic route for lanthanacarboranes

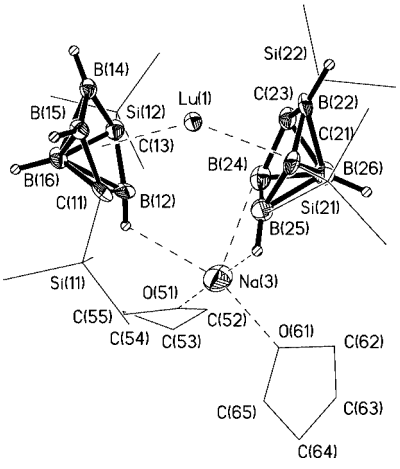

Figure 1. Crystal structure of a full-sandwiched lutetiacarborane complex

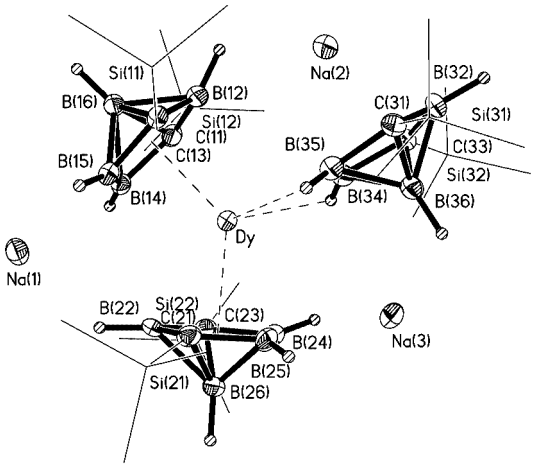

Figure 2. Crystal structure of a full-sandwiched dysprosacarborane complex

yield (Scheme 3 and Figure 3).[41] It is noteworthy that, under the same reaction conditions, neither the Er or K metals alone, nor the one generated in situ by treating K with $ErCl_3$ in a 3:1 ratio, underwent reductive cage opening; in both cases the *closo*-carborane precursor was recovered. Although the Na/Hg alloy has been widely used in coupling reactions of many organometallic species,[42] there have been no reports of its use either in the reductive cage opening of the carboranes or in the synthesis of mercuracarborane complexes. Therefore, the reaction shown in Scheme 3 is an unprecedented example of a new reductive cage-opening process that could prove applicable to the *closo*-carboranes in both the icosahedral and sub-icosahedral cage systems, thus affording hitherto unknown metallacarborane species.

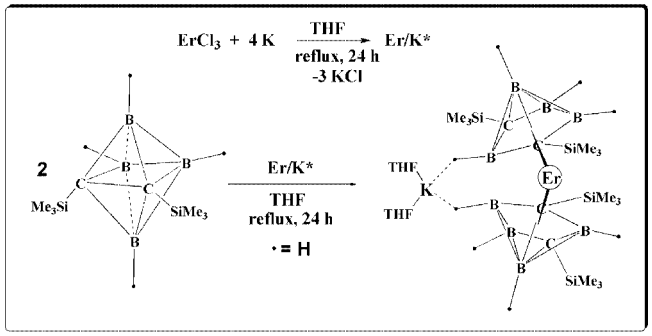

Scheme 3. One-pot two-electron reductive cage opening with concomitant metalation of the carborane ligand

 © 2003 Wiley-VCH Verlag GmbH & Co. KGaA, Weinheim

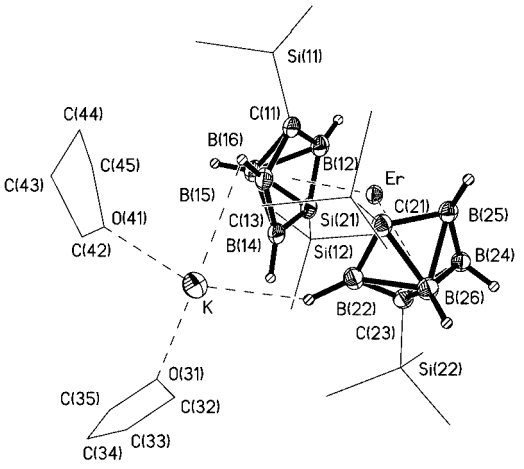

Figure 3. Crystal structure of a full-sandwiched erbacarborane complex

3. Chemistry of Half-Sandwich, Constrained-Geometry C_2B_9 Metallacarboranes

The potential applications of functionalized carborane clusters in catalytic organic reactions have resulted in reports of the syntheses and reactivities of several new metallacarboranes.[43] Our preliminary research has shown that the trianionic ligand [*nido*-7-(CH_2NH)-7,8-$C_2B_9H_{10}$]$^{3-}$, prepared from the reaction of [*nido*-7-(CH_2NH_2)-7,8-$C_2B_9H_{11}$]$^-$ with 2 equiv. of *n*BuLi, reacts with MCl_4 (M = Ti, Zr) to give the corresponding half-sandwich metallacarboranes (Scheme 4).[44]

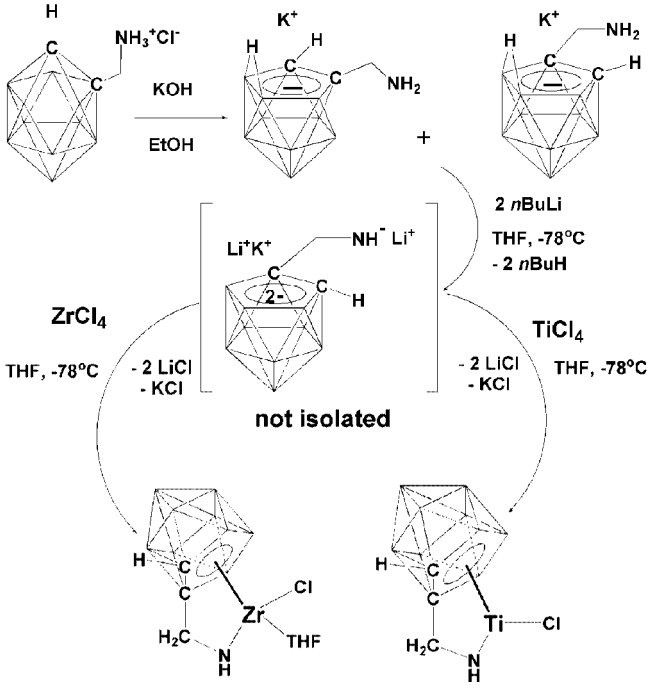

Scheme 4. Synthesis of *ansa*-alkylamidometallacarboranes; unlabelled vertices are BH groups

Of the handful of reports in which the appended moiety forms either a coordinate covalent bond or another delocalized π-bond with the metal atom *exo*-polyhedrally, none have demonstrated the additional stabilization of the metal atom by σ-bonding to the $C_{(cage)}$-appended moiety.[43] Therefore, our results are the first examples of half-sandwiched group-4 metallacarboranes in which the nitrogen atom of the *exo*-polyhedral $C_{(cage)}$-alkylamido unit is $\eta^1(\sigma)$-bonded to the metal atom that is complexed with the open C_2B_3-bonding face of the carborane ligand (Scheme 4). Other constrained-geometry ligands, such as the *ansa*-alkyloxocarborane, can thus be used to prepare a series of $C_{(cage)}$-appended half-sandwich alkyloxometallacarboranes (Scheme 5)[45] In these syntheses, the in situ generated trianionic ligand is treated with anhydrous $MeMCl_3$ (M = Si, Ge), followed by re-crystallization from a toluene/heptane solution to form the corresponding half-sandwich group-14 metallacarboranes, *closo*-1-M(Me)-2-[1-$\eta^1(\sigma)$-OCH_2]-3-Me-η^5-2,3-$C_2B_9H_9$ (M = Si, Ge), in 48 and 56% yields, respectively. The NMR spectra, IR spectra and the microanalytical data for these species confirmed the formulations shown in Scheme 5.[45]

4. Syntheses and Reactivities of $B_{(cage)}$-Alkyl- and -Silylamido C_2B_4 Carborane Ligands

The usefulness of the carborane ligands would be extended if substituents could be systematically introduced on the boron atoms of both 2,3- and 2,4-C_2B_4 carboranes. While there have been several isolated reports of the syntheses of such derivatives,[46–48] only Davis and Grimes have reported a systematic study of the *B*-alkylation of the *nido*-C_2B_4 cage.[49] They found that the reactions of the [*nido*-2,3-$R_2C_2B_4H_5$]$^-$ (R = Et, CH_2Ph) anion with the organic halides R′X [R′ = Me, Et, CH_2Ph, $(CH_2)_3Ph$ and $CH_2C_6H_4Me$; X = Cl or Br] gave exclusively *nido*-4-(R′)-2,3-$(R)_2$-2,3-$C_2B_4H_5$ products. The triethyl- and tribenzyl-alkylated carboranes undergo both metalation and cage-fusion reactions. However, this study was not systematically extended to further alkylation reactions. To investigate the reactivities of alkylated and polyalkylated carboranes, we examined the regiospecific alkylation of the *nido*-2,3-$(SiMe_3)_2$-2,3-$C_2B_4H_6$ carborane and investigated the chemical behavior of any *B*-alkylated products. The following questions were addressed: (1) Is it possible to systematically alkylate and/or polyalkylate carboranes having such bulky substituents as the $SiMe_3$ groups? (2) If so, what is the effect of the $SiMe_3$ groups in determining the distribution of products? (3) Could any alkylated product undergo standard deprotonation and oxidation reactions preparatory to the formation of metallacarboranes and the "carbon atoms apart" analogues, respectively? (4) How effective are the standard techniques of ^1H, ^{11}B, and ^{13}C NMR spectroscopy in identifying the structures of any alkylated products? To address these concerns, the sodium compound of *nido*-2,3-$(SiMe_3)_2$-2,3-$C_2B_4H_6$ was treated with standard alkylating agents, MeI and *i*BuBr, to produce the corresponding neutral monoalkylated carboranes, *nido*-5-(*R*)-2,3-$(SiMe_3)_2$-2,3-$C_2B_4H_5$ (R = Me and *i*Bu) in 75% yields (see Scheme 6).[50]

 © 2003 Wiley-VCH Verlag GmbH & Co. KGaA, Weinheim

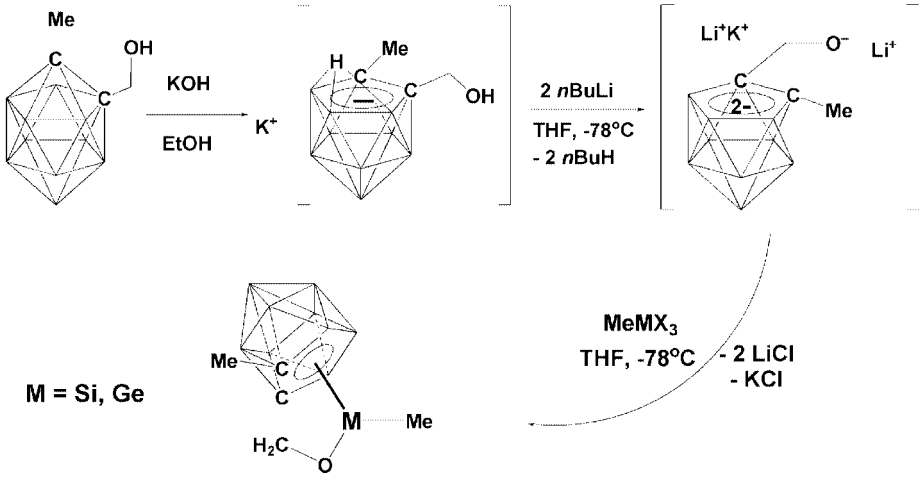

Scheme 5. Synthesis of *ansa*-alkyloxometallacarboranes; unlabelled vertices are BH groups

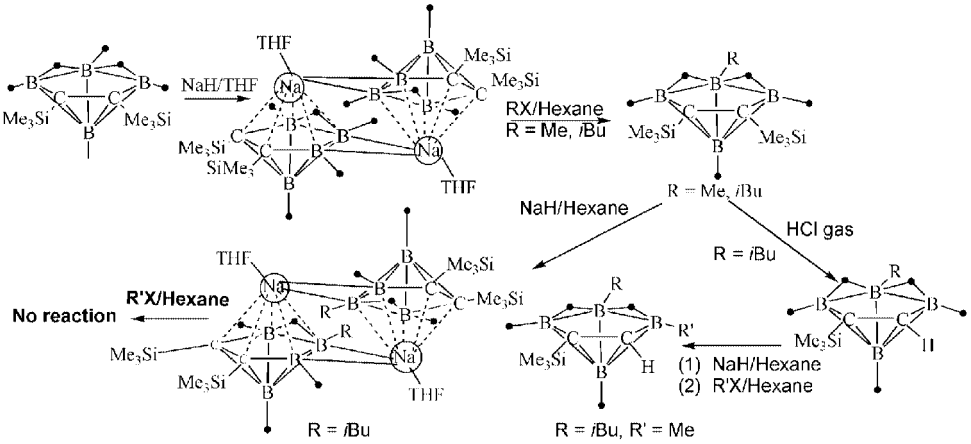

Scheme 6. Systematic $B_{(cage)}$-alkylation of *nido*-2,3-$(SiMe_3)_2$-2,3-$C_2B_4H_6$

The alkylation reaction seems to be a general one that leads exclusively to $B_{(unique)}$-alkylated products. These reactions presumably proceed through an intermediate in which the incoming alkyl unit is bridged between the unique boron atom and one of its neighboring basal boron atoms. The intermediate then collapses with the alkyl group migrating to the terminal position of one of the two boron atoms, changing places with its terminal hydrogen atom. The difference in the directing ability of $SiMe_3$ compared with *C*-alkyl groups is probably due to the steric bulk of the former. This unique directive property of the $SiMe_3$ group was profitably exploited in the synthesis of the corresponding $B_{(cage)}$-silylamido-substituted carborane derivatives. The reactions of $RNHSi(Me)_2Cl$ [R = *t*Bu, 2,6-$(Me_2CH)_2C_6H_3$] with the carborane ligands *nido*-1-Na-(C_4H_8O)-2,3-$(SiMe_3)_2$-2,3-$C_2B_4H_5$ and Li[*closo*-1-R′-1,2-$C_2B_{10}H_{10}$] produced two kinds of neutral ligand precursors, *nido*-5-[$Si(Me)_2N(H)R$]-2,3-$(SiMe_3)_2$-2,3-$C_2B_4H_5$ (R = *t*Bu) and *closo*-1-R′-2-[$Si(Me)_2N(H)R$]-1,2-$C_2B_{10}H_{10}$ [R = *t*Bu, R′ = Ph; R = 2,6-$(Me_2CH)_2C_6H_3$, R′ = H], in 85, 92, and 95% yields, respectively (Scheme 7).[51] Treatment of *closo*-2-[$Si(Me)_2NH$(2,6-$(Me_2CH)_2C_6H_3$)]-1,2-$C_2B_{10}H_{11}$ with 3 equiv. of freshly cut sodium metal in the presence of naphthalene produced, in almost quantitative yield, the corresponding cage-opened sodium salt of the "carbon atoms apart" carborane trianion, [*nido*-3-{$Si(Me)_2N$(2,6-$(Me_2CH)_2C_6H_3$)}-1,3-$C_2B_{10}H_{11}$]$^{3-}$, whose reaction with anhydrous MCl_4 (M = Ti and Zr) in 1:1 molar ratios gave the corresponding half-sandwich neutral d^0-metallacarboranes, *closo*-1-M[$(Cl)(THF)_n$]-2-{1′-η^1,σ-N[2,6-$(Me_2CH)_2C_6H_3$]$(Me)_2Si$}-2,4-η^6-$C_2B_{10}H_{11}$ (M = Ti, *n* = 0; M = Zr, *n* = 1) in 47 and 36% yields, respectively (Scheme 7).[51] Conversely, the small-cage species 5-*t*BuNHSi$(Me)_2$-2,3-$(SiMe_3)_2$-2,3-$C_2B_4H_5$ had limited use as a ligand since it could not withstand deprotonation with a strong base. Therefore, the reactivity of the neutral carborane with $M(NMe_2)_4$ (M = Zr and Ti) was studied. However, while possible metalation occurred, no characterizable products could be isolated.[51] All compounds were characterized by elemental analysis, ^1H, ^{11}B, and ^{13}C NMR spectra and IR spectra, and the ligand processor, *closo*-2-[$Si(Me)_2NH${2,6-$(Me_2CH)_2C_6H_3$}]-1,2-$C_2B_{10}H_{11}$, was also characterized by single-crystal X-ray diffraction.

The crystal structure (Figure 4) of this *ansa* ligand shows that it consists of a closed C_2B_{10} polyhedron with a distorted icosahedral cage geometry. The intracage bond

 © 2003 Wiley-VCH Verlag GmbH & Co. KGaA, Weinheim

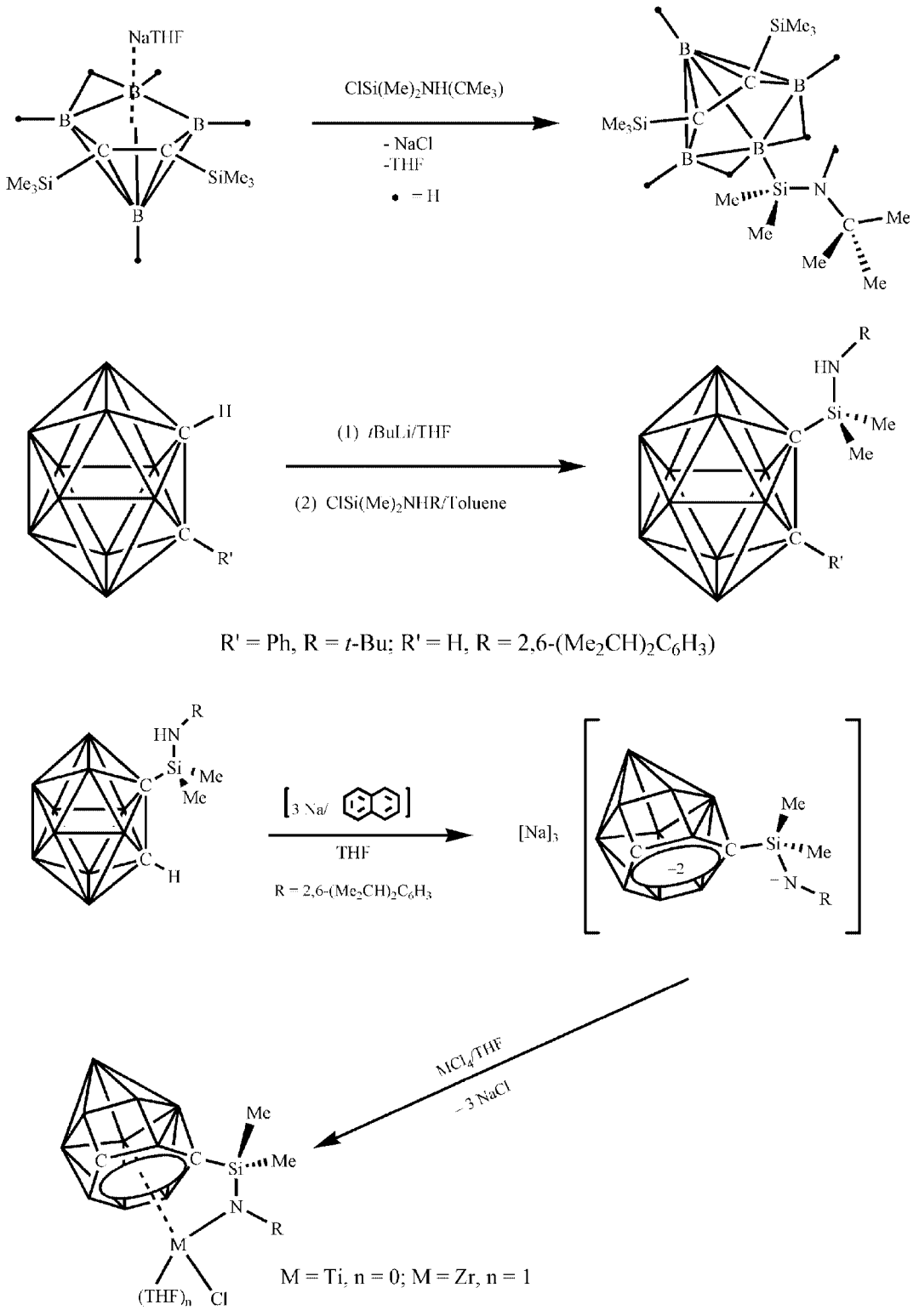

Scheme 7. Syntheses, cage-opening and concomitant metalation of the $B_{(cage)}$- and $C_{(cage)}$-substituted silylamidocarborane ligands; unlabelled vertices are BH groups

lengths are quite similar to those reported for *closo*-1-(methyl)-2-(phthalimidomethyl)-1,2-$C_2B_{10}H_{10}$.[52] The *exo*-polyhedral $Si(Me)_2NH[2,6\text{-}(Me_2CH)_2C_6H_3]$ group is attached to a cage carbon atom by a standard 2*c*2*e* bond, and the Si−C(02) bond of 1.911(3) Å is longer than the Si−C bonds in $(C_5Me_4SiMe_2NtBu)$Ti(prone-2,4-hexadiene) [1.869(6) Å],[53] and $\eta^5{:}\sigma\text{-}Me_2Si(C_9H_6)\text{-}\eta^6\text{-}(C_2B_{10}H_{10}\text{-}CH_2NMe)Zr(NC_5H_5)]$ [1.861(6) Å].[54] The four groups on

 © 2003 Wiley-VCH Verlag GmbH & Co. KGaA, Weinheim

the silicon atom are in a distorted tetrahedral arrangement, with X−Si−Y angles ranging from 103.53° for N−Si−C(02) to 114° for N−Si−C(03/04). The most interesting aspect of this structure is the large C(1)−N−Si angle of 125.5(2)°.[51] This is probably due to repulsion between the Si−Me groups and the large diisopropylphenyl moiety. Such an angle indicates that the lone pair on the nitrogen atom would not be particularly available for bonding. However, from its conversion to the corresponding half-sandwich neutral d^0-metallacarborane, *closo*-1-M[(Cl)(THF)$_n$]-2-{1′-η^1,σ-N[2,6-$(Me_2CH)_2C_6H_3$](Me)$_2$Si}-2,4-η^6-$C_2B_{10}H_{11}$ (M = Ti, n = 0; M = Zr, n = 1), it seems that η^1-coordination of the N atom is possible after removal of its H atom to form the amido group.

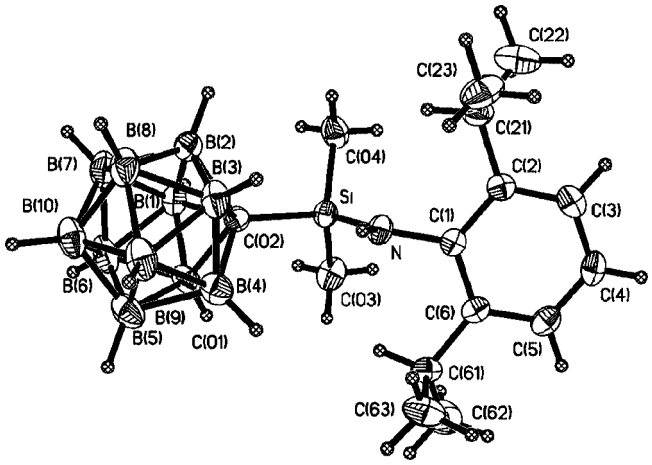

Figure 4. Crystal structure of the *ansa*-carborane ligand, *closo*-2-[Si(Me)$_2$NH{2,6-$(Me_2CH)_2C_6H_3$}]-1,2-$C_2B_{10}H_{11}$

5. Novel Synthetic Approach to Heavier Group-2 Metallacarboranes

The reaction of tetrakis(tetrahydrofuran)barium bis[tris(trimethylsilylmethyl)zincate] with 2,3-bis(trimethylsilyl)-2,3-dicarba-*nido*-hexaborane in THF yielded nearly quantitatively the bis(carborane)barium complex (Scheme 8).[55]

Only one of the trimethylsilylmethyl groups of the zincate is active in this metalation. The formed bis(trimethylsilylmethyl)zinc neither reacts with the carborane nor with the bis(carborane)barium complex. Each barium atom in the dimeric complex shows a coordination number of nine (Figure 5).[55]

The Ba−O bond lengths (ca. 2.74 Å) lie in the expected range. Furthermore, two carborane ligands are bonded via hydride bridges with Ba−H distances of approximately 2.90 Å, which were refined isotropically and can be interpreted as Ba−H−B three-center bonds. A third carborane ligand is coordinated with Ba−C distances of 3.16 Å and a bridging hydrogen atom [Ba1−H356 = 2.93(4) Å]. This corre-

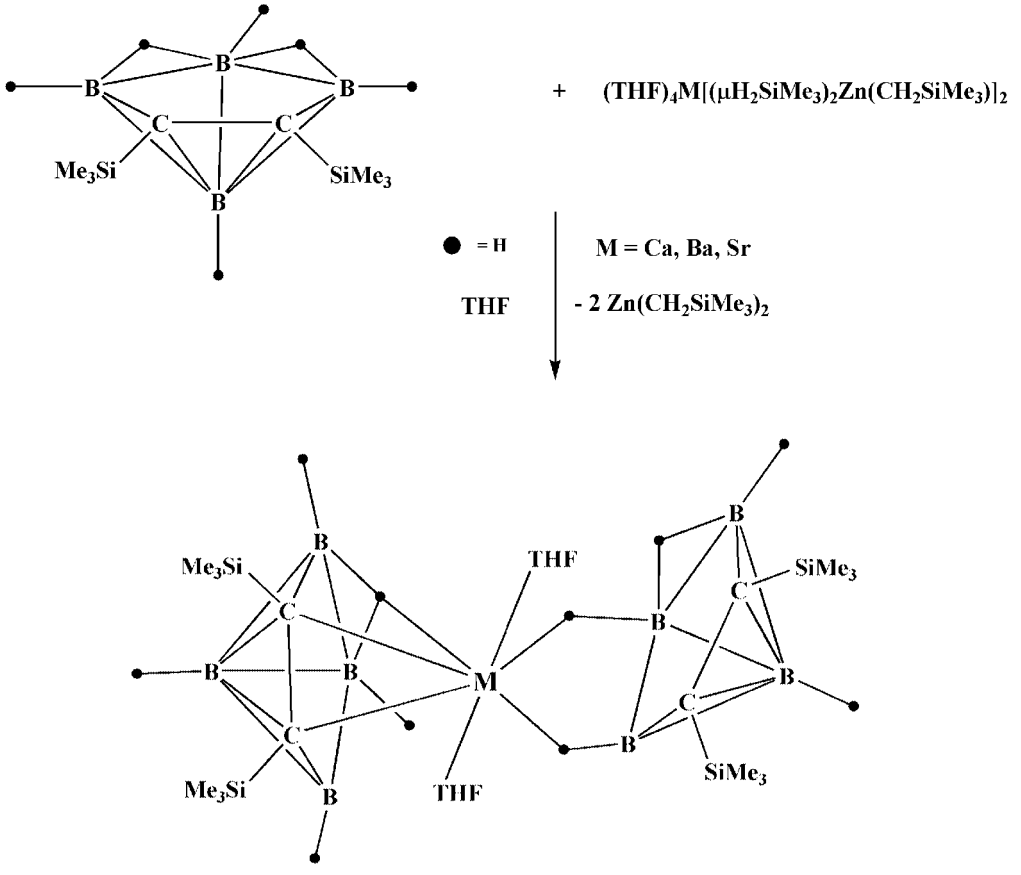

Scheme 8. Synthesis of heavier group-2 metallacarboranes of the C_2B_4 cage systems

 © 2003 Wiley-VCH Verlag GmbH & Co. KGaA, Weinheim

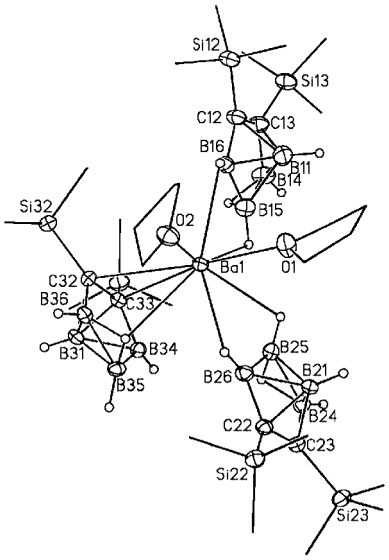

Figure 5. Crystal structure of a baracarborane complex

sponds to a four-center $BaHB_2$ bond. In the highly ionic solvated $Ba(BH_4)_2$ the boranate anions coordinate via three H atoms to the alkaline earth metal atom, thus forming three-center Ba−H−B bonds.[56] The Ba−C distances are similar to those of barium bis[tris(trimethylsilylmethyl)zincates][57] where bridging trimethylsilylmethyl moieties between barium and zinc atoms were found. The Ba−C distances of substituted barocenes vary between 2.90 and 3.00 Å.[58] This coordination of the carborane to the barium center is quite different from that of (carborane)magnesium and -calcium complexes.[31,59−61] In the magnesacarborane complex the metal center bonds to the hydride substituents but not to the carbon atoms. With the doubly deprotonated carborane ligands the metal centers show shorter contacts to the boron atoms than to the carbon atoms. The barium complex has very long Ba−B bonds due to the coordination geometry about the metal center. Nevertheless, this baracarborane was the first example of the heaviest group-2 metallacarborane. Similarly, the corresponding calca- and strontacarboranes have been synthesized and structurally characterized.[62]

Conclusions

Our recent work on carborane chemistry has concentrated on developing synthetic routes to new carborane ligands in both large and small cage systems. The aim is to establish general procedures for the systematic production of specific metallacarboranes that have potentially useful and interesting properties. We have also developed synthetic routes to precursor boranes that might otherwise be unavailable. Such routes invite chemists to explore the properties of these fascinating molecules.

Acknowledgments

This work was supported by grants from the National Science Foundation (CHE-9988045 and CHE-0241319), the donors of the Petroleum Research Fund, administered by the American Chemical Society, The Robert A. Welch Foundation (N-1322 to J. A. M.) and Northern Illinois University through a Presidential Research Professorship. The Forschungspreis der Alexander von Humboldt-Stiftung and the nominating Professors, Dr. Herbert W. Roesky of Universität Göttingen and Dr. Wolfgang Kaim of Universität Stuttgart, are also hereby gratefully acknowledged.

[1] For general references see: [1a] *Comprehensive Organometallic Chemistry II* (Eds,: E. W. Abel, F. G. A. Stone, G. Wilkinson), Elsevier Science Ltd., Oxford, **1995**, vol 1, chapters 6−9. [1b] N. S. Hosmane, J. A. Maguire in *Electron Deficient Boron and Carbon Clusters* (Eds.: G. A. Olah, K. Wade, R. E. Williams), John Wiley & Sons, New York, **1991**, chapter 9, pp. 215−235. [1c] N. S. Hosmane, J. A. Maguire, *Adv. Organomet. Chem.* **1990**, *30*, 99−150. [1d] N. S. Hosmane, *Pure Appl. Chem.* **1991**, *63*, 375−378.

[2] [2a] A. K. Saxena, J. A. Maguire, N. S. Hosmane, *Chem. Rev.* **1997**, *97*, 2421−2462 and references therein. [2b] N. S. Hosmane, K.-J. Lu, H. Zhang, J. A. Maguire, *Organometallics* **1997**, *16*, 5163−5170. [2c] N. S. Hosmane, J. Yang, K.-J. Lu, H. Zhang, U. Siriwardane, M. S. Islam, J. L. C. Thomas, J. A. Maguire, *Organometallics* **1998**, *17*, 2784−2796.

[3] [3a] N. S. Hosmane, Y. Wang, H. Zhang, K.-J. Lu, J. A. Maguire, T. G. Gray, K. A. Brooks, E. Waldhör, W. Kaim, R. K. Kremer, *Organometallics* **1997**, *16*, 1365−1377. [3b] H. Zhang, Y. Wang, A. K. Saxena, A. R. Oki, J. A. Maguire, N. S. Hosmane, *Organometallics* **1993**, *12*, 3933−3944. [3c] N. S. Hosmane, Y. Wang, H. Zhang, J. A. Maguire, E. Waldhör, W. Kaim, *Organometallics* **1993**, *12*, 3785−3787. [3d] A. K. Saxena, N. S. Hosmane, *Chem. Rev.* **1993**, *93*, 1081−1124. [3e] N. S. Hosmane, Y. Wang, H. Zhang, J. A. Maguire, E. Waldhör, W. Kaim, H. Binder, R. K. Kremer, *Organometallics* **1994**, *13*, 4156−4158. [3f] A. R. Oki, H. Zhang, N. S. Hosmane, H. Ro, W. E. Hatfield, *J. Am. Chem. Soc.* **1991**, *113*, 8531−8532. [3g] H. Zhang, L. Jia, N. S. Hosmane, *Acta Crystallogr., Cryst. Struct. Commun.* **1993**, *C49*, 453−456. [3h] T. J. Colacot, L. Jia, H. Zhang, U. Siriwardane, J. A. Maguire, Y. Wang, K. A. Brooks, V. P. Weiss, N. S. Hosmane, *Organometallics* **1995**, *14*, 1365−1376. [3i] N. S. Hosmane, D. Zhu, H. Zhang, A. R. Oki, J. A. Maguire, *Organometallics* **1998**, *17*, 3196−3203.

[4] [4a] N. S. Hosmane, Y. Wang, A. R. Oki, H. Zhang, D. Zhu, E. M. McDonald, J. A. Maguire, *Phosphorus, Sulfur, Silicon* **1994**, *93−94*, 253−256. [4b] N. S. Hosmane, Y. Wang, A. R. Oki, H. Zhang, J. A. Maguire, *Organometallics* **1996**, *15*, 626−638. [4c] N. S. Hosmane, Y. Wang, H. Zhang, J. A. Maguire, M. McInnis, T. G. Gray, J. D. Collins, R. K. Kremer, H. Binder, E. Waldhör, W. Kaim, *Organometallics* **1996**, *15*, 1006−1013. [4d] H. Zhang, A. R. Oki, Y. Wang, J. A. Maguire, N. S. Hosmane, *Acta Crystallogr., Cryst. Struct. Commun.* **1995**, *C51*, 635−638. [4e] N. S. Hosmane, Y. Wang, H. Zhang, A. R. Oki, J. A. Maguire, E. Waldhör, W. Kaim, H. Binder, R. K. Kremer, *Organometallics* **1995**, *14*, 1101−1103. [4f] H. Zhang, Y. Wang, J. A. Maguire, N. S. Hosmane, *Acta Crystallogr., Cryst. Struct. Commun.* **1996**, *C52*, 640−643. [4g] H. Zhang, Y. Wang, J. A. Maguire, N. S. Hosmane, *Acta Crystallogr., Cryst. Struct. Commun.* **1996**, *C52*, 8−11. [4h] N. S. Hosmane, A. R. Oki, H. Zhang, *Inorg. Chem. Commun.* **1998**, *1*, 101−104.

[5] *Edwards Air Force Base RTS Bulletin*, Aug/Sept **1999** and references therein (http://www.edwards.af.mil/penvmng/NewsInfo/RTS/1999RTS/AugSep99/augsep99p5.htm).

[6] M. G. H. Wallbridge, C. G. Savory, *J. Chem. Soc., Dalton Trans.* **1973**, 179−184.

 © 2003 Wiley-VCH Verlag GmbH & Co. KGaA, Weinheim

[7] N. S. Hosmane, J. R. Wermer, H. Zhu, T. D. Getman, S. G. Shore, *Inorg. Chem.* **1987**, *26*, 3638−3639.

[8] [8a] R. L. Middaugh, in *Boron Hydride Chemistry* (Ed.: E. L. Muetterties), Academic Press, New York; **1975**, chapter 8, pp. 273−300. [8b] S. G. Shore, in *Clusters, Rings and Polymers of the Main Group Elements* (Ed.: A. H. Cowley), ACS Symposium Series, American Chemical Society, Washington, DC, **1983**, chapter 1. [8c] S. H. Lawrence, J. R. Wermer, S. K. Boocock, M. A. Banks, P. C. Keller, S. G. Shore, *Inorg. Chem.* **1986**, *25*, 367−372.

[9] M. A. Toft, J. B. Leach, F. L. Himpsl, S. G. Shore, *Inorg. Chem.* **1982**, *21*, 1952−1957.

[10] Natural and ^{10}B-enriched decaborane ($B_{10}H_{14}$), and *anti*-$B_{18}H_{22}$ are commercially available from KATCHEM LTD., Czech Republic, for $15, $250, $151 and $510 per gram, respectively.

[11] H. I. Schlesinger, H. C. Brown, D. L. Mayfield, J. R. Gilbreath, *J. Am. Chem. Soc.* **1953**, *75*, 213−215.

[12] H. I. Schlesinger, H. C. Brown, A. E. Finholt,, *J. Am. Chem. Soc.* **1953**, *75*, 205−209.

[13] [13a] K. C. Nainan, G. E. Ryschkewitsch, *Inorg. Nucl. Chem. Lett.* **1970**, *6*, 765−766. [13b] G. E. Ryschkewitsch, K. C. Nainan, *Inorg. Synth.* **1974**, *15*, 111−118.

[14] L. Adams, S. N. Hosmane, J. E. Eklund, J. Wang, N. S. Hosmane, *J. Am. Chem. Soc.* **2002**, *124*, 7292−7293.

[15] L. V. McCarty, P. A. Di Giorgio, *J. Am. Chem. Soc.* **1951**, *73*, 3138−3143.

[16] [16a] G. E. Ryschkewitsch, V. R. Miller, *J. Am. Chem. Soc.* **1975**, *97*, 6258−6259. [16b] V. R. Miller, G. E. Ryschkewitsch, *Inorg. Synth.* **1974**, *15*, 118−122. [16c] N. S. Hosmane, R. N. Grimes, *Inorg. Chem.* **1979**, *18*, 3294−3297.

[17] [17a] A. H. Soloway, W. Tjarks, B. A. Bauman, F. G. Rong, R. F. Barth, I. M. Codogni, J. G. Wilson, *Chem. Rev.* **1998**, *98*, 1515−1562. [17b] *Advances in Neutron Capture Therapy, Vol. II, Chemistry and Biology* (Eds.: B. Larsson, J. Crawford, R. Weinreich), Elsevier Science, New York, **1997**.

[18] [18a]L. Adams, S. Tomlinson, J. Wang, S. N. Hosmane, J. A. Maguire, N. S. Hosmane, *Inorg. Chem. Commun.* **2002**, *5*, 765−767. [18b] C. T. Brewer, R. N. Grimes, *J. Am. Chem. Soc.* **1985**, *107*, 3552−3557.

[19] [19a] L. I. Zakharkin, L. S. Podvisotskaya, *Zh. Obshch. Khim.* **1967**, *37*, 506−507. [19b] L. I. Zakharkin, V. N. Kalinin, L. S. Podvisotskaya, *Izv. Akad. Nauk, Ser. Khim.* **1967**, 2310−2316. [19c] V. I. Stanko, Yu. V. Goltyapin, V. A. Brattsev, *Zh. Obshch. Khim.* **1969**, *39*, 1175.

[20] N. S. Hosmane, L. Jia, H. Zhang, J. W. Bausch, G. K. S. Prakash, R. E. Williams, T. P. Onak, *Inorg. Chem.* **1991**, *30*, 3793−3795.

[21] M. B. Ezhova, H. Zhang, J. A. Maguire, N. S. Hosmane, *J. Organomet. Chem.* **1998**, *550*, 409−422.

[22] [22a] J. L. Spencer, M. Green, F. G. A. Stone, *J. Chem. Soc., Chem. Commun.* **1972**, 1178−1179. [22b] M. Green, J. L. Spencer, F. G. A. Stone, A. J. Welch, *J. Chem. Soc., Dalton Trans.* **1975**, 179−184. [22c] M. Green, J. L. Spencer, F. G. A. Stone, *J. Chem. Soc., Dalton Trans.* **1979**, 1679−1686.

[23] W. E. Carroll, M. Green, F. G. A. Stone, A. J. Welch, *J. Chem. Soc., Dalton Trans.* **1975**, 2263−2270.

[24] [24a] M. F. Hawthorne, G. B. Dunks, M. M. McKown, *J. Am. Chem. Soc.* **1971**, *93*, 2541−2543. [24b] T. D. Getman, C. B. Knobler, M. F. Hawthorne, *J. Am. Chem. Soc.* **1990**, *112*, 4593−4594.

[25] [25a] N. M. M. Wilson, D. Ellis, A. S. F. Boyd, B. T. Giles, S. A. MacGregor, G. M. Rosair, A. J. Welch, *Chem. Commun.* **2002**, 464−465. [25b] Z. Xie, C. Yan, Q. Yang, T. C. W. Mak, *Angew. Chem. Int. Ed.* **1999**, *38*, 1761−1763. [25c] K. Chui, H.-W. Li, Z. Xie, *Organometallics* **2000**, *19*, 5447−5453. [25d] G. Zi, H.-W. Li, Z. Xie, *Chem. Commun.* **2001**, 1110−1111.

[26] C. Viñas, G. Barberà, F. Teixidor, *J. Organomet. Chem.* **2002**, *642*, 16−19.

[27] K. Chui, Q. Yang, T. C. W. Mak, Z. Xie, *Organometallics* **2000**, *19*, 1391−1401.

[28] [28a] G. Zi, H.-W. Li, Z. Xie, *Organometallics* **2001**, *20*, 3836−3838. [28b] Y. Wang, H. Wang, H.-W. Li, Z. Xie, *Organometallics* **2002**, *21*, 3311−3313. [28c] G. Zi, H.-W. Li, Z. Xie, *Organometallics* **2002**, *21*, 3464−3470.

[29] B. Lockman, T. Onak, *J. Am. Chem. Soc.* **1972**, *94*, 7923−7924.

[30] V. R. Miller, L. G. Sneddon, D. C. Beer, R. N. Grimes, *J. Am. Chem. Soc.* **1974**, *96*, 3090−3098.

[31] N. S. Hosmane, D. Zhu, J. E. McDonald, H. Zhang, J. A. Maguire, T. G. Gray, S. C. Helfert, *Organometallics* **1998**, *17*, 1426−1437.

[32] N. S. Hosmane, D. Zhu, H. Zhang, A. R. Oki, J. A. Maguire, *Organometallics* **1998**, *17*, 3196−3203.

[33] C. Zheng, J.-Q. Wang, J. A. Maguire, N. S. Hosmane, *Main Group Met. Chem.* **1999**, *22*, 361−366.

[34] N. S. Hosmane, *J. Organomet. Chem.* **1999**, *581*, 13−27.

[35] N. S. Hosmane, *Curr. Sci.* **2000**, *78*, 475−486.

[36] G. Rana, J. A. Maguire, S. N. Hosmane, N. S. Hosmane, *Main Group Met. Chem.* **2000**, *23*, 527−547.

[37] N. S. Hosmane, S.-J. Li, C. Zheng, J. A. Maguire, *Inorg. Chem. Commun.* **2001**, *4*, 104−107.

[38] N. S. Hosmane, H. Zhang, J. A. Maguire, T. Demissie, A. R. Oki, A. K. Saxena, W. N. Lipscomb, *Main Group Met. Chem.* **2001**, *24*, 589−596.

[39] J. Wang, S.-L. Li, C. Zheng, J. A. Maguire, N. S. Hosmane, *Organometallics* **2002**, *21*, 3314−3316.

[40] J. Wang, S.-L. Li, C. Zheng, J. A. Maguire, N. S. Hosmane, *Inorg. Chem. Commun.* **2002**, *5*, 602−605.

[41] J. Wang, S. Li, C. Zheng, J. A. Maguire, N. S. Hosmane, *Organometallics* **2002**, *21*, 5149−5151.

[42] [42a] E. Wiberg, O. Stecher, H. J. Andraschek, L. Kreuzbichler, E. Staude, *Angew. Chem. Int. Ed. Engl.* **1963**, *2*, 507. [42b] C. Eaborn, R. A. Jackson, R. W. Walsingham, *J. Chem. Soc., C.* **1967**, 2188−2191. [42c] J. L. Wardell, *Comp. Organomet. Chem.* **1982**, *1*, 52−54. [42d] D. C. Billington, *Comp. Org. Syn.* in *Comprehensive Organic Chemistry* (Eds. B. M. Trost, I. Fleming), Pergamon Press, U. K., **1991**, vol. 3, p. 413−434.

[43] [43a] T. P. Fehlner, N. S. Hosmane (Guest Eds.), *J. Organomet. Chem.* **2000**, *614−615*, 1−333 (special volume). [43b] Z. Xie, *Coord. Chem. Rev.* **2002**, *231*, 23−46.

[44] Y. Zhu, K. Vyakaranam, J. A. Maguire, W. Quintana, F. Teixidor, C. Viñas, N. S. Hosmane, *Inorg. Chem. Commun.* **2001**, *4*, 486−489.

[45] Y. Zhu, J. A. Maguire, N. S. Hosmane, *Inorg. Chem. Commun.* **2002**, *5*, 296−299.

[46] T. Onak, D. Marynick, P. Mattschei, G. B. Dunks, *Inorg. Chem.* **1968**, *7*, 1754−1757.

[47] N. S. Hosmane, R. N. Grimes, *Inorg. Chem.* **1979**, *18*, 2886−2891.

[48] R. Wilczynski, L. G. Sneddon, *Inorg. Chem.* **1982**, *21*, 506−514.

[49] J. H. Davis, R. N. Grimes, *Inorg. Chem.* **1988**, *27*, 4213−4219, and references therein.

[50] J. A. Maguire, J.-Q. Wang, C. Zheng, C. Li, N. S. Hosmane, *Inorg. Chim. Acta* **2002**, *334C*, 91−104.

[51] J. Wang, Y. Zhu, S.-J. Li, C. Zheng, J. A. Maguire, N. S. Hosmane, *J. Organomet. Chem.*, in press.

[52] Y. Zhu, J. A. Maguire, C. Zheng, S.-L. Li, N. S. Hosmane, *Main Group Met. Chem.* **2002**, *25*, 173−174.

[53] D. D. Devore, F. J. Timmers, D. L. Hasha, R. K. Rosen, T. J. Marks, P. A. Deck, C. L. Stern, *Organometallics* **1995**, *14*, 3132−3134.

[54] Y. Wang, H. Wang, H.-W. Li, Z. Xie, *Organometallics* **2002**, *21*, 3311−3313.

[55] M. Westerhausen, C. Gückel, S. Schneiderbauer, H. Nöth, N. S. Hosmane, *Angew. Chem. Int. Ed.* **2001**, *40*, 1902−1904.

[56] M. Bremer, H. Nöth, M. Thomann, M. Schmidt, *Chem. Ber.* **1995**, *128*, 455−460.

[57] M. Westerhausen, C. Gückel, T. Habereder, M. Vogt, M. Warchhold, H. Nöth, *Organometallics* **2001**, *20*, 893−899.

[58] [58a] P. Jutzi, *J. Organomet. Chem.* **1990**, *400*, 1−17. [58b] T. P.

 © 2003 Wiley-VCH Verlag GmbH & Co. KGaA, Weinheim

Hanusa, *Chem. Rev.* **1993**, *93*, 1023−1036. [58c] D. J. Burkey, T. P. Hanusa, *Comments Inorg. Chem.* **1995**, *17*, 41−47. [58d] P. Jutzi, *Chem. Rev.* **1999**, *99*, 969−990.
[59] R. Khattar, C. B. Knobler, M. F. Hawthorne, *J. Am. Chem. Soc.* **1990**, *112*, 4962−4963.
[60] R. Khattar, C. B. Knobler, M. F. Hawthorne, *Inorg. Chem.* **1990**, *29*, 2191−2192.
[61] N. S. Hosmane, D. Zhu, J. E. McDonald, H. Zhang, J. A. Maguire, T. G. Gray, S. C. Helfert, *J. Am. Chem. Soc.* **1995**, *117*, 12362−12363.
[62] M. Westerhausen, C. Gückel, S. Schneiderbauer, H. Nöth, N. S. Hosmane, to be published.

Received May 2, 2003
Early View Article
Published Online September 12, 2003

 © 2003 Wiley-VCH Verlag GmbH & Co. KGaA, Weinheim

Self-Assembly and Characterisation of Grid-Type Iron(II), Cobalt(II) and Zinc(II) Complexes

Violetta Patroniak,[a,b] Paul N. W. Baxter,[a,d] Jean-Marie Lehn,*[a] Maciej Kubicki,[b] Maija Nissinen,[c] and Kari Rissanen[c]

Keywords: Grid-type complexes / Iron / Cobalt / Zinc / Supramolecular chemistry / Self-assembly

The reaction of the ligands **5** and **6**, containing two tridentate binding units, with iron(II), cobalt(II) and zinc(II) leads to the self-assembly of supramolecular architectures of [2 × 2] grid type containing four ions in octahedral coordination sites. The grid-type structures have been assigned on the basis of the spectroscopic data in solution, and confirmed in the solid state in the case of complexes **6b** and **6c** by X-ray crystallography. The latter study revealed that each metal ion is situated in a distorted octahedral coordination environment comprising two N,N,O ligand donor sets.
(© Wiley-VCH Verlag GmbH & Co. KGaA, 69451 Weinheim, Germany, 2003)

Introduction

Self-assembly has been defined as the spontaneous but directed formation of a closed superstructure or polymer from a mixture of components (organic ligands, salt crystals, and sometimes molecules of solvents).[1] The product exhibits a notable thermodynamic and kinetic stability and its components should contain all the information necessary for a correct assembly to occur. Self-assembly has recently been achieved in many types of organic and inorganic systems.[2] Inorganic self-assembly involves the spontaneous generation of well-defined metallo-supramolecular architectures from mixtures of organic ligands and metal ions. This latter approach has proven particularly successful for the generation of a wide spectrum of architectural types such as, for example, inorganic double and triple helicates,[1,3] rotaxanes,[4] clusters,[5] racks,[6] cages,[7] grids[8] etc., based on ligand design and on the application of suitable coordination geometries for the assembly process. Among them, there is an increasing interest in grid-shaped complexes, based on ligands containing oligopyridine-type groups and various transition metal ions. The grids are the thermodynamically most stable motif when metal ions of octahedral coordination geometry are combined with a linear ligand containing two tridentate binding subunits. Such compounds may exhibit novel physical (electronic,[8a] magnetic[8g−8i]) and chemical properties with potential applications in supramolecular engineering, nanotechnology, biomedical inorganic chemistry or biological catalysis. Transistors incorporating complexes containing a cobalt ion bonded to polypyridyl ligands have been reported recently, and this development is expected to be important in molecular electronics and in the study of the physics of nanoscale systems.[9]

In this paper we describe the syntheses, structural characterisation and luminescence properties of some polynuclear metal complexes prepared from hexadentate ligands **5** and **6** containing pyridine, pyrimidine, and carbonyl donor groups. The syntheses of the new ligands and their precursors have been achieved in good overall yield. The coordination chemical investigations of **5** and **6** with metal ions of preferred octahedral coordination geometry, such as Fe^{II}, Co^{II} and Zn^{II} revealed that the ligands are correctly preorganised for the assembly of tetranuclear grid-type complexes.

Results and Discussion

Synthesis of Ligands 5 and 6

We have designed heterotopic ligands **5** and **6**, which each possess two unusual N,N,O tridentate binding subunits for the complexation of ions of octahedral coordination geometry. Ligands **5** and **6** comprise heterocyclic pyrimidine and pyridine units synthesised as outlined in Scheme 1.

2-Methyl-6-(trimethylstannyl)pyridine **(1)** was obtained from 2-bromo-6-methylpyridine by a halogen/lithium ex-

[a] ISIS, Université Louis Pasteur,
8, Allée Gaspard Monge, BP 70028, 67083 Strasbourg, France
E-mail: lehn@isis.u-strasbg.fr
[b] Faculty of Chemistry, Adam Mickiewicz University,
Grunwaldzka 6, 60780 Poznań, Poland
[c] Department of Chemistry, University of Jyväskylä,
P. O. Box 35, 40351, Jyväskylä, Finland
[d] Current address: Institut Charles Sadron
6 Rue Boussingault, 67083 Strasbourg, France

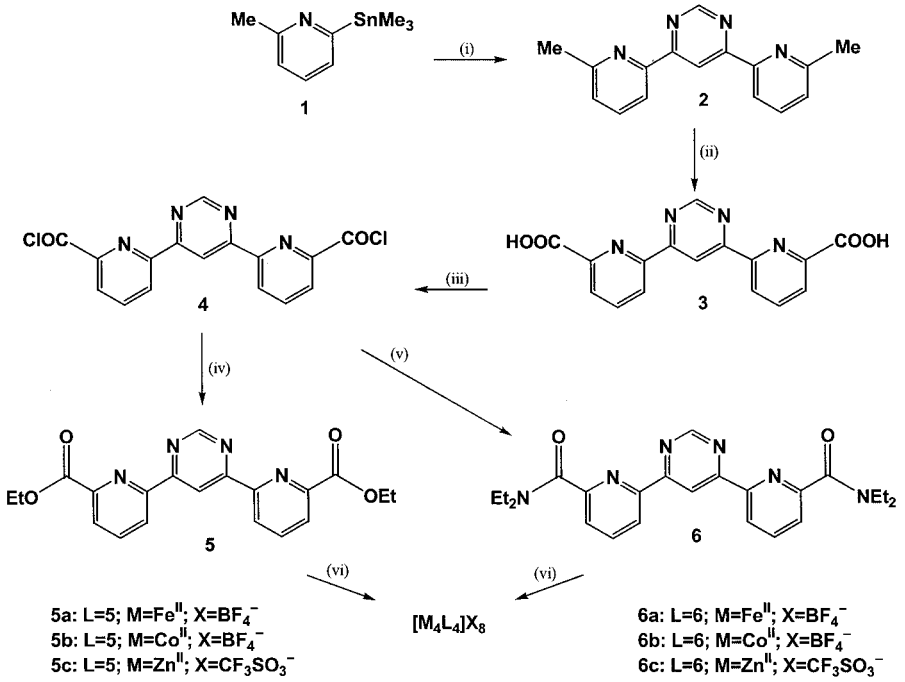

Scheme 1. Reaction scheme for the synthesis of the [2 × 2] grid complexes **5a**−**c** and **6a**−**c**. i) 4,6-dichloropyrimidine, LiCl, $Pd(PPh_3)_4$, toluene (90%), ii) H_2SO_4, CrO_3 (81%), iii) $SOCl_2$, iv) EtOH, (88%), v) Et_2NH, THF (38%), vi) $Fe(BF_4)_2$, $Co(BF_4)_2$ or $Zn(CF_3SO_3)_2$, CH_3CN

change protocol at low temperature in THF with *n*-butyllithium, followed by quenching the pyridyllithium intermediate with $ClSnMe_3$.[10] The twofold Stille-type[11] coupling reaction of **1** with 4,6-dichloropyrimidine in toluene using $[Pd(PPh_3)_4]$ as a catalyst furnished **2** in 90% yield after workup. The methyl groups of **2** were further oxidized with CrO_3 in concentrated H_2SO_4 to afford diacid **3** in 81% yield. The acid is insoluble in most organic solvents and only slightly soluble in DMSO. Precursor **3** was converted into the diacid dichloride **4** upon refluxing in $SOCl_2$. The diacid dichloride **4** was used subsequently in further transformations without purification. Thus, when **4** was refluxed with EtOH or stirred with Et_2NH in THF ligands **5** and **6** were obtained in 88% and 38% yields, respectively, after purification. The structures of **5**, **6** and precursors were confirmed by NMR spectroscopy, FAB-MS and elemental analysis. Ligands **5** and **6** were also structurally characterised by X-ray crystallography (Figure 1 and 2).

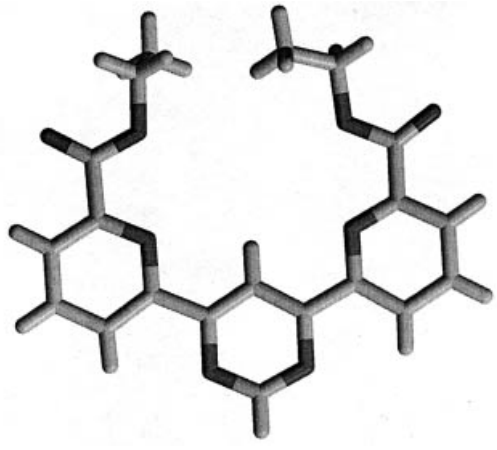

Figure 1. Single-crystal X-ray structure of ligand **5**

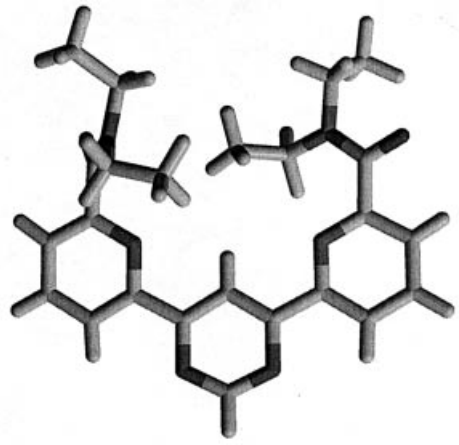

Figure 2. Single-crystal X-ray structure of ligand **6**

Both **5** and **6** exist in the solid state as *transoid* conformers (Figure 1 and 2) for N−C−C−N torsion angles (Table 1). This conformation is energetically favoured, as shown in earlier work.[12] It presents C−H···N intramolecular hydrogen bond interactions for further stabilisation (Table 2). However, in the metal complexes presented below the ligands exist in a *cisoid* conformation in which the terminal carbonyl oxygens form chelating coordination bonds with metal ions.

 © 2003 Wiley-VCH Verlag GmbH & Co. KGaA, Weinheim

Table 1. Relevant torsion angles in the crystal structures of ligands **5** and **6**

	5A	5B	6
N1−C6−C7−N8	−178.9(5)	177.8(5)	−178.4(2)
N3−C4−C13−N14	177.6(5)	−179.9(5)	−169.7(2)
N14−C15−C19−O20	175.3(7)	178.0(6)	−119.5(2)
N8−C9−C24−O25	−172.8(6)	−172.6(7)	
N8−C9−C26−O27			−151.3(2)
C19−O21−C22−C23	159.9(7)	−98.0(7)	
C24−O26−C27−C28	97.6(7)	−162.3(6)	

The aromatic rings of **5** and **6** are essentially planar, with a maximal deviation from the least-squares plane of 0.022(3) Å. In **5** the dihedral angles between the aromatic ring planes are small [up to 5(1)°], and the ester COO fragments are almost coplanar with the ring plane. The carbonyl oxygen atoms are *trans* with respect to the nitrogen atoms of the neighbouring pyridine rings, suggesting that weak intramolecular C−H···O=C interactions stabilise this conformation (in a carboxylate group the carbonyl oxygen atom is a better hydrogen bond acceptor than the ester one). In both symmetry-independent molecules the ethoxy fragments on either side of the molecule are differently oriented. This is probably a result of steric interactions between the ethyl groups within the bay region of the molecule. In one of the ethyl groups, the terminal C−C bond is almost coplanar with the main plane of the molecule, while in the other it is almost perpendicular (Figure 1, Table 1).

In **6** the amide groups are essentially planar, but they are more twisted with respect to the respective pyridine ring planes. The twist angles are as large as 58.2(5)° — this may be caused by the steric requirements of four relatively bulky CH_2CH_3 groups. Interestingly, even in this case the carbonyl oxygen atoms are in a *pseudo-trans* orientation with respect to the pyridine nitrogen atom (Table 1). The steric stress is transferred to some extent to the central part of the molecule, and therefore the dihedral angles between the aromatic ring planes are in this case much larger than in **5**, up to 12.02(14)°. The space between the oxygen atoms in the *transoid* conformation of ligand **6** is 8.58 Å.

The bond lengths and angles are unexceptional, and similar in both compounds. The differences between the intraannular bond angles in the terminal pyridine rings can be attributed to the presence of the different substituents.[13] The intraannular angles show a difference between C−C−C and N−C−C angles, the former being about 5°

Table 2. Crystal structures of ligands **5** and **6**; hydrogen bond data [including weak intramolecular C−H···N(O) interactions]

Compound **5**				
D−H···A[a]	D−H (Å)	H···A (Å)	D···A (Å)	D−H···A(θ °)
C(2A)−H(2A)···O(20A)#1	0.93	2.67	3.578(9)	165
C(2B)−H(2B)···O(25B)#1	0.93	2.69	3.604(9)	167
C(11B)−H(11B)···O(20A)#3	0.93	2.54	3.139(7)	123
C(17B)−H(17B)···O(25A)#4	0.93	2.62	3.286(7)	129
C(5A)−H(5A)···N(8A)	0.93	2.54	2.830(8)	99
C(5A)−H(5A)···N(14A)	0.93	2.50	2.814(8)	98
C(18A)−H(18A)···N(3A)	0.93	2.52	2.797(10)	99
C(12A)−H(12A)···N(1A)	0.93	2.45	2.764(9)	100
C(5B)−H(5B)···N(8B)	0.93	2.52	2.778(8)	96
C(5B)−H(5B)···N(14B)	0.93	2.53	2.820(8)	98
C(18B)−H(18B)···N(3B)	0.93	2.43	2.767(9)	102
C(12B)−H(12B)···N(1B)	0.93	2.44	2.743(10)	99
Compound 6				
D−H···A[b]	D−H (Å)	H···A (Å)	D···A (Å)	D−H···A(θ °)
C(23)−H(23C)···O(27)#1	1.03(3)	2.47(3)	3.480(4)	165(2)
C(24)−H(24A)···O(27)#1	0.99(2)	2.63(3)	3.606(3)	168.3(19)
C(29)−H(29A)···O(20)#2	1.04(3)	2.71(3)	3.431(3)	126.5(18)
C(30)−H(30C)···O(20)#2	1.04(4)	2.67(4)	3.337(4)	122(2)
C(31)−H(31A)···O(20)#2	0.99(3)	2.67(3)	3.465(3)	138(2)
C(5)−H(5)···N(8)	0.91(2)	2.51(2)	2.800(3)	99.3(17)
C(5)−H(5)···N(14)	0.91(2)	2.49(2)	2.786(3)	99.6(16)
C(22)−H(22B)···N(14)	1.00(2)	2.74(2)	3.066(3)	99.6(16)
C(23)−H(23B)···N(14)	1.01(3)	2.70(3)	3.318(4)	119(2)
C(18)−H(18)···N(3)	0.94(2)	2.52(2)	2.849(3)	100.5(16)
C(29)−H(29B)···N(8)	1.08(2)	2.26(2)	2.902(3)	116.0(17)
C(30)−H(30B)···N(8)	1.05(3)	2.97(3)	3.380(4)	104(2)

[a] Symmetry transformations used to generate equivalent atoms: #1 $x - 1/2, -y + 1/2, z$; #2 $x + 1/2, -y + 1/2, z$; #3 $x - 1/2, -y - 1/2, z$; #4 $-x + 3/2, y + 1/2, z + 1/2$. [b] Symmetry transformations used to generate equivalent atoms: #1 $-x + 1, -y + 1, -z + 1$; #2 $-x + 1, -y + 1, -z$.

 © 2003 Wiley-VCH Verlag GmbH & Co. KGaA, Weinheim

greater than the latter; similar differences have been observed in related compounds.[14]

The crystal packing is governed by van der Waals interactions, weak intermolecular C−H···O(N) interactions (Table 2) and, to some extent, by the π-stacking between the heterocyclic rings.

Synthesis and Characterisation of the Complexes

Multitopic ligands with N,N,O(carbonyl) type donor sets have only infrequently been employed in the metal ion directed assembly of coordination architectures. However, such ligands have been successfully demonstrated to form helicate complexes, in particular with lanthanide metal ions.[3a] The reason for the propensity of the N,N,O (carbonyl) donor set to bind to lanthanides presumably originates from the strong hard-hard, oxygen-lanthanide(III) interaction. The following account describes the successful utilisation of ligands of this type (**5** and **6**) for the generation of [2 × 2] grid architectures with certain first row transition metal ions. Specifically, the syntheses of the new [2 × 2] grid-type complexes **5a**−**c** and **6a**−**c** were performed by reaction of **5** and **6** with iron(II), cobalt(II) and zinc(II) salts (Scheme 2).

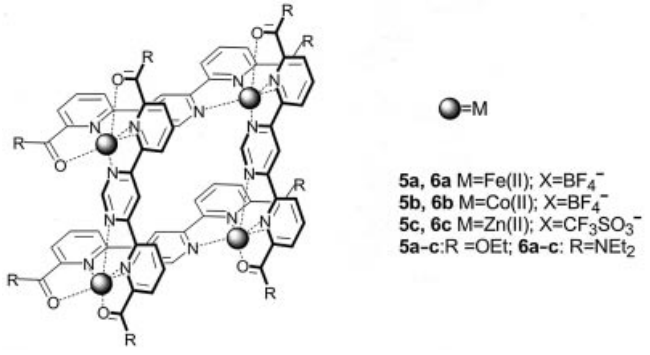

Scheme 2. Schematic representation of the self-assembly of the [2 × 2] grids

The self-assembly of [2 × 2] grid-type compounds was achieved by reaction at room temperature or under reflux in acetonitrile, using the triflate or tetrafluoroborate salt of the corresponding metal ion. The complexation reactions were followed by ESI-MS and NMR spectroscopy. The ^{1}H NMR spectra of the paramagnetic complexes (**5a**, **5b**, **6a**, and **6b**) show strongly shifted signals, as expected, and are strongly supportive of the grid-type structures. In the case of the iron complexes **5a** and **6a**, signals are observed between δ = 88.25 and 1.42 ppm, and δ = 90.96 and −7.79 ppm, respectively, indicating the presence of high-spin iron centres, similar to related grid structures with N,N,N donor sets reported earlier.[15] For the cobalt complexes **5b** and **6b** the signals were found to be shifted to an even greater extent, lying between δ = 130.27 and 1.40 ppm and between δ = 114.33 and −15.23 ppm, respectively. The ^{1}H NMR spectra of the diamagnetic zinc complexes **5c** and **6c** show the signals of a symmetrically coordinated ligand in a single chemical and magnetic environment, in agreement with the grid structure. Interestingly, significant coordination-induced shifts of the signals are observed when the spectra of **5c** and **6c** are compared to those of uncomplexed ligands **5** and **6**.

ESI-MS is a highly sensitive and accurate analytical tool widely used for the characterisation of large, charged biomolecules such as proteins and DNA. The technique has also been found to be particularly successful for the identification of large metallosupramolecular architectures in solution, in which multiply charged ions are generated by sequential loss of counterions, resulting in characteristic isotopic patterns in the spectrum. The ESI-MS investigations of all complexes were performed on acetonitrile solutions at approximately 10^{-4} M. For example, the ESI mass spectrum of **5c** shows peaks corresponding to the multiply charged species: *m/z* = 839.2 (5%, $\{[Zn_4(\mathbf{5})_4](CF_3SO_3)_5\}^{3+}$), 591.0 (100%, $\{[Zn_4(\mathbf{5})_4](CF_3SO_3)_4\}^{4+}$) and 345.2 (5%, $\{[Zn_4(\mathbf{5})_4](CF_3SO_3)_2\}^{6+}$. These data confirm the presence of the grid **5c** in solution. At higher dilutions, significant dissociation of the grid complexes to mononuclear species was found to occur.

The UV/Visible spectrum of complex **6c** in acetonitrile shows an absorption band at around 300 nm. Complex **6c** also affords an intense emission at 372 nm upon excitation at 270 nm at room temperature (Figure 3). The luminescence of this complex may be attributed to emission from the lowest ligand-centred excited singlet level. The absence of emission for the cobalt complex **6b** is due to the presence of the low-lying nonemissive Co^{II}-centred MLCT excited state which inhibits luminescence.[16]

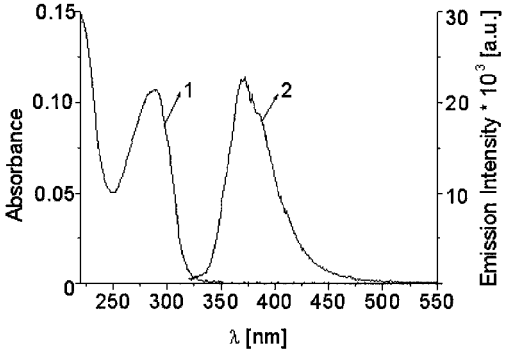

Figure 3. Absorption (1) and emission (2) spectra of $Zn_4L_4(OTf)_8$ complex **6c** at 1×10^{-5} mol/dm^{-3} in CH_3CN solution (λ_{exc} = 270 nm, λ_{em} = 372 nm)

Crystallographic Characterisation of Grid Complexes 6b and 6c

Complexes **6b** and **6c** were crystallographically characterised by X-ray diffraction. The results unambiguously demonstrated the [2 × 2] tetranuclear grid-type structure of the complexes in which the metal ions are hexacoordinated by four nitrogen atoms and the remaining outer positions by oxygen atoms of the carbonyl groups.

 © 2003 Wiley-VCH Verlag GmbH & Co. KGaA, Weinheim

Crystal Data for Complex 6b

Crystals of complex **6b** were obtained by diffusion of benzene into a solution of the complex in acetonitrile and its structure was determined by X-ray crystallography (Figure 4 and Table 3). The architecture of this grid is similar to that of the structures of similar compounds.[15,16] The complex **6b** crystallises with two cations per unit cell. The size of this grid is within nanoscopic dimensions, as the intraligand methyl-methyl and pyridine H4-pyridine H4 distances are respectively 15.9−17.9 Å (width) and 9.2−9.4 Å (height). The ligands in the grid are not totally planar but somewhat distorted. The distortion angle varies from 4.4° to 14.5°. There are two anions partially encapsulated inside the cavity of the grid. The size of the cavity is between 6.39 and 6.75 Å. In addition, each anion inside the cavity is surrounded by two molecules of acetonitrile. These molecules of solvent are sandwiched between opposite pyridine moieties. The rest of the anions are positioned between adjacent grids in a layer-like fashion. A limited degree of van der Waals contact between aromatic groups and ethyl chains of adjacent grids is also observed. The Co^{II} ions are situated in a distorted octahedral coordination polyhedron and the Co−Co distances are in the range 6.328−6.395 Å. The Co−N and Co−O bond lengths lie between 2.033 and 2.200 Å and 2.068 and 2.135 Å, respectively.

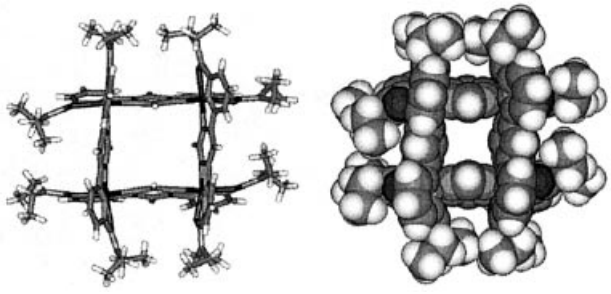

Figure 4. Crystal structure of [2 × 2] grid-type complex **6b**; counterions and solvent molecules are omitted for clarity

Table 3. Selected averaged bond lengths [Å] and angles [°] for complex **6b** (each of the two molecules in the asymmetric unit are presented) and for complex **6c**

Bond/angle[a]	6b	6c
$M-N_{ax}$	2.043 2.043	2.058
$M-N_{eq}$	2.168 2.166	2.170
M−O	2.110 2.106	2.157
$N_{ax}-M-N_{ax}$	163.8 162.4	156.7
$N_{eq}-M-N_{eq}$	95.5 95.9	101.3
O−M−O	100.6 102.2	97.2

[a] M = Co^{II} in **6b** and Zn^{II} in **6c**. ax = M−N bonds to the pyridine moiety, eq = M−N bonds to the pyrimidine moiety.

Crystal Data for Complex 6c

Crystals of complex **6c** were obtained by diffusion of *tert*-butyl methyl ether into a solution of the complex in acetonitrile and its structure was determined by X-ray crystallography (Figure 5 and Table 3). The Zn^{II} ions in complex **6c** also display a distorted octahedral coordination. The Zn−Zn distances are in the range 6.255−6.390 Å. The lengths of the coordinative Zn−N bonds vary from 2.052 to 2.199 Å and the Zn−O bond lengths lie between 2.134 and 2.188 Å. Two CF_3SO_3 ions are partially encapsulated in the cavity of this grid.

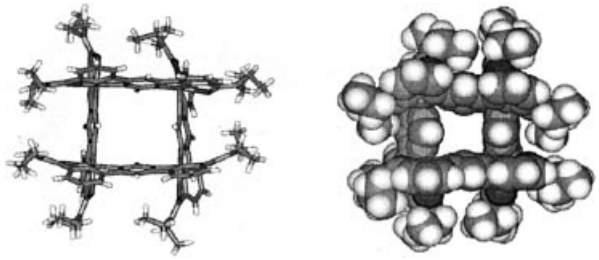

Figure 5. Crystal structure of [2 × 2] grid-type complex **6c**; counterions and solvent molecules are omitted for clarity

Conclusion

The two novel ligands **5** and **6** containing two tridentate N,N,O(carbonyl) binding subunits, have been prepared and their solid-state conformational properties characterised by X-ray crystallography. Reaction of **5** and **6** with Fe^{II}, Co^{II} and Zn^{II} resulted in the clean and quantitative formation of [2 × 2] grid-type complexes, which were characterised in solution on the basis of ESI-MS and ^1H NMR spectroscopy. The structures of the Zn^{II} and Co^{II} complexes **6b** and **6c** were also investigated by X-ray crystallography which confirmed that they were indeed [2 × 2] grid-type architectures with each metal ion octahedrally coordinated by two N,N,O donors. The above work therefore details a particularly facile and rapid synthetic protocol for the preparation of [2 × 2] grid-type coordination scaffolds with first row transition metal ions. Of particular significance is the fact that the N,N,O(carbonyl) donor set approach should enable a wide range of substituents to be externally connected onto the outer surface of the grid. Such substituents may for example be electroactive or mesogenic, or may enable attachment of the complex to gold or graphite surfaces. Many potential future applications may be envisioned for materials of this type, for example, as functional components of molecular electronic devices. These and related avenues of exploration will be reported in due course.

Experimental Section

General: CH_3CN was freshly distilled under argon from CaH_2. 2-Methyl-6-(trimethylstannyl)pyridine (**1**) was prepared according to a literature procedure.[10] The reagents were used as received from Aldrich or Acros without further purification. The NMR spectra were run on a Bruker AC 200 at 200.1 MHz, a Varian Gemini 300, and 500 MHz spectrometer, and were calibrated against residual protonated solvent signal ($CDCl_3$: δ = 7.24 ppm; $[D_6]$DMSO: δ = 2.50 ppm; CD_3CN: δ = 1.94 ppm). Mass spectra were determined by FAB^+ using a ZAB-HF VG apparatus in a *m*-nitrobenzyl alcohol matrix and by ESI-MS using a Waters Micromass ZQ spec-

 © 2003 Wiley-VCH Verlag GmbH & Co. KGaA, Weinheim

trometer in acetonitrile. IR spectra were obtained with a Perkin−Elmer 580 spectrophotometer and are reported in cm^{-1}. The electronic absorption spectrum of **6c** was measured on a Shimadzu UV 2401 PC spectrometer in acetonitrile, with λ_{max} in nm and ε ($\times 10^4$) in $M^{-1}cm^{-1}$. The luminescence spectrum for complex **6c** was recorded in CH_3CN using a Perkin−Elmer MPF-3 spectrofluorimeter. Microanalyses were obtained using a Perkin−Elmer 2400 CHN microanalyzer. Melting points were recorded on an Electrothermal Digital melting point apparatus.

4,6-Bis[6-(2-methylpyridyl)]pyrimidine (2): 2-Methyl-6-(trimethylstannyl)pyridine (**1**; 5 g, 20 mmol) and degassed toluene (45 mL) were added consecutively by syringe to a mixture of 4,6-dichloropyrimidine (0.9818 g, 6 mmol), $Pd(PPh_3)_4$ (0.27 g, 0.9 mmol) and LiCl (1.7 g, 29 mmol) under an argon atmosphere. The reaction was refluxed and stirred at 120 °C for 24 h, and the toluene was then evaporated on a water bath under reduced pressure. The residue was purified by column chromatography on alumina, eluting with dichloromethane, to afford 1.547 g (90%) **2**. ^1H NMR (400 MHz, $CDCl_3$): δ = 9.32 (s, 1 H, H2), 9.30 (s, 1 H, H5), 8.26 (d′, *J* = 5.49 Hz, 2 H, H5′, -5′), 7.75 (t, *J* = 5.95 Hz, 2 H, H4′, -4′′), 7.28 (d, *J* = 5.19 Hz, 2 H, H3′, -3′′), 2.75 (s, CH_3) ppm. ^{13}C NMR (75 MHz, $CDCl_3$): δ = 164.07, 158.46, 158.34, 153.49, 136.98, 124.78, 118.77, 113.85, 24.70 ppm. FAB-MS: *m*/*z* (%) = 263.0 (100) [**2** + H]. IR (KBr): ṽ = 3408, 2917, 1597, 1571, 1530, 1448, 1379, 1228, 1158, 1090, 989, 904, 808, 771, 640, 438 cm^{-1}. $C_{16}H_{14}N_4$ (262.31): calcd. C 73.26, H 5.38, N 21.36; found C 73.04, H 5.46, N 21.24. M.p. 126−128 °C.

2,2′-Bis(4,6-pyrimidinediyl)pyridine-6,6′-dicarboxylic Acid (3): Product **2** (0.35 g, 1.3 mmol) was added to concentrated H_2SO_4 (10 mL) and cooled to 0 °C with stirring in an ice-bath. Chromium(VI) oxide (0.80 g, 8 mmol) was then added in 0.1 g portions to the stirred solution of **2** at a rate that maintained the reaction temperature below 3 °C. When the addition of CrO_3 was completed (about 5 h) the mixture was stirred for 9 hours at 0−5 °C, and 42 hours at room temperature. The viscous reaction solution was then poured onto excess crushed ice with stirring. The precipitated product was finally isolated by filtration under reduced pressure, washed with distilled water and air dried to yield 0.348 g (81%) of **3**. ^1H NMR (200 MHz, DMSO): δ = 9.50 (s, 1 H, H2), 9.35 (s, 1 H, H5), 8.72 (t′, *J* = 4.75 Hz, 2 H, H4′, -4′), 8.27 (d, *J* = 4.57 Hz, 4 H, H3′, -3′′, -5′, -5′′) ppm. IR (KBr): ṽ = 3411, 2926, 1746, 1646, 1581, 1533, 1452, 1367, 1252, 1168, 1086, 995, 905, 838, 752, 636, 607, 471, 427 cm^{-1}. $C_{16}H_{10}N_4O_4{\cdot}2H_2O$ (358.31): calcd. C 53.63, H 3.91, N 15.64; found C 53.25, H 3.70, N 15.03. M.p. 253 °C

2,2′-Bis(4,6-pyrimidinediyl)pyridine-6,6′-dicarboxylic Acid Chloride (4): Compound **3** (0.133 g, 0.4 mmol) was refluxed for 5 h in thionyl chloride (20 mL) and then the $SOCl_2$ evaporated under reduced pressure on a water bath. The crude **4** was then used immediately for the subsequent synthesis of diester **5** and diamide **6** without further purification.

Diethyl 2,2′-Bis(4,6-pyrimidinediyl)pyridine-6,6′-dicarboxylate (5): EtOH (20 mL) was added to **4** (0.148 g, 0.41 mmol) and the resulting mixture refluxed for 15 h and subsequently cooled to room temperature. The reaction was then reduced in volume to 8 mL under pressure on a water bath, and the mixture cooled in an ice-bath. The crystalline solid was isolated by filtration under vacuum, washed with a small quantity of ice-cold EtOH and air dried to yield 0.138 g (88%) **5** as white needles. ^1H NMR (300 MHz, $CDCl_3$): δ = 9.51 (s, 1 H, H2), 9.38 (s, 1 H, H5), 8.70 (d, *J* = 8.1 Hz, 2 H, H5′, -5′′), 8.24 (d, *J* = 7.8 Hz, 2 H, H3′, -3′′), 8.05 (t, *J* = 7.8 Hz, 2 H, H4, -4′), 4.52 (q, *J* = 6.9 Hz, 4 H, CH_2), 1.51 (t, *J* = 7.2 Hz, 6 H, CH_3) ppm. ^{13}C NMR (DEPT, 75 MHz, $CDCl_3$): δ = 165.16, 163.57, 158.55 (CH), 154.51, 148.70, 138.09 (CH), 126.40 (CH), 124.84 (CH), 115.05 (CH), 61.95 (CH_2), 14.29 (CH_3) ppm. FAB-MS: *m*/*z* (%) = 379.4 (100) [**5** + H]. IR (KBr): ṽ = 3410, 2982, 1715, 1646, 1575, 1529, 1447, 1318, 1259, 1150, 1083, 992, 919, 838, 756, 701, 636, 471, 433 cm^{-1}. $C_{20}H_{18}N_4O_4$ (378.39): calcd. C 63.49, H 4.79, N 14.81; found C 63.17, H 4.82, N 14.44. M.p. 162 °C.

2,2′-Bis(4,6-pyrimidinediyl)pyridine-6,6′-diethyl Diamide (6): Anhydrous THF (5 mL), and a solution of Et_2NH (10 mL) in anhydrous THF (50 mL) were added consecutively by syringe to **4** (0.2592 g, 0.72 mmol) under an atmosphere of argon. The resulting mixture (pale brown suspended solid) was then stirred for 20 h at ambient temperature, and filtered under gravity. The filtrate was evaporated to dryness and the remaining solid dissolved in boiling *n*-hexane (100 mL), filtered under gravity, and left to stand overnight. The crystalline solid which formed was isolated by filtration under vacuum, washed with ice-cold hexane and air dried to yield 0.118 g (38%) **6** as white needles. ^1H NMR (300 MHz, $CDCl_3$): δ = 9.37 (s, 2 H, H2, H5), 8.58 (d, *J* = 7.8 Hz, 2 H, H5′, -5′′), 8.00 (t′, *J* = 7.8 Hz, 2 H, H4′, -4′), 7.79 (d′, *J* = 7.8 Hz, 2 H, H3′, -3′), 3.62 (q, *J* = 7.2 Hz, 4 H, CH_2), 3.47 (q, *J* = 7.2 Hz, 4 H, CH_2), 1.33 (t, *J* = 6.9 Hz, 6 H, CH_3), 1.29 (t, *J* = 7.2 Hz, 6 H, CH_3) ppm. ^{13}C NMR (DEPT, 75 MHz, $CDCl_3$): δ = 167.70, 163.42, 158.36 (CH), 154.83, 152.42, 137.60 (CH), 125.05 (CH), 122.04 (CH), 113.93 (CH), 43.48 (CH_2), 40.52 (CH_2), 14.69 (CH_3), 13.01 (CH_3) ppm. FAB-MS: *m*/*z* (%) = 433.2 (100) [**6** + H]. IR (KBr): ṽ = 3412, 2975, 1636, 1569, 1477, 1443, 1377, 1316, 1117, 1080, 993, 827, 756, 636, 608, 472, 409 cm^{-1}. $C_{24}H_{28}N_6O_2$ (432.53): calcd. C 66.58, H 6.52, N 19.43; found C 66.39, H 6.42, N 18.50. M.p. 123 °C.

Fe Complex (5a): An equimolar mixture of $Fe(BF_4)_2{\cdot}6H_2O$ (9.8 mg, 29 μmol) and ligand **5** (11.0 mg, 29 μmol) in MeCN (5 mL) was stirred at room temperature for 10 h. The solvent was evaporated under reduced pressure to give a quantitative yield of **5a** as a blue powder. ^1H NMR (300 MHz, CD_3CN): δ = 88.25, 64.59, 34.53, 31.15, 9.36 (d), 8.75, 8.75, 8.27, 4.47, 3.75, 2.57, 1.42 ppm. IR (KBr): ṽ = 3349, 2991, 1635, 1577, 1533, 1444, 1381, 1247, 1219, 1033, 929, 875, 795, 755, 703, 657, 581, 417 cm^{-1}. $Fe_4(\mathbf{5})_4(BF_4)_8$ (2469.34): calcd. C 38.91, H 2.44, N 9.08; found C 39.21, H 2.53, N 9.78.

Co Complex (5b): A solution of ligand **5** (10.0 mg, 26 μmol) and $Co(BF_4)_2{\cdot}6H_2O$ (9.0 mg, 26 μmol) in MeCN (5 mL) was heated under reflux for 10 h. The red complex **5b** was isolated in quantitative yield by evaporation of the solvent. ESI-MS: *m*/*z* = 1135 $\{[Co_4(\mathbf{5})_4](BF_4)_6\}^{2+}$, 218 $\{[Co_4(\mathbf{5})_4]\}^{8+}$. ^1H NMR (300 MHz, CD_3CN): δ = 130.27, 100.79, 97.26, 87.88, 72.57, 68.41, 62.20, 34.07, 14.48, 11.42, 9.49 (d), 8.75, 8.27, 8.04, 6.56, 5.98, 4.45, 3.56, 2.95, 1.76, 1.42, 1.40 ppm. IR (KBr): ṽ = 3371, 3084, 1613, 1573, 1531, 1442, 1385, 1265, 1212, 1158, 1034, 928, 878, 794, 759, 701, 672, 657, 587, 444 cm^{-1}. $Co_4(\mathbf{5})_4(BF_4)_8$ (2481.69): calcd. C 38.72, H 2.92, N 9.03; found C 39.07, H 2.98, N 9.65.

Zn Complex (5c): An equimolar mixture of $Zn(CF_3SO_3)_2$ (9.6 mg, 26 μmol) and ligand **5** (10.0 mg, 26 μmol) in MeCN (5 mL) was stirred at room temperature for 22 h. The solvent was evaporated under reduced pressure to yield the dark yellow complex **5c** in quantitative yield. ESI-MS: *m*/*z* = 839.2 $\{[Zn_4(\mathbf{5})_4](CF_3SO_3)_5\}^{3+}$, 591.0 $\{[Zn_4(\mathbf{5})_4](CF_3SO_3)_4\}^{4+}$, 345.2 $\{[Zn_4(\mathbf{5})_4](CF_3SO_3)_2\}^{6+}$. ^1H NMR (300 MHz, CD_3CN): δ = 9.71 (s), 9.57 (d), 9.36 (s), 8.70 (d), 8.33 (t), 4.50 (m), 1.71 (t, *J* = 5.1 Hz) ppm. IR (KBr): ṽ = 3452, 3095, 1724, 1693, 1620, 1582, 1538, 1475, 1452, 1404, 1381, 1342, 1263, 1163, 1100, 1031, 857, 840, 758, 723, 704, 638, 574, 518, 446,

 © 2003 Wiley-VCH Verlag GmbH & Co. KGaA, Weinheim

405 cm^{-1}. $Zn_4(\mathbf{5})_4(CF_3SO_3)_8$ (2967.65): calcd. C 35.62, H 2.45, N 7.55; found C 36.12, H 2.44, N 7.07.

Fe Complex (6a): An equimolar mixture of $Fe(BF_4)_2{\cdot}6H_2O$ (5.5 mg, 16 μmol) and ligand **6** (7.1 mg, 16 μmol) in MeCN (4 mL) was stirred at room temperature for 16 h. The solvent was evaporated under reduced pressure to give a quantitative yield of **6a** as a blue powder. ESI-MS: *m*/*z* = 1236.9 $\{[Fe_4(\mathbf{6})_4](BF_4)_6\}^{2+}$, 291.1 $\{[Fe_4(\mathbf{6})_4](BF_4)\}^{7+}$. ^{1}H NMR (200 MHz, CD_3CN): δ = 90.96, 87.54, 74.31, 63.69, 48.69, 32.52, 29.96, 27.64, 18.19, 16.91, 14.04, 12.03, 9.89, 7.64, 5.32, 3.98, 0.07, −4.80, −5.54, −7.79 ppm. IR (KBr): $\tilde{\nu}$ = 3403, 2926, 2854, 1632, 1570, 1530, 1485, 1447, 1379, 1363, 1299, 1259, 1221, 1182, 1120, 1084, 1071, 1042, 993, 827, 810, 756, 640, 574, 533, 522 cm^{-1}. $Fe_4(\mathbf{6})_4(BF_4)_8$ (2647.89): calcd. C 43.55, H 4.26, N 12.70; found C 40.36, H 4.03, N 12.53.

Co Complex (6b): A solution of ligand **6** (14.8 mg, 34 μmol) and $Co(BF_4)_2{\cdot}6H_2O$ (11.7 mg, 34μmol) in MeCN (7 mL) was heated under reflux for 19 h. The red complex **6b** was isolated in quantitative yield upon evaporation of the solvent. ESI-MS: *m*/*z* = 799.9 $\{[Co_4(\mathbf{6})_4](BF_4)_5\}^{3+}$, 578.1 $\{[Co_4(\mathbf{6})_4](BF_4)_4\}^{4+}$, 356 $\{[Co_4(\mathbf{6})_4](BF_4)_2\}^{6+}$. ^{1}H NMR (200 MHz, CD_3CN): δ = 114.33, 71.57, 21.68, 14.66, 10.51, 6.30, 5.45, 4.72, −2.11, −4.31, −10.13, −13.40, −15.23 ppm. IR (KBr): $\tilde{\nu}$ = 3439, 2978, 2931, 1719, 1636, 1609, 1572, 1534, 1485, 1442, 1386, 1363, 1266, 1208, 1083, 1033, 827, 756, 657, 522 cm^{-1}. $Co_4(\mathbf{6})_4(BF_4)_8$ (2660.24): calcd. C 43.34, H 4.24, N 12.64; found C 46.95, H 4.31, N 11.84.

Zn Complex (6c): A solution of ligand **6** (6.2 mg, 14 μmol) and $Zn(CF_3SO_3)_2$ (5.2 mg, 14μmol) in MeCN (3 mL) was stirred at room temperature for 19 h. The pale yellow complex **6c** was isolated in quantitative yield upon evaporation of the solvent. ^{1}H NMR (300 MHz, CD_3CN): δ = 9.70 (s), 9.42(s), 9.23 (d, *J* = 7.8 Hz), 8.68 (t, *J* = 7.8 Hz), 8.29 (d, *J* = 7.8 Hz), 3.48 (q), 3.12 (q, *J* = 6.3 Hz), 1.32 (t, *J* = 6.9 Hz) ppm. IR (KBr): $\tilde{\nu}$ = 3441, 2981, 1613, 1533, 1487, 1461, 1377, 1364, 1279, 1259, 1224, 1159, 1031, 993, 829, 757, 638, 574, 517 cm^{-1}. $Zn_4(\mathbf{6})_4(CF_3SO_3)_8{\cdot}10CH_3CN{\cdot}H_2O$ (3612.72): calcd. C 41.22, H 4.02, N 13.18; found C 44.01, H 4.30, N 12.21. UV/Vis: 298.0 (1.1).

Crystal Structure Determination of Ligands 5 and 6: Colourless crystals of dimensions 0.05 × 0.1 × 0.5 mm (compound **5**) and 0.2 × 0.25 × 0.25 mm (compound **6**) were chosen for X-ray data collection (see also Table 4). For ligand **5**, diffraction data were collected at room temperature by the ω-scan technique up to 2Θ = 40°, on a KUMA KM4CCD four-circle diffractometer with graphite-monochromated Mo-K_α radiation (λ = 0.71073Å). For ligand **6**, the data collection was performed with KUMA KM4 κ-geometry diffractometer equipped with point detector, using graphite-monochromated Cu-K_α radiation (λ = 1.54178Å) and ω-2θ scan method. All data were corrected for Lorentz-polarisation effects. The structures were solved with direct methods with SHELXS-97[17] and refined by full-matrix least-squares procedures on F^2 with SHELXL-97.[17] All non-hydrogen atoms were refined anisotropically, for **5** hydrogen atoms were located at calculated positions and refined as a ''riding model' with isotropic thermal parameters fixed at 1.2-times the U_{eq}'s of appropriate carrier atom, while for **6** both positional and thermal parameters of hydrogen atoms were refined.

Table 4. Crystallographic data for the structural analyses of ligands **5** and **6**

	5	**6**
Empirical formula	$C_{20}H_{16}N_4O_4$	$C_{24}H_{28}N_6O_2$
Molecular weight	376.7	432.5
a (Å)	18.675(3)	10.457(5)
b (Å)	4.3936(13)	10.713(3)
c (Å)	44.604(5)	11.242(3)
α (°)	90	86.98(2)
β (°)	90	77.11(3)
γ (°)	90	67.49(3)
V (Å^3)	3659.8(13)	1133.4(5)
Z	8	2
Space group	$Pna2_1$ (No. 33)	$P\bar{1}$ (No.2)
D_{calc} (g·cm^{-3})	1.37	1.27
μ(Mo-K_α) (mm^{-1})	0.10	0.67
$R(F)$ [$F^2 > 2\sigma(F^2)$][a]	0.0508	0.0445
$R_w(F^2)$ [all data][b]	0.0876	0.1209

[a] $R(F) = \Sigma||F_o| - |F_c||/\Sigma|F_o|$. [b] $Rw(F^2) = (\Sigma[w(F_o^2 - F_c^2)^2/\Sigma[w(F_o^2)^2])^{1/2}$.

Table 5. Crystallographic data for the structural analyses of complexes **6b** and **6c**

	6b	**6c**
Empirical formula	$2[C_{96}H_{112}O_8N_{24}Co_4]^{8+}{\cdot}16BF_4^-{\cdot}14.5CH_3CN{\cdot}8C_6H_6{\cdot}H_2O$	$[C_{96}H_{112}O_8N_{24}Zn_4]^{8+}{\cdot}8CF_3SO_3^-{\cdot}5CH_3CN{\cdot}4C_6H_6{\cdot}H_2O$
Molecular weight	6553.66	3405.41
a (Å)	23.2752(2)	18.3628(1)
b (Å)	26.7290(2)	20.6511(2)
c (Å)	27.1194(3)	23.0437(2)
α (°)	77.0095(3)	108.0590(3)
β (°)	85.0779(3)	112.4300(4)
γ (°)	74.7044(6)	95.6630(3)
V (Å^3)	15851.2(3)	7441.7(1)
Z	2	2
Space group	$P\bar{1}$ (No.2)	$P\bar{1}$ (No. 2)
D_{calc} (g·cm^{-3})	1.373	1.520
μ(Mo-K_α) (mm^{-1})	0.512	0.859
$R(F)$ [$F^2 > 2\sigma(F^2)$][a]	0.0918	0.0816
$R_w(F^2)$ [all data][b]	0.2515	0.2256

[a] $R(F) = \Sigma||F_o| - |F_c||/\Sigma|F_o|$for 28779 and 15857 observed reflections for **6b** and **6c**, respectively. [b] $Rw(F^2) = (\Sigma[w(F_o^2 - F_c^2)^2/\Sigma[w(F_o^2)^2])^{1/2}$.

 © 2003 Wiley-VCH Verlag GmbH & Co. KGaA, Weinheim

Compound **5** crystallises with two molecules in the asymmetric part of the unit cell. A normal probability plot shows that the differences in geometrical parameters between these two symmetry-independent molecules are of a statistical nature.

Crystal Structure Determination of Complexes 6b and 6c: A summary of crystal data and refinement parameters is given in Table 5. Data were collected on a Nonius Kappa CCD diffractometer at 173.0 ± 0.1 K using graphite-monochromated Mo-K_α radiation (λ = 0.71073 Å). The CCD data were processed with Denzo-SMN v0.95.373.[18] Corrections for Lorentz and polarisation effects were applied. The structures were solved by Patterson method (SHELXS-97)[17] and refined on F^2 by full-matrix least-squares techniques (SHELXL-97).[17] Empirical absorption correction from multiple reflections was performed for both data (Platon for Windows).[19] Scattering factors, corrected for anomalous dispersion, were used as implemented in the refinement program.

The asymmetric unit of complex **6b** contains two of each species. Of 150268 measured reflections in the range 2.10−50.04° in 2θ (and ω scans), 54918 were unique (R_{int} = 0.1215). A red 0.20 × 0.20 × 0.40 mm block-shaped crystal of $2[C_{96}H_{112}Co_4N_{24}O_8]^{8+}\cdot 16BF_4^-\cdot 14.5CH_3CN\cdot 8C_6H_6\cdot H_2O$ was used for data collection. Minimum and maximum transmission factors of 0.758/0.824. All non-hydrogen atoms were refined with anisotropic displacement parameters, except for seven anions, five acetonitriles, a benzene molecule and a water molecule, which were refined isotropically owing to large thermal movement and disorder. Thirteen anions, two acetonitriles, the water molecule and carbon C23H of one of the grids are disordered over two positions. One acetonitrile molecule was refined with population parameter 0.5. A bond restraint in the C−N bond of the disordered part of the grid had to be used to keep the disorder model chemically reasonable. Hydrogen atoms were calculated to their idealised positions with isotropic temperature factors (1.2- or 1.5-times C temperature factor) and refined as riding atoms. No hydrogen atoms were determined for water and one of the disordered acetonitriles. Final agreement factors were obtained for 3865 parameters and one restraint; GOF 1.023. The largest peak and hole in the final difference map were 1.257 and −0.945 e·Å^{-3} and are located near disordered benzene and disordered anion.

A pale yellow 0.20 × 0.30 × 0.30 mm block-shaped crystal of $[C_{96}H_{112}O_8N_{24}Zn_4]^{8+}\cdot 8CF_3SO_3^-\cdot 5CH_3CN\cdot 4C_6H_6\cdot H_2O$ was used for data collection. Of 67176 measured reflections in the range 2.34−50.02° in 2θ (and ω scans), 25963 were unique (R_{int} = 0.0713). Minimum and maximum transmission factors of 0.646/0.710. All non-hydrogen atoms were refined with anisotropic displacement parameters, except for five anions, which were refined partly isotropically owing to large thermal movement and disorder. Two acetonitrile molecules were refined with population parameter 0.5. Five anions and two methyl carbons (C22B and C24) of the grid are disordered over two positions. Temperature factor of disordered methyl C22F was equalised with C22B. Hydrogen atoms were calculated to their idealised positions with isotropic temperature factors (1.2- or 1.5-times C temperature factor) and refined as riding atoms. No hydrogen atoms were determined for water. Final agreement factors were obtained for 1898 parameters; GOF 1.027. The largest peak and hole in the final difference map were 1.330 and −1.100 e·Å^{-3} and are located near one of the disordered anions.

CCDC-205374 (**5**), -205375 (**6**), -205462 (**6b**) and -205463 (**6c**). contain the supplementary crystallographic data for this paper. These data can be obtained free of charge at www.ccdc.cam.ac.uk/conts/retrieving.html [or from the Cambridge Crystallographic Data Centre, 12, Union Road, Cambridge CB2 1EZ, UK; Fax: (internat.) +44-1223/336-033; E-mail: deposit@ccdc.cam.ac.uk].

Acknowledgments

We thank NATO for postdoctoral fellowship to V. P. We also thank Dr. Zbigniew Hnatejko for absorption and fluorescence measurements. This work was partly supported by the Polish State Committee for Scientific Research (grant no. 4 T09A 049 24).

[1] [1a] J.-M. Lehn, *Angew. Chem. Int. Ed. Engl.* **1990**, *29*, 1304−1319. [1b] J.-M. Lehn, *Supramolecular Chemistry-Concepts and Perspectives*, VCH, Weinheim, **1995**.

[2] [2a] J. S. Lindsey, *New J. Chem.* **1991**, *15*, 153−180. [2b] P. Molenveld, J. F. J. Engbersen, D. N. Reinhoudt, *Chem. Soc. Rev.* **2000**, *29*, 75−86. [2c] S. Leininger, B. Olenyuk, P. J. Stang, *Chem. Rev.* **2000**, *100*, 853−908. [2d] G. F. Swiegers, T. J. Malefetse, *Chem. Rev.* **2000**, *100*, 3483−3537. [2e] L. M. Greig, D. Philp, *Chem. Soc. Rev.* **2001**, *30*, 287−302. [2f] C. V. K. Sharma, *J. Chem. Ed.* **2001**, *78*, 617−622.

[3] [3a] C. Piguet, G. Bernardinelli, G. Hopfgartner, *Chem. Rev.* **1997**, *97*, 2005−2062. [3b] M. Albrecht, *Chem. Rev.* **2001**, *101*, 3457−3497. [3c] R. Krämer, J.-M. Lehn, A. Marquis-Rigault, *Proc. Natl. Acad. Sci. USA* **1993**, *90*, 5394−5398. [3d] E. C. Constable, *Tetrahedron* **1992**, *48*, 10013−10059.

[4] [4a] P. N. W. Baxter, H. Sleiman, J.-M. Lehn, K. Rissanen, *Angew. Chem. Int. Ed. Engl.* **1997**, *36*, 1294−1296. [4b] H. Sleiman, P. N. W. Baxter, J.-M. Lehn, K. Airola, K. Rissanen, *Inorg. Chem.* **1997**, *36*, 4734−4742. [4c] M. C. Jimenez-Molero, Ch. Dietrich-Buchecker, J.-P. Sauvage, *Chem. Eur. J.* **2002**, *8*, 1455−1466.

[5] [5a] D. Freedman, S. Sayan, T. J. Emge, M. Croft, J. G. Brennan, *J. Am. Chem. Soc.* **1999**, *121*, 11713−11719. [5b] J. Xu, K. N. Raymond, *Angew. Chem. Int. Ed.* **2000**, *39*, 2745−2747. [5c] B. K. Roland, H. D. Selby, M. D. Carducci, Z. Zheng, *J. Am. Chem. Soc.* **2002**, *124*, 3222−3223. [5d] R. W. Saalfrank, U. Reimann, M. Göritz, F. Hampel, A. Scheurer, F. W. Heinemann, M. Büschel, J. Daub, V. Schünemann, A. X. Trautwein, *Chem. Eur. J.* **2002**, *8*, 3614−3619.

[6] [6a] M. Fujita, Y. J. Kwon, O. Sasaki, K. Yamaguchi, K. Ogura, *J. Am. Chem. Soc.* **1995**, *117*, 7287−7288. [6b] R. L. Paul, S. M. Couchman, J. C. Jeffery, J. A. McCleverty, Z. R. Reeves, M. D. Ward, *J. Chem. Soc., Dalton Trans.* **2000**, 845−851.

[7] [7a] A. M. Garcia, D. M. Bassani, J.-M. Lehn, G. Baum, D. Fenske, *Chem. Eur. J.* **1999**, *5*, 1234−1238. [7b] M. Yoshizawa, T. Kusukawa, M. Fujita, S. Sakamoto, K. Yamaguchi, *J. Am. Chem. Soc.* **2001**, *123*, 10454−10459. [7c] M. Yoshizawa, Y. Takeyama, T. Kusukawa, M. Fujita, *Angew. Chem. Int. Ed.* **2002**, *41*, 1347−1349.

[8] For example: [8a] M.-T. Youinou, N. Rahmouni, J. Fischer, J. A. Osborn, *Angew. Chem. Int. Ed. Engl.* **1992**, *31*, 733−735. [8b] P. N. W. Baxter, G. S. Hanan, J.-M. Lehn, *Chem. Commun.* **1996**, 2019−2020. [8c] M. Fujita, Y. J. Kwon, S. Washizu, K. Ogura, *J. Am. Chem. Soc.* **1994**, *116*, 1151−1152. [8d] P. N. W. Baxter, J.-M. Lehn, B. Kneisel, D. Fenske, *Chem. Commun.* **1997**, 2231−2232. [8e] J. Rojo, M. Ruben, E. Breuning, J.-P. Giesselbrecht, J.-M. Lehn, *Angew. Chem. Int. Ed.* **2000**, *39*, 4139−4142. [8f] G. S. Hanan, D. Volkmer, U. S. Schubert, J.-M. Lehn, G. Baum, D. Fenske, *Angew. Chem. Int. Ed. Engl.* **1997**, *36*, 1842−1844. [8g] O. Waldmann, J. Hassmann, P. Müller, G. S. Hanan, D. Volkmer, U. S. Schubert, J.-M. Lehn, *Physical Rev. Lett.* **1997**, *17*, 3390−3393. [8h] J. Rojo, J.-M. Lehn, G. Baum, D. Fenske, O. Waldmann, P. Müller, *Eur. J. Inorg. Chem.* **1999**, 517−522. [8i] E. Breuning, M. Ruben, J.-M. Lehn, F. Renz, Y. Garcia, V. Ksenofontov, P. Gütlich, E. Wegelius, K. Rissanen, *Angew. Chem. Int. Ed.* **2000**, *39*, 2504−2505.

 © 2003 Wiley-VCH Verlag GmbH & Co. KGaA, Weinheim

[8j] H. Oshio, H. Onodera, O. Tamada, H. Mizutani, T. Hikichi, T. Ito, *Chem. Eur. J.* **2000**, 2523−2530. [8k] P. N. W. Baxter, J.-M. Lehn, K. Rissanen, *Chem. Commun.* **1997**, 1323−1324. [8l] P. N. W. Baxter, R. G. Khoury, J.-M. Lehn, G. Baum, D. Fenske, *Chem. Eur. J.* **2000**, *6*, 4140−4148. [8m] A. Marquis, J.-P. Kintzinger, R. Graff, P. N. W. Baxter, J.-M. Lehn, *Angew. Chem. Int. Ed.* **2002**, *41*, 2760−2764. [8n] J. P. Plante, P. D. Jones, D. R. Powell, T. E. Glass, *Chem. Commun.* **2003**, 336−337. [8o] M. Ruben, E. Breuning, M. Barboiu, J.-P. Gisselbrecht, J.-M. Lehn, *Chem. Eur. J.* **2003**, *9*, 291−299.

[9] J. Park, A. N. Pasupathy, J. I. Goldsmith, C. Chang, Y. Yaish, J. R. Petta, M. Rinkoski, J. P. Sethna, H. D. Abruña, P. L. McEuen, D. C. Ralph, *Nature* **2002**, *417*, 722−725.

[10] [10a] P. Jutzi, U. J. Gilge, *Organomet. Chem.* **1983**, *246*, 163. [10b] G. V. Long, S. E. Boyd, M. M. Harding, I. E. Buys, T. W. Hambley, *J. Chem. Soc., Dalton Trans.* **1993**, 3175−3180.

[11] J. K. Stille, *Angew. Chem. Int. Ed. Engl.* **1986**, *25*, 508−524.

[12] G. S. Hannan, J.-M. Lehn, N. Kyritsakas, J. Fischer, *J. Chem. Soc., Chem. Commun.* **1995**, 765−766; D. M. Bassani, J.-M. Lehn, G. Baum, D. Fenske, *Angew. Chem. Int. Ed. Engl.* **1997**, *36*, 1845−1847; D. M. Bassani, J.-M. Lehn, *Bull. Soc. Chim. Fr.* **1997**, *134*, 897−906; M. Ohkita, J.-M. Lehn, G. Baum, D. Fenske, *Chem. Eur. J.* **1999**, *12*, 3471−3481.

[13] A. Domenicano, P. Murray-Rust, *Tetrahedron Lett.* **1979**, *24*, 2283−2286.

[14] G. S. Hanan, U. S. Schubert, D. Volkmer, E. Rivière, J.-M. Lehn, N. Kyritsakas, J. Fischer, *Can. J. Chem.* **1997**, *75*, 169−182.

[15] E. Breuning, U. Ziener, J.-M. Lehn, E. Wegelius, K. Rissanen, *Eur. J. Inorg. Chem.* **2001**, 1515−1521.

[16] J. Rojo, F. J. Romero-Salguero, J.-M. Lehn, G. Baum, D. Fenske, *Eur. J. Inorg. Chem.* **1999**, 1421−1428.

[17] SHELX97 − Programs for Crystal Structure Analysis (Release 97−2). Sheldrick, G. M., Institüt für Anorganische Chemie der Universität, Tammanstrasse 4, 3400 Göttingen, Germany, **1998**.

[18] Z. Otwinowski, W. Minor, "Processing of X-ray Diffraction Data Collected in Oscillation Mode", Methods in Enzymology, Volume 276: Macromolecular Crystallography, part A, p. 307−326, **1997**, C. W. Carter, Jr. & R. M. Sweet, Eds., Academic Press.

[19] R. H. Blessing, *Acta Crystallogr., Sect. A* **1995**, *51*, 33−38; PLATON, A Multipurpose Crystallographic Tool, Utrecht University, Utrecht, The Netherlands, Spek, A. L. **1998**.

Received May 26, 2003
Early View Article
Published Online October 2, 2003

 © 2003 Wiley-VCH Verlag GmbH & Co. KGaA, Weinheim

Novel Complexes of Ligands Containing Phenol and Alcohol Groups: From Polynuclear Cluster, 1D Coordination Polymer to 2D Supramolecular Assemblies

Yongshu Xie,[a] Qingliang Liu,*[a] Hui Jiang,[a] and Jia Ni[a]

Keywords: Copper / Cobalt / Silver / Coordination polymers / N,O ligands

A series of Co^{II}, Cu^{II}, Zn^{II}, Ag^{I} and mixed-valence cobalt complexes **1**–**9** with tridentate and tetradentate chelating ligands containing oxygen-bridging and hydrogen-bonding groups have been synthesized, four of which have been structurally characterized: $[Co_6L^1_6(OH)(H_2O)_3]Cl_2{\cdot}10H_2O$ (**1**) [H_2L^1 = *N*-(2-hydroxybenzyl)ethanolamine] is a hexanuclear $Co^{III}_3Co^{II}_3$ complex, with a core of quadruple face-sharing defective cubane-like units; $[CuNaL^2(ClO_4)]_\infty$ (**3**) [H_2L^2 = *N*,*N*′-bis(2-hyroxybenzyl)ethylenediamine] is a μ_3-phenoxo- and μ_4-perchlorato-bridged 1D heterometallic $Cu^{II}Na^{I}$ coordination polymer; the coordination moieties of $[CuL^3]_4{\cdot}4H_2O$ (**6**) [H_2L^3 = *N*,*N*′-bis(2-hyroxy-5-methylbenzyl)ethylenediamine] form a 2D hydrogen-bonded network structure of monophenoxo-bridged dimeric moieties; and the molecules of $[Ag(H_2L^2)(HL^2)]$ (**9**) are connected to give an undulated 2D structure, consisting of hydrogen-bonded hexagonal units. The variety of these structures is discussed on the basis of the stereoelectronic preferences of the metal atoms, hydrogen bonds, disposition of the bridging groups, steric effect, and conformational flexibility of the ligands. Variable-temperature magnetic properties of **1** and **6** are also reported.

(© Wiley-VCH Verlag GmbH & Co. KGaA, 69451 Weinheim, Germany, 2003)

Introduction

Assemblies of polynuclear complexes, coordination polymers and hydrogen-bonded supramolecular coordination networks have potential applications and are aesthetically appealing.[1−3] The assemblies of these frameworks are influenced by factors such as the structures of the ligands and the stereoelectronic preferences of the metal ions.[4] The assembly of metal atoms with chelating ligands containing endogenous bridging atoms is one promising route to unexpected, interesting coordination structures, wherein the most commonly utilized bridging atoms are from carboxylate functionalities.[5] In contrast, chelating ligands containing phenol groups have been much less explored.[6] We demonstrate here the successful construction of various novel coordination architectures, utilizing chelating ligands containing phenol and/or alkoxy groups (H_2L^1 − H_2L^3) (Scheme 1), which have been synthesized by the reduction of the corresponding Schiff bases. The phenol and the alkoxy groups can act as bridging and hydrogen-bonding functionalities. Compared with the corresponding Schiff bases, $H_2L^1-H_2L^3$ have greater flexibility and conformational freedom. In addition, the amino groups, which are absent in the Schiff bases, may also affect the structures of the products via intermolecular hydrogen bonds. Consequently, these ligands may be promising for the construction of novel coordination assemblies, and so we have investigated several of their metal complexes. Our interest in ligands containing phenoxy and alkoxy groups also lie in their relevance to the coordination environments of active sites of metalloenzymes.[7]

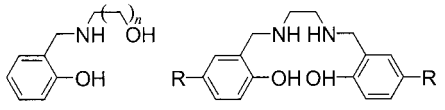

Scheme 1. Molecular structures of the ligands (H_2L^1: n = 1, H_2L': n = 2, H_2L^2: R = H, H_2L^3: R = CH_3)

Divalent metals with pseudooctahedral coordination preferences, namely, Co^{II}, Cu^{II} and Zn^{II}, have been used for the synthesis of the complexes. For comparison, the soft metal Ag^{I}, which has a tetrahedral preference, has also been used. Thus, a series of Co^{II}, Cu^{II}, Zn^{II}, Ag^{I} and mixed-valence cobalt complexes have been synthesized, four of which have been characterized by X-ray crystal analyses to reveal structures varying from hexanuclear cluster, 1D bimetallic coordination polymers to 2D supramolecular assemblies. The structures of the complexes are discussed on the basis of various structure-directing factors, including the metal coordination preferences, hydrogen bonds, bridging groups, steric effect, and conformational flexibility of the ligands. Variable-temperature magnetic properties of two of the complexes are also reported. The results ob-

[a] Department of Chemistry, University of Science and Technology of China,
Hefei, 230026, P. R. China
E-mail: yshxie@ustc.edu.cn

Supporting information for this article is available on the WWW under http://www.eurjic.org or from the author.

 © 2003 Wiley-VCH Verlag GmbH & Co. KGaA, Weinheim **DOI: 10.1002/ejic.200300384**

tained are valuable for the design and synthesis of further such novel complexes.

Results

Synthesis and Spectroscopic Results: To promote the deprotonation and subsequent coordination of the phenol and the alkoxy groups, complexes **1**−**8** were synthesized at alkaline pH by the addition of stoichiometric aqueous NaOH solution. For the Ag^I complex (**9**), Ag_2O precipitates upon the addition of NaOH, and the direct reaction of H_2L^2 with $AgNO_3$ in methanol resulted in a white precipitate of **9**, which was gradually dissolved by the addition of an excess of concentrated ammoniacal solution. Probably, the coordinated H_2L^2 is initially displaced by NH_3, which then evaporates to allow H_2L^2 to reform complex **9**, which gradually crystallized. Attempts to synthesize Ag^I complexes of H_2L^1 and H_2L^3 gave only the free ligands, possibly due to the weak coordinating abilities of the ligands and the instability of the resulting complexes.

In the IR spectra of complexes **1**−**8**, the coordination of the phenol groups is exhibited by the shifting of ν(C−O) to higher wavenumbers. For complexes **3**−**5**, and **7**, the intense bands near 1100 cm^{-1} show distinct splittings, indicative of coordinated ClO_4^-.

Isotropic EPR spectra of complex **3** and **6** in DMF containing four copper hyperfine lines are observed at 300 K (Figure 1), while the spectra at 100 K have axial symmetries, with four hyperfine peaks in the parallel region derived from the coupling of the copper nucleus and the unpaired electron. The EPR parameters (**3**: $g_{//} = 2.229$, $g_{\perp} = 2.004$, $A_{//} = 186.4$ G, $A_{iso} = 85.7$ G; **6**: $g_{//} = 2.231$, $g_{\perp} = 2.006$, $A_{//} = 188.7$ G) are indicative of tetragonal coordination environments with $(d_{x^2-y^2})^1$ ground states for complexes **3** and **6**.[8]

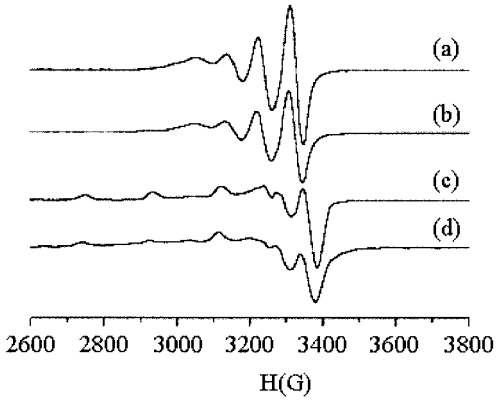

Figure 1. EPR spectra of the complexes in DMF: (a) **3**, 300 K; (b) **6**, 300 K; (c) **3**, 100 K; (d) **6**, 100 K

The electronic spectra of the copper and cobalt complexes in DMF (Table 1) exhibit intraligand transitions, and d−d transitions in addition to strong LMCT bands, confirming the coordination of the deprotonated phenoxy groups.

Structural Results: The crystal structure of **1** consists of a discrete $[Co_6L^1_6(OH)(H_2O)_3]^{2+}$ hexameric entity (Figure 2, a, Table S1 of the Supporting Information; see also the footnote on the first page of this article), two noncoordinated chloride counter anions, and ten water molecules of crystallization. Bond lengths, charge balance considerations

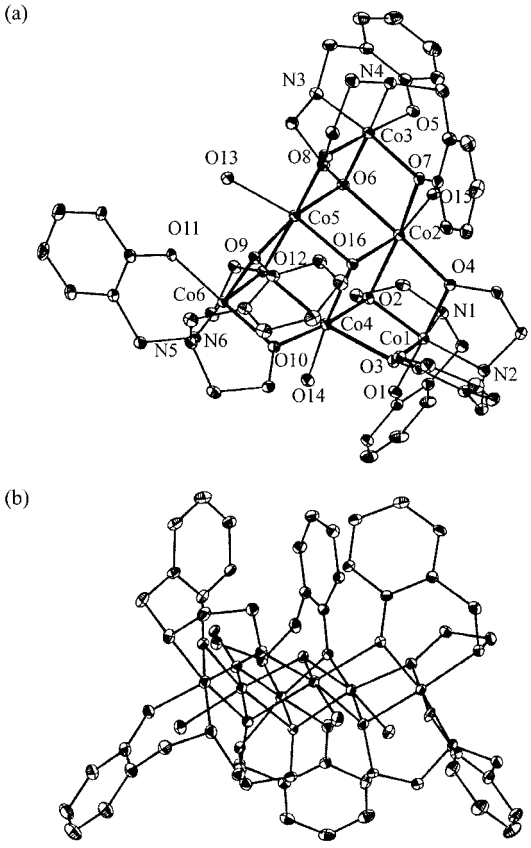

Figure 2. Complementary views of the structure of **1** showing 20% probability displacement ellipsoids. H atoms have been omitted for clarity

Table 1. Electronic spectra of the complexes in DMF

Complexes	λ_{max}/nm (ε/$dm^3 \cdot mol^{-1} \cdot cm^{-1}$)			
$\pi \rightarrow \pi^*$	$n \rightarrow \pi^*$	$L \rightarrow M$	$d \rightarrow d$	
1	264 (9.63×10^3)	290 (5.30×10^3)	358 (1.35×10^3)	598 (100)
3		290 (1.37×10^4)	390 (1.22×10^3)	605 (283)
4		252 (2.46×10^4)	373 (3.01×10^3)	584 (323)
6	268 (6.00×10^3)	286 (5.33×10^3)	340 (704), 398 (781)	598 (296)
7	213 (1.51×10^4)	247 (1.42×10^4)	384 (1.55×10^3)	592 (205)

 © 2003 Wiley-VCH Verlag GmbH & Co. KGaA, Weinheim

and magnetic measurements (vide infra) reveal that the three inner cobalt atoms are Co^{II}, and the outer ones are Co^{III}. Each Co^{III} has an N_2O_4 ligation, namely the two phenoxo, two alkoxo and two amino groups of two *fac*-$(L^1)^{2-}$ ligands. The phenoxo and alkoxo groups of the $(L^1)^{2-}$ ligands, together with a μ_3-hydroxo ligand, bridge the six cobalt atoms, resulting in, apparently, the first Co_6O_{10} face-sharing quadruple defective cubane-like complex. The whole hexameric entity adopts a crown shape (Figure 2, b), with the three phenyl rings at the upper rim tilted inward, and the phenyl rings at the lower rim tilted outward. According to the "Harris" notation,[9] the upper $(L^1)^{2-}$ and lower $(L^1)^{2-}$ ligands are involved in $32_{12}2_{13}1_1$ and $31_13_{123}1_1$ bridging modes, respectively (Figure 3). The $Co^{III}-N$ and $Co^{III}-O$ distances are in the ranges 1.944(7)−1.980(7) and 1.862(5)−1.956(5) Å, respectively. The $Co^{II}-O$ distances are in the range 1.991(5)−2.286(5) Å, and the $Co^{II}-O-Co^{II}$ angles are 94.44(19)−107.8(3)°, with $Co^{II}\cdots Co^{II}$ separations of 3.240, 3.253 and 3.270 Å, respectively.

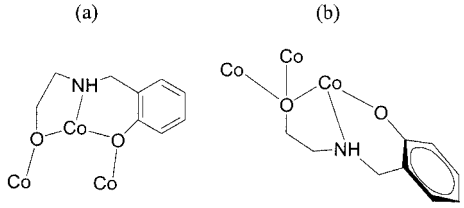

Figure 3. Bridging modes of $(L^1)^{2-}$ in complex **1**

Table 2. Selected bond lengths and angles for **3**

Bond lengths (Å)			
Cu(1)−O(2)	1.914(3)	Cu(1)−O(1)	1.924(4)
Cu(1)−O(6)	2.640(5)	Cu(1)−O(3)[a]	2.672(5)
Cu(1)−N(2)	2.005(5)	Cu(1)−N(1)	2.007(4)
Na(1)−O(1)	2.433(4)	Na(1)−O(6)	2.450(5)
Na(1)−O(2)	2.616(4)	Na(2)−O(3)[b]	2.327(5)
Na(2)−O(2)	2.453(4)	Na(2)−O(1)	2.569(4)
Bond angles (°)			
O(2)−Cu(1)−O(1)	84.4(2)	O(2)−Cu(1)−N(2)	95.6(2)
O(1)−Cu(1)−N(2)	175.7(2)	O(2)−Cu(1)−N(1)	176.4(2)
O(1)−Cu(1)−N(1)	93.9(2)	N(2)−Cu(1)−N(1)	86.4(2)
O(1)−Na(1)−O(1)[b]	180.0	O(1)−Na(1)−O(6)[b]	96.66(14)
O(1)[b]−Na(1)−O(6)[b]	83.34(14)	O(1)−Na(1)−O(6)	83.34(14)
O(1)[b]−Na(1)−O(6)	96.66(14)	O(6)[b]−Na(1)−O(6)	180.000(1)
O(1)−Na(1)−O(2)	61.28(12)	O(1)[b]−Na(1)−O(2)	118.72(12)
O(6)[b]−Na(1)−O(2)	105.80(13)	O(6)−Na(1)−O(2)	74.20(13)
O(1)−Na(1)−O(2)[b]	118.72(12)	O(1)[b]−Na(1)−O(2)[b]	61.28(12)
O(6)[b]−Na(1)−O(2)[b]	74.20(13)	O(6)−Na(1)−O(2)[b]	105.80(13)
O(2)−Na(1)−O(2)[b]	180.0	O(3)[b]−Na(2)−O(3)[a]	180.000(1)
O(3)[b]−Na(2)−O(2)	96.6(2)	O(3)[b]−Na(2)−O(2)[c]	83.4(2)
O(3)[a]−Na(2)−O(2)	83.4(2)	O(3)[a]−Na(2)−O(2)[c]	96.6(2)
O(2)−Na(2)−O(2)[c]	180.000(1)	O(3)[b]−Na(2)−O(1)[c]	78.91(14)
O(3)[a]−Na(2)−O(1)[c]	101.09(14)	O(2)−Na(2)−O(1)[c]	118.28(11)
O(2)[c]−Na(2)−O(1)[c]	61.72(11)	O(3)[b]−Na(2)−O(1)	101.09(14)
O(3)[a]−Na(2)−O(1)	78.91(14)	O(2)−Na(2)−O(1)	61.72(11)
O(2)[c]−Na(2)−O(1)	118.28(11)	O(1)[c]−Na(2)−O(1)	180.0

[a] Symmetry transformations used to generate equivalent atoms: $-1+x, y, z$. [b] $2-x, 2-y, 2-z$. [c] $1-x, 2-y, 2-z$.

The asymmetric unit of **3** (Table 2) consists of one Cu^{II}, one $(L^2)^{2-}$, one ClO_4^- anion and two partially occupied Na^I atoms lying on the special positions of the inversion centers with occupation factors of 50%. Thus, **3** can be understood as a 1:1 adduct of CuL^2 with $NaClO_4$, wherein $(L^2)^{2-}$ coordinates with Cu^{II} as a tetradentate ligand in the equatorial plane. The neighboring CuL^2 units are arranged in an alternating up/down-up/down mode, and act as neutral ligands to coordinate Na^I atoms via the phenoxo O atoms, affording an infinite zigzag arrangement of alternating Cu^{II} and Na^I centers along the *a* axis (Figure 4). The final coordination polymer involves phenoxo and perchlorato groups in the unusual μ_3- and μ_4-bridging modes, respectively, and the final coordination geometries around Cu^{II} and Na^I are elongated octahedral and irregular octahedral, respectively. This appears to be the first coordination polymer of H_2L^2.[10]

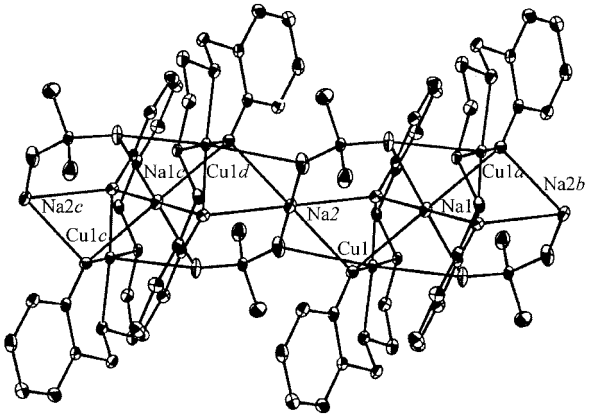

Figure 4. One-dimensional linear structure of **3**, showing the atom labeling scheme at the 20% probability level with H atoms omitted for clarity

The asymmetric unit of crystal **6** (Table 3) consists of four crystallographically independent, and chemically similar, CuL^3 moieties and four water molecules of crystallization. In each CuL^3 moiety, the tetradentate $(L^3)^{2-}$ ligand is coordinated in the basal plane of Cu^{II}. The four CuL^3 units are connected into two dimers via axial monophenoxo bridging, with Cu−O bridging distances of 2.562(2) and 2.490(3) Å, and Cu−O−Cu angles of 98.49(10) and 103.56(10)°, respectively. The dimers are further connected by multiple hydrogen bonds, i.e., every two water molecules are connected via hydrogen bonds to form a structural unit, which in turn connects the amino and the phenoxo functionalities to form a 2D sheet approximately along the *ab* plane (Figure 5). In the final structure, half of the water molecules are quadruple-connecting, and the other half are triple-connecting. Interestingly, a nearly planar six-membered ring is formed by Cu(4), O(7), O(8), and the water molecule via hydrogen bonds.

In the crystal structure of the Ag^I complex **9** (Figure 6, and Table 4), Ag^I is coordinated with four N atoms from two L^2 ligands, with one ligand in the protonated H_2L^2 form, and the other in mono-deprotonated $(HL^2)^-$. The noncoordinated phenol and phenolate groups are involved

 © 2003 Wiley-VCH Verlag GmbH & Co. KGaA, Weinheim

Table 3. Selected bond lengths and angles for **6**

Bond lengths (Å)			
Cu(1)−O(1)	1.911(2)	Cu(1)−O(2)	1.913(2)
Cu(1)−N(1)	1.989(3)	Cu(1)−N(2)	2.005(3)
Cu(2)−O(3)	1.925(2)	Cu(2)−O(4)	1.952(3)
Cu(2)−N(4)	2.016(3)	Cu(2)−N(3)	2.019(3)
Cu(3)−O(5)	1.918(2)	Cu(3)−O(6)	1.919(2)
Cu(3)−N(5)	1.990(3)	Cu(3)−N(6)	1.994(3)
Cu(4)−O(8)	1.923(3)	Cu(4)−O(7)	1.953(2)
Cu(4)−N(8)	2.009(3)	Cu(4)−N(7)	2.027(3)
Cu(4)−O(6)[a]	2.490(2)	Cu(2)−O(1)	2.562(3)
Bond Angles (°)			
O(1)−Cu(1)−O(2)	88.88(10)	O(1)−Cu(1)−N(1)	94.06(11)
O(2)−Cu(1)−N(1)	169.22(11)	O(1)−Cu(1)−N(2)	167.52(12)
O(2)−Cu(1)−N(2)	92.85(11)	N(1)−Cu(1)−N(2)	86.52(12)
O(3)−Cu(2)−O(4)	89.01(10)	O(3)−Cu(2)−N(4)	177.63(12)
O(4)−Cu(2)−N(4)	162.48(12)	O(3)−Cu(2)−N(3)	93.81(11)
O(4)−Cu(2)−N(3)	92.12(11)	N(4)−Cu(2)−N(3)	85.74(12)
O(5)−Cu(3)−O(6)	89.52(10)	O(5)−Cu(3)−N(5)	93.57(11)
O(6)−Cu(3)−N(5)	166.20(11)	O(5)−Cu(3)−N(6)	167.66(11)
O(6)−Cu(3)−N(6)	93.90(11)	N(5)−Cu(3)−N(6)	85.93(12)
O(8)−Cu(4)−O(7)	89.23(11)	O(8)−Cu(4)−N(8)	94.19(12)
O(7)−Cu(4)−N(8)	160.38(11)	O(8)−Cu(4)−N(7)	177.69(11)
O(7)−Cu(4)−N(7)	92.40(11)	N(8)−Cu(4)−N(7)	84.81(12)
Cu(4)−O(6)[a]−Cu(3)[a]	103.56(11)	Cu(2)−O(1)−Cu(1)	98.49(10)

[a] Symmetry transformations used to generate equivalent atoms: x, $-1 + y$, z.

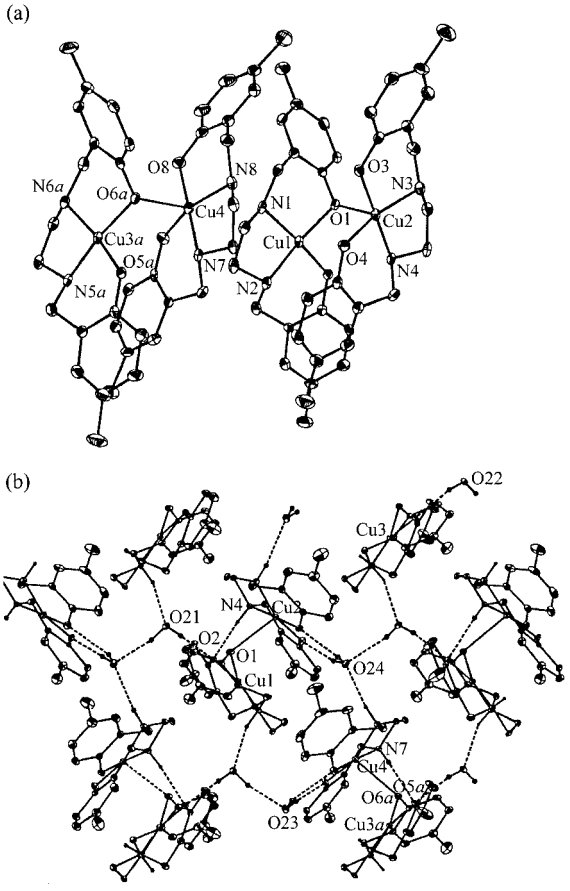

Figure 5. Molecular structure and 2-D sheet of complex **6**, approximately along the *ab* plane

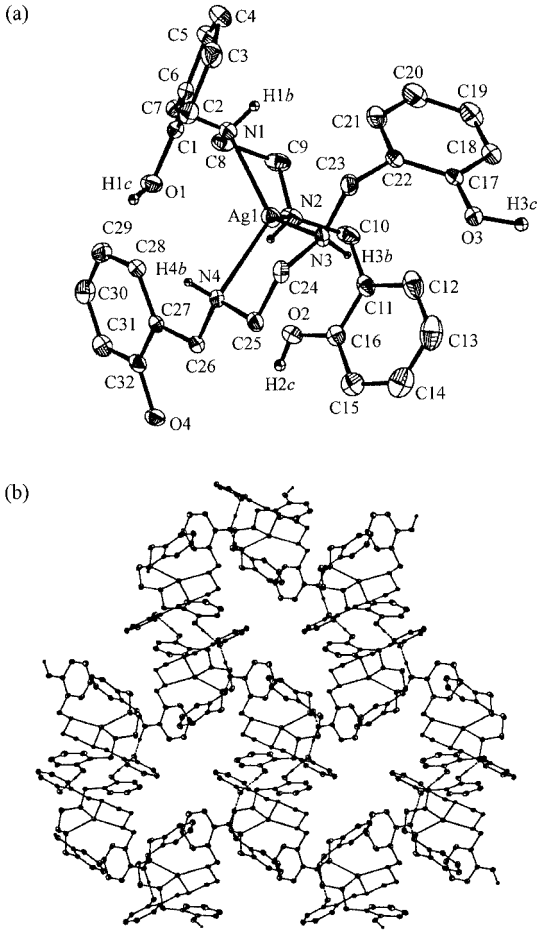

Figure 6. Molecular structure and undulated 2-D sheet of complex **9**, approximately along the *bc* plane

Table 4. Selected bond lengths and angles for **9**

Bond lengths (Å)			
Ag1−N3	2.298(3)	Ag1−N2	2.331(2)
Ag1−N1	2.410(2)	Ag1−N4	2.424(2)
Bond Angles (deg)			
N3−Ag1−N2	135.88(11)	N3−Ag1−N1	130.47(9)
N2−Ag1−N1	76.48(9)	N3−Ag1−N4	77.94(8)
N2−Ag1−N4	118.59(9)	N1−Ag1−N4	124.34(8)

in intermolecular hydrogen bonds, resulting in an undulated 2D network of hexagonal units; each corner of the hexagons is occupied by an Ag^{I} atom. Interestingly, the hydrogen bond O3···H···O4A [O3···O4A 2.444(3) Å, bond angle of 173.56°] can be regarded as a (−)CAHB type; such strong bonds have been observed mostly in systems containing carboxylate and carboxylic acid molecules.[11] Their occurrence between the phenolate and the phenol groups is rather unusual.

Magnetic Studies: The magnetic behavior of **1** and **6** was studied. With the decreasing of temperature, the observed $\chi_M T$ for **1** (Figure S1, see Supporting Information) gradually decreases from 8.47 (300 K) to 3.02 $cm^3 \cdot mol^{-1} \cdot K$ at 5 K, which is characteristic of an antiferromagnetically cou-

 © 2003 Wiley-VCH Verlag GmbH & Co. KGaA, Weinheim

pled Co^{II}_3 moiety, and is consistent with the crystal structure (vide supra). For **6**, however, $\chi_M T$ (Figure S2, Supporting Information) increases slowly from 0.633 (300 K) to a maximum of 0.737 $cm^3 \cdot mol^{-1} \cdot K$ at 9 K, and then decreased to 0.730 $cm^3 \cdot mol^{-1} \cdot K$ at 5 K, indicating a net weak ferromagnetic interaction between the Cu^{II} centers due to the coexistence of ferro- and antiferromagnetic interactions, which can be assigned to interactions within the dimers with the bridging angles of 98.49° and 103.56° (vide supra), respectively.

Discussion

The unsymmetrical tridentate ligand H_2L^1 contains both phenol and alkoxy groups. It forms the hexanuclear cluster **1**, with both the phenoxy and alkoxy groups involved in bridging. A few polynuclear clusters have also been reported for similar tridentate unsymmetrical ligands.[12,13] While the number of polynuclear transition metal complexes reported continues to grow rapidly, some nuclearities remain rare. Only a few hexanuclear cobalt complexes containing N or O donors have been reported,[14] along with some larger cobalt cages[15] and a number of hexanuclear cobalt-chalcogen clusters.[16] The occurrence of complex **1** may be related to the properly disposed bridging functionalities from the $(L^1)^{2-}$ ligand and the suitable chelate ring size. In contrast to the *fac*-coordination mode of $(L^1)^{2-}$ in **1**, in the related tetranuclear cubane Cu^{II} complex $[Cu_4L'_4]$ [L′ = *N*-(2-hydroxybenzyl)propanolamine, Scheme 1],[12] the two O atoms from $(L')^{2-}$ occupy the *trans* positions in the basal plane of the square pyramidal coordination polyhedron of Cu^{II}, which can be ascribed to the tendency for the six-membered chelate ring in $[Cu_4L'_4]$ to span a larger distance, as compared to the corresponding five-membered ring in complex **1**. In $[Cu_4L'_4]$, all the alkoxo groups act as μ_3-bridges, with the phenoxo groups at the *trans* positions not involved in bridging. In contrast, the neighboring alkoxo and phenoxo groups in complex **1** are involved in more complicated bridging modes (vide supra), resulting in the larger nuclearity.

Considering the distances between the O, N, and Cl^- atoms, the water molecules, and the chlorides, form complicated hydrogen-bond networks with the amino, phenoxo, and alkoxo groups of the $(L^1)^{2-}$ ligands. These multiple hydrogen bonds may contribute to the stability of the complex, and thus the crystal structure can readily be determined at room temperature. For the polynuclear Cu^{II} complex of $(L^1)^{2-}$, the crystal structure cannot be obtained due to its efflorescence during measurement.[8] In the Zn^{II} complex $[ZnHL^1Cl]$ (**2**), the alkoxy group is not deprotonated, even if an excess of NaOH is added, which can be ascribed to the weaker coordination of Zn^{II}, as compared to Co^{II} and Cu^{II}. The positive charge of Zn^{II} is balanced by a chloride, in addition to the deprotonated phenoxo group.

In contrast to H_2L^1, the tetradentate ligand H_2L^2 has an additional phenyl ring, and H_2L^3 has a further two methyl groups on the two phenyl rings − severe steric hindrance can be anticipated if similar polynuclear clusters of these two ligands are formed. Thus, the 1D heterometallic coordination polymer and the weak axial monophenoxo-bridged binuclear moieties are seen for **3** and **6**, respectively. For $[CoL^2NaClO_4] \cdot CH_3OH$ (**4**), $[ZnL^2 \cdot NaClO_4] \cdot H_2O$ (**5**), and $[CoL^3NaClO_4] \cdot 1.5H_2O$ (**7**), structures similar to that of **3** may also be assigned.

For the complex of H_2L^2 with the soft Ag^I atom, which prefers a tetrahedral coordination, the ligand acts in bidentate mode in complex **9** via coordination of the N atoms. H_2L^2 is usually a tetradentate ligand,[10] but the unusual bidentate coordination mode can be rationalized by the tendency of Ag^I to coordinate with N rather than O atoms, and by the tetrahedral preference of four-coordinate Ag^I, which cannot be satisfied without great strain if the ligand coordinates in a tetradentate mode. Thus, the 1:2 complex $[Ag(H_2L^2)(HL^2)]$ is formed, irrespective of the molar ratio of the reagents, and the noncoordinated phenol groups are involved in intermolecular hydrogen bonds, resulting in an undulated 2D network.

The rich coordination modes of the ligands can also be related to their conformational flexibility, as evidenced by the large values of 36.9°, 52.0° and 84.9° for the dihedral angles between the two mean planes through the aromatic rings of the same ligands in complexes **3**, **6**, and **9**, respectively. In contrast to the approximately planar trinuclear salen adduct $[Cu(salen)]_2NaClO_4$,[17] the totally different arrangement in complex **3** provides a perfect match between the coordination environment provided by the donor atoms of $(L^2)^{2-}$ and the pseudooctahedral coordination preferences of the Cu^{II} and Na^I centers, and, also, the positive and the negative charges are exactly balanced. This perfect match gives extreme thermal stability to the novel coordination polymer: no weight loss was observed for **3** until about 328 °C. These subtle matching factors are delicate, and extremely sensitive to the structures of the ligands. As for H_2L^2, similar complexes with other divalent metals, namely, the Co^{II} complex $[CoL^2] \cdot NaClO_4 \cdot CH_3OH$ (**4**) and the Zn^{II} complex $[ZnL^2 \cdot NaClO_4] \cdot H_2O$ (**5**) were also obtained; however, for H_2L^3, only the corresponding Co^{II} complex $[CoL^3NaClO_4] \cdot 1.5H_2O$ (**7**) was obtained. No $NaClO_4$ is included in the Cu^{II} and Zn^{II} complexes of H_2L^3.

Conclusions

Various novel coordination assemblies can be successfully obtained by altering the ligands and metal atoms. For metal atoms with octahedral coordination preferences, with increasing steric hindrance and the decreasing bridging ability of the ligands, the structures of the products vary from polynuclear cluster and 1D heterometallic coordination polymer to weak axial monophenoxo-bridged binuclear moieties. For the soft Ag^I atom, which prefers tetrahedral coordination, H_2L^2 coordinates bidentately via the N atoms to give a 1:2 complex. These results provide further insight into the subtle structure-directing factors of metal complexes, including the metal coordination preferences, the

 © 2003 Wiley-VCH Verlag GmbH & Co. KGaA, Weinheim

disposition of the bridging groups, the conformational flexibility, the hydrogen bonds, and the steric effect of the ligands. This work may be valuable in our aim to design and synthesize novel complexes; for example, coordination assemblies could arise by modifying the aliphatic chains or the phenyl rings of the ligands or by adding further donor groups into the phenyl rings.

Experimental Section

Physical Measurements: IR spectra were recorded with a Bruker Vector-22 spectrometer (KBr Disc.). UV-Vis spectra were obtained with a Shimadzu UV-Vis 2401 PC spectrophotometer. EPR measurements were performed with a Bruker ER200D-SRC spectrometer at X-band (9.46 GHz). Microanalyses of C, H and N were carried out with a GmbH VarioEL elemental analyzer. Magnetic susceptibility data were collected with a Quantum Design Squid magnetometer in the temperature range 5−300 K. The data were corrected for the diamagnetism of the sample holder and for diamagnetic contributions with Pascal's constants.

Caution! *Perchlorate salts of metal complexes with organic ligands are potentially explosive. Only a small amount of the material should be used and it should be handled with extreme care.*

5-Methylsalicylaldehyde was prepared by the reaction of *p*-cresol and $CHCl_3$ in aqueous ethanol according to the Reimer−Tiemann procedure. $H_2L^1{\cdot}HCl{\cdot}1.5H_2O$ was synthesized by the method reported earlier;[8] H_2L^2 was prepared by a similar method., and H_2L^3 was prepared in analogues fashion starting from 5-methylsalicylaldehyde and ethylenediamine.

$[Co_6L^1_6(OH)(H_2O)_3]Cl_2{\cdot}10H_2O$ (1): $Co(OAc)_2{\cdot}4H_2O$ (100 mg, 0.40 mmol), $H_2L^1{\cdot}HCl{\cdot}1.5H_2O$ (89 mg, 0.40 mmol), aqueous NaOH (0.3 mL, 4 M, 1.2 mmol), and a few drops of H_2O_2 were added successively to methanol (100 mL). The resulting solution was then boiled under reflux for 3 h, and concentrated in vacuo. The so-obtained microcrystalline brown solid was collected and washed with diethyl ether and dried (yield 97 mg, 87%). $C_{54}H_{93}Cl_2Co_6N_6O_{26}$: calcd. C 38.91, H 5.62, N 5.04; found C 38.69, H 5.63, N 4.89. IR (KBr pellet, cm^{-1}): $\tilde{\nu}$ 3386 br. (H_2O), 3190 s (N−H), 1596 s, 1567 m, 1483 s, 1448 s, 1304 m, 1284 s (C−O), 1270 vs (C−O), 882 m, 759 s, 685 s, 630 m, 602 w, 535 w.

$[ZnHL^1Cl]$ (2): A solution of $Zn(ClO_4)_2{\cdot}6H_2O$ (149 mg, 0.40 mmol), $H_2L^1{\cdot}HCl{\cdot}1.5H_2O$ (89 mg, 0.40 mmol), and aqueous NaOH (0.2 mL, 4 M, 0.8 mmol) was boiled under reflux for 4 h, and then concentrated in vacuo. The resulting colorless solid was collected and washed with diethyl ether and dried (yield 91 mg, 85%). $C_9H_{12}ClNO_2Zn$: calcd. C 40.48, H 4.53, N 5.25; found C 40.59, H, 4.75, N 5.06. IR (KBr pellet, cm^{-1}): $\tilde{\nu}$ = 3260 m (N−H), 2922 w, 2859 w, 1597 s, 1569 m, 1483 s, 1453 s, 1277 s (C−O), 1086 s, 1021 s, 874 m, 760 s, 623 m, 592 w, 528 w.

$[CuNaL^2(ClO_4)]_\infty$ (3): The microcrystalline brown solid complex **3** was prepared by a procedure similar to that of **2**, starting from $Cu(ClO_4)_2{\cdot}6H_2O$ (0.142 g, 0.40 mmol), H_2L^2 (117 mg, 0.40 mmol), and NaOH (0.2 mL, 4 M, 0.8 mmol) (yield 170 mg, 93%). $C_{16}H_{18}ClCuN_2NaO_6$: calcd. C 42.12, H 3.98, N 6.14; found C 42.04, H 4.01, N 5.88. IR (KBr pellet, cm^{-1}): $\tilde{\nu}$ = 3263 s (N−H), 3059 w, 2884 w, 1597 w, 1566 w, 1483 s, 1451 s, 1290 s, 1270 s (C−O), 1116 s, 1108 s, 1088 s, 1055 m, 1038 m, 992 m, 958 w, 926 w, 883 m, 858 w, 755 s, 729 m, 626 s, 596 w, 570 m, 530 w, 408 w.

$[CoL^2NaClO_4]{\cdot}CH_3OH$ (4): $Co(OAc)_2{\cdot}4H_2O$ (100 mg, 0.40 mmol), H_2L^2 (117 mg, 0.40 mmol), aqueous NaOH (0.2 mL, 4 M, 0.8 mmol) and $NaClO_4$ (49 mg, 0.40 mmol) were added successively to methanol (50 mL). The resulting solution was boiled under reflux for 4 h, and then concentrated in vacuo to give a yellowish green powder that was collected and washed with diethyl ether and dried (yield 153 mg, 79%). $C_{17}H_{22}ClCoN_2NaO_7$: calcd. C 42.21, H 4.58, N 5.79; found C 42.63, H 4.67, N 5.77. IR (KBr pellet, cm^{-1}): $\tilde{\nu}$ = 3424 br., 3226 m (N−H), 2927 m, 1598 s, 1481 s, 1451 s, 1399 m, 1272 s (C−O), 1116 s, 1106 s, 1085 s, 881 m, 759 s, 625 m, 594 w, 508 w.

$[ZnL^2{\cdot}NaClO_4]{\cdot}H_2O$ (5): Complex **5** was prepared by a procedure similar to that of **3**, using $Zn(ClO_4)_2{\cdot}6H_2O$ instead of $Cu(ClO_4)_2{\cdot}6H_2O$ (yield 173 mg, 91%). $C_{16}H_{20}ClN_2NaO_7Zn$: calcd. C 40.36, H 4.23, N 5.88; found C 40.23, H 4.34, N 6.05. IR (KBr pellet, cm^{-1}): $\tilde{\nu}$ = 3440 br., 3254 m (N−H), 2922 m, 1597 s, 1481 s, 1452 s, 1366 m, 1272 s (C−O), 1110 s, 1039 s, 928 m, 877 m, 760 s, 733 m, 623 m, 591 m.

$[CuL^3]_4{\cdot}4H_2O$ (6): The microcrystalline green solid complex **6** was prepared by a procedure similar to that of **3**, using H_2L^3 instead of H_2L^2 (yield 128 mg, 84%). $C_{72}H_{96}Cu_4N_8O_{12}$: calcd. C 56.90, H 6.37, N 7.37; found C 56.69, H 6.07, N 7.01. IR (KBr pellet, cm^{-1}): $\tilde{\nu}$ = 3443 br. (H_2O), 3256 s (N−H), 2919 m, 1642 w, 1488 vs, 1290 s, 1272 s (C−O), 1254 s (C−O), 1122 s, 1093 s, 1055 s, 998 w, 957 w, 863 m, 818 s, 796 s, 635 m, 500 m.

Single crystals of **1**, **3**, and **6** were grown by slow evaporation of their methanol solutions.

$CoL^3NaClO_4{\cdot}1.5H_2O$ (7): Complex **7** is a yellowish green powder that was prepared by a procedure similar to that of **4**, using H_2L^3 instead of H_2L^2 (yield 158 mg, 78%). $C_{36}H_{50}Cl_2Co_2N_4Na_2O_{15}$: calcd. C 42.66, H 5.53, N 4.97; found C 42.69, H 5.21, N 5.36. IR (KBr pellet, cm^{-1}): $\tilde{\nu}$ = 3442 br., 3226 m (N−H), 2919 m, 1612 s, 1487 s, 1272 s (C−O), 1118 s, 1108 s, 1082 s, 1046 s, 969 w, 927 w, 798 m, 625 m, 517 m.

$[ZnL^3]{\cdot}2H_2O$ (8): Complex **8** was prepared by a procedure similar to that of **7**, using H_2L^3 instead of H_2L^2 (yield 128 mg, 80%). $C_{18}H_{26}N_2O_4Zn$: calcd. C 54.08, H 6.55, N 7.01; found C 54.24, H 6.24, N 7.05. IR (KBr pellet, cm^{-1}): $\tilde{\nu}$ = 3408 br., 3253 m (N−H), 2916 m, 2859 m, 1611 s, 1488 s, 1269 s (C−O), 1127 m, 1047 m, 825 s, 790 s, 756 m, 726 w, 531 w, 492 m.

$[Ag(H_2L^2)(HL^2)]$ (9): A solution of $AgNO_3$ (68 mg, 0.40 mmol) in H_2O (5 mL) was added to a solution of H_2L^2 (117 mg, 0.40 mmol) in methanol (5 mL). The resultant precipitate was redissolved by the addition of concentrated ammoniacal solution (5 mL). The resulting solution was then filtered and left in a P_2O_5 desiccator in a dark place to slowly evaporate. Single crystals were obtained after several days in 35% yield (91 mg). $C_{32}H_{39}AgN_4O_4$: calcd. C 58.99, H 6.03, N 8.60; found C 58.80, H 5.78, N 8.31. IR (KBr pellet, cm^{-1}): $\tilde{\nu}$ = 3300 m (N−H), 2922 m, 2857 m, 1595 s, 1454 s, 1385 m, 1329 w, 1251 s (C−O), 1186 m, 876 m, 829 m, 752 s, 504 m.

X-ray Crystallography: All measurements were made with a Rigaku RAXIS-IV image plate area detector with Mo-K_α radiation (λ = 0.71073 Å). The structures were solved by direct methods and expanded using Fourier techniques. The non-hydrogen atoms were refined anisotropically. Hydrogen atoms were included but not refined. The final cycle of full-matrix least-squares refinement was based on observed reflections [$I > 2.00\sigma(I)$] and variable parameters. All calculations were performed by using the SHELX-97 software package.[18] A summary of the crystal data is presented in Table 5.

 © 2003 Wiley-VCH Verlag GmbH & Co. KGaA, Weinheim

Table 5. Details of X-ray structure determinations

Complexes	**1**	**3**	**6**	**9**
Empirical formula	$C_{54}H_{93}Cl_2Co_6N_6O_{26}$	$C_{16}H_{18}ClCuN_2NaO_6$	$C_{72}H_{96}Cu_4N_8O_{12}$	$C_{32}H_{39}AgN_4O_4$
Formula mass	1666.85	456.30	1519.73	651.54
Crystal System	triclinic	triclinic	monoclinic	monoclinic
Space group	$P\bar{1}$	$P\bar{1}$	$P2_1/c$	$P2_1/c$
T (K)	293(2)	291(2)	291(2)	291(2)
a (Å)	15.363(3)	7.456(2)	20.524(4)	11.395(2)
b (Å)	16.161(3)	11.283(2)	12.765(3)	13.044(3)
c (Å)	14.981(3)	11.326(2)	28.181(6)	21.277(4)
α (°)	91.54(3)	78.15(3)	90.00	90.00
β (°)	106.17(3)	89.07(3)	98.64°	95.00(3)
γ (°)	96.85(3)°	88.32(3)°	90.00	90.00
V (Å^3)	3539.7(12)	932.0(3)	7299(3)	3150.5(11)
Z	2	2	4	4
$D_{calcd.}$ (Mg/m^3)	1.541	1.626	1.383	1.374
μ (mm^{-1})	1.528	1.374	1.214	0.681
No. of reflns. [$I > 2\sigma(I)$]	7703	1757	7318	4585
Final $R1$ [$I > 2\sigma(I)$]	0.0842	0.0683	0.0736	0.0424
wR_2 (all data)	0.2550	0.1703	0.1098	0.0767
Goodness of fit	1.064	1.080	1.032	1.031

CCDC-183121 to -183124 contain the supplementary crystallographic data for this paper. These data can be obtained free of charge at www.ccdc.cam.ac. uk/cont/retrieving.html [or from the Cambridge Crystallographic Data center, 12 Union Road, Cambridge, CB2 1EZ, UK; fax: (internat.) +44-1223/336-033; E-mail: deposit@ccdc.cam.ac.uk].

Acknowledgments

This work was supported by the National Natural Science Foundation of China (30270321) and the Natural Science Foundation of Anhui Province (No. 01045408).

[1] R. Y. Wang, H. D. Selby, H. Liu, M. D. Carducci, T. Z. Jin, Z. P. Zheng, J. W. Anthis, R. J. Staples, *Inorg. Chem.* **2002**, *41*, 278−286.
[2] [2a] M. C. Brandys, R. J. Puddephatt, *J. Am. Chem. Soc.* **2002**, *124*, 3946−3950. [2b] C. Richardson, P. J. Steel, *Eur. J. Inorg. Chem.* **2003**, 405−408.
[3] [3a] C. B. Aakeroy, A. M. Beatty, B. A. Helfrich, *Angew. Chem. Int. Ed.* **2001**, *40*, 3240−3242. [3b] D. G. Kurth, K. M. Fromm, J. M. Lehn, *Eur. J. Inorg. Chem.* **2001**, 1523−1526.
[4] [4a] O. D. Fox, M. G. B. Drew, P. D. Beer, *Angew. Chem. Int. Ed.* **2000**, *39*, 135−140. [4b] N. Takeda, K. Umemoto, K. Yamaguchi, M. Fujita, *Nature* **1999**, *398*, 794−796.
[5] [5a] F. Hohn, I. Pantenburg, U. Ruschewitz, *Chem. Eur. J.* **2002**, *8*, 4536−4541. [5b] D. M. Ciurtin, M. D. Smith, H. C. zur Loye, *Chem. Commun.* **2002**, 74−75. [5c] J. G. Mao, Z. K. Wang, A. Clearfield, *New J. Chem.* **2002**, *26*, 1010−1014.
[6] [6a] C. T. Yang, B. Moubaraki, K. S. Murray, J. D. Ranford, J. J. Vittal, *Inorg. Chem.* **2001**, *40*, 5934−5941. [6b] M. L. Tong, X. M. Chen, B. H. Ye, L. N. Ji, *Angew. Chem. Int. Ed.* **1999**, *38*, 2237−2240.
[7] [7a] A. E. M. Boelrijk, G. C. Dismukes, *Inorg. Chem.* **2000**, *39*, 3020−3028. [7b] J. A. Cappuccio, I. Ayala, G. I. Elliott, I. Szundi, J. Lewis, J. P. Konopelski, B. A. Barry, O. Einarsdottir, *J. Am. Chem. Soc.* **2002**, *124*, 1750−1760. [7c] C. Belle, I. Gautier-Luneau, L. Karmazin, J. L. Pierre, S. Albedyhl, B. Krebs, M. Bonin, *Eur. J. Inorg. Chem.* **2002**, 3087−3090.
[8] Y. S. Xie, W. M. Bu, A. S. C. Chan, X. L. Xu, Q. L. Liu, Z. D. Zhang, Y. G. Fan, *Inorg. Chim. Acta* **2000**, *310*, 257−260.
[9] R. A. Coxall, S. G. Harris, D. K. Henderson, S. Parsons, P. A. Tasker, R. E. P. Winpenny, *J. Chem. Soc., Dalton Trans.* **2000**, 2349−2356.
[10] [10a] D. A. Atwood, M. P. Remington, D. Rutherford, *Organometallics* **1996**, *15*, 4763−4769. [10b] D. A. Atwood, *Coord. Chem. Rev.* **1997**, *165*, 267−296.
[11] [11a] P. Gilli, V. Bertolasi, V. Ferretti, G. Gilli, *J. Am. Chem. Soc.* **2000**, *122*, 10405−10417. [11b] T. Steiner, C. C. Wilson, I. Majerz, *Chem. Commun.* **2000**, 1231−1232.
[12] Y. S. Xie, H. Jiang, A. S. C. Chan, Q. L. Liu, X. L. Xu, C. X. Du, Y. Zhu, *Inorg. Chim. Acta* **2002**, *333*, 138−143.
[13] R. W. Saalfrank, I. Bernt, F. Hampel, *Chem. Eur. J.* **2001**, *7*, 2770−2774.
[14] [14a] I. Kim, B. Kwak, M. S. Lah, *Inorg. Chim. Acta* **2001**, *317*, 12−20. [14b] M. A. Golubnichaya, A. A. Sidorov, I. G. Fomina, M. O. Ponina, S. M. Deomidov, S. E. Nefedov, I. L. Eremenko, I. I. Moiseev, *Russ. Chem. Bull.* **1999**, *48*, 1751−1756. [14c] M. Mikuriya, M. Fukuya, *Chem. Lett.* **1998**, 421−422.
[15] [15a] V. A. Grillo, Z. M. Sun, K. Folting, D. N. Hendrickson, G. Christou, *Chem. Commun.* **1996**, 2233−2234. [15b] E. K. Brechin, R. A. Coxall, A. Parkin, S. Parsons, P. A. Tasker, R. E. P. Winpenny, *Angew. Chem. Int. Ed.* **2001**, *40*, 2700−2703.
[16] B. S. Kang, T. B. Wen, X. Y. Yu, H. X. Zhang, Y. X. Tong, C. Y. Su, Z. N. Chen, H. Q. Liu, *J. Clust. Sci.* **1999**, *10*, 429−443.
[17] G. H. W. Milburn, M. R. Truter, B. L. Vickery, *J. Chem. Soc., Chem. Commun.* **1968**, 1188.
[18] G. M. Sheldrick, *SHELXL-97 Program for Crystal Structure Refinement*, University of Göttingen, Germany, **1997**.

Received June 20, 2003

 © 2003 Wiley-VCH Verlag GmbH & Co. KGaA, Weinheim

New Ag^{I} Organometallic Coordination Polymers and M^{II} ($M = Cu^{II}$ and Co^{II}) Inorganic Supramolecular Complexes Generated from New Fulvene-Type Ligands

Yu-Bin Dong,*[a,b] Xia Zhao,[a] Guo-Xia Jin,[a] Ru-Qi Huang,[a] and Mark D. Smith[c]

Keywords: Coordination polymers / Supramolecular chemistry / Silver / Cobalt / Copper

Two novel fulvene-type organic ligands **L1** and **L2** have been synthesized by aroylation reaction of substituted cyclopentadienyl anions. **L1** crystallized in the monoclinic space group $P2_1$, a = 6.7498(4), b = 20.5769(11), c = 8.9532(5) Å, β = 109.5060(10)°, and Z = 2. **L2** crystallized in the triclinic space group $P\bar{1}$, a = 11.4126(10), b = 11.4763(10), c = 11.7719(10) Å, α = 67.050(2), β = 74.509(2), γ = 61.148(2)°, and Z = 2. The coordination chemistry of **L1** and **L2** has been investigated. One novel Ag^{I}-containing organometallic coordination polymer **3**, based on both Ag^{I}–C and Ag^{I}–N interactions, has been synthesized by combination of **L1** and $AgClO_4$ in a benzene/dichloromethane mixed-solvent system. Two new M^{II}-containing [M = Cu^{II} (**4**) and Co^{II} (**5**)] supramolecular complexes with seven-membered metalla-ring unit have been prepared by combination of **L2** and the corresponding $M(OAc)_2{\cdot}2H_2O$ (M = Cu^{II} and Co^{II}) salts in ethanol. The isostructural compounds **4** and **5** crystallized in the triclinic space group $P\bar{1}$ [**4**: a = 8.8808(5), b = 10.9928(7), c = 14.2196(9) Å, α = 99.9750(10), β = 95.8190(10), γ = 93.5610(10)°, and Z = 1; **5**: a = 8.7964(10), b = 10.8103(12), c = 14.3765(15) Å, α = 99.681(2), β = 95.930(2), γ = 93.429(2)°, and Z = 1]. In the solid state, molecular complexes **4** and **5** are bound by strong intermolecular N···O–H hydrogen bonds in a hand-in-hand fashion to give a novel one-dimensional chain motif.
(© Wiley-VCH Verlag GmbH & Co. KGaA, 69451 Weinheim, Germany, 2003)

Introduction

The construction of new inorganic−organic coordination polymers and supramolecular complexes through the rational combination of organic ligands and metal ions is of intense current interest.[1−3] Two types of organic ligands have proven popular in construction of coordination polymers or supramolecular complexes. The first type contains heteroatom donors separated by various spacers such as bipyridine-type or biphenyl-cyanide-type ligands,[4] and the second type contains sp^2 electron-rich carbon atoms, such as small aromatic molecules and polycyclic aromatic hydrocarbons.[5] During the past decade, a number of inorganic coordination polymers based on metal−heteroatom bonding interactions and organometallic coordination polymers based on metal−carbon bonding interactions have been generated successfully with various structural motifs. In contrast, coordination polymers or supramolecular complexes based on both metal−heteroatom and metal−carbon bonding interactions have received considerably less attention. In principle, such materials might exhibit enhanced physical properties, such as electrical conductivity or fluorescence resulting from the synergy between the two distinctly different types of interactions. We are investigating the coordination chemistry of fulvene-type ligands that could provide both heteroatom and carbon atoms as coordination sites (Scheme 1). Recently, a series of novel organometallic coordination polymers based on both metal−carbon and metal−heteroatom interactions were obtained in our laboratory.[6] Conversely, fulvene-type organic spacers act not only as multidentate ligands but also as chelating ligands. Their specific geometry affords a good opportunity to synthesize seven-membered metalla-ring complexes that are not achievable easily with other 1,4-diketone organic ligands.

We report here the synthesis and characterization of two new fulvene-type ligands (**L1** and **L2**), one new organometallic coordination polymer $[Ag(\mathbf{L1})(ClO_4)]{\cdot}CH_2Cl_2$ (**3**), based on both metal−heteroatom and metal−carbon interactions, and two new M^{II} ($M = Co^{II}$, Cu^{II}) seven-membered metalla-ring supramolecular complexes, $[Co(\mathbf{L2})_2(C_2H_5OH)_2]$ (**4**) and $[Cu(\mathbf{L2})_2(C_2H_5OH)_2]$ (**5**), based on them.

[a] College of Chemistry, Chemical Engineering and Materials Scinece, and Shandong Key Laboratory of Chemical Functional Materials, Shandong Normal University, Jinan 250014, P. R. China
[b] State Key Laboratory of Crystal Materials, Jinan 250014, P. R. China
E-mail: yubindong@sdnu.edu.cn
[c] Department of Chemistry and Biochemistry, The University of South Carolina, Columbia, South Carolina 29208, USA

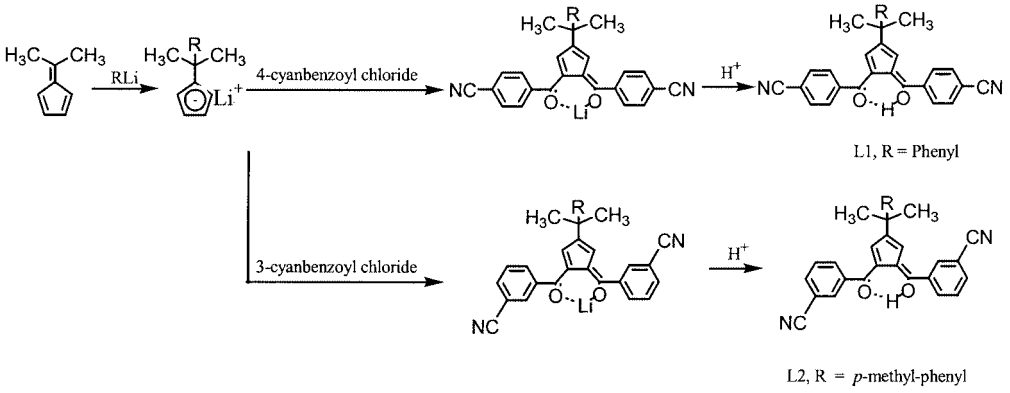

Scheme 1. Synthesis of ligands **L1** and **L2**

Results and Discussion

Synthesis and Structural Analysis of L1 and L2

Ligands **L1** and **L2** were prepared in moderate yields as deep-yellow crystalline solids by the respective reactions of 4- and 3-cyanobenzoyl chloride with substituted cyclopentadienyl anions, derived from 6,6′-dimethylfulvene and *p*-methylphenyllithium and phenyllithium in diethyl ether at 0 °C (Scheme 1). **L1** and **L2** are very soluble in common organic solvents, such as CH_2Cl_2, $CHCl_3$, THF, and C_6H_6. Their structures were determined by ^1H NMR and IR spectroscopy, elemental analyses, and standard single-crystal X-ray diffraction techniques. Their IR spectra show −CN absorption bands at $\tilde{\nu}$ = 2250 cm^{-1}. In the ^1H NMR spectrum of **L1** and **L2** the proton resonances at δ = 18.20 and 17.79 ppm as singlets, respectively, are due to the chelated proton, which is hydrogen-bonded to the neighboring carbonyl group on the 1-benzoyl group.[6,9] Their IR spectra do not show absorptions above 1630 cm^{-1} in the region normally assigned to organic carbonyl groups. However, the strong band at 1615 cm^{-1} is consistent with the hydrogen-bonded enol structure since conjugation and chelation lead to a large shift of the carbonyl infrared band. The structures of **L1** and **L2** were further confirmed by X-ray diffraction techniques. The corresponding molecular structures of **L1** and **L2** are shown in Figures 1 and 2, respectively; that of **L2** reveals that the two aroyl groups on the substituted cyclopentadienylenyl ring are adjacent. The C−C bonds on

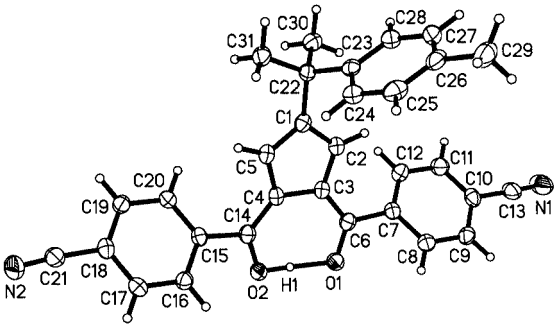

Figure 1. ORTEP plot of compound **L1** with 30% probability ellipsoids

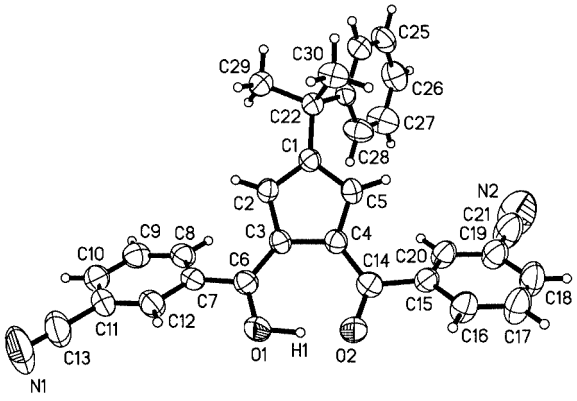

Figure 2. ORTEP plot of compound **L2** with 30% probability ellipsoids

the substituted Cp ring and also C(3)−C(6) and C(4)−C(14) range from 1.377(2) to 1.468(2) Å, which are significantly shorter than a normal C−C single bond. Thus, **L2** is a fulvene[6,8] – an important organometallic moiety.[10] The enol hydrogen atom [H(1)] is hydrogen-bonded to the carbonyl oxygen atom [O(2), $d_{O(2)\cdots H(1)}$ = 1.35(3) Å, ∠O(1)−H(1)···O(2) = 171(2)° and $d_{O(1)\cdots O(2)}$ = 2.464(18) Å] to provide a hydrogen-bonded seven-membered ring. Interestingly, two $-C_6H_4-$CN-*m* rings and the hydrogen-bonded seven-membered ring are not in the same plane. The dihedral angles between the $-C_6H_4-$CN-*m* ring and the seven-membered ring are 10.4(3) and 13.4(3)°, respectively. In the solid state, two −*m*-CN functional groups on **L2** are oriented in opposite directions and the terminal (−CN) N···N separation is 17.32(5) Å. A similar molecular structure was found for **L1**, with a slightly shorter terminal (−CN) N···N separation [16.88(5) Å]. In addition to the two −CN groups, the carbonyl and enol groups in **L1** and **L2** could act as potential chelating coordinating sites to bind transition metal ions into seven-membered metalla-ring-containing complexes; they could also potentially be transferred to other types of organic functional groups, such as heterocycles, by reaction with hydroxylamine, hydrazine or the like.[6b] Compounds **L1** and **L2** are a new type of ligands that can be used to construct polymeric compounds containing both inorganic and organometallic moieties.

 © 2003 Wiley-VCH Verlag GmbH & Co. KGaA, Weinheim

Synthesis and Structural Analysis of 3

Silver-containing polymeric compound **3**, $[Ag(\mathbf{L1})(ClO_4)]\cdot CH_2Cl_2$, was synthesized in 85% yield by the combination of **L1** and $Ag(ClO_4)\cdot H_2O$ in a benzene/dichloromethane mixed-solvent system at ambient temperature. Crystals of **3** lose solvent molecules and turn opaque within several minutes under ambient atmosphere, preventing investigation of the host-guest chemistry of **3**. Single-crystal analysis revealed (Figure 3) a distorted tetrahedral coordination sphere around the silver atom, consisting of two N-donors [N(1) and N(2)] from two ligands **L1** [Ag−N(1) = 2.242(2) and Ag−N(1) = 2.242(2) 2.190(2) Å], one O-donor [O(11)] from the ClO_4^- counterion [Ag−O(11) = 2.416(2) Å], and one carbon atom [C(27)] from the *p*-methylphenyl group on the third ligand **L1**. The Ag−C distance is 2.763(3) Å while the remaining Ag−C contacts (> 2.958 Å) are beyond the limits (2.47−2.80 Å) commonly observed in Ag^I−aromatic complexes. Thus, the benzene ring in **L1** coordinates to the Ag^I ion with an η^1-bonding mode, which is normally observed in arene−metal complexes.[11]

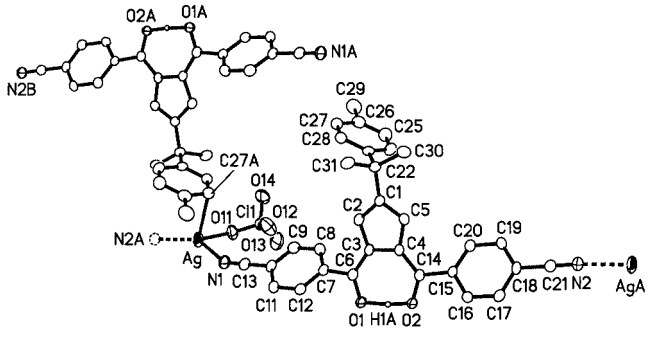

Figure 3. ORTEP plot of compound **3** with 30% probability ellipsoids

In the solid state, the silver centers are connected by **L1** through the two terminal −CN groups into mild zigzag one-dimensional chains which further associate into inversion-related pairs by Ag−C organometallic interactions along the crystallographic [211] direction (Figure 4). In addition, the ladder-like chains stack together to create two kinds of rectangular channels: large ones along the crystallographic [100] direction (crystallographic dimensions of the rings ca. 14 × 12 Å), which are filled by CH_2Cl_2 guest

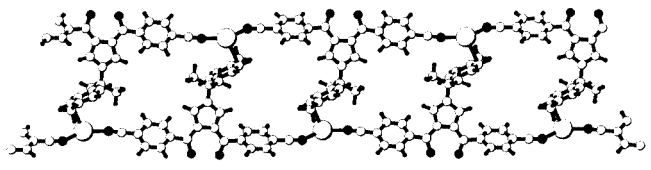

Figure 4. One-dimensional organometallic chain found in **3** (along crystallographic [211] direction), H atoms, ClO_4^- counterions and CH_2Cl_2 guest molecules are omitted for clarity

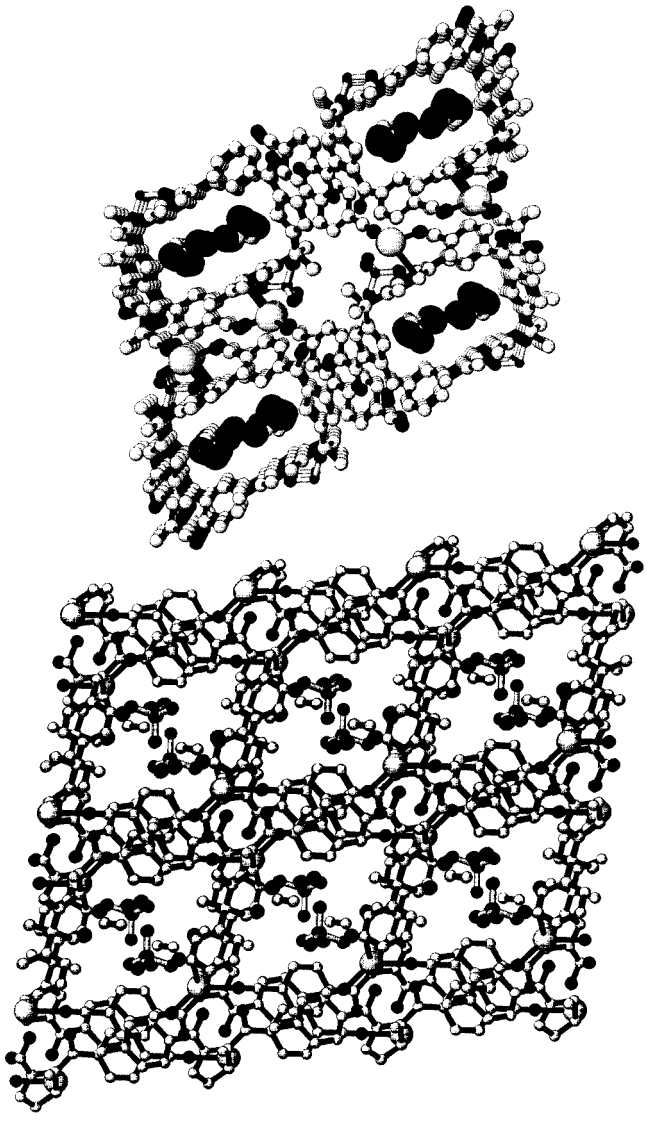

Figure 5. Top: channels in **3** (down the *a* axis), H atoms are omitted for clarity; bottom: channels in **3** (down the [011] direction), H atoms are omitted for clarity

molecules (Figure 5, a), and small ones (around 10 × 10 Å) that extend along the crystallographic [011] direction, in which both ClO_4^- counterions and CH_2Cl_2 guest molecules are located (Figure 5, b). Extended frameworks composed of organic spacers containing heteroatom donors via metal−heteroatom coordination bonds[4] and organometallic coordination polymers generated from smaller aromatics and also polycyclic aromatic hydrocarbons based on cation−π interactions[5] are well established; however, supramolecular complexes based on both metal−aromatic carbon and metal−heteroatom interactions appear to be quite unusual. A related example is the coordination of the rigid tridentate ligand 1-(4-cyanobenzoyl)-6-(4-cyanophenyl)-6-hydroxy-3-(4-phenylcyclohexyl)fulvene with Ag-OTf in benzene that led to the open-framework material $[Ag_2(C_{33}H_{26}N_2O_2)(H_2O)_2(SO_3CF_3)_2]\cdot 0.5C_6H_6$,[6a] which contains 21 × 15 Å parallelogram-like channels in which benzene guest molecules are located.[6a] The smaller chan-

 © 2003 Wiley-VCH Verlag GmbH & Co. KGaA, Weinheim

nels found in **3**, however, differ in shape (rectangle-like in **3**, Figure 5) due to the different coordination mode of the silver(I) ion and the different templating effect of counterions.

To confirm **L1** as a chelating ligand to bind metal ions by two carbonyl oxygen atoms, $M(OAc)_2{\cdot}2H_2O$ ($M = Cu^{II}$, Co^{II}) were used instead of inorganic Ag^I salts in the reactions in ethanol. Elemental analyses and IR spectra showed that the resultant compounds have the chemical formula $[M(\mathbf{L1})_2(C_2H_5OH)_2]$. Unfortunately, no single-crystal structures were obtained. To confirm the structures by single-crystal X-ray diffraction, ligand **L2** was treated instead of **L1** under the same conditions.

Synthesis and Structural Analysis of 4 and 5

Synthesis

Complexes **4** and **5** were synthesized by solution reactions between the new **L2** and $Cu(OAc)_2{\cdot}2H_2O$ and $Co(OAc)_2{\cdot}2H_2O$ in ethanol, respectively. When a solution of **L2** in ethanol was treated with $Cu(OAc)_2{\cdot}2H_2O$ and $Co(OAc)_2{\cdot}2H_2O$, respectively, in a metal/ligand molar ratio of 1:2, compounds **4** and **5** were obtained as neutral molecular compounds with seven-membered metalla-rings. It is noteworthy that the coordination chemistry of **L2** with transition metal templates Cu^{II} and Co^{II} is independent of the metal/ligand molar ratio. For example, ratios of 2:1 and even 3:1 yielded **4** and **5** as the only products.

Structural Analysis of Compounds 4 and 5

Compounds **4** and **5** are isostructural and crystallize in the triclinic system. For example, the Cu^{II} center lies in an octahedral coordination environment defined by four O-donors from two bidentate ligands **L1** and two O-donors from two coordinated ethanol solvent molecules (Figure 6). The octahedral coordination polyhedron is slightly distorted — all angles around the copper center deviate significantly from 90° [O(1)−Cu−O(2) = 93.85(7)°, O(1)−Cu−O(3) = 87.77(8)°, O(2)−Cu−O(3) = 96.99(8)°]. The Cu−O bond lengths on the basal plane are 1.9318(15) and 1.9451(16) Å, respectively, which compare well with the Cu−O distance found in copper−oxygen complexes (e.g., $[Cu(C_6O_4Cl_2)(C_4H_4N_2)]$,[12] $[Cu(HLOX)Ni(N_3)]_2{\cdot}2CH_3OH$[13]). The distances between the copper center and the two axial O-donor atoms are the same [d_{Cu-O} = 2.390(2) Å], again consistent with the corresponding bond lengths in, for example, $Ag[Cu(2\text{-pyrazinecarboxylate})_2](H_2O)(NO_3)$[14] and $[Cu(HBIP)(C_2O_4)(H_2O)]{\cdot}2H_2O$.[15] 1,2-Diketone or 1,3-diketone compounds are known to chelate transition metal ions into five- or six-membered metalla-ring systems which engender less strain (Scheme 2),[16] because the atoms on the rings are allowed to adopt more closely their natural bond angles. However, seven-membered metalla-ring complexes generated from 1,4-diketone-containing ligands and transition metal ions are much less known, probably due to conformational strain.[16] **L2** reported herein, however, is perfect for the synthesis of such complexes because of its specific molecular geometry. In **4**, the carbon−carbon bond lengths on the substituted Cp ring and also the exocyclic carbon−carbon double bonds are almost the same as their corresponding bond lengths in the free ligand **L2** [ranging from 1.393(2) to 1.457(2) Å]. The four −CN groups in **4** are uncoordinated as two pairs oriented in opposite directions. The IR spectrum of **4** shows that the −C≡N stretch (2260 cm^{-1}) in **4** is essentially unchanged from that of the free ligand **L2**, indicating that the nitrile nitrogen atom does not enter the coordination sphere of the Cu^{II} center. A similar phenomenon occurs in the reaction of $[Ru_2\{O_2C(CH_2)_6CH_3\}_4]$ in toluene and $[Cu(hfacac)_2]{\cdot}H_2O$ (hfacac = hexafluoroacetylacetonate) in dichloromethane with 4-cyanopyridine and 3-cyanopyridine, respectively.[17] The discrete molecular 1:2 adducts $[Ru_2\{O_2C(CH_2)_6CH_3\}_4(4\text{-cyanopyridine})_2]$ and $[Cu(hfacac)_2(3\text{-cyanopyridine})_2]$ were obtained instead of the expected 4-cyanopyridine- and 3-cyanopyridine-bridged transition metal complexes. 4-Cyanopyridine and 3-cyanopyridine spacers have been used as bridging ligands to link transition metal species into dimers and polymers.[18,19] It appears that the nitrile N-donor atom has a poor coordinating ability to effectively link 3d metal ions. For example, in $[Cu(4\text{-cyanopyridine})_4(H_2O)(ClO_4)_2]_n$ the nitrile nitrogen atom only weakly coordinates with copper centers through a "semi-coordinated" bond [Cu−N≡C 2.649(4) Å], which is much longer than a normal Cu−N coordinative bond.[20] It is noteworthy that **4** contains uncoordinated N-donors, which have recently been suggested as potential new metal-containing building blocks,[21] that could be connected by other suitable metal ions (Ag^+ or Cd^{2+}, for example) or unsaturated metal complexes via bonding interactions with the free nitrile nitrogen atoms in **L2** (a possibility that we are pursuing).

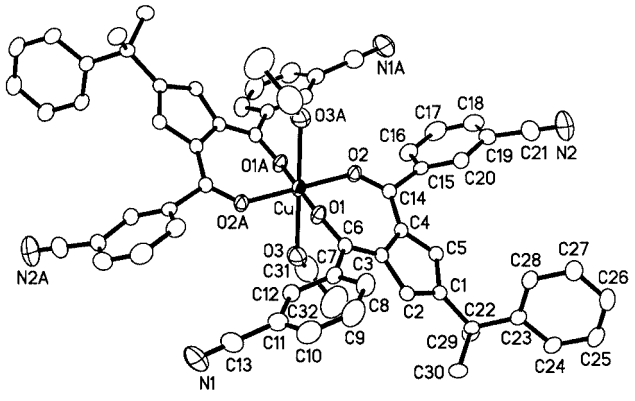

Figure 6. ORTEP plot of compound **4** with 30% probability ellipsoids

In the solid state (Figure 7) the neutral building blocks **4** arrange parallel to the crystallographic *c* axis, and moreover are bound by strong intermolecular N···O−H hydrogen bonds in a hand-in-hand fashion to create a one-dimensional chain motif along the crystallographic *b* axis. The hydrogen-bonding system in **4** consists of the one uncoordi-

 © 2003 Wiley-VCH Verlag GmbH & Co. KGaA, Weinheim

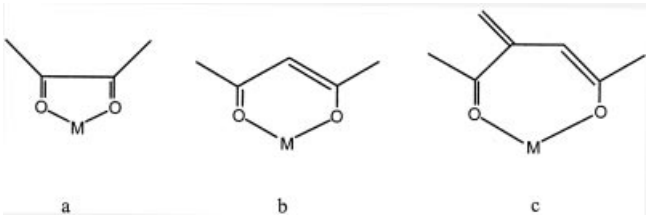

Scheme 2. Five-membered metalla-ring (a); six-membered metalla-ring (b); seven-membered-ring (c)

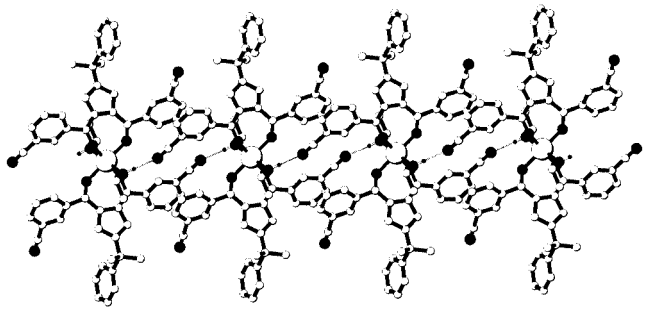

Figure 7. Hydrogen-bonded one-dimensional chain motif found in compounds **4** and **5**; hydrogen bonds are shown as dotted lines; this view is down the *a* axis

nated nitrogen atom N(1) on a −CN group with the hydrogen atom H(3) on the coordinated ethanol molecule O(3) of a neighboring Cu^{II} complex. The N(1)···H(3) distance is 1.94(2) Å. The corresponding O(3)···N(1) distance is 2.906(4) Å, and the corresponding O(3)−H(3)···N(1) angle is 170(4)°. The existence and structural importance of strong hydrogen-bonding interactions generated from −CN (as the hydrogen-bond acceptor) are now well established and have been observed in many compounds.[22] These strong hydrogen-bonding interactions contribute significantly to the alignment of the molecules of **4** in the crystalline state. The intrachain Cu···Cu distance is 10.99(3) Å.

In compound **5**, the Co^{II} center adopts a distorted octahedral $\{CoO_6\}$ coordination sphere, which is identical with the $\{CuO_6\}$ coordination environment found in **4**. In the corresponding single-crystal structure of **5** (Figure 8) the Co−O bond lengths on the basal plane lie in the range of 2.0059(19)−2.0226(16) Å. The distance between the Co^{II} center atom and the axial O-donor atom is 2.1385(19) Å, which is significantly longer than the equatorial Co−O distance. However, it is similar to the bond lengths in other Co^{II} compounds.[23]

In the solid state, compound **5** presents the same hydrogen-bonded one-dimensional chain as in **4** (Figure 7). The N···H distance is 1.94(2) Å and the corresponding O···N distance is 2.906(4) Å, with a corresponding O−H···N angle of 170(4)°.

Luminescent Properties

The fluorescence properties and potential applications as light-emitting diodes (LEDs) of aromatic organic molecules, all-organic polymers and mixed inorganic−organic hybrid coordination polymers have been investigated.[24] Owing to the higher thermal stability of inorganic−organic coordination polymers and the ability to alter the emission wavelength of organic materials, syntheses of inorganic−organic coordination polymers by the judicious choice of organic spacers and transition metal centers can be an efficient method for obtaining new electroluminescent materials.[25] The luminescent properties of the free ligand **L2**, and its metal complexes **4** and **5** have been investigated in the solid state and CH_2Cl_2 solution. In the solid-state spectra of **L2**, **4**, and **5** (Figure 9) **L2** exhibits one emission maximum at 523 nm and complexes **4** and **5** exhibit emission bands that are blue-shifted to 346 nm and 347 nm, respectively; however, the fluorescence intensity was not enhanced. The emission maximum of **L2** in CH_2Cl_2 is at 542 nm, and those of complexes **4** and **5** in CH_2Cl_2 are blue-shift to 518 nm and 521 nm, respectively (Figure 10). Due to its instability, the luminescent properties of **3** could not be investigated. In summary, the emission color of free **L2** is significantly affected by its incorporation into the M-containing (M = Co^{II} and Cu^{II}) complexes.

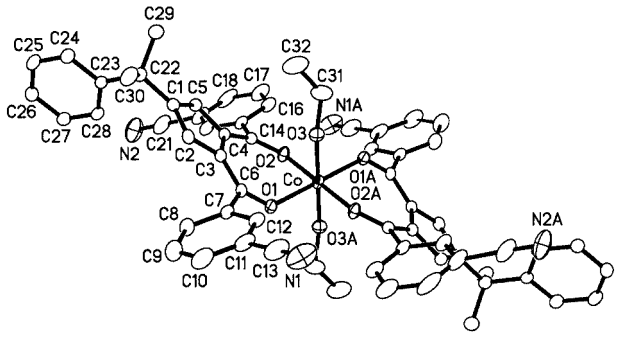

Figure 8. ORTEP plot of compound **5** with 30% probability ellipsoids

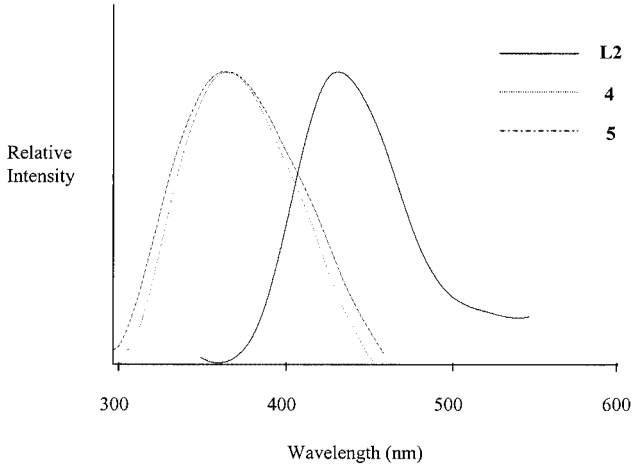

Figure 9. Photo-induced emission spectra of **L2**, **4**, and **5** in the solid state at room temperature

 © 2003 Wiley-VCH Verlag GmbH & Co. KGaA, Weinheim

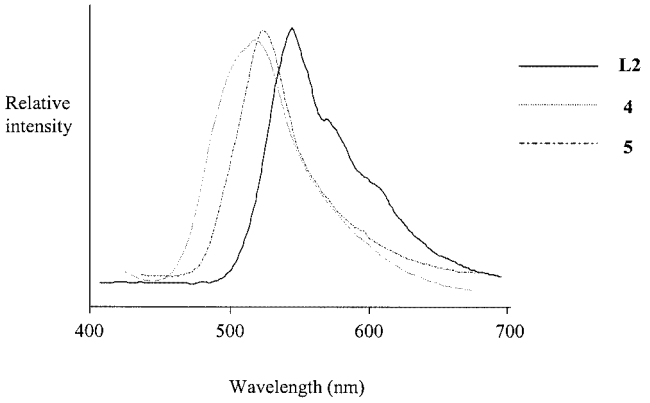

Figure 10. Photo-induced emission spectra of **L2**, **4**, and **5** in CH_2Cl_2 at room temperature

Conclusions

The two new fulvene-type ligands **L1** and **L2**, synthesized by the aroylation of substituted cyclopentadienyl anions, have been shown to be tridentate or bidentate chelating ligands to coordinate transition metal ions into coordination polymers or supramolecular complexes. The specific coordination behavior of ligand **1** resulted in a novel a Ag^{I}-containing organometallic coordination polymer (**3**) based on both metal−carbon and metal−heteroatom interactions. The special geometry of **2** resulted in complexes **4** and **5** with unusual seven-membered metalla-ring structures. In the solid state, **4** and **5** adopt a novel hydrogen-bonded one-dimensional chain motif. We are currently preparing new such fulvene ligands, with different substituted organic functional groups, so as to construct various new transition metal complexes and coordination polymers (including dimetallic polymeric compounds) with potentially novel structures.

Experimental Section

Materials and Methods: 4-Cyanobenzoyl chloride, 3-cyanobenzoyl chloride, 6,6′-dimethylfulvene, and aryllithium were prepared according to literature methods.[7] Inorganic metal salts were purchased from Acros and used without further purification. Infrared (IR) samples were prepared as KBr pellets, and spectra were obtained in the 400−4000 cm^{-1} range using a Perkin−Elmer 1600 FTIR spectrometer. ^1H NMR spectroscopic data were collected using a JEOL FX 90Q NMR spectrometer. Chemical shifts (δ) are relative to TMS. Element analyses were performed with a Perkin−Elmer Model 240C analyzer.

Preparation of L1: A solution of 4-cyanobenzoyl chloride (1.80 g, 10.8 mmol) in anhydrous diethyl ether (20 mL) was added dropwise to a solution of substituted cyclopentadienyl anions (16.2 mmol) in anhydrous diethyl ether at 0 °C, which in turn was derived from 6,6′-dimethylfulvene (16.2 mmol) and 4-methylphenyllithium (16.2 mmol) in anhydrous diethyl ether. The mixture was then stirred at room temperature overnight. The solvent was then reduced to about 10 mL under vacuum. Hexane was added and an orange solid precipitated that was washed with hexane several times and stirred in HCl (5% in water) overnight. The final product was purified by column chromatography on silica gel (CH_2Cl_2/hexane, 6:5) to afford an orange crystalline solid in 50% yield. IR (KBr pellet, cm^{-1}): $\tilde{\nu}$ = 3110 (w), 2250 (s), 1635 (s), 1600 (s), 1575 (m), 1540 (vs), 1500 (m), 1475 (s), 1413 (vs), 1410 (s), 1365 (s), 845 (m). ^1H NMR (90 MHz, $CDCl_3$, 25 °C, TMS, ppm): δ = 18.20 (s, 1 H, OH), 7.85 (s, 8 H, C_6H_4), 7.25, 7.20 (d, 2 H, C_5H_3), 6.57 (t, 1 H, C_5H_3). $C_{21}H_{13}N_2O_2$ (456.52): calcd. C 77.78, H 4.01, N 8.64; found C 77.80, H 4.00, N 8.66.

Preparation of L2: A solution of 3-cyanobenzoyl chloride (1.47 g, 8.87 mmol) in anhydrous diethyl ether (20 mL) was added dropwise into a solution of substituted cyclopentadienyl anions (13.3 mmol) in anhydrous diethyl ether (20 mL) at 0 °C, which derived from 6,6′-dimethylfulvene (13.3 mmol) and phenyllithium (13.3 mmol) in anhydrous diethyl ether. The mixture was then stirred at room temperature overnight, and the solvent then reduced to about 10 mL under vacuum. Hexane was subsequently added and an orange solid precipitated, which was then washed with hexane several times and stirred in HCl (5% in water) overnight. The final product was purified by column chromatography on silica gel (CH_2Cl_2/hexane, 3:2) to afford an orange crystalline solid (1.0 g, 51%). IR (KBr pellet, cm^{-1}) $\tilde{\nu}$ = 2995 (m), 2885 (w), 2250 (s), 1615 (s), 1590 (s), 1555 (m), 1525 (s), 1490 (m), 1435 (s), 1415 (s), 1347 (s), 760 (s). ^1H NMR (90 MHz, $CDCl_3$, 25 °C, TMS, ppm): δ = 17.74 (s, 1 H, -OH), 7.99−7.51 (m, 8 H, C_6H_4), 7.25 (s, 5 H, C_6H_5), 6.96 (s, 2 H, C_5H_2), 1.61 (s, 6 H, CH_3). $C_{30}H_{22}N_2O_2{\cdot}0.5CH_3OH$ (458.52): calcd. C 79.82, H 5.23, N 6.11; found C 79.80, H 5.22, N 6.10.

Preparation of 3: Compound **3** was synthesized in 85% yield by layering a benzene solution (4 mL) of $Ag(ClO_4){\cdot}H_2O$ (9.5 mg, 0.046 mmol) over a dichloromethane solution (4 mL) of **L1** (13.9 mg, 0.03 mmol). IR (KBr pellet, cm^{-1}): $\tilde{\nu}$ = 2998 (s), 2920 (w), 2280 (s), 2250 (m), 1615 (w), 1595 (s), 1540 (w), 1510 (s), 1435 (m), 1410 (m), 1350(s), 1255 (vs), 1180 (s), 1100 (vs), 850 (s). $C_{32}H_{26}AgCl_3N_2O_6$ (748.77): calcd. C 51.28, H 3.47, N 3.74; found C 51.49, H 3.54, N 3.75. Crystals of **3** lose solvent molecules and turn opaque within several minutes under ambient atmosphere, and so the host-guest chemistry of **3** could not be investigated.

Preparation of 4: A mixture of **L2** (24 mg, 0.054 mmol) and $Cu(OAc)_2{\cdot}2H_2O$ (5 mg, 0.027 mmol) in anhydrous EtOH (15 mL) was heated under reflux for 5 min and allowed to cool. The resultant clear red-brown solution was allowed to stand for a week at room temperature. Deep brown crystals were then collected, washed with hexane and dried in air (80% yield). IR (KBr pellet, cm^{-1}): $\tilde{\nu}$ = 3510 (br), 2990 (m), 2260 (s), 1600 (m), 1584 (s), 1555 (vs), 1530 (s), 1490 (w), 1450 (w), 1415 (s), 1360 (m), 1335 (s), 1310 (s), 775 (s). $C_{64}H_{54}CuN_4O_6$ (1038.65): calcd. C 73.94, H 5.20, N 5.39; found C 74.01, H 5.30, N 5.36.

Preparation of 5: A mixture of **L2** (24 mg, 0.054 mmol) and $Co(OAc)_2{\cdot}2H_2O$ (7 mg, 0.027 mmol) in anhydrous EtOH (15 mL) was heated under reflux for 5 min and allowed to cool. The clear red solution was allowed to stand at room temperature for 3 d. Deep red crystals were collected, washed with hexane and dried in air (95% yield). IR (KBr pellet, cm^{-1}): $\tilde{\nu}$ = 3475 (br), 2995 (m), 2260 (s), 1600 (m), 1585 (s), 1560 (vs), 1530 (s), 1494 (s), 1440 (w), 1430 (m), 1415 (s), 1360 (m), 1315 (s), 775 (s). $C_{64}H_{54}CoN_4O_6$ (1034.04): calcd. C 74.27, H 5.22, N 5.42; found C 74.27, H 5.23, N 5.38.

Crystal Structure Determination: Suitable single crystals of **L1**, **L2** and **3**−**5** were selected and epoxied in inert oil onto thin glass fibers. X-ray intensity data were measured with a Bruker SMART

 © 2003 Wiley-VCH Verlag GmbH & Co. KGaA, Weinheim

Table 1. Crystallographic data for **L1**, **L2**, and **3**

	L1	**L2**	**3**
Empirical formula	$C_{31}H_{24}N_2O_2$	$C_{30}H_{22}N_2O_2{\cdot}0.5CH_3OH$	$C_{32}H_{26}AgCl_3N_2O_6$
Formula mass	456.52	458.52	748.77
Crystal system	monoclinic	triclinic	triclinic
Space group	$P2_1$	$P\bar{1}$	$P\bar{1}$
a [Å]	6.7498(4)	11.4126(10)	10.0147(8)
b [Å]	20.5769(11)	11.4763(10)	12.6221(10)
c [Å]	8.9532(5)	11.7719(10)	14.1054(11)
α [°]	90	67.050(2)	108.9110(10)
β [°]	109.5060(10)	74.509(2)	92.025(2)
γ [°]	90	61.148(2)	112.2560(10)
V [Å^3]	1172.14(11)	1237.57(19)	1535.5(2)
Z	2	2	2
ρ(calcd.) [g/cm^3]	1.293	1.230	1.620
μ(Mo-K_α) [mm^{-1}]	0.079	0.079	0.378
Temperature [K]	150	293	150
No. of refl. ($I > 3\sigma$)	5247	5084	6280
Residuals:			
*R*1; *wR*2 (all data)	0.0434; 0.0868	0.0919; 0.1066	0.0428; 0.0866

APEX CCD-based diffractometer system (Mo-K_α radiation, λ = 0.71073 Å). Recollection of the first 50 frames at the end of the process revealed no significant crystal decay. The raw frame data for all new compounds were integrated into SHELX-format reflection files and corrected for Lorentz and polarization effects using SAINT.[8] Corrections for incident and diffracted beam absorption effects were applied using SADABS.[8] All structures were solved by direct methods and refined against F^2 by the full-matrix least-squares technique. Hydrogen atoms were calculated and refined as riding atoms; all non-hydrogen atoms were refined with anisotropic displacement parameters. For compounds **4** and **5**, one C_6H_4CN group of the $C_{30}H_{21}N_2O_2$ ligand was found to be rotationally disordered over two orientations in ratios of 0.675:0.325 (**4**) and 0.78:0.22 (**5**). Solution and refinement in the space group *P*1 did not remove the disorder; the space group $P\bar{1}$ was therefore retained. Crystal data, data collection parameters, and refinement statistics for **L1** and **L2** and **3**−**5** are listed in Tables 1 and 2. Selected interatomic bond lengths and bond angles for **L1** and **L2** and **3**−**5** are given in Tables 3, 4, 5, 6, and 7. CCDC-175505 (**L1**), -191568 (**L2**), -175506 (**3**), -191569 (**4**), and -191570 (**5**) contain the supplementary crystallographic data for this paper. These data can be obtained free of charge at www.ccdc.cam.ac.uk/conts/retrieving.

Table 2. Crystallographic data for **4** and **5**

	4	**5**
Empirical formula	$CuC_{64}H_{54}N_4O_6$	$CoC_{64}H_{54}N_4O_6$
Formula mass	1038.65	1034.04
Crystal system	triclinic	triclinic
Space group	$P\bar{1}$	$P\bar{1}$
a [Å]	8.8803(5)	8.7946(10)
b [Å]	10.9928(7)	10.8103(12)
c [Å]	14.2156(9)	14.3765(15)
α [°]	99.9750(10)	99.681(2)
β [°]	95.8190(10)	95.930(2)
γ [°]	93.5610(10)	93.429(2)
V [Å^3]	1355.19(14)	1336.0(3)
Z	1	1
ρ(calcd.) [g/cm^3]	1.273	1.285
μ(Mo-K_α) [mm^{-1}]	0.459	0.378
Temperature [°C]	293	190
No. of refl. ($I > 3\sigma$)	5525	4706
Residuals:		
*R*1; *wR*2 (all data)	0.0655; 0.1330	0.0728; 0.0939

Table 3. Interatomic distances [Å] and bond angles [°] with estimated standard deviations (in parentheses) for **1**

C(1)−C(2)	1.414(2)	C(1)−C(5)	1.378(2)
C(1)−C(22)	1.516(2)	C(2)−C(3)	1.386(2)
C(3)−C(6)	1.419(2)	C(3)−C(4)	1.476(2)
C(6)−O(1)	1.270(2)	C(6)−C(7)	1.488(2)
C(7)−C(8)	1.396(2)	C(13)−N(1)	1.136(2)
C(2)−C(1)−C(5)	107.02(14)	C(2)−C(1)−C(22)	124.76(14)
C(1)−C(2)−C(3)	110.87(13)	C(6)−C(3)−C(2)	125.69(14)
O(1)−C(6)−C(7)	114.23(14)	C(9)−C(10)−C(11)	120.77(15)
C(10)−C(11)−C(12)	119.90(15)	N(1)−C(13)−C(10)	177.6(2)

Table 4. Interatomic distances [Å] and bond angles [°] with estimated standard deviations (in parentheses) for **2**

C(1)−C(2)	1.337(2)	C(1)−C(5)	1.415(2)
C(1)−C(22)	1.513(2)	C(2)−C(3)	1.427(2)
C(3)−C(6)	1.386(2)	C(3)−C(4)	1.468(2)
C(6)−O(1)	1.307(2)	C(6)−C(7)	1.483(2)
C(7)−C(8)	1.380(3)	C(13)−N(1)	1.134(3)
C(2)−C(1)−C(5)	106.94(16)	C(2)−C(1)−C(22)	128.09(16)
C(1)−C(2)−C(3)	110.42(16)	C(6)−C(3)−C(2)	125.46(17)
O(1)−C(6)−C(7)	112.90(16)	C(9)−C(10)−C(11)	119.5(2)
C(10)−C(11)−C(13)	118.9(2)	N(1)−C(13)−C(11)	178.2(3)

Table 5. Interatomic distances [Å] and bond angles [°] with estimated standard deviations (in parentheses) for **3** (symmetry transformations used to generate equivalent atoms: #1: $x - 2$, $y - 1$, $z - 1$; #2: $-x + 1$, $-y + 1$, $-z + 1$; #3: $-x + 1$, $-y$, $-z + 1$; #4: $x + 2$, $y + 1$, $z + 1$)

Ag−N(2)#1	2.190(2)	Ag−N(1)	2.242(2)
Ag−O(11)	2.390(2)	Ag−O(11)	2.416(2)
Ag−C(27)#2	2.763(3)		
N(2)#1−Ag−N(1)	136.21(8)	N(2)#1−Ag−O(11)	117.55(7)
N(1)−Ag−O(11)	100.86(8)	N(2)#1−Ag−C(27)#2	108.55(8)
N(1)−Ag−C(27)#2	82.23(8)	O(11)−Ag−C(27)#2	100.75(7)

 © 2003 Wiley-VCH Verlag GmbH & Co. KGaA, Weinheim

html [or from the Cambridge Crystallographic Data Centre, 12 Union Road, Cambridge CB2 1EZ, UK; Fax: (internat.) + 44-1223/336-033; E-mail: deposit@ccdc.cam.ac.uk].

Table 6. Interatomic distances [Å] and bond angles [°] with estimated standard deviations (in parantehses) for **4** (symmetry transformations used to generate equivalent atoms: #1: $-x+1, -y+1, -z+1$)

Cu(1)−O(1)	1.9318(15)	Cu−O(2)	1.9451(16)
Cu−O(3)	2.390(2)		
O(1)#1−Cu−O(1)	180.00(7)	O(1)#1−Cu−O(2)#1	93.58(7)
O(2)#1−Cu−O(3)	83.01(7)	O(2)−Cu−O(3)	96.99(8)
O(1)−Cu−O(3)	87.77(8)	O(3)−C(31)−C(32)	112.2(8)
C(6)−O(1)−Cu	131.58(15)	C(14)−O(2)−Cu	135.22(15)
C(31)−O(3)−Cu	131.7 (5)	O(2)−C(14)−C(15)	113.7(2)

Table 7. Interatomic distances [Å] and bond angles [°] with estimated standard deviations (in parantehses) for **5** (symmetry transformations used to generate equivalent atoms: #1: $-x+1, -y+1, -z+1$)

Co(1)−O(1)	2.0059(19)	Co−O(2)	2.0226(16)
Co−O(3)	2.1385(19)		
O(1)#1−Co−O(1)	180.00(7)	O(1)#1−Co−O(2)#1	90.98(7)
O(2)#1−Co−O(3)	85.82(7)	O(2)−Co−O(3)	94.18(7)
O(1)−Co−O(3)	88.28(8)	O(3)−C(31)−C(32)	114.0(3)
C(6)−O(1)−Co	130.50(18)	C(14)−O(2)−Co	137.03(18)
C(31)−O(3)−Co	126.83(18)	O(2)−C(14)−C(15)	113.9(2)

Acknowledgments

We are grateful for financial support from the National Natural Science Foundation of China (No. 20174023), Shangdong Natural Science Foundation (No. Z2001B01) and Young Scientists Funding of Shandong Province of P. R. China; we also acknowledge financial support from the Starting Funding of China for overseas scholar.

[1] [1a] T. Iwamoto, in: *Inclusion Compounds: Inorganic and physical Aspects of Inclusion* (Eds.: T. Iwamoto, J. L. Atwood, J. E. D. Davies, D. D. MacNicol), Oxford University Press, Oxford, **1991**, vol. 5, chapter 6, pp. 177. [1b] R. Robson, B. F. Abrahms, S. R. Batten, R. W. Gable, B. F. Hoskin, F. Liu, in: *Supramolecular Architecture* (Ed.: T. Bein), American Chemical Society, Washington, DC, **1992**, pp. 256. [1c]K. A. Hirsch, S. R. Wilson, J. S. Moore, *Inorg. Chem.* **1997**, *36*, 2960−2974.

[2] [2a] O. M. Yaghi, H. Li, *J. Am. Chem. Soc.* **1995**, *117*, 10401−10402. [2b] O. M. Yaghi, H. Li, T. L. Groy, *J. Am. Chem. Soc.* **1996**, *118*, 9096−9101.

[3] [3a] M. Fujita, Y. J. Kwon, O. Sasaki, K. Yamaguchi, K. Ogura, *J. Am. Chem. Soc.* **1995**, *117*, 7287−7288. [3b] K. N. Power, T. L. Hennigar, M. J. Zaworotko, *Chem. Commun.* **1998**, 595−596.

[4] [4a] P. J. Hagrman, D. Hagrman, J. Zubieta, *Angew. Chem.* **1999**, *111*, 2798−2848; *Angew. Chem. Int. Ed.* **1999**, *38*, 2638−2684, and references cited therein. [4b] A. J. Blake, N. R. Champness, P. Hubberstey, W.-S. Li, M. A. Withersby, M. Schröder, *Coord. Chem. Rev.* **1999**, *183*, 117−138, and references cited therein.

[5] [5a] G. L. Ning, L. P. Wu, K. Sugimoto, M. Munakata, T. Kuroda-Sowa, M. Mackawa, *J. Chem. Soc., Dalton Trans.* **1999**, 2529−2536, and references cited therein. [5b] M. Munakata, L. P. Wu, T. Kuroda-Sowa, M. Maekawa, Y. Suenaga, G. L. Ning, T. Kojima, *J. Am. Chem. Soc.* **1998**, *120*, 8610−8618.

[6] [6a] Y.-B. Dong, G.-X. Jin, M. D. Smith, R-Q. Huang, B. Tang, H.-C. zur Loye, *Inorg. Chem.* **2002**, *41*, 4909−4914. [6b] Y.-B. Dong et al., unpublished results.

[7] [7a] A. Dormond, *J. Organomet. Chem.* **1975**, *101*, 71−78. [7b] R. A. Howie, *J. Organomet. Chem.* **1986**, *303*, 213−216.

[8] Bruker Analytical X-ray Systems, Inc., Madison, WI, **1999**.

[9] J. L. William, H. S. William, *J. Am. Chem. Soc.* **1957**, *79*, 4970−4973.

[10] K. J. Stone, R. D. Little, *J. Org. Chem.* **1984**, *49*, 1849−1852.

[11] M. Munakata, L. P. Wu, G. L. Ning, *Coord. Chem. Rev.* **2000**, *198*, 171−203.

[12] S. Kawata, S. Kitagawa, M. Kondo, I. Furuchi, M. Munakata, *Angew. Chem. Int. Ed. Engel.* **1994**, *33*, 1759−1761.

[13] C. N. Verani, E. Rentschler, T. Weyhermüller, E. Bill, P. Chaudhuri, *J. Chem. Soc., Dalton Trans.* **2000**, 251−258.

[14] Y.-B. Dong, M. D. Smith, H.-C. zur Loye, *Solid State Sci.* **2000**, *2*, 335−341.

[15] Y. Akhriff, J. Server, A. Sancho, J. Garcia, E. Escriva, J. V. Folgado, L. Soto, *Inorg. Chem.* **1999**, *38*, 1174−1185.

[16] P. Guerriero, S. Tamburini, P. A. Vigato, *Coord. Chem. Rev.* **1995**, *139*, 17−243.

[17] J. L. Wesemann, M. H. Chisholm, *Inorg. Chem.* **1997**, *36*, 3258−3267.

[18] [18a] H. Y. Hung, W. J. Chen, G. C. Yang, A. Yeh, *Inorg. Chem.* **1991**, *30*, 1862−1868. [18b] A. Benaltabef, S. B. R. Degllo, M. E. Folquer, N. E. Katz, *Inorg. Chim. Acta* **1991**, *188*, 67−70. [18c] A. E. Almaraz, L. A. Gentil, L. M. Baraldo, J. A. Olabe, *Inorg. Chem.* **1996**, *35*, 7718−7727.

[19] [19a] R. D. Bailey, L. L. Hook, W. T. Pennington, *Chem. Commun.* **1998**, 1181−1182. [19b] L. Carlucci, G. Ciani, D. M. Proserpio, A. Sironi, *J. Chem. Soc., Chem. Commun.* **1994**, 2755−2756.

[20] W. R. Zhang, J. R. Jeitler, M. M. Turnbull, C. P. Landee, M. Y. Wei, R. D. Willet, *Inorg. Chim. Acta* **1997**, *256*, 183−198.

[21] H.-P. Wu, C. Janiak, G. Rheinwald, H. Lang, *J. Chem. Soc., Dalton Trans.* **1999**, 183−190.

[22] G. R. Desiraju, *Chem. Rev.* **1998**, *98*, 1375−1405.

[23] Y.-B. Dong, M. D. Smith, H.-C. zur Loye, *Solid State Sci.* **2000**, *2*, 861−870.

[24] U. H. F. Bunz, *Chem. Rev.* **2000**, *100*, 1605−1644.

[25] [25a] D. M. Ciurtin, N. G. Pschirer, M. D. Smith, U. H. F. Bunz, H.-C. zur Loye, *Chem. Mater.* **2001**, *13*, 2743−2745. [25b] E. Cariati, X. Bu, P. C. Ford, *Chem. Mater.* **2000**, *12*, 3385−3391. [25c] F. Würthner, A. Sautter, *Chem. Commun.* **2000**, 445−446.

Received June 12, 2003
Early View Article
Published Online October 2, 2003

 © 2003 Wiley-VCH Verlag GmbH & Co. KGaA, Weinheim

A New Diazacyclooctane Dihydroxamate as a Siderophore Analogue − Synthesis and Equilibrium Studies of Iron(III) and Copper(II) Complexes

Margarida Gaspar,[a,b] J. Paulo Telo,[a] and M. Amélia Santos*[a]

Keywords: Copper / Iron / Aminohydroxamates / Hydroxamic acids / Siderophores

A new siderophore analogue based on the mesocyclic diamine 1,5-diazacyclooctane (DACO) functionalized with two additional hydroxamate donor pendant groups, 1,5-diazacyclooctane-1,5-bis(*N*-methylacetohydroxamic acid) (DACODMAHA), has been synthesized from the corresponding diacetate derivative (DACODA). The complexation behaviour of this ligand towards Cu^{II} and Fe^{III} in aqueous solution has been studied by potentiometry, UV/Vis and EPR spectroscopy and magnetic moment measurements. The Cu^{II} complexation involves the formation of a mononuclear species with a tetradentate mixed amine/hydroxamate coordination mode, whereas the Fe^{III} complexation involves a binuclear species with Fe_2L_3 stoichiometry and normal {*O*,*O*}-hydroxamate coordination mode. The redox potential of the iron complexes and the corresponding electron transfer mechanism are also evaluated.
(© Wiley-VCH Verlag GmbH & Co. KGaA, 69451 Weinheim, Germany, 2003)

Introduction

Hydroxamic acid derivatives have been objects of interest for many years due to their natural occurrence and role as microbial iron-transporting compounds (siderophores).[1] Hydroxamate biomimetics have been developed with the aim of obtaining potential constituents of therapeutic agents, for use in chelating therapy (due to their ability to complex iron(III) and related metal ions)[2,3] or as metalloenzyme inhibitors (associated with their complexation with M^{II} transition metal ions).[4,5]

We have been involved in the development and study of a series of polyamine-polyhydroxamate acids as potential siderophore analogues. Their design has been based on macrocyclic or mesocyclic polyamine backbones with *N*-methylacetohydroxamic acids as pendant arms.[6−9] Some of those cyclic diamine-hydroxamate biomimetics − PIPDMAHA and DACHDMAHA (see Scheme 1) − proved to possess interesting properties as siderophore analogues of rhodotorulic acid, a naturally occurring dihydroxamate siderophore.[9] We therefore decided to extend this set of cyclic diamine-dihydroxamic acids by including a PIPDMAHA homologue with a larger backbone skeleton: 1,5-diazacyclooctane-1,5-bis(*N*-methylacetohydroxamic acid) (DACODMAHA, see Scheme 1). Its mesocyclic backbone, 1,5-diazacyclooctane (DACO), presents interesting "boat/chair/crown" configurations and some of its derivatives, those bearing donor pendants such as acetate,[10] thiolate[11] and many other groups,[12−14] have attracted special attention in recent years.

Here we report the preparation of this new ligand (DACODMAHA) as well as the study of its acid−base and complexing properties towards iron(III) and copper(II), mostly by potentiometric and spectroscopic methods. In the absence of X-ray data, because of a lack of suitable crystals, molecular modelling calculations were performed to provide information about the probable topology of the binuclear iron(III)-DACODMAHA complex with 2:3 (metal:ligand) stoichiometry, which can be a mono- or a three-bridged dimer. Since the reduction of the Fe^{III} siderophore complexes has been proposed for the mechanism of microbial Fe release, the redox properties of the iron complexes were studied by voltammetric methods. This set of results is discussed and compared with previous reports on some of the corresponding synthetic or naturally occurring dihydroxamate siderophores.

Results and Discussion

Synthesis

1,5-diazacyclooctane-1,5-bis(*N*-methylacetohydroxamic acid) (DACODMAHA) was prepared by a two-step strategy, starting from the corresponding dicarboxylic acid derivative, 1,5-diazacyclooctane-*N*,*N*′-diacetic acid (DACODA), which was synthesized as described previously.[15] The carboxylic acid groups were condensed with *O*-benzyl-*N*-methylhydroxylamine, in the presence of 1-ethyl-3,3-di-

[a] Centro de Química Estrutural, Complexo I, Instituto Superior Técnico,
1049-001 Lisboa, Portugal
Fax: (internat.) + 351-(0)21-8464455
E-mail: masantos@ist.utl.pt
[b] Centro de Investigação e Desenvolvimento da Universitas, Instituto Superior de Educação e Ciências,
Alameda das Linhas de Torres, 179, 1750-142 Lisboa, Portugal

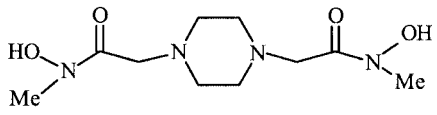

PIPDMAHA

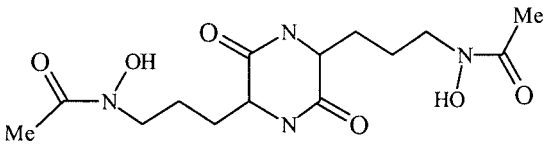

Rhodotorulic acid (RA)

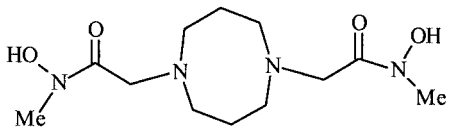

DACODMAHA

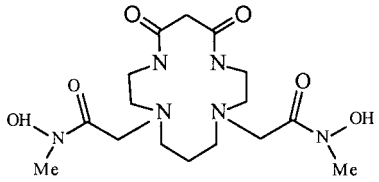

DOCYDMAHA

Scheme 1

methylaminopropyl-carbodiimide (EDC), at room temperature and pH 4.8. Next, standard catalytic hydrogenolysis (P_{H_2} = 1 atm) of this bis(*O*-benzylhydroxamate) derivative afforded the free dihydroxamate ligand (DACODMAHA). It is noteworthy that the synthetic scheme used for this ligand is quite different from that previously reported for the smaller size analogues (ex. PIPDMAHA),[6] which involved the coupling of the previously synthesized hydroxamate arms to the amine groups of the cyclic backbones. In the case of the current ligand, however, one of the amine groups in DACO is much more basic than the corresponding groups in the backbones of the previously reported ligands (see below), so the use of the same coupling reaction in the synthesis of DACODMAHA would require more drastic basic conditions, which would probably result in the subsequent hydrolytic scission of the hydroxamate peptidic bond.

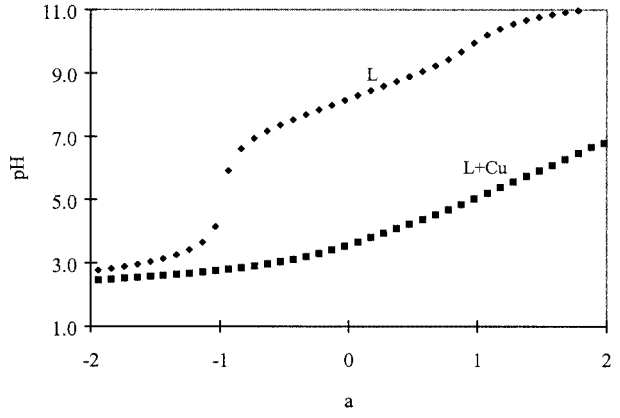

Figure 1. Potentiometric titration curves (experimental points) for the ligand H_2L (DACODMAHA) and for the copper(II)-H_2L system; C_L= 2.4 × 10^{-3} M, C_L/C_{Cu} = 1:1, I = 0.1 M (KNO_3); T = 25.0 °C

Protonation Studies

The acid−base behaviour of this *N*,*N*′-bis(hydroxamate)-diazacyclooctane derivative (DACODMAHA) was studied by potentiometry. A representative pH titration curve for the ligand is presented in Figure 1. The fully protonated form of this ligand can release four protons, although only three protonation constants can be calculated from direct potentiometric data, since the first is too high to be accurately determined by this method (under our experimental conditions it is limited to the range 2−12).[16]

Thus, to achieve a full acid−base characterization of the ligand, a ^{1}H NMR titration was carried out (Figure 2). The indicated peak attribution was based on the corresponding integration areas and multiplicity. The ^{1}H NMR titrations curves corresponding to the three sets of methylenic protons show two well defined inflections at pD* ≈ 2 ($\Delta\delta_a$ = 0.47 ppm, $\Delta\delta_c$ = 0.37 ppm, $\Delta\delta_d$ = 0.40 ppm) and pD* ≈ 13 ($\Delta\delta_a$ = 0.21 ppm, $\Delta\delta_c$ = 0.38 ppm, $\Delta\delta_d$ = 0.33 ppm) regions. A small inflection at pD* ≈ 8 ($\Delta\delta_a$ = 0.04 ppm, $\Delta\delta_c$ = 0.05 ppm, $\Delta\delta_d$ = 0.135 ppm) region is due to the hydroxamate methyl protons, as would be expected. As in the cases studied previously,[17] attribution of the protonation processes (and stepwise protonation constants) to individual basic centres in the ligand is straightforward. The first and last constants (K_1 and K_4) are mainly associated with the protonation of the macrocyclic amines, while the remaining two (K_2 and K_3) are attributable to the protonation of the hydroxamate groups. Further analysis of the sequence of protonation of the four basic sites and calculation of the corresponding microconstants is beyond the scope of this work.

As mentioned above, only three protonation macroconstants (K_2, K_3, K_4) could be determined through fitting analysis of the potentiometric titration data (with the aid of the SUPERQUAD program[18]), while the first protonation constant (K_1) was obtained from fitting of the ^{1}H NMR

 © 2003 Wiley-VCH Verlag GmbH & Co. KGaA, Weinheim

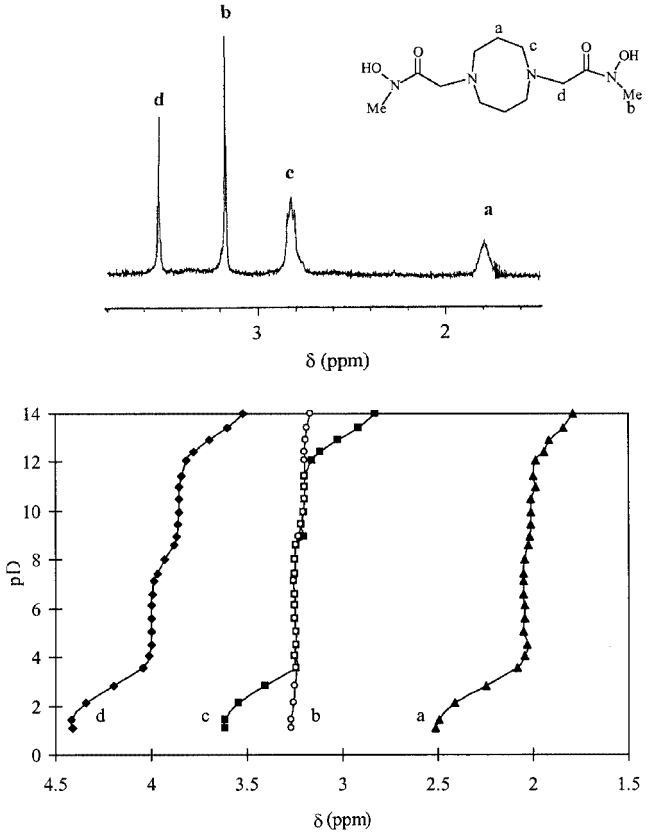

Figure 2. Proton NMR titration curves for DACODMAHA (C_L = 2×10^{-2} M); the pD* of the solution was adjusted with DCl and KOD

titration curves (Figure 2) with the aid of the PSEQUAD program.[16] The refined logarithmic stepwise protonation constants (log K) are listed in Table 1, together with the corresponding values for two structural analogues.

The first protonation constant of DACODMAHA (log K_1 = 13.04), attributable to the protonation of an amine group, is higher than the corresponding value for the cyclic backbone, DACO (log K_1 = 10.74).[19] This feature may be due to the formation of a very stable hydrogen bond between the corresponding ammonium proton and the nearby nitrogen atom of the cyclic backbone, which should be stronger in DACODMAHA than in DACO. The corresponding dicarboxylic derivative, DACODA, showed similar behaviour (log K_1 = 12.27)[15] and it was proposed that the introduction of the acetate groups induces the "boat" as the major macrocyclic conformation, while DACO shows three conformations (boat, chair and crown). Furthermore, of the three conformations of the monoprotonated macrocycle, the "boat" presented the strongest *NH···N* hydrogen bond. Therefore, for similar reasons, the introduction of the hydroxamate arms should favour the "boat" conformation in DACODMAHA. On the other hand, there is an additional stabilization of the DACODMAHA monoprotonated species, due to the hydrogen bond between the ammonium proton and the deprotonated oxygen atom of the adjacent hydroxamate group, through a six-membered ring interaction. The quite low protonation constant of the second nitrogen atom of DACODMAHA (log K_4 = 2.22) supports the existence of such a strong hydrogen bond network, namely between the ammonium proton and the amine *N* atom (>N^+-*H*···*N*<) as well as between the deprotonated amine nitrogen atom and the adjacent hydroxamic proton (>*N*···*HO*−). The remaining protonation constants (log K_2 = 8.91, log K_3 = 7.45) agree with the expected values for hydroxamate groups (log K = 8−10),[20] although their values are slightly lowered by inductive/electrostatic effects of the α-amino/ammonium groups.

Table 1. Stepwise protonation constants of DACODMAHA, DACO and DACODA; global stability constants and spectroscopic data of the corresponding copper(II) complexes

Ligand	H^+ log K_i	Cu^{2+} log $\beta_{Cu_pH_qL_r}$[a]	λ_{max}/nm (ε/$M^{-1}cm^{-1}$)
DACODMAHA	13.0(3)	(1,2,1) = 29.7(1)	640 (112); pH = 2.99
	8.91(1)	(1,1,1) = 24.7(1)	595 (170); pH = 8.40
	7.45(2)		
	2.22(5)		
DACO	10.74[b]	(1,1,1) = 17.84[b]	637 (116)[c]
	7.25	(1,0,1) = 10.56	
DACODA	12.27[d]		
	4.70	(1,0,1) = 16.44[e]	621 (152)[c]
	1.84		

[a] The (*p*,*q*,*r*) symbolism means a species with stoichiometry ($Cu_pH_qL_r$) [b] From ref.[19] [c] From ref.[23] [d] From ref.[15] [e] From ref.[28]

Copper(II) Complexation

The complexation behaviour of DACODMAHA toward copper(II) in aqueous solution was studied by potentiometry and UV/Vis spectrophotometry. A representative pH-metric titration curve of this binary system (C_{Cu} = 2.4 × 10^{-3} M, C_L/C_{Cu} = 1:1) is shown in Figure 1. Some precipitation was observed above pH 5. Analysis of the potentiometric titration curves shows that, in the presence of copper(II), the fully protonated form of the ligand is able to dissociate four protons. The global formation constants (Table 1) were calculated from fitting analysis of the titration curve by use of the SUPERQUAD computer program.[18] Below pH ≈ 5, the best model, included only two species, $[CuH_2L]^{2+}$ and $[CuHL]^+$; their overall stability constants (log β) are 29.7 and 24.7, respectively. For higher pH values, neutral species (ex. CuL) or mixed metal-ligand-hydroxo complexes are formed but they are insoluble under our experimental conditions. On the assumption that the last equivalent of base consumption corresponds mainly to the release of the last labile ligand proton, the drastic decrease in the corresponding pH (ca. 5−6) indicates that this proton is being pushed by the metal ion. A rough evaluation of the stability constant of the neutral species (log $\beta_{CuL} \approx 19$) indicates that it would be quite high and closer to the corresponding overall constants of the 1:2 complex (log β_{CuL_2}) for α-aminohydroxamic acids (19.89 for glycinehydroxamic acid)[21] than for simple hydroxamic acids (14.06 for acetohydroxamic acid).[22]

 © 2003 Wiley-VCH Verlag GmbH & Co. KGaA, Weinheim

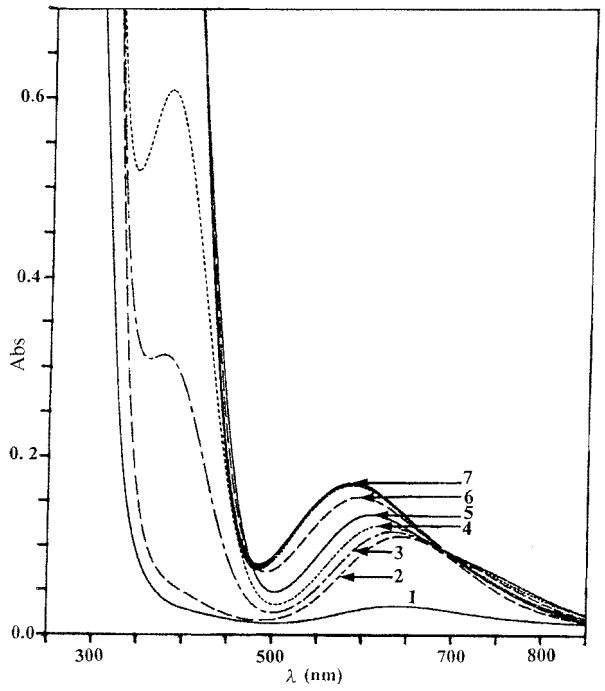

Figure 3. Absorbance spectra of Cu^{II}-DACODMAHA system as function of pH: 1.56 (1), 2.44 (2), 3.73 (3), 4.34 (4), 5.52 (5), 6.36 (6), 7.42−12.03 (7); $C_L = 3 \times 10^{-3}$ M, $C_L/C_M = 3{:}1$, $I = 0.1$ M (KNO_3), $T = 25.0$ °C

In order to obtain further insight into the coordination modes involved in the Cu^{II}-DACODMAHA complexes, UV/Vis spectra were recorded for solutions with $C_L = 3 \times 10^{-3}$ M and 1:3 copper-to-ligand molar ratio at different pH values. We did not observe any precipitate in this study, probably due to the excess of ligand and/or to the higher dilution conditions. The Cu^{II}-DACODMAHA spectra (Figure 3) each exhibit a broad band in the visible region, attributable to the copper d-d transition energy (for pH = 1.6, $\lambda_{max} = 635$ nm, $\varepsilon_{max} = 48$ $dm^3 \cdot mol^{-1} \cdot cm^{-1}$; for pH = 7.4−12.0, $\lambda_{max} = 595$ nm, $\varepsilon_{max} = 170$ $dm^3 \cdot mol^{-1} \cdot cm^{-1}$). At pH = 3.7, a charge transfer (c.t.) band started to appear at $\lambda_{max} = 400$ nm, its intensity increasing with the pH (for pH = 5.52, $\lambda_{max} = 400$ nm, $\varepsilon_{max} = 960$ $dm^3 \cdot mol^{-1} \cdot cm^{-1}$). The isosbestic point at $\lambda = 680$ nm observed for $4 < pH < 7$ suggests the interconversion of two major chromophoric species in that pH range.

Conjugation of spectroscopic and potentiometric data was analysed with care, since different stoichiometries were used. Spectral analysis indicates that, in the highly acidic pH range (pH 1.6−2.4), there is only one major chromophoric species ($\lambda_{max} = 635-640$ nm), which should correspond to the CuH_2L species [or possibly $Cu(H_2L)_2$ for excess of ligand]. Spectra at pH 2.44 ($\lambda_{max} = 640$ nm and the absence of the c.t. band at 400 nm, but around 300 nm) suggest for that complex species a copper coordination sphere involving just one or two amine groups of the macrocycle and water molecules (see Scheme 2). In fact, the DACO-Cu^{II} complex, with Cu^{II} coordinated to the amine groups of the macrocycle, exhibits $\lambda_{max} = 637$ nm,[23] and also some Cu^{II}-α-aminohydroxamic acid complexes with Cu^{II} coordinated to two nitrogen atoms and two water molecules, exhibit $\lambda_{max} = 647-650$ nm.[24] In the pH range around ca. 4−7 there is an interconversion of two species, which is accompanied by a probable change in the coordination mode. In fact the spectral changes that occurred along this pH range − the blue shift and the intensity increase in the d-d transition band, together with the appearance of the band at 400 nm − suggest an increase in the hydroxamate coordination with pH. For some aminohydroxamate ligands, UV bands identical to those seen in the oxygen-hydroxamate to Cu^{II} charge transfer were assigned.[8,25] On the other hand, visible bands with similar λ_{max} values were also found for Cu^{II} complexes with other cyclic polyaminopoly(*N*-methyl-hydroxamate) ligands, for which a mixed coordination of *N*-amine atoms of cyclic backbones and of *O*-hydroxamate atoms of the side arms was considered: $\lambda_{max} = 600$ nm for 1,4-diaazacycloheptane-*N*,*N*′-bis(*N*-methylacetohydroxamic acid);[26] $\lambda_{max} = 590$ nm for 4,8-(12,14-dioxo-1,4,8,11-tetraazacyclotetradecane)bis(*N*-methylacetohydroxamic acid) (DOCYDMAHA).[27] The UV/Vis spectroscopic data of copper(II) complexes with other DACO derivatives bearing different substituents also show absorption maxima around 594−637 nm, attributed to five-coordinate Cu^{II} complex, with distortion from square-pyramidal towards trigonal structures.[12] Furthermore, metal ion coordination through the amine nitrogen atoms and the acetate oxygen atoms has also been proposed for the DACODA-Cu^{II} complexes possessing acetate groups bonded to the macrocycle.[28] Thus, for the CuHL and CuL species, the coordination of Cu^{II} to the ligand should involve not only the mesocyclic amines but also one or two hydroxamate groups, respectively, and one water molecule that occupies the fifth coordination position. The absence of the sixth coordination position, as happens in other similar complexes with DACO derivatives, may also be assumed, consistently with the expected boat-chair conformation of the ligand. The central methylene C−H groups of the boat form in DACO shields the Cu^{II} centre, thus blocking the sixth coordination position.[13]

Electron Paramagnetic Resonance: To advance the study of the type of coordination involved in the DACODMAHA-Cu^{II} complexes further, EPR spectra were obtained over a wide pH range (2−10). No EPR-silent pH region was detected in that pH range, thus suggesting the absence of binuclear species under our experimental conditions. Two EPR spectra were selected (pH 2.99 and 8.40), because the major species under these pH conditions should be CuH_2L and CuL, respectively. All the recorded spectra (Figure 4) present the four lines due to the copper coupling.

The corresponding EPR parameters present $g_{//} > g_{\perp}$ ($g_{//} \cong 2.40$, $g_{\perp} \cong 2.08$, $A_{//} \cong 164 \times 10^{-4}$ cm^{-1}, $A_{\perp} \cong 35 \times 10^{-4}$ cm^{-1}, for pH = 2.99, and $g_{//} \cong 2.26$, $g_{\perp} \cong 2.07$, $A_{//} \cong 167 \times 10^{-4}$ cm^{-1}, $A_{\perp} \cong 30 \times 10^{-4}$ cm^{-1}, for pH = 8.40), indicating an axially elongated-tetragonal copper(II) environment, as is the case with most of the Cu^{II} complexes in solution. For pH = 2.99, the calculated spectral param-

 © 2003 Wiley-VCH Verlag GmbH & Co. KGaA, Weinheim

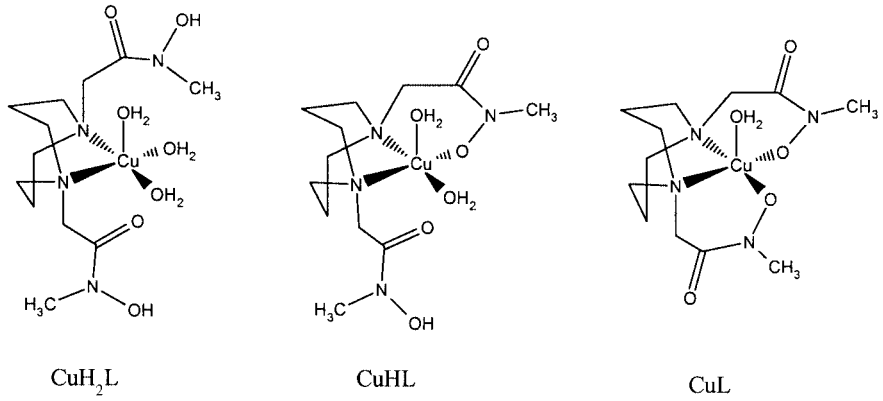

Scheme 2

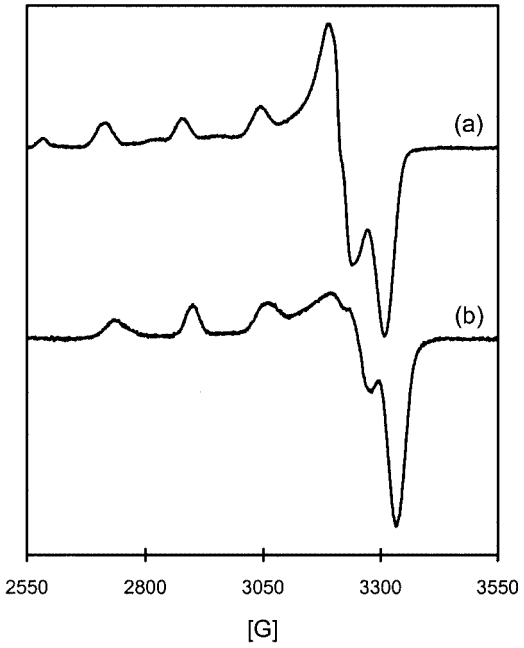

Figure 4. EPR spectra of frozen D_2O solutions with 20% ethylene glycol containing the Cu^{II}-DACODMAHA complexes at: pD* = 2.99 (a), pD* = 8.40 (b) ($C_{Cu} = 6.0 \times 10^{-3}$ M, $C_L/C_{Cu} = 1{:}1$; $T = 100$ K; frequency 9.34 GHz and modulation frequency 100 kHz)

eters indicate complex formation. However, Cu^{II} still seems to be in equilibrium with water molecules ($g_{//} = 2.401$ and $A_{//} = 146 \times 10^{-4}$ cm^{-1} for the Cu^{II} aquo complex)[29] and it is possible that the copper cation is coordinated by two ligand nitrogen atoms. At pD* = 8.40, there is one predominant species, for which the EPR parameters are close to those reported in the literature for some forms of Cu^{II}-α-aminohydroxamic acids complexes ($g_{//} \cong 2.33$; $A_{//} \cong 167 \times 10^{-4}$ cm^{-1}).[29] In this species Cu^{II} is coordinated through mixed (*N*,*N*) and (*O*,*O*) bonding modes. On the other hand, the parameters calculated for this major species, namely $A_{//}$, do not seem to give support to the hypothesis of Cu^{II} being coordinated by two hydroxamate groups ($g_{//} \cong 2.25-2.29$; $A_{//} \cong 189-190 \times 10^{-4}$ cm^{-1}).[30] Furthermore, the difference between $g_{//}$ and $g_{\perp}$ (Δg) is slightly higher at pH 2.99 ($\Delta g = 0.23$) than at pD* 8.40 ($\Delta g = 0.21$), thus suggesting that the presence of the hydroxamate groups in the copper coordination sphere induces less distortion from the square-planar geometry towards the tetragonal than its absence. In conclusion, the EPR spectra support the hypothesis suggested by the UV/Vis spectra, that DACODMAHA-Cu^{II} complexes have a five-coordinate structure with distorted square-pyramidal geometry. In the acid range, CuH_2L should have Cu^{II} coordinated only to the amine groups of the macrocycle and possibly three water molecules; at neutral pH, besides the coordination to the amine groups of the macrocycle, the metal centre should be also coordinated to one and two hydroxamate groups in CuHL and CuL, respectively, with one water molecule in the fifth apical position (see Scheme 2).

Iron Complexion

The interaction of DACODMAHA with iron(III) was studied by UV/Vis spectrophotometric titration ($C_{Fe} = 1.80 \times 10^{-4}$ M with tenfold ligand excess to avoid precipitation of hydroxo complexes). The set of visible spectra registered for the DACODMAHA-Fe^{III} system (Figure 5) shows that complex formation begins at a very low pH (pH < 2). There is a typical ferric-hydroxamate charge-transfer (*c.t.*) band, the intensity enhancement of which and its blue shift with increasing pH indicate greater coordination to the ferric ion (at pH 2.08, $\lambda_{max} = 475$ nm, $\varepsilon = 1660$ M^{-1}·cm^{-1}/Fe; at pH 8.5, $\lambda_{max.} = 420$ nm, $\varepsilon = 2666$ M^{-1}·cm^{-1}/Fe). The isosbestic point at $\lambda = 475$ nm suggests the existence of only two major species in the pH range 3−5. For pH 5−9, $\lambda_{max.}$ and $\varepsilon_{max.}$ are practically pH-independent, indicating the existence of one predominant complex species. Its spectroscopic data is consistent with three hydroxamate moieties coordinated to Fe^{III} [31] (probably as a dimeric structure with Fe_2L_3 stoichiometry). At ca. pH 2.1, according to the spectroscopic data presented above, the major species should already have two hydroxamate moieties coordinated to each ferric centre (probably as a monomeric species). The isosbestic point should therefore be the result of an equilibrium between the monomeric and the dimeric species. Above

 © 2003 Wiley-VCH Verlag GmbH & Co. KGaA, Weinheim

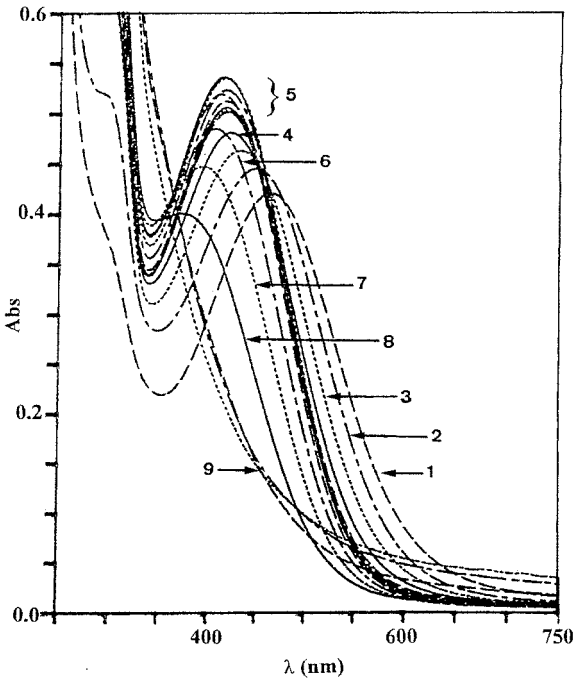

Figure 5. Absorbance spectra of Fe^{III}-DACODMAHA as a function of pH: 2.08 (1), 3.20 (2), 3.77 (3), 4.31(4), 4.91−8.97 (5), 9.38 (6), 9.92 (7), 10.48 (8), 10.92−11.83 (9). $C_{Fe} = 1.8 \times 10^{-4}$ M, $C_L/C_{Fe} = 10:1$; $I = 0.1$ (KNO_3); $T = 25.0$ °C

pH = 9, the corresponding ferric complexes exhibit decreases in their $\varepsilon_{max.}$ and $\lambda_{max.}$ values (orange colour lightens to yellowish) with increasing pH, which is attributable to mixed hydroxo-hydroxamate complexes with only two hydroxamate moieties coordinated to each ferric centre. These results are similar to previously reported for rhodotorulic acid[32] and other synthetic dihydroxamic acids.[6,26,33]

The stability constants of the DACODMAHA-iron(III) complexes were determined by fitting analysis of the spectrophotometric titration data with the aid of the PSEQUAD[16] program. In the pH range from 2−9, the best-fitting model includes one monomeric species $[Fe(HL)]^{2+}$ and two dimeric species ($[Fe_2H_3L_3]^{3+}$ and $[Fe_2H_2L_3]^{2+}$), the global stability constants of which are 28.91, 86.77 and 76.83, respectively. The corresponding species distribution diagram (Figure 6) is consistent with the spectral observations, namely the existence of the monomeric species (FeHL) in the acidic pH range and of the dimeric complex ($Fe_2H_3L_3$) in the neutral zone. The assigned $Fe_2H_2L_3$ species that started to form at ca pH 8 could also be attributable to a mixed $Fe_2H_3L_3(OH)$ complex, or both may possibly occur, but these species are not distinguishable by the PSEQUAD program. Although the first assumption seems consistent with the spectral analysis, above pH = 9, hydrolytic processes compete with the further deprotonation of the complexed ligand.

A brief comparative analysis of the iron affinity of DACODMAHA and other related dihydroxamate ligands can be made from the set of results presented (Table 2), namely from the corresponding pFe values at pH = 7 (pFe = -log [Fe] for $C_L/C_{Fe} = 10$ and $C_L = 10^{-5}$ M), to take account of

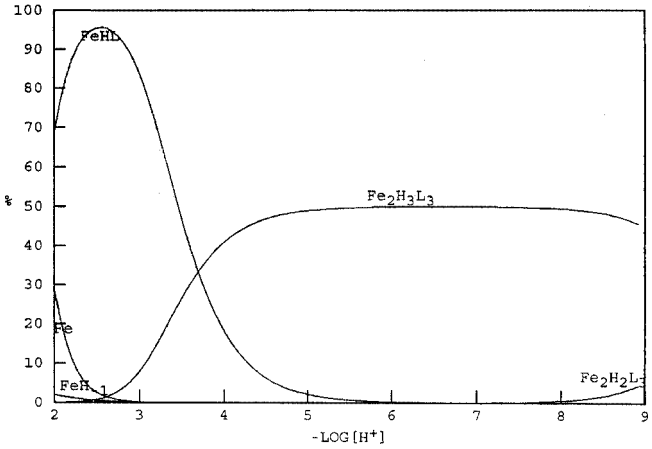

Figure 6. Distribution species diagram for the Fe^{III}-DACODMAHA system as a function of pH ($C_L/C_{Fe} = 10:1$; $C_{Fe} = 1.8 \times 10^{-4}$ M; $I = 0.1$ M (KNO_3); $T = 25$ °C)

the different proton concentration dependency of the different ligands. It is clearly shown that at neutral pH DACODMAHA has less affinity for Fe^{III} (pFe ≈ 17) than the related dihydroxamate derivatives (pFe ≈ 21 for PIPDMAHA and DOCYDMAHA).[9,33]

Since all these ligands form dimeric diiron complexes with the same stoichiometry and probably identical structures under these experimental conditions (the triply ligand-bridged coordination mode, see below), there are no relevant differences in the interaction between the two metal centres. Therefore, the *ca* 4 orders of magnitude difference in the pFe values should be attributable to overall charge differences due to pK_a differences. In fact, protonated DACODMAHA is positively charged as a ligand, whereas the others are neutral Fe^{III} binding ligands. At neutral pH, the current complex ($Fe_2H_3L_3$) therefore has the ligand protonated with the concomitant Fe^{3+}-H^+ electrostatic repulsions and an overall decrease in the stability of the complex, while for the analogous ligands the corresponding complex species are deprotonated. Furthermore, comparison between the calculated pFe values associated with the ferric complexation with the current ligand and *N*-methyl-acetohydroxamic acid (pFe = 16)[34] indicates that the entropic factors associated with the polydenticity of the ligand in this study hardly overcome the destabilizing charge effects on the overall binding interaction. Furthermore, the weaker *O*-donor capacity of the hydroxamate groups is consistent with lower protonation constant found for one of the hydroxamate groups (log $K_3 = 7.45$), due to the electronic effect of the α-ammonium moiety.

Electron Paramagnetic Resonance: To obtain extra information on the dimeric complex of DACODMAHA with iron, the EPR spectrum of DACODMAHA-Fe^{III} system was registered at neutral pH (Figure 7), together with the corresponding spectra for DOCYDMAHA and PIPDMAHA iron complexes, for purposes of comparison.

Each of these spectra shows one single signal at $g = 4.3$, a characteristic value of high-spin octahedral ferric complexes, as previously found for the naturally occurring di-

 © 2003 Wiley-VCH Verlag GmbH & Co. KGaA, Weinheim

Table 2. Global formation constants (log $\beta_{Fe_pH_qL_r}$), electronic spectroscopic data, pFe values, magnetic moments, and half-wave reduction potentials for the ferric complexes with DACODMAHA, DOCYDMAHA, PIPDMAHA and rhodotorulic acid

Ligand	log $\beta_{Fe_pH_qL_r}$[a]	λ_{max}/nm, (ε/M^{-1}cm^{-1})	pFe[b]	μ_{Fe} (BM)	$E_{1/2}$ (mV)
DACODMAHA	(1,1,1) = 28.91(3)	420	16.6	5.8	−502
	(2,3,3) = 86.77(8)	(2666)			
	(2,2,3) = 76.83(8)				
DOCYDMAHA	(2,0,3) = 60.50[c]				
	(1,2,1) = 27.94				
	(1,1,1) = 24.50	425	21.1[c]	5.8[c]	−603[c]
	(1,0,1) = 21.33	(2995)[d]			
	(1,-2,1) = 5.07				
PIPDMAHA	(2,0,3) = 61.7[e]	425	21.5[c]	5.5[e]	−560[c]
		(2880)[e]			
Rhodotorulic acid[f]	(1,0,1) = 21.55	425	21.9	5.9	−601[c]
	(2,0,3) = 62.3	(2700)			

[a] The (p,q,r) symbology means a species with stoichiometry ($Fe_pH_qL_r$). [b] pFe = −log [Fe^{3+}] at pH = 7.4, C_{Fe} = 1 × 10^{-6} M, C_L = 1 × 10^{-5} M. [c] From ref.[9] [d] From ref.[33] [e] From ref.[6] [f] From ref.[35]

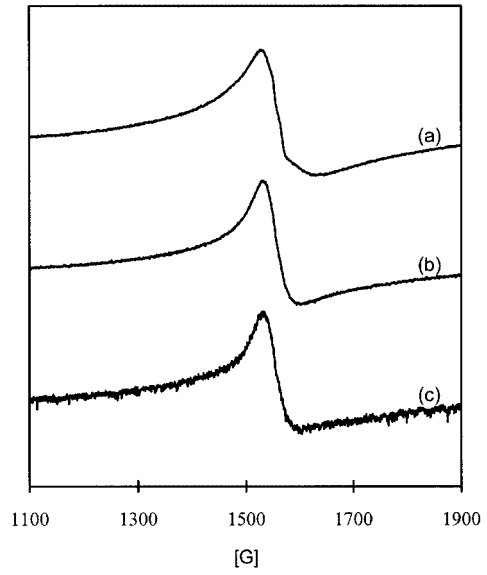

Figure 7. EPR spectra of frozen D_2O solutions containing: (a) ferric-PIPDMAHA, (b) ferric-DOCYDMAHA and (c) ferric-DACODMAHA complexes (C_{Fe}/C_L = 2:3, pD* = 7; C_{Fe} = 1.00 × 10^{-3} M); T = 100 K; frequency 9.34 GHz and modulation frequency 100 kHz)

hydroxamate rhodotorulic acid.[35] The signal linewidth obtained for the dimeric ferric-DACODMAHA complex (72 G) is close to the value found for the DOCYDHAMA-Fe^{III} complex (70 G)[33] and for the ferric rhodotorulate in methanol (51 G), but much lower than the corresponding value for the PIPDMAHA-Fe complex (120 G). The ferric rhodotorulate complex has a distance of ca. 9−10 Å between the two ferric centres, which may be regarded as enough for the existence of significant metal interactions,[35] while the results obtained for the PIPDMAHA dimeric complex indicated dipole-dipole interactions between the metal centres.[6] This type of interaction has also been observed in ferric dimeric complexes of other dihydroxamate ligands, analogues of rhodotorulic acid.[31] These results therefore support the assumption that DACODMAHA forms dimeric species with iron(III), although with weak magnetic interactions between the two metal centres.

Magnetic Properties: The molar magnetic susceptibility (χ_M) and magnetic moment (μ_{Fe}) of the DACODMAHA ferric complexes were measured in D_2O solution as a function of pH (pD*), by Evans' method.[36] In the pH 5−8 range ($Fe_2H_3L_3$ is the major species), the values found for the magnetic moments (μ_{Fe} = 5.83−5.74 BM) are consistent with the existence of a high-spin octahedral complex. They are just between the value for an octahedral unimolecular spin-free iron(III) complex (5.92 BM) and the literature value (5.7 BM) reported for some binuclear iron(III) complexes with very weak interactions between the ferric centres.[31] The ferric rhodotorulate and other dihydroxamate complexes have μ_{Fe} = 5.9 BM, while the ferric PIPDMAHA complex presented μ_{Fe} = 5.5 BM.[6] These results, together with the EPR spectra, suggest that, in the neutral pH range, the DACODMAHA diferric complex has the iron sites enough apart from one another and so only weak or negligible metal−metal interactions.

Molecular Simulation: In order to gain further insight into the $Fe_2H_3L_3$ complex structure, molecular mechanics modelling calculations were performed, through the use of the CERIUS-2 program[37] and also by a previously reported approach.[7] This study was aimed at determining the most probable configuration involved in the DACODMAHA-Fe^{III} dimeric complex, considering two different hypothesis (see Figure 8): (a) three-bridge conformation, similar to that found for the ferric-rhodotorulic acid complex,[38] in which the three ligand molecules each have a hydroxamate moiety coordinated to a different metal centre, and (b) one-bridge conformation, similar to that in the ferric-alcaligin complex,[39] in which only one ligand molecule is coordinated to two metal centres, while the remaining two ligand molecules have both the hydroxamate moieties with intramolecular coordination to the same metal ion.

These theoretical modelling studies showed that, for the dimeric ferric-DACODMAHA complex, conformation (a) is more stable than conformation (b), and that the distance

 © 2003 Wiley-VCH Verlag GmbH & Co. KGaA, Weinheim

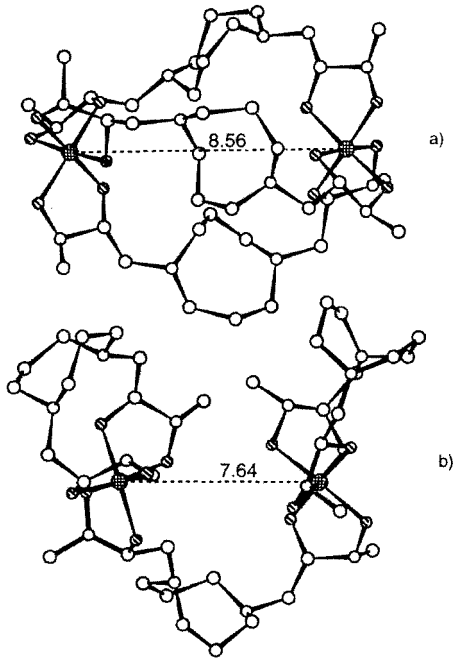

Figure 8. Low-energy conformations simulated for the dimeric complexes of the Fe^{III}/DACODMAHA system

between the ferric centres should be ca. 8.6 Å. This result supports the hypothesis that DACODMAHA forms a binuclear complex with weak interactions between the ferric centres. It is noteworthy that similar theoretical conformational preferences were found for DOCYDHAMA and PIPDHAMA ferric complexes, in which distances between the ferric centres were ca 8.5 Å and 7.7 Å, respectively. The lower stability associated with the structure with the monobridged coordination mode (b) should be mainly due to the existence of some steric strain involved in two ligand molecules, each one tetracoordinate to the same metal centre.

Electrochemistry of the Fe_2L_3 Complex: Cyclic voltammetry studies were carried out for the iron-DACODMAHA system in aqueous solution ($C_{Fe} = 2.5 \times 10^{-4}$ M) containing a 20-fold ligand excess, at pH = 7.0. A cathodic peak and the corresponding anodic counterpart were found. Analysis of the scan-rate effect on the voltammograms suggested a global mechanism involving an electrochemical reversible step (*E*) followed by an irreversible chemical reaction (*C*), perhaps a dissociation. In fact, the diagnostic criteria for (*EC*) global mechanisms are followed because: E_p^c shifts cathodically by around 30/*n* mV (16 mV) for a tenfold increase on *v*, for low scan rates; $i_p/v^{1/2}$ is virtually constant, in the absence of adsorption ($v < 5$ V/s) and the i_p^a/i_p^c ratio approximates to unity with increasing scan rate. The electrochemical reaction should involve a two-electron transfer because for $v = 20$ V/s, where the chemical reaction practically has no time to occur, $\Delta E_p = 30$ mV ($\Delta E_p = 60/n$ for a reversible reaction).[40,41]

This two-electron transfer agrees with $Fe_2H_3L_3$ being the major species at pH = 7 and the expected change of one electron per ferric centre. The fact that E_p^c presented a cathodic shift with increasing pH (pH = 5−8), as a linear variation with a slope of ca 60 mV indicates that the global electrochemistry reaction involves the transfer of two electrons and two protons. On the other hand, the independence of E_p^a and E_p^c of the ligand concentration (C_L/C_{Fe} = 10−30) indicates that both the reduced and oxidized complexes have the same coordination number in relation to the ligand. Thus, the global electrochemical reaction can be represented by the equilibrium Equation (1). The overall stability constant for the reduced species was derived from Equation (2), by the same approach as reported previously.[6,42]

$$[Fe_2^{III}H_3L_3]^{3+} + 2H^+ + 2\bar{e} \rightleftharpoons [Fe_2^{II}H_5L_3]^{3+} \quad (1)$$

$$E_p^c - E_p^s = -\frac{59.15}{2} \times \log\frac{\beta^{III}_{Fe_2H_3L_3}}{\beta^{II}_{Fe_2H_5L_3}} - 59.15 \times pH\ (25\ ^\circ C) \quad (2)$$

The lower stability of the reduced complex ($\log \beta^{II}_{Fe_2H_5L_3} = 67.01$) relative to the oxidized one [$\log \beta^{II}_{Fe_2H_5L_3} = 86.65$) is consistent with the assumed easy dissociation of that species. The reduction potential obtained for the Fe^{III}-DACODMAHA system ($E_{1/2} = -502$ mV) is lower than the corresponding values for other dihydroxamate analogues and rhodotorulic acid[43] (see Table 2). This is not a surprising feature, however, in view of its lower affinity for the iron. Since this potential is closer to the range of physiological reducing agents such as NADH, the complex species is easily reduced and some differences in its possible biological activity are probable. Since many factors influence the biological activity of a siderophore, biological assays need to be done to evaluate the potential of this new siderophore model.

Conclusions

This study reports the preparation of a DACO derivative bearing two hydroxamate arms (DACODMAHA) and its complexation behaviour towards Cu^{II} and Fe^{III} in relation to that of previously reported analogues. With regard to its complexation with copper(II), this ligand can act as a tetradentate ligand, forming stable five-coordinate mononuclear complexes, with the involvement of amine/hydroxamate and H_2O coordination. In the case of iron(III), DACODMAHA-metal binding occurs exclusively through the hydroxamate groups, leaving the amine groups free for potential extra interactions. Although it can act as a tetradentate ligand towards Fe^{III}, forming a mononuclear species under acidic conditions, under conditions of ligand excess and around the physiological pH zone, the Fe^{III} coordination sphere can be completed by formation of a binuclear complex [$Fe_2(HL)_3$] with a triply ligand-bridged structure, in analogy with rhodotorulic acid. At neutral pH, that complex is a three-protonated species, with inherent charge effects, which should account for the lower stability of the DACODMAHA-Fe^{III} complexes, relative to other dihydro-

 © 2003 Wiley-VCH Verlag GmbH & Co. KGaA, Weinheim

xamate siderophore analogues reported previously. This effect is further reflected in the redox potential, which becomes more positive and therefore closer to the range of the physiological reducing agents.

Experimental Section

Chemicals: Analytical grade reagents were used as supplied. The solvents were dried by standard methods.[44] 1,5-Diazacyclooctane-*N*,*N*′-diacetic acid was synthesized as described previously.[15]

Potentiometric Measurements: The pH potentiometric titrations were conducted at 25.0 ± 0.1 °C and at constant ionic strength (0.1 M, KNO_3) by use of a Crison Digital 517 instrument with an Ingold U1330 glass electrode and an Orion 90−00.11 Ag/AgCl reference electrode. The electrode calibration was carried out daily by titration of a strong acid (HNO_3, 0.1 M) with a strong base (KOH, 0.1 M) at the same ionic strength to ensure that we obtained adequate responses in the studied pH range and to control the exact concentration of the ligand (Gran's method).[45] The ligand was weighed directly into the potentiometric cell ($C_L = 2.4 \times 10^{-3}$ M) and the Cu^{II} solution was pipetted from a stock solution of 0.1 M $Cu(NO_3)_2$ in HNO_3 (C_L/C_{Cu} = 1:1). Calculations from potentiometric data were performed with the aid of the superquad[18] program.

Spectrophotometric Measurements: All spectra were measured with a Lambda 9 Perkin−Elmer spectrophotometer at 25 °C and at constant ionic strength (I = 0.1 M, KNO_3). Solutions of the metal complexes were generated in situ by addition, to an excess of the ligand, of a standard metal ion nitrate solution: 5×10^{-2} M $Cu(NO_3)_2$ in HNO_3 (1M) and 1000 ppm $Fe(NO_3)_3$ in HNO_3 (0.5 M). The pH measurements were carried out by use of a 420A Orion pH-meter, equipped with an Orion 91−03 glass calomel combination electrode. The stability constants for the iron(III) complexes were evaluated from the spectrophotometric titration data, by use of the PSEQUAD[16] computer program and speciation curves with the SPEA program.[46]

Electrochemical Measurements: Cyclic voltammograms were recorded with a three-electrode system with a hanging mercury drop working electrode, a platinum auxiliary electrode, and a saturated calomel reference electrode (SCE). All measurements were performed by use of an autolab ecochemie instrument coupled with a computer running the GPES-3 program. The complex in study was generated in situ, in a solution of iron(III) ($C_{Fe} = 2.5 \times 10^{-4}$ M) with a 20-fold excess of ligand, at pH 7.0, with constant ionic strength (I = 1.0 M, KNO_3), thermostatted at 25 °C and degassed with N_2. The pH measurements were performed with a 420A Orion pH meter equipped with an Orion 91−03 combined electrode.

Other Measurements: ^{1}H NMR spectra were recorded with a Varian Unity 300 spectrometer at 25 °C. Chemical shifts are reported in ppm (δ) from internal references {tetramethylsilane (TMS) in $CDCl_3$ solutions and sodium 3-(trimethylsilyl)[2,2,3,3-$^2H_4$]propionate (DSS) in D_2O solutions}. EPR studies were performed with a Bruker ESP ER 200D spectrometer (X-band) in frozen D_2O solutions with 20% ethylene glycol to ensure a good glass (C_L/C_{Cu} = 1:1, $C_{Cu} = 6.0 \times 10^{-3}$ M, T = 100 K, modulation frequency 100 kHz; C_L/C_{Fe} = 3:2, $C_{Fe} = 1.0 \times 10^{-3}$ M, pD* = 7.0, T = 100 K, modulation frequency 100 kHz). The spectra were simulated with the EPR program (version 1.0 by Frank Neese)[47] to calculate the g and A parameters. IR spectra were recorded with a Perkin−Elmer 683 spectrophotometer. Melting temperatures were measured with a Kofler hot-stage apparatus and are uncorrected. Elemental analyses were performed on a Fifons EA1108 CHNF/O instrument. Mass spectra were performed in a VG TRIO-2000 GC/MS instrument.

1,5-Diazacyclooctane-*N*,*N*′-bis(*N*-methyl-*O*-benzyl-acetohydroxamic Acid) (DACODMAHA-Bz): 1-Ethyl-3,3-(dimethylaminopropyl)-carbodiimide (3.60 g, 19 mmol) was added to a solution of 1,5-diazacyclooctane-*N*,*N*′-diacetic acid (1.10 g, 4.7 mmol) and *O*-benzyl-*N*-(methyl)hydroxylamine (2.40 g, 14 mmol) in THF/H_2O (2:1). The pH was adjusted to a constant 4.8 and the mixture was stirred at room temperature for 12 h. The end of the reaction was detected by TLC. The reaction mixture was dissolved in ethyl acetate, washed with saturated NaCl solution and dried with Na_2SO_4. Purification with a silica gel column yielded the pure final product (0.51 g, η = 25%) as a pale oil. IR (film): $\tilde{\nu}$ = 1675 cm^{-1} (C=O). ^{1}H NMR ($CDCl_3$/TMS): δ = 1.96 (t, 4 H, $NCH_2CH_2CH_2N$), 3.01 (br. t, 4 H, $NCH_2CH_2CH_2N$), 3.20 (s, 6 H, CH_3), 3.46 (br. t, 4 H, $NCH'_2CH_2CH'_2N$), 4.01 (s, 4 H, NCH_2CO), 4.95 (s, 4 H, CH_2Ph), 7.39−7.49 (m, 10 H, Ph*H*) ppm. FAB-MS: m/z = 469 [M + 1].

1,5-Diazacyclooctane-*N*,*N*′-bis(*N*-methylacetohydroxamic Acid) (DACODMAHA): Pd/C (10%, 161 mg) was added to a solution of 1,5-diazacyclooctane-*N*,*N*′-bis(*N*-methyl-*O*-benzyl-acetohydroxamic acid) (0.48 g, 1.0 mmol) in dry methanol and the mixture was stirred under H_2 (1 atm) at room temperature for 4 h. After filtration of the solid residue, the solvent was evaporated under reduced pressure and the product was obtained as a white powder, which was then recrystallized from ethanol/acetonitrile (288 mg, η = 98%), m.p. 175 °C (dec.). IR (KBr): $\tilde{\nu}$ = 1640 cm^{-1} (C=O). ^{1}H NMR (D_2O/DSS): δ (ppm) 2.04 (m, 4 H, $NCH_2CH_2CH_2N$), 3.25 (br. s, 14 H, $NCH_2CH_2CH_2N$; CH_3), 4.00 (s, 4 H, NCH_2CO) ppm. (FAB-MS): m/z = 289 [M + 1]. $C_{12}H_{24}N_4O_4 \cdot 2H_2O$: calcd. C 44.43, H 8.70, N 17.27; found C 44.42, H 8.75, N 17.18.

Acknowledgments

The authors are grateful to the Fundação de Ciência e Tecnologia (FCT) and to the COST-D21−001 project program for financial support. One of the authors (M. A. S.) would like also to take the opportunity of Prof. Fraústo da Silva's jubilee to express her acknowledgment for all the encouragement given in introducing her into the bioinorganic chemistry area and for suggestions on biologically relevant ligands.

[1] J. B. Neilands, *J. Biol. Chem.* **1995**, *270*, 2672.
[2] A.-M. Albrecht-Gary, A. L. Crumbliss, in: *Iron Transport and Storage in Microroganisms, Plants and Animals* (Eds. A. Sigel, H. Sigel), Metal Ions in Biological Systems, vol. 35, M. Decker, New York, **1998**, p. 239.
[3] F. Aouad, A. Florence, Y. Zhang, F. Collins, C. Henry, R. J. Ward, R. R. Crichton, *Inorg. Chim. Acta* **2002**, *339*, 470−480.
[4] C. T. Supuran, A. Scozzafava, Matrix metalloproteinases (MMPs). In: *Proteinase and Peptidase Inhibition: Recent Potential Targets for Drug Development* (Eds. H. J. Smith, C. Simons), Taylor & Francis, London, New York, **2002**, pp. 35−61.
[5] M. Whittaker, C. D. Floyd, P. Brown, A. J. H. Gearing, *Chem. Rev.* **1999**, *99*, 2735−2776. D. A. Brown, H. Bogge, R. Coogan, D. Doocey, T. J. Kemp, A. Müller, B. Neumann, *Inorg. Chem.* **1996**, *35*, 1674.
[6] M. A. Santos, M. A. Esteves, M. C. T. Vaz, M. L. S Gonçalves, *J. Chem. Soc., Dalton Trans.* **1993**, 927−932.
[7] M. A. Esteves, M. C. T Vaz, M. L. S. Gonçalves, E. Farkas, M. A. Santos, *J. Chem. Soc., Dalton Trans.* **1995**, 2565−2573.
[8] M. Gaspar, R. Grazina, A. Bodor, E. Farkas, M. A. Santos, *J. Chem. Soc., Dalton Trans.* **1999**, 799−806.

 © 2003 Wiley-VCH Verlag GmbH & Co. KGaA, Weinheim

[9] M. Gaspar, M. A. Santos, K. Krauter, G. Winkelmann, *BioMetals* **1999**, *12*, 209−218. M. A. Santos, "Polyamino-Polyhydroxamic Acids as Siderophore Analogues", *Coordination Chemistry at the Turn of the Century* (Eds. G. Ondrejovic, A. Sirota), Slovac Technical University press, Bratislava, **1999**, p. 327−332.
[10] D. O. Nielson, M. L. Larsen, R. D. Willet, J. I. Legg, *J. Am. Chem. Soc.* **1971**, *93*, 5079. J. I. Legg, D. O. Nielson, D. Smith, M. L. Larson, *J. Am. Chem. Soc.* **1968**, *90*, 5030−5031.
[11] M. Y. Darengsbourg, I. Font, D. K. Mills, M. Pala, J. H. Reibenspies, *Inorg. Chem.* **1992**, *31*, 4965−4971. C. A. Grapperhaus, J. A. Bellefeuille, J. H. Rebenspies, M. Y. Darensbourg, *Inorg. Chem.* **1999**, *38*, 3698−3703.
[12] X.-H. Bu, M. Du, L. Zang, Z.-L. Shang, R.-H. Zhang, M. Shionoya,, *J. Chem. Soc., Dalton Trans.* **2001**, 729.
[13] X.-H. Bu, Z.-L. Shang, W. Weng, R.-H. Zhang, H.-P. Zhu, Q.-T. Liu, *Acta Chem. Scand.* **1999**, *53*, 295. M. Du, Z.-L. Shang, X.-B. Leng, X.-H. Bu, *Polyhedron* **2001**, *20*, 3065.
[14] W. K. Musker, *Coord. Chem. Rev.* **1992**, *117*, 133−157.
[15] J. R. Ascenso, M. A. Santos, J. J. R. Fraústo da Silva, M. C. Vaz, M. G. B. Drew, *J. Chem. Soc., Perkin Trans. 2* **1990**, 2211−2218.
[16] L. Zékány, I. Nagypál, in: *Computational Methods for the Determination of Stability Constants*" (Ed. D. Legget), Plenum, New York, **1985**.
[17] M. A. Santos, M. A. Esteves, M. C. Vaz, J. J. R. Fraústo da Silva, B. Noszal, E. Farkas, *J. Chem. Soc., Perkin Trans. 2* **1997**, 1977−1983.
[18] P. Gans, A. Sabatini, A. Vacca, *J. Chem. Soc., Dalton Trans.* **1985**, 1195.
[19] W. K. Musker, M. S. Hussain, *Inorg. Chem.* **1966**, *5*, 1416.
[20] K. Myoshi, H. Tanaka, E. Kimura, S. Tsuboyama, S. Murata, H. Shimizu, K. Ishizu, *Inorg. Chim. Acta* **1983**, *78*, 23.
[21] D. A. Brown, A. L. Roche, *Inorg. Chem.* **1983**, *22*, 2199−2202.
[22] R. Karlicek, V. Jokl, *Chem. Zvesti* **1980**, *34*, 762.
[23] D. F. Averill, J. I. Legg, D. L. Smith, *Inorg. Chem.* **1972**, *10*, 2344.
[24] B. Kurzak, K. Kurzak, J. Jezierska, *Inorg. Chim. Acta* **1986**, *125*, 77.
[25] B. Kurzak, E. Farkas, T. Glowiak, H. Kozlowski, *J. Chem. Soc., Dalton Trans.* **1991**, 163. E. B. Paniago, S. Carvalho, *Inorg. Chim. Acta* **1984**, *92*, 253.
[26] M. A. Santos, M. A. Esteves, M. C. T. Vaz, M. L. S. Gonçalves, *Inorg. Chim. Acta* **1993**, *214*, 47−53.
[27] M. A. Santos, M. Gaspar, M. T. Amorim, *Inorg. Chim. Acta* **1999**, *284*, 20−29.
[28] M. A. Santos, J. J. R. Fraústo da Silva, M. C. T. Vaz, *II Italian-Spanish Congress on Thermodinamics of Metal Complexes*, Palermo, Italy, **1991**.
[29] B. Kurzak, H. Kozlowski, E. Farkas, *Coord. Chem. Rev.* **1992**, *114*, 169−200.
[30] E. Farkas, H. Csóka, G. Micera, A. Dessi, *J. Inorg. Biochem.* **1997**, *65*, 281−286.
[31] S. J. Barclay, B. H. Huynh, K. N. Raymond, *Inorg. Chem.* **1984**, *23*, 2011.
[32] C. J. Carrano, K. N. Raymond, *J. Am. Chem. Soc.* **1978**, *100*, 5371.
[33] M. A. Santos, M. Gaspar, M. L. S. Gonçalves, M. T. Amorim, *Inorg. Chim. Acta* **1998**, *278*, 51−60.
[34] I. Spasojevic, S. K. Armstrong, T. J. Brickman, A. L. Crumbliss, *Inorg. Chem.* **1999**, *38*, 449−454.
[35] C. J. Carrano, S. R. Cooper, K. N. Raymond, *J. Am. Chem. Soc.* **1979**, *101*, 599.
[36] D. F. Evans, *J. Chem. Soc.* **1959**, 2003.
[37] CERIUS-2 Program, Version 3.0, Molecular Simulation Inc., Cambridge, **1998**.
[38] R. C. Scarrow, D. L. White, K. N. Raymond, *J. Am. Chem. Soc.* **1985**, *107*, 6540.
[39] Z. Hou, C. J. Sunderland, T. Nishio, K. N. Raymond, *J. Am. Chem. Soc.* **1996**, *118*, 5148.
[40] R. S. Nicholson, I. Shain, *Anal. Chem.* **1964**, *36*, 706.
[41] A. Weissberger, B. W. Rossiter, "Part II, Electrochemical Methods" E. R. Brown, R. F. Large, "Physical Methods of Chemistry", Wiley Interscience, New York, **1971**.
[42] D. DeFord, D. H. Hume, *J. Am. Chem. Soc.* **1951**, *73*, 532.
[43] K. N. Raymond, C. J. Carrano, *Acc. Chem. Res.* **1979**, *12*, 183.
[44] W. L. Almarego, D. D. Perin, "Purification of Laboratory Chemicals", 4th Edition, Butterworth−Heinemann Press, Oxford, **1999**.
[45] G. Gran, *Analyst* **1952**, *77*, 661.
[46] A. E. Martell, R. J. Motekaitis, "The Determination and Use of Stability Constants", VCH Publishers Inc., New York, **1988**.
[47] F. NEESE, EPR Program − A Modeling Approach, version 1.0; F. Martell, PhD Thesis, University of Konstanz, Department of Biology, 78434 Konstanz, Germany, **1993**.

Received March 21, 2003
Early View Article
Published Online October 2, 2003

 © 2003 Wiley-VCH Verlag GmbH & Co. KGaA, Weinheim

Preparation, Photo-luminescence and Electro-Luminescence Behavior of Langmuir−Blodgett Films of Bipyridylrhenium(I) Surfactant Complexes

Vivian Wing-Wah Yam,*[a] Bin Li,[a] Yu Yang,[a] Ben Wai-Kin Chu,[a] Keith Man-Chung Wong,[a] and Kung-Kai Cheung[a]

Keywords: Luminescence / Surfactants / Langmuir−Blodgett films / Rhenium

Several bipyridylrhenium(I) surfactant complexes, *fac*-[Re(CO)$_3$(bpy)(L)]PF$_6$ [bpy = 2,2′-bipyridine, L = *trans*-4-dodecyloxy-4′-stilbazole (**L1**), *trans*-4-octadecyloxy-4′-stilbazole (**L2**), 4-(4′-dodecyloxyphenylethynyl)pyridine (**L3**)] were synthesized and characterised. The X-ray crystal structure of *fac*-[Re(CO)$_3$(bpy)(**L1**)]PF$_6$ has been determined. The complexes exhibited intense photo-luminescence which has been ascribed to the dπ(Re) → π*(bpy) metal-to-ligand charge transfer (MLCT) triplet emission. The complexes were found to form stable Langmuir–Blodgett (LB) films with relatively high collapse pressures. The organic light-emitting diodes (OLEDs) fabricated by employing the LB films of various complexes as the emitting layer exhibited electroluminescence (EL) behavior. The luminances of the EL devices were found to vary as a function of the number of LB film layers, hydrocarbon chain length and the deposition types.
(© Wiley-VCH Verlag GmbH & Co. KGaA, 69451 Weinheim, Germany, 2003)

Introduction

Efficient electroluminescence (EL) from organic films at low voltages was first reported in 1987.[1] Since then, a variety of EL materials have been synthesised,[1,2] and various techniques for device fabrication have been optimised.[2f,3] Recent works on the fabrication of thin-film devices for organic light-emitting diodes (OLEDs) have mainly concentrated on the use of vacuum deposition,[1,3b,4] spin coating,[5] self-assembly[3g,6,7a] and Langmuir−Blodgett (LB) techniques.[7,8] The LB film technique is interesting in that it is possible to prepare organic functional ultra-thin films with controlled thickness of a molecular size and well-defined molecular orientation.[9] In some circumstances LB films may produce films of higher quality than the general vacuum deposited or spin-coat films and may have potential applications in molecular electronic devices.[9,10]

Employment of transition metal complexes as the emissive layer in OLEDs has become one of the important subjects in recent years,[5,11] since many of them have excellent photoluminescence properties and potential advantages of achieving a maximum internal quantum efficiency of 100%.[2f] The formation efficiency of the triplet state will be triple that of the singlet state in the non-geminate pair electron combination (as in ELs), thus an improvement in the EL yield should be predicted by using triplet state materials as the emitting layer, which makes them promising candidates for OLEDs, and a number of related studies have been reported.[5,11,12] Amongst the transition metal complexes studied, those of the bipyridylruthenium(II) systems, which show ^{3}MLCT emission, have been extensively studied.[5a,5b] Other relatively less studied systems involving ^{3}MLCT emissive states include the well-known tricarbonyl(diimine)rhenium(I) complexes.[13−15]

In order to explore the potential applications of metal-based ultra-thin films in the design and construction of molecular electronic devices and to better understand the mechanism of ELs displayed by transition metal complexes in LB films, it is important to design, fabricate, and study OLEDs using LB films of metal complexes as the emissive layer. However, little attention has been devoted to this area.[8] Herein we report the synthesis of luminescent bipyridylrhenium(I) complexes with long hydrocarbon chain-containing pyridine ligands, *fac*-[Re(CO)$_3$(bpy)(L)]PF$_6$ [bpy = 2,2′-bipyridine, L = *trans*-4-dodecyloxy-4′-stilbazole (**L1**), *trans*-4-octadecyl-4′-stilbazole (**L2**), 4-(4′-dodecyloxyphenylethynyl) pyridine (**L3**); Scheme 1]. The successful preparation of stable LB films of these complexes renders their employment as the emitting layer for OLED fabrication possible and such devices have been found to exhibit electroluminescence, typical of the ^{3}MLCT emission of diiminerhenium(I) complexes. The influence of various factors on the OLEDs performance involving LB films of the complexes has also been described.

[a] Center for Carbon-Rich Molecular and Nano-Scale Metal-Based Materials Research, Department of Chemistry, and HKU-CAS Joint Laboratory on New Materials, The University of Hong Kong,
Pokfulam Road, Hong Kong
Fax: (internat.) + 852-28571586
E-mail: wwyam@hku.hk

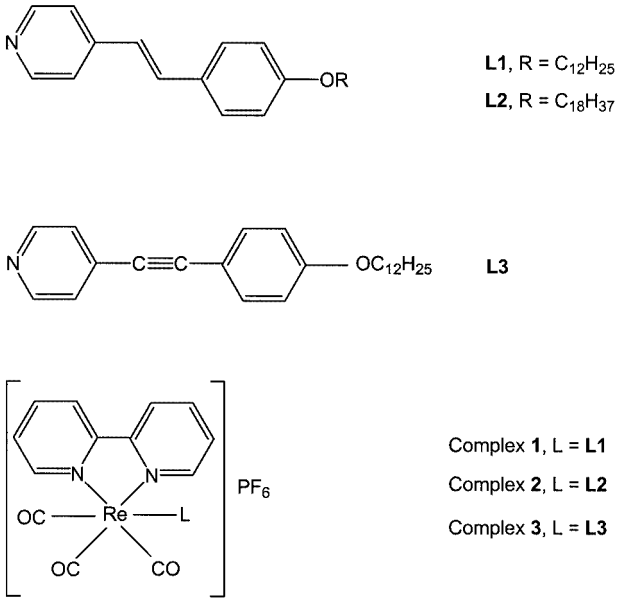

Scheme 1. Structures of ligands and corresponding surfactant Re^{I} diimine complexes

Results and Discussion

Synthesis and Characterization

The ligands **L1**,[16] **L2**,[16] **L3**[17] and the corresponding rhenium(I) complexes **1**, **2**, **3**[14e,18] were prepared according to literature methods, and their structures are shown in Scheme 1. The purity and composition of the rhenium(I) complexes were confirmed by ^{1}H NMR, IR spectroscopy, positive-ion FAB-MS and elemental analyses. The structure of **1** was determined by X-ray crystallography. The observation of three strong bands between 1900 and 2100 cm^{-1} in the infrared spectra for all rhenium(I) complexes confirms that the tricarbonyl Re^{I} moiety is in the facial arrangement.[19]

X-ray Crystal Structure

The perspective drawing of the complex cation of **1** with atomic numbering is shown in Figure 1, and selected bond lengths and angles are given in Table 1. The coordination geometry at the Re atom is distorted octahedral with the three carbonyl ligands arranged in a facial fashion. The N(1)−Re−N(2) angle of 75° is a result of the steric requirement of the bidentate diimine ligand. The C(19)−C(20) bond length of 1.342(8) Å and the bond angles of C(16)−C(19)−C(20) at 121.3(6)° and C(19)−C(20)−C(21) at 126.5(6)° are typical of the sp^2 hybridization of the styryl group. All other bond lengths and bond angles are unremarkable and are similar to those found for other related Re^{I} polypyridyl complexes.[14,19,20] The hydrophobic aliphatic chain is running along an axis that is almost perpendicular to the plane containing the Re atom and the bipyridine unit, which leads to the good LB film forming capability of the complexes.

Table 1. Selected bond lengths (Å) and angles (°) for **1**

Distances			
Re(1)−N(1)	2.171(5)	Re(1)−C(1)	1.919(7)
Re(1)−N(3)	2.230(4)	Re(1)−C(3)	1.930(8)
Re(1)−C(2)	1.941(8)	O(2)−C(2)	1.143(8)
O(1)−C(1)	1.148(7)	C(19)−C(20)	1.342(8)
O(3)−C(3)	1.145(7)	C(20)−C(21)	1.463(8)
Re(1)−N(2)	2.173(5)		
Angles			
N(1)−Re(1)−N(2)	75.0(2)	N(1)−Re(1)−C(2)	99.4(2)
N(1)−Re(1)−C(1)	95.1(2)	N(2)−Re(1)−N(3)	82.9(2)
N(1)−Re(1)−C(3)	173.8(2)	N(2)−Re(1)−C(2)	174.4(2)
N(2)−Re(1)−C(1)	93.9(3)	N(3)−Re(1)−C(1)	176.6(3)
N(2)−Re(1)−C(3)	98.8(3)	N(3)−Re(1)−C(3)	93.4(2)
N(3)−Re(1)−C(2)	96.3(2)	C(1)−Re(1)−C(3)	86.1(3)
C(1)−Re(1)−C(2)	87.0(3)	C(16)−C(19)−C(20)	121.3(6)
C(2)−Re(1)−C(3)	86.7(3)	C(19)−C(20)−C(21)	126.5(6)
N(1)−Re(1)−N(3)	85.0(2)	C(20)−C(21)−C(22)	124.6(5)

Surface Pressure−Area (π−A) Isotherms and LB Film Deposition

The π−A isotherms of the Re^{I} complexes which spread from chloroform solutions onto ultrapure water at room temperature were recorded, and are shown in Figure 2. The curves show one well-defined condensed region.

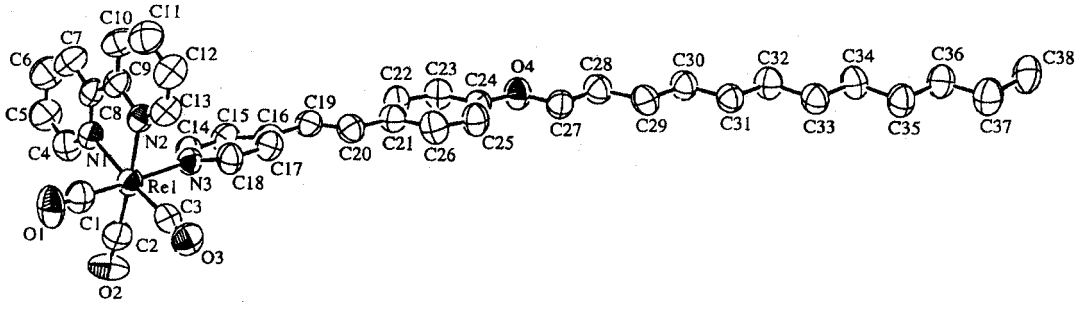

Figure 1. Perspective drawing of the complex cation of **1** with atomic numbering scheme; hydrogen atoms were omitted for clarity; the thermal ellipsoids are shown at the 50% probability level

 © 2003 Wiley-VCH Verlag GmbH & Co. KGaA, Weinheim

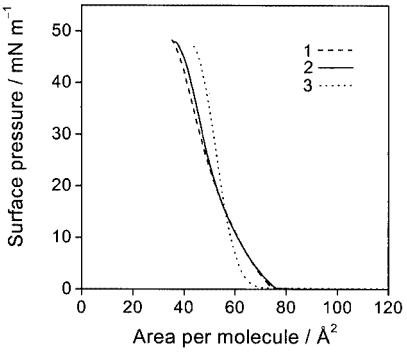

Figure 2. Surface pressure-area (π−A) isotherms of **1** (− − −), **2** (···) and **3** (---)

The molecular areas for these Re^I complexes are obtained by the extrapolation of the condensed region to zero surface pressure. The data are summarized in Table 2. It is worth noting that these complexes have similar π−A isotherms with fairly high collapse pressures as a result of the similarity in their structures.

Table 2. LB film-forming properties for complexes **1**−**3**

Complex	Molecular area (Å)^2	Collapse pressure (mN m^{-1})	Transfer ratio
1	61.5	48	0.65−1
2	60.5	49	0.80−1
3	62	48	0.65−1

The almost identical molecular areas of 61 Å^2 for these Re^I complexes match fairly well with the calculated value of 55 Å^2 based on the crystal structure of **1**. This indicates the formation of a close-packed stable monolayer at the air-water interface, probably with the long alkyl chain vertically oriented with respect to the water surface, resulting in almost no change in the area per molecule upon increasing the chain length of the hydrocarbon. Despite **1** and **3** only containing 12 -CH_2- units, their LB film-forming properties are good and similar to those of **2** which has an alkyl chain

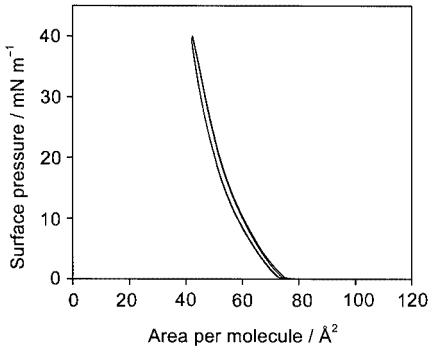

Figure 3. Compression-expanding isotherms for **1**

of 18 -CH_2- units. The formation of stable LB films with relatively short hydrocarbon chains may be advantageous in that it may minimize the resistance of the LB films in the construction of the OLED devices. The compression-expanding cycle isotherms of **1** are shown in Figure 3. No obvious hysteresis was observed, further confirming the good monolayer forming properties of the complexes.

UV/Vis Absorption Spectroscopy

The electronic absorption spectra of **1**−**3** in dichloromethane and in LB films show a high-energy absorption band at ca. 248 nm and a low-energy absorption band at ca. 364−370 nm. The high-energy absorption band is tentatively assigned as a π → π* intra-ligand transition (IL) of bipyridine. With reference to previous spectroscopic studies of the related cationic diiminerhenium(I) complexes, $[Re(CO)_3(diimine)(pyridine)]^+$,[13,14] which also exhibit a low-energy absorption band in a similar region, the low-energy absorption is ascribed to the dπ(Re) → π*(bpy) metal-to-ligand charge transfer (MLCT) transition. However, the extinction coefficients of these low-energy absorption bands in the order of 10^4 dm^3 mol^{-1} cm^{-1} in complexes **1**−**3** are much larger than those for typical MLCT transitions (approx. 10^3 dm^3 mol^{-1} cm^{-1}). In view of the similar absorption energies and extinction coefficients of the free ligands **L1**, **L2** and **L3**, the low-energy absorption band of **1**−**3** is accordingly assigned as an admixture of π → π* IL transitions of **L1**, **L2** and **L3** and dπ(Re) → π*(bpy) MLCT transitions.

Photoluminescence Properties

Complexes **1**−**3** exhibit intense greenish yellow luminescence in solution, solid state and as an LB film. The emission data for the complexes are summarized in Table 3. In general, the emission spectra of the complexes in dichloromethane and in an LB film at room temperature show broad emission bands at ca. 527−548 nm. On the basis of the previous spectroscopic assignments on the related cationic diiminerhenium(I) complexes, $[Re(CO)_3(diimine)(pyridine)]^+$,[13,14] the emission origin is assigned to be derived from the ^{3}MLCT excited state. The emission energies of the complexes in glass at 77 K were found to be blue-shifted with respect to those in solution and in LB films, and are attributed to the phenomenon of luminescence rigidochromism.[21] The emission spectra of **1** in dichloromethane and in LB films at room temperature and in EtOH/MeOH (4:1 v/v) glass at 77 K are shown in Figure 4. It is noteworthy that the luminescence quantum yield (Φ_{lum}) of **3** in fluid solution is larger than those of **1** and **2** by one order of magnitude. The lower luminescence quantum yield observed in **1** and **2** is probably due to the presence of the energy-accepting *trans*-styryl group, which would provide an additional non-radiative decay pathway for the quenching of the ^{3}MLCT excited state via an intramolecular energy transfer process, rendering the lower luminescence quantum yield. Similar observation has also been reported in the related azo- or styryl-containing rhenium(I) complexes.[15g]

 © 2003 Wiley-VCH Verlag GmbH & Co. KGaA, Weinheim

Table 3. Photophysical and EL data for complex **1**−**3**

Complexes	Medium (*T*/K)	Absorption λ_{max}/nm ($\varepsilon \times 10^{-4}$/dm^3 mol^{-1}cm^{-1})	Emission λ_{em}/nm (τ_o/μs)	Luminescence quantum yield ($\Phi_{lum} \times 10^3$)	EL Luminance (cd/cm^2)[a]
1	CH_2Cl_2 (298), LB film (298), Glass[b] (77)	248 (3.38), 282 (2.12), 310 (1.83), 322 (1.80), 370 (3.91) 324, 368	539 (0.66) 527 499	6.9	6
2	CH_2Cl_2 (298), LB film (298), Glass[b] (77)	248 (3.57), 282 (2.22), 312 (1.92), 320 (2.09), 370 (3.92) 324, 366	540 (0.70) 530 492	5.7	1
3	CH_2Cl_2 (298), LB film (298), Glass[b] (77)	248 (3.29), 280 (2.12), 311 (1.98), 322 (2.56), 364 (4.44) 324, 354	548 (0.93) 546 491, 528, 555	78.0	<1

[a] ITO/LB film (25-layer)/Al. [b] EtOH/MeOH (4:1, v/v).

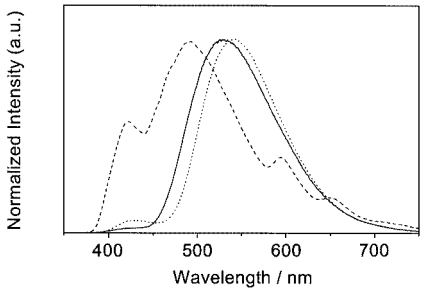

Figure 4. Normalized emission spectra of **1** (---) in EtOH/MeOH (4:1 v/v) glass at 77 K; (− − −) in 25-layer LB film; (···) in CH_2Cl_2

Electroluminescence Properties

The rhenium(I) surfactant complexes were deposited as Y-type LB films and were used as the emissive layer in single-layer OLED devices (ITO/LB film/Al; Scheme 2). An LB film thickness of at least 10 monolayers was required to prevent the possibility of a short circuit between the ITO and the aluminium electrode. Upon being forward biased with ITO at positive polarity in a continuous DC mode, the EL devices with a 25-layer LB film of **1**−**3** exhibit yellow electroluminescence (EL) with turn-on voltages of ca. 10 V. The close resemblance of the EL and PL spectra suggests that the EL of these rhenium(I) surfactant complexes involves the same excited state as PL, i.e. the triplet MLCT state or exciton. Upon forward bias, holes injected from ITO and electrons from Al migrate in the LB films and EL is generated upon recombination form excitons. The EL and PL spectra of **1** in a 25-layer LB film are shown in Figure 5.

Scheme 2. Configuration of EL cells

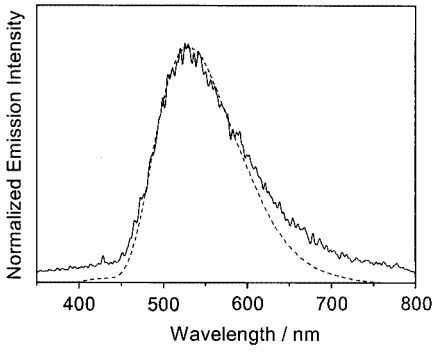

Figure 5. EL (−) and PL (···) spectra of **1** in 25-layer LB films

The EL intensity was found to vary as a function of the number of monolayers in the LB films and the relationship between the LB film layer number and the luminance of the EL devices of **1** is summarized in Table 4. The EL intensity increases with increasing layer numbers in the range of 10−20 layers, reaching a maximum at ca. 20−30 layers and then decrease upon further increase in the layer numbers of 30−40 and beyond. The EL behavior was hardly detectable for the device with an 80-layer LB film. Upon increasing the number of LB film layers, two opposite effects governing EL intensity come into effect. One is an increase in the concentration of charge carriers (both hole and electron) generated by applying DC voltage and hence an increase in the recombination probability, leading to the intensification of EL luminance. The other is an increase in the energy loss for the charge carriers passing through the LB layers, due to the larger resistance across the LB film, resulting in the diminishing of the EL intensity. For devices with 20 layers or less, it is likely that the first effect plays a more important role with such a short distance and the EL intensity is therefore increased. When the number of layers increases further (> 30 layers), the charge carrier concentration reaches a saturation level. On the other hand, fewer charge carriers can pass through the LB layers as a result of the energy loss from the long distance transporting process. Eventually, the

Table 4. Layer number-luminance relations of the EL devices of **1**

Layer number	10	20	30	40	80
Luminance (cd/cm^2)	<1	5	6	3	<1

 © 2003 Wiley-VCH Verlag GmbH & Co. KGaA, Weinheim

EL intensity drops for a device with greater than 30 LB film layers. A similar phenomenon has been reported for the EL device using LB films of bis[*N*-hexadecyl-8-hydroxy-2-quinoline carboxamide]cadmium as the emitting layer.[8e,22] Optimum EL efficiency of the present EL device is obtained for the LB film in the range of 20−30 layers. It is interesting to find that complex **1**, with the shorter hydrocarbon chain, shows a higher EL intensity than **2** by a factor greater than four for the same number of LB film layers. This may be attributed to the larger energy loss for the charge carriers transporting the LB film layers with higher resistance in the longer hydrocarbon chain of **2**.

On the other hand, the EL intensity is found to depend on the deposition types of the LB films. For example, an EL device constructed of a 25-layer LB film of complex **1** in the Y-type shows an approximately 180-fold increase in EL intensity relative to that of the same device in the Z-deposition type. It is likely that the head-to-head arrangement in LB films of rhenium(I) complexes may facilitate the charge transport processes, giving rise to better EL performance (Scheme 3).[23]

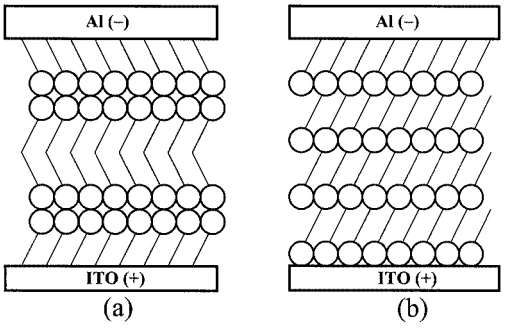

Scheme 3. Scheme of devices with different deposition types: (a) device in Y-type LB film; (b) device in Z-type LB film

In view of the poor stability of these single-layer devices, a double-layer configuration of ITO/PVK/LB film/Al was employed in order to improve the stability of the EL device. By taking advantage of the LB deposition technique which can control the deposition range, a device using the LB film of **1** was fabricated to cover only half of the area of the ITO glass. One half of the device is the ITO/PVK/Al (single-layer structure) and the other half is the ITO/PVK/**1**(LB film)/Al (double-layer structure). When the device was subjected to a forward bias using a DC power supply, the two halves of the device simultaneously emitted two different colors, a characteristic yellow EL coming from the ITO/PVK/**1**(LB film)/Al and a purple EL from the ITO/PVK/Al, typical of EL arising from PVK. In the double-layer device, PVK itself did not give rise to EL but rather acted as the hole transporting layer. The relatively even distribution of luminance indicates that uniform assemblies are formed by LB deposition on ITO/PVK. An improved performance was observed in the double-layer device. Relatively stable characteristic emission of the Re^{I} complex under the driving voltage of 7 V was observed and a maximum luminance of 9 cd/cm^2 at 18 V was achieved from the ITO/PVK/**1**(LB film)/Al device with a 25-layer LB film of **1**. The forward bias current could be obtained when the ITO electrode was positively biased and aluminium electrode negatively biased. The current increased when the forward bias voltage increased and the reverse current remained small when the ITO electrode was applied, a negative bias voltage and the Al electrode a positive bias. Figure 6 shows the current-voltage characteristics of the double-layer EL device of **1**.

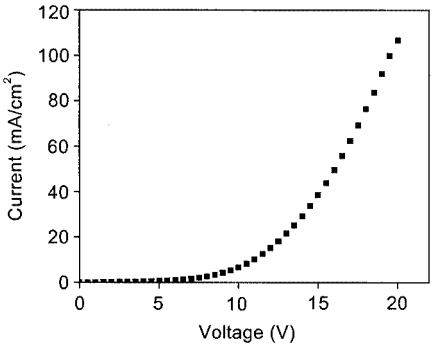

Figure 6. Current-voltage characteristics for the devices of [ITO/PVK/LB film/Al] for **1**

It is interesting to note that the luminance of the single layer device ITO/PVK/Al was 0.8 cd/m^2 when a driving voltage of 18 V was applied. Double-layer devices prepared other than using the LB technique of spin-coating of the rhenium complexes were also fabricated. The luminance of ITO/PVK:**1**/Al, ITO/PVK:**2**/Al and ITO/PVK:**3**/Al are 16, 0.7 and 0.3 cm/m^2, respectively, when the voltage applied is 18 V, similar to that obtained from LB deposition of the complexes.

Conclusions

Three Re^{I} bipyridyl surfactant complexes with hydrocarbon chain lengths of 12 and 18 were synthesised. Yellow luminescence was observed upon visible light excitation and attributed to ^{3}MLCT emission. All of them exhibit stable air-water interface behavior and are capable of forming stable multi-layer LB films on ITO substrates in an electroluminescence (EL) device. The LB films of these complexes were found to show EL behaviors with emission energies similar to those of the photo-luminescence. A decrease in the hydrocarbon chain length of the ligands in the complexes increases the EL intensity. The thickness and the deposition types of the LB films are shown to affect the luminance of the EL devices.

Experimental Section

Materials and Synthesis: 1-Bromododecane (97%, Lancaster), 1-bromooctadecane (98%, Lancaster) and $Re(CO)_5Cl$ (98%, Strem) were used as received. Piperidine (99%, Acros) was distilled over CaH_2. All other solvents for synthesis were of analytical grade and were used without further purification. The ligands **L1**,[16] **L2**,[16]

 © 2003 Wiley-VCH Verlag GmbH & Co. KGaA, Weinheim

L3[17] and the corresponding rhenium(I) complexes[14e,18] were prepared according to literature methods.

The Re^{I} complexes were prepared by reaction of [Re(bpy)-$(CO)_3(CH_3CN)$]OTf with the corresponding ligand L in THF solution.[14]

***fac*-[Re(CO)$_3$(bpy)(L1)]PF$_6$ (1):** Yellow crystalline solid. Yield: 85%. Mp: 155 °C. ^{1}H NMR (300 MHz, $CDCl_3$, relative to Me_4Si): δ = 9.06 (d, *J* = 5.3 Hz, 2 H, 6,6′-H of bpy), 8.59 (d, *J* = 8.1 Hz, 2 H, 3,3′-H of bpy), 8.30 (t, *J* = 7.9 Hz, 2 H, 4,4′-H of bpy), 7.93 (d, *J* = 5.6 Hz, 2 H, pyridyl H *ortho* to N), 7.72 (d, *J* = 6.5 Hz, 2 H, 5,5′-H of bpy), 7.42 (d, *J* = 8.2 Hz, 2 H, aryl H of **L1**), 7.31 (d, *J* = 5.9 Hz, 2 H, pyridyl H *meta* to N), 7.27 (d, *J* = 15.9 Hz, 1 H, −CH=CH−), 6.86 (d, *J* = 8.1 Hz, 2 H, aryl H of **L1**), 6.71 (d, *J* = 16.1 Hz, 1 H, −CH=CH−), 3.96 (t, *J* = 6.4 Hz, 2 H, $-OCH_2-$), 1.77 (m, 2 H, $-CH_2-$), 1.44 (m, 2 H, $-CH_2-$), 1.26 [m, 16 H, $-(CH_2)_8-$], 0.87 (t, *J* = 6.2 Hz, 3 H, $-CH_3$) ppm. UV/Vis [CH_2Cl_2 λ/nm (ε × 10^{-4}/dm^{3}mol^{-1}cm^{-1})]: 248 (3.38), 282 (2.12), 310 (1.83), 322 (1.80), 370 (3.91). UV/Vis (LB film, λ/nm): 324, 368. IR (Nujol): 2028 cm^{-1} (s) ν(CO), 1927 (s) ν(CO), 1918 (s) ν(CO). Positive FAB-MS: *m*/*z* = 792 [M$^+$], 427 [M − **L1**]$^+$. $C_{38}H_{43}F_6N_3O_4PRe$ (936.9): calcd. C 48.72, H 4.59, N 4.49; found C 48.40, H 4.42, N 4.25.

***fac*-[Re(CO)$_3$(bpy)(L2)]PF$_6$ (2):** Yellow crystalline solid. Yield: 84%. Mp: 142 °C. ^{1}H NMR (300 MHz, $CDCl_3$): δ = 9.07 (d, *J* = 5.4 Hz, 2 H, 6,6′-H of bpy), 8.54 (d, *J* = 8.2 Hz, 2 H, 3,3′-H of bpy), 8.27 (d, *J* = 7.9 Hz, 2 H, 4,4′-H of bpy), 7.95 (d, *J* = 6.7 Hz, 2 H, pyridyl H *ortho* to N), 7.73 (m, 2 H, 5,5′-H of bpy), 7.41 (d, *J* = 8.8 Hz, 2 H, phenyl H of **L2**), 7.31 (d, *J* = 6.7 Hz, 2 H, pyridyl H *meta* to N), 7.25 (d, *J* = 16 Hz, 1 H, vinyl H of **L2**), 6.85 (d, *J* = 8.8 Hz, 2 H, phenyl H of **L2**), 6.70 (d, *J* = 16 Hz, 1 H, vinyl H of **L2**), 3.95 (t, *J* = 6.5 Hz, 2 H, $-OCH_2-$), 1.77 (m, 2 H, $-CH_2-$), 1.43 (m, 2 H, $-CH_2-$), 1.25 [m, 28 H, $-(CH_2)_{14}-$], 0.87 (t, *J* = 6.4 Hz, 3 H, $-CH_3$) ppm. UV/Vis [CH_2Cl_2, λ/nm (ε × 10^{-4}/dm^{3}mol^{-1}cm^{-1})]: 248 (3.57), 282 (2.22), 312 (1.92), 320 (2.09), 370 (3.92). UV/Vis (LB film, λ/nm): 366. IR (Nujol): 2028 cm^{-1} (s) ν(CO), 1929 (s) ν(CO), 1919 (s) ν(CO). Positive FAB-MS: *m*/*z* = 877 [M]$^+$, 427 [M − **L2**]$^+$. $C_{44}H_{55}F_6N_3O_4PRe$ (1021.1): calcd. C 51.76, H 5.39, N 4.12; found C 51.50, H 5.35, N 3.83.

***fac*-[Re(CO)$_3$(bpy)(L3)]PF$_6$ (3):** Yellow-orange crystalline solid. Yield: 81%. ^{1}H NMR (300 MHz, $CDCl_3$): δ = 9.05 (d, *J* = 4.6 Hz, 2 H, 6,6′-H of bpy), 8.61 (d, *J* = 8.2 Hz, 2 H, 3,3′-H of bpy), 8.32 (m, 2 H, 4,4′-H of bpy), 8.02 (d, *J* = 6.7 Hz, 2 H, pyridyl H *ortho* to N), 7.73 (m, 2 H, 5,5′-H of bpy), 7.42 (d, *J* = 8.8 Hz, 2 H, phenyl H of **L3**), 7.33 (d, *J* = 6.7 Hz, 2 H, pyridyl H *meta* to N), 6.85 (d, *J* = 8.9 Hz, 2 H, phenyl H of **L3**), 3.96 (t, *J* = 6.5 Hz, 2 H, $-OCH_2-$), 1.77 (m, 2 H, $-CH_2-$), 1.44 (m, 2 H, $-CH_2-$), 1.25 [m, 16 H, $-(CH_2)_8-$], 0.87 (t, *J* = 6.6 Hz, 3 H, $-CH_3$) ppm. UV/Vis [CH_2Cl_2, λ/nm (ε × 10^{-4}/dm^{3}mol^{-1}cm^{-1})]: 248 (3.29), 280 (2.12), 311 (1.98), 322 (2.56), 364 (4.44). UV/Vis (LB film, λ/nm): 354. IR (Nujol): 2034 cm^{-1} (s) ν(CO), 1942 (s) ν(CO), 1909 (s) ν(CO), 2185(ν), 2219 (m) ν(C≡C). Positive FAB-MS: *m*/*z* = 790 [M]$^+$, 427 [M − **L3**]$^+$. $C_{38}H_{41}F_6N_3O_4PRe$ (934.9): calcd. C 48.82, H 4.39, N 4.49; found C 48.96, H 4.34, N 4.48.

Instrumentation and Physical Characterization: The UV/Vis spectra were obtained on a Hewlett−Packard 8452A diode array spectrophotometer, IR spectra as Nujol mulls on a Bio-Rad FTS-7 spectrophotometer. ^{1}H NMR spectra were recorded on a Bruker DPX-300 NMR spectrometer with chemical shifts reported relative to tetramethylsilane. Positive-ion fast-atom bombardment (FAB) mass spectra were recorded on a Finnigan MAT95 mass spectrometer. Elemental analyses were performed on a Carlo Erba 1106 elemental analyzer at the Institute of Chemistry, Chinese Academy of Sciences. Steady-state excitation and emission spectra were obtained on a Spex Fluorolog-2 111 spectrofluorometer with or without Corning filters. Low-temperature (77 K) spectra were recorded using an optical Dewar sample holder. The OLED devices were driven at room temperature in air with a DC power supply. The EL spectra were collected on an Oriel Instruments intensified charge-coupled device (ICCD) detector (Model DH520) and were analyzed using the InstaSpec V software. The emission signal was collected by an optical fiber and dispersed onto the CCD detector with an Oriel MultiSpec 115 imaging spectrograph (Model 77480). The system was operated at −15 °C by the single-stage system in order to reduce the dark current signal. The luminance of the OLED devices was measured with a Minolta LS-110 luminance meter. The current-voltage (*I*−*V*) characteristics were studied by a Keithley 2400 autoranging sourcemeter.

X-ray Crystal Structure Determination: Crystals of **1** were obtained by slow diffusion of diethyl ether vapour into a chloroform solution of the complex. A yellow needle-shaped crystal of dimensions of 0.35 × 0.25 × 0.15 mm was used for data collection at 28 °C on a Rigaku AFC7R diffractometer with graphite monochromated Mo-K_α radiation (λ = 0.71073 Å). The space group was uniquely determined based on systematic absences and the structure was solved by direct methods (SIR92)[24a] and expanded by Fourier method and refinement by full-matrix least-squares using the software package TeXsan[24b] on a Silicon Graphics Indy computer. One crystallographic asymmetric unit consists of one formula unit. The F atoms were disordered and were placed at 12 positions with F(1) to F(12) having occupation numbers 0.87, 0.82, 0.52, 0.35, 0.64, 0.43, 0.44, 0.37, 0.49, 0.37, 0.44 and 0.26 respectively. In the least-squares refinement, 47 non-H atoms were refined anisotropically, the 12 disordered F atoms were refined isotropically, and 41 H atoms at calculated positions with thermal parameters equal to 1.3 times that of the attached C atoms were not refined. Crystal and structure determination data of **1** are collected in Table 5. CCDC-

Table 5. Crystal and structure determination data for **1**

Formula	$[C_{38}H_{41}N_3O_4Re]PF_6$
M_r (g·mol^{-1})	934.93
Crystal system	Monoclinic
Space group	$P2_1/a$ (No.14)
T, (K)	301
D_c (g cm^{-3})	1.564
V (Å^3)	3969(1)
Z	4
a (Å)	20.922(3)
b (Å)	9.104(2)
c (Å)	23.302(4)
α (deg)	90
β (deg)	116.573(2)
γ (deg)	90
F(000)	1864
Collection range	$2\theta_{max}$ = 52° (0 > *h* > 25; 0 > *k* > 11; −28 > *l* > 25)
Reflections collected	8553
Independent reflections	8321
Parameters	472
Goodness-of-fit	1.96
Final *R* indices	$R1 = 0.034$, $wR2 = 0.045$[a]
Largest difference peak/hole [e·Å^{-3}]	1.04/−0.66

[a] $w = 4\ F_o^2/\sigma^2(F_o)^2$, where $\sigma^2(F_o)2 = [\sigma^2(I) + (0.024\ F_o^2)^2]$ for 5066 reflections with $I > 3\sigma(I)$.

 © 2003 Wiley-VCH Verlag GmbH & Co. KGaA, Weinheim

208904 contains the supplementary crystallographic data for this paper. These data can be obtained free of charge via www.ccdc.cam.ac.uk/conts/retrieving.html or from CCDC, 12 Union Road, Cambridge CB2 1EZ, UK [Fax: (internat.) +44-1223/336-033; E-mail: deposit@ccdc.cam.ac.uk].

LB Film Preparation and OLED Device Fabrication: Indium tin oxide (ITO) glass slides with a sheet resistance of about 30 Ω/□ were used as the positive electrode of the OLEDs. The cleaning procedure included sonication in detergent for 30 min and acetone for 30 min, rinsing in de-ionized water and isopropyl alcohol, boiling in $CHCl_3$, treatment by UV-ozone exposure, and repeated rinsing with copious amounts of ultrapure water.[25] The cleaned ITO-coated glass slides present good hydrophilic properties. The quartz substrates were cleaned by well-known standard procedures.[15j] The complexes in chloroform with concentrations of 1.00 mg cm^{-3} were spread onto a pure water sub-phase with a conductivity of 18 MΩ cm (pH, 5.6, 20 °C) using a Nima model-622 computer-controlled trough. After a 15 min. period to allow for the evaporation of chloroform, surface pressure-area (π−A) isotherms were recorded at a barrier compression speed of 150 cm^2 min^{-1}. The monolayers formed under a constant surface pressure of 25 mN m^{-1} were transferred onto hydrophilically treated substrates after maintaining the pressure constant at the transfer pressure for 10 min for stabilization, at a dipping speed of 15 mm min^{-1}. The transfer ratios of these complex films were between 0.6 and 1 (see Table 2). After the LB films were deposited, aluminium was deposited at 10^{-5} Torr to a thickness of 150 nm onto the LB film surface with a deposition rate of 1.0 nm s^{-1}. The devices ITO/[$Re(CO)_3$(bpy)(L)]PF_6/Al were obtained. The emitting area was 20 mm^2. For ITO/PVK/[$Re(CO)_3$(bpy)(L)]PF_6/Al, the [poly(9-vinylcarbazole) (PVK) layer was inserted between the LB films and the ITO electrode by spin casting solutions of PVK in $CHCl_3$ (5 mg/mL) onto the treated ITO-coated glass with a spin speed of 2400 rpm. The PVK surface is regarded as hydrophobic. The first monolayer was transferred onto a hydrophobic PVK surface on the down path. In the fabrication of double-layer devices using the spin-coating technique, the emissive layer was spin-coated onto ITO glass from a 1,1,2,2,-tetrachloroethane solution of the respective complex and PVK (10 mg:5 mg in 1 mL $C_2H_2Cl_4$) followed by deposition of aluminium by vacuum evaporation. The other procedures are the same as described above.

Acknowledgments

V. W. W. Y. acknowledges financial support from The University of Hong Kong Foundation for Educational Development and Research Limited, the Research Grants Council of the Hong Kong Special Administrative Region, China (Project No. HKU 7123/00P) and the receipt of a Croucher Senior Research Fellowship from the Croucher Foundation. B. W. K. C. and K. M. C. W. are grateful for the receipt of University Postdoctoral Fellowships, both of which are administered by The University of Hong Kong. Special thanks are due to Dr. W.-K. Chan and Miss L. S.-M Lam for their assistance in the Al electrode deposition.

[1] C. W. Tang, S. A. Vanslyke, *Appl. Phys. Lett.* **1987**, *51*, 913−915.

[2] [2a] C. W. Tang, S. A. Vanslyke, C. H. Chen, *J. Appl. Phys. Lett.* **1989**, *65*, 3610−3616. [2b] N. C. Greenham, S. C. Moratti, D. D. C. Bradley, R. H. Friend, A. B. Holmes, *Nature* **1993**, *365*, 628−630. [2c] J. Kido, C. Ohtaki, K. Hongawa, K. Okuyama, K. Nagai, *Jpn. J. Appl. Phys.* **1993**, *32*, L917−L920. [2d] C. Hosokawa, H. Higashi, H. Nakamura, T. Kusumoto, *Appl. Phys. Lett.* **1995**, *67*, 3853−3855. [2e] H. Tokuhisa, M. Era, T. Tsutsui, *Appl. Phys. Lett.* **1998**, *72*, 2639−2641. [2f] M. A. Baldo, D. F. O'Brien, Y. You, A. Shoustikov, S. Sibley, M. E. Thompson, S. R. Forrest, *Nature* **1998**, *395*, 151−154. [2g] U. Mitschke, P. Bauerle, *J. Mater. Chem.* **2000**, *10*, 1471−1507. [2h] F. G. Gao, A. J. Bard, *J. Am. Chem. Soc.* **2000**, *122*, 7426−7427. [2i] S. Lamansky, P. Djurovich, D. Murphy, F. Abdel-Razzaq, H. E. Lee, C. Adachi, P. E. Burrows, S. R. Forrest, M. E. Thompson, *J. Am. Chem. Soc.* **2001**, *123*, 4304−4312.

[3] [3a] A. Stocking, *Science* **1996**, *273*, 884−888. [3b] P. E. Burrows, V. Bulovic, G. Gu, V. Kozlov, S. R. Forrest, M. E. Thompon, *Thin Solid Films* **1998**, *331*, 101−105. [3c] T. Justel, T. H. Nikol, C. Ronda, *Angew. Chem. Int. Ed.* **1998**, *37*, 3085−3103. [3d] V. E. Choong, S. Shi, J. Curless, C. L. Shieh, H. C. Lee, J. Shen, J. Yang, *Appl. Phys. Lett.* **1999**, *75*, 172−174. [3e] G. Gu, G. Parthasarathy, P. Tian, P. E. Burrows, S. R. Forrest, *Appl. Phys. Lett.* **1999**, *86*, 4067−4075. [3f] C. J. Liang, D. Zhao, Z. R. Hong, D. X. Zhao, X. Y. Liu, W. L. Li, J. B. Peng, J. Q. Yu, C. S. Lee, S. T. Lee, *Appl. Phys. Lett.* **2000**, *76*, 67−69. [3g] J. Cui, Q. L. Huang, Q. W. Wang, T. J. Marks, *Langmuir* **2001**, *17*, 2051−2054. [3h] J. Cui, A. C. Wang, N. L. Edleman, J. Ni, P. Lee, N. R. Armstrong, T. J. Marks, *Adv. Mater.* **2001**, *13*, 1476−1480. [3i] Z. R. Hong, C. J. Liang, R. G. Li, W. L. Li, D. Zhao, D. Fan, D. Y. Wang, B. Chu, F. X. Zang, L. S. Hong, S. T. Lee, *Adv. Mater.* **2001**, *13*, 1241−1245.

[4] [4a] J. H. Burroughes, D. D. C. Bradley, A. R. Brown, R. N. Marks, K. Mackay, P. L. Burns, A. B. Holmes, *Nature* **1990**, *347*, 539−541. [4b] J. Kido, H. Hayase, K. Honogawa, K. Okuyama, K. Nagai, *Appl. Phys. Lett.* **1994**, *64*, 815−817. [4c] C. Vaterlein, H. Neureiter, W. Gebauer, B. Ziegler, M. Sokolowski, P. Bauerle, E. Umbach, *J. Appl. Phys.* **1997**, *82*, 3003−3013.

[5] [5a] F. G. Gao, A. J. Bard, *J. Am. Chem. Soc.* **2000**, *122*, 7426−7427. [5b] A. Wu, D. Yoo, J. K. Lee, M. F. Rubner, *J. Am. Chem. Soc.* **1999**, *121*, 4883−4891. [5c] V. W. W. Yam, C. L. Chan, S. W. K. Choi, K. M. C. Wong, E. C. C. Cheng, S. C. Yu, P. K. Ng, W. K. Chan, K. K. Cheung, *J. Chem. Soc., Chem. Commun.* **2000**, 53−54. [5d] Y. G. Ma, C. M. Che, H. Y. Chao, X. M. Zhou, W. H. Chan, J. C. Shen, *Adv. Mater.* **1999**, *11*, 852−857.

[6] [6a] J. K. Lee, D. Yoo, M. F. Rubner, *Chem. Mater.* **1997**, *9*, 1710−1712. [6b] M. Onoda, K. Yoshino, *Jpn. J. Appl. Phys.* **1995**, *34*, L260−L263. [6c] M. Onoda, K. Yoshino, *J. Appl. Phys.* **1995**, *78*, 4456−4462. [6d] H. Hong, D. Davidov, H. Chayet, E. Z. Faraggi, M. Tarabia, Y. Avny, R. Neumann, S. Kirstein, *Supramol. Sci.* **1997**, *4*, 67−73.

[7] [7a] E. Arias-Marin, J. C. Arnault, D. Guillon, T. Maillou, J. Le Moigne, B. Geffory, J. M. Nunzi, *Langmuir* **2000**, *16*, 4309−4318. [7b] R. Osterbacka, G. Juska, K. Arlauskas, A. J. Pal, K. M. Kalman, H. Stubb, *J. Appl. Phys.* **1998**, *84*, 3359−3363. [7c] R. Osterbacka, A. J. Pal, H. Stubb, *Thin Solid Films* **1998**, *327*, 668−670.

[8] [8a] Y. Hua, J. Peng, D. Cui, L. Li, Z. Xu, X. Xu, *Thin Solid Films* **1992**, *210*, 219−220. [8b] M. S. Weaver, D. G. Lidzey, M. A. Pavier, H. Mellor, S. L. Thope, D. D. C. Bradley, T. Richardson, T. M. Searle, C. H. Huang, H. Lui, D. Zhou, *Synth. Met.* **1996**, *76*, 91−93. [8c] A. P. Wu, T. Fujuwara, M. Jikei, M. A. Kakimoto, Y. Imai, T. Kubota, M. Iwamoto, *Thin Solid Films* **1996**, *284*, 901−903. [8d] J. M. Ouyang, L. Li, Z. H. Tai, Z. H. Lu, G. M. Wang, *Chem. Commun.* **1997**, 815−816. [8e] J. M. Ouyang, L. Li, Z. H. Tai, Z. H. Lu, G. M. Wang, *Chem. Lett.* **1997**, 199−204.

[9] F. L. Carter, " *Molecular Electronic Devices I* " Dekker, New York, **1982**.

[10] M. Schmelzer, S. Roth, C. P. Niesert, F. Effenberger, R. Li, *Thin Solid Films* **1993**, *235*, 210−214.

[11] [11a] Y. Koide, Q. W. Wang, J. Cui, D. D. Benson, T. J. Marks, *J. Am. Chem. Soc.* **2000**, *122*, 11266−11267. [11b] E. S. Handy, A. J. Pal, M. F. Rubner, *J. Am. Chem. Soc.* **1999**, *121*, 3525−3528. [11c] X. Gong, P. K. Ng, W. K. Chan, *Adv. Mater.* **1998**, *10*, 1337−1340. [11d] W. K. Chan, P. K. Ng, X. Gong, S. J. Hou, *Appl. Phys. Lett.* **1999**, *75*, 3920−3922. [11e] Y. G. Ma,

 © 2003 Wiley-VCH Verlag GmbH & Co. KGaA, Weinheim

X. Zhou, J. Shen, H. Y. Chao, C. M. Che, *Appl. Phys. Lett.* **1999**, *74*, 1361−1363. [11f] J. K. Lee, D. S. Yo, E. S. Handy, M. F. Rubner, *Appl. Phys. Lett.* **1996**, *69*, 1686−1688. [11g] Y. Q. Li, Y. Wang, Y. Zhang, Y. Wu, J. C. Shen, *Synth. Met.* **1999**, 257−260.

[12] [12a] M. A. Baldo, S. Lamansky, P. E. Burrows, M. E. Thompson, S. R. Forrest, *Appl. Phys. Lett.* **1999**, *75*, 4−6. [12b] C. H. Lyons, E. D. Abbas, J. K. Lee, M. F. Rubner, *J. Am. Chem. Soc.* **1998**, *120*, 12100−12107.

[13] [13a] A. Juris, V. Balzani, F. Barigelletti, S. Campagna, P. Belser, A. V. Zelewsky, *Coord. Chem. Rev.* **1988**, *84*, 85−277. [13b] D. J. Stufkens, A. Vlcek, *Coord. Chem. Rev.* **1998**, *171*, 93−105. [13c] V. W. W. Yam, K. K. W. Lo, K. M. C. Wong, *J. Organomet. Chem.* **1999**, *578*, 3−30. [13d] M. D. Ward, F. Barigelletti, *Coord. Chem. Rev.* **2001**, *216*, 127−154.

[14] [14a] M. S. Wrighton, D. L. Morse, *J. Am. Chem. Soc.* **1974**, *96*, 998−1003. [14b] G. Sprintschnik, H. W. Sprintschnik, P. P. Kirsch, D. G. Whitten, *J. Am. Chem. Soc.* **1976**, *98*, 2337−2338. [14c] J. C. Luong, L. Nadjo, M. S. Wrighton, *J. Am. Chem. Soc.* **1978**, *100*, 5790−5795. [14d] S. M. Fredericks, J. C. Luong, M. S. Wrighton, *J. Am. Chem. Soc.* **1979**, *101*, 7415−7417. [14e] R. H. Schmehl, L. G. Whiteside, D. G. Whitten, *J. Am. Chem. Soc.* **1981**, *103*, 3761−3764. [14f] J. V. Caspar, T. J. Meter, *J. Phys. Chem.* **1983**, *87*, 952−957. [14g] P. Chen, R. Duesing, G. Tapolsky, T. J. Meyer, *J. Am. Chem. Soc.* **1989**, *111*, 8305−8306. [14h] W. M. Xue, N. Goswami, D. M. Eichhorn, P. L. Orizondo, D. P. Rillema, *Inorg. Chem.* **2000**, *39*, 4460−4467.

[15] [15a] V. W. W. Yam, V. C. Y. Lau, K. K. Cheung, *Organometallics* **1995**, *14*, 2749−2753. [15b] V. W. W. Yam, V. C. Y. Lau, K. K. Cheung, *J. Chem. Soc. Chem. Commun.* **1995**, *259*, 1195−1195. [15c] V. W. W. Yam, K. M. C. Wong, V. W. M. Lee, K. K. W. Lo, K. K. Cheung, *Organometallics* **1995**, *14*, 4043−4036. [15d] V. W. W. Yam, K. K. W. Lo, K. K. Cheung, R. Y. C. Kong, *J. Chem. Soc. Chem. Commun.* **1995**, 1191−1193. [15e] V. W. W. Yam, V. C. Y. Lau, K. K. Cheung, *Organometallics* **1996**, *15*, 1740−1744. [15f] V. W. W. Yam, K. M. C. Wong, K. K. Cheung, *Organometallics* **1997**, *16*, 1729−1734. [15g] V. W. W. Yam, V. C. Y. Lau, L. X. Wu, *J. Chem. Soc., Dalton Trans.* **1998**, 1461−1468. [15h] V. W. W. Yam, V. C. Y. Lau, K. Z. Wang, K. K. Cheung, C. H. Huang, *J. Mater. Chem.* **1998**, *8*, 89−97. [15i] V. W. W. Yam, K. Z. Wang, C. R. Wang, Y. Yang, K. K. Cheung, *Organometallics* **1998**, *17*, 2440−2446. [15j] V. W. W. Yam, Y. Yang, H. P. Yang, K. K. Cheung, *Organometallics* **1999**, *18*, 5252−5258.

[16] D. W. Bruce, D. A. Dunmur, E. Lalinde, P. M. Maitlis, P. Stying, *Liq. Cryst.* **1988**, *3*, 385−395.

[17] A. EIGhayoury, L. Douce, R. Ziessel, *Liq. Cryst.* **1996**, *21*, 143−146.

[18] G. Tapolsky, R. Duesing, T. J. Meyer, *J. Phys. Chem.* **1989**, *93*, 3885−3887.

[19] P. J. Giordano, M. S. Wrighton, *J. Am. Chem. Soc.* **1979**, *101*, 2888−2897.

[20] S. A. Moya, J. Guerrero, R. Pastene, R. Schmidt, R. Sariego, R. Sartori, J. Sanzaparicio, I. Fonseca, M. Maertiez-ripoll, *Inorg. Chem.* **1994**, *33*, 2341−2346.

[21] [21a] T. G. Kotch, A. J. Lees, *Inorg. Chem.* **1993**, *32*, 2570−2575. [21b] S. A. Moya, R. Schmidt, U. Muller, G. Frenzen, *Organometallics* **1996**, *15*, 3463−3465.

[22] G. M. Wang, C. W. Yuan, H. M. Wu, Y. Wei, *Jpn. J. Appl. Phys.* **1995**, *34*, L182−L184.

[23] G. L. Zhong, K. Z. Yang, *Langmuir* **1998**, *14*, 5502−5506.

[24] [24a] *SIR92:* A. Altomare, M. Cascarano, C. Giacovazzo, A. Guagliardi, M. C. Burla, G. Polidori, M. Camalli, *J. Appl. Cryst.* **1994**, *27*, 435−439. [24b] TeXsan: *Crystal Structure Analysis Package*; Molecular Structure Corporation. The Woodlands TX, **1985** and **1992**.

[25] M. G. Mason, L. S. Hung, C. W. Tang, S. T. Lee, K. W. Wong, W. Wang, *J. Appl. Phys.* **1999**, *86*, 1688−1692.

Received April 16, 2003
Early View Article
Published Online October 2, 2003

 © 2003 Wiley-VCH Verlag GmbH & Co. KGaA, Weinheim

Synthesis, Structure and Characterization of New Olivacine Derivatives and Their Platinum(II) Complexes

Anna Romaniewska,[a] Ryszard Jasztold-Howorko,[b] Andrzej Regiec,[b] Tadeusz Lis,[a] and Janina Kuduk-Jaworska*[a]

Keywords: Antitumor agents / Template synthesis / Platinum / Structure elucidation / Conformational analysis

Three unknown olivacine derivatives (L-OCH_3, L-OH, L-OAc) were synthesized according to a procedure that involves only a few steps, and used as ligands in the synthesis of neutral chelate platinum(II) complexes. The ligands, as well as their platinum complexes were spectroscopically characterized with IR, $^1H/^{13}C$ NMR and UV/Vis spectroscopic techniques. The solid state structures of two ligands (L-OCH_3, L-OAc) and one complex {[(L-OCH_3)$PtCl_2$]} were determined by X-ray diffraction. Molecular structure analysis of the ligands and the complex indicated that complexation resulted in a change in the conformation of the bipyridine fragment of the compounds studied and caused other interesting effects. Two crystallographically independent molecules of the complex were revealed in the measured crystal, with short intramolecular H···H distances. The structural and energetic aspects of the conformational behavior of the ligand L-OCH_3 and the complex [(L-OCH_3)$PtCl_2$] have been analyzed using semiempirical PM3 methods. In vitro antiproliferative activity was preliminarily estimated.

(© Wiley-VCH Verlag GmbH & Co. KGaA, 69451 Weinheim, Germany, 2003)

Introduction

The quest for new antitumor agents among the platinum complexes is still active and seems to be deeply grounded because of the fact that two compounds from this group, cisplatin and carboplatin, belong to the most effective and widely used platinum anticancer drugs. However, there are limitations to their applicability because of the high level of resistance observed in various tumors.[1] Moreover, these drugs are cross-resistant to each other which may be as a result of their similarity as they are both compounds of type $[Pt(NH_3)_2X_2]$ and have the same neutral ligands.

The in vivo cisplatin resistance may be caused by three major mechanisms. Firstly, the intracellular concentrations of the drug may be lower as a result of increased efflux or blocked uptake. Secondly, the drug can be inactivated through the quenching of the monofunctional Pt-DNA adducts before the formation of cross-links through reaction with metallothioneins, glutathione or other intracellular ligands. Finally, the removal of the drug-DNA adducts may occur through cell-based repair, which includes nucleotide excision repair.[2] The need to circumvent these processes has led to a search for analogs which avoid the cross-resistance but achieve a similar level of effectiveness. Considering that carboplatin does not fulfil such requirements, probably because of the formation of DNA adducts identical to those formed by cisplatin, one strategy to overcome cisplatin (and carboplatin) resistance would be to employ platinum complexes with bulky neutral ligands that form very different types of DNA lesions and inhibit nucleotide excision repair.[3]

In fact, in vitro studies of complexes that have at least one neutral ligand that is bulkier than NH_3, such as aminocyclohexane or pyridine derivatives, showed diminished cross-resistance to cisplatin.[4,5]

Moreover, it has also been suggested that the bulkier ligand may inhibit the reactivity of the platinum drug with cellular glutathione and other sulfur donors in vivo, and in this way diminish the concentration of GSH-platinum complexes. These complexes are actively transported out of cells and contribute to cisplatin efflux.[6,7]

If the mode of resistance to cisplatin is the efficient repair of specific adducts, then the other effective means of circumventing such resistance might be to prepare platinum complexes with ligands that have intercalative properties.[8,9] This led to the idea of using three new olivacine derivatives (L-OCH_3, L-OH, L-OAc, Figure 1) as ligands in the neutral platinum(II) complexes.

Olivacine is an isomeric form of ellipticine, which is a well-known cytostatic that acts through intercalation. Ellipticine is used as an anticancer drug in the form of elliptinium acetate (Figure 2, **NMHE**).[10,11] Recently, a series of new very promising antitumor olivacine derivatives, such as 9-hydroxy-5,6-dimethyl-6*H*-pyrido[4,3-*b*]carbazole-1-*N*-

[a] Faculty of Chemistry, University of Wroclaw,
14 F. Joliot-Curie St., 50-383 Wroclaw, Poland
E-mail: radek@wchuwr.chem.uni.wroc.pl
[b] Faculty of Pharmacy, Wroclaw University of Medicine,
9 Grodzka Str., 50-137 Wroclaw, Poland

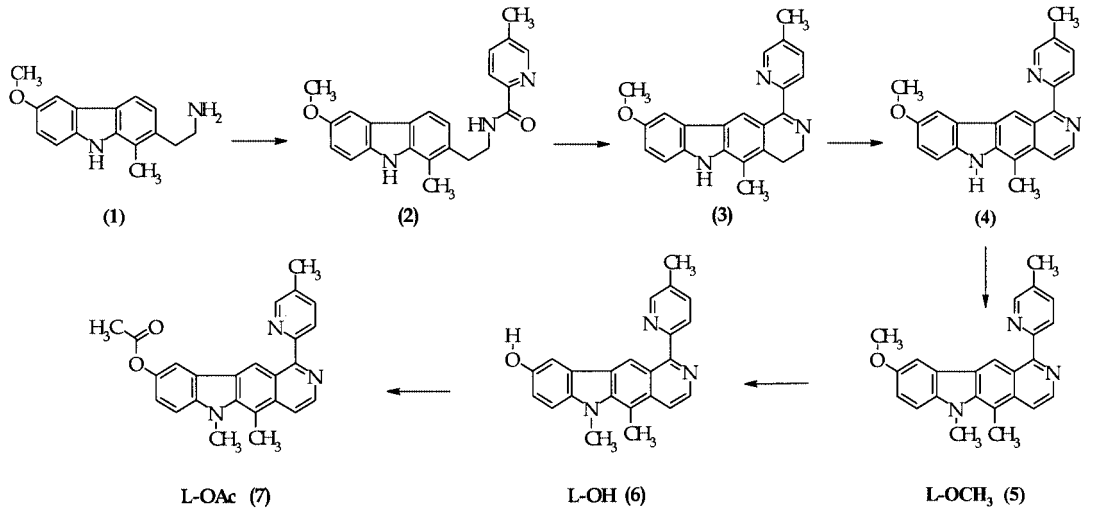

Figure 1. Synthetic pathway for the preparation of the ligands

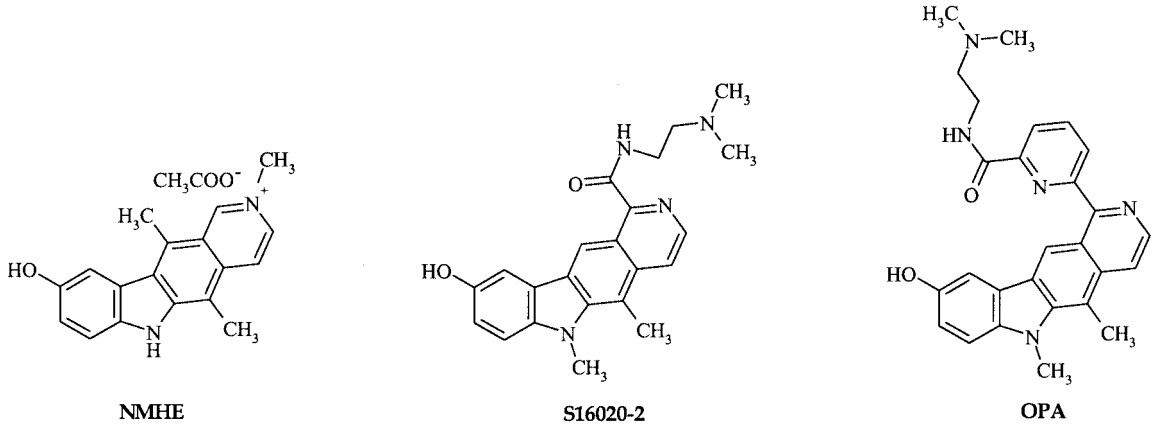

Figure 2. Ellipticine and olivacine derivatives: elliptinium acetate (**NMHE**); NSC-6596871 (**S16020−2**); olivacine picolinic amide (**OPA**)

(dimethylaminoethyl) carboxamide (Figure 2, **S16020−2**) and 6-(9-hydroxy-5,6-dimethyl)-6*H*-pyrido[4,3-*b*]carbazol-1-yl)picolinic (dimethylamino)ethylamide (Figure 2, **OPA**), has been synthesized and analyzed.[12−14]

The high antitumor activity of the above-mentioned olivacine derivatives encouraged us to search for new analogues which have already been preliminarily tested by us, and which have been shown to have significant cytotoxic activity in vitro.[15] In this paper, we present the synthesis of these analogues.

In Conclusion, we believe that the use of heterocyclic sterically hindered olivacine derivatives as ligands of metal complexes leads to a new group of effective platinum-containing cytostatics that would not be cross-resistant with the platinum-based drugs used so far.

Results and Discussion

Synthesis and Identification

Olivacine derivatives (L-OCH_3, L-OH, L-OAc) were synthesized as shown in Figure 1. The synthesis involved the use of 2-(6-methoxy-1-methylcarbazol-2-yl)ethylamine (**1**) as the starting compound, which was obtained according to an earlier procedure.[12] The reaction of **1** with 5-methyl-2-pyridinecarboxylic acid, and cyclization of the resulting new amide **2** using phosphorous oxychloride in boiling toluene, led to the formation of 9-methoxy-5-methyl-1-(5′-methylpyridin-2-yl)-3,4-dihydro-6*H*-pyrido[4,3-*b*]carbazole (**3**). This was aromatized to **4** by dehydrogenation over 10% palladium on charcoal in boiling diphenyl ether. *N*-6-methylation of **4** to (L-OCH_3) was then performed using an excess of dimethyl carbonate in dimethyl formamide, in the presence of potassium carbonate and 18-crown-6. Compound (L-OCH_3) was 9-*O*-demethylated to give 9-hydroxy-5,6-dimethyl-1-(5′-methylpyridin-2-yl)-6*H*-pyrido[4,3-*b*]carbazole (L-OH), by heating with a 48% aqueous solution of hydrobromic acid. The 9-hydroxy derivative, (L-OH), was allowed to react with a mixture of acetic anhydride/pyridine (1:1) at room temperature. This led to the formation of 9-acetoxy-5,6-dimethyl-1-(5′-methylpyridin-2-yl)-6*H*-pyrido[4,3-*b*]carbazole (L-OAc).

The new platinum(II) complexes, [(L-OCH_3)$PtCl_2$], [(L-OH)$PtCl_2$], [(L-OAc)$PtCl_2$], were prepared from K_2PtCl_4

 © 2003 Wiley-VCH Verlag GmbH & Co. KGaA, Weinheim

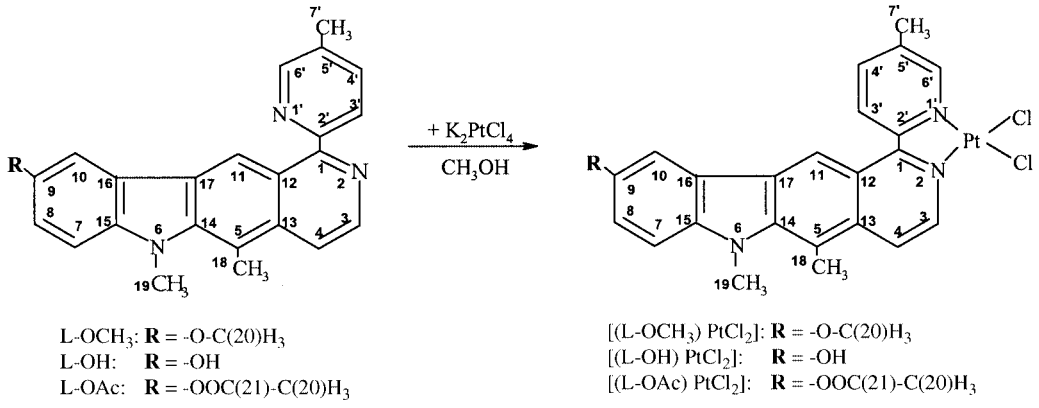

Figure 3. Scheme showing the formation of the complexes and the numbered atoms

and the olivacine derivatives, L-OCH_3, L-OH and L-OAc (Figure 3), respectively, according to a modified version of previously published methods.[16,17]

Chemical analyses, TLC, and spectroscopic techniques [MS (*m*/*z*), ^{13}C and/or ^{1}H NMR, UV/Vis, IR] were used for the characterization of the olivacine derivatives, as well as their platinum complexes. The platinum complexes were characterized additionally using electric conductivity measurements, which showed their neutral character. On the basis of the above physico-chemical studies, the molecular formulae of all the investigated compounds were postulated. The structures of the two ligands (L-OAc, L-OCH_3) and one platinum complex {[(L-OCH_3)$PtCl_2$]} were established by X-ray analysis. The structural and energetic aspects of the conformational behavior of the ligand/complex system have been analyzed.

FT-IR Characterization

The bands were assigned using literature data for the vibrational spectra of pyridine and its derivatives,[18−21] bipyridine,[22] carbazole derivatives [23] and platinum complexes.[24−35] Despite the general similarity of the spectra of the ligands, a few significant differences were noticed. Namely, only the IR spectrum of L-OH contains peaks that are characteristic for ν(C-OH) (at 1235 cm^{-1}) and for δ(O−H) (doublet at 852 and 843 cm^{-1} and band at 665 cm^{-1}). The IR spectrum of L-OAc shows a characteristic strong band at 1753 cm^{-1}, which is assigned to ν(C=O) of the 9-($OOCCH_3$) substituent, whereas the in the IR spectrum of L-OCH_3, a band at 2824 cm^{-1} is assigned to ν_s(C−H) of the OCH_3 group.

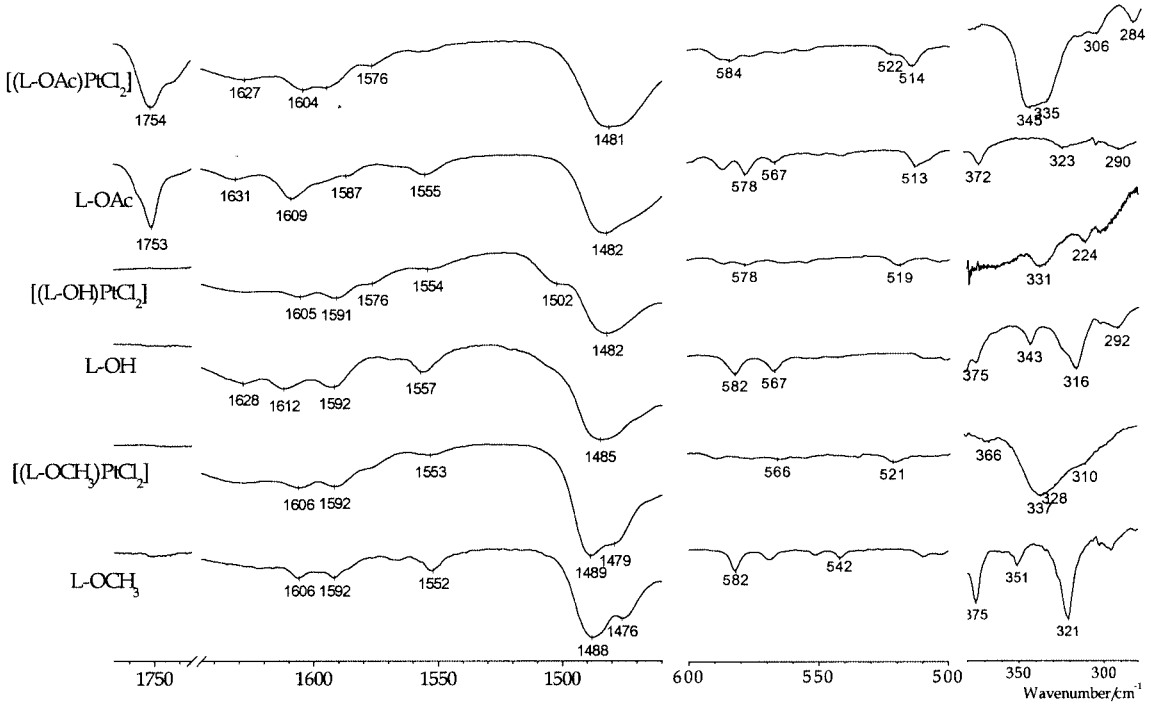

Figure 4. IR spectra of the ligands and Pt complexes

 © 2003 Wiley-VCH Verlag GmbH & Co. KGaA, Weinheim

After complexation, changes in the position and intensity of some of the above bands and the appearance of new bands are observed (Figure 4). The new bands in the complexes that appear in the range 514−521 cm^{-1} and 330−350 cm^{-1} are assigned to ν(py) + ν(Pt−N) and ν(Pt−Cl), respectively. We can also identify the new bands at around 300 cm^{-1} and below; they seem to occur as a result of the bending vibrations of the N−Pt−N and/or N−Pt−Cl bonds. In general, the IR results show that the N(1′) and N(2) atoms donate electron density to the Pt^{2+} ion that is simultaneously bonded to the Cl anions.

NMR Spectroscopic Characterization

The ^{1}H NMR spectroscopic data for the 9-olivacine derivatives (ligands) and their platinum complexes are listed in Table 1. The ^{13}C NMR spectroscopic data, which were gathered only for the ligands, are presented in Table 2. The atom (H and C) numbering is according to Figure 3. The ^{1}H NMR spectra of the 9-olivacine derivatives were recorded using CD_2Cl_2 and [D_7]DMF as solvents. CD_2Cl_2 was the more convenient solvent since its signals does not overlap those of the olivacine derivatives. However, the Pt

Table 1. Chemical shift values (δ [ppm]), integrals, and coupling constants (*J* [Hz]) in the ^{1}H NMR spectra of the ligands and their platinum complexes

	−**CH**$_3$				−**CH**								
Proton's number	7′	18	19	20	3	4	7	8	10	11	3′	4′	6′
L-OCH_3 (CD_2Cl_2)	2.49 s, 3H	3.12 s, 3H	4.13 s, 3H	3.89 s, 3H	8.52 d, 1H $J_{3,4}$ = 6.4	7.97 d, 1H $J_{4,3}$ = 6.2	7.31 d, 1H $J_{7,8}$ = 8.7	7.17 dd, 1H $J_{8,7}$ = 8.7 $J_{8,10}$ = 2.5	7.60 d, 1H $J_{10,8}$ = 2.5	9.15 s, 1H	7.90 d, 1H $J_{3',4'}$ = 8.2	7.75 dd, 1H $J_{4',3'}$ = 8.2 $J_{4',6'}$ = 1.9	8.69 s, 1H
L-OH (CD_2Cl_2)	2.43 s, 3H	3.08 s, 3H	4.05 s, 3H	−	8.51 d, 1H $J_{3,4}$ = 6.2	7.97 d, 1H $J_{4,3}$ = 6.2	7.12 d, 1H $J_{7,8}$ = 8.6	6.89 dd, 1H $J_{8,7}$ = 8.5 $J_{8,10}$ = 2.3	7.49 d, 1H $J_{10,8}$ = 2.2	9.00 s, 1H	7.91 d, 1H $J_{3',4'}$ = 7.8	7.76 dd, 1H $J_{4',3'}$ = 7.8 $J_{4',6'}$ = 1.5	8.61 s, 1H
L-OAc (CD_2Cl_2)	2.49 s, 3H	3.13 s, 3H	4.16 s, 3H	2.32 s, 3H	8.54 d, 1H $J_{3,4}$ = 6.3	7.98 d, 1H $J_{4,3}$ = 6.3	7.37 d, 1H $J_{7,8}$ = 8.6	7.25 dd, 1H $J_{8,7}$ = 8.7 $J_{8,10}$ = 2.4	7.80 d, 1H $J_{10,8}$ = 2.2	9.17 s, 1H	7.90 d, 1H $J_{3',4'}$ = 7.8	7.74 dd, 1H $J_{4',3'}$ = 7.8 $J_{4',6'}$ = 2.2	8.67 s, 1H
L-OCH_3 ([D_7]DMF)	2.52 s, 3H	3.21 s, 3H	4.27 s, 3H	3.94 s, 3H	8.58 d, 1H $J_{3,4}$ = 6.2	8.17 d, 1H $J_{4,3}$ = 6.2	7.61 d, 1H $J_{7,8}$ = 8.9	7.27 dd, 1H $J_{8,7}$ = 8.6 $J_{8,10}$ = 2.8	7.89 d, 1H $J_{10,8}$ = 2.6	9.43 s, 1H	8.03 d, 1H partly covered	7.94 dd, 1H $J_{4',3'}$ = 7.9 $J_{4',6'}$ = 1.4	8.72 s, 1H
[(L-OCH_3)$PtCl_2$] ([D_7]DMF)	2.55 s, 3H	3.29 s, 3H	4.39 s, 3H	3.99 s, 3H	8.30 d, 1H $J_{3,4}$ = 8.5	8.24 d, 1H $J_{4,3}$ = 8.4	7.71 d, 1H $J_{7,8}$ = 8.9	7.38 dd, 1H $J_{8,7}$ = 8.8 $J_{8,10}$ = 2.6	8.16 d, 1H $J_{10,8}$ = 2.5	9.51 s, 1H	9.35 d, 1H $J_{3',4'}$ = 7.0	8.36 d, 1H $J_{4',3'}$ = 7.1	9.46 s, 1H
L-OH ([D_7]DMF)	2.53 s, 3H	3.18 s, 3H	4.22 s, 3H	−	8.57 d, 1H $J_{3,4}$ = 4.7	8.13 d, 1H $J_{4,3}$ = 5.9	7.50 d, 1H $J_{7,8}$ = 8.7	7.19 dd, 1H $J_{8,7}$ = 8.7 $J_{8,10}$ = 2.4	7.65 d, 1H $J_{10,8}$ = 2.4	9.33 s, 1H	d, 1H partly covered	7.94 dd, 1H $J_{4',3'}$ = 7.9 $J_{4',6'}$ = 1.2	8.74 s, 1H
[(L-OH)$PtCl_2$] ([D_7]DMF	2.57 s, 3H	3.25 s, 3H	4.33 s, 3H	−	8.81 d, 1H $J_{3,4}$ = 8.5	8.26 d, 1H $J_{4,3}$ = 7.5	7.59 d, 1H $J_{7,8}$ = 8.9	7.31 dd, 1H $J_{8,10}$ = 2.3	7,92 s, 1H	9.40 s, 1H	9.32 d, 1H $J_{3',4'}$ = 6.9	8.31 d, 1H $J_{4',3'}$ = 6.9	9.35 s, 1H
L-OAc ([D_7]DMF)	2.50 s, 3H	3.15 s, 3H	4.22 s, 3H	2.35 s, 3H	8.60 s, 1H	8.19 d, 1H $J_{4,3}$ = 5.1	7.66 d, 1H $J_{7,8}$ = 8.8	7.37 dd, 1H $J_{8,7}$ = 8.7 $J_{8,10}$ = 2.3	8.01 d, 1H $J_{10,8}$ = 2.3	9.42 s, 1H	covered	7.91 d, 1H $J_{4',3'}$ = 7.9	8.73 s, 1H
[(L-OAc)$PtCl_2$] ([D_7]DMF)	2.46 s, 3H	3.23 s, 3H	4.35 s, 3H	2.45 s, 3H	8.90 d, 1H $J_{3,4}$ = 5.2	8.08 d, 1H $J_{4,3}$ = 5.6	7.74 d, 1H $J_{7,8}$ = 9.0	7.49 d, 1H $J_{8,7}$ = 8.5	8.45 s, 1H	9.57 s, 1H	9.35 s, 1H	8.24 s, 1H	9.46 s, 1H

Table 2. Chemical shift values (δ [ppm]) in the ^{13}C NMR spectra of the ligands

Carbon's number	1	3	4	5	7	8	9	10	11	12	13	16	18	19	20	21	2′	3′	4′	5′	6′	7′
L-OCH_3 (CD_2Cl_2)	158.82	140.49	116.36	111.55	109.69	116.40	154.41	104.49	117.73	135.68	121.64	126.67	14.15	34.12	56.33	−	157.10	125.16	137.49	132.97	149.22	18.46
L-OH (CD_2Cl_2)	158.08	141.24	116.60	111.80	109.63	116.57	150.58	106.88	117.75	135.63	121.12	126.56	14.06	33.85	−	−	156.59	125.44	137.77	133.33	148.63	18.41
L-OAc (CD_2Cl_2)	158.83	140.68	116.45	111.89	109.23	121.50	142.96	113.86	118.23	135.93	121.83	126.15	14.10	34.12	21.21	170.42	156.91	125.15	137.50	133.06	149.17	18.44

 © 2003 Wiley-VCH Verlag GmbH & Co. KGaA, Weinheim

complexes are sparingly soluble in CD_2Cl_2, hence their ^1H NMR spectra were recorded in [D_7]DMF. The use of two solvents was intentional since it allowed us to assign all the proton chemical shift values of the ligands, and in this way help in the analysis of the ^1H NMR spectra of the Pt complexes. The ^{13}C NMR spectra could be recorded only for the ligands since the Pt complexes were relatively insoluble in all the solvents used.

The assignments of the ^1H and ^{13}C NMR chemical shifts for the ligands were completed using two-dimensional HMQC, HMBC and COSY techniques; however, for the Pt complexes, only the ^1H NMR peaks could be assigned by comparing the spectra of the complexes with that of the corresponding ligands, and using data from the literature.[12,14] The proton chemical shift values for compounds **2**, **3** and **4** were measured and the data is presented in the Exp. Sect.

There is an appreciable downfield shift of almost all the signals in the ^1H NMR spectra of the Pt complexes relative to those in the spectra of the free ligands. However, there is a greater downfield shift of the signals for the protons at position 3′, 4′ and 6′. This is in agreement with IR results and leads to the conclusion that ligands exhibit a neutral bidentate function through the N2 and N1′ atoms. The downfield shift of the signals for the protons in neighboring region of the nitrogen atoms that are coordinated to the platinum ion has been reported for other chelate platinum complexes with nitrogen ligands.[36−38]

UV/Vis Characterization

Data obtained from the electronic spectra of the ligands (L-OCH_3, L-OH, L-OAc) and their Pt complexes ([(L-OCH_3)$PtCl_2$], [(L-OH)$PtCl_2$], [(L-OAc)$PtCl_2$]) in methanol and chlorobenzene solutions are presented in Table 3.

The UV/Vis bands of the ligands and Pt complexes were assigned using data from the literature for free bipyridine derivatives and their Pt complexes.[39−47] The authors in the above-mentioned references usually observed two bands, which were assigned as charge transfer transitions from the platinum d-orbital to π-anti-bonding orbitals of the bipyridyl group (MLCT); the energies were strongly dependent on the identity of the other ligands coordinated to the platinum ion and the solvent (e.g. in water, the first MLCT band appeared at 345 nm, whereas in chlorobenzene the band was at 413 nm).[39] In our studies on platinum complexes, in methanol, the band appears between 420−428 nm, and in chlorobenzene, the band appears at 440 nm. These were assigned to the first MLCT. This absorption band, which is correlated to the polarity of solvents, must be due to the platinum d → bipyridyl π* transition.

The second MLCT band in the spectra of our complexes also show a solvent dependency; in methanol, the band appears between 272−278 nm, whereas in chlorobenzene, the band is shifted to 288−292 nm.

According to the data published for other bipyridine platinum complexes, we assigned the intensive band in the

Table 3. Data from the UV/Vis measurements of the ligands and their platinum complexes in two solvents

Wavelength [nm] (ε [$mol^{-1}\cdot dm^3\cdot cm^{-1}$])						Assignments
L-OCH_3	[(L-OCH_3)$PtCl_2$]	L-OH	[(L-OH)$PtCl_2$]	L-OAc	[(L-OAc)$PtCl_2$]	
212[a]	210[a]	212[a]	208[a]	210[a]	210[a]	
($1.1\cdot10^5$)	($1.7\cdot10^4$)	($8.4\cdot10^4$)	($1.7\cdot10^4$)	($8.6\cdot10^4$)	($3.7\cdot10^4$)	
solvent abs.[b]	solvent abs.[b]	solvent abs.[b]	solvent abs.[b]	solvent abs.[b]	solvent abs.[b]	π → π*
274[a]		274[a]		272[a]		(intra ligand)
($1.4\cdot10^5$)		($8.7\cdot10^4$)		($1.2\cdot10^5$)		
solvent abs.[b]		solvent abs.[b]				
	278[a]		272[a]		278[a]	MLCT
	($1.3\cdot10^4$)		($1.1\cdot10^4$)		($3.2\cdot10^4$)	(spin
	292[b]		290[b]		288[b]	forbidden)
	($2.0\cdot10^4$)		($1.1\cdot10^4$)		($1.8\cdot10^4$)	
306[a]		308[a]		302[a]		
($2.0\cdot10^5$)		($1.2\cdot10^5$)		($2.1\cdot10^5$)		
312		312[b]		306[b]		
($1.5\cdot10^5$)		($3.9\cdot10^4$)		($9.83\cdot10^4$)		π → π*
	350[a]		348[a]		342[a]	(intra ligand)
	($1.3\cdot10^4$)		($8.7\cdot10^3$)		($3.3\cdot10^4$)	
	356[b]		354[b]		348[b]	
	($2.6\cdot10^4$)		($6.7\cdot10^3$)		($2.8\cdot10^4$)	
	420[a]		428[a]		420[a]	MLCT
	($6.7\cdot10^3$)		($3.8\cdot10^3$)		($1.4\cdot10^4$)	(spin
	440[b]		440[b]		440[b]	allowed)
	($7.7\cdot10^3$)		($2.0\cdot10^3$)		($6.7\cdot10^3$)	

[a] Methanol solution. [b] Chlorobenzene solution.

 © 2003 Wiley-VCH Verlag GmbH & Co. KGaA, Weinheim

Table 4. Crystal data and structure refinement for **5**, **7** and **8**

Compound	L-OCH_3 (**5**)	L-OAc (**7**)	[(L-OCH_3)$PtCl_2$] (**8**)
CCDC no.	203648	203649	203650
Empirical formula	$C_{24}H_{21}N_3O$	$C_{25}H_{21}N_3O_2$	$C_{24}H_{21}Cl_2N_3OPt \times C_3H_7NO \times 0.25H_2O$
Formula mass	367.44	395.45	711.03
Crystal system	monoclinic	monoclinic	monoclinic
Space group	$P2_1/c$	$P2_1/n$	$P2_1/n$
a (Å)	7.175(3)	14.369(3)	14.233(3)
b (Å)	20.072(7)	8.050(2)	25.569(4)
c (Å)	13.105(5)	17.074(3)	14.700(3)
β [°]	101.51(4)	96.18(2)	107.83(3)
V (Å^3)	1849.4(12)	1963.5(7)	5092.7(17)
Z	4	4	8
$d_{calcd.}$ [g·cm^{-3}]	1.320	1.338	1.855
T [K]	100	100	100
μ [mm^{-1}]	0.082	0.086	5.76
F(000)	776	832	2788
Crystal size [mm]	0.8 × 0.1 × 0.06	0.6 × 0.2 × 0.1	0.06 × 0.05 × 0.02
θ range [°]	3.5 to 28.5	3.5 to 28.7	3.3 to 28.5
Reflections measured	11673	12818	29166
Unique reflections ($R_{int.}$)	4318 (0.0721)	4643 (0.0265)	11396 (0.1085)
Absorptio correction	none	none	analytical
Transmission, max./min.			0.904/0.695
Extinction	0.0121(15)		
Parameters/constraints	317/0	355/0	349/27
R_1 [$I > 2\sigma(I)$]	0.0590	0.0396	0.0699
Data with $I > 2\sigma(I)$	2897	3615	6015
R_1(all data)	0.1086	0.0570	0.1769
wR_2(all data, on F^2)	0.1208	0.1044	0.1048
S	1.039	1.095	0.874
Residual density [e·Å^{-3}]	−0.26/0.22	−0.22/0.20	−1.63/1.18

Table 5. Shortest intra- and intermolecular hydrogen bonds for **5**, **7**, and **8**, with standard deviations in parentheses; square brackets denote short contacts for disordered atoms; symmetry codes: i ($x-1, y, z$); ii ($2-x, 1-y, 1-z$); iii ($1+x, 0.5-y, z-0.5$); iv ($0.5+x, 0.5-y, z-0.5$); v ($x-0.5, 0.5-y, 0.5+z$); vi ($1.5-x, 0.5+y, 1.5-z$); vii ($x+0.5, -y+0.5, z+0.5$); viii ($x-0.5, 0.5-y, z-0.5$)

Compound	D−H···A	D···A [Å]	<(DHA) [°]
L-OCH_3 (**5**)	C(11)−H(11)···N(18)	2.976(3)	115.6(13)
	C(20)−H(20)···N(2)	2.820(3)	94.5(13)
	C(23)−H(23)···N(2)^{i}	3.445(3)	150.8(14)
	C(20)−H(20)···C(9)^{ii}	3.412(3)	115.3(14)
	C(3)−H(3)···C(01)^{iii}	3.582(3)	138.9(15)
	C(92)−H(922)···C(12)^{i}	3.801(3)	162.8(15)
	C(92)−H(922)···C(13)^{i}	3.814(3)	149.3(15)
L-OAc (**7**)	C(11)−H(11)···N(18)	2.917(2)	120.7(10)
	C(20)−H(20)···N(2)	2.810(2)	96.5(9)
	C(21)−H(21)···O(94)^{iv}	3.330(2)	124.7(11)
	C(8)−H(8)···N(2)^{v}	3.544(2)	161.6(11)
	C(93)−H(933)···N(18)^{vi}	3.409(2)	134.0(13)
[(L-OCH_3)$PtCl_2$] (**8**)	C(3a)−H(3a)···Cl(2a)	3.193(12)	123
	C(23a)−H(23a)···Cl(1a)	3.253(12)	122
	[C(21a)−H(21a)···O(1e)]	3.14(2)	154
	[C(21a)−H(21a)···O(1d)]	3.24(2)	156
	C(3b)−H(3b)···Cl(2b)	3.207(13)	120
	C(23b)−H(23b)···Cl(1b)	3.299(11)	121
	[C(10b)−H(10b)···O(1d)]^{vii}	3.40(2)	130
	[C(20b)−H(20b)···O(1d)]^{vii}	3.44(2)	132
	[C(20b)−H(20b)···O(1e)]^{vii}	3.15(2)	128
	[C(21b)−H(21b)···O(1c)]^{vii}	3.38(2)	136
	[O(1f)−H(1f1)···O(1c)]	2.70(2)	116
	O(1f)−H(1f2)···Cl(2a)^{viii}	3.78(2)	139

 © 2003 Wiley-VCH Verlag GmbH & Co. KGaA, Weinheim

spectra of the ligands at 306 nm to an internal bipyridine ring transition.[38−40] In complexes [(L-OCH_3)$PtCl_2$], [(L-OH)$PtCl_2$] and [(L-OAc)$PtCl_2$], this band is bathochromic shifted by about 40 nm. Such a shift is consistent with reports in the literature on complexation or reduction of bipyridines.[39,46−50]

X-ray Structure

Details of the crystal parameters, data collection and structure refinement for L-OCH_3 (**5**), L-OAc (**7**) and [(L-OCH_3)$PtCl_2$] × DMF × 0.25H_2O (**8**), are given in Table 4. Selected hydrogen interactions are listed in Table 5.

The asymmetric unit of **8** contains two crystallographically independent complex molecules [(L-OCH_3)$PtCl_2$] (hereafter referred to as **a** and **b**), two molecules of DMF (one is disordered) and half a molecule of water.

Both molecular structures of ligands **5** and **7** (presented in Figure 5 and 6) reveal the intramolecular hydrogen bond between C(11)−H(11) and N(18), and a fairly short contact between C(20)−H(20) and N(2). The picoline ring in both ligands is twisted from the core formed by four other rings, with dihedral angles of 38.0(1)° and 36.3(1)° in **5** and **7**, respectively.

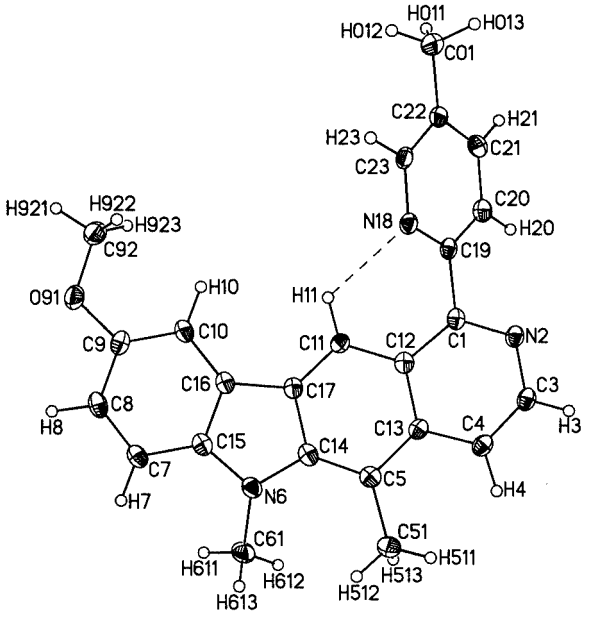

Figure 5. Molecular structure of **5**, showing the atom numbering scheme and displacement ellipsoid plotted at the 50% probability; four fused rings of the molecular core are in the plane of the sheet; the shortest intramolecular C−H···N hydrogen bond is shown as a dashed line

Analysis of the crystal packing reveals stacking interactions between consecutive parallel molecules; these are often observed for compounds with extended π-systems.[51] In the crystal cells of both ligands, columnar structures of the molecules are formed with the nearest neighbors, with a head-to-head orientation, and the distances between them allow for the C···C and C···H and N···H stacking interactions. In both ligands, mutual arene−arene interactions are

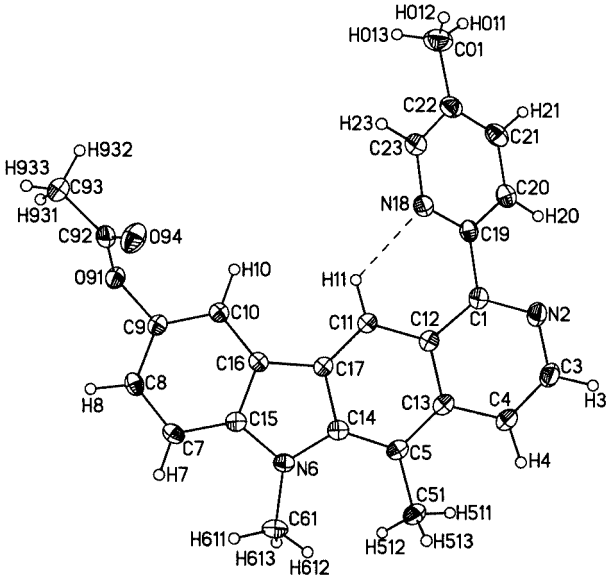

Figure 6. Molecular structure of **7**, showing the atom numbering scheme and displacement ellipsoid plotted at the 50% probability; four fused rings of the molecular core are in the plane of the sheet; the shortest intramolecular C−H···N hydrogen bond is shown as a dashed line

also observed through weak C−H···C and C−H···N intermolecular hydrogen bonds. However, as shown in Figure 7 and 8, some differences are seen in the crystal packing. The adjacent columns of bow-like shaped molecules of **5** are in a head-to-tail nonparallel mutual arrangement, and intermolecular hydrogen bonds are observed between them. In the crystal cell of **7**, the adjacent columns are oriented in an almost perpendicular manner.

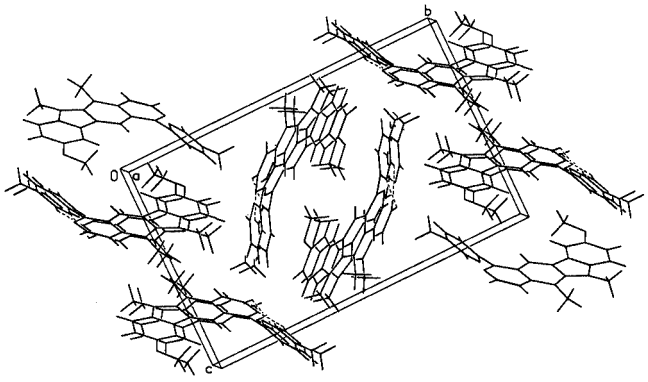

Figure 7. Crystal packing diagram for **5** along axis *a*

The relatively planar molecular structure and stacking interactions seen in **5** and **7** meet the structural requirements for the intercalative type of biological activity mechanism predicted for this type of compounds.[52]

The molecular structure of complex **8** obtained by X-ray diffraction unequivocally confirms that the bipyridine fragment is chelated to the platinum center; the remaining coordination sites are occupied by two *cis* chloride ligands. In molecules **a** and **b**, the coordination geometry around the platinum center is square planar. Although molecules **a** and

 © 2003 Wiley-VCH Verlag GmbH & Co. KGaA, Weinheim

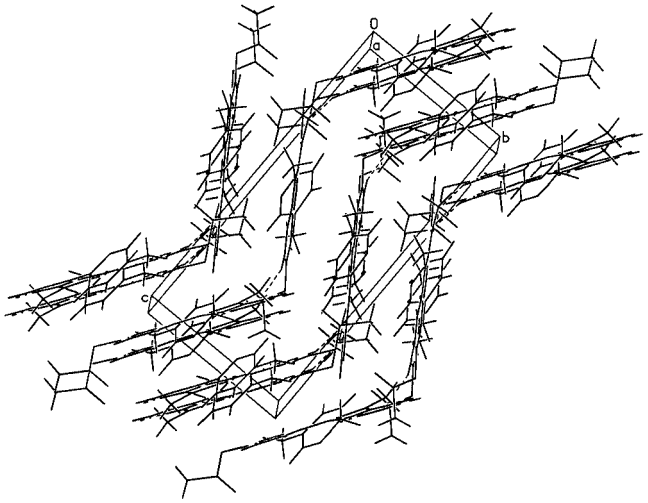

Figure 8. Crystal packing diagram for **7** along axis *a*

b are very similar, as seen in Figure 9, some differences can be observed.

Firstly, the methoxy substituent in molecule **b**, as in **5**, is in a *cis* configuration relative to C(10)−H(10), whereas in **a**, it is in a *trans* configuration.

Another difference is related to the value of dihedral angle between the picoline ring and the skeleton of the molecule (formed by four other rings); 13.9(3)° in **a**, and 16.7(3)° in **b**. This is further related to the proximity of the H(11) and H(20) atoms. Complexation resulted in picoline ring rotation, thus this distance is 1.67 in **a** and 1.88 Å in **b** (with the C−H distance assumed as 1.08 Å). The geometric effect forced by coordination and/or the crystal packing effect cannot be excluded as a reason for achieving such a short contact between H(11) and H(20) and for the appearance of two independent molecules observed in the crystalline state of **8**.

A comparison of the bond lengths reveals the next difference between **a** and **b** (and **5**). The differences in the bond lengths may be due to the change in the conjugation of the π-bonds, and might be related to the above-mentioned H(11)···H(20) interaction.

The Pt−N bond lengths in molecules **a** and **b** are similar to those in other chloro-platinum complexes with bisisoquinoline,[53] as well as with bipyridines.[35,54,55] In molecule **a**, both Pt−Cl bond lengths are within the expected range, whereas in molecule **b**, the Pt−Cl(1) bond is slightly longer [2.315(3) Å]. The chloride ligands are also engaged in weak intramolecular hydrogen bonds with C(23)−H(23) and C(3)−H(3).

The mode of π-π stacking interactions in the unit cell of **8** is more complicated than in **5**. Molecules **a** and **b** show alternative coordination modes of *cis*-[PtN_2Cl_2]. Consecutive molecules of **a** and **b** are not parallel and overlap each other, either with through the bipyridine fragments or through the "tails" of the molecules.

C···C and H···C stacking interactions are observed. Furthermore, N(6)···Pt and Pt···C(14) interactions can also be seen . In contrast to some other Pt complexes with similarly coordinated bipyridine ligands, there is no linear stacking

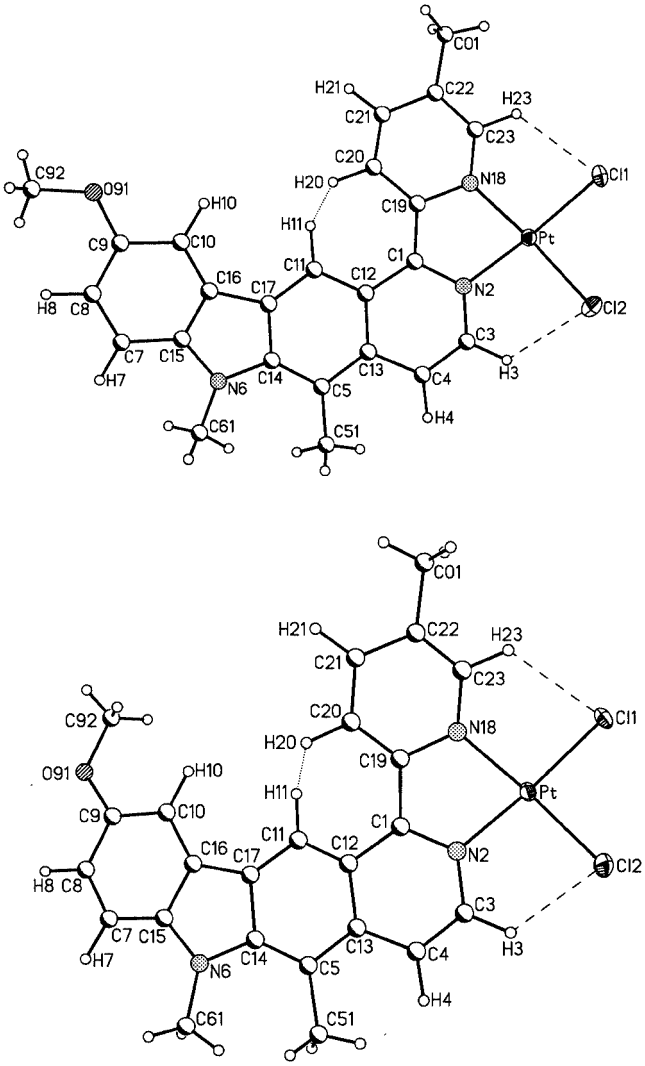

Figure 9. Molecular structure of **8 a** and **8 b**, showing the atom numbering scheme and displacement ellipsoid plotted at the 50% probability for the platinum center and the chloride ligands; the coordination plane defined by [PtN_2Cl_2] is in the plane of the sheet; the intramolecular C−H···Cl hydrogen bonds are shown as dashed lines; the shortest intramolecular distances between the hydrogen atoms are shown as a dotted line

arrangement of the platinum centers.[54] The shortest distance between the platinum centers in **a** and **b** is 6.2 Å, and suggests no significant Pt−Pt interaction (relative to the reported value 3.45 Å in ref.[54]).

Conformational Analysis of L-OCH_3

Due to symmetry, two conformers of the ligand L-OCH_3 can exist in a global energy minimum in the one molecule model gas state, with calculated torsion angles N(2)−C(1)−C(19)−N(18) of approximately −91° or 93,° respectively, for conformers in an energy minimum. The calculated binding energy of these conformers is −5537.71 kcal/mol (Table 6). The calculated standard enthalpy is 56.35 kcal/mol. In the crystalline state, the measured torsion angle N(2)−C(1)−C(19)−N(18) is −141.5(2)°, so the difference between the calculated torsion angle

 © 2003 Wiley-VCH Verlag GmbH & Co. KGaA, Weinheim

Table 6. Calculated binding energies, heats of formation and energy barriers for rotation for the conformers of L-OCH_3

Conformers of L-OCH_3	Respected torsion angle N(2)−C(1)−C(19)−N(18)[a] [°]	Binding energy [kcal/mol]	Standard heat (enthalpy) of formation ΔH^{298} [kcal/mol]	Rotational barrier E_{rot} [kcal/mol]
In energy minimum	−91.16 or 92.64[b]	−5537.71	56.35	0.00
Antiplanar	180.0 (−180.0)	−5535.60	58.46	2.11
Synplanar	0.00	−5511.37	82.69	26.34
in [(L-OCH_3)$PtCl_2$] molecule **a**	−11.7(14)[c]	−5531.32	62.74	6.39

[a] Atom numbering according to that used for the X-ray structure. [b] Calculated. [c] From X-ray diffraction measurements.

N(2)−C(1)−C(19)−N(18) in the model gas state and that measured in the crystals is −50.49°. The observed difference might be caused by the fact that intermolecular interactions (e.g. electrostatic, Van der Waals, dispersion, hydrogen bonds) that exist in the real crystalline state, are not taken into consideration in the calculated method. The estimated binding energy for one of the planar conformers, for which N(2)−C(1)−C(19)−N(18) is 180° (or −180°), is −5535.60 kcal/mol, and the standard enthalpy is 58.46 kcal/mol. Moreover, the energy barrier for rotation around the C(1)−C(19) bond (when the torsion angle N(2)−C(1)−C(19)−N(18) changes from −91° to 180°), calculated from the difference in the enthalpies of formation of the proper conformers, is : E_{rot} = 2.11 kcal/mol (E_{rot} = ΔH_{rot} rotational enthalpy). This low energy barrier indicates that the antiplanar conformation of L-OCH_3 is easily achieved, and this may also explain the significant difference between the measured and calculated torsion angles because this fragment of the molecule is flexible enough [in this range for the torsion angle N(2)−C(1)−C(19)−N(18)], although rotation around the C(1)−C(19) bond is not completely free since the energy required is higher than the thermal energy (translation) at 298 K ($E_{rot} > RT$ = 0.592 kcal/mol). The energy barrier for rotation around the C(1)−C(19) bond (torsion angle N(2)−C(1)−C(19)−N(18) changes from −91° or 92° to 0°) in order to adopt a synplanar conformation is very high, E_{rot} = 26.34 kcal/mol (= rotational enthalpy), so this conformation is almost impossible to achieve at standard temperature, hence there is absolutely no rotation around this bond. If the Pt^{2+} ion required a synplanar [torsion angle N(2)−C(1)−C(19)−N(18) = 0°] conformation of the ligand L-OCH_3 for complexation, complex formation would probably not occur. However, according to the literature, the known complexes of Pt^{2+} with 1,1′-biisoquinoline[53] and 2,2′-bipyridines[56] have analogous torsion angles that are not planar. X-ray diffraction measurements show that in the case of [(1,1′-biisoquinoline)$PtCl_2$], these angles are 35.18° and 41.12°, and thus the molecule is very twisted.[53] In the case of unsubstituted [(2,2′-bipyridine)$PtCl_2$], the torsion angle indicated an almost planar molecule and the torsion angle was estimated to be 4.8(6)°, but 3,3′-bisubstituted [(2,2′-bipyridine)$PtCl_2$] is markedly non-planar [25.5(3)°].[56] The measured torsion angle N(2)−C(1)−C(19)−N(18) in the crystal of [(L-OCH_3)$PtCl_2$] for molecule **a** is −11.7(14)°; this shows that the molecule is twisted, however, to a lesser extent than in the complex [(1,1′-biisoquinoline)$PtCl_2$] and the 3,3′-bisubstituted 2,2′-bipyridine complexes. The calculated rotational barrier required to adopt this conformation (torsion angle N(2)−C(1)−C(19)−N(18) equals −11.7(14)°) has been estimated to be E_{rot} = 6.39 kcal/mol. Neglecting the effects of entropy, $E_{rot} \approx \Delta G_{rot} = -RT\ln K$ (ΔG_{rot} is free enthalpy of rotation), hence, the equilibrium constant, K, for rotation between the conformers can be estimated. Therefore, $K_{rot} \approx 2.06 \times 10^{-5}$, which indicates that there is one molecule of the less stable conformer for every 48500 molecules of the more stable conformer. (For comparison, the rotational barrier E_{rot} for 1,1′-biisoquinoline (from 85.06° to 35.18°) is 4.97 kcal/mol; $K_{rot} = 2.28 \times 10^{-4}$; 1 molecule of the less stable conformer for every 4387 molecules of the more stable conformer.)

The results obtained indicate that the concentration of the proper conformer of L-OCH_3 [torsion angle N(2)−C(1)−C(19)−N(18) equals −11.7(14)°] is sufficient for complexation to occur at standard temperatures. Moreover, protogenic polar solvents can stabilize this conformation by the formation of hydrogen bonds, thus the energy barrier for rotation may decrease and complex formation is made easier. This is supported by the experiment in which [(L-OCH_3)$PtCl_2$] is formed.

Antiproliferative Activity

The in vitro growth-inhibitory effect of the ligands L-OH, L-OAc, L-OMe were tested on four human cancer cell lines: A549, SW707, HCV29T, T47D and on mice leukemia L1210. The results, expressed as the IC_{50} values, are presented in Table 7. In general, the ligands are much more

Table 7. The in vitro antiproliferative activity against human cancer cell lines and mice leukemia

Cell line: Compound	A549 IC_{50} [μmol/dm³]	SW707	HCV29T	T47D	L1210
L-OH	9.56	10.19	9.25	9.79	1.7
L-OAc	18.97	21.24	17.83	11.66	2.3
L-OCH_3	neg.	25.04	20.55	17.47	−
[Pt(L-OH)Cl_2][a]	−	−	−	−	ca. 10
[Pt(L-OAc)Cl_2][a]	−	−	−	−	ca. 10
Carboplatin	108.00	210.00	68.70	202.00[b]	−
Adriamycin	−	−	−	−	0.03
Elliptinium acetate	−	−	−	−	0.07

[a] Slurry in DMSO. [b] IC_{30}; neg. inactive; − not measured.

 © 2003 Wiley-VCH Verlag GmbH & Co. KGaA, Weinheim

active against the human lines than the reference carboplatin. The most active was L-OH (ID_{50} against all human cancer cell lines and against L1210). The least active was L-OCH_3 (negative against A549).

The relatively insoluble platinum complexes, [(L-OH)$PtCl_2$] and [(L-OAc)$PtCl_2$], were tested against L1210; they could be measured only as a slurry in DMSO. Although IC_{50} values for the complexes are less than those for the reference compounds, as well as for the ligands, their activity seems to be significant, taking into account that the cytotoxic effect was only caused by a soluble part of sample. More advanced studies will be described elsewhere.[15]

The results obtained indicate that the new olivacine derivatives and their neutral platinum complexes are promising cytotoxic agents of a new class; however, improvement on the solubility of the chloro complexes is necessary. This may be achieved by exchanging the chloride ligands for chosen dicarboxylate ligands, according to our earlier methodology.[57]

Experimental Section

Materials: The starting material for the synthesis of the new 9-olivacine derivatives was 2-(6-methoxy-1-methylcarbazol-2-yl)-ethylamine, which was synthesized from 5-methoxyindol and 4-acetylpyridine, both purchased from Aldrich.

The starting material for the synthesis of the platinum complexes were the new 9-olivacine derivatives, and K_2PtCl_4, which was prepared from metallic Pt by known procedure.[58] Synthetic procedures for the platinum complexes were carried out in the dark. All other chemicals obtained from commercial suppliers were used as received and were of analytical grade.

Physical Measurements: Elemental analyses (C,H,N) were performed on a model Perkin−Elmer Elemental Analyzer 2400 CHN. Pt was analyzed by ICP-AES method on ARL 3410 instrument (with permissible deviation ± 5%), with previous mineralization by microwaves on MDS 200 CEM mineralizator. Thin-layer chromatography was carried out on pre-coated silica gel plates (Poligram) and on plates with the UV marker (Silufol, Cavalier). (A) 1-propanol-1:acetic acid:water (4:16:1) and (B) acetone/chloroform (1:4) were used as developing mixtures. The spots were visualized with rubeanic acid (VEB Laborchemie Apolda) (10% in acetone) and with UV radiation (254 and 366 nm).

Conductivity data (Λ_0 = immediate, Λ_{24} = after twenty four hours [$\Omega^{-1}\cdot mol^{-1}\cdot cm^2$]) were obtained at 298 K in DMF solutions (c = 4.7×10^{-5} M), on a Radelkis OK-104 conductometer.

IR and FIR spectra were run as KBr pellets and nujol mulls, respectively, on a Bruker JFS 113 V FT-IR spectrometer. UV spectra were obtained on Hewlett Packard HP8452A diode array spectrophotometer. ESI-MS measurements were done on a Finnigan MAT TSQ-700 triple-quadrupole mass spectrometer (equipped with a 20 kV conversion dynode for enhanced sensitivity). The ion signals were recorded by a Finnigan ICIS data system operated on a DEC station 3000. The ^1H spectra were recorded at 500.13 MHz and ^{13}C NMR spectra at 125.72 MHz on a Bruker Avance 500 instrument (all at 298 K). Spectra were referenced to the internal solvent peaks.

X-ray Structure Determination: X-ray diffraction data were collected at 100 K on a KUMA KM4CCD diffractometer with graphite−monochromated Mo-K_α radiation (λ = 0.71073 Å) using the ω scan technique. The crystal structures were solved with SHELXS-97 and refined against $|F|^2$ using SHELXL-97.[59]

In the ligands L-OCH_3 (**5**) and L-OAc (**7**), all hydrogen atoms were found from the difference maps and refined isotropically. In the complex [(L-OCH_3)$PtCl_2$] (**8**) all hydrogen atoms were placed in their geometrically calculated positions d(C−H) = 1.08 Å. Platinum atoms and chloride ligands were refined anisotropically. One of the DMF molecules is disordered, with an occupation factor of 0.5. Refinement of the water molecule gave an occupation factor of 0.5.

Single crystals of the ligands were obtained at ambient temperature by slow evaporation of solvents. L-OCH_3 (**5**) was crystallized from dichloromethane and L-OAc (**7**) from methanol. The nucleation process of [(L-OCH_3)$PtCl_2$] (**8**) crystallization was started after dropwise addition of diethyl ether to the DMF solution of **8**. CCDC-203648, -203649, and -203650 contain the supplementary crystallographic data for this paper. These data can be obtained free of charge at www.ccdc.cam.ac.uk/conts/ retrieving.html [or from the Cambridge Crystallographic Data Centre, 12 Union Road, Cambridge CB2 1EZ, UK; Fax: (internat.) + 44-1223-336-033; E-mail: deposit@ccdc.cam.ac.uk].

Computational Methods: Quantum mechanical calculations were performed using semiempirical PM3 methods[60][61] with the computer software − HyperChem. Pro ver. 7.[62] SCF and geometry optimization − Polak−Ribiere (conjugate gradient) minimization algorithm, SCF convergence limit was set to 10^{-6}, energy optimization gradient was set to 0.01 kcal/(mol × Å).

In-Vitro Cytotoxicity Assays: Test on human cancer cell lines (A549, SW707, HCV29T, T47D) were performed at the Institute of Immunology and Experimental Therapy, Polish Academy of Sciences, in Wroclaw, Poland, as described.[15] The test on mice leukemia L1210 was performed at the Curie Institute − Orsay (France), as described.[15]

2-(6-Methoxy-1-methylcarbazol-2-yl)ethylamine (1): Compound **1** was obtained in accordance with ref.[12]

***N*-[2-(6-Methoxy-1-methyl-9*H*-carbazol-2-yl)ethyl]-5-methyl-2-pyridinecarboxamide (2):** Triethylamine (506 mg, 5.0 mmol) was added to the 5-methyl-2-pyridinecarboxylic acid (603 mg, 4.4 mmol) in dry dichloromethane (100 mL). To the resulting mixture, after cooling to 263 K, a solution of ethyl chloroformate (543 mg, 5.0 mmol) in dry dichloromethane (10 mL) was added, whilst stirring. This was stirred for a further 30 min and then 2-(6-methoxy-1-methylcarbazol-2-yl)ethylamine (**1**) (1017 mg, 4.0 mmol) in THF (100 mL) was added dropwise at 263 K, and left to reach room temperature (20 h) whilst stirring. The precipitate was collected and the filtrate was evaporated to dryness. The residue dissolved in water (50 mL), was made basic with concentrated aqueous ammonia and extracted with dichloromethane and dried over magnesium sulfate. Evaporation of the solvent provided a solid residue, which was recrystallized from ethanol to give 900 mg, (60%) of amide **2**. M.p. 458 K. $C_{23}H_{23}N_3O_2$ (373.5): calcd. C 73.97, H 6.21, N 11.25; found C 73.56, H 6.54, N 10.91. ^1H NMR ($CDCl_3$, 298 K): δ = 2.36 (s, 3 H, 5′-CH_3), 2.52 (s, 3 H, 1-CH_3), 3.12 [t, J(α-CH_2−β-CH_2) = 6.2 Hz, 2 H, α-CH_2], 3.70 (t, 2 H, β-CH_2), 3.90 (s, 3 H, 6-OCH_3), 7.05−7.11 (m, 2 H, 3-H +7-H), 7.40 (d, $J_{8,7}$ = 8.7 Hz, 1 H, 8-H), 7.50 (d, $J_{5,7}$ = 2.5 Hz, 1 H, 5-H), 7.74 (dd, $J_{4',3'}$ = 8 Hz, 1 H, 4′-H), 7.84 (d, $J_{4,3}$ = 7.8 Hz, 1 H, 4-H),

 © 2003 Wiley-VCH Verlag GmbH & Co. KGaA, Weinheim

8.03 (d, $J_{3',4'}$ = 8 Hz, 1 H, 3′-H), 8.31 (s, 1 H, 6′-H), 8.75 (s, 1 H, 9-H).

9-Methoxy-5-methyl-1-(5′-methylpyridin-2-yl)-3,4-dihydro-6*H*-pyrido[4,3-*b*]carbazole (3): The preceding amide (**2**) (1867 mg, 5.0 mmol) was dissolved in boiling toluene (150 mL) and treated dropwise with phosphorous oxychloride (12 mL). Reflux was continued for a 12 h, and evaporation under reduced pressure afforded a residue, which was dissolved in water (100 mL), was made basic to pH 9−10 with concentrated aqueous ammonia, and extracted with dichloromethane. Evaporation of the solvent provided a solid residue, which was recrystallized from ethanol to give yellow crystals (1320 mg, 74%). M.p. 554 K. $C_{23}H_{21}N_3O$ (355.4): calcd. C 77.72, H 5.96, N 11.82; found C 77.52, H 6.03, N 11.91. ^{1}H NMR ($CDCl_3$, 298 K): δ = 2.45 (s, 3 H, 5′-CH_3), 2.68 (s, 3 H, 5-CH_3), 2.83 (t, $J_{4,3}$ = 6.5 Hz, 2 H, 4-H), 3.85 (s, 3 H, 6-OCH_3), 3.90 (t, $J_{3,4}$ = 6.5 Hz, 2 H, 3-H), 7.00 (dd, $J_{8,7}$ = 8.7, $J_{8,10}$ = 2.4 Hz, 1 H, 8-H), 7.34 (d, $J_{7,8}$ = 8.8 Hz, 1 H, 7-H), 7.41 (d, $J_{10,8}$ = 2.3 Hz, 1 H, 10-H), 7.52 (dd, $J_{4',3'}$ = 8.5 Hz, 1 H, 4′-H), 7.88 (d, $J_{3',4'}$ = 8.6 Hz, 1 H, 3′-H), 8.38 (br. s, 1 H, 6-H), 8.70 (s, 1 H, 6′-H), 9.07 (s, 1 H, 11-H).

9-Methoxy-5-methyl-1-(5′-methylpyridin-2-yl)-6*H*-pyrido[4,3-*b*]carbazole (4): Compound **3** (1422 mg, 4.0 mmol) was refluxed in diphenyl ether (50 mL) in the presence of 10% palladized charcoal (100 mg) for 30 min. After removal of the catalyst, the filtrate was cooled and diluted with hexane. The resulting precipitate was collected and washed with hexane and recrystallized from ethyl acetate to give yellow crystals (1060 mg, 75%). M.p. 544 K. $C_{23}H_{19}N_3O$ (353.4): calcd. C 78.17, H 5.42, N 11.89; found C 77.97, H 5.66, N 11.73. ^{1}H NMR ($CDCl_3$, 298 K): δ = 2.34 (s, 3 H, 5′-CH_3), 2.56 (s, 3 H, 5-CH_3), 3.85 (s, 3 H, 9-OCH_3), 7.12 (dd, $J_{8,7}$ = 8.8, $J_{8,10}$ = 2.4 Hz, 1 H, 8-H), 7.26 (d, $J_{7,8}$ = 8.7 Hz, 1 H, 7-H), 7.65 (d, $J_{10,8}$ = 2.4 Hz, 1 H, 10-H), 7.87 (dd, $J_{4',3'}$ = 8.4 Hz, 1 H, 4′-H), 7.97 (m, 2 H, 4H +3′-H), 8.49 (d, $J_{3,4}$ = 6.5 Hz, 1 H, 3-H), 8.55 (s, 1 H, 6-H), 8.81 (s, 1 H, 6′-H), 9.12 (s, 1 H, 11-H).

9-Methoxy-5,6-dimethyl-1-(5′-methylpyridin-2-yl)-6*H*-pyrido[4,3-*b*]carbazole (5, L-OCH_3): A mixture of **4** (1060 mg, 3.0 mmol), fine powdered dry potassium carbonate (750 mg), dimethyl carbonate (20 mL), dimethyl formamide (3 mL) and 18-crown-6-ether (3 drops) was heated under reflux, whilst stirring for a 12 h. After evaporation to dryness, the residue was dissolved in water. The solid was collected, air-dried, and recrystallized from isopropyl acetate to give yellow crystals (880 mg, 80%). M.p. 497−498 K. R_f = 0.82 (A), 0.34 (B). $C_{24}H_{21}N_3O$ (367.45): calcd. C 78.45, H 5.76, N 11.44; found C 77.09, H 5.93, N 11.50. MS: *m*/*z* (%) = 368 (100).

9-Hydroxy-5,6-dimethyl-1-(5′-methylpyridin-2-yl)-6*H*-pyrido[4,3-*b*]carbazole (6, L-OH): A mixture of (**L-OCH_3**) (735 mg, 2 mmol) and hydrobromic acid (48%, 30 mL) was heated under reflux, whilst stirring for 3 h. After evaporation to dryness, the residue was dissolved in water. The resulting mixture was made basic with concentrated ammonia and extracted with dichloromethane. The extract was dried over magnesium sulfate and the solvents evaporated. The solid was recrystallized from dichloromethane to give yellow crystals (676 mg, 96%). M.p. 522−524 K. R_f = 0.82 (A). $C_{23}H_{19}N_3O$ (353.42): calcd. C 78.17, H 5.42, N 11.89; found C 78.01, H 5.61, N 11.72. MS: *m*/*z* (%) = 354 (100).

9-Acetoxy-5,6-dimethyl-1-(5′-methylpyridin-2-yl)-6*H*-pyrido[4,3-*b*]carbazole (7, L-OAc): A solution of (**L-OH**) (106 mg, 0.3 mmol) in dry pyridine (1 mL) was cooled to 263 K and then treated dropwise with acetic anhydride (1 mL). The mixture was stirred at 263 K for 30 min and allowed to reach room temperature over 3 h. The mixture was then poured into cold water (10 mL) and extracted with dichloromethane. Evaporation of the solvent provided a solid residue, which was recrystallized from isopropyl acetate to give yellow crystals (105 mg, 89%). M.p. 529−530 K. R_f = 0.80 (A); 0.31 (B). $C_{25}H_{21}N_3O_2$ (395.46): calcd. C 75.93, H 5.35, N 10.62; found C 75.18, H 5.41, N 10.43. MS: *m*/*z* (%) = 396 (100).

Dichloro[(9-methoxy-5,6-dimethyl-1-(5′-methyl-pyridin-2-yl)-6*H*-pyrido[4,3-*b*]carbazole]platinum(II) [8, (L-OCH_3)$PtCl_2$]: 9-Methoxy-5,6-dimethyl-1-(5-methylpyridin-2-yl)-6*H*-pyrido[4,3-*b*]carbazole (**L-OCH_3**) (150 mg, 0.41 mmol) was dissolved in methanol (250 mL) and an aqueous solution (8 mL) of K_2PtCl_4 (169 mg, 0.41 mmol) was added dropwise. The mixture was stirred at room temperature for several hours and left for 5 weeks. The precipitate obtained was centrifuged, washed with a small amount of water to remove KCl (tested with $AgNO_3$). The platinum complex was dried over P_4O_{10} in vacuo. Yield 239 mg (92%). R_f = 0.88 (A), 0.76 (B). $C_{24}H_{21}Cl_2N_3OPt$ (633.44): calcd. C 45.51, H 3.34, Cl 11.19, N 6.63, Pt 30.68; found C 44.77, H 3.29, N 6.42, Cl 11.08, Pt 30.68. MS: *m*/*z* (%) = 633 (100). $\Lambda_{0\ and\ 24}$ = 4.2 [$\Omega^{-1}\cdot mol^{-1}\cdot cm^2$].

Dichloro[(9-hydroxy-5,6-dimethyl-1-(5′-methylpyridin-2-yl)-6*H*-pyrido[4,3-*b*]carbazole]platinum(II) [9, (L-OH)$PtCl_2$]: 9-hydroxy-5,6-dimethyl-1-(5′-methylpyridin-2-yl)-6*H*-pyrido[4,3-*b*]carbazole (**L-OH**) (149 mg, 0.42 mmol) was dissolved in methanol (200 mL), an aqueous solution (8 mL) of K_2PtCl_4 (175 mg, 0.42 mmol) was then added. The mixture was stirred at room temperature for several hours and left for 4 weeks. The precipitate obtained was centrifuged, washed with a small amount of water to remove KCl (tested with $AgNO_3$) and dried over P_4O_{10} in vacuo. Yield 221 mg (85%). R_f = 0.94 (A). $C_{23}H_{19}Cl_2N_3OPt$ (619.41): calcd. C 44.6, H 3.09, Cl 11.45, N 6.78, Pt 31.49; C 44.33, H 3.68, Cl 10.68, N 6.46, Pt 28.44. MS: *m*/*z* (%) = 620 (100). $\Lambda_{0\ and\ 24}$ = 5.0 [$\Omega^{-1}\cdot mol^{-1}\cdot cm^2$].

Dichloro[9-acetoxy-5,6-dimethyl-1-(5′-methyl-pyridin-2-yl)-6*H*-pyrido[4,3-*b*]carbazole]platinum(II) [10, (L-OAc)$PtCl_2$]: 9-Acetoxy-5,6-dimethyl-1-(5-methylpyridin-2-yl)-6*H*-pyrido[4,3-*b*]carbazol] (**L-OAc**) (140 mg, 0.35 mmol) was dissolved in methanol (150 mL), an aqueous solution (9 mL) of K_2PtCl_4 (145 mg, 0.35 mmol) was then added. The mixture was stirred at room temperature for several hours and then left for about 4 weeks. The precipitate obtained was centrifuged, washed with a small amount of water to remove KCl (tested with $AgNO_3$). The platinum complex was dried over P_4O_{10} in vacuo. Yield 190 mg (82%). R_f = 0.72 (B). $C_{25}H_{21}Cl_2N_3O_2Pt$ (661.45): calcd. C 45.40, H 3.20, Cl 10.72, N 6.35, Pt 29.49; found C 44.58, H 3.74, Cl 10.05, N 6.00, Pt 25.49. MS: *m*/*z* (%) = 663 (100). $\Lambda_{0\ and\ 24}$ = 3.3 [$\Omega^{-1}\cdot mol^{-1}\cdot cm^2$].

Acknowledgments

Financial support from the State Committee for Scientific Research KBN of Poland (Grants 3 T09A 126 19 and 4 P05F 032 19) is kindly acknowledged.

[1] B. J. S. Sanderson, L. R. Ferguson, W. A. Denny, Mutat Res-Fundam Mol Mech Mutage, **1996**, 355−359.
[2] D. P. Gately, S. B. Howell, *Brit. J. Cancer* **1993**, *67*, 1171−1176.
[3] T. Matsumoto, K. Endoh, K. Akamatsu, K. Kamisango, H. Mitsui, K. Koizumi, K. Morikawa, M. Koizumi, T. Matsuno, *Brit. J. Cancer* **1991**, *64*, 41−46.
[4] J. Holford, S. Y. Sharp, B. A Murrer, M. Abrams, L. R. Kelland, *Brit. J. Cancer* **1998**, *77*, 366−373.
[5] E. Cvitkovic, *Brit. J. Cancer* **1998**, *77*, 8−11.
[6] R. P. Perez, *Eur. J. Cancer* **1998**, *34*, 1535−1542.
[7] J. Holford, F. Raynaud, B. A. Murrer, K. Grimaldi, J. A. Hart-

 © 2003 Wiley-VCH Verlag GmbH & Co. KGaA, Weinheim

ley, M. Abrams, L. R. Kelland, *Anti-Cancer Drugs Des.* **1998**, *13*, 1−18.
[8] D. Gibson, N. Mansur, K. F. Gean, *J. Inorg. Biochem.* **1995**, *58*, 79−88.
[9] B. E. Bowler, K. J. Ahmed, W. I. Sundquist, L. S. Hollis, E. E. Whang, S. J. Lippard, *J. Am. Chem. Soc.* **1989**, *111*, 1299−1306.
[10] J. B. Le Pecq, N. D. Xuong, C. Gosse, C. Paoletti, *Proc. Natl. Acad. Sci. USA* **1974**, *71(12)*, 5078−5082.
[11] M. Maftouh, R. Besselievre, B. Monserrat, P. Lesca, B. Meunier, H. P. Husson, C. Paoletti;, *J. Med. Chem.* **1985**, *28*, 708−714.
[12] R. Jasztold-Howorko, C. Landras, A. Pierré, G. Atassi, N. Guilbaud, L. Kraus-Berhier, S. Léonce, Y. Rolland, J.-F. Prost, E. Bisagni, *J. Med. Chem.* **1994**, *37*, 2445−2452.
[13] E. Bisagni, R. Jasztold-Howorko, G. Atassi, A. Pierré, *Eur. Pat. Appl.* EP591, *051, Chem. Abstr.* **1994**, *121, 109*, 365r.
[14] C. Landras, R. Jasztold-Howorko, A. Pierre, S. Leonce, N. Guilbaud, L. Kraus-Berthier, C. Guillonneau, Y. Rolland, G. Atassi, E. Bisagni, *Chem. Pharm. Bull.* **1996**, *44(11)*, 2169−2172.
[15] A. Opolski, R. Jasztold-Howorko, A. Croisy, article to be published.
[16] M. J. Cleare, *Platinum Met. Rev.* **1974**, *18*, 122−129.
[17] J. Kuduk-Jaworska, *Polish J. Chem.* **1985**, *59*, 705−712.
[18] G. L. Cook, F. M. Church, *J. Phys. Chem.* **1957**, *61*, 458−402.
[19] A. R. Katritzky, A. R. Hands, R. A. Jones, *J. Chem. Soc.* **1958**, 3165−3167.
[20] J. H. Green, W. Kynaston, H. M. Paisley, *Spectrochim. Acta* **1963**, *19*, 549−564.
[21] E. Spinner, *J. Chem. Soc.* **1963**, 3860−3870.
[22] J. S. Strukl, J. L. Walter, *Spectrochim. Acta, Part A* **1971**, *27*, 209−221.
[23] W. Lao, Ch. Xu, J. Jinmao You, Q. Ou, *Spectrochim. Acta, Part A* **2000**, *56*, 2049−2060.
[24] A. D. Allen, T. Theophanides, *Can. J. Chem.* **1964**, *42*, 1551−1554.
[25] D. M. Adams, J. Chatt, J. Gerratt, A. D. Westland, *J. Chem. Soc.* **1964**, 734−739.
[26] K. Nakamoto, P. J. McCarthy, J. Fujita, R. A. Condrate, G. T. Behnke, *Inorg. Chem.* **1965**, *4*, 36−42.
[27] R. J. H. Clark, C. S. Williams, *Inorg. Chem.* **1965**, *4*, 350−357.
[28] R. A. Walton, *J. Inorg. Nucl. Chem.* **1966**, *28*, 2229−2241.
[29] J. R. Durig, B. R. Mitchell, D. W. Sink, J. N. Willis, A. S. Wilson, *Spectrochim. Acta, Part A* **1967**, *23*, 1121−1135.
[30] T. Boshi, G. Deganello, G. Carturan, *J. Inorg. Nucl. Chem.* **1969**, *31*, 2423−2426.
[31] P. Haake, S. H. Mastin, *J. Am. Chem. Soc.* **1971**, *93*, 6823−6828.
[32] C. Engelter, A. T. Hutton, D. A. Thornton, *J. Mol. Struct.* **1978**, *44*, 22−30.
[33] M. Pfeffer, P. Braunstein, J. Dehand, *Spectrochim. Acta, Part A* **1974**, *30*, 331−340.
[34] E. Bielli, P. M. Gidney, R. D. Gillard, B. T. Heaton, *J. Chem. Soc., Dalton Trans.* **1974**, 2133−2139.
[35] R. H. Herber, M. Croft, M. J. Coyer, B. Bilash, A. Sahiner, *Inorg. Chem.* **1994**, *33*;2422−2426.
[36] M. K. Cooper, D. W. Yaniuk, M. McPartlin, *J. Organomet. Chem.* **1979**, *166*, 241−249.
[37] J. Yoo, J.-H. Kim, Y. S. Sohn, Y. Do, *Inorg. Chim. Acta* **1997**, *263*, 53−60.
[38] S. S. Kamath, V. Uma, T. S. Srivastava, *Inorg. Chim. Acta* **1989**, *161*, 49−56.
[39] P. M. Gidney, R. D. Gillard, B. T Heaton, *J. Chem. Soc., Dalton Trans.* **1973**, 132−134.
[40] N. Chaudhury, R. J. Puddephatt, *J. Organomet. Chem.* **1975**, *84*, 105−115.
[41] V. M. Miskowski, V. H. Houlding, *Inorg. Chem.* **1989**, *28*, 1529−1533.
[42] V. H. Houlding, V. M. Miskowski, *Coord. Chem. Rev.* **1991**, *111*, 145−152.
[43] J. K. Jawad, R. J. Puddephatt, *J. Organomet. Chem.* **1976**, *117*, 297−302.
[44] S. Wimmer, P. Castan, F. L. Wimmer, N. P. Johnson, *J. Chem. Soc., Dalton Trans.* **1989**, 403−412.
[45] J. K. Jawad, F. N. K. Al-Obaidy, J. A. Hammud, F. Al-Azab, *J. Organomet. Chem.* **2000**, *599*, 166−169.
[46] L. Yang, F. M. Wimmer, S. Wimmer, J. Zhao, P. S. Braterman, *J. Organomet. Chem.* **1996**, *525*, 1−8.
[47] P. S. Braterman, J.-I. Song, *Inorg. Chim. Acta* **1991**, *183*, 131−132.
[48] B. Martin, W. R. McWhinnie, G. M. Waind, *J. Inorg. Nucl. Chem.* **1961**, *23*, 207−223.
[49] K. Sone, P. Krumholz, H. Stammreich, *J. Am. Chem. Soc.* **1955**, *77*, 777−780.
[50] L. Gil, E. Moraga, S. Bunel, *Mol. Phys.* **1967**, *12*, 333−339.
[51] G. R. Desiraju, A. Gavezzotti, *Acta Crystallogr., Sect. B* **1989**, *45*, 473−482.
[52] W. I. Sunquist, S. J. Lippart, *Coord. Chem. Rev.* **1990**, *100*, 293−322.
[53] L.-K. Cheng, K.-S. Yeung, C.-M. Che, M.-C. Cheng, Y. Wang, *Polyhedron* **1993**, *12*, 1201−1207.
[54] R. S. Osborn, D. Rogers, *J. Chem. Soc., Dalton Trans.* **1974**, *9*, 1002−1004.
[55] J. Yoo, J.-H. Kim, Y. S. Sohn, Y. Do, *Inorg. Chim. Acta* **1997**, *263*, 53−60.
[56] V. M. Miskowski, V. H. Houlding, Ch.-M. Che, Y. Wang, *Inorg. Chem.* **1993**, *32*, 2518−2524.
[57] J. Kuduk-Jaworska, K. Waszkiewicz, *Transit. Metal Chem.* **2000**, *25*, 443−449.
[58] G. B. Kauffman, D. O. Cowan, *Inorg. Synth.* **1963**, *7*, 239−241, 249−250.
[59] G. M. Sheldrick, SHELXL-97, *Program for Crystal Structure Refinement*, University of Göttingen, Germany, **1997**.
[60] J. J. P. Stewart, *J. Comp. Chem.* **1989**, *10*, 209−220.
[61] J. J. P. Stewart, *J. Comp. Chem.* **1989**, *10*, 221−264.
[62] HyperChem Pro software package by Hypercube, Inc.

Received May 17, 2003
Early View Article
Published Online October 2, 2003

 © 2003 Wiley-VCH Verlag GmbH & Co. KGaA, Weinheim

New $[Ru_3(CO)_{12}]$-Based Catalysts with Imidazolinium Salt, Diimine, or Bis(oxazoline) Ligands and Ruthenium Bis(oxazoline) Complex for Tandem Isomerisation/Claisen Rearrangement of Dienyl Ethers − X-ray Structure of [RuCl{(*R*,*R*)-bis(isopropyloxazoline)}(*p*-cymene)]BF_4

Hamed Ben Ammar,[a] Jérôme Le Nôtre,[a] Mansour Salem,[b] Mohamed T. Kaddachi,[b] Loïc Toupet,[c] Jean-Luc Renaud,[a] Christian Bruneau,[a] and Pierre H. Dixneuf*[a]

Keywords: Ruthenium / Isomerisation / Claisen reaction / Aldehydes / N ligands

The reaction of various 1,7-dienes in the presence of the three-component catalyst **A**: $[Ru_3(CO)_{12}]$/imidazolinium salt/Cs_2CO_3 (1:1:2) leads to the tandem alkene isomerisation/Claisen rearrangement affording γ,δ-unsaturated aldehydes. Other three component catalysts: $[Ru_3(CO)_{12}]$/diimine/Cs_2CO_3 and $[Ru_3(CO)_{12}]$/benzoxazoline or chiral bis(oxazoline)/Cs_2CO_3 offer new active catalytic systems for these tandem reactions. Two ruthenium complexes containing optically active bis(oxazoline), [RuCl{(*R*,*R*)-bis(oxazoline)}(*p*-cymene)]BF_4, were prepared and the X-ray structure of one of them (**18**) was established. The combination of chiral **18**/imidazolinium salt/Cs_2CO_3 (1:1:2) catalysed the above reaction of 1,6-dienes and the results suggest initial catalytic isomerisation followed by a thermal Claisen rearrangement.
(© Wiley-VCH Verlag GmbH & Co. KGaA, 69451 Weinheim, Germany, 2003)

Introduction

The [3,3]-sigmatropic rearrangement of allyl vinyl ethers constitutes a powerful method for accessing γ,δ-unsaturated aldehydes[1] since its discovery by Claisen.[2] This reaction is often limited by the difficulty of introducing the vinyl ether group. The most general routes to vinyl ethers involve organometallic intermediates or acid-catalysed reactions.[3] An alternative method is emerging. It is based on selective isomerisation of allyl groups into vinyl heteroatom intermediates. Ruthenium complexes, such as ruthenium hydride[4] or ruthenium carbonyl[5] derivatives have been used for selective alkene isomerisation. This isomerisation process was also applied to enantioselective catalysis.[6] Recently alkene metathesis ruthenium catalysts have shown a propensity to isomerise alkenes, but leading to competition between isomerisation and metathesis.[7,8]

The $[RuCl_2(PPh_3)_3]$-catalysed Claisen rearrangement of diallyl ethers occur at a high temperature (150 °C),[9] whereas selected iridium[10] and rhodium[11] complexes tend to promote this transformation under milder conditions. It is worth noting that an indenylidene ruthenium catalyst has performed ring closing metathesis (RCM), isomerisation and a Claisen rearrangement, successively.[8]

By contrast we found that ruthenium catalysts prepared in situ for the RCM of 1,6-dienes and 1,6-enynes[12−14] did not perform RCM of 1,7-dienyl ethers but selectively led to tandem isomerisation/Claisen rearrangement affording γ,δ-unsaturated aldehydes[15] [Equation (1)]. The in situ generated catalyst, was originally prepared with $[RuCl_2(p\text{-cymene})]_2$ as a ruthenium source,[12] but the combination of $[Ru_3(CO)_{12}]$, with an imidazolinium salt appeared to be more efficient as reported in our preliminary communication.[15]

(1)

We now wish to report (i) the detailed study of in situ prepared catalysts for isomerisation/Claisen rearrangement of 1,7- and 1,6-dienyl ethers into γ,δ-unsaturated aldehydes, (ii) we show that new $[Ru_3(CO)_{12}]$-based catalysts containing sterically hindered diimine or the bis(oxazoline) ligand, and bis(oxazoline)ruthenium complex as the ruthenium source and imidazolinium salt in the presence of Cs_2CO_3, are active catalysts for these tandem catalytic reactions. (iii) The synthesis of new chiral bis(oxazoline)ruthenium arene derivatives, used as catalyst precursors, is described with the X-ray structure of one of them.

[a] Institut de Chimie de Rennes, UMR 6509 CNRS-Université de Rennes 1, "Organométalliques et Catalyse", Campus de Beaulieu, 35042 Rennes Cedex, France
[b] Laboratoire de Chimie Appliquée, Faculté des Sciences de Sfax, 3000, Tunisia
[c] UMR 6626 CNRS-Université de Rennes 1 − "Groupe Matière Condensée et Matériaux", Campus de Beaulieu, 35042 Rennes, France

Results and Discussion

1. Catalytic Reaction Principle and Influence Factors

Recently, in a preliminary study[15] it was revealed that the in situ prepared three-component catalyst for the ring closing metathesis (RCM) reaction of 1,6-dienes and 1,6-enynes: $[RuCl_2(p\text{-cymene})]_2$/a hindered imidazolinium chloride/Cs_2CO_3, when applied to allyl homoallyl ethers with a 1,7-diene structure, the latter were catalytically transformed into γ,δ-unsaturated aldehydes rather than the expected RCM six-membered cyclic compounds. The new three-component system consisting of **A** = $[Ru_3(CO)_{12}]$, 1,3-bis(2,6-diisopropylphenyl)imidazolinium chloride, and cesium carbonate appeared to be the most active catalyst for this transformation of 1,7-dienes **1** into unsaturated aldehydes **4** (Scheme 1). The reaction takes place via a double C=C isomerisation of allyl and homoallyl branches via the intermediates **2** and **3**, followed by a Claisen rearrangement to give **4**.

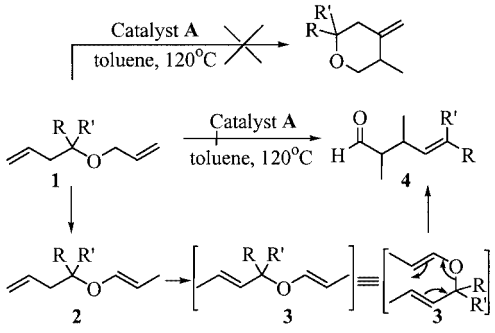

Scheme 1

The use of the three-component catalytic system **A** has now been applied to the selective transformation of various 1,7-dienes. The etherated dienes **5** and **6** were easily prepared from the corresponding ketones, in two steps, by addition of allylmagnesium bromide, followed by allylation of the corresponding homoallyl alcohols (Scheme 2).

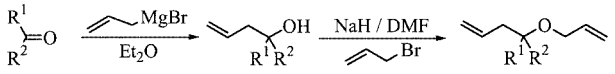

5 : R^1 = Ph, R^2 = Me, 57%
6 : R^1, R^2 = -$(CH_2)_5$-, 82%

Scheme 2

In the presence of the catalytic system **A** based on $[Ru_3(CO)_{12}]$ (1.67 mol %, that is 5 mol % of ruthenium atoms), 1,3-bis(2,6-diisopropylphenyl)imidazolinium chloride (5 mol %) and cesium carbonate (10 mol %) in toluene, these dienes have been totally converted into their corresponding γ,δ-unsaturated aldehydes after 1 hour at 120 °C (Scheme 3). The aldehydes **7** and **8** were obtained in 78% and 71% yield, respectively, as a mixture of diastereoisomers due to the formation of stereogenic centres, and their

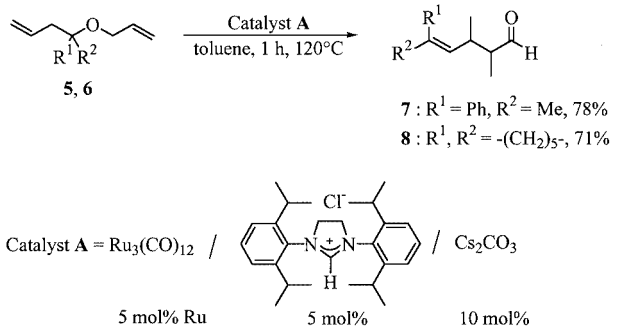

Scheme 3

NMR spectroscopic analyses were in accordance with those in the literature.[10b]

The absence of one of the three components of the catalytic system A gave no conversion, not even isomerisation. This observed reaction indicates that the isomerisation of the terminal alkene branches is faster than the RCM and cycloisomerisation reactions leading to six-membered rings. The RCM involving disubstituted C=C bonds is known to be disfavoured, thus in that case, after isomerisation no competition occurs between isomerisation and metathesis, and hence high selectivity in aldehyde formation is observed.

It is noteworthy that the above in situ generated ruthenium catalyst **A** selectively isomerises terminal alkene branches, by displacing the C=C bond towards the heteroatom, to produce a vinyl ether group.

The influence of the catalyst concentration and temperature has been investigated. This study was performed on the 1,6-diene **9** which is more easily transformed into the corresponding γ,δ-unsaturated aldehyde **10**, than the dienes **5** and **6**. It involves one simple allyl to vinyl isomerisation followed by a Claisen rearrangement (Scheme 4).

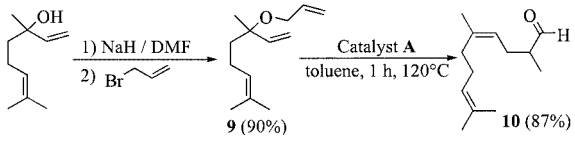

Scheme 4

The commercially available linalol was first converted by allylation in 90% yield to the 1,6-diene **9**. In the presence of the catalytic system **A,** using 5 mol % of ruthenium, this diene was transformed into the aldehyde **10**[16] at various temperatures. The transformation of **9** into aldehyde **10** was very slow at 60 °C, it reached completion at 80 °C for 3 h and alternatively within 1 h at 120 °C (see Table l).

A minimum temperature of 80 °C was required to reach completion (Table 1). By performing the transformation at 80 °C, but varying the diene/catalyst ratio, it was observed that decreasing this ratio under 5 mol % (3%, 0.5%) led to longer reaction times (Entries 3,5,6). Thus, for further tandem isomerisation/Claisen reaction of unsaturated ethers, 5 mol % of ruthenium catalyst was used between 80 °C and

 © 2003 Wiley-VCH Verlag GmbH & Co. KGaA, Weinheim

Table 1. Influence of temperature, time and ruthenium loading on the transformation **9** → **10**

Entry	Mol-% [Ru]	Temp. (°C)	Reaction time (h)	Conversion (%)
1	5	40	16	0
2	5	60	16	22
3	5	80	3	100
4	5	120	1	100
5	3	80	60	80
6	0.5	80	96	20

120 °C, and a reaction time of 1−3 h was expected according to the nature of the substrate.

2. Use of Dinitrogen Chelating Ligands in Ruthenium Catalyst Precursors

With the objective of finding new efficient catalysts for the above tandem catalytic reactions several catalytic modifications were investigated. Since well-defined chelating dinitrogen containing ruthenium complexes of type [RuCl{bis(oxazoline)}(arene)]$^+$ X^- have already shown some activity for this reaction,[17] we have explored the catalyst modification based on [$Ru_3(CO)_{12}$], as a ruthenium source, by replacing the bulky imidazolinylidene precursor by a sterically hindered diimine or bis(oxazoline)ligand.

2.1 Diimine Ruthenium Precursors

Catalyst **B** was generated in situ by a combination of [$Ru_3(CO)_{12}$] (5 mol % of Ru atoms), diimine **L** (5 mol %) and Cs_2CO_3 (10 mol %) and was evaluated on the transformation of the diene **9** into the aldehyde **10** in toluene at 80 °C and the conversions were monitored using proton NMR spectroscopy by measuring the **10/9** ratio (Scheme 5). Several diimines **L1**−**L6**[18] containing bulky R groups were evaluated.

The results show that the diimines lead to an in situ generated catalyst performing the tandem reactions at 80 °C for 16 h. The nature of the diimine drastically influences the catalytic activity. The diimines $\mathbf{L_6}$ (96%) $\mathbf{L_2}$ (84%) and $\mathbf{L_1}$ (76%) offer the best catalyst efficiencies. Especially when the reaction is performed at 120 °C, the ferrocenyl containing diimine $\mathbf{L_6}$ leads to the best activity and the corresponding catalyst **B** completely converts **9** into **10** within 6 hours.

However, the resulting catalyst **B** requires a longer reaction time to reach suitable conversion into aldehyde **10** than catalyst **A**; catalyst **B** requires 16 h at 80 °C with the most activating diimine. These results indicate that the preliminary catalytic alkene isomerisation and the overall tandem reaction are not at all restricted to imidazolinium ruthenium intermediates. Moreover they show that the presence of cesium carbonate does allow the reaction to proceed. Cs_2CO_3 was originally used for the deprotonation of the imidazolinium salt to generate an imidazolinylidene ligand. In the absence of Cs_2CO_3 in catalyst **B** no isomerisation takes place. Although its role is not elucidated, cesium carbonate thus has a crucial influence on the ruthenium-catalysed isomerisation reaction.

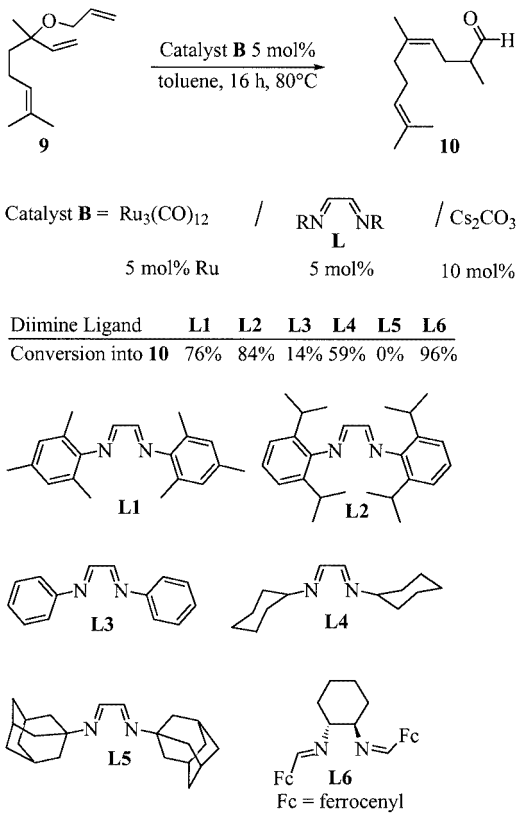

Scheme 5

It is noteworthy that profit can be taken from the slightly lower catalytic activity of catalyst **B** to perform the selective isomerisation without Claisen rearrangement. The isomerisation of the diene **5**, containing a phenyl and methyl groups at the homoallylic position, is more difficult to perform than that of **9**. The reaction of **5** with catalyst **B,** containing the $\mathbf{L_1}$ diimine, in toluene, at 120 °C for 16 h does not afford the expected unsaturated aldehyde **7** but is completely transformed into the vinyl homoallyl ether **11** resulting simply from the allyl to vinyl isomerisation (Scheme 6). Thus, the phenyl group inhibits the homoallyl to allyl isomerisation with catalyst **B** that readily takes place with catalyst **A** (Scheme 3). This experiment shows that the *O*-allyl branch of the 1,7-diene **1** is first isomerised to give an intermediate of type **2** and that the ease of the second isomerisation further controls the Claisen rearrangement. It also reveals the interest of less active catalysts to perform only one reaction step.

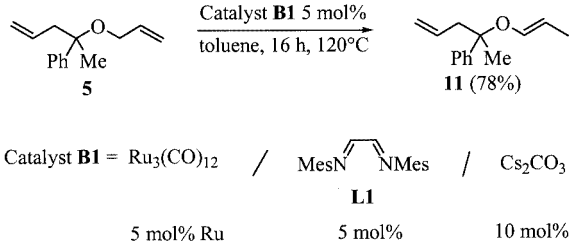

Scheme 6

 © 2003 Wiley-VCH Verlag GmbH & Co. KGaA, Weinheim

The large influence of the nature of the ligand on catalyst activity and the ease of generating these catalysts in situ suggest that the association of various ruthenium sources with various ligands, should be investigated to reveal new active catalysts.

2.2 Bis(oxazoline) Ruthenium Precursors

Achiral or chiral bis(oxazolines) are commonly used as chelating nitrogen ligands in catalysis nowadays,[19] because they are easily prepared and have been shown to significantly modify the catalytic metal site with respect to phosphane or carbene ligands.[20] Thus, catalyst **C** analogous to catalyst **B**, by replacing the diimine **L** by the benzoxazoline derivative **12**,[21] has been evaluated for the transformation of 1,6-diene **13** into aldehyde **14** (Scheme 9). The results show that the bis(oxazoline)ligand **12** associated with $[Ru_3(CO)_{12}]$ in the presence of Cs_2CO_3 promotes the tandem reactions with an activity analogous to that of the most active diimine-containing catalysts. The efficiency of catalyst **C** is analogous to that of catalyst **B**, as the transformation was complete after 16 h at 120 °C and led to the isolation of 87% of aldehyde **14**[22] (Scheme 7).

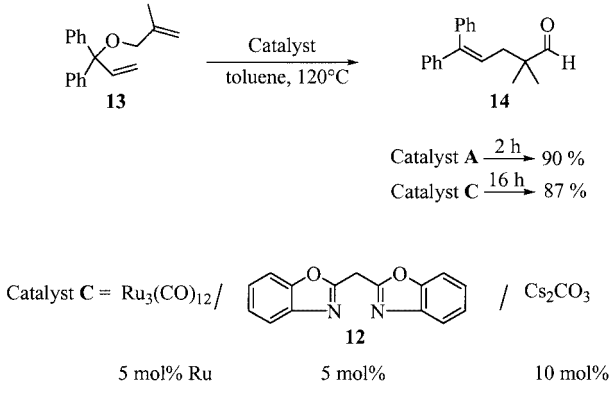

Scheme 7

An advantage to generating a catalyst in situ, from a metal source and a ligand, is related to the easy access of the chiral version of the catalyst. Catalysts of type **C** could thus easily be transformed into chiral catalysts using an optically active bis(oxazoline). The transformation of the 1,6-diene **15** into the aldehyde **16**, containing only one chiral centre, was first considered.

The interest in using a chiral catalyst was to investigate whether, after isomerisation, the Claisen step leading to the creation of a chiral centre, was influenced by the catalyst or essentially a thermal process. An enantiomeric excess is expected to be observed in the first process and not in the second. The achiral catalyst **A** performed the tandem reaction at 120 °C, and after 3 h the racemic aldehyde **16** was isolated (78%) (Scheme 8). Then catalyst **C** was modified into catalyst **D** by the introduction of the optically active (*R*,*R*)-bis(oxazoline)**17**,[19] instead of **12**. Catalyst **D** gave an activity similar to that of catalyst **C** and afforded 60% of aldehyde **16**. The isolated aldehyde **16** *showed no enantiomeric excess,* thus indicating that the chiral catalyst **D** gave no stereochemical induction, unless the racemization of the aldehyde takes place (Scheme 8).

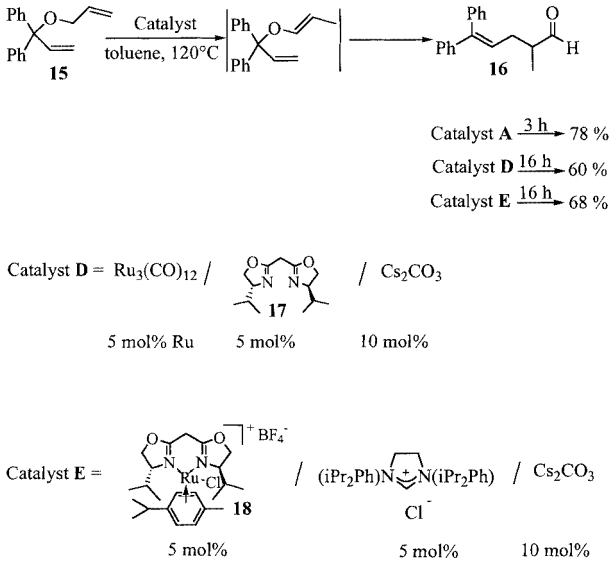

Scheme 8

The bis(oxazoline) **17** was then used to prepare a well-defined ruthenium(II) (arene) complex according to the procedure we previously used for *achiral* bis(oxazoline)ruthenium complexes.[17] Two equiv. of the bis(oxazoline) **17** were reacted with the ruthenium complex $[RuCl_2(p\text{-cymene})]_2$ in methanol at room temperature with two equiv. of NH_4BF_4 and the orange complex **18** was isolated in 98% yield (Scheme 9). Analogously, the optically active bis(oxazoline) **19**[19f] led to the ruthenium complex **20.**

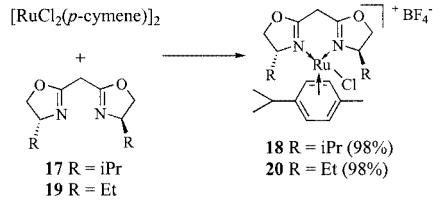

Scheme 9

Complex **18** does not catalyse the **15** → **16** transformation, even in the presence of two equiv. of Cs_2CO_3. By contrast complex **18** with one equiv. of imidazolinium salt and two equiv. of Cs_2CO_3 (Catalyst **E**), allowed the transformation of **15** into **16**, isolated in 68% yield after 1 h at 120 °C (Scheme 8). It is worth noting that with the well-defined chiral ruthenium complex **18**, the resulting aldehyde **16,** did not exhibit an enantiomeric excess.

The above results show that a bis(oxazoline) associated with $[Ru_3(CO)_{12}]$ and a bis(oxazoline)ruthenium complex associated with an imidazolinium salt performed the isomerisation of 1,6-dienes, in the presence of Cs_2CO_3. But no enantiomeric excess was observed when a chiral centre was formed in the presence of an optically active catalytic species. This suggests that the ruthenium complex, associated with Cs_2CO_3, plays an isomerisation catalyst role and when the required 1,5-diene is formed in situ, a thermal Claisen

 © 2003 Wiley-VCH Verlag GmbH & Co. KGaA, Weinheim

rearrangement takes place, unless the imidazolylidene ligand displaces the chiral ligand from the ruthenium site.

3. Crystal Structure of Complex 18

The structure of these bis(oxazoline)ruthenium complexes is confirmed by the crystal structure of the complex **18**. The ORTEP is presented in Figure 1 and the principal bond lengths and angles are reported in Table 2. The crystal data and structure refinement are gathered in Table 3.

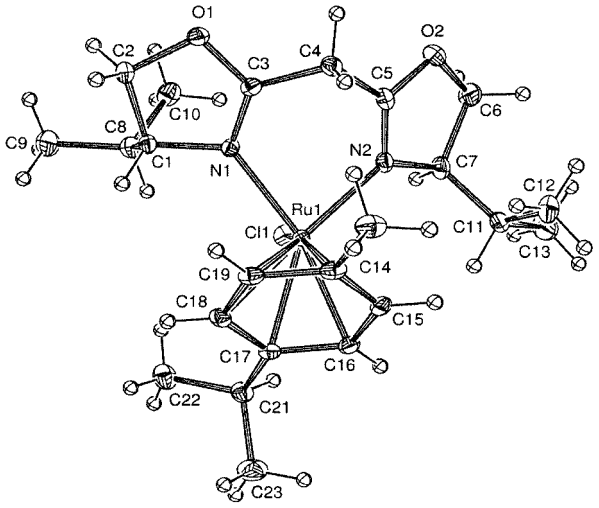

Figure 1. X-ray structure of complex **18**

Table 2. Selected bond lengths and angles

Bond lengths	Å	Angles	°
Ru(1)−N(2)	2.129(2)	C(3)−C(4)−C(5)	110.9(2)
Ru(1)−N(1)	2.130(2)	N(1)−C(3)−C(4)	125.8(2)
N(1)−C(3)	1.285(4)	N(2)−C(5)−C(4)	126.2(2)
N(2)−C(5)	1.279(4)		

The structure shows the chirality of the complex with a classical piano stool geometry. This structure reveals that the bis(oxazoline) ligand presents only slight distortions due to the coordination to the metal centre. Indeed, the C(3)−C(4)−C(5) angle of 110.9° is close to the expected value for an sp^3 carbon atom and the N(1)−C(3)−C(4) and N(2)−C(5)−C(4) angles (125.8(2) and 162.2(2)°) correspond to the value of an sp^2 carbon atom. The two oxazoline rings are nearly in the same plane and the distortion between the two planes is around 10°. The ruthenium-nitrogen bonds have similar distances to those of related complexes.[23]

Conclusion

The above results show that tandem isomerisation/Claisen reactions of etherated 1,7-dienes and 1,6-dienes are catalysed by in situ prepared ruthenium catalysts to selectively produce γ,δ-unsaturated aldehydes. The best catalyst appears to consist of the combination of [$Ru_3(CO)_{12}$], an imidazolinium salt that is a bulky heterocyclic carbene precursor and Cs_2CO_3. However the combination of [$Ru_3(CO)_{12}$], a bulky diimine or bis(benzoxazoline) ligand, in the presence of Cs_2CO_3 results in a slightly less efficient catalyst, which is still able to operate at 80 °C. The use of the optically active bis(oxazoline) ligand or complex in the formation of a chiral centre, in the unsaturated aldehyde product, gave no enantiomeric excess, and thus there is no evidence that the Claisen rearrangement step is also catalysed by the chiral ruthenium catalyst under these conditions. The ease of in situ preparation of such catalysts from a ruthenium source and a variety of ligands open the route to the use of high throughput experiment tools to discover new or more efficient catalysts.

Table 3. Crystal data and structure refinement of **18**·$(CH_3)_2CO$

Chemical formula[a]	$RuC_{23}H_{36}BClO_2$, BF_4, C_3H_6O
Formula mass	653.95
Wavelength (Å)	0.71073
T (K)	120(1)
Crystal size (mm)	0.25 × 0.22 × 0.12
Crystal system	orthorhombic
a (Å)	10.9218(2)
b (Å)	13.6861(2)
c (Å)	19.8514(4)
V (Å^3)	2967.3(9)
Z	4
$D_{calcd.}$ (mg m^{-3})	1.464
μ (mm^{-1})	0.673
F(000)	1352
2Θ range (deg)	1.0−27.48
No. of reflections collected	23815
No. of indep. reflections	6792
R_{int}	0.038
Refined method	full-matrix least-square on F^2
Refined parameters	344
Goodness of fit on F^2	1.097
Final R indices [$I > 2\sigma(I)$]	
$R1$[a], $wR2$[b]	0.0312, 0.0682
(all data)	0.0388, 0.0724
Largest diff. peak/hole (e·Å^{-3})	1.136/−0.503

[a] $R1 = \Sigma(||F_o| - |F_c||)/\Sigma|F_o|$. [b] $wR2 = \{\Sigma w(F_o^2 - F_c^2)^2]/\Sigma w(F_o^2)^2]^{1/2}$.

Experimental Section

General Experimental Procedures: All experiments were carried out in Schlenk tubes under nitrogen. Diethyl ether and tetrahydrofuran were dried by refluxing over sodium/benzophenone under argon, while toluene was dried with sodium, and dichloromethane was purified over calcium hydride. Methanol was used without further purification and degassed before use.

^1H and ^{13}C NMR spectra were recorded with a Bruker AC 200 MHz spectrometer. GC-MS were performed with a CE Instrument GC 8000 Top (capillary column OV1, 25 m × 0.35 mm, 0.1−0.15 μm) chromatograph linked to an Automass II Finnigan MAT (70 eV) apparatus. Infra-red spectra were recorded in KBr pellets using a Nicolet 205 FT-IR. UV/Visible spectra were recorded with a KONTRON UVIKON 941 spectrometer in diluted dichloromethane (*ca*, 10^{-4} mol·L^{-1}). Microanalyses were performed by the Service Central d'Analyses du CNRS (Vernaison, France).

 © 2003 Wiley-VCH Verlag GmbH & Co. KGaA, Weinheim

General Procedures. Procedure A − Synthesis of the Homoallylic Alcohols via Allylmagnesium Addition to a Ketone: In a two-necked flask under nitrogen, equipped with a reflux condenser, magnesium turnings (2 equiv.) were heated under vacuum for 5 minutes by means of a heat gun. After cooling to room temperature, diethyl ether (1 mL per 2 mmol of magnesium) was added. Allyl bromide (1.2 equiv.) was then slowly added to the vigorously stirred mixture and the flask was introduced into an ice bath as soon as the diethyl ether ebullition started. After the addition was complete the reaction mixture was stirred for 1 h at 0 °C. The ketone (1 equiv.) was then added dropwise in diethyl ether (1 mL per 3 mmol of ketone). The reaction mixture was stirred for 30 minutes at 0 °C, followed by 4 h at room temperature. After addition of a 1 N HCl solution and extraction with diethyl ether, the corresponding homoallylic alcohol was obtained and used without purification.

Procedure B − Alcohol Allylation Reaction: Sodium hydride (1.2 equiv.) and dry dimethylformamide (1.5 mL per mmol of alcohol) were introduced into a Schlenk tube under nitrogen. The alcohol (1 equiv.) in dimethylformamide (1 mL per mmol of alcohol) was slowly added at 0 °C. After 30 minutes, allyl bromide (1.3 equiv.) was added dropwise and the stirring was continued at 0 °C for 30 minutes and at room temperature for 4 h. After hydrolysis extraction with diethyl ether and drying over $MgSO_4$, the crude product was then purified by flash chromatography over silica gel using a low polar mixture of diethyl ether and heptane.

Procedure C − Synthesis of the Allylic Alcohols via Vinylation of Aldehydes and Ketones: A Schlenk tube under nitrogen containing anhydrous $CeCl_3$ (0.1 equiv.) was first heated at 150 °C for 5 minutes and then cooled down to room temperature. Tetrahydrofuran (2 mL per mmol of ketone or aldehyde) was introduced followed by the ketone or the aldehyde (1 equiv.) and the reaction mixture was stirred at room temperature for 30 minutes. After cooling to 0 °C, vinylmagnesium bromide (1.0 M solution in tetrahydrofuran, 1.2 equiv.) was added dropwise. The reaction mixture was stirred at 0 °C for 1 h and then at room temperature 16 h. After quenching by slow addition of a 1 N HCl solution and extraction with diethyl ether, the corresponding allylic alcohol was obtained and used in the following step without purification.

Procedure D − General Procedure using the $[Ru_3(CO)_{12}]$-Based Catalyst for Tandem Isomerisation/Claisen Reaction: $[Ru_3(CO)_{12}]$ (5/3 mol % = 5 mol % of Ru atoms), 1,3-bis(2,6-diisopropylphenyl)imidazolinium chloride (5 mol %), cesium carbonate (10 mol %) and toluene (7.5 mL per mmol of diene) were introduced into a Schlenk tube under nitrogen. The reaction mixture was stirred for 5 minutes at room temperature and the diene was then added. After 1 hour of heating at 120 °C, the solvent was removed under reduced pressure and the crude product was extracted with heptane, filtered and the solvents evaporated to dryness. After chromatography on silica using a mixture of diethyl ether/heptane as eluent and/or bubble-to-bubble distillation the corresponding aldehyde was isolated as a colourless oil as a mixture of diastereoisomers.

Preparation of the 1,7-Dienes

2-Allyloxy-2-phenylpent-4-ene (5):[10b]

Following Procedure A: Allyl bromide (1.92 mL, 20.6 mmol) was added to a solution of magnesium turnings (0.83 g, 34.2 mmol) in diethyl ether (15 mL). Acetophenone (2.0 mL, 17.3 mmol) in diethyl ether (6 mL) was then added. Subsequent treatment gave the corresponding homoallylic alcohol as a yellow oil, which was used without purification for the next step.

Following Procedure B: Homoallylic alcohol (17.3 mmol) in dimethylformamide (17 mL) was added to a solution of sodium hydride (60% in mineral oil, 0.82 g, 20.6 mmol) in of dimethylformamide (30 mL). After addition of allyl bromide (2.0 mL, 22.5 mmol) and subsequent treatment, the crude was purified by flash chromatography over silica gel using diethyl ether/heptane (1:40) as eluent to afford the corresponding 1,7-diene **5** as a colourless oil (2.01 g, 57% yield). ^{1}H NMR (200 MHz, $CDCl_3$): δ = 1.53 (s, 3 H, CH_3), 2.53−2.64 [m, 2 H, CH_2C(Ph)(Me)OR], 3.61−3.85 (m, 2 H, OCH_2CH=CH$_2$), 4.94−5.45 [m, 4 H, 2 × (CH=CH_2)], 5.58−5.98 [m, 2 H, 2 × (CH=CH$_2$)], 7.20−7.48 (m, 5 H, Ph) ppm. ^{13}C NMR (50 MHz, $CDCl_3$): δ = 23.5 (CH_3), 47.9 [CH$_2$C(Ph)(Me)OR], 63.9 (OCH$_2$CH=CH$_2$), 78.9 [C(Ph)(Me)], 115.6 (OCH$_2$CH=CH$_2$), 117.7 [C(Ph)(Me)CH$_2$CH=CH$_2$], 126.3, 127.1, 128.3 (CH arom.), 134.3 (OCH$_2$$C$H=CH$_2$), 135.7 [C(Ph)(Me)CH$_2$$C$H=CH$_2$], 145.1 (C arom.) ppm. MS (EI): *m*/*z* (%) = 202 (<1) $[M]^+$, 161 (35), 143 (11), 129 (52), 115 (25), 105 (15), 103 (18), 91 (19), 77 (48), 65 (15), 63 (15), 57 (15), 51 (35), 43 (100), 41 (56).

1-Allyl-1-allyloxycyclohexane (6):[10b]

Following Procedure A: Allyl bromide (0.96 mL, 10.3 mmol) was added to a solution of magnesium turnings (0.42 g, 17.1 mmol) in diethyl ether (10 mL). Cyclohexanone (0.9 mL, 8.6 mmol) in diethyl ether (3 mL) was then added. Subsequent treatment gave the corresponding homoallylic alcohol as a yellow oil, which was used without purification for the next step.

Following Procedure B: Homoallylic alcohol (8.6 mmol) in dimethylformamide (9 mL) was added to a solution of sodium hydride (60% in mineral oil, 0.41 g, 10.3 mmol) in dimethylformamide (15 mL). After addition of allyl bromide (1.0 mL, 11.3 mmol) and subsequent treatment, the crude was purified by flash chromatography over silica gel using diethyl ether/heptane (1:40) as eluent to afford the corresponding 1,7-diene **6** as a colourless oil (1.32 g, 85% yield). ^{1}H NMR (200 MHz, $CDCl_3$): δ = 1.61−1.79 (m, 10 H, 5 × CH_2), 2.31−2.43 [m, 2 H, CH_2C(Cy)OR], 3.85−3.91 (m, 2 H, OCH_2CH=CH$_2$), 4.95−5.34[m, 4 H, 2 × (CH=CH_2)], 5.55−6.02 [m, 2 H, 2 × (CH=CH$_2$)] ppm. ^{13}C NMR (50 MHz, $CDCl_3$): δ = 22.0 (2 × *m*-CH_2 of Cy), 26.7 (*p*-CH_2 of Cy), 34.5 (2 × *o*-CH_2 of Cy), 51.2 [CH$_2$C(Cy)OR], 61.3 (OCH$_2$CH=CH$_2$), 74.8 [C(Cy)], 114.6 (OCH$_2$CH=CH$_2$), 116.9 [C(Cy)CH$_2$CH=CH$_2$], 134.3 (OCH$_2$$C$H=CH$_2$), 136.9 [C(Cy)CH$_2$$C$H=CH$_2$] ppm. MS (EI): *m*/*z* (%) = 180 (<1) $[M]^+$, 147 (14), 133 (24), 119 (11), 105 (12), 93 (26), 91 (31), 79 (58), 77 (29), 67 (40), 65 (19), 55 (19), 53 (25), 41 (100), 39 (44).

Tandem Isomerisation/Claisen Rearrangement Reactions

2,3-Dimethyl-5-phenylhex-4-enal (7):[10b]

Following Procedure D: $[Ru_3(CO)_{12}]$ (26.3 mg, 5 mol % of ruthenium), 1,3-bis(2,6-diisopropylphenyl)imidazolinium chloride (52.7 mg, 5 mol %), Cs_2CO_3 (80.5 mg, 10 mol %), toluene (25 mL) and diene **5** (0.5 g, 2.47 mmol) were stirred at 120 °C for 1 h. After treatment and distillation, the aldehyde **7** was obtained as a colourless oil as a mixture of diastereoisomers (0.39 g, 78% yield). ^{1}H NMR (200 MHz, $CDCl_3$): δ = 1.08−1.19 [m, 6 H, 2 × [CH(CH_3)], 2.07 [s, 3 H, (CH_3)(Ph)C=CH], 2.28−2.43 [m, 1 H, CH(CH$_3$)CH-(CH$_3$)CHO], 2.89−3.05 [m, 1 H, CH(CH$_3$)CH(CH$_3$)CHO], 5.52−5.66 [m, 1 H, (CH$_3$)(Ph)C=CH)], 7.22−7.39 (m, 5 H, Ph), 9.40−9.70 (m, 1 H, CHO) ppm. ^{13}C NMR (50 MHz, $CDCl_3$): δ = 11.2 [CH(CH$_3$)CHO], 16.3 [CH(CH$_3$)CH(CH$_3$)CHO], 18.9 [(CH$_3$)-(Ph)C=CH], 34.0 [CH(CH$_3$)CH(CH$_3$)CH], 52.3 [CH(CH$_3$)CH-(CH$_3$)CH], 125.7, 126.9, 128.2 (CH arom.), 130.2 [(CH$_3$)(Ph)C=C], 136.2 [(CH$_3$)(Ph)C=CH], 143.5 (C arom.), 205.2 (CHO) ppm.

 © 2003 Wiley-VCH Verlag GmbH & Co. KGaA, Weinheim

MS (EI): *m*/*z* (%) = 202 (8) $[M]^+$, 145 (64), 143 (12), 131 (12), 129 (30), 118 (100), 117 (52), 115 (34), 91 (65), 79 (13), 77 (44), 65 (22), 63 (13), 53 (13), 51 (26), 41 (35), 39 (31).

4-Cyclohexylidene-2,3-dimethylbutyraldehyde (8):[10b]

Following Procedure D: [$Ru_3(CO)_{12}$] (26.3 mg, 5mol % of ruthenium), 1,3-bis(2,6-diisopropylphenyl)imidazolinium chloride (52.7 mg, 5 mol %), Cs_2CO_3 (80.5 mg, 10 mol %), toluene (25 mL) and diene **6** (0.45 g, 2.47 mmol) were stirred at 120 °C for 1 h. After treatment and distillation, the aldehyde **8** (0.32 g, 71% yield) was obtained as a colourless oil as a mixture of diastereoisomers. ^{1}H NMR (200 MHz, $CDCl_3$): δ = 0.91−1.10 [m, 6 H, CH(C*H*$_3$)-CH(C*H*$_3$)CHO], 1.40−1.85 (m, 10 H, 5 × C*H*$_2$), 2.25−2.50 [m, 1 H, CH(CH$_3$)C*H*(CH$_3$)CHO], 2.62−2.82 [m, 1 H, C*H*(CH$_3$)-CH(CH$_3$)CHO], 5.69−5.91 [m, 1 H, (Cy)C=C*H*], 9.55−9.60 (m, 1 H, C*H*O) ppm. ^{13}C NMR (50 MHz, $CDCl_3$): δ = 10.1 [CH(*C*H$_3$)CHO], 17.3 [CH(*C*H$_3$)CH(CH$_3$)CHO], 22.8 (2 × *m*-*C*H$_2$ of Cy), 26.2 (*p*-*C*H$_2$ of Cy), 33.2 [*C*H(CH$_3$)CH(CH$_3$)CHO], 33.5 [(*E*)-*o*-*C*H$_2$ of Cy], 41.2 [(*Z*)-*o*-*C*H$_2$ of Cy], 52.3 [CH(CH$_3$)*C*H(CH$_3$)CH], 123.7 [(Cy)C=*C*H], 140.5 [(Cy)*C*=CH], 205.7 (*C*HO) ppm. MS (EI): *m*/*z* (%) = 180 (1) $[M]^+$, 162 (10), 81 (74), 79 (26), 77 (21), 69 (17), 67 (69), 65 (15), 55 (100), 53 (31), 51 (11), 43 (16), 41 (92), 39 (43).

Preparation of the 1,6-Dienes

3-Allyloxy-3,7-dimethylocta-1,6-diene (9):

Following Procedure B: Linalol (6.5 mmol) in dimethylformamide (7 mL) was added to a solution of sodium hydride (60% in mineral oil, 0.31 g, 7.8 mmol) in dimethylformamide (15 mL). After addition of allyl bromide (0.73 mL, 8.4 mmol) and subsequent treatment, the crude was purified by flash chromatography over silica gel using diethyl ether/heptane (1:30) as eluent to afford the corresponding 1,6-diene **9** (1.13 g, 90% yield) as a colourless oil. ^{1}H NMR (200 MHz, $CDCl_3$): δ = 1.22 (s, 3 H, C*H*$_3$), 1.49−1.58 [m, 5 H, CH$_2$C*H*$_2$CH=C(CH$_3$)$_2$, (*E*) CH$_2$CH$_2$CH=C(C*H*$_3$)$_2$], 1.63−1.69 [m, 3 H, (*Z*) CH$_2$CH$_2$CH=C(C*H*$_3$)$_2$], 1.92−2.05 [m, 2 H, C*H*$_2$CH$_2$CH=C(CH$_3$)$_2$], 3.80 (dt, ^3J = 5.2, ^4J = 1.6 Hz, 2 H, OC*H*$_2$CH=CH$_2$), 5.04−5.30 [m, 5 H, C*H*=C(CH$_3$)$_2$, C(CH$_3$)(R)$_2$-CH=C*H*$_2$, OCH$_2$CH=C*H*$_2$], 5.70−5.99 [m, 2 H, C(CH$_3$)(R)$_2$C*H*=CH$_2$, OCH$_2$C*H*=CH$_2$] ppm. ^{13}C NMR (50 MHz, $CDCl_3$): δ = 17.7 (*C*H$_3$), 22.3 [(*E*)-CH$_2$CH$_2$CH=C(*C*H$_3$)$_2$], 22.4 [CH$_2$*C*H$_2$CH=C(CH$_3$)$_2$], 25.7 [(*Z*)-CH$_2$CH$_2$CH=C(*C*H$_3$)$_2$], 39.8 [*C*H$_2$CH$_2$CH=C(CH$_3$)$_2$], 63.5 (O*C*H$_2$CH=CH$_2$), 77.5 [*C*(CH$_3$)(R)$_2$CH=CH$_2$], 114.5 [C(CH$_3$)(R)$_2$CH=*C*H], 115.5 (OCH$_2$CH=*C*H$_2$), 124.5 [*C*H=C(CH$_3$)$_2$], 131.4 [CH=*C*(CH$_3$)$_2$], 136.0 (OCH$_2$*C*H=CH$_2$), 143.0 [C(CH$_3$)(R)$_2$*C*H=CH$_2$] ppm. MS (EI): *m*/*z* (%) = 194 (<1) $[M]^+$, 136 (25), 121 (44), 111 (50), 107 (15), 95 (23), 93 (36), 91 (17), 82 (13), 80 (100), 71 (12), 69 (49), 67 (39), 55 (44), 53 (22), 42 (40), 40 (34).

{1-[Isoprop-2-enyl)oxy]-1-(phenyl)prop-2-enyl}benzene (13):

Following Procedure C: Benzophenone (3.0 g, 16.5 mmol) was added to $CeCl_3$ (0.41 g, 1.65 mmol) in tetrahydrofuran (30 mL) at room temperature. Vinylmagnesium bromide (20.0 mL, 20.0 mmol) was then added at 0 °C. Subsequent treatment afforded the corresponding allylic alcohol as a pale yellow oil used without purification for the next step.

Following Procedure B: Allylic alcohol (16.5 mmol) in dimethylformamide (15 mL) was added to a solution of sodium hydride (60% in mineral oil, 0.86 g, 19.8 mmol) in dimethylformamide (25 mL). After the addition of 2-methylpropenyl chloride (2.2 mL, 19.8 mmol) and subsequent treatment, the crude was purified by flash chromatography over silica gel using diethyl ether/heptane (1:20) as eluent to afford an orange oil which was then bubble-to-bubble distilled to give the corresponding 1,6-diene **13** (3.74 g, 86% yield) as a colourless oil. ^{1}H NMR (200 MHz, $CDCl_3$): δ = 2.00 (s, 3 H, C*H*$_3$), 3.94−4.00 [m, 2 H, OC*H*$_2$C(CH$_3$)=CH$_2$], 5.15−5.63 [m, 4 H, C(CH$_3$)=C*H*$_2$, C(Ph)$_2$CH=C*H*$_2$], 6.69−6.84 [m, 1 H, C(Ph)$_2$C*H*=CH$_2$], 7.42−7.55 (m, 6 H, H arom.), 7.62−7.72 (m, 4 H, H arom.) ppm. ^{13}C NMR (50 MHz, $CDCl_3$): δ = 20.6 (*C*H$_3$), 68.0 [O*C*H$_2$C(CH$_3$)=CH$_2$], 84.8 [*C*(Ph)$_2$(R)$_2$], 111.1 [C(Ph)$_2$CH=*C*H$_2$], 117.0 [OCH$_2$C(CH$_3$)=*C*H$_2$], 127.8, 128.5, 128.7 (*C*H arom.), 141.0 [C(Ph)$_2$*C*H=CH$_2$], 143.4 (*C* quat. arom.), 144.9 [OCH$_2$*C*(CH$_3$)=CH$_2$] ppm. MS (EI): *m*/*z* (%) = 264 (1) $[M]^+$, 193 (32), 191 (15), 178 (18), 165 (14), 144 (12), 116 (19), 115 (100), 106 (43), 103 (19), 91 (40), 77 (45), 55 (69), 41 (13), 39 (25).

(1-Allyloxy-1-phenylprop-1-enyl)benzene (15):

Following Procedure C: Benzophenone (1.67 g, 9.2 mmol) was added to $CeCl_3$ (0.23 g, 0.92 mmol) in tetrahydrofuran (20 mL) at room temperature. Vinylmagnesium bromide (11.1 mL, 11.1 mmol) was then added at 0 °C. Subsequent treatment afforded the corresponding allylic alcohol as a pale yellow oil used without purification for the next step.

Following Procedure B: Allylic alcohol (9.2 mmol) in 10 mL of dimethylformamide was added to a solution of sodium hydride (60% in mineral oil, 0.44 g, 11.1 mmol) in dimethylformamide (15 mL). After addition of allyl bromide (1.1 mL, 12.0 mmol) and subsequent treatment, the crude was purified by flash chromatography over silica gel using diethyl ether/heptane (1:20) as eluent to afford an orange oil which was then bubble-to-bubble distilled to give the corresponding 1,6-diene **15** (1.88 g, 82% yield) as a colourless oil. ^{1}H NMR (200 MHz, $CDCl_3$): δ = 3.84−3.90 (m, 2 H, OC*H*$_2$CH=CH$_2$), 5.20−5.53 [m, 4 H, CH=C*H*$_2$, C(Ph)$_2$CH=C*H*$_2$], 5.95−6.12 (m, 1 H, OCH$_2$C*H*=CH$_2$), 6.49−6.63 [m, 1 H, C(Ph)$_2$C*H*=CH$_2$], 7.29−7.50 (m, 10 H, H arom.) ppm. ^{13}C NMR (50 MHz, $CDCl_3$): δ = 64.8 (O*C*H$_2$CH=CH$_2$), 84.2 [*C*(Ph)$_2$(R)$_2$], 115.3 [C(Ph)$_2$CH=*C*H$_2$], 116.2 (OCH$_2$CH=*C*H$_2$), 127.1, 127.8, 127.9 (*C*H arom.), 135.6 (OCH$_2$*C*H=CH$_2$), 140.2 [C(Ph)$_2$*C*H=CH], 144.0 (*C* quat. arom.) MS (EI): *m*/*z* (%) = 250 (<1) $[M]^+$, 211 (15), 210 (65), 192 (17), 165 (17), 133 (25), 115 (23), 106 (40), 104 (21), 91 (38), 79 (40), 77 (18), 63 (14), 55 (100), 51 (43), 39 (10).

Tandem Isomerisation/Claisen Rearrangement Reactions

2,5,9-Trimethyldeca-4,8-dienal (10):[16]

Following Procedure D: [$Ru_3(CO)_{12}$] (27.4 mg, 5mol % of ruthenium), 1,3-bis(2,6-diisopropylphenyl)imidazolinium chloride (54.9 mg, 5mol %), Cs_2CO_3 (83.8 mg, 10mol %), toluene (25 mL) and diene **9** (0.5 g, 2.6 mmol). After 1 h at 120 °C, treatment and distillation, the aldehyde **10** (0.435 g, 87% yield) was obtained as a colourless oil as a mixture of diastereoisomers. ^{1}H NMR (200 MHz, $CDCl_3$): δ = 1.00 [d, ^3J = 7.6 Hz, 3 H, CH(C*H*$_3$)CHO], 1.15−1.24 [m, 1 H, C*H*(CH$_3$)CHO], 1.50−1.66 [m, 9 H, CH=C(C*H*$_3$)CH$_2$CH$_2$CH=C(C*H*$_3$)$_2$], 1.90−2.10 [m, 4 H, C*H*$_2$C*H*$_2$CH=C(CH$_3$)$_2$], 2.21−2.39 [m, 2 H, C*H*$_2$CH(CH$_3$)CHO], 4.95−5.06 [m, 2 H, C*H*=C(CH$_3$)CH$_2$CH$_2$C*H*=C(CH$_3$)$_2$], 9.56 (d, ^4J = 1.5 Hz, 1 H, C*H*O) ppm. ^{13}C NMR (50 MHz, $CDCl_3$): δ = 12.6/12.8 [CH(*C*H$_3$)CH], 17.2/17.3 [(*E*)-CH$_2$CH$_2$CH=C(*C*H$_3$)$_2$], 23.1 [CH=C(*C*H$_3$)], 26.1/26.2 [(*Z*)-CH$_2$CH$_2$CH=C(*C*H$_3$)$_2$], 28.6/28.8 [CH$_2$*C*H$_2$CH=C(CH$_3$)$_2$], 31.7 [*C*H$_2$CH$_2$CH=C(CH$_3$)$_2$], 39.4 [*C*H$_2$CH(CH$_3$)CHO], 46.4/46.5 [*C*H(CH$_3$)CH], 120.7/121.1 [*C*H=C(CH3)], 123.8/123.9 [*C*H=C(CH$_3$)$_2$], 131.0/131.3 [CH=*C*(CH$_3$)$_2$], 137.2/137.3 [CH=*C*(CH3)], 204.30/204.35 (*C*HO) ppm. MS (EI):

 © 2003 Wiley-VCH Verlag GmbH & Co. KGaA, Weinheim

m/*z* (%) = 194 (1.5) $[M]^+$, 107 (10), 95 (12), 81 (16), 69 (100), 67 (14), 55 (30), 53 (14), 43 (30), 41 (85), 39 (22).

2,2-Dimethyl-5,5-diphenylpent-4-enal (14):[22]

Following Procedure D: $[Ru_3(CO)_{12}]$ (10.0 mg, 5mol % of ruthenium), 1,3-bis(2,6-diisopropylphenyl)imidazolinium chloride (16.2 mg, 5mol %), Cs_2CO_3 (30.7 mg, 10mol %), toluene (7.5 mL) and diene **13** (250 mg, 0.94 mmol). After 1 h at 120 °C, treatment and distillation, the aldehyde **14** (225 mg, 90% yield) was obtained as a colourless oil as a mixture of diastereoisomers. ^{1}H NMR (200 MHz, $CDCl_3$): δ = 1.12 (s, 6 H, 2 × CH_3), 2.39 (d, ^3J = 7.6 Hz, 2 H, CH_2), 6.09 [t, ^3J = 7.6 Hz, 1 H, $(Ph)_2C{=}CHCH_2$], 7.18−7.30 (m, 6 H, C*H* arom.), 7.38−7.49 (m, 4 H, C*H* arom.), 9.48 (s, 1 H, C*H*O) ppm. ^{13}C NMR (50 MHz, $CDCl_3$): δ = 21.2 (2 × CH_3), 36.6 (CH_2), 46.5 [$C(CH_3)_2$], 123.6 [$(Ph)_2C{=}CHCH_2$], 127.0, 127.1, 128.0, 128.2, 129.7 (*C*H arom.), 139.5, 142.2 (*C* arom.), 144.3 [$(Ph)_2C{=}CH$], 205.5 (*C*HO) ppm. MS (EI): *m*/*z* (%) = 264 (2) $[M]^+$, 193 (43), 180 (100), 178 (36), 165 (37), 115 (87), 91 (38), 51 (10), 43 (14), 41 (16), 39 (14).

2-Methyl-5,5-diphenylpent-4-enal (16):

Following Procedure D: $[Ru_3(CO)_{12}]$ (4.3 mg, 5mol % per ruthenium atom), 1,3-bis(2,6-diisopropylphenyl)imidazolinium chloride (8.5 mg, 5mol %), Cs_2CO_3 (13.0 mg, 10mol %), toluene (5 mL) and diene **15** (100 mg, 0.40 mmol). After 3 h at 120 °C, treatment and distillation, the aldehyde **16** (78 mg, 78% yield) was obtained as a colourless oil as a mixture of diastereoisomers. ^{1}H NMR (200 MHz, $CDCl_3$): δ = 1.14 (d, ^3J = 6.9 Hz, 3 H, CH_3), 2.16−2.39 [m, 1 H, C*H*(CH_3)], 2.44−2.64 (m, 2 H, CH_2), 6.08 [t, ^3J = 7.5 Hz, 1 H, $(Ph)_2C{=}CHCH_2$], 7.19−7.44 (m, 10 H, C*H* arom.), 9.63 (d, ^3J = 1.4 Hz, 1 H, C*H*O) ppm. ^{13}C NMR (50 MHz, $CDCl_3$): δ = 13.1 (CH_3), 30.5 (CH_2), 46.7 [C*H*(CH_3)], 125.5 $[(Ph)_2C{=}CHCH_2]$, 127.1, 128.1, 128.3, 129.7 (*C*H arom.), 139.6, 142.1 (*C* arom.), 144.9 $[(Ph)_2C{=}CH]$, 204.4 (*C*HO) ppm. MS (EI): *m*/*z* (%) = 250 (39) $[M]^+$, 219 (24), 204 (18), 203 (19), 193 (100), 191 (55), 189 (45), 177 (17), 167 (20), 166 (37), 152 (33), 129 (25), 128 (38), 116 (38), 105 (16), 103 (15), 89 (26), 77 (27), 65 (25), 51 (17), 39 (20).

{1-Methyl-1-[prop-1-enyloxy]but-3-enyl}benzene (11) Using Catalyst B1 with the Diimine L1: $[Ru_3(CO)_{12}]$ (13.2 mg, 5mol % per ruthenium atom), bis(imine) **L1** (18.1 mg, 5mol %), cesium carbonate (40.3 mg, 10mol %) and of toluene (10 mL) were introduced into a Schlenk tube under nitrogen. The reaction mixture was stirred at room temperature for 5 minutes and the diene **5** (250 mg, 1.24 mmol) was then added. After heating at 120 °C for 16 hours, the solvent was removed under reduced pressure and NMR spectroscopic analysis of the crude gave a complete conversion into the homoallyl vinyl ether **11**. The crude was dissolved in heptane, filtered and the solvents evaporated to dryness. This material was then purified by a bubble-to-bubble distillation to afford the corresponding compound **11** (195 mg, 78%) as a colourless oil. ^{1}H NMR (200 MHz, $CDCl_3$): δ = 1.55−1.62 [m, 3 H, C(Ph)(CH_3)], 1.65−1.72 (m, 3 H, OCH=CHCH_3), 2.52−2.65 [m, 2 H, OC(Ph)(Me)CH_2CH=CH_2], 4.33−4.49 (m, 1 H, OCH=C*H*CH_3), 4.96−5.10 (m, 2 H, CH=CH_2), 5.54−5.76 [m, 1 H, OC(Ph)(Me)CH_2C*H*=CH_2], 5.81−5.92 (m, 1 H, OC*H*=$CHCH_3$), 7.20−7.38 (m, 5 H, Ph) ppm. ^{13}C NMR (50 MHz, $CDCl_3$): δ = 11.8 (OCH=CH*C*H_3), 25.4 (CH_3), 47.1 [CH_2C(Ph)(Me)OR], 76.2 [*C*(Ph)(Me)], 97.8 (OCH=*C*HCH_3), 117.3 [C(Ph)(Me)CH_2CH=*C*H], 126.1, 126.8, 127.8 (*C*H arom.), 133.9 [C(Ph)(Me)CH_2*C*H=CH], 143.7 (O*C*H=$CHCH_3$), 144.8 (*C* arom.) ppm. MS (EI): *m*/*z* (%) = 202 (7) $[M]^+$, 143 (13), 131 (13), 129 (45), 115 (100), 113 (37), 91 (69), 78 (21), 65 (24), 63 (14), 53 (16), 51 (31), 41 (38), 39 (37).

2,2-Dimethyl-5,5-diphenylpent-4-enal (14) by Using Catalyst D and the 2,2′-Bis(oxazoline) Ligand 17: $[Ru_3(CO)_{12}]$ (10.6 mg, 5mol % ruthenium atom), 2,2′-bis(oxazoline) **17**[19d] (11.9 mg, 5 mol %), cesium carbonate (32.5 mg, 10 mol %) and toluene (10 mL) were introduced into a Schlenk tube under nitrogen. The reaction mixture was stirred at room temperature for 5 minutes and the diene **13** (250 mg, 1.01 mmol) was then added. After heating at 120 °C for 16 hours, the solvent was removed under reduced pressure and NMR spectroscopic analysis of the crude gave 60% of conversion into the aldehyde **14**.

General Procedure for the Preparation of [RuCl{bis(oxazoline)}(*p*-cymene)][BF_4]: A solution of bis(oxazoline) ligand (2 equiv.) in MeOH (10 mL) was added to $[RuCl_2(p\text{-cymene})]_2$ (1 equiv.) and NH_4BF_4 (2 equiv.), and the resulting suspension was stirred at room temperature for 2 h. An orange-brown solution was obtained, which was then evaporated and the crude residue dissolved in CH_2Cl_2. Filtration through celite gave a brown solution, which was evaporated, and the crude complex was washed with diethyl ether (2 × 15 mL) and dried under vacuum. The scale and the yields for individual complexes are shown below.

[RuCl{(*R*,*R*)-4,4′-Diisopropyl-2,2′-methylenebis(1,3-oxazoline)}(*p*-cymene)][BF_4] (18): Complex **18** was prepared in methanol (10 mL) from $[RuCl_2(p\text{-cymene})]_2$ (100 mg, 0.163 mmol), (*R*,*R*)-4,4′-diisopropyl-2,2′-methylenebis(1,3-oxazoline) (**17**) (77 mg, 0.32 mmol) and NH_4BF_4 (34 mg, 0.32 mmol) in a 94 mg yield (98%). Recrystallisation in a mixture of acetone/heptane afforded complex **18** as orange needles. $C_{23}H_{36}BClF_4N_2O_2Ru$: calcd. C 46.36, H 6.09, N 4.70, Cl 5.95; found C 46.45, H 6.33, N 4.51, Cl 5.95. ^{1}H NMR (200 MHz, $CDCl_3$): δ = 0.52, 0.87, 1.00, 1.07 [4 × d, 12 H, ^3J = 6.6, ^3J = 7.2, ^3J = 7.0, ^3J = 6.8 Hz, 2 $CH(CH_3)_2$], 1.31 [d, ^3J = 7.0 Hz, 6 H, $CH(CH_3)_2$ of *p*-cymene], 2.30 (s, 3 H, $CH_3C_6H_4$), 2.28−2.33 [m, 1 H, C*H*$(CH_3)_2$], 2.60−2.66 [m, 1 H, C*H*$(CH_3)_2$], 3.01−3.09 [m, 1 H, C*H*$(CH_3)_2$ of *p*-cymene], 3.45, 4.00 (AB, 2 H, J_{AB} = 19.7 Hz, CH_2), 4.30−4.92 [m, 6 H, OCH_2C*H*(*i*Pr)N], 5.40−6.05 (m, 4 H, C*H* *p*-cymene) ppm. ^{13}C NMR (50 MHz, $CDCl_3$): δ = 14.4, 14.7 [$CH(CH_3)_2$], 18.4 ($CH_3C_6H_4$), 18.9, 19.5 [$CH(CH_3)_2$], 20.9, 22.9 [$CH(CH_3)_2$ of *p*-cymene], 27.0 (CH_2), 28.1, 28.6, 30.9 [C*H*$(CH_3)_2$], 69.4, 70.3 [2 × *C*H(*i*Pr)], 71.3, 71.7 [OCH_2-CH(*i*Pr)], 79.4, 80.8, 83.8, 85.7 (4 *C*H *p*-cymene), 99.5, 110.0 (2 × *C* *p*-cymene), 165.4, 165.6 (2 × *C*=N) ppm. IR: $\tilde{\nu}$ = 1173 (ν B−F), 1540 (ν C=C), 1602 (ν C=N), 1670 (ν C=N) cm^{-1}. UV: λ (ε, $L{\cdot}mol^{-1}{\cdot}cm^{-1}$) = 422 (910) nm, 325 (1245), 278 (5465) 246 n(5465), 230 (5326).

[RuCl{(*S*,*S*)-4,4′-Diethyl-2,2′-methylenebis(1,3-oxazoline)}(*p*-cymene)][BF_4] (20): Complex **20** was prepared in methanol (10 mL) from $[RuCl_2(p\text{-cymene})]_2$ (100 mg, 0.163 mmol), (*S*,*S*)-4,4′-diethyl-2,2′-methylenebis(1,3-oxazoline) (**19**)[19f] (69 mg, 0.32 mmol) and NH_4BF_4 (34 mg, 0.32 mmol) in a 91 mg yield (98%). $C_{21}H_{32}BClF_4N_2O_2Ru$: calcd. C 44.42, H 5.68, N 4.93; found C 44.17, H 5.76, N 4.93. ^{1} H NMR (200 MHz, $CDCl_3$): δ = 0.79 (t, ^3J = 7.4 Hz, 3 H, CH_3CH_2), 0.96 (t, ^3J = 7.4 Hz, 3 H, CH_3CH_2), 1.28 [d, ^3J = 6.9 Hz, 6 H, $CH(CH_3)_2$], 1.57 (m, 2 H, CH_3CH_2), 2.11 (m, 2 H, CH_3CH_2), 2.19 (s, 3 H, $CH_3C_6H_4$), 2.91 (m, 1 H, C*H*Me_2), 3.49, 3.68 (AB, 2 H, J_{AB} = 20.0 Hz and J_{AB} = 20.1 Hz, CH_2), 4.27−4.88 [m, 6 H, OCH_2C*H*(Et)N], 5.51−5.61 (m, 4 H, C_6H_4) ppm. ^{13}C NMR (50 MHz, $CDCl_3$): δ = 8.8, 9.4 (CH_3CH_2), 18.4 ($CH_3C_6H_4$), 21.3, 22.7 [$CH(CH_3)_2$], 27.1, 27.2, 27.3 (2 × CH_3CH_2, CH_2), 31.1 (*C*HMe_2), 68.5, 72.2 (2 × *C*HEt), 74.0, 74.2 (OCH_2CHEt), 80.6, 82.5, 83.1, 83.8 (4 *C*H *p*-cymene), 98.4, 108.0 (2 *C* *p*-cymene), 165.1, 165.4 (*C*=N) ppm. IR: $\tilde{\nu}$ = 1097 (ν B−F), 1534 (ν C=C), 1601 (ν C=N), 1670 (ν C=N) cm^{-1}. UV: λ (ε,

 © 2003 Wiley-VCH Verlag GmbH & Co. KGaA, Weinheim

$L \cdot mol^{-1} \cdot cm^{-1}$) = 421 nm (1012), 322 (1587), 278 (7524), 245 (6780), 230 (7252).

2,2-Dimethyl-5,5-diphenylpent-4-enal (14) by Using Catalyst E with Complex (18) as the Metal Source: Complex **18** (29.7 mg, 5 mol %), 1,3-bis(2,6-diisopropylphenyl)imidazolinium chloride (21.3 mg, 5 mol %), cesium carbonate (32.5 mg, 10 mol %) and toluene (10 mL) were introduced into a Schlenk tube under nitrogen. The reaction mixture was stirred at room temperature for 5 minutes and the diene **13** (250 mg, 1.01 mmol) was then added. After heating at 120 °C for 16 hours, the solvent was removed under reduced pressure and NMR spectroscopic analysis of the crude gave 90% of conversion into the aldehyde **14**. After a column chromatography over silica gel using a mixture diethyl ether/heptane (1/20), the aldehyde **14** (170 mg) was isolated in 68% yield.

X-ray Crystallographic Study of Complex 18: Crystallographic and data collection information as well as a description of the structural analyses and refinements are summarised in Table 3. Single crystals of **18** were obtained by slow diffusion of heptane into an acetone solution of the complex. Data were collected with a Nonius−Kappa CCD diffractometer with graphite-monochromatised Mo-K_α radiation. The cell parameters were obtained with Denzo and Scalepack[24] using 10 frames (psi rotation: 1° per frame). The data collection[25] ($2\Theta_{max}$ = 54°, 128 frames via 21.7° omega rotation and 50 s per frame, *hkl* range: h −14,14; k −17,17; l −25,25) gives 23815 reflections. The data reduction[24] leads to 6792 independent reflections from which 6112 with $I > 2.0\sigma(I)$. The structure was solved with SIR-97,[26] which reveals the non-hydrogen atoms of the structure. After anisotropic refinement, many hydrogen atoms could be found with a Fourier Difference. The whole structure was refined with SHELXL-97[27] by the full-matrix least-squares techniques.

Atomic scattering factors were obtained from International Tables for X-ray Crystallography.[28] ORTEP views were realised with PLATON98.[29]

CCDC-210758 contains the supplementary crystallographic data for this paper. These data can be obtained free of charge at www.ccdc.cam.ac.uk/conts/retrieving.html [or from the Cambridge Crystallographic Data Centre, 12, Union Road, Cambridge CB2 1EZ, UK; Fax: (internat.) +44-1223-336-033; E-mail: deposit@ccdc.cam.ac.uk].

Acknowledgments

The authors are grateful to the Région Bretagne for the award of a doctoral grant to JLN and a PRIR program (691 no. AOC316), and to the EU COST-chemistry program (Action D17/0003/00).

[1] [1a] F. E. Ziegler, *Chem. Rev.* **1988**, *88*, 1423. [1b] H. Frauenrath in *Methods Org. Chem.* (Houben-Weyl) 4th ed., **1952**, *vol. E21d*, **1995**, 3301.
[2] L. Claisen, *Ber. Dtsch. Chem. Ges.* **1912**, *45*, 3157.
[3] [3a] C. J. Burrows, B. K. Carpenter, *J. Am. Chem. Soc.* **1981**, *103*, 6983. [3b] D. E. Vogel, G. H. Büchi, *Org. Synth.* **1987**, *66*, 29. [3c] R. E. Ireland, D. J. Dawson, *Org. Synth. VI* **1988**, 298. [3d] J. S. Swenton, D. Bradin, B. D. Gates, *J. Org. Chem.* **1991**, *56*, 6156. [3e] M. Sugiura, M. Yanagisawa, T. Nakai, *Synlett* **1995**, 447.
[4] [4a] H. Suzuki, Y. Koyama, *Tetrahedron Lett.* **1979**, *16*, 1415. [4b] H. Wakamatsu, M. Nishida, N. Adachi, M. Mori, *J. Org. Chem.* **2000**, *65*, 3966. [4c] S. Krompiec, M. Pigulla, W. Szczepankiewicz, T. Bieg, N. Kuznik, K. Leszczynska-Sedja, M. Kubichi, T. Borowiak, *Tetrahedron Lett.* **2001**, *42*, 7095.
[5] [5a] A. Salvini, P. Frediani, F. Piacenti, *J. Mol. Catal. A: Chemical* **2000**, *159*, 185. [5b] A. Salvini, F. Piacenti, P. Frediani, A. Devescovi, M. Caporali, *J. Organomet. Chem.* **2001**, *625*, 255. [5c] K. Dallmann, R. Buffon, *J. Mol. Catal. A: Chemical* **2002**, *185*, 187. [5d] K. Dallmann, R. Buffon, *J. Mol. Catal. A: Chemical* **2001**, *172*, 81.
[6] [6a] R. Noyori, H. Takaya, *Acc. Chem. Res.* **1990**, *23*, 345. [6b] K. Tani, T. Yamagata, S. Otsuka, S. Akutagawa, H. Kumobayashi, T. Taketomi, H. Takaya, A. Miyashita, R. Noyori, *J. Chem. Soc., Chem. Commun.* **1982**, 600. [6c] K. Tani, T. Yamagata, S. Akutagawa, H. Kumobayashi, T. Taketomi, H. Takaya, A. Miyashita, R. Noyori, S. Otsuka, *J. Am. Chem. Soc.* **1984**, *106*, 5208. [6d] H. Frauenrath, M. Kaulard, *Synlett* **1994**, 517.
[7] [7a] C. Cadot, P. I. Dalko, J. Cossy, *Tetrahedron Lett.* **2002**, *43*, 1839. [7b] D. Bourgeois, A. Pancrazi, S. P. Nolan, J. Prunet, *J. Organomet. Chem.* **2002**, *643−644*, 247. [7c] A. E. Sutton, B. A. Seigal, D. F. Finnegan, M. L. Snapper, *J. Am. Chem. Soc.* **2002**, *124*, 13390.
[8] B. Schmidt, H. Wildemann, *J. Org. Chem.* **2000**, *65*, 5817.
[9] [9a] J. M. Reuter, R. G. Salomon, *J. Org. Chem.* **1977**, *42*, 3360. [9b] R. S. Iyer, M. E. Kobierski, R. G. Salomon, *J. Org. Chem.* **1994**, *59*, 6038. [9c] T. N. Mitchell, F. Giesselmann, *Synlett* **1996**, 475.
[10] [10a] J. S. Swenton, D. Bradin, B. D. Gates, *J. Org. Chem.* **1991**, *56*, 6156. [10b] T. Higashino, S. Sakaguchi, Y. Ishii, *Org. Lett.* **2000**, *2*, 4193.
[11] S. P. Miller, J. P. Morken, *Org. Lett.* **2002**, *4*, 2743.
[12] D. Sémeril, M. Cléran, C. Bruneau, P. H. Dixneuf, *Adv. Synth. Catal.* **2001**, *343*, 184.
[13] D. Sémeril, M. Cléran, A. Jimenez Perez, C. Bruneau, P. H. Dixneuf, *J. Mol. Catal. A: Chemical* **2002**, 9.
[14] D. Sémeril, C. Bruneau, P. H. Dixneuf, *Helv. Chim. Acta* **2001**, *84*, 3335.
[15] J. Le Nôtre, L. Brissieux, D. Sémeril, C. Bruneau, P. H. Dixneuf, *Chem. Commun.* **2002**, 1772.
[16] R. Marbet, G. Saucy, *Helv. Chim. Acta* **1967**, *50*, 2095.
[17] H. Ben Ammar, J. Le Nôtre, M. Salem, M. T. Kaddachi, P. H. Dixneuf, *J. Organomet. Chem.* **2002**, *662*, 63.
[18] For general synthesis of **L1**−**L6** from glyoxal and the corresponding amine see: [18a] J. M. Kliegman, R. K. Barnes, *Tetrahedron* **1970**, *26*, 2555. [18b] H. Tom Dieck, I. W. Renk, *Chem. Ber.* **1971**, *104*, 92. [18c] M. Zettlitzer, H. Tom Dieck, E. T. K. Haupt, *Chem. Ber.* **1986**, *119*, 1868. [18d] A. J. Arduengo, III, R. Krafczyk, R. Schmutzler, *Tetrahedron* **1999**, *55*, 14523.
[19] [19a] A. K. Ghosh, P. Mathivanan, J. Cappiello, *Tetrahedron: Asymmetry* **1998**, *9*, 1. [19b] C. Bolm, *Angew. Chem. Int. Ed. Engl.* **1991**, *103*, 556. [19c] D. Mueller, G. Umbricht, B. Weber, A. Pfaltz, *Helv. Chim. Acta* **1991**, *74*, 232. [19d] D. A. Evans, K. A. Woerpel, M. M. Hinman, M. M. Faul, *J. Am. Chem. Soc.* **1991**, *113*, 726. [19e] D. A. Evans, J. S. Johnson, E. J. Olhava, *J. Am. Chem. Soc.* **2000**, *122*, 1635. [19f] R. E. Lowenthal, A. Abiko, S. Masamune, *Tetrahedron Lett.* **1990**, *31*, 6005.
[20] [20a] D. A. Evans, K. A. Worepel, M. M. Hinman, M. M. Faul, *J. Am. Chem. Soc.* **1991**, *113*, 726. [20b] D. A. Evans, K. A. Woerpel, M. J. Scott, *Angew. Chem. Int. Ed. Engl.* **1992**, *31*, 430.
[21] [21a] A. S. Waggoner, B. M. Karandikar, R. B. Mujumdar, *Eur. Pat. Appl.* **1996**, 37. [21b] A. Abbotto, S. Bradamante, G. A. Pagani, *J. Org. Chem.* **1996**, *61*, 1761. [21c] A. Abbotto, S. Bradamante, N. Capri, H. Rzepa, D. J. Williams, A. White, *J. Org. Chem.* **1996**, *61*, 1770.
[22] K. Peterfy, M. A. Garcia-Garibay, *J. Am. Chem. Soc.* **1998**, *120*, 4540.
[23] [23a] H. Takaya, T. Ohta, R. Noyori, in *Catalytic Asymmetric Synthesis*, (Ed.: I. Ojima), Wiley-VCH, New York, **1993**, p. 1−39. [23b] R. Noyori, H. Takaya, *Acc. Chem. Res.* **1990**, *23*, 345. [23c] T. Ohta, H. Takaya, R. Noyori, *Inorg. Chem.* **1988**, *27*, 566. [23d] M. T. Ashby, *J. Am. Chem. Soc.* **1995**, *117*, 2000.

 © 2003 Wiley-VCH Verlag GmbH & Co. KGaA, Weinheim

[23e] M. T. Ashby, S. S. Alguindigue, M. A. Khan, *Organometallics* **2000**, *19*, 547. [23f] P. Frediani, C. Giannelli, A. Salvini, S. Ianelli, *J. Organomet. Chem.* **2003**, *667*, 197.
[24] Z. Otwinowski, W. Minor, *Processing of X-ray Diffraction Data Collected in Oscillation Mode*, in *Methods in Enzymology, Vol. 276, Macromolecular Crystallography*, **1997**, Part A, edited by C. W. Carter & R. M. Sweet, pp. 307−326. London: Academic Press.
[25] Nonius **1999**, *KappaCCD Software*, Nonius BV, Delft, The Netherlands.
[26] A. Altomare, M. C. Burla, M. Camalli, G. Cascarano, C. Giacovazzo, A. Guagliardi, A. G. G. Moliterni, G. Polidori, R. Spagna, *J. of Appl. Cryst.* **1998**, *31*, 74.
[27] G. M. Sheldrick, SHELX97, *Program for the Refinement of Crystal Structures*, **1997**, Univ. of Göttingen, Germany.
[28] International Tables for X-ray Crystallography **1992**, *vol. C.*, Ed. A. J. C. (Kluwer Academic Publishers, Dordrecht).
[29] A. L. Spek, PLATON, *A multipurpose crystallographic tool*, **1998**, Utrecht University, Utrecht, The Netherlands.

Received May 28, 2003
Early View Article
Published Online October 2, 2003

 © 2003 Wiley-VCH Verlag GmbH & Co. KGaA, Weinheim

Structural, Photophysical and Chiro-Optical Properties of Lanthanide Complexes with a Bis(benzimidazole)pyridine-Based Chiral Ligand

Gilles Muller,[a,b] Christine L. Maupin,[b] James P. Riehl,[b] Henrik Birkedal,[c,d] Claude Piguet,[e] and Jean-Claude G. Bünzli*[a,b]

Keywords: Lanthanides / Luminescence / Chirality / Complexes / Terdentate ligand

The neutral Ln^{III} 1:1 nitrato complexes with the chiral ligand 2,6-bis(1-*S*-neopentylbenzimidazol-2-yl)pyridine (L^{11}) have been synthesised and their stability constants measured in acetonitrile (log K_1 = 4.0–6.4). The crystal and molecular structure of $[Eu(NO_3)_3(L^{11})(MeCN)]$ shows the typical meridional planar coordination of L^{11} to the metal ion and low symmetry of the coordination polyhedron. The influence of the steric hindrance generated by the substituent at R^2 on the crystal packing and bond lengths is discussed. Photophysical measurements show that ligand L^{11} induces a $^3\pi\pi^*$-to-Ln energy-transfer process in the Eu^{III} complex, while the Tb^{III} compound is ten times less luminescent. Addition of a second molecule of L^{11} to give $[Ln(ClO_4)_2(L^{11})_2]^+$ leads to a large quenching of the Eu^{III} luminescence (140-fold) due to several factors: a less efficient $^1\pi\pi^* \rightarrow {}^3\pi\pi^*$ transfer (ca. fourfold), a smaller intrinsic quantum yield Q^{Eu} (ca. threefold), and a substantially less efficient ligand-to-metal transfer (ca. 12-fold). In the case of the Tb^{III} complex, the decrease in the energy of the triplet state reduces further the Tb^{III} emission through increased back transfer. The specific rotary dispersion of the 1:1 and 1:2 complexes points to the chirality of the complexes arising mainly from the ligand, while the circularly polarized luminescence of these complexes with Eu^{III} and Tb^{III} displays a weak effect, pointing to a small diastereomeric excess in solution. Altogether, this study demonstrates that electronic, thermodynamic and photophysical properties of lanthanide complexes with aromatic terdentate ligands can be tuned by modifying the number and the arrangement of the ligands, as well as their substituents, particularly those in the R^2 and R^3 positions.
(© Wiley-VCH Verlag GmbH & Co. KGaA, 69451 Weinheim, Germany, 2003)

Introduction

Present interest in luminescent lanthanide complexes[1] is primarily motivated by applications in life sciences, mainly for developing chemical sensors[2] or tools for medical diagnosis and therapy.[3,4] In this context, the design and use of enantiopure lanthanide compounds present a special advantage with respect to the chiral recognition of biological substrates.[5,6] Lanthanides are subject to fast ligand- and solvent-exchange reactions so that easy interconversion between optical isomers often occurs. Therefore, the use of ligands leading to kinetically inert complexes, such as those derived from the dota (1,4,7,10-tetraazadodecane *N*,*N*′,*N*″,*N*‴,-tetraacetic acid) framework favours the isolation of enantiopure compounds.[7] We have recently reported on the first diastereoselective formation in solution of lanthanide triple helical complexes with a terdentate chiral C_2-symmetric ligand **L(−)** (Scheme 1) derived from terpyridine, as was suggested by their specific rotary dispersion, circularly polarized luminescence (CPL) and NMR spectra.[8] We have also investigated the influence of chiral groups grafted onto aromatic tridentate ligands on the diastereomeric induction in solution. For instance, ligands **L*** and $\mathbf{L^{12}}$, with a chiral group in the pyridine 4-position, form thermodynamically stable 1:3 triple helical complexes with Ln^{III} ions in acetonitrile, and chiro-optical measurements suggest the helical wrapping of the ligand strands around the Ln^{III} ions, while the CPL data are in agreement with a small diastereomeric excess in solution.[9,10]

Working along these lines, we have introduced a chiral substituent onto the benzimidazole sidearms of bis(benzimidazole)pyridine to yield $\mathbf{L^{11}}$. However, the bulky neopentyl group precludes the formation of stable triple helical com-

[a] Institute of Molecular and Biological Chemistry, Swiss Federal Institute of Technology, BCH 1402, CH-1015 Lausanne, Switzerland
E-mail: jean-claude.bunzli@epfl.ch
[b] Department of Chemistry, University of Minnesota Duluth, Duluth, MN, 55812-3020, USA
[c] Institute of Crystallography, BSP, University of Lausanne, CH-1015 Lausanne, Switzerland
[d] Department of Chemistry and Biochemistry, University of California, Santa Barbara, CA 93106, USA
[e] Department of Inorganic, Analytical and Applied Chemistry, University of Geneva, 30 quai E. Ansermet, CH-1211 Geneva 4, Switzerland
Supporting information for this article is available on the WWW under http://www.eurjic.org or from the author.

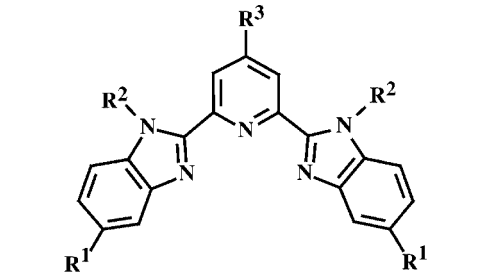

R^1	R^2	R^3	L^i
H	H	H	L^0
H	Me	H	L^1
H	$Bz(OMe)_2$	$PhNO_2$	L^7
H	Oct	H	L^{10}
H		H	L^{11}
H	Me	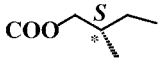	L^{12}

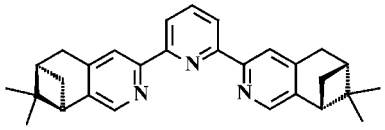

L(-)

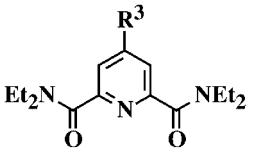

$R^3 = CH_2C^*H(CO_2Me)(NHCO_2CMe_3)$: L*

Scheme 1

plexes: in the X-ray structure of $[Eu(\mathbf{L^{11}})_3](ClO_4)_3 \cdot 4.28MeCN$, two of the ligand molecules are wrapped around the Eu^{III} ion in a helical fashion, much as they are in the 1:2 complex with La^{III}, while the third one lies more or less perpendicular to the other two.[11] To further our understanding of the influence of helical wrapping on diastereomeric induction, we investigate here the thermodynamic, structural, luminescent and chiro-optical properties of the neutral nitrato complexes $[Ln(NO_3)_3(\mathbf{L^{11}})]$ (Ln = La, Eu, Tb) and compare them to those of $[Ln(ClO_4)_2(\mathbf{L^{11}})_2]^+$ complexes in solution.

Results and Discussion

Isolation, Structure and Stability of the 1:1 Nitrato Complexes

Neutral 1:1 complexes form easily upon mixing equivalent amounts of hydrated lanthanide nitrate and $\mathbf{L^{11}}$ in dichloromethane/acetonitrile. The general formula of the isolated complexes is $[Ln(NO_3)_3(\mathbf{L^{11}})(MeCN)_x]$ [x = 0, La (**1**), Gd (**3**), Tb (**4**); x = 1, Eu (**2**)] where the acetonitrile molecule sometimes completes the inner-sphere of the Ln^{III} ion to a coordination number of 10 (see below), but can be removed by heating under vacuum. Complexation is evidenced in the IR spectra by the blue shift of the two C=C benzimidazole and pyridine vibrational modes by 2−5 and 11−14 cm^{-1}, respectively (Table S1). Nitrate ions behave as bidentate ligands with local C_{2v} symmetry as exemplified by energy differences $\Delta(\nu_1 - \nu_4)$ larger than 180 cm^{-1}:[12] 221, 228, 229, and 230 cm^{-1} for La, Eu, Gd, and Tb, respectively. Single crystals suitable for X-ray diffraction analysis were obtained for the Eu complex **2**. The atom-numbering scheme is displayed in Figure 1 and selected bond lengths and angles are reported in Table 1, while interplanar angles are listed in Table S2. The structure consists of neutral molecules with 10-coordinate Eu^{III}, the metal ion being bound to six O atoms from the three bidentate nitrate anions, one N atom from the solvating molecule and three N atoms from $\mathbf{L^{11}}$. The ligand is coordinated in the usual meridional planar way, as was observed for $[Eu(NO_3)_3(\mathbf{L^1})(MeOH)]$,[13] with two small and very similar interplanar angles between the pyridine and benzimidazole moieties, α_{pb} = 6.5° and 6.2°, as compared to 3.3° and 5.5° for $\mathbf{L^{11}}$, but in contrast to the situation found in $[Eu(NO_3)_3(\mathbf{L^7})(MeCN)] \cdot 2.5MeCN$[14] and $[Eu(NO_3)_3(\mathbf{L^{10}})]$.[13] Indeed, in the former, $\mathbf{L^7}$ is bent with two different angles

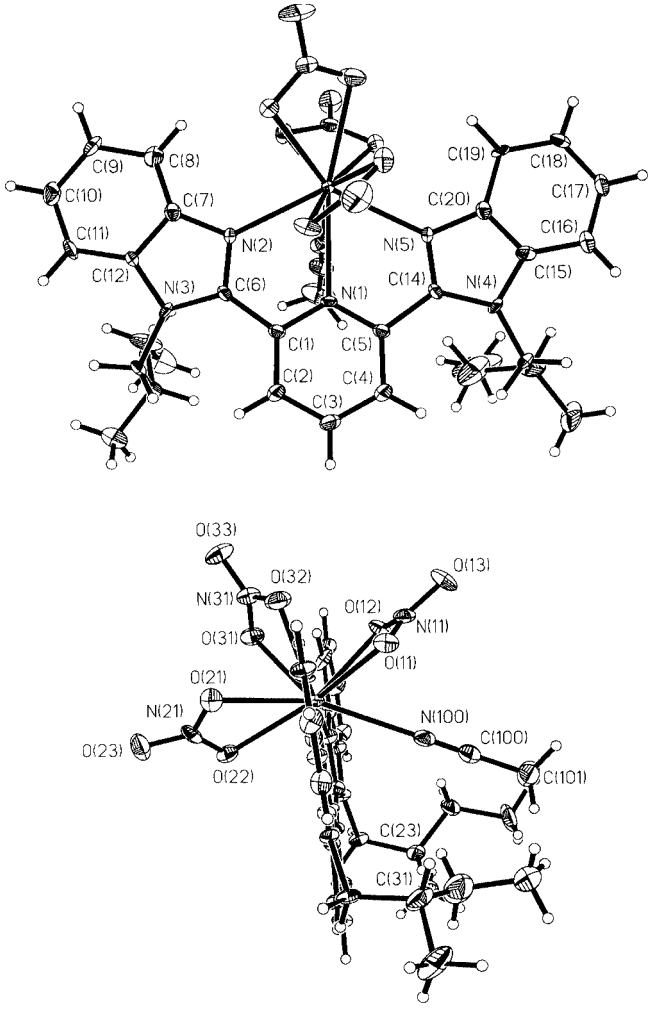

Figure 1. Two views of the molecular structure of $[Eu(NO_3)_3(\mathbf{L^{11}})(MeCN)]$ showing the atom-numbering scheme

 © 2003 Wiley-VCH Verlag GmbH & Co. KGaA, Weinheim

Table 1. Bond lengths (Å) and angles (deg) in the coordination polyhedron of $[Eu(NO_3)_3(\mathbf{L^{11}})(MeCN)]$

Bond lengths					
Eu1−N1	2.627(4)	Eu1−N100	2.735(5)	Eu1−O21	2.592(5)
Eu1−N2	2.470(7)	Eu1−O11	2.486(7)	Eu1−O22	2.535(5)
Eu1−N5	2.470(7)	Eu1−O12	2.478(7)	Eu1−O31	2.492(5)
				Eu1−O32	2.562(6)
Bond angles					
N1−Eu1−N2	63.8(3)	N5−Eu1−O21	70.8(2)	O21−Eu1−N100	151.7(2)
N1−Eu1−N5	63.1(3)	N5−Eu1−O22	88.8(2)	O22−Eu1−O31	71.9(2)
N2−Eu1−N5	126.9(1)	N5−Eu1−O31	139.1(2)	O22−Eu1−O32	104.7(2)
N1−Eu1−O11	117.8(2)	N5−Eu1−O32	103.9(2)	O22−Eu1−N100	127.1(2)
N1−Eu1−O12	124.8(2)	N5−Eu1−N100	81.2(3)	O31−Eu1−O32	50.7(2)
N1−Eu1−O21	99.6(2)	O11−Eu1−O12	52.1(2)	O31−Eu1−N100	139.2(2)
N1−Eu1−O22	66.6(2)	O11−Eu1−O21	112.2(2)	O32−Eu1−N100	128.2(1)
N1−Eu1−O31	132.1(2)	O11−Eu1−O22	161.5(2)	N1−Eu1−N11	125.2(1)
N1−Eu1−O32	163.5(2)	O11−Eu1−O31	109.2(2)	N2−Eu1−N11	104.9(3)
N1−Eu1−N100	62.6(1)	O11−Eu1−O32	66.0(2)	N5−Eu1−N11	103.6(3)
N2−Eu1−O11	126.4(2)	O11−Eu1−N100	64.7(2)	N100−Eu1−N11	162.9(1)
N2−Eu1−O12	82.0(2)	O12−Eu1−O21	135.5(2)	N31−Eu1−N11	79.9(2)
N2−Eu1−O21	120.3(2)	O12−Eu1−O22	142.3(2)	N1−Eu1−N31	153.9(2)
N2−Eu1−O22	72.0(2)	O12−Eu1−O31	77.9(2)	N2−Eu1−N31	105.9(2)
N2−Eu1−O31	81.8(2)	O12−Eu1−O32	70.9(2)	N5−Eu1−N31	122.7(2)
N2−Eu1−O32	128.5(2)	O12−Eu1−N100	67.0(2)	N100−Eu1−N31	140.4(1)
N2−Eu1−N100	73.5(3)	O21−Eu1−O22	50.1(2)	O11−Eu1−N11	25.8(3)
N5−Eu1−O11	78.6(2)	O21−Eu1−O31	69.1(2)	O21−Eu1−N11	127.4(2)
N5−Eu1−O12	128.8(2)	O21−Eu1−O32	65.3(2)	O31−Eu1−N11	94.0(2)

α_{pb} = 4.3° and 13.1°, while in the latter the two benzimidazole arms of $\mathbf{L^{10}}$ are not coplanar with the central pyridine (α_{pb} = 29.7° and 28.3°). The observation of different conformations for these ligands may be explained by the crystal packing and the steric hindrance generated by the R^2 groups. In $[Eu(NO_3)_3(\mathbf{L^{11}})(MeCN)]$, the crystal packing is governed by several weak intermolecular CH···O H-bonds, involving the O-atoms of the nitrate anion N2 (Figure 2 and Table S3). Each coordinated O atom generates one interaction with H atoms located on the neopentyl arms or on the phenyl groups of another complex molecule, while the non-coordinated O-atom is involved in similar interactions with H atoms from acetonitrile or from the neopentyl groups of a different complex molecule. The steric hindrance of the neopentyl groups increases the bend of the ligand slightly, as previously observed for $[Eu(NO_3)_3(\mathbf{L^{10}})]$, so that the interstrand π-stacking interactions evidenced in $[Eu(NO_3)_3(\mathbf{L^1})(MeOH)]$ are lost.[13] Furthermore, the asymmetric conformation of the two benzimidazole units in $[Eu(NO_3)_3(\mathbf{L^7})(MeCN)]\cdot 2.5MeCN$ can be explained by the presence of strong intermolecular interactions, induced by the bulky dimethoxybenzyl substituents, with nitrate anions.[14]

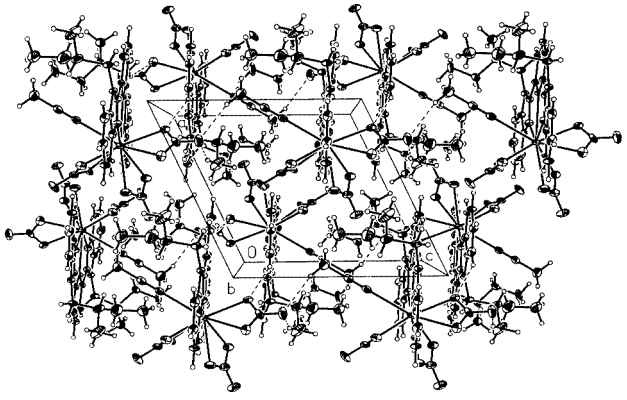

Figure 2. Intermolecular CH···O interactions observed in the crystal structure of $[Eu(NO_3)_3(\mathbf{L^{11}})(MeCN)]$

The coordination environment of the Eu^{III} ion in **2** is best described as a distorted 4:5:1 polyhedron (Figure S1) similar to the arrangement observed in the complexes with $\mathbf{L^1}$ [13] and $\mathbf{L^7}$.[14] In comparison with $[Eu(NO_3)_3(\mathbf{L^1})(MeOH)]$, the complexes with $\mathbf{L^7}$ and $\mathbf{L^{11}}$ feature an acetonitrile molecule coordinated to the Eu^{III} ion instead of a methanol molecule. This difference does not influence the characteristics of the coordination polyhedron. However, the Eu−N(MeCN) distance in **2** (2.735 Å) is substantially longer than those found in the complex with $\mathbf{L^7}$ (2.555 Å)[14] and in the solvate $[Sm(MeCN)_9]^{3+}$ (2.54 Å).[15] This lengthening is a consequence of the acetonitrile molecule in **2** being implied in an intermolecular interaction with a nitrate anion (see above). The capping position of the polyhedron is occupied by N2 from one of the benzimidazole units, while the two planes are defined by O11, O21 and O31 from the three nitrate anions and N5 from the second benzimidazole substituent, and O12, O22 and O32 from the nitrates, N1 from the central pyridine, and N100 from the coordinated acetonitrile molecule. The two Eu−N(benzimidazole) bonds are symmetric (Table 1), in contrast to the situation

 © 2003 Wiley-VCH Verlag GmbH & Co. KGaA, Weinheim

with **L¹**, **L⁷** and **L¹⁰** where the two Eu−N(benzimidazole) distances are different, but in all cases shorter than the Eu−N(pyridine) bond. On the other hand, we note that the mean Eu−N distances in the complexes with **L¹⁰** and **L¹¹** are similar (2.52 Å) and shorter than in the complexes with ligands bearing small R^2 groups such as hydrogen {2.58 Å, $[Eu(NO_3)_2(\mathbf{L^0})_2](NO_3)$[16]} or methyl (2.54 Å, **L¹**).[13] Generally speaking, this mean value decreases with the increase of the steric hindrance generated by the R^2 substituents. However, the mean Eu−N distance of 2.57 Å in the complex with **L⁷**, which contains the bulky dimethoxybenzyl groups, is quite close to the value determined for the complex with **L⁰**, a consequence of the influence of the electron-attracting *p*-nitrophenyl group substituted in the R^3 position of the central pyridine ring.

All three bidentate nitrate anions bound to the metal ion in **2** have an approximate C_{2v} local symmetry and present Eu−O bonds in the range 2.48−2.59 Å, with an average distance of 2.52 Å, similar to the values observed in related nitrato complexes (2.46−2.55 Å).[13,14,16] The ionic radius calculated according to Shannon's definition (1.17 Å) is the same as in the other 10-coordinate complexes (1.16−1.17 Å)[13,14,16] and is close to the expected value of 1.18 Å.[17] Finally, it should be mentioned that the two asymmetric carbon atoms, C21 and C23, retain their absolute configuration *S* in the complex, as was observed in the free ligand.[11]

In order to gain information on the stability of the 1:1 nitrato complexes, we performed spectrophotometric and luminescence titrations of **L¹¹** with $Ln(NO_3)_3$ (Ln = La, Eu, Tb, Lu) at 298 K in MeCN, in the presence of 0.1 M Et_4NClO_4, under N_2 atmosphere. Factor analysis[18] indicates the presence of two absorbing species and the fit converges for $\log K_1 = 4.0 \pm 0.4$, 4.0 ± 0.5, 4.0 ± 0.5, and 6.4 ± 0.2 for La, Eu, Tb, and Lu, respectively. For La, the stability constant is similar to the value determined for **L¹** (4.2 ± 0.3).[19] The $\log K_1$ value of the Eu^{III} complex determined by luminescence titration is in good agreement with that extracted from the spectrophotometric data: 4.1 ± 0.4.

Luminescent Properties of the Nitrato 1:1 and Perchlorato 1:2 Complexes in Solution

The electronic spectrum of **L¹¹** in MeCN displays one intense band centred at 31385 cm^{-1}, which splits into two components upon complexation, reflecting the electronic transformations associated with the *trans-trans* → *cis-cis* conformational change and the complexation of the Ln^{III} metal to the tridentate binding unit (Table 2).[13,20] UV irradiation of **L¹¹** at room temperature yields one broad unresolved fluorescence band, centred around 27100 cm^{-1}, and originating from the $^1\pi\pi^*$ state (Figure 3). Upon complexation to non-luminescent Ln^{III} ions, the energy of the ligand $^1\pi\pi^*$ state decreases by about 2000 and 2770 cm^{-1} in the 1:1 and 1:2 complexes, respectively. At 77 K, the ligand triplet state appears at 21120 cm^{-1} and undergoes a bathochromic shift of 90−185 cm^{-1} in the nitrato complexes and of 755 cm^{-1} in the La^{III} 1:2 perchlorato complex (Table 2); lifetimes decrease from 389 ± 4 ms for the free ligand to 215 ± 1 and 93 ± 5 ms for the La 1:1 and 1:2 complexes, respectively. In addition to the weak metal-centred emission bands, the luminescence spectra of the Eu^{III} and Tb^{III} solutions reveal emission from the ligand $^1\pi\pi^*$ state. The latter is more intense in the case of the 1:2 complexes (see Figure 3), for which the ratio between the integrated ligand-centred singlet state and metal-centred emission bands reaches a factor of 280, compared to about one in the nitrato complexes. The mechanism by which energy is transferred from the ligand to the metal ion involves two essential steps, an intersystem crossing (isc) from the singlet to the triplet state of the ligand and energy transfer to the long-lived excited $^5D_0$(Eu) or $^5D_4$(Tb) states.[1] To get a better insight into the various energy migration processes occurring in the 1:1 and 1:2 complexes, we determined the quantum yield of both the ligand- and metal-centred luminescence of 10^{-4} to 10^{-3} M solutions at 293 K upon ligand excitation, and the ratio between the integrated triplet and singlet state emissions, $R_{TS} = I^T/I^S$, for the free ligand and its La (or Gd) complexes at 77 K.

The fluorescence quantum yield of the free ligand, $Q^F = 78\%$, is smaller than for **L¹**, for which it is close to 100%. It is substantially reduced by factors of 55 (La) and 83 (Gd) in the 1:1 nitrato complexes, but only by a factor of nine in the perchlorato 1:2 complex with La. Simultaneously, the ligand-centred phosphorescence is enhanced upon complexation as shown by R_{TS} which increases from 1.5×10^{-4} for uncomplexed **L¹¹** to 5.5×10^{-3} (La) and 1.5×10^{-2} (Gd) in the nitrato complexes, and to 1.5×10^{-3} in the La 1:2 complex. The better isc efficiency in 1:1 complexes results (i) from a more favourable energy gap between the $^1\pi\pi^*$ and $^3\pi\pi^*$ states: $\Delta E(^3\pi\pi^* - {}^1\pi\pi^*) = 4640$ (La) and 4450 (Gd) cm^{-1}, as compared to 6660 cm^{-1} in the free ligand and to 5690 cm^{-1} in its 1:2 complex with La (ideal value of 5000 cm^{-1}, Figure 4),[21] and (ii) from the mixing of the ligand-centred singlet and triplet wavefunctions promoted by spin-orbit and/or paramagnetic effects.[22]

The overall quantum yield of the europium-centred luminescence obtained upon ligand excitation, Q_L^{Eu}, amounts to 1.4% for the nitrato 1:1 complex, as compared to 2.8% for the corresponding compound with **L¹**.[19] This quantum yield can be broken down according to the following equation:

$$Q_{tot}^{Eu} = \eta_{ISC} \cdot \eta_{ET} \cdot Q^{Eu} = \eta_{sens} \cdot Q^{Eu}$$

where Q^{Eu} is the intrinsic luminescence quantum yield of the Eu^{III} ion, η_{sens} the efficiency of the luminescence sensitisation by the ligand, and η_{ISC} and η_{ET} the yields of the intersystem crossing and of the ligand-to-metal energy transfer, respectively. The intrinsic quantum yield Q^{Eu} is simply the ratio between the observed and radiative lifetimes of the Eu($^5D_0$) level:

$$Q^{Eu} = \tau_{obs}/\tau_R$$

In turn, in the special case of Eu^{III}, for which the intensity of the magnetic dipole $^5D_0 \rightarrow {}^7F_1$ transition is in prin-

 © 2003 Wiley-VCH Verlag GmbH & Co. KGaA, Weinheim

Table 2. Ligand-centred absorptions in acetonitrile, ligand-centred singlet- and triplet-state energies as determined from emission spectra of solutions 10^{-3} M in MeCN for the ligand **L^{11}** and its 1:1 and 1:2 complexes

Compound	$E(x\rightarrow\pi^*)$/cm^{-1} 293 K	$E(^1\pi\pi^*)$/cm^{-1} 293 K	77 K[c]	$E(^3\pi\pi^*)$/cm^{-1} 77 K [c]
L^{11}	31385 (4.48)			21120
			27780	19685
		27100	26810	18780
$[La(NO_3)_3(\mathbf{L^{11}})]$	31950 (4.44)			*20935*
	30120 (4.44)	27250 sh	25575	19640
		25250	24750	18360
$[Eu(NO_3)_3(\mathbf{L^{11}})(MeCN)]$	32465 (4.41)	26845	[d]	[e]
	28925 (4.46)	25445		
$[Gd(NO_3)_3(\mathbf{L^{11}})]$	32260 (4.41)			21030
	28820 (4.46)	27360 sh	25480	19630
		25000	24600	18315
$[Tb(NO_3)_3(\mathbf{L^{11}})]$	32465 (4.44)		[d]	[e]
	28820 (4.44)	24785		
$[La(ClO_4)_2(\mathbf{L^{11}})_2]^+$	32050 (4.69)		26055	
	29585 (4.71)		24845	20365
		24330	23895	18330
$[Eu(ClO_4)_2(\mathbf{L^{11}})_2]^+$	32585 (4.60)	26845 sh	[d]	[e]
	28530 (4.57)	23875		
$[Tb(ClO_4)_2(\mathbf{L^{11}})_2]^+$	32580 (4.69)		[d]	[e]

[a] sh = shoulder; at the concentration used, about 97, and 72−77% of the metal ion is under the form of the 1:2 and 1:1 complexes and 3, and 23−28% under the form of the 1:1 complex and free ligand in 1:2 and 1:1 solutions, respectively. [b] x = n or π; Logε values are given between parentheses. [c] The 0-phonon transition is given in italics for frozen solutions in MeCN. [d] Not measured. [e] Not observed because of the **L11**-to-Ln energy transfer process.

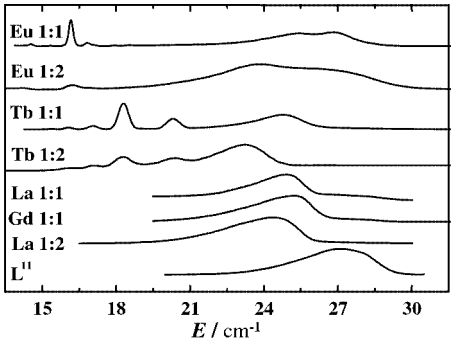

Figure 3. Emission spectra of $[Ln(NO_3)_3(\mathbf{L^{11}})(MeCN)_x]$ (x = 0, 1), $[Ln(ClO_4)_2(\mathbf{L^{11}})_2]^+$, and **L^{11}** 10^{-3} M in MeCN at 293 K

ciple independent of the chemical environment, the radiative lifetime τ_R can be estimated from:[23]

$$\tau_R = [1/(A_{MD,0}\cdot n^3)]\cdot(I_{MD}/I_{tot})$$

in which $A_{MD,0}$ is the spontaneous emission probability of the Eu($^5D_0\rightarrow{}^7F_1$) transition (14.65 s^{-1}), n is the refractive index (1.34 for the acetonitrile solution) and I_{MD}/I_{tot} is the intensity ratio of the Eu($^5D_0\rightarrow{}^7F_1$) transition to the total emission of the $^5D_0$ level. For the 1:1 complex, I_{MD}/I_{tot} = 0.1, leading to τ_R = 2.8 ms, Q^{Eu} = 0.47 (τ_{obs} = 1.32 ± 0.01 ms) and η_{sens} = 0.03. The isc efficiency in $[La(NO_3)_3\mathbf{L^{11}}]$ is about three times larger than in the nitrato La complex with **L^1**. Since the energy gaps $\Delta E(^3\pi\pi^*\text{-}^5D_0)$ are comparable — ca. 3600 cm^{-1} and 3700 cm^{-1} for the complexes with **L^1** and **L^{11}**, respectively, as estimated from $E(^3\pi\pi^*)$ in the La complexes — the smaller overall quantum

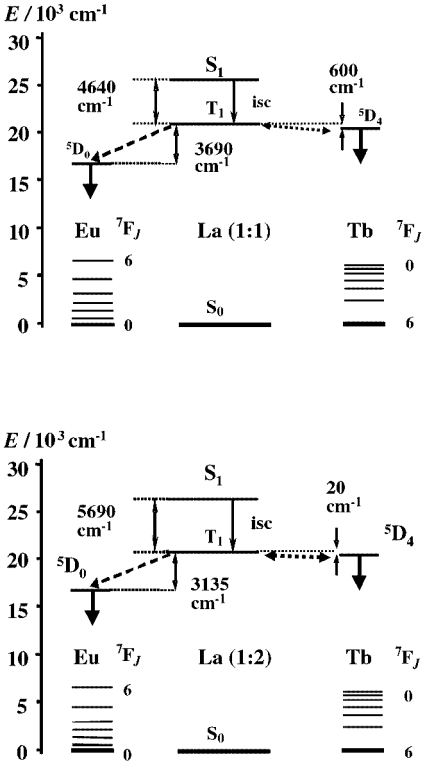

Figure 4. Schematic energy diagram for $[Ln(NO_3)_3(\mathbf{L^{11}})(MeCN)_x]$ (x = 0, 1) and $[Ln(ClO_4)_2(\mathbf{L^{11}})_2]^+$ complexes; data for S_1 and T_1 are those of the La^{III} complexes in frozen solution at 77 K (0-phonon transitions)

 © 2003 Wiley-VCH Verlag GmbH & Co. KGaA, Weinheim

yield of $[Eu(NO_3)_3\mathbf{L^{11}}]$ compared with the $\mathbf{L^1}$ complex can be traced back to more efficient non-radiative deactivation processes taking place in the former complex, probably in view of the larger fluxionality induced by the neopentyl substituents.

The situation is different in the Eu 1:2 complexes with $\mathbf{L^{11}}$ for which the quantum yield drops to 1×10^{-2} %. With respect to the nitrato 1:1 complex, the $\Delta(^3\pi\pi^* - {}^5D_0)$ gap decreases from ca. 3700 cm^{-1} to ca. 3100 cm^{-1}, which should be more favourable for the sensitisation of the metal luminescence. On the other hand, the isc process is about four times less efficient (compare the R_{TS} values given above for the La complexes) and the intrinsic quantum yield is smaller: a calculation similar to the one above leads to $I_{MD}/I_{tot} = 0.18$, $\tau_R = 5.1$ ms, $Q^{Eu} = 0.14$ ($\tau_{obs} = 0.73 \pm 0.01$ ms). Consequently, $\eta_{sens} = 7 \times 10^{-4}$, that is 42-fold smaller than in the 1:1 complex. Therefore, the 140-fold drop in the overall quantum yield of the 1:2 complex compared with the 1:1 compound can be roughly broken into three contributions: a less-efficient $^1\pi\pi^* \rightarrow {}^3\pi\pi^*$ transfer (ca. fourfold), a smaller intrinsic quantum yield Q^{Eu} (ca. threefold), and a substantially less efficient ligand-to-metal transfer (ca. 12-fold). A similar, but much more dramatic decrease in the overall quantum yield (3400-fold) has been reported for $[Eu(\mathbf{L^1})_3]^{3+}$ compared with $[Eu(NO_3)_3(\mathbf{L^1})(MeOH)]$. This effect was assigned, both on the basis of experimental data[19] and theoretical modelling,[24] to the presence of a ligand-to-metal charge transfer (LMCT) state with an energy close to that of the ligand singlet state.

The Tb^{III} complexes are about ten times less luminescent than the Eu^{III} analogues, with $Q_L^{Tb} = 1.1 \times 10^{-1}$ and 1.3×10^{-3} % for the 1:1 and 1:2 complexes, respectively. The main reason is a deactivation through energy back-transfer onto the ligand since the energy gap $\Delta(^3\pi\pi^* - {}^5D_4)$ amounts to only 600 and 20 cm^{-1}, respectively. The more efficient back-transfer taking place in the 1:2 complex compared with the nitrato compound is exemplified by the temperature dependence of the $^5D_4$(Tb) lifetimes, which are longer, for solid state samples, than for the nitrato complex.[25]

Chiro-Optical Properties

The specific rotary dispersion of solutions of the $[Ln(NO_3)_3(\mathbf{L^{11}})(MeCN)_x]$ ($x = 0, 1$) complexes (10^{-3} M in anhydrous acetonitrile) amounts to 18.8 ± 0.8 (La), 17.1 ± 0.2 (Eu), 16.8 ± 0.3 (Gd) and 19.1 ± 0.3 (Tb) deg·dm^2·mol^{-1}. These values are close to the one measured for the free ligand (15.1 ± 0.3 deg dm^2 mol^{-1}), pointing essentially to no structural contribution to the chiro-optical effect. For the 1:2 complexes, a similarly small structural contribution (4−5 deg dm^2 mol^{-1}) has been evidenced.[11] As a comparison, 4- to 10-fold larger rotary dispersion values have been observed for 1:3 complexes with ligands $\mathbf{L^{12}}$[10] and $\mathbf{L^*}$[9] compared with the free ligand value, pointing to the importance of the structural contribution in triple-stranded chiral helical complexes.

We have resorted to circularly polarized luminescence (CPL) to determine whether or not the 1:3 complex with $\mathbf{L^{11}}$ presents an enantiomeric excess of one isomer. CPL spectra were measured for solutions of $[Eu(NO_3)_3(\mathbf{L^{11}})(MeCN)]$, $[Ln(ClO_4)_2(\mathbf{L^{11}})_2]^+$ (Ln = Eu, Tb) $1-1.6 \times 10^{-3}$ M and for a perchlorate solution containing an Eu:$\mathbf{L^{11}}$ ratio equal to 1:34. In the latter, high resolution luminescence spectra (in a mixture of anhydrous MeCN:CH_2Cl_2, 97:3) show that the 1:3 species exists in a proportion of about 20% (Figure S2), the remaining Eu-containing species being the 1:2 complex, while only 1% of the Eu^{III} ions are in the 1:3 form in a 10^{-3} M perchlorate solution with a stoichiometric 1:3 ratio. The excitation spectrum of $[Eu(ClO_4)_2(\mathbf{L^{11}})_2]^+$ 10^{-3} M in the range of the $^5D_0 \leftarrow {}^7F_0$ transition reveals the presence of two bands at 17260 and 17244 cm^{-1} originating from the 1:1 and 1:2 complexes, respectively (Figure S3). The presence of the 1:1 species in the 10^{-3} M $[Eu(ClO_4)_2(\mathbf{L^{11}})_2]^+$ solution is confirmed by the speciation that can be calculated from the stability constants:[11] a 10^{-3} M solution contains 97% of the 1:2 species and about 3% of the 1:1 species. However, the quantum yield of the latter is 140 times larger than for the 1:2 compound, which explains the observation of both species in the excitation spectrum with similar intensity.

The emission of the magnetic dipolar $^5D_0 \rightarrow {}^7F_1$ transition is circularly polarized for the three Eu^{III} solutions with very small ΔI values, the smallest effect occurring, as expected, for the 1:1 species (Figure 5). We interpret these data as follows. The CPL properties observed for $[Eu(NO_3)_3(\mathbf{L^{11}})(MeCN)]$ result solely from the effect of the chirality of the ligand, while for the 1:2 and 1:3 compounds, the structural contribution of the helical wrapping of the ligands also contributes to ΔI. It is noteworthy that for the solutions of the perchlorato complexes, ΔI depends on the polarisation of the excitation light, indicating the presence of more than a single species in solution.[26] The CPL spectrum of the corresponding terbium 1:2 perchlorato complex displays a low ΔI value (Figure S4), which also demonstrates that the compound is not a racemic mixture in solution. Therefore, the chiro-optical data presented here are consistent with the presence of small diastereomeric excesses in solutions of the 1:2 and 1:3 complexes, on the short time scale of optical

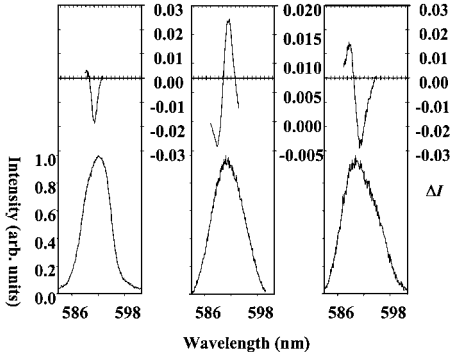

Figure 5. CPL spectrum of the $^5D_0 \rightarrow {}^7F_1$ transition of $1-1.6 \times 10^{-3}$ M solutions of $[Eu(NO_3)_3(\mathbf{L^{11}})(MeCN)]$ (left), $[Eu(ClO_4)_2(\mathbf{L^{11}})_2]^+$ (middle) in anhydrous MeCN and one with an Eu:$\mathbf{L^{11}}$ ratio of 1:34 (right) in a mixture of anhydrous MeCN and CH_2Cl_2 (97:3) at 293 K

 © 2003 Wiley-VCH Verlag GmbH & Co. KGaA, Weinheim

measurements, as previously observed for 1:3 complexes with **L12** [10] and **L***.[9]

Conclusion

The structural properties of $[Eu(NO_3)_3(\mathbf{L^{11}})(MeCN)]$ are similar to those of the Eu^{III} complexes with ligands **L1** and **L7**. Upon complexation, the ligand adopts a *cis-cis* configuration which implies a meridional planar coordination of the Eu^{III} metal. The introduction of various substituents in the R^2 position influences both the inner coordination sphere of the metal ion and the crystal packing, which is mainly governed by intermolecular interactions involving hydrogen bonds. The addition of a second ligand in the perchlorato 1:2 complexes significantly modifies the photophysical properties. For Eu^{III}, an efficient quenching of the metal-centred luminescence occurs which is due to several factors, one of which could be lowering of the energy of the LMCT state. Ligand **L11** is not a good sensitizer of the Tb^{III} luminescence in view of its too low-lying triplet state, and the introduction of a second ligand molecule lowers the energy of this state still further, leading to increased energy back-transfer. This study confirms that electronic, thermodynamic and photophysical properties of lanthanide complexes with aromatic terdentate ligands can be tuned by modifying the number, the arrangement and the nature of the ligands. In particular, the nature of electron-attracting or -withdrawing R^2 or R^3 groups influences critically the physicochemical properties of the complexes. Contrary to what was observed for the tris complexes with **L12**,[10] **L*** [9] and **L(−)**,[8] the chiro-optical properties of the 1:2 and 1:3 complexes mainly arise from the chirality of the ligand and not from a structural contribution due to the helical wrapping of the ligand strands around the Ln^{III} ions. On the other hand, small enantiomeric excesses are generated in solutions of 1:2 and 1:3 complexes.

Experimental Section

Solvents and Starting Materials: Acetonitrile and dichloromethane were distilled from CaH_2. Other products were purchased from Fluka AG (Buchs, Switzerland) or Merck and used without further purification. The ligand **L11**, its 1:2 complexes and lanthanide perchlorates and nitrates were synthesised as described previously.[11,27]

Caution: *Dry perchlorates and their complexes with aromatic amines may easily explode and should be handled in small quantities and with extreme precaution.*[28]

Spectroscopic and Analytical Measurements: Electronic spectra in the UV/Vis range were recorded at 293 K with a Perkin−Elmer Lambda 900 spectrometer using 1.0 and 0.1 cm quartz cells. Specific rotary dispersion values were measured from 10^{-3} M solutions in degassed anhydrous acetonitrile at 298 K with the help of a JASCO DIP-370 polarimeter (sodium D line). IR spectra were obtained from KBr pellets with a Mattson α-Centauri FT-IR spectrometer. Ligand excitation and emission spectra were recorded on a Perkin−Elmer LS-50B spectrometer equipped for low temperature (77 K) measurements. The experimental procedures for high resolution, laser excited luminescence studies have been published previously.[29] Emission spectra are corrected for the instrument function. Quantum yields of the ligand-centred emission were measured relative to quinine sulfate in 0.05 M H_2SO_4 ($A_{347} = 0.05$, absolute quantum yield: 0.546).[30] Quantum yields of the metal-centred emission were determined as described previously[19] at excitation wavelengths at which (i) the Lambert−Beer law is obeyed, and (ii) the absorption of the reference $[Ln(terpy)_3]^{3+}$ closely matches that of the sample. CPL measurements were made on an instrument described previously, operating in a differential photon-counting mode.[26] Elemental analyses were performed by Dr H. Eder (Microchemical Laboratory, University of Geneva).

Spectrophotometric Titrations: The electronic spectra in the UV/Visible range were recorded at 298 K from 10^{-4} M solutions in acetonitrile containing Et_4NClO_4 0.1 M as inert electrolyte with a Perkin−Elmer Lambda 7 spectrometer connected to an external personal computer and using quartz cells of 0.100 cm path length. Solutions were prepared in a thermostatted vessel (Metrohm 6.1418.220) and the titrating solution was added with an automated burette from Metrohm (6.1569.150 or -.210) fitted with an anti-diffusion device. In a typical experiment, 5−10 cm^3 of **L11** were titrated with a solution of Ln^{III} nitrate 10^{-4} M in acetonitrile, under N_2 atmosphere. After each addition of 0.10 cm^3 and a delay of 2 min, the spectrum was measured and transferred to the computer. Factor analysis and stability constant determinations were carried out with the program SPECFIT, version 2.10 (± 2σ).[31]

Crystal Structure of $[Eu(NO_3)_3(\mathbf{L^{11}})(MeCN)]$: The block-shaped crystals were directly transferred from the mother liquor into a drop of Hostinert 216 and kept at 210 K. A specimen was selected and placed in a glass capillary. The data collection took place at 150 K on a Stoe IPDS system equipped with Mo-K_α radiation. The detector-crystal distance was set to 80 mm, and a φ interval of 1° was chosen. Two hundred images were collected with an exposure time of 10 min/image. The integration was based on an effective mosaic spread of 0.011 and a profile of between 9 and 21 pixels. The intensities were corrected for Lorentz and polarisation effects. No absorption correction could be applied since the crystal was all but invisible in the frozen oil, but the absorption coefficient appears to be small. The decay during the measurement was negligible. The structure was solved and refined on F^2 with the help of the SHELX system.[32] In the final model, a part of the ligand was described with isotropic atomic displacement parameters and all atoms in **L11** were submitted to rigid link restraints. All hydrogen atoms were clearly visible in the difference electron density maps, and were included in a riding atom model. The last cycles continued to show a non-zero maximal parameter chance over σ. This is due to the fact that the Flack parameter[33] (refined as a component in the least-squares) turns negative at the end of each of the final cycles; it is then reset to zero by the program. The structure was analysed using SHELXTL 5.05[34] and PLATON.[35] The refinement favours the *S* configuration for the chirality centres C21 and C23, as expected from the synthesis.

Crystal Data: $C_{31}H_{36}EuN_9O_9$, $M = 830.65$, monoclinic, space group $P2_1$ (N_0 4), $a = 10.172(2)$, $b = 16.804(3)$, $c = 10.989(2)$ Å, $U = 1697.2(6)$ Å^3, $T = 150(2)$ K, $Z = 2$, $\mu(\text{Mo-}K_\alpha) = 1.915$ mm^{-1}, 10740 reflections measured, 5205 unique ($R_{int} = 0.1013$) which were used in all calculations. The final $wR(F^2)$ was 0.0347 (all data). CCDC-217485 contains the supplementary crystallographic data for this paper. These data can be obtained free of charge at www.ccdc.cam.ac.uk/conts/retrieving.html [or from the Cambridge Crystallographic Data Centre, 12, Union Road, Cambridge CB2 1EZ, UK; Fax: (internat.) + 44-1223/336-033; E-mail: deposit@ccdc.cam.ac.uk].

 © 2003 Wiley-VCH Verlag GmbH & Co. KGaA, Weinheim

Preparation of the 1:1 Nitrato Complexes: The 1:1 complexes $[Ln(NO_3)_3(\mathbf{L^{11}})(MeCN)_x]$ [x = 0, La (**1**), Gd (**3**), Tb (**4**); x = 1, Eu (**2**)] were prepared by mixing equivalent amounts of $Ln(NO_3)_3{\cdot}nH_2O$ (Ln = La, Eu, Gd, Tb and n = 5−6) and $\mathbf{L^{11}}$ in dichloromethane/acetonitrile (1:4 v/v) and the residual suspension was refluxed for 30 min. The complexes were crystallised in 70−80% yield by slow evaporation of the solvent and were characterised by their IR spectra (Table S1) and elemental analyses. [$C_{29}H_{33}LaN_8O_9$ (776.53): calcd. C 44.9, H 4.3, N 14.4; found C 44.9, H 4.3, N 14.3. $C_{31}H_{36}EuN_9O_9$ (830.64): calcd. C 44.8, H 4.4, N 15.2; found C 44.6, H 4.3, N 15.0. $C_{29}H_{33}GdN_8O_9$ (794.88): calcd. C 43.8, H 4.2, N 14.1; found C 43.9, H 4.3, N 14.1. $C_{29}H_{33}N_8O_9Tb$ (796.55): calcd. C 43.7, H 4.2, N 14.1; found C 43.7, H 4.1, N 14.1].

Acknowledgments

This work is supported through grants from the Swiss National Science Foundation. HB thanks the Danish Training Council for additional funding. We thank Prof. Pierre Vogel for the use of his polarimeter.

[1] J.-C. G. Bünzli, *Spectroscopic* Pr*operties of Rare Earths in Optical Materials* (Eds.: G. K. Liu and B. Jacquier), Springer Verlag, Berlin, **2003**, Ch. 11, in press.
[2] D. Parker, *Coord. Chem. Rev.* **2000**, *205*, 109−130.
[3] J.-C. G. Bünzli, in *Metal Ions in Biological Systems* (Eds.: A. Sigel and H. Sigel), Marcel Dekker Inc., New York, **2003**, Vol. 42, Ch. 2, in press.
[4] V. W. W. Yam, K. K. W. Lo, *Coord. Chem. Rev.* **1998**, *184*, 157−240.
[5] G. Bobba, R. S. Dickins, S. D. Kean, C. E. Mathieu, D. Parker, R. D. Peacock, G. Siligardi, M. J. Smith, J. A. G. Williams, C. F. G. C. Geraldes, *J. Chem. Soc., Perkin Trans. 2* **2001**, 1729−1737.
[6] H. Tsukube, S. Shinoda, *Chem. Rev.* **2002**, *102*, 2389−2403.
[7] D. Parker, R. S. Dickins, H. Puschmann, C. Crossland, J. A. K. Howard, *Chem. Rev.* **2002**, *102*, 1977−2010.
[8] G. Muller, J.-C. G. Bünzli, J. P. Riehl, D. Suhr, A. von Zelewsky, H.-R. Mürner, *Chem. Commun.* **2002**, 1522−1523.
[9] G. Muller, B. Schmidt, J. Jiricek, G. Hopfgartner, J. P. Riehl, J.-C. G. Bünzli, C. Piguet, *J. Chem. Soc., Dalton Trans.* **2001**, 2655−2662.
[10] G. Muller, J. P. Riehl, K. J. Schenk, G. Hopfgartner, C. Piguet, J.-C. G. Bünzli, *Eur. J. Inorg. Chem.* **2002**, 3101−3110.
[11] G. Muller, J.-C. G. Bünzli, K. J. Schenk, C. Piguet, G. Hopfgartner, *Inorg. Chem.* **2001**, *40*, 2642−2651.
[12] K. Nakamoto, *Infrared and Raman Spectra of Inorganic and Coordination Compounds. Part A. Theory and Applications in Inorganic Chemistry*, Wiley Interscience, New York, **1997**.
[13] C. Piguet, A. F. Williams, G. Bernardinelli, E. Moret, J.-C. G. Bünzli, *Helv. Chim. Acta* **1992**, *75*, 1697−1717.
[14] S. Petoud, J.-C. G. Bünzli, K. J. Schenk, C. Piguet, *Inorg. Chem.* **1997**, *36*, 1345−1353.
[15] H. Jingyu, S. Qi, J. Zhongsheng, *Kexue Tongbao (Chin. Sci. Bull.)* **1990**, *35*, 1090−1092.
[16] W. Shuangxi, Z. Ying, C. Yuxin, W. Liufang, L. Qinhui, *J. Chem. Soc., Dalton Trans.* **1994**, 2523−2530.
[17] R. D. Shannon, *Acta Crystallogr., Sect. A* **1976**, *32*, 751−767.
[18] E. R. Malinowski and D. G. Howery, *Factor Analysis in Chemistry*, John Wiley, New York, Chichester, Brisbane, Toronto, **1980**.
[19] S. Petoud, J.-C. G. Bünzli, T. Glanzman, C. Piguet, Q. Xiang, R. P. Thummel, *J. Lumin.* **1999**, *82*, 69−79.
[20] C. Piguet, J.-C. G. Bünzli, G. Bernardinelli, C. G. Bochet, P. Froidevaux, *J. Chem. Soc., Dalton Trans.* **1995**, 83−97.
[21] F. J. Steemers, W. Verboom, D. N. Reinhoudt, E. B. van der Tol, J. W. Verhoeven, *J. Am. Chem. Soc.* **1995**, *117*, 9408−9414.
[22] S. Tobita, M. Arakawa, I. Tanaka, *J. Phys. Chem.* **1984**, *88*, 2697−2702. S. Tobita, M. Arakawa, I. Tanaka, *J. Phys. Chem.* **1985**, *89*, 5649−5654.
[23] M. H. V. Wertz, R. T. F. Jukes, J. W. Verhoeven, *Phys. Chem. Chem. Phys.* **2002**, *4*, 1542−1548.
[24] F. R. Gonçalves e Silva, R. Longo, O. L. Malta, C. Piguet, J.-C. G. Bünzli, *Phys. Chem. Chem. Phys.* **2000**, *2*, 5400−5403.
[25] G. Muller, PhD. Dissertation, University of Lausanne, **2000**.
[26] J. P. Riehl, F. S. Richardson, *Chem. Rev.* **1986**, *86*, 1−16.
[27] J.-C. G. Bünzli, J.-R. Yersin, C. Mabillard, *Inorg. Chem.* **1982**, *21*, 1471−1476.
[28] W. C. Wolsey, *J. Chem. Educ.* **1973**, *50*, A335−A337.
[29] R. Rodríguez-Cortiñas, F. Avecilla, C. Platas-Iglesias, D. Imbert, J.-C. G. Bünzli, A. de Blas, T. Rodríguez-Blas, *Inorg. Chem.* **2002**, *41*, 5336−5349.
[30] S. R. Meech, D. C. Phillips, *J. Photochem.* **1983**, *23*, 193−217.
[31] H. Gampp, M. Maeder, C. J. Meyer, A. D. Zuberbühler, *Talanta* **1985**, *23*, 1133−1139.
[32] G. M. Sheldrick, *Acta Crystallogr., Sect. A* **1997**, *46*, 467−473.
[33] H. D. Flack, *Acta Crystallogr., Sect. A* **1983**, *39*, 876−881.
[34] G. M. Sheldrick, SHELXTL 5.05 Siemens Analytical X-ray Instruments Inc., Madison, WI, **1996**.
[35] A. L. Spek, *Acta Crystallogr., Sect. A* **1990**, *46*, C34.

Received June 26, 2003
Early View Article
Published Online October 2, 2003

 © 2003 Wiley-VCH Verlag GmbH & Co. KGaA, Weinheim

Structure and Magnetism of a New Dodecanuclear Cu^{II} Complex with Acetato and Imidazolato Bridges, Formed by Oxidation of the Chelating Ligand 1,1,7,7-Tetrakis(imidazol-2-yl)-2,6-diazaheptane

Yufei Song,[a] Patrick Gamez,[a] Arno F. Stassen,[a] Martin Lutz,[b] Anthony L. Spek,[b] and Jan Reedijk*[a]

Keywords: Copper / Magnetic properties / N ligands / Chelates

A novel dodecanuclear copper(II) complex $[Cu_{12}(tidhd)_4(MeOH)_8(CH_3COO)_8](MeOH)_{0.8}$ (Htidhd = 1,1,7,7-tetrakis-(imidazol-2-yl)-2,6-diaza-1,6-heptadiene) with imidazolato and acetato bridging ligands was synthesized by reaction of polyimidazole 1,1,7,7-tetrakis(imidazol-2-yl)-2,6-diazaheptane (Htidahp) with copper acetate in a methanol solution. The complex crystallized in the triclinic space group $P\bar{1}$ with a = 9.1204(1), b = 13.5139(2), c = 27.6925(5), α = 76.8006(6)°, β = 82.8066(7)°, γ = 76.4594(9)°, Z = 1. Structure analysis shows that the unit cell of the complex contains twelve copper(II) ions in three different coordination environments. The complex is centrosymmetric and the two hexanuclear units are linked by two μ_3-acetate anions [the Cu1–Cu1a distance is 3.5507(7) Å]. The magnetic superexchange interaction via the bridging imidazolate ligand appears to be the most important magnetic interaction in this complex. Magnetic susceptibility measurement vs. temperature in the range of 6–300 K were fitted to the parameters g = 2.05, J_a = –32.0 cm^{-1} and J_b = –5.45 cm^{-1}.

(© Wiley-VCH Verlag GmbH & Co. KGaA, 69451 Weinheim, Germany, 2003)

Introduction

There has been great interest in the magnetostructural studies carried out on polynuclear divalent first-row transition metal complexes in recent years.[1] One of the main interests in this field comes from the need for the design and synthesis of novel functional materials with highly ordered structures in order to provide new molecular-based magnets.[2] Furthermore, many such systems are potential model compounds of multi-metal proteins.[3] This is especially relevant when imidazole is used as a ligand, since it is ubiquitous in proteins.[4]

Over the past decades, much progress has been made in the structural characterisation of copper proteins by different methods,[5] although the specific reaction pathways and mechanisms of action have remained unclear. In order to understand their catalytic mechanisms and their unusual spectroscopic characteristics, the development of relatively simple synthetic models of the active sites of copper proteins is of considerable interest.[6] The ligands most frequently used are based on pyrazole, imidazole and pyridine moieties.[7,8] Since imidazole is present in many natural enzyme and proteins, we have chosen to design and synthesize model compounds of copper proteins with imidazole-containing ligands.[9]

The reaction of 1,1,7,7-tetrakis(imidazol-2-yl)-2,6-diazaheptane (Htidahp) with $Cu(OAc)_2$ leads to an unprecedented imidazolato- and acetato-bridged dodecanuclear complex. In this paper, the synthesis, crystal structure, spectroscopic and magnetic properties of this compound are discussed. Figure 1 shows the schematic structure of the ligand Htidahp.

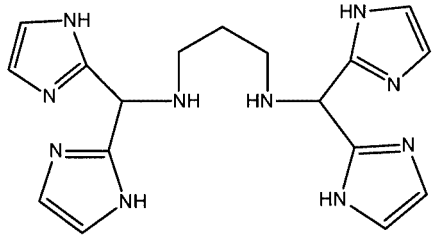

Figure 1. The structure of the ligand1,1,7,7-tetrakis(imidazol-2-yl)-2,6-diazaheptane (Htidahp)

Results and Discussion

The dodecanuclear complex was obtained by reaction of one equivalent of Htidahp with three equivalent of copper(II) acetate in methanol. Diethyl ether diffusion into the methanolic solution led to the formation of deep green,

[a] Leiden Institute of Chemistry, Gorlaeus Laboratories, Leiden University, P. O. Box 9502, 2300 RA Leiden, The Netherlands
[b] Bijvoet Center for Biomolecular Research, Utrecht University, Padualaan 8, 3584 CH Utrecht, The Netherlands

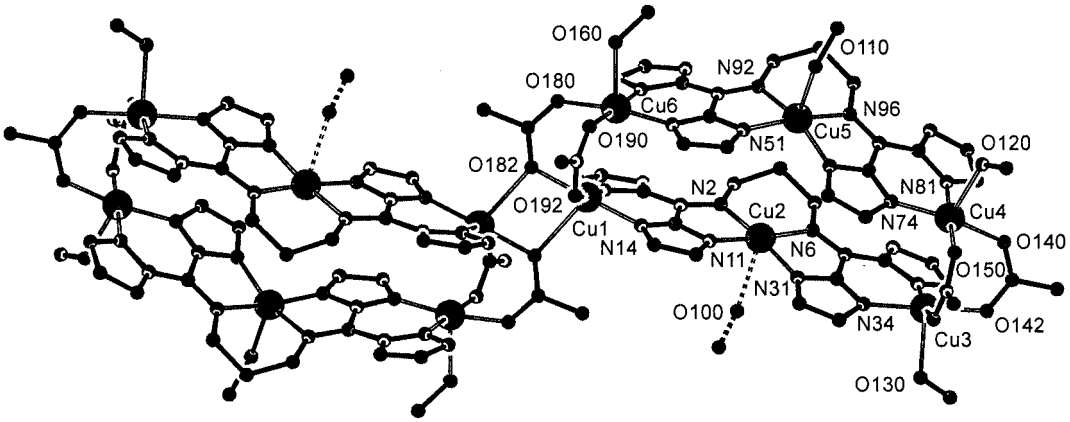

Figure 2. Platon projection[14] of the crystal structure of $[Cu_{12}(tidhd)_4(CH_3OH)_8(CH_3COO)_8](CH_3OH)_{0.8}$; hydrogen atoms are omitted for clarity; only the major component of the disordered methanol molecule at O130 is shown; the methanol molecule at O100 is only partially occupied

square crystals suitable for X-ray crystal structure determination (Figure 2).

The unit cell of the structure encloses one dodecanuclear unit, which is centrosymmetric. The asymmetric unit of the complex contains one $[Cu_6(tidhd)_2]^{4+}$ cation, five methanol molecules, of which one is disordered and one only partially occupied, and four $[CH_3COO]^-$ anions. Disordered solvent molecules occupy 13.5% of the unit cell volume, and they were treated as diffuse electron density (see Exp. Sect.). In the asymmetric unit, the six copper atoms are in different environments. Four dehydronated imidazole groups bridge Cu1 and Cu2 [5.6889(8) Å], Cu2 and Cu3 [5.6731(8) Å], Cu4 and Cu5 [5.7224(8) Å], and Cu5 and Cu6 [5.7148(7) Å], while the acetate anions bridge Cu1 and Cu6 [2.9926(8) Å], and Cu3 and Cu4 [3.0393(8) Å]. Cu1 is coordinated by a bridging imidazolate nitrogen atom, an imidazole nitrogen atom and three bridging acetate oxygen atoms in a distorted square-pyramidal geometry {O192−Cu1−N21 170.23(14)°, O182−Cu1−N14 175.87(14)°; $\tau_1 = 0.094$, where $\tau = 0$ and 1 are for the perfect square pyramidal and trigonal bipyramidal geometries, respectively[10]}, with a N_2O_3 donor set. Cu2 and Cu5 are each coordinated by a bridging imidazolate nitrogen atom, an imidazole nitrogen atom, two nitrogen atoms from the diamine unit, and one oxygen atom from a methanol molecule (N_4O donor set; $\tau_2 = 0.057$, $\tau_5 = 0.194$). The Cu3, Cu4 and Cu6 atoms are coordinated by a bridging imidazolate nitrogen atom, an imidazole nitrogen atom, two oxygen atoms from acetate oxygen atoms and one oxygen from a methanol molecule (N_2O_3 donor set; $\tau_3 = 0.170$, $\tau_4 = 0.123$, $\tau_6 = 0.124$). All the coordination spheres of these six copper atoms are distorted square-pyramidal. The Cu−O distances for the coordinated methanol molecules are in the range of 2.265(3) to 2.294(3) Å. On Cu2 the methanol molecule is only very weakly bound with a Cu−O distance of 2.706(10) Å. It can therefore easily evaporate, which explains the partial occupancy in the crystal. In all cases the methanol ligand is in an axial position. The complex consists of two hexanuclear units bridged by two acetate groups; the distance between Cu1 and Cu1a is 3.5507(7) Å.

It has to be pointed out that the C−N bonds in the original ligand have been oxidized to C=N upon coordination with copper acetate. Such oxidation and dehydrogenation reactions are not uncommon.[9,11] This compound is further stabilized by intramolecular and intermolecular hydrogen bonds. The different molecules are linked by intermolecular stacking between the imidazole rings, and by several hydrogen bonds.

A crystal structure of a related ligand, namely 1,1,6,6-tetrakis(imidazol-2-yl)-2,5-diazahexane (Htidah) was reported by our group with six copper ions in three different coordination environments.[11] The asymmetric unit in that complex consists of three copper ions, a negative tidah ligand, five chloride ions, two coordinated water molecules involved in hydrogen bonding and three lattice water molecules. The imidazole only bridges two copper atoms and the two trinuclear units are linked by two asymmetric chloride bridges (Cl6 and Cl6a) and two further bridges (Cl4 and Cl4a). The present dodecanuclear copper complex has both imidazolato and acetato bridging ligands. Its magnetic and electronic properties are described below.

Electronic Properties

The ligand field diffusion reflectance spectrum of the complex shows three d-d absorption bands centered at approximately $\lambda = 252$ nm (39.6×10^3 cm^{-1}), $\lambda = 368$ nm (27.2×10^3 cm^{-1}) and $\lambda = 603$ nm (16.6×10^3 cm^{-1}) in agreement with such geometries. The intensity of the absorptions at 368 nm and at 252 nm are assigned to the charge-transfer transition from the imidazolate nitrogen atoms to Cu^{II},[12] while the absorption at 603 nm is assigned to d-d transitions.[13]

 © 2003 Wiley-VCH Verlag GmbH & Co. KGaA, Weinheim

EPR and Magnetic Susceptibility

The EPR spectrum of a powered polycrystalline sample of the complex at room temperature shows a broad isotropic copper(II) signal centered around a g value of 2.1034. At 77 K, the signals of the powder and a frozen solution of the complex in CH_3CN/MeOH are sharper, but no resolution of $g_{//}$ and $g_{\perp}$ is observed.

Magnetic susceptibility measurements have been performed on crystals of the complex (m = 34.87 mg) at 0.1 Tesla in the temperature range of 6 to 300 K. The plot of χ^{-1} and χT versus the temperature [with χ being the magnetization per copper(II) ion] is shown in Figure 3. At 300 K, $\chi T = 0.35$ cm^3·K·mol^{-1}, which is slightly lower than the expected value for a single, uncoupled copper(II) ion ($\chi T \approx 0.42$ cm^3·K·mol^{-1} for paramagnetic systems). The value of χT decreases upon cooling, with an even sharper decline below 60 K, to a value of $\chi T = 0.06$ cm^3·K·mol^{-1} at 6 K. This decrease indicates the presence of a quite strong antiferromagnetic coupling. The shape of the curve of both χT, and of χ^{-1} vs. the temperature is characteristic for a linear arrangement of three copper(II) ions.[14−16]

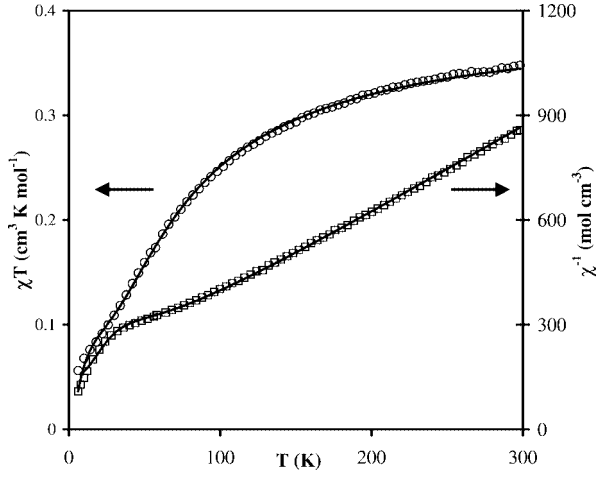

Figure 3. χT vs. T (○) and χ^{-1} vs. T curves (□) of **1**; the solid lines represent the calculated curves with parameters g = 2.05, J_a = −32.0 cm^{-1}, J_b = −5.45 cm^{-2} and $R = 7.6\cdot10^{-5}$ ($J_a = J_1 = J_2 = J_3 = J_4$; $J_b = J_5 = J_6$; $J_7 = 0$)

The fitting of the linear part of the χ^{-1} vs. T curve (between 80 and 300 K) results in a Curie constant, C, of 0.45 cm^3 mol^{-1} and a Curie Weiss temperature, θ, of −80.0 K with $R < 1.6\cdot10^{-4}$. [The fit was accompanied by minimisation of the reliability factor, defined as $R = {}^1/_n\cdot\Sigma(\chi^{-1}_{calc}/\chi^{-1}_{obs})^2/(\chi^{-1}_{obs})^2$, by least-squares procedure.] The Curie constant is in good agreement with the g value measured by EPR spectroscopy.[17] To interpret the magnetic data, the possible magnetic-exchange pathways have to be examined in some detail (Figure 4).

Along with six different magnetic superexchange interactions within the hexanuclear ring, coupling (J_7) between the two hexanuclear units is possible via the acetate anion bridging between Cu1 and Cu6, Cu1 and Cu1a. This interaction is expected to be small, as no equatorial links are involved, and is therefore not taken into account.[18]

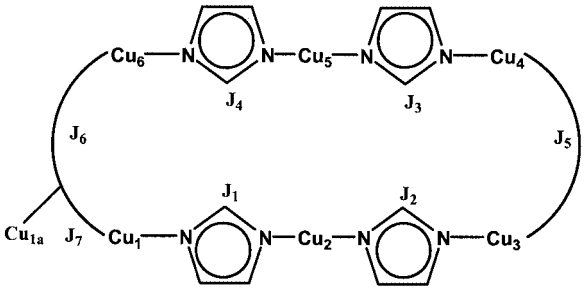

Figure 4. Possible magnetic superexchange pathways of the complex

Magnetic superexchange interaction via a bridging imidazole ligand is known to be relatively strong.[18,19] It is concluded from the short copper-imidazole distances (all between 1.948 Å and 2.022 Å) that the magnetic orbitals of the copper(II) ions are directed in such a way that a considerable electron delocalization occurs over the imidazolate nitrogen atoms. Therefore, an antiferromagnetic interaction is expected between Cu1−Cu2−Cu3 and between Cu4−Cu5−Cu6. Because the difference in Cu−Cu distances and the angles between the copper centers and the C2-atom of the imidazole ring are small (5.698 ± 0.025 Å, 172.12 ± 1.35°), the magnetic-exchange pathways J_{1-4} are considered to be identical (J_a).

These considerations lead to the first part of the expression (1), to describe the magnetic behaviour of this bis-hexanuclear cluster.

$$\chi = \frac{N\beta^2 g^2}{4kT}\,\frac{1+\exp[-2J_a/kT]+10\exp[J_a/kT]}{3+3\exp[-2J_a/kT]+6\exp[J_a/kT]}\times\exp[J_b/kT] \qquad (1)$$

In this formula, N, β and k have their normal value and g is assumed to be equal for all individual metal ions. The first term is an equation for an A-B-A copper(II) trinuclear species.[14,17] A trinuclear copper(II) species will normally lead to spin frustration, resulting in a χT value at low temperature equivalent to that of one uncoupled copper(II) ion.[17] As can be seen in Figure 3, the value of χT at low temperature is even lower than would be expected for such a trinuclear species. The superexchange interactions over the bridging acetate anions (J_5 and J_6) will be virtually identical and are therefore not expected to be equal to zero, and will be called J_b. This interaction forces the two trinuclear units to behave as two antiferromagnetic coupled units. The coupling constant J_b expresses this intertrinuclear superexchange interaction.

A good fit has been obtained for the parameters g = 2.05, J_a = −32.0 cm^{-1}, J_b = −5.45 cm^{-2} and $R = 7.6\times10^{-5}$. [$R = {}^1/_n\cdot\Sigma(\chi^{-1}_{calc}/\chi^{-1}_{obs})^2/(\chi^{-1}_{obs})^2$, where n is the number of points, χ_{calc} is the magnetic susceptibility calculated by formula 1 and χ_{obs} the measured susceptibility]. The magnetic behaviour of the complex can therefore be described as antiferromagnetic dimers of linear antiferromagnetic linear trimers. The value of J_a is in the range commonly observed for imidazolato-bridged Cu^{II} ions.[17−19]

 © 2003 Wiley-VCH Verlag GmbH & Co. KGaA, Weinheim

Conclusions

In this paper, the synthesis and the structural and magnetic study of a novel dodecanuclear copper complex $[Cu_{12}(tidhd)_4(MeOH)_8(CH_3COO)_8](MeOH)_{0.8}$ are presented. The imidazole groups of the Htidhd ligand are dehydronated. The C−N bonds from the starting ligands have been oxidatively converted into C=N bonds upon coordination with copper acetate, which results in an unprecedented complex with a unique architecture. The unit cell of the dodecanuclear complex is centrosymmetric. Each asymmetric unit of the complex is composed by one $[Cu_6(tidhd)_2]^{4+}$, four methanol molecules and four acetate anions, and six copper atoms are in different coordination environment. All the coordination spheres of the six copper atoms are of a distorted square-pyramidal geometry. The two hexanuclear units are linked by two μ_3-acetate groups. The magnetic superexchange interaction via the bridging imidazolate ligand plays an important role in the magnetic interaction. The study here provides not only a novel dodecanuclear complex with imidazolato- and acetato- group as bridges, but also more information about the magnetic and structural data for imidazolato-bridged complexes.

Experimental Section

All reagents and solvents were purchased from commercial sources and used as received. C, H and N analyses were carried out in Leiden University. Infrared spectra were recorded on a Perkin−Elmer Paragon 1000 spectrophotometer equipped with a Golden Gate diamond ATR as a sample support. X-band EPR spectra were recorded on a JEOL ESR spectrometer equipped with an Esprit 330 data system, at room temperature and at 77 K, with dpph as internal reference (g = 2.0036). The ligand-field spectra of the solid samples were recorded in the 300−2000 nm range on a Perkin−Elmer Lambda 900 UV/Vis/NIR spectrometer in the diffuse reflectance mode with MgO as reference. Bulk magnetizations of polycrystalline samples were measured in the range 6−300 K with a Quantum Design MPMS-5S SQUID magnetometer, in a 1 kG applied field. The data were corrected for the experimentally determined contribution of the sample holder. Corrections for the diamagnetic responses of the complex, as estimated from Pascal's constants, were applied.[20]

The ligand 1,1,7,7-tetrakis(imidazol-2-yl)-2,6-diazaheptane (Htidahp) was prepared as follows: 1,3-Diaminopropane (0.32 g, 4.34 mmol) was added to a solution of the hydrochloride salt of bis(imidazol-2-yl)nitromethane[21] (2.0 g, 8.69 mmol) in 10 mL of ethanol and 10 mL of sodium hydroxide solution (2.0 M). The solution was stirred for 45 min at 80 °C, during which time the product crystallised from the reaction mixture. After cooling to room temperature, the reaction mixture was filtered. The product was washed with water, ethanol and dried with diethyl ether. Yield 76%. ^{1}H NMR (200 MHz, 1 M DCl, 25 °C): δ = 7.40 (s, 8 H, imidazole), 5.85 (s, 2 H, CH), 2.58 (d, 4 H, CH_2), 1.67 (m, 2 H, CH_2) ppm.

Preparation of the Complex: A solution of the ligand Htidahp (14.64 mg, 0.01 mmol) in 3 mL of methanol was added to a solution of $Cu(CH_3COO)_2$ (24.00 mg, 0.03 mmol) in 5 mL of methanol. The reaction mixture was stirred at room temperature for 10 min and filtered. Diethyl ether diffusion into the filtered solution led to the formation of deep green crystals of sufficient quality for X-ray structure determination. Yield: 11%. $C_{92.8}H_{114.4}Cu_{12}N_{40}O_{24.8}$ (2949.5): calcd. C 37.8, H 3.9, N 19.0; found C 37.5, H 3.7, N 18.4. IR (solid): $\tilde{\nu}$ = 1557.9, 1455.3, 1414.3, 1373.0, 1199.4, 937.9, 764.4, 623.1, 480.4 cm^{-1}. UV/Vis/NIR (solid): λ_{max} = 368 nm (strong); λ = 252 nm and λ = 603 nm (weak). EPR (solid, room temp): g = 2.1034.

X-ray Crystal Structure Determination: $C_{92.8}H_{114.4}Cu_{12}N_{40}O_{24.8}$ + solvent, Fw = 2949.52, green needle, 0.30 × 0.12 × 0.06 mm^3, triclinic, $P\bar{1}$ (no. 2), a = 9.1204(1), b = 13.5139(2), c = 27.6925(5) Å, α = 76.8006(6)°, β = 82.8066(7)°, γ = 76.4594(9)°, V = 3221.33(8) Å^3, Z = 1, ρ_x = 1.520 g cm^{-3}, 36255 measured reflections, 11025 unique reflections (R_{int} = 0.0656), 7472 observed reflections [$I > 2\sigma(I)$]. 785 refined parameters, 16 restraints. R (obs. refl.): $R1$ = 0.0416, $wR2$ = 0.1143. R (all data): $R1$ = 0.0674, $wR2$ = 0.1285. S = 1.038. Intensities were measured on a Nonius KappaCCD diffractometer with rotating anode (Mo-K_α, λ = 0.71073 Å) at a temperature of 150 K. An absorption correction based on multiple measured reflections was applied (μ = 2.014 mm^{-1}, 0.76−0.89 transmission). The structure was solved by direct

Table 1. Selected bond lengths (Å) and angles (°) of $[Cu_{12}(tidhd)_4(CH_3OH)_8(CH_3COO)_8](CH_3OH)_{0.8}$

Bond lengths (Å)			
Cu1−Cu6	2.9925(8)	Cu3−Cu4	3.0392(8)
Cu1−O182	2.007(3)	Cu4−O120	2.294(3)
Cu1−O181a	2.484(3)	Cu4−O140	1.975(3)
Cu1−O192	1.970(3)	Cu4−O150	2.009(3)
Cu1−N14	1.961(4)	Cu4−N74	1.961(3)
Cu1−N21	1.964(4)	Cu4−N81	1.992(3)
Cu1−Cu2	5.6885(8)	Cu4−Cu5	5.7225(8)
Cu2−N2	2.004(4)	Cu5−O110	2.287(3)
Cu2−N6	2.002(3)	Cu5−N51	1.966(3)
Cu2−N11	1.968(3)	Cu5−N71	1.966(3)
Cu2−N31	1.948(4)	Cu5−N92	2.022(4)
Cu2−O100	2.706(10)	Cu5−N96	2.013(3)
Cu2−Cu3	5.6732(8)	Cu5−Cu6	5.7147(8)
Cu3−O130	2.265(3)	Cu6−O160	2.292(3)
Cu3−O142	1.968(3)	Cu6−O180	1.978(3)
Cu3−O152	1.975(3)	Cu6−O190	1.981(3)
Cu3−N34	1.958(4)	Cu6−N54	1.949(4)
Cu3−N41	1.968(4)	Cu6−N61	1.977(4)
Bond angles (°)			
O182−Cu1−O192	87.22(12)	O120−Cu4−O140	92.92(12)
O182−Cu1−N14	175.87(14)	O140−Cu4−O150	88.79(12)
O182−Cu1−N21	93.55(14)	O140−Cu4−N74	170.52(14)
O182−Cu1−O182a	76.01(13)	O140−Cu4−N81	90.72(13)
O192−Cu1−N14	88.94(14)	O150−Cu4−N74	91.40(13)
O192−Cu1−N21	170.23(14)	O150−Cu4−N81	177.93(14)
N2−Cu2−N6	96.86(14)	O110−Cu5−N51	91.69(13)
N2−Cu2−N11	81.77(15)	N51−Cu5−N71	96.82(14)
N2−Cu2−N31	171.82(15)	N51−Cu5−N92	81.82(14)
N2−Cu2−O100	90.8(2)	N51−cu5−N96	170.34(14)
N6−Cu2−N11	175.25(15)	N71−Cu5−N92	158.76(15)
N6−Cu2−O100	93.7(2)	N71−Cu5−N96	81.84(14)
O130−Cu3−O142	89.55(12)	O160−Cu6−N54	96.08(13)
O142−Cu3−O152	88.28(13)	O180−Cu6−O190	86.46(13)
O142−Cu3−N34	177.31(14)	O180−Cu6−N54	171.11(14)
O142−Cu3−N41	91.62(13)	O180−Cu6−N61	92.15(14)
N34−Cu3−N41	89.63(15)	O190−Cu6−N54	91.52(15)
O152−Cu3−N41	167.12(14)	O190−Cu6−N61	178.55(14)

 © 2003 Wiley-VCH Verlag GmbH & Co. KGaA, Weinheim

methods using the program SHELXS-97,[22] and refined with the program SHELXL-97[23] against F^2 of all reflections up to a resolution of $(\sin\theta/\lambda)_{max} = 0.59$ Å^{-1}. Non-hydrogen atoms were refined freely with anisotropic displacement parameters. O-H hydrogen atoms were fixed in their located positions, all other hydrogen atoms were refined as rigid groups. One weakly coordinated methanol molecule was only partially occupied in the crystal (occupancy 40%); its O-H hydrogen atom could not be located in the difference Fourier map and was therefore not included in the refinement. The crystal structure contains large voids (435.5 Å^3) filled with disordered solvent molecules. Their contribution to the structure factors was secured by back-Fourier transformation (program PLATON,[24] CALC SQUEEZE, 56 e$^-$/unit cell). The drawings, structure calculations, and checking for higher symmetry were performed with the program PLATON.[24]

The Platon projection[24] of the crystal structure of $Cu_{12}(tidhd)_4(CH_3OH)_8(CH_3COO)_8](CH_3OH)_{0.8}$ is shown in Figure 2. Selected bond lengths and angles are given in Table 1.

CCDC-213532 contains the supplementary crystallographic data for this paper. These data can be obtained free of charge at www.ccdc.cam.ac.uk/conts/retrieving.html [or from the Cambridge Crystallographic Data Centre, 12, Union Road, Cambridge CB2 1EZ, UK; Fax: (internat.) +44-1223/336-033; E-mail: deposit@ccdc.cam.ac.uk].

Acknowledgments

The work described here has been supported by the Leiden University Study group WFMO (Werkgroep Fundamenteel Materialen Onderzoek), the CNRS and the Conseil Régional d'Aquitaine. Support from the NRSC Catalysis (a Research School Combination of HRSMC and NIOK) is kindly acknowledged. This ECOX project is financially supported by the Dutch Economy, Ecology, Technology (EET) programme, a joint programme of the Ministry of Economic Affairs, the Ministry of Education, Culture and Science, and the Ministry of Housing, Spatial Planning and the Environment. This work was partially supported (M.L., A.L.S.) by The Netherlands Foundation for Chemical Sciences (CW) with financial aid from The Netherlands Organization for Scientific Research (NWO).

[1] [1a] G. De Munno, M. Julve, G. Viau, F. Lloret, J. Faus, D. Viterbo, *Angew. Chem. Int. Ed. Engl.* **1996**, *35*, 1807. [1b] R. Cortés, L. Lezama, J. L. Pizarro, M. I. Arriortua, T. Rojo, *Angew. Chem. Int. Ed. Engl.* **1996**, *35*, 1810. [1c] J. Ribas, M. Monfort, I. Resino, X. Solans, P. Rabu, F. Maingot, M. Drillon, *Angew. Chem. Int. Ed. Engl.* **1996**, *35*, 2520. [1d] J. A. R. Navarro, M. Angustias Romero, J. M. Salas, M. Quiós, E. R. T. Tiekink, *Inorg. Chem.* **1997**, *36*, 4988.

[2] [2a] A. Escuer, M. A. S. Goher, F. A. Mautner, R. Vicente, *Inorg. Chem.* **2000**, *39*, 2107. [2b] O. Castillo, A. Luque, J. Sertucha, P. Román, F. Lloret, *Inorg. Chem.* **2000**, *39*, 6142. [2c] J. Cano, P. Alemany, S. Alvarez, M. Verdaguer, E. Ruiz, *Chem. Eur. J.* **1998**, *4*, 476.

[3] [3a] Y. Akhriff, J. Server-Carrió, A. Sancho, J. García-Lozano, E. Escrivá, L. Soto, *Inorg. Chem.* **2001**, *40*, 6832. [3b] R. H. Holm, P. Kennepohl, E. I. Solomon, *Chem. Rev.* **1996**, *96*, 2239. [3c] G. Tabbi, W. L. Driessen, J. Reedijk, R. P. Bonomo, N. Veldman, A. L. Spek, *Inorg. Chem.* **1997**, *36*, 1168.

[4] [4a] R. Bhalla, M. Helliwell, C. D. Garner, *Inorg. Chem.* **1997**, *36*, 2944. [4b] C. Place, J. L. Zimmermann, E. Mulliez, G. Guillot, C. Bois, J. C. Chottard, *Inorg. Chem.* **1998**, *37*, 4030.

[5] W. Kaim, J. Rall, *Angew. Chem. Int. Ed. Engl.* **1996**, *35*, 43.

[6] N. K. Kitajima, Y. Moro-oka, *Chem. Rev.* **1994**, *94*, 737.

[7] N. K. Kitajima, K. Fujisabbla, Y. Moro-oka, *J. Mol. Catal.* **1992**, *74*, 143.

[8] I. Sanyal, M. Mahroof-Tahir, M. S. G. P. Nasir, B. Cohen, Y. Gulthey, R. W. Cruse, A. Farooq, K. D. Karlin, S. Liu, J. Zubieta, *Inorg. Chem.* **1992**, *31*, 4322.

[9] [9a] C. J. Campbell, W. L. Driessen, J. Reedijk, W. J. J. Smeets, A. L. Spek, *J. Chem. Soc., Dalton Trans.* **1998**, 2703. [9b] G. J. A. A. Koolhaas, P. M. van Berkel, S. C. van der Slot, G. Mendoza-Diaz, W. L. Driessen, J. Reedijk, H. Kooijman, N. Veldman, A. L. Spek, *Inorg. Chem.* **1996**, *35*, 3525. [9c] G. J. A. A. Koolhaas, W. L. Driessen, J. Reedijk, J. van der Plas, R. A. G. de Graaff, D. Gattesch, H. Kooijman, A. L. Spek, *Inorg. Chem.* **1996**, *35*, 1509. [9d] M. C. Mimmi, F. Micciche, H. Kooijman, A. L. Spek, S. T. Warzeska, E. Bouwman, *Inorg. Chim. Acta* **2002**, *340*, 197. [9e] G. Tabbi, T. Nauser, W. H. Koppenol, J. Reedijk, *Eur. J. Inorg. Chem.* **1998**, 1939. [9f] G. A. van Albada, W. J. J. Smeets, A. L. Spek, J. Reedijk, *J. Coord. Chem.* **1999**, *48*, 375. [9g] G. A. van Albada, W. J. J. Smeets, A. L. Spek, J. Reedijk, *Inog. Chim. Acta* **1999**, *288*, 220. [9h] G. A. van Albada, W. J. J. Smeets, N. Veldman, A. L. Spek, J. Reedijk, *Inorg. Chim. Acta* **1999**, *290*, 105.

[10] A. W. Addison, T. N. Rao, J. Reedijk, J. van Rijn, G. C. Verschoor, *J. Chem. Soc., Dalton Trans.* **1984**, 1349.

[11] G. J. A. A. Koolhaas, W. L. Driessen, J. Reedijk, H. Kooijman, A. L. Spek, *J. Chem. Soc., Chem. Commun.* **1995**, 517.

[12] M. H. W. Lam, Y. Y. Tang, K. M. Fung, X. Z. You, W. T. Wong, *Chem. Commun.* **1997**, *21*, 957.

[13] B. J. Hathaway, *Comprehensive Coordination Chemistry*; Pergamon Press Oxford, **1987**, Vol. 5.

[14] D. B. Brown, J. R. Wasson, J. W. Hall, W. E. Hatfield, *Inorg. Chem.* **1977**, *16*, 2526.

[15] G. Vos, J. G. Haasnoot, G. C. Verschoor, J. Reedijk, P. E. L. Schaminee, *Inorg. Chim. Acta* **1985**, *105*, 31.

[16] P. J. van Koningsbruggen, J. G. Haasnoot, W. Vreugdenhill, J. Reedijk, O. Kahn, *Inorg. Chim. Acta* **1995**, *239*, 5.

[17] O. Kahn, *Molecular Magnetism*; Wiley-VCH, New York, **1993**.

[18] G. J. A. A. Koolhaas, W. L. Driessen, P. J. van Koningsbruggen, J. Reedijk, A. L. Spek, *J. Chem. Soc., Dalton Trans.* **1993**, 3803.

[19] N. Matsumoto, S. Yamashita, A. Ohyoshi, S. Kohata, H. Okawa, *J. Chem. Soc., Dalton Trans.* **1988**, 1943.

[20] I. M. Kolthoff, P. J. Elving, *Treatise on Analytical Chemistry.,* New York, **1963**, vol. 4.

[21] M. Joseph, T. Leigh, M. L. Swain, *Synthesis* **1977**, 459.

[22] G. M. Sheldrick. SHELXS-97. *Program for crystal structure solution.* University of Göttingen, Germany, **1997**.

[23] G. M. Sheldrick. *SHELXL-97. Program for crystal structure refinement.* University of Göttingen, Germany, **1997**.

[24] A. L. Spek, *J. Appl. Cryst.* **2003**, *36*, 7.

Received July 16, 2003
Early View Article
Published Online October 10, 2003

 © 2003 Wiley-VCH Verlag GmbH & Co. KGaA, Weinheim

Dimensionality Variation in Polymeric Metallo-Organic Frameworks

Kalle I. Nättinen,[a] Juha Linnanto,[a] and Kari Rissanen*[a]

Keywords: Crystal engineering / X-ray diffraction / Self-assembly / Coordination polymers

Single crystal X-ray crystallography was used to determine the structures of four metallo-organic complexes derived from pyridyl ligands and the metal ions, Cu^{2+}, Zn^{2+} and Ag^{+}. Two metallo-organic layer framework structures (**1** and **3**), a strand (**2**) and a dimer (**4**) structure were formed when the tetradentate ligands, tetrakis(nicotinoxymethyl)methane (TNM) and tetrakis(isonicotinoxymethyl)methane (TINM), were reacted with the first and second row transition metal cations, copper, silver, and zinc. The choice of anion and ligand was found to affect the outcome of the structure. Contrary to our previous results with the same ligands and similar transition metal cations, no genuine 3D metallo-organic frameworks (MOFs) were obtained. Several factors were found to affect MOF formation: the coordination geometry, the *meta*- or *para*-configuration of the coordinating pyridyl moieties and the size and type of the counter anion. In **1**, the use of TNM (with a shorter "coordination arm" than TINM), in combination with an octahedral coordination geometry (4 Py, SO_4^{2-} and H_2O) and a relatively large sulfate anion, leads to a sandwich-like layer structure with the anions between the MOF layers. The layers have a thickness of 2.1 nm. In complex **3**, similar layer structures are assembled from four- and five-coordinate (2 Py, NO_3^-, H_2O/2 Py, 3 NO_3^-) Ag^+ ions with TINM and nitrate anions. However, in complex **2**, the Zn^{2+} ion is tetrahedrally (2 Py, 2 Cl^-) coordinated, creating an infinite strand structure. Most surprisingly, in complex **4**, two arms of the ligand are uncoordinated and a binuclear square-planar coordination geometry (2 Py, 2 CH_3COO^-) around the Cu^{2+} ions, as well as the acetate anions, create a non-polymeric dimeric structure.
(© Wiley-VCH Verlag GmbH & Co. KGaA, 69451 Weinheim, Germany, 2003)

Introduction

The ease with which new polymeric metallo-organic materials can be analyzed and synthesized, as well as their potential capacity for a range of applications, have in the last decade created an interesting field of chemistry dealing with supramolecular, polymeric strands, sheets, and 3D networks. Possible applications include trapping (or chlathrating) of guest molecules,[1] chemical sensing,[2] light element ceramics,[3] electronic switches, and gas-storage.[4,5] Molecular self-assembly enables the synthesis of these complexes by the utilization of molecular tectons[6] and supramolecular synthons[7] to create infinite polymers that form crystals. The tectons are held together by a variety of interactions such as metal−ligand coordination bonds,[8−11] hydrogen-bonds,[12−15] stacking interactions,[16] S− S bonds,[11] metal-metal contacts,[17] weak hydrogen−bonds,[16,18] π··· π interactions or mixtures of these.[9,19] The networks created from the tectons come in many forms such as one-dimensional rods, ladders and tubes,[20] two-dimensional grids, sheets or honeycombs,[9] three-dimensional diamondoid (tetrahedral centers),[12,17,21,22] or simple cubic lattices (octahedral centers).[23−25] The coordination networks offer some attractive properties which include modularity (i.e. the availability of a large number of identical sites), regioselectivity, stereoselectivity, shape selectivity, and exact information on the nature of binding (i.e. position in the crystal lattice), as opposed to absorption or adsorption on the surface.[26] Although crystal engineers try to control the properties of the crystal,[27] the majority of crystallizations lead to unexpected results, such as the formation of two different structures from one crystallization method,[8] or the formation of different MOFs from the *cis*- and *trans*-isomers of a ligand.[28]

We have previously studied the interpenetrating 3D MOFs formed by TINM and the first row transition metal cations, copper, nickel and cobalt.[29] This work deals with metallo-organic complexes that form architectures with fewer dimensions than the MOFs studied in our previous work. Despite some examples of tetradentate ligands used in the synthesis of one- or two-dimensional structures, most of the structures are synthesized from bidentate ligands, such as 4,4′-bipyridine, or tridentate ligands.[17,23,30−32] This is partly due to ease with which the starting materials for the bidentate MOFs are synthesized, and the fact that the tetrahedral conformation typical of tetradentate MOFs tend to lead to 3D networks.[29,33] In this work, we investigate the effect of using the *meta*- (TNM) and *para*-isomers (TINM) of the same ligand with a selection of anions and the first and second row transition metal cations, copper, zinc, and silver. The effects on MOF formation, and on the

[a] Department of Chemistry, University of Jyväskylä,
P. O. Box 35, 40351 Jyväskylä, Finland
E-mail: Kalle.Nattinen@cc.jyu.fi
juha.linnanto@c.c.jyu.fi
Kari.Rissanen@cc.jyu.fi

Supporting information for this article is available on the WWW under http://www.eurjic.org or from the author.

 © 2003 Wiley-VCH Verlag GmbH & Co. KGaA, Weinheim **DOI: 10.1002/ejic.200300280**

geometry and dimensions of the formed frameworks were investigated. The use of flexible organic ligands adds an element of freedom to the coordination geometry of the metal atoms. Therefore, one would expect a deviation from the structures based on rigid bidentate ligands.

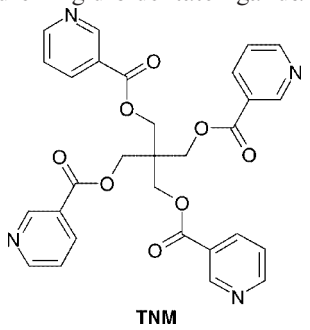

TNM

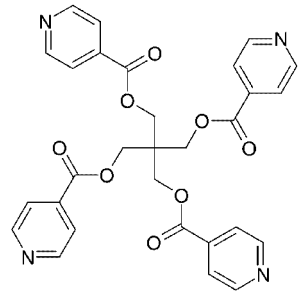

TINM

Results and Discussion

Synthesis: X-ray quality crystalline solids of complexes **1**−**4** were obtained by evaporation of the solvents. All combinations of the ligands, TNM and TINM, and the metal salts, copper diacetate, copper- and silver nitrate, zinc, cobalt, and nickel chloride, and copper sulfate, and the solvents and solvents mixtures, MeOH, MeCN, CH_2Cl_2, and H_2O, were tried. Almost all the complexation attempts produced fine microcrystalline precipitates. Complexes **1**−**4** were the only single crystalline solids that could be collected. The structures were further confirmed using elemental analysis and TGA. Since complexes **1**−**4** only exist as solid crystalline material, no NMR measurements were performed.

X-ray Single Crystal Structures

The crystal data for complexes **1**−**4** are presented in the Table 1. No unusual metal coordination angles or bond lengths were found in the structures.

Layer Structure 1: The asymmetric unit of **1** consists of half a molecule of TNM, with skewed tetrahedral coordination of the arms, one copper cation, one coordinated disordered sulfate anion, five water molecules, and one methanol molecule. A model to describe the sulfate disorder was built by splitting the sulfate molecule into two positionsr. Two water molecule halves were located in special positions, two were disordered to two and three positions, respectively.

Table 1. Crystallographic parameters for complexes **1**−**4**

Complex	**1**	**2**	**3**	**4**
Empirical formula	$[Cu(C_{29}H_{24}N_4O_8)(SO_4)(H_2O)_2]$-$(CH_3OH)_2(H_2O)_8$ [a]	$[Zn_2(C_{29}H_{24}N_4O_8)Cl_4]$-$(CH_3CN)_{2/3}(H_2O)_{1/3}$	$[Ag_2(C_{29}H_{24}N_4O_8)$-$(NO_3)_2(H_2O)]$	$[Cu(C_{29}H_{24}N_4O_8)$-$(O_2CCH_3)_2](H_2O)_4$
Formula mass	952.30	855.74	914.30	810.22
Crystal color, shape	blue, plates	yellow, blocks	colorless, blocks	blue, prisms
Crystal dimensions (mm)	0.08 × 0.2 × 0.3	0.15 × 0.15 × 0.3	0.20 × 0.25 × 0.4	0.08 × 0.15 × 0.5
Crystal system	Monoclinic	Trigonal	triclinic	triclinic
Space group	*P*2/*c* (No.13)	$P3(2)2_1$ (No.154)	$P\bar{1}$ No.2	$P\bar{1}$ (No.2)
a (Å)	10.5626(4)	12.511(2)	9.1111(2)	10.8279(4)
b (Å)	15.3884(6)	12.511(2)	11.1364(2)	10.8228(4)
c (Å)	13.7398(5)	21.472(4)	15.4384(4)	18.7422(9)
α (°)	90	90	91.057(1)	77.639(2)
β (°)	100.219(2)	90	90.350(1)	74.946(2)
γ (°)	90	120	90.218(2)	60.785(2)
V (Å^3)	2197.9(2)	2910.6(9)	1566.15(6)	1841.2(2)
Calcd. density (Mg/m^3)	1.439	1.465	1.939	1.461
Temp. during data collection (K)	173	173	173	173
Z	2	3	2	2
$R_{obsd.}$	$R1 = 0.0642$, $wR2 = 0.1678$	$R1 = 0.0362$, $wR2 = 0.0998$	$R1 = 0.0302$, $wR2 = 0.0677$	$R1 = 0.0560$, $wR2 = 0.1244$
R_{all}	$R1 = 0.0891$, $wR2 = 0.1861$	$R1 = 0.0429$, $wR2 = 0.1039$	$R1 = 0.0382$, $wR2 = 0.0708$	$R1 = 0.0835$, $wR2 = 0.1363$
GooF	1.060	1.128	1.082	1.075
θ range for data collection (°)	2.98 to 25.69	3.26 to 25.02	2.24 to 25.00	3.29 to 25.70
Scan type	Φ/Ω, 2°	Φ/Ω, 2°	Φ/Ω, 2°	Φ/Ω, 1°
Refl. collected/unique/cell refinement	14322/4313/4010	29711/10200/9491	14486/5488/5006	11447/6830/5779
Refined parameters	372	225	475	513
Residual electron density e/Å^3	0.611/−0.686	0.738/−0.229	0.402/−0.518	0.858/−0.576
min./max. abs. correction	0.8902/0.9407	0.7397/0.7753	0.7304/0.7489	−

[a] The hydrogens could not be located for all the water and methanol molecules.

 © 2003 Wiley-VCH Verlag GmbH & Co. KGaA, Weinheim

Hydrogen atoms could not be located for the disordered water molecules. The TNM ligand is coordinated by the copper cations through the four aromatic nitrogen atoms. The coordination geometry around the copper atom is octahedral.

A schematic presentation of the ligand and its surroundings in complex **1** is displayed in Scheme 1. The 2D MOF of **1** is a grid that is puckered so that the equatorial copper coordination planes are placed both on top and bottom of the layer that is formed. The TNM ligands form the inside of the layer. The equatorial coordination bonds of the copper atoms are coplanar with the layer. Therefore, all the arms of TNM are directed towards center of the layer (Figure 1). The puckering arises as a result of the *meta*-position of the nitrogen atom of TNM and the relatively large size of the sulfate anion. The puckered structure results in the formation of open channels on top and bottom of the layers. The channels are filled by water molecules and occupied by sulfate anions from the neighboring layer (Figure 2).

In our previous work we synthesized two complexes of TINM with copper nitrate.[29] Both of these complexes are two-fold interpenetrating 3D MOF structures with channels formed by cavities that contain nitrate anions and solvent water molecules. The "effective" length (distance between central carbon atom and the coordinating nitrogen atom) of the TINM ligand is longer than that of the TNM ligand. The nitrate anion is also smaller than the sulfate anion. In addition, with the nitrogen atom in the *meta*-position of TNM, the arms of the ligand cannot be straightened so as to satisfy the square-planar coordination geometry around the copper cation. Due to the distorted tetrahedral conformation of the arms, combined with the *meta*-position of the aromatic nitrogen atom, complex **1** forms a pseudo 3D MOF that does not elongate infinitely in all dimensions, but instead creates thick layers perpendicular to the crystallographic *b*-axis. Therefore, it is not a true 3D MOF in this respect. However, its third dimension is in the nanoscale range: the thickness of the layers is 2.1 nm.

In order to provide enough space for the sulfate anion, the structural components of **1** should create a non-interpenetrating MOF rather than the two-fold interpenetrating MOF previously observed with $Cu(NO_3)_2$ and TINM.[29] However, the difference in the size of the anions is probably not enough to allow for the formation of a stable non-interpenetrating MOF: the sulfate anions are not large enough to support the formation of a framework that would not collapse without a second interpenetrating framework. We have performed molecular modeling, the results of which support this hypothesis. The channels contain water molecules with hydrogen atoms pointed towards the highly negative electron potential of the sulfate anions. The negative electron potential of the sulfate anion requires too much space for the 3D network to be formed. All attempts to crystallize a 3D MOF from TNM and a metal cation with octahedral coordination (Cu, Ni, Co) failed, thereby also supporting the spatial and conformational requirements of the TNM ligand.

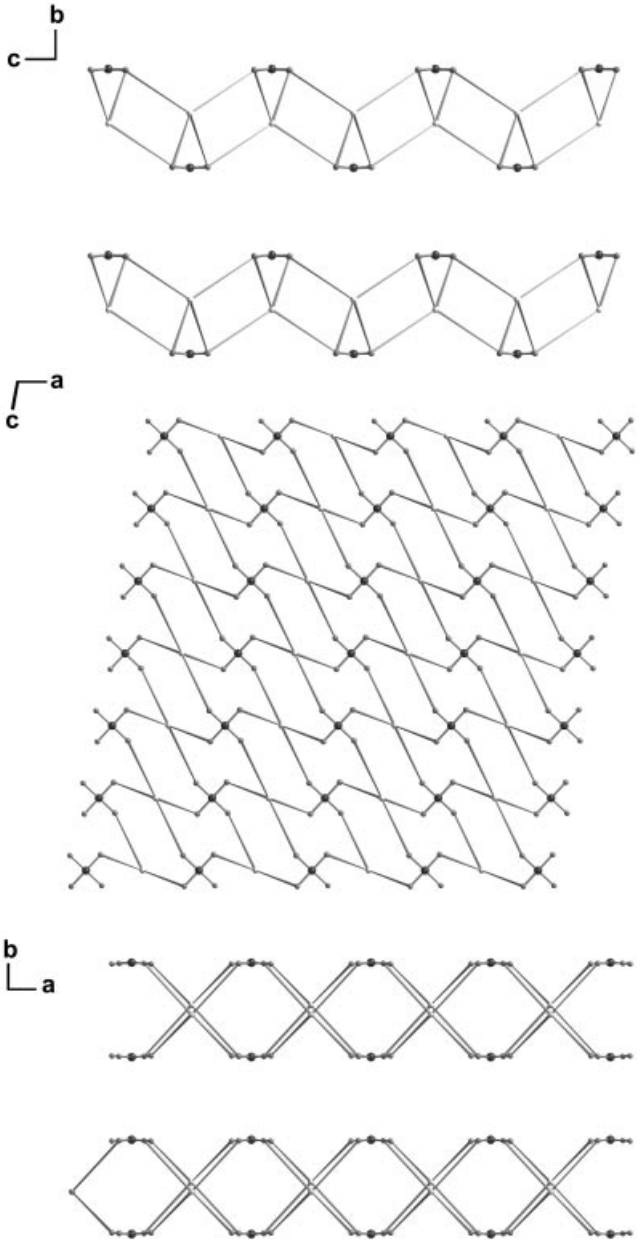

Figure 1. A view of the ball-and-stick model of two layers of **1** along the crystallographic unit cell axes *a, b*, and *c*. Only the central carbon atoms, terminal nitrogen atoms of TNM, the copper atoms, and the bonds between them are shown. The separation between the two layers is 3.5 Å

Strand Structure 2: The asymmetric unit of **2** consists of a Zn atom, half a molecule of TNM coordinated by it, two chloride anions coordinated by the zinc atom, a water molecule, and an acetonitrile molecule. The water molecule is situated in a special position and was located with a population parameter 1/2 and a site occupancy of 1/3. The terminal carbon atom of the acetonitrile molecule is also in a special position. The acetonitrile was located with a population parameter 1/2 (besides the terminal carbon atom for which a population parameter 1/2 and a site occupancy of 1/3 were applied). The solvent molecules are located inside

 © 2003 Wiley-VCH Verlag GmbH & Co. KGaA, Weinheim

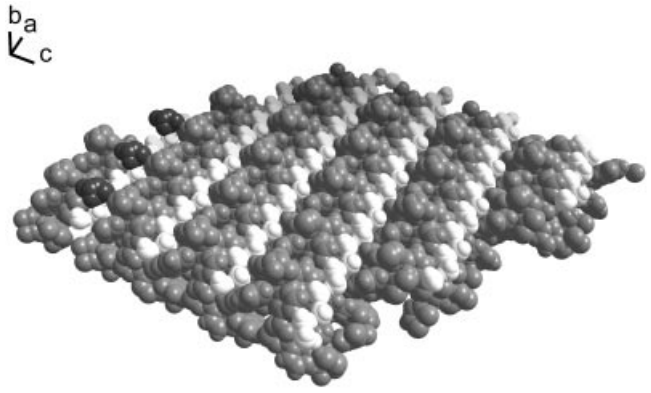

Figure 2. A perspective view of the space-filling model of a square section of the layer in **1**. The oxygen atoms of the water molecules are shown. The sulfate anions of the neighboring layer are displayed on top of the leftmost channel

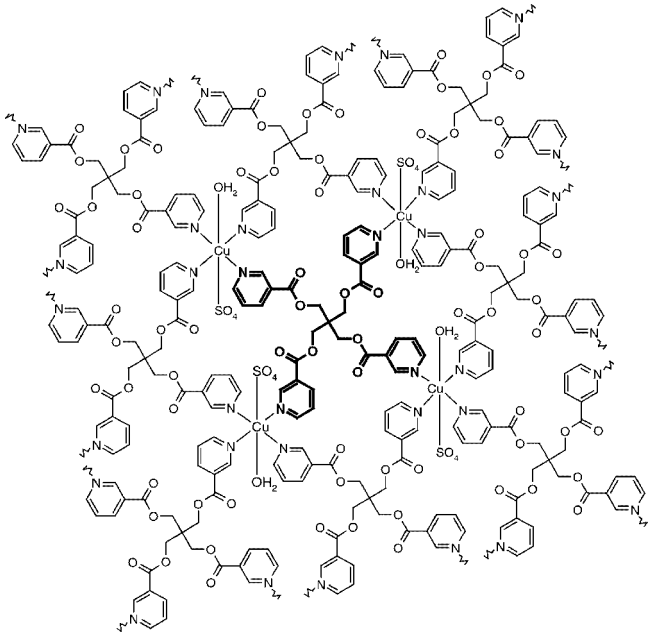

Scheme 1. A schematic representation of the layer network of **1**, with the central ligand shown in bold font

the cavity formed by the links of the chains. The coordination geometry around the zinc atom is tetrahedral.

A schematic representation of a polymeric unit of **2** is presented in Scheme 2. Due to the trigonal symmetry of the structure, each layer of stacked chains forms a 60° angle with those above and below it. The layers are formed perpendicular to the crystallographic *c*-axis (Figure 3).

The formation of a 3D MOF is prevented by two factors: the zinc cation has only two available coordination sites from its tetrahedral coordination sphere for the TNM ligand, and the arms of TNM are paired, i.e. their orientation is not tetrahedral. Therefore, the polymeric structure only grows in one dimension and there are no coordination bonds between individual chains (Scheme 2). Additionally, the chloride anion is not able to act as a bridging anion between two adjacent Cu centers, unlike the acetate or nitrate anions. The planar, cross-like conformation of the ligand arms could create a 2D MOF, with four ligands forming one large square in the grid. This type of structure would probably need to be interpenetrated so as to stabilize the framework. However, only the strand structure **2** could be obtained from the complexation experiments. A probable explanation for not obtaining the 2D layer MOF is the high complementarity requirements of interpenetrating frameworks in the solid state. In our experiments, interpenetration was not observed in the single crystals that were obtained.

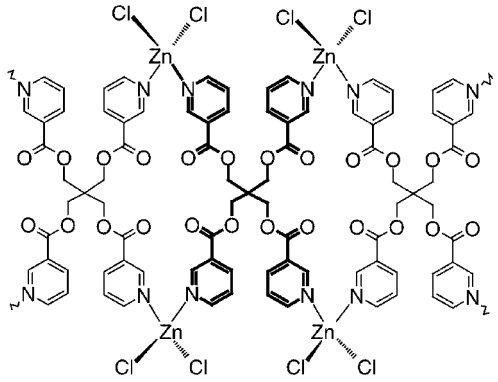

Scheme 2. A schematic representation of **2**, with the central ligand shown in bold font

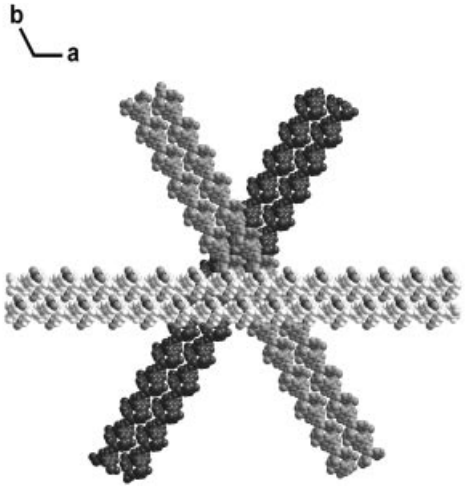

Figure 3. Two chains from each of the three layers with a unique orientation in complex **2** (the planes of the layers are in the plane of the paper). The orientation of the fourth layer is identical to that of the first layer. The chain pairs are displayed with the color intensity increasing along the *c*-axis. The solvent molecules are excluded

Layer Structure 3: The asymmetric unit of **3** consists of a non-tetrahedral TINM ligand that is coordinated to four silver cations, two of which belong to the asymmetric unit. There are also two nitrate anions and one water molecule that are coordinated to the silver cations. A plot with thermal ellipsoids of structure **3** is presented in Figure 4. The linear conformation of TINM is stabilized by π···π interactions between the pyridine rings C36−C41 and C26−C31 (separation between the centroids of the rings is 3.89 Å), as well as CH···π interactions between the remaining two arms [d = 2.72 Å for C17−H17··· centroid (C6−C11)]. The π···π

 © 2003 Wiley-VCH Verlag GmbH & Co. KGaA, Weinheim

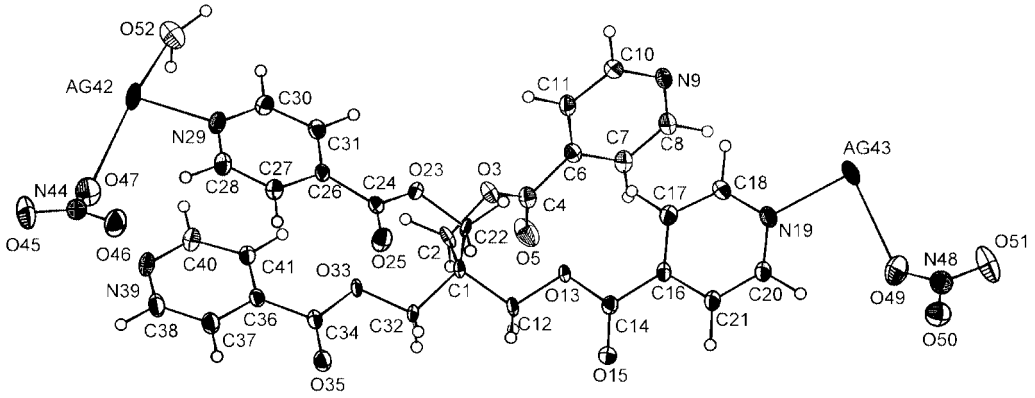

Figure 4. A plot with thermal ellipsoids shown at the 50% probability level for **3**. The non-hydrogen atoms of the asymmetric unit are numbered

interactions between the aromatic rings are attractive forces that bring the Ag^+ cations closer (within a distance of 4.07 Å from each other).

A schematic representation of the structure of **3** is displayed in Scheme 3. The neighboring chains provide additional nitrate anions for coordination by the Ag^+ cations. This coordination creates additional connections in another direction of the lattice, thus forming a link between the chains of **3**, and leading to the formation of 2D layers (Figure 5) with a thickness of 13.2 Å. One silver cation (Ag42) exhibits a distorted square-planar coordination geometry, while the other (Ag43) exhibits a square-pyramidal ge-

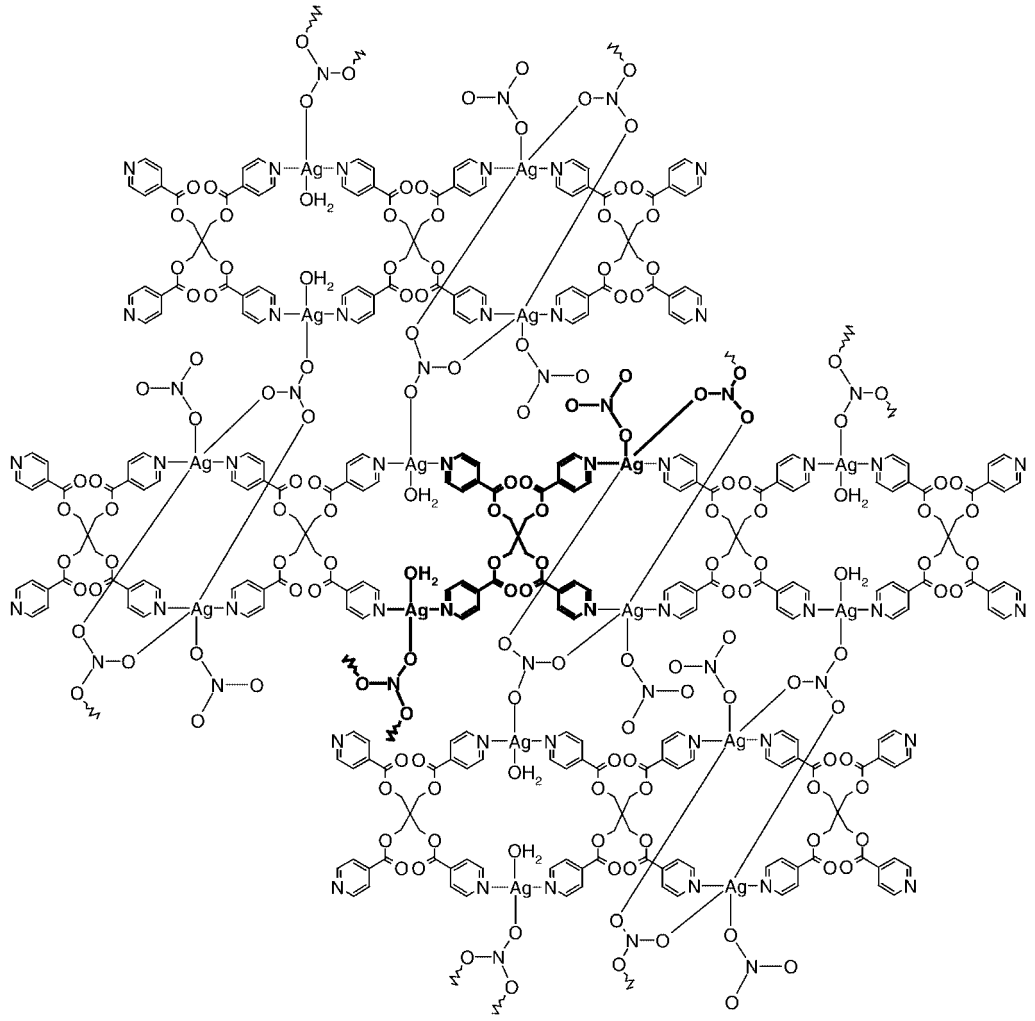

Scheme 3. A schematic representation of the structure of **3**. The central asymmetric unit is shown in bold font. The chains run in a horizontal direction

 © 2003 Wiley-VCH Verlag GmbH & Co. KGaA, Weinheim

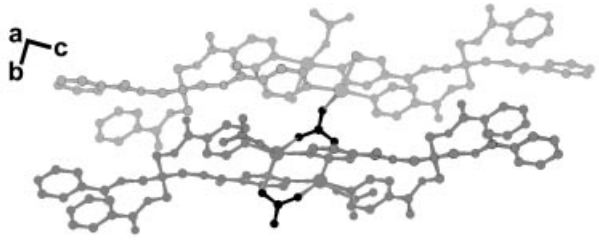

Figure 5. The links between the chains of **3**. Four TINM ligands and silver cations are shown. The different chains are shown in light and medium gray. For clarity, the bridging nitrate anions are shown in black ink and the hydrogen atoms are omitted

ometry. The two symmetry equivalent Ag43 cations are bridged by two nitrate anions (N44−O47 and its symmetry equivalent). They are also bridged to the neighboring chain Ag42 cations by the same nitrate anions, through the remaining oxygen atom of the nitrate anions. The other nitrate anion coordinated to the Ag43 cation does not form a bridge.

With the planar, cross-like conformation of the ligand arms, a 2D grid-like MOF could hypothetically be created by N−Ag bonds alone (see discussion of complex **2**). Anion coordination between layers could extend this structure into a 3D MOF, assuming that the anions would be suitably positioned. However, neither of these structures are observed. As with complex **2,** the probable explanation for not obtaining the 2D MOF is the high complementarity requirements of the interpenetrating frameworks. These requirements were not met by any quantitative combination of the TINM ligand and silver nitrate, since the layer structure **3** was the only single crystalline material that could be obtained. Since the arms of the TINM are paired, thereby providing an extension of the structure only in one dimension, the structure remains as a stack of anion-bridged 2D layers.

The three bond lengths involving the bridging nitrate anion are both shorter [Ag43−O46: 2.608(1) Å] and longer [Ag42−O47: 2.797(3) Å and Ag43−O45: 3.025(2) Å] than the bond length of the singly coordinated nitrate anion [Ag43−O49 of 2.651(1) Å]. The layers of **3** stack along the crystallographic *a*-axis, forming a dense lattice with no voids.

Dimeric Structure 4: Each asymmetric unit of **4** contains one Cu atom, one TINM ligand coordinated by the copper atom, two coordinated acetate anions and four water molecules. The four water molecules are hydrogen-bonded to the carbonyl oxygen atoms of the acetate anions or to those of the TINM core, except one, which is hydrogen-bonded to one of the water molecules. The coordination geometry around the copper atom is square-planar (Figure 6). The formation of dimers and the π···π interactions between the pyridine rings (3.66 Å between the centroids) of parallel arms (as in **3**) brings the copper cations to within 3.43 Å of each other. A schematic representation of the structure of **4** is displayed in Scheme 4.

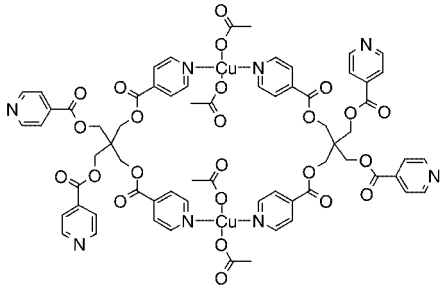

Scheme 4. A schematic representation of **4**

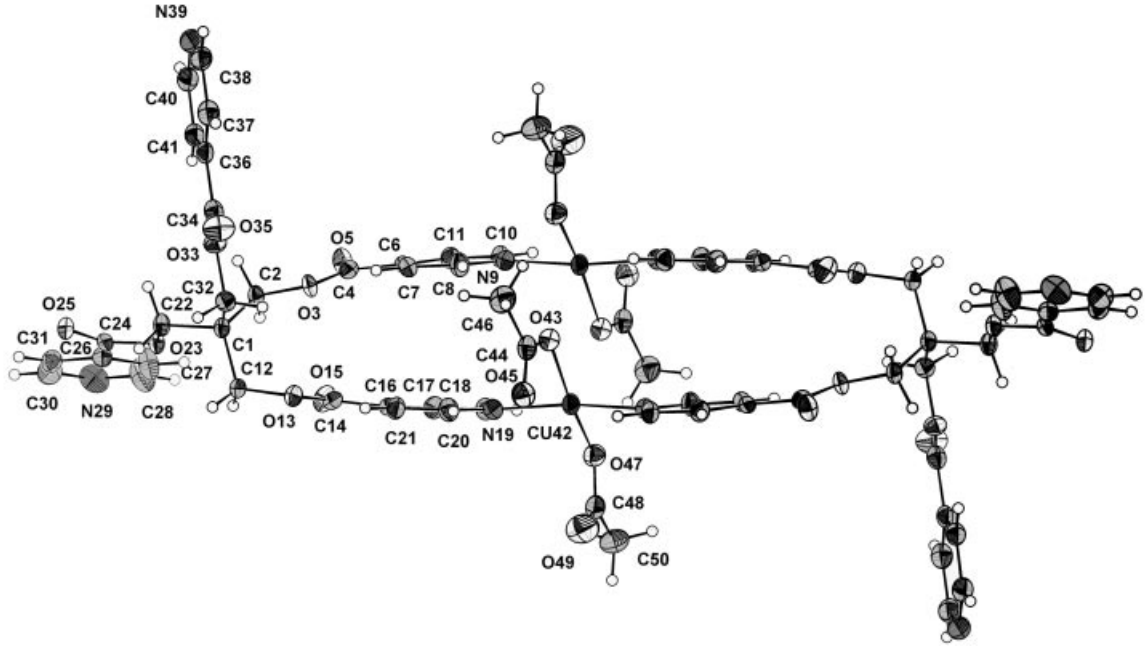

Figure 6. A plot with thermal ellipsoids shown at the 50% probability level for **4**, with the numbering of the non-hydrogen atoms of the asymmetric unit. The solvent water molecules are excluded

 © 2003 Wiley-VCH Verlag GmbH & Co. KGaA, Weinheim

Several hydrogen bonds and other weak interactions such as CH···π and π···π interactions are involved in the packing of **4**. Despite the available coordinating sites of the terminal nitrogen atoms, only two arms of each TINM are coordinated. Although the use of copper acetate instead of copper nitrate is the only difference between the synthesis of the 3D MOF in our previous work[29] and the synthesis of **4**, a dimeric rather than a polymeric complex is obtained. A 3D MOF is not formed because the coordination geometry around the copper cation is square-planar. Despite the availability of nitrogen atoms for coordination, the complex remains a dimer, and does not form chains as in structures **2** and **3**. The multiple weak intermolecular interactions between the uncomplexed pyridyl moieties of the dimers could possibly be the reason for the lack of strand or layer formation. A strong hydrogen-bond is formed between the uncoordinated nitrogen atom N29 and a water molecule (DH···A: 2.017Å, D−H−A: 171.3°). The other uncoordinated nitrogen atom N39 is blocked since it intertwines with the ends of neighboring molecules (Figure 7).

The completely different architectures of the layer structure of **3** and the dimeric structure of **4** can be explained by the greater bridging ability of the nitrate anion relative to that of the acetate anion. Since the nitrate anions in the previously reported structures do not participate significantly in the formation of the framework,[29] the difference between these 3D MOF structures and **4** is probably due to polymorphism, rather than differences between the acetate and nitrate anions.

TGA Studies: As expected, the TGA studies do not show the removal of solvents before high temperatures were reached. In complex **1**, a weight loss of 15% is observed before decomposition at 280 °C. This approximately corresponds to the eight uncoordinated water molecules in the lattice (Figure 8). The TGA curve of **2** reveals stepwise decomposition of the structure beginning at 260 °C, and for complex **3**, at 280 °C. In complex **3**, the only solvent molecule is coordinated by the silver cation, thus its removal

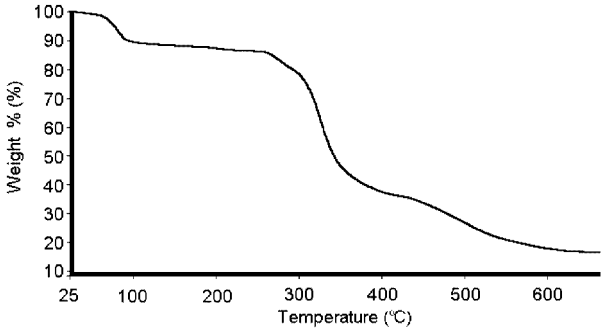

Figure 8. The TGA curve for **1**

results in the rapid collapse of the structure. In the TGA analysis of **4**, no intermediate products are seen. The decomposition occurs in one step, in contrast with the TGA results of the MOFs **1**, **2** and **3**, all of which display stepwise thermal decomposition.

Conclusions

The pseudo 3D MOF structure **1** is in fact a 2D MOF since it does not have an infinite third dimension. The thickness of the layers in **1** is 2.1 nm. In spite of the octahedral coordination geometry around the copper cations and the skewed tetrahedral conformation of the pyridyl moieties of TNM, a 3D MOF is not formed. This is because the branching from the metal center is directed only towards the center of the layer from the metal centers on both the top and bottom of the layer. This is probably due to the lack of space for the sulfate anion. The relatively short arms of TNM, and the large size and long bond length of the sulfate anion relative to the anions used in the synthesis of the 3D MOFs with copper and TNM/TINM ligands in our previous study, prevent the formation of a 3D MOF with suitable cavities for the sulfate anions.[29] Ad-

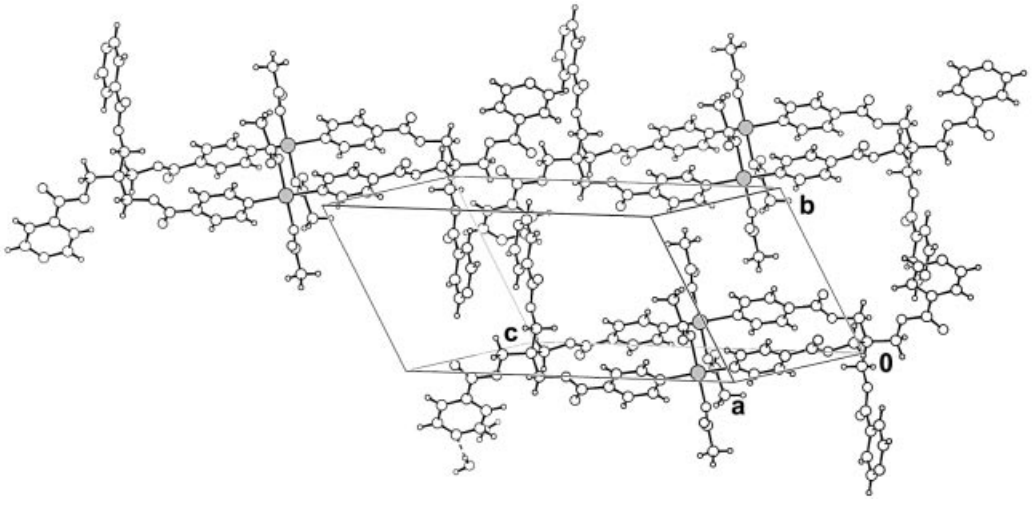

Figure 7. Three dimers of **4** showing the unit cell and the hydrogen-bond between water and N29

 © 2003 Wiley-VCH Verlag GmbH & Co. KGaA, Weinheim

ditionally, due to the *meta*-position of the nitrogen atom, the TNM ligands are incapable of aligning in a co-planar manner to the equatorial metal coordination plane, and therefore are unable to assume a conformation similar to that of the ligands in the 3D MOFs in our previous study.

Structure **2**, a polymeric complex of zinc chloride and TNM, is composed of infinite, flat, linear chains of TINM ligands linked by zinc cations. Despite the potential ability of **2** and **3** to form 2D layers through metal−nitrogen bonds alone, only 1D chain structures are obtained from these interactions. The formation of 3D MOFs is prevented because the zinc cation in **2** has only two coordination sites for the ligand, and the pyridyl moieties of the TNM are paired, i.e. they are not tetrahedrally oriented. In contrast with the nitrate anions in **3**, the chloride anion in **2** is incapable of promoting layer formation by creating links between individual chains. The layers of chains in **2** are tightly packed, and each layer of chains forms a 60° angle with its neighbors. A probable explanation for not obtaining 2D layers (besides those created by the anion bridging in **3**) is the low packing efficiency of these grid structures. The high complementarity requirements for interpenetrating frameworks may not be fulfilled.

The π···π interactions between the pyridyl rings of adjacent arms are probably the driving force for the formation of the structure **3**. A polymeric chain of the TINM ligands, with paired pyridyl moieties coordinated by the silver cations in one dimension is formed. However, by coordinating three silver cations, the nitrate anions create a link between the chains, and thereby form a 2D layer structure with a thickness of 13.2 Å. The cyclic dimeric metal complex formed between TINM and copper acetate, structure **4,** provides interesting possibilities for heterometallic complexation. This is because the remaining, uncomplexed four arms of the dimer are available for further coordination. The completely different architecture of **4** with respect to previous structures[29] with the nitrate anion instead of the acetate anion probably arises as a result of polymorphism.

Experimental Section

Materials and Measurements: All commercially available chemicals were of reagent grade and used as received without further purification. TINM and TNM were synthesized as previously reported.[34] The purity of the complexes was confirmed by elemental analysis. TGA experiments were carried out at a heating rate of 5 °C/min under nitrogen using a Perkin−Elmer TGA 7 instrument. The elemental analyses were performed at the University of Joensuu using CE-Instruments EA1110. The elemental analyses revealed a loss of solvent for structure **1**, and some solvent residuals for **2** and **4**, thus giving inaccurate results for the chemical compositions. Therefore, only the results for the elemental analyses of **1** and **3** are presented. The complexes were not vacuum dried before elemental analysis, so as to avoid decomposition.

Preparation of the Complexes $[Cu(TNM)(SO_4)(H_2O)_2]\cdot(MeOH)_2(H_2O)_8$ (1): $CuSO_4\cdot 5H_2O$ (22.4 mg, 89.8 μmol) in water (10 mL) was added to TINM (50 mg, 89.8 μmol) dissolved in MeOH (30 mL). The solution was evaporated slowly, and the crystalline solid was collected from the solution before complete evaporation of the solvents. The solid was washed with water and dried in air. Yield 54.6% (46.7 mg). $C_{31}H_{44}Cu_1N_4O_{24}S_1$ − ($8H_2O$ + 2MeOH), $[Cu(TNM)(SO_4)(H_2O)_2]$: calcd. C 46.3, H 3.8, N 7.5; found C 46.2, H 3.6, N 7.5.

$[Zn_2(TNM)Cl_4](MeCN)_{2/3}(H_2O)_{1/3}$ (2): $ZnCl_2$ (24.5 mg, 89.8 μmol) in water (10 mL) was added to TNM (50 mg, 89.8 μmol) dissolved in MeCN (35 mL). The solution was evaporated slowly, and the crystalline solid was collected from the solution before complete evaporation of the solvents. The solid was washed with water and dried in air. Yield 100% (76.8 mg).

$[Ag_2(TINM)(NO_3)_2(H_2O)]$ (3): $AgNO_3$ (30.5 mg, 89.8 μmol) in water (10 mL) was added to TINM (50 mg, 89.8 μmol) dissolved in MeCN (30 mL). The solution was evaporated slowly, and the crystalline solid was collected from the solution before complete evaporation of the solvents. The solid was washed with water and dried in air. Yield 100% (82.1 mg). $C_{29}H_{26}Ag_2N_6O_{15}$: calcd. C 38.1, H 2.9, N 9.2; found: C 38.9, H 2.9, N 9.2.

$[Cu(TINM)(O_2CCH_3)_2](H_2O)_4$ (4): $Cu(O_2CCH_3)_2\cdot 3H_2O$ (16.3 mg, 89.8 μmol) in water (5 mL) was added to TINM (50 mg, 89.8 μmol) dissolved in MeOH (30 mL). The solution was evaporated slowly, and the blue crystalline solid was collected from the solution before complete evaporation of the solvents. The solid was dried in air. Yield 20.7% (15.1 mg).

X-ray Diffraction: The single crystal X-ray diffraction was performed using a Nonius−KappaCCD diffractometer with graphite-monochromatized Mo-K_α (λ = 0.71073 Å) radiation. Collect software was used for the measurement and DENZO-SMN[35] for the processing of the data. The structures were solved and refined by full-matrix least-squares on F^2 using the WinGX-software package which utilizes the SHELXS-97 and SHELXL-97 modules.[36−38] Hydrogen atoms were refined using a riding model. Empirical absorption correction was performed for complexes **1**, **2**, and **3**. The graphic presentations of the structures were created with the software package Diamond.[39] CCDC-206599, -206600, -206601 and -206602 contain the supplementary crystallographic data for this paper. These data can be obtained free of charge on applicaton to The Director, CCDC, 12 Union Road, Cambridge CB2 1EZ, UK [Fax: (internat.) +44-1223- 336-033; E-mail: deposit@ccdc.cam.ac.uk.

Acknowledgments

K. N. thanks the Graduate School of Bioorganic Chemistry for financial support. K. R. thanks the Finnish Academy (proj. no. 777871) for financial support.

[1] M.-L. Tong, B-H. Ye, J-W. Cai, X-M. Chen, S. W. Ng, *Inorg. Chem.* **1998**, *37*, 2645.
[2] O-S Jung, Y. J. Kim, Y-A. Lee, J. K. Park, H. K. Chae, *J. Am. Chem. Soc.* **2000**, *122*, 9921.
[3] D. Williams, B. Pleune, J. Kouvetakis, M. D. Williams, R. A. Andersen, *J. Am. Chem. Soc.* **2000**, *122*, 7735.
[4] G. J. Halder, C. J. Kepert, B. Maoubaraki, K. S. Murray, J. D. Cashion, *Science* **2002**, *298*, 1762.
[5] M. Eddaoudi, J. Kim, N. Rosi, D. Vodak, J. Wachter, M. O'Keefe, O. M. Yaghi, *Science* **2002**, *295*, 469.
[6] X. Wang, M. Simard, J. D. Wuest, *J. Am. Chem. Soc.* **1994**, *116*, 12119.

 © 2003 Wiley-VCH Verlag GmbH & Co. KGaA, Weinheim

[7] G. R. Desiraju, *Angew. Chem. Int. Ed. Engl.* **1995**, *34*, 2311.
[8] S. Kheradmandan, H. W. Schmalle, H. Jacobsen, O. Blacque, T. Fox, H. Berke, M. Gross, S. Decurtins, *Chem. Eur. J.* **2002**, *8*, 2526.
[9] P. Jensen, S. R. Batten, B. Moubaraki, K. S. Murray, *J. Chem. Soc., Dalton Trans.* **2002**, 3712.
[10] S. Muthu, J. H. K. Yip, J. J. Vittal, *J. Chem. Soc., Dalton Trans.* **2002**, 4561.
[11] I. Ino, J. C. Zhong, M. Munakata, T. Kuroda-Sowa, M. Maekawa, Y. Suenaga, Y. Kitamori, *Inorg. Chem.* **2000**, *39*, 4273.
[12] O. Ermer, L. Lindenberg, *Helv. Chim. Acta* **1991**, *74*, 825.
[13] M. Simard, D. Su, J. D. Wuest, *J. Am. Chem. Soc.* **1991**, *113*, 4696.
[14] D. Venkatamaran, S. Lee, J. Zhang, J. S. Moore, *Nature* **1994**, *371*, 591.
[15] H. Sauriat-Dorizon, T. Maris, J. D. Wuest, *J. Org. Chem.* **2003**, *68*, 240.
[16] K. Biradha, K. V. Domasevitch, B. Moulton, C. Seward, M. J. Zaworotko, *Chem. Commun.* **1999**, 1327.
[17] K. A. Hirsch, S. R. Wilson, J. S. Moore, *Inorg. Chem.* **1997**, *36*, 2960.
[18] M. A. Withersby, A. J. Blake, N. R. Champness, P. A. Cooke, P. Hubberstey, A. L. Realf, S. J. Teat, M. Schröder, *J. Chem. Soc., Dalton Trans.* **2000**, 3261.
[19] M-L. Tong, S-L. Zheng, X-M. Chen, *Polyhedron* **2000**, *19*, 1809.
[20] S. Muthu, J. H. K. Yip, J. J. Vittal, *J. Chem. Soc., Dalton Trans.* **2002**, 4561.
[21] K. A. Hirsch, S. R. Wilson, J. S. Moore, *Chem. Commun.* **1998**, 13.
[22] O. M. Yaghi, H. Li, *J. Am. Chem. Soc.* **1995**, *117*, 10401.
[23] M. J. Plater, M. R. St J. Foreman, J. M. S. Skakle, *Cryst. Eng.* **2001**, *4*, 293.
[24] D. M. L. Goodgame, D. A. Grachvogel, A. J. P. White, D. J. Williams, *Inorg. Chem.* **2001**, *40*, 6180.
[25] B. F. Hoskins, R. Robson, *J. Am. Chem. Soc.* **1990**, *112*, 1546.
[26] F. Gröhn, G. Kim, B. J. Bauer, E. J. Emis, *Macromolecules* **2001**, *34*, 2179.
[27] G. M. J. Schmidt, *Pure Appl. Chem.* **1971**, *27*, 647.
[28] J. Fan, H-F. Zhu, T-a. Okamura, W-Y. Sun, W-X. Tang, N. Ueyama, *Inorg. Chem.* **2003**, *42*, 158.
[29] K. Nättinen, K. Rissanen, *Inorg. Chem.* **2003**, *42*, 5126.
[30] L. Carlucci, G. Ciani, D. Proserpio, S. Rizzato, *CrystEngCommun.* **2002**, *4*, 121.
[31] C. Janiak, *Angew. Chem. Int. Ed. Engl.* **1997**, *36*, 1431.
[32] G. B. Gardner, D. Venkatamaran, J. F. Moore, S. Lee, *Nature* **1995**, *374*, 792.
[33] J. Kim, B. Chen, T. M. Reineke, H. Li, M. Eddaoudi, D. B. Moler, M. O'Keeffe, O. M. Yaghi, *J. Am. Chem. Soc.* **2001**, *123*, 8239.
[34] K. Nättinen, K. Rissanen, *Cryst. Growth Des.* **2003**, *3*, 339.
[35] Z. Otwinowski, W. Minor, *Methods in Enzymology, Macromolecular Crystallography, Part A*, (Eds.: C. W. Carter, Jr., M. Sweet), **1997**, pp. 307−326, Academic Press, New York.
[36] L. J. Farrugia, *J. Appl. Cryst.* **32**, 837.
[37] G. M. Sheldrick, *Acta Crystallogr., Sect. A* **1990**, *46*, 467.
[38] G. M. Sheldrick, SHELXL-97 − *A program for crystal structure refinement*, **1997**, University of Göttingen, Germany.
[39] DIAMOND − Visual Crystal Structure Information System, Prof. Dr. G. Bergerhoff, Gerhard-Domagk-Str. 1, 53121 Bonn, Germany.

Received May 12, 2003
Early View Article
Published Online October 2, 2003

 © 2003 Wiley-VCH Verlag GmbH & Co. KGaA, Weinheim

C−H Activation by AlCl Monomers: Characterization of $HAl(Cl)CH_3$ as the Product of the Photoactivated Reaction Between AlCl and CH_4 in a Solid Ar Matrix at 12 K

Hans-Jörg Himmel*[a]

Keywords: Aluminum / Hydrides / Matrix isolation / C−H activation / Reaction mechanisms / Photochemistry

In a solid Ar matrix at 12 K and upon photoactivation AlCl inserts into the C–H bond of CH_4 to give the new monomeric aluminium hydride $HAl(Cl)CH_3$, which was identified and characterized with the aid of the IR spectra recorded for several isotopomers [$Cl(H)Al^{12}CH_3$, $Cl(D)Al^{12}CD_3$, and $Cl(H)Al^{13}CH_3$], comparison with the known IR properties of related molecules and detailed quantum chemical calculations. Calculations yield a C_s symmetric global energy minimum structure for this compound, and that the reaction is slightly exothermic (reaction energy of –43.2 kJ·mol^{-1}). This work demonstrates impressively how reactive photoactivated AlCl molecules are.
(© Wiley-VCH Verlag GmbH & Co. KGaA, 69451 Weinheim, Germany, 2003)

Introduction

Subvalent compounds of the general formula MX [M = Al, Ga or In, and X = F, Cl, I, or a cyclopentadienyl (Cp) derivative] react readily, when photoactivated, with a number of molecules.[1] Examples include the reaction of AlCl with H_2 to give H_2AlCl,[2] with O atoms to give OAlCl,[3] with O_2 to give $ClAlO_2$ [4] or, when the concentration of O_2 is increased, $ClAl(O_2)_2$,[5] and with HX (X = F, Cl or Br) to give HAl(Cl)X.[6,7] With GaCl[8] and InCl,[9] reactions with H_2 and with HCl afford the hydrides H_2MCl and $HMCl_2$ (M = Ga or In), respectively. GaF reacts with O atoms to give OGaF.[10] Finally, matrix-isolated AlCp* reacts with H_2 upon photoactivation to yield H_2AlCp^*.[11] Although these species are generally highly reactive, there are some remarkable differences between AlX, GaX and InX with respect to their reactivities and the structures and composition of the end-products. Whereas AlCl reacts, as already mentioned, upon photoactivation with O_2 [Equation (1)], GaCl or InCl show no matrix reaction, photoactivated or not, with O_2 [Equation (2)].[12]

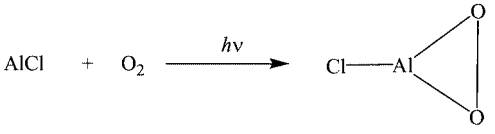

(1)

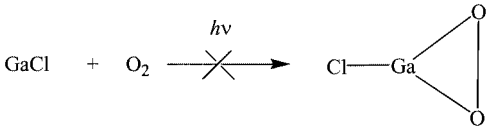

(2)

Some of the differences can be explained by an "inert-pair" effect. The strength of the bonds in the lighter homologues is usually higher than in their heavier counterparts and can thus more easily compensate the loss of one binding interaction in the reactant. In other cases it might be of some importance that Al prefers a higher coordination number than Ga. For example, a bis(superoxo) complex, $[XM(O_2)_2]$, can be formed for M = Al, but not for M = Ga.

To study in more depth the reactions with small model hydrocarbons we have looked at the reaction with C_2H_2 leading to the acetylide species HAl(Cl)CCH. Interestingly, the cyclic alumina-cyclopropene derivative [see Equation (3)] is not formed.[13] That comparatively small modifications of the reactants can lead to different products is shown by comparing the reaction between AlCl and HCCH with that between AlCl and H_3CCCCH_3. Photoactivated AlCl reacts with 2-butyne to give two products, one of them being the alumina-cyclopropene derivative.[13] Thus, the replacement of the hydrogen atoms in C_2H_2 by methyl groups alters the structures (cyclic vs. acetylide form) of the reaction products.

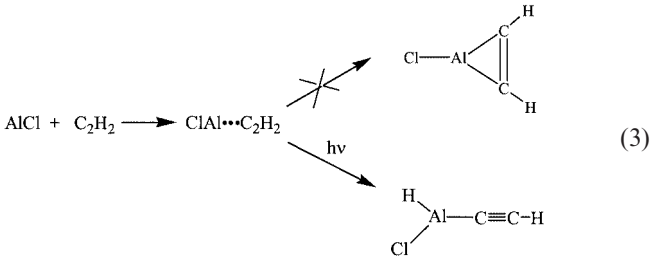

(3)

We are also currently studying the reaction of AlCl with CpH (C_5H_6).[14] The reaction of AlCp* with H_2 gives H_2AlCp^*, in which the C_5 ring is coordinated in η^5-fashion

[a] Institut für Anorganische Chemie, Universität Karlsruhe
Engesserstr., Geb 30.45, 76128 Karlsruhe
Fax: (internat.) +49-(0)721-608-4854
E-mail: himmel@chemie.uni-karlsruhe.de

to the Al center.[11] Theoretical studies and a series of experimental results obtained with suitable derivatives suggest that the energy differences between η^5-, η^3-, η^2- and η^1-coordination for $CpAlH_2$ are very small ($<$ 13 kJ·mol^{-1}).[15] The coordination mode of the Cp ring in HAl(Cl)Cp, the likely product of the reaction between AlCl and CpH, is therefore difficult to predict. It should, though, be easy to distinguish between these forms on the basis of the matrix IR spectra.

Here it will be shown that matrix-isolated AlCl inserts on photoactivation into the C−H bond of CH_4 to give the new species $Cl(H)AlCH_3$. This reaction shows impressively how reactive photoactivated AlCl molecules are. Such C−H activation mechanisms are important in catalytic processes.

Results

The IR spectrum taken upon deposition of AlCl together with 2% CH_4 in an Ar matrix showed strong absorptions due to CH_4 and AlCl. However, there are no bands due to a reaction product. The matrix was therefore exposed for a period of 10 min to broad-band UV/Visible radiation ($200 < \lambda < 800$ nm). Several new bands in the spectrum recorded after the photolysis period indicate that the photoactivated AlCl molecules readily react with CH_4. The difference between a spectrum taken after and before photolysis is shown in Figure 1, a. A family of bands appears at 3015.2, 2998.1, 2984.4, 1905.2, 1199.7, 743.7, 672.8, 657.7, 604.4, 488.1/482.8, and 421.4 cm^{-1}. With different concentrations of CH_4 and AlCl in the matrix the relative intensities of these bands remain unchanged, indicating that they all belong to the same absorber. The strongest band is at 1905.2 cm^{-1}, a region characteristic of the ν(Al−H) stretching fundamentals of Al^{III} compounds [cf. AlH_3 1882.9,[16] H_2AlNH_2 1899.3,[17,18] H_2AlPH 1874.7/1866.1,[19] $HAlCl_2$ 1967.6,[6] H_2AlCl 1928.1/1915.9,[2] HAl(Cl)CCH 1952.2 cm^{-1} [13]]. Strong, but somewhat broader, features are at 743.7, 672.8 and 657.7 cm^{-1} (the second one being a shoulder of the more intense band at 657.7 cm^{-1}). The band at 743.7 cm^{-1} occurs in the region of the ρ(CH_3) rocking mode of a methyl group (cf. $HGaCH_3$ 752.9,[20] $HBeCH_3$ 704.1 cm^{-1} [21]). The bands at 3015.2, 2998.1 and 2984.4 cm^{-1} qualify for ν(C−H) stretching vibrations.

A weak additional feature at 1965.7 cm^{-1}, which grew in on photolysis, can be assigned to the ν(Al−H) stretching fundamental of HAl(Cl)OH.[13] This species is formed from reaction of AlCl with H_2O that is present as a trace impurity. Additionally, a sharp relatively intense band appeared at 769.9 cm^{-1} and very weak ones at 1928.1, 1915.9, 604.9, 549.9, and 518.6 cm^{-1}. These were previously assigned to H_2AlCl,[2] representing the product of the photoactivated reaction between AlCl and H_2. Traces of H_2 in the matrix are a consequence of the generation of AlCl in the oven, from reaction between liquid Al and HCl at ca. 1000 °C to give AlCl and H_2. Finally, some experiments revealed very small amounts of $HAlCl_2$ in the matrix, arising from traces of HCl in the matrix (HCl that has not reacted with the liquid Al in the oven).[6] These bands were, however, extremely weak.

The experiment was repeated with CD_4 in place of CH_4. Again, no reaction product was evident from the spectrum recorded immediately after deposition. However, photolysis furnished a family of new bands at 2212.0, 1386.1, 947.1, 630.1, 569.0, 518.4, 471.7, 435.4/430.6, and 308.1 cm^{-1} (Figure 2). All the features were red-shifted with respect to their counterparts with CH_4. The strongest band in the spectrum is at 1386.1 cm^{-1}, which can confidently be attributed to a ν(Al−D) stretching fundamental, experienced a marked shift, corresponding to a ν(H):ν(D) ratio of 1.3745:1. The absorptions at 743.7, 672.8 and 657.7 cm^{-1} in the experiments with $^{12}CH_4$ now occurred at 630.1, 518.4 and 569.0 cm^{-1}, respectively. A band at 2212.0 cm^{-1} appeared in a region characteristic of ν(C−D) stretching fundamentals.

Finally, in experiments conducted with $^{13}CH_4$, as with CH_4 and CD_4, no absorption due to any product of a thermal reaction between AlCl and $^{13}CH_4$ appeared in the IR spectrum recorded immediately after deposition. Photolysis

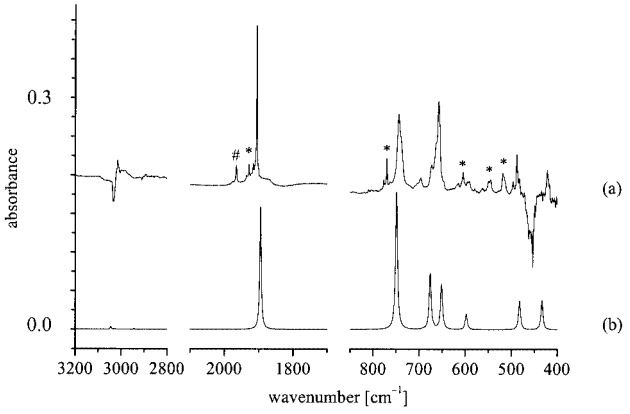

Figure 1. (a) IR difference spectrum, between the spectra after and before 40 min of photolysis of an Ar matrix containing AlCl together with $^{12}CH_4$. (b) Calculated IR spectrum for $HAl(Cl)^{12}CH_3$. #: Band due to HAl(Cl)OH. *: Bands due to H_2AlCl

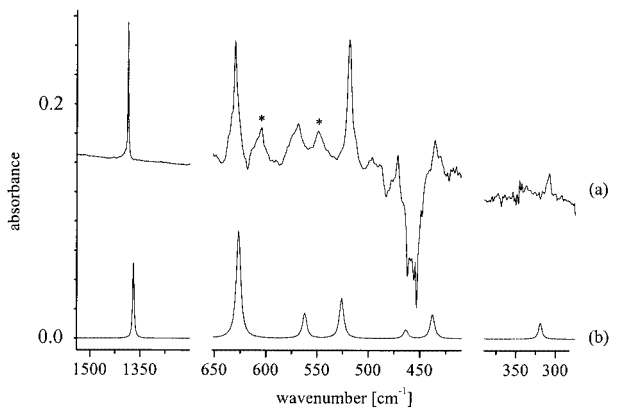

Figure 2. (a) IR difference spectrum, between the spectra after and before 40 min of photolysis of an Ar matrix containing AlCl together with $^{12}CD_4$. (b) Calculated IR spectrum for $DAl(Cl)^{12}CD_3$. *: Bands due to H_2AlCl

 © 2003 Wiley-VCH Verlag GmbH & Co. KGaA, Weinheim

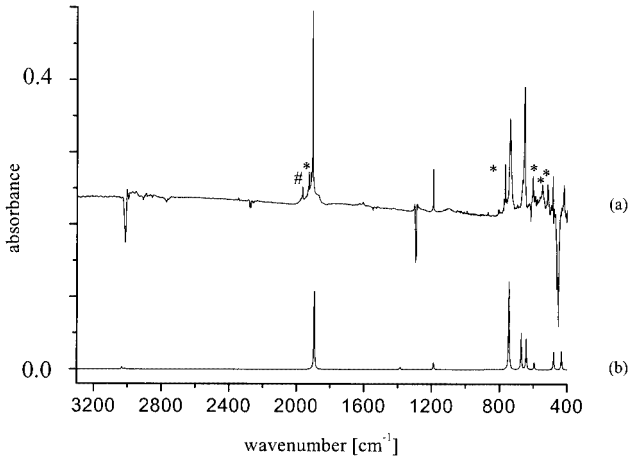

Figure 3. (a) IR difference spectrum, between the spectra after and before 40 min of photolysis of an Ar matrix containing AlCl together with $^{13}CH_4$. (b) Calculated IR spectrum for $HAl(Cl)^{13}CH_3$. #: Band due to HAl(Cl)OH. *: Bands due to H_2AlCl

was needed to initiate a reaction. Figure 3 shows the difference between the IR spectrum taken after photolysis and the one taken before photolysis. In its ^{13}C version, the product of the reaction between AlCl and methane is the author of bands at 3003.9, 2972.6, 2951.9, 1905.2, 1375.5, 1191.0, 739.9, 667.2, 652.7, 604.7, 486.5, and 421.1 cm^{-1}.

Discussion

The experimental results clearly show that AlCl reacts with CH_4 upon photoactivation to give a single reaction product.[22] The detection of a ν(Al−H) stretching fundamental and its location indicate that this product contains a terminal Al−H bond; it also shows all the hallmarks of a species featuring a methyl (CH_3) group. Finally, the band at 482.0 cm^{-1} indicates a terminal Al−Cl bond. The obvious inference is that photoactivated AlCl inserts into one of the C−H bonds of CH_4 to give the new monomeric Al hydride species $HAl(Cl)CH_3$.

Quantum chemical calculations on the possible structure of such a product suggest that $HAl(Cl)CH_3$ exhibits a C_s symmetric global energy minimum structure characterized by the bond lengths (in pm) Al−Cl 212.7, Al−H 160.1, C−H 111.2/111.4, Al−C 195.5. The H−Al−Cl, Cl−Al−C and H−Al−C bond angles are 115.8°, 118.5° and 125.7°, respectively. Thus, in agreement with the predictions of VSEPR theory,[23] the smallest angle at the Al center is for H−Al−Cl.

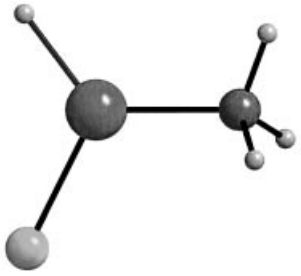

At 195.5 pm, the Al−C bond length is in pleasing agreement with those measured for several compounds containing Al−C bonds. Thus, on the basis of gas-phase electron diffraction studies, the Al−C distance in monomeric $Al(CH_3)_3$ was determined to be 195.7(3) pm.[24] In $(Me_2AlNC_6H_{12})_2$, an example for Al with a coordination number of 4, Al−C bond lengths of 196.3(4) and 198.0(6) pm are adopted according to an X-ray diffraction analysis.[25] One further example is the compound $[(tmpCO_2)_2AlMe]_2$, which features an Al atom with a coordination number of 5 and an Al−C distance of 195.2(4) pm.[26] In general, the Al−C bond lengths cover a large range (189.7 to 236.6 pm) with an average of 198.3 pm according to the Cambridge Structural Database.[27] However, these statistics include compounds with different coordination numbers. Some structurally characterized monomeric alanes containing terminal Al−H bonds are now known. The Al−H bond length (r_0 value) in $(Ar^*)_2AlH$ [Ar* = (*tert*-butyl)$_3C_6H_2$] is 153(4) pm,[28] whereas in $Mes^*Al(H)N(SiMe_3)_2$ an Al−H distance of 151(3) pm was found by X-ray diffraction.[29] However, X-ray measurements give, at best, estimates significantly different from r_e. For AlH_3, an Al−H bond length (r_e value) of 157.1−159.7 was calculated, depending on the applied theoretical method.[16,30] These values compare satisfactorily with the r_e of 160.1 pm calculated for $HAl(Cl)CH_3$. The Al−H bond lengths in general cover a large range, adopting values as low as ca. 125 pm and up to more than 180 pm.[31] Finally, electron diffraction measurements yielded an Al−Cl distance of 206.2(3) pm in monomeric $AlCl_3$ (which is in equilibrium with its dimer in the gas-phase at 400 °C),[32] which is reasonably close to that calculated for $HAl(Cl)CH_3$ (212.7 pm). Thus the dimensions derived for $HAl(Cl)CH_3$ from quantum chemical calculations are wholly reasonable.

Table 1 compares the experimentally observed wavenumbers with those forecast by the DFT calculations, and also includes an attempt to describe the molecular motions of the modes. Obviously any such attempt is limited by the degree of mode coupling in this rather unsymmetrical molecule (C_s symmetry). The ν(C−H) stretching region showed a sharp band at 3015.2 cm^{-1}, red-shifted from the ν(C−H) stretching mode of CH_4, which can be assigned to one of the antisymmetric ν(C−H) stretching modes, namely $\nu_1(a')$. The calculations predict a wavenumber of 3044.4 cm^{-1} for this mode. The calculated shifts upon $^{12}C/^{13}C$ and H/D substitution agree well with the experimental ones (Table 1). Additional weaker bands at 2998.1 and 2984.4 cm^{-1} can be assigned to the second antisymmetric and the symmetric ν(C−H) stretching fundamental, $\nu_{11}(a'')$ and $\nu_2(a')$, respectively. Again, the calculated wavenumbers of 3026.5 and 2944.0 cm^{-1} pleasingly match the experimental ones.

As already mentioned, the wavenumber of the ν(Al−H) stretching mode comes in a region that is characteristic of Al^{III} compounds (ca. 1850−2000 cm^{-1}). The only exception is H_2AlCp^*, for which the antisymmetric and symmetric ν(Al−H) stretching fundamentals were detected at 1801.5 and 1773.7 cm^{-1}, respectively.[11] Such low values can be explained by the back-donation from the Cp* ring

 © 2003 Wiley-VCH Verlag GmbH & Co. KGaA, Weinheim

Table 1. Comparison of IR properties observed and calculated for $HAl(Cl)CH_3$ and isotopomers (wavenumbers in cm^{-1}, intensities in km mol^{-1})

$HAl(Cl)^{12}CH_3$		$HAl(Cl)^{13}CH_3$		$DAl(Cl)^{12}CD_3$			
obsd.	calcd.	obsd.	calcd.	obsd.	calcd.	assign.	approx. descrip.
3015.2	3044.4 (4)	3003.9	3033.6 (5)	2212.0	2260.8 (1)	$\nu_1(a')$	$\nu_{asym}(C-H)$
2984.4	2944.0 (1)	2951.9	2940.8 (1)	[a]	2121.9 (0.03)	$\nu_2(a')$	$\nu_{sym}(C-H)$
1905.2	1894.6 (172)	1905.2	1894.7 (172)	1386.1	1369.4 (104)	$\nu_3(a')$	$\nu(Al-H)$
[a]	1390.3 (3)	[a]	1388.1 (3)	[a]	1006.8 (3)	$\nu_4(a')$	$\delta_{asym}(CH_3)$
1199.7	1196.9 (18)	1191.0	1187.9 (16)	947.1	941.9 (27)	$\nu_5(a')$	$\delta_{sym(}CH_3)$
743.7	748.7 (191)	739.9	744.8 (192)	630.1	626.7 (146)	$\nu_6(a')$	$\rho(CH_3)$
657.7	651.0 (62)	652.7	642.3 (67)	569.0	562.2 (34)	$\nu_7(a')$	$\delta(Cl-Al-H)$
604.4	597.6 (22)	604.7	594.8 (16)	471.7	463.7 (12)	$\nu_8(a')$	$\nu(Al-C)$
488.1/ 482.8	482.0 (39)	486.5	479.9 (38)	435.4/430.6	437.8 (33)	$\nu_9(a')$	ν(Al-Cl)
[b]	176.8 (5)	[b]	174.7 (5)	[b]	160.0 (4)	$\nu_{10}(a')$	δ(ClAlC
2998.1	3026.5 (1)	2972.6	3016.1 (2)	[a]	2244.6 (0.03)	$\nu_{11}(a'')$	$\nu_{asym}(C-H)$
[a]	1386.0 (4)	1375.5	1383.4 (4)	[a]	1006.1 (4)	$\nu_{12}(a'')$	$\delta(CH_3)$
672.8	675.6 (79)	667.2	671.9 (78)	518.4	526.0 (54)	$\nu_{13}(a'')$	γ
421.4	433.1 (40)	421.1	433.1 (40)	308.1	319.1 (22)	$\nu_{14}(a'')$	$\rho(Al-H)$
[a]	230.5 (0.1)	[a]	230.4 (0.2)	[b]	162.8 (0.1)	$\nu_{15}(a'')$	

[a] Too weak to be observed. [b] Outside the experimental detection range.

to the Al center which leads to a significant weakening of the Al−H bonds. At 1894.6 cm^{-1}, the calculated wavenumber for the ν(Al−H) mode is in excellent agreement with the experimental one. Calculation and experiment also agree that this mode shows virtually no shift upon $^{12}C/^{13}C$ isotopic substitution. Conversely, H/D substitution strongly affects this mode [calculated and experimental ν(H):ν(D) ratios of 1.3835:1 and 1.3745:1 respectively].

The weak feature at 1199.7 cm^{-1} can be assigned to a mode with a high CH_3 "umbrella" [$\delta_{sym}(CH_3)$] character. Wavenumbers of 1158, 1179, 1147.9 and 1115.3 cm^{-1} have been reported for the $\delta_{sym}(CH_3)$ mode in $LiCH_3$,[33] $BeCH_3$,[21] $GaCH_3$ [20,34] and $InCH_3$,[20,34] respectively. For $Al(CH_3)_3$ and $HGa(CH_3)_2$, isolated in Ar matrices, the "umbrella" mode shows up at 1196[35] and 1202.5 cm^{-1},[36] respectively. The calculations yielded 1196.9 cm^{-1} for this mode in $HAl(Cl)CH_3$. The experimental and calculated ν(H):ν(D) ratios are 1.2667:1 and 1.2707:1, respectively. Unfortunately, with only one exception, the other two $\delta(CH_3)$ deformation fundamentals [$\nu_4(a')$ and $\nu_{12}(a'')$] escaped experimental detection. The only sign of the $\nu_{12}(a'')$ mode was a very weak feature at 1375.5 cm^{-1} in the experiments with $^{13}CH_4$. The calculations predict wavenumbers of 1390.3 and 1386.0 cm^{-1} and very low intensities for these modes.

The 657.7 cm^{-1} band can be assigned to the δ(HAlCl) deformation fundamental. This is close to that measured for the corresponding mode in HAl(Cl)CCH (671.4 cm^{-1}).[13] The calculated value of 651.0 cm^{-1} pleasingly matches the experimental value. As anticipated, the effect of $^{12}C/^{13}C$ substitution is again relatively small. In $Cl(H)Al^{13}CH_3$, the mode appears at 652.7 cm^{-1}, shifted by not more than 5.0 cm^{-1} to lower wavenumbers. Conversely, the large ν(H):ν(D) ratio (observed 1.1559:1 and calculated 1.1580) again indicates substantial H atom motion in this vibration.

The strong band at 672.8 cm^{-1} in the spectra recorded for $^{12}CH_4$ belongs to a mode which can be approximately described as the *out-of-plane* Al−H bending mode, γ. The corresponding mode in H_2AlCl[2] and $HAlCl_2$ [6] occurs at 604.9 and 654 cm^{-1}, respectively. The calculations yielded 675.6 cm^{-1}. This approximate description of this mode is supported by the substantial ν(H):ν(D) ratio (observed 1.2978:1 and calculated 1.2844:1).

The spectra also gave evidence for a band at 604.4 cm^{-1} in the experiments with $^{12}CH_4$ and the corresponding mode should have a high contribution from the ν(Al−C) stretching mode. The value compares with 615.9 cm^{-1} for a mode of HAl(Cl)CCH also with a high contribution from the ν(Al−C) stretching vibration.[13] In the radical $HAlCH_3$, which can be generated by the matrix reaction between Al atoms and CH_4, the ν(Al−C) stretching mode appears at 610 cm^{-1}.[37] In $Al(CH_3)_3$, the ν(Al−C) stretching fundamentals were observed at 691 (e′ mode) and 530 cm^{-1} (a_1' mode) for the molecule in the gas phase.[38] Obviously, this mode couples significantly with other modes of the same symmetry and therefore these wavenumbers cannot be compared directly. The calculations yielded 597.6 cm^{-1}, in close conformity with the experimental value.

The bands at 488.1/482.8, 486.5 and 435.4/430.6 cm^{-1} in the experiments with $^{12}CH_4$, $^{13}CH_4$ and $^{12}CD_4$ are obvious candidates for modes with a significant degree of ν(Al-Cl) stretching. Modes in related molecules which also exhibit high ν(Al-Cl) stretching mode character have the wavenumbers (in cm^{-1}) H_2AlCl 549.9,[2] $HAlCl_2$ 579,[6] HAl(Cl)CCH 505.8.[13] The small ν(H):ν(D) ratios observed and calculated (1.1210:1 and 1.1010:1, respectively) agree with this assignment. The doublet pattern seen in experiments with $^{12}CH_4$ and $^{12}CD_4$ probably arises from $^{35}Cl/^{37}Cl$ isotopic splitting. The relative intensities of the two components at 488.1 and 482.8 cm^{-1} for $^{12}CH_4$ and at 435.4 and 430.6 cm^{-1} for $^{12}CD_4$ are in good agreement with the relative abundances of ^{35}Cl and ^{37}Cl.

Overall, the comparison of the data measured for the three isotopomers with the properties measured previously for related molecules and the results of quantum chemical

 © 2003 Wiley-VCH Verlag GmbH & Co. KGaA, Weinheim

calculations affirm that $HAl(Cl)CH_3$ is the product of the photolytically induced matrix reaction between AlCl and CH_4.

AlCl in its ground electronic state is expected to interact only very weakly with CH_4. Quantum chemical calculations suggest, as anticipated, that a complex of the form $ClAl{\cdot}CH_4$ is, if at all, only very weakly bound. The binding energy seems to be even smaller than that calculated for an $Al{\cdot}CH_4$ complex (2.6 kJ·mol^{-1} according to MP2 calculations and a TZVPP basis set, ZPVE corrections included).[39] The effect of photolysis has been discussed previously.[1] The electronic transition in the AlCl molecule is mainly metal atom-centered and leads to the population of a vacant π-orbital that is expected to be ideally suited to interact with a σ* orbital of an E−H bond. As a consequence, the E−H bond is weakened and the Al atom inserts into the bond yielding the $HAl(Cl)CH_3$ end-product.

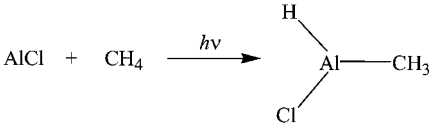

(4)

The overall reaction [Equation (4)] is slightly exothermic. According to the calculations, the reaction energy amounts to −43.2 kJ·mol^{-1}. The analogous reaction of GaCl with CH_4 to give $HGa(Cl)CH_3$ is, by contrast, *endothermic* and requires, according to DFT calculations, an energy of +32.6 kJ·mol^{-1}. This again shows the differences in reactivity between AlCl and GaCl. The reaction energy calculated for $AlCl/CH_4$ is nevertheless smaller than that calculated for $AlCl/H_2$ (−75.6 kJ·mol^{-1}).[1,2]

Conclusions

Experiments have shown that matrix-isolated and photoactivated AlCl molecules insert readily into a C−H bond of methane to give the new monomeric Al hydride $HAl(Cl)CH_3$. IR spectra of this C_s-symmetric molecule in its $HAl(Cl)^{12}CH_3$, $DAl(Cl)^{12}CD_3$ and $HAl(Cl)^{13}CH_3$ isomeric forms were recorded. The experiments were accompanied by detailed quantum chemical calculations, according to which the reaction of AlCl with CH_4 to give $HAl(Cl)CH_3$ is slightly exothermic (−43.2 kJ·mol^{-1}).

The reaction with CH_4 demonstrates the potential for detailed exploration of the photochemistry of subvalent compounds like AlCl. The experience gained from the matrix-isolated molecules could be vital in developing the photochemistry on a preparative scale.

Experimental Section

Details of the matrix isolation method can be found elsewhere.[40] Very briefly, in a high vacuum apparatus, HCl was passed over liquid Al (at 1000 °C) inside a Knudsen-type graphite container. Hence AlCl was formed and the vapor emitted from the cell. The AlCl vapor was co-deposited with methane in an excess of Ar onto a freshly polished Cu block kept at 12 K (with a Leybold LB510 refrigerator).

IR spectra were recorded with a Bruker 113v spectrometer equipped with a DTGS and a MCT detector, allowing measurements in the region 5000−200 cm^{-1}. The spectra were recorded with a resolution of 0.5 cm^{-1}. A Ge/KBr beam splitter was used for the 5000−400 cm^{-1} range, and a Mylar 3.5 beam splitter for measurements down to 200 cm^{-1}. Photolysis was achieved with the aid of a medium-pressure mercury lamp (Philips LP 125) operating at 100 W.

$^{12}CH_4$ (99.995 Vol-%) was used as purchased from Messer. $^{12}CD_4$ (98 atom% D) and $^{13}CH_4$ (99 atom% ^{13}C) were used as delivered from Aldrich.

Quantum chemical calculations were carried out with the aid of the TURBOMOLE program package.[41] The BP method in combination with a TZVPP basis set for Al (and Ga) and a SV(P) basis set for the other elements was used in all calculations. The reaction energies are given with ZPVE corrections.

Acknowledgments

Financial support from the Deutsche Forschungsgemeinschaft (DFG) and the Fonds der Chemischen Industrie is gratefully acknowledged.

[1] H.-J. Himmel, *J. Chem. Soc., Dalton Trans.* **2002**, 2678.
[2] H.-J. Himmel, C. Klaus, *Z. Anorg. Allg. Chemie* **2003**, *629*, 1477.
[3] H. Schnöckel, *J. Mol. Struct.* **1978**, *50*, 267.
[4] J. Bahlo, H.-J. Himmel, H. Schnöckel, *Inorg. Chem.* **2002**, *41*, 2678.
[5] J. Bahlo, H.-J. Himmel, H. Schnöckel, *Inorg. Chem.* **2002**, *41*, 4488.
[6] H. Schnöckel, *J. Mol. Struct.* **1978**, *50*, 275.
[7] H.-J. Himmel, J. Bahlo, M. Haussmann, F. Kurth, G. Stösser, H. Schnöckel, *Inorg. Chem.* **2002**, *41*, 4952.
[8] [8a] R. Köppe, M. Tacke, H. Schnöckel, *Z. Anorg. Allg. Chem.* **1991**, *605*, 35. [8b] R. Köppe, H. Schnöckel, *J. Chem. Soc., Dalton Trans.* **1992**, 3393.
[9] H.-J. Himmel, A. J. Downs, T. M. Greene, *J. Am. Chem. Soc.* **2000**, *122*, 922.
[10] H. Schnöckel, H. J. Goecke, *J. Mol. Struct.* **1978**, *50*, 281.
[11] H.-J. Himmel, J. Vollet, *Organometallics* **2002**, *21*, 5972.
[12] H.-J. Himmel, unpublished results.
[13] H.-J. Himmel, *Organometallics* **2003**, *22*, 2679.
[14] H.-J. Himmel, C. Klaus, unpublished results.
[15] P. H. M. Budzelaar, J. J. Engelberts, J. H. van Lenthe, *Organometallics* **2003**, *22*, 1562. Eichkorn, O. Treutler, H. Öhm, M. Häser, R. Ahlrichs, *Chem. Phys. Lett.* **1995**, *240*, 283. K. Eichkorn, O. Treutler, H. Öhm, M. Häser, R. Ahlrichs, *Chem. Phys. Lett.* **1995**, *242*, 652. K. Eichkorn, F. Weigend, O. Treutler, R. Ahlrichs, *Theor. Chem. Acc.* **1997**, *97*, 119. F. Weigend, M. Häser, *Theor. Chem. Acc.* **1997**, *97*, 331. F. Weigend, M. Häser, H. Patzelt, R. Ahlrichs, *Chem. Phys. Lett.* **1998**, *294*, 143.
[16] P. Pullumbi, Y. Bouteiller, L. Manceron, C. Mijoule, *Chem. Phys.* **1994**, *185*, 25.
[17] H.-J. Himmel, A. J. Downs, T. M. Greene, *J. Am. Chem. Soc.* **2000**, *122*, 9793.
[18] H.-J. Himmel, A. J. Downs, J. C. Green, T. M. Greene, *J. Chem. Soc., Dalton Trans.* **2001**, 535.
[19] H.-J. Himmel, A. J. Downs, T. M. Greene, *Inorg. Chem.* **2001**, *40*, 396.
[20] H.-J. Himmel, A. J. Downs, T. M. Greene, L. Andrews, *Organometallics* **2000**, *19*, 1060.

 © 2003 Wiley-VCH Verlag GmbH & Co. KGaA, Weinheim

[21] T. M. Greene, D. V. Lanzisera, L. Andrews, A. J. Downs, *J. Am. Chem. Soc.* **1998**, *120*, 6097.
[22] The relative intensities of the bands remained unchanged in experiments in which the concentrations of the reactants in the matrix were varied.
[23] R. J. Gillespie, I. Hargittai, *The VSEPR Model of Molecular Geometry*; Allyn and Bacon: Boston, **1991**, R. J. Gillespie, *Chem. Soc. Rev.* **1992**, *21*, 59.
[24] A. Almenningen, S. Halvorsen, A. Haaland, *Acta Chem. Scand.* **1971**, *25*, 1937.
[25] C. B. Lagrone, S. J. Schauer, C. J. Thomas, G. M. Gray, C. L. Watkins, L. K. Kranich, *Organometallics* **1996**, *15*, 2458.
[26] K. Knabel, I. Krossing, H. Nöth, H. Schwenk-Kircher, M. Schmidt-Amelunxen, T. Seifert, *Eur. J. Inorg. Chem.* **1998**, 1095.
[27] Cambridge Structural Database, Release April **2003**. Only compounds with *R* smaller than 5% and no disorder and errors were considered.
[28] A. H. Cowley, H. S. Isom, A. Decken, *Organometallics* **1995**, *14*, 2589.
[29] R. J. Wehmschulte, P. P. Power, *Inorg. Chem.* **1998**, *37*, 2106.
[30] See: [30a] A. J. Downs, C. M. Pulham, *Chem. Soc. Rev.* **1994**, *23*, 175. [30b] S. Aldridge, A. J. Downs, *Chem. Rev.* **2001**, *101*, 3305. [30c] F. A. Kurth, R. A. Eberlein, H. Schnöckel, A. J. Downs, C. R. Pulham, *J. Chem. Soc., Chem. Commun.* **1993**, 1302.
[31] C. Y. Tang, A. J. Downs, T. M. Greene, S. Parsons, *Dalton Trans.* **2003**, 540.
[32] K. Aarset, Q. Shen, H. Thomassen, A. D. Richardson, K. Hedberg, *J. Phys. Chem. A* **1999**, *103*, 1644.
[33] [33a] L. Andrews, G. C. Pimentel, *J. Chem. Phys.* **1967**, *47*, 3637. [33b] L. Andrews, *J. Chem. Phys.* **1967**, *47*, 4834.
[34] H.-J. Himmel, A. J. Downs, T. M. Greene, L. Andrews, *Chem. Commun.* **1999**, 2243.
[35] S. Kvisle, E. Rytter, *Spectrochim. Acta* **1984**, *40A*, 939.
[36] J. Müller, H. Sternkicker, U. Bergmann, B. Atakan, *J. Phys. Chem. A* **2000**, *104*, 3627.
[37] J. M. Parnis, G. A. Ozin, *J. Phys. Chem.* **1989**, *93*, 1204 and 1220.
[38] G. A. Atiya, A. S. Grady, D. K. Russell, T. A. Claxton, *Spectrochim. Acta* **1991**, *47A*, 467.
[39] B. Gaertner, H.-J. Himmel, V. A. Macrae, A. J. Downs, T. M. Greene, *Chem. Eur. J.*, submitted for publication.
[40] H.-J. Himmel, A. J. Downs, T. M. Greene, *Chem. Rev.* **2002**, *102*, 4191.
[41] R. Ahlrichs, M. Bär, M. Häser, H. Horn, C. Kölmel, *Chem. Phys. Lett.* **1989**, *162*, 165. K.

Received May 26, 2003

 © 2003 Wiley-VCH Verlag GmbH & Co. KGaA, Weinheim

X-ray Crystal Structure and Electrical Conductivity of $[Au(ppy)(C_8H_4S_8)]_2[PF_6]$ [$ppy^- = C$-deprotonated 2-phenylpyridine(−); $C_8H_4S_8^{2-}$ = 2-{(4,5-ethylenedithio)-1,3-dithiol-2-ylidene}-1,3-dithiole-4,5-dithionate(2−)]

Kazuya Kubo,[a] Motohiro Nakano,[a] Hatsue Tamura,[a] and Gen-etsu Matsubayashi*[a]

Keywords: Gold / S ligands / Oxidation / Sulfur / Electrochemistry

Crystals of $[Au(ppy)(C_8H_4S_8)]_2[PF_6]$ [ppy^- = *C*-deprotonated 2-phenylpyridine(−); $C_8H_4S_8^{2-}$ = 2-{(4,5-ethylenedithio)-1,3-dithiol-2-ylidene}-1,3-dithiole-4,5-dithiolate(2−)] were prepared by current-controlled electrolysis of a benzonitrile solution of $[Au(ppy)(C_8H_4S_8)]$ with $[NEt_4][PF_6]$ as an electrolyte. The X-ray crystal structure analysis revealed the formation of a columnar stacking of two crystallographically independent cations in formally the 0.5-electron-oxidized state. Cation moieties with some S–S non-bonded contacts (< 3.7 Å) along the *a* and *b* axes form a two-dimensional sheet, with the molecular interaction parallel to the *ab* plane. The electrical conductivities measured for a crystal at room temperature were 9.2 and 0.0028 S cm^{-1} along the *a* and *c* axes, respectively. From the activation energy for the electron conduction determined by the conductivities measured for a compacted pellet the complex was estimated to be metallic from room temperature to 110 K. The energy-band calculation for the oxidized species showed two-dimensional electron conduction through the column.

(© Wiley-VCH Verlag GmbH & Co. KGaA, 69451 Weinheim, Germany, 2003)

Introduction

Many molecular electron-conducting compounds made from metal complexes containing sulfur-rich dithiolate ligands, such as $C_3S_5^{2-}$ and $C_8H_4S_8^{2-}$, have been extensively studied; their oxidized metal complexes become good electrical conductors and superconductors.[1−6] They construct effective electron-conduction pathways through some sulfur-sulfur non-bonding contacts in the solid state.

Polarized metal complexes containing both a sulfur-rich dithiolate ligand and an N−N or N−C chelating ligand are expected to form unique molecular stackings and/or layered arrangements through electrostatic interaction of the polarized metal-center moieties, metal-metal interactions and some S−S non-bonding contacts in the solid state behaving as an inorganic/organic molecular composite. Recently, we reported the preparation and crystal structures of planar, asymmetric metal complexes of the [M(N−N)(S−S)] type [M = Pd^{II} and Pt^{II}; N−N = diimine ligands and S−S = sulfur-rich dithiolate ligands(2−)][7,8] and of the [Au^{III}(C−N)(S−S)] type [C−N = *C*-deprotonated 2-phenylpyridine(−) (ppy^-); S−S = sulfur-rich dithiolate ligands(2−)];[9] their chemically oxidized species exhibit high electrical conductivities.

This paper reports the crystal structure of the title oxidized species prepared by electrocrystallization of $[Au(ppy)(C_8H_4S_8)]$ in benzonitrile in the presence of $[NEt_4][PF_6]$, together with the electrical conductivities measured for the crystal and energy bands calculated based on the crystal structure.

Results and Discussion

Preparation of the 0.5-Electron-Oxidized Species $[Au(ppy)(C_8H_4S_8)]_2[PF_6]$

The cyclic voltammogram of $[Au(ppy)(C_8H_4S_8)]$ measured in *N*,*N*-dimethylformamide exhibits two oxidation peaks at −60 and +430 mV (versus Ag/Ag^+);[9] the first oxidation occurs on the $C_8H_4S_8$ ligand. The first oxidation potential is slightly higher than that of the diimine/$C_8H_4S_8$-Pt^{II} complex $[Pt(bpy)(C_8H_4S_8)]$ (−180 mV versus Ag/Ag^+).[8] Reactions of $[Au(ppy)(C_8H_4S_8)]$ with iodine and tetracyano-*p*-quinodimethane (TCNQ) also gave the one-electron-oxidized species $[Au(ppy)(C_8H_4S_8)](I_3)$ and the essentially 0.5-electron-oxidized complex $[Au(ppy)(C_8H_4S_8)](TCNQ^{\cdot -})_{0.6}$, respectively.[9] The present 0.5-electron-oxidized species prepared by the electrocrystallization exhibits almost an isotropic ESR signal with g = 2.007 (peak-to-peak linewidth, 5 mT), as observed for other oxidized $C_8H_4S_8$-metal complexes.[7−13] This finding suggests the $C_8H_4S_8$ ligand-centered oxidation, as confirmed from the

[a] Department of Molecular Chemistry & Frontier Research Center, Graduate School of Engineering, Osaka University, 1-16, Machikaneyama, Toyonaka, Osaka 560-0043, Japan
E-mail: matsu@ch.wani.osaka-u.ac.jp

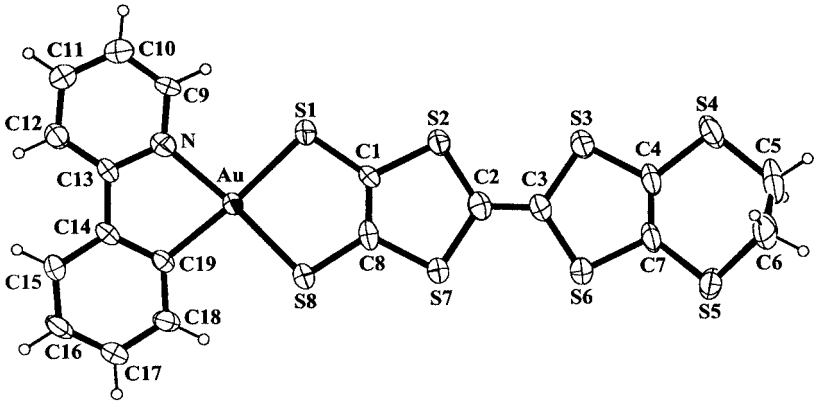

Figure 1. Geometry of one of the cation moieties of $[Au(ppy)(C_8H_4S_8)]_2[PF_6]$ together with the atom-labeling scheme

spin densities calculated for the one-electron-oxidized $C_8H_4S_8$-Ti^{IV} complex.[13]

The powder reflectance spectrum of the present oxidized species exhibits a band at 900 nm due to the metal-to-dithiolate ligand charge-transfer transition[7–9] and broad bands at longer wavelengths. They suggest intermolecular interactions through some S−S non-bonding contacts in the solid state.

Molecular and Crystal Structures of $[Au(ppy)(C_8H_4S_8)]_2[PF_6]$

The crystal structure of the complex consists of two crystallographically independent cations and octahedral anions. The molecular structure of one of the cation moieties of the complex is shown in Figure 1, together with the atom-labeling scheme. The other cation has also almost the same geometry as this. Selected bond lengths and angles are listed in Table 1.

The Au^{III} ion shows a square-planar coordination, as expected for d^8-metal complexes. The Au(1)−N(1) [2.069(6) Å] and Au(1)−C(19) [2.054(7) Å] distances are close to those of the unoxidized species $[Au(ppy)(C_8H_4S_8)]$ [Au−N = 2.063(3) Å and Au−C = 2.041(5) Å].[9] They are also similar to those of [Au(ppy)(tdt)] [tdt^{2-} = 3,4-toluenedithiolate(2−)] [Au−N = 2.079(5) Å and Au−C = 2.035(7) Å][14] and $[Au(ppy)(S_2CNEt_2)]^+$ [Au−N = 2.058(11) Å and Au−C = 2.036(7) Å].[15] The Au(1)−S(1) bond [2.316(2) Å] trans to the Au(1)−C(19) bond is longer than the Au(1)−S(8) bond [2.298(2) Å] trans to Au(1)−N(1) owing to the structural trans influence. This structural trans influence has also been observed for other $[Au^{III}(C-N)(S-S)]$-type complexes.[9,14–17] The $C_8H_4S_8$

Table 1. Selected bond lengths (Å) and angles (°) of $[Au(ppy)(C_8H_4S_8)]_2[PF_6]$

Au(1)−S(1)	2.316(2)	Au(1)−S(8)	2.298(2)	Au(2)−S(9)	2.324(2)
Au(2)−S(16)	2.294(2)	Au(1)−N(1)	2.069(6)	Au(2)−N(2)	2.065(7)
Au(1)−C(19)	2.054(7)	Au(2)−C(38)	2.035(6)	S(1)−C(1)	1.735(7)
S(2)−C(1)	1.753(6)	S(2)−C(2)	1.719(8)	S(3)−C(3)	1.742(8)
S(3)−C(4)	1.744(8)	S(4)−C(4)	1.759(8)	S(4)−C(5)	1.801(11)
S(5)−C(6)	1.790(10)	S(5)−C(7)	1.735(8)	S(6)−C(3)	1.731(8)
S(6)−C(7)	1.746(7)	S(7)−C(2)	1.760(8)	S(7)−C(8)	1.749(7)
S(8)−C(8)	1.731(7)	S(9)−C(20)	1.731(7)	S(10)−C(20)	1.747(7)
S(10)−C(21)	1.739(7)	S(11)−C(22)	1.747(7)	S(11)−C(23)	1.753(6)
S(12)−C(23)	1.756(7)	S(12)−C(24)	1.803(8)	S(13)−C(25)	1.774(9)
S(13)−C(26)	1.741(7)	S(14)−C(22)	1.737(8)	S(14)−C(26)	1.758(7)
S(15)−C(21)	1.746(7)	S(15)−C(27)	1.736(7)	S(16)−C(27)	1.745(7)
C(1)−C(8)	1.344(10)	C(2)−C(3)	1.370(10)	C(4)−C(7)	1.34(1)
C(5)−C(6)	1.49(1)	C(20)−C(27)	1.365(10)	C(21)−C(22)	1.36(1)
C(23)−C(26)	1.325(10)	C(24)−C(25)	1.50(1)		
S(1)−S(4*)[a]	3.579(3)	S(2)−S(4*)[a]	3.636(4)	S(5)−S(10**)[a]	3.339(3)
S(5)−S(9**)[a]	3.441(3)	S(9)−S(12′)[a]	3.665(3)	S(13)−S(16′′)[a]	3.351(3)
S(13)−S(15′′)[a]	3.408(3)				
S(1)−Au(1)−S(8)	91.44(7)	S(1)−Au(1)−N(1)	93.9(2)		
S(8)−Au(1)−C(19)	93.7(3)	N(1)−Au(1)−C(19)	81.1(3)		
S(9)−Au(2)−S(16)	90.93(6)	S(9)−Au(2)−N(2)	95.7(2)		
S(16)−Au(2)−C(38)	93.3(2)	N(2)−Au(2)−C(38)	80.4(2)		
Au(1)−S(1)−C(1)	99.3(3)	Au(1)−S(8)−C(8)	100.3(3)		
S(1)−C(1)−C(8)	124.9(5)	S(8)−C(8)−C(1)	123.8(5)		
Au(2)−S(9)−C(20)	100.5(2)	Au(2)−S(16)−C(27)	101.0(2)		
S(9)−C(20)−C(27)	124.0(5)	S(16)−C(27)−C(20)	123.3(6)		

[a] Symmetry code: * 1 − x, 1 − y, 1 − z; ** 1 − x, −y, 1 − z; ′ −x, −y, 1 − z; ′′ −x, 1 − y, 1 − z.

 © 2003 Wiley-VCH Verlag GmbH & Co. KGaA, Weinheim

moiety of $[Au(ppy)(C_8H_4S_8)]_2[PF_6]$ is almost planar, and is similar to that of the one-electron-oxidized complex $[Pt(bpy)(C_8H_4S_8)][BF_4]$.[8] The planar $C_8H_4S_8$ ligand of the oxidized species is in great contrast to the bent geometries of this ligand observed for unoxidized $C_8H_4S_8$-metal complexes such as $[Au(ppy)(C_8H_4S_8)]$[9] and $[Ti(C_5Me_5)_2(C_8H_4S_8)]$.[12] The C(2)−C(3) bond [1.37(1) Å] of the $C_8H_4S_8$ ligands is somewhat longer than the corresponding bond (1.349 Å) in $[Au(ppy)(C_8H_4S_8)]$.[9] This is consistent with the $C_8H_4S_8$ ligand-centered oxidation in the complex, as described above.

The perspective view of the packing diagram of $[Au(ppy)(C_8H_4S_8)]_2[PF_6]$ along the *a* axis is shown in Figure 2. The ppy and $C_8H_4S_8$ ligand moieties of the cations are almost overlapped with themselves in the same molecular orientations along the *a* axis to form a dimer unit with an Au(1)−Au(2) contact of 3.812 Å. This is in a contrast to the unoxidized species $[Au(ppy)(C_8H_4S_8)]$, which has a zigzag arrangement with alternating ppy and $C_8H_4S_8$ ligands because of the polarized orientation around the metal ion.[9] In the present case the cation moieties overlap with one another in the same molecular direction. A similar stacking pattern has also been seen in the cation moieties of $[Pt(bpy)(C_8H_4S_8)][BF_4]$.[8] For these oxidized complexes, some S−S non-bonding contacts (< 3.7 Å) between the oxidized $C_8H_4S_8$ moieties seem to contribute to such molecular arrangements: S(2)−S(14) = 3.682(3); S(6)−S(11) = 3.616(3); S(7)−S(10) = 3.679(2) Å.

As illustrated in Figure 3, the dimer units form a columnar structure along the *a* axis through an S−S non-bonding contact [S(3)−S(15) (1 + *x*, *y*, *z*) = 3.655(3) Å]. Furthermore, there are many S−S non-bonding contacts between the columns (3.339−3.616 Å, in Table 1), resulting in a two-dimensional sheet of molecular interactions parallel to the *ab* plane.

Energy-Band Calculation and Electron Conduction

Figure 4 shows the resultant energy dispersions of several orbitals calculated by the extended Hückel method for the crystal structure of $[Au(ppy)(C_8H_4S_8)]_2[PF_6]$ along the symmetry lines *Γ*-*X*, *X*-*V* and *V*-*C*.[18]

Appreciably significant dispersions are found in the *Γ*-*X* zone, which reflects a large orbital overlapping along the column of the cation moieties parallel to the *a* axis. Fur-

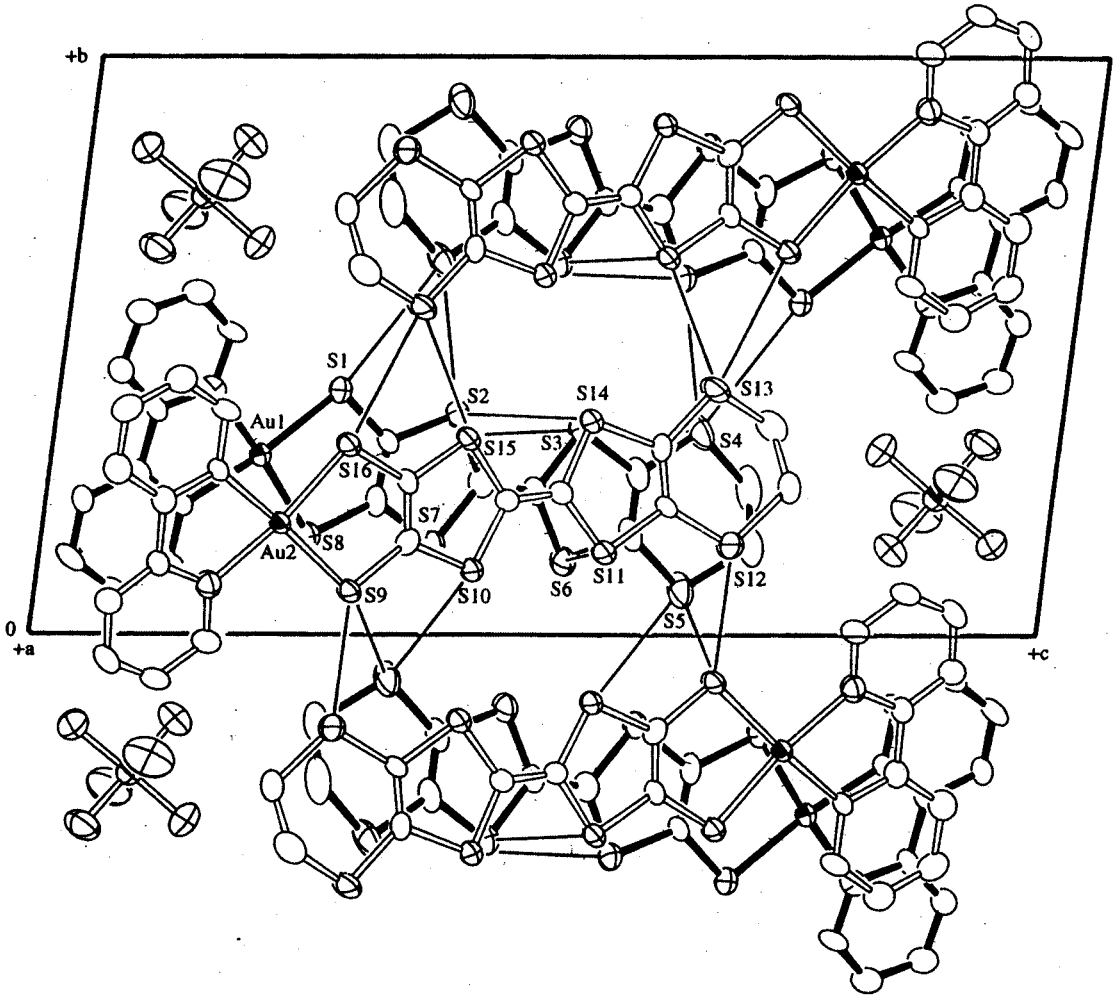

Figure 2. Crystal structure of $[Au(ppy)(C_8H_4S_8)]_2[PF_6]$ projected along the *a* axis; fine lines represent S−S non-bonding contacts of less than 3.7 Å

 © 2003 Wiley-VCH Verlag GmbH & Co. KGaA, Weinheim

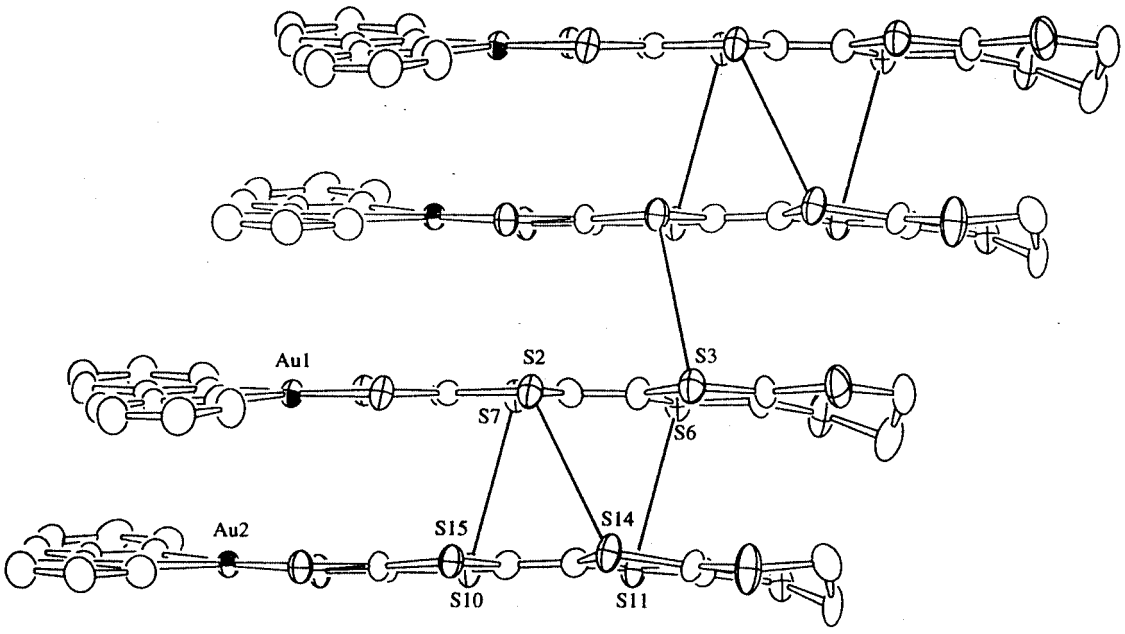

Figure 3. Projection of the overlapping mode of the cation moieties of $[Au(ppy)(C_8H_4S_8)]_2[PF_6]$ along the *a* axis; fine lines represent S−S non-bonding contacts of less than 3.7 Å

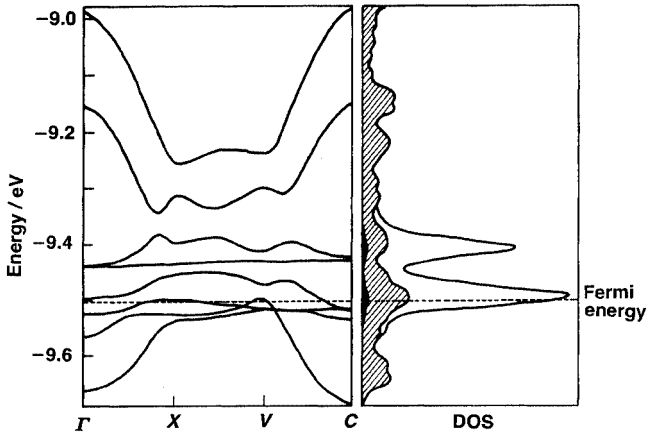

Figure 4. Dispersion of energy bands near the Fermi energy calculated for a crystal of $[Au(ppy)(C_8H_4S_8)]_2[PF_6]$, together with total densities of states (DOS) for gold (dark), ppy (open), and $C_8H_4S_8$ moieties (diagonal lines): *Γ, X, V* and *C* refer to the symmetry points with wave vectors 0, $a^*/2$, $(a^* + b^*)/2$ and $(b^* + c^*)/2$, respectively

thermore, large dispersions of some orbitals are observed in the *V*-*C* zone along the *b* axis, which are attributable to a side-by-side overlap of the $C_8H_4S_8$ moieties in neighboring columns. However, no significant dispersions of orbitals are observed in the *X*-*V* zone along the axis including the *c* component. The ppy ligands and PF_6^- anions are located parallel to the *bc* plane. Thus, no significant dispersions are found between the $C_8H_4S_8$ ligand moieties in the neighboring columns along the *c* axis. The Fermi energy level is located in the sharp ppy band, which is overlapped with $C_8H_4S_8$ bands with large dispersions. This band character, as well as the overlapping among the $C_8H_4S_8$ moieties observed in the crystal structure, suggests a metallic character of the complex along the *a* and *b* axes.

The electrical conductivities of the complex measured for a crystal are 9.2 and 0.0028 S cm^{-1} along almost the *a* and *c* axes, respectively, at room temperature. The activation energy for the electron conduction determined by the electrical conductivities measured for a compacted pellet was 0.0 eV from room temperature to 110 K. Thus, the complex is estimated to be metallic along the *a* axis. This finding, together with extremely low conductivity measured along almost the *c* axis, is consistent with the energy-band dispersions calculated based on the crystal structure of the complex, as described above. The present complex exhibits a much higher electrical conductivity than that (2.0×10^{-2} S cm^{-1} for a compacted pellet) of the essentially 0.5-electron-oxidized species $[Au(ppy)(C_8H_4S_8)](TCNQ^{\cdot -})_{0.6}$,[9] which may be due to a variance of molecular packing of these $[Au(ppy)(C_8H_4S_8)]$ moieties in the crystal.

Experimental Section

Preparation of $[Au(ppy)(C_8H_4S_8)]_2[PF_6]$: A benzonitrile (15 mL) solution of $[Au(ppy)(C_8H_4S_8)]$[9] (3.0 mg, 4.2 μmol) containing $[NEt_4][PF_6]$ (20 mg, 7.2 mmol) as an electrolyte was electrolyzed under current-controlled conditions (0.1 μA) for 10 days in an H-shaped cell equipped with platinum wire electrodes under an argon atmosphere at 30 C. Black needles of the oxidized species that formed on the surface of the anode were collected and dried in vacuo. The chemical formula of the complex was confirmed by the X-ray crystal structure analysis.

Physical Measurements and Energy-Band Calculations: Electronic absorption, powder reflectance and ESR spectra were recorded as described previously.[19,20] Electrical conductivities were measured

 © 2003 Wiley-VCH Verlag GmbH & Co. KGaA, Weinheim

for a crystal at room temperature. To determine the activation energy for the electron-conduction the conductivities were measured for a compacted pellet from room temperature to 110 K using an apparatus consisting of a Hioki 3552 LCR Hi-tester and a digital temperature controller (Scientific Instrument Model 9650).[21]

Energy-band calculations based on the extended Hückel method[22,23] for the crystal structure of the cation moieties of $[Au(ppy)(C_8H_4S_8)]_2[PF_6]$ were carried out using standard extended Hückel parameters[23,24] and the conventional weight of 1.75 for the Wolfsberg−Helmholtz relation.[25−27] In the calculations the PF_6^- parts of the crystal were disregarded since they have negligible contributions to the orbitals near the Fermi energy.

Crystal Structure Determination of $[Au(ppy)(C_8H_4S_8)]_2[PF_6]$: A single crystal of the complex of dimensions 0.10 × 0.06 × 0.025 mm obtained electrolytically was used for the crystal structure determination. Diffraction data were collected on a Rigaku RAXIS-RAPID imaging plate diffractometer equipped with a Rigaku low temperature device (liquid nitrogen as the coolant) and graphite-monochromated Mo-K_α (λ = 0.71069 Å) radiation at the Graduate School of Engineering, Osaka University. Indexing was performed for reflections obtained from three oscillations exposed for 200 s. Final values of the cell parameters were obtained from least-squares refinement of the positions of 23225 observed reflections. Equivalent reflections were merged by use of the PROCESS-AUTO program package. Of 24467 reflections collected, 12826 were unique (R_{int} = 0.060), which were corrected for absorption using the program ABSCOR[28] (transmission factor: 0.449−0.834) and for Lorenz and polarization effects. Crystallographic data are summarized in Table 2.

Table 2. Experimental crystallographic data for $[Au(ppy)(C_8H_4S_8)]_2[PF_6]$

Formula	$C_{38}H_{24}Au_2F_6N_2PS_{16}$
M	1560.48
Crystal size (mm)	0.10 × 0.06 × 0.025
Crystal system	triclinic
Space group	$P\bar{1}$
a (Å)	8.2731(2)
b (Å)	12.8828(5)
c (Å)	21.6185(7)
α (°)	83.375(1)
β (°)	87.937(1)
γ (°)	85.809(2)
V (Å^3)	2281.7(1)
Z	2
D_{calc} (g cm^{-3})	2.271
F(000)	1498
μ(Mo-K_α) (mm^{-1})	7.251
T (°C)	−40
Measured 2θ range (°)	6.1−60.0
No. of reflections collected	24467
Independent reflections	12826
Observed reflections	9521
R[a]	0.055
R_w [b]	0.117

[a] $R = \Sigma(|F_o| - |F_c|)/\Sigma|F_o|$. [b] $R_w^2 = \Sigma w(F_o^2 - F_c^2)^2/\Sigma w(F_o^2)^2$; $w^{-1} = \sigma^2(F_o^2) + (0.0575P)^2 + 1.8569P$, where $P = (F_o^2 + 2F_c^2)/3$.

The structure was solved by the Patterson method (PATTY)[29] and expanded using Fourier techniques (DIRDIF94)[30] and refined on F^2 by the full-matrix least-squares method (SHELXL-97).[31] Non-hydrogen atoms were refined anisotropically with 1.2-times equivalent temperature factors of the parent atoms. Hydrogen atoms were placed on the positions calculated geometrically. Atomic scattering factors were taken from the usual sources.[32] Figures 1 and 2 were drawn with ORTEP II.[33]

CCDC-208606 contains the supplementary crystallographic data for this paper. These data can be obtained free of charge at www.ccdc.cam.ac.uk/conts/retrieving.html [or from the Cambridge Crystallographic Data Centre, 12, Union Road, Cambridge CB2 1EZ, UK; Fax: (internat.) +44-1223/336-033; E-mail: deposit@ccdc.cam.ac.uk].

Acknowledgments

This research was supported in part by grants-in-Aid for scientific research (no. 14044056) from Ministry of Education, Science, Sports and Culture, Japan and by a Strategic Research Base Upbringing Special Coordination Fund for Promoting Science and Technology.

[1] P. Cassoux, L. Valade, H. Kobayashi, A. Kobayashi, R. A. Clark, A. E. Underhill, *Coord. Chem. Rev.* **1991**, *110*, 115−160.
[2] G. Matsubayashi, *Reviews on Heteroatom Chemistry*, vol. 4, My, Tokyo, **1991**, 171−194.
[3] R.-M. Olk, B. Olk, W. Dietzsch, R. Kirmse, E. Hoyer, *Coord. Chem. Rev.* **1992**, *117*, 99−131.
[4] A. E. Pullen, R.-M. Olk, *Coord. Chem. Rev.* **1999**, *188*, 211−262.
[5] H. Tanaka, Y. Okano, H. Kobayashi, W. Suzuki, A. Kobayashi, *Science* **2001**, *291*, 285−287.
[6] G. Matsubayashi, M. Nakano, H. Tamura, *Coord. Chem. Rev.* **2002**, *226*, 143−151.
[7] K. Kubo, M. Nakano, G. Matsubayashi, *Inorg. Chim. Acta* **2000**, *311*, 6−14.
[8] K. Kubo, N. Nakano, H. Tamura, G. Matsubayashi, *Inorg. Chim. Acta* **2002**, *336*, 120−124.
[9] K. Kubo, N. Nakano, H. Tamura, G. Matsubayashi, M. Nakamoto, *J. Organomet. Chem.* **2003**, *669*, 141−148.
[10] M. Nakano, A. Kuroda, H. Tamura, R. Arakawa, G. Matsubayashi, *Inorg. Chim. Acta* **1998**, *279*, 165−171.
[11] H. Mori, M. Nakano, H. Tamura, G. Matsubayashi, *J. Organomet. Chem.* **1999**, *574*, 77−85.
[12] K. Saito, M. Nakano, H. Tamura, G. Matsubayashi, *Inorg. Chem.* **2000**, *39*, 4815−4820.
[13] K. Saito, M. Nakano, H. Tamura, G. Matsubayashi, *J. Organomet. Chem.* **2001**, *625*, 7−12.
[14] M. A. Mansour, R. J. Lachicotte, H. J. Gysling, R. Eisenberg, *Inorg. Chem.* **1998**, *37*, 4625−4632.
[15] R. V. Parish, J. P. Wright, R. G. Pritchard, *J. Organomet. Chem.* **2000**, *596*, 165−176.
[16] J. Mack, K. Ortner, U. Abram, R. V. Parsh, *Z. Anorg. Allg. Chem.* **1997**, *623*, 873−879.
[17] S.-W. Audi Fong, J. J. Vittal, W. Henderson, T. S. A. Hor, A. G. Oliver, C. E. F. Rickard, *Chem. Commun.* **2001**, 421−422.
[18] M. Lax, *Symmetry Principles in Solid State and Molecular Physics*, Appendix E, John-Wiley, New York, 1974.
[19] T. Nakazono, M. Nakano, H. Tamura, G. Matsubayashi, *J. Mater. Chem.* **1999**, *9*, 2413−2417.
[20] K. Natsuaki, M. Nakano, G. Matsubayashi, *Inorg. Chim. Acta* **2000**, *299*, 112−117.
[21] N. Fujita, K. Nakahama, M. Nakano, H. Tamura, G. Matsubayashi, W. Mori, *2000 Int. Chem. Congress of Pacific Basin Societies (Honolulu)*, INOR 369, 2000; *Mol. Cryst. Liq. Cryst.* **2002**, *379*, 365−370.
[22] R. Hoffmann, *J. Chem. Phys.* **1963**, *39*, 1397−1412.

 © 2003 Wiley-VCH Verlag GmbH & Co. KGaA, Weinheim

[23] G. A. Landrum, W. V. Glassey, *Bind (v. 3.0)*. *Bind* is distributed as a part of the *YAeHMOP* extend Huckel molecular orbital package and is freely available on the www at: http://overlap.-chem.cornell.edu:8080/yaehmop.html
[24] T. Mori, *Bull. Chem. Soc. Jpn.* **1988**, *71*, 2509−2526.
[25] M. Wolfsberg, L. Helmholtz, *J. Chem. Phys.* **1952**, *20*, 837−843.
[26] M.-H. Whagbo, R. Hoffmann, *J. Chem. Phys.* **1978**, *68*, 5498−5500.
[27] J. H. Ammeter, H.-B. Burgi, J. C. Thibeault, R. Hoffmann, *J. Am. Chem. Soc.* **1978**, *100*, 3686−3692.
[28] T. Higashi, ABSCOR, a computer program for absorption correction, Rigaku Corporation, Tokyo, Japan, **1995**.
[29] PATTY: P. T. Beurskens, G. Admiraal, G. Beurskens, W. P. Bosman, R. de Gelder, R. Israel, J. M. M. Smits, DIRDIF94 program system, Technical report of the Crystallography laboratory, University of Nijmegen, The Netherlands, **1994**.
[30] P. T. Beurskens, G. Admiraal, G. Beurskens, W. P. Bosman, R. de Gelder, R. Israel, J. M. M. Smits, DIRDIF94 program system, Technical report of the Crystallography laboratory, University of Nijmegen, The Netherlands, **1994**.
[31] G. M. Sheldrick, SHELXL 97, a computer program for the refinement of crystal structures, University of Göttingen, Germany, **1997**.
[32] *International Tables for X-ray Crystallography*, vol. 4, Kynoch Press, Birmingham, England, **1974**.
[33] C. K. Johnson, ORTEP-II, Report ORNL-5138, Oak Ridge National Laboratory, Oak Ridge, TN, **1976**.

Received June 16, 2003

 © 2003 Wiley-VCH Verlag GmbH & Co. KGaA, Weinheim

General Synthesis and Characterization of Monocrystalline Lanthanide Orthophosphate Nanowires

Ya-Wen Zhang,[a] Zheng-Guang Yan,[a] Li-Ping You,[b] Rui Si,[a] and Chun-Hua Yan*[a]

Keywords: Nanostructures / Lanthanides / Orthophosphates / Solvothermal synthesis

Monocrystalline $LnPO_4$ (Ln = La, Ce, Pr, Nd, Sm, Eu, Gd, Tb) nanowires have been prepared in bulk quantities by a simple, facile, and clean solution-based hydrothermal method at 220–240 °C by finely tuning the acidity of the stock solutions. The length and width of the nanowires were in the range of 1–10 μm and 10–200 nm, respectively.
(© Wiley-VCH Verlag GmbH & Co. KGaA, 69451 Weinheim, Germany, 2003)

Introduction

In recent years, one-dimensional (1D) nanomaterials such as nanowires, nanobelts, nanotubes, and nanorods have attracted growing interest not only because of their unique properties with respect to their bulk materials, but also because of their promising applications in mesoscopic physics and fabrication of nanodevices of electronics, optoelectronics, and biochemical sensing.[1−9] Among the 1D nanomaterials, nanowires have played key roles as both interconnectors and active components in fabricating the nanodevices.[1,2,5] Therefore, to synthesize diverse nanowires with well-controlled shape, size, phase purity, crystallinity, and chemical composition on a large scale has become one of the most challenging issues faced by synthetic inorganic chemists.[10] So far, a rich variety of nanowires such as elemental semiconductors, II−VI and III−V semiconductors, metal oxides, and metals have been prepared by methods including templating direction, catalytic growth, electrochemistry, chemical vapor deposition, and solution-based solvothermal or hydrothermal treatment.[1−4]

Based on the electronic, optical, and chemical characteristics originating from their unique 4*f* electron configurations, lanthanides have promised various applications in magnets, phosphors, catalysts, biochemical probes, and medical diagnostics, and thus are of rapidly growing importance. In lanthanide chemistry, much of the recent attention has been focused on the fields of the coordination chemistry of lanthanides, organic transformations mediated or catalyzed by rare-earth compounds, and the preparation and properties of new lanthanide-related materials.[11] More recently, some lanthanide-related materials (oxides, borates, and fluorides) were reported to show exceptional electrical or luminescent behaviors when their grain sizes were reduced to the nanometer regime.[12−14] Nevertheless, the advance in the studies of 1D-nanostructured rare earth related compounds is still very limited, only nanowires/nanotubes of rare earth hydroxides/oxides have been prepared and characterized.[15−18] Amongst the large number of lanthanide inorganic salts, lanthanide phosphates are widely used in the production of luminescent or laser materials, moisture sensors, heat-resistant materials, and hosts for radioactive nuclear waste.[19−23] In this paper, we will report the general synthesis of monocrystalline lanthanide orthophosphate nanowires by a solution-based hydrothermal route by finely tuning the acidity of the stock solutions.

Lanthanide orthophosphates with the chemical formula $LnPO_4{\cdot}nH_2O$ ($n = 0-3$) (Ln^{3+} = lanthanide ion) have five polymorphs: monazite (monoclinic), xenotime (tetragonal), rhabdophane (hexagonal), weinschenkite (monoclinic), and orthorhombic.[23] In this research, $LnPO_4{\cdot}nH_2O$ ($n = 0-0.5$) were hydrothermally prepared at 220−240 °C for 17−24 h, using H_3PO_4, $NH_4H_2PO_4$, $(NH_4)_2HPO_4$, $(NH_4)_3PO_4$, or their mixtures, as both the precipitators and the mediators of acidity. Experimentally, monazite-type $LnPO_4$ (Ln = La, Ce, Pr, Nd, Sm, Eu, Gd) nanowires, rhabdophane-type $TbPO_4{\cdot}0.5H_2O$ nanowires/nanorods, and xenotime-type $LnPO_4$ (Ln = Dy, Ho, Er, Tm, Yb, Lu, Y) nanocrystals were obtained.

Results and Discussion

The crystal structures of the products have been identified by X-ray diffraction analysis (XRD). In Figure 1(a), we show the typical XRD pattern of the $LaPO_4$ nanowires. All the reflections can be distinctly indexed to a pure mono-

[a] State Key Laboratory of Rare Earth Materials Chemistry and Applications, PKU-HKU Joint Laboratory in Rare Earth Materials and Bioinorganic Chemistry, Peking University, Beijing 100871, China
Fax: (internat.) + 86-10-62754179
E-mail: chyan@chem.pku.edu.cn
[b] Electron Microscopy Laboratory
Peking University, Beijing 100871, China

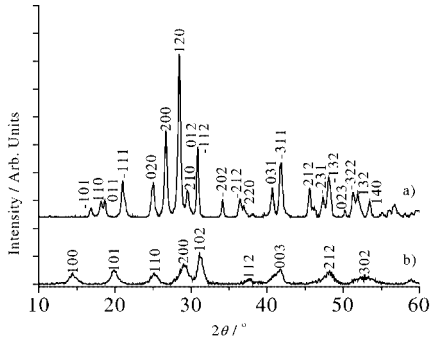

Figure 1. XRD patterns of $LaPO_4$: (a) nanowires; (b) colloidal precipitate

clinic phase (space group $P2_1/n$) with lattice constants a = 6.868 Å, b = 7.104 Å, c = 6.521 Å, and β = 103.6° (JC,PDS No. 32-493). Such a monoclinic structure was also identified for the other $LnPO_4$ nanowires. From Figure 1(b), we noted that the $LaPO_4$ colloid precipitate prior to hydrothermal treatment shows a hexagonal structure (JC,PDS No. 46-1439) and consists of nanoparticles as suggested by the line broadening of the diffraction peaks. The XRD pattern shown in Figure 2 informs us that the $TbPO_4{\cdot}0.5H_2O$ product is of hexagonal structure (space group $P3_121$) with lattice constants a = 6.799 Å and c = 6.332 Å (JC,PDS No. 20-1244). XRD analysis also showed that the as-synthesized $LnPO_4$ products of heavy lanthanides exhibit a zircon-type structure with tetragonal symmetry (space group $I4_1/amd$) with grain sizes in the range of 20−150 nm, as estimated by transmission electron microscopy (TEM).

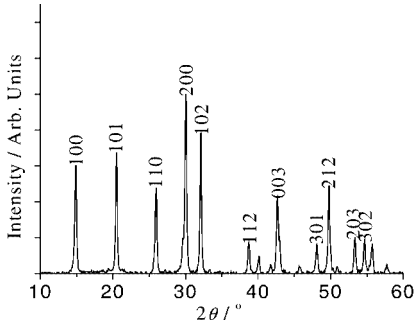

Figure 2. XRD pattern of $TbPO_4{\cdot}0.5H_2O$ nanowires/nanorods

By TEM and high resolution TEM (HRTEM), the morphology, crystallinity, and growth directions of the nanowires were carefully examined. From Figure 3, we can see that the as-prepared monoclinic $LnPO_4$ nanowires have a length of between 1 and 10 μm and a width of between 10 and 200 nm, are pure without any appreciable amount of particulate by-products, and are of a single-crystal nature. The surfaces of the nanowires are perfect without any stacking faults, and clean without any sheathed amorphous phase even at the edges. The preferred growth direction of the monazite-type nanowires was determined along the c axis [001]. Figure 4 shows that the $TbPO_4{\cdot}0.5H_2O$ nanowires/nanorods are perfect single crystals with a length of between 0.5 and 2 μm and a width of between 20 and

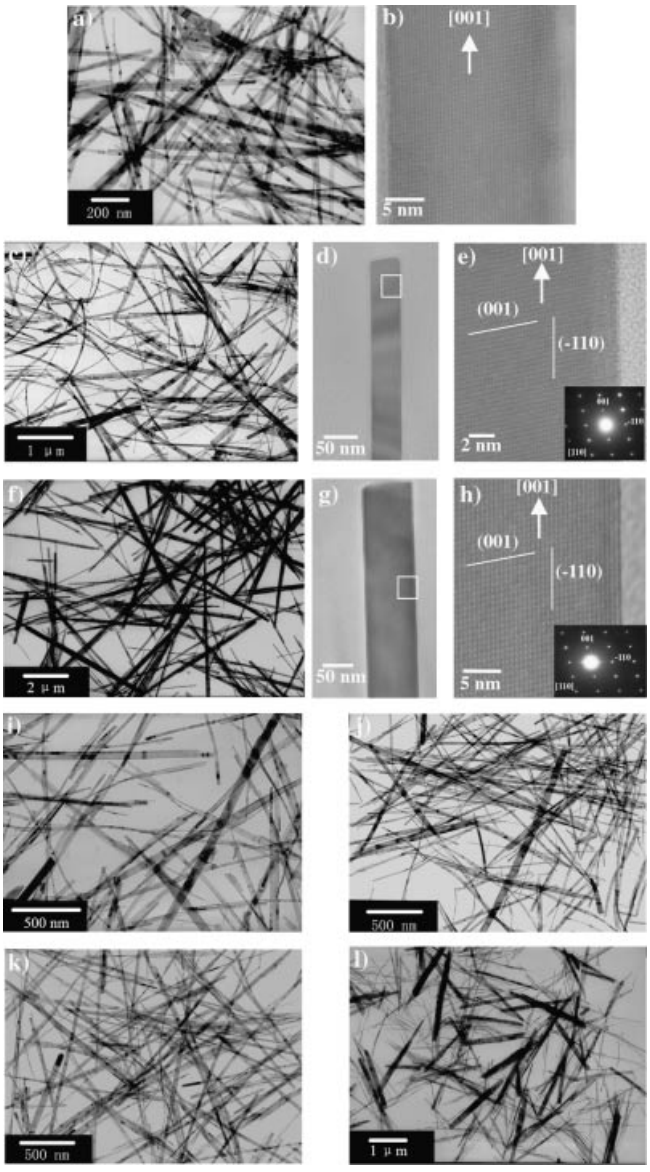

Figure 3. (a) TEM image of $LaPO_4$ nanowires; (b) HRTEM image of a single 23 nm $LaPO_4$ nanowire; (c) TEM image of $SmPO_4$ nanowires; (d) TEM image of a uniform 50 nm $SmPO_4$ nanowire; (e) HRTEM image of a single $SmPO_4$ nanowire taken from the highlighted section with inset showing the electron diffraction pattern; (f) TEM image of $EuPO_4$ nanowires; (g) TEM image of a uniform 80 nm $EuPO_4$ nanowire; (h) HRTEM image of a single $EuPO_4$ nanowire taken from the highlighted section with inset showing the electron diffraction pattern; (i) TEM image of $CePO_4$ nanowires; (j) TEM image of $PrPO_4$ nanowires; (k) TEM image of $NdPO_4$ nanowires; and (l) TEM image of $GdPO_4$ nanowires/nanorods

150 nm. The HRTEM image and selected area electron diffraction (SAED) pattern shown in Figure 4(b) and (c), respectively, suggest that the $TbPO_4{\cdot}0.5H_2O$ single crystals also grow along the c axis. From Figures 3 and 4, we can see that the nanowires of light lanthanides are more uniform than those of middle lanthanides, possibly resulting from the differences in their intrinsic properties such as solubility, ionic mobility and growth rate in solution associated with the lanthanide contraction.[24] In addition, the smooth morphology and perfect monocrystalline nature of

 © 2003 Wiley-VCH Verlag GmbH & Co. KGaA, Weinheim

the as-synthesized nanowires indicate that a reversible pathway between the solution phase and the solid phase, which allows building blocks in $LnPO_4$ crystals to adopt the correct positions, was established during the hydrothermal treatment employed. The optimal preparative conditions, crystal structures, length, and width of the $LnPO_4$ nanowires are summarized in Table 1.

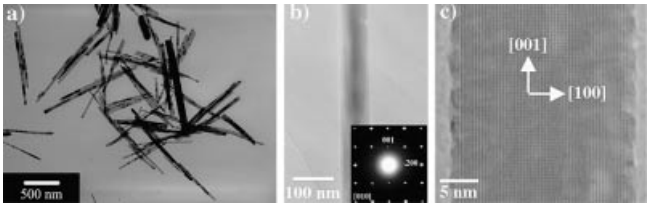

Figure 4. (a) TEM image of $TbPO_4 \cdot 0.5H_2O$ nanowires/nanorods; (b) TEM image of a uniform 70 nm $TbPO_4 \cdot 0.5H_2O$ nanorod with inset showing the electron diffraction pattern; and (c) HRTEM image of a single 25 nm $TbPO_4 \cdot 0.5H_2O$ nanowire

Solution-based hydrothermal/solvothermal methods have already become a commonly used methodology for preparing shaped/sized/oriented nanomaterials, but a quantitative thermodynamic prediction of the crystallization in the nanometer regime for growing 1D nanomaterials by this method is still very difficult and requires extensive research.[2] Herein, the preferred growth direction of the $LnPO_4$ nanowires was understood from the viewpoint of energy by simulating the coordination fashion of the rare earth ions in the monazite structure based on the Kossel model of crystal growth on completely smooth surfaces.[25] As is well-known, the lanthanide atoms in the monazite structure are coordinated to nine oxygen atoms forming a polyhedron of pentagonal interpenetrating tetrahedra, and the nine-coordinate lanthanide atoms are apically combined by the distorted tetrahedral PO_4^{3-} groups forming chains.[26] Figure 5 shows the growth models of $LaPO_4$ nanowires along the [001] (*c* axis) and [100] (*a* axis) directions, which were constructed using the CERIUS2 software package.[27] From Figure 5(a), we can see that two La−O bonds form as a PO_4^{3-} tetrahedron is attached along the [001] direction. However, only one La−O bond forms when

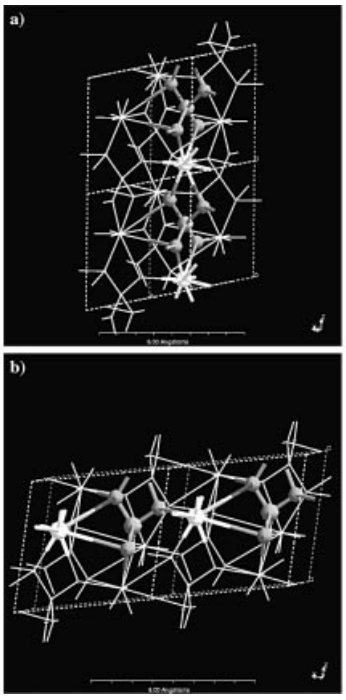

Figure 5. Growth models for $LaPO_4$ along different directions built up by CERIUS2 software: (a) [001] and (b) [100]

the growth is along the [100] direction (Figure 5, b). The growth along the [001] direction can release more energy, and the La−O bond lengths in the two cases show slight differences.[26] Thus, the [001] direction should be preferably taken when $LnPO_4$ nanowires are growing. Moreover, it is inferred that the anisotropic nature of the building blocks in the monazite structure should be one source of the driving forces for the growth of the $LnPO_4$ nanowires.

Control experiments were carried out to screen the optimal conditions for preparing phase-pure monocrystalline $LnPO_4$ nanowires. It was shown that the temperature and the starting acidity in the mother liquors are the major factors governing the crystallinity and the phase purity of the products. Temperature-dependent experiments showed that pure dehydrated monocrystalline nanowires could only be prepared at temperatures above 200 °C, and the dehydration temperature for middle lanthanides is higher than that for light lanthanides. When heat-treated at 220−240

Table 1. Optimal preparative conditions, crystal structures and morphologies of the $LnPO_4$ nanowires

Sample	Preparative conditions		Structure	Morphology	
	pH	Temperature [°C]		Length [μm]	Width [nm]
$LaPO_4$	0.8	220	monoclinic	1−3	20−50
$CePO_4$	0.8	220	monoclinic	2−5	20−100
$PrPO_4$	0.8	220	monoclinic	1−4	10−60
$NdPO_4$	0.8	220	monoclinic	1−3	20−60
$SmPO_4$	0.8	220	monoclinic	2−6	50−150
$EuPO_4$	1	240	monoclinic	3−10	50−200
$GdPO_4$	2	240	monoclinic	1−3	20−200
$TbPO_4 \cdot 0.5H_2O$	1.6	240	hexagonal	0.5−2	20−150

 © 2003 Wiley-VCH Verlag GmbH & Co. KGaA, Weinheim

°C, $LnPO_4$ (Ln = La, Pr, Nd, Sm, Eu) products exhibit the monazite structure under the acidities investigated. However, at the same temperatures, pure monazite $CePO_4$ could only be synthesized at pHs less than 1. When the pH is greater than 1, cubic CeO_2 will coexist with monazite-type $CePO_4$ due to the partial oxidization of Ce^{3+} at the reduced acidity in solution. Pure monazite-type $GdPO_4$ instead of mixed phases of rhabdophane and monazite could only be prepared at pHs between 1.5 and 6 at 240 °C. In the case of $TbPO_4$, no monazite phase was obtained under the acidities used at 240 °C; instead, pure rhabdophane and xenotime phase were obtained at pHs greater than 1.5 and lower than 1.5, respectively.

At a given heat-treatment temperature, it was observed that the morphologies of the products depend strongly upon the starting acidity and the formation of colloidal precipitates in the mother liquors. As an example, the effects of the preparative conditions on the morphologies of the $LaPO_4$ products are given in Table 2. It can be seen that $LaPO_4$ nanowires could only be obtained in a fairly narrow pH range (between 0.5 and 1.5) in the presence of the colloidal precipitate. In fact, the acidity of the stock solutions was finely tuned according to the following equation:

$$Ln^{3+} + (NH_4)_mH_{3-m}PO_4 \rightarrow LnPO_4 \downarrow + (3 - m)\cdot H^+ + m\cdot NH_4^+ \quad (m = 0-3)$$

The hexagonal $LaPO_4$ colloidal precipitate was confirmed to be an aggregate of nearly spherical nanoparticles with sizes around 80 nm (Figure 6). Those nanoparticles could serve as anisotropic seeds for the growth of highly anisotropic nanostructures in the solution solid process by a dissolution and crystallization mechanism during the hydrothermal treatment employed.[15,28,29] At pH values between 0.8 and 6, the colloidal precipitate formed instantly in the stock solution. After hydrothermal treatment, the morphologies of the $LaPO_4$ products changed from nanoparticles/nanorods (at pH 6, Figure 7, a) to nanowires/nanorods (at pH 1.6, Figure 7, b), then to nanowires (at pH 0.8−1.3, Figures 3 and 7, a and c, respectively), along with the increasing aspect ratio (also see Table 2). When the starting acidity of the stock solution was further enhanced by the addition of H_3PO_4, the colloidal precipitate formed gradually over a few minutes or even disappeared. After hydrothermal treatment, the morphologies of the $LaPO_4$ products changed from nanowires (at pH 0.8−1.3, Figures 3 and 7, a and c, respectively) to nanowires/nanorods (at 1 mol·L^{-1} H_3PO_4, Figure 7, d), then to nanorods (at 2 mol·L^{-1} H_3PO_4, Figure 7, e), along with the decreasing aspect ratio (see also Table 2).

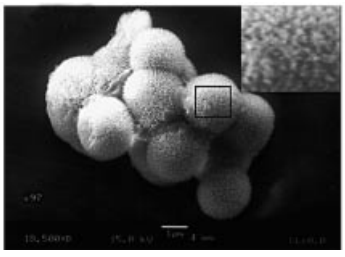

Figure 6. SEM images at different magnifications of the $LaPO_4$ colloidal precipitate prepared at pH 0.8 (inset was taken from the highlighted section)

Previously, Peng et al. have investigated the effects of chemical potential on the shape evolution of CdSe nanocrystals with the wurtzite structure, and observed that the high chemical potential generated by a high monomer concentration in the growth solution favors the growth of elongated nanocrystals.[30] Very recently, Li et al. found that a higher chemical potential was a dominant driving force for the growth of hexagonal lanthanide hydroxide nanowires during hydrothermal treatment.[15] In the present case, the concept of chemical potential was also used to explain the above experimental phenomenon related to the formation of $LnPO_4$ nanowires. We think that the chemical potential of the monoclinic $LnPO_4$ crystals is mainly determined by the apparent concentration of $LnPO_4$ in the solutions, which depends thermodynamically upon the acidity of the reaction system. Previously, the apparent solubility of $LnPO_4$ in aqueous solution was found to decrease upon increasing the precipitation temperature.[31] Under mild to strongly acidic conditions, the apparent concentration of $LnPO_4$ in boiling H_3PO_4 solution decreases gradually upon increasing the concentration of H_3PO_4 from 0.5 to 2 M, and decreases drastically when it is higher than 2 M.[31] Under weakly acidic conditions, Ln^{3+} ions are known to hydrolyze slightly in solution with the formation of both mononuclear and polynuclear species in small amounts before the precipitation of the hydroxide occurs above pH 6.[32] In ad-

Table 2. Effect of the preparative conditions on the morphologies of the $LaPO_4$ products prepared at 220 °C for 17 h

Acidity	Precipitating[a]	Morphology Length [μm]	Width [nm]	
pH = 6	instantly	0.05−0.2	10−20	nanoparticles/nanorods
pH = 1.6	instantly	0.2−0.7	10−60	nanowires/nanorods
pH = 1.3	instantly	0.5−3	30−70	nanowires
pH = 1	instantly	1−3	20−90	nanowires
pH = 0.8	instantly	1−3	20−50	nanowires
1 mol·L^{-1} H_3PO_4	gradually	0.1−0.3	20−200	nanowires/nanorods
2 mol·L^{-1} H_3PO_4	−	0.08−0.3	40−100	nanorods
4 mol·L^{-1} H_3PO_4	−	0.04−0.12	50−300	nanorods

[a] Formation of colloidal precipitates before hydrothermal treatment.

 © 2003 Wiley-VCH Verlag GmbH & Co. KGaA, Weinheim

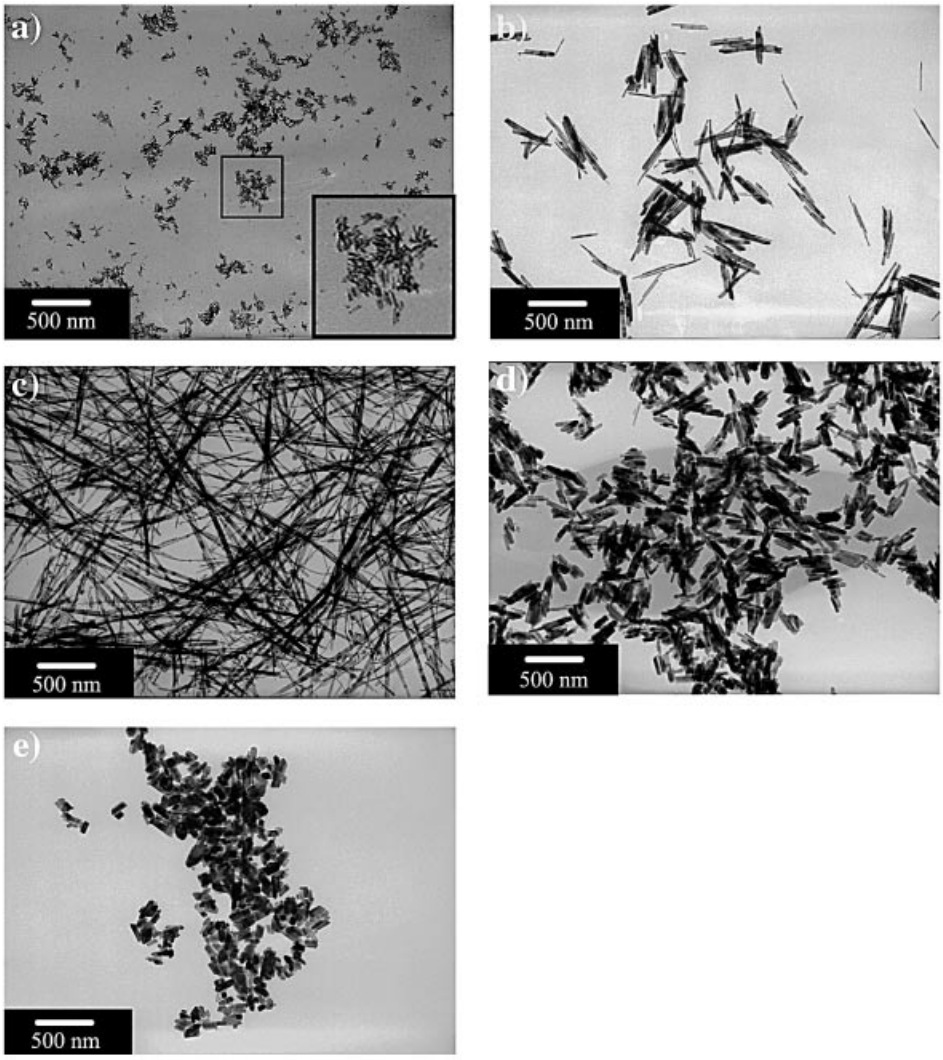

Figure 7. TEM images of the hydrothermal products of $LaPO_4$ prepared at 220 °C for 17 h: (a) pH 6 (inset was taken from the highlighted section); (b) pH 1.6; (c) pH 1.3; (d) 1 mol·L^{-1} H_3PO_4; (e) 2 mol·L^{-1} H_3PO_4

dition, the hydrolysis rate increases with pH value. In the present experiments, both the increasing hydrolysis of La^{3+} ions at pH values greater than 1.5 and the increasing acidity by addition of H_3PO_4 ($\geq$ 0.5 M) are thought to reduce the apparent concentration of $LaPO_4$ and thus its chemical potential in solution. As a result, the $LaPO_4$ nanowires could only be prepared in a fairly narrow pH range (0.5−1.5) where the chemical potential of $LaPO_4$ crystals is higher. Interestingly, the coexistence of the $LaPO_4$ nanorods/nanoparticles (at pH 6, Figure 7, a) or nanowires/nanorods (at pH 1.6 or at 1 M H_3PO_4, Figure 7, b and d) might indicate the mixed-shape evolution of 1D/2D ripening.[30] Conclusively, a high chemical potential of $LnPO_4$ crystals in solution should be another major driving force for the growth of the $LnPO_4$ nanowires.

As demonstrated above by XRD analysis, there is a structural transition from monazite to rhabdophane, then to xenotime with the ionic radius of Ln^{3+} decreasing from La to Lu, and rhabdophane-type $TbPO_4$ sits on the borderline for this transition. Under the synthetic conditions investigated, we found that $LnPO_4$ with larger Ln^{3+} ions could be synthesized in the form of nanowires at suitable pH values, whereas $LnPO_4$ with the heavier and smaller Ln^{3+} ions could only be prepared in the form of nanocrystals. This result might hint that xenotime-type $LnPO_4$ crystals have lower structural anisotropy and lower chemical potential in solution than monazite-type $LnPO_4$ crystals, probably as a result of their lower coordination number and increasing solubility induced by the lanthanide contraction.[31,33] In the xenotime-type structure, Ln ions are eight-coordinate to oxygen atoms from the somewhat-distorted tetrahedral PO_4^{3-} groups to form a polyhedron of bis-bisphenoid.[33]

Conclusion

We have demonstrated the general synthesis of $LnPO_4$ monocrystalline nanowires in bulk quantities and high purity by a simple, facile, and clean solution-based hydrothermal method by finely tuning the acidity of the stock solu-

 © 2003 Wiley-VCH Verlag GmbH & Co. KGaA, Weinheim

tions. This successful demonstration can assist us to understand the fundamentals of the reaction and nanowire growth mechanisms under hydrothermal conditions. Our recent experiments also showed that monocrystalline rhabdophane and orthorhombic hydrated $LnPO_4$ 1D nanomaterials and luminescent-active $LaPO_4$:Eu and $LaPO_4$:CeTb nanowires can be also prepared by the same synthetic approach. It is expected that the hydrothermal route employed in this work can be extended to the preparation of other pure and doped 1D nanomaterials with highly anisotropic structures. Moreover, the as-synthesized monocrystalline lanthanide orthophosphate nanowires may promote both academic interest in lanthanide chemistry and novel applications in nanotechnology. Further research on the luminescent behavior of doped $LnPO_4 \cdot nH_2O$ 1D nanomaterials associated with the reduced dimensionality are in progress.

Experimental Section

Synthesis of the $LnPO_4$ Nanowires: Quantitative solutions of $Ln(NO_3)_3$ (AR, > 99.9%) and H_3PO_4 [$NH_4H_2PO_4$/$(NH_4)_2HPO_4$/$(NH_4)_3PO_4$ or their mixtures] of analytical grade in a given molar ratio (usually 1:1.1) were employed to prepare a stock solution (40 mL) with a cation concentration of 0.05 M in a Teflon cup (50 mL). After 15 min of stirring, the cup was transferred into a stainless steel autoclave, and subjected to hydrothermal treatment at 220−240 °C for 17−24 h under autogenous pressure in an electric oven. As the autoclave cooled to room temperature, precipitates with the color of lanthanide ions were formed and collected. The precipitates were washed with deionized water, centrifugally filtered off, and dried at 60 °C for 24 h. The yields of the products were about 80−90%.

The water content in the products was determined with a thermogravimetry and differential thermal analyzer (Du Pont 2100) in air at a heating rate of 10 °C/min, using α-Al_2O_3 as a reference. The crystal structures of the products were obtained on a powder X-ray diffractometer (Rigaku D/max-2000, Japan), employing Cu-K_α radiation (λ = 1.5418 Å). The sizes and morphologies of the products were characterized by scanning electron microscopy (AMARY 1910FE, USA) at 15 kV, transmission electronic spectroscopy (200CX, JEOL, Japan) at 160 kV and high-resolution transmission electronic spectroscopy (H-9000, Hitachi, Japan) at 400 kV.

Acknowledgments

Grants-in-aids from NSFC (Nos. 20171003, 20221101, 50272006, and 20023005), MOST of China (G19980613), and Founder Foundation of Peking University are gratefully acknowledged.

[1] J. T. Hu, T. W. Odom, C. M. Lieber, *Acc. Chem. Res.* **1999**, *32*, 435−445.
[2] Y. N. Xia, P. D. Yang, Y. G. Sun, Y. Y. Wu, B. Mayers, B. Gates, Y. D. Yin, F. Kim, H. Q. Yan, *Adv. Mater.* **2003**, *15*, 353−389.
[3] Y. Y. Wu, H. Q. Yan, M. Huang, B. Messer, J. H. Song, P. D. Yang, *Chem. Eur. J.* **2002**, *8*, 1260−1268.
[4] G. R. Partzke, F. Krumeich, R. Nesper, *Angew. Chem. Int. Ed.* **2002**, *41*, 2446−2461.
[5] X. F. Duan, Y. Hang, R. Agarwal, C. M. Lieber, *Nature* **2003**, *421*, 241−245.
[6] M. S. Arnold, P. Avouris, Z. W. Pan, Z. L. Wang, *J. Phys. Chem. B* **2003**, *107*, 659−663.
[7] R. Martel, T. Schmidt, H. R. Shea, T. Hertel, Ph. Avouris, *Appl. Phys. Lett.* **1998**, *73*, 2447−2449.
[8] S. J. Trans, R. M. Verschueren, C. Dekker, *Nature* **1998**, *393*, 49−52.
[9] S. S. Wong, E. Joselevich, A. T. Woolley, C. L. Cheung, C. M. Lieber, *Nature* **1998**, *394*, 52−55.
[10] Y. N. Xia, P. D. Yang, *Adv. Mater.* **2003**, *15*, 351−352.
[11] H. B. Kagan, *Chem. Rev.* **2002**, *102*, 1805−1806.
[12] Y. W. Zhang, Y. Yang, S. Jin, S. J. Tian, G. B. Li, J. T. Jia, C. S. Liao, C. H. Yan, *Chem. Mater.* **2001**, *13*, 372−378.
[13] Z. G. Wei, L. D. Sun, C. S. Liao, J. L. Yin, X. C. Jiang, C. H. Yan, S. Z. Lu, *J. Phys. Chem. B* **2003**, *106*, 10610−10617.
[14] J. W. Stouwdam, F. C. J. M. van Veggel, *Nano Lett.* **2002**, *2*, 733−737.
[15] X. Wang, Y. D. Li, *Angew. Chem. Int. Ed.* **2002**, *41*, 4790−4793.
[16] A. W. Xu, Y. P. Fang, L. P. You, H. Q. Lin, *J. Am. Chem. Soc.* **2003**, *125*, 1494−1495.
[17] C. F. Wu, W. P. Qin, G. S. Qin, D. Zhao, J. S. Zhang, S. H. Huang, S. Z. Lu, H. Q. Liu, H. Y. Lin, *Appl. Phys. Lett.* **2003**, *82*, 520−522.
[18] M. Yada, M. Mihara, S. Mouri, M. Kuroki, T. Kijima, *Adv. Mater.* **2002**, *14*, 309−313.
[19] K. Riwotzki, H. Meyssamy, H. Schnablegger, A. Kornowski, M. Haase, *Angew. Chem. Int. Ed.* **2001**, *40*, 573−576.
[20] K. Riwotzki, H. Meyssamy, A. Kornowski, M. Haase, *J. Phys. Chem. B* **2000**, *104*, 2824−2828.
[21] H. Meyssamy, K. Riwotzki, *Adv. Mater.* **1999**, *11*, 840−844.
[22] S. Nishihama, T. Hirai, I. Komasawa, *J. Mater. Chem.* **2002**, *12*, 1053−1057.
[23] H. Ito, Y. Fujishiro, T. Sato, A. Okuwaki, *Br. Ceram. Trans.* **1995**, *94*, 146−150.
[24] N. N. Greenwood, A. Earnshaw, *Chemistry of the Elements*, 2nd ed.; Oxford: Butterworth-Heinemann, **1998**, p.1235−1237.
[25] A. W. Vere, *Crystal Growth, Principles and Progress*, Plenum, New York, **1987**, p. 14−15.
[26] D. F. Mullica, W. O. Milligan, D. A. Grossie, G. W. Beall, L. A. Boatner, *Inorg. Chim. Acta* **1984**, *95*, 231−236.
[27] http://www.accelrys.com/cerius2
[28] B. Gates, Y. D. Yin, Y. N. Xia, *J. Am. Chem. Soc.* **2000**, *122*, 12582−12583.
[29] J. Lu, Y. Xie, F. Xu, L. Y. Zhu, *J. Mater. Chem.* **2002**, *12*, 2755−2761.
[30] Z. A. Peng, X. G. Peng, *J. Am. Chem. Soc.* **2001**, *123*, 1389−1395.
[31] R. Kijkowska, *J. Mater. Sci.* **2003**, *38*, 229−233.
[32] C. F. J. Baes, R. E. Mesmer, *The Hydrolysis of Cations*, John Wiley & Sons, New York, **1976**, p. 129−146.
[33] W. O. Milligan, D. F. Mullica, G. W. Beall, L. A. Boatner, *Inorg. Chim. Acta* **1982**, *60*, 39−43.

Received June 25, 2003

 © 2003 Wiley-VCH Verlag GmbH & Co. KGaA, Weinheim

Mechanism of Reduction of 2,2-Dibromomethyl-1,3-propanediol by Ni^{I}-Tetraazamacrocyclic Complexes in Aqueous Solution − A Pulse Radiolysis and Electrochemical Study

Elisabetha Shandalov,[a] Israel Zilbermann,[a,b] Eric Maimon,[a,b] Yeoshua Nahmani,[a,b] Haim Cohen,[a,b] Eilon Adar,[c] and Dan Meyerstein*[a,d]

Keywords: Halogenated compounds / Pulse radiolysis / Reduction / Electrochemistry / Macrocycles

The reduction, catalytic reduction and the electrocatalytic reduction of halo-organic compounds are of major interest due to their role as pollutants. The mechanism and kinetics of reduction of 2,2-dibromomethyl-1,3-propanediol by several Ni^{I} tetraazamacrocyclic complexes, $(Ni^{I}L^{i})^{+}$ (i = 1–4), in aqueous solutions to yield Br^{-} and the non-halogenated compound was studied using the pulse radiolysis technique. The rate constants $k = 5.3 \times 10^{8}$, 1.6×10^{7}, 6.0×10^{5} and 3.5×10^{4} $M^{-1}s^{-1}$ for L^{1}, L^{2}, L^{3} and L^{4} respectively, of the reactions $(Ni^{I}L^{i})^{+} + RBr \rightarrow (Ni^{II}L^{i})^{2+} + Br^{-} + R^{\cdot}$ increase with the free-energy gain in the reaction. All these complexes are good electrocatalysts for the reduction of this substrate. The mechanisms of the reductions is are discussed.

(© Wiley-VCH Verlag GmbH & Co. KGaA, 69451 Weinheim, Germany, 2003)

Introduction

Recently, the underground water of many sites all over the world has become heavily contaminated by halogenated organic compounds.[1,2] Halogenated hydrocarbons such as halogenated methanes and ethanes are mainly used as solvents and are produced on a scale of 10^{6} tons per year.[3] Release of these hazardous compounds into the environment by leakage from industrial effluents causes ecological damage to the subsurface water reservoirs. Thus, the reduction, catalytic reduction and the electrocatalytic reduction of halo-organic compounds is of major interest for the removal of such compounds either from the raw effluents or for remediation of contaminated water. The kinetics and mechanisms of the reactions of nickel(I) macrocyclic complexes with alkyl halides have been investigated.[4,5] Moreover these complexes have attracted considerable attention because they enable the electrocatalytic reduction of alkyl halides.[6,7] $Ni^{II}L^{i}$ complexes, with macrocyclic ligands, are reduced reversibly to relatively stable nickel(I) species in aqueous solution.[8] The redox potentials and lifetimes of the $Ni^{I}L$ complexes are affected mainly by three factors: 1) substitution on the macrocyclic ring (especially on the nitrogens), 2) ring size, and 3) saturation of the macrocyclic ring. Thermodynamic and/or kinetic stabilization of the monovalent nickel complexes is achieved by N-alkylation of the macrocyclic ligands.[8,9]

It seemed of interest to study the effect of the redox potential, and plausibly of steric hindrance, of the nickel complexes on the rate of dehalogenation and on the detailed mechanism of the process. In this framework it was decided to study the reduction of 2,2-dibromomethyl-1,3-propanediol (as a representative contaminant found in the polluted groundwater in the Beer-Sheva region of Israel) by $(Ni^{I}L^{i})^{+}$ in aqueous solution. The tetraazamacrocyclic ligands L^{i} (i = 1−4) were chosen as they affect both the redox potential of the central cation and impose different steric strains on the complex and on the approach of the substrate to the central nickel cation.

[a] Chemistry Department, Ben-Gurion Univ. of the Negev, Beer-Sheva, Israel
E-mail: danmeyer@bgumail.bgu.ac.il
[b] Nuclear Research Centre Negev, Beer-Sheva, Israel
[c] Department of Environmental Hydrology and Microbiology, Institute for Water Sciences and Technologies − The J. B. Institutes for Desert Research, Ben-Gurion Univ. of the Negev, Beer-Sheva, Israel
[d] Department of Biological Chemistry, College of Judea and Samaria, Ariel, Israel

Results and Discussion

Pulse-Radiolysis Studies

He-saturated aqueous solutions containing 0.1 M HCOONa, $2 \times 10^{-4} - 1 \times 10^{-3}$ M $(Ni^{II}L^{i})^{2+}$ and 1×10^{-4} to 2×10^{-3} M $(CH_2Br)_2C(CH_2OH)_2$, at pH 10.0 ± 0.3, were irradiated by a short electron pulse from the linear

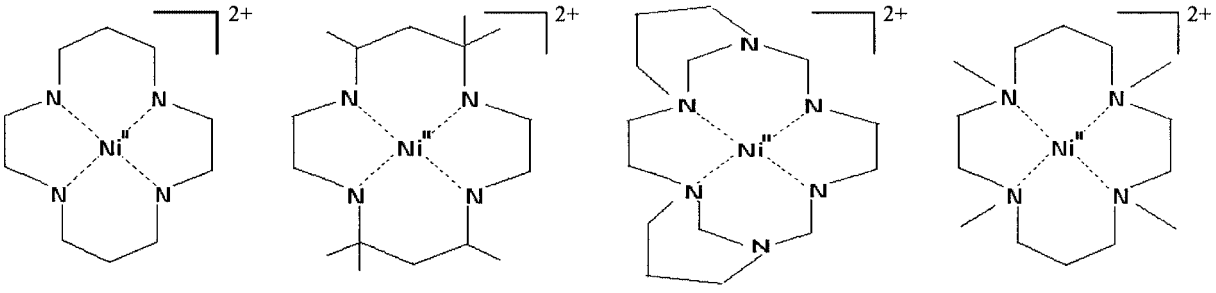

accelerator. When ionizing radiation is absorbed by a dilute aqueous solution the following initial products are formed:[10]

$$H_2O \xrightarrow{e^-,\gamma} {}^{\bullet}OH\ (2.65);\ {}^{\bullet}H\ (0.60);\ e^-_{aq}\ (2.65);\ H_2O_2\ (0.75);\ H_2\ (0.45);\ H_3O^+;\ OH^- \quad (1)$$

Where the G values are given in parentheses (G values are defined as the number of molecules of each product per 100 eV of radiation absorbed by the solution).[10]

In the presence of formate ($HCOO^-$), both $H^{\cdot}$ and $^{\cdot}OH$, are scavenged by $HCOO^-$ to generate the $CO_2^{\cdot -}$ radical.

$$^{\cdot}H/^{\cdot}OH + HCOO^- \rightarrow CO_2^{\cdot -} + H_2/H_2O$$
$$(k_{\cdot OH} = 3.2\cdot10^9\ M^{-1}sec^{-1};[11]\ k_{\cdot H} = 2.1\cdot10^8\ M^{-1}sec^{-1}\ [11]) \quad (2)$$

The $CO_2^{\cdot -}$ radical generated and the hydrated electron, e^-_{aq}, are powerful single-electron reducing agents, $E^0 = -1.90$ V[12,13] and $E^0 = -2.87$ V[11] vs. NHE respectively. $CO_2^{\cdot -}$ is an inner-sphere reducing agent[14] due to the fact that it is bent and the product, CO_2, is linear.

The $CO_2^{\cdot -}$ radical and e^-_{aq} react rapidly with $(Ni^{II}L^i)^{2+}$ to produce $(Ni^{I}L^i)^{+}$ [8,15] which, in turn, reacts with the organic substrate in the next step. A typical experimental result is shown in Figure 1.

These results indicate that reactions (3) obey pseudo-first order rate laws. The rates of the dehalogenation reactions depend linearly on the $(CH_2Br)_2C(CH_2OH)_2$ concentration, Figure 2; the rate constants (k) derived from the slopes of the lines are summed up in Table 1.

$$(Ni^{I}L^i)^+ + RBr \xrightarrow{k} (Ni^{II}L^i)^{2+} + R^{\bullet} + Br^- \quad (3)$$

Thus the results are in agreement with the suggestion that the reactions observed are reactions (3).

When the radical yield of reaction (3) is relatively low, i.e. when low pulse intensities are applied, and in the presence of a relatively high concentration of $(Ni^{II}L^1)^{2+}$, the formation of a second intermediate is observed (Figure 3). It is proposed that this intermediate is $L^1Ni^{III}-R$, which is formed by

$$(Ni^{II}L^1)^{2+} + R^{\cdot} \rightarrow (L^1Ni^{III}\text{-}R)^{2+} \quad (4)$$

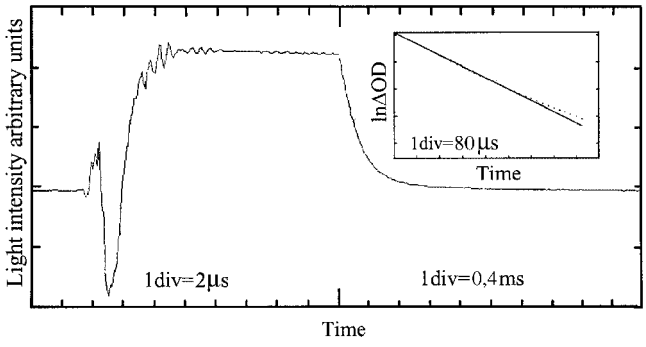

Figure 1. Decrease of the absorbance (at 380 nm) due to the reaction of $(Ni^{I}L^2)^+$ with $(CH_2Br)_2C(CH_2OH)_2$ and first order fit of the data (insert); solution composition: 1×10^{-3} M $(Ni^{II}L^2)^{2+}$, 0.1 M HCOONa and 3×10^{-4} M $(CH_2Br)_2C(CH_2OH)_2$ at pH 10.0 ± 0.3, He sat, pulse intensity (17.2 ± 3.4) Gy/pulse

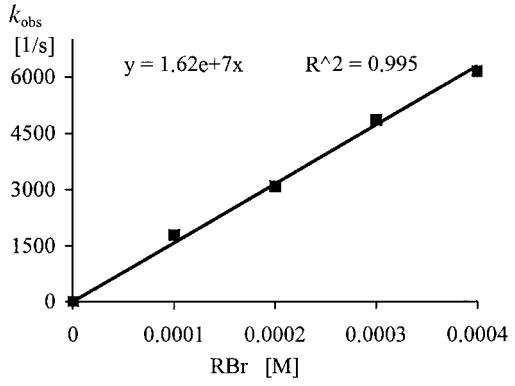

Figure 2. Dependence of k_{obs} on $[(CH_2Br)_2C(CH_2OH)_2]$, for the reaction of $(Ni^{I}L^2)^+$ with $(CH_2Br)_2C(CH_2OH)_2$

Table 1. Rate constants of the debromination reactions by the different nickel complexes

L^i	$E^0_{1/2}$ $Ni^{2+/+}$ [V]	k [$M^{-1}s^{-1}$]
L^1	−1.58	$(5.3 \pm 0.8) \times 10^8$
L^2	−1.42	$(1.6 \pm 0.2) \times 10^7$
L^3	−1.25	$(6.0 \pm 0.9) \times 10^5$
L^4	−1.15	$(3.5 \pm 0.5) \times 10^4$

This suggestion is supported by the observation that the absorbance due to the second intermediate increases with

 © 2003 Wiley-VCH Verlag GmbH & Co. KGaA, Weinheim

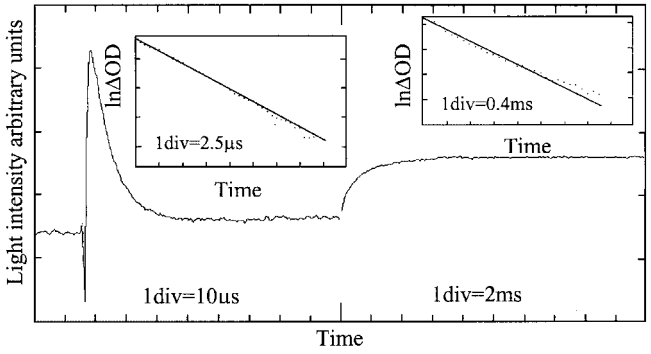

Figure 3. Decay of the absorption (at 370 nm) due to the reaction of $(Ni^{I}L^{1})^{+}$ with $(CH_2Br)_2C(CH_2OH)_2$ followed by increase of the absorption due to the formation of $(L^{1}Ni^{III}\ R)^{2+}$; solution composition: 1×10^{-3} M $(Ni^{II}L^{1})^{2+}$, 0.1 M HCOONa and 4×10^{-4} M $(CH_2Br)_2C(CH_2OH)_2$, pH 10.0 ± 0.3, He sat, pulse intensity (5.9 ± 1.2) Gy/pulse

concentration of $(Ni^{II}L^{1})^{2+}$, as reaction (4) has to compete with reaction (5)

$$2R^{\cdot} \rightarrow R_2 \quad (5)$$

The analogous reaction

$$(Ni^{II}L^{1})^{2+} + {}^{\cdot}CH_3 \rightleftarrows (L^{1}Ni^{III}\text{-}CH_3)^{2+} \quad [k_{4a} = (6.5 \pm 0.7) \times 10^{8}\ M^{-1}s^{-1}]\ k_{-4a} = 57 \pm 6\ s^{-1} \quad (4a)$$

is well documented in the literature.[16,17]

This competition also explains why this intermediate is not observed at high pulse intensities. The lifetime of $(L^{1}Ni^{III}\text{-}R)^{2+}$ is considerably longer than 40 sec, in agreement with the reported lifetime of $(L^{1}Ni^{III}\text{-}CH_3)^{2+}$.[16]

The formation of the second intermediate is not observed for the other complexes studied, probably due to steric hindrance, which slows down reactions analogous to reaction (4), and to the fact that k_3 is slower for these complexes.

It is of interest to note that a plot of log k vs. $E°(Ni^{II/I}L)$ yields a straight line (Figure 4). As the self-exchange rate for the $Ni^{II/I}L^{i}$ couples is relatively slow,[8,15] and as the self exchange for the $RBr/RBr^{\cdot -}$ couple is probably not high and the free energy gain in the outer sphere reduction

$$(Ni^{I}L^{i})^{+} + RBr \rightarrow (Ni^{II}L^{i})^{2+} + RBr^{\cdot -} \quad (3a)$$

is also not high, due to the instability of $RBr^{\cdot -}$, it is proposed that reaction (3) probably proceeds via an inner-sphere mechanism. However, the straight line observed in Figure 4 suggests that steric hindrance does not slow down reaction (3) considerably.

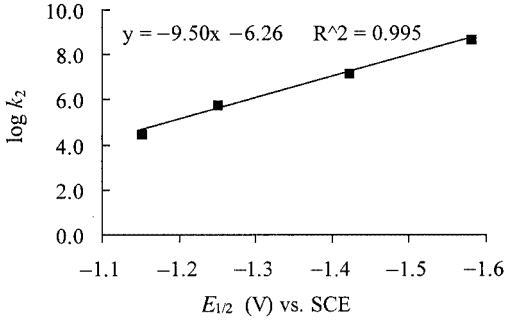

Figure 4. Dependence of log k_2 on $E_{1/2}$ of the complexes

Yield of Bromide

He-saturated aqueous solutions containing 0.1 M HCOONa, 5×10^{-4} M $(Ni^{II}L^{1})^{2+}$ and 2.5×10^{-4} to 7×10^{-3} M $(CH_2Br)_2C(CH_2OH)_2$, at pH 10, were irradiated in the ^{60}Co γ source with a dose rate of 4 Gy/min to an overall dose of 720 Gy. The yields of bromide obtained by the γ irradiation in the ^{60}Co source are summed up in Table 2.

Table 2. Bromide yield as a function of $(CH_2Br)_2C(CH_2OH)_2$ concentration; solution composition: 0.1 M HCOONa, 5×10^{-4} M $(Ni^{II}L^{1})^{2+}$ and 2.5×10^{-4} to 7×10^{-3} M $(CH_2Br)_2C(CH_2OH)_2$, pH 10.0 ± 0.3, He sat., dose 720 Gy at 4 Gy/min; experimental error: ±20%

[RBr] (M)	$[Br^{-}]$ (M)	G (Br^{-})
2.5×10^{-4}	4.9×10^{-4}	> 7.8
5.0×10^{-4}	9.8×10^{-4}	> 15
1.0×10^{-3}	2.0×10^{-3}	> 32
3.0×10^{-3}	2.2×10^{-3}	35
5.0×10^{-3}	2.6×10^{-3}	41
7.0×10^{-3}	2.6×10^{-3}	41

The results clearly indicate that total debromination is obtained at low concentrations of $(CH_2Br)_2C(CH_2OH)_2$ and therefore only lower limits of G(Br^{-}) can be derived. The yield of Br^{-} is considerably larger than the primary yield of radicals, G = 6.0,[10] therefore it has to be concluded that the debromination occurs via a chain reaction.

When blank experiments were performed (in the absence of $(Ni^{II}L^{1})^{2+}$ surprisingly G(Br^{-}) = 112 was obtained.[18]

These results are in agreement with the following mechanism:[18]

$$RBr + CO_2^{\cdot -} \rightarrow R^{\cdot} + CO_2 + Br^{-} \quad (6)$$

$$R^{\cdot} + HCO_2^{-} \rightarrow RH + CO_2^{\cdot -} \quad (7)$$

and the termination reactions:

$$2R^{\cdot} \rightarrow R_2 \text{ or } RH + R_{-H} \quad (8)$$

$$2CO_2^{\cdot -} \rightarrow C_2O_4^{2-} \quad (9)$$

$$CO_2^{\cdot -} + R^{\cdot} \rightarrow RCO_2^{-} \quad (10)$$

In the presence of $(Ni^{II}L^{i})^{2+}$ the following reactions have to be added:

$$(Ni^{II}L^{i})^{2+} + CO_2^{\bullet -} \longrightarrow (Ni^{I}L^{i})^{+} + CO_2 \quad (11)$$

$$(Ni^{I}L^{i})^{+} + RBr \longrightarrow R^{\bullet} + Br^{-} + (Ni^{II}L^{i})^{2+} \quad (3)$$

$$R^{\bullet} + (Ni^{I}L^{i})^{+} \rightleftarrows (L^{i}Ni^{II}\text{–}R)^{+} \quad (12)$$

$$(L^{i}Ni^{II}\text{–}R)^{+} \xrightarrow{H^{+}} RH + (Ni^{II}L^{i})^{2+} \quad (13)$$

$$R^{\bullet} + (Ni^{II}L^{i})^{2+} \rightleftarrows (L^{i}Ni^{III}\text{–}R)^{2+} \quad (14)$$

$$R^{\bullet} + (L^{i}Ni^{III}\text{–}R)^{2+} \longrightarrow (Ni^{II}L^{i})^{2+} + R_2 \text{ or } RH + R_{-H} \quad (15)$$

$$(Ni^{I}L^{i})^{+} + (L^{i}Ni^{III}\text{–}R)^{2+} \longrightarrow (Ni^{II}L^{i})^{2+} + (L^{i}Ni^{II}\text{–}R)^{+} \quad (16)$$

 © 2003 Wiley-VCH Verlag GmbH & Co. KGaA, Weinheim

Thus the nickel complex "retards" the radiolytic debromination reactions, as reactions (13) and (15) are also termination steps.

Electrochemical Studies

The complexes $(Ni^{II}L^i)^{2+}$ were electrochemically (CV experiments) reduced on a glassy carbon electrode in He-saturated aqueous solutions, at pH 10, using $NaClO_4$ as the supporting electrolyte. Cyclic voltammograms show pseudo-reversible waves which correspond to the $Ni^{II/I}L^i$ redox couples. Under the same conditions $(CH_2Br)_2C(CH_2OH)_2$ is not reduced in the voltage range required for the reduction of the $(Ni^{II}L^i)^{2+}$ complexes. When $(CH_2Br)_2C(CH_2OH)_2$ is added, at different concentrations — $(2-7) \times 10^{-3}$ M — to a solution containing 5×10^{-4} M $(Ni^{II}L^i)^{2+}$ complex, the voltammetric behavior of $(Ni^{II}L^i)^{2+}$ changes. On addition of low concentrations of $(CH_2Br)_2C(CH_2OH)_2$, the reduction current of the cathodic peak $(Ni^{II/I}L^i)$ is enhanced in comparison with the reference voltammogram of $(Ni^{II}L^i)^{2+}$ alone, whereas that of the anodic peak decreases. On further addition of substrate, the cathodic peak current increases further and no anodic current is observed on the reverse scan, showing that $(CH_2Br)_2C(CH_2OH)_2$ is efficiently reduced electrocatalytically (Figure 5).

The increase in the cathodic peak current is linearly proportional to the concentration of the substrate, suggesting that the electrochemical process is diffusion controlled. This conclusion is in agreement with the rate constants of reaction (3) in Table 1. Thus, the nickel complexes are good electrocatalysts for the reduction of $(CH_2Br)_2C(CH_2OH)_2$.

As the concentration of $(Ni^{II}L^i)^{2+}$ is expected to be low near the electrode, the electrochemical process is probably best described by reaction:

$$(Ni^{II}L^i)^{2+} + e^- \rightarrow (Ni^{I}L^i)^{+} \quad (18)$$

followed by reactions (3), (12) or (14) + (16) and (13).

Preparative electrolysis was carried out at several potentials in the presence of $(Ni^{II}L^3)^{2+}$ as the electrocatalyst. The maximum of the reduction peak for this complex, using a graphite electrode, is observed at −1.15V. The concentration ratio $RBr/(Ni^{II}L^3)^{2+}$ was 10. The results of the yield of Br^- as a function of the applied potentials are summarized in Table 3. As expected, the yield of Br^- increases upon shifting the potential cathodically.

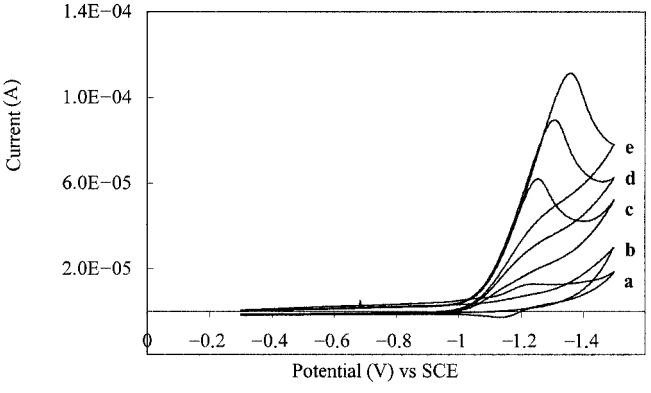

Figure 5. Cyclic voltammograms at pH 10.0 ± 0.3, supporting electrolyte 0.01 M $NaClO_4$, scan rate 50mV/s: (a) 5×10^{-4} M $(Ni^{II}L^3)^{2+}$; (b) 7×10^{-3} M $(CH_2Br)_2C(CH_2OH)_2$; (c) (a) + 3×10^{-3} M $(CH_2Br)_2C(CH_2OH)_2$; (d) (a) + 5×10^{-3} M $(CH_2Br)_2C(CH_2OH)_2$; (e) (a)+ 7×10^{-3} M $(CH_2Br)_2C(CH_2OH)_2$

Table 3. Bromide yield as function of potential; solution composition: 0.1 M $NaClO_4$, 5×10^{-4} M $(Ni^{II}L^3)^{2+}$ and 5×10^{-3} M $(CH_2Br)_2C(CH_2OH)_2$, pH 10.0 ± 0.3, He sat.; experimental error: ±20%

Potential (V)	−1.00	−1.05	−1.10	−1.15	−1.22	−1.30
$[Br^-]$ (M)	0.00026	0.00055	0.0013	0.0022	0.0028	0.0034

Concluding Remarks

The results presented here elucidate the mechanism of the electrocatalytic debromination processes. The rate of the debromination step, reaction (3), depends mainly on the redox potential of the $Ni^{II/I}L^i$ couple. It is proposed that these nickel complexes may be bound to modified electrodes, and might be useful as electrocatalysts for the dehalogenation of aliphatic halo-organic compounds.

Surprisingly enough it is shown that formate reduces $(CH_2Br)_2C(CH_2OH)_2$ in a radical-induced catalytic process, i.e. formate acts via a hydrogen-atom-transfer mechanism.

Experimental Section

Materials: All solutions were prepared from analytical-grade chemicals and distilled water that was passed through a Millipore setup, the final resistance being above 10 MΩ.

The complexes $Ni^{II}L^i(ClO_4)_2$ (i = 1−4) were prepared according to literature procedures,[8,19] and were characterized by NMR, UV/Vis and IR spectroscopy.

***Warning*:** Transition metal perchlorates are potentially explosive and have to be handled with care.

Pulse Radiolysis: The solutions were handled by the syringe technique.[20] The experiments were carried out using the Varian 7715 linear accelerator facility of the Hebrew University of Jerusalem. The pulse duration was 0.5−1.5 μs with a 200 mA current of 5 MeV electrons. The dose per pulse was in the range of 10−30 Gy/pulse. The experimental setup and the techniques used for evaluating the results have been described in detail elsewhere.[21,22]

Electrochemical Measurements: The electrochemical experiments were carried out using an EG&G Potentiostat/Galvanostat Model 263. A three-electrode cell was used. The working electrode was a glassy carbon electrode of 3 mm diameter, the auxiliary electrode was a Pt wire and an SCE was used as the reference electrode.
The preparative electrolyses were performed at controlled potential conditions in a three-electrode cell. A graphite electrode was used as the cathode. The counter electrode was a Pt wire and the satu-

 © 2003 Wiley-VCH Verlag GmbH & Co. KGaA, Weinheim

rated calomel electrode (SCE) served as a reference electrode. 0.1 M $NaClO_4$ was used as a support electrolyte. The experiments were performed with constant stirring.

Product Analysis: Quantitative analysis of bromide was performed by ion chromatography on a Hamilton-PRP-X100 column (250 × 4.1 mm^2) using a Jasco PU-980 Intelligent HPLC Pump and was optimized utilizing $H_5C_6CO_2Na$ (4 mM) as the eluent. The flow rate was 1.5 mL/min and a suppressed conductivity detector was used.

Irradiation: γ-Irradiations were carried out in a ^{60}Co γ source, Noratom, with a dose rate of about 4.0 Gy/min, which was determined by means of Fricke dosimetry, using a G value of G = 15.6.[23,24]

Acknowledgments

This study was supported in part by a grant from the Budgeting and Planning Committee of The Council of Higher Education and the Israel Atomic Energy Commission. D. M. wishes to express his thanks to Mrs. Irene Evens for her ongoing interest and support.

[1] National Academy of Sciences. *Alternatives for ground water cleanup*; National Academy Press: Washington, DC **1994**.
[2] H. Kerndorff, in *Chemie und Biologie der Altlasten*; Fachgruppe Wasserchemie der GDCh, VCH: Weinheim **1997**, 1−41.
[3] R. Mertens, C. Sonntag, *J. Chem. Soc., Perkin Trans. 2* **1994**, 2181−2185.
[4] A. Bakac, J. H. Espenson, *J. Am. Chem. Soc.* **1986**, *108*, 713−719.
[5] M. S. Ram, A. Bakac, J. H. Espenson, *Inorg. Chem.* **1986**, *25*, 3267−3272.
[6] J. Y. Becker, J. B. Kerr, D. Pletcher, R. Rosas, *J. Electroanal. Chem.* **1981**, *117*, 87−99.
[7] C. Gosden, J. B. Kerr, D. Pletcher, R. Rosas, *J. Electroanal. Chem.* **1981**, *117*, 101−107.
[8] N. Jubran, G. Ginzburg, H. Cohen, Y. Korehs, D. Meyerstein, *Inorg. Chem.* **1985**, *24*, 251−258.
[9] D. Meyerstein, *Coordin, Chem. Rev.* **1999**, 185−186, 141−147.
[10] M. S. Matheson, L. M. Dorfman, *Pulse Radiolysis*, MIT Press, Cambridge, MA, **1969**.
[11] G. V. Buxton, C. L. Greenstock, W. P. Helman, A. B. Ross, *J. Phys. Chem. Ref. Data* **1988**, *17*, 513−886.
[12] P. Wardman, *J. Phys. Chem. Ref. Data* **1989**, *18*, 1637−1755.
[13] H. A. Schwarz, R. W. Dodson, *J. Phys. Chem.* **1989**, *93*, 409−414.
[14] C. Creutz, H. A. Schwarz, J. F. Wishart, E. Fujita, N. Sutin, *J. Am. Chem. Soc.* **1991**, *113*, 3361−3371.
[15] I. Zilbermann, M. Winnik, D. Sagiv, A. Rotman, H. Cohen, D. Meyerstein, *Inorg. Chim. Acta* **1995**, *240*, 503−514.
[16] A. Sauer, H. Cohen, D. Meyerstein, *Inorg. Chem.* **1988**, *27*, 4578−4581.
[17] R. V. Eldik, H. Cohen, A. Meshulam, D. Meyerstein, *Inorg. Chem.* **1990**, *29*, 4156−4158.
[18] E. Shandalov, I. Zilbermann, E. Maimon, Y. Nahmani, H. Cohen, E. Adar, D. Meyerstein, to be published.
[19] M. P. Suh, H. Y. Kim, M. J. Kim, K. Y. Oh, *Inorg. Chem.* **1992**, *31*, 3620−3625.
[20] E. J. Hart, S. Gordon, J. K. Thomas, *J. Phys. Chem.* **1964**, *68*, 1271−1274.
[21] S. Goldstein, G. Czapski, H. Cohen, D. Meyerstein, J. K. Cho, S. S. Shaik, *Inorg. Chem.* **1992**, *31*, 798−803.
[22] N. Shaham, A. Masarwa, Y. Matana, H. Cohen, D. Meyerstein, *Eur. J. Inorg. Chem.* **2002**, 87−92.
[23] E. J. Hart, *Radiat. Res.* **1955**, *2*, 33−46.
[24] H. Fricke and E. J. Hart, in *Radiation Dosimetry* (Eds.: F. H. Attix, W. C. Roesch and E. Tochilin), Academic Press, New York, **1966**, p. 167.

Received February 27, 2003
Early View Article
Published Online October 2, 2003

 © 2003 Wiley-VCH Verlag GmbH & Co. KGaA, Weinheim

Design of Calixarene-Type Ligands for Second Sphere Complexation of Noble Metal Ions

Kamel Belhamel,[a] T. K. Dzung Nguyen,[b,c] Mohamed Benamor,[a] and Rainer Ludwig*[c]

Keywords: Macrocyclic ligands / Host-guest systems / Calixarenes / Gold / Solvent extraction

Macrocyclic ligands were designed according to the principle of ion recognition, synthesized and tested in their capability to extract Au^{III}. Different from other complexants which require ligand exchange prior to complexation, the reported ligands bind the complexes $AuCl_3$ and $AuCl_4^-$. With a sufficiently sized macrocyclic cavity, hydrophobic calix[6]arenes derivatized at the "lower rim' were employed for that purpose. Their ligating functionalities contain pyridino, amide or thioamide groups in order to achieve electron donor-acceptor and electrostatic host-guest interactions. We report the synthesis route and results on extraction, selectivity, kinetics and back-extraction and compare with commercial extractants. Quantitative extraction from hydrochloric acid solutions was achieved as well as over 99% recovery in back-extraction in one step each. Data on the selectivity over base metals, which are representative for the matrix in gold ores are provided. The ligands are powerful extractants for Au^{III} and show fast complexation kinetics.
(© Wiley-VCH Verlag GmbH & Co. KGaA, 69451 Weinheim, Germany, 2003)

Introduction

The molecular recognition of metal cations,[1] anions[2,3] and of organic molecules[4] can be achieved with macrocyclic ligands having tailor-made structures. Among the design features are complementary interactions, size compatibility, complementary coordination geometry and balanced complex stability which allows decomplexation. Calixarenes are suited to act as a molecular backbone for subsequent derivatizations to achieve these goals as shown by more than 500 papers on complexation of metal ions.[1,5−10] Solvent extraction is useful to test the molecular recognition mechanism and can be applied for chemical separations, as summarized recently.[11−16]

The complexation and extraction of anions such as oxyanions by calixarenes has been investigated to a smaller extent compared with cations. Complexation was for example achieved by incorporating amino-,[17,18] amido-,[19,20] pyridino-[21] or Schiff base groups,[22] or alternatively metal centers.[23,24]

[a] Laboratory of Analytical Chemistry, Chemical Engineering Department, University of Bejaia
DZ-06000, Algeria
Fax: (internat.) +213-3420-5193
[b] Institute for Technology on Rare Elements, Centre for Analyt. Chemistry and Environment, Vietnam Atomic Energy Commission
48 Lang Ha Street, Hanoi, Vietnam
Fax: (internat.) +84-48/835-0966
[c] Freie Universität Berlin, Institute of Chemistry, Inorg. and Analyt. Chemistry
Fabeckstr. 34−36, 14195 Berlin, Germany
Fax: (internat.) +49-30/838-52424
E-mail: rludwig@mail.chemie.fu-berlin.de

For the complexation of Au^{III}, S-donor[25−27] or P-donor atoms[28−30] were tethered to either the lower or the upper rim of the calixarene backbone. Some of these ligands quantitatively extract Au^{III} from water. If substituted at the upper rim of a calix[4]arene, the cavity is large enough to accommodate the chloro complex. Data for the extraction of Au^{III} by these ligands at different pH values, especially from very acidic solutions, were not reported.

On the other hand, commercial extractants were investigated with respect to Au^{III}. These contain ketones or alcohols,[31] phosphane oxides,[32] amines[33,34] or thiophosphinic acids.[35,36] Some of them have disadvantages, such as low extraction power from strongly acidic solutions, difficult back-extraction and loss of reagent, low selectivity, slight solubility in water, or degradation during use. One aim of this work was to show whether or not calixarenes can compete with those commercial extractants, and which molecular structures may be suitable for that purpose.

In our previous works, we investigated the complexation abilities of various calix[4]arenes towards noble metal ions.[37] We found that calix[4]arenes bearing both acidic and amido groups at the lower rim extract Au^{III}, Pd^{II} and Pt^{IV} ions from acidic solutions, but in case of Au^{III} not quantitatively ($\log D < 2$ at optimum pH 1). Moreover, in the presence of excess sodium ions, Au^{III} is no longer extracted ($\log D < -1$). These results can be interpreted that the ligand cavity size is too small for the Au^{III} complex anion, but matches the size and coordination sphere of the interfering Na^+. In order to improve the selectivity, we changed to calix[6]arenes[38] and would like to report on the ligands, which are able to selectively extract the chloro

 © 2003 Wiley-VCH Verlag GmbH & Co. KGaA, Weinheim **DOI: 10.1002/ejic.200300219**

complexes of metal ions and allow the pH control of extraction and back-extraction.

As the new ligands extract Au^{III} selectively from highly acidic media, there is an environmentally friendly application in hydrometallurgy: ores can be leached with acidic thiourea solution and oxidized[39] as an alternative to cyanide leaching.[40] Sulfidic ores are also subjected to acid-leaching. The extractant in this case must both be very selective and chemically stable. Metals present in gold ores such as the one from Algeria are Fe (4.6%), Al (4.5%), Ca (2.5%), Zn (0.02%), Pb(0.02%), alkali etc. and Au (0.001%). Therefore a high selectivity for gold is required for an extractant to be applied.

Results and Discussion

Ligand Structures

Figure 1 shows the structures of the calix[6]arenes used for this study. Their preparation proceeds smoothly in high yields. Ligand **1** was not applied to extraction because of low solubility in organic solvents. This is probably caused by hydrogen bonding and improves significantly upon thionation (ligand **3**). The solubility can also be improved by changing *tert*-butyl to *tert*-octyl groups (ligand **2**), which render the molecule more hydrophobic. The ^1H and ^{13}C NMR spectra of ligands **2** and **3** show sharp signals at room temperature, indicating the predominance of one conformation. From the symmetrical spectral pattern we concluded this to be the cone[41] conformation. It is rare that uncomplexed calix[6]arenes exist in a symmetrical cone shape at room temperature, because of the molecular flexibility. Ligands **4** to **6** and many other calix[6]arenes with smaller functional groups attached to the ethereal oxygens display broadened NMR spectra with temperature-dependent presence of various conformers.

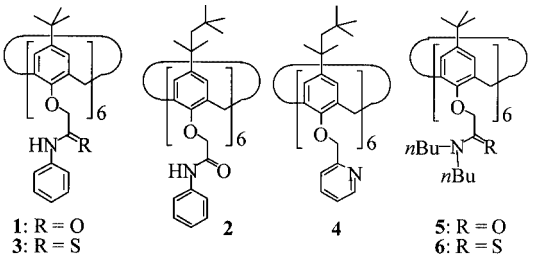

Figure 1. Structures of the investigated calixarenes and numbering

The binding of $AuCl_4^-$ is reflected by changes in the NMR spectra as confirmed for ligand **4**. Compared with the uncomplexed, protonated ligand, the -O-CH_2 and the N-CH_{py} C-signals broaden and shift, the other C_{py} signals shift as well. The C_{Ar} signals of the calixarene backbone shift to a smaller extent. In ^1H NMR spectrum, the δ = 3.3 ppm shift of equatorial Ar-CH_2-Ar protons changes to δ = 3.55 ppm upon complexation, partly off-setting the ring current. The axial and the O-CH_2 protons also shift downfield. The H_{py} signals shift as well and two of them broaden, while H_{Ar} and H_{Oct} of the calixarene backbone scarcely change upon complexation. These results indicate that $AuCl_4^-$ interacts with all the py groups inside the molecular cavity. Probably it coordinates not to all of them at the same time, but exchanges rapidly on the NMR timescale.

In the aqueous phase (>0.1 M Cl^-), the complex ion $AuCl_4^-$ exists exclusively (log β_4 = 25 [42]). The ligand cavity (0.3 × 0.8 nm at the ether oxygens,[6] or 0.5 nm as the inner circle) is large enough and retains conformational freedom to match the size of $AuCl_4^-$ (ca. 0.57 nm diameter). In order to render the complex hydrophobic and to avoid tensidic properties, the upper rim of the calixarene bears branched alkyl groups.

Extraction Properties

Figure 2 shows the distribution ratio D of Au^{III} on a logarithmic scale as a function of the pH in the aqueous phase after extraction for ligands **3**−**6**. D is defined as $c_{Au,org}/c_{Au,aq}$ at equilibrium. In order to characterize and to compare the ligands, their concentration was kept in high excess compared to the concentration of Au^{III}. The pH range was selected to allow protonation of the ligands [approx. pK_a of monomeric functional groups: 5.1 (pyridine), 0.1 (DMF),[43] −0.46 (acetanilide),[44] ≤0 (thioamide)]. pK_a Values of these macrocycles are not known. If more than one N-atom protonates under the experimental conditions (e.g. ligand **4**), this charge is neutralized by Cl^-. The conditional extraction constants take these equilibria into account, because the concentration of Cl^- is nearly constant.

Ligand **3** is characterized by a very high extractability towards Au^{III} (log $D \geq 3$, which was the upper measurement limit), over the investigated pH range. A variation of D could therefore not be observed. Ligands **4**−**6** display a pH dependency in accordance with their ability to pro-

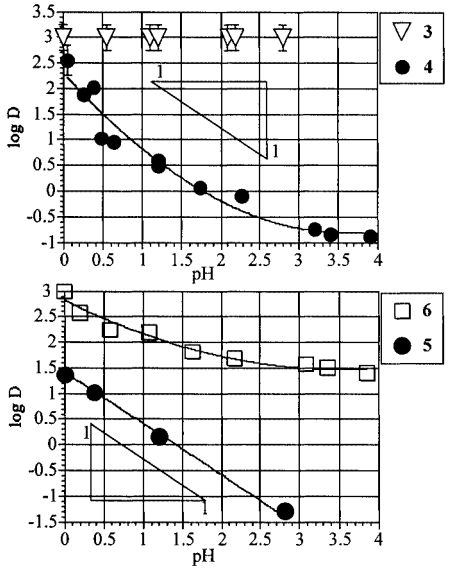

Figure 2. Effect of the pH of the aqueous phase on the extraction of Au^{III} by the ligands **3**−**6**; aq phase: 14 ppm $AuCl_3$ in HCl/NH_4Cl, pH measured at equilibrium; org. phase: 5 mM ligand in $CHCl_3$

 © 2003 Wiley-VCH Verlag GmbH & Co. KGaA, Weinheim

tonate. The protonated ligands form ion-pair complexes with $AuCl_4^-$. In cases of **4** (at higher acidity) and **5** the slope of log *D* vs. pH corresponds to (−1) as expected for monoprotonation.

The high extraction power of ligands **3** and **6** is interpreted as the result of the thioamide groups. It resembles synergistic extraction systems, in which an ammonium and a sulfur-donor ligand are mixed in the organic phase and achieve better extraction than the individual ligands.[35] The coordination of the unprotonated ligands **3**, **4**, and **6** to $AuCl_4^-$ via N or S, accompanied by dissociation of one Cl^- from the complex ion (ligand exchange) is concluded from the data, which show remaining extraction power even at pH >2. The neutral ligands probably extract $AuCl_3$, similar to the neutral commercial extractants Cyanex® 301, 302 and 471X.

The capability of the ligands to extract Au^{III} from HCl solutions into the organic phase serves as a measure to estimate their complexation power, although solvent effects during extraction (dehydration, solvation and ion pairing), which were not investigated here, also play a role. Hence, the extraction constant serves as a quantitative measure, assuming comparable solvent effects in the investigated extraction systems.

Complexation Equilibria

By changing the ligand concentration, the extraction mechanism and the stoichiometry can be derived. As concluded from slope 2 in the plot of log *D* vs. log *c* in Figure 3, all investigated extractants form complexes with a stoichiometry of 1:2 (metal/ligand) at low concentrations of Au^{III}. This is interpreted as being due to Au^{III} being sandwiched by two calixarene molecules, although size and charge of one calixarene molecule should be sufficient and the Au^{III}-coordination sphere is saturated with one counterion. However, commercial extractants such as thiophosphinic acid (protonated), phosphane oxide and -sulfide extract Au^{III} also as 1:2 complexes as can be concluded from slope analysis.[35]

Taking into account the ligand protonation, we can derive the following, simplified extraction equilibrium [Equation (1)]:

$$AuCl_4^- + 2L_{(org)} + H^+ \rightleftarrows [AuCl_4^- \cdot L \cdot LH^+]_{(org)} \quad (1)$$

The extraction constants are defined as shown in Equation (2):

$$K_{ex} = \frac{\left[AuCl_4^- \cdot L \cdot LH^+\right]_{(org)}}{\left[AuCl_4^-\right]\left[H^+\right]\left[L_{(org)}\right]^2} \quad (2)$$

In order to compare the four ligands with different pH dependencies, we refer K_{ex} as conditional constants to pH = 0 as well as to the other conditions. Table 1 lists the results, obtained by fitting the experimental data in Figure 3 with Equation (3), which is derived from Equation (2). Among the investigated ligands, the amide **5** is characterized by the lowest extraction. This is, however, not a disadvantage, because 96% extracted Au^{III} at pH 0 can be further increased at higher acidity in the aqueous phase.

$$\log D = \log K_{ex} + 2 \cdot \log[c_L]_{(org)} \quad (3)$$

The stoichiometry at high loading of the organic phase was tested by contacting equal volumes of equimolar (20 mM) Au^{III} with ligand **4** at pH 0. The extraction was near quantitative. The extract was dried and subjected to elemental analysis: found C 69.1, H 7.70, N 3.73%. This corresponds to a stoichiometry of 1:1 ($[AuCl_4]^-$:$[ligandH]^+$): calcd. C 68.9, H 7.48, N 3.83%. We conclude that the stoichiometry changes as a function of metal concentration in the organic phase: From diluted solutions, a second ligand molecule can shield the 'bottom' of the 1:1 complex. At high metal concentration there is no excess of ligand available and the 1:1 complex is extracted. Figure 4 schematically depicts that complex.

Table 1. Calculated extraction constants

Ligand	log K_{ex}
3	7.45
4	8.59
5	6.0
6	8.08

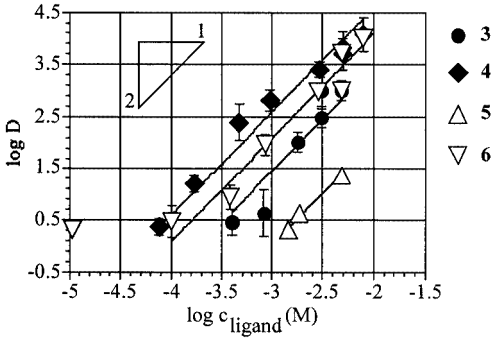

Figure 3. Estimation of the extraction power of the ligands; data are fitted by $\log D = 2 \cdot \log(c) + \log(K_{ex})$ with K_{ex} being the extraction constant at pH = 0; aq. phase: 14 ppm $AuCl_3$ in 1 M HCl; org. phase: $CHCl_3$ containing the corresponding ligand

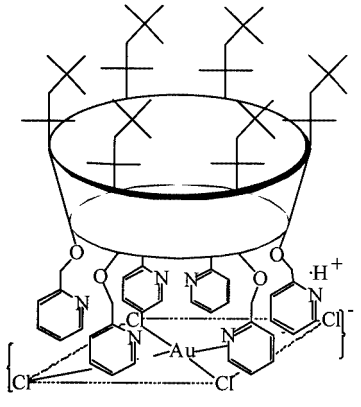

Figure 4 Schematic drawing of the extracted complex between Au^{III} and protonated **4** at high loading

 © 2003 Wiley-VCH Verlag GmbH & Co. KGaA, Weinheim

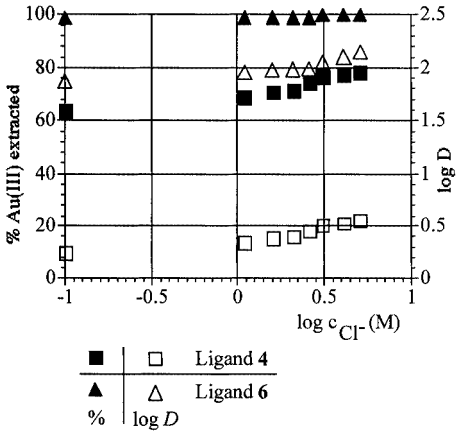

Figure 5. Influence of the chloride concentration on the extraction of Au^{III}; aq. phase: 17 ppm Au^{III} in 0.1 M HCl, up to 5 M NaCl; org. phase: $CHCl_3$ with 5 mM ligand

Variation of the chloride concentration at constant pH of the aqueous phase only causes small changes in the distribution ratio, as tested for ligands **4** and **6** (Figure 5). It is interpreted by the change of activity coefficients (salting-out effect). No change in the extraction mechanism takes place, as concluded from the slope of log D vs. log c_{Cl^-} being $<< +1$.

Back-Extraction

Ligands **4** and **5** have a pronounced pH dependency in their extraction ability (Figure 1). The organic phase, loaded with gold during extraction can therefore be regenerated by contacting with an aqueous phase of higher pH. The metal is back-extracted and, by using a small aqueous volume, enriched for a second time. The sulfur-containing ligands release their complexed metal only partly when the pH is increased. It is possible to completely recover all the metal by repeated mixing with water. More effective for the purpose of back-extraction is a competing, water-soluble ligand (e.g. thiourea, tu). Table 2 lists the results and shows that the ligands may be applicable not only for separation but also for analytical purposes, because both extraction and back-extraction are quantitative. The ligands were stable during four weeks of continuous extraction/back-extraction as concluded from the NMR spectra.

Table 2. Recovery of Au^{III} (in %) from the complexed ligands

Ligand	Buffer (pH, 5.5)	10 mM tu in H_2O	10 mM tu in 1 M HCl
3	5%	64.8%	> 99%
4	86%	89%	> 99%
5	80%	85%	> 99%
6	3.8%	0.1%	> 97%

Selectivity

Taking into account the composition from acidic ore leaching, it is important to achieve a high selectivity for Au over the other metal ions, especially Fe(III). Figure 6 depicts results obtained in competitive extraction tests with ligands **3**, **4** and **6**. Under a 30-fold excess of Fe^{III}, ligand **3** still extracts Au^{III} quantitatively, while Fe^{III} is not extracted over the whole pH range. The separation factor S_f, defined as D_{Au}/D_{Fe} is $> 10^5$. Among the investigated metal ions only Zn^{II}, which has some thiophilic character, is extracted up to 7 and 13% by ligands **4** and **6** respectively. Alkali, alkaline earth and Al^{III} ions were not extracted from 1 M HCl. The overall high selectivity is discussed in terms of the ligand design: (i) the preferred binding of anions over metal cations due to electrostatic interactions, (ii) the suitable cavity, (iii) the preference for class "B" metal ions due to the presence of S and/or aromatic π-systems, and (iv) the macrocyclic effect. On the other hand, various monodentate ligands (except quaternary amines) extract Au^{I} without selectivity over Fe^{III}: a dithiophosphinic acid (91%:99%), a thiophosphinic acid (93%:99%), a phosphinic acid (93%:99%), DEHPA (76%:99%), an 8-hydroxyquinoline (87%:70%), and a bisphosphonic acid (90%:99%) at pH 2.[36]

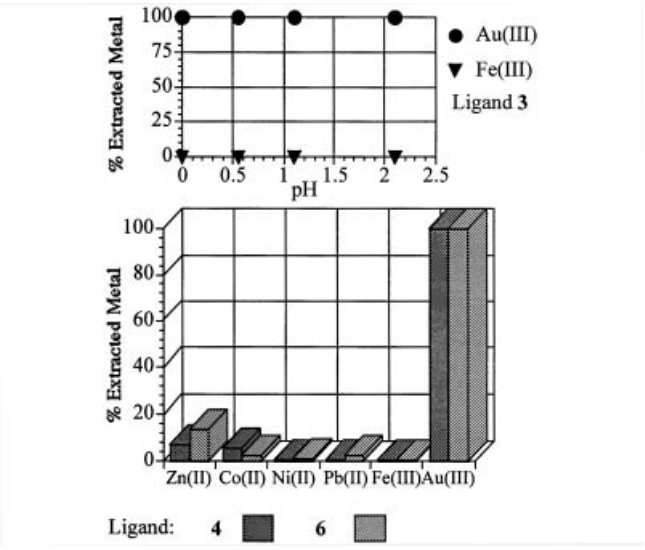

Figure 6 Selectivity of the ligands in competitive extraction; aq. phase:14 ppm Au^{III} and 2 mM Fe^{III} (upper part) or 0.1 mM of each M^{n+} (M = Zn^{2+}, Ni^{2+}, Pb^{2+}, Fe^{3+}, lower part) in 1 M HCl; org. phase: $CHCl_3$ containing 5 mM Ligand

Kinetics

Because the ligands are completely water-insoluble, the extraction consists of complexation at the interface followed by transport into the bulk organic phase. The extraction equilibria are reached very fast as expected for ion pairing in the absence of any interfacial resistance to mass transfer: Ligands **3**−**6** extract > 98% Au within 1 min and > 99% within 5 min. The short contact times required are advantageous for analytical as well as scaled up separation purposes.

Comparison with Cation Exchangers

We tested thiacalix[4]arene **7** [45] and the analogue **8** (CH_2 instead of S)[37], which are known to extract metal ions by

 © 2003 Wiley-VCH Verlag GmbH & Co. KGaA, Weinheim

cation exchange. The distribution ratio D_{Au} changed scarcely from 0.18 to 0.28 (**7**) when the pH was varied from 2 to 0 while that for **8** was even lower. It indicates that these ligands can hardly compete with Cl^- due to the high pK_a of the acid groups and that the S-bridges in **7** are inaccessible to binding due to steric reasons.

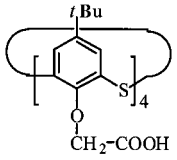

Ligand **7**

Figure 7

Conclusion

High distribution ratios of Au^{III} are observed when ligands based on the calix[6]arene contain sulfur and/or nitrogen atoms, resulting in quantitative extraction from strongly acidic solution. Ligands containing only nitrogen as donor atoms extract Au^{III} quantitatively when they are protonated. Thioamide derivatives extract Au^{III} over a wider pH range. The loaded metal is quantitatively back-extracted by pH change or by competing ligands. The ligands have high selectivity which allows potential application in separation chemistry. Further works will be devoted to the extraction of other noble metals by these ligands and to the determination of their protonation constants.

Experimental Section

Complexation Experiments: Metal extraction was carried out batchwise with equal volumes at 298 K. The agitation speed was 54 rpm in an overhead shaker. Metal contents before and after extraction were analyzed by means of AAS (Shimadzu AA 6500) after dilution with 1 M HCl. Solutions were prepared by handling $AuCl_3$ under N_2 in a glove bag and dissolving in HCl. For the pH dependent extraction, the pH was adjusted by adding 1 M NH_3 or 8 M HCl to 0.1 M HCl solutions and mixing them with Au-stock solution. $CHCl_3$ saturated with water served as organic solvent for which reference data are available. The extractants are however, also soluble in less-polar solvents. Equilibrium pH values were measured with a combination glass electrode (Schott N42) after extraction and phase separation. The concentration of uncomplexed ligand ($c_{corrected}$) in Figures showing concentration-dependencies was calculated by taking into account the complexation. Selectivities were determined in competitive extraction. Quantitative stripping was done with 10 mM thiourea solution in 1 M HCl and a 100% mass balance was obtained. Using water or thiourea in water complete stripping was achieved for ligands **4** and **5** after three repetitions. The chemical stability was tested by repeated extraction and stripping cycles, in the course of which no decomposition of the ligands was observed. Metal complex NMR spectra (ligand **4**) were measured after contact with excess amounts of Au^{III} at pH 0 and compared with those of the protonated ligand. These concentrated organic Au^{III} complexes did not decompose. In the case of calix[4]arenes, complexed Au^{III} slowly oxidized thiocarbamoyl groups.[25]

NMR spectra were recorded at room temperature on a Bruker AC-250 instrument at 250 (^1H) or 63 MHz (^{13}C), chemical shifts are referenced to TMS and correspond to the neutral (non-protonated) ligands. H_{Ar}/C_{Ar} indicates the calixarene backbone rather than substituents if not stated otherwise. Mass spectra were measured in the EI mode (200 °C, 80 eV, 8 keV, MAT 711 instrument). Analytical TLC was carried out on dry Merck Silicagel $60F_{254}$, the R_f-values somewhat depend on the concentration. Melting points were determined on a Gallenkamp apparatus under air and are uncorrected. They were reconfirmed by DSC, measured with a Netzsch DSC 200 type calorimeter under N_2 atmosphere at 10 K/min. IR spectra were recorded on a Nicolet 5 SCX instrument with a DTGS detector. All solvents were dried and freshly distilled, chemicals were of synthesis grade. NaH (80% in oil) was washed with hexane prior to use. The air-sensitive reactions were carried out under N_2 atmosphere using transfer techniques. Yields are given for purified products. Parent calix[6]arenes were synthesized according to the literature.[46,47] Their purity was greater than 96%.

Ligand 1: The hexakis(carbomethoxy) derivative[48] of *tert*-butylcalix[6]arene (2.5 g, 1.9 mmol) was dried and treated with $(COCl)_2$ (45 equiv.) in CCl_4 under N_2 for 12 h at 75 °C. Volatiles were completely removed in vacuo, the residue dissolved in dry THF and treated with a mixture of pyridine (28 mmol) and aniline (28 mmol) under cooling with an ice bath. After stirring for 24 h at 35 °C the mixture was filtered. The residue was stirred with CH_2Cl_2/H_2O and filtered to give the pure product as a white residue, which is very insoluble in common organic solvents. Yield 87%.5,11,17,23,29,35-Hexakis(*t*ert-butyl)-37,38,39,40,41,42-hexakis(N-phenylcarbamoylmethoxy)calix[6]arene. $C_{114}H_{126}N_6O_{12}$ (M_r = 1772.21): calcd. C 77.26, H 7.17, N 4.74; found C 76.82, H 7.13, N 4.86; m.p. 277−279 °C. ^1H NMR [$CDCl_3/CD_3C(O)CD_3/CD_3OD$, 3:1:1]: δ = 1.15 (s, *t*Bu, 54 H), 3.56 and 4.76 (2 d, Ar-CH_2, each 6 H, J = 16.5 Hz), 4.33 (s, O-CH_2, 12 H), 6.69 (m, pH_{Ar}, 6 H), 6.83 (m, mH_{Ar}, 12 H), 7.10 (s, H_{Ar} of calix, 12 H), 7.31 (m, oH_{Ar}, 12 H), 8.6 (s, NH) ppm, in [D_8]THF/[D_6]ethanol the spectrum indicates a mixture of conformers frozen on the NMR timescale. IR (KBr): $\tilde{\nu}$ = 1690 cm^{-1} (νCO amide I), 753 and 692 (γCH, 5 neighboring H of aniline), 1531 (Amide II), 3396 (NH); TLC ($CHCl_3$/EtOH, 9:1) R_f = 0.82. Because of the low solubility of 1, we also synthesized the *tert*-octyl analogue and characterized it for reasons of comparison.

Ligand 2: The hexakis(carbomethoxy) derivative of *tert*-octylcalix-[6]arene[47] (3.2 g, 1.9 mmol) was treated with $(COCl)_2$ (45 equiv.) in CCl_4 under N_2 for 8 h at 75 °C. Volatiles were completely removed under reduced N_2 pressure, the residue was dissolved in dry THF and treated with a mixture of triethylamine (23 mmol) and aniline (23 mmol) under cooling with an ice bath. The mixture was filtered after stirring for 24 h at 38 °C. The filtrate was evaporated in vacuo, dissolved in CH_2Cl_2, washed 4 times with 1 M HCl, dried and crystallized by addition of EtOH to a CH_2Cl_2 solution. Yield 83%.5,11,17,23,29,35-Hexakis(*tert*-octyl)-37,38,39,40,41,42-hexakis(*N*-phenylcarbamoylmethoxy)calix[6]arene $C_{138}H_{174}N_6O_{12}$ (M_r = 2108.8): calcd. C 78.59, H 8.32, N 3.99; found C 77.88, H 8.24, N 3.76; m.p. 218−220 °C (dec.); DSC: 25.8 J/g at m.p., endothermic phase transition at 167 °C (−18.2 J/g). This is interpreted as the break-up of hydrogen bonds in the solid state (intramolecular H-bonding was concluded from the NMR spectroscopy), and conformational change from the symmetrical to an unsymmetrical, energetically favoured conformation. The ^1H and

 © 2003 Wiley-VCH Verlag GmbH & Co. KGaA, Weinheim

^{13}C spectra ($CDCl_3$) are characterized by sharp signals, this indicates rigidified and symmetrical conformation (intramolecular H-bonding), while calix[6]arenes with smaller O-substituents usually show broadened peaks in the NMR spectra at room temp. due to conformational flexibility, as do the investigated thioamides. ^1H NMR: δ = 0.72 (s, *t*Oct, 54 H), 1.12 (s, *t*Oct, 36 H), 1.60 (s, *t*Oct, 12 H), 3.57 and 5.03 (2 d, Ar-CH_2, each H, J = 16.5 Hz), 4.31 (s, O-CH_2, 2 H), 6.83 (*m*, *p*$H_{aniline}$, 3 H), 7.08 (s, H_{Ar} of calixarene backbone, 2 H), 7.21 (*o*$H_{aniline}$, 2 H), 8.66 (s, NH, 1 H) ppm, ^{13}C NMR: δ = 29.7 (Ar-CH_2), 31.3 (1,1 dimethyl of *t*Oct), 31.8 (3 × CH_3 of *t*Oct), 32.4 (C_3 of *t*Oct), 38.1 (C_1 of *t*Oct), 57.2 (CH_2 of *t*Oct), 72.0 (O-CH_2), 120.8 (*o*C_{Ar} of aniline), 124.3 (*p*C_{Ar} of aniline), 127.4 (C_{Ar}-H of calix), 128.4 (*m*C_{Ar} of aniline), 131.6 (***C***$_{Ar}$-CH_2), 136.8 (C_{Ar}-NH), 146.0 (C_{Ar}-*t*Oct), 151.1 (C_{Ar}-O), 167.3 (CO) ppm. IR (KBr): $\tilde{\nu}$ = 1691 cm^{-1} (νCO amide I), 752 and 691 (γCH, 5 neighboring H's of aniline), 1533 (Amide II), 3391 (NH); TLC (CH_2Cl_2) R_f = 0.30 (tailing), ($CHCl_3$/EtOH, 9:1) R_f = 0.86.

Ligand 3: The precursor **1** (1 g, 0.56 mmol) was dissolved in dry toluene and treated with 2,4-bis(4-methoxyphenyl)-1,3-dithia-2,4-diphosphetane-2,4-disulfide (4 mmol) at 90 °C for 40 h. After cooling, the mixture was filtered and the solvents evaporated. The product precipitated from the residue upon adding MeOH and was recrystallized twice by addition of MeOH to a CH_2Cl_2 solution. Yield 68%. No interfering side products are formed during thionation reactions even in less polar solvents. 5,11,17,23,29,35-Hexakis(*tert*-butyl)-37,38,39,40,41,42-hexakis(*N*-phenylthiocarbamoylmethoxy)calix[6]arene, $C_{114}H_{126}N_6O_6S_6$ (M_r = 1868.6) calcd. C 73.27, H 6.8, N 4.50, S 10.28; found C 72.02, H 6.86, N 4.35, S 9.8; m.p. 240−242 °C (dec.). In the NMR spectra ($CDCl_3$) chemical shifts in *italics* indicate some of the characteristic changes upon thionation. ^1H NMR: δ = 1.12 (s, 54 H, *t*Bu), 3.62 and 4.41 (2 d, J = 16.25 Hz, 6 H each, CH_2-Ar), 4.5 (s, -O-CH_2, 12 H), 7.0 (s, 12 H, H_{Ar} of calix backbone), 7.13 (m, 18 H, *m* and *p*H_{Ar}), 7.53 (d, 12 H, *o*H_{Ar}), 9.8 (s, 6 H, NH) ppm. ^{13}C NMR: δ = 29.9 (CH_2-Ar), 31.3 (*t*Bu), 34.2 (quart C), *80.0* (-O-CH_2), 123.0 (*o*C_{Ar} of aniline), 126.6 (*p*C_{Ar} of aniline), 126.9 (C_{Ar}−H of calix), 128.6 (*m*C_{Ar} of aniline), 131.3 (*C*$_{Ar}$-CH_2), 137.3 (C_{Ar}-NH), 146.9 (C_{Ar}-*t*Oct), 151.8 (C_{Ar}-O), *194.4* (CS) ppm, no CO. IR (KBr): $\tilde{\nu}$ = 1394 cm^{-1} (thioamide I), 997 (thioamide IV), disappeared 1690; TLC ($CHCl_3$/EtOH, 9:1) R_f = 0.92.

Ligand 4: *tert*-Octylcalix[6]arene (6 g, 4.6 mmol) was deprotonated with NaH (18 equiv.) in dry THF for 12 h at 60 °C under N_2. A filtered mixture of triethylamine (18 equiv., 11.5 mL) and 2-picolyl chloride hydrochloride (9 equiv., 76.8 g), which had been stirred for 3 h, was added dropwise to the grey suspension under N_2 with ice-cooling. The reaction was completed by warming to 50 °C for 48 h, quenched with EtOH after cooling and the solvents evaporated. The residue was dissolved in CH_2Cl_2/EtOH (9:1), washed with brine and 0.1 M HCl, filtered through a Whatman phase separator and crystallized from hexane. Yield 54%. The *tert*-butylcalix[6]-arene analogue was described earlier.[49] 5,11,17,23,29,35-Hexakis-(*tert*-octyl)-37,38,39,40,41,42-hexakis[(2-pyridylmethyl)oxy]-calix[6]arene $C_{126}H_{162}N_6O_6$ (M_r = 1856.62): calcd. C 81.5, H 8.8, N 4.53; found C 81.60, H 8.79, N 3.98; MS (EI), [M^+], 1856 (L); m.p. 243−245 °C. The ^1H NMR spectroscopy ($CDCl_3$): broadened peaks of Ar-CH_2, O-CH_2 and H_{Ar} indicated conformational flexibility, adding CD_3OD (30%) stabilizes a mixture of conformational isomers. ^1H NMR: δ = 0.62 (s, 54H Me of *t*Oct), 1.29 (s, 36 H, dimethyl), 1.77 (s, 12 H, CH_2 of *t*Oct), 3.49 (br., 6 H, Ar-CH_2), 4.0 to 5.0 (br., 18 H, Ar-CH_2 and O-CH_2), 6.79 (s, 6 H, H_{py}), 6.9 to 7.1 (br. s, 24 H, H_{calix} and H_{py}), 8.24 [br. s, 6 H, H_{py}(N-CH)] ppm. ^{13}C NMR: δ = 31.5 (1,1 dimethyl of *t*Oct), 32.1 (3 × CH_3 of *t*Oct), 32.2 (Ar-CH_2), 32.4 (C_3 of *t*Oct), 37.9 (C_1 of *t*Oct), 56.9 (CH_2 of *t*Oct), 75.3 (O-CH_2), 122.0 (*m*C_{py}), 126.5 (C_{Ar}-H of calix), 132.6 (*C*$_{Ar}$-CH_2), 136.6 (*m*C_{py}), 140.2 (*p*C_{py}), 145.3(N-CH_{py}), 147.9 (C_{Ar}-*t*Oct), 151.8 (C_{Ar}-O), 157.9 (CH_2-*C*$_{py}$) ppm. IR (KBr): new (py) 753, 994, 1032, 1147, 1435 cm^{-1}; TLC ($CHCl_3$/EtOH, 9:1) R_f = 0.63 (1 spot); (CH_2Cl_2) R_f = 0 (no starting material).

Ligand 5: The hexakis(carbomethoxy) derivative of *tert*-butylcalix-[6]arene[48] (3 g, 2.27 mmol) was dried and treated with $(COCl)_2$ (60 equiv.) in CCl_4 under N_2 for 12 h at 75 °C. Volatiles were completely removed under reduced N_2 pressure, the residue dissolved in dry THF and treated with a mixture of triethylamine (46 mmol) and di-*n*butylamine (46 mmol) under cooling with an ice bath. After stirring for 12 at 30 °C the mixture was filtered, evaporated to dryness, dissolved in CH_2Cl_2 and washed five times with 1 M HCl. The product crystallized from MeOH and was dried in vacuo at 80 °C. Yield 90%. 5,11,17,23,29,35-Hexaakis(*tert*-butyl)-37,38,39,40,41,42-hexakis[(*N*,*N*-di-*n*butylcarbamoylmethoxy)-calix[6]arene, $C_{126}H_{198}N_6O_{12}$ (M_r = 1988.9): calcd. C 76.08, H 10.03, N 4.23; found C 75.74, H 9.72, N 4.06; m.p. 197−199 °C; DSC: 36 J/g. Within the NMR spectra ($CDCl_3$), the presence of two separate, equal H_{Ar} and two -O-CH_2-signals are interpreted in terms of two conformations present, probably due to H-bonding. The structurally similar *N*,*N*-diethylamide derivative also exists as a mixture of conformers at 298 K in $CDCl_3$.[50] In the case of ligand **5**, the more bulky groups may restrict the number of co-existing conformers to two. ^1H NMR: δ = 0.70 (br. s), 0.95 (q), 1.34 (m), 1.62 (br. s), (Σ23 H); 3.34 and 3.63 (m, 4 H), 3.9−5.1 (br. m, O-CH_2 and CH_2-Ar, 4 H), 7.18 and 7.49 (2 s, H_{Ar}, 1H each) ppm. ^{13}C NMR: δ = 13.8 (CH_3 of *n*Bu), 20.0 and 20.2 (*n*Bu), 29.7 (Ar−CH_2-Ar), 31.1 (*t*Bu), 31.5 (*n*Bu), 34.0 (quart C of *t*Bu), 45.5 (N−CH_2), 71.6 (-O-CH_2), C_{Ar}: 124.7, 127.1, 133.2, 146.4, 151.9; 168.0 (CO) ppm. IR (KBr):1646 cm^{-1} (νCO), no 1755 (COOH); TLC ($CHCl_3$/EtOH 9:1) R_f = 0.28 (characteristic short tailing).

Ligand 6: The ligand **5** (0.5 g, 0.25 mmol) was dissolved in dry toluene and treated with 2,4-bis(4-methoxyphenyl)-1,3-dithia-2,4-diphosphetane-2,4-disulfide (2.5 mmol) at 85 °C for 24 h. After cooling, the mixture was filtered and the solvents evaporated. The product was precipitated from hot acetone by adding 3% water, and was crystallized twice from hexane and washed with hot MeOH/H_2O (1:1). Yield 72%. 5,11,17,23,29,35-Hexakis(*tert*-butyl)-37,38,39,40,41,42-hexakis[(*N*,*N*-di-*n*butylthiocarbamoylmethoxy)-calix[6]arene, $C_{126}H_{198}N_6O_6S_6$ (M_r 2085.3): calcd. C 72.57, H 9.57, N 4.03, S 9.21; found C 71.99, H 9.27, N 3.87, S 8.82; m.p. 171−173 °C. In the NMR spectra ($CDCl_3$) chemical shifts in *italics* indicate some of the characteristic changes upon thionation. Similar to ligand **5**, a conformational mixture exists at 298 K. ^1H NMR: δ = 0.80 (d), 0.96 (s), 1.40 (m), 1.80 (br), (Σ138 H), 2.88 (br. d) and 3.43 (d, Ar-CH_2), 3.9 (br. m, N-CH_2), 4.75−5.05 (br., O-CH_2 and Ar-CH_2) (Σ48 H), H_{Ar}: 6.4, 6.53, 7.28, 7.55 (Σ12 H) ppm. ^{13}C NMR: δ = 13.7 (CH_3 of *n*Bu), 20.2 (*n*Bu), 27.8 (Ar−CH_2-Ar), 31.6 (*t*Bu), 32.0 (*n*Bu), 34.1 (quart C of *t*Bu), *53.5* (N-CH_2), *79.2* (-O-CH_2), 123.1 (C_{Ar}), 128.3 (C_{Ar}), 132.3 (C_{Ar}), 145.4 (C_{Ar}), 153.3 (C_{Ar}), *195.2* (CS), IR (KBr): νCO disappeared, new 1505 cm^{-1} (νCS I), 990 (νCS IV), TLC ($CHCl_3$/EtOH, 9:1) R_f = 0.95 (one spot, no partially substituted material), (CH_2Cl_2) R_f = 0.74 (1 spot, no thionation reagent).

Acknowledgments

A fruitful discussion on pyridine-type calixarenes and their spectral properties with Ass. Prof. K. Ohto (Saga Univ., Japan) is appreciated. We thank Prof. H. Hartl and Ms. Friese (FU Berlin) for the

 © 2003 Wiley-VCH Verlag GmbH & Co. KGaA, Weinheim

DSC measurements and discussions. Financial support for this work by DAAD (German Academic Exchange Office), by German foundations Stiftung Industrieforschung (Köln) and Fonds d. Chem. Industrie (Frankfurt) as well as from the Vietnamese National Science Council/Fundamental Research Projects are appreciated.

[1] *Molecular Recognition: Receptors for Cationic Guests (Comprehensive Supramolecular Chemistry Vol. 1)*, (Ed.) G. W. Gokel, Pergamon Press, New York, Oxford, **1996**.
[2] P. D. Beer, in *Calixarenes in Action*, (Eds.) L. Mandolini, R. Ungaro, Imperial College Press, Lonon, 111−143, **2000**.
[3] P. D. Beer, in ref.[5], pp 421−439.
[4] *Molecular Recognition: Receptors for Molecular Guest (Comprehensive Supramolecular Chemistry Vol. 2)*, (Ed.) F. Vögtle, Pergamon Press, New York, Oxford, **1996**.
[5] *Calixarenes 2001*, (Eds.) Z. Asfari, V. Böhmer, J. Harrowfield, J. Vicens, Kluwer Acad. Publ., Dordrecht, **2001**.
[6] C. D. Gutsche, *Calixarenes Revisited*, The Royal Society of Chemistry, Cambridge, **1998**.
[7] *Calixarenes. A Versatile Class of Macrocyclic Compounds*, (Eds.) J. Vicens, V. Böhmer, Kluwer Acad. Publ., Dordrecht/Boston/London, **1991**.
[8] *Calixarenes 50th Anniversary: Commemorative Issue*, (Eds.) J. Vicens, Z. Asfari, J. M. Harrowfield, Kluwer Acad. Publ., Dordrecht, **1994**.
[9] *Calixarene Molecules for Separations*, (Eds.) G. J. Lumetta, R. D. Rogers, *Am. Chem.* Soc., Washington DC, **1999**.
[10] N. Iki, S. Miyano, *J. Inclusion Phenon. Macrocyclic Chem.* **2001**, *41*, 99−105.
[11] R. Ludwig, JAERI-Review 95−022, JAERI, Japan, **1995**.
[12] M. A. McKervey, M. J. Schwing-Weill, F. Arnaud-Neu in [6], pp 537−603.
[13] A. T. Yordanov, D. M. Roundhill, *Coord. Chem. Rev.* **1998**, *170*, 93−124.
[14] D. M. Roundhill in *Prog. Inorg. Chem.* K. D. Karlin (Ed.), Wiley, New York, **1995**, Vol. 43, pp 533−591.
[15] M. Lauterbach, E. Engler, N. Muzet, L. Troxler, G. Wipff, *J. Phys. Chem. B* **1998**, *102*, 245−256.
[16] R. Ludwig, *Fresenius J. Anal. Chem.* **2000**, *367*, 103−128.
[17] E. M. Georgiev, N. Wolf, D. M. Roundhill, *Polyhedron* **1997**, *16*, 1581−1584.
[18] N. J. Wolf, E. M. Georgiev, A. T. Yordanov, B. R. Whittlesey, H. F. Koch, D. M. Roundhill, *Polyhedron* **1999**, *18*, 885−896.
[19] O. M. Falana, H. F. Koch, D. M. Roundhill, G. L. Lumetta, B. P. Hay, *Chem. Commun.* **1998**, 503−504.
[20] V. Stastny, P. Lhotak, V. Michlova, I. Stibor, J. Sykora, *Tetrahedron* **2002**, *58*, 7207−7211.
[21] P. D. Beer, M. G. B. Drew, K. Gradwell, *J. Chem. Soc., Perkin Trans. 2* **2000**, 511−519.
[22] A. Yilmaz, S. Memon, M. Yilmaz, *Tetrahedron* **2002**, *58*, 7735−7740.
[23] P. D. Beer, M. Shade, *Gazz. Chim. Ital.* **1997**, *127*, 651−652.
[24] P. D. Beer, M. G. B. Drew, D. Hesek, K. C. Nam, *Chem. Commun.* **1997**, 107−108.
[25] A. T. Yordanov, B. R. Whittlesey, D. M. Roundhill, *Inorg. Chem.* **1998**, *37*, 3526−3531.
[26] A. T. Yordanov, D. M. Roundhill, *New J. Chem.* **1996**, *20*, 447−451.
[27] A. T. Yordanov, O. M. Falana, H. F. Koch, D. M. Roundhill, *Inorg. Chem.* **1997**, *36*, 6468−6471.
[28] M. Lejeune, C. Jeunesse, D. Matt, N. Kyritsakas, R. Welter, J.-P. Kintzinger, *J. Chem. Soc., Dalton Trans.* **2002**, 1642−1650.
[29] C. D. Dieleman, D. Matt, A. Harriman, *Eur. J. Inorg. Chem.* **2000**, 831−834.
[30] P. Faidherbe, C. Wieser, D. Matt, A. Harriman, A. D. Cian, J. Fischer, *Eur. J. Inorg. Chem.* **1998**, 451−457.
[31] R. A. Grant, V. A. Drake, in *Proc. ISEC 2002*, (Eds.) K. C. Sole, P. M. Cole, J. S. Preston, D. J. Robinsons, 940−945, C. v. Rensburg Publ., Melville, **2002**.
[32] S. Martinez, A. M. Sastre, F. J. Alguacil, *Hydrometallurgy* **2001**, *46*, 205−214.
[33] S. Martinez, A. M. Sastre, F. J. Alguacil, *Hydrometallurgy* **2001**, *52*, 63−70.
[34] F. J. Alguacil, S. Martinez, A. M. Sastre, *J. Chem. Res. Synop.* **2001**, 384−386.
[35] R. Haddad, A. Kumar, F. J. Alguacil, A. M. Sastre, in *Proc. ISEC 1999*, (Eds.) M. Cox, M. Hidalgo, M. Valientes, 1155−1160, SCI, London, **2001**.
[36] M. S. D. Erosa, R. N. Mendoza, T. I. S. Medina, G. L. Lavine, M. Avila-Rodriguez, in *Proc. ISEC 2002*, (Eds.) K. C. Sole, P. M. Cole, J. S. Preston, D. J. Robinsons, 902−907, C. v. Rensburg Publ., Melville, **2002**.
[37] R. Ludwig, S. Tachimori, *Solvent Extr. Res. Dev. Jpn.* **1996**, *3*, 244−254.
[38] K. Belhamel, T. K. D. Nguyen, M. Benamor, R. Ludwig, in *Proc. ISEC 2002*, (Eds.) K. C. Sole, P. M. Cole, J. S. Preston, D. J. Robinsons, 307−312, C. v. Rensburg Publ., Melville, **2002**.
[39] S. Örgül, Ü. Atalay, *Hydrometallurgy* **2002**, *67*, 71−77.
[40] A. C. Grosse, G. W. Dicinoski, M. J. Shaw, P. R. Haddad, *Hydrometallurgy* **2003**, *69*, 1−21.
[41] M. Perrin, D. Oehler in [7], 65−85.
[42] K. J. Powell, *The IUPAC Stability Constants Database*, Academic Software, **2000**.
[43] L. Kisova, *Scr Fac. Sci. Nat. Univ. Purkynianae Brun.* **1975**, *5*, 53−59.
[44] H. Kuura, M. Tamme, U. Haldna, *Reak. Sposob. Org. Soedin.* **1971**, *8*, 1201−1206.
[45] N. Iki, T. Narumi, A. Suzuki, A. Sugawara, S. Miyano, *Chem. Lett.* **1998**, 1065−1066.
[46] C. D. Gutsche, B. Dhawan, M. Leonis, D. Stewart, *Org. Synth.* **1990**, *68*, 238−242.
[47] K. Ohto, M. Yano, K. Inoue, T. Yamamoto, M. Goto, F. Nakashio, S. Shinkai, T. Nagasaki, *Anal. Sci.* **1995**, *11*, 893−902.
[48] S. Shinkai, Y. Shiramama, H. Satoh, O. Manabe, T. Arimura, K. Fujimoto, T. Matsuda, *J. Chem. Soc., Perkin Trans. 2* **1989**, 1167−1171.
[49] S. Shinkai, T. Otsuka, K. Araki, T. Matsuda, *Bull. Chem. Soc., Japan* **1989**, *62*, 4055−4057.
[50] A. Casnati, P. Minari, A. Pochini, R. Ungaro, W. F. Nijenhuis, F. deJong, D. N. Reinhoudt, *Isr. J. Chem.* **1992**, *32*, 79−87.

Received April 16, 2003

 © 2003 Wiley-VCH Verlag GmbH & Co. KGaA, Weinheim

Synthesis and Structures of Fe^{III} Complexes Bridged by Cyanorhenium Clusters

Seon-Mi Park,[a] Youngmee Kim,[a] and Sung-Jin Kim*[a]

Keywords: Cluster compounds / Nanostructures / Magnetic properties / Rhenium / Iron

The reaction of FeCl(L1) and FeCl(L2) [L1 = bis(3-salicylideneaminopropyl)amine, L2 = bis(3-salicylideneaminopropyl)-methylamine] with the Re_6 clusters $[Re_6Q_8(CN)_6]^{4-}$ (Q = Se, Te) led to the formation of the nanomolecular (≈2.5 nm) compounds $[(CN)_2Re_6Se_8\{(CN)Fe(L1)\}_4]\cdot 7H_2O$ (**1**) and $[(CN)_2Re_6Te_8\{(CN)Fe(L2)\}_4]\cdot 4CH_3CN\cdot 4H_2O$ (**2**). Both compounds were characterized by single-crystal X-ray diffraction analysis. Compound **1** crystallizes in the triclinic space group $P\bar{1}$ with a = 12.2822(10), b = 14.2524(10), c = 15.8474(10) Å, α = 106.093(10)°, β = 101.992(10)°, γ = 92.438(10)°, and Z = 1. Compound **2** crystallizes in the orthorhombic space group *Pbca* with a = 19.3024(2), b = 16.8134(3), c = 35.9842(6) Å, and Z = 4. In these two compounds, only four pentadentate compartments are bonded to the Re_6 cluster for charge balancing. The magnetic-susceptibility data show that there is no evidence for interactions between Fe^{III} ions via the central Re_6 cluster in either compound. The observed effective magnetic moments suggest that there are low-spin Fe^{III} ions and high-spin Fe^{III} ions mixed in each compound.

(© Wiley-VCH Verlag GmbH & Co. KGaA, 69451 Weinheim, Germany, 2003)

Introduction

Over the past decade, molecule-based magnetic materials have been investigated extensively in the fields of physics and chemistry. A major target in these fields is to obtain discrete polynuclear compounds with high-spin ground states.[1−5] The well-known high-spin molecules were prepared by connecting a Prussian-blue-like hexacyanometallate and multidentate metal complexes via metal-CN-metal bonding;[6−17] the bridging cyanide ligand plays an important role in the spin interaction between metals.

Recently, water-soluble hexanuclear clusters $[Re_6Q_8(CN)_6]^{4-}$ (Q = S, Se, Te), which are an extended analogue of the Prussian-blue cluster $[Fe(CN)_6]^{4-}$, have been used to synthesize extended solid frameworks.[18−22] In these extended solid frameworks the metal ions are bridged by Re_6 clusters instead of Fe^{II} ions to form bigger cubic cavities which can include plenty of small solvent molecules as well as metal ions.[23−30] In a recent study we synthesized two- and three-dimensional frameworks containing $Mn(salen)^+$ units bridged by Re_6 clusters.[31,32] We found that changing the chalcogen Q in a $[Re_6Q_8(CN)_6]^{4-}$ cluster can control the dimensionality of infinite frameworks. We also synthesized discrete molecules, containing manganese porphyrin complexes instead of extended frameworks, which show a high catalytic activity in the epoxidation reaction of olefins by iodosylbenzene.[33] These results demonstrate that multinuclear metal clusters are good candidates as building blocks in the preparation of new heterogeneous catalysts and high-spin nanomolecules.

We now report new discrete nanomolecules containing high-spin Fe^{III} complexes linked to the Re_6 clusters $[(CN)_2Re_6Se_8\{(CN)Fe^{III}(L1)\}_4]\cdot 7H_2O$ and $[(CN)_2Re_6Te_8\{(CN)Fe^{III}(L2)\}_4]\cdot 4CH_3CN\cdot 4H_2O$ [L1 = bis(3-salicylideneaminopropyl)amine, L2 = bis(3-salicylideneaminopropyl)-methylamine]. These molecules can be described as expanded versions of $[Fe^{II}\{CNFe^{III}(L2)\}_6]Cl_2$.[16,17]

Results and Discussion

Synthesis and Characterization

Recently, a mixed-valence, mixed-spin, Prussian-blue-like heptanuclear complex was synthesized that contains a central low-spin S = 0 Fe^{II} ion linked to six high-spin S = 5/2 $Fe^{III}(L)$ species through cyanide bridges[16,17] [Equation (1)].

$$K_4[Fe(CN)_6] + Fe(L2)Cl \rightarrow [Fe^{II}\{CNFe^{III}(L2)\}_6]Cl_2 \quad (1)$$

The pentadentate ligand L2 [bis(3-salycylideneaminopropyl)methylamine], shown below, was used in this reaction.

[a] Department of Chemistry, Ewha Women's University, Seoul 120-750, Korea
Fax: (internat.) + 82-2/3277-2384
E-mail: sjkim@ewha.ac.kr

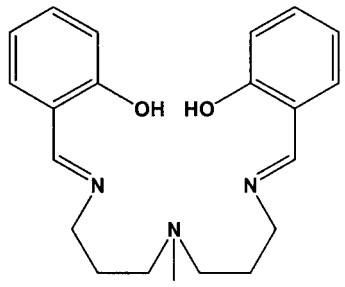

To obtain larger nanomolecules with similar pentadentate ligands, we used a face-capped octahedral Re_6 cluster ion instead of an Fe^{II} central ion. A similar reaction results in enlarged nanomolecules [Equation (2)].

$$Na_4[Re_6Q_8(CN)_6] + Fe(L1 \text{ or } L2)Cl \rightarrow [(CN)_2Re_6Q_8\{(CN)Fe(L1 \text{ or } L2)\}_4] \quad (2)$$

Nanomolecules $[(CN)_2Re_6Se_8\{(CN)Fe(L1)\}_4]\cdot 7H_2O$ (**1**) and $[(CN)_2Re_6Te_8\{(CN)Fe(L2)\}_4]\cdot 4CH_3CN\cdot 4H_2O$ (**2**) were prepared by a direct diffusion technique in which aqueous solutions of $Na_4[Re_6Se_8(CN)_6]$ and $Na_4[Re_6Te_8(CN)_6]$ were carefully layered with ethanol and acetonitrile solutions of FeCl(L1) and FeCl(L2), respectively. Single crystals of **1** and **2** were obtained within three days. We also tried to prepare $[(CN)_2Re_6Se_8\{(CN)Fe(L2)\}_4]$ and $[(CN)_2Re_6Te_8\{(CN)Fe(L1)\}_4]$, but we couldn't obtain suitable single crystals for a single crystal study. The IR spectra of **1** and **2** show all the peaks expected for the L1 and L2 ligand together with two peaks at 2117 and 2130 cm^{-1} originating from the vibrations of bridging and non-bridging cyanides.

Structure Description

$[(CN)_2Re_6Se_8\{(CN)Fe(L1)\}_4]\cdot 7H_2O$ (1, L1 = $C_{20}H_{23}N_3O_2$)

The asymmetric unit contains half an Re_6Se_8 cluster, two Fe(L1) units, and 3.5 water solvent molecules in a triclinic cell with $Z = 1$. A crystallographic center of inversion is located at the center of a Re_6Se_8 cluster. The structure of a complete molecule is shown in Figure 1. Four cyano groups of the Re_6Se_8 cluster are linked to the Fe(L1) unit with Fe−N(cyano) distances of 2.125(9) and 2.146(9) Å. The C(cyano)−N(cyano)−Fe angles are 154.6(9) and 154.1(9)°. The two oxygen atoms of the hydroxyl groups of the pentadentate ligand in $Fe(C_{20}H_{23}N_3O_2)$ unit are coordinated to the Fe^{III} ion, and are trans to the cyano group of the Re_6Se_8 cluster with O(hydroxy)−Fe−N(cyano) angles of 177.9(4)° and 177.6(4)°. Two salicylate groups are perpendicular to each other in linked Fe(L1) units. The distance between two Fe^{III} ions in the trans positions of the Re_6Se_8 cluster is around 14.1 Å. The largest distance between two atoms within compound **1** is over 2.5 nm, making it a nanosized molecule.

$[(CN)_2Re_6Te_8\{(CN)Fe(L2)\}_4]\cdot 4CH_3CN\cdot 4H_2O$ [2; L2 = $C_{20}H_{23}(NCH_3)N_2O_2$]

The asymmetric unit contains half an Re_6Te_8 cluster, two Fe(L2) units, and two acetonitrile and water solvent molecules in the space group *Pbca* with $Z = 4$. The complete

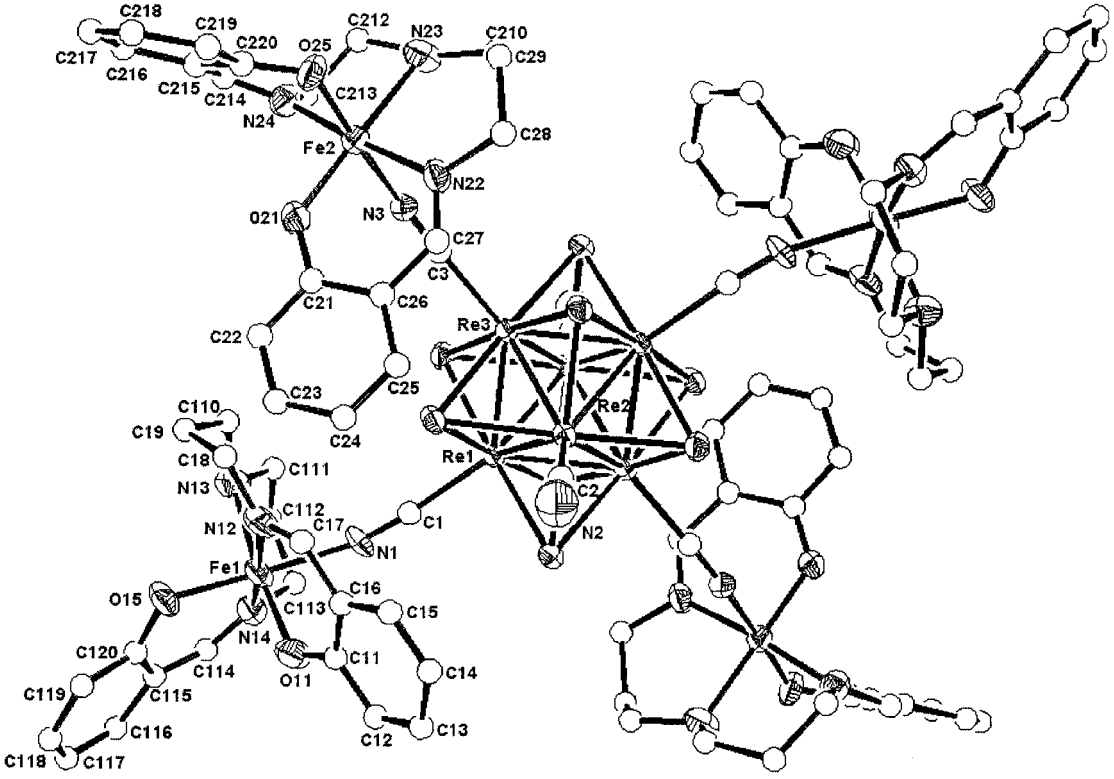

Figure 1. The structure of $[(CN)_2Re_6Se_8\{(CN)Fe(L1)\}_4]$; all hydrogen atoms have been omitted for clarity

 © 2003 Wiley-VCH Verlag GmbH & Co. KGaA, Weinheim

structure is generated by the symmetry operation ($-x$, $-y + 1$, $-z + 1$). Figure 2 shows a whole molecule with Fe−N(cyano) distances of 2.070(10) and 2.070(9) Å. In contrast to compound **1**, The C(cyano)−N(cyano)−Fe angles in compound **2** are almost linear at 175.1(10)° and 177.8(11)°. The O(hydroxy)−Fe−N(cyano) angles are 177.9(4)° and 179.0(4)°. The distance between two Fe^{III} ions in the trans positions of the Re_6Te_8 cluster is around 14.4 Å. The largest distance between two atoms within the compound **2** is over 2.4 nm.

In the Re_6 cluster-centered compounds **1** and **2** the Re_6 clusters are linked to only four Fe^{III} complexes, whereas in the Fe^{II}-centered compound there are six Fe^{III} complexes attached in $[Fe^{II}\{CNFe^{III}(L2)\}_6]Cl_2$. The Re_6 cluster-centered compounds do not need any cations or anions to balance the charge while the Fe^{II}-centered compound contains two chloro anions. It is known that the Fe−N distance of low-spin complexes is shorter(ca. 1.9 Å) than that of high-spin complexes (ca. 2.2 Å). The Fe−N distances observed in the title compounds are between those reported in high-spin Fe^{III} complexes and low-spin Fe^{III} complexes.[40,41] In the Re_6 cluster-centered molecule, the distance between Fe^{III} ions through the central Re_6 cluster is about 14 Å, which is much longer than in the Fe^{II}-containing molecule (ca. 10 Å). The size of the Re_6 cluster-centered molecule is more than 2.5 nm, as compared to that of the Fe^{II}-centered molecule (2 nm).

Magnetic Properties

The temperature-dependent magnetic data of both compounds **1** and **2** are shown in Figure 3. The magnetic susceptibility data of both **1** and **2** can be clearly described using the Curie−Weiss law $\chi = \chi_o + C/(T - \theta)$. At room temperature, the effective magnetic moments of compounds **1** and **2** are 9.97 and 9.91 μ_B, respectively. These values are close to the value for a molecule with two uncoupled high-spin and two uncoupled low-spin Fe^{III} ions. There is no evidence of magnetic exchange coupling between Fe^{III} ions via the central Re_6 cluster in either compound, while the magnetic properties of the Fe^{II} ion-centered compound revealed a ferromagnetic interaction between the high-spin Fe^{III} ions of six ligands around Fe^{II}. The reason for the absence of magnetic coupling between Fe^{III} ligands in the title compounds is because the central diamagnetic Re_6 cluster core is too large to mediate magnetic interactions.

In summary, we have synthesized new Re_6 cluster-centered nanosize molecules with four Fe^{III} complexes connected to $[Re_6Q_8]^{2+}$ (Q = Se, Te) clusters. This demonstrates that an Re_6-type multinuclear metal cluster can be an effective basis to make new molecules by bridging multidentate

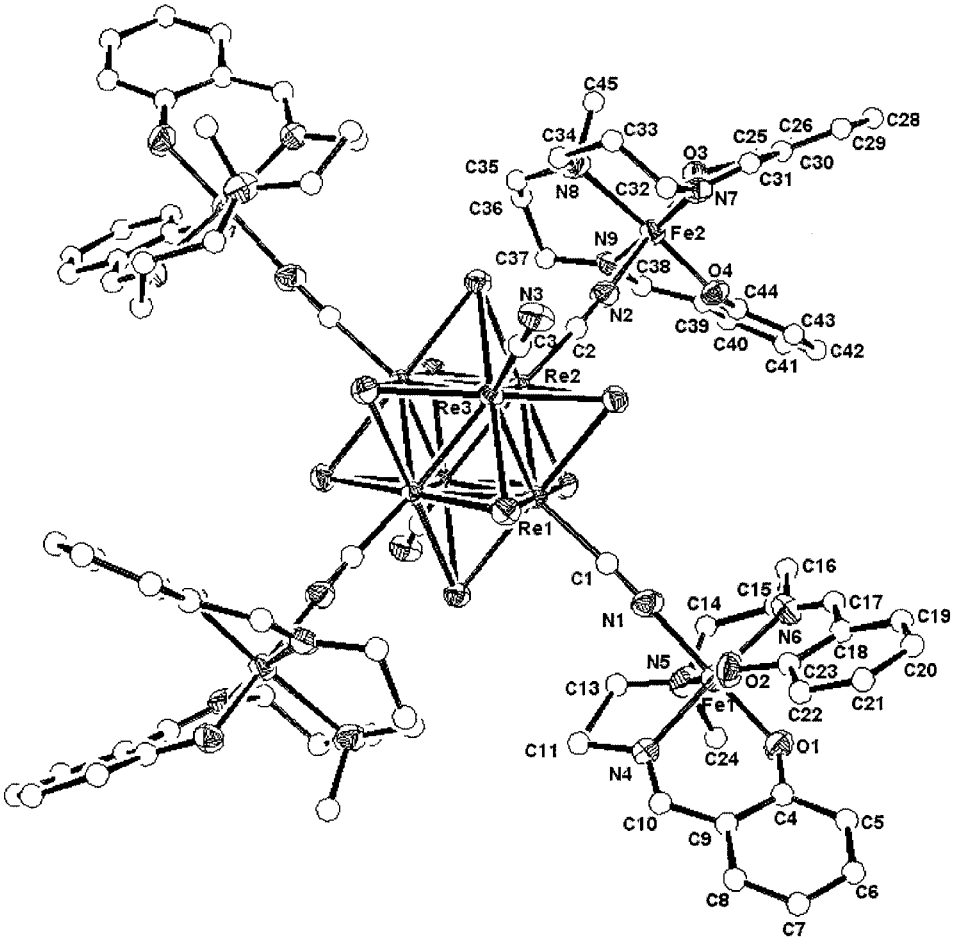

Figure 2. The structure of $[(CN)_2Re_6Te_8\{(CN)Fe(L2)\}_4]$; all hydrogen atoms have been omitted for clarity

 © 2003 Wiley-VCH Verlag GmbH & Co. KGaA, Weinheim

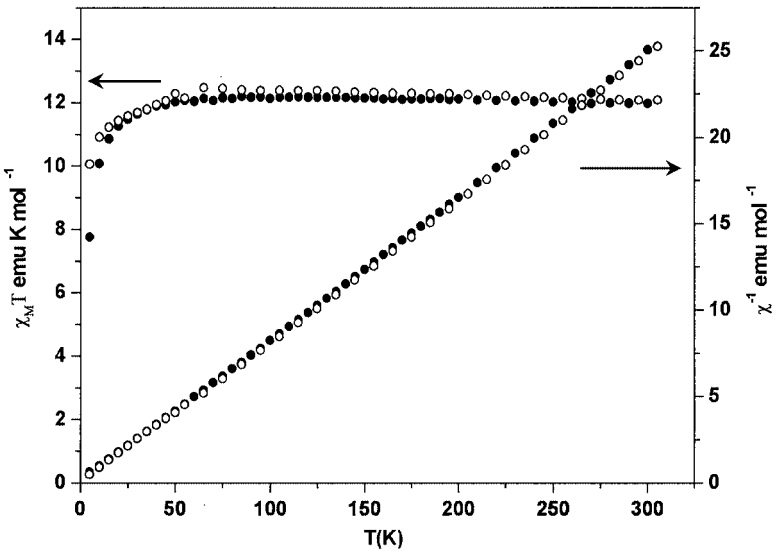

Figure 3. The magnetic susceptibility data and reciprocal susceptibility data of compound **1** (filled circle) and compound **2** (open circle) as a function of temperature

ligands. These results also suggest that if we choose proper magnetic elements for the similar M_6-type (M = transition metals such as Mo, Nb, W) multinuclear metal clusters, magnetic coupling between the M_6-type cluster and the ligand metal complex could be achieved.

Experimental Section

General Remarks: All experimental manipulations were performed in air. The compounds FeCl(L1), FeCl(L2), and $Na_4[Re_6Q_8(CN)_6]$ (Q = Se, Te) were prepared as described previously.[11,18] Other reagents were purchased from Aldrich and used as received. IR spectra were measured on a BIO RAD FTS 135 spectrometer as KBr pellets. Elemental analysis for carbon, nitrogen, and hydrogen was carried by using an EA1108 (Carlo Erba Instrument, Italy). Magnetic susceptibility data were obtained with an MPMS5 Quantum Design SQUID magnetometer. The magnetic measurements on single crystals were carried out under increasing temperatures (5−300 K) with a 5000 G applied field.

FeCl(L1): A typical preparation produced black crystals (yield: 75%). $C_{20}H_{23}ClFeN_3O_2$ (428.7): calcd. C 56.03, H 5.40, N 9.80; found C 55.92, H 5.60, N 9.94.

FeCl(L2): A typical preparation produced black crystals (yield: 78%). $C_{21}H_{25}ClFeN_3O_2$ (442.7): calcd. C 57.99, H 5.82, N 9.56; found C 56.97, H 5.69, N 9.49.

$[(CN)_2Re_6Se_8\{(CN)Fe(L1)\}_4]\cdot 7H_2O$ (1): Dark purple rod-type crystals were obtained by the direct diffusion technique. A water solution of $Na_4[Re_6Se_8(CN)_6]$ was carefully layered with an ethanol solution of FeCl(L1). IR (KBr): ν(CN) 2117 cm^{-1}.

Table 1. Crystallographic data for compound **1** and **2**

	1	**2**
Empirical formula	$C_{86}H_{88}Fe_4N_{18}O_{15}Re_6Se_8$	$C_{98}H_{124}Fe_4N_{22}O_{12}Re_6Te_8$
Molecular weight	3586.02	4163.59
Temperature	293(2) K	150(2) K
Wavelength	0.71074 Å	0.71073 Å
Crystal system, space group	Triclinic, $P\bar{1}$	Orthorhombic, *Pbca*
a (Å)	12.2822(10)	19.3024(2)
b (Å)	14.2524(10)	16.8134(3)
c (Å)	15.8474(10)	35.9842(6)
α (°)	106.093(10)	90
β (°)	101.992(10)	90
γ (°)	92.438(10)	90
Volume (Å^3)	2592.4(3)	11678.3(3)
Z, calculated density (mg/m^3)	1, 2.297	4, 2.368
Reflections collected/unique	10881/10162 [*R*(int) = 0.0347]	48836/10285 [*R*(int) = 0.0913]
Data/restraints/parameters	10162/0/612	10285/0/677
Goodness-of-fit on F^2	1.036	1.065
Final *R* indices [$I > 2\sigma(I)$]	*R*1 = 0.0521, *wR*2 = 0.1446	*R*1 = 0.0507, *wR*2 = 0.1186
R indices (all data)	*R*1 = 0.0793, *wR*2 = 0.1600	*R*1 = 0.0737, *wR*2 = 0.1301
Largest diff. peak	3.935	1.707

 © 2003 Wiley-VCH Verlag GmbH & Co. KGaA, Weinheim

$C_{86}H_{88}Fe_4N_{18}O_{15}Re_6Se_8$ (3586.0): calcd. C 29.34, H 2.65, N 7.11; found C 29.70, H 2.67, N 7.25.

$[(CN)_2Re_6Te_8\{(CN)Fe(L2)\}_4]\cdot 4CH_3CN\cdot 4H_2O$ (2): Dark purple plate crystals were also obtained by the direct diffusion technique. A water solution of $Na_4[Re_6Te_8(CN)_6]$ was carefully layered with an acetonitrile solution of FeCl(L2). IR (KBr): ν(CN) 2117 cm^{-1}. $C_{98}H_{124}Fe_4N_{22}O_{12}Re_6Te_8$ (4163.6): calcd. C 27.44, H 2.51, N 6.36; found C 27.55, H 2.57, N 6.43.

X-ray Crystallographic Study: The X-ray diffraction data for compound **1** were collected on an Enraf−Nonius CAD-4 Mach3 diffractometer equipped with a monochromator in the Mo-K_α (λ = 0.71073 Å) incident beam. The crystal was mounted on a glass fiber. A description of the data collection techniques for this diffractometer has been given before.[34] The final cell parameters for **1** were obtained from least-squares fit to 25 reflections in the range $9.44 \leq \theta \leq 10.62°$. Intensities were corrected for Lorentz and polarization effects but not for absorption. The crystal structure was determined by direct methods and Fourier techniques. All the calculations were performed on an IBM Pentium computer using SHELXS-97 and SHELXL-97, and atomic scattering factors for all non-hydrogen atoms were supplied by SHELXS-97.[35] All hydrogen atoms were located in the calculated positions. The molecular structure was drawn with the Ortep-3 for Windows program.[36] The diffraction data for compound **2** were collected on a Nonius Kappa-CCD diffractometer using Mo-K_α (λ = 0.71073 Å) radiation.[37] The crystals were mounted on glass fibers in epoxy resin. The CCD data were integrated and scaled using the DENZO-SMN software package,[38] and the structures were solved and refined by using SHEXTL V5.0.[39] All non-hydrogen atoms were located in the calculated positions. The crystallographic data for compounds **1** and **2** are listed in Table 1.

CCDC-206671 (**1**) and -206672 (**2**) contain the supplementary crystallographic data for this paper. These data can be obtained free of charge at www.ccdc.cam.ac.uk/conts/retrieving.html [or from the Cambridge Crystallographic Data Centre, 12, Union Road, Cambridge CB2 1EZ, UK; fax: (internat.) +44-1223/336-033; E-mail: deposit@ccdc.cam.ac.uk].

Acknowledgments

Financial support from the Ministry of Science and Technology (MOST) of KOREA is gratefully acknowledged.

[1] E. D. Dahlberg, J.-G. Zhu, *Phys. Today* **1995**, *48*, 34−40.
[2] D. D. Awschalom, D. P. Di Vicenzo, *Phys. Today* **1995**, *48*, 43−48.
[3] R. Sessoli, H.-L. Tsai, A. R. Schake, S. Wang, J. B. Vincent, K. Folting, D. Gatteschi, G. Christou, D. N. Hendrickson, *J. Am. Chem. Soc.* **1993**, *115*, 1804−1816.
[4] R. Sessoli, D. Gatteschi, A. Caneschi, M. A. Novak, *Nature* **1993**, *365*, 141−143.
[5] L. Thomas, F. Ballou, D. Gatteschi, R. Sessoli, B. Babara, *Nature* **1996**, *383*, 145−147.
[6] J. L. Heinrich, P. A. Berseth, J. R. Long, *Chem. Commun.* **1998**, 1231−1232.
[7] F. Bodadio, M. Gross, H. Stoeckli-Evans, S. Decurtins, *Inorg. Chem.* **2002**, *41*, 5891−5896.
[8] R. J. Parker, L. Spiccia, B. Moubaraki, K. S. Murray, D. C. Hockless, A. D. Rae, A. C. Willis, *Inorg. Chem.* **2002**, *41*, 2489−2495.
[9] J. Y. Yang, M. P. Shores, J. J. Sokol, J. R. Long, *Inorg. Chem.* **2003**, *42*, 1403−1419.
[10] J. J. Sokol, M. P. Shores, J. R. Long, *Inorg. Chem.* **2002**, *41*, 3052−3054.
[11] H.-Z. Kou, S. Gao, C.-H. Li, D.-Z. Liao, B.-C. Zhou, R.-J. Wang, Y. Li, *Inorg. Chem.* **2002**, *41*, 4756−4762.
[12] J. J. Sokol, A. G. Hee, J. R. Long, *J. Am. Chem. Soc.* **2002**, *124*, 7656−7657.
[13] P. A. Berseth, J. J. Sokol, M. P. Shores, J. L. Heinrich, J. R. Long, *J. Am. Chem. Soc.* **2000**, *120*, 9655−9662.
[14] R. J. Parker, L. Spiccia, K. J. Berry, G. D. Fallon, B. Moubaraki, K. S. Murray, *Chem. Commun.* **2001**, 333−334.
[15] Z. J. Zhong, H. Seino, Y. Mizobe, M. Hidai, A. Fujishima, S. Ohkoshi, K. Hashimoto, *J. Am. Chem. Soc.* **2000**, *122*, 2952−2953.
[16] G. Rogez, A. Marvilliers, E. Riviere, J.-P. Audiere, F. Lloret, F. Varret, A. Goujon, N. Mendenez, J.-J. Girered, T. Mallah, *Angew. Chem. Int. Ed.* **2000**, *39*, 2885−2887.
[17] G. Rogez, S. Parsons, C. Paulsen, V. Villar, T. Mallah, *Inorg. Chem.* **2001**, *40*, 3836−3837.
[18] Y. V. Mironov, J. A. Cody, T. E. Albrecht-Schmitt, J. A. Ibers, *J. Am. Chem. Soc.* **1997**, *119*, 493−498.
[19] J. P. Gabriel, K. Boubekeur, S. Uriel, P. Batail, *Chem. Rev.* **2001**, *101*, 2037−2066.
[20] K. R. Dunbar, R. A. Heintz, *Prog. Inorg. Chem.* **1997**, *45* 283−392.
[21] W. P. Fehlhammer, M. Fritz, *Chem. Rev.* **1993**, *93*, 1243−1280.
[22] M. P. Shores, L. G. Beauvais, J. R. Long, *J. Am. Chem. Soc.* **1999**, *121*, 775−779.
[23] M. V. Bennett, L. G. Beauvais, M. P. Shores, J. R. Long, *J. Am. Chem. Soc.* **2001**, *123*, 8022−8032.
[24] L. G. Beauvais, M. P. Shores, J. R. Long, *Chem. Mater.* **1998**, *10*, 3783−3786.
[25] N. G. Naumov, A. V. Virovets, M. N. Sokolov, S. B. Artemkina, V. E. Fedorov, *Angew. Chem. Int. Ed.* **1998**, *37*, 1943−1945.
[26] L. G. Beauvais, M. P. Shores, J. R. Long, *J. Am. Chem. Soc.* **2000**, *122*, 2763−2772.
[27] M. V. Bennett, M. P. Shores, L. G. Beauvais, J. R. Long, *J. Am. Chem. Soc.* **2000**, *122*, 6664−6668.
[28] N. G. Naumov, A. V. Virvets, V. E. Fedorov, *Inorg. Chem. Commun.* **2000**, *3*, 71−72.
[29] M. P. Shores, L. G. Beauvais, J. R. Long, *Inorg. Chem.* **1999**, *38*, 1648−1649.
[30] N. G. Naumov, D. V. Soldatov, J. A. Ripmeester, S. B. Artemkina, V. E. Fedorov, *Chem. Commun.* **2001**, 571−572.
[31] Y. Kim, S.-M. Park, W. Nam, S.-J. Kim, *Chem. Commun.* **2001**, 1470−1471.
[32] Y. Kim, S.-M. Park, S.-J. Kim, *Inorg. Chem. Commun.* **2002**, *5*, 592−595.
[33] Y. Kim, S. K. Choi, S.-M. Park, W. Nam, S.-J. Kim, *Inorg. Chem. Commun.* **2002**, *5*, 612−615.
[34] A. Bino, F. A. Cotton, P. E. Fanwick, *Inorg. Chem.* **1979**, *18*, 3558−3562.
[35] G. M. Sheldrick, *SHELXS-97* Universität Göttingen, **1997**; *SHELXL-97*, Universität Göttingen, **1997**.
[36] L. J. Farrugia, *J. Appl. Cryst.* **1997**, 565.
[37] Nonius. Kappa-CCD Server software. Nonius B. V., Delft, The Netherlands. **1997**.
[38] Z. Otwinowski, W. Minor, *Methods Enzymol.* **1997**, *176*, 307−325.
[39] G. M. Sheldrick, *SHELXTL/PC.* Version 5.1 Windows NT Version. Bruker AXS Inc., Madisin, USA. **1998**.
[40] J. Baker, L. M. Engelhardt, B. N. Figgis, A. H. White, *J. Chem. Soc., Dalton Trans.* **1975**, 530.
[41] J. C. A. Boeyens, A. G. S. Forbes, R. D. Hancock, K. Wieghardt, *Inorg. Chem.* **1985**, *24*, 2926.

Received May 1, 2003
Early View Article
Published Online October 2, 2003

 © 2003 Wiley-VCH Verlag GmbH & Co. KGaA, Weinheim

EurJIC
European Journal of Inorganic Chemistry

Issue 23/2003

Pages 4123–4262

Papers available ahead of print in Early View at www.interscience.wiley.com

Earliest available Table of Contents:
Automatically, free of charge by e-mail through
www.interscience.wiley.com/alerts

COVER PICTURE

The cover picture shows the structures of two new types of calix[4]arene complexes obtained by deprotonating the calixarene with an alkaline earth metal, or potassium metal, followed by reaction with selected titanium(IV) compounds. The alkaline earth metals form dimeric alkaline earth-titanium(IV) complexes, containing at the core a rhombus of alternating alkaline earth metal and μ_3-oxo centres. Each oxo centre of the rhombic core is the apical ligand of a square-pyramidal titanium(IV) centre, whose basal plane donors are the four phenolate oxygen atoms from a calix[4]arene arrayed in the symmetrical cone conformation. Terminal methanol ligands surround the alkaline earth centres, and simultaneously hydrogen-bond to the adjacent phenolate oxygen atoms. Potassium reacts with calix[4]arene and the titanium(IV) source to give a monomeric mixed potassium-titanium complex. The potassium cation binds within the π-basic calix[4]arene cavity, whilst the titanium centre is octahedrally complexed in the *exo* position by four phenolate and one acetylacetonate ligands. A solution pathway exists for the interconversion between the potassium-titanium calix[4]arene monomer and the alkaline earth-titanium dimers, where the product is dictated by the choice of solvent. Details are discussed in the article by R. N. Lamb et al. on p. 4153 ff.

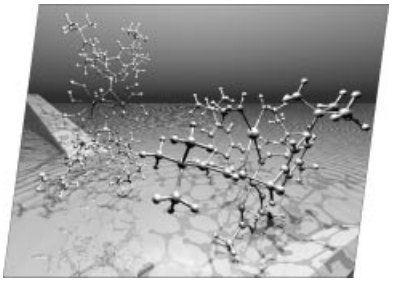

MICROREVIEW

Contents

4137 **C. Belle,* J.-L. Pierre***

Asymmetry in Bridged Binuclear Metalloenzymes: Lessons for the Chemist

Keywords: Unsymmetrical binuclear metalloenzymes / Superoxide dismutase / Purple acid phosphatases / Catechol oxidases / Model complexes

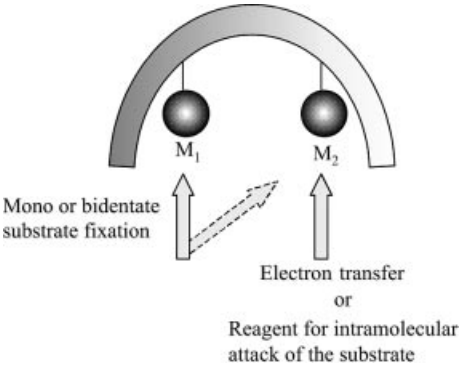

 © 2003 Wiley-VCH Verlag GmbH & Co. KGaA, Weinheim

SHORT COMMUNICATION

4147 **J. Duran, A. Polo,* J. Real,* J. Benet-Buchholz, A. Poater, M. Solà**

Stereodiscrimination in Phosphanylthiolato Nickel(II) Complexes

Keywords: Nickel / P,S ligands / Conformation Analysis / Chiral resolution / Density functional calculations

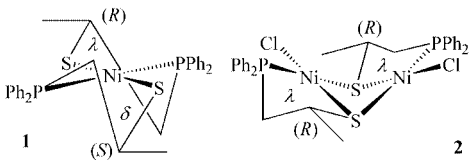

FULL PAPERS

4153 **A. J. Petrella, N. K. Roberts, C. L. Raston, D. C. Craig, M. Thornton-Pett, R. N. Lamb***

Heterobimetallic Calix[4]arene Complexes: Interconversion of Dimeric (Ca, Sr or Ba)/Ti^{IV} Complexes with a Monomeric K/Ti^{IV} Complex

Keywords: Calixarenes / Heterometallic complexes / Alkaline earth metals / Potassium / Titanium

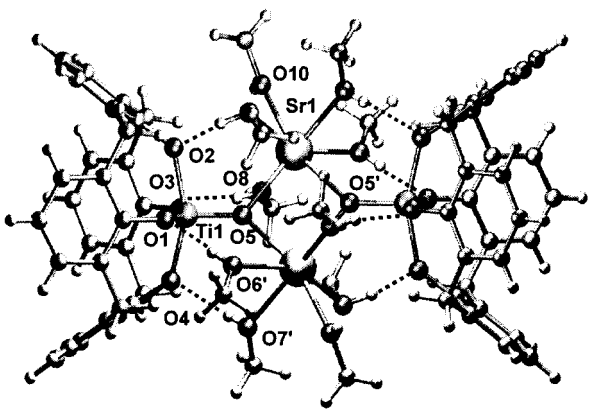

4159 **J. A. Cabeza,* I. del Río, V. Riera, M. Suárez, C. Álvarez-Rúa, S. García-Granda, S. H. Chuang, J. R. Hwu***

Di- and Trinuclear Ruthenium and Osmium Bis(2-pyridyl) Ketone Oximate Derivatives

Keywords: Ruthenium / Osmium / Cluster compounds / Oximes / DNA cleavage

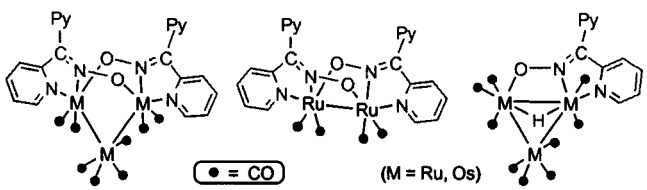

4166 **P. Barbaro,* C. Bianchini, G. Giambastiani,* A. Togni**

Ruthenium(II) Complexes with Triphosphane Ligands Combining Planar, Phosphorus, and Carbon Chirality: Application to Asymmetric Reduction of Trifluoroacetophenone

Keywords: Asymmetric catalysis / Tridentate ligands / Ruthenium / Hydrogen transfer / Chiral ferrocenyls

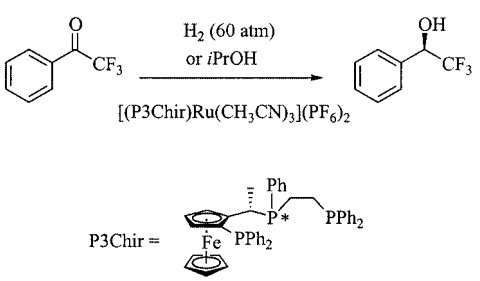

4173 **J.-M. Rueff, S. Pillet, G. Bonaventure, M. Souhassou, P. Rabu***

Synthesis, Structure and Magnetic Properties of the Cobalt(II) 1,1′-Biphenyl-2,2′-dicarboxylate Hydroxide Chain Compound $[Co_3\{O_2CC_{12}H_8\text{-}CO_2\}_{2.5}(OH)(H_2O)_2]_n$

Keywords: Carboxylate ligands / Hydrothermal synthesis / Cobalt / Magnetic properties

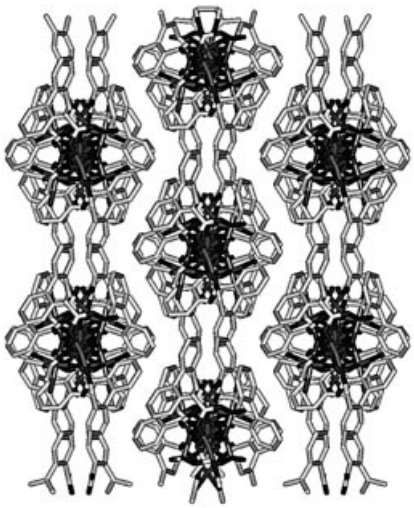

4179 **F. Avecilla,* J. A. Peters, C. F. G. C. Geraldes***

X-ray Crystal Structure of a Sodium Salt of $[Gd(DOTP)]^{5-}$: Implications for Its Second-Sphere Relaxivity and the ^{23}Na NMR Hyperfine Shift Effects of $[Tm(DOTP)]^{5-}$

Keywords: Gadolinium / Imaging agents / Solid-state structures / Hydration / NMR shift reagents

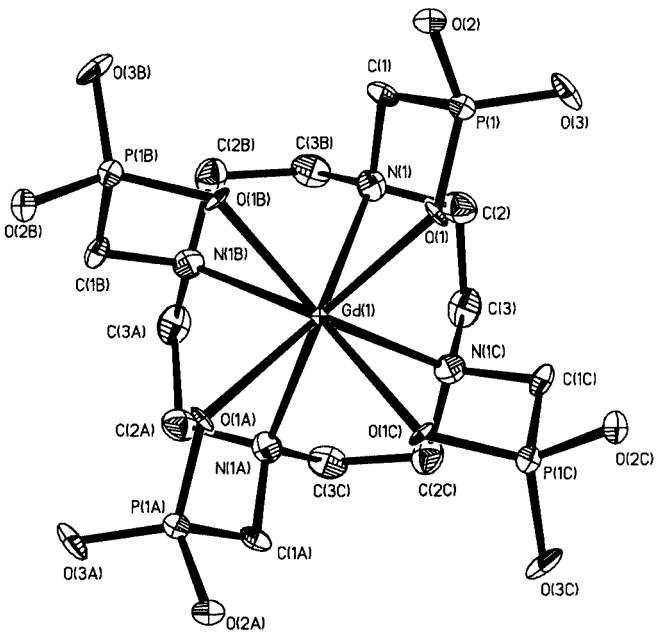

4187 **A. Lledós,* M. Moreno-Mañas,* M. Sodupe, A. Vallribera, I. Mata, B. Martínez, E. Molins***

Bent and Linear Forms of the (μ-Oxo)bis[trichloroferrate(III)] Dianion: An Intermolecular Effect − Structural, Electronic and Magnetic Properties

Keywords: Iron / Oxygen / (μ-Oxo)trichloroferrate dianion / Packing effects / Magnetic properties / DFT calculations

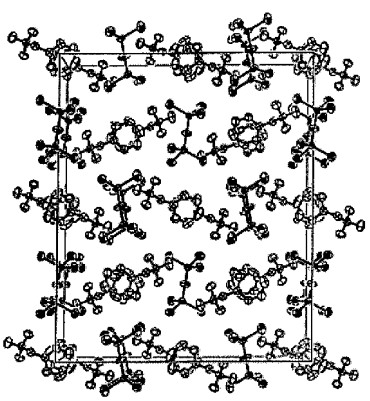

 © 2003 Wiley-VCH Verlag GmbH & Co. KGaA, Weinheim

4195 **J. Arpalahti,* K. D. Klika**

Platinum−Nitrogen Bond Rearrangements in Isomeric *cis*-$Pt^{II}(NH_3)_2$-bis(9-methyladenine) Complexes under Alkaline Conditions

Keywords: Platinum / Nucleobases / Antitumor agents / N ligands

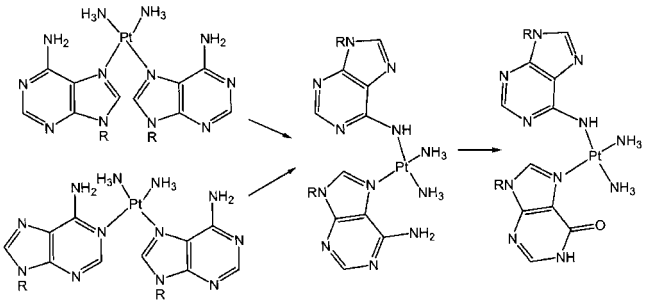

4202 **Q.-J. Pan, H.-X. Zhang***

Ab initio Study on Luminescence and Aurophilicity of a Dinuclear $[(AuPH_3)_2$(i-mnt)] Complex (i-mnt = isomer-Malononitriledithiolate)

Keywords: Ab initio calculations / Luminescence / Aurophilicity / Excited state

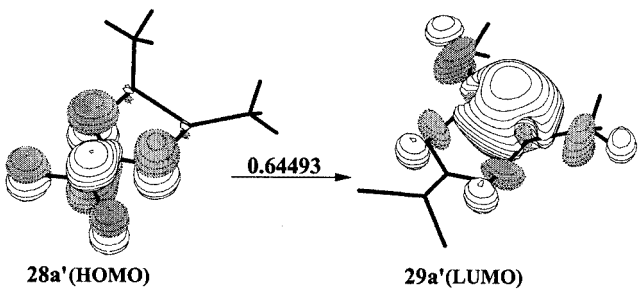

4211 **B.-P. Yang, J.-G. Mao,* Y.-Q. Sun, H.-H. Zhao, A. Clearfield**

Syntheses, Characterizations, and Crystal Structures of Three New Metal Phosphonocarboxylates with a Layered and a Microporous Structure

Keywords: Metal phosphonates / Hydrothermal reactions / Lead / Layered compounds / Cluster compounds

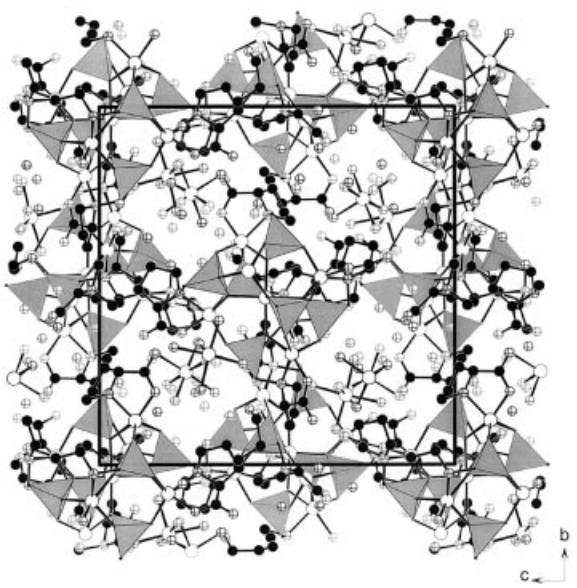

4218 **J.-L. Song, J.-G. Mao,* Y. Q. Sun, A. Clearfield**

Novel Hybrid Porous 3D Networks of Lead(II) Diphosphonate and Triphosphonate Containing 1,3,5-Benzenetricarboxylate

Keywords: Synthetic methods / Lead / Carboxylate ligands / P ligands

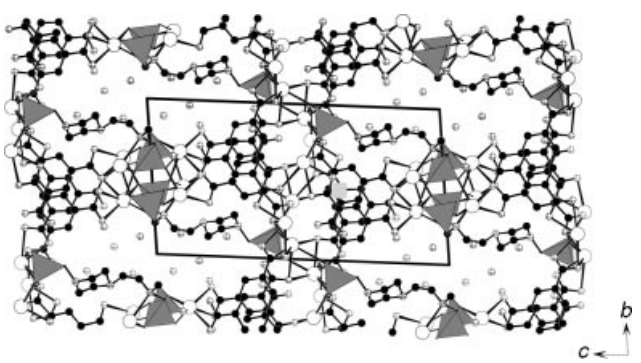

 © 2003 Wiley-VCH Verlag GmbH & Co. KGaA, Weinheim

4227 **I. Rusonik, H. Polat, H. Cohen, D. Meyerstein***

Reaction of Methyl Radicals with Metal Powders Immersed in Aqueous Solutions

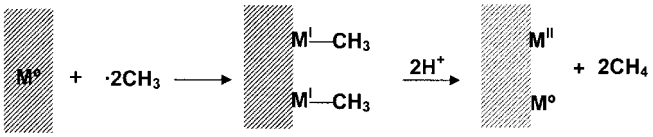

Keywords: Carbon / Energy transfer / Radicals / Oxidation

4234 **W. Chen, F. Liu, T. Nishioka, K. Matsumoto***

Heterotrimetallic Complexes [{Pt(RNH_2)$_2$(μ-NHCO*t*Bu)$_2$}$_2$M](ClO_4)*n* (M = Mn, Co, Cu, Ni, Cd, and Zn, *n* = 2; M = In, *n* = 3), [{Pt(NH_3)(μ-DACHCO*t*Bu)(μ-NHCO*t*Bu)}$_2$-Ni](ClO_4)$_2$, and [{Pt(RNH_2)$_2$(NHCO*t*Bu)$_2$}$_3$-Ag_3](ClO_4)$_3$ Bridged by Amidate Ligands: A Novel Amidate−Amine Interligand Reaction During the Pt−Ni Bond Formation

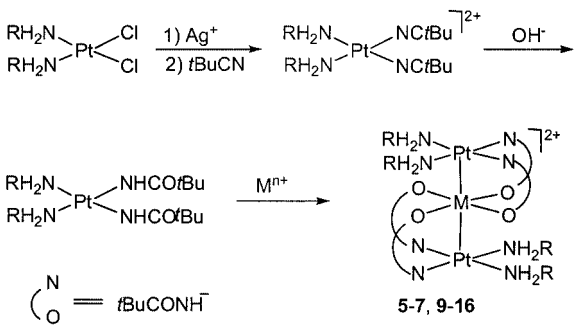

Keywords: Platinum / Amidate ligand / Metal−metal interaction / Heterotrimetallic complexes / Nickel

4244 **Sat. Pal, Sam. Pal***

Ruthenium(III) Complexes with a Phenolate-O, Imine-N, and Amide-O Coordinating Ligand: Syntheses, Structures, Properties, and Protonation Studies of Coordinated Amide

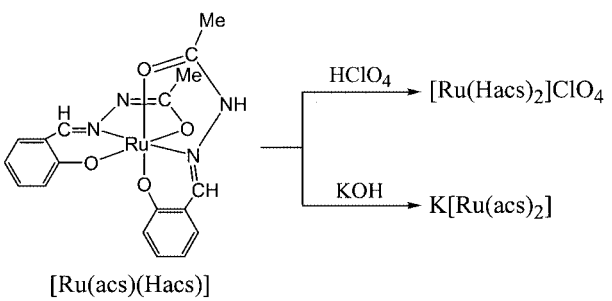

Keywords: Ruthenium / Acetylhydrazone / Crystal structures / Protonation / Redox chemistry

4253 **R. Bhattacharya, A. Ghosh,* M. S. Ray, L. Righi, G. Bocelli, S. Chaudhuri, R. D. Willet, J. M. Clemente-Juan, E. Coronado, C. J. Goméz-Garcia**

Synthesis, Crystal Structure, Thermal Analysis and Magnetic Behavior of a Novel One-Dimensional Polymeric Pyridinium Chlorocuprate(II): $(Hpy)_2[Cu_3Cl_8(H_2O)_2]$

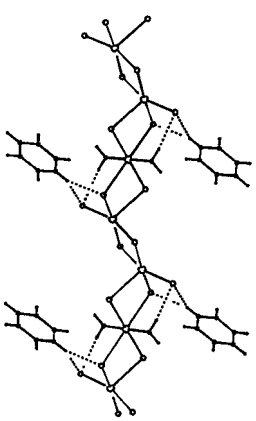

Keywords: Coordination polymers / Copper / Magnetic properties / N ligands / X-ray crystallography

 © 2003 Wiley-VCH Verlag GmbH & Co. KGaA, Weinheim

CORRECTIONS

4261 **P. Liptau, L. Tebben, G. Kehr, B. Wibbeling, R. Fröhlich, G. Erker***

Preparation of Optically Active α-Amino[3]-ferrocenophanes − Building Blocks for Chelate Ligands in Asymmetric Catalysis

Keywords: Ferrocenes / Ferrocenophanes / Chelate ligands

4262 **M. Heitzmann, J.-C. Moutet,* J. Pécaut, O. Reynes, G. Royal,* E. Saint-Aman, G. Serratrice**

Modulation of the Communication between Redox Centers in a Tris(ferrocene)-tren Ligand by Complexation of Lanthanide Ions

Keywords: Sandwich complexes / Electrostatic interactions / Electrochemistry / Lanthanides

 © 2003 Wiley-VCH Verlag GmbH & Co. KGaA, Weinheim

Asymmetry in Bridged Binuclear Metalloenzymes: Lessons for the Chemist

Catherine Belle,*[a] and Jean-Louis Pierre*[a]

Keywords: Unsymmetrical binuclear metalloenzymes / Superoxide dismutase / Purple acid phosphatases / Catechol oxidases / Model complexes

This microreview describes the structures, properties and mechanisms of three selected bimetallic enzymes: Cu-Zn superoxide dismutase (SOD), purple acid phosphatases (PAPs) and catechol oxidases (COs). The relevance of the unsymmetrical structures in the binucleating environment to the reaction mechanism and the respective roles of each metal center of these enzymes are discussed. Relevant model compounds are also considered.
(© Wiley-VCH Verlag GmbH & Co. KGaA, 69451 Weinheim, Germany, 2003)

Introduction

The active site of numerous homobinuclear and heterobinuclear metalloenzymes contains two metal centers, bridged by oxo, hydroxo, carboxylate or imidazolate groups. Even for homobinuclear sites the two metal centers usually reside in chemically different environments, an asymmetry that may also involve the coordination numbers and the geometry of the metal centers. One, two or three bridging groups may be encountered, for example: one imidazolate bridge in Cu-Zn superoxide dismutase, one oxygen and one carboxylate in the diiron enzyme ribonucleotide reductase B_2, one hydroxy and two carboxylates in the diiron enzyme deoxyhemerythrin.

[a] LEDSS, Chimie Biomimétique, UMR CNRS 5616, Université J. Fourier,
B. P. 53, 38041 Grenoble Cedex, France
Fax: (internat.) +33-4-76514836
E-mail: Catherine.Belle@ujf-grenoble.fr
Jean-Louis.Pierre@ujf-grenoble.fr

One challenging problem presented by these binuclear enzymes and their models is to elucidate the overall catalytic mechanism and to identify the roles of the metal ions. These may include:

– activation (fixation) of the substrate,

– stabilization of a transition state by metal ion coordination, hydrogen bonding or proton transfer,

– nucleophile generation via proton abstraction by a basic group,

– nucleophilic attack on the substrate by a functional group or by metal-coordinated hydroxide.

We will focus here on the respective roles of the two metal centers of the selected metalloenzymes (whose essential features are summarized in Table 1). The electronic structures of the metal centers of the enzymes have been described in recent reviews.[1−4] We also indicate selected synthetic models for these enzymes. The identification of small well-defined molecules with unsymmetrical bimetallic centers is

Jean-Louis Pierre was born in France in 1939. He is Professor of Chemistry at the Joseph Fourier University in Grenoble. He worked for several years in the field of stereochemistry before turning to bioinorganic chemistry. His current research interests include iron transport and metabolism in living systems, and biomimetism of redox metalloenzymes. He is the author of several books on Chemistry and Stereochemistry.

Catherine Belle received her Chemical Engineering degree in 1985 in Marseilles. She obtained her PhD in 1988 at the University of Marseilles under the supervision of Pr. R. Gallo. After a two-year postdoctoral stay at the University of Firenze (Italy) with Pr. A. Guarna she joined the research group of Pr. J. L. Pierre in Grenoble in 1991, where she now works as a CNRS researcher (senior researcher). She has launched new research axes in biomimetic chemistry, especially on purple acid phosphatases and catechol oxidases models.

MICROREVIEWS: This feature introduces the readers to the author's research through a concise overview of the selected topic. Reference to important work from others in the field is included.

Table 1. Three selected enzymes with unsymmetrical binuclear sites

Enzyme	Function	Nature of the bridge(s) (Intermetallic distance)	Nature of the asymmetry	Ref.
Cu^{II}-Zn^{II} Superoxide dismutase (SOD)	O_2^- dismutation	Imidazolate (6.3 Å)	Heterobinuclear Cu^{II} ligands: four His and one H_2O removed by substrate Zn^{II} ligands: three His and one carboxylate	[5]
Fe^{II}-Fe^{III} or Zn^{II}-Fe^{III} Purple acid phosphatases (PAP)	Hydrolysis of phosphoric esters	One hydroxo and one monodentate carboxylate (3.31 Å [Fe^{II}-Fe^{III}]) (3.26 Å [Zn^{II}-Fe^{III}])	Mixed valence or heterobinuclear Fe^{III} ligands: one His, one Tyr, one hydroxo and one carboxylate (Asp) Fe^{II} (or Zn^{II}) ligands: two His, one carboxylate (Asp) and one H_2O	[4,6–10]
Cu^{II}-Cu^{II} Catechol oxidase (CO)	Oxidation of *o*-diphenols to quinones	One hydroxo (2.87 Å)	Cu_A ligands: three His, one of them covalently linked by an unusual thioether bond to a cystein Cu_B ligands: three His	[11–13]

relevant in catalysis and in understanding the enzymatic processes, and will increase our understanding of the advantages of asymmetry in binuclear metallocatalysts.

Cu-Zn Superoxide Dismutase: A Redox Heterobinuclear Enzyme with only One Metal Center Involved in the Catalytic Cycle

Structural and Functional Aspects of Cu-Zn SOD

Copper-zinc superoxide dismutase (SOD) is composed of two identical subunits, each containing in its active site an imidazolate-bridged bimetallic center with one copper(II) and one zinc(II) ion.[5] It occurs in the cytosol of eukaryotic cells and protects them from the toxic effects of superoxide ions. It catalyzes the dismutation of superoxide via two diffusion-controlled one-electron redox processes ("ping-pong" mechanism):

$$O_2^- + [Cu^{II}] \rightarrow O_2 + [Cu^{I}]$$

$$O_2^- + [Cu^{I}] + 2\,H^+ \rightarrow H_2O_2 + [Cu^{II}]$$

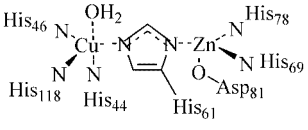

Figure 1. The active site in Cu-Zn SOD

In the metal-binding site (Figure 1) the Cu^{II} ion is coordinated by four histidines in a distorted square-planar coordination sphere and by a fifth axial water ligand, while the tetrahedral zinc ion is coordinated by three histidines, one of them bridging to the copper, and by a carboxylate group. The SOD Cu^{II} center exhibits type-2 copper protein characteristics: a d → d transition in the 500 to 1 μm region and normal EPR signals for tetragonal copper(II) ($g_{//} = 2.229$, $g_{\perp} = 2.041$, $A_{//} = 137 \times 10^{-4}$ cm^{-1}).[3]

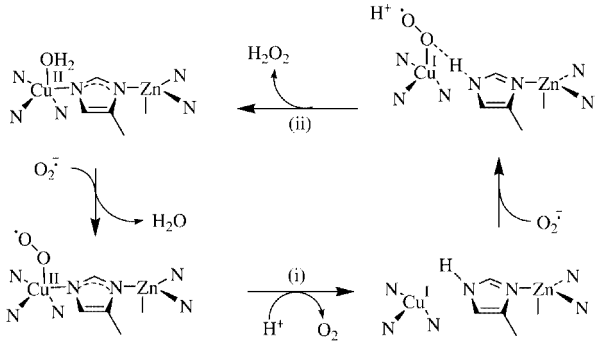

Figure 2. Mechanism for Cu-Zn SOD[5]

The superoxide ion is electrostatically guided by a deep (≈ 13 Å), narrow (≈ 4 Å) channel lined by positively charged amino acid residues. The zinc ion probably assists the protein in adopting the required coordination environment and confers stability to the protein, which is remarkably stable to heat and is active from pH 4.5 to 10. The catalytic mechanism is depicted in Figure 2. The oxidation step (i) is an inner-sphere electron transfer between the coordinated superoxide and the copper(II) center. The concomitant cleavage of the copper-imidazolate bond is assisted by protonation of the imidazolate by the solvent, and oxygen is released. Reoxidation of Cu^{I} to Cu^{II} by the next superoxide reforms the bridge with transfer of a proton to the peroxide ion.

A modified enzyme, having copper in both metal binding sites, Cu-Cu SOD, exhibits the same catalytic activity as native SOD,[14] demonstrating clearly that a copper ion located in the zinc site does not exert catalytic activity.

Cu-Zn SOD Models

Many low-molecular weight copper chelates exhibit, in vitro, superoxide dismutase-like activity. Most lose their activity in the presence of bovine serum albumin (BSA), which can mobilize the complexed copper(II) ions (BSA, a plasmatic protein, is one of the strongest biological chelators of cupric ions; log $K = 16.2$). One of us had described

 © 2003 Wiley-VCH Verlag GmbH & Co. KGaA, Weinheim

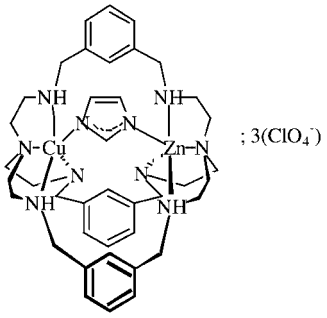

Figure 3. Biomimetic model for the Cu-Zn SOD active site[15]

a biomimetic model[15] that catalyzes the dismutation of superoxide at biological pH and retains its activity in the presence of BSA. Moreover this model shares many of the spectroscopic properties of the enzyme. It is an imidazolate-bridged heterobinuclear copper(II)-zinc(II) complex of a macrobicyclic ligand (Figure 3). The closed bicyclic structure of the ligand is more selective than monocyclic or open-chain ligands: only small ligands (e.g. O_2^-) can access the copper center and the bicyclic structure is expected to mimic the SOD protein channel.

X-ray diffraction studies show a Cu−Zn distance of 5.93 Å (6.3 Å for the enzyme). The EPR and electronic spectral parameters are close to those of the protein. The imidazolate bridge is remarkably stable over a large pH range (6 to 10.5), which is significantly better than other abiotic models that do not involve a protecting bicyclic structure,[16] and is close to that of the enzyme (pH: 4.5 to 10). This is a good structural and functional model, but it does not evidence cooperation between copper and zinc.

An imidazolate-bridged heterobinuclear Cu-Zn complex with a symmetrical ligand, exhibiting SOD activities, has been recently described by Fukuzumi et al.,[17] who tried to clarify the role of the zinc ion (Figure 4). The X-ray structure indicates that the Cu^{II} and Zn^{II} ions have a slightly distorted trigonal-bipyramidal coordination geometry. The cyclic voltammogram in acetonitrile exhibited only one reversible Cu^{I}/Cu^{II} redox couple, at $E_{1/2} = -0.03$ V (vs. Ag/AgCl). This is 0.2 V more positive than for a Cu^{II} mononuclear complex homologue. The authors ascribe this shift to the electronic effect of the imidazolate-bound zinc ion. They conclude that the zinc ion in the heterobinuclear complex may accelerate an outer-sphere electron transfer from superoxide to the Cu^{II}-Zn^{II} complex to produce the Cu^{I}-Zn^{II} complex. The free energy change of electron transfer for the complex is thermodynamically more favorable than that without the Zn^{II} ion. The Zn^{II} ion, which can act as a Lewis acid, may also accelerate electron transfer from the Cu^{I}-Zn^{II} complex to superoxide, since superoxide can form a complex with metal ions acting as a Lewis acid to accelerate the electron transfer reduction of superoxide. Thus, the essential role of Zn^{II} in SOD may be to accelerate both the oxidation and the reduction of superoxide by controlling the redox potential of the Cu^{II} ion and superoxide in the SOD catalytic cycle.

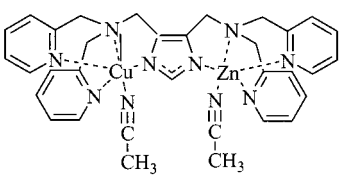

Figure 4. SOD model of Fukuzumi et al.[17]

Purple Acid Phosphatases: An Example of Non-Redox Bimetallic Catalysis

Structural and Functional Aspects of Purple Acid Phosphatases

Purple acid phosphatases (PAPs, Table 1) have been isolated from mammals, plants and fungal sources. They catalyze in vitro the hydrolysis of phosphate esters such as ATP, at a pH range of 4−7.[4,7−9] Their function in vivo is still subject to debate but has been proposed to involve fetal iron transport, control of bone resorption, and phosphate homeostatis in plants.[4] This class of acid phosphatases are purple due to a tyrosinate-to-Fe^{III} charge-transfer at about 560 nm ($\varepsilon \geq 3000$ $M^{-1}\cdot cm^{-1}$ per iron) for their inactive form. The crystal structure of the red kidney bean purple acid phosphatase (kbPAP)[8,10] displays a heterobinuclear $Zn^{II}Fe^{III}$ core, while those of the mammalian PAPs, determined from rat,[18] rat bone[19] and porcine uterus (UfPAP),[20] contain an $Fe^{III}Fe^{III}$ site in the oxidized non-active state.

The crystal structure of kbPAP, first determined at a resolution of 2.9 Å[10] and subsequently at 2.65 Å,[8] reveals a homodimeric 111 kDa enzyme, with two domains in each subunit. In the active site, located in the carboxyl-terminal domain, the two metal ions are 3.26 Å apart, and bridged monodentately by Asp164, each one involving octahedral coordination.

The iron is further coordinated by Tyr167, His325 and Asp135 residues, and the zinc by His286, His323 and Asn201 (Figure 5). Three exogenous ligands are also included in the X-ray model to complete the coordination sphere: one terminal hydroxo ligand to iron, one terminal water ligand to zinc, and one hydroxo bridge (also supported by physical measurements[21]) between the metal ions. In the μ-phosphato derivative structures of mammalian PAPs, the dimetallic ligation appears to be identical and confirms the similarities observed with kbPAP from sequence homologies and spectroscopic studies. The detailed electronic structure of the oxidized and reduced di-iron centers have been characterized by magnetic suscepti-

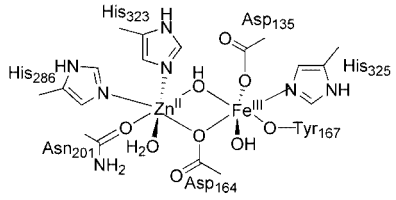

Figure 5. Active site in Zn-Fe kbPAP

 © 2003 Wiley-VCH Verlag GmbH & Co. KGaA, Weinheim

bility and EPR measurements, which showed a strong antiferromagnetic interaction ($-2J > 80$ cm^{-1}) in the $Fe^{III}Fe^{III}$ ($S = 0$ ground state) forms and a weaker value in the reduced $Fe^{II}Fe^{III}$ ($S = 1/2$ ground state) forms (typically $-2J = 11$ to 22 cm^{-1}).[2,22] The active forms exhibit a pH-dependent rhombic EPR signal[23] ($g_{av} \approx 1.75$) whereas the inactive forms are EPR silent. Native kbPAP shows a signal at $g = 4.3$, which is characteristic for isolated high-spin Fe^{III} with a $S = 5/2$ ground state, as expected for the $Zn^{II}Fe^{III}$ center.[24]

The crystal structures of kbPAP complexed with μ-phosphate, the product of the reaction, (2.7 Å resolution) and with μ-tungstate inhibitor (3.0 Å) have also been determined, allowing a proposed mechanism for the hydrolysis of phosphomonoesters (Figure 6).[8] In this mechanism, which has not been experimentally demonstrated in such detail, the phosphate group of the substrate binds zinc in monodentate fashion by displacing the presumed water ligand. The terminal Fe^{III}-bound hydroxide ion attacks the phosphorus to form a pentacoordinate intermediate, and the P−O bond opposite the hydroxide ion attack breaks to form the leaving group and phosphate, which is consistent with the inversion at phosphorus. In addition, the three histidines (His202, His295 and His296) located near the bimetallic center can interact with the phosphate. In mammalian PAPs the corresponding residues are two histidines and a glutamate. No similar role is envisaged for the glutamate, which points away from the active site, but the histidines are hydrogen bonded to the bridging phosphate.[18−20]

This proposed mechanism underlines the respective roles of the two metal centers: The substrate first binds the Fe^{II} or Zn^{II} center by removal of the exchangeable water ligand, followed by intramolecular nucleophilic attack of the hydroxide group bound to the Fe^{III} center on the phosphorus P−O bond (activated by its binding to the electrophilic metal center). The well-fitted intermetallic distance allows the overall mechanism. The essential features of the respective roles of the two metal centers are: (*i*) a metal center (bearing an exchangeable ligand) that firstly binds the substrate; (*ii*) a second metal center bearing a reactive OH group that allows the assisted intramolecular reaction; (*iii*) a geometry that allows an intermediate in which the substrate is bound to both metal centers.

Alternative proposed reaction pathways of M^{II}/Fe^{III} purple acid phosphatases have been reviewed recently.[25] Merkx and co-workers propose that the terminal bound hydroxide deprotonates another water molecule from the second coordination sphere of the ferric ion, which then acts as an intramolecular base catalyst (Figure 7, A).[26,27]

As proposed for Fe^{II}/Fe^{III} uteroferrin,[28,29] the two metallic centers are bridged by the phosphate ester. The μ-OH may act as a nucleophile and attack the phosphate (Figure 7, B). When coordinated to one metal ion (Figure 7, A), the hydroxide is expected to be much more nucleophilic

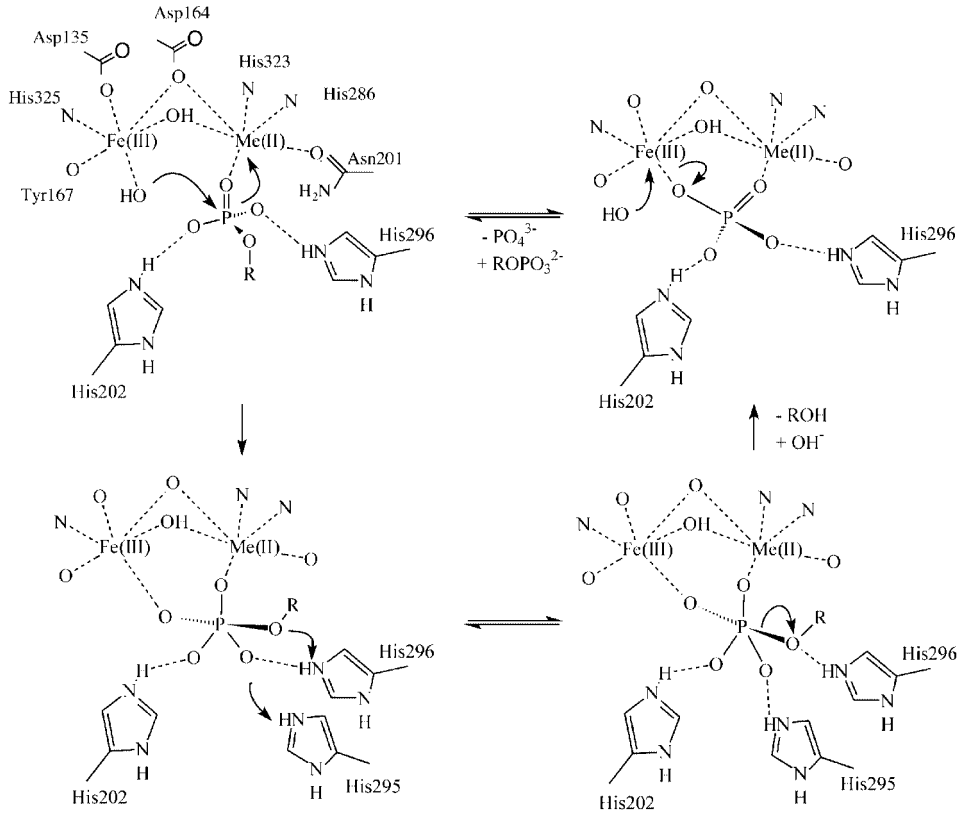

Figure 6. Proposed mechanism of phosphate ester hydrolysis in kbPAP (based on B. Krebs[8])

 © 2003 Wiley-VCH Verlag GmbH & Co. KGaA, Weinheim

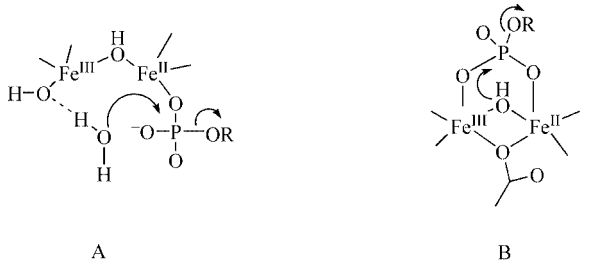

A B

Figure 7. Proposed reaction intermediates for the hydrolysis of phosphomonoesters by PAPs

than when it bridges two metal ions.[7] The second metal ion may help to generate the nucleophilic hydroxide by lowering the p*K*a of the bridging hydroxo and by converting the hydroxo bridge into a quasi-terminal $M^{II}-OH$ moiety.[29]

However, it is not known whether the phosphate ester binds to both metal ions in a bridging mode (as in the structurally characterized phosphato derivatives of PAPs)[8,18−20] or only to the divalent metal ion. For bovine spleen PAP (bsPAP), the bridging phosphate complex reportedly represents an inactive form of the enzyme−substrate complex.[27] No decisive evidence is available about the fixation mode of the substrate during the enzymatic cycle.

Although the exact mechanism has not been clearly elucidated, in all proposed reaction pathways the two metal centers act cooperatively, with a precise role for each. These proposed mechanisms are fascinating examples of bimetallic catalysis.

To explore the role of each metal center, the Fe^{II} has been selectively substituted with various divalent metal ions, leading to changes in catalytic activity[7] (e.g. the $Zn^{II}Fe^{III}$ Uf reacts with $H_2PO_4^-$ 35 times faster than does the native $Fe^{II}Fe^{III}$ form[30]). Conversely, replacing the Fe^{III} center with Ga^{III} results in small but consistent changes in catalytic activities.[31]

Purple Acid Phosphatase Models

A View on PAPs Models

Most reported model complexes of binuclear metallobiosites imply equivalent environments for the two metal ions, since symmetrical dinucleating ligands greatly simplify the synthetic problem.[32] The structural and functional model compounds of PAPs have been reviewed.[9] To mimic the reactivity of PAPs, two isostructural binuclear complexes, Zn^{II}-Fe^{III} and Fe^{II}-Fe^{III}, of the phenolate-hinged dinucleating ligand H-BPMOP [2,6-bis{[bis(2-pyridylmethyl)-amino]methyl}-4-methoxyphenol] have been prepared and studied to compare their activity towards phosphate ester cleavage, and to allow comparisons between kbPAP and bsPAP.[33] The pH dependence of the acceleration in cleavage of the activated phosphodiester 2-hydroxypropyl-*p*-nitrophenyl phosphate (HPNP) was investigated in acetonitrile/water 1:1 (optimum pH 8.5 ± 0.2). The Zn^{II}-Fe^{III} complex of H-BPMOP shows a twofold higher rate acceleration than the complex with H-BPMP [2,6-bis{[bis(2-pyridylmethyl)amino]methyl}-4-methylphenol], and the di-iron complex from BPMOP is 10-fold more reactive than the homologous complexes from BPMP. As observed with the Zn^{II} substituted $Fe^{II}Fe^{III}$ UfPAP enzyme,[30,31] the heterobinuclear catalyst exhibits a higher reaction rate than the homobinuclear catalyst.

Unsymmetrical Models for PAPs

The rational design of dinucleating ligands that induce a controlled synthesis of the targeted unsymmetrical complexes is a prerequisite for a better understanding of spectroscopic and chemical properties related to metalloenzymes. The search for unsymmetrical dinucleating ligands has been reviewed and discussed by Fenton.[34]

Two essential factors in designing dinucleating ligands are:

– The ligand, which has to accommodate two metals with a well-suited metal−metal separation, allowing bridging by the designed ligand(s).

– The coordination environment, which dictates steric and electronic features, especially the redox properties of each metal center.

Table 2 shows some example ligands and their corresponding unsymmetrical complexes that have been characterized by X-ray structures.

An unsymmetrical binuclear iron complex from a symmetrical ligand, reported by Krebs et al.,[35] involves a monodentate coordinated phosphato ligand. Phosphate (and arsenate) anions have also been found as bidentate bridges between the two metal centers in other model complexes (Table 2). Thus, these biomimetic models do not allow decisive arguments regarding the substrate coordination to the enzyme.

In the complexes described by Latour et al.,[36] the unsymmetrical environment mimics the coordination of the tyrosine residue at the PAP active site. This work shows how the introduction in the iron environment of a single terminal phenolate influences the redox properties (i.e. noticeable destabilization of the diferrous state, less pronounced stabilization of the diferric one, and enhanced stability domain for the mixed valence state). A similar effect has been observed Neves.[42] The stabilizing effect of the mixed valence state compared to the symmetric ligands is attributed to a stereochemical effect of the ligand and to coulombic interactions.

We have described a zinc(II)-iron(III) complex involving two chemically distinct coordination sites, one suited for iron(III) complexation and bearing two phenolate nonbridging ligands, the other bearing pyridine nitrogen donor sites (half part of BPMP); the two sites being connected by the classical bridging phenolate group.[41] We used our previously described unsymmetrical ligand LH_3 (Table 2, last Entry).[43] A heterobinuclear Zn^{II}-Fe^{III} complex has been obtained by the addition (in methanol) of one equivalent of iron(III) perchlorate in the presence of triethylamine to a solution of the zinc complex, followed by the addition of two equivalents of diphenylphosphate. This complex in-

 © 2003 Wiley-VCH Verlag GmbH & Co. KGaA, Weinheim

Table 2. Selected unsymmetrical complexes as models for PAPs

Ligand (LH_n)	Dimetallic core and Structural formulas	Bridging mode	Coordination mode	Ref.
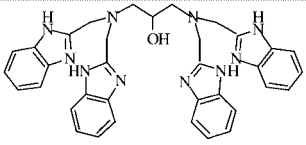	$Fe^{III}Fe^{III}$ $[Fe_2Cl_2(L)(O_2P(OPh)_2(MeOH)](ClO_4)_2$	μ-alkoxo	Fe^{III}: N3O2Cl Fe^{III}: N3O2Cl	[35]
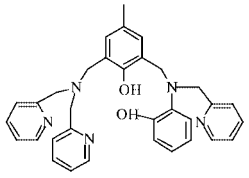	$Fe^{II}Fe^{III}$ $[Fe_2(L)(O_2P(mpdp)^{[a]}]BPh_4$	μ-phenoxo, bis μ-carboxylato	Fe^{II}: N3O3 Fe^{III}: N2O4	[36]
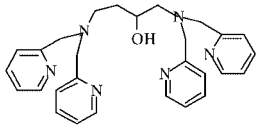	$Fe^{II}Fe^{III}$ $[Fe_2(L)(C_6H_5CO_2)_2](ClO_4)_2$	μ-alkoxo, bis μ-carboxylato	Fe^{II}: N3O3 Fe^{III}: N3O3	[37]
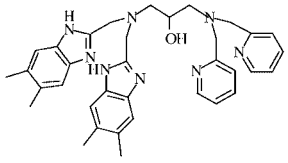	$Zn^{II}Fe^{III}$ $[ZnFe(L)(O_2AsMe_2)(MeOH)](ClO_4)_3$	μ-alkoxo, μ-dimethylarsinato	Zn^{II}: N3O2 Fe^{III}: N3O3	[38]
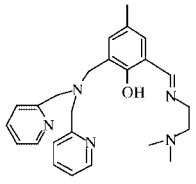	$Zn^{II}Fe^{III}$ $[ZnFe(L)(AcO)_3)]BPh_4$	μ-phenoxo, bis μ-acetato	Zn^{II}: N3O3 Fe^{III}: N2O4	[39]
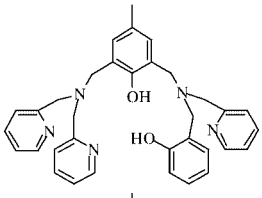	$Zn^{II}Fe^{III}$ $[ZnFe(L)(AcO)_2)]ClO_4$	μ-phenoxo, bis μ-acetato	Zn^{II}: N3O3 Fe^{III}: N2O4	[40]
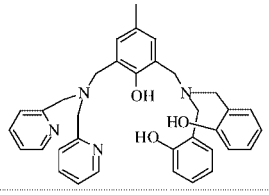	$Zn^{II}Fe^{III}$ $[ZnFe(L)(O_2P(OPh)_2]$	μ-phenoxo,bis μ-diphenylphosphato	Zn^{II}: N3O3 Fe^{III}: NO5	[41]

[a] *m*-Phenylenedipropionate.

volves two phosphate bridges, as shown in the X-ray structure.[41] The main feature of the electronic absorption in CH_3CN, at 501 nm ($\varepsilon \approx 3077\ cm^{-1}$), is assigned to charge-transfer transitions from the terminal and the bridging phenolates to the iron(III). This complex can act as a structural model of the substrate bound to the active site of kbPAP (a phosphate-bridged species has been tentatively proposed during the catalytic cycle of kbPAP). Moreover, the NO5 coordination sphere around the Fe^{III} reproduces the kbPAP oxygen-rich NO5 coordination sphere of iron.

Functional models have been prepared by a combinational method using a mixture of distinct bidentate ligands, the best activity being obtained with unsymmetrical models.[44]

Catechol Oxidase: Two Copper(II) Ions with Distinct Roles for a Two-Electron Oxidation

Structural and Functional Aspects of Catechol Oxidase

Catechol oxidases (COs) are ubiquitous plant enzymes that catalyze the oxidation of a broad range of *ortho*-diphenols into *ortho*-quinones in the presence of oxygen.[4,11−13,45] They belong to the family of type-3 copper proteins, containing a binuclear copper active site that is EPR silent in the native *met* Cu^{II}-Cu^{II} form, due to a strong antiferromagnetic coupling between the copper(II) atoms. The other prominent type-3 copper proteins are hemocyanins (Hc), the dioxygen carrier for arthropods and mollusks, and tyrosinases (Tyr).[3] The crystal structure of

 © 2003 Wiley-VCH Verlag GmbH & Co. KGaA, Weinheim

CO from sweet potatoes (*Ipomoea batatas*, ibCO) was resolved in 1998.[13] Both metal binding sites in the *met* form involve three histidine ligands. The two cupric ions, probably bridged by a hydroxide ion, are 2.87 Å apart in a trigonal pyramidal coordination sphere. Interestingly, the binuclear metal center has a covalent thioether bond between a carbon atom of His109 (one of the copper ligands) and the sulfur atom of Cys92 (Figure 8).

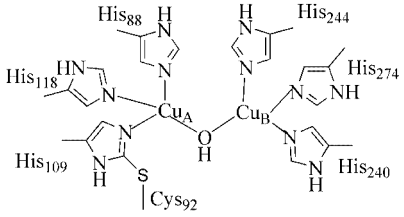

Figure 8. Active site of catechol oxidase from *Ipomoea batatas* (*met* form)[13]

The crystal structure of catechol oxidase reveals that this covalent bond puts additional structural restraints on the ligand sphere of the Cu_A center. Cys-His thioether bridges have been reported for the sequences of ncTyr (*Neurospora crassa* Tyr),[46] odgHc (*Octopus dofleini* Hc),[47] hpHc (*Helix pomatia* Hc)[48] and in all known COs. The absence of the covalent thioether bond in Hcs from arthropods and human Tyr does not support its direct involvement in the catalytic process.[4,11] A thioether bond between cysteine and tyrosine has also been reported for the mononuclear copper enzyme galactose oxidase.[49] In COs, this Cys-His unit may optimize the redox potential of the metal needed for the oxidation of the *ortho*-diphenol substrate and (or) prevents the displacement of His109 and therefore tunes the binding mode of the substrate.

The crystal structure was solved in the *deoxy* Cu^I Cu^I state and with a substrate analogue inhibitor (phenylthiourea, PTU) relevant to the mechanism.[13,45] In the reduced state a water molecule was coordinated to Cu_A. The coordination sphere is a distorted trigonal pyramidal whereas that of Cu_B (three histidine ligands) can be described as square planar with a vacant coordination site. The copper−copper distance is 4.4 Å. In the dimetallic center for the PTU-enzyme complex, the hydroxo bridge is replaced by a sulfur bridge from PTU, increasing the $Cu^{II}-Cu^{II}$ separation to 4.2 Å compared to the *met* form. The amide nitrogen interacts weakly with Cu_B, leading to still more unsymmetrical coordination spheres for the two copper centers.

A catalytic cycle for catechol oxidase activity (Figure 9) has been proposed from a combination of biochemical, spectroscopic, structural data[11] and by comparison with the tyrosinase-related cycle.[3] It begins with the native *met* form. The monodentate binding of the diphenolic substrate to the Cu_B is suggested from the crystal structure of the ibCO-PTU complex.[13] Nevertheless, a bidentate bridging of catechol has also been proposed.[3,45] Stoichiometric amounts of the quinone product are formed immediately after addition of catechol, even in the absence of dioxygen. This excludes the *oxy* form at the start of the catalytic cycle. The *oxy* form may arise from the *deoxy* form in the presence of oxygen. The *oxy* form has been experimentally obtained upon addition of H_2O_2 to the *met* form. In the proposed catalytic cycles, catecholate binds either monodentately or bidentately the *oxy* form, for a two-electron transfer

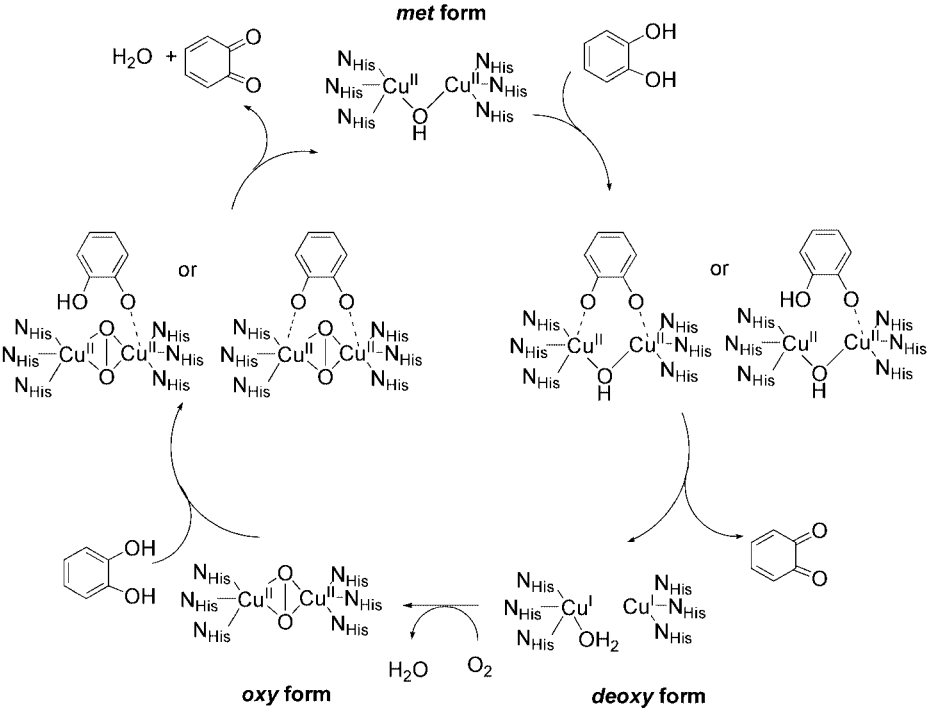

Figure 9. Proposed catalytic cycle for catechol oxidase activity[3,11,45]

 © 2003 Wiley-VCH Verlag GmbH & Co. KGaA, Weinheim

leading to the release of the quinone product and to the *met* form.

Interestingly, Krebs et al.[11] have noted that in copper type-3 proteins the Cu_B site is always strictly conserved, while the varying Cu_A environment seems to tune the proteins to specific activities. Comparison of the metal coordination region from structural data on ibCO and Hcs evidences high similarities. The active site of odgHc has an identical coordination for Cu_A as in ibCO.[45] As no detailed structural information was available for any tyrosinase, it would be of great interest to explain the difference between CO and Tyr, which may be related to the respective roles of each metal center.

Catechol Oxidase Models

Catecholase activity on a model substrate (3,5-di-*tert*-butylcatechol, 3,5-dtbc) has been described, in particular for binuclear compounds.[50,51] A complex with a bridging tetrachlorocatechol between the two Cu^{II} ions has been characterized, by X-ray diffraction studies, and suggested as a model for a substrate-binding intermediate in catechol oxidation.[52] Our group has investigated a series of dicopper(II) complexes as model systems for the catechol oxidase active site. We have described the pH-controlled changes of the metal coordination in one such complex, with a H-BPMP ligand, and shown that its catecholase activity depends on the copper−copper distance, which was modified according to pH changes (Figure 10).[53]

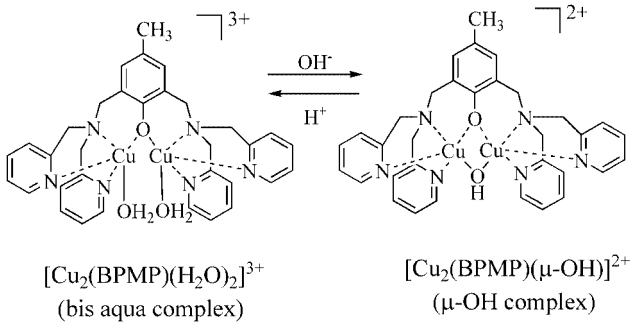

Figure 10. pH-Driven change in dicopper(II) complexes model of catechol oxidase[53]

The complex $[Cu_2(BPMP)(\mu\text{-}OH)](ClO_4)_2$ is EPR silent, in agreement with the antiferromagnetic coupling ($J = -112\ cm^{-1}$) between the two copper(II) atoms, with a very short Cu−Cu distance of 2.87 Å, similar to the enzyme in the *met* form.[12,13,54] Only the μ-OH complex $[Cu_2(BPMP)(\mu\text{-}OH)](ClO_4)_2$ exhibits catecholase activity compared to the bis aqua compound $[Cu_2(BPMP)(H_2O)_2](ClO_4)_3$. Substitution at the 4-position of the bridging phenolate with an electron-donating or an electron-withdrawing group drastically influences the catecholase activity, even though the structural properties are only slightly affected.[55]

These, models, and others in the literature, involve symmetrical ligands leading to the same coordination sphere for each metal center. Nevertheless, mechanistic studies with our model series have shown distinct roles for each metal center. First, a monodentate coordination on one copper center, associated with an interaction between the second phenol group of the catechol substrate and the hydroxy group bound to the second copper center (arising from cleavage of the initial hydroxo bridge). Then the proton transfer occurs followed by displacement of a water molecule and the bridging coordination of the catecholate (Figure 11).[56]

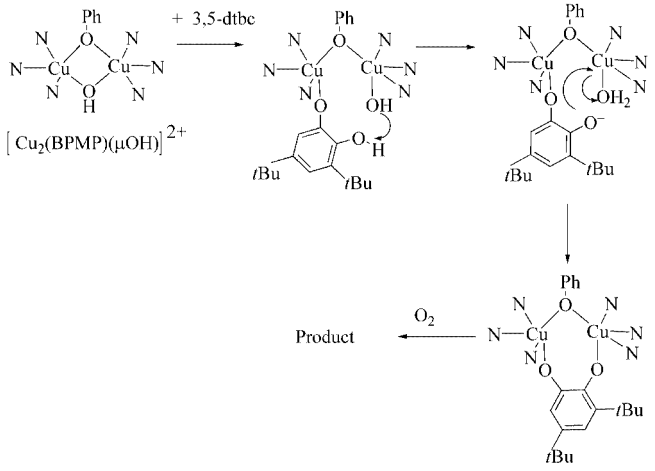

Figure 11. Proposed mechanism for the interaction between dinuclear copper(II) μ-OH complexes and the 3,5-dtbc substrate[56]

It is of interest to prepare CO models from unsymmetrical ligands, differentiating, in a controlled manner, the two metal centers as it is done in the enzyme. Few model complexes for catechol oxidase from unsymmetrical ligands have been reported (Figure 12).[51,57] With such models further studies to identify the roles of each metal ions could shed light on the likely behavior of the two copper atoms in dissimilar environments.

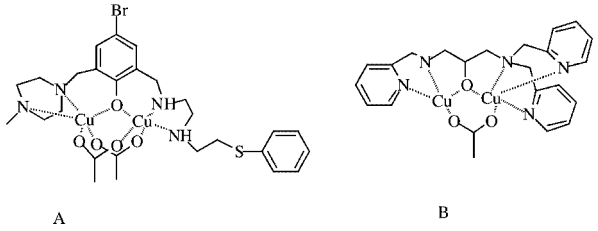

Figure 12. Unsymmetrical dicopper(II) complexes as models of catechol oxidase. (A) from,[57] (B) from[51]

Conclusion

From our briefly developed examples of μ-bridged binuclear metalloenzymes, focusing on the asymmetry of the two metal centers and their respective roles, we can underline the following aspects:

– One redox catalytic metal center; the second metal helps maintain the structural integrity and possibly accelerates the redox processes by controlling the redox potential of the first metal center. This has been observed for Cu-

 © 2003 Wiley-VCH Verlag GmbH & Co. KGaA, Weinheim

Zn superoxide dismutase (moreover, the coordination of the bridging histidine nitrogen to the Zn ion lowers the p*K*a of the other nitrogen, which consequently prefers to bind to a proton rather than to Cu^{I} after the first step of the catalytic cycle).

– Coordination number asymmetry that presents the possibility of "open coordination sites" for direct interaction of one metal center with the substrate. The reactant can be bound to the second metal center. Alternatively, the second metal center can "assist" the reaction. This has been encountered with PAPs.

– In another possibility, the substrate is coordinated to both metal centers simultaneously in a bridging manner. The substrate is then activated and reacts with another molecule, either bound or not to one metal center.

– A very tenuous and subtle asymmetry with catechol oxidase (CO): a simple substitution of one ligand of one metal center may confer to CO a distinct reactivity compared with that of the closely related copper type-3 proteins.

Bimetallic catalysis is a fascinating aspect of chemical catalysis.[32] Chemists can even envisage the self-assembly of bimetallic sites during the catalytic event and, in this sense, outdo Nature. Of course, our limiting the discussion to the active site and to the first coordination spheres of the metal centers is an over-simplification. Nevertheless, this approach partly answers the question: Asymmetry in binuclear metalloenzymes: what and why?

[1] R. H. Holm, P. Kennepohl, E. I. Solomon, *Chem. Rev.* **1996**, *96*, 2239−2314.
[2] D. E. Wilcox, *Chem. Rev.* **1996**, *96*, 2435−2458.
[3] E. I. Solomon, U. M. Sundaram, T. E. Machonkin, *Chem. Rev.* **1996**, *96*, 2563−2605.
[4] A. Rompel, C. Gerdemann, A. Vogel, B. Krebs, in *Inorganic Chemistry Highlights*, Wiley-VCH Verlag, Weinheim, **2002**, pp. 155−163.
[5] J. A. Tainer, E. D. Getzoff, J. S. Richardson, D. C. Richardson, *Nature* **1983**, *306*, 284.
[6] N. Sträter, W. N. Lipscomb, T. Klabunde, B. Krebs, *Angew. Chem. Int. Ed. Engl.* **1996**, *35*, 2024−2055; *Angew. Chem.* **1996**, *108*, 2158−2191.
[7] M. B. Twitchett, A. G. Sykes, *Eur. J. Inorg. Chem.* **1999**, 2105−2115.
[8] T. Klabunde, N. Sträter, R. Frohlich, H. Witzel, B. Krebs, *J. Mol. Biol.* **1996**, *259*, 737−748.
[9] R. Than, A. A. Feldmann, B. Krebs, *Coord. Chem. Rev.* **1999**, *182*, 211−241.
[10] N. Sträter, T. Klabunde, P. Tucker, H. Witzel, B. Krebs, *Science* **1995**, *268*, 1489−1492.
[11] C. Eicken, B. Krebs, J. C. Sacchettini, *Curr. Opin. Struc. Biol.* **1999**, *96*, 677−683.
[12] C. Eicken, F. Zippel, K. Buldt-Karentzopoulos, B. Krebs, *FEBS Letters* **1998**, *436*, 293−299.
[13] T. Klabunde, C. Eicken, J. C. Sacchettini, B. Krebs, *Nat. Struct. Biol.* **1998**, *5*, 1084−1090.
[14] K. G. Strothkamp, S. J. Lippard, *Acc. Chem. Res.* **1982**, *15*, 318−326.
[15] J. L. Pierre, P. Chautemps, S. Refaif, C. Beguin, A. El Marzouki, G. Serratrice, E. Saint Aman, P. Rey, *J. Am. Chem. Soc.* **1995**, *117*, 1965−1973.
[16] C. Béguin, P. Chautemps, J. L. Pierre, E. Saint Aman, G. Serratrice, *Bull. Soc. Chim. Fr.* **1997**, *134*, 635−640.
[17] H. Ohtsu, Y. Shimazaki, A. Odani, O. Yamauchi, W. Mori, S. Itoh, S. Fukuzumi, *J. Am. Chem. Soc.* **2000**, *122*, 5733−5741.
[18] J. Uppenberg, F. Lindqvist, C. Svensson, B. Ek-Rylander, G. Andersson, *J. Mol. Biol.* **1999**, *290*, 201−211.
[19] Y. Lindqvist, E. Johansson, H. Kaija, P. Vihko, G. Schneider, *J. Biol. Chem.* **1999**, *291*, 135−147.
[20] L. W. Guddat, A. S. McAlpine, D. Hume, S. Hamilton, J. de Jersey, J. L. Martin, *Structure* **1999**, *7*, 757−767.
[21] M. A. S. Aquino, J. S. Lim, A. G. Sykes, *J. Chem. Soc., Dalton Trans.* **1994**, 429−436.
[22] B. A. Averill, J. C. Davis, S. Burman, T. Ziniro, J. Sanders-Loehr, T. M. Loehr, J. T. Sage, P. G. Debrunner, *J. Am. Chem. Soc.* **1987**, *109*, 3760−3767.
[23] M. Dietrich, H. Münstermann, H. Suerbaum, H. Witzel, *Eur. J. Biochem.* **1991**, *199*, 105−113.
[24] J. L. Beck, J. de Jersey, B. Zerner, M. P. Hendrich, P. G. Debrunner, *J. Am. Chem. Soc.* **1988**, *110*.
[25] E. Kimura, *Curr. Opin. Chem. Biol.* **2000**, *4*, 207−213.
[26] M. Merkx, B. A. Averill, *J. Am. Chem. Soc.* **1999**, *121*, 6683−6689.
[27] M. Merkx, M. W. H. Pinkse, B. A. Averill, *Biochemistry* **1999**, *38*, 9914−9925.
[28] X. D. Wang, C. R. Randall, A. E. True, L. Que, *Biochemistry* **1996**, *35*, 13946−13954.
[29] X. D. Wang, R. Y. N. Ho, A. K. Whiting, L. Que, *J. Am. Chem. Soc.* **1999**, *121*, 9235−9236.
[30] J. S. Lim, M. A. S. Aquino, A. G. Sykes, *Inorg. Chem.* **1996**, *35*, 614−618.
[31] M. Merkx, B. A. Averill, *Biochemistry* **1998**, *37*, 8490−8497.
[32] E. K. Van den Beuken, B. L. Feringa, *Tetrahedron* **1998**, *54*, 12985−13011.
[33] S. Albedyhl, M. T. Averbuch Pouchot, C. Belle, B. Krebs, J. L. Pierre, E. Saint Aman, S. Torelli, *Eur. J. Inorg. Chem.* **2001**, 1457−1464.
[34] D. E. Fenton, *Chem. Soc. Rev.* **1999**, *28*, 159−168.
[35] B. Bremer, K. Schepers, P. Fleischhauer, W. Haase, G. Henkel, B. Krebs, *J. Chem. Soc., Chem. Commun.* **1991**, 510−512.
[36] [36a] E. Bernard, W. Moneta, J. Laugier, S. Chardon-Noblat, A. Deronzier, J. L. Tuchagues, J. M. Latour, *Angew. Chem. Int. Ed. Engl.* **1994**, *33*, 887−889; *Angew. Chem.* **1994**, *106*, 914−917. [36b] E. Lambert, B. Chabut, S. Chardon-Noblat, A. Deronzier, G. Chottard, A. Bousseksou, J. P. Tuchagues, J. Laugier, M. Bardet, J. M. Latour, *J. Am. Chem. Soc.* **1997**, *119*, 9424−9437.
[37] M. Suzuki, S. Fujinami, T. Hibino, H. Hori, Y. Maeda, A. Uehara, *Inorg. Chim. Acta* **1998**, *283*, 124−135.
[38] S. Albedyhl, D. Schnieders, A. Jancso, T. Gajda, B. Krebs, *Eur. J. Inorg. Chem.* **2002**, 1400−1409.
[39] H. Machiniga, K. Matsufuji, M. Ohba, M. Kodera, H. Okawa, *Chem. Lett.* **2002**, 716−717.
[40] M. Lanznaster, A. Neves, A. J. Bortoluzzi, B. Szpoganicz, E. Schwingel, *Inorg. Chem.* **2002**, *41*, 5641−5643.
[41] C. Belle, I. Gautier Luneau, L. Karmazin, J. L. Pierre, S. Albedyhl, B. Krebs, M. Bonin, *Eur. J. Inorg. Chem.* **2002**, 3087−3090.
[42] A. Neves, L. M. Rossi, I. Vencato, W. Haase, R. Werner, *J. Chem. Soc., Dalton Trans.* **2000**, 707−712.
[43] C. Belle, G. Gellon, C. Scheer, J.-L. Pierre, *Tetrahedron Lett.* **1994**, *35*, 7019−7022.
[44] F. Verge, C. Lebrun, M. Fontecave, S. Ménage, *Inorg. Chem.* **2003**, 499−507.
[45] C. Gerdemann, C. Eicken, B. Krebs, *Acc. Chem. Res.* **2002**, *35*, 183−191.
[46] K. Lerch, *J. Biol. Chem.* **1982**, *257*, 6414−6419.
[47] K. I. Miller, M. E. Cuff, W. F. Lang, P. Varga-Weisz, K. G. Field, K. E. van Holde, *J. Mol. Biol.* **1998**, *278*, 827−842.
[48] C. Gielens, N. De Geest, X. Q. Xin, B. Devreese, J. Van Beeumen, G. Preaux, *Eur. J. Biochem.* **1997**, *248*, 879−888.
[49] N. Ito, S. E. V. Phillips, K. D. S. Yadav, P. F. Knowles, *J. Mol. Biol.* **1994**, *238*, 794−814.
[50] For example see: [50a] N. Oshi, Y. Nishida, K. Ida, S. Kida,

 © 2003 Wiley-VCH Verlag GmbH & Co. KGaA, Weinheim

Bull. Chem. Soc., Jpn. **1980**, *53*, 2847−2850. [50b] J. Reim, B. Krebs, *J. Chem. Soc., Dalton Trans.* **1997**, *1997*, 3793−3804. [50c] E. Monzani, L. Quinti, A. Perotti, L. Casella, M. Gullotti, L. Randaccio, S. Geremia, G. Nardin, P. Faleschini, G. Tabbi, *Inorg. Chem.* **1998**, *37*, 553−562. [50d] J. Manzur, A. M. Garcia, A. Vega, E. Spodine, *Polyhedron* **1999**, *18*, 2399−2404. [50e] M. R. Malachowski, H. B. Huynh, L. J. Tomlinson, M. G. Davidson, R. S. Kelly, J. W. Furbee, *J. Chem. Soc., Dalton Trans.* **1995**, 31−36. [50f] M. Gupta, P. Mathur, R. J. Butcher, *Inorg. Chem.* **2001**, *40*, 878−885. [50g] J. Ackermann, F. Meyer, E. Kaifer, H. Pritzkow, *Chem. Eur. J.* **2002**, *8*, 247−258.

[51] C. Fernandes, A. Neves, A. J. Bortoluzzi, A. S. Mangrich, E. Rentschler, B. Szpoganicz, E. Schwingel, *Inorg. Chim. Acta* **2001**, *320*, 12−21.

[52] K. D. Karlin, Y. Guiltneth, T. Nicholson, J. Zubieta, *Inorg. Chem.* **1985**, *24*, 3725−3727.

[53] S. Torelli, C. Belle, I. Gautier Luneau, J. L. Pierre, E. Saint Aman, J. M. Latour, L. Le Pape, D. Luneau, *Inorg. Chem.* **2000**, *39*, 3526−3536.

[54] A. Rompel, H. Fischer, D. Meiwes, K. Buldt-Karentzopoulos, R. Dillinger, F. Tuczek, H. Witzel, B. Krebs, *J. Biol. Inorg. Chem.* **1999**, *4*, 56−63.

[55] C. Belle, C. Beguin, I. Gautier-Luneau, S. Hamman, C. Philouze, J. L. Pierre, F. Thomas, S. Torelli, E. Saint Aman, M. Bonin, *Inorg. Chem.* **2002**, *41*, 479−491.

[56] S. Torelli, C. Belle, S. Hamman, J. L. Pierre, E. Saint Aman, *Inorg. Chem.* **2002**, *41*, 3983−3989.

[57] N. Möller, M. Lücken, B. Krebs, *J. Inorg. Biochem.* **2001**, *86*, 344.

Received April 22, 2003
Early View Article
Published Online October 2, 2003

 © 2003 Wiley-VCH Verlag GmbH & Co. KGaA, Weinheim

Stereodiscrimination in Phosphanylthiolato Nickel(II) Complexes

Josep Duran,[a] Alfonso Polo,*[a] Julio Real,*[b] Jordi Benet-Buchholz,[c] Albert Poater,[a,d] and Miquel Solà[a,d]

Keywords: Nickel / P,S ligands / Conformation analysis / Chiral resolution / Density functional calculations

The presence of a stereogenic carbon centre (*R* or *S*) in the racemic ligand 1-(diphenylphosphanyl)propane-2-thiol induces a conformational preference (λ or δ) in the five-membered chelate ring of its 2:1 and 2:2 coordination compounds with Ni^{II}: the mononuclear *trans*-[Ni{SCH(CH_3)CH_2PPh_2-*P*,*S*}$_2$] (**1**) and the binuclear *trans*-[Ni{μ-SCH(CH_3)CH_2PPh_2-*P*,*S*}(Cl)]$_2$ (**2**). Both complexes exist as mixtures of two diastereomers: racemic-*trans* (R_λ, R_λ and S_δ, S_δ) and *meso*-*trans* (R_λ, S_δ), in an equilibrium displaced towards the more stable isomer, the *meso*-*trans* for **1** (calculated $\Delta E = < -0.1$ kcal·mol^{-1}) and the racemic-*trans* for **2** (calculated $\Delta E = -5.1$ kcal·mol^{-1}). This phenomenon is especially evident for complex **2**, in which an efficient chiral recognition between the two enantiomeric forms of the racemic ligand was observed. (© Wiley-VCH Verlag GmbH & Co. KGaA, 69451 Weinheim, Germany, 2003)

Introduction

The reactivity of 2-phosphanylthiolato nickel(II) complexes has been studied because of their relevance in *S*-alkylation/*S*-dealkylation reactions[1] and their applications in desulfurisation technologies[2] and in understanding the biological pathways of certain sulfur-containing metalloproteins.[3] However, less attention has been given to the importance of the ligand-based stereoelectronic effects in determining the coordination conformations around the metal and the stereochemistries of these compounds.[4] Thus, we decided to focus our attention on these particular aspects. The bis(phosphanylthiolato)nickel(II) complexes *trans*-[Ni($SCH_2CH_2PR_2$-*P*,*S*)$_2$][4,5] exist as mixtures of diastereomers because the five-membered chelate ring can adopt two different conformations (λ and δ) and therefore is able to form three optically isomeric complexes. When both chelate rings are in a λ-conformation, and the two chelate rings of the enantiomer are in a δ-conformation, we have the racemic-*trans* complex and when each chelate ring is in a different conformation, we have the *meso*-*trans* diastereomer (see Scheme 1). These two stereoisomers can be distinguished when a racemic chiral ligand is present, such as in complex [Ni($SCH_2CH_2PMePh)_2$], which has a racemic ligand chiral at the phosphorus centre. This compound exists in solution as a mixture of the racemic-*trans* and the *meso*-*trans* forms that equilibrate slowly ($t_{1/2}$ ca. 12 h) through an intermolecular process to form a 1:1 mixture, since the two diastereomers have very close energies.[4]

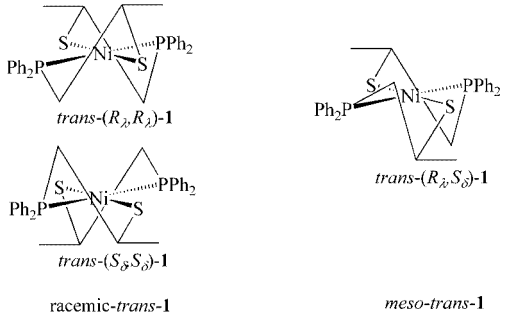

Scheme 1. Stereoisomers of mononuclear five-membered ring bis(phosphanylthiolato)nickel(II) complexes exemplified by complex **1**

The same stereochemical analysis can be applied to the 2-phosphanylthiolato-bridged binuclear nickel(II) complexes [Ni(μ-$SCH_2CH_2PR_2$)(X)]$_2$, which form bent *syn*-*endo*-*trans* structures.[6,7] Theoretical studies have shown that for this class of compounds the stabilisation of folded structures with respect to the planar arrangement can be

[a] Departament de Química, Universitat de Girona, Campus de Montilivi s/n, 17071 Girona, Spain
Fax: (internat.) +34-9724-18150
E-mail: alfons.polo@udg.es
[b] Departament de Química, Universitat Autònoma de Barcelona, 08193 Bellaterra, Spain
Fax: (internat.) +34-9358-13101
E-mail: Juli.real@uab.es
[c] Bayer AG, Bayer Industry Services, Analytics X-ray Laboratory, Geb. Q18, Raum 490, 51368 Leverkusen, Germany
Fax: (internat.) +49-2143-050677
E-mail: jordi.benet-buchholz.jb@bayerindustry.de
[d] Institut de Química Computational, Universitat de Girona, Campus de Montilivi s/n, 17071Girona, Spain
Fax: (internat.) +34-9724-18356
E-mail: miquel@iqc.udg.es
Supporting information for this article is available on the WWW under http://www.eurjic.org or from the author.

 DOI: 10.1002/ejic.200300508 © 2003 Wiley-VCH Verlag GmbH & Co. KGaA, Weinheim

ascribed to the pyramidalisation of the sulfur bridge compounded with a weak Ni−Ni interaction. Furthermore, it has been proposed that in a bent structure the chelate ring involving the bridging sulfur would be highly strained in *syn-exo* or *anti* conformations.[7] As in the case of bis(phosphanylthiolato) complexes, the chelate chain introduces some degree of structural variation, also producing the racemic-*trans* and *meso-trans* diastereomers (see Scheme 2). Nevertheless, it should be noted that the *anti* conformation of the bridging sulfur substituents would be necessary for the *meso-trans* isomer to be formed and that, for this type of complexes, the bent-*anti* structure has been observed neither in the solid state nor in solution.

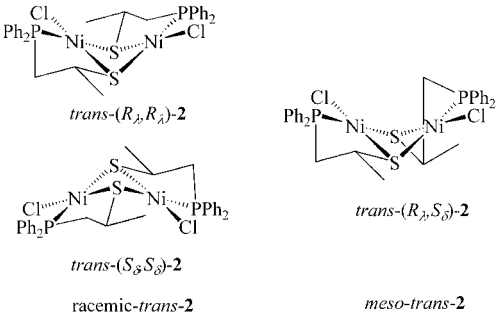

Scheme 2. Stereoisomers of double 2-phosphanylthiolato-bridged binuclear nickel(II) complexes with bent structures exemplified by complex **2**

For these reasons, we propose that the energy difference between the racemic-*trans* and *meso-trans* diastereomers of bis(phosphanylthiolato) complexes, and the strong tendency of the phosphanylthiolato-bridged binuclear complexes to adopt the folded *syn-endo-trans* conformation, could produce a chiral discrimination between the two enantiomeric conformations of the five-membered chelate ring. In order to demonstrate this hypothesis, we synthesised and characterised the 2:1 and 1:1 coordination compounds of the racemic ligand 1-(diphenylphosphanyl)propane-2-thiol[8] with nickel(II).

Results and Discussion

An alternative method to the literature procedures for the syntheses of $[Ni(SCH_2CH_2PPh_2)_2]$[5,9] and $[Ni(\mu\text{-}SCH_2CH_2PPh_2)(Br)]_2$[9] was applied to prepare the mononuclear bis-chelate *trans*-$[Ni\{SCH(CH_3)CH_2PPh_2\}_2]$ (**1**) and the binuclear *trans*-$[Ni(\mu\text{-}SCH(CH_3)CH_2PPh_2)(Cl)]_2$ (**2**) complexes. Addition of a CH_2Cl_2 solution of two equiv. of racemic 1-(diphenylphosphanyl)propane-2-thiol to a solution of nickel chloride in methanol resulted in the formation of solid **1**, which was isolated in 85 % yield. The same base-free procedure was used for **2**, which was isolated in 80 % yield upon addition of one equiv. of the racemic ligand and precipitation with diethyl ether.[10]

The *trans* geometry of the mononuclear complex **1** was determined by NMR analysis. In the $^{13}C\{^1H\}$ NMR spectra all aliphatic carbon atoms appear as triplets owing to virtual coupling with two equivalent mutually *trans* phosphorus nuclei (see Figure 1). According to the $^{31}P\{^1H\}$ NMR spectrum, bis-chelate **1** exists as a mixture of two diastereomers: freshly prepared $CDCl_3$ solutions of complex **1** show two resonances at δ_P = 52.6 and 54.2 ppm in about an 11:5 intensity ratio. The similar δ_P values point to two diastereomers with the same configuration but different conformations.

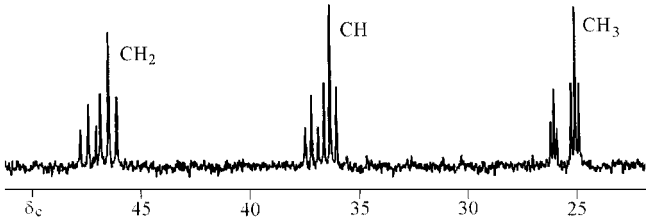

Figure 1. The aliphatic $^{13}C\{^1H\}$ NMR signals of complex **1** appear as triplets owing to virtual coupling with 2 equiv. mutually *trans* phosphorus nuclei

In keeping with the conformational analysis for compound **1** (see Scheme 1), the preferred conformation for the chiral chelate ring depends on the configuration at the stereogenic carbon centre of the ligand.[10a] Thus, the ligand with *R* configuration adopts the λ-conformation, which places the substituent of the chelate ring in the equatorial position. For the same reasons, the ligand with *S* configuration adopts the δ-conformation. As a result of these conformational preferences, complexes carrying two ligands with the same configuration, *trans*-(*R*,*R*)-**1** and *trans*-(*S*,*S*)-**1** are enantiomers (racemic-*trans*-**1**) giving a single $^{31}P\{^1H\}$ NMR signal. The second resonance is then assigned to the diastereomeric complex carrying one ligand in each configuration, *trans*-(*R*,*S*)-**1** (*meso-trans*-**1**). By comparison with the related complex $[Ni(SCH_2CH_2PMePh)_2]$,[4] the major signal could be initially assigned to the racemic-*trans*-**1** stereoisomer, which was claimed to be the kinetic product. However, the intensity ratio of the $^{31}P\{^1H\}$ NMR signals remains constant after 72 h at 50 °C. This behaviour contrasts with that observed for other similar Group VIII metal bis(phosphanylthiolato) complexes, in which the two signals become equal after 24 h at room temperature. In the latter case the two diastereomers have very close energies,[4,10a] suggesting that for complex **1** they have a slight, but significant, difference in energy (experimental $\Delta E \approx 0.41$ kcal·mol^{-1}). The BP86 energy calculations on complex **1** (see below) reveal that this energy difference is really small (less than 0.1 kcal·mol^{-1}) and predict the stabilisation of the *meso-trans*-**1** isomer over the racemic-*trans*-**1**, owing most probably to the steric interactions between the *pseudo*-axial phenyl groups that are mutually *syn* in racemic-*trans*-**1** and *anti* in *meso-trans*-**1** (see Scheme 3).

Binuclear complex **2** adopts a bent *syn-endo-trans* conformation in the solid state (see below) and shows a single, sharp resonance in the $^{31}P\{^1H\}$ NMR spectrum at δ_P = 36.3 ppm, both for freshly prepared and aged solutions,

 © 2003 Wiley-VCH Verlag GmbH & Co. KGaA, Weinheim

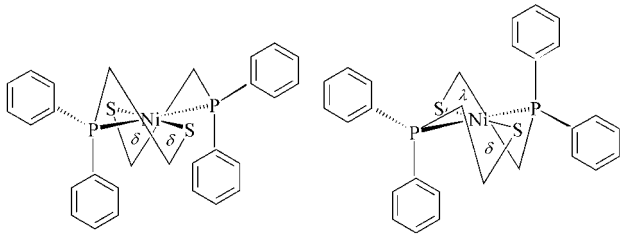

Scheme 3. The pseudo-axial phenyl groups of the *trans*-bis(2-diphenylphosphanylthiolato)nickel(II) complexes are mutually *syn* in the stereoisomers carrying both chelate rings in the same conformation (λ, λ or δ, δ) and *anti* in the stereoisomer with one chelate ring in each conformation (λ, δ)

pointing to the presence of only one of the possible diastereomers. It is noteworthy that in the $^{13}C\{^1H\}$ NMR spectrum of binuclear **2**, two of the aromatic carbon atoms (C_o and C_m) show two signals each, and all are pseudo-triplets (see Figure 2). The doubling of these signals is assigned to the different surroundings of each phenyl ring in the same diphenylphosphanyl group, while the fine splitting could be ascribed to a somewhat surprisingly similar coupling to both phosphorus nuclei generated by the P−Ni−Ni−P connection, a special case of the known phenomenon of virtual coupling.[7]

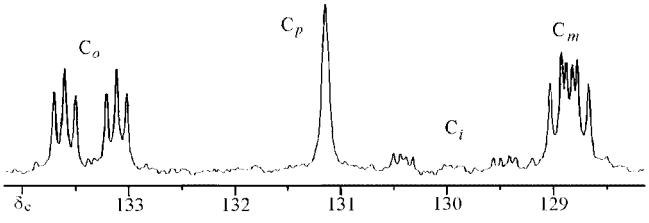

Figure 2. Two of the aromatic $^{13}C\{^1H\}$ NMR signals of complex **2** appear as pseudo-triplets (C_o and C_m), probably owing to a P−Ni−Ni−P coupling; complex **2** is not soluble enough to obtain quality signals for the quaternary carbon atoms, but an unfolded doublet of doublets can be glimpsed in the spectral trace

The conformational analysis of complex **2** shows, as in the case of **1**, that ligands with *R* and *S* configuration adopt λ and δ conformations, respectively, thereby placing the chelate chain substituent in the equatorial position. Thus, two diastereomeric forms of **2** could exist (racemic-*trans*-**2** and *meso*-*trans*-**2**: see Scheme 2), but only one of them was observed in solution. The BP86 energy calculations on complex **2** (see below) gave an energy difference of 5.1 kcal·mol^{-1} between the racemic-*trans*-**2** and the *meso*-*trans*-**2** isomers, in agreement with an equilibrium strongly displaced towards the racemic-*trans*-**2** diastereomer (experimental $\Delta E \geq 2.3$ kcal·mol^{-1}).[11] Furthermore, the minimum in energy for the *meso*-*trans*-**2** isomer represents a folded *syn*-*endo*-*trans* structure with one of the chelate chain substituents in the equatorial position and the other in the axial. This result is in agreement with the instability of the bent *anti* conformations predicted for this type of complex.[7]

An XRD study was carried out on crystals of **2**·$CHCl_3$ (see Figure 3). The crystal structure contains only the racemic-*trans*-**2** diastereomer and reveals an edge-sharing binuclear complex with square-planar coordination geometry around the nickel atoms. The molecule adopts a folded *syn*-*endo*-*trans* conformation (see Figure 3). Although the Ni−S, Ni−P and Ni−Cl distances are in the range observed for the isostructural $[Ni(\mu\text{-}SCH_2CH_2PPh_2)(X)]_2$ complexes (where X = Cl, Br), the fold angle of the central four-membered Ni_2S_2 cycle is appreciably greater (118.1 vs. 100.7−104.1°), increasing the Ni−Ni distance from 2.681−2.695 to 2.906 Å.[6] The reason for this geometrical alteration must be attributed to the presence of the substituent in the chelate chain, because there are no other structural changes. In complex **2**, the requirement to locate the methyl group in the equatorial position increases the bending of the tertiary carbon atom away from the S−S hinge (33.6 vs. 27.1−27.8°) and, since this bending is related to the arching of the Ni_2S_2 group,[7] the central core must unfold.

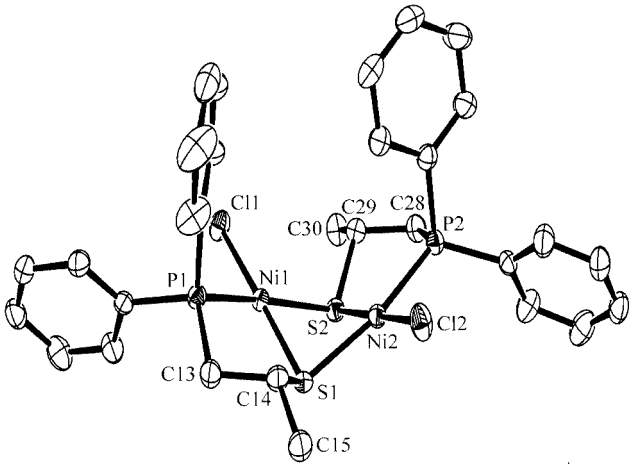

Figure 3. ORTEP plot (50 %) of complex **2**, hydrogen atoms are omitted; selected distances (Å) and angles (°): Ni1−Ni2 2.9065(4), Ni1−S1 2.1556(6), Ni1−S2 2.2244(7), Ni1−P1 2.1705(7), Ni1−Cl1 2.1910(7), Ni2−S1 2.2081(7), Ni2−S2 2.1558(7), Ni2−P2 2.1559(7), Ni2−Cl2 2.1811(7), S1−C14 1.841(3), C13−C14 1.531(4), C14−C15 1.516(4), P1−C13 1.834(3), S2−C29 1.854(3), C28−C29 1.520(4), C29−C30 1.521(4), P2−C28 1.833(3), S1−Ni1−P1 87.99(3), P1−Ni1−Cl1 95.22(3), S1−Ni1−S2 79.51(2), Cl1−Ni−S2 97.74(3), S2−Ni2−P2 88.29(3), P2−Ni2−Cl2 92.58 (3), S2−Ni2−S1 79.81(3), Cl2−Ni2−S1 99.15 (3), Ni1−S1−Ni2 83.52(2), C14−S1−Ni1 105.94(8), C14−S1−Ni2 112.74(9), Ni2−S2−Ni1 83.13(2), C29−S2−Ni2 105.38(8), C29−S2−Ni1 112.77(9).

Computational Results

The reported calculations were carried out by using the Amsterdam density functional (ADF2002.03) program system, developed by Baerends et al.[12−14] The numerical integration scheme employed was that of te Velde and Baerends.[15] An uncontracted triple-ζ basis set[16] was used

 © 2003 Wiley-VCH Verlag GmbH & Co. KGaA, Weinheim

for describing the 3s, 3p, 3d, 4s, and 4p orbitals of nickel. For carbon (2s,2p), phosphorus (3s,3p), sulfur (3s,3p), and hydrogen (1s), double-ζ basis sets[16] were employed and augmented by an extra polarisation function. Electrons in lower shells were treated within the frozen core approximation.[13a] A set of auxiliary s, p, d, f, and g functions,[17] centred in all nuclei, was introduced in order to fit the molecular density and Coulomb potential accurately in each SCF cycle. Both geometry optimisations and energy evaluations have been fully carried out within a generalised gradient approximation (GGA) that includes a GGA exchange and correlation corrections of Becke[18] and Perdew (BP86).[19]

In order to validate the method, the XRD data of complex **2** was geometrically optimised by excluding the solvent molecules. The results show good agreement between the experimental and theoretical data. The experimental and theoretical bond lengths and angles differ by less than 0.08 Å and 3.6°, respectively. The standard deviations for the selected distances and angles listed in Figure 3 were 0.04 Å and 2.1°, respectively, which confirm the validity of the chosen computational method.

All the experimental compounds were analysed computationally. It was found experimentally that both mononuclear and binuclear species are diamagnetic. For this reason, optimisations were carried out for neutral closed-shell singlet ground-state structures. However, since it has been found that the triplet state is close in energy to the singlet state, or it can be even more stable than the singlet state, we checked the relative stability of both states for all compounds by optimising the triplet state. In all cases the triplet state geometry presented a higher energy, indicating that the singlet states are the most favourable. This is in agreement with the sharp peaks in the NMR spectra. The difference between these two states is around 20 kcal·mol^{-1} (*racemic-trans*-**1** 22.2 kcal·mol^{-1}; *meso-trans*-**1** 21.4 kcal·mol^{-1}; *racemic-trans*-**2** 19.4 kcal·mol^{-1}; *meso-trans*-**2** 21.6 kcal·mol^{-1}).

Energy calculations predicted a slight stabilisation, by less than 0.1 kcal·mol^{-1}, of the *meso-trans*-**1** isomer relative to the racemic-*trans*-**1**, showing that the two isomers have similar energies, in line with the fact that experimentally the two isomers are present as final products. On the other hand, the energy calculations on complex **2** gave an energy difference of 5.1 kcal·mol^{-1} between the racemic-*trans*-**2** and the *meso-trans*-**2** isomers, in agreement with an equilibrium strongly displaced towards the racemic-*trans*-**2** diastereomer (experimental $\Delta E \geq 2.3$ kcal·mol^{-1}).[11]

We also attempted to optimise an *anti* conformation for the binuclear complex, but the optimisation process evolved towards the racemic-*trans*-**2** species, as the *anti* conformations are even less stable than the *syn* ones because of the steric requirements of the ligands.

Conclusion

In conclusion, the calculated energy differences between the racemic-*trans* and *meso-trans* diastereomers of these phosphanylthiolato complexes of Ni^{II} are in agreement with the experimentally observed racemic-*trans*/*meso-trans* ratios and are responsible for the chiral recognition between the two enantiomeric forms of the racemic ligand. This phenomenon is especially important in the binuclear complex **2**, in which a destabilised *anti* conformation of the bridging sulfurs would be necessary in order for the *meso-trans* isomer to be stable.

Experimental Section

General Remarks: The complexes were synthesised using standard Schlenk techniques under nitrogen atmosphere. The solvents were dried by standard methods and distilled and deoxygenated before use. The C, H and S analyses were carried out using a Carlo−Erba microanalyser. $CDCl_3$ for NMR measurements was dried over molecular sieves. Proton NMR spectra were recorded at 200 MHz on a Bruker DPX-200 spectrometer. Peak positions are relative to tetramethylsilane as internal reference. $^{31}P\{^1H\}$ NMR spectra were recorded on the same instrument operating at 81.0 MHz. Chemical shifts are relative to external 85 % H_3PO_4 and downfield values are reported as positive. $^{13}C\{^1H\}$ NMR spectra were recorded on the same instrument operating at 50.3 MHz. Chemical shifts are relative to tetramethylsilane as internal reference.

[Ni{SCH(CH$_3$)CH$_2$PPh$_2$-*P*,*S*}$_2$] (1): 1-(diphenylphosphanyl)propane-2-thiol (205.4 mg, 0.79 mmol) in CH_2Cl_2 (1 mL) was added to a solution of $NiCl_2{\cdot}6H_2O$ (75.1 mg, 0.316 mmol) in methanol (2 mL) under a nitrogen atmosphere to produce a green precipitate. The precipitate was washed with hexane yielding complex **1** (155.1 mg, 80 %). ^1H NMR (200 MHz, $CDCl_3$, TMS): δ = 1.31 (d, ^3J = 6.4 Hz, 2.72 H, CH_3 racemic-*trans*-**1**); 1.40 (d, ^3J = 6.2 Hz, 6 H, CH_3 *meso-trans*-**1**); 2.33 (tt, ^2J = −13.4, ^3J = 13.4, $^2J_{H,P} \approx$ 2.8 Hz, 2 H, $CH_{2ax.}$ *meso-trans*-**1**); 2.47 (ddt, ^2J = −13.1, ^3J = 10.1, $^2J_{H,P} \approx$ 3.0 Hz, 0.92 H, $CH_{2ax.}$ racemic-*trans*-**1**); 2.6−3.0 (m, 5.8 H, $CH_{2\ equiv.}$, CH, *meso-trans*-**1** and racemic-*trans*-**1**); 7.1−8.3 (m, 29 H, H_{ar}) ppm. $^{13}C\{^1H\}$ NMR (50.3 MHz, $CDCl_3$, TMS): δ = 25.10 (t, $J_{C,P}$ = 9.0 Hz, CH_3 *meso-trans*-**1**); 26.08 (t, $J_{C,P}$ = 7.4 Hz, CH_3 racemic-*trans*-**1**); 36.37 (t, $J_{C,P}$ = 12.3 Hz, CH *meso-trans*-**1**); 37.22 (t, $J_{C,P}$ = 14.4 Hz, CH racemic-*trans*-**1**); 46.51 (t, $J_{C,P}$ = 18.5 Hz, CH_2 *meso-trans*-**1**); 47.44 (t, $J_{C,P}$ = 18.2 Hz, CH_2 racemic-*trans*-**1**); 128.5−129.2 (m, C_m *meso-trans*-**1** and racemic-*trans*-**1**); 129.2−132.3 (m, C_i *meso-trans*-**1** and racemic-*trans*-**1**); 130.66 (s, C_p *meso-trans*-**1**); 130.79 (s, C_p racemic-*trans*-**1**); 131.23 (s, C'_p racemic-*trans*-**1**); 131.41 (s, C'_p *meso-trans*-**1**); 132.85 (t, $J_{C,P}$ = 5.4 Hz, C_o *meso-trans*-**1**); 133.41 (t, $J_{C,P}$ = 5.6 Hz, C_o racemic-*trans*-**1**); 134.58 (t, $J_{C,P}$ = 6.1 Hz, C'_o racemic-*trans*-**1**); 135.10 (t, $J_{C,P}$ = 6.1 Hz, C'_o *meso-trans*-**1**) ppm. $^{31}P\{^1H\}$ NMR (81 MHz, $CDCl_3$, H_3PO_4): δ = 52.56 (s, 1P, *meso-trans*-**1**); 54.23 (s, 0.46P, racemic-*trans*-**1**) ppm. $C_{30}H_{32}NiP_2S_2$ (577.4): calcd. C 62.41, H 5.59, S 11.11; found C 62.22, H 5.70, S 10.99 %.

[Ni{μ-SCH(CH$_3$)CH$_2$PPh$_2$-*P*,*S*}(Cl)]$_2$ (2): 1-(diphenylphosphanyl)-propane-2-thiol (88.1 mg, 0.338 mmol) in CH_2Cl_2 (1 mL) was added to a solution of $NiCl_2{\cdot}6H_2O$ (80.5 mg, 0.338 mmol) in methanol (2 mL) under a nitrogen atmosphere. The green precipitate obtained had redissolved after 3 h stirring, yielding a brown solution. The product was crystallised by addition of diethyl ether to afford complex **2** as brown crystals (91.3 mg, 80 %). ^1H NMR (200 MHz, $CDCl_3$, TMS): δ = 1.34 (d, ^3J = 8.0 Hz, 6 H, CH_3); 2.34 (td, ^2J = −13.7, ^3J = 13.7, $^2J_{H,P}$ = 6.4 Hz, 2 H, $CH_{2ax.}$); 2.63

 © 2003 Wiley-VCH Verlag GmbH & Co. KGaA, Weinheim

(ddpseudo-t, $^2J = -13.7$, $^3J = 4.5$, $^2J_{H,P} \approx 4.4$ Hz, 2 H, $CH_{2\,equiv.}$); 3.24 (m, 2 H, CH); 7.2−8.4 (m, 20 H, H_{ar}) ppm. $^{13}C\{^1H\}$ NMR (50.3 MHz, $CDCl_3$, TMS): δ = 22.96 (m, CH_3); 39.16 (pseudo-t, $J \approx 3.0$ Hz, CH); 44.97 (d, $^1J_{C,P} = 38.8$ Hz, CH_2); 128.80 (pseudo-t, $^3J_{C,P} = 5.2$ Hz, C_m); 128.95 (pseudot, $^3J_{C,P} = 5.2$ Hz, C'_m); 130.12 (dd, $^1J_{C,P} = 6.7$, $^4J_{C,P} \approx 3.1$ Hz, C_i); 131.09 (dd, $^1J_{C,P} = 5.6$, $^4J_{C,P} \approx 3.0$ Hz, C'_i); 131.84 (s, C_p); 133.14 (pseudo-t, $J_{C,P} \approx 4.9$ Hz, C_o); 133.63 (pseudo-t, $J_{C,P} \approx 5.1$ Hz, C_o) ppm. $^{31}P\{^1H\}$ NMR (81 MHz, $CDCl_3$, H_3PO_4): δ = 36.28 (s) ppm. $C_{30}H_{32}Cl_2Ni_2P_2S_2$ (707.0): calcd. C 50.97, H 4.56, S 9.07; found C 50.66, H 4.69, S 8.93 %.

X-ray Structure Determination of 2: Brown crystals of **2** were obtained by slow evaporation of a chloroform/dichloromethane (1:1) solution at room temperature. Molecular formula: $C_{31}H_{33}Cl_5Ni_2P_2S_2$; $M = 826.30$; monoclinic; $a = 12.8894(4)$, $b = 11.8883(3)$, $c = 22.5265(7)$ Å, β = 96.5500(10)°, $V = 3429.27(17)$ Å^3; space group $P2_1/n$; $Z = 4$, μ = 1.725 mm^{-1}, $D_{calcd.} = 1.600$ g cm^{-3}. The measurements were made on a Siemens P4 diffractometer equipped with a SMART-CCD-1000 area detector, a MAC Science Co. rotating anode with Mo-K_α radiation, a graphite monochromator and a Siemens low temperature device LT2 (T = −120 °C). In the range 1.74 to 31.50°, 49317 reflections were collected, of which 10947 were unique ($R_{int} = 0.0838$). Full-sphere data was collected using ω and scans. Programs used: Data collection Smart V. 5.060 (Bruker AXS, 1999), data reduction Saint + Version 6.02 (Bruker AXS 1999) and absorption correction SADABS (max/min transmission: 1.000000/0.356109, Bruker AXS 1999). Structure solution and refinement was done using SHELXTL Version 5.10 (Sheldrick, Universität Göttingen, Göttingen (Germany), 1998). The structure was solved by direct methods and refined by full-matrix least-squares methods on F^2. All hydrogen atoms were refined without constraints. Final $R_1[I > 2\sigma(I)] = 0.0452$ and $wR(F^2)[I > 2\sigma(I)] = 0.1037$. The number of refined parameters was 511. CCDC-216078 contains the supplementary crystallographic data for this paper. These data can be obtained free of charge at www.ccdc.cam.ac.uk/conts/retrieving.html [or from the Cambridge Crystallographic Data Centre, 12, Union Road, Cambridge CB2 1EZ, UK; Fax: (internat.) +44-1223/336-033; E-mail: deposit@ccdc.cam.ac.uk].

Acknowledgments

This work was financially supported by the DGESIC, projects PB98-0913-C02, BQU2002-04070-C02 and BQU2002-04112-C02-02. M. S. would like to thank the DURSI (Generalitat de Catalunya) for financial support through the Distinguished University Research Promotion, 2001.

[1] J. S. Kim, J. H. Reibenspies, M. Y. Darensbourg, *J. Am. Chem. Soc.* **1996**, *118*, 4115−4423.
[2] D. A. Vicic, W. D. Jones, *J. Am. Chem. Soc.* **1999**, *121*, 7606−7617.
[3] [3a] L. C. Myers, M. P. Terranova, A. E. Ferentz, G. Wagner, G. L. Verdine, *Science* **1993**, *261*, 1164−1167. [3b] T. Ohkubo, H. Sakashita, T. Sakuma, M. Kainosho, M. Sekiguchi, K. Morikawa, *J. Am. Chem. Soc.* **1994**, *116*, 6035−6036.
[4] P. H. Leung, J. W. L. Martin, S. B. Wild, *Inorg. Chem.* **1986**, *25*, 3396−3400.
[5] [5a] Y.-M. Hsiao, S. S. Chojnacki, P. Hinton, J. H. Reibenspies, M. Y. Darensbourg, *Organometallics* **1993**, *12*, 870−875. [5b] M. Kita, T. Yamamoto, K. Kashiwabara, J. Fujita, *Bull. Chem. Soc. Jpn.* **1992**, *65*, 2272−2274.
[6] [6a] T. Gerdau, W. Klein, R. Kramolowsky, *Acta Crystallogr., Sect. C: Cryst. Struct. Commun.* **1982**, *11*, 1663−1669. [6b] K. Aurvillius, G. Bertinsson, *Acta Crystallogr., Sect. B* **1982**, *38*, 1295−1298.
[7] [7a] G. Aullón, G. Ujaque, A. Lledós, S. Alvarez, *Chem. Eur. J.* **1999**, *5*, 1391−1410. [7b] G. Aullón, G. Ujaque, A. Lledós, S. Alvarez, P. Alemany, *Inorg. Chem.* **1998**, *37*, 804−813.
[8] M. Wieber, T. Z. Clarius, *Z. Anorg. Allg. Chem.* **1995**, *621*, 1288−1292.
[9] E. Pfeiffer, M. L. Pasquier, W. Marty, *Helv. Chim. Acta* **1984**, *67*, 654−663.
[10] [10a] N. Brugat, J. Duran, A. Polo, J. Real, A. Álvarez-Larena, J. F. Piniella, *Tetrahedron: Asymmetry* **2002**, *13*, 569−577. [10b] N. Brugat, A. Polo, A. Álvarez-Larena, J. F. Piniella, J. Real, *Inorg. Chem.* **1999**, *38*, 4829−4837.
[11] The experimental difference of energy between the two diastereomers was calculated from the $^{31}P\{^1H\}$ NMR spectra using the relative signal intensities for complex **1** and the signal to noise ratio for complex **2**.
[12] G. te Velde, F. M. Bickelhaupt, E. J. Baerends, C. Fonseca Guerra, S. J. A. Van Gisbergen, G. J. Snijders, T. Ziegler, *J. Comput. Chem.* **2001**, *22*, 931−967.
[13] [13a] E. J. Baerends, D. E. Ellis, P. Ros, *Chem. Phys.* **1973**, *2*, 41−51. [13b] E. J. Baerends, PhD Thesis, Vrije Universiteit, Amsterdam, **1975**.
[14] W. Ravenek, *Algorithms and Applications on Vector and Parallel Computers* (Eds.: H. J. J. te Riele, Th. J. Dekker, H. A. van de Vorst), Elsevier, Amsterdam, **1987**.
[15] G. te Velde, E. J. Baerends, *J. Comput. Phys.* **1992**, *99*, 84−98.
[16] [16a] G. J. Snijders, E. J. Baerends, P. Vernooijs, *At. Nucl. Data Tables* **1982**, *26*, 483−509. [16b] P. Vernooijs, G. J. Snijders, E. J. Baerends, *Slater Type Basis Functions for the Whole Periodic System. Internal Report*, Vrije Universiteit of Amsterdam, The Netherlands, **1981**.
[17] J. Krijn, E. J. Baerends, *Fit functions in the HFS method. Internal Report (in Dutch)*, Vrije Universiteit of Amsterdam, The Netherlands, **1984**.
[18] A. D. Becke, *Phys. Rev. A* **1988**, *38*, 3098−3100.
[19] J. P. Perdew, *Phys. Rev. B* **1986**, *33*, 8822−8824.

Received July 25, 2003

 © 2003 Wiley-VCH Verlag GmbH & Co. KGaA, Weinheim

Heterobimetallic Calix[4]arene Complexes: Interconversion of Dimeric (Ca, Sr or Ba)/Ti^{IV} Complexes with a Monomeric K/Ti^{IV} Complex

Antonella J. Petrella,[a] Nicholas K. Roberts,[a] Colin L. Raston,[b] Donald C. Craig,[a] Mark Thornton-Pett,[c] and Robert N. Lamb*[a]

Keywords: Calixarenes / Heterometallic complexes / Alkaline earth metals / Potassium / Titanium

Reaction of calix[4]arene with alkaline earth metals (Ca/Sr/Ba) in methanol followed by the addition of various titanium(IV) sources afforded novel dimeric 1:1 alkaline earth/titanium(IV) calix[4]arene complexes. In each complex the central core of the crystallographically imposed centrosymmetric dimer consists of a rhombus of alternating alkaline earth metals and μ_3-oxo-centres. Five terminal methanol ligands form seven-coordinate calcium and strontium centres, while the barium centres are bridged by two additional methanol ligands, making them nine-coordinate. Each oxo centre is the apical ligand of a square-pyramidal titanium(IV) centre, whose basal plane ligands are the four phenolate oxygens from a calix[4]arene in the symmetrical cone-conformation. Deprotonation of calix[4]arene with potassium metal, followed by the addition of a titanium(IV) source containing at least one acetylacetonate ligand, formed a mixed potassium/titanium complex based on one calix[4]arene. The potassium cation in this complex binds within the π-basic calix[4]arene cavity, whilst titanium is octahedrally complexed in the *exo*-position, by four phenolates and one acetylacetonate. The alkaline earth titanium dimers and potassium/titanium monomers could be interconverted merely by changing the solvent, with the appropriate cations and ligands present in solution.
(© Wiley-VCH Verlag GmbH & Co. KGaA, 69451 Weinheim, Germany, 2003)

Introduction

There is currently much interest in the formation and characterisation of heterobimetallic alkoxide species with well-defined stoichiometries.[1] Such complexes have potential as single source precursors to ultra-pure oxide ceramics,[2] or as molecular catalysts.[3] The synthesis and structural characterisation of heterobimetallic alkoxides has typically required the use of inert atmosphere techniques, owing to the inherent instability of such complexes towards hydrolysis and/or facile redistribution reactions.[1] We sought to explore alternative synthetic approaches, using macrocyclic calix[n]arenes as multidentate alkoxy ligands to circumvent the above decomposition reactions, and to impart high thermal stability.

Calix[4]arenes provide a set of four contiguous phenolic oxygen centres poised for metal ion chelation, and their complexes show a wide range of structural types, usually with the macrocycle in the bowl-shaped conformation.[4] While there are many structurally authenticated calix[4]arene transition metal complexes, those for the main group metals are limited. In the case of alkali and alkaline earth metals there are few examples of complexes of calix[*n*]arenes, the main focus of the chemistry concerned with ion extraction processes. In the case of calix[4]arenes there are a few examples of alkali metal[5] and alkaline earth metal[6] complexes, and a few examples of mixed transition-alkali metal complexes,[4,7] yet there are no examples of mixed transition metal alkaline earth complexes.

Herein we report a simple route to the preparation of dimeric alkaline earth/titanium(IV) calix[4]arene complexes, **1**−**3**, and the formation of a monomeric potassium/titanium(IV) calix[4]arene complex, **4** (Scheme 1). The complexes are formed rapidly in good yield, and do not require the use of an inert atmosphere, or dry solvents, although the yield of the dimeric calcium/titanium(IV) complex is higher in dry solvent. We also show that the alkaline earth/titanium(IV) dimers may be inter-converted into the potassium/titanium(IV) monomers by merely changing the solvent, with the appropriate cations and ligands present in solution. Seemingly the relative disposition of the alkoxide groups in the calix[4]arene stabilises these novel structures, with their formation also depending on the nature of the alkali/alkaline earth metal as well as the choice of solvent.

Addition of one equivalent of alkaline earth metal (Ca, Sr or Ba) to a suspension of *p*-*t*Bu-calix[4]arene, *p*-*t*Bu-

[a] School of Chemical Sciences, University of New South Wales
Sydney, NSW, Australia
E-mail: r.lamb@unsw.edu.au
[b] School of Biomedical and Chemical Sciences, University of Western Australia
Crawley, Perth, Australia
E-mail: clraston@chem.uwa.edu.au
[c] Department of Chemistry, University of Leeds,
Leeds LS2 9JT, UK

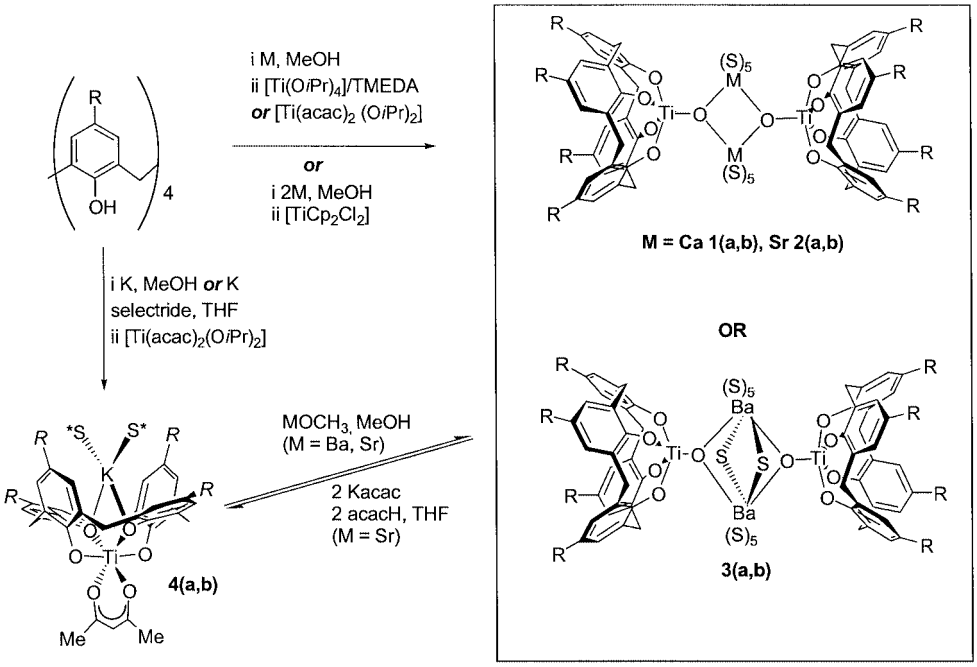

Scheme 1. S = MeOH, S* = MeOH or THF; (a) R = *t*Bu, (b) R = H

$L[OH]_4$, or calix[4]arene, $L[OH]_4$, in methanol, followed by addition of a 1:1 solution of $[Ti(OiPr)_4]$ and TMEDA (*N*,*N*,*N*′,*N*′-tetramethylethylenediamine) in methanol afforded complexes **1**−**3** (Scheme 1). In the case of reactions involving calcium metal, dry methanol was used (see below). Premixing the $[Ti(OiPr)_4]$ and TMEDA before addition of methanol avoids the precipitation of titanium hydroxides/methoxides.

Alternative preparations of **1**−**3** were also established, where $[Ti(acac)_2(OiPr)_2]$ (acac = acetylacetonate) or $[TiCp_2Cl_2]$ (Cp = cyclopentadienyl) and an extra equivalent of alkaline earth metal were used in place of $[Ti(OiPr)_4]$/TMEDA. Base cleavage of both Cp ligands from $[TiCp_2Cl_2]$ is consistent with previous reports that Cp groups are cleaved from titanocene reagents under basic conditions.[8] The success of this synthetic route suggests that the relatively slow reaction of $[TiCp_2Cl_2]$ provides a synthetically engineered pathway for gradually delivering labile titanium(IV) into the reaction mixture, which presumably allows ligation with calix[4]arene to compete successfully against hydrolysis/methanolysis. Similarly, the successful use of $[Ti(OiPr)_4]$/TMEDA or $[Ti(acac)_2(OiPr)_2]$ reagents appears to rely on the chelation of titanium(IV) by TMEDA or acetylacetonate ligand to provide the same slow delivery of titanium(IV).

When TMEDA was omitted from the reaction of $[Ti(OiPr)_4]$ with calix[4]arene deprotonated by strontium or barium, the respective yields of **2(a,b)** and **3(a,b)** were low (< 20%, identified by ^{1}H NMR spectroscopy) and the complexes were contaminated by insoluble titanium hydrolysis/alcoholysis products. For calcium metal, under the same conditions, some dimer products **1(a,b)** precipitated, ca. 50% yield, along with unchanged calix[4]arene. The same modest yield results for calcium, even in the presence of TMEDA, in contrast to the good yields, ca. 80%, for the strontium and barium analogues. However, the yield of the Ca/Ti dimers **1(a,b)** can be improved to ca. 70% by using dry methanol. These findings can be rationalised by the poor solubility of calcium hydroxide in wet methanol, compared to strontium and barium hydroxides. Thus, whereas solutions containing strontium and barium ions and calix[4]arenes in wet methanol remain clear, the corresponding calcium solutions deposit considerable amounts of white material. However, when the latter mixture is formed in dry methanol the solution remains clear. For all three structures oxo-bridges are possibly derived from adventitious water; alternatively they could result from the presence of oxides/hydroxides on the surface of the metal.

The dimeric structures of **1b**, **2b** and **3a** were established using single-crystal X-ray diffraction data. Complexes **1b** and **2b** crystallise in the space group $P2_1/n$ having similar cell dimensions and are strictly isomophous, with the cell volume of the calcium complex slightly smaller than that of the strontium analogue, as expected. Major differences in the molecular structures of **1b** and **2b** (Figure 1, Table 1),[9] relative to that of **3a** (Figure 2, Table 2),[9] other than those associated with the substituents on the calixarene, include two additional methanol ligands which bridge the two barium centres in **3a** and the resulting coordination environment of the alkaline earth metal centres. The ^{1}H NMR spectra of **1b**, **2b** and **3a** are consistent with the persistence of the solid-state structures in solution.

The central cores of the crystallographically imposed centrosymmetric dimers in **1b** and **2b** consist of a rhombus of alternating alkaline earth metals and μ_3 oxo-centres, with each oxygen atom forming the apical ligand to a square-pyramidal titanium(IV) centre. The basal plane ligands are the four phenolate oxygen centres from a calix[4]arene in a

 © 2003 Wiley-VCH Verlag GmbH & Co. KGaA, Weinheim

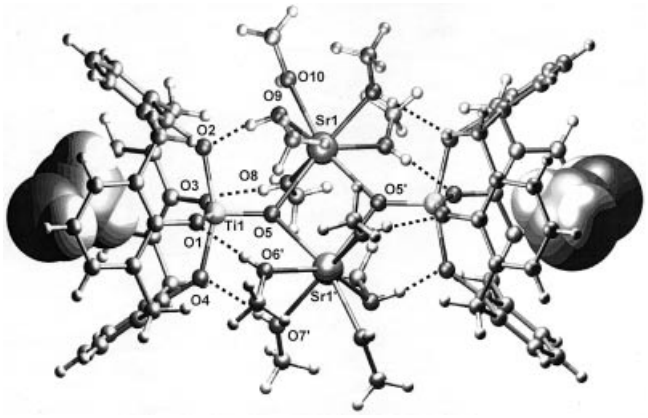

Figure 1. Molecular projection of the strontium/titanium(IV) complex, **2b**, showing included methanol (space filling) and intramolecular H-bonds

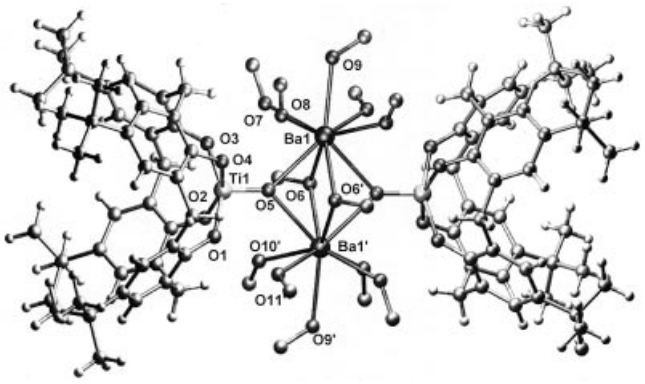

Figure 2. Molecular projection of the barium/titanium(IV) complex, **3a**, excluding methanol hydrogen atoms.

Table 1. Selected bond lengths (Å) and angles (°) for **2b**, values in parentheses are for the isomorphous calcium complex **1b**

Ti(1)−O(1, 2, 3, 4, 5)	1.9706(19), 1.9548(19), 1.9413(19), 1.9481(19), 1.7056(18), [1.9707(15), 1.9459(16), 1.9359(15), 1.9433(16),1.7078(14)]
Sr(1)−O(5, 5′, 6, 7, 8, 9, 10)	2.6019(18), 2.5426(17), 2.510(2), 2.549(2), 2.533(2), 2.578(2), 2.509(2), [2.5358(15), 2.4066(15), 2.3747(17), 2.4231(18), 2.4036(17), 2.4177(16), 2.3724(17)]
O(1)−Ti(1)−O(2, 3, 4, 5)	86.90(8), 156.36(8), 87.14(8), 102.07(8), [86.62(6), 155.18(6), 86.67(7), 102.87(7)]
O(2)−Ti(1)-(3, 4, 5)	87.86(8), 156.15(8), 100.50(8), [87.72(7), 154.40(6), 101.57(7)]
O(3)−Ti(1)−O(4, 5)	88.41(8), 101.55(8), [88.09(7), 101.94(7)]
O(4)−Ti(1)−O(5)	103.33(8), [104.00(7)]
O(5)−Sr(1)−O(5′, 6, 7, 8, 9, 10)	77.61(6), 133.63(7), 130.93(8), 75.46(7), 72.80(6), 120.02(7), [77.76(5), 134.70(6), 134.43(6), 75.32(6), 73.14(5), 116.97(6)]
O(5′)−Sr(1)−O(6, 7, 8, 9, 10)	78.41(6), 78.19(7), 111.67(7), 103.04(6), 162.30(7), [80.52(5), 81.32(6), 112.24(6), 104.45(7), 165.14(6)]
O(6)−Sr(1)−O(7, 8, 9, 10)	80.91(8), 77.47(7), 151.83(8), 88.85(7), [79.54(7), 76.98(6), 151.47(6), 89.28(6)]
O(7)−Sr(1)−O(8, 9, 10)	153.59(8), 72.06(8), 87.79(8), [150.21(7), 73.64(6), 86.23(7)]
O(8)−Sr(1)−O(9, 10)	125.72(7), 76.86(8), [124.21(6), 75.46(6)]
O(9)−Sr(1)−O(10)	82.46(7), [79.57(6)]

Table 2. Selected bond lengths (Å) and angles (°) for **3a**

Ti(1)−O(1, 2, 3, 4, 5)	1.961(4), 1.977(4), 1.938(4), 2.035(4), 1.680(4)
Ba(1)−O(5, 5′, 6, 6′ 7, 8, 9, 10, 11)	2.816(4), 2.861(4), 2.907(4), 2.889(4), 2.751(4), 2.742(4), 2.799(5), 2.743(4), 2.704(4)
O(1)−Ti(1)−O(2, 3, 4, 5)	87.7(2), 153.3(2), 87.3(2), 104.0(2)
O(2)−Ti(1)-(3, 4, 5)	88.2(2), 159.6(2), 101.5(2)
O(3)−Ti(1)−O(4, 5)	87.5(2), 102.7(2)
O(4)−Ti(1)−O(5)	98.9(2)
O(5)−Ba(1)−O(5′, 6, 6′, 7, 8, 9, 10, 11)	91.7(1), 61.0(71), 62.8(1), 72.1(1), 75.1(1), 137.0(1), 135.2(1), 132.6(1)
O(5′)−Ba(1)−O(6, 6′, 7, 8, 9, 10, 11)	62.1(1), 60.7(1), 140.2(1), 134.5(1), 131.3(1), 70.9(1), 73.6(1)
O(6)−Ba(1)−O(6′, 7, 8, 9, 10, 11)	94.0(1), 78.5(1), 134.5(1), 132.0(2), 131.3(1), 72.6(1)
O(6′)−Ba(1)−O(7, 8, 9, 10, 11)	131.6(1), 74.8(1), 133.8(2), 72.8(1), 133.0(1)
O(7)−Ba(1)−O(8, 9, 10, 11)	77.3(2), 72.2(2), 144.5(1), 90.7(1)
O(8)−Ba(1)−O(9, 10, 11)	7304 (2), 88.1(1), 144.9(1)
O(9)−Ba(1)−O(10, 11)	72.7(2), 70.7(2)
O(10)−Ba(1)−O(11)	82.9(1)

symmetrical cone-conformation, as shown in Figure 1, along with key bond lengths and angles, which are unexceptional. Deviation of the titanium centres from the plane defined by the four phenolate oxygen centres is 0.4016 and 0.4250 Å for **2b** and **1b** respectively. The calcium/strontium centres are seven-coordinate, having a distorted pentagonal bipyramidal geometry with two bridging oxo- and five terminal methanol ligands. An oxo group and one methanol ligand are in apical positions, with the other methanol ligands associated with hydrogen bonding to the oxygen atoms of the calix[4]arene, this presumably contributes to the stability and favourable formation/crystallisation of the complexes from methanol. The calixarene-methanol O···O distances and corresponding O···HO distances (in parentheses) are 2.676, (2.006), 2.645, (1.759), 2.649, (1.881), 2.603, (1.889) for **1b**; and 2.684, (1.920), 2.649, (1.769), 2.648,

 © 2003 Wiley-VCH Verlag GmbH & Co. KGaA, Weinheim

(1.910) 2.689, (2.026) for **2b**. There are 15 methanol solvates per dimer, of which 10 are coordinated to the strontium metal centres, two are located within the cavities of the calixarenes, and the remainder are found at interstitial sites in the structure.

Complex **3a** crystallises in the space group *Pbca*. The molecular structure of the complex is essentially the same as in **1b** and **2b**, being also comprised of centrosymmetric dimers. The titanium centres are in a similar environment, the metal centres deviating from the basal plane of four oxygen centres by 0.4021 Å. The expanded coordination sphere of the barium centres, each now with nine ligands, two bridging oxo, two bridging methanol and five terminal methanol solvates, is best described as capped square antiprismatic (Figure 2). The square face opposite the unique capping methanol is comprised of two *trans*-μ_3-oxo groups and two *trans*-μ_2-methanol ligands, which is common to both barium centres, and replaces the rhombus oxo-Ca/Sr core in **1b** and **2b**. Intramolecular hydrogen bonding is also prevalent, with calixarene-methanol O···O distances 2.688, 2.723, 2.631, 2.667Å, and additional interactions between bridging oxo and bridging methanol ligands, O5···O1, O1′ 2.904, 2.974 Å. Overall there are 24 methanol solvent molecules per dimer: 12 are coordinated to barium centres, two are located in the cavities of the calix[4]arenes, and the remaining 10 are located in the interstitial sites in the structure, along with one molecule of water. The titanium(IV) centres have similar geometries to those in **1b** and **2b**.

Previous examples of mixed-metal M/Ti species (M = Ba, Sr, Ca) based on simple alkoxide ligands do not generally have 1:1 stoichiometry,[10] but this is the case for complexes based on β-diketonates (M = Sr, Ba),[11] catecholate (M = Sr, Ba),[12] and aryloxy ligands [M = Ba].[13] The structures of such complexes are similar to the present structures in being dimeric, but are dissimilar in that the titanium centres are octahedrally coordinated. Also, whilst there are several examples of larger M/Ti aggregates displaying oxo-bridging between alkaline earth and titanium(IV) centres,[14] examples of oxo-bridged 2:2 complexes (as in the present structures) have the oxo groups between the titanium centres. Thus our structures are unique in the interplay of the oxo groups with the two different metal centres. This, and the lower coordination number of the titanium centres, possibly relates to the steric constraints imposed by the four phenolato groups of the calixarene, and also the intramolecular hydrogen bonds between the coordinated methanol molecules and the calixarene oxygens.

The monomeric heterobimetallic K/Ti calix[4]arene complexes, **4(a,b)**, were prepared by addition of one equivalent of potassium metal to *p*-*t*Bu-L[OH]$_4$ in either methanol, for **4a**, or THF for **4b**, followed by the addition of one equivalent of [Ti(acac)$_2$(O*i*Pr)$_2$]. The complexes were structurally authenticated using X-ray diffraction data. They crystallise in the space groups *C*2/*c* and *P*2$_1$/*n*, respectively, **4a** having half a molecule in the asymmetric unit, the other half being generated by a twofold rotation operation, whereas **4b** has a full molecule as the asymmetric unit. A molecular projection of **4a** is shown in Figure 3.[9] For both complexes the titanium(IV) centres are octahedral, bound by a bidentate β-diketonate and four phenolato oxygen atoms of a pinched cone conformation calix[4]arene (the pitch of the phenol planes relative to the plane through the oxygens of the calixarene being 18.2° and 70.1° for **4a** and 12.0°, 13.2°, 67.7°, 66.1° for **4b**; see also Table 3). The potassium is accommodated within the cavity of the calix[4]arene, interacting with two of the phenolate oxygen atoms and forming π-interactions to two opposite aromatic rings. Additionally two terminal methanol or THF ligands result in six-coordinate potassium centres. The K^+-η^6-arene(centroid) distances in **4a** and **4b** are 3.142 and 3.180, 3.253 Å, respectively, which are similar to previously reported values for a mixed *endo*-*exo*-potassium *exo* titanium dimeric calix[4]arene complex (3.217 Å).[7b]

The formation of the monomeric species **4(a,b)** is favoured by the incorporation of a chelating β-diketonate ligand, which provides steric protection against the formation of metallo-bridged structures, and predisposes titanium to chelate to only one calix[4]arene. In addition, the potassium ion is bound within the calix[4]arene cavity. Analogous monomeric alkaline earth/titanium calix[4]arene complexes could not be obtained, the dimers **1(a,b)**−**3(a,b)** being formed instead, even in the presence of acetylacetonate. This difference is consistent with the more polarising divalent alkaline earth cations preferring *exo*-cavity coordination, where they can obtain higher coordination numbers relative to the coordination available in the *endo*-cavity.

Dimers **1a**−**3a** possessing the *p*-*t*Bu substituents are sparingly soluble in methanol, and they precipitate from solution in good yield when prepared in this solvent. In contrast, these same dimers are highly soluble in solvents such

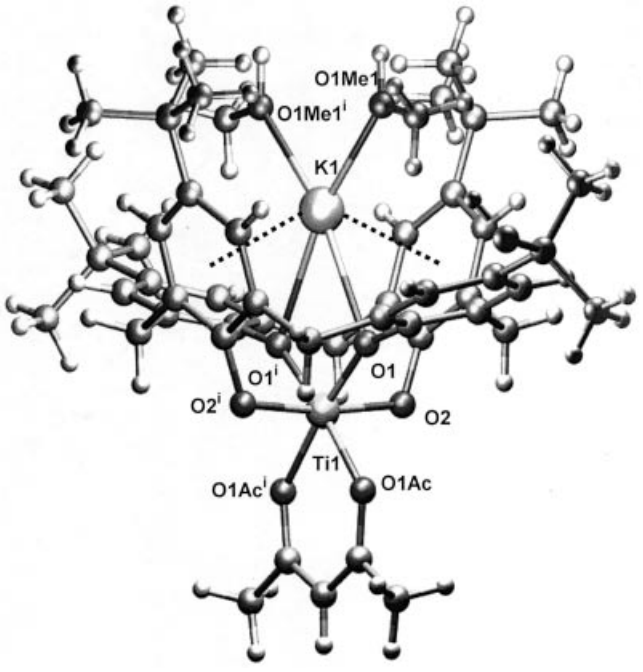

Figure 3. Molecular projection of the potassium/titanium(IV) complex **4a**

 © 2003 Wiley-VCH Verlag GmbH & Co. KGaA, Weinheim

Table 3. Selected bond lengths (Å) and angles (°) for **4a** and **4b**

	4a
Ti(1)−O(1, 1Ac, 2)	1.8307(19), 1.999(2), 1.9907(18)
K(1)−O(1, 1Me)	2.833(2), 2.68(3)
O(2)−Ti(1)−O(1Ac, 1Ac[i], 2[i])	94.24(13), 86.51(8), 88.75(8), 91.45(9), 173.76(9)
O(1Ac)−Ti(1)−O(1Ac[i])	82.99(14)
O(1)−K(1)−O(1[i], 1Me, 1Me[i])	56.53(8), 108.78(8), 165.29(8)
O(1Me)−K(1)−O(1Me[i])	85.91(15)
	4b
Ti(1)−O(1, 2, 3, 4, 7, 8)	1.8593(16), 1.9503(17), 1.8547(16), 1.9622(17), 1.9989(17), 2.0130(17)
K(1)−O(1, 3, 5, 6)	2.7476(17), 2.7479(17), 2.706(2), 2.693(2)
O(1)−Ti(1)−O(2, 3, 4, 7, 8)	87.89(7), 90.86(7), 87.44(7), 173.94(7), 91.04(7)
O(2)−Ti(1)−O(3, 4, 7, 8)	87.81(7), 172.90(7), 94.79(7), 92.04(7)
O(3)−Ti(1)−O(4, 7, 8)	86.91(7), 94.66(7), 178.09(7)
O(4)−Ti(1)−O(7, 8)	90.37(7), 93.40(7),
O(7)−Ti(1)−O(8)	83.45(7)
O(1)−K(1)−O(3, 5, 6)	57.56(5), 110.84(6), 162.04(6),
O(3)−K(1)−O(5, 6)	168.40(7), 104.62(6)
O(5)−K(1)−O(6)	86.98(7)

as toluene, dichloromethane or THF. We utilised solubility differences to devise methods to interconvert the dimers, in general, with the corresponding K/Ti monomers, **4(a,b)**, the latter being readily recrystallised from a variety of solvents. Thus, the K/Ti monomer **4a** crystallises from THF on addition of two equivalents of K(acetylacetonate) and acetylacetone to the alkaline earth/Ti dimers **2a** or **3a** (Scheme 1). No conversion into monomer could be effected in methanol. In THF, both the K/Ti monomer and Ba/Ti, Sr/Ti dimers are soluble, hence both monomeric and dimeric species can be present in equilibrium in solution. The K/Ti monomer can then be isolated from the mixture by selective crystallisation in the presence of additional ligand, since the Ba/Ti and Sr/Ti dimers cannot be crystallised from THF. Dissolution of the dimers in THF presumably results in ligand solvent displacement with disruption of the tightly coordinated methanol-calix[4]arene hydrogen bonding array (Figure 1).

Conversely the K/Ti monomer **4b** can be converted simply to the dimers by addition of methanolic solutions of Ba/Sr methoxides (>90%). Evidently the insolubility of the Ba/Ti and Sr/Ti dimers in methanol drives their formation. Attempts to interconvert the Ca/Ti dimers with monomers were thwarted by the precipitation of $Ca(OH)_2$.

Dimers **1**−**3** have been tested for application as single source precursors for CVD of perovskite titanate films. Preliminary results indicate that the compounds sublime under high vacuum and that annealing of this sublimate indeed gives a crystalline perovskite phase, and further investigations are underway. This aspect aside, the significance of the above results include (i) the simplicity and versatility of the synthetic approach in gaining access to heterobimetallic complexes, which should have a profound impact on synthetic strategies for gaining access to a wide range of mixed metal complexes, (ii) the novelty of the structures, and (iii) the remarkable control of the interconversion of monomeric and dimeric complexes.

Experimental Section

Synthesis of 1(a,b) 2(a,b) and 3(a,b): Full experimental details are given for **3a**, the synthesis of **1**, **2** and **3b** being very similar. Barium (0.12 g, 0.87 mmol) was added to a suspension of *p*-*t*Bu-calix[4]arene (0.50 g, 0.77 mmol) in methanol (30 mL). The mixture was stirred, affording a clear pale yellow solution on complete reaction of the metal. [Ti(O*i*Pr)$_4$] (0.25 mL, 97%, 0.84 mmol) and TMEDA (0.15 mL, 1 mmol) were mixed together and then diluted in approximately 5 mL methanol and this solution was added to the barium calix[4]arene complex. A fine white solid formed, which was collected after 15 min and recrystallised from 10 mL dichloromethane by the addition of 15 mL of boiling methanol, yielding colorless prisms of **3a** (0.7 g, 80%). The analogous Sr/Ti **2a** (85% yield) and Ca/Ti (**1a**, 51% yield), were prepared as for **3a**. For **1a**, the solution formed by reaction of calcium with *p*-*t*Bu-calix[4]arene required filtering. Also, the solution of crude **1a** in dichloromethane required filtering to remove some precipitated *p*-*t*Bu-calix[4]arene. Crystals of **3a** suitable for X-ray crystallography were grown by layering methanol onto a dichloromethane solution of the complex. Compounds **1b**, **2b**, and **3b** were prepared similarly, calix[4]arene being used in place of *p*-*t*Bu-calix[4]arene, except that recrystallisation was performed directly from hot methanol,[15] yield 71% **1b**,[16] 80% **2b**, 82% **3b**. ^{1}H NMR ($CDCl_3$, 300 MHz, 298 K): δ = **1a**: 6.90 (s, 16 H, aryl), 4.73 (br., 8 H, CH_2), 3.40, (s, 66 H, methanol), 2.88 (br., 8 H, CH_2), 1.15 (s, 72 H, *t*Bu); **2a**: 6.92 (s, 16 H, aryl), 4.64 (d, J = 12 Hz, 8 H, CH_2), 3.33 (s, 66 H, methanol), 2.94 (d, J = 12 Hz, 8 H, CH_2), 1.15 (s, 72 H, *t*Bu); **3a**: 6.94 (s, 16 H, aryl), 4.63 (d, J = 12 Hz, 8 H, CH_2), 3.35 (s, 72 H, methanol), 3.00 (d, J = 12 Hz, 8 H, CH_2), 1.15 (s, 72 H, *t*Bu); **1b**: 6.98 (d, 16 H, J = 6 Hz, aryl), 6.49 (t, J = 6 Hz, 8 H, aryl), 4.79 (d, J = 12 Hz, 8 H, CH_2), 3.40 (s, 45 H, methanol), 3.16 (d, J = 12 Hz, 8 H, CH_2); **2b**: 6.96 (d, 16 H, J = 6 Hz, aryl), 6.51 (t, J = 6 Hz, 8 H, aryl), 4.74 (d, J = 12 Hz, 8 H, CH_2), 3.40 (s, 45 H, methanol), 3.03 (d, J = 12 Hz, 8 H, CH_2); **3b**: 6.96 (d, 16 H, J = 6 Hz, aryl), 6.50 (t, J = 6 Hz, 8 H, aryl), 4.74 (d, J = 12 Hz, 8 H, CH_2), 3.40 (s, 51 H, methanol), 3.06 (d, J = 12 Hz, 8 H, CH_2) ppm.

Synthesis of 4a and 4b: Potassium was added (0.04 g, 1.0 mmol) to a suspension of *p*-*t*Bu-calix[4]arene (0.50 g, 0.77 mmol) in methanol (20 mL). The mixture was stirred, resulting in a clear pale yellow solution on complete reaction of the metal. The addition of [Ti(acac)$_2$(O*i*Pr)$_2$] (0.40 mL, 75%, 0.82 mmol) gave an orange solution, which was concentrated by boiling to incipient crystallisation. On slow cooling to 0 °C orange prisms of **4a** formed[15] (0.6 g, 72%). **4b**: This THF adduct was prepared using dry THF and K-selectride (1 M in THF) in place of methanol and potassium metal, giving **4b** (0.45, 56%). ^{1}H NMR ($CDCl_3$, 300 MHz, 298 K): δ = **4a** 7.13 (s, 4 H, aryl), 6.91 (s, 4 H, aryl), 5.94 (s, 1 H, CH), 4.53 (d, J = 15 Hz, 4 H, CH_2), 3.45 (s, 24 H, methanol), 3.12 (d, J = 15 Hz, 4 H, CH_2), 2.00 (s, 6 H, CH_3), 1.37 (s, 18 H, *t*Bu), 1.10 (s, 18 H, *t*Bu); **4b:** 7.13 (s, 4 H, aryl), 6.93 (s, 4 H, aryl), 5.93 (s, 1 H, CH), 4.52 (d, J = 15 Hz, 4 H, CH_2), 3.69 (m, 12 H, THF), 3.14 (d, J = 15 Hz, 4 H, CH_2), 1.98 (s, 6 H, CH_3), 1.83 (m, 12 H, THF), 1.37 (s, 18 H, *t*Bu), 1.10 (s, 18 H, *t*Bu) ppm.

 © 2003 Wiley-VCH Verlag GmbH & Co. KGaA, Weinheim

Conversion of Ba/Ti Dimers to K/Ti Monomers: Acetylacetone (0.12 mL, 1.2 mmol) in methanol (ca. 2 mL) was treated with potassium metal (0.025 g, 0.64 mmol) and the solution was added to a solution of the Ba/Ti dimer **3a** (0.7 g 0.30 mmol) dissolved in THF (20 mL). The orange solution was concentrated by heating until incipient crystallisation. On cooling slowly to room temperature, crystals of **4b** formed (0.22 g, 36%). The Sr/Ti dimer **2a** could be converted into **4b** analogously (38% yield).

Conversion of K/Ti Monomer to Ba/Ti or Sr/Ti Dimer: A solution of **4b** (0.5 g, 0.48 mmol) in methanol (50 mL) was treated with a solution of Ba in methanol (0.07 g, 0.50 mmol) to give a white precipitate of **1a** (0.49 g, 96%); **4b** could be similarly converted into **1b** using Sr in place of Ba (94%).

Crystal Data: The intensity data was collected at 150(1)K on an Enraf−Nonius Kappa CCD diffractometer with Mo-K_α (λ = 0.71073Å) radiation. Structures **1b**, **2b**, **4a** and **4b** were solved by direct methods (SHELXL-97) and refined with a full-matrix least-squares fit refinement on F^2 (SHELXL-97). Structure **3a** was solved by direct methods (SIR92) and refined with a full-matrix least-squares fit on F (RAELS).

1b: $C_{28}H_{20}O_5CaTi{\cdot}7.5(CH_3OH)$ M_r = 764.74, monoclinic, space group $P2_1/n$, a = 11.4550(2), b = 17.2957(2), c = 18.9410(3) Å, β = 94.497(2), V = 3741.08(11) Å^3, Z = 4, $\rho_{calcd.}$ = 1.358 Mg/m^3, μ(Mo-K_α) = 0.427 mm^{-1}, F(000) = 1620, 32671 reflections collected, 7344 independent reflections, GooF = 1.041, R_1 = 0.0416, wR_2 = 0.1061 (observed data).

2b: $C_{28}H_{20}O_5SrTi{\cdot}7.5(CH_3OH)$, M_r = 812.28, monoclinic, space group $P2_1/n$, a = 11.5578(2), b = 17.3628(2), c = 19.0148(3) Å, β = 94.253(2), V = 3805.30(10) Å^3, Z = 4, $\rho_{calcd.}$ = 1.418 Mg/m^3, μ(Mo-K_α) = 1.672 mm^{-1}, F(000) = 1692, 14265 reflections collected, 7476 independent reflections, GooF = 1.053, R_1 = 0.038, wR_2 = 0.0998 (observed data).

3a: $C_{44}H_{52}BaO_5Ti{\cdot}12(CH_3OH){\cdot}H_2O$, M_r = 1248.7, orthorhombic, space group *Pbca*, a = 21.3817(2), b = 22.4084(2), c = 27.7100(3) Å, V = 13277(1) Å^3, Z = 8, $\rho_{calcd.}$ = 1.25 Mg/m^3, μ(Mo-K_α) = 0.766 mm^{-1}, F(000) = 5280.0, 121528 reflections collected, 15053 independent reflections, GooF = 1.37, R_1 = 0.077, wR_2 = 0.109 (observed data).

4a: $C_{49}H_{59}KO_6Ti{\cdot}8(CH_3OH)$, M = 1087.3, monoclinic, space group $C2/c$, a = 14.2018(5), b = 21.9002(9), c = 21.1284(8) Å, β = 106.461(2)°, V = 6302.1(4) Å^3, T = 150(2) K, Z = 4, μ(Mo-K_α) = 0.259mm^{-1}, 12718 reflections collected, 4209 independent reflections, GooF = 1.112, R_1 = 0.0503, wR_2 = 0.1324 (observed data).

4b: $C_{49}H_{59}KO_6Ti{\cdot}3(THF)$, M = 1047.27, monoclinic, space group $P2_1/n$, a = 13.8800(2), b = 20.3074(3) c = 21.3492(3) Å, β = 96.309(2)°, V = 5981.18(15) Å^3, T = 150(2) K, Z = 4, μ(Mo-K_α) = 0.265mm^{-1}, 66468 reflections collected, 11731 independent reflections, GooF = 1.058, R_1 = 0.0562, wR_2 = 0.1455 (observed data).

CCDC-208110−208114 (for **2b**, **1b**, **4a**, **4b** and **3a** respectively) contains the supplementary crystallographic data for this paper. These data can be obtained free of charge at www.ccdc.cam.ac.uk/conts/retrieving.html [or from the Cambridge Crystallographic Data Centre, 12, Union Road, Cambridge CB2 1EZ, UK; Fax: (internat.) +44-1223/336-033; E-mail: deposit@ccdc.cam.ac.uk].

[1] M. Veith, S. Mathur, C. Mathur, *Polyhedron* **1998**, *17*, 1005−1034; K. G. Caulton, L. G. Hubert-Pfalzgraf, *Chem. Rev.* **1990**, *90*, 969−995.

[2] D. C. Bradley, *Chem. Rev.* **1989**, *89*, 1317−1322.

[3] L. Hocks, P. Durbut, P. Teyssie, *J. Mol. Catal.* **1980**, *7*, 75−80; Y. Iwasawa, *Tailored Molecular Catalysts*; Reidel: Dordrecht **1986.**

[4] S. Steyer, C. Jeunesse, D. Armspach, D. Matt, J. Harrowfield; C. Floriani, R. Floriani-Morro, *Calixarenes 2001* (Eds: Z. Asfari,V. Bohmer, J. Harrowfield, J. Vicens), Kluwer, Dordrecht, **2001**; Chapters 28 & 29, p. 513−560; C. Wieser, C. B. Dieleman, D. Matt, *Coord. Chem. Rev.* **1997**, *165*, 93−136.

[5] S. R. Dubberley, A. J. Blake, P. Mountford, *Chem. Commun.* **1997**, 1603−1604; M. G. Davidson, J. A. K. Howard, S. Lamb, C. W. Lehmann, *Chem. Commun.* **1997**, 1607−1608; J. M. Harrowfield, M. I. Ogden, W. R. Richmond, A. H. White, *J. Chem. Soc., Chem. Commun.* **1991**, 1159−1160; T. A. Hanna, L. Liu, A. M. Angeles-Boza, X. Kou, C. D. Gutsche, K. Ejsmont, W. H. Watson, L. N. Zakharov, C. D. Incarvito, A. L. Rheingold, *J. Am. Chem. Soc.* **2003**, *125*, 6228−6238; T. A. Hanna, L. Liu, L. N. Zakharov, A. L. Rheingold, W. H. Watson, C. D. Gutsche, *Tetrahedron* **2002**, *58*, 9751−9757; E. D. Gueneau, K. M. Fromm, H. Goesmann, *Chem. Eur. J.* **2003**, *9*, 509−514; S. R. Dubberley, A. J. Blake, P. Mountford, *Dalton Trans.* **2003**, 2418−2427; P. Thuery, Z. Asfari, J. Vicens, V. Lamare, J.-F. Dozol, *Polyhedron* **2002**, *21*, 2497−2503.

[6] G. Guillemot, E. Solari, C. Rizzoli, C. Floriani, *Chem. Eur. J.* **2002**, *8*, 2072−2080.

[7] [7a] A. Zanotti-Gerosa, E. Solari, L. Giannini, C. Floriani, A. Chiesi-Villa, C. Rizzoli, *Chem. Commun.* **1997**, 183−184. [7b] F. A. Cotton, E. V. Dikarev, C. Murillo, M. A. Petrukhina, *Inorg. Chim. Acta* **2002**, *332*, 41−46. [7c] A. J. Petrella, N. K. Roberts, D. C. Craig, C. L. Raston, R. N. Lamb, *Chem. Commun.* **2003**, 1728−1729.

[8] M. Bottrill, P. D. Gavens, J. W. Kelland, J. McMeeking, *Comprehensive Organometallic Chemistry* (Eds.: G. Wilkinson, F. G. A. Stone, E. W. Abel), Pergamon Press, **1982**, 331.

[9] W. Humphrey, A. Dalke, K. Schulten, "VMD − Visual Molecular Dynamics" J. Molec. Graphics **1996**, 14.1, 33−38; http://www.povray.org.

[10] E. P. Turevskaya, V. G. Kessler, N. Ya. Turova, A. P. Pisarevsky, A. I. Yanovsy, Y. T. Struchkov, *J. Chem. Soc., Chem. Commun.* **1994**, 2303; Z. A. Starikova, A. I. Yanovsky, N. M. Kotova, M. I. Yanovskaya, N. Ya. Turova, D. Benlian, *Polyhedron* **1997**, *16*, 4347−4351; I. Baxter, S. R. Drake, M. B. Hursthouse, K. M. Abdul Malik, D. M. P. Mingos, J. C. Plakatouras, D. J. Otway, *Polyhedron* **1998**, *17*, 625−639.

[11] V. G. Kessler, L. G. Hubert-Pfalzgraf, S. Daniele, *Chem. Mater.* **1994**, 2336−2342; L. G. Hubert-Pfalzgraf, S. Daniele, J. M. Decams, *J. Sol-Gel Sci. Technol.* **1997**, *8*, 49−53.

[12] Y. Chi, P.-F. Hsu, J.-W. Lan, C.-L. Chen, S.-M. Peng, G.-H. Lee, *J. Phys. Chem. Solids* **2001**, *62*, 1871−1879.

[13] V. W. Day, T. A. Eberspacher, W. G. Klemperer, S. Liang, *Chem. Mater.* **1995**, *7*, 1607−1608.

[14] A. I. Yanovsy, M. I. Yanovskaya, V. K. Limar, V. G. Kessler, N. Ya. Turova, Y. T. Struchkov, *J. Chem. Soc., Chem. Commun.* **1991**, 1605−1606; J. F. Campion, D. A. Payne, H. K. Chae, J. K. Maurin, S. R. Wilson, *Inorg. Chem.* **1991**, *30*, 3244−3245.

[15] Crystals suitable for X-ray structural analysis were obtained from this sample.

[16] Dry methanol was used in this synthesis.

Received April 10, 2003
Early View Article
Published Online October 2, 2003

 © 2003 Wiley-VCH Verlag GmbH & Co. KGaA, Weinheim

Di- and Trinuclear Ruthenium and Osmium Bis(2-pyridyl) Ketone Oximate Derivatives

Javier A. Cabeza,*[a] Ignacio del Río,[a] Víctor Riera,[a] Marta Suárez,[a] Carmen Álvarez-Rúa,[b] Santiago García-Granda,[b] Shih Hsien Chuang,[c] and Jih Ru Hwu*[c]

Keywords: Ruthenium / Osmium / Cluster compounds / Oximes / DNA cleavage

Treatment of $[Ru_3(CO)_{12}]$ with bis(2-pyridyl) ketone oxime (Hdpko) in refluxing THF leads to a separable mixture of $[Ru_3(\mu,\eta^3\text{-dpko-}N,N,O)_2(CO)_8]$ (**1**) and $[Ru_2(\mu,\eta^3\text{-dpko-}N,N,O)_2(CO)_4]$ (**2**). In both complexes, two Ru atoms are doubly bridged by two dpko ligands, which are attached to a Ru atom through the oximate O atom while chelating the other Ru atom through the N atoms of a pyridyl group and the oximate fragment. While the Ru–Ru distance of the bridged edge of complex **1** is very long [3.5388(9) Å], that of complex **2** is very short [2.620(1) Å]. The acetonitrile complexes $[M_3(CO)_{10}(MeCN)_2]$ (M = Ru, Os) react with Hdpko in THF at room temperature to give $[M_3(\mu\text{-H})(\mu,\eta^3\text{-dpko-}N,N,O)(CO)_9]$ [M = Ru (**3**) Os (**4**)], in which the dpko ligand behaves in the same way as in **1** and **2**. The thermal reaction of **3** with Hdpko leads to a mixture of **1** and **2**, while an analogous treatment of complex **4** gives $[Os_3(\mu,\eta^3\text{-dpko-}N,N,O)_2(CO)_8]$ (**5**), which is isostructural with complex **1**. Compounds **1** and **3** are the first examples of ruthenium clusters containing oximate ligands. These oximate complexes display low activity as DNA cleavage agents, requiring high complex concentrations, long incubation times, and the use of UV light as a trigger.
(© Wiley-VCH Verlag GmbH & Co. KGaA, 69451 Weinheim, Germany, 2003)

Introduction

Oximes and oximates are attractive ligands because they can interact with metal atoms through either one or both N and O atoms, acting as terminal (monodentate or chelating)[1,2] or, less frequently, as bridging ligands.[3−6] In addition, oximes can remain intact in the coordination sphere of the metals or undergo O−H bond cleavage to afford oximate derivatives.[1−6] In some cases they can also suffer N−OH bond activation to form nitrenium fragments.[2b,2c,3,4] The osmium cluster-promoted O−H vs. N−O bond cleavage of these ligands has been studied.[4] Despite this rich derivative chemistry and the large number of oximate complexes of transition metals known to date,[1−6] it is noteworthy that no ruthenium and only a few osmium[4−6] cluster complexes containing oximate ligands have been reported.

Herein we report the synthesis and structural characterization of triruthenium and triosmium carbonyl clusters derived from bis(2-pyridyl) ketone oxime (Hdpko). We decided to use this oxime because, in addition to its varied coordination possibilities, its chemistry has been little explored.[7]

[a] Departamento de Química Orgánica e Inorgánica, Instituto de Química Organometálica "Enrique Moles", Universidad de Oviedo-CSIC,
33071 Oviedo, Spain
Fax: (internat.) + 34-985/103446
E-mail: jac@sauron.quimica.uniovi.es
[b] Departamento de Química Física y Analítica, Universidad de Oviedo,
33071 Oviedo, Spain
[c] Department of Chemistry, National Tsing Hua University, Hsinchu 30013, Taiwan, Republic of China
E-mail: jrhwu@mx.nthu.edu.tw

Results and Discussion

Synthesis and Structural Characterization of Oximate Complexes

Treatment of $[Ru_3(CO)_{12}]$ with one equivalent of Hdpko, in THF at reflux temperature, gave a complex mixture of compounds containing some ruthenium carbonyl starting material. When two equivalents of Hdpko were used under the same reaction conditions, the novel trinuclear derivative $[Ru_3(\mu,\eta^3\text{-dpko-}N,N,O)_2(CO)_8]$ (**1**) and the dioximate-bridged binuclear complex $[Ru_2(\mu,\eta^3\text{-dpko-}N,N,O)_2(CO)_4]$ (**2**) were obtained as the major reaction products (Scheme 1).

The ^{1}H NMR spectra of both complexes display no signals attributable to hydride ligands, while the aromatic regions reflect, in both cases, the presence of two inequivalent pyridyl groups. Their IR spectra confirm the absence of bridging carbonyl ligands and display no bands in the O−H stretching region, suggesting O−H bond activation.

The trinuclear nature of **1** was clearly indicated by its microanalysis and FAB MS spectrum, which also show the presence of eight CO ligands and the incorporation of two

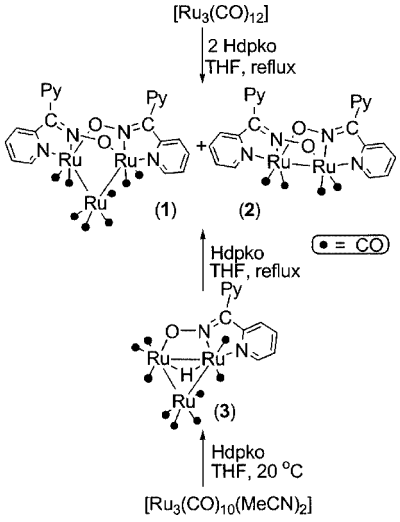

Scheme 1. Synthesis of compounds **1**−**3**

oximate ligands to the cluster shell. The structure of **1** was established by X-ray diffraction methods (Figure 1, Table 1). In addition to eight terminal CO ligands, the complex contains two oximate ligands spanning the same edge of the trimetallic core, in a head-to-tail arrangement, through both the N and O atoms. Each dpko ligand is also attached through a pyridine N-atom to one of the metal atoms of the bridged edge, in such a way that the complex

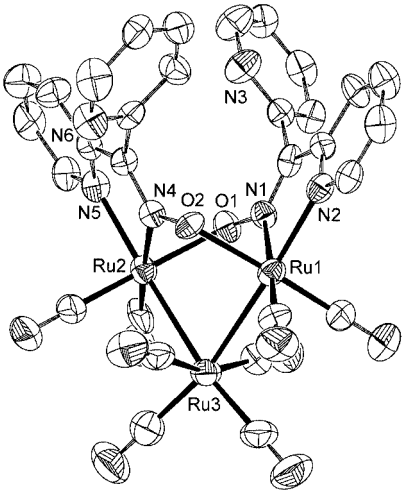

Figure 1. Molecular structure of compound **1** (50% probability level ellipsoids); H atoms omitted for clarity

Table 1. Selected interatomic distances (Å) in complex **1**

Ru(1)−Ru(2)	3.5388(9)	Ru(1)−Ru(3)	2.8137(9)
Ru(2)−Ru(3)	2.8170(9)	Ru(1)−N(1)	2.131(6)
Ru(1)−N(2)	2.173(7)	Ru(2)−N(4)	2.115(6)
Ru(2)−N(5)	2.154(7)	Ru(1)−O(2)	2.131(5)
Ru(2)−O(1)	2.124(5)	N(1)−O(1)	1.350(8)
N(4)−O(2)	1.363(8)		

presents a non-crystallographic twofold axis. Such a symmetry was also indicated by its $^{13}C\{^1H\}$ NMR spectrum, which displays only four carbonyl resonances. The length of the bridged edge [Ru(1)−Ru(2) = 3.5388(9) Å] indicates the absence of a metal−metal bond, as expected for a 50-electron trinuclear cluster.[8]

The $^{13}C\{^1H\}$ NMR spectrum of **2** shows only two signals attributable to terminal carbonyl ligands. Its binuclear character and the incorporation of one dpko ligand per Ru atom were pointed out by its microanalysis and FAB MS. Its structure was confirmed by an X-ray diffraction study (Figure 2, Table 2). The ligand arrangement in compound **2** is analogous to that described above for complex **1**, but the $Ru(CO)_4$ fragment present in **1** is now missing. The Ru(1)−Ru(2) distance in **2**, 2.620(1) Å, is in the range expected for a single metal−metal bond, in accordance with the 34-electron count for the complex.[8] It is noteworthy that the oximate NO fragment is able to bridge two metal atoms which are either close to each other (complex **2**) or very far apart (complex **1**).

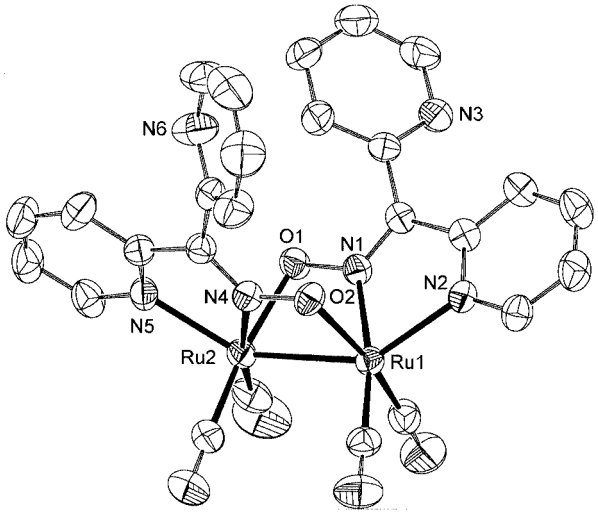

Figure 2. Molecular structure of compound **2** (50% probability level ellipsoids); H atoms omitted for clarity

Table 2. Selected interatomic distances (Å) in complex **2**

Ru(1)−Ru(2)	2.620(1)	Ru(1)−N(1)	2.061(3)
Ru(1)−N(2)	2.209(4)	Ru(2)−N(4)	2.060(4)
Ru(2)−N(5)	2.176(4)	Ru(1)−O(2)	2.162(4)
Ru(2)−O(1)	2.135(3)	N(1)−O(1)	1.341(4)
N(4)−O(2)	1.334(4)		

IR monitoring of the reaction of $[Ru_3(CO)_{12}]$ with Hdpko showed that an intermediate, probably arising from the incorporation of only one equivalent of Hdpko to the cluster, is formed prior to compounds **1** and **2**. Its isolation was not possible under the thermal conditions applied, since it readily reacted with more Hdpko to give **1** and **2** as the two major final products. Fortunately, we managed to isolate this intermediate working at room temperature, using the reactive complex $[Ru_3(CO)_{10}(MeCN)_2]$[9] as starting material. The product was characterized as the novel

 © 2003 Wiley-VCH Verlag GmbH & Co. KGaA, Weinheim

trinuclear derivative $[Ru_3(\mu\text{-H})(\mu,\eta^3\text{-dpko-}N,N,O)(CO)_9]$ (**3**; Scheme 1).

The IR spectrum of **3** strongly suggests O−H bond scission. This was further supported by its ^{1}H NMR spectrum, which shows a singlet resonance at $\delta = -18.85$ ppm attributable to a hydride ligand, while the inequivalence of two pyridine rings is evident in the aromatic region. The incorporation of one equivalent of the oxime to the trinuclear framework and the presence of nine carbonyl ligands were confirmed by its microanalysis and FAB MS.

The structure proposed for **3**, and its role as an intermediate in the formation of **1** and **2** from $[Ru_3(CO)_{12}]$, were further corroborated by treating **3** with one equivalent of the oxime in THF at reflux temperature. This reaction led to complexes **1** and **2**, along with a small amount of $[Ru_3(CO)_{12}]$.

To the best of our knowledge, **1** and **3** are the first ruthenium cluster complexes containing oximate ligands. Some diruthenium(I) complexes structurally related to **2**, namely $[Ru_2(\mu,\eta^2\text{-ONCR}^1\text{R}^2\text{-}O,N)_2(CO)_4L_2]$ (L = intact oxime or other neutral two-electron donor ligands), have been reported.[10] It has also been reported that the reaction of $[Ru_3(CO)_{12}]$ with 1-nitrous-2-naphthol gives a triruthenium cluster structurally related to complex **1**, which also contains two NO bridges.[11]

The triosmium acetonitrile complex $[Os_3(CO)_{10}(MeCN)_2]$[12] reacts with Hdpko in THF at room temperature to give the monohydrido derivative $[Os_3(\mu\text{-H})(\mu,\eta^3\text{-dpko-}N,N,O)(CO)_9]$ (**4**; Scheme 2). The structure of this compound was established by X-ray diffraction methods (Figure 3, Table 3). The cluster consists of a nearly equilateral triangle of Os atoms in which two metal atoms are attached to a dpko ligand in the same way as that found previously for compounds **1** and **2**. A hydride ligand spans the same Os−Os edge as the oximate NO fragment. The cluster shell is completed by nine CO ligands. Therefore, the cluster is a closed-shell, 48-electron trinuclear species.[8] The spectroscopic data of **4** are similar to those of the ruthenium complex **3**, indicating that both compounds are isostructural.

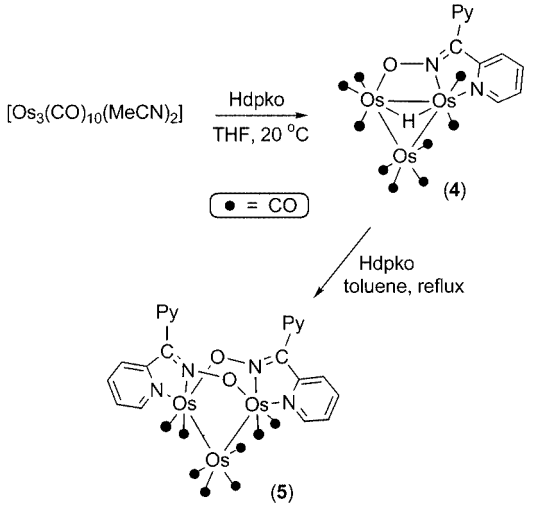

Scheme 2. Synthesis of compounds **4** and **5**

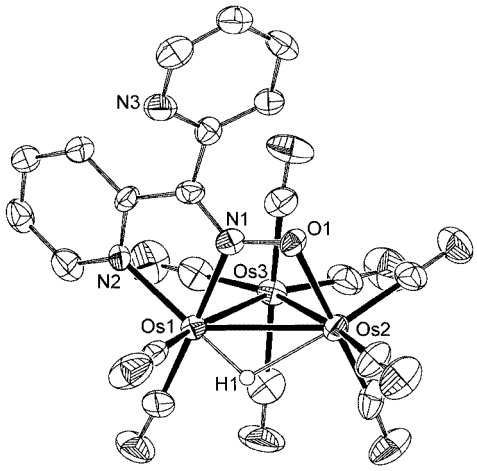

Figure 3. Molecular structure of compound **4** (50% probability level ellipsoids); H atoms (except the hydride) omitted for clarity

Table 3. Selected interatomic distances (Å) in complex **4**

Os(1)−Os(2)	2.861(5)	Os(1)−Os(3)	2.876(1)
Os(2)−Os(3)	2.855(2)	Os(1)−N(1)	2.062(9)
Os(1)−N(2)	2.078(9)	Os(2)−O(1)	2.170(7)
N(1)−O(1)	1.31(1)		

Therefore, the oxime Hdpko reacts with the triruthenium bis(acetonitrile) cluster in the same way as its triosmium analogue, giving isostructural products. However, this is not always the case for other ligands, such as bis(2-pyridyl)-amine,[13] 2-amino-7,8-benzoquinoline,[14] or 2,2′-diamino-1,1′-binaphthalene.[15]

Bearing in mind that the triruthenium complex **3** is an intermediate in the formation of **1**, we reasoned that complex **4** could be a suitable precursor of a triosmium cluster isostructural with complex **1**. Indeed, treatment of complex **4** with Hdpko in toluene at reflux temperature allowed the isolation of $[Os_3(\mu,\eta^3\text{-dpko-}N,N,O)_2(CO)_8]$ (**5**). The structure depicted for this complex in Scheme 2, which is similar to that of the triruthenium complex **1**, was determined by X-ray diffraction methods (Figure 4, Table 4). Accordingly, its IR and NMR spectroscopic data are also similar to those of complex **1**.

Very few triosmium clusters containing oximate ligands have been reported prior to this work. They contain oximate fragments that span two metal atoms through the N and O atoms.[4,5] During the preparation of this manuscript, some triosmium clusters related to compounds **4** and **5**, derived from diphenyl ketone oxime and phenyl (2-pyridyl) ketone oxime, have been reported.[6]

DNA-Cleavage Ability of the Oximate Complexes

Although most metal complex-mediated DNA cleavage reactions use mononuclear complexes as promoters,[16,17] a few interesting results have been reported using bi-[18] and trinuclear[19] complexes. Prompted by the fact that prior to

 © 2003 Wiley-VCH Verlag GmbH & Co. KGaA, Weinheim

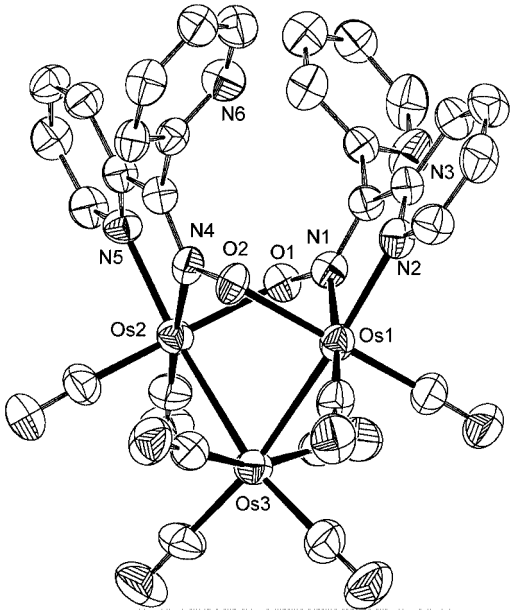

Figure 4. Molecular structure of compound **5** (50% probability level ellipsoids); H atoms omitted for clarity

Table 4. Selected interatomic distances (Å) in complex **5**

Os(1)−Os(2)	3.5903(5)	Os(1)−Os(3)	2.8318(6)
Os(2)−Os(3)	2.8274(5)	Os(1)−N(1)	2.125(7)
Os(1)−N(2)	2.130(7)	Os(2)−N(4)	2.145(8)
Os(2)−N(5)	2.148(7)	Os(1)−O(2)	2.130(6)
Os(2)−O(1)	2.124(6)	N(1)−O(1)	1.359(9)
N(4)−O(2)	1.346(9)		

this work no metal complexes of oximes had been studied as DNA cleaving agents, the ruthenium and osmium oximate complexes **1**−**5** were tested by studying the nicking of supercoiled circular φ*X174* RFI DNA (form I; 50 μM/base pair) into relaxed circular DNA (form II).

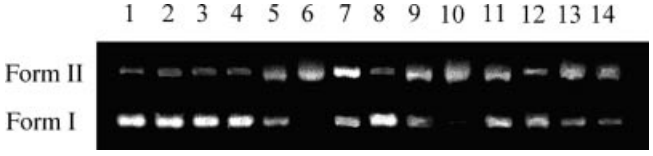

Figure 5. Electrophoresis separation of supercoiled circular φ*X174* RFI DNA (form I) and relaxed circular DNA (form II) after treatment of form I DNA with the ruthenium complexes **1**−**3**; lanes 1, 4, 8, 12 were run in the dark, the remaining ones involved UV light irradiation; lane 1, DNA alone (dark, pH = 7.0); lane 2, DNA alone (pH = 7.0); lane 3, DNA alone (pH = 5.0); lane 4, **1** (1000 μM, pH = 7.0, dark); lane 5, **1** (1000 μM, pH = 7.0); lane 6, **1** (1000 μM, pH = 5.0); lane 7, **1** (500 nM, pH = 5.0); lane 8, **2** (1000 μM, pH = 7.0, dark); lane 9, **2** (1000 μM, pH = 7.0); lane 10, **2** (1000 μM, pH = 5.0); lane 11, **2** (1.0 μM, pH = 5.0); lane 12, **3** (1000 μM, pH = 7.0, dark); lane 13, **3** (1000 μM, pH = 7.0); lane 14, **3** (1000 μM, pH = 5.0)

Figure 5 shows the results obtained with the ruthenium complexes. After UV irradiation of complexes **1**−**3** (1000 μM) and form I DNA, in pH 7.0 buffer for 8.0 h, ratios of (form II)/(form I) of 1.78, 1.63 and 2.57 were found (see lanes 5, 9, and 13). The cleaving ability of **1** and **2** was found to be pH dependent and is greater under slightly acidic conditions, cleaving DNA at pH 5.0 at concentrations of 500 nM (**1**) and 1.0 μM (**2**), with ratios of (form II)/(form I) of 1.27 and 1.08, respectively (lanes 7 and 11).

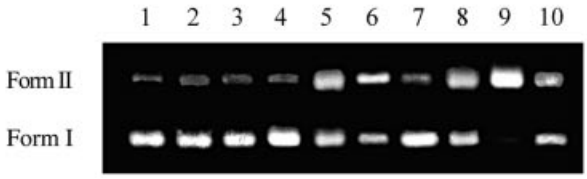

Figure 6. Electrophoresis separation of supercoiled circular φ*X174* RFI DNA (form I) and relaxed circular DNA (form II) after treatment of form I DNA with the osmium complexes **4** and **5**; lanes 1, 4, 7 were run in the dark, the remaining ones involved UV light irradiation; lane 1, DNA alone (dark, pH = 7.0); lane 2, DNA alone (pH = 7.0); lane 3, DNA alone (pH = 5.0); lane 4, **4** (1000 μM, pH = 7.0, dark); lane 5, **4** (1000 μM, pH = 7.0); lane 6, **4** (1000 μM, pH = 5.0); lane 7, **5** (1000 μM, pH = 7.0, dark); lane 8, **5** (1000 μM, pH = 7.0); lane 9, **5** (1000 μM, pH = 5.0); lane 10, **5** (1.0 μM, pH = 5.0)

For the osmium oximate complexes **4** and **5** (Figure 6), it was found that they can also cleave DNA upon UV activation. The ratios of (form II)/(form I) were 1.13 and 1.44 for **4** and **5** (1000 μM), respectively, in pH 7.0 buffer (see lanes 5 and 8). Complex **5** also cleaved DNA at pH 5.0 in concentrations of 1.0 μM to give a (form II)/(form I) ratio of 1.04 (see lane 10).

A comparison of the cleavage activity of the pairs of isostructural clusters **1**, **5** and **3**, **4** indicates that the ruthenium clusters (**1** and **3**) are more active than the osmium ones (**4** and **5**). In addition, the binuclear complex **2** is less active than the trinuclear ones **1** and **3**.

Although the cleaving ability of the Ru cluster complexes **1** and **3** is higher than that reported for other triruthenium carbonyl clusters,[19c] their activity is very low when compared to that of many mono- and binuclear compounds previously studied.[17,18] The high complex concentrations needed (millimolar range), along with long incubation times (8 h) and UV activation, hamper the use of these complexes for experiments in vivo.

Concluding Remarks

By using the oxime Hdpko as a ligand precursor, we have prepared one diruthenium, two triruthenium and two triosmium carbonyl complexes, all containing the oximate ligand dpko η^3-coordinated to two metal atoms through the N and O atoms of the oximate fragment and the N atom of the pyridyl group. Compounds **1** and **3** are the first ruthenium cluster complexes derived from oximes.

The first DNA cleaving studies using oximate metal complexes are described. Unfortunately, the observed activity is very low when compared to those of many mono- and binuclear compounds previously studied.

 © 2003 Wiley-VCH Verlag GmbH & Co. KGaA, Weinheim

Experimental Section

General Synthetic and Characterization Data: Solvents were dried over sodium diphenyl ketyl (THF, Et_2O, hydrocarbons) or CaH_2 (dichloromethane) and distilled under nitrogen prior to use. The reactions were carried out under nitrogen, using Schlenk-vacuum line techniques, and were routinely monitored by solution IR spectroscopy (carbonyl stretching region) and spot TLC (silica gel). $[Os_3(CO)_{10}(MeCN)_2]$ was prepared as described previously;[12] the remaining reagents were purchased from commercial suppliers. IR: Perkin−Elmer Paragon 1000 FT. NMR: Bruker AC-200 and DPX-300, room temperature, TMS as internal standard. Microanalyses: Perkin−Elmer 2400. MS: VG Autospec double-focussing mass spectrometer operating in the FAB+ mode; ions were produced with a standard Cs^+ gun at ca. 30 kV; 3-nitrobenzyl alcohol (NBA) was used as matrix; data given refer to the most abundant molecular ion isotopomer.

$[Ru_3(\mu,\eta^3$-dpko-*N,N,O*$)_2(CO)_8]$ (1) and $[Ru_2(\mu,\eta^3$-dpko-*N,N,O*$)_2(CO)_4]$ (2): A solution of $[Ru_3(CO)_{12}]$ (104 mg, 0.163 mmol) and Hdpko (66 mg, 0.331 mmol) in THF (20 mL) was heated under reflux for 20 min. The color changed from orange to black. The solvent was concentrated under reduced pressure to ca. 2 mL and transferred onto TLC silica plates. Dichloromethane/THF (95:5) eluted four bands. The first two were very weak and were discarded. The third (orange) and fourth (pink) bands afforded compounds **1** (21 mg, 14%) and **2** (14 mg, 12%), respectively. A black residue remained uneluted at the base line.
1: FAB+ MS: *m/z* = 925 [M^+]. $C_{30}H_{16}N_6O_{10}Ru_3$ (923.74): calcd. C 39.01, H 1.75, N 9.09; found C 38.78, H 1.85, N 8.92. IR (CH_2Cl_2): ν(CO) = 2069 (m), 2007 (vs), 1990 (m), 1935 (w) cm^{-1}. ^1H NMR ([D_6]acetone): δ = 8.84 (ddd, *J* = 5.4, 1.7, 0.8 Hz, 1 H), 8.42 (ddd, *J* = 4.8, 1.7, 0.8 Hz, 1 H), 8.00 (td, *J* = 8.0, 1.7 Hz, 1 H), 7.54 (ddd, *J* = 8.0, 5.4, 1.1 Hz, 1 H), 7.52 (td, *J* = 7.7, 1.7 Hz, 1 H), 7.26 (ddd, *J* = 7.7, 4.8, 1.1 Hz, 1 H), 7.21 (ddd, *J* = 8.0, 1.1, 0.8 Hz, 1 H), 7.05 (ddd, *J* = 7.7, 1.1, 0.8 Hz, 1 H) ppm. $^{13}C\{^1H\}$ NMR (DEPT, CD_2Cl_2): δ = 206.1, 206.0, 202.6, 194.0 (COs); 160.3 (*C*=N); 156.2 (C_{ipso}), 152.3 (*C*H), 150.3 (C_{ipso}), 149.8 (*C*H), 137.8 (*C*H), 136.1 (*C*H), 126.4 (*C*H), 124.8 (*C*H), 123.9 (*C*H), 123.6 (*C*H) ppm.
2: FAB+ MS: *m/z* = 712 [M^+]. $C_{26}H_{16}N_6O_6Ru_2$ (710.59): calcd. C 43.94, H 2.27, N 11.83; found C 43.83, H 2.42, N 11.74. IR (CH_2Cl_2): ν(CO) = 2018 (vs), 1971 (w), 1943 (s) cm^{-1}. ^1H NMR ([D_6]acetone): δ = 9.04 (ddd, *J* = 5.2, 1.6, 0.8 Hz, 1 H), 8.65 (dt, *J* = 4.8, 1.6 Hz, 1 H), 7.91 (td, *J* = 8.3, 1.6 Hz, 1 H), 7.79−7.73 (m, 3 H), 7.47 (ddd, *J* = 7.6, 5.2, 1.6 Hz, 1 H), 7.34−7.30 (m, 1 H) ppm. $^{13}C\{^1H\}$ NMR (DEPT, CD_2Cl_2): δ = 211.9, 203.9 (COs); 155.7 (*C*=N); 153.7 (*C*H), 153.3 (C_{ipso}), 149.8 (*C*H), 149.0 (C_{ipso}), 137.5 (*C*H), 136.6 (*C*H), 127.3 (*C*H), 124.3 (*C*H), 124.2 (*C*H), 124.1 (*C*H) ppm.

$[Ru_3(\mu$-H$)(\mu,\eta^3$-dpko-*N,N,O*$)(CO)_9]$ (3): A solution of Me_3NO (40 mg, 0.533 mmol) in acetonitrile (10 mL) was slowly added to a solution of $[Ru_3(CO)_{12}]$ (150 mg, 0.235 mmol) in dichloromethane/acetonitrile (10:1, 20 mL) at −78 °C. Once the formation of $[Ru_3(CO)_{10}(MeCN)_2]$ was achieved (IR monitoring), Hdpko (51 mg, 0.256 mmol) was added and the solution was allowed to warm up to room temperature. Solvents were removed under reduced pressure and the residue was redissolved in THF (25 mL), whereupon the color changed from brown to black. The solvent was removed under reduced pressure, the residue was dissolved in ca. 1 mL of toluene and this solution was placed onto a silica gel column (2 × 8 cm) packed in hexanes. Elution with hexanes afforded some unchanged $[Ru_3(CO)_{12}]$. Elution with dichloromethane afforded complex **3** (40 mg, 23%). A black residue remained uneluted at the top of the column. FAB+ MS: *m/z* = 756 [M^+]. $C_{20}H_9N_3O_{10}Ru_3$ (754.55): calcd. C 31.84, H 1.20, N 5.57; found C 31.78, H 1.35, N 5.52. IR (CH_2Cl_2): ν(CO) = 2087 (m), 2047 (s), 2021 (vs), 2000 (s), 1978 (sh), 1959 (sh) cm^{-1}. ^1H NMR ($CDCl_3$): δ = 8.75 (d, *J* = 5.6 Hz, 1 H), 8.72 (dd, *J* = 5.2, 1.2 Hz, 1 H), 8.17 (br. d, *J* = 8.8 Hz, 1 H), 8.11 (d, *J* = 7.8 Hz, 1 H), 7.85 (td, *J* = 7.8, 1.6 Hz, 1 H), 7.71 (td, *J* = 8.8, 1.6 Hz, 1 H), 7.35 (td, *J* = 5.2, 1.2 Hz, 1 H), 7.20 (td, *J* = 5.2, 1.2 Hz, 1 H), −18.88 (s, μ-H) ppm.

$[Os_3(\mu$-H$)(\mu,\eta^3$-dpko-*N,N,O*$)(CO)_9]$ (4): Hdpko (85 mg, 0.427 mmol) was added to a solution of $[Os_3(CO)_{10}(MeCN)_2]$ (270 mg, 0.290 mmol) in THF (25 mL). The solution was stirred at room temperature for 2 h. The color changed from lemon yellow to red. The solvent was removed under reduced pressure, the residue was dissolved in ca. 2 mL of toluene and this solution was placed onto a silica gel column (2 × 10 cm) packed in hexanes. Elution with hexanes afforded some $[Os_3(CO)_{12}]$. Elution with hexanes/dichloromethane (1:1) afforded two bands. The first band (blue) was very weak and was not investigated. The second band (red) afforded complex **4** (125 mg, 42%). FAB+ MS: *m/z* = 1023 [M^+]. $C_{20}H_9N_3O_{10}Os_3$ (1021.90): calcd. C 23.51, H 0.89, N 4.11; found C 23.62, H 0.94, N 4.02. IR (CH_2Cl_2): ν(CO) = 2091 (m), 2051 (m), 2014 (vs), 1994 (m), 1964 (w), 1945 (w) cm^{-1}. ^1H NMR (CD_2Cl_2): δ = 9.04 (br. d, *J* = 5.9 Hz, 1 H), 8.73 (ddd, *J* = 4.7, 1.6, 0.8 Hz, 1 H), 8.40 (br. d, *J* = 8.4 Hz, 1 H), 8.12 (dt, *J* = 7.7, 1.2 Hz, 1 H), 7.87 (td, *J* = 7.7, 1.8 Hz, 1 H), 7.82 (ddd, *J* = 8.4, 7.7, 1.2 Hz, 1 H), 7.40 (ddd, *J* = 7.5, 4.7, 1.2 Hz, 1 H), 7.30 (ddd, *J* = 7.5, 5.9, 1.2 Hz, 1 H), −18.14 (s, μ-H) ppm. $^{13}C\{^1H\}$ NMR (DEPT, CD_2Cl_2): δ = 187.7, 186.7, 184.4, 181.0, 179.9, 177.8, 177.7, 175.0, 168.4 (COs); 154.8 (*C*=N); 154.7 (*C*H), 153.7 (C_{ipso}), 149.3 (*C*H), 148.2 (C_{ipso}), 136.7 (*C*H), 136.5 (*C*H), 127.6 (*C*H), 126.0 (*C*H), 124.6 (*C*H), 124.4 (*C*H) ppm.

$[Os_3(\mu,\eta^3$-dpko-*N,N,O*$)_2(CO)_8]$ (5): A solution of Hdpko (16 mg, 0.080 mmol) and complex **4** (80 mg, 0.078 mmol) in toluene (10 mL) was heated to reflux temperature for 75 min. The color changed from red to black. The solvent was partially removed under reduced pressure (to ca. 2 mL) and this solution was placed onto a silica gel column (2 × 10 cm) packed in hexanes. Elution with hexanes afforded some $[Os_3(CO)_{12}]$. Elution with hexanes/dichloromethane (1:2) afforded two weak bands, which were not investigated. Dichloromethane/THF (20:1) eluted a red band, which afforded complex **5** (18 mg, 19%). A black residue remained uneluted at the top of the column. FAB+ MS: *m/z* = 1192 [M^+]. $C_{30}H_{16}N_6O_{10}Os_3$ (1190.70): calcd. C 30.25, H 1.35, N 7.06; found C 30.42, H 1.42, N 7.06. IR (CH_2Cl_2): ν(CO) = 2071 (m), 1993 (vs), 1921 (m) cm^{-1}. ^1H NMR (CD_2Cl_2): δ = 8.73 (dd, *J* = 4.8, 0.8 Hz, 1 H), 8.33 (dd, *J* = 4.8, 0.8 Hz, 1 H), 7.74 (td, *J* = 8.0, 1.6 Hz, 1 H), 7.45 (td, *J* = 8.0, 2.0 Hz, 1 H), 7.24−7.06 (m, 4 H) ppm.

X-ray Diffraction Studies: Suitable crystals of **1**·C_6H_{14}, **2** and **5**·CH_2Cl_2 were obtained by slow diffusion of hexanes into dichloromethane solutions of the appropriate complexes. Crystals of **4** were obtained by slow diffusion of pentane into a solution of the complex in diethyl ether. Diffraction data for **1**·C_6H_{14} and **5**·CH_2Cl_2 were collected on a Nonius Kappa-CCD diffractometer equipped with a 95-mm CCD camera on a κ-goniostat, using graphite-monochromated Cu-K_α radiation. Diffraction data for **2** and **4** were collected on a Nonius CAD-4 diffractometer, with the ω-2θ scan technique and a variable scan rate, using graphite-monochromated Mo-K_α radiation, applying Lorentz and polarization corrections, and reducing the data to F_o^2 values. All structures were solved by Patterson interpretation using the program DIRDIF-96.[20] Absorption corrections were applied using XABS2[21] (**1**·C_6H_{14}, **2**, and

 © 2003 Wiley-VCH Verlag GmbH & Co. KGaA, Weinheim

Table 5. Crystal, measurement, and refinement data for **1**·C_6H_{14}, **2**, **4**, and **5**·CH_2Cl_2

	1·C_6H_{14}	**2**	**4**	**5**·CH_2Cl_2
Empirical formula	$C_{30}H_{16}N_6O_{10}Ru_3$·$C_6H_{14}$	$C_{26}H_{16}N_6O_6Ru_2$	$C_{20}H_9N_3O_{10}Os_3$	$C_{30}H_{16}N_6O_{10}Os_3$·$CH_2Cl_2$
Formula mass	1009.87	710.59	1021.90	1276.01
Cryst. system	triclinic	monoclinic	monoclinic	triclinic
Space group	$P\bar{1}$	$P2_1/c$	$P2_1/a$	$P\bar{1}$
a, Å	10.6768(3)	9.029(2)	18.92(3)	10.8194(4)
b, Å	12.4667(4)	21.231(7)	7.566(2)	12.4036(4)
c, Å	15.6330(6)	13.43(2)	18.95(1)	15.4080(6)
α, deg	83.596(3)	90	90	85.049(2)
β, deg	79.614(2)	92.31(6)	120.05(7)	80.843(2)
γ, deg	72.495(2)	90	90	71.770(2)
V, Å^3	1948.3(1)	2573(4)	2349(4)	1937.4(1)
Z	2	4	4	2
F(000)	1000	1400	1832	1176
D_{calcd}, g cm^{-3}	1.721	1.835	2.889	2.187
Radiation (λ, Å)	Cu-K_α (1.54180)	Mo-K_α (0.71073)	Mo-K_α (0.71073)	Cu-K_α (1.54180)
μ, mm^{-1}	9.838	1.229	16.246	19.960
Cryst size, mm	0.33 × 0.20 × 0.13	0.33 × 0.10 × 0.10	0.27 × 0.10 × 0.07	0.17 × 0.07 × 0.07
Temp., K	200(2)	293(2)	293(2)	200(2)
θ limits, deg	2.88 to 69.76	1.80 to 25.98	1.24 to 25.98	2.91 to 69.93
Min/max *h*, *k*, *l*	−12/12, −14/15, −13/18	−11/0, −26/0, −16/16	−23/0, −9/0, −20/23	−12/13, −14/15, 0/18
No. of collected rflns.	9338	5361	4764	22303
No. of unique rflns. (R_{int})	6866 (0.0525)	5037 (0.0280)	4608 (0.0415)	7242 (0.0783)
No. of rflns. with $I > 2\sigma(I)$	6121	3399	3415	5680
Absorption correction	XABS2	XABS2	XABS2	SORTAV
Max/min transmission	0.278/0.141	0.884/0.863	0.321/0.156	1.249/0.744
No. of restraints/params.	83/515	0/361	0/326	0/496
GOF (on F^2)	1.106	1.015	1.030	0.962
Final *R*1 [on *F*, $I > 2\sigma(I)$]	0.0630	0.0317	0.0384	0.0481
Final *wR*2 (on F^2, all data)	0.2319	0.0884	0.1102	0.1291
Max/min residuals, e·Å^{-3}	1.266/−1.487	0.617/−0.554	1.974/−2.404	1.986/−1.708

4) or SORTAV[22] (**5**·CH_2Cl_2). Isotropic and full-matrix anisotropic least-squares refinements were carried out using SHELXL-97.[23] All non H atoms were refined anisotropically. Hydrogen atom positions were geometrically calculated and refined riding on their parent atoms, except the hydride H atom of **4**, which was located by Fourier difference maps. The disordered solvent molecule of **1**·C_6H_{14} was treated with a mixture of constraints and restraints as described elsewhere.[24] The solvent molecule of **5**·CH_2Cl_2 was found disordered over two positions, with partial occupancies of 0.5. The molecular plots were made with the EUCLID program package.[25] The WINGX program system[26] was used thorough the structure determinations. Selected crystal, measurement, and refinement data for the four X-ray structures are given in Table 5. CCDC-182375 (**1**·C_6H_{14}), -182376 (**2**), -203169 (**4**) and -203170 (**5**·CH_2Cl_2) contain the supplementary crystallographic data for this paper. These data can be obtained free of charge at www.ccdc.cam.ac.uk/conts/retrieving.html [or from the Cambridge Crystallographic Data Centre, 12, Union Road, Cambridge CB2 1EZ, UK; Fax: (internat.) +44-1223/336-033; E-mail: deposit@ccdc.cam.ac.uk].

DNA-Cleavage Experiments: All reactions were carried out in oven-dried (120 °C) or autoclaved glassware and eppendorf tubes. Supercoiled circular φ*X174* RFI DNA (molecular weight 3.50 × 10^6, 5386 base pairs in length) was purchased from New England Biolabs Co. The remaining reagents were also purchased from commercial suppliers. Photolytic experiments were carried out at 37 °C, using a medium pressure mercury lamp (350 nm, 32-W). The NIH 1.60 image program, provided by Dr. R. Wayne of National Institutes of Health, U. S. A., was used for the quantitative analysis of DNA cleavage.

In a typical experiment, a reaction mixture (10 μL) containing supercoiled circular φ*X174* RFI DNA stock solution (form I, 50 μM/base pair, 1.0 μL), an oximate complex (10 mM, 1.0 μL), and a phosphate buffer (0.10 M, 8.0 μL) was preincubated at 37 °C in a Pyrex vial and irradiated with UV light (350 nm, 32-W) under aerobic conditions for 8.0 h. After addition of the gel-loading buffer (0.25% bromophenol blue, 0.25% xylene cyanol, and 30% glycerol), the reaction mixture was loaded onto a 1% agarose gel with ethidium bromide staining. The electrophoresis tank was attached to a power supply at a constant current of about 100 mA). The gel was visualized by 312-nm UV transilluminator and photographed by an FB-PDC-34 camera. Quantification of DNA cleavage activity was performed by integration of the optical density of the spot as a function of the band area by use of a Microtek scanner and the NIH 1.60 image program.

Acknowledgments

This work has been supported by the Spanish MECD (grant PB98-1555 to J. A. C.), MCYT (grants BQU2000-2019 to S. G.-G. and BQU2002-2623 to J. A. C.), and Principado de Asturias (grant PR-01-GE-7 to V. R.), and by the Republic of China's National Science Council (to J. R. H.).

[1] A. Chakravorty, *Coord. Chem. Rev.* **1974**, *13*, 1−46.
[2] [2a] A. R. Middleton, J. R. Thornback, G. Wilkinson, *J. Chem. Soc., Dalton Trans.* **1980**, 174−179. [2b] T. Daniel, W. Knaup, M. Dziallas, H. Werner, *Chem. Ber.* **1993**, *126*, 1981−1993. [2c] H. Werner, T. Daniel, W. Knaup, O. Nürnberg, *J. Organomet. Chem.* **1993**, *462*, 309−318. [2d] R. Castarlenas, M. A. Es-

 © 2003 Wiley-VCH Verlag GmbH & Co. KGaA, Weinheim

teruelas, E. Gutiérrez-Puebla, Y. Jean, A. Lledós, M. Martín, J. Tomás, *Organometallics* **1999**, *18*, 4296−4303.
[3] T. Carofiglio, S. Stella, C. Floriani, A. Chiesi-Villa, C. Guastini, *J. Chem. Soc., Dalton Trans.* **1989**, 1957−1962.
[4] A. J. Deeming, D. W. Owen, N. I. Powell, *J. Organomet. Chem.* **1990**, *398*, 299−310.
[5] M. H. Chao, S. Kumaresan, Y. S. Wen, S. C. Lin, J. R. Hwu, K.-L. Lu, *Organometallics* **2000**, *19*, 714−717.
[6] J. S. Y. Wong, W. T. Wong, *New J. Chem.* **2002**, *26*, 94−104.
[7] Hdpko has heretofore been used to prepare Ag,[11a] Cu,[11a,11b] Zn[11c] and Ni[11d] derivatives. [7a] S. O. Sommerer, B. L. Westcott, A. J. Jircitano, K. A. Abboud, *Inorg. Chim. Acta* **1995**, *238*, 149−153. [7b] M. A. S. Goher, F. A. Mautner, *Polyhedron* **1999**, *18*, 3425−3431. [7c] A. J. Stemmler, J. W. Kampf, V. L. Pecoraro, *Inorg. Chem.* **1995**, *34*, 2271−2272. [7d] G. Psomas, C. Dendrinou-Samara, M. Alexiou, A. Tsohos, C. P. Raptopoulou, A. Terzis, D. P. Kessissoglou, *Inorg. Chem.* **1998**, *37*, 6556−6557.
[8] D. M. P. Mingos, D. J. Wales, *Introduction to Cluster Chemistry*, Prentice-Hall International, Englewood Cliffs, NJ, **1990**.
[9] G. A. Foulds, B. F. G. Johnson, J. Lewis, *J. Organomet. Chem.* **1985**, *296*, 147−153.
[10] [10a] M. Langenbahn, H. Stoeckli-Evans, G. Süss-Fink, *J. Organomet. Chem.* **1990**, *397*, 347−358. [10b] M. Langenbahn, H. Stoeckli-Evans, G. Süss-Fink, *Helv. Chim. Acta* **1991**, *74*, 549−553.
[11] K. K. H. Lee, W. T. Wong, *J. Chem. Soc., Dalton Trans.* **1997**, 2987−2996.
[12] M. J. Nicholls, M. D. Vargas, *Inorg. Synth.* **1990**, *28*, 232−235.
[13] J. A. Cabeza, I. del Río, S. García-Granda, V. Riera, M. Suárez, *Organometallics* **2002**, *21*, 2540−2543.
[14] J. A. Cabeza, I. del Río, S. García-Granda, V. Riera, M. Suárez, *Organometallics* **2002**, *21*, 5055−5059.
[15] J. A. Cabeza, I. da Silva, I. del Río, S. García-Granda, V. Riera, M. G. Sánchez-Vega, *Organometallics* **2003**, *22*, 1519−1525.
[16] [16a] N. Farrell, in *Catalysis by Metal Complexes* (Eds.: R. Ugo, B. R. James), Kluwer Academic Publishers, Dordrecht, The Netherlands, **1989**, Vol. 11, p. 17. [16b] J. Kim, M. F. Sistare, P. J. Carter, H. H. Thorp, *Coord. Chem. Rev.* **1998**, *171*, 341−349. [16c] A. Sreedhara, J. D. Freed, J. A. Cowan, *J. Am. Chem. Soc.* **2000**, *122*, 8814−8824. [16d] G. Roelfes, M. E. Branum, W. Li, L. Que, B. L. Feringa, *J. Am. Chem. Soc.* **2000**, *122*, 11517−11518. [16e] S. Dhar, A. R. Chakravarty, *Inorg. Chem.* **2003**, *42*, 2483−2485.
[17] For recent reviews, see: [17a] G. Pratviel, J. Bernadou, B. Meunier, *Adv. Inorg. Chem.* **1997**, *45*, 251−312. [17b] B. Armitage, *Chem. Rev.* **1998**, *98*, 1171−1200. [17c] Z. Guo, P. J. Sadler, *Angew. Chem. Int. Ed.* **1999**, *38*, 1512−1531. [17d] K. E. Erkkila, D. T. Odom, J. K. Barton, *Chem. Rev.* **1999**, *99*, 2777−2796. [17e] G. Pratviel, J. Bernadou, B. Meunier, *Angew. Chem. Int. Ed. Engl.* **1995**, *34*, 746−769. [17f] S. J. Franklin, *Cur. Op. Chem. Biol.* **2001**, *5*, 201−208.
[18] [18a] F. O'Reilly, J. Kelly, A. Kirsch-De-Mesmaeker, *Chem. Commun.* **1996**, 1013−1014. [18b] M. E. Branum, L. Que, *J. Biol. Inorg. Chem.* **1999**, *4*, 593−600. [18c] M. E. Branum, A. K. Tipton, S. Zhu, L. Que, *J. Am. Chem. Soc.* **2001**, *123*, 1898−1904.
[19] [19a] K. J. Humphreys, K. D. Karlin, S. E. Rokita, *J. Am. Chem. Soc.* **2001**, *123*, 5588−5589. [19b] C. S. Allardyce, P. J. Dyson, *J. Cluster Sci.* **2001**, *12*, 563−569. [19c] J. R. Hwu, K.-L. Lu, S.-F. Yu, L.-J. Yu, S. Kumaresan, K.-J. Lin, S.-C. Tsay, *Photochem. Photobiol.* **2002**, *75*, 457−461. [19d] E. Rosenberg, F. Spada, K. Sugden, B. Martin, L. Milone, R. Gobetto, A. Viale, J. Fiedler, *J. Organomet. Chem.* **2003**, *668*, 51−58.
[20] P. T. Beurskens, G. Beurskens, W. P. Bosman, R. de Gelder, S. García-Granda, R. O. Gould, R. Israël, J. M. M. Smits, *The DIRDIF-96 Program System, Crystallography Laboratory*, University of Nijmegen, The Netherlands, **1996**.
[21] S. Parkin, B. Moezzi, H. Hope, *J. Appl. Cryst.* **1995**, *28*, 53−56.
[22] R. H. Blessing, *Acta Crystallogr., Sect. A* **1995**, *51*, 33−38.
[23] G. M. Sheldrick, *SHELXL-97, version 97−2*, University of Göttingen, Germany, **1997**.
[24] J. F. van der Maelen, *Cryst. Rev.* **1999**, *7*, 125−187.
[25] A. L. Spek, *The EUCLID Package*, in *Computational Crystallography* (Ed.: D. Sayre), Clarendon Press, Oxford, UK, **1982**, p. 528.
[26] L. J. Farrugia, *J. Appl. Crystallogr.* **1999**, *32*, 837−838.

Received June 4, 2003
Early View Article
Published Online October 10, 2003

 © 2003 Wiley-VCH Verlag GmbH & Co. KGaA, Weinheim

Ruthenium(II) Complexes with Triphosphane Ligands Combining Planar, Phosphorus, and Carbon Chirality: Application to Asymmetric Reduction of Trifluoroacetophenone

Pierluigi Barbaro,*[a] Claudio Bianchini,[a] Giuliano Giambastiani,*[a] and Antonio Togni[b]

Keywords: Asymmetric catalysis / Tridentate ligands / Ruthenium / Hydrogen transfer / Chiral ferrocenyls

Dichloro-, bis(acetonitrile)chloro-, and tris(acetonitrile)ruthenium(II) complexes with the triphosphane ligands $(R)_C$-$(S)_{Fe}$-$(S)_P$-P3Chir and $(R)_C$-$(S)_{Fe}$-$(R)_P$-P3Chir, combining planar, phosphorus, and carbon chirality, were prepared and structurally characterized in solution. The complexes were tested as catalyst precursors for the reduction of trifluoroacetophenone to (*R*)-α-(trifluoromethyl)benzyl alcohol by either hydrogenation or hydrogen transfer from *i*PrOH. The best conversion and enantioselectivity was obtained with the tris(acetonitrile) precursor [{$(R)_C$-$(S)_{Fe}$-$(S)_P$-P3Chir}Ru-$(CH_3CN)_3$]$(PF_6)_2$ in hydrogen-transfer conditions using a basic co-catalyst.
(© Wiley-VCH Verlag GmbH & Co. KGaA, 69451 Weinheim, Germany, 2003)

Introduction

The design of new, enantiomerically pure ligands leading to highly efficient and selective processes is a challenging issue attracting constant attention in the field of asymmetric catalysis. The large majority of stereoselective reactions catalysed by transition metal complexes involve chiral chelating diphosphane ligands, in particular those with C_2 symmetry.[1] Some attempts have been made to use chiral tridentate phosphanes, aimed at exploiting the superior stabilising effect and coordination versatility of tridentate ligands over bidentate ones.[2] However, due to the inherent difficulty of their synthesis, chiral stereohomogeneous triphosphanes have been scarcely investigated so far,[3] which has prevented an in-depth study of their great potential in asymmetric catalysis. In view of the large diversity of coordination modes accessible through tridentate ligands, the characterization and the knowledge of the structure of their metal complexes is of particular importance for the fine tuning of the catalytic activity and for the design of new active species.

The understanding of the chemical and physical factors that control the source of chiral information in metal complexes with tridentate phosphanes is a current research objective in our laboratories. As part of these studies, we have recently reported the synthesis of the *pseudo*-C_2-symmetric bis(ferrocenyl)triphosphanes Pigiphos (Figure 1), together with some applications of their Ru^{II}, Ni^{II} and Rh^{III} complexes in asymmetric catalysis.[4]

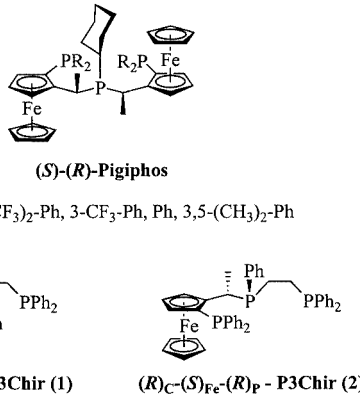

Figure 1. Sketch of the tridentate phosphane ligands (*S*)-(*R*)-Pigiphos = bis{(*S*)-1-[(*R*)-2-(diphenylphosphanyl)ferrocenyl]ethyl}-cyclohexylphosphane, $(R)_C$-$(S)_{Fe}$-$(S)_P$-P3Chir (**1**) and $(R)_C$-$(S)_{Fe}$-$(R)_P$-P3Chir (**2**) = (*R*)-1-[(*S*)-2-diphenylphosphanyl)ferrocenyl]-ethyl-(*R*)-[phenylphosphanyl-2-(diphenylphosphanyl)ethane]

The enantiomeric excesses (*ee*) obtained in the hydrogen-transfer reduction of acetophenone by (Pigiphos)Ru^{II} catalysis were relatively good, yet hardly comparable with those reported for the most efficient Ru^{II} systems modified with chiral chelating ligands.[5]

Since the tendency of Pigiphos to adopt a meridional (*mer*) coordination geometry and a *pseudo*-C_2 symmetry have been suggested to be unfavourable features for high asymmetric induction,[4b] we decided to design triphosphane ligands devoid of C_2 symmetry. Two ligands with these characteristics, namely $(R)_C$-$(S)_{Fe}$-$(S)_P$-P3Chir (**1**) and

[a] Istituto di Chimica dei Composti Organometallici − CNR, Via Madonna del Piano, 50019 Sesto Fiorentino, Italy
Fax: (internat.) + 39-055/5225203
E-mail: pierluigi.barbaro@iccom.cnr.it
giuliano.giambastiani@iccom.cnr.it
[b] Department of Chemistry and Applied Biosciences, Swiss Federal Institute of Technology, ETH Hönggerberg, 8093 Zürich, Switzerland

 © 2003 Wiley-VCH Verlag GmbH & Co. KGaA, Weinheim **DOI: 10.1002/ejic.200300264**

$(R)_C$-$(S)_{Fe}$-$(R)_P$-P3Chir (**2**), have been recently synthesized in diastereomerically pure form through an original procedure developed in our laboratories.[6] The peculiarity of the P3Chir ligands is to combine the planar chirality of the ferrocenyl moiety with phosphorus and carbon stereocenters in an unprecedented molecular assembly.

In this paper, we describe the synthesis and characterisation of the first ruthenium(II) complexes with the P3Chir ligands and also report a preliminary study of their use as catalyst precursors for the asymmetric reduction of trifluoroacetophenone by either hydrogenation or hydrogen transfer from *i*PrOH.

Results and Discussion

Synthesis and Characterization of the Dichlororuthenium Complexes

The diastereomeric, mononuclear Ru^{II} complexes [{$(R)_C$-$(S)_{Fe}$-$(S)_P$-P3Chir}$RuCl_2$] (**3**) and [{$(R)_C$-$(S)_{Fe}$-$(R)_P$-P3Chir}$RuCl_2$] (**4**) were straightforwardly synthesized by treating $[RuCl_2(PPh_3)_3]$ in toluene with $(R)_C$-$(S)_{Fe}$-$(S)_P$-P3Chir and $(R)_C$-$(S)_{Fe}$-$(R)_P$-P3Chir, respectively (Figure 1). Both compounds were isolated in excellent yields as orange solids that are air-stable and soluble in solutions of non-coordinating, non-chlorinated solvents.

The $^{31}P\{^1H\}$ NMR spectroscopic data in [D_4]methanol for all the complexes described in this paper are listed in Table 1, whereas selected ^1H NMR spectroscopic data are reported in the Exp. Sect.

The $^{31}P\{^1H\}$ NMR spectra of **3** and **4** show the presence of several isomers in methanol solution at room temperature, in particular three isomers A/B/C in about a 5:2:1 molar ratio for **3** and four isomers A/B/C/D in about a 6:2:1.5:1 ratio for **4**. Stereochemical nonrigidity, leading to the formation of isomers in solution, is typical for five-coordinate Ru^{II} complexes with linear tridentate phosphane ligands.[7] Irrespective of the complex, the $^{31}P\{^1H\}$ NMR spectrum of each isomer consists of an AMQ pattern with $^2J_{P,P}$ values ranging from 19.2 to 41 Hz, which anticipates a facial (*fac*) arrangement of the tridentate ligands about the metal center (see Table 1 for the labelling scheme).[8,9]

Based on *trans* influence criteria,[3d,4b,7,10] all isomers have been assigned a square-pyramidal coordination geometry with an apical PhP(2) group (Scheme 1), though considerable distortions from an idealized geometry are possible due to the constraints imposed by the polydentate nature of the ligands. Indeed, from a comparison of the $^{31}P\{^1H\}$ NMR spectra of the Ru^{II} complexes **3** and **4** with those of the free ligands,[6] one may readily distinguish the apical phosphorus atoms (with no *trans* ligand) from the phosphorus atom *trans* to the chloride ion that experience a high-field shift of ca. 30−40 ppm, as previously reported for other dichloro(polyphosphane)ruthenium complexes.[3d,9,11] Once disregarded the formation of trigonal-bipyramidal Ru^{II} species, the isomers observed for **3** and **4** are apparently originated by the two chelate rings that may adopt either a boat or envelope conformation in each complex. A similar behaviour has already been observed in other Ru^{II} and Ir^{I} chiral ferrocenyltriphosphane complexes.[4b,12]

3, 4 **5, 6**

S = CH_3CN

Scheme 1

Conductivity measurements show the complexes to behave as non-electrolytes in methanol solution. In CD_3CN solution, the $^{31}P\{^1H\}$ NMR spectra of **3** and **4** are dramatically different from those recorded in [D_4]methanol due to the formation of acetonitrile adducts (see below).[13]

Synthesis and Characterization of the (Acetonitrile)ruthenium Complexes

Complexes **3** and **4** react at very different rates with acetonitrile to give the six-coordinate bis(acetonitrile)chloro

Table 1. $^{31}P\{^1H\}$ NMR spectroscopic data for the ruthenium complexes

Complex[a]	Isomer	δ(P1)	δ(P2)	δ(P3)	$^2J_{P1P2}$	$^2J_{P1P3}$	$^2J_{P2P3}$
3	A	41.48 (dd)	93.25 (dd)	65.38 (*t*)	40.7	27.5	24.0
	B	38.44 (dd)	95.15 (dd)	67.90 (*t*)	36.3	30.0	26.3
	C	35.51 (dd)	96.25 (dd)	60.90 (*t*)	40.0	29.1	22.9
4	A	35.63 (*t*)	100.14 (dd)	67.91 (dd)	37.2	32.0	19.8
	B	38.80 (dd)	106.12 (dd)	79.58 (dd)	41.0	31.9	18.8
	C	36.12 (dd)	104.02 (dd)	70.02 (*t*)	36.1	26.8	19.2
	D	36.91 (*t*)	100.82 (dd)	66.98 (dd)	34.5	29.1	21.3
5		35.92 (*t*)	95.64 (dd)	54.21 (dd)	38.9	32.7	21.2
6		41.21 (*t*)	92.77 (dd)	47.45 (dd)	34.1	31.6	19.2
7		39.03 (*t*)	92.53 (dd)	55.95 (dd)	34.2	33.4	19.6
8		38.65 (*t*)	91.34 (dd)	55.07 (dd)	34.8	29.8	18.8

[a] [D_4]Methanol, 161.98 MHz, 294 K. Chemical shifts in ppm, coupling constants in Hz. The labeling scheme adopted is: P(1) = Cp*P*Ph2, P(2) = *P*Ph, P(3) = *P*Ph_2 (see Figure 1). Isomers concentration A > B > C > D.

 © 2003 Wiley-VCH Verlag GmbH & Co. KGaA, Weinheim

cationic derivatives [{$(R)_C$-$(S)_{Fe}$-$(S)_P$-P3Chir}RuCl-$(CH_3CN)_2$]Cl (**5**) and [{$(R)_C$-$(S)_{Fe}$-$(R)_P$-P3Chir}RuCl-$(CH_3CN)_2$]Cl (**6**), respectively. Monitoring the reactions by $^{31}P\{^1H\}$ NMR spectroscopy in CD_3CN showed the conversion of **3** to occur within seconds at room temperature. In contrast, the quantitative conversion of **4** into **6** was achieved only by heating the solution at 75 °C for 2 h. In CD_3CN solution at room temperature, **5** and **6** exist as single isomers as shown by the $^{31}P\{^1H\}$ NMR spectra in which canonical AMQ spin systems are displayed,[13] with $^2J_{P,P}$ values indicative of a *fac* arrangement of the triphosphane ligands about the metal center.[8,9] The coordination geometry of **5** and **6** in solution can be established on the basis of the *trans* influence of the coligands discussed above, which decreases in the order $CH_3CN > Cl$.[9,11,14,15] In particular, from a comparison of the ^{31}P NMR chemical shifts in each complex with those observed for the corresponding nuclei in the free ligands and in the dichloro complexes **3** and **4**, the PhP(2) group is assigned a *trans* position to the chloride ion in both **5** and **6** (Scheme 1).

Compounds **5** and **6** behave as 1:1 electrolytes in acetonitrile solution, from which they can be isolated in the solid state by addition of diethyl ether (molar conductance in acetonitrile is 61 $\Omega^{-1}\cdot cm^2\cdot mol^{-1}$ and 68 $\Omega^{-1}\cdot cm^2\cdot mol^{-1}$ for **5** and **6**, respectively). The IR spectra show weak absorptions in the region 2280−2360 cm^{-1}, where the ν(C≡N) absorption of coordinated CH_3CN is usually observed (see Exp. Sect.).[16] Both **5** and **6** dissolve in methanol generating a dissociation equilibrium concentration with the corresponding dichloro complexes. At room temperature, an approximate 30:70 molar ratio of the bis(acetonitrile) and dichloro complexes was determined on the basis of $^{31}P\{^1H\}$ NMR integration (Scheme 2). $^{31}P\{^1H\}$ NMR spectroscopic data for **5** and **6** in [D_4]methanol are listed in Table 1, whereas selected ^1H NMR spectroscopic data are reported in the Exp. Sect. When CH_3CN is used as solvent the bis(acetonitrile) adducts are stabilized and the equilibrium is completely shifted to the left.

$$\underset{\mathbf{5,\,6}}{[(P3Chir)RuCl(CH_3CN)_2]Cl} \rightleftharpoons \underset{\mathbf{3,\,4}}{(P3Chir)RuCl_2} + 2\,CH_3CN$$

P3Chir = $(R)_C$-$(S)_{Fe}$-$(S)_P$-P3Chir **3, 5**
P3Chir = $(R)_C$-$(S)_{Fe}$-$(R)_P$-P3Chir **4, 6**

Scheme 2

The occurrence of the equilibrium shown in Scheme 2 was further substantiated by a ^1H NOESY experiment carried out in [D_4]methanol, where the resonances due to the coordinated acetonitrile molecules can be detected. A section of the ^1H NOESY spectrum of **5** is shown in Figure 2. Strong exchange cross-peaks between coordinated [δ = 1.73 and 1.45 ppm (both s)] and free CH_3CN [δ = 2.06 ppm (s)] molecules are observed together with exchange peaks relating the CHCH_3 signals of **5** [δ = 1.59 ppm (dd)] with those of the A, B and C isomers of **3** [δ = 1.22, 1.16 and 0.94 ppm (all dd), respectively].

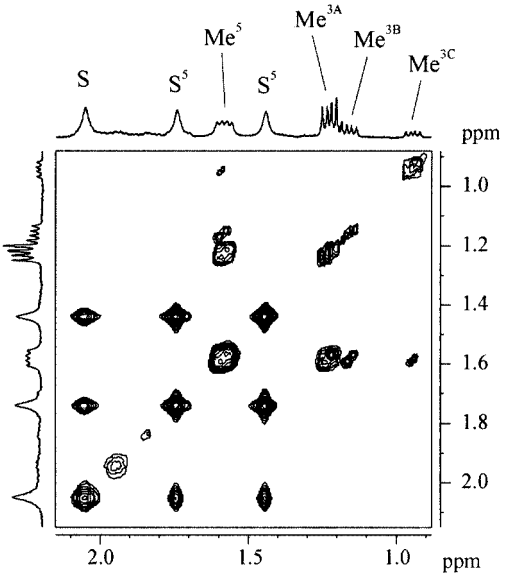

Figure 2. Section of the ^1H NOESY spectrum of **5** ([D_4]methanol, 294 K, 400.13 MHz, τ_m = 0.80 s); signals due to coordinated (S^5) and free (S) CH_3CN molecules and to the CHCH_3 protons of **5** (Me^5) and the A, B and C isomers of **3** (Me^{3A}, Me^{3B}, Me^{3C}) are displayed

The ^1H and ^{13}C NMR resonances of the acetonitrile molecules in each complex could be unambiguously assigned by means of ^1H,^{13}C correlations. $^{13}C\{^1H\}$ NMR spectroscopic data for **5** and **6** in methanol solution are reported in the Exp. Sect.

The dicationic, tris(acetonitrile) adducts [{$(R)_C$-$(S)_{Fe}$-$(S)_P$-P3Chir}Ru$(CH_3CN)_3$]$(PF_6)_2$ (**7**) and [{$(R)_C$-$(S)_{Fe}$-$(R)_P$-P3Chir}Ru$(CH_3CN)_3$]$(PF_6)_2$ (**8**) were obtained as orange microcrystals by treatment of the corresponding dichloro complexes **3** and **4** in CH_3CN with $TlPF_6$. The isolated compounds are quite stable in both the solid state and in deaerated methanol solution. The nujol IR spectra show absorptions in the range 2320−2390 cm^{-1}, characteristic of coordinated CH_3CN molecules (see Exp. Sect.).[16] Compounds **7** and **8** are stereochemically rigid on the NMR timescale at room temperature in [D_4]methanol, as shown by the $^{31}P\{^1H\}$ NMR spectra, which consist of canonical AMQ spin systems. A *fac* arrangement of the triphosphane ligands in the octahedral compounds can be assigned on the basis of the $^2J_{P,P}$ values, which range between 18.8 and 38.9 Hz.[8,9] The preservation of a *fac* arrangement of the tridentate ligand on going from chloro to acetonitrile complexes has been previously reported for other (triphosphane)Ru^{II} complexes.[4b,16a] The ^1H and ^{13}C NMR resonances of the acetonitrile molecules in **7** and **8** were readily assigned using ^1H,^{13}C correlations. The $^{13}C\{^1H\}$ NMR spectroscopic data in [D_4]methanol are reported in the Exp. Sect. Due to the small contribution of a neighbouring anisotropy effect,[9,17] ^{13}C chemical shifts generally provide more direct information concerning the electronic environment of a given ligand than proton shifts do. In the case at hand, the observed low-field shift of 0.43−2.01 ppm for the ^{13}C resonances of the CH_3CN carbon atoms, compared to the corresponding signals of free acetonitrile, is unequivo-

 © 2003 Wiley-VCH Verlag GmbH & Co. KGaA, Weinheim

cally indicative of coordinated acetonitrile molecules.[4b,12,18]

Catalytic Reduction of Trifluoroacetophenone

Experiments with 2,2,2-trifluoroacetophenone showed that the Ru^{II} precursors with the P3Chir ligands can form effective asymmetric catalysts for the homogeneous reduction of prochiral ketones to optically pure secondary alcohols by either hydrogenation or hydrogen transfer (Scheme 3 and Table 2).

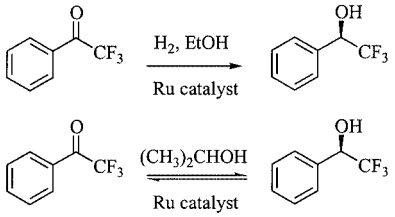

Scheme 3

The reduction of 2,2,2-trifluoroacetophenone to (*R*)-α-(trifluoromethyl)benzyl alcohol (Scheme 2) is a typical probe reaction to test the efficiency of chiral Ru^{II} catalysts. Indeed, asymmetric reductions of prochiral ketones can be carried out with Ru^{II} compounds through hydrogenation, hydrosilylation or hydrogen transfer. Most examples in the literature involve Ru^{II} complexes stabilised by bidentate ligands with P, N and O donor atoms.[1,19] The reduction of ketones catalyzed by complexes containing tri- and tetradentate ligands has been much less intensely studied.[4b,20]

The hydrogenation reactions were performed in ethanol at 60 °C under a H_2 pressure of 60 atm, while *i*PrOH was the solvent for the hydrogen-transfer reactions which, however, require the addition of *i*PrOK as basic co-catalyst to achieve the reduction of the ketone.[21] Irrespective of the hydrogen source, the yields of (*R*)-α-(trifluoromethyl)benzyl alcohol increased with the number of coordinated acetonitrile molecules in the {$(R)_C$-$(S)_{Fe}$-$(S)_P$-P3Chir}ruthenium(II) precursors, which reflects the easier displacement of acetonitrile by the ketone as compared to the chloride ion (Table 2). Under the same experimental conditions, 2,2,2-trifluoroacetophenone was quantitatively hydrogenated after 19 h only with the tris(acetonitrile) complex **7** (Table 2, Entry 3), whereas a 78.7% and 23.4% yield was observed using the bis(acetonitrile) complex **5** and the dichloro complex **3**, respectively (Table 2, Entries 2 and 1). Although the hydrogen-transfer reactions occurred even at room temperature, relatively high temperatures (68 °C) were required to obtain appreciable reaction rates. Again, the best results were obtained with the tris(acetonitrile) complex **7**, which gave a nearly complete conversion of the ketone after 2.5 h (Table 2, Entry 6). Under these conditions, the yield of (*R*)-α-(trifluoromethyl)benzyl alcohol using **5** and **3** were 79.2% and 36.2%, respectively (Table 2, Entries 5 and 4). Besides higher activity, the hydrogen-transfer reactions also gave higher enantioselectivities (38−41%) than the hydrogenation reactions (19−23%). This finding prompted us to investigate the behaviour of the $(R)_C$-$(S)_{Fe}$-$(R)_P$-P3Chir derivative **8** as a hydrogen-transfer catalyst precursor as well. This latter epimer gave a slightly better productivity than **7** in the same experimental conditions, yet the *ee* was almost negligible (Table 2, Entry 7). To summarise, the ruthenium(II) complexes described in this paper are efficient catalyst precursors either for the hydrogenation and the hydrogen-transfer reactions to prochiral ketones under mild conditions. In general, however, the *ee* values are lower than those achieved with other Ru^{II} chiral catalysts.[21a,22] The above results are consistent with those previously obtained in the transfer hydrogenation to acetophenone mediated by the dicationic Ru^{II} complex with the chiral triphosphane Pigiphos.[4b] This latter compound, however, was found to be the best preformed catalyst precursor containing a chiral tridentate ligand reported so far in terms of enantioselectivity for this reaction.[20d]

From a comparison of the results obtained with the P3Chir and Pigiphos ligands, one can see that the design of chiral tridentate ligands for diverse applications in asymmetric catalysis is still a challenging task. Indeed, other factors besides the presence/absence of C_2 symmetry or geometrical (*mer*/*fac*) isomerism of the tridentate ligand, seem to play an important role in controlling the chiral transfer ability.

Conclusion

Five- and six-coordinate Ru^{II} complexes with the first chiral tridentate phosphane ligands combining planar, phosphorus, and carbon chirality have been synthesized

Table 2. Asymmetric catalytic reduction of 2,2,2-trifluoroacetophenone with Ru^{II} complexes

Entry	Complex	*T* [°C]	Hydrogen source	*t* [h]	Yield [%][a]	*ee* [%][a]
1[b]	[{$(R)_C$-$(S)_{Fe}$-$(S)_P$-P3Chir}$RuCl_2$] (**3**)	60	H_2, 60 atm	19	22.0	21.9
2[b]	[{$(R)_C$-$(S)_{Fe}$-$(S)_P$-P3Chir}$RuCl(CH_3CN)_2$]Cl (**5**)	60	H_2, 60 atm	19	77.3	22.8
3[b]	[{$(R)_C$-$(S)_{Fe}$-$(S)_P$-P3Chir}$Ru(CH_3C)_3$]$(PF_6)_2$ (**7**)	60	H_2, 60 atm	19	99.0	19.0
4[c]	[{$(R)_C$-$(S)_{Fe}$-$(S)_P$-P3Chir}$RuCl_2$] (**3**)	68	*i*PrOH	2.5	35.3	38.2
5[c]	[{$(R)_C$-$(S)_{Fe}$-$(S)_P$-P3Chir}$RuCl(CH_3CN)_2$]Cl (**5**)	68	*i*PrOH	2.5	78.7	41.0
6[c]	[{$(R)_C$-$(S)_{Fe}$-$(S)_P$-P3Chir}$Ru(CH_3CN)_3$]$(PF_6)_2$ (**7**)	68	*i*PrOH	2.5	93.7	40.9
7[c]	[{$(R)_C$-$(S)_{Fe}$-$(R)_P$-P3Chir}$Ru(CH_3CN)_3$]$(PF_6)_2$ (**8**)	68	*i*PrOH	2.5	98.1	5.0

[a] Isolated yields. [b] Reaction conditions: Ru (0.0022 mmol), solvent ethanol (4 mL), 500 rpm, substrate/Ru mol. ratio 100:1. [c] Reaction conditions: Ru (0.0022 mmol), solvent *i*PrOH (4 mL), substrate/Ru/*i*PrO^-K^+ mol. ratio 100:1:1.

 © 2003 Wiley-VCH Verlag GmbH & Co. KGaA, Weinheim

and fully characterized in solution. Irrespective of the co-ligands (chloro or acetonitrile), the absolute configuration of the stereocentres and the temperature, the triphosphane ligands wrap the metal centre in a facial arrangement.

The dichloro, bis(acetonitrile)chloro and tris(acetonitrile) complexes with $(R)_C$-$(S)_{Fe}$-$(S)_P$-P3Chir and the tris(acetonitrile) complex with $(R)_C$-$(S)_{Fe}$-$(R)_P$-P3Chir have been tested as catalyst precursors for the reduction of 2,2,2-trifluoroacetophenone to (*R*)-α-(trifluoromethyl)benzyl alcohol by either hydrogenation and hydrogen transfer from *i*PrOH. The catalytic activity was fairly good, particularly using the precursors bearing only acetonitrile co-ligands, yet the asymmetric induction was quite low.

To gain some insight into the chemical and physical factors (ligand conformation, steric and electronic properties of the donor groups) that may control the asymmetric induction by tridentate phosphane complexes, studies are presently ongoing in our laboratories and will be published in due course.

Experimental Section

General Remarks: All manipulations were performed under pure nitrogen unless otherwise stated. Diethyl ether was distilled from Na/benzophenone. Acetonitrile was distilled from CaH_2. Toluene was distilled from sodium. $[RuCl_2(PPh_3)_3]$,[23] $(R)_C$-$(S)_{Fe}$-$(S)_P$-P3Chir (**1**) and $(R)_C$-$(S)_{Fe}$-$(R)_P$-P3Chir (**2**)[6] were synthesized as previously reported. Unless otherwise stated, all the other chemicals were obtained from commercial suppliers and were used as received without further purification. The solid compounds were collected on sintered glass frits before being dried in a stream of nitrogen. $^{31}P\{^1H\}$ NMR spectra were recorded with a Bruker Avance DRX-400 spectrometer operating at 161.98 MHz. Chemical shifts are relative to external 85% H_3PO_4 with downfield values reported as positive. ^1H and $^{13}C\{^1H\}$ NMR spectra were recorded at 400.13 and 100.61 MHz, respectively, with a Bruker Avance DRX-400 spectrometer. Chemical shifts are calibrated against solvent resonances. The spectrometer was equipped with a variable-temperature control unit accurate to ±0.1 °C. The assignments of the signals were made from 1D spectra, $^1H\{^{31}P\}$ heteronuclear decoupling experiments, ^1H COSY and proton detected ^1H,^{13}C and ^1H,^{31}P correlations using degassed nonspinning samples. 2D NMR spectra were recorded using pulse sequences suitable for phase-sensitive representations using TPPI. The ^1H,^{13}C and ^1H,^{31}P correlations[24] were recorded using an HMQC sequence with decoupling during acquisition. A standard pulse sequence was used for the ^1H-NOESY[25] experiments. Infrared spectra were recorded with a Perkin−Elmer 1600 Series FT-IR spectrometer using samples mulled in Nujol between KBr plates. Reactions under a controlled pressure of hydrogen were performed with a stainless steel autoclave (10 mL internal volume) constructed at ICCOM-CNR (Firenze, Italy) and equipped with a magnetic stirrer, a Teflon inset and a pressure controller. The temperature control was achieved by an oil-bath thermostat accurate to ±0.2 °C. GC analyses were performed with a Shimadzu GC-17A gas chromatograph equipped with a flame-ionization detector and a 30-m (0.25 mm ID, 0.25 μm FT) SPB-1 Supelco fused-silica capillary column. The *ee* values were determined by GC analyses with a Shimadzu GC-17A gas chromatograph equipped with a flame-ionization detector and a 50 m × 0.25 mm ID Chiraldex G-TA capillary column and coupled with a Shimadzu C-R7A Chromatopac. Conductivities were measured with a Model 990101 Orion conductance cell connected to a Model 101 conductivity meter.

$[\{(R)_C$-$(S)_{Fe}$-$(S)_P$-P3Chir$\}RuCl_2]$ (3): Solid $[RuCl_2(PPh_3)_3]$ (0.08 g, 0.08 mmol) was added to a solution of **1** (0.06 g, 0.08 mmol) in toluene (3 mL) and the suspension was refluxed with stirring for 3 h. During this time, a red solution was obtained from which red microcrystals separated slowly. After cooling to room temperature, the solid obtained was filtered off and washed with diethyl ether (25 mL). Yield: 62 mg (87%). ^1H NMR ([D$_4$]methanol, 400.13 MHz, 294 K): isomer A: δ = 4.51 (m, 1 H, C_5H_3), 4.18 (m, 1 H, C_5H_3), 3.85 (*s*, 5 H, C_5H_5), 3.63 (m, 1 H, C_5H_3), 3.61 (quint, $^3J_{H,H} = {}^2J_{H,P}$ = 7.0 Hz, 1 H, C*H*CH$_3$), 1.22 (dd, $^3J_{H,H}$ = 6.7, $^3J_{H,P}$ = 12.6 Hz, 3 H, CHC*H*$_3$); isomer B: δ = 4.62 (m, 1 H, C_5H_3), 4.46 (m, 1 H, C_5H_3), 4.07 (s, 5 H, C_5H_5), 3.98 (m, 1 H, C_5H_3), 3.75 (quint, $^3J_{H,H} = {}^2J_{H,P}$ = 7.4 Hz, 1 H, C*H*CH$_3$,), 1.16 (dd, $^3J_{H,H}$ = 6.7, $^3J_{H,P}$ = 12.8 Hz, 3 H, CHC*H*$_3$); isomer C: δ = 4.32 (m, 1 H, C_5H_3), 3.96 (s, 5 H, C_5H_5), 3.69 (m, 1 H, C_5H_3), 2.90 (quint, $^3J_{H,H} = {}^2J_{H,P}$ = 7.1 Hz, 1 H, C*H*CH$_3$), 0.94 (dd, $^3J_{H,H}$ = 7.1, $^3J_{H,P}$ = 12.4 Hz, 3 H, CHC*H*$_3$) ppm. $C_{44}H_{41}Cl_2FeP_3Ru$ (890.6): calcd. C 59.34, H 4.64; found C 59.40, H 4.65.

$[\{(R)_C$-$(S)_{Fe}$-$(R)_P$-P3Chir$\}RuCl_2]$ (4): This compound was prepared as described above for **3** by using $(R)_C$-$(S)_{Fe}$-$(R)_P$-P3Chir (**2**) instead of $(R)_C$-$(S)_{Fe}$-$(S)_P$-P3Chir (**1**). Yield: 56 mg (78%). ^1H NMR ([D$_4$]methanol, 400.13 MHz, 294 K): isomer A: δ = 4.31 (s, 5 H, C_5H_5), 0.86 (dd, $^3J_{H,H}$ = 6.7, $^3J_{H,P}$ = 12.5 Hz, 3 H, CHC*H*$_3$); isomer B: δ = 4.52 (s, 5 H, C_5H_5), 1.42 (dd, $^3J_{H,H}$ = 6.8, $^3J_{H,P}$ = 13.2 Hz, 3 H, CHC*H*$_3$); isomer C: δ = 4.25 (s, 5 H, C_5H_5), 1.50 (dd, $^3J_{H,H}$ = 7.4, $^3J_{H,P}$ = 13.3 Hz, 3 H, CHC*H*$_3$); isomer D: δ = 4.20 (s, 5 H, C_5H_5), 1.62 (dd, $^3J_{H,H}$ = 7.8, $^3J_{H,P}$ = 13.5 Hz, 3 H, CHC*H*$_3$) ppm. $C_{44}H_{41}Cl_2FeP_3Ru$ (890.6): calcd. C 59.34, H 4.64; found C 59.28, H 4.63.

$[\{(R)_C$-$(S)_{Fe}$-$(S)_P$-P3Chir$\}RuCl(CH_3CN)_2]Cl$ (5): A solution of **3** (0.07 g, 0.08 mmol) in CH_3CN (2 mL) was stirred at room temperature for 1 h. Slow addition of diethyl ether (10 mL) caused the precipitation of an orange solid which was filtered off and washed with diethyl ether (15 mL). Yield: 72 mg (93%). ^1H NMR ([D$_4$]methanol, 400.13 MHz, 294 K): δ = 8.13 (m, 2 H, Ph), 7.91 (m, 2 H, Ph), 7.80 (m, 2 H, Ph), 7.6−7.1 (m, 17 H, Ph), 6.98 (m, 2 H, Ph), 4.86 (m, 1 H, C_5H_3), 4.62 (m, 1 H, C_5H_3), 4.41 (s, 5 H, C_5H_5), 3.80 (quint, $^3J_{H,H} = {}^2J_{H,P}$ = 7.1 Hz, 1 H, C*H*CH$_3$), 3.42 (m, 1 H, C_5H_3), 2.60 (ddddd, $^3J_{H,H}$ = 2.7, $^3J_{H,H}$ = 5.5, $^3J_{H,P}$ = 12.2, $^2J_{H,H}$ = 14.6, $^2J_{H,P}$ = 43.9 Hz, 1 H, PC*H*H), 2.38 (ddddd, $^3J_{H,H}$ = 2.3, $^3J_{H,H}$ = 5.8, $^3J_{H,P}$ = 10.8, $^2J_{H,H}$ = 14.1, $^2J_{H,P}$ = 42.9 Hz, 1 H, PC*H*H), 1.84 (m, 1 H, PCH*H*), 1.73 (s, 3 H, CH_3CN), 1.59 (dd, $^3J_{H,H}$ = 7.1, $^3J_{H,P}$ = 13.2 Hz, 3 H, CHC*H*$_3$), 1.45 (s, 3 H, CH_3CN), 0.74 (tdt, $^3J_{H,H}$ = 5.6, $^2J_{H,H}$ = 14.7, $J_{H,P}$ = 19.2 Hz, 1 H, PCH*H*) ppm. $^{13}C\{^1H\}$ NMR ([D$_4$]methanol, 100.61 MHz, 294 K): δ = 76.79 (d, $J_{C,P}$ = 7.2 Hz, 1 C, C_5H_3), 70.65 (s, 5 C, C_5H_5), 70.15 (d, $J_{C,P}$ = 7.7 Hz, 1 C, C_5H_3), 68.71 (d, C_5H_3, $J_{C,P}$ = 7.5 Hz, 1 C), 32.00 (d, $^1J_{C,P}$ = 19.9 Hz, 1 C, *C*HCH$_3$), 22.80 (dd, $^1J_{C,P}$ = 34.0, $^2J_{C,P}$ = 10.8 Hz, 1 C, PCH$_2$), 15.70 (dd, $^1J_{C,P}$ = 28.8, $^2J_{C,P}$ = 8.6 Hz, 1 C, PCH$_2$), 13.08 (s, 1 C, CH*C*H$_3$), 1.67 (s, 1 C, *C*H$_3$CN), 1.58 (s, 1 C, *C*H$_3$CN) ppm. $C_{48}H_{47}Cl_2FeN_2P_3Ru$ (972.7): calcd. C 59.27, H 4.87, N 2.88; found C 59.35, H 4.81, N 2.85. IR: $\tilde{\nu}$ = 2319 ν(C≡N) cm^{-1}.

$[\{(R)_C$-$(S)_{Fe}$-$(R)_P$-P3Chir$\}RuCl(CH_3CN)_2]Cl$ (6): A solution of **4** (0.07 g, 0.08 mmol) in CH_3CN (3 mL) was heated with stirring at 70 °C for 2 h. After cooling to room temperature, diethyl ether (15 mL) was added causing the precipitation of an orange solid. This was filtered off and washed with diethyl ether (15 mL). Yield: 66 mg (85%). ^1H NMR ([D$_4$]methanol, 400.13 MHz, 294 K): δ =

 © 2003 Wiley-VCH Verlag GmbH & Co. KGaA, Weinheim

8.25 (m, 2 H, Ph), 8.06 (m, 2 H, Ph), 7.63 (m, 2 H, Ph), 7.6−7.2 (m, 17 H, Ph), 7.12 (m, 2 H, Ph), 5.03 (m, 1 H, C_5H_3), 4.44 (m, 1 H, C_5H_3), 4.32 (s, 5 H, C_5H_5), 3.94 (quint, $^3J_{H,H} = {}^2J_{H,P} = 6.8$ Hz, 1 H, C*H*CH_3), 3.29 (m, 1 H, C_5H_3), 2.73 (m, 1 H, PC*H*H), 2.45 (m, 1 H, PC*H*H), 1.87 (m, 1 H, PCH*H*), 1.72 (s, 3 H, CH_3CN), 1.61 (dd, $^3J_{H,H} = 6.8$, $^3J_{H,P} = 13.8$ Hz, 3 H, CHC*H*$_3$), 1.37 (s, 3 H, CH_3CN), 0.88 (m, 1 H, PCH*H*) ppm. $^{13}C\{^1H\}$ NMR ([D$_4$]methanol, 100.61 MHz, 294 K): δ = 76.82 (d, $J_{C,P} = 7.3$ Hz, 1 C, C_5H_3), 70.45 (s, 5 C, C_5H_5), 70.22 (d, $J_{C,P} = 7.8$ Hz, 1 C, C_5H_3), 68.69 (d, $J_{C,P} = 7.5$ Hz, 1 C, C_5H_3), 31.88 (d, $^1J_{C,P} = 19.7$ Hz, 1 C, *C*HCH$_3$), 23.30 (dd, $^1J_{C,P} = 33.8$, $^2J_{C,P} = 10.6$ Hz, 1 C, PCH_2), 15.52 (dd, $^1J_{C,P} = 28.6$, $^2J_{C,P} = 8.6$ Hz, 1 C, PCH_2), 12.87 (s, 1 C, CH*C*H$_3$), 1.88 (s, 1 C, *C*H$_3$CN), 1.68 (s, 1 C, *C*H$_3$CN) ppm. $C_{48}H_{47}Cl_2FeN_2P_3Ru$ (972.7): calcd. C 59.27, H 4.87, N 2.88; found C 59.28, H 4.85, N 2.84. IR: $\tilde{\nu}$ = 2323 ν(C≡N) cm^{-1}.

[{(R)$_C$-(S)$_{Fe}$-(S)$_P$-P3Chir}Ru(CH$_3$CN)$_3$](PF$_6$)$_2$ (7): Solid $TlPF_6$ (0.06 g, 0.16 mmol) was added to a solution of **3** (0.07 g, 0.08 mmol) in CH_3CN (5 mL). After stirring for 20 min, the mixture was decanted and TlCl was filtered off. Upon addition of diethyl ether (20 mL) to the resulting solution, orange microcrystals separated. The crystals were filtered and washed with diethyl ether (20 mL). Yield: 175 mg (89%). ^1H NMR ([D$_4$]methanol, 400.13 MHz, 294 K): δ = 7.9−7.8 (m, 4 H, Ph), 7.7−7.4 (m, 12 H, Ph), 7.3−7.1 (m, 9 H, Ph), 5.02 (m, 1 H, C_5H_3), 4.73 (m, 1 H, C_5H_3), 4.46 (s, 5 H, C_5H_5), 4.03 (quint, $^3J_{H,H} = {}^2J_{H,P} = 7.1$ Hz, 1 H, C*H*CH$_3$), 3.70 (m, 1 H, C_5H_3), 2.76 (m, 1 H, PC*H*H), 2.64 (s, 3 H, CH_3CN), 2.44 (m, 1 H, PCH*H*), 2.18 (m, 1 H, PC*H*H), 1.79 (s, 3 H, CH_3CN), 1.65 (dd, $^3J_{H,H} = 7.1$, $^3J_{H,P} = 13.9$ Hz, 3 H, CHC*H*$_3$), 1.54 (s, 3 H, CH_3CN), 1.22 (m, 1 H, PCH*H*) ppm. $^{13}C\{^1H\}$ NMR ([D$_4$]methanol, 100.61 MHz, 294 K): δ = 89.77 (m, 1 C, C_5), 84.52 (m, 1 C, C_5), 76.89 (s, 1 C, C_5H_3), 70.81 (s, 5 C, C_5H_5), 70.50 (s, 1 C, C_5H_3), 68.89 (s, 1 C, C_5H_3), 31.59 (d, $^1J_{C,P}$ = 17.7 Hz), 1 C, *C*HCH$_3$, 24.02 (d, $^1J_{C,P} = 42.3$ Hz, 1 C, PCH_2), 15.51 (dd, $^1J_{C,P} = 30.7$, $^2J_{C,P} = 8.6$ Hz, 1 C, PCH_2), 12.46 (s, 1 C, CH*C*H$_3$), 1.72 (s, 1 C, *C*H$_3$CN), 0.95 (s, 1 C, *C*H$_3$CN), 0.87 (s, 1 C, *C*H$_3$CN) ppm. $C_{50}H_{50}F_{12}FeN_3P_5Ru$ (1232.7): calcd. C 48.72, H 4.09, N 3.41; found C 48.69, H 4.02, N 3.52. IR: $\tilde{\nu}$ = 2319, 2388 ν(C≡N), 832 (P−F) cm^{-1}.

[{(R)$_C$-(S)$_{Fe}$-(R)$_P$-P3Chir}Ru(CH$_3$CN)$_3$](PF$_6$)$_2$ (8): Solid $TlPF_6$ (0.03 g, 0.08 mmol) was added to a solution of **4** (0.04 g, 0.04 mmol) in CH_3CN (5 mL). After stirring at 50 °C for 30 min, the mixture was cooled to room temperature, decanted and TlCl was filtered off. Upon addition of diethyl ether (20 mL) to the resulting solution, an orange solid separated which was filtered and washed with diethyl ether (20 mL). Yield: 84 mg (85%). ^1H NMR ([D$_4$]methanol, 400.13 MHz, 294 K): δ = 7.8−7.7 (m, 2 H, Ph), 7.6−7.2 (m, 14 H, Ph), 7.1−7.0 (m, 9 H, Ph), 5.13 (m, 1 H, C_5H_3), 4.44 (m, 1 H, C_5H_3), 4.15 (s, 5 H, C_5H_5), 3.40 (quint, $^3J_{H,H} = {}^2J_{H,P} = 6.5$ Hz, 1 H, C*H*CH$_3$), 2.96 (m, 1 H, C_5H_3), 2.75 (s, 3 H, CH_3CN), 2.50 (m, 1 H, PC*H*H), 2.46 (m, 1 H, PCH*H*), 2.18 (s, 3 H, CH_3CN), 1.78 (m, 1 H, PC*H*H), 1.55 (dd, $^3J_{H,H} = 6.7$, $^3J_{H,P} = 13.7$ Hz, 3 H, CHC*H*$_3$), 1.47 (m, 1 H, PCH*H*), 1.39 (s, 3 H, CH_3CN) ppm. $^{13}C\{^1H\}$ NMR ([D$_4$]methanol, 100.61 MHz, 294 K): δ = 92.10 (m, 1 C, C_5), 87.45(m, 1 C, C_5), 77.02 (s, 1 C, C_5H_3), 69.86 (s, 5 C, C_5H_5), 69.54 (s, 1 C, C_5H_3), 68.74 (s, 1 C, C_5H_3), 32.54 (d, $^1J_{C,P} = 17.8$ Hz, 1 C, *C*HCH$_3$), 25.08 (d, 1 C, PCH_2, $^1J_{C,P} = 41.9$ Hz), 15.47 (dd, $^1J_{C,P} = 30.5$, $^2J_{C,P} = 8.8$ Hz, 1 C, PCH_2), 12.44 (s, 1 C, CH*C*H$_3$), 2.31 (s, 1 C, *C*H$_3$CN), 1.12 (s, 1 C, *C*H$_3$CN), 0.73 (s, 1 C, *C*H$_3$CN) ppm. $C_{50}H_{50}F_{12}FeN_3P_5Ru$ (1232.7): calcd. C 48.72, H 4.09, N 3.41; found C 48.68, H 4.05, N 3.50. IR: $\tilde{\nu}$ = 2321, 2384 ν(C≡N); 840 (P−F) cm^{-1}.

General Procedure for the Reduction of 2,2,2-Trifluoroacetophenone by Hydrogen Transfer: In a typical reaction, a catalyst precursor (0.002 mmol) and freshly distilled 2,2,2-trifluoroacetophenone (28 μL, 0.2 mmol) were introduced under Ar into a flask equipped with a condenser and containing 5 mL of anhydrous *i*PrOH. The mixture was heated at 68 °C with stirring. After 10 min, freshly prepared *i*PrOK (0.1 M in *i*PrOH, 22 μL, 0.002 mmol) was introduced. The addition of *i*PrOK was considered as the starting time of the reaction. The solution was stirred at 68 °C for 3 h. During this time the reaction progress was monitored by GC (SPB-1 capillary column). After cooling the reaction mixture to room temperature, the solvent was removed in vacuo. The residue was dissolved in 1 mL of diethyl ether and chromatographed by short-column chromatography on silica gel using diethyl ether as eluent. The enantiomeric excess was determined on the resulting solution by GC analysis.

General Procedure for the Enantioselective Hydrogenation of 2,2,2-Trifluoroacetophenone: In a typical experiment, a suspension of the catalyst precursor (0.002 mmol) in ethanol (4 mL) was stirred at 60 °C under argon until the complete dissolution of the starting complex occurred (ca. 15 min). 2,2,2-Trifluoroacetophenone (28 μL, 0.2 mmol) was added at room temperature and the resulting solution was transferred via a Teflon capillary into a 10-mL autoclave under argon. Argon was then replaced by hydrogen with three cycles of 5 bar/normal pressure. The autoclave was finally charged with the desired pressure of H_2 and then heated using a thermostatted oil bath with magnetic stirring. After the desired time, the reactor was cooled to room temperature and a sample of the reaction mixture was analyzed by GC.

Acknowledgments

Thanks are due to COST D24 chemistry action for support.

[1] [1a] H. Brunner, W. Zettlmeier, *Handbook of Enantioselective Catalysis with Transition Metal Compounds*, Wiley-VCH, Weinheim, **1993**, vol. 1. [1b] R. Noyori, *Asymmetric Catalysis in Organic Synthesis*, John Wiley & Sons, New York, **1994**.
[2] F. A. Cotton, B. Hong, *Progr. Inorg. Chem.* **1992**, *40*, 179.
[3] [3a] M. J. Burk, R. L. Harlow, *Angew. Chem. Int. Ed. Engl.* **1990**, *29*, 1462. [3b] M. J. Burk, J. E. Feaster, R. L. Harlow, *Tetrahedron: Asymmetry* **1991**, *2*, 569. [3c] T. R. Ward, L. M. Venanzi, A. Albinati, F. Lianza, T. Gerfin, V. Gramlich, G. M. Ramos Tombo, *Helv. Chim. Acta* **1991**, *74*, 983. [3d] G. Jia, H. M. Lee, I. D. Williams, *Organometallics* **1996**, *15*, 4235. [3e] H. Heidel, J. Scherer, A. Asam, G. Huttner, O. Walter, L. Zsolnai, *Chem. Ber.* **1995**, *128*, 293. [3f] R. B. King, J. Bakos, C. D. Hoff, L. Markó, *J. Org. Chem.* **1979**, *44*, 3095. [3g] C. R. Johnson, T. Imamoto, *J. Org. Chem.* **1987**, *52*, 2170. [3h] H. M. Lee, C. Bianchini, G. Jia, P. Barbaro, *Organometallics* **1999**, *18*, 1961.
[4] [4a] P. Barbaro, A. Togni, *Organometallics* **1995**, *14*, 3570. [4b] P. Barbaro, C. Bianchini, A. Togni, *Organometallics* **1997**, *16*, 3004. [4c] P. Barbaro, C. Bianchini, W. Oberhauser, A. Togni, *J. Mol. Cat. A, Chem.* **1999**, *145*, 139. [4d] L. Fadini, A. Togni, *Chem. Commun.* **2003**, 30.
[5] For a review on asymmetric, catalytic reduction of ketones, see: [5a] G. Zassinovich, G. Mestroni, S. Gladiali, *Chem. Rev.* **1992**, *92*, 1051. [5b] *Catalytic Asymmetric Synthesis* (Ed.: I. Ojima), Wiley-VCH, Weinheim, **2000**. [5c] *Comprehensive Asymmetric Catalysis* (Eds.: E. N. Jacobsen, A. Pfaltz, H. Yamamoto), Springer-Verlag, Heidelberg, **2000**, vol. 1, chapter 6. [5d] R. Noyori, M. Yamakawa, S. Hashiguchi, *J. Org. Chem.* **2001**, *66*, 7931. [5e] R. Noyori, T. Ohkuma, *Angew. Chem. Int. Ed.* **2001**, *40*, 41. [5f] H. U. Blaser, C. Malan, B. Pugin, F. Spindler, H. Steiner, M. Studer, *Adv. Synth. Catal.* **2003**, *345*, 103.
[6] [6a] P. Barbaro, C. Bianchini, G. Giambastiani, A. Togni, *Chem.*

 © 2003 Wiley-VCH Verlag GmbH & Co. KGaA, Weinheim

Commun. **2002**, 2672. [6b] P. Barbaro, C. Bianchini, G. Giambastiani, A. Togni, manuscript in preparation.
[7] G. Jia, I. Lee, D. W. Meek, J. C. Gallucci, *Inorg. Chim. Acta* **1990**, *177*, 81.
[8] A. L. Crumbliss, R. J. Topping, in *Methods in Stereochemical Analysis*, vol. 8 ("Phosphorus-31 NMR Spectroscopy in Stereochemical Analysis") (Eds.: J. G. Verkade, L. D. Quin), Wiley-VCH, Weinheim, **1987**, chapter 15, p. 531.
[9] P. S. Pregosin, R. W. Kunz, *^{31}P and ^{13}C NMR of Transition Metal Phosphane Complexes* (Eds.: P. Diehl, E. Fluck, R. Kosfeld), Springer-Verlag, Berlin, **1979**.
[10] W. J. Sime, T. A. Stephenson, *J. Organomet. Chem.* **1978**, *161*, 245.
[11] T. G. Appleton, H. C. Clark, L. E. Manzer, *Coord. Chem. Rev.* **1973**, *10*, 335.
[12] L. Hintermann, M. Perseghini, P. Barbaro, A. Togni, *Eur. J. Inorg. Chem.* **2003**, 601.
[13] **3**: $^{31}P\{^1H\}$ NMR (161.98 MHz, CD_3CN, 294 K): $\delta = -36.04$ (*t*, P1), 94.69 (dd, P2), 54.26 (dd, P3), $^2J_{P1P2} = 37.4$, $^2J_{P1P3} = 32.8$, $^2J_{P2P3} = 19.8$ Hz. **4**: $^{31}P\{^1H\}$ NMR (161.98 MHz, CD_3CN, 294 K, after heating at 75 °C for 2 h): $\delta = -40.06$ (*t*, P1), 93.82 (dd, P2), 47.72 (dd, P3), $^2J_{P1P2} = 33.3$, $^2J_{P1P3} = 32.0$, $^2J_{P2P3} = 19.1$ Hz.
[14] D. W. Meek, T. J. Mazanec, *Acc. Chem. Res.* **1981**, *14*, 266.
[15] J. G. Verkade, R. J. A. Mosbo, in *Methods in Stereochemical Analysis*, vol. 8 ("Phosphorus-31 NMR Spectroscopy in Stereochemical Analysis") (Eds.: J. G. Verkade, L. D. Quin), Wiley-VCH, Weinheim, **1987**, chapter 13, p. 432.
[16] [16a] A. Albinati, Q. Jiang, H. Rügger, L. M. Venanzi, *Inorg. Chem.* **1993**, *32*, 4940. [16b] K. Nakamoto, *Infrared and Raman Spectra of Inorganic and Coordination Compounds*, John Wiley & Sons, New York, **1986**. [16c] M. Sekine, W. D. Harman, H. Taube, *Inorg. Chem.* **1988**, *27*, 3604. [16d] C. Sorato, Dissertation, Nr. 8775, ETH, Zürich, **1989**.
[17] E. Breitmaier, W. Voelter, *Carbon-13 NMR Spectroscopy*, Wiley-VCH, Weinheim, **1989**.
[18] [18a] P. G. Andersson, A. Harden, D. Tanner, P. O. Norrby, *Helv. Chim. Acta* **1995**, *1*, 12. [18b] P. von Matt, G. C. Lloyd-Jones, A. B. E. Minidis, A. Pfaltz, L. Macko, M. Neuburger, M. Zehnder, H. Rüegger, P. S. Pregosin, *Helv. Chim. Acta* **1995**, *78*, 265. [18c] P. Barbaro, P. S. Pregosin, R. Salzmann, A. Albinati, R. W. Kunz, *Organometallics* **1995**, *14*, 5160.
[19] For recent examples of Ru-catalyzed asymmetric reduction of ketones see: [19a] Y. Nishibayashi, I. Takei, S. Uemura, M. Hidai, *Organometallics* **1998**, *17*, 3420. [19b] C. Moreau, C. G. Frost, B. Murrer, *Tetrahedron Lett.* **1999**, *40*, 5617. [19c] R. Noyori, T. Ohkuma, *Pure Appl. Chem.* **1999**, *71*, 1493. [19d] A. Marinetti, J. P. Genet, S. Jus, D. Blanc, V. Ratovelomanana-Vidal, *Chem. Eur. J.* **1999**, *5*, 1160. [19e] T. Ohkuma, D. Ishii, H. Takeno, R. Noyori, *J. Am. Chem. Soc.* **2000**, *122*, 6510. [19f] C. C. Pai, C. W. Lin, C. C. Lin, C. C. Chen, A. S. C. Chan, *J. Am. Chem. Soc.* **2000**, *122*, 11513. [19g] R. Noyori, M. Koizumi, D. Ishii, T. Ohkuma, *Pure Appl. Chem.* **2001**, *73*, 227. [19h] K. Abdur-Rashid, M. Faatz, A. J. Lough, R. H. Morris, *J. Am. Chem. Soc.* **2001**, *123*, 7473. [19i] J. W. Faller, A. R. Lavoie, *Organometallics* **2001**, *20*, 5245. [19j] L. Xiao, K. Mereiter, F. Spindler, W. Weissensteiner, *Tetrahedron: Asymmetry* **2001**, *12*, 1105. [19k] S. J. M. Nordin, P. Roth, T. Tarnai, D. A. Alonso, P. Brandt, P. G. Andersson, *Chem. Eur. J.* **2001**, *7*, 1431. [19l] I. M. Pastor, P. Västilä, H. Adolfsson, *Chem. Commun.* **2002**, 2046. [19m] C. J. A. Daley, S. H. Bergens, *J. Am. Chem. Soc.* **2002**, *124*, 3680.
[20] [20a] C. Bianchini, E. Farnetti, M. Graziani, M. Peruzzini, A. Polo, *Organometallics* **1993**, *12*, 3753. [20b] C. Bianchini, E. Farnetti, L. Glendenning, M. Graziani, G. Nardini, M. Peruzzini, E. Rocchini, F. Zanobini, *Organometallics* **1995**, *14*, 1489. [20c] J. X. Gao, T. Ikariya, R. Noyori, *Organometallics* **1996**, *15*, 1087. [20d] P. Braunstein, F. Naud, A. Pfaltz, S. J. Rettig, *Organometallics* **2000**, *19*, 2676.
[21] For examples of base-assisted hydrogenations of ketones see: [21a] T. Ohkuma, H. Ooka, S. Hashiguchi, T. Ikariya, R. Noyori, *J. Am. Chem. Soc.* **1995**, *117*, 2675. [21b] M. Kitamura, M. Tokunaga, T. Ohkuma, R. Noyori, *Org. Synth.* **1993**, *71*, 1. [21c] J. Takehara, S. Hashiguchi, A. Fujii, S. Inoue, T. Ikariya, R. Noyori, *Chem. Commun.* **1996**, 233. [21d] P. Gamez, S. Fache, M. Lemaire, *Tetrahedron: Asymmetry* **1995**, *6*, 705.
[22] [22a] S. Hashiguchi, A. Fujii, J. Takehara, T. Ikariya, R. Noyori, *J. Am. Chem. Soc.* **1995**, *117*, 7562. [22b] Y. Jiang, Q. Jiang, G. Zhu, X. Zhang, *Tetrahedron Lett.* **1997**, *38*, 215.
[23] T. A. Stephenson, G. Wilkinson, *J. Inorg. Nucl. Chem.* **1966**, *28*, 945.
[24] A. Bax, R. H. Griffey, B. L. Hawkins, *J. Magn. Reson.* **1983**, *55*, 301.
[25] [25a] V. Sklener, H. Miyashiro, G. Zon, H. T. Miles, A. Bax, *FEBS Lett.* **1986**, *208*, 94. [25b] J. Jeener, B. H. Meier, P. Bachmann, R. R. Ernst, *J. Chem. Phys.* **1979**, *71*, 4546.

Received May 2, 2003
Early View Article
Published Online October 22, 2003

 © 2003 Wiley-VCH Verlag GmbH & Co. KGaA, Weinheim

Synthesis, Structure and Magnetic Properties of the Cobalt(II) 1,1′-Biphenyl-2,2′-dicarboxylate Hydroxide Chain Compound $[Co_3\{O_2CC_{12}H_8CO_2\}_{2.5}(OH)(H_2O)_2]_n$

Jean-Michel Rueff,[a] Sébastien Pillet,[b] Gautier Bonaventure,[a] Mohamed Souhassou,[b] and Pierre Rabu*[a]

Keywords: Carboxylate ligands / Hydrothermal synthesis / Cobalt / Magnetic properties

A new 1D compound $[Co_3(O_2CC_{12}H_8CO_2)_{2.5}(OH)(H_2O)_2]$ (**2**) was synthesised with the hydrothermal method from $Co(NO_3)_2{\cdot}6H_2O$, 1,1′-biphenyl-2,2′-dicarboxylic acid, and KOH under hydrothermal conditions. Its structure was solved by single-crystal X-ray diffraction analysis. Compound **2** crystallises as purple crystals with the monoclinic cell (*C*2/*c*) a = 19.370(1), b = 14.5350(9), c = 22.583(1) Å, β = 89.910(4)°. The structure consists of chains of butterfly motifs of Co^{II} ions in both octahedral and tetrahedral oxygen sites. The structural, IR and UV spectroscopic data and magnetic behaviour are presented and compared to that of the parent pink compound **1**, obtained under slightly different stoichiometric conditions. Ligand-field characteristics, $Dq \approx 1146$ cm^{-1} and $B \approx 811$ cm^{-1} for the octahedral sites, and $Dq \approx 434$ cm^{-1} and $B \approx 782$ cm^{-1} for Co^{II} in the tetrahedral sites, were deduced from the electronic spectra and related to the structural and magnetic findings. From the magnetic point of view, the occurrence of efficient Co–O–Co superexchange pathways contributes to significant antiferromagnetic coupling between the cobalt(II) ions along the chains.
(© Wiley-VCH Verlag GmbH & Co. KGaA, 69451 Weinheim, Germany, 2003)

Introduction

The design and construction of new polymeric compounds of tuneable dimensionality, through adapted synthetic routes, is of strong interest in materials chemistry.[1] In particular, the solvothermal or hydrothermal route is currently being developed in solid-state and coordination chemistry,[2,3] for the design of new architectures, such as layered compounds,[4,5] helical chain polymers,[6−9] organic-inorganic compounds,[10−12] or mesoporous materials.[13−15] In this method, the organic ligand acts as a template, the structure of the product being closely related to the geometry and the number of coordination sites provided by the ligand. It has also been shown that solvothermal conditions are quite versatile, slight variations in temperature, reaction time, concentration or molar ratio between reactants may lead to very different products.[13] Nowadays these techniques are applied in the design of new low-dimensional (1D, 2D) magnetic compounds, whose study is particularly useful for a better understanding of the mechanisms responsible for magnetic coupling in solids.[16−19] Indeed, correlations between the magnetic properties of molecule-based solids and their structure, or the nature of the chemical bond between magnetic centres is largely used for the design of new magnetic materials, including high T_C magnets.[20−23] For the synthesis of new coordination compounds with extended structures, the use of dicarboxylate ligands provides many examples where magnetic transition-metal ions are arranged within various kinds of networks. The structural variety of these compounds arises from the carboxylate ligand, which is able to adopt different coordination modes, exhibiting either unidentate or chelating or bridging bidentate modes.

In a previous study[24] we reported on the structural and magnetic properties of two isostructural 1D polymers, obtained from the reaction of 1,1′-biphenyl-2,2′-dicarboxylic acid (diphenic acid) with KOH and $Co(NO_3)_2{\cdot}6H_2O$ and $Ni(NO_3)_2{\cdot}6H_2O$ under hydrothermal conditions. Their structure consists in the stacking of helical chains of M^{II} ions in octahedral coordination. In the case of the Co^{II} analogue, $[Co_2(O_2CC_{12}H_8CO_2)_2(H_2O)_8]$ (**1**), another phase was observed, depending on the synthesis conditions, and appearing as purple needle-shaped crystals. After slightly varying the synthesis conditions, we were able to isolate this purple phase and this paper describes its crystal structure and magnetic properties. A comparison is also made with the previous pink compound **1**.

[a] Institut de Physique et Chimie des Matériaux de Strasbourg, UMR 75040 du CNRS,
23 rue du Loess, 67034 Strasbourg, France
Fax: (internat.) + 33-3/88107247
E-mail: Pierre.rabu@ipcms.u-strasbg.fr
[b] Laboratoire de crystallographie et modélisation des matériaux minéraux et biologiques, Faculté des Sciences, UHP,
B. P. 239, 54506 Vandoeuvre-les-Nancy Cedex

Results and Discussion

Structural Results

$C_{35}H_{25}Co_3O_{13}$ crystallises in the monoclinic *C*2/*c* space group with $a = 19.370(1)$, $b = 14.5350(9)$, $c = 22.583(1)$ Å, $\beta = 89.910(4)°$. Selected bond lengths and angles are summarised in Table 1. The asymmetric unit (see Figure 1) consists of four non-equivalent cobalt atoms of octahedral and tetrahedral coordination, 2.5 biphenyl dicarboxylate ligands, one hydroxy ion and two water molecules. Moreover, two of the cobalt atoms are located on symmetry elements: Co2 on a centre of symmetry and Co4 on a twofold axis. Three Co atoms (Co1, Co2 and Co3) are located in octahedral environments CoO_6, whereas Co4 lies in a quasi-perfect tetrahedral oxygen surrounding (see Figure 2). The hydroxy ion, the water molecules and the two carboxylate groups of each biphenyl dicarboxylate ligand are involved in the Co coordination.

Table 1. Selected bond lengths (Å) and angles (°) for compound **2**

Co1−O1	2.178(4)	Co3−O2	2.047(3)
Co1−O2	2.046(3)	Co3−O12	2.074(4)
Co1−O3	2.329(4)	Co3−O11	2.078(4)
Co1−O4	2.067(3)	Co3−O7	2.111(4)
Co1−O5	2.142(3)	Co3−O8	2.143(5)
Co1−O6	2.037(3)	Co3−O9	2.134(4)
Co2−O2	2.068(3)	Co4−O5	1.959(3)
Co2−O1	2.222(3)	Co4−O10	1.922(4)
Co2−O7	2.124(3)		
C1−O6	1.258(6)	C8−O12	1.250(6)
C1−O11	1.250(6)	C20−O3	1.244(6)
C2−O13	1.235(6)	C20−O5	1.304(6)
C2−O7	1.296(6)	C27−O4	1.263(6)
C8−O1	1.286(6)	C27−O10	1.266(6)
Co1···Co2	3.2883(7)	Co1···Co4	3.2028(8)
Co1···Co3	3.4370(9)	Co2···Co3	3.1416(7)
O9(H20)···O11	2.704(5)	O9(H24)···O13	2.686(6)
O8(H17)···O12	3.065(6)	O8(H25)···O9	3.240(6)
Co1−O1−Co2	96.70(14)	Co3−O2−Co2	99.50(13)
Co1−O2−Co3	114.24(15)	Co4−O5−Co1	102.62(16)
Co1−O2−Co2	106.11(16)	Co2−O7−Co3	95.75(13)
O9−H20−O11	114(4)	O9−H24−O13	174(5)
O8−H17−O12	118(3)	O8−H25−O9	127(4)

The C−O bond lengths in the five carboxylate fragments of the asymmetric unit range from 1.235(6) Å to 1.304(6) Å. This dispersion reflects the weakening of the C−O bonds due to the Co···O interactions. The only oxygen atom, O13, which is not coordinated to a cobalt atom presents the shortest C−O bond [1.235(6) Å], whereas the longest bond lengths, 1.286(6) Å, 1.304(6) Å and 1.296(6) Å, correspond to O1, O5 and O7, respectively, which are all involved in the coordination polyhedron of two Co atoms. The mean C−O bond length for oxygen atoms coordinated to only one cobalt atom is 1.258(10) Å.

Two oxygen octahedra (around Co1 in position *8f* and Co2 in *4a*) and the tetrahedron (around Co4 in *4e*) are connected through chains along the crystallographic *c* axis (see Figure 2) as a repetition of the symmetry block ··Co4···Co1···Co2···Co1···Co4···. The last octahedron around Co3 in the *8f* position is located on the side of the chain. The Co−Co distances range from 3.1416(7) Å to 3.4370(9) Å for Co2−Co3 and Co1−Co3, respectively. Contrary to the tetrahedron, the octahedral sites are far from being regular. As shown by the dispersion in bond lengths given in Table 2, the Co−O bond lengths range

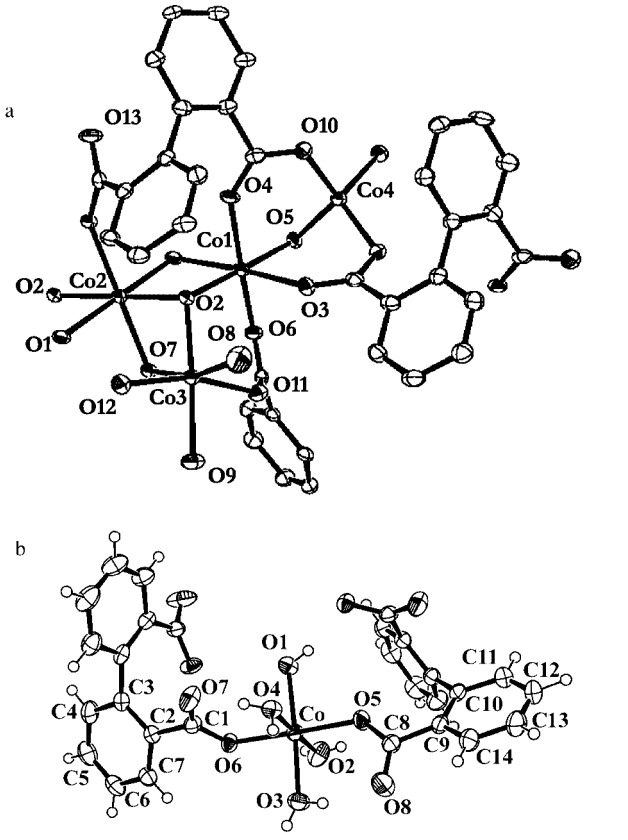

Figure 1. ORTEP drawing of the asymmetric unit of a) compound **2** $Co_3C_{35}O_{13}H_{25}$ and b) for compound **1**, with the atom labelling (some equivalent O atoms have been generated to complete the Co coordination, H atoms omitted; the ellipsoids are plotted at 50% level)

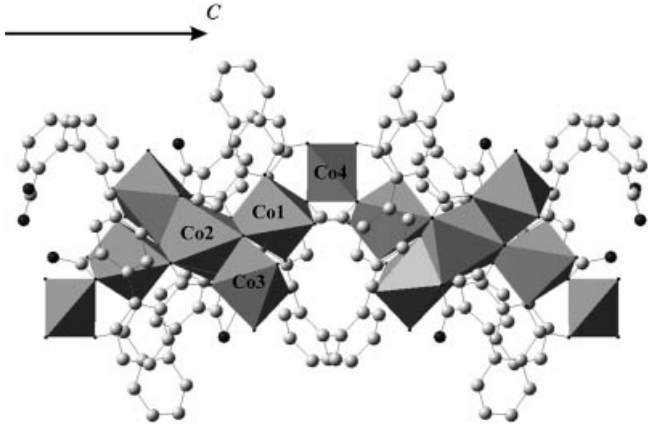

Figure 2. Octahedra and tetrahedron connectivity along one chain in compound **2**

 © 2003 Wiley-VCH Verlag GmbH & Co. KGaA, Weinheim

from 2.037(3) Å to 2.329(4) Å for the octahedra, while the metal-oxygen distances for the tetrahedron are 1.922(4) Å and 1.959(3) Å. The particular geometry exhibited by the chain thus implies four specific exchange pathways, with different characteristics (see Table 2). Co1 and Co2 are connected through one oxygen atom from a hydroxy group (O2) and one oxygen from a carboxylate group. The Co2−Co3 pathway involves an identical geometric configuration. The Co1 and Co3 atoms are connected by a hydroxy ion (O2) and through an O−C−O bridge of a carboxylate group. Finally, one oxygen atom from a carboxylate group (O5) and two O−C−O pathways are involved in the Co1−Co4 connection. Based only on these geometric considerations, one can expect a rather complex situation for the Co-Co magnetic interactions along the chain.

As shown in Figure 3, no contact, and especially no hydrogen bonds, are observed between the chains, the phenyl rings of the biphenyl dicarboxylate ligands being located away from the chain axis. The two water molecules are nevertheless involved in four intra-chain hydrogen bonds whose geometrical characteristics are given in Table 1.

Interestingly, the formerly characterised compound **1**, whose structure is shown in Figure 1b, exhibits a helical arrangement of the dicarboxylate ligands. The Co^{II} atoms are interconnected through carboxylate bridges and surrounded by four water molecules. The Co-Co distance along the chains is 4.9981(3) Å.[24] By comparison, the present structure thus corresponds to the condensation of the Co^{II} chains resulting in shorter contacts between magnetic centres and in the occurrence of more efficient metal-oxygen-metal exchange pathways. Another difference is the occurrence of tetrahedral coordination for Co4.

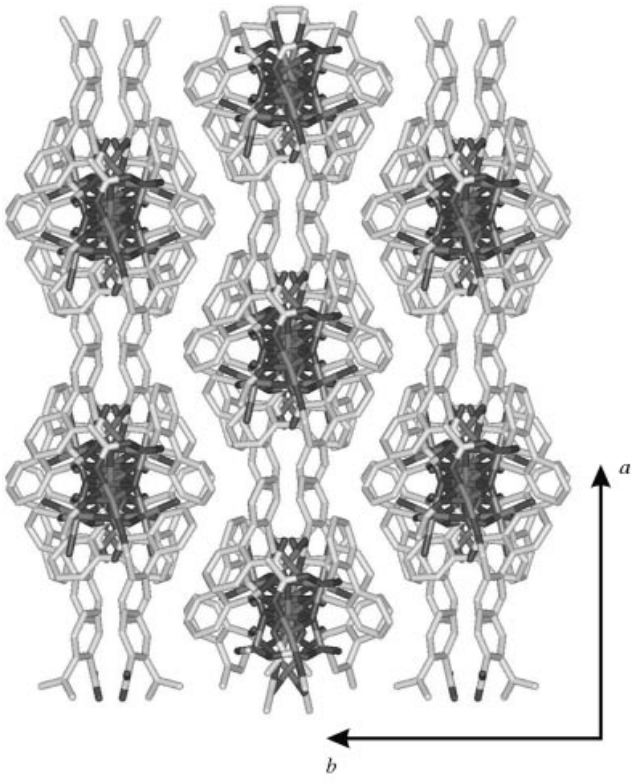

Figure 3. Crystal structure viewed along the chains in the crystallographic *c* direction for compound **2**

Spectroscopic Properties

The IR spectrum of compound **2** shows the characteristic bands of the 1,1′-biphenyl-2,2′-dicarboxylate. The fre-

Table 2. Geometric details of the different Co···Co exchange pathways in compound **2**

Co···Co connection	Co1···Co2 [3.2883(7) Å]	Co1···Co3 [3.4370(9) Å]	Co1···Co4 [3.2028(8) Å]	Co2···Co3 [3.1416(7) Å]
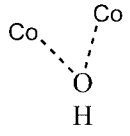	X	X		X
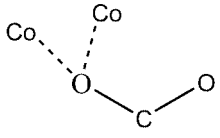	X		X	X
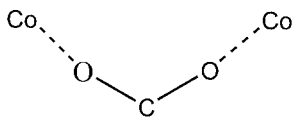		X	X X	

 © 2003 Wiley-VCH Verlag GmbH & Co. KGaA, Weinheim

quency difference between the symmetrical and antisymmetrical carboxylate vibrations, $\Delta\nu = 135\ cm^{-1}$, is in agreement with the bridging bidentate coordination mode of the carboxylate groups found in the structure.[25−27] The experimental spectra do not allow to distinguish a doublet corresponding to the minority unidentate mode of one of the carboxylate functions. The presence of broad ν_{O-H} bands at 3429 cm^{-1} is related to the hydrogen-bonded aqua ligands. UV/Vis spectra (reflectance) shown in Figure 4 are consistent with the presence of both octahedral coordination {λ = 1090 nm ($^4T_{1g} \rightarrow {}^4T_{2g}$), 525 nm, [$^4T_{1g} \rightarrow {}^4T_{1g}(P)$]}, and tetrahedral coordination of Co^{II} {λ = 1280 nm [$^4A_2 \rightarrow {}^4T_1(P)$], 590 nm [$^4A_2 \rightarrow {}^4T_1(F)$]}.[28,29] The comparison with the spectrum of compound **1** (see Figure 4) indicates a different octahedral geometry for the Co^{II} ions in compound **2**, where the octahedra are found to be significantly distorted. The corresponding values of Dq (≈ 1146 cm^{-1} for **2**) and Racah's parameter B (≈811 cm^{-1}), deduced from the transitions assigned to the octahedral sites, agree with a low octahedral crystal field ($Dq/B = 1.4$) and high-spin configuration for the metal centres, also inferred from the magnetic findings (see below). The other set of transitions gives $Dq \approx 434\ cm^{-1}$ and $B \approx 782\ cm^{-1}$ in agreement with the presence of Co^{II} in a tetrahedral site.[28,29]

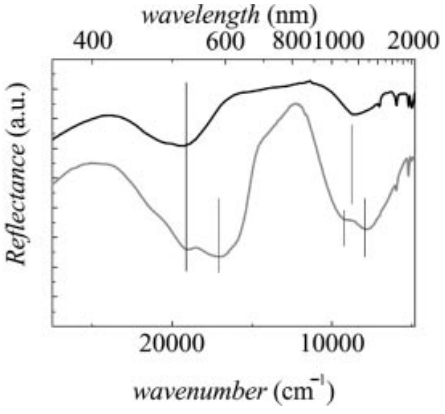

Figure 4. Reflectance UV spectra of compounds **1** (above) and **2** (below); vertical lines are guides for the eyes

Magnetic Properties

The magnetic properties of compound **2** were investigated as described in the Exp. Sect. The temperature variation of the magnetic susceptibilities, χ, is shown in Figure 5. Upon cooling down, $\chi = f(T)$ increases continuously up to a maximum of 1.9 emu·mol^{-1} at 2 K. The χT product exhibits a regular decrease from 8.35 emu·K·mol^{-1} at 300 K without tending to zero but to 2.46 emu·K·mol^{-1} at 2 K. The inverse susceptibility (not shown) varies linearly with the temperature in the high temperature regime ($T >$ 180 K) and is well fitted in this region by using the Curie−Weiss law, giving $C = 8.96$ emu·K·mol^{-1} and θ = −18.6 K. The Curie constant deduced for three metal ions per formula unit agrees with that expected for 5/6 octahedral high spin and 1/6 tetrahedral Co^{II} ions[30,31] with

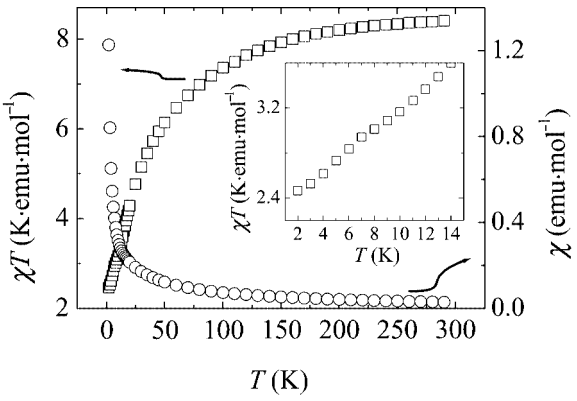

Figure 5. Temperature variation of the magnetic susceptibility (scaled to 1 formula unit) for compound **2**

$C_{octa} = 3.21$ emu·K per Co^{II} mol and $C_{tetra} = 1.875$ emu·K per Co^{II} mol.

The decrease of the χT product together with the negative value of θ might be related to the effect of the spin-orbit coupling for isolated Co^{II} ions in the octahedral crystal field. This results in the splitting of the energy levels arising from the $^4T_{1g}$ ground term, stabilizing the $J = \pm 1/2$ doublet well separated from the excited states.[30] However, the χT value of 2.46 emu·K·mol^{-1} at 2 K is much smaller than the minimum value expected for isolated high-spin octahedral and tetrahedral cobalt(II) centres [ca. 3 × (5/6 × 1.8 + 1/6 × 1.875) = 5.44 K.emu·mol^{-1}],[30] which suggests the occurrence of an antiferromagnetic coupling between the Co^{II} ions. It is also inferred by the magnetisation vs. field curve at 2 K (see Figure 6) that exhibits a very small "saturation" moment, $Ms = 3.3\ \mu_B.mol^{-1}$ for three Co^{II} ions (expected: 2−3 μ_B per cobalt)[30,31] with a slight increase toward the high fields. However, no long-range magnetic order occurs down to 2 K.

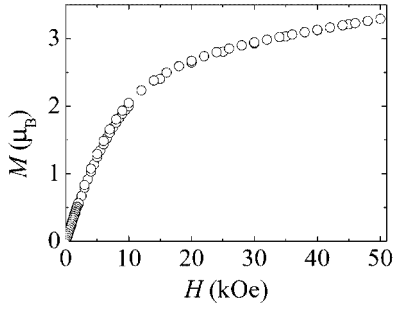

Figure 6. Magnetisation versus field variation at 2 K for compound **2** (scaled to 1 formula unit)

Magnetostructural Relationship

As summarised in Scheme 1, compound **2** can be viewed as chains formed by butterfly motifs of five octahedral Co^{II} centres interconnected through tetrahedral Co4. We identified four different exchange pathways, connecting the cobalt atoms along the chains (see Table 2), corresponding to

 © 2003 Wiley-VCH Verlag GmbH & Co. KGaA, Weinheim

four magnetic coupling constants: J_1, J_2, J_3 and J_4, each of which corresponds to double or triple bridges between the magnetic centres (see above). Exchange between the Co^{II} ions through the carboxylate bridge is expected to be small and antiferromagnetic.[32,33] All exchange pathways involve at least one Co−O−Co bridge that can lead either to antiferromagnetic or ferromagnetic coupling, as found in hydroxide[14,34−37] or carboxylate[38,39] compounds. The situation is thus rather complex and no analytical expression is available for computing the magnetic behaviour of Co^{II} chains by taking the spin-orbit coupling for the magnetic centres in an octahedral site into account. Also the numerical approach is limited here because of the size of the elemental unit involving six Co^{II} atoms, except for the low temperature region ($T < 30$ K), where the effect of octahedral crystal field and spin-orbit coupling results in a doublet ground-state (effective $S = 1/2$ spin). However, the system appears largely over-parameterized and attempts to fit the susceptibility data in a limited low temperature range, where no anomaly occurs, would be meaningless. What is expected is that J_2 and J_3, which correspond to an exchange through corners of neighbouring coordination polyhedra, are less efficient than J_1 and J_4, which occur through the octahedron's edges. In addition, the Co1−Co2 distance is large (3.437 Å, see Table 2) and J_2 should be negligible compared to J_1 and J_4. In this scheme, and assuming that all the interactions along the chains are antiferromagnetic (the effect of J_2 is neglected), it is worth noticing that an antiferromagnetic arrangement between neighbouring Co^{II} ions would stabilize two resulting moments within the six-centre unit, that is, the moment of one Co^{II} ion per formula unit at low temperature This fits well with the value of ca 3 μ_B observed in the magnetisation versus field curve at 2 K.

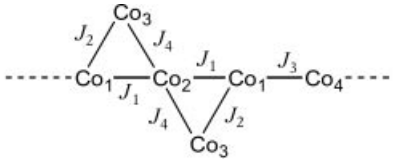

Scheme 1

Finally, compared to compound **1**, which was found to be quasi paramagnetic, the present compound, **2**, corresponds to a condensation of the structure along the chains with occurrence of efficient Co−O−Co exchange pathways. This leads to a significant antiferromagnetic interaction between neighbouring Co^{II} ions in the present compound.

Conclusion

A new one-dimensional cobalt(II) 1,1′-biphenyl-2,2′-dicarboxylate was synthesised by the hydrothermal method. The structure was solved on single crystals and consists of decorated chains of Co^{II} ions in octahedral and tetrahedral sites. Compound **2** was obtained by slightly varying the reaction conditions with respect to the previous derivative **1**, thus showing the versatility of the simple 1,1′-biphenyl-2,2′-dicarboxylate bridging ligand towards synthesis conditions. The two compounds can be considered as the result of two competing driving forces, namely templating by the ligand that stabilizes the helical chains in **1**, on the one hand, and templating through the metal coordination that leads to a more compact interconnection of the metal ions in **2**, on the other hand. The IR and UV/Vis data of the two compounds were compared and ligand field characteristics were deduced from the electronic spectra and related to the structural findings. From the magnetic point of view, the diphenic ligand is not good for magnetic exchange-coupling, as shown in compound **1**. However the occurrence of efficient Co−O−Co super-exchange pathways in compound **2** contributes to significant antiferromagnetic coupling between the cobalt(II) ions along the chains.

Experimental Section

General Remarks: The temperature variation of the magnetic moment between 2 K and 300 K was measured by using an MPMS*XL*-Quantum Design SQUID magnetometer at 200 Oe, in the field range corresponding to linear variation of magnetisation versus field. These data were corrected for sample diamagnetism by using Pascal's constants and for diamagnetism of the sample holder consisting of a gel cap. Magnetisation versus field data were recorded in the whole range between −5 and +5 T. UV/Vis-NIR studies were performed with a Perkin−Elmer Lambda 19 instrument (spectra recorded by reflection). FT-IR studies were performed with an ATI Mattson Genesis computer-driven instrument (0.1 mm thick powder samples in KBr). Thermogravimetric (TG) experiments were performed using a Setaram TG92 instrument (heating rate of 3 °C/min, air stream).

$Co_3(O_2CC_{12}H_8CO_2)_{2.5}(OH)(H_2O)_2$ (2): $C_3H_{255}Co_3O_{13}$ was synthesised by the hydrothermal method from $Co(NO_3)_2{\cdot}6H_2O$ (98% Aldrich), diphenic acid (1,1′-biphenyl-2,2′-dicarboxylic acid, 98% Across), and KOH (85%, SDS). The starting mixture corresponding to the molar composition 1:1.5:3.5:195 of $Co(NO_3)_2{\cdot}6H_2O$, $C_{14}H_{10}O_4$, KOH and H_2O was homogenized and transferred into a sealed 23 cm^3 hydrothermal bomb, walled with a Teflon liner, and heated at 170 °C for 74 h under autogenous pressure. The purple needle-shaped crystals obtained were washed with deionized water and rinsed with absolute ethanol [yield > 50% on the basis of $Co(NO_3)_2{\cdot}6H_2O$]. As mentioned above, some platelet-shaped crystals of the pink compound $C_{28}H_{32}Co_2O_{16}$ were also observed and pure compound **2** was isolated by manual separation of the largest crystals. The purity and the chemical formula were confirmed by elemental analysis and are consistent with the structural and magnetic findings: $C_{35}H_{25}Co_3O_{13}$ (830.4): calcd. C 50.63, H 3.03; found C 50.24, H 3.44. Oxidative pyrolysis (TG Analysis, heating in air from 20 to 700 °C at 3 °C/min, maintaining at 700 °C for 30 min to transform cobalt into Co_3O_4, and cooling to 20 °C at 10 °C/min: calcd. Co 21.3; found 21.6). IR (KBr pellet): $\tilde{\nu}$ = 3580 cm^{-1} (ν OH), 3429 (ν OH−O), 3056 (ν C−H), 1612 (δ H_2O), 1579 (ν C−C), 1540 (ν_{as} C=O), 1475 (ν C−C), 1442 (ν C−C), 1405 (ν_s C−O), 1267 (in plane δ_b C−H), 1151 (in plane δ_b C−H), 1108 (in plane δ_b C−H), 1049 (in plane δ_b C−H). UV/Vis (reflectance): see text.

X-ray Crystallographic Study: X-ray data collection was performed on a Nonius Kappa CCD at low temperature (T = 104 K) using a

 © 2003 Wiley-VCH Verlag GmbH & Co. KGaA, Weinheim

needle-shaped single crystal. 124314 Reflections were measured up to a resolution of 0.70 $Å^{-1}$ and merged into 9210 unique reflections (R_{int} = 0.097). Crystal faces were indexed and a gaussian integration absorption correction[40] was applied (μ = 1.62mm^{-1}, T_{min} = 0.387, T_{max} = 0.798). The structure was solved by direct methods using SHELX,[41] the H atoms being localised in difference Fourier maps. The structure was refined by full-matrix least-squares on F^2 with anisotropic temperature factors for non H atoms and isotropic ones for H atoms and gave $R[F^2 > 2\sigma(F^2)]$ = 0.062, S = 0.85] final agreement factors. *Crystal data:* $C_{35}H_{25}Co_3O_{13}$, 830.32, monoclinic, *C*2/*c*, a = 19.370(1) Å, b = 14.5350(9) Å, c = 22.583(1) Å, β = 89.910(4)°, V = 6358.1(6) $Å^3$, Z = 8, D_x (g cm^{-3}) 1.727, Mo-K_α, 124314 reflections for cell parameters, μ (mm^{-1}) 1.618, temperature (K) 104(2), crystal form, needle, colour, purple, crystal size (mm) 0.14 × 0.14 × 0.52. *Data collection*: Diffractometer Nonius Kappa CCD; data collection method, ω scans; absorption correction, gaussian integration (DeTitta, 1985), T_{min} = 0.387, T_{max},= 0.798. No. of measured, independent and observed reflections, 124314, 9210, 4544; criterion for observed reflections, $I > 2\sigma(I)$; R_{int} = 0.097; θ_{max} (°) 30.03; range of *h, k, l,* $-27 \geq h \geq 27$, $0 \geq k \geq 20$, $0 \geq l \geq 31$; refinement on F^2, $R[F^2 > 2\sigma(F^2)]$ = 0.0623, $wR(F^2)$ = 0.1332, S = 0.852; no. of reflections and parameters used in refinement, 9210, 552; weighting scheme, $w = 1/[\sigma^2(F_o^2)]$, $(\Delta/\sigma)_{max}$ = 0.004, $\Delta\rho_{max}$ = 1.0984, $\Delta\rho_{min}$ = −1.074. CCDC-209800 contains the supplementary crystallographic data for this paper. These data can be obtained free of charge at www.ccdc.cam.ac.uk/conts/retrieving.html [or from the Cambridge Crystallographic Data Centre, 12, Union Road, Cambridge CB2 1EZ, UK; Fax: (internat.) + 44-1223/336-033; E-mail: deposit@ccdc.cam.ac.uk].

Acknowledgments

We thank Dr. M. Drillon, Institut de Physique et Chimie des Matériaux de Strasbourg, France, and Prof. C. Lecomte, Laboratoire de crystallographie et modélisation des matériaux minéraux et biologiques, Nancy, France, for helpful discussions.

[1] O. Yaghi, H. Li, C. Davis, D. Richardson, T. L. Groy, *Acc. Chem. Res.* **1998**, *31*, 474−484.
[2] P. J. Hagrman, J. Zubieta, *Inorg. Chem.* **2000**, *39*, 5218.
[3] R. P. Hammond, D. J. Chesnut, J. Zubieta, *J. Solid State Chem.* **2001**, *158*, 55.
[4] Z.-L. Huang, M. Drillon, N. Masciocchi, A. Sironi, J.-T. Zhao, P. Rabu, P. Panissod, *Chem. Mater.* **2000**, *12*, 2805.
[5] P. Rabu, P. Janvier, B. Bujoli, *J. Mater. Chem.* **1999**, *9*, 1323.
[6] S. O. H. Gutschke, D. J. Price, A. K. Powell, P. T. Wood, *Angew. Chem. Int. Ed.* **2001**, *40*, 1920.
[7] D. J. Price, S. Tripp, A. K. Powell, P. T. Wood, *Chem. Eur. J.* **2001**, *7*, 200.
[8] L.-M. Zheng, T. Whitfield, X. Wang, A. J. Jacobson, *Angew. Chem. Int. Ed.* **2000**, *39*, 4528.
[9] Z. Shi, S. Feng, S. Gao, L. Zhang, G. Yang, J. Hua, *Angew. Chem. Int. Ed.* **2000**, *39*, 2325.
[10] Y. Zhou, L. Zhang, H.-K. Fun, X. You, *Inorg. Chem. Commun.* **2000**, *3*, 114.
[11] J. Tao, X.-M. Zhang, M.-L. Tong, X.-M. Chen, *J. Chem. Soc., Dalton Trans.* **2001**, 770.
[12] P. J. Zapf, R. C. Haushalter, J. Zubieta, *Chem. Mater.* **1997**, *9*, 2019.
[13] C. Livage, C. Egger, G. Férey, *Chem. Mater.* **2001**, *13*, 410, and references cited therein.
[14] A. Rujiwatra, C. J. Kepert, M. J. Rosseinsky, *Chem. Commun.* **1999**, 2307.
[15] S. Fernández, J. L. Mesa, J. L. Pizaro, L. Lezama, M. I. Arriortua, R. Olazcuaga, T. Rojo, *Chem. Mater.* **2000**, *12*, 2092.
[16] *Research Frontiers in Magnetochemistry* (Ed.: C. O'Connor), World Scientific Publishers, **1993**.
[17] *Magnetic Properties of Layered Transition Metal Compounds* (Ed.: L. J. de Jongh), Physics and Chemistry of Materials with Low-dimensional Structures 9A, Kluwer Academic Publishers: Dordrecht, **1990**.
[18] *Magnetic Molecular Materials* (Eds.: D. Gatteschi, O. Kahn, J. S. Miller, F. Palacio), Kluwer, Dordrecht, **1991**.
[19] O. Kahn, *Molecular Magnetism*, VCH, Weinheim, **1993**.
[20] D. Babel, *Comments Inorg. Chem.* **1986**, *5*, 285.
[21] M. Verdaguer, *Science* **1996**, *272*, 698.
[22] O. Sato, T. Iyoda, A. Fujishima, K. Hashimoto, *Science* **1996**, *272*, 704.
[23] O. Hatlevik, W. E. Buschmann, J. Zhang, J. L. Manson, J. S. Miller, *Adv. Mater.* **1999**, *11*, 914.
[24] J.-M. Rueff, S. Pillet, N. Claiser, G. Bonaventure, M. Souhassou, P. Rabu, *Eur. J. Inorg. Chem.* **2002**, 895−900.
[25] K. Nakamoto, *Infrared and Raman Spectra of Organic and Coordination Compounds*, 4th Ed., Wiley Interscience Publication, New York **1986**, 231.
[26] C. Dendrinou-Samara, G. Tsotsou, L. V. Ekateriniadou, A. H. Kortsaris, C. P. Raptopoulou, A. Terzis, D. A. Kyriakidis, D. P. Kessissoglou, *J. Inorg. Biochem.* **1998**, *71*, 171−179.
[27] J.-J. Max, C. Chapados, J. Phys. Chem. A **2002**, *106*, 6452−6461.
[28] A. B. P. Lever, *Inorganic Electronic Spectroscopy*, 2nd Ed., Elsevier, Amsterdam **1984**.
[29] S.-I. Aizawa, S. Funahashi, *Inorg. Chem.* **2002**, *41*, 4555−4559.
[30] F. E. Mabbs and D. J. Machin, *Magnetism and Transition Metal Complexes*, Chapman and Hall Ltd., London **1973**.
[31] R. L. Carlin, *Magnetochemistry*, Springer-Verlag, Berlin-Heidelberg **1986**.
[32] J.-M. Rueff, N. Masciocchi, P. Rabu, A. Sironi, A. Skoulios, *Chem. Eur. J.* **2002**, *8*, 1813−1820.
[33] E. Coronado, M. Drillon, D. Beltran, J.-C. Bernier, *Inorg. Chem.* **1984**, *23*, 4000−4004.
[34] R.-K. Chiang, N.-T. Chuang, C.-S. Wur, M.-F Chong, C.-R. Lin, *J. Solid State Chem.* **2002**, *166*, 158−163.
[35] M. Drillon, P. Rabu, P. Legoll, *Trends Inorg. Chem.* **1993**, *3*, 581−592.
[36] P. Rabu, S. Angelov, P. Legoll, M. Belaiche, M. Drillon, *Inorg. Chem.* **1993**, *32*, 2463.
[37] P. Chaudhuri, J. Querbach, K. Wieghardt, B. Nuber, J. Weiss, *J. Chem. Soc., Dalton Trans.* **1990**, *1*, 271−8.
[38] S. Konar, P. S. Mukherjee, M. G. B. Drew, J. Ribas, N. R. Chaudhuri, *Inorg. Chem.* **2003**, *42*, 2545−2552.
[39] N. Snejko, E. Gutiérrez-Puebla, J. L. Martínez, M. A. Monge, C. Ruiz-Valero, *Chem. Mater.* **2002**, *14*, 1879−1883.
[40] G. T. DeTitta, *J. Appl. Crystallogr.* **1985**, *18*, 75−79.
[41] Sheldrick, G. M. **1993**. SHELXS-96 and SHELXL-96. University of Gottingen, Germany.

Received May 6, 2003
Early View Article
Published Online October 10, 2003

 © 2003 Wiley-VCH Verlag GmbH & Co. KGaA, Weinheim

X-ray Crystal Structure of a Sodium Salt of $[Gd(DOTP)]^{5-}$: Implications for Its Second-Sphere Relaxivity and the ^{23}Na NMR Hyperfine Shift Effects of $[Tm(DOTP)]^{5-}$

Fernando Avecilla,*[a] Joop A. Peters,[b] and Carlos F. G. C. Geraldes*[c]

Keywords: Gadolinium / Imaging agents / Solid-state structures / Hydration / NMR shift reagents

The X-ray structure of the sodium salt of $[Gd(DOTP)]^{5-}$ shows two different chelates, $[Gd^{(1)}(DOTP)]^{5-}$ and $[Gd^{(2)}(DOTP)]^{5-}$, bound at either surface of a sheet formed by a cluster of hydrated Na^+ ions. Each $[Gd^{(1)}(DOTP)]^{5-}$ anion binds directly to four Na^+ ions of this cluster through the free oxygen atoms of the phosphonate groups of the adjacent ligand, while each $[Gd^{(2)}(DOTP)]^{5-}$ unit is connected to the cluster via hydrogen bonds only. The Gd^{3+} ions in the two moieties do not have any inner-sphere water molecules, and are eight-coordinate. Their coordination polyhedra are twisted square antiprisms, with slightly different twist angles. These **m**′ isomers are found in the crystal structure as racemic mixtures of enantiomers. Only one set of NMR resonances is observed in aqueous solution, corresponding to an averaged **m**′ isomer. In this crystal structure, the Na^+ ions bind the phosphonate oxygen atoms of the $[Gd^{(1)}(DOTP)]^{5-}$ anion at positions far removed from the main symmetry axis. This is significantly different from the binding mode(s) previously proposed to be occurring in solution between Na^+ and $[Tm(DOTP)]^{5-}$, based on the interpretation of solution paramagnetic ^{23}Na NMR shifts. This could arise as a result of the effects of the cluster of hydrated Na^+ ions that are present, which may hinder axial binding modes and distort lateral binding modes. Further, in the crystal structure, both types of Gd^{3+} centers have four second-sphere water molecules that are located at distances (4.2–4.5 Å) significantly longer than those previously proposed from the analysis of the NMRD data of $[Gd^{(1)}(DOTP)]^{5-}$. This is a result of the coordination of Na^+ by these water molecules, thus preventing their direct interaction with the phosphonate oxygen atoms. However, in solution such second-sphere water molecules can interact strongly with the phosphonate ligand oxygen atoms, resulting in efficient relaxation if their binding has relatively long lifetimes (> 50 ps). Rotational immobilization will amplify this contribution, thus making it similar to outer-sphere relaxation.
(© Wiley-VCH Verlag GmbH & Co. KGaA, 69451 Weinheim, Germany, 2003)

Introduction

Stable lanthanide chelates of polyazamacrocyclic ligands have been widely used as paramagnetic shift reagents for the in vivo NMR spectroscopy of cations,[1] and as contrast agents for magnetic resonance imaging (MRI).[2–5] The Tm^{3+} complex of 1,4,7,10-tetraazacyclododecane-1,4,7,10-tetrakis(methylenephosphonic acid) (H_8DOTP) has proved to be a particularly favorable NMR shift reagent for the $^{23}Na^+$ NMR spectroscopic study of isolated cells,[6] perfused tissues,[7–11] and intact animals.[12–15] It is also useful as an extracellular in vivo marker of tissues.[16,17] The relaxation properties of the Gd^{3+} complex, $[Gd(DOTP)]^{5-}$, a potential MRI contrast agent, have also been studied.[18–20] Although the solution structures of the Ln^{3+} complexes of this ligand[21–24] have been thoroughly investigated using multinuclear NMR spectroscopic techniques by exploiting the structural information content of the paramagnetic effects of these ions,[25,26] only a preliminary X-ray crystal structure of the $[(NH_4)_5Tm(DOTP)]$ complex has been reported.[27] Here we report on the single-crystal X-ray structural determination of $[Na_5Gd(DOTP)]$. The structural data are used to compare the configuration of the bound ligand with that found in solution.[22] The binding of the Na^+ ions and the positions of the water molecules found in this crystal structure are compared with what has been proposed in solution from ^{23}Na NMR spectroscopic[28,29] and relaxivity studies.[18–20]

[a] Departamento de Química Fundamental, Universidade da Coruña,
Campus de A Zapateira s/n, 15071 A Coruña, Spain
[b] Laboratory for Applied Organic Chemistry and Catalysis, Delft University of Technology,
Julianalaan 136, 2628 BL Delft, The Netherlands
[c] Departamento de Bioquímica, Faculdade de Ciências e Tecnologia, Universidade de Coimbra,
Apartado 3126, 3049 Coimbra, Portugal
Fax: (internat.) + 351-239/853607
E-mail:geraldes@ci.uc.pt
Supporting information for this article is available on the WWW under http://www.eurjic.org or from the author.

Results and Discussion

X-ray Crystal Structure of the Na^+ Salt of $[Gd(DOTP)]^{5-}$

The chemical formula of the compound in the crystal form, as obtained from the X-ray diffraction crystal structural analysis, is $[\{Na_{13}(OH)_3(H_2O)_{29}\}\{Gd^{(1)}(DOTP)\}][Gd^{(2)}(DOTP)]\cdot 7H_2O\cdot 2CH_3CH_2OH$. The overall structure of the crystal is shown in Figure 1, where the asymmetric unit contains two different $[Gd(DOTP)]^{5-}$ moieties, with the $Gd^{(1)}$ and $Gd^{(2)}$ atoms as centers. Within this unit, there are 0.25 $Gd^{(1)}(DOTP)$ moieties, 3.25 Na^+ ions, 0.75 hydroxide groups and 7.25 water molecules that form a hydrated Na^+ cluster. $Gd^{(2)}$ also contributes to the asymmetric unit with an isolated quarter of $Gd^{(2)}(DOTP)$, in which the oxygen atoms of its phosphonate groups are directed to the hydrated Na^+ cluster. 1.75 water and 0.5 ethanol molecules of crystallization complete the structure. This basic unit is repeated according to the crystal symmetry, with the formation of the complete structure.

The $[Gd^{(1)}(DOTP)]^{5-}$ anion, along with the associated Na^+ ions and water molecules is presented in more detail in Figure 2. Four Na^+ ions [Na(4)] are coordinated directly to $[Gd^{(1)}(DOTP)]^{5-}$, each Na^+ ion forms a bridge between the two Gd^{3+}-unbound oxygen atoms of the phosphonate groups of the adjacent ligand. One of these oxygen atoms points towards the azamacrocycle, while the other points towards a cluster of hydrated Na^+ ions that is located next to the methylenephosphonate pendant arms of the macrocycle, connected to the four phosphonate-bound Na^+ ions through four bridging water molecules. The sodium ions are either eight-coordinate [e.g. Na(2)], as in the center of the cluster, six-coordinate at the edges of the cluster [e.g. Na(1)], or four-coordinate when bound to the oxygen atoms of the ligand phosphonate groups [Na(4) in Figure 2]. There are no water molecules directly coordinated to the $[Gd^{(1)}(DOTP)]^{5-}$ moiety. The $[Gd^{(2)}(DOTP)]^{5-}$ anion can also be seen in detail in Figure 2. Although there are many water molecules in the vicinity of the Na^+ ions, no water molecule is directly coordinated by the $[Gd^{(2)}(DOTP)]^{5-}$ chelates. The isolated $[Gd^{(2)}(DOTP)]^{5-}$ unit is connected via hydrogen-bond interactions to the hydrated $[\{Na_{13}(OH)_3(H_2O)_{29}\}\{Gd^{(1)}(DOTP)\}]$ cluster. Table 1 lists some selected interatomic distances. The close proximity of O(1W) to the O(4) and O(5) atoms may indicate a hydrogen-bond between these atoms. The calculated values for the O(1W)···O(4) and O(1W)···O(5) distances, 2.860(13) and 2.966(14), and the angles O(1W)H(1W1)···O(4) and O(1W)H(1W2)···O(5), 169.0 and 149.4°, respectively, fall within the expected ranges.

The molecular geometries of the $[Gd^{(1)}(DOTP)]^{5-}$ and $[Gd^{(2)}(DOTP)]^{5-}$ anions are shown in Figure 3. The Gd^{3+} ion is eight-coordinate, four nitrogen atoms of the macrocycle and four phosphonate oxygen atoms of the pendant arms are bound by it. No inner-sphere water molecule is coordinated by the center. The coordination polyhedra around the Gd^{3+} ions can be described as a twisted intermediate between a prism and a square antiprism. A geometric analysis of the structure was performed in order to

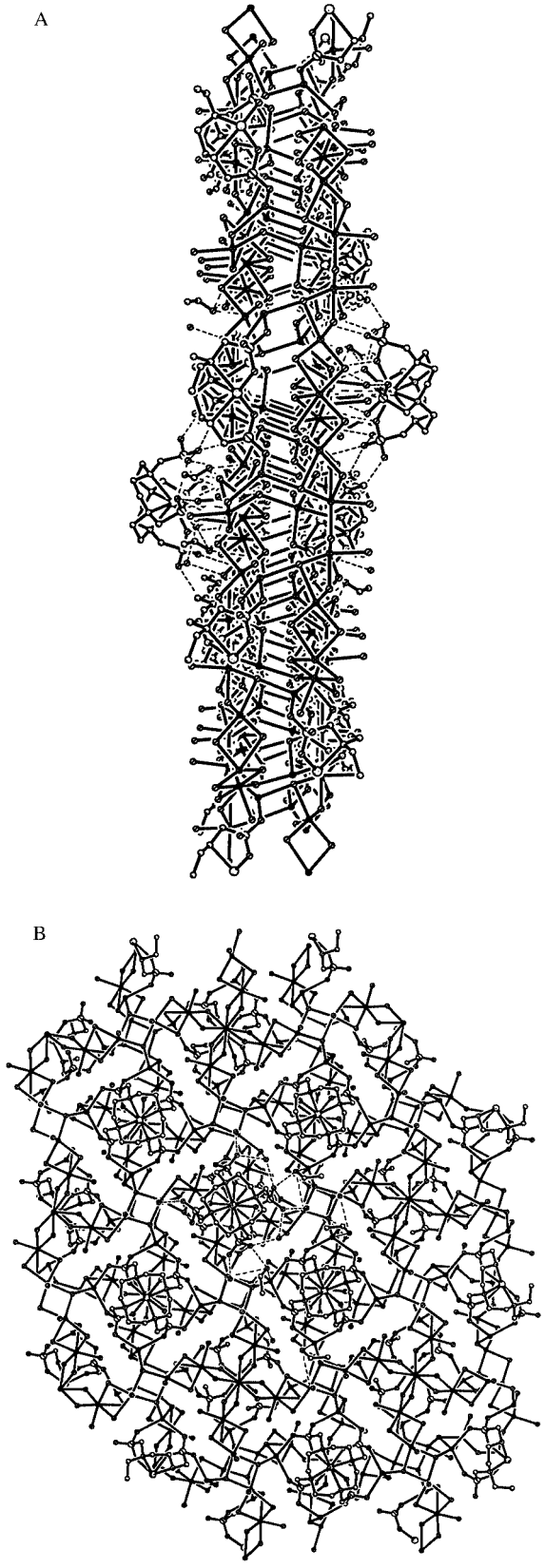

Figure 1. Packing views of the crystal structure of $[\{Na_{13}(OH)_3(H_2O)_{29}\}\{Gd^{(1)}(DOTP)\}][Gd^{(2)}(DOTP)]\cdot 7H_2O\cdot 2CH_3CH_2OH$; the cluster of hydrated Na^+ ions is shown in the middle of two layers in parallel planes perpendicular to the axis connecting $Gd^{(2)}$ and $Gd^{(1)}$: (A) side view; (B) top view

 © 2003 Wiley-VCH Verlag GmbH & Co. KGaA, Weinheim

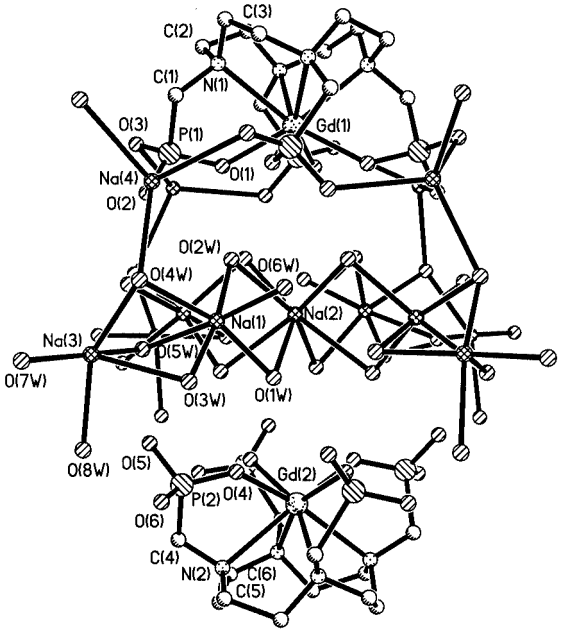

Figure 2. A general view of the supramolecule in the solid state, including the external spheres of the $[Gd^{(1)}(DOTP)]^{5-}$ and $[Gd^{(2)}(DOTP)]^{5-}$ moieties; hydrogen atoms are omitted for simplicity

Table 1. Selected interatomic distances [Å] for $[\{Na_{13}(OH)_3(H_2O)_{29}\}\{Gd^{(1)}(DOTP)\}]\,[Gd^{(2)}(DOTP)]\cdot 7H_2O\cdot 2CH_3CH_2OH$

Gd(1)−O(1)	2.312(6)	Gd(2)−O(4)	2.314(9)
Gd(1)−N(1)	2.652(10)	Gd(2)−N(2)	2.667(16)
P(1)−O(1)	1.533(7)	P(2)−O(4)	1.492(10)
P(1)−O(2)	1.545(10)	P(2)−O(5)	1.525(12)
P(1)−O(3)	1.486(9)	P(2)−O(6)	1.473(12)
P(1)−C(1)	1.842(15)	P(2)−C(4)	1.904(15)
Na(1)−O(1 W)	2.377(9)	Na(3)−O(3 W)	2.691(18)
Na(1)−O(2 W)	2.360(11)	Na(3)−O(4 W)	2.325(15)
Na(1)−O(3 W)	2.367(14)	Na(3)−O(5 W)	2.414(10)
Na(1)−O(4 W)	2.625(17)	Na(3)−O(7 W)	2.387(11)
Na(1)−O(5 W)	2.425(10)	Na(3)−O(8 W)	2.44(2)
Na(1)−O(6 W)	2.413(10)	Na(4)−O(2)	2.700(12)
Na(2)−O(1 W)	2.671(11)	Na(4)−O(3)	2.842(14)
Na(2)−O(2 W)	2.664(11)	Na(4)−O(4 W)	2.744(15)
		Na(4)−O(7 W)	2.743(14)

determine the degree of torsion of the prism around the pseudo C_4 axis.[30] The resulting geometry of the coordinated atoms is almost midway between prismatic (twist angle between the planes: 0°) and antiprismatic (twist angle: 45°). Negative twist angles of −27.07 and −23.67° are found in the structures for $[Gd^{(1)}(DOTP)]^{5-}$ and $[Gd^{(2)}(DOTP)]^{5-}$, respectively, which can both be defined as eight-coordinate twisted (or inverted) square-antiprismatic (TSAP) structures, also known as **m′** isomers.[31a] A twisted antiprismatic structure has also been reported for $[La(DOTA)]^-$ crystals: a nine-coordinate twisted capped square-antiprismatic (TCSAP) structure with a twist angle of about −22°, and a water molecule at the capping position.[31b] The two slightly different twist angles observed for the two types of $[Gd(DOTP)]^{5-}$ chelates probably result from their different interactions with the cluster of hydrated Na^+ ions in the crystal structure, and have not been reported in a previous preliminary crystal structural study.[27]

The inherent structural features of the $[Gd(DOTP)]^{5-}$ chelate give rise to two independent sources of chirality, associated with the conformation of each of the four Gd-NCCN chelate moieties in the macrocyclic ring (the helicity of the four C−C bonds relative to the respective Gd^{3+}−N−N planes is defined by two possible forms, δ and λ) and the helicity of the pendant arms (Δ or Λ).[26] The two twisted square-antiprismatic **m′** isomers found in the crystal structure appear both as racemic mixtures of the two Δ(δ,δ,δ,δ) and Λ(λ,λ,λ,λ) enantiomers.

In the coordination polyhedra, the Gd−N bond lengths are 2.660(1) Å (ave.) and the Gd−O bond lengths are 2.314(8) Å (ave.), while in the twisted square-antiprismatic Tm^{3+} coordination polyhedron of $[(NH_4)_5Tm(DOTP)]$, the Tm−N bond lengths were found to be 2.63(1) Å (ave.) and the Gd−O bond lengths 2.26(1) Å (ave.).[27]

These solid-state structural data agree with the results of the solution structural studies on the $[Ln(DOTP)]^{5-}$ complexes carried out using multinuclear and paramagnetic NMR spectroscopy.[21−24] ^{17}O NMR spectroscopic measurements of $[Dy(DOTP)]^{5-}$ in solution have shown that this complex lacks an inner-sphere water molecule.[23] The diamagnetic $[La(DOTP)]^{5-}$ and $[Lu(DOTP)]^{5-}$ complexes have been studied by ^1H and ^{13}C NMR spectroscopy, while the complete paramagnetic series of the $[Ln(DOTP)]^{5-}$ complexes has been studied by ^1H, ^{13}C, ^{31}P, and ^{23}Na NMR spectroscopy, as well as molecular mechanics calculations.[22] Unlike DOTA complexes, which appear in solution as enantiomeric pairs of nine-coordinate capped square-antiprismatic (CSAP, also called **M**) and twisted capped square-antiprismatic (TCSAP, also called **m**) isomers,[25,26,31a] $[Ln(DOTP)]^{5-}$ complexes exist in solution as a single enantiomeric pair. Although the coordination cage appears to be locked into a single conformation, variable-temperature ^1H and ^{13}C NMR spectra suggested dynamic behavior related to the interconversion of the ethylenediamine chelate rings, coupled with the concerted flipping motion of the arms. As a result, $[Ln(DOTP)]^{5-}$ complexes exist as racemic mixtures in solution, and the two enantiomers give indistinguishable NMR signals at room temperature when using conventional NMR spectroscopic techniques.[22,23] Structural analysis of the dipolar contribution to the LIS values and MMX force-field calculations initially suggested a distorted square-antiprismatic (SAP) **M′** arrangement of the ligand, with only minor structural changes throughout the Ln series.[22] However, a recent re-evaluation of the data and of the assignments of the methylenephosphonate protons led to the conclusion that the enantiomeric pair present in solution corresponds to a twisted square-antiprismatic (TSAP) **m′** structure.[32] Thus, the two slightly different **m′**-type enantiomeric pair structures observed in the solid state are replaced by just one pair in solution, as the interaction between the $[Gd(DOTP)]^{5-}$ chelates and the cluster of the hydrated Na^+ ions breaks down

 © 2003 Wiley-VCH Verlag GmbH & Co. KGaA, Weinheim

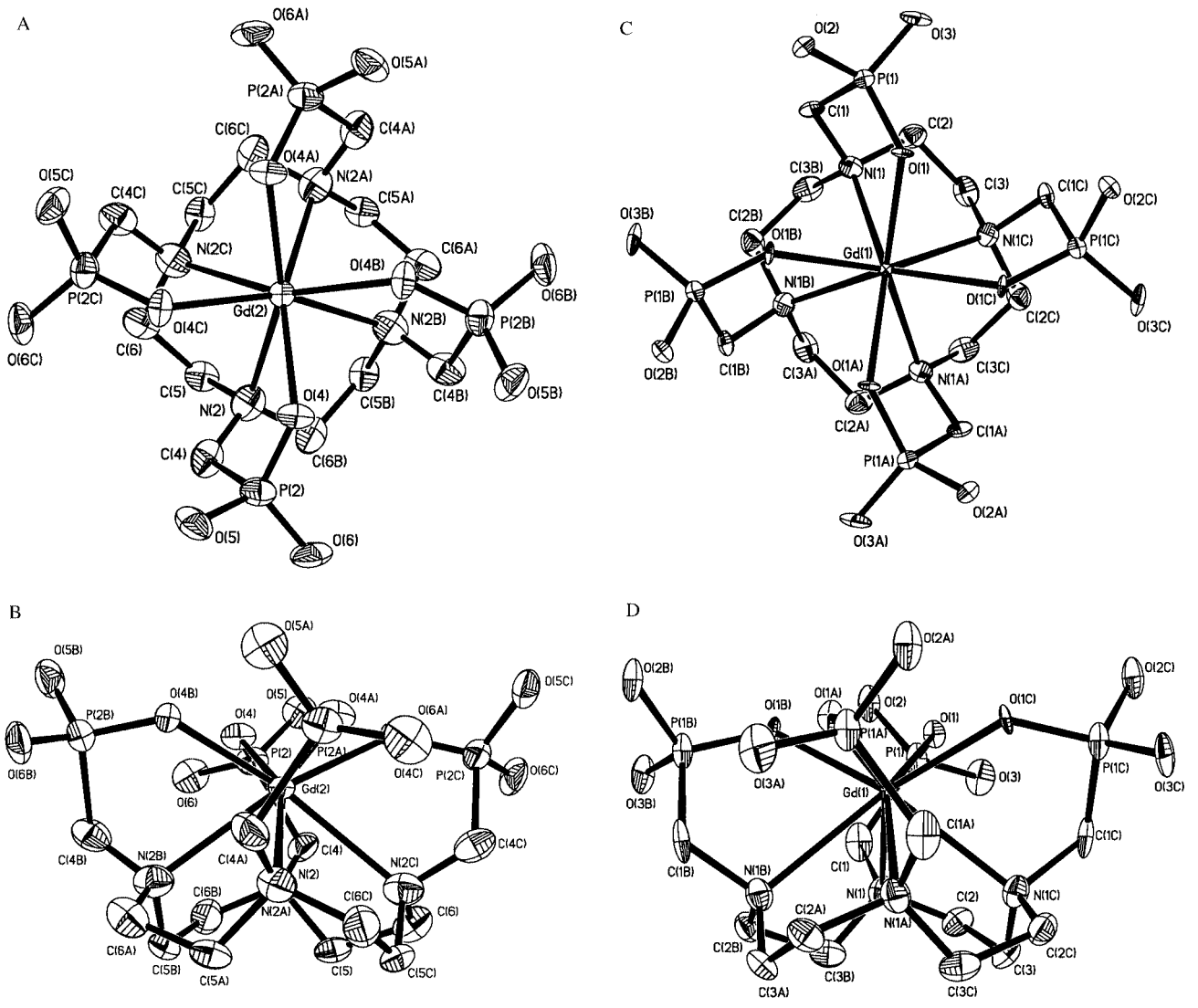

Figure 3. ORTEP diagrams with the top (A, C) and side (B, D) views of the anion complexes $[Gd^{(2)}(DOTP)]^{5-}$ (A, B) and $[Gd^{(1)}(DOTP)]^{5-}$ (C, D), representing the two square-antiprismatic **m**′ isomers; hydrogen atoms have been omitted for simplicity, the ORTEP plots are at the 30% probability level

in solution. Chiral NMR resolution, using the formation of diastereomeric adducts between the two enantiomers of $[Ln(DOTP)]^{5-}$ and a chiral substrate, has provided indirect, but conclusive, evidence for the existence of the two enantiomers of **m**′ in solution.[33−36]

Structural Evaluation of the $[Tm(DOTP)]^{5-}$-Induced ^{23}Na NMR Shifts

The magnitudes of the solution ^{23}Na LIS induced by $[Ln(DOTP)]^{5-}$ complexes, in particular by $[Tm(DOTP)]^{5-}$, are very large and are most likely due to the formation of strong ion-pairs resulting from the high negative charge on the DOTP complexes. Consequently, $[Tm(DOTP)]^{5-}$ is a very efficient shift reagent for in vivo $^{23}Na^+$ NMR spectroscopic studies. The binding sites of the Na^+ ions found in the present crystal structure of the Na^+ salt of $[Gd(DOTP)]^{5-}$ can be used to check the interpretation of the ^{23}Na LIS induced in solution by $[Tm(DOTP)]^{5-}$.[28,29] In this solid-state structure, the $[Gd^{(1)}DOTP)]^{5-}$ center displays four Na^+ ions [Na(4)] that are directly coordinated to the bound ligand and that form bridges between two Gd^{3+}-unbound oxygen atoms of the phosphonate groups of the adjacent ligand (Figure 2). The experimental structural parameters of this binding mode are $\theta = 72.6°$ and $r = 5.29$ Å, where θ is the angle between the four-fold symmetry axis of the $[Gd(DOTP)]^{5-}$ moiety and the $Gd^{3+}-Na^+$ vector, and r is the $Gd^{3+}-Na^+$ distance. The $[Gd^{(2)}(DOTP)]^{5-}$ moiety has no Na^+ ions directly coordinated to the bound ligand (Figure 2), but several of them can be found in its vicinity that belong to the hydrated Na^+ cluster. These ions form two layers in parallel planes perpendicular to the axis

 © 2003 Wiley-VCH Verlag GmbH & Co. KGaA, Weinheim

connecting $Gd^{(2)}$ and $Gd^{(1)}$, which is the main susceptibility axis of $Gd^{(2)}$. Five Na^+ ions can be found in a layer further away from $Gd^{(2)}$.

Two different types of binding sites for the Na^+ counterions have been proposed in order to interpret the solution ^{23}Na LIS induced by $[Tm(DOTP)]^{5-}$.[28,29] The extremely large ^{23}Na LIS (ca. 420 ppm) observed at low $Na^+/[Tm(DOTP)]^{5-}$ ratios was interpreted as resulting from a type of binding (type A) at a position near the four-fold symmetry axis (low θ). In particular, MMX calculations generated an optimal model where the Na^+ ion interacts with one Tm-bound oxygen atom and another oxygen atom of an adjacent phosphonate group which points away from the tetraazamacrocycle (model A_4, with dipolar angle θ = 26°, $Tm^{3+}-Na^+$ distance r = 3.78 Å).[29] The much smaller shifts (ca. 160 ppm) observed at high $Na^+/[Tm(DOTP)]^{5-}$ ratios were interpreted as resulting from four binding sites of a second type (type B) at higher θ and r values. An MMX-optimized model suggested that the Na^+ ions are associated with two unbound oxygen atoms of adjacent phosphonate groups that point away from the tetraazamacrocycle, with an average θ = 36°, and r = 4.56 Å (model B_2).[29] Both proposed binding sites are located within the positive shift cone of the lanthanide ion.

The structural parameters of the four $Na^+(4)$ ions bound to the $[Gd^{(1)}(DOTP)]^{5-}$ moiety in the crystal show that this binding is similar to the second proposed (type B) binding mode (model B_2), rather than to the first (type A), but with a much larger angle θ (θ > 54.5°) and distance r, thus, the Na^+ ions are located in the negative shift cone of the lanthanide ion. This would lead to a small negative ^{23}Na LIS value for $[Tm(DOTP)]^{5-}$, thereby contradicting the NMR spectroscopic data.[6−15] The $Na^+(4)$ binding mode is very similar to the B_3 model (Na^+ binding to the two oxygen atoms of the same phosphonate group), which has not been considered to contribute to the experimental ^{23}Na LIS.[28,29]

The Na^+ ions in the cluster, near the $[Gd^{(2)}(DOTP)]^{5-}$ moiety but not directly bound to it, occupy three different types of sites. One Na^+ ion [Na(2), θ = 0°, r = 5.17 Å] is located along that susceptibility axis of $Gd^{(2)}$, thus at equal distances from the four phosphonate moieties. It occupies a type-A position, but at a significantly larger distance than the proposed binding model A_1 (θ = 0° and r = 3.22 Å). Four Na^+ ions [Na(1), θ = 36.7°, r = 6.37 Å] occupy a type-B position, but at a larger distance than model B_1, and coordinate one of the metal-unbound oxygen atoms of one bound phosphonate group (θ = 36.7°, r = 5.42 Å). Another four Na^+ ions [Na(3), θ = 56.6°, r = 7.92 Å], which are part of the layer closer to $Gd^{(2)}$, are located at wider angles from the main axis and at larger distances from $Gd^{(2)}$; a position that is similar to the binding model B_3 (θ = 65.5°, r = 6.05 Å), but also at a larger distance.[29]

Therefore, from this analysis we can conclude that the Na^+ binding sites detected in the crystal structure of the Na^+ salt of $[Gd(DOTP)]^{5-}$ at a high $Na^+/[Gd(DOTP)]^{5-}$ ratio of 5 do not represent the binding mode(s) previously proposed to be occurring in solution. This could arise as a result of the effects of the cluster of hydrated Na^+ ions that are present, which may hinder the axial binding mode (type A) and also distort the lateral binding mode (type B).

Simulation of the Parameter Dependence of the Second-Sphere and Outer-Sphere Contributions to the Relaxivity of a Gd^{3+} Complex

The unexpectedly high relaxivities displayed by the NMRD profiles of some small Gd^{3+} chelates such as $[Gd(DOTP)]^{5-}$,[18,19] and also of some small Gd^{3+} chelates bound to macromolecules such as HSA,[37−43] led to the proposal that second-sphere water molecules may, in some cases, significantly contribute to the measured relaxivities.[43−45] Such second-sphere relaxivity contributions could become as important as well-recognized outer-sphere contributions. The Solomon−Bloembergen−Morgan equations, which usually describe the field dependency of the inner-sphere relaxivity, can be adapted to describe second-sphere effects, while Freed's equation is used to describe the outer-sphere contribution of the relaxivity.[46] Both equations depend on a variety of molecular parameters. In order to obtain an insight into the factors that determine the relative importance of both contributions, the values of the second-sphere and outer-sphere relaxivities of the water protons of a Gd^{3+} complex in aqueous solution were simulated at 298 K and at the 0.01 MHz and 40 MHz Larmor frequencies, as a function of various relevant parameters. The set of equations used is given in the Supporting Information.

Second-sphere relaxivity depends on a variety of parameters, some of which were fixed at reasonable values, such as the number of second-sphere water molecules (q' = 1) and the electronic relaxation parameters ($\Delta^2 = 6.94\cdot10^{19}$ s^2, τ_v = 15 ps). The distance (r') from Gd^{3+} to a second-sphere water proton was varied between two reasonable values, 3.5 and 3.9 Å, while its exchange lifetime $\tau_{M'}$ was varied between 10 and 100 ps, assuming fast (τ_R = 50 ps) and slow ($\tau_R = 10^4$ ps) rotational diffusion of the complex. The outer-sphere contribution has been simulated before as a function of the distance of closest approach of a water molecule to Gd^{3+} (a^H), the diffusion constant (D) and the electronic relaxation time at zero field (τ_{S0}), which is a function of the crystal-field parameter Δ^2.[47] Here, the outer-sphere contribution was calculated as a function of the parameter a^H, which took on the values of 3.5, 3.9, and 4.5 Å, with the same electronic relaxation parameters as assumed for second-sphere relaxation and a typical value of the diffusion constant, $D = 2.28\cdot10^{-9}$ $m^2\cdot s^{-1}$. These simulations (Figure 4) show that the second-sphere relaxation is efficient only if the second-sphere water molecules have a reasonably long lifetime $\tau_{M'}$. In such a case, rotational immobilization (long τ_R) may amplify this contribution, so that it becomes similar to outer-sphere relaxation. Thus, the long-lived second-sphere hydration water molecules trapped in the interface of a Gd^{3+} chelate binding at a pocket of a protein such as HSA, together with exchangeable protons from protein residues nearby, have very sizeable contributions to the large relaxivities observed.[5,43]

 © 2003 Wiley-VCH Verlag GmbH & Co. KGaA, Weinheim

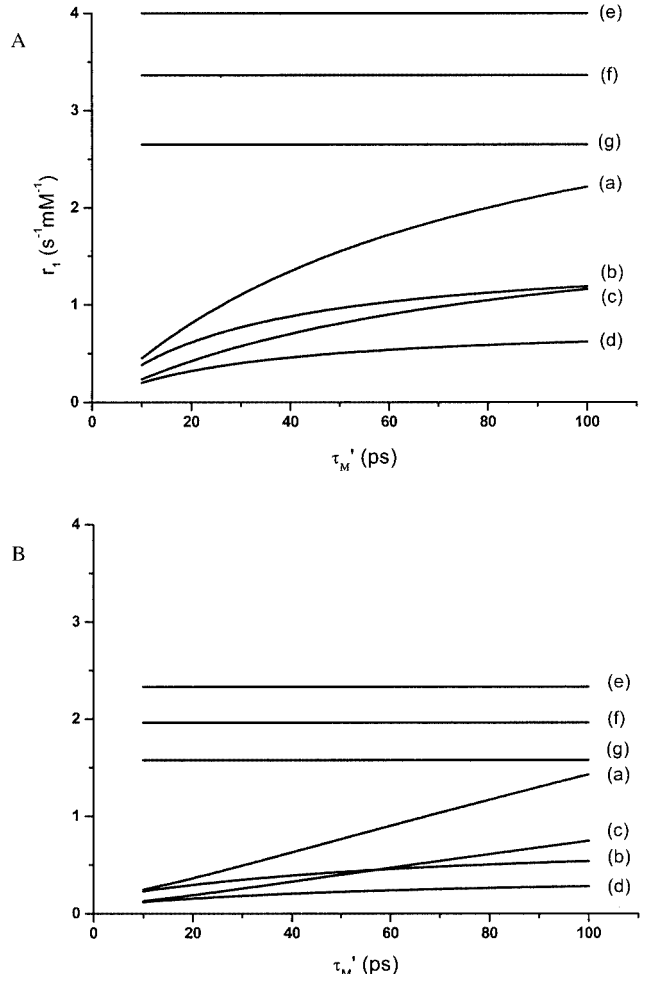

Figure 4. Calculated values at 0.01 MHz (A) and 40 MHz (B) of the parameter dependencies of the contributions to the proton relaxivity r_1 of a Gd^{3+} complex in aqueous solution: (a)−(d) second-sphere relaxivity as a function of $\tau_{M'}$ for $\tau_R = 50$ ps, $r' = 3.5$ Å (b) and $r' = 3.9$ Å (d) and for $\tau_R = 10^4$ ps, $r' = 3.5$ Å (a) and $r' = 3.9$ Å (c) ($q' = 1$, $\Delta^2 = 6.94 \cdot 10^{19}$ s^2, $\tau_v = 15$ ps); (e)−(g) outer-sphere relaxivity for $a^H = 3.5$ Å (e), $a^H = 3.9$ Å (f), and $a^H = 4.5$ Å (g) ($D = 2.28 \cdot 10^{-9}$ $m^2 \cdot s^{-1}$, $\Delta^2 = 6.94 \cdot 10^{19}$ s^2, $\tau_v = 15$ ps)

Structural Evaluation of the Second-Sphere Hydration of Gd^{3+} in $[Gd(DOTP)]^{5-}$ and of Its Contribution to Its Relaxivity

The NMRD profile of $[Gd(DOTP)]^{5-}$ shows a relatively high relaxivity,[18,19] and its unusual features have led to conflicting explanations. Initially, the formation of oligomers containing a mixture of isomers with different q (inner-sphere water molecules) values were considered, leading to fractional q values.[18] Later, the same curve was interpreted on the basis of the collective contributions of one coordinated water molecule ($q = 1$) with an unusually long distance, $r_{GdH} = 3.26$ Å (instead of the standard 2.9 Å value) and a residence time, $\tau_M = 3000$ ps, together with an outer-sphere contribution calculated using a rather short distance of closest approach $a_{GdH} = 3.76$ Å,[19,20] instead of the more commonly used value of $a_{GdH} = 4.5$ Å.[44] As it became evident that this system has $q = 0$,[23] the same data were well-fitted when considering a strong second-sphere contribution, with two water molecules ($q' = 2$) located at a somewhat longer distance ($r'_{GdH} = 3.89$ Å) with short residence times ($\tau'_M \approx 100$ ps), corresponding to water molecules hydrogen-bonded to the phosphonate oxygen atoms of $[Gd(DOTP)]^{5-}$, together with an outer-sphere contribution calculated using standard values of D and $a_{GdH} = 4.5$ Å.[45] The important contribution of second-sphere water molecules to the relaxivity of $[Gd(DOTP)]^{5-}$ was also pinpointed by a reasonable fit of its NMRD curve to a calculated curve based on an outer-sphere hydration model obtained by molecular dynamics simulations. This hydration model was defined by a radial distribution function which contains a second-sphere of four water molecules on the hydrophilic hemisphere encasing the phosphonate groups of the complex, at an average distance $r'_{GdH} = 3.4$ Å, and residence time $\tau'_M = 56$ ps.[48]

We tried to find experimental evidence of the solution hydration model of $[Gd(DOTP)]^{5-}$ from the low-temperature (−100 °C) X-ray structure, in a similar way to what was done previously for $K_2[Yb(DTPA)(H_2O)]$.[44] However, this was not as successful since the presence of the Na^+ counterions in close contact with the complex (Figure 2) significantly affects its hydration. Eight water molecules that are coordinated to the four Na^+ ions, which are bound to the phosphonate groups, are at 7.0−7.3 Å away from $Gd^{(1)}$. Half of these connect the four Na^+ ions to the main hydrated Na^+ cluster. Another four water molecules belonging to the cluster that connect the $Na^+(1)$ and $Na^+(2)$ ions are at 4.5 Å from $Gd^{(1)}$. The $[Gd^{(2)}DOTP]^{5-}$ chelates interact with the hydrated Na^+ cluster through the hydrogen-bonding interaction between one Gd-unbound oxygen atom of each phosphonate group and a water molecule that is coordinated to the $Na^+(3)$ ions of the cluster. These water molecules are located 7.0 Å from $Gd^{(2)}$. However, the layer of eight water molecules within the cluster are closer to $Gd^{(2)}$: four water molecules at 4.2 Å from $Gd^{(2)}$, which connect the $Na^+(1)$ and $Na^+(2)$ ions, and four water molecules at 6.7 Å from $Gd^{(2)}$, which connect the two $Na^+(1)$ and $Na^+(3)$ ions. Thus, in the crystal structure, both the $Gd^{(1)}$ and $Gd^{(2)}$ centers have four second-sphere water molecules located at 4.5 and 4.2 Å, respectively, from them. These distances are significantly longer than those proposed from the analysis of NMRD data.[45,48] The water molecules in the crystal coordinate the Na^+ ions, which prevents their direct interaction with the phosphonate oxygen atoms, significantly increasing their distances from the Gd^{3+} ions.

In summary, the structural information obtained in the solid state for the Na^+ salt of $[Gd(DOTP)]^{5-}$ provides significant clues to the location of Na^+ ions and water molecules around the chelate, which are of value for the rationalization of the solution ^{23}Na paramagnetic NMR shifts induced by $[Tm(DOTP)]^{5-}$, and of the second-sphere water relaxivity of $[Gd(DOTP)]^{5-}$.

Experimental Section

X-ray Crystallographic Study: $Na_5Gd(DOTP) \cdot 2.75\ H_2O$ was provided by Macrocyclics, Richardson, Texas, USA. Single crystals of

 © 2003 Wiley-VCH Verlag GmbH & Co. KGaA, Weinheim

$[\{Na_{13}(OH)_3(H_2O)_{29}\}\{Gd^{(1)}(DOTP)\}][Gd^{(2)}(DOTP)]\cdot 7H_2O\cdot 2CH_3CH_2OH$ were recrystallized from a water/ethanol solution of the sodium salt of $[Gd(DOTP)]^{5-}$ and grown by slow diffusion of 2-propanol into this solution, and slow evaporation of the solvent. Colorless crystals of X-ray quality were obtained. A suitable crystal of $[\{Na_{13}(OH)_3(H_2O)_{29}\}\{Gd^{(1)}(DOTP)\}][Gd^{(2)}(DOTP)]\cdot 7H_2O\cdot 2CH_3CH_2OH$ was coated with Fomblin oil, placed on the end of a silica fiber and mounted on a goniometer head of a Bruker SMART CCD diffractometer with a stream of cold nitrogen gas. The crystal was centered optically, and the unit cell parameters and an orientation matrix for data collection were obtained at −100 °C by using the centering program in the SMART system. Details of the crystal data are given in Table 2. The default hemisphere runs required about 3.5 h for full data collection (with 5-s-per-frame scan time) and comprised 3 runs totaling about 1250 frames. They were set up assuming a sample-to-detector distance of about 5 cm, which provided full coverage to better than 0.75 Å (56.6° with Mo radiation). Three-dimensional X-ray data were collected by 3-circle hemisphere runs in the θ-range method. Lorentz, polarization and decay corrections were applied to the data, as well as an absorption correction based on a series of ψ scans. Reflections were measured from a hemisphere of data collected in frames of 0.3°. A total of 35498 reflections was collected, of which 4568 independent reflections exceeded the significance level $|F|/\sigma(|F|) > 4.0$. Complex scattering factors were taken from the program package SHELXTL/PC V5.1.[49] The structure was solved by direct methods and refined by full-matrix least-squares methods on F^2 using SHELXTL/PC V5.1.[49] Due to the crystal nature and diffraction capabilities, some disagreeable reflections were suppressed. All non-hydrogen atoms were refined anisotropically. Hydrogen atoms were included in calculated positions and refined with the riding model on their respective heteroatoms, except for the H atoms involved in hydrogen-bonding interactions with the $[Gd^{(2)}(DOTP)]^{5-}$ moieties, which were first located in geometrically calculated positions, left freely and then refined riding on the oxygen atoms of the water molecules. The H atoms of some water molecules and of the ethanol molecule were not included. Minimum and maximum final electron-densities (−1.571 and 3.976 e·Å^{-3}) were 0.84 Å from $Gd^{(1)}$ and 0.76 Å from $Gd^{(2)}$. The weighting scheme used during refinement is given in Table 2. Structure refinement and preparation of figures and tables for publication were carried out on PCs using SHELXTL/PC V5.1.[49] A complete list of atomic coordinates, bond lengths and angles, thermal parameters, and hydrogen atom coordinates are available from the Cambridge Crystallographic Data Centre. CCDC-213923 contains the supplementary crystallographic data for this paper. These data can be obtained free of charge at www.ccdc.cam.ac.uk/conts/retrieving.html [or from the Cambridge Crystallographic Data Centre, 12 Union Road, Cambridge CB2 1EZ, UK; Fax: (internat.) + 44-1223/336-033; E-mail: deposit@ccdc.cam.ac.uk].

Table 2. Crystal data and structure refinement for $[\{Na_{13}(OH)_3(H_2O)_{29}\}\{Gd^{(1)}(DOTP)\}][Gd^{(2)}(DOTP)]\cdot 7H_2O\cdot 2CH_3CH_2OH$

	Gd(DOTP)
Empirical formula	$C_{28}H_{133}Gd_2N_8Na_{13}O_{65}P_8$
Formula mass	2483.56
Temperature [K]	173(2)
λ(Mo-K_α) [Å]	0.71073
Crystal system	tetragonal
Space group	*P*4/*n*
a [Å]	16.4809(12)
b [Å]	16.4809(12)
c [Å]	21.989(2)
V [Å^3]	5972.7(9)
Z	4
$D_{calcd.}$ [g/cm^3]	1.381
μ [mm^{-1}]	1.342
F(000)	2536
Crystal size [mm]	0.49 × 0.44 × 0.10
θ range for data collection	2.23−28.30°
Index range	$-16 \le h \le 21$, $-20 \le k \le 21$, $-29 \le l \le 28$
Reflections collected	35498
Independent reflections	7042 [R(int) = 0.1124]
Max./min. transmission	0.8775/0.5594
Refinement method	full-matrix least squares on F^2
Data/restraints/parameters	7042/0/302
Goodness-of-fit on F^2	1.030
Final R indices [$I > 2\sigma(I)$]	R_1 = 0.1091[a], wR_2 = 0.2604[b]
R indices (all data)	R_1 = 0.1660[a], wR_2 = 0.2979[b]
Largest diff. peak and hole	3.976 and −1.571 e·Å^{-3}

[a] $R_1 = \Sigma||F_o| - |F_c||/\Sigma|F_o|$. [b] $wR_2 = \{\Sigma[w(||F_o|^2 - |F_c|^2|)^2]|/\Sigma[w(F_o^4)]\}^{1/2}$.

Acknowledgments

We thank Fundação da Ciência e Tecnologia (F.C.T.), Portugal (project POCTI/QUI/47005/2002), and Universidade da Coruña, Spain, for financial support, and the COST D18 Action of the E. U.

[1] A. D. Sherry, C. F. G. C. Geraldes, in: *Lanthanide Probes in Life, Chemical and Earth Sciences* (Eds.: J.-C. Bünzli, G. R. Choppin), Elsevier, Amsterdam, **1989**, pp. 93−126.
[2] R. B. Lauffer, *Chem. Rev.* **1987**, *87*, 901−927.
[3] M. F. Tweedle, in: *Lanthanide Probes in Life, Chemical and Earth Sciences* (Eds.: J.-C. Bünzli, G. R. Choppin), Elsevier, Amsterdam, **1989**, pp. 127−179.
[4] P. Caravan, J. J. Ellison, T. J. McMurry, R. B. Lauffer, *Chem. Rev.* **1999**, *99*, 2293−2352.
[5] [5a] S. Aime, M. Botta, M. Fasano, E. Terreno, *Chem. Soc. Rev.* **1998**, *27*, 19−29. [5b] S. Aime, M. Botta, M. Fasano, S. Geninnatti Crich, E. Terreno, *Coord. Chem. Rev.* **1999**, *185−186*, 321−333.
[6] A. D. Sherry, C. R. Malloy, F. M. H. Jeffrey, W. P. Cacheris, C. F. G. C. Geraldes, *J. Magn. Reson.* **1988**, *76*, 528−533.
[7] D. C. Buster, M. M. C. A. Castro, C. F. G. C. Geraldes, C. R. Malloy, A. D. Sherry, T. C. Siemers, *Magn. Reson. Med.* **1990**, *15*, 25−32.
[8] C. R. Malloy, D. C. Buster, M. M. C. A. Castro, C. F. G. C. Geraldes, F. M. H. Jeffrey, A. D. Sherry, *Magn. Reson. Med.* **1990**, *15*, 33−44.
[9] N. B. Butwell, R. Ramasamy, A. D. Sherry, C. R. Malloy, *Invest. Radiol.* **1991**, *26*, 1079−1082.
[10] N. B. Butwell, R. Ramasamy, I. Lazar, A. D. Sherry, C. R. Malloy, *Am. J. Physiol.* **1993**, *264*, H1884−H1889.
[11] M. M. Pike, C. Su Luo, M. D. Clark, K. A. Kirk, M. Kitakaze, M. C. Madden, E. J. Cragoe Jr., G. M. Pohost, *Am. J. Physiol.* **1993**, *265*, H2017−H2026.
[12] N. Bansal, M. J. Germann, I. Lazar, C. R. Malloy, A. D. Sherry, *J. Magn. Reson. Imag.* **1992**, *2*, 385−391.
[13] N. Bansal, M. J. Germann, V. Seshan, G. T. Shires III, C. R. Malloy, A. D. Sherry, *Biochemistry* **1993**, *32*, 5638−5643.
[14] Z.-F. Xia, J. W. Horton, P.-Y. Zhao, N. Bansal, E. E. Babcock, A. D. Sherry, C. R. Malloy, *J. Appl. Physiol.* **1994**, *76*, 1507−1511.
[15] V. Seshan, M. J. Germann, P. Preisig, C. R. Malloy, A. D. Sherry, N. Bansal, *Magn. Reson. Med.* **1995**, *34*, 25−32.
[16] J. D. Makos, C. R. Malloy, A. D. Sherry, *J. Appl. Physiol.* **1998**, *85*, 1800−1805.

 © 2003 Wiley-VCH Verlag GmbH & Co. KGaA, Weinheim

[17] P. M. Winter, V. Seshan, J. D. Makos, A. D. Sherry, C. R. Malloy, N. Bansal, *J. Appl. Physiol.* **1998**, *85*, 1806−1812.
[18] C. F. G. C. Geraldes, R. D. Brown III, W. P. Cacheris, S. Koenig, A. D. Sherry, M. Spiller, *Magn. Res. Med.* **1989**, *9*, 94−104.
[19] S. Aime, M. Botta, E. Terreno, P. L. Anelli, F. Uggeri, *Magn. Res. Med.* **1993**, *30*, 583−591.
[20] S. Aime, M. Botta, D. Parker, J. A. G. Williams, *J. Chem. Soc., Dalton Trans.* **1996**, 17−23.
[21] A. D. Sherry, C. F. G. C. Geraldes, W. P. Cacheris, *Inorg. Chim. Acta* **1987**, *139*, 137−139.
[22] C. F. G. C. Geraldes, A. D. Sherry, G. E. Kiefer, *J. Magn. Reson.* **1992**, *97*, 290−304.
[23] J. Ren, A. D. Sherry, *J. Magn. Reson.* **1996**, *B111*, 178−182.
[24] S. Aime, M. Botta, E. Garino, S. G. Crich, G. B. Giovenzana, R. Pagliarin, G. Palmisano, M. Sisti, *Chem. Eur. J.* **2000**, *6*, 2609−2617.
[25] J. A. Peters, J. Huskens, D. J. Raber, *Prog. NMR Spectrosc.* **1996**, *28*, 283−350.
[26] J. A. Peters, E. Zitha-Bovens, D. M. Corsi, C. F. G. C. Geraldes, in: *The Chemistry of Contrast Agents in Medical Magnetic Resonance Imaging* (Eds.: A. E. Merbach, É. Tóth), John Wiley & Sons, Chichester, **2001**, chapter 8.
[27] E. F. Paulus, P. Juretschke, J. Lang, *3. Jahrestag der Deutschen Gesellschaft für Kristallographie*, Darmstadt, **1995**.
[28] A. D. Sherry, J. Ren, J. Huskens, E. Brücher, É. Tóth, C. F. G. C. Geraldes, M. M. C. A. Castro, W. P. Cacheris, *Inorg. Chem.* **1996**, *35*, 4604−4612.
[29] J. Ren, A. D. Sherry, *Inorg. Chim. Acta* **1996**, *246*, 331−341.
[30] [30a] C. Piguet, J.-C. G. Bünzli, G. Bernardinelli, C. G. Bochet, P. Froidevaux, *J. Chem. Soc., Dalton Trans.* **1995**, 83−97; M. Elhabiri, R. Scopelliti, J.-C. G. Bünzli, C. Piguet, *J. Am. Chem. Soc.* **1999**, *121*, 10747−10762. [30b] C. Platas, F. Avecilla, A. de Blas, T. Rodríguez-Blas, R. Bastida, A. Macías, A. Rodríguez, H. Adams, *J. Chem. Soc., Dalton Trans.* **2001**, 1699−1705.
[31] [31a] S. Aime, M. Botta, M. Fasano, M. P. M. Marques, C. F. G. C. Geraldes, D. Pubanz, A. E. Merbach, *Inorg. Chem.* **1997**, *36*, 2059−2068. [31b] S. Aime, A. Barge, F. Benetollo, G. Bombieri, M. Botta, F. Uggeri, *Inorg. Chem.* **1997**, *36*, 4287−4289.
[32] J. Ren, S. Zhang, A. D. Sherry, C. F. G. C. Geraldes, *Inorg. Chim. Acta* **2002**, *339C*, 273−282.
[33] J. Ren, C. S. Springer, A. D. Sherry, *Inorg. Chem.* **1997**, *36*, 3493−3498.
[34] S. Aime, M. Botta, S. G. Crich, E. Terreno, P. L. Anelli, F. Uggeri, *Chem. Eur. J.* **1999**, *5*, 1261−1266.
[35] D. M. Corsi, H. van Bekkum, J. A. Peters, *Inorg. Chem.* **2000**, *39*, 4802−4808.
[36] R. A. Carvalho, J. A. Peters, C. F. G. C. Geraldes, *Inorg. Chim. Acta* **1997**, *262*, 167−176.
[37] S. Aime, M. Botta, M. Fasano, S. G. Crich, E. Terreno, *J. Biol. Inorg. Chem.* **1996**, *1*, 312−319.
[38] L. Vander Elst, F. Maton, S. Laurent, F. Seghi, F. Chapelle, R. N. Muller, *Magn. Reson. Med.* **1997**, *38*, 604−614.
[39] R. B. Lauffer, D. J. Parmelee, S. U. Dunham, H. S. Ouellet, R. P. Dolan, S. Witte, T. J. McMurry, R. C. Walovitch, *Radiology* **1998**, *207*, 529−538.
[40] R. N. Muller, B. Radüchel, S. Laurent, J. Platzek, C. Piérart, P. Mareski, L. Vander Elst, *Eur. J. Inorg. Chem.* **1999**, 1949−1955.
[41] S. Aime, M. Chiaussa, G. Digilio, E. Gianolo, E. Terreno, *J. Biol. Inorg. Chem.* **1999**, *4*, 766−774.
[42] S. Aime, M. Botta, L. Frullano, S. G. Crich, G. B. Giovenzana, R. Pagliarin, G. Palmisano, M. Sisti, *Chem. Eur. J.* **1999**, *5*, 1253−1260.
[43] P. Caravan, M. T. Greenfield, X. Li, A. D. Sherry, *Inorg. Chem.* **2001**, *40*, 6580−6587.
[44] K. I. Hardcastle, M. Botta, M. Fasano, G. Digilio, *Eur. J. Inorg. Chem.* **2000**, 971−977.
[45] M. Botta, *Eur. J. Inorg. Chem.* **2000**, 399−407.
[46] [46a] É. Tóth, L. Helm, A. E. Merbach, in: *The Chemistry of Contrast Agents in Medical Magnetic Resonance Imaging* (Eds.: A. E. Merbach, É. Tóth), John Wiley & Sons, Chichester, England, **2001**, chapter 2, p. 45. [46b] D. H. Powell, O. M. N. Dhubhghaill, D. Pubanz, L. Helm, Y. S. Lebedev, W. Schlaepfer, A. E. Merbach, *J. Am. Chem. Soc.* **1996**, *118*, 9333−9346.
[47] S. Aime, A. S. Batsanov, M. Botta, J. A. K. Howard, D. Parker, K. Senanayake, G. Williams, *Inorg. Chem.* **1994**, *33*, 4696−4706.
[48] A. Borel, L. Helm, A. Merbach, *Chem. Eur. J.* **2001**, *7*, 600−610.
[49] G. M. Sheldrick, *SHELXTL: An Integrated System for Solving and Refining Crystal Structures from Diffraction Data (Revision 5.1)*, University of Göttingen, Germany, **1997**.

Received May 27, 2003
Early View Article
Published Online October 10, 2003

 © 2003 Wiley-VCH Verlag GmbH & Co. KGaA, Weinheim

Bent and Linear Forms of the (μ-Oxo)bis[trichloroferrate(III)] Dianion: An Intermolecular Effect − Structural, Electronic and Magnetic Properties

Agustí Lledós,*[a] Marcial Moreno-Mañas,*[a] Mariona Sodupe,[a] Adelina Vallribera,[a] Ignasi Mata,[b] Benjamín Martínez,[b] and Elies Molins*[b]

Keywords: Iron / Oxygen / (μ-Oxo)trichloroferrate dianion / Packing effects / Magnetic properties / DFT calculations

We have analyzed the great diversity of Fe–O–Fe angles, 140–180°, found in the X-ray structures of the (μ-oxo)bis-[trichloroferrate(III)] dianion $[Cl_3FeOFeCl_3]^{2-}$ from both experimental and theoretical points of view. Theoretical calculations show that only the linear isomer is found as a minimum on the potential energy surface. Detailed analysis of the crystal packing indicates that the angular form is due to attractive intermolecular interactions. Analysis of a selected reduced set of the 45 crystal structures retrieved from the Cambridge Structural Database allowed us to classify the bending of the $[Cl_3FeOFeCl_3]^{2-}$ dianion in three categories, depending on the balance and strength of the intermolecular O···H–X contacts. A crystal diffraction study on the bis(benzyltrimethylammonium) salt has shown both bent (144.6°) and linear (180°) forms of the (μ-oxo)bis[trichloroferrate(III)] dianion. The magnetic susceptibility of this compound has been fitted by assuming two equally weighted contributions (J_{ang} and J_{lin}) of the two forms, considering $J_{ang} - J_{lin}$ estimated by theoretical calculations. The obtained J_{ang} and J_{lin} of −117 and −133 cm^{-1} respectively, agree well with B3LYP results.

(© Wiley-VCH Verlag GmbH & Co. KGaA, 69451 Weinheim, Germany, 2003)

Introduction

Understanding spin coupling in condensed matter is of fundamental interest. Strategies to control this coupling are of paramount importance for several material applications. Colossal magnetoresistive manganites, high T_c superconductors or superparamagnetic clusters like Fe8 and Mn12 are impressive examples of how spin coupling can be fine-tuned to promote outstanding material properties.

Uncoupled transition metal atoms with unpaired electrons behave as paramagnets. When two atoms interact, the most stable ground state usually corresponds to the singlet $S = 0$ state. In metals and alloys, the metal atoms are directly linked, but in ceramic materials they are usually bridged by other atoms. Oxygen is a very suitable bridging atom; it is a two-electron acceptor, and its flexibility allows the transformation of a linear into a square configuration. The very simple M−O−M system is ideal to study the spin coupling between metal atoms through a bridging atom, acting as a model for more complicated systems.

In particular, oxo-bridged iron(III) complexes have received considerable attention as both simple and useful models for non-heme metalloproteins containing dinuclear iron units in their active site,[1,2] and in studies of the intramolecular antiferromagnetic spin exchange coupling between two high-spin ferric ions.[1,3,4] Within this family, the (μ-oxo)bis[trichloroferrate(III)] dianion **1** (Figure 1) is ubiquitous. X-ray diffraction studies on salts of **1** have been described with various different cations.[3,5−7] An interesting feature of the crystal structure determinations is that the Fe−O−Fe angle in the solid state ranges from 180 to ca. 140° depending on the respective countercation (Figure 1). In general, bent structures **1a** have been considered for the anions with Fe−O−Fe angles of 146−171°. The apparently linear conformations **1b** (Fe−O−Fe 180°) found in a few cases have been attributed to orientational disorder.[3] In spite of the different Fe−O−Fe angles found in these structure determinations, only one type of anion (i.e. with a unique angle) was found in each crystal.

Interest in (μ-oxo)bis[trichloroferrate(III)] salts has been renewed by the discovery that the two different forms (bent

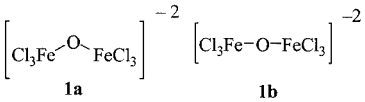

1a **1b**

$[PhCH_2N(CH_3)_3]_2\ [Fe_2OCl_6]$

2

Figure 1. Compound **2** with coexisting bent **1a** and linear **1b** anions

[a] Department of Chemistry, Universitat Autònoma de Barcelona
Cerdanyola, 08193 Barcelona, Spain
Fax: (internat.) + 34-93/5811265
E-mail: marcial.moreno@uab.es
agusti@klingon.uab.es
[b] Institut de Ciència de Materials de Barcelona (CSIC),
Campus de la UAB, 08193 Bellaterra, Barcelona, Spain
E-mail: elies.molins@icmab.es

and linear) can be simultaneously present in the crystal. A crystal diffraction study on the bis(benzyltrimethylammonium) salt **2** showed that both bent (144.6°) and linear (180°) anions were present in the solid, in a ratio of 1:1.[8] Instead of a linear arrangement, the elongated shape of the ellipsoids at the oxygen atoms is also compatible with the presence of two angular conformers (> 165°). However, the ellipsoids' shape, which could be due to either vibrational behavior or some disorder between two quasi-linear conformers, was not explained. In any case, Mössbauer spectroscopy of **2** showed a doublet exhibiting notorious peak asymmetry. The spectrum was fitted with two symmetric doublets associated with two different environments for the iron atoms in the crystal.[8] Thus, from crystal structure and Mössbauer spectroscopy two different Fe−O−Fe forms were identified. Recently, two different types of crystals were obtained for tetramethylformamidinium disulfide (μ-oxo)bis[trichloroferrate(III)] (Form I: orthorhombic; Form II: monoclinic).[9] Two independent (μ-oxo)bis[trichloroferrate(III)] ions, with Fe−O−Fe angles of 146.4 and 180°, were found in the asymmetric unit of Form I, whereas only one ion (Fe−O−Fe 167.9°) was found in Form II. The Fe−O−Fe antisymmetric vibrations in the IR spectra, at 845 and 890 cm^{-1} for Form I crystals and 875 cm^{-1} for Form II crystals, are consistent with such variations in the Fe−O−Fe bond angles.[9]

The concurrent presence of both bent and linear forms of anion **1** in the same crystal raises the possibility of two minima on the Fe−O−Fe potential energy curve. Moreover, given the small separation between the low-spin ground state ($S = 0$) and the high-spin excited state ($S = 5$), the two minima might be spin isomers, corresponding to antiferromagnetic and ferromagnetic couplings of the $S = 5/2$ Fe^{III} spins, respectively.

The magnetic properties of (μ-oxo)bis[trichloroferrate(III)] salts have been extensively studied,[1,3] but in all cases only one anion was present. Therefore, we decided to study the magnetism of two coexisting $[Cl_3FeOFeCl_3]^{2-}$ anions. In the early 1990s a systematic theoretical study on the geometry dependence of the magnetic exchange constant J of $[Fe_2OCl_6]^{2-}$ was performed by means of UHF calculations.[10] Nowadays, quantitative calculations of the exchange coupling constants in dinuclear transition metal complexes are possible. The application of broken symmetry DFT calculations produces very good estimates of J, as compared to experimental data.[11] However, in most calculations the magnetic coupling constant is related to the singlet/triplet energy difference. In the (μ-oxo)bis[trichloroferrate(III)] anion the low- and high-spin states are singlet and undecaplet, respectively. Therefore, obtaining a good estimate of this energy difference is a challenge for DFT methods. Recent studies[12] on the magnetic exchange interaction in $[Fe_2OCl_6]^{2-}$ using pure density functional methods computed an exchange coupling of -244 cm^{-1} (Hamiltonian $\hat{H} = -2J\ \hat{S}_1\ \hat{S}_2$), which is much larger than the experimental -134 cm^{-1}. It is interesting to analyze how hybrid functionals behave for the present systems because previous theoretical studies[13] for singlet/triplet energy differences have shown that the related magnetic exchange coupling is quite sensitive to the amount of exact exchange included in the functional.

We have two goals here: First to clarify whether two separated minima are present on the potential energy surface of the isolated $[Cl_3FeOFeCl_3]^{2-}$ dianion using theoretical calculations and, if not, to search for possible mechanisms that result in the anion bending. The second goal is to study the dianion's magnetic properties, taking into account the existence of two isomers or forms and combining experimental and theoretical hybrid density functional methods.

Results and Discussion

Structural Aspects

Fe−O−Fe Potential Energy Curve

Regarding the first goal given above, geometry optimizations of $[Cl_3FeOFeCl_3]^{2-}$, both for the high-spin ($S = 5$) and low-spin (broken symmetry) states, led to only one isomer as minimum on the potential energy surface: the linear one with the chlorine atoms in an alternate conformation (dihedral angles between planes Cl−Fe1−O and O−Fe2−Cl are 60°). The optimized geometrical parameters for the high- and low-spin states (Figure 2) show that Fe−O is longer in the former ground state (1.826 vs. 1.788 Å). Even though the optimizations of the low-spin state were performed using a broken symmetry (BS) approach and, e.g., not using a pure singlet wave function, the obtained values are in quite good agreement with those determined experimentally, which range from 1.752 to 1.765 Å.[3,6,7] Moreover, the computed harmonic vibrational frequencies provide an asymmetric Fe−O−Fe stretching frequency of 861 cm^{-1}, which is in very good agreement with

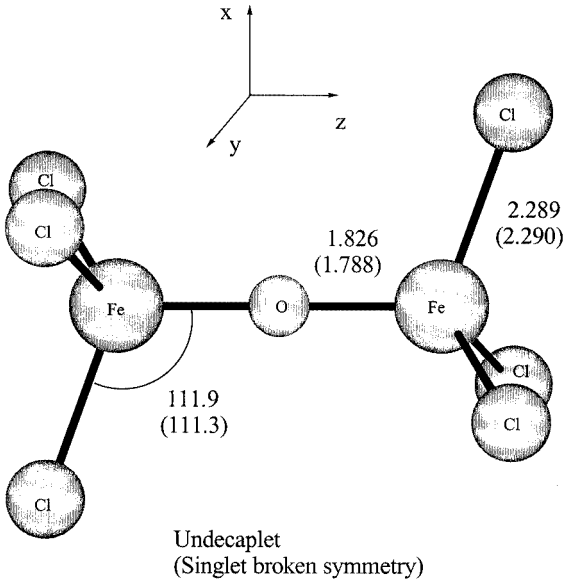

Figure 2. B3LYP-optimized geometries for the undecaplet and singlet (broken symmetry, in parentheses) ground states; distances are in Å and angles in °

 © 2003 Wiley-VCH Verlag GmbH & Co. KGaA, Weinheim

that determined experimentally for several (μ-oxo)diiron complexes (850−880 cm^{-1}). In fact, intense IR absorption in this region is commonly used as a diagnostic criterion to identify monooxo-bridged Fe^{III} complexes.[3,14]

The Fe−O−Fe angular dependence has been analyzed by optimizing the geometry of the anion $[Cl_3FeOFeCl_3]^{2-}$ at different Fe−O−Fe angles (from 180.0 to 130.0°). We have considered both the in-plane (*xz*) and out-of-plane (*yz*) Fe−O−Fe bending. Figure 3 shows that for both the high- and low-spin states the energy slightly increases as the angle is reduced and that no minimum is found at about 140.0°. This behavior is similar to that found in a previous theoretical study.[10] Conversely, the energy cost for the in-plane Fe−O−Fe bending, from 180.0 to 140.0°, is < 3 kcal/mol for the singlet (BS) and < 2 kcal/mol for the undecaplet; indicating a very flat potential energy surface along this direction. The energy cost is even smaller for the out-of-plane bending. Therefore, the presence of two forms, linear and angular, in $([BzlMe_3N]^+)_2$ $[Cl_3FeOFeCl_3]^{2-}$ seems to be due not to electronic effects but probably to packing effects in the crystal.

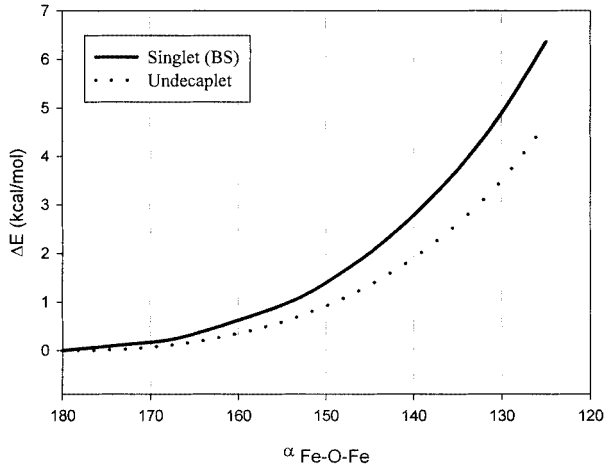

Figure 3. Relative energies of the singlet (BS) (—) and undecaplet (···) states as a function of O−Fe−O angle; in-plane bending (*xz*)

Crystal Packing Effects

The molecular structure, as well as the Mössbauer and vibrational spectroscopy results, of **2** have been reported previously.[8] However, the crystal packing effects were not analyzed. The crystal packing can be rationalized as a parallel piling of waved sheets along the unique axis *b* (Figure 4). Rows along the *a* axis can be distinguished within each sheet; they are formed of alternating cations and anions. In the five rows depicted in Figure 4 the linear anions lie in the odd ones whereas the angular ones are in the even ones. Although the neighborhood of each anion seems to be very similar, only O4 of the angular anion is involved in hydrogen bonds (numbering of ref.[8]). For symmetry reasons, this oxygen atom is bonded to two HC′3 atoms, which ride on their respective CC′ atoms. Then, while the geometry around O8 is strictly linear, for symmetry reasons, O4 has a tetrahedral bonding scheme

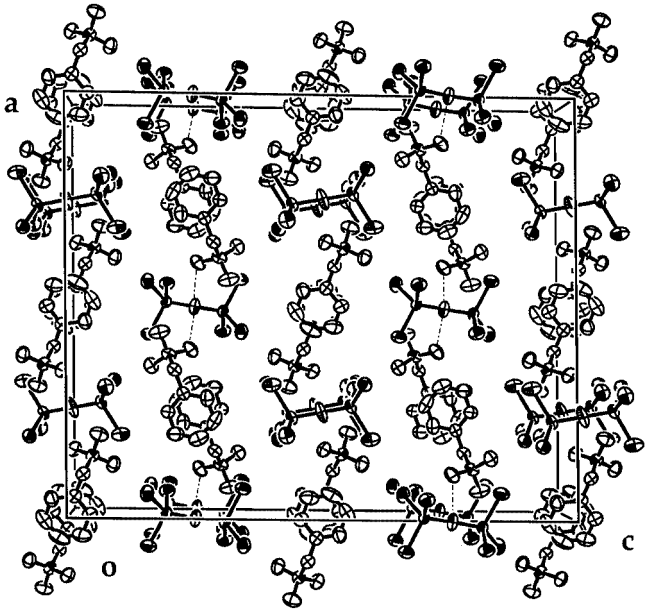

Figure 4. Perspective view of the crystal packing of **2** along the unique axis *b*

(Fe1−O4−Fe1 144.6°, HC′3···O4···HC′3 95°), with their lone pairs roughly pointing to the hydrogen atoms. These two hydrogen bonds, indicated by dashed lines in Figure 4, stabilize the angular conformation of this anion. To estimate the energy involved in this stretching process, the Espinosa model can be used.[15]

As is well known, the position of the hydrogen atoms obtained from conventional X-ray diffraction experiments are biased to their riding atom due to the polarization of the bond and the absence of core electrons in the hydrogen atoms. A correction of this effect[16] available in the PARST program[17] reduces HC′3···O4 from 2.712(6) to 2.603 Å. Introducing this value into the expression of the dissociation energy, D_e, of the Espinosa model gives 0.5 kcal/mol. As O4 is involved in two such hydrogen bonds, the energy afforded by the hydrogen bonds to distort the anion is about 1 kcal/mol, which is in close agreement with the theoretical value obtained from the potential energy curve (Figure 3), and within the range of previous estimations for CH···O hydrogen bonds.[18]

The intermolecular contacts involving the O atom in the $[Cl_3FeOFeCl_3]^{2-}$ anion were then analyzed in a set of structures[3,5−7] taken from the Cambridge Structural Database.[19] The set was formed by 17 structures selected to have no disorder and $R \leq 0.07$. In the 21 $[Fe_2OCl_6]^{2-}$ anions included in the structure set, the environment of the O atom was analyzed. The results allow the structures to be classified as three groups, showing the correlation between Fe−O−Fe angle and the presence of intermolecular interactions involving the O atom (Table 1).

Group I corresponds to anions in the bent configuration that show one or two C−H···O hydrogen bonds. Group III corresponds to linear configurations, and the intermolecular contacts, if they exist, involve pairs of short contacts related by symmetry and situated in opposite directions at

 © 2003 Wiley-VCH Verlag GmbH & Co. KGaA, Weinheim

Table 1. Fe−O−Fe angle and intermolecular C···O distances in the set of 21 $[Fe_2OCl_6]^{2-}$ anions, which are classified in three groups depending on the three O-atom environments (*: corresponds to two contacts with the same C···O distance due to the crystal symmetry)

Group	Structure	Fe−O−Fe angle [°]	Shortest intermolecular C···O distances [Å]
I	DEKHUW01	148.06	3.432, 3.789
	FEDMSC01	146.54	3.547, 3.836
	SIRBAW	147.68	3.460, 3.641, 3.947
	TIQNEM	145.16	3.610, 3.653
	UBENUK	144.58	3.607
	YAFQOL01	146.42	3.430
II	COPTUW	162.14	3.683, 3.734*
	FACTEI	160.17	3.654, 3.918
	NADTAN	164.80	3.813, 3.899, 3.956
	PYDCFO	155.65	3.960
	SUJWEZ	170.23	3.987
	YAFQOL	167.87	3.566, 3.705, 3.771
III	BUTROX	180.00	3.817*
	HEBTEN	180.00	no contact
	HIRTIL	180.00	no contact
	HIRTIL	180.00	no contact
	ICAHUP	180.00	no contact
	KEBYOF	180.00	no contact
	UBENUK	180.00	no contact
	XEDHAP	180.00	3.699*
	YAFQOL01	180.00	3.977*

both sides of the anion. In group II, consisting of anions halfway between those of groups I and III, the Fe−O−Fe angles are in the range 155−170° and the intermolecular contacts are very weak or they pull the oxygen atom from different directions (Figure 5).

Thus, there is a clear dependence between intermolecular interactions and anion configuration. In group I, where the interactions are strong and cooperative, the oxygen atom is displaced from its center position and bending is produced. In group II the interactions are weak or non-cooperative, and the bending is smaller. Finally, in group III there are no interactions or they are opposed and the configuration remains linear at the potential minimum.

Magnetic Behavior

Calculation of the Magnetic Coupling Constants

The magnetic behavior of a complex can be analyzed by using the Heisenberg−Dirac−Van Vleck HDVV spin hamiltonian, where J is the magnetic coupling constant and $\hat{S}_1$ and $\hat{S}_2$ are the spin operators of the magnetically interacting centers 1 and 2 [Equation (1)].

$$\hat{H}_{HDVV} = -2J\hat{S}_1\hat{S}_2 \quad (1)$$

The magnetic coupling constant, which is positive for a ferromagnetic interaction, can be obtained from the energy differences of pure spin sates, by using ab initio configuration interaction procedures [Equation (2)].

$$E(S-1) - E(S) = 2JS \quad (2)$$

Alternatively, one can also efficiently determine magnetic coupling constants by performing unrestricted density functional calculations. However, due to the single determinant nature of the Kohn−Shan procedure, the low-spin state must be treated using the broken symmetry approach, in which the open-shell magnetic orbitals are localized in different centers, with the magnetic electrons having opposite spins. The broken symmetry approach does not lead to a pure spin state and so it is necessary to relate the energy of the broken symmetry solution to that of the pure state.[11a] For a system with two magnetic centers with spins S_1 and S_2, and considering that the overlap between magnetic orbitals is very small (weak bonding regime), J can be obtained by Equation (3).[21]

$$J = \frac{E(Broken-symmetry) - E(high-spin)}{4S_1S_2} \quad (3)$$

For the system considered here, $[Fe_2Cl_6O]^{2-}$, both Fe ions carry a local high spin of $S = 5/2$. The two centers can couple ferromagnetically to give an overall high-spin state with $S = 5$ or antiferromagnetically to provide a low-spin $S = 0$ singlet state. Whereas the high-spin state (undecaplet) can be reasonably described by a single determinant, for the low-spin state (singlet) we have used the broken symmetry approach and the magnetic coupling constant has been obtained according to Equation (4).

$$J = \frac{E(Broken-symmetry) - E(S=5)}{25} \quad (4)$$

 © 2003 Wiley-VCH Verlag GmbH & Co. KGaA, Weinheim

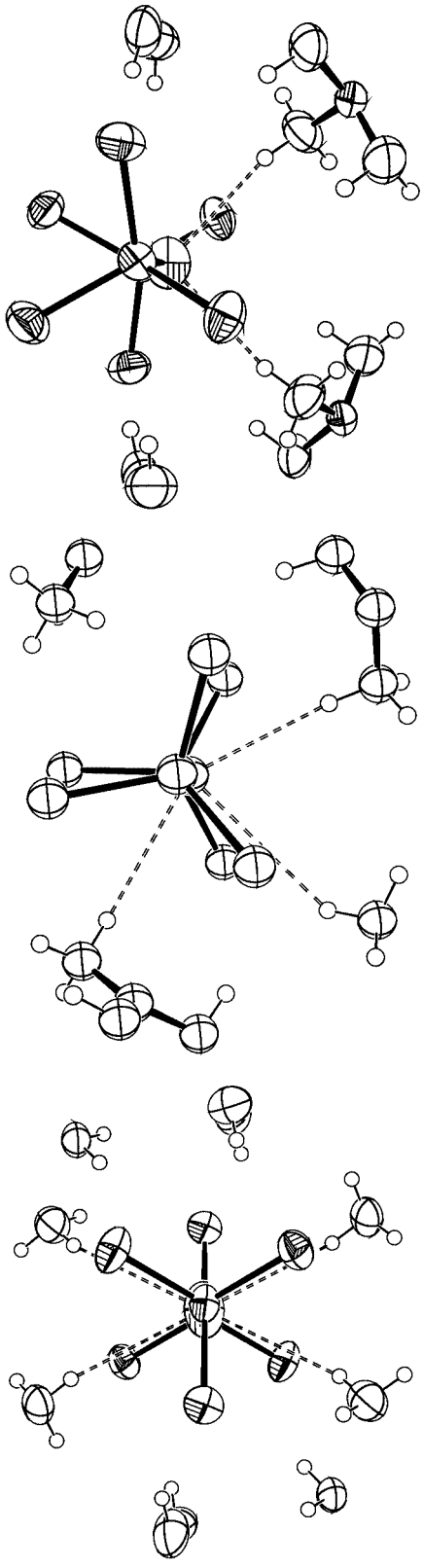

Figure 5. Perspective view of the oxygen environment of $[Cl_3FeOFeCl_3]^{2-}$ anions in a plane perpendicular to the Fe···Fe direction of representative examples of each bending-degree group: a) I, b) II and c) III; a) and c) show the two anions in **2** and b) corresponds to the NADTAN structure; diagrams generated with ORTEP-3 for Windows[20]

In addition to the B3LYP density functional approach, we have also performed calculations using the BHLYP method as previous theoretical studies have shown that the magnetic coupling constant is strongly dependent on the amount of exact exchange introduced in the functional.[13]

The magnetic coupling constants for the linear and angular forms have been computed at the experimentally determined geometry of **2**, using Equation (4). All the performed calculations indicate that antiferromagnetic exchange coupling is the most favorable interaction. Table 2 shows the computed values of J at the B3LYP and BHLYP levels for the two forms. Further enlarging the basis set in the calculation at the B3LYP level had a very small effect on the coupling constant. In contrast, the J value strongly depends on the amount of exact exchange introduced in the used functional. The value determined with the BHLYP functional, for which the amount of exact exchange is 50%, is about half of that obtained using the B3LYP functional with a ca. 20% mixture of exact exchange. Moreover, the B3LYP value is much smaller (in absolute value) than that reported recently[12] using pure density functional methods (-244 cm^{-1}). Similar behavior observed for other complexes has been attributed to the tendency of LDA and even GGA to overstabilize the antiferromagnetic coupling. This trend has been related to an overestimation of the delocalization of the spin density, which is reduced by increasing the percentage of Hartree−Fock mixture in the exchange functional.[13] Spin densities on the metal for the low-spin broken symmetry solution at the B3LYP (3.9) and BHLYP level (4.2) confirm this fact.

Table 2. Magnetic coupling constants [cm^{-1}] for the linear and angular forms at different levels of theory

Method	J_{lin}	J_{ang}
B3LYP/B1	−161	−145
B3LYP/B2	−160	−145
BHLYP/B1	−84	−73
Experimental[a]	−133	−117
	(−130)	(−119)

[a] From the magnetic susceptibility fitting by using the B3LYP/B1 (BHLYP/B1) $J_{ang} - J_{lin}$ difference.

It is also worth noting that the magnetic coupling constant of the linear form is larger than the angular one. This is not due to the different Fe−O−Fe angle, since calculations show a very small dependence of J with the Fe−O−Fe angle,[10] in agreement with experimental observations.[3] The observed difference arises from the different Fe−O distances, which are larger in the angular form due to the larger repulsive interactions between the chlorine atoms. Previous theoretical studies have shown that the absolute value of J decreases sharply as the Fe−O distance increases.[10,12]

Magnetic Measurements

The sample magnetization can be understood as a result of the magnetic coupling among the iron spins. Iron atoms

 © 2003 Wiley-VCH Verlag GmbH & Co. KGaA, Weinheim

in **2** are in the ferric valence state Fe^{3+}, as confirmed by Mössbauer spectroscopy,[8] and are in a distorted tetrahedral environment. The unpaired ferric spins are coupled through the bridging oxygen atom, with the ground state corresponding to an antiferromagnetic spin interaction.

The magnetic susceptibility of powdered samples, $\chi(T)$, has been measured from 5 to 300 K by using a SQUID magnetometer (Figure 6).

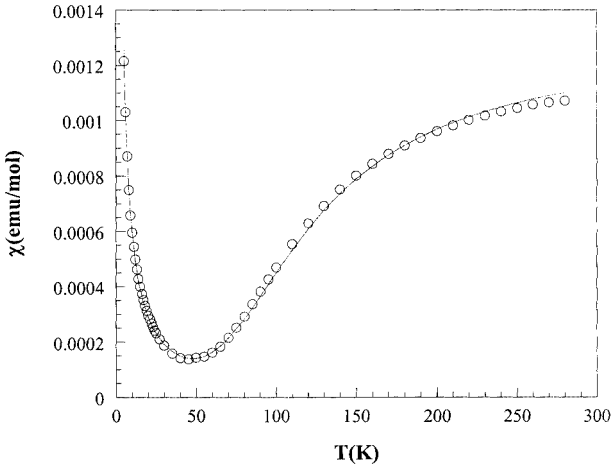

Figure 6. Magnetic susceptibility of compound **2**; the solid line corresponds to the fitting using Equation (5)

The hyperbolic tail in the low-temperature range has been attributed to paramagnetic impurities and treated as a free parameter in fitting the experimental data. After the fitting, the amount of paramagnetic impurities in the sample turns out to be only ca. 0.13 wt%.

The antiferromagnetic nature of the $[Fe_2Cl_6O]^{2-}$ anion is clearly established in the literature and is usually described by Equation (5).[22]

$$\chi_M = \frac{Ng^2\beta^2}{kT}\left[\frac{2e^{2x}+10e^{6x}+28e^{12x}+60e^{20x}+110e^{30x}}{1+3e^{2x}+5e^{6x}+7e^{12x}+9e^{20x}+11e^{30x}}\right](1-p)+p\frac{35N\beta^2}{k(T-\theta)} \quad (5)$$

In Equation (5), p represents the fraction of the paramagnetic impurity,[3] $x = J/k_BT$, J being the intensity of the magnetic coupling. The g value was fixed to 2.00 in all cases and the only fitting parameters were J, P, and θ. Because two different forms with different Fe−O−Fe bonding angles exist, namely 180 and 144.6°, it was not possible to reach an acceptable fitting of the experimental data using a single coupling constant.

The solid line in Figure 6 corresponds to the fitting of the experimental data using Equation (5), but assuming two equally weighted contributions (J_{ang} and J_{lin}) that correspond to the two different forms. As the strong correlation between the coupling constants impedes an independent determination of either of them separately, we used the computed B3LYP/B1 differences between them ($J_{ang} - J_{lin} = 16$ cm^{-1}) to obtain $J_{ang} \approx -117$ cm^{-1} and $J_{lin} \approx -133$ cm^{-1}. Even though the J values significantly depend on the density functional approach used, we expect the difference between coupling constants to be less sensitive and more accurate than the absolute values. The BHLYP values are about half of the B3LYP ones, but the $J_{ang} - J_{lin}$ differences at this level of theory (11 cm^{-1}) is only 5 cm^{-1} smaller.

By using the BHLYP computed difference as the starting point for the magnetic susceptibility fitting, the obtained coupling constants are $J_{ang} \approx -119$ cm^{-1} and $J_{lin} \approx -130$ cm^{-1} and the quality of the fitting is practically the same as that obtained with the B3LYP values. This concordance confirms the validity of the procedure used to determine the magnetic coupling constants from the fitting of the susceptibility. These values lie within the B3LYP and BHLYP values, and even the B3LYP results are in better agreement with that obtained from the fit; the BHLYP values cannot be disregarded.

These results seem to indicate that, at least for this system, a functional with an exact exchange mixing between BHLYP and B3LYP will provide results in close agreement with experiment. Unfortunately, it is not easy to know a priori how much exact exchange needs to be included in the functional to obtain an accurate answer.

Conclusion

Two different forms (bent and linear) of $[Cl_3FeOFeCl_3]^{2-}$ anions coexist in the crystal structure of $(BzlMe_3N)_2^+[Fe_2OCl_6]^{2-}$. Theoretical calculations for the low- and high-spin state of the dianion indicate that only the linear isomer is a minimum on the potential energy surface, although the energy cost for Fe−O−Fe bending is small. A detailed analysis of the crystal packing shows that the oxygen atom of the angular form is involved in two O···HC hydrogen bonds with the $BzlMe_3N$ cation. Therefore, the presence of both linear and angular forms in $([BzlMe_3N]^+)_2$ $[Fe_2OCl_6]^{2-}$ is due to crystal packing rather than electronic effects.

Moreover, analysis of those crystal structures showing bent conformations (Fe−O−Fe angle < 160°) of (μ-oxo)bis-[trichloroferrate(III)] anions shows that the bridging O atom is always involved in at least one intermolecular attractive contact. This contact, although soft, affords enough tension to bend the Fe−O−Fe angle, because the angle potential is flat, while the bulky $FeCl_3$ groups remain anchored in the crystal. The steric contribution to the Fe−O−Fe bending, related to the accommodation of the cation in the anion network holes, which is driven by attractive and repulsive contacts to chlorine atoms, must be included. The very shallow minimum of the Fe−O−Fe angle potential also explains the large vibration of oxygen atoms in the linear conformations.

The magnetic properties of $[Fe_2OCl_6]^{2-}$ have been investigated both experimentally and theoretically. The coexistence of the two forms prevented an acceptable fitting of the magnetic susceptibility when a single coupling constant was used. However, a good fit was possible by assuming two equally weighted contributions (J_{ang} and J_{lin}) that corre-

 © 2003 Wiley-VCH Verlag GmbH & Co. KGaA, Weinheim

spond to the two different forms, and by considering $J_{ang} - J_{lin}$ determined by theoretical calculations. The J_{ang} and J_{lin} values were found to be −117 and −133 cm^{-1}, respectively, and are in reasonably good agreement with those obtained with the B3LYP density functional approach (−145 and −161 cm^{-1}). Considering the low computational cost of density functional methods, compared to conventional post-Hartree−Fock ones, B3LYP appears to be an efficient tool to estimate magnetic coupling constants in such systems.

Experimental Section

General: The magnetic susceptibility of the powder samples, $\chi(T)$, was measured by using a commercial SQUID magnetometer (Quantum Design MPMS-5T), over the temperature range 5−300 K, under an applied field of 5 kOe. Corrections for the diamagnetic response of the sample holder and for the diamagnetic contribution of the samples (Pascal's constants) were carried out.

Computational Details: Calculations were performed using the nonlocal hybrid three-parameter B3LYP density functional method[23] and the following basis sets. For O and Cl we used the Dunning's (9s5p)/[4s2p] and (11s7p)/[6s4p] sets,[24] respectively, supplemented with one d polarization function (ζ = 0.85 for oxygen and ζ = 0.60 for chlorine). The Fe basis set is the [8s4p3d] contraction of the (14s9p5d) primitive set of Wachters[25] supplemented with two diffuse p and one diffuse d functions,[26] the final basis sets were of the form (14s11p6d)/[8s6p4d]. This basis set is referred as Basis1 (B1). To check the effect of further enlarging the basis set, in some calculations the metal basis set was increased by adding one f polarization function,[27] i.e. based on a three-term fit to a Slater orbital of exponent 3.6, and the Cl and O atom basis sets were supplemented with one valence diffuse function. This basis set is referred as Basis2 (B2). The *J* calculations were performed using both the B3LYP and BHLYP[28] density functional methods. All calculations were performed with the Gaussian 98 package.[29]

Acknowledgments

Financial support from MEC and MCyT of Spain (Projects BQU2002-04002, PB98-0916-C02-01, PB98-0912, and MAT2000-2016) and Generalitat de Catalunya (Projects SGR2001-0181 and SGR2001-0335) is gratefully acknowledged. Professor Y. Jean (Orsay) is also acknowledged for helpful discussions.

[1] [1a] D. M. Kurtz, *Chem. Rev.* **1990**, *90*, 585−606. [1b] S. M. Gorun, S. J. Lippard, *Inorg. Chem.* **1991**, *30*, 1625−1630.
[2] R. M. Davydov, S. Ménage, M. Fontecave, A. Gräslund, A. Ehrenberg, *J. Biol. Inorg. Chem.* **1997**, *2*, 242−255.
[3] G. Haselhorst, K. Wieghardt, S. Keller, B. Schrader, *Inorg. Chem.* **1993**, *32*, 520−525 and references cited therein.
[4] D. Gatteschi, R. Sessoli, A. Cornia, *Chem. Commun.* **2000**, 725−732.
[5] M. G. B. Drew, V. McKee, S. M. Nelson, *J. Chem. Soc., Dalton Trans.* **1978**, 80−84.
[6] [6a] H. Schmidbaur, C. E. Zybill, D. Neugebauer, *Angew. Chem. Int. Ed. Engl.* **1983**, *22*, 156−157. [6b] K. Dehnicke, H. Prinz, W. Massa, J. Pebler, R. Z. Schmidt, *Anorg. Allg. Chem.* **1983**, *499*, 20−30. [6c] P. C. Healy, B. W. Skelton, A. H. White, *Aust. J. Chem.* **1983**, *36*, 2057−2064. [6d] W. M. Reiff, E. H. Witten, K. Mottle, T. F. Brennan, A. R. Garafalo, *Inorg. Chim. Acta* **1983**, *77*, L83−L88. [6e] L. Huang, F. Jiang, J. Lu, *Huaxue Tongbao* **1984**, 14; *Chem. Abstr.* **1984**, *101*, 63979a. [6f] V. I. Ponomarev, L. D. Arutyunyan, L. O. Atovmyan, *Kristallografiya* **1984**, *29*, 910−922. *Sov. Phys. Crystallog.* **1984**, *29*, 538. [6g] H. Weiss, J. Sträle, *Z. Naturforsch., Teil B* **1984**, *39*, 1453−1455. [6h] J. C. A. Boeyens, F. B. D. Khan, E. W. S. Neuse, *S. Afr. J. Chem.* **1984**, *37*, 187−192. [6i] E. W. Neuse, F. B. W. Khan, K. Berhalter, U. Thewalt, *J. Crystallogr. Spectrosc. Res.* **1986**, *16*, 483−493. [6j] P. Carty, K. C. Clare, J. R. Creighton, E. Metcalfe, E. S. Raper, H. M. Dawes, *Inorg. Chim. Acta* **1986**, *112*, 113−117. [6k] D. Petridis, A. Terzis, *Inorg. Chim. Acta* **1986**, *118*, 129−134. [6l] G. J. Bullen, B. J. Howlin, J. Silver, B. W. Fitzsimmons, I. Sayer, L. F. Larkworthy, *J. Chem. Soc., Dalton Trans.* **1986**, 1937−1940. [6m] I. Vasilevsky, R. E. Stenkamp, E. C. Lingafelter, N. J. Rose, *J. Coord. Chem.* **1988**, *19*, 171−187. [6n] S. Bernès, F. Sécheresse, Y. Jeannin, *Inorg. Chim. Acta* **1992**, *194*, 105−112.
[7] [7a] I. G. Gusakova, S. I. Pirumova, N. S. Ovanesyan, N. I. Golovina, R. F. Tofimova, G. V. Shilov, E. A. Lavrent'eva, *Zh. Obshch. Khim.* **1996**, *66*, 1436−1443. [7b] R. D. Köhn, G. Seifert, G. Kociok-Köhn, *Angew. Chem. Int. Ed. Engl.* **1997**, *35*, 2879−2881. [7c] M. James, H. Kawaguchi, K. Tatsumi, *Polyhedron* **1997**, *16*, 4279−4282. [7d] N. Kuhn, H. Kotowski, C. Maichle-Moessmer, U. Abram, *Z. Anorg. Allg. Chem.* **1998**, *624*, 1653−1656. [7e] I. Ondrejkovicová, T. Lis, J. Mrozinski, V. Vancová, M. Melník, *Polyhedron* **1998**, *17*, 3181−3192. [7f] I. G. Gusakovskaya, S. I. Pirumova, N. I. Golovina, R. F. Trofimova, G. V. Shilov, N. S. Ovanesyan, E. A. Lavrent'eva, *Russ. J. Gen. Chem.* **1999**, *69*, 175−181. [7g] B. Yan, Z.-D. Chen, S.-X. Wang, *J. Chin. Chem. Soc. (Taipei)* **2000**, *47*, 1211−1214. [7h] S. Ameerunisha, J. Schneider, T. Meyer, P. S. Zacharias, E. Bill, G. Henkel, *Chem. Commun.* **2000**, 2155−2156.
[8] E. Molins, A. Roig, C. Miravitlles, M. Moreno-Mañas, A. Vallribera, N. Gálvez, N. Serra, *Struct. Chem.* **1998**, *9*, 203−208.
[9] H. Senda, S. Kitoh, T. Suganami, K.-K. Kunimoto, *Anal. Sci.* **2000**, 1003−1004.
[10] J. R. Hart, A. K. Rappé, S. M. Gorun, T. H. Upton, *Inorg. Chem.* **1992**, *31*, 5254−5259.
[11] [11a] F. Illas, I. de P. R. Moreira, C. de Graaf, V. Barone, *J. Phys. Chem.* **1997**, *101*, 1526−1531. [11b] E. Ruiz, P. Alemany, S. Alvarez, J. Cano, *J. Am. Chem. Soc.* **1997**, *119*, 1297−1303. [11c] J. Cano, P. Alemany, S. Alvarez, M. Verdaguer, E. Ruiz, *Chem. Eur. J.* **1998**, *4*, 476−484.
[12] Z. Chen, Z. Xu, L. Zhang, F. Yan, Z. Lin, *J. Phys. Chem. A* **2001**, *105*, 9710−9716.
[13] [13a] J. Cabrero, N. Ben Amor, C. de Graaf, F. Illas, R. Caballol, *J. Phys. Chem. A* **2000**, *104*, 9983−9989. [13b] C. de Graaf, I. de P. R. Moreira, F. Illas, R. L. Martin, *Phys. Rev. B* **1999**, *60*, 3457−3464.
[14] P. Gomez-Romero, E. H. Witten, W. M. Reiff, G. B. Jameson, *Inorg. Chem.* **1990**, *29*, 5211−5217.
[15] E. Espinosa, E. Molins, C. Lecomte, *Chem. Phys. Lett.* **1998**, *285*, 170−173.
[16] G. A. Jeffrey, L. Lewis, *Carbohydr. Res.* **1978**, *60*, 179−182.
[17] [17a] M. Nardelli, *Comput. Chem.* **1983**, *7*, 95−98. [17b] M. Nardelli, *J. Appl. Crystallogr.* **1995**, *28*, 659.
[18] J. Steiner, *Angew. Chem. Int. Ed.* **2002**, *41*, 48−76.
[19] F. H. Allen, *Acta Crystallogr., Sect. B* **2002**, *58*, 380−388.
[20] L. J. Farrugia, *J. Appl. Crystallogr.* **1997**, *30*, 565.
[21] [21a] L. Noodleman, *J. Chem. Phys.* **1981**, *74*, 5737−5743. [21b] L. Noodleman, E. R. Davidson, *Chem. Phys.* **1986**, *109*, 131−143. [21c] T. Onishi, Y. Takano, Y. Kitagawa, T. Kawakami, Y. Yoshioka, K. Yamaguchi, *Polyhedron* **2001**, *20*, 1177−1184.
[22] C. J. O'Connor, *Prog. Inorg. Chem.* **1982**, *29*, 203−283.
[23] [23a] A. D. Becke, *J. Chem. Phys.* **1993**, *98*, 5648−5652. [23b] C. Lee, W. Yang, R. G. Parr, *Phys. Rev. B* **1988**, *37*, 785−789.
[24] T. H. Dunning, P. J. Hay, *Modern Theoretical Chemistry* (Ed.: H. F. Schaefer III), Plenum, New York, **1976**, vol 3, p.1.
[25] A. J. H. Wachters, *J. Chem. Phys.* **1970**, *52*, 1033−1036.

 © 2003 Wiley-VCH Verlag GmbH & Co. KGaA, Weinheim

[26] P. J. Hay, *J. Chem. Phys.* **1977**, *66*, 4377−4384.
[27] C. W. Jr. Bauschlicher, S. R. Langhoff, H. Partridge, L. A. Barnes, *J. Chem. Phys.* **1989**, *91*, 2399−2411.
[28] A. D. Becke, *J. Chem. Phys.* **1993**, *98*, 1372−1377.
[29] M. J. Frisch, G. W. Trucks, H. B. Schlegel, G. E. Scuseria, M. A. Robb, J. R. Cheeseman, V. G. Zakrzewski, J. A. Montgomery, Jr., R. E. Stratmann, J. C. Burant, S. Dapprich, J. M. Millam, A. D. Daniels, K. N. Kudin, M. C. Strain, O. Farkas, J. Tomasi, V. Barone, M. Cossi, R. Cammi, B. Mennucci, C. Pomelli, C. Adamo, S. Clifford, J. Ochterski, G. A. Petersson, P. Y. Ayala, Q. Cui, K. Morokuma, D. K. Malick, A. D. Rabuck, K. Raghavachari, J. B. Foresman, J. J. V. Cioslowski, A. G. Ortiz, B. B. Baboul, G. Stefanov, A. Liu, Liashenko, P. Piskorz, I. Komaromi, R. Gomperts, R. L. Martin, D. J. Fox, T. Keith, M. A. Al-Laham, C. Y. Peng, A. Nanayakkara, C. Gonzalez, M. Challacombe, P. M. W. Gill, B. Johnson, W. Chen, M. W. Wong, J. L. Andres, C. Gonzalez, M. Head-Gordon, E. S. Replogle, J. A. Pople, *Gaussian 98, Revision A.7*, Gaussian, Inc., Pittsburgh PA, **1998**.

Received June 3, 2003
Early View Article
Published Online October 2, 2003

 © 2003 Wiley-VCH Verlag GmbH & Co. KGaA, Weinheim

Platinum−Nitrogen Bond Rearrangements in Isomeric *cis*-$Pt^{II}(NH_3)_2$-bis(9-methyladenine) Complexes under Alkaline Conditions

Jorma Arpalahti*[a] and Karel D. Klika[a]

Keywords: Platinum / Nucleobases / Antitumor agents / N ligands

The migration of coordinated Pt^{II} in the adenine ring was studied in basic aqueous solutions for the isomeric bis(9-methyladenine) complexes: *cis*-$[Pt(NH_3)_2(9\text{-made-N7})_2]^{2+}$ (**1**) and *cis*-$[Pt(NH_3)_2(9\text{-made-N1})(9\text{-made-N7})]^{2+}$ (**2**). In both compounds, coordinated Pt^{II} migrates from the endocyclic nitrogen N(7) or N(1), respectively, to the exocyclic amino group, upon displacement of an NH_2 proton, to give the same first-generation product, viz. *cis*-$[Pt(NH_3)_2(9\text{-made-N6})(9\text{-made-N7})]^{2+}$ (**3**). Although both reactions undergo an intramolecular reaction, the N(1)→N(6) step is faster and far more efficient than the N(7)→N(6) step. This may be attributed to the more favorable electronic effects and to the spatial positioning of the N(1)-bound Pt^{II} in comparison to the platinum coordinated to the N(7) site. However, the contribution of a Dimroth-type rearrangement to the overall N(1)→N(6) conversion cannot be completely ruled out. Attempts to obtain second migration in the N(6),N(7)-bound species to give the N(6),N(6) species were unsuccessful. Rather, prolonged treatment of the N(6),N(7)-bound complex in strongly basic solution resulted in the deamination of the N(7)-bound 9-methyladenine yielding a mixed ligand complex consisting of N(6)-bound 9-methyladenine and N(7)-bound 9-methylhypoxanthine, i.e. *cis*-$[Pt(NH_3)_2(9\text{-made-N6})(9\text{-mhyp-N7})]^{2+}$ (**4**). To the best of our knowledge, this is the first example of such a deamination reaction in Pt^{II} complexes. Both reaction products, **3** and **4**, were characterized by ^1H and ^{195}Pt NMR spectroscopy and by X-ray crystallography of the diperchlorate. In dicationic **3** and **4**, the N(6)-bound 9-made exists in the rare imino tautomer with the N(1) site bearing a proton.

(© Wiley-VCH Verlag GmbH & Co. KGaA, 69451 Weinheim, Germany, 2003)

Introduction

The discovery of the anticarcinogenic activity of *cis*-$[PtCl_2(NH_3)_2]$ (cisplatin) by B. Rosenberg in 1969 has led to research interests being focused on the interactions of Pt compounds with nucleic acids and their constituents.[1−3] From a chemical point of view, considerable effort has been paid to the various binding modes[4] of Pt and to the kinetics of complexation.[1,5,6] Due to the general inertness of Pt^{II} and Pt^{IV}, and the high thermodynamic stability of the Pt−N bond, the factors affecting the initial binding step of Pt to DNA are considered crucial for understanding the biological activity of Pt drugs[1,5] and, in this respect, findings on relatively facile Pt−N bond rearrangements at the oligonucleotide level are of prime interest.[7−9] For example, rearrangement of *trans*-$[Pt(NH_3)_2\{d(G^*XG^*)\}]$ intrastrand adducts (where X = A, T, C; * denotes the platination site) into interstrand crosslinks appears as soon as the platinated oligonucleotides are hybridized with their complementary ribonucleotide or deoxyribonucleotide strands.[7] Unfortunately, the exact mechanism for this type of rearrangement is unknown, rendering model studies in this field highly desirable. There have been, however, a few reports on Pt−N bond rearrangements in simple complexes, either within the nucleobase moiety[10,11] or within the auxiliary[12] ligand. Other types of Pt−N bond rearrangements include oxidative Pt migration from the ring nitrogen to the exocyclic amino group in platinated pyrimidine complexes, which involve Pt^{IV} as an intermediate.[13−15] A clear picture, though, is not apparent as regards the factors controlling the migration reactions, and the latter may even require the cooperation of other nucleophiles.[8] In addition, Pt^{II} coordinated to different bioligands has also been found to migrate from the soft S atom to the hard N atom,[16−21] or vice versa.[22]

We have previously examined[23−25] the distribution of Pt^{II} in the adenine ring between the N(7) (kinetically preferred) and N(1) (thermodynamically preferred) binding modes in neutral solutions. Under basic conditions, though, migration of coordinated Pt^{II} to N(6) was observed from both N(1)[10] and N(7)[11] binding sites. In this study we wanted to compare the behavior of *cis*-N(7),N(7) coordinated Pt to the previously examined[11] *trans*-N(7),N(7) system and to contrast directly the N(1) and N(7) binding modes by using a mixed system, namely, *cis*-N(1),N(7) coordinated Pt, by following the reactions of *cis*-$[Pt(NH_3)_2(9\text{-made-N7})_2]^{2+}$ (**1**) and *cis*-$[Pt(NH_3)_2(9\text{-made-N1})(9\text{-made-N7})]^{2+}$ (**2**) under alkaline conditions (9-made = 9-methyl-

[a] Department of Chemistry, University of Turku,
20014 Turku, Finland
Fax: (internat.) + 358-2-333 6700
E-mail: jorma.arpalahti@utu.fi

Supporting information for this article is available on the WWW under http://www.eurjic.org or from the author.

adenine). In both complexes **1** and **2**, Pt^{II} migrates from an endocyclic nitrogen atom to the exocyclic amino group upon displacement of an N(6) proton to give a first-generation product, *cis*-$[Pt(NH_3)_2$(9-made-N6)(9-made-N7)$]^{2+}$ (**3**), which is common to the reactions of both **1** and **2**.[26] Further treatment of **3** at high pH results in the deamination of the N(7)-bound 9-made providing the corresponding 9-methylhypoxanthine (9-mhyp) complex, *cis*-$[Pt(NH_3)_2$(9-made-N6)(9-mhyp-N7)$]^{2+}$ (**4**).[26] Both reaction products **3** and **4** were characterized by ^1H and ^{195}Pt NMR spectroscopy and by X-ray crystallography of the diperchlorate.

Results and Discussion

General Considerations

The reactions of the isomeric *cis*-$Pt^{II}(NH_3)_2$-bis(9-methyladenine) complexes **1** and **2** were studied in strongly alkaline aqueous solutions at 65 and 85 °C employing HPLC equipped with an RP-18 column as an analytical tool. Both complexes **1** and **2** were found to undergo two distinct, consecutive reaction steps, the products of which were well resolved from each other, and from the starting material in both cases. Quite interestingly, the major first-generation product, **3**, is the same for the reactions of both **1** and **2** and possesses a much longer retention time than either of the starting compounds. This first-generation product slowly reacts further to yield the major second-generation product, **4**, which elutes earlier than either of the original complexes (see Figure 1). Both reaction steps also produced a small amount of free 9-methyladenine and several unidentified, weakly UV-absorbing (at 260 nm) side products with short retention times. Since the two consecutive reaction steps differ considerably, they are discussed separately.

Intramolecular Migration of Pt^{II}

Although both **1** and **2** give the same major first-generation product **3**, kinetically they behave in a very different manner. While the reaction **2**→**3** is clean and efficient, the reaction **1**→**3** proceeds less efficiently and produces a number of unidentified side products, particularly under more forcing conditions (see Tables S1 and S2). For example, at 338.2 K the overall decomposition of **1** in 1.0 M NaOH solution is rather fast [$k_{obs} = (4.10 \pm 0.04) \times 10^{-3}$ s^{-1}], but only about 6% of the starting material is converted into **3**, with weakly UV-absorbing side products constituting the remainder. At 358.2 K and in 1.0 M NaOH solution, the overall reaction is about five times faster than at 338.2 K, with **3** representing ca. 15% conversion. By contrast, in all cases the efficacy of the reaction **2**→**3** is greater than 95% of the overall decomposition of **2**, with free 9-methyladenine as the principal side product according to HPLC analysis. In 0.03 M NaOH solution, the reaction **2**→**3** is about 30 times faster than the **1**→**3** conversion (at 338.2 K), whereas in 1.0 M NaOH solution this reactivity difference is only a factor of three (see Figure 2). A similar trend is also in place

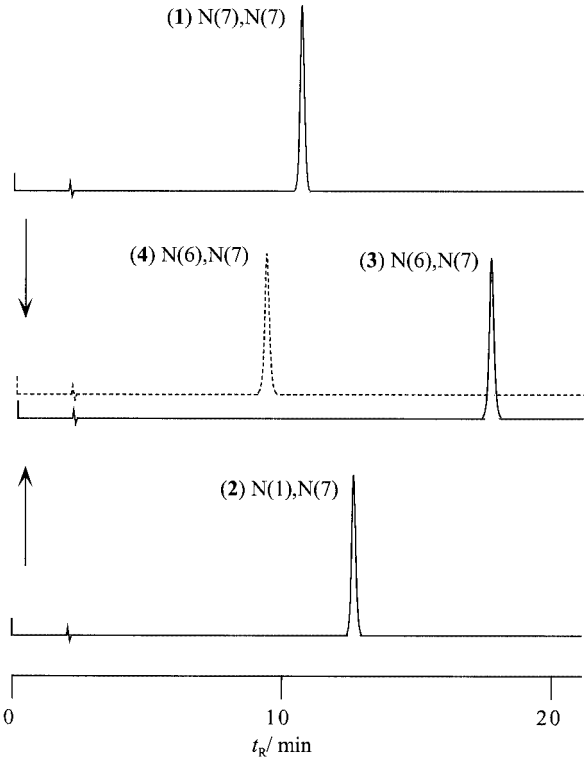

Figure 1. Simplified HPLC traces showing the conversion of **1**→**3** and **2**→**3** under alkaline conditions; the dotted line refers to the second reaction step **3**→**4**; the labeling of the signals refers to the binding sites of Pt^{II}

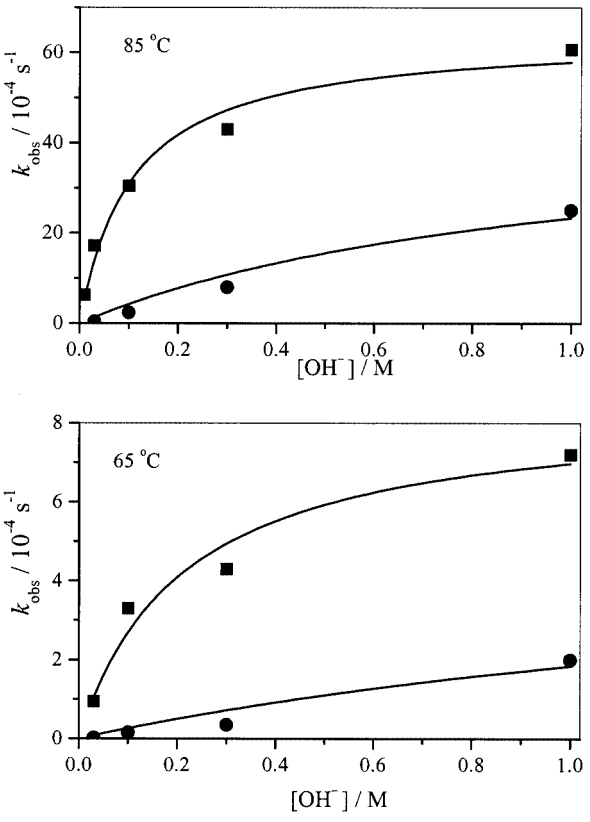

Figure 2. Observed rate constants for the reactions **1**→**3** (●) and **2**→**3** (■) as a function of pH at two different temperatures

 © 2003 Wiley-VCH Verlag GmbH & Co. KGaA, Weinheim

Table 1. ^{1}H and ^{195}Pt NMR chemical shifts in ppm for **3**, **4**, and some reference compounds[a]

Compounds		δ_{Pt}	δ_H(H2)	δ_H(H8)	δ_H(CH_3)
3	N(6)[b]	−2530 {−2457}	8.172 {7.995}[c]	7.995[c] {8.224}	3.780 {3.873}[d]
	N(7)[b]		8.328 {8.309}	8.702 {8.576}	3.897 {3.873}[d]
[e]	N(6)[b]	−2463 {−2520}	8.220 {8.315}	8.055 {8.302}	3.861 {3.878}
	N(7)[b]		8.593 {8.611}	8.999 {9.041}	4.023 {4.050}
4	9-made-N(6)[b]	−2524	8.111	7.994	3.785
	9-mhyp-N(7)[b]		8.318	8.570	3.872
[f]			8.30	8.55	3.89

[a] Spectra recorded in D_2O (^{1}H) or in H_2O/D_2O (^{195}Pt); minor species with an intensity of ca. 20% of the major one in braces. [b] Binding site of the nucleobase derivative and associated ^{1}H chemical shifts. [c] Overlapped. [d] Overlapped. [e] *trans*-[Pt(NH_3)$_2$(9-made-N6)(9-made-N7)]$^{2+}$.[11] [f] Pt(dien)(mhyp-N7)]$^{2+}$.[32]

at 358.2 K, where the reaction **2**→**3** is favored over the reaction **1**→**3** by a factor of 20 in 0.03 M NaOH, and by a factor of 2 in 1.0 M NaOH. It is worth noting that the first step in the conversion **2**→**3** was unequivocal: no other product with a retention time close to that of **3** could be detected by HPLC analysis.

Table 2. Crystal data and structure refinement for the complexes *cis*-[Pt(NH_3)$_2$(9-made-N6)(9-made-N7)](ClO_4)$_2$·H_2O (**3**) and *cis*-[Pt(NH_3)$_2$(9-made-N6)(9-mhyp-N7)](ClO_4)$_2$·H_2O (**4**)

	3	**4**
Empirical formula	$C_{12}H_{22}Cl_2N_{12}O_9Pt$	$C_{12}H_{21}Cl_2N_{11}O_{10}Pt$
Molecular mass	744.41	745.39
Crystal system	monoclinic	triclinic
Space group	*P*21/*c*	$P\bar{1}$
a (Å)	13.406(3)	11.428(3)
b (Å)	13.1230(17)	13.878(4)
c (Å)	13.9926(19)	8.2638(14)
α (°)		92.90(2)
β [°]	108.302(14)	108.941(14)
γ (°)		74.94(3)
V (Å^3)	2337.2(7)	1196.3(5)
Z	4	2
$D_{calcd.}$ (g cm^{-3})	2.116	2.069
μ (mm^{-1})	6.304	6.160
F(000)	1448	724
Crystal size (mm)	0.16 × 0.18 × 0.22	0.26 × 0.36 × 0.40
θ_{range} (°)	1.60−25.00	2.71−25.00
Index ranges	+16, +16, ±17	+14, ±17, ±10
Reflections coll.	4302	4432
Independent (R_{int})	4117 (0.0535)	4202 (0.0167)
Observed ($I > 2\sigma I$)	2697	3794
Absorption correction	ψ scan	ψ scan
Transmission	1.000−0.636	1.000−0.594
Refinement method	Full-matrix least-squares on F^2	
Data/restraints/parameters	4117/−/342	4202/−/354
Goodness-of-fit on F^2	1.014	1.045
R indices[a] ($I > 2\sigma I$)	R_1 = 0.0488	R_1 = 0.0336
	wR_2 = 0.1052	wR_2 = 0.0818
R indices (all data)	R_1 = 0.1076	R_1 = 0.0407
	wR_2 = 0.1219	wR_2 = 0.0845
Largest diff. peak and hole (eÅ^{-3})	1.514 and −1.598	1.623 and −2.248

[a] $R_1 = \Sigma||F_o| - |F_c||/\Sigma|F_o|$, $wR_2 = \{\Sigma[w(F_o^2-F_c^2)^2]/\Sigma\,[w(F_o^2)^2]\}^{1/2}$ and $w = 1/[\sigma^2(F_o^2) + (aP)^2 + bP)]$, where $P = (2F_c^2 + F_o^2)/3$.

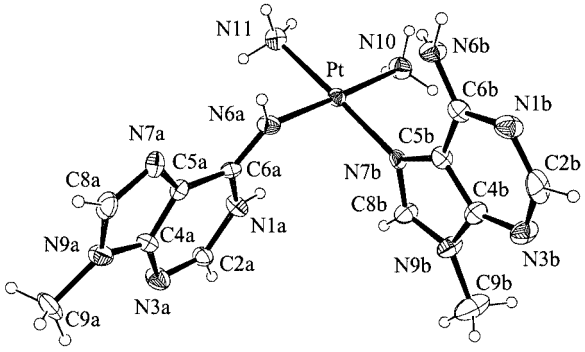

Figure 3. ORTEP plot showing 30% probability ellipsoids of the cation of *cis*-[Pt(NH_3)$_2$(9-made-N6)(9-made-N7)](ClO_4)$_2$·H2O (**3**) with its atom labeling scheme; selected interatomic distances (Å) and angles (°) with estimated deviations in parentheses: Pt−N(6a) 2.016(10), Pt−N(7b) 2.030(9), Pt−N(10) 2.056(9), Pt−N(11) 2.072(10), N(6a)−Pt−N(7b) 93.3(4), N(6a)−Pt−N(10) 177.8(4), N(7b)−Pt−N(10) 88.9(4), N(6a)−Pt−N(11) 86.8(4), N(7b)−Pt−N(11) 177.4(4), N(10)−Pt−N(11) 91.1(4), C(6a)−N(6a)−Pt 129.7(8)

We were able to purify and isolate **3** by fractionating the neutralized reaction solution. It was characterized using ^{1}H and ^{195}Pt NMR spectroscopy (Table 1) and by X-ray crystallography of the diperchlorate (Table 2), thus revealing that the compound is a bis(9-methyladenine) complex of *cis*-$Pt^{II}(NH_3)_2$ where one 9-methyladenine is coordinated to Pt through N(7) and the other through the exocyclic amino group upon displacement of an NH_2 proton which is translocated to N(1) upon acidification. A thermal ellipsoid diagram for the dication of **3** is presented in Figure 3. The platinum atom has nearly square-planar geometry, as is typical for these types of complexes, and lies virtually in the plane defined by the four coordinating nitrogen atoms deviating less than 0.02 Å from this plane. However, the N(6a)−Pt−N(7b) angle is widened [93.3(4)°] at the expense of the N(6a)−Pt−N(11) angle [86.8(4)°]. The Pt−N bond lengths in **3** are comparable to those in **1** and **2** and also to those in the corresponding N(6),N(7)-bound *trans* isomer.[11] It is notable that the Pt−N(6a) bond appears to be significantly shorter by more than three standard deviations[27] than the Pt−NH_3 bonds. Protonation of N(1a) also slightly widens the C(2)−N(1)−C(6) angle [C(2a)−N(1a)−C(6a) 124.5(11)°; C(2b)−N(1b)−C(6b)

 © 2003 Wiley-VCH Verlag GmbH & Co. KGaA, Weinheim

119.8(11)°]; a similar widening was also observed in the corresponding *trans* compound.[11] The packing of **3** is stabilized by hydrogen bonding involving primarily the am(m)ine hydrogens and perchlorate oxygens, e.g. N(11)···O(21) 2.974(16) Å, N(6a)···O(24) 3.223(15) Å, and N(10)···O(22[a]) 3.192(17) Å. Other possible H-bonds include: N(6b)···N(1b[b]) 3.105(14) Å, N(1a)···O(14[c]) 2.849(15) Å, and O(1w)···N(3a[d]) 3.285(29) Å. [Symmetry operations: a) $-x + 1, y - 1/2, -z + 1/2$; b) $-x + 1, -y, -z + 1$; c) $x, -y + 1/2, z + 1/2$; d) $-x, y + 1/2, -z + 1/2$.] However, stacking of the base moieties does not play a significant role in stabilizing the crystal lattice.

In aqueous solution, the dication of **3** shows evidence of dynamic processes as indicated by the splitting of the ^{1}H and ^{195}Pt signals. Most probably, the dynamic process in effect is the restricted rotation of the nucleobase(s) about the Pt−N bond, as has been observed frequently with Pt^{II} complexes of adenine derivatives.[10,11,23] The ^{1}H chemical shifts are in line with the proposed binding modes showing significant downfield shifts for those signals near the proposed Pt^{II} coordination site, whereas the δ_{Pt} values close to −2500 ppm are typical for a PtN_4 coordination sphere[28] and are in agreement with those reported earlier for the corresponding *trans* isomer.[11]

Mechanistically, the formation of **3** is interesting since it forms directly from supposedly inert, isomeric species. The readiness of the reactions **1**→**3** and **2**→**3** rules out the likelihood that the reaction proceeds via hydrolysis of the initial Pt−N bonds and then formation of the Pt−N(6) bond by taking into account the reasoning given earlier for the N(7)→N(6) migration in the N(7)-bound bis(9-methyladenine) complex of *trans*-Pt^{II}(NH$_3$)$_2$.[11] Moreover, the nonlinear dependency of the reactions **1**→**3** and **2**→**3** on [OH$^-$] indicates that the OH$^-$ ion (known as a poor *trans*-labilizing group) does not act as nucleophile on Pt^{II}.[29,30] Rather, the proposed mechanism involves an intramolecular migration of coordinated Pt from endocyclic ring nitrogens, N(7) in **1** or N(1) in **2**, to the exocyclic amino group upon displacement of an NH_2 proton, as depicted in Scheme 1 for the reaction **1**→**3**.

As the first step, deprotonation of the exocyclic amino group provides an imino group close to Pt^{II}, albeit fleetingly transient. Values of 3.430(7) Å and 3.515(7) Å have been reported for the N(6)···Pt distances in the two crystallographically distinct cations of **1**, whilst for **2**, the N(6)···Pt distances are 3.149(8) Å and 3.446(8) Å for the N(1)- and N(7)-bound 9-methyladenines, respectively. For **1**, the attack of the imino group on Pt results in a five-coordinate intermediate, where subsequent cleavage of the presumably weaker Pt−N(7) bond furnishes the N(7)→N(6) migration of Pt in an analogous fashion to the *trans* isomer.[11] Most probably, the same mechanism is also valid for **2** to effect the N(1)→N(6) migration, or at least partly so. Here the efficacy of the migration can be attributed to the shorter N(6)···Pt distance in the N(1)-bound 9-methyladenine and also to the supposedly stronger influence of Pt^{II} on the acidity of the NH_2 protons. However, an alternative mechanistic explanation for the N(1)→N(6) migration of coordinated Pt involves exchanging of the N(1) and N(6) atoms via a Dimroth-type bond rearrangement. It has been proposed that in adenine derivatives, OH$^-$ attacks both protonated (amino form) and deprotonated (imino form) species at C(2), the former being significantly faster than the latter.[31] Although a Dimroth-type bond rearrangement cannot be completely ruled out for **2**, according to our current knowledge, the rate profile nevertheless indicates that the nucleophilic action of the OH$^-$ ion on deprotonated **2** does not play any significant role in the overall migration reaction.

The Second Reaction Step

In **3**, the comparable N(6b)···Pt distance of 3.54(1) Å provided the impetus for attempting a second Pt migration to obtain the N(6),N(6)-bound species. Prolonged treatment of the reaction mixtures of both **1** and **2** ([OH$^-$] > 0.1 M) slowly yielded one major second-generation product, **4**, common to both initial complexes, together with free 9-methyladenine and several unidentified side products. In a 0.1 M NaOH solution (358.2 K), the reaction **3**→**4** is rather inefficient and yields only ca. 15% conversion of **3** to **4**, using **3** as a starting material with the principal side product being 9-methyladenine. However, in 1.0 M NaOH (358.2 K), the yield of **4** rises to ca. 75% and the amount of free 9-methyladenine produced is negligible.

Serendipitously, **4** is virtually insoluble in cold alkali and can thus be easily separated from the reaction mixture. The crude product converts to sparingly soluble in dilute perchloric acid and can be recrystallized as the diperchlorate. The structure provided by X-ray analysis showed Pt^{II} to be bound now to two distinct ligands: 9-made through N(6) and 9-methylhypoxanthine (9-mhyp) through N(7), that is, the N(6),N(7)→N(6),N(6) transformation does not occur and prolonged treatment only results in N(6) deamination of the N(7)-bound ligand. This transformation has not been observed previously for Pt-bound adenines, but substrates have never been subjected to such forcing conditions as they

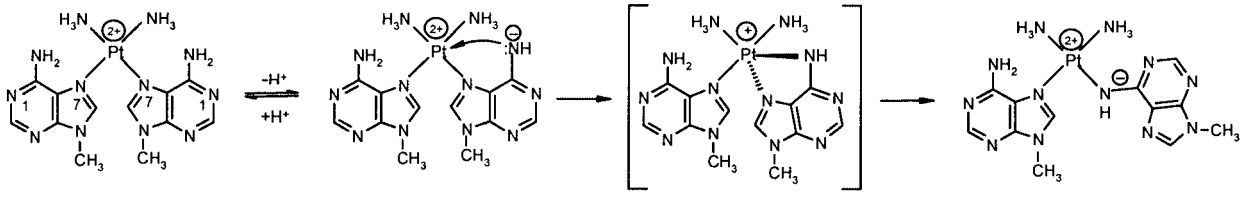

Scheme 1. Intramolecular N(7)→N(6) migration (**1**→**3**) of coordinated Pt upon displacement of an NH_2 proton

 © 2003 Wiley-VCH Verlag GmbH & Co. KGaA, Weinheim

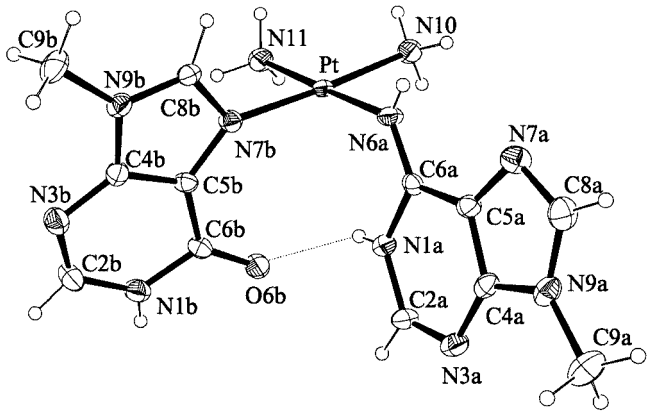

Figure 4. ORTEP plot showing 30% probability ellipsoids of the cation of *cis*-[Pt(NH_3)$_2$(9-made-N6)(9-mhyp-N7)](ClO_4)$_2$·H_2O (**4**) with its atom labeling scheme; selected interatomic distances (Å) and angles (°) with estimated deviations in parentheses: Pt−N(6a) 2.005(6), Pt−N(7b) 2.020(5), Pt−N(10) 2.040(6), Pt−N(11) 2.060(6), N(6a)−Pt−N(7b) 91.6(2), N(6a)−Pt−N(10) 89.3(2), N(7b)−Pt−N(10) 176.9(2), N(6a)−Pt−N(11) 178.6(2), N(7b)−Pt−N(11) 89.6(2), N(10)−Pt−N(11) 89.5(2) C(6a)−N(6a)−Pt 128.4(5)

were here.[11] A thermal ellipsoid diagram for the dication of **4** is shown in Figure 4. The atom bound to C(6b) is best identified as oxygen rather than nitrogen according to the thermal displacement parameters and the *R* values of least-squares refinements. This is supported by the elemental analysis, which provided a composition consistent with this structure.

Only a single platinum signal resonating at δ = −2524 ppm was observed for **4**, which is consistent with a PtN_4 coordination sphere. This species singularity was also evident in the ^{1}H NMR spectrum of **4** where four aromatic protons within the range δ = 7.99−8.57 ppm with nearly equal intensities, together with two methyl groups in a 1:1 ratio further upfield, were observed. These chemical shifts are apt for this structure in comparison to the reference compounds (see Table 2). Finally, treatment of **4** with thiourea (tu), which is known[25] to displace nitrogen-bound ligands from Pt^{II}, provided three HPLC-detectable end products in approximately stoichiometric amounts, namely, $[Pt(tu)_4]^{2+}$-ion, 9-made, and 9-mhyp, identified as such by coelution with authentic samples.

According to the X-ray analysis, the platinum atom in **4** has an almost idealized square-planar geometry with the Pt atom lying in the plane defined by the four coordinating nitrogen atoms, deviating by less than 0.03 Å from this plane. The Pt−N bond lengths in **4** are similar to those in **3**, with the Pt−N(6a) bond being significantly shorter by $> 4.1\sigma$[27] than the Pt−NH_3 distances. The packing of **4** is stabilized by hydrogen bonding involving primarily the am(m)ine hydrogens and the perchlorate oxygens, e.g. N(10)···O(21^a) 3.102(11) Å, N(6a)···O(23^a) 3.092(9) Å, and N(1b)···O(12^b) 2.938(11) Å. Most notable, though, is the intramolecular H-bond N(1a)···O(6b) 2.889(8) Å, where the proton involved was located from the electron density map. Other possible H-bonds include N(10)···O(1w^a) 3.050(9) Å and N(11)···O^a 3.038(12) Å. [Symmetry operations: a) $-x$, $-y+1$, $-z+1$; b) $-x+1$, $-y$, $-z+1$.] The intramolecular H-bond may affect the orientation of the bases in **4**, as seen in the dihedral angle between the base moieties and the Pt coordination sphere, namely 72.5(2)° for the N(6)-bound 9-made and 82.7(2)° for the N(7)-bound 9-mhyp. In **3**, the corresponding angles are 80.5(2) and 86.8(3)°, respectively. Also the dihedral angle between the base moieties is different; 76.5(2)° in **4** and 89.2(2) in **3**. The crystal lattice of **4** is further stabilized by stacking of the six-membered rings of adjacent hypoxanthine bases in a head-to-tail fashion with a distance of 3.44(2) Å between the centers of the rings. Deamination of the N(7)-bound 9-methyladenine and subsequent protonation of N(1b) widens the C(2b)−N(1b)−C(6b) angle from 119.8(11)° to 125.3(7)°, a widening similar to that observed for the N(6)-bound ligand in **3**.

Conclusions

Coordinated Pt^{II} has been found to migrate in the adenine ring from both the N(1) and N(7) sites to the exocyclic amino group, upon displacement of an NH_2 proton in basic aqueous solution. Although both isomeric bis(complexes) of 9-methyladenine with N(7),N(7) and N(1),N(7) binding modes of Pt^{II} undergo an intramolecular reaction and provide the same first-generation product, the N(1)→N(6) migration is faster and far more efficient than the N(7)→N(6) migration. This may be attributed to more favorable electronic effects and to the spatial positioning of the N(1)-bound Pt^{II} in comparison to platinum coordinated to the N(7) site. However, the contribution of a Dimroth-type mechanism to the overall N(1)→N(6) conversion cannot be completely ruled out. Attempts to obtain a second platinum migration from the N(6),N(7)-bound species to produce the N(6),N(6) species were unsuccessful. Rather, the prolonged treatment of the N(6),N(7)-bound complex in strongly basic solution resulted in the deamination of the N(7)-bound 9-methyladenine and yielded the mixed ligand complex consisting of N(6)-bound 9-methyladenine and N(7)-bound 9-methylhypoxanthine. To the best of our knowledge this is the first example of such a deamination reaction in Pt^{II} complexes. By comparison, treatment of free 9-methyladenine in 1.0 M NaOH for 8 h at 85 °C did not provide 9-methylhypoxanthine, though this reaction is known to proceed in the presence of oxidizing agents,[32,33] and thereby it can be concluded that Pt complexation facilitates adenine deamination when migration is not favored. This is quite interesting when considering that for the two major DNA adducts of cisplatin, that is, A-N(7),G-N(7) and G-N(7),G-N(7) (where A = adenine, G = guanine), the former is more mutagenic than the latter, which is cytotoxic.[1,34,35] In addition, in dicationic **3** and **4**, the N(6)-bound 9-made exists in the rare imino tautomer with the N(1) site bearing a proton in an analogous fashion to other N(6)-metalated adenine derivatives.[4,10,11]

 © 2003 Wiley-VCH Verlag GmbH & Co. KGaA, Weinheim

Experimental Section

Materials: 9-Methylhypoxanthine (9-mhyp) from Chemogen was used as received. The compounds 9-methyladenine[36] (9-made), $[Pt(tu)_4]Cl_2$[37] (tu = thiourea), *cis*-$[Pt(NH_3)_2(9\text{-made-}N7)_2](ClO_4)_2$ (**1**),[24] and *cis*-$[Pt(NH_3)_2(9\text{-made-}N1)(9\text{-made-}N7)](ClO_4)_2$ (**2**)[24] were obtained as described previously. All other chemicals were of the highest purity available and were used as received. For the preparation of *cis*-$[Pt(NH_3)_2(9\text{-made-}N6)(9\text{-made-}N7)](ClO_4)_2\cdot H_2O$ (**3**), 65 mg of **2** was dissolved in 5 mL of 0.1 M NaOH and the mixture was stirred for 30 min at 85 °C in a stoppered tube. The mixture was neutralized (pH 6) using 1 M $HClO_4$ and the resulting solution concentrated to ca. 1 mL, prior to fractionation using a preparative RP-18 column.[38] After concentration, the combined fractions of **3** afforded 30 mg (50%) of crystalline product upon cooling on ice. $C_{12}H_{22}Cl_2N_{12}O_9Pt$ (744.41): calcd. C 19.36, H 2.98, N 22.58; found C 19.42, H 2.94, N 22.60.

The compound *cis*-$[Pt(NH_3)_2(9\text{-made-}N6)(9\text{-mhyp-}N7)](ClO_4)_2\cdot H_2O$ (**4**) was obtained in a similar manner by dissolving 55 mg of **3** in 5 mL of 1 M NaOH and stirring the mixture for 6 h at 85 °C. Upon cooling to room temperature, crude **4** precipitated from the reaction mixture and was separated by centrifugation. The collected product was first dissolved using a calculated amount of 1 M $HClO_4$ to provide a solution of pH 6 which afforded 28 mg (51%) of **4** as colorless prisms suitable for X-ray analysis upon cooling on ice. $C_{12}H_{21}Cl_2N_{11}O_{10}Pt$ (745.39): calcd. C 19.34, H 2.84, N20.67; found C 19.14, H 2.90, N 20.67.

Methods: NMR measurements were conducted in D_2O (^1H) or in H_2O/D_2O (^{195}Pt) at ambient temperature. Spectra were acquired on a JEOL Alpha 500 spectrometer equipped with a 5 mm tunable probe operating at 500.16 MHz for ^1H, and 107.21 MHz for ^{195}Pt as described earlier.[23,24,38] ^1H spectra were referenced internally to sodium 4,4-dimethyl-4-silapentanesulfonate (δ_H = 0.015 ppm); ^{195}Pt spectra were referenced externally to $[PtCl_4]^{2-}$ (δ_{Pt} = −1625 ppm from $[PtCl_6]^{2-}$). HPLC analyses were conducted on a Merck-Hitachi chromatograph using an end-capped RP-18 column (5 μm, E. Merck AG) and water−methanol mixtures (0.05 M $NaClO_4$, pH 3) as eluents.

Migration Studies: The reactions of the Pt^{II} complexes were followed at 65 and 85 °C at various $[OH^-]$ by HPLC. Samples withdrawn from the aqueous reaction mixtures (I = 1 M, adjusted with $NaClO_4$) were diluted with an appropriate mixture of cold 1 M $HClO_4$ and HOAc/NaOAc buffer (pH 4) prior to chromatographic analysis. First-order rate constants, $k_{1,obs}$, for the disappearance of the starting material were obtained by Equation (1), where $[S]_0$ denotes the initial concentration of the complex and $[S]_t$ the concentration at time t.

$$\ln[S]_t = -k_{1,obs}t + \ln[S]_0 \quad (1)$$

In a few cases the rate constants, $k_{2,obs}$, for the decomposition of **3** were obtained by Equation (2) from the time-dependent concentration of **3**, denoted as $[P]_t$, using $k_{1,obs}$ values obtained from Equation (1) where $[P]_{max}$ is the maximum observed concentration of **3** at moment t_{max}.

$$\frac{[P]_t}{[P]_{max}} = \frac{e^{-k_{1,obs}t} - e^{k_{2,obs}t}}{e^{-k_{1,obs}t_{max}} - e^{k_{2,obs}t_{max}}} \quad (2)$$

When possible, the amount of **3** or **4** formed was approximated by HPLC analysis employing a standard solution of the desired species. In all cases, the signal area was used as the measure of the concentration.

X-ray Diffraction Studies: All X-ray data were collected on a Rigaku AFC5S diffractometer at ambient temperature using Mo−K_α radiation (λ = 0.71069 Å). Unit cell parameters were obtained from a least-squares fit of 20 reflections [11.07 < 2θ < 15.96° (**3**) and 10.70 < 2θ < 16.14° (**4**)]. Intensity data were collected by the ω/2θ scan technique to a maximum 2θ value of 50°. The intensities of three standard reflections were measured every 150 data points in all cases [intensity decays, 3.4% (**3**) and 1.2% (**4**)]. The intensities of the reflections were corrected for Lorenz, polarization, and absorption (empirical) effects.[39] The structures were solved by standard Patterson and difference Fourier methods and refined by full-matrix least-squares calculations employing SHELXL-97.[40] All atoms other than hydrogen were refined with anisotropic temperature factors. The positions of the hydrogen atoms in **3** were calculated except for those located at N(1a), N(6a) and N(6b) which were found from electron density maps. For **4**, the proton at N(6a) and those at the C and N atoms of the aromatic rings were also found from the electron density maps. The water hydrogens could not be located. The final cycle of refinement yielded for the structure of **3**, R_1 = 0.0448 and wR_2 = 0.1052 for the observed data [$I > 2\sigma(I)$] and 342 parameters, and R_1 = 0.1076 and wR_2 = 0.1219 for all data. For **4**, refinement converged at R_1 = 0.0336 and wR_2 = 0.0819 for the observed data and 354 parameters, and R_1 = 0.0407 and wR_2 = 0.0846 for all data. Crystallographic data and experimental details are presented in Table 2. Data reduction and subsequent calculations were performed with *teXsan for Windows*.[41] Figures were drawn with *Ortep-3 for Windows*.[42] CCDC-212435 and CCDC-212436 for **3** and **4**, respectively, contain the supplementary crystallographic data for this paper. These data can be obtained free of charge at www.ccdc.cam.ac.uk/conts/retrieving.html [or from the Cambridge Crystallographic Data Centre, 12, Union Road, Cambridge CB2 1EZ, UK; Fax: (internat.) +44-1223/336-033; E-mail: deposit@ccdc.cam.ac.uk].

[1] For a recent and comprehensive collection of review articles, see: *Cisplatin − Chemistry and Biochemistry of a Leading Anticancer Drug* (Ed.: B. Lippert), Verlag Helvetica Chimica Acta Zürich, **1999**.
[2] Z. Guo, P. J. Sadler, *Angew. Chem. Int. Ed.* **1999**, *38*, 1512−1531.
[3] J. Reedijk, *Chem. Rev.* **1999**, *99*, 2499−2510.
[4] B. Lippert, *Coord. Chem. Rev.* **2000**, *200−202*, 487−516.
[5] J. Arpalahti, *Perspectives on Bioinorganic Chemistry, Vol. 4.* (Eds.: R. W. Hay, J. R. Dilworth, K. B. Nolan), JAI Press Inc., Stamford, Connecticut, **1999**, 165−208.
[6] J. Reedijk, *Proc. Natl. Acad. Sci. U. S. A.* **2003**, *100*, 3611−3616.
[7] M. Boudvillain, R. Dalbiès, M. Leng, *Met. Ions Biol. Syst.* **1996**, *33*, 87−103.
[8] D. Yang, S. S. G. E. van Boom, J. Reedijk, J. H. van Boom, A. H.-J. Wang, *Biochemistry* **1995**, *34*, 12912−12920.
[9] S. L. Bruhn, J. H. Toney, S. J. Lippard, *Prog. Inorg. Chem.* **1990**, *38*, 477−516.
[10] J. Arpalahti, K. D. Klika, *Eur. J. Inorg. Chem.* **1999**, 1199−1201.
[11] J. Viljanen, K. D. Klika, R. Sillanpää, J. Arpalahti, *Inorg. Chem.* **1999**, *38*, 4924−4925.
[12] S. Komeda, M. Lutz, A. L. Spek, Y. Yamanaka, T. Sato, M. Chikuma, J. Reedijk, *J. Am. Chem. Soc.* **2002**, *124*, 4738−4746.
[13] B. Lippert, H. Schöllhorn, U. Thewalt, *J. Am. Chem. Soc.* **1986**, *108*, 6616−6621.

 © 2003 Wiley-VCH Verlag GmbH & Co. KGaA, Weinheim

[14] F. Pichierri, D. Holtenrich, E. Zangrando, B. Lippert, L. Randaccio, *J. Biol. Inorg. Chem.* **1996**, *1*, 439−445.
[15] J. Müller, E. Zangrando, N. Pahlke, E. Freisinger, L. Randaccio, B. Lippert, *Chem. Eur. J.* **1998**, *4*, 397−405.
[16] S. S. G. E. van Boom, J. Reedijk, *J. Chem. Soc., Chem. Commun.* **1993**, 1397−1398.[10f]
[17] K. J. Barnham, M. I. Djuran, P. del S. Murdoch, P. J. Sadler, *J. Chem. Soc., Chem. Commun.* **1994**, 721−722.
[18] K. J. Barnham, M. I. Djuran, P. del S. Murdoch, P. J. Sadler, *J. Chem. Soc., Dalton Trans.* **1995**, 3721−3725.
[19] C. D. W. Fröhling, W. S. Sheldrick, *Chem. Commun.* **1997**, 1737−1738.
[20] M. Hahn, D. Wolters, W. S. Sheldrick, F. B. Hulsbergen, J. Reedijk, *J. Biol. Inorg. Chem.* **1999**, *4*, 412−420.
[21] M. I. Djuran, S. U. Milinkovic, *Aust. J. Chem.* **2000**, *53*, 645−649.
[22] E. L. M. Lempers, J. Reedijk, *Inorg. Chem.* **1990**, *29*, 1880−1884.
[23] J. Arpalahti, K. D. Klika, R. Sillanpää, R. Kivekäs, *J. Chem. Soc., Dalton Trans.* **1998**, 1397−1402.
[24] J. Arpalahti, K. D. Klika, S. Molander, *Eur. J. Inorg. Chem.* **2000**, 1007−1013.
[25] M. Mikola, K. D. Klika, J. Arpalahti, *Chem. Eur. J.* **2000**, *6*, 3404−3413.
[26] The charge of the complex is pH dependent with the proton being reintroduced at N(1) at lower pH.
[27] σ is defined as $\sigma = (\sigma_1^2 + \sigma_2^2)^{1/2}$ where σ_1 and σ_2 represent the errors in interatomic distances or angles that are being compared, see F. Zamora, M. Kunsman, M. Sabat, B. Lippert, *Inorg. Chem.* **1997**, *36*, 1583−1587.
[28] T. G. Appleton, J. R. Hall, S. F. Ralph, *Inorg. Chem.* **1985**, *24*, 4685−4693.
[29] M. Mikola, J. Arpalahti, *Inorg. Chem.* **1996**, *35*, 7556−7562.
[30] J. Arpalahti, E. Niskanen, R. Sillanpää, *Chem. Eur. J.* **1999**, *5*, 2306−2311.
[31] T. Fujii, T. Itaya, *Heterocycles.* **1998**, *48*, 359−390.
[32] E. G. Talman, W. Brüning, J. Reedijk, A. L. Spek, N. Veldman, *Inorg. Chem.* **1997**, *36*, 854−861.
[33] J. H. J. den Hartog, M. L. Salm, J. Reedijk, *Inorg. Chem.* **1984**, *23*, 2001−2005.
[34] L. J. N. Bradley, K. J. Yarema, S. J. Lippard, J. M. Essigmann, *Biochemistry* **1993**, *32*, 982−988.
[35] K. J. Yarema, S. J. Lippard, J. M. Essigmann, *Nucleic Acids Res.* **1995**, *23*, 4066−4072.
[36] H. Lönnberg, J. Ylikoski, J. Arpalahti, E. Ottoila, A. Vesala, *Acta Chem. Scand., Ser. A* **1985**, *39*, 171−180.
[37] J. Arpalahti, B. Lippert, H. Schöllhorn, U. Thewalt, *Inorg. Chim. Acta* **1988**, *153*, 51−55.
[38] M. Mikola, K. D. Klika, J. Arpalahti, *Chem. Eur. J.* **2000**, *6*, 3404−3413.
[39] A. C. T. North, D. C. Phillips, F. S. Mathews, *Acta Crystallogr., Sect. A* **1968**, *24*, 351−359.
[40] G. M. Sheldrick, *SHELXL 97, Program for the Refinement of Crystal Structures*, University of Göttingen, **1997**.
[41] *teXsan for Windows. Structure Analysis Software.* Molecular Structure Corporation, Texas 77381, USA, **1997**.
[42] L. J. Farrugia, *J. App. Cryst.* **1997**, *30*, 565.

Received June 12, 2003
Early View Article
Published Online October 10, 2003

 © 2003 Wiley-VCH Verlag GmbH & Co. KGaA, Weinheim

Ab initio Study on Luminescence and Aurophilicity of a Dinuclear $[(AuPH_3)_2(i\text{-}mnt)]$ Complex (i-mnt = isomer-Malononitriledithiolate)

Qing-Jiang Pan,[a,b] and Hong-Xing Zhang*[a]

Keywords: Ab initio calculations / Luminescence / Aurophilicity / Excited state

The luminescence and Au–Au aurophilicity of the model complex, $[(AuPH_3)_2(i\text{-}mnt)]$ (i-mnt = isomer-malononitriledithiolate in both solid state and solution have been studied by ab initio methods. The structures of the Au^I complex were fully optimized by the MP2 method for the ground state and the CIS method for the excited state. The b^3A' excited-state Au–Au (2.946 Å) and the corresponding Au–Au stretching frequency (83 cm^{-1}) indicate intramolecular Au–Au aurophilicity. Using $[(AuPH_3)_2(i\text{-}mnt)]_2$ to rationalize the solid-state emission to the $[(AuPPh_3)_2(i\text{-}mnt)]$ complex at 20 K we assigned the experimental emission (462 nm) to an Au–Au→i-mnt charge-transfer (^{3}MMLCT) transition from the triplet excited state to the ground state. In the ^{3}MMLCT emissive excited state, the Au–Au aurophilicity, including intra- and intermolecular Au–Au interactions, results in a ca. 120 nm red shift in emission relative to that of mononuclear PH_3AuSH. The calculated absorption and emission in dichloromethane solution agree with the experimental results. These results, combined with our previous studies on both $[Au_2(dpm)_2]^{2+}$ [dpm = bis(diphosphanyl)methane] and $[Au_2(dpm)(i\text{-}mnt)]$, indicate a clear correlation between Au–Au aurophilicity and the excited-state properties of the dinuclear Au^I complexes.
(© Wiley-VCH Verlag GmbH & Co. KGaA, 69451 Weinheim, Germany, 2003)

Introduction

The luminescence and aurophilicity of Au^I complexes have been extensively studied over the last two decades.[1−10] Many Au^I complexes luminesce in the solid state and/or in solution, mostly accompanied by intra- and/or intermolecular Au−Au interactions.[11−18] By experiments and accurate theoretical calculations containing electron correlation and relativistic effects, the energy of the Au−Au attraction was estimated to be 5−15 kcal/mol, similar to that of hydrogen bonds.[19−23] The photoluminescence properties of di- and polynuclear Au^I complexes are highly diversified. For various bridging and ancillary ligands, the luminescence properties of such complexes have been suggested to range from MLCT (metal-to-ligand charge transfer), LMCT (ligand-to-metal charge transfer), MCCT (metal-centered charge transfer) and ILCT (intraligand charge transfer).[24−27]

The Au−Au aurophilicity is correlated with the excited-state properties, especially for MCCT in dinuclear Au^I complexes such as those with bridging phosphane ligands, which possess a lower-energy phosphorescence (500−600 nm) in acetonitrile.[26,27] Ab initio calculations indicated that the $^3(d_{\sigma^*}s_\sigma)$ excited state corresponding to the lower-energy emission presents an Au−Au distance of ca. 2.72 Å, which is much shorter than the ca. 3.16 Å in the ground state.[28] The promotion of electron from the d_{σ^*} antibonding orbital to the s_σ bonding orbital affords an Au−Au σ single bond in the MCCT emissive excited state. In addition, for the well-known dinuclear Pt^{II} complex $[Pt_2(pop)_4]^{4-}$ (pop = pyrophosphate), Pt−Pt in the $^3(d_{\sigma^*}p_\sigma)$ excited state shortens by ca. 0.29 Å relative to that in the ground state, which is supported by both the excited-state structure from time-resolved X-ray diffraction and ab initio studies.[29,30]

For Au^I complexes containing both phosphane and thiolate ligands, the lower-energy emissions in the solid state have been experimentally attributed to Au→thiolate charge transfer (MLCT).[11,17,24,31−36] Bruce's studies on a series of dinuclear (phosphane)Au^I thiolates with or without Au−Au interaction showed that the interaction is not a necessary condition for luminescence and that its presence does not significantly perturb the luminescence;[32] however, Fackler and co-workers found that the emission maximum in the luminescence of many mononuclear (phosphane)Au^I thiolate complexes can be affected by an Au−Au interaction.[11] In fact, such studies are not incompatible. The charge transfer from metal to ligand should be divided into metal−metal-to-ligand charge transfer (MMLCT) and metal-to-ligand charge transfer (MLCT).[12,18,37] The former is clearly correlated with the Au−Au interaction but the latter does not.

[a] State Key Lab of Theoretical and Computational Chemistry, Institute of Theoretical Chemistry, Jilin University, Changchun 130023, P. R. China
Fax: (internat.) + 86-431/8945942
E-mail: hxzhang@mail.jlu.edu.cn
[b] College of Chemistry and Chemical Engineering, Heilongjiang University, HaerBin 150080, China

 © 2003 Wiley-VCH Verlag GmbH & Co. KGaA, Weinheim **DOI: 10.1002/ejic.200300389**

Unlike those of dinuclear Au^I complexes with bridging phosphane ligands, the excited-state properties of dinuclear (phosphane)Au^I thiolates are clearly related to MMLCT or MLCT, in which the thiolate ligands are greatly involved in the luminescence.[31−36] This is because phosphane ligands always provide lone-pair electrons to form the dative P→Au bond while thiolates, usually as anions, prefer the covalent S−Au bond to coordinating. These different electronic properties may lead to differences in luminescence and aurophilicity when thiolates are introduced into (phosphane)Au^I complexes to form (phosphane)Au^I thiolate complexes.

To study both their luminescent properties and Au−Au aurophilicity, several dinuclear Au^I complexes have been designed, with at least two different structural arrangements: the more common dinuclear Au^I dimers, in which the aurophilicity is sterically imposed,[26,27,38,39] and the open-ring structural disposition, in which the interaction between two Au^I atoms, if it appears, is not sterically imposed.[31−34,40,41] The structurally characterized (phosphane)Au^I thiolate [$(AuPPh_3)_2$(i-mnt)] (i-mnt = isomer-malononitriledithiolate has a nonimposed intramolecular Au−Au interaction.[41] The intense 462 nm phosphorescence of the solid-state complex at 20 K was assigned as an Au→thiolate charge transfer (^{3}MLCT) from the triplet excited state to the ground state.[33,34] Since the π-conjugated i-mnt ligand is greatly involved in the emission and Au−Au aurophilicity is possibly present in the corresponding excited state, the [$(AuPPh_3)_2$(i-mnt)] complex may be an ideal candidate for the ^{3}MMLCT emissive excited state.

Dinuclear Au^I thiolates have also been widely applied in medicine,[42] optical sensors,[12,13,43] and photoredox chemistry.[22,24,27,44] For example, the therapeutic action of gold drugs for rheumatoid arthritis may be related to the ability of the Au^I complexes to quench the singlet oxygen $^1\Delta_g$ state at 7752 cm^{-1}.[42c] Eisenberg and co-workers have reported that [Au{$S_2CN(C_5H_{11})_2$}]$_2$ can be used to monitor efficiently volatile organic compounds (VOCs), by a reversible interaction with VOC vapors that results in both a dramatic color change and a positive "switching on" of luminescence.[13] Such applications make use of excited-state properties. Thus, theoretical investigation of the electronic structures of the ground and excited states for the Au^I complexes is also of practical significance.

Here, ab initio methods have been employed to study the spectroscopic properties and Au−Au aurophilicity of [$(AuPH_3)_2$(i-mnt)] in both solid state and solution. In the solid state, the calculated 450-nm phosphorescence of [$(AuPH_3)_2$(i-mnt)]$_2$ was assigned as an Au−Au→i-mnt charge transfer (^{3}MMLCT) from the triplet excited state to the ground state, similar to the 462-nm solid-state emission of the [$(AuPPh_3)_2$(i-mnt)] complex at 20 K. In the ^{3}MMLCT emissive excited state of polynuclear [$(AuPH_3)_2$(i-mnt)]$_2$, both intra- and intermolecular Au−Au interactions strongly affect the solid-state emission, causing a ca. 120 nm red shift with respect to the 332-nm emission of mononuclear PH_3AuSH. The studies of $[Au_2(dpm)_2]^{2+}$ [dpm = bis(diphosphanyl)methane],[28] [$(AuPH_3)_2$(i-mnt)] and [Au_2(dpm)(i-mnt)] show that the Au−Au aurophilicity is clearly correlated with the excited-state properties of these Au^I complexes.

Computational Details and Theory

In the calculations, [$(AuPH_3)_2$(i-mnt)] was employed to represent the real [$(AuPPh_3)_2$(i-mnt)] complex. A similar model was applied in our previous work[28] by using dpm to stand for dmpm, dppm and dcpm in the $[Au_2(dmpm)_2]^{2+}$, $[Au_2(dppm)_2]^{2+}$ and $[Au_2(dcpm)_2]^{2+}$ complexes respectively [dmpm = bis(dimethylphosphanyl)methane, dppm = bis(diphenylphosphanyl)methane and dcpm = bis(dicyclohexylphosphanyl)methane]. Hydrogen is generally used in place of methyl, phenyl substituents etc. in ab initio studies to save computational resources. Häberlen and Rösch[45] have proved that PH_3 provided a satisfactory model for PMe_3 or PPh_3 for the structural properties of Au^I complexes. Bruce[22] and other researchers[26,46,47] have successfully used such a kind of model in their theoretical studies on the related topics of (phosphane)Au^I complexes.

Here, the C_s symmetry was adopted to settle the conformation of [$(AuPH_3)_2$(i-mnt)] in both the ground and excited states. The structures of the ground and excited states were fully optimized by the second-order Møller−Plesset perturbation (MP2)[48] and the single excitation configuration interaction (CIS)[49] methods, respectively, in which electron correlation effects were considered.[22,23] Based on such calculations, the isodensity-polarized continuum model (IPCM) in the self-consistent reaction field (SCRF) method[50−53] was employed to account for the solvent effect of dichloromethane, by considering the dramatic red shift of emission due to the solvation of acetonitrile on $[Au_2(dpm)_2]^{2+}$ indicated previously.[28] Therefore, the electronic structure of the excited state and the absorption and emission in CH_2Cl_2 solution were obtained.

In the calculations, the quasi-relativistic pseudopotentials of the Au, S and P atoms proposed by Hay and Wadt[54] with 19, 6 and 5 valence electrons, respectively, were employed and the LANL2DZ basis sets associated with the pseudopotential were adopted and implemented by one additional f-type function for Au (α_f = 0.2), and a d-type function for S (α_d = 0.421) and P (α_d = 0.34).[23] The basis sets were taken as Au(8s6p3d1f/3s3p2d1f), S(3s3p1d/2s2p1d), P(3s3p1d/2s2p1d), N(10s5p/3s2p), C(10s5p/3s2p) and H(4s/2s). Thus, 176 basis functions and 104 electrons were included for [$(AuPH_3)_2$(i-mnt)] in the calculations. All the calculations were performed with the Gaussian98 program package[53] using an Origin/3800 server.

Result and Discussion

A. Structures of the Ground and Excited States of [$(AuPH_3)_2$(i-mnt)]

The full MP2 optimizations on [$(AuPH_3)_2$(i-mnt)] indicate that the complex has a $^1A'$ ground state with [(28a′^{2})-

 © 2003 Wiley-VCH Verlag GmbH & Co. KGaA, Weinheim

Table 1. Optimized geometry parameters of the $^1A'$ ground state using the MP2 method and the a^3A' and b^3A' excited states using the CIS method for $[(AuPH_3)_2(i\text{-}mnt)]$, together with the experimental data of $[(AuPPh_3)_2(i\text{-}mnt)]$

Parameters	Ground state $^1A'$	Experiment	Excited state a^3A'	b^3A'
Bond lengths [Å]:				
Au1−Au2	2.945	3.156	4.753	2.946
Au1−P3	2.327	2.257	2.390	2.477
Au1−S5	2.335	2.313	2.380	2.506
S5−C7	1.782	1.729	1.771	1.740
C7−C8	1.406	1.372	1.490	1.402
C8−C9	1.455	1.432	1.423	1.434
C9−N11	1.216	1.132	1.158	1.154
P3···P4	3.826		6.657	5.966
S5···S6	3.223		3.108	3.152
Bond angles [°]:				
P3−Au1−S5	165.7	172.1	176.7	140.1
P3−Au1−Au2	100.9		113.5	127.6
S5−Au1−Au2	93.4		69.8	92.4
S5−C7−S6	129.4	123.2	122.6	129.9
Dihedral angles [°]:				
P3−Au1−Au2−S6	180.0		179.4	−179.8
S5−C7−C8−S6	−179.4		176.2	−180.0
Au1−S5−S6−C7	−178.1		−87.9	−179.9

$(24a''^2)$] electronic configuration. The calculated main geometry parameters are listed in Table 1, associated with the data from X-ray crystal diffraction for the $[(AuPPh_3)_2(i\text{-}mnt)]$ complex.[41] The structure of the $^1A'$ ground state (Figure 1, a) consists of two $AuPH_3$ units bridged by an i-mnt ligand. The calculated dihedral angles of 180.0° (P3−Au1−Au2−S6), −179.4° (S5−C7−C8−S6) and −178.1° (Au1−S5−S6−C7) indicate that the molecule is nearly coplanar. The Au^I atom has a linear two-coordinate structure with a P3−Au1−S5 angle of 165.7°, which is similar to the experimental 172.1°. The calculated Au−Au (2.945 Å) bond is shorter than the 3.156 Å determined by experiment for $[(AuPPh_3)_2(i\text{-}mnt)]$ (Table 1) because we used the hydrogen atom in place of the phenyl ligand on the P atoms − the bulky phenyl ligand does not facilitate the approach of two Au^I atoms. Bruce et al.[22] have studied theoretically the luminescent properties and Au−Au aurophilicity of *cis*- and *trans*-$[Au_2X_2CH_2(PH_2)_2]$ (X = Cl, Br and I) complexes, in which the same approximation was employed. Their calculated results agreed well with experimental observations and revealed the nature of the excited states of the real $[Au_2X_2CH_2(PPh_2)_2]$ complex. Thus, our approximation applied here may have little effect on the excited-state properties of the $[(AuPPh_3)_2(i\text{-}mnt)]$ complex. The other distances in the $^1A'$ ground state presented by MP2 calculations accord with those determined experimentally (Table 1).

The frequencies calculated for the ground state of $[(AuPH_3)_2(i\text{-}mnt)]$, performed at the MP2 level, are all low relative to experiment (Table 2), but parallel them because of the ratio of calculation to experiment of 0.80−0.84, excluding the C=C stretching vibration. The 42 cm^{-1} frequency was assigned as the Au−Au stretching vibration and fell

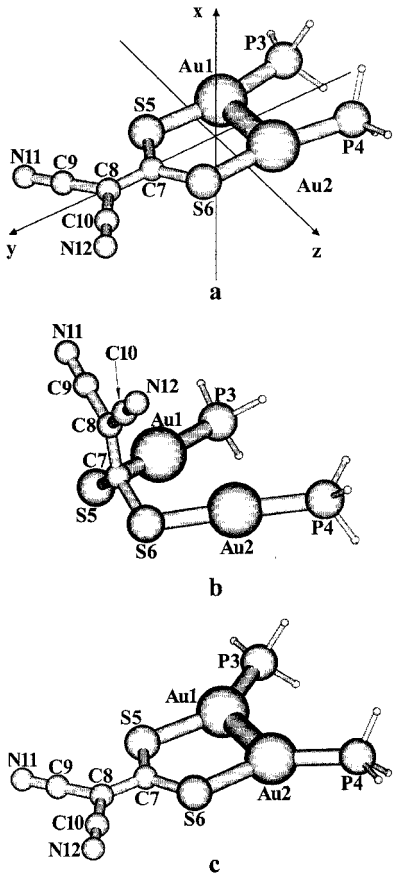

Figure 1. Optimized $^1A'$ (a) ground-state structure using the MP2 method, and the optimized a^3A' (b) and b^3A' (c) excited-state structures using the CIS method for $[(AuPH_3)_2(i\text{-}mnt)]$

Table 2. Calculated frequencies at the MP2 level for the $^1A'$ ground state of $[(AuPH_3)_2(i\text{-}mnt)]$, associated with Raman frequencies of $[(AuPPh_3)_2(i\text{-}mnt)]$

Assignment	Frequencies [cm^{-1}] Calcd.	Exp.	Calcd./exp.
ν(Au-Au)	42	36−71[a]	
ν(Au−P)	324	385	0.8416
ν(Au−S)	396	480	0.8250
ν(C−S)	695	865	0.8035
ν(C=C)	1372	1410	0.9730
ν(C≡N)	1856	2209	0.8402

[a] Frequencies of ν(Au−Au) from ref.[55]

well within the experimental range reported for such vibrations,[55] suggesting weak aurophilicity between the two Au^I atoms in the $^1A'$ ground state.

The CIS method was used to optimize the structure of the excited state of $[(AuPH_3)_2(i\text{-}mnt)]$. Two triplet excited states were obtained with a^3A' and b^3A' symmetries. The calculated geometry parameters (Table 1) and the corresponding structures (Figure 1, b and c) are given here. Apparently, the geometry of the excited states changes greatly with respect to that of the ground state. In the a^3A' excited state the i-mnt ligand deviates from the $Au_2S_2P_2$ plane due to the dihedral angle of −87.9° for Au1−S5−S6−C7, and

 © 2003 Wiley-VCH Verlag GmbH & Co. KGaA, Weinheim

almost all the ligand bonds are longer than those in the $^1A'$ ground state (Table 1). The two Au atoms are much farther apart (4.753 Å) than in the $^1A'$ ground state (2.945 Å), suggesting no Au−Au aurophilicity as the separation is much more than the van der Waals contact (3.4 Å).[56] Thus, the a^3A' excited state may be related to i-mnt intraligand charge-transfer character.

Unlike the a^3A' excited state, the geometry of the b^3A' excited state is still in a plane, which is intuitively depicted in Figure 1 (c) and quantitatively reflected in Table 1. The Au−Au (2.946 Å) is close to that in the $^1A'$ ground state, but the P···P distance (5.966 Å) in the excited state is far longer than the 3.826 Å in the ground state. This implies a significant Au−Au aurophilicity in the b^3A' excited state as the two P atoms tend to separate in opposite directions. To characterize the Au−Au interaction in the b^3A' excited state of $[(AuPH_3)_2$(i-mnt)], we also carried out frequency calculations. Through vibrational-mode analysis, the calculated frequency of 83 cm^{-1} was attributed to the Au−Au stretching frequency in the excited state, which is much higher than the 42 cm^{-1} frequency in the $^1A'$ ground state. The Au−Au stretching frequency provides evidence of aurophilic attraction between the two gold atoms in both the b^3A' excited state and the $^1A'$ ground state. In addition, the calculated overlap population between the two Au atoms is 0.062 and 0.036 for the b^3A' excited state and $^1A'$ ground state respectively. From such calculated frequencies and overlap populations between the two Au atoms, it is easily seen that although the Au−Au distances are very close in the b^3A' excited state (2.946 Å) and the $^1A'$ ground state (2.945 Å), the Au−Au aurophilicity in the former is stronger. This suggests that there may be some electron transfer to the 6s and/or 6p bonding orbitals of Au atoms in the b^3A' excited state, which then reinforces the Au−Au interaction.

B. Absorption Spectra of $[(AuPH_3)_2$(i-mnt)] in the CH_2Cl_2 Solution

Keeping the optimized structure of the ground state constant, the CIS method was used to calculate the excited state related to absorption. Based on such calculations, the solvent effect of dichloromethane was taken into account by the IPCM in the SCRF method[50−53] and absorption spectra of $[(AuPH_3)_2$(i-mnt)] in solution were obtained. The calculated absorption and the corresponding oscillator strength are given in Table 3, together with the experimental results of $[(AuPPh_3)_2$(i-mnt)] available in the CH_2Cl_2 solution at room temperature.

To assign the absorption in solution, the partial molecular orbital compositions (%) involved in the absorption transition are listed in Table 4, associated with the orbital components. The coordinate orientation of $[(AuPH_3)_2$(i-mnt)] is depicted in Figure 1 (a), in which the z axis parallels the line through the two Au atoms.

The calculated absorption maximum in CH_2Cl_2 solution is at 303 nm with the nature of an $X^1A'\rightarrow A^1A''$ transition. In the excitation, the $24a''\rightarrow 29a'$ configuration has the largest coefficient (ca. 0.6) in the CI wavefunctions, and is responsible for the absorption. The 24a′′ orbital (HOMO-1) has 68% i-mnt ligand composition, mainly contributed by the $S(p_y)$ orbital, while the metal (62%) plays an important role in the 29a′ orbital (LUMO), mainly from the $Au(p_z)$ character (Table 4). Thus, the 303-nm absorption, arising from the $X^1A'\rightarrow A^1A''$ transition, is attributed to $S(p_y)\rightarrow Au(p_z)$ charge transfer (LMCT) mixed with some $Au(d_{z^2})\rightarrow Au(p_z)$ charge transfer (MCCT), which corresponds to the 365-nm absorption observed experimentally for $[(AuPPh_3)_2$(i-mnt)] at room temperature.[33] The large difference between calculated and experimental absorption wavelength is caused mainly by the use of a hydrogen atom to represent the bulky phenyl ligand on P atoms. In a real $[(AuPPh_3)_2$(i-mnt)] system, the relatively longer Au−Au distance may result in less metal participation in the 24a′′ (HOMO-1) orbital. Because the order of the energy level in occupied orbitals is $S(p_\pi) > Au(d_{\sigma^*})$ by analyzing the wavefunctions, the lesser Au contribution to the transition wound reduce the excitation energy. Therefore, if the steric bulk of the phenyl ligands on P atoms was taken into account, the calculated absorption maximum would red-shift relative to the 303 nm of $[(AuPH_3)_2$(i-mnt)] and approach the experimental value of 365 nm.

For the B^1A' excited state, the corresponding absorption was calculated at 295 nm with an oscillator strength of 0.765, which is similar to the 310-nm absorption of the experiment[33] (Table 3). The transition arises mainly from the $28a'\rightarrow 30a'$ configuration with the largest CI coefficient of ca. −0.6. From Table 4, the 295 nm absorption from an $X^1A'\rightarrow B^1A'$ transition was assigned as i-mnt intraligand charge transfer (ILCT) with some LMCT. Because the B^1A' excited state has ILCT character and less metal participation, the approximation overestimating the metal−metal interaction does not significantly perturb the absorption, i.e. the calculated absorption wavelength of 295 nm agrees with the experimental absorption (310 nm).[33] To intuitively understand the absorption process, the density diagrams of the frontier molecular orbitals are depicted in Figure 2. In the 28a′ orbital (HOMO) the electron density mainly focuses around the i-mnt ligand, with the C7−C8 π-bonding orbitals, while in the 30a′ (LUMO+1) and 31a′ (LUMO+3) orbitals the electron density is still distributed on the i-mnt ligand and π* antibonding orbitals form between the two carbon atoms. Thus, we can further assign the 295-nm absorption to a $\pi\rightarrow\pi^*$ transition involving the C=C double bond. Gray et al.[57] have studied the electronic spectra of a series of metal complexes containing the i-mnt ligand in acetonitrile and attributed the absorptions in the range 250−350 nm to $L\rightarrow L^*$ charge transfer.

As a reference, the same methods and basis sets as those of $[(AuPH_3)_2$(i-mnt)] were used to calculate electronic spectra of the organic i-mnt ligand. The ligand also has a C_s symmetry in the calculations of both ground and excited states. The calculated absorption maximum in CH_2Cl_2 solution of 268 nm (Table 3), arising from a $\pi\rightarrow\pi^*$ transition localized on the C=C double bond, supports our assignment for the 295 nm absorption of $[(AuPH_3)_2$(i-mnt)].

 © 2003 Wiley-VCH Verlag GmbH & Co. KGaA, Weinheim

Table 3. Calculated absorption and emission of $[(AuPH_3)_2(i\text{-mnt})]$ and i-mnt ligand in the solid state and CH_2Cl_2 solution under the CIS calculations, together with experimental results

		Solid state Calcd. [nm]	Exp. [nm]	CH_2Cl_2 solution Calcd. [nm]	Exp. [nm]
$[(AuPH_3)_2(i\text{-mnt})]$	absorption			303 (0.068)[a]	365[b]
				295 (0.765)[a]	310[b]
				238 (0.364)[a]	225[b]
	emission	593	595[c]	702	
		414/450[d]	462[e]	333	
i-mnt ligand	absorption			268 (0.512)[a]	275[f]
	emission	611	595[c]	714	

[a] Oscillator strength in parentheses. [b] Absorptions of $[(AuPPh_3)_2(i\text{-mnt})]$ in CH_2Cl_2 solution at room temperature from ref.[33] [c] Solid-state emission of $K_2(i\text{-mnt})$ at 20 K from refs.[33,34] [d] 414- and 450-nm emissions from $[(AuPH_3)_2(i\text{-mnt})]$ and $[(AuPH_3)_2(i\text{-mnt})]_2$, respectively, from the present work. [e] Solid-state emission of $[(AuPPh_3)_2(i\text{-mnt})]$ at 20 K from ref.[33] [f] Average value of absorptions of a series of metal complexes with the i-mnt ligand in acetonitrile from ref.[57]

Table 4. Partial molecular orbital compositions (%) of $[(AuPH_3)_2(i\text{-mnt})]$ in CH_2Cl_2 solution under the CIS calculations

MO	Energy [eV]	Composition (%) 2 Au	i-mnt	2 PH_3	Components of orbital
34a′	3.1563	54.7	0.6	44.6	$Au(p_x) + P(p_x)$
33a′	2.8292	69.1	25.8	5.1	$Au(p_y) + S(p_y) + C7(p_y) + C8(p_y)$
32a′	2.2251	59.7	7.6	32.7	$Au(p_z) + P(p_z)$
26a"	1.9171	78.3	18.7	3.0	$Au(s,p_z)$
31a′	1.7527	15.2	72.1	12.7	$S(p_x) + C7(p_x) + Au(p_x)$
25a"	1.6085	75.4	4.6	20.0	$Au(p_x)$
30a′	0.1195	27.8	54.1	18.2	$C7(p_x) + C8(p_x) + N11(p_x) + Au(p_x)$
29a′ (LUMO)	0.0656	62.1	18.7	19.2	$Au(p_z)$
28a′ (HOMO)	−8.2323	5.5	94.1	0.4	$S(p_x) + C8(p_x) + N11(p_x)$
24a"	−8.6168	24.4	68.4	7.2	$S(p_y) + Au(d_{z^2})$
23a"	−9.0136	12.0	87.4	0.7	$S(p_x)$
22a"	−10.1012	40.2	14.8	45.0	$Au(d_{xy},p_y) + P(p_y)$
27a′	−10.3045	16.4	79.1	4.6	$S(p_y)$
26a′	−11.9418	44.1	17.9	37.9	$Au(d_{x^2-y^2},s) + P(p_y)$
25a′	−12.2743	8.8	90.5	0.7	$C7(p_x) + C9(p_x) + N11(p_x) + S(p_x)$
21a"	−12.3432	8.9	89.9	1.2	$S(p_y) + N7(p_y) + C9(p_y) + N11(p_y)$

The calculated 238-nm absorption from $X^1A' \rightarrow C^1A''$ is related to charge transfer between Au atoms and phosphane ligands. The main configuration 22a′′→29a′, gives rise to the absorption. The 22a′′ orbital has 45% PH_3 and 40% Au orbital character. Therefore, the 238-nm absorption was assigned as $P(p_y) \rightarrow Au(p_z)$ charge transfer (LMCT) mixed with MCCT transitions, which is similar to the observed 225-nm absorption.[33]

C. Emission Spectra of $[(AuPH_3)_2(i\text{-mnt})]$ in the Solid State and CH_2Cl_2 Solution

The excited-state structure was fully optimized by the CIS method to describe the emissive properties of $[(AuPH_3)_2(i\text{-mnt})]$. Two triplet a^3A' and b^3A' excited states were obtained in the CIS calculations and the corresponding emissions were at 593 and 414 nm, respectively, for a single $[(AuPH_3)_2(i\text{-mnt})]$ molecule (Table 3).

By analyzing the wavefunctions of the a^3A' excited state, the calculated 593-nm emission was assigned as a $\pi^* \rightarrow \pi$ charge transfer (i-mnt ^{3}ILCT) involved in the C=C double bond from the triplet excited state to the $^1A'$ ground state, similar to the 595-nm emission of $K_2(i\text{-mnt})$ in the solid state at 20 K.[33] The $\pi^* \rightarrow \pi$ transition is reflected in the structural change of the a^3A' excited state (Table 1). The calculated C7=C8 distance (1.490 Å) in the excited state is longer than that in the $^1A'$ ground state (1.406 Å), suggesting a π^*-orbital character between the two carbon atoms in the excited state. By the combination of the CIS method and the IPCM in the SCRF method, the $[(AuPH_3)_2(i\text{-mnt})]$ complex has a 702-nm emission in the CH_2Cl_2 solution. The solvent effect results in a red shift of ca. 110 nm relative to the emission in the solid state (593 nm). Using the same methods, the lowest-energy emission of the organic i-mnt ligand was calculated at 611 nm, originating from a $^3A' \rightarrow {}^1A'$ transition in the solid state, and at 714 nm in CH_2Cl_2 solution (Table 3), which supports our assignment for such emissions of $[(AuPH_3)_2(i\text{-mnt})]$.

With respect to the $b^3A' \rightarrow {}^1A'$ transition, the corresponding emission is calculated at 414 nm for the single $[(AuPH_3)_2(i\text{-mnt})]$ molecule. To characterize the emission process, we used the difference in the natural atomic orbital populations for the b^3A' excited state and the correspond-

 © 2003 Wiley-VCH Verlag GmbH & Co. KGaA, Weinheim

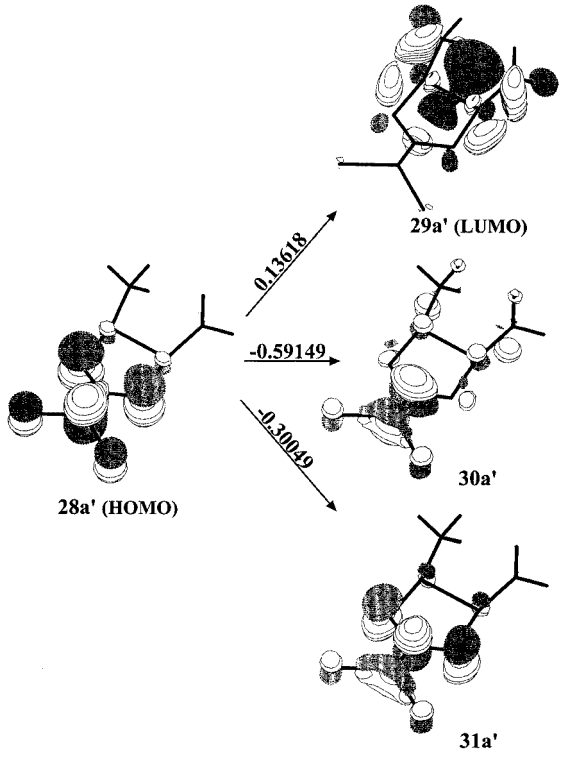

Figure 2. Single-electron transitions with (CI coefficient) > 0.1 in the CIS calculations for the 295 nm absorption of $[(AuPH_3)_2$(i-mnt)] in CH_2Cl_2 solution

Table 5. Natural atomic orbital populations of the b^3A' excited state and the corresponding $^1A'$ ground state for the 414 nm emission of $[(AuPH_3)_2$(i-mnt)] under the CIS calculations

	Atom	Orbital	$^1A'$	b^3A'
	Au	6s	0.647	0.889
		6p	0.024	0.080
		5d	9.863	9.860
		4f	0.003	0.004
i-mnt ligand	S	3s	1.711	1.713
		3p	4.563	4.383
		3d	0.025	0.025
	C7	2s	1.055	1.079
		2p	3.128	3.155
	C8	2s	0.902	0.904
		2p	3.490	3.165
	C9	2s	0.845	0.851
		2p	2.799	2.818
	N11	2s	1.594	1.595
		2p	3.814	3.743
PH_3 ligand	P	3s	1.418	1.433
		3p	3.332	3.374
		3d	0.055	0.055
	H_{P1}	1s	0.990	1.003
	H_{P2}	1s	1.014	1.012

ing $^1A'$ ground state for $[(AuPH_3)_2$(i-mnt)] (Table 5). The electron transition is dominated by the metal centers and the i-mnt ligand (Table 5), while the charge transfer localized on the PH_3 ligand changes little. There are ca. 0.59 electrons to transfer from two Au atoms to the i-mnt ligand in the emissive process, in which 6s and 6p orbitals of Au

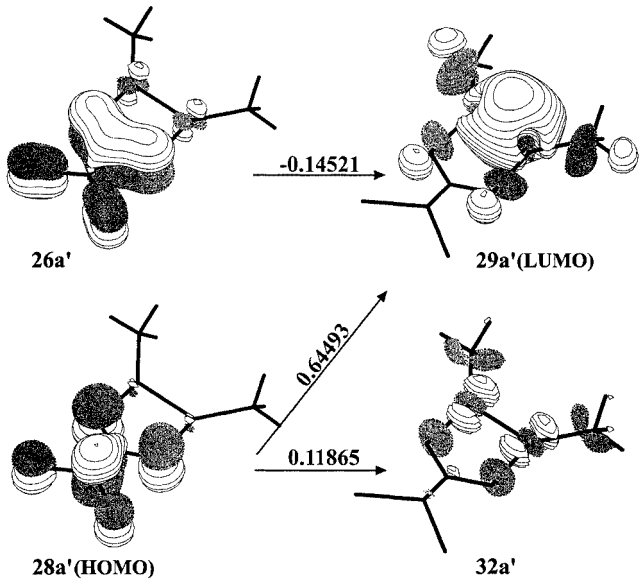

Figure 3. Single-electron transitions with (CI coefficient) > 0.1 in the CIS calculations for the 414-nm phosphorescence of $[(AuPH_3)_2$(i-mnt)]

atom lose ca. 0.24 and 0.06 electrons, respectively, and the $3p_x$ orbital of the S atom and the $2p_x$ orbital of the C8 atom increase by ca. 0.18 and 0.32 electrons, respectively. Therefore, we attributed the 414-nm emission to an Au→i-mnt charge transfer (^{3}MLCT) from the triplet b^3A' excited state to the $^1A'$ ground state. Density diagrams of the frontier molecular orbitals (Figure 3) help us intuitively understand the transition process. In the 26a′ and 28a′ orbitals, the electron density mainly focuses around the i-mnt ligand while the electron density transfers to Au centers to form a σ-bonding orbital in 29a′. Electron promotion from the i-mnt ligand orbitals to s_σ and p_σ orbitals of the Au atoms results in an Au−Au σ bond in the b^3A' excited state. The density diagrams seem to show significant Au−Au aurophilicity in the excited state, and that the Au−Au aurophilicity is relatively stronger in the b^3A' excited state than in the $^1A'$ ground state. Therefore, the 414-nm emission corresponding to the b^3A' excited state should have Au−Au→i-mnt charge transfer (^{3}MMLCT) character.

To reveal the effect of Au−Au aurophilicity on the luminescence in the b^3A' excited state of a $[(AuPH_3)_2$(i-mnt)] molecule, the mononuclear PH_3AuSH molecule was calculated using the same methods and basis sets as those of the dinuclear $[(AuPH_3)_2$(i-mnt)] complex. The 332-nm emission of PH_3AuSH arising from an Au(s,p)→S transition corresponds to the 414-nm phosphorescent emission of $[(AuPH_3)_2$(i-mnt)] from Au−Au[$(sp)_\sigma$]→i-mnt charge transfer. Apparently, there is no Au−Au aurophilicity in the mononuclear PH_3AuSH molecule, but the emissions of 332 nm for PH_3AuSH and 414 nm for $[(AuPH_3)_2$(i-mnt)] are both MLCT in nature. It is the Au−Au aurophilicity in $[(AuPH_3)_2$(i-mnt)] that results in a ca. 80 nm red shift relative to the emission of PH_3AuSH. Bruce and co-workers[22] have studied the relationship between the Au−Au aurophilicity and the spectrum of the excited state for *cis*- and *trans*-

 © 2003 Wiley-VCH Verlag GmbH & Co. KGaA, Weinheim

$[Au_2X_2C_2H_2(PH_2)_2]$ (X = Cl, Br and I) using ab initio methods. The calculations indicated that the aurophilic interaction stabilizes the first singlet excited state in the *cis* complex and leads to a red shift in the spectrum of the *cis* isomers relative to the *trans* isomers.

The intense 462-nm emission of the $[(AuPPh_3)_2$(i-mnt)] complex observed in the solid state at 20 K, and experimentally attributed to an Au→i-mnt charge transfer (^{3}MLCT),[33] agrees with our assignment for the 414-nm emission of $[(AuPH_3)_2$(i-mnt)]. The 50 nm difference between calculated and experimental emission wavelength may be because the single $[(AuPH_3)_2$(i-mnt)] molecule is not accurate enough to describe the solid-state emission of the $[(AuPPh_3)_2$(i-mnt)] complex at 20 K.

Recent studies on dinuclear $[AuS_2PR(OR)]_2$ (R = alkyl or aryl) complexes with MLCT excited-state properties have shown, by determining emissions of the Au^I complexes at different temperature (298 and 77 K), that the intermolecular Au−Au interaction in the solid state causes a red shift in emissive wavelengths.[14,15] The Au^I complexes were divided into two types: one, containing intermolecular Au−Au interactions in the solid state, has one emission at 298 K and two emissions at 77 K; and the other, without the intermolecular interaction in the solid, has no emissive band at 298 K but one band at 77 K. Apparently, the $[(AuPPh_3)_2$(i-mnt)] complex belongs to the second type because X-ray crystal-diffraction studies showed that it has no intermolecular Au−Au interaction in the solid state (shortest Au−Au of ca. 8.1 Å) and it possesses one emission of 462 nm in the solid state at 20 K.[33,41] Since the Au−Au separation is strongly related to the temperature,[14,15] there may be intermolecular Au−Au interactions between two adjacent $[(AuPPh_3)_2$(i-mnt)] molecules at 20 K. Therefore, the red shift of 50 nm for the solid-state emission at 20 K relative to the calculation can be rationalized by shortening the intermolecular Au−Au separations in the crystal lattice, which results in a lower-energy ^{3}MMLCT emission.

Since an intermolecular Au−Au interaction would affect the solid-state emission, we chose $[(AuPH_3)_2$(i-mnt)$]_2$ to simulate the solid-state luminescent properties of the Au^I complex at 20 K. The intermolecular Au−Au separation changes from 10.0 to 3.5 Å on keeping four Au atoms collinear and considering the least steric hindrance; the calculated emission wavelength varies from 412 to 450 nm. This shows that the intermolecular Au−Au interaction between two adjacent $[(AuPH_3)_2$(i-mnt)] molecules causes a ca. 40-nm red shift in the emission spectrum, which agrees with Fackler's studies mentioned above.[14,15] As the repeating unit of $[(AuPH_3)_2$(i-mnt)] increases it tends to the case of $[(AuPH_3)_2$(i-mnt)] in the solid state. Accordingly, the number of the intermolecular Au−Au interaction in the solid state at 20 K increases and the emission is anticipated to show a larger red shift. In fact, for MMLCT or MLCT transitions the Au−Au interactions have a systematic influence on the energies of the frontier orbitals responsible for the emission. The increasing number of intermolecular interactions in the solid state causes a net decrease of HOMO−LUMO energy gap. Therefore, the calculated 450-nm emission of $[(AuPH_3)_2$(i-mnt)$]_2$ agrees with the experimental 462-nm emission of the $[(AuPPh_3)_2$(i-mnt)] complex in the solid state at 20 K, and both have ^{3}MMLCT character.

The spectroscopic properties of $[(AuPH_3)_2$(i-mnt)] in the CH_2Cl_2 solution corresponding to the b^3A' excited state were also obtained by the CIS/IPCM methods. The calculated 333-nm emission arises from an ^{3}MLCT transition from the triplet excited state to the ground state, which blue-shifts ca. 120 nm relative to the 450-nm emission in the solid state. No emission has been found experimentally in the visible region for the $[(AuPPh_3)_2$(i-mnt)] complex in CH_2Cl_2 solution.[33,34]

Comparison of the calculated solid-state emissions with experiment shows that the single molecule $[(AuPH_3)_2$(i-mnt)] model is satisfactory for the ^{3}ILCT excited state (a^3A'). Because the intermolecular Au−Au interaction between two adjacent $[(AuPH_3)_2$(i-mnt)] molecules has almost no effect on the ^{3}ILCT excited state, the 593-nm phosphorescence corresponding to the excited state (Table 3) agrees well with the 595-nm emission of K_2(i-mnt) in the solid state at 20 K. However, the two-molecule $[(AuPH_3)_2$(i-mnt)$]_2$ model is required to rationalize the ^{3}MMLCT excited state as this excited state is strongly related to intermolecular Au−Au interactions. In the excited state, both intra- and intermolecular Au−Au interactions dramatically affect the solid-state emission, which ranges from 332 nm for mononuclear PH_3AuSH to 414 nm for dinuclear $[(AuPH_3)_2$(i-mnt)] to 450 nm for polynuclear $[(AuPH_3)_2$(i-mnt)$]_2$. Thus, the 450 nm phosphorescence of $[(AuPH_3)_2$(i-mnt)$]_2$ corresponds to the 462-nm emission of the $[(AuPPh_3)_2$(i-mnt)] complex in the solid state at 20 K, and both

Table 6. Excited state, corresponding Au−Au distance, emission wavelength and property of the excited state for $[Au_2(dpm)_2]^{2+}$, $[(AuPH_3)_2$(i-mnt)] and $[Au_2$(dpm)(i-mnt)]

	$[Au_2(dpm)_2]^{2+}$	$[(AuPH_3)_2$(i-mnt)]	$[Au_2$(dpm)(i-mnt)]
Excited state	^3A_u	$^3A'$	$^3A''$
Au−Au [Å]	2.74	2.95	3.39
Wavelength [nm]	331	414	411
Excited-state property	MCCT	MMLCT[a]	ILCT (MLCT)[a] [b]

[a] For MMLCT and ILCT (MLCT), L refers to i-mnt ligand. [b] Excited-state property of $[Au_2$(dpm)(i-mnt)] is i-mnt ILCT, modified by MLCT.

 © 2003 Wiley-VCH Verlag GmbH & Co. KGaA, Weinheim

are ^{3}MMLCT in nature (triplet excited state to the ground state).

D. Comparison of the Luminescent Properties of $[Au_2(dpm)_2]^{2+}$, $[(AuPH_3)_2(i\text{-}mnt)]$ and $[Au_2(dpm)(i\text{-}mnt)]$

To reveal the luminescence regularity of the dinuclear Au^I complexes with the interchange of phosphane ligand and thiolate ligand, the calculated excited-state properties of $[Au_2(dpm)_2]^{2+}$,[28] $[(AuPH_3)_2(i\text{-}mnt)]$ and $[Au_2(dpm)(i\text{-}mnt)]$[58] are presented in Table 6. The phosphane ligand has little participation in the luminescence while the thiolate ligand is greatly involved in the transition. The excited-state properties of $[Au_2(dpm)_2]^{2+}$, $[(AuPH_3)_2(i\text{-}mnt)]$ and $[Au_2(dpm)(i\text{-}mnt)]$ change from MCCT to MMLCT to ILCT (MLCT), and the corresponding Au−Au distances vary from 2.74 to 2.95 to 3.39 Å. For $[Au_2(dpm)_2]^{2+}$ and $[(AuPH_3)_2(i\text{-}mnt)]$, the promotion of an electron from the antibonding orbitals to the s_σ and/or p_σ bonding orbitals of Au atoms results in an Au−Au σ-bond between the two Au atoms in the excited state; however, the charge transfer only occurs inside the i-mnt ligand and the metal simply modifies the i-mnt ILCT in the emission corresponding to the $^3A''$ excited state of the $[Au_2(dpm)(i\text{-}mnt)]$ complex. The stronger Au−Au aurophilicity causes the greater Au contribution to the transition, favoring an MCCT emissive excited state such as $[Au_2(dpm)_2]^{2+}$. Conversely, the excited state with the weaker Au−Au aurophilicity has less metal contribution and tends to be ILCT in character, such as $[Au_2(dpm)(i\text{-}mnt)]$.

In brief, ab initio investigations on $[Au_2(dpm)_2]^{2+}$, $[(AuPH_3)_2(i\text{-}mnt)]$ and $[Au_2(dpm)(i\text{-}mnt)]$ indicate that the Au−Au aurophilicity has no clear correlation with the emission wavelength but with the excited-state property. With the interchange of phosphane and thiolate ligands, the excited-state properties of such Au^I complexes regularly change from MCCT to MMLCT to ILCT.

Conclusions

The luminescence and Au−Au aurophilicity of $[(AuPH_3)_2(i\text{-}mnt)]$ in both the solid state and CH_2Cl_2 solution have been studied by ab initio methods. For the solid state, $[(AuPH_3)_2(i\text{-}mnt)]$ and $[(AuPH_3)_2(i\text{-}mnt)]_2$ models were employed to describe the spectroscopic properties. The former has been used to accurately calculate the ^{3}ILCT emissive excited state, because the intermolecular Au−Au interaction between the two adjacent $[(AuPH_3)_2(i\text{-}mnt)]$ molecules plays a minor role in the excited state. However, the ^{3}MMLCT emissive excited state is strongly related to the intermolecular Au−Au interaction between the two neighboring $[(AuPH_3)_2(i\text{-}mnt)]$ molecules in the solid state, especially at lower temperatures (20 K). The two-molecular model, $[(AuPH_3)_2(i\text{-}mnt)]_2$, can satisfactorily rationalize the solid-state emission of the $[(AuPPh_3)_2(i\text{-}mnt)]$ complex at 20 K. For dilute CH_2Cl_2 solutions, we used the single $[(AuPH_3)_2(i\text{-}mnt)]$ molecule associated with the IPCM in the SCRF method to calculate the absorption and emission. Most calculated spectra in solution agree with the experimental results.[33]

Studies on $[Au_2(dpm)_2]^{2+}$,[28] $[(AuPH_3)_2(i\text{-}mnt)]$ and $[Au_2(dpm)(i\text{-}mnt)]$ [58] show that the Au−Au aurophilicity is clearly correlated with the excited-state properties. With the interchange of phosphane and thiolate ligands, the excited-state properties of such Au^I complexes regularly change from MCCT to MMLCT to ILCT.

Acknowledgments

This work was supported by the Natural Science Foundation of China (20173021).

[1] [1a] R. L. White-Morris, M. M. Olmstead, F. Jiang, D. S. Tinti, A. L. Balch, *J. Am. Chem. Soc.* **2002**, *124*, 2327. [1b] R. L. White-Morris, M. M. Olmstead, A. L. Balch, *J. Am. Chem. Soc.* **2003**, *125*, 1033. [1c] R. L. White-Morris, M. M. Olmstead, F. Jiang, D. S. Tinti, A. L. Balch, *Inorg. Chem.* **2002**, *41*, 2313. [1d] M. M. Olmstead, F. Jiang, S. Attar, A. L. Balch, *J. Am. Chem. Soc.* **2001**, *123*, 3260. [1e] J. C. Vickery, M. M. Lomstead, E. Y. Fung, A. L. Balch, *Angew. Chem. Int. Ed. Engl.* **1997**, *36*, 1179.
[2] R. E. Bachman, S. A. Bodolosky-Bettis, S. C. Glennon, S. A. Sirchio, *J. Am. Chem. Soc.* **2000**, *122*, 7146.
[3] V. W.-W. Yam, E. C.-C. Cheng, *Angew. Chem. Int. Ed.* **2000**, *39*, 4240.
[4] M. Bardají, A. Laguna, V. M. Orera, M. D. Villacampa, *Inorg. Chem.* **1998**, *37*, 5125.
[5] J. M. Forward, Z. Assefa, J. P. Facker, Jr., *J. Am. Chem. Soc.* **1995**, *177*, 9103.
[6] Md. N. I. Khan, C. King, D. D. Heinrich, J. P. Fackler, Jr., L. C. Porter, *Inorg. Chem.* **1989**, *28*, 2150.
[7] B. Trzcinska-Bancroft, Md. N. I. Khan, J. P. Fackler, Jr., *Organometallics* **1988**, *7*, 993.
[8] S. Wang, G. Garzón, C. King, J.-C. Wang, J. P. Fackler, Jr., *Inorg. Chem.* **1989**, *28*, 4623.
[9] S. K. Chastain, W. R. Mason, *Inorg. Chem.* **1982**, *21*, 3717.
[10] J. Kozelka, H. R. Oswald, E. Dubler, *Acta Crystallogr., Sect. C* **1986**, *42*, 1007.
[11] J. M. Forward, D. Bohmann, J. P. Fackler, Jr., R. J. Staples, *Inorg. Chem.* **1995**, *34*, 6330.
[12] Y.-A. Lee, J. E. McGarrah, R. J. Lachicotte, R. Eisenberg, *J. Am. Chem. Soc.* **2002**, *124*, 10662.
[13] M. A. Mansour, W. B. Connick, R. J. Lachicotte, H. J. Gysling, R. Eisenberg, *J. Am. Chem. Soc.* **1998**, *120*, 1329.
[14] W. E. van Zyl, J. M. López-de-Luzuriaga, A. A. Mohamed, R. J. Staples, J. P. Fackler, Jr., *Inorg. Chem.* **2002**, *41*, 4579.
[15] W. E. van Zyl, J. M. López-de-Luzuriaga, J. P. Fackler, Jr., *J. Mol. Struct.* **2000**, *516*, 99.
[16] E. J. Fernández, C. Gimeno, A. Laguna, J. M. López-de-Luzuriaga, M. Monge, P. Pyykkö, D. Sundholm, *J. Am. Chem. Soc.* **2000**, *122*, 7287.
[17] S. S. Tang, C. P. Chang, I. J. B. Lin, L. S. Liou, J. C. Wang, *Inorg. Chem.* **1997**, *36*, 2294.
[18] V. W.-W. Yam, C.-K. Li, C.-L. Chan, *Angew. Chem. Int. Ed.* **1998**, *37*, 2857.
[19] H. Schmidbaur, *Gold Bull.* **1990**, *23*, 11.
[20] S. S. Pathaneni, G. R. Desiraju, *J. Chem. Soc., Dalton Trans.* **1993**, 319.
[21] M. A. Rawashdeh-Omary, M. A. Omary, H. H. Patterson, J. P. Fackler, Jr., *J. Am. Chem. Soc.* **2001**, *123*, 11237.
[22] P. Schwerdtfeger, A. E. Bruce, M. R. M. Bruce, *J. Am. Chem. Soc.* **1998**, *120*, 6587.
[23] [23a] P. Pyykkö, N. Runeberg, F. Mendizabal, *Chem. Eur. J.* **1997**, *3*, 1451. [23b] P. Pyykkö, F. Mendizabal, *Chem. Eur. J.* **1997**, *3*, 1458. [23c] P. Pyykkö, F. Mendizabal, *Inorg. Chem.* **1998**, *37*, 3018. [23d] P. Pyykkö, *Chem. Rev.* **1997**, *97*, 597. [23e]

 © 2003 Wiley-VCH Verlag GmbH & Co. KGaA, Weinheim

P. Pyykkö, Y.-F. Zhao, *Angw. Chem.* **1991**, *103*, 622; *Angew. Chem. Int. Ed. Engl.* **1991**, *30*, 604. [23f] J. Li, P. Pyykkö, *Chem. Phys. Lett.* **1992**, *197*, 586. [23g] J. Li, P. Pyykkö, *Inorg. Chem.* **1993**, *32*, 2630.
[24] V. -W. W. Yam, K. K. W. Lo, *Chem. Soc. Rev.* **1999**, *28*, 323.
[25] S. Watase, M. Nakamoto, T. Kitamura, N. Kanehisa, Y. Kai, *J. Chem. Soc., Dalton Trans.* **2000**, 3585.
[26] C. King, J. C. Wang, M. N. I. Khan, J. P. Fackler, Jr., *Inorg. Chem.* **1989**, *28*, 2145.
[27] [27a] W.-F. Fu, K.-C. Chan, V. M. Miskowski, C.-M. Che, *Angew. Chem. Int. Ed.* **1999**, *38*, 2783. [27b] K. H. Leung, D. L. Phillips, M.-C. Tse, C.-M. Che, V. M. Miskowski, *J. Am. Chem. Soc.* **1999**, *121*, 4799. [27c] C.-M. Che, H.-L. Kwong, V. W.-W. Yam, K.-C. Cho, *J. Chem. Soc., Chem. Commun.* **1989**, 885. [27d] C.-M. Che, H.-L. Kwong, C.-K. Poon, *J. Chem. Soc., Dalton Trans.* **1990**, 3215.
[28] H.-X. Zhang, C.-M. Che, *Chem. Eur. J.* **2001**, *7*, 4887.
[29] C. D. Kim, S. Pillet, G. Wu, W. K. Fullagar, P. Coppens, *Acta Crystallogr., Sect. A* **2002**, *58*, 133.
[30] I. V. Novozhilova, A. V. Volkov, P. Coppens, *J. Am. Chem. Soc.* **2003**, *125*, 1079.
[31] R. Narayanaswamy, M. A. Young, E. Parkhurst, M. Ouellette, M. E. Kerr, K. M. Ho, R. C. Elder, A. E. Bruce, M. R. M. Bruce, *Inorg. Chem.* **1993**, *32*, 2506.
[32] W. B. Jones, J. Yuan, R. Narayanaswamy, M. A. Young, R. C. Elder, A. E. Bruce, M. R. M. Bruce, *Inorg. Chem.* **1995**, *34*, 1996.
[33] S. D. Hanna, J. I. Zink, *Inorg. Chem.* **1996**, *35*, 297.
[34] S. D. Hanna, S. I. Khan, J. I. Zink, *Inorg. Chem.* **1996**, *35*, 5813.
[35] M. Bardají, A. Laguna, P. G. Jones, A. K. Fischer, *Inorg. Chem.* **2000**, *39*, 3560.
[36] M. Bardají, A. Laguna, J. Vicente, *Inorg. Chem.* **2001**, *40*, 2675.
[37] V. -W. W. Yam, E. C. -C. Cheng, Z. -Y. Zhou, *Angew. Chem. Int. Ed.* **2000**, *39*, 1683.
[38] E. J. Fernández, J. M. López-de-Luzuriaga, M. Monge, M. A. Rodríguez, O. Crespo, M. C. Gimeno, A. Laguna, P. G. Jones, *Chem. Eur. J.* **2000**, *6*, 636.
[39] E. J. Fernández, J. M. López-de-Luzuraga, M. Monge, M. A. Rodríguez, O. Crespo, M. C. Gimeno, A. Laguna, P. G. Jones, *Inorg. Chem.* **1998**, *37*, 6002.
[40] O. Crespo, A. Laguna, E. J. Fernández, J. M. López-de-Luzuriaga, P. G. Jones, M. Teichert, M. Monge, P. Pyykkö, N. Runeberg, M. Schütz, H. -J. Werner, *Inorg. Chem.* **2000**, *39*, 4786.
[41] M. N. I. Khan, S. Wang, D. D. Heinrich, J. P. Fackler, Jr., *Acta Crystallogr., Sect. C* **1998**, *44*, 822.
[42] [42a] M. J. McKeage, L. Maharaj, S. J. Berners-Price, *Coord. Chem. Rev.* **2002**, *232*, 127. [42b] S. J. Berners-Price, G. R. Girard, D. T. Hill, B. M. Sutton, P. S. Jarrett, L. F. Faucette, R. K. Johnson, C. K. Mirabelli, P. J. Sadler, *J. Med. Chem.* **1990**, *33*, 1386. [42c] E. J. Corey, M. M. Mahrotra, A. U. Khan, *Science* **1987**, *236*, 68. [42d] C. K. Mirabelli, R. K. Johnson, D. T. Hill, L. F. Faucette, G. R. Girard, G. Y. Kuo, C. M. Sung, S. T. Crooke, *J. Med. Chem.* **1986**, *29*, 218. [42e] J. Weinstock, B. M. Sutton, G. Y. Kuo, D. T. Walz, M. J. Dimartino, *J. Med. Chem.* **1974**, *17*, 139. [42f] C. F. Shaw, III, A. Beery, *Inorg. Chim. Acta* **1986**, *123*, 213.
[43] L. Hao, R. J. Lachicotte, H. J. Gysling, R. Eisenberg, *Inorg. Chem.* **1999**, *38*, 4616.
[44] M. O. Wolf, M. A. Fox, *J. Am. Chem. Soc.* **1995**, *117*, 1845.
[45] O. D. Häberlen, N. Rösch, *J. Phys. Chem.* **1993**, *97*, 4970.
[46] E. J. Fernández, M. C. Gimeno, P. G. Jones, A. Laguna, M. Laguna, J. M. López-de-Luzuriaga, M. A. Rodriguez, *Chem. Ber.* **1995**, *128*, 121.
[47] B. I. Dunlap, N. Rösch, *Adv. Quantum Chem.* **1990**, *21*, 317.
[48] C. Møller, M. S. Plesset, *Phys. Rev.* **1934**, *46*, 618.
[49] [49a] J. B. Foresman, M. Head-Gordon, J. A. Pople, M. J. Frisch, *J. Phys. Chem.* **1992**, *96*, 135. [49b] K. Raghavachari, J. A. Pople, *Int. J. Quant. Chem.* **1981**, *20*, 167.
[50] J. B. Foresman, T. A. Keith, K. B. Wiberg, J. Snoonian, M. J. Frisch, *J. Phys. Chem.* **1996**, *100*, 16098.
[51] L. E. Sanscores, R. Salcedo, H. Flores, A. Martinez, *J. Mol. Struct. (TheoChem)* **2000**, *530*, 125.
[52] J. B. Foresman, A. Frisch, *Exploring Chemistry with Electronic Structure Method*, Gaussian, Inc., Pittsburgh, PA **1996**.
[53] M. J. Frisch, G. W. Trucks, H. B. Schlegel, G. E. Scuseria, M. A. Robb, J. R. Cheeseman, V. G. Zakrzewski, J. A. Montgomery, Jr., R. E. Stratmann, J. C. Burant, S. Dapprich, J. M. Millam, A. D. Daniels, K. N. Kudin, M. C. Strain, O. Farkas, J. Tomasi, V. Barone, M. Cossi, R. Cammi, B. Mennucci, C. Pomelli, C. Adamo, S. Clifford, J. Ochterski, G. A. Petersson, P. Y. Ayala, Q. Cui, K. Morokuma, D. K. Malick, A. D. Rabuck, K. Raghavachari, J. B. Foresman, J. Cioslowski, J. V. Ortiz, A. G. Baboul, B. B. Stefanov, G. Liu, A. Liashenko, P. Piskorz, I. Komaromi, R. Gomperts, R. L. Martin, D. J. Fox, T. Keith, M. A. Al-Laham, C. Y. Peng, A. Nanayakkara, M. Challacombe, P. M. W. Gill, B. Johnson, W. Chen, M. W. Wong, J. L. Andres, C. Gonzalez, M. Head-Gordon, E. S. Replogle, and J. A. Pople, *Gaussian 98, Revision A.9*, Gaussian, Inc., Pittsburgh PA, **1998**.
[54] [54a] W. R. Wadt, P. J. Hay, *J. Chem. Phys.* **1985**, *82*, 284. [54b] P. J. Hay, W. R. Wadt, *J. Chem. Phys.* **1985**, *82*, 299.
[55] D. Perreault, M. Drouin, A. Michel, V. M. Miskowski, W. P. Schaefer, P. D. Harvey, *Inorg. Chem.* **1992**, *31*, 695.
[56] A. Bondi, *J. Phys. Chem.* **1964**, *68*, 441.
[57] B. G. Werden, E. Billig, H. B. Gray, *Inorg. Chem.* **1966**, *5*, 78.
[58] Q.-J. Pan, H. -X. Zhang, submitted to *J. Phys. Chem.*

Received June 23, 2003
Early View Article
Published Online October 2, 2003

 © 2003 Wiley-VCH Verlag GmbH & Co. KGaA, Weinheim

Syntheses, Characterizations, and Crystal Structures of Three New Metal Phosphonocarboxylates with a Layered and a Microporous Structure

Bing-Ping Yang,[a] Jiang-Gao Mao,*[a] Yan-Qiong Sun,[a] Han-Hua Zhao,[b] and Abraham Clearfield[b]

Keywords: Metal phosphonates / Hydrothermal reactions / Lead / Layered compounds / Cluster compounds

Hydrothermal reactions of *N*-(phosphonomethyl)proline (H_3L) with M^{II} (M = Cd, Pb, and Zn) chlorides resulted in three new metal amino-phosphono-carboxylates, namely, $[Cd_2LCl(H_2O)]$ (**1**) and $[Pb_2Cl_2(HL)]$ (**2**) with a layered structure, and $[Zn_7L_6][Zn(H_2O)_6]_2{\cdot}16H_2O$ (**3**) featuring a microporous structure built from centered octahedral $Zn_6(Zn)$ cluster anions. The cadmium(II) ions in complex **1** are octahedrally coordinated [Cd(1)O_5Cl, Cd(2)O_4NCl]. These cadmium octahedra form a 1D zigzag chain along the *b*-axis through edge sharing, and such chains are further interconnected via phosphonate tetrahedra to form a <002> layer. The organic rings of the ligands are orientated to the interlayer space. Complex **2** also has a layered structure, in which Pb(1) is six-coordinated by four phosphonate oxygen atoms and two carboxylate oxygen atoms from four ligands in a distorted octahedral geometry, three Pb–O distances are relatively longer than those of the remaining ones, whereas Pb(2) is six coordinated by three phosphonate oxygen atoms and one carboxylate oxygen from four ligands as well as two chloride anions in a distorted octahedral geometry, one Pb–O bond is much longer than the remaining ones. These two different types of Pb^{II} ions are further interconnected through bridging carboxylate and phosphonate groups to form a <200> layer. Complex **3** contains a novel heptanuclear zinc phosphonate cluster anion $[Zn_7L_6]^{4-}$ and two hexahydrated zinc(II) cations as well as 16 lattice water molecules. The seven Zn^{II} cations in an anion form an unusual centered $Zn_6(Zn)$ octahedron, packing of such cluster anions creates micropores that are occupied by the hexahydrated zinc(II) cations and lattice water molecules.
(© Wiley-VCH Verlag GmbH & Co. KGaA, 69451 Weinheim, Germany, 2003)

Introduction

The chemistry of metal phosphonates has been an active research area in recent years due to its potential applications in the areas of catalysis, ion exchange, proton conductivity, intercalation chemistry, photochemistry and materials chemistry.[1] Metal phosphonates also exhibit a variety of open frameworks such as layered and microporous structures.[1] Materials with open-framework and microporous structures are expected to find their use as hybrid composite materials in electro-optical and sensing applications in the future.[2] Attaching additional functional groups such as crown ethers and carboxylate groups to the phosphonic acid has been proved to be very useful methods in building open-framework and microporous structures. A number of porous metal phosphonates with crown ether moieties have been reported recently.[3,4] A series of metal carboxylate-phosphonates with a framework structure, using $H_2O_3PCH_2CO_2H$ and $H_2O_3PCH_2CH_2CO_2H$ as ligands, have also been isolated mainly by the Cheetham, Bujoli, and Sevov groups.[2,5,6] Results of our research and others indicate that amino-carboxylic-phosphonic acids are also capable of forming open frameworks. The structures of amino-carboxylate-phosphonates depend on the extent of deprotonation of the ligands as well as on the nature of the metal ions.[7–10] For example, *N*-(phosphonomethyl)iminodiacetic acid (H_4PMIDA) has been found to be able to adopt various kinds of coordination modes under different reaction conditions.[7–10] A layered zirconium compound of 4-[bis(phosphonomethyl)amino]butanoic acid was reported by the Vivani group,[11a] and two zinc(II) complexes with *N*,*N*-bis(phosphonomethyl)aminoacetic acid and *N*-(phosphonomethyl)-*N*-methylglycine have been also obtained in our laboratory.[11b,11c] The structure of the latter zinc(II) amino-carboxylate-phosphonate features a microporous structure built from heptanuclear $Zn_6(Zn)(ligand)_6$ cluster anions.[11c] A layered Co^{II} compound of *N*-(phosphonomethyl)proline (H_3L) with a 3:2 metal/ligand ratio, $Co_3L_2{\cdot}5H_2O$ and a layered Pb^{II} complex with $H_2O_3PCH_2NHCH_2CO_2H$ have been reported very recently.[11d,11e] Hydrothermal reactions of *N*-(phosphonomethyl)proline with other divalent metal salts resulted in two types of layered materials containing chloride anions, $[Cd_2LCl(H_2O)]$ (**1**) and $[Pb_2Cl_2(HL)]$ (**2**), and a microporous compound, $[Zn_7L_6][Zn(H_2O)_6]_2{\cdot}16H_2O$ (**3**). Herein we

[a] State Key Laboratory of Structural Chemistry, Fujian Institute of Research on the Structure of Matter, Chinese Academy of Sciences,
Fuzhou 350002, P. R. China
Fax: (internat.) + 86-591-371-4946
E-mail: mjg@ms.fjirsm.ac.cn
[b] Department of Chemistry, Texas A&M University,
P. O. Box 30012, College Station, Texas 77843-3255, USA

report their syntheses, characterizations and crystal structures.

Results and Discussion

Crystal Structure of $[Cd_2LCl(H_2O)]$ (1)

Complex **1** features a 2D layer built from a zigzag chain of edge-sharing cadmium(II) octahedra. As shown in Figure 1, Cd2 is octahedrally coordinated by a tridentate chelating ligand (O11, N1, O2), one carboxylate (O1b), and one phosphonate oxygen (O12d) atom from two neighboring [Cd(L)] units and a chloride anion (Cl1), whereas Cd1 is octahedrally coordinated by two carboxylate (O1c, O2b) and two phosphonate oxygen (O11, O13a) atoms from four neighboring [Cd(L)] units, an aqua ligand and a chloride anion. These octahedra are severely distorted, probably due to the edge-sharing of the octahedra and the larger size of the chloride anion. The average Cd−N distance is 2.37(1) Å; Cd−O distances range from 2.18(1) to 2.48(1) Å, and the Cd−Cl bonds are in the range from 2.527(3) to 2.665(3) Å. These bond lengths are similar to those reported for other Cd^{II} phosphonates.[3c,12] The phosphonate-carboxylate ligand adopts a coordination mode different from those in the Co^{II} complex.[11d] Both carboxylate oxygen atoms are bidentately bridging, whereas one phosphonate oxygen (O11) is bidentate and the other two are unidentate.

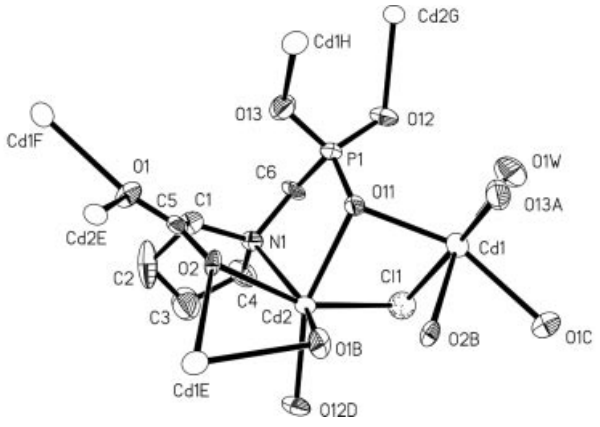

Figure 1. ORTEP representation of the asymmetric unit of complex **1**; thermal ellipsoids are drawn at 50% probability; symmetry codes for generated atoms: a. $x + 1, y + 1/2, -z + 1$; b. $x + 2, y + 1/2, -z + 1$; c. $x, y + 1, z$; d. $x + 1, y, z$; e. $x + 2, -1/2 + y, -z + 1$; f. $x, y - 1, z$; g. $x - 1, y, z$; h. $1 - x, -1/2 + y, 1 - z$

These two types of Cd^{II} octahedra are condensed by edge-sharing (O11−Cl1 and O2−O1b) to form a 1D zigzag chain along the *b* axis. Two types of four-membered rings are found: one is formed by Cd1−O11−Cd2−Cl1 and the other one is composed of Cd2, O2, Cd1e, and O1b atoms. Such 1D chains are further interconnected by bridging phosphonate tetrahedra to form a <002> 2D layer (Figure 2). There are small cavities formed within the 2D layer, each cavity is formed by three edge-sharing Cd^{II} octahedra from one chain and another Cd^{II} octahedron from a neighboring

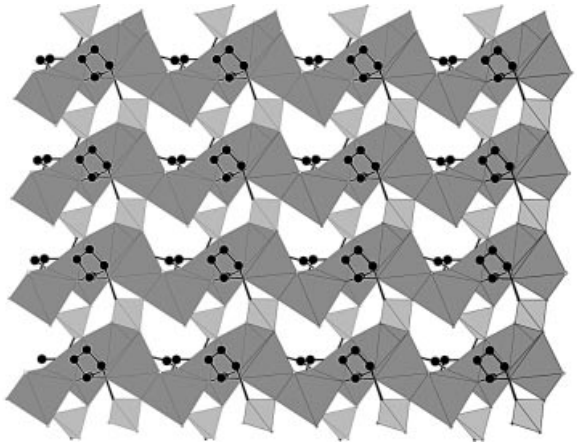

Figure 2. A <002> layer of complex **1**; the Cd^{II} octahedra and $C-PO_3$ tetrahedra are shaded in medium and light gray, respectively, and C atoms are drawn as black circles

chain interconnected by two phosphonate tetrahedra. In the Co^{II} complex, the Co octahedra form a dimer by edge-sharing, and these dimers are interconnected into a 1D chain by corner-sharing. The 1D chains are interconnected through isolated dimers by bridging $C-PO_3$ tetrahedra, hence the cavities of the layered Co^{II} compound are much larger than those in the Cd^{II} complex.[11d] Similar to those in the Co^{II} complex, the double layers of complex **1** are held together by weak Van der Waals forces (Figure 3). The interlayer distance is about 10.3 Å, which is much smaller than that of the Co^{II} compound (11.9 Å) reported previously.[11d]

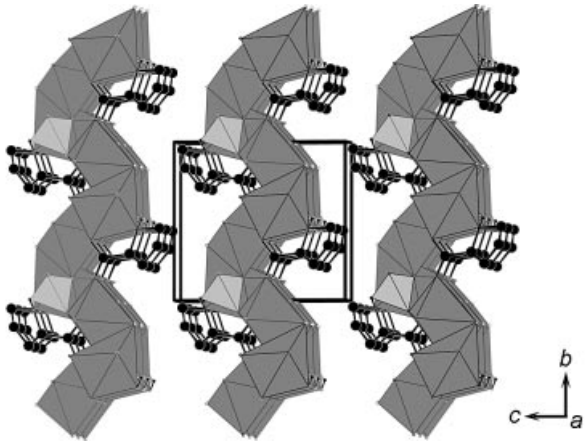

Figure 3. View of structure of complex **1** down the *a* axis; the Cd^{II} octahedra and $C-PO_3$ tetrahedra are shaded in medium and light gray, respectively; the C atoms are drawn as black circles

Crystal Structure of $[Pb_2Cl_2(HL)]$ (2)

Complex **2** has a layered structure quite different from that of complex **1**. The asymmetric unit of complex **2** contains one $[Pb_2Cl_2(HL)]$ unit (Figure 4). In addition to three regular Pb−O bonds (O1b, O11, O12a) with Pb−O distances ranging from 2.400(14) to 2.572(18) Å, the Pb(1) atom also forms three much weaker Pb−O bonds with the O2c, O13a, and O13c atoms. These weak bonds range from

 © 2003 Wiley-VCH Verlag GmbH & Co. KGaA, Weinheim

2.824(14) to 2.851(19) Å (Table 1). Long Pb−O weak bonds have also been reported in other lead(II) phosphonates and lead(II) carboxylates — they are needed to satisfy the bond valences of the Pb^{II} ion.[9b,11e,13] Considering all these bonds, the coordination geometry around Pb(1) can be described as a severely distorted octahedron. Pb(2) is six-coordinated by three phosphonate and one carboxyl oxygen atoms, as well as two chloride anions, and also has a distorted octahedral geometry. The Pb2−O13b distance of 2.811(15) Å is much longer than those of the remaining Pb−O bonds, which range from 2.421(13) to 2.749(14) Å. The Pb−Cl distances are in the range of 2.684(7) to 2.767(5) Å (Table 1). The distortion of the lead polyhedron is due to the presence of the lone pair electrons of the lead(II) ion.

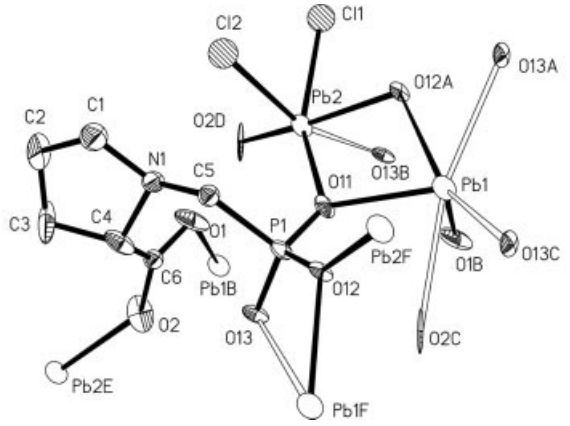

Figure 4. ORTEP representation of the asymmetric unit of complex **2**; thermal ellipsoids are drawn at 50% probability; the longer Pb−O contacts are represented by the open line; symmetry codes for generated atoms: a. $x, -y + 1/2, z - 1/2$; b. $x + 1, -y + 1, -z$; c. $x + 1, y - 1/2, -z + 1/2$; d. $x, -y + 3/2, z - 1/2$; e. $x, 3/2 - y, 1/2 + z$; f. $x, 1/2 - y, 1/2 + z$

The phosphonate-carboxylate ligand adopts a coordination mode that is different from those in its Co^{II} and Cd^{II} complexes. The amine group is protonated, hence it remains non-coordinated. Two phosphonate oxygen atoms (O11 and O12) are bidentate, whereas the third one (O13) forms a weak Pb−O bond. Each carboxylate oxygen atom is bridged to one Pb^{II} ion, however O(2) also forms a weak Pb−O bond with the Pb(1) center.

The interconnection of the above two types of Pb^{II} ions via bridging carboxylate and phosphonate groups results in a <200> layer (Figure 5), and such layers are packed together by weak Van der Waals forces (Figure 6). The d-spacing is about 12.0 Å, very close to that of complex **1**.

Crystal Structure of $[Zn_7L_6][Zn(H_2O)_6]_2 \cdot 16H_2O$ (3)

The structure of complex **3** is similar to that of the Zn^{II} complex with $CH_3N(CH_2CO_2H)CH_2PO_3H_2$ that we reported recently,[11] although the symmetry of the structure is lower due to the presence of the pyrrolidine ring in the ligand. The compound contains a novel heptanuclear zinc(II) phosphonate anion, two hexahydrated zinc(II) cations and 16 lattice water molecules. As shown in Figure 7, Zn1 is five-coordinated by a chelate ligand (N2, O3, O23), and two phosphonate oxygen atoms (O11a and O22a) from neighboring [ZnL] units in a distorted trigonal bipyramidal geometry. The Zn1−N2 and Zn1−O3 distances are 2.138(9) and 2.061(8) Å, respectively. The Zn1−O (phosphonate) distances are in the range of 1.966(8) to 2.125(7) Å. Zn3 is also five-coordinated by a chelate ligand (N1, O2, O13), and two phosphonate oxygen atoms (O21 and O12a) from two neighboring [ZnL] units in a distorted trigonal bipyramidal geometry. The Zn3−N1 and Zn3−O2 bond

Table 1. Selected bond lengths (Å) for complexes **1**, **2**, and **3**

Complex **1**[a]			
Cd(1)−O(13)#1	2.181(10)	Cd(1)−O(1 W)	2.294(10)
Cd(1)−O(11)	2.299(10)	Cd(1)−O(2)#2	2.440(7)
Cd(1)−O(1)#3	2.447(10)	Cd(1)−Cl(1)	2.527(3)
Cd(1)−Cd(2)	3.4148(12)	Cd(2)−O(12)#4	2.205(8)
Cd(2)−O(1)#2	2.336(8)	Cd(2)−O(11)	2.371(7)
Cd(2)−O(2)	2.372(9)	Cd(2)−N(1)	2.374(11)
Cd(2)−Cl(1)	2.665(3)		
Complex **2**[b]			
Pb(1)−O(11)	2.400(14)	Pb(1)−O(12)#1	2.482(13)
Pb(1)−O(1)#2	2.572(18)	Pb(1)−O(13)#1	2.824(14)
Pb(1)−O(13)#3	2.842(13)	Pb(1)−O(2)#3	2.851(19)
Pb(2)−O(12)#1	2.421(13)	Pb(2)−Cl(2)	2.684(7)
Pb(2)−O(2)#4	2.747(16)	Pb(2)−O(11)	2.749(14)
Pb(2)−Cl(1)	2.767(5)	Pb(2)−O(13)#2	2.811(15)
Complex **3**[c]			
Zn(1)−O(11)#1	1.966(8)	Zn(1)−O(22)#1	1.982(7)
Zn(1)−O(3)	2.061(8)	Zn(1)−O(23)	2.125(7)
Zn(1)−N(2)	2.138(9)	Zn(2)−O(23)#2	2.115(7)
Zn(2)−O(23)	2.115(7)	Zn(2)−O(23)#1	2.115(7)
Zn(2)−O(13)	2.122(7)	Zn(2)−O(13)#2	2.122(7)
Zn(2)−O(13)#1	2.122(7)	Zn(3)−O(12)#1	1.955(7)
Zn(3)−O(21)	1.985(8)	Zn(3)−O(2)	2.033(8)
Zn(3)−O(13)	2.135(7)	Zn(3)−N(1)	2.165(9)
Zn(4)−O(1 W)#3	2.089(13)	Zn(4)−O(1 W)#4	2.089(13)
Zn(4)−O(1 W)	2.089(13)	Zn(4)−O(2 W)#3	2.110(12)
Zn(4)−O(2 W)	2.110(12)	Zn(4)−O(2 W)#4	2.110(12)
Zn(5)−O(3 W)#1	2.093(10)	Zn(5)−O(3 W)	2.093(10)
Zn(5)−O(3 W)#2	2.093(10)	Zn(5)−O(4 W)#2	2.099(11)
Zn(5)−O(4 W)	2.099(11)	Zn(5)−O(4 W)#1	2.099(11)
Hydrogen bonds:			
O(1)···O(3w)#5	2.650(13)	O(4)···O(2w)	2.817(15)
O(4)···O(8w)#6	2.792(15)	O(2w)···O(5w)#7	2.691(17)
O(3w)···O(4w)#1	2.819(15)	O(4w)···O(6w)#8	2.839(16)
O(5w)···O(7w)#9	2.785(15)	O(6w)···O(7w)#9	2.716(14)
O(6w)···O(7w)#2	2.824(15)	O(7w)···O(8w)	2.780(18)
O(9w)···O(10w)	2.830(30)		

[a] Symmetry transformations used to generate equivalent atoms: For **1**: #1: $-x + 1, y + 1/2, -z + 1$; #2: $-x + 2, y + 1/2, -z + 1$; #3: $x, y + 1, z$; #4: $x + 1, y, z$. [b] For **2**: #1: $x, -y + 1/2, z - 1/2$; #2: $-x + 1, -y + 1, -z$; #3: $-x + 1, y - 1/2, -z + 1/2$; #4: $x, -y + 3/2, z - 1/2$. [c] For **3**: #1: $y - 1, z, x + 1$; #2: $z - 1, x + 1, y$; #3: $y - 1/2, -z + 3/2, -x+1$; #4: $-z + 1, x + 1/2, -y + 3/2$; #5: $-z + 1, x + 3/2, -y + 3/2$; #6: $-x + 1/2, -y + 2, z - 1/2$; #7: $-x, y - 1/2, -z + 3/2$; #8: $-x - 1/2, -y + 2, z - 1/2$; #9 $x - 1/2, -y + 5/2, -z + 2$.

 © 2003 Wiley-VCH Verlag GmbH & Co. KGaA, Weinheim

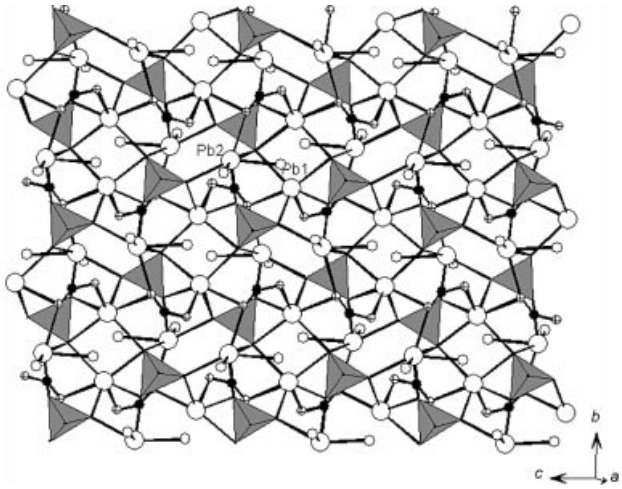

Figure 5. A <200> layer of lead(II) phosphonocarboxylate in complex **2**; the C−PO_3 tetrahedra are shaded in gray, Pb, Cl, C, and O atoms are drawn as open (large), open (small), black, and crossed circles, respectively; the pyrrolidine ring of the ligand has been omitted for clarity

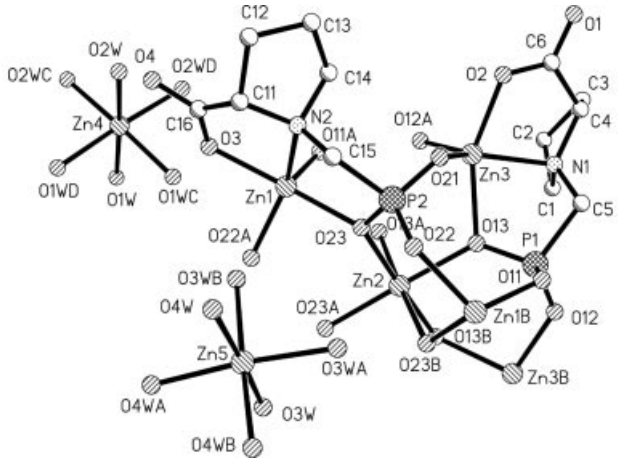

Figure 7. The asymmetric unit of complex **3** with atomic labeling; the lattice water molecules have been omitted for clarity; symmetry codes for generated atoms: a. $y - 1, z, x + 1$; b. $z - 1, x + 1, y$; c. $y - 1/2, -z + 3/2, -x+1$; d. $z + 1, x + 1/2, -y + 3/2$

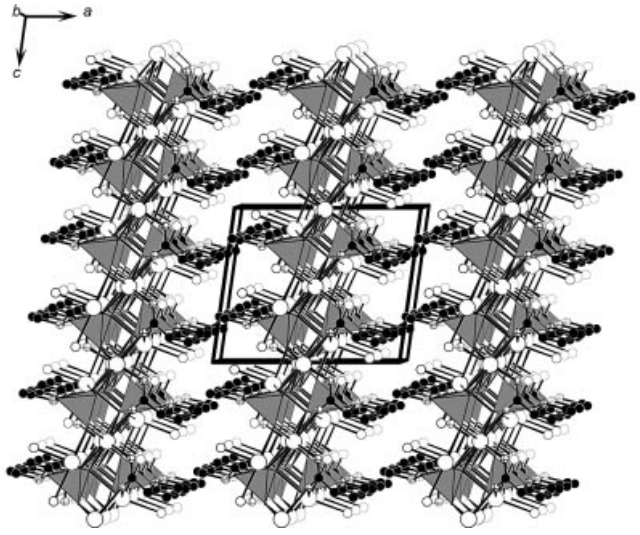

Figure 6. View of the structure of complex **2** down the *b* axis; the C−PO_3 tetrahedra are shaded in gray, Pb, Cl, N, C, and O atoms are drawn as open (large), open (small), octand, black, and crossed circles, respectively

lengths are 2.165(9) and 2.033(8) Å, respectively. The Zn3−O (phosphonate) distances range from 1.955(7) to 2.135(7) Å (Table 1); these distances are similar to those reported for other zinc(II) amino-carboxylate-phosphonates.[9,11]

The Zn2 atom lies on a position with threefold symmetry; it is octahedrally coordinated by six phosphonate oxygen atoms from three [Zn(1)(L)] and three [Zn(3)(L)] units. The Zn−O distances of 2.115(7) Å and 2.122(7) Å are close to those for the Zn1 and Zn3 atoms. The *N*-(phosphonomethyl)proline acts as a hexadentate ligand. It chelates to a Zn1 or a Zn3 atom and bridges three neighboring Zn^{II} ions. The O23 of P(2)O_3C group bridges one Zn1 and one Zn2 atom, and O13 of the P(1)O_3C group connects one Zn3 and one Zn2 atom. Such a coordination mode has been found in Co^{II} and Zn^{II} complexes with *N*-(phosphonomethyl)iminodiacetic acid.[9] Two carboxylate oxygen atoms (O1 and O4) remain non-coordinated. Since all C−O and P−O bonds have very short distances, we would expect both phosphonate and carboxylate groups of the ligand to be completely deprotonated. Each ligand carries three negative charges, thus the heptanuclear anion has a 4− charge.

The seven Zn^{II} cations in the anion form an unusual centered octahedron similar to the Zn^{II} complex with $CH_3N(CH_2CO_2H)CH_2PO_3H_2$. The octahedron is created by six five-coordinate zinc(II) cations (Zn1 and Zn3) with the six-coordinate Zn2 atom as the central atom. The edge Zn···Zn contacts are in the range of 4.515(2) to 5.758(2) Å, and the distances from the central Zn to the octahedral apexes range from 3.610(2) to 3.665(2) Å. It is interesting to compare our heptanuclear zinc(II) phosphonate anions with the hexanuclear zinc(II) cages containing phosphonate and pyrazole reported by the Chandrasekhar group, in which the six zinc atoms are arranged in a chair-like conformation.[14]

The four negative charges of the cluster are balanced by two hexa-hydrated zinc(II) cations. These zinc(II) ions (Zn4 and Zn5) are located at positions with a threefold symmetry. The Zn4−O distances are 2.089(13) and 2.110(12) Å, respectively, and the Zn5−O distances are 2.093(10) and 2.099(11) Å, respectively. Its coordination geometry is a slightly distorted octahedron.

In a similar fashion to the Zn^{II} complex with $CH_3N(CH_2CO_2H)CH_2PO_3H_2$,[11] packing of the cluster anions create large cavities occupied by the hexahydrated zinc(II) cations as well as lattice water molecules (Figure 8). The diameter of the pore is estimated to be around 8.0 Å. The polynuclear cluster anions are located at the centers of the cell edges and the cell body center. A number of hydrogen bonds are formed among the non-coordinated carboxylate oxygen atoms, and coordinated and lattice water molecules (Table 1).

 © 2003 Wiley-VCH Verlag GmbH & Co. KGaA, Weinheim

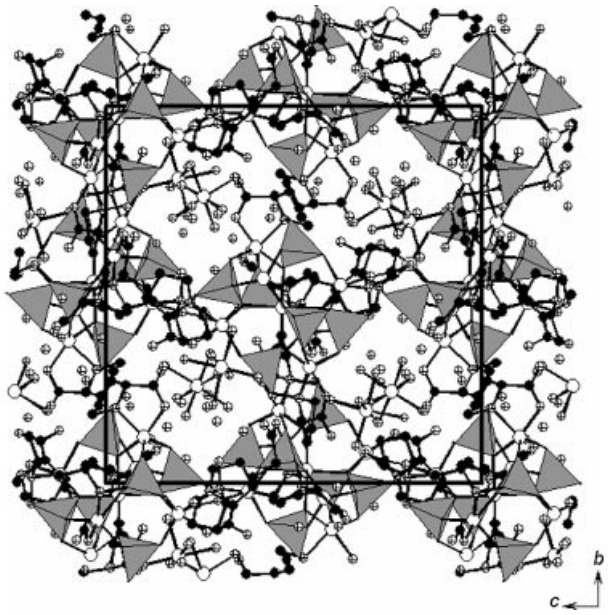

Figure 8. View of structure of complex **3** down the *a* axis; the $C-PO_3$ tetrahedra are shaded in gray, the Zn, N, C, and O atoms are drawn as open, octand, black, and crossed circles, respectively

Thermogravimetric Analysis

1The TGA diagram for complex **1** shows two main steps of weight loss. The first step, which corresponds to the loss of one aqua ligand and the chloride anion, starts at about 150 °C and ends at about 350 °C. The weight loss of 9.9% is slightly less than the calculated weight loss of 11.2%. The second step corresponds to the decomposition of the organic groups that starts at about 441 °C and is complete at 926 °C. The final products are $Cd_3(PO_4)_2$ and CdO in a 1:1 molar ratio. The total weight loss of 31.4% is close to the calculated weight loss of 32.3%. The TGA curves of the Pb^{II} complex show only one main weight loss. The compound is stable up to 240 °C. It then starts to decompose from 240 °C and continues up to 800 °C; this process corresponds to the loss of the chloride anions and the burning of the organic groups of the carboxylate-phosphonate ligand. The total weight loss is 32.4%, which is slightly less than the calculated one (35.5%) if the final products are assumed to be PbO. However, the total weight loss is much larger than the calculated value (25.3%) if the final products are $Pb_2P_2O_7$ and PbO in a 1:2 molar ratio. Thus we think our final products are mainly PbO mixed with a small amount of $Pb_2P_2O_7$. The TGA diagram for complex **3** shows two main steps of weight loss. The first step, which corresponds to the loss of 16 lattice water molecules and 12 coordinated water molecules, starts at about 60 °C and is complete at about 250 °C. The weight loss of 28.9% is slightly less than the calculated value (29.6%). The second step corresponds to the decomposition of organic groups starting at about 360 °C and continues up to 800 °C. The total weight loss of 33.7% is less than the calculated weight loss of 50.3% if the final products are assumed to be $Zn_2P_2O_7$ and ZnO; hence, the decomposition process is not complete at 800 °C. The use of N_2 gas to provide an inert atmosphere may be another reason for the incomplete decomposition.

Conclusion

Hydrothermal reactions of *N*-(phosphonomethyl)proline (H_3L) with divalent metal ions afforded four different complexes, $[Cd_2LCl(H_2O)]$ (**1**), $[Pb_2Cl_2(HL)]$ (**2**), a microporous compound, $[Zn_7L_6][Zn(H_2O)_6]_2 \cdot 16H_2O$ (**3**), and the previously reported layered $Co_3L_2 \cdot 5H_2O$.[11d] *N*-(phosphonomethyl)proline (H_3L) exists as a zwitterion where one proton of a phosphonate group has been transferred to the amine group. The molecular units of *N*-(phosphonomethyl)-proline (H_3L) are further interconnected by O−H···O and N−H···O hydrogen bonds into a 2D layer.[15] Upon partial or complete replacement of protons by divalent metal ions, three types of layered structures and a microporous structure are formed. As shown in Scheme 1, the carboxylate-phosphonate ligand adopts five different coordination modes in these four complexes. In the Cd^{II} complex, the phosphonate-carboxylate ligand chelates a Cd^{II} ion and bridges six other metal ions, both carboxylate oxygen atoms are bidentate, and one of the phosphonate oxygen atoms is also bidentate. The other two phosphonate oxygen atoms are unidentate (Scheme 1, a). In the lead(II) complex, the amine group of the ligand is protonated, hence it is not coordinated to the Pb^{II} ion. Without consideration of those weak Pb−O contacts, its coordination mode can be described as a hexadentate bridging mode, where two phosphonate O atoms behave as μ^2 metal linkers and the third phosphonate O remains non-coordinated (Scheme 1, b). In the zinc(II) cluster compound, the ligand chelates in a tridentate manner with a Zn^{II} ion and bridges three other Zn^{II} ions; only one phosphonate O is a μ^2 metal linker (Scheme 1, c). In the layered cobalt(II) complex,

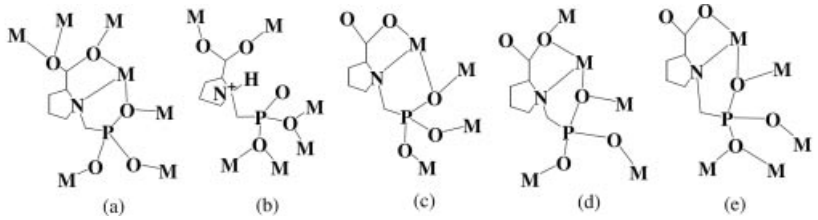

Scheme 1. Coordination modes of amino-carboxylate phosphonate ligand in complexes **1** (a), **2** (b), and **3** (c) as well as in its Co^{II} complex (d and e)

 © 2003 Wiley-VCH Verlag GmbH & Co. KGaA, Weinheim

$Co_3L_2{\cdot}5H_2O$, two types of chelating and bridging modes are found, the ligand in one CoL unit chelates with a Co^{II} ion in a tridentate fashion (one N, one carboxyl O and one phosphonate O) and bridges other four metal ions; one carboxyl O and one phosphonate O act as bidentate metal linkers (Scheme 1, d). In another CoL unit, the ligand also chelates a Co^{II} ion and bridges four other metal ions. However, two phosphonate O atoms behave as μ^2 metal linkers (Scheme 1, e).[11d] Transition metal ions such as Co^{II}, Zn^{II}, and Cd^{II} ions have a greater affinity for the nitrogen atom than the Pb^{II} ion, thus the ligand can form a chelate ring with a Co^{II} (or Cd^{II} or Zn^{II}) ion through the amine nitrogen, a phosphonate, and a carboxylate oxygen atom, whereas in the lead(II) complex the amine group remains protonated. The lead(II) complexes also have a coordination geometry different from the transition metal complexes due to the presence of the lone pair of electrons.

We are especially interested in the cluster unit and microporous structure in the zinc(II) complex. This complex has a structure similar to that of zinc(II) complexes with *N*-(phosphonomethyl)-*N*-methylglycine previously reported by us.[11c] Thus, we would expect that each Zn_6(Zn) cluster unit and the microporous structure built from the packing of the cluster units should be relatively stable. Currently, we are investigating the possibility of isolating a similar cluster unit with other magnetic transition metal ions, such as Mn^{II}, Cu^{II}, Ni^{II}, etc.; such materials may be used as single molecular magnets. Due to the number of lattice water molecules and hexahydrated zinc(II) cations located in the micropore of the structure, it would be interesting to replace the hydrated zinc(II) cations with alkaline earth cations or diamines such as ethylenediamine, methylenediamine etc. Such research efforts are in progress and the results will be published later.

Experimental Section

Materials and Methods: All of the starting materials were of reagent grade and were used without further purification. *N*-(Phosphonomethyl)proline (H_3L) was synthesized by a Mannich-type reaction according to the procedures previously described.[11d,15] Elemental analyses were performed on a German Elementary Vario EL III instrument. The FT-IR spectra were recorded on a Nicolet Magna 750 FT-IR spectrometer on KBr pellets in the range of 4000−400 cm^{-1}. Thermogravimetric analyses were carried out with a TGA/SBTA851 unit, at a heating rate of 15 °C/ min under a nitrogen atmosphere.

Synthesis of $[Cd_2LCl(H_2O)]$ (1): $CdCl_2{\cdot}2{\cdot}5H_2O$ (0.4 mmol, 0.091 g), H_3L (0.2 mmol, 0.042 g) and 25% ethanol aqueous solution (13 cm^3) were mixed and the pH was adjusted to between 4 and 5 by addition of Bu_4NOH. The resultant solution was heated at 170 °C in a Teflon-lined stainless steel autoclave for four days. Colorless plate-shaped crystals of **1** were collected in about 86% yield (83 mg). $C_6H_{11}Cd_2ClNO_6P$ (484.38): calcd. C 14.86, H 2.29, N 2.89; found C 15.58, H 1.89, N 2.94%. IR data (KBr, cm^{-1}): 3502−2899 (br), 1535 (s), 1417 (m), 1115 (s), 1051 (s), 964 (s), 559 (s).

Synthesis of $[Pb_2Cl_2(HL)]$ (2): A mixture of $PbCl_2$ (0.4 mmol, 0.111 g), H_3L (0.2 mmol, 0.042 g), and H_2O (10 cm^3) with the pH value adjusted to between 4 and 5 by addition of Bu_4NOH, was heated at 160 °C in a Teflon-lined stainless steel autoclave for two days. Colorless plate crystals were recovered in about 26% yield (36 mg). $C_6H_{10}Cl_2NO_5PPb_2$ (692.40): calcd. C 10.41, H 1.46, N 2.02; found C 10.29, H 1.10, N 1.85%. IR data (KBr, cm^{-1}): 3600−2825 (br), 1566 (s), 1400 (m), 1340 (m), 1292 (w), 1030 (s), 964 (s), 764 (m), 569(m), 478 (m) cm^{-1}.

Synthesis of $[Zn_7L_6][Zn(H_2O)_6]_2{\cdot}16H_2O$ (3): Complex **3** was synthesized by a method similar to that of complex **2**. Yield: 80% (155 mg) based on L. $C_{36}H_{110}N_6O_{58}P_6Zn_9$ (2329.45): calcd. C 18.56, H 4.76, N 3.61; found C 18.65, H 4.64, N 3.57%. IR (KBr, cm^{-1}): 3600−2864 (br), 1605 (s), 1400 (m), 1333 (w), 1234 (w), 1111 (s), 1078 (s), 989 (s), 931 (m), 580 (m).

X-ray Crystallographic Study: Data collections were performed on a Siemens Smart CCD diffractometer, using graphite-monochromated Mo-K_α radiation (λ = 0.71073 Å). Intensity data were collected by using narrow frame method with 0.3° per frame in at 293 K. A total of 1389, 2179 and 4713 independent reflections, respectively, for **1**, **2**, and **3**, were collected among which 1361 (for **1**), 1520 (for **2**), and 3341 (for **3**) with $I > 2.0\sigma(I)$ were considered observed. For data of complexes **1** and **3**, absorption corrections

Table 2. Summary of crystal data and details of intensity collection and refinement

	1	**2**	**3**
Empirical formula	$C_6H_{11}Cd_2ClNO_6P$	$C_6H_{10}Cl_2NO_5PPb_2$	$C_{36}H_{110}N_6O_{58}P_6Zn_9$
Formula mass	484.38	692.40	2329.45
Space group	$P2_1$	$P2_1/c$	$P2_13$
a, Å	6.5038(9)	11.9851(8)	20.203(2)
b, Å	8.9677(12)	10.4696(4)	20.203(2)
c, Å	10.3081(14)	10.0066(6)	20.203(2)
β, °	90	98.039(3)	90
V, Å^3	577.01(14)	1243.28(12)	8245.6(16)
Z	2	4	4
D_{calcd}, g·cm^{-3}	2.788	3.699	1.876
T, K	293(2)	293(2)	293(2)
μ, mm^{-1}	4.069	27.612	2.798
GOF	1.121	1.076	1.126
*R*1,*wR*2 $[I > 2\sigma(I)]$[a]	0.0427, 0.1225	0.0597, 0.0999	0.0651, 0.1096
*R*1,*wR*2 (all data)	0.0435, 0.1239	0.1050, 0.1198	0.1159, 0.1336

[a] $R1 = \Sigma(\Sigma F_o - F_c)/\Sigma F_o$; $wR2 = [\Sigma w(F_o - F_c)^2/\Sigma wF_o^2]^{1/2}$.

 © 2003 Wiley-VCH Verlag GmbH & Co. KGaA, Weinheim

were performed by using the SADABS program.[12] Absorption corrections based on the Ψ scan technique were applied to the data set of complex **2**. From E-value statistics and systematic absence, the space group is either $P2_1$ or $P2_1/m$ for **1**, $P2_1/c$ for **2**, and $P213$ for **3**. When $P2_1/m$ was used for the refinements of complex **1**, the structure was severely distorted, even for the cadmium atom, thus we refined the structure in the non-centrosymmetric $P2_1$ and the results were satisfactory. All three structures were solved by direct methods and refined by full-matrix least-square fitting on F^2 by SHEXLS.[16] All of the non-hydrogen atoms, except C(1), C(5), and C(6) atoms in **2**, were refined anisotropically. All hydrogen atoms were located at geometrically calculated positions and refined with isotropic thermal parameters. The hydrogen atoms for the aqua ligands and lattice water molecules in all three complexes were not refined. A summary of the crystallographic data for these three complexes is listed in Table 2. Selected bond lengths for complexes **1**, **2**, and **3** are given in Table 1.

CCDC-212383 (**1**), -212384 (**2**), and -212385 (**3**) contain the supplementary crystallographic data for this paper. These data can be obtained free of charge at www.ccdc.cam.ac.uk/conts/retrieving.html [or from the Cambridge Crystallographic Data Centre, 12, Union Road, Cambridge CB2 1EZ, UK; Fax: (internat.) +44-1223-336-033; E-mail: deposit@ccdc.cam.ac.uk].

Acknowledgments

This work was supported by the Innovative Project and the Introduction of Overseas Elitists Program by Chinese Academy of Sciences, and the Scientific Research Foundation for the Returned Overseas Chinese Scholars, State Education Ministry. We thank Prof. Kim Dunbar for her valuable suggestions and corrections of the manuscript.

[1] [1a] E. Stein, A. Clearfield, M. A. Subramanian, *Solid State Ionics.* **1996**, *83*, 113−124. [1b] G. Alberti, U. Costantino, in: *Comprehensive Supramolecular Chemistry* (Ed.: J. M. Lehn), Pergamon−Elsevier Science Ltd., London, **1996**, p. 1. [1c] A. Clearfield, *Curr. Opin. Solid State Mater. Sci.* **1996**, *1*, 268−278. [1d] A. Clearfield, Metal phosphonate chemistry, in: *Progress in Inorganic Chemistry* (Ed.: K. D. Karlin), John Wiley & Sons, New York, **1998**, *vol. 47*, pp. 371−510 (and references cited therein).

[2] [2a] A. K. Cheetham, G. Ferey, T. Loiseau, *Angew. Chem. Int. Ed.* **1999**, *38*, 3269−3292. [2b] J. Zhu, X. Bu, P. Feng, G. D. Stucky, *J. Am. Chem. Soc.* **2000**, *122*, 11563−11564.

[3] [3a] B. Zhang, A. Clearfield, *J. Am. Chem. Soc.* **1997**, *119*, 2751−2752. [3b] A. Clearfield, C. V. K. Sharma, B. Zhang, *Chem. Mater.* **2001**, *13*, 3099−3112. [3c] J.-G. Mao, Z. Wang, A. Clearfield, *Inorg. Chem.* **2002**, *41*, 3713−3720.

[4] H. L. Ngo, W. Lin, *J. Am. Chem. Soc.* **2002**, *124*, 14298−14299.

[5] [5a] F. Fredoueil, M. Evain, D. Massiot, M. Bujoli-Doeuff, P. Janvier, A. Clearfield, B. Bujoli, *J. Chem. Soc., Dalton Trans.* **2002**, 1508−1512. [5b] P. Rabu, P. Janvier, B. Bujoli, *J. Mater. Chem.* **1999**, *9*, 1323−1326. [5c] S. Drumel, P. Janiver, P. Barboux, M. Bujoli-Doeuff, B. Bujoli, *Inorg. Chem.* **1995**, *34*, 148−156.

[6] [6a] N. Stock, S. A. Frey, G. D. Stucky, A. K. Cheetham, *J. Chem. Soc., Dalton Trans.* **2000**, 4292−4296. [6b] S. Ayyappan, G. D. de Delgado, A. K. Cheetham, G. Ferey, C. N. R. Rao, *J. Chem. Soc., Dalton Trans.* **1999**, 2905−2907. [6c] A. Distler, S. C. Sevov, *Chem. Commun.* **1998**, 959−960.

[7] [7a] B. Zhang, D. M. Poojary, A. Clearfield, G.-Z. Peng, *Chem. Mater.* **1996**, *8*, 1333−1340. [7b] D. M. Poojary, A. Clearfield, *J. Organomet. Chem.* **1996**, *512*, 237−242. [7c] D. M. Poojary, B. Zhang, A. Clearfield, *Angew. Chem. Int. Ed. Engl.* **1994**, *33*, 2324−2326.

[8] B. Zhang, D. M. Poojary, A. Clearfield, *Inorg. Chem.* **1998**, *37*, 249−254.

[9] [9a] J.-G. Mao, A. Clearfield, *Inorg. Chem.* **2002**, *41*, 2319−2324. [9b] J.-G. Mao, Z. Wang, A. Clearfield, *Inorg. Chem.* **2002**, *41*, 6106−6111.

[10] S. O. H. Gutschke, D. J. Price, A. K. Powell, P. T. Wood, *Angew. Chem. Int. Ed.* **1999**, *38*, 1088−1090.

[11] [11a] R. Vivani, U. Costantino, M. Nocchetti, *J. Mater. Chem.* **2002**, *12*, 3254−3260. [11b] J.-G. Mao, Z. Wang, A. Clearfield, *New J. Chem.* **2002**, *26*, 1010−1014. [11c] J.-G. Mao, C. Lei, Y.-Q. Sun, H.-Y. Zeng, A. Clearfield, *Inorg. Chem.* **2003**, manuscript accepted for publication. [11d] A. Turner, P. A. Jaffrès, E. J. MacLean, D. Villemin, V. Mckee, *Dalton Trans.* **2003**, 1314−1319. [11e] N. Stock, *Solid State Sci.* **2002**, *4*, 1089−1094.

[12] [12a] C. V. K. Sharma, A. Clearfield, *J. Am. Chem. Soc.* **2000**, *122*, 1558−1559. [12b] J. G. Mao, Z. Wang, A. Clearfield, *J. Chem. Soc., Dalton Trans.* **2002**, 4457−4463. [12c] N· Stock, T. Bein, *J. Solid. State. Chem.* **2002**, *167*, 330−336.

[13] [13a] M. R. St. J. Foreman, T. Gelbrich, M. B. Hursthouse, M. J. Plater, *Inorg. Chem. Commun.* **2000**, *3*, 234−238. [13b] S. Ayyappan, G. D. de Delgado, A. K. Cheetham, G. Férey, C. N. R. Rao, *J. Chem. Soc., Dalton Trans.* **1999**, 2905−2907. [13c] A. Cabeza, M. A. G. Aranda, S. Bruque, *J. Mater. Chem.* **1999**, *9*, 571−578.

[14] V. Chandrasekhar, S. Kingsley, B. Rhatigan, M. K. Lam, A. L. Rheingold, *Inorg. Chem.* **2002**, *41*, 1030−1032.

[15] W. Sawka-Dobrowolska, J. Barychi, *Acta Crystallogr., Sect. C* **1989**, *45*, 606−609.

[16] [16a] G. M. Sheldrick, *Program SADABS*, Universität Göttingen, **1995**. [16b] G. M. Sheldrick, *SHELXTL, Crystallographic Software Package*, SHELXTL, Version 5.1, Bruker-AXS, Madison, WI, **1998**.

Received June 11, 2003
Early View Article
Published Online October 10, 2003

 © 2003 Wiley-VCH Verlag GmbH & Co. KGaA, Weinheim

Novel Hybrid Porous 3D Networks of Lead(II) Diphosphonate and Triphosphonate Containing 1,3,5-Benzenetricarboxylate

Jun-Ling Song,[a] Jiang-Gao Mao,*[a] Yan-Qiong Sun,[a] and Abraham Clearfield[b]

Keywords: Synthetic methods / Lead / Carboxylate ligands / P ligands

Hydrothermal reactions of lead(II) acetate with 1,3,5-benzenetricarboxylic acid (H_3BTC) and a new aminodiphosphonic acid, [3-pyridyl-$CH_2N(CH_2PO_3H_2)_2$] (H_4L^1), or a new aminotriphosphonic acid, [1-{$(H_2O_3PCH_2)_2NCH_2CH_2$-}-piperazine-4-$CH_2PO_3H_2$] (H_6L^2), afforded two novel porous carboxylate–phosphonate hybrids, $[Pb_4(BTC)(HBTC)(HL^1)]\cdot 3H_2O$ (**1**) and $[Pb_6(BTC)_2(HBTC)(H_2L^2)]\cdot 4.5H_2O$ (**2**). The structure of **1** is built from a 3D porous network of lead(II) tricarboxylate and 1D double chains of lead(II) aminodiphosphonate. The structure of **2** contains <002> lead(II) carboxylate–phosphonate hybrid layers, which are cross-linked by 1D double chains of lead(II) phosphonate through the organic groups of both types of ligands, resulting in the formation of a complex 3D porous network. The lattice water molecules in both compounds are located at the micropores of the structures.
(© Wiley-VCH Verlag GmbH & Co. KGaA, 69451 Weinheim, Germany, 2003)

Introduction

Open-framework and microporous materials are very important compounds due to their traditional applications in catalysis, separations, sorbents, and ion exchange, as well as their expected future use as hybrid composite materials in electro-optical and sensing applications.[1,2] Recently a number of metal carboxylates with open-framework network structure have been reported.[3] In the chemistry of metal phosphonates, the use of bifunctional or multifunctional anionic units, such as diphosphonates, aminophosphonates or phosphonocarboxylates has led to a number of new materials with microporous or open-framework structures.[4−7] Recently we have also reported a microporous Cd^{II} complex with *N*,*N*′-bis(phosphonomethyl)-1,10-diaza-18-crown ether.[8] Several porous Zr^{IV} complexes with aza-crown ether functionalised phosphonic acids have been synthesized by using phosphoric acid as the spacer group.[9] Direct use of two types of ligands in the preparation, such as a phosphonic acid and a carboxylic acid, has been found to be a useful method to build hybrid open frameworks, though such reports are still rare.[2,10] A 3D open-framework tin(II) phosphonopropionate oxalate and a layered tin(II) methylphosphonate oxalate have been reported by the Cheetham group,[10] and a microporous zinc(II) complex of phosphonopropionic acid and 1,3,5-benzenetricarboxylic acid (H_3BTC) was isolated; however, the tricarboxylate moiety remains noncoordinated and is also severely disordered.[2] We have synthesized a new amino diphosphonic acid, [3-pyridyl-$CH_2N(CH_2PO_3H_2)_2$] (H_4L^1) and a new amino triphosphonic acid, 1-[{$(H_2O_3PCH2)_2NCH_2CH_2$-}-piperazine-4-$CH_2PO_3H_2$] (H_6L^2) (Scheme 1). These two ligands are different from the aminodiphosphonic and -triphosphonic acids, which we had used previously: H_4L^1 contains an additional nitrogen atom for coordination; H_6L^2 has three methylenephosphonate groups attached to two different amine groups which are far apart, whereas the aminotriphosphonate ligand such as nitrilotris(methylenephosphonic acid) has three phosphonate groups attached to the same amine group.[11,12] Thus these new types of ligands are expected to be more likely to form novel hybrid materials with porous 3D network architectures. Hydrothermal reactions of the above two ligands with lead(II) acetate and 1,3,5-benzenetricarboxylic acid afforded two novel porous

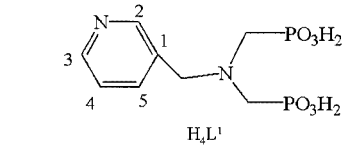

H_4L^1

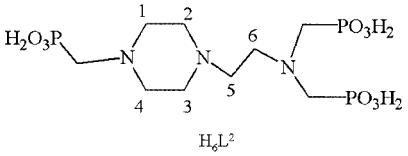

H_6L^2

Scheme 1. The structures of H_4L^1 and H_6L^2

[a] State Key Laboratory of Structural Chemistry,
Fujian Institute of Research on the Structure of Matter,
Chinese Academy of Sciences,
Fuzhou 350002, P. R. China
Fax: (internat.) +86-591-3714946
E-mail: mjg@ms.fjirsm.ac.cn
[b] Department of Chemistry, Texas A&M University,
P. O. Box 30012, College Station,
Texas 77843-3255

 © 2003 Wiley-VCH Verlag GmbH & Co. KGaA, Weinheim **DOI: 10.1002/ejic.200300417**

lead(II) carboxylate-phosphonates in which both types of ligands act as multidentate metal linkers, $[Pb_4(BTC)(HBTC)(HL^1)]\cdot 3H_2O$ (**1**) and $[Pb_6(BTC)_2(HBTC)(H_2L^2)]\cdot 4.5H_2O$ (**2**). Herein we report their syntheses, characterizations and crystal structures.

Results and Discussion

The crystal structure of **1** features a 3D porous network of lead(II) tricarboxylate and a 1D double chain of lead diphosphonate, which are interconnected by sharing some Pb^{II} ions. There are four Pb^{II} atoms, one fully deprotonated tricarboxylate anion (BTC, O7 to O12), one 1H-protonated tricarboxylate (HBTC, O1 to O6), one 1H-protonated diphosphonate (HL^1) anion, and three lattice water molecules in an asymmetric unit of **1**. The coordination geometries around the lead(II) ions are shown in Figure 1. Pb1 is four-coordinated by three phosphonate oxygen atoms from three HL^1 ligands and one carboxylate oxygen atom from a BTC anion, whereas Pb3 is four-coordinated by two phosphonate and two carboxylate oxygen atoms from two HL^1 and two HBTC ligands, respectively. Their coordination geometry can be described as a ψ-square pyramidal PbO_4 in which the lone pair occupies the fifth coordination site. Pb2 is solely coordinated by diphosphonate ligands; it is four-coordinated by a tridentate chelating HL^1 ligand (ligating through two O and one N atoms) and a phosphonate oxygen atom from another HL^1 anion with a ψ-square pyramidal PbO_3N, similar to those of Pb1 and Pb3.

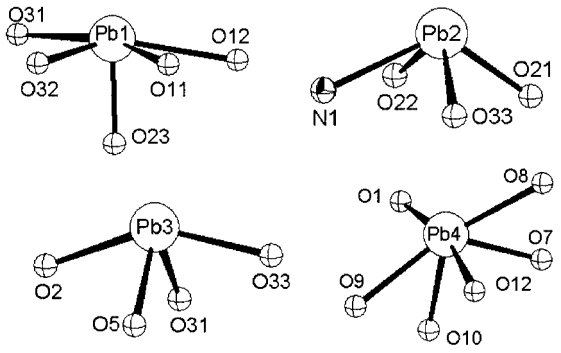

Figure 1. Coordination geometries of the lead(II) ions in **1**

This kind of coordination geometry has been reported in tin(II) phosphonopropionate oxalate and lead phosphonopropionate.[6,10] Pb4 is solely coordinated by tricarboxylate ligands; it is six-coordinated by two bidentate chelating carboxylate groups and two unidentate carboxylate groups from four carboxylate ligands. The coordination geometry around Pb4 can be described as a severely distorted ψ-pentagonal bipyramidal PbO_6 in which the seventh coordination site is occupied by the lone pair of the Pb^{II} ion. The coordination modes of the diphosphonate and BTC ligands are shown in Figure 2.

Each diphosphonate anion chelates with one Pb^{II} ion and bridges six other Pb^{II} ions. Atoms O31 and O33 are bidentate, whereas the remaining phosphonate oxygen atoms are unidentate. The Pb−O distances range from 2.30(2) Å to 2.71(2) Å, similar to those reported for other lead(II) phosphonates and lead(II) carboxylates.[6,7,12,13] The $[BTC]^{3-}$ anion is hexadentate and chelates with two lead(II) ions and also bridges two other lead(II) ions, whereas the $[HBTC]^{2-}$ anion acts as a tridentate ligand and bridges three Pb^{II} ions through two carboxylate groups. The third carboxylate group remains noncoordinated and protonated, as indicated by the longer C18−O4 distance. Based on charge balance, P−O distances, and its coordination mode, the diphosphonate anion should have a charge of −3; hence the pyridyl N atom must be also protonated.

It was noticed that diphosphonate or BTC ligands in $[Pb_4(BTC)(HBTC)(HL^1)]\cdot 3H_2O$ alone can form a coordination polymer with the lead(II) ions. Each pair of $[Pb(HL^1)]$ chelating units is bridged by a pair of phosphonate groups to form a dimer. Such dimers are further interconnected by Pb1 and Pb3 atoms, resulting in the formation of a $[Pb_3(HL^1)]^{3-}$ anionic double chain along the *a*-axis (Figure 3a). The interconnection of lead(II) ions (Pb1, Pb3 and Pb4) by bridging BTC and HBTC ligands results in a $[Pb_3(BTC)(HBTC)]^+$ cation whose structure is also a 3D porous network with two types of tunnels (Figure 3b).

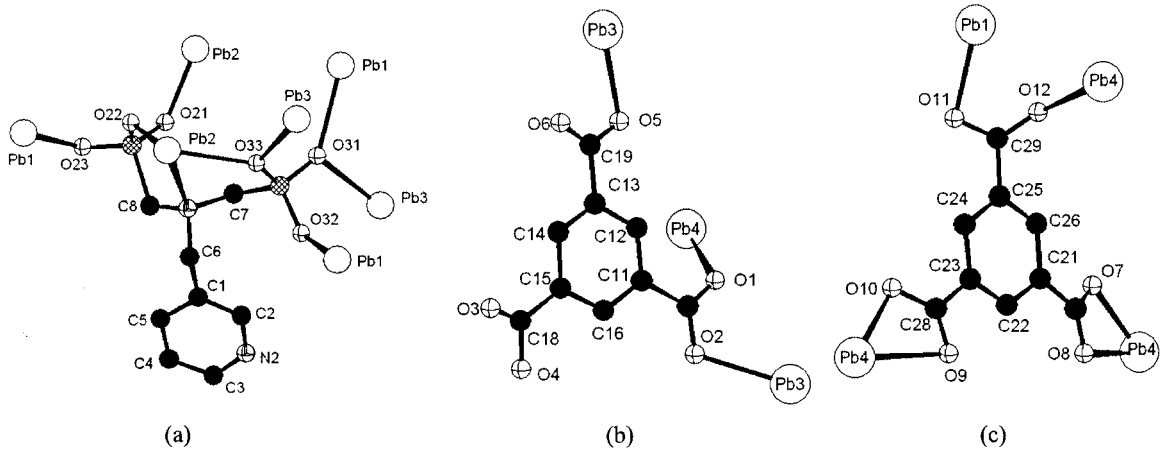

Figure 2. Coordination modes for the diphosphonate and BTC ligands in **1**: (a) HL^1; (b) $[BTC]^{3-}$; (c) $[HBTC]^{2-}$

 © 2003 Wiley-VCH Verlag GmbH & Co. KGaA, Weinheim

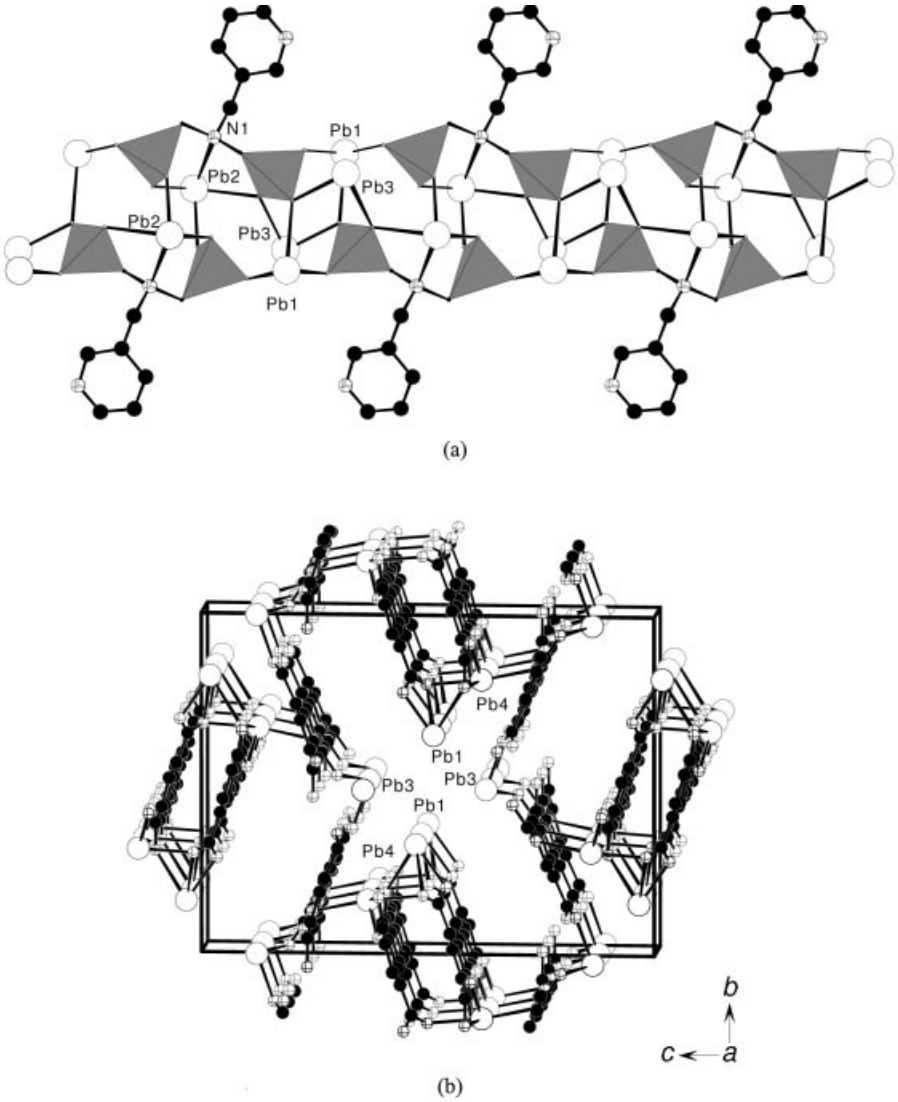

Figure 3. The 1D double chain of lead(II) diphosphonate along the *a*-axis in **1**(a) and the porous 3D network of lead(II) 1,3,5-benzenetricarboxylate in **1** (b); the C-PO_3 tetrahedra are shaded in gray, Pb, N, O and C atoms are represented by open, octanded, crossed and black circles, respectively

The smaller cavity is ca 8.0 $Å^2$ wide and is formed by 16-member rings, each of which is composed of two Pb1 atoms and two BTC ligands. The larger cavity is formed by 54-membered rings, each of which is formed by 8 Pb atoms and 8 BTC ligands. The size of the larger channel is estimated to be about 1/4 of the cell volume. This kind of arrangement is similar to that reported in $Pb_3(BTC)_2{\cdot}H_2O$.[13] These two types of coordination polymeric anions and cations are interconnected through atoms Pb1 and Pb3, resulting in the formation of a new porous network (Figure 4). Such linkage cuts the large cavity of $[Pb_3(BTC)(HBTC)]^+$ in half, thus greatly reducing the cavity size. The pyridine and noncoordinated carboxylate groups are directed towards the micropores. The lattice water molecules also occupy the cavity of the pores, forming hydrogen bonds with noncoordinated carboxylate oxygen atoms, which further increase the stability of the structure (Table 1).

The structure of **2** contains six Pb^{II} ions, two $[BTC]^{3-}$ anions, one $[HBTC]^{2-}$ anion and a 2H-protonated triphosphonate ligand (H_2L^2) in an asymmetric unit. Both Pb1 and Pb3 are five-coordinated by four carboxylate oxygen atoms from two BTC and one HBTC ligands as well as a phosphonate oxygen atom (Figure 5).

Pb2 is six-coordinated by four carboxylate oxygen atoms from one HBTC and two BTC ligands, and two phosphoate oxygen atoms from a bidentate chelating phosphonate group. Pb4 is five-coordinated by three carboxylate oxygen atoms from one BTC and one HBTC anions, and two phosphonate oxygen atoms from two phosphonate groups. Pb5 is four-coordinated by a chelating carboxylate group of a HBTC ligand and two phosphonate oxygen atoms from two L^2 ligands. Pb6 is five-coordinated by a tridentate chelating L^2 ligand (through N2, O41 and O33), a phosphonate oxygen from a neighboring L^2 ligand and a carboxylate oxygen atom of a BTC anion. The four-, five- and six-coordinate

 © 2003 Wiley-VCH Verlag GmbH & Co. KGaA, Weinheim

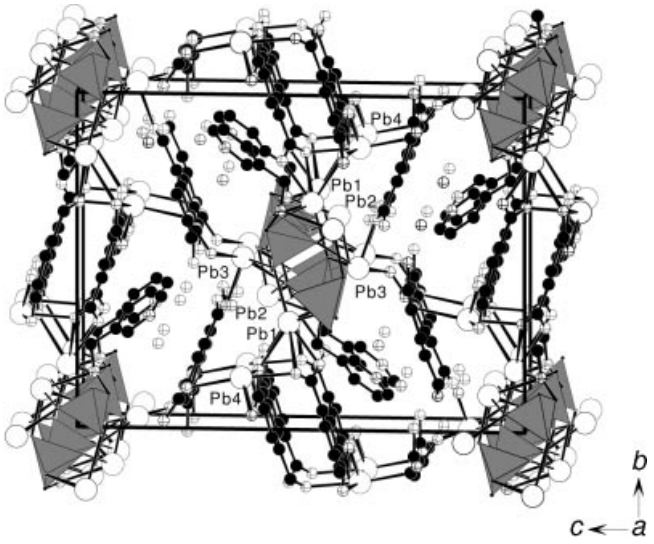

Figure 4. View of the structure of **1** down the *a*-axis; the C-PO_3 tetrahedra are shaded in gray, Pb, N, O and C atoms are represented by open, octanded, crossed and black circles, respectively

lead(II) ions have quite different coordination geometries: ψ-square pyramidal PbO_4, ψ-octahedral PbO_5 (or PbO_4N) and ψ-pentagonal bipyramidal PbO_6 (the lone pairs occupying the fifth, sixth and seventh coordination sites), which are similar to those in compound **1**. The Pb−O distances range from 2.27(1) to 2.75(1) Å and the P−N distance is 2.67(2) Å, which are similar to those in **1** and other lead(II) phosphonates.[6,7,12]

The aminotriphosphonate ligand adopts an interesting coordination mode (Figure 6). The phosphonate group containing P2 forms a chelate with the Pb2 atom (through O21 and O23) and bridges the Pb1 and the Pb3 atom. The O22 atom remains noncoordinated and forms a hydrogen bond with the noncoordinated carboxylate oxygen atom (O10; Table 2). The $N(CH_2PO_3)_2$ moiety of the L^2 ligand is octadentate; it chelates with Pb6 as a tridentate ligand (through N2, O33 and O41) and also bridges five other Pb^{II} ions (two Pb5, two Pb4 and one Pb6 atom). Three phosphonate oxygen atoms (O21, O23 and O41) are bidentate metal linkers. The two nitrogen atoms of the piperazine ring are 1H-

Table 1. Selected bond lengths (Å) and angles (°) for complex **1**

Selected Bonds[a]			
Pb1−O32	2.300(15)	Pb1−O(23)#1	2.341(15)
Pb1−O11	2.460(17)	Pb1−O(31)#2	2.684(15)
Pb2−O(21)#3	2.275(15)	Pb2−O22	2.320(15)
Pb2−O33	2.570(15)	Pb2−N1	2.711(17)
Pb3−O5	2.420(16)	Pb3−O31	2.428(13)
Pb3−O(33)#2	2.575(15)	Pb3−O(2)#4	2.586(18)
Pb4−O(7)#5	2.32(2)	Pb4−O(10)#6	2.36(2)
Pb4−O(12)#2	2.59(2)	Pb4−O(8)#5	2.62(2)
Pb4−O(9)#6	2.70(3)	Pb4−O1	2.70(3)
	Hydrogen bonds		
O4···O(2w)#7	2.86(4)	O4···O(6)#8	2.67(3)
O(1w)···O(2w)	2.41(5)	O(2w)···O(3w)	2.77(4)
O3···O(1w)#1	2.73(5)		
O32−Pb1−O(23)#1	79.4(5)	O32−Pb1−O11	77.1(5)
O(23)#1−Pb1−O11	78.7(6)	O32−Pb1−O(31)#2	80.7(5)
O(23)#1−Pb1−O(31)#2	90.8(5)	O11−Pb1−O(31)#2	156.8(5)
O(21)#3−Pb2−O22	83.2(6)	O(21)#3−Pb2−O33	76.5(5)
O22−Pb2−O33	115.7(5)	O(21)#3−Pb2−N1	120.8(5)
O22−Pb2−N1	71.5(5)	O33−Pb2−N1	68.9(5)
O5−Pb3−O31	83.7(5)	O5−Pb3−O(33)#2	82.9(6)
O31−Pb3−O(33)#2	79.0(5)	O5−Pb3−O(2)#4	76.0(6)
O31−Pb3−O(2)#4	74.5(6)	O(33)#2−Pb3−O(2)#4	147.6(5)
O(7)#5−Pb4−O(10)#6	81.7(9)	O(7)#5−Pb4−O(12)#2	80.3(8)
O(10)#6−Pb4−O(12)#2	81.5(7)	O(7)#5−Pb4−O(8)#5	51.7(8)
O(10)#6−Pb4−O(8)#5	130.9(7)	O(12)#2−Pb4−O(8)#5	76.9(6)
O(7)#5−Pb4−O(9)#6	128.5(8)	O(10)#6−Pb4−O(9)#6	51.3(8)
O(12)#2−Pb4−O(9)#6	73.8(6)	O(8)#5−Pb4−O(9)#6	149.8(7)
O(7)#5−Pb4−O1	102.7(8)	O(10)#6−Pb4−O1	85.0(8)
O(12)#2−Pb4−O1	165.6(7)	O(8)#5−Pb4−O1	116.2(7)
O(9)#6−Pb4−O1	93.8(7)		

[a] Symmetry transformations used to generate equivalent atoms: #1 $x-1, y, z$; #2 $-x, -y+1, -z+1$; #3 $-x+1, -y+1, -z+1$; #4 $-x+1/2, y+1/2, -z+3/2$; #5 $x+1, y-1, z$; #6 $x, y-1, z$; #7 $1/2-x, -1/2+y, 3/2-z$; #8 $-1/2-x, -1/2+y, 3/2-z$.

 © 2003 Wiley-VCH Verlag GmbH & Co. KGaA, Weinheim

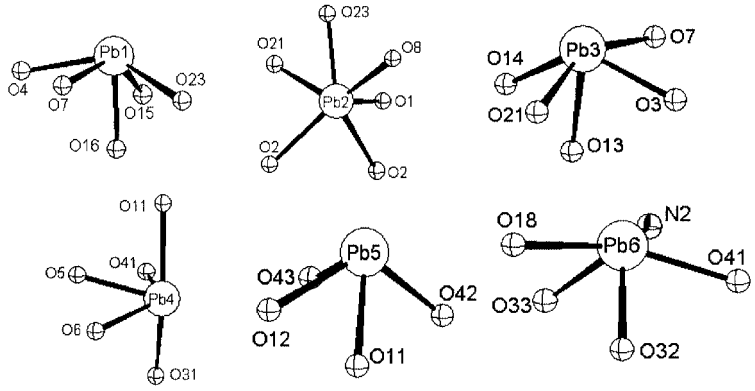

Figure 5. The coordination geometries around the lead(II) ions in **2**

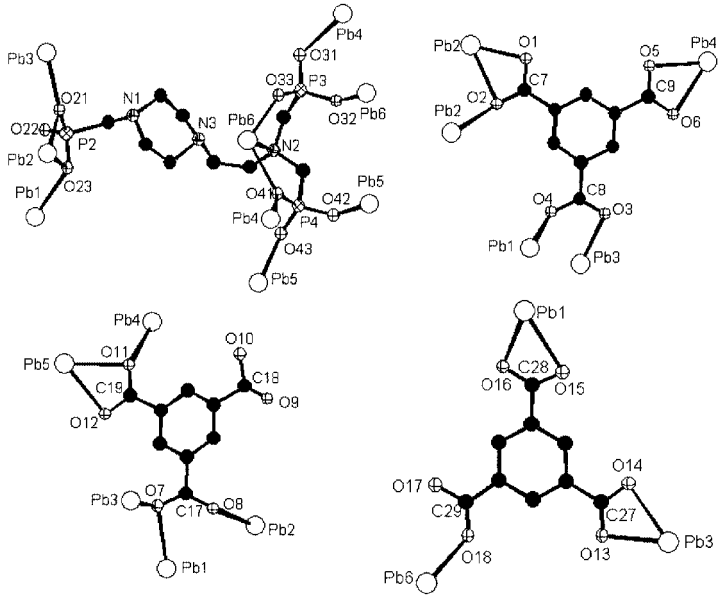

Figure 6. The coordination modes of L^2 and 1,3,5-benzenetricarboxylate ligands in **2**

protonated and remain noncoordinated. The three 1,3,5-benzyltricarboxylate ligands in **2** adopt three different types of coordination modes (Figure 6).

The BTC ligand containing O1 to O6 is heptadentate and bridges five Pb^{II} ions. The carboxylate group CO1O2 forms three bonds, a chelate to one Pb2 atom and a bridge between the two Pb2 atoms, the one containing CO3O4 bridges Pb1 and Pb3 (two-coordinated), whereas the one composed of CO5O6 forms a chelate with Pb4 (two-coordinated). The second tricarboxylate ligand containing O7 to O12 is hexadentate. One carboxylate group CO7O8 bridges three Pb^{II} ions (three bonds to Pb1, Pb2, and Pb3), the second carboxylate group CO11O12 forms three bonds (a chelate with Pb5 and a bridge between Pb4 and Pb5). The third carboxylate group CO9O10 is noncoordinated, and the O10 atom remains protonated as indicated by its longer C−O distance. Thus it is a $[HBTC]^{2-}$ anion. The third BTC ligand (O13 to O18) is pentadentate two carboxylate groups (CO13O14 and CO15O16) are bidentate chelating whereas the third (CO17O18) is unidentate. The atoms O2, O7 and O11 are bidentate metal linkers.

The interconnection of Pb4, Pb5 and Pb6 atoms by the $N(CH_2PO_3)_2$ moieties of L^2 ligands resulted in a 1D double chain along the *a*-axis (Figure 7a). Pb1, Pb2 and Pb3 atoms form a <002> corrugated carboxylate−phosphonate hybrid layer with carboxylate ligands and the phosphonate groups containing P2 atoms (Figure 7b), resulting in the formation of several types of rings. One is the four-membered ring formed by Pb1, O4, Pb3 and O7 atoms. The second type is the six-membered ring formed by Pb1, O23, Pb2, O8, C17 and O7 atoms. The third one is the 12-membered ring composed of four Pb^{II} ions (two Pb2 and two Pb3), two bridging carboxylate groups (two CO7O8) and two bidentate O14 atoms.

The above 1D lead(II) phosphonate double chains and <002> hybrid layers are cross-linked through the organic

 © 2003 Wiley-VCH Verlag GmbH & Co. KGaA, Weinheim

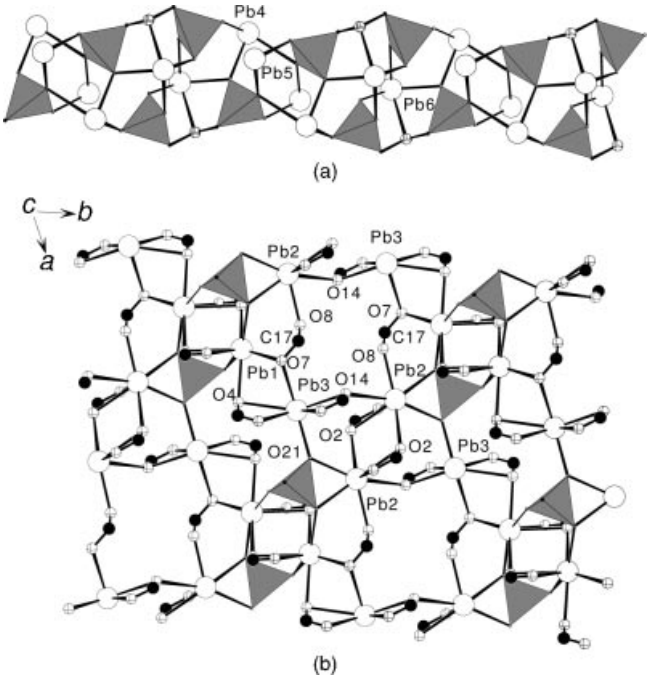

Figure 7. The 1D double chain of lead(II) diphosphonate along the *a*-axis (a) and a <002> lead(II) carboxylate−phosphonate hybrid 2D layer (b) in complex **2**; the C-PO_3 tetrahedra are shaded in gray, Pb, N, O and C atoms are represented by open, octanded, crossed and black circles, respectively.

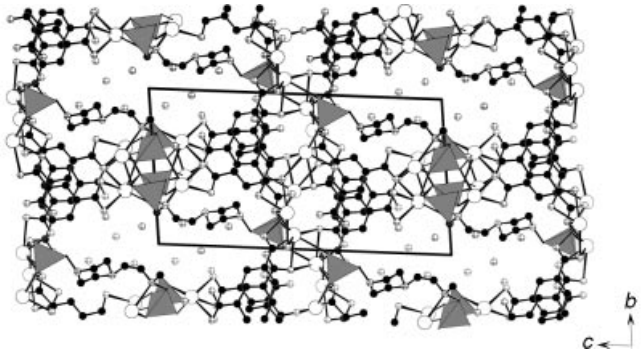

Figure 8. View of the porous 3D network of **2** down the *a*-axis; the C-PO_3 tetrahedra are shaded in gray, Pb, N, O and C atoms are represented by open, octanded, crossed and black circles, respectively

groups of HBTC, BTC and H_2L^2 ligands to form a porous 3D network (Figure 8). The size of the pore is estimated to be 4.0 × 16.0 Å^2. The lattice water molecules are located at these micropores and are involved in hydrogen bonding (Table 2).

The XRD powder patterns for compounds **1** and **2** were collected on a Philips X'Pert-MPD diffractometer using graphite-monochromated Cu-K_α radiation in the angular range $2\theta = 5-70°$. Their powder patterns match with the ones calculated from their single crystal structure data, thus both compounds exist as a single phase.

IR spectra of compounds **1** and **2** show the asymmetric and symmetric vibrations of the carboxyl group at 1543 and 1431 cm^{-1} for **1**, and 1531 and 1433 cm^{-1} for **2**, respectively. The vibrations of the phosphonic groups are in the region 900−1100 cm^{-1}.[7] The broad bands at 3392 cm^{-1} (**1**) and 3396 cm^{-1} (**2**) indicate the presence of the water molecules in both compounds.

The TGA diagram of **1** shows three main steps of the weight losses. The first step is loss of three lattice water molecules, which started at 62 °C and was completed at 165 °C, the observed weight loss of 3.2% is in good agreement with the calculated value (3.4%). The second step covering a temperature range of 320 °C to 633 °C corresponds to the burning of BTC and diphosphonate ligands. The third step overlapped with the second one, corresponding to further decomposition of organic groups. The final products are $Pb_2P_2O_7$ and PbO in a 1:2 molar ratio. The total weight loss of 33.0% is close to the calculated value (35%). The TGA curves of **2** also exhibit three steps of weight loss. The first step is the release of the lattice water molecules, which started at 33°C and was completed at 155°C; the observed weight loss of 3.46% matches with the theoretical one (3.44%). The second and third steps are overlapped, starting at 340 °C and continued up to 1000 °C, during which two processes occurred, firstly, the decomposition of the BTC ligands, and secondly, the burning of the triphosphonate ligand. The final products are assumed to be $Pb_2P_2O_7$ and PbO in a molar ratio of 1:2. The total weight loss of 31.8% is close to the calculated one (34.1%).

Conclusion

In summary, the hydrothermal reactions of lead(II) acetate with an aminodiphosphonic or an aminotriphosphonic acid and 1,3,5-benzenetricarboxylic acid resulted in two novel porous lead(II) carboxylate−phosphonate hybrids in which both ligands act as multidentate metal linkers. The 1,3,5-benzenetricarboxylate ligand may also act as a pillar agent or an intercalated species between two metal phosphonate layers. Thus we believe that a wide range of new open frameworks and microporous materials can be developed by using this technique.

Experimental Section

Materials and Methods: All chemicals were obtained from commercial sources and used without further purification. Elemental analyses were performed on a Vario EL III elemental analyzer. Thermogravimetric analyses were carried out with a TGA/SBTA851 unit at a heating rate of 15 °C/min under an oxygen atmosphere. IR spectra were recorded on a Magna 750 FT-IR spectrometer photometer as KBr pellets in the range 4000−400 cm^{-1}. ^{1}H and ^{31}P NMR spectra were recorded on a Varian Unity 500 NMR in D_2O. H_3PO_4 was used as the ^{31}P standard reference. The XRD powder patterns were collected on a Philips X'Pert-MPD diffractometer using graphite-monochromated Cu-K_α radiation in the angular range $2\theta = 5-70°$ with a step size of 0.02° and a counting time of 3 s per step.

Preparation of H_4L^1 and H_6L^2: H_4L^1 was prepared by a Mannich type reaction according to the procedures previously described.[11] 3-(Aminomethyl)pyridine (100 mmol, 12.6 mL) was mixed with

 © 2003 Wiley-VCH Verlag GmbH & Co. KGaA, Weinheim

Table 2. Selected bond lengths (Å) and angles (°) for complex **2**.

Selected bonds[a]			
Pb1−O7	2.545(12)	Pb1−O(4)#1	2.569(11)
Pb1−O(16)#1	2.569(12)	Pb1−O23	2.587(11)
Pb1−O(15)#1	2.753(13)	Pb2−O1	2.437(13)
Pb2−O8	2.520(11)	Pb2−O21	2.573(11)
Pb2−O23	2.596(12)	Pb2−O2	2.679(12)
Pb2−O(2)#2	2.704(11)	Pb3−O21	2.400(11)
Pb3−O(3)#3	2.430(12)	Pb3−O13	2.506(13)
Pb3−O14	2.571(13)	Pb3−O(7)#4	2.647(12)
Pb4−O41	2.445(11)	Pb4−O(31)#5	2.472(15)
Pb4−O5	2.530(13)	Pb4−O6	2.598(14)
Pb4−O11	2.751(13)	Pb5−O(42)#6	2.331(14)
Pb5−O43	2.355(13)	Pb5−O11	2.615(14)
Pb5−O12	2.646(15)	Pb6−O33	2.274(13)
Pb6−O(32)#5	2.438(14)	Pb6−O41	2.510(11)
Pb6−O18	2.663(13)	Pb6−N2	2.671(16)
Hydrogen bonds			
O10···O(22)#7	2.587(19)	O(1w)···O(3w)#1	2.80(5)
O(1w)···O(6w)	2.57(9)	O(2w)···O(7w)	2.51(8)
O(3w)···O(4w)	2.51(6)	O(4w)···O(7w)#6	2.44(8)
O7−Pb1−O(4)#1	74.5(4)	O7−Pb1−O(16)#1	89.7(4)
O(4)#1−Pb1−O(16)#1	76.6(4)	O7−Pb1−O23	76.2(4)
O(4)#1−Pb1−O23	139.3(4)	O(16)#1−Pb1−O23	75.5(4)
O7−Pb1−O(15)#1	138.1(4)	O(4)#1−Pb1−O(15)#1	84.7(4)
O(16)#1−Pb1−O(15)#1	49.7(4)	O23−Pb1−O(15)#1	99.0(4)
O1−Pb2−O8	93.3(4)	O1−Pb2−O21	86.5(4)
O8−Pb2−O21	124.2(4)	O1−Pb2−O23	88.5(4)
O8−Pb2−O23	67.4(4)	O21−Pb2−O23	56.8(3)
O1−Pb2−O2	50.4(4)	O8−Pb2−O2	109.8(4)
O21−Pb2−O2	112.1(4)	O23−Pb2−O2	138.9(4)
O1−Pb2−O(2)#2	109.8(4)	O8−Pb2−O(2)#2	151.7(4)
O21−Pb2−O(2)#2	74.9(4)	O23−Pb2−O(2)#2	127.2(4)
O2−Pb2−O(2)#2	75.7(4)	O21−Pb3−O(3)#3	83.5(4)
O21−Pb3−O13	74.1(4)	O(3)#3−Pb3−O13	77.6(4)
O21−Pb3−O14	91.2(4)	O(3)#3−Pb3−O(14)	127.6(4)
O13−Pb3−O14	51.2(4)	O21−Pb3−O(7)#4	150.0(4)
O(3)#3−Pb3−O(7)#4	76.5(4)	O13−Pb3−O(7)#4	79.9(4)
O14−Pb3−O(7)#4	83.8(4)	O41−Pb4−O(31)#5	81.4(5)
O41−Pb4−O5	76.4(4)	O(31)#5−Pb4−O5	100.8(4)
O41−Pb4−O6	120.9(4)	O(31)#5−Pb4−O6	83.2(5)
O5−Pb4−O6	51.3(4)	O41−Pb4−O11	81.6(5)
O(31)#5−Pb4−O11	162.9(5)	O5−Pb4−O11	74.4(4)
O6−Pb4−O11	105.1(5)	O(42)#6−Pb5−O43	81.8(4)
O(42)#6−Pb5−O11	71.6(4)	O43−Pb5−O11	95.9(5)
O(42)#6−Pb5−O12	118.4(5)	O43−Pb5−O12	86.5(5)
O11−Pb5−O12	49.8(5)	O33−Pb6−O(32)#5	79.4(5)
O33−Pb6−O41	116.0(4)	O(32)#5−Pb6−O41	79.9(4)
O33−Pb6−O18	73.0(4)	O(32)#5−Pb6−O18	74.5(4)
O41−Pb6−O18	150.8(4)	O33−Pb6−N2	73.4(5)
O(32)#5−Pb6−N2	127.0(4)	O41−Pb6−N2	72.9(4)
O18−Pb6−N2	134.7(4)		

[a] Symmetry transformations used to generate equivalent atoms: #1 $x-1, y+1, z$; #2 $-x+1, -y+1, -z+1$; #3 $x, y+1, z$; #4 $x+1, y, z$, #5 $-x+1, -y+1, -z$; #6 $-x, -y+1, -z$; #7 $x, -1+y, z$.

37% hydrochloric acid (16.0 mL), deionized water (20 mL) and phosphorous acid (400 mmol, 32.8 g). The mixture was allowed to reflux at 120 °C for 1 h, then paraformaldehyde (300 mmol, 9 g) was added in small portions over a period of 1 h, and the mixture was refluxed for an additional hour. Removal of the solvents afforded 26.4 g of a white powder of H_4L^1 (yield 89.2%). Its purity was confirmed by NMR measurements and elemental analysis. ^{31}P NMR spectrocopy shows a single peak at $\delta = 7.97$ ppm. ^1H NMR: $\delta = 3.51$ ppm (N-CH_2-PO_3, d, 4 H, $J_{H,P} = 12.5$ Hz), 5.02 ppm (pyridine-CH_2-N, s, 2 H), 8.21 ppm [C(4)H, 1 H, t], 8.91 ppm [C(5)H, 1 H, d, $J_{H,H} = 5.5$ Hz], 8.93 ppm [C(3)H, d, $J_{H,H} = 8.5$ Hz], 9.15 ppm [C(2)H, 1 H, s], refer to Scheme 1 for the labeling of the carbon atoms. $C_8H_{14}N_2O_6P_2$ (296.2): calcd. C 32.45, H 4.76, N 9.46; found C 32.53, H 4.98, N 9.23. IR (KBr): $\tilde{\nu} = 3428$ cm^{-1} s, 3317 w, 3093 m, 3002 w, 2162 m, 2009 w, 1678 m, 1574 w, 1518 s, 1431 m, 1296 m, 1225 m, 1173 s, 1124 s, 1074 s, 1049 s, 1003 vs,

 © 2003 Wiley-VCH Verlag GmbH & Co. KGaA, Weinheim

Table 3. Crystal data and structure refinement for complexes **1** and **2**

Compound	**1**	**2**
Formula	$C_{26}H_{24}N_2O_{21}P_2Pb_4$	$C_{36}H_{39}N_3O_{31.5}P_3Pb_6$
M_r	1591.17	2353.75
Space group	$P2_1/n$	$P\bar{1}$
a (Å)	10.1516(4)	10.3370(2)
b (Å)	15.8101(6)	12.5019(3)
c (Å)	21.7442(9)	21.8254(3)
α (°)	90.0	83.473(1)
β (°)	102.252(2)	86.896(1)
γ (°)	90.0	68.040(1)
V (Å^3)	3410.4(2)	2598.74(9)
Z	4	2
$D_{calcd.}$ (g.cm^{-3})	3.099	3.008
μ (mm^{-1})	19.875	19.560
Total reflections	11442	13226
Unique reflections	5946	8937
No. of parameters refined	497	653
GooF on F^2	1.054	1.106
$R1$, $wR2$ [$I > 2\sigma(I)$][a]	0.0716/0.1896	0.055/0.1042
$R1$, $wR2$ (all data)	0.0901/0.2070	0.0941/0.1231

[a] $R1 = \Sigma(F_o - F_c)/\Sigma F_o$; $wR2 = \{\Sigma w[(F_o)^2 - (F_c)^2]^2/\Sigma w[(F_o)^2]^2\}^{1/2}$.

951 vs, 920 s, 833 m, 816 m, 802 m, 760 m, 717 m, 692 m, 636 m, 627 m, 553 m, 476 s.

H_6L^2 was prepared in a yield of 86.8% by a Mannich type reaction of 1-(2-aminomethyl)piperazine (100 mmol, 13.2 mL), 37% hydrochloric acid (30 mmol), deionized water (32.0 mL), phosphorous acid (700 mmol, 57.4 g) and paraformaldehyde (500 mmol, 15 g) in a similar method to that of H_4L^1. ^{31}P NMR spectroscopy shows two peaks at δ = 7.18 ppm (for piperazine-CH_2-PO_3H_2) and 11.00 ppm [for $N(CH_2PO_3H_2)_2$], respectively. ^1H NMR: δ = 3.50 ppm (N-CH_2-PO_3, d, 6 H, $J_{H,P}$ = 12.5 Hz), 3.66 ppm [C(5)H_2 and C(6)H_2, t, 4 H], 3.86 ppm [C(1)H_2-C(4)H_2, t, 8 H]. $C_9H_{24}N_3O_{12}P_3$ (459.2): calcd. C 23.54, H 5.27, N 9.15; found. C 23.62, H 5.60, N 9.06. IR (KBr): $\tilde{\nu}$ = 3498 cm^{-1} m, 3392 m, 3342 m, 3016 m, 3016 m, 1662 w, 1629 w, 1521 w, 1458 m, 1433 m, 1383 w, 1271 m, 1174 s, 1119 vs, 1057 m, 1024 m, 985 s, 947 s, 923 m, 769 m, 548 s, 455 m.

Synthesis of $[Pb_4(BTC)(HBTC)(HL^1)]\cdot 3H_2O$ (1) and $[Pb_6(BTC)_2(HBTC)(H_2L^2)]\cdot 4.5H_2O$ (2): $[Pb_4(BTC)(HBTC)(HL^1)]\cdot 3H_2O$ (**1**) was prepared by hydrothermal reaction of lead(II) acetate trihydrate (0.75 mmol, 0.29 g), H_4L^1 (0.25 mmol, 0.08 g) and H_3BTC (0.5 mmol, 0.10 g) in a 3:1:2 molar ratio in 10.0 mL of deionized water at 150 °C for 3 days. Colorless crystals of **1** were recovered in 45.8% yield (based on Pb). $C_{26}H_{22}N_2O_{21}P_2Pb_4$ (1591.17): calcd C 19.65, H 1.40, N 1.76; found C 19.53, H 1.27, N 1.72. IR (KBr): $\tilde{\nu}$ = 3392 cm^{-1} m, 1697 m, 1610 s, 1543 s, 1527 s, 1431 s, 1354 vs, 1261 m, 1190 m, 1095 m, 1061 s, 989 w, 939 w, 843 w, 816 w, 760 w, 721 s, 683 w, 586 m, 569 w, 515 m. $[Pb_6(BTC)_2(HBTC)(H_2L^2)]\cdot 4.5H_2O$ (**2**) was prepared by hydrothermal reactions of lead(II) acetate trihydrate (0.75 mmol, 0.29 g) H_6L^2 (0.25 mmol, 0.11 g) and H_3BTC (0.5 mmol, 0.10 g) in a 3:1:2 molar ratio in 10.0 mL of deionized water at 180 °C for 3 days. Colorless crystals of **2** were recovered in 46.4% yield (based on Pb). $C_{36}H_{40}N_3O_{32}P_3Pb_6$ (2353.75): calcd. C 18.30, H 1.71, N 1.78; found C 18.43, H 1.98, N 1.64. IR (KBr): $\tilde{\nu}$ = 3396 cm^{-1} m, 1651 w, 1610 m, 1531 s, 1433 s, 1361 vs, 1311 m, 1219 w, 1095 s, 1039 s, 966 s, 817 w, 802 w, 758 m, 721 s, 694 w, 572 m, 555 w, 509 w, 482 w.

Crystal Structure Determination: Single crystals of **1** and **2** were mounted on a Siemens Smart CCD diffractometer equipped with a graphite-monochromated Mo-K_α radiation (λ = 0.71073 Å). Intensity data were collected by the narrow frame method at 293 K. The data sets were corrected for Lorentz and polarization as well as for absorption by ψ scan technique. Both structures were solved by direct methods and refined by full-matrix least-squares fitting on F^2 by SHELX-97.[14] All non-hydrogen atoms, except for C7, C11, and O32 in **1**, and C6, C22, C25, C31, C32, C33, C34, C35 and O(7 W) in **2,** were refined with anisotropic thermal parameters. The carbon atoms of the piperazine ring in **2** have large thermal parameters and were refined with a rigid model. Lattice water molecules [O(3 W) to O(7 W)] also have large thermal parameters, and each was assigned with an occupancy factor of 50%. Despite these problems, the refinement of **2** can still be considered satisfactory for such a complicated structure. The final difference Fourier maps showed featureless residual peaks of 2.88 [for, **1**, 1.15 Å from the Pb4 atom] and 1.78 e·Å^{-3} [for **2**, 0.84 from the Pb6 atom], respectively. All hydrogen atoms were located at geometrically calculated positions. The hydrogen atoms for the water molecules were not included in the refinement. Crystallographic data and structural refinement are summarized in Table 3. Important bond lengths and angles are listed in Table 1 for complex **1** and Table 2 for complex **2**. CCDC-209007 and -209008 contain the supplementary crystallographic data for this paper. These data can be obtained free of charge at www.ccdc.cam.ac.uk/conts/retrieving.html [or from the Cambridge Crystallographic Data Centre, 12 Union Road, Cambridge CB2 1EZ, UK; Fax: (internat.) + 44-1223-336-033; E-mail: deposit@ccdc.cam.ac.uk].

Acknowledgments

This work was supported by the Innovative Project, "The Introduction of Overseas Elitists Program by the Chinese Academy of Sciences and the Scientific Research Foundation for the Returned Overseas Chinese Scholars, State Education Ministry."

[1] A. K. Cheetham, G. Ferey, T. Loiseau, *Angew. Chem. Int. Ed.* **1999**, *38*, 3268−3292.

 © 2003 Wiley-VCH Verlag GmbH & Co. KGaA, Weinheim

[2] J. Zhu, X. Bu, P. Feng, G. D. Stucky, *J. Am. Chem. Soc.* **2000**, *122*, 11563−11564.
[3] N. L. Rosi, M. Eddaoudi, J. Kim, M. O'Keeffe, O. M. Yaghi, *Angew. Chem. Int. Ed.* **2001**, *41*, 284−310; M. Eddaoudi, J. Kim, M. O'Keeffe, O. M. Yaghi, *J. Am. Chem. Soc.* **2002**, *124*, 376−377; M. E. Braun, C. D. Steffek, J. Kim, P. G. Rasmussen, O. M. Yaghi, *Chem. Commun.* **2001**, 2532−2533.
[4] A. Distler, L. Lohse, S. C. Sevov, *J. Chem. Soc., Dalton Trans.* **1999**, 1805−1812; V. Soghomonian, Q. Chen, R. C. Haushalter, J. Zubieta, *Angew. Chem. Int. Ed. Engl.* **1995**, *34*, 223−226.
[5] S. Drumel, P. Janvier, D. Deniaud, B. Bujoli, *Chem. Commun.* **1995**, 1051−1052; U. Costantino, M. Nocchetti, R. Vivani, *J. Am. Chem. Soc.* **2002**, *124*, 8428−8434; S. O. H. Gutschke, D. J. Price, A. K. Powell, P. T. Wood, *Angew. Chem. Int. Ed.* **1999**, *38*, 1088−1090; E. Galdecka, Z. Galdecki, P. Gawryszewska, J. Legendziewicz, *New J. Chem.* **2000**, *24*, 387−391; L.-M. Zheng, P. Yin, X.-Q. Xin, *Inorg. Chem.* **2002**, *41*, 4084−4086.
[6] N. Stock, S. A. Frey, G. D. Stucky, A. K. Cheetham, *J. Chem. Soc., Dalton Trans.* **2000**, 4292−4296; S. Ayyappan, G. D. Delgado, A. K. Cheetham, G. Ferey, C. N. R. Rao, *J. Chem. Soc., Dalton Trans.* **1999**, 2905−2907; F. Fredoueil, M. Evain, D. Massiot, M. Bujoli-Doeuff, P. Janvier, A. Clearfield, B. Bujoli, *J. Chem. Soc., Dalton Trans.* **2002**, 1508−1512; S. Drumel, M. Bujolidoeuff, P. Janvier, B. Bujoli, *New J. Chem.* **1995**, *19*, 239−242.
[7] A. Distler, S. C. Sevov, *Chem. Commun.* **1998**, 959−960; S. J. Hartman, E. Todorov, C. Cruz, S. C. Sevov, *Chem. Commun.* **2000**, 1213−1214; J.-G. Mao, Z. Wang, A. Clearfield, *Inorg. Chem.* **2002**, *41*, 6106−6111; R. Vivani, U. Costantino, M. Nocchetti, *J. Mater. Chem.* **2002**, *12*, 3254−3260.
[8] J.-G. Mao, Z. Wang, A. Clearfield, *Inorg. Chem.* **2002**, *41*, 3713−3720.
[9] B. Zhang, A. Clearfield, *J. Am. Chem. Soc.* **1997**, *119*, 2751−2752; A. Clearfield, D. M. Poojary, B. Zhang, B. Zhao, A. Derecskei-Kovacs, *Chem. Mater.* **2000**, *12*, 2745−2752.
[10] N. Stock, G. D. Stucky, A. K. Cheetham, *Chem. Commun.* **2000**, 2277−2278; B. Adair, S. Natarajan, A. K. Cheetham, *J. Mater. Chem.* **1998**, *8*, 1477−1479.
[11] J.-G. Mao, Z. Wang, A. Clearfield, *Inorg. Chem.* **2002**, *41*, 2334−2340; J.-G. Mao, Z. Wang, A. Clearfield, *J. Chem. Soc., Dalton Trans.* **2002**, 4541−4546.
[12] A. Cabeza, M. A. G. Aranda, S. Bruque, A. Clearfield, *J. Mater. Chem.* **1999**, *9*, 571−578; J.-G. Mao, Z. Wang, A. Clearfield, *New J. Chem.* **2002**, *26*, 1010−1014; C. V. K. Sharma, A. Clearfield, A. Cabeza, M. A. G. Aranda, S. Bruque, *J. Am. Chem. Soc.* **2001**, *123*, 2885−2886; A. Cabeza, O. Y. Xiang, C. V. K. Sharma, M. A. G. Aranda, S. Bruque, A. Clearfield, *Inorg. Chem.* **2002**, *41*, 2325−2333.
[13] M. R. St J. Foreman, T. Gelbrich, M. B. Hursthouse, M. J. Plater, *Inorg. Chem. Commun.* **2000**, *3*, 234−238.
[14] G. M. Sheldrick, *SHELXTL*, *Crystallographic Software Package*, version 5.1, Bruker-AXS, Madison, WI, **1998**.

Received June 30, 2003
Early View Article
Published Online October 10, 2003

 © 2003 Wiley-VCH Verlag GmbH & Co. KGaA, Weinheim

Reaction of Methyl Radicals with Metal Powders Immersed in Aqueous Solutions

Irena Rusonik,[a] Hurriyet Polat,[a,b] Haim Cohen,[a,c] and Dan Meyerstein*[a,d]

Keywords: Carbon / Energy transfer / Radicals / Oxidation

Methyl radicals radiolytically produced in aqueous solutions react efficiently with Cr^0, Mn^0, Fe^0, Ni^0, Cu^0 and Zn^0 powders immersed in the solution. The Cr^0, Mn^0, Fe^0, Ni^0 and Zn^0 powders reduce the radicals to form methane. On the other hand the Cu^0 powder seems to oxidize the radicals. Surprisingly a part of the energy absorbed by the Cr^0, Fe^0, Ni^0 and Zn^0 powders is transferred to the aqueous solution, thus increasing the radical yield. CH_4, C_2H_4, C_2H_6, C_3H_6 and C_3H_8 are formed when an aqueous deaerated buffer solution, pH 4–5, is added to powders of analytical iron, zinc, manganese and chromium. The source of these gases is carbon traces present, as atoms or atom clusters, in the "analytical" metal powders. These carbon atoms, when present on the surface of the metals, are reduced by the metal particles in aqueous solutions. This mechanism might be the source of light alkanes and alkenes in the prebiotic era.
(© Wiley-VCH Verlag GmbH & Co. KGaA, 69451 Weinheim, Germany, 2003)

Introduction

Extensive use of halogenated aliphatic compounds, as solvents and degreasing agents in industry, and as pesticides in agriculture, has led to environmental problems of contamination of groundwater systems. Therefore, there is considerable interest in developing methods for removing halogenated organic compounds from industrial and agricultural wastes. Zero-valent iron,[1−11] Fe^0, is an effective reagent for the dehalogenation process of contaminated water streams. Despite recent significant progress in the elucidation of this mechanism,[9,12,13] many basic questions remain unanswered. The principle goal of our research program is a detailed investigation of the dehalogenation mechanism. The elucidation of this mechanism is of scientific interest and might enable to improve the process.

The mechanism of the dehalogenation process probably involves in the first stage the reactions:[2,6,14]

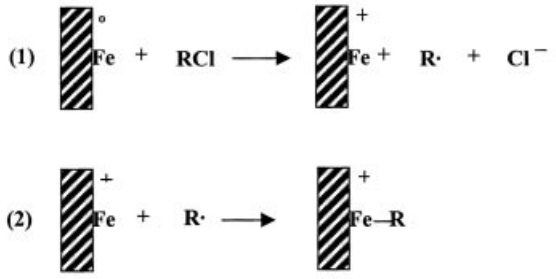

Thus, it seemed of interest to study the mechanism of reaction 2 and the mechanism of the decomposition of the transient I formed in it. For this purpose it was decided to form the radicals R˙ in the vicinity of iron powder using radiation chemical techniques. The methyl radical was chosen due to its simplicity and reactivity as a strong oxidizing and reducing agent.[15,16] However blank experiments revealed that light alkanes and alkenes are formed when "analytical" iron is dissolved in slightly acidic aqueous solutions. This observation, which partially corroborates an earlier study,[17] might affect the nature of the final products obtained and was therefore also studied. For comparison purposes the analogous processes in the presence of other metal powders were also studied.

[a] Department of Chemistry, Ben-Gurion University of the Negev, Beer-Sheva, Israel
[b] Department of Chemistry, Ismir Institute of Technology, Ulra-Izmir, Turkey
[c] Nuclear Research Centre Negev, Beer-Sheva, Israel
[d] Department of Biological Chemistry College of Judea and Samaria, Ariel, Israel
Fax: (internat.) +972 39067440
E-mail: danmeyer@bgumail.bgu.ac.il

Results and Discussion

Formation of Alkanes during the Dissolution of Analytical Metals in Aqueous Solution

Light alkanes and alkenes are formed when analytical iron is dissolved in He-saturated, CO_2-free, slightly acidic

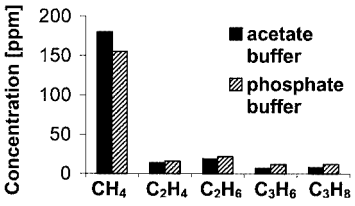

Figure 1. Yield of alkanes and alkenes in the gas phase: 10 g Fe^0, 2.5 mL 0.5 M acetate buffer pH 4.0 or 10 g Fe^0, 2.5 mL 0.1 M phosphate buffer pH 4.0; t = 3 h, T = 25 °C

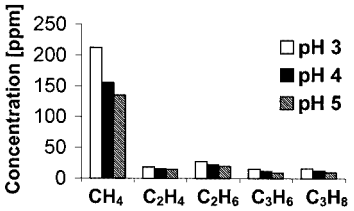

Figure 2. pH dependence of the dissolution of iron in phosphate buffer 0.1 M: 10 g Fe^0, 2.5 mL phosphate buffer 0.1 M; t = 3 h, T = 25 °C; error limit ± 15%

buffers. Typical results are summed up in Figure 1. The major product is always methane. The results suggest that the nature of the buffer slightly affects the relative yields of the different products. The larger methane yield in the acetate buffer is tentatively attributed to the larger buffer capacity of acetate at this pH.

As, at least in the phosphate buffer, the source of the organic gases has to be the iron, an analysis of the carbon content of the iron powder was performed. Indeed the results point out that the carbon/carbide content of the analytical iron is 450 ppm by weight, though this is not mentioned in the analytical data given by Merck. As expected, analysis of the iron ions formed indicates that over 95% of the iron is present as $Fe^{II}_{(aq)}$ and not as $Fe^{III}_{(aq)}$. The yield of $H_{2(g)}$, not shown, is very similar to that of $Fe^{II}_{(aq)}$ and corroborates the previous observation.

Analysis of the time dependence of the process shows that no induction period is observed and the product gases are formed within the first 20 min of the process, during which the pH at the metal surface presumably increases thus stopping, or slowing down, the process. The observation that the process is over within the first 20 min could alternatively suggest that the carbon atoms are present only at the surface of the iron particles. In order to check this possibility, the iron powder was activated in sulfuric acid (0.1 M) for 30 min, it was then washed with excess distilled water, and was bubbled with He for one hour. The water was then removed and the bulb was closed and deaerated with He before adding the phosphate buffer. After a further 20 min the gas phase was analyzed. The gas composition and concentrations were the same as in the previous experiments. This result points out that the carbon atoms are present in the iron bulk.

The emission of organic gases during the dissolution of iron powder in slightly acidic aqueous solutions is surprising. The yield of the organic gases increases with the decrease in pH of the solution (see Figure 2). It seemed of interest to check whether similar results are obtained for other analytical metal powders. The results obtained are summed up in Table 1. The results clearly demonstrate that light alkanes and alkenes are also formed during the dissolution of "analytical" Cr^0, Mn^0 and Zn^0. However, the relative yields of the different gases depend on the nature of the metal.

As the main purpose of our research was to study the mechanism of reaction 2 and the mechanism of decomposition of the transient **I** formed in it, the influence of radiation on the dissolution process of the metal power was studied. When the samples (10 g activated metal powder, 2.5 mL water at pH 4.0) are irradiated in a ^{60}Co γ-source with a dose of 480 Gy, the yield of the alkanes and alkenes increases somewhat. Typical results are shown in Table 1. Clearly the radiation enhances the rate of dissolution of the metals; this might be due to the reactions of the radicals formed by irradiating the aqueous solutions (see below) with the metals.

The mechanism of formation of the alkanes and alkenes probably involves in the first stage one of the following steps:

Table 1. The relative yields of the different gases depend on the nature of the metal and of the radiation[a]

Metal	Radiation	E [V]	Carbon [ppm]	CH_4 [ppm]	C_2H_4 [ppm]	C_2H_6 [ppm]	C_3H_6 [ppm]	C_3H_8 [ppm]
Cr^0	+	−0.41	3000	30.8	16.9	8	9	−
Cr^0	−			28	14	6	8	−
Fe^0	+	−0.44	450	29	17	11	4.9	3.9
Fe^0	−			21	10.1	8	−	3.7
Zn^0	+	−0.76	40	23.6	−	1.8	−	3.2
Zn^0	−			22.2	−	1.8	−	−
Mn^0	+	−1.18	50	87.8	−	5.1	0.4	−
Mn^0	−			72.9	−	3.1	−	−

[a] All samples contained 10 g of activated metal powder and 2.5 mL of water at pH 4.0, t = 3 hours, radiation dose 480 Gy. No buffer was added to these experiments.Error limit ± 15%.

 © 2003 Wiley-VCH Verlag GmbH & Co. KGaA, Weinheim

1. Hydrogen atoms adsorbed to the iron particles migrate to exposed carbon atoms forming

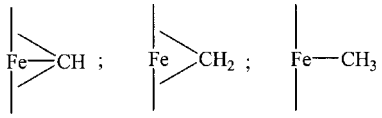

groups.

The migration of the hydrogen atoms is equivalent to that involved in the formation of $H_{2(g)}$ via the migration of two hydrogen atoms. The formation of transients containing Fe−alkyl bonds is analogous to the formation of transient complexes in the reaction of alkyl radicals with iron(II) complexes,[18] and other low valent transition metal complexes,[16] in homogeneous solutions.

2. The iron particles act as microelectrodes charging negatively the less electropositive exposed carbon atoms that then reduce the water.

These two mechanisms might contribute in parallel to the process observed.

In addition, the next step might occur via two mechanisms:

1. Migration of the alkyl groups of

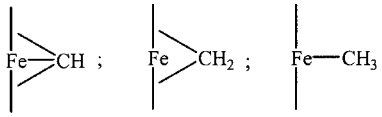

in parallel to hydrogen atom migration, to form

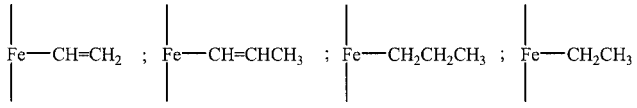

2. The carbon atoms might be dispersed in the metal particles as C_1, C_2 and C_3, which are then reduced. This mechanism does not require migration of alkyl groups which at least for

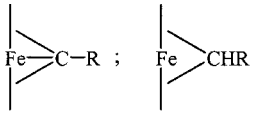

seems to be difficult.

The results of the study of the mechanism of the reaction of $^{\cdot}CH_3$ radicals with metal powders (see below) seems to suggest that the latter mechanism is more probable. However the considerably smaller ratios of $[CH_4]/[C_2H_4]$ and $[CH_4]/[C_2H_6]$ in non-buffered solutions than in buffered solutions (see Table 2), suggests that the acid-catalyzed heterolysis of the metal−carbon σ-bonds[19,20] in the dissolution process of the metal powder, inhibits alkyl migration, thus increasing these ratios.

Table 2. Ratio comparison of gas concentrations formed in the dissolution process of analytical iron in the presence of a buffer and in its absence[a]

Presence of buffer	$[CH_4]/[C_2H_4]$	$[CH_4]/[C_2H_6]$
+	9.8	7.1
−	2.1	2.6

[a] Every sample contains 10 g of activated iron powder, 2.5 mL H_2O or 0.1 M phosphatebuffer pH 4.0, t = 3 hours, T = 25 °C, No radiation. Error limit ± 15%.

The last step of the mechanism clearly involves the heterolysis of the M−C σ-bonds, in an analogous mechanism to that observed for homogeneously dissolved complexes with metal−carbon σ bonds.[21−23]

The results clearly demonstrate that whenever the reduction of haloalkanes by metals is studied by following the kinetics of formation of the organic products,[24,25] the corresponding blank experiments, in the absence of organic substrates, have to be carried out.

Finally it is tempting to suggest that the production of alkanes and alkenes via this mechanism might have contributed to the formation of light organic compounds[26] including petroleum,[27] in the prebiotic era. Clearly this mechanism does not require the harsh conditions required by many alternative mechanisms.[28]

Reaction of Methyl Radicals

At first the reaction of activated iron powder with methyl radicals was studied. The results (see Table 3) clearly demonstrate that considerably more CH_4 is formed in the irradiated sample containing iron powder than in the sum of the blank experiments (non-irradiated sample and irradiated sample without iron powder). The gases formed in the non-irradiated blank experiment are due to the dissolution process of the iron powder, which contains 450 ppm of carbon by weight. A comparison of the yields of the gases formed in the irradiated sample containing iron powder and the same non-irradiated experiment (see Table 3), demonstrates that the C_2H_4, C_3H_6 and C_3H_8 gases formed in irradiated experiments originate from the dissolution of Fe^0. However the yield of CH_4 and C_2H_6 in this experiment is considerably larger than that in the non-irradiated experiment. It is suggested that the excess CH_4 and C_2H_6 formed in the irradiated samples containing iron powder are

Table 3. Emitted gas composition in reaction with $(CH_3)_2SO$[a]

Presence of Iron	Radiation	CH_4	C_2H_4	C_2H_6	C_3H_6	C_3H_8
+	+	1598	18	147	4	5.7
+	−	45	17	11	3.9	5.7
−	+	990	−	122	−	−

[a] 10 g activated iron, 2.5 mL solution containing buffer acetate 0.1 M and $(CH_3)_2SO$ 0.05 M, pH 4.0, radiation dose 480 Gy, N_2O saturated. Error limit ± 15%.

 © 2003 Wiley-VCH Verlag GmbH & Co. KGaA, Weinheim

formed via the mechanism outlined in Scheme 1. It is proposed that the reaction proceeds via the inner-sphere mechanism, as the formation of CH_3^- is endothermic in analogy to oxidations by hydrogen atoms.[30,31] The formation of M^I-CH_3 σ-bonds is analogous to the observed mechanism of reaction of $^{\cdot}CH_3$ radicals with a variety of low valent transition metal complexes.[16,21]

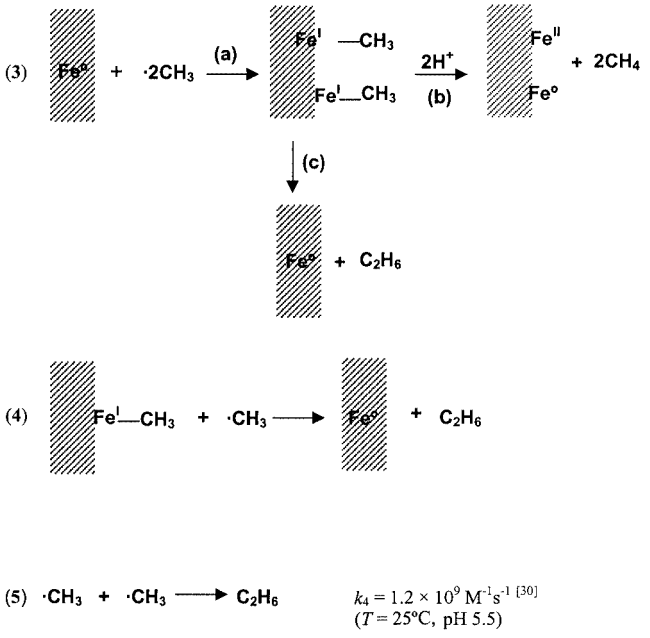

Scheme 1. CH_4 and C_2H_6 formation via reaction of methyl radicals with iron powder

It is of interest to note that the yield of $[CH_4] + 2[C_2H_6]$ in irradiated samples containing iron powder is considerably larger than in irradiated samples without iron powder, by at least a factor of two. This result proves that more methyl radicals are formed by radiation in the solution containing the iron powder. This result points out that some of the energy absorbed by the metal powder is transferred to the aqueous solution or to$(CH_3)_2SO$ molecules adsorbed to the powder surface. Energy transfer and charge transfer from irradiated solids to the solvent or to adsorbed molecules is a well-known phenomenon in the literature.[32−37] But the solid systems studied were porous silica, zeolites, porous glass and clay systems i.e. insulators. Nothing is known about energy transfer or charge transfer from irradiated metals to adsorbed molecules or to the solution. Obviously, the present results point out that, surprisingly, this phenomenon occurs also for iron, i.e. for a metal. This means that a band gap between the ground state and the excited state is not required for this process.

The dependence of the yield of CH_4 and C_2H_6 on $(CH_3)_2SO$, in the range 0.02−0.08 M, was studied. The results (not shown) point out that the gas yields are independent of $(CH_3)_2SO$. This suggests that either the energy is transferred from the iron to the solution or that even at the lowest concentration the iron surface is saturated with adsorbed $(CH_3)_2SO$. The latter alternative seems less probable.

The results are pH independent in the range 4−6. Therefore it was decided to omit the acetate buffer from the solutions. This action decreases the $[CH_4]/[C_2H_6]$ ratio in the blank experiments that do not contain iron powder, because reaction 6 contributes to the methane yield.

(6) $^{\cdot}CH_3 + CH_3COO^- \longrightarrow CH_4 + {}^{\cdot}CH_2CO_2^-$ $k_6 = 600\ M^{-1}s^{-1}$ [38] ($T = 25°C$, pH 1.0)

When N_2O-saturated blank solutions containing only 0.05 M $(CH_3)_2SO$ are irradiated, the methane and ethane are formed via reactions 7 and 5. Using the radiation dose 480 Gy and k_5 one can calculate k_7 from the results.

(7) $^{\cdot}CH_3 + (CH_3)_2SO \longrightarrow CH_4 + {}^{\cdot}CH_2S(O)CH_3$ $k_7 = 100 \pm 20\ M^{-1}s^{-1}$ ($T = 25\ °C$, pH 4.0)

The calculated value of k_7 is smaller than the k_6 value, therefore, in the absence of acetate buffer, the contribution of reaction 5 is larger and the yield of ethane is increased in comparison to the methane yield.

At the end of all the reactions the Fe^{II} and Fe^{III} concentrations were measured using a colorimetric method.[39] The measured concentrations of Fe^{III} ions are negligible [$(5 \pm 0.8) \times 10^{-5}$ M] compared to Fe^{II} [$(1.2 \pm 0.2) \times 10^{-3}$ M]. The Fe^{II} and Fe^{III} concentrations were the same at all pHs and for irradiated and non irradiated systems. The calculated concentration of Fe^{II} due to reaction 3, which yields 2100 ppm CH_4 (see Table 4) in the irradiated system is 1.1×10^{-4} M, i.e. within the experimental error of the non-irradiated sample.

Next it was checked whether the methane is formed via the reaction:

(8) $Fe^{2+}_{aq} + {}^{\cdot}CH_3 \xrightarrow{H^+} Fe^{3+}_{aq} + CH_4$

For this purpose N_2O-saturated solutions containing $FeSO_4$ were irradiated. The results (see Table 5) clearly point out that reaction 8 involving the Fe^{2+}_{aq} ions, formed in the corrosion process, is not the source of the methane formed in the presence of the iron powder.

Thus the results illustrate that methyl radicals react with the iron powder to form CH_4 and probably some C_2H_6. Assuming that all the ethane is formed via reaction 5, i.e. that reactions 3c and 4 do not contribute to the ethane yield, one can calculate the apparent rate of reaction 3a from the known dose rate and k_4. Thus $k_{3a} = 20 \pm 10\ s^{-1}$ and is calculated for this powder.

A considerably larger $[CH_4]/[C_2H_6]$ ratio is observed in the irradiated samples containing iron powder than in the blank non-irradiated samples (see Table 4). In the irradiated samples the density of -CH_3 groups bound to the iron particles is clearly considerably higher than in the blank non-irradiated experiments. These observations suggest that the C_2H_6 formed in the blank experiments does not stem from the reaction:

 © 2003 Wiley-VCH Verlag GmbH & Co. KGaA, Weinheim

Table 4. The role of metal powder activation and irradiation on the gas yields[a]

Metal	Activated	Irradiated	E^0 [V]	Carbon [ppm]	CH_4 [ppm]	C_2H_4 [ppm]	C_2H_6 [ppm]	C_3H_6 [ppm]	C_3H_8 [ppm]
$(CH_3)_2SO$	−	+			500		370		
$Cu^{0[a]}$	+	+	0.34	560	41		20		
	+	−			17		5.6		
	−	+			44		82		
	−	−			2				
$Cr^{0[b]}$	+	+	−0.41	3000	1500	72	160	32	30
	+	−			75	19	15	8	7.4
	−	+			466	28	37		
	−	−			58	13.7	5.3		
$Fe^{0[c]}$	+	+	−0.44	450	2100	63	240	1.2	4
	+	−			28.4	13	8.6	4.7	5
	−	+			753	22	85	2.7	1.7
	−	−			30	20	8.8	8	3.2
$Zn^{0[d]}$	+	+	−0.76	40	2060		553		
	+	−			12	2.6	1.6		
	−	+			903		150		
	−	−			1.8				
$Mn^{0[e]}$	+	+	−1.18	50	790		90		
	+	−			170		32		
	−	+			780		132		
	−	−			140		8		

[a] Composition of the gases formed in the reaction of 10 g activated/ non activated metal powders with 2.5 mL $(CH_3)_2SO$ 0.05 M solution, pH 4.0, t = 3 hours (radiation dose 480 Gy), T = 25 °C. All samples N_2O saturated. Error limit ± 15%. Cu^0 powder (Aldrich 99%, <10 μm). [b] Cr^0 powder (Alfa Aesar 99.8%, <10 μm). [c] Fe^0 powder (Merck 99%, ≤10 μm). [d] Zn^0 powder (Aldrich 98%, <10 μm). [e] Mn^0 powder (Aldrich 99%, 325 mesh).

Table 5. Dependence of gas formation in the presence of $Fe^{2+}{}_{aq}$ ions[a]

Sample composition	Irradiated	CH_4 [ppm]	C_2H_6 [ppm]
$FeSO_4$, $(CH_3)_2SO$	+	480	190
$FeSO_4$, $(CH_3)_2SO$	−	−	−
$(CH_3)_2SO$	+	500	370

[a] 2.5 mL of N_2O saturated solutions containing $FeSO_4$ (5×10^{-3} M), $(CH_3)_2SO$ (0.05 M), pH 4.0, t = 3 hours (radiation dose 480 Gy), T = 25 °C. Error limit ± 15%.

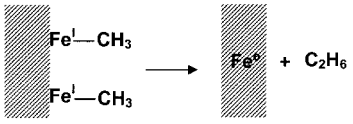

i.e. from the migration of -CH_3 groups bound to the iron particle. Thus the results corroborate the suggestion that the C_2H_4, C_2H_6, C_3H_6 and C_3H_8 gases formed in the non-irradiated blank experiments containing iron powder, originate from small carbon clusters present in the iron metal.

It was interesting to check whether analogous reactions of methyl radicals also take place with other metal powders. For this purpose the reactions of Cu, Cr, Zn and Mn powders with methyl radicals were studied. In addition, the role of metal powder activation on the gas yields was investigated; the results are summed up in Table 4. The effect of irradiating metal powders immersed in water at pH 4.0, in the absence of $(CH_3)_2SO$, on the yield of light alkanes is minor (see Table 1).

Conclusions

According to the experimental results the following conclusions can be drawn:

1. For all metals, except for Cu^0 and Mn^0, in the {M^0, $(CH_3)_2SO$, Ra} system the radiolytic yield of methane is considerably larger than that obtained in the absence of the metal powder but the ethane yield decreases, except for the system containing activated Zn. Thus, the results point out that under the experimental condition the rate of reaction 9 is considerably higher than that of reaction 5.

$$(9)\ M^o + \cdot CH_3 \xrightarrow{H^+} CH_4 + M^I$$

2. For all metals except for Cu^0, the total radiolytic alkane yield, $[CH_4] + 2\,[C_2H_6]$, in solutions containing $(CH_3)_2SO$ and metal powder, is considerably larger than the sum of the yields of the two blank experiment, i.e. the non-irradiated solution containing metal powder and the irradiated solution containing only $(CH_3)_2SO$ without the metal. This result points out that some energy transfer from the irradiated metal to the solution or to adsorbed $(CH_3)_2SO$ occurs.

3. The addition of copper powder to $(CH_3)_2SO$ decreases the total radiolytic gas yield considerably (see Table 4). The logic explanation for this observation is that methyl radicals are oxidized by the copper particles. A mechanism for this process is presented in Scheme 2. It should be noted that the oxidation potential of $\cdot CH_3$ radicals is considerably higher than that of $Cu^0{}_{(s)}$. Thus, thermodynamically the methyl radicals can oxidize copper as they oxidize the other

 © 2003 Wiley-VCH Verlag GmbH & Co. KGaA, Weinheim

metals. The copper system is still under investigation and the yield of the methanol and dihydrogen in the system will be determined.

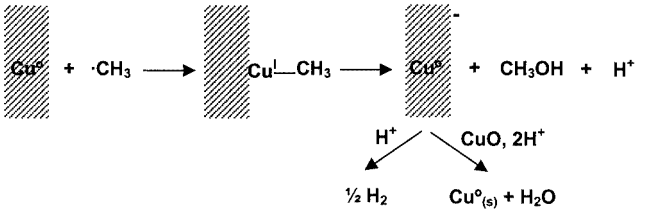

Scheme 2. Reaction of methyl radicals with copper powder

4. Activation of the metal powders leads to an increase in the radiolytic gas yield. In the activation step oxides are removed from the metal surface, this probably transforms the metal particle into a stronger reducing agent. Oxides present on the surface might react via:

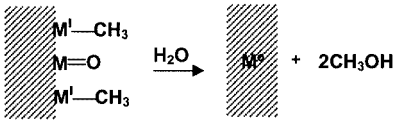

thus decreasing the yields of CH_4 and C_2H_6. Nevertheless, the activation step does not contribute to an increase in the radiolytic gas yield in the case of Cu^0 and Mn^0. The explanation for the Cu^0 system was outlined above. Mn^0 is the strongest reducing metal studied ($E^0 = -1.18$ V) thus, it probably tends to act only as a reductant.

It seemed of interest to check whether the use of metal nano-particles, prepared via reduction of the metal ions with BH_4^-,[40] affects the results. The results of these experiments are summed up in Table 6. A comparison of the results for iron in Tables 4 and 6 reveals that indeed the smaller particles scavenge a larger part of the methyl radicals thus increasing the methane yield and decreasing the ethane yield. Furthermore, the total gas yield, $[CH_4] + 2[C_2H_6]$, is larger for the "nano" particles, that is the smaller particles induce a larger energy transfer from the metal to the solution, as expected.

Table 6. Reaction of methyl radicals with synthesized metal powders[a]

Metal	Irradiated	CH_4 [ppm]	C_2H_6 [ppm]
Fe^0 (synth)	+	2600	152
	−	14	
Ni^0 (synth)	+	25000	606
	−	18	

[a] Gas product composition in reaction of 10 g activated nanoparticle metal powders with 2.5 mL N_2O saturated solution containing 0.05 M $(CH_3)_2SO$ solution, pH 4.0, t = 3 hours (2 h of radiation, 480 Gy), $T = 25$ °C. Error limit ± 15%.

Finally it should be pointed out that:

1. Methyl radicals which are strong reducing and oxidizing agents[15,16] oxidize Cr^0, Mn^0, Fe^0, Ni^0 and Zn^0 powders. The products of these reactions are methane and the corresponding $M^{2+}_{(aq)}$ ions. The analogous reaction with Cu^0 powders probably yields methanol and dihydrogen.

2. As the radicals formed in the dehalogenation reaction 1 are formed in the vicinity of the metal surface, it is clear that, since reaction 9 is fast, reaction 1 is followed by reaction 9.

3. The results suggest that if radioactive wastes are stored as aqueous solutions containing organic materials in metal containers, the formation of alkyl radicals will contribute to the corrosion of the container.

Experimental Section

The sources and properties of the metal powders used in this study are summed up in the footnotes of Table 4. All other chemicals were of AR grade and were used without further purification. The water used was deionized water, which was further purified by a Millipore Milli-Q setup with a final resistivity of > 10 MΩ. The solutions were deaerated by bubbling with N_2O (He was used for studying alkane formation during the dissolution of analytical metals in aqueous solutions) for 15 min using the syringe technique. Then 2.5 mL of the solution were added to a glass bulb (15 mL) sealed with a rubber septum containing 10 g of the metal powder, which was previously activated by H_2SO_4 (0.1 M) for two minutes and then washed 7−8 times by 8 mL portions of water. This bulb was also deaerated by N_2O (or He was used for studying alkane formation during the dissolution of the analytical metals in aqueous solutions) prior to the injection of the solution.

After three hours of reaction the gas phase above the metal was analyzed using an HP 5890 GC fitted with a FID detector (Poropaq QS GC column 10Ft 1/8 in, Supelco). The carrying gas was He (30 mL/min, $T = 70$ °C). Hydrogen was determined using a TCD detector (12 mL/min of N_2, 40 °C). Some of the samples were irradiated for two hours, within the three hour time span, in a ^{60}Co γ source with a dose rate of 4 Gy/min.

The Fe^{II} yield was measured using a colorimetric procedure based on *ortho*-phenanthroline.[39]

The amount of carbon in the metals was determinate using a Carbon-Elementary Analyzer, of LECO.

Metal nanoparticles were synthesized was by reducing $M^{II}/M^{III}_{(aq)}$ ions with $NaBH_4$ in He-saturated aqueous solutions.[40,41]

Formation of Radicals with Ionizing Radiation: When ionizing radiation (γ -radiation) is absorbed by a dilute aqueous solution, the following initial products are formed:[42]

$$\textbf{(10)}\ H_2O \xrightarrow{\gamma,\ e^-} \cdot H\ (0.60), \cdot OH\ (2.65), e^-_{aq}\ (2.65), H_2O_2\ (0.75), H_2\ (0.45)$$

where the G values are given in parentheses (G values are defined as the number of molecules of each product per 100 eV of radiation absorbed by the solution). In concentrated solutions the yields of the radicals are somewhat higher while those of H_2O_2 and H_2 are somewhat lower. In N_2O-saturated solutions the hydrated electron is converted into the hydroxyl radical:[43]

$$\textbf{(11)}\ e^-_{aq} + N_2O \xrightarrow{H^+} N_2 + \cdot OH \qquad k = 8.7 \times 10^9\ M^{-1}\ s^{-1}$$

 © 2003 Wiley-VCH Verlag GmbH & Co. KGaA, Weinheim

At pH > 3 the solvated electrons will all react with N_2O yielding ·OH as the major radical.

Preparation of the $\cdot CH_3$ Radicals: The methyl radicals were formed[44] via the following reactions in N_2O-saturated solutions:

(12) $\cdot OH + (CH_3)_2SO \longrightarrow (CH_3)_2S^{\cdot}(O)OH \qquad k = 7.0 \times 10^9\ M^{-1}\ s^{-1}$

(13) $(CH_3)_2S^{\cdot}(O)OH \longrightarrow (CH_3)_2S(O)OH + \cdot CH_3 \quad k = 1.5 \times 10^7\ M^{-1}\ s^{-1}$

Acknowledgments

This study was supported in part by a grant from the Budgeting and Planning Committee of The Council of Higher Education and the Israel Atomic Energy Commission. D. M. wishes to express his thanks to Mrs. Irene Evens for her ongoing interest and support.

[1] R. W. Gillham, S. F. O'Hannesin, *Groundwater* **1994**, *32*, 958−967.
[2] L. J. Matheson, P. G. Tratnyek, *Environ. Sci. Technol.* **1994**, *28*, 2045−2053.
[3] C. Su, R. W. Puls, *Environ. Sci. Technol.* **1999**, *33*, 163−168.
[4] T. Bigg, S. J. Judd, *Environ. Technol.* **2000**, *21*, 661−670.
[5] J. L. Chen, S. R. Al-Abed, J. A. Ryan, Z. Li, *J. Hazard. Mater.* **2001**, *83*, 243−254.
[6] T. Li, J. Farrell, *Environ. Sci. Technol.* **2000**, *34*, 173−179.
[7] S. M. Ponder, J. G. Darab, J. Bucher, D. Caulder, I. Craig, L. Davis, N. Edelstein, W. Lukens, H. Nitsche, L. Rao, D. K. Shuh, *Chem. Mater.* **2001**, *13*, 479−486.
[8] R. Muftikian, Q. Fernando, N. Korte, *Water Resour.* **1995**, *29*, 2434−2439.
[9] B. R. Helland, P. J. J. Alvarez, J. L. Schnoor, *J. Hazard. Mater.* **1995**, *41*, 205−216.
[10] T. L. Jonson, M. M. Scherer, P. G. Tratnyek, *Environ. Sci. Technol.* **1996**, *30*, 2634−2640.
[11] B. Deng, D. R. Burris, T. J. Campbell, *Environ. Sci. Technol.* **1999**, *33*, 2651−2656.
[12] K. D. Warren, R. G. Arnold, T. L. Bishop, L. C. Lindholm, E. A. Betterton, *J. Hazard. Mater.* **1995**, *41*, 217−227.
[13] L. A. Totten, U. Jans, A. L. Roberts, *Environ. Sci. Technol.* **2001**, *35*, 2268−2274.
[14] J. P. Fennelly, A. L. Roberts, *Environ. Sci. Technol.* **1998**, *32*, 1980−1988.
[15] The redox potentials of $\cdot CH_3$ radicals were not determined. However they can be estimated using the redox potentials of hydrogen atoms and the bond dissociation energies of H−H (104 kcal/mol), H−CH_3 (105 kcal/mol), H−OH (119 kcal/mol) and CH_3−OH (91 kcal/ mol) [Branchaud, B. P. Free radicals as a result of dioxygen metabolism in *Metal Ions in Biological Systems* (Eds.: A. Sigel, H. Sigel), **1999**, *36*, 79−102].
[16] P. Neta, J. Grodkowski, A. B. Ross, *J. Phys. Chem. Ref. Data.* **1996**, *25*, 709−1050.
[17] B. Deng, T. J. Campbell, D. R. Burris, *Environ. Sci. Technol.* **1997**, *31*, 1185−1190.
[18] D. M. Guldi, M. Kumar, P. Neta, P. Hambright, *J. Phys. Chem.* **1992**, *96*, 9576−9581.
[19] A. Rotman, H. Cohen, D. Meyerstein, *Inorg. Chem.* **1985**, *24*, 4158−4164.
[20] W. Gaede, R. van Eldik, *Inorg. Chim. Acta* **1994**, *215*, 173−178.
[21] N. Shaham, A. Masarwa, Y. Matana, H. Cohen, D. Meyerstein, *Eur. J. Inorg. Chem.* **2002**, *1*, 87−92.
[22] H. Cohen, D. Meyerstein, *Isr. J. Chem.* **1974**, *12*, 1049−1057.
[23] R. van Eldik, D. Meyerstein, *Acc. Chem. Res.* **2000**, *33*, 207−214.
[24] K. D. Warren, R. G. Arnold, T. L. Bishop, L. C. Lindholm, E. A. Betterton, *J. Hazard. Mater.* **1995**, *41*, 217−227.
[25] J. Farrell, M. Kason, N. Melites, T. Li, *Environ. Sci. Technol.* **2000**, *34*, 514−521.
[26] M. Maurette, P. Bonny, A. Brack, C. Jouret, M. Pourchet, P. Siry, *Lect. Notes in Phys.* **1991**, *390*, 124−132.
[27] S. Abbas, *Curr. Sci.* **1996**, *71*, 677−684.
[28] G. D. Cody, N. Z. Boctor, R. M. Hazen, J. A. Brandes, H. J. Harold, H. S Yoder, *Geochim. Cosmochim. Acta* **2001**, *65*, 3557−3576.
[29] G. C. Stevens, R. M. Clarke, E. J. Hart, *J. Phys. Chem.* **1972**, *76*, 3863−3867.
[30] J. Halpern, G. Czapski, J. Jortner, G. Stein, *Nature* **1960**, *186*, 629−630.
[31] H. Cohen, D. Meyerstein, *J. Chem. Soc., Dalton Trans.* **1974**, *23*, 2559−2564.
[32] T. Schatz, A. R. Cook, D. Meisel, *J. Phys. Chem. B* **1998**, *102*, 7225−7230.
[33] J. K. Thomas, *Chem. Rev.* **1993**, *93*, 301−320.
[34] P. K. Wong, A. O. Allen, *J. Phys. Chem.* **1970**, *74*, 774−778.
[35] J. M. Caffrey, A. O. Allen, *J. Phys. Chem.* **1958**, *62*, 33−37.
[36] P. K. Wong, J. E. Willard, *J. Phys. Chem.* **1969**, *73*, 2226−2230.
[37] P. K. Wong, J. E. Willard, *J. Phys. Chem.* **1968**, *72*, 2623−2627.
[38] M. J. Davies, B. Gilbert, C. B. Thomas, J. Young, *J. Chem. Soc., Perkin Trans. 2* **1985**, *8*, 1199−1204.
[39] A. E. Harrey, J. A. Smart, E. S. Amis, *Anal. Chem.* **1995**, *27*, 26−28.
[40] I. Rusonik, H. Polat, H. Cohen, D. Meyerstein, submitted for publication.
[41] S. M. Ponder, J. G. Darab, T. E. Mallouk, *Environ. Sci. Technol.* **2000**, *34*, 2564−2569.
[42] M. Matheson, L. Dorfman, Pulse Radiolysis, MIT Press, Cambridge, MA, **1969**.
[43] G. V. Buxton, C. L. Greenstock, W. P. Helman, A. B. Ross, *J. Phys. Chem. Ref. Data* **1988**, *17*, 513−886.
[44] D. Veltwisch, E. Janata, K. D. Asmus, *J. Chem. Soc., Perkin Trans. 2* **1980**, 146−153.

Received June 26, 2003
Early View Article
Published Online October 10, 2003

 © 2003 Wiley-VCH Verlag GmbH & Co. KGaA, Weinheim

Heterotrimetallic Complexes $[\{Pt(RNH_2)_2(\mu\text{-}NHCOtBu)_2\}_2M](ClO_4)_n$ (M = Mn, Co, Cu, Ni, Cd, and Zn, n = 2; M = In, n = 3), $[\{Pt(NH_3)(\mu\text{-}DACHCOtBu)(\mu\text{-}NHCOtBu)\}_2Ni](ClO_4)_2$, and $[\{Pt(RNH_2)_2(NHCOtBu)_2\}_3Ag_3](ClO_4)_3$ Bridged by Amidate Ligands: A Novel Amidate−Amine Interligand Reaction During the Pt−Ni Bond Formation

Wanzhi Chen,[a] Fenghui Liu,[a] Takuya Nishioka,[a] and Kazulo Matsumoto*[a]

Keywords: Platinum / Amidate ligand / Metal−metal interaction / Heterotrimetallic complexes / Nickel

The neutral square-planar complexes $[Pt(NH_2CH_2CH_2OCH_3)_2(NHCOtBu)_2]$, $[Pt(DACH)(NHCOtBu)_2]$ (DACH = *trans*-1,2-diaminocyclohexane), and $[Pt(NH_2CH_2CH_2NMe_2)(NHCOtBu)_2]$ have been prepared by hydrolysis of the corresponding $[Pt(RNH_2)_2(NCtBu)_2](ClO_4)_2$ with NaOH. Reactions of $[Pt(RNH_2)_2(NHCOtBu)_2]$ with metal ions afforded Pt–M–Pt clusters $[\{Pt(RNH_2)_2(\mu\text{-}NHCOtBu)_2\}_2M](ClO_4)_n$ (M = Mn, Co, Cu, Ni, Cd, Zn, and In; n = 2 or 3) and $[\{Pt(NH_2CH_2CH_2NMe_2)(\mu\text{-}NHCOtBu)_2\}_2M](ClO_4)_2$ (M = Co, Ni). The Pt_2M (M = Mn, Co, Cu, Ni, Zn, and In) complexes consist of a linear Pt–M–Pt core bridged by four pivalamidate ligands. The Pt–M–Pt angles are 180° or nearly so. The central metal ions with an octahedral geometry are coordinated by four equatorial amidate oxygen atoms and two platinum atoms occupy the axial site. One of the two *t*-BuCO group shifts to the neighboring nitrogen atom of DACH (DACH = *trans*-1,2-diaminocyclohexane) in the reaction of $[Pt(DACH)(NHCOtBu)_2]\cdot 4H_2O$ with Ni^{2+} to generate the unexpected $[\{Pt(NH_3)(DACHCOtBu)(\mu\text{-}NHCOtBu)\}_2Ni](ClO_4)_2$. The central Cd ion in $[\{Pt(RNH_2)_2(\mu\text{-}NHCOtBu)_2\}_2Cd](ClO_4)_2$ is trigonal-bipyramidal and the Pt–Cd–Pt is bent. Treatment of $[Pt(NH_2CH_2CH_2OCH_3)_2(NHCOtBu)_2]$ with an equimolar amount of $AgClO_4$ yielded the Pt_4Ag_3 cluster consisting of alternate Pt and Ag atoms either doubly or singly bridged by amidate ligands. The spectroscopic and electrochemical studies show that the metal–metal interactions between platinum and the heterometal ions are very weak.

(© Wiley-VCH Verlag GmbH & Co. KGaA, 69451 Weinheim, Germany, 2003)

Introduction

Heteronuclear metal complexes of linearly arranged metal arrays with metal−metal bonds may act as multifunctional catalysts for organic transformation processes and multifunctional materials with versatile physical and chemical properties.[1−6] Heterometallic cluster systems involving platinum(II) and other metal ions of d^{10} and s^2 electronic configuration exhibit unique physicochemical properties such as luminescence based on the d^8 and the closed-shell metal−metal interactions, and have potential applications in chemical devices. The metallophilic interactions are important in determining the solid-state structures and also contribute to the properties of such complexes in solution. Many complexes containing Pt−M bonds, such as $Pt^{II}-Cu^{I}$,[3,4] $Pt^{II}-Cd^{II}$,[7] and $Pt^{II}-Tl^{I}$,[2,7−9] display intense luminescence that is correlated with the metal−metal bonds through metallophilic interactions.[10]

We have found that amidate-bridged dimeric Pt^{III} complexes are efficient catalysts for the epoxidation and dihydroxylation of olefins and can activate the C−H bonds of ketones.[11] The versatile role of transition metal ions of the first row in many organic oxidation reactions suggests it would be of interest to prepare amidate-bridged heterometallic complexes having various Pt−M bonds.

The electron-rich platinum atom in $[Pt(RNH_2)_2(NHCOR')_2]$ can act as a soft base through donating its d_{z^2} electrons to transition metal ions to form Pt−M bonds. Heterometallic Pt−M (M = Mn, Co, Ni, Cu) complexes are potentially useful reagents or catalysts for some organic oxidation processes since the role of these metals in oxidation reactions is well known. Few examples of symmetrical heterotrinuclear Pt−M−Pt complexes have been reported.[2,6] We reported recently that reactions of $[Pt(NH_3)_2(NHCOtBu)_2]$ with M^{2+} (M = Mn, Fe, Co, Ni, and Cu) ions afforded trinuclear complexes $[\{Pt(NH_3)_2(NHCOtBu)_2\}_2M]^{n+}$ exclusively.[6] The present work examines how different substituents on the amine ligands alter the metal−metal interactions and the possibility of obtaining new cluster compounds by introducing additional functional groups such as MeO and Me_2N. The

[a] Department of Chemistry, Advanced Research Institute of Science and Engineering, Waseda University,
Okubo, Shinjuku-Ku 169-8555, Tokyo, Japan
Fax: (internat.) + 81-3/5273-3489
E-mail: kmatsu@waseda.jp

 © 2003 Wiley-VCH Verlag GmbH & Co. KGaA, Weinheim **DOI: 10.1002/ejic.200200684**

compound $[Pt(RNH_2)_2(NHCOR')_2]$ is expected to have better donating abilities than $[Pt(NH_3)_2(NHCOR')_2]$. To further investigate such metal−metal bonds, we describe herein the synthesis and structural characterization, including X-ray diffraction analysis, of the trinuclear complexes $[\{Pt(DACH)(\mu\text{-}NHCOtBu)_2\}_2M](ClO_4)_n$ (M = Cu, Co, Mn, and Cd, n = 2; M = In, n = 3), $[\{Pt(\mu\text{-}DACHNHCOtBu)(\mu\text{-}NHCOtBu)\}_2Ni](ClO_4)_2$, $[\{Pt(NH_3)_2(\mu\text{-}NHCOtBu)_2\}_2M](ClO_4)_n$ (M = Cd, n = 2; M = In, n = 3), $[\{Pt(NH_2CH_2CH_2NMe_2)(\mu\text{-}NHCOtBu)_2\}_2M](ClO_4)_2$ (M = Co, Ni), $[\{Pt(NH_2CH_2CH_2OCH_3)_2(\mu\text{-}NHCOtBu)_2\}_2M](ClO_4)_2$ (M = Co, Zn), and heptanuclear $[\{Pt(NH_2CH_2CH_2OCH_3)_2(\mu\text{-}NHCOtBu)_2\}_4Ag_3](ClO_4)_2\cdot 2H_2O$. The electrochemistry of the trinuclear heterometallic complexes as well as their parent platinum complexes has also been studied.

Results and Discussion

Synthesis and Spectroscopic Characterization

The complexes synthesized are depicted in Schemes 1−3. $[Pt(DACH)(NHCOtBu)_2]$ (**2**), $[Pt(NH_2CH_2CH_2OCH_3)_2(NHCOtBu)_2]$ (**3**), and $[Pt(NH_2CH_2CH_2NMe_2)(NHCOtBu)_2]$ (**4**) were easily prepared by basic hydrolysis of the corresponding $[Pt(RNH_2)_2(NCtBu)_2]^{2+}$ in good yields.[12] The heteronuclear complexes **5**−**17** were readily obtained by mixing $[Pt(RNH_2)_2(NHCOtBu)_2]$ and the corresponding metal salts in water or water/acetone. Regardless of the Pt/M ratio used, the trinuclear Pt_2M (M = Mn, Co, Ni, Cu, Zn, Cd, and In) complexes were exclusively obtained in high yields. Attempts to prepare dimeric Pt−M complexes by using a large excess of M ions were unsuccessful. All the compounds were characterized by elemental analyses.

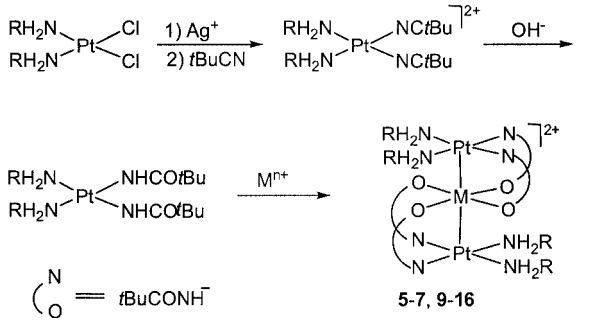

5, RNH_2 = 1/2 DACH, M = Mn^{2+}
6, RNH_2 = 1/2 DACH, M = Co^{2+}
7, RNH_2 = 1/2 DACH, M = Cu^{2+}
9, RNH_2 = 1/2 DACH, M = In^{3+}
10, RNH_2 = 1/2 DACH, M = Cd^{2+}
11, RNH_2 = NH_3, M = In^{3+}
12, RNH_2 = NH_3, M = Cd^{2+}
13, RNH_2 = 1/2 $NH_2CH_2CH_2NMe_2$, M = Co^{2+}
14, RNH_2 = 1/2 $NH_2CH_2CH_2NMe_2$, M = Ni^{2+}
15, RNH_2 = $NH_2CH_2CH_2OCH_3$, M = Zn^{2+}
16, RNH_2 = $NH_2CH_2CH_2OCH_3$, M = Co^{2+}

Scheme 1

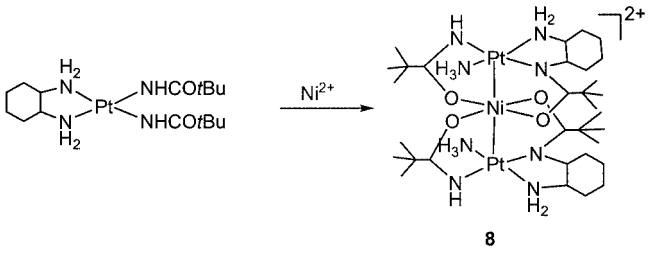

Scheme 2

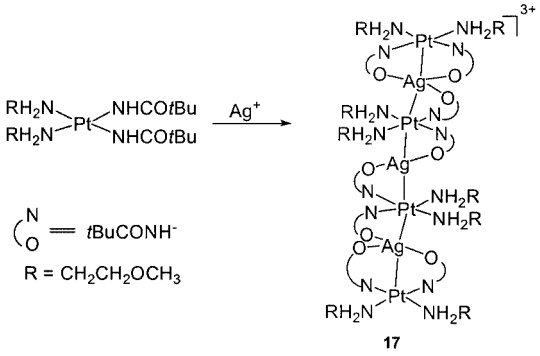

Scheme 3

The reaction of $[Pt(DACH)(NHCOtBu)_2]$ (**2**) and Ni^{2+} under the same conditions did not afford the expected Pt−Ni−Pt complex $[\{Pt(DACH)(\mu\text{-}NHCOtBu)_2\}_2Ni]^{2+}$, but, instead, $[\{Pt(NH_3)(\mu\text{-}DACHCOtBu)(\mu\text{-}NHCOtBu)\}_2Ni]^{2+}$ (**8**) through migration of a BuCO group to the DACH ligand (Scheme 2).

The oligomeric Pt_4Ag_3 complex $[\{Pt(NH_2CH_2CH_2OCH_3)_2(\mu\text{-}NHCOtBu)_2\}_4Ag_3](ClO_4)_2\cdot 2H_2O$ (**17**) was isolated as colorless crystals when $[Pt(NH_2CH_2CH_2OCH_3)_2(NHCOtBu)_2]$ was treated with 1 equiv. of $AgClO_4$ in water (Scheme 3). The compound is moderately soluble in acetone and ethanol and is light-sensitive. Silver(I) tends to form platinum(II)−silver(I) coordination polymers, which have been studied.[13,14]

The ^{195}Pt NMR resonances of $[Pt(DACH)(NCtBu)_2](ClO_4)_2$ (**1**) and $[Pt(DACH)(NHCOtBu)_2]$ (**2**) in [D_6]acetone appear at δ = −2857 and −2625 ppm as singlets, respectively, which are typical for a PtN_4 coordination sphere.[12,15] Both the ^1H NMR spectra of $[\{Pt(DACH)(\mu\text{-}NHCOtBu)_2\}_2In](ClO_4)_3\cdot(CH_3)_2CO$ (**9**) and $[\{Pt(DACH)(\mu\text{-}NHCOtBu)_2\}_2Cd](ClO_4)_2$ (**10**) in [D_6]DMSO show two sets of signals corresponding to the NH protons of amidate ligands, and four sets of signals each corresponding to two NH_2 protons of *trans*-1,2-diaminocyclohexane, respectively, indicating that these protons are magnetically unequal. Simultaneously, the ^1H NMR spectra exhibit two singlets (1:1) assigned to *t*Bu protons for **10**. Singlets at δ = −2429 (**9**) and −2562 ppm (**10**) appear in their ^{195}Pt NMR spectra. The ^1H NMR spectrum of $[\{Pt(NH_3)_2(\mu\text{-}NHCOtBu)_2\}_2In]^{3+}$ (**11**) consists of singlets at δ = 6.46, 4.12, 2.06, and 1.10 ppm assignable to NH, NH_3, $(CH_3)_2CO$, and *t*Bu, respectively. The ^1H NMR spectrum of $[\{Pt(NH_3)_2(\mu\text{-}NHCOtBu)_2\}_2Cd](ClO_4)_2$ (**12**) exhib-

 © 2003 Wiley-VCH Verlag GmbH & Co. KGaA, Weinheim

its signals at δ = 5.42, 4.51, and 1.06 ppm due to NH_3, NH, and *t*Bu groups. The ^{195}Pt NMR spectra of **11** and **12** show singlets at δ = −2474 and −2561 ppm, respectively. No Pt−Cd coupling was observed. For comparison, the ^{195}Pt resonance of the starting compound $[Pt(NH_3)_2(NHCOtBu)_2]\cdot 2H_2O$ appears at δ = −2428 ppm in [D_6]DMSO. The change in chemical shifts of NH and NH_3 between complexes **11**, **12**, and $[Pt(NH_3)_2(NHCOtBu)_2]$ is clearly due to the complexation of Pt. Spin−spin coupling between ^{195}Pt and ^{113}Cd was not observed for the two cadmium complexes, probably because the interaction between the two metals is too weak. The small variation in ^{195}Pt chemical shifts compared to their parent platinum complexes suggests that the metal−metal interactions are weak in **9**−**12**.

The IR spectra of the trinuclear Pt_2M complexes **5**−**16** are very similar to their parent platinum compounds. There are two bands at $\tilde{\nu}$ = 3400 and 3245 cm^{-1} assignable to ν(N−H) of amine and amidate groups, respectively. The amidate bands at $\tilde{\nu}$ = 1556 ($[Pt(NH_3)_2(NHCOtBu)_2]$), 1562 (**2**), 1568 (**3**), and 1560 cm^{-1} (**4**) are assignable to the carbonyl stretching of the amidate ligands and are in the typical range of amidate anions. The δ(N−H) bands appear as shoulder peaks at $\tilde{\nu} \approx 1600$ cm^{-1}. The amide vibrations are only slightly shifted due to the complexation of the transition metal ions, and appear in the narrow range $\tilde{\nu}$ = 1562−1569 cm^{-1}. The carbonyl stretching band of the oligomeric Pt−Ag complex **17** shifts to a lower wavenumber, $\tilde{\nu}$ = 1531 cm^{-1}, showing enhanced electron delocalization within the amidate group. The skeletal vibrations at $\tilde{\nu}$ = 1481−1490 cm^{-1} and δ(NCO) bands at $\tilde{\nu} \approx 600$ cm^{-1} of $[Pt(RNH_2)_2(NHCOtBu)_2]$ complexes are essentially unaffected by heterometal coordination. These observations are consistent with the reported amidate complexes.[14]

Structure of $[\{Pt(RNH_2)(\mu\text{-}NHCOtBu)_2\}_2M](ClO_4)_2$ (M = Mn, Co, and Cu)

A few trimeric Pt_2M complexes derived from $[Pt(NH_3)_2(NHCOtBu)_2]$ have been described.[6] The compounds $[\{Pt(DACH)(\mu\text{-}NHCOtBu)_2\}_2M]^{2+}$ (M = Mn, **5**; Co, **6**, Cu **7**), $[\{Pt(NH_2CH_2CH_2NMe_2)(\mu\text{-}NHCOtBu)_2\}_2Co]^{2+}$ (**13**), and $[\{Pt(NH_2CH_2CH_2OCH_3)_2(\mu\text{-}NHCOtBu)_2\}_2Co]^{2+}$ (**16**) have essentially the same structures (Figures 1−5), and are discussed together below. Selected bond lengths and bond angles are given in Table 1. Overall, despite the different space groups, compounds **5**−**7**, **13**, and **16** have essentially the same structure, which consists of the trimetallic Pt−M−Pt (M = Mn, Co, and Cu) cations. Within the cations the heterometal ions are located at the center, and the three metal atoms are held together through Pt−M interactions and four bridging pivalamidate ligands. The Pt−N distances range from 1.985(8) to 2.052(10) Å, which are normal. The N−Pt−N angles indicate that the geometry about the platinum atom is square-planar. The O−M−O angles suggest that the geometry about the central metal atoms is slightly distorted from an octahedron. The sum of the neighboring O−M−O angles is, or is close to, 360°. The two platinum atoms within a cation sit above and below the coordination planes of MO_4 with Pt−M−Pt angles of 180° or nearly so. The cyclohexyl rings exhibit pseudo-coplanarity due to their disorder.

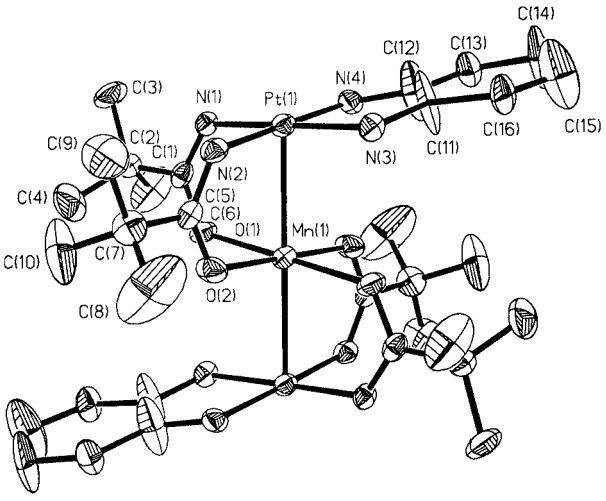

Figure 1. ORTEP plot of $[\{Pt(DACH)(\mu\text{-}NHCOtBu)_2\}_2Mn]^{2+}$ (**5**) with thermal ellipsoids plotted at 30% probability level

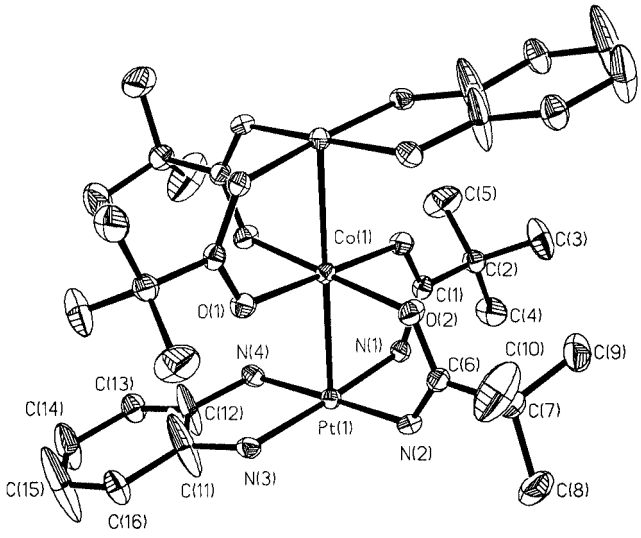

Figure 2. ORTEP plot of $[\{Pt(DACH)(\mu\text{-}NHCOtBu)_2\}_2Co]^{2+}$ (**6**) with thermal ellipsoids plotted at 30% probability level

The Pt−Mn distances [2.643(3) Å] of **5** are shorter than those found in $[\{Pt(NH_3)_2(\mu\text{-}MeT)_2\}_2Mn]^{2+}$ (MeT = 1-methylthymine) [2.704(1) Å], which has a similar Mn^{II} coordination geometry.[16] The Pt−Mn distances of **5** are also shorter than that in $[(dppe)(CH_3)PtMn(CO)_5]$ [2.795 Å] which contains a typical Pt−Mn covalent single bond.[17] The Pt−Cu distances in **7** are 2.6529(8) Å, which are shorter than that in both the PtCu dimer *cis*-$[(NH_3)_2Pt(1\text{-}MeU)_2Cu(H_2O)_2]^{2+}$ [2.756(3) Å] and the Pt_2Cu trimer *cis*-$[(NH_3)_2Pt(1\text{-}MeU)_2Cu(1\text{-}MeU)_2Pt(NH_3)_2]^{2+}$ [2.681(1) Å, 1-MeU = 1-methyluracilato],[18] and much shorter than those in the platinum−copper complexes bridged by alkynyl ligands.[19]

 © 2003 Wiley-VCH Verlag GmbH & Co. KGaA, Weinheim

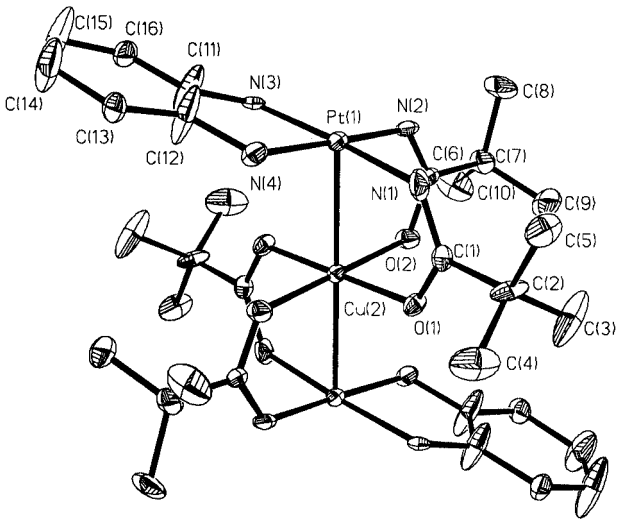

Figure 3. ORTEP plot of $[\{Pt(DACH)(\mu\text{-}NHCO\textit{t}Bu)_2\}_2Cu]^{2+}$ (**7**) with thermal ellipsoids plotted at 30% probability level

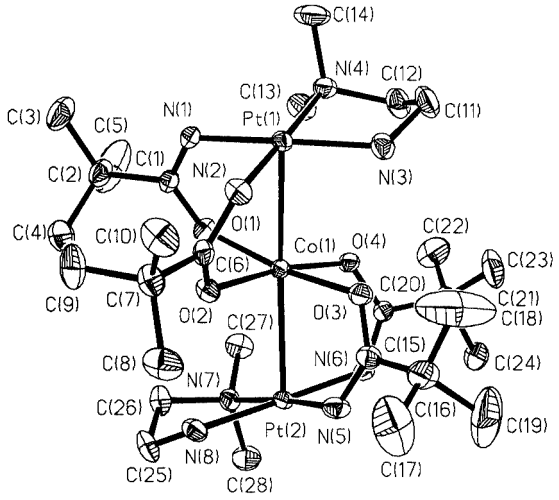

Figure 4. ORTEP plot of $[\{Pt(NH_2CH_2CH_2NMe_2)(\mu\text{-}NHCO\textit{t}Bu)_2\}_2Co]^{2+}$ (**13**) with thermal ellipsoids plotted at 30% probability level

The Pt−Co bonds of **13** [2.6902(10) and 2.6830(9) Å] are slightly longer than those of **6** [2.6087(6) Å] and **16** [2.6031(7) Å] because of the large steric hindrance of the NMe_2 groups. They are also longer than those in the Pt−Co clusters $[PtCo_2(CO)_7(cod)]$ [2.515(1) and 2.514(1) Å] and $[Pt_2Co_2(CO)_8(\mu_3\text{-}EtC_2Et)]$ [2.551(1) and 2.556(1) Å],[20] and in the $(Ph_2P)_2NH$-bridged Pt−Co carbonyl complexes [2.531(2)−2.508(2) Å],[21] indicating weak metal−metal interactions in the amidate-bridged platinum−cobalt complexes **6**, **13**, and **16**.

Structures of 8 and 14

When compound **2** was treated with Ni^{2+} in H_2O/acetone under the same conditions as for **5**−**7**, the expected product $[\{Pt(DACH)(\mu\text{-}NHCO\textit{t}Bu)_2\}_2Ni](ClO_4)_2$ was not obtained, but, instead, $[\{Pt(NH_3)(\mu\text{-}DACHCO\textit{t}Bu)(\mu\text{-}NHCO\textit{t}Bu)\}_2Ni](ClO_4)_2$ (**8**) was isolated in high yield as light green crystals, the structure of which was revealed by X-ray diffraction analysis (Figure 6). One of the two *t*BuCO groups shifts to the adjacent nitrogen atom of 1,2-diaminocyclohexane. This rearrangement is remarkable since the large *t*BuCO group and two hydrogen atoms have to exchange simultaneously. The most striking feature of compound **8** is that, although it has the same linear Pt−M−Pt arrangement, the two amidate bridging ligands are *trans* about the platinum atom. The Pt−Ni distance, 2.5750(14) Å, is slightly shorter than for the closely related trinuclear Pt_2Ni complex $[\{Pt(NH_3)_2(\mu\text{-}NHCO\textit{t}Bu)_2\}_2Ni](ClO_4)_2$.[6]

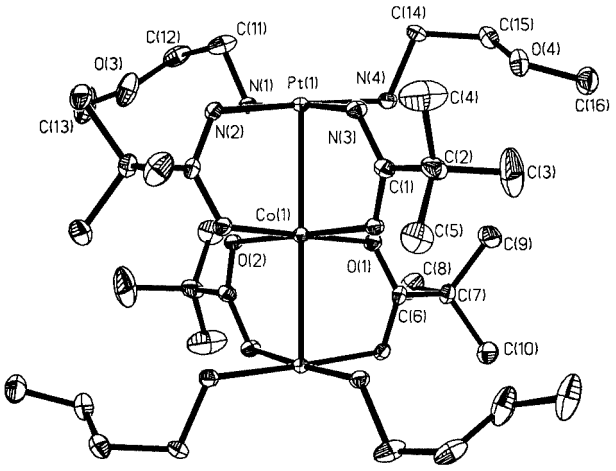

Figure 5. ORTEP plot of $[\{Pt(NH_2CH_2CH_2OCH_3)_2(\mu\text{-}NHCO\textit{t}Bu)_2\}_2Co]^{2+}$ (**16**) with thermal ellipsoids plotted at 30% probability level

Table 1. Important bond lengths [Å] and angles [°] of **5**−**9** and **11**−**17**

	M ion	Pt−M	Pt−M−Pt
5	Mn^{2+}	2.643(3)	180.0
6	Co^{2+}	2.6087(6)	180.0
7	Cu^{2+}	2.6529(8)	180.0
8	Ni^{2+}	2.5750(14)	179.48(17)
9	In^{3+}	2.6358(8)	180.0
11	In^{3+}	2.6422(6), 2.6278(6)	174.78(3)
12	Cd^{2+}	2.8156(9), 2.8196(9)	145.50(3)
13	Co^{2+}	2.6830(9), 2.6902(10)	168.13(2)
14	Ni^{2+}	2.6466(9), 2.6544(10)	169.33(2)
15	Zn^{2+}	2.5932(5)	180.0
16	Co^{2+}	2.6031(7)	180.0
17	Ag^{+}	2.8203(14), 2.8531(14), 2.9161(7)	167.52(6), 180.0

The rearrangement reaction is not generally seen, as illustrated by the isolation and characterization of $[\{Pt(NH_3)_2(\mu\text{-}NHCO\textit{t}Bu)_2\}_2Ni](ClO_4)_2$[6] and $[\{Pt(NH_2CH_2CH_2NMe_2)(\mu\text{-}NHCO\textit{t}Bu)_2\}_2Ni](ClO_4)_2$ (**14**). Both **14** and **15** are the expected Pt_2Ni products. The amine exchange reaction between a free amine and an acetamide is well known, unlike the migration of the BuCO group. It is not clear why such a rearrangement occurs only for complex **8**. The structure of **14** is shown in Figure 7. Because of the steric hindrance of the NMe_2 units, the Pt−Ni distances [2.6466(9), 2.6544(10) Å] of **14** are longer than those of **8**

 © 2003 Wiley-VCH Verlag GmbH & Co. KGaA, Weinheim

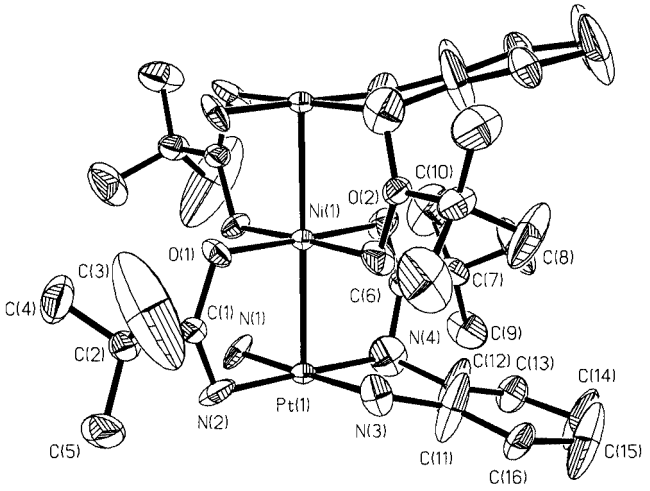

Figure 6. ORTEP plot of $[\{Pt(NH_3)(DACHCO\textit{t}Bu)(\mu\text{-}NHCO\textit{t}Bu)\}_2Ni]^{2+}$ (**8**) with thermal ellipsoids plotted at 30% probability level

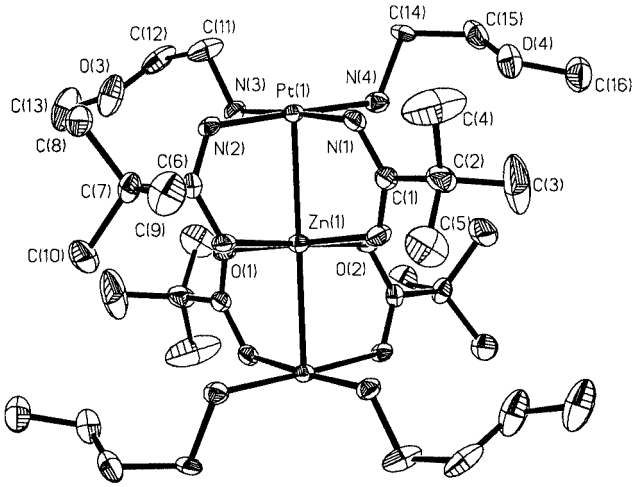

Figure 8. ORTEP plot of $[\{Pt(NH_2CH_2CH_2OCH_3)_2(\mu\text{-}NHCO\textit{t}Bu)\}_2Zn]^{2+}$ (**15**) with thermal ellipsoids plotted at 30% probability level

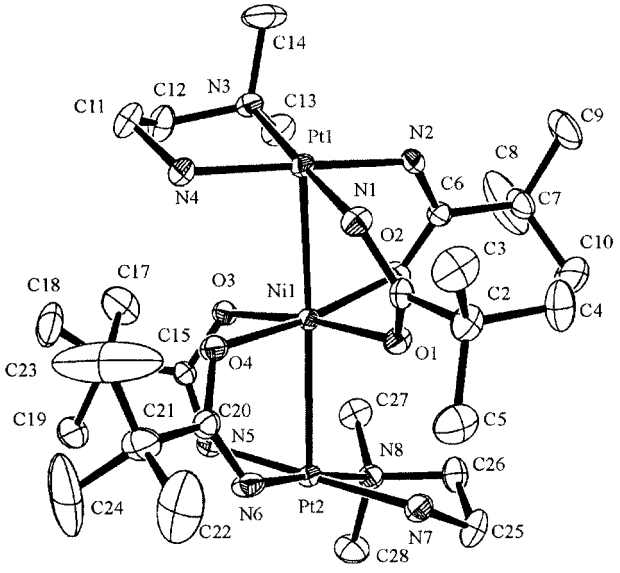

Figure 7. ORTEP plot of $[\{Pt(NH_2CH_2CH_2NMe_2)(\mu\text{-}NHCO\textit{t}Bu)\}_2Ni]^{2+}$ (**14**) with thermal ellipsoids plotted at 30% probability level

[2.5750(14) Å], and the Pt−Ni−Pt vector [169.33(2)°] is more bent.

Structure of 15

The trinuclear Pt_2Zn complex $[\{Pt(NH_2CH_2CH_2OMe)_2(\mu\text{-}NHCO\textit{t}Bu)_2\}_2Zn]^{2+}$ (**15**) was isolated as colorless crystals, and its structure is shown in Figure 8. Similar to other heteronuclear Pt_2M (M = Mn, Co, Ni, Cu) complexes, **15** contains a linear trimetallic core, in which Pt and Zn are doubly bridged by the amidate ligands. The methoxy groups remain uncoordinated. The Pt−Zn bond lengths are 2.5932(5) Å — comparable to the sum of covalent radii of the two metals (2.55 Å). Heteronuclear complexes containing direct Pt−Zn interaction have not been reported, but PtZn alloys are known catalysts for the dehydrogenation of alkanes.[22]

Structure of 12

The platinum−cadmium complex $[\{Pt(NH_3)_2(\mu\text{-}NHCO\textit{t}Bu)_2\}_2Cd]^{2+}$ (**12**) crystallizes in the space group $P2_1/n$. Its structure is shown in Figure 9. The platinum and cadmium centers are held together by four amidate ligands, which act as bridging units via their NCO groups. Unlike the analogous Pt_2Zn compound, the central Cd atom adopts tetrahedral geometry, which is completed by the four amidate oxygen atoms, or bicapped tetrahedron when the two rather long Pt−Cd contacts are also considered. The Pt−Cd distances [2.8156(9) and 2.8196(9) Å] are close to the sum of the metallic radii of platinum and cadmium (2.88 Å), indicating some Pt−Cd interaction. However, the Pt−Cd distances in **12** are much longer than the Pt−Cd dative bonds [2.6389(8) and 2.6101(8) Å] found in the complexes $[\{Pt(phpy)_2\}\{Cd(cyclen)\}](ClO_4)_2$ and

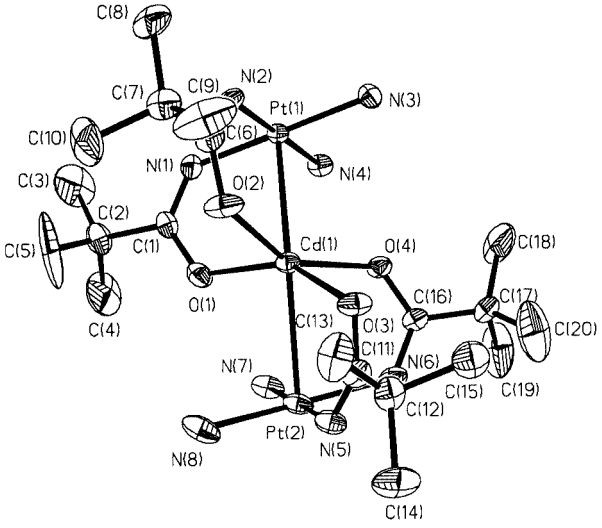

Figure 9. ORTEP plot of $[\{Pt(NH_3)_2(\mu\text{-}NHCO\textit{t}Bu)\}_2Cd]^{2+}$ (**12**) with thermal ellipsoids plotted at 30% probability level

 © 2003 Wiley-VCH Verlag GmbH & Co. KGaA, Weinheim

[{$PtMe_2$(bipy)}{Cd(cyclen)}]$(ClO_4)_2$ (Hphpy = 2-phenylpyridine, bipy = 2,2′-bipyridine; cyclen = 1,4,7,10-tetraazacyclododecane).[23] Pt−Cd distances in **12** are much shorter than those in $(NBu_4)_2$[{Pt(μ-C≡CPh)$_4$}$_2$($CdCl_2$)] [2.960(1) Å][24] and [Pt_4Cd_6(C≡CPh)$_4$(μ-C≡CPh)$_{12}$(μ$_3$-OH)$_4$] [2.8570(14)−3.2234(8) Å].[25] The Pt−Cd−Pt is bent [145.50(3)°]. The Cd−O distances fall in the range 2.214(8)−2.263(9) Å, which are not unusual.[25]

Structures of 9 and 11

[{Pt(DACH)(μ-NHCO*t*Bu)$_2$}$_2$In]$^{3+}$ (**9**) crystallizes in a triclinic space group $P\bar{1}$, whereas [{Pt(NH_3)$_2$(μ-NHCO*t*Bu)$_2$}$_2$In]$^{3+}$ (**11**) crystallizes in a chiral orthorhombic space group $P2_12_12_1$. The indium(III) ions in both **9** and **11** are approximately octahedrally coordinated by four equatorial oxygen atoms of the amidate ligands, and two platinum atoms occupy the axial sites. The structures of **9** and **11** are shown in Figures 10 and 11, respectively. The indium atom and the four oxygen atoms are almost co-planar, with the sum of the neighboring O−In−O angles being 360°. The Pt−In bond lengths are 2.6358(8) Å for **9** and 2.6279(8) and 2.6412(8) Å for **11**. The Pt−In−Pt angle for **9** is 180°, whereas that of **11** (174.81°) deviates slightly from 180°. The two [Pt(RNH_2)$_2$($NHCOtBu$)$_2$] units maintain a square-planar geometry.

The In−O bonds of **9** [2.128(6)−2.167(6) Å] and **11** [2.128(6)−2.16786] Å] are only slightly longer than those in the indium alkoxide complexes [In(μ-OR)(OR)$_2$]$_2$ (R = *t*Bu, CMe_2Et, $CMeEt_2$, and CMe_2iPr) [1.985(4)−2.152(6) Å].[26] Platinum−indium heterometallic complexes containing Pt−In donor−acceptor interactions have been rarely studied. The Pt−In distances of **9** and **11** are similar to those in $LaPtIn_3$ (Pt−In, 2.694 Å),[27] [{$Cy_2P(CH_2CH_2)PCy_2$}Pt(InR_2)(R)] (R = CH_2SiMe_3, Pt−In, 2.601 Å),[28] but longer than those in [Pt{$InC(SiMe_3)_3$}$_4$] (2.441 Å).[29]

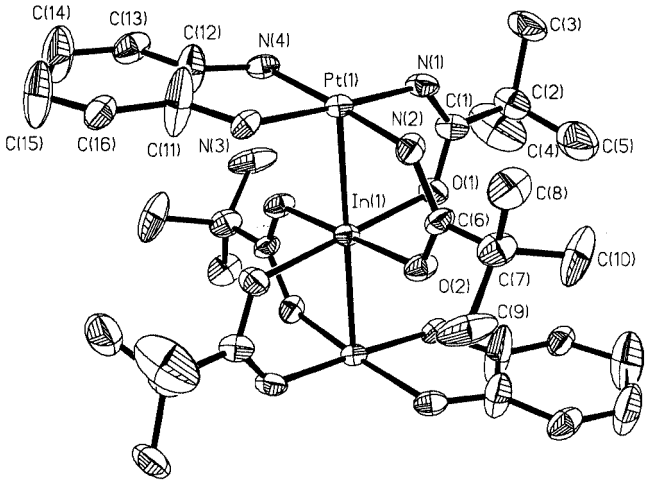

Figure 10. ORTEP plot of [{Pt(DACH)(μ-NHCO*t*Bu)$_2$}$_2$In]$^{3+}$ (**9**) with thermal ellipsoids plotted at 30% probability level

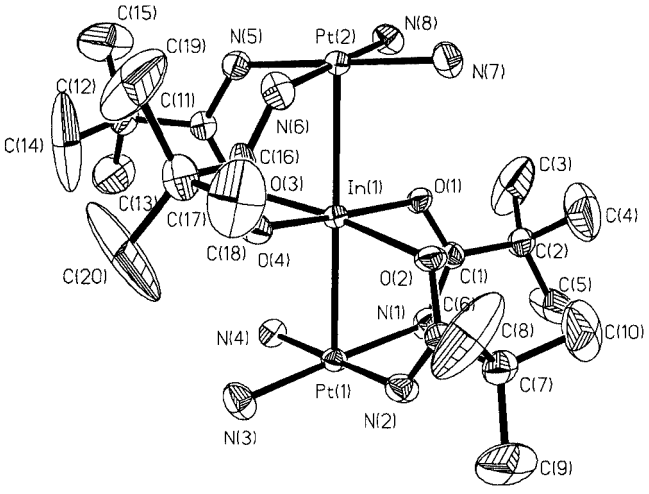

Figure 11. ORTEP plot of [{Pt(NH_3)$_2$(μ-NHCO*t*Bu)$_2$}$_2$In]$^{3+}$ (**11**) with thermal ellipsoids plotted at 30% probability level

Structure of 17

In the structure of the platinum−silver complex [{Pt($NH_2CH_2CH_2OCH_3$)$_2$(μ-NHCO*t*Bu)$_2$}$_4$$Ag_3$]$^{3+}$ (**17**) (Figure 12) the Pt_4Ag_3 cation is a chain of limited length, consisting of alternating Pt and Ag atoms bridged by amidate ligands. The metal−metal distances in the chain are 2.8203(14), 2.8531(14), and 2.9161(7) Å. There are two independent silver atoms, and Ag(2) is at the crystallographic inversion center. Ag(1) adopts a distorted trigonal-bipyramidal geometry with three amidate oxygen atoms at the equatorial positions and two Pt atoms occupying the two axial positions; the Pt(1)−Ag(1)−Pt(2) angle is 167.52(6)°. The coordination geometry around the Ag(2) atom is square-planar, and the Ag atom is linearly coordinated by two amidate oxygen and two Pt atoms, with a Pt(2)−Ag(2)−Pt(2a) angle of 180°. The Pt−Ag [2.8203(17), 2.8531(14), and 2.9161(7) Å] are close to those in other heteronuclear Pt−Ag complexes.[13] In contrast, the reaction

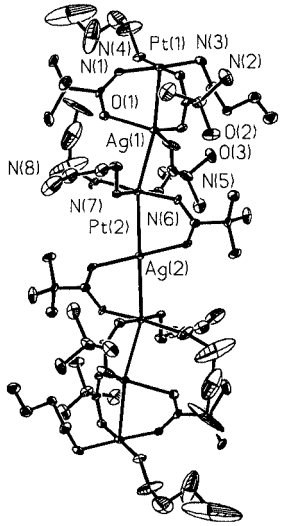

Figure 12. ORTEP plot of [{Pt($NH_2CH_2CH_2OCH_3$)-($NHCOtBu$)$_2$}$_4$$Ag_3$]$^{3+}$ (**17**) with thermal ellipsoids plotted at 30% probability level

 © 2003 Wiley-VCH Verlag GmbH & Co. KGaA, Weinheim

of $AgNO_3$ with *trans*- and *cis*-$[Pt(NH_3)_2(NHCOMe)_2]$ yielded the heteronuclear polymeric complexes *cis*- and *trans*-$[(NH_3)_2Pt(NHCOMe)_2Ag]NO_3$, in which Pt and Ag atoms are all singly bridged by acetamidate ligands.[14]

Electrochemistry

Electrochemical data were obtained from freshly prepared nitrogen-purged DMSO, and CH_3CN, solutions of the trinuclear complexes, and for their parent platinum complexes. The cyclic voltammograms of all the compounds exhibit an irreversible oxidation, whose peak potentials in DMSO at 50 $mV \cdot s^{-1}$ are 0.50 ($[Pt(NH_3)_2(NHCOtBu)_2]$), 0.44 (**2**), ca. 0.48 (**3**), and 0.56 V (**4**) versus Fc/Fc^+. The electron-transfer behaviour of the trinuclear complexes **5**−**15** is essentially identical to that of the parent platinum complexes, which involve oxidation potentials in the range 0.41−0.49 V. Thus, the complexation of $[Pt(RNH_2)_2(NHCOtBu)_2]$ to a heterometal ions does not significantly change the platinum-based redox potentials. Obviously, metal−metal charge transfer is not important for these trinuclear complexes and the Pt−M interactions within **5**−**15** are very weak.

Conclusion

A number of amidate-bridged trinuclear complexes containing a trimetallic Pt−M−Pt core, either linear or bent, have been prepared in good yield by reactions between $[Pt(RNH_2)_2(NHCOtBu)_2]$ and the corresponding metal ions. The platinum units can bind heterometal ions through amidate oxygen atoms. The cyclic voltammograms, ^{195}Pt NMR spectra, and solid-state infrared spectra suggest that metal−metal interactions between platinum and the heterometals are limited. The short Pt−M distances of the Pt_2M (M = Mn, Co, Ni, Cu, Cd, Zn, and In) and Pt_4Ag_3 complexes, revealed by X-ray diffraction analyses, may be attributed to geometric requirement of the bridging amidate ligands, although attractions between the platinum and the heterometal ions could not be excluded. The two $[Pt(RNH_2)_2(NHCOtBu)_2]$ units and an M ion are held together mainly by the amidate functionality. The substituents on the amine ligands do not affect significantly the Pt−M interactions.

Experimental Section

General Remarks: $[Pt(NH_3)_2(NHCOtBu)_2]\cdot 2H_2O$[12] and $PtCl_2(DACH)$[30] were prepared according to the published procedure. All other chemicals were of A. R. grade and used as received. Elemental analyses were performed with a Perkin−Elmer PE 2400II analyzer. IR spectra as KBr pellets were recorded with a Perkin−Elmer 2000 spectrophotometer. ^1H and ^{195}Pt NMR spectra were recorded with a Bruker 500 MHz spectrometer. The NMR chemical shifts are given in ppm relative to TMS (^1H) and K_2PtCl_4 (^{195}Pt), and referenced either to residual solvent signals (^1H) or externally (^{195}Pt). UV/Vis spectra were recorded with a JASCO v-570 spectrophotometer. Cyclic voltammograms were obtained by use of a BAS CV-50 W instrument, in 10^{-5} M DMSO solutions containing 0.05 M $(Bu_4N)ClO_4$ as supporting electrolyte at a scan rate of 50 $mV \cdot s^{-1}$, and a three-electrode cell composed of an Ag/$AgNO_3$ reference electrode, a 3.0-mm glassy carbon working electrode, and a platinum counter electrode. The potentials were referenced to the ferrocenium/ferrocene couple.

$[Pt(DACH)(NCtBu)_2](ClO_4)_2\cdot H_2O$ (1): A suspension of $PtCl_2(DACH)$ (1.14 g, 3.0 mmol) in water (15 mL) was treated with $AgClO_4$ (1.24 g, 6.0 mmol), and the resultant mixture was stirred overnight in the dark. After removal of AgCl, *t*BuCN (1.0 g, 12.0 mmol) was added to the filtrate. The so-obtained white precipitate was then separated and washed with H_2O, EtOH, and Et_2O, and dried in air. Yield: 1.95 g (94%). $C_{16}H_{32}Cl_2N_4O_8Pt\cdot H_2O$ (692.45): calcd. C 27.75, H 4.95, N 8.09; found C 27.55, H 4.93, N 7.94. ^1H NMR (500 MHz, [D$_6$]acetone): δ = 1.20−2.75 (m, C_6H_{10}, 10 H), 3.01 (s, H_2O), 1.52 [s, $C(CH_3)_3$, 18 H] ppm. ^{195}Pt NMR (107.00 MHz, [D$_6$]acetone): δ = −2857.2 ppm.

$[Pt(DACH)(NHCOtBu)_2]\cdot 4H_2O$ (2): A suspension of **1** (1.45 g, 2.0 mmol) in water (10 mL) was treated with NaOH (0.20 g, 5.0 mmol). The resultant mixture was then stirred at room temperature overnight to give a white solid that was collected by filtration, washed with cold water, and dried in air. Yield: 1.12 g (96%). $C_{16}H_{34}N_4O_2Pt\cdot 4H_2O$ (581.61): calcd. C 33.04, H 7.28; N 9.63; found C 33.29, H 6.78, N 9.57. ^1H NMR (500 MHz, [D$_6$]DMSO): δ = 6.50, 4.65 (each d, $J_{H,H}$ = 9 Hz, NH_2, each 2 H), 5.59 (s, NH, 2 H), 3.38 (s, H_2O), 1.07 [s, $C(CH_3)_3$, 18 H], 2.21, 1.91, 1.51, 1.29, 1.10 (m, C_6H_{10}, each 2 H) ppm. ^{195}Pt (107.00 MHz, [D$_6$]DMSO): δ = −2625.2 ppm.

$[Pt(NH_2CH_2CH_2OCH_3)_2(NHCOtBu)_2]$ (3): This compound was isolated as a white hygroscopic solid according to the method described for **2**, but starting from $PtCl_2(NH_2CH_2CH_2OCH_3)_2$ (1.20 g, 2.0 mmol). Yield: 0.73 g (67%). $C_{16}H_{38}N_4O_4Pt$ (545.58): calcd. C 35.22, H 7.02, N 10.27; found C 34.89, H 7.46, N 9.72.

$[Pt(NH_2CH_2CH_2NMe_2)(NHCOtBu)_2]$ (4): As described for **3**, but starting from $PtI_2(NH_2CH_2CH_2NMe_2)$ (0.54 g, 1.0 mmol), compound **4** was isolated as a white hygroscopic solid. Yield: 0.20 g (42%). $C_{14}H_{32}N_4O_2Pt$ (483.51): calcd. C 34.78, H 6.67, N 11.59; found C 33.26, H 7.02, N 11.12; the elemental analysis is unsatisfactory due to the compound's hygroscopic properties. ^1H NMR (270.05 MHz, [D$_6$]acetone): δ = 5.21 (s, NH_2, 2 H), 4.89, 4.63 (both s, NH, each 1 H), 2.92, 2.74 (both t, CH_2, $J_{H,H}$ = 6.0 Hz, each 2 H), 2.83 [s, $N(CH_3)_2$, 6 H], 1.15, 1.05 [both s, $C(CH_3)_3$, each 9 H] ppm. ^{195}Pt (57.95 MHz, [D$_6$]DMSO): δ = −2657 ppm.

$[\{Pt(DACH)(\mu\text{-}NHCOtBu)_2\}_2Mn](ClO_4)_2\cdot 2(CH_3)_2CO$ (5): $[Pt(DACH)(NHCOtBu)_2]\cdot 4H_2O$ (58 mg, 0.10 mmol) in acetone (2 mL) was added to a solution of $MnCl_2\cdot 4H_2O$ (20 mg, 0.10 mmol) and $NaClO_4$ (50 mg) in water (2 mL). Pale-yellow crystals were grown by slow concentration of the resultant solution. Yield: 57 mg (81%). $C_{32}H_{68}Cl_2N_8O_{12}Pt_2Mn\cdot 2(CH_3)_2CO$ (1389.09): calcd. C 32.86, H 5.80, N 8.07; found C 32.73; H 5.91, N 7.94.

$[\{Pt(DACH)(\mu\text{-}NHCOtBu)_2\}_2Co](ClO_4)_2\cdot 2(CH_3)_2CO$ (6): This compound was prepared in a similar manner to **5** except that $Co(NO_3)_2\cdot 6H_2O$ (29 mg, 0.10 mmol) was used in place of $MnCl_2\cdot 4H_2O$. Yield: 60 mg (86%). $C_{32}H_{68}Cl_2N_8O_{12}Pt_2Co\cdot 2(CH_3)_2CO$ (1393.08): calcd. C 32.76, H 5.79, N 8.04; found C 32.94; H 6.02; N 7.87.

$[\{Pt(DACH)(\mu\text{-}NHCOtBu)_2\}_2Cu](ClO_4)_2$ (7): The method employed for compound **5** was used to prepare **7**, except that $Cu(ClO_4)_2\cdot 6H_2O$ (37 mg, 0.10 mmol) was used in place of

 © 2003 Wiley-VCH Verlag GmbH & Co. KGaA, Weinheim

$MnCl_2·4H_2O$. Yield: 52.5 mg (82%). $C_{32}H_{68}Cl_2N_8O_{12}Pt_2Cu$ (1281.54): calcd. C 29.99, H 5.35, N 8.74; found C 30.03, H 5.15, N 8.67.

[{Pt(NH$_3$)(μ-DACHCO*t*Bu)(μ-NHCO*t*Bu)}$_2$Ni](ClO$_4$)$_2$ (8): Compound **8** was prepared in a similar manner as for **5** except that $Ni(NO_3)_2·6H_2O$ (29 mg, 0.10 mmol) was used instead of $MnCl_2·4H_2O$. Yield: 54 mg (84%). $C_{32}H_{68}Cl_2N_8O_{12}Pt_2Ni$ (1276.68): calcd. C 30.10, H 5.37, N 8.78; found C 30.06; H 5.35; N 8.66.

[{Pt(DACH)(μ-NHCO*t*Bu)$_2$}$_2$In](ClO$_4$)$_3$ (9): Here the method used to synthesize **5** was employed, with $In(NO_3)_3·6H_2O$ (41 mg, 0.10 mmol) in place of $MnCl_2·4H_2O$, to give **9** in 63% yield (45 mg). $C_{32}H_{68}Cl_3N_8O_{16}Pt_2In$ (1432.26): calcd. C 26.83, H 4.79, N 7.82; found C 26.79, H 4.68, N 7.68. ^{1}H NMR (500 MHz, [D$_6$]DMSO): δ = 6.85, 6.01 (both d, $J_{H,H}$ = 9.0 Hz, NH_2, each 2 H), 6.33, 6.30 (both s, NH, each 2 H), 5.70, 4.44 (both t, $J_{H,H}$ = 9.0 Hz, each 2 H), 1.01−2.72 (m, C_6H_{10}, 20 H), 1.12 [s, $C(CH_3)_3$, 36 H] ppm. ^{195}Pt (107.00 MHz, [D$_6$]DMSO): δ = −2439 ppm.

[{Pt(DACH)(μ-NHCO*t*Bu)$_2$}$_2$Cd](ClO$_4$)$_2$ (10): Compound **10** was prepared in a similar manner as for **3**, starting from $CdSO_4·6H_2O$ (32 mg, 0.10 mmol). Yield: 51 mg (76%). $C_{32}H_{68}Cl_2N_8O_{12}Pt_2Cd$ (1330.4): calcd. C 28.89, H 5.15, N 8.42; found C 28.45, H 5.30, N 8.36. ^{1}H NMR (500 MHz, [D$_6$]DMSO): δ = 6.06, 5.55, 5.38, 4.60 (all s, NH_2, each 2 H), 5.57, 5.41 (both s, NH, each 2 H), 1.40−2.73 (m, C_6H_{10}, 20 H), 1.13, 1.04 [both s, $C(CH_3)_3$, each 18 H] ppm. ^{195}Pt (107.00 MHz, [D$_6$]DMSO): δ = −2562 ppm.

[[Pt(NH$_3$)$_2$(NHCO*t*Bu)$_2$]$_2$In](ClO$_4$)$_3$·C$_3$H$_6$O (11): $[Pt(NH_3)_2(NHCOtBu)_2]·2H_2O$ (47 mg, 0.10 mmol) was added to a solution of $In(NO_3)_3·6H_2O$ (41 mg, 0.10 mmol) in H_2O (2 mL). The resultant colorless solution yielded a colorless precipitate immediately after subsequent addition of $NaClO_4$. Cooling at 5 °C overnight gave colorless crystals, which were filtered off and then washed with cold water, EtOH, and Et_2O. Yield: 53 mg (79%). $C_{20}H_{52}Cl_3InN_8O_{16}Pt_2·(CH_3)_2CO$ (1330.08): calcd. C 20.77, H 4.40, N 8.42; found C 20.39, H 4.25, N 8.58. ^{1}H NMR (500.00 MHz, [D$_6$]DMSO): δ = 6.46 (s, NH, 2 H), 4.13 (s, NH_3, 6 H), 2.07 [s, $(CH_3)_2CO$, 6 H), 1.10 [s, $C(CH_3)_3$, 18 H] ppm. ^{195}Pt NMR (107.30 MHz, [D$_6$]DMSO): δ = −2474 ppm.

[{Pt(NH$_3$)$_2$(μ-NHCO*t*Bu)$_2$}$_2$Cd](ClO$_4$)$_2$·2H$_2$O (12): This compound was obtained similarly to **11** by using the corresponding materials $Cd(NO_3)_2·4H_2O$ (24 mg, 0.10 mmol), $NaClO_4$ (50 mg, 0.43 mmol), and $[Pt(NH_3)_2(NHCOtBu)_2]·2H_2O$ (47 mg, 0.10 mmol). Yield: 51 mg (84%). $C_{20}H_{52}CdCl_2N_8O_{12}Pt_2·2H_2O$ (1206.18): calcd. C 19.92, H 4.68, N 9.29; found C 19.79, H 4.83, N 9.20. ^{1}H NMR (500.00 MHz, [D$_6$]DMSO): δ = 5.42 (br. NH_3, 12 H), 4.51 (br. NH, 4 H), 1.06 [s, $C(CH_3)_3$, 36 H] ppm. ^{195}Pt NMR (107.30 MHz, [D$_6$]DMSO): δ = −2561 ppm.

[{Pt(NH$_2$CH$_2$CH$_2$NMe$_2$)(μ-NHCO*t*Bu)$_2$}$_2$Co](ClO$_4$)$_2$·H$_2$O (13): Compound **13** was prepared by an analogous procedure to that of **6** but using **4** (48 mg, 0.10 mmol) and $Co(NO_3)_2·6H_2O$ (29 mg, 0.10 mmol) to isolate **13** as a blue solid. Yield: 50 mg (81%). $C_{28}H_{64}CoCl_2N_8O_{12}Pt_2·H_2O$ (1242.86): calcd. C 27.06, H 5.35, N 9.02; found C 27.30, H 5.30, N 9.20.

[{Pt(NH$_2$CH$_2$CH$_2$NMe$_2$)(μ-NHCO*t*Bu)$_2$}$_2$Ni](ClO$_4$)$_2$·H$_2$O (14): By a similar procedure to that used for **13**, but using $Ni(NO_3)_2·6H_2O$ (29 mg, 0.10 mmol), **14** was isolated as a green solid. Yield: 53 mg (86%). $C_{28}H_{64}Cl_2N_8NiO_{12}Pt_2·H_2O$ (1242.62): calcd. C 27.06, H 5.35, N 9.02; found C 26.93, H 5.47, N 8.96.

[{Pt(NH$_2$CH$_2$CH$_2$OCH$_3$)$_2$(μ-NHCO*t*Bu)$_2$}$_2$Zn](ClO$_4$)$_2$ (15): This compound was prepared as described for **5** but starting from **3** (55 mg, 0.10 mmol) and $Zn(ClO_4)_2·6H_2O$ (37 mg, 0.10 mmol), and was isolated as a white solid. Yield: 52 mg (76%). $C_{32}H_{76}Cl_2N_8O_{16}Pt_2Zn$ (1355.4): calcd. C 28.36, H 5.65, N 8.27; found C 28.34, H 5.42, N 8.05.

[{Pt(NH$_2$CH$_2$CH$_2$OCH$_3$)(μ-NHCO*t*Bu)$_2$}$_2$Co](ClO$_4$)$_2$ (16): Using the method described for **5**, but starting from **3** (55 mg, 0.10 mmol) and $Co(NO_3)_2·6H_2O$ (29 mg, 0.10 mmol), **16** was isolated as a blue solid in 78% yield (53 mg). $C_{32}H_{76}Cl_2CoN_8O_{16}Pt_2$ (1348.98): calcd. C 28.49, H 5.68, N 8.31; found C 28.22, H 5.79, N 8.20.

[{Pt(NH$_2$CH$_2$CH$_2$OCH$_3$)(NHCO*t*Bu)$_2$}$_4$Ag$_3$](ClO$_4$)$_3$·2H$_2$O (17): Compound **17** was prepared from **3** (55 mg, 0.10 mmol) and an equimolar amount of $AgClO_4$ (21 mg, 0.10 mmol) in water. Slow concentration of the resultant colorless solution yielded colorless crystals. Yield: 44 mg (63%). $C_{64}H_{152}Ag_3Cl_3N_{16}O_{28}Pt_4·2H_2O$ (2840.3): calcd. C 27.06, H 5.54, N 7.89; found C 26.82, H 5.63, N 7.45.

Table 2. Crystal data and structure refinement for compounds **5**−**9**, **17**

	5	**6**	**7**	**8**	**9**	**17**
Empirical formula	$C_{38}H_{80}Cl_2MnN_8O_{14}Pt_2$	$C_{38}H_{80}Cl_2CoN_8O_{14}Pt_2$	$C_{32}H_{68}Cl_2CuN_8O_{12}Pt_2$	$C_{32}H_{68}Cl_2N_8NiO_{12}Pt_2$	$C_{34}H_{74}Cl_3InN_8O_{17}Pt_2$	$C_{64}H_{152}Ag_3Cl_3N_{16}O_{28}Pt_4$
Formula mass	1389.12	1393.11	1281.56	1276.73	1478.33	2804.34
Crystal system	monoclinic	monoclinic	monoclinic	monoclinic	triclinic	monoclinic
Space group	$P2_1/c$	$P2_1/c$	$P2_1/n$	$C2$	$P\bar{1}$	$P2_1/n$
a [Å]	11.367(13)	11.273(3)	12.181(4)	21.847(12)	12.998(4)	14.235(4)
b [Å]	19.51(2)	19.415(5)	12.056(4)	11.883(7)	13.148(4)	24.889(6)
c [Å]	12.897(16)	12.888(3)	16.454(5)	11.302(6)	17.925(5)	16.097(4)
α [°]	90	90	90	90	74.715(5)	90
β [°]	100.88(2)	101.055(4)	93.753(6)	121.124(8)	79.638(5)	94.982(5)
γ [°]	90	90	90	90	73.405(5)	90
V [Å^3]	2809(6)	2768.5(13)	2411.1(14)	2512(2)	2813.7(14)	5682(3)
Z	2	2	2	2	2	2
$D_{calcd.}$ [Mg/m^3]	1.643	1.671	1.765	1.688	1.704	1.639
Refls. collected	16455	16689	14886	7444	14102	32411
Refls. unique	6226 (0.1854)	6157 (0.069)	5506 (0.0489)	9934 (0.0319)	10052 (0.0598)	12446 (0.0932)
GOF	0.959	1.193	1.475	1.043	0.957	1.066
$R1$, $wR2$ [$I > 2\sigma(I)$]	0.0626, 0.1370	0.0399, 0.0954	0.0653, 0.1417	0.0251, 0.0684	0.0580, 0.1337	0.0958, 0.2520
$R1$, $wR2$ (all data)	0.1208, 0.1562	0.0463, 0.0977	0.0765, 0.1446	0.0291, 0.0712	0.1087, 0.1478	0.1416, 0.2810

 © 2003 Wiley-VCH Verlag GmbH & Co. KGaA, Weinheim

Table 3. Crystallographic data and structure refinement for compounds **11**−**16**

	11	**12**	**13**	**14**	**15**	**16**
Empirical formula	$C_{23}H_{58}Cl_3InN_8O_{17}Pt_2$	$C_{20}H_{56}CdCl_2N_8O_{14}Pt_2$	$C_{28}H_{66}Cl_2CoN_8O_{13}Pt_2$	$C_{28}H_{66}Cl_2N_8NiO_{13}Pt_2$	$C_{32}H_{76}Cl_2N_8O_{16}Pt_2Zn$	$C_{32}H_{76}Cl_2CoN_8O_{16}Pt_2$
Formula mass	1330.12	1206.21	1242.90	1242.68	1355.46	1349.02
Crystal system	orthorhombic	monoclinic	monoclinic	monoclinic	orthorhombic	orthorhombic
Space group	$P2_12_12_1$	$P2_1/n$	$P2_1/n$	$P2_1/n$	*Pbca*	*Pbca*
a [Å]	10.9233(9)	13.656(3)	12.878(5)	12.906(6)	14.067(2)	14.054(4)
b [Å]	18.5229(16)	19.988(5)	16.048(7)	16.144(7)	18.615(3)	18.491(5)
c [Å]	22.5474(19)	15.154(4)	21.637(9)	21.624(10)	20.106(3)	19.977(6)
β [°]	90	92.010(4)	98.644(7)	99.075(8)	90	90
V [Å^3]	4562.0(7)	4133.7(16)	4421(3)	4449(3)	5265.0(16)	5192(3)
Z	4	4	4	4	4	4
$D_{calcd.}$ [g/cm^3]	1.937	1.938	1.867	1.855	1.710	1.726
Refls. collected	28711	25791	27147	25851	29970	28599
Refls. uniqe (R_{int})	10434 (0.0850)	9391 (0.1313)	9966 (0.0312)	9934 (0.0319)	5969 (0.1092)	5821 (0.0585)
Goodness-of-fit	1.023	0.995	1.039	1.043	0.927	0.938
*R*1, *Rw* [$I > 2\sigma(I)$]	0.0435, 0.1002	0.0669, 0.1680	0.0272, 0.0631	0.0289, 0.0638	0.0427, 0.0908	0.0361, 0.0771
*R*1, *Rw* (all data)	0.0535, 0.1048	0.0901, 0.1841	0.0409, 0.0690	0.0481, 0.0712	0.1073, 0.1122	0.0717, 0.0935

X-ray Crystallographic Study: Data collection was performed with a Bruker Smart-CCD diffractometer using monochromatized Mo-K_α radiation, λ = 0.71073 Å, at room temperature. Data reduction was performed using SAINT+ Version 6.02 software.[31] The data were corrected for absorption by using the program SADBAS within the SAINTPLUS package. Structures were solved by the direct method. This solution yielded metal atoms, N, O, and some C atoms. Subsequent Fourier synthesis gave the remaining C-atom positions. The hydrogen atoms were geometrically fixed and allowed to ride on their attached atoms, and refined with the XSHELL software.[32] The final refinement included anisotropic thermal parameters for all of the non-hydrogen atoms and converged to the *R*1 and *wR*2 values listed in Tables 2 and 3. The crystal data collection and refinement parameters are summarized in Tables 2 and 3. CCDC-187851 (**5**), -187852 (**6**), -187853 (**7**), -187854 (**8**), -187855 (**9**), -188637 (**11**), -188638 (**12**), -195593 (**13**), -195594 (**14**), -195595 (**15**), -195596 (**16**), and -195597 (**17**) contain the supplementary crystallographic data for this paper. These data can be obtained free of charge at www.ccdc.cam.ac.uk/conts/retrieving.html [or from the Cambridge Crystallographic Data Centre, 12 Union Road, Cambridge CB2 1EZ, UK; Fax: (internat.) + 44-1223/336-033; E-mail: deposit@ccdc.cam.ac.uk].

[1] T. Tanase, R. A. Begum, H. Toda, Y. Yamamoto, *Organometallics* **2001**, *20*, 968−979.
[2] H. Song, Z. Zhang, Z. Hui, C. Che, T. C. W. Mak, *Inorg. Chem.* **2002**, *41*, 3146−3154.
[3] R. Clerac, F. A. Cotton, K. R. Dunbar, T. B. Lu, C. A. Murillo, X. P. Wang, *J. Am. Chem. Soc.* **2000**, *122*, 2272−2278.
[4] A. L. Balch, V. J. Catalano, M. M. Olmstead, *J. Am. Chem. Soc.* **1990**, *112*, 2010−2011.
[5] H. Xiao, Y. Weng, W. Wong, T. C. W. Mak, C. Che, *J. Chem. Soc., Dalton Trans.* **1997**, 221−226.
[6] W. Chen, K. Matsumoto, *Eur. J. Inorg. Chem.* **2002**, 2664−2670.
[7] J. R. Berenguer, J. Forniés, J. Gómez, E. Lalinde, M. T. Moreno, *Organometallics* **2001**, *20*, 4847−4851.
[8] J. K. Nagle, A. L. Balch, M. M. Olmstead, *J. Am. Chem. Soc.* **1988**, *110*, 319−321.
[9] A. L. Balch, S. P. Rowley, *J. Am. Chem. Soc.* **1990**, *112*, 6139−6140.
[10] P. Pyykkö, *Chem. Rev.* **1997**, *97*, 597−636.
[11] [11a] Y. Lin, S. Takeda, K. Matsumoto, *Organometallics* **1999**, *18*, 4897−4899. [11b] Y. Lin, H. Misawa, K. Matsumoto, *J. Am. Chem. Soc.* **2001**, *123*, 569−575. [11c] K. Matsumoto, J. Matsunami, K. Mizuno, H. Uemura, *J. Am. Chem. Soc.* **1996**, *118*, 8959−8960. [11d] K. Matsumoto, Y. Nagai, J. Matsunami, K. Mizuno, T. Abe, R. Somazawa, J. Kinoshita, H. Shimura, *J. Am. Chem. Soc.* **1998**, *120*, 2900−2907.
[12] W. Chen, K. Matsumoto, *Inorg. Chim. Acta* **2002**, *342*, 88−96.
[13] [13a] F. Zamora, H. Witkowski, E. Freisinger, J. Muller, B. Thormann, A. Albinati, B. Lippert, *J. Chem. Soc., Dalton Trans.* **1999**, 175−182. [13b] D. Holthenrich, M. Krumm, E. Zangrando, F. Pichierri, L. Randaccio, B. Lippert, *J. Chem. Soc., Dalton Trans.* **1995**, 3275−3279.
[14] A. Erxleben, B. Lippert, *J. Chem. Soc., Dalton Trans.* **1996**, 2329−2333.
[15] J. Arpalahti, K. D. Klika, S. Molander, *Eur. J. Inorg. Chem.* **2000**, 1007−1013.
[16] B. Lippert, U. Schubert, *Inorg. Chim. Acta* **1981**, *56*, 15−20.
[17] S. Komiya, S. Muroi, M. Furuya, M. Hirano, *J. Am. Chem. Soc.* **2000**, *122*, 170−171.
[18] B. Lippert, U. Thewalt, H. Schoellhorn, D. M. L. Goodgame, R. W. Rollins, *Inorg. Chem.* **1984**, *23*, 2807−2813.
[19] [19a] V. W. W. Yam, K. L. Yu, K. K. Cheung, *J. Chem. Soc., Dalton Trans.* **1999**, 2913−2915. [19b] J. P. H. Charmant, J. Forniés, J. Gomez, E. Lalinde, R. I. Merino, M. T. Moreno, A. C. Orpen, *Organometallics* **1999**, *18*, 3353−3358.
[20] R. D. Adams, G. Chen, W. G. Wu, J. G. Yin, *Inorg. Chem.* **1990**, *29*, 4208−4214.
[21] [21a] I. Bachert, I. Bartusseck, P. Braunstein, E. Guillon, J. Rose, G. Kickelbick, *J. Organomet. Chem.* **1999**, *588*, 144−151. [21b] I. Bachert, I. Bartusseck, P. Braunstein, E. Guillon, J. Rose, G. Kickelbick, *J. Organom. Chem.* **1999**, *580*, 257−264.
[22] J. Silvestre-Albero, M. A. Sanchez-Castillo, R. He, A. Sepulveda-Escribano, F. Rodriguez-Reinoso, J. A. Dumesic, *Catal. Lett.* **2001**, *74*, 17−25.
[23] T. Yamaguchi, F. Yamazaki, T. Ito, *J. Am. Chem. Soc.* **1999**, *121*, 7405−7406.
[24] J. P. H. Charmant, L. R. Falvello, J. Forniés, J. Gómez, E. Lalinde, M. T. Moreno, A. G. Orphen, A. Rueda, *Chem. Commun.* **1999**, 2045−2046.
[25] J. Forniés, J. Gómez, E. Lalinde, M. T. Moreno, *Inorg. Chem.* **2001**, *40*, 5415−5419.
[26] [26a] S. Suh, D. M. Hoffman, *J. Am. Chem. Soc.* **2000**, *122*, 9396−9404. [26b] T. J. Trentler, S. C. Goel, K. M. Hickman, A. M. Viano, M. Y. Chiang, A. M. Beatty, P. C. Gibbons, W. E. Buhro, *J. Am. Chem. Soc.* **1997**, *119*, 2172−2181.

 © 2003 Wiley-VCH Verlag GmbH & Co. KGaA, Weinheim

[27] Y. V. Galadzhun, R. Pottgen, *Z. Angorg. Allg. Chem.* **1999**, *625*, 481−487.
[28] R. A. Fischer, J. Behm, *J. Organomet. Chem.* **1991**, *413*, C10−C14.
[29] W. Uhl, S. Melle, *Z. Anorg. Allg. Chem.* **2000**, *626*, 2043−2045.
[30] A. H. Talebian, D. Bensely, A. Ghiorghis, C. F. Hammer, P. S. Schein, D. Green, *Inorg. Chim. Acta* **1991**, *179*, 281−287.
[31] G. M. Sheldrick, *SHELXS-97, Program for X-ray Crystal Structure Solution*, University of Göttingen, Göttingen, Germany, **1997**.
[32] G. M. Sheldrick, *SHELXL-97, Program for X-ray Crystal Structure Refinement*, University of Götingen, Götingen, Germany, **1997**.

Received December 13, 2002
Early View Article
Published Online October 22, 2003

 © 2003 Wiley-VCH Verlag GmbH & Co. KGaA, Weinheim

Ruthenium(III) Complexes with a Phenolate-O, Imine-N, and Amide-O Coordinating Ligand: Syntheses, Structures, Properties, and Protonation Studies of Coordinated Amide

Satyanarayan Pal,[a] and Samudranil Pal*[a]

Keywords: Ruthenium / Acetylhydrazone / Crystal structures / Protonation / Redox chemistry

The reaction of *cis*-[$RuCl_2(dmso)_4$], *N*-(acetyl)-*N′*-(salicylidene)hydrazine (H_2acs), and KOH (1:2:2 molar ratio) in methanol under aerobic conditions produces a ruthenium(III) complex, [Ru(acs)(Hacs)]·H_2O. Addition of one mol equivalent of $HClO_4$ to this complex in methanol affords [$Ru(Hacs)_2$]ClO_4. On the other hand, reaction of one mol equivalent of KOH with [Ru(acs)(Hacs)]·H_2O in methanol produces K[$Ru(acs)_2$]. All three complexes have been characterised by elemental analyses, magnetic, spectroscopic, and electrochemical techniques. In solution, except for [Ru(acs)(Hacs)]·H_2O, the other two complexes are 1:1 electrolytes. Solid state magnetic moments (at 298 K) of the complexes are in the range 1.91–2.15 μ_B. These values reflect a spin state $S = 1/2$ and hence low-spin ruthenium(III) within each complex is observed. X-ray structures of [Ru(acs)(Hacs)]·H_2O and the tetraphenylphosphonium salt of [$Ru(acs)_2$]$^-$ have been determined. In both complexes, the ligands bind to the metal ion meridionally through the phenolate-O, the imine-N and the amide-O atoms. In [Ru(acs)(Hacs)]·H_2O, the amide functionality of one of the ligands is protonated, and in [PPh_4][$Ru(acs)_2$] the amide functionalities of both ligands are deprotonated. Electronic spectra of the complexes display ligand-to-metal charge-transfer bands in the range 626–699 nm. Cyclic voltammetry reveals a $Ru^{III} \rightarrow Ru^{IV}$ oxidation change in the potential range of 0.56–0.84 V (vs. SCE) for these complexes. The charge-transfer band positions and the oxidation potentials are significantly influenced by the protonation state of the O-coordinating amide functionality present in each ligand. The pK_a values of the coordinated amide functionalities have been determined by spectrophotometric titration.
(© Wiley-VCH Verlag GmbH & Co. KGaA, 69451 Weinheim, Germany, 2003)

Introduction

The interest in ruthenium chemistry stems from its ability to have a wide range of oxidation states (−2 to +8) and various coordination geometries. Due to these characteristics complexes of ruthenium exhibit versatile electron-transfer properties and hence a wide range of reactivities.[1]

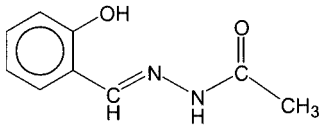

H_2acs

As a result a large variety of ruthenium complexes have been utilized in studies on artificial photosynthesis, photomolecular devices, elucidation of structural and electron-transfer properties of proteins and DNA, catalytic oxidation of water and organic substrates and stoichiometric as well as catalytic reactions for organic synthesis.[1l−1t] Due to such a broad array of applications there is a continuous pursuit for new complexes of ruthenium with diverse types of ligands. The primary objective is to tune the properties of the complex by alteration of the coordination geometry and the nature of the coordinating functionalities. Recently we have reported a series of ruthenium(II) bis complexes with a tridentate pyridine-N, imine-N, and amide-O donor deprotonated Schiff-base system, *N*-(aroyl)-*N′*-(picolinylidene)hydrazines.[2] In these complexes, the energy separation between the metal-dπ and ligand-π* level remains constant regardless of the variation in the polar effect of the substituent on the aroyl fragment of the ligand. In this report, we have explored the coordination chemistry of ruthenium with a similar kind of Schiff base *N*-(acetyl)-*N′*-(salicylidene)hydrazine (H_2acs, the two H′s representing the dissociable phenolic and amide protons). In the deprotonated state the Schiff base acs^{2-} can coordinate to a metal ion via the phenolate-O, the imine-N, and the deprotonated amide-O atoms forming a six- and a five-membered chelate ring. This type of coordination mode by acs^{2-} and similar ligands is known.[3] The reasons for the choice of this Schiff base are as follows: it contains high oxidation state promoting[4] phenolic hydroxy and amide functionalities; the O-coordinating amide functionality provides a rare opportunity to study the influence of the amide protonation state on the coordination geometry and physical properties of the complex, which is not easy for amide-N coordinated species. Herein, we describe three new ruthenium(III) bis-chelates with H_2acs. These complexes differ only in the protonation state

[a] School of Chemistry, University of Hyderabad, Hyderabad 500 046, India
Fax: (internat.) +91-40/2301-2460
E-mail: spsc@uohyd.ernet.in

 © 2003 Wiley-VCH Verlag GmbH & Co. KGaA, Weinheim **DOI: 10.1002/ejic.200300232**

of the coordinated amide functionalities. Solid state molecular structures for two of these three complexes have been determined by X-ray crystallography In solution, dependence of the spectral and the redox features on the amide protonation state has been scrutinized.

Results and Discussion

Syntheses and Characterisation of the Complexes

The neutral complex [Ru(acs)(Hacs)] was isolated from a methanolic medium by reacting *cis*-[$RuCl_2(dmso)_4$], H_2acs and KOH in 1:2:2 molar ratio under aerobic conditions. The monohydrated complex precipitates from the reaction mixture as a green solid in reasonable yield. Atmospheric oxygen is the most likely oxidizing agent in the oxidation of the metal ion during the formation of the complex. If the stoichiometrically required molar ratio (1:2:3) is taken, the amount of the precipitated complex is significantly lower. However, the potassium salt of the anionic complex $[Ru(acs)_2]^-$ can be recovered from the filtrate. The dissociation of the phenolic-OH proton may happen in the absence of a strong base like OH^-. Most likely for this reason the 1:2:2 mol ratio gives a better yield of the neutral complex and for stoichiometric mol ratio (1:2:3) formation of $[Ru(acs)_2]^-$ has been observed. A more convenient and clean method for the synthesis of $K[Ru(acs)_2]$ is the treatment of [Ru(acs)(Hacs)]·H_2O with one molar equivalent of KOH in methanol. By using a similar approach the perchlorate salt of the cationic complex $[Ru(Hacs)_2]^+$ can be prepared by reacting [Ru(acs)(Hacs)]·H_2O and $HClO_4$ in a 1:1 molar ratio in methanol. The elemental analysis data (Table 1) for all three complexes agree with the proposed molecular formulae. Molar conductivity values (Table 1) of the complexes in solutions are consistent with the neutral character of [Ru(acs)(Hacs)]·H_2O and 1:1 electrolyte nature[5] of both $K[Ru(acs)_2]$ and $[Ru(Hacs)_2]ClO_4$. The solid-state magnetic moments (Table 1) of these complexes at 298 K are in the range 1.91−2.15 μ_B. Thus, in each complex, the ruthenium centre is in the +3 oxidation state and is low-spin in character.

Spectral Characteristics

The infrared spectra of [Ru(acs)(Hacs)]·H_2O and $[Ru(Hacs)_2]ClO_4$ display multiple peaks in the range 3206−2710 cm^{-1}. These peaks are most likely associated with the N−H group of the protonated amide functionalities in these complexes.[6a] On the other hand, absence of any such peak in this region of the spectrum of $K[Ru(acs)_2]$ confirms deprotonation of the amide functionalities in both ligands. In addition to the above mentioned peaks, [Ru(acs)(Hacs)]·H_2O displays a broad peak centred at 3427 cm^{-1} ascribable to the lattice water molecules.[6b] All three complexes display three medium to strong peaks at about 1597, 1550 and 1520 cm^{-1}. These peaks are possibly due to the metal-coordinated azomethine and protonated/deprotonated amide functionalities of the ligands.[2,3,6a] The presence of perchlorate ion in $[Ru(Hacs)_2]ClO_4$ is indicated by a broad and strong peak at ca. 1100 cm^{-1} and a sharp peak at ca. 620 cm^{-1}.

The electronic spectroscopic data of the complexes in acetonitrile solutions are listed in Table 1. The spectral profiles are quite similar. In the visible region, the major features displayed by these complexes are a band in the range 626−699 nm and a shoulder within the range 487−504 nm (Table 1). These absorptions are assigned to the phenolate-pπ to the metal-dπ charge-transfer transitions.[7] Interestingly, $[Ru(Hacs)_2]ClO_4$, where both the amide functionalities of the ligands are protonated, displays the first band at lower energy (699 nm) whereas the completely deprotonated species $K[Ru(acs)_2]$ displays the same band at higher energy (626 nm). The band position shift suggests that the energy gap between the phenolate-pπ and the metal-dπ levels is significantly decreased due to the protonation of the O-coordinating amide functionalities of the two ligands. The band position of the neutral complex [Ru(acs)(Hacs)], where only one amide functionality is protonated, shows the same trend but to a much smaller extent. The strong absorptions (Table 1) observed in the ultraviolet region of the spectra are most likely due to transitions involving only ligand orbitals.

The EPR spectra of the complexes in frozen (103 K) methanol/toluene (1:1) solutions are very similar. A representative spectrum is shown in Figure 1. Each of them display three distinct signals (Table 2) indicating the distortion of the N_2O_4 coordination sphere around the metal centre from octahedral symmetry. This distortion can be measured in terms of axial (Δ) and rhombic (V) components. The axial distortion (Δ) splits t_2 into "a" and "e" and the rhombic component again splits "e" into nondegenerate

Table 1. Elemental analysis,[a] molar conductivity, magnetic moment[b] and electronic spectral[c] data

Compound	%C	%H	%N	Λ_M (Ω^{-1} cm^2 M^{-1})	μ_{eff}/μ_B	λ_{max} nm ($\varepsilon/10^3$ M^{-1} cm^{-1})
[Ru(acs)(Hacs)]·H_2O	45.53 (45.76)	3.87 (4.05)	11.63 (11.86)	15[d]	1.91	630 (1.1), 504[e] (1.2), 375 (15.4), 343 (15.5), 271[e] (19.6)
$[Ru(Hacs)_2]ClO_4$	38.61 (38.96)	3.42 (3.27)	9.85 (10.10)	117[f]	2.15	699 (2.0), 496[e] (1.1), 365 (13.6), 267 (18.6), 235 (26.1)
$K[Ru(acs)_2]$	43.58 (43.90)	3.13 (3.27)	11.04 (11.37)	138[f]	2.01	626 (0.7), 487[e] (1.2), 380 (14.7), 342 (16.4), 282[e] (15.6), 241 (28.3)

[a] Calculated values are in parentheses. [b] In powder phase at 298 K. [c] In CH_3CN solvent. [d] In $HCON(CH_3)_2/CH_3CN$ (1:4) solvent. [e] Shoulder. [f] In CH_3CN solvent.

 © 2003 Wiley-VCH Verlag GmbH & Co. KGaA, Weinheim

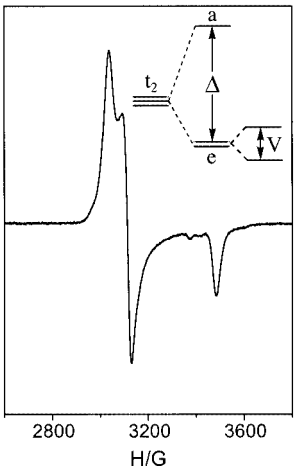

Figure 1. EPR spectrum of $[Ru(Hacs)_2]ClO_4$ in frozen (103 K) methanol/toluene (1:1) solvent mixture and t_2 splitting pattern

Table 2. EPR *g*-values,[a] calculated distortion parameters and near-IR transitions[b]

Compound	g_1	g_2	g_3	Δ/λ	V/λ	$\Delta E_1/\lambda$	$\Delta E_2/\lambda$
$[Ru(acs)(Hacs)]\cdot H_2O$	2.186	2.133	1.876	4.849	−0.935	4.377	5.659
$[Ru(Hacs)_2]ClO_4$	2.166	2.114	1.888	5.069	−1.064	4.540	5.921
$K[Ru(acs)_2]$	2.208	2.161	1.854	4.492	−0.670	4.125	5.225

[a] In 1:1 methanol/toluene at 103 K. [b] The calculations are based on spin-orbit coupling constant (λ) = 1000 cm^{-1}.

components (Figure 1). In addition to Δ and V, spin-orbit coupling also influences the extent of the energy gaps between these levels. Thus, two ligand-field transitions of energies ΔE_1 and ΔE_2 ($\Delta E_1 < \Delta E_2$) are possible within these three levels. The distortion parameters and the transition energies have been quantified using the observed *g* values and the *g* tensor theory of low-spin d^5 complexes (Table 2).[8] The distortion parameters suggest that the axial component is significantly larger than the rhombic component in all of the complexes. The ΔE_1 and ΔE_2 transitions are expected to occur in the range 4100−4600 and 5200−6000 cm^{-1} (Table 2), respectively. No absorption was detected in either of the above two regions due to non-transparency of the solvent. Similar EPR spectral profiles and the comparable values of the distortion parameters calculated from the EPR data indicate that the nature and extent of distortions from the octahedral geometry are not very different in these complexes. Thus there is no significant change in the distortion pattern of the N_2O_4 coordination sphere around the low-spin ruthenium(III) centre due to protonation or deprotonation of the amide functionalities of the ligands. Earlier we reported a similar series of three high-spin iron(III) complexes with enolate-O, imine-N, and amide-O donor deprotonated acetylacetone benzoylhydrazone. It may be noted that unlike the present series of complexes, the variation of the protonation state of the amide functionalities changes the distortion pattern from rhombic to near-axial in the iron(III) complexes.[3b]

Description of Structures

The solid-state molecular structure of $[Ru(acs)(Hacs)]\cdot H_2O$ has been determined by X-ray crystallography. The complex crystallises in the *C*2/*c* space group. The structure of the complex molecule is depicted in Figure 2. The bond parameters associated with the metal centre are listed in Table 3. Each ligand binds the metal ion meridionally through the phenolate-O, the imine-N, and the amide-O atoms forming a six- and a five-membered chelate ring. Two ligands are related by a crystallographically imposed twofold axis of symmetry passing through Ru and bisecting the angles O1−Ru−O1′ and O2−Ru−O2′ (Figure 2). The presence of this twofold axis of symmetry indicates that two ligands are crystallographically equivalent. This could also indicate that both ligands are chemically equivalent. Taking into account the neutral character of the complex, this will be possible if the oxidation state of the metal centre is +2 and the ligands are monoanionic ($Hacs^-$). Considering the more acidic character of the phenolic-OH the amide functionality in each ligand has to be protonated. The second possibility is that the oxidation state of the metal centre is +4 and the ligands are dianionic (acs^{2-}). However, the physical properties (vide supra) of the complexes clearly

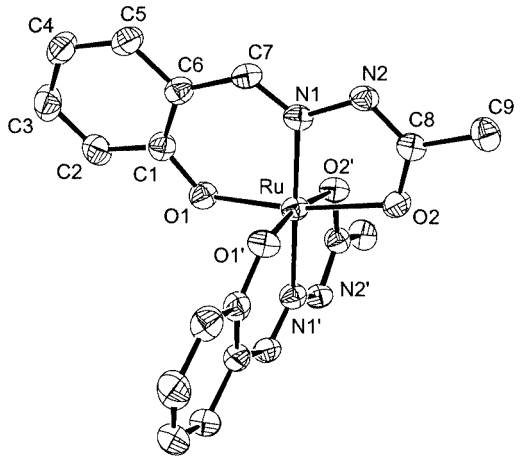

Figure 2. The structure of [Ru(acs)(Hacs)] showing the 35% probability thermal ellipsoids and the atom-labelling scheme; hydrogen atoms are omitted for clarity

Table 3. Selected bond lengths (Å), and angles (°) for $[Ru(acs)(Hacs)]\cdot H_2O$[a]

Ru−O(1)	1.961(2)	Ru−O(1)′	1.961(2)
Ru−N(1)	1.983(3)	Ru−N(1)′	1.983(3)
Ru−O(2)	2.063(2)	Ru−O(2)′	2.063(2)
O(1)−Ru−O(1)′	95.12(14)	O(1)−Ru−O(2)	169.57(9)
O(1)−Ru−O(2)′	90.46(11)	O(1)−Ru−N(1)	93.16(9)
O(1)−Ru−N(1)′	87.45(9)	O(1)′−Ru−O(2)	90.46(11)
O(1)′−Ru−O(2)′	169.57(9)	O(1)′−Ru−N(1)	87.45(9)
O(1)′−Ru−N(1)′	93.16(9)	O(2)−Ru−O(2)′	85.45(14)
O(2)−Ru−N(1)	78.27(10)	O(2)−Ru−N(1)′	101.06(9)
O(2)′−Ru−N(1)	101.06(9)	O(2)′−Ru−N(1)′	78.27(10)
N(1)−Ru−N(1)′	179.11(13)		

[a] Symmetry transformation used to generate equivalent atoms: $-x, y, -z + 1/2$.

 © 2003 Wiley-VCH Verlag GmbH & Co. KGaA, Weinheim

suggest a +3 oxidation state of the metal ion in all of the complexes. In addition, the observed (Table 3) Ru−O(phenolate) and Ru−N(imine) distances are similar to the distances reported for Ru^{III} complexes with ligands that provide the deprotonated salicylaldimine or similar moiety for metal ion binding.[9] The significantly shorter Ru−O(amide) distance compared to the distances observed in ruthenium(II) complexes[2] containing the same coordinating atom is also consistent with the +3 oxidation state of the metal ion. Thus the two ligands are not chemically equivalent, one of them is dianionic acs^{2-} and the other one is monoanionic $Hacs^{-}$. The origin of the crystallographic equivalence of the two ligands is therefore due to either a static disorder resulting from the crystallographic superposition of an equal number of $Hacs^{-}$ and acs^{2-}, or a dynamic disorder due to rapid (on the crystallographic time scale) H-atom transfer between the two amide-N centres. Rapid H-atom transfer in the solid state is highly unlikely to occur and hence the observed crystallographic equivalence of the two ligands can be attributed solely to a static disorder. The lattice water molecule is also similarly disordered and the O-atom sits at a special position with half occupancy. The distance (2.754 Å) between the amide-N atom (N2) and the water O-atom suggests an N−H···O hydrogen bonding interaction. Due to disorder the amide-N atoms of both ligands show the same interaction. In the crystal lattice, a one-dimensional chain of an alternating complex molecule and a water molecule is formed via this hydrogen bonding. The H_2O hydrogen atoms are also involved in inter-chain weak H-bonding interactions with the amide-O and phenolate-O atoms (O−H···O distances are 3.370 and 3.250 Å, respectively) forming a two-dimensional network of $[Ru(acs)(Hacs)]\cdot H_2O$ in the crystal lattice (Figure 3).

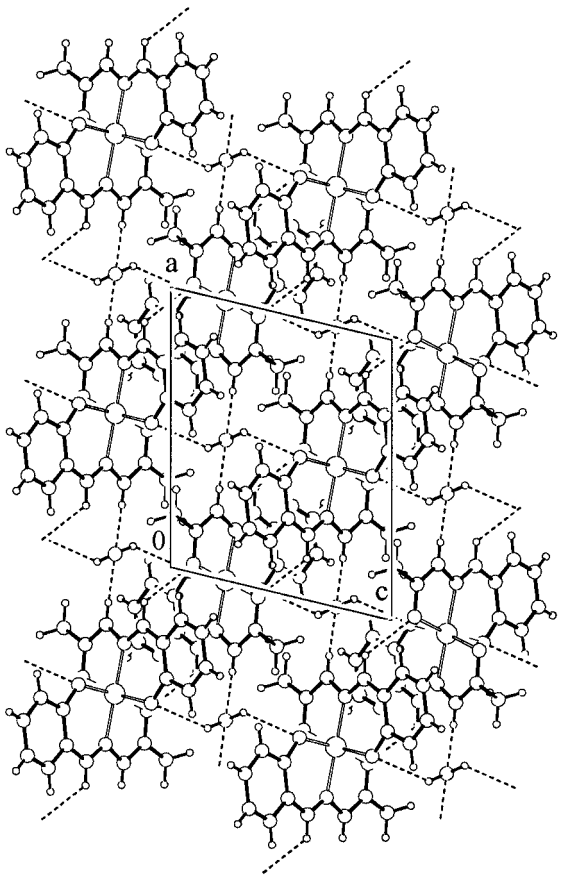

Figure 3. Two dimensional network of $[Ru(acs)(Hacs)]\cdot H_2O$ along *b* axis

We were unable to grow X-ray quality single crystals of $K[Ru(acs)_2]$. However, the tetraphenylphosphonium salt of $[Ru(acs)_2]^{-}$ crystallises in the $P\bar{1}$ space group. Single crystals of $[PPh_4][Ru(acs)_2]$ were obtained by the reaction of $K[Ru(acs)_2]$ and PPh_4Cl in acetonitrile followed by addition of toluene and slow evaporation of the mixture in air. The asymmetric unit contains a PPh_4^{+} cation, a complex anion $[Ru(acs)_2]^{-}$, and a toluene molecule that has been located at two sites. The structure of $[PPh_4][Ru(acs)_2]$ is shown in Figure 4 and selected bond parameters involving the metal centre are collected in Table 4. As in the previous structure the ligands bind the metal ion meridionally. The Ru−O(amide), Ru−O(phenolate) and Ru−N(imine) distances are typical for a ruthenium(III) species.[2,9] These distances clearly indicate that there is essentially no difference with respect to the binding strength of the two ligands. The dianionic nature of both ligands and hence the single negative charge on the complex and the +3 oxidation state of the metal ion are further confirmed by the presence of the PPh_4^{+} ion. The bond parameters of the cation are unexceptional.[10]

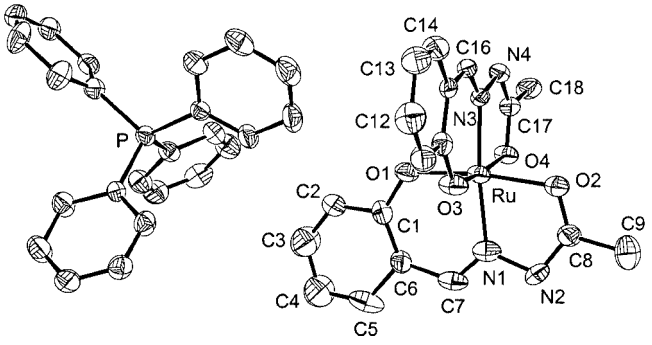

Figure 4. Structure of $[PPh_4][Ru(acs)_2]$ with the atom-labelling scheme; all atoms are represented by their 25% probability thermal ellipsoids; the labelling of the carbon atoms in the cation and hydrogen atoms are not shown for clarity

In contrast to $[Ru(acs)(Hacs)]\cdot H_2O$, there are no good, conventional hydrogen-bond acceptors or donors in $[PPh_4][Ru(acs)_2]\cdot C_6H_5CH_3$. However, this species also forms a two-dimensional network in the crystal lattice via several C−H···π interactions.[11] The H···centroid distances and the C−H···centroid angles are within the ranges 2.742−3.177 Å and 134.98−169.48°, respectively. The methyl group C-H, the aromatic C-H of the ligand and that of the phenyl groups of the cation are involved in these interactions with the π-electrons of the toluene, PPh_4^{+} phenyl groups, ligand phenolate ring and the chelate rings. A few of these interactions are depicted in Figure 5.

 © 2003 Wiley-VCH Verlag GmbH & Co. KGaA, Weinheim

Table 4. Selected bond lengths (Å), and angles (°) for $[PPh_4][Ru(acs)_2]\cdot C_6H_5CH_3$

Ru−O(1)	1.971(7)	Ru−O(2)	2.021(7)
Ru−O(3)	1.975(7)	Ru−O(4)	2.024(6)
Ru−N(1)	2.020(9)	Ru−N(3)	1.999(7)
O(1)−Ru−O(2)	171.7(3)	O(1)−Ru−O(3)	92.5(3)
O(1)−Ru−O(4)	90.4(3)	O(1)−Ru−N(1)	95.2(3)
O(1)−Ru−N(3)	90.9(3)	O(2)−Ru−O(3)	90.4(3)
O(2)−Ru−O(4)	87.7(3)	O(2)−Ru−N(1)	77.1(3)
O(2)−Ru−N(3)	96.6(3)	O(3)−Ru−O(4)	172.1(3)
O(3)−Ru−N(1)	87.8(3)	O(3)−Ru−N(3)	93.9(3)
O(4)−Ru−N(1)	99.3(3)	O(4)−Ru−N(3)	78.7(3)
N(1)−Ru−N(3)	173.6(4)		

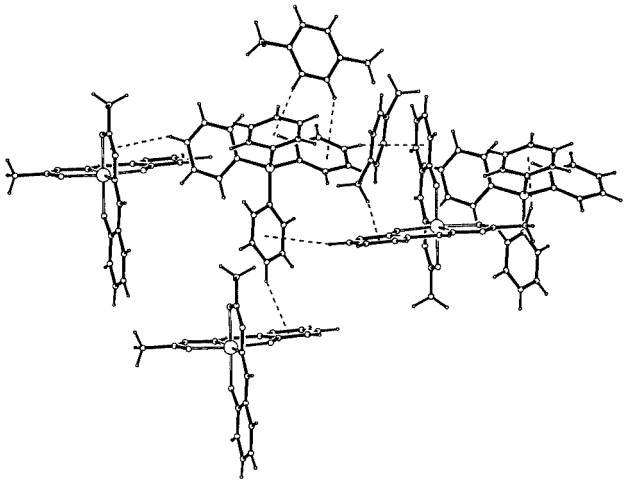

Figure 5. Various C−H···π interactions in the crystal lattice of $[PPh_4][Ru(acs)_2]\cdot C_6H_5CH_3$

Electrochemical Properties

Electron transfer properties of the complexes in acetonitrile/dimethylformamide (9:1) solutions (0.1 M TBAP) have been investigated with the help of cyclic voltammetry. Each of the three complexes displays an oxidation response on the anodic side of SCE (Figure 6). The one-electron stoichiometry for these oxidation processes is ascertained by comparing the current heights with known one-electron redox processes under identical conditions.[2,9a] The anionic complex $[Ru(acs)_2]^-$ has the lowest potential ($E_{1/2}$ = 0.56 V and ΔE_p = 70 mV)[12] and the cationic complex $[Ru(Hacs)_2]^+$ has the highest potential ($E_{1/2}$ = 0.84 V and ΔE_p = 150 mV). The potential ($E_{1/2}$ = 0.76 V and ΔE_p = 240 mV) for the neutral complex [Ru(acs)(Hacs)] is in between the above two values. The free Schiff base H_2acs shows an irreversible oxidation with comparatively much higher current at +1.38 V under identical conditions. Thus the oxidation responses observed for the complexes are assigned to the $Ru^{III} \rightarrow Ru^{IV}$ process. The trend in the $E_{1/2}$ values indicates that the oxidation of the metal centre in the anionic complex where the amide functionality for each of the two ligands is deprotonated, is most favourable, and that in the cationic complex where the amide functionalities are protonated, is most difficult. This behaviour is likely to be primarily due to electrostatic reasons.

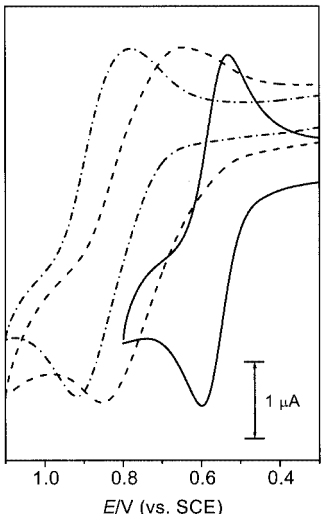

Figure 6. Cyclic voltammograms of $K[Ru(acs)_2]$ (−), $[Ru(acs)(Hacs)]\cdot H_2O$ (-----), and $[Ru(Hacs)_2]ClO_4$ (−·−·−) in acetonitrile/dimethylformamide (9:1) solvent mixture (0.1 M TBAP) at scan rates of 50 mV s^{-1}

On the cathodic side of the SCE, both $K[Ru(acs)_2]$ and [Ru(acs)(Hacs)] display a reduction response. The $E_{1/2}$ values are −1.11 V (ΔE_p = 80 mV) and −1.13 V (ΔE_p = 80 mV), respectively. In both cases, the anodic (i_{pa}) and cathodic (i_{pc}) peak currents are very similar to the current heights observed for the $Ru^{III} \rightarrow Ru^{IV}$ processes. On the other hand, $[Ru(Hacs)_2]ClO_4$ displays three reduction responses at $E_{1/2}$ = −0.20 V (ΔE_p = 100 mV), E_{pc} = −0.90 and −1.63 V. For the highest potential reduction i_{pc} is much larger than the i_{pa}. However, the i_{pc} is similar to that of the $Ru^{III} \rightarrow Ru^{IV}$ process. This first reduction response of $[Ru(Hacs)_2]ClO_4$ and the reduction responses observed for [Ru(acs)(Hacs)] and $K[Ru(acs)_2]$ may be assigned to the $Ru^{III} \rightarrow Ru^{II}$ process and the differences in the potential values can be rationalised considering the electrostatic effect. However, the trend in the reduction potential values is significantly different than that of the oxidation potential values. The reduction potentials observed for $K[Ru(acs)_2]$ (−1.11 V) and [Ru(acs)(Hacs)] (−1.13 V) are very similar and much lower than the first reduction potential (−0.20 V) observed for $[Ru(Hacs)_2]ClO_4$, whereas the $Ru^{III} \rightarrow Ru^{IV}$ potentials are observed in a comparatively smaller range (0.56−0.84 V). Under identical conditions, free perchloric acid also shows a reduction response ($E_{1/2}$ = −0.25 V, ΔE_p = 100 mV). This voltammogram is very similar to that of the first reduction displayed by $[Ru(Hacs)_2]ClO_4$. The free Schiff base (H_2acs) also displays a reduction response under the same conditions. E_{pc} and E_{pa} values for this reduction response are −1.37 and −0.96 V, respectively. Considering all the above, the reductions displayed by the present series of complexes cannot be assigned to the $Ru^{III} \rightarrow Ru^{II}$ process unambiguously.

Protonation and Deprotonation of Coordinated Amide

Spectrophotometric titrations have been performed using acetonitrile solutions of $K[Ru(acs)_2]$ and CF_3SO_3H to study

 © 2003 Wiley-VCH Verlag GmbH & Co. KGaA, Weinheim

the protonation behaviour of the coordinated amide functionalities in the complex. With the progressive addition of the acid the change of spectral profiles is characteristic of successive protonation of the two amide functionalities present in the two acs^{2-} ligands of $K[Ru(acs)_2]$.[2,13] The initial change in the spectral profile gradually decreases and becomes a minimum when the complex/acid mol ratio reaches 1:1.2. At this stage the spectral profile is akin to that of the neutral complex [Ru(acs)(Hacs)] indicating the protonation of the first ligand amide functionality. In this portion of the titration, the shift of band positions occurs through eight isosbestic points (455, 378, 361, 284, 250, 242, 222, and 207 nm) (Figure 7a). Continued addition of the acid causes a further shift of band positions through another set of five isosbestic points (584, 344, 374, 299, and 263 nm) (Figure 7b). The spectral profile becomes constant and similar to that of $[Ru(Hacs)_2]^+$ at a complex/acid molar ratio of about 1:2.6. Quantitative reversibility of this protonation

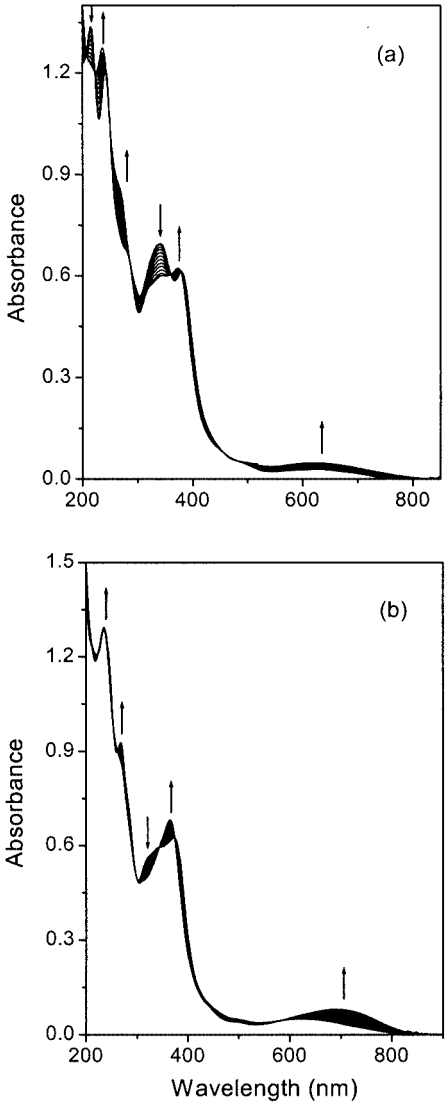

Figure 7. Spectrophotometric titration of $K[Ru(acs)_2]$ in acetonitrile with CF_3SO_3H; (a) first segment and (b) second segment of the titration (see text)

behaviour was confirmed by spectrophotometric back-titration with triethylamine. The values of pK_{a1} and pK_{a2} determined from the two segments of the titration are 6.64(4) and 7.19(1), respectively. These values are much lower than the pK_a ($\approx$15) of the free amide functionality in organic compounds.[14] This difference in the pK_a values is likely to be due to a combination of several factors. Among various explanations one possibility could be the following: the electron deficiency at the imine-N adjacent to the amide-N arising out of coordination of the former to the metal centre is compensated by the amide functionality and thereby contributes to the increase of the amide N−H acidity.[2,15] Interestingly the pK_a values determined in this work are very similar to those [pK_{a1} = 6.85(5) and pK_{a2} = 7.44(9)] determined for the ruthenium(II) complex, $[RuL_2]$, where HL is *N*-(benzoyl)-*N*′-(picolinylidene)hydrazine.[2] It seems there is no effect of the difference in the oxidation states (+3 and +2) on the acidities of the ligand amide functionalities. However, there are two very distinct dissimilarities between the two systems. In the ruthenium(II) complex, after protonation the amide functionalities are no longer bound to the metal centre which is not the case for the present complexes of acs^{2-} and $Hacs^-$ (vide supra). The ligand L^- is a pyridine-N, imine-N, and deprotonated amide-O donor whereas acs^{2-} is a phenolate-O, imine-N, and deprotonated amide-O donor. Perhaps these dissimilarities offset the effect of oxidation state on the acidity of ligand amide functionalities and similar pK_a values are observed for both systems.

Conclusion

In this article, syntheses and physical properties of three new ruthenium(III) complexes with *N*-(acetyl)-*N*′-(salicylidene)hydrazine (H_2acs) have been described. The bis complexes vary in the protonation state of the amide functionality of the ligands. The crystal structures of [Ru(acs)(Hacs)] and $[Ru(acs)_2]^-$ reveal the meridionally spanning phenolate-O, imine-N and amide-O coordinating mode of both $Hacs^-$ and acs^{2-}. In frozen solutions, all the three complexes display the typical rhombic EPR spectra for low-spin ruthenium(III) species, indicating no significant variation in the distortion pattern from octahedral symmetry of the N_2O_4 coordination spheres around the metal centre due to protonation or deprotonation of the amide functionalities. However, the potentials of the $Ru^{III} \rightarrow Ru^{IV}$ oxidation are markedly affected by the protonation state of the amide functionalities. Reversible protonation and deprotonation of the O-coordinating amide functionalities present in the ligands have been demonstrated.

Experimental Section

Materials: The Schiff base H_2acs[3a] and *cis*-$[RuCl_2(dmso)_4]$[16] were prepared by following reported procedures. All other chemicals and

 © 2003 Wiley-VCH Verlag GmbH & Co. KGaA, Weinheim

solvents were of commercially available analytical grade and were used as received.

Physical Measurements: Elemental (C, H, N) analysis data were obtained with a Perkin−Elmer Model 240C elemental analyzer. Infrared spectra were collected by using KBr pellets on a Jasco-5300 FT-IR spectrophotometer. A Shimadzu 3101-PC UV/Vis/NIR spectrophotometer was used to record the electronic spectra. Room temperature solid-state magnetic susceptibilities were measured by using a Sherwood Scientific magnetic susceptibility balance. Diamagnetic corrections calculated from Pascal's constants[17] were used to obtain the molar paramagnetic susceptibilities. EPR spectra were recorded on a Jeol JES-FA200 spectrometer. Solution electrical conductivities were measured with a Digisun DI-909 conductivity meter. A CH-Instruments model 620A electrochemical analyzer was used for cyclic voltammetric experiments with acetonitrile/dimethylformamide (9:1) solutions of the complexes containing $[(n\text{-}C_4H_9)_4N]ClO_4$ (TBAP) as supporting electrolyte. The three-electrode measurements were carried out at 298 K under a dinitrogen atmosphere with a platinum disk working electrode, a platinum wire auxiliary electrode and a saturated calomel reference electrode (SCE). The potentials reported in this work are uncorrected for junction contributions.

Synthesis of the Ruthenium Complexes

[Ru(acs)(Hacs)]·H_2O: Solid *cis*-$[RuCl_2(dmso)_4]$ (242 mg, 0.5 mmol) was added to a methanol solution (40 mL) of H_2acs (178 mg, 1 mmol) and KOH (56 mg, 1 mmol). The mixture was heated under reflux for 8 h. The hot brown solution was cooled to room temperature and left in air for 5 h. The colour of the solution changed to green and the complex was precipitated as a dark green solid. It was collected by filtration, washed with methanol followed by diethyl ether and finally dried in air. The yield was 95 mg (40%). Single crystals suitable for X-ray structure determination were obtained by storing the filtrate at 5 °C for about 3−4 days.

[Ru(Hacs)$_2$]ClO_4: A methanol solution (10 mL) of 70% aqueous $HClO_4$ (0.2 mL) was prepared. To a suspension of [Ru(acs)(Hacs)]·H_2O (118 mg, 0.25 mmol) in 25 mL methanol 1 mL of the above $HClO_4$ solution was added and the mixture was magnetically stirred in air. Initially a clear green solution was obtained and after about 1/2 h a green solid separated. The complex thus obtained was collected by filtration, washed with diethyl ether and dried in air. The isolated yield was 70 mg (49%).

K[Ru(Hacs)$_2$]: [Ru(acs)(Hacs)]·H_2O (150 mg, 0.32 mmol) was dissolved in 50 mL of methanol and KOH (18 mg, 0.32 mmol) was added to the suspension. The mixture was magnetically stirred in air for 6 h. The green solution thus obtained was filtered to remove any unreacted starting complex and the filtrate was evaporated to about ca. 4−5 mL in vacuo. The green solid obtained was collected by filtration, washed with diethyl ether and dried in air. The yield obtained by this procedure was 120 mg (76%).

Spectrophotometric Titration: In a typical titration, a 3 mL aliquot of a stock solution of K[Ru(acs)$_2$] in acetonitrile {3.74×10^{-5} M, prepared by dissolving 1.84 mg (3.74 μmol) of K[Ru(acs)$_2$] in 10 mL of acetonitrile and then diluting 1 mL of this solution to 10 mL by adding the same solvent} was placed in an air-tight cuvette. Protonation of K[Ru(acs)$_2$] was performed by addition of aliquots (1 μL) of an acetonitrile solution of CF_3SO_3H [1.13×10^{-2} M, prepared by dissolving 0.5 mL (5.65 mmol) in 10 mL of acetonitrile and then diluting 0.2 mL of this solution to 10 mL by adding the same solvent] with a gas-tight syringe. Protonation was considered complete when no significant change of the electronic spectrum was observed by further addition of CF_3SO_3H solution. The effective pK_{ai} (i = 1 and 2) values were determined from the two segments (Figure 7a for pK_{a2} and Figure 7b for pK_{a1}) of the spectrophotometric titration curves using Equations (1)−(3).[2,18] The value of $K_a(CF_3SO_3H)$ in acetonitrile used to calculate the pK_{ai} values is 2.512×10^{-3}.[19] The change in absorbance at 364 nm and that at 340 nm were used to calculate K_{c1} and K_{c2}, respectively.

$$K_{ai} = K_a(CF_3SO_3H)/K_{ci} \quad (1)$$

$$K_{c1} = [Ru(Hacs)_2^+][CF_3SO_3^-]/[Ru(acs)(Hacs)][CF_3SO_3H] \quad (2)$$

$$K_{c2} = [Ru(acs)(Hacs)][CF_3SO_3^-]/[Ru(acs)_2^-][CF_3SO_3H] \quad (3)$$

Table 5. Crystallographic data

Compound	[Ru(acs)(Hacs)]·H_2O	[PPh_4][Ru(acs)$_2$]·$C_6H_5CH_3$
Empirical formula	$RuC_{18}H_{19}N_4O_5$	$RuPC_{49}H_{44}N_4O_4$
Crystal system	monoclinic	triclinic
Space group	*C*2/*c*	$P\bar{1}$
a (Å)	10.789(3)	11.910(3)
b (Å)	19.872(2)	13.437(3)
c (Å)	8.768(2)	15.227(7)
α (°)	90	91.93(3)
β (°)	103.46(3)	109.650(19)
γ (°)	90	106.50(3)
V (Å^3)	1828.2(7)	2177.7(12)
Z	4	2
$D_{calcd.}$ (g cm^{-3})	1.716	1.350
μ (mm^{-1})	0.897	0.445
Reflections collected	4178	7617
Reflections unique	4020	7617
Reflections [$I > 2\sigma(I)$]	3267	3819
Parameters	131	535
*R*1, *wR*2 [$I > 2\sigma(I)$]	0.0545, 0.1394	0.0840, 0.1913
Goodness-of-fit on F^2	1.083	1.022
Largest peak, hole [e·Å^{-3}]	1.487, −1.989	0.850, −0.361

 © 2003 Wiley-VCH Verlag GmbH & Co. KGaA, Weinheim

X-ray Crystallography: X-ray data for crystals of both [Ru(acs)(Hacs)]·H_2O and [PPh_4][Ru(acs)$_2$]·$C_6H_5CH_3$ were collected on an Enraf−Nonius Mach-3 single crystal diffractometer using graphite monochromated Mo-K_α radiation (λ = 0.71073 Å) by ω-scan method at 298 K. In each case, unit-cell parameters were determined by least-squares fit of 25 reflections having 2θ values in the range 10−22°. Intensities of three check reflections were measured after every 1.5 h during the data collection to monitor the crystal stability. In both cases, there was no significant change in the intensities of the check reflections. Empirical absorption corrections were applied to both datasets based on the ψ-scans.[20] The structures were solved by direct methods and refined on F^2 by full-matrix least-squares procedures. In each case, the asymmetric unit contains one molecule of the complex and one solvent molecule. All non-hydrogen atoms having full occupancy were refined using anisotropic thermal parameters. For both molecules the methyl group H-atoms and the aromatic H-atoms were placed geometrically by using a riding model. In the case of [Ru(acs)(Hacs)]·H_2O, H-atoms attached to the water oxygen atom and the amide nitrogen atom were located in a difference map. For both structures all the H-atoms were included in the structure factor calculation at idealised positions [with U_{iso}(methyl-H) = 1.5U_{eq}(C), U_{iso}(aromatic-H) = 1.2U_{eq}(C), U_{iso}(water-H) = 1.5U_{eq}(O), and U_{iso}(amide-H) = 1.2U_{eq}(N)], but not refined. The programs of WinGX[21] were used for data reduction and absorption correction. Structure solution and refinement were performed with the SHELXL-97 programs.[22] The Ortex6a[23] and Platon98[24] packages were used for molecular graphics. Selected crystal and refinement data are listed in Table 5.

CCDC-208845 for [Ru(acs)(Hacs)]·H_2O and CCDC-208846 for [PPh_4][Ru(acs)$_2$]·$C_6H_5CH_3$ contain the supplementary crystallographic data for this paper. These data can be obtained free of charge at www.ccdc.cam.ac.uk/conts/retrieving.html [or from the Cambridge Crystallographic Data Centre, 12, Union Road, Cambridge CB2 1EZ, UK; Fax: (internat.) +44-1223/336-033; E-mail: deposit@ccdc.cam.ac.uk].

Acknowledgments

Financial assistance for this work was provided by the Department of Science and Technology (DST), New Delhi (Grant No. SP/S1/F23/99). X-ray crystallographic studies were performed at the National Single Crystal Diffractometer Facility, School of Chemistry, University of Hyderabad (funded by the DST). We thank the University Grants Commission, New Delhi for the facilities provided under the Universities with potential for excellence program. Mr. Satyanarayan Pal thanks the Council of Scientific and Industrial Research, New Delhi for a research fellowship.

[1] [1a] E. A. Seddon, K. R. Seddon, *The Chemistry of Ruthenium*, Elsevier, New York, **1984**. [1b] G. Wilkinson, R. D. Gillard, J. A. McCleverty, *Comprehensive Coordination Chemistry*, Pergamon, Oxford, **1987**, *4*, 277. [1c] B. K. Ghosh, A. Chakravorty, *Coord. Chem. Rev.* **1989**, *95*, 239. [1d] A. B. P. Lever, H. Masui, R. A. Metcalfe, D. J. Stufkens, E. S. Dodsworth, P. R. Auburn, *Coord. Chem. Rev.* **1993**, *125*, 317. [1e] V. Balzani, A. Juris, M. Venturi, S. Campagna, S. Serroni, *Chem. Rev.* **1996**, *96*, 759. [1f] S.-M. Lee, W.-T. Wong, *Coord. Chem. Rev.* **1997**, *164*, 415. [1g] L. De Cola, P. Belser, *Coord. Chem. Rev.* **1998**, *177*, 301. [1h] D. B. Grotjahn, *Coord. Chem. Rev.* **1999**, *190−192*, 1125. [1i] K. Szaciowski, W. Macyk, G. Stochel, Z. Stasicka, S. Sostero, O. Traverso, *Coord. Chem. Rev.* **2000**, *208*, 277. [1j] B.-Z. Shan, Q. Zhao, N. Goswami, D. M. Eichhorn, D. P. Rillema, *Coord. Chem. Rev.* **2001**, *211*, 117. [1k] M. J. Clarke, *Coord. Chem. Rev.* **2002**, *232*, 69. [1l] L. Sun, L. Hammarström, B. Åkermark, S. Styring, *Chem. Soc. Rev.* **2001**, *30*, 36. [1m] P. D. Beer, *Acc. Chem. Res.* **1998**, *31*, 71. [1n] N. Sardesai, S. C. Lin, K. Zimmermann, J. K. Barton, *Bioconjugate Chem.* **1995**, *6*, 302. [1o] H. B. Grey, J. R. Winkler, *Annu. Rev. Biochem.* **1996**, *65*, 537. [1p] P. Lincoln, E. Tuite, B. Nordén, *J. Am. Chem. Soc.* **1997**, *119*, 1454. [1q] S. Goswami, A. R. Chakravarty, A. Chakravorty, *J. Chem. Soc., Chem. Commun.* **1982**, 1288. [1r] J. A. Gilbert, D. S. Eggleston, W. R. Murphy, Jr., D. A. Geselowitz, S. W. Gersten, D. J. Hodgson, T. J. Meyer, *J. Am. Chem. Soc.* **1985**, *107*, 3855. [1s] C.-M. Che, *Pure Appl. Chem.* **1995**, *67*, 225. [1t] T. Naota, H. Takaya, S.-I. Murahashi, *Chem. Rev.* **1998**, *98*, 2599.

[2] S. N. Pal, S. Pal, *J. Chem. Soc., Dalton Trans.* **2002**, 2102.

[3] [3a] S. C. Chan, L. L. Koh, P. -H. Leung, J. D. Ranford, K. Y. Sim, *Inorg. Chim. Acta* **1995**, *236*, 101. [3b] N. R. Sangeetha, C. K. Pal, P. Ghosh, S. Pal, *J. Chem. Soc., Dalton Trans.* **1996**, 3293. [3c] S. P. Rath, S. Mondal, A. Chakravorty, *Inorg. Chim. Acta* **1997**, *263*, 247. [3d] N. R. Sangeetha, S. Pal, *Bull. Chem. Soc. Jpn.* **2000**, *73*, 357. [3e] M. R. Maurya, S. Khurana, C. Schulzke, D. Rehder, *Eur. J. Inorg. Chem.* **2001**, 779.

[4] [4a] D. W. Margerum, *Pure Appl. Chem.* **1983**, *55*, 23. [4b] K. L. Kotska, B. G. Fox, M. P. Hendrich, T. J. Collins, C. E. Pickard, L. J. Wright, E. Münck, *J. Am. Chem. Soc.* **1993**, *115*, 6746. [4c] M. Mikuriya, D. Jie, Y. Kakuta, T. Tokii, *Bull. Chem. Soc. Jpn.* **1993**, *66*, 1132.

[5] W. J. Geary, *Coord. Chem. Rev.* **1971**, *7*, 81.

[6] [6a] R. M. Silverstein, F. X. Webster, *Spectrometric Identification of Organic Compounds*, Wiley, New York, **1998**, 6th ed., p 101. [6b] K. Nakamoto, *Infrared and Raman Spectra of Inorganic and Coordination Compounds*, Wiley, New York, **1986**, 4th ed., p 228.

[7] F. Basuli, A. K. Das, G. Mostafa, S.-M. Peng, S. Bhattacharya, *Polyhedron* **2000**, *19*, 1663.

[8] [8a] B. Bleany, M. C. M. O'Brien, *Proc. Phys. Soc., London, Sect. B* **1956**, *69*, 1216. [8b] J. S. Griffith, *The Theory of Transition Metal Ions*, Cambridge University Press, London, **1961**, p. 364. [8c] S. Bhattacharya, A. Chakravorty, *Proc. Indian Acad. Sci. (Chem. Sci.)* **1985**, *95*, 159.

[9] [9a] S. N. Pal, S. Pal, *Inorg. Chem.* **2001**, *40*, 4807. [9b] A. K. Das, S. -M. Peng, S. Bhattacharya, *J. Chem. Soc., Dalton Trans.* **2000**, 181. [9c] B. Mondal, S. Chakraborty, P. Munshi, M. G. Walawalkar, G. K. Lahiri, *J. Chem. Soc., Dalton Trans.* **2000**, 2327. [9d] K. Nakajima, Y. Ando, H. Mano, M. Kojima, *Inorg. Chim. Acta* **1998**, *274*, 184. [9e] S. Pattanayak, K. Pramanik, N. Bag, P. Ghosh, A. Chakravorty, *Polyhedron* **1997**, *16*, 2951.

[10] H. Miyasaka, H.-C. Chang, K. Mochizuki, S. Kitagawa, *Inorg. Chem.* **2001**, *40*, 3544.

[11] [11a] M. Nishio, Y. Umezawa, M. Hirota, Y. Takeuchi, *Tetrahedron* **1995**, *51*, 8665. [11b] K. S. B. Hancock, J. W. Steed, *Chem. Commun.* **1998**, 1409. [11c] K. Biradha, M. J. Zaworotko, *J. Am. Chem. Soc.* **1998**, *120*, 6431.

[12] $E_{1/2}$ = (E_{pa} + E_{pc})/2, ΔE_p = E_{pa} − E_{pc} where E_{pa} and E_{pc} are anodic and cathodic peak potentials. Scan rate is 50 mVs^{-1}.

[13] [13a] C. Long, J. G. Vos, *Inorg. Chim. Acta* **1984**, *89*, 125. [13b] S. Baitalik, U. Flörke, K. Nag, *Inorg. Chem.* **1999**, *38*, 3296.

[14] D. D. Perrin, B. Dempsey, E. P. Serjeant, *pK_a Prediction for Organic Acids and Bases, Chapman and Hall, London and New York,* **1981**.

[15] B. Mondal, S. Chakraborty, P. Munshi, M. G. Walawalkar, G. K. Lahiri, *J. Chem. Soc., Dalton Trans.* **2000**, 2327.

 © 2003 Wiley-VCH Verlag GmbH & Co. KGaA, Weinheim

[16] I. P. Evans, A. Spencer, G. Wilkinson, *J. Chem. Soc., Dalton Trans.* **1973**, 204.
[17] W. E. Hatfield, *Theory and Applications of Molecular Paramagnetism* (Eds.: E. A. Boudreaux, L. N. Mulay), Wiley, New York, **1976**, p. 491.
[18] C. E. Dubé, D. W. Wright, S. Pal, P. J. Bonitatebus, Jr., W. H. Armstrong, *J. Am. Chem. Soc.* **1998**, *120*, 3704.
[19] K. Izutsu, *Acid-Base Dissociation Constants in Dipolar Aprotic Solvents*, Blackwell, Oxford, **1990**, p. 28.
[20] A. C. T. North, D. C. Philips, F. S. Mathews, *Acta Crystallogr., Sect. A* **1968**, *24*, 351.
[21] L. J. Farrugia, *J. Appl. Crystallogr.* **1999**, *32*, 837.
[22] G. M. Sheldrick, *SHELXL-97, Programs for Structure Determination and Refinement*, University of Göttingen, Göttingen, Germany.
[23] P. McArdle, *J. Appl. Crystallogr.* **1995**, *28*, 65.
[24] A. L. Spek, *Platon98, Molecular Graphics Software*, University of Glasgow, UK, **1998**.

Received April 23, 2003
Early View Article
Published Online October 2, 2003

 © 2003 Wiley-VCH Verlag GmbH & Co. KGaA, Weinheim

Synthesis, Crystal Structure, Thermal Analysis and Magnetic Behavior of a Novel One-Dimensional Polymeric Pyridinium Chlorocuprate(II): $(Hpy)_2[Cu_3Cl_8(H_2O)_2]$

Rahul Bhattacharya,[a] Ashutosh Ghosh,*[a] Mau Sinha Ray,[a] Lara Righi,[b] Gabriele Bocelli,[b] Siddhartha Chaudhuri,[c] Roger D. Willett,[d] Juan M. Clemente-Juan,[e] Eugenio Coronado,[e] and Carlos J. Goméz-Garcia[e]

Keywords: Coordination polymers / Copper / Magnetic properties / N ligands / X-ray crystallography

A one-dimensional polymeric pyridinium chlorocuprate $(HPy)_2[Cu_3Cl_8(H_2O)_2]$, an intermediate between $(HPy)CuCl_3$ and $CuCl_2{\cdot}2H_2O$, has been synthesized and characterized by X-ray analysis [monoclinic, $P2_1/c$, a = 7.8950(10), b = 14.144(2), c = 9.921(10) Å, β = 99.20(2)°]. The structure contains $[Cu_3Cl_8(H_2O)_2]_n^{2n-}$ chains in which both square-pyramidal and octahedral Cu^{II} exist. The chains are composed of linked $[Cu_2Cl_6]^{2-}$ dimers and $CuCl_2(H_2O)_2$ monomeric units. On being heated in the solid state the compound undergoes dehydration followed by dehydrohalogenation to produce a pyridine complex of Cu^{II}: $[Cu_3Py_2Cl_6]$. Other compounds, $(HPy)_2[CuCl_4]$, $CuPyCl_2$ and $CuPy_2Cl_2$, also produce $[Cu_3Py_2Cl_6]$ as an intermediate on thermal analysis. Magnetic studies reveal ferromagnetic coupling within the chains with an intradimer exchange coupling of 12.1 cm^{-1} and a dimer-monomer exchange coupling of 1.34 cm^{-1}.
(© Wiley-VCH Verlag GmbH & Co. KGaA, 69451 Weinheim, Germany, 2003)

Introduction

The structural properties of chlorocuprates continue to be of interest, because of a wide variety of stereochemical features as well as unexpected oligomeric species.[1,2] However, most complexes for which structures have so far been reported contain copper atoms with a single coordination geometry, both in polymeric and in monomeric chlorocuprates.[3−7] Distorted octahedral, square-pyramidal, and trigonal-bipyramidal geometries of copper are known in polymeric chlorocuprates, whereas square-planar, square-pyramidal, and distorted tetrahedral anions have been reported with the monomeric $CuCl_{n+2}^{n-}$ complexes.[8−10] Among the hydrated chlorocuprates, the $CuCl_3(H_2O)^-$ species provides a novel intermediate between $CuCl_2(H_2O)_2$ and the $[CuCl_4]^{2-}$ anion.[11] On the other hand, the complexation of $CuCl_2{\cdot}2H_2O$ with pyridine and its derivatives has been studied extensively and the copper atoms in those complexes exhibit interesting structures.[12] With 2-picoline *N*-oxide it is found that $CuCl_2$ (when mixed in exactly 1:1 stoichiometric ratio) does not produce the expected 1:1 complex; instead a complex with empirical formula $Cu_3Cl_6(C_6H_7NO)_2{\cdot}2H_2O$ results, in which two types of copper atoms are present, one in an octahedral environment and the other in a square-pyramidal one. Here we report the synthesis, structure, and magnetic properties of the first example of a one-dimensional polymeric chain of hydrated chlorocuprates containing both hexa- and pentacoordinate copper atoms and possessing the empirical formula $(HPy)_2[Cu_3Cl_8(H_2O)_2]$, which can be regarded as a novel intermediate between $CuCl_2{\cdot}2H_2O$ and $(HPy)CuCl_3$, together with the solid-state synthesis of a new pyridine complex of Cu^{II}, $\{[Cu_3Py_2Cl_6]\}$, by thermal analysis.

Results and Discussion

The general method for the preparation of trichlorocuprates with cations of organic bases is to mix solutions containing the copper compound and a 1:1 molar ratios of the respective base acidified with HCl in aqueous or ethanolic medium. In the current case, however, the expected compound, $(HPy)CuCl_3$, is not produced by this method; instead a complex with empirical formula $(HPy)_2[Cu_3Cl_8(H_2O)_2]$ results. All attempts to prepare $(HPy)CuCl_3$ by changing the acidity of the solution and the ratio of pyridine:$CuCl_2{\cdot}2H_2O$ were unsuccessful.

[a] Department of Chemistry, University College of Science and Technology, University of Calcutta,
92, A. P. C. Road, 700 009 Kolkata, India
E-mail: ghosh_59@yahoo.com
[b] Centro di Studio per la Strutturistica Diffratometrica del CNR, 43100 Parma, Italy
[c] R.S.I.C, Bose Institute,
700 009 Kolkata, India
[d] Department of Chemistry, Washington State University, Pullman, WA 99164, USA
[e] Instituto de Ciencia Molecular, Universidad de Valencia, Dr. Moliner 50, 46100 Burjasot (Valencia), Spain

Description of the Structure of $(Hpy)_2[Cu_3Cl_8(H_2O)_2]$ (1): An ORTEP view of the complex **1** is shown in Figure 1. The complex consists of one-dimensional infinite chains that run parallel to the *c*-axis. These chains contain both six-coordinate (elongated octahedral) and five-coordinate (elongated square-pyramidal) copper ions bridged by the chlorine atoms. The six-coordinate copper ion (Cu1) is located on a center of inversion and bridged to two adjacent copper ions (Cu2) by pairs of chloride ions (Cl1, Cl2) and their inversion-related chloride ions. Two water molecules complete the distorted octahedral coordination around Cu1. Each five-coordinate copper ion (Cu2) is bridged to another five-coordinate copper ion by a pair of chloride ions (Cl4 and its inversion-related counterpart) with a center of symmetry between the pairs of Cu2 ions. Each Cu2 ion is bridged asymmetrically to Cu1 by two chloride ions. A non-bridging chloride ion (Cl3) occupies the fifth coordination site. The symmetry about the pentacoordinate copper ion (Cu2) is that of a square pyramid, with the three bridging chlorine atoms Cl2, Cl4, and Cl4 ($-x + 1$, $-y$, $-z$), and the non-bridging chlorine atom Cl3 forming the base of the pyramid and a bridging chlorine atom (Cl1) at the apex. The basal Cu−Cl distances lie in the 2.2681(8) to 2.3125(7) Å range and the apical Cu−Cl distance is 2.6770(8) Å (Table 1). The least-squares plane through Cl2, Cl3, Cl4, and Cl4($-x + 1$, $-y$, $-z$) is slightly puckered, with a maximum deviation of ±0.1447(8) Å for the two symmetry-related Cl4 atoms. The Cu2 atom is 0.2479(3) Å out of plane in the direction of the apex. The bond from the Cu2 ion to the chlorine atom Cl1 makes an angle of 88.9° with the basal plane. In the case of the hexacoordinate copper atom Cu1, the two chlorine atoms [Cl1 and Cl1($-x + 1$, $-y$, $-z - 1$)] and the two oxygen atoms [O and O($-x + 1$, $-y$, $-z - 1$)] define a perfect plane, since they lie on a center of symmetry. The apical chlorine atoms [Cl2 and Cl2 ($-x + 1$, $-y$, $-z - 1$)] on either side lie at a Cu−Cl distance of 2.8763(8) Å from the base plane. The compound, $(HPy)_2[Cu_3Cl_8(H_2O)_2]$, thus consists of $Cu_2Cl_6^{2-}$ dimers bridged by $CuCl_2{\cdot}2H_2O$ groups through two chlorine atoms, one from each unit, to form infinite chains. In other words, it can be regarded as an intermediate between $CuCl_2{\cdot}2H_2O$ and $CuCl_3^-$, since, of the three molecules of $CuCl_2{\cdot}2H_2O$, two form the dimeric trichlorocuprate anions $Cu_2Cl_6^{2-}$, while the third remains as a monomeric $CuCl_2{\cdot}2H_2O$ species. To the best of our knowledge, no chlorocuprate possessing this composition and structure has been reported to date. On the other hand, the structure of the 2-picoline *N*-oxide complex of Cu^{II}, $[Cu_3Cl_6(C_6H_7NO)_2]{\cdot}2H_2O$, is similar to that of the current complex.[12] It also consists of infinite chains containing both square-pyramidal five-coordinate and distorted octahedral six-coordinate copper ions. The only difference is that the two square-pyramidal copper ions are bridged by the oxygen atoms of two 2-picoline *N*-oxide ligands instead of the chloride ions in the present case.

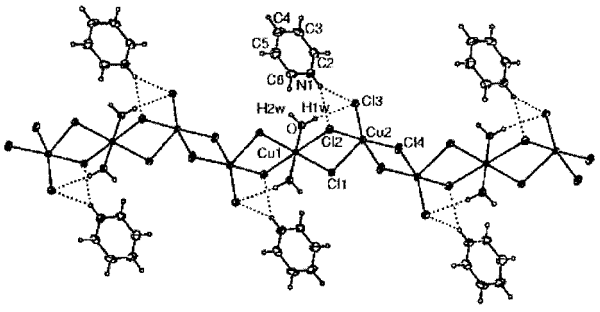

Figure 1. ORTEP drawing of the complex **1** with the atom numbering scheme; the bonds shown by dashed lines indicate hydrogen bonds; thermal ellipsoids shown at 50% probability

Table 1. Bond lengths (Å) and angles (°) with e.s.d.s in parentheses for $(HPy)_2[Cu_3Cl_8(H_2O)_2]$

Cu(1)−O	1.978(2)
Cu(1)−Cl(2)	2.8763(8)
Cu(2)−Cl(2)	2.2681(8)
Cu(2)−Cl(4)	2.2952(8)
O−Cu(1)−Cl(1)	88.78(6)
O−Cu(1)−Cl(2)	93.90(7)
Cl(1)−Cu(1)−Cl(2)	84.00(3)
Cl(2)−Cu(2)−Cl(3)	91.43(2)
Cl(2)−Cu(2)−Cl(4)	172.80(3)
Cl(3)−Cu(2)−Cl(4)	90.77(2)
Cl(2)−Cu(2)−Cl(4)[a]	91.30(3)
Cl(3)−Cu(2)−Cl(4)[a]	160.76(3)
Cl(4)−Cu(2)−Cl(4)[a]	84.40(3)
Cl(2)−Cu(2)−Cl(1)	89.01(2)
Cl(3)−Cu(2)−Cl(1)	100.28(3)
Cl(4)−Cu(2)−Cl(1)	97.33(3)
Cl(1)−Cu(2)−Cl(4)[a]	98.80(3)
Cu(1)−Cl(2)−Cu(2)	87.97(3)
Cu(1)−Cl(1)−Cu(2)	92.78(3)
Cu(2)−Cl(4)−Cu(2)[a]	95.60(4)
Cu(1)−Cl(1)	2.2801(7)
Cu(2)−Cl(1)	2.6770(8)
Cu(2)−Cl(3)	2.2940(7)
Cu(2)−Cl(4)[a]	2.3125(7)

[a] Symmetry transformation used to generate equivalent atoms: $-x + 1$, $-y$, $-z$.

The crystal structure is stabilized by an extensive network of hydrogen bonds, with the Cl3 atom playing a key role, and also by stacking interactions (Figure 2, and Figure 3, Table 2). The Cl3 atom is the acceptor of two O−H···Cl hydrogen bonds, one from a water molecule of its own chain and the other from a water molecule of an adjacent chain related by a c glide plane. The pyridinium nitrogen atom is involved in a pair of bifurcated N−H···Cl hydrogen bonds with the Cl2 and Cl3 atoms of a polymeric chain acting as acceptors. The Cl3 atom thus accepts three hydrogen bonds: two from water molecules and one from a pyridinium ion. This is a good example of the principle of charge compensation that has been used to interpret the structures of copper(II) halides, in which the negatively charged halide ions compete for electrostatic interactions with the Cu^{II} ions and hydrogen bonding with the organoammonium ions.[13] It can also be observed that the pyridinium rings

 © 2003 Wiley-VCH Verlag GmbH & Co. KGaA, Weinheim

are stacked with the shortest distance between the centroids of two adjacent rings being 4.998(2) Å while the shortest perpendicular distance between the rings is 3.421 Å. This indicates a strong π-π interaction between the aromatic pyridinium moieties.

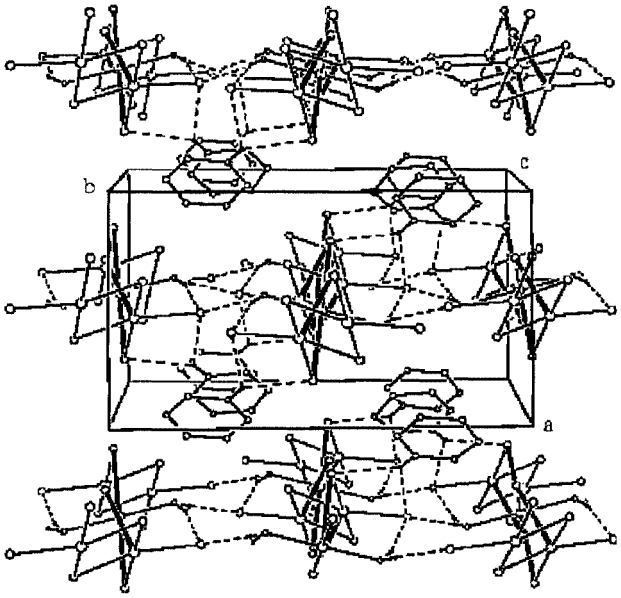

Figure 2. Crystal packing arrangement showing hydrogen bonding scheme and the stacking of pyridinium moieties; the dashed lines indicate hydrogen bonds

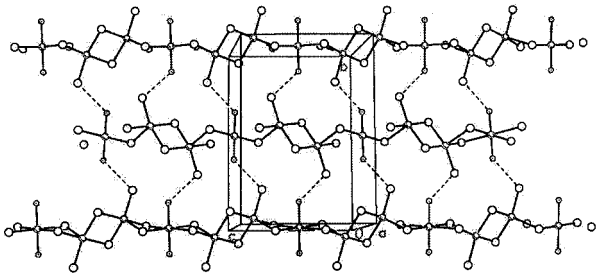

Figure 3. The interchain hydrogen bonding interaction; the dashed lines represent hydrogen bonds

Table 2. Hydrogen bonding distances (Å) and angles (°) for $(HPy)_2[Cu_3Cl_8(H_2O)_2]$

D−H··· A	D−H	D···A	H···A	∠ D−H···A
O−H(1 W) ···Cl(3)	0.81(3)	3.132(2)	2.34(3)	165(3)
O−H(2 W) ···Cl(3)[a]	0.82(2)	3.184(2)	2.38(3)	169(2)
N(1)−H(1)···Cl(2)	0.860	3.189(3)	2.469	141.8
N(1)−H(1)···Cl(3)	0.860	3.345(3)	2.650	138.8

[a] Symmetry equivalents: x, $1/2 - y$, $-1/2 + z$.

IR and Electronic Spectroscopy

The electronic spectrum of compound **1** in Nujol mull shows three peaks with λ_{max} values at 24096, 18692, and 12004 cm^{-1}. The spectral pattern and peak positions are quite similar to those of brown dimeric trichlorocuprate ($Cu_2Cl_6^{2-}$), with a square-pyramidal structure and an empirical formula of $(HBz)_2Cu_2Cl_6$ {Bz = benzimidazolium[6]}. The spectrum of **1** is therefore totally dominated by the square-pyramidal copper(II), which obscures the weak Laporte-forbidden transitions originating from the centrosymmetric octahedral copper(II) portion of compound **1**.

The spectrum of $[Cu_3Py_2Cl_6]$ (**1a**) shows two peaks with λ_{max} values at 23981 and 11723 cm^{-1}. Although it is very difficult to infer the exact structure of this type of complex, the presence of flattened tetrahedral (D_{2d}) copper(II) may be predicted from the lower energy of the d−d transition.[1] In addition, the band in the 24000 cm^{-1} region is indicative of the presence of doubly bridged Cu−$(Cl)_2$−Cu or Cu−$(Cl)_3$−Cu linkage.

IR spectra of **1** show a broad band due to the OH stretching modes of water molecules at 3301cm^{-1}. The appearance of the peak at lower wavelength corroborates the presence of extensive hydrogen bonding as found by single-crystal X-ray diffraction.

Thermal Analyses

The TG curves of the compounds $(HPy)_2[Cu_3Cl_8(H_2O)]_2$, $(HPy)_2[CuCl_4]$, $CuPyCl_2$, and $CuPy_2Cl_2$ are given in Figure 4. The thermal behavior of compound **1** shows that the compound loses its water molecules at ca. 105 °C (obsd. loss 5.6%; calcd. 5.4%) to produce the dehydrated compound $(HPy)_2Cu_3Cl_8$ (Table 3), which on being kept in a humid atmosphere (relative humidity > 50%) for several hours at ambient temperature absorbs exactly two molecules of water per three copper atoms to revert to **1**. The process is thus reversible. The X-ray powder diffraction pattern of **1** differs considerably from that of its anhydrous analogue $(HPy)_2Cu_3Cl_8$, but is identical to that of the rehydrated species. As the coordinated water molecules from the hexacoordinate copper (Cu1) are removed on dehydration, there should be a drastic change in the coordination geometry around this copper atom, and it is probably this that is reflected in the difference between the diffraction patterns. However, the structural skeleton of **1** must be retained on dehydration because on being kept in moist atmosphere, compound **1** is obtained again, as is confirmed by the identical diffraction patterns of the re-hydrated species and **1**. It is a reasonable assumption that the structure collapses to one analogous to the $A_nCu_{n+1}Cl_{3n+2}$ structures, in which a repeat sequence of n tribridged units and one bibridged unit occurs in the chain structure.[14] On further heating, $(HPy)_2Cu_3Cl_8$ undergoes dehydrohalogenation (obsd. loss 11.40%; calcd. 10.9%) at ca. 190 °C to produce $[Cu_3Py_2Cl_6]$. It is to be noted here that the pyridine ligand, after losing its proton as HCl, enters into the coordination sphere of the copper(II) in the solid state to yield the pyridine complex **1a**. This compound is thermally stable up to ca. 240 °C, after which it finally decomposes to $CuCl_2$.

 © 2003 Wiley-VCH Verlag GmbH & Co. KGaA, Weinheim

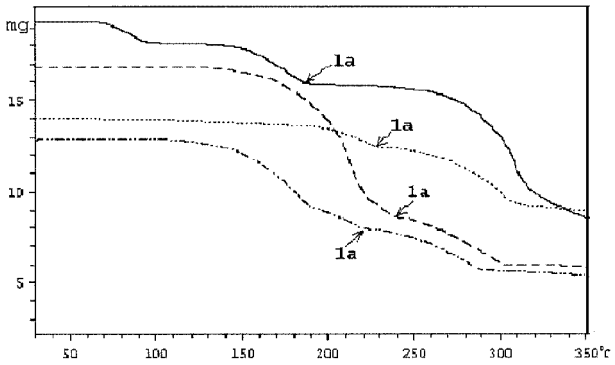

Figure 4. The TG curves: −−, $(HPy)_2[Cu_3Cl_8(H_2O)_2]$; -----, $(HPy)_2[CuCl_4]$; •••••••, $[CuPyCl_2]$ and - •• - •• −, $[CuPy_2Cl_2]$; the labels **1a** denote the temperature at which $[Cu_3Py_2Cl_6]$ is formed

Table 3. Results of thermal analysis of compounds **2, 3** and **4**

Thermal reactions	Temp. range (°C)	Weight loss (%) Obsd.	Calcd.
$(PyH)_2[CuCl_4]$ (2) → $CuPyCl_2$	150−220	42.20	41.59
$3CuPyCl_2 \rightarrow [Cu_3Py_2Cl_6]$	220−250	6.60	7.20
$[Cu_3Py_2Cl_6] \rightarrow 3CuCl_2$	250−305	14.50	14.41
$3CuPyCl_2$ (3) → $[Cu_3Py_2Cl_6]$	190−235	11.40	12.33
$[Cu_3Py_2Cl_6] \rightarrow 3CuCl_2$	245−310	25.50	24.67
$CuPy_2Cl_2$ (4) → $CuPyCl_2$	125−190	26.80	27.00
$3CuPyCl_2 \rightarrow [Cu_3Py_2Cl_6]$	190−220	9.30	9.00
$[Cu_3Py_2Cl_6] \rightarrow 3CuCl_2$	225−293	18.25	18.00

The interesting feature of the thermal analysis is the isolation of $[Cu_3Py_2Cl_6]$ (**1a**), which can be synthesized in the solid state from **1** as discussed in the preceding paragraph. Any attempt to synthesize compound **1a** in solution, either by the addition of pyridine and $CuCl_2 \cdot 2H_2O$ in 2:3 ratio or by crystallization of the title compound from common solvents (methanol, ethanol, water etc.) always results in $CuPyCl_2$ (see Exp. Sect.). Recrystallization of **1a** also results in $CuPyCl_2$. The X-ray powder diffraction results for compounds **1a**, **3**, and anhydrous $CuCl_2$ show that $[Cu_3Py_2Cl_6]$ is not a mixture of $CuPyCl_2$ and $CuCl_2$. It is relevant to mention here that complexes of composition $[M_3Py_2Cl_6]$ have been prepared by pyrolytic techniques with Cr^{II}, Mn^{II}, Co^{II}, Ni^{II}, and Cd^{II}.[15] With copper(II), though, it was thought that the existence of such complexes is not possible, as it does not form regular octahedral complexes because of Jahn−Teller effects.[16] Also, in a recent paper, no isolable intermediate was detected in the thermal analysis of $(Hpy)_2[CuCl_4]$.[17] However, the thermal analysis results for $(HPy)_2[Cu_3Cl_8(H_2O)_2]$, $(HPy)_2[CuCl_4]$, $CuPyCl_2$, and $CuPy_2Cl_2$ presented in this paper show that all of them finally decompose to $CuCl_2$ via the intermediate species $[Cu_3Py_2Cl_6]$. Only compound **1** permits isolation of **1a** in the pure state upon being heated, however, as the TG curve for **1** shows a plateau in the temperature range in which **1a** is stable. Earlier failure in its isolation was therefore a result of the decomposition temperature of copper(II)-pyridine complexes and had nothing to do with the Jahn−Teller effect.

Magnetic Behavior

The plot of $\chi_M T$ vs. T in Figure 5 reveals the presence of ferromagnetic interactions within the system. The value of $\chi_M T$ increases monotonically as T is lowered, with no maximum observed down to 1.9 K. Thus, no significant antiferromagnetic coupling appears to exist in this material. The M vs. H curve at 2.0 K (Figure 6) rises smoothly to a saturation value of $M_{satd.} \approx 3.05\ \mu_\beta$, giving no evidence for significant spin canting nor for a ferrimagnetic ground state of the chain system.

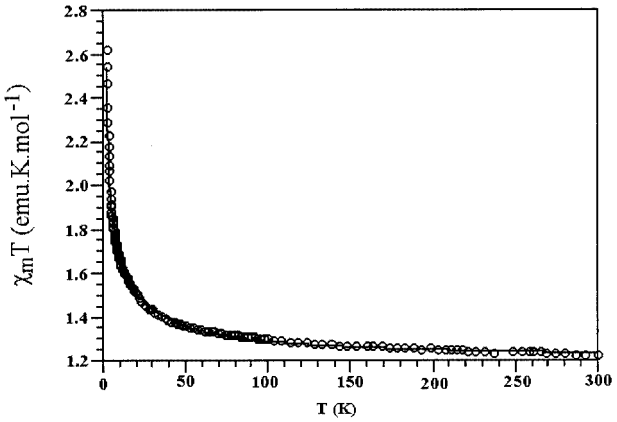

Figure 5. Plot of $\chi_M T$ vs. T for $(HPy)_2[Cu_3Cl_8(H_2O)_2]$; solid line is the calculated curve

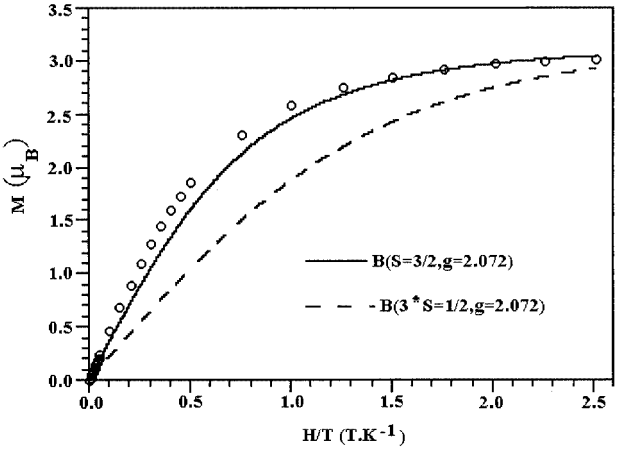

Figure 6. Plot of M vs. H/T at 1.8 K for $(HPy)_2[Cu_3Cl_8(H_2O)_2]$; solid line and dashed line are the calculated Brillouin functions

The data in Figure 5 can be fitted very satisfactorily by use of a model for a chain of alternating dimer and monomer units. The procedure consisted of treatment of the infinite chain as a ring of finite length by use of a closed-chain computational procedure. The infinite chain behavior can be obtained by extrapolation from the exact result for increasing ring length.

$$\hat{H} = -2\sum_{i=0}^{N-1}\left[J_1\hat{S}_{3i}\hat{S}_{3i+1} + J_2\left(\hat{S}_{3i+1}\hat{S}_{3i+2} + \hat{S}_{3i+2}\hat{S}_{3i+3}\right)\right]$$

 © 2003 Wiley-VCH Verlag GmbH & Co. KGaA, Weinheim

The exchange Hamiltonian may be written as where 3 N corresponds to the number of interacting spins. J_1 is the intradimer exchange interaction, and J_2 is the interaction between the dimer and the monomer. The calculations are limited up to 18 spins ($N = 6$). Evaluation of the susceptibility curves was performed by use of the MAGPACK programs package.[18] The differences between the curves with $N = 4$ and 6 are less than 0.2% over the full range of temperatures, so the $N = 6$ ring is taken as the exact solution for the infinite change in the experimental temperature range. Under these considerations the best fit obtained by a least-squares analysis of the $\chi_m T$ data is $J_1 = 17.35$ K = 12.1 cm^{-1} (intradimer exchange constant), $J_2 = 1.93$ K = 1.34 cm^{-1} (dimer−monomer exchange constant), $g = 2.072$, and $R = 5.76 \times 10^{-5}$.

The magnetization data (Figure 6) can be compared with the Brillouin function expected for three independent Cu^{II} ions (dashed line) and with a $S = 3/2$ system (solid line). As can be seen, the agreement is much better, as would be expected, for a $S = 3/2$ system, although the experimentally measured values are slightly above the theoretical ones at low fields. This may be due to the presence of the extended interactions within chains that cannot be taken into account with a simple Brillouin function.

Magneto-Structural Correlations

The magnetic studies indicate the presence of ferromagnetic coupling both within the dimeric species and between the dimer and monomer units. Correlation of the exchange coupling with structural parameters in $Cu_2Cl_6^{2-}$ dimers has received considerable attention in the past.[19] The coupling is antiferromagnetic, with $J/k \approx 50$ K for the planar conformation (based on the interaction Hamiltonian $H = -J \mathbf{S}_1 \cdot \mathbf{S}_2$), with the coupling becoming ferromagnetic as distortion from planarity occurs. In particular, for the type of bifold distortion observed in this structure, the crossover is estimated to occur at a bifold angle near 20°. Thus, with a bifold angle of 19.7°, the presence of ferromagnetic coupling within the dimer is consistent with the previous studies. For the dimer/monomer coupling, this pathway is analogous to those found in asymmetric bibridged dimers and chains.[20] This coupling can be either ferro- or antiferromagnetic, depending on details of the pathway (although no simple magneto-structural correlations exist). When the coupling is ferromagnetic, the magnitude of the coupling is invariably small, in agreement with these results.

Finally, it should be noted that hydrogen-bonded Cu−Cl···H_2O−Cu linkages occur between chains (Figure 3). In the absence of any decrease in $\chi_M T$ as $T \rightarrow 0$ K, it is clear that this interaction must also be ferromagnetic. The J' value may thus also include some small contribution from this pathway.

Discussion

The magnetic properties of this system can be compared with those of several other previously examined trimer-type chain systems. The $(Cu_2X_6)Cu(TMSO)_4$ system (TMSO = tetramethylenesulfone) contains chains of $Cu_2X_6^{2-}$ anions bridged by $Cu(TMSO)_4^{2+}$ cations.[21] For these compounds, the Cu^{II} ions in the cations have distorted tetrahedral geometries, which results in quite strong ferromagnetic coupling within the $Cu_2X_6^{2-}$ dimers. The cations and anions are linked by bent Cu−X···Cu interactions, giving ferromagnetic dimer/monomer coupling for the chloride salt, but weak antiferromagnetic coupling is observed at low temperatures in the bromide salt (although this antiferromagnetic coupling may, in reality, be propagated through a short interchain Br···S contact). Thus, the chloride salt behaves as a ferromagnetic chain, while the bromide exhibits ferrimagnetic behavior.

In $[Cu_3Cl_6(dioxane)_2]$, a complex bi-bridged chain with a ferro/ferro/antiferro repeat pattern exists.[22] With J(ferro) >> J(antiferro), the system effectively behaves as an antiferromagnetic $S = 3/2$ chain at low temperature. This can be contrasted with the behavior of the ferrimagnetic trimer chain in (N-methyl-2-picolinium)$_2Cu_3Br_8$.[23] Here, strong antiferromagnetic interactions exist within the planar bibridged $Cu_3Br_8^{2-}$ trimer units, stabilizing a $S = 1/2$ ground state. These are then coupled together in a ferromagnetic fashion, to give a system that behaves as a $S = 1/2$ ferromagnetic chain at low temperature. In addition, there are numerous other known $A_2Cu_3X_8$ salts containing planar bibridged trimers, in which the antiferromagnetically coupled trimers stack in complex fashions, for which the magnetic properties have not been thoroughly analyzed.[24]

Experimental Section

Materials and Measurements: High purity (98%) pyridine and copper(II) chloride dihydrate were purchased from E. Merck, Germany and were used as received. Elemental analyses (carbon, hydrogen, and nitrogen) were performed with a Perkin−Elmer 240C elemental analyzer and the copper contents in all the complexes were estimated spectrophotometrically.[25] IR spectra in KBr (4500−500 cm^{-1}) were recorded with a Perkin−Elmer RXI FT-IR spectrophotometer. Electronic spectra (1200−350 nm) were recorded with a Hitachi U-3501 spectrophotometer in Nujol mull. The thermal analyses (TG-DTA) were carried out with a Mettler Toledo TGA/SDTA 851 thermal analyzer in a dynamic atmosphere of dinitrogen (flow rate: 30 cm^3 min^{-1}). The sample was heated in an alumina crucible at a rate of 5 °C min^{-1}. The X-ray powder diffraction experiments were carried out on a Philips PW 3710 diffractometer equipped with a copper tube anode. Variable-temperature susceptibility measurements were carried out for $(HPy)_2Cu_3Cl_8 \cdot 2H_2O$ in the 2−300 K temperature range at a magnetic field of 0.1 T on ground polycrystalline samples with a SQUID magnetometer (Quantum Design MPMS-XL-5). The susceptibility data were corrected for the diamagnetic contributions deduced by use of Pascal's constant tables. Isothermal magnetization and hysteresis measurements were made for $(HPy)_2Cu_3Cl_8 \cdot 2H_2O$ at different temperatures, after zero field cooling between 0 and 5 T in the SQUID magnetometer.

Preparations

$(HPy)_2[Cu_3Cl_8(H_2O)_2]$ (Brown) (1): $CuCl_2 \cdot 2H_2O$ (5 mmol) was dissolved in a minimum volume of water. Pyridine (5 mmol) was

 © 2003 Wiley-VCH Verlag GmbH & Co. KGaA, Weinheim

mixed into this solution, along with concentrated HCl (4 mL). The resulting solution was concentrated in a water bath to ca. 5 mL and kept in a desiccator. After a few days reddish-brown shiny single crystals suitable for X-ray diffraction were obtained. $C_{10}H_{16}Cl_8Cu_3N_2O_2$ (670.5): calcd. C 17.9, H 2.4, N 4.2, Cu 28.4; found C 18.0, H 2.3, N 4.3, Cu 27.8. λ_{max} = 24096, 18692, 12005 cm^{-1}

[$Cu_3Py_2Cl_6$] (Pale Green) (1a): This compound was prepared by heating of compound **1** for 30 min at ca. 190 °C. $C_{10}H_{10}Cl_6Cu_3N_2$ (561.5) : calcd. C 21.4, H 1.8, N 5.0, Cu 33.9; found C 21.2, H 1.9, N 5.1, Cu 33.6. λ_{max} = 23981 and 11723 cm^{-1}.

$(HPy)_2[CuCl_4]$ (Yellow) (2): This compound was prepared by the same procedure as used in the case of compound **1** except that $CuCl_2{\cdot}2H_2O$ and pyridine were used here in 1:2 molar ratio. $C_{10}H_{12}Cl_4CuN_2$ (365.5): calcd. C 32.8, H 3.3, N 7.7, Cu 17.4; found C 32.5, H 3.2, N 7.4, Cu 17.0. λ_{max} = 24390 and 9200 cm^{-1}.

$CuPyCl_2$ (Pale Yellow) (3) and $CuPy_2Cl_2$ (Blue) (4): The compounds were synthesized by mixing of ethanol solutions of $CuCl_2{\cdot}2H_2O$ and pyridine in the required molar ratios. The compounds can also be synthesized by shaking the compounds **1** and **2** respectively in ethanol. **3:** $C_5H_5Cl_2CuN$ (213.5): calcd. C 28.1, H 2.4, N 6.6, Cu 29.7; found C 28.0, H 2.1, N 6.4, Cu 29.5. UV: λ_{max} = 23585, 20747, 14970, 11723, 10953 cm^{-1}. **4:** $C_{10}H_{10}Cl_2CuN_2$ (292.7): calcd. C 41.0, H 3.4, N 9.6, Cu 21.7; found C 41.0, H 3.6, N 9.4, Cu 21.5. λ_{max} values are as reported in the literature[26] for **4**.

X-ray Crystallography: A suitable single crystal of the complex **1** was mounted on a Bruker AXS CCD area detector system for data collection. The crystal data of the complex were collected at 293(2) K. Intensity data were collected in the ω scan mode by use of graphite-monochromated Mo-K_α radiation (0.71073 Å). The empirical absorption corrections were based on Ψ scans. The structure was solved by SIR-97[27] methods and refinement was made with the SHELXL-97 suite of programs. Anisotropic full-matrix refinements based on F^2 were carried out for all non-hydrogen atoms. The hydrogen atoms were placed geometrically and refined in the "riding" model with isotropic thermal parameters 1.2 times U_{eq} of the atom to which they were attached. Complex neutral atom scattering factors were used throughout the refinement. All calculations were carried out with the aid of the SHELX 97,[28] PLATON 99[29] and ORTEP[30] programs. Selected crystallographic data for complex **1** are displayed in Table 4, while selected bond lengths and bond angles of the complex are presented in Table 1. The H-bonding and non-bonding contacts of **1** are listed in Table 2. CCDC-170243 contains the supplementary crystallographic data for this paper. These data can be obtained free of charge at www.ccdc.cam.ac.uk/conts/retrieving.html [or from the Cambridge Crystallographic Data Centre, 12, Union Road, Cambridge CB2 1EZ, UK; Fax: (internat.) +44−1223/336−033; E-mail: deposit@ccdc.cam.ac.uk].

Table 4. Crystal data and structure refinement details of $(HPy)_2[Cu_3Cl_8(H_2O)_2]$

Empirical formula	$C_5H_8Cl_4Cu_{1.5}ON$
Molecular mass	335.23
Temperature	293(2) K
Wavelength	0.71069 Å
Crystal system, space group	monoclinic, $P2_1/c$
Unit cell dimensions	a = 7.8950(10) Å
	b = 14.144(2) Å
	c = 9.9210(10) Å
	β = 99.20(2)°
V	1093.6(2) $Å^3$
Z, calculated density	4, 2.036 Mg/m^3
Absorption coefficient	3.876 mm^{-1}
F(000)	658
Crystal size	0.21 × 0.17 × 0.11 mm
Crystal color	brown
θ range for data collection	2.53 to 28.09°
Limiting indices	$-10 \le h \le 10$
	$-18 \le k \le 18$
	$-12 \le l \le 12$
Reflections collected/unique	11396/2460
R(int)	0.0406
Completeness to θ = 28.09°	92.2%
Refinement method	Full-matrix least-squares on F^2
Data/restraints/parameters	2460/2/121
Goodness-of-fit on F^2	1.105
Final R indices [$I > 2\sigma(I)$]	R_1 = 0.0277, wR_2 = 0.0708
R indices (all data)	R_1 = 0.0329, wR_2 = 0.0740
Largest diff. peak and hole	0.467 and −0.610 $eÅ^{-3}$

Acknowledgments

We would like to thank the University Grant Commission, India for the financial support (Sanction No. UGC/2976/GRW(UNG) 99−00). The work is also supported in part by ACS-PRF 34779-AC5 and by the Spanish project MAT2001−3507. R. D. Willett thanks the University of Valencia for a visitors grant.

[1] D. W. Smith, *Coord. Chem. Rev.* **1976**, *21*, 93.
[2] U. Geiser, R. D. Willett, M. Lindbeck, J. Emerson, *J. Am. Chem. Soc.* **1986**, *108*, 1173.
[3] M. R. Bond, R. D. Willett, *Inorg. Chem.* **1989**, *28*, 3267.
[4] S. H. Simonsen, G. W. Watt, *J. Chem. Soc., Chem. Commn.* **1979**, 632.
[5] M. Bukowska-Strzyzewska, J. Skoweranda, *Acta Crystallogr., Sect. C* **1987**, *43*, 2290.
[6] M. Bukowska-Strzyzewska, J. Wnek, A. Tosik, T. Glowiak, *Acta Crystallogr., Sect. C* **1985**, 41, 1184.
[7] S. Haddad, R. D. Willett, *Inorg. Chem.* **2001**, *40*, 2457.
[8] M. Wei, R. D. Willett, *Inorg. Chem.* **1996**, *35*, 6381.
[9] R. D. Willett, H. Place, M. Middleton, *J. Am. Chem. Soc.* **1988**, *110*, 8639.
[10] U. Geiser, R. M. Gaura, R. D. Willett, D. X. West, *Inorg. Chem.* **1986**, *25*, 4203.
[11] T. Manfredini, G. C. Pellacani, A. B. Corradi, L. P. Battaglia, G. G. T. Guarini, J. G. Giusti, G. Pon, R. D. Willett, *Inorg. Chem.* **1990**, *29*, 2221.
[12] R. S. Sager, W. H. Watson, *Inorg. Chem.* **1968**, 7, 2035.
[13] R. D. Willett, U. Geiser, *Croat. Chem. Acta* **1984**, *57*, 737.
[14] Y. Fujii, Z. Wang, R. D. Willett, W. Zhang, C. P. Landee, *Inorg. Chem.* **1995**, *34*, 2870; M. R. Bond, R. D. Willett, G. V. Rubenacker, *Inorg. Chem.* **1990**, *29*, 2713.
[15] J. R. Allan, D. H. Brown, R. H. Nuttall, D. W. A. Sharp, *J. Chem. Soc.(A)* **1966**, 1031.
[16] S. W. Peterson, H. A. Levy, *J. Chem. Phys.* **1957**, *26*, 220.
[17] A. Purkayashtha, J. B. Baruah, *Thermochim. Acta* **2002**, *390*, 187.
[18] J. J. Borrás-Almenar, J. M. Clemente-Juan, E. Coronado, B. S. Tsukerblat, *Inorg. Chem.* **1999**, *38*, 6081; J. J. Borrás-Almenar, J. M. Clemente-Juan, E. Coronado, B. S. Tsukerblat, *J. Comput. Chem.* **2001**, *22*, 985.
[19] B. Scott, R. D. Willett, *Inorg. Chim. Acta* **1988**, *141*, 193.
[20] W. E. Hatfield, in "Magneto-Structural Correlations in Exchange Coupled Systems" (R. D. Willett, D. Gatteschi, O. Kahn, Eds.), NATO ASI Series, Plenum, New York, **1985**, p. 555.

 © 2003 Wiley-VCH Verlag GmbH & Co. KGaA, Weinheim

[21] C. P. Landee, A. Djili, D. F. Mudgett, M. Newhall, H. Place, B. Scott, R. D. Willett, *Inorg. Chem.* **1988**, *27*, 620.
[22] J. C. Livermore, R. D. Willett, R. M. Gaura, C. P. Landee, *Inorg. Chem.* **1982**, *21*, 1403.
[23] M. R. Bond, H. Place, Z. Wang, R. D. Willett, Y. Liu, T. E. Grigereit, J. E. Drumheller, G. F. Tuthill, *Inorg. Chem.* **1995**, *34*, 3141.
[24] M. R. Bond, R. D. Willett, R. S. Rubins, P. Zhou, C. E. Zaspel, S. L. Hutton, J. E Drumheller, *Phys. Rev. B* **1990**, *42*, 10280.
[25] A. I. Vogel, *A Text book of Quantitative Inorganic Analysis*, 4th edition, Longman, New York, **1978**.
[26] N. S. Gill, R. S. Nyholm, *J. Inorg. Nucl. Chem.* **1961**, *18*, 88.
[27] A. Altomare, G. Cascarano, C. Giacovazzo, A. Guagliardi, A. G. G. Moliterni, M. C. Burla, G. Polidori, M. Camalli, R. Spagna, *Private Communication*, **1997**.
[28] G. M. Sheldrick, SHELX 97, Program for the refinement of crystal structure, University of Göttingen, Germany.
[29] A. L. Spek, PLATON, A Multipurpose Crystallographic Tool, University of Utrecht, Utrecht, The Netherlands, **2001**.
[30] L. J. Farrugia, ORTEP-3, *J. Appl. Crystallogr.* **1997**, 30, 565.

Received February 26, 2003
Early View Article
Published Online October 10, 2003

 © 2003 Wiley-VCH Verlag GmbH & Co. KGaA, Weinheim

Preparation of Optically Active α-Amino[3]ferrocenophanes − Building Blocks for Chelate Ligands in Asymmetric Catalysis

Patrick Liptau, Ludger Tebben, Gerald Kehr, Birgit Wibbeling, Roland Fröhlich, and Gerhard Erker*

Keywords: Ferrocenes / Ferrocenophanes / Chelate ligands

We noticed that some mistakes were made in the determination of the Δε and $[\alpha]_D^{20}$ values of compounds ***6*** *and* ***11*** *in our article[1] that need to be corrected. The correct values for* ***6*** *(p. 3597) and* ***11*** *(p. 3598f.) (including the corrected Figure 8, p. 3596) are as follows:*

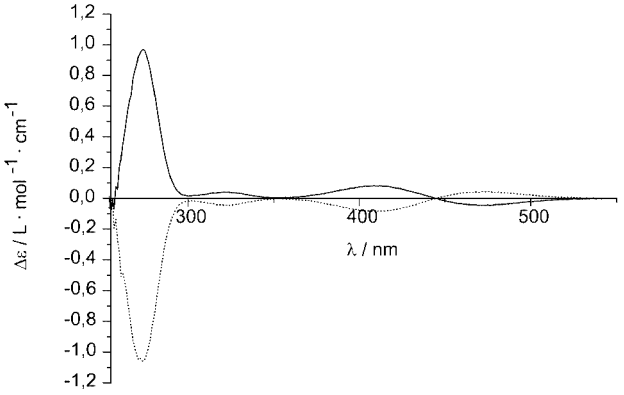

Figure 8. CD spectra of (1*R*,3*R*)-**6** (solid line, 4×10^{-4} g mL^{-1}) and (1*S*,3*S*)-**6** (dotted line, 4×10^{-4} g mL^{-1}) in CH_3CN

(1*S*,3*S*)-**6**: $[\alpha]_D^{20} = -89$ ($c = 2 \times 10^{-3}$ g mL^{-1}, CH_3CN). CD: Δε (λ_{max}) = −1.06 (274), −0.04 (326), −0.08 (412), +0.04 (476) ($c = 4 \times 10^{-4}$ g mL^{-1}, CH_3CN). (1*R*,3*R*)-**6**: $[\alpha]_D^{20} = +91$ ($c = 2 \times 10^{-3}$ g mL^{-1}, CH_3CN). CD: Δε (λ_{max}) = +0.97 (274), +0.04 (326), +0.08 (412), −0.04 (476) ($c = 4 \times 10^{-4}$ g mL^{-1}, CH_3CN).

(1*S*,3*S*)-**11**: $[\alpha]_D^{20} = -109$ ($c = 2 \times 10^{-3}$ g mL^{-1}, CH_3CN). CD: Δε (λ_{max}) = −0.23 (275), +0.02 (334), −0.10 (416), +0.03 (483) ($c = 4 \times 10^{-4}$ g mL^{-1}, CH_3CN). (1*R*,3*R*)-**11**: $[\alpha]_D^{20} = +111$ ($c = 2 \times 10^{-3}$ g mL^{-1}, CH_3CN). CD: Δε (λ_{max}) = +0.23 (275), −0.02 (334), +0.10 (416), −0.02 (483) ($c = 4 \times 10^{-4}$ g mL^{-1}, CH_3CN).

[1] P. Liptau, L. Tebben, G. Kehr, B. Wibbeling, R. Fröhlich, G. Erker, *Eur. J. Inorg. Chem.* **2003**, 3590−3600.

Received October 23, 2003
G. Erker

 DOI: 10.1002/ejic.200300782 © 2003 Wiley-VCH Verlag GmbH & Co. KGaA, Weinheim

Modulation of the Communication between Redox Centers in a Tris(ferrocene)-tren Ligand by Complexation of Lanthanide Ions

Marie Heitzmann, Jean-Claude Moutet,* Jaques Pécaut, Olivier Reynes, Guy Royal,* Eric Saint-Aman, and Guy Serratrice

Keywords: Sandwich complexes / Electrostatic interactions / Electrochemistry / Lanthanides

In our article,[1] on page 3769, second column, line 14 from bottom, the expression for ΔE^o is erroneous and should read:

$(RT/F)\ln 3^2$

[1] M. Heitzmann, J.-C. Moutet, J. Pécaut, O. Reynes, G. Royal, E. Saint-Aman, G. Serratrice, *Eur. J. Inorg. Chem.* **2003**, 3767−3773.

Received October 29, 2003
G. Royal

 © 2003 Wiley-VCH Verlag GmbH & Co. KGaA, Weinheim **DOI: 10.1002/ejic.200300797**

EurJIC
European Journal of Inorganic Chemistry

Issue 24/2003

Pages 4263–4410

Papers available ahead of print in Early View at www.interscience.wiley.com

Earliest available Table of Contents:
Automatically, free of charge by e-mail through
www.interscience.wiley.com/alerts

COVER PICTURE

The cover picture shows the multiple characterization methods used to unravel the electronic and geometrical structures of the unit $M_A^{III}M_B^{II}$, in which three oximato groups $(=N-O)^-$ are present as bridging ligands. Variable-temperature magnetic susceptibility and EPR measurements provide a consistent answer to the question of electronic ground states for different heterometallic combinations. Mößbauer spectroscopy helps to differentiate between the species Co^{III}(l.s.)Fe^{II}(l.s.) and Fe^{II}(h.s.)Co^{III}(l.s.). Details on the preparation and characterization of the species $Fe^{III}M^{II}$ and related heterometallic compounds are presented in a forthcoming article by P. Chaudhuri et al.: Asymmetric Heterodinuclear $Fe^{III}M^{II}$ (M = Zn, Cu, Ni, Fe, Mn), $Co^{III}Fe^{II}$ and $Fe^{II}Co^{III}$ Species: Synthesis, Structure, Redox Behaviour and Magnetism.

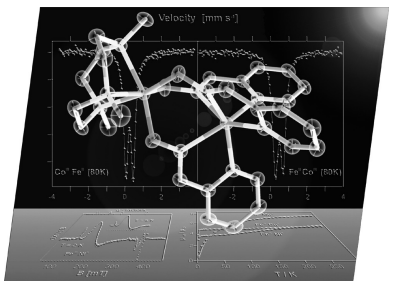

MICROREVIEW

Contents

4275 **W. Beck**

The First Chemical Achievements and Publications by Justus von Liebig (1803–1873) on Metal Fulminates and Some Further Developments in Metal Fulminates and Related Areas of Chemistry

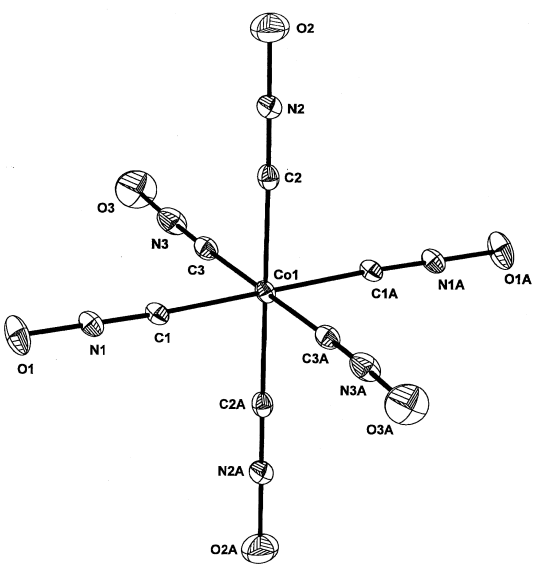

Keywords: Liebig / Fulminates / Silver / Structure elucidation

 © 2003 Wiley-VCH Verlag GmbH & Co. KGaA, Weinheim

The First Chemical Achievements and Publications by Justus von Liebig (1803−1873) on Metal Fulminates and Some Further Developments in Metal Fulminates and Related Areas of Chemistry[‡]

Wolfgang Beck[a]

Dedicated to Professor Wolfgang Steglich on the occasion of his 70th birthday for his great friendship, collaboration and support[‡‡]

Keywords: Liebig / Fulminates / Silver / Structure elucidation

The first chemical investigations and publications by Justus von Liebig dealt with the fulminates of silver and mercury. Even as a boy Liebig had learnt how to prepare silver fulminate, and as student of chemistry in Erlangen (1821) he studied the properties and reactions of silver fulminate. In Paris in 1823 (together with Gay-Lussac) he succeeded in analyzing quantitatively the highly explosive silver compound. This great experimental success with the dangerous silver fulminate was most important in three respects: i. The development of the experimental method later culminated in Liebig's perfected and well-known C,H,N analysis of organic compounds (1830). ii. It led to the concept of isomerism when F. Wöhler found that silver cyanate had the same composition as silver fulminate. iii. It was decisive for furthering the scientific career of Liebig, since Alexander von Humboldt was highly impressed by the great skill and talent of Liebig and — by recommendation of Humboldt — Liebig became Professor in Gießen in 1824 (at the young age of 21). The first (fulminato)metal complex, $K[Ag(CNO)_2]$, was also isolated by Liebig. Later, explosive (fulminato)metal complexes were prepared by Nef, Wieland, and especially by Lothar Wöhler and co-workers. In Munich the HCNO structure of fulminic acid was established by its IR spectrum and the spectroscopic properties of (fulminato)metal complexes were studied. A series of new nonexplosive complexes could be obtained by dilution of the energy-rich species with large cations or ligands. Recent X-ray structure determinations have revealed the almost perfect linear, tetrahedral, square-planar, or octahedral structures of these complexes with linear metal–C≡NO bonds, e.g. $[Au(CNO)_2]^-$, $[Zn(CNO)_4]^{2-}$, $[Ni(CNO)_4]^{2-}$, $[Co(CNO)_6]^{3-}$. DFT calculations have given very good agreement between the calculated and experimental structural parameters and CNO stretching frequencies. The (fulminato)metal complexes closely resemble the analogous cyano compounds.

(© Wiley-VCH Verlag GmbH & Co. KGaA, 69451 Weinheim, Germany, 2003)

Liebig's Work on Metal Fulminates

Justus Liebig was born on May 12, 1803 in Darmstadt, Germany. His father owned a pigment and drug shop. Even as a boy he was fascinated by the crackers sold by the pedlars at the market,[1−7] and he watched the preparation of this explosive. Liebig recognised that it was nitric acid

[‡] On the occasion of Liebig's 200th birthday.

[a] Department Chemie der Ludwig-Maximilians-Universität Butenandtstr. 5−13, 81377 München, Germany

[‡‡] Professor Steglich currently holds the chair of Organic Chemistry of the University of Munich, a position previously occupied by J. v. Liebig, A. v. Baeyer, R. Willstätter, H. Wieland, and R. Huisgen.

Wolfgang Beck, born in 1932, received his Ph.D. in 1960 at the Technische Hochschule (TH), München, under the supervision of Prof. W. Hieber. In 1968 he was appointed to the Chair of Inorganic and Analytical Chemistry at the Ludwig-Maximilians-Universität in München (LMU) and is now Emeritus Professor. His research interests are coordination and organometallic chemistry. He started his studies with metal complexes of pseudohalides (fulminato and azido ligands) and later proceeded to (among other topics) complexes of biologically important ligands. He has published over 600 papers and has been awarded the Liebig Medal of the Gesellschaft Deutscher Chemiker.

MICROREVIEWS: This feature introduces the readers to the author's research through a concise overview of the selected topic. Reference to important work from others in the field is included.

which was used for the dissolution of silver or mercury with evolution of brown gases, and that the liquid which was added smelt of brandy and was alcohol. He probably repeated the preparation of silver fulminate in his father's small laboratory, where pigments were usually made and probably the metal fulminates were sold in his father's shop.[5b] The synthesis of mercury and silver fulminate from ethanol, nitric acid, and mercury or silver was reported in 1800 by the English chemist Howard,[8] and 107 years later the complicated process of fulminate formation was interpreted by Wieland in Munich.[9] The young Liebig didn't like to study languages at the gymasium in Darmstadt, so he left in 1817 aged 14 and started an apprenticeship in a pharmacy near Darmstadt where he stayed, although only for a few months. It is only a tale that Liebig caused an explosion (with metal fulminates?) in the school and in the pharmacy and therefore had to leave both.[1,2] (However, the Liebig biography by Brock[3] contains a painting of the explosion).

In these times — during the Napoleonic wars — there was a great demand for mercury fulminate. F. F. Runge has given an amusing report (F. Franz, Grundriß der Chemie, II. Teil, München, **1847**) on his experience and accidents with mercury fulminate when he was a pharmacy apprentice in Lübeck in 1813.

Aged $17^1/_2$, in 1820 Liebig was accepted by Karl Kastner — at that time one of the leading professors of chemistry — to study at the University of Bonn. Liebig (Figure 1) followed Kastner one year later to the University

Figure 1. Justus Liebig in 1821

5.

Einige Bemerkungen über die Bereitung und Zusammensetzung des Brugnatellischen und Howardschen Knallsilbers.

(Vom Herrn Liebig, der Chemie Beflissenen aus Darmstadt *).

Es scheint vielleicht überflüssig, zu den vielen Vorschriften und Bereitungsarten dieses merkwürdigen Salzes noch eine neue hinzuzufügen; allein die älteren Angaben sind mehr oder weniger unbestimmt und unsicher, so, daſs wenn man darnach arbeitet, ohne besondere Uebung das Präparat meistentheils mifslingt. Schon seit 2 Jahren verfertige ich nach der unten gegebenen Vorschrift eine

*) Die Leser mögen diese erste Probe des experimentellen Fleifses eines jungen Chemikers mit Nachsicht aufnehmen. Der Hr. Verf. widmete sich der Chemie bereits in Bonn mit achtungswerthem Eifer und setzte hier seine Studien in gleichem Geiste fort. Kastner.

Figure 2. Liebig's first publication

of Erlangen. In 1822 Liebig published his first paper[10] on the safe preparation and some properties of silver fulminate (Figure 2). This paper contains also some chemical observations on silver fulminate by Kastner, and a kind remark on the skill and dedication of Liebig. In a subsequent, very short paper,[11] Liebig reported that silver fulminate is soluble in aqueous ammonia solution and that NH_3 is formed on reaction with KOH.

In 1822 Liebig got into trouble with the citizens and the police as a member of a student unit, and he left Erlangen. With the aid of Kastner he was awarded a stipend by the Duke of Hessen, Ludwig I, for the study of chemistry at the Sorbonne in Paris, at that time the centre of the scientific study of chemistry, which was founded by Lavoisier. In Paris he could listen to the lectures of famous scientists such as Gay-Lussac, Thenard, Dulong, and Biot.[1−3,5] In the small laboratory of Gaultier de Claubry (who discovered the reaction of iodine with starch) and with the support of Thenard, Liebig could continue his experiments with silver and mercury fulminate. Gay-Lussac presented Liebig's results before the Academy of Science in Paris, which attracted great attention. He himself demonstrated his new compounds at the meeting of the academy. In the publications on these results[12,13] some very interesting remarks on fulminates are to be found: "It is now clear, that the detonating principle is due to a special acid." Liebig recognised the analogy between metal cyanides and metal fulminates, perhaps somewhat instinctively and said: "Although we find in detonating acids (fulminic acid) and det-

 © 2003 Wiley-VCH Verlag GmbH & Co. KGaA, Weinheim

onating salts (metal fulminates) all the elements of cyanic acid they are not cyanides.''

Liebig[13] reported the reactions of silver fulminate and of mercury fulminate with CaO, MgO, KOH, and NaOH. With copper, zinc, and iron he obtained explosive compounds which he called, for example, ''real fulminating copper'' (''wahres Knallkupfer'') and stated that the salts of fulminic acid (metal fulminates) belong to the most beautiful compounds in chemistry. He correctly formulated the products from the reaction of silver fulminate with, for example, CaO or KOH as double salts {in today's terminology (fulminato)metal complexes like $K[Ag(CNO)_2]$} and compared these compounds with (in our words) complexes of cyanide or of tartaric acid. Also the first experiments to analyze silver fulminate were carried out by Liebig,[12,13] for instance, using 100 g (!) of silver fulminate and 400 g of magnesia (MgO) in a retort. Liebig found that the organic parts of silver fulminate and mercury fulminate have the same composition.[12]

With AgCNO and aqueous ammonia Liebig obtained white crystals which proved to be so explosive and dangerous that they could not be handled. He reported several ''terrible'' explosions.[13] Later several binary metal fulminates were obtained from $Hg(CNO)_2$ and amalgams of Na, K, Mn, Cu, Tl, and Cd.[14]

Liebig was very courageous in his studies with the highly explosive and sensitive silver fulminate and used rather large quantities. In later days he admitted that any study with fulminates usually ended with an explosion, and further work was only started when the accident was gradually thrust into the background.[2,15] In November 1830 — after a big explosion with solid silver fulminate and ammonium sulfide solution — Liebig wrote to Wöhler that he didn't want to handle ''fulminic acid'' any more [''Liebig's and Wöhler's Briefwechsel in den Jahren 1829−1873'' (Eds.: A. W. Hoffmann, E. Wöhler), Braunschweig, **1888**; November 18th, 1830]. But Liebig obviously was a most skilful chemist and no serious injury was reported.

Liebig found that Berliner Blau (''Berlin Blue'') is formed from silver fulminate, KOH, and iron sulfate.[13] Later this was confirmed by Schischkoff.[16] Together with F. Lux it was shown[16] that hexa(fulminato)ferrate(II) $[Fe(CNO)_6]^{4-}$ {and also $[Fe(CN)_5CNO]^{4-}$ [16]} is quantitatively reduced (deoxygenated) by $Fe(OH)_2$ to $[Fe(CN)_6]^{4-}$.

At the session of the academy, where Liebig's results were so successfully presented,[13] Alexander von Humboldt was present. Gay-Lussac and von Humboldt were close friends and they worked together on the law of combining gases (Gay-Lussac law).

Humboldt was highly impressed by the talent of Liebig and upon his recommendation Liebig was accepted in the laboratory of Gay-Lussac (Figure 3), where he could profit from Gay-Lussac's and Thenard's vast experience in the elemental analysis of organic compounds (Figure 4). In a short time the collaboration of Liebig and Gay-Lussac led to the perfect analysis of silver fulminate,[17] a masterpiece of exact chemical work. Silver fulminate (200 mg) and copper oxide (8 g) were mixed and heated and gave CO_2 and

Figure 3. Joseph Louis Gay-Lussac (1778−1850)

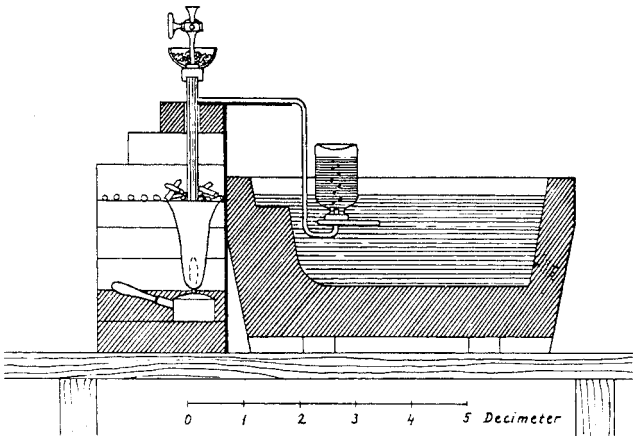

Figure 4. Gay-Lussac and Thenard's apparatus for the combustion and analysis of organic substances (1810)

N_2 in the exact volume ratio 2:1 according to the equation

$$2\ AgCNO + 2\ CuO \rightarrow 2\ Ag + 2\ Cu + 2\ CO_2 + N_2$$

Previously, Gay-Lussac had analyzed hydrocyanic acid (HCN) by combustion with CuO to give CO_2/N_2 in the volume ratio 2:1 (Gay-Lussac, *Ann. Chim.* **1815**, *XCV*, 136−251).

In another quantitative experiment Liebig and Gay-Lussac determined the Ag content of silver fulminate after decomposition with hydrochloric acid, according to the equation

$$AgCNO + 2\ HCl \rightarrow AgCl + Cl(H)C{=}NOH$$

mass of AgCNO used: 2.266 g

mass of AgCl produced: 2.171 g (theoretical value 2.167 g)

They also correctly analyzed the reaction of silver fulminate with KCl according to the equation

$$2\ AgCNO + KCl \rightarrow K[Ag(CNO)_2] + AgCl$$

mass of AgCNO used: 2.552 g

mass of AgCl found: 1.202 g (theoretical value 1.220 g)

In the latter case, the silver complex $[Ag(CNO)_2]^-$ is formed (which was called by Liebig ''knallsaures Kali'').

Only half of the silver present in AgCNO was found in AgCl. The $K[Ag(CNO)_2]$ (''knallsaures Kali'') gave 1.210 g of AgCl after decomposition with HCl (compared with the theoretical value of 1.220 g). Thus, Liebig had discovered the first (fulminato)metal complex. Interestingly, $K[Ag(CNO)_2]$ is also formed by reaction with KBr in the solid state, as monitored by IR spectroscoppy.[18]

 © 2003 Wiley-VCH Verlag GmbH & Co. KGaA, Weinheim

Next, Liebig and Gay-Lussac[17] determined the carbon and nitrogen content of silver fulminate. A mixture of silver fulminate and copper oxide was carefully dried with $CaCl_2$ in a tube in vacuo using an air-pump. The measurements were carried out with the apparatus shown in Figure 5. The volumes of CO_2 and N_2 were measured with the apparatus developed by Gay-Lussac and Thenard (Figure 4).

It was found by five analyses (using 30 g of AgCNO for each analysis) from the volumes of CO_2 (which then was absorbed with KOH) and N_2 that 100 mg of AgCNO gave 17.16 mg (theory 17.35 mg) of cyanogen (CN). These analyses of AgCNO were really excellent: Ag: found 72.187, calcd. 71.97, CN: found 17.160, calcd. 17.35, O: found 10.653, calcd. 10.67.

Liebig and Gay-Lussac had carefully eliminated the possibility that silver fulminate contained hydrogen — this was confirmed by decomposition of a mixture of silver fulminate and K_2SO_4.

Twenty years later Berzelius[19] again questioned whether silver fulminate could contain hydrogen; this was immediately rejected by Liebig,[19] as other arguments against his formulation were refuted with irony.[20]

Liebig and Gay-Lussac[17] also measured the gases which are formed from silver fulminate on detonation; they diluted AgCNO with KCl or K_2SO_4 and correctly concluded that the residue must contain a "cyan" compound of silver (AgNCO!).

Finally, Liebig and Gay-Lussac[17] came to the conclusion "that the various salts of fulminic acid contain the same acid which comprises one atom of cyanogen (CN) and one atom of oxygen". In other words they had found the correct formulation (AgCNO). It is quite surprising and somewhat strange that it took about 70−80 years before Nef[24] formulated fulminic acid as the monomeric oxime of carbon monoxide C=N−OH, and Lothar Wöhler proved the monomeric nature of the fulminate ion $C{\equiv}N{-}O^-$.[25]

It was as late as 1965 that, together with K. Feldl,[26] the structure of fulminic acid as formonitrile oxide H−C≡N−O could be proven by its IR spectrum and that Winnewisser et al.[27,32] confirmed this structure by microwave spectroscopy and high resolution IR spectra. The HCNO structure could be deducted from the Huisgen[31] 1,3-dipolar cycloaddition reactions of fulminic acid with unsaturated carbon compounds,[22] which were performed by Quilico,[28] and Huisgen and Christl.[28] More recently, the mechanism of the cycloaddition reactions of HCNO was studied theoretically.[29] L. Pauling[30] calculated in 1926 from the mutual potential energy of the positive cores that fulminic acid has the formula HCNO rather than the tautomer CNOH, which was the possibility accepted at that time.

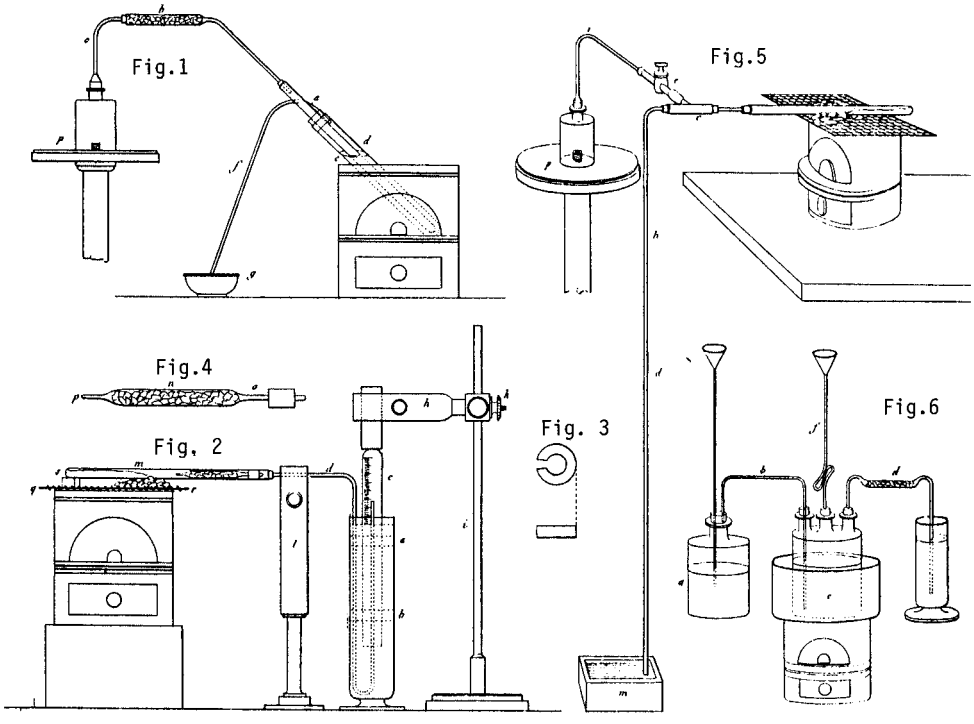

Figure 5. Apparatus used by Liebig and Gay-Lussac for the analysis of silver fulminate; legends in the figure itself (selection): *Fig. 1*: Drying of AgCNO with $CaCl_2$ and with an air-pump; *Fig. 2*: Determination of the volumes of CO_2 and N_2 after combustion of AgCNO with CuO using mercury; *Fig. 4*: Tube with $CaCl_2$ for the absorption of H_2O; *Fig. 5*: Determination of the volumes of gases after thermal decomposition of an $AgCNO/K_2SO_4$ mixture; *Fig. 6*: Experiments to measure HCN from AgCNO and HCl (HCN was not observed); a) $AgNO_3$ for forming AgCN from HCN; d) formation of H_2 from Zn and H_2SO_4 (in order to float HCN from the tube c); f) HCl

 © 2003 Wiley-VCH Verlag GmbH & Co. KGaA, Weinheim

For excellent reviews of the long and fascinating history of fulminic acid, see refs.[8,21−23] Interestingly in Munich there is a tradition of fulminic acid chemistry: J. v. Liebig, H. Wieland (who first proved the existence of the free fulminic acid[9]) and R. Huisgen (1,3-dipolar cycloaddition reactions of HCNO[28,31]). Fulminic acid and its derivatives have been studied extensively by many chemists. A list of citations on fulminic acid (which was kindly forwarded to the present author by M. Winnewisser) contains 140 titles from 1800 to 1966. After 1966 (ca. 180 papers were published up until 2003), fulminic acid attracted great attention from spectroscopists and theoreticians — mainly through the many important studies by M. and B. Winnewisser[27,32] — because it proved to be a highly interesting unusual quasilinear molecule. The possible CHNO isomers and their stability attracted the interest of theoreticians.[23,33]

HCNO can be prepared by several methods:[22] a) By treatment of aqueous NaCNO solutions with sulfuric acid.[9,26,27] b) From iodoformhydroxime [I(H)C=CNOH] and base (NEt_3);[28] this is obviously a method for preparative work; I(H)C=NOH has been obtained from NaCNO solutions and HI[34] or more conveniently by Huisgen and Christl (avoiding the highly explosive NaCNO), directly from $Hg(CNO)_2$ and HI.[28] c) By gas-phase pyrolysis of 3-phenyl-4-oxoiminoisoxazol-5(4*H*)-one[35] (high yield) for spectroscopic measurements of HCNO.[27] d) In situ preparation of HCNO by hydrolysis of trimethylsilylnitrile oxide Me_3SiCNO,[36] which is accessible from $Hg(CNO)_2$ and Me_3SiBr.[37] A reinvestigation of cycloaddition and polymerisation reactions of HCNO using this method has been reported.[37]

In 1824, Friedrich Wöhler reported the synthesis of silver cyanate,[38] which showed an identical analysis to silver fulminate. This proved to be one of the first examples of isomerism, a term which was coined after some discussion by Berzelius.[39] However, at first Liebig[40] did not believe these results (and at first Berzelius did not believe the silver fulminate analysis).

For a detailed discussion of the history of isomerism see: J. R. Partington, *A History of Chemistry*, Macmillan, London, **1964**, vol. 4, p. 256; C. Graebe, *Geschichte der Organischen Chemie*, Springer, Berlin, **1920**, p. 49.

Liebig[40] repeated Wöhler's work and found a smaller content of oxygen in his silver cyanate sample which he called "cyanichte Säure". But Liebig had probably analyzed an impure sample of silver cyanate (containing AgCN), and later he confirmed Wöhler's findings, together with another analysis of silver fulminate.[41] As it is well known,[1−7] this was the beginning of a close and long-lasting friendship between Liebig and Wöhler. It may be mentioned that the present author has verified the fulminate ($C{\equiv}N{-}O^-$) to cyanate ($N{=}C{=}O^-$) isomerisation,[42] for which a cyclic intermediate seems plausible.[43]

To summarise, these experiments of Liebig were most important, mainly for three reasons:

− Through his studies of silver fulminate, Liebig was introduced to the field of elemental analysis, which, in 1830, he developed into a general method in organic chemistry, by means of his ingenious five-sphere apparatus (Kali-Apparat; Figure 6).

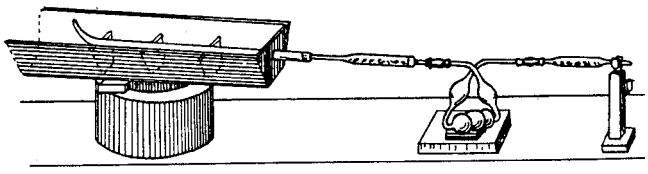

Figure 6. Liebig's method for elemental analysis for the absorption of H_2O ($CaCl_2$) and of CO_2 (KOH) with the five-spheres apparatus

− The identical analyses (but completely different properties) of silver fulminate (Liebig) and silver cyanate (Wöhler) led to the concept of isomerism.

− The work with metal fulminates decided Liebig's future scientific career, and won him − upon recommendation by Humboldt − a professorship at the University of Gießen at a very young age.

In the publication with Gay-Lussac,[17] Liebig also reported reactions of silver fulminate with hydrochloric acid, hydroiodic acid, and hydrogen sulfide. The reaction of AgCNO with H_2S was later separately described by Liebig.[45] This reaction was clarified later.[45]

Liebig had wondered why no gas (HCN) was observed on reaction with hydrochloric acid (Figure 5). It was later found to be due to the formation of Cl(H)C=NOH.[9,21,22,24]

In 1838, Liebig defined acids as compounds in which hydrogen can be replaced by metals (e.g. silver).[46] Following this important definition, fulminic acid was considered by Liebig[47] as a compound in which hydrogen can be substituted by a metal and in which hydrogen is bound to an oxygen-containing "radical".

Liebig published his last paper on metal fulminates in 1855[48] and reported the oligomerisation of fulminic acid (by heating mercury fulminate in a diluted aqueous solution of KCl) to fulminuric acid; this was later studied by Wieland[9,21] and Grundmann.[22,49] Interestingly, Liebig gave, in his first and last publications on metal fulminates, a detailed and safe description for the preparation of silver[10] and mercury[48] fulminate. The preparation of the latter compound was later optimised,[48] and mercury fulminate was also studied by Liebig's student August Kekulé in his habilitation thesis.[50]

Further Developments

Structure of Silver Fulminate and Silver Cyanate

The interesting structure of silver fulminate, Liebig's favourite compound in his young years, was determined by Britton and Dunitz[51] by X-ray crystallography. These X-ray structure determinations were later repeated and confirmed.[51] It was found that AgCNO crystallises in two

 © 2003 Wiley-VCH Verlag GmbH & Co. KGaA, Weinheim

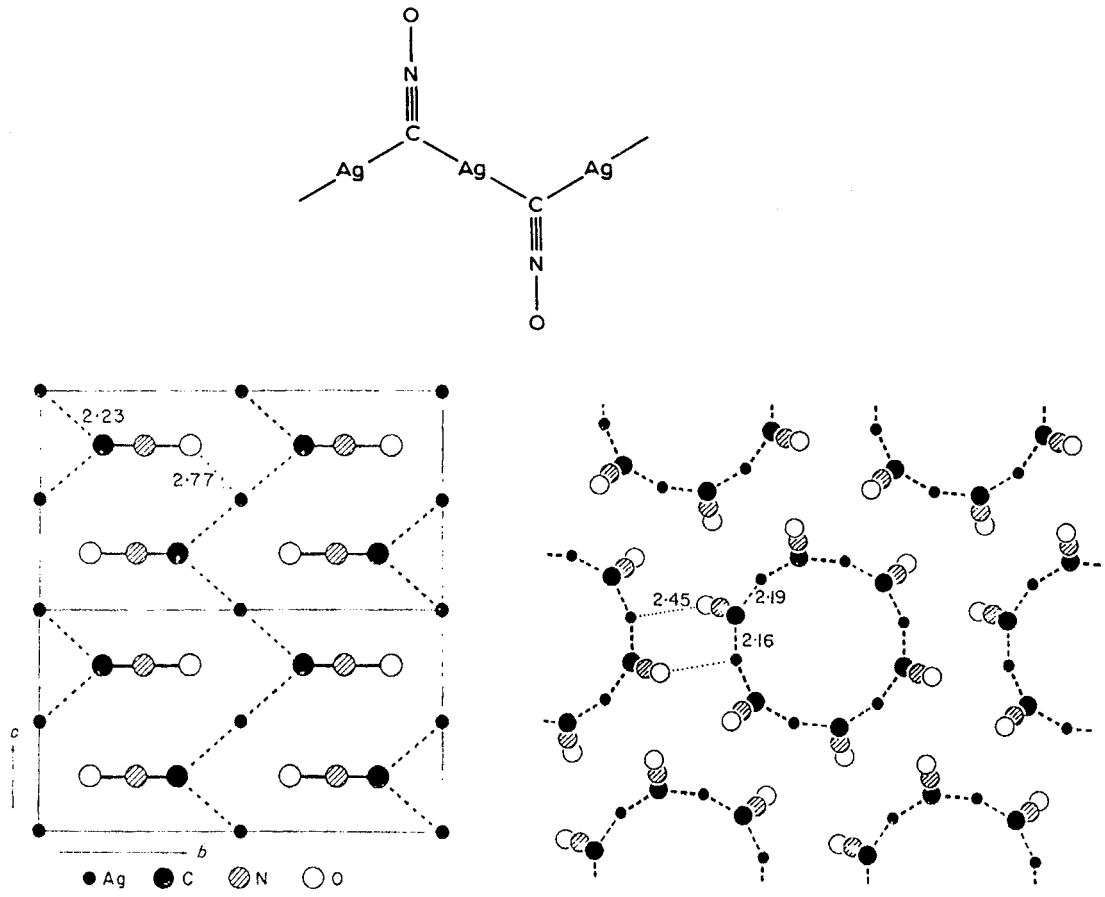

Figure 7. Structural element of orthorhombic (left) and trigonal (right) AgCNO in the crystal

polymorphic forms. In the orthorhombic form, infinite chains with fulminate bridges and three-centred Ag−C−Ag bonds are present (Figure 7), whereas the trigonal silver fulminate structure contains cyclic hexameric units, again with Ag−C−Ag bonds. The crystal structure of the isomeric silver cyanate AgNCO was also determined by Britton and Dunitz[52] and shows Ag−N−Ag−N chains with NCO bridges, where each silver ion has two linearly coordinated N atoms. To the best of our knowledge a full crystal structure determination of mercury fulminate $Hg(CNO)_2$ has not been carried out.[53] Mercury fulminate was widely used as explosive and was introduced by A. Nobel in 1867 as primary explosive to detonate dynamite.[8,54] For this purpose it is now replaced in most industrial countries by lead azide, which is more stable to storage; mercury fulminate can react with metals in moist atmosphere.[55]

Decomposition of Metal Fulminates

Liebig[41] mentioned that oxides of metals (Ag, Hg) which readily loose oxygen form explosive salts of fulminic acid ("Oxide, welche ihren Sauerstoff leicht fahren lassen").

The thermal and photochemical decomposition of $Hg(CNO)_2$, AgCNO, and NaCNO was studied by Boddington and Iqball.[56] Gaseous metal, metal cyanate,[42] CO_2, CO, N_2, and a polymeric material were identified as products by IR and mass spectra.[56] Of interest is the extremely high sensitivity of the ionic fulminates NaCNO or KCNO (in contrast to sodium azide, for example). It was suggested[56] that electron transfer from the fulminate anion to sodium may be involved, to give CNO radicals. Recently, CNO radicals have been generated from anionic precursors in the gas phase.[57] The dimer cyanogen di-*N*-oxide with the linear structure O−N≡C−C≡N−O was also generated in the gas phase.[58] This compound was isolated by Grundmann[22] from dichloroglyoxime and has a rich chemistry.[22,58]

(Fulminato)metal Complexes

Formation of (Fulminato)metal Complexes

As mentioned, the first metal complex with fulminato ligands, $K[Ag(CNO)_2]$, was obtained by Liebig[12,13,17] from the reaction of silver fulminate with potassium chloride. This silver complex was later studied by Wieland.[59] The hexa(fulminato)iron complex $Na_4[Fe(CNO)_6]\cdot 18H_2O$, the analogue of the cyanide $[Fe(CN)_6]^{4-}$, was discovered by Nef.[24] It crystallises with 18 molecules of water, and one can speculate that its structure contains hydrogen bonds between the fulminato ligands and the water molecules (Figure 8).

 © 2003 Wiley-VCH Verlag GmbH & Co. KGaA, Weinheim

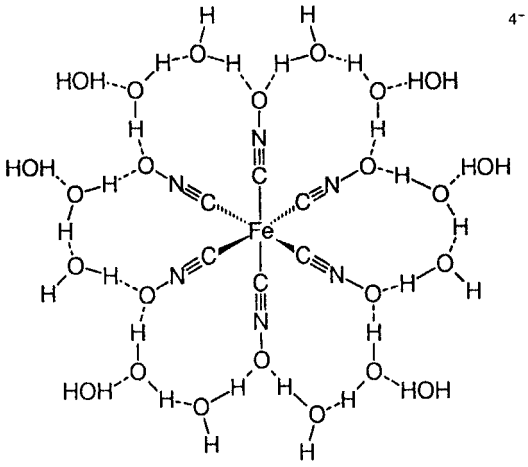

Figure 8. Possible hydrogen bonding in $Na_4[Fe(CNO)_6]\cdot 18\ H_2O$

We found by IR spectroscopy that several (fulminato)-metal complexes like $[Ni(phen)_3][Ru(CNO)_6]\cdot H_2O$, $Na_4[Fe(CNO)_6]\cdot 18H_2O$, and $Na_4[Fe(CN)_5CNO]\cdot H_2O$ are only stable when water of crystallisation is present. On drying, the complexes decompose, with the formation of cyanate.[18,60] Wieland described the explosive mercury complex $Na_2[Hg(CNO)_4]$.[61] The foundations for the coordination chemistry of the fulminate ion were laid by Lothar Wöhler in Darmstadt who, between 1914 and 1929, reported (with his coworkers Martin, Weber, and Berthmann) a series of homoleptic anionic (fulminato)metal complexes, isolated as highly explosive alkali or alkaline earth metal salts.[62] Since that time (about 1930) fulminate complexes did not attract a great deal of attention. The present author studied these complexes in his habilitation work,[18] because a metal−carbon bond had to be assumed, as in transition-metal complexes involving carbon monoxide, isocyanide, cyanide, and acetylide ligands. The coordination chemistry of the metal fulminates up until 1970 has been summarised.[63,64] Therefore, in the following discussion, only the most important features and the newer results will be described. In our group,[60,63] we found that fulminate complexes of transition metals can be stabilised by "diluting" the energy-rich metal−fulminate groups with large cations ($AsPh_4^+$, PPh_4^+, NR_4^+) or with large neutral ligands (e.g. PPh_3). This strategy was also very successfully applied to the isolation and characterisation of (azido)metal complexes, for example $[AsPh_4]_2[Pt(N_3)_6]$.[65]

Usually, these (fulminato)metal complexes were prepared from aqueous sodium fulminate solutions and transition-metal salts, followed by the addition of tetraphenylarsonium chloride.[60,63] The aqueous solution of NaCNO can be prepared from $Hg(CNO)_2$ and sodium amalgam under water.[14,25,62,63] The known homoleptic anionic (fulminato)metal complexes are shown in Table 1; all correspond in their composition to cyano complexes, as it was first pointed out by Liebig[12,13,17] (Table 1). The (fulminato)platinum complex *trans*-$[(Ph_3P)_2Pt(CNO)_2]$ could be obtained by oxidative addition of nitromethane to $[Pt(PPh_3)_4]$ in benzene/ethanol/water.[66] Similarly, Ercolani et al.[67] found that C−C cleavage of α-nitro ketones by platinum(II) and -(0) gives (fulminato)- and (carboxylato)-platinum(II) complexes. Presumably, the formation of fulminate occurs here via a (hydrido)(nitromethyl) complex. The isolation of σ-bonded nitromethyl complexes $[R(R_3P)_2PtCH_2NO_2]$ from zerovalent platinum complexes and nitromethane[68] and the observed conversion of $[R(dppe)PtCH_2NO_2]$ to [R(dppe)PtCNO] by Bennett and co-workers[69] support this assumption. Examples of other nitromethanide compounds are $[R_3SnON(O)CR_2]$[70] and $[(terpy)PtCH_2NO_2]^+$.[71]

Nef[24] and Wöhler[25] showed that mercury fulminate is formed from the sodium salt of nitromethane and $HgCl_2$. In addition, organomercury fulminate compounds RHgCNO can be prepared from RHgOH and CH_3NO_2.[72] Organomercury fulminates RHgCNO are easily formed by synproportionation of diorganylmercury and mercury fulminate[73][74] and can undergo Huisgen[31] [2+3] cycloaddition reactions.[74]

$[(Ph_3P)_2Pt(CNO)_2]$ {which is also accessible from $[Pt(CNO)_4]^{2-}$ and PPh_3 [75]} is best prepared by reaction of $[(Ph_3P)_2Pt(C_2H_4)]$ with nitromethane,[76] since with $[Pt(PPh_3)_4]$ an excess of PPh_3 can lead to reduction of fulminate to give the (cyano)metal complex $[(Ph_3P)_2Pt(CN)_2]$.

A very interesting source of the fulminato ligand is CH_2Cl_2, CO, and nitrate. Bos, Steggerda et al.[77] discovered the formation of the (fulminato)metal complex $[Ph_3PAuCNO]$ and the cluster compound $[Au_{11}(PPh_3)_8(CNO)_2]^+NO_3^-$ by reaction of $[Ph_3PAuNO_3]$ or of $[Au_{9(8)}(PPh_3)_{8(7)}NO_3]$ with carbon monoxide in dichloromethane. It was suggested that the fulminate ligand is formed by reduction of $[Ph_3PAuNO_3]$ with CO to $[Ph_3PAuNO]$, which reacts with CH_2Cl_2 to afford chloroformoxime (Scheme 1). It was demonstrated by ^{13}CO

$$Ph_3PAuNO_3 \xrightarrow[-\ CO_2]{CO} Ph_3PAuNO \xrightarrow{CH_2Cl_2} Ph_3PAuCl + ClHC{=}NOH$$

$$ClHC{=}NOH \xrightarrow{-\ HCl} HCNO \xrightarrow{Ph_3PAuNO_3} Ph_3PAuCNO$$

Scheme 1

Table 1. Homoleptic anionic (fulminato)metal complexes

$[Fe(CNO)_6]^{4-}$	$[Co(CNO)_6]^{3-}$	$[Ni(CNO)_4]^{2-}$	$[Cu(CNO)_2]^-$ $[Cu(CNO)_3]^{2-}$	$[Zn(CNO)_4]^{2-}$
$[Ru(CNO)_6]^{4-}$	$[Rh(CNO)_6]^{3-}$	$[Pd(CNO)_4]^{2-}$	$[Ag(CNO)_2]^-$	$[Cd(CNO)_4]^{2-}$
−	$[Ir(CNO)_6]^{3-}$	$[Pt(CNO)_4]^{2-}$	$[Au(CNO)_2]^-$	$[Hg(CNO)_4]^{2-}$

 © 2003 Wiley-VCH Verlag GmbH & Co. KGaA, Weinheim

experiments that the carbon atom of CNO^- originates from CH_2Cl_2.[77] Dehydrochlorination of chloroformoxime with base gives fulminic acid, which can form the (fulminato)-metal complexes. Already Nef[21,22,24] had reported the formation of AgCNO from chloroformoxime and a silver salt.

An unexpected metal cluster with a fulminate bridge $[(C_5Me_5)_3Mo_3(CO)_4(\mu_3\text{-}O)(\mu_2\text{-}CNO)]$ was reported by Dahl et al.[78] from the photochemical reaction of $[(C_5Me_5)_3Mo_3(CO)_4(O)(N)]$ with CO.

Some (fulminato)metal complexes with the metal atom in a low oxidation state could be obtained from the reaction of the hexacarbonyl compounds of Cr, Mo, and W with sodium fulminate[60] as well as from the reaction of $Et_4N[W(CO)_5Br]$ with AgCNO (***Caution!***),[79] for example $[M(CO)_5CNO]^-$ and $[M(CO)_4(CNO)_2]^{2-}$ (as $AsPh_4^+$ or NEt_4^+ salts; M = Cr, Mo, W).

Reactivity of (Fulminato)metal Complexes

Reduction $M-C\equiv N-O \rightarrow M-C\equiv N$

The fulminate ligand can be reduced to the cyano group; for example, $[Fe(CNO)_6]^{4-}$ and $[Fe(CN)_5(CNO)]^{4-}$ can be deoxygenated with $Fe(OH)_2$ to give $[Fe(CN)_6]^{4-}$.[16] Like nitrile oxides,[22] the metal-coordinated fulminate ion can also be deoxygenated with phosphanes; for example, the (cyano)metal complex *trans*-$[(Ph_3P)_2Pt(CN)_2]$ is formed from the reaction of *trans*-$[(Ph_3P)_2Pt(CNO)_2]$ with PR_3 (R = Ph, OEt). The intermediate $[(Ph_3P)_2Pt(CNO)(CN)]$ could be detected by its IR spectrum.[80] The deoxygenation of the fulminato ligand at the metal atom is chemical proof that the fulminate ion is bonded to the metal atom through the carbon atom.[16,18,64a]

Isomerisation $M-C\equiv N-O \rightarrow M-N=C=O$

Thermal isomerisation of fulminate (at temperatures above 200 °C) to the much more stable[81] isocyanate has been observed for several complexes.[60,63,67,79] As for the fulminate anion[42,43] and nitrile oxides,[22,82] the rearrangement may occur via a cyclic intermediate.

The isomerisation of CNO to NCO was also observed during attempts to stabilise the isofulminic acid or fulminic acid ether complexes ($M-C\equiv N-OH$ or $M-C\equiv N-OR$) by reaction of $[(Ph_3P)_2Pt(CNO)_2]$ with acetic acid or Et_3OBF_4,[79][80] in a similar manner to the formation of hydrogen isocyanide by protonation of cyano complexes.[83] Until now isofulminic acid (HONC) could not be detected, even not by the elegant and thorough studies of Maier and co-workers.[84] However, Wentrup and co-workers[85] were able to generate "organic fulminates" $R-O-N\equiv C$ from 4-oximinoisoxazol-5(4*H*)-ones.

The isomerisation of $[(Ph_3P)_2Pt(CNO)_2]$ to $[(Ph_3P)_2Pt(NCO)_2]$ occurs in the presence of organic carbonyl compounds (e.g. acetone, benzaldehyde) at much lower temperatures.[80] This can be explained by a Huisgen [2+3] cycloaddition of the carbonyl group to the fulminato ligand, to give an (unstable) dioxazolone, similar to nitrile oxides.[22,31,86] The formation of $[(Ph_3P)_2Pt(NCS)_2]$[80] from $[(Ph_3P)_2Pt(CNO)_2]$ and CS_2 or thiobenzophenone can be attributed to a [2+3] cycloaddition of the C−S group to the fulminato ligand — as occurs with organic nitrile oxides[22] — and subsequent elimination of COS or benzophenone, respectively.

Substitution of the fulminato ligand in $[(Ph_3P)_2Pt(CNO)_2]$ by Ph_4AsCN led to Ph_4AsCNO, from which several (fulminato)metal complexes could be safely prepared.[80]

Reactions of Nitrile Oxides with Metal Complexes

The reactions of nitrile oxides with $Co_2(CO)_8$ resulted in deoxygenation to the corresponding nitriles.[87] By reaction of stable nitrile oxides with zerovalent platinum complexes $[(Ph_3P)_2Pt(L)]$ (L = 2 × PPh_3, C_2H_4) the nitrile oxide is deoxygenated and one of the phenyl groups on PPh_3 migrates to the platinum atom to give the complexes $[(Ph_3P)(RCN)Pt(OPPh_2)(Ph)]$,[88] in which the $OPPh_2$ group is bonded by the P atom to the metal atom. The only complex in which an intact RCNO group is present appears to be the cluster $[Cp_3Co_3(\mu_3\text{-}CR)(\mu_2\text{-}RCNO)]$ which is formed from $Cp_3Co_3(\mu_3\text{-}CR)_2$ and NO^+.[89]

With electron-rich carbonyliridium complexes, nitrile oxides undergo Huisgen [2+3] cycloadditions (with the metal−carbon bond as the 1,3-dipolarophile) to give metallacycles $[L_nM-C^a(R)=N-O-C^b(O)(M-C^b)]$.[90] Interestingly, decomposition of these metallacycles gives π-bonded nitrile complexes and can lead to activation of C−H bonds.[90]

Spectra

The IR spectra of binary metal fulminates[42,91] and of (fulminato)metal complexes[18,63,64b,92] are particularly characteristic. The overtone of the ν_s(CNO) [ν(NO)] stretching vibration (at ca. 1100 cm^{-1}) absorbs near the ν_{as}(CNO) band. So, Fermi resonance occurs, and two strong bands appear in the region 2000−2200 cm^{-1}. This is typical for metal fulminates, which can thus be easily identified by their IR spectra. It was observed that ν_{as}(CNO) and ν_s(CNO) are coupled, that is, they move in the same direction for various metal fulminates.[63] Also ^{15}N-containing metal fulminates[93a] and (fulminato)metal complexes[92] have been studied and the frequencies of coordinated cyanate and fulminate groups have been theoretically analyzed.[64b,94] The metal isotope technique was employed to assign the iron−CNO stretching vibration at 533 cm^{-1} of Fe(*o*-phenanthroline)$_2$(CNO)$_2$.[93b] DFT calculations of ν_{as}(CNO) and ν_s(CNO) frequencies of (fulminato)metal complexes are in very good agreement with the observed data.[95]

The ^{14}N chemical shifts in the NMR spectra of metal fulminates are similar to those of nitrile oxides and differ considerably from those of isomeric isocyanate complexes.[96]

The electronic spectra of fulminate complexes reveal that the fulminato ligand is near cyanide in the spectrochemical series[97] (just a little lower in ligand field strength) and also has a similarly strong *trans* influence.[98]

 © 2003 Wiley-VCH Verlag GmbH & Co. KGaA, Weinheim

Table 2. Bond lengths [pm] and angles [°] in metal fulminates

	Ref.	M−C	C≡N	N−O	M−C≡N	C≡N−O
$(Ph_3P)_2Pt(CNO)_2$	[76]	198	113	127	179	178
$[Au(CNO)_2]^-$	[103]	201	110	125	179	178
$[Ph_3PAuCNO]$	[104]	194	115	127	163	179
AgCNO	[51]	218	116	125		180
$[Hg(CNO)_4]^{2-}$	[100]	219	114	125	173	179
$[Co(CNO)_6]^{3-}$	[101]	191	113	127	178	178
$[Ni(CNO)_4]^{2-}$	[102]	187	114	126	174	179
$[Pt(CNO)_4]^{2-}$	[102]	199	115	126	179	179
$[Zn(CNO)_4]^{2-}$	[102]	200	114	125	178	179

The formation constant of $[Hg(CNO)_4]^{2-}$ has been determined ($K_2 = 10^{36}$). This is smaller than that for $[Hg(CN)_4]^{2-}$ by a factor of 10^5, but it is nevertheless still high.[99]

Crystal and Molecular Structures of (Fulminato)metal Complexes

Recently, a series of (fulminato)metal complexes, which had been prepared about 35 years ago and which "survived", were structurally characterised by X-ray diffraction.[100−102]

Table 2 shows the (fulminato)metal complexes, which have so far been studied by X-ray diffraction. In the crystals of, for example, $[AsPh_4][Au(CNO)_2]$, $[AsPh_4]_2[Hg(CNO)_4]$, $[N(C_3H_7)_4]_2[Ni(CNO)_4]$, and $[N(C_3H_7)_4][Pt(CNO)_4]$, it is clearly evident that in the crystal the energy-rich (fulminato)metallate anions are separated and surrounded by the large cations (Figures 9−12). So the metal fulminate groups are "diluted" and the fulminate compounds are thermally stabilised. Already the IR and Raman spectra had indicated the high symmetry of the homoleptic anionic (fulminato)-metal complexes, since only one ν_{as}(CNO) and ν_s(CNO) absorption was observed in the solutions of these compounds.[18,63,92] The X-ray structure determinations of the $AsPh_4^+$ salts of $[Au(CNO)_2]^-$,[103] $[Hg(CNO)_4]^{2-}$,[100] $[Ni(CNO)_4]^{2-}$,[102] $[Pt(CNO)_4]^{2-}$,[102] $[Zn(CNO)_4]^{2-}$,[102] and $[Co(CNO)_6]^{3-}$ [101] reveal the almost ideal linear, tetrahedral, square-planar or octahedral structure of these anions (Figures 9−14).

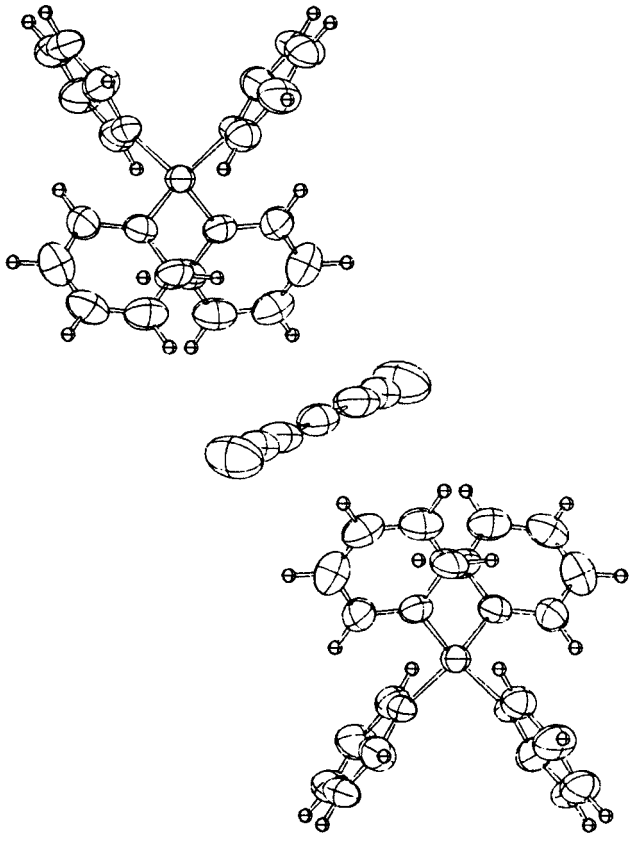

Figure 9. Crystal structure of $AsPh_4[Au(CNO)_2]$

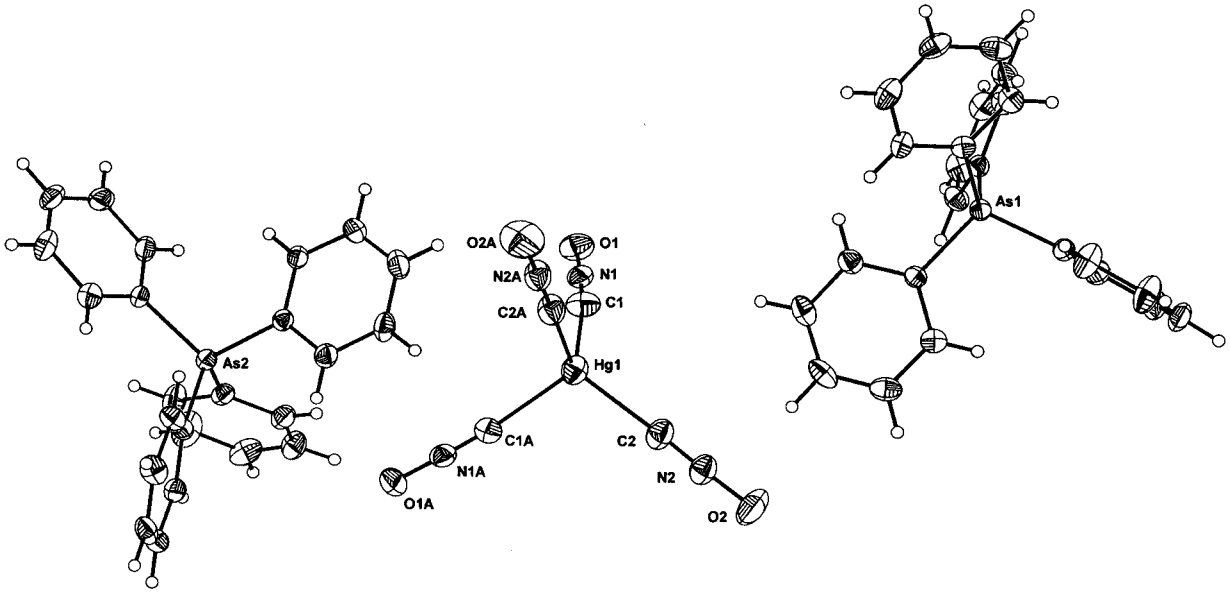

Figure 10. Crystal structure of $[AsPh_4]_2[Hg(CNO)_2]$

 © 2003 Wiley-VCH Verlag GmbH & Co. KGaA, Weinheim

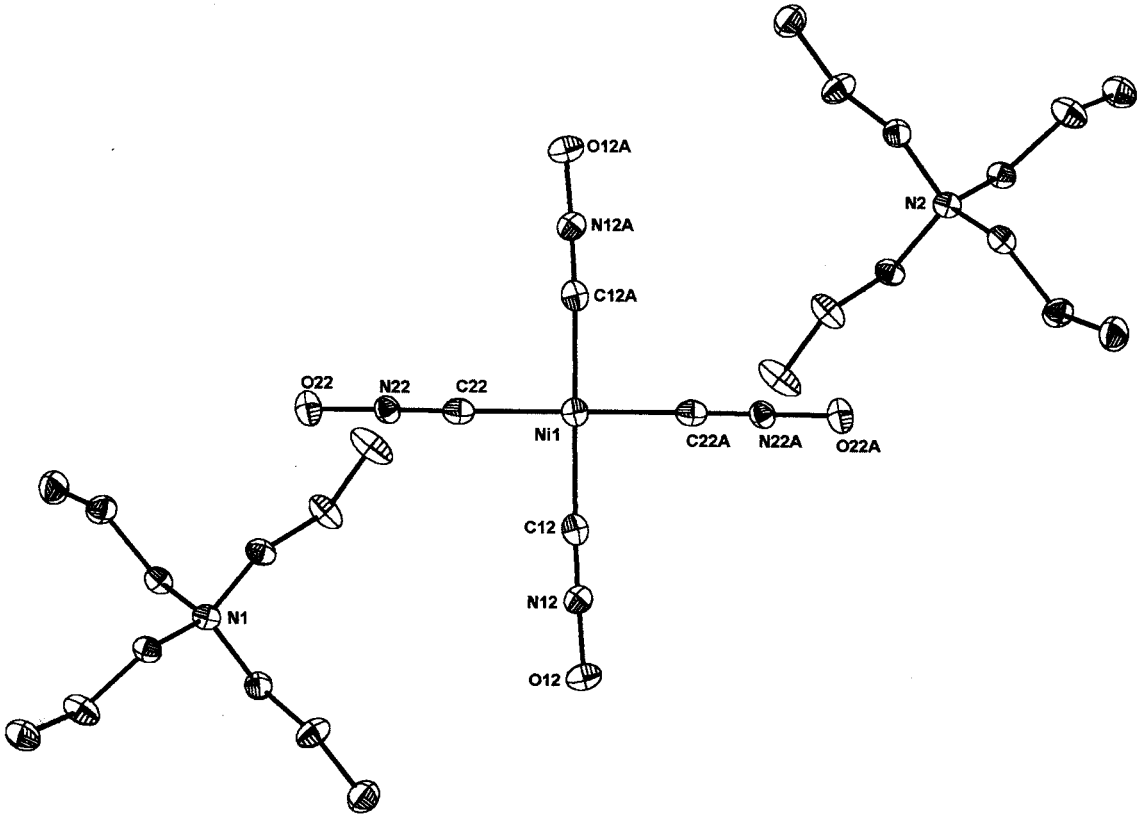

Figure 11. Crystal structure of $[N(C_3H_7)_4]_2[Ni(CNO)_4]$

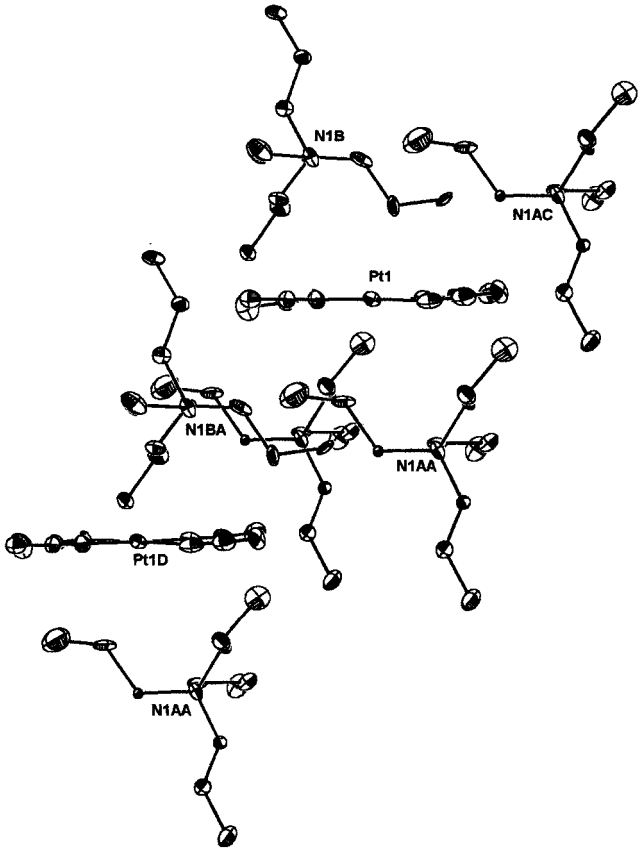

Figure 12. Crystal structure of $[N(C_3H_7)_4]_2[Pt(CNO)_4]$

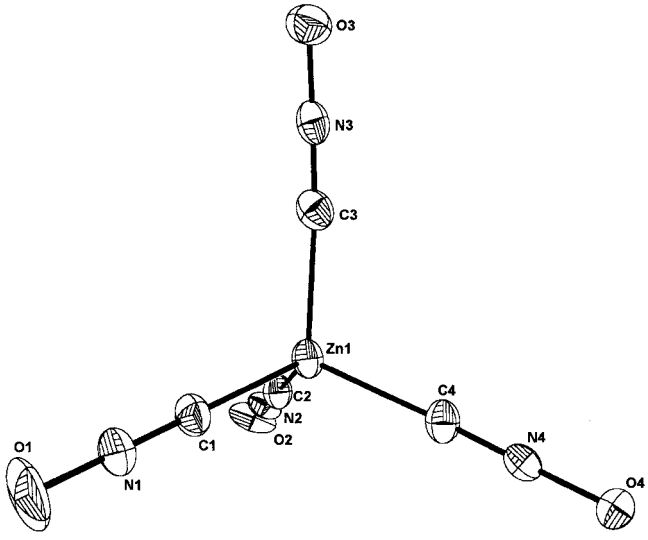

Figure 13. Crystal structure of $[Zn(CNO)_4]^{2-}$

The bonding parameters of the (fulminato)metal complexes are very similar (Table 2) with C≡N and N−O bond lengths of 114−116 pm and 125−126 pm, respectively, and M−C≡N and C≡N−O angles close to 180°. Remarkably, the metal−C and C≡N bond lengths in corresponding (fulminato)- and (cyano)metal complexes are almost identical (Table 3). Therefore, the formula M−C≡N−O| is a good description for the bonding in fulminato complexes. As mentioned earlier, Liebig emphasised the analogy be-

 © 2003 Wiley-VCH Verlag GmbH & Co. KGaA, Weinheim

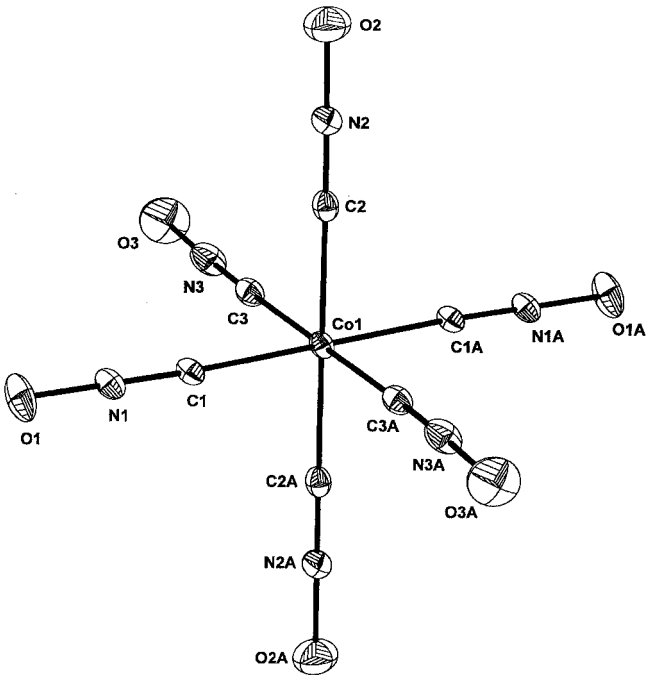

Figure 14. Crystal structure of $[Co(CNO)_6]^{3-}$

Table 3. Bond lengths [pm] in (cyano)- and (fulminato)metal complexes

	Ref.	M−C	C≡N
$[Hg(CNO)_4]^{2-}$	[100]	219	114
$[Hg(CN)_4]^{2-}$	[105]	218	114
$[Co(CNO)_6]^{3-}$	[101]	191	113
$[Co(CN)_6]^{3-}$	[106]	189	115
$[Ni(CNO)_4]^{2-}$	[102]	187	114
$[Ni(CN)_4]^{2-}$	[107]	186	113
$[Pt(CNO)_4]^{2-}$	[102]	199	115
$[Pt(CN)_4]^{2-}$	[108]	ca.200	ca.115
$[Zn(CNO)_4]^{2-}$	[102]	200	114
$[Zn(CN)_4]^{2-}$	[109]	202	116

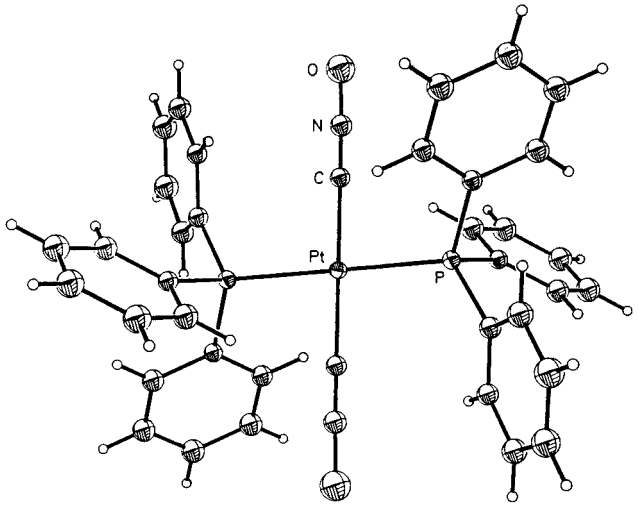

Figure 15. Crystal structure of *trans*-$[(Ph_3P)_2Pt(CNO)_2]$

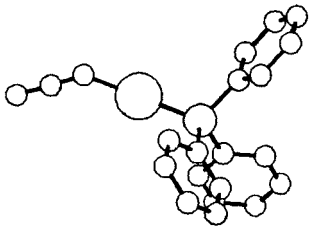

Figure 16. Crystal structure of $[Ph_3PAuNCO]$

tween metal cyanides and fulminates.[12,13,17] The fulminate ion, which is best formulated as C≡N−O$^-$,[42,91,93] behaves predominantly as a σ-donor to the metal ion through an sp-carbon atom in the linear M−C≡N−O group (Figures 9−15), whereas the metal isocyanate group M−N=C=O is bent with an sp^2-nitrogen atom (e.g. in $Ph_3PAu-N=C=O$,[104] Figure 16). DFT (Density Functional Theory) calculations by Klapötke[95] are in good agreement with the observed structural parameters (Table 4).

Table 4. Observed (X-ray) and computed structural parameters

Complex anion	Sym.	*d*(M−C) [Å] calcd./exptl.	*d*(C−N) [Å] calcd./exptl.	*d*(N−O) [Å] calcd./exptl.
$[Co(CNO)_6]^{3-}$	O_h	1.919/1.915(6)	1.181/1.130(6)	1.269/1.269(6)
$[Ni(CNO)_4]^{2-}$	D_{4h}	1.863/1.875(5)	1.184/1.138(5)	1.259/1.261(4)
$[Zn(CNO)_4]^{2-}$	T_d	2.044/2.005(4)	1.187/1.140(4)	1.253/1.250(4)
$[Pt(CNO)_4]^{2-}$	D_{4h}	2.008/2.00(2)	1.184/1.16(3)	1.257/1.25(2)
$[Au(CNO)_2]^-$	$D_{\infty h}$	1.985/2.01(2)	1.187/1.10(3)	1.241/1.25(2)
$[Hg(CNO)_4]^{2-}$	T_d	2.248/2.218(8)	1.188/1.150(9)	1.252/1.256(8)

Acknowledgments

Generous support over many years by the Technische Hochschule München, the Ludwig-Maximilians-Universität München, the Deutsche Forschungsgemeinschaft and the Fonds der Chemischen Industrie and Wacker Chemie München GmbH is gratefully acknowledged. I thank Drs. Erich Schuierer, Klaus Feldl, Peter Swoboda, Claus Oetker, Karl Schorpp, Werner Becker, Florian Holsboer, Wolfgang Weigand, Walter Ponikwar, Professor Franz Lux and the X-ray crystallographers Ulrich Nagel, Peter Mayer, and Holger Pietrowski for their great enthusiasm, skill, and dedication while working with me on metal fulminates. I thank Professor Fritz Eiden for literature on Liebig and Professor Karlheinz Sünkel for looking through the manuscript.

[1] G. von Liebig (J. von Liebig's son), "Liebigs eigenhändige biographische Aufzeichnungen", *Ber. Dtsch. Chem. Ges.* (Referate, Patente, Nekrologe) **1890**, *23*, 817−828; A. W. v. Hofmann, *Ber. Dtsch. Chem. Ges.* **1890**, *23*, 792−811. For Liebig's autobiographical reminiscenses see also: H. von Dechend, *Justus von Liebig, in eigenen Zeugnissen und seine Zeitgenossen*, Verlag Chemie, Weinheim, **1963**; F. Heinrich, "Justus Liebig's year of learning and traveling", *Z. Angew. Chem.* **1929**, *42*, 1173−1176.

[2] J. Volhard, *Justus von Liebig*, Verlag J. A. Barth, Leipzig **1909**, vol. 1 and 2; J. Vollhard, "Justus von Liebig, sein Leben und Wirken, *Justus Liebigs Ann. Chem.* **1903**, *328*, 1−40.

[3] W. H. Brock, *Justus von Liebig − The Chemical Gatekeeper*,

 © 2003 Wiley-VCH Verlag GmbH & Co. KGaA, Weinheim

Cambridge University Press, **1997**. German translation by G. E. Siebeneicher: W. H. Brock, *Justus von Liebig: eine Biografie des großen Wissenschaftlers und Europäers*, Vieweg, Braunschweig, **1999**; W. H. Brock, "Justus von Liebig, Gatekeeper of Chemistry", *Chem. Soc. Rev.* **1995**, 383−389.

[4] C. Paoloni, *Justus von Liebig, eine Bibliogaphie sämtlicher Veröffentlichungen*, Carl Winter, Heidelberg, **1968**; *Justus von Liebig zum 200. Geburtstag*, Antiquariat G. Gruber, Heilbronn, **2003**, Katalog 96.

[5] [5a] G. Schwedt, *Liebig und seine Schüler, die neue Schule der Chemie*, Springer, Berlin, **2002**. [5b] Justus Liebig, Ausstellung der Justus-Liebig-Universität Gießen zum 200. Geburtstag, **2003**, ISBN 3-9808949-1-6, p. 28. [5c] E. Heilbronner, C. Maikoff, "Justus von Liebig and His Kali-Apparat", *Philatelia Chimica et Physica*, **2003**, *25*, 232−240.

[6] T. Heuss, *Justus von Liebig, vom Genius der Forschung*, Hoffmann and Campe, Hamburg **1942**; F. Haber, "Gedächtnisrede auf Justus von Liebig", *Angew. Chem.* **1928**, *33*, 891−897.

[7] R. Winderlich, in: *Das Buch der großen Chemiker* (Ed.: G. Bugge), Verlag Chemie, Weinheim **1955**, vol. 2, p. 1−30; I. Strube, *Justus von Liebig*, Teubner, Leipzig, **1973**.

[8] F. Kurzer, "Fulminic Acid in the History of Organic Chemistry", *J. Chem. Educ.* **2000**, *77*, 851−857; F. Kurzer, "The Life and Work of Edward Charles Howard", *Ann. Sci.* **1999**, *56*, 113−141.

[9] H. Wieland, *Ber. Dtsch. Chem. Ges.* **1907**, *40*, 418−422; H. Wieland, *Ber. Dtsch. Chem. Ges.* **1910**, *43*, 3362−3364; H. Wieland, B. Hess, *Ber. Dtsch. Chem. Ges.* **1909**, *42*, 1346−1363; *Justus Liebigs Ann. Chem.* **1925**, *444*, 7−40; Review on the work of H. Wieland on fulminic acid: F. Klages, *Naturwissenschaften* **1942**, *30*, 351−358.

[10] J. Liebig, "Einige Bemerkungen über die Bereitung und Zusammensetzung des Brugnatellischen und Howardschen Knallsilber", *Buchners Repertorium der Pharmacie* **1822**, vol. XII, p. 412−426.

[11] J. Liebig, "Bemerkungen über das Knallsilber und Einfluß des Lichtes auf Schwefelkalk", *Buchners Repertorium der Pharmacie* **1822**, vol. XIII, p. 300−301.

[12] J. Liebig, "Über das Knallsilber und das Knallquecksilber", *Buchners Repertorium der Pharmacie* **1823**, vol. XV, p. 361−391.

[13] J. Liebig, "Über das Knall-Silber und Knall-Quecksilber und über ihre, und anderer Knall-Metalle wahre Natur", *Gilbert Annalen der Physik und Chemie* **1823**, vol. LXXV, p. 393−420; J. Liebig, "Sur l'Argent et le Mercure fulminans", *Ann. Chim. Phys.* **1823**, *XXIV*, 294−317; presented by Gay-Lussac before the Royal Academy in Paris, Sept. 1823.

[14] E. Carstanjen, A. Ehrenberg, *J. Prakt. Chem.* **1882**, *25*, 232−248; L. Wöhler, F. Martin, *Ber. Dtsch. Chem. Ges.* **1917**, *50*, 586−596; L. Wöhler, *Z. Angew. Chem.* **1914**, *27*, 335−336.

[15] J. Liebig, *Schweiggers Jahrbuch der Chemie und Physik* **1826**, vol. XVIII, p. 380.

[16] L. Schischkoff, *Annalen der Chemie und Pharmacie* **1861**, suppl. vol. I, p. 108; W. Beck, F. Lux, "Über die Reduktion von Hexafulminatoferrat(II) to Hexacyanoferrat(II)", *Chem. Ber.* **1962**, *95*, 1683−1686; W. Beck, *Z. Anorg. Allg. Chem.* **1964**, *333*, 115−119.

[17] J. Liebig, Gay-Lussac, "Analyse du Fulminate d'argent", *Ann. Chim. Phys.* **1824**, *XXV*, 285−311 (presented at the Royal Academy of Science in Paris on March 22, 1824); Prof. Gay-Lussac, Dr. Liebig, "Analyse des knallsauren Silberoxydes", *Kastners Archiv* **1824**, vol. II, p. 58−91; Liebig, Gay-Lussac, "Zerlegung des Knallsilbers", *Schweiggers Jahrbuch* **1824**, vol. XI, p. 129−157; Liebig, Gay-Lussac, "Zerlegung des knallsauren Silberoxydes", *Poggendorffs Annalen der Physik und Chemie*, **1824**, vol. I, p. 87−116.

[18] W. Beck, Habilitationsschrift, "Zur Kenntnis der Fulminato-Komplexe der Übergangsmetalle", Technische Hochschule München, **1963**; W. Beck, *Z. Naturforsch.* **1962**, *17b*, 130−131.

[19] J. Berzelius, "Über die knallsauren Salze", *Ann. Chem. Pharm.* **1844**, *L*, 426−429; J. Liebig, "Bemerkungen zu obiger Notiz", *Ann. Chem. Pharm.* **1844**, *L*, 429−431.

[20] J. Liebig, *Mag. Pharm.* **1831**, *36*, 227−232.

[21] H. Wieland, "Die Knallsäure", *Sammlung Chemischer und Chemisch-Technischer Vorträge*, Enke, **1909**, vol. 14, p. 385−461.

[22] C. Grundmann, P. Grünanger, *The Nitrile Oxids*, Springer, Berlin, **1971**.

[23] M. Winnewisser, B. P. Winnewisser, "Why it took 174 years to understand the structure of fulminic acid", *Chem. Listy* **1976**, *70*, 785−807; J. H. Teles, G. Maier, B. A. Hess, L. J. Schaad, M. Winnewisser, B. Winnewisser, *Chem. Ber.* **1989**, *122*, 753−766, 1219.

[24] J. U. Nef, *Ann. Chem.* **1894**, *280*, 263−342; see also: R. Scholl, *Ber. Dtsch. Chem. Ges.* **1890**, *23*, 3509.

[25] L. Wöhler, *Ber. Dtsch. Chem. Ges.* **1910**, *43*, 754−756; L. Wöhler, *Ber. Dtsch. Chem. Ges.* **1905**, *38*, 1351−1359.

[26] W. Beck, K. Feldl, *Angew. Chem.* **1966**, *78*, 746−747; *Angew. Chem. Int. Ed. Engl.* **1966**, *5*, 722−723; W. Beck, P. Swoboda, K. Feld, R. S. Tobias, *Chem. Ber.* **1971**, *104*, 533−543; H. Ley, H. Kissel suggested in 1899 that fulminic acid could have the HCNO structure (*Ber. Dtsch. Chem. Ges.* **1899**, *32*, 1365), and the tautomerism between CNOH and HCNO was discussed by F. C. Palazzo (*Gazz. Chim. Ital.* **1913**, *43*, 563−570).

[27] G. Schulze, O. Koja, B. P. Winnewisser, M. Winnewisser, *J. Mol. Struct.* **2000**, *517−518*, 307−325; P. R. Bunker, B. M. Landsberg, B. P. Winnewisser, *J. Mol. Spectrosc.* **1979**, *74*, 9−25; M. Winnewisser, H. K. Bodenseh, *Z. Naturforsch.* **1967**, *22a*, 1724−1737; M. Winnewisser, H. K. Bodenseh, *Z. Naturforsch.* **1969**, *24a*, 1966−1973; M. Winnewisser, H. K. Bodenseh, *Z. Naturforsch.* **1969**, *24a*, 1973−1979; S. Albert, M. Winnewisser, "The colorful world of quasilinearity" in: B. Winnewisser, *Mikrochim. Acta Suppl.* **1997**, *14*, 79−88; *Ber. Bunsen-Ges.* **1996**, *100*, 1876−1898; S. Albert, U. Keppler, M. Winnewisser, B. Winnewisser, *J. Mol. Struct.* **2001**, *599*, 347−369; V. E. Bondybey, J. H. English, C. W. Mathews, R. J. Contolini, *J. Mol. Spectrosc.* **1982**, *92*, 431−441.

[28] A Quilico, G. Sgtagna d'Alcontres, *Gazz. Chim. Ital.* **1949**, *79*, 654; A. Quilico, G. Speroni, *Gazz. Chim. Ital.* **1946**, *76*, 148; R. Huisgen, M. Christl, *Angew. Chem.* **1967**, *79*, 471; *Angew. Chem. Int. Ed. Engl.* **1967**, *6*, 456−457; R. Huisgen, M. Christl, *Tetrahedron Lett.* **1968**, 5209−5213; R. Huisgen, M. Christl, *Chem. Ber.* **1973**, *106*, 3291−3311; M. Christl, R. Huisgen, *Chem. Ber.* **1973**, *106*, 3345−3367.

[29] See e.g.: R. D. Harcourt, *J. Phys. Chem. A* **2001**, *105*, 10947−10948; M. T. Nguyen, A. K. Chandra, T. Uchimaru, S. Sakai, *J. Phys. Chem. A* **2001**, *105*, 10943−10946; P. B. Karadakov, D. L. Cooper, *J. Phys. Chem. A* **2001**, *105*, 10946; E. C. Magnuson, J. Pranata, *J. Comput. Chem.* **1998**, *19*, 1795−1804.

[30] L. Pauling, S. B. Hendricks, *J. Am. Chem. Soc.* **1926**, *48*, 641−651; L. Pauling, *J. Chem. Educ.* **1975**, *52*, 577.

[31] R. Huisgen, *Angew. Chem.* **1963**, *75*, 604−637, 742−754; *Angew. Chem. Int. Ed. Engl.* **1963**, *2*, 565, 633; *J. Org. Chem.* **1976**, *41*, 403−419; R. Huisgen, *The Adventure Playground of Mechanisms and Novel Reactions*, ACS, Washington, DC, **1994**; R. Huisgen, in: *1,3-Dipolar Cycloaddition Chemistry* (Ed.: A. Pawda), Wiley, **1984**, vol. 1, p. 653.

[32] J. Koput, B. P. Winnewisser, M. Winnewisser, *Chem. Phys. Lett.* **1996**, *255*, 357−362; M. Winnewisser, R. Schermaul, *Berichte der Justus Liebig Gesellschaft* **1994**, vol. 3, p. 37−53.

[33] D. Poppinger, L. Radom, *J. Am. Chem. Soc.* **1978**, *100*, 3674−3685; N. Pinnavaia, M. J. Branley, M. D. Su, W. H. Green, N. C. Handy, *Mol. Phys.* **1993**, *78*, 319−343; M. Fehér, T. Pasinszki, T. Veszpremi, *Inorg. Chem.* **1995**, *34*, 945−951; T. Pasinszki, N. P. C. Westwood, *J. Am. Chem. Soc.* **1995**, *117*, 8428−8430; A. M. Mebel, A. Luna, M. C. Lin, K. Morokuma, *J. Chem. Phys.* **1996**, *105*, 6439−6454; D. A. Pantazis, A. Tsipis, C. A. Tsipis, *J. Phys. Chem. A* **2002**, *106*, 1425−1440; W. A. Shapley, G. B. Bacskay, *J. Phys. Chem. A* **1999**, *103*, 6624−6631.

[34] A. Quilico, L. Panizzi, *Gazz. Chim. Ital.* **1942**, *72*, 155−164.

 © 2003 Wiley-VCH Verlag GmbH & Co. KGaA, Weinheim

[35] C. Wentrup, B. Gerecht, H. Briehl, *Angew. Chem.* **1979**, *91*, 503−504; *Angew. Chem. Int. Ed. Engl.* **1979**, *18*, 467.

[36] F. De Sarló, A. Brandi, A. Guarna, A. Goti, S. Corezzi, *Tetrahedron Lett.* **1983**, *24*, 1815−1816.

[37] A. Brandi, F. De Sarló, A. Guarna, G. Speroni, *Synthesis* **1982**, 719−721; F. De Sarlo, A. Guarna, A. Brandi, A. Gotti, *Tetrahedron* **1985**, *41*, 5181−5185.

[38] F. Wöhler, *Poggendorffs Ann. Phys. Chem.* **1824**, *1*, 117−124; F. Wöhler, *Poggendorffs Ann. Phys. Chem.* **1825**, *V*, 385−389.

[39] J. Berzelius, *Mag. Pharm.* **1830**, *31*, 260; J. Berzelius, *Poggendorffs Ann. Phys. Chem.* **1830**, *19*, 305.

[40] J. Liebig, "Ueber Wöhler's Cyansäure", *Kastners Archiv* **1825**, vol. VI, p. 145−153.

[41] J. Liebig, "Ueber Cyan- und Knallsäure", *Schweiggers Jahrbuch der Chemie und Physik* **1826**, vol. XVIII, p. 376−381; J. Liebig, "Sur quelque Cyanates", *Ann. Chim. Phys.* **1826**, *XXXIII*, 207−214.

[42] W. Beck, *Chem. Ber.* **1962**, *95*, 341−344; K. Singh, *J. Chem. Soc.* **1959**, 459−461.

[43] F. Holsboer, W. Beck, *J. Chem. Soc., Chem. Commun.* **1970**, 262−263; W. K. Li, J. Baker, L. Randow, *Aust. J. Chem.* **1986**, *39*, 913−921; Y.-S. Cheung, W.-K. Li, *Aust. J. Chem.* **1997**, *50*, 169−172; Y. Pak, R. C. Woods, K. A. Peterson, A. Kirk, *J. Chem. Phys.* **1997**, *106*, 5123−5132; S. Rani, N. K. Ray, *Ind. J. Chem. Sect. A* **1998**, *37*, 811−812.

[44] J. Liebig, "Sur un nouvel Appareil pour l'analyse des substances organique", *Ann. Chim. Phys.* **1831**, *XLVII*, 147−197; J. Liebig, "Ueber einen neuen Apparat zur Analyse organischer Körner und über die Zusammensetzung einiger organischer Substanzen", *Poggendorffs Ann. Phys. Chem.* **1931**, *21*, 1−43.

[45] J. Liebig, "Ueber die Zerlegung des knallsauren Silbers durch Schwefelwasserstoff", *Kastners Archiv* **1825**, vol. VI, p. 327−332; L. Gambi, *Gazz. Chim. Ital.* **1911**, *41*, 166−173; D. Kjiersgaard, A. Kjaer, *Acta Chem. Scand.* **1970**, *24*, 1367−1372.

[46] J. Liebig, "Ueber die Constitution organischer Säuren", *Ann. Pharm.* **1838**, *XXVI*, 113−189.

[47] J. Liebig, "Über die Constitution der knallsauren Salze", *Ann. Pharm.* **1838**, *XXVII*, 133−134.

[48] J. Liebig, "Ueber die Fulminursäure, eine neue Cyansäure", *Ann. Chem. Pharm.* **1855**, *XCV*, 282−290; E. Beckmann, *Ber. Dtsch. Chem. Ges.* **1886**, *19*, 993−995; C. A. Lobry de Bruyn, *Ber. Dtsch. Chem. Ges.* **1886**, *19*, 1370−1372.

[49] [49a] C. Grundmann, R. K. Bansal, P. S. Osmanski, *Justus Liebigs Ann. Chem.* **1973**, 898−909. [49b] C. Grundmann, G. W. Nickel, R. K. Bansal, K. Rai, *Justus Liebigs Ann. Chem.* **1975**, 1029−1075. Recently, in the mass spectrum of a specimen of an oligomer dating from 1970,[26] the trimer $(HCNO)_3$ (m/z = 129) [previously isolated by Wieland,[9,21] Grundmann (ref.[22] and citations therein), Wentrup,[35] and De Sarlo[37]] was identified as main product (G. Fischer, P. Swoboda, W. Beck, unpublished results).

[50] A. Kekulé, *Liebigs Ann. Chem.* **1857**, *101*, 200−213.

[51] D. Britton, J. D. Dunitz, *Acta Crystallogr.* **1965**, *19*, 662−668; J. C. Barrick, D. Canfield, B. C. Giessen, *Acta Crystallogr., Sect. B* **1979**, *35*, 464−465; D. Britton, *Acta Crystallogr., Sect. C* **1991**, *47*, 2646−2647.

[52] D. Britton, J. D. Dunitz, *Acta Crystallogr.* **1965**, *18*, 424−428.

[53] A. Suzuki, *J. Ind. Explos. Soc., Jpn.* **1953**, *14*, 142; Z. Iqbal, A. D. Joffer, *Proc. Roy. Soc.* **1967**, *A302*, 35. A polymeric structure with CNO bridges as in the orthorhombic form of AgCNO[42] may be also present in $Hg(CNO)_2$ since the cell parameters of AgCNO and $Hg(CNO)_2$ are similar (K. Sünkel, personal communication).

[54] A. Nobel, *J. Soc. Arts* **1875**, *23*, 611−626.

[55] J. Boileau, in: "Explosives", *Ullmanns Encyclopedia of Industrial Chemistry*, Wiley Interscience, **2003**.

[56] T. Boddington, Z. Iqball, *Trans. Faraday Soc.* **1969**, *65*, 509−518.

[57] S. Dun, J. H. Bowie, *J. Phys. Chem. A* **2003**, *107*, 76−82.

[58] T. Pasinszki, N. P. C. Westwood, *J. Am. Chem. Soc.* **1995**, *117*, 8425−8430.

[59] H. Wieland, *Ber. Dtsch. Chem. Ges.* **1909**, *42*, 820.

[60] W. Beck, P. Swoboda, K. Feldl, E. Schuierer, *Chem. Ber.* **1970**, *103*, 3591−3604.

[61] H. Wieland, *Justus Liebigs Ann. Chem.* **1925**, *444*, 19.

[62] L. Wöhler, *Angew. Chem.* **1914**, *27*, 335−336; L. Wöhler, F. Martin, *Ber. Dtsch. Chem. Ges.* **1917**, *50*, 586−596; L. Wöhler, A. Weber, *Ber. Dtsch. Chem. Ges.* **1929**, *62*, 2742−2748; L. Wöhler, A. Berthmann, *Ber. Dtsch. Chem. Ges.* **1929**, *62*, 2748−2758.

[63] W. Beck, *Organomet. Chem. Rev., Sect A* **1971**, *7*, 159−190. See also: W. Beck, *Berichte der Liebig-Gesellschaft* **1994**, vol. 3, p. 21−35; W. Beck, *Jahrbuch der Akademie der Wissenschaften in Göttingen*, Vandenhoeck, Göttingen, **1967**, p. 13−16.

[64] Other reviews on (fulminato)metal complexes: [64a] A. G. Sharpe, in: *Comprehensive Coordination Chemistry*, Pergamon Press, Oxford, **1987**, vol. 2, p. 12−14. [64b] G. V. Tsintsadze, in: *Chemie der Pseudohalide* (Eds.: A. M. Golub, H. Köhler), Hüthig Verlag, Heidelberg, **1979**, p. 176−217 and in: *Chemistry of Pseudohalides*, Amsterdam, **1986**. [64c] W. Beck, W. P. Fehlhammer, in: *MTP International Review of Science, Inorg. Chem. Ser. 1*, **1972**, vol. 2, p. 253−300.

[65] W. Beck, W. P. Fehlhammer, P. Pöllmann, E. Schuierer, K. Feldl, *Chem. Ber.* **1967**, *100*, 2335; H. H. Schmidtke, D. Garhoff, *J. Am. Chem. Soc.* **1967**, *89*, 1317; W. Beck, W. P. Fehlhammer, K. Feldl, T. M. Klapötke, G. Kramer, P. Mayer, H. Piotrowski, P. Pöllmann, W. Ponikwar, T. Schütt, M. Vogt, *Z. Anorg. Allg. Chem.* **2001**, *627*, 1751−1758; B. Neumüller, E. Schöck, S. Schlecht, K. Dehnicke, *Z. Anorg. Allg. Chem.* **2000**, *626*, 1792; S. Schröder, W. Preetz, *Z. Anorg. Allg. Chem.* **2001**, *627*, 390−397; A Karnath, *Angew. Chem.* **2001**, *113*, 3231−3232; *Angew. Chem. Int. Ed.* **2001**, *40*, 3135−3136.

[66] W. Beck, K. Schorpp, F. Kern, *Angew. Chem.* **1971**, *83*, 43; *Angew. Chem. Int. Ed. Engl.* **1971**, *10*, 66; K. Schorpp, W. Beck, *Chem. Ber.* **1974**, *107*, 1371−1379.

[67] S. Alessandrini, I. Collamati, C. Ercolani, *J. Chem. Soc., Dalton Trans.* **1973**, 2409−2413.

[68] M. A. Bennett, T. Yoshida, *J. Am. Chem. Soc.* **1978**, *100*, 1750−1759; D. P. Arnold, M. A. Bennett, *J. Organomet. Chem.* **1980**, *199*, 119−135.

[69] T. G. Appleton, M. A. Bennett, *Inorg. Chem.* **1978**, *17*, 738−749.

[70] J. Lorberth, J. Pebler, G. Lange, *J. Organomet. Chem.* **1973**, *54*, 165−190.

[71] M. Akiba, Y. Sasaki, *Inorg. Chem. Commun.* **1998**, *1*, 61−63 and references cited therein.

[72] M. V. Kashutina, O. Y. Okhlobystin, *J. Organomet. Chem.* **1967**, *9*, 5−9; M. V. Kashutina, O. Y. Okhlobystin, *Izvestiya Akademi Nauk SSSR, Ser. Khim.* **1968**, 2311−2314 (*Chem. Abstr.* **1969**, *70*, 29025).

[73] W. Beck, E. Schuierer, *J. Organomet. Chem.* **1965**, *3*, 55−61.

[74] F. De Sarlo, A. Guarna, A. Goti, A. Brandi, *J. Organomet. Chem.* **1984**, *269*, 115−121; F. De Sarlo, A. Brandi, L. Fabrizi, A. Guarna, N. Niccolai, *Org. Magn. Res.* **1984**, *22*, 372−375 (*Chem. Abstr.* **1984**, *101*, 151983).

[75] W. Beck, E. Schuierer, *Chem. Ber.* **1965**, *98*, 298−306.

[76] W. Weigand, U. Nagel, W. Beck, *J. Organomet. Chem.* **1986**, *314*, C55−C58.

[77] W. Bos, J. J. Bour, J. J. Steggerda, L. H. Pignolet, *Inorg. Chem.* **1985**, *24*, 4298−4301; W. Bos, PhD thesis, ISBN 90-9001558-2, **1987**.

[78] C-P. Gibson, B. A. Adams, L. F. Dahl, 190th ACS National Meeting, Chicago, **1985**, abstract no. 73.

[79] F. Beck, W. P. Fehlhammer, W. Beck, *J. Organomet. Chem.* **1985**, *279*, C22−C24.

[80] W. Beck, K. Schorpp, C. Oetker, *Chem. Ber.* **1974**, *107*, 1380−1388.

[81] By 1926 L. Pauling had already calculated the stability of CNO^- and NCO^- ions.[30]

[82] C. Grundmann, P. Kochs, J. R. Boal, *Justus Liebigs Ann. Chem.*

 © 2003 Wiley-VCH Verlag GmbH & Co. KGaA, Weinheim

1972, 162−181; L. W. Gibbs, D. K. Wedegaertner, *J. Org. Chem.* **1991**, *56*, 7320−7322.
[83] W. P. Fehlhammer, M. Fritz, *Chem. Rev.* **1993**, *93*, 1243−1280.
[84] G. Maier, A. Bothur, J. Eckwert, H. P. Reisenauer, T. Stumpf, *Liebigs Ann./Recueil* **1997**, 2505−2517; G. Maier, *Berichte der Justus-Liebig-Gesellschaft*, **1994**, vol. 3, p. 123−135.
[85] C. Wentrup, B. Gerecht, D. Laqua, H. Briehl, H. W. Winter, H. P. Reisenauer, M. Winnewisser, *J. Org. Chem.* **1981**, *46*, 1046−1048; Wentrup used the name fulminate for RONC; G. I. Yranzo, J. Elguro, R. Flammang, C. Wentrup, *Eur. J. Org. Chem.* **2001**, 2209−2220.
[86] R. Huisgen, W. Mack, *Tetrahedron Lett.* **1961**, 581; R. Huisgen, W. Mack, E. Aneser, *Angew. Chem.* **1961**, *73*, 656.
[87] W. Beck, A. Mielert, E. Schier, *Z. Naturforsch., Teil B* **1969**, *24*, 936.
[88] W. Beck, M. Keubler, E. Leidl, U. Nagel, M. Schaal, S. Cenini, P. del Buttero, E. Licandro, S. Maiorana, *J. Chem. Soc., Chem. Commun.* **1981**, 446−448.
[89] A. Goldhaber, K. P. C. Vollhardt, E. C. Walborsky, M. Wolfgruber, *J. Am. Chem. Soc.* **1986**, *108*, 516−518.
[90] J. A. Walker, C. B. Knobler, M. F. Hawthorne, *J. Am. Chem. Soc.* **1983**, *105*, 3370; P. A. Chetcuti, M. F. Hawthorne, *J. Am. Chem. Soc.* **1987**, *109*, 942−943; P. A. Chetcuti, J. A. Walker, C. B. Knobler, *Organometallics* **1988**, *7*, 641, 650.
[91] Z. Iqball, A. D. Yoffe, *Proc. R. Soc.* **1967**, *302*, 35−49.
[92] W. Beck, C. Oetker, P. Swoboda, *Z. Naturforsch., Teil B* **1973**, *28*, 229−233.
[93] [93a] K. Sing, N. N. Banerji, *J. Chem. Soc.* **1965**, 1513−1515. [93b] J. H. Takemoto, B. Streusand, B. Hutchinson, *Spectrochim. Acta* **1974**, *30A*, 827−834.
[94] A. Yu. Tsivadze, Yu. Kharitonov, G. V. Tsintsadze, *Zh. Neorg. Khim.* **1972**, *17*, 2706−2712; *Chem. Abstr.* **1973**, *78*, 35634.
[95] W. Beck, T. M. Klapötke, *Z. Naturforsch., Teil B* **2001**, *56*, 1376−1378.
[96] W. Becker, W. Beck, *Z. Naturforsch., Teil B* **1970**, *25*, 101−102.
[97] W. Beck, K. Feldl, *Z. Anorg. Allg. Chem.* **1965**, *341*, 113−123.
[98] W. Beck, K. Feldl, *Z. Naturforsch., Teil B* **1966**, *21*, 588−589.
[99] B. Klatt, K. Schwabe, *J. Electroanal. Chem.* **1970**, *24*, 61−78.
[100] W. Ponikwar, E. Schuierer, W. Beck, *Z. Anorg. Allg. Chem.* **2000**, *626*, 1282−1284.
[101] P. Mayer, W. Ponikwar, P. Swoboda, W. Beck, *Z. Anorg. Allg. Chem.* **2000**, *626*, 2038−2039.
[102] W. Ponikwar, P. Mayer, H. Pietrowski, P. Swoboda, C.-J. Oetker, W. Beck, *Z. Anorg. Allg. Chem.* **2002**, *628*, 15−19.
[103] U. Nagel, K. Peters, H. G. von Schnering, W. Beck, *J. Organomet. Chem.* **1980**, *185*, 427−432.
[104] W. P. Bosman, W. Bos, J. M. M. Smits, P. T. Beurskens, J. J. Bour, J. J. Steggerda, *Inorg. Chem.* **1986**, *25*, 2093−2095.
[105] P. Klüfers, H. Fuess, S. Haussühl, *Z. Kristallogr.* **1981**, *156*, 255.
[106] M. Konno, F. Murumo, Y. Saito, *Acta Crystallogr., Sect. B* **1979**, *29*, 739.
[107] M. G. Clark, J. R. Cancedo, A. G. Maddock, A. F. Williams, *J. Chem. Soc., Dalton Trans.* **1975**, 120.
[108] W. Holzapfel, H. Yersin, G. Gliemann, *Z. Kristallogr.* **1981**, *157*, 47; G. Gliemann, H. Yersin, *Struct. Bonding (Berlin)* **1985**, *62*, 89.
[109] A. Sequeira, R. Chidambaram, *Acta Crystallogr.* **1966**, *20*, 910.

Received July 16, 2003

 © 2003 Wiley-VCH Verlag GmbH & Co. KGaA, Weinheim

Stoichiometric Control of the Magnetic Properties in Copper(II) Cyano-Bridged Bimetallic Complexes

Eugenio Coronado,[a] Carlos Giménez-Saiz,[a] Alicia Nuez,[a] Víctor Sánchez,[a] and Francisco M. Romero*[a]

Keywords: Magnetic properties / Heterometallic complexes / N ligands / Copper / Iron

Control of the Cu^{2+} ion coordination environment affords a 1D, magnetically diluted compound, $[Cu(cis\text{-chxn})_2]_3[Fe(CN)_6]_2\cdot 7H_2O$ (**1**) and the 2D ferromagnetic material $[Cu(cis\text{-chxn})]_3[Fe(CN)_6]_2\cdot 6H_2O$ (**2**) with a critical temperature, T_c, of 3.5 K.

(© Wiley-VCH Verlag GmbH & Co. KGaA, 69451 Weinheim, Germany, 2003)

Introduction

The search for bimetallic cyanide systems based on Prussian blue has given rise to a rich and well-documented family of molecule-based magnets. Most of these systems are obtained from the assembly of unsaturated cations of the $[M^{II}(L)_n]^{2+}$ type (where M = Ni[1−9] or Cu;[1,9−18] L = polydentate ligand) and hexacyanometallate anions: $[M^{II}(CN)_6]^{4-}$ or $[M^{III}(CN)_6]^{3-}$ (where M^{II} = Fe^{II}; M^{III} = Fe^{III}, Mn^{III}, Co^{III}, or Cr^{III}). The choice of the polydentate ligand, the metal ion and its number of free coordination sites in the cationic unit endow us with potential control over the dimensionality and magnetic properties of these systems. Ni^{2+} ions invariably present six-coordination, whereas d^9 Cu^{2+} ions are stereochemically more versatile and can be either tetra-, penta- or hexacoordinate. Therefore, the use of $[Cu(L)_n]^{2+}$ building blocks should enable the preparation of new compounds with novel structures and perhaps improved magnetic properties. However, not very many examples of these have been reported to date. Only two of such copper-containing compounds, $[Cu(EtOH)_2][Cu(en)]_2[Cr(CN)_6]_2$ (en = 1,2-diaminoethane)[15] and $[Cu(tn)]_3[Cr(CN)_6]_2\cdot 3H_2O$ (tn = 1,3-diaminopropane),[18] have been structurally characterised and exhibit spontaneous magnetisation, with critical temperatures, T_c, of 57 K and 9.5 K, respectively. To the best of our knowledge, no $Cu^{II}-Fe^{III}$ cyanide-bridged compounds showing magnetic ordering have been reported so far, as most of the $Cu^{II}-Fe$ bimetallic systems are indeed formed by diamagnetic hexacyanoferrate(II) units. By stoichiometric control of the copper-coordination environment, allowing either axial or equatorial coordination of the hexacyanometallate anions, the compounds $[Cu(cis\text{-chxn})_2]_3[Fe(CN)_6]_2\cdot 7H_2O$ (**1**) and $[Cu(cis\text{-chxn})]_3[Fe(CN)_6]_2\cdot 6H_2O$ (**2**) (where *cis*-chxn = *cis*-cyclohexane-1,2-diamine), respectively, were obtained. Herein we report their syntheses, structural characterizations and magnetic properties.

[a] Institut de Ciència Molecular, Universitat de València, Dr. Moliner 50, 46100 Burjassot, Spain
Fax: (internat.) + 34-963544859
E-mail: fmrm@uv.es

Results and Discussion

Compound **1** crystallises in the centrosymmetric $P\bar{1}$ space group. A view of the crystal structure along the *a* axis (see Figure 1) shows the existence of Cu(1)−NC−Fe(1)−CN−Cu(2) zigzag chains running along the [011] direction and composed of alternating *trans*-$[Cu(cis\text{-chxn})_2]^{2+}$ cations and $[Fe(CN)_6]^{3-}$ anions. The latter exhibit an octahedral environment and bind axially to the copper ions in a μ^2-mode. The Cu(1) and Cu(2) atoms of the cationic unit show centrosymmetric, elongated, octahedral geometries due to Jahn−Teller effects, with long axial Cu−N distances as compared to those of equatorial ligands [Cu(1)−N(ax): 2.818(3) Å; Cu(1)−N(eq): 1.995(3) Å and 2.027(2) Å; Cu(2)−N(ax): 2.676(3) Å; Cu(2)−N(eq): 1.996(3) Å and 2.017(2) Å]. Cu−N−C angles within the chain deviate greatly form linearity, with values ranging between 120.8° and 109.4°. Similar values have been reported for other copper-containing compounds.[4,12−14,17,18] Isolated from the chain, square planar $[Cu(cis\text{-chxn})_2]^{2+}$ cations compensate the charge of the polymer. The shortest Cu(3)−N[Fe(1)] distances is 3.123(3) Å. Seven water molecules of crystallisation are present in the structure per formula unit. Four of them [O(1) and O(2)] are hydrogen-bonded to each other and to terminal cyanide groups belonging to adjacent chains, leading to a two-dimensional network.

The thermal variation of the $\chi_m T$ product for **1** is shown in Figure 2. At room temperature $\chi_m T$ equals 2.42 emu·K·mol^{-1}. This value differs from the spin-only value

 DOI: 10.1002/ejic.200300641 © 2003 Wiley-VCH Verlag GmbH & Co. KGaA, Weinheim

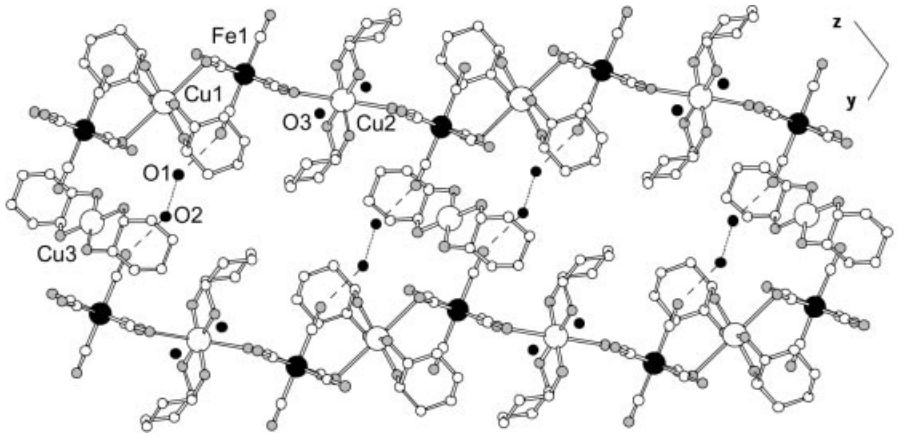

Figure 1. View of the crystal molecular structure of **1** along the *a* axis; dashed and dotted lines refer to hydrogen bonds

of 1.875 emu·K·mol^{-1} calculated for uncorrelated spins, owing to the orbital contribution in low-spin Fe^{III} complexes. Spin-orbit coupling accounts for the smooth decrease in $\chi_m T$ observed on cooling. Below 4 K, $\chi_m T$ decreases on lowering the temperature, indicating the existence of weak intermolecular magnetic interactions.

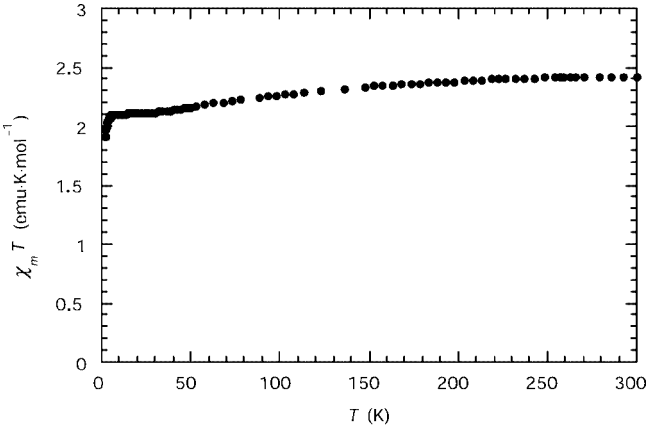

Figure 2. Temperature dependence of the χT product for **1**

Compound **2** also crystallises in the $P\bar{1}$ space group. It presents a structure similar to that reported previously for compound [Cu(tn)]$_2$[Fe(CN)$_6$]·KCl·5H$_2$O[18] (see Figure 3). The binding of [Cu(*cis*-chxn)]$^{2+}$ cations and [Fe(CN)$_6$]$^{3-}$ anions yields a two-dimensional [Cu(*cis*-chxn)]$_2$[Fe(CN)$_6$] monocationic assembly made up of defective cubane units. The structure can also be viewed as a hexagonal close packing of copper ions, in which the iron atoms occupy the octahedral sites ($CdCl_2$-type layered structure). Thus, every [Fe(CN)$_6$]$^{3-}$ moiety links to six copper atoms in a μ^6-mode, whereas each copper ion presents a square-based pyramidal geometry and links to three iron units. Two cyanide ligands and a bidentate *cis*-chxn ligand bind to the equatorial positions of the square-based pyramids and the apical sites are occupied by the third bridging CN$^-$ anion (see Table 1). One *cis*-chxn ligand is disordered over two positions in the coordination sphere of the Cu(3) metal centre. Cu−N−C angles are close to linear; the values range between 163.9° and 177.3°. Fe(2) ions occupy an inversion centre in the structure. A view along the *b* axis (see Figure 3) shows all iron atoms lying in the same *ab* plane and all copper atoms, as well as bulky cyclohexane rings, lying on both sides of this central plane. A very long interlayer Cu···Cu separation of 12.290 Å results. It should be noted that the presence of isolated [Fe(CN)$_6$]$^{3-}$ anions between the layers ensures electroneutrality and yields an overall two-component material.

The value of the $\chi_m T$ product of **2** at room temperature (2.32 emu·K·mol^{-1}) is slightly higher than the spin-only value and accounts for the orbital contribution of the low-spin iron(III) ions. A continuous decrease of $\chi_m T$ is observed on cooling (see Figure 4), as expected from the spin-orbit coupling of the iron sites. Below 15 K, $\chi_m T$ increases sharply, pointing to the onset of long-range ferromagnetic order. The first magnetisation curve performed at 2 K reaches a value of 4.69 μ_B at 5 T, close to the one expected for complete saturation. AC susceptibility measurements performed between 2 and 5 K show the appearance of an out-of-phase signal below the critical temperature, T_c = 3.5 K (Figure 4, inset). The frequency dependence of this signal appears to be a common feature in bimetallic magnets based on chxn ligands.[7,8] Finally, the magnetic order was confirmed by specific-heat measurements. The typical metamagnetic behaviour reported for several bimetallic cyanide systems was not observed in our case, a result that is attributed to the large interplanar distance induced by the presence of the bulky chxn ligands.[1,8]

Conclusion

Simple molecular orbital considerations predict the observation of ferromagnetic interactions between hexacyanoferrate(III) anions (t_{2g}^5 electronic configuration) and copper(II) ions (t_{2g}^6 e_g^3) in octahedral geometry. Surprisingly, this type of interaction has rarely been observed in such bimetallic systems and there is no previously reported example of a Cu^{II}−Fe^{III} cyano-bridged magnet, despite the fact that several two-dimensional structures have been de-

 © 2003 Wiley-VCH Verlag GmbH & Co. KGaA, Weinheim

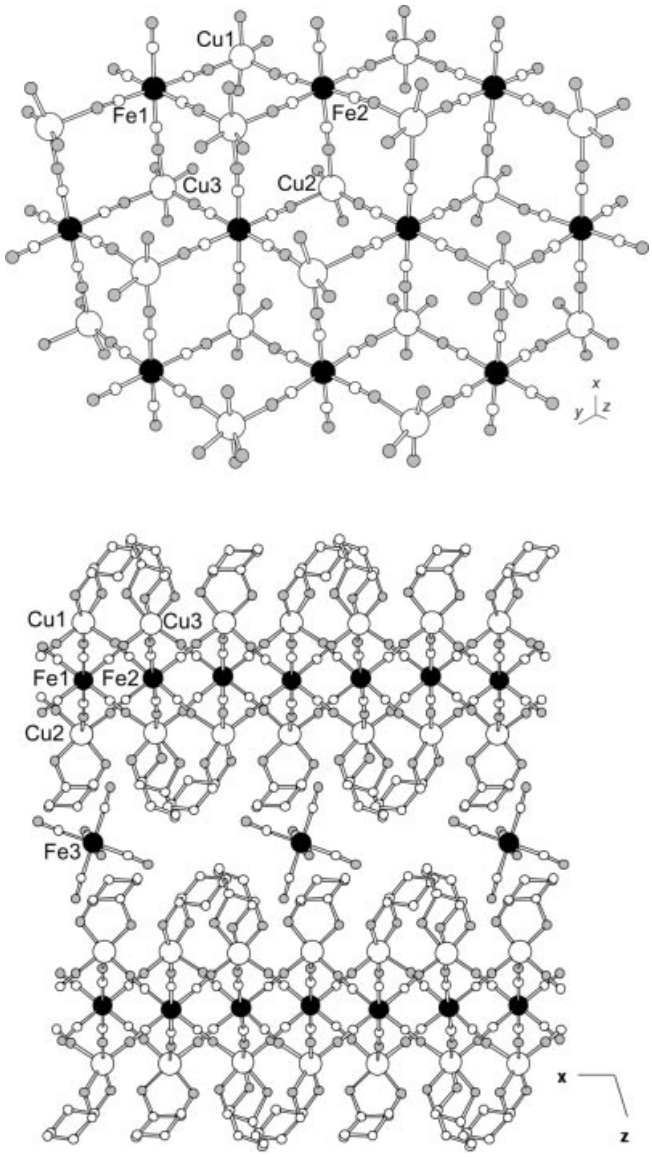

Figure 3. Crystal structure of **2**: (top) projection of the 2D monocationic network showing the defective cubane units (cyclohexane rings have been omitted for clarity); (bottom) view along the *b* axis of the interlayer arrangement and the isolated hexacyanoferrate(III) anions

scribed. It can be anticipated that the use of $[Cu(L)_2]^{2+}$ precursors (where L = diamine) in the synthesis of Cu_3Fe_2 bimetallic complexes compels axial coordination of the cyanide ligands. In fact, the soft, stronger diamine ligands are expected to occupy the equatorial positions of the Cu^{2+} coordination sphere. Due to the Jahn−Teller effect, long intrachain Cu···N(Fe) distances result and a magnetic behaviour of quasi-isolated spins is observed. As shown here, compound **1**, obtained from the $[Cu(cis\text{-chxn})_2]^{2+}$ precursor (either prepared in situ or isolated), follows exactly the same behaviour. These occurrences are overcome by the use of $[Cu(cis\text{-chxn})]^{2+}$ building blocks, enabling cyanide-bridging ligands to bind to the equatorial positions in the Cu^{II} coordination environment. Shorter Cu···N(Fe) distances and higher dimensionality are achieved in this coordination

Table 1. Cu−N distances (Å) for compound **2**

Bond	Distance (Å)
Cu(1)−N(1)	2.012(3)
Cu(1)−N(2)	2.024(2)
Cu(1)−N(3)	1.977(2)
Cu(1)−N(4)	1.987(2)
Cu(1)−N(5)	2.209(3)
Cu(2)−N(6)	2.017(2)
Cu(2)−N(7)	2.004(3)
Cu(2)−N(8)	2.235(3)
Cu(2)−N(9)	1.981(2)
Cu(2)−N(10)	1.971(3)
Cu(3)−N(11)	2.021(4)
Cu(3)−N(11′)	2.031(7)
Cu(3)−N(12)	2.007(3)
Cu(3)−N(13)	2.111(3)
Cu(3)−N(14)	1.967(2)
Cu(3)−N(15)	2.024(3)

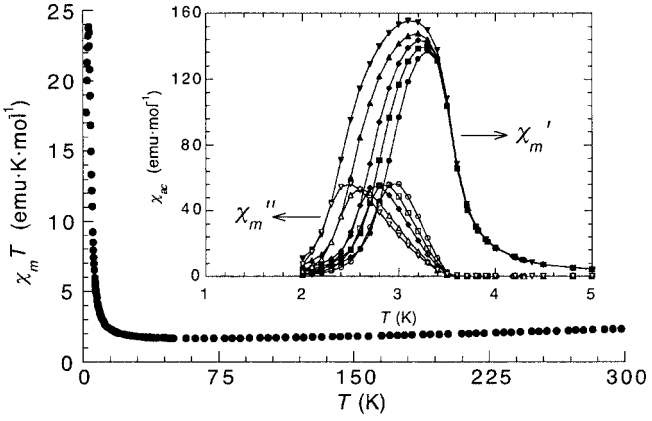

Figure 4. Temperature dependence of the *dc* $\chi_m T$ product for **2**; inset: real (filled symbols) and imaginary (open symbols) components of the *ac* magnetic susceptibility for **2** at frequencies of 997 (circles), 332 (squares), 110 (rhombuses), 10 (up triangles) and 1 Hz (dow

mode. It is also interesting to compare the quasi-linear Cu···Fe bridges of **2** with the extremely bent angles observed in **1**. This is expected to enhance the ferromagnetic components of the magnetic interactions for the former compound. All these features allow the observation of long-range magnetic ordering, despite the poor energy match between the orbitals of the different metal centres. Indeed, compound **2** is the only $Cu^{II}-Fe^{III}$ cyano-bridged ferromagnet reported to date. In addition, it exhibits a two-component structure comprising ferromagnetic layers and paramagnetic ferricyanide anions located in between. Experiments in progress (Mössbauer and single-crystal EPR) may provide information about the magnetic environment of the different sites present in the structure.

Experimental Section

General Remarks: Compounds $Cu(NO_3)_2{\cdot}3H_2O$ (Panreac), $K_3[Fe(CN)_6]$ (Fluka) and *cis*-chxn (Fluka) were of reagent grade and used without further purification.

 © 2003 Wiley-VCH Verlag GmbH & Co. KGaA, Weinheim

[Cu(*cis*-chxn)$_2$(NO$_3$)$_2$]: This precursor was prepared by a method similar to that reported previously for the *trans*-chxn analogue.[19] A solution of *cis*-chxn (228 mg, 2 mmol) in methanol (5 mL) was added dropwise to a stirred solution of Cu(NO$_3$)$_2$·3H$_2$O (242 mg, 1 mmol) in the same amount of methanol. The violet precipitate was filtered off, washed with methanol and air-dried. $C_{12}H_{28}CuN_6O_6$ (415.94): calcd. C 34.65, H 6.79, N 20.2; found C 34.60, H 7.08, N 20.91. IR (KBr): $\tilde{\nu}$ = 3288, 3237, 2935, 2858, 1603 cm^{-1}.

[Cu(*cis*-chxn)$_2$]$_3$[Fe(CN)$_6$]$_2$·7H$_2$O (1): Cu(NO$_3$)$_2$·3H$_2$O (72 mg, 0.3 mmol) and *cis*-chxn (68 mg, 0.6 mmol) were dissolved in the minimum amount of water. Slow diffusion of this solution and an aqueous solution of K$_3$[Fe(CN)$_6$] (66 mg, 0.2 mmol) produced brown crystals of the title compound. Complex **1** was also obtained by slow diffusion of [Cu(*cis*-chxn)$_2$(NO$_3$)$_2$] (125 mg, 0.3 mmol) and K$_3$[Fe(CN)$_6$] (66 mg, 0.2 mmol) in water. $C_{48}H_{98}Cu_3Fe_2N_{24}O_7$ (1425.80): calcd. C 40.44, H 6.93, N 23.58; found C 40.27, H 6.78, N 24.13. IR (KBr): $\tilde{\nu}$ = 3309 cm^{-1}, 3242 (N−H), 2930, 2853 (C−H), 2118, 2105 (C≡N).

[Cu(*cis*-chxn)]$_3$[Fe(CN)$_6$]$_2$·6H$_2$O (2): This compound was obtained by slow diffusion of Cu(NO$_3$)$_2$·3H$_2$O (72 mg, 0.3 mmol), *cis*-chxn (34 mg, 0.3 mmol) and K$_3$[Fe(CN)$_6$] (66 mg, 0.2 mmol) in water as described above for **1**. IR (KBr): $\tilde{\nu}$ = 3309 cm^{-1}, 3145 (N−H), 2925, 2853 (C−H), 2172, 2141, 2105, 2100, 2090 (C≡N).

Magnetic Measurements: Variable-temperature susceptibility measurements were carried out on polycrystalline samples in the 2−300 K temperature range at magnetic fields of 1 T (**1**) and 0.1 T (**2**) using a magnetometer (Quantum Design MPMS-XL-5) equipped with a SQUID sensor. Diamagnetic contributions were corrected with Pascal's constants. Isothermal magnetization measurements at 2 K were carried out up to 5 T by using the same equipment.

X-ray Crystallographic Study: X-ray diffraction data of **1** and **2** were collected at room temperature with a Nonius−KappaCCD diffractometer using a graphite monochromated Mo-K_α radiation source (λ = 0.71073 Å). Denzo and Scalepack[20] programs were used for cell refinements and data reduction. The structures were solved by direct methods using the SIR97[21] program with the WinGX[22] graphical user interface. The structure refinements were carried out with SHELX-97.[23] All non-hydrogen atoms were refined anisotropically. Multiscan absorption corrections, based on equivalent reflections, were applied to the data using the program SORTAV.[24] Crystallographic data are summarized in Table 2.

For **1**, three independent H$_2$O solvent molecules were found in the asymmetric unit and were well behaved. The sample, however, showed the presence of further disordered water molecules. Calculations with PLATON[25] indicated a solvent-accessible void centred around the inversion point (*1/2*, *1/2*, *1/2*) with an area of 73 Å^3. There was some indication of electron density at this site. The presumed solvent was heavily disordered and no realistic atomic model could be satisfactorily refined. Therefore, the SQUEEZE procedure of Spek and van der Sluis[26] was used to accommodate this extra density. A total of 20 electrons per unit cell were recovered and they fit quite well with one water molecule. This extra H$_2$O molecule was added to the final formula of **1**. H atoms of water molecules were found in difference maps and refined positionally with geometric restraints (O−H = 0.82 Å, N−H = 0.90 Å and H···H = 1.35 Å) and with U_{iso}(H) = 1.2U_{eq}(O). The remaining H atoms were placed in calculated positions and refined with a riding model, with C−H = 0.97 Å, N−H = 0.90 Å and U_{iso}(H) = 1.2U_{eq}(C, N).

In compound **2**, one of the three independent cyclohexanediamine ligands [coordinating to Cu(3)] shows a positional disorder over two sets of sites having refined occupancies of 0.668 and 0.332. This disorder only affects three atoms of the ligand: N(11), C(28) and C(29). H atoms on O(1 W), O(2 W), O(3 W) and N atoms were found in difference maps and refined positionally with geometric restraints as described previously. The H atoms on atoms O(4 W), O(5 W) and O(6 W) could not be found clearly in difference maps.

For both compounds, six low-angle reflections were omitted from the final cycles of refinement because the observed intensities were much lower than the calculated values, as a result of being partially obscured by the beam stop.

CCDC-213881 and -213882 contain the supplementary crystallographic data for this paper. These data can be obtained free of

Table 2. Crystal data and structure refinement for **1−2**

Compound	**1**	**2**
Empirical formula	$C_{48}H_{100}Cu_3Fe_2N_{24}O_8$	$C_{30}H_{48}Cu_3Fe_2N_{18}O_6$
Molecular mass	1443.84	1065.23
a (Å)	8.4720(2)	12.3931(8)
b (Å)	13.4430(3)	12.7006(7)
c (Å)	15.7510(4)	18.2838(5)
α (°)	106.304(5)	102.751(3)
β (°)	103.865(5)	96.370(2)
γ (°)	90.586(5)	119.062(3)
Z	1	2
d (mg·m^{-3})	1.439	1.492
Crystal system	triclinic	triclinic
Space group	$P\bar{1}$	$P\bar{1}$
Crystal dimensions (mm)	0.40 × 0.30 × 0.20	0.20 × 0.10 × 0.10
T (K)	293(2)	293(2)
Θ range	1.78 < Θ < 27.44	2 < Θ < 27.70
Reflections collected	15772	103797
Independent reflections	7270	10862
Data/restraints/parameters	7270/10/398	10862/43/623
Final *R* indices [$I > 2\sigma(I)$]	R_1 = 0.0465, wR_2 = 0.1445	R_1 = 0.0427, wR_2 = 0.1190
R indices (all data)	R_1 = 0.0592, wR_2 = 0.1512	R_1 = 0.0587, wR_2 = 0.1314

 © 2003 Wiley-VCH Verlag GmbH & Co. KGaA, Weinheim

charge at www.ccdc.cam.ac.uk/conts/retrieving.html [or from the Cambridge Crystallographic Data Centre, 12 Union Road, Cambridge CB2 1EZ, UK; Fax: (internat.) + 44-1223-336-033; E-mail: deposit@ccdc.cam.ac.uk].

Acknowledgments

This work was supported by the Ministerio de Ciencia y Tecnología (MCT) (Project n° MAT2001−3507-C02−01). AN thanks the Generalitat Valenciana for a PhD fellowship. CGS and FMR acknowledge research contracts from MCT (Programa "Ramón y Cajal").

[1] M. Ohba, H. Okawa, *Coord. Chem. Rev.* **2000**, *198*, 313, and references cited therein.
[2] H.-Z. Kou, W.-M. Bu, D.-Z. Liao, Z.-H. Jiang, S.-P. Yan, Y.-G. Fan, G.-L. Wang, *J. Chem. Soc., Dalton Trans.* **1998**, 4161.
[3] E. Colacio, J. M. Domínguez-Vera, M. Ghazi, R. Kivekas, F. Lloret, J. M. Moreno, H. Stoeckli-Evans, *Mol. Cryst. Liq. Cryst.* **1999**, *335*, 283.
[4] H.-Z. Kou, S. Gao, W.-M. Bu, D.-Z. Liao, B.-Q. Ma, Z.-H. Jiang, S.-P. Yan, Y.-G. Fan, G.-L. Wang, *J. Chem. Soc., Dalton Trans.* **1999**, 2477.
[5] E. Colacio, J. M. Domínguez-Vera, M. Ghazi, R. Kivekäs, F. Lloret, J. M. Moreno, H. Stoeckli-Evans, *Chem. Commun.* **1999**, 987.
[6] H.-Z. Kou, W.-M. Bu, S. Gao, D.-Z. Liao, Z.-H. Jiang, S.-P. Yan, Y.-G. Fan, G.-L. Wang, *J. Chem. Soc., Dalton Trans.* **2000**, 2996.
[7] F. Bellouard, M. Clemente-León, E. Coronado, J. R. Galán-Mascarós, C. J. Gómez-García, F. M. Romero, K. R. Dunbar, *Eur. J. Inorg. Chem.* **2002**, 1603.
[8] E. Coronado, C. J. Gómez-García, A. Nuez, F. M. Romero, E. Rusanov, H. Stoeckli-Evans, *Inorg. Chem.* **2002**, *41*, 4615.
[9] E. Coronado, C. J. Giménez-Saiz, J. M. Martínez-Agudo, A. Nuez, F. M. Romero, H. Stoeckli-Evans, *Polyhedron* **2003**, *22*, 2435−2440.
[10] H-Z. Kou, d-Z. Liao, P. Cheng, Z-H. Jiang, S-P. Yan, G-L. Wang, X-K. Yao, H-G. Wang, *J. Chem. Soc., Dalton Trans.* **1997**, 1503.
[11] D.-G. Fu, J. Chen, X.-S. Tan, L.-J. Jiang, S.-W. Zhang, P.-J. Zheng, W.-X. Tang, *Inorg. Chem.* **1997**, *36*, 220.
[12] E. Colacio, J. M. Domínguez-Vera, M. Ghazi, R. Kivekäs, J. M. Moreno, A. Pajunen, *J. Chem. Soc., Dalton Trans.* **2000**, 505.
[13] N. Mondal, M. K. Saha, B. Bag, S. Mitra, V. Gramlich, J. Ribas, M. S. El Fallah, *J. Chem. Soc., Dalton Trans.* **2000**, 1601.
[14] M. S. El Fallah, J. Ribas, X. Solans, M. Font-Bardia, *J. Chem. Soc., Dalton Trans.* **2001**, 247.
[15] H-Z. Kou, S. Gao, J. Zhang, G-H. Wen, G. Su, R. K. Zheng, X. X. Zhang, *J. Am. Chem. Soc.* **2001**, *123*, 11809.
[16] F. Thétiot, S. Triki, J. S. Pala, *New J. Chem.* **2002**, *26*, 196.
[17] J. Luo, M. Hong, C. Chen, M. Wu, D. Gao, *Inorg. Chim. Acta* **2002**, *328*, 185.
[18] F. Thétiot, S. Triki, J. S. Pala, C. J. Gómez-García, S. Golhen, *Chem. Commun.* **2002**, 1078.
[19] C. Pariya, F-L. Liao, S-L. Wang, C-S. Chung, *Polyhedron* **1998**, *17*, 547.
[20] Z. Otwinowski, W. Minor, *Methods Enzymol.* **1997**, *276*, 307.
[21] A. Altomare, M. C. Burla, M. Camalli, G. Cascarano, C. Giacovazzo, A. Guagliardi, A. G. G. Moliterni, G. Polidori, R. Spagna, *J. Appl. Crystallogr.* **1999**, *32*, 115.
[22] L. J. Farrugia, *J. Appl. Crystallogr.* **1999**, *32*, 837.
[23] G. M. Sheldrick, *SHELX-97, an integrated system for solving and refining crystal structures from diffraction data*, University of Göttingen (Germany), **1997**.
[24] R. H. Blessing, *J. Appl. Crystallogr.* **1997**, *30*, 421.
[25] A. L. Spek, *PLATON.* University of Utrecht, The Netherlands, **2001**.
[26] P. Van der Sluis, A. L. Spek, *Acta Crystallogr., Sect. A* **1990**, *46*, 194.

Received September 10, 2003

 © 2003 Wiley-VCH Verlag GmbH & Co. KGaA, Weinheim

Analysis of Coordination and Organometallic Compounds Using Photoionisation Mass Spectrometric Techniques

Antoine Dorcier,[a] Paul J. Dyson,*[a] and J. Scott McIndoe[a,b]

Keywords: Atmospheric chemistry / Electrospray ionisation / Mass spectrometry / Transition metals

A range of coordination and organometallic compounds have been analysed by quadrupole ion-trap mass spectrometry using various photoionisation methods. Atmospheric-pressure photo ionisation (APPI), which combines atmospheric-pressure chemical ionisation (APCI) with a photolysis lamp, was compared with the new technique photo-assisted electrospray ionisation (PAESI). Additionally, the atmospheric-pressure matrix-assisted laser desorption ionisation (AP-MALDI) was also evaluated and compared to MALDI quadrupole ion-trap time-of-flight (MALDI-QIT-TOF) mass spectrometry.
(© Wiley-VCH Verlag GmbH & Co. KGaA, 69451 Weinheim, Germany, 2003)

Introduction

An armoury of mass spectrometric techniques is already available for determining the molecular weight and obtaining structural data on a plethora of different types of compounds. Coordination and organometallic chemists once relied almost exclusively on electron impact, chemical ionisation and fast-atom bombardment methods, but now they routinely employ electrospray ionisation (ESI) and matrix-assisted laser desorption ionisation (MALDI) techniques.[1] Although these techniques were largely developed with biomolecules and polymers in mind, various strategies have been developed to assist the analysis of coordination and organometallic compounds. For example, MALDI is sometimes most effective in the absence of a matrix; hence, LDI is a better description of the experiment. ESI mass spectrometry seems to be ideally suited to naturally charged coordination and organometallic compounds, although variations including ambient temperature ESI[2] and cold-spray ionisation[3] have been applied to compounds with labile ligands and unstable reaction intermediates, and instrument modifications made for high-throughput catalyst screening.[4] Apart from charged compounds, neutral compounds with ligands that have basic pendant groups are readily protonated and analysed; however, where such ligands are not present, a range of derivatisation reagents have been evaluated, which are now in widespread use.[5] Clearly, chemical derivatisation complicates the experiment and alternative ionisation sources would be advantageous. Since many coordination and organometallic compounds are photoactive, we have evaluated a series of photoionisation methods and indicate where they exhibit greatest utility.

A range of coordination and organometallic compounds, including metallocenes, phosphane compounds, metal-carbonyl complexes and clusters, porphyrin and phthalocyanine complexes, and bi- and tripyridine complexes (see Exp. Sect. for a full list), were investigated using a quadrupole ion-trap mass spectrometer. Initial experiments were carried out using an atmospheric-pressure photoionisation (APPI) source,[6] which comprises a krypton photolysis lamp that emits photons with energies of 10.0 and 10.6 eV combined with an atmospheric-pressure chemical-ionisation (APCI) source. APCI mass spectrometry has been previously applied to the analysis of coordination[7] and organometallic[8] compounds and we find that essentially any compound that is amenable to APCI can be analysed by APPI. The lamp can be switched on or off as the analyte enters the mass spectrometer and in certain cases large increases in the signal intensity can be obtained when the lamp is on. Perhaps the most interesting results were provided by the analysis of ruthenocene in aromatic solvents. Figure 1 shows a series of spectra of ruthenocene in toluene recorded using APCI only, APPI (i.e. APCI with PI) and APPI in which the plasma source of the APCI unit was switched off. In the APCI spectrum the dominant peak at m/z = 232 corresponds to the ruthenocenium cation $[Ru(C_5H_5)_2]^+$, but in addition, a peak of quite high relative intensity is observed at m/z = 259 and corresponds to a complex in which one cyclopentadienyl ligand has been replaced by a toluene molecule, viz. $[Ru(C_5H_5)(C_7H_8)]^+$. This type of arene exchange reaction has been observed previously, but under very different conditions, with $AlCl_3$ as a Lewis acid catalyst.[9]

[a] Institut de Chimie Moléculaire et Biologique,
Ecole Polytechnique Fédérale de Lausanne, EPFL-BCH,
1015 Lausanne, Switzerland
Fax: (internat.) + 41-(0)21-693-9885
E-mail: paul.dyson@epfl.ch
[b] Department of Chemistry, University of Victoria,
P. O. Box 3065, Victoria, BC V8 W 3V6, Canada

 © 2003 Wiley-VCH Verlag GmbH & Co. KGaA, Weinheim **DOI: 10.1002/ejic.200300459**

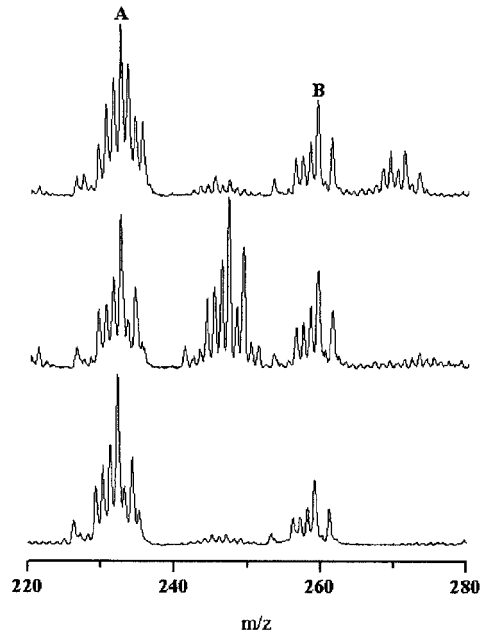

Figure 1. The positive ion mass spectra of ruthenocene in toluene recorded using (top) APCI, (middle) APPI and (bottom) APPI without the plasma: **A** corresponds to $[Ru(C_5H_5)_2]^+$ and **B** to $[Ru(C_5H_5)(C_7H_8)]^+$

Other peaks are also present, but these are less readily assigned. Using APPI the same two peaks are present, but the most intense is observed at $m/z = 247$ which cannot be assigned to any simple species (see below). However, if the APCI plasma is turned off and PI is used alone, the spectrum becomes much cleaner with the dominant peaks corresponding to $[Ru(C_5H_5)_2]^+$ and $[Ru(C_5H_5)(C_7H_8)]^+$. If the PI lamp is switched off, no peaks are observed. Clearly, the PI lamp has a significant effect, but it is very difficult to separate from the thermal effect of the APCI source (even when the plasma is off the source is maintained at a very high temperature) and the ligand exchange reaction is thermally driven. The same arene exchange process occurs with other arenes when these are used as the solvent. Solvent has already been shown to be very important in APPI mass spectrometry,[6] and here it seems probable that the PI source ionises the solvent molecules, and the solvent ions then ionise the ruthenocene. The peak of highest relative intensity obtained under APPI conditions is 15 mass units above the parent ion and might correspond to the parent ion with a methyl group attached, possibly arising from a side reaction related to the primary ionisation mechanism.

In general, most of the compounds analysed by APPI afforded spectra, but the effect of PI was minimal compared to the effect of the APCI source, which is too harsh for most coordination and organometallic compounds, resulting in extensive fragmentation and reactivity. As such, we combined PI with the considerably softer ESI source, which, as far as we are aware, has not been attempted before, and we term the technique photo-assisted ESI (PAESI). In keeping with ESI, no peaks were observed when neutral compounds were studied using PAESI mass spectrometry, but any compound that can be analysed with

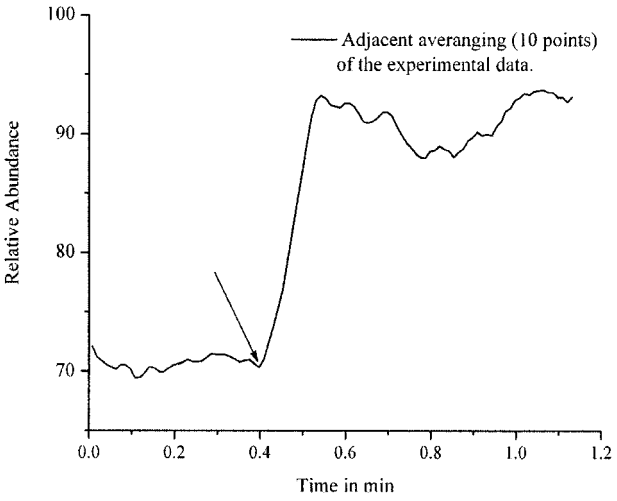

Figure 2. The effect of PI on ESI; the arrow indicates when the PI lamp was switched on, resulting in a higher ion current and hence an improved signal-to-noise ratio

ESI mass spectrometry, can be analysed by PAESI. The main effect was found for some positively and negatively charged coordination and organometallic compounds which tended to give higher ion currents, and hence improved the signal-to-noise ratio (Figure 2). However, characteristic photolysis products, such as carbonyl dissociation products, were not observed. In comparison to APPI, where photoionisation takes place in the gas-phase, in the PAESI experiment the analyte remains in the solvent during photolysis. As such, it is likely that the PI effect will be relatively dilute, since the exposure of the ions in the solvent spray is very short. As in APPI, it is likely that the solvent will play an important role and further experiments are required in this respect.

MALDI mass spectrometry, in which a laser is used to photolyse the analyte, has been used for the analysis of coordination and organometallic compounds. Atmospheric-pressure MALDI has been developed recently,[10] but the types of compounds considered here have not been analysed using this method. Since the AP-MALDI source is compatible with the quadrupole ion-trap instrument, we evaluated the method for coordination and organometallic compounds. The same method was used to great success for coordination and organometallic compounds, (viz. when no matrix[11] was present). In general, the only compounds that could be detected were those with strong chromophores such as porphyrin and phthalocyanine complexes. Metal-carbonyl compounds, for example, gave only very weak signals in AP-LDI in contrast to those in spectra obtained from LDI-TOF experiments, which reveal extensive gas-phase reaction products.[12] In the LDI-TOF experiments, the energetic ions formed by the laser desorption process undergo gas-phase reactions with little interference from other molecules or ions, because the experiment is conducted under a high vacuum. In contrast, the ions formed in the AP-LDI experiment may undergo collisional deactivation by reaction with the gas molecules present in the source. Porphyrin and phthalocyanine complexes have also

 © 2003 Wiley-VCH Verlag GmbH & Co. KGaA, Weinheim

been shown to dimerise and oligomerise in LDI mass spectrometry,[12] although no MS/MS experiments have been conducted on the gas-phase products, which would help to confirm their identity.

Using AP-LDI, the mass spectrum of manganese phthalocyanine showed four main peaks, the parent ion $[Mn(phthalocyanine)]^+$ at $m/z = 567$ and the dimeric species $[\{Mn(phthalocyanine)\}_2]^+$ at $m/z = 1134$, (Figure 3). In addition, a peak centred at $m/z = 1153$ corresponds to two overlapping species, these being the hydroxide $[\{Mn(phthalocyanine)\}_2(OH)]^+$ and $[\{Mn(phthalocyanine)\}_2(H_3O)]^+$, and the peak at $m/z = 1168$ corresponds to $[\{Mn(phthalocyanine)\}_2(O_2H_3)]^+$, (i.e. probably an adduct with both OH and H_2O interactions). Oxidation products such as these are not unexpected for these types of compounds.[13] These products result from the presence of oxygen and water in the source, which are removed in conventional MALDI since it operates under high vacuum. In Figure 3 spectrum (ii) was obtained using exactly the same conditions, except the source was purged with nitrogen for five minutes before acquiring the data, and during data acquisition. The amount of products resulting from reactions with oxygen and water is reduced considerably. MS/MS of the simple dimer product resulted in regeneration of the parent ion only (**A**; Figure 3) indicating that the aggregate is held together by noncovalent interactions.

The same compound was analysed by MALDI quadrupole ion-trap time-of-flight (MALDI-QIT-TOF) mass spectrometry without matrix. Like the AP-MALDI experiment, a parent ion peak was observed at $m/z = 567$; however, a dimer was observed at $m/z = 1132$, which corresponds to the dimer with loss of two hydrogen atoms, probably corresponding to the formation of a C−C bond. This hypothesis is given greater weight as the MS/MS of the dimer does not result in the reformation of the monomer, but instead, a complicated series of fragmentation products are observed.

Again, the differences between the LDI-QIT-TOF and AP-LDI experiments may be attributed to the differences in pressure at which these experiments take place (see above).

Overall, the new techniques described herein cannot be applied to a wide range of coordination and organometallic compounds; APPI and PAESI give good spectra for any compound that can be analysed by APCI and ESI mass spectrometry, respectively. In addition, LDI-QIT-TOF can also be applied to any sample which is amenable to LDI, whereas AP-LDI is only suited to compounds with very strong chromophores. These various photoionisation techniques also give rise to some interesting features not accessible with other techniques currently used. For example, certain gas-phase products that form can be deciphered using the ion-trap, which allows information to be gained that would otherwise be inaccessible. We also found that for best results with AP-MALDI it is essential that the source is purged with nitrogen or another inert gas in order to reduce gas-phase reactions with oxygen or other reactive contaminants in the atmosphere. As yet, we have not evaluated in detail the influence of matrices in AP-MALDI and it is possible that their application may increase the range of compounds that can be studied.

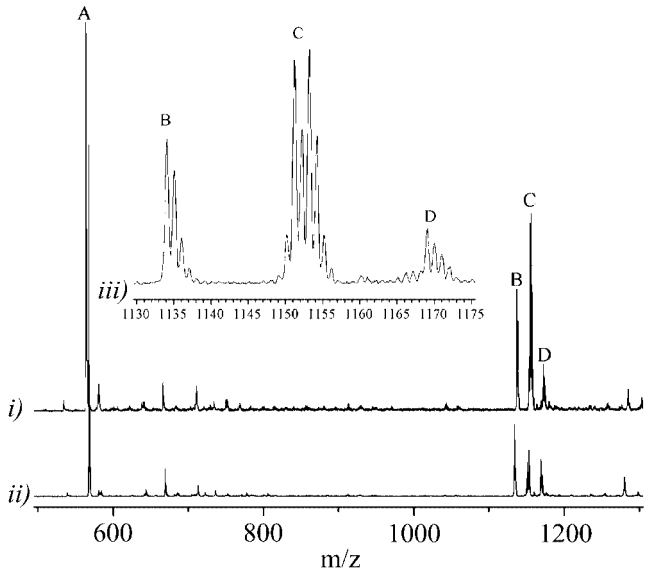

Figure 3. The positive ion AP-MALDI mass spectrum of Mn(phthalocyanine): (i) corresponds to the spectrum recorded under ambient atmospheric pressure, (ii) is the spectrum recorded when the source is purged with N_2: **A** corresponds to $[Mn(phthalocyanine)]^+$, **B** to $[\{Mn(phthalocyanine)\}_2]^+$, **C** to two overlapping ions $[\{Mn(phthalocyanine)\}_2(O)(H)]^+$ and $[\{Mn(phthalocyanine)\}_2(H_3O)]^+$, **D** to $[\{Mn(phthalocyanine)\}_2(O)(H_3O)]^+$; note that the amount of oxide and H_3O adducts reduced when the system is purged with N_2; trimers of low relative intensity are also observed (not shown)

Experimental Section

The compounds evaluated $[Fe(\eta\text{-}C_5H_5)_2]$, $[Fe(\eta\text{-}C_5H_5)(\eta\text{-}C_5H_4BOH_2)]$, $[Ru(\eta\text{-}C_5H_5)_2]$, $[Zr(\eta\text{-}C_5H_5)_2Cl_2]$, $[RhCl(PPh_3)_3]$, $[IrCl(CO)(PPh_3)_2]$, $[Ru(\eta\text{-}p\text{-cymene})(dppe)]^+$,[14] $[RuCl_2(\eta\text{-}p\text{-cymene})(pta)]$,[15] $Mo(CO)_6$ and $M_2(CO)_{10}$ (M = Mn or Re), $M_3(CO)_{12}$ (M = Fe, Ru or Os), $[Cr(\eta\text{-}C_6H_6)(CO)_3]$, $[Cr(\eta\text{-}C_{16}H_{16})(CO)_3]$,[16] $[Cr(\eta\text{-}C_7H_{10})(CO)_3]^+$, $Rh(Me)O_3$, [phthalocyanito manganese(II)], [chloro(5,10,15,20-tetraphenylporphyrinatok^4-$N^{21,22,23,24}$)iron(III)], [(5,10,15,20-tetraphenylporphyrinato-$k^4N^{21,22,23,24}$)nickel(II)], [(5,10,15,20-tetraphenylporphyrinato-$k^4N^{21,22,23,24}$)zinc(II)], *cis*-$PtCl_2(NH_3)_2$, auranofin (ICN Biomedicals Inc), ruthenium(II)tris(2,2′-bipyridyl-4,4′-dicarboxylato) dichloride (Solaronix), ruthenium(II)*cis*-bis(isocyanato)(2,2′-bipyridyl-4,4′-dicarboxylato) (Solaronix), tris(isothiocyanato)-ruthenium(II)-2,2′:6′,2"-terpyridine-4,4′,4"-tricarboxylic acid (Solaronix), ruthenium(II)*cis*-bis(isothiocyanato)bis(2,2′-bipyridyl-4,4′-dicarboxylato) (Solaronix) and tris(isothiocyanato)-ruthenium(II)-2,2′:6′,2"-terpyridine-4,4′,4"-tricarboxylic acid (Solaronix) were obtained from commercial sources (indicated when not a common supplier) or prepared by literature methods (indicated). Mass spectra were collected on a ThermoFinnigan LCQ DecaXP Plus quadrupole ion-trap instrument (APPI, APCI, PAESI and AP-MALDI) or a Shimadzu AXIMA-QIT (MALDI-OTI-TOF) mass spectrometer.

APPI, APCI and PAESI: All sources are commercially available from Thermo-Finnigan, although the PAESI must be constructed by combining the PI lamp with the ESI source. This is straightforward given the similar designs of the APCI and ESI sources. The

 © 2003 Wiley-VCH Verlag GmbH & Co. KGaA, Weinheim

PI lamp is based on a photo-Mate ion source using a Krypton lamp which emits photons at 10.0 and 10.6 eV. Samples were infused directly into the source at 5 μL·min^{-1} using a syringe pump with nitrogen as drying gas. For the ESI source the temperature was set to 50 °C and the cone voltage within the range 4.50−5 kV. The MS detector was tuned automatically on the base peak, which optimised the remaining parameters. Samples were prepared by dissolving the complex (10−100 mg) in the appropriate mobile phase (1 mL).

AP-MALDI and MALDI-QIT-TOF: Samples were dissolved in dichloromethane solvent and deposited onto the sample probe. The solvent was allowed to evaporate leaving a thin layer of the pure sample. Several layers were added in this manner. The laser power was optimised for each sample. The spectra were recorded under air or N_2 at atmospheric pressure.

Peaks were assigned from the *m*/*z* values and from the isotope distribution patterns which were simulated using the ISOTOPE program.[17] The *m*/*z* values given are for the most intense peak in the envelope in each case.

Acknowledgments

We thank Dr. Rachel Martin (Shimadzu, Manchester, UK) for conducting the LDI-QIT-TOF experiment and the referees for their helpful comments. We thank the EPFL and Swiss National Science Foundation for financial support and JSM thanks Trinity and Newnham Colleges (Cambridge) for a college lectureship.

[1] [1a] W. Henderson, L. J. McCaffery, B. K. Nicholson, *Polyhedron* **1998**, *17*, 4291. [1b] R. Colton, A. D'Agostino, J. C. Traeger, *Mass Spectrom. Rev.* **1995**, *14*, 79. [1c] J. C. Traeger, *Int. J. Mass Spectrom.* **2000**, *200*, 387:[c] J. S. McIndoe, *Trans. Met. Chem.* **2003**, *28*, 122.
[2] P. J. Dyson, J. S. McIndoe, *Inorg. Chim. Acta.* **2003**, *354*, 68.
[3] [3a] J. Kim, Y. Dong, E. Larka, L. Que Jr., *Inorg. Chem.* **1996**, *35*, 2369. [3b] S. Sakamoto, M. Fujita, K. Kim, K. Yamaguchi, *Tetrahedron* **2000**, *56*, 955.
[4] P. Chen, *Angew. Chem. Int. Ed.* **2003**, *42*, 2832.
[5] [5a] W. Henderson, J. S. McIndoe, B. K. Nicholson, P. J. Dyson, *Chem. Commun.* **1996**, 1183. [5b] W. Henderson, J. S. McIndoe, B. K. Nicholson, P. J. Dyson, *J. Chem. Soc., Dalton Trans.* **1998**, 519.
[6] [6a] D. B. Robb, T. R. Covey, A. P. Bruins, *Anal. Chem.* **2000**, *72*, 3653. [6b] J. P. Rauha, H. Vuorela, R. Kostiainen, *J. Mass Spectrom.* **2001**, *36*, 1269. [6c] T. J. Kauppila, T. Kuuranne, E. C. Meurer, M. N. Eberlin, T. Kotiaho, R. Kostiainen, *Anal. Chem.* **2002**, *74*, 5470. [6d] H. Keski-Hynnila, M. Kurkela, E. Elovaara, L. Antonio, J. Magdalou, L. Luukkanen, J. Taskinen, R. Kostiainen, *Anal. Chem.* **2002**, *74*, 3449.
[7] [7a] L. Agocs, G. G. Briand, N. Burford, T. S. Cameron, W. Kwiatkowski, K. N. Robertson, *Inorg. Chem.* **1997**, *36*, 2855. [7b] J. M. Hough, C. A. Haney, R. D. Bereman, C. E. Keefer, *J. Coord. Chem.* **2000**, *51*, 45.
[8] [8a] G. Esquius, J. Pons, R. Yanez, J. Ros, *J. Organomet. Chem.* **2001**, *619*, 14. [8b] M. Tsuchlya, *Mass Spectrom. Rev.* **1998**, *17*, 51.
[9] C. C. Lee, R. G. Sutherland, B. J. Thomson, *J. Chem. Soc., Chem. Commun.* **1972**, 907.
[10] [10a] V. V. Laiko, S. C. Moyer, R. J. Cotter, *Anal. Chem.* **2000**, *72*, 5239. [10b] J. J. Coon, K. J. McHale, W. W. Harrison, *Rapid Commun. Mass spectrom.* **2002**, *16*, 681. [10c] V. M. Doroshenko, V. V. Laiko, N. I. Taranenko, V. D. Berkout, H. S. Lee, *Int. J. Mass Spectrom.* **2002**, *221*, 39.
[11] G. Critchley, P. J. Dyson, B. F. G. Johnson, J. S. McIndoe, R. K. O'Reilly, P. R. R. Langridge-Smith, *Organometallics* **1999**, *18*, 4090.
[12] E. Stulz, C. C. Mak, J. K. M. Sanders, *J. Chem. Soc., Dalton Trans.* **2001**, 604.
[13] G. Engelsma, A. Yamamoto, E. Markham, M. Calvin, *J. Phys. Chem.* **1962**, *66*, 2517.
[14] C. Daguenet, P. J. Dyson, *Catal. Commun.* **2003**, *4*, 153.
[15] C. S. Allardyce, P. J. Dyson, D. J. Ellis, S. L. Heath, *Chem. Commun.* **2001**, 1396.
[16] P. J. Dyson, D. G. Humphrey, J. E. McGrady, D. M. P. Mingos, D. J. Wilson, *J. Chem. Soc., Dalton Trans.* **1995**, 4039.
[17] L. J. Arnold, *J. Chem. Educ.* **1992**, *69*, 811.

Received July 14, 2003

 © 2003 Wiley-VCH Verlag GmbH & Co. KGaA, Weinheim

Non-Oxo Vanadium(IV) Complexes of Aminebis(phenolate) [O,N,O] Donor Ligands and Solution Studies of Isostructural V^{IV} and Mn^{IV} Complexes

Tapan K. Paine,[a] Thomas Weyhermüller,[a] Eckhard Bill,[a] Eberhard Bothe,[a] and Phalguni Chaudhuri*[a]

Keywords: Vanadium / Manganese / EPR spectroscopy / Cyclic voltammetry / Isomerism

Mononuclear non-oxo vanadium(IV) complexes, $[V^{IV}L^{Me}_2]$ (**1**) and $[V^{IV}LtBu_2]$ (**2**), with a tridentate bis(phenol) ligand H_2L bearing the O_2N donor atoms and with either dimethyl or di-*tert*-butyl substituents have been synthesized and the X-ray structures of **1** and **2** are reported. Additionally, **3**, an Mn^{IV} complex $[Mn^{IV}L^{Me}_2]$, and **4**, the anion containing the Mn^{III} center $[Mn^{III}L^{Me}_2]^-$, are discussed. The X-ray structure of **4** present as an anion in **4a**, $[(Me_3tacn)_2Mn^{II}_2(\mu\text{-}OOCCH_3)_3][Mn^{III}L^{Me}_2]$, where Me_3tacn = 1,4,7-trimethyl-1,4,7-triazacyclononane, confirms the magnetic susceptibility results of the high-spin d^4 nature of the manganese center in **4**. The compounds were characterized by elemental analysis, IR, UV/Vis, mass spectrometry, EPR spectroscopy, electrochemical and variable-temperature (2–295 K) magnetic susceptibility measurements. The electrochemical results of **1** and **2** suggest the metal-centered oxidation, i.e. the generation of a V^V–phenolate species, prior to the second oxidation attributable to the formation of a V^V–phenoxyl radical species. Isomerization of the meridional form for the bis(ligand)-metal species to the facial form has been observed for **1** and **3** in solution. The EPR spectroscopic data of **1** and **2** clearly show a considerable increase in the in-plane π bonding, as is expected for a phenolate ligand.

(© Wiley-VCH Verlag GmbH & Co. KGaA, 69451 Weinheim, Germany, 2003)

Introduction

We have been exploring the feasibility of using tridentate bis(phenol) ligands,[1] which comprise the three donor atoms [O,X,O], where X = S, Se, P, P=O or N for generating novel transition metal complexes.[2] These types of bis(phenol) ligands are expected to yield homoleptic bis(ligand) non-oxo vanadium(IV) complexes, whose relevance to bioinorganic chemistry has been mentioned quite often in the literature.[3]

It is now well established that vanadium occurs in a variety of biological systems,[3] e.g. in amavadin, a compound isolated from the mushroom *Amanita muscaria*. Amavadin has been shown to contain an eight-coordinate V^{5+} ion without oxo ligands; so-called "bare" or non-oxo vanadium species are still scarce.[4] Non-oxo vanadium centers have also been reported for the cofactor in vanadium nitrogenase. Although the chemistry of oxovanadium(IV) and -(V) complexes is well developed,[5] far less information is available for non-oxo (so-called "bare") complexes, particularly the EPR spectroscopic properties. The vanadyl ion ranks among the most stable of diatomic cations and dominates the chemistry of vanadium. Here we describe two mononuclear octahedral vanadium(IV) complexes ML_2, **1** and **2**, with the ligands H_2L^{Me} and H_2L^{tBu} (X = N) which are depicted in Scheme 1. Our expectation of non-oxo vanadium(IV) complexes was confirmed, as is authenticated by structure determinations, the results of which together with the EPR spectroscopic and electrochemical investigations are described herein. The solution properties of complex **1** and the manganese(IV) complex **3** with the same ligand are also discussed in comparison with the Mn^{III} anion complex **4**. Complex **3** and the anion complex **4** have recently been reported by us.[1c] As the structural characterization of **4** was lacking,[1c] we report it to be the same as the anion in **4a**. Scheme 1 shows the complexes to be described with their labels and the ligands.

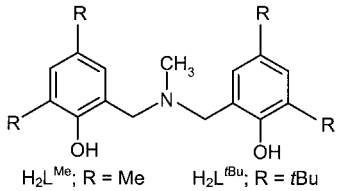

H_2L^{Me}; R = Me H_2L^{tBu}; R = *t*Bu

1 $V^{IV}L^{Me}_2$ **2** $V^{IV}L^{tBu}_2$ **3** $Mn^{IV}L^{Me}_2$ **4** $[Mn^{III}L^{Me}_2]^-$
4a $[(Me_3tacn)_2Mn^{II}_2(\mu\text{-}OOCCH_3)_3][Mn^{III}L^{Me}_2]$
Me_3tacn = 1,4,7-trimethyl-1,4,7-triazacyclononane

Scheme 1

[a] Max-Planck-Institut für Bioanorganische Chemie
Stiftstrasse 34–36, 45470 Mülheim an der Ruhr, Germany
E-mail: chaudh@mpi-muelheim.mpg.de
Supporting information for this article is available on the WWW under http://www.eurjIc.org or from the author.

Results and Discussion

The general method for the synthesis of complexes **1** and **2** involves an anaerobic reaction of $[V^{III}(THF)_3Cl_3]$ with the ligands H_2L and Et_3N as a base in dry acetonitrile. Exposing the resulting solution to air for a while ensures the conversion of V^{iii} to V^{IV} and subsequent storage of the solution under an argon stream, to avoid further oxidation and to concentrate the solution, yields the desired product. The reactions are clean, affording large quantities of pure crystalline products in good yield (50−80%).

$$2\ H_2L^x + V(THF)_3Cl_3 + 4\ Et_3N \xrightarrow[\text{ii) Air}]{\text{i) } CH_3CN,\ Ar} V^{IV}L^x{}_2 + 4\ Et_3NH^+ + 3\ Cl^- + 1\ e^- + 3\ THF$$

X = Me (**1**), *t*Bu (**2**)

Scheme 2

Selected IR data for complexes **1** and **2** are given in the Exp. Sect. There are several strong bands in the region 3000−2800 cm^{-1} due to the ν(C−H) stretchings of the *tert*-butyl or methyl groups. Absence of a strong ν(V=O) stretch at ca. 950 cm^{-1} in **1** and **2** indicates that the complexes are non-oxo species.

EI and ESI mass spectrometry were found to be very important analytical techniques for the characterization of complexes **1** and **2**. The EI mass spectrum of **1** shows a molecular ion peak at *m*/*z* = 645 with only 42% abundance. The base peak at *m*/*z* = 377 is a fragmentation product. The ESI (positive ion mode in CH_2Cl_2) mass spectrum for **2** clearly confirms the composition of the complex showing *m*/*z* (%) = 981 (100).

The electronic spectra (250−1200 nm) of complexes **1** and **2** in CH_2Cl_2 solution primarily consist of two transitions: a band at ca. 550 nm and the second band at ca. 400 nm. The lowest energy band at 550 nm is assigned to phenolate-to-vanadium(IV) CT transitions, by analogy with other reported "bare" vanadium(IV) complexes.[4a−4o] The higher energy transitions at ca. 400 nm, which are absent in the free ligands, are also assigned to the phenolate-to-vanadium(IV) CT transition. There is also a shoulder at ca. 700 nm for complexes **1** and **2**.

Single Crystal X-ray Diffraction Studies

Complexes **1** and **2** are structurally very similar and hence detailed structural aspects of only **1** are discussed here. The molecular structure of **3** has recently been reported.[1c] The structural parameters for the anionic unit **4** are obtained from the structural characterization of $[(Me_3tacn)_2Mn^{II}{}_2(\mu\text{-}OOCCH_3)_3][Mn^{III}L^{Me}{}_2]$ (**4a**), where Me_3tacn represents 1,4,7-trimethyl-1,4,7-triazacyclononane. The cation $[(Me_3tacn)_2Mn^{II}{}_2[\mu\text{-}OOCCH_3)_3]^+$ has been structurally characterized previously.[6]

Molecular Structure of 1

Single crystals of deep blue *mer-trans*-(*N*,*N*)-$[VL^{Me}{}_2]\cdot{}^2/_3CH_3CN$ were obtained from acetonitrile solution by slow evaporation of the solvent. As no substantial differences in bond lengths and angles are found between the crystallographically nonequivalent molecules, only one ORTEP diagram for the structure of compound **1** is displayed in Figure 1, while selected bond lengths and angles are summarized in Table 1.

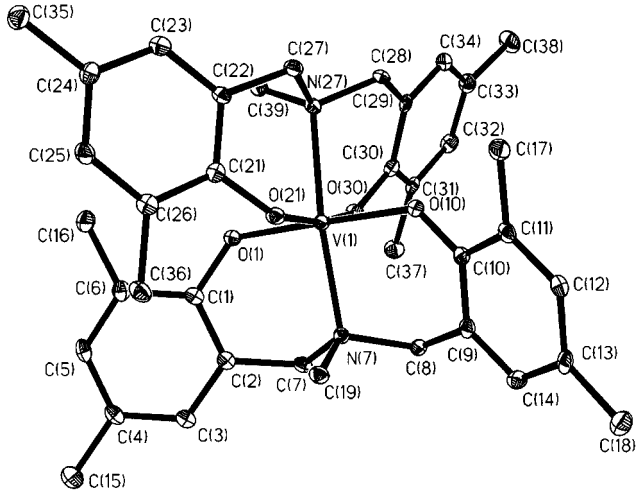

Figure 1. Molecular structure of $[VL^{Me}{}_2]\cdot{}^2/_3CH_3CN$ (**1**)

Table 1. Selected bond lengths [Å] and bond angles [°] for $[VL^{Me}{}_2]\cdot{}^2/_3CH_3CN$ (**1**) (#: center of symmetry-related atoms)

V(1)−O(30)	1.851(2)	O(21)−C(21)	1.353(4)
V(1)−O(21)	1.835(2)	O(30)−C(30)	1.344(4)
V(1)−O(10)	1.919(2)	O(10)−C(10)	1.339(4)
V(1)−O(1)	1.916(3)	O(1)−C(1)	1.346(4)
V(1)−N(27)	2.209(3)	V(1)−N(7)	2.160(3)
O(30)−V(1)−O(21)	168.88(11)	O(30)−V(1)−O(10)	91.46(11)
O(21)−V(1)−O(10)	92.20(11)	O(30)−V(1)−O(1)	87.71(11)
O(21)−V(1)−O(1)	88.84(11)	O(10)−V(1)−O(1)	178.51(11)
O(30)−V(1)−N(27)	83.12(11)	O(21)−V(1)−N(27)	86.59(11)
O(10)−V(1)−N(27)	87.13(11)	O(1)−V(1)−N(27)	94.00(11)
O(30)−V(1)−N(7)	93.31(11)	O(21)−V(1)−N(7)	97.31(11)
O(10)−V(1)−N(7)	88.00(11)	O(1)−V(1)−N(7)	90.81(11)
N(27)−V(1)−N(7)	173.88(11)		
V(2)−O(41)	1.921(3)	O(41)−C(41)	1.342(4)
V(2)−O(41)#	1.921(3)	O(50)−C(50)	1.357(4)
V(2)−O(50)	1.849(2)	V(2)−O(50)#	1.849(2)
V(2)−N(47)#	2.167(3)	V(2)−N(47)	2.167(3)
O(50)−V(2)−O(50)#	180.0	O(41)#−V(2)−O(50)#	90.40(11)
O(41)#−V(2)−O(50)	89.60(11)	O(41)−V(2)−O(50)#	89.60(11)
O(50)−V(2)−O(41)	90.40(11)	O(41#)−V(2)−O(41)	180.0
O(50)#−V(2)−N(47)#	85.35(11)	O(50)−V(2)−N(47)#	94.65(11)
O(41#)−V(2)−N(47)#	91.29(11)	O(41)−V(2)−N(47)#	88.71(11)
O(50)#−V(2)−N(47)	94.65(11)	O(50)−V(2)−N(47)	85.35(11)
O(41)#−V(2)−N(47)	88.71(11)	O(41)−V(2)−N(47)	91.29(11)
N(47)#−V(2)−N(47)	180.00		

The overall geometry around the vanadium ion V(1) is best described as a distorted octahedron with *trans*-positioned nitrogen atoms N(7) and N(27) of the two amine bis(phenolate) ligands. The doubly deprotonated ligand with an [O,N,O] donor set is bound in a meridional manner.

 © 2003 Wiley-VCH Verlag GmbH & Co. KGaA, Weinheim

All the phenyl rings attached to the phenolate oxygen atoms are found to be planar, indicating that upon coordination the aromaticity of the phenyl rings is retained. The small distortion from octahedral geometry is mainly caused by the bite angles between the phenolate O atom and the N atom of the $[ONO]^{2-}$ ligand: N(7)−V(1)−O(10) 88.00(11)°, N(7)−V(1)−O(30) 93.31(11)°. The O(30)−V(1)−O(21) and O(10)−V(1)−O(1) angles are 168.88(11) and 178.51(11)°, respectively, while the corresponding N(27)−V(1)−N(7) angle at 173.88(11)° deviates from linearity. All the C−O bond lengths found in compound **1** are normal, the average being 1.345(4) Å. The average V−O and V−N distances of 1.879(3) and 2.185(3) Å fall in the range reported for other structurally characterized mononuclear vanadium(IV) complexes; the V−O bond is a little shorter.[4a] The V−N and V−O bond lengths are in agreement with those of a d^1 V^{IV} complex,[4] which also corroborate with the EPR measurements.

Molecular Structure of 2

This complex is isostructural with complex **1** having overall distorted octahedral geometry around the vanadium ion with two meridionally spanning ligands and two *trans* positioned nitrogen atoms. The ORTEP plot with the atom labeling scheme is shown in Figure 2. The structural parameters are given in Table 2.

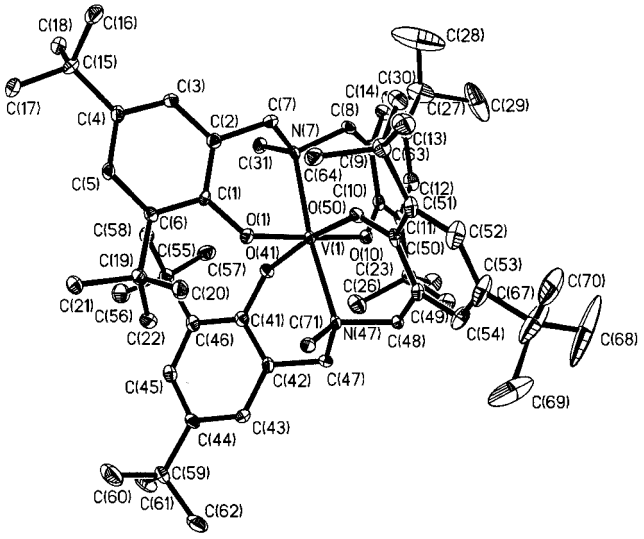

Figure 2. ORTEP representation of $[VLtBu_2]$ (**2**)

Molecular Structure of Complex 4a

The lattice of the crystal used for structural determination consists of discrete $[(Me_3tacn)_2Mn_2(\mu\text{-}OOCCH_3)_3]^+$ and $[ML^{Me}{}_2]^-$ ions. The bond lengths and angles in the cation $[(Me_3tacn)_2Mn_2(\mu\text{-}OOCCH_3)_3]^+$ are comparable (Table 3) with the reported values[6] and hence we have not described the cation in detail. An ORTEP diagram of the anion, **4** in **4a** with the atom labeling scheme is shown in Figure 3. Selected bond parameters are listed in Table 4.

Table 2. Selected bond lengths [Å] and bond angles [°] for $[VLtBu_2]$ (**2**)

V(1)−O(41)	1.854(2)	O(21)−C(21)	1.358(4)
V(1)−O(50)	1.867(2)	O(41)−C(41)	1.359(4)
V(1)−O(1)	1.923(2)	O(10)−C(10)	1.347(4)
V(1)−O(10)	1.938(2)	O(1)−C(1)	1.348(4)
V(1)−N(47)	2.193(3)	V(1)−N(7)	2.159(3)
O(41)−V(1)−O(50)	169.82(10)	O(41)−V(1)−O(10)	87.25(10)
O(41)−V(1)−O(1)	89.31(10)	O(50)−V(1)−O(10)	94.79(10)
O(50)−V(1)−O(1)	89.18(10)	O(10)−V(1)−O(1)	175.20(11)
O(41)−V(1)−N(7)	98.95(11)	O(41)−V(1)−N(47)	87.34(11)
O(50)−V(1)−N(7)	91.11(11)	O(50)−V(1)−N(47)	82.71(10)
O(1)−V(1)−N(7)	89.82(10)	O(1)−V(1)−N(7)	93.56(10)
O(10)−V(1)−N(7)	87.41(10)	O(10)−V(1)−N(47)	89.62(10)
N(7)−V(1)−N(47)	172.91(11)		
V(2)−O(130)	1.862(2)	O(41)−C(41)	1.342(4)
V(2)−O(141)	1.877(2)	O(50)−C(50)	1.357(4)
V(2)−O(101)	1.917(2)	V(2)−O(110)	1.917(2)
V(2)−N(107)	2.174(3)	V(2)−N(147)	2.198(3)
O(130)−V(2)−O(141)	170.58(11)	O(130)−V(2)−O(110)	88.04(10)
O(130)−V(2)−O(101)	88.97(11)	O(141)−V(2)−O(110)	94.84(10)
O(141)−V(2)−O(101)	88.70(10)	O(101)−V(2)−O(110)	175.19(11)
O(130)−V(2)−N(107)	97.16(11)	O(130)−V(2)−N(147)	87.89(10)
O(141)−V(2)−N(107)	91.97(11)	O(141)−V(2)−N(147)	83.15(10)
O(101)−V(2)−N(107)	90.34(10)	O(101)−V(2)−N(147)	93.58(10)
O(110)−V(2)−N(107)	86.30(10)	O(110)−V(2)−N(147)	90.07(10)
N(107)−V(2)−N(147)	173.66(11)		

Table 3. Selected bond lengths [Å] and angles [°] for the complex cation ($[(Me_3tacn)_2Mn_2(\mu\text{-}OOCCH_3)_3]^+$) of **4a**

Mn(2)−O(60)	2.102(3)		
Mn(2)−O(80)	2.102(3)		
Mn(2)−O(70)	2.107(3)		
Mn(2)−N(42)	2.345(3)		
Mn(2)−N(41)	2.359(3)		
Mn(2)−N(40)	2.362(3)		
Mn(3)−O(61)	2.098(3)		
Mn(3)−O(71)	2.107(3)		
Mn(3)−O(81)	2.117(3)		
Mn(3)−N(50)	2.314(3)		
Mn(3)−N(51)	2.332(3)		
Mn(3)−N(52)	2.368(3)		
O(60)−Mn(2)−O(80)	100.5(2)	O(60)−Mn(2)−O(70)	107.02(13)
O(80)−Mn(2)−O(70)	101.23(14)	O(60)−Mn(2)−N(42)	87.48(13)
O(80)−Mn(2)−N(42)	162.59(12)	O(70)−Mn(2)−N(42)	91.01(12)
O(60)−Mn(2)−N(41)	159.79(13)	O(80)−Mn(2)−N(41)	92.80(14)
O(70)−Mn(2)−N(41)	84.93(13)	N(42)−Mn(2)−N(41)	75.84(12)
O(60)−Mn(2)−N(40)	88.74(13)	O(80)−Mn(2)−N(40)	89.20(13)
O(70)−Mn(2)−N(40)	158.90(12)	N(42)−Mn(2)−N(40)	75.41(12)
N(41)−Mn(2)−N(40)	76.21(13)		
O(61)−Mn(3)−O(71)	106.70(11)	O(61)−Mn(3)−O(81)	100.55(12)
O(71)−Mn(3)−O(81)	100.55(12)	O(61)−Mn(3)−N(50)	91.85(11)
O(71)−Mn(3)−N(50)	88.80(11)	O(81)−Mn(3)−N(50)	164.22(11)
O(61)−Mn(3)−N(51)	159.55(11)	O(71)−Mn(3)−N(51)	90.38(11)
O(81)−Mn(3)−N(51)	90.11(11)	N(50)−Mn(3)−N(51)	77.02(10)
O(61)−Mn(3)−N(52)	85.14(12)	O(71)−Mn(3)−N(52)	161.29(11)
O(81)−Mn(3)−N(52)	91.95(12)	N(50)−Mn(3)−N(52)	76.15(11)
N(51)−Mn(3)−N(52)	75.62(11)		

 © 2003 Wiley-VCH Verlag GmbH & Co. KGaA, Weinheim

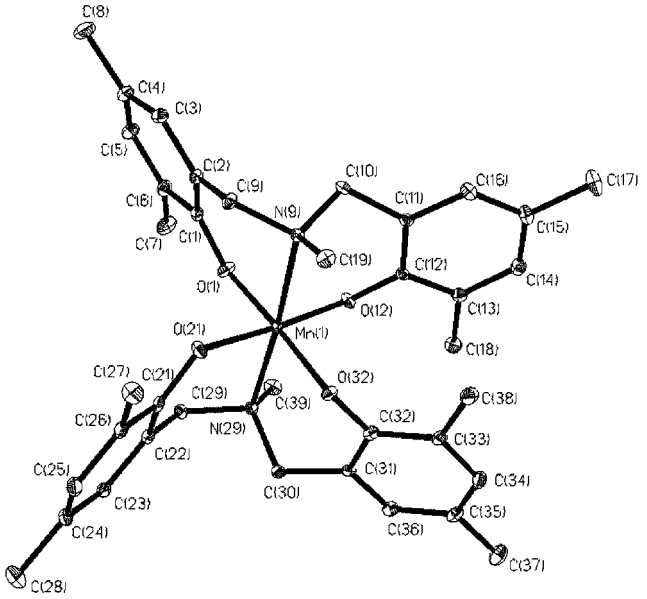

Figure 3. Perspective view of the anionic unit $[MnL_2^{Me}]^-$ (**4**) in **4a**

Table 4. Selected bond lengths [Å] and angles [°] for $[Mn^{III}L_2^N]^-$(**4**) in **4a**

Mn(1)−O(12)	1.913(2)	O(1)−C(1)	1.318(4)
Mn(1)−O(1)	1.919(2)	O(12)−C(12)	1.326(3)
Mn(1)−O(32)	1.920(2)	O(32)−C(32)	1.340(4)
Mn(1)−O(21)	1.926(2)	O(21)−C(21)	1.328(4)
Mn(1)−N(9)	2.317(2)		
Mn(1)−N(29)	2.322(3)		
O(12)−Mn(1)−O(1)	87.52(10)	O(12)−Mn(1)−O(32)	92.35(9)
O(1)−Mn(1)−O(32)	175.80(9)	O(12)−Mn(1)−O(21)	176.50(10)
O(1)−Mn(1)−O(21)	89.96(10)	O(32)−Mn(1)−O(21)	90.33(10)
O(12)−Mn(1)−N(9)	89.34(9)	O(1)−Mn(1)−N(9)	87.64(9)
O(32)−Mn(1)−N(9)	96.56(9)	O(21)−Mn(1)−N(9)	88.13(9)
O(12)−Mn(1)−N(29)	92.24(9)	O(1)−Mn(1)−N(29)	88.14(9)
O(32)−Mn(1)−N(29)	87.66(9)	O(21)−Mn(1)−N(29)	90.10(9)
N(29)−Mn(1)−N(9)	175.43(9)		

Each ligand acts as a facial [O,N,O] donor. In terms of angles within the coordination sphere, MnN_2O_4 is very close to an ideal octahedron. The ranges of *cis* and *trans* angles at the manganese center Mn(1) are 87.5(1)−92.4(1)° and 175.4(1)−176.5(1)°, respectively. The MnO_4 fragment is planar within experimental error, the mean deviation is 0.046 Å.

That the manganese center Mn(1) is in the +3 oxidation state is evident from the axial elongation of the octahedron along the N(29)−Mn(1)−N(9) axis with Mn(1)−N(29) 2.322(3) and Mn(1)−N(9) 2.317(2) Å as is expected for a Jahn−Teller distorted high-spin d^4 ion. The Mn−O [average 1.920(6) Å] and Mn−N [average 2.319(3) Å] distances fall in the range reported for the structurally characterized d^4 Mn^{III} complexes.[7] As expected, the average distances Mn(1)−O and Mn(1)−N are significantly longer than the corresponding bond lengths in complex **3** containing a +4 charged manganese center.[1c]

The anion **4**, being one of the numerous structurally characterized bis(homoleptic) manganese(III) complexes,[7] does not warrant any other special discussion.

Magnetic Susceptibility Studies

Magnetic susceptibility data for polycrystalline samples of complexes **1**, **2** and **4a** were collected over the temperature range 2−290 K in an applied magnetic field of 1 T. Above 10 K the temperature-independent magnetic moments of solids **1** and **2** are 1.69 (± 0.05) μ_B, and 1.70 (± 0.04) μ_B, respectively. These results are consistent with the formulation of the complexes as vanadium(IV) d^1 species (spin-only μ_{eff} = 1.73 μ_B) with no or very small intermolecular coupling and are in complete agreement with the X-ray and EPR spectroscopy results. Simulations (Figure S1 of Supporting Information; see also the footnote on the first page of this article) of the experimental magnetic moment data yield g_v = 1.89, temperature-independent paramagnetism (TIP) = 145 × 10^{-6} emu for **1** and g_v = 1.92, TIP = 200 × 10^{-6} emu for **2**. We note that the *g* values thus evaluated differ from those obtained from the EPR spectroscopic studies (see later).

The magnetic behavior of **4a**, $[(Me_3tacn)_2Mn_2(\mu\text{-}OOCCH_3)_3]^+[MnL_2^{Me}]^-$, is characteristic of an antiferromagnetically coupled complex (Figure 4). At 290 K the μ_{eff} value of 9.24 μ_B ($X_M{\cdot}T$ = 10.686 $cm^3{\cdot}K{\cdot}mol^{-1}$) decreases monotonically with decreasing temperature until it reaches a value of 4.12 μ_B ($X_M{\cdot}T$ = 2.127 $cm^3{\cdot}K{\cdot}mol^{-1}$) at 2 K; this is a clear indication of exchange coupling between two paramagnetic Mn^{II} centers present in the cation of **4a**, with a residual spin moment of ca. 4 μ_B due to the presence of the mononuclear $[MnL_2^{Me}]^-$ anion. The experimental magnetic data were simulated using a least-squares fitting computer program[8] involving three spins $S_1 = {}^5/_2$, $S_2 = {}^5/_2$ and $S_3 = {}^4/_2$ and applying a model in which the coupling between the S_1 and S_2 spins is only prevailing, and there is no exchange interactions between the S_3 and S_1 or S_2 spins. We use the Heisenberg spin-Hamiltonian in the form $\hat{H} = -2J\,\hat{S}_1{\cdot}\hat{S}_2$ for an isotropic exchange coupling between two spins $S_1 = S_2 = {}^5/_2$. The solid line in Figure 4 represents the best fit with the following parameters: J_{12} = −2.14 cm^{-1}, g_1 = g_2 = $g_{Mn^{II}}$ = 2.00, g_3 = $g_{Mn^{III}}$ = 1.95 and *TIP* = 185 ×

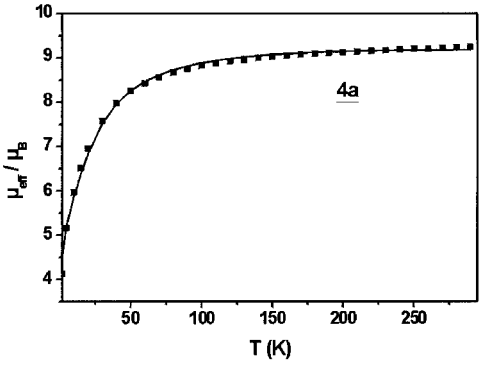

Figure 4. Plots of μ_{eff} vs. *T* for solid **4a**; the solid line represents the best fit of the data to the exchange coupling model

 © 2003 Wiley-VCH Verlag GmbH & Co. KGaA, Weinheim

10^{-6} $cm^3 \cdot K \cdot mol^{-1}$. The evaluated antiparallel exchange coupling is very similar to that observed earlier[6] for the cation $[(Me_3tacn)_2Mn_2(\mu\text{-}OOCCH_3)_3]^+$. Thus, the magnetic susceptibility study also corroborates with the structural data of **4a**, whose anion contains the bis(ligand) manganese(III) unit (**4**) with a d^4 high-spin ion.

Electrochemical Results

Cyclic voltammograms (CVs) of complexes **1** and **2** have been measured in CH_2Cl_2 solutions containing 0.1 M nBu$_4$NPF$_6$ as supporting electrolyte at a glassy carbon working electrode and an Ag/AgNO$_3$ reference electrode. Ferrocene (Fc) was used as an internal standard, and the potentials are referenced vs. the ferrocenium/ferrocene couple (Fc^+/Fc). From the voltammograms redox potentials $E_{1/2}$ of the complexes were obtained and are compiled in Table 5.

Table 5. Redox potentials $E_{1/2}$ [V] (vs. Fc^+/Fc) of complexes **1** and **2**, obtained from cyclic voltammograms in CH_2Cl_2 solutions

Complex	$E_{1/2}^{red}$	$E_{1/2}^{ox1}$	$E_{1/2}^{ox2}$
1	−0.882	+0.177	+0.950
2	ca. −0.85[a]	+0.226	+0.875

[a] Slow heterogeneous electron transfer; electrochemically quasi-reversible.

The cyclic voltammogram of **1** displays two reversible and one irreversible wave, whereas that of **2** displays three reversible waves (Figure 5). Coulometric experiments show that the waves are due to one-electron transfer processes. The redox potentials $E_{1/2}$ for the reductions are observed in a narrow range (−0.85 to −0.88 V), irrespective of the nature of the heterodonor, i.e. N, S, Se or P [2] and since, moreover, phenolato ligands are not reduced in this potential range we assign all of these reductions to metal-centered reductions, the V^{III} form of the complexes.

For complexes **1** and **2** we performed controlled potential coulometric experiments at appropriate potentials (at −25 °C) in order to generate the reduced and oxidized forms of the complexes and recorded their electronic spectra. In each of the experiments referring to $E_{1/2}^{red}$ and $E_{1/2}^{ox1}$ the current dropped to background levels when one electron per molecule had passed. The stability of the oxidized and reduced forms was confirmed by recording a CV after the electrolysis or by the recovery of the starting material's electronic spectrum upon voltage reversal. The stabilities of the species were sufficient for the coulometric experiments (duration ca. 30 min at −25 °C).

In all reductions it was found that the broad absorption band which extends from 400 to 700 nm greatly diminishes during electrolysis. Likewise, the changes in the UV/Vis spectra during oxidations exhibit similar features for complexes **1** and **2**: new and very intense absorption grows in two regions, viz. at ca. 300−370 nm (for **1**) or 407 nm (for **2**) and in a second very broad range which extends typically from 500 to 1100 nm. These similarities of the spectral

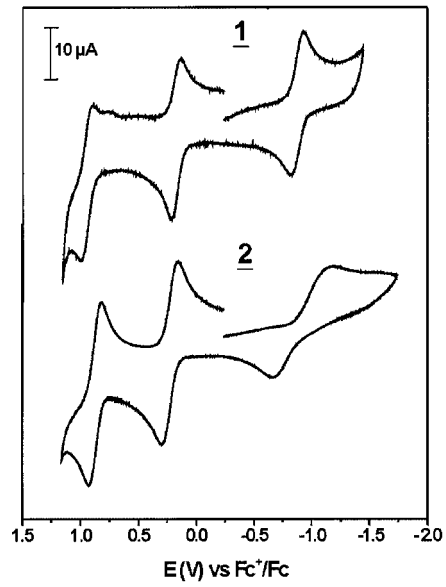

Figure 5. Cyclic voltammograms of complexes **1** and **2** in CH_2Cl_2 solution containing ca. 1 mM complex and 0.1 M nBu$_4$NPF$_6$ (scan rate = 0.2 V/s)

changes provide evidence that the oxidation mechanism is the same for compounds **1** and **2**. Since all monocations (oxidized species) were found to be EPR-silent in the temperature range 2−30 K two mechanisms appear to be feasible: a metal-centered oxidation to a V^V species or formation of an antiferromagnetically coupled V^{IV}−phenoxyl radical system.

However, phenoxyl radicals exhibit a very characteristic electronic spectrum: a band at 400−420 nm and often a single broad band at longer wavelengths with lower intensity. In the present monocations these features are not present: most of the low wavelength bands are at 300−370 nm, they are spread over a much broader range and the bands at higher wavelengths are very intense. Therefore we assign the cations to V^V species.

To gain information about the oxidation mechanism represented by $E_{1/2}^{ox2}$ we performed a $2e^-$ coulometric oxidation on **2**. During the coulometry the current approached a constant value, which indicates that the dication is not stable and there is a concomitant formation and decay of the $2e^-$-oxidized species. However, after two electrons had passed, the frozen solution showed an almost isotropic EPR signal (Figure 6) typical for an organic radical ($S = {}^1/_2$; no vanadium hyperfine coupling; $g_x = g_y = 2.0078$, $g_z = 2.0027$, $\langle g_{iso} \rangle = 2.0061$). Therefore the second oxidation represents the formation of a V^V−phenoxyl radical species.

Solution Properties and EPR Spectroscopy

Although the crystallographically characterized complex was found to be meridional in nature, complex **1** {$[VL_2^{Me}]$}separated out, from the acetonitrile reaction solution, as a mixture of two isomers (*fac* and *mer*). The solid isolated from the reaction solution after 75 h also exists in

 © 2003 Wiley-VCH Verlag GmbH & Co. KGaA, Weinheim

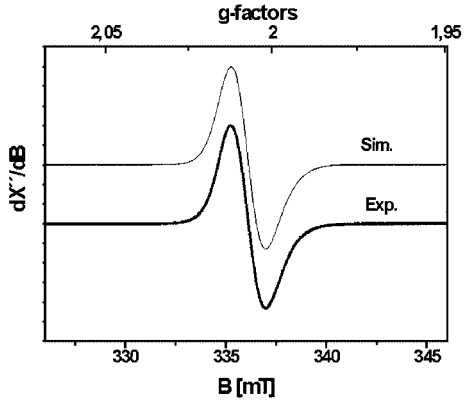

Figure 6. X-band EPR spectrum for the electrochemically $2e^-$-oxidized species of complex **2** at 30 K in CH_2Cl_2; experimental conditions (—): microwave frequency 9.44 GHz, microwave power 0.16 mW, modulation amplitude 6 G; simulations (---): g_{iso} = 2.0061; Gaussian line with angular-dependent line width W = {18, 22, 26} G

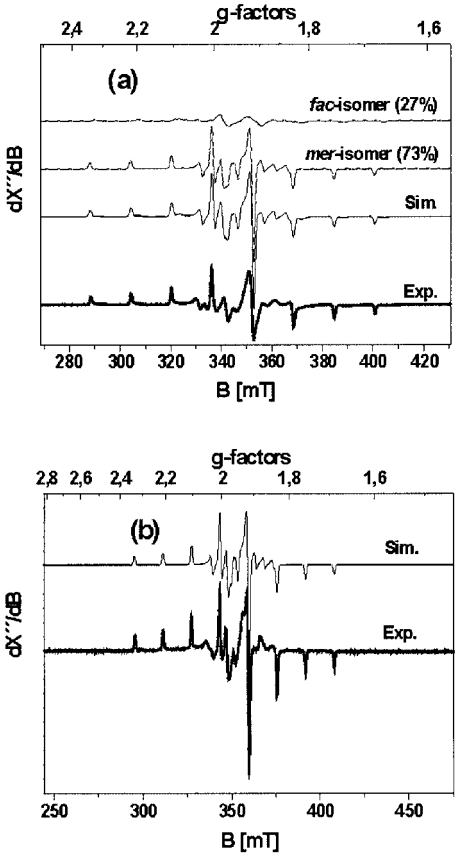

Figure 7. X-band EPR spectra of complex **1** at t = 0, T = 9.9 K (a) and at t = 90 h in CH_2Cl_2 + toluene, T = 33.8 K (b); experimental conditions (—): microwave frequency 9.44 GHz (a), 9.64 GHz (b); microwave power 0.01 μW (a), 0.2 μW (b); modulation amplitude 5 G (a), 5 G (b); simulations for spectrum (a) (---): g = {1.930, 1.960, 1.940}, A = {44, 14, 147} × 10^{-4} cm^{-1} (*fac* isomer); g = {1.932, 1.966, 1.958}, A = {44, 14, 147} × 10^{-4} cm^{-1} (*mer* isomer); Gaussian line with frequency-dependent line width W_f = 80 G (*fac*) and 30 G (*mer*)

two isomeric forms in CH_2Cl_2 solution. When the complex obtained after 75 h was dissolved in CH_2Cl_2 at room temperature followed immediately by LC analysis, both *fac* and *mer* isomers were seen. The LC analyses were performed as a function of time to monitor the change of the relative isomer percentage of **1** in solution.

With time the percentage of the *fac* isomer decreases whereas that of the *mer* isomer increases. 100% *mer* isomer is obtained after 90 h. The LC-MS, clearly indicating the two isomers present in the solution at initial or intermediate times, confirms the presence of only the *mer* form after ca. 90 h. For a qualitative comparison, the UV/Vis spectra of *mer* and *fac* isomers obtained from the LC analyses are provided as Supporting Information (Figure S2).

This change can also be observed in the solution EPR spectra recorded at low temperature. At the very beginning, the spectrum shows a mixture of two isomers, whereas at t = 90 h, only one isomer is seen. The spectrum taken at the beginning can be simulated by considering two isomers in the ratio obtained from the LC analysis (*fac*/*mer* = 27:73). On the other hand, the EPR spectrum of the same solution after 90 h shows only one isomer (meridional) in 100% and can be simulated as seen in Figure 7. The parameters found after simulations with the components x, y and z, respectively, are: g = {1.930, 1.960, 1.940} and A = {44, 14, 147} × 10^{-4} cm^{-1} for the facial isomer and g = {1.932, 1.966, 1.958} and A = {44, 14, 147} × 10^{-4} cm^{-1} for the meridional isomer. The same set of parameters for the meridional isomer was found from the simulation of the EPR spectrum taken after 90 h, containing 100% of the meridional form. Complex **2** on the contrary remains only in the *mer* form presumably due to steric reasons. The EPR spectrum of **2** was simulated with the parameters: g = {1.920, 1.945, 1.954} and A = {50, 10, 146} × 10^{-4} cm^{-1}.

Complexes **1** and **2** belong to the class with a $(d_{xy})^1$ ground state. Six-membered ring formation and steric availability favors the coordination of the ligands in a meridional manner. This results in a small increase in the equatorial σ bonding but considerable increase in the in-plane π bonding.

On the other hand, complex **3**, the Mn^{IV} complex, shows solution behavior in which the nature of the change is the opposite. When complex **3** is dissolved in methanol and the LC analysis is performed, only one isomer is found (100%). This is the *mer* isomer as confirmed from the solid-state crystal structure analysis. But with time the percentage of the *mer* isomer decreases and that of a second isomer (*fac*) increases (Figure 8). After 80 min, there is no more change and the percentage of the two isomers becomes constant with a *fac*/*mer* ratio of 1:4. At this stage the two isomers equilibrate in solution with the K_{eq} value found to be 4.

$$fac \rightleftharpoons mer$$

$$K_{eq} = [mer]/[fac] = 4$$

The isomerization processes for the isostructural **1** and **3** can be rationalized on the basis of the effective ionic radii for V^{IV} and Mn^{IV}. V^{IV}, with a larger ionic radius (0.58 Å)

 © 2003 Wiley-VCH Verlag GmbH & Co. KGaA, Weinheim

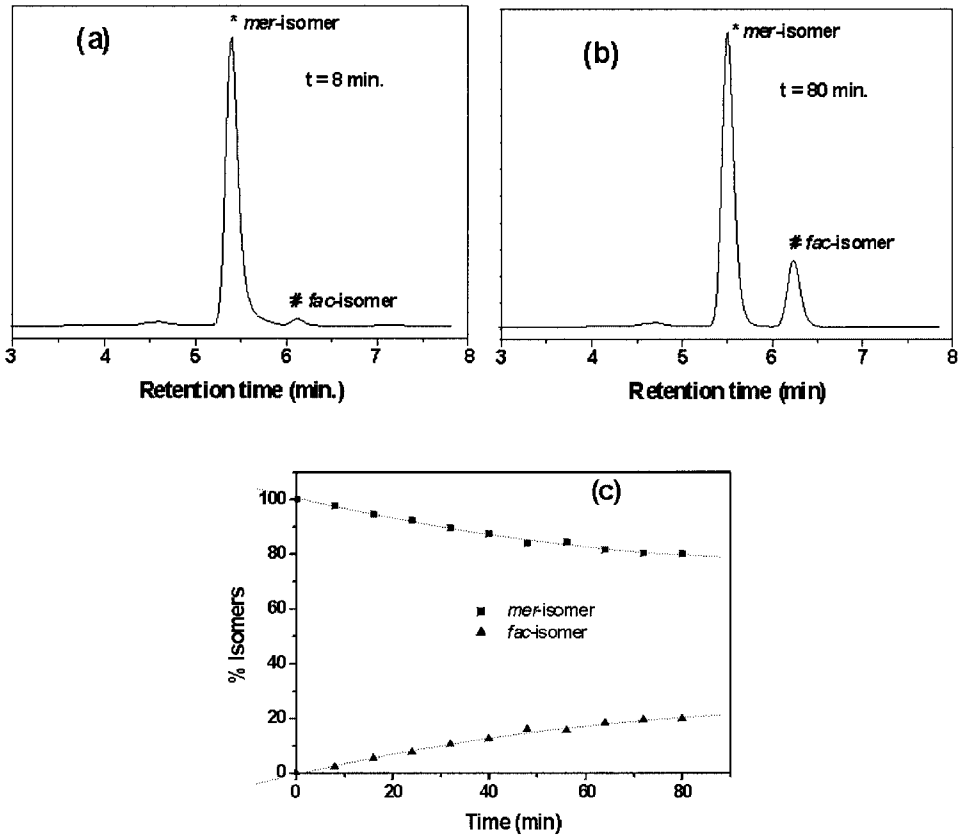

Figure 8. Liquid chromatograms of **3** (a) at t = 8 min and (b) at t = 80 min and (c) change of the isomer percentage with time for complex **3** in CH_2Cl_2 solution; the percentage of isomers is obtained from LC analysis

than that of Mn^{IV} (0.53 Å),[9] is prone to changing the coordination mode of the ligand from facial to meridional because of the steric availability in the meridional form.

This line of argument is in agreement with the observation that the Mn^{III} anion complex **4**, whose structure determination in the solid state shows the presence of only the facial form, also remains facial in solution. Mn^{III} has the largest ionic radius of 0.65 Å amongst these three ions and thus stabilizes the more sterically demanding facial form.

Conclusions

To conclude, the following points of this study deserve particular attention:

(i) The tridentate aminebis(phenolate) ligands with different substituents are capable of generating non-oxo vanadium(IV) complexes, VL_2, in which the ligands are coordinated to the V^{IV} metal center mainly meridionally. A similar geometrical isomer, i.e. meridional, is obtained with the manganese(IV) ions. On the contrary, manganese(III) exclusively yields the facial form. A rationale based on the metal ionic radii has been forwarded to explain the difference in geometrical isomers.

(ii) The investigation emphasizes the observation of the presence of two geometrical isomers, meridional and facial, in solution, albeit the structure determined in the solid state to be meridional.

(iii) Electrochemical measurements indicate that the reversibility of the redox processes is profoundly affected by the substituent on the ligand. Thus, the ligand with *tert*-butyl groups yields reversible redox behavior for the metal complexes. No stabilization of the V^{IV}–phenoxyl radical species has been observed. On the other hand, the formation of a V^{V}–phenoxyl radical complex has been clearly shown by an EPR spectroscopic experiment.

Experimental Section

Materials and Physical Measurements: Commercial grade chemicals were used for the synthetic purposes and solvents were distilled and dried before use. Fourier transform IR spectroscopy on KBr pellets was performed with a Perkin–Elmer 2000 FT-IR instrument. Solution UV/Vis spectra were measured with a Perkin–Elmer Lambda 19 spectrophotometer. Mass spectra were recorded either in the EI or ESI (in CH_2Cl_2) mode with a Finnigan MAT 95 or 8200 spectrometer. Magnetic susceptibilities of the polycrystalline samples were recorded with a SQUID magnetometer (MPMS, Quantum Design) in the temperature range 2–290 K with an applied field of 1 T. The resulting volume magnetization from the sample had its diamagnetic contribution compensated and was recalculated as volume susceptibility. Diamagnetic contributions were estimated for each compound by using Pascal's constants.

 © 2003 Wiley-VCH Verlag GmbH & Co. KGaA, Weinheim

Cyclic voltammetry and coulometric experiments were performed using an EG&G potentiostat/galvanostat. X-band EPR spectra were recorded with a Bruker ESP 300E spectrometer equipped with a helium flow cryostat (Oxford Instruments ESR 910), an NMR field probe (Bruker 035M), and a microwave frequency counter HP5352B. Spin-Hamiltonian simulations of the EPR spectra were performed with a program that was developed from the routines of Gaffney and Silverstone[10] and that specifically makes use of the resonance-search procedure based on a Newton−Raphson algorithm as described therein. LC experiments were performed with HPLC instrumentation using a Gilson M305 pump, and the Diode Array Detector (DAD) SPDM 10 AV(Shimadzu Corporation). CH_3OH (0.8 mL/min) was used as eluent through a Nucleodor-5μ-(100A)-C18 column. LC-MS was performed using the above column with a mass spectrometer having a mass-selective detector.

X-ray Crystallographic Data Collection and Refinement of the Structures: Single crystals of **1**, **2** and **4a** were coated with perfluoropolyether, picked up with glass fibers, and mounted on a Nonius Kappa-CCD diffractometer equipped with a cryogenic nitrogen cold stream operating at 100(2) K. Graphite-monochromated Mo-K_α radiation (λ = 0.71073 Å) was used. Intensity data were corrected for Lorentz and polarization effects. The intensity data set of **1** was corrected for absorption with the use of the program Gaussian face-indexed and that for **2** and **4a** were not corrected. The Siemens SHELXTL software package (G. M. Sheldrick, Universität Göttingen[13] was used for solution, refinement, and artwork of the structure, and neutral atom scattering factors of the program were used. All structures were solved and refined by direct methods and difference Fourier techniques. Non-hydrogen atoms were refined anisotropically, and hydrogen atoms were placed at calculated positions and refined as riding atoms with isotropic displacement parameters. Details of data collection and structure refinements are summarized in Table 6. CCDC-211067 (**1**), -211068 (**2**) and -211069 (**4a**) contain the supplementary crystallographic data for this paper. These data can be obtained free of charge at www.ccdc.cam.ac.uk/conts/retrieving.html [or from the Cambridge Crystallographic Data Centre, 12 Union Road, Cambridge CB2 1EZ, UK; Fax: (internat.) + 44-1223/336-033. E-mail: deposit@ccdc.cam.ac.uk].

Ligand Synthesis: The ligands H_2L^{Me},[1c,11] and H_2LtBu[11] were synthesized according to the published procedure. Syntheses of the complexes **3** and the complex anion **4** have recently been reported by us.[1c]

General Method for the Synthesis of V^{IV} Complexes 1 and 2: $V(THF)_3Cl_3$ (0.5 mmol, 0.186 g) was dissolved in a degassed CH_3CN solution (40 mL) of ligand (1 mmol). Et_3N (0.5 mL) was added to the violet solution and the resulting solution was refluxed under argon for 0.5 h. After cooling to room temperature, the solution was opened to air and stirred for 5 min. The solution was then concentrated by passing argon over the surface of the solution to yield a crystalline solid.

Complex $[VL^{Me}_2]\cdot{}^2/_3CH_3CN$ (1): Yield: 0.23 g (68%). $C_{38}H_{46}N_2O_4V\cdot{}^2/_3CH_3CN$ (673.1): calcd. C 70.19, H 7.19, N 5.55, V 7.57; found C 69.9, H 7.1, N 5.5, V 8.7. IR: $\tilde{\nu}$ = 3422 (br), 2902 (s), 1473 (s), 1249 (s), 1158, 813, 596, 559 cm^{-1}. UV/Vis (CH_2Cl_2): λ_{max} (ε) = 362 (6900), 562 nm (9200 $M^{-1}\cdot cm^{-1}$). EI MS: *m*/*z* (%) = 645 (42) [M^+], 377 (100).

Complex [VL*t*Bu$_2$] (2): Yield: 0.26 g (53%). $C_{62}H_{94}N_2O_4V$ (982.38): calcd. C 75.80, H 9.64, N 2.85, V 5.19; found C 75.6, H 9.5, N 2.8, V 5.3. IR: $\tilde{\nu}$ = 3454 (br), 2953−2868 (s), 1465 (s), 1237 (s), 1166,

Table 6. Crystallographic data for $[VL^{Me}_2]\cdot{}^2/_3CH_3CN$ (**1**), [VL*t*Bu$_2$] (**2**) and $[(Me_3tacn)_2Mn_2(\mu\text{-}OOCCH_3)_3][MnL^{Me}_2]$ (**4a**)

	1	**2**	**4a**
Empirical formula	$C_{38}H_{46}VN_2O_4\cdot{}^2/_3CH_3CN$	$C_{62}H_{94}VN_2O_4$	$C_{62}H_{97}Mn_3N_8O_{10}$
Formula mass	673.08	982.33	1279.30
Temperature	100(2) K	100(2) K	100(2) K
Wavelength (Mo-K_α)	0.71073 Å	0.71073 Å	0.71073 Å
Crystal system	monoclinic	monoclinic	monoclinic
Space group	$P2_1/c$	P2(1)	$P2_1/n$
Unit cell dimensions	a = 22.5319(12) Å	a = 11.8937(3) Å	a = 16.3023(6) Å
	b = 16.1089(9) Å	b = 28.1316(9) Å	b = 21.7165(9) Å
	c = 14.5134(9) Å	c = 18.4680(6) Å	c = 18.1744(6) Å
	β = 97.90(1)°	β = 90.57(1)°	β = 93.90(1)°
Volume, Z	5217.8(5) $Å^3$, 6	6178.9(3) $Å^3$, 4	6419.4(4) $Å^3$, 4
Density (calcd.)	1.285 Mg/m^3	1.056 Mg/m^3	1.324 Mg/m^3
Absorption coeff.	0.329 mm^{-1}	0.203 mm^{-1}	0.643 mm^{-1}
F(000)	2146	2140	2720
Crystal size	0.15 × 0.15 × 0.04 mm	0.16 × 0.12 × 0.08 mm	0.27 × 0.16 × 0.14 mm
θ range for data collect.	4.44−26.00°	3.10−24.79°	2.43−30.00°
Index range	$-29 \le h \le 29$,	$-14 \le h \le 14$,	$-22 \le h \le 25$,
	$-20 \le k \le 20$,	$-33 \le k \le 33$,	$-32 \le k \le 33$,
	$-18 \le l \le 18$	$-21 \le l \le 21$	$-25 \le l \le 28$
Reflections collected	33024	105111	83533
Independent reflect.	10170	21124	18699
	[R(int) = 0.0970]	[R(int) = 0.0903]	[R(int) = 0.1217]
Absorption correction	Gaussian, face-indexed	not corrected	not indexed
Data/restraints/parameter	10137/0/638	21123/31/1254	18644/0/748
Goodness-of-fit on F^2	1.019	1.029	1.024
Final R indices [$I > 2\sigma(I)$]	$R1$ = 0.0691,	$R1$ = 0.0548,	$R1$ = 0.0745,
	$wR2$ = 0.1616	$wR2$ = 0.1106	$wR2$ = 0.1675
R indices (all data)	$R1$ = 0.1014,	R = 0.0720,	$R1$ = 0.1069,
	$wR2$ = 0.1798	$wR2$ = 0.1188	$wR2$ = 0.1851
Largest diff. peak/hole	0.652/−0.641 e·$Å^{-3}$	0.597/−0.318 e·$Å^{-3}$	1.261/−1.086 e·$Å^{-3}$

 © 2003 Wiley-VCH Verlag GmbH & Co. KGaA, Weinheim

833, 746, 551 cm^{-1}. UV/Vis (CH_2Cl_2): λ_{max} (ε) = 383 (10900), 603 (11800) 814 nm (4100 $M^{-1}\cdot cm^{-1}$, sh). MS (ESI positive ion, CH_2Cl_2): *m*/*z* (%) = 981 (100) [M^+].

Complex [(Me$_3$tacn)$_2$Mn$_2$(μ-OOCCH$_3$)$_3$][MnL$^{Me}_2$] (4a): The ligand (0.15 g, 0.5 mmol) was dissolved in dry methanol (20 mL) and treated with a manganese(III) complex[12] [(Me$_3$tacn)$_2$Mn$_2$(μ-OOCCH$_3$)$_2$(μ-O)](ClO$_4$)$_2$ (0.17 g, 0.25 mmol) and triethylamine (0.5 mL). The resulting red solution was then refluxed under argon for 0.5 h. After cooling to room temperature, the solution was filtered under argon and the isolated solid was dried. X-ray quality crystals were grown from a methanolic solution under a slow sweep of argon. Yield: 0.030 g (10%). $C_{62}H_{97}Mn_3N_8O_{10}$ (1279.30): calcd. C 58.21, H 7.64, Mn 12.88, N 8.76; found C 58.6, H 7.4, Mn 12.5, N 8.5. IR: $\tilde{\nu}$ = 3448 (br), 2990−2814 (s), 1634−1607 (s), 1472 (s), 1314 (s), 1273 (s), 1016, 812, 546·cm^{-1}. UV/Vis (CH_2Cl_2): λ_{max} (ε) = 352 (sh), 427 (2900), 656 (380), 962 nm (200 $M^{-1}\cdot cm^{-1}$). MS (ESI, CH_2Cl_2): *m*/*z* = 629 (positive ion) and 649 (negative ion).

Acknowledgments

Skilful technical assistance of Mrs. H. Schucht, Mr. A. Göbels, Mrs. R. Wagner and Mrs. M. Trinoga is thankfully acknowledged. We are grateful to the German Research Council (DFG) for the financial support (Project: Priority Program Ch 111/2-2).

[1] [1a] P. Chaudhuri, M. Hess, U. Flörke, K. Wieghardt, *Angew. Chem. Int. Ed.* **1998**, *110*, 2217. [1b] R. Siefert, T. Weyhermüller, P. Chaudhuri, *J. Chem. Soc., Dalton Trans.* **2000**, 4656. [1c] T. Weyhermüller, T. K. Paine, E. Bothe, E. Bill, P. Chaudhuri, *Inorg. Chim. Acta* **2002**, *337*, 344. [1d] T. K. Paine, T. Weyhermüller, K. Wieghardt, P. Chaudhuri, *Inorg. Chem.* **2002**, *41*, 6538. [1e] T. K. Paine, E. Rentschler, T. Weyhermüller, P. Chaudhuri, *Eur. J. Inorg. Chem.* **2003**, 3167.

[2] T. K. Paine, PhD thesis, Universität Paderborn, **2002**.

[3] [3a] K. Kustin, G. C. McLeod, *Struct. Bonding (Berlin)* **1983**, *53*, 140. [3b] D. Rehder, *Angew. Chem. Int. Ed. Engl.* **1991**, *30*, 148. [3c] D. Rehder, *Coord. Chem. Rev.* **1999**, *182*, 297. [3d] *Metal Ions in Biological Systems*, vol. 31 ("Vanadium and its Role in Live") (Eds.: H. Sigel, A. Sigel), Marcel Dekker, New York, **1995**. [3e] *J. Inorg. Biochem.* **2000**, *80* (special issue dedicated to biological aspects of vanadium).

[4] [4a] S. R. Cooper, Y. B. Koh, K. N. Raymond, *J. Am. Chem. Soc.* **1982**, *104*, 5092. [4b] U. Auerbach, B. P. C. Della Vedova, K. Wieghardt, B. Nuber, J. Weiss, *J. Chem. Soc., Chem. Commun.* **1990**, 1004. [4c] T. A. Kabanas, A. J. P. White, D. J. Williams, J. D. Woollins, *J. Chem. Soc., Chem. Commun.* **1992**, 17. [4d] A. Neves, A. S. Ceccato, I. Vencato, Y. P. Mascarenhas, C. Erasmus-Buhr, *J. Chem. Soc., Chem. Commun.* **1992**, 652. [4e] T. A. Kabanos, A. M. Z. Slawin, D. J. Williams, J. D. Woollins, *J. Chem. Soc., Dalton Trans.* **1992**, 1423. [4f] S. Bruni, A. Caneschi, F. Cariatia, C. Delfs, A. Dei, D. Gatteschi, *J. Am. Chem. Soc.* **1994**, *116*, 1388. [4g] V. Gergopoulos, S. Jantzen, D. Rodewald, D. Rehder, *J. Chem. Soc., Chem. Commun.* **1995**, 377. [4h] P. R. Klich, A. D. Daniher, P. R. Challen, D. B. McConville, W. J. Youngs, *Inorg. Chem.* **1996**, *35*, 347. [4i] M. Farahbakhsh, H. Schmidt, D. Rehder, *Chem. Commun.* **1998**, 2009. [4j] B. Kang, L. Wenig, H. Liu, D. Wu, L. Huang, C. Lu, J. Cai, X. Chen, J. Lu, *Inorg. Chem.* **1990**, *29*, 4873. [4k] E. Ludwig, H. Hefele, E. Uhlemann, F. Weller, W. Z. Kläui, *Z. Anorg. Allg. Chem.* **1995**, *621*, 23. [4l] H. Hefele, E. Ludwig, E. Uhlemann, F. Weller, *Z. Anorg. Allg. Chem.* **1995**, *621*, 1973. [4m] A. A. Diamantis, M. R. Snow, J. A. Vanzo, *J. Chem. Soc., Chem. Commun.* **1976**, 264. [4n] P. Comba, L. M. Engelhardt, J. M. Harrowfield, G. A. Lawrence, L. L. Martin, A. M. Sargeson, A. H. White, *J. Chem. Soc., Chem. Commun.* **1985**, 174. [4o] A. A. Diamantis, M. Manikas, M. A. Salam, M. R. Snow, E. R. T. Tiekink, *Aust. J. Chem.* **1988**, *41*, 453.

[5] [5a] *Comprehensive Coordination Chemistry* (Eds.: G. Wilkins, R. D. Gillard, J. A. McCleverty), Pergamon Press, England, **1987**, vol. 3, p. 453. [5b] *Encyclopedia of Inorganic Chemistry* (Ed.: R. B. King), John Wiley & Sons, New York, **1994**, vol. 8, p. 4296. [5c] F. A. Cotton, G. Wilkinson, *Advanced Inorganic Chemistry*, 5th ed., John Wiley & Sons, New York, **1988**, p. 665.

[6] K. Wieghardt, U. Bossek, B. Nuber, J. Weiss, J. Bonvoisin, M. Corbella, S. E. Vitols, J. J. Girerd, *J. Am. Chem. Soc.* **1998**, *110*, 7398.

[7] [7a] F. A. Cotton, G. Wilkinson, in *Advanced Inorganic Chemistry*, 5th ed., John Wiley & Sons, New York, **1988**. [7b] *Comprehensive Coordination Chemistry* (Ed.: G. Wilkinson), Pergamon, England, **1987**, vol. 4.

[8] F. Birkelbach, C. Krebs, V. Staemmler, Bochum, Germany, **1997**, unpublished results.

[9] R. D. Shannon, *Acta Crystallogr., Sect. A* **1976**, *32*, 751.

[10] B. J. Gaffney, H. J. Silverstone, in *EMR of Paramagnetic Molecules* (Eds.: L. J. Berliner, J. Reuben), Plenum Press, New York, **1993**, vol. 13.

[11] N. N. Timosheva, A. Chandrasekharan, R. O. Day, R. R. Holmes, *Inorg. Chem.* **1998**, *37*, 4945.

[12] K. Wieghardt, U. Bossek, D. Ventur, J. Weiss, *J. Chem. Soc., Chem. Commun.* **1995**, 347.

[13] ShelXTL V.5: Siemens Analytical X-ray Instruments, **1994**; ShelXL 97: G. M. Sheldrick, University of Göttingen, **1997**.

Received June 25, 2003
Early View Article
Published Online November 4, 2003

 © 2003 Wiley-VCH Verlag GmbH & Co. KGaA, Weinheim

Kinetics of Oxidation of Azide by [Ethylenebis(biguanide)]silver(III) in Aqueous Acidic Media

Prabir Bandyopadhyay,[a] Basab Bijayi Dhar,[a] Jhimli Bhattacharyya,[a] and Subrata Mukhopadhyay*[a]

Keywords: Kinetics / Mechanisms / Redox chemistry / Silver / Azides

In aqueous acidic media sodium azide and the orange-yellow title complex react quantitatively generating N_2 gas along with a colourless solution of Ag^+ ion and the ligand, ethylenebis(biguanide). The parent complex, $[Ag(H_2L)]^{3+}$, and one of its conjugate bases, $[Ag(HL)]^{2+}$, participate in the reaction with N_3^- as the kinetically reactive reductant. Ag^+ has no catalytic effect. At 25.0 °C, I = 1.0 M ($NaNO_3$), rate constants for the reactions $[Ag(H_2L)]^{3+} + N_3^-$ and that for $[Ag(HL)]^{2+} + N_3^-$ are (12.3±0.5) and (3.8±0.6) $M^{-1}\cdot s^{-1}$, respectively. The high rate constants along with the very low equilibrium constant (10^{-15} M^{-1}) calculated for the first reaction strongly suggest inner-sphere redox mechanism.
(© Wiley-VCH Verlag GmbH & Co. KGaA, 69451 Weinheim, Germany, 2003)

Introduction

Ethylenebis(biguanide)silver(III) (Figure 1) represents the simplest cationic complex[1−3] of Ag^{III} stable in aqueous solution over a wide pH range against dechelation and intramolecular redox decomposition.[4] The square-planar acyclic tetraaza ligand imparts fascinating thermodynamic stability[5] to the Ag^{III} state and renders the title complex a milder oxidant[6] than Ag^+. It is a potential inner-sphere oxidant,[7−11] which may bind a reducing ligand in its vacant axial coordination sites. But in this strong-field d^8 system such ligand binding is likely to be weak or at best moderate. Hence, outer-sphere reactions may be energetically more favourable[12,13] for weakly basic but strongly reducing ligands with the Ag^{III} complex. In redox reactions the complex may act as either a one-[7] or a two-electron[10] oxidant. In solution the title complex undergoes ligand-based protic equilibria.[14] Also, the Ag^{III}-bound ligand, H_2L may form hydrogen bonds with a suitable reducing agent, like $HC_2O_4^-$ and lead to a dead-end adduct in the electron-transfer pathway.[15] The mechanistic versatility of oxidations of various organic and inorganic species by the title Ag^{III} complex is an outcome of such properties as discussed above.

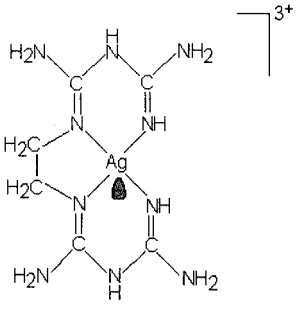

Figure 1. Structure of $[Ag(H_2L)]^{3+}$; the gray-shaded area represents a weakly bonded ClO_4^- ion at the axial site

Kirschenbaum et al. studied[16] the oxidation of N_3^- by $Ag(OH)_4^-$ in strongly alkaline media. They found that the N_3^- ion replaced a coordinated hydroxide ion in $Ag(OH)_4^-$ and the azido complex so produced underwent subsequent redox decay with another N_3^- ion. Sengupta et al. proposed an analogous mechanism[17] for the oxidation of N_3^- by $[Ag(H_2TeO_6)_2]^{5-}$, again in strongly alkaline media. We are not aware of any mechanistic study of azide oxidation by higher valent silver species in acidic media. The exceptional stability of the title complex towards redox decomposition in acidic media affords a good chance to examine for the first time the reactivity of HN_3 and N_3^- towards a cationic Ag^{III} complex in acidic solutions. Moreover, the ligand H_2L in $[Ag(H_2L)]^{3+}$ is substitution-inert so that Ag^{III} never comes free in solution to open up extra, complicating pathways in its kinetics.

Results and Discussion

Preliminary Observations

In the absence of any external buffer, the media pH before and after the reactions did not change by more than 0.05 units. Autodecomposition of the Ag^{III} complex was insignificant under the experimental conditions of pH and temperature. No Ag^+ catalysis (studied up to 0.01 M) was found in the reactions. We did not extend the reaction pH

[a] Department of Chemistry, Jadavpur University, Calcutta 700032, India
E-mail: subrataju@vsnl.net

 © 2003 Wiley-VCH Verlag GmbH & Co. KGaA, Weinheim DOI: 10.1002/ejic.200300300

> ca. 4.05, as reaction mixtures above pH ≈ 4.2 turn turbid probably due to formation of insoluble silver azide after ca. 30% decrease in their initial absorbances, thus seriously interfering with the kinetic measurements.

Stoichiometry and Reaction Products

Stoichiometric measurements yielded $\Delta[Ag^{III}]_T/\Delta T_R = 0.52\pm0.05$. The principal conversion can thus be represented by Equation (1).

$$Ag^{III} + 2\ N_3^- \rightarrow Ag^{I} + 3\ N_2 \quad (1)$$

The oxidation of azide to dinitrogen was qualitatively confirmed by GC analysis. Immediately after completion of the reaction (absorbance < 0.01 at 380 nm), the solution pH was raised to ca. 5 by adding NaOH solutions when all Ag^+ was precipitated as AgN_3 and removed by filtration. From the filtrate, the free ligand ethylenebis(biguanide) was quantitatively isolated[18] as the sparingly soluble [ethylenebis(biguanide)]copper(II) sulfate, and the amount of Cu^{II} thus held was estimated iodometrically after decomposing the Cu^{II} complex. The results showed that more than 95% of the free ligand (H_2L) was recovered.

Kinetics

No immediate spectral changes were observed on mixing the reactants over the entire experimental range of pH. But the absorbance of the reaction mixtures at $\lambda \geq 380$ nm gradually decreased to less than 0.01 and the $\log_{10}$(absorbance)/time plots were found to be linear to 90% completion of the reactions. The first-order rate constants, k_{obs}, defined by Equation (2) were obtained from least-squares slopes of these plots.

$$-d[Ag^{III}]/dt = k_{obs}[Ag^{III}] \quad (2)$$

Averages of the k_{obs} values (Table 1) from at least three independent runs were taken and the average coefficients of variation (CV) for these measurements were within 3%.

The reaction was found to be first-order in T_R (= $[HN_3] + [N_3^-]$) and there is no T_R-independent term. The following changes of the reaction conditions had, within the limits of experimental uncertainties, no influence on the values of k_{obs}: a fivefold variation in $[Ag^{III}]$ from 0.10 to 0.50 mM, addition of $AgNO_3$ up to 0.01 M, addition of ethylenebis(biguanide) up to 1.0 mM, occasional shaking of the spectrophotometer cell, presence or absence of dissolved oxygen and diffused light, and a variation in the monitoring wavelength in the range 380−480 nm.

No polymer formed when 6% (v/v) acrylonitrile was added to the reaction mixture and the entire reaction course was EPR-silent. These experiments therefore indicate that free radicals or other paramagnetic species like Ag^{II} do not accumulate in the reaction media in concentrations detectable by either of these two methods.

The value of k_{obs} sharply decreases with increasing $[H^+]$. A plot of k_{obs} versus $[H^+]^{-1}$ at a fixed T_R (Figure 2) is a

Table 1. Some representative first-order rate constants for the oxidation of azide by the Ag^{III} complex

pH	T_R [mM]	$10^4 k_0$ [s^{-1}][a]	CV in%[b]
1.00	3.0	0.24 (0.24)	3.0
1.50		0.76 (0.76)	3.0
2.00		2.35 (2.34)	2.5
2.65		10.0 (9.9)	2.6
2.90		16.8 (16.7)	2.1
3.35		39.2 (38.4)	2.3
3.70		60.0 (62.8)	2.3
4.05		84.0[c] (86.8)	3.0
1.01	30.0	2.29 (2.44)	2.8
1.50	6.0	1.56 (1.51)	3.0
1.50	12.0	3.10 (3.02)	2.9
2.00	12.0	9.20 (9.36)	2.2
2.02	6.0	5.00 (4.93)	2.6
2.05	24.0	22.0 (21.1)	2.6
2.05	30.0	25.8 (26.4)	2.7
2.50	15.0	34.2 (36.0)	2.0
2.52	30.0	70.0 (74.9)	2.1
2.90	1.5	8.30 (8.35)	3.0
2.90	6.0	33.0 (33.4)	2.1
2.90	12.0	65.5 (66.8)	1.8
3.05	6.0	44.5 (44.9)	1.9
3.05	12.0	88.0 (89.8)	1.9
3.10	1.5	12.1 (12.4)	2.0
3.10	3.0	24.2 (24.8)	2.0
3.35	3.0	37.3 (38.4)	2.8
3.35	6.0	76.0 (76.8)	1.9
3.55	1.5	25.4 (26.0)	2.9
3.55	6.0	107 (104)	1.8
3.85	1.5	36.2 (37.0)	2.2
3.85	6.0	143 (148)	1.9
4.05	1.5	42.5 (43.4)	2.8

[a] [complex] = 0.20 mM, T = 25.0 °C, I = 1.0 M ($NaNO_3$). Calculated k_{obs} values are given in parentheses. [b] CV was measured using the relation: CV = sd × 100/x, where sd = standard deviation of the measurements of k_{obs} and x = average k_{obs}. See ref.[19], p. 1123. [c] 10^4 k_{obs} [s^{-1}] values are 91.0, 97.0 and 106 at I = 0.5, 0.2 and 0.1 M respectively.

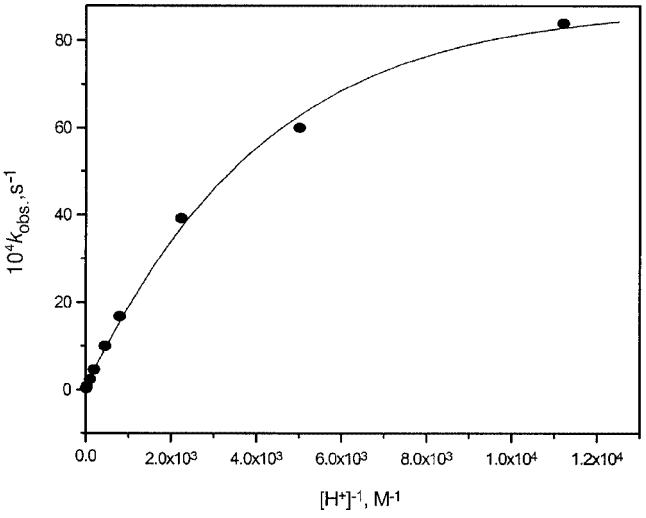

Figure 2. Plot of k_{obs} versus $[H^+]^{-1}$ at T_R = 3.0 mM; the solid line represents the fit of Equation (7)

 © 2003 Wiley-VCH Verlag GmbH & Co. KGaA, Weinheim

good straight line for pH ≤ 2.9 ($[H^+] \geq 1.26\cdot10^{-3}$ M) with zero intercept but droops at higher $[H^+]^{-1}$. Such $[H^+]$ dependence of k_{obs} indicates that the conjugate base form of one of the reactants is more reactive while that of the other is less reactive than the parent acid. We infer that N_3^- is much more reactive than HN_3 while $[Ag(H_2L)]^{3+}$ is more reactive than its conjugate base, $[Ag(HL)]^{2+}$. This is expected from known kinetic behaviour[11,12,19,20] of these species and the fact[21,22] that protonation generally increases the reactivity of metal complex oxidants whereas the anionic forms of protolytic reductants are much more reactive than the uncharged molecular compounds.[23–25] The near-zero value for k_{obs} at high $[H^+]$ further suggests that kinetic activity of HN_3 is negligible for the present system. The scheme in Equations (3) to (6) most simply accommodates the kinetic observations and the known acid/base equilibria K_{a1} and K_a.

$$[Ag(H_2L)]^{3+} \overset{K_{a1}}{\rightleftharpoons} [Ag(HL)]^{2+} + H^+ \quad (3)$$

$$HN_3 \overset{K_a}{\rightleftharpoons} H^+ + N_3^- \quad (4)$$

$$[Ag(H_2L)]^{3+} + N_3^- \xrightarrow{k_1} \text{Products, } Ag^+ + H_2L + N_2 \quad (5)$$

$$[Ag(HL)]^{2+} + N_3^- \xrightarrow{k_2} \text{Products, } Ag^+ + HL + N_2 \quad (6)$$

The derived rate-law for this scheme is Equation (7).

$$k_{obs}(K_{a1} + [H^+])(K_a + [H^+])/T_R = k_1K_a[H^+] + k_2K_{a1}K_a \quad (7)$$

A plot of the left hand side of Equation (7) versus $[H^+]$ is a good straight line (Figure 3, $r = 0.99$) with slope = $(8.0\pm0.3) \times10^{-4}$ s^{-1} and intercept = $(3.9\pm0.6) \times10^{-8}$ M·s^{-1}. Using known K_a (= $6.5\cdot10^{-5}$ M)[26] and K_{a1} (= $1.585\cdot10^{-4}$ M)[14] values, these lead to $k_1 = (12.3\pm0.5)$ $M^{-1}\cdot s^{-1}$ and $k_2 = (3.8 \pm 0.6)$ $M^{-1}\cdot s^{-1}$. These rate constants reproduced all experimental k_{obs} values satisfactorily (Table 1).

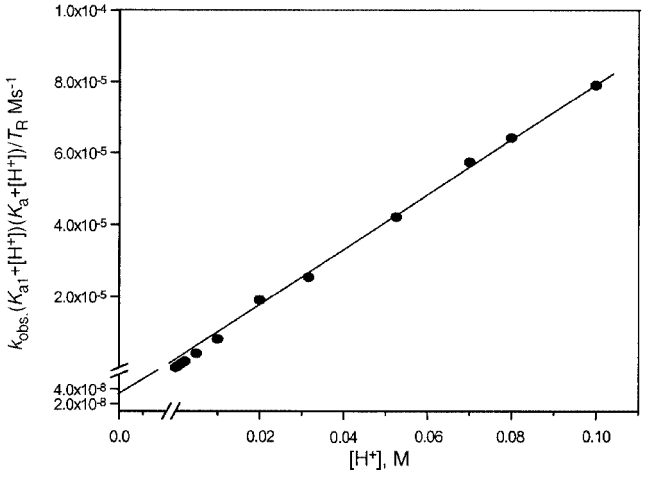

Figure 3. Plot of $k_{obs}(K_{a1} + [H^+])(K_a + [H^+])/T_R$ versus $[H^+]$; the solid line represents the fit of Equation (7)

Mechanism

The redox potentials for the couple $[Ag(H_2L)]^{3+/2+}$ and that for N_3^-/N_3 are 0.43 V[27,6] and 1.33 V,[28] respectively. The self-exchange rate constant[28] for N_3^-/N_3 is $4\cdot10^4$ $M^{-1}\cdot s^{-1}$ and the upper limit for the self-exchange rate for $[Ag(H_2L)]^{3+/2+}$ has been estimated[27] to be $10^{6.6}$. With these values and using the Marcus cross-relation,[29] $k_{12} = (k_{11}k_{22}K)^{1/2}$, the calculated maximum value of the outer-sphere oxidation rate of N_3^- by $[Ag(H_2L)]^{3+}$ is 10^{-4} $M^{-1}\cdot s^{-1}$, considerable less (10^5 times) than k_1 and we therefore propose an inner-sphere mechanism for the k_1 path. An inner-sphere mechanism appears very likely for the k_2 path, too. Indeed, the very high thermodynamic price for the oxidation of N_3^- to N_3 essentially requires strong oxidants[30,31] like $[Ni(bipy)_3]^{3+}$ or $[CoW_{12}O_{40}]^{5-}$ for outer-sphere reactions to occur.

Coordination of the azide ion to the metal centers[16,17,32–34] in $[Ag^{III}(OH)_4]^-$, $[Ag^{III}(H_2TeO_6)_2]^{5-}$, $[Cu^{III}(H_2TeO_6)_2]^{5-}$, $[Mn^{III}(bipy)_2(OH)]^{2+}$, $[Mn^{III}(edta)(H_2O)]^-$, or in Mn_{aq}^{3+} are well documented with the formation constants of azido complexes lying in the range 10^{-1} to 10^2. A similar azide binding is likely for the Ag^{III} complex under investigation. X-ray photoelectron spectroscopic measurements[35] have shown that the silver(III) centre in the title complex has a high degree of positive charge resulting in a high electron affinity of the Ag^{III} ion. Expectedly, therefore, structural[36–38] and kinetic studies[8,9,11] indicated axial coordination by Ag^{III} with low molecular weight alcohols, H_2O_2, SO_4^{2-}, NO_3^-, or even ClO_4^-. The kinetic steps (5) and (6) are therefore most likely to proceed via intermediate adduct formations between Ag^{III} and N_3^- followed by intramolecular redox decomposition to form the final products. The present results cannot straightaway eliminate the possibility of proton-ambiguous paths like

$$[Ag(H_2L)]^{3+} + HN_3 \rightleftarrows \{[Ag(H_2L)]^{3+}\cdot N_3^-\} + H^+;$$
$$\{[Ag(H_2L)]^{3+}\cdot N_3^-\} \rightarrow \text{Products, etc.}$$

Nevertheless, the observed increase in reaction rate with decreased ionic strength of the reaction media does not fit into this alternative reaction scheme, rather it directs the reaction between oppositely charged ions. Also, it has been established that N_3^- is kinetically far more reactive than HN_3 and may exhibit overwhelming kinetic dominance over HN_3[30,39] even for redox reactions in 1 M acid.

In the lower pH range (pH ≤ 2.9), where $[Ag(H_2L)]^{3+}$ is the only active and sole oxidant, the rate law simplifies to $k_{obs}/T_R = kK_a/[H^+]$. The observed linearity of the k_{obs} versus $[H^+]^{-1}$ plot at higher $[H^+]$ demands a maximum value of the order of 10^1 M^{-1} for preequilibrium formation of any adduct between $[Ag(H_2L)]^{3+}$ and N_3^-. $[Ag(HL)]^{2+}$, a possible weaker Lewis acid than its conjugate acid should bind N_3^- even less tightly.

The present kinetic observations cannot unambiguously settle the question of one- or two-electron transfer. The immediate one-electron oxidation product[28,40–44] of azide is N_3, as firmly established by pulse radiolysis, flash photolysis or by molecular beam studies. The azidyl radical (N_3)

 © 2003 Wiley-VCH Verlag GmbH & Co. KGaA, Weinheim

may decay to N_2 in several ways, like by fragmentation[45] to N_2 and N, the process, although spin-forbidden, is close to thermoneutral[46] with a rate constant[47,48] around 10^6 s^{-1}. In yet another possibility, N_3 can combine with N_3^- forming[49−51] N_6^- (however, attempts to observe the radical dimer N_6^- using pulse radiolysis met with no success,[48b] but nanosecond laser flash photolysis[50,51] and kinetic evidences[16] suggest involvement of N_6^- in some instances) and then rapid reaction of N_6^- with the oxidant species or a rapid direct reaction of two mol of N_3 radical could produce three mol of N_2 ($2\ N_3 \rightarrow 3\ N_2$, $2k = 9\cdot10^9$ $M^{-1}\cdot s^{-1}$).[28] The absence of EPR evidence for Ag^{II} or N_3 radicals in our study cannot conclusively eliminate the formation of such species as it may only indicate that such species are formed but decayed too rapidly before they can diffuse into the bulk solvent sufficiently quickly to permit detection. For example, Equations (8) to (12) are one conceivable expansion for the k_1 path.

$$[Ag(H_2L)]^{3+} + N_3^- \overset{K}{\rightleftharpoons} \{[Ag(H_2L)]\cdot N_3\}^{2+} \quad (8)$$

$$\{[Ag(H_2L)]\cdot N_3\}^{2+} \xrightarrow{k_1'} [Ag^{II}(H_2L)]^{2+} + N_3 \quad (9)$$

$$[Ag^{II}(H_2L)]^{2+} + N_3^- \xrightarrow{fast} Ag^I + H_2L + N_3 \quad (10)$$

$$N_3 \xrightarrow{k_d} N_2 + N \quad (11)$$

$$2\ N \xrightarrow{fast} N_2 \quad (12)$$

Reaction (9) requires a very high thermodynamic price and is as such unfavourable. Yet, the very high protonation constants[52] of the ligand H_2L drag the overall reaction to completion in acidic media.

An alternative for the assigned fate of the azidyl radical could be the dimerisation to produce N_6 that ultimately produces N_2. But, this appears unlikely here as, if it were the actual pathway, then sufficient accumulation of N_3 to cause appreciable reversal of reaction (9) and hence rate retardation (deviation from simple first-order kinetics) could be anticipated.[48b,53] No such retardation could be detected and thus the dimerisation pathway is neglected in the present study.

Though the silver(III) complex under investigation is far more stable than $[Ag(OH)_4]^-$ or $[Ag(TeO_4)_2(OH)_4]^{5-}$, it oxidises N_3^- at a faster rate. This can be attributed to a difference in mechanism operating in these oxidations, for example, two-electron transfer in $[Ag(OH)_3N_3]^-$ or in $[Ag(TeO_4)_2(OH)_3(N_3)]^{5-}$ and the proposed one-electron transfer in our inner-sphere adducts. A reactive species ambiguity (HN_3 versus N_3^-) may also be a reason for obtaining a higher rate in the present investigation. However, of these two alternatives, the first appears more logical but the proton-ambiguity situation is unresolvable. The tetraaza ligand is expected to stabilise Ag^{II} much more than that by hydroxide or tellurate.

Direct two-electron changes in these redox steps to form N_3^+ which reacts with N_3^- forming N_6 and ultimately decays to N_2 cannot be ruled out in principle. Formation of N_3^+ has been proposed for the thermal decomposition[54] of $[Mn(N_3)_2]^{2+}$ and photoinduced reductive decomposition of *cis*-$[Pt(N_3)_2(PPh_3)_2]$ has provided distinct spectral evidence for the intermediate formation[55] of neutral cyclic hexazine, N_6.

Experimental Section

Materials: The silver(III) complex, $[Ag(H_2L)]^{3+}$, was prepared by a known procedure.[3,56] Sodium azide (G. R., E. Merck) solutions were standardised by Ce^{IV} titration.[57] $NaNO_3$ (G. R., E. Merck) solutions were standardised by passing an aliquot through a Dowex 50W X-8 strong cation exchange resin in the H^+ form and titrating the liberated acid with standard NaOH to a phenolphthalein endpoint. To avoid any possible interaction of azide with oxides of nitrogen,[58] the stock HNO_3 solutions were purged with argon before use. All measurements were made at 25.0 °C and I = 1.0 M ($NaNO_3$). All solutions were prepared in water which was deionised and then doubly distilled.

Physical Measurements and Kinetics: UV/Vis spectra were recorded with a Shimadzu (1601 PC) spectrophotometer using 1.00-cm quartz cells. Kinetics were generally monitored at 380 nm in situ in the thermostatted (25.0±0.1 °C) cell-housing (CPS, 240A). For faster reactions sodium azide solutions (adjusted to the desired pH) were directly injected into the spectrophotometer cell containing other components of the reaction mixture at the same pH. The desired concentrations of the complex and the reducing agent were achieved after mixing which was immediately followed by automatic monitoring of the change in absorbance with time. We used capped quartz cells with minimum vacant space left and thus avoided escape of volatile HN_3. The solution pH (1.00−4.05) was measured with a Systronics (India) pH meter (model 335) with electrodes calibrated as described earlier.[59] All such pH measurements were done quickly to ensure minimum evaporation of volatile HN_3. Spectrophotometric determination[60] of azide in blank experiments indicated a near quantitative (≥ 97%) recovery of total azide under our experimental conditions. Excess reducing agent, T_R (= $[HN_3] + [N_3^-]$), 1.5−30.0 mM over the complex (0.20 mM) was used in all kinetic runs.

Stoichiometry and Reaction Products: The reaction stoichiometry was determined under kinetic conditions in the pH range 3.5−4.0 by estimating unchanged azide spectrophotometrically. Excess azide was mixed with the complex solutions and stored until the reaction mixtures turned colourless indicating complete reduction of Ag^{III} to Ag^I. $Fe(NO_3)_3$ solution in 0.5 M HNO_3 was then added to the product mixtures[60] to achieve $[Fe^{III}]/T_R$ in the final solutions within the range 1.5−2.5. The pH of the solutions was then adjusted[60] to 1.5−2.0 using HNO_3 or NaOH, as needed. A red complex, $[Fe(H_2O)_5N_3]^{2+}$, generated within minutes. Its absorbance at 460 nm yielded the concentration of unchanged azide from a calibration curve constructed under comparable conditions (ε = 3570 $M^{-1}\cdot cm^{-1}$, literature value,[60] 3680 $M^{-1}\cdot cm^{-1}$). We verified that Ag^+ or the ligand, ethylenebis(biguanide), do not interfere with the measurement of the azide concentration. The gaseous product formed during the reactions was collected over a saturated sodium chloride solution as described earlier[61] and analysed by gas chromatography using a Chemito (India) GCHT 8610 equipped with TCD, a Porapack Q and molecular sieves 13 X column. Splitless mode injection of 500 μL of sample was used. The oven temperature, injector and detector temperature were kept at 40, 55, and 100 °C, respectively. The carrier hydrogen gas flow was adjusted to 30 mL/min.

 © 2003 Wiley-VCH Verlag GmbH & Co. KGaA, Weinheim

Acknowledgments

We are grateful to Professor Rupendranath Banerjee for helpful advice. Financial assistance from Jadavpur University Research Fund is gratefully acknowledged.

[1] P. Ray, *Nature (London)* **1943**, *151*, 643.
[2] P. Ray, K. Chakravarty, *J. Indian Chem. Soc.* **1944**, *21*, 47−50.
[3] P. Ray, *Inorg. Synth.* **1960**, *6*, 74−79.
[4] R. Banerjee, D. Banerjea, *Indian J. Chem.* **1979**, *17A*, 246−249.
[5] D. Sen, N. N. Ghosh, P. Ray, *J. Indian Chem. Soc.* **1950**, *27*, 619−626.
[6] K. Das, R. Banerjee, A. Das, S. Dasgupta, *Bull. Electrochem.* **1989**, *5*, 477−482.
[7] R. Banerjee, R. Das, S. Mukhopadhyay, *J. Chem. Soc., Dalton Trans.* **1992**, 1317−1321.
[8] R. Banerjee, A. Das, S. Dasgupta, *J. Chem. Soc., Dalton Trans.* **1990**, 1207−1212.
[9] R. Banerjee, A. Das, S. Dasgupta, *J. Chem. Soc., Dalton Trans.* **1989**, 1645−1649.
[10] S. Dasgupta, E. Herlinger, W. Linert, *J. Chem. Soc., Dalton Trans.* **1993**, 567−570.
[11] P. Bandyopadhyay, S. Mukhopadhyay, *Polyhedron* **2002**, *21*, 1893−1898.
[12] S. Mukhopadhyay, R. Banerjee, *J. Chem. Soc., Dalton Trans.* **1994**, 1349−1353.
[13] R. Banerjee, *Proc. Indian Acad. Sci. (Chem. Sci.)* **1994**, *106*, 655−664.
[14] S. Mukhopadhyay, R. Banerjee, *Polyhedron* **1994**, *13*, 53−56.
[15] S. Mukhopadhyay, S. Kundu, R. Banerjee, *Proc. Indian Acad. Sci. (Chem. Sci.)* **1995**, *107*, 403−410.
[16] E. T. Borish, L. J. Kirschenbaum, *Inorg. Chem.* **1984**, *23*, 2355−2359.
[17] K. K. Sen Gupta, A. Sanyal, S. P. Ghosh, *J. Chem. Soc., Dalton Trans.* **1995**, 1227−1232.
[18] P. Ray, *Chem. Rev.* **1961**, *61*, 313−359.
[19] T. W. Swaddle, G. Guastalla, *Inorg. Chem.* **1969**, *8*, 1604−1609.
[20] [20a] G. Stedman, *Adv. Inorg. Chem. Radiochem.* **1979**, *22*, 113−143. [20b] Z. B. Alfassi, R. H. Schuter, *J. Phys. Chem.* **1985**, *89*, 3359−3363.
[21] S. K. Ghosh, R. N. Bose, E. S. Gould, *Inorg. Chem.* **1987**, *26*, 2688−2692.
[22] K. D. Asmus, M. Bonifacic, P. Toffel, P. O'Neill, D. S. Frohlinde, S. Steenken, *J. Chem. Soc., Faraday Trans. 1* **1978**, 1820−1826.
[23] K. Lemma, A. M. Sargeson, L. I. Elding, *J. Chem. Soc., Dalton Trans.* **2000**, 1167−1172.
[24] T. Shi, J. Berglund, L. I. Elding, *Inorg. Chem.* **1996**, *35*, 3498−3503.
[25] J. Berglund, L. I. Elding, *Inorg. Chem.* **1995**, *34*, 513−519.
[26] [26a] C. F. Wells, M. A. Salam, *Chem. Ind.* **1967**, 2079−2080. [26b] C. F. Wells, M. A. Salam, *J. Chem. Soc., A* **1968**, 1568−1575.
[27] S. P. Ghosh, M. C. Ghosh, E. S. Gould, *Inorg. Chim. Acta* **1994**, *225*, 83−88.
[28] [28a] M. S. Ram, D. M. Stanbury, *Inorg. Chem.* **1985**, *24*, 4233−4234. [28b] M. S. Ram, D. M. Stanbury, *J. Phys. Chem.* **1986**, *90*, 3691−3696.
[29] [29a] R. A. Marcus, *Annu. Rev. Phys. Chem.* **1964**, *15*, 155−196. [29b] R. A. Marcus, N. Sutin, *Inorg. Chem.* **1975**, *14*, 213−216.
[30] J. K. Brown, D. Fox, M. P. Heyward, C. F. Wells, *J. Chem. Soc., Dalton Trans.* **1979**, 735−739.
[31] B. Goyal, M. Mehrotra, A. Prakash, R. N. Mehrotra, *Inorg. React. Mech.* **2000**, *1*, 289−299.
[32] M. P. Heyward, C. F. Wells, *J. Chem. Soc., Dalton Trans.* **1988**, 1331−1335.
[33] M. A. Suwyn, R. E. Hamm, *Inorg. Chem.* **1967**, *6*, 2150−2154.
[34] C. F. Wells, D. Mays, *J. Chem. Soc., A* **1968**, 1622−1625.
[35] D. A. Zatko, J. P. Prather, *J. Electron Spectrosc. Relat. Phenom.* **1973**, *2*, 191−197.
[36] N. R. Kunchur, *Nature (London)* **1968**, *217*, 539−541.
[37] M. L. Simms, J. L. Atwood, D. A. Zatko, *J. Chem. Soc., Chem. Commun.* **1973**, 46−47.
[38] L. Coghi, G. Pelizzi, *Acta Crystallogr., Sect. B* **1975**, *31*, 131−134.
[39] K. D. Whitburn, G. S. Laurence, *J. Chem. Soc., Dalton Trans.* **1979**, 334−337.
[40] E. Hayon, M. Simic, *J. Am. Chem. Soc.* **1970**, *92*, 7486−7487.
[41] D. M. Stanbury, L. A. Lednicky, *J. Am. Chem. Soc.* **1984**, *106*, 2847−2853.
[42] G. V. Buxton, I. Janovsky, *J. Chem. Soc., Faraday Trans. 1* **1976**, *72*, 1884−1886.
[43] A. Treinin, E. Hayon, *J. Chem. Phys.* **1969**, *50*, 538−539.
[44] A. G. Griesbeck, J. Lex, K. M. Saygin, J. Steinwascher, *Chem. Commun.* **2000**, 2205−2206.
[45] R. K. Murmann, J. C. Sullivan, R. C. Thompson, *Inorg. Chem.* **1968**, *7*, 1876−1879.
[46] P. Gray, *Q. Rev. Chem. Soc.* **1963**, *17*, 441−473.
[47] J. Butler, E. J. Land, A. J. Swallow, W. Prutz, *Radiat. Phys. Chem.* **1984**, *23*, 265−270.
[48] [48a] S. W. Benson, *Thermochemical Kinetics*, 2nd ed., Wiley, New York, **1976**, p. 206. [48b] W. K. Wilmarth, D. M. Stanbury, J. E. Byrd, H. N. Po, C. P. Chua, *Coord. Chem. Rev.* **1983**, *51*, 155−179.
[49] C. F. Wells, D. Mays, *J. Chem. Soc., A* **1969**, 2175−2179.
[50] M. S. Workentin, B. D. Wagner, F. Negri, M. Z. Zgierski, J. Lusztyk, W. Siebrand, D. D. M. Wayner, *J. Phys. Chem.* **1995**, *99*, 94−101.
[51] M. S. Workentin, B. D. Wagner, J. Lusztyk, D. D. M. Wayner, *J. Am. Chem. Soc.* **1995**, *117*, 119−126.
[52] B. Das Sarma, *J. Indian Chem. Soc.* **1952**, *29*, 217−224.
[53] B. Chaudhuri, R. Banerjee, *J. Chem. Soc., Dalton Trans.* **1998**, 3451−3455.
[54] G. Davies, L. J. Kirschenbaum, K. Kustin, *Inorg. Chem.* **1969**, *8*, 663−669.
[55] A. Vogler, R. E. Wright, H. Kunkely, *Angew. Chem. Int. Ed. Engl.* **1980**, *19*, 717−718.
[56] R. Banerjee, K. Das, A. Das, S. Dasgupta, *Inorg. Chem.* **1989**, *28*, 585−588.
[57] A. I. Vogel, *A Textbook of Quantitative Inorganic Analysis including Elementary Instrumental Analysis*, 3rd ed., The English Language Book Society and Longmans, Green & Co. Ltd., London, **1964**, p. 314.
[58] G. Stedman, *J. Chem. Soc.* **1960**, 1702−1709 and references cited therein.
[59] [59a] S. Banerjee, U. Roy Choudhury, R. Banerjee, S. Mukhopadhyay, *J. Chem. Soc., Dalton Trans.* **2002**, 2047−2052. [59b] S. Banerjee, U. Roy Choudhury, B. C. Ray, R. Banerjee, S. Mukhopadhyay, *Anal. Lett.* **2001**, *34*, 2797−2815.
[60] R. M. Wallace, E. K. Dukes, *J. Phys. Chem.* **1961**, *65*, 2094−2097.
[61] K. Dutta, S. Bhattacharjee, B. Chaudhuri, S. Mukhopadhyay, *J. Environ. Monit.* **2002**, *4*, 754−760.

Received May 20, 2003
Early View Article
Published Online October 22, 2003

 © 2003 Wiley-VCH Verlag GmbH & Co. KGaA, Weinheim

η^1-Vinylidene to η^2-Alkyne Isomerization of Tungsten and Molybdenum Complexes

Junes Ipaktschi,*[a] Javad Mohsseni-Ala,[a] and Sascha Uhlig[a]

Keywords: Vinylidene ligands / Alkyne ligands / Isomerization / Kinetics / Isotope effects

The thermal isomerizations of η^1-vinylidene complexes [(η^5-C_5H_5)(CO)(NO)W=C=CHR] [**5a**, R = $Si(CH_3)_2C(CH_3)_3$; **5c**, R = $C(CH_3)_3$] as well as [(η^5-C_5H_5)(CO)(NO)Mo=C=CHC$(CH_3)_3$] (**8**), to the corresponding η^2-1-alkyne complexes [(η^5-C_5H_5)(CO)(NO)W(η^2-H–C≡C–R)] [**7a**, R = $Si(CH_3)_2C(CH_3)_3$; **7c**, R = $C(CH_3)_3$] and [(η^5-C_5H_5)(CO)(NO)Mo{η^2-H–C≡C–CHC$(CH_3)_3$}] (**9**) has been investigated. Activation parameters for the isomerization of **5a** in [D_6]benzene and **8** in [D_8]toluene and [D_5]ethanol were determined. In [D_8]toluene η^1-vinylidene complex **5a** undergoes a single step 1,2-shift of the silyl group from C_β to C_α. However, complex **8** shows dichotomous behavior. The isomerization **8** → **9**, dependent upon the solvent applied, occurs by means of two different pathways: in a nonpolar solvent, **8** tautomerizes via the 1,2-migration of the hydrogen atom to **9** and in ethanol this tautomerization proceeds by a multi-step process via deprotonation-protonation and subsequent reductive elimination.
(© Wiley-VCH Verlag GmbH & Co. KGaA, 69451 Weinheim, Germany, 2003)

Introduction

A great deal of attention has been devoted to the isomerization of transition metal η^1-vinylidene and η^2-1-alkyne complexes over the past two decades.[1] Thus, it is now well established that the thermodynamic stabilities and properties of such derivatives are essentially a function of the nature of both the metal center and its ancillary ligands.[1,2] It is well-known that η^1-vinylidene complexes of electron-rich transition metals are thermodynamically more stable than the corresponding η^2-1-alkyne derivatives.[1,3] This fact is widely used in the preparation of η^1-vinylidene complexes.[4]

The mechanism of the η^2-1-alkyne → η^1-vinylidene rearrangement has been extensively studied both experimentally and theoretically.[2,4,5–8] Two alternative pathways are discussed so far in the literature (Scheme 1): via either an intramolecular 1,2-hydrogen shift (A–B–D)[2,4e,6a,6b] or by the formation of a hydride alkynyl species C and concomitant 1,3-hydrogen shift.[4a,4c,4d,4f,5a,8,6b] Electron-rich metal complexes favor the A–C–D[4a,4d,8b] pathway whereas electron poor complexes prefer the A–B–D[4e,5a,6a] pathway.

The reaction order for the 1,3-hydrogen shift is also a matter of active debate. Recent experimental and theoretical studies demonstrated a bimolecular mode for this process[4c,4a,4d,9] while others support a unimolecular reaction.[2]

The isomerization of η^1-vinylidene transition metal complexes into the corresponding η^2-alkyne complexes has rarely been described in the literature.[5] Bly et al.[5g,5h] have observed the isomerization of the cationic complexes [Fe(=C=CR^1R^2)(η^5-C_5H_5)$(CO)_2]^+OTf^-$ to the corresponding η^2-alkyne derivatives [Fe(η^2-R^1C≡CR^2)(η^5-C_5H_5)-$(CO)_2]^+OTf^-$ by an alkyl shift from the β- to α-carbon atom. In the same way, Connelly et al.[5b,5g,5i] have observed η^1-vinylidene → η^2-alkyne rearrangements induced by one-electron oxidation of the 18-electron complexes [M=C=$C(SiMe_3)_2$(η^6-C_6R_6)$(CO)_2]^+$ (M = Cr, Mo).

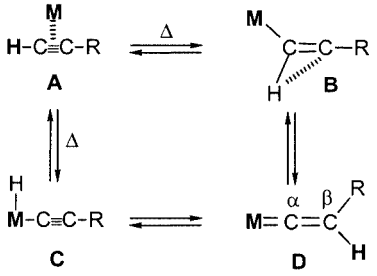

Scheme 1. Alternative pathways for the η^2-1-alkyne → η^1-vinylidene rearrangement

To shed some light on the mechanism of the η^1-vinylidene → η^2-alkyne isomerization we have studied the thermal isomerization of the tungsten η^1-vinylidene complexes **5a–c**, as well as of the molybdenum derivatives **8**.

Results

Synthesis and Characterization of 5a,b

The reaction of the tungsten carbonyl complex **1** with lithium alkynyl **2a,b** in THF at −30 °C led to a deep green

[a] Institute of Organic Chemistry, Justus-Liebig University, Heinrich-Buff-Ring 58, 35392 Giessen, Germany
Fax: (internat.) +49-(0)641-9934309
E-mail: junes.ipaktschi@org.chemie.uni-giessen.de

solution of the lithium metalate **3a,b** (Scheme 2). Treatment of this solution with dilute HCl resulted, after purification through chromatography, in the formation of the η^1-vinylidene complexes **5a,b** as a mixture of two rotamers. It is interesting to note that, after protonation the C−Si bond is cleaved, in the course of the reaction of **3b**, yielding the η^1-vinylidene complex **6** (21% yield).[10] This behavior has precedents in the literature, i.e., the formation of [CpRu=C=CH_2(dippe)][BPh_4] from [CpRuCl(dippe)] with H−C≡C−$SiMe_3$,[4g] and the formation of [CpFe=C=CH_2(dppm)][BF_4] from [CpFe−C≡C−$SiMe_3$(dppm)].[11]

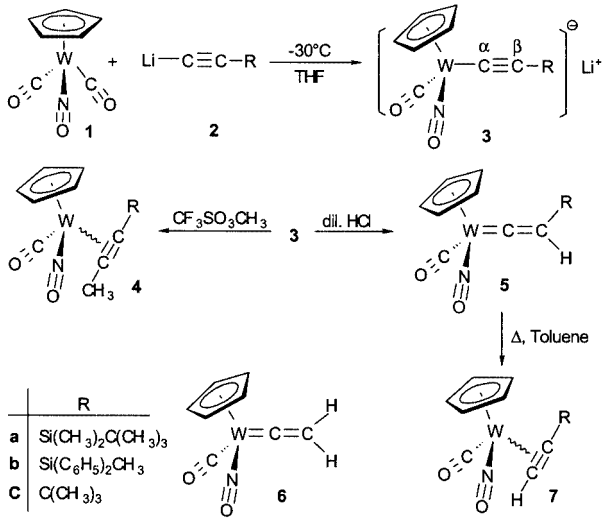

Scheme 2. Synthesis of vinylidene complexes **5** and **6** from the tungsten complexes **1**

Compound **5a** is an orange crystalline solid, whereas **5b** is a dark red oil. These η^1-vinylidenes can be stored under argon at −20 °C for several months. Their unequivocal characterization was achieved by means of standard spectroscopic techniques and, in particular, by the ^{13}C NMR signal at δ = 331−335 ppm that is characteristic for the α-carbon atom of the η^1-vinylidene moiety.

Upon treatment of the deep green solution of lithium metalate **3a,b** with methyltrifluoromethanesulfonate at −30 °C, the η^2-alkynes **4a,b** were obtained (Scheme 2). We suppose that the alkylation of the metalate anion occurs at the β-carbon atom generating the corresponding η^1-vinylidene complexes, which then isomerize by migration of the silyl group to **4a,b**. Structural assignment of the η^2-alkynes **4a,b** are based on NMR spectroscopic data and by the characteristic C≡C stretching vibration in IR spectra, respectively.[12]

Isomerization of η^1-Vinylidene Complexes

Molybdenum-vinylidene complex **8** and tungsten derivatives **5a,b** rearrange under refluxing toluene to the corresponding η^2-alkyne complexes **9** and **7a,b**. Whereas the tungsten η^1-vinylidene complex **5c** with a *tert*-butyl group at the β-carbon atom, is much more stable than **5a,b** and **8** and rearranges very poorly upon heating at 110 °C to the corresponding η^2-alkyne complex **7c**. The η^1-vinylidene/η^2-alkyne ratios of the interconversion of **8**, **5a,b** and **5c** after heating in toluene for 24 h are reported in Table 1. Longer reaction times lead to the decomposition of **5b** and **5c**. Interestingly the isomerization rate of **8** is highly dependent on the nature of the solvent. In ethanol as the solvent the transformation occurs quantitatively after heating for 2 h at 79 °C.[13]

Table 1. Product ratios of the thermal interconversion of the η^1-vinylidenes **8, 5a−c** after 24 h at 110 °C

η^1-Vinylidene complexes	Product ratio[a] η^2-alkyne: η^1-vinylidene[b]
[Mo{=C=CHC(CH_3)$_3$}(η^5-C_5H_5)(CO)(NO)] (**8**)	100:0
[W{=C=CHSi(CH_3)$_2$C(CH_3)$_3$}(η^5-C_5H_5)(CO)(NO)] (**5a**)	79:21
[W{=C=CHSi(C_6H_5)$_2$$CH_3$}($\eta^5$-$C_5H_5$)(CO)(NO] (**5b**)	63:37
[W{=C=CHC(CH_3)$_3$}(η^5-C_5H_5)(CO)(NO)] (**5c**)	6:94

[a] All reactions were carried out in toluene. [b] The product ratios were determined by measuring the relative peak integration of the ^1H NMR signals of the η^2-alkyne and η^1-vinylidene complexes in the crude product spectra.

Also a quantitative isomerization to **9** is observed by treating the THF solution of **8** at room temperature with 10% aqueous NaOH for 20 min (Scheme 3).

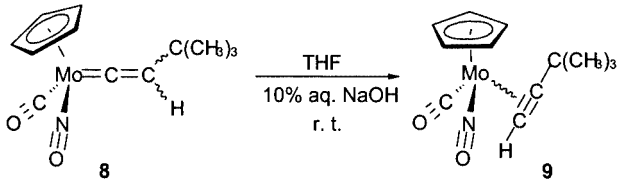

Scheme 3. Base-catalyzed isomerization of vinylidene complexes **8**

Kinetic Studies

a) Isomerization in a Nonpolar Solvent

The isomerization rates of **8** to **9** were measured at fixed temperatures between 80 °C and 140 °C in [D_8]toluene while the rate of transformation of **5a** to **7a** was measured between 130 °C and 150 °C in [D_6]benzene by varying the starting concentration of the η^1-vinylidene complexes.[14] The results indicate that the η^1-vinylidene → η^2-alkyne isomerization is first-order. The first-order rate constants measured at five different temperatures are listed in Table 2 and 3. From the Eyring plot, we derived the activation parameters for **8** → **9**: $\Delta H^{\#}$ = 29.0 ± 0.5 (kcal·mol^{-1}) and $\Delta S^{\#}$ = −1.8 ± 0.2 (cal/mol·K) and for **5a** → **7a**: $\Delta H^{\#}$ = 27.2 ± 0.4 (kcal·mol^{-1}) and $\Delta S^{\#}$ = −9.7 ± 0.9 (cal/mol·K). For the rearrangement of [RuCp(H−C≡C−Me)(PMe_3)$_2$]PF_6 to [RuCp(=C=CHMe)(PMe_3)$_2$]PF_6 the kinetic study in CH_3CN by Bullock gave $\Delta H^{\#}$ = 23.4 ± 0.3 kcal·mol^{-1} and $\Delta S^{\#}$ = 3.9 ± 0.9 (cal/mol·K).[15]

 © 2003 Wiley-VCH Verlag GmbH & Co. KGaA, Weinheim

Table 2. Rates of the isomerization and kinetic deuterium isotope effect of **5a** to **7a** and **5a-D** to **7a-D** in [D_6]benzene

Temp. (°C)	$10^4 k_H$ (s^{-1})	r[a]	$10^4 k_D$ (s^{-1})	r[a]	k_H/k_D
130	1.174	0.999	0.957	0.999	1.227
135	1.731	0.999	1.482	0.999	1.168
140	2.706	0.998	2.310	0.999	1.172
145	4.037	0.999	3.414	0.999	1.182
150	6.067	0.999	4.939	0.999	1.228
					average: 1.196 ± 0.030

[a] Correlation coefficient for the first-order plot.

Table 3. Rates of the isomerization and kinetic deuterium isotope effect of **8** to **9** and **8-D** to **9-D** in [D_8]toluene

Temp. (°C)	$10^5 k_H$ (s^{-1})	r[a]	$10^5 k_D$ (s^{-1})	r[a]	k_H/k_D
80.0	0.558	0.999	0.280	0.999	2.0
90.2	1.733	0.998	0.920	0.998	1.9
106.2	11.483	0.999	5.266	0.999	2.2
121.4	43.883	0.998	22.070	0.998	2.0
139.6	236.516	0.999	123.489	0.999	1.9
					average: 2.00 ± 0.2

[a] Correlation coefficient for the first-order plot.

Principally the isomerization of **5a** to **7a** can occur either by migration of the silyl group or of the hydrogen atom from C_β to C_α, however, a priori it is not possible to differentiate between one or the other reaction path. In order to distinguish between these two possibilities, we determined the kinetic deuterium isotope effect for the conversion of $[(\eta^5\text{-}C_5H_5)(CO)(NO)W{=}C{=}CDSi(CH_3)_2C(CH_3)_3]$ (**5a-D**) to $[(\eta^5\text{-}C_5H_5)(CO)(NO)W\{\eta^2\text{-}DC{\equiv}CSi(CH_3)_2C(CH_3)_3\}]$ (**7a-D**) and as a comparison the kinetic deuterium isotope effect for the transformation **8-D** to **9-D** (Scheme 4).

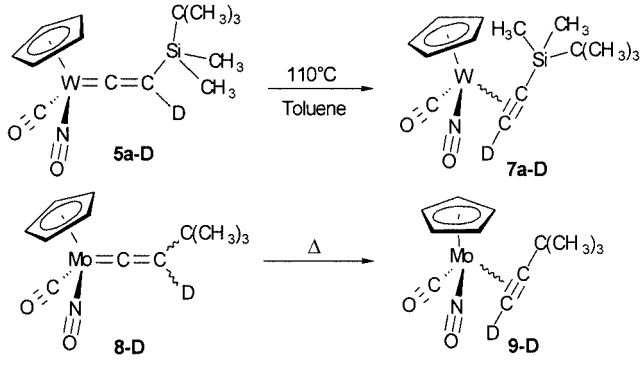

Scheme 4. Thermal isomerization of **5a-D** and **8-D**

The $k_{\mathbf{5a\rightarrow 7a}}/k_{\mathbf{5a\text{-}D\rightarrow 7a\text{-}D}}$ in [D_8]toluene was found to be 1.20 ± 0.03 and $k_{\mathbf{8\rightarrow 9}}/k_{\mathbf{8\text{-}D\rightarrow 9\text{-}D}}$ = 2.00 ± 0.2 (Table 2 and 3), both effects show very minor temperature dependency. The kinetic isotope effect for the former reaction is in the range of normal secondary isotope effects,[16] and is the result of a hybridization change from sp^2 to sp of the C_β of the η^1-vinylidene ligand in the transition state during the migration of the silyl group. Contrary, for the later isomerization, k_H/k_D suggests that the bond to the isotopically substituted hydrogen atom is being broken in the rate-determining step. The 1,2-shift of the silyl group is also supported by the comparison of the isomerization ability of **5a** and **5b** versus **5c** where the reaction rate decreases in the order: $Si(CH_3)_2C(CH_3)_3 > Si(C_6H_5)_2(CH_3) > C(CH_3)_3$.[17]

b) Isomerization in Ethanol

In order to obtain more information on the mechanism of the η^1-vinylidene → η^2-alkyne isomerization we examined the isomerization of **8** in ethanol as the solvent. The isomerization rate of **8** in C_2D_5OH, measured in a 0.1 M solution at fixed temperatures between 60 °C and 100 °C, is much faster than the reaction rate in [D_8]toluene. The pseudo first-order rate constants are listed in Table 4. From Eyring plots we have obtained the activation parameters for the isomerization **8** → **9** in C_2D_5OH, $\Delta S^{\#} = -21.3 \pm 0.5$ (cal/mol·K) and $\Delta H^{\#} = 19.6 \pm 1.6$ kcal·mol^{-1}. Compared to the isomerization in [D_8]toluene, the most striking point of the thermodynamics of the reaction, is the high negative value of $\Delta S^{\#}$ in C_2D_5OH. This leads one to suppose, that in toluene and ethanol two different mechanisms govern the reaction. This presumption is further strongly supported by the large differences of the kinetic isotope effect for $k_{\mathbf{8\rightarrow 9}}$ measured in C_2D_5OH and $k_{\mathbf{8\text{-}D\rightarrow 9\text{-}D}}$ in C_2D_5OD versus the $k_{\mathbf{8\rightarrow 9}}/k_{\mathbf{8\text{-}D\rightarrow 9\text{-}D}}$ measured in [D_8]toluene as the solvent. The $k_{\mathbf{8\rightarrow 9}}/k_{\mathbf{8\text{-}D\rightarrow 9\text{-}D}}$ ratio also shows a large temperature dependency in ethanol contrary to the value in toluene. From extrapolation of the reaction rate the values k_H/k_D = 15.7 at 60 °C and k_H/k_D = 7.1 at 100 °C, are obtained.

Table 4. Rates of the isomerization and kinetic deuterium isotope effect of **8** to **9** in [D_5]ethanol and **8-D** to **9-D** in [D_6]ethanol (k_H/k_D = 15.7 at 60 °C and 7.1 at 100 °C)

8 → 9			**8-D → 9-D**		
Temp. (°C)	$10^4 k_H$ (s^{-1})	r[a]	Temp. (°C)	$10^4 k_D$ (s^{-1})	r[a]
59.0	1.070	0.998	83.7	0.717	0.998
69.0	2.200	0.998	94.4	2.233	0.999
79.3	4.450	0.999	106.2	5.417	0.998
88.5	8.833	0.999	116.2	12.867	0.999
97.6	24.920	0.998	125.0	25.68	0.999

[a] Correlation coefficient for the first-order plot.

 © 2003 Wiley-VCH Verlag GmbH & Co. KGaA, Weinheim

H/D Exchange

The η^1-Vinylidene derivatives **8** and **5a** undergo H/D exchange at the C_β atom without isomerization. Treatment of tetrahydrofuran solutions of **5a** at room temperature and **8** at 45 °C with D_2O produces the corresponding deuterated derivatives **8-D** and **5a-D** (Scheme 5).

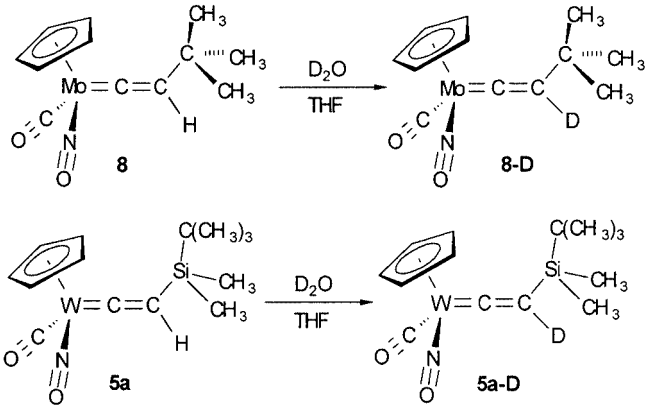

Scheme 5. H/D exchange of vinylidene complexes **8** and **5a**

Besides the deprotonation-deuteration pathway, it is conceivable that the H/D exchange occurs by the prior addition of deuterium to yield a carbyne derivative (Scheme 6).

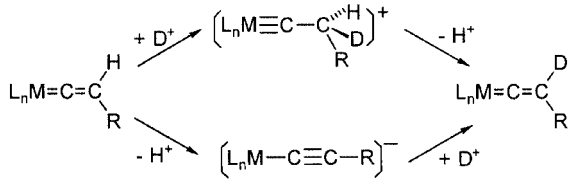

Scheme 6. Alternative mechanisms for the H/D exchange of vinylidene complexes

Theoretical studies on vinylidene transition metal complexes have identified the electron density on the C_β atom,[18] and the protonation of vinylidene complexes to the carbyne derivatives occurs via another mechanism.[9,19] In order to distinguish between these two possibilities we investigated the exchange rate in the presence of D_2O and C_6D_5OD, respectively. While after 3 h at 45 °C the H/D exchange in 10 molar D_2O/[D_8]THF was complete, no exchange occurred in the presence of C_6D_5OD. The result of this experiment clearly shows that the H/D exchange occurs by a dissociative pathway.

Discussion

Our kinetic study of the isomerization of **8** → **9** and **5a** → **7a** suggests that the η^1-vinylidene → η^2-alkyne isomerization of the molybdenum and tungsten complexes studied here, follows two different pathways.

In nonpolar solvents such as toluene or benzene, starting from the η^1-vinylidene **5a**, a 1,2-shift of the silyl group takes place by forming the transition state **10** (Scheme 7). Slippage processes of the silyl group as well as the metal, followed by C−Si σ bonding and π coordination of the metal center generated the η^2-alkyne complexes **7**. The magnitude of the kinetic isotope effect and the activation entropy observed for the isomerization **5a** → **7a** are in good agreement with an isomerization mechanism of least motion; namely, the 1,2-silyl group shifts in a concerted fashion.[20,21] In the same manner the thermal tautomerization of **8** in nonpolar solvents occurs by a 1,2-migration of the hydrogen atom leading to the transition state **11**, followed by a slippage of the metal to yield the η^2-1-alkyne complex **9**. The observed kinetic isotope effect supports the isomerization pathway, **D**→**B**→**A** (Scheme 1) with an asymmetrically bonded transition state in a single-step hydrogen or silyl transfer reaction for both transformations depicted as **10** and **11**.[22,23]

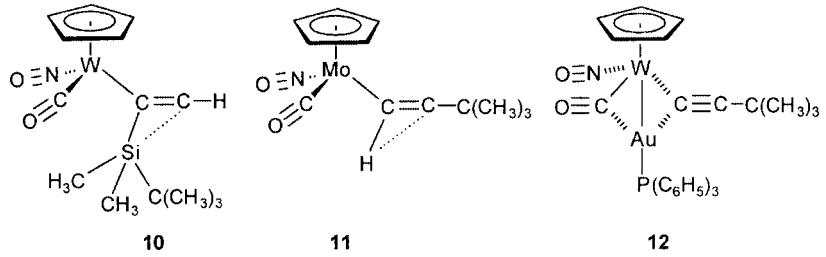

Scheme 7. Postulated transition states **10** and **11** and structure of gold complexes **12**

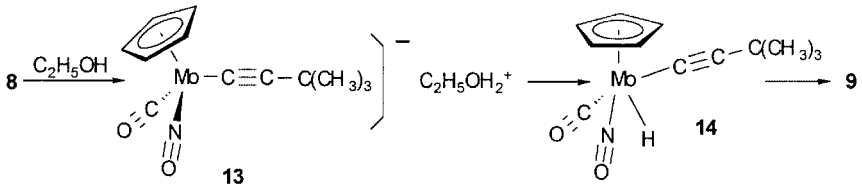

Scheme 8. Postulated mechanism for the isomerization of vinylidene complexes **8** in ethanol

 © 2003 Wiley-VCH Verlag GmbH & Co. KGaA, Weinheim

Additionally we have recently synthesized and structurally characterized the gold-tungsten complex **12** which has similar structural features to **10** and **11** and shows a fluxional behavior.[24]

Contrary to the isomerization in nonpolar solvents, the kinetic data of the isomerization **8** → **9** in ethanol suggests a two-step dissociation-addition process (Scheme 8). The high value of $k_{\mathbf{8}\rightarrow\mathbf{9}}/k_{\mathbf{8\text{-}D}\rightarrow\mathbf{9\text{-}D}}$ and its temperature dependency supports this mode of isomerization and suggests that it is even more likely that a tunneling process takes place for this reaction.[22,23] According to this data we suppose that the tautomerization of **8** occurs via a deprotonation step generating the η^1-alkynyl complex **13** followed by the protonation on molybdenum to the hydrido-alkynyl complex **14** which undergoes reductive elimination to the η^2-1-alkyne isomer **9**. The NaOH catalyzed isomerization of **8** (see Scheme 3) is in agreement with this hypothesis as it supports a deprotonation-protonation process. All attempts to isolate the hydrido-alkynyl complex were unsuccessful.

The tautomerization of η^2-1-alkyne via hydrido-alkynyl complexes is often postulated in the literature as a concerted 1,3-hydrogen shift.[1,4f] However, this mechanism was found to be, in general, energetically too costly.[4b,4h] Our results, however, support the findings that isomerization via a hydrido-alkynyl complex proceeds in a nonconcerted fashion.

Experimental Section

General Remarks: All reactions were carried out under argon (99.99%, by Messer−Griesheim) with the use of standard Schlenk techniques. Solvents were purified by standard methods and distilled under argon prior to use. Literature methods were used to prepare $[(\eta^5\text{-}C_5H_5)Mo(CO)_2(NO)]$ and $[(\eta^5\text{-}C_5H_5)W(CO)_2(NO)]$,[25] (*tert*-butyldimethylsilyl)acetylene,[26] (methyldiphenylsilyl)acetylene,[26] $[(\eta^5\text{-}C_5H_5)(CO)(NO)Mo{=}C{=}CHC(CH_3)_3]$ (**8**);[12] **7c**, and **5c**[12] and $[(\eta^5\text{-}C_5H_5)(CO)(NO)W{=}C{=}CHSi(CH_3)_2C(CH_3)_3]$ (**5a**).[27] All other compounds were commercially available. NMR spectra were obtained with a Bruker AM 400 spectrometer (^{1}H NMR, 400.13 MHz. ^{13}C NMR, 100.61 MHz). Proton and carbon chemical shifts are reported in ppm relative to the residual proton resonance (δ = 7.24 ppm) or the carbon multiplet (δ = 77.0 ppm) of the NMR solvent $CDCl_3$. When [D$_6$]benzene is used as solvent for a ^{1}H NMR spectrum, the shifts are reported in ppm relative to the residual proton resonance at δ = 7.17 ppm. ^{13}C DEPT experiments were run with the Bruker AM 400 spectrometer. MS measurements (70 eV) were performed with a Varian MAT 311-A. IR spectra were recorded with a Bruker FT-IR IFS 85. Microanalyses were done with a Carlo Erba 1104 elemental analyzer.

Synthesis of the Vinylidene Complexes. $[(\eta^5\text{-}C_5H_5)(CO)(NO)W{=}C{=}CHSi(C_6H_5)_2CH_3]$ (5b): At −78 °C *n*BuLi (3 mL, 4.5 mmol; a solution of 1.5 mmol/mL in hexane) was added to a solution of (methyldiphenylsilyl)acetylene (1.00 g, 4.5 mmol) in THF (10 mL). This solution was added dropwise to $[(\eta^5\text{-}C_5H_5)(CO)_2(NO)W]$ (1.0 g, 3.0 mmol) in THF (60 mL) at −30 °C, whereby the color changed from orange to deep green. The reaction mixture was stirred for 4 h at −30 °C. Addition of 1 mL of concentrated HCl diluted with 20 mL of water led to a dark red solution. After the reaction mixture was allowed to reach room temperature, the THF was removed under reduced pressure. The residue was extracted with diethyl ether, washed with saturated aqueous sodium chloride and dried with magnesium sulfate. The dark red oil was filtered through silica gel (*n*-pentane/diethyl ether, 5:1) to remove decomposition products. Chromatography on silica gel (*n*-pentane/diethyl ether, 5:1) yielded 341 mg (21%) of **5b** as dark red oil and 230 mg (15%) of the unsubstituted vinylidene complex **6** as orange crystals.[12]

Compound 5b: Two rotamers (5:2) were found in the NMR spectra. ^{1}H NMR ($CDCl_3$, 25 °C): δ = 7.65−7.38 (m, 10 H, C_6H_5), 6.02 and 5.93 (2 s, 2:5, 1 H, $C_\beta H$), 5.73 and 5.40 (2 s, 2:5, 5 H, Cp), 0.71 and 0.69 (2 s, 5:2, 3 H, CH_3) ppm. ^{13}C NMR ($CDCl_3$, 25 °C): δ = 334.9 and 333.6 [$^1J_{C-W}$ = 183.1 Hz, C_α], 212.3 ($^1J_{C-W}$ = 202.6 Hz), 212.0 (CO), 136.0−127.9 (C_6H_5), 118.3 and 117.2 [$^2J_{C-W}$ = 34.5 Hz, C_β], 95.4 and 95.3 (Cp), −2.0 and −2.2 (CH_3) ppm. IR (KBr): $\tilde{\nu}$ = 1990 (s, C=O), 1636 (s, N≡O), 1595 (s, C=C) cm^{-1}. MS (70 eV): *m*/*z* = 529 [M$^+$, ^{184}W], 501 [M$^+$ − CO], 471 [M$^+$ − CO − NO]. $C_{21}H_{19}NO_2SiW$: calcd. C 47.65, H 3.62, N 2.65; found C 47.28, H 3.32, N 2.89. High-resolution mass spectrum: *m*/*z* calcd. for $C_{21}H_{19}NO_2Si^{182}W$ [M$^+$] 527.0668, found 527.0667.

Compound 6: ^{1}H NMR ($CDCl_3$, 25 °C): δ = 5.87 (s, 5 H, Cp), 5.28 ($^3J_{W-H}$ = 6 Hz), 5.21 [2 d, 2 H, $^2J_{H,H}$ = 19 Hz, CH_2] ppm. ^{13}C NMR ($CDCl_3$, 25 °C): δ = 341.2 (C_α), 209.9 (CO), 112.2 (C_β), 96.3 (Cp) ppm. IR (KBr): $\tilde{\nu}$ = 1998 (CO), 1635 (NO), 1591 (C=C) cm^{-1}. IR (CCl_4): $\tilde{\nu}$ = 2008 (CO), 1654 (NO), 1618 (C=C) cm^{-1}. MS (70 eV): *m*/*z* = 333 [M$^+$, ^{184}W], 305 [M$^+$ − CO], 275 [M$^+$ − CO − NO]. $C_{14}H_{11}NO_2W$: calcd. C 28.86, H 2.12, N 4.21; found C 29.17, H 1.74, N 4.29. High-resolution mass spectrum: *m*/*z* calcd. for $C_{14}H_{11}NO_2{}^{186}W$ [M$^+$] 335.0021, found 335.0027.

$[(\eta^5\text{-}C_5H_5)(CO)(NO)W{=}C{=}CDSi(CH_3)_2C(CH_3)_3]$ (5a-D): A solution of vinylidene **5a** (300 mg) in THF (5 mL) and D_2O (5 mL) was stirred for 2 h at room temperature. After removal of THF and D_2O under reduced pressure, the residue was dried under vacuum for several hours. Spectroscopically pure orange crystals of **5a-D** were obtained (m.p. 60 °C). $C_{14}DH_{20}NO_2SiW$: calcd. C 37.51, H 4.50, N 3.12; found C 37.32, H 4.53, N 3.28. Two rotamers were found in the NMR spectra. ^{1}H NMR ($CDCl_3$, 25 °C): δ = 5.76 (s, 5 H, Cp), 0.91 and 0.89 [2 s, 3:2, 9 H, $C(CH_3)_3$], 0.13, 0.10 and 0.09 (3 s, overlapping, diastereotopic methyl groups, 6 H, $Si[CH_3)_2C(CH_3)_3]$ ppm. ^{13}C NMR ($CDCl_3$, 25 °C): δ = 333.0 and 331.0 (C_α), 213.8 and 212.0 (CO), 118.5 ($^1J_{C-D}$ = 20.8 Hz) and 117.5 ($^1J_{C-D}$ = 22.2 Hz) (C_β), 95.4 and 95.2 (Cp), 26.1 [$C(CH_3)_3$], 17.6 and 17.1 [$C(CH_3)_3$], −4.4, −4.5 and −4.8 [$Si(CH_3)_2C(CH_3)_3$] ppm. IR (KBr): $\tilde{\nu}$ = 1999 and 1975 (s, C=O), 1635 and 1617 (s, N≡O), 1584 (s, C=C) cm^{-1}. MS (70 eV): *m*/*z* = 448 [M$^+$, ^{184}W], 420 [M$^+$ − CO]. High-resolution mass spectrum: *m*/*z* calcd. for $C_{14}DH_{20}NO_2Si^{182}W$ [M$^+$] 446.0887, found 446.0884.

Synthesis of the η^2-Alkyne Complexes. $[(\eta^5\text{-}C_5H_5)(CO)(NO)W\{\eta^2\text{-}H_3C{-}C{\equiv}C{-}Si(CH_3)_2C(CH_3)_3\}]$ (4a): The preparation of **4a** is analogous to that of **5a**, but, instead of diluted HCl, (0.5 mL, 4.5 mmol) trifluoromethanesulfonate was used. This solution was stirred for 1 h at −30 °C. After usual workup the dark red oil was chromatographed on silica gel (*n*-pentane/diethyl ether, 3:1) to yield 927 mg (67%) of **4a** as orange crystals (m.p. 119 °C). $C_{15}H_{23}NO_2SiW$: calcd. C 39.06, H 5.03, N 3.04; found C 39.02, H 4.73, N 2.78. Two rotamers were found in the NMR spectra. ^{1}H NMR ($CDCl_3$, 25 °C): δ = 5.65 and 5.60 ppm (2 s, 6:1, 5 H, Cp), 2.92 and 2.87 (2 s, 1:6, 3 H, $C{\equiv}CCH_3$), 0.96 and 0.90 [2 s, 6:1, 9 H, $C(CH_3)_3$], 0.30 ($^2J_{H-Si}$ = 6.3 Hz), 0.24 and 0.16 [3 s, overlapping,

 © 2003 Wiley-VCH Verlag GmbH & Co. KGaA, Weinheim

diastereotopic methyl groups, 6 H, $Si(CH_3)_2C(CH_3)_3$] ppm. ^{13}C NMR ($CDCl_3$, 25 °C): δ = 220.0 (CO), 122.5 (alkyne C), 95.9 and 95.8 (Cp), 90.7 (alkyne C), 26.6 and 26.5 [$C(CH_3)_3$], 20.6 and 18.6 [$C(CH_3)_3$], 18.2 and 15.7 ($C{\equiv}CCH_3$), −3.8 and −3.9 [$Si(CH_3)_2C(CH_3)_3$] ppm. IR (KBr): $\tilde{\nu}$ = 1986 (s, C=O), 1827 (m, C≡C), 1558 (s, N≡O) cm^{-1}. MS (70 eV): *m/z* = 461 [M^+, ^{184}W], 433 [M^+ − CO]. High-resolution mass spectrum: *m/z* calcd. for $C_{15}H_{23}NO_2Si^{182}W$ [M^+] 459.0981, found 459.0974.

[(η⁵-C_5H_5)(CO)(NO)W{η²-$H_3C-C{\equiv}C-Si(C_6H_5)_2CH_3$}] (4b): The preparation was carried out as described for **4a**, but, instead of (*tert*-butyldimethylsilyl)acetylene, (1.00 g, 4.5 mmol) (methyldiphenylsilyl)acetylene was used. After usual workup the dark red oil was chromatographed on silica gel (*n*-pentane/diethyl ether, 7:1) to yield 760 mg (47%) of **4b** as a dark red oil. $C_{22}H_{21}NO_2SiW$: calcd. C 48.63, H 3.90, N 2.58; found C 48.90, H 3.58, N 2.77. Two rotamers were found in the NMR spectra. ^1H NMR ($CDCl_3$, 25 °C): δ = 7.62−7.33 (m, 10 H, C_6H_5), 5.57 and 5.37 [2 s, 1:8, $^2J_{H-W}$ = 9.5 Hz, , 5 H, Cp], 2.88 and 2.82 (2 s, 8:1, 3 H, $C{\equiv}CCH_3$), 0.83 ($^2J_{H-Si}$ = 6.6 Hz) and 0.79 [2 s, 8:1, 3 H, $Si(C_6H_5)_2CH_3$] ppm. ^{13}C NMR ($CDCl_3$, 25 °C): δ = 219.1 ($^1J_{C-W}$ = 183.1 Hz) and 217.5 (CO), 136.8−127.8 (C_6H_5), 127.4 [$^1J_{C-W}$ = 13.9 Hz, alkyne C], 96.0 and 95.8 (Cp), 90.7 [$^1J_{C-W}$ = 38.9 Hz, alkyne C], 20.4 and 15.5 ($C{\equiv}CCH_3$), −2.0 ($^1J_{C-Si}$ = 56.9 Hz) and −2.9 [$Si(C_6H_5)_2CH_3$] ppm. IR (KBr): $\tilde{\nu}$ = 1966 (s, C=O), 1806 (s, C≡C), 1575 (s, N≡O) cm^{-1}. MS (70 eV): *m/z* = 543 [M^+, ^{184}W], 515 [M^+ − CO], 485 [M^+ − CO − NO]. High-resolution mass spectrum: *m/z* calcd. for $C_{22}H_{21}NO_2Si^{182}W$ [M^+] 541.0820, found 541.0817.

[(η⁵-C_5H_5)(CO)(NO)W{η²-$H-C{\equiv}C-Si(CH_3)_2C(CH_3)_3$} (7a): A solution of vinylidene **5a** (300 mg) in toluene (30 mL) was heated for 24 h under reflux. After removal of the solvent under reduced pressure at room temperature, the dark red oily residue was chromatographed on silica gel (*n*-pentane/diethyl ether, 7:1) to yield 152 mg (51%) of **7a** as orange crystals (m.p. 66 °C). $C_{14}H_{21}NO_2SiW$: calcd. C 37.60, H 4.73, N 3.13; found C 37.87, H 4.57, N 2.90. Two rotamers were found in the NMR spectra. ^1H NMR ($CDCl_3$, 25 °C): δ = 8.74 ($^2J_{H-W}$ = 7.8 Hz) and 8.12 [2s, 1:5, $^2J_{H-W}$ = 8.8 Hz, 1 H, C≡CH], 5.67 and 5.62 (2 s, 5:1, 5 H, Cp), 0.97 and 0.93 [2 s, 5:1, 9 H, $C(CH_3)_3$], 0.32 ($^2J_{H-Si}$ = 6.1 Hz), 0.27, 0.25 (6.0 Hz) and 0.18 [4 s, diastereotopic methyl groups, 5:1:5:1, 6 H, $Si(CH_3)_2C(CH_3)_3$] ppm. ^{13}C NMR ($CDCl_3$, 25 °C): δ = 219.2 and 218.4 [$^1J_{C-W}$ = 178.4 Hz, CO], 121.9 and 115.7 [$^1J_{C-W}$ = 15.4 Hz, C≡CH], 105.1 ($^1J_{C-W}$ = 40.3 Hz) and 97.1 (C≡CH), 95.9 (Cp), 26.5 and 26.4 [$C(CH_3)_3$], 18.2 and 17.8 [$C(CH_3)_3$], −3.6 ($^1J_{C-Si}$ = 52.2 Hz), −4.1 ($^1J_{C-Si}$ = 54.5 Hz), −4.5 and −4.8 [$Si(CH_3)_2C(CH_3)_3$] ppm. IR (KBr): $\tilde{\nu}$ = 1965 (s, C=O), 1713 (m, C≡C), 1565 (s, N≡O) cm^{-1}. MS (70 eV): *m/z* = 447 [M^+, ^{184}W], 419 [M^+ − CO]. High-resolution mass spectrum: *m/z* calcd. for $C_{14}H_{21}NO_2Si^{182}W$ [M^+] 445.0825, found 445.0824.

[(η⁵-C_5H_5)(CO)(NO)W{η²-$H-C{\equiv}C-Si(C_6H_5)_2CH_3$}] (7b): The preparation of **7b** is analogous to that of **7a**, but, instead of complex **5a**, vinylidene **5b** (300 mg) was used. Chromatography on silica gel (*n*-pentane/diethyl ether, 7:1) yielded 60 mg (20%) of **7b** as dark red oil and 40 mg (13%) of the starting material **5b** as orange crystals. $C_{21}H_{19}NO_2SiW$: calcd. C 47.65, H 3.62, N 2.65; found C 47.20, H 3.34, N 2.86. Two rotamers were found in the NMR spectra. ^1H NMR ($CDCl_3$, 25 °C): δ = 9.10 ($^2J_{H-W}$ = 7.4 Hz) and 8.54 ($^2J_{H-W}$ = 8.8 Hz) (2s, 1:5, 1 H, C≡CH), 7.64 and 7.33 (m, 10 H, C_6H_5), 5.59 and 5.38 (2 s, 5:1, 5 H, Cp), 0.84 ($^2J_{H-Si}$ = 6.5 Hz) and 0.83 (2 s, 5:1, 3 H, CH_3) ppm. ^{13}C NMR ($CDCl_3$, 25 °C): δ = 217.6 ($^1J_{C-W}$ = 177.6 Hz) and 217.0 (CO), 136.4−126.7 (C_6H_5), 120.1 [$^1J_{C-W}$ = 15.3 Hz, C≡CH], 105.2 [$^1J_{C-W}$ = 40.2 Hz, C≡CH], 96.0 and 95.9 (Cp), −1.9 ($^1J_{C-Si}$ = 58.3 Hz), −2.9 (CH_3) ppm. IR (KBr): $\tilde{\nu}$ = 1983 (s, C=O), 1699 (m, C≡C), 1594 (s, N≡O) cm^{-1}. MS (70 eV): *m/z* = 529 [M^+, ^{184}W], 501 [M^+ − CO], 471 [M^+ − CO − NO]. High-resolution mass spectrum: *m/z* calcd. for $C_{21}H_{19}NO_2Si^{182}W$ [M^+] 527.0668, found 527.0681.

[(η⁵-C_5H_5)(CO)(NO)W{η²-$H-C{\equiv}C-C(CH_3)_3$}] (7c): The preparation of **7c** is analogous to that of **7a**, but, instead of complex **5a**, vinylidene **5c** (1000 mg) was used. Chromatography on silica gel with 10:1 *n*-pentane/diethyl ether yielded 24 mg (2%) of **7c** as light orange crystals and 563 mg (56%) of the starting material **5c** as orange crystals. $C_{12}H_{15}NO_2W$: calcd. C 37.04, H 3.89, N 3.60; found C 37.32, H 3.70, N 3.40. Two rotamers were found in the NMR spectra. ^1H NMR ($CDCl_3$, 25 °C): δ = 7.45 ($^2J_{H-W}$ = 8.0 Hz) and 6.98 ($^2J_{H-W}$ = 9.2 Hz) (2 s, 1:6, 1 H, C≡CH), 5.77 and 5.68 (2 s, 6:1, 5 H, Cp), 1.35 and 1.32 [2 s, 6:1, 9 H, $C(CH_3)_3$] ppm. ^{13}C NMR ($CDCl_3$, 25 °C): δ = 215.5 (CO), 133.7 ($^1J_{C-W}$ = 52.0 Hz) and 124.4 ($^1J_{C-W}$ = 13.6 Hz) (alkyne C), 96.4 and 96.0 (Cp), 91.0 ($^1J_{C-W}$ = 43.1 Hz) and 88.1 ($^1J_{C-W}$ = 8.9 Hz) (alkyne C), 36.4 and 34.6 [$C(CH_3)_3$], 31.9 and 31.0 [$C(CH_3)_3$] ppm. IR (KBr): $\tilde{\nu}$ = 1977 (s, C=O), 1736 (m, C≡C), 1556 (s, N≡O) cm^{-1}. MS (70 eV): *m/z* = 389 [M^+, ^{184}W], 361 [M^+ − CO]. High-resolution mass spectrum: *m/z* calcd. for $C_{12}H_{15}NO_2{}^{182}W$ [M^+] 387.0585, found 387.0553.

Isomerization of 8 to 9 with NaOH: 10% aqueous NaOH (3 mL) was added to a solution of **8** (0.4 mmol) in THF (10 mL). After the reaction mixture was stirred for 20 min at room temperature, the organic layer was separated and the solvent was removed under reduced pressure. The residue was dissolved in diethyl ether and dried with $MgSO_4$. The diethyl ether was removed under reduced pressure, and the ^1H NMR spectrum of the residue was collected. **8** was 100% isomerized to **9**.

Treatment of 8 with D_2O and C_6D_5OD: 8 (0.6 mL, 0.1 mmol) and D_2O (0.2 mL, 10 mmol) in [D_8]THF (1 mL) were heated at 45 °C. At regular time intervals the probe was cooled to −20 °C, which was followed by the measuring of the relative peak integration of the ^1H NMR $C_\beta-H$ signal [([D_8]THF) δ = 5.93 and 5.91 ppm] of **8**. After 3 h the H/D exchange was complete. The same experiment with perdeuterated phenol (C_6D_5OD) instead of D_2O showed no exchange.

[(η⁵-C_5H_5)(CO)(NO)Mo{η²-H-C≡C-$C(CH_3)_3$}] (9): At −30 °C, a solution of 7.5 mmol of (*tert*-butylethynyl)lithium in THF (15 mL) was added dropwise to an orange solution of (η⁵-C_5H_5)Mo(CO)₂(NO) (1.24 g, 5 mmol) in THF (50 mL). The progress of the reaction was monitored by IR spectroscopy. After complete disappearance of [(η⁵-C_5H_5)Mo(CO)₂(NO)], at 5 °C, saturated aq. sodium carbonate (30 mL) was added to the deep green reaction mixture, whereby the color changed to red. The solution was concentrated under vacuum and extracted with diethyl ether. The organic layer was dried with $MgSO_4$. The diethyl ether was removed under reduced pressure and the residue was chromatographed (silica gel, pentane) to yield 714 mg (47%) of **9**, as orange crystals, m.p. 71−72 °C (dec, pentane:dichloromethane, 10:1). $C_{12}H_{15}MoNO_2$: calcd. C 47.85, H 5.02, N 4.65; found C 47.84, H 4.83, N 4.72. Two rotamers (ratio 1:5). ^1H NMR ($CDCl_3$, 25 °C): δ = 6.69 and 6.09 ppm (2 s, 1:5, 1 H, C≡CH), 5.65 and 5.55 (2 s, 5:1, 5 H, Cp), 1.37 and 1.34 [2 s, 5:1, 9 H, $C(CH_3)$]. ^{13}C NMR ($CDCl_3$, 25 °C): δ = 226.7 (C=O), 128.0 (C≡C), 97.0 and 96.7 (Cp), 80.5 (C≡C), 35.8 [$C(CH_3)_3$], 32.2 and 31.3 (CH_3) ppm. IR (KBr): $\tilde{\nu}$ = 1982 (C=O), 1785 (C≡C), 1581 (N=O) cm^{-1}. MS (70 eV): *m/z* = 301 [M^+, ^{96}Mo], 273 [M^+ − CO], 243 [M^+ − CO − NO]. High resolution mass spectrum calcd. for $C_{12}H_{15}{}^{92}MoNO_2$ [M^+]: *m/z* = 297.0171, found *m/z* = 297.0141.

 © 2003 Wiley-VCH Verlag GmbH & Co. KGaA, Weinheim

Kinetic Studies of the η¹-Vinylidene → η²-Alkyne Isomerization of 8 → 9; 8-D → 9-D in [D₈]Toluene and 5a → 7a and 5a-D → 7a-D in [D₆]Benzene: A typical experiment was done in the following way. **8** or **8-D** (0.8 mL, 0.1 M) in [D_8]toluene as well as a weighted amount of the vinylidene **5a** or **5a-D** (in the range of 20−120 mg) in [D_6]benzene (0.8 mL) (measured with a gas-tight syringe) were placed in a dried sealable NMR tube. The solution was freeze-pump-thaw degassed and the NMR tube was sealed under vacuum. The sample was then placed into a thermostat at a fixed temperature (reproducibility ± 0.1 °C). At regular time intervals, the tube was removed and the reaction quenched at room temperature. The reaction time was followed by measuring the relative peak integration of the ^{1}H NMR of the cyclopentadienyl signals of **8** (δ = 5.18 and 5.16 ppm); **9** (δ = 5.06 and 4.92 ppm); **8-D** (δ = 5.18 and 5.16 ppm); **9-D** (δ = 5.06 and 4.92 ppm); *tert*-butyl signals of **5a** (δ = 0.95 ppm); **7a** (δ = 1.01 and 0.99 ppm); **5a-D** (δ = 0.94 ppm) and **7a-D** (δ = 1.01 and 0.99 ppm).

First-order rate constants were derived from least-squares best-fit lines of the ln(%) versus time plots. The uncertainty in the isomerization rate constants was derived from the slope of the best-fit line. Uncertainties in the activation enthalpies and entropies were calculated from the uncertainties in the slope of the best-fit line of the Eyring plot.

Kinetic Studies of the η¹-Vinylidene → η²-Alkyne. Isomerization of 8 → 9 in [D₅]Ethanol and 8-D → 9-D in [D₆]Ethanol: The kinetic studies of isomerization of **8** → **9** in [D_5]ethanol and **8-D** → **9-D** in [D_6]ethanol are analogous to that for the isomerization of **8** → **9** and **8-D** → **9-D** in [D_8]toluene. The time course of the reaction was followed by measuring the relative peak integration of the ^{1}H NMR of cyclopentadienyl signals **8** [(C_2D_5OH) δ = 5.83 and 5.81 ppm], **9** [(C_2D_5OH) δ = 5.70 and 5.60 ppm], **8-D** [(C_2D_5OD) δ = 5.82 and 5.81 ppm] and **9-D** [(C_2D_5OD) δ = 5.67 and 5.59 ppm]. Uncertainties in the activation enthalpies and entropies were calculated from the uncertainties in the slope of the best-fit line of the Eyring plot.

Acknowledgments

We gratefully acknowledge financial support from the Deutsche Forschungsgemeinschaft.

[1] For comprehensive reviews see: [1a] M. C. Puerta, P. Valerga, *Coord. Chem. Rev.* **1999**, *193−195*, 977−1025. [1b] C. Bruneau, P. H. Dixneuf, *Acc. Chem. Res.* **1999**, *32*, 311−323. [1c] H. Werner, *J. Organomet. Chem.* **1994**, *47*, 45−55. [1d] H. Werner, *Nachr. Chem. Technol. Lab.* **1992**, *40*, 435−444. [1e] M. I. Bruce, *Chem. Rev.* **1991**, *91*, 197−257. [1f] H. Werner, *Angew. Chem.* **1990**, *102*, 1109−1121; *Angew. Chem. Int. Ed. Engl.* **1990**, *29*, 1077. [1g] S. G. Davies, J. P. McNally, A. J. Smallridge, *Adv. Organomet. Chem.* **1990**, *30*, 1. [1h] A. B. Antonova, A. A. Johansson, *Russ. Chem. Rev.* **1989**, *58*, 693−710. [1i] M. I. Bruce, A. G. Swincer, *Adv. Organomet. Chem.* **1983**, *22*, 59−128.

[2] [2a] E. Bustelo, J. J. Carbo, A. Lledos, K. Mereiter, M. C. Puerta, P. Valerga, *J. Am. Chem. Soc.* **2003**, *125*, 3311−3321. [2b] F. De Angelis, A. Sgamellotti, N. Re, *Organometallics* **2002**, *21*, 2715−2723. [2c] V. Cadierno, M. P. Gamasa, J. Gimeno, C. González-Bernardo, E. Pérez- Carreño, S. García-Granda, *Organometallics* **2001**, *20*, 5177−5188.

[3] [3a] J. L. Templeton, P. B. Winston, B. C. Ward, *J. Am. Chem. Soc.* **1981**, *103*, 7713−7721. [3b] J. L. Templeton, B. C. Ward, *J. Am. Chem. Soc.* **1980**, *102*, 3288−3290.

[4] η²-alkyne → η¹-vinylidene isomerization: [4a] E. Bustelo, M. Jiménez-Tenorio, M. C. Puerta, P. Valerga, *Eur. J. Inorg. Chem.* **2001**, 2391−2398. [4b] M. Tokunaga, T. Suzuki, N. Koga, T. Fukushima, A. Horiuchi, Y. Wakatsuki, *J. Am. Chem. Soc.* **2001**, *123*, 11917−11924. [4c] M. Baya, P. Crochet, M. A. Esteruelas, A. M. López, J. Modrego, E. Oñate, *Organometallics* **2001**, *20*, 4291−4294. [4d] E. Bustelo, I. De los Ríos, M. Jiménez-Tenorio, M. C. Puerta, P. Valerga, *Monatsheft. Chem.* **2000**, *131*, 1311−1320. [4e] V. Cadierno, M. P. Gamasa, J. Gimeno, E. Peréz-Carreño, S. García-Granda, *Organometallics* **1999**, *18*, 2821−2832. [4f] E. Peréz-Carreño, P. Paoli, A. Ienco, C. Mealli, *Eur. J. Inorg. Chem.* **1999**, 1315−1324. [4g] I. De los Ríos, M. Jiménez-Tenorio, M. C. Puerta, P. Valerga, *J. Am. Chem. Soc.* **1997**, *119*, 6529−6538. [4h] Y. Wakatsuki, N. Koga, H. Yamazaki, K. Morokuma, *J. Am. Chem. Soc.* **1994**, *116*, 8105−8111.

[5] η¹-vinylidene → η²-alkyne isomerization: [5a] C. García-Yebra, C. López-Mardomingo, M. Fajardo, A. Antiñolo, A. Otero, A. Rodríguez, A. Vallat, D. Lucas, Y. Mugnier, J. J. Carbó, A. Lledós, C. Bo, *Organometallics* **2000**, *19*, 1749−1765. [5b] I. M. Bartlett, N. G. Connelly, A. J. Martín, A. G. Orpen, T. J. Paget, A. L. Rieger, P. H. Rieger, *J. Chem. Soc., Dalton Trans.* **1999**, 691−698. [5c] M. P. Gamasa, J. Gimeno, C. González-Bernando, J. Borge, S. García-Granda, *Organometallics* **1997**, *16*, 2483−2485. [5d] H. Katayama, K. Onitsuka, F. Ozawa, *Organometallics* **1996**, *15*, 4642−4645. [5e] N. G. Connelly, W. E. Geiger, C. Lagunas, B. Metz, A. L. Rieger, P. H. Rieger, M. J. Shaw, *J. Am. Chem. Soc.* **1995**, *117*, 12202−12208. [5f] P. Nombel, N. Lugan, R. Mathieu, *J. Organomet. Chem.* **1995**, *503*, C22−C25. [5g] R. S. Bly, Z. Zhong, C. Kane, R. K. Bly, *Organometallics* **1994**, *13*, 899−905. [5h] R. S. Bly, M. Raja, R. K. Bly, *Organometallics* **1992**, *11*, 1220−1228. [5i] N. G. Connelly, A. G. Orpen, A. L. Rieger, P. H. Rieger, C. J. Scott, G. M. Rosair, *J. Chem. Soc., Chem. Commun.* **1992**, 1293−1295.

[6] [6a] F. De Angelis, A. Sgamellotti, N. Re, *Organometallics* **2002**, *21*, 2715−2723. [6b] R. Stegmann, G. Frenking, *Organometallics* **1998**, *17*, 2089−2095. [6c] I. De los Ríos, M. J. Tenorio, M. C. Puerta, P. Valerga, *J. Am. Chem. Soc.* **1997**, *119*, 6529−6538. [6d] Y. Wakatsuki, N. Koga, H. Werner, K. Morokuma, *J. Am. Chem. Soc.* **1997**, *119*, 360−366.

[7] For earlier theoretical studies see: J. Silvestre, R. Hoffmann, *Helv. Chim. Acta* **1985**, *68*, 1461.

[8] [8a] M. Baya, P. Crochet, M. A. Esteruelas, E. Gutiérrez-Puebla, A. M. López, J. Modrego, E. Oñate, N. Vela, *Organometallics* **2000**, *19*, 2585−2596. [8b] E. Bustelo, M. Jiménez-Tenorio, M. C. Puerta, P. Valerla, *Organometallics* **1999**, *18*, 4563−4573. [8c] M. Oliván, E. Clot, O. Eisenstein, K. G. Caulton, *Organometallics* **1998**, *17*, 897−901.

[9] M. Baya, M. A. Esteruelas, E. Oñate, *Organometallics* **2001**, *20*, 4875−4886.

[10] The formation of complex **18** can be explained by cleavage of the C−Si bond of the methyldiphenyl-substituted vinylidene complex **17b**.

[11] M. P. Gamasa, J. Gimeno, E. Lastra, B. M. Martín, A. Anillo, A. Tiripicchio, *Organometallics* **1992**, *11*, 1373−1381.

[12] J. Ipaktschi, G. Demuth-Eberle, F. Mirzaei, B. G. Müller, J. Beck, M. Serafin, *Organometallics* **1995**, *14*, 3335−3341.

[13] In toluene at 80 °C after 3 h, **8** isomerizes only 25% to **9**.

[14] [14a] Below 130 °C the isomerization of **5a** was too slow and above 150 °C the decomposition was too fast. [14b] Due to precipitation of decomposition products during the rate measurement of **5b** and **5c**, only the reaction rate of the isomerization of **5a** could be determined.

[15] For further kinetic studies of isomerization see: [15a] R. M. Bullock, *J. Chem. Soc., Chem. Commun.* **1989**, *3*, 165−167. [15b] C. Bianchini, M. Peruzzini, A. Vacca, F. Zanobini, *Organometallics* **1991**, *10*, 3697−3707. [15c] See ref. 5d.

[16] Secondary isotope effects are usually in the range of k_H/k_D = 0.7−1.5 (normal effect $k_H/k_D > 1$, inverse effect $k_H/k_D < 1$), see: F. A. Carey, R. J. Sundberg, *Advanced Organic Chemistry,*

 © 2003 Wiley-VCH Verlag GmbH & Co. KGaA, Weinheim

Third Edition; Plenum Press: New York, London, **1990**; pp. 216−218.
[17] For the migratory aptitude of silyl group compared to hydrogen see: [17a] S. S. Rigby, H. K. Gupta, N. K. Werstiuk, A. D. Bain, M. J. McGlinchey, *Polyhedron* **1995**, *14*, 2787−2796. [17b] A. Bonny, R. D. Holmes-Smith, G. Hunter, S. R. Stobart, *J. Am. Chem. Soc.* **1982**, *104*, 1855−1859. [17c] A. J. Ashe, III, *J. Am. Chem. Soc.* **1970**, *92*, 1233−1235.
[18] N. M. Kostic, R. F. Fenske, *Organometallics* **1982**, *1*, 974−982.
[19] K. R. Birdwhistell, S. J. N. Burgmeyer, J. L. Templeton, *J. Am. Chem. Soc.* **1983**, *105*, 7789−7790.
[20] The values of activation entropy are in the typical range for the 1,2-sigmatropic shift of silyl groups in organic systems ($\Delta S^{\#} = -9.2$ to -3.8 cal/mol K) see: C. W. Spangler, *Chem. Rev.* **1976**, *76*, 187−217.
[21] The activation parameters of the transformation **5c** to **7c** are in excellent accord with the values of the interconversion of [*trans*-Rh{=C=C(Fc)SiMe$_3$}{PCH(CH$_3$)$_2$}$_2$Cl] to [*trans*-Rh(η^2-FcC≡CSiMe$_3$) {PCH(CH$_3$)$_2$}$_2$Cl] ($\Delta H^{\#} = 22.7 \pm 0.1$ kcal mol^{-1} and $\Delta S^{\#} = -8.6 \pm 0.4$ cal/mol K).[5e]
[22] [22a] H. Kwart, *Acc. Chem. Res.* **1982**, *15*, 401−408. [22b] F. H. Westheimer, *Chem. Rev.* **1961**, *61*, 265−273.
[23] A. V. Willi, *Isotopeneffekte bei chemischen Reaktionen*, Georg Thieme Verlag, Stuttgart, **1983**.
[24] J. Ipaktschi, F. Munz, *Organometallics* **2002**, *21*, 977−981.
[25] T. T. Chin, J. K. Hoyano, P. Legzdins, J. T. Malito, *Inorg. Synth.* **1990**, *28*, 196− 198.
[26] A. B. Holmes, C. N. Sporikou, *Organic Syntheses*; John Wiley & Sons: New York, **1983**; Collect. Vol. VIII, pp. 606−609.
[27] J. Ipaktschi, S. Uhlig, A. Dülmer, *Organometallics* **2001**, *20*, 4840−4846.

Received May 28, 2003
Early View Article
Published Online October 10, 2003

 © 2003 Wiley-VCH Verlag GmbH & Co. KGaA, Weinheim

2,3-Bis(diarylphosphanyl)-1,4-diazadienes: P,P Coordination of Pd^{II}, Pt^{II} and a Nickelacyclopentanone with Subsequent Formation of Quinoxalines by a Ring-Closure Reaction at the Periphery

Dirk Walther,*[a] Stefan Liesicke,[a] Reinald Fischer,[a] Helmar Görls,[a] Jennie Weston,[b] and Ariadna Batista[b]

Keywords: Chelates / Cycloadditions / Metallacycles / N,P ligands / Transition metals

The solid-state structures of several 2,3-bis(phosphanyl)-1,4-diazadiene ligands of the general formula RN=C(PPh_2)–C(PPh_2)=NR (**B**: R = 4-tolyl; **C**: R = 4-*tert*-butylphenyl; **D**: R = mesityl) were determined by single-crystal X-ray diffraction. The ligands **B** and **C** are nonplanar and lie between the (*E*) and the (*Z*) form (N=C–C=N is 99.5° in **B**, 94.0° in **C**, and 128.2° in **D**). In the presence of air, **B** is oxidized to its corresponding phosphane oxide. Reaction of **D** with elemental sulfur yields the corresponding phosphane sulfide. Furthermore, ligand **C** reacts with [$PtCl_2$(cod)] and [$PdCl_2(CH_3CN)_2$] to form mononuclear complexes (**1** and **2**, respectively) in which the two P atoms are bound to the metal center. X-ray structural analysis showed that in both complexes the 1,4-diazadiene functionality at the periphery had undergone a ring-closure reaction with one of the aromatic N-substituents thus resulting in a quinoxaline ring. The bulkier ligand **D** reacts with [$PdCl_2(CH_3CN)_2$] to form the mononuclear complex **3**. In the solid state, the two phosphorus atoms are coordinated to the metal center in a five-membered chelate ring. In contrast to **1** or **2**, a cyclohexadiene system is formed as result of a cycloaddition reaction of one aromatic N-substituent with the 1,4-diazadiene system. The nickel complex [Ni(tmeda)(C_2H_4COO)] reacts with **D** by displacement of tmeda to form a mononuclear complex **4a** with P,P coordination. A subsequent ring-closure reaction (cycloaddition) at the periphery does not occur in **4a**. If the ligand is sterically less demanding (**B** or **C**), a cycloaddition between the 1,4-diazadiene system and one aromatic substituent takes place in the nickel complex to form complexes of the type **5** containing a quinoxaline ring. This reaction could be monitored by ^{31}P NMR spectroscopy for ligand **C**.

(© Wiley-VCH Verlag GmbH & Co. KGaA, 69451 Weinheim, Germany, 2003)

Introduction

2,3-Bis(phosphanyl)-1,4-diazadienes contain perhaps the two most important chelating functionalities, a conjugated 1,4-diazadiene and a 1,2-bis(phosphanyl)ethane, within the same ligand. Both of these structural units are known to form stable five-membered metal chelate ring systems which have general importance in organometallic and coordination chemistry. Numerous catalysts for homogeneous reactions are, for example, based on these chelate complexes.[1–16]

In an initial communication, we reported a synthetic procedure for obtaining hitherto unknown 2,3-bis(diarylphosphanyl)-1,4-diazadienes.[17] These are the first experimentally accessible representatives that unify the two functionalities mentioned above. As one would expect, they react readily with Ni^{II}, Cu^{I}, and Mo^{0} fragments thus giving rise to a rich complex chemistry. Some of these chelating ligands chelate by P,P complexation with nickel(II) bromide and then subsequently undergo a rather unusual ring-closure reaction at the periphery of the ligand to form a quinoxaline.[17] This opens a simple route for the synthesis of bis(diphenylphosphanyl)ethylenes containing a quinoxaline backbone. Continuing with our investigations, we now report an alternative synthesis for obtaining these ligands. We have further investigated their structural and electronic properties as well as their behavior towards oxygen and sulfur. In order to gain a deeper understanding of their coordination behavior, as well as their interesting peripheral ring-closure reaction, we have extended the palette of metal fragments employed to include Pd^{II} and Pt^{II} as well as an organometallic derivative of Ni^{II}.

[a] Institut für Anorganische und Analytische Chemie der Friedrich-Schiller-Universität Jena, 07743 Jena, Germany
[b] Institut für Organische Chemie und Makromolekulare Chemie der Friedrich-Schiller-Universität Jena, 07743 Jena, Germany

Results and Discussion

Synthesis of the Bis(diarylphosphanyl)-1,4-diazadienes A–D

In analogy to the previously reported 2,3-bis(diarylphosphanyl)-1,4-diazadienes **B**–**D**,[17] we succeeded in preparing

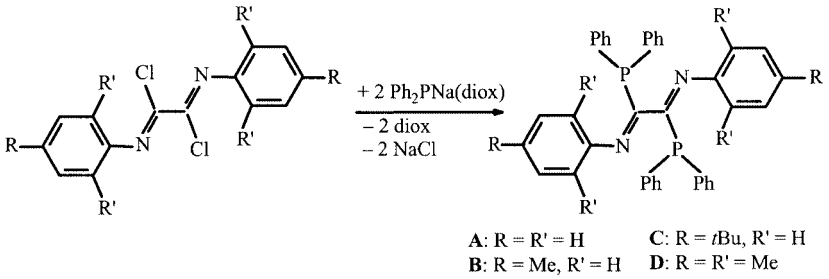

Scheme 1

the 2,3-bis(diphenylphosphanyl)-1,4-diphenyl-1,4-diazadiene (**A**) in 40% yield from sodium diphenylphosphide and the corresponding imidoyl chloride in THF (Scheme 1).

This new ligand has one singlet $^{31}P\{^1H\}$ resonance (δ = 4.7 ppm) in the same spectral region as the ^{31}P NMR signals of ligands **B**–**D**. The ^1H and ^{13}C NMR spectra of **A** are very simple, typical for a symmetrical structure in solution, and are directly comparable with those reported for the ligands **B**–**D**.[17]

An alternative route to **D** is the reaction of the corresponding imidoyl chloride with diphenyl(trimethylsilyl)phosphane (Scheme 2).

This preparative route leads to pure **D** in a much higher yield (64%) without the time-consuming necessity of purifying the raw material. The reaction mixture for this alternative route contained, in addition to **D**, a small amount of the hitherto unknown 2-(diphenylphosphanyl)-1,4-dimesityl-1,4-diazabutadiene (**G**) which could be isolated as yellow crystals and fully characterized by NMR spectroscopy and X-ray diffraction analysis.

The Structure and Electronic Properties of Ligands A–D

Single crystals of **B**–**D** suitable for an X-ray diffraction analysis could be grown from a solution in either toluene or chloroform. All of these ligands possess the same structural motif in the solid state. As a representative example, Figure 1 illustrates the molecular structure of compound **D**, which co-crystallizes with 1 equiv. of $CHCl_3$. Selected geometrical parameters can be found in the figure caption.

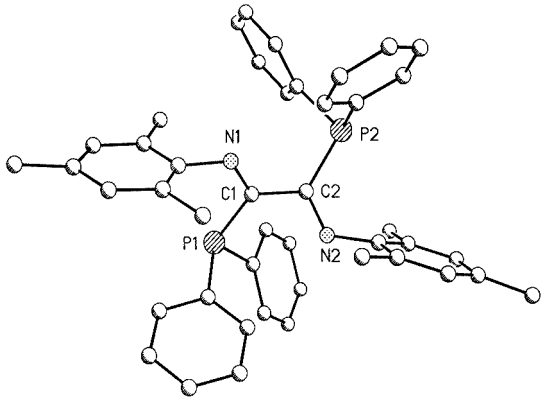

Figure 1. Solid-state structure of compound **D**; selected bond lengths [Å] and bond angles [°]: C1–P1 1.874(2), C1–N1 1.280(2), C1–C2 1.517(2), C2–P2 1.875(2), C2–N2 1.266(2); P1–C1–N1 119.5(1), P2–C2–N2 121.7(1), P1–C1–C2 125.4(1), N1–C1–C2 114.9(1), P2–C2–C1 124.7(1), N2–C2–C1 113.5(1)

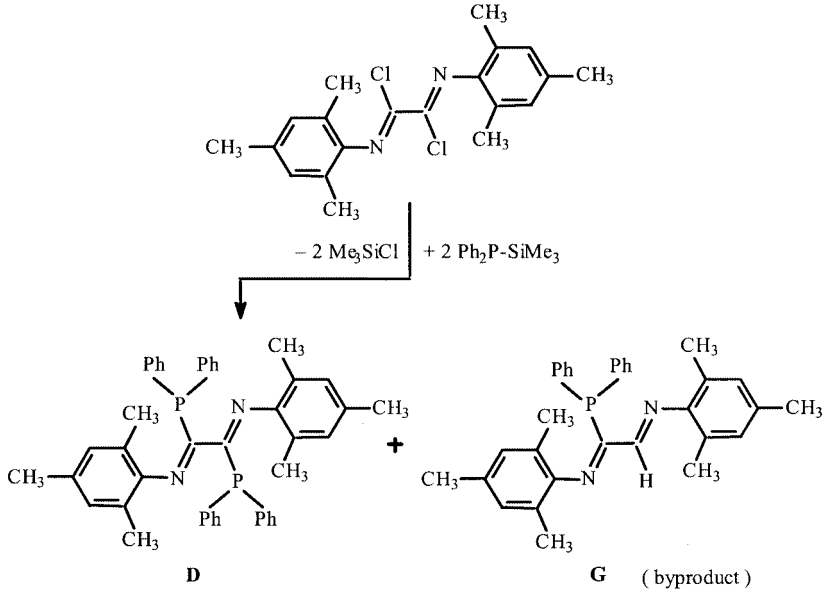

Scheme 2

 © 2003 Wiley-VCH Verlag GmbH & Co. KGaA, Weinheim

The central C−C bond in **D** is a typical single bond (1.517 Å) and the C−N bond lengths are typical of double bonds (1.280 and 1.266 Å). The bulky PPh_2 group results in large P−C−C bond angles (125.4 and 124.7°); the N−C−C angles (114.9 and 113.5°) are rather small due to the effect of the lone pair on the nitrogen atom. Perhaps the most unusual feature of ligand **D** is that, in spite of the 1,4 diazabutadiene unit, it is not planar and assumes a twisted (*E*) conformation (the N−C−C−N dihedral angle is 128.2°). The twist angle is even larger in **B** (N−C−C−N = 99.5°) and **C** (N−C−C−N = 94.0°), leading to an almost orthogonal conformation. A conformational search for **D** at the B3LYP/lanl2dz level of theory confirmed that this nonplanar geometry is the global minimum (and the only stable conformation on the hypersurface). All calculated geometrical parameters agree quite satisfactorily with the solid-state values. An NBO analysis for **D** showed that a residual delocalization between the two C=N double bonds is present [$\pi_{C=N} \rightarrow \pi^*_{C=N}$ = 10.2 kcal/mol] in spite of the relatively large twist angle.

The by-product 2-(diphenylphosphanyl)-1,4-dimesityl-1,4-diazabutadiene (**G**, Scheme 2), which lacks the bulk of a second PPh_2 group, assumes a planar (*E*) conformation in the solid state (not depicted; the N−C−C−N torsion angle is 158.8°). This prompted us to explore the rotational process about the central C−C bond in the absence of steric hindrance (Figure 2).

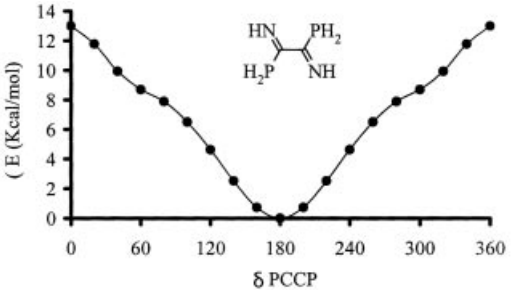

Figure 2. Torsional potential for rotation about the central C−C bond in a simple diphosphanyl-diazabutadiene, calculated at the B3LYP/6-311++G(3df,3pd) level of theory

The (*E*) conformation (P−C−C−P = 180°) is the only stable minimum on the hypersurface of this bifunctional chelating unit. The (*Z*) conformer is the transition structure for rotation about the C−C bond due to strong electronic repulsions between the lone electron pairs on the nitrogen atom in this orientation. It is interesting that two inflection points occur in the rotational barrier at ca. 60 and 300°. In the neighborhood of these points, the repulsion between the lone pairs of the nitrogen atoms is becoming quite weak and a $\pi_{C=N} \rightarrow \pi^*_{C=N}$ delocalization is beginning to appear. This delocalization is responsible for the preferred (E) conformation. If bulky substituents on P are introduced, these inflection points are stabilized and become minima on the hypersurface at the expense of the planar (E) conformation.

There are several possibilities for the coordination of **D** to a metal ion (P,P, N,N and two P,N modes) but, as discussed below, P,P coordination is generally favored. In each case, a lone pair on the heteroatom functions as a donor orbital to the metal ion. The NBO analysis of **D** (Table 1) shows that the lone pair orbital on P lies significantly higher in energy (−7.7 eV) than on N (−8.6 eV). This difference is probably responsible for the observed preference of a P,P coordination mode since the lone electron pair on P can interact more effectively with low-lying unoccupied orbitals on the metal ion.

Table 1. Selected electronic properties of ligand **D**, calculated at the B3LYP/6-31+G(d,p)//B3LYP/lanl2dz level of theory

Atomic charge		Orbital	Occupancy	Energy [eV]
q_C	0.05	n_N	1.82	−8.6
q_N	−0.46	n_P	1.80	−7.7
q_P	+0.76			

Reactivity towards Oxygen and Sulfur

The ligands **B**−**D** all decompose in the presence of water and are oxidized by air to yield the corresponding phosphane oxides. We succeeded in isolating the phosphane oxide **E**, resulting from the reaction of **B** with hydroperoxide or with oxygen, as single crystals. Its solid-state structure and relevant geometrical parameters can be found in Figure 3.

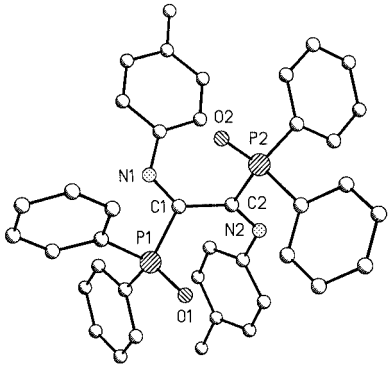

Figure 3. Solid-state structure of compound **E**; selected bond lengths [Å] and bond angles [°]: P1−O1 1.484(2), P1−C1 1.857(3), C1−N1 1.285(3), C1−C2 1.522(4), P2−O2 1.483(2), P2−C2 1.857(3), C2−N2 1.280(3); O1−P1−C1 112.1(1), O2−P2−C2 111.1(1), P1−C1−N1 113.0(2), P2−C2−N2 116.4(2), P1−C1−C2 115.9(2), N1−C1−C2 130.9(3), P2−C2−C1 115.9(2), N2−C2−C1 127.2(3)

Ligand **E** also assumes a nonplanar conformation. Rather than being almost orthogonal, the torsion angle (N−C−C−N = 118.6°) is significantly shifted towards an (*E*) conformation (N−C−C−N in **B** is 99.5°). This may possibly be due to the higher coordination number and thus increased steric bulk of the phosphorus functionalities which force them to be (*E*) to each other.

Adding elemental sulfur to a solution of **D** resulted in the formation of the corresponding disulfide **F**, which could then be characterized by MS and NMR spectroscopy. In the $^{31}P\{^1H\}$ NMR spectrum of **F**, a singlet at δ = 34.9 ppm (shifted downfield relative to **D**) was observed. In the ^{13}C NMR spectrum at room temperature, all expected 11 sig-

 © 2003 Wiley-VCH Verlag GmbH & Co. KGaA, Weinheim

nals were detected. Surprisingly, the resonance of the P−C=N carbon atoms occurs at δ = 159.3 ppm as a broad signal, thus suggesting the presence of a hindered rotation about the central PNC−CNP single bond.

Pd^{II} and Pt^{II} Complexes of These Ligands

We observed in our initial investigation that a ring-closure reaction at the periphery of a metal-complexed 2,3-bis(diarylphosphanyl)-1,4-diazadiene unit only occurred when P,P coordination is present and only when the metal ion was Ni^{II}.[17] Corresponding Cu^{I} or $Mo(CO)_4$ complexes did not promote this reaction. This fact prompted us to investigate the coordination chemistry of the related d^8 metal ions Pd^{II} and Pt^{II}.

Ligand **C** reacts with $[PtCl_2(cod)]$ to yield the mononuclear complex **1** as the only product. The two phosphorus atoms are nonequivalent as can be seen from two resonances (δ = 25.0 and 20.0 ppm) in the $^{31}P\{^1H\}$ spectrum of **1**. In addition, the ^1H and ^{13}C NMR spectra of **1** in $[D_8]$THF are in agreement with the unsymmetrical structure shown in Scheme 3.

For example, two different signals, each integrating to nine protons, were observed at δ = 1.05 and 1.24 ppm for the two *tert*-butyl groups. The NMR spectroscopic data suggest that **1** is the product of a ring-closure reaction between the 1,4-diazadiene system at the periphery of the complex with one *tert*-butylphenyl substituent of a nitrogen atom yielding a quinoxaline system by subsequent tautomerization (Scheme 3).

Figure 4 shows the solid-state structure of **1**, which confirms the existence of a mononuclear complex in which a ring-closure reaction to form a quinoxaline ring has occurred. The coordination geometry of the platinum center is square-planar with two *cis*-chloro ligands. The two phosphorus donor atoms form a five-membered chelate ring. Typical for this structure is the C1−C2 double bond (1.342 Å). As expected, the C−C bond lengths in the peripheral benzene ring are equivalent to each other within experimental errors and correspond to typical C−C bond lengths in aromatic systems. The C1−N1 and the C3−N1 bond lengths are those of typical single bonds [1.448(6), and 1.449(7) Å]. In contrast, the C2−N2 and C4−N2 bonds [1.380(7), 1.404(6) Å] are slightly shortened, indicating

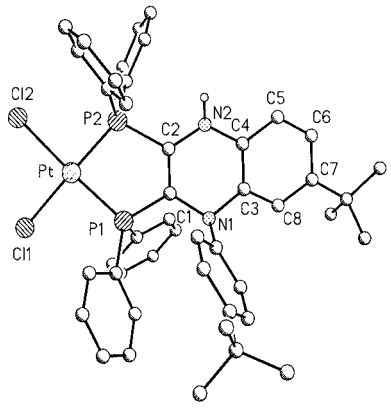

Figure 4. Solid-state structure of complex **1**; selected bond lengths [Å] and bond angles [°]: Pt−Cl1 2.361(1), Pt−Cl2 2.360(1), Pt−P1 2.214(1), Pt−P2 2.206(1), P1−C1 1.795(6), C1−C2 1.342(8), C1−N1 1.448(6), N1−C3 1.449(7), P2−C2 1.830(5), C2−N2 1.380(7), N2−C4 1.404(6), C4−C3 1.387(8), C4−C5 1.390(8), C5−C6 1.390(8), C6−C7 1.392(8), C7−C8 1.391(8), C8−C3 1.399(7); Cl1−Pt−Cl2 91.31(5), Cl1−Pt−P1 91.42(5), Cl1−Pt−P2 178.48(5), Cl2−Pt−P1 177.04(6), Cl2−Pt−P2 89.77(5), P1−Pt−P2 87.48(5)

charge delocalization in the C1−C2−N2−C4 part of the quinoxaline ring. Consequently, N1 is pyramidal and N2 is planar. This difference may be explained by steric reasons: N1 bears an aryl substituent in the neighborhood of the Ph_2P group whereas N2 bears the much smaller hydrogen substituent.

Ligand **C** also reacts with $[PdCl_2(CH_3CN)_2]$ to form the mononuclear complex **2** even if an excess of the palladium compound was employed. Analogous to the Pt compound, the $^{31}P\{^1H\}$ spectrum show that the two phosphorus atoms are unsymmetrical (two doublets at δ = 43.5 and 37.6 ppm). The ^1H and ^{13}C NMR spectra also indicate that a ring-closure reaction has taken place (see Exp. Sect.). Brown crystals of the palladium complex **2** could be isolated from THF. However, their quality was insufficient for the exact determination of bond lengths and bond angles in the solid state. Only the structure motif of the planar complex containing a peripheral quinoxaline ring could be unequivocally confirmed in the solid state.

Ligand **D** contains, in contrast to **C**, methyl groups in both *ortho* positions of the N substituents. This effectively prevents tautomerization to form a benzene ring. Coordi-

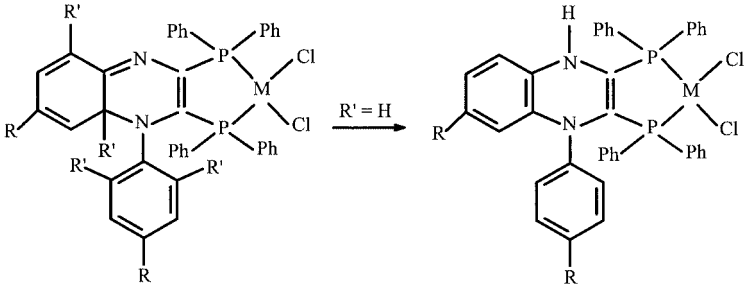

3: R = R' = Me, M = Pd

1: R = *t*Bu, R' = H, M = Pt

2: R = *t*Bu, R' = H, M = Pd

Scheme 3

 © 2003 Wiley-VCH Verlag GmbH & Co. KGaA, Weinheim

nation of a metal ion to both phosphorus atoms, followed by a peripheral ring closure, must then stop at the cyclohexadiene stage of the reaction.[17]

Ligand **D** does indeed react with $[PdCl_2(CH_3CN)_2]$ in THF to form the mononuclear complex **3**. ^1H, ^{13}C, and $^{31}P\{^1H\}$ NMR spectra are in complete agreement with a 1,3-cyclohexadiene ring at the periphery of the metal complex. The solid-state structure of **3** confirmed the presence of the expected 1,3-cyclohexadiene ring with its typically alternating bond lengths (Figure 5). The N1−C3 bond length (1.300 Å) is that of a double bond and therefore much shorter than the corresponding bond length in the N1−C1 single bond of **1** (1.448 Å). Bond lengths and angles in the (P,P)Pd chelate ring are very similar to those in **1**.

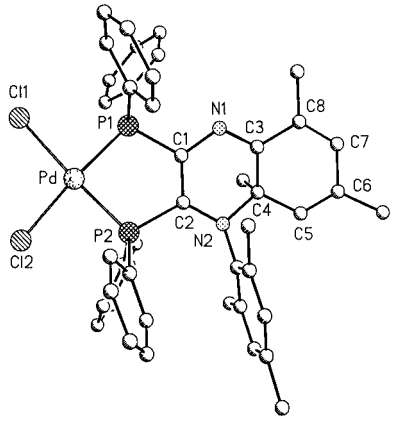

Figure 5. Solid-state structure of complex **3**; selected bond lengths [Å] and bond angles [°]: Pd−Cl1 2.354(1), Pd−Cl2 2.346(1), Pd−P1 2.194(1), Pd−P2 2.227(1), P1−C1 1.789(5), C1−N1 1.394(7), C1−C2 1.350(7), N1−C3 1.300(7), C2−N2 1.386(7), N2−C4 1.530(7), C4−C3 1.520(7), C4−C5 1.460(7), C5−C6 1.331(8), C6−C7 1.447(9), C7−C8 1.331(8), C8−C3 1.459(8); Cl1−Pd−Cl2 95.26(6), Cl1−Pd−P1 89.62(6), Cl1−Pd−P2 176.20(6), Cl2−Pd−P1 174.31(6), Cl2−Pd−P2 88.07(6), P1−Pd−P2 87.14(5), P1−C1−N1 116.8(4), P2−C2−N2 125.0(4), P1−C1−C2 120.9(4), P2−C2−C1 114.8(4), N1−C1−C2 122.0(5), N2−C2−C1 120.1(5)

These results allow us to conclude that bromides and chlorides of d^8 systems (Ni^{II}, Pd^{II}, and Pt^{II}) generally favor P,P coordination with 2,3-bis(phosphanyl)-1,4-diazadienes over P,N or N,N coordination. The formation of a mononuclear complex is then directly followed by an unusual peripheral ring-closure reaction to form a quinoxaline derivative, independent of the size of the metal ion.

Reaction of These Ligands with a Nickelacycle

We then modified the metal fragment employed to find out if the peripheral ring-closure reaction depends on the nature of the additional ligand(s) coordinated to the metal ion. Our metal fragment of choice was the nickelacycle [Ni(tmeda)(C_2H_4COO)], which contains a doubly negatively charged 1-oxo-2-nickelacyclopentan-5-one chelate ring on one side of the square-planar complex. On the other side is the neutral chelating ligand *N*,*N*,*N*′,*N*′-tetramethylethylenediamine (tmeda). Displacement of tmeda by either **B**, **C**, or **D** should result in the initial formation of an [Ni{2,3-bis(diarylphosphanyl)-1,4-diazadiene}(C_2H_4COO)] complex. If the ring closure is affected by the additional metal ligands, one would expect a different reactivity of this complex compared to the related $NiBr_2$ complex, which undergoes a fast ring-closure reaction.

Treatment of the nickelacycle with the bulk ligand **D** in a solution of DMF followed by removal of tmeda by distillation in vacuo resulted in the expected organometallic complex [Ni(**D**)(C_2H_4COO)] (**4a**; Scheme 4) which turned out to be dark red. There are theoretically four possibilities for the coordination of **D** to the nickelacyclic fragment in this compound (P,P, N,N, and two P,N coordination modes). NMR spectroscopic data show that both phosphorus donor atoms coordinate to the nickelacycle in a different chemical environment (double signal sets for the mesityl groups in the ^1H NMR spectrum and two doublets at δ = 19.8 and 44.8 ppm in the $^{31}P\{^1H\}$ NMR spectrum of **4a**). Isolation of single crystals of **4a** from benzene and subsequent X-ray diffraction analysis (Figure 6) showed that both phosphorus atoms are coordinated to the nickel center (square-planar P,P mode) in the solid state. In addition, an oxygen and a carbon atom of the C_2HC_4COO moiety are bound to the nickel center. The 1,4-diazadiene unit of **D** is not involved in coordination. A ring-closure reaction of the 1,4-diazadiene and one mesityl substituent at the nitrogen atom to yield a quinoxaline ring *did not take place* upon coordination of the diphosphane unit to the nickelacycle.

The diazabutadiene unit in ligand **D** is not planar (N−C−C−N torsional angle is 52.4°) but is definitely closer to a (*Z*) arrangement than to the *twist*-(*E*) conformation of the free ligand **D** (N−C−C−N = 128.2°). Ligand bond lengths do not differ significantly between the free ligand **D** and the coordinated complex **4a**.

The less bulky ligand **B** also reacted with the nickelacycle [Ni(tmeda)(C_2H_4COO)] to yield an orange chelate complex, which could be isolated in good yields (54%) from dichloromethane as an adduct of the composition "[Ni(**B**)(C_2H_4-COO)(CH_2Cl_2)]". Analogous to **4a**, the $^{31}P\{^1H\}$ NMR spectrum of this complex in $CDCl_3$ shows a low-field shift relative to the free ligand and indicates a P,P coordination mode but, in this case, *two* sets of two doublets are observed at δ = 28.3 [d, $^2J(^{31}P^{31}P)$ = 19.0 Hz], 39.0 [d, $^2J(^{31}P^{31}P)$ = 24.2 Hz], 46.1 [d, $^2J(^{31}P^{31}P)$ = 24.2 Hz], and 48.9 [d, $^2J(^{31}P^{31}P)$ = 19.0 Hz] ppm.

This is not compatible with the "open coordination form" observed for **4a** but can be rationalized by an unsymmetrical chelate ring system formed by ring-closure reaction between the 1,4-diazadiene unit and an aromatic N-substituent to form the regioisomers **5b/5b′** (Scheme 4).

The ^1H NMR spectroscopic data support this conclusion. In the ^1H NMR spectrum two sets of signals for the CH_3 protons at δ = 1.84, 1.91, 2.11, and 2.15 ppm were found whereas the CH_2 protons of the metallacyclic ring appear as multiplets. The $^{13}C\{^1H\}$ NMR spectrum is very complicated due to the ^{31}P coupling pattern of the ^{13}C signals of the two very similar regioisomers. Therefore, not all expected signals could be resolved (see Exp. Sect.).

 © 2003 Wiley-VCH Verlag GmbH & Co. KGaA, Weinheim

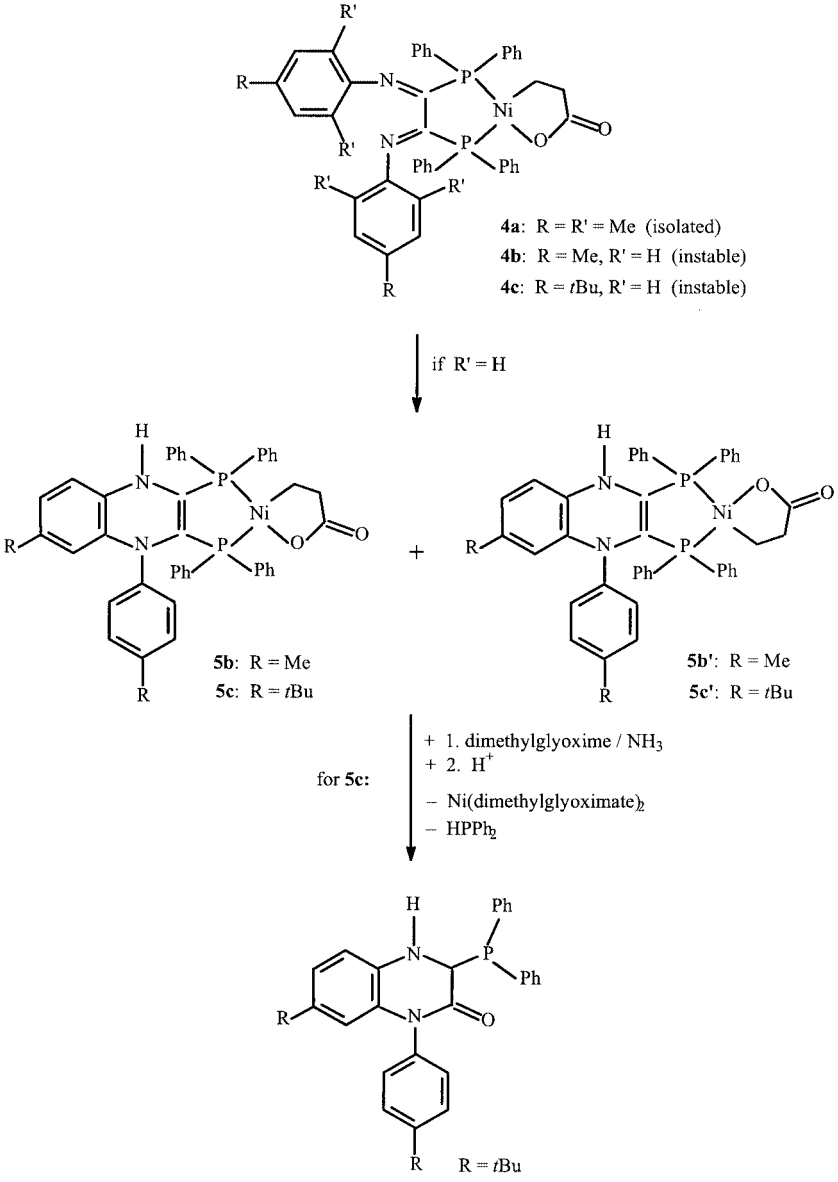

Scheme 4

The formation of a quinoxaline system at the periphery was confirmed by X-ray diffraction analysis. Figure 7 shows the molecule structure of a single crystal of the regioisomer **5b·CH_2Cl_2** grown from dichloromethane. Unfortunately, the quality of the crystals was insufficient for satisfactory refinement of all parameters.

Ligand **B** thus behaves in a fundamentally different way to ligand **D**. This clearly demonstrates the subtle dependence of the ring-closure reaction upon ligand environment and identity in the metal complex. Both the nature of the metal and the coordination geometry of the complex formed in the first step of the complex formation, and the nature of the other ligands surrounding the metal center, influence the subsequent cycloaddition reaction at the periphery.

When the closely related ligand **C** was treated with the nickelacycle [Ni(tmeda)(C_2H_4COO)], an initial intermediate was formed which could be monitored by time-resolved $^{31}P\{^1H\}$ NMR spectroscopy at 5 °C. The "open coordination form", characterized by two doublets at δ = 42.7 and 60.9 ppm, could be assigned to this intermediate [Ni(**C**)(C_2H_4COO)] (**4c**; Scheme 4).

As the reaction progressed, two sets of two doublets appeared at δ = 30.5/51.0 and 37.7/49.0 ppm and grew in intensity over time. The signals assigned to the "open form" intermediate **4c** completely disappeared after 2 h at room temperature, and, except for a very small amount of the free ligand, only the two sets of two doublets were observed, which we concluded was the "quinoxaline form" **5c/5c′** resulting from the peripheral ring-closure reaction. A com-

 © 2003 Wiley-VCH Verlag GmbH & Co. KGaA, Weinheim

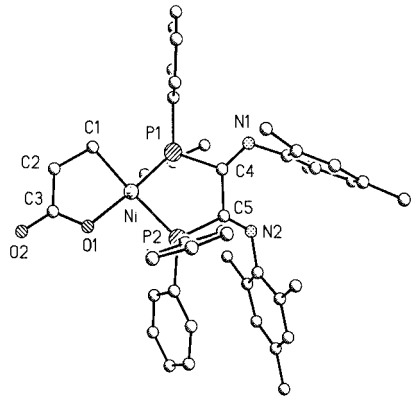

Figure 6. Solid -state structure of complex **4a**; selected bond lengths [Å] and bond angles [°]: Ni−P1 2.096(1), Ni−P2 2.170(1), Ni−O1 1.882(3), Ni−C1 1.952(4), C1−C2 1.526(6), C2−C3 1.512(6), C3−O1 1.306(5), C3−O2 1.227(5), P1−C4 1.853(4), P2−C5 1.864(4), C4−C5 1.530(5), C4−N1 1.271(5), C5−N2 1.267(5); P1−Ni−P2 90.30(4), P1−Ni−O1 170.55(9), P1−Ni−C1 88.6(1), P2−Ni−O1 96.00(9), P2−Ni−C1 171.5(1), O1−Ni−C1 86.2(1), P1−C4−N1 120.9(3), P2−C5−N2 133.4(3), P1−C4−C5 110.1(2), P2−C5−C4 110.4(2), N1−C4−C5 128.9(3), N2−C5−C4 115.0(3)

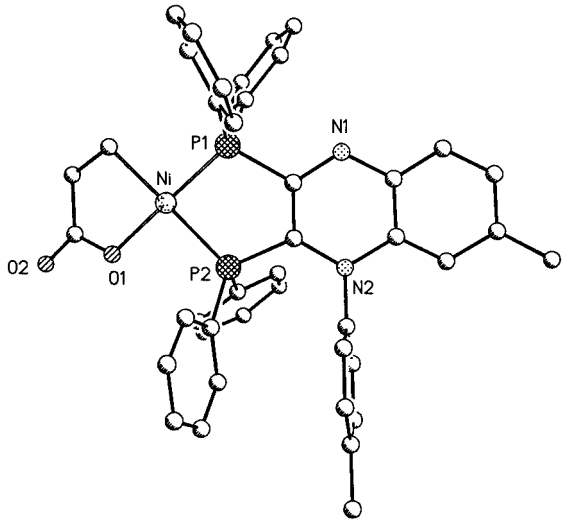

Figure 7. Solid-state structural motif of complex **5b** (the solvent CH_2Cl_2 has been omitted for clarity)

parison of the ^{31}P NMR spectrum of the closely related complex pair **5b/5b′** completely supports this assignment. There is no evidence for any other stable intermediate occurring during the ring-closure reaction.

In order to separate the quinoxaline ligand from the nickelacycle, the reaction mixture was treated with a solution of dimethylglyoxime in ethanol and aqueous ammonia. After separation of bis(dimethylgyoximato)nickel(II), thin white needles of 4-(*p*-*tert*-butylphenyl)-9-*tert*-butyl-3,4-dihydro-3-(diphenylphosphanyl)-1*H*-quinoxalin-2-one were isolated from the mother liquor, and were identified by IR measurements, mass spectra, ^1H, ^{13}C, and ^{31}P NMR spectra. The formation of this product can easily be explained by hydrolysis of the free 1,2-bis(diphenylphosphanyl)quinoxaline according to Scheme 4.

Experimental Section

General: ^1H, ^{13}C, and $^{31}P\{^1H\}$ NMR spectra were recorded at ambient temperature with a Bruker AC 200 MHz spectrometer unless otherwise stated. All spectra were referenced to TMS or deuterated solvent as an internal standard. FAB mass spectra were obtained with a Finnigan MAT SSQ 710 system (2,4-dimethoxybenzyl alcohol as matrix), ESI mass spectra were recorded with a Finnigan MAT, MAT 95 XL. IR measurements were carried out with a Perkin−Elmer System 2000 FT-IR. All manipulations were carried out by using Schlenk techniques under argon. Prior to use, tetrahydrofuran, diethyl ether, and toluene were dried with potassium hydroxide and distilled from Na/benzophenone. $[PtCl_2(cod)]$ and $[PdCl_2(CH_3CN)_2]$ (Aldrich) were used as received. Oxalic imidoyl chlorides R−N=C(Cl)−C(Cl)=N−R,[18,19] $NaPPh_2$(dioxane) and $K(PPh_2)(dioxane)_n$,[20] and the nickelacycle [Ni{(tmeda)-C_2H_4COO}][21] were prepared according to the literature.

Computational Methods: All calculations reported in this article were performed using the Gaussian 98[22] program package using the gradient-corrected B3LYP[23−25] density functional. Default convergence criteria were used for all optimizations. The size of ligand **D** limited optimizations and frequency calculations to the lanl2dz basis set developed by Hay and Wadt[26] as implemented in Gaussian 98. Atomic charges, orbital and hyperconjugative interaction energies were obtained at the B3LYP/6-31+G(d,p)//B3LYP/lanl2dz level using the natural bond orbital (NBO) analysis of Reed et al.[27] as implemented in Gaussian 98. The torsional barrier of diphosphanyl-diazabutadiene (Figure 2) was calculated using the very large 6-311++G(3df,3pd) basis set.

Crystal Structure Determination: The intensity data for the compounds were collected with a Nonius KappaCCD diffractometer, using graphite-monochromated Mo-K_α radiation. Data were corrected for Lorentz and polarization effects, and (only for **1**) for absorption effects.[28,29] The structures were solved by direct methods (SHELXS[30]) and refined by full-matrix least-squares techniques against F_o^2 (SHELXL-97[31]). For the molecules **B**, **C**, **D**, **E**, and **G**, the hydrogen atoms were located by difference Fourier synthesis and refined isotropically. All other hydrogen atoms were included at calculated positions with fixed thermal parameters. All non-hydrogen atoms were refined anisotropically.[4] Since the quality of the data of compounds **2** and **5c** was too low, we will only publish the conformation of **5b** and the crystallographic data of **2** and **5b**. We have not deposited the data in the Cambridge Crystallographic Data Centre. XP (SIEMENS Analytical X-ray Instruments, Inc.) was used for structure representations.

Crystal Data for B:[32] $C_{40}H_{34}N_2P_2$, M_r = 604.63 g·mol^{-1}, colourless prism, size 0.21 × 0.18 × 0.10 mm, monoclinic, space group *C*2, *a* = 21.7489(8), *b* = 6.3620(2), *c* = 12.8609(6) Å, β = 115.479(2)°, *V* = 1606.4(1) Å^3, *T* = −90 °C, *Z* = 2, $\rho_{calcd.}$ = 1.250 g·cm^{-3}, μ(Mo-K_α) = 1.67 cm^{-1}, *F*(000) = 636, 4265 reflections in *h*(−30/30),*k*(0/7),*l*(−18/18), measured in the range 3.22° ≤ Θ ≤ 30.54°, completeness to Θ_{max} 95%, 2532 independent reflections, R_{int} = 0.029, 2233 reflections with $F_o > 4\sigma(F_o)$, 267 parameters, 1 restraint, $R1_{obs}$ = 0.038, $wR2_{obs}$ = 0.083, $R1_{all}$ = 0.048, $wR2_{all}$ = 0.087, GOOF = 1.004, Flack parameter 0.1(1), largest difference peak/hole 0.240/−0.199 e·Å^{-3}.

Crystal Data for C:[32] $C_{46}H_{46}N_2P_2$, M_r = 688.79 g·mol^{-1}, colourless prism, size 0.32 × 0.30 × 0.28 mm, orthorhombic, space group *Fdd*2, *a* = 31.3604(9), *b* = 38.780(1), *c* = 6.3478(2) Å, *V* = 7719.9(4) Å^3, *T* = −90 °C, *Z* = 8, $\rho_{calcd.}$ = 1.185 g·cm^{-3}, μ(Mo-K_α) = 1.47 cm^{-1}, *F*(000) = 2928, 9627 reflections in *h*(−43/

 © 2003 Wiley-VCH Verlag GmbH & Co. KGaA, Weinheim

44),*k*(−55/55),*l*(−9/0), measured in the range 3.34° ≤ Θ ≤ 30.49°, completeness to Θ_{max} 99.2%, 3155 independent reflections, R_{int} = 0.049, 2727 reflections with $F_o > 4\sigma(F_o)$, 318 parameters, 1 restraint, $R1_{obs}$ = 0.047, $wR2_{obs}$ = 0.090, $R1_{all}$ = 0.061, $wR2_{all}$ = 0.094, GOOF = 1.060, Flack parameter 0.07(9), largest difference peak/hole: 0.220/−0.278 e·Å^{-3}.

Crystal Data for D:[32] $C_{44}H_{42}N_2P_2{\cdot}CHCl_3$, M_r = 780.10 g·mol^{-1}, yellow prism, size 0.10 × 0.10 × 0.06 mm, triclinic, space group $P\bar{1}$, *a* = 10.9955(2), *b* = 11.0908(4), *c* = 18.6186(6) Å, α = 88.207(1), β = 77.765(2), γ = 65.120(2)°, *V* = 2008.7(1) Å^3, *T* = −90 °C, *Z* = 2, $\rho_{calcd.}$ = 1.290 g·cm^{-3}, μ(Mo-K_α) = 3.42 cm^{-1}, *F*(000) = 816, 14121 reflections in *h*(−11/14),*k*(−14/13),*l*(−20/24), measured in the range 2.03° ≤ Θ ≤ 27.48°, completeness to Θ_{max} 98.3%, 9053 independent reflections, R_{int} = 0.055, 6598 reflections with $F_o > 4\sigma(F_o)$, 641 parameters, 0 restraints, $R1_{obs}$ = 0.047, $wR2_{obs}$ = 0.131, $R1_{all}$ = 0.067, $wR2_{all}$ = 0.140, GOOF = 1.059, largest difference peak/hole 0.287/−0.461 e·Å^{-3}.

Crystal Data for E:[32] $C_{40}H_{34}N_2O_2P_2$, M_r = 636.63 g·mol^{-1}, orange prism, size 0.32 × 0.20 × 0.10 mm, monoclinic, space group $P2_1/c$, *a* = 16.4345(5), *b* = 12.3660(5), *c* = 16.3540(4) Å, β = 94.429(3)°, *V* = 3313.68(19) Å^3, *T* = −90 °C, *Z* = 4, $\rho_{calcd.}$ = 1.276 g·cm^{-3}, μ(Mo-K_α) = 1.7 cm^{-1}, *F*(000) = 1336, 24310 reflections in *h*(−18/20),*k*(−15/15),*l*(−20/20), measured in the range 3.16° ≤ Θ ≤ 26.33°, completeness to Θ_{max} 99.7%, 6730 independent reflections, R_{int} = 0.128, 4229 reflections with $F_o > 4\sigma(F_o)$, 551 parameters, 0 restraints, $R1_{obs}$ = 0.061, $wR2_{obs}$ = 0.115, $R1_{all}$ = 0.119, $wR2_{all}$ = 0.134, GOOF = 1.015, largest difference peak/hole 0.215/−0.344 e·Å^{-3}.

Crystal Data for G:[32] $C_{32}H_{33}N_2P$, M_r = 476.57 g·mol^{-1}, orange prism, size 0.20 × 0.18 × 0.12 mm, triclinic, space group $P\bar{1}$, *a* = 11.3416(6), *b* = 11.7240(5), *c* = 12.1736(7) Å, α = 116.217(3), β = 103.457(2), γ = 95.600(3)°, *V* = 1374.6(1) Å^3, *T* = −90 °C, *Z* = 2, $\rho_{calcd.}$ = 1.151 g·cm^{-3}, μ(Mo-K_α) = 1.22 cm^{-1}, *F*(000) = 508, 9420 reflections in *h*(−11/14),*k*(−15/12),*l*(−15/14), measured in the range 2.01° ≤ Θ ≤ 27.49°, completeness to Θ_{max} 97.3%, 6133 independent reflections, R_{int} = 0.030, 4556 reflections with $F_o > 4\sigma(F_o)$, 448 parameters, 0 restraints, $R1_{obs}$ = 0.060, $wR2_{obs}$ = 0.116, $R1_{all}$ = 0.091, $wR2_{all}$ = 0.128, GOOF = 1.049, largest difference peak/hole 0.208/−0.277 e·Å^{-3}.

Crystal Data for 1:[32] $C_{46}H_{46}Cl_2N_2P_2Pt{\cdot}2C_4H_8O$, M_r = 1098.99 g·mol^{-1}, yellow prism, size 0.20 × 0.18 × 0.10 mm, monoclinic, space group $P2_1/n$, *a* = 18.5552(9), *b* = 14.0777(6), *c* = 21.6152(7) Å, β = 104.845(2)°, *V* = 5457.7(4) Å^3, *T* = −90 °C, *Z* = 4, $\rho_{calcd.}$ = 1.337 g·cm^{-3}, μ(Mo-K_α) = 27.66 cm^{-1}, semiempirical,[2] trans(min) 0.507, trans(max) 0.849, *F*(000) = 2232, 21216 reflections in *h*(−24/24),*k*(−18/17),*l*(−26/25), measured in the range 1.84° ≤ Θ ≤ 27.55°, completeness to Θ_{max} 95.7%, 12062 independent reflections, R_{int} = 0.060, 6529 reflections with $F_o > 4\sigma(F_o)$, 563 parameters, 0 restraints, $R1_{obs}$ = 0.044, $wR2_{obs}$ = 0.101, $R1_{all}$ = 0.095, $wR2_{all}$ = 0.109, GOOF = 0.886, largest difference peak/hole 1.120/−0.853 e·Å^{-3}.

Crystal Data for 2: $C_{46}H_{46}Cl_2N_2P_2Pd{\cdot}3C_4H_8O$, M_r = 1082.40 g·mol^{-1}, brown prism, size 0.18 × 0.12 × 0.10 mm, monoclinic, space group $P2_1/n$, *a* = 18.5913(3), *b* = 14.0835(4), *c* = 21.5903(6) Å, β = 104.930(1)°, *V* = 5462.2(2) Å^3, *T* = −90 °C, *Z* = 4, $\rho_{calcd.}$ = 1.316 g·cm^{-3}, μ(Mo-K_α) = 5.41 cm^{-1}, *F*(000) = 2264, 20954 reflections in *h*(−23/24),*k*(−17/18),*l*(−28/28), measured in the range 1.84° ≤ Θ ≤ 27.49°, completeness to Θ_{max} 99.2%, 12444 independent reflections, R_{int} = 0.077.

Crystal Data for 3:[32] $C_{44}H_{42}Cl_2N_2P_2Pd{\cdot}1.5C_4H_8O$, M_r = 946.19 g·mol^{-1}, yellow prism, size 0.18 × 0.12 × 0.10 mm, monoclinic, space group $P2_1/n$, *a* = 14.4502(6), *b* = 24.9850(10), *c* = 14.6521(5) Å, β = 112.360(3)°, *V* = 4892.2(3) Å^3, *T* = −90 °C, *Z* = 4, $\rho_{calcd.}$ = 1.285 g·cm^{-3}, μ(Mo-K_α) = 5.91 cm^{-1}, *F*(000) = 1960, 13135 reflections in *h*(−16/16),*k*(−28/28),*l*(−16/16), measured in the range 1.73° ≤ Θ ≤ 24.09°, completeness to Θ_{max} 96.7%, 7502 independent reflections, R_{int} = 0.037, 4810 reflections with $F_o > 4\sigma(F_o)$, 508 parameters, 8 restraints, $R1_{obs}$ = 0.057, $wR2_{obs}$ = 0.165, $R1_{all}$ = 0.081, $wR2_{all}$ = 0.177, GOOF = 0.953, largest difference peak/hole 1.069/−0.475 e·Å^{-3}.

Crystal Data for 4a:[32] $C_{47}H_{46}N_2NiO_2P_2{\cdot}0.5C_6H_6$, M_r = 830.56 g·mol^{-1}, red prism, size 0.10 × 0.10 × 0.08 mm, monoclinic, space group $P2_1/n$, *a* = 12.6055(3), *b* = 16.4881(4), *c* = 20.9493(6) Å, β = 99.186(2)°, *V* = 4298.3(2) Å^3, *T* = −90 °C, *Z* = 4, $\rho_{calcd.}$ = 1.283 g·cm^{-3}, μ(Mo-K_α) = 5.68 cm^{-1}, *F*(000) = 1748, 45176 reflections in *h*(−15/16),*k*(−21/21),*l*(−22/27), measured in the range 2.39° ≤ Θ ≤ 27.42°, completeness to Θ_{max} 98.6%, 9656 independent reflections, R_{int} = 0.115, 6543 reflections with $F_o > 4\sigma(F_o)$, 499 parameters, 0 restraints, $R1_{obs}$ = 0.069, $wR2_{obs}$ = 0.162, $R1_{all}$ = 0.114, $wR2_{all}$ = 0.191, GOOF = 1.055, largest difference peak/hole 1.412/−0.611 e·Å^{-3}.

Crystal Data for 5b: $C_{43}H_{38}N_2NiO_2P_2{\cdot}2CH_2Cl_2$, M_r = 904.70 g·mol^{-1}, prism, size 0.20 × 0.18 × 0.12 mm, monoclinic, space group $P2_1/c$, *a* = 8.8883(3), *b* = 26.1761(9), *c* = 19.3778(6) Å, β = 95.384(2)°, *V* = 4488.6(3) Å^3, *T* = −90 °C, *Z* = 4, $\rho_{calcd.}$ = 1.391 g·cm^{-3}, μ(Mo-K_α) = 8.4 cm^{-1}, *F*(000) = 1936, 16022 reflections in *h*(−11/11),*k*(−33/31),*l*(−25/25), measured in the range 2.89° ≤ Θ ≤ 27.46°, completeness to Θ_{max} 93.9%, 9655 independent reflections, R_{int} = 0.101.

Preparation of the Ligands

Ph−N=C(PPh$_2$)−C(PPh$_2$)=N−Ph (Ligand A): A solution of $NaPPh_2$ (7.17 mmol 15% excess) in 10 mL of cold THF (−78 °C) was added dropwise to a solution of diphenyloxalylimidoyl chloride (0.9 g, 3.24 mmol) in 50 mL of THF at −78 °C. The reaction mixture was then allowed to warm to room temperature. After removing the solvent in vacuo and recrystallization from toluene 0.75 g (40%) of **A** was isolated as a light yellow powder. ^{1}H NMR ([D$_8$]THF, 25 °C, 200 MHz): δ = 7.04 (m, CH-phenyl) ppm. $^{31}P\{^1H\}$ NMR ([D$_8$]THF, 25 °C, 81 MHz): δ = 4.59 (s) ppm. MS (CI): 577 (basic peak $[M+1]^+$ ($C_{38}H_{30}N_2P_2 + H^+$), 499 ($[M+1]^+ - C_6H_6$, 3%), 409 ($[M+1]^+ - C_{12}H_{12}N$, 3%), 393 ($[M+1]^+ - C_{12}H_9P$, 16%), 288 ($[M+1]^+ - C_{19}H_{16}NP$, 37%), 185 ($[M+1]^+ - C_{26}H_{21}N_2P$, 15%).

Mes−N=C(PPh$_2$)−C(PPh$_2$)=N−Mes·CHCl$_3$ [D(CHCl$_3$)]

a) From Mes−N=CCl−CCl=N−Mes and KPPh$_2$: A solution of dimesityloxalylimidoyl chloride (2.7 g, 7.5 mmol) and $Pd(OAc)_2$ (85 mg, 0.038 mmol) in 100 mL of toluene was cooled to −40 °C in a three-necked flask equipped with a stirrer and a dropping funnel. Over 1 h, a solution of $KPPh_2$ (15.0 mmol) in 42 mL of dioxane/THF (1:1) was added. The color of the solution turned from yellow to dark red. The dry-ice bath was then removed and the reaction mixture was kept at room temperature overnight. The precipitated KCl was then filtered off. The solvent was removed in vacuo and the residue dissolved in hexane. The mixture was then filtered through Celite and the filtrate concentrated to dryness. The

 © 2003 Wiley-VCH Verlag GmbH & Co. KGaA, Weinheim

residue is a slowly crystallizing oil. Recrystallization from chloroform/hexane gave 3.96 g (80%) of **D(CHCl$_3$)** as yellow crystals. M.p. 170 °C. $C_{45}H_{43}N_2P_2Cl_3$ (780.1): calcd. C 69.28, H 5.56, Cl 13.63, N 3.59; found C 69.97, H 5.67, Cl 13.18, N 3.55. ^{1}H NMR ($CDCl_3$, 200.13 MHz, 298 K): δ = 1.42 (s, 12 H, *o*-CH_3), 2.17 (s, 6 H, *p*-CH_3), 6.45 (s, 4 H, *m*-H, Mes), 7.19−7.21 (m, 12 H, Ph), 7.50−7.54 (m, 8 H, Ph) ppm. ^{13}C{^{1}H} NMR ($CDCl_3$, 50.32 MHz, 298 K): δ = 17.7 [t, $J(^{13}C^{31}P)$ = 2.5 Hz, CH_3), 20.6 (CH_3), 124.4 (C), 128.1 (CH), 128.1 [d, $J(^{13}C^{31}P)$ = 8.3 Hz, CH], 128.8 (CH), 132.8 (C), 133.8 [br., d, $J(^{13}C^{31}P)$ = 10.5 Hz, C], 135.2 [br., d, $J(^{13}C^{31}P)$ = 23.4 Hz, C], 145.3 [br., d, $J(^{13}C^{31}P)$ = 9.3 Hz, C], 175.2 [dd, $J(^{13}C^{31}P)$ = 58.1, $J(^{13}C^{31}P)$ = 4.5 Hz, C] ppm. ^{31}P{^{1}H} NMR ($CDCl_3$, 81.01 MHz, 298 K): δ = 9.0 (s) ppm. MS (EI): *m*/*z* = 660 [M^+], 330 [M^+/2]. **G** was separated by column chromatography (Florisil, hexane, toluene) as the most nonpolar compound from the residue of the mother liquor. Yield: 0.18 g (5%) of yellow crystals. The yield can be increased up to 44% by addition of $HPPh_2$ *before* $KPPh_2$. ^{1}H NMR ($CDCl_3$, 200.13 MHz, 298 K): δ = 1.55 (s, 6 H, *o*-CH_3), 2.02 (s, 6 H, *o*-CH_3), 2.14 (s, 3 H, *p*-CH_3), 2.17 (s, 3 H, *p*-CH_3), 6.65 (s, 2 H, *m*-H), 6.73 (s, 2 H, *m*-H), 7.34−7.64 (m, 11 H, Ph, =CH−) ppm. ^{13}C{^{1}H} NMR ($CDCl_3$, 50.32 MHz, 298 K): δ = 17.5 (CH_3), 17.6 (CH_3), 20.6 (CH_3), 124.4 [d, $J(^{13}C^{31}P)$ = 1.8 Hz, C], 126.7 (C), 128.4 [d, $J(^{13}C^{31}P)$ = 18.8 Hz, CH], 128.4 (*m*-CH, Mes), 128.6 (*m*-CH, Mes), 129.1 (CH), 132.7 (C), 133.8 (C), 134.4 [d, $J(^{13}C^{31}P)$ = 6.6 Hz, C], 135.0 (CH), 135.2 (CH), 135.1 [d, $J(^{13}C^{31}P)$ = 20.1 Hz, C], 157.5 [d, $J(^{13}C^{31}P)$ = 23.4 Hz, C], 175.5 [d, $J(^{13}C^{31}P)$ = 14.2 Hz, C] ppm. ^{31}P{^{1}H} NMR ($CDCl_3$, 81.01 MHz, 298 K): δ = 2.4 (s) ppm. ^{31}P{^{1}H} NMR (C_6D_6, 81.01 MHz, 298 K): δ = 5.7 (s) ppm. MS (EI): *m*/*z* = 446 [M^+], 330 [$Ph_2PCNMes^+$], 146 [$MesNCH^+$].

b) From Mes−N=CCl−CCl=N−Mes and Me$_3$Si−PPh$_2$: A mixture of dimesityloxalylimidoyl chloride (2.25 g, 6.23 mmol) and diphenyl(trimethylsilyl)phosphane (3.25 g, 12.58 mmol) was held at 100 °C in a water bath for 12 h. Trimethylsilyl chloride was then distilled off the reaction mixture, which became more and more solid. The residue was then extracted with *n*-hexane. Yield: 2.63 g (64%) of **D** as yellow crystals. M.p. 170 °C.

Phosphane Oxide E by Oxidation of B: A solution of **B** in THF was treated with an equimolar amount of hydrogen peroxide at room temperature and a few milligrams of $CuSO_4$ were added. After 6 h, the solvent was removed and the residue was treated with chloroform. The organic phase was separated and dried with $NaSO_4$. After removing the solvent, a yellow product was isolated. White single crystals of **E** were obtained from THF at −20 °C. Similarly, the oxidation can also be carried out with air in the presence of a copper salt. MS (EI): *m*/*z* = 636 [$M^+ = C_{40}H_{34}N_2O_2P_2$], 402 [$(Ph_2PO)_2$], 318 [$M^+$/2], 201 [$Ph_2PO$]. ^{31}P{^{1}H} NMR ($CDCl_3$, 81.01 MHz, 298 K): δ = 23.56 ppm. ^{1}H NMR ($CDCl_3$, 200.13 MHz, 298 K): δ = 2.14 (s, 6 H, *p*-CH_3), 6.62. 6.78 (AA′BB′, 8 H, CH-tolyl), 7.24−7.70 (m, phenyl, solvent) ppm.

Phosphane Sulfide F by Oxidation of D with Sulfur: A solution of **D(CHCl$_3$)** (1.01 g, 1.30 mmol) in toluene was treated with sulfur (85 mg, 2.65 mmol) and stirred at room temperature for 24 h. The solution slowly turned dark red. The signal of **D** in the ^{31}P{^{1}H} NMR spectrum of the reaction mixture disappeared and a new signal at δ = 33.8 ppm appeared. The solvent was removed in vacuo. Recrystallization of the crude product from diethyl ether gave 0.60 g of Mes−N=C[P(S)Ph$_2$]−C[P(S)Ph$_2$]=N−Mes (**F**) (63.6%) as dark red thin plates. M.p. 242−243 °C. $C_{44}H_{42}N_2P_2S_2$ (724.8): calcd. C 72.90, H 5.84, N 3.86, S 8.85; found C 72.55, H 6.08, N 3.83, S 8.43. IR (nujol mull): ν(C=N) = 1640 cm^{-1}. ^{1}H NMR ($CDCl_3$, 200.13 MHz, 298 K): δ = 1.74 (s, 12 H, *o*-CH_3), 1.97 (s, 6 H, *p*-CH_3), 6.20 (s, 4 H, *m*-H), 1.74 (s, 12 H, *o*-CH_3), 7.17 (m, 8 H, *m*-H), 7.24 (m, 4 H, *p*-H), 7.81 (m, 8 H, *o*-H) ppm. ^{13}C{^{1}H} NMR ($CDCl_3$, 50.32 MHz, 298 K): δ = 19.0 (*o*-CH_3), 20.3 (*p*-CH_3), 123.5 (*o*-C), 127.8 (m, *o*-CH), 129.1 (*i*-C), 130.5 (*p*-CH), 131.5 (m, *m*-CH), 132.4 (*p*-C), 133.2 (*m*-CH), 142.5 (m, *i*-C), 159.3 [br., t, *J* ≈ 29 Hz, $(N=C-P)_2$] ppm. ^{31}P{^{1}H} NMR ($CDCl_3$, 81.01 MHz, 298 K): δ = 34.9 (s) ppm. MS *m*/*z* = 725 [M^+ + H].

Complex 1 [PdCl$_2$(C$_{46}$H$_{46}$N$_2$P$_2$)]: A solution of **C** (0.873 mmol, 0.601 g) in 25 mL of THF was added dropwise to a solution of $[PdCl_2(CH_3CN)_2]$ (0.873 mmol, 0.226 g) in 25 mL of THF whilst stirring. Shortly after warming the solution up to 60 °C, complex **1** precipitated almost quantitatively. After filtration, the compound was dried in vacuo at room temperature. It is only very slightly soluble in organic solvents. $C_{50}H_{54}Cl_2N_2OP_2Pd$ [**1(THF)**] (938.26): calcd. C 64.01, H 5.80, N 2.99; found C 63.25, 62.94, H 6.24, 5.98, N 2.89. ^{1}H NMR ([D$_8$]THF, 25 °C, 200 MHz): δ = 1.06, 1.15 (s, 18 H, CH_3-*t*Bu), 6.79−7.67 (m, 28 H, Ph) ppm. ^{31}P{^{1}H} NMR ([D$_8$]THF, 25 °C, 81 MHz): δ = 37.67 (d), 43.54 (d) ppm.

Complex 2 [PtCl$_2$(C$_{46}$H$_{46}$N$_2$P$_2$)]: A solution of **B** (0.32 mmol) in 10 mL of THF was added to [PtCl$_2$(cod)] (0.32 mmol, 0.12 g), dissolved in 10 mL of THF. Shortly after warming the solution up to 60 °C, complex **2** crystallized in more than 95% yield. $C_{50}H_{54}Cl_2N_2OP_2Pt$ [**2(THF)**] (954.82): calcd. C 58.48, H 5.30, N 2.73; found C 58.44, H 5.61, 5.44, N 2.65. ^{1}H NMR ([D$_8$]THF, 27 °C, 200 MHz): δ = 1.11, 1.15 (s, 18 H,CH_3), 6.38−8.01 (m, 25 H, Ph and NH); ^{31}P{^{1}H} NMR ([D$_8$]THF, 27 °C, 81 MHz): δ = −1.49 (d), 4.38 (d), 20.16 (d, *J* = 12 Hz), 25.05 (d, *J* = 13 Hz), 41.82 (d), 45.80 (d) ppm. MS (DEI): 953 [$M^+ = C_{46}H_{46}N_2P_2Cl_2Pt$], 918 [$M^+$ − Cl], 784 [$M^+ - C_{10}H_{13}Cl$], 696 [$M^+ - C_{12}H_{11}PCl_2$].

Complex 3 [PdCl$_2$(C$_{44}$H$_{42}$N$_2$P$_2$)]: A solution of 1.17 mmol of **D** in 20 mL of THF was added dropwise to a solution of [PdCl$_2$(acetonitrile)$_2$] (1.17 mmol, 0.292 g) in 25 mL of THF whilst stirring at room temperature. The complex precipitated after a short time in almost quantitative yield. After filtration, the product was washed with cold THF and dried in vacuo. $C_{48}H_{50}Cl_2N_2OP_2Pd$ [**3(THF)**] (910.21): calcd. C 63.34, H 5.53, N 3.08; found C 63.37, H 6.06, N 3.12. ^{1}H NMR ([D$_8$]THF, 27 °C, 200 MHz): δ = 0.89, 0.99, 1.46, 1.59; 1.89, 2.17 (s, each 3 H, CH_3), 5.13, 5.97 (s, each 1 H, olefin-H), 6.08, 6.70 (s, each 1 H, mesityl-CH), 7.06−8.30 (m, 20 H, Ph), ^{31}P{^{1}H} NMR ([D$_6$]DMSO, 25 °C, 81 MHz): δ = 46.86 (d, *J* = 46 Hz), 53.63 (d, *J* = 46 Hz) ppm. MS (EI): *m*/*z* = 802 [$C_{44}H_{42}N_2P_2ClPd = M^+ - Cl$].

Ligand Exchange Reaction of [Ni(C$_2$H$_4$COO)(tmeda)] with B, C, and D

[Ni{Mes−N=C(PPh$_2$)−C(PPh$_2$)=N−Mes}(C$_2$H$_4$COO)] (4a): [Ni(tmeda)(C_2H_4COO)] (1.05 g, 4.26 mmol) and **D** (2.82 g, 4.26 mmol) in 20 mL of DMF were stirred for 20 min. During this time, the solution (initially light green) turned dark red. The volatile part of the reaction mixture was then removed at 50 °C in vacuo. The residue was washed with diethyl ether, extracted with benzene and crystallized at 5 °C by addition of diethyl ether. Yield 1.22 g (33.5%) red crystals of **4a(C$_6$H$_6$)$_{0.5}$**. ^{1}H NMR ($CDCl_3$, 200.13 MHz, 298 K): δ = 0.91 (m, 2 H, Ni−CH_2), 1.33 (s, 6 H, CH_3), 1.37 (s, 6 H, *o*-CH_3), 1.74 (s, 3 H, *p*-CH_3), 2.10 (s, 3 H, *p*-CH_3), 2.10 (m, 2 H, COO-CH_2), 5.67 (s, 2 H, CH Mes), 6.56 (s, 2 H, CH Mes), 7.20−7.64 (m, 20 H, Ph) ppm. ^{31}P{^{1}H} NMR ($CDCl_3$, 81.01 MHz, 298 K): δ = 19.8 [br. d, $^2J(^{31}P^{31}P)$ = 19.3 Hz], 44.8 [br. d, $^2J(^{31}P^{31}P)$ = 19.3 Hz] ppm.

 © 2003 Wiley-VCH Verlag GmbH & Co. KGaA, Weinheim

Preparation of [Ni($C_{40}H_{34}N_2P_2$)(C_2H_4COO)] (5b/5b′): A mixture of [Ni(tmeda)(C_2H_4COO)] (0.76 g, 3.08 mmol) and **B** (1.85 g, 3.08 mmol) in 20 mL of THF was warmed up until both compounds dissolved. A few minutes later, an orange-colored compound precipitated. Recrystallization from dichloromethane gave 1.36 g (54%) of **5b/5b′(CH_2Cl_2)** as orange crystals. This compound loses dichloromethane very easily in vacuo. $C_{43}H_{38}N_2NiO_2P_2$ (735.4): calcd. C 70.22, H 5.21, N 3.81; found C 69.83, H 5.61, N 3.74. IR (nujol): ν(C=O) = 1606 cm^{-1} (s), ν(N−H) = 3140 cm^{-1} (w). ^1H NMR ($CDCl_3$, 200.13 MHz, 298 K): δ = 0.70 (m, 2 H, CH_2-Ni), 1.84 (s, 3 H, CH_3), 1.91 (s, 3 H, CH_3), 2.11 (s, 3 H, CH_3), 2.15 (s, 3 H, CH_3), 2.20 (m, 2 H, CH_2−COO) ppm. $^{13}C\{^1H\}$ NMR ($CDCl_3$, 50.32 MHz, 298 K): δ = 20.6 (CH_3), 20.8 (CH_3); CH: δ = 128.2 [d, $J(^{13}C^{31}P)$ = 2.4 Hz], 128.2 [d, $J(^{13}C^{31}P)$ = 2.4 Hz], 129.3 [d, $J(^{13}C^{31}P)$ = 4.9 Hz], 129.4 [d, $J(^{13}C^{31}P)$ = 4.9 Hz], 129.5 (s), 129.9 [d, $J(^{13}C^{31}P)$ = 2.4 Hz], 130.4 (s), 132.5 [d, $J(^{13}C^{31}P)$ = 1.8 Hz], 132.7 (s), 132.8 [d, $J(^{13}C^{31}P)$ = 4.7 Hz], 133.1 [d, $J(^{13}C^{31}P)$ = 5.9 Hz]; C: δ = 113.4 (s), 113.6 (s), 117.7 (s), 119.6 (s), 123.7 (s), 124.4 (s), 127.5 (s), 131.4 [t, $^1J(^{13}C^{31}P)$ = 22.0 Hz, $(NPC=)_2$], 133.3 [d, $J(^{13}C^{31}P)$ = 8.2 Hz], 136.3 (s), 136.7 (s), 137.2 (s), 139.8 (s), 142.0 (s) ppm. $^{31}P\{^1H\}$ NMR ($CDCl_3$, 81.01 MHz, 298 K): δ = 28.3 [d, $^2J(^{31}P^{31}P)$ = 19.0 Hz], 39.0 [d, $^2J(^{31}P^{31}P)$ = 24.2 Hz], 46.1 [d, $^2J(^{31}P^{31}P)$ = 24.2 Hz], 48.9 [d, $^2J(^{31}P^{31}P)$ = 19.0 Hz] ppm.

In situ Preparation of 5c/5c′ and Reaction with Dimethylglyoxime and Aqueous Ammonia: A mixture of [Ni(tmeda)(C_2H_4COO)] (175 mg, 0.71 mmol) and **C** (484 mg, 0.70 mmol) in 20 mL of THF was stirred at 5 °C for 30 min. All of the starting materials dissolved and the color of the solution changed from light green to yellow. The complete ring-closure reaction of the intermediate [Ni(**C**)(C_2H_4COO)] to the orange-colored product [Ni($C_{46}H_{46}N_2P_2$)(C_2H_4COO)] was monitored by $^{31}P\{^1H\}$ NMR spectroscopy. $^{31}P\{^1H\}$ NMR (C_6D_6/THF, 81.01 MHz, 298 K): δ = 30.5 [d, $^2J(^{31}P^{31}P)$ = 18.7 Hz], 37.7 [d, $^2J(^{31}P^{31}P)$ = 24.7 Hz], 49.0 [d, $^2J(^{31}P^{31}P)$ = 24.7 Hz], 51.0 [d, $^2J(^{31}P^{31}P)$ = 18.7 Hz] ppm. Intermediate [Ni{*p*-*t*Bu−Ph−N=C(PPh_2)−C(PPh_2)=N−Ph-*p*-*t*Bu}(C_2H_4COO)]: $^{31}P\{^1H\}$ NMR (C_6D_6/THF, 81.01 MHz, 298 K): δ = 42.7 [d, $^2J(^{31}P^{31}P)$ = 23.0 Hz], 60.9 [d, $^2J(^{31}P^{31}P)$ = 23.0 Hz] ppm.

9-*tert*-Butyl-4-(*p*-*tert*-butylphenyl)-3,4-dihydro-3-(diphenylphosphanyl)-1*H*-quinoxalin-2-one: A solution of dimethylgyoxime (165 mg, 1.42 mmol in 20 mL of methanol), followed by 10 drops of concentrated aqueous ammonia, were added dropwise to a solution of [Ni($C_{46}H_{46}N_2P_2$)(C_2H_4COO)] (0.70 mmol in 5 mL THF). Red bis(dimethylglyoximato)nickel(II) precipitated from the reaction mixture and was then filtered off. The filtrate was distilled to dryness in a rotary condenser and the residue recrystallized from alcohol/chloroform. Yield 0.21 g (57%) of 9-*tert*-butyl-4-(*p*-*tert*-butylphenyl)-3,4-dihydro-3-(diphenylphosphanyl)-1*H*-quinoxalin-2-one. M.p. 288−292 °C. $C_{34}H_{37}N_2OP$ (520.6): calcd. C 78.43, H 7.16, N 5.38; found C 77.88, H 6.83, N 5.34. IR (nujol): ν(C=O) = 1663 cm^{-1}. ^1H NMR ($CDCl_3$, 200.13 MHz, 298 K): δ = 1.18 (s, 9 H, *t*Bu), 1.35 (s, 9 H, *t*Bu), 6.70 (s, 1 H), 7.14−7.70 (m, 16 H), 8.00 (br., 1 H) ppm. $^{13}C\{^1H\}$ NMR ($CDCl_3$, 50.32 MHz, 298 K): δ = 30.8 (*t*Bu), 30.9 (*t*Bu), 34.8 (C, *t*Bu), 35.2 (C, *t*Bu), 112.0 (CH), 121.2 (CH), 127.0 (C), 127.3 [d, $J(^{31}P^{13}C)$ = 42.3 Hz], 127.8 (CH), 128.3 [d, $J(^{31}P^{13}C)$ = 5.5 Hz, CH], 128.9 (CH), 129.7 (CH), 132.0 (CH), 132.2 [d, $J(^{31}P^{13}C)$ = 9.7 Hz], 132.6 (CH), 133.5 (C), 134.5 (C), 134.7 (CH), 152.3 (C), 154.0 (C) ppm. $^{31}P\{^1H\}$ NMR ($CDCl_3$, 81.01 MHz, 298 K): δ = 0.0 (br) ppm. MS (CI) (m/z): 519 $[M-1]^+$.

Acknowledgments

We are grateful to the Deutsche Forschungsgemeinschaft and the Fonds der Chemische Industrie for supporting this research.

[1] A. Togni, L. M. Venanzi, *Angew. Chem.* **1994**, *106*, 517−547; *Angew. Chem. Int. Ed. Engl.* **1994**, *33*, 497−526.
[2] G. J. P. Britovsek, V. C. Gibson, D. F. Wass, *Angew. Chem.* **1999**, *111*, 448−468; *Angew. Chem. Int. Ed.* **1999**, *38*, 428−447.
[3] C. M. Killian, L. K. Johnson, M. Brookhart, *Organometallics* **1997**, *16*, 2005 and references cited therein.
[4] S. D. Ittel, L. K. Johnson, M. Brookhart, *Chem. Rev.* **2000**, *100*, 1169 −1203.
[5] Y. Chen, R. M. B. Kiattansakul, J. K. Synder, *J. Org. Chem.* **2001**, *66*, 6932−6942.
[6] K. Tanaka, G. C. Fu, *Angew. Chem.* **2002**, *114*, 1677−1679; *Angew. Chem. Int. Ed.* **2002**, *41*, 1607−1609.
[7] C. S. Shultz, J. M. DeSimone, M. Brookhart, *Organometallics* **2001**, *20*, 16−18.
[8] S. Rigaut, O. Maury, D. Touchard, P. H. Dixneuf, *Chem. Commun.* **2001**, 373−374.
[9] R. Rigaut, F. Monnier, F. Mousset, D. Touchard, P. H. Dixneuf, *Organometallics* **2002**, *21*, 2654−2661.
[10] M. H. Garcia, M. P. Robalo, A. R. Dias, M. T. Duarte, W. Wenseelers, G. Aerts, E. Goovaerts, M. P. Cifuntes, S. Hurst, M. G. Humphrey, M. Samoc, B. Luther-Davies, *Organometallics* **2002**, *21*, 2107−2118.
[11] M. H. Garcia, M. P. Robalo, A. R. Dias, M. F. M. Piedade, A. Galvao, W. Wenseelers, E. Goovaerts, *J. Organomet. Chem.* **2001**, *619*, 252−264.
[12] R. H. Heyn, C. H. Görbitz, *Organometallics* **2002**, *21*, 2781−2784.
[13] R. Melenkivitz, D. J. Mindiola, G. L. Hillhouse, *J. Am. Chem. Soc.* **2002**, *124*, 3846−3847.
[14] D. J. Mindiola, G. L. Hillhouse, *J. Am. Chem. Soc.* **2001**, *123*, 4623−4624.
[15] S. Sjoevall, C. Andersson, O. F. Wendt, *Organometallics* **2001**, *20*, 4919−4926.
[16] W. S. Knowles, *Angew. Chem.* **2002**, *114*, 2096−2106; *Angew. Chem. Int. Ed.* **2002**, *41*, 1998−2007 and references cited therein.
[17] D. Walther, S. Liesicke, L. Böttcher, R. Fischer, H. Görls, G. Vaughan, *Inorg. Chem.* **2003**, *42*, 625−632.
[18] D. Lindauer, R. Beckert, M. Döring, P. Fehling, H. Görls, *J. Prakt. Chem.* **1995**, *337*, 143−152.
[19] R. Bauer, *Ber. Dtsch. Chem. Ges.* **1907**, *40*, 2650−2662.
[20] K. Issleib, A. Tzschach, *Chem. Ber.* **1959**, *92*, 1118−1126.
[21] R. Fischer, B. Nestler, H. Schütz, *Z. Anorg. Allg. Chem.* **1989**, *577*, 111−114.
[22] M. J. Frisch, G. W. Trucks, H. B. Schlegel, G. E. Scuseria, M. A. Robb, J. R. Cheeseman, V. G. Zakrzewski, J. A. Montgomery, Jr., R. E. Stratmann, J. C. Burant, S. Dapprich, J. M. Millam, A. D. Daniels, K. N. Kudin, M. C. Strain, O. Farkas, J. Tomasi, V. Barone, M. Cossi, R. Cammi, B. Mennucci, C. Pomelli, C. Adamo, S. Clifford, J. Ochterski, G. A. Petersson, P. Y. Ayala, Q. Cui, K. Morokuma, D. K. Malick, A. D. Rabuck, K. Raghavachari, J. B. Foresman, J. Cioslowski, J. V. Ortiz, A. G. Baboul, B. B. Stefanov, G. Liu, A. Liashenko, P. Piskorz, I. Komaromi, R. Gomperts, R. L. Martin, D. J. Fox, T. Keith, M. A. Al-Laham, C. Y. Peng, A. Nanayakkara, C. Gonzalez, M. Challacombe, P. M. W. Gill, B. Johnson, W. Chen, M. W. Wong, J. L. Andres, C. Gonzalez, M. Head-Gordon, E. S. Replogle, J. A. Pople, *Gaussian 98, Revision A.7*, Gaussian, Inc., Pittsburgh PA, **1998**.
[23] A. D. Becke, *J. Chem. Phys.* **1993**, *98*, 1372−1377; A. D. Becke, *J. Chem. Phys.* **1993**, *98*, 5648−5652.
[24] C. Lee, W. Yang, R. G. Parr, *Phys. Rev. B* **1988**, *37*, 785−789.

 © 2003 Wiley-VCH Verlag GmbH & Co. KGaA, Weinheim

[25] A. D. Becke, *Phys. Rev. A* **1988**, *38*, 3098−3100.
[26] Lanl2dz basis set.
[27] A. E. Reed, R. B. Weinstock, F. Weinhold, *J. Chem. Phys.* **1985**, *83*, 735.
[28] *COLLECT, Data Collection Software*, Nonius B. V., The Netherlands, **1998**.
[29] Z. Otwinowski, W. Minor, "Processing of X-ray Diffraction Data Collected in Oscillation Mode", in: *Methods in Enzymology*, vol. 276 (Macromolecular Crystallography), part A (Eds.: C. W. Carter, R. M. Sweet), Academic Press, San Diego, **1997**, pp. 307−326.
[30] G. M. Sheldrick, *Acta Crystallogr., Sect. A* **1990**, *46*, 467−473.
[31] G. M. Sheldrick, *SHELXL-97*, Release 97-2, University of Göttingen, Germany, **1997**.
[32] CCDC-202223 (**B**), -202224 (**C**), -202225 (**D**), -202226 (**E**), -202227 (**G**), -202228 (**1**), -202229 (**3**) and -202230 (**4a**) contain the supplementary crystallographic data for this paper. These data can be obtained free of charge via www.ccdc.cam.ac.uk/conts/retrieving.html (or from the Cambridge Crystallographic Data Centre, 12 Union Road, Cambridge CB2 1EZ, UK; Fax: (internat.) + 44-1223/336-033; E-mail: deposit@ccdc.cam.ac.uk).

Received June 6, 2003
Early View Article
Published Online October 10, 2003

 © 2003 Wiley-VCH Verlag GmbH & Co. KGaA, Weinheim

Synthesis and Reaction of Mn^{II} Iodides Bearing the β-Diketiminate Ligand: the First Divalent Manganese N-Heterocyclic Carbene Complexes [{HC(CMeNAr)$_2$}MnI{C[N(*i*Pr)CMe]$_2$}] and [{HC(CMeNAr)$_2$}MnNHAr{C[N(*i*Pr)CMe]$_2$}] (Ar = 2,6-*i*Pr$_2$C$_6$H$_3$)

Jianfang Chai,[a] Hongping Zhu,[a] Kerstin Most,[a] Herbert W. Roesky,*[a] Denis Vidovic,[a] Hans-Georg Schmidt,[a] and Mathias Noltemeyer[a]

Keywords: Manganese / Iodine / N ligands / Heterocycles / Carbene ligands

The manganese mono-iodide [HC(CMeNAr)$_2$]MnI(THF) (Ar = 2,6-*i*Pr$_2$C$_6$H$_3$) (**3**) was prepared in good yield from the reaction of [HC(CMeNAr)$_2$]K with MnI_2 in THF. Treatment of **3** under reflux in toluene and removing all the volatiles in vacuo afforded the dimeric compound [{HC(CMeNAr)$_2$}-Mn]$_2$(μ-I)$_2$ (**4**). Displacement of the coordinated THF in **3** by a strong Lewis base C[N(*i*Pr)CMe]$_2$ or by adding C[N(*i*Pr)CMe]$_2$ to the toluene solution of **4** readily gave the N-heterocyclic carbene adduct [{HC(CMeNAr)$_2$}]MnI{C-[N(*i*Pr)CMe]$_2$} (**5**). Reduction of **5** with sodium/potassium alloy at room temperature unexpectedly resulted in the formation of the monomeric compound [{HC(CMeNAr)$_2$}]MnNHAr{C[N(*i*Pr)CMe]$_2$} (**6**). Alternatively **6** was obtained by the salt elimination reaction of **5** with LiNHAr. Compounds **5** and **6** are the first examples of divalent manganese N-heterocyclic carbene adducts and the first manganese non-carbonyl carbene complexes. The single crystal X-ray structural analyses reveal that compounds **3** and **6** are monomeric and compound **4** is dimeric in the solid state. The manganese centers in these compounds exhibit a distorted tetrahedral geometry.

(© Wiley-VCH Verlag GmbH & Co. KGaA, 69451 Weinheim, Germany, 2003)

Introduction

Manganese carbene complexes are important due to their applications in organic synthesis, synthetic methodology and theoretical implications and have been studied extensively.[1−4] N-Heterocyclic carbenes have attracted great attention in ligand design and homogeneous catalysis since Arduengo et al. reported the first stable crystalline N-heterocyclic carbene in 1991.[5−8] A variety of transition metal N-heterocyclic carbene complexes have been synthesized and isolated and some of them have been successfully applied as catalysts in a number of organic reactions such as iridium-catalyzed transfer hydrogenation,[6] ruthenium-catalyzed olefin metathesis, and especially palladium-catalyzed C−C coupling reactions: the Heck, Suzuki and Kumada reactions.[7,9] However, manganese N-heterocyclic carbene complexes are rare and have not attracted much attention to date.[9a] To the best of our knowledge, only a few monovalent manganese N-heterocyclic carbene complexes are known, including [$MeC_5H_4(CO)_2MnC(NMeCH_2)_2$],[10] [$(CO)_3MnBr\{C(NMeCH_2)_2\}_2$][10] and [$(CO)_5MnC\{N(BH_3)CMeCMeNMe\}$][11] and so far no higher oxidation state manganese N-heterocyclic carbene complexes have been reported. Furthermore, no X-ray structural data of manganese N-heterocyclic carbene complexes are available.

Organometallic iodide complexes have unique chemical properties due to their labile M−I bond compared to the M−Cl congener.[12] Recent results in our group proved that aluminum diiodide bearing a β-diketiminate ligand [AlI_2\{HC(CMeNAr)$_2$\}] (Ar = 2,6-*i*Pr$_2$C$_6$H$_3$) is a good starting material for some interesting reactions such as reduction and hydrolysis. For instance, we reported the monomeric [Al\{HC(CMeNAr)$_2$\}] as a stable carbene analogue by reduction of [AlI_2\{HC(CMeNAr)$_2$\}] with potassium.[13a] Furthermore, the aluminum dihydroxide complex [$Al(OH)_2$\{HC(CMeNAr)$_2$\}], with terminal OH groups, was obtained by hydrolysis of [AlI_2\{HC(CMeNAr)$_2$\}] using a liquid NH_3/toluene two-phase system.[13b] Consequently we became interested in transition metals and investigated the behavior of Mn iodides bearing a β-diketiminate ligand. However, our efforts to reduce [{HC(CMeNAr)$_2$}Mn(μ-I)$_2$Li(OEt$_2$)$_2$] were unsuccessful with sodium or potassium due maybe to the existence of the stable lithium salt.[14] Herein we report the preparation of manganese iodides bearing β-diketiminate ligand free of lithium salt of composition [LMnI(THF)] (**3**), [(LMn)$_2$(μ-I)$_2$] (**4**) and [LMnI\{C[N(*i*Pr)CMe]$_2$\}] (**5**) [L = HC(CMeNAr)$_2$, Ar = 2,6-*i*Pr$_2$C$_6$H$_3$] and the derivative [LMnNHAr\{C-[N(*i*Pr)CMe]$_2$\}] (**6**), in which compounds **5** and **6** are the

[a] Institut für Anorganische Chemie, Universität Göttingen, Tammannstrasse 4, 37077 Göttingen, Germany
Fax: (internat.) + 49-551/393373
E-mail: hroesky@gwdg.de

 © 2003 Wiley-VCH Verlag GmbH & Co. KGaA, Weinheim DOI: 10.1002/ejic.200300289

first examples of divalent manganese N-heterocyclic carbene adducts and the first manganese non-carbonyl carbene complexes. Compound **6** is the first structurally characterized manganese N-heterocyclic carbene complex.

Results and Discussion

Synthesis of Compounds 2−6

KL (**2**) was prepared from the reaction of HL (**1**) with $KN(SiMe_3)_2$ in relatively low yield (27%).[15] Herein we report that this compound can be conveniently obtained as a crystalline solid in good yield (87%) by the reaction of HL with KH in diethyl ether at room temperature (Scheme 1). The ^1H NMR spectrum and elemental analysis are identical with those of the literature.[15] Compound **2** is stable under an inert atmosphere and can be kept for a long time without obvious decomposition.

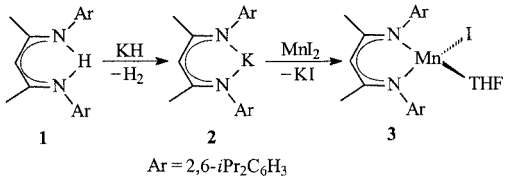

Scheme 1

The reaction of MnI_2 with one equiv. of $[LiL(Et_2O)]$ in diethyl ether afforded the heterobimetallic complex $[LMn(\mu\text{-}I)_2Li(OEt_2)_2]$.[14] Attempts to remove the coordinated lithium salt from the manganese center were unsuccessful. However, the reaction of MnI_2 with one equiv. of **2** in THF easily gave the monomeric compound [LMnI(THF)] (**3**) in high yield (87%) with a coordinated THF at the metal center. EI-MS of **3** exhibits $[LMnI]^+$ (m/z = 599, 100%) without the coordinated THF. The formula of **3** was confirmed by the crystal structure (Figure 1).

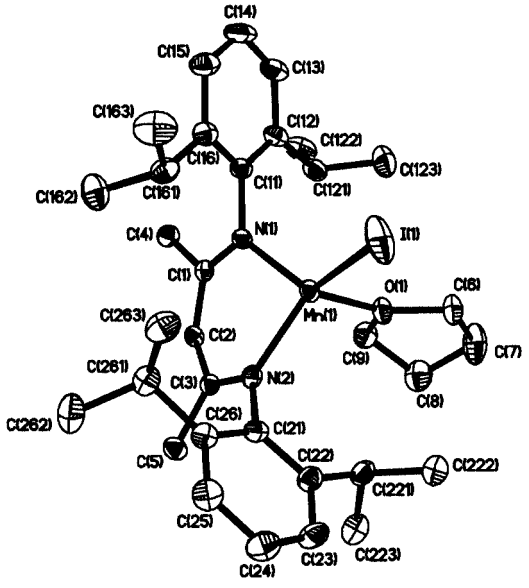

Figure 1. Molecular structure of **3** (30% probability thermal ellipsoids); hydrogen atoms are omitted for clarity

Attempts to prepare the di-β-diketiminato complex by using two equiv. of **2** were unsuccessful.

Refluxing of **3** in toluene for 0.5 h and removing all the volatiles in vacuo afforded the dimeric compound $[(LMn)_2(\mu\text{-}I)_2]$ (**4**). Crystals suitable for X-ray analysis were obtained by recrystallization from toluene. EI-MS of **4** did not give the molecular ion peak M^+ whereas half of the molecular mass $[LMnI]^+$ is observed at m/z = 599 (100%), which shows that **4** is monomeric in the gas phase, and no indication of fragments containing a Mn−Mn species, which is consistent with the X-ray structural analysis. Compound **3** can easily be obtained by dissolving **4** in THF (Scheme 2).

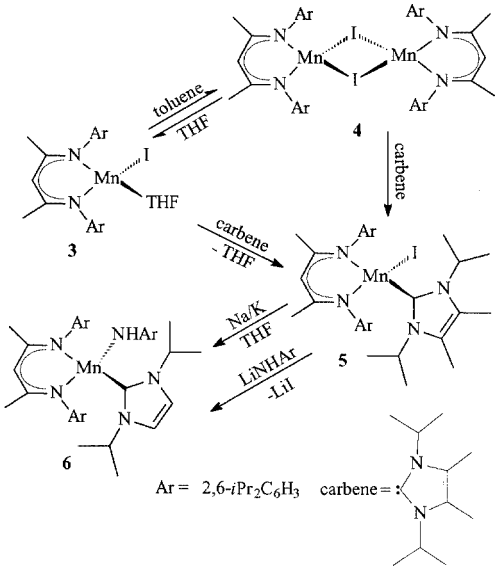

Scheme 2

Compound **3** can be considered as an adduct of a Lewis acid LMnI and a weak Lewis base THF. Displacement of the THF by a strong Lewis base $[C\{N(i\text{Pr})CMe\}_2]$ readily afforded the N-heterocyclic carbene adduct $[LMnI\{C[N(i\text{Pr})CMe]_2\}]$ (**5**), which can also be obtained by adding $[C\{N(i\text{Pr})CMe\}_2]$ to a solution of **4** in toluene. On the other hand we were not able to prepare **4** by removing the carbene in **5**, which shows that the N-heterocyclic carbene is a much stronger σ-donor ligand. Compounds **3**, **4**, and **5** are all soluble in polar solvents such as THF and CH_2Cl_2 and have poor solubility in hydrocarbon solvents.

The chemistry of organometallic dinuclear complexes containing a metal-metal bond is a burgeoning field.[16] We are interested in preparing L′MML′ (L′ = ligands, M = metal) type compounds by reduction of L′MX (X = halide). The first three-coordinate dinuclear manganese(I) compound LMnMnL [L = $HC(CMeNAr)_2$, Ar = 2,6-$i\text{Pr}_2C_6H_3$] has been successfully synthesized by reduction of **4** with sodium/potassium alloy.[17] However, further reduction of **5** by sodium/potassium alloy at room temperature, unexpectedly resulted in the formation of the monomeric compound $[LMnNHAr\{C[N(i\text{Pr})CMe]_2\}]$ (**6**) in low yield. The efforts to identify other species were unsuccessful. Given that Mn^{II} complexes are used as radical initiators

 © 2003 Wiley-VCH Verlag GmbH & Co. KGaA, Weinheim

for radical polymerisation processes,[18] it is tempting to propose that the formation of compound **6** is due to the partial decomposition of the intermediate radical [LMnC{N(*i*Pr)CMe}$_2$], which cannot aggregate due to the presence of the bulky N-heterocyclic carbene. In the mass spectrum, [LMnNHAr]$^+$ was observed at m/z = 648 (52%), followed by [LMn]$^+$ (m/z = 472, 100%). The elemental analyses are consistent with the solid-state structure. Compound **6** can also be prepared in good yield (76%) by the reaction of **5** with LiNHAr.

X-ray Diffraction Analyses for 3, 4, and 6

The single-crystal X-ray diffraction analyses for compounds **3**, **4**, and **6** have been undertaken. For **3** and **4**, there are two molecules in the unit cell, one of which is shown in Figures 1 and 2, respectively. The structure of **6** is presented in Figure 3. Crystallographic data for **3**, **4**, and **6** are given in Table 1 and selected bond lengths and angles in Table 2.

The X-ray structural analyses reveal that the [LMnI(THF)] (**3**), [LMnNHAr{C[N(*i*Pr)CMe]$_2$}] (**6**) are monomeric and [(LMn)$_2$(μ-I)$_2$] (**4**) is dimeric in the solid state (Figures 1−3). In all three compounds the manganese centers are four-coordinate and display a distorted tetrahedral geometry. The backbone of the chelating ligand is nearly planar and the manganese atom in all the reported compounds is out of the C_3N_2 plane (0.62 Å in **3**, 0.43 Å in **4**, 0.78 Å in **6**). The N(1)−Mn(1)−N(2) angle in **6** [88.94(7)°] is significantly smaller than the corresponding angles in **3** [93.56(13)°] and **4** [95.57(14)°], while the Mn(1)−N(1) and Mn(1)−N(2) bond lengths in **6** [2.166(2) and 2.133(2) Å] are obviously longer than those in **3** [2.079(3) and 2.070(3) Å] and **4** [2.067(2) and 2.067(2) Å], which indicates that the metal center in **6** is more weakly bonded to the chelating ligand possibly due to the different substituents that cause a stronger trans effect.

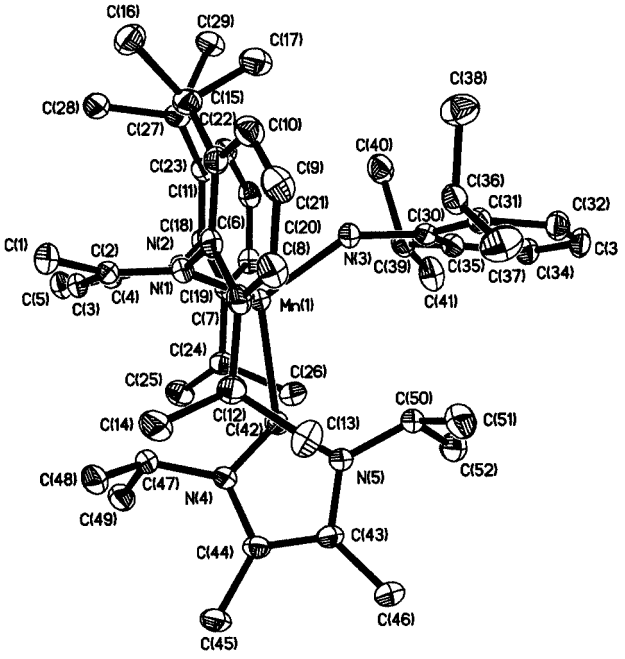

Figure 3. Molecular structure of **6** (30% probability thermal ellipsoids); hydrogen atoms are omitted for clarity

The terminal Mn(1)−I(1) distance [2.6272(8) Å] in **3** is similar to the reported values for the terminal Mn−I bond such as those in [MnI(sima)$_2$] [2.6233(6) Å] [sima = N(SiMe$_3$)C(Ph)N(SiMe$_3$)][19] and [MnI$_2$(PEt$_3$)$_2$] [av. 2.666(2) Å],[20] which is significantly shorter than the bridging Mn−I bond length in **4** [2.7688(7) and 2.7484(8) Å] and [LMn(μ-I)$_2$Li(OEt$_2$)$_2$] [2.716(9) and 2.733(9) Å].[14] The two manganese atoms are bridged by two iodine atoms in **4** and the distance between two manganese atoms is 3.615 Å, which is out of the range of a Mn−Mn bond. The Mn$_2$I$_2$

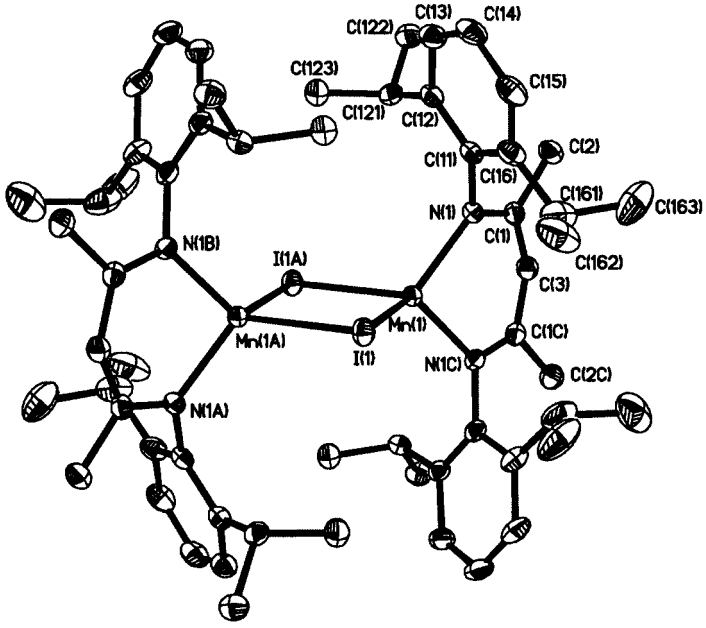

Figure 2. Molecular structure of **4** (30% probability thermal ellipsoids); hydrogen atoms are omitted for clarity

 © 2003 Wiley-VCH Verlag GmbH & Co. KGaA, Weinheim

Table 1. Crystallographic data for compounds **3**, **4**, and **6**

	3	1/2 **4** incl. toluene	**6**
Empirical formula	$C_{33}H_{49}IMnN_2O$	$C_{36}H_{49}IMnN_2$	$C_{52}H_{79}MnN_5$
Molecular weight	671.58	691.61	829.14
Temperature (K)	203(2)	203(2)	133(2)
Wavelength (Å)	0.71073	0.71073	0.71073
Crystal system	monoclinic	monoclinic	monoclinic
Space group	$P2_1/c$	$C2/m$	$P2_1/c$
Unit cell dimensions (a, b, c = Å, α, β, γ = °)	a = 16.752(2)	a = 19.188(3)	a = 11.694(2)
	b = 20.290(6)	b = 21.000(4)	b = 19.388(4)
	c = 19.620(3)	c = 16.5839(13)	c = 22.168(4)
	α = 90	α = 90	α = 90
	β = 91.317(14)	β = 100.053(8)	β = 102.59(3)
	γ = 90	γ = 90	γ = 90
Volume (Å^3)	6670(1)	6580.0(16)	4905.3(17)
Z	8	8	4
Absorption coefficient (mm^{-1})	1.348	1.366	0.307
θ range for data collection	3.52 to 25.03°	3.57 to 25.00°	1.78 to 24.72°
F(000)	2776	2856	1804
Reflections collected	14274	7832	34511
Independent reflections	11722 (R_{int} = 0.0616)	5952 (R_{int} = 0.0425)	8269 (R_{int} = 0.0717)
Data/restraints/parameters	11722/0/705	5952/0/374	8269/0/543
Goodness-of-fit on F^2	1.053	1.018	0.932
Final R indices [$I > 2\sigma(I)$]	0.0534, 0.1296	0.0349, 0.0900	0.0422, 0.0983
R (all data)	0.0714, 0.1457	0.0388, 0.0936	0.0616, 0.1044
Largest diff. peak/hole (e·Å^{-3})	0.971 /-1.279	0.977/-0.788	0.431/-0.469

Table 2. Selected bond lengths (Å) and bond angles (deg) for compounds **3**, **4**, and **6**

Compound **3**			
Mn(1)−N(1)	2.079(3)	N(2)−Mn(1)−O(1)	104.28(12)
Mn(1)−N(2)	2.070(3)	N(1)−Mn(1)−O(1)	101.90(1)
Mn(1)−O(1)	2.155(3)	N(2)−Mn(1)−I(1)	124.79(9)
Mn(1)−I(1)	2.6272(8)	N(1)−Mn(1)−I(1)	124.12(9)
N(2)−Mn(1)−N(1)	93.56(13)	I(1)−Mn(1)−O(1)	104.96(8)
Compound **4**			
Mn(1)−N(1)	2.067(2)	N(1)−Mn(1)−I(1)	119.04(7)
Mn(1)−N(1C)	2.067(2)	N(1C)−Mn(1)−I(1)	119.04(7)
Mn(1)−I(1)	2.7484(8)	N(1)−Mn(1)−I(1A)	113.02(7)
Mn(1)−I(1A)	2.7688(7)	I(1)−Mn(1)−I(1A)	98.14(2)
Mn(1A)−I(1)	2.7688(7)	Mn(1)−I(1)−Mn(1A)	81.86(2)
N(1)−Mn(1)−N(1C)	95.57(14)		
Compound **6**			
Mn(1)−N(1)	2.166(2)	N(3)−Mn(1)−N(1)	99.25(7)
Mn(1)−N(2)	2.133(2)	N(2)−Mn(1)−N(1)	88.94(7)
Mn(1)−N(3)	2.055(2)	N(3)−Mn(1)−C(42)	117.46(8)
Mn(1)−C(42)	2.270(2)	N(2)−Mn(1)−C(42)	111.68(8)
N(3)−Mn(1)−N(2)	123.25(7)	N(1)−Mn(1)−C(42)	109.83(7)

four-membered ring is exactly planar, bisecting and perpendicular to the two chelating ligands around them.

[LMnNHAr{C[N(*i*Pr)CMe]$_2$}] (**6**) is, to the best of our knowledge, the first structurally characterized manganese N-heterocyclic carbene complex. The Mn−C(carbene) distance [2.270(2) Å] is in the normal range of those in the manganates [Li(TMEDA)]$_2$[MnR$_4$] [2.22(6)−2.28(1) Å] (R = Me, Et, Bu or CH_2SiMe_3, TMEDA = tetramethylethylenediamine).[21] However, it is significantly longer than the Mn−C (carbene) distance in extensively studied manganese carbonyl carbene complexes [CpMn(CO)$_2$CXY] [X = Y = Me, 1.872(10) Å;[22] X = Y = Ph, 1.885(2) Å;[23] X = F, Y = Ph, 1.830(5) Å;[24] X = OEt, Y = Ph, 1.865(14) Å[25]]. This could result from two reasons: one is the steric repulsion between the bulky substituents; the other is the very weak Mn→C back bonding in **6** due to the relatively high energy of the formal empty p(π) orbital of the N-heterocyclic carbene carbon, which is increased by the N→C bond.[9a,26] In this respect N-heterocyclic carbenes are different from the usual carbenes, which have rather strong M→C(carbene) back bonding.[25,27] The manganese atom in **6** is out of the carbene plane (0.41 Å) and the dihedral angle between the carbene plane and the chelating ligand plane is 108.8°. The Mn(1)−N(3) bond length in **6** is 2.055(2) Å, which is close to that reported in Mn^{II} amide.[28]

Conclusion

As an extension of our previous work, manganese iodides bearing β-diketiminate ligand free of lithium salt, and their derivatives, were successfully synthesized and characterized. Compounds **5** and **6** are the first examples of divalent manganese N-heterocyclic carbene adducts and the first manganese non-carbonyl carbene complexes. The structure of **6** shows that the Mn−C (carbene) bond length in **6** is significantly longer than that of a "real" manganese carbene bond and π-backbonding is considered to be negligible in this system.

 © 2003 Wiley-VCH Verlag GmbH & Co. KGaA, Weinheim

Experimental Section

General: All reactions were performed using standard Schlenk and dry box techniques. Solvents were appropriately dried and distilled under dinitrogen prior to use. Elemental analyses were performed by the Analytisches Labor des Instituts für Anorganische Chemie der Universität Göttingen. Mass spectra were obtained on a Finnigan Mat 8230. IR spectra were recorded on a Bio-Rad Digilab FTS-7 spectrometer as Nujol mulls between KBr plates. HL (**1**) [L = $HC(CMeNAr)_2$, Ar = 2,6-*i*$Pr_2C_6H_3$][29] and $C[N(iPr)CMe]_2$[30] were prepared by literature procedures.

KL (2): A suspension of KH (0.18 g, 4.5 mmol) and **1** (1.67 g, 4 mmol) in diethyl ether (50 mL) was stirred at room temperature for 3 days. After filtration the light yellow filtrate was concentrated to ca. 10 mL and kept at −26 °C for 24 h to afford crystalline solid. Yield: 1.59 g (87%). The ^1H NMR spectrum and elemental analyses are identical with those of the literature.[15]

[LMnI(THF)] (3): A solution of **2** (0.91 g, 2 mmol) in THF (10 mL) was added to a suspension of MnI_2 (0.62 g, 2 mmol) in THF (35 mL) at −78 °C. The mixture was allowed to warm to room temperature and stirred for 14 h. The precipitate was removed by filtration. The yellow filtrate was concentrated to ca. 5 mL and kept at −26 °C for 24 h to give yellow crystals. Yield: 1.17 g (87%). M.p. 379−381 °C. $C_{33}H_{49}IMnN_2O$ (670.84): calcd. C 59.03, H 7.30, N 4.17; found C 58.95, H 7.24, N 4.16. EI-MS: *m*/*z* (%) = 599 (100) $[LMnI]^+$. IR (KBr, Nujol mull): $\tilde{\nu}$ = 1624 cm^{-1} (w), 1552 (w), 1520.62 (m), 1314 (m), 1262 (m), 1174 (w), 1100 (w), 1024 (m), 935 (w), 870 (w), 852 (w), 794 (m), 757 (w), 721 (w), 600 (vw), 524 (w), 468 (vw).

[$(LMn)_2(\mu\text{-}I)_2$] (4): A solution of **3** (1.34 g, 2 mmol) in toluene (40 mL) was refluxed for 0.5 h. All volatiles were removed in vacuo and bright yellow micro crystals were obtained. Yield: 1.15 g (96%). M.p. 271−273 °C (dec). $C_{58}H_{82}I_2Mn_2N_4$ (1197.68): calcd. C 58.11, H 6.84, N 4.67; found C 58.34, H 6.92, N 4.85. EI-MS: *m*/*z* (%) = 599 (100) $[LMnI]^+$. IR (KBr, Nujol mull): $\tilde{\nu}$ = 1657 cm^{-1} (w), 1625 (w), 1552 (w), 1262 (m), 1097 (m), 1023 (m), 875 (w), 800 (m), 722 (w), 659 (vw), 536 (w), 468 (w).

[LMnI{C[N(*i*Pr)CMe]$_2$}] (5): A solution of $C[N(iPr)CMe]_2$ (0.18 g, 1 mmol) in THF (10 mL) was added to a THF (20 mL) solution of **3** (0.67 g, 1 mmol) at room temperature. The resulting mixture was stirred for 1 h. After removal of all volatiles in vacuo, a yellow solid was obtained. Yield: 0.76 g (98%). M.p. 271 °C (dec). $C_{40}H_{61}IMnN_4$ (778.8): calcd. C 61.63, H 7.83, N 7.19; found C 61.78, H 8.02, N 7.20. EI-MS: *m*/*z* (%) = 599 (100) $[LMnI]^+$. IR (KBr, Nujol mull): $\tilde{\nu}$ = 1625 cm^{-1} (m), 1552 (s), 1505 (m), 1318 (m), 1261 (s), 1232 (w), 1218 (vw), 1190 (vw), 1171 (m), 1105 (m), 1071 (vw), 1020 (m), 936 (w), 929 (w), 793 (s), 763 (m), 758 (m), 722 (m).

[LMnNHAr{C[N(*i*Pr)CMe]$_2$}] (6). Method a: A solution of **5** (0.78 g, 1 mmol) in THF (20 mL) was added to a suspension of sodium/potassium alloy (Na, 0.01 g, 0.5 mmol; K 0.04 g, 1 mmol) in THF (10 mL). The mixture was stirred for 6 days at room temperature. All volatiles were removed in vacuo and the residue was extracted with *n*-hexane (10 mL). Yellow crystals were obtained after cooling for one week at 4 °C. The crystals were collected by filtration and the mother liquor was concentrated to ca. 4 mL and kept at 4 °C for 4 days to give yellow crystals. Total yield: 0.19 g (23%). M.p. 170−172 °C. $C_{52}H_{79}MnN_5$ (829.14): calcd. C 75.26, H 9.53, N 8.44; found C 74.84, H 9.92, N 8.85. EI-MS: *m*/*z* (%) = 472 (100) $[LMn]^+$, 648 (52) $[LMnNHAr]^+$. IR (KBr, Nujol mull): $\tilde{\nu}$ = 3173 cm^{-1} (vw), 1633 (w), 1588 (w), 1543 (w), 1512 (m), 1420 (s), 1406 (m), 1316 (m), 1261 (m), 1169 (m), 1102 (w), 1019 (w), 929 (w), 886 (vw), 841 (w), 794 (m), 758 (w), 737 (m), 722 (m), 600 (vw), 565 (vw), 543(vw).

Method b: A THF (10 mL) solution of LiNHAr (0.18 g, 1 mmol) was added to a THF (20 mL) solution of **5** (0.78 g, 1 mmol) at −78 °C. The mixture was allowed to warm to room temperature and stirred for 14 h. After removal of all volatiles in vacuo, the residue was extracted with diethyl ether (10 mL). After filtration, the yellow filtrate was concentrated to ca. 5 mL and stored at −26 °C for 3 days to give yellow crystals. Yield: 0.63 g (76%). The spectroscopic characterization of the compound is identical to that of the compound prepared by method a.

X-ray Crystallography: Crystallographic data for **3** and **4** were collected on a Stoe−Siemens−Huber four-circle diffractometer coupled to a Siemens CCD area detector and for **6** on a Stoe IPDS II-array detector system. In both cases graphite-monochromated Mo-K_α radiation (λ = 0.71073 Å) was used. All structures were solved by direct methods (SHELXS-97)[31] and refined against F^2 using SHELXL-97.[32] All non-hydrogen atoms were refined anisotropically. The hydrogen atoms were included at geometrically calculated positions and refined using a riding model. Atomic coordinates, thermal parameters, bond lengths and angles. CCDC-207299 (**3**), -207298 (**4**), and -207297 (**6**) contain the supplementary crystallographic data for this paper. These data can be obtained free of charge at www.ccdc.cam.ac.uk/conts/retrieving.html or from the Cambridge Crystallographic Data Centre, 12, Union Road, Cambridge CB2 1EZ, UK [Fax: (internat.) + 44-1223/336-033; E-mail: deposit@ccdc.cam.ac.uk].

Acknowledgments

This work was supported by the Deutsche Forschungsgemeinschaft and Ciba company. We thank Dr. Frauendorf (Institut für organische Chemie, Universität Göttingen) for MS(DCI) and helpful discussions.

[1] K. H. Dötz, H. Fischer, P. Hoffmann, F. R. Kreissl, U. Schubert, K. Weiss, *Transition Metal Carbene Complexes*, Verlag Chemie, Weinheim, **1983**.
[2] N. M. Kostić, R. F. Fenske, *J. Am. Chem. Soc.* **1982**, *104*, 3879−3884.
[3] N. Lugan, C. Kelley, M. R. Terry, G. L. Geoffroy, A. L. Rheingold, *J. Am. Chem. Soc.* **1990**, *112*, 3220−3221.
[4] T. R. Hoye, G. M. Rehberg, *Organometallics* **1990**, *9*, 3014−3015.
[5] C. D. Abernethy, G. M. Codd, M. D. Spicer, M. K. Taylor, *J. Am. Chem. Soc.* **2003**, *125*, 1128−1129.
[6] M. Albrecht, J. R. Miecznikowski, A. Samuel, J. W. Faller, R. H. Crabtree, *Organometallics* **2002**, *21*, 3596−3604.
[7] V. César, S. Bellemin-Laponnaz, L. H. Gade, *Organometallics* **2002**, *21*, 5204−5208.
[8] A. J. Arduengo, III, R. L. Harlow, M. Kline, *J. Am. Chem. Soc.* **1991**, *113*, 361−363.
[9] [9a] D. Bourissou, O. Guerret, F. P. Gabbaï, G. Bertrand, *Chem. Rev.* **2000**, *100*, 39−91. [9b] L. Jafarpour, S. P. Nolan, *Adv. Organomet. Chem.* **2000**, *46*, 181−222. [9c] W. A. Herrmann, T. Weskamp, V. P. W. Böhm, *Adv. Organomet. Chem.* **2002**, *48*, 1−69.
[10] M. F. Lappert, P. L. Pye, *J. Chem. Soc., Dalton Trans.* **1977**, 2172−2180.
[11] A. Wacker, H. Pritzkow, W. Siebert, *Eur. J. Inorg. Chem.* **1998**, 843−849.

 © 2003 Wiley-VCH Verlag GmbH & Co. KGaA, Weinheim

[12] G. B. Nikiforov, H. W. Roesky, T. Labahn, D. Vidovic, D. Nicolei, *Eur. J. Inorg. Chem.* **2003**, 433−436.
[13] [13a] C. Cui, H. W. Roesky, H.-G. Schmidt, M. Noltemeyer, H. Hao, F. Cimpoesu, *Angew. Chem.* **2000**, *112*, 4444−4446; *Angew. Chem. Int. Ed.* **2000**, *39*, 4274−4276. [13b] G. Bai, Y. Peng, H. W. Roesky, J. Li, H.-G. Schmidt, M. Noltemeyer, *Angew. Chem.* **2003**, *115*, 1164−1167; *Angew. Chem. Int. Ed.* **2003**, *42*, 1126−1132.
[14] J. Prust, K. Most, I. Müller, A. Stasch, H. W. Roesky, I. Usón, *Eur. J. Inorg. Chem.* **2001**, 1613−1616.
[15] W. Clegg, E. K. Cope, A. J. Edwards, F. S. Mair, *Inorg. Chem.* **1998**, *37*, 2317−2319.
[16] S. K. Hurst, T. Ren, *J. Organomet. Chem.* **2003**, *670*, 188−197.
[17] J. Chai, H. W. Roesky, unpublished results.
[18] D. Reardon, G. Aharonian, S. Gambarotta, G. P. A. Yap, *Organometallics* **2002**, *21*, 786−788 and references cited therein.
[19] D. Walther, P. Gebhardt, R. Fischer, U. Kreher, H. Görls, *Inorg. Chim. Acta* **1998**, *281*, 181−189.
[20] N. Hebendanz, F. H. Köhler, G. Müller, *Inorg. Chem.* **1984**, *23*, 3043−3044.
[21] C. Eaborn, P. B. Hitchcock, J. D. Smith, S. Zhang, W. Clegg, K. Izod, P. O'Shaughnessy, *Organometallics* **2000**, *19*, 1190−1193 and references cited therein.
[22] P. Friedrich, G. Besl, E. O. Fischer, G. Huttner, *J. Organomet. Chem.* **1977**, *139*, C68−C72.
[23] W. A. Herrmann, J. L. Hubbard, I. Bernal, J. D. Korp, B. L. Haymore, G. L. Hillhouse, *Inorg. Chem.* **1984**, *23*, 2978−2983.
[24] E. O. Fischer, W. Kleine, W. Schambeck, U. Schubert, *Z. Naturforsch., Teil B* **1981**, *36*, 1575−1579.
[25] U. Schubert, *Organometallics* **1982**, *1*, 1085−1088.
[26] D. S. McGuinness, B. F. Yates, K. J. Cavell, *Organometallics* **2002**, *21*, 5408−5414 and references cited therein.
[27] B. L. Balzer, M. Cazanoue, M. Sabat, M. G. Finn, *Organometallics* **1992**, *11*, 1759−1761.
[28] H. Chen, R. A. Bartlett, H. V. R. Dias, M. M. Olmstead, P. P. Power, *Inorg. Chem.* **1991**, *30*, 2487−2494 and references cited therein.
[29] J. Feldman, S. J. McLain, A. Parthasarathy, W. J. Marshall, J. C. Calabrese, S. D. Arthur, *Organometallics* **1997**, *16*, 1514−1516.
[30] N. Kuhn, T. Kratz, *Synthesis* **1993**, 561−562.
[31] G. M. Sheldrick, *Acta Crystallogr., Sect. A* **1990**, *46*, 467−473.
[32] G. M. Sheldrick, SHELXL-97, *Program for Crystal Structure Refinement*, Universität Göttingen, **1997**.

Received May 15, 2003
Early View Article
Published Online October 10, 2003

 © 2003 Wiley-VCH Verlag GmbH & Co. KGaA, Weinheim

The First Stable Monomeric Triaminostannane of Composition $[(Me_3Si)_3CSn(NHtBu)_3]$ Containing Three Substituted NH Groups

Jörg Janssen,[a] Hans-Georg Schmidt,[a] Mathias Noltemeyer,[a] and Herbert W. Roesky*[a]

Dedicated to Professor G. Ourisson for his outstanding contributions to chemistry

Keywords: N ligands / Ammonolysis / Tin

Triaminostannanes of secondary amines have been known since 1977 and are widely used in tin organic chemistry. However, the corresponding nitrogen substituted stannanes of primary amines are not cited in the literature. Herein we report on the ammonolysis reaction of $[(Me_3Si)_3CSnCl_3]$ with $tBuNH_2$ in the presence of a strong base and the X-ray structural analysis of $[(Me_3Si)_3CSn(NHtBu)_3]$, the first monomeric triaminostannane containing protons at the nitrogen atoms.
(© Wiley-VCH Verlag GmbH & Co. KGaA, 69451 Weinheim, Germany, 2003)

Introduction

Hydrolysis as well as ammonolysis of mono-organotrihalides of the heavier group 14 elements has been a topic of interest for a long time. In the case of silicon there are many compounds of composition $RSi(OH)_3$ and $RSi(NH_2)_3$ (R = organic substituent) known, which can be used as precursors for generating molecular building blocks of heterosilicates or zeolite-like materials. These systems containing silicon, nitrogen and various metal atoms are often much more stable than the oxygen-based ceramics.[1]

Although hydroxy-substituted compounds of the congener tin are widely used in organic synthesis,[2] there is only one example known of a structurally characterized mono-organotin acid, the trimeric $[TsiSn(OH)O]_3$ [Tsi = $C(SiMe_3)_3$].[3] A monomeric trihydroxystannane has not been reported so far.

The corresponding isoelectronic nitrogen compounds of tin $[RSn(NH_2)(NH)]_3$ and $RSn(NH_2)_3$ are not reported in the literature, whereas tin compounds of composition $RSn(NR'_2)_3$ have been known since 1977 and are widely used as precursors in organometallic reactions.[4] Moreover, tin compounds of primary amines such as $RSn(NHR')_3$ are also unknown.

Finally a computer-based literature search showed that there are no known tin-nitrogen compounds with four-coordinate tin atoms, containing substituted NH groups. This fact indicates the instability of those compounds against condensation reactions.

The successful recently published hydrolysis reaction of $TsiSnCl_3$, which yields the trimeric mono-organotin acid chloride $[TsiSn(Cl)O]_3$,[3] showed that the so-called trisyl ligand[5] is able to stabilise unusual tin organic compounds.

Results and Discussion

Previously we tried ammonolysis reactions under mild conditions with liquid ammonia, but we were not able to isolate any products except the starting material $TsiSnCl_3$. However, the reaction of $TsiSnCl_3$ with an excess of $tBuNH_2$ in toluene containing three equivalents of nBuLi yields the first monomeric, triaminostannane $[TsiSn(NHtBu)_3]$ (**1**), with four-coordinate tin bound to primary amine groups. Compound **1** is stable against condensation reactions (Scheme 1).

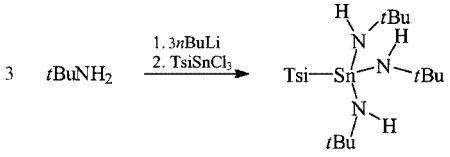

Tsi = $C(SiMe_3)_3$ **1**

Scheme 1

We were able to confirm the tetrahedral coordination site of the tin atom in compound **1** by characteristic resonances in the ^{119}Sn NMR spectrum ($\delta = -94.7$ ppm). There are similar ^{119}Sn NMR resonances reported in the literature.[6] Crystallisation of the crude product from *n*-pentane resulted in single crystals of **1**, which could be characterized

[a] Institut für Anorganische Chemie der Universität Göttingen, Tammannstraße 4, 37077 Göttingen, Germany
Fax: (internat.) +49−551/39−3373
E-mail: hroesky@gwdg.de

 © 2003 Wiley-VCH Verlag GmbH & Co. KGaA, Weinheim DOI: 10.1002/ejic.200300397

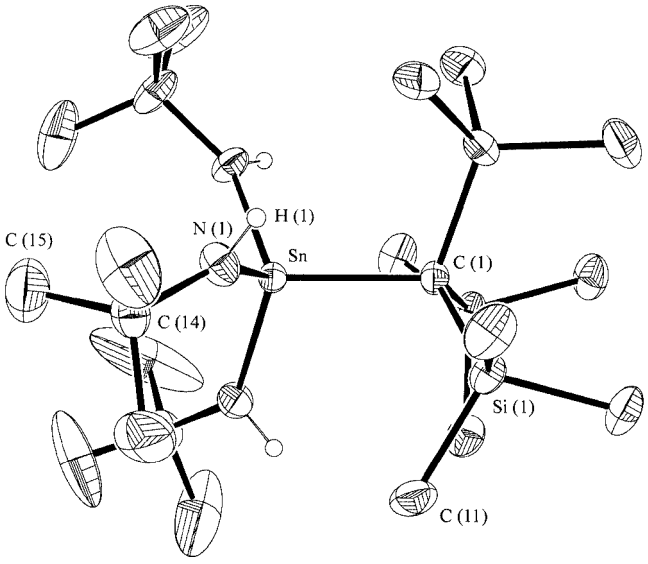

Figure 1. Molecular structure of **1** [ORTEP drawing[8] thermal ellipsoids (30% probability)]; the methyl groups are omitted for clarity; selected bond lengths [Å] and angles [°]: Sn(1)−N(1) 2.028(4), Sn(1)−C(1) 2.212(4), N(1)−C(14) 1.466(6), C(1)−Si(1) 1.895(5); N(1)−Sn(1)−C(1) 107.4(16), Sn(1)−C(1)−Si(1) 109.5(2), N(1)−Sn(1)−N(2) 110.2(17), C(1)− Si(1)−C(11) 113.4(2), Si(1)−C(1)−Si (2) 110.4(2), C(14)−N (1)−Sn (1) 135.0(3), C(15)−C (14)−N (1) 110.8(5)

for the first time by single-crystal X-ray structural analysis (Figure 1).[7]

Compound **1** exhibits a very high symmetrical arrangement and is built up by two staggered tetrahedral centers of carbon and tin. The angles between the C, N and Sn atoms range from 135.0 to 137.9° whereas the others are close to 108° (103.8−113.9°). This finding demonstrates distinctly the high symmetry of **1**. The tin-nitrogen bond lengths range from 2.017 to 2.028 Å and are similar to those in known tin-nitrogen systems of the type $[RSn(NR'R'')_3]$.[9] The Sn(1)−C(1) bond length amounts to 2.212 Å and could be compared with that in $[TsiSn(OH)O]_3$.[3] The N−C bond lengths range from 1.466 to 1.510 Å. They are similar to those in *tert*-butyl-substituted organometallic nitrogen compounds.[10]

Interactions between two molecules of **1** through hydrogen bonding were not observed. This crystallographic observation could be additionally supported by the determination of the molecular mass of **1** in liquid toluene, which is close to the calculated value for **1**. The mass spectrum shows a characteristic signal at $m/z = 567$. Furthermore the ^{1}H NMR investigation exhibits one resonance for the three nitrogen-bonded, chemically identical *tert*-butyl groups. The NH resonance was assigned as a singlet at $\delta = 0.5$ ppm, whereas in the IR spectrum the NH stretching frequency was observed at 3371 cm^{-1}.

Conclusion

The herein presented synthesis and single-crystal X-ray analysis of the monomeric, four-coordinate triaminostannane $[TsiSn(NHtBu)_3]$ (**1**) is the first example of a tetrahedral tin-nitrogen system with N-bonded protons. Now we are looking forward to a multitude of new reactions with this compound. Presently we are studying the chemistry of **1** using this compound as a precursor for preparing zeolite-like materials, but based on nitrogen and tin instead of silicon and oxygen.

Experimental Section

General Remarks: Solvents were dried and distilled under nitrogen prior to use. All reactions were carried out under dry nitrogen, using standard Schlenk techniques. NMR spectra were recorded using a Bruker Avance 200, Bruker MSL 400 or a Bruker Avance 500 spectrometer and referenced to the resonances of the residual protons in deuterated benzene. ^{1}H NMR: internal standard C_6D_6, external standard TMS. ^{13}C NMR: internal standard C_6D_6, external standard TMS. ^{29}Si NMR: internal standard C_6D_6, external standard TMS. ^{119}Sn NMR: internal standard C_6D_6, external standard $SnMe_4$. Infrared spectra were recorded on a BIO-RAD Digilab FTS 7 spectrometer as solution in *n*-pentane. The starting material $TsiSnCl_3$ was prepared as described in the literature.[3]

[Tris(trimethylsilyl)methyl]tri(*tert*-butylamino)stannane (1): At 0 °C tBuNH$_2$ (2.26 mL, 21.5 mmol) was dissolved in toluene (30 mL) and a solution of *n*BuLi in hexane (2 M, 2.60 mL, 6.45 mmol) was slowly added. The mixture was stirred for 0.5 h at this temperature to complete the lithiation reaction. A solution of $TsiSnCl_3$ (0.98 g, 2.15 mmol) in toluene (30 mL) was added to the resulting fine suspension of LiNH*t*Bu. After the addition was complete, the reaction mixture was allowed to warm to room temperature and was stirred for an additional 48 h. While warming the solution, the mixture was intensively yellow colored and a gel-like consistence resulted. After the reaction was completed a colorless liquid was obtained. Finally all volatile components were removed in vacuo and the residue was dissolved in *n*-pentane. The insoluble components were removed by filtration and the resulting colorless solution was concentrated under reduced pressure. The concentrated solution was stored for 2 days at −26 °C and **1** crystallised as a colorless solid (1.16 g, 2.04 mmol, 95%). M.p. 132−136 °C. ^{1}H NMR (C_6D_6, 300 K, 500 MHz): δ = 0.42 [s, 27 H, $(H_3C)_3Si$], 0.50 (br., 3 H, N*H*), 1.42 [s, 27 H, $(H_3C)C$]. ^{13}C NMR (C_6D_6, 300 K, 125 MHz): δ = 6.27 [s, $(H_3C)_3Si$], 11.34 [s, $\{(H_3C)_3Si\}_3C$], 35.68 [s, $(H_3C)_3C$], 53.94 [s, $(H_3C)_3C$]. ^{29}Si NMR (C_6D_6, 300 K, 99 MHz): δ = −1.66 [s, $(H_3C)_3Si$]. ^{119}Sn NMR (C_6D_6, 300 K, 186 MHz): δ = −94.7. $C_{22}H_{57}N_3Si_3Sn$ (566.65): calcd. C 46.6, H 10.1, N 7.4; found C 46.8, H 10.0, N 7.6. IR (*n*-pentane) $\tilde{\nu}$ = 468 w cm^{-1}, 615 w, 660 w, 676 w, 718 w, 800 w, 852 vs, 970 s, 1024 w, 1096 w, 1190 s, 1257 s, 1358 vs, 3371 w. MS (70 eV): *m*/*z* (%) = 567 (3) [M$^+$], 494 (10) [M$^+$ − TMS], 479 (8) [M$^+$ − TMS − Me], 422 (100) [M$^+$ − TMS − Me − *t*Bu].

Crystal Data for 1: A colorless crystal of compound **1** was mounted onto a STOE Siemens Huber Diffractometer System equipped with a four-circle goniometer and a graphite monochromator. Data collection was performed at 200 K using Mo-K_α radiation (λ = 0.71073 Å). The structure was solved by direct methods and refined using full-matrix least-squares on F^2 with SHELX-97.[11a] The hydrogen atoms were included in calculated positions and treated as riding atoms using the SHELXL-97 default parameters.[11b] Monomeric, space group $P2_1/n$, a = 9.6292(15), b = 32.260(3), c = 11.006(3) Å, α = 90, β = 113, γ = 90°, V =

 © 2003 Wiley-VCH Verlag GmbH & Co. KGaA, Weinheim

3150.0(1) Å^3. $Z = 4$, $\rho_{calcd.} = 1.194$ Mg·m^{-3}, $T = 200(2)$ K, 7770 measured, 5485 crystallographic independent reflections, $\theta_{max} = 25.03°$, numeric absorption correction ($\mu = 0.937$ mm^{-1}), $wR = 0.0481$, $wR2 = 0.1355$ (all data). The figures were drawn with ORTEP-3 for Windows.[8]

Table 1. Crystallographic data for **1**

Empirical formula	$C_{22}H_{57}N_3Si_3Sn$
Molecular mass [gmol^{-1}]	566.65
Temperature [K]	200 (2)
Wavelength λ [Å]	0.71073
Crystal system	monoclinic
Space group	$P2_1/n$
a [Å]	9.6292 (15)
b [Å]	32.260 (3)
c [Å]	11.006 (3)
α [°]	90
β [°]	113
γ [°]	90
Volume [Å^3]	3150.0 (1)
Z	4
D_c [gcm^{-3}]	1.194
μ [mm^{-1}]	0.937
F(000)	1208
θ range [°]	3.59−25.03
Unique refl. with [$I > 2\sigma(I)$]	5485
GooF	1.073
Final *R*1, *wR*2	0.0444, 0.1306
Residual density (max/min) [e·Å^{-3}]	1.073/− 0.976

Acknowledgments

This work was supported by the Deutsche Forschungsgemeinschaft and the Fonds der Chemischen Industrie.

[1] [1a] R. Murugavel, A. Voigt, M. G. Walawalkar, H. W. Roesky, *Chem. Rev.* **1996**, *96*, 2205−2236. [1b] T. Schlieper, W. Schnick, *Z. Anorg. Allg. Chem.* **1995**, *621*, 1037−1041. [1c] T. Schlieper, W. Milius, W. Schnick, *Z. Anorg. Allg. Chem.* **1995**, *621*, 1380−1384. [1d] T. Schlieper, W. Schnick, *Z. Anorg. Allg. Chem.* **1995**, *621*, 1535−1538. [1e] H. Huppertz, W. Schnick, *Angew. Chem.* **1996**, *108*, 2115−2116; *Angew. Chem. Int. Ed. Engl.* **1996**, *35*, 1983−1984. [1f] H. Huppertz, W. Schnick, *Chem. Eur. J.* **1997**, *3*, 249−252. [1g] R. Riedel, A. Greiner, G. Miehe, W. Dreßler, H. Fuess, J. Bill, F. Aldinger, *Angew. Chem.* **1997**, *109*, 657−660; *Angew. Chem. Int. Ed. Engl.* **1997**, *36*, 603−606. [1h] H.-P. Baldus, M. Jansen, *Angew. Chem.* **1997**, *109*, 338−353; *Angew. Chem. Int. Ed. Engl.* **1997**, *36*, 328−343. [1i] M. L. Montero, I. Usón, H. W. Roesky, *Angew. Chem.* **1994**, *106*, 2198−2200; *Angew. Chem. Int. Ed. Engl.* **1994**, *33*, 2103−2104. [1j] M. L. Montero, A. Voigt, M. Teichert, I. Usón, H. W. Roesky, *Angew. Chem.* **1995**, *107*, 2761−2763; *Angew. Chem. Int. Ed. Engl.* **1995**, *34*, 2504−2506. [1k] K. Wraage, A. Künzel, M. Noltemeyer, H.-G. Schmidt, H. W. Roesky, *Angew. Chem.* **1995**, *107*, 2954−2556; *Angew. Chem. Int. Ed. Engl.* **1995**, *34*, 2645−2647. [1l] C. Rennekamp, A. Gouzyr, A. Klemp, H. W. Roesky, C. Brönneke, J. Kärcher, R. Herbst-Irmer, *Angew. Chem.* **1997**, *109*, 413−415; *Angew. Chem. Int. Ed. Engl.* **1997**, *36*, 404−406.

[2] [2a] I. Shibata, T. Yoshida, T. Kawakami, A. Baba, M. Matsuda, *J. Org. Chem.* **1992**, *57*, 4049−4051. [2b] K. Nozaki, K. Oshima, K. Utimoto, *Tetrahedron* **1989**, *45*, 923−933. [2c] S. Hanessian, R. Léger, *J. Am. Chem. Soc.* **1992**, *114*, 3115−3117. [2d] E. Nakamura, K. Tanaka, S. Aoki, *J. Am. Chem. Soc.* **1992**, *114*, 9715−9716. [2e] L. Plamondon, J. D. Wuest, *J. Org. Chem.* **1991**, *56*, 2066−2075. [2f] M. Ochiai, S. Iwaki, T. Ukita, Y. Matsuura, M. Shiro, Y. Nagao, *J. Am. Chem. Soc.* **1988**, *110*, 4606−4610. [2g] J. W. Herndon, C. Wu, *Tetrahedron Lett.* **1989**, *30*, 6461−6464. [2h] B. M. Trost, S. A. King, T. Schmidt, *J. Am. Chem. Soc.* **1989**, *111*, 5902−5915. [2i] N. Nagashima, M. Ohno, *Chem. Pharm. Bull.* **1991**, *39*, 1972−1982. [2j] T. Sato, Y. Wakahara, J. Otera, H. Nozaki, *Tetrahedron* **1991**, *47*, 9773−9782.

[3] J. Janssen, J. Magull, H. W. Roesky, *Angew. Chem.* **2002**, *114*, 1435−1437; *Angew. Chem. Int. Ed.* **2002**, *41*, 1365−1367.

[4] [4a] M. E. Bishop, J. J. Zuckerman, *Inorg. Chem.* **1977**, *16*, 1749−1762. [4b] A. Roubineau, J.-C. Pommier, *C. R. Hebd. Seances Acad. Sci.* **1975**, *281*, 47−49. [4c] A. Roubineau, J.-C. Pommier, *C. R. Hebd. Seances Acad. Sci.* **1973**, *277*, 579−582. [4d] A. G. Davies, J. D. Kennedy, *J. Chem. Soc., (C)* **1970**, 759−765. [4e] J.-M. Brocas, B. de Jeso, J.-C. Pommier, *J. Organomet. Chem.* **1976**, *120*, 217−222. [4f] W. Storch, W. Jackstiess, H. Nöth, G. Winter, *Angew. Chem.* **1977**, *89*, 494−495; *Angew. Chem. Int. Ed. Engl.* **1977**, *16*, 478−479.

[5] [5a] R. L. Merker, M. J. Scott, *J. Am. Chem. Soc.* **1963**, *85*, 2243−2244. [5b] R. L. Merker, M. J. Scott, *J. Organomet. Chem.* **1965**, *4*, 98−100. [5c] C. Eaborn, P. B. Hitchcock, J. D. Smith, A. C. Sullivan, *J. Chem. Soc., Chem. Commun.* **1983**, *15*, 827−828.

[6] B. Wrackmeyer in *Annual Reports on NMR Spectroscopy*, Academic Press, London, **1999**, Vol. *38*, 203−264.

[7] CCDC-211229 contains the supplementary crystallographic data for this paper. These data can be obtained free of charge at www.ccdc.cam.ac.uk/conts/retrieving.html [or from the Cambridge Crystallographic Data Centre, 12, Union Road, Cambridge CB2 1EZ, UK; Fax: (internat.) +44−1223/336−033; E-mail: deposit@ccdc.cam.ac.uk].

[8] ORTEP3 for Windows: L. J. Farrugia, *J. Appl. Crystallogr.* **1997**, *30*, 565.

[9] C. E. Laplaza, W. M. Davis, C. C. Cummins, *Organometallics* **1995**, *14*, 577−580.

[10] [10a] P. J. Wilson, A. J. Blake, P. Mountford, M. Schroder, *J. Organomet. Chem.* **2000**, *600*, 71−83. [10b] A. Tzschach, K. Jurkschat, M. Scheer, J. Meunier-Piret, M. van Meerssche, *J. Organomet. Chem.* **1983**, *259*, 165−170.

[11] [11a] G. M. Sheldrick, SHELX-97, Program for Crystal Structure Analysis, Institut für Anorganische Chemie der Universität Göttingen, **1998**. [11b] G. M. Sheldrick, SHELXL-97, *Program for Crystal Structure Refinement*, Institut für Anorganische Chemie der Universität Göttingen, **1998**.

Received June 20, 2003
Early View Article
Published Online October 22, 2003

 © 2003 Wiley-VCH Verlag GmbH & Co. KGaA, Weinheim

High Molecular Weight Phosphazene Copolymers Having Chemical Functions Inside Chiral Pockets Formed by (*R*)-(1,1′-Binaphthyl-2,2′-dioxy)phosphazene Units

Gabino A. Carriedo,*[a] Francisco J. García Alonso,[a] and Alejandro Presa-Soto[a]

Keywords: Polymers / Polyphosphazenes / Ligand effects / Chirality

The polyphosphazene $\{[NPCl_2]_x[NP(O_2C_{20}H_{12})]_{1-x}\}_n$ ($O_2C_{20}H_{12}$ = 1,1′-binaphthyl-2,2′-dioxy) reacted in refluxing THF in the presence of Cs_2CO_3 with HOC_5H_4N or *para*-substituted phenols HOC_6H_4R to give the random copolymers $\{[NP(OC_5H_4N)_2]_x[NP(O_2C_{20}H_{12})]_{1-x}\}_n$ (**1**) or $\{[NP(OC_6H_4R)_2]_x[NP(O_2C_{20}H_{12})]_{1-x}\}_n$ [R = CN (**2**), COMe (**3**), CO_2nPr (**4**), PPh_2 (**5**)] and with H_2NnBu to give $\{[NP(NHnBu)_2]_x[NP(O_2C_{20}H_{12})]_{1-x}\}_n$ (**6**). The reaction of the polymer $\{[NPCl_2]_x[NP(O_2C_{20}H_{10}Br_2)]_{1-x}\}_n$ ($O_2C_{20}H_{10}Br_2$ = 6,6′-dibromo-1,1′-binaphthyl-2,2′-dioxy) with $HOC_6H_4PPh_2$ and Cs_2CO_3 gave $\{[NP(OC_6H_4PPh_2)_2]_x[NP(O_2C_{20}H_{10}Br_2)]_{1-x}\}_n$ (**7**). Those polymers have a very high glass-transition temperature (*Tg*) and a chemical function or ligand that is in the interior of a chiral pocket.
(© Wiley-VCH Verlag GmbH & Co. KGaA, 69451 Weinheim, Germany, 2003)

Introduction

Due to their growing interest in materials science, the chemistry of linear polyphosphazenes $(N{=}PX_2)_n$ containing halogen, pseudohalogen, alkoxy, aryloxy, amino, alkyl or aryl group have been very extensively reviewed.[1] Recently, a new type of phosphazene polymer was discovered containing cyclic repeating units with biphenyldioxy[2] $[NP(O_2C_{12}H_8)]_n$ or binaphthyldioxy[3] $[NP(O_2C_{20}H_{12})]_n$ groups. The latter could be obtained as isotactic chiral (*R*) or (*S*) polymers, or as (*R*/*S*) copolymers with different proportions of both chiral units.[3] The structural data of those polymers revealed that both in solution[4,5] and in the solid state[6] their chains are helicoidal and therefore they are a new type of interesting synthetic helical polymers.[7] These results led us to attempt the preparation of well-defined copolymeric phosphazenes of the general type $\{[NPX_2]_x[NP(O_2C_{20}H_{12})]_{1-x}\}_n$, where the X group supports a chemical functionality, useful as precursors for other derivatives or as ligands for transition metal complexes. As shown in Scheme 1, these polymers contain their chemical functions within a chiral environment that could be considered as a chiral pocket,[8] and therefore they may be potentially useful as supported catalysts (soluble or insoluble) for enantiomeric synthesis. From our previous knowledge[2,3] we anticipated that these polymers would have very high transition temperatures, i.e. they are stereochemically very rigid and the efficiency to induce chirality of the pocket could be modified by using derivatized binaphthols. Herein we describe the synthesis and full characterization of several chiral copolymers having (binaphthyldioxy)- or (dibromobinaphthyldioxy)phosphazene units and pyridine, nitrile, ketone, ester, phosphane or amine functions.

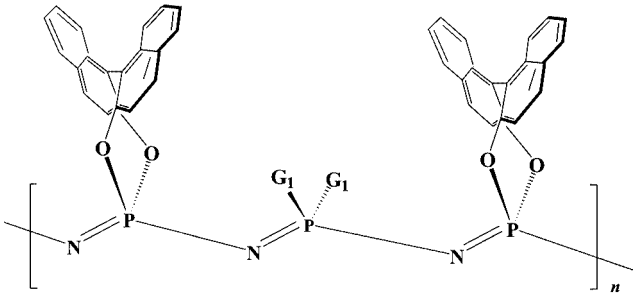

Scheme 1

Results and Discussion

According to the partial substitution method previously described by us for functionalized phosphazene copolymers with biphenyldioxy[2,3] or binaphthyldioxy[4] units, the poly(dichlorophosphazene) $[NPCl_2]_n$ was treated first with *x* equiv. of (*R*)-(+)-1,1′-binaphthyl-2,2′-diol in the presence of Cs_2CO_3 [9] to give a THF solution of the intermediate $\{[NPCl_2]_x[NP(OC_{20}H_{12})]_{1-x}\}_n$ (see Scheme 2). The addition of 4-hydroxypiridine, a 4-substituted phenol HOC_6H_4R, or *n*-butylamine H_2NnBu, led to the new functionalized phosphazene random copolymers $\{[NP(OC_5H_4N)_2]_{0.1}[NP(O_2C_{20}H_{12})]_{0.9}\}_n$ (**1**), $\{[NP(OC_6H_4R)_2]_x[NP(O_2C_{20}H_{12})]_{1-x}\}_n$ [R = CN, *x* = 0.15 (**2**); R = COMe, *x* = 0.2 (**3**); R = CO_2nPr, *x* = 0.2 (**4**);

[a] Departamento de Química Orgánica e Inorgánica, Facultad de Química, Universidad de Oviedo
Oviedo 33071 Spain
E-mail: gac@sauron.quimica.uniovi.es

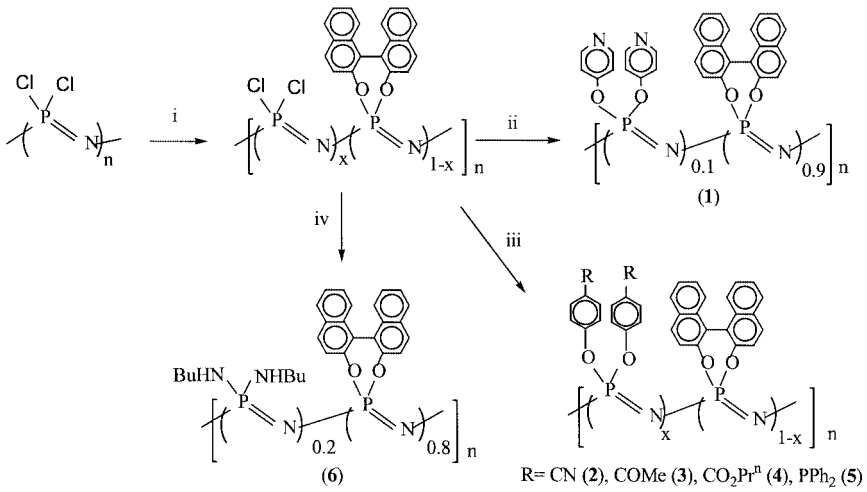

Scheme 2. i) (*R*)-(+)-$C_{20}H_{12}(OH)_2$, Cs_2CO_3; ii) HOC_5H_4N, Cs_2CO_3; iii) HOC_6H_4R, Cs_2CO_3; iv) H_2NnBu; for conditions see text

R = PPh_2, x = 0.1 (**5**)] and {$[NP(NHnBu)_2]_{0.2}[NP(O_2C_{20}H_{12})]_{0.8}\}_n$ (**6**) (see Scheme 2, Table 1).

The actual x values observed in the isolated materials (see below) were close to the 0.2:0.8 ratio initially intended. The deviations in the cases of **1**, **2** and **5** are within the limits normally encountered in the synthesis of this kind of copolymer.[4]

The average *Mw* values, as determined by GPC, were of the order of 10^6. That of the amine derivative **6** was lower, however, in agreement with previous observations,[10] and this is due to some degradation of the chains during the aminolysis step. On the other hand, polymer **7** (Scheme 3) exhibits a higher *Mw*, namely 1.7×10^6. In all cases the specific rotation of the isolated polymers revealed their optical activity (Table 2).

All the spectroscopic data of the new polymers (Exp. Sect., Tables 2 and 3) are in agreement with their formulation and confirmed their expected stereochemical rigidity. The IR spectra (in KBr pellets) show, along with the expected bands of the $[NP(O_2C_{20}H_{12})]$ units, the specific absorptions corresponding to the other $[NP(OC_5H_4N)_2]$, $[NP(OC_6H_4R)_2]$ or $[NP(NHnBu)_2]$ repeating units (see Exp. Sect.). No significant changes on either group of frequencies were observed when compared with those of the $[NP(O_2C_{20}H_{12})]_n$ homopolymer (given in the Exp. Sect.) or other copolymers containing similar pyridinoxy[11] or (diphenylphosphanyl)phenoxy groups.[12] However, a rather conspicuous difference was observed between the ν(NH) stretching frequency in **6** (3396 cm^{-1}), and that normally found in poly[(dibutylamino)phosphazenes] (3330 cm^{-1}).[13] This might be due to the effects of the environment on the NPNHBu groups provided by the two binaphthoxyphosphazene units surrounding them, but it could also indicate that, being more isolated within the chains, their participation in H-bonding interactions is precluded. In fact, the ν(NH) band in **6** is rather sharp in contrast with the broad one observed in the poly[(dibutylamino)phosphazenes] previously reported by us.[10]

The ^1H, ^{13}C and ^{31}P NMR spectra are broad, as expected for these types of polymers, but they sharpen significantly upon heating above 110 °C in [D_6]DMSO. The integration of the ^1H and ^{31}P NMR spectra at high temperature confirmed the chemical composition of the copolymer and allowed the quantitative determination of the relative amounts of the two repeating units. In those cases where x could be obtained form both the ^1H and the ^{31}P NMR spectra (i.e. polymers **3** and **4**), the results were practically identical. Moreover, in the case of the high-temperature ^{31}P NMR spectrum (Figure 1) the distribution of the chemical shifts of the phosphorus atom bearing the $[NP(O_2C_{20}H_{12})]$ units along the chain ($\delta \approx -5$ ppm) was clearly evidenced by two distinct main signals, one sharper (units mainly surrounded by the same units) and another much broader (units nearer the other repeating units).

Similarly, the high-temperature ^1H and ^{13}C NMR spectra show the main signals for the statistical distribution of the (binaphthoxy)phosphazene units and, among them, the much weaker signals corresponding to the other aryl groups present in the chain (see Exp. Sect.). Only in the

Table 1. Experimental data for the synthesis of the polymers **2**−**5**

Polymer	PDCP [g (mmol)]	THF [mL]	RBIN [g (mmol)]	Cs_2CO_3 [g (mmol)]	t_1 [h]	HOC_6H_4R [g (mmol)]	t_2 [h]	DT [d]	Yield [g (%)]
2	1.50 (12.94)	200	2.96 (10.34)	16.87 (51.78)	4	0.92 (7.72)	18	1	3.20 (77)
3	1.40 (12.08)	150	2.77 (9.70)	17.96 (55.12)	12	0.99 (7.27)	83	3	2.62 (66)
4	2.12 (18.29)	250	4.19 (14.63)	23.84 (73.17)	4	1.98 (11.00)	13	1	5.3 (80)
5	2.40 (20.71)	230	4.75 (16.59)	29.24 (89.74)	17	3.46 (12.43)	46	1	3.53 (48)

 © 2003 Wiley-VCH Verlag GmbH & Co. KGaA, Weinheim

Table 2. Analytical, molecular weight, glass transition, and specific rotation for the polymers

Polymer	Colour	C calcd. (found)	H calcd. (found)	N calcd. (found)	Cl	Mw (*Mw*/*Mn*)	*Tg* [°C] (ΔC_p [J $g^{-1}K^{-1}$])	$[\alpha]_D^{20}$ [a]
1	white	71.4 (67.0)	3.66 (3.65)	5.26 (5.36)	0.11	930 000 (2.4)	296 (0.24)	−160
2	pale creme	71.2 (71.3)	3.57 (3.42)	5.65 (5.16)	0.21	1 100 000 (1.8)	293 (0.17)	−145
3	white	70.6 (68.3)	3.83 (3.90)	4.29 (4.25)	0.17	1 100 000 (2.3)	271 (0.14)	−150
4	white	69.8 (69.2)	4.10 (3.96)	4.07 (4.14)	0.04	1 200 000 (2.5)	227 (0.18)	−116
5	white	72.7 (70.1)	3.84 (3.24)	3.92 (3.71)	0.07	940 000 (2.3)	268 (0.29)	−66
6	white	70.2 (67.8)	4.55 (4.77)	6.51 (6.94)	0.1	470 000 (4.9)	236 (0.12)	−186
7	yellow	54.6 (53.7)	2.69 (2.68)	2.74 (2.85)	[b]	1 760 000 (1.9)	256 (0.20)	9.7[c]

[a] [° $mL \cdot dm^{-1} \cdot g^{-1}$]. [b] Br calcd. 25.05; found 24.02. [c] At Hg line (578 nm).

Table 3. $^{31}P\{^1H\}$ NMR spectroscopic data of the polymers (see Figure 1)

Polymer	In $CDCl_3$ at room temp. NPOAr	$NP(O_2C_{20}H_{12})$	In $[D_6]$DMSO at 110 °C **A**[a]	**B**	**C**
1	−26	−2.6	−26.2, −25.6, −25.1	−5.0, −4.7,	−4.0, −3.7
2	−25	−2.5	−26.6, −26.0, −25.4	−5.4	−4.0
3	−25.1	−2.7, −4.0	−25.1	−5.0	−3.9
4	−25.0	−3.0	−25.6, −25.1, −24.5	−5.1	−4
5	−25.0	−3.0[b]	−25.7[c], −25.0, −24.3	−6.0	−4.0
7[d]	−22.3	−4.0[e]	−23[f]	−5.7	−4.4

[a] The signals A correspond to $NP(OAr)_2$ groups, where Ar = C_5H_4N or C_6H_5-R. The signals B are due to $NP(O_2C_{20}H_{12})$ units surrounded by $NP(OAr)_2$ groups. The peaks C correspond to $NP(O_2C_{20}H_{12})$ units which are located between other $NP(O_2C_{20}H_{12})$ units. [b] At δ = −6.2 $[OC_6H_4P(C_6H_5)_2]$, 28.3 $[OC_6H_4P\{O\}(C_6H_5)_2]$ ppm. [c] At δ = −4.4 $[OC_6H_4P(C_6H_5)_2]$, 25.1 $[OC_6H_4P\{O\}(C_6H_5)_2]$ ppm. [d] Polymer **6** exhibits a very broad signal with two maxima at δ = −2.7 and −1.6 ppm in its $CDCl_3$ spectrum, measured at room temp.; in $[D_6]$DMSO at 120 °C its spectrum shows a very broad peak centered at δ = −3.4 ppm. [e] At δ = −6.3 $[OC_6H_4P(C_6H_5)_2]$, 28.0 $[OC_6H_4P\{O\}(C_6H_5)_2]$ ppm. [f] At δ = −4.4 $[OC_6H_4P(C_6H_5)_2]$, 25 $[OC_6H_4P\{O\}(C_6H_5)_2]$ ppm.

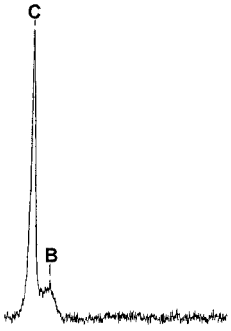

Figure 1. $^{31}P\{^1H\}$ NMR spectrum of $\{[NP(O_2C_{20}H_{12})]_{0.85}[NP(OC_6H_4CN)_2]_{0.15}\}_n$ (**2**) in $[D_6]$DMSO at 110 °C; δ_A = −26.6, −26.0, −25.4 ppm; δ_B = −5.4 ppm; δ_C = −4.0 ppm (see Table 3)

case of **6** are significant differences found between the signals corresponding to the butyl protons of NHBu (δ = 2.2, 0.6 and 0.4 ppm) and those observed in other poly-[(dibutylamino)phosphazene] polymers (δ = 3.0, 1.5 and 1.05 ppm).[10] However, the shift of the amine proton PNHR in **6** (δ = 2.6 ppm), which was unambiguously identified by its disappearance in the presence of D_2O, is very similar to that of the other aminophosphazenes (e.g., δ = 2.67 ppm in ref.[10]).

The *n*-butyl group was also easily detected in the ^{13}C NMR spectrum by the signals at δ = 15, 21, 35 and 42 ppm, of decreasing intensity, that are very close to those published for other polymers containing (butylamino)phosphazene units.[14]

The ^1H and ^{13}C NMR spectra also showed that all the isolated materials were perfectly free of any solvents, a fact that was confirmed by the TGA analysis (see below). This is important since poly(binaphthoxyphosphazene) polymers tend to retain solvent molecules even after having been dried in vacuo at 70 °C.[3,4] The only impurity present was a very small amount of the cyclic trimer $[N_3P_3(O_2C_{20}H_{12})_3]$ that in no case was higher than one molecule of the trimer for every 100 polymeric units [to be exact 1 (**1**), 0.5 (**2**), 0 (**3**), 1 (**4**), 1 (**5**), 0 (**6**), and 0.1 (**7**) molecules of the trimer].

In the case of the phosphane derivative **5**, the ^{31}P NMR spectrum (Table 3) revealed that 20% of the PPh_2 groups had been oxidized to $P(O)Ph_2$. Therefore, the exact chemical formula of **5** would be $\{[NP(OC_6H_4PPh_2)_{1.6}$-

 © 2003 Wiley-VCH Verlag GmbH & Co. KGaA, Weinheim

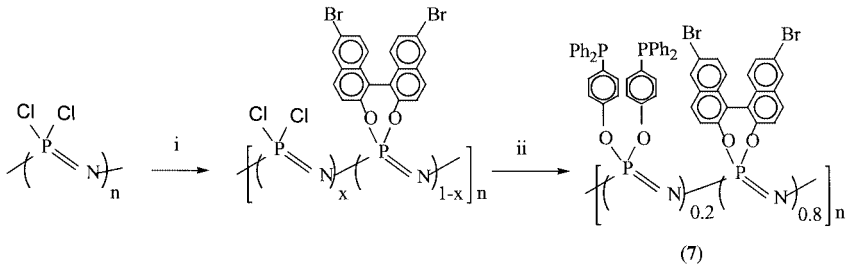

Scheme 3

$(OC_6H_4POPh_2)_{0.4}]_{0.1}[NP(O_2C_{20}H_{12})]_{0.9}\}_n$. The formation of oxidized phosphane sites also noted in other similar phosphazene polymers with PPh_2 ligands could not be prevented even under careful workup.[15]

All the polymers exhibit an increase in C_p corresponding to the glass transition at rather high temperatures ranging from 227 to 296 °C (Table 2) in their DSC thermograms. In fact, the *Tg* of **1** (296 °C) is the highest glass transition recorded for a phosphazene high molecular weight polymer [up to now the highest reported *Tg* is 220 °C for a poly(aminophosphazene)].[16] This, together with the broad NMR spectra at room temperature and the observed sharpness upon heating evidenced the high stereochemical rigidity of the polymeric chains, which, in principle, is helpful in their potential use as ligands to support catalysts for asymmetric reactions.

In order to synthesize similar polymers with a chiral pocket with different electronic and steric characteristics, we extended the reactions of Scheme 2 to the preparation of the polymer **7** (see Scheme 3), which is a brominated derivative of **5**. The data of the isolated product are in agreement with the formula given in the Scheme 3. In spite of the presence of the Br atoms in the binaphthyl units, the *Tg* of **7** (256 °C) is not higher than that of **5**. However, this is due to the lower content of binaphthyl groups — 0.8 in **7** and 0.9 in **5**. The oxidized phosphanes make up 12.5% of the PPh_2 groups, and therefore the exact formula is $\{[NP(OC_6H_4PPh_2)_{1.75}(OC_6H_4POPh_2)_{0.25}]_{0.2}[NP(O_2C_{20}H_{10}Br_2)]_{0.8}\}_n$.

The TGA thermograms show that the copolymers **1**−**3**, **5** and **7** have a high thermal stability, losing weight around 500 °C, near to the decomposition temperature of the poly(binaphthoxy) homopolymer $[NP(O_2C_{20}H_{12})]_n$ (540 °C).[3] The polymer **4** has two further losses at 380 and 440 °C. On the other hand, polymer **6** shows a stepped and continuous loss of weight starting at ca. 150 °C (see Exp. Sect.), which is typical of the poly(phosphazene)s containing amino side groups.[17] The final residues at 800 °C, of the order of 50−65%, are comparable or higher than the 50% residue observed for $[NP(O_2C_{20}H_{12})]_n$ under the same experimental conditions.[3]

Experimental Section

General: All the reactions were carried out under nitrogen. Cs_2CO_3 (Aldrich) was dried at 140 °C prior to use. THF (VWR International) was treated with KOH and distilled twice from Na in the presence of benzophenone. Hexane (VWR intern), (*R*)-(+)-1,1′-bis(2-naphthol) [(*R*)-(+)-$C_{20}H_{10}(OH)_2$], HOC_5H_4N, and the phenols HOC_6H_4R (R = CN, COMe and CO_2nPr) were used as purchased (Aldrich); the amine H_2NnBu (Aldrich) was distilled from CaH_2. The starting polymer $[NPCl_2]_n$ was prepared as described by Magill et al.[18] The phosphane $HOC_6H_4PPh_2$ [12] and (*R*)-(+)-6,6′-dibromo-1,1′-binaphthalene-2,2′-diol [(*R*)-(+)-$C_{20}H_{10}Br_2(OH)_2$][19] were prepared as described previously. The IR spectra were recorded with a Perkin−Elmer FT Paragon 1000 spectrometer. NMR spectra were recorded with Bruker AC-200, AV-300 and DPX 300 instruments, using $CDCl_3$ as solvent unless otherwise stated. Chemical shifts (^1H and $^{13}C\{^1H\}$) are given in δ relative to TMS. $^{31}P\{^1H\}$ NMR values are given in δ relative to external 85% aqueous H_3PO_4. C, H, N analyses were performed with a Perkin−Elmer 2400 microanalyzer. Chlorine analyses were performed by Galbraith Laboratories. GPC were measured with a Perkin−Elmer equipment with a Model LC 250 pump, a Model LC 290 UV, and a Model LC 30 refractive index detector. The samples were eluted with a 0.1% by weight solution of tetra-*n*-butylammonium bromide in THF through Perkin−Elmer PLGel (Guard, 10^5, 10^4 and 10^3 Å) at 30 °C. Approximate molecular weight calibrations were obtained using narrow molecular weight distribution polystyrene standards. *Tg* values were measured with a Mettler 3000 differential scanning calorimeter DSC. Thermal gravimetric analyses were performed with a Mettler TA 4000 instrument. The polymer samples were heated at a rate of 10 °C/min from ambient temperature to 800 °C under a constant flow of nitrogen. The specific rotation [α] was measured with a Perkin−Elmer 343 or 241 in $CHCl_3$ at c = 1 at 20 °C using the Na-D or the 578-nm Hg lines, respectively. The colour, analytical, *Mw* (GPC), glass transition and specific rotation data for the polymers are given in Table 2. The IR spectra (KBr pellet) of all the copolymers **1**−**6** showed the expected bands of the $[NP(O_2C_{20}H_{12})]$ units. These were identical to those found in the homopolymer $[NP(O_2C_{20}H_{12})]_n$: $\tilde{\nu}$ = 3054 cm^{-1} [w, ν_{CH} aromatic), 1622 w, 1590 m,1507 w, 1465 sh, 1433 sh,1403 w, 1362 m (aryl rings), 1318 (s, ν_{C-OP}), 1267 sh, 1220 vs (ν_{NP}), 1190 sh, 1155 w, 1072 (m, ν_{P-OC}), 964, 946 sh, (s, δ_{POC}), 896 w, 868 m, 812 (s, δ_{PNP}), 772 w, 746 m, 714 m, 695 w, 655 w, 571 (s, δ_{NPO}), 531 w, 487 w. The specific absorptions corresponding to the other repeating units present in the copolymers are given below. The ^{31}P NMR spectroscopic data are given in Table 3. The ^1H and ^{13}C NMR and TGA data for each compound are given below.

Preparation of $\{[NP(OC_5H_4N)_2]_{0.1}[NP(O_2C_{20}H_{12})]_{0.9}\}_n$ (1): (*R*)-(+)-$(HO)_2(C_{20}H_{12})$ (8.16 g, 28.50 mmol) and Cs_2CO_3 (46.4 g, 142.5 mmol) were added to a solution of $[NPCl_2]_n$ (4.13 g, 35.65 mmol) in THF (440 mL) and the mixture was refluxed with vigorous mechanical stirring for 35 h. Then, the pyridone HOC_5H_4N (2.03 g, 21.34 mmol) was added and the refluxing was maintained for another 48 h. The resulting mixture was poured into water (1.5 L) to give a solid residue that was extracted at room

 © 2003 Wiley-VCH Verlag GmbH & Co. KGaA, Weinheim

temperature in THF (500 mL) for 4 h. The mixture was filtered and concentrated into a viscous liquid that was poured slowly into water (1.5 L). The product was reprecipitated in the same way from THF/IPA (isopropyl alcohol), and THF/hexane. Finally, the product was dried under vacuum at 70 °C for 7 d to give the polymer **1** as a white solid. Yield [5.41 g (47%)]. IR (KBr): $\tilde{\nu}$ = 1580 w cm^{-1} (ν_{CC}-ν_{CN}, OC_5H_4N) (seen as a shoulder of the band at 1591 cm^{-1} of the binaphthoxy group). ^{1}H NMR ($CDCl_3$, 25 °C): δ = 5.5−8.0 (very br. m, aromatic rings) ppm. ^{1}H NMR ([D$_6$]DMSO, 110 °C): δ = 6.7, 6.8, 7.1, 7.6 (br. m, $O_2C_{20}H_{12}$), 6.9, 7.9 (br. m, OC_5H_4N-4) ppm. ^{13}C{^{1}H} NMR ($CDCl_3$, 25 °C): δ = 118 (C-3 of OC_5H_4N), 153 (C-2 of OC_5H_4N), 159 (NPO*C*, OC_5H_4N), 124, 128−131, 133−135 (br. peaks, naphthalene rings), 150 (NPO$C_{\text{naphthalene ring}}$) ppm. TGA: −48% (500 °C); residue at 800 °C (52%).

Preparation of {[NP(OC$_6$H$_4$R)$_2$]$_x$[NP(O$_2$C$_{20}$H$_{12}$)]$_{1-x}$}$_n$ [R = CN, *x* = 0.15 (2); R = COMe, *x* = 0.20 (3); R = CO$_2$*n*Pr, *x* = 0.20 (4); R = PPh$_2$, *x* = 0.10 (5)]: The following procedure for **2** is representative for all the polymers using the data given in Table 1. (*R*)-(+)-$(HO)_2(C_{20}H_{12})$ (2.96 g, 10.34 mmol) and Cs_2CO_3 (16.87 g, 51.78 mmol) were added to a solution of $[NPCl_2]_n$ (PDCP) (1.5 g, 12.94 mmol) in THF (200 mL), and the mixture was refluxed for 4 h (t_1) with vigorous mechanical stirring. After that, the phenol HOC_6H_4CN (0.92 g, 7.72 mmol) was added and the refluxing was continued for another 18 h (t_2). The resulting mixture was poured into water (1.5 L) and the precipitate was washed with water (3 × 0.5 L), IPA (2 × 0.2 L) and diethyl ether (2 × 0.2 L). This crude product was purified from THF/H_2O, THF/IPA, and THF/hexane as explained for **1**. Finally, the product was dried under vacuum at 70 °C for 1 d (DT) to give the polymer as a pale creamy solid. Yield [3.2 g 77 (%)].

{[NP(OC$_6$H$_4$CN)$_2$]$_{0.15}$[NP(O$_2$C$_{20}$H$_{12}$)]$_{0.85}$}$_n$ (2): IR (KBr): $\tilde{\nu}$ = 2227 w cm^{-1} (ν_{CN}). ^{1}H NMR ($CDCl_3$, 25 °C): δ = 6.0−8.0 (very br. m, aromatic rings) ppm. ^{1}H NMR ([D$_6$]DMSO, 110 °C): δ = 6.6, 6.8, 7.1, 7.6 (br. m, $O_2C_{20}H_{12}$), 7.2, 7.8 (br. m, OC_6H_4CN) ppm. ^{13}C{^{1}H} NMR ($CDCl_3$, 25 °C): δ = 107, 119 (OC_6H_4CN), 154 (NPO*C*, OC_6H_4CN), 122, 125−130, 132−133 (br. peaks, aromatic C), 148 (NPO$C_{\text{naphthalene ring}}$) ppm. TGA: −45.5% (530 °C); residue at 800 °C 54.5%.

{[NP(OC$_6$H$_4$COMe)$_2$]$_{0.2}$[NP(O$_2$C$_{20}$H$_{12}$)]$_{0.8}$}$_n$ (3): IR (KBr): $\tilde{\nu}$ = 1683 m cm^{-1} (ν_{CO}), 1266 s, 1164 m. ^{1}H NMR ($CDCl_3$, 25 °C): δ = 1.9 (3 H, CO*CH*$_3$), 6.0−9.0 (very br. m, aromatic rings) ppm. ^{1}H NMR ([D$_6$]DMSO, 110 °C): δ = 2.1 (3 H, CO*CH*$_3$), 6.7, 6.8, 7.2, 7.6 (br. m, $O_2C_{20}H_{12}$) 7.4, 7.8 (br. m, $OC_6H_4COCH_3$) ppm. ^{13}C{^{1}H} NMR ($CDCl_3$): δ = 29 (CO*C*H$_3$), 157 (NOP*C*, OC_6H_4-$COCH_3$), 199 (*C*OMe), 125, 128−132, 133, 134, (br. peaks, aromatic rings), 150 (NPO$C_{\text{naphthalene ring}}$) ppm. TGA: −34.5% (485 °C); residue at 800 °C: 65.5%.

{[NP(OC$_6$H$_4$CO$_2$*n*Pr)$_2$]$_{0.2}$[NP(O$_2$C$_{20}$H$_{12}$)]$_{0.8}$}$_n$ (4): IR (KBr): $\tilde{\nu}$ = 2964 w cm^{-1}, 2877 w (ν_{CH} alkylic), 1717 (s, ν_{CO}), 1109 s. ^{1}H NMR ($CDCl_3$, 25 °C): δ = 0.8 (3 H, $OCH_2CH_2CH_3$), 1.5 (2 H, $OCH_2CH_2CH_3$), 4.0 (2 H, $OCH_2CH_2CH_3$), 6.0−8.0 (very br. m, aromatic rings) ppm. ^{1}H NMR ([D$_6$]DMSO, 110 °C): δ = 0.8 (3 H, $OCH_2CH_2CH_3$), 1.5 (2 H, $OCH_2CH_2CH_3$), 4.0 (2 H, $OCH_2CH_2CH_3$), 6.7, 6.8, 7.1, 7.5 (br. m, $O_2C_{20}H_{12}$), 7.3, 7.8 (br. m, OC_6H_4COO) ppm. ^{13}C{^{1}H} NMR ($CDCl_3$): δ = 11 ($OCH_2CH_2CH_3$), 23 ($OCH_2CH_2CH_3$), 67 ($OCH_2CH_2CH_3$), 121 [$OC_6H_4C(O)OPr$], 155 (NPO*C*, $OC_6H_4C(O)OPr$], 166 (*C*OOPr), 122, 125−130, 132, 133 (br. peaks, aromatic rings), 148 (NPO$C_{\text{naphthalene ring}}$) ppm. TGA: −13.5% (380 °C), −11.5% (440 °C), −32% (516 °C); residue at 800 °C: 43%.

{[NP(OC$_6$H$_4$PPh$_2$)$_2$]$_{0.1}$[NP(O$_2$C$_{20}$H$_{12}$)]$_{0.9}$}$_n$ (5): IR (KBr): $\tilde{\nu}$ = 1490 cm^{-1} sh, 1434 m, 694 m. ^{1}H NMR ($CDCl_3$, 25 °C): δ = 5.5−8.5 (very br. m, aromatic rings). ^{1}H NMR ([D$_6$]DMSO, 110 °C): δ = 6.4 (br. m, OC_6H_4P), 7.0 [br. m $P(C_6H_5)_2$], 6.6, 6.7, 7.0, 7.6 (br. m, $O_2C_{20}H_{12}$) ppm. ^{13}C{^{1}H} NMR ($CDCl_3$): δ = 128, 138 [$P(C_6H_5)_2$], 122, 127, 128, 131, 132, 134, (br. peaks, naphthalene and phosphane rings), 148 (NPO$C_{\text{naphthalene ring}}$) ppm. TGA: −42% (509 °C); residue at 800 °C: 58%.

Preparation of {[NP(NH*n*Bu)$_2$]$_{0.2}$[NP(O$_2$C$_{20}$H$_{12}$)]$_{0.8}$}$_n$ (6): (*R*)-(+)-$(HO)_2(C_{20}H_{12})$ (2.73 g, 9.54 mmol) and Cs_2CO_3 (29.24 g, 24.86 mmol) were added to a solution of $[NPCl_2]_n$ (1.38 g, 11.91 mmol) in THF (150 mL), and the mixture was refluxed with vigorous mechanical stirring for 21 h. After that, *n*-butylamine (H_2NnBu) (3.28 mL, 2.43 g, 33.22 mmol) was added at 0 °C and stirring was continued at room temp. for 54 h. The mixture was then poured into water (1.5 L) giving a white solid which was purified by re-precipitating it from THF/H_2O, THF/IPA, and THF/hexane. The resulting white polymer was dried under vacuum at 70 °C for 1 d and later at 90 °C for 2 d. Yield 3 g, 84%. IR (KBr): $\tilde{\nu}$ = 3396 w cm^{-1} (ν_{NH} amine), 2952 m, 2927 m, 2868w (ν_{CH} alkyl), 1508 m, 1094 w. ^{1}H NMR ([D$_8$]THF, 25 °C): δ = 0.36, 0.58 (br., $NHCH_2CH_2CH_2CH_3$), 2.2 (very br., $NHCH_2CH_2CH_2CH_3$), 2.6 (br., N*H*Bu), 7.3, 7.8 (very br. m, aromatic rings) ppm. ^{1}H NMR ([D$_6$]DMSO, 120 °C): δ = 0.4 (br., $NHCH_2CH_2CH_2CH_3$), 0.7 (br., $NHCH_2CH_2CH_2CH_3$), 2.3 (very br., $NHCH_2CH_2CH_2CH_3$), 2.9 (br., N*H*Bu), 7.2, 7.3, 7.6, 7.7 (br. m, aromatic rings) ppm. ^{13}C{^{1}H} NMR ([D$_8$]THF, 25 °C): δ = 15 (br., $NHCH_2CH_2CH_2CH_3$), 21 (br., $NHCH_2CH_2CH_2CH_3$), 35 (br., $NHCH_2CH_2CH_2CH_3$), 42 (br., $NHCH_2CH_2CH_2CH_3$), 123, 126, 127, 128, 130, 132, 133, 134 (br. peaks, naphthalene rings) 150 (NPO$C_{\text{naphthalene ring}}$) ppm. TGA: −4% (210 °C), −12% (370 °C), 28% (507 °C); residue at 800 °C: 56%.

Preparation of {[NP(OC$_6$H$_4$PPh$_2$)$_2$]$_{0.2}$[NP(O$_2$C$_{20}$H$_{10}$Br$_2$)]$_{0.8}$}$_n$ (7): (*R*)-(+)-$(HO)_2(C_{20}H_{10}Br_2)$ (6.4 g, 14.41 mmol) and Cs_2CO_3 (23.5 g, 72.13 mmol) were added to a solution of $[NPCl_2]_n$ (2.09 g, 18.03 mmol) in THF (300 mL), and the mixture was refluxed with vigorous mechanical stirring for 14 h. After that, the phenol ($HOC_6H_4PPh_2$) (3 g, 10.78 mmol) was added and refluxing was continued for 30 h. The mixture was then poured into water (1.5 L) giving a yellow solid which was washed with water (2 × 1 L) and then purified by re-precipitating it from THF/H_2O, THF/IPA, and THF/hexane. The resulting yellow polymer was dried under vacuum at 70 °C for 1 d. Yield 6.86 g, 74%. IR (KBr): $\tilde{\nu}$ = 3052 (w, ν_{CH} aromatic) cm^{-1}, 1585 m, 1493 m, 1434 w, 1396 w, 1354 w (aryl rings), 1317 (m, ν_{C-OP}), 1255 sh, 1217 (vs, ν_{NP}) 1186 sh, 1170 sh, 1066 (m, ν_{P-OC}), 960 (s, δ_{POC}), 942 s, 874 m, 826 m, 807 (m, δ_{PNP}), 778 w, 742 w, 728 w, 692 w, 655 w, 601 w, 570 (m, δ_{NPO}), 533 w, 493 w, 472 w. ^{1}H NMR ($CDCl_3$, 25 °C): δ = 5.5−9.5 (very br. m, aromatic rings). ^{1}H NMR ([D$_6$]DMSO, 110 °C): δ = 6.4 (br. m, OC_6H_4P), 7.0 (br. m, $P(C_6H_5)_2$], 6.4, 6.8, 7.4, 7.7 (br. m, $O_2C_{20}H_{10}Br_2$) ppm. ^{13}C{^{1}H} NMR ($CDCl_3$, 25 °C): δ = 120 (br., Br*C*), 121−122, 129−134 (br. peaks, naphthalene and phosphane rings), 148 (NPO$C_{\text{naphthalene ring}}$), 129, 138 [$P(C_6H_5)_2$], 152 [NPO*C*, $P(C_6H_5)_2$] ppm. TGA: −48% (477 °C); residue at 800 °C: 52%.

Acknowledgments

The authors thank the Spanish DGICYT (Project BQU-2001-3676) and to the FICYT (Project PB-EXPO1-15) for financial support.

[1] [1a] C. W. Allen, *Coord. Chem. Rev.* **1994**, *130*, 137−172. [1b] I. Manners, *Angew. Chem. Int. Ed. Engl.* **1996**, *35*, 1602−1621. [1c] R. De Jaeger, M. Gleria, *Prog. Polym. Sci.* **1998**, *23*, 179−276. [1d] R. De Jaeger, M. Gleria (Eds.), *Phosphazenes: A Worldwide Insight*, NOVA Publishers, New York, in press.

 © 2003 Wiley-VCH Verlag GmbH & Co. KGaA, Weinheim

[2] G. A. Carriedo, L. Fernández-Catuxo, F. J. García Alonso, P. Gómez Elipe, P. A. González, *Macromolecules* **1996**, *29*, 5320−5325.
[3] G. A. Carriedo, F. J. García Alonso, P. A. González, J. L. García Álvarez, *Macromolecules* **1998**, *31*, 3189−3196.
[4] G. A. Carriedo, F. J. García Alonso, P. Gómez Elipe, J. L. García Álvarez, M. P. Tarazona, M. Teresa Rodriguez, E. Sáiz, J. T. Vázquez, J. L. Padrón, *Macromolecules* **2000**, *33*, 3671−3679.
[5] G. A. Carriedo, F. J. García Alonso, J. L. García Álvarez, A. Presa Soto, in preparation.
[6] G. C. Pappalardo, G. A. Carriedo, in preparation.
[7] [7a] I. M. Khan (Ed.), *Synthetic Macromolecules with Higher Structural Order*, ACS Symposium Series 812, Oxford University Press, Oxford, **2002**. [7b] T. Nakano, Y. Okamoto, *Chem. Rev.* **2001**, *101*, 4013−4038. [7c] Y. Okamoto, T. Nakano, *Chem. Rev.* **1994**, *94*, 349−372.
[8] [8a] S-L. You, X-L. Hou, L.-X. Dai, X-Z. Zhu, *Org. Lett.* **2001**, *3*, 149−151. [8b] P. Lustenberger, F. Diederich, *Helv. Chim. Acta* **2000**, *83*, 2865−2883. [8c] S. D. Dreher, T. J. Katz, K-C. Lam, A. L. Rheingold, *J. Org. Chem.* **2000**, *65*, 815−822.
[9] G. A. Carriedo, F. J. García Alonso, P. A. González, *Macromol. Rapid Commun.* **1997**, *18*, 371−377.
[10] G. A. Carriedo, J. I. Fidalgo Martínez, F. J. García Alonso, E. Rodicio, A. Presa Soto, *Eur. J. Inorg. Chem.* **2002**, 1502−1510.
[11] G. A. Carriedo, F. J. García Alonso, J. L. García Álvarez, C. Díaz Valenzuela, N. Yutronic Sáez, *Polyhedron* **2002**, *21*, 2587−2592.
[12] G. A. Carriedo, F. J. García Alonso, P. A. González, C. Díaz Valenzuela, N. Yutronic Sáez, *Polyhedron* **2002**, *21*, 2579−2586.
[13] [13a] S. Ganapathiappan, S. S. Krishnamurthy, *J. Chem. Soc., Dalton Trans.* **1987**, 579−584. [13b] S. Ganapathiappan, S. S. Krishnamurthy, *J. Chem. Soc., Dalton Trans.* **1987**, 585−590. [13c] J. Y. Chang, S. B. Rhee, S. Cheong, M. Yoon, *Macromolecules* **1992**, *25*, 2666−2670.
[14] Y. Ni, P. Park, M. Liang, J. Massey, C. Waddling, I. Manners, *Macromolecules* **1996**, *29*, 3401−3408.
[15] G. A. Carriedo, F. J. García Alonso, P. A. González, P. Gómez Elipe, *Polyhedron* **1999**, *18*, 2853−2859.
[16] V. Chandrasekhar, K. Vivekanandan, S. Nagendran, G. T. Senthil Andavan, N. R. Weathers, J. C. Yarbrough, A. W. Cordes, *Inorg. Chem.* **1998**, *37*, 6192.
[17] H. R. Allcock, G. S. Mc Donnell, G. H. Riding, I. Manners, *Chem. Mater.* **1990**, *2*, 425−432.
[18] A. N. Mujumdar, S. G. Young, R. L. Merker, J. H. Magill, *Macromolecules* **1990**, *23*, 14−21.
[19] G. D. Sogah, D. J. Cram, *J. Am. Chem. Soc.* **1979**, *101*, 3035−3042.

Received June 26, 2003
Early View Article
Published Online October 22, 2003

 © 2003 Wiley-VCH Verlag GmbH & Co. KGaA, Weinheim

Synthesis, Structure, and Biological Activity of New Azine-Bridged Dinuclear Platinum(II) Complexes − a New Class of Anticancer Compounds

Ganna V. Kalayda,[a] Seiji Komeda,[a] Kyoko Ikeda,[b] Takaji Sato,[b] Masahiko Chikuma,[b] and Jan Reedijk*[a]

Keywords: Platinum / Antitumor agents / Structure-activity relationships / Cytotoxicity / Apoptosis / Guanine binding

A recently described new class of dinuclear platinum anticancer compounds, represented so far by the isomeric azine-bridged complexes [{*cis*-Pt(NH_3)$_2$Cl}$_2$(μ-pzn)]Cl_2 (**1**) (pzn = pyrazine), [{*cis*-Pt(NH_3)$_2$Cl}$_2$(μ-pmn)]Cl_2 (**2**) (pmn = pyrimidine) and [{*cis*-Pt(NH_3)$_2$Cl}$_2$(μ-pdn)](NO_3)$_2$ (**3**) (pdn = pyridazine), has been added to. Three new dinuclear complexes of this type, [{*cis*-Pt(NH_3)$_2$Cl}$_2$(μ-2,5pzn)]Cl_2 (**4**) (2,5pzn = 2,5-dimethylpyrazine), [{*cis*-Pt(NH_3)$_2$Cl}$_2$(μ-qzn)]Cl_2 (**5**) (qzn = quinazoline), and [{*cis*-Pt(NH_3)$_2$Cl}$_2$(μ-pht)](NO_3)$_2$ (**6**) (pht = phthalazine), have been newly synthesized and characterized by ^{1}H and ^{195}Pt NMR spectroscopy. The interaction of the new compounds with 2 equiv. of 9EtG in D_2O at 310 K has been investigated. Complexes **4** and **5** undergo substitution of both chloride ligands by 9EtG similarly to the related complexes **1** and **2**, respectively. The methyl substituents on the pyrazine ring induce steric hindrance in **4** resulting in a slower reaction rate as compared to **1**. Similarly to the case of **3**, interaction of complex **6** with 9EtG results in cleavage of the Pt–N(pht) bond and subsequent formation of the polymeric species. A cytotoxicity assay of **4**–**6** has been performed on seven human tumor cell lines and on L1210 murine leukemia cell lines, sensitive and resistant to cisplatin. Compounds **4** and **5** exhibit lower cytotoxicity than the analogous complexes with unsubstituted azines. Complex **6** is more active: its cytotoxicity in the L1210 cell lines is similar to that of cisplatin. Analysis of nuclear DNA fragmentation in L1210 cells treated with the azine-bridged complexes **1**–**6** has been carried out. The results clearly indicate induction of apoptosis by all the compounds, implying considerable anticancer potential. The structure-activity relationship for this class of dinuclear platinum(II) complexes is discussed.
(© Wiley-VCH Verlag GmbH & Co. KGaA, 69451 Weinheim, Germany, 2003)

Introduction

cis-Diamminedichloroplatinum(II), usually referred to as cisplatin, has been used in cancer chemotherapy ever since its approval for the treatment of testicular cancer in 1978.[1] At present, it is one of the most widely utilized antitumor drugs, with especially high efficacy against solid tumors, such as testicular and ovarian cancer.[2] However, several problems have been encountered in clinical use. Firstly, cisplatin treatment is accompanied by severe side effects, e.g. nausea, vomiting, and nephrotoxicity. Secondly, cisplatin anticancer activity is limited to a relatively narrow range of tumors. Besides, some tumors develop resistance after repeated cisplatin administrations.[3,4] These drawbacks have stimulated intensive search for new potential antitumor drugs.

One of the most successful approaches in platinum-based anticancer drug design is the synthesis of polynuclear platinum complexes with bridging linkers.[5] Its success is based on the ability of such complexes to form DNA adducts, which are structurally different from those of cisplatin. The major product of cisplatin interaction with genomic DNA is a 1,2-intrastrand cross-link, which induces a kink on a DNA double helix.[6−9] These conformational changes are believed to play an important role in the development of cisplatin resistance.[10] Thus, the compounds capable of binding to DNA in a significantly different way are expected to overcome the resistance problem. Some of the polynuclear (mostly dinuclear) antitumor active platinum(II) complexes described in the literature contain flexible bridging ligands,[11−15] while others possess rigid linkers together with bridging leaving groups.[16−19] The complexes with flexible linkers (for instance, aliphatic diamines) are designed to form long-range cross-links on DNA,[20,21] and the complexes possessing rigid bridging ligands, such as hydrazine and azoles, are developed to minimize distortion of the DNA double helix in a 1,2-intrastrand cross-link.[22]

Recently, we described a new class of dinuclear platinum(II) complexes with azines as bridging ligands.[23] These complexes present a combination of the two above-mentioned types of compounds: they utilize rigid aromatic rings of azines as linkers between two platinum atoms, featuring

[a] Leiden Institute of Chemistry, Gorlaeus Laboratories, Leiden University,
P. O. Box 9502, 2300 RA Leiden, The Netherlands,
Fax: (internat.) + 31-71/527-4671
E-mail: reedijk@chem.leidenuniv.nl
[b] Osaka University of Pharmaceutical Sciences
4-20-1 Nasahara, Takatsuki 569-1094, Japan

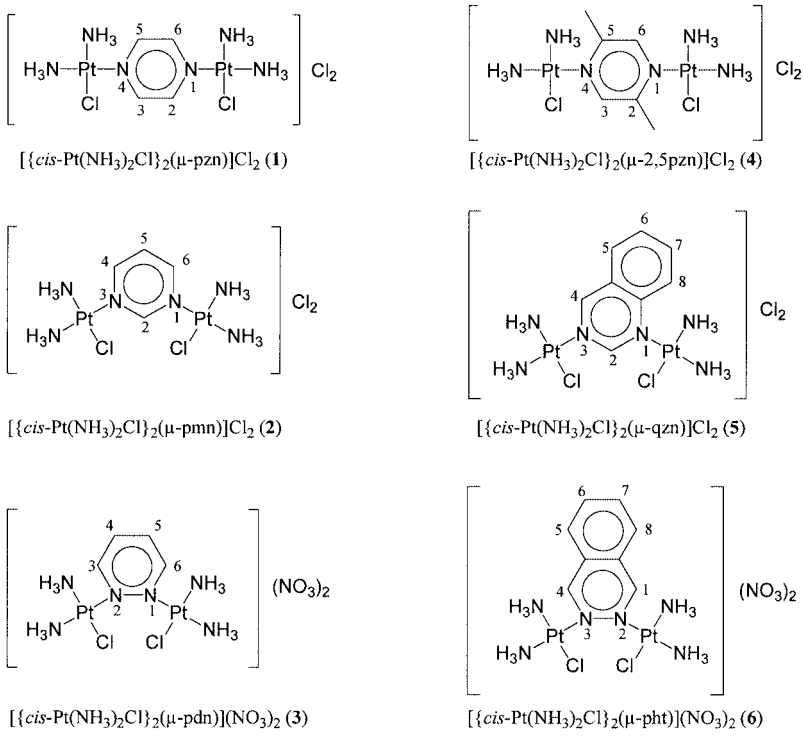

Figure 1. Schematic representation of the azine-bridged dinuclear platinum complexes [{*cis*-$Pt(NH_3)_2Cl\}_2$(μ-pzn)]Cl_2 (**1**), [{*cis*-$Pt(NH_3)_2Cl\}_2$(μ-pmn)]Cl_2 (**2**), [{*cis*-$Pt(NH_3)_2Cl\}_2$(μ-pdn)]$(NO_3)_2$ (**3**), [{*cis*-$Pt(NH_3)_2Cl\}_2$(μ-2,5pzn)]Cl_2 (**4**), [{*cis*-$Pt(NH_3)_2Cl\}_2$(μ-qzn)]Cl_2 (**5**), and [{*cis*-$Pt(NH_3)_2Cl\}_2$(μ-pht)]$(NO_3)_2$ (**6**)

at the same time non-bridging chloride ions as leaving groups. These compounds exhibit considerable activity in vitro in several human tumor cell lines. The complex [{*cis*-$Pt(NH_3)_2Cl\}_2$(μ-pzn)]Cl_2 (pzn = pyrazine) overcomes cisplatin resistance in the L1210/DDP murine leukemia cell line (Figure 1). We have now extended this new class of dinuclear platinum complexes applying other azines, such as quinazoline (qzn), phthalazine (pht), and 2,5-dimethylpyrazine (2,5pzn), as bridging ligands. These azines have different streric and electronic properties caused by substituents on the aromatic ring. In this paper, we describe the synthesis and characterization of three new azine-bridged dinuclear platinum(II) complexes, their interaction with 9-ethylguanine (9EtG), the results of cytotoxicity tests for these compounds, and the analysis of nuclear DNA fragmentation induced by the azine-bridged complexes. Structure-activity correlations for azine-bridged dinuclear platinum(II) complexes are presented.

Results

Synthesis and Characterization of the Complexes

The synthetic procedure used for the preparation of the new azine-bridged dinuclear platinum(II) complexes is similar to the previously described method for the synthesis of **1**−**3**.[23] In all cases the formation of the desired compounds was accompanied by a series of side reactions, and repeated recrystallizations were necessary to purify the complexes.

The complexes were characterized by ^1H and ^{195}Pt NMR spectroscopy (Table 1) and elemental analysis. ^1H NMR spectra show a downfield shift of the signals of the aromatic protons of the ligands as compared to the respective signals for the free azines. ^{195}Pt NMR shifts are in the range typical for an $[N_3Cl]$ coordination environment around the platinum atom.[24] The smaller upfield shift of **6** (δ = −2232 ppm) compared to the shifts of the two other platinum complexes (δ ≈ −2330 ppm) might result from the close proximity of the platinum atoms in **6**. Thus, NMR spectroscopy presents clear evidence of the formation of the desired dinuclear platinum(II) complexes.

Interaction with 9EtG

^1H NMR spectra, run over the course of the reaction, of the complexes **1** and **4**−**6** with 2 equiv. of 9EtG in 0.1 M $NaClO_4$ solution in D_2O at 310 K are shown in Figure 2, a−d, respectively. The ^1H and ^{195}Pt NMR spectroscopic data for the final products are given in Table 2.

Complex 1

As the reaction proceeds, the intensity of the 9EtG signal (δ = 7.82 ppm) decreases, and a signal at δ = 8.27 ppm from the H8 protons of the guanines in the disubstituted product **I** increases in intensity (Figure 2, a). The structure of **I** was confirmed by ^{195}Pt NMR spectroscopy: the ^{195}Pt chemical shift of the product is typical of the $[PtN_4]$ unit.[19,25] In the first hours of interaction of **1** with 9EtG a signal at δ = 8.34 ppm corresponding to the intermediate

 © 2003 Wiley-VCH Verlag GmbH & Co. KGaA, Weinheim

Table 1. ^{1}H and ^{195}Pt NMR spectroscopic data for the dinuclear azine-bridged complexes **4**−**6** and the respective free ligands (D_2O)

Free azines, δ(^{1}H) [ppm]	Complex	Coordinated azine ligands, δ(^{1}H) [ppm]	δ(^{195}Pt) [ppm]
8.27, s (H3, H5); 2.47, s (CH_3)	**4**	9.11, s (H3, H5); 3.09, s (CH_3)	−2346
9.08, s (H2); 8.84, s (H4); 7.85, t (H7); 7.76, d (H8); 7.62, d (H5); 7.59, t (H6)	**5**	10.21, s (H2); 10.09, s (H4); 9.56, d (H8); 8.53, t (H7); 8.41, d (H5); 8.12, t (H6)	−2317, −2339
9.44.08, s (H3, H8); 8.05, m (H4, H7, H5, H6)	**6**	10.08, s (H3, H8); 8.41, m (H4, H7); 8.36, m (H5, H6)	−2232

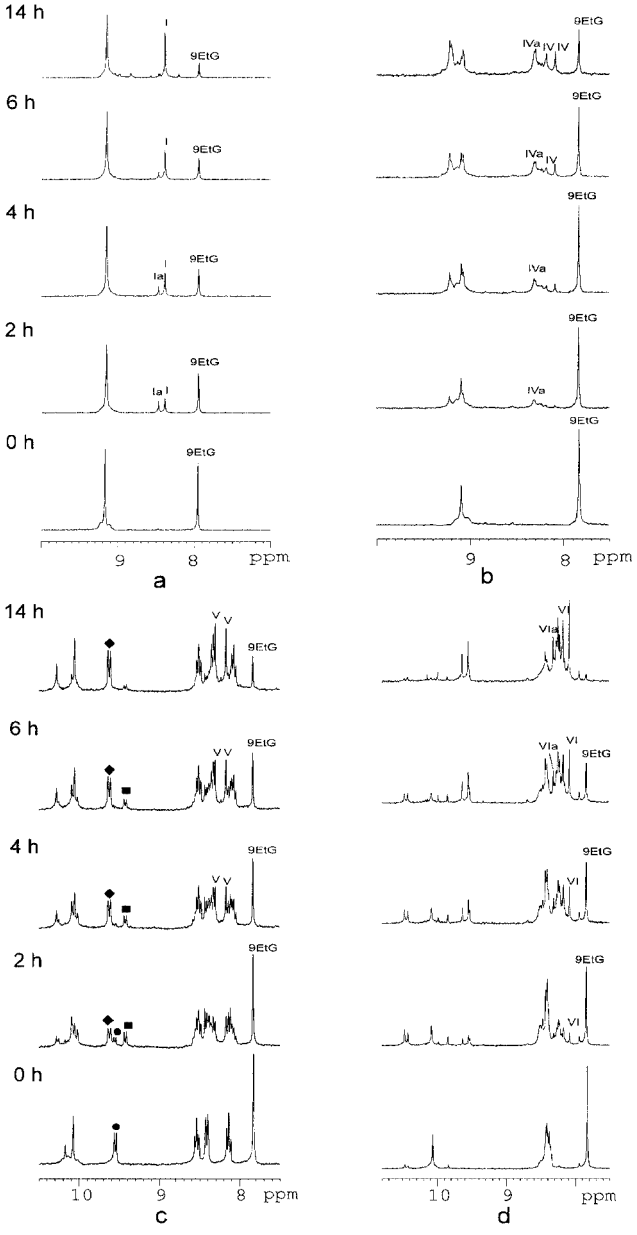

Figure 2. ^{1}H NMR spectra taken over the course of the reaction of **1** (a), **4** (b), **5** (c), and **6** (d) with 2 equiv. of 9EtG in 0.1 M $NaClO_4$ solution in D_2O at 310 K; the H8 signals of the reaction products **I**, **Ia**, **IV**, **IVa**, **V**, **VI**, and **VIa** are shown with the respective roman numbers; the symbols refer to $H8_{(qzn)}$ protons in **5** (circle), **Va** (square), and **V** (diamond)

product **Ia** (see Scheme 1) was also observed, while during the reaction of this complex with GMP no intermediate species were detected.

Table 2. ^{1}H and ^{195}Pt NMR spectroscopic data for the final products of the reaction with 9EtG, **I**, **IV**, **V**, **VI** and **VIa**, in 0.1 M $NaClO_4$ solution in D_2O at 298K

Complex	H8 of 9EtG, δ(^{1}H) [ppm]	δ(^{195}Pt) [ppm]
I	8.27	−2438
IV	8.08; 8.18	−2458
V	8.19; 8.31	−2456
VI	8.10	n.o.[a]
VIa	8.33	−2422

[a] Not observed.

The half-life of 9EtG was determined graphically based on relative integration values of the H8 proton, and is presented in Table 3. As compared to the reaction with GMP [$t_{1/2}$(GMP) = 100 min] previously described,[23] binding of 9EtG to **1** is slower than GMP binding to this complex. A certain amount of the monosubstituted complex was observed in the case of 9EtG, indicating a slower substitution of the second chloride ion as compared to the reaction with GMP.

Table 3. The times of disappearance of 50% 9EtG ($t_{1/2}$) during the reactions of **1** and **4** with 2 equiv. of 9EtG in 0.1 M $NaClO_4$ solution in D_2O at 310 K

Complex	$t_{1/2}$ [min]
1	160
4	210

Complex 4

The substitution of the first chloride ion by a 9EtG molecule yields an intermediate complex **IVa** (see Scheme 1). As the reaction proceeds further, two new signals at δ = 8.08 and 8.18 ppm appear and gradually increase in intensity. One of them was initially tentatively assigned to the hydrolyzed intermediate **IVb**. However, no peaks corresponding to the platinum nucleus in the [N_3O] coordination environment[19,23,25] were found in the ^{195}Pt NMR spectrum. Thus, **IVb** is not present in the reaction mixture, and the signals at δ = 8.08 and 8.18 ppm can only be assigned to the non-equivalent H8 protons of the two guanine bases in the disubstituted product **IV**. In contrast to **I** where free rotation around Pt−N bonds is present, complex **IV** is sterically hindered, and it might exist in a certain thermo-

 © 2003 Wiley-VCH Verlag GmbH & Co. KGaA, Weinheim

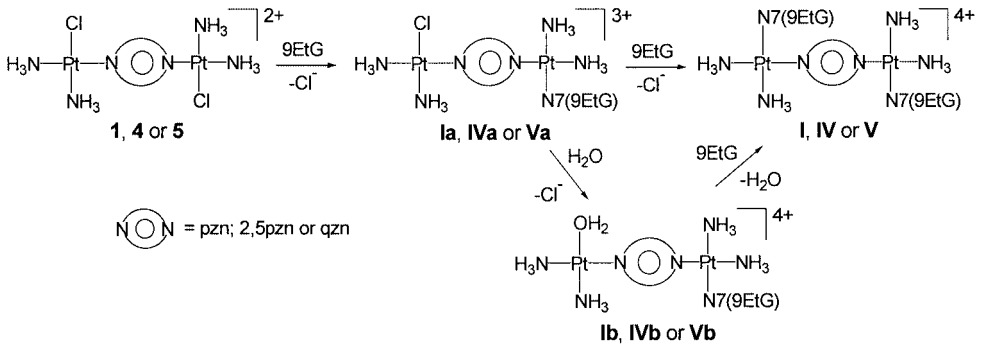

Scheme 1. The reaction scheme for the interaction of complexes **1**, **4**, and **5** with 2 equiv. of 9EtG in aqueous solution

dynamically favored conformation, in which the two guanine molecules have a different configuration with respect to the CH_3 groups.

The half-life of 9EtG was determined graphically based on relative integration values of the H8 proton, and is given in Table 3. As is clear from Table 3, complex **4** reacts much slower with 9EtG than the analogous complex **1**, without methyl substituents on the azine ring. It has been shown previously that the rate-limiting step of guanine binding to the azine-bridged complexes is a direct substitution of the chloride ion by N7 of a guanine base, and therefore the reaction rate is mainly determined by steric factors.[23] Apparently, methyl groups of the 2,5-dimethylpyrazine in **4** hamper chloride substitution by 9EtG, resulting in a much slower interaction as compared to **1**.

Complex 5

The reaction of **5** with 9EtG provides the disubstituted complex **V** as confirmed by ^1H and ^{195}Pt NMR spectroscopy (Table 2). An interesting feature of **V** is that the H8 protons of the two guanine molecules in this complex are not equivalent. This is not unexpected, as one of them is shielded by an aromatic ring of quinazoline and its signal is, therefore, shifted upfield. Complex **5** reacts with guanine via the intermediate species **Va**. This is clearly seen from the signals of the $H8_{(qzn)}$ proton of the quinazoline. As the reaction proceeds, the intensity of the peak corresponding to the starting complex **5** ($\delta = 9.56$ ppm) decreases, and at first the signal of the $H8_{(qzn)}$ proton of the intermediate **Va**, at $\delta = 9.42$ ppm, increases in intensity. Later in the course of the reaction the intensity of this signal diminishes, while the peak ($\delta = 9.63$ ppm) corresponding to the $H8_{(qzn)}$ proton of the final product **V** builds up in intensity. It should be noted that only one intermediate was observed, whereas two different intermediates would be expected due to the asymmetry of the starting complex. This indicates that the least hindered chloride ion is substituted first. The substitution of the second chloride ion is more difficult for steric reasons and is, therefore, slower. It may be concluded that the reaction of 9EtG with complex **5** proceeds slower than the same reaction with the related compound **2**. However, no quantitative confirmation was possible due to an overlap between the signals of the aromatic protons of quinazoline and H8 signals of the guanine bases of the products.

Complex 6

Complex **6** interacts with 9EtG in a similar manner to that previously found for the reaction of the related compound **3** with GMP,[23] i.e. with the cleavage of the Pt−N(pht) bond and subsequent polymerization. First, the N7,O6-platinated 1:1 complex $[\{cis\text{-}Pt(NH_3)_2\}_2(\mu\text{-}9EtG\text{-}N7,O6)(\mu\text{-}pht)]^{4+}$ is formed. Binding of another 9EtG molecule to this complex breaks the Pt−N(pht) bond, yielding two mononuclear fragments, $[cis\text{-}Pt(NH_3)_2(pht)(9EtG\text{-}N7)]^{2+}$ (**VIa**) and $[cis\text{-}Pt(NH_3)_2(9EtG)(H_2O)]^{2+}$. The latter species polymerizes to form product **VI**, $[\{cis\text{-}Pt(NH_3)_2\}(\mu\text{-}9EtG\text{-}N7,O6)\{cis\text{-}Pt(NH_3)_2\}(\mu\text{-}9EtG\text{-}N7,O6)]_n$ (see Scheme 2).

In contrast to the previously described reaction of **3** with GMP, in the case of interaction between **6** and 9EtG the second guanine molecule predominantly attacks the platinum atom bound to O6 of the bridging guanine. The Pt−N7(9EtG) bond of the initially formed 1:1 complex $[\{cis\text{-}Pt(NH_3)_2\}_2(\mu\text{-}9EtG\text{-}N7,O6)(\mu\text{-}pht)]^{4+}$ remains intact, and therefore, the mononuclear complex $[cis\text{-}Pt(NH_3)_2(pht)(9EtG\text{-}O6)]^{2+}$ was not observed. This phenomenon appears to be related to the guanine base rather than to the bridging azine, as during the reaction of **3** with 9EtG no species $[cis\text{-}Pt(NH_3)_2(pdn)(9EtG\text{-}O6)]^{2+}$ was detected (spectra not shown).

The structures of the products were confirmed by ^1H and ^{195}Pt NMR spectroscopy, mass spectrometry and pH titration. The ^1H NMR spectrum of **VIa** shows an asymmetric profile of the pht ligand. The ^{195}Pt shift of this complex is typical of $[N_4]$ coordination surrounding a platinum atom.[18,23,25] A signal assigned to $[cis\text{-}Pt(NH_3)_2(pht)(9EtG)]^+$ was observed in the mass spectrum of **VIa**. ^1H NMR spectroscopic data for **VI** confirm the absence of phthalazine. The H8 signal of this complex is shifted by 0.26 ppm downfield compared with free 9EtG, indicating an inductive effect of platinum coordinated to guanine. As in the case of the similar complex $[\{cis\text{-}Pt(NH_3)_2\}(\mu\text{-}GMP\text{-}N7,O6)\{cis\text{-}Pt(NH_3)_2\}(\mu\text{-}GMP\text{-}N7,O6)]_n$,[23] no signal was found in the ^{195}Pt NMR spectrum of **VI**. This phenomenon

 © 2003 Wiley-VCH Verlag GmbH & Co. KGaA, Weinheim

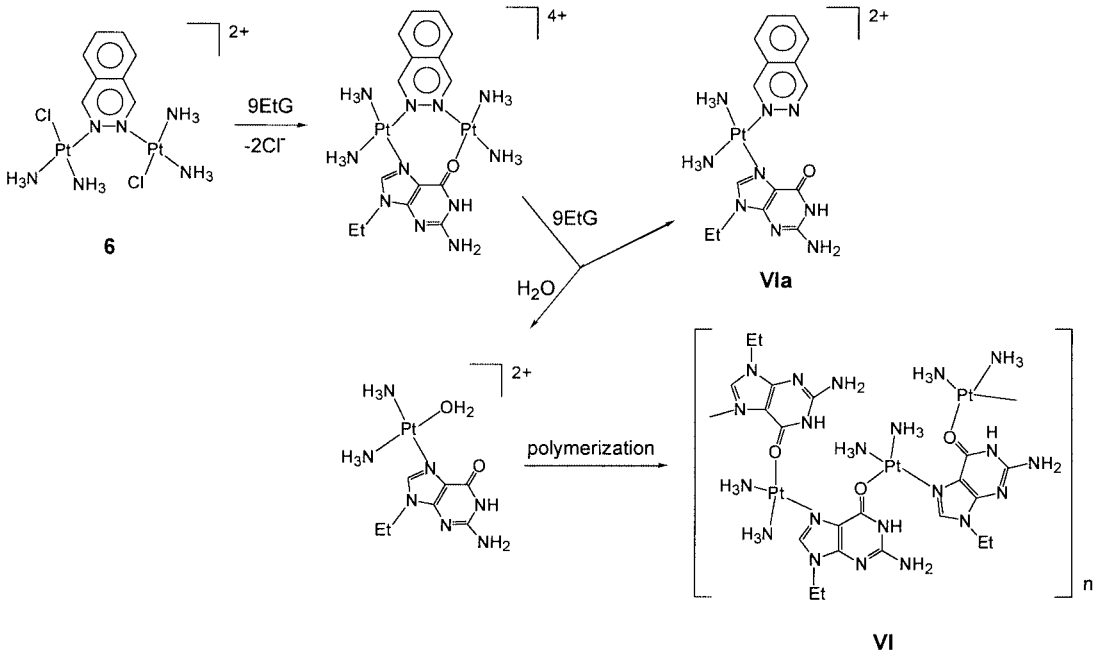

Scheme 2. The proposed reaction scheme for the interaction of **6** with 2 equiv. of 9EtG in aqueous solution

is a result of ^{195}Pt relaxation, and is often observed in the case of polymerized compounds.[26] The mass spectrum of complex **VI** gives a signal, which corresponds to $[Pt(\mu\text{-}9EtG)Pt(NH_3)]^+$.

Thus, the close proximity of the platinum atoms does not allow coordination of two 9EtG ligands to the Pt−(μ-pht)−Pt moiety resulting in cleavage of the Pt−N(pht) bond upon binding of the second 9EtG, followed by polymerization. It should be noted that this is the first example of the formation of polymeric species in the reactions involving platinum complexes with 9EtG.

pH Titrations

The chemical shift of the signal of the H8 proton of 9EtG is strongly dependent on (de)protonation of the heterocyclic nitrogen atoms. Therefore, a pH titration is a very convenient method of determining the platinum binding position of the guanine.[27,28] The pH titration was performed on the final products of the reaction of 9EtG with compounds **1** and **4**−**6**. The plots of the chemical shifts of the signal of the H8 protons as a function of pD are shown in Figure 3. For all the products analyzed, the N7 (de)protonation in the acidic area, as it is known for free 9EtG, is absent. This clearly indicates that in all of these compounds the platinum atoms are bound to the guanines at the N7 position. The N1 (de)protonation in basic solution was observed for **I**, **IV**, and **VIa**, confirming the proposed structures. Complex **V** was found to be unstable at pD > 8.5, therefore, the (de)protonation process at N1 in the basic region could not be detected.

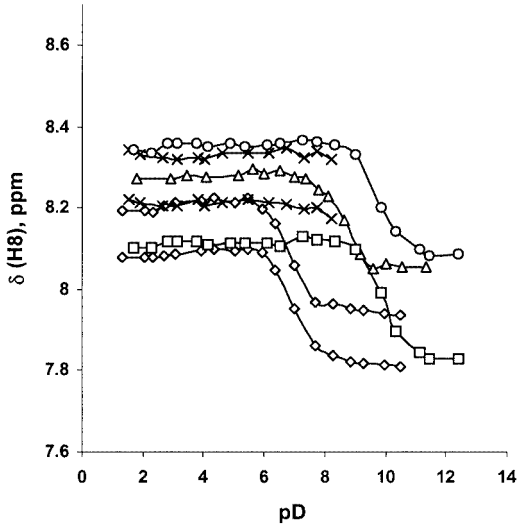

Figure 3. Plots of the chemical shift of H8 protons vs. pD for **I** (triangle), **IV** (diamond), **V** (cross), **VI** (square), and **VIa** (circle); pH titrations were performed in 0.1 M $NaClO_4$ solutions in D_2O at 298 K; pD was adjusted with 1 M and 0.1 M DCl, 1 M and 0.1 M NaOD

The results from the pH titration of **VI** present evidence of the binding positions of the platinum atoms in this complex. For **VI**, the N7 (de)protonation process was not observed indicating that platinum binds to guanine at the N7 position. Another platinum atom can possibly be bound to either N1 or the O6 position. N1 (de)protonation was detected upon pH titration of **VI**, strongly suggesting that the binding position of another platinum atom is the O6 atom of a guanine ligand.

 © 2003 Wiley-VCH Verlag GmbH & Co. KGaA, Weinheim

In vitro Cytotoxicity Assay in Human Tumor Cell Lines

The cytotoxicity of **4**−**6**, and cisplatin as a reference, in several human tumor cell lines, MCF and EVSA-T (breast cancer), WIDR (colon cancer), IGROV (ovarian cancer), M19 (melanoma), A498 (renal cancer), and H226 (non-small cell lung cancer), is summarized in Table 4. All three azine-bridged complexes were found to be in the active range in all the cell lines, except for **4** in A498. Among the three dinuclear compounds tested, **4** was the least cytotoxic in all of the cell lines, and **6** exhibited a slightly higher activity than **5** in five cell lines. The cytotoxicity of the complexes is lower than that of cisplatin. However, similarly to the related complexes **1**−**3**,[23] compounds **4**−**6** show a high specificity for the IGROV cell line. They are approximately half as cytotoxic as cisplatin in this cell line, whereas their activity compared to cisplatin in the other cell lines is 4−5 times lower.

Table 4. In vitro cytotoxicity assay of complexes **4**−**6** and cisplatin on human tumor cell lines

Test compound	IC_{50} [μM]						
	A498	EVSA-T	H226	IGROV	M19	MCF-7	WIDR
4	11.9	6.3	19.6	1.1	8.4	9.0	5.4
5	21.8	5.7	17.8	1.0	5.8	7.3	5.8
6	> 88.3	16.7	53.7	3.2	23.5	23.4	7.5
Cisplatin	5.7	1.4	4.5	0.4	1.8	1.4	1.8

In vitro Cytotoxicity Assay in L1210 Cell Lines Sensitive and Resistant to Cisplatin

The cytotoxicity tests of complexes **4**−**6** were performed on L1210 murine leukemia cells, sensitive (L1210/0) and resistant (L1210/DDP) to cisplatin. Cisplatin and the azine-bridged complexes **1**−**3** were included as reference compounds. The results are presented in Table 5. The IC_{50} values for the reference complexes **1**−**3** correlate with the previously reported data.[23] Complex **4** exhibits significantly lower activity compared with the related compound **1** in both L1210/0 and L1210/DDP cell lines. Compound **5** is half as active as the analogous complex **2**. Both **4** and **5** are approximately 5 times less cytotoxic than cisplatin. Nevertheless, these complexes are still in the active range. Compound **6** was found to be twice as active as the related complex **3**. Its cytotoxicity is similar to that of cisplatin. As expected, in the resistant cell line cisplatin is significantly less active, with the resistance factor (*RF*) equal to 4.7. The resistant factors of the azine-bridged complexes are lower (around 3) indicating that they partially circumvent cisplatin resistance.

Table 5. In vitro cytotoxicity assay of complexes **1**−**6** and cisplatin on L1210 murine leukemia cell lines, sensitive (L1210/0) and resistant (L1210/DDP) to cisplatin

Test compound	IC_{50} [μM] L1210/0	L1210/DDP	*RF*[a]
1	1.0±0.1	3.5±0.1	3.5
2	5.2±0.2	18.4±1.0	3.5
3	5.7±0.6	21.3±3.0	3.7
4	9.3±1.6	> 38	> 4
5	12.2±0.4	34.6±1.0	2.8
6	2.8±0.1	8.4±0.3	3.0
Cisplatin	2.0±0.2	9.4±0.8	4.7

[a] *RF* − resistance factor, $RF = IC_{50}(L1210/DDP)/IC_{50}(L1210/0)$.

Induction of Apoptosis by the Platinum Complexes in L1210/0 Cells

One potentially important manner by which platinum−DNA adducts may kill the cells is by induction of programmed cell death or apoptosis. Activation of apoptosis results in nuclear disintegration and eventual fragmentation of the dying cell. Irreversible cleavage of nuclear DNA into nucleosomal oligomers is a distinct feature of apoptotic cell death.

The L1210/0 cells were exposed to the azine-bridged complexes **1**−**6** and cisplatin for 48 h at the concentrations equal to their IC_{50}. The low-molecular weight DNA extracted from the cells was taken for agarose electrophoresis. As shown in Figure 4, DNA fragmentation with a characteristic laddering pattern was observed for all the compounds. DNA laddering is a frequently used indicator of apoptosis.[29,30] Therefore, it can be concluded that all the azine-bridged complexes as well as cisplatin trigger apoptotic pathways in L1210/0 cells.

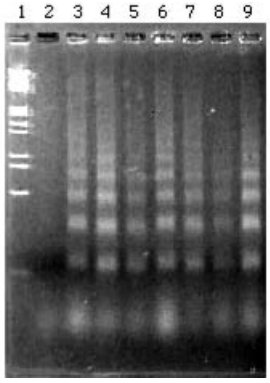

Figure 4. Analysis of nuclear DNA fragmentation induced by the azine-bridged dinuclear platinum complexes **1**−**6** and cisplatin; gel analysis was carried out as described in the Exp. Sect.; cells were incubated for 48 h with cisplatin (lane 3) and compounds **1**−**6** (lane 4−9, respectively) at the concentrations equal to their IC_{50}; lane 1: DNA marker; lane 2: control

Discussion

Compared to the previously described azine-bridged dinuclear complexes **1**−**3**, the newly synthesized complexes **4**−**6** possess additional substituents (e.g. additional aromatic ring or methyl groups) on the azine ligand. Investigation of their interaction with 9EtG shows that the steric hindrance induced by additional groups hampers the substitution of chloro ligands by guanine molecules. Binding

 © 2003 Wiley-VCH Verlag GmbH & Co. KGaA, Weinheim

of these complexes to DNA is supposed to be sterically even more restricted, and they might prefer to react with relatively flexible protein molecules than with rather rigid dsDNA. Therefore, a very small amount of Pt−DNA adducts is expected to be formed resulting in a lower cytotoxicity as compared to the parent compounds. This was observed for complexes **4** and **5**, which were found to be less active than their analogues **1** and **2**, respectively. The methyl groups of 2,5-methylpyrazine in **4** induce steric hindrance on both platinum atoms, while in the case of **5** only the second substitution step is supposed to be affected by the presence of an additional aromatic ring. This difference reflects on the activity of the complexes: **4** is much less cytotoxic than **5**.

In the case of **6**, the close proximity of two platinum atoms rather than the presence of an additional aromatic ring determines the outcome of the interaction with 9EtG. In contrast to the reaction with 9EtG, it is unlikely that complex **6** would form an N7,O6-platinated complex [{*cis*-$Pt(NH_3)_2$}$_2${μ-G(dsDNA)-N7,O6}(μ-pht)] on double-stranded DNA, because the O6 atom of the guanine is involved in Watson−Crick base paring. As suggested earlier for the related complex **3**,[23] the initial substitution of the first chloride ion will probably be followed by the Pt−N(pht) bond cleavage upon nucleophilic attack of the neighbouring guanine molecule. This will result in the formation of the two mononuclear fragments, [*cis*-$Pt(NH_3)_2$-(pht){G(dsDNA)-N7}] and [*cis*-$Pt(NH_3)_2${G(dsDNA)-N7}(H_2O)]. The latter one is expected to coordinate to another nucleobase producing cross-links on DNA similarly to cisplatin. The former will apparently stay as a monofunctional adduct as in the case of the analogous complex **3**. Since in this monofunctional adduct the phthalazine ligand occupies the *cis* position with respect to the guanine base, it might act as an intercalator on DNA improving the cytotoxicity of **6** compared with complex **3**, which cannot provide any additional interaction with nuclear DNA.

The azine-bridged dinuclear platinum(II) complexes present a new class of platinum anticancer compounds. In human tumor cell lines they exhibit cytotoxic profiles, which differ from that of cisplatin, and some of them largely or partly circumvent the cross-resistance with cisplatin in murine leukemia cells, due to the formation of DNA adducts different from those of cisplatin. Our results clearly show that the azine-bridged complexes induce apoptosis in L1210/0 cells. Apoptosis in cancer cells is more difficult to trigger because of their ability to either block pro-apoptotic pathways or stimulate anti-apoptotic ones. Thus, induction of apoptosis in tumor cells by the azine-bridged complexes presents clear evidence of considerable anticancer activity of these compounds.

Conclusion

In this paper, we have described the synthesis of three new azine-bridged dinuclear platinum complexes, their interaction with 9EtG, and biological activity of these compounds. The structure-activity relationship within this class of dinuclear platinum anticancer compounds has been established. The complexes possessing additional groups in the azine ring, which induce steric hindrance and hamper binding of the complex to nuclear DNA, are less cytotoxic than the complexes with unsubstituted azines. The substituents on the ligand, that can provide additional interaction with DNA such as intercalation, significantly improve antitumor properties of the complex. In this study, we have also shown that all the azine-bridged dinuclear platinum complexes are able to induce apoptosis in tumor cells indicating a considerable anticancer potential of this class of compounds.

Experimental Section

General: K_2PtCl_4 was used as obtained from Johnson&Matthey (Reading, U.K). Silver nitrate was purchased from Acros, 2,5-dimethylpyrazine, quinazoline, and phthalazine were received from Aldrich, 9EtG was purchased from Sigma, and further purification was not carried out. *cis*-$[Pt(NH_3)_2Cl_2]$ was synthesized according to a literature method.[31] The dinuclear platinum complexes [{*cis*-$Pt(NH_3)_2Cl$}$_2$(μ-pzn)]Cl_2 (**1**), [{*cis*-$Pt(NH_3)_2Cl$}$_2$(μ-pmn)]Cl_2 (**2**), [{*cis*-$Pt(NH_3)_2Cl$}$_2$(μ-pdn)]$(NO_3)_2$ (**3**) were prepared as described previously.[23]

Instrumentation: All NMR spectra were recorded with a 300-MHz Bruker DPX300 spectrometer with a 5-mm multi-nucleus probe. The temperature was kept constant by a variable-temperature unit. ^1H and ^{195}Pt chemical shifts were referenced to TSP and $Na_2[PtCl_6]$ (δ = 0 ppm), respectively. C, H, and N analyses were performed with a Perkin−Elmer 240B microanalyzer. Mass spectrometric measurements were performed with a ThermoFinnigan AQA spectrometer using an Electrospray Interface ionization technique.

***cis*-$[Pt(NH_3)_2Cl(dmf)](NO_3)$:** A solution of $AgNO_3$ (0.08 g, 0.47 mmol) in 3 mL of dimethylformamide (DMF) was added dropwise over 3 h to a stirred solution of *cis*-$[Pt(NH_3)_2Cl_2]$ (0.15 g, 0.5 mmol) in DMF (7 mL) at room temperature in the dark. The mixture was stirred overnight in the dark, and the AgCl precipitate was then filtered off. The resulting pale-yellow DMF solution of *cis*-$[Pt(NH_3)_2Cl(dmf)](NO_3)$ was used as a starting material for the preparation of each azine-bridged dinuclear platinum(II) complex described below.

[{*cis*-$Pt(NH_3)_2Cl$}$_2$(μ-2,5pzn)]Cl_2 (4): 2,5pzn (23.0 mg, 0.21 mmol) in DMF (1 mL) was added dropwise to the stirred DMF solution of *cis*-$[Pt(NH_3)_2Cl(dmf)](NO_3)$, obtained as above. The resulting solution was stirred at room temperature for 6 h in the dark, then concentrated in a rotary evaporator, and the residue was washed with diethyl ether. A crude product was recrystallized twice from a minimal amount of 0.5 M aqueous solution of LiCl yielding a pale-yellow powder of **4**, which was washed with MeOH and diethyl ether, dried in vacuo. Yield: 0.03 g (17%). $C_6H_{20}Cl_4N_6Pt_2$ (708.2): calcd. C 10.18, H 2.85, N 11.87; found C 10.13, H 2.82, N 11.94. ^1H NMR (D_2O): δ (2,5pzn resonance) = 3.09 (s, 6 H), 9.11 (s, 2 H) ppm. ^{195}Pt NMR (D_2O): δ = −2346 ppm.

[{*cis*-$Pt(NH_3)_2Cl$}$_2$(μ-qzn)]Cl_2 (5): qzn (28.3 mg, 0.22 mmol) in DMF (1 mL) was added dropwise to the stirred DMF solution of *cis*-$[Pt(NH_3)_2Cl(dmf)](NO_3)$, obtained as above. The resulting solution was stirred at room temperature for 6 h in the dark. This solution was then concentrated in a rotary evaporator, and the resi-

 © 2003 Wiley-VCH Verlag GmbH & Co. KGaA, Weinheim

due was washed with diethyl ether. The crude product was dissolved in a minimal amount of 1 M aqueous solution of LiCl, then excess of MeOH was added. The volume of the resulting solution was reduced to yield a yellow precipitate, which was purified in the same way once more to obtain a yellow precipitate of **5**. This precipitate was collected, washed with MeOH and diethyl ether, and dried in a dessicator over KOH. Yield: 0.05 g (25%). $C_8H_{18}Cl_4N_6Pt_2$ (730.2): calcd. C 13.16, H 2.48, N 11.51; found C 13.02, H 2.27, N 11.41. ^{1}H NMR (D_2O): δ (qzn resonance) = 8.13 (t, 1 H), 8.41 (d, 1 H), 8.53 (t, 1 H), 9.56 (d, 1 H), 10.09 (s, 1 H), 10.21 (s, 1 H) ppm. ^{195}Pt NMR (D_2O): δ = −2317, −2339 ppm.

[{*cis*-Pt(NH$_3$)$_2$Cl}$_2$(μ-pht)](NO$_3$)$_2$ (6): pht (28.3 mg, 0.22 mmol) in DMF (1 mL) was added dropwise to the stirred DMF solution of *cis*-[Pt(NH$_3$)$_2$Cl(dmf)](NO$_3$), obtained as above. The resulting solution was stirred overnight in the dark at room temperature. Then it was concentrated in a rotary evaporator and the residue extracted with MeOH (15 mL). The extract was filtered, concentrated in a rotary evaporator, and extracted again with MeOH (15 mL). The resulting extract was filtered, concentrated in a rotary evaporator, and the residue washed with a small amount of EtOH, and thoroughly washed with diethyl ether to obtain a yellow powder of **6** which was dried in a dessicator over KOH. Yield: 0.06 g (30%). $C_8H_{18}Cl_2N_8O_6Pt_2$ (783.3): calcd. C 12.27, H 2.32, N 14.30; found C 12.22, H 2.40, N 14.40. ^{1}H NMR (D_2O): δ (pht resonance) = 8.36 (m, 2 H), 8.41 (m, 2 H), 10.08 (s, 2 H) ppm. ^{195}Pt NMR (D_2O): δ = −2232 ppm.

Reactions with 9EtG: The reactions of the complexes **1**, **4**, **5**, and **6** (4 mM) with 2 equiv. of 9EtG (8 mM) were monitored over 14 h at 310 K by ^{1}H NMR spectroscopy in a 0.1 M $NaClO_4$ solution in D_2O (pD ≈ 7). The reactions of **1** and **4** with 9EtG were quantified using relative integration values of the signals of the H8 protons.

pH Titrations: The pH titrations were carried out in 0.1 M $NaClO_4$ solutions in D_2O by adjustment of the pD with 0.1 M and 1 M DCl, 0.1 M and 1 M NaOD. The pD values were measured at 298 K using a PHM 80 pH meter (Radiometer) before and after each ^{1}H NMR measurement. The pH values were not corrected for H/D isotope effects.

In vitro Cytotoxicity Assay in Human Tumor Cell Lines: In vitro cytotoxicity assays in human tumor cell lines were performed at the Dr. Daniel den Hoed Kliniek (Rotterdam Cancer Institute), Department of Medical Oncology (Rotterdam, the Netherlands). The seven well-characterized cell lines used were MCF7 and EVSA-T (breast cancer), WIDR (colon cancer), IGROV (ovarian cancer), M19 (melanoma), A498 (renal cancer), and H226 (non-small cell lung cancer). All cell lines were maintained in a continuous logarithmic culture in RPMI 1640 medium with Hepes and phenol red (Paisley, Scotland). The medium was supplemented with 10% FCS (Paisley, Scotland), penicillin 100 IU/mL and streptomycin 100 μg/mL (Sigma). Cisplatin and the dinuclear platinum complexes **4** and **5** were dissolved in water (1 mg/200 μL), complex **6** was dissolved in DMSO (1 mg/200 μL) and finally diluted in full medium. After 48 h of preincubation of the tumor cells in 96-well flatbottom microtiter plates, the solutions of the test compounds were added. The plates were incubated at 37 °C, 8.5% CO_2 for 120 h. IC_{50} values were determined using the microculture sulforhodamine-B test (SRB).[32]

In vitro Cytotoxicity Assay in L1210 Cell Lines Sensitive and Resistant to Cisplatin: The L1210/0 murine leukemia cell line (JCRB 9026) was obtained from the Health Science Research Resources Bank (Osaka, Japan). The cisplatin-resistant L1210/DDP cell line was obtained by exposure of L1210/0 cells to cisplatin at the concentration of 10 μM over a period of 3 months and subsequent cloning. L1210/0 and L1210/DDP were cultured in a suspension in RPMI 1640 medium (Sigma) supplemented with 10% heat-inactivated fetal calf serum and no antibiotics. The cells were grown at 37 °C in a 5% CO_2 humidified atmosphere. Cell growth inhibition was determined by an MTT assay [MTT = 3-(4,5-dimethylthiazol-2-yl)-2,5-diphenyl-2*H*-tetrazolium bromide].[33] In brief, the cells were divided into 96 well plates at the concentrations of 10^5 cells/mL in 100 μL of growth medium and were allowed to attach for 16 h at 37 °C in a 5% CO_2 humidified atmosphere. Then the cells were incubated with the platinum complexes at various concentrations for 48 h. Following exposure to the drugs, 10 μL of a 5 mg/mL MTT solution was added to each well, and the cells were incubated for 4 h. Then the culture media were removed, and the plates were washed with PBS. 200-μL aliquots of 2-propanol containing 0.04 M HCl were pipetted into each well. The absorbance was measured at 570 nm using a Biorad 550 microplate reader. The IC_{50} values were defined as the drug concentrations that reduced the absorbance by 50% compared to the drug-free control.

Induction of Apoptosis by the Platinum Complexes in L1210/0 Cells: The cells were exposed to the concentrations equal to IC_{50} of each azine-bridged complex. For the analysis of DNA fragmentation, DNA of a low molecular weight extracted from the cells was taken for agarose electrophoresis. The cells were cultured at the concentrations of 10^5 cells/mL in 24 mL for 16 h, followed by incubation with complexes **1**−**6** for 48 h. The cells (10^7 cells) were then harvested by centrifugation and resuspended in 0.1 mL of lysis buffer [0.5% Triton X-100, 1 mM EDTA, 10 mM Tris-HCl buffer (pH = 7.4)]. Afterwards the suspension was incubated at 4 °C for 10 min. In order to remove DNA of a high molecular weight, the suspension was centrifuged at 16300 rpm at 4 °C for 5 min. Then 10 μL of RNase A (10 mg/mL) in Tris-EDTA buffer [1 mM EDTA, 10 mM Tris-HCl buffer (pH = 8.0)] was added to the supernatant and incubated at 37 °C for 1 h. 10 μL of Proteinase K solution (10 mg / mL) was then added, and further incubation was performed at 50 °C for 30 min. Afterwards 20 μL of 5 M NaCl and 120 μL of 2-propanol were added, and the resulting mixture was left overnight at −20 °C. After centrifuging at 16300 rpm at 4 °C for 15 min, the DNA pellet was obtained and subsequently resuspended in 100 μL of 10 mM loading buffer [2 mM EDTA, 90 mM Tris-boric acid buffer (pH = 8.0)]. The DNA was loaded onto a 2% agarose gel, and electrophoresis was carried out in a loading buffer at 100 V for 1 h. The DNA was observed by ethidium bromide solution staining (1 μg/mL, 20 min). The photographs were obtained under UV illumination by a Kodak EDAS-120 system.

Acknowledgments

The authors are grateful to Johnson & Matthey (Reading, UK) for their generous donation of K_2PtCl_4 and to PCN/Pharmachemie BV (Haarlem, The Netherlands) for cytotoxicity tests. Also the support and sponsorship concerted by COST Actions D20/0001/00, D20/0002/00, and D20/003/01 is kindly acknowledged. This work has been performed under the auspices of the joint BIOMAC Research Graduate School of Leiden University and Delft University of Technology.

[1] B. Rosenberg, L. van Camp, J. E. Trosko, V. H. Mansour, *Nature* **1969**, *222*, 385−386.
[2] G. Giaccone, *Drugs* **2000**, *59*, 9−17.
[3] L. R. Kelland, *Drugs* **2000**, *59*, 1−8.
[4] W. Dempke, W. Voigt, A. Grothey, B. T. Hill, H. J. Schmoll, *Anti-Cancer Drugs* **2000**, *11*, 225−236.

 © 2003 Wiley-VCH Verlag GmbH & Co. KGaA, Weinheim

[5] J. Reedijk, *Proc. Natl. Acad. Sci. U. S. A.* **2003**, *100*, 3611−3616.
[6] A. M. J. Fichtinger-Schepman, J. L. Van der Veer, J. H. J. Den Hartog, P. H. M. Lohman, J. Reedijk, *Biochemistry* **1985**, *24*, 707−713.
[7] E. Reed, Y. Ostchega, S. M. Steinberg, S. H. Yuspa, R. C. Young, R. F. Ozols, M. C. Poirier, *Cancer Res.* **1990**, *50*, 2256−2260.
[8] P. M. Pil, S. J. Lippard, *Science* **1992**, *256*, 234−237.
[9] S. V. D. Z. Yang, J. Reedijk, J. H. Vanboom, N. Farrell, A. H. J. Wang, *Nat. Struct. Biol.* **1995**, *2*, 577−586.
[10] A. Eastman, N. Schulte, *Biochemistry* **1988**, *27*, 4730−4734.
[11] N. Farrell, Y. Qu, M. P. Hacker, *J. Med. Chem.* **1990**, *33*, 2179−2184.
[12] N. Farrell, Y. Qu, U. Bierbach, M. Valsecchi, E. Menta, in: *Cisplatin, Chemistry and Biochemistry of a Leading Anticancer Drug* (Ed.: B. Ed.), Wiley VCH, Weinheim, **1999**, pp. 479−496.
[13] P. Di Blasi, A. Bernareggi, G. Beggiolin, L. Piazzoni, E. Menta, M. L. Formento, *Anticancer Res.* **1998**, *18*, 3113−3117.
[14] R. D. D. H. Rauter, E. Menta, A. Oliva, Y. Qu, N. Farrell, *Inorg. Chem.* **1997**, *36*, 3919−3927.
[15] S. van Zutphen, M. S. Robillard, G. A. van der Marel, H. S. Overkleeft, H. den Dulk, J. Brouwer, J. Reedijk, *Chem. Commun.* **2003**, 634−635.
[16] J. Kozelka, E. Segal, C. Bois, *J. Inorg. Biochem.* **1992**, *47*, 67−80.
[17] Y. Montet, J. Kozelka, *Inorg. Chim. Acta* **1999**, *284*, 103−106.
[18] S. Komeda, M. Lutz, A. L. Spek, M. Chikuma, J. Reedijk, *Inorg. Chem.* **2000**, *39*, 4230−4236.
[19] S. Komeda, M. Lutz, A. L. Spek, Y. Yamanaka, T. Sato, M. Chikuma, J. Reedijk, *J. Am. Chem. Soc.* **2002**, *124*, 4738−4746.
[20] N. Farrell, T. G. Appleton, Y. Qu, J. D. Roberts, A. P. S. Fontes, K. A. Skov, P. Wu, Y. Zou, *Biochemistry* **1995**, *34*, 15480−15486.
[21] V. Brabec, J. Kasparkova, O. Vrana, O. Novakova, J. W. Cox, Y. Qu, N. Farrell, *Biochemistry* **1999**, *38*, 6781−6790.
[22] S. Komeda, H. Ohishi, H. Yamane, M. Harikawa, K. Sakaguchi, M. Chikuma, *J. Chem. Soc., Dalton Trans.* **1999**, 2959−2962.
[23] S. Komeda, G. V. Kalayda, M. Lutz, A. L. Spek, Y. Yamanaka, T. Sato, M. Chikuma, J. Reedijk, *J. Med. Chem.* **2003**, *46*, 1210−1219.
[24] T. G. Appleton, J. R. Hall, S. F. Ralph, *Inorg. Chem.* **1985**, *24*, 4685−4693.
[25] C. A. L. D. P. Bancroft, S. J. Lippard, *J. Am. Chem. Soc.* **1990**, *112*, 6860−6871.
[26] S. J. Berners-Price, P. W. Kuchel, *J. Inorg. Biochem.* **1990**, *38*, 305−326.
[27] F. J. Dijt, G. W. Canters, J. H. J. Den Hartog, A. T. M. Marcelis, J. Reedijk, *J. Am. Chem. Soc.* **1984**, *106*, 3644−3647.
[28] J. Reedijk, *Chem. Commun.* **1996**, 801−806.
[29] J. D. Robertson, S. Orrenius, B. Zhivotovsky, *J. Struct. Biol.* **2000**, *129*, 346−358.
[30] A. M. Martelli, M. Zweyer, R. L. Ochs, P. L. Tazzari, G. Tabellini, P. Narducci, R. Bortul, *J. Cell. Biochem.* **2001**, *82*, 634−646.
[31] S. C. Dhara, *Indian J. Chem.* **1970**, *8*, 193−194.
[32] Y. P. Keepers, P. E. Pizao, G. J. Peters, J. Vanarkotte, B. Winograd, H. M. Pinedo, *Eur. J. Cancer* **1991**, *27*, 897−900.
[33] T. Mossmann, *J. Immunol. Methods* **1983**, *83*, 55−63.

Received May 28, 2003
Early View Article
Published Online October 10, 2003

 © 2003 Wiley-VCH Verlag GmbH & Co. KGaA, Weinheim

The Isoelectronic Replacement of E = P^+ and Si in the Trinuclear Organotin−Oxo Clusters $[Ph_2E(OSntBu_2)_2O{\cdot}tBu_2Sn(OH)_2]$

Jens Beckmann,*[a] Dainis Dakternieks,[a] Andrew Duthie,[a] Klaus Jurkschat,*[b] Michael Mehring,[b] Cassandra Mitchell,[a] and Markus Schürmann[b]

Keywords: Tin / Phosphorous / NMR spectroscopy / Cluster compounds

The trinuclear organotin–oxo cluster $[Ph_2P(OSntBu_2)_2O{\cdot}tBu_2Sn(OH)_2][O_3SCF_3]$ (**6**), was prepared in good yield by the consecutive reaction of $(tBu_2SnO)_3$ with F_3CSO_3H and Ph_2PO_2H, and adopts a common tricyclic $ESn_3O_3X_2$ structural motif with E = P; X = OH, similar to those found in the recently reported species $[M(OSntBu_2)_2O{\cdot}tBu_2Sn(OH)_2]$ [M = Ph_2Si (**1**), Me_2Si (**2**), CO (**3**), MesB (**4**)] and $[Ph_2Si(OSntBu_2)_2O{\cdot}tBu_2SnF_2]$ (**5**) where E = Si, C, B and X = OH, F. Compound **6** was characterized by multinuclear NMR spectroscopy, IR spectroscopy, electrospray mass spectrometry and single-crystal X-ray diffraction analysis. A natural population analysis (NPA) performed on the B3LYP/LANL2DZ level of theory for the molecular structures of the isoelectronic species $[Ph_2Si(OSntBu_2)_2O{\cdot}tBu_2Sn(OH)_2]$ (**1**) and $[Ph_2P(OSntBu_2)_2O{\cdot}tBu_2Sn(OH)_2]^+$ (**6a**) suggests that the positive charge of the latter is partially delocalised over the phenyl rings.

(© Wiley-VCH Verlag GmbH & Co. KGaA, 69451 Weinheim, Germany, 2003)

Introduction

In the last two decades there has been considerable interest in the chemistry of organotin−oxo clusters,[1] and particularly in those with Sn−O−P linkages.[1−8] In this regard, we and others have reported a variety of trinuclear organotin−oxo clusters $[M(OSntBu_2)_2O{\cdot}tBu_2Sn(OH)_2]$ [M = Ph_2Si (**1**),[9] Me_2Si (**2**),[10] CO (**3**),[11] and MesB (**4**)[12]] and $[Ph_2Si(OSntBu_2)_2O{\cdot}tBu_2SnF_2]$ (**5**)[13] that adopt a common tricyclic, almost planar $ESn_3O_3X_2$ (E = Si, C, B; X = OH, F) structural motif (Scheme 1). It was proposed that further examples of this class of compound might be accessible upon replacement of E by other organometallic fragments.[13]

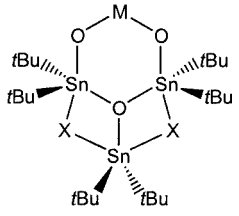

1, M = Ph_2Si, X = OH
2, M = Me_2Si, X = OH
3, M = OC, X = OH
4, M = MesB, X = OH
5, M = Ph_2Si, X = F
6a, M = Ph_2P^+, X = OH

Scheme 1

[a] Centre for Chiral and Molecular Technologies, Deakin University,
Geelong 3217, Australia
Fax: (internat.) +61-3-5227-1040
E-mail: beckmann@deakin.edu.au
[b] Lehrstuhl für Anorganische Chemie II, Universität Dortmund, 44221 Dortmund, Germany.
Fax: (internat.) +49-231-7553800
E-mail: kjur@platon.chemie.uni-dortmund.de

We now describe the synthesis and structure of $[Ph_2P(OSntBu_2)_2O{\cdot}tBu_2Sn(OH)_2](O_3SCF_3)$ (**6**), which features a cation, $[Ph_2P(OSntBu_2)_2O{\cdot}tBu_2Sn(OH)_2]^+$ (**6a**), that is isoelectronic to **1** and possesses a $PSn_3O_3(OH)_2$ structural motif in solution and in the solid state. The existence of the cation **6a** was recently suggested on the basis of a prominent mass cluster found in the electrospray mass spectrum of the eight-membered heterocycle *cyclo*-$[Ph_2P(OSntBu_2O)_2PPh_2](O_3SCF_3)_2$.[7]

Results and Discussion

The consecutive reaction of di-*tert*-butyltin oxide with triflic acid and diphenylphosphinic acid provided the trinuclear organotin−oxo cluster $[Ph_2P(OSntBu_2)_2O{\cdot}tBu_2Sn(OH)_2](O_3SCF_3)$ (**6**) in good yield [Equation (1)].

$$(tBu_2SnO)_3 + F_3CSO_3H + Ph_2PO_2H \longrightarrow [Ph_2P(OSntBu_2)_2O{\cdot}tBu_2Sn(OH)_2](O_3SCF_3)\ \mathbf{6} \quad (1)$$

Compound **6** comprises air-stable colourless crystals that are readily soluble in most common organic solvents. The ^{119}Sn NMR spectrum of **6** in $[D_3]MeCN$ reveals a singlet at $\delta = -240.4$ and a doublet at $\delta = -269.1$ with a $^2J(^{119}Sn\text{-}O\text{-}^{31}P)$ coupling constant of 134 Hz, with an integral ratio of 1:2. The ^{119}Sn chemical shifts are consistent with pentacoordinate tin atoms. The ^{119}Sn NMR spectrum of **6** in

 © 2003 Wiley-VCH Verlag GmbH & Co. KGaA, Weinheim DOI: 10.1002/ejic.200300401

[D_8]toluene shows almost identical signals at δ = −243.3 and −271.9 ppm [$^2J(^{119}Sn\text{-}O\text{-}^{31}P)$ = 140 Hz], which apparently suggests that acetonitrile is not involved in strong coordination to the tin atoms. High temperature ^{119}Sn NMR measurements (T = 90 °C) in [D_8]toluene indicate the high configurative stability of **6**, which contrasts with the tendency of [$Ph_2Si(OSn{t}Bu_2)_2O{\cdot}{t}Bu_2Sn(OH)_2$] (**1**) to undergo a reversible dissociation in chloroform into [$Ph_2Si(OSn{t}Bu_2)_2O$], ($t$$Bu_2SnO)_3$ and water, even at room temperature.[9] The ^{31}P NMR spectrum of **6** in [D_3]MeCN shows a signal at δ = 33.1 ppm with unresolved tin satellites [$^2J(^{31}P\text{-}O\text{-}^{119/117}Sn)$ = 136 Hz]. The electrospray mass spectrum (positive mode, cone voltage 20 V) of **6** displays two intense mass clusters at 965.2 and 700.1 Da that were unambiguously assigned to the organotin cations $[Ph_2P(OSn{t}Bu_2)_2O{\cdot}{t}Bu_2Sn(OH)_2]^+$ (**6a**) and $[Ph_2P(OSn{t}Bu_2)_2O]^+$ (**6b**), respectively. A conductivity measurement (372 μS cm^{-1}; c = 3.33 mmol·L^{-1}, Λ = 112 S cm^2 mol^{-1}) of **6** confirms the electrolytic dissociation into **6a** and triflate anions in MeCN.[14]

Solid-State Structure of $[Ph_2P(OSntBu_2)_2O{\cdot}tBu_2Sn(OH)_2][O_3SCF_3]$ (6)

The molecular structure of $[Ph_2P(OSn{t}Bu_2)_2O{\cdot}{t}Bu_2Sn(OH)_2](O_3SCF_3)$ (**6**) is shown in Figure 1; selected bond lengths and angles are collected in Table 1. Like its closely related stannasiloxane derivatives [$Ph_2Si(OSn{t}Bu_2)_2O{\cdot}{t}Bu_2SnX_2$] [X = OH (**1**),[9] F (**5**)[13]], the [$PSn_3O_3(OH)_2$] structural motif of **6a** is almost planar, the largest deviation from the plane being 0.033(3) Å. All three tin atoms show slightly distorted trigonal bipyramidal configurations [geometrical goodness[15] ΔΣ(θ) = 89.0° for Sn(1), 89.6° for Sn(2), 90.1° for Sn(3)], in which two carbon atoms and an oxygen atom occupy the equatorial positions [C(10), C(20) and O(1) for Sn(1); C(30), C(40) and O(1) for Sn(2); C(50), C(60) and O(1) for Sn(3)]. The axial positions are occupied by O(2) and O(4) for Sn(1), O(3) and O(5) for Sn(2), and O(4) and O(5) for Sn(3).

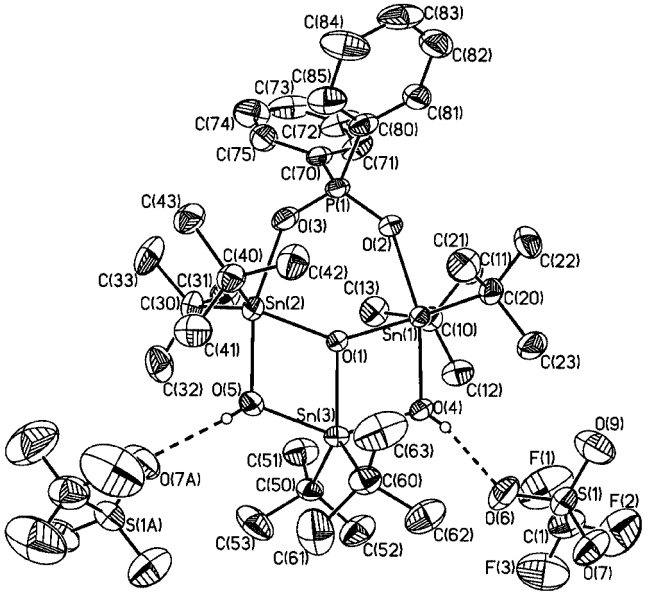

Figure 1. ORTEP diagram of the cation **6a** and two associated triflate anions showing 30% probability displacement ellipsoids and the atom numbering scheme (symmetry transformations used to generate equivalent atoms: a = $-x$, y −1/2, −1/2 − z)

Table 1. Selected bond lengths [Å] and bond angles [°] for **6**; symmetry operation used to generate equivalent atoms: a = $-x$, y −1/2, −1/2 − z.

Sn(1)−O(1)	2.076(2)	Sn(1)−O(2)	2.192(3)
Sn(1)−O(4)	2.138(2)	Sn(1)−C(10)	2.183(4)
Sn(1)−C(20)	2.187(4)	Sn(2)−O(1)	2.075(2)
Sn(2)−O(3)	2.200(3)	Sn(2)−O(5)	2.134(3)
Sn(2)−C(30)	2.181(4)	Sn(2)−C(40)	2.185(4)
Sn(3)−O(1)	2.152(2)	Sn(3)−O(4)	2.109(3)
Sn(3)−O(5)	2.106(3)	Sn(3)−C(50)	2.188(4)
Sn(3)−C(60)	2.180(4)	P(1)−O(2)	1.509(3)
P(1)−O(3)	1.493(3)	P(1)−C(70)	1.795(4)
P(1)−C(80)	1.818(3)	O(4)−O(6)	2.787(5)
O(5)−O(7a)	2.786(5)		
O(1)−Sn(1)−O(2)	89.93(9)	O(1)−Sn(1)−O(4)	72.53(9)
O(2)−Sn(1)−O(4)	162.45(10)	O(1)−Sn(1)−C(10)	117.27(12)
O(1)−Sn(1)−C(20)	118.24(13)	O(2)−Sn(1)−C(10)	90.67(13)
O(2)−Sn(1)−C(20)	90.33(13)	O(4)−Sn(1)−C(10)	96.83(13)
O(4)−Sn(1)−C(20)	98.34(13)	C(20)−Sn(1)−C(10)	124.48(16)
O(1)−Sn(2)−O(3)	89.02(9)	O(1)−Sn(2)−O(5)	72.61(10)
O(3)−Sn(2)−O(5)	161.47(12)	O(1)−Sn(2)−C(30)	117.26(12)
O(1)−Sn(2)−C(40)	118.13(13)	O(3)−Sn(2)−C(30)	91.81(16)
O(3)−Sn(2)−C(40)	89.30(14)	O(5)−Sn(2)−C(30)	98.87(16)
O(5)−Sn(2)−C(40)	96.91(14)	C(30)−Sn(2)−C(40)	124.69(16)
O(1)−Sn(3)−O(4)	71.59(9)	O(1)−Sn(3)−O(5)	71.66(10)
O(4)−Sn(3)−O(5)	143.20(11)	O(1)−Sn(3)−C(50)	119.97(13)
O(1)−Sn(3)−C(60)	119.79(14)	O(4)−Sn(3)−C(50)	101.03(14)
O(4)−Sn(3)−C(60)	97.14(15)	O(5)−Sn(3)−C(50)	98.77(14)
O(5)−Sn(3)−C(60)	99.20(15)	C(50)−Sn(3)−C(60)	120.24(16)
O(2)−P(1)−O(3)	115.22(14)	O(2)−P(1)−C(70)	108.52(18)
O(2)−P(1)−C(80)	105.28(18)	O(3)−P(1)−C(70)	110.30(19)
O(3)−P(1)−C(80)	113.3(2)	C(70)−P(1)−C(80)	103.40(18)
Sn(1)−O(1)−Sn(2)	143.63(11)	Sn(1)−O(1)−Sn(3)	108.29(9)
Sn(1)−O(4)−Sn(3)	108.29(9)	Sn(2)−O(1)−Sn(3)	108.07(10)
Sn(2)−O(5)−Sn(3)	107.59(14)	Sn(1)−O(2)−P(1)	140.30(16)
Sn(2)−O(3)−P(1)	141.72(16)		

The effects of the variation of E and X upon the overall geometry of the tristannoxane motif of [$Ph_2E(OSn{t}Bu_2)_2O{\cdot}{t}Bu_2Sn(X)_2$] [E = P^+, X = OH (**6a**); E = Si, X = OH (**1**); E = Si, X = F (**5**)] is shown in Table 2 and can be summarized as follows: (*i*) The Sn(1)−O(1) and Sn(2)−O(1) distances show only marginal differences. The Sn(3)−O(1) distances decrease in the order **6** > **1** > **5**. (*ii*) The Sn(1)−X(1) and Sn(2)−X(2) distances increase on going from **6** to **1** and then **5**, which is consistent with the dissociation of compound **1** in solution, as shown by variable temperature ^{119}Sn NMR spectroscopy.[9] (*iii*) The Sn(1)−O(2) and Sn(2)−O(3) distances also decrease in the order **6** > **1** > **5**. (*iv*) The geometrical goodness ΔΣ(θ)[15] of the trigonal bipyramidal configurations for Sn(1) and Sn(2), is best for compound **6**. For the Sn(3) atom there is almost no difference between compounds **1**, **5** and **6** .

Consistent with the ^{119}Sn chemical shifts in solution and the molecular structure established by X-ray diffraction, the ^{119}Sn MAS NMR spectrum of **6** shows two signals at δ =

 © 2003 Wiley-VCH Verlag GmbH & Co. KGaA, Weinheim

Table 2. Comparison of selected bond lengths [Å] and geometrical goodness' [°]; [definition: $\Delta\Sigma(\theta) = \Sigma(\theta_{eq}) - \Sigma(\theta_{ax})$; 0°(tetrahedron) $\leq \Delta\Sigma(\theta) \leq$ 90°(trigonal bipyramid)][15] for **1**, **5** and **6a**

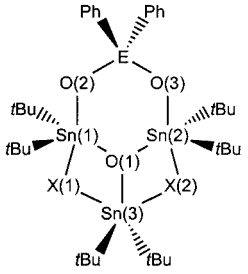

1, E = Si, X = OH
5, E = Si, X = F
6a, E = P^+, X = OH

	6a, E = P^+, X(1) = X(2) = O	**1**, E = Si,[9] X(1) = X(2) = O	**5**, E = Si,[13] X(1) = X(2) = F
Sn(1)−O(1)	2.076(2)	2.092(2)	2.098(4)
Sn(2)−O(1)	2.075(2)	2.093(2)	2.109(4)
Sn(3)−O(1)	2.153(2)	2.091(2)	2.064(4)
Sn(1)−X(1)	2.138(2)	2.261(3)	2.399(3)
Sn(3)−X(1)	2.109(3)	2.106(3)	2.074(3)
Sn(2)−X(2)	2.134(3)	2.264(3)	2.353(3)
Sn(3)−X(2)	2.109(3)	2.103(3)	2.073(3)
Sn(1)−O(2)	2.192(3)	2.020(2)	1.981(4)
Sn(2)−O(3)	2.200(3)	2.018(3)	1.999(4)
$\Delta\Sigma(\theta)$ for Sn(1)	89.0	73.7	65.9
$\Delta\Sigma(\theta)$ for Sn(2)	89.6	74.2	64.5
$\Delta\Sigma(\theta)$ for Sn(3)	90.1	89.7	88.2

−246.1 and −277.9 with an integral ratio of 39:61 and accompanying sets of spinning sidebands. The sets of spinning sidebands were used to perform a tensor analysis according to the method of Herzfeld and Berger;[16] the results are collected along with those of the stannasiloxane **1** in Table 3. In view of the similar molecular structures of compounds **1** and **6**, it is not surprising that the anisotropy (ζ) and asymmetry (η) parameters are also comparable. With the data at hand, it appears that the anisotropy (ζ) somewhat correlates with an increasing geometrical goodness $\Delta\Sigma(\theta)$; however, this tentative observation may be subject to revision when more examples are available for comparison. The individual P−O bond lengths of the organotin phosphinate **6** [1.493(3), 1.509(3) Å] differ only slightly.

Table 3. Selected ^{119}Sn MAS NMR parameters for **1** and **6**.

	δ_{iso} [ppm][a]	%	ζ [ppm]	η	σ_{11} [ppm]	σ_{22} [ppm]	σ_{33} [ppm]
1[9]	−265.7	33	471	0.61	−115	175	737
	−273.7	67	417	0.68	−78	207	692
6	−246.1	39	508	0.45	−123	106	755
	−277.9	61	522	0.60	−140	174	800

[a] Definitions: $\delta_{iso} = -\sigma_{iso} = -(\sigma_{11} + \sigma_{22} + \sigma_{33})/3$; $\zeta = \sigma_{33} - \sigma_{iso}$ and $\eta = \sigma_{22} - \sigma_{11}/\sigma_{33} - \sigma_{iso}$ where σ_{11}, σ_{22} and σ_{33} are the principal tensor components on the shielding anisotropy (SA), sorted as follows $\sigma_{33} - \sigma_{iso} > \sigma_{11} - \sigma_{iso} > \sigma_{22} - \sigma_{iso}$.

In the crystal lattice, the cations **6a** are associated with the triflate anions through O(4)-H(4)···O(6) and O(5)-H(5)···O(7a) hydrogen bonds giving rise to the formation of an infinite chain (symmetry operation: $a = -x, y - 1/2, -1/2 - z$), as shown in Figure 2. The O(4)···O(6) and O(5)···O(7a) distance of 2.789(6) and 2.791(6) Å, respectively, and the position of the corresponding OH stretching vibration ν(OH) at 3338 cm^{-1} in the IR spectrum of **6** are indicative of medium-strength hydrogen bonding.[17] The fact that the triflate anions are not involved in coordination to tin atoms is also reflected by IR spectroscopy. Generally, for the free triflate anion (C_{3v} symmetry) the asymmetric SO_3 stretching vibration $\nu_{as}(SO_3)$ is doubly degenerate, whereas in the presence of sufficiently large cation−anion interactions the axial symmetry is diminished (C_s symmetry), and the asymmetric SO_3 stretching vibration $\nu_{as}(SO_3)$ splits into two components.[18] Thus, for $[Ph_2P(OSn\textit{t}Bu_2)_2O{\cdot}\textit{t}Bu_2Sn(OH)_2](O_3SCF_3)$ (**6**), the non-coordinating triflate anion gives rise to only one IR absorption (KBr) for the asymmetric SO_3 stretching vibration $\nu_{as}(SO_3)$ at 1285 cm^{-1}. The symmetric SO_3 stretching vibration $\nu_s(SO_3)$ is found at 1034 cm^{-1}.

Charge Distribution in $[Ph_2E(OSn\textit{t}Bu_2)_2O{\cdot}\textit{t}Bu_2Sn(OH)_2]$ [E = Si (1), P^+ (6a)]

Considering the structural similarity of $[Ph_2E(OSn\textit{t}Bu_2)_2O{\cdot}\textit{t}Bu_2Sn(OH)_2]$ with E = Si (**1**) and E = P^+ (**6a**), the question arises as to where the positive charge of **6a** is situated. In an effort to answer this question a natural population analysis (NPA)[19] was performed at the B3LYP/LANL2DZ level of theory and the atomic charges are given in Scheme 2. Somewhat unexpected, the atomic charges of the Si and P atoms are almost alike at about 2.2 (variation < 0.1). Moreover, the atomic charges of all Sn atoms are almost identical at about 2.5 for both compounds (variation < 0.05). However, this result is essentially in agreement with the results obtained by single-crystal X-ray structure determination. In compound **1** the Sn(1)−O(2) and Sn(2)−O(3) bond lengths of 2.020(2) and 2.018(3) Å, respectively, are somewhat shorter than the corresponding values of 2.192(3) and 2.200(3) Å in **6a**. The Sn−O bonding situation is reversed for the Sn(1)−X(1) and Sn(2)−X(2) bond lengths [2.261(3) and 2.264(3) Å in **1**; 2.138(2) and 2.134(3) Å in **6a**]. A minor difference of +0.26 is found for the atomic charges of the two E−O oxygen atoms (E = Si, P). A more significant change of +0.48 is observed for the group atomic charges of the two phenyl groups on going from **1** to **6a**. The remainder of the atomic charge difference of +0.24 is almost equally divided over the six *tert*-butyl groups (variation per *tert*-butyl group smaller than 0.05). Thus, it appears that the largest fraction of the positive charge in **6a** is delocalised over the polarisable phenyl groups. Apparently, this observation provides a reasonable explanation for the absence of strong cation−anion interactions in **6**, which is in marked contrast to the related eight-membered heterocycle *cyclo*-$[Ph_2P(OSn\textit{t}Bu_2O)_2PPh_2](O_3SCF_3)_2$.[7]

 © 2003 Wiley-VCH Verlag GmbH & Co. KGaA, Weinheim

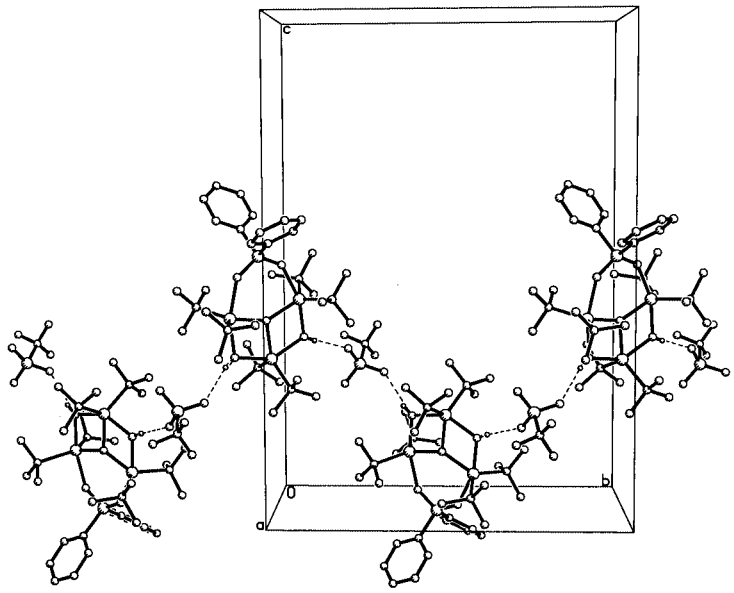

Figure 2. Perspective view through the *c*-axis of **6** showing the hydrogen bond interaction in the crystal lattice

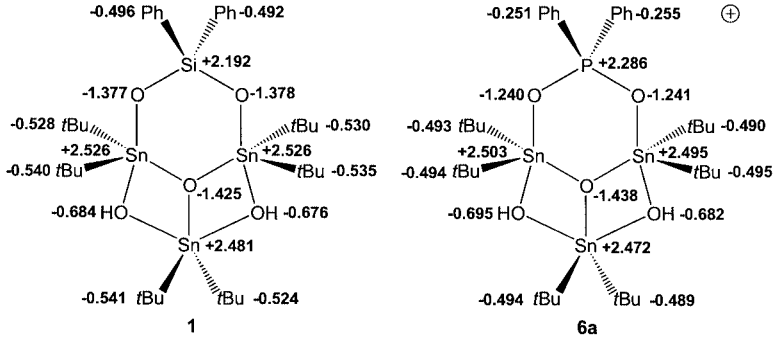

Scheme 2

Experimental Section

General Remarks: (tBu$_2$SnO)$_3$ was prepared according to the literature.[20] F_3CSO_3H and Ph_2PO_2H were purchased from Aldrich. The solution NMR spectra (conc. 50 mg/300 μL; 25 °C) were measured using a Jeol Eclipse Plus 400 spectrometer [at 399.78 MHz (^{1}H) 100.54 (^{13}C) 161.84 (^{31}P) 149.05 (^{119}Sn)] and were referenced against $SiMe_4$, aqueous H_3PO_4 (90%) and $SnMe_4$. The solid-state NMR spectra were measured using the same instrument equipped with a 4 mm MAS probe. Crystalline $NH_4H_2PO_4$ (δ = 0.95 ppm) and c-Hex$_4$Sn (δ = −97.35 ppm) were used as secondary references. The ^{119}Sn MAS NMR spectra were obtained using cross polarization (contact time 5 ms, recycle delay 10s). The isotropic chemical shifts δ_{iso} were determined by comparison of two acquisitions measured at sufficiently different spinning frequencies. The tensor analyses were performed using the method of Herzfeld and Berger[16] implemented in DmFit 2002.[21] The IR spectrum was recorded using a BioRad FTIR spectrometer. The ESMS spectrum was obtained with a Platform II single quadrupole mass spectrometer (Micromass, Altrincham, UK) using an acetonitrile mobile phase. MeCN solutions (0.1 mM) were injected directly into the spectrometer with a Rheodyne injector equipped with a 50 μL loop. A Harvard 22 syringe pump delivered the solutions to the vaporisation nozzle of the electrospray ion source at a flow rate of 10 μL min^{-1}. Nitrogen was used both as a drying gas and for nebulization with flow rates of approx. 200 mL min^{-1} and 20 mL min^{-1} respectively. The pressure in the mass analyser region was usually about 4×10^{-5} mbar. The conductivity measurement was performed using a CDM80 Conductivity Meter equipped with a CDC104 Conductivity Cell (Radiometer Copenhagen, DK) at 25 °C. Microanalysis was carried out by CMAS, Belmont, Australia.

[Ph$_2$P(OSntBu$_2$)$_2$O·tBu$_2$Sn(OH)$_2$](O$_3$SCF$_3$) (6): F_3CSO_3H (150 mg, 1.00 mmol) was added to a suspension of (tBu$_2$SnO)$_3$ (747 mg, 1.00 mmol) in MeCN (20 mL) whilst stirring at room temperature. After 10 min, solid Ph_2PO_2H (218 mg, 1.00 mmol) was added, and the mixture heated at 85 °C for 12 h. The solvent was removed in vacuo, to yield a white powder, which was recrystallized from $CHCl_3$/MeCN to give colourless crystals of **6** [959 mg, 0.86 mmol, 86%; m.p. 220 °C (dec)].

^{119}Sn NMR ([D$_3$]MeCN): δ = −240.4 (1Sn), −269.1 [d, 2Sn; ^2J(^{119}Sn-O-^{31}P) = 134 Hz] ppm. ^{119}Sn NMR ([D$_8$]toluene): δ = −243.3 (1Sn), −271.9 [d, 2Sn; ^2J(^{119}Sn-O-^{31}P) = 140 Hz] ppm. ^{31}P NMR ([D$_3$]MeCN): δ = 33.1 [^2J(^{31}P-O-$^{119/117}$Sn) = 136 Hz] ppm. ^{13}C NMR ([D$_3$]MeCN): δ = 133.0, 131.0, 129.9, 127.4, 119.2, 41.8, 38.9, 28.7, 28.5 ppm. ^{1}H NMR ([D$_3$]MeCN): δ = 8.00−7.50 (m,

 © 2003 Wiley-VCH Verlag GmbH & Co. KGaA, Weinheim

10 H), 1.52 (s, 9 H, $^3J(^1H\text{-}^{119}Sn)$ = 112 Hz), 1.48 (s, 18 H, $^3J(^1H\text{-}^{119}Sn)$ = 119 Hz) ppm. ^{119}Sn MAS NMR: δ = −246.1 (1 Sn), −277.9 (2 Sn) ppm. ^{31}P MAS NMR: δ = 27.4 ppm. IR (KBr): $\tilde{\nu}$ = 3338 br, 3064 w, 2976 m, 2947 m, 2853 s, 1466 m, 1441 w, 1396 w, 1366 w, 1285 s, 1253 s, 1224 w, 1166 s, 1131 vs, 1048 s, 1034 m, 1014 m, 998 w, 941 w, 802 w, 756 w, 721 m, 698 w, 665 w, 638 m, 548 m, 532 m, 448 m cm^{-1}. $C_{37}H_{66}F_3O_8PSSn_3$ (1115.16): calcd. C 39.85, H, 5.97; found C 39.82, H 6.00. ES MS (positive mode, cone voltage 20 V): *m*/*z* = 700.1 $[Ph_2P(OSntBu_2)_2O]^+$, 965.2 $[Ph_2P(OSntBu_2)_2O{\cdot}tBu_2Sn(OH)_2]^+$. Conductivity measurement (MeCN; *c* = 3.33 mmol·L^{-1}): 372 μS cm^{-1}.

X-ray Crystallographic Study: Single crystals of $[Ph_2P(OSntBu_2)_2O{\cdot}tBu_2Sn(OH)_2](O_3SCF_3)$ (**6**) suitable for X-ray crystallography were obtained by slow evaporation of a CH_2Cl_2/*n*-hexane solution. Data and structure solution at *T* = 293(2) K: $C_{37}H_{66}F_3O_8PSSn_3$, (1115.00), orthorhombic, $P2_12_12_1$, crystal dimensions: 0.20 × 0.25 × 0.45 mm^3, *a* = 10.7376(6), *b* = 17.9769(10), *c* = 25.4598(14) Å, *V* = 4914.5(5) $Å^3$, *Z* = 4, $\rho_{calcd.}$ = 1.507 Mg·m^{-3}, *F*(000) = 2240, μ = 1.640 mm^{-1}. Intensity data were collected on a Bruker SMART Apex CCD diffractometer fitted with Mo-K_α radiation (graphite crystal monochromator, λ = 0.71073 Å) to a maximum of θ_{max} = 27.52° via ω scans (completeness 99.6% to θ_{max}). Data were reduced and corrected for absorption using the programs SAINT and SADABS.[22] The structure was solved by direct methods and difference Fourier synthesis using SHELX-97 implemented in the program WinGX 2002.[23] Full-matrix least-squares refinement on F^2 using all data was carried out with anisotropic displacement parameters applied to all non-hydrogen atoms. The hydrogen atoms H(4) and H(5) were located in the Fourier density map and refined isotropically, whereas all other hydrogen atoms were included in geometrically calculated positions using a riding model and were refined isotropically. One phenyl group is disordered over two positions with occupancies of 0.8 [C(80) to C(85)] and 0.2 [C(80′) to C(85′)], which were refined as regular hexagons (AFIX66). One carbon atom of a *tert*-butyl group is also disordered and was refined over two sites with occupancies of 0.7 C(61) and 0.3 C(61′). The weighting scheme employed was of the type $w = [\sigma^2(F_o^2) + (0.0404\ P)^2 + 0.6740\ P]^{-1}$ where $P = (F_o^2 + 2\ F_c^2)/3$. R_1 = 0.0284 for 10422 [$I > 2\sigma(I)$] reflections and wR_2 = 0.0692 for 11216 independent reflections; GooF = 1.035. The Flack parameter was −0.002(17).[24] The max. and min. residual electron densities were 0.900/−0.233 e·$Å^{-3}$. CCDC-213484 contains the supplementary crystallographic data for this paper. These data can be obtained free of charge at www.ccdc.cam.ac.uk/conts/retrieving.html [or from the Cambridge Crystallographic Data Centre, 12, Union Road, Cambridge CB2 1EZ, UK; Fax: (internat.) +44-1223-336-033; E-mail: deposit@ccdc.cam.ac.uk].

MO Calculation: Single point calculations based on the coordinates of the molecular structures of $[Ph_2E(OSntBu_2)_2O{\cdot}tBu_2Sn(OH)_2]$ with E = Si (**1**) and E = P^+ (**6a**) were performed at the B3LYP/LANL2DZ level of theory using Gaussian 98.[25] Natural bond orbital charges were obtained using NBO 5.0.[26]

Acknowledgments

The Australian Research Council (ARC) and the Deutsche Forschungsgemeinschaft (DFG) are thanked for financial support. Dr. Jonathan White (The University of Melbourne) is gratefully acknowledged for the X-ray crystallography data collection.

[1] V. Chandrasekhar, S. Nagendran, V. Baskar, *Coord. Chem. Rev.* **2002**, *235*, 1−52.
[2] R. R. Holmes, *Acc. Chem. Res.* **1989**, *22*, 190−197.
[3] V. K. Jain, *Coord. Chem. Rev.* **1994**, *135*/*136*, 809−843.
[4] F. Ribot, C. Sanchez, M. Biesemans, F. A. G. Mercier, J. C. Martins, M. Gielen, R. Willem, *Organometallics* **2001**, *20*, 2593−2603.
[5] A. F. Shihada, F. Weller, *Z. Anorg. Allg. Chem.* **2001**, *627*, 638−644.
[6] V. Chandrasekhar, V. Baskar, A. Steiner, S. Zacchini, *Organometallics* **2002**, *21*, 4528−4532.
[7] J. Beckmann, D. Dakternieks, A. Duthie, C. Mitchell, *Organometallics* **2003**, *22*, 2161−2164.
[8] J. Beckmann, D. Dakternieks, A. Duthie, C. Mitchell, *Dalton Trans.* **2003**, 3258−3263.
[9] J. Beckmann, K. Jurkschat, B. Mahieu, M. Schürmann, *Main Group Met. Chem.* **1998**, *21*, 113−122.
[10] F. Cervantes-Lee, H. K. Sharma, I. Haiduc, K. H. Pannell, *J. Chem. Soc., Dalton Trans.* **1998**, 1−2.
[11] H. Reuter, PhD thesis, University of Bonn, Germany, **1986**.
[12] P. Brown, M. F. Mahon, K. C. Molloy, *J. Chem. Soc., Dalton Trans.* **1992**, 3503−3509.
[13] J. Beckmann, K. Jurkschat, M. Schürmann, D. Suter, R. Willem, *Organometallics* **2002**, *21*, 3819−3822.
[14] W. J. Geary, *Coord. Chem. Rev.* **1971**, *7*, 81−122.
[15] U. Kolb, M. Beuter, M. Dräger, *Inorg. Chem.* **1994**, *33*, 4522−4530.
[16] J. Herzfeld, X. Chen *Encyclopedia of Nuclear Magnetic Resonance, Vol. 7*, Eds.; D. M. Grant, R. K. Harris, John Wiley & Sons, Chichester, **1996**, 6021−6030.
[17] G. A. Jeffrey, *An Introduction to Hydrogen Bonding*, Oxford University Press, New York, **1997**.
[18] G. A. Lawrance, *Chem. Rev.* **1986**, *86*, 17−33.
[19] A. E. Reed, L. A. Curtiss, F. Weinhold, *Chem. Rev.* **1988**, *88*, 899−926.
[20] H. Puff, W. Schuh, R. Sievers, W. Wald, R. Zimmer, *J. Organomet. Chem.* **1984**, *260*, 271−280.
[21] D. Massiot, F. Fayon, M. Capron, I. King, S. Le Calvé, B. Alonso, J.-O. Durand, B. Bujoli, Z. Gan, G. Hoatson, *Mag. Res. Chem.* **2002**, *40*, 70−76.
[22] SMART, SAINT and SADABS, Siemens Analytical X-ray Instruments Inc. Madison, Wisconsin USA, **1999**.
[23] L. J. Farrugia, *J. Appl. Crystallogr.* **1997**, *20*, 565.
[24] H. D. Flack, *Acta Crystallogr., Sect. A* **1983**, *39* 876−881.
[25] Gaussian 98, Revision A.7, M. J. Frisch, G. W. Trucks, H. B. Schlegel, G. E. Scuseria, M. A. Robb, J. R. Cheeseman, V. G. Zakrzewski, J. A. Montgomery, R. E. Stratmann, J. C. Burant, S. Dapprich, J. M. Millam, A. D. Daniels, K. N. Kudin, M. C. Strain, O. Farkas, J. Tomasi, V. Barone, M. Cossi, R. Cammi, B. Mennucci, C. Pomelli, C. Adamo, S. Clifford, J. Ochterski, G. A. Petersson, P. Y. Ayala, Q. Cui, K. Morokuma, D. K. Malick, A. D. Rabuck, K. Raghavachari, J. B. Foresman, J. Cioslowski, J. V. Ortiz, B. B. Stefanov, G. Liu, A. Liashenko, P. Piskorz, I. Komaromi, R. Gomperts, R. L. Martin, D. J. Fox, T. Keith, M. A. Al-Laham, C. Y. Peng, A. Nanayakkara, C. Gonzalez, M. Challachombe, P. M. W. Gill, B. G. Johnson, W. Chen, M. W. Wong, J. L. Andres, M. Head-Gordon, E. S. Replogle, J. A. Pople, Gaussian, Inc., Pittsburgh, **1998**.
[26] NBO 5.0. E. D. Glendening, J. K. Badenhoop, A. E. Reed, J. E. Carpenter, J. A. Bohmann, C. M. Morales, F. Weinhold (Theoretical Chemistry Institute, University of Wisconsin, Madison, WI, **2001**.

Received June 26, 2003
Early View Article
Published Online October 10, 2003

 © 2003 Wiley-VCH Verlag GmbH & Co. KGaA, Weinheim

New Diphosphane Ligands Based on Bisphenol A Backbones − Synthesis and Coordination Chemistry

Jarl Ivar van der Vlugt,[a] Michiel M. P. Grutters,[a] Allison M. Mills,[b] Huub Kooijman,[b] Anthony L. Spek,[b] and Dieter Vogt*[a]

Keywords: Ligand design / Phosphanes / Coordination modes / Structure elucidation / Transition metals

A series of easily accessible diphosphane compounds **1**–**4**, based on bisphenol A derived backbones, has been prepared. A straightforward two-step synthetic route has been employed to obtain these new ligands in good yields from cheap starting materials. Molecular structures for both compound **2** and its oxidized form (**5**·H_2O) have been determined and are discussed in detail. The coordination of ligand **2** to palladium, platinum, and rhodium precursors has been studied by NMR spectroscopy as well as X-ray crystallography. The molecular structures of the face-to-face dimeric species [{$PdCl(CH_3)$(**2**)}$_2$] (**6**), [{$PtCl_2$(**2**)}$_2$] (**7**), and [{$RhCl(CO)$(**2**)}$_2$] (**8**) are described in detail.
(© Wiley-VCH Verlag GmbH & Co. KGaA, 69451 Weinheim, Germany, 2003)

Introduction

The coordination chemistry of diphosphane ligands with a variety of transition metals has been widely studied and several types of coordination modes have been established over the years.[1,2] Numerous families of novel ligands have been synthesized,[3] with emphasis on *cis*-chelation to form monomeric metal complexes. As well as designing ligands based on desired behaviour towards transition metals and the catalytic activity of the resultant systems, the approach of modular design and availability from cheap resources has gained significant importance.

We have chosen Bisphenol A as a somewhat neglected yet promising starting material for the synthesis of a new ligand class.[4,5] A wide range of these bisphenols is commercially available at low price since they are used as components in epoxy resins. Generic structures are easily available by simple acid catalyzed condensation of a ketone with two molecules of a phenol.[6] Based on these versatile compounds we employed a straightforward two-step synthetic route to novel P-containing compounds (Scheme 1).

In the first step, the phenol groups were protected by methylation with iodomethane. Subsequently, selective *ortho*-lithiation of both phenyl rings was followed by reaction with the phosphane source $ClPPh_2$. Filtration and evaporation of the solvent followed by washing of the crude product with methanol afforded the pure compounds in overall yields of 40−50%. Using this method, we obtained compounds **1**−**3** based on derivatives of the Bisphenol A backbone. Furthermore, the silicon derivative **4** was synthesized in good yield starting from 4-bromoanisole and dichlorodimethylsilane via a modified two-step route. Compounds **1**−**4** were characterized by ^1H, ^{13}C, and ^{31}P NMR spectroscopy, as well as by elemental analysis. We have previously reported this synthetic route, focussing on the synthesis and catalytic applicability of a ligand derived from 1,2-diphenylbenzene as the backbone.[5]

We were able to obtain single crystals, suitable for X-ray analysis, for compounds **1**−**3**, by recrystallization of the pure solids from hot 1-propanol or hot acetonitrile. Only the molecular structure of compound **2** is depicted in Figure 1, while selected bond lengths and bond angles for all three compounds are summarized in Table 1.

Because of the rotational freedom of the aromatic rings in the backbone, the diphenylphosphane groups are not constrained to any particular mutual orientation. Compound **2** shows approximate C_2 symmetry. The bond distances between the *ipso*-carbons of the backbone with the phosphorus atoms are normal at around 1.84 Å [P^1-C^3 1.840(2) Å and P^2-C^9 1.845(2) Å]. The central-carbon (C^{15}) of the backbone is clearly tetrahedrally surrounded. The through-space P^1-O^1 and P^2-O^2 distances are around 2.8−2.9 Å. The intramolecular P−P distance is 9.7664(8) Å.

To obtain the corresponding diphosphane oxide, we reacted compound **2** with hydrogen peroxide to yield compound **5**. In the ^{31}P NMR spectrum a singlet was observed at $\delta = 27.7$ ppm which is a typical value for a phosphane oxide.[7] We were able to obtain single crystals, suitable for

[a] Schuit Institute of Catalysis, Laboratory of Homogeneous Catalysis, Eindhoven University of Technology,
P. O. Box 513, 5600 MB Eindhoven, The Netherlands
Fax: (internat.) + 31-40-2455054
E-mail: d.vogt@tue.nl
[b] Laboratory for Crystal and Structural Chemistry, Department of Chemistry, Utrecht University,
Padualaan 8, 3584 CH, Utrecht, The Netherlands

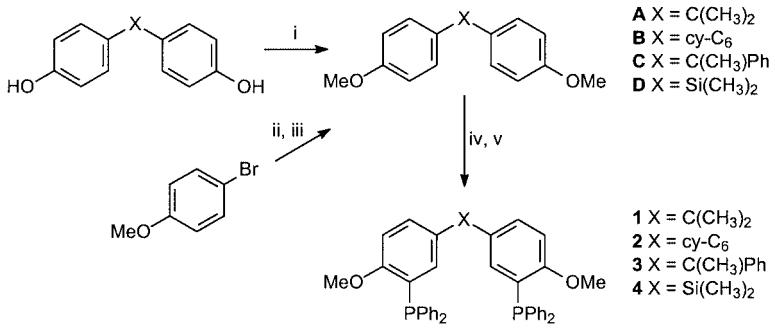

Scheme 1. Synthetic route to BPphos

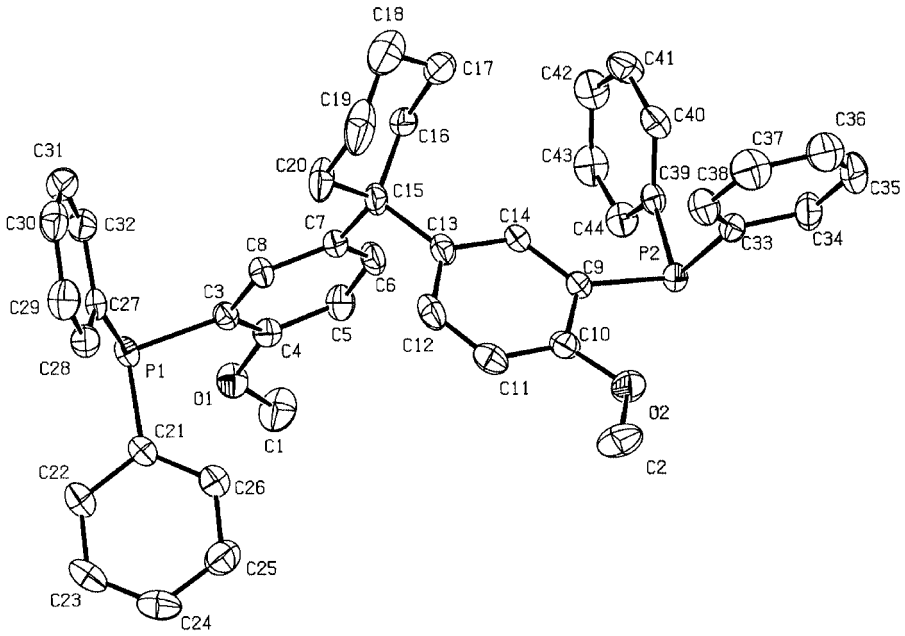

Figure 1. Molecular structure of compound **2**

Table 1. Selected bond lengths and angles for compounds **1**−**3**

	1	**2**	**3**
Bond lengths [Å]			
P^1-C^3	1.8484(15)	1.840(2)	1.8354(16)
P^2-C^9	1.8428(16)	1.845(2)	1.8385(17)
O^1-C^1	1.429(2)	1.431(3)	1.413(3)
O^1-C^4	1.374(2)	1.370(2)	1.375(2)
O^2-C^2	1.429(3)	1.425(3)	1.424(2)
O^2-C^{10}	1.372(2)	1.372(2)	1.376(2)
P^1-P^2	9.8510(6)	9.7664(8)	6.7749(6)
Angles [°]			
$C^1-O^1-C^4$	117.64(13)	117.52(17)	118.25(14)
$C^2-O^2-C^{10}$	118.26(14)	117.86(16)	117.61(14)
$P^1-C^3-C^4$	118.25(11)	118.01(14)	116.89(12)
$P^2-C^9-C^{10}$	117.17(13)	118.72(15)	116.99(13)
$C^7-C^{15}-C^{13}$	111.30(13)	106.96(14)	110.23(13)

X-ray analysis, from a THF solution. The molecular structure is depicted in Figure 2, with selected bond lengths and angles listed in Table 2.

The structure of compound **5** represents the diphosphane oxide of **2** but with an additional molecule of water present. There is hydrogen-bonding between the oxo groups of compound **5** and the hydrogen atoms of the water molecule.[8] The O−H···O(P) contacts are almost equivalent with $H^{\#}-O(P)$ bond lengths of 1.99(5) Å ($H^{\#}-O^3$) and 2.01(5) Å ($H^{\#}-O^4$), which are much smaller than the calculated sum of the van der Waals radii of 2.72 Å. The $O^5-O(P)$ distances are 2.835(7) Å (O^3-O^5) and 2.822(7) Å (O^4-O^5) and the $O^5-H^{\#}-O(P)$ angles are 166(5)° (P^1) and 168(6)° (P^2), respectively. Furthermore, the orientation of the two phosphorus atoms is dramatically altered relative to the structure of the free ligand (vide supra). Due to the template effect of the water molecule, both P-atoms are located on the same side of the molecule with the oxygen atoms pointing towards one another. This leads to a decreased P^1-P^2 distance of 6.579(2) Å. The bond lengths between the phosphorus and carbon atoms of the ligand backbone (P^1-C^3 and P^2-C^9) are slightly shorter than the corresponding distances in compound **2**, due to a decrease of electron density on the phosphorus atoms in the oxidized state. The P−O bond lengths found for both phosphane oxide moieties, 1.491(4) Å (P^1-O^3) and 1.492(5) Å (P^2-O^4), are similar to those found in triphenylphosphane oxide hemihydrate[8] and tris(*p*-tolyl)phosphane oxide[9] but slightly lower in comparison with the mono oxide of

 © 2003 Wiley-VCH Verlag GmbH & Co. KGaA, Weinheim

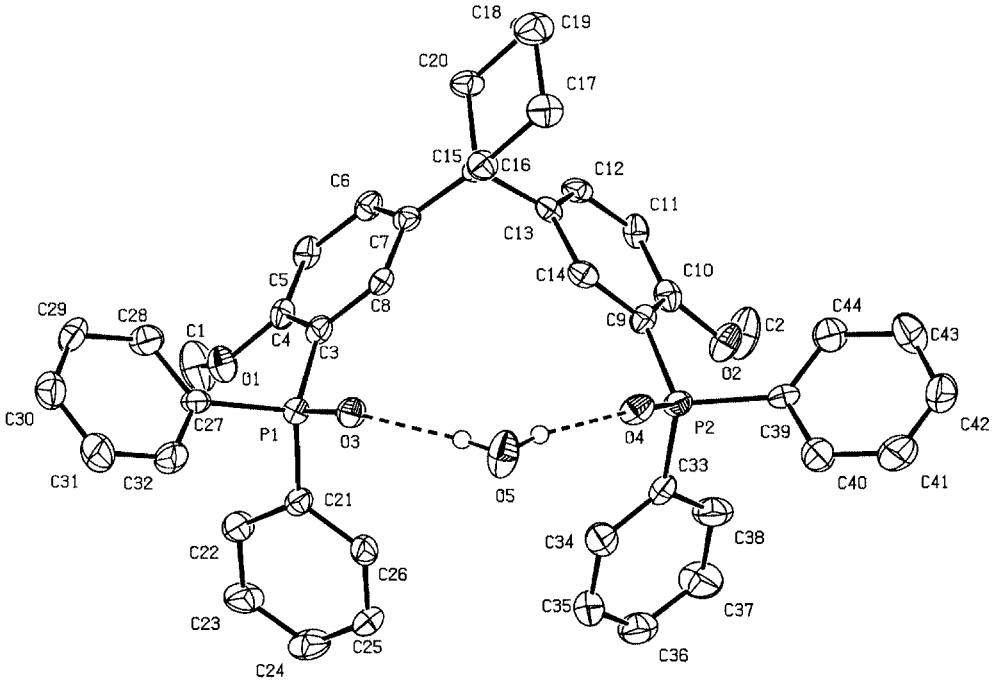

Figure 2. Crystal structure of compound **5**

Table 2. Selected bond lengths and angles for compound **5**·H_2O

Bond lengths [Å]		Angles [°]	
P^1-C^3	1.810(7)	$C^1-O^1-C^4$	117.4(6)
P^2-C^9	1.803(9)	$C^2-O^2-C^{10}$	118.9(6)
O^1-C^1	1.427(9)	$P^1-C^3-C^4$	125.4(5)
O^1-C^4	1.378(8)	$P^2-C^9-C^{10}$	125.6(5)
O^2-C^2	1.416(9)	$C^7-C^{15}-C^{13}$	105.1(5)
O^2-C^{10}	1.383(9)	$O^3-P^1-C^3$	110.1(3)
P^1-O^3	1.491(4)	$O^4-P^2-C^9$	109.9(3)
P^2-O^4	1.492(5)		
P^1-P^2	6.579(2)		

BINAP.[10] We are currently investigating the inclusion of other molecules capable of forming hydrogen bonds in order to form three-dimensional networks. The coordination behaviour of the phosphane oxide, which is still a weakly coordinating group,[11] has also been studied.

We were interested in the coordination of the novel diphosphane compounds to various transition metals and, in particular, whether the chelate ring size of 9 atoms (including the two P-atoms) would have implications for the mode of coordination and if bidentate mononuclear complexes would be formed.

Rauchfuss et al. have already investigated the monophosphane (diphenylphosphanyl)anisole and they concluded that coordination to a metal, such as palladium and platinum, took place only through the phosphorus.[12] In order to study the coordination chemistry of the new family of BPphos ligands to Pd, Pt, and Rh, we used ligand **2** as a representative example. Marty et al. have reported some experimental evidence for the formation of a monomeric, *trans*-coordinated $PdCl_2$ complex using 3,3′-oxybis[(diphenylphosphanyl)methyl]benzene, which is structurally related to compounds **1**−**4**.[13]

From the reaction of **2** with [$PdClCH_3$(cod)] as a starting material, only a singlet at δ = 25.0 ppm was observed in the ^{31}P NMR spectrum. In the ^1H NMR spectrum, a broad triplet was present at δ = −0.05 ppm and a singlet at δ = 3.8 ppm was seen in the ^{13}C NMR spectrum. These observations are clear indications that a *trans*-coordinated species is present, either monomeric or dimeric. For monomeric *trans*-coordinated [$PdClCH_3$(Xantphos)] complexes, Zuideveld et al. have reported proton methyl signals at around δ = −0.2 ppm.[14] Upon slow evaporation of the deuterated solvent, yellow block-shaped single crystals, suitable for X-ray analysis, were obtained for this compound. The crystallographic study undertaken, indicated formation of the dimeric macrocyclic complex **6** which did indeed display a *trans*-coordination for each of the two phosphorus atoms and two bridging palladium atoms. The molecular structure of complex **6** is depicted in Figure 3, while Table 3 contains selected bond lengths and bond angles.

The complex is centrosymmetric and the geometry around the palladium atoms is distorted square planar, as indicated by the corresponding angles listed in Table 2. The P^1-Pd-P^2 angle is 172.94(3)°, while the $C^1-Pd^1-Cl^1$ angle is 171.64(13)°. The Pd−P bond lengths of 2.3250(9) Å ($Pd-P^1$) and 2.3248(9) Å ($Pd-P^2$) are typical for triarylphosphanes[15,16] as are the lengths of the palladium to chlorine and palladium to methyl bonds.[17] The P^1-P^{2a} distance was found to be 7.4470(13) Å. Other binuclear palladium complexes with a face-to-face structure that have been described in literature most often have two chlorine ligands coordinated to the metal center instead of one

 © 2003 Wiley-VCH Verlag GmbH & Co. KGaA, Weinheim

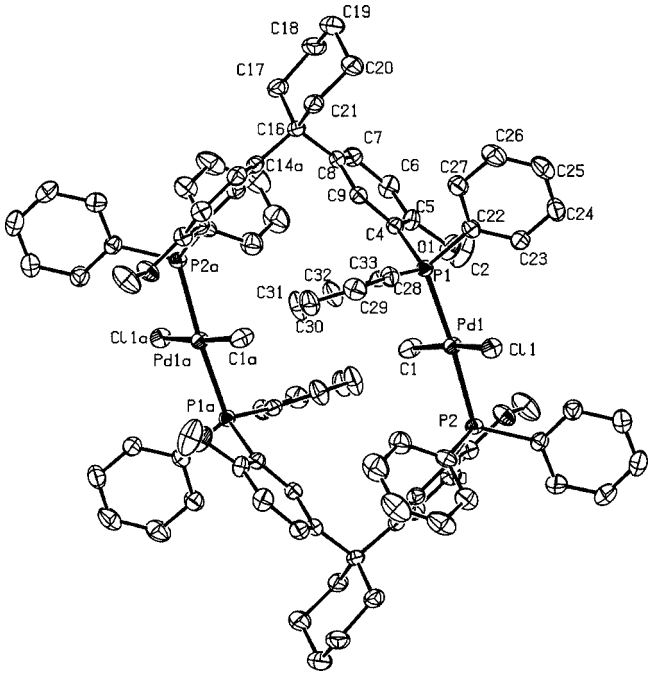

Figure 3. X-ray structure of complex **6**

Table 3. Selected bond lengths and angles for complex **6**, *trans,trans*-[{PdCl(CH_3)(μ-**2**)}$_2$]

Bond lengths [Å]		Angles [°]	
Pd^1-P^1	2.3250(9)	$P^1-Pd^1-P^2$	172.94(3)
Pd^1-P^2	2.3248(9)	$C^1-Pd^1-Cl^1$	171.64(13)
Pd^1-Cl^1	2.4330(10)	$P^1-Pd^1-Cl^1$	88.18(3)
Pd^1-C^1	2.075(4)	$P^2-Pd^1-Cl^1$	88.41(3)
P^1-C^4	1.836(3)	$P^1-Pd^1-C^1$	92.30(9)
P^2-C^{10}	1.830(3)	$P^2-Pd^1-C^1$	90.17(9)
P^1-P^{2a}	7.4470(13)	$C^8-C^{16}-C^{14a}$	105.2(3)
Pd^1-Pd^{1a}	7.4972(4)		

chlorine and one methyl ligand.[18,19] Davies et al. have described the face-to-face dimer [$Pd_2Cl_2(CH_2NO_2)$(μ-dmpm)$_2$] (dmpm = $Me_2PCH_2PMe_2$). The bond lengths between the palladium and the chlorine or the carbon atom of the nitromethyl group turned out to be slightly shorter than in the case of complex **6**, due to the electronic withdrawing effect of the nitro unit.[20] Only very recently the group of James published the synthesis and structural characterization of the Pd_2Cl_4 derivative of dmpm.[20b] Kemmitt and co-workers quite recently reported various dimeric palladium-diphosphane complexes with a chlorine and a phenyl group attached to the palladium atoms.[16]

In order to verify if the formation of face-to-face dimeric complexes is always favoured, regardless of the transition metal, we decided to study the complexation of ligand **2** with a platinum precursor. After reaction with [$PtCl_2(CH_3CN)_2$], an off-white solid was obtained. After dissolving this compound in acetone and slow evaporation of the solvent, one product could be isolated as yellow single crystals in good yield. The ^{31}P NMR spectrum of this compound showed a singlet at δ = 15.8 ppm, flanked by ^{195}Pt-satellites, and a coupling constant J_{Pt-P} of 2705 Hz. This clearly indicates a *trans*-coordination of two phosphorus atoms.[21] These block-shaped crystals turned out to be suitable for X-ray analysis. The molecular structure for complex **7** is depicted in Figure 4. Selected bond lengths and bond angles are listed in Table 4.

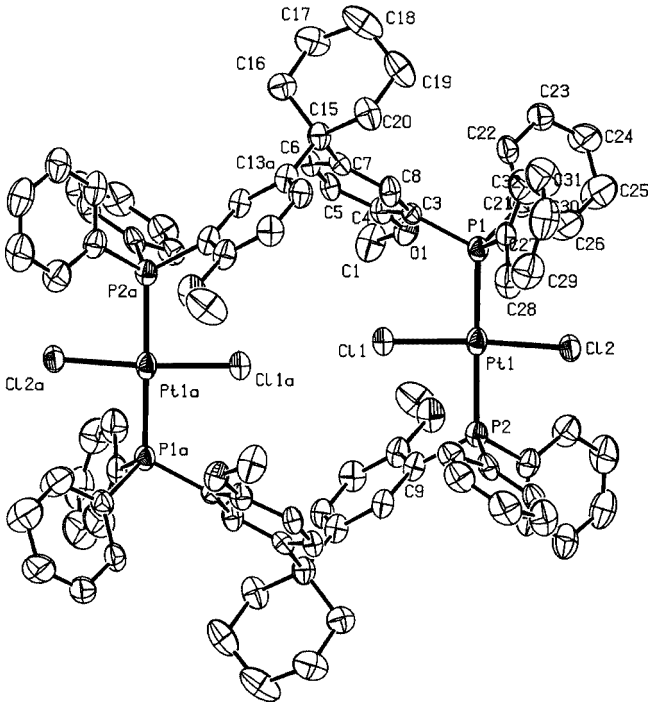

Figure 4. X-ray structure of complex **7**

Table 4. Selected bond lengths and angles for complex **7**, *trans,trans*-[{$PtCl_2$(μ-**2**)$_2$}$_2$]

Bond lengths [Å]		Angles [°]	
Pt^1-P^1	2.320(2)	$P^1-Pt^1-P^2$	176.78(7)
Pt^1-P^2	2.315(2)	$P^1-Pt^1-Cl^1$	92.33(8)
Pt^1-Cl^1	2.294(2)	$P^1-Pt^1-Cl^2$	90.09(7)
Pt^1-Cl^2	2.3270(18)	$Cl^1-Pt^1-Cl^2$	171.77(7)
P^1-C^3	1.835(7)	$P^2-Pt^1-Cl^1$	88.80(7)
P^2-C^9	1.827(7)	$P^2-Pt^1-Cl^2$	88.38(7)
P^1-P^{2a}	8.627(3)	$C^7-C^{15}-C^{13a}$	108.9(7)
Pt^1-Pt^{1a}	8.6391(5)		

Like the palladium complex **6**, the molecular structure of complex **7** also turned out to be dimeric and centrosymmetric. The geometry around the platinum atoms is distorted square planar, with a P^1-Pt-P^2 angle of 176.78(7)° and a $Cl^1-Pt-Cl^2$ angle of 171.77(7)°. The geometry around the central atom C^{15} of the ligand backbone is nearly perfectly tetrahedral, as indicated by the angle of 108.9(7)° for both phenyl rings. Interestingly, the P^1-P^{2a} distance of 8.627(3) Å is larger than in the palladium-dimer **6**. The P−Pt and Cl−Pt bond lengths are in their expected ranges, compared with similar structures previously reported.[22,23] Wood et al. showed that the reaction of 2,6-bis(diphenylphosphanyl)pyridine with $PtCl_2$ yielded a *cis*-

 © 2003 Wiley-VCH Verlag GmbH & Co. KGaA, Weinheim

dimer. When the chlorine-ligands were substituted for iodine-ligands, however, the phosphorus atoms were coordinated in a *trans*-fashion.[24]

To further understand the formation of these face-to-face dimers, we chose the rhodium precursor [{Rh(μ-Cl)$(CO)_2$}$_2$]. Complexes prepared from this metal source normally exhibit a *trans*-coordination for the phosphorus atoms. After reaction of this rhodium species with ligand **2**, a doublet was observed in the ^{31}P NMR spectrum at δ = 23.7 ppm, with a coupling constant J_{Rh-P} of 128.3 Hz. This value is typical of those seen in rhodium diphenylphosphane complexes.[25] In the carbonyl region of the IR spectrum (ATR-mode) obtained from the solid product, the CO-stretching vibration was present at ν_{CO} = 1976 cm^{-1}. This is in good agreement with the value of ν_{CO} = 1974 cm^{-1} reported for [RhCl(CO){P(*o*-An)Ph_2}] (An = anisole).[26] Compared with the value of ν_{CO} = 1982 cm^{-1} found for [RhCl(CO){$PPh_2(C_6F_5)$}][27] and ν_{CO} = 1980 cm^{-1} for [Rh(Cl)(CO)$(PPh_3)_2$][28], the value found for our Rh complex is slightly low. *Note:* Moloy and Petersen have touched upon the discrepancy arising in literature with respect to the CO stretching frequency for [Rh(Cl)(CO)$(PPh_3)_2$]. Their own experiments showed a single band at ν_{CO} = 1965 cm^{-1} in CH_2Cl_2.[29] The value of 1976 cm^{-1} demonstrates that the ligands from the BPphos family are slightly more basic than the aforementioned two ligand systems. However the value is signifcantly higher than that found for Rh(Cl)(CO) complexes with alkyldiarylphosphanes such as those described by Zhang et al.[30] and by the group of Dilworth (ν = 1957 cm^{-1}).[31]

By slow diffusion of acetonitrile into a dichloromethane solution of the compound, single crystals could be grown that were suitable for an X-ray crystallographic study. The molecular structure for centrosymmetric complex **8** is shown in Figure 5. Similar to the Pd and Pt complexes, a face-to-face dimeric structure can be observed. Selected bond lengths and bond angles are listed in Table 5.

The geometry around the rhodium atoms is distorted square planar, with a P−Rh−P angle of 171.01(3)° and a Cl−Rh−C(O) angle of 176.99(7)°. These distances are in the expected range with an average Rh−P bond length of 2.32 Å. The Rh−Cl and Rh−C(O) bond lengths are 2.3795(5) Å and 1.810(2) Å, respectively. The C−O distance is typical at 1.145(2) Å.[30−34] The P^1-P^{2a} distance of 8.8150(12) Å as well as the corresponding Rh−Rh distance of 9.0005(11) Å are in the range found for the palladium and platinum complexes.

Many *trans*-[RhCl(CO)] complexes with (di)phosphane ligands have been described in the literature, yet most of these systems are solely mononuclear. Relatively few examples are known where a dimeric compound has been formed exclusively and subsequently structurally characterized by X-ray crystallography.[35−39]

In summary, we have described the easy synthesis of a new class of diphosphane ligands based on commercially available, cheap raw materials derived from Bisphenol A and in good overall yields. In addition to NMR spectroscopy, X-ray crystallography has been used to study the structural differences between compound **2** and its oxidised form, **5**. In the structure of the latter compound, water acts as a template orientating both phosphorus-atoms to the same side of the molecule in the same direction. Complexation studies undertaken with ligand **2** yielded face-to-face dimeric macrocycles with palladium, platinum and rhodium, as was shown by NMR spectroscopy as well as X-ray crystallography.

We are currently investigating the options available for modifying the ligand backbone to further control and enforce a certain orientation of the phosphane-moieties as well as the modification of these ligands in order to gain access to chelating variants.

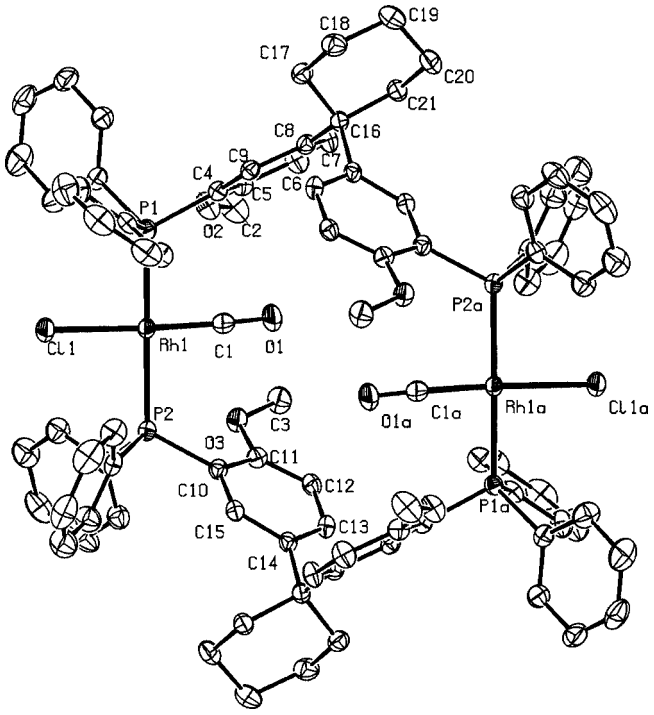

Figure 5. X-ray structure of complex **8**

Table 5. Selected bond lengths and angles for complex **8**, *trans,trans*-[{RhCl(CO)(μ-**2**)$_2$}$_2$]

Bond lengths [Å]		Angles [°]	
Rh^1-P^1	2.3153(5)	$P^1-Rh^1-P^2$	171.01(3)
Rh^1-P^2	2.3345(6)	$P^1-Rh^1-Cl^1$	87.85(3)
Rh^1-Cl^1	2.3795(5)	$P^2-Rh^1-Cl^1$	90.36(3)
Rh^1-C^1	1.810(2)	$Cl^1-Rh^1-C^1$	176.99(7)
C^1-O^1	1.145(2)	$P^1-Rh^1-C^1$	89.80(7)
P^1-C^4	1.8349(17)	$P^2-Rh^1-C^1$	92.24(7)
P^2-C^{10}	1.8352(18)	$Rh^1-C^1-O^1$	177.33(18)
P^1-P^{2a}	8.8150(12)	$Rh^1-P^1-C^4$	116.75(6)
Rh^1-Rh^{1a}	9.0005(11)	$C^8-C^{16}-C^{14a}$	110.19(15)

Experimental Section

Chemicals were purchased from Aldrich, Acros, and Merck and used as received. All preparations were carried out under an argon

 © 2003 Wiley-VCH Verlag GmbH & Co. KGaA, Weinheim

atmosphere using standard Schlenk techniques. Solvents were distilled from sodium/benzophenone (THF, diethyl ether, toluene, hexanes, and ethanol) or calcium hydride (CH_2Cl_2 and $CDCl_3$) prior to use. $[PdCl_2(cod)]$,[40] $[PdClMe(cod)]$[41] and $[PtCl_2(cod)]$[42] were synthesized according to literature procedures. All glassware was dried by heating under vacuum. The NMR spectra were recorded on a Varian Mercury 400 spectrometer (^1H, $^{13}C\{^1H\}$, $^{31}P\{^1H\}$). Chemical shifts are given in ppm referenced to the deuterated solvent (^1H, $^{13}C\{^1H\}$) or 85% H_3PO_4 ($^{31}P\{^1H\}$).

2,2-Bis(4-methoxyphenyl)propane (A): This is a modification of the literature procedure.[43] To a solution of Bisphenol A [2,2′-bis(4-hydroxyphenyl)propane] (11.48 g, 0.050 mol) in acetone (120 mL) were added K_2CO_3 (27.69 g, 0.20 mol) and CH_3I (21.69 g, 0.15 mol) as well as NBu_4I (0.88 g, 2.38 mmol). The heterogeneous mixture was stirred for 16 h under reflux. The suspension was filtered through celite and poured into a mixture of diethyl ether (100 mL) and a 15 w% aqueous KOH solution (100 mL). The organic phase was further washed with saturated brine (100 mL) and water (50 mL) after which $MgSO_4$ was added and the organic phase stirred for about 10 h. After filtration through Celite the solvent was removed in vacuo and ethanol (40 mL) was added to the remaining oil. After stirring, the ethanol was removed in vacuo to yield a pure off-white powder (9.44 g, 36.8 mmol) (73%). ^1H NMR (400 MHz, $CDCl_3$, 300 K, ppm): δ = 1.65 (s, 6 H, CCH_3), 3.79 (s, 6 H, OCH_3), 6.81 (d, ^1J = 8.8 Hz, 4 H, *m*-H^2), 7.15 (d, ^1J = 8.8 Hz, 4 H, *o*-H^1) (Numbering scheme see Figure 6). ^{13}C NMR (100 MHz, $CDCl_3$, 300 K, ppm): δ = 31.1, 41.6, 55.2, 113.2, 127.7, 143.1, 157.4.

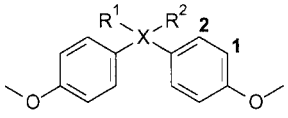

Figure 6. Numbering scheme for protons H^1 and H^2 of compounds **A**−**D**

1,1-Bis(4-methoxyphenyl)cyclohexane (B): This is a modification of the literature procedure.[44] Starting from Bisphenol *Z* [1,1-bis(4-hydroxyphenyl)cyclohexane] (28.8 g, 0.11 mol), compound **B** was obtained as a white crystalline solid, using the same procedure as described for **A**. Yield 83.5% (27.7 g, 93.5 mmol). ^1H NMR (400 MHz, $CDCl_3$, 300 K, ppm): δ = 1.55 (m, 6 H, *m*-,*p*-CH_2, *c*-C^6), 2.23 (m, 4 H, *o*-CH_2, *c*-C^6), 3.77 (s, 6 H, OCH_3), 6.81 (d, ^1J = 8.8 Hz, 4 H, *m*-H^2), 7.18 (d, ^1J = 8.8 Hz, 4 H, *o*-H^1). ^{13}C NMR (100 MHz, $CDCl_3$, 300 K, ppm): δ = 22.9, 26.4, 37.4, 45.0, 55.1, 113.4, 128.0, 141.0, 157.1.

2,2-Bis(4-methoxyphenyl)ethylbenzene (C): This is a modification of the literature procedure.[45] Starting from Bisphenol AP {[2,2-bis(4-hydroxyphenyl)ethyl]benzene} (20.0 g, 68.9 mmol), compound **C** was obtained as a pure off-white powder, using the same procedure as described for **A**. Yield 64% (13.92 g, 43.7 mmol). ^1H NMR (400 MHz, $CDCl_3$, 300 K, ppm): δ = 2.14 [s, 6 H, $C(CH_3)$], 3.79, (s, 6 H, OCH_3), 6.79 (d, ^1J = 8.8 Hz, 4 H, H^2), 7.00 (d, ^1J = 8.8 Hz, 4 H, H^1), 7.09 (m, 2 H, *o*-CH, Ph), 7.20 (m, 1 H, *p*-CH, Ph), 7.26 (m, 2 H, *m*-CH, Ph). ^{13}C NMR (100 MHz, $CDCl_3$, 300 K, ppm): δ = 30.7, 55.2, 113.1, 125.8, 127.8, 128.6, 129.7, 141.5, 157.6.

Bis(4-methoxyphenyl)dimethylsilane (D): This is a modification of the literature procedure.[46] 4-Bromoanisole (5.79 g, 0.031 mmol) was dissolved in THF (100 mL) and the solution was cooled to −78 °C whereupon *n*BuLi (2.5 M solution in hexanes) (12.4 mL, 31.0 mmol) was added dropwise by syringe. The reaction mixture was stirred for 1 h followed by addition of $SiCl_2(CH_3)_2$ (2.0 g, 31.0 mmol) by syringe. The reaction mixture was allowed to warm up to room temp. and stirring was continued for about 10 h. Solvents were removed in vacuo and the crude product was dissolved in CH_2Cl_2 (30 mL). Washing with distilled water (40 mL) afforded a turbid white organic layer. The organic phase was separated and the solvent removed in vacuo to leave a yellow oil. Upon addition of hexanes (25 mL), a brown precipitate was formed. The solution was isolated and dried with $MgSO_4$. After filtration and subsequent removal of solvent, an off-white solid was obtained. Yield 71% (3.00 g, 22.0 mmol). ^1H NMR (400 MHz, $CDCl_3$, 300 K, ppm): δ = 0.54 [s, 6 H, $Si(CH_3)$], 3.83 (s, 6 H, OCH_3), 6.93 (d, ^1J = 8.8 Hz, 4 H, H^2), 7.48 (d, ^1J = 8.8 Hz, 4 H, H^1). ^{13}C NMR (100 MHz, $CDCl_3$, 300 K, ppm): δ = −2.0, 55.0, 113.5, 129.4, 135.6, 155.0. 160.4.

2,2-Bis[(3-diphenylphosphanyl-4-methoxy)phenyl]propane (1): TMEDA (12.95 g, 0.11 mol) was added to *n*BuLi (2.5 M solution in hexanes) (44.6 mL, 0.11 mol). At −15 °C a solution of **A** (13.29 g, 0.052 mol) in diethyl ether (75 mL) was added dropwise over a period of 1.5 h. The mixture was allowed to slowly warm up to room temp. and was stirred for about 10 h to yield a yellow suspension. At 0 °C $ClPPh_2$ (24.6 g, 0.11 mol) in hexanes (30 mL) was added dropwise over a period of 1 h. Solvents were removed in vacuo and CH_2Cl_2 (60 mL) was added together with saturated brine (50 mL). The organic phase was separated and dried with $MgSO_4$. After filtration through celite, the solvents were removed in vacuo to yield a pink oil that solidified on standing for about 10 h at room temp. under argon. Ethanol (40 mL) was added to give an orange solution and a white precipitate. The solid was washed with ethanol, filtered, and dried. Yield 54% (17.46 g, 28.1 mmol). ^1H NMR (400 MHz, $CDCl_3$, 300 K, ppm): δ = 1.24 (s, 6 H, CCH_3), 3.73 (s, 6 H, OCH_3), 6.40 (dd, ^1J = 5.2, ^2J = 2.4 Hz, 2 H, H^1), 6.73 (dd, ^1J = 8.8, ^2J = 4.8 Hz, 2 H, H^2), 7.04 (dd, ^1J = 8.8, ^2J = 2 Hz, 2 H, H^3), 7.24 (m, 20 H, PPh_2) (Numbering scheme see Figure 7). ^{13}C NMR (100 MHz, $CDCl_3$, 300 K, ppm): δ = 30.3 [$C(CH_3)_2$], 41.6 [$C(CH_3)_2$], 55.7 (OCH_3), 109.5, 124.3, 128.2 (d, $J_{P,C}$ = 6.8 Hz), 128.3, 128.4, 132.4, 133.7 (d, $J_{P,C}$ = 19.8 Hz), 136.9 (d, $J_{P,C}$ = 10.7 Hz), 143.0, 159.0 (d, $J_{P,C}$ = 14.5 Hz). $^{31}P\{^1H\}$ NMR (162 MHz, $CDCl_3$, 300 K, ppm): δ = −14.8 (s). $C_{41}H_{38}O_2P_2$: calcd. C 78.83, H 6.13; P, 9.92; found C 78.65, H 6.08; P, 9.98.

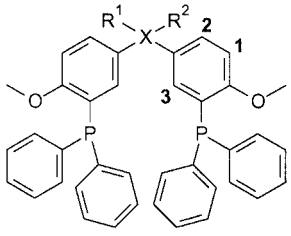

Figure 7. Numbering scheme for protons H^1, H^2, and H^3 of compounds **1**−**8**

1,1-Bis[(3-diphenylphosphanyl-4-methoxy)phenyl]cyclohexane (2): Starting from **B** (4.99 g, 0.017 mol), compound **2** was obtained as a white powder using the same procedure as described for compound **1**. Yield 56% (6.34 g, 9.4 mmol). ^1H NMR (400 MHz, $CDCl_3$, 300 K, ppm): δ = 1.23 (m, 6 H, *m*,*p*-CH_2, *c*-C^6), 1.73 (m,

 © 2003 Wiley-VCH Verlag GmbH & Co. KGaA, Weinheim

4 H, *o*-CH_2, *c*-C^6), 3.71 (s, 6 H, OCH_3), 6.47 (dd, ^1J = 5.6, ^2J = 2.4 Hz, 2 H, H^1), 6.72 (dd, ^1J = 8.8, ^2J = 4.8 Hz, 2 H, Ar-H^2), 6.99 (dd, ^1J = 8.8, ^2J = 2.4 Hz, 2 H, H^3), 7.24 (m, 20 H, PPh_2). ^{13}C NMR (100 MHz, $CDCl_3$, 300 K, ppm): δ = 22.7, 26.2, 37.0, 45.2, 55.6, 109.8, 125.7, 128.2, 128.3 (d, $J_{P,C}$ = 13.0 Hz), 128.8, 132.9, 133.7 (d, $J_{P,C}$ = 19.8 Hz), 137.0, 140.9, 159.0 (d, $J_{P,C}$ = −15.2 (s). $C_{44}H_{42}O_2P_2$: calcd. C 79.50, H 6.37; P, 9.32; found C 79.39, H 6.39; P, 9.31

2,2-Bis[(3-diphenylphosphanyl-4-methoxy)phenyl]ethylbenzene (3): Starting from **C** (12.4 g, 38.9 mmol), compound **3** was obtained as a white powder using the same procedure as described for compound **1**. Yield 61% (16.5 g, 23.7 mmol). ^1H NMR (400 MHz, $CDCl_3$, 300 K, ppm): δ = 1.74 (s, 3 H, CCH_3), 3.72 (s, 6 H, OCH_3), 6.33 (dd, ^1J = 5.6, ^2J = 2.4 Hz, 2 H, H^1), 6.67 (dd, ^1J = 8.8, ^2J = 4.8 Hz, 2 H, H^2), 6.81 (m, 2 H, *o*-CH, Ph), 6.91 (dd, ^1J = 8.8, ^2J = 2.4 Hz, 2 H, H^3), 7.07 (m, 3 H, *m*-,*p*-CH, Ph), 7.18 (m, 20 H, PPh_2). ^{13}C NMR (100 MHz, $CDCl_3$, 300 K, ppm): δ = 30.0, 51.2, 55.6, 109.3, 124.2 (d, $J_{P,C}$ = 13.0 Hz), 125.5, 127.6, 128.2 (d, $J_{P,C}$ = 6.8 Hz), 128.3 (d, $J_{P,C}$ = 3.1 Hz), 130.2, 133.6 (d, $J_{P,C}$ = 19.8 Hz), 134.1, 136.7 (d, $J_{P,C}$ = 10.7 Hz), 141.3, 149.0, 159.1 (d, $J_{P,C}$ = 14.5 Hz). $^{31}P\{^1H\}$ NMR (162 MHz, $CDCl_3$, 300 K, ppm): δ = −15.3 (s). $C_{46}H_{40}O_2P_2$: calcd. C 80.45, H 5.87; P, 9.02; found C 80.52, H 5.76; P, 9.05.

Bis[(3-diphenylphosphanyl-4-methoxy)phenyl]dimethylsilane (4): Starting from **D** (3.00 g, 0.011 mol), compound **4** was obtained as a white powder using the same procedure as described for compound **1**. Yield 65% (4.58 g, 7.20 mmol). ^1H NMR (400 MHz, $CDCl_3$, 300 K, ppm): δ = 0.09 [s, 6 H, $Si(CH_3)$], 3.75 (s, 6 H, OCH_3), 6.69 (dd, ^1J = 8.0, ^2J = 4.4 Hz, 2 H, H^1), 6.81 (dd, ^1J = 8.0, ^2J = 4.4 Hz, 4 H, H^2, H^3), 7.28 (m, 20 H, PPh_2). ^{13}C NMR (100 MHz, $CDCl_3$, 300 K, ppm): δ = −2.6, 55.5, 109.7, 124.7, 128.2 (d, $J_{P,C}$ = 6.8 Hz), 128.5, 129.5, 133.8 (d, $J_{P,C}$ = 19.8 Hz), 136.3, 136.7 (d, $J_{P,C}$ = 9.9 Hz), 139.5, 161.9 (d, $J_{P,C}$ = 15.9 Hz). $^{31}P\{^1H\}$ NMR (162 MHz, $CDCl_3$, 300 K, ppm): δ = −16.1 (s). $C_{40}H_{38}O_2P_2Si$: calcd. C 74.98, H 5.98; P, 9.67; found C 75.06, H 5.93; P, 9.63.

Bis(2,2′-methoxy-5,5′-cyclohexyl)diphenylphosphane Oxide (5): Ligand **2** (0.65 g, 0.98 mmol) was dissolved in CH_2Cl_2 (25 mL) and H_2O_2 (30 wt% aqueous solution) (0.20 mL, 1.96 mmol) in H_2O (20 mL) was added dropwise at 0 °C after which the two-phase system was stirred for about 10 h at room temp. The organic layer was washed with 0.1 M NaOH solution (20 mL) and water (20 mL). After drying with $MgSO_4$ and subsequent filtration, the solvent was removed in vacuo to leave a white powder. Yield 85% (0.58 g, 0.83 mmol). ^1H NMR (400 MHz, $CDCl_3$, 300 K, ppm): δ = 1.46 (s, 6 H, *m*,*p*-CH_2, *c*-C^6), 2.18 (s, 4 H, *o*-CH_2, *c*-C^6), 3.55 (s, 6 H, O*C*H_3), 6.81 (dd, ^1J = 8.8, ^2J = 5.6 Hz, 2 H, H^1), 7.32 (dd, ^1J = 8.8, ^2J = 2.4 Hz, 2 H, H^2), 7.41 (dt, ^1J = 8.0, ^2J = 2.4 Hz, 8 H, *o*-CH, PPh), 7.51 (dt, ^1J = 8.4, ^2J = 1.2 Hz, 4 H, *p*-CH, PPh), 7.65 (d, ^1J = 2.4 Hz, 2 H, H^3), 7.69 (q, ^1J = 4.8 Hz, 8 H, *m*-CH, PPh). ^{13}C NMR (100 MHz, $CDCl_3$, 300 K, ppm): δ = 22.7, 26.1, 37.0, 45.3, 55.2, 111.3 (d, $J_{P,C}$ = 7.6 Hz), 128.0 (d, $J_{P,C}$ = 12.3 Hz), 131.3 (d, $J_{P,C}$ = 10.8 Hz), 132.8, 133.2, 133.9, 141.0, 158.6 (d, $J_{P,C}$ = 3.7 Hz). $^{31}P\{^1H\}$ NMR (162 MHz, $CDCl_3$, 300 K, ppm): δ = 27.7 (s). $C_{44}H_{42}O_4P_2$: calcd. C 75.85, H 6.08; found C 76.04, H 6.14.

***trans,trans*-[$PdClCH_3$-2]$_2$, Complex 6:** Ligand **2** (40.2 mg, 60.5 μmol) and [$PdClCH_3$(cod)] (13.9 mg, 52.4 μmol) were dissolved in $CDCl_3$ (0.5 mL) and the solution was stirred for 2 h before the solution was analyzed by NMR spectroscopy. Single crystals were obtained by slow evaporation of the solvent from the NMR solution. ^1H NMR (400 MHz, $CDCl_3$, 300 K, ppm): δ = −0.05 (t, 6 H, PdCH_3), 1.26 (br. s, 12 H, *m*,*p*-CH_2, *c*-C^6), 1.80 (br. s, 8 H, *o*-CH_2, *c*-C^6), 3.61 (s, 12 H, OCH_3), 6.71 (d, ^1J = 8.0 Hz, 4 H, H^3), 7.04 (d, ^1J = 8.0 Hz, 8 H, H^1, H^2), 7.30 (m, 24 H, PPh_2), 7.71 (br. s, 16 H, PPh_2). ^{13}C NMR (100 MHz, $CDCl_3$, 300 K, ppm): δ = 3.8, 22.8, 26.3, 37.1, 45.1, 55.5, 110.8, 119.0, 119.2, 127.5, 129.2, 130.9, 131.6, 133.3, 135.0, 140.4, 157.9. $^{31}P\{^1H\}$ NMR (162 MHz, $CDCl_3$, 300 K, ppm): δ = 25.0 (s). $C_{90}H_{90}Cl_2O_4P_4Pd_2$: calcd. C 65.78, H 5.52; found C 65.60, H 5.46.

***trans,trans*-[$PtCl_2$-2]$_2$, Complex 7:** $PtCl_2$ (170.3 mg, 640.5 μmol) was heated to reflux in acetonitrile (10 mL) until the solid had completely dissolved. Ligand **2** (425.8 mg, 640.5 μmol) was added and the mixture stirred under reflux for about 10 h. After cooling to room temp., the solvent was evaporated in vacuo to leave a yellow powder. Single crystals were obtained from acetone, by slow evaporation of the solvent. ^1H NMR (400 MHz, $CDCl_3$, 300 K, ppm): δ = 1.23 (m, 12 H, *m*,*p*-CH_2, *c*-C^6), 1.71 (br. s, 8 H, *o*-CH_2, *c*-C^6), 3.63 (s, 12 H, OCH_3), 6.67 (d, ^1J = 8.0 Hz,4 H, H^1), 7.00 (br. s, 4 H, H^2), 7.09 (d, ^1J = 8.8 Hz, 4 H, H^3), 7.37 (br. m, 24 H, PPh_2), 7.73 (q, ^1J = 5.6 Hz, 16 H, PPh_2). $^{31}P\{^1H\}$ NMR (162 MHz, $CDCl_3$, 300 K, ppm): δ = 15.8 (s, J_{Pt-P} = 2705 Hz). $C_{88}H_{84}Cl_4O_4P_4Pt_2$: calcd. C 56.78, H 4.55; found C 56.65, H 4.45.

***trans,trans*-RhCl(CO)-2, Complex 8:** [$RhCl(CO)_2$]$_2$ (170.3 mg, 640.5 μmol) and ligand **2** (425.8 mg, 640.5 μmol) were dissolved in CH_2Cl_2 (10 mL) and the mixture was stirred for 2 h. Evaporation of the solvent in vacuo yielded a yellow solid. Single crystals were obtained by slow diffusion of CH_3CN into a CH_2Cl_2 solution of the solid. ^1H NMR (400 MHz, $CDCl_3$, 300 K, ppm): δ = 1.20 (br. s, 12 H, *m*,*p*-CH_2, *c*-C^6), 1.64 (br. s, 8 H, *o*-CH_2, *c*-C^6), 3.61 (s, 12 H, OCH_3), 6.65 (d, ^1J = 8.8 Hz, 4 H), 6.87 (br. s, 4 H), 7.00 (d, ^1J = 6.4 Hz, 4 H), 7.38 (t, ^1J = 7.2 Hz, 16 H, PPh_2), 7.46 (q, ^1J = 7.2 Hz, 8 H, PPh_2), 7.82 (br. s, 16 H, PPh_2). $^{31}P\{^1H\}$ NMR (162 MHz, $CDCl_3$, 300 K, ppm): δ = 23.7 (d, J_{Rh-P} = 128 Hz). IR (ATR mode, solid, carbonyl region, cm^{-1}): $\tilde{\nu}$ = 1976 (Rh*CO*). $C_{90}H_{84}Cl_2O_6P_4Rh_2$: calcd. C 65.03, H 5.09; found C 64.88, H 4.96.

Molecular Structures of 1−3 and 5−8: The data were collected on a Nonius−Kappa CCD diffractometer with a rotating anode. The structures were solved by direct methods using SHELXS-97 (**2**, **3**)[47] or DIRDIF99 (**1**, **6**−**8**)[48] and refined by least-squares procedures on F^2 using SHELXL-97.[49] All non-hydrogen atoms were refined with anisotropic displacement parameters. Hydrogen atoms were constrained to idealized geometries and allowed to ride on their carrier atoms with an isotropic displacement parameter related to the equivalent displacement parameter of their carrier atoms. Compound **3** contained one phenyl ring on one of the phosphanes which is disordered over two positions. Compound **6** contained four molecules of $CDCl_3$ in the unit cell. Compound **7** contained two acetone molecules which were disordered over two positions. Compound **8** contained disordered dichloromethane molecules. Their contribution was taken into account using the PLATON/SQUEEZE procedure. Structure validation and molecular graphics preparation were performed with the PLATON package.[50] Crystal data are given in Tables 6 and 7. CCDC-213681 (**1**), -213682 (**2**), -213683 (**3**), -213684 (**5**), -213685 (**6**), -213686 (**7**), and -213687 (**8**) contain the supplementary crystallographic data for this paper. These data can be obtained free of charge via www.ccdc.cam.ac.uk/conts/retrieving.html [or from the CCDC, 12 Union Road, Cambridge CB2 1EZ, UK; Fax: (internat.) + 44-1223-336033; E-mail: deposit@ccdc.cam.ac.uk].

 © 2003 Wiley-VCH Verlag GmbH & Co. KGaA, Weinheim

Table 6. Selected crystallographic data for compounds **1**−**3** and **5**

	1	**2**	**3**	**5**
Formula	$C_{41}H_{38}O_2P_2$	$C_{44}H_{42}O_2P_2$	$C_{46}H_{40}O_2P_2$	$C_{44}H_{42}O_4P_2{\cdot}H_2O$
FW/M_r	624.65	664.72	686.72	714.73
Crystal size [mm]	0.12 × 0.27 × 0.42	0.12 × 0.15 × 0.45	0.21 × 0.39 × 0.48	0.09 × 0.21 × 0.24
Crystal system	monoclinic	monoclinic	triclinic	monoclinic
Space group	*C*2/*c* (no. 15)	$P2_1/c$ (no. 14)	$P\bar{1}$ (no. 2)	$P2_1/c$ (no. 14)
a [Å]	28.1693(3)	17.4156(2)	11.1456(1)	12.2410(10)
b [Å]	8.2166(1)	7.8636(1)	12.0144(2)	11.9950(10)
c [Å]	32.3533(4)	28.3503(4)	15.0980(2)	27.398(3)
α [°]			89.1746(9)	
β [°]	115.7420(4)	113.2940(10)	70.6049(9)	114.279(11)
γ [°]			80.4301(5)	
V [Å^3]	6745.21(14)	3566.08(8)	1878.66(4)	3667.1(7)
μ (Mo-K_α) [mm^{-1}]	0.164	0.159	0.153	0.165
Z	8	4	2	4
$d_{calcd.}$ [g cm^{-3}]	1.230	1.238	1.214	1.295
T [K]	150	150	150	150
Reflections collected	26580	28637	27481	4661
Unique reflections (R_{int})[a]	7617 (0.058)	8121 (0.055)	8452 (0.054)	4661 (0.085)
Observed data [$I>2.0\sigma(I)$]	5758	5506	6384	3645
wR_2 of F^2 (all data)	0.1025	0.1063	0.1159	0.1921
λ [Å]	0.71073	0.71073	0.71073	0.71073
R_1	0.0411	0.0452	0.0431	0.0785
S	1.02	1.03	1.03	1.13
Min., max. residual electron density [e/Å^3]	−0.27, 0.32	−0.28, 0.28	−0.38, 0.35	−0.41, 0.53

[a] $Rint = \Sigma[|F_o^2 - F_o^2(\text{mean})|]/\Sigma[F_o^2]$; $wR(F^2) = \{\Sigma[w(F_o^2 - F_c^2)^2]/\Sigma[w(F_o^2)^2]\}^{1/2}$; $R(F) = \Sigma(||F_o| - |F_c||)/\Sigma|F_o|$.

Table 7. Selected crystallographic data for complexes **6**−**8**

	6	**7**	**8**
Formula	$C_{90}H_{90}Cl_2O_4P_4Pd_2{\cdot}4\ CDCl_3$	$C_{88}H_{84}O_4P_4Pt_2{\cdot}2\ C_3H_6O$	$C_{90}H_{84}O_6P_4Cl_2Rh_2{\cdot}2\ CH_2Cl_2$
FW/M_r	2124.68	1977.57	1832.13
Crystal size [mm]	0.06 × 0.12 × 0.18	0.21 × 0.30 × 0.36	0.21 × 0.30 × 0.36
Crystal system	triclinic	monoclinic	monoclinic
Space group	$P\bar{1}$ (no.2)	$P2_1/c$ (no.14)	$P2_1/c$ (no.14)
a [Å]	11.3951(2)	14.4501(2)	14.3323(10)
b [Å]	14.6487(2)	19.5893(3)	19.9531(12)
c [Å]	16.5314(2)	16.5611(2)	16.4423(19)
α [°]	63.8137(6)		
β [°]	77.9245(6)	112.0310(6)	112.66(2)
γ [°]	79.6576(8)		
V (Å^3)	2409.47(6)	4345.60(11)	4339.1(9)
μ (Mo-K_α) [mm^{-1}]	0.877	3.465	0.682
Z	1	2	2
$d_{calcd.}$ [g cm^{-3}]	1.462	1.511	1.272
T [K]	150	150	150
Reflections collected	37005	42286	82640
Unique reflections (R_{int})[a]	10960 (0.061)	8532 (0.072)	9954 (0.0505)
Observed data [$I>2.0\sigma(I)$]	8417	6829	8179
wR_2 of F^2 (all data)	0.1176	0.1106	0.070
λ [Å]	0.71073	0.71073	0.71073
R_1	0.0479	0.0587	0.029
S	1.07	1.36	1.05
Min., max. residual electron density [e/Å^3]	−0.73, 1.17	−0.91, 1.40	−0.49, 0.37

[a] $R_{int} = \Sigma[|F_o^2 - F_o^2(\text{mean})|]/\Sigma[F_o^2]$; $wR(F^2) = \{\Sigma[w(F_o^2 - F_c^2)^2]/\Sigma[w(F_o^2)^2]\}^{1/2}$; $R(F) = \Sigma(||F_o| - |F_c||)/\Sigma|F_o|$.

Acknowledgments

This work was financially supported by the National Research School Combination for Catalysis (NRSCC) and in part (A.M.M. and A.L.S.) by the Netherlands Foundation of Chemical Research (SON) with financial aid from the Netherlands Organisation for Scientific Research (CW-NWO). OMG is gratefully acknowledged for a generous loan of metal precursors. We would like to thank Dr. Rafael Sablong and Dr. Christian Müller (TU/e) for scientific discussions.

 © 2003 Wiley-VCH Verlag GmbH & Co. KGaA, Weinheim

[1] C. A. Bessel, P. Aggarwal, A. C. Marschilok, K. J. Takeuchi, *Chem. Rev.* **2001**, *101*, 1031−1066.

[2] [2a] C. A. McAuliffe, *Transition Metal Complexes of Phosphorus, Arsenic and Antimony Ligands*; New York, **1973**. [2b] C. A. McAuliffe, W. Levason, *Phosphane, Arsane and Stibine Complexes of the Transition Elements*; Elsevier Science: New York, **1978**. [2c]D. M. A. Minahan, W. E. Hill, C. A. McAuliffe, *Coord. Chem. Rev.* **1984**, *55*, 31.

[3] W. Tang, X. Zhang, *Chem. Rev.* **2003**, *103*, 3029−3069.

[4] W. Ahlers, R. Paciello, D. Vogt, J. I. van der Vlugt (to BASF AG), US Patent Appl. 20020111517 [*Chem. Abstract.* **2002**, 169060].

[5] J. I. van der Vlugt, J. M. Bonet, A. M. Mills, A. L. Spek, D. Vogt, *Tetrahedron Lett.* **2003**, *44*, 4389−4392.

[6] Ullmann's Encyclopedia of Industrial Chemistry, 6th electronic edition, Wiley-VCH, Weinheim, **2002**.

[7] *^{31}P NMR spectroscopy in stereochemical analysis* (Ed.: J. G Verkade, L. D. Quin); VCH, Weinheim, **1987**.

[8] [8a] P. W. Baures, J. V. Silverton, *Acta Crystallogr., Sect. C* **1990**, *46*, 715−717. [8b] P. W. Baures, *Acta Crystallogr., Sect. C* **1991**, *47*, 2715−2716. [8c] C. Lariucci, R. Helena de Almeida Santos, J. R. Lechat, *Acta Crystallogr., Sect. C* **1986**, *42*, 1825−1828.

[9] M. R. Churchill, R. F. See, S. L. Randall, J. D. Atwood, *Acta Crystallogr., Sect. C* **1993**, *49*, 345−347.

[10] S. Gladiali, S. Pulacchini, D. Fabbri, M. Manassero, M. Sansoni, *Tetrahedron: Asymmetry* **1998**, *9*, 391−395.

[11] [11a] W. J. Marshall, V. V. Grushin, *Organometallics* **2003**, *22*, 555−562. [11b] S. Priya, M. S. Balakrishna, J. T. Mague, S. M. Mobin, *Inorg. Chem.* **2003**, *42*, 1272−1281. [11c] T.-W. Teo, S. Selvaratnam, J. J. Vittal, P.-H. Leung, *Inorg. Chim. Acta* **2003**, *352*, 213−219.

[12] T. B. Rauchfuss, F. T. Patino, D. M. Roundhill, *Inorg. Chem.* **1975**, *14*, 652−656.

[13] W. Marty, P. N. Kapoor, H. B. Bürgi, E. Fischer, *Helv. Chim. Acta* **1987**, *70*, 158−170.

[14] M. A. Zuideveld, B. H. G. Swennenhuis, M. D. K. Boele, Y. Guari, G. P. F. van Strijdonck, J. N. H. Reek, P. C. J. Kamer, K. Goubitz, J. Fraanje, M. Lutz, A. L. Spek, P. W. N. M. van Leeuwen, *J. Chem. Soc., Dalton Trans.* **2002**, 2308−2317.

[15] K. Takenaka, Y. Obora, L. H. Jiang, Y. Tsuji, *Organometallics* **2002**, *21*, 1158−1166.

[16] A. Mentes, R. D. W. Kemmitt, J. Fawcett, D. R. Russeli, *Polyhedron* **1999**, *18*, 1141−1145.

[17] S. J. Young, B. Kellenberger, J. H. Reibenspies, S. E. Himmel, M. Manning, O. P. Anderson, J. K. Stille, *J. Am. Chem. Soc.* **1988**, *110*, 5744−5753.

[18] A. Pryde, B. L. Shaw, B. Weeks, *J. Chem. Soc., Dalton Trans.* **1976**, 322−327.

[19] C. E. Housecroft, B. A. M. Shaykh, A. L. Rheingold, B. S. Haggerty, *Inorg. Chem.* **1991**, *30*, 125−130.

[20] [20a] J. A. Davies, S. Dutremez, A. A. Pinkerton, M. Vilmer, *Organometallics* **1991**, *10*, 2956−2958. [20b] C. B. Pamplin, S. J. Rettig, B. O. Patrick, B. R. James, *Inorg. Chem.* **2003**, *42*, 4117−4126.

[21] C. J. Cobley, P. G. Pringle, *Inorg. Chim. Acta* **1997**, *265*, 107−115.

[22] N. W. Alcock, L. Judd, P. G. Pringle, *Inorg. Chim. Acta* **1986**, *113*, L13−L15.

[23] F. C. March, R. Mason, K. M. Thomas, B. L. Shaw, *J. Chem. Soc., Chem. Commun.* **1975**, 584−585.

[24] F. E. Wood, J. Hvoslef, H. Hope, A. L. Balch, *Inorg. Chem.* **1984**, *23*, 4309−4315.

[25] B. E. Mann, C. Masters, B. L. Shaw, *J. Chem. Soc.* **1971**, 1104−1106.

[26] P. Suomalainen, S. Jääskeläinen, M. Haukka, R. H. Laitinen, J. Pursiainen, T. A. Pakkanen, *Eur. J. Inorg. Chem.* **2000**, 2607−2613.

[27] M. J. Atherton, K. S. Coleman, J. Fawcett, J. H. Holloway, E. G. Hope, A. Karaçar, L. A. Peck, G. C. Saunders, *J. Chem. Soc., Dalton Trans.* **1995**, 4029−4038.

[28] L. Vaska, J. Peone Jr., *J. Chem. Soc., Chem. Commun.* **1971**, 418−419.

[29] K. G. Moloy, J. L. Petersen, *J. Am. Chem. Soc.* **1995**, *117*, 7696−7710.

[30] F.-B. Xu, Q.-S. Li, X.-S. Zeng, X.-B. Leng, Z.-Z. Zhang, *Organometallics* **2002**, *21*, 4894−4896.

[31] J. R. Dilworth, Y. Zheng, D. V. Griffiths, *J. Chem. Soc., Dalton Trans.* **1999**, 1877−1882.

[32] C. M. Thomas, R. Mafua, B. Therrien, E. Rusanov, H. Stœckli-Evans, G. Süss-Fink, *Chem. Eur. J.* **2002**, *8*, 3343−3352.

[33] T. W. Graham, A. Llamazares, R. McDonald, M. Cowie, *Organometallics* **1999**, *18*, 3502−3510.

[34] N. W. Alcock, J. M. Brown, J. C. Jeffery, *J. Chem. Soc., Dalton Trans.* **1977**, 888−893.

[35] M. Cowie, S. K. Dwight, *Inorg. Chem.* **1980**, *19*, 2500−2507.

[36] A. L. Balch, L. A. Fossett, M. M. Olmstead, D. E. Oram, P. E. Reedy Jr., *J. Am. Chem. Soc.* **1985**, *107*, 5272−5274.

[37] X. Liu, A. H. Eisenberg, C. L. Stern, C. A. Mirkin, *Inorg. Chem.* **2001**, *40*, 2940−2941.

[38] M. F. M. Al-Dulaymmi, D. L. Hughes, R. L. Richards, *J. Organomet. Chem.* **1992**, *424*, 79−86.

[39] M. Cowie, S. K. Dwight, A. R. Sanger, *Inorg. Chim. Acta* **1978**, *31*, L407−L409.

[40] D. R. Drew, J. R. Doyle, *Inorg. Synth.* **1990**, *28*, 346−349.

[41] F. T. Ladipo, G. K. Anderson, *Organometallics* **1994**, *13*, 303−306.

[42] H. C. Clark, L. E. Manzer, *J. Organomet. Chem.* **1973**, *59*, 411−428.

[43] [43a] N. Yonezawa, T. Hino, Y. Tokita, K. Matsuda, T. Ikeda, *Tetrahedron* **1997**, *53*, 14287−14296. [43b] S. H. Dai, C. Y. Lin, D. V. Rao, F. A. Stuber, P. S. Carleton, H. Ulrich, *J. Org. Chem.* **1985**, *50*, 1722−1725.

[44] B. Gerharz, G. Meier, E. W. Fischer, *J. Chem. Phys.* **1990**, *92*, 7110−7122.

[45] I. E. Marko, J. M. Southern, M. L. Kantam, *Synlett* **1991**, *4*, 235−237. [45a] I. E. Marko, M. L. Kantam, *Tetrahedron Lett.* **1991**, *32*, 2255−2258.

[46] [46a] A. Studer, M. Bossart, T. Vasella, *Org. Lett.* **2000**, *2*, 985−988. [46b] C. A. van Walree, X. Y. Lauteslager, A. M. A. van Wageningen, J. W. Zwikker, L. W. Jenneskens, *J. Organomet. Chem.* **1995**, *496*, 117−125.

[47] G. M. Sheldrick, *SHELXS-97.* University of Göttingen, Germany, **1997**.

[48] P. T. Beurskens, G. Beurskens, R. de Gelder, S. Garçia-Granda, R. O. Gould, R. Israel, J. M. M. Smits, *The DIRDIF99 Program System*, University of Nijmegen, The Netherlands, **1999**.

[49] G. M. Sheldrick, *SHELXL-97.* University of Göttingen, Germany, **1997**.

[50] A. L. Spek, *PLATON*, A Multipurpose Crystallographic Tool, Utrecht University, The Netherlands, **2002**.

Received June 30, 2003
Early View Article
Published Online October 10, 2003

 © 2003 Wiley-VCH Verlag GmbH & Co. KGaA, Weinheim

Investigation of the Crystallization Stages of LTA-Type Zeolite by Complementary Characterization Techniques

Monique Smaihi,*[a] Olivier Barida,[a] and Valentin Valtchev[b]

Keywords: Zeolites / Hydrothermal synthesis / NMR spectroscopy / Crystal growth

This paper reports on the physicochemical reorganizations, at 40 °C, of a template-free aluminosilicate system yielding an LTA-type zeolite. The events that take place in the system during the transformations of the amorphous material into a crystalline material were monitored by various characterization techniques which provide information from the molecular to the micrometer scale. High-resolution solid-state ^{29}Si and ^{27}Al MAS NMR spectroscopy, small-angle X-ray scattering (SAXS), X-ray diffraction (XRD), and scanning electron microscopy (SEM) were used in order to achieve a better understanding of the structural properties of the precursor gel and its transformation into a crystalline zeolite-type material. The experimental results show that the first crystallization stage proceeds by reorganization of the amorphous aluminosilicate units formed during the mixing of the precursors. This reorganization involves an ordering of the Si–O–Al bond angles and operates on aggregates of constant volume. The crystallization process takes place in the volume of the aggregates by propagation through the gel phase. This propagation through the gel continues to complete the transformation of the particles into crystalline zeolite Na-A nanocrystals with a rough surface. After this stage, the growth in the system is dominated by the solution-mediated transport, which leads to the formation of well-shaped zeolite A crystals.
(© Wiley-VCH Verlag GmbH & Co. KGaA, 69451 Weinheim, Germany, 2003)

Introduction

Zeolites are crystalline solids that have a highly regular and open microporous structure.[1] More than 130 microporous structure types are known,[2] each with its own distinct pore size, shape, and interconnectivity. The sizes of these pore openings range from 0.3 to 1 nm. The framework composition (Si/Al ratio) can give rise to different ion-exchange properties, to a hydrophilic or hydrophobic character of the material, and to acid sites with different strengths and densities.

Owing to its excellent ion-exchange capacity and consequent use as a water-softening agent in modern-day washing powders, zeolite A boasts the greatest world-wide industrial tonnage of any zeolite. Besides the important industrial applications, zeolite A attracts the interest of researchers with its relatively simple composition and fast crystallization kinetics, which makes it very useful for fundamental studies.

Many techniques have been used to gain an insight into the complex processes occurring during the nucleation and subsequent crystal-growth processes.[3−26] Recently, the use of various non-intrusive and in-situ techniques have provided evidence to support the theory of zeolite crystallization through gel transformation, even for situations considered before as homogeneous.[20,22] The presence of aluminosilicate nanoparticles in the early stages of nucleation of zeolite A has been confirmed by quasi-elastic light scattering and SAXS,[11] dynamic light scattering (DLS),[17,18] TEM,[8] and AFM.[7,14] SAXS observations[19−21] have suggested that some physical rearrangements occur within the amorphous aluminosilicate particles during the nucleation process. A number of studies on the transformations occurring on a molecular scale during the nucleation and crystal-growth processes were based on Nuclear Magnetic Resonance (NMR) spectroscopy.[22−25] Such a spectroscopic method is complementary to those presented above; it fills the gaps in the information needed between the molecular scale entities and the crystal structure formed. Several studies[23−26] showed how the initial reactant sources greatly affect the intermediates observed during the crystallization process. These investigations showed the complexity of the zeolite nucleation/crystallization process, which is dependent on the overall composition of the initial system and the silica and alumina sources used.

Although it was proven that the nucleation of zeolite A is related to the presence of aluminosilicate gel, many questions concerning different stages of evolution of the system remain to be met. The crystal growth can take place by propagation through the gel phase or by solution-mediated transport. In a particular reaction system, the true mechanism could lie somewhere between these two extremes, where one of those might be dominant at a certain stage. In

[a] IEM, UMR 5635, CNRS,
1919 route de Mende, 34293 Montpellier Cedex 5, France
[b] LMM, UMR 7016, CNRS, ENSC Mulhouse, Université de Haute Alsace,
3 rue Alfred Werner, 68093 Mulhouse Cedex, France

 © 2003 Wiley-VCH Verlag GmbH & Co. KGaA, Weinheim DOI: 10.1002/ejic.200300154

order to highlight the mechanism that controls the zeolite formation in a particular system, a link between events taking place on an atomic and on a large scale has to be established. Therefore, valuable information on the mechanism governing crystal growth could be obtained only by a combination of methods which provide information from the molecular to the micrometric scale.

The goal of the present study was to distinguish different stages of zeolite A formation at low temperature, and to investigate the mechanism controlling each of these stages for a conventional organic-free system. The experiments were performed at 40 °C in order to slow down crystal growth so as to distinguish different stages of zeolite formation. High-resolution solid-state ^{29}Si and ^{27}Al MAS NMR spectroscopy, SAXS, X-ray diffraction (XRD), and scanning electron microscopy (SEM) were used to provide information from the molecular to the micrometer scale, and thus to achieve a better understanding of the structural properties of the solid gel phase and its transformation into a crystalline LTA-type material.

Results

The XRD patterns of the samples after different crystallization times are shown in Figure 1. Traces of crystalline LTA-type material were detected after 14 h of hydrothermal synthesis, whereas after 16 h, the XRD pattern showed all the characteristic peaks of zeolite A. A gradual increase in the crystallinity was observed between 14 and 20 h. Further increase in the synthesis time did not yield material with higher X-ray crystallinity.

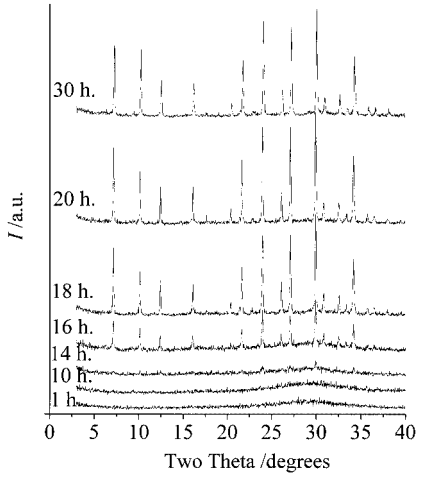

Figure 1. X-ray diffractograms of samples prepared at 40 °C for various heating times: a) 1 h; b) 10 h; c) 14 h; d) 16 h; e) 18 h; f) 20 h; g) 30 h

The electron micrographs shown in Figure 2 represent the morphological features of the materials taken after 1, 16, and 20 h of hydrothermal treatment. The micrograph of the material taken after 1 h shows that the material does not have a crystalline appearance. However, isometric particles of similar sizes, which form large aggregates can be seen. The sizes of these primary particles are in the range 40−100 nm. The micrograph of the sample taken after 16 h shows isolated particles with a round shape and sizes from 40 to 300 nm. All samples that were treated hydrothermally for more than 18 h contained crystals that are of similar sizes, with cubic morphology typical of zeolite A. The sizes of the crystals are in the range 300−400 nm. A small fraction of 40−100 nm crystallites can also be seen.

The morphologies and interfaces of the samples crystallized for different periods of time were characterized by SAXS. The SAXS data provide information on the presence of different particle populations, and on some of their properties such as particle-size distribution, their shape and the type of interactions they are involved in. The intensity of the small-angle X-ray scattering, $I(Q)$, is given by the general equation

$$I(Q) = \varphi P(Q)S(Q)$$

where φ is the number density of the particles in the sample and Q is the momentum transfer [$Q = 4\pi\cdot\lambda^{-1}\cdot\sin(\theta/2)$, θ the scattering angle, λ the X-ray wavelength]. The form factor $P(Q)$ reflects the distribution of the scattering material in the scattering particle, and the structure factor $S(Q)$ is related to the spatial distribution of the scattering particles in the material. The relation between a scattering spectrum and the species responsible for the scattering is shown schematically in Figure 3. On the scale of the primary building units (Porod region, $QR_g >> 1 >> Qa$, where a is the monomer size), the form factor of the primary building units becomes dominant in the scattering pattern, thus providing information about the surface structure of these particles. In many cases, the concept of fractal geometry[27] is used to describe scattering curves in the Porod region. Basi-

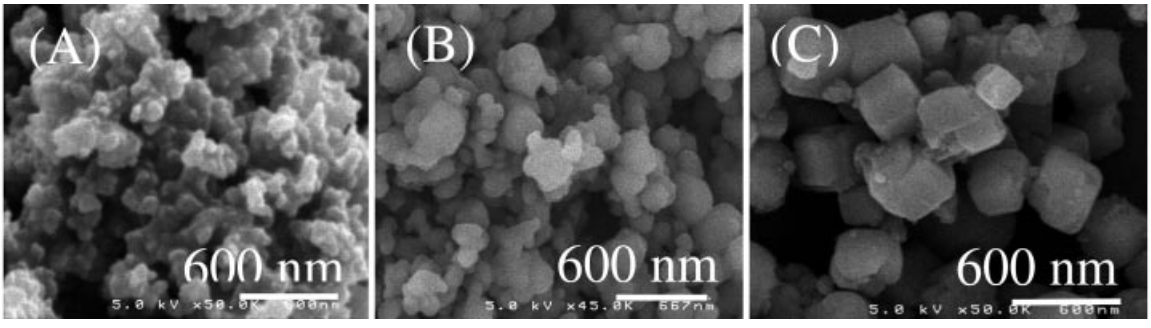

Figure 2. SEM micrographs of samples prepared at 40 °C for various heating times: (A) 1 h; (B) 16 h; (C) 20 h

 © 2003 Wiley-VCH Verlag GmbH & Co. KGaA, Weinheim

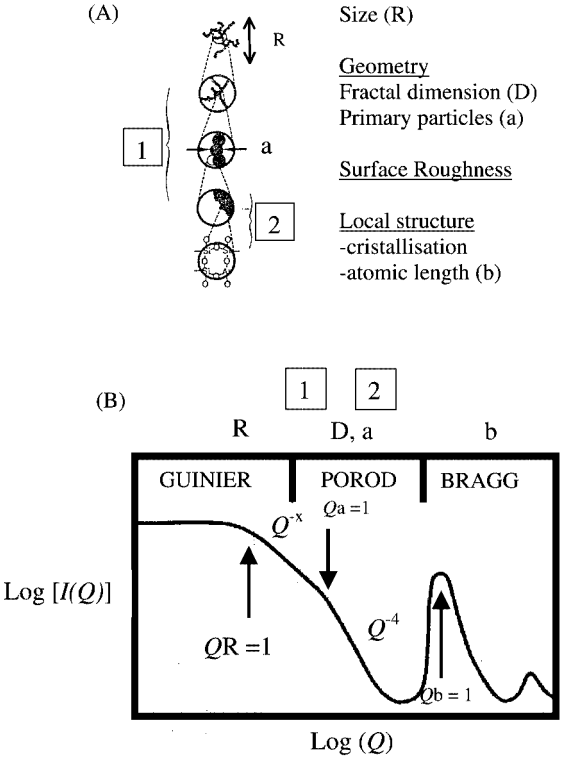

Figure 3. Relation between a scattering spectrum and the species responsible for the scattering: A) aggregate structure at various scales; B) scattering profile of the aggregates presented in A) (according to ref.[34])

cally, all fractals show a power law dependence of the scattered intensity I on the scattering vector Q: $I(Q) \propto Q^{-x}$. For 3-dimensional objects with fractal surfaces,[28] $x = 6 - D_s$, where D_s is the fractal dimension of the surface ($2 \leq D_s \leq 3$). D_s provides a quantitative measure of the roughness; if the roughness of the surface increases, D_s will increase. Thus, $D_s = 2$ represents a classical smooth surface. The $I(Q)$ curves (Figure 4) are similar for all samples with slopes ranging from -3.8 (± 0.05) for samples with "short" synthesis time (1−14 h) to -4 (± 0.05) for those obtained after

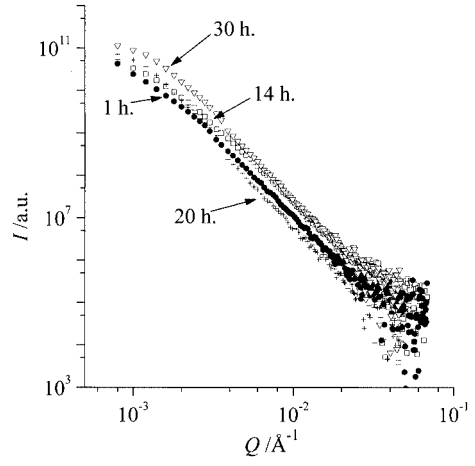

Figure 4. SAXS profiles of samples obtained after different synthesis times at 40 °C

20−30 h of thermal treatment. The initial decay of the intensity in the Guinier region also varies slightly with hydrothermal treatment of the samples.

The molecular organization in the samples was studied by ^{29}Si and ^{27}Al NMR spectroscopy. The ^{29}Si NMR and ^{27}Al NMR spectra of the precursor solutions were recorded in order to characterize the initial species before mixing. Each spectrum presents a single line at $\delta = -72.2$ and 79.5 ppm, which are assigned to the monomeric $Si(OH)_4$ and $Al(OH)_4^-$ species, respectively. The ^{29}Si and ^{27}Al NMR chemical shifts (δ) and line-widths ($\Delta\nu_{1/2}$) recorded for all solid samples are summarized in Table 1. The ^{29}Si MAS NMR spectra of samples obtained after a short synthesis time exhibit broad signals between $\delta = -78$ and -92 ppm (Figure 5). Sample 1 (Table 1) presents a relatively broad signal (half-width = 668 Hz) with a chemical shift of the peak maximum at $\delta = -83.5$ ppm. With increasing synthesis time, the resonance signal becomes narrower and also shows a change in the chemical shift distribution. After 8 h of synthesis, the resonance signal is centered at $\delta = -85.9$ ppm, and after 14 h of thermal treatment, an additional shoulder appears at $\delta = -88.4$ ppm. The latter increases with synthesis time at the expense of the higher frequency resonances. After 20 h of synthesis, the spectrum presents a single narrow signal centered at $\delta = -89.5$ ppm, which does not change with further thermal treatment. The ^{27}Al MAS NMR spectra have been recorded using the same samples (Figure 6). They all present a single signal centered at $\delta = +58$ ppm. The width of this resonance signal then decreases with the time of thermal treatment. The spectrum collected after 1 h of synthesis presents a broad signal (half-width = 1197 Hz), whereas the spectrum recorded after 20 h presents a narrow signal (half-width = 400 Hz) which does not change with further thermal treatment.

Discussion

The TEM study of the initial gel showed that the 40−100 nm particles formed non-uniform gel aggregates (Figure 7). The large-scale changes observed by SEM show that aggregates composed of nanoparticles with a random form are seen in the system during the induction period. The characteristic morphological features of the product did not change substantially after 14 h of hydrothermal treatment, when traces of crystalline LTA-type material were detected in the XRD pattern of the product. In the sample crystallized for 16 h, which displayed a relatively high crystallinity (approximately 30%) (Figure 2, B), particles without the specific morphological features of LTA-type zeolite were observed. All these data show that the first stage of the crystallization process is not coupled with substantial morphological changes in the solid. This result could be considered as reasonable if the crystallization takes place in the volume of the gel phase. Bearing in mind the mass of the crystallites at this stage, and the fact that the density of the zeolite and the gel is about 2.0 and 1.0,

 © 2003 Wiley-VCH Verlag GmbH & Co. KGaA, Weinheim

Table 1. ^{29}Si and ^{27}Al NMR spectroscopic data of the samples obtained after 1−30 h of hydrothermal treatment at 40 °C

Sample	Reaction time at 40 °C [h]	δ(Si) [ppm] (±0.1)	$\Delta\nu_{1/2}$(Si) [ppm] (±5%)	δ(Al) [ppm] (±0.1)	$\Delta\nu_{1/2}$(Al) [ppm] (±5%)	Nature of the solid
1	1	−83.5	668	57.9	1197	amorphous
2	8	−85.9	668	58.4	1271	amorphous
3	14	−83.5/−88.4	802	57.7	1152	amorphous > LTA
4	16	−89.5	99.3	58.5	556	LTA > amorphous
5	18	−89.2	69	58.6	477	LTA
6	20	−89.5	74	58.3	387	LTA
7	30	−89.4	136	58.4	451	LTA

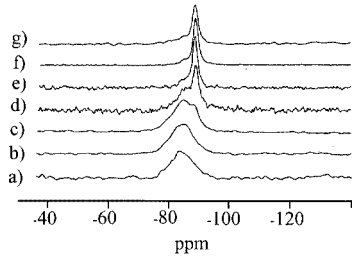

Figure 5. ^{29}Si MAS NMR spectra of samples obtained after different synthesis times at 40 °C: a) 1 h; b) 10 h; c) 14 h; d) 16 h; e) 18 h; f) 20 h; g) 30 h

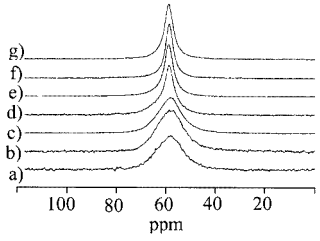

Figure 6. ^{27}Al MAS NMR spectra of samples obtained after different synthesis times at 40 °C: a) 1 h; b) 10 h; c) 14 h; d) 16 h; e) 18 h; f) 20 h; g) 30 h

respectively, a substantial decrease in the volume could not be expected. On the other hand, if the zeolite nuclei are released by the gel phase and grown in the mother liquor, at 30% conversion, the formation of new particles would be observed in the product.

Complementary information on the morphological changes in the course of the transformation of the initial gel into crystalline zeolite A was obtained by the SAXS investigation. From the initial decay of the SAXS intensity in the Guinier region, the electronic radius of gyration, Rg, can be deduced using the Guinier approximation for scattering particles $I(Q) = N{\cdot}n^2{\cdot}\exp(-Q^2{\cdot}\mathrm{Rg}^2/3)$, where N is the number density of particles and n the number of excess electrons in each particle.

The Guinier radius (Figure 8) is about 100 nm and does not drastically vary with the time of thermal treatment. In spite of the limitations of the Guinier method due to the restricted Q range and the possible interference effects due to multiple particle scattering, the obtained values for samples that were heated for up to 20 h are not unreason-

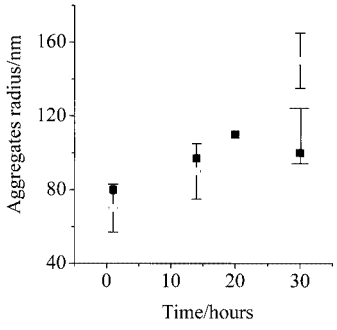

Figure 8. Aggregates radius obtained from SAXS profiles (solid squares), SEM micrographs (open circles) as a function of heating time at 40 °C

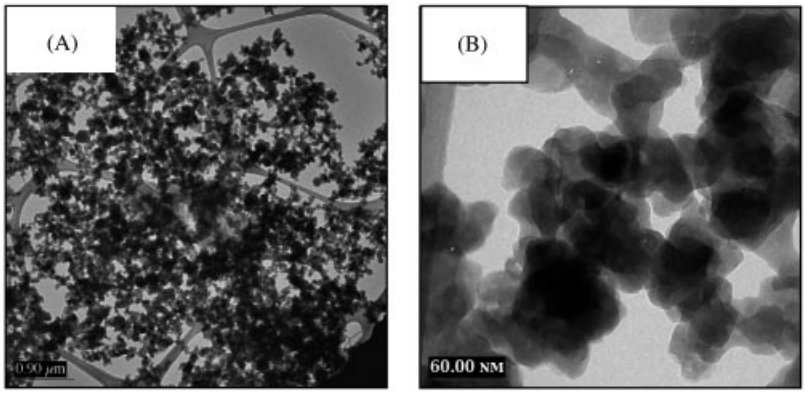

Figure 7. Low (A) and high (B) magnification TEM images of the zeolite A precursor gel

 © 2003 Wiley-VCH Verlag GmbH & Co. KGaA, Weinheim

able and the estimated errors are ±10 nm. For crystalline samples (30 h of thermal treatment), the restricted Q range of the experimental set-up may underestimate the Guinier radius of particles larger than 250 nm, and leads to larger experimental errors (±30 nm). However, the sizes observed by SEM are consistent with the Guinier radii for all samples treated for up to 30 h, and similarly do not significantly vary during the first 14 h of thermal treatment.

Porod plots for all samples (Figure 4) show a single region with a slope of about −3.8 for the noncrystalline samples and −4 for the crystalline samples. The SAXS profiles observed for all samples are rather similar and insensitive to the crystallization stage. The observed Porod slopes of about −4 indicate that the particle surfaces are smooth. Several studies have been devoted to the characterization of silicate networks obtained under different conditions, and show that the scattering curves display fractal dimensions varying from −2 to −4 depending on the polymerization conditions.[28b,28c] Further, with regard to the specific case of zeolite crystallization, there have been many studies involving the crystallization of silicalite under different conditions.[29] Slopes observed during crystallization of these systems ranged between −2 and −4, depending on the composition of the system and the aging of the system.

In our case, it can be concluded that the SAXS investigation is in agreement with the SEM observation, i.e. on the morphological scale there were no changes during the first stage of zeolite formation. In other words, as the SAXS measurements did not detect the formation of new particles, the nucleation and the subsequent growth of the nuclei takes place in the volume of the gel. Thus, it appears that the nucleation and subsequent crystallization occur with aggregates of constant size. A close association of the initially formed nuclei with the gel particles has already been described by Gora et al.[17] However, it is difficult, to discuss the transport of the nutrient during this stage.

On a molecular scale amorphous highly disordered species were detected during this stage. The broad resonance observed between δ = −78 and −92 ppm in the ^{29}Si MAS NMR spectra of sample 1 is typical of amorphous aluminosilicates.[30] This broadness is mainly caused by the overlapping of individual peaks with slightly different δ values, due to the small differences in the structural arrangements in the SiO_4 tetrahedra of the gel skeleton. The ^{29}Si and ^{27}Al NMR spectra of aluminosilicate solutions, pertinent to zeolite synthesis, indicate the formation of Si−O−Al linkages by the appearance of up to four peaks assigned to the Al(OSi), $Al(OSi)_2$, $Al(OSi)_3$, and $Al(OSi)_4$ species.[31] For solid samples, characteristic ^{29}Si NMR chemical shift ranges for the five $Q^4(m\text{Al})$ [i.e. $Si(OSi)_{4-m}(OAl)_m$] units in framework silicates have been established by comparison between calculated and experimental chemical shifts.[32] They range from δ = −112 to −94 ppm for $1 \leq m \leq 4$. Thus, the presence of such units in our samples can be excluded. Further, hydroxylated units, such as $HOSi(OAl)_3$, for which chemical shift values may be expected in the range of the observed signal, should be present only in minor amounts since no noticeable signal enhancement is observed in the ^{1}H-^{29}Si cross-polarization spectrum.

For sample 6 (20 h, 40 °C), the chemical shift of δ = −89.5 ppm reveals that the framework of the gel consists mainly of $Si(OAl)_4$ building units, i.e. of silicon atoms linked by oxygen bridges to four tetrahedral aluminum atoms. This chemical shift is consistent with the presence of crystalline zeolite Na-LTA (Si/Al = 1).[33]

Since the ^{29}Si NMR spectra can be analyzed quantitatively (the total area of the peaks corresponds to 100% of the observed nuclei), the signal centered at δ = −89.5 ppm corresponding to $Si(OAl)_4$ units in crystalline Na-A zeolite can be deconvoluted from the spectra in order to follow the kinetics of the formation of these units. Figure 9 presents the proportion of $Si(OAl)_4$ crystalline units as a function of crystallization time. This curve shows an "induction" period of about 10 h, which precedes a steep rise. After 20 h of synthesis (t/t_c = 1), 95% of the silicon species are $Si(OAl)_4$ crystalline units. Nevertheless, an increase in the size of the crystals and the formation of crystals with well-defined crystal morphology was observed after this period.

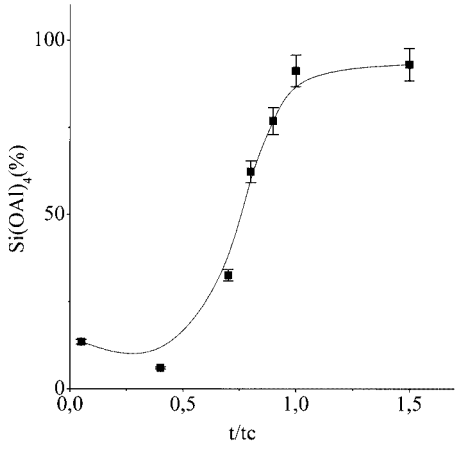

Figure 9. Proportion of crystalline $Si(OAl)_4$ units as a function of crystallization time (t_c: time needed to obtain pure crystalline Na-A zeolite)

The single signal centered at δ = +58 ppm in the ^{27}Al MAS NMR spectra is typical of $Al(OSi)_4$ units. The highly symmetrical line shape indicates that the presence of hydroxylated AlO_4 species is unlikely. Moreover, no signals corresponding to octahedral AlO_6 or tetrahedral $Al(OAl)_4$ aluminate species are detected. For the latter two units, ^{27}Al NMR chemical shifts of δ ≈ 0 and +75 ppm, respectively, were found in previous studies.[34] The observed line broadening is probably caused by residual quadrupolar interactions due to slight symmetry distortions in the vicinity of the Al atoms. However, these quadrupolar interactions are small enough such that they do not modify the line shape.

Short-range ordering in the samples can also be estimated from the line-widths of the ^{29}Si and ^{27}Al NMR resonance signals. The most likely contributing factor to the line-width ($\Delta\nu_{1/2}$) is the structural disorder which involves

 © 2003 Wiley-VCH Verlag GmbH & Co. KGaA, Weinheim

a large number of slightly different environments around nominally equivalent $Q^n(m\text{Al})$ type silicon atoms, thus leading to many overlapping lines with slightly different chemical shifts. The different environments are created by distortion of bond angles and bond lengths due to lattice imperfections. Hence, very broad signals ($\Delta\nu_{1/2} \approx 10-20$ ppm) are observed for highly disordered systems such as amorphous materials, whereas narrow peaks ($\Delta\nu_{1/2} \approx 0.2-3$ ppm) are obtained for perfectly ordered systems. Figure 10 presents the evolution of the ^{29}Si and ^{27}Al MAS NMR signal line-width as a function of the synthesis time for the $Si(OAl)_4$ and $Al(OSi)_4$ species. Both curves present two regions where a slight decrease in the line-width is observed for up to 14 h, followed by a significant decrease in the line-width after 16 h of synthesis.

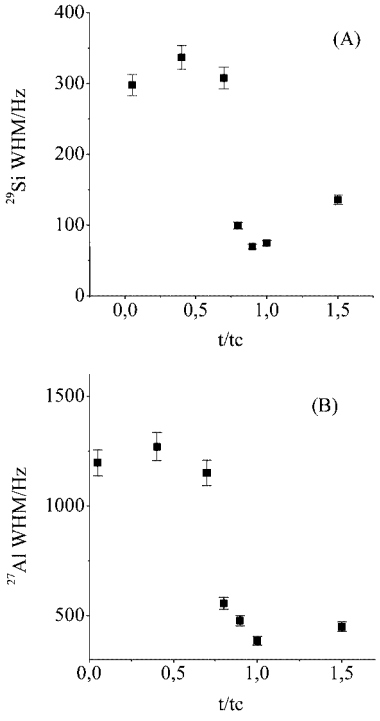

Figure 10. Width at half maximum of the $Si(OAl)_4$ (A) and $Al(OSi)_4$ (B) resonance signals of the ^{29}Si and ^{27}Al MAS NMR spectra, respectively, as a function of crystallization time at 40 °C (t_c: time needed to obtain pure crystalline Na-A zeolite)

Thus, the information collected on the molecular scale shows that during the first 16 h, while no large-scale morphological changes were observed, the first crystallization stage involves a rearrangement of the Si−O−T bonds in the amorphous phase formed after precursor mixing prior to crystallization. After this induction period when a product with zero crystallinity was observed, the above-mentioned transformation in the system takes place. This stage includes the time period 12−16 h, when the increase in the crystallinity is not coupled with large-scale changes in the system, i.e. the crystalline particles retain the size and morphology of the initial amorphous gel precursors. Obviously, during this first stage, the dominant mechanism of crystal growth is propagation through the gel. Growth by propagation through the gel network has already been observed in the formation of zeolite L.[16] During this first stage, the solid is about 30% crystalline, according to the XRD measurements (Figure 1). The nutrients for the crystal growth are provided mainly by the amorphous gel phase, although an extensive exchange between the solid and liquid parts of the system is likely.

After the first stage, a very rapid increase in crystallinity was observed which was coupled with significant changes in the size and morphological features of the particles. Well-shaped zeolite A crystals in the product indicate a change in the crystal growth process. This distinct change in the system occurred during the period 16−18 h, when the crystallinity is about 50%. At this stage, a substantial part of the amorphous material is consumed and crystallites are either released by the gel or are in contact with the mother liquor.[34] The SEM study of the 18-h product does not show much material with an amorphous appearance. At this stage the product already contains well-distinguished individual particles. During this latter stage, a solution-mediated growth mechanism seems to be dominant in the system. This crystallization stage, where a layer growth mechanism controls the zeolite A formation, has been studied and described in detail by Agger et al.[7] The nutrients for this crystallization stage are provided by the amorphous part of the gel and the less stable zeolite nanoparticles. The crystallization during this second stage was completed between 16 and 20 h, and further hydrothermal treatment did not influence the morphology nor the crystallinity of the product. The disappearance of the small crystallites and the increase in the size of the well-shaped cubic crystals were observed during the 20−30-h period, thus resembling Ostwald ripening.

Conclusions

The present study reports on the results obtained during the formation and transformations of precursor particles for the whole course of the template-free Na-A zeolite crystallization process at 40 °C, using various characterization techniques that provide information from the molecular to the micron scale.

The experimental results showed that in the system under investigation the crystallization process could be subdivided into two stages, during which the crystallization process is controlled by different crystallization mechanisms. After the formation of viable nuclei, the first stage of the crystal growth process proceeded by reorganization of the amorphous homogeneous aluminosilicate phase formed during the mixing of the initial precursors. This reorganization involves an ordering of the Si−O−Al bond angles of the $Si(OAl)_4$ units and operates on aggregates of constant volume to form nanocrystals with a rough surface at the end of the process. The zeolite formation in the system was

 © 2003 Wiley-VCH Verlag GmbH & Co. KGaA, Weinheim

completed by the second crystallization stage when a fully crystalline product containing well-shaped zeolite crystals was obtained. A layer growth, where a solution-mediated transport of nutrients dominates, is the controlling mechanism during the second stage.

Experimental Section

Samples Preparation: The Na-A zeolite samples were prepared from an initial gel with the following composition: $7.5Na_2O/0.5Al_2O_3/SiO_2/200H_2O$. Sodium silicate solution (overall composition $SiO_2/7.5NaOH/102H_2O$) was prepared by dissolving sodium silicate (2.22 g, $Na_2Si_3O_7$, 27% SiO_2, 17% NaOH, Aldrich) and sodium hydroxide (2.69 g) in H_2O (17.1 g). A sodium aluminate solution (overall composition $Al_2O_3/15NaOH/197H_2O$) was prepared by dissolving sodium aluminate (0.963 g, $NaAlO_2$, 53% Al_2O_3, 42% Na_2O, Riedel−de Haën) and sodium hydroxide (2.465 g) in H_2O (17.69 g). The solutions were stirred in closed polyethylene bottles at room temperature until complete dissolution of the solid. After mixing of the initial solutions, the resultant mixture was stirred vigorously for 15 min. During mixing, the solution became opaque. The syntheses were performed at 40 °C for different periods of time ranging from 1 to 30 h. At this temperature, the crystallization of the zeolite A was relatively slow, but still fast enough to be achieved in a reasonable period of time. The solid phase was recovered after 5−8 cycles of centrifugation (8000 rpm, 15 min), decanting and ultrasonic redispersion in distilled water. The solid phase was dried over silica gel at room temperature for 48 h. The yield based on the silica conversion was ca. 70%. A similar (slightly higher) yield (76%) was obtained in the reference experiment performed with the same initial system at 90 °C for 5 h.

Samples Characterization: Scanning electron micrographs were obtained with a Hitachi S-4500 microscope. All samples were platinum-coated (2−3 nm) and mounted on aluminum mounts with carbon conducting tape. X-ray diffraction measurements were performed with a Bruker diffractometer D-5000 (Cu-$K_{\alpha 1}$ radiation, 0.154 nm). Small-angle X-ray scattering experiments were performed with an instrument that has an incident wavelength of 0.154 nm (Cu-$K_{\alpha 1}$ radiation) using a high-resolution Bonse-Hart camera. The monochromator was a three-reflection channel-cut scattered beam. These experimental parameters allow studies in a range of wave vectors Q from 0.02 to 1 nm^{-1}. The ^{29}Si and ^{27}Al NMR spectra of the precursor solutions were obtained at 49.68 and 65.17 MHz, respectively, with a Bruker spectrometer. The ^{29}Si spectra were recorded using a 12-μs pulse width (corresponding to a 60° flip angle), 10 s pulse repetition time and 128 scans. The ^{27}Al spectra were recorded using a 4-μs pulse width (corresponding to a 45° flip angle), 0.1 s pulse repetition time and 256 scans. The ^{29}Si MAS NMR spectra of the solid samples were recorded with a Bruker spectrometer at 39.73 MHz, using 4-μs single pulses (60° flip angle) with 60 s repetition rate, and employing high-power proton decoupling and magic-angle spinning at 3.5 kHz; 1000 scans were accumulated. The powder samples were filled into zirconia rotors of 4 mm diameter. The ^{27}Al MAS NMR spectra were measured at 104.26 MHz, using single pulses of 1 μs duration with 1 s repetition rate, and employing magic-angle spinning at 10 kHz; 512 scans were accumulated. All ^{27}Al and ^{29}Si chemical shifts were referenced to a 1% aqueous $Al(H_2O)_6^{3+}$ solution and tetramethylsilane (TMS), respectively.

Acknowledgments

The authors thank Dr. H. Kessler for helpful discussions and D. Cot for the SEM micrographs.

[1] R. M. Barrer, *Zeolites and Clay Minerals and Sorbents and Molecular Sieves*, Academic Press, New York, **1978**.
[2] W. M. Meier, D. H. Olson, *Atlas of Zeolite Structure Types*, 3rd ed., Butterworth-Heinemann, London, **1992**.
[3] S. P. Zhdanov, in: *Molecular Sieve Zeolites* (Eds.: E. M. Flanigen, L. B. Sand), Adv. Chem. Ser. 101, ACS, Washington, DC, **1971**, p. 20−43.
[4] R. J. Francis, D. O'Hoare, *J. Chem. Soc., Dalton Trans.* **1998**, 3133−3148.
[5] A. K. Cheetham, C. F. Mellot, *Chem. Mater.* **1997**, *9*, 2269−2279.
[6] M. E. Davis, R. F. Lobo, *Chem. Mater.* **1992**, *4*, 756−768.
[7] J. R. Agger, N. Pervaiz, A. K. Cheetham, M. W. Anderson, *J. Am. Chem. Soc.* **1998**, *120*, 10754−10759.
[8] S. Mintova, N. H. Olson, V. Valtchev, T. Bein, *Science* **1999**, *283*, 958−960.
[9] R. I. Walton, R. I. Smith, D. O'Hare, *Microporous Mesoporous Mater.* **2001**, *48*, 79−88.
[10] Y. Marui, R. Irie, H. Takiyama, H. Uchida, M. Matsuoka, *J. Cryst. Growth* **2002**, 237−239, 2148−2152.
[11] P. S. Singh, T. L. Dowling, J. N. Watson, J. M. White, *Phys. Chem. Chem. Phys.* **1999**, *1*, 4125−4130.
[12] R. Grizetti, G. Artioli, *Microporous Mesoporous Mater.* **2002**, *54*, 105−112.
[13] V. Nikolakis, D. G. Vlacho, M. Tsapatsis, *Microporous Mesoporous Mater.* **1998**, *21*, 337−346.
[14] S. Sugiyama, S. Yamamoto, O. Matsukoa, H. Noroye, J. Yu, G. Zhu, S. Qiu, O. Terasaki, *Microporous Mesoporous Mater.* **1999**, *28*, 1−7.
[15] M. Smaihi, S. Kallus, J. D. F. Ramsay, *Stud. Surf. Sci. Catal.* **2001**, *135*, 183.
[16] M. Tsapatsis, M. Lovallo, M. E. Davis, *Microporous Mater.* **1996**, *5*, 381−388.
[17] L. Gora, K. Streletzky, R. W. Thompson, G. D. J. Phillies, *Zeolites* **1997**, *18*, 119−131.
[18] B. J. Schoeman, O. Regev, *Zeolites* **1996**, *17*, 447−456.
[19] P. W. J. G. Wijnen, T. P. M. Beelen, R. A. Van Santen, in: *The Colloidal Chemistry of Silica*, Advances in Chemistry Series, **1994**, vol. 234, p. 517.
[20] W. H. Dokter, H. F. Van Garderen, T. P. M. Beelen, R. A. Van Santen, W. Bras, *Angew. Chem. Int. Ed. Engl.* **1995**, *34*, 73−75.
[21] O. Regev, Y. Cohen, E. Kehat, Y. Talmon, *Zeolites* **1994**, *14*, 314−319.
[22] S. L. Burkett, M. E. Davis, *J. Phys. Chem.* **1994**, *98*, 4647−4653.
[23] G. Engelhardt, B. Fahlke, M. Mägi, E. Lippmaa, *Zeolites* **1985**, *5*, 49−52.
[24] J. Shi, M. W. Anderson, *Chem. Mater.* **1996**, *8*, 369−375.
[25] G. Engelhardt, B. Fahlke, M. Mägi, E. Lippmaa, *Zeolites* **1983**, *3*, 292−294.
[26] S. Mintova, V. Valtchev, *Microporous Mesoporous Mater.* **2002**, *55*, 171−179.
[27] B. B. Mandelbrot, *Fractals, Form and Chance*, Freeman, San Francisco, **1977**.
[28] [28a] H. D. Bale, P. W. Schmidt, *Phys. Rev. Lett.* **1984**, *53*, 596−599. [28b] D. W. Schaeffer, K. D. Keefer, *Fractals in Physics* (Eds.: L. Pietronero, E. Tosatti), Elsevier B. V., Amsterdam, **1986**, p. 39−45. [28c] D. W. Schaeffer, K. D. Keefer, *Phys. Rev. Lett.* **1984**, *53*, 1383−1386.
[29] P. P. E. A. de Moor, T. P. M. Beelen, R. A. van Santen, *Microporous Mater.* **1997**, *9*, 117−130.
[30] E. Lipmaa, A. Mägi, A. Samoson, M. Tarmak, G. Engelhardt, *J. Am. Chem. Soc.* **1981**, *103*, 4992−4996.

 © 2003 Wiley-VCH Verlag GmbH & Co. KGaA, Weinheim

[31] L. S. Dent-Glasser, G. Harvey, *Proceedings of the 6th International Zeolite Conference* (Reno, 1983), Butterworth, Guildford, **1985**, p. 925.
[32] J. M. Bennett, C. S. Blaskwell, D. F. Fox, *J. Phys. Chem.* **1983**, *87*, 3783−3790.
[33] G. Engelhardt, D. Michel, *High-Resolution Solid State NMR of Silicates and Zeolites* John Wiley & Sons, New York, **1987**.
[34] S. Gontier, L. Gora, I. Güray, R. W. Thompson, *Zeolites* **1993**, *13*, 414−418.

Received March 24, 2003
Early View Article
Published Online October 10, 2003

 © 2003 Wiley-VCH Verlag GmbH & Co. KGaA, Weinheim

Thermal Stability and Absorption Spectroscopic Behavior of (μ-Peroxo)dicopper Complexes Regulated with Intramolecular Hydrogen Bonding Interactions

Syuhei Yamaguchi,[a] Akira Wada,[a] Yasuhiro Funahashi,[a] Shigenori Nagatomo,[b] Teizo Kitagawa,[b] Koichiro Jitsukawa,*[a] and Hideki Masuda*[a]

Keywords: Copper / Peroxides / Tripodal ligands / Hydrogen bonding interactions

In order to clarify the effect of hydrogen bonding on the stabilities of (μ-peroxo)dicopper complexes with a *trans*-μ-1,2-peroxo form, novel copper complexes with intramolecular hydrogen bonding interaction sites have been synthesized, and their spectroscopic properties and thermal stabilities studied. The selected tripodal tetradentate ligands were tris(2-pyridylmethyl)amine (TPA) derivatives bearing pivalamido and amino groups at the 6-position of the pyridine ring in TPA, {[6-(pivalamido)pyrid-2-yl]methyl}bis(pyrid-2-ylmethyl)amine (MPPA) and [(6-aminopyrid-2-yl)methyl]bis(pyrid-2-ylmethyl)amine (MAPA). The single-crystal X-ray structure of a monomeric Cu^{II} complex with N_3^- namely $[Cu(mppa)N_3]ClO_4$ (**1a**), revealed an interligand hydrogen bonding interaction between the substituent NH group of MPPA and the azide nitrogen atom in the axial position. The Cu^I complexes of MPPA and MAPA were immediately oxygenated with dioxygen in acetone solution at –78 °C to give the μ-peroxo dinuclear copper(II) complexes $[\{Cu(mppa)\}_2(O_2)]^{2+}$ (**1b**) and $[\{Cu(mapa)\}_2(O_2)]^{2+}$ (**2b**). These complexes exhibited two kinds of characteristic absorption bands ($\pi^*_\sigma \rightarrow d_\sigma$, $\pi^*_v \rightarrow d_\sigma$) originating from the ligand–metal charge transfer (LMCT) of O_2^{2-} to Cu. Affected by the hydrogen bonding interaction, the $\pi^*_\sigma \rightarrow d_\sigma$ CT band shifted significantly to a higher energy region and the $\pi^*_v \rightarrow d_\sigma$ CT absorbance decreased due to stabilization of the π^*_σ orbital and restriction of the Cu–O bond rotation. The thermal stabilities of the (μ-peroxo)dicopper(II) complexes were estimated from their decomposition rates which decreased in the order, **2b** ≈ $[\{Cu(tpa)\}_2(O_2)]^{2+}$ (**3b**) > **1b** >> $[\{Cu(6\text{-}metpa)\}_2(O_2)]^{2+}$ (**4b**) {6-MeTPA = [(6-methylpyrid-2-yl)methyl]bis(pyrid-2-ylmethyl)amine}. The above findings indicate that the interligand hydrogen bonding interaction, although overcome to some extent by the adverse effect of the steric bulk of the NH group, is inclined to stabilize (μ-peroxo)dicopper(II) complexes.

(© Wiley-VCH Verlag GmbH & Co. KGaA, 69451 Weinheim, Germany, 2003)

Introduction

In biological systems, O_2 binding and its activation by metalloenzymes are important processes for respiratory and metabolic systems.[1] Detailed examinations using biomimetic model systems are required for understanding the natural processes, such as dioxygen transport, oxidation, oxygenation, and dehydrogenation.[1–3] These processes are catalyzed by heme iron,[4,5] non-heme iron[6,7] and copper centers[8–13] at the active sites of the metalloenzymes. In order to clarify the catalytic reaction mechanism of the dicopper-containing enzymes, dicopper–dioxygen adduct complexes have been investigated as biomimetic models.[14–35] The binding of dioxygen to dinuclear copper complexes has been previously found to result in (*trans*-μ-1,2-peroxo)dicopper(II),[14–25] [μ-(η^2:η^2)-peroxo]dicopper(II),[14,26–31] and [bis(μ-oxo)]dicopper(III) forms.[14,32–35] These coordination modes in dicopper sites are known to depend on the stereochemistry of the coordination environment. The geometries of dicopper–dioxygen complexes are likely to be regulated by the number of coordinating ligands;[14–35] (*trans*-μ-1,2-peroxo)dicopper(II) complexes[14–25] have been generally formed using tetradentate ligands and the structural and spectroscopic properties of (*trans*-μ-1,2-peroxo)dicopper(II) complexes were first systematically investigated by Karlin and co-workers.[16–23]

In biological catalysts, environmental factors such as the proximal effect of amino acid residues are frequently required for regulating reaction intermediates and activating substrates. We have demonstrated that the hydrogen bonding interaction can control the reactivity of metal–dioxygen species, and have succeeded in the preparation of the stable monomeric (hydroperoxo)copper(II) complex $[Cu^{II}(bppa)(OOH)]^+$ [BPPA = bis{[6-(pivalamido)pyrid-2-yl]methyl}-(pyrid-2-ylmethyl)amine].[36] The crystal structure of this

[a] Department of Applied Chemistry, Nagoya Institute of Technology,
Gokiso-cho, Showa-ku, Nagoya 466-8555, Japan
Fax: (internat.) + 81-52-7355228
E-mail: masuda@ach.nitech.ac.jp
[b] Center of Integrative Bioscience, Okazaki National Research Institutes,
Myodaiji, Okazaki 444-8585, Japan

 © 2003 Wiley-VCH Verlag GmbH & Co. KGaA, Weinheim **DOI: 10.1002/ejic.200300178**

complex revealed a hydrogen bonding interaction between the pivalamido NH group of BPPA and the ligating hydroperoxo oxygen atom.[36] The remarkable stability of $[Cu^{II}(bppa)(OOH)]^+$ was acquired by the intramolecular hydrogen bonding interaction. From this point of view, it has been previously discussed that the interligand hydrogen bonding interaction can stabilize (superoxo)-, (alkylperoxo)-, and (hydroxo)metal complexes with tripodal tetradentate ligands.[37−43]

As an expansion of our previous research, tripodal ligands having the hydrogen bonding feature, such as {[6-(pivalamido)pyrid-2-yl]methy}bis(pyrid-2-ylmethyl)amine (MPPA) and [(6-amino-2-pyridyl)methyl]bis(pyrid-2-ylmethyl)amine (MAPA) (Scheme 1), have been newly prepared for complexation with copper ions. It was expected that these tetradentate ligands would form (*trans*-μ-1,2-peroxo)dicopper(II) complexes that would be dominated by their coordination numbers. In this paper, we describe details of the following: (i) the coordination structures and hydrogen bonding modes of copper complexes with MPPA and MAPA and (ii) formation of the corresponding μ-peroxo dinuclear copper complexes and their characteristic absorption spectroscopic behavior and thermal stabilities. We also discuss the intrinsic effect of the proximal hydrogen bonding interaction in μ-peroxo dinuclear copper complexes in detail and compare these with the cases of copper complex systems of TPA and Cu-6-MeTPA {6-MeTPA = [(6-methyl-2-pyridyl)methyl]bis(pyrid-2-ylmethyl)amine} without a hydrogen bonding site (Scheme 1).[44,45]

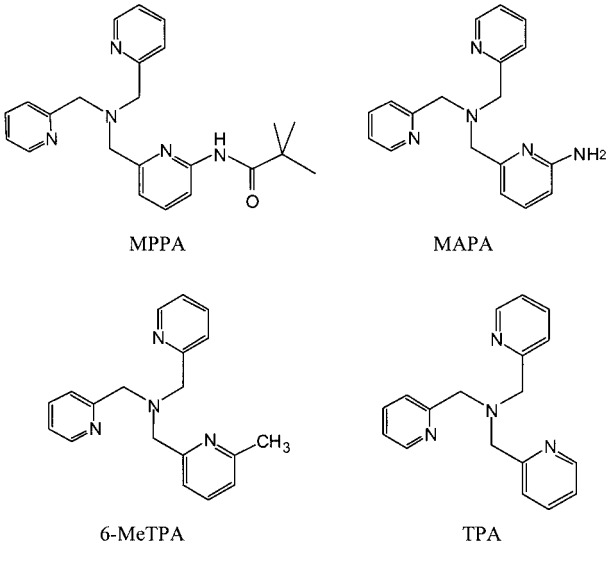

MPPA: {[6-(pivalamido)pyrid-2-yl]methyl}bis(pyrid-2-ylmethyl)amine
MAPA: [(6-aminopyrid-2-yl)methyl]bis(pyrid-2-ylmethyl)amine
6-MeTPA: [(6-methyl-2-pyridyl)methyl]bis(pyrid-2-ylmethyl)amine
TPA: tris(pyrid-2-ylmethyl)amine

Scheme 1. Tripodal pyridylamine ligands

Results and Discussion

Formation of $Cu^{II}-L-N_3$ Complexes (L = mppa, mapa, tpa, 6-metpa) and Their Spectroscopic Properties

$[Cu^{II}(mppa)](ClO_4)_2$ (**1**) [mppa = bis(pyrid-2-ylmethyl){[6-(pivalamido)pyrid-2-yl]methyl}amine] was synthesized by mixing equimolar amounts of $Cu^{II}(ClO_4)_2 \cdot 6H_2O$ and MPPA in methanol. Addition of NaN_3 to **1** in CH_3CN results in a color change of the solution from blue to green, indicating formation of $[Cu^{II}(mppa)(N_3)]^+$ (**1a**). $[Cu^{II}(L)(N_3)]^+$ complexes [L = mapa (**2a**), tpa (**3a**),[46] and 6-metpa (**4a**)] were also prepared in CH_3CN solution by a similar procedure and the azide complexes all showed almost the same spectroscopic properties corresponding to the analogous coordination geometries. Electronic absorption and ESR spectroscopic data for $[Cu^{II}(L)(N_3)]^+$, **1a**, **2a**, **3a** and **4a**, are listed in Tables 1 and 2, respectively. The electronic absorption spectrum of **1a** exhibited d-d transition bands centered at 647 nm (300 $M^{-1}cm^{-1}$) and 833 nm (220 $M^{-1}cm^{-1}$), and an intense absorption band at 395 nm (2700 $M^{-1}cm^{-1}$). The latter intense absorption band in the UV region can be assigned to LMCT since the other azide complexes, $[Cu(mapa)(N_3)]^+$ (**2a**) and $[Cu(tpa)(N_3)]^+$ (**3a**), exhibited intense LMCT bands between the bound N_3^- anion and the copper ion in the same region [at 403 nm (2940 $M^{-1}cm^{-1}$) [46] and 413 nm (2130 $M^{-1}cm^{-1}$), respectively] (Table 1).

$[Cu^{II}(6\text{-metpa})(N_3)]^+$ (**4a**) also showed the same characteristic LMCT band at 414 nm (2600 $M^{-1}cm^{-1}$), indicating that the azide ion is bound to the Cu^{II} center. The frozen solution ESR spectrum of the azide complex **1a** at 77 K gave signals typical for a Cu^{II} complex with a d_{z^2} ground state ($g_{\|} = 2.03 < g_{\perp} = 2.20$, $|A_{\|}| = 71$ G, and $|A_{\perp}| = 130$ G). Including other azide complexes, the ESR spectroscopic patterns of **1a**, **2a**, and **3a** are characteristic of a trigonal-bipyramidal geometry ($g_{\|} < g_{\perp}$) which agrees well with those speculated from their absorption spectroscopic features showing lower d-d transition energies (Table 2).

Crystal Structures of $[Cu(mppa)](ClO_4)_2$ (1) and $[Cu(mppa)(N_3)]ClO_4$ (1a)

$[Cu(mppa)](ClO_4)_2$ (**1**) and $[Cu(mppa)(N_3)]ClO_4$ (**1a**) were obtained as blue and green crystals, respectively, which were suitable for X-ray structural analysis. The molecular structures of the cationic parts of **1** and **1a** are shown in Figures 1 and 2, respectively. Selected bond lengths and angles around the copper cores are listed together in Table 3. The Cu^{II} ion in **1** is coordinated by three pyridine nitrogen atoms of MPPA [Cu−N(2) = 1.970(6) Å, Cu−N(3) = 2.062(6) Å, Cu−N(4) = 2.079(6) Å] in the trigonal plane and by one tertiary amine nitrogen and one pivalamido oxygen atom of MPPA [Cu−N(1) = 2.006(7) Å and Cu−O(1) = 1.940(6) Å] in the axial positions. The Cu^{II} ion in the azide complex **1a** has almost the same coordination mode as in **1** except for substitution of an azide ion for the pivalamido oxygen atom of MPPA. The copper

 © 2003 Wiley-VCH Verlag GmbH & Co. KGaA, Weinheim

Table 1. UV/Vis spectroscopic data for $[Cu(L)(N_3)]^+$ in MeCN

Complex	LMCT ($N_3^- \rightarrow Cu^{II}$) λ_{max}/nm (ε/$M^{-1}cm^{-1}$)	d-d bands λ_{max}/nm (ε/$M^{-1}cm^{-1}$)
$[Cu(mppa)(N_3)]^+$ (**1a**)	395 (2700)	647 (300), 833 (220)
$[Cu(mapa)(N_3)]^+$ (**2a**)	403 (2940)	670 (300), 878 (250)
$[Cu(tpa)(N_3)]^+$ (**3a**)	413 (2130)[a]	674 (277), 882 (275)[a]
$[Cu(6\text{-metpa})(N_3)]^+$ (**4a**)	414 (2600)	670 (300), 845 (210)

[a] Ref.[46]

Table 2. ESR spectroscopic data for $[Cu(L)(N_3)]^+$ in MeCN

Complex	$g_{\parallel}$	$\lvert A_{\parallel}\rvert$/Gauss	$G_{\perp}$	$\lvert A_{\perp}\rvert$/Gauss
$[Cu(mppa)(N_3)]^+$ (**1a**)	2.03	71	2.20	130
$[Cu(mapa)(N_3)]^+$ (**2a**)	2.00	76	2.21	100
$[Cu(tpa)(N_3)]^+$ (**3a**)	2.00	82	2.19	92
$[Cu(6\text{-metpa})(N_3)]^+$ (**4a**)	—[a]	—[a]	—[a]	—[a]

[a] Broadened signal.

Table 3. Selected bond lengths [Å] and angles [°] for $[Cu(mppa)](ClO_4)_2$ (**1**) and $[Cu(mppa)(N_3)]ClO_4$ (**1a**)

$[Cu(mppa)](ClO_4)_2$ (**1**)

Bond length [Å]

Cu(1)−O(1)	1.940(6)	Cu(1)−N(3)	2.062(6)
Cu(1)−N(1)	2.006(7)	Cu(1)−N(4)	2.079(6)
Cu(1)−N(2)	1.970(6)		

Bond angle [°]

O(1)−Cu(1)−N(1)	176.0(2)	N(1)−Cu(1)−N(2)	85.3(3)
O(1)−Cu(1)−N(2)	90.8(2)	N(1)−Cu(1)−N(3)	83.8(3)
O(1)−Cu(1)−N(3)	98.6(3)	N(1)−Cu(1)−N(4)	82.6(3)
O(1)−Cu(1)−N(4)	99.8(3)	N(2)−Cu(1)−N(3)	127.3(3)
		N(2)−Cu(1)−N(4)	125.3(3)
		N(3)−Cu(1)−N(4)	104.0(2)

$[Cu(mppa)(N_3)]ClO_4$ (**1a**)

Bond length [Å]

Cu(1)−N(6)	1.936(5)	Cu(1)−N(3)	2.050(6)
Cu(1)−N(1)	2.010(5)	Cu(1)−N(4)	2.070(5)
Cu(1)−N(2)	2.180(5)	N(5)···N(6)	2.893(6)

Bond angle [°]

N(6)−Cu(1)−N(1)	175.3(2)	N(1)−Cu(1)−N(2)	80.0(2)
N(6)−Cu(1)−N(2)	96.5(2)	N(1)−Cu(1)−N(3)	81.0(2)
N(6)−Cu(1)−N(3)	98.0(2)	N(1)−Cu(1)−N(4)	81.2(2)
N(6)−Cu(1)−N(4)	103.2(2)	N(2)−Cu(1)−N(3)	116.7(2)
		N(2)−Cu(1)−N(4)	116.5(2)
		N(3)−Cu(1)−N(4)	119.2(2)

center is surrounded by three pyridine nitrogen atoms from MPPA [Cu−N(2) = 2.180(5) Å, Cu−N(3) = 2.050(5) Å, Cu−N(4) = 2.070(5) Å] in the trigonal plane and one tertiary amine nitrogen atom [Cu−N(1) = 2.010(5) Å] from MPPA and one azide nitrogen atom [Cu−N(6) = 1.936(5) Å] in the axial positions. Judging from the coordination geometric parameter τ around the Cu^{II} ion [$\tau = (\beta - \alpha)/60$, where α and β represent two basal angles ($\beta \geq \alpha$)],[47] the coordination structures for **1** (0.81) and **1a** (0.94) are both almost trigonal-bipyramidal as listed in Table 3. As shown by the above spectroscopic and structural results, it is clear that the Cu^{II} complexes with an azide group exhibit a trigonal-bipyramidal structure both in solution and in the solid state. In the molecular structure of **1a**, a hydrogen bond was observed between the pivalamido NH group of MPPA and the coordinated azide ion. The distance between N(5) and N(6) [2.893(6) Å] corresponds well to a hydrogen bonding interaction (Figure 2), which apparently contributes to the fixation of the azide ion, as found in the previously reported Cu-TPPA and Cu-BPPA complexes with the pivalamido group [TPPA: tris{[6-(pivalamido)pyrid-2-yl]methyl}amine; BPPA: bis{[6-(pivalamido)pyrid-2-yl]methyl}(pyrid-2-ylmethyl)amine].[36−41]

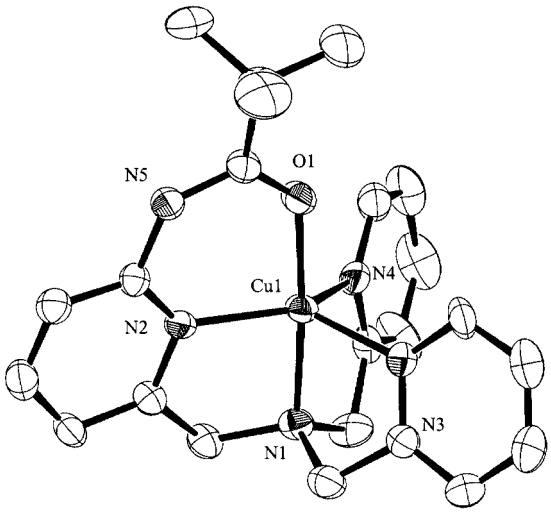

Figure 1. ORTEP plots of $[Cu(mppa)]^{2+}$ (**1**) with the atomic labeling scheme; hydrogen atoms have been omitted for clarity

Electrochemical Properties

In order to understand the electrochemical properties of the Cu^{II} complexes with tripodal tetradentate ligands, the cyclic voltammograms of the azide complexes were measured in MeCN under argon relative to the SCE. The cyclic voltammograms of **1a**, **2a**, **3a**, and **4a** showed a reversible one-electron redox potential wave. The redox potential values were converted into the NHE scale by adding 244.4 mV,[48] and the electrochemical data are listed in Table 4. The $E_{1/2}$ values of the azide complexes are significantly dif-

 © 2003 Wiley-VCH Verlag GmbH & Co. KGaA, Weinheim

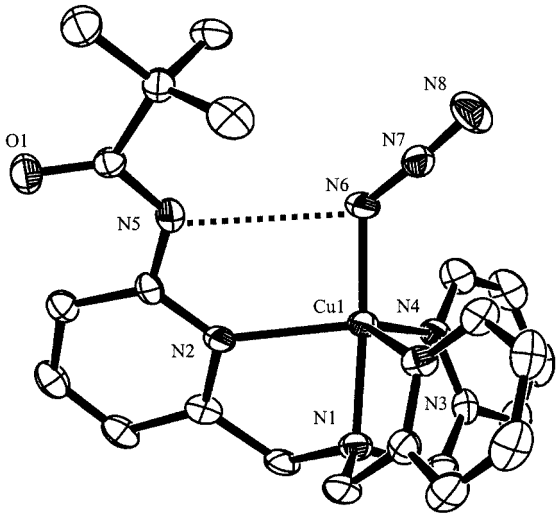

Figure 2. ORTEP plots of $[Cu(mppa)(N_3)]^+$ (**1a**) with the atomic labeling scheme; hydrogen atoms have been omitted for clarity

ferent from each other: those of **1a** and **4a** are in the range of −40 mV whilst those of **2a** and **3a** are −138 and −89 mV, respectively (vs. NHE).

Table 4. Electrochemical parameters for $[Cu(L)(N_3)]^+$ in MeCN (reduction and oxidation potentials are given relative to the NHE)

Complex	E_{pa}/mV	E_{pc}/mV	ΔE/mV	$E_{1/2}$/mV
$[Cu(mppa)(N_3)]^+$ (**1a**)	−4	−84	80	−44
$[Cu(mapa)(N_3)]^+$ (**2a**)	−98	−178	80	−138
$[Cu(tpa)(N_3)]^+$ (**3a**)	−37	−140	103	−89
$[Cu(6\text{-}metpa)(N_3)]^+$ (**4a**)	+16	−85	101	−34

Reaction of Copper(I) Complexes with Dioxygen and Characterization of the Oxygenated Complexes

The reactions of the Cu^I-MPPA or -MAPA complexes with dioxygen were performed in acetone and EtCN solutions, which were monitored by spectroscopic methods such as electronic absorption, resonance Raman and ESR spectroscopy. Bubbling dioxygen into the solution of each Cu^I complex at −78 °C resulted in an intense color change from light yellow to violet. The absorption spectra of these violet species in acetone solution showed intense bands at 517 nm (ε = 5600 $M^{-1}cm^{-1}$) and 503 nm (ε = 7500 $M^{-1}cm^{-1}$) for the Cu-MPPA and Cu-MAPA systems, respectively. These bands exhibited shoulder bands around 600 nm (ε = 1500 $M^{-1}cm^{-1}$). The intense absorption bands in the visible region have been tentatively assigned as resulting from charge transfer (CT) transitions from the *trans*-μ-1,2-peroxo groups to the copper(II) centers.[14−25] A detailed interpretation of the spectroscopic features of these CT bands for the Cu-MPPA and Cu-MAPA systems will be discussed in the following section together with those of the Cu-TPA system.[16−23] The resonance Raman spectra of EtCN or acetone solutions containing these copper−dioxygen adduct complexes measured at −78 °C (514 nm laser excitation) showed a strong resonance enhanced Raman peak at 837 cm^{-1} for the Cu-MPPA system, which shifted to 792 cm^{-1} ($\Delta\nu$ = 45 cm^{-1}) when ^{18}O-labeled dioxygen was used and a corresponding peak for the Cu-MAPA complex was observed at 847 cm^{-1}, which shifted to 800 cm^{-1} ($\Delta\nu$ = 45 cm^{-1}) when $^{18}O_2$ was used. The frequencies and ^{18}O-isotope shifts of these bands are characteristic of (*trans*-μ-1,2-peroxo)dicopper(II) complexes.[14−25] The ESR spectra of these oxygenated complexes in solution were silent which also suggests that two copper(II) ions are bridged by a dioxygen molecule and are antiferromagnetically coupled.

On the basis of these spectroscopic observations, we conclude that the (*trans*-μ-1,2-peroxo)dicopper(II) complexes $[\{Cu(mppa)\}_2(O_2)]^{2+}$ (**1b**) and $[\{Cu(mapa)\}_2(O_2)]^{2+}$ (**2b**) have formed in solution.

Spectral Changes in the LMCT Bands of O_2 Adduct Complexes Affected by a Hydrogen Bonding Interaction

Bubbling dioxygen into an acetone solution containing $[Cu(L)]PF_6$ complexes with L = MPPA or MAPA afforded $[\{Cu(mppa)\}_2(O_2)]^{2+}$ (**1b**) or $[\{Cu(mapa)\}_2(O_2)]^{2+}$ (**2b**), respectively, as described above. The intense charge-transfer bands (LMCT) observed at 517 nm for the Cu-MPPA system and at 503 nm for the Cu-MAPA system can be attributed to the formation of a (*trans*-μ-peroxo)dicopper(II) core in each case. The absorption spectra of four kinds of μ-peroxide complexes namely **1b**, **2b**, $[\{Cu(tpa)\}_2(O_2)]^{2+}$ (**3b**),[16−23] and $[\{Cu(6\text{-}metpa)\}_2(O_2)]^{2+}$ (**4b**),[44] are shown in Figure 3 and Table 5. Interesting spectroscopic behavior was observed as follows: the LMCT bands of the complexes exhibited blue shifts in the order **4b** < **3b** < **1b** < **2b**. The intensities of the shoulder peaks of the LMCT bands observed in the former two complexes **1b** and **2b** at about 600 nm were quite weak compared with those in the latter two complexes **3b** and **4b**. In the following section we discuss this by use of Solomon's theoretical consideration.

Solomon et al. first explained the LMCT bands of copper(II) peroxide complexes using a mononuclear copper(II) model with a peroxide ion in the end-on mode (Figure 4).[49] The highest occupied molecular orbitals of the peroxide have two degenerate π* sets which split into two energy levels upon binding to the copper(II) ion. One π* orbital (π^*_σ) along the Cu−O bond has a larger overlap with the d_σ orbital of the copper ion and is critically stabilized by this interaction. The other π* orbital (π^*_v) perpendicular to the d_σ orbital undergoes a weaker d-π interaction. On the basis of this consideration, there are two types of CT transitions from the peroxide to the copper(II) ion, that is, the band in the shorter wavelength region (500−540 nm) corresponds to a $\pi^*_\sigma \rightarrow d_\sigma$ transition and the shoulder band at longer wavelength (≈ 600 nm) can be ascribed to a $\pi^*_v \rightarrow d_\sigma$ transition.

Firstly, considering the $\pi^*_\sigma \rightarrow d_\sigma$ transition wavelength region (500−540 nm), the LMCT band for **4b** was observed at 537 nm, indicating that the energy gap between the π^*_σ and the d_σ orbitals is relatively small in comparison with that of **3b** at 523 nm, as shown in Table 5. This low energy shift of the $\pi^*_\sigma \rightarrow d_\sigma$ transition band can be explained by a decrease in the energy splitting of the d orbitals because the

 © 2003 Wiley-VCH Verlag GmbH & Co. KGaA, Weinheim

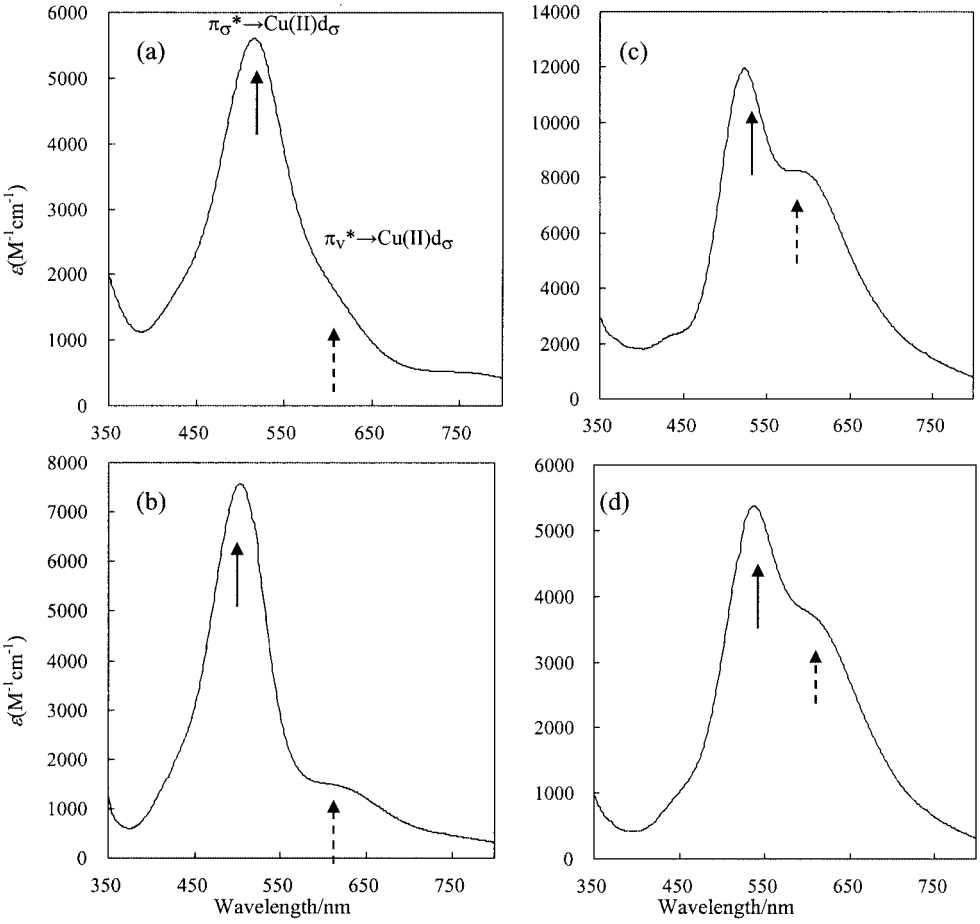

Figure 3. Absorption spectra of $[(CuL)_2(O_2)]^{2+}$ complexes in acetone at −78 °C [L = MPPA (a), MAPA (b), TPA (c), 6-MeTPA(d)]

Table 5. Absorption spectroscopic data for $[(CuL)_2(O_2)]^{2+}$ complexes

L (Ligand)	λ_{max}/nm (ε/M^{-1}cm^{-1})	Ref.
MPPA (**1b**)	517 (5600), 600 (1500)	this work
MAPA (**2b**)	503 (7500), 600 (1500)	this work
TPA (**3b**)	524 (12000), 600 (8000)	[16−23]
6-MeTPA (**4b**)	537 (5500), 600 (4000)	[44]

ligation of the pyridine nitrogen atoms to the copper(II) ion is weakened by the steric hindrance of the methyl group substituents at the 6-position of the pyridine ring.[44,45] On the other hand, the $\pi^*_\sigma\rightarrow d_\sigma$ CT bands of **1b** (517 nm) and **2b** (503 nm) were observed in a higher energy region than that of **3b** (523 nm) in spite of the larger steric hindrance of the 6-(pivalamido)- and 6-amino substituted derivatived. In these cases, the pivalamido and amino groups in the 6-positions of the pyridine ring in MPPA and MAPA can be considered to form intramolecular hydrogen bonding interactions with the ligating peroxide ion in the same mode as in the previously reported monomeric (hydroperoxo)-copper(II) complex $[Cu^{II}(bppa)(OOH)]^+$ [BPPA = bis{[6-(pivalamido)pyrid-2-yl]methyl}(2-pyridylmethyl)amine].[36] The electronic absorption spectra of the azide complexes,

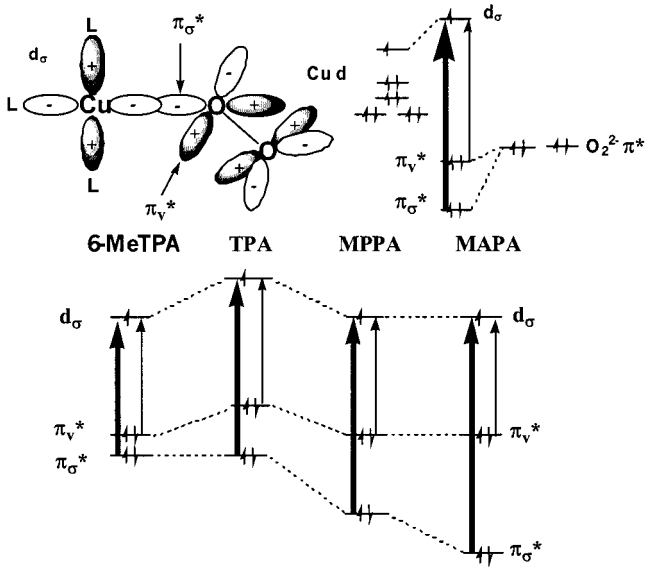

Figure 4. Schematic diagram of the energy levels of the molecular orbitals participating in the copper−peroxo bond

1a, **2a**, **3a and 4a**, also exhibited a similar tendency: the LMCT energies of the azide complexes with MPPA and MAPA detected at 395 and 403 nm are relatively larger than

 © 2003 Wiley-VCH Verlag GmbH & Co. KGaA, Weinheim

those of the azide complexes with TPA and 6-MeTPA observed at 413 and 414 nm. Indeed, in the crystal structures of the azide complexes with MPPA and MAPA, **1a** and **2a**, the intramolecular hydrogen bonding interactions were clearly formed between the 6-amido/amino NH hydrogen and the axially bound azide nitrogen atoms. These findings suggest that similar hydrogen bonds can also be formed in the corresponding (peroxo)dicopper(II) complexes, **1b** and **2b**. Taking this into account, it can be understood that the higher energy shifts of the $\pi^*_\sigma \rightarrow d_\sigma$ CT bands in the (peroxo)dicopper(II) species, **1b** and **2b**, were caused by a stabilizing π^*_σ orbital energy level giving the larger $\pi^*_\sigma - d_\sigma$ CT energy gap.

In the $\pi^*_v \rightarrow d_\sigma$ transition wavelength region ($\approx$ 600 nm), the shoulder LMCT bands of **1b** and **2b** are broadened as shown in Figure 4. The shoulder LMCT absorbances of **1b** and **2b** at 600 and 600 nm (ε = 1500 and 1500 $M^{-1}cm^{-1}$) are smaller than those of **3b** and **4b** at 600 and 600 nm (ε = 8000 and 4000 $M^{-1}cm^{-1}$), respectively. The decrease in the $\pi^*_v \rightarrow d_\sigma$ CT absorbance would also be affected by the intramolecular hydrogen bonding interaction. In the case of **3b** and **4b** without a hydrogen bonding moiety, the π^*_v orbital of the peroxide can overlap well with the d_σ orbital of copper because of the free rotation of the Cu−O bond in these (peroxo)dicopper(II) complexes. In **1b** and **2b**, however, such a rotation around the Cu−O bond is apparently inhibited by the hydrogen bond formed between the groups in the 6-position of the pyridine ring and the ligating peroxide ion with the result that overlap of the π^*_v and the d_σ orbitals would become small enough so as to decrease the CT transition probability.

In summary, the absorption spectroscopic behavior of the (peroxo)dicopper(II) complexes in question can be interpreted in terms of the contribution of the hydrogen bonding ability of the NH group of the pivalamido or amino groups introduced into pyridine 6-position of the ligands.

Thermal Stability of the (μ-Peroxo)dicopper Complexes with Hydrogen Bonding Interaction Sites

In our previous report, we found that the copper(II) complex with pivalamido at the 6-position of pyridine ring in the ligand forms the stable (hydroperoxo)copper(II) complex, $[Cu^{II}(bppa)(OOH)]^+$ [BPPA = bis{[6-(pivalamido)pyrid-2-yl]methyl}(2-pyridylmethyl)amine][36] which remains stable in solution at room temperature for more than one month. The first crystal structure of a monomeric (hydroperoxo)copper(II) complex $[Cu^{II}(bppa)(OOH)]^+$ revealed that the pivalamido NH group of BPPA interacts with the ligated hydroperoxide oxygen atom by hydrogen bonding, thus promoting its thermal stability.[36] Based on this study, we expected that the hydrogen bond interaction might stabilize (μ-peroxo)dicopper(II) species generated from the Cu-MPPA and -MAPA systems. The thermal stability of these peroxo species at 183 or 213 K was established by monitoring the decrease in their LMCT absorbances. The reduction of the LMCT bands occurred with first-order kinetics, demonstrating the decomposition of the (μ-peroxo)dicopper(II) species. The decomposition rate constants are listed in Table 6. The effects on the thermal stabilities of the (μ-peroxo)dicopper(II) species as a result of substitution at the 6-position of pyridine ring are described in detail in the following discussion.

Table 6. Decomposition rate constants of $[(CuL)_2(O_2)]^{2+}$ complexes

L (Ligand)	λ_{max}/nm	$k_{obsd.}$/min^{-1} [a]	T/K
MPPA (**1b**)	517	0.2×10^{-3}	183
6-MeTPA (**4b**)	537	39.4×10^{-3}	183
MPPA (**1b**)	517	13.3×10^{-3}	213
MAPA (**2b**)	503	2.5×10^{-3}	213
TPA (**3b**)	523	2.9×10^{-3}	213

[a] The $k_{obsd.}$ values are estimated by following the decrease of absorption band (λ_{max}).

The (μ-peroxo)dicopper(II) complex **4b** is remarkably unstable and its decomposition rate is the fastest of all the complexes listed in Table 6 ($k_{obsd.}$ = 39.4×10^{-3} min^{-1} at 183 K). Unlike the other systems, the decomposition of **4b** at 213 K was too fast to allow estimation of the rate constant. This clearly indicates that the thermal stability of the (μ-peroxo)dicopper(II) complex is extensively decreased by the sterically hindered 6-methyl substituent around the metal center.[44,45] Substitution of the 6-pivalamido group in place of the 6-methyl substituent dramatically improves the thermal stability and stabilized the (μ-peroxo)dicopper(II) complex, **1b** ($k_{obsd.}$ = 0.2×10^{-3} min^{-1} at 183 K). Furthermore, the analogous 6-amino-substituted (μ-peroxo)dicopper(II) complex **2b** ($k_{obsd.}$ = 2.5×10^{-3} min^{-1}) is more stable than **1b** ($k_{obsd.}$ = 13.3×10^{-3} min^{-1} at 213 K) and its thermal stability was improved to the same extent as that of **3b** ($k_{obsd.}$ = 2.9×10^{-3} min^{-1}), although the amino group in the 6-position of pyridine ring is as bulky as the methyl group in **4b**.

The order of the thermal stability of these peroxo complexes can therefore be determined as follows: **2b** $\approx$ **3b** > **1b** >> **4b**.The (μ-peroxo)dicopper complexes are partially stabilized by the hydrogen bonding interaction, although the stability was reduced by the adverse effect of the steric bulk around the metal ion.

Conclusion

In order to examine the mode of the hydrogen bonding interaction and its effect on the (μ-peroxo)dicopper(II) species, we have prepared copper complexes with the tripodal tetradentate ligands MPPA and MAPA which bear a hydrogen bonding site . The crystal structures of the azide complexes **1a** and **2a** revealed that pivalamido and amino NH groups in 6-position of the pyridine ring can interact with the axially coordinated azide ion via the hydrogen bond. The tripodal ligands with a hydrogen bonding ability exerted significant influence on two LMCT bands of the (μ-peroxo)dicopper(II) species. The energy of the $\pi^*_\sigma \rightarrow d_\sigma$ CT transition was raised and the absorbance of the $\pi^*_v \rightarrow d_\sigma$ CT band was decreased. Such characteristic spectroscopic

 © 2003 Wiley-VCH Verlag GmbH & Co. KGaA, Weinheim

behavior was interpreted in terms of stabilization of the π^*_σ orbital and restriction of rotation of the Cu−O bond by the hydrogen bond between the NH group and the axially coordinated peroxide groups of the copper complexes. Finally, the hydrogen bonding interaction was found to overcome the adverse effect of steric bulk and thus stabilize the (μ-peroxo)dicopper(II) complexes.

Experimental Section

Materials and Measurements: Reagents and solvents employed were of the highest grade available. All solvents for spectroscopy were further purified by distillation before use. Other chemicals were used without further purification. Tris(pyrid-2-ylmethyl)amine (TPA) and [(6-methylpyrid-2-yl)methyl]bis(pyrid-2-ylmethyl)amine (6-MeTPA) were prepared using literature methods.[16,44] Electronic absorption spectra were recorded at low temperature with a JASCO Ubest-35 spectrophotometer equipped with an Oxford Variable Temperature Liquid Nitrogen Cryostat Optistant. X-Band ESR spectra of frozen solutions were recorded at 77 K by using a JEOL RE-1X ESR spectrometer. ^{1}H NMR spectra were measured with a Bruker Avance-600 spectrometer with chemical shift values referenced relative to TMS as an internal standard. Cyclic voltammetric measurements were performed using a Bioanalytical Systems (BAS) CV-1B electrochemical analyzer. A three-electrode system was used with a 3-mm diameter glassy carbon electrode as the working electrode, a saturated calomel electrode (SCE) as the reference electrode and a Pt-wire electrode as the counter electrode in a glass cell having a working compartment of approximately 3 mL in volume. All measurements were made in solution at 25 °C under argon with tetra(*n*-butyl)ammonium tetrafluoroborate (0.1 M) as a supporting electrolyte at a scan rate of 100 mVs^{-1}. The potential of the regular ferrocene/ferrocenium (Fc/Fc^+) redox couple in acetonitrile was −0.33 V under our experimental conditions. In order to discuss the electrochemical values in comparison with other data, all the electrochemical potentials were converted into values with the normal hydrogen electrode (NHE) as a standard by adding 244.4 mV. Resonance Raman spectra were recorded with a liquid-nitrogen-cooled CCD detector (Model LN/CCD-1300-PB, Princeton Instrument) attached to a 100-cm single polychromator (Model MC-100DG, Ritsu Oyo Kogaku). The excitation was provided by the 476.5-nm line of an Ar laser (Model GLG3200, NEC). $^{16}O_2$ samples were prepared by bubbling dry dioxygen into acetone or EtCN solutions of the copper(I) complexes with tetradentate ligands at −78 °C. Isotopic substitution of the peroxo oxygen atoms bridged to the dicopper ions was accomplished by oxygenation of the copper(I) complexes with $^{18}O_2$. All measurements were carried out with a spinning cell maintained at −78 °C by a stream of liquid N_2 vapor.

Synthesis of Ligands

{[6-(Pivalamido)-2-pyridyl]methyl}bis(pyrid-2-ylmethyl)amine (MPPA): Reaction of the primary amine, 2-(aminomethyl)-6-(pivalamido)pyridine,[37,38] (2.80 g, 13.5 mmol) with 2 equiv. of 2-(chloromethyl)pyridine (5.25 g, 32.0 mmol) was carried out in a dioxane/H_2O (4:1) solution (300 mL) containing KOH (2.92 g, 52.0 mmol). The solution was stirred at 50 °C for 3 d followed by removal of the solvent by evaporation in vacuo. Dissolving the resultant crude brownish oil in diethyl ether and allowing it to stand at room temperature gave colorless needle-like crystals of MPPA (2.32 g, 45.9% yield). ^{1}H NMR ($CDCl_3$): δ = 1.33 (s, 9 H), 3.78 (s, 2 H), 3.89 (s, 2 H), 7.15 (m, 2 H), 7.28 (d, 2 H), 7.56 (d, 2 H), 7.66 (t, 3 H), 7.95 (b, 1 H), 8.06 (b,1 H), 8.10 (d, 1 H), 8.53 (d, 2 H) ppm.

[(6-Aminopyrid-2-yl)methyl]bis(pyrid-2-ylmethyl)amine (MAPA): To an ethanol solution (500 mL) of MPPA (3.89 g, 10.0 mmol) was added KOH (28.1 g, 0.50 mol). The solution was stirred at 50 °C for 1 week. After removal of the solvent from the reaction mixture by evaporation in vacuo, the resultant crude brownish oil was dissolved in dichloromethane (100 mL) which was washed with water and dried with $MgSO_4$. The resultant solution was concentrated in vacuo to give the crude product as an oil. Pure MAPA was obtained as colorless needle-like crystals by recrystallization from diethyl ether (2.13 g, 70.0% yield). ^{1}H NMR ($CDCl_3$): δ = 3.54 (s, 2 H), 3.76 (s, 4 H), 5.79 (s, 2 H), 6.30 (d, 1 H), 6.73 (d, 1 H), 7.24 (t, 2 H), 7.35 (t, 1 H), 7.62 (d, 2 H), 7.77 (t, 1 H), 8.48 (d, 2 H) ppm.

Synthesis of Cu Complexes

Preparation of [Cu(mppa)](ClO$_4$)$_2$: To a stirred MeOH solution (10 mL) of $Cu(ClO_4)_2 \cdot 6H_2O$ (74.1 mg, 0.2 mmol) was added MPPA (77.8 mg, 0.2 mmol). After the resultant mixture was allowed to stand at room temperature for a few days, blue crystals of $[Cu(mppa)](ClO_4)_2$, suitable for X-ray structural analysis, were obtained. Yield: 109 mg (85%). $C_{23}H_{27}Cl_2CuN_5O_9$ (651.94): calcd. C 42.37, H 4.17, N 10.73; found C 42.57, H 4.16, N 11.05.

Preparation of [Cu(mppa)(N$_3$)]ClO$_4$: To a stirred MeCN solution (10 mL) of $[Cu(mppa)](ClO_4)_2$ (151.9 mg, 0.2 mmol) was added NaN_3 (13.0 mg, 0.2 mmol). A green precipitate formed immediately. After filtration, recrystallization of the precipitate from MeCN gave plate-like green single crystals, suitable for X-ray structural analysis. Yield: 85 mg (71%). $C_{23}H_{27}ClCuN_8O_5$ (594.51): calcd. C 46.46, H 4.47, N 18.84; found C 46.38, H 4.47, N 19.15.

X-ray Structural Analysis of [Cu(mppa)](ClO$_4$)$_2$ and [Cu(mppa)(N$_3$)]ClO$_4$: Crystals suitable for X-ray diffraction measurements were mounted on glass fibers. The diffraction data were collected with a Rigaku Mercury diffractometer using graphite-monochromated Mo-K_α radiation at −100 °C with the oscillation technique. Crystal data and experimental details are listed in Table 7. All structures were solved by a combination of direct methods and Fourier techniques. Non-hydrogen atoms were anisotropically refined by full-matrix least-squares calculations. Hydrogen atoms were included but not refined. Refinements were continued until all shifts were smaller than one-third of the standard deviations of the parameters involved. Atomic scattering factors and anomalous dispersion terms were taken from the International Tables for X-ray Crystallography.[50] All calculations were carried out with a Japan SGI workstation computer using the teXsan crystallographic software package.[51] CCDC-211622 and -211623 contain the crystallographic data for this paper. This data can be obtained free of charge at www.ccdc.cam.ac.uk/conts/ or from the Cambridge Crystallographic Data Centre, 12 Union Road, Cambridge CB2 1EZ [Fax: (internat.) + 44-1223-336-033; E-mail: depost@ccdc.cam.ac.uk].

Reaction of [Cu(L)]PF$_6$ (L = MPPA, MAPA, TPA, 6-MeTPA) with Dioxygen: Sample solutions of $[Cu(L)]PF_6$ (L = MPPA, MAPA, TPA, 6-MeTPA) were prepared by mixing $[Cu(MeCN)_4]PF_6$ (0.7 mg, 2.0 mmol) and each ligand (2.1 mmol) in acetone (4 mL) at room temperature under nitrogen. The resultant solutions containing $[Cu(L)]PF_6$ were oxygenated by bubbling dioxygen through them at −78 °C. The formation and decomposition of the peroxo intermediates were monitored by following the increase or decrease in their characteristic ligand−metal change transfer (LMCT) absorption bands at λ_{max} = 517, 503, 524, and 537 nm, for $[\{Cu(L)\}_2(O_2)]^{2+}$ [L = MPPA (**1b**), MAPA (**2b**), TPA (**3b**), 6-

 © 2003 Wiley-VCH Verlag GmbH & Co. KGaA, Weinheim

Table 7. Crystallographic data for $[Cu(mppa)](ClO_4)_2$ (**1**) and $[Cu(mppa)(N_3)]ClO_4$ (**1a**)

	$[Cu(mppa)](ClO_4)_2$ (**1**)	$[Cu(mppa)(N_3)]ClO_4$ (**1a**)
Empirical formula	$C_{21}H_{26}Cl_2CuN_5O_9$	$C_{23}H_{27}ClCuN_8O_5$
Formula mass	743.64	594.52
Crystal system	triclinic	monoclinic
Space group	$P\bar{1}$ (No. 2)	$P2_1/a$ (No. 14)
a [Å]	11.721(4)	14.156(2)
b [Å]	14.191(2)	10.032(1)
c [Å]	9.897(1)	18.645(2)
α [°]	103.058(10)	90
β [°]	90.34(2)	102.262(7)
γ [°]	73.26(2)	90
V [Å^3]	1535.6200	2587.5(6)
Z	2	4
$D_{calcd.}$ [g cm^{-3}]	1.608	1.526
$F(000)$	752.00	1228.00
μ [cm^{-1}]	14.39	9.98
λ [Å]	0.71070	0.71070
T [K]	298	173
No. of refls. measured	4361	5832
No. of refls. used [$I > 2\sigma(I_0)$]	2616	4452
R_1 [a]/R_w [b]	0.081/0.111	0.094/0.235
GOF	1.02	1.61

[a] $R_1 = \Sigma||F_o| - |F_c||/\Sigma|F_o|$. [b] $Rw = [\Sigma w(|F_o| - |F_o|)^2/\Sigma w|F_o|^2]^{1/2}$; $w = 4F_o^2/\sigma^2(F_o)^2$.

MeTPA (**4b**)], respectively. The thermal stability of the peroxo species was examined under constant temperature (183 or 213 K) by following the absorption intensity at 5-min intervals for 12 or 24 h. The decomposition process of the respective complex was analyzed using first order kinetics in which $\ln([A]/[A_0])$ values were plotted according to the time course (where $[A_0]$ and $[A]$ are absorption intensities of the LMCT bands observed initially and at a given time). It was observed that decreasing of the LMCT bands exhibited good first-order kinetics for each peroxo complex.

Acknowledgments

This work was supported partly by a Grant-in-Aid for Scientific Research (No. 11228203, 12304039) from the Ministry of Education, Science, Sports, and Culture of Japan and in part by a grant from the NITECH 21st Century COE Program (S. Y. and H. M.) to which our thanks are due. A. W. is grateful to the Japan Society for the Promotion of Science for a JSPS Research Fellowship for Young Scientists.

[1] *Handbook on Metalloproteins* (Eds.: I. Bertini, A. Sigel, H. Sigel), Marcel Dekker, Inc., New York, **2001**.
[2] J. P. Klinman, *Chem. Rev.* **1996**, *96*, 2541−2561.
[3] *Mechanistic Bioinoganic Chemistry* (Eds.: H. H. Thorp, V. L. Pecoraro), American Chemical Society, Washington, D.C., **1995**.
[4] M. Momenteau, C. A. Reed, *Chem. Rev.* **1994**, *94*, 659−698.
[5] J. H. Dawson, *Science* **1988**, *240*, 433−439.
[6] A. L. Feig, S. J. Lippard, *Chem. Rev.* **1994**, *94*, 759−805.
[7] L. Que, Jr., in *Bioinorganic Catalysis* (Ed.: J. Reedijk), Marcel Dekker, Inc., New York, **1999**, p. 269.
[8] S. Fox, K. D. Karlin, in *Active Oxygen in Biochemistry* (Eds.: J. S. Valentine, C. S. Foote, A. Greenberg, J. F. Liebman), Blackie Academic & Professional, Chapman & Hall, Glasgow, **1995**, p. 188.
[9] N. Kitajima, Y. Moro-oka, *Chem. Rev.* **1994**, *94*, 737−757.
[10] *Bioinorganic Chemistry of Copper* (Eds.: K. D. Karlin, Z. Tyeklar), Chapman & Hall, New York, **1993**.
[11] K. D. Karlin, Z. Tyeklar, A. D. Zuberbuhler, in *Bioinorganic Chemistry* (Ed.: J. Reedijk), Marcel Dekker, Inc., New York, **1993**, p. 261.
[12] E. I. Solomon, F. Tuczek, D. E. Root, C. A. Brown, *Chem. Rev.* **1994**, *94*, 827−856.
[13] E. I. Solomon, M. D. Lowery, *Science* **1993**, *259*, 1575−1581.
[14] A. G. Blackman, W. B. Tolman, in *Structure and Bonding* (Ed.: B. Meunier), Springer Verlag, Berlin, **2000**, 97, p. 179−211.
[15] S. Schindler, *Eur. J. Inorg. Chem.* **2000**, 2311−2326.
[16] R. R. Jacobson, Z. Tyeklár, A. Farooq, K. D. Karlin, S. Liu, J. Zubieta, *J. Am. Chem. Soc.* **1988**, *110*, 3690−3692.
[17] M. J. Baldwin, P. K. Ross, J. E. Pate, Z. Tyeklár, K. D. Karlin, E. I. Solomon, *J. Am. Chem. Soc.* **1991**, *113*, 8671−8679.
[18] N. Wei, N. N. Murthy, Q. Chen, J. Zubieta, K. D. Karlin, *Inorg. Chem.* **1994**, *33*, 1953−1965.
[19] D.-H. Lee, N. Wei, N. N. Murthy, Z. Tyeklár, K. D. Karlin, S. Kaderli, B. Jung, A. D. Zuberbühler, *J. Am. Chem. Soc.* **1995**, *117*, 12498−12513.
[20] K. D. Karlin, D.-H. Lee, S. Kaderli, A. D. Zuberbühler, *Chem. Commun.* **1997**, 475−476.
[21] K. D. Karlin, S. Kaderli, A. D. Zuberbühler, *Acc. Chem. Res.* **1997**, *30*, 139−147.
[22] C. X. Zhang, S. Kaderli, M. Costas, E. Kim, Y.-M. Neuhold, K. D. Karlin, *Inorg. Chem.* **2003**, *42*, 1807−1824.
[23] M. Schatz, M. Becker, F. Thaler, F. Hampel, S. Schindler, R. R. Jacobson, Z. Tyeklar, N. N. Murthy, P. Ghosh, Q. Chen, J. Zubieta, K. D. Karlin, *Inorg. Chem.* **2001**, *40*, 2312−2322.
[24] M. Becker, F. W. Heinemann, S. Schindler, *Chem. Eur. J.* **1999**, *5*, 3124−3129.
[25] M. Weitzer, S. Schindler, G. Brehm, S. Schneider, E. Hoermann, B. Jung, S. Kaderli, A. D. Zuberbuehler, *Inorg. Chem.* **2003**, *42*, 1800−1806.
[26] S. Mahaptra, S. Kaderli, A. Llobet, Y.-M. Neuhold, T. Palanché, J. A. Halfen, V. G. Young, Jr., T. A. Kaden, L. Que, Jr., A. D. Zuberbühler, W. B. Tolman, *Inorg. Chem.* **1997**, *36*, 6343−6356.
[27] P. L. Holland, K. R. Rodgers, W. B. Tolman, *Angew. Chem. Int. Ed.* **1999**, *38*, 1139−1142.
[28] H. V. Obias, Y. Lin, N. N. Murthy, E. Pidcock, E. I. Solomon, M. Ralle, N. J. Blackburn, Y.-M. Neuhold, A. D. Zuberbühler, K. D. Karlin, *J. Am. Chem. Soc.* **1998**, *120*, 12960−12961.

 © 2003 Wiley-VCH Verlag GmbH & Co. KGaA, Weinheim

[29] J. A. Halfen, S. Mahapatra, E. C. Wilkinson, S. Kaderli, V. G. Young, Jr., L. Que, Jr., A. D. Zuberbühler, W. B. Tolman, *Science* **1996**, *217*, 1397−1400.
[30] S. Mahapatra, J. A. Halfen, E. C. Wilkinson, G. Pan, X. Wang, V. G. Young, Jr., C. J. Cramer, L. Que, Jr., W. B. Tolman, *J. Am. Chem. Soc.* **1996**, *118*, 11555−11574.
[31] P. L. Holland, W. B. Tolman, *Coord. Chem. Rev.* **1999**, *190*, 855−869.
[32] P. L. Holland, C. J. Cramer, E. C. Wilkinson, S. Mahapatra, K. R. Rodgers, S. Itoh, M. Taki, S. Fukuzumi, L. Que, Jr., W. B. Tolman, *J. Am. Chem. Soc.* **2000**, *122*, 792−802.
[33] S. Itoh, M. Taki, H. Nakao, P. L. Holland, W. B. Tolman, L. Que, Jr., S. Fukuzumi, *Angew. Chem. Int. Ed.* **2000**, *39*, 398−400.
[34] S. Itoh, H. Nakao, L. M. Berreau, T. Kondo, M. Komatsu, S. Fukuzumi, *J. Am. Chem. Soc.* **1998**, *120*, 2890−2899.
[35] V. Mahadevan, Z. Hou, A. P. Cole, D. E. Root, T. K. Lal, E. I. Solomon, T. D. P. Stack, *J. Am. Chem. Soc.* **1997**, *119*, 11996−11997.
[36] A. Wada, M. Harata, K. Hasegawa, K. Jitsukawa, H. Masuda, M. Mukai, T. Kitagawa, H. Einaga, *Angew. Chem. Int. Ed.* **1998**, *37*, 798−799.
[37] M. Harata, K. Jitsukawa, H. Masuda, H. Einaga, *J. Am. Chem. Soc.* **1994**, *116*, 10817−10818.
[38] M. Harata, K. Jitsukawa, H. Masuda, H. Einaga, *Chem. Lett.* **1995**, 61−62.
[39] M. Harata, K. Jitsukawa, H. Masuda, H. Einaga, *Bull. Chem. Soc. Jpn.* **1998**, *71*, 637−645.
[40] M. Harata, K. Jitsukawa, H. Masuda, H. Einaga, *Bull. Chem. Soc. Jpn.* **1998**, *71*, 1031−1038.
[41] M. Harata, K. Jitsukawa, H. Masuda, H. Einaga, *Chem. Lett.* **1996**, 813−814.
[42] L. M. Berreau, S. Mahapatra, J. A. Halfen, V. G. Young, Jr., W. B. Tolman, *Inorg. Chem.* **1996**, *135*, 6339−6342.
[43] C. E. MacBeth, A. P. Golombek, V. G. Young, Jr., C. Yang, K. Kuczera, M. P. Hendrich, A. S. Borovik, *Science* **2000**, *289*, 938−941.
[44] K. Uozumi, Y. Hayashi, M. Suzuki, A. Uehara, *Chem. Lett.* **1993**, 963−966.
[45] H. Nagao, N. Komeda, M. Mukaida, M. Suzuki, K. Tanaka, *Inorg. Chem.* **1996**, *35*, 6809−6815.
[46] D. -H. Lee, N. N. Murthy, K. D. Karlin, *Inorg. Chem.* **1997**, *36*, 5785−5792.
[47] A. W. Addison, T. N. Rao, J. Reedijk, J. Rijn, G. C. Verschoor, *J. Chem. Soc., Dalton Trans.* **1984**, 1349−1356.
[48] J. O'M. Bockris, A. K. N. Reddy, *Modern Electrochemistry*, Plenum Press, New York, **1970**.
[49] J. E. Pate, R. W. Cruse, K. D. Karlin, E. I. Solomon, *J. Am. Chem. Soc.* **1987**, *109*, 2624−2630.
[50] *International Tables for X-ray Crystallography* (Eds.: J. A. Ibers, W. C. Hamilton), Kynoch Press, Birmingham, U. K., **1974**, vol. IV.
[51] *Texsan, Crystal Structure Analysis Package*, Molecular Structure Corporation (1985), **1992**.

Received April 1, 2003
Early View Article
Published Online October 22, 2003

 © 2003 Wiley-VCH Verlag GmbH & Co. KGaA, Weinheim

The Metastable, Glasslike Solid-State Phase of HAlO and Its Transformation to Al/Al_2O_3 Using a CO_2 Laser

Michael Veith,*[a] Kathrin Andres,[a] Stefan Faber ,[a] Joel Blin,[a] Michael Zimmer,[a] Yan Wolf,[a] Hansgeorg Schnöckel,[b] Ralf Köppe,[b] Remo de Masi,[c] and Stefan Hüfner[c]

Keywords: Metastable phase / Aluminum / Laser chemistry / Solid-state structures

Bis(*tert*-butoxyaluminum dihydride) $(t\text{BuOAlH}_2)_2$ decomposes on metal surfaces heated to 250 °C (Fe, Ni, Cu, Pt) and under reduced pressures of 0.01–0.1 atm with elimination of dihydrogen and isobutene to form a glasslike, amorphous film, which is composed of equimolar parts of hydrogen, aluminum and oxygen (elemental analysis, EDX analysis). The gases eliminated during this process were characterized by mass spectroscopy (H_2, isobutene) or by infrared matrix techniques (isobutene). The exclusive binding of hydrogen to aluminum is deduced from IR spectroscopy of the HAlO film and of its deuterated form DAlO. The HAlO layer (which shows no X-ray diffraction pattern), when heated to 450 °C or when exposed to a CO_2 laser, loses hydrogen and transforms to an almost stoichiometric composite with nanoscale crystalline aluminum and aluminum oxide (Al/Al_2O_3) as ingredients. This transformation may be followed by IR spectroscopy, by ^{27}Al MAS NMR or by XPS, the latter showing different signals (Al, 2p electrons, Mg-K_α, $\theta = 0°$) for HAlO (74.2 eV) and for the composite (Al: 72.1 eV, Al_2O_3: 75.3 eV). Microstructures that are characterized by different chemical compositions and different optical contrasts of the "drawing", relative to the surrounding matrix, may be generated with an X/Y-table and a CO_2 laser.

(© Wiley-VCH Verlag GmbH & Co. KGaA, 69451 Weinheim, Germany, 2003)

Introduction

Aluminum hydride (AlH_3)[1,2] and aluminum oxide (Al_2O_3)[3] are well-characterized, crystalline compounds. In the first case, the compound may be considered a coordination polymer from a molecular point of view. For aluminum oxide, several crystalline and amorphous phases, which are often described as ionic structures, are known.[4] Well-established compounds of aluminum simultaneously containing hydrogen and oxygen are aluminum hydroxide, $[Al(OH)_3$, for example: bayerite] and other oxohydroxides such as boehmite, AlO(OH).[5,6] It is interesting to note that no chemically pure compounds in which hydrogen is directly bound to aluminum have yet been described (for recent developments see the next paragraph). This is even more surprising because aluminum oxohalides with the general formula XAlO (where X = Cl, Br, I) have been well-established for many years and have been structurally characterized by X-ray diffraction[7–9] (and for molecular OAlX species in matrix by spectroscopy[10]).

We were intrigued by the possible existence of HAlO, a compound that may be derived from the oxohalide by formal substitution of the halide by hydride. Instead of using a classical solid-state reaction to synthesize this compound, we chose a molecular route, which seemed to open up the access to metastable compounds or phases. When revising the manuscript in June, we learned that R.J. Wehmschulte and his co-workers have described a powder, obtained in organic solvents, in which HAlO also seems to be present.[29] This mixed compound, which also contains some organic residues, is synthesized by treating AlH_3*NMe_3 with siloxanes [such as $(Me_2SiH)_2O$]; the oxygen is thus transposed from silicon to aluminum, while the hydride is partly transferred to silicon, forming Me_2SiH_2. Indeed, some of the spectroscopic data given in this paper[29] are similar to our results, while others seem to be different. This difference may also be due to the fact that we describe a layer, whereas the alternative route gives a powder.

[a] Institut für Anorganische Chemie, Universität des Saarlandes, 66123 Saarbrücken, Germany
Fax: (internat.) +49-(0)681-302-3995
E-mail: veith@mx.uni-saarland.de
[b] Institut für Anorganische Chemie, Universität Karlsruhe, 76128 Karlsruhe, Germany
Fax: (internat.) +49-(0)721-608-4854
[c] Experimenthalpysik, Universität des Saarlandes, 66041 Saarbrücken, Germany
Fax: (internat.) +49-(0)681-302-2773

Results and Discussion

Synthesis and Elemental Composition of HAlO

For the synthesis of HAlO, the gas-phase decomposition of $(t\text{BuOAlH}_2)_2$ on metallic substrates heated to 240–250

°C at low pressures (0.01−0.1 atm) was used.[11,12] HAlO is formed as a transparent layer on the metallic surface of the sample and may be separated as a glasslike film from the metal surface using cold shock in a liquid-nitrogen bath. Prior to the gas-phase process the whole apparatus is heated, flooded, and pumped several times with nitrogen, argon, or helium, in order to eliminate residual oxygen and water in the apparatus. The most simple way to generate HAlO layers is to direct a constant stream of $(t\text{BuOAlH}_2)_2$ on inductively heated copper, nickel, iron, or platinum substrates in a CVD cold-wall reactor, the principle construction of which was described earlier.[13] The obtained layers stick well to the metal surfaces if their thickness does not exceed 2−3 μm, and they are stable towards the atmosphere (H_2O, O_2, H_2S, CO_2) for longer periods of time. The synthetic route used has to be different from the route producing the composite Al/Al_2O_3, which requires distinctly higher temperatures (450−500 °C) at the surface of the metallic target, with $(t\text{BuOAlH}_2)_2$ as a precursor[14,15] (see also next chapters and reference [16]).

In order to get some insight in the thermal reaction discussed above and in order to analyze the gaseous products of the reaction, we ran the same process with the deuterated molecule $(t\text{BuOAlD}_2)_2$ parallel to $(t\text{BuOAlH}_2)_2$ (where D = ^{2}H). The mass spectra of the two reactions only differ in one mass peak at m/z = 3 (HD), which is the signal of highest intensity for the deuterated compound, whereas this peak is completely absent in the mass spectrum when $(t\text{BuOAlH}_2)_2$ is the precursor. A mass fragment m/z = 4 is not found in the case of $(t\text{BuOAlD}_2)_2$ (as long as 270 °C is not exceeded), and all signals in both spectra, besides hydrogen, are those of isobutene.

Conducting a constant stream of $(t\text{BuOAlH}_2)_2$ through a quartz tube heated to 300−700 °C and subsequent trapping of the gaseous products in a cold argon matrix leads exclusively to isobutene, in accordance with the mass spectrometry (see Figure 1).

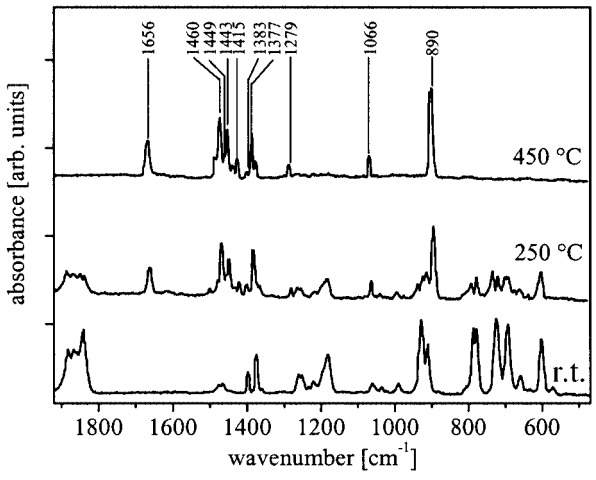

Figure 1. IR spectra of the argon matrix isolated isobutene with identification of the lines (spectrum obtained at 450 °C) and the precursor spectra of $(t\text{Bu−O−AlH}_2)_2$ obtained at room temperature (r.t.) and at 250 °C; already at 250 °C the evolution of isobutene, together with residual $(t\text{Bu−O−AlH}_2)_2$, is found

No $(HAlO)_n$ species or any other aluminum compound is trapped in the matrix under these experimental conditions. This observation is a first hint that HAlO must have a high molecular mass and perhaps a complex structure. On the basis of these findings, the reactions may be formulated as in Equation (1).

$$\begin{aligned}[H_3C-C(CH_3)_2-O-AlH_2]_2 &\rightarrow H-H + H_2C=C(CH_3)_2 \\ &\quad + 2/n\,(HAlO)_n \\ [H_3C-C(CH_3)_2-O-AlD_2]_2 &\rightarrow H-D + H_2C=C(CH_3)_2 \\ &\quad + 2/n\,(DAlO)_n\end{aligned} \quad (1)$$

The splitting off of dihydrogen from $(t\text{BuOAlH}_2)_2$ can be explained by the recombination of a partially negatively charged hydrogen at aluminum with a partially positively charged hydrogen in the *tert*-butyl group, forming isobutene as a complementary molecule (β-elimination). The observed reaction is very similar to the process when $[Mg\{(Ot\text{Bu})_2AlH_2\}_2]$ is transformed to $MgAl_2O_4$.[17]

Whereas the structural and analytical characterization of the gaseous products of Equation (1) is straightforward, the structure and composition of HAlO is not yet clear. From the EDX analysis, the Al to O ratio in HAlO is 0.96(3) to 1.00(3). The carbon content of the film determined by classical elemental analysis is C = 0.2(1)%, and the hydrogen content has a high standard deviation with a lower threshold value of 0.8% (see also below). The aluminum content, determined by complexometry, is found to be 60.5(1.0)% near to the 61.4% calculated for HAlO.

In order to make the elemental determination of hydrogen and its relation to the other elements more accurate, we developed a new analytical method. First we deposited a layer of HAlO (around 1.8 mg) on a thin platinum sheet of approximately 30 mg. The layer was then dissolved in a defined volume of 2 N HCl heated to 80 °C. To avoid hydrolysis of the aluminum ion, sodium fluoride was added to the solution. Some aliquots of the solution were taken to determine the former hydroxide content (after HCl addition and by back-titration with NaOH) and others for the determination of the aluminum content by complexometry. The hydrogen content can be deduced from volumetric measurements of the gas developed from the contact with the acid in a calibrated vessel [see also Equation (2)]. It should be pointed out that freshly prepared samples have to be used and that the HAlO layer should be produced at moderate temperatures (240−250 °C). If higher temperatures are used on the platinum sheet during the deposition process, slightly yellow layers with a significant decrease in the hydrogen content of the layer are obtained.[18]

$$\begin{aligned}1/n(H-AlO)_n + 3\,H_3O^+Cl^- + 6\,NaF &\rightarrow H_2 + 4\,H_2O \\ &\quad + 3\,NaCl + Na_3(AlF_6)\end{aligned} \quad (2)$$

From these analyses, the experimental molar ratio of the elements in the layers on platinum are H:Al:O = 0.95(8):0.95(8):1.0.

 © 2003 Wiley-VCH Verlag GmbH & Co. KGaA, Weinheim

Properties of HAlO

The HAlO layers do not show any reflections when exposed to X-rays. In the infrared spectrum of HAlO (see Figure 2), two signals of different width are found in the 1100−2000 cm^{-1} region: one of these absorption bands at 1925 cm^{-1} is sharp while the other seems to be broad, with a shoulder around 1670 cm^{-1}.

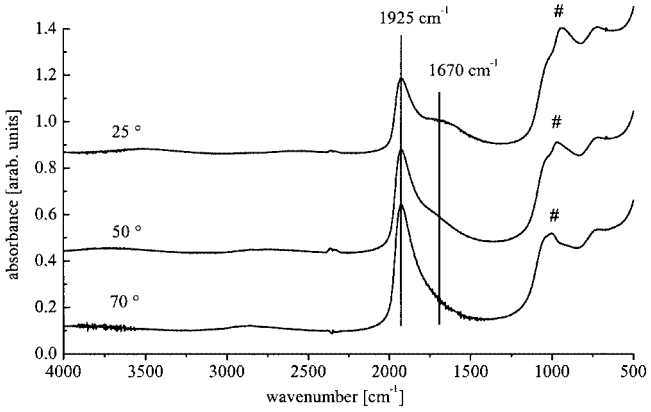

Figure 2. IR spectra of an HAlO layer deposited on a plain copper target in angle-dependent reflection (angles taken between the perpendicular line to the surface and the incoming beam); the signals indicated by # do not belong to the layer and are due to the spectrometer setting

In the deuterated sample DAlO, these absorption bands are found at 1400 and 1223 cm^{-1}, respectively (see Figure 3). The observed isotopic shifts are only understandable for vibrations in which hydrogen takes part, and the values indicate that terminal Al−H (higher wavenumbers) and bridging Al−H···Al entities are both present.[19,20] From the spectra, shown in Figures 2 and 3, obtained in the reflection mode on films deposited on plain metal substrates, it is evident that there is a correlation between the incident angle of the IR beam and the width and the intensities of the absorptions.

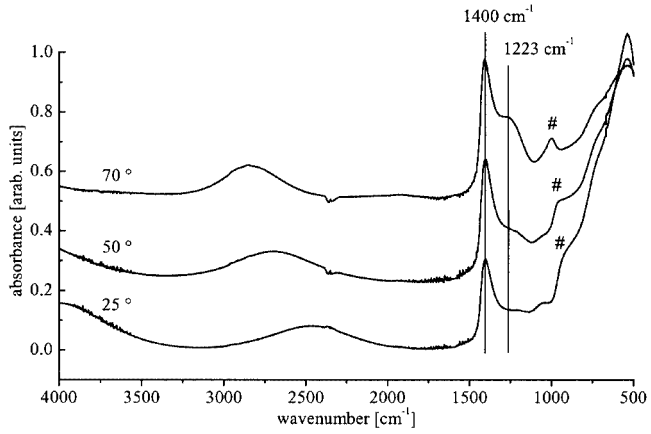

Figure 3. IR spectra of a DAlO layer in angle-dependent reflection with "wrings"; cf. the comments of Figure 2

Although we have not yet finished our systematic studies, we have noticed that, for example, the relative intensities of the hydrogen-based and oxygen-based vibrations (found in between 600−900 cm^{-1} with a characteristic shoulder at 730 cm^{-1}) change with the angle of incidence of the IR beam. This change could indicate different orientations between the Al−H and Al−O bonds with respect to the plain surface of the film.[18]

In the ^1H NMR (MAS) spectrum of the glassy HAlO film separated from the metal target by the shock technique (see above), a broad, structured absorption at approximately 4.0 ppm appears [hydride in $(t\text{BuOAlH}_2)_2$ at δ = 4.48 ppm].[12] In the ^{27}Al NMR spectrum [see spectrum (e) in Figure 4] absorption peaks are found at δ = 6 (sixfold), 30 (fivefold) and 58 ppm (fourfold coordinated aluminum) indicating an amorphous or complex structure for HAlO.[21] For comparison, ^{27}Al NMR spectra for amorphous Al_2O_3 {obtained from the thermolysis of $[(t\text{BuO})_2\text{AlH}]_2$ (a)}, for aluminum metal [obtained from the thermolysis of AlH_3 (b)] and for composites Al/Al_2O_3 [obtained from HAlO at 600 °C (c) and 450 °C (d)] are shown in Figure 4. The aluminum metal is nicely characterized through its Knight shift, whereas in the Al−O (Al−H) region (due to more, or less crystallinity and different compositions) the maxima of the peaks are of different intensities. These data, as well as the IR spectrum and the matrix-isolation experiments, indicate that HAlO is not a simple mixing of the distinct phases AlH_3 and Al_2O_3 (compare data in references [2,4,19,20,22]), but could be composed of different structural units.

The XPS analysis of an HAlO film obtained at 250 °C is consistent with the findings of the spectroscopic methods described so far. In Figure 5, the spectrum (2p-band of aluminum) of an HAlO layer (deposited at 250 °C) is compared to a surface of bulk aluminum that has been partly oxidized (lower part of the figure) and to an HAlO film

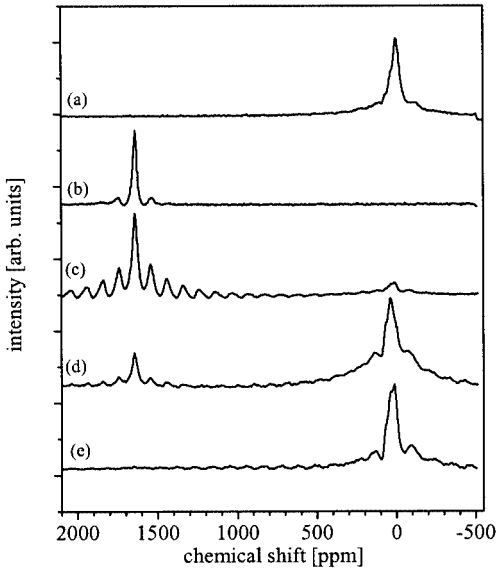

Figure 4. ^{27}Al NMR MAS spectra of (a) amorphous Al_2O_3 obtained from decomposition of $[(t\text{BuO})_2\text{AlH}]_2$, (b) aluminum obtained by decomposition of AlH_3, (c) solid phase after heating HAlO to 600 °C under argon, (d) solid phase after heating HAlO to 420 °C under argon, (e) HAlO obtained from $(t\text{BuOAlH}_2)_2$ at 250 °C

 © 2003 Wiley-VCH Verlag GmbH & Co. KGaA, Weinheim

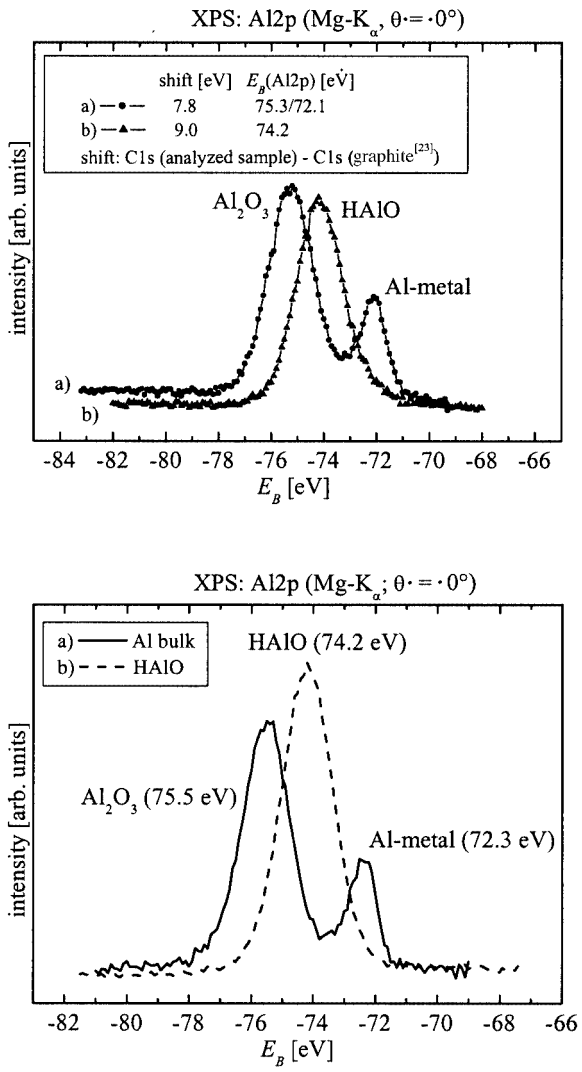

Figure 5. XPS spectra (measured in normal emission); top: the HAlO film obtained at 250 °C from (tBu−O−AlH_2)$_2$ (b) and an Al/Al_2O_3-composite, obtained by heating the HAlO film to 550 °C for comparison (a); bottom: the same HAlO film (b) and a partly oxidized aluminum sheet for comparison (a)

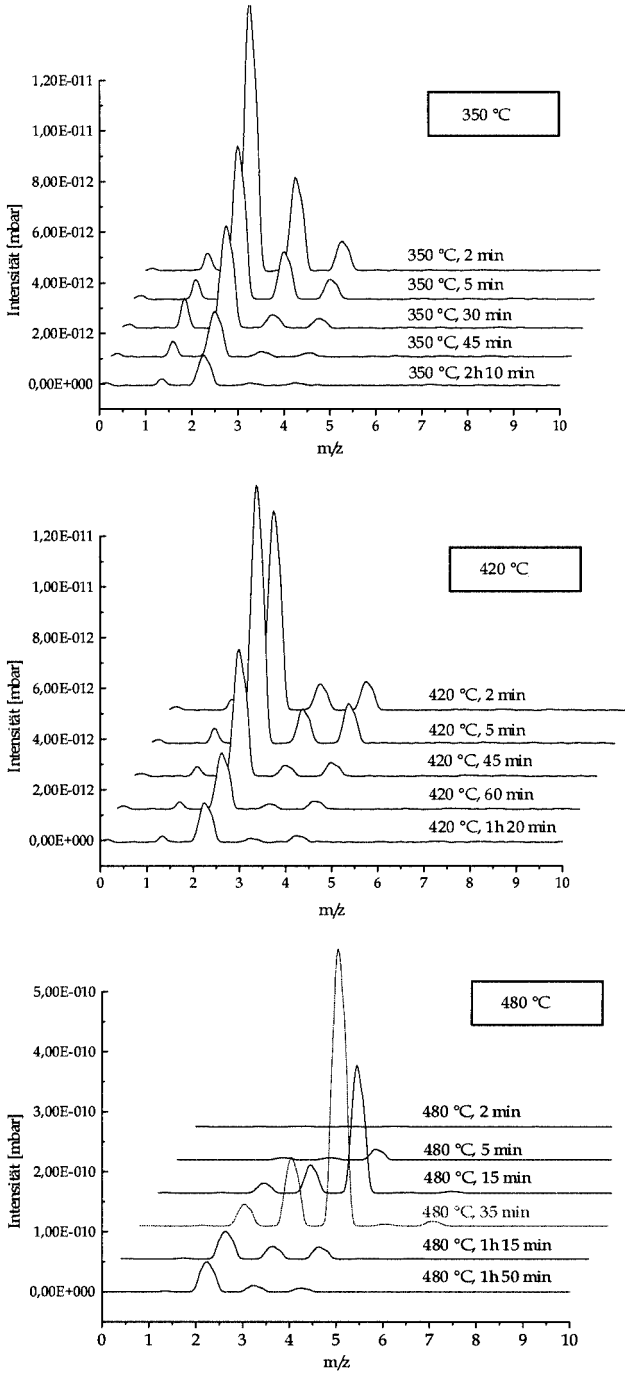

Figure 6. Evolution of H_2 or D_2 from H(D)AlO films (H:D = 8:92) heated at different temperatures, determined by mass spectrometry

that has been heated up to about 600 °C under exclusion of air (see also next paragraph). Compared to Al_2O_3 (Al, 2p-peak found at 75.3 eV), the Al atom in HAlO has a 2p-peak maximum at 74.2 eV, and is shifted towards the energy of the bulk Al metal (Al, 2p-band found at 72.1 eV in the corresponding samples), which is in accordance with the lower electronegativity of hydrogen compared to oxygen.

The bonding of hydrogen to aluminum and the metastable property of HAlO can be easily demonstrated by thermolysis of the film.[16,29] This experiment was repeated with DAlO containing approximately 8% HAlO. In the mass spectrum run simultaneously during decomposition, the evolution of the signal at m/z = 4(D_2) could be followed with increasing temperature and time (see Figure 6).

The hydrogen observed at the beginning may come from the HAlO mixing in the deuterated sample, or may be attributed to residuals on the surfaces of the sample and the apparatus. During the temper process, the color of the layer changed from transparent to black. The temperature- and time-dependent liberation of hydrogen may also be followed in the infrared spectrum of the film coated on the target, in which the Al−H valence vibration constantly decreases. At the end of the heating process the IR absorption at 1925 cm^{-1} had completely disappeared (see Figure 7).

At this stage the HAlO film had turned into a biphasic composite film of almost stoichiometric composition, Al/Al_2O_3. Figure 8 contains an X-ray powder diffractogram, which, apart from some non-indexed lines of low intensities

 © 2003 Wiley-VCH Verlag GmbH & Co. KGaA, Weinheim

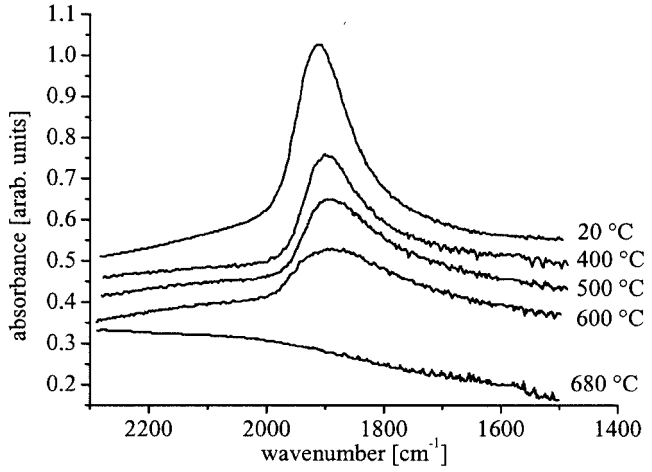

Figure 7. FT-IR spectra of HAlO layers in the 2200−1500 cm^{-1} region heated at different temperatures (heated for 3 minutes before the registration of each spectrum)

at low diffraction angles, consists of two phases: Al and γ-Al_2O_3 (aluminum forms nanoscale crystals; from the reflex profiles in the powder pattern 30−40 nm particles can be deduced;[24] compare also[14,15]).

The chemical equations for the tempering are assembled in Equation (3):

$$\begin{aligned} HAlO &\rightarrow 1/2\ H_2 + 1/3\ Al/Al_2O_3 \\ DAlO &\rightarrow 1/2\ D_2 + 1/3\ Al/Al_2O_3 \end{aligned} \quad (3)$$

The chemical equations in Equation (3) may be interpreted as follows: H (H_2) or D (D_2) is eliminated after breaking of the Al−H or Al−D bonds. The remaining "AlO" (with formal Al^{II}) seems to be unstable at the high processing temperatures and disproportionates to zero- and three-valent aluminum. Accordingly, the aluminum/oxygen ratio is maintained during the tempering process with an EDX analysis of the composite Al:O = 0.95(9):1.00 (similar to the precursor HAlO). In the classical CHN analysis, the carbon content remains 0.2(1)%, while no hydrogen can be detected.

Instead of transforming the whole surface by heating, locally defined regions may be tranformed using a 12.5-W CO_2 laser together with a motor driven *x*/*y*-table. By this technique various structures may be produced on the surface of the film.

In Figure 9, a 600 μm large letter, with a line width of approximately 70 μm, which is dark gray and is composed of Al/Al_2O_3 composite, is seen. The area around the letter is still made up of metastable HAlO, whereas in the infrared spectrum taken within the letter, no vibrations due to Al−H can be detected.

Conclusions

The formation of HAlO (DAlO) films by thermolysis of (tBuOAlH_2)$_2$ on hot metallic substrates has been shown to proceed via β-elimination of dihydrogen and isobutene. Although the HAlO layers are almost stoichiometric in hydrogen, aluminum and oxygen, their structure is not yet clear. Like in other amorphous glasses, there may be different structure entities present, which, according to NMR spectroscopy, seem to have four, five, and sixfold coordination sites around aluminum. HAlO films are metastable and lose hydrogen when heated. At a certain point disproportionation of intermediate Al(II) is observed, forming aluminum and aluminum oxide. From the infrared spectra, the presence of Al−H(D) bonding is beyond doubt; even under high reflection angles we have not yet been able to detect hydroxide on the surface of the films by infrared

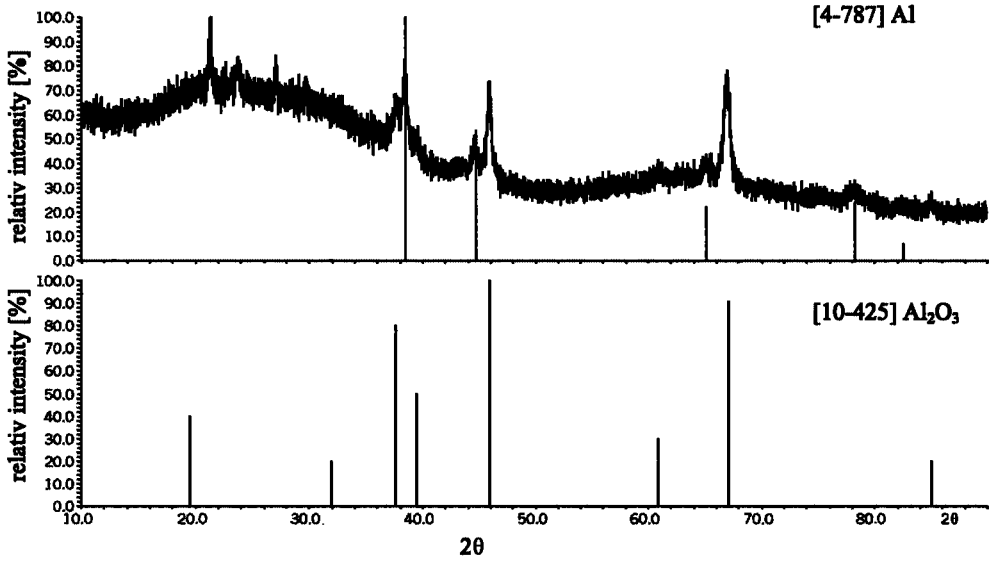

Figure 8. X-ray powder pattern of an HAlO layer on steel tempered at 510 °C; the reflections at lower 2-θ values seem to come from reactions of the iron surface, as they are almost absent on other metal surfaces; the reflections at higher angles can be indexed with Al[27] and γ-Al_2O_3[28]

 © 2003 Wiley-VCH Verlag GmbH & Co. KGaA, Weinheim

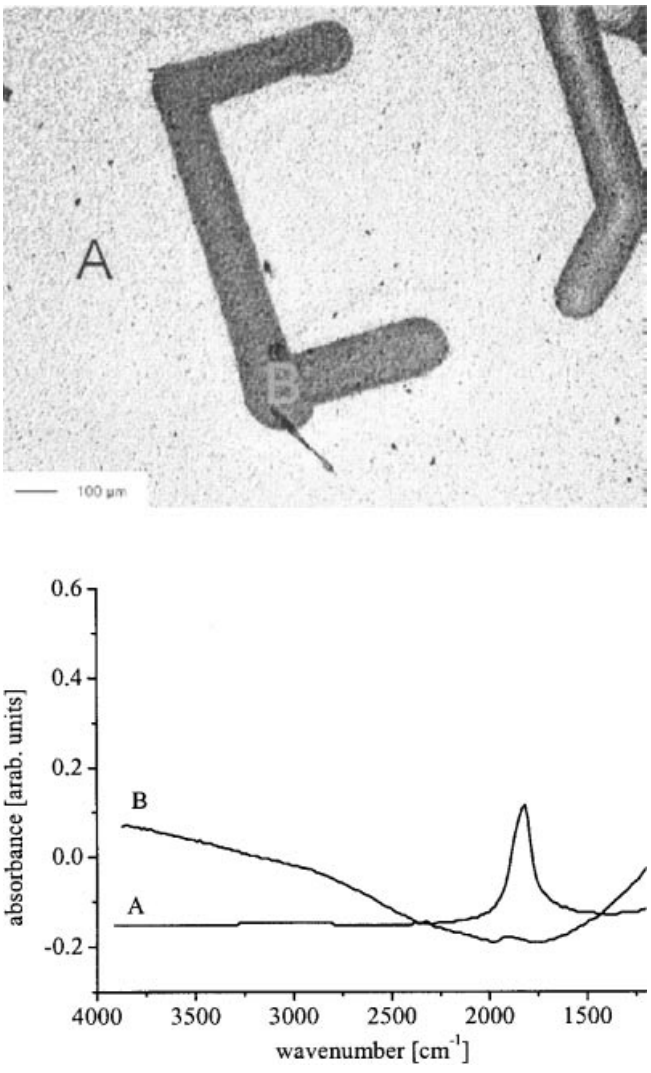

Figure 9. Light microscopy picture of a 3 µm thick HAlO layer, on which an Al/Al_2O_3-microstructure has been produced with a CO_2 laser (the sample was moved with respect to the laser beam with a velocity of 200 µm/s); the transparent (A) and the dark (B) spots show different absorptions in the Al−H region of the IR spectrum (reflection mode)

spectroscopy, although we cannot exclude it completely. More sophisticated measurements on the structure of HAlO are on the way.

Experimental Section

General Remarks: The precursor compound $(t\text{BuOAlH}_2)_2$ is synthesized following the routes described before[11,12] under dry N_2 using standard Schlenk techniques. The deuterated sample $(t\text{BuOAlD}_2)_2$ was obtained from $LiAlD_4$ instead of $LiAlH_4$. Solvents were dried by refluxing with appropriate drying agents and were distilled before being used. CVD was carried out in a cold-wall reactor as described in an earlier publication[13]. The CVD reactor consists of a cylindrical reaction tube in which the metal substrate is situated on a glass support. The substrate is heated inductively at temperatures ranging from 250−500 °C. The temperature of the substrate is measured by a thermocouple and is connected to the high frequency source to monitor the temperature. The quadrupole mass spectrometer is linked to the system and enables monitoring of the reaction gases.

Physical Measurements: The C, H analyses were carried out using a CHN analyzer from LECO™ Corporation, St. Joseph, MI., U.S.A. IR spectra of the produced solid film were obtained using a Bio-Rad FTS 165 with a mirror unit for direct reflection. ^{27}Al solid-state MAS NMR spectra were measured on a Bruker 200 MHz-MSL 200 with magic angle spinning (MAS). The powder X-ray diffraction measurements were performed in a glass capillary on a STOE diffractometer using Cu-K_α and a linear PSD detector. The XRD patterns of layer material were compared with literature values.[27,28] Electron microscopy and energy dispersive X-ray (EDX) analyses were performed on a scanning electron microscope CAMSCAN S4 with Si(Li)-semiconductor detectors and with thin windows (Cameca and Noran). The mass spectra of the pyrolysis gases were recorded on a quadrupole mass spectrometer QMS 200 (Balzer). The cryostat used for the matrix isolation of the pyrolysis gases and the deposition conditions are described in an earlier publication.[25,26] The IR spectra of the pyrolysis products were obtained with a Bruker IFS 113 v FT-IR spectrometer. The XPS spectra were recorded on a VG ESCA MKII spectrometer with a Mg-K_α-source (E_{kin} = 1253.6 eV, E_{Pass} = 10 eV, $\Delta E \approx$ 0.8 eV). The HAlO film was heated successively up to 600 °C on a micro-heating table TS 1400 (Linkham) under N_2 atmosphere. The tempering was monitored by IR spectrometry. Laser-structuring of the HAlO film was achieved by a CO_2laser (LC-25, DEOS) of 25 W. In the optical pathway between laser and film surface, layer gold-coated, optical lenses (f = 2.5 mm) were used for focussing, while the target was positioned by use of a micro-driven mechanical X/Y-table.

Preparation of Compounds

CVD Process of $(t\text{BuOAlH}_2)_2$ [$(t\text{BuOAlD}_2)_2$] and Synthesis of HAlO (DAlO): The thermal decomposition of the alkoxide precursor $(t\text{BuOAlH}_2)_2$ [$(t\text{BuOAlD}_2)_2$] was performed in a CVD apparatus. The experimental setup consists of a high vacuum line with Ar as the inert gas and a metal (steel, copper, nickel, platinum) support, which is inductively heated at 250 °C. The volatile precursor is transported to the substrate at pressures around 6.0×10^{-2} mbar. The volatile decomposition products (hydrogen, isobutene) were analyzed by online mass spectrometry. The precursor deposits on the substrate as a transparent HAlO layer. The CHN analysis of HAlO (43.989 g/Mol) gave a mean C value of 0.2(1), a range for H of 0.8 to 2.1% (calculated: 2.31%) and a value for N of 0(0.1)%. EDX analysis agrees with an Al/O ratio of 0.96(3):1.00(3). The titrimetric analysis of Al content (with titriplex as complexing ligand) gave a value of 60.5 (1.0) wt% (calculated Al in HAlO: 61.4 wt%). In order to determine the content of aluminum with respect to hydroxide in the same sample (after hydrolysis of HAlO, see also Equation 2), we used a known concentration of aqueous HCl and a standard solution of NaOH for back-titration. In a typical experiment, a layer of HAlO (1.212 mg, 0.0276 mMol) deposited on a platinum sheet gave 0.028(4) mMol aluminum and 0.087(4) mMol of hydroxide, consistent with a H:Al:O ratio of 1.05:1.01:1.05. The volumetric determination of the hydrogen evolved during hydrolysis in a calibrated tube (under standard conditions), gave typically 95% of the assumed hydrogen content. The reflectance IR spectra of the HAlO thin layer show an absorption at 1925 cm^{-1} (valence vibration for terminal Al−H groups), a shoulder at 1670 cm^{-1} for bridging Al−H···Al groups, and a broad band between 900 and 600 cm^{-1} with a typical shoulder at 730 cm^{-1} (Al-O groups). The ^1H-MAS solid NMR spectrum of HAlO shows a wide, structured absorption with a maximum at 4.0 ppm. The ^{27}Al-MAS solid NMR spectrum shows peaks at 6, 30 and 58 ppm. The binding

 © 2003 Wiley-VCH Verlag GmbH & Co. KGaA, Weinheim

energy of the 2p-signal of aluminum in HAlO was found at 74.2 eV in the XPS spectrum.

Synthesis of Al/Al_2O_3 by Annealing of HAlO: The HAlO sample was tempered on a micro-heating table under N_2 atmosphere or was heated inductively in the CVD reactor under vacuum conditions (1×10^{-2} mbar). The annealing of the HAlO at 500 °C for one hour transforms the transparent layer into a black Al/Al_2O_3 composite. The XRD pattern of the Al/Al_2O_3 is shown in Figure 8. EDX analysis agrees with an Al/O ratio of 0.95(9):1.00. The CHN analysis of the composite gave a mean C value of 0.2(1)%, and almost no H and N. In the IR spectrum a broad absorption is found between 900 cm^{-1} and 600 cm^{-1}. During the temper process of HAlO (DAlO) the hydrogen elimination was detected online by a quadrupole mass spectrometer linked to the CVD apparatus (see also Figure 6). The XPS analysis shows the binding energies of two 2p-signals of aluminum: at 75.3 eV for Al_2O_3 and at 72.1 eV for Al, in agreement with the literature.[23] The peaks were shifted towards the C1s peak (E_B = 284.3 eV).

Synthesis of Al/Al_2O_3 by CO_2 Laser Treatment of HAlO: The HAlO sample was laser-treated by a CO_2 laser (12.5 W) in air. The transparent HAlO layer changes to display black Al/Al_2O_3 composite patterns. In the IR spectra (microscopic setup) of the Al/Al_2O_3 patterns, the Al−H valence bands at 1925 cm^{-1} and 1670 cm^{-1} disappear, whereas the broad absorption between 900 cm^{-1} and 600 cm^{-1} is maintained.

Acknowledgments

This work has been supported by the Deutsche Forschungsgemeinschaft (DFG) in the frameworks of the SFB 277 and the "Europäisches Graduiertenkolleg" 532 as well as by Fonds der chemischen Industrie.

[1] E. Wiberg, H. Graf, M. Schmidt, R. Uson, *Z. Naturforsch., Teil B* **1952**, *7*, 578−579.
[2] J. W. Turley, H. W. Rinn, *Inorg. Chem.* **1969**, *8*, 18−22.
[3] B. Schepers, H. D. Neuwinger, R. Sroka, *Aluminium Oxide (Ullmann)* **1974**, *7*, 293−332.
[4] A. R. West, *Solid State Chemistry and its Applications*, John Wiley & Sons, Chichester, **1984**.
[5] H. C. Stumpf, A. S. Russel, J. W. Newsome, C. M. Tucker, *Ind. Eng. Chem. (New York)* **1950**, *42*, 1398−1403.
[6] B. C. Lippens, J. H. de Boer, *Acta Crystallogr.* **1964**, *17*, 1312−1321.
[7] J. Rouxel, *Acad. Sci.* **1959**, *248*, 810−812.
[8] H. Schäfer, F. E. Wittig, W. Wilborn, *Z. Anorg. Allg. Chem.* **1958**, *297*, 48−58.
[9] P. Hagenmüller, J. Rouxel, J. David, A. Colin, B. Le Neindre, *Z. Anorg. Allg. Chem.* **1963**, *323*, 1−12.
[10] H. Schnöckel, *J. Mol. Struct.* **1978**, *50*, 267−273.
[11] H. Nöth, H. Suchy, *Z. Anorg. Allg. Chem.* **1968**, *358*, 44−66.
[12] M. Veith, S. Faber, H. Wolfganger, V. Huch, *Chem. Ber.* **1996**, *129*, 381−384.
[13] M. Veith, S. J. Kneip, *J. Mater. Sci. Lett.* **1994**, *13*, 335−337.
[14] M. Veith, S. Faber, R. Hempelmann, S. Janssen, J. Prewo, H. Eckerlebe, *J. Mater. Sci.* **1996**, *31*, 2009−2017.
[15] M. Veith, S. J. Kneip, S. Faber, E. Fritscher, *Mater. Sci. Forum* **1998**, *303*, 269−272.
[16] M. Veith, K. Andres, *J. Metastable and Nanocrystalline Materials* **2003**, *15−16*, 279 −282.
[17] M. Veith, A. Altherr, H. Wolfanger, *Chem. Vap. Deposition* **1999**, *5*, 87−90.
[18] M. Veith, Y. Wolf, N. Köhler, to be published.
[19] H. Roszinski, R. Dautel, W. Zeil, *Z. Physik. Chem.* **1963**, *36*, 26−52.
[20] E. P. Go, K. Thuermer, J. E. Reutt-Robey, *Surf. Sci.* **1999**, *437*, 377−385.
[21] M. Balmer, H. Eckert, N. Das, F. F. Lange, *J. Am. Ceram. Soc.* **1996**, *29*, 321−26.
[22] F. A. Kurth, R. A. Eberlein, H. Schnöckel, A. J. Downs, C. R. Pulham, *J. Chem. Soc., Chem. Commun.* **1993**, 1302−1304.
[23] *Handbook of X-ray Photoelectron Spectroscopy* (Ed.: G. E. Muilenberg), Perkin−Elmer Corporation, Eden Prairie, Minnesota, USA, **1978**, S. 50.
[24] T. H. de Keijser, E. J. Mittelmeijer, H. C. F. Rozendaal, *J. Appl. Crystallogr.* **1983**, *16*, 309.
[25] H. J. Becher, H. Schnöckel, H. Willner, *Z. Physik. Chem. (München)* **1974**, *92*, 160.
[26] H. Schnöckel, *Z. Anorg. Allg. Chem.* **1980**, *460*, 37.
[27] JC,PDA-Datei [4−787]: Al
[28] JC,PDA-Datei [10−425]: Al_2O_3
[29] Note added in proof: S. Liu, U. Fooken, C. M. Burba, M. A. Eastman, R. J. Wehmschulte, *Chem. Mater.* **2003**, online version published on the WWW in June 2003; **2003**, *15*, 2803−2808.

Received March 8, 2003
Early View Article
Published Online October 22, 2003

 © 2003 Wiley-VCH Verlag GmbH & Co. KGaA, Weinheim

Synthesis, Structure and Magnetic Properties of a New Iron Arsenate, $[C_{10}N_4H_{28}][\{FeF(OH)(HAsO_4)\}_4]$, with a Layer Structure

Sandip Chakrabarti,[a] Swapan K. Pati,[b] Mark A. Green,[c] and Srinivasan Natarajan*[a]

Keywords: Iron / Arsenic / Solvothermal synthesis / N ligands

Through an unfortunate series of events, the Figures in this article[1] do not correspond with their captions. The correct version is given below.

[1] S. Chakrabarti, S. K. Pati, M. A. Green, S. Natarajan, *Eur. J. Inorg. Chem.* **2003**, 3820−3825.

Received November 12, 2003
S. Natarajan
The Editors

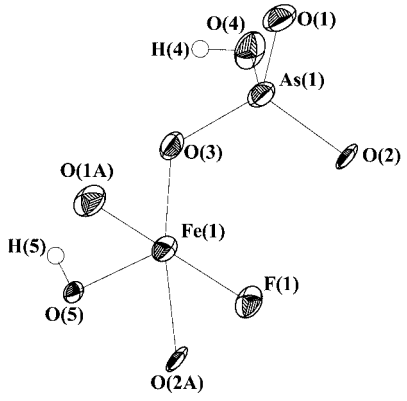

Figure 1. ORTEP diagram of $[C_{10}N_4H_{28}][\{FeF(OH)(HAsO_4)\}_4]$ showing the atoms that constitute the layer; thermal ellipsoids are given at 50% probability

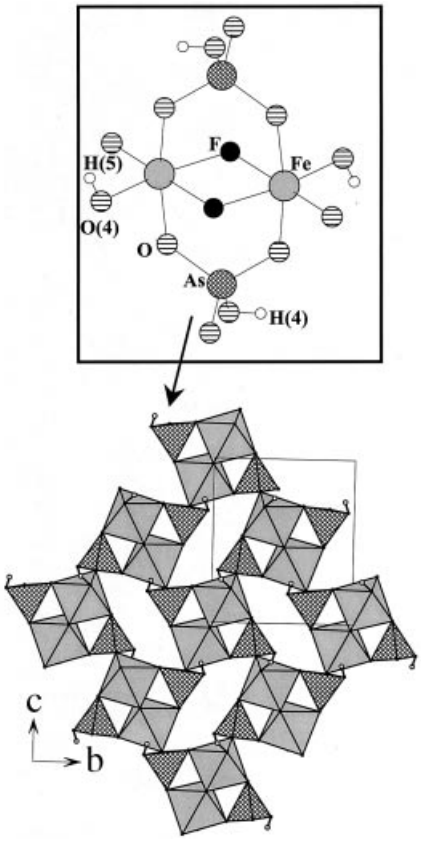

Figure 2. Polyhedral view of the structure of $[C_{10}N_4H_{28}]$-$[\{FeF(OH)(HAsO_4)\}_4]$ in the *bc* plane showing a single layer; the inset shows the SBU-4 units; the amine molecules are not shown

 DOI: 10.1002/ejic.200300838 © 2003 Wiley-VCH Verlag GmbH & Co. KGaA, Weinheim

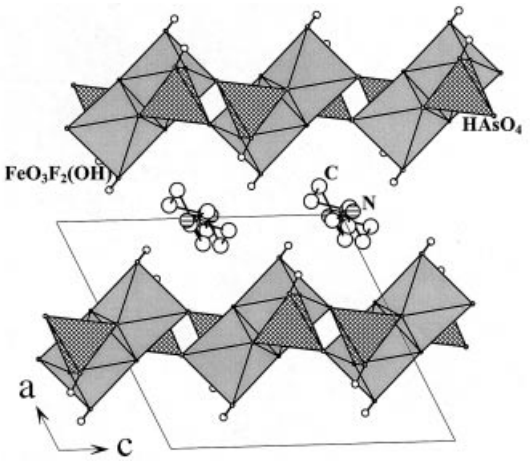

Figure 3. Polyhedral view of the structure of $[C_{10}N_4H_{28}][\{FeF(OH)(HAsO_4)\}_4]$ in the *ac* plane showing the arrangement of layers

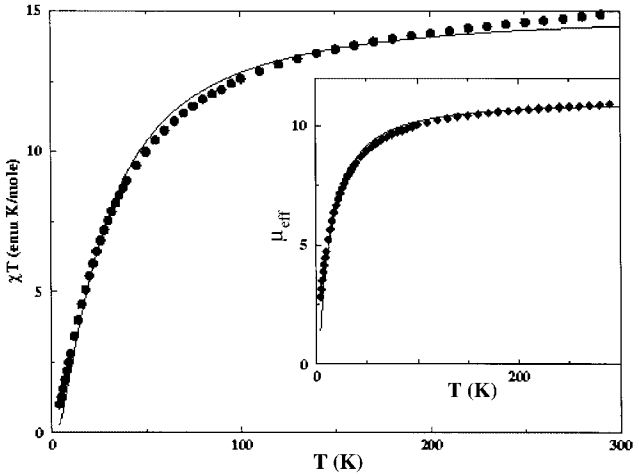

Figure 5. The variation of the χT as a function of temperature for $[C_{10}N_4H_{28}][\{FeF(OH)(HAsO_4)\}_4]$; the inset shows the variation of $\mu_{eff.}$ as a function of temperature; the solid line in both the cases shows the dimer-model fit to the experimental data

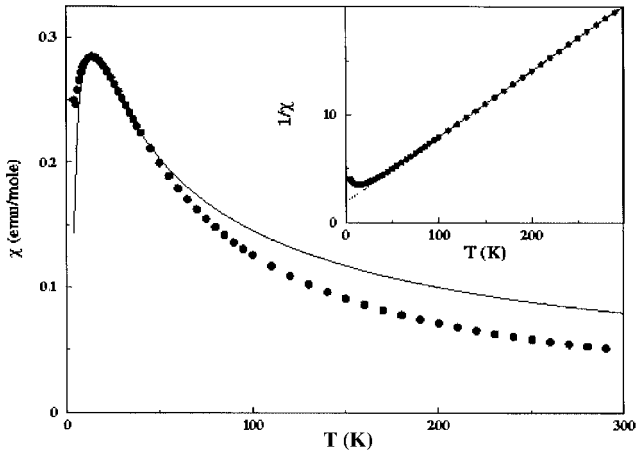

Figure 4. Thermal variation of the experimental magnetic susceptibility (χ) of $[C_{10}N_4H_{28}][\{FeF(OH)(HAsO_4)\}_4]$; the solid line is a fit using the exponential form (see text); the inset shows the variation of inverse magnetic susceptibility (χ^{-1}) with temperature; the Curie−Weiss fit is shown as dotted lines

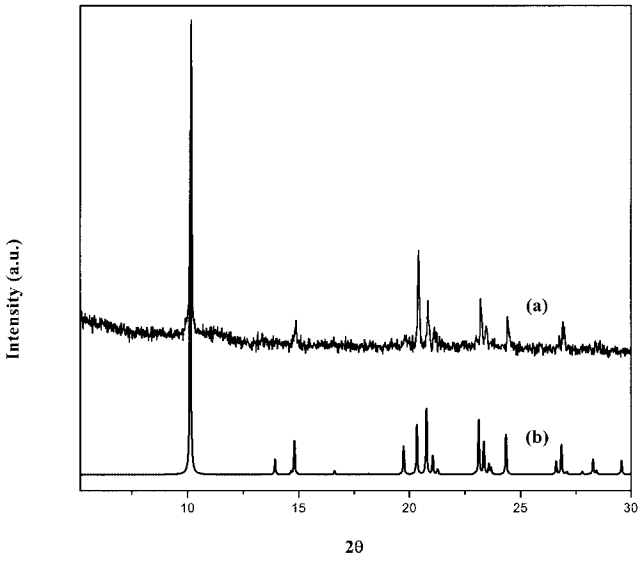

Figure 6. Powder XRD pattern of $[C_{10}N_4H_{28}]$-$[\{FeF(OH)(HAsO_4)\}_4]$ (a) experimental (Cu *Kα*) and (b) simulated

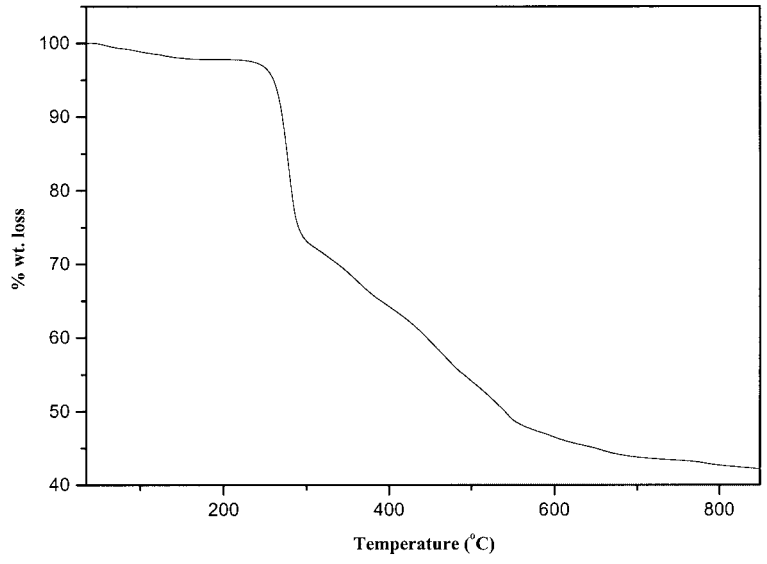

Figure 7. Thermogravimetric analysis (TGA) of $[C_{10}N_4H_{28}][\{FeF(OH)(HAsO_4)\}_4]$

 © 2003 Wiley-VCH Verlag GmbH & Co. KGaA, Weinheim

EurJIC
European Journal of Inorganic Chemistry
2003

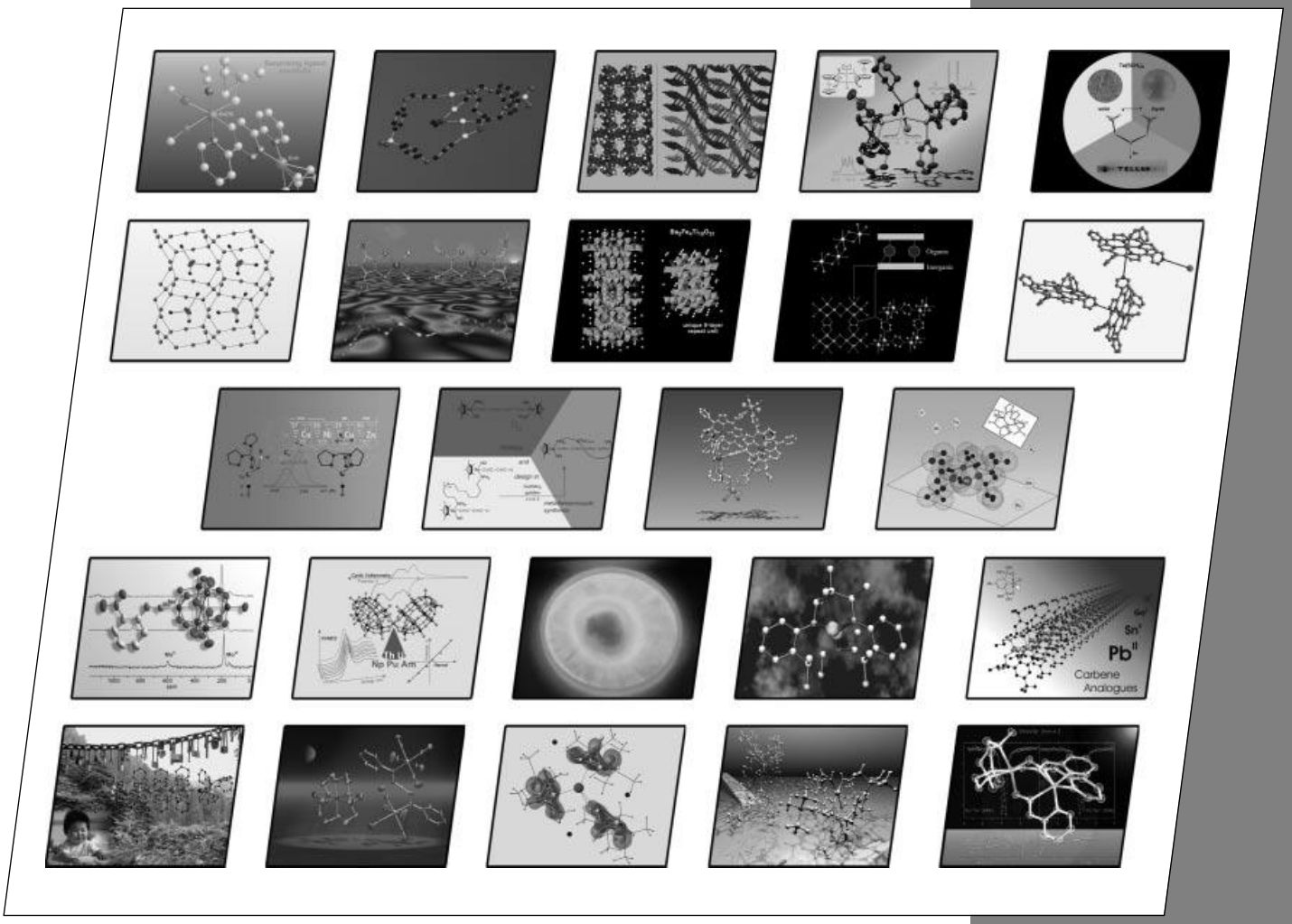

INDEX

WILEY-VCH
EU ChemSoc
DOI: 10.1002/ejic.200312345

EurJIC
European Journal of Inorganic Chemistry

The Belgian, French, German, Greek, Italian, Netherlands, Portuguese and Spanish Chemical Societies, and the Hungarian Academy of Sciences together with the Hungarian Chemical Society have taken a significant step into the future by merging their traditional journals to form two leading chemistry journals, the *European Journal of Inorganic Chemistry* and the *European Journal of Organic Chemistry*. Each one of the founding society owned journals brings decades of past excellence to this merger as a guarantee for future excellence. Three further European societies, those of Austria, the Czech Republic, and Sweden, are associate members.

EDITOR:
Karen J. Hindson

MANAGING EDITOR:
Udo Eberhardt

EDITORIAL ASSISTANTS:
Ursula Lerch
Linda Nocera
Fay Wolter

ASSOCIATE EDITOR:
Robert Temme

ASSISTANT EDITORS:
David Barden
Anthony Meredith

ADMINISTRATION:
Audrey Bauer
Carola Goldenstein

PRODUCTION:
Meike Blaschke
Silke Lautenschläger
Margitta Schmitt

EDITORIAL BOARD:
Jaime Casabó, Barcelona
Bernard Meunier, Toulouse
Jan Reedijk, Leiden
Günter Schmid, Essen

CHAIRMAN OF THE EDITORIAL BOARD:
Ivano Bertini, Firenze

INTERNATIONAL ADVISORY BOARD:
Giulio Alberti, Perugia
Robert G. Bergman, Berkeley
Guy Bertrand, Riverside
Jean-Luc Brédas, Atlanta
Henri Brunner, Regensburg
Chi-Ming Che, Hong Kong
Dimitri Coucouvanis, Ann Arbor
Eric Derouane, Liverpool
Michel Devillers, Louvain-la-Neuve
Kim R. Dunbar, College Station
Cornelis J. Elsevier, Amsterdam
Gerhard Erker, Münster
Pablo Espinet, Valladolid
Anton W. Gal, Nijmegen
José M. González-Calbet, Madrid
Hansjörg Grützmacher, Zürich
Brian F. G. Johnson, Cambridge
Nikos Katsaros, Athens
Tamás Kiss, Szeged
Thomas M. Klapötke, München
Peter Klüfers, München
Bernt Krebs, Münster
Lechoslaw Latos-Grażyński, Wroclaw
Kazuko Matsumoto, Tokyo
Dan Meyerstein, Beer-Sheva
Giovanni Natile, Bari
Paul O'Brien, Manchester
Luis A. Oro, Zaragoza
Maurizio Peruzzini, Firenze
Michel Pfeffer, Strasbourg
Fernando Pina, Monte da Caparica
Rinaldo Poli, Dijon
Carlos C. Romão, Oeiras
Eduardo Ruiz-Hitzky, Madrid
Myunghyun P. Suh, Seoul
Alejandro J. Vila, Rosario
Dieter Vogt, Eindhoven
Dirk Walther, Jena
Yoshihito Watanabe, Nagoya

MANUSCRIPTS MAY BE SUBMITTED ONLINE AT
http://webeos.wiley-vch.de/osm

EDITORIAL OFFICE:
Dr. Karen J. Hindson
P. O. Box 10 11 61
69451 Weinheim
Germany
For Courier Services:
Boschstraße 12
69469 Weinheim
Germany
Phone: +49 (0) 62 01/606-255
Fax: +49 (0) 62 01/606-203
E-mail: ejic-ejoc@wiley-vch.de

HOMEPAGE:
http://www.eurjic.org

SUBSCRIPTIONS:
Customer Service
(Phone: +49 (0) 6201/606-400
Fax: +49 (0) 6201/606-184
E-mail: service@wiley-vch.de)

MARKETING:
Claudia Barzen
(E-mail: cbarzen@wiley-vch.de)

COORDINATING MANAGING EDITOR EUROPEAN JOURNALS:
Karen J. Hindson

PUBLISHER:
Eva-E. Wille

PUBLISHERS:
WILEY-VCH Verlag GmbH & Co. KGaA
Postfach 10 11 61
69451 Weinheim
Germany
Phone: +49 (0) 62 01/606-0
Fax: +49 (0) 62 01/606-328
http://www.wiley-vch.de/

PUBLICATION:
twice monthly

© 2003 WILEY-VCH Verlag GmbH & Co. KGaA, Weinheim

BELGIUM
FRANCE
GERMANY
GREECE
HUNGARY
ITALY
NETHERLANDS
PORTUGAL
SPAIN
AUSTRIA
CZECH REPUBLIC
SWEDEN

Issue number	Pagination	Date of publication	
		Print	Online (if not otherwise indicated in the article)
1	1–180	January 3	December 12–December 16
2	181–378	January 17	December 23–January 8
3	379–568	February 3	January 16–January 20
4	569–776	February 13	January 29–February 5
5	777–1012	March 3	Feburary 17–February 18
6	1013–1254	March 17	March 3–March 6
7	1255–1468	April 4	March 20–March 24
8	1469–1644	April 17	April 2–April 7
9	1645–1828	May 9	April 28
10	1829–2000	May 23	May 7–May 13
11	2001–2184	June 6	May 21–May 23
12	2185–2356	June 25	June 10
13	2357–2536	July 7	June 24
14	2537–2718	July 23	July 8–July 10
15	2719–2888	August 4	July 17–July 21
16	2889–3056	August 18	July 29–August 1
17	3057–3256	September 5	August 14–August 22
18	3257–3500	September 23	September 12
19	3501–3668	October 6	September 12–September 18
20	3669–3832	October 27	October 13
21	3833–3974	November 7	October 28
22	3975–4122	November 25	November 6
23	4123–4262	December 5	November 26
24	4263–4410	December 18	December 9

 © 2003 Wiley-VCH Verlag GmbH & Co. KGaA, Weinheim

Author Index

REMINISCENCE

Snaith, R. (by R. E. Mulvey, K. Wade), 3271

Abakumov, G. A., 2519
Accorsi, G., 467
Ackerhans, C., 66
Adams, M. J., 3639
Adar, E., 4105
Ahlrichs, R., 1518
Aime, S., 2045, 3530
Aizoubi, B. M., 2972
Akkerman, O. S., 638
Albertin, G., 2845, 2855
Albinati, A., 3958
Albrecht-Gary, A.-M., 2596
Alessio, E., 2371, 3160
Alonso, J., 2986
Alonso, J. A., 2839
Alvarado-Rodríguez, J. G., 3554
Alvarez, S., 1756
Alvarez-Rúa, C., 4159
Alvarez-Toledano, C., 562
Alzoubi, B. M., 3738
Amador, U., 2419
Ammar, H. B., 4055
Amouri, H., 499, 3055
An, C., 3250
Anddrushko, V., 54
Anderson, M. W., 1175
Anderson, T. M., 3924
Andersson, C., 377
Andrade-López, N., 3554
Andres, K., 4387
Andrews, P. C., 3305
Andrikopoulos, P. C., 3354
Andruh, M., 1995
Anson, C. E., 2283
Antiñolo, A., 17, 2438, 2626, 3233
Antipin, M. Yu., 29, 1053
Antolini, F., 3391
Antoniadis, C. D., 1635
Antonio, M. R., 2663, 2929
Antoniutti, S., 2845, 2855
Anxolabéhère-Mallart, E., 1900, 2529
Aplincourt, M., 1984, 3007
Aplincourt, P., 3007
Appelt, R., 3731
Aragoni, M. C., 1291, 1939
Aranda, P., 1242
Arca, M., 1232, 1291, 1939
Arii, H., 2917
Arillo, M. A., 2397
Arion, V., 2619
Armaroli, N., 467
Armspach, D., 805
Armstrong, C. M., 1145
Armstrong, D. R., 3354, 3363
Arnaiz, F. J., 2639
Arnold, D. P., 1555
Aromí, G., 1394
Arpalahti, J., 4195
Arquier, D., 960
Arrais, A., 1186
Arriortua, M. I., 518
Arsenyan, P., 3139
Artaud, I., 759
Asenjo, A., 1608
Asselberghs, I., 3895
Auffrant, A., 3895
Aukauloo, A., 1900
Autzen, S., 1401
Avecilla, F., 4179
Azam, A., 1966
Bacchi, A., 1523
Badura, D., 3723
Bagryanskaya, I. Y., 77
Baird, M. C., 175
Bakardjiev, M., 2524
Baker, R. J., 2446
Balazs, L., 1361
Balland, V., 2529
Ballester, L., 3034
Balogh-Hergovich, E., 1735
Bandini, A. L., 3958
Banditelli, G., 3958
Bandyopadhyay, P., 4308
Banerjee, P., 1540
Banse, F., 2529
Baranov, A. I., 1053
Barbaro, P., 601, 4166
Barberà, G., 1511
Barberio, G., 3649
Barbier, J.-P., 1984
Barbieri, A., 324
Bardají, M., 3069
Baret, P., 2596
Barge, A., 2045
Barida, O., 4370
Barigelletti, F., 3752
Barral, M. C., 2339
Bartolomé, C., 3127
Baruah, B., 2299
Basset, J.-M., 2139
Batis, H., 2486
Batista, A., 4321
Bats, J. W., 2049
Battaini, G., 1197
Bauer, W., 822, 1253
Baumgartner, C., 2619
Baxter, P. N. W., 4001
Bayot, D., 737
Bazzicalupi, C., 1974
Beatty, A. M., 3325
Beck, A., 339
Beck, R., 232, 240, 853, 1380
Beck, W., 3745, 4275
Beckmann, J., 164, 4356
Beckmann, U., 1768
Belhamel, K., 4110
Belle, C., 2452, 4137
Beller, M., 3513
Belsky, V., 3034
Belyakov, S., 3139
Ben-David, Y., 70
Benamor, M., 4110
Bencini, A., 1974
Beneš, L., 1577, 3662
Benet-Buchholz, J., 4147
Benisch, C., 1099
Bensch, W., 506
Beraldo, S., 2845
Berente, Z., 556
Berg, K. E., 1890
Bergamini, P., 918
Bergander, K., 1599
Berggrund, M., 2352
Berghahn, M., 2059
Berke, H., 2463
Bermejo, M. R., 1128, 3193, 3703, 3905
Bernhardt, P. V., 1145, 2512
Berni, E., 1974
Bertagnolli, H., 839, 2082
Bertolasi, V., 918
Besse, J.-P., 1242
Bettentrup, H., 2446
Bhasin, K. K., 744
Bhattacharya, R., 4253
Bhattacharyya, J., 4308
Bhattacharyya, P., 1461, 2426
Bi, W., 38, 94, 1303
Bialas, H., 3929
Bianchi, A., 1974
Bianchini, C., 1620, 4166
Biaso, F., 2596
Bickelhaupt, F., 638
Biesemans, M., 1315, 3803
Bill, E., 541, 1768, 4299
Binnemans, K., 3021, 3028
Birkedal, H., 4065
Birkelbach, F., 541
Blacque, O., 2463
Blacue, O., 633
Blair, S., 3319
Blake, A. J., 1232, 2389
Blanc, S., 2596
Blazina, D., 2901
Blin, J., 4387
Blockhuys, F., 77
Blom, M., 1307
Blondin, G., 1900
Blum, D. C. F., 418
Bocelli, G., 4253
Bockmeyer, M., 458
Bodes, G., 281
Boese, R., 1401
Böhme, U., 751
Boldron, C., 528
Bolte, M., 666, 2049
Bolton, P. D., 3445
Bonaventure, G., 4173
Bonchio, M., 699
Boni, G., 633
Boniforte, P., 3530
Borrmann, T., 3211
Bortolini, O., 42, 699
Bothe, E., 863, 1956, 4299
Botta, M., 3530
Boulahya, K., 2419, 2986
Bouwman, E., 453, 3968
Bozoglian, F., 2512
Brandão, P., 1175
Brauer, D. J., 1748
Braunschweig, H., 393
Bravic, G., 356
Brégeault, J.-M., 908
Bremer, M., 111
Bressan, M., 1807
Breunig, H. J., 1361
Bricout, H., 595
Brown, D., 3547
Brown, K. L., 268, 2095
Browne, W. R., 1503
Brücher, E., 3601
Bruhn, C., 143
Bruneau, C., 4055
Brunner, B. M., 876
Bruno, G., 2612
Brus, J., 143
Bruschetta, G., 2612
Brussee, E. A. C., 427
Bu, H.-W., 618
Bubnov, M. P., 2519
Buchold, D. H. M., 3453
Buder, I., 1340
Budzelaar, P. H. M., 648, 656
Bünzli, J.-C. G., 1332, 4065
Burger, S., 3099
Burghaus, O., 1445
Burgos, M., 2170
Burling, S., 3179
Burrows, A. D., 766, 1433
Burzlaff, N., 339, 409
Bustos, C., 2757
Butcher, R. J., 1540
Butler, I. S., 1635
Cabeza, J. A., 4159
Calligaris, M., 3160
Campo, J., 2397
Campos-Fernández, C. S., 988
Canales, J. C., 3221
Canipelle, M., 595
Cano, J., 2463
Cano, M., 2693, 3831
Cao, J., 644
Cao, R., 38, 94, 1303, 1778, 2705, 3623
Carey, D. T., 3464
Carfagna, C., 2683
Carlos, L. D., 3609
Carmona, L., 2139
Caron, L., 595
Carpio, S. M., 1614
Carraro, M., 42
Carriedo, G. A., 2413, 4341
Carrillo-Hermosilla, F., 3233
Caruso, F., 3221
Casais, M. T., 2839
Casanova, M. I., 678
Casas, J. C., 2790
Casella, L., 1197, 3934
Caspar, R., 499, 3055
Cassano, T., 1939
Cassoux, P., 2333, 2880
Castiñeiras, A., 2790
Cattabriga, M., 918
Cavallo, L., 892
Cendrowski-Guillaume, S. M., 1388
Cenini, S., 1452
Chai, J., 3113, 4332
Chaichit, N., 263
Chakrabarti, S., 3820, 4395
Chakraborty, I., 1157
Chakravarty, A. R., 2318
Chakravorty, A., 1157, 2299
Chalbot, M.-C., 453
Chambron, J.-C., 3752
Chang, H.-C., 2385
Chantrapromma, S., 947
Chaplais, G., 1193
Chasseau, D., 356
Chaudhuri, N. R., 3929
Chaudhuri, P., 541, 863, 1956, 3167, 4253, 4299
Chaudhuri, S., 4253
Chauvin, R., 207
Chavignon, R., 3895
Che, C.-M., 255, 2749
Chen, C., 1227, 2872
Chen, F., 2872
Chen, N., 1822
Chen, W., 4234
Chen, X.-M., 138, 413, 2385, 2959, 2965
Chen, X.-P., 3539
Chen, Z.-F., 2920
Chérioux, F., 1043
Cherkasov, V. K., 2519
Cheung, K.-K., 255, 4035
Chézeau, J.-M., 1366
Chiang, M.-H., 2663, 2929
Chik, T.-W., 3539

 © 2003 Wiley-VCH Verlag GmbH & Co. KGaA, Weinheim

INDEX

Chikuma, M., 4347
Chimisso, F., 2845
Chin, P., 1145
Chiotellis, E., 3826
Chiusoli, G. P., 1523
Chivers, T., 1857, 3314
Chmielewski, P. J., 1548
Chodorowski-Kimmes, S., 331
Choi, H. J., 1373
Choi, M. T. M., 1555
Chottard, J.-C., 1641
Chouai, L., 2774
Choukroun, R., 628
Chu, B. W.-K., 4035
Chu, D.-Q., 1514
Chuang, S.-H., 4159
Chuburu, F., 1984
Chudakova, V. A., 3336
Chung, Y. K., 2311
Cinellu, M. A., 2304
Císařová, I., 1533
Ciunik, Z., 89, 1548, 2475
Claramunt, R. M., 2693, 3831
Clark, T., 1562
Clark, T. J., 1857
Clearfield, A., 4211, 4218
Clegg, W., 3319
Clemente-Juan, J. M., 1005, 4253
Clérac, R., 1866
Cohen, H., 4105, 4227
Collin, J.-P., 467
Colling, M., 393
Colognesi, D., 3958
Comba, P., 34, 1703, 1711, 3042
Comensoli, E., 213
Commenges, G., 207
Comte, V., 1893, 3731
Comuzzi, C., 1948
Conato, C., 1694
Condori, F., 2790
Conradson, S., 3843
Conte, V., 42, 699
Coppel, Y., 960
Coppens, P., 3914
Corain, B., 3080
Corban, G. J., 1635
Cordier, C., 499, 3055
Cornago, P., 2693, 3831
Coronado, E., 2290, 2880, 4253, 4289
Correia, I., 2113
Costa, M., 1523
Costa Pessoa, J., 2113
Costamagna, J., 3221
Couce, M. D., 2790
Coumans, R. G. E., 1072
Craig, D. C., 4153
Crespo, O., 2170
Crispini, A., 3649
Cui, X., 1555
Cui, X.-B., 2578
Cusumano, M., 2612
d'Alessandro, N., 1807
Dahlenburg, L., 2733
Dai, J.-C., 2670
Daknernieks, D., 164, 4356
Daran, J.-C., 2820
Darensbourg, D. J., 3639
Davidson, M. G., 3445
Davies, R. P., 3363, 3409
Day, P., 720
de Biani, F. F., 449
de Bruin, B., 648
De Cian, A., 1299
de Gelder, R., 47, 648, 656, 1072
De Gioia, L., 3934
de Greef, M., 3811
de Groot, H., 1401
de Kanter, F. J. J., 638
de Masi, R., 4387
De Proft, F., 1315, 3803
de Sousa, R. A., 759
Déchamps-Olivier, I., 1984
Dechert, S., 3336
Declercq, J.-P., 737
Deelman, B.-J., 2798
del Hierro, I., 2438
del Río, I., 4159
Delgado, E., 562
Della Pergola, R., 213, 2108
Demartin, F., 1452
Demertzis, M. A., 1761
Demleitner, B., 822, 1253
Demsar, A., 437
Den Auwer, C., 3843
Denk, M. K., 224
Denotti, C., 1291, 1939
Desplanches, C., 1756
Devillanova, F. A., 1291, 1939
Devillers, M., 737
Dey, S., 744
Dhar, B. B., 4308
Diana, E., 1186
Dias, A. R., 3895
Di Bella, S., 2606
Di Pietro, M. L., 2612
Di Vaira, M., 3185
Dijkstra, H. P., 830
Dijkstra, P. J., 3432
Dinda, R., 363
Dinger, M. B., 2827
Dioury, F., 2834
Dixneuf, P. H., 4055
Do, Y., 2563
Dolgushin, F. M., 29
Dong, Y.-B., 4017
Donnadieu, B., 518, 528, 562, 628, 960, 1866
Dorbes, S., 2880
Dorcier, A., 4294
Döring, S., 1599
Dörnyei, A., 2113
Dorta, R., 70
Doux, M., 687, 3878
Dova, E., 2273
Doyle, E. L., 3279
Drabent, K., 1548
Dragani, L. K., 1807
Dreßel, B., 1088
Drichko, N. V., 3914
Driess, M., 51
Driessen, W. L., 47, 1394
Du, W.-X., 1798
Duan, L.-M., 2578
Duati, M., 1503
Dücker-Benfer, C., 2972
Duckett, S. B., 2901
Duin, M. A., 3811
Dunbar, K. R., 988
Dunne, J. P., 458, 1416
Duran, J., 4147
Durán, M. L., 678
Duthie, A., 164, 4356
Dutta, S. K., 2812
Duvail, J.-L., 610
Duval, R., 499, 3055
Dybal, J., 3662
Dyson, P. J., 3527, 4294
Eaborn, C., 3332
Eckert, J., 3958
Efremova, O. A., 2591
Eichele, K., 705
Eichhöfer, A., 1307
Eichhorn, C., 339
Eisner, D., 2133
Elsegood, M. R. J., 120, 2071
Elsevier, C. J., 3811
Elst, L. V., 3021
Engelke, L., 506
Ephritikhine, M., 1388
Erker, G., 1599, 3583, 3590, 4261
Ernst, L., 1815
Erras-Hanauer, H., 1562
Escuer, A., 3929
Espenson, J. H., 1911
Espinet, P., 3127
Esquivias, L., 1608
Esterhuysen, M. W., 3861
Expósito, T., 3233
Faber, S., 4387
Faissner, R., 1681, 2219, 2239
Fajardo, M., 17, 2438
Fakih, S., 1206
Fan, J., 3783
Fan, Y., 2325
Fandos, R., 493
Fanizzi, F. P., 1136
Fatin-Rouge, N., 1332
Faulmann, C., 2333, 2880
Favre-Réguillon, A., 2834
Fedeli, F., 3530
Fedorov, V. E., 2591
Fedushkin, I. L., 3336
Fei, B.-L., 618
Fei, Z., 3527
Feijen, J., 3432
Feil, F., 3401
Felluga, A., 3738
Feng, Y. S., 1794
Fereira, A., 1175
Fernandes, M. A., 2095
Fernández, N., 2458
Fernández-Baeza, J., 3233
Fernández-Galán, R., 2438, 2626
Ferretti, V., 918
Feth, M., 2082
Feth, M. P., 839
Field, L. D., 3179
Findeis, R. A., 99
Fischer, A., 2352
Fischer, R., 4321
Flay, M.-L., 1719
Fleischer, H., 815
Flinzner, K., 671
Flörke, U., 240, 541, 853, 1380
Flower, K. R., 1929
Fonari, M., 3034
Fondo, M., 1128, 3703, 3905
Font-Bardia, M., 2992
Font-Bardía, M., 1591, 3929, 3952
Fontani, M., 3201
Foos, J., 2834
Fornasari, P., 1974
Fragalà, I., 2606
Francescangeli, O., 3649
Frank, W., 1340, 2059, 3945
Frapart, Y., 759
Frau, R., 1939
Friese, K., 1411
Fröhlich, R., 1088, 1599, 3583, 3590, 4261
Fromm, K. M., 3440
Fu, R.-B., 1798
Fu, W.-F., 255
Fu, Z.-Y., 1798, 2670
Fukin, G. K., 3336
Fun, H.-K., 947
Funahashi, Y., 2917, 4378
Gade, L. H., 99, 1161
Gal, A. W., 648, 656, 1072
Galán-Mascarós, J. R., 988, 2290
Galani, A., 1761
Galanski, M., 2619
Galeev, R., 1995
Gallego, B., 2626
Gallego, L. M., 3831
Gallego, M. L., 2693
Galli, P., 1577
Gallo, E., 1452
Gamer, M. T., 2145
Gamez, P., 47, 1394, 1669, 2924, 4073
Gan, D., 2812
Gao, S., 149, 726, 731, 1822, 2393
Garcia, M. H., 3895
García, M.-F., 2458
Garcia, Y., 356
García Alonso, F. J., 4341
Garcia-Alonso, F. J., 2413
García-Alvarez, J. L., 2413
García-Antón, J., 2992, 3952
García-Deibe, A. M., 1128, 3193, 3703, 3905
García-Granda, S., 1113, 4159
García-Rodríguez, E., 1113
García-Tojal, J., 518, 2123, 2639
García-Vázquez, J. A., 678
Garlaschelli, L., 213, 2108
Gaspar, M., 4025
Gatilov, Y. V., 77
Gatteschi, D., 1128
Geerlings, P., 1315, 3803
Gellon, G., 2596
Gencaslan, S., 1873
Genêt, J.-P., 2583
Geraldes, C. F. G. C., 4179
Geue, R. J., 1340
Ghedini, M., 3649
Ghosh, A., 4253
Ghosh, S., 363
Ghoshal, D., 3929
Giacobbi, E., 1523
Giambastiani, G., 4166
Gianolio, E., 2045
Gil, A. M., 3034
Gil de Muro, I., 2948
Giménez-Saiz, C., 2290, 4289
Gimeno, M. C., 2170
Gindulyte, A., 3221
Giordano, R., 610
Giorgi, C., 1974
Giorgi, M., 1735
Giorgi, M. T., 2855
Girerd, J.-J., 2529
Girgsdies, F., 301
Gladiali, S., 556
Gladysz, J. A., 2211
Glaser, H., 822, 1253
Gleiter, R., 1099
Gobetto, R., 1186, 2108
Goderis, B., 3028
Golan, J. A., 2767
Goldberg, I., 969
Golub, V. O., 2299
Gómez, M., 3681
Gómez, M. A., 562
Gómez-Coca, R. B., 2937
Goméz-Garcia, C. J., 4253
Gómez-García, C. J., 2290
Gómez-Saiz, P., 518, 2123, 2639
Gonçalves, I. S., 3870
Gong, M.-L., 138
Gonsalvi, L., 1614
González, G., 2512
González, I., 978

González-Calbet, J. M., 2419, 2986
González-Montiel, S., 3554
González-Noya, A. M., 3193
González-Prieto, R., 2339
González-Vílchez, F., 2937
Görls, H., 4321
Gornitzka, H., 528
Gorrell, I. B., 3332
Görz, D., 2783
Gou, S. 947, 2054
Gougeon, R. D., 1366
Gouygou, M., 2820
Gouzerh, P., 2406, 2757
Goze, C., 3752
Graf, E., 1299
Graiff, C., 1659
Greco, F., 2108
Green, M. A., 3820, 4395
Grepioni, F., 556
Grigiotti, E., 1291
Grimme, S., 1088
Grüner, B., 1533
Grunert, M., 2273
Gruselle, M., 499, 3055
Grüßing, A., 1503
Grutters, M. M. P., 4361
Guérin, C., 1866
Guillon, E., 1984, 3007
Gullotti, M., 1197, 3934
Gun, J., 482, 2264
Günther, B., 751
Guo, J.-P., 3539
Gupta, S., 1540
Gutiérrez, A., 3034
Guy, A., 2834
Haas, K., 3745
Haasnoot, J. G., 671, 713, 2273
Habermacher, D. D., 1296
Hadjikakou, S. K., 1635
Hadjiliadis, N., 1635, 2045
Hageman, P. R., 656
Haigh, R., 3363
Hampe, O., 1307
Hampel, F., 822, 1253
Hamza, M. S. A., 268, 2972, 3738
Han, L., 2705, 3623
Handel, H., 1984
Hanusa, T. P., 3383
Hao, N., 2567
Hardcastle, K. I., 3924
Harder, S., 3401
Harmer, J., 1340
Harms, K., 1507
Harriman, A., 955
Harrington, R. W., 766, 1433, 3319
Harrop, T. C., 475
Harrowfield, J., 2913
Hartenbach, I., 876
Hartmann, S., 876
Harvey, M. J., 3383
Hasenknopf, B., 2406, 2757
Hatano, K., 224
Haupt, H.-J., 240, 853, 1380
Heck, J., 313, 936
Hegelmann, I., 339, 409
Hegetschweiler, K., 1340
Heinemann, F. W., 281, 418, 903, 1197
Heinze, K., 3918
Heitz, V., 3752
Heitzmann, M., 3767, 4262
Hekking, K. F. W., 648
Hemmert, C., 528
Henderson, K. W., 3325
Hendy, M. A., 3363
Henke, H., 2283
Henkel, G., 1727
Henner, B., 1866
Heras, J. V., 2693, 3831
Herberich, G. E., 2175
Herbst-Irmer, R., 3120
Herdtweck, E., 1802, 2463
Hermans, S., 1325
Hernández, C., 493
Hernández, E., 562
Hernando, M., 2419
Herráiz, M., 2458
Herson, P., 908
Hessen, B., 427
Hetche, O., 232
Hevia, E., 1113, 3347
Hideg, K., 3601
Hill, C. L., 3924
Hill, M., 3583
Himmel, H.-J., 2153, 4087
Hintermann, L., 601
Hissler, M., 955
Hitchcock, P. B., 3332, 3391
Hoffmann, N., 1815
Hoffmann, R.-D., 3425
Holmes, K. E., 120
Holub, J., 1533, 2524
Holý, A., 2937
Hong, D., 3242
Hong, M., 38, 94, 1303, 1778, 2705, 3623
Hoogboom, J., 1072
Hor, T. S. A., 277
Horn, C. R., 2211
Horn, D., 164
Horton, A. D., 638
Hosmane, N. S., 3989
Hosseini, M. W., 57, 1299
Hou, H., 2325
Hu, C., 370
Hu, C.-W., 2567
Hu, D., 947
Hu, H., 3699
Hu, H.-M., 51, 3618
Hu, N.-H., 1570
Hu, Q.-M., 2164, 320
Hu, S.-M., 1798, 2670
Hu, Z., 1632
Hua, G., 2426
Huang, J.-H., 1440
Huang, J.-S., 2867
Huang, R.-B., 2678
Huang, R.-L., 731
Huang, R.-Q., 4017
Huang, S.-P., 810
Huang, W., 947, 2054
Hüfner, S., 4387
Hung, C.-H., 1440
Huniar, U., 1518
Hupp, J. T., 2348
Huttner, G., 1681, 2219, 2239
Hwu, J.-R., 4159
Iengo, E., 2371
Igau, A., 960
Ikeda, K., 4347
Iliescu, M., 1445
Ilyin, E. G., 437
Imbert, D., 1332
Inoue, H., 1785
Insausti, M., 2948
Ipaktschi, J., 4313
Isaia, F., 1291, 1939
Ishihara, K., 1785
Ishii, A., 3716
Izod, K., 3319
Izquierdo-Barba, I., 1608
Jacob, V., 3918
Jacobsen, H., 892, 2463
Jacobsohn, O., 1445
Jain, V. K., 744
Jakusch, T., 2113
Jang, Y., 2774
Jansen, M., 3759
Janssen, J., 4338
Jászberényi, Z., 3601
Jasztold-Howorko, R., 4043
Jeandet, P., 1366
Jehle, H., 2133
Jekő, J., 3601
Jennings, M. C., 217
Jentoft, R. E., 301, 1058
Jia, G., 2551
Jiang, H., 4010
Jiang, J., 1555
Jiang, M., 370
Jiang, Y.-B., 2678
Jiang, Z., 62
Jiménez-Aparicio, R., 2339
Jin, G.-X., 1570, 4017
Jin, L., 3572
Jin, L.-P., 1355
Jitsukawa, K., 2917, 4378
Jobi, G., 281
Johansson, M. H., 377
Johnson, A. L., 3445
Johnson, B. F. G., 1325
Jones, C., 2446
Jones, M., 175
Jones, P. G., 1815, 2170
Jouaiti, A., 57
Jurkschat, K., 164, 3563, 4356
Jus, S., 2583
Justyniak, I., 2753
Jutand, A., 2017
Kaddachi, M. T., 4055
Kahn, O., 356
Kaifer, E., 1681, 2219
Kálai, T., 3601
Kalayda, G. V., 4347
Kalck, P., 610
Kamiński, D., 1741
Kamysz, W., 1694
Kang, Z., 370
Karlov, S. S., 1507
Kaskel, S., 1193
Kataeva, O., 1599
Katsaros, N., 3001
Kazaryan, R. K., 1861
Kehr, G., 1599, 3583, 3590, 4261
Keita, B., 3924
Kelly, P. F., 120
Kempe, R., 791
Kenley, F. R., 3347
Kennedy, A. R., 3347, 3354
Keppler, B. K., 2619
Khanna, M., 1193
Khatyr, A., 955
Khimyak, T., 1325
Khurana, S., 1966
Khvostov, A. V., 3391
Kihn, Y., 610
Kilian, P., 249, 1461
Kim, J., 2563
Kim, S.-J., 4117
Kim, Y., 2913, 4117
Kimpe, K., 3021
Király, R., 3601
Kircher, P., 2219
Kirchner, K., 1883
Kirschhock, C. E. A., 1296
Kiss, T., 2113
Kitagawa, S., 2385
Kitagawa, T., 4378
Kivekäs, R., 1511
Kläui, W., 2059, 3945
Klein, A., 839, 1917
Klein, C., 1299
Klein, H.-F., 232, 240, 853, 1380
Klett, J., 3417
Klika, K. D., 4195
Klinkhammer, K. W., 3417
Klinowski, J., 3609
Klodwig, J., 281
Kloo, L., 2352
Klopper, W., 830
Knapp, C., 3211
Knödler, A., 876
Kneifel, A. N., 3432
Kniep, R., 1632
Knijnenburg, Q., 648
Knorr, M., 514
Knyazev, V. V., 77
Ko, J. W., 1373
Köckerling, M., 1727
Köhler, K., 449
Kokozay, V. N., 1426
Kokunov, Y. B., 437
Kollár, L., 556
Komeda, S., 4347
Konarev, D. V., 3914
Konstantinovski, L., 70
Kooijman, H., 1394, 2798, 4361
Kooistra, T. M., 648
Kopitzky, R., 1727
Köppe, R., 4387
Korobchenko, L., 1995
Korth, H.-G., 1401
Korybut-Daszkiewicz, B., 1741
Kostakis, D., 2045
Kostyanovsky, R. G., 2979
Kotov, V. V., 1599
Kottsieper, K. W., 1748
Kou, H.-Z., 731
Koval, I. A., 1669
Kovala-Demertzi, D., 1761
Kovalevsky, A. Y., 3914
Kozlevčar, B., 47
Kozłowski, H., 1694
Krahn, M., 1857
Krautscheid, H., 822, 1253
Krebs, B., 1669
Krebs, C., 541
Kreiter, R., 830
Kremer, S. P. B., 1296
Krom, M., 1072
Krossing, I., 666
Krüger, S., 3144
Kruithof, C. A., 830
Kryatov, S. V., 1581
Kubicki, M., 1635, 1761, 4001
Kubicki, M. M., 514, 633
Kubo, K., 4093
Kuduk-Jaworska, J., 4043
Kühn, F. E., 449
Kumar, S. S., 442
Kunz, P. C., 3945
Kuo, P.-C., 1440
Kurtikyan, T. S., 1861
Kuzmann, E., 1735
Kyritsakas, N., 57, 1299
La Deda, M., 3649
Labahn, T., 433
Labrue, F., 2583
Laemmel, A.-C., 467
Lafuma, A., 331
Laguna, A., 2170, 3069
Lai, S.-W., 2749
Lam, A. W.-H., 149
Lamb, R. N., 4153
Lampeka, Y. D., 34
Lamy, F., 2820
Lang, H., 1703, 2059
Lappert, M. F., 3391
Lapshin, A. N., 3914

 © 2003 Wiley-VCH Verlag GmbH & Co. KGaA, Weinheim

INDEX

Larionova, J., 1866
Laschi, F., 1291, 1620, 3201
Lattman, M., 1169
Lau, C. P., 2551
Laurent, S., 3021
Le Baccon, M., 1984
Le Dred, R., 1366
Le Floch, P., 687, 3878
Le Gland, G., 1388
Le Goff, X. F., 1866
Le Nôtre, J., 4055
Lébl, T., 143
Lee, E. Y., 3242
Lee, F.-W., 3539
Lee, G.-H., 1440
Lee, I. S., 2311
Lee, Y. H., 2913
Lehmann, C. W., 1193
Lehn, J.-M., 4001
Leibl, W., 1900
Leith, J. S., 1529
Lelj, F., 1939
Lenev, D. A., 2979
Leng, M., 1641
Leovac, V. M., 1222
Lepetit, C., 207
Lerner, H.-W., 666
Leroux, F., 1242
Leung, W.-H., 583
Lev, O., 482, 2264
Leveque, H., 499, 3055
Lewiński, J., 2753
Lezama, L., 518, 2123, 2639, 2948, 3703
Lhuachan, S., 263
Li, B., 4035
Li, C., 644, 3534, 3699
Li, G., 2325
Li, G.-H., 1514
Li, H. L., 3179
Li, J., 3110
Li, J.-F., 810
Li, J.-R., 731
Li, L., 62, 1227, 2872
Li, Q., 3699
Li, X., 38, 94
Li, Y., 370, 2054, 2393, 2651
Li, Y.-G., 2567
Li, Y.-Z., 3783
Liable-Sands, L. M., 2767
Lian, S., 370
Liao, D., 62, 1227, 2872
Liehr, G., 1562
Liesicke, S., 4321
Lim, A. E. K., 164
Lim, J. M., 2563
Lin, Z., 2164, 2551, 2705, 3623
Lindel, T., 2255
Lindner, E., 705
Linert, W., 2273
Linnanto, J., 4078
Lipkowski, J., 2753
Lippolis, V., 1232, 1291, 1939
Liptau, P., 3590, 4261
Lis, T., 4043
Litvinov, A. L., 3914
Liu, C.-M., 3618
Liu, D.-S., 810
Liu, F., 4234
Liu, G.-F., 2965
Liu, J., 1181
Liu, J.-T., 3201
Liu, P.-C., 2164, 3201
Liu, Q., 1227, 2872
Liu, Q.-D., 731
Liu, S.-T., 3152
Liu, W., 2393
Liu, X., 3250
Liu, Y., 644, 4010
Liu, Y.-H., 3152
Liu, Z., 62
Lledós, A., 4187
Lloret, F., 1005
Llusar, R., 1271
Lodewyckx, K., 3028
Long, G. J., 453
Longato, B., 128
Lopes, A. D., 3870
López, M. L., 2397
López-Magaña, C., 348
López-Solera, I., 3233
López-Torres, E., 2711
Loprieno, U., 918
Lorber, C., 628
Lorberth, J., 1507
Lork, E., 54, 1361, 3211
Lötzbeyer, L., 34
Lough, A. J., 224
Lu, C., 1181, 2393
Lu, C.-Z., 2867
Lu, J., 1822
Lu, S., 1181
Lu, W., 2749
Lu, Y., 2567
Łuczkowski, M., 1694
Ludwig, R., 4110
Lugan, N., 3047
Lügger, T., 1088
Lukevics, E., 3139
Luo, J., 1778, 2705, 3623
Luo, J.-L., 3618
Luo, Y., 318
Lutz, M., 830, 2798, 2924, 3968, 4073
Lutz, P., 805
Lyssenko, K. A., 2979
Lyubovskaya, R. N., 3914
Ma, B.-Q., 731
Ma, C., 1227, 2872
Ma, Y., 2054
Maas, O., 1340
Macchioni, A., 195
Mackiewicz, Z., 1694
MacLean, E. J., 120
Macpherson, B. P., 2512
Mad'arová, M., 2075
Madakyan, V. N., 1861
Madalan, A. M., 1995
Madic, C., 2834, 3943
Maestro, M., 2123
Maestro, M. A., 2639
Maguire, J. A., 3989
Maguire, M., 3305
Magull, J., 66, 437, 442, 1995, 3110, 3113, 3120
Mahía, J., 2123, 2639
Mahon, M. F., 766, 1433
Maid, H., 822, 1253
Maimon, E., 4105
Mair, F. S., 3464
Maji, T. K., 1005, 3929
Majoral, J.-P., 960
Makarov, A. Y., 77
Maksimov, A. M., 77
Malézieux, B., 499, 3055
Malisch, W., 2133
Maluenga, M., 822. 1253
Mañas, S., 348
Manassero, M., 213, 2108, 2304, 3958
Mancini, F., 1694
Maneiro, M., 3193
Mani, F., 3185
Manoury, E., 2820
Mantovani, G., 1620
Mantovani, N., 918
Mao, J.-G., 4211, 4218
Mao, Z.-W., 1562
Maqueda, O., 2458
Maraval, A., 960
Marcão, S., 2113
Marchal, R., 1366
Marchetti, F., 3221
Marciniak, W., 2753
Marcoux, P. R., 2406
Marek, J., 2075
Margiotta, N., 1136
Marhic, C., 610
Marinetti, A., 2583
Marin-Becerra, A., 2389
Marques, H. M., 2095
Martens, J. A., 1296
Martín, G., 562
Martin, J. M. L., 3803
Martín-Alvarez, J. M., 3127
Martinelli, M. G., 3409
Martínez, B., 4187
Martínez, J. L., 2397
Martínez, M., 2512
Martínez-Lope, M. J., 2839
Martínez-Sarrión, M.-L., 2458
Martynova, E. V., 29, 2041
Marvelli, L., 918
Mas-Marzá, E., 1215
Mas-Torrent, M., 720
Mascharak, P. K., 475
Massa, L., 3221
Massari, A. M., 2348
Masuda, H., 2917, 4378
Mata, I., 4187
Mata, J. A., 1215
Matějka, P., 3662
Mathey, F., 687
Mathieu, B., 737
Mathieu, R., 3047
Matsubayashi, G., 4093
Matsumoto, K., 1785, 3716, 4234
Matt, D., 805
Matyjaszewski, K., 2082
Maudez, W., 3440
Mauphin, C. L., 4065
Maurya, M. P., 1966
Mayboroda, A., 1703, 3042
Mayer, I., 1445
Mayer, P., 3432
Mazet, C., 1161
Mbomekalle, I. M., 3924
McDonald, A., 830
McIndoe, J. S., 4294
McMaster, J., 1232, 2389
Medici, S., 556
Meetsma, A., 427
Mehring, M., 4356
Melánová, K., 1577, 3662
Melchior, A., 1948
Meli, A., 1620
Mendia, A., 518
Mendiola, M. A., 2711
Meng, Q., 947, 2393
Mereiter, K., 1883
Merino, G., 3554
Merz, K., 51
Merz, M., 1711
Messerle, B. A., 293, 3179
Mestres, L., 2458
Mestroni, G., 2683
Meunier, B., 528
Mews, R., 3211
Meyer, F., 1581
Meyer-Friedrichsen, T., 313, 936
Meyerstein, D., 4105, 4227
Mézailles, N., 687, 3878
Miehé-Brendlé, J., 1366
Migliacci, F., 1620
Miguel, D., 995, 1113, 2183
Mikhalina, T. V., 77
Milanesio, M., 1186
Milani, B., 2683
Mills, A. M., 453, 671, 830, 4361
Milone, L., 3530
Milstein, D., 70
Mimmi, M. C., 3934
Min, K. S., 1373
Minghetti, G., 2304
Mironov, Y. V., 2591
Mitchell, C., 4356
Mitzel, N. W., 815
Modestov, A., 482, 2264
Mohr, F., 217
Mohsseni-Ala, J., 4313
Moïse, C., 633, 1893
Mol, J. C., 2827
Molina, R. M., 903
Molins, E., 4187
Monflier, E., 595
Montesu, D. R., 1232
Monzani, E., 1197, 3934
Morales, A. F., 3752
Moreau, J., 3007
Moreno-Mañas, M., 4187
Moro, S., 42
Morris, G. A., 2348
Mortillaro, A., 3530
Morvillo, A., 1807
Most, K., 4332
Mostafa, G., 1005
Moulin, C., 2834
Mourgues, S., 2820
Moutet, J.-C., 3767, 4262
Mucci, A., 128
Mukherjee, S., 863, 1956
Mukhopadhyay, S., 4308
Muller, G., 4065
Müller, I. M., 1873
Müller, M., 2273
Muller, R. N., 2495, 3021
Mulvey, R. E., 3271, 3347, 3354
Munk, V. P., 1206
Muranjan, S., 3547
Murata, M., 3716
Murdoch, P. del S., 1206
Musella, D., 1452
Młynarz, P., 1694
Nabavizadeh, S. M., 1911
Nadjo, L., 3924
Nagatomo, S., 4378
Nahmani, Y., 4105
Nair, B. U., 3633
Nakano, M., 4093
Nakayama, J., 3716
Nardin, G., 1197
Nassar, R., 3325
Natarajan, S., 1675, 3820, 4395
Natile, G., 1136
Nättinen, K. I., 4078
Naumov, D. Y., 2591
Navarro, D., 3905
Navarro-Ranninger, C., 1591
Neculai, A. M., 3120
Neculai, D., 433, 3120
Neiwert, W. A., 3924
Neretin, I. S., 2041
Nethaji, M., 2318
Neumann, S., 281
Ng, D. K. P., 1555
Nguyen, S. B. T. 2348
Nguyen, T. K. D., 4110
Ni, C., 2393
Ni, J., 4010
Niazov, T., 1445
Nieger, M., 2133
Nierlich, M., 1388, 2529

Niewa, R., 1632
Nijbacker, T., 638
Nikiforov, G. B., 433, 437, 3120
Nishioka, T., 4234
Nissinen, M., 4001
Nitti, L., 1939
Nogueira, H. I. S., 3609
Noltemeyer, M., 437, 442, 3113, 3120, 4332, 4338
Nöth, H., 111, 666, 2254, 3432
Novikov, Yu. N., 29, 2041
Novio, F., 3905
Nuez, A., 4289
Nunes, C. D., 3870
O'Connor, C. J., 2299
O'Hara, C. T., 3354
Ochal, Z., 2753
Oeser, T., 1099
Ogden, J. S., 1861
Okamoto, K., 1005
Okamura, T., 618, 3783
Okuda, J., 926
Olenev, A. V., 1053
Oleneva, O. S., 1053
Olmstead, M. M., 475, 3495
Ortega-Jiménez, F., 562
Oshida, H., 3716
Otero, A., 17, 493, 2438, 2626, 3233
Ouyang, L., 731
Ouyang, X.-M., 618
Owsianik, K., 960
Ozawa, T., 2917
Pagliarin, R., 3934
Paine, T. K., 3167, 4299
Pal, Sam., 4244
Pal, Sat., 4244
Pala, L., 1291
Pan, C.-L., 1514, 2578
Pan, Q.-J., 4202
Panina, N. S., 3160
Panja, A., 1540
Papachristou, M., 3826
Papadia, P., 1136
Papadopoulos, M., 3826
Papakyriakou, A., 3001
Pappalardo, G. C., 2413
Parac-Vogt, T. N., 3021, 3028
Paredes, P., 995, 2183
Park, H. W., 3242
Park, S.-M., 4117
Parkinson, J. A., 1206
Parr, J., 120
Parras, M., 2419, 2986
Parvez, M., 1857
Pasquato, L., 128
Pastor, C. J., 2711
Pati, S. K., 3820, 4395
Patra, G. K., 969
Patroniak, V., 4001
Patrono, P., 1577
Paulsson, H., 2352
Pavlík, I., 2524
Paz, F. A. A., 3609
Pécaut, J., 3767, 4262
Pedrido, R., 1128, 3193
Pelecanou, M., 3826
Peli, G., 2108
Pellegrin, Y., 1890
Peng, S.-M., 1440, 3152
Peng, Y., 726, 3110
Penoni, A., 1452
Peregudov, A. S., 29, 2041
Pérez, J., 1113
Pérez, J. M., 1591
Peris, E., 1215
Perkovic, M. W., 2812
Perotti, A., 1197
Perpiñán, M. F., 3034
Perrey, D., 633
Perrier, S., 1641
Perry, C. B., 2095
Perseghini, M., 601
Persoons, A., 3895
Peruch, F., 805
Peruzzini, M., 1614
Peters, J. A., 4179
Peters, K. P., 903
Peters, T. P. J., 1072
Petrella, A. J., 4153
Petrusenko, S. R., 1426
Pettinari, C., 3221
Pettinari, R., 3221
Peveling, K., 3563
Phelps, A. L., 3639
Philippou, A., 1175
Phillips, A. D., 3495
Philouze, C., 2452
Philp, D., 249
Pico, C., 2397
Piérart, C., 3021
Pierrard, J.-P., 3007
Pierre, J.-L., 2452, 2596, 4137
Piguet, C., 4065
Pillet, S., 4173
Pillinger, M., 3870
Pinilla, E., 2693, 3831
Pinna, M. V., 2304
Pintauer, T., 2082
Piotrowski, H., 2255
Pirmettis, I., 3826
Pitié, M., 528
Pizarro, J. L., 518
Plakatouras, I. C., 2045
Plancque, G., 2834
Platonov, V. E., 77
Poater, A., 4147
Pokorni, S. V., 1222
Polat, H., 4227
Polese, P., 1948
Poleshchuk, O. Kh., 1507
Poli, R., 482, 2264
Polo, A., 4147
Polo, E., 324
Pombo-Villar, E., 3305
Pomeranc, D., 3752
Pons, B., 2583
Pons, J., 2992, 3952
Poppitz, W., 1503
Porsch, F., 506
Port, M., 2495, 3007
Portanova, R., 1948
Pöttgen, R., 3425
Poulard, C., 633
Powell, A. K., 2283
Power, P. P., 3495
Poyatos, M., 1215
Prashar, S., 17, 2438, 2626
Predieri, G., 1659
Presa-Soto, A., 4341
Priego, J. L., 2339
Prikhod'ko, A. I., 34
Prim, D., 3895
Pritchard, R. G., 1929, 3464
Pritzkow, H., 1581, 1703, 1711, 2783, 3042
Procopio, J. R., 2711
Prosenc, M. H., 313, 936
Proust, A., 2757
Provendier, H., 2139
Pryma, O. V., 1426
Pucci, D., 3649
Puddephatt, R. J., 217
Pudova, O., 3139
Punzo, F., 2413
Pursche, D., 1669
Qian, H., 947
Qian, Y., 644, 3250, 3534, 3699
Qu, Z.-R., 2920, 3712
Quinn, F. X., 331
Quiroga, A. G., 713, 1591
Quisenberry, K. T., 3383
Rabu, P., 4173
Ragaini, F., 1452
Ragel, C. V., 1029
Raithby, P. R. 3363, 3445
Rammal, W., 2452
Ramos-Lima, F. J., 1591
Randaccio, L., 1197, 3738
Rao, C. N. R., 1675
Raptopoulou, C. P., 3826
Raston, C. L., 4153
Rat, M., 759
Rau, S., 1503
Raubenheimer, H. G., 3861
Ray, M. S., 4253
Ray Chaudhuri, N., 1005
Raynal, I., 2495
Real, J., 4147
Reddy, N. D., 442
Reddy, P. A. N., 2318
Redshaw, C., 2071
Reedijk, J., 47, 671, 713, 1394, 1529, 1669, 2273, 2924, 4073, 4347
Reger, D. L., 3480
Regiec, A., 4043
Réglier, M., 1735
Rehder, D., 1966
Reihs, S., 822, 1253
Reiland, V., 1340
Reina, E., 2348
Reinen, D., 1445
Reinöhl, U., 2082
Reinholdt, M., 1366
Reiß, G. J., 2059, 3945
Rell, S., 51
Remelli, M., 1694
Ren, X., 2393
Renaud, J.-L., 4055
Rentschler, E., 541, 3167
Ressler, T., 301, 1058
Reynes, O., 3767, 4262
Rheingold, A. L., 2767
Rheinwald, G., 1703, 2059
Ribas, J., 1005, 3929
Ricard, L., 687, 2583, 3878
Ricciutelli, M., 3221
Richard, D. P. P., 1893
Richard-Plouet, M., 1445
Richardson, C., 405
Richardson, D. R., 1145
Riehl, J. P., 4065
Riera, L., 1113, 3279
Riera, V., 1113, 4159
Righi, L., 4253
Rimbault, J., 3007
Rissanen, K., 4001, 4078
Rittmeister, B., 751
Rivals, F., 3309
Rivière, E., 2880
Robalo, M. P., 3895
Roberts, N. K., 4153
Robillard, M. S., 1529
Rocha, J., 1175, 3870
Rodrigues, L., 2113
Rodríguez, A., 493
Rodríguez, A. M., 2438, 2626
Roesky, H. W., 66, 332, 437, 442, 2145, 3110, 3113, 3120, 4332, 4338
Rojas, S., 3233
Rojo, T., 518, 2123, 2639, 2948, 3703
Romaniello, P., 1939
Romaniewska, A., 4043
Romero, F. M., 4289
Romero, J., 678
Romerosa, A., 348, 1614
Rominger, F., 1099
Rong, J., 3110
Ros, J., 2992, 3952
Rösch, N., 3144
Rosche, F., 164
Röschenthaler, G.-V., 54, 1169
Rose, E., 1893, 3895
Rose-Munch, F., 1893, 3895
Roßenbach, S., 1748
Rossi, M., 3221
Rossi, P., 2413
Rotondo, A., 2612
Rotondo, E., 2612
Roubeau, O., 2924
Rovira, C., 720
Rowlings, R. B., 3347, 3354
Royal, G., 3767, 4262
Royer, S., 3895
Royo, P., 2463
Rueff, J.-M., 4173
Ruhlandt-Senge, K., 3472
Ruiz, E., 1756
Ruiz, M. J., 493
Ruiz-González, L., 2986
Ruiz-Hitzky, E., 1242
Ruiz-Pérez, C., 2290
Ruman, T., 89, 2475
Rusonik, I., 4227
Russo, U., 2790
Rutsch, P., 1681, 2219
Rybak-Akimova, E. V., 1581
Sá Ferreira, R. A., 3609
Saalfrank, R. W., 822, 1253
Sadler, P. J., 1206
Saeki, N., 1785
Saint-Aman, E., 2452, 3767, 4262
Saito, Y., 2917
Salassa, L., 2108
Salem, M., 4055
Salinas, A. J., 1029
Salom-Roig, X. J., 3752
Sanaú, M., 1215
Sánchez, A., 2790
Sánchez, A. E., 3034
Sanchez, C., 331
Sánchez, V., 4289
Sanmartín, J., 1128, 3703, 3905
Sansoni, M., 213, 2108
Santagostini, L., 1197, 3934
Santini, C. C., 2139
Santos, A. M., 449
Santos, M. A., 4025
Santrich-Badal, A., 2397
Saoud, M., 348, 1614
Sargeson, A. M., 1340
Sarkar, B., 876
Sartorel, A., 699
Sato, T., 4347
Saurenz, D., 482
Sauvage, J.-P., 467, 3752
Sawicka, A., 3790
Schaefer, M., 506
Schäfer, B., 1503
Schapp, J., 3745
Schatte, G., 1857, 3314
Schebesta, S., 1503
Scheer, M., 1518
Scheibitz, M., 2049
Schenetti, L., 128
Schenk, H., 2273
Schiebel, H., 1815
Schildbach, D., 3453
Schindler, S., 1197
Schlebos, P. P. J., 1072
Schlecht, S., 1411

 © 2003 Wiley-VCH Verlag GmbH & Co. KGaA, Weinheim

INDEX

Schlichte, K., 1193
Schlicker, C., 3120
Schlosser, D., 2245
Schlosser, F., 3144
Schmid, A., 2255
Schmid, G., 1121, 3080
Schmid, R., 1883
Schmidt, H.-G., 437, 442, 3113, 4332, 4338
Schmiedeskamp, B., 2133
Schmitt, G., 514
Schmitt, O., 3105
Schneider, J., 1727
Schneiderbauer, S., 3432
Schnöckel, H., 4387
Schoeller, W. W., 2133
Schollmeyer, D., 815
Scholz, S., 666
Schönherr, T., 2059
Schreiber, J., 610
Schreuder Goedheijt, M., 638
Schröder, K., 427
Schröder, M., 1232, 2389
Schumacher, D., 2133
Schumann, H., 3336
Schürmann, M., 164, 3563, 4356
Schwartz, A., 1641
Schweiger, A., 1340
Schwitzgebel, G., 1340
Sciarone, T. J. J., 1072
Scopelliti, R., 3527
Seebacher, J., 2502
Seela, F., 1641
Seibel, T., 3453
Sekar, P., 1518
Sekiya, H., 1785
Selinka, C., 1416, 3376
Sellmann, D., 418, 903
Semeniuc, R. F., 3480
Sengupta, P., 363
Sengupta, S., 1157
Seniori Costantini, S., 3185
Senocq, F., 2880
Serli, B., 3160
Serp, P., 610
Serra, D., 2820
Serratrice, G., 2596, 3767, 4262
Shaikh, N., 1540
Shailendra, 1966
Shakhnin, D., 1169
Shakirov, M. M., 77
Shandalov, E., 4105
Sheldrick, W. S., 363, 1873, 2591
Shen, Q., 318
Sheng, T., 3731
Shevchenko, I., 54, 1169
Shevelkov, A. V., 1053
Shi, Q., 1778
Shimazaki, K., 1785
Shimon, L. J. W., 70
Shin, D. M., 2311
Shipman, M. A., 1206
Shishkin, O. V., 1426
Shu, M., 2502
Shul'pin, G. B., 908
Shutov, P. L., 1507
Si, R., 4099
Sian, S., 370
Siatra-Papastaikoudi, T., 3826
Siaugue, J.-M., 2834
Siebert, W., 2783
Siegrist, T., 1483
Sienra, B., 2512
Sigel, H., 2937
Silaghi-Dumitrescu, R., 1048
Sillanpää, R., 1511
Silver, J., 678
Silvestru, C., 1361
Simon, U., 1121
Simoni, E., 3843
Simonot, C., 2495
Singh, J., 744
Siren, K., 2633
Siripaisarnpipat, S., 263
Sitzmann, H., 3105
Siu, P. K. M., 2749
Sivák, M., 2075
Sjövall, S., 377
Skatova, A. A., 3336
Skelton, B. W., 1426
Skurski, P., 3790
Slagt, M. Q., 830
Slawin, A. M. Z., 249, 1291, 1461, 2426
Slovokhotov, Yu. L., 2041
Smaihi, M., 4370
Smička, A., 143
Smith, J. D., 3332
Smith, M. D., 3480, 4017
Smits, J. M. M., 648, 656, 1072
Smucker, B. W., 988
Snaith, R., 3363
Soares-Santos, P. C. R., 3609
Sobczyk, M., 3790
Soderholm, L., 2663, 2929
Sodupe, M., 4187
Soibinet, M., 1984
Solà, M., 4147
Solans, X., 1591, 2992, 3929, 3952
Soleilhavoup, M., 207
Söltl, Y., 3432
Sommazzi, A., 1620
Song, D., 3774
Song, J.-L., 4218
Song, L.-C., 2164, 3201
Song, Y., 2325, 2924, 4073
Sorace, L., 1128
Sordo, J., 2790
Sosa-Torres, M. E., 978
Souhassou, M., 4173
Soulard, M., 1366
Sousa, A., 678
Sousa-Pedrares, A., 678
Spaniol, T. P., 926
Speier, G., 1735
Spek, A. L., 453, 671, 830, 1394, 2798, 2924, 3968, 4073, 4361
Splan, K. E., 2348
Sprengers, J. W., 3811
Stabon, E., 2683
Stalke, D., 1416, 3376
Stam, M., 2798
Stanciu, C., 3495
Standfest-Hauser, C. M., 1883
Stanghellini, P. L., 1186
Stassen, A. F., 671, 1669, 2273, 4073
Steel, P. J., 405
Steiner, A., 3309
Stelzer, O., 1748
Stender, M., 3495
Stenson, P. A., 2389
Steudel, R., 2149, 3798
Steudel, Y., 2149, 3798
Štíbr, B., 1533, 2524
Stoccoro, S., 2304
Stodt, R., 1873
Stohrer, W.-D., 3211
Stonehouse, J. M., 120
Stoppioni, P., 3185
Strassner, T., 1802
Streubel, R., 1815
Ströbele, M., 705
Strohmann, C., 3453
Strumolo, D., 213
Su, F.-H., 3201
Suades, J., 3047
Suárez, M., 4159
Sugimoto, H., 2633
Sugimoto, T., 2333
Suh, M. P., 1373. 3242
Sun, D., 38, 94, 1303
Sun, L., 2872
Sun, S.-S., 2348
Sun, W.-Y., 618, 3783
Sun, X., 1555
Sun, Y., 38, 94, 1303
Sun, Y. Q., 4218
Sun, Y.-Q., 4211
Sundermeier, M., 3513
Sünkel, K., 3745
Süss-Fink, G., 1043, 3099, 3707
Sustmann, R., 1401
Sutter, J., 418
Suwinska, K., 3034
Tacke, M., 458, 1416
Tamm, M., 1088
Tamura, H., 4093
Tanaka, K., 2633
Tang, K., 3250
Tang, W.-X., 618
Tanski, J., 3221
Tao, J., 2678
Taraszewska, J., 1741
Tatiersky, J., 2075
Tauzher, G., 3738
Teat, S. J., 766, 1433
Tebben, L., 3590, 4261
Tei, L., 1232
Teichert, M., 822, 1253
Teixidor, F., 1511
Tellenbach, A., 3759
Telo, J. P., 4025
Teplova, I. A., 2519
Teplytska, T. S., 1426
ter Beek, S. I., 1072
Terreno, E., 3530
Terreros, P., 493, 3233
Terzis, A., 3826
Teuben, J. H., 427
Therrien, B., 1043, 3099, 3707
Theunissen, E., 1296
Thomas, F., 2596
Thompson, D. M., 175
Thornton-Pett, M., 4153
Thouvenot, R., 2757
Thuéry, P., 2913
Thummel, R. P., 2774, 3547
Tilloy, S., 595
Tinant, B., 737, 3028
Tiripicchio, A., 1659
Titler, P. J., 678
Togni, A., 601, 4166
Tok, O. L., 2524
Tolazzi, M., 1948
Tolhurst, V.-A., 293
Tollari, S., 1452
Tomas, A., 759
Tomic, Z. D., 1222
Tommasi, R., 1939
Tong, M.-L., 138, 2385
Tong, Y.-X., 2385
Tonucci, L., 1807
Torelli, S., 2452
Torma, V., 1121
Torres, M. R., 2339, 2693, 3831
Tóth, G. K., 2113
Toupet, L., 4055
Tranchier, J. P., 1893, 3895
Trani, M., 2683
Traverso, O., 324
Trchová, M., 3662
Trehan, V., 744
Trifonov, A. T., 926
Trindade, T., 3609
Trofimenko, S., 2767
Tsoukalas, C., 3826
Tsukube, H., 2633
Tuchagues, J.-P., 759
Turner, P., 293, 3179
Turner, S. S., 62, 720
Tyler, L. A., 475
Ueda, K., 2333
Ueyama, N., 618, 3783
Ugalde-Saldivar, V. M., 978
Uhlig, S., 4313
Urbanos, F. A., 2339
Uriel, S., 1271
Usatov, A. V., 29, 2041
Vacca, A., 3185
Vahrenkamp, H., 1719, 2502, 3723, 2731
Vaidhyanathan, R., 1675
Vaidyanathan, V. G., 3633
Vaissermann, J., 2406, 2757, 3895
Valensin, D., 1694
Valensin, G., 1694
Valente, A., 1175
Valente, A. A., 3870
Valente, E. J., 2095
Vallet-Regí, M., 1029, 1608
Vallribera, A., 4187
Valls, E., 3047
Valtancoli, B., 1974
Valtchev, V., 4370
Van Alsenoy, C., 77
van Boom, J. H., 1529
van den Broeke, J., 2798
van der Marel, G. A., 1529
van der Vlugt, J. I., 4361
Van Deun, R., 3028
van Eldik, R., 268, 1562, 2972, 3738
Van Hecke, K., 3028
van Klink, G. P. M., 830
van Koningsbruggen, P. J., 356
van Koten, G., 830, 1703, 2798
van Meerendonk, W. J., 427
Van Meervelt, L., 3028
van Slageren, J., 1917
Vander Elst, L., 2495
Vanderah, T. A., 1483
Varela, J. M., 2790
Vargas, W., 3472
Varghese, B., 744
Vázquez, M., 1128, 3193
Veciana, J., 720
Veiga, M. L., 2397
Veith, M., 4387
Vela, A., 3554
Velders, A. H., 713
Vennat, M., 908
Verani, G., 1939
Verhagen, J. A. W., 3968
Vértes, A., 1735
Viau, L., 207
Vicente, R., 3929
Vidal-Gancedo, J., 720
Vidoni, O., 1121
Vidovic, D., 66, 433, 443, 3110, 3113, 4332
Vieille-Petit, L., 3707
Viertelhaus, M., 2283
Vigier, E., 514, 633
Vilaplana, R. A., 2937
Villafañe, F., 995, 2183, 3127
Viñas, C., 1511
Vincendeau, S., 2820
Viterbo, D., 1186

Vittal, J. J., 277
Vivas-Reyes, R., 1315, 3803
Vogel, U., 1518
Vogt, D., 4361
von Hänisch, C., 2955
Voronkova, V., 1995
Vorontsov, I. I., 1053
Vorotyntsev, M. A., 482
Vos, J. G., 1503
Wada, A., 4378
Wade, K., 3271
Wagner, M., 2049
Walther, D., 1503, 4321
Walz, R., 2502
Wan, S.-Y., 3783
Wang, E., 370
Wang, E.-B., 2567
Wang, G.-F., 3201
Wang, N.-L., 3618
Wang, R., 1778, 2705, 3623
Wang, S., 3774
Wang, T.-G., 1514. 2578
Wang, X.-S., 2920, 3712
Wang, Y., 3572
Wang, Y.-B., 1355, 2164
Wanke, R., 1452
Warchhold, M., 111
Warner, S., 1635
Warren, J. E., 1929, 3464
Weber, L., 1843
Weibert, B., 339
Weinberger, P., 2273
Weisser, U., 705
Wen, G., 149
Weng, J., 1778
Weng, L., 318
Weng, L.-H., 810
Werckmann, J., 1445
Werz, D. B., 1099
Westerhausen, M., 3432
Weston, J., 4321
Weyhermüller, T., 541, 863, 1768, 1956, 3167, 4299
Wheatley, A. E. H., 3291, 3363,
White, A. J. P., 3409
Wibbeling, B., 3590, 4261
Wiberg, N., 666
Wieghardt, K., 863, 1768
Wienold, J., 301, 1058
Wiesinger, G., 2273
Wild, K., 3453
Willem, R., 1315, 3803
Willemin, S., 1866
Willet, R. D., 4253
Williams, C. W., 2663
Williams, D. J., 3409
Wilson, C., 2389
Winter, R. F., 876
Wismach, C., 1815
Wolf, Y., 4387
Wolff, F., 628
Wolmershäuser, G., 3105
Wołowiec, S., 2475
Wołwiec, S., 89
Wong, H., 936
Wong, K. M.-C., 4035
Wong, W. K., 3539
Wong, W.-T., 149, 2651
Wong, W.-Y., 3539
Woods, R. J., 3464
Woollins, J. D., 249, 1291, 1461, 2426
Woźniak, K., 1741
Wrackmeyer, B., 2524
Wright, D. S., 3279
Wu, B., 2502
Wu, C.-D., 2867
Wu, F., 2774
Wu, H.-R., 3152
Wu, H.-S., 2959
Wu, X.-T., 1798, 2670
Wu, Y.-M., 2385
Wu, Z., 3425
Wurst, K., 720
Xia, S.-Q., 1798
Xie, F.-T., 2578
Xie, J., 2393
Xie, Y., 1822, 4010
Xie, Y.-R., 2572, 3712
Xin, X.-Q., 726
Xing, L.-X., 2920
Xiong, R.-G., 2572, 2920, 3712
Xiong, Y., 3417
Xu, J.-Q., 1514, 2578
Xu, L., 2567
Xu, X., 2054
Xu, Y., 3623
Xue, X., 3712
Xue, Z., 2572, 3712
Yahia, M., 2486
Yam, V. W.-W., 4035
Yamaguchi, S., 4378
Yan, C.-H., 4099
Yan, S., 62
Yan, Y., 3534
Yan, Z.-G., 4099
Yang, B., 3534, 3699
Yang, B.-P., 4211
Yang, L.-F., 2678
Yang, W., 1181
Yang, X., 3534, 3699
Yang, Y., 4035
Yao, S., 3417
Yao, Y., 318, 2393
Yarbrough, J. C., 3639
Ye, B.-H., 2965
Ye, Q., 2572
Yeo, J. S. L., 277
Yin, P., 726
Yin, X., 2678
You, L.-P., 4099
You, X.-Z., 2572, 2920, 3712
Young, Jr., V. G., 3383
Yu, K., 318
Yu, K.-B., 731
Yu, Z., 2920
Yuan, D., 3623
Yudanova, E. I., 3914
Zablocka, M., 960
Zachwieja, U., 164
Zaitseva, G. S., 1507
Záliš, S., 1917
Zamora, F., 562
Zanello, P., 1291, 3201
Zangrando, E., 2371, 2683, 3160, 3929
Zanobini, F., 1620
Zapf, A., 3513
Zarić, S. D., 1222, 2197
Zeller, A., 1802
Zeng, J., 644
Zenneck, U., 281
Zhang, D., 1570
Zhang, D.-Q., 3618
Zhang, H., 1169
Zhang, H.-H., 2867
Zhang, H.-X., 4202
Zhang, J., 2572
Zhang, J.-J., 1798, 2670
Zhang, L., 3924
Zhang, L. D., 1794
Zhang, L.-Y., 2965
Zhang, Q., 1181, 2426
Zhang, S., 644
Zhang, W., 1966, 2393
Zhang, X., 313, 1181
Zhang, X.-M., 138, 149, 413, 731, 2959, 2965
Zhang, Y., 656
Zhang, Y.-W., 4099
Zhao, H., 2920, 3712
Zhao, H.-H., 4211
Zhao, X., 4017
Zhao, Y., 38, 94, 1822
Zheng, L.-M., 726
Zheng, L.-S., 2678
Zheng, S.-L., 2965
Zheng, X., 2175, 3572
Zheng, X.-J., 1355
Zhong, Z., 3432
Zhou, S. M., 1794
Zhu, D.-B., 3618
Zhu, H., 3113, 4332
Zhu, L., 2325
Zhu, N., 2749
Zhu, Y., 2325
Zhuang, H., 1181
Zhuang, W., 3572
Zhuang, W.-J., 1355
Zibarev, A. V., 77
Zięba, K., 1741
Ziessel, R., 955
Zilbermann, I., 4105
Zima, V., 1577, 3662
Zimmer, A., 1340
Zimmer, M., 4387
Zobel, D., 1222
Zong, R., 705
Zou, X., 2095
Zou, Y., 268
Zsolnai, L., 2219
Zucca, A., 556, 2304
Zuo, J.-L., 255, 449

 © 2003 Wiley-VCH Verlag GmbH & Co. KGaA, Weinheim

Microreview Index

A. Antiñolo, M. Fajardo, A. Otero, S. Prashar
Sandwich and Half-Sandwich (Imido)niobium Complexes
Eur. J. Inorg. Chem. **2003**, 17−28

A. Macchioni
Elucidation of the Solution Structures of Transition Metal Complex Ion Pairs by NOE NMR Experiments
Eur. J. Inorg. Chem. **2003**, 195−205

H. Braunschweig,* M. Colling
The Chemistry of Borylene Complexes
Eur. J. Inorg. Chem. **2003**, 393−403

W.-H. Leung
Synthesis and Reactivity of Organoimido Complexes of Chromium
Eur. J. Inorg. Chem. **2003**, 583−593

R. Kempe
The Strained η^2-$N_{Amido}-N_{Pyridine}$ Coordination of Aminopyridinato Ligands
Eur. J. Inorg. Chem. **2003**, 791−803

M. Vallet-Regí,* C. V. Ragel, A. J. Salinas
Glasses with Medical Applications
Eur. J. Inorg. Chem. **2003**, 1029−1042

R. Llusar,* S. Uriel
Heterodimetallic Chalcogen-Bridged Cubane-Type Clusters of Molybdenum and Tungsten Containing First-Row Transition Metals
Eur. J. Inorg. Chem. **2003**, 1271−1290

T. Siegrist,* T. A. Vanderah
Combining Magnets and Dielectrics: Crystal Chemistry in the $BaO-Fe_2O_3-TiO_2$ System
Eur. J. Inorg. Chem. **2003**, 1483−1501

C. Graiff, G. Predieri, A. Tiripicchio*
Phosphane-Substituted Selenido−(carbonyl)iron and −(carbonyl)ruthenium Clusters: Structures, Fluxionality and Reactivity
Eur. J. Inorg. Chem. **2003**, 1659−1668

L. Weber
The Quest for Isophosphaalkynes (Isophosphocyanides) C≡P−R — Still an Elusive Class of Compounds
Eur. J. Inorg. Chem. **2003**, 1843−1856

A. Jutand
The Use of Conductivity Measurements for the Characterization of Cationic Palladium(II) Complexes and for the Determination of Kinetic and Thermodynamic Data in Palladium-Catalyzed Reactions
Eur. J. Inorg. Chem. **2003**, 2017−2040

S. D. Zarić
Metal Ligand Aromatic Cation−π Interactions
Eur. J. Inorg. Chem. **2003**, 2197−2209

E. Iengo, E. Zangrando, E. Alessio*
Discrete Supramolecular Assemblies of Porphyrins Mediated by Coordination Compounds
Eur. J. Inorg. Chem. **2003**, 2371−2384

G. Jia,* Z. Lin, C. P. Lau
Reactions of Dihydrogen(norbornadiene) Complexes
Eur. J. Inorg. Chem. **2003**, 2551−2562

L. Dahlenburg
P-Modular Homochiral Bis(phosphanes) with 1,2-Disubstituted Cyclopentane Backbones in Asymmetric Hydrogenation
Eur. J. Inorg. Chem. **2003**, 2733−2747

S. B. Duckett,* D. Blazina
The Study of Inorganic Systems by NMR Spectroscopy in Conjunction with Parahydrogen-Induced Polarisation
Eur. J. Inorg. Chem. **2003**, 2901−2912

 © 2003 Wiley-VCH Verlag GmbH & Co. KGaA, Weinheim

MICROREVIEW

M. Bardají, A. Laguna*
Heteronuclear Metal−Metal Contacts between Gold(I) and Group-11, -12, and -13 Centers
Eur. J. Inorg. Chem. **2003**, 3069−3079

G. Schmid,* B. Corain
Nanoparticulated Gold: Syntheses, Structures, Electronics, and Reactivities
Eur. J. Inorg. Chem. **2003**, 3080−3098

E. L. Doyle, L. Riera, D. S. Wright*
Toroidal Main Group Macrocycles: New Opportunities for Cation and Anion Coordination
Eur. J. Inorg. Chem. **2003**, 3279−3289

A. E. H. Wheatley
The Directed Lithiation of Benzenoid Aromatic Systems
Eur. J. Inorg. Chem. **2003**, 3291−3303

M. Sundermeier, A. Zapf, M. Beller*
Palladium-Catalyzed Cyanation of Aryl Halides: Recent Developments and Perspectives
Eur. J. Inorg. Chem. **2003**, 3513−3526

M. Gómez
(Alkyl)(monocyclopentadienyl)niobium and -tantalum Complexes in Insertion Processes
Eur. J. Inorg. Chem. **2003**, 3681−3697

C. Den Auwer,* E. Simoni, S. Conradson, C. Madic
Investigating Actinyl Oxo Cations by X-ray Absorption Spectroscopy
Eur. J. Inorg. Chem. **2003**, 3843−3859

N. S. Hosmane,* J. A. Maguire
Recent Advances in the Chemistry of Metallacarboranes
Eur. J. Inorg. Chem. **2003**, 3989−3999

C. Belle,* J.-L. Pierre*
Asymmetry in Bridged Binuclear Metalloenzymes: Lessons for the Chemist
Eur. J. Inorg. Chem. **2003**, 4137−4146

W. Beck
The First Chemical Achievements and Publications by Justus von Liebig (1803−1873) on Metal Fulminates and Some Further Developments in Metal Fulminates and Related Areas of Chemistry
Eur. J. Inorg. Chem. **2003**, 4275−4288

 © 2003 Wiley-VCH Verlag GmbH & Co. KGaA, Weinheim